Available online at www.sciencedirect.com
ScienceDirect
Polyhedron 27 (2008) 2007–2014
POLYHEDRON
www.elsevier.com/locate/poly

Synthesis, crystal structure and some properties of new perrhenate and pertechnetate complexes of Nd^{3+} and Am^{3+} with 2,6-bis(tetramethylfurano)-1,2,4-triazin-3-yl)-pyridine, tris(2-pyridylmethyl)amine and *N*,*N*′-tetraethylmalonamide

A.M. Fedosseev [a,*], M.S. Grigoriev [a], I.A. Charushnikova [a], N.A. Budantseva [a], Z.A. Starikova [b], Ph. Moisy [c,*]

[a] *Frumkin Institute of Physical Chemistry and Electrochemistry, Russian Academy of Sciences, Leninskii pr. 31, Moscow 119991, Russia*
[b] *Nesmeyanov Institute of Organoelement Compounds, Russian Academy of Sciences, ul. Vavilova, 28, Moscow 119991, Russia*
[c] *Commissariat à l'Énergie Atomique (CEA), Valrhô, DEN/DRCP/SCPS, BP 17171, 30207 Bagnols sur Cèze, France*

Received 21 August 2007; accepted 9 December 2007

Abstract

The coordination complexes of trivalent f-element pertechnetates and perrhenates with some N-donor ligands were determined by using X-ray structural analysis: Nd^{3+} perrhenate with 2,6-bis(tetramethylfurano)-1,2,4-triazin-3-yl)-pyridine ($[Nd(FBTP)_3ReO_4](ReO_4)_2 \cdot 2H_2O$ (**I**)), tris(2-pyridylmethyl)amine ($[Nd(TPA)(ReO_4)_3]$ (**II**)) and *N*,*N*′-tetraethylmalonamide ($[Nd(TEMA)_4](ReO_4)_3$ (**III**)). The coordination number of Nd is 10 in **I**, 9 in **II** and 8 in **III**. The complexes of Nd^{3+} pertechnetate and Am^{3+} pertechnetate with TPA have been also synthesized ($Nd(TPA)(TcO_4)_3$ (**IV**) and $Am(TPA)(TcO_4)_3$ (**V**)). The structure **II** does not change on replacement of perrhenate by pertechnetate and neodymium by americium.
© 2008 Elsevier Ltd. All rights reserved.

Keywords: Trivalent f-element; Pertechnetates; Perrhenates; Coordination complexes; N-donor ligands

1. Introduction

Interactions between the pertechnetate anion and actinide cations can occur in the course of nuclear fuel processing and nuclear waste treatment and can interfere with some stages of nuclear fuel processing. Structural characterization of actinide compounds with the pertechnetate anion could clarify to some extent the role of such interactions in technology. Complexes of uranyl [1,2], neptunyl [3] and thorium [1] with pertechnetate have been prepared and structurally characterized. Complexes of uranyl [2,4], neptunium(V) [5] and uranium(IV) [6] with the perrhenate anion, an excellent analogue of the pertechnetate anion, have also been investigated. In these complexes, both the pertechnetate and the perrhenate anions directly coordinate to the actinide metal center, demonstrating the high affinity of these tetraoxoanions toward ions of actinides with different oxidation states.

We have investigated coordination complexes of trivalent f-element pertechnetates and perrhenates with some N-donor ligands which are considered as promising agents for new separation processes such as SANEX and related projects. Such complexes could be useful as precursors for ceramic–metallic (cermet) composite preparations. Regarding targets for minor actinide incineration, cermet composites have been identified [7,8] as the materials with the best thermal conductivity that can help to reduce the operating temperature.

* Corresponding authors.
E-mail addresses: fedosseev@ipc.rssi.ru (A.M. Fedosseev), philippe.moisy@cea.fr (Ph. Moisy).

0277-5387/$ - see front matter © 2008 Elsevier Ltd. All rights reserved.
doi:10.1016/j.poly.2007.12.029

Table 1
Crystal data and structure determination details for $[Nd(FBTP)_3ReO_4](ReO_4)_2 \cdot 4H_2O$ (**I**), $[Nd(TPA)(ReO_4)_3]$ (**II**) and $[Nd(TEMA)_4](ReO_4)_3$ (**III**)

	I	II	III
Empirical formula	$C_{69}H_{89}N_{21}NdO_{22}Re_3$	$C_{18}H_{18}N_4NdO_{12}Re_3$	$C_{44}H_{88}N_8NdO_{20}Re_3$
Fw (g mol^{-1})	2277.53	1185.20	1752.06
T (K)	298(2)	298(2)	120(2)
Space group	$P2_1/n$	$Pna2_1$	$P2_1/n$
a (Å)	23.7329(5)	10.7227(2)	25.584(2)
b (Å)	14.1893(2)	21.1177(4)	13.3184(12)
c (Å)	27.7959(5)	11.8048(1)	37.340(3)
α (°)	90	90	90
β (°)	109.9608(10)	90	91.697(2)
γ (°)	90	90	90
V (Å^3)	8798.0(3)	2673.06(7)	12718(2)
Z	4	4	8
ρ_{calc} (g cm^{-1})	1.712	2.945	1.830
μ (mm^{-1})	4.773	15.516	6.565
θ_{max} (°)	25	27.5	30
Reflections collected	91053	29929	113629
Independent reflections	15512	5933	34368
Observed reflections [$I > 2\sigma(I)$]	8613	5153	14206
R_{int}	0.1067	0.0623	0.1584
T_{min}, T_{max}	0.6396, 0.6731	0.1914, 0.3303	0.2072, 0.6217
Number of parameters/ restraints	1045/0	343/1	1380/30
R_1, wR_2 [$I > 2\sigma(I)$][a]	0.0468, 0.0908	0.0329, 0.0672	0.0731, 0.1234
R_1, wR_2 (all data)	0.1238, 0.1141	0.0443, 0.0718	0.1400, 0.1754
GOOF	1.007	1.030	0.938
$\Delta\rho_{max}$, $\Delta\rho_{min}$ (e Å^{-3})	0.953, −1.268	1.205, −1.838	8.178, −4.147

[a] $R_1 = \sum||F_o| - |F_c||/\sum|F_o|$; $wR_2 = \{\sum[w(F_o^2 - F_c^2)^2]/[\sum F_o^4]\}^{1/2}$.

2. Experimental

2.1. Synthesis of Nd^{3+} and Am^{3+} perrhenate and pertechnetate complexes with N-bearing neutral ligands

Nd^{3+} perrhenate complexes with 2,6-bis(tetramethylfurano)-1,2,4-triazin-3-yl)-pyridine (FBTP), tris(2-pyridylmethyl)amine (TPA) and *N*,*N*′-tetraethylmalonamide (TEMA) were synthesized and their structures were determined by X-ray structural analysis. The compositions of the new complexes were $[Nd(FBTP)_3ReO_4](ReO_4)_2 \cdot 2H_2O$ (**I**), $[Nd(TPA)(ReO_4)_3]$ (**II**) and $[Nd(TEMA)_4](ReO_4)_3$ (**III**). Nd^{3+} pertechnetate and americium pertechnetate complexes with TPA were also synthesized ($Nd(TPA)(TcO_4)_3$ (**IV**) and $Am(TPA)(TcO_4)_3$ (**V**)). All compounds were formed during the isothermal evaporation ($T \sim 20$ °C) of solutions, prepared in the following manner: freshly prepared $Nd(OH)_3$ or $Am(OH)_3$ was dissolved in a calculated amount of 0.01 M $HReO_4$ or $HTcO_4$ in H_2O and this solution was evaporated to dryness at $T \leqslant 100$ °C. The residue was dissolved in a minimal quantity of ethanol and a solution of the ligand in ethanol was added to obtain a 1:3 Nd:ligand molar ratio.

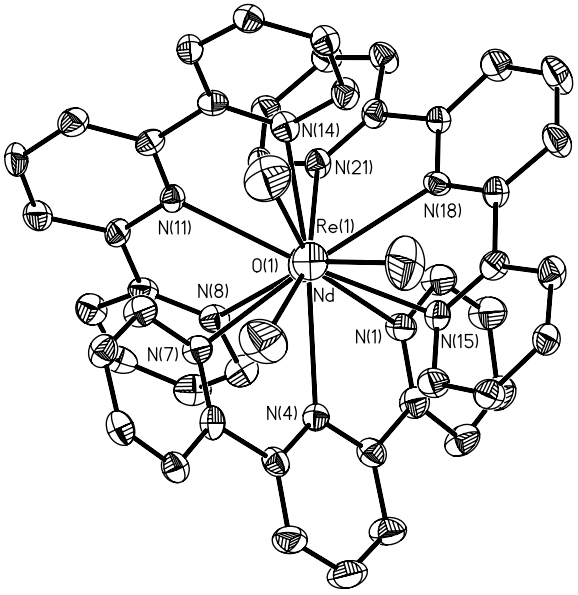

Fig. 2. Complex cation $[Nd(FBTP)_3ReO_4]^{2+}$ in **I**. Outer rings, CH_3 groups and H atoms of the central rings of the FBTP ligands are omitted.

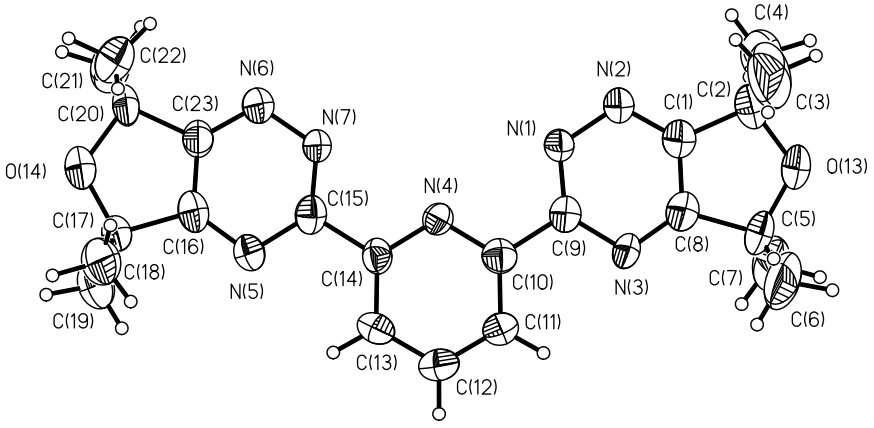

Fig. 1. A view of one of the three FBTP ligands in **I**, showing the atom labelling scheme. Displacement ellipsoids are drawn at the 30% probability level and H atoms are represented by circles of arbitrary size.

Table 2
Selected bond lengths (Å) in **I**, **II** and **III**

I		**II**		**III**	
Nd–O(1)	2.464(5)	Nd–O(11)	2.496(7)	Nd(1)–O(1)	2.400(7)
Nd–N(1)	2.622(6)	Nd–O(21)	2.501(7)	Nd(1)–O(2)	2.408(6)
Nd–N(4)	2.608(6)	Nd–O(31)	2.399(7)	Nd(1)–O(3)	2.453(6)
Nd–N(7)	2.660(6)	Nd–O(12[a])	2.458(7)	Nd(1)–O(4)	2.438(6)
Nd–N(8)	2.655(6)	Nd–O(22[b])	2.463(7)	Nd(1)–O(5)	2.427(7)
Nd–N(11)	2.621(5)	Nd–N(1)	2.671(8)	Nd(1)–O(6)	2.399(7)
Nd–N(14)	2.655(6)	Nd–N(2)	2.700(9)	Nd(1)–O(7)	2.429(6)
Nd–N(15)	2.682(6)	Nd–N(3)	2.646(8)	Nd(1)–O(8)	2.434(6)
Nd–N(18)	2.635(6)	Nd–N(4)	2.686(8)		
Nd–N(21)	2.609(5)			Nd(2)–O(9)	2.401(6)
				Nd(2)–O(10)	2.403(6)
				Nd(2)–O(11)	2.446(6)
				Nd(2)–O(12)	2.441(6)
				Nd(2)–O(13)	2.399(6)
				Nd(2)–O(14)	2.432(5)
				Nd(2)–O(15)	2.430(5)
				Nd(2)–O(16)	2.396(6)

Symmetry codes: (a) $1-x$, $1-y$, $1/2+z$; (b) $1-x$, $1-y$, $1/2+z$.

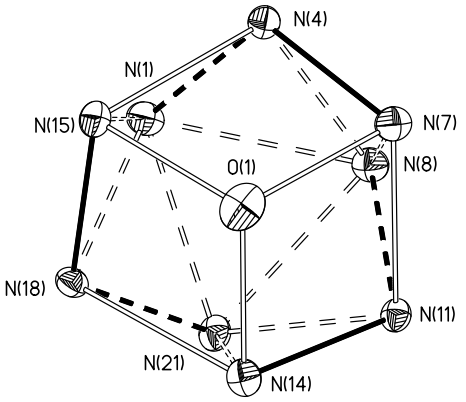

Fig. 3. Coordination polyhedron of the Nd atom in **I**. The edges connecting the N atoms of the same ligand are shown with solid lines.

2.2. X-ray analysis

Data for $[Nd(FBTP)_3ReO_4](ReO_4)_2 \cdot 4H_2O$ (**I**) and $[Nd(TPA)(ReO_4)_3]$ (**II**) were collected on a Nonius Kappa CCD area detector diffractometer (Mo $K\alpha$ radiation, graphite monochromator). The lattice parameters were determined from 10 images recorded with 1° ϕ-scans and later refined on all data. A hemisphere of the reciprocal space was measured. The crystal-to-detector distance was fixed at 30 mm. The data were processed with the HKL package [9]. Absorption effects were empirically corrected with the MULABS routine in PLATON [10]. The structures were solved by the heavy-atom method with SHELXS97 [11] and subsequent difference Fourier-syntheses and refined by full-matrix least-squares on F^2 with SHELXL97 [11]. All non-hydrogen atoms were refined anisotropically. The hydrogen atoms of organic ligands were placed in idealized calculated positions and refined as riding atoms with displacement parameters equal to 1.2 (CH and CH_2) or 1.5 (CH_3) times that of the attached carbon atom. The hydrogen atoms of crystallization water molecules in **I** were not located. The value of the Flack parameter [12] for **II** was −0.014(9) showing the correctness of the determination

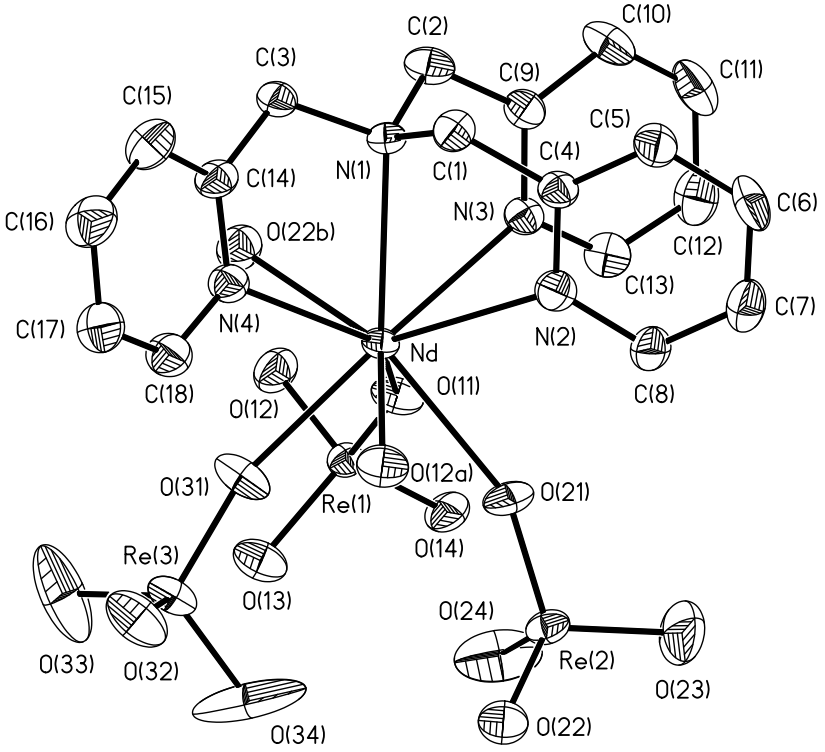

Fig. 4. A view of **II**, showing the atom labelling scheme. Displacement ellipsoids are drawn at the 30% probability level and H atoms are omitted.

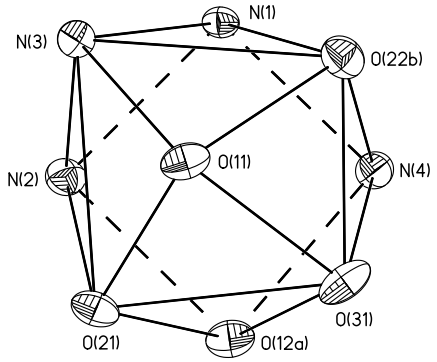

Fig. 5. Coordination polyhedron of the Nd atom in **II**.

of the absolute structure. Crystal data for the structures are given in Table 1.

X-ray diffraction analysis of $[Nd(TEMA)_4](ReO_4)_3$ (**III**) was performed with a single-crystal fragment. The main crystal data, data collection, and refinement for **III** are presented in Table 1. Experimental data were collected on a Bruker AXS SMART 1000 CCD automated diffractometer (Mo Kα radiation, graphite monochromator). The experimental intensities were empirically corrected for absorption using SADABS [13]. The structure was solved by direct methods (SHELXS97) and refined by full-matrix least-squares procedure on F^2 (SHELXL97) in an anisotropic approximation for all the non-hydrogen atoms. The perrhenate anions are partially disordered. This disordering was indicated by the shape and size of the thermal vibration ellipsoids. Attempts to refine the structure with the perrhenate anions disordered over two positions failed. The $Re(1)O_4$, $Re(2)O_4$ and $Re(3)O_4$ groups were restrained using DFIX (free variable 3) and refined as regular tetrahedra. The $Re(2)O_4$ group was refined with the same anisotropic displacement parameters for all atoms. The positions of the hydrogen atoms in TEMA were added in calculated positions and refined using a riding model. The H atoms of CH_2 groups were refined with $U_{iso}(H) = 1.2U_{eq}(C)$. The H atoms of CH_3 groups were refined including free rotation about C–C bonds with $U_{iso}(H) = 1.5U_{eq}(C)$.

The molecular drawings for **I**, **II** and **III** were done with SHELXTL [14].

The X-ray powder patterns were measured with a model XDC-700 focusing Guinier-Hägg camera (Jungner Instrument, Sweden) using Cu Kα1 radiation, with Si as an internal standard. The X-ray patterns were indexed and cell parameters were refined using the CRYSFIRE program suite [15].

The IR spectra were recorded in the range 4000–400 cm^{-1} using a Specord M80 spectrophotometer at room temperature in the NaCl matrix.

3. Results and discussion

One of three FBTP ligands in the structure of **I** is shown in Fig. 1. Three tridentate ligands linked to a Nd atom together with a monodentate perrhenate anion form the complex cation $[Nd(FBTP)_3ReO_4]^{2+}$ (Fig. 2). Interatomic distances for the Nd atom environment are given in Table 2. The complex cation is close to (non-crystallographic) C_3 symmetry (Fig. 2). The Nd, Re(1) and O(1) atoms are on a pseudo-threefold axis. Symmetric coordination of the FBTP ligands results in the formation of a rather unusual coordination polyhedron (coordination number 10) having three quadrilateral faces (Fig. 3). A similar coordination

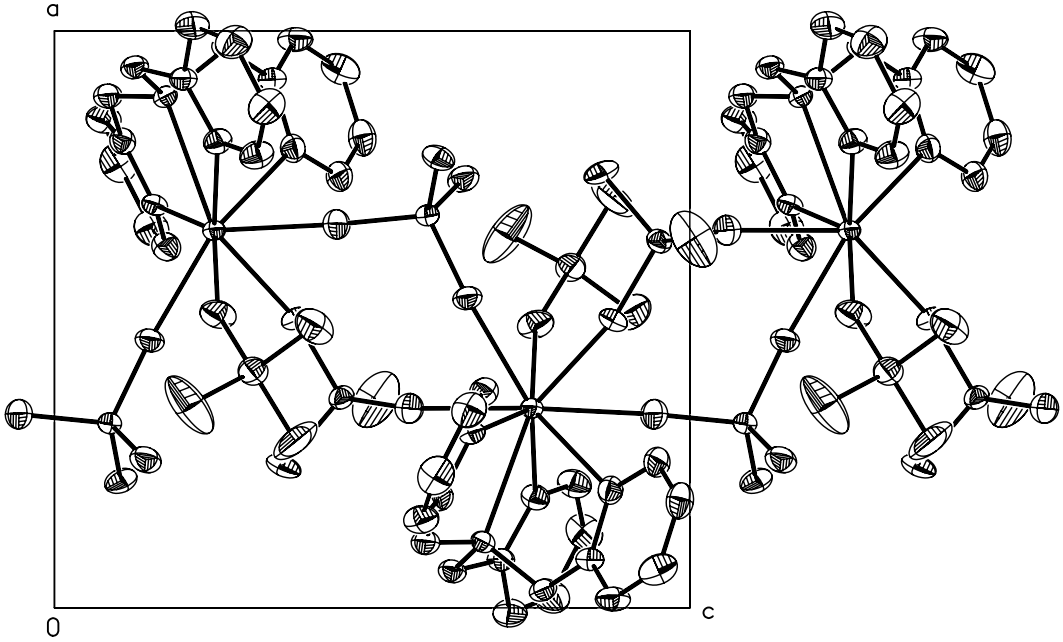

Fig. 6. Electroneutral chain in **II**.

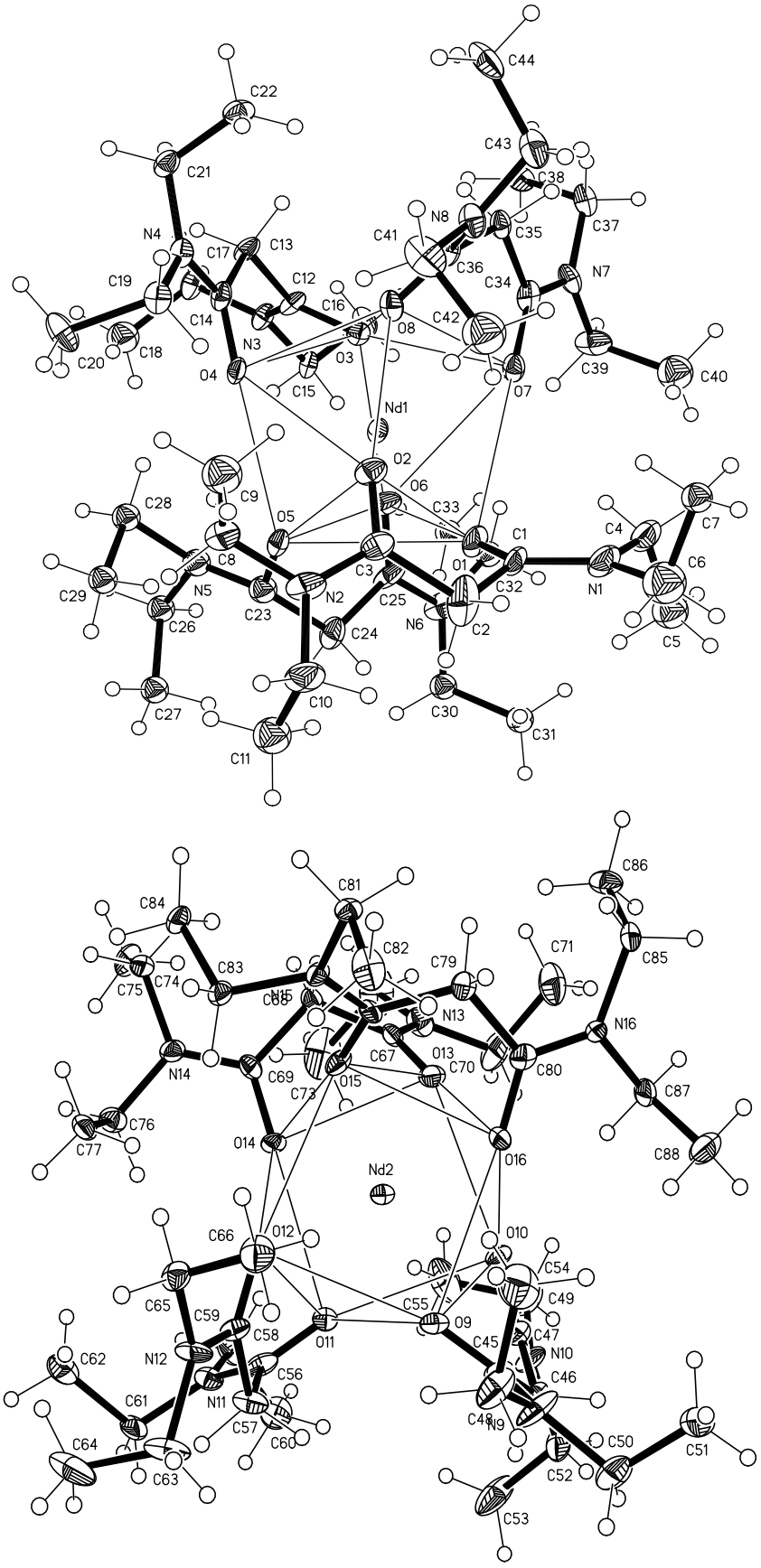

Fig. 7. Coordination environment of Nd(1) and Nd(2) in **III**

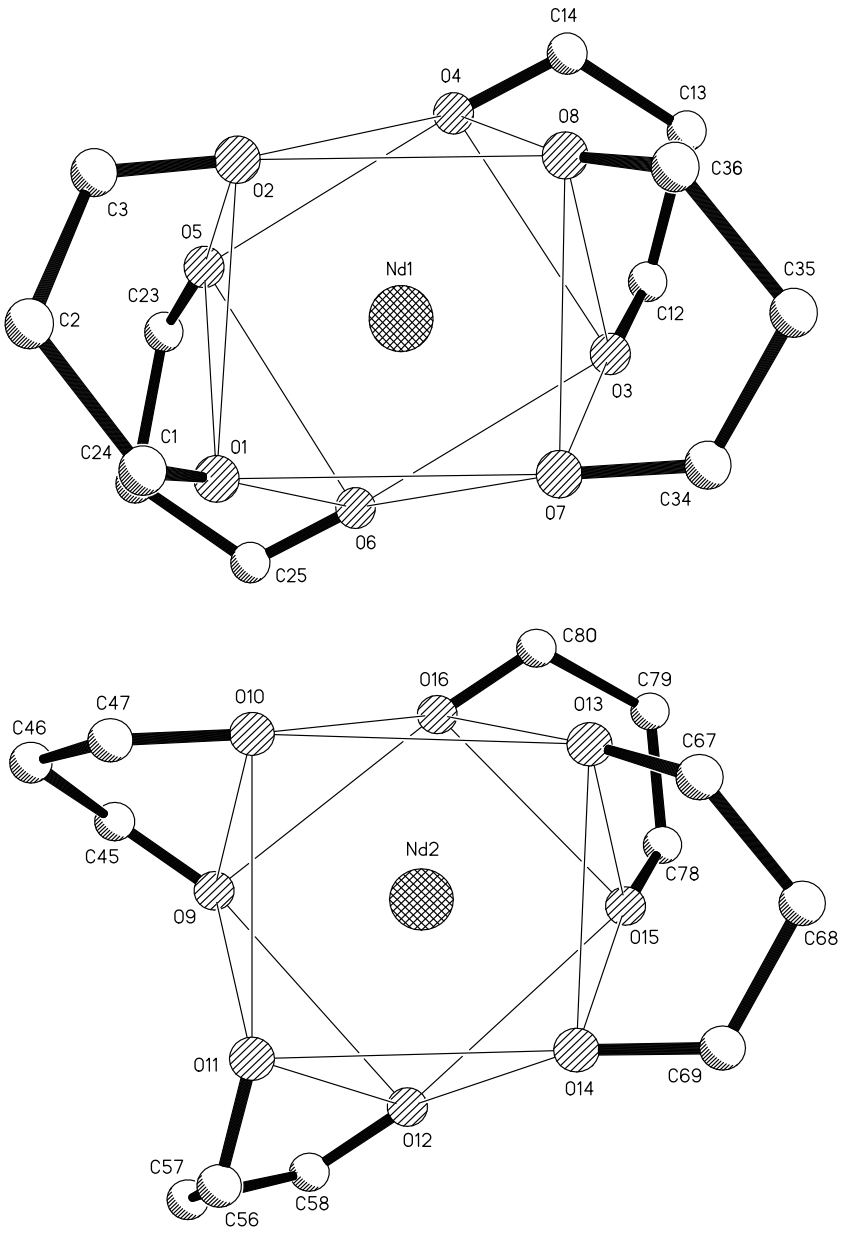

Fig. 8. Coordination polyhedra of Nd(1) and Nd(2) in **III**.

Table 3
Unit cell constants for $Nd(TPA)(TcO_4)_3$ (**IV**) and $Am(TPA)(TcO_4)_3$ (**V**)

$Pna2_1$	**IV**	**V**
a (Å)	10.7048(9)	10.7022(9)
b (Å)	21.039(3)	21.0545(15)
c (Å)	11.7528(10)	11.7608(7)
V (Å^3)	2646.9(5)	2650.1(3)

polyhedron can be found in La^{3+} complexes containing three terpyridine molecules and coordinated water or acetonitrile [16], but the authors of that work did not discuss the coordination polyhedra. Two ReO_4 groups in **I** are outer sphere anions. Four crystallization water molecules are, possibly, partially disordered.

The Nd atom in **II** is nine-coordinated. All four N atoms of the TPA ligand enter the coordination sphere of the Nd atom. Such coordination is typical of TPA with Ln^{3+}, U^{3+} or U^{4+} [17–19]. In contrast to **I**, all three perrhenate anions in **II** are involved in coordination with the Nd atom (Fig. 4). One anion acts as a monodentate ligand, whilst two others are bidentate-bridging ones. The Nd–N and Nd–O distances are given in Table 2. The coordination polyhedron of the Nd atom in **II** can be described as a distorted capped square antiprism (Fig. 5). The bridging function of the two perrhenate anions results in the formation of chains along the [0 0 1] direction (Fig. 6).

Two crystallographically independent Nd(1) and Nd(2) atoms in **III** have coordination environments formed by oxygen atoms of four TEMA ligands (coordination number 8) (Fig. 7). Each TEMA ligand links to the Nd atom in a

Table 4
Probable assignment of some characteristic absorption bands of $[Nd(FBTP)_3ReO_4](ReO_4)_2 \cdot 4H_2O$ (**I**), $[Nd(TPA)(ReO_4)_3]$ (**II**) and $[Nd(TEMA)_4](ReO_4)_3$ (**III**)

Assignment	The maxima of the absorption bands (cm^{-1})		
	I	**II**	**III**
ν(HOH); ν(CH)	3480	3636–3396	3502–3416
$\nu(CH_3)$	2978,2928, 2872	2916, 2856	2980, 2940
ν(CC); ν(NC); δ(CCN); $\Delta(CH_3)$;	1636, 1588, 1556, 1540, 1528, 1496, 1476, 1456,1436, 1364, 1300, 1268, 1212, 1178, 1128, 1092, 1022	1624, 1604, 1446, 1396, 1380, 1156, 1100, 1088	1608, 1580, 1508, 1476, 1460, 1382, 1360, 1264, 1212, 1152, 1100, 1076
$\nu(ReO_4^-)$	932, 909	952, 936, 922	908, 904
$\rho(CH)_{Pyr}$	616	634	622

bidentate mode. Structure **III** contains $[Nd(TEMA)_4]^{3+}$ complex cations. The perrhenate anions are not involved in the coordination sphere of the Nd(1) and Nd(2) atoms. Interatomic distances in the Nd(1) and Nd(2) atom environments are given in Table 2. The coordination polyhedra of the Nd(1) and Nd(2) atoms can be described as distorted square antiprisms. The average bond distance in the coordination sphere of Nd(1) is 2.424 Å, the largest deviation of oxygen atoms from the square faces is 0.109(4) Å. The average Nd(2) bond length is 2.418 Å, both square faces are planar within the 0.096(4) Å limit.

There are three different ways of arranging bidentate ligands along the various edges of a tetragonal antiprism and two of them result in D_{2d} molecular symmetry [20]. In **III** both possibilities of the TEMA fitting are realized, as shown in Fig. 8.

FBTP with neodymium pertechnetate gives a crystalline complex, but its X-ray powder diffraction pattern differs from that of complex **I**. In contrast to **I** and **III**, structure **II** does not change due to replacement of perrhenate by pertechnetate and neodymium by americium. Thus the corresponding compounds can be given the formulas $[Nd(TPA)(TcO_4)_3]$ (**IV**) and $[Am(TPA)(TcO_4)_3]$ (**V**). X-ray pattern indexing gives the unit cell constants indicated in Table 3 for **IV** and **V**.

The conditions under which complex **III** was prepared using neodymium pertechnetate yielded only amorphous products.

The IR spectra of complexes **I**–**III** consist of numerous bands due to the large organic ligands containing different functional groups which are active in the spectra. Table 4 indicates the probable assignments for some characteristic absorption bands that should be taken into account; in the 1700–1000 cm^{-1} range are situated vibration frequencies of the furan and pyridine rings, which are hardly mixed ν(CC), ν(NC), δ(CCN) and δ(CH) [21].

In the range of valent vibrations of the perrhenate ion, in all the spectra high-intensity split $\nu(ReO_4^-)$ absorption bands are observed, for which the maxima are largely shifted towards the low-frequency region in comparison with the non-coordinated ion [22].

4. Conclusions

1. The complexes $[Nd(FBTP)_3ReO_4](ReO_4)_2 \cdot 2H_2O$ (I), $[Nd(TPA)(ReO_4)_3]$ (**II**) and $[Nd(TEMA)_4](ReO_4)_3$ (**III**) were synthesized and their structures were determined by X-ray diffraction [FBTP is 2,6-bis(tetramethylfurano)-1,2,4-triazin-3-yl)-pyridine, TPA is tris(2-pyridylmethyl)amine and TEMA is *N*,*N*′-tetraethylmalonamide.
2. Pertechnetate analogue complexes were synthesized with Nd or Am, and only $[M(III)(TPA)(TcO_4)_3]$ are isostructural to **II**.

Acknowledgements

We are grateful to Dr. Ch. Den Auwer and Dr. D. Meyer for their aid in XRD studies. This work was supported by DEN/DDIN/DPSF/CCC and DEN/DSOE/RB (CEA, France).

Appendix A. Supplementary material

Supplementary data associated with this article can be found, in the online version, at doi:10.1016/j.poly.2007.12.029.

References

[1] M.J. Sarsfield, A.D. Sutton, G.H. May John, C. Sharrad, M. Helliwell, Chem. Commun. 2320 (2004).
[2] A.D. Sutton, G.H. John, M.J. Sarsfield, J.C. Renshaw, I. May, L.R. Martin, A.J. Selvage, D. Collinson, M. Helliwell, Inorg. Chem. 43 (2004) 5480.
[3] A.M. Fedosseev, N.A. Budantseva, M.S. Grigoriev, K.E. Guerman, J.-C. Krupa, Radiochim. Acta 91 (2003) 147.
[4] G.H. John, I. May, M.J. Sarsfield, M.H. Steele, D. Collinson, M. Helliwell, J. McKinney, J. Chem. Soc., Dalton Trans. 743 (2004).
[5] N.A. Budantseva, G.B. Andreev, A.M. Fedosseev, M.Yu. Antipin, Koord. Khim. 29 (2003) 346 (in Russian).
[6] G.H. John, I. May, C.A. Sharrad, A.D. Sutton, D. Collinson, M. Helliwell, M.J. Sarsfield, Inorg. Chem. 44 (21) (2005) 7606.
[7] A. Fernandez, D. Haas, R.J.M. Konings, J. Somers, in: Proceedings of the 6th Information exchange meeting on Actinide and Fission Product Partitioning and Transmutation, 11–13 December 2000, Madrid, Spain, pp. 427–434.

[8] R.J.M. Konings, D. Haas, CR Phys. 3 (NN7-8 Sept–Oct) (2002) 1013–1022.
[9] Z. Otwinowski, W. Minor, Methods in enzymology, in: C.W. CarterJr., R.M. Sweet (Eds.), Macromolecular Crystallography Part A, vol. 276, Academic Press, New York, 1997, pp. 307–326.
[10] A.L. Spek, PLATON – A Multipurpose Crystallographic Tool, Utrecht University, Utrecht, The Netherlands, 2003.
[11] G.M. Sheldrick, SHELXL97 and SHELXS97, University of Göttingen, Germany, 1997.
[12] H.D. Flack, Acta Crystallogr. A 39 (1983) 876.
[13] G.M. Sheldrick, SADABS, v. 2.01. Bruker/Siemens Area Detector Absorption Correction Program, Bruker AXS Inc., Madison, WI, USA, 1998.
[14] G.M. Sheldrick, SHELXTL, v. 5.10, Bruker AXS Inc., Madison, WI, USA, 1997.
[15] R. Shirley, The CRYSFIRE System for Automatic Power Indexing: User's Manual, The Lattice Press, Surrey, England, 2000.
[16] L.I. Semenova, A.N. Sobolev, B.W. Skelton, A.H. White, Aust. J. Chem. 52 (1999) 519.
[17] L. Karmazin, M. Mazzanti, J. Pecaut, Inorg. Chem. 42 (2003) 5900.
[18] R. Wietzke, M. Mazzanti, J.-M. Latour, J. Pecaut, P.-Y. Cordier, C. Madic, Inorg. Chem. 37 (1998) 6690.
[19] R. Wietzke, M. Mazzanti, J.-M. Latour, J. Pecaut, J. Chem. Soc., Dalton Trans. 4167 (2000).
[20] D.L. Kepert, Inorganic Stereochemistry, Springer-Verlag, Berlin, Heidelberg, NY, 1982, p. 227.
[21] H. Van der Poel, G. Van Koten, K. Vriese, Inorg. Chem. 19 (1980) 1145.
[22] R. Busey, O. Keller, J. Chem. Phys. 41 (1964) 215.

Polyhedron 27 (2008) 2015–2021

Contents lists available at ScienceDirect

Polyhedron

journal homepage: www.elsevier.com/locate/poly

Structural, theoretical and multinuclear NMR study of mercury(II) complexes of phosphorus ylides: Mono and binuclear complexes

Seyyed Javad Sabounchei [a,*], Hassan Nemattalab [a], Sadegh Salehzadeh [a], Sima Khani [a], Mehdi Bayat [a], Hamid Reza Khavasi [b]

[a] Faculty of Chemistry, Bu-Ali Sina University, Hamedan 65174, Iran
[b] Department of Chemistry, Shahid Beheshti University, Evin, Tehran 19839-63113, Iran

ARTICLE INFO

Article history:
Received 10 February 2008
Accepted 4 March 2008
Available online 21 April 2008

Keywords:
Mercury(II) halide
Phosphorus ylide
DMSO
Triphenylphosphine
Triparatolylphosphine

ABSTRACT

Reaction of phosphorus ylide $Ph_3PCHC(O)C_6H_4Cl$ ($\mathbf{Y}_1$) with HgX_2 (X = Cl, Br and I) and ylide $(p\text{-tolyl})_3PCHC(O)CH_3$ ($\mathbf{Y}_2$) with HgI_2 in equimolar ratios using methanol as solvent leads to binuclear products. The bridge-splitting reaction of binuclear complex $[(Y_1)\cdot HgCl_2]_2$ by DMSO yields a mononuclear complex containing DMSO as ligand. O-coordination of DMSO is revealed by single crystal X-ray analysis in mononuclear complex of $[(Y_1)\cdot HgCl_2\cdot DMSO]$. C-coordination of ylides is confirmed by X-ray structure of binuclear complex $[(Y_2)\cdot HgI_2]_2$. Characterization of the obtained compounds was also performed by elemental analysis, IR, ^1H, ^{31}P, and ^{13}C NMR. Theoretical studies on mercury(II) complexes of Y_1 show that formation of mononuclear complexes in DMSO solution in which DMSO acts as a ligand, energetically is more favorable than that of binuclear complexes.

© 2008 Elsevier Ltd. All rights reserved.

1. Introduction

The utility of metalated phosphorus ylides in synthetic chemistry has been well documented [1,2]. Synthesis of complexes derived from phosphorus ylides and Hg(II) halides was started in 1965 by Nesmeyanov et al. [3]. In 1975, Weleski et al. [4] proposed a symmetric halide-bridged dimeric structure for Hg(II) halide complexes whereas Kalyanasundari et al. [5] reported an asymmetric halide-bridged dimeric structure in 1995. In 1985, Sanehi et al. [6] reported a mononuclear Hg(II) complex of phosphorus ylides without any structural characterization. We have recently focused on the synthesis of binuclear and polynuclear complexes derived from mercury(II) salts and phosphorus ylides [7–9]. The α-keto-stabilized phosphorus ylides $R_3P{=}C(R')COR''$ show interesting properties such as their high stability and their ambidentate character as ligands (C- versus O-coordination) [10]. This ambidentate character can be rationalized in terms of the resonance forms A–C, together with the isomeric form D (Chart 1).

Form B can be considered as leading to coordination by the carbon atom to give a complex of form E, whereas isomers C and D would both lead to coordination by the oxygen atom, affording structures F (*transoid*) and form G (*cisoid*), respectively. Although many coordination modes are possible for keto ylides [11], coordination through carbon is more predominant and observed with soft metal ions, *e.g.*, Pd(II), Pt(II), Ag(I), Hg(II), Au(I) and Au(III) [5,12–15], whereas, O-coordination dominates when the metals involved are hard, *e.g.*, Ti(IV), Zr(IV), and Hf(IV) [16]. Only W(0) complexes of the type $W(CO)_5L$ (L = ylide) [17] and Pd(II) complexes of stoichiometry $[Pd(C_6F_5)(L_2)(APPY)](ClO_4)$ [12] [APPY = $Ph_3PCHCOMe$; L = PPh_3 and PBu_3; L_2 = bipy] contain stable ylides O-linked to a soft metal centre.

2. Experimental

2.1. Materials

All reactions were performed in air. Starting materials were purchased from commercial sources and used without further purification. The ligands were synthesized by the reaction of related phosphine with 2-bromo-4′-chloroacetophenone or chloroacetone and concomitant elimination of HBr by NaOH [18].

2.2. Physical measurements

Melting points were measured on a SMPI apparatus. Elemental analysis for C and H atoms were performed using a Perkin–Elmer 2400 series analyzer. IR spectra were recorded on a Shimadzu 435-U-04 FT spectrophotometer from KBr pellets. ^1H, ^{13}C, and ^{31}P NMR spectra were recorded on a 300 MHz Bruker spectrometer in DMSO-d_6 or $CDCl_3$ as solvent at 25 °C. Chemical shifts (ppm) are reported according to internal TMS and external 85% phosphoric acid. Coupling constants are given in Hz. The single crystal X-ray diffraction analyses were performed on a STOE IPDS-II two

* Corresponding author.
E-mail address: jsabounchei@yahoo.co.uk (S.J. Sabounchei).

0277-5387/$ - see front matter © 2008 Elsevier Ltd. All rights reserved.
doi:10.1016/j.poly.2008.03.009

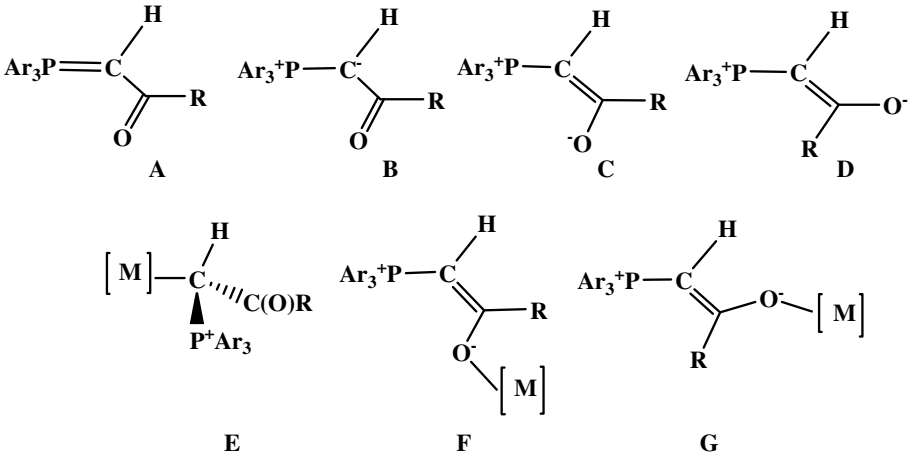

Chart 1.

circle diffractometer at 293(2) K, using graphite monochromated Mo Kα X-ray radiation ($\lambda = 0.7107$ nm). The data collection were performed at room temperature using the ω-scan technique and using the STOE X-AREA software package [19]. The crystal structures were solved by direct methods and refined by full-matrix least-squares on F^2 by SHELX [20] and using the X-STEP32 crystallographic software package [21]. All non-hydrogen atoms were refined anisotropically using reflections $I > 2\sigma(I)$. Hydrogen atoms were located in ideal positions.

2.3. Theoretical studies

The geometries of compounds were fully optimized at the Hartree–Fock (HF) level of theory using the GAUSSIAN98 program [22] on a Pentium-PC computer with 3600 MHz processor. The standard LanL2mb basis set was used for all complexes [23]. This basis set includes effective core potentials (ECP) for both the mercury and phosphorus as well as halide (Cl, Br and I) ions. Vibrational frequency analyses, calculated at the same level of theory, indicate that optimized structures are at the stationary points corresponding to local minima, without any imaginary frequency. Atomic coordinates for ab initio calculations were obtained from the data of the X-ray crystal structure analyses.

2.4. Preparation of $Ph_3PCHCOC_6H_4Cl$ (Y_1), general procedure for ylides [24]

A solution of triphenylphosphine (0.131 g, 0.5 mmol) and 2-bromo-4′-chloroacetophenone (0.117 g, 0.5 mmol) in acetone (15 ml) was stirred at room temperature for 4 h. The resulting white precipitate was filtered off, washed with diethylether and dried. Further treatment with aqueous solution of NaOH (0.5 M, 50 ml) led to elimination of HBr, giving the free ligand Y_1. IR (KBr, cm^{-1}): ν 1579 (C=O), 1522, 1480, 1435, 1404, 1383, 1175, 1104, 1085, 1009, 882 (P–C), 848. ^{1}H NMR ($CDCl_3$) δ_H: 4.38 (d, $^2J_{PH}$ = 23.75 Hz, 1H, C*H*); 7.25–7.94 (m, 19H, Ph). ^{31}P NMR ($CDCl_3$) δ_P: 14.19 (s). ^{13}C NMR ($CDCl_3$) δ_C: 50.65 (d, $^1J_{PC}$ = 110.3 Hz, *C*H); 126.0 (d, $^1J_{PC}$ = 91.40 Hz, PPh_3 (*i*)); 127.31 (COPh (*m*)); 128.03 (PPh_3 (*p*)); 128.48 (d, $^3J_{PC}$ = 12.41 Hz, PPh_3 (*m*)); 131.80 (d, $^4J_{PC}$ = 2.73 Hz, COPh (*o*)); 132.60 (d, $^2J_{PC}$ = 10.25 Hz, PPh_3 (*o*)); 134.71 (COPh (*p*)); 139.15 (d, $^2J_{PC}$ = 14.69 Hz, COPh (*i*)); 182.84 (d, $^2J_{PC}$ = 3.1 Hz, CO).

2.5. $(p\text{-tolyl})_3PCHCOCH_3$ (Y_2)

Anal. Calc. for $C_{24}H_{25}OP$: C, 80.00; H, 7.00. Found: C, 79.51; H, 7.01%. Yield 0.364 g (92%). m.p., 100–102 °C. IR (KBr disk): ν (cm^{-1}) 1711, 1599 (C=O), 1502, 1448, 1425, 1402, 1363, 1313, 1193, 1156, 1111, 1038, 1002, 848 (P–C), 808 and 777. ^{1}H NMR ($CDCl_3$): δ (ppm) 2.04 (3H, s, $COCH_3$), 2.36 (9H, s, $3CH_3$), 3.65 (1H, d, $^2J_{PH}$ = 24.8 Hz, C*H*); 7.24–7.52 (12H, m, Ph). ^{31}P NMR ($CDCl_3$) δ_P: 10.59 (s). ^{13}C NMR ($CDCl_3$) δ_C: 21.49 (s, $3CH_3$); 28.43 (d, $^3J_{PC}$ = 15.1 Hz, $COCH_3$); 52.53 (d, $^1J_{PC}$ = 107.7 Hz, C*H*); 124.29 (d, $^1J_{PC}$ = 92.7 Hz, *p*-tolyl, (*i*)); 133.05 (d, $^2J_{PC}$ = 10.5 Hz, *p*-tolyl, (*o*)); 129.51 (d, $^3J_{PC}$ = 12.3 Hz, *p*-tolyl, (*m*)); 142.32 (*p*-tolyl, (*p*)); 190.38 (CO).

2.6. Synthesis of the complexes

The binuclear complexes **1**–**4** were prepared based on a general procedure as follows (Scheme 1). According to various papers [5,7,8,25], the binuclear structures are suggested for above compounds, as shown in Scheme 1. X-ray quality crystals of the complexes **4** and **5** (Schemes 1 and 2) were grown from a

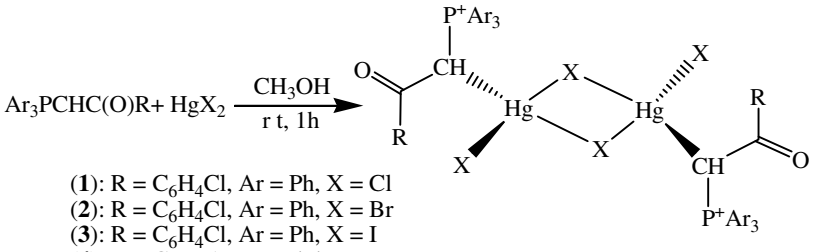

(**1**): R = C_6H_4Cl, Ar = Ph, X = Cl
(**2**): R = C_6H_4Cl, Ar = Ph, X = Br
(**3**): R = C_6H_4Cl, Ar = Ph, X = I
(**4**): R = CH_3, Ar = *p*-tolyl, X = I

Scheme 1.

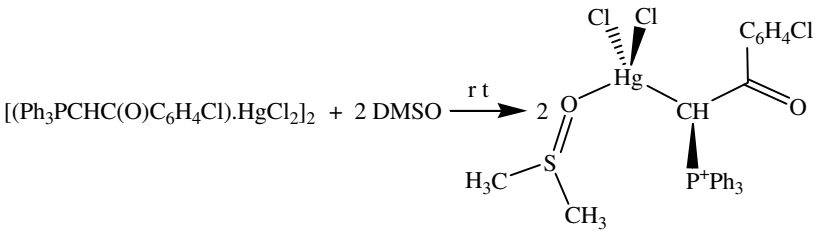

Scheme 2.

dimethylsulfoxide solution of compounds **4** and **1**, respectively. This was carried out by the slow evaporation of the solvent over several days.

*2.6.1. Synthesis of [(Y_1) · $HgCl_2$]$_2$ (**1**), general procedure for dimeric structures*

To a methanolic solution (15 ml) of $HgCl_2$ (0.082 g, 0.3 mmol) was added a methanolic solution (10 ml) of Y_1 (0.124 g, 0.3 mmol). The mixture was stirred for 1 h. The separated solid was filtered and washed with diethyl ether. *Anal.* Calc. for $C_{26}H_{20}Cl_3HgOP$: C, 45.50; H, 2.94. Found: C, 44.41; H, 2.81%. Yield 0.115 g (56%). m.p. 215–217 °C. IR (KBr, cm^{-1}): ν 1635 (C=O), 1586, 1567, 1483, 1437, 1398, 1312, 1284, 1184, 1108, 1091, 1005, 823 (P–C). ^{1}H NMR (DMSO-d_6) δ_H: 5.46 (d, $^2J_{PH}$ = 6.36 Hz, 1H, C*H*); 7.46–8.10 (m, 19H, Ph). ^{31}P NMR (DMSO-d_6) δ_p: 22.16 (s). ^{13}C NMR (DMSO-d_6) δ_c: 46.77 (d, $^1J_{PC}$ = 75.58 Hz, *C*H); 123.33 (d, $^1J_{PC}$ = 89.46 Hz, PPh_3 (*i*)); 127.81 (COPh (*m*)); 129.16 (d, $^3J_{PC}$ = 12.35 Hz, PPh_3 (*m*)); 129.16 (COPh (*p*)); 129.74 (PPh_3 (*p*)); 133.10 (d, $^2J_{PC}$ = 9.46 Hz, PPh_3 (*o*)); 136.22 (COPh (*o*)); 136.63 (COPh (*i*)); 188.82 (s, CO).

*2.6.2. [(Y_1) · $HgBr_2$]$_2$ (**2**)*

Anal. Calc. for $C_{26}H_{20}Br_2ClHgOP$: C, 40.28; H, 2.60. Found: C, 40.13; H, 2.57%. Yield 0.193 g (83%). m.p. 195–197 °C. IR (KBr, cm^{-1}): ν 1625 (C=O), 1586, 1566, 1482, 1435, 1398, 1317, 1292, 1195, 1108, 1030, 1010, 997, 885, 819 (P–C) and 805. ^{1}H NMR (DMSO-d_6) δ_H: 5.38 (d, $^2J_{PH}$ = 7.62 Hz, 1H, C*H*); 7.45–8.08 (m, 19H, Ph). ^{31}P NMR (DMSO-d_6) δ_p: 22.72 (s). ^{13}C NMR (DMSO-d_6) δ_c: 48.04 (d, $^1J_{PC}$ = 79.40 Hz, *C*H); 124.13 (d, $^1J_{PC}$ = 89.97 Hz, PPh_3 (*i*)); 128.52 (COPh (*m*)); 129.92 (d, $^3J_{PC}$ = 11.40 Hz, PPh_3 (*m*)); 130.54 (PPh_3 (*p*)); 133.87 (d, $^2J_{PC}$ = 9.28 Hz, PPh_3 (*o*)); 133.93 (COPh (*p*)); 136.96 (COPh (*o*)); 137.22 (COPh (*i*)); 189.41 (s, CO).

*2.6.3. [(Y_1) · HgI_2]$_2$ (**3**)*

Anal. Calc. for $C_{26}H_{20}ClHgI_2OP$: C, 35.92; H, 2.32. Found: C, 35.86; H, 2.17%. Yield 0.170 g (82%). m.p. 192–194 °C. IR (KBr, cm^{-1}): ν 1620 (C=O), 1586, 1565, 1482, 1434, 1398, 1316, 1291, 1266, 1193, 1108, 1092, 1030, 1009, 998, 878, 820 (P–C) and 802. ^{1}H NMR (DMSO-d_6) δ_H: 5.12 (d, $^2J_{PH}$ = 12.46 Hz, 1H, C*H*); 7.42–8.05 (m, 19H, Ph). ^{31}P NMR (DMSO-d_6) δ_p: 20.64 (s). ^{13}C NMR (DMSO-d_6) δ_c: 48.90 (d, $^1J_{PC}$ = 83.25 Hz, *C*H); 124.71 (d, $^1J_{PC}$ = 89.74 Hz, PPh_3 (*i*)); 128.45 (COPh (*m*)); 129.85 (d, $^3J_{PC}$ = 12.15 Hz, PPh_3 (*m*)); 130.24 (PPh_3 (*p*)); 133.75 (d, $^2J_{PC}$ = 9.13 Hz, PPh_3 (*o*)); 133.81 (COPh (*p*)); 136.66 (COPh (*o*)); 137.67 (d, $^3J_{PC}$ = 10.64 Hz, COPh (*i*)); 187.81 (s, CO).

*2.6.4. [(Y_2) · HgI_2]$_2$ (**4**)*

Anal. Calc. for $C_{24}H_{25}HgI_2OP$: C, 35.38; H, 3.09. Found: C, 35.24; H, 3.54%. Yield 0.218 g, 89%. m.p. 206–208 °C. IR (KBr, cm^{-1}): ν 1655 (C=O), 1596, 1497, 1399, 1350, 1289, 1192, 1149, 1106, 964, 902, 852 and 805. ^{1}H NMR (DMSO-d_6): δ (ppm) 2.14 (3H, s, $COCH_3$); 2.39 (9H, s, $3CH_3$); 4.59 (1H, br, C*H*); 7.44–7.66 (12H, m, Ph). ^{31}P NMR (DMSO-d_6) δ_p: 20.63 (s). ^{13}C NMR (DMSO-d_6) δ_c: 21.03 ($3CH_3$); 30.54 (d, $^3J_{PC}$ = 11.2 Hz, $COCH_3$); 50.39 (d, $^1J_{PC}$ = 63.8 Hz, *C*H); 119.97 (d, $^1J_{PC}$ = 92.6 Hz, *p*-tolyl (*i*)); 129.84 (d, $^3J_{PC}$ = 12.6 Hz, *p*-tolyl (*m*)); 133.09 (d, $^2J_{PC}$ = 10.2 Hz, *p*-tolyl (*o*)); 143.81 ((*p*-tolyl) (*p*)); 197.91 (*C*O).

*2.6.5. [(Y_1) · $HgCl_2$ · DMSO] (**5**)*

0.137 g (0.1 mmol) of binuclear complex **1** was dissolved in DMSO (2 ml). The pale yellow crystals formed by the slow evaporation of the solvent over several days. Yield 0.147 g (96%). Decomposition at 180 °C. IR (KBr, cm^{-1}): ν 1635 (C=O), 1586, 1567, 1483, 1437, 1398, 1312, 1284, 1184, 1108, 1091, 1005, 823 (P–C). ^{1}H NMR (DMSO-d_6) δ_H: 5.46 (d, $^2J_{PH}$ = 6.36 Hz, 1H, C*H*); 7.46–8.10 (m, 19H, Ph). ^{31}P NMR (DMSO-d_6) δ_p: 22.16 (s). ^{13}C NMR (DMSO-d_6) δ_c: 46.77 (d, $^1J_{PC}$ = 75.58 Hz, *C*H); 123.33 (d, $^1J_{PC}$ = 89.46 Hz, PPh_3 (*i*)); 127.81 (COPh (*m*)); 129.16 (d, $^3J_{PC}$ = 12.35 Hz, PPh_3 (*m*)); 129.16 (COPh (*p*)); 129.74 (PPh_3 (*p*)); 133.10 (d, $^2J_{PC}$ = 9.46 Hz, PPh_3 (*o*)); 136.22 (COPh (*o*)); 136.63 (COPh (*i*)); 188.82 (s, CO).

3. Results and discussion

3.1. Spectroscopy

The ν (CO) band, which is sensitive to complexation, is observed for complexes at higher frequencies compared to the parent ylides, indicating coordination of the ylide thorough carbon atom in each case [26]. The ν (P^+–C^-) band, (823, 819 and 820 cm^{-1} for complexes **1**–**3**, respectively) which is also diagnostic of the coordination modes, occurs at lower frequencies (882 cm^{-1}) in comparison to the parent ylide (Y_1), consistent with some removal of electron density in the P–C bonds [7–9]. C-coordination causes an increase in ν (CO) and decrease in ν (P^+–C^-) while for O-coordination a lowering for both frequencies is expected [15]. It should be noted that there is not any significant difference in the IR absorption bands for binuclear complex **1** and related mononuclear complex **5**.

In the ^{1}H NMR spectra, the signals due to the methinic protons for complexes are doublet or broad. Similar behavior was observed earlier in the case of ylide complexes of platinum(II) chloride [27]. The expected downfield shifts of ^{31}P and ^{1}H signals for the PCH group upon complexation in the case of C-coordination were observed in their corresponding spectra. The proton decoupled ^{31}P NMR spectra show only one sharp singlet between 20.63 and 22.72 ppm in the complexes. The appearance of a single signal for the PCH group in each of the ^{31}P and ^{1}H NMR spectra indicates that all ligands are in the same environment in these complexes, as expected for C-coordination. It must be noted that O-coordination of the ylide generally leads to the formation of a mixture of *cisoid* and *transoid* isomers, giving rise to two different signals in ^{31}P and ^{1}H NMR spectra (Chart 1) [12]. The ^{31}P chemical shift values for the complexes appear to be shifted downfield by about 6.5–10 ppm with respect to the parent ylides also indicating that coordination of the ylide has occurred [5,7–9,25]. Satellites due to coupling to ^{199}Hg for ylidic complexes of Hg(II) are only observed at low temperature [7,25] or by solid-state ^{31}P NMR [25] and also in the case of $Hg(NO_3)_2 \cdot H_2O$ as metal source [9]. Failure to observe satellites

in above spectra was previously noted in the complexes of Hg(II) [28] and Ag(I) [15] and was assigned to fast exchange of the ylide with the metal at higher temperatures.

The most interesting aspect of the ^{13}C NMR spectra of the complexes is the upfield shift of the signals due to the ylidic carbon atoms. Such an upfield shift was observed in [PdCl(η^3-2-XC_3H_4)$(C_6H_5)_3$PCHCOR] (X = H, CH_3; R = CH_3, C_6H_5), and is due to the change in hybridization of the ylidic carbon atom on coordination [29]. Similar up field shifts of 2–3 ppm with reference to the parent ylide were also observed in the case of $[(C_6H_5)_3PC_5H_4HgI_2]_2$ [28]. The downfield shifts of the carbonyl C atom in the complexes compared to the same carbon atom in the parent ylides, indicate a much lower shielding of the CO group in these complexes.

3.2. X-ray crystallography

Table 1 provides the crystallographic results and refinement information for complexes **4** and **5**. The molecular structures are shown in Figs. 1 and 2. Pertinent bond distances and angles for **4** and **5** are given in Tables 2 and 3, respectively. Packing diagrams, fractional atomic coordinates and equivalent isotropic displacement coefficients (Ueq) for the non-hydrogen atoms of complexes are shown in Supplementary materials.

The Hg(II) centre in complex **4** forms four-coordinate with sp^3 hybridization. This environment is contained of one short terminal Hg–I bond, one Hg–C bond and two asymmetric bridging Hg–I bonds. The Hg–C and terminal Hg–I bond lengths in **4** (2.279(8) and 2.7036(8) Å) are comparable to analogous distances in $[(Ph_3PCHCOPh)\cdot HgI_2]_2$ (2.312(13) and 2.705(1) Å, respectively) [5].

Table 1
Crystallographic data summary for complexes **4** and **5**

Compound	**4**	**5**
Empirical formula	$C_{48}H_{50}Hg_2I_4O_2P_2$	$C_{28}H_{26}Cl_3HgO_2PS$
F_w	1629.6	764.47
Temperature (K)	293(2)	293(2)
Wavelength (Å)	0.71073	0.71073
Crystal system	triclinic	orthorhombic
Space group	$P\bar{1}$	*Pbca*
a (Å)	11.697(2)	11.1014(11)
b (Å)	11.968(3)	18.7168(14)
c (Å)	11.933(2)	28.292(3)
α (°)	105.371(16)	90
β (°)	106.160(16)	90
γ (°)	115.223(15)	90
Volume (Å^3)	1302.4(5)	5878.5(9)
Z	1	8
D_{Calcd} (Mg/m^3)	2.078	1.727
Absorption coefficient (mm^{-1})	8.353	5.658
F(000)	752	2976
Crystal size (mm)	0.35 × 0.22 × 0.12	0.50 × 0.30 × 0.04
Theta range for data collection (°)	1.98–26.76	2.25–26.82
Limiting indices	$-14 \leqslant h \leqslant 14$, $-15 \leqslant k \leqslant 15$, $-15 \leqslant l \leqslant 15$	$-13 \leqslant h \leqslant 14$, $-23 \leqslant k \leqslant 20$, $-31 \leqslant l \leqslant 35$
Reflections collected/ unique [*R*(int)]	7728/5006 [0.0304]	22647/6214 [0.0359]
Completeness to theta (%)	26.76, 90.5	26.82, 98.8
Absorption correction	numerical	numerical
Maximum and minimum transmission	0.370 and 0.131	0.800 and 0.145
Refinement method	full-matrix least-squares on F^2	full-matrix least-squares on F^2
Data/restraints/ parameters	5006/0/262	6214/0/327
Goodness-of-fit on F^2	1.113	1.161
Final *R* indices [$I > 2$sigma(I)]	$R_1 = 0.0375$, $wR_2 = 0.1240$	$R_1 = 0.0372$, $wR_2 = 0.0619$
R indices (all data)	$R_1 = 0.0456$, $wR_2 = 0.1362$	$R_1 = 0.0524$, $wR_2 = 0.0658$
Largest difference peak and hole (e Å^{-3})	0.891 and −1.003	0.870 and −0.597

The angles subtended by the ligands at the Hg(II) centre in **4** vary from 95.53(3) to 121.7(2) indicating a much distorted tetrahedral environment. The widening of the IHgC angle from the tetrahedral angle must be due to the higher s character of the sp^3 hybrid mercury orbitals involved in the above bonds and the formation of a strong halide-bridge between Hg atoms which requires the internal IHgI angle (95.53(3)) to be considerably smaller. The two mercury atoms and two bridging halides are perfectly coplanar. The internuclear distance between mercury atoms in complex **4** were found to be 3.926 Å, which is much longer than the sum of Van der Waals radii (3 Å) of the two mercury atoms [30], indicating the absence of significant bonding interactions between the mercury atoms in the molecular structures.

The Hg(II) centre in complex **5** is coordinated by one carbon, one oxygen and two chloro atoms in a distorted tetrahedral geometry. The two different Hg–Cl distances in **5** (2.3986(13) and 2.5106(12) Å) are less than those of found in mononuclear complex of $[HgCl_2(PPh_3)_2]$ [31] (2.559(2) and 2.545(3) Å), indicating relatively strong Hg–Cl bonds in **5**. Difference between two distances in these complexes might be arising from steric effects of the large ylidic groups. The angles around mercury in complex **5** vary from 87.39(13) to 139.45(11), indicating a much distorted tetrahedral environment. This distortion must be due to the higher s character of the sp^3 hybrid mercury orbitals involved in the above bonds and the steric effects of phosphine group needing the C–Hg–Cl angle to be larger.

The stabilized resonance structure for the parent ylides are destroyed by the complex formation, thus, the C(H)–C bond lengths, 1.473(12) Å (**4**) and 1.491(5) Å (**5**) are significantly longer than the corresponding distances found in the uncomplexed similar phosphoranes (1.407(8) Å [32] and 1.401(2) Å [33]). On the other hand, the bond length of P–C(H) in the similar ylide is 1.7194(17) Å [33] which shows that the corresponding bonds are considerably elongated to 1.786(8) Å (**4**) and 1.787(4) Å (**5**).

The C-coordination of the title ylides is in contrast to the O-coordination of the phosphorus ylide $Ph_3PC(COMe)(COPh)$ (ABPPY) in a different Hg(II) complex [34]. The difference in coordination mode between ABPPY and present ylides to Hg(II) can be rationalized in terms of the electronic properties, steric requirements and size and shape of the ligand in the final bonding mode. This may also explain by the electronic nature of the metal (Pd, Pt, Ru, Au, etc.) and even the position of the coordination site (*trans* to a C atom, *trans* to a N atom, *trans* to an O atom, and so on). The nucleophilicity of the carbanion in ABPPY is less than in our ylides; this is due to the additional delocalization of the ylide electron density in ABPPY which is facilitated by the second carbonyl group. This will reduce the ability of ABPPY to bind via the ylidic carbon. Belluco et al. have studied steric influences on the coordination modes of ylide molecules to Pt(II) systems [35]. These authors concluded that the preferred coordination mode is via the ylidic carbon, but that steric hindrance around the metal centre or the ylidic carbon will necessitate O-coordination. Indeed, this trend is reflected here, these ylides are slightly less sterically demanding than ABPPY and are C-coordinated to Hg(II).

3.3. DMSO as ligand

Literature data show that the coordination mode of dimethylsulfoxide (DMSO) to relatively soft metal atoms depends on both electronic and steric factors deriving from the DMSO moderate π-acceptor properties and its greater steric demand in the case of S-bonding [36]. In the case of ruthenium(II) complexes, coordination through sulfur (DMSO–S) seems to be preferred over

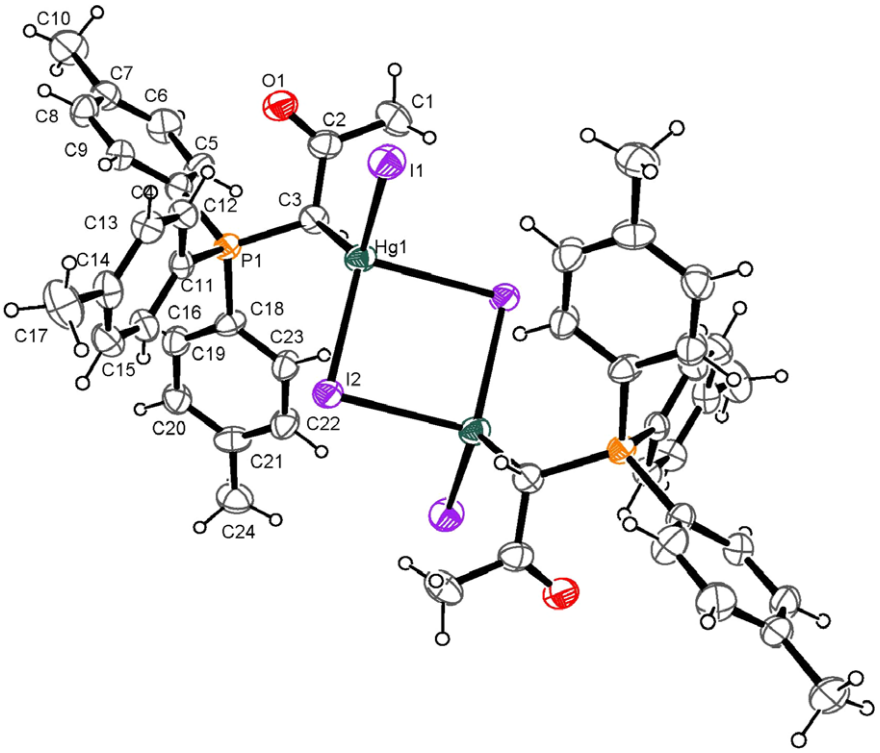

Fig. 1. ORTEP view of X-ray crystal structure of $[(Y_2) \cdot HgI_2]_2$ (**4**).

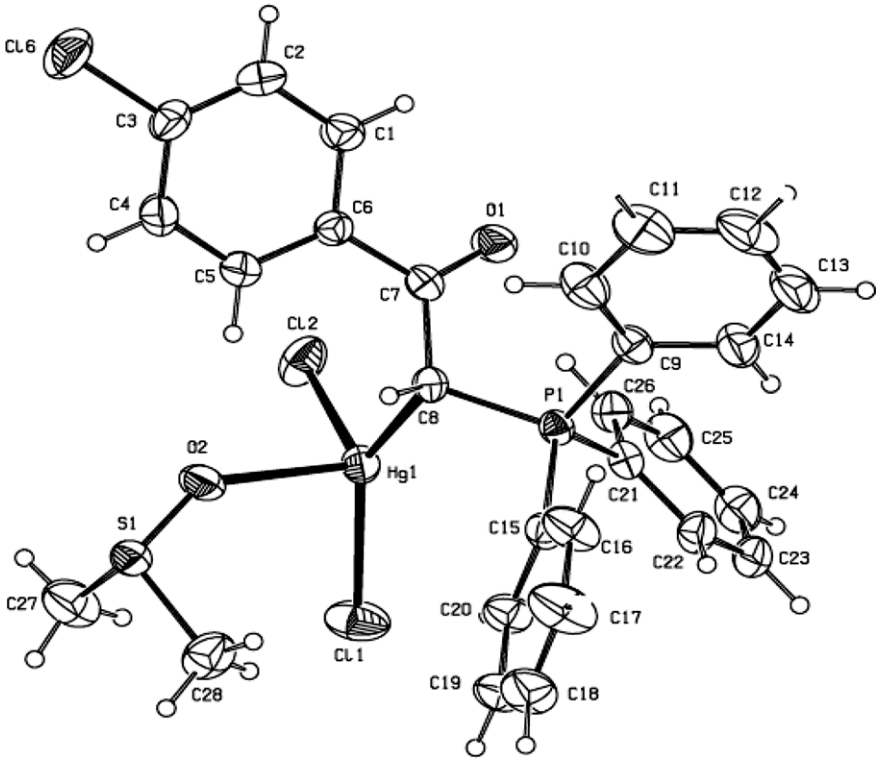

Fig. 2. ORTEP view of X-ray crystal structure of $[(Y_1) \cdot HgCl_2 \cdot DMSO]$ (**5**).

coordination through oxygen (DMSO–O) to get stable species, unless ligand overcrowding occurs [37] or DMSO is trans to strong π-acceptors like CO [38] and NO [39,40]. A similar overestimate is found for the calculated S–O distance in 'free' DMSO (1.509 Å), which results 0.018 Å longer than the experimental reference value of 1.492(1) Å [41]. The significant elongation of the S–O distance upon O-coordination is further confirmed by the recent X-ray structure determination of a disulfoxide and related copper(II) complexes, where the average S–O distances are of 1.487(4) Å (free) and 1.520(3) Å (O-bonded) [42]. This work reports the example of

Table 2
Selected bond lengths (Å) and angles (°) for **4**

Bond lengths	**4**
C(3)–C(2)	1.473(12)
C(3)–P(1)	1.786(8)
C(3)–Hg(1)	2.279(8)
C(2)–O(1)	1.214(12)
I(1)–Hg(1)	2.7036(8)
I(2)–Hg(1)	2.7795(9)
I(2)–Hg(1)#1	3.0544(12)
Bond angles	
C(2)–C(3)–Hg(1)	101.3(6)
P(1)–C(3)–Hg(1)	111.2(4)
Hg(1)–I(2)–Hg(1)#1	84.47(3)
C(2)–Hg(1)–I(1)	119.1(2)
C(2)–Hg(1)–I(2)	121.7(2)
I(1)–Hg(1)–I(2)	111.08(3)
C(3)–Hg(1)–I(2)#1	98.4(2)
I(1)–Hg(1)–I(2)#1	104.96(3)
I(2)–Hg(1)–I(2)#1	95.53(3)

Table 3
Selected bond lengths (Å) and angles (°) for **5**

Bond lengths	**5**
Hg(1)–C(8)	2.208(4)
Hg(1)–Cl(1)	2.3986(13)
Hg(1)–Cl(2)	2.5106(12)
Hg(1)–O(2)	2.548(3)
P(1)–C(8)	1.787(4)
O(1)–C(7)	1.220(5)
C(8)–C(7)	1.491(5)
O(2)–S(1)	1.507(3)
Bond angles	
Cl(2)–Hg(1)–Cl(1)	105.46(6)
C(8)–Hg(1)–Cl(2)	112.91(11)
C(8)–Hg(1)–Cl(1)	139.45(11)
C(8)–Hg(1)–O(2)	87.39(13)
O(2)–Hg(1)–Cl(2)	104.32(9)
O(2)–Hg(1)–Cl(1)	95.67(8)
C(7)–C(8)–P(1)	114.4(3)
C(7)–C(8)–Hg(1)	108.5(3)
P(1)–C(8)–Hg(1)	109.29(19)

a mercury(II) complex containing DMSO as ligand with an O-coordination mode. It is worth noting that in **5**, the S–O bond distance of 1.507(3) Å, is about 0.015 Å longer than the experimental reference value of 1.492(1) Å for free DMSO ligand [41].

3.4. Theoretical studies

We were interested to determine whether the formation of mononuclear complexes in the gas phase in which DMSO acts as ligand, energetically is more favorable than those of binuclear complexes. The analytical and spectroscopic data for compound **5** can be similar to those of the other complexes synthesized here containing ylide Y_1. Thus the observed geometry of compound **5** was considered for ab initio calculations. The optimized structure of compounds **5** is shown in Fig. 3. A comparison between the calculated bond lengths (Å) and bond angles (°) for this compound with corresponding experimental values are presented in Table 4. A list of calculated key bond lengths and bond angles and the optimized structure of compounds $[(Y_1)\cdot HgX_2\cdot DMSO]$ (where X = Br and I) are presented in Supplementary materials.

As can be seen, the calculated bond lengths are slightly longer than measured ones but the similarity of calculated and measured bond angles reflects the similar geometrical structures for these compounds in both the solid state and gas-phase. The results of calculations (Table 5) show that the products of following proposed reaction (Eq. (1)) are more stable than reactants. These stabilities are about 32, 34 and 40 kcal/mol where X is Cl, Br and I, respectively.

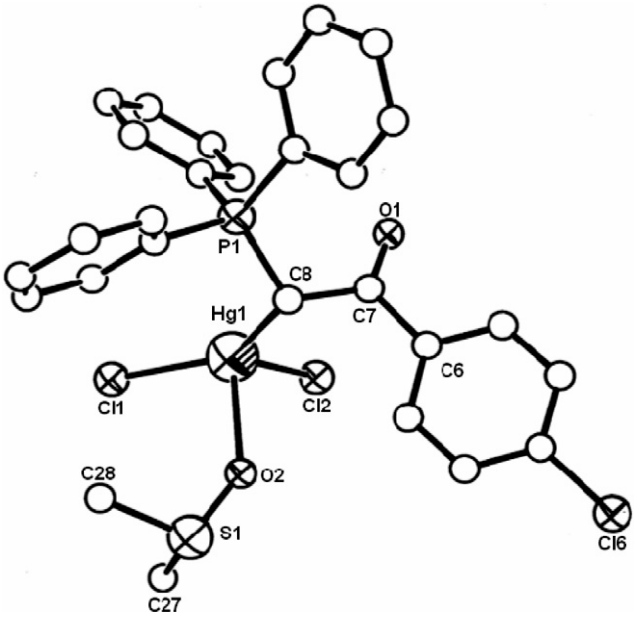

Fig. 3. The optimized structure of compound **5**.

Table 4
A comparison between the calculated bond lengths (Å) and bond angles (°) for compound **5** with corresponding experimental values

$[(Y_1)\cdot HgCl_2\cdot DMSO]$ (**5**)	X-ray	HF/Lanl2mb
Bond lengths		
Hg(1)–Cl(2)	2.511(12)	2.676
Hg(1)–Cl(1)	2.399(13)	2.688
Hg(1)–O(2)	2.548(3)	2.301
C(8)–Hg(1)	2.207(4)	2.272
P(1)–C(8)	1.788(4)	1.919
C(8)–C(7)	1.491(5)	1.538
C(7)–O(1)	1.220(5)	1.222
Bond angles		
C(8)–Hg(1)–Cl(1)	139.451	121.872
C(8)–Hg(1)–Cl(2)	112.912	106.614
Cl(1)–Hg(1)–Cl(2)	105.452	120.035
Cl(1)–Hg(1)–O(2)	95.677	95.351
Cl(2)–Hg(1)–O(2)	104.327	99.840
C(8)–C(7)–O(1)	121.186	122.329
Hg(1)–O(2)–S(1)	139.574	117.325

$$[(Y_1)\cdot HgX_2]_2 + 2DMSO \xrightarrow{rt} 2[(Y_1)\cdot HgX_2\cdot DMSO] \quad (1)$$

The similarity of calculated energies for latter reaction of Y_1 complexes indicate that the reaction energy mainly depends on the bridging halide atom. Therefore it is clear that for all compounds synthesized here, the gas-phase reaction shown in Eq. (1) is an exothermic reaction, thus it seems that the bridge-splitting reaction in

Table 5
Calculated electronic energies for binuclear complexes, DMSO and mononuclear complexes involved in Eq. (1)

Compounds	$[(Y)\cdot HgX_2]_2$ (hartree)	DMSO (hartree)	$[(Y)\cdot HgX_2\cdot DMSO]$ (hartree)	ΔE (kcal.mol^{-1})
X = Cl	−2299.4410769	−161.8305649	−1311.5770188	32.524
X = Br	−2292.3597909	−161.8305649	−1308.0376782	34.159
X = I	−2285.2766229	−161.8305649	−1304.5010169	40.337

DMSO solution is potentially possible for all dimeric complexes of Y_1 in which DMSO acts as a ligand. The data show that in the case of iodine complex, the formation of mononuclear complexes is relatively more favorable than corresponding chlorine and bromine complexes (Table 5).

4. Conclusions

Present study describes the synthesis and characterization of mononuclear and binuclear Hg(II) complexes of phosphorus ylides. On the basis of the physico-chemical and spectroscopic data we propose that ligands herein exhibit monodentate C-coordination to the metal centre, which is further confirmed by the X-ray crystal structure of the complexes. This study also presents a method for synthesis of mononuclear Hg(II) complexes of phosphorus ylides via bridge-splitting reaction using DMSO as ligand. Theoretical studies on the gas-phase structure of the complexes, confirm that, the bridge-splitting reaction in DMSO solution is potentially possible for all dimeric complexes in which DMSO acts as a ligand.

Acknowledgements

We are grateful to the Bu-Ali Sina University for a grant and Mr. Zebarjadian for recording the NMR spectra.

Appendix A. Supplementary data

CCDC 648212 and 648213 contain the supplementary crystallographic data for $[(Y_1) \cdot HgCl_2 \cdot DMSO]$ and $[(Y_2) \cdot HgI_2]_2$. These data can be obtained free of charge via http://www.ccdc.cam.ac.uk/conts/retrieving.html, or from the Cambridge Crystallographic Data Centre, 12 Union Road, Cambridge CB2 1EZ, UK; fax: (+44) 1223-336-033, or e-mail: deposit@ccdc.cam.ac.uk. Supplementary data associated with this article can be found, in the online version, at doi:10.1016/j.poly.2008.03.009.

References

[1] H.J. Christau, Chem. Rev. 94 (1994) 1299.
[2] O.I. Kolodiazhnyi, Tetrahedron 52 (1996) 1855.
[3] N.A. Nesmeyanov, V.M. Novikov, Q.A. Reutov, J. Organomet. Chem. 4 (1965) 202.
[4] E.T. Weleski, J.L. Silver, M.D. Jansson, J.L. Burmeister, J. Organomet. Chem. 102 (1975) 365.
[5] M. Kalyanasundari, K. Panchanatheswaran, W.T. Robinson, H. Wen, J. Organomet. Chem. 491 (1995) 103.
[6] R. Sanehi, R.K. Bansal, R.C. Mehrotra, Indian J. Chem. 24a (N12) (1985) 1031.
[7] S.J. Sabounchei, A. Dadrass, M. Jafarzadeh, S. Salehzadeh, H.R. Khavasi, J. Organomet. Chem. 692 (2007) 2500.
[8] S.J. Sabounchei, V. Jodaian, H.R. Khavasi, Polyhedron 26 (2007) 2845.
[9] S.J. Sabounchei, H. Nemattalab, H.R. Khavasi, J. Organomet. Chem. 692 (2007) 5440.
[10] J. Vicente, M.T. Chicote, J.A. Cayuelas, J. Fernandez-Baeza, P.G. Jones, G.M. Sheldrick, P. Espinet, J. Chem. Soc., Dalton Trans. (1985) 1163.
[11] J.A. Albanese, A.L. Rheingold, J.L. Burmeister, Inorg. Chim. Acta 150 (1988) 213.
[12] R. Usón, J. Forniés, R. Navarro, P. Espinet, C. Mendívil, J. Organomet. Chem. 290 (1985) 125.
[13] J. Vicente, M.T. Chicote, I. Saura-Llamas, J. Turpin, J. Fernandez-Baeza, J. Organomet. Chem. 333 (1987) 129.
[14] J. Vicente, M.T. Chicote, J. Fernandez-Baeza, J. Martin, I. Saura-Llamas, J. Turpin, P.G. Jones, J. Organomet. Chem. 331 (1987) 409.
[15] H. Koezuka, G. Matsubayashi, T. Tanaka, Inorg. Chem. 25 (1976) 417.
[16] J.A. Albanese, D.L. Staley, A.L. Rheingold, J.L. Burmeister, Inorg. Chem. 29 (1990) 2209.
[17] I. Kawafune, G.E. Matsubayashi, Inorg. Chim. Acta 70 (1983) 1.
[18] F. Ramirez, S. Dershowitz, J. Organomet. Chem. 22 (1957) 41.
[19] Stoe & Cie, X-AREA, version 1.30: Program for the Acquisition and Analysis of Data, Stoe & Cie GmbH, Darmatadt, Germany, 2005.
[20] G.M. Sheldrick, SHELX97. Program for Crystal Structure Solution and Refinement, University of Göttingen, Germany, 1997.
[21] Stoe & Cie, X-STEP32, Version 1.07b: Crystallographic Package, Stoe & Cie GmbH, Darmatadt, Germany, 2000.
[22] M.J. Frisch, G.W. Trucks, H.B. Schlegel, G.E. Scuseria, M.A. Robb, J.R. Cheeseman, V.G. Zakrzewski, J.A. Montgomery, R.E. Stratman, J.C. Burant, S. Dapprich, J.M. Millam, A.D. Daniels, K.N. Kudin, M.C. Strain, O. Farkas, J. Tomasi, V. Barone, M. Cossi, R. Cammi, B. Menucci, C. Pomelli, C. Adamo, S. Clifford, J. Ochterski, G.A. Petersson, P.Y. Ayala, Q. Cui, K. Morokuma, D.K. Malick, A.D. Rabuck, K. Raghavachari, J.B. Foresman, J. Ciolowski, J.V. Ortiz, B.B. Stefanov, G. Liu, A. Liashenko, P. Piskorz, I. Komaromi, R. Gomperts, R.L. Martin, D.J. Fox, T. Keith, M.A. Al-Laham, C.Y. Peng, A. Nanayakkara, C. Gonzales, M. Challacombe, P.M.W. Gill, B.G. Jonhson, W. Chen, M.W. Wong, J.L. Andres, M. Head-Gordon, E.S. Repogle, J.A. Pople, GAUSSIAN 98, Revision A.6, Gaussian Inc., Pittsburgh, PA, 1998.
[23] J.B. Collins, P.V.R. Schleyer, J.S. Binkley, J.A. Pople, J. Chem. Phys. 64 (1976) 5142.
[24] H.J. Bestmann, B. Arnason, Chem. Ber. 95 (1962) 1513.
[25] E.C. Spencer, M.B. Mariyatra, J.A.K. Howard, A.M. Kenwright, K. Panchanatheswaran, J. Organomet. Chem. 692 (2007) 1081.
[26] J. Vicente, M.T. Chicote, M.C. Lagunas, P.G. Jones, J. Chem. Soc., Dalton Trans. (1991) 2579.
[27] J.A. Teagle, J.L. Burmeister, Inorg. Chim. Acta 118 (1986) 65.
[28] N.L. Holy, N.C. Baenziger, R.M. Flynn, D.C. Swenson, J. Am. Chem. Soc. 98 (1976) 7823.
[29] G. Facchin, R. Bertani, M. Calligaris, G. Nardin, M. Mari, J. Chem. Soc., Dalton Trans. (1987) 1381.
[30] J.E. Huheey, Inorganic Chemistry – Principles of Structure and Reactivity, 2nd ed., Harper Int. Ed., New York, 1978. p. 233.
[31] N.A. Bell, T.D. Dee, M. Goldstein, P.J. McKenna, I.W. Novel, Inorg. Chim. Acta 71 (1983) 135.
[32] M. Kalyanasundari, K. Panchanatheswaran, V. Parthasarathi, W.T. Robinson, H. Wen, Acta Crystallogr. 50 (1994) 1738.
[33] S.J. Sabounchei, A. Dadrass, M. Jafarzadeh, H.R. Khavasi, Acta Crystallogr., Sect. E 63 (2007) o3160.
[34] P. Laavanya, U. Venkatasubramanian, K. Panchanatheswaran, J.A.K. Bauer, Chem. Commun. (2001) 1660.
[35] U. Belluco, R.A. Michelin, R. Bertani, G. Facchin, G. Pace, L. Zanotto, M. Mozzon, M. Furlan, E. Zangrando, Inorg. Chim. Acta 252 (1996) 355.
[36] M. Calligaris, O. Carugo, Coord. Chem. Rev. 153 (1996) 83.
[37] E. Alessio, G. Mestroni, G. Nardin, W.M. Attia, M. Calligaris, G. Sava, S. Zorzet, Inorg. Chem. 27 (1988) 4099.
[38] E. Alessio, B. Milani, M. Bolle, G. Mestroni, P. Faleschini, F. Todone, S. Geremia, M. Calligaris, Inorg. Chem. 34 (1995) 4722.
[39] B. Serli, E. Zangrando, E. Iengo, G. Mestroni, L. Yellowlees, E. Alessio, Inorg. Chem. 41 (2002) 4033.
[40] B. Serli, E. Zangrando, E. Iengo, E. Alessio, Inorg. Chim. Acta 339 (2002) 265.
[41] M. Calligaris, N.S. Panina, J. Mol. Struct. 646 (2003) 61.
[42] M. Calligaris, A. Melchior, S. Geremia, Inorg. Chim. Acta 323 (2001) 89.

Polyhedron 27 (2008) 2022–2028

Contents lists available at ScienceDirect

Polyhedron

journal homepage: www.elsevier.com/locate/poly

Studies on zinc(II) complexes with *N*-thioacylamidophosphates: X-ray crystal structure of the [Zn(RC(S)NP(O)(O*i*Pr)$_2$)$_2$] (R = NH_2, *t*BuNH, *c*-$C_6H_{11}NH$)

Damir A. Safin [a,*], Felix D. Sokolov [a], Heinrich Nöth [b], Maria G. Babashkina [a], Timur R. Gimadiev [a], Joanna Galezowska [c], Henryk Kozlowski [c]

[a] *A.M. Butlerov Chemistry Institute, Kazan State University, Kremlevskaya Street 18, 420008 Kazan, Russia*
[b] *Department für Chemie der Universität München, Butenandtstrasse 5-13 (Haus D), 81377 München, Germany*
[c] *University of Wroclaw, Faculty of Chemistry, 50-383 Wroclaw, Poland*

ARTICLE INFO

Article history:
Received 27 September 2007
Accepted 12 March 2008

Keywords:
Organoelement analogues of β-dicarbonyl ligands
(Thioacylamido)phosphates
Zn(II) chelates
Heteroligand complexes
1,10-Phenanthroline
2,2′-Bipyridine

ABSTRACT

The photoluminescent properties of 17 zinc(II) chelates [Zn(RC(S)NP(O)(O*i*Pr)$_2$-*O*,*S*)$_2$] (R = Ph (**1a**), PhNH (**1b**), *p*-BrPh (**1c**), *p*-MeOC$_6$H$_4$NH (**1d**), *p*-BrC$_6$H$_4$NH (**1e**), NH_2 (**1f**), *i*PrNH (**1g**), *t*BuNH (**1h**), Et_2N (**1i**), *c*-$C_5H_{10}N$ (**1j**), *c*-OC_4H_8N (**1k**), *c*-$C_6H_{11}NH$ (**1l**), aminobenzo-15-crown-5 (**1m**)) and [Zn(B)(RC(S)NP(O)(O*i*Pr)$_2$-*O*,*S*)$_2$] (R = Ph, B = 2,2′-bipyridine (**2a**); R = Ph, B = 1,10-phenanthroline (**2b**); R = PhNH, B = 2,2′-bipyridine (**2c**); R = PhNH, B = 1,10-phenanthroline (**2d**)), are reported. Colorless and air/moisture stable chelate complexes of divalent zinc show blue emission in the solid state when excited with UV light. Complexes **1f**, **1h**, **1l** were investigated by single crystal X-ray diffraction. The zinc(II) atom in complexes **1f**, **1h**, **1l** is in a distorted tetrahedral O_2S_2 environment formed by the C=S sulphur atoms and the P=O oxygen atoms of two deprotonated ligands.

© 2008 Elsevier Ltd. All rights reserved.

1. Introduction

Up to now, large numbers of coordination complexes of the Zn(II) cation have been prepared by taking certain factors into account, such as the functionality, flexibility, symmetry and nature of donor centers of organic ligands and the coordination ability of the metal ion [1]. Among these, the construction of complexes with changeable geometry and structure, to the best of our knowledge, has become a widely propagated and popular subject. Such complexes are important in advanced materials such as optical devices, especially with luminescence properties [2]. One of the effective strategies to vary luminescent activity is to change the geometry and structure. This requires the synthesis of complexes by addition of a heteroligand to homoligand luminescence active complexes. These compounds might find applications as receptors with optical detecting properties.

The late transition metal ion complexes of *N*-acylthioureas $R_2NC(S)NHC(O)R'$ [3] and their phosphoryl analogues based on thioureas $R_2NC(S)NHP(O)(OR')_2$ and thioamides $RC(S)NHP(O)(OR')_2$ [4,5, and references therein] are of interest due to their magnetic and photophysical properties. The 1,5-*X*,*S*-coordination of these ligand anions is typical for chelate complexes (e.g. [4–6]).

However, recent investigations have shown that the coordination mode of these ligands containing the RNH group towards Ni(II), Pd(II), Pt(II) [7,8], Cu(II) [9] and Cd(II) [10] cations depends on the presence of strong intramolecular NH···O=P or NH···O=C bonds. The thiourea ligands of common formula $RNHC(S)NHP(O)(OR')_2$ (NPTU) [8,9] are able to bind Ni(II), Pd(II) and Cu(II) cations through the C=S sulfur and P–N nitrogen atoms. The thiourea *n*PrNHC(S)NHC(O)*n*Pr [7] forms similar 1,3-*N*,*S*-chelate with the Pt(II) cation through the C=S sulfur and NC(O) nitrogen atoms.

Interestingly, the *N*-(*o*-nitrophenyl)-*N*′-(methoxycarbonyl)thiourea (HQ) in complex of formula [Cd(2,2′-bpy)Q_2] is also bound in the 1,3-*N*,*S*-fashion via the C=S sulfur and NC(O) nitrogen atoms [10]. However, the sulfur atom of the thiourea HQ does not coordinate to the Zn(II) ion. A monodentate coordination through the deprotonated nitrogen atom of the C(S)NC(O) moiety occurs in the chelate [Zn(2,2′-bpy)Q_2].

In the literature there is no information on crystal structure of NPTU complexes with the Zn(II) cation. In this connection it was interesting to investigate the structure and properties of some complexes of phosphorylated thioureas and thioamides and compares these with heteroligand analogues with participation of 2,2′-bipyridine (bpy) and 1,10-phenanthroline (phen) as additional donor ligands.

* Corresponding author. Tel./fax: +7 843 2543734.
E-mail addresses: damir.safin@ksu.ru (D.A. Safin), felix.sokolov@ksu.ru (F.D. Sokolov).

0277-5387/$ - see front matter © 2008 Elsevier Ltd. All rights reserved.
doi:10.1016/j.poly.2008.03.005

In this paper, we report on the photoluminescence properties at room temperature of thirteen solid zinc-containing chelating complexes with HL of composition Zn[RC(S)NP(O)(O*i*Pr)$_2$-*O*,*S*]$_2$ (R = Ph **1a**, PhNH **1b**, *p*-BrPh **1c**, *p*-MeOC$_6$H$_4$NH **1d**, *p*-BrC$_6$H$_4$NH **1e**, NH$_2$ **1f**, *i*PrNH **1g**, *t*BuNH **1h**, Et$_2$N **1i**, *c*-C$_5$H$_{10}$N **1j**, *c*-OC$_4$H$_8$N **1k**, *c*-C$_6$H$_{11}$NH **1l**, aminobenzo-15-crown-5 **1m**) and four novel heteroligand complexes of composition Zn(B)[RC(S)NP(O)(O*i*Pr)$_2$-*O*,*S*]$_2$ (R = Ph, B = 2,2′-bipyridine **2a**; R = Ph, B = 1,10-phenanthroline **2b**; R = PhNH, B = 2,2′-bipyridine **2c**; R = PhNH, B = 1,10-phenanthroline **2d**).

2. Experimental

2.1. Physical measurements

Infrared spectra (Nujol) were recorded on a Specord M-80 spectrometer in the range 400–3600 cm^{-1}. NMR spectra were obtained on a Varian Unity-300 NMR spectrometer at 25 °C. ^{1}H and ^{31}P{^{1}H} spectra were recorded at 299.948 and 121.420 MHz, respectively. Chemical shifts are reported with reference to $SiMe_4$ (^{1}H) and H_3PO_4 (^{31}P{^{1}H}). Electron ionization mass spectra were measured on the TRACE MS Finnigan MAT instrument. Ionization energy was 70 eV. The substance was injected directly into the ion source at 150 °C. Heating was carried out in a programmed mode from 35 to 200 °C at a rate of 35 °C/min. Electrospray ionization mass spectra were measured with a Finnigan-Mat TCQ 700 mass spectrometer on a 10^{-6} M solution in CH_3OH. The speed of a sample submission was 2 μL/min. The ionization energy was 4.5 kV. The capillary temperature was 200 °C. Fluorescence measurements were made on a SLM Aminco 500 spectrofluorometer at room temperature. Elemental analyses were performed on a Perkin–Elmer 2400 CHN microanalyser. An ENRAF NONIUS four circle diffractometer, operating with Mo Kα radiation and a graphite monochromator was used for determining the crystallographic parameters and collecting the data sets.

2.2. Synthesis of [ZnL$_2$] (**1a**–**1m**)

Complexes **1a**, **1b**, **1d**, **1e**, **1g**–**1l** were prepared according to the previously described techniques [4,5,11].

Complexes **1c** and **1f** were synthesized for the first time by the method used in [4,5]. A suspension of HL, R = *p*-BrC$_6$H$_4$ (1.900 g, 5 mmol) or R = NH$_2$ (1.200 g, 5 mmol) in aqueous ethanol (20 mL) was mixed with an ethanol solution of potassium hydroxide (0.28 g, 5 mmol). An aqueous (20 mL) solution of $ZnCl_2$ (0.381 g, 2.8 mmol) was added dropwise under vigorous stirring at room temperature for a further 3 h and left overnight. The resulting complex was extracted with dichloromethane, washed with water and dried with anhydrous $MgSO_4$. The solvent was then removed in vacuo. A colourless precipitate was isolated from dichloromethane by *n*-hexane.

2.2.1. [Zn(*p*-BrC$_6$H$_4$C(S)NP(O)(O*i*Pr)$_2$)$_2$] (**1c**)

Yield: 1.73 g (84%), m.p. 143 °C. ^{1}H NMR ($CDCl_3$): δ (ppm) = 1.35 (d, $^3J_{H,H}$ = 5.6 Hz, 12 H, CH_3), 1.36 (d, $^3J_{H,H}$ = 5.6 Hz, 12H, CH_3), 4.71 (d. sept, $^3J_{POCH} \approx {}^3J_{H,H} \approx 6.2$ Hz, 4H, OCH), 7.50 (m, 4H, *o*-H, C$_6$H$_4$), 8.14 (m, 4H, *m*-H, C$_6$H$_4$). ^{31}P{^{1}H} NMR ($CDCl_3$): 6.9 ppm. IR (cm^{-1}): 1000 (b, vs) (POC); 1152 (vb, s) (P═O); 1544 (s) (SCN). *Anal.* Calc. for $C_{26}H_{36}Br_2N_2O_6P_2S_2Zn$ (823.85): C, 37.90; H, 4.40; N, 3.40. Found: C, 37.86; H, 4.45; N, 3.38%.

2.2.2. [Zn(NH$_2$C(S)NP(O)(O*i*Pr)$_2$)$_2$] (**1f**)

Yield: 1.24 g (91%), m.p. 182 °C. ^{1}H NMR ($CDCl_3$): δ (ppm) = 1.29 (d, $^3J_{H,H}$ = 6.2 Hz, 12H, CH_3), 1.30 (d, $^3J_{H,H}$ = 6.2 Hz, 12H, CH_3), 4.58 (d. sept, $^3J_{POCH}$ = 7.6 Hz, $^3J_{H,H}$ = 6.2 Hz, 4H, OCH), 5.81 (br. s, 1H, NH$_2$), 5.97 (br. s, 1H, NH$_2$). ^{31}P{^{1}H} NMR ($CDCl_3$): 6.2 ppm. IR (cm^{-1}): 992 (b, vs) (POC); 1132 (vb, s) (P═O); 1512 (s) (SCN); 1620 (s), 3136 (b, s), 3272 (s); 3496 (s) (NH$_2$). *Anal.* Calc. for $C_{14}H_{32}N_4O_6P_2S_2Zn$ (542.05): C, 30.92; H, 5.93; N, 10.30. Found: C, 30.90; H, 5.91; N, 10.33%.

2.3. Synthesis of [Zn(B)L$_2$] (**2a**–**2d**)

A solution of complexes **1a** (0.30 g, 0.45 mmol) or **1b** (0.31 g, 0.45 mmol) in benzene (10 mL) was added dropwise whilst stirring to a solution of 2,2′-bipyridine (0.07 g, 0.45 mmol) or 1,10-phenanthroline (0.08 g, 0.45 mmol) in benzene (10 mL). After complete addition, the solution was stirred for an hour. The solvent was then removed in vacuo. The residue was recrystallized from a methylene chloride/*n*-hexane mixture. The complexes **2a**-**2d** were isolated as colorless powders.

2.3.1. [Zn(2,2′-bpy)(PhC(S)NP(O)(OiPr)$_2$)$_2$] (**2a**)

Yield: 0.28 g (75%), m.p. 102 °C. ^{1}H NMR ($CDCl_3$): δ (ppm) = 1.36 (d, $^3J_{H,H}$ = 6.1 Hz, 24H, CH_3), 4.74 (d. sept, $^3J_{POCH} \approx {}^3J_{H,H} \approx 6.5$ Hz, 4H, OCH), 7.21–8.76 (m, 18H, C$_6$H$_5$ + bpy). ^{31}P{^{1}H} NMR ($CDCl_3$): 5.9 ppm. IR (cm^{-1}): 996 (b, vs) (POC); 1168 (b, s) (P═O); 1464 (s) (SCN). EI-MS: *m*/*z* (%) = 665 (73) [ZnL$_2$]$^+$, 301 (61) [HL]$^+$, 156 (13) [bpy]$^+$. ES (positive ion): *m*/*z* (%) = 522.2 (100) [M−PhC(S)NP(O)(O*i*Pr)$_2$]$^+$. *Anal.* Calc. for $C_{36}H_{46}N_4O_6P_2S_2Zn$ (820.16): C, 52.59; H, 5.64; N, 6.81. Found: C, 52.62; H, 5.60; N, 6.78%.

2.3.2. [Zn(1,10-phen)(PhC(S)NP(O)(OiPr)$_2$)$_2$] (**2b**)

Yield: 0.31 g (82%), m.p. 154 °C. ^{1}H NMR ($CDCl_3$): δ (ppm) = 1.32 (d, $^3J_{H,H}$ = 6.0 Hz, 24H, CH_3), 4.72 (d. sept, $^3J_{POCH} \approx {}^3J_{H,H} \approx 6.5$ Hz, 4H, OCH), 7.28–8.42 (m, 18H, C$_6$H$_5$ + phen). ^{31}P{^{1}H} NMR ($CDCl_3$): 6.1 ppm. IR (cm^{-1}): 996 (b, vs) (POC); 1172 (b, s) (P═O); 1492 (s) (SCN). EI-MS: *m*/*z* (%) = 665 (100) [ZnL$_2$]$^+$, 301 (29) [HL]$^+$, 180 (54) [phen]$^+$. ES (positive ion): *m*/*z* (%) = 546.3 (100) [M−PhC(S)NP(O)(O*i*Pr)$_2$]$^+$. *Anal.* Calc. for $C_{38}H_{46}N_4O_6P_2S_2Zn$ (844.16): C, 53.93; H, 5.48; N, 6.62. Found: C, 53.96; H, 5.51; N, 6.59%.

2.3.3. [Zn(2,2′-bpy)(PhNHC(S)NP(O)(OiPr)$_2$)$_2$] (**2c**)

Yield: 0.25 g (65%), m.p. 101 °C. ^{1}H NMR ($CDCl_3$): δ (ppm) = 1.15–1.33 (m, 24H, CH_3), 4.48–4.65 (m, 4H, OCH), 6.89–8.46 (m, 18H, C$_6$H$_5$ + bpy), 8.58–8.63 (m, 2H, PhNH). ^{31}P{^{1}H} NMR ($CDCl_3$): 6.5 ppm. IR (cm^{-1}): 1008 (b, vs) (POC); 1140 (b, s) (P═O); 1560 (s) (SCN); 3312 (NH). EI-MS: *m*/*z* (%) = 695 (22) [ZnL$_2$]$^+$, 316 (100) [HL]$^+$, 56 (74) [bpy]$^+$. ES (positive ion): *m*/*z* (%) = 537.3 (100) [M−PhNHC(S)NP(O)(O*i*Pr)$_2$]$^+$. *Anal.* Calc. for $C_{36}H_{48}N_6O_6P_2S_2Zn$ (850.18): C, 50.73; H, 5.68; N, 9.86. Found: C, 50.70; H, 5.72; N, 9.84%.

2.3.4. [Zn(1,10-phen)(PhNHC(S)NP(O)(OiPr)$_2$)$_2$] (**2d**)

Yield: 0.31 g (82%), m.p. 104 °C. ^{1}H NMR ($CDCl_3$): δ (ppm) = 0.96–1.32 (m, 24H, CH_3), 4.39–4.66 (m, 4H, OCH), 6.85–8.45 (m, 18H, C$_6$H$_5$ + phen), 9.18–9.40 (m, 2H, PhNH). ^{31}P{^{1}H} NMR ($CDCl_3$): 6.6 ppm. IR (cm^{-1}): 1020 (b, vs) (POC); 1144 (b, s) (P═O); 1504 (s) (SCN); 3288 (NH). EI-MS: *m*/*z* (%) = 695 (34) [ZnL$_2$]$^+$, 316 (57) [HL]$^+$, 180 (91) [phen]$^+$. ES (positive ion): *m*/*z* (%) = 561.2 (100) [M−PhNHC(S)NP(O)(O*i*Pr)$_2$]$^+$. *Anal.* Calc. for $C_{38}H_{48}N_6O_6P_2S_2Zn$ (874.18): C, 52.08; H, 5.52; N, 9.59. Found: C, 52.04; H, 5.47; N, 9.64%.

2.4. Crystal structure determination and refinement

The selected crystal was coerced with lithelene and mounted on a glass fibre. It was then cooled to −60 °C on the goniometer head of a Kappa Nonius diffractometer operated with a rotating anode. After alignment the unit cell parameters were calculated from a se-

lected data set, and data collection was performed by using an area detector. For data reduction the program SMART was used, and for structure solution and refinement the program package SHELXTL PLUS. All plots of the molecules are shown with a 50% probability for the thermal ellipsoids. The numbering of the atoms is shown in Figs. 1–3 (ORTEP) [12] (see Table 1).

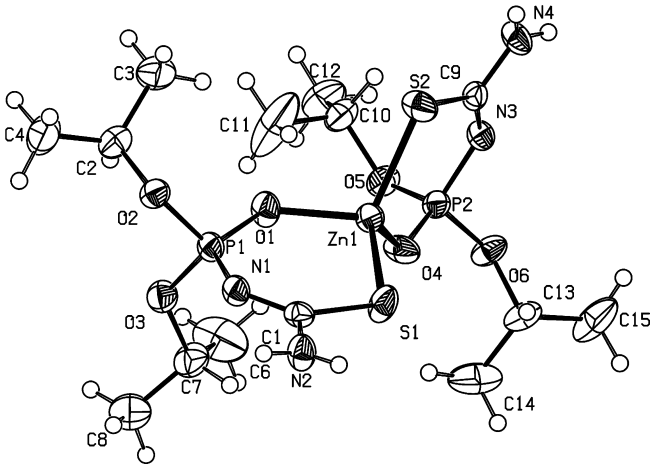

Fig. 1. An ORTEP view of $[Zn(H_2NC(S)NP(O)(OiPr)_2)_2]$ (**1f**). Displacement ellipsoids are drawn at the 50% probability level.

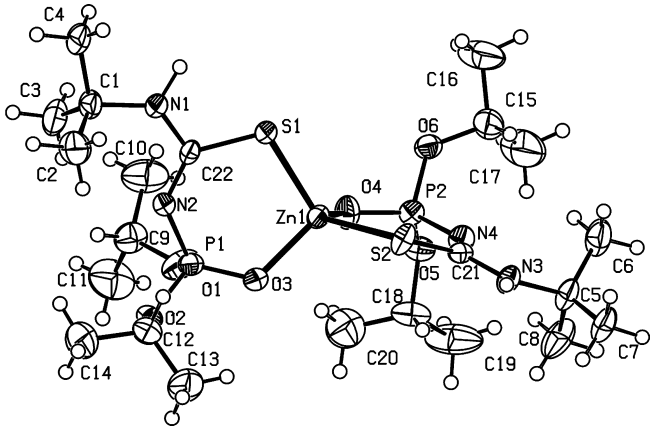

Fig. 2. An ORTEP view of $[Zn(t\text{BuNHC}(S)NP(O)(OiPr)_2)_2]$ (**1h**). Displacement ellipsoids are drawn at the 50% probability level.

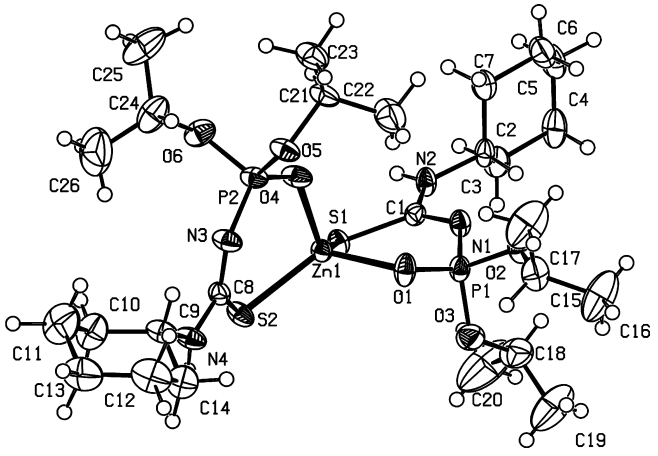

Fig. 3. An ORTEP view of $[Zn(c\text{-}C_6H_{11}NHC(S)NP(O)(OiPr)_2)_2]$ (**1l**). Displacement ellipsoids are drawn at the 50% probability level.

3. Results and discussion

3.1. Synthesis

Complexes **1a**–**1m** were prepared by the following procedure: the ligand was converted to the potassium salt, followed by reaction with $ZnCl_2$ (Scheme 1). The compounds obtained are crystalline solids soluble in most polar solvents.

Unsaturation of the ZnO_2S_2 coordination environment opens up possibilities for the synthesis of a large number of heteroligand complexes. They are obtained by the interaction of these complexes with various donor agents.

In order to obtain the heteroligand complexes, we have combined HL and two aromatic chelate ligands, (2,2′-bipyridine or 1,10-phenanthroline) in experiments based on the following considerations: (i) the steric hindrance at the metal center will be increased when the aromatic 1,4-donor ligand binds to the metal ion; this ensures the formation of the lower dimensional structure and on the other hand (ii) metal complexes of 2,2′-bipyridine or 1,10-phenanthroline and their derivatives exhibit excellent luminescent properties [13], which can be used not only as efficient blue emitters in electroluminescent devices but also as chemical sensors for specific organic molecules [14].

Complexes **2a**–**2d** were prepared by the following procedure: a benzene solution of 2,2′-bipyridine or 1,10-phenanthroline was added dropwise to a benzene solution of **1a** or **1b** (Scheme 1). The compounds obtained **2a**–**2d** are crystalline solids soluble in most polar solvents.

3.2. IR and NMR spectroscopy

It is shown that all listed complexes **1a**–**1m** have a similar coordination environment at the zinc atom. The IR, ^1H, $^{31}P\{^1H\}$ NMR [4,11] and X-ray [4] data confirm that in a $CDCl_3$ solution and in the solid state only $[ZnL_2]$ chelates with a tetrahedral ZnO_2S_2 core exist. The 1,5-*O*,*S*-coordination appears to be the most steric favorable in this case because it provides a maximal bite angle for the ligand's anionic form L^-.

The additional ligands bpy or phen in a molecule of complex could affect on the coordination mode of the anionic thiourea ligands. The bond angles in the cation environment decrease in comparison with the tetrahedral core and requirements to the bite angle are softened, thus the situation becomes ambiguous. The structures of the thiourea HQ chelates with the Zn(II) and Cd(II) cations demonstrate the examples of such changes in the coordination modes [10].

There is a strong (20–25 kJ/mol) hydrogen bond of type PhNH···O=P in the thiourea $PhNHC(S)NHP(O)(OiPr)_2$ and its complexes [8,9]. It prevents the coordination through the P=O group in square planar complexes of the Ni(II), Pd(II) and Cu(II) cations.

Thus, the presence the bpy or phen in the coordination sphere of Zn(II) makes possible the three coordination modes of $PhNHC(S)NHP(O)(OiPr)_2$ (HL): (i) preservation of the 1,5-*O*,*S*-coordination for L^- (Scheme 2A); (ii) 1,3-*N*,*S*-coordination of L^- (Scheme 2B); (iii) monodentate *N*-coordination (Scheme 2C). Neither of them could be discarded *a priori*.

The 1,5-*O*,*S*-coordination (Scheme 2A) is a unique variant is for complexes of the thioamide $PhC(S)NHP(O)(OiPr)_2$ due to absence of the intramolecular H-bonds.

Unfortunately, we could not get suitable crystals of complexes **2a**–**2d**, for X-ray structure analysis. However, according to the IR, ^1H, $^{31}P\{^1H\}$ NMR and luminescence data, obtained in a $CDCl_3$ solution and in the solid state, complexes **2a**–**2d** have a $ZnO_2S_2N_2$ core (Scheme 2A). The comparative analysis of IR spectra of the initial ligands $RC(S)NHP(O)(OiPr)_2$ (R = Ph and PhNH), their complexes

Table 1
Crystal data and data collection parameters for **1f**, **1h** and **1l**

	Compound		
	1f	**1h**	**1l**
Chemical formula	$C_{14}H_{32}N_4O_6P_2S_2Zn$	$C_{22}H_{48}N_4O_6P_2S_2Zn$	$C_{26}H_{52}N_4O_6P_2S_2Zn$
Formula weight	543.91	656.11	708.19
Crystal size (mm)	0.06 × 0.14 × 0.19	0.22 × 0.30 × 0.35	0.15 × 0.21 × 0.25
Crystal system	monoclinic	monoclinic	monoclinic
Space group	$P2_1/n$	Cc	$P2_1/c$
a (Å)	15.9479(4)	24.776(5)	14.912(5)
b (Å)	9.1698(2)	9.350(2)	17.531(5)
c (Å)	17.4946(4)	14.476(3)	15.153(5)
β (°)	104.0098(1)	98.41(3)	115.410(5)
V (Å^3)	2482.29(10)	3317.3(12)	3578(2)
Z	4	4	4
ρ(calc.) (Mg/m^3)	1.455	1.314	1.315
μ (mm^{-1})	1.321	1.001	0.933
F(000)	1136	1392	1504
Index range	$-18 \leqslant h \leqslant 18$, $-10 \leqslant k \leqslant 10$, $-20 \leqslant l \leqslant 20$	$-30 \leqslant h \leqslant 30$, $-11 \leqslant k \leqslant 11$, $-17 \leqslant l \leqslant 17$	$-18 \leqslant h \leqslant 18$, $-21 \leqslant k \leqslant 20$, $-18 \leqslant l \leqslant 18$
2θ (°)	50.02	52.22	52.02
Temperature (K)	200	193	193
Reflections collected	8389	6192	13268
Reflections unique	4358	6187	7020
Reflections observed (4σ)	3598	5724	5853
R(int.)	0.017	0.005	0.026
Number of variables	294	337	538
Weight. scheme[a], x/y	0.0511/1.1243	0.0495/7.0103	0.0500/0.8394
Goodness-of-fit	1.05	1.01	1.02
Final R (4σ)	0.0337	0.0387	0.0319
Final wR_2	0.0927	0.1028	0.0882
Larg. res. peak (ε/Å^3)	0.29	0.43	0.38

[a] $w^{-1} = \sigma^2F^2_o + (xP)^2 + yP$; $P = (F^2_o + 2F^2_c)/3$.

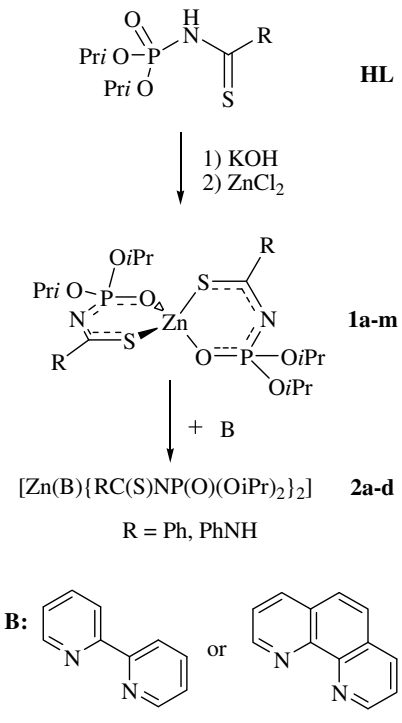

Scheme 1.

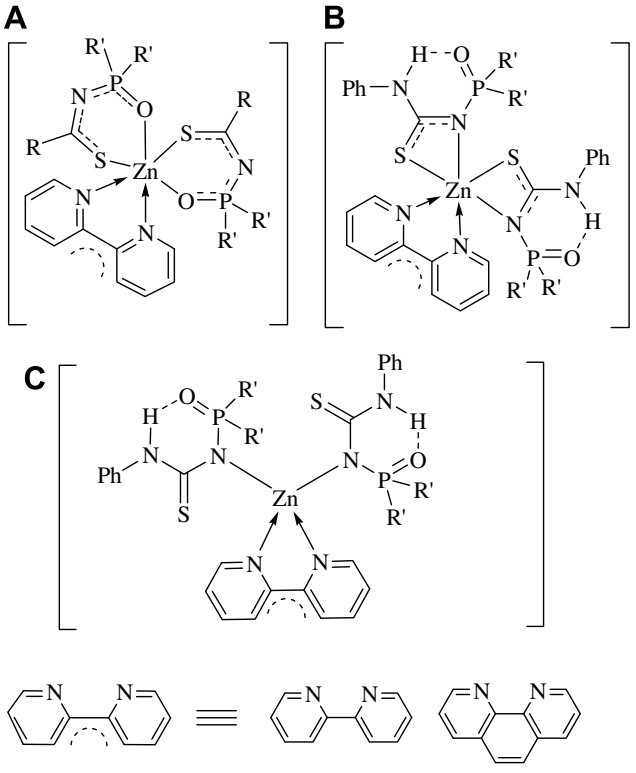

Scheme 2. Proposed modes of the ligand coordination in complexes [Zn(B)L_2] (2). R′ = O*i*Pr.

with the Zn(II) cation **1a** and **1b**, and adducts **2a**–**2d** confirms the preservation of the 1,5-*O*,*S*-coordination in the [ZnL_2] core of **2a**–**2d**.

There is a series of the P═O group absorption bands in the IR spectra of complexes **2a**–**2d** in the area close to the appropriate 1,5-*O*,*S*-chelate complexes of type [ML_2] [4–6], and there is also an intense absorption band of the SCN fragment. This confirms the 1,5-*O*,*S*-coordination of the ligand anions.

It is important to note, that the band of the PhNH group in **2c**, **2d** is in the field of 3288–3312 cm^{-1}, which is characteristic for

1,5-*O*,*S*-isomers, showing the weak intermolecular H-bonding in the solid state [5,8]. The isomers B and C must have the NH-group absorption band up to 3100–3160 cm^{-1} [8] due to formation of the strong intramolecular hydrogen bond (Scheme 2).

The $^{31}P\{^1H\}$ NMR signals of complexes **2a**–**2d** appear at δ = 5.9–6.7 ppm, i. e. there is a down-field shift relative to that of the free ligand RC(S)NP(O)(O*i*Pr)$_2$ (R = Ph, δ = −5.6 ppm and PhNH, δ = −5.3 ppm). Full width at half peak heights is in the range 3.0–9.0 Hz. However, the shift of the signals in **2a**–**2d** is more than 0.2–0.4 ppm, compared to the complexes **1a** and **1b** [11]. The signals are in the region that is characteristic to the amidophosphate environment in complexes of *N*-acylamidophosphate anions.

The ^1H NMR spectra of complexes **2a**–**2d** contain a set of signals for the (*i*PrO)$_2$P(O) and C_6H_5 protons. There are also signals corresponding to the polyaromatic chelate ligand. Analysis of the integral intensities of the proton signal testifies about complexes **2a**–**2d** structure of [Zn(2,2′-bpy)L_2] (**2a**, **2c**) or [Zn(1,10-phen)L_2] (**2b**,**2d**).

Thus, IR and NMR spectroscopy data confirm the structure of the adducts **2a**–**2d** in solution and solid state. The donor polyaromatic ligands, as well as anionic ligands, are coordinated to the Zn(II) cation.

3.3. EI mass spectrometry

Molecular ions of complexes **2a**–**2d** are unstable under the conditions of measurement, and the heaviest molecular ion, observed in the spectra of **2a**–**2d**, corresponds to the neutral [ZnL_2] complex core. In the EI mass spectra there are also peaks of the parent amidophosphate ligands, 2,2′-bipyridine and 1,10-phenanthroline, respectively.

3.4. Molecular structure of ZnL_2 complexes *1f*, *1h*, *1l*

According to the X-ray data complexes **1f**, **1h**, **1l** are spirocycling bis-chelates with a distorted-tetrahedral ZnO_2S_2 core. All complexes contain structurally independent ligand moieties. The selected bond lengths and torsion angles are given in Table 2. Intermolecular hydrogen bond parameters are given in Table 3.

Bond lengths (S)C–N and P–N in complexes are shortened (Table 2) and the C=S and P=O(Zn) distances are considerably lengthened in comparison with typical interatomic distances reported for *N*-phosphorylated thioureas [6]. The bond lengths distribution in the ligand moieties confirms the superiority of *S*-enolic tautomeric form S–C=N–P=O for all compounds.

Six-membered Zn–O–P–N–C–S cycles have the asymmetrical boat conformation. The maximal deviation of atoms from the least square plane (LSP) of the cycles is observed for the phosphorus, sulphur and zinc atoms. Chelate cycles in **1f** are almost planar; the deviation from LSP is the smallest among the presented structures.

Complexes **1f**, **1l** show a remarkably different H-bonding pattern in the crystal (Scheme 3). Molecules of **1f** are connected to endless chains by H-bonds between the NH_2 group proton and the nitrogen atom of the N–P group. The chelates **1h** and **1l** form hydrogen-bonded chains with the RNH proton and the sulphur atom of neighbor chelate molecule.

3.5. Photoluminescent properties

The data of the emission spectra for complexes **1a**–**1m** and **2a**–**2d** in the solid state at room temperature are listed in Table 4 (note that the parent ligands have no emission). Interestingly, they exhibit practically the same fluorescent properties.

Complexes **1a**–**1m** show a blue emission band with the maximum intensity at 394–399 nm upon excitation at 249 nm (Table 4 and Fig. 4). Complexes **2a**–**2d** give a strong blue emission band at 413–419 nm when irradiated at wavelength 249 nm (Table 4 and Fig. 4). In order to understand the nature of these emission bands, we analyzed the photoluminescence properties of free HL. For excitation wavelengths between 300 and 500 nm, there is no obvious emission observed for free HL under the same experimental conditions. Therefore, the fluorescent emissions in the compounds **1a**–**1m** are proposed to originate from the coordination of two L^- to the zinc atom and according to the literature [15], these emission bands can be assigned to the emission of ligand-to-metal charge transfer (LMCT).

Table 2
Selected bond distances (Å) bond and torsion angles (°) for six-membered cycles Zn–S–C–N–P–O in complexes **1f**, **1h** and **1l**[a]

	Complexes of general formula [ZnL_2]		
	1f	**1h**	**1l**
Zn–O	1.957(2) 1.954(2)	1.964(3) 1.948(3)	1.973(2) 1.973(2)
Zn–S	2.2945(9) 2.2890(8)	2.2894(12) 2.2850(11)	2.3077(9) 2.2970(9)
C–S	1.749(2) 1.751(2)	1.767(4) 1.752(4)	1.770(2) 1.766(2)
(S)C–N	1.315(3) 1.314(3)	1.314(5) 1.302(5)	1.310(3) 1.303(3)
(S)C–N (exocyclic)	1.329(4) 1.334(4)	1.349(4) 1.338(4)	1.331(3) 1.330(3)
P–N	1.598(2) 1.606(2)	1.603(3) 1.599(4)	1.602(2) 1.593(2)
P–O	1.494(2) 1.496(2)	1.495(3) 1.492(3)	1.4996(14) 1.4961(14)
S–Zn–O (endocyclic)	109.53(6) 102.00(6)	103.00(9) 101.89(9)	101.38(4) 99.70(4)
P–N–C–S	3.5(4) 4.5(4)	−7.0(6) −8.0(7)	7.8(3) 3.5(3)
O–P–N–C	−17.1(3) −25.9(3)	32.6(4) −13.5(5)	−45.3(2) −23.8(3)
Zn–S–C–N	11.7(3) 11.0(3)	176.3(2) 16.1(4)	29.1(2) 26.5(2)
N–P–O–Zn	10.4(2) 27.0(2)	21.1(3) −42.9(3)	29.50(14) 2.20(2)
S–Zn–O–P	3.20(14) −11.19(14)	28.8(2) −10.1(2)	6.50(11) 23.41(12)
O–Zn–S–C	−12.49(11) −6.77(11)	−6.1(2) −6.6(2)	−31.18(9) −33.51(9)

[a] Presented data relate to the two independent ligand moieties with P(1) and P(2) atoms, respectively.

Table 3
Intermolecular hydrogen bond parameters for **1f**, **1h** and **1l**

D–H···A	D–H	H···A	D···A	D–H···A
1f				
N(2)–H(2N)···N(3)#[a]	0.83(3)	2.30(3)	3.131(3)	175(3)
N(4)–H(4N)···N(1)#[b]	0.83(3)	2.20(3)	3.007(3)	166(3)
1h				
N(1)–H(1N)···S(2)#[c]	1.02(4)	2.56(4)	3.559(4)	169(3)
N(3)–H(3N)···S(1)#[d]	0.68(5)	2.87(5)	3.536(4)	167(4)
1l				
N(2)–H(2)···S(2)#[e]	0.80(2)	2.65(2)	3.400(2)	158(2)
N(4)–H(4)···S(1)#[f]	0.78(3)	2.77(3)	3.531(2)	166(2)

[a] [−1/2 + *x*, 1/2 − *y*, −1/2 + *z*].
[b] [1/2 + *x*, 1/2 − *y*, 1/2 + *z*].
[c] [*x*, 1 − *y*, −1/2 + *z*].
[d] [*x*, 1 − *y*, 1/2 + *z*].
[e] [*x*, 1/2 − *y*, −1/2 + *z*].
[f] [*x*, 1/2 − *y*, 1/2 + *z*].

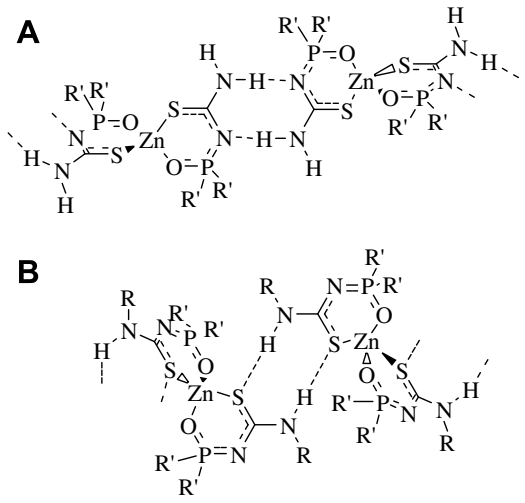

Scheme 3. Intermolecular hydrogen bonds patterns in a crystal of **1f** (A) and **1h** (R = *t*Bu), **1l** (R = *c*-C_6H_{11}) (B). R′ = O*i*Pr.

Table 4
Photophysical data for complexes **1a**–**1m** and **2a**–**2d**[a]

	Emission max (nm)		Emission max (nm)
1a	394	**1j**	398
1b	397	**1k**	399
1c	395	**1l**	399
1d	398	**1m**	398
1e	398	**2a**	415
1f	397	**2b**	418
1g	398	**2c**	413
1h	399	**2d**	419
1i	398		

[a] Excitation at 249 nm.

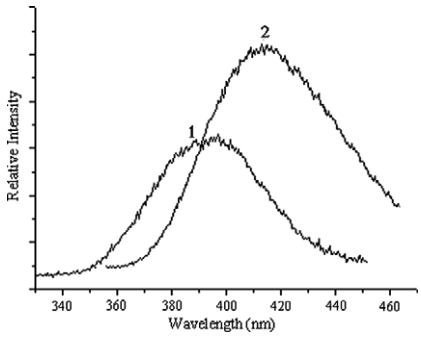

Fig. 4. Fluorescent emission spectra of complexes **1a** (curve 1; spectra of complexes **1b**–**1m** are similar) and **2a** (curve 2; spectra of complexes **2b**–**2d** are similar).

In the solid state, the emission bands increase in intensity and with a notable shift in energy. As it has been told above, there are no emission bands of HL found at 300–500 nm and it is known that the free 2,2′-bipyridine molecule displays a very weak luminescence at 530 nm in the solid state at room temperature [15b]. Thus, compared with **1a**, **1b**, the emission peaks of **2a**–**2d** exhibit a clear bathochromic shift, which may be due to σ-donations from both the L^- and 2,2′-bipyridine or 1,10-phenanthroline ligands to the Zn(II) ion.

Easily synthesized *N*-thioacylamidophosphates HL do not have absorption in the visible region and their Zn(II) chelates are colourless. Therefore they could be excited with UV light that has been shown by us during the experiment. The presence of the bpy or phen ligands in the coordination sphere of the Zn(II) cation allows increasing the emission that might be easily used in non-linear optical devices.

4. Conclusion

N-Phosphorylated thioamides and thioureas HL form with the Zn(II) cation only [ZnL_2] chelates with a tetrahedral ZnO_2S_2 core. 1,5-*O*,*S*-Coordination of the deprotonated form of the ligand, generating a maximal bite angle for L^-, appears as much as possible favorable on the steric reasons.

The ZnO_2S_2 core in these complexes shows a coordination unsaturation. The [ZnL_2] complexes tends to increase the coordination number of the central atom with neutral donor ligands like 2,2′-bipyridine or 1,10-phenanthroline. The adducts of common formula [Zn(bpy)L_2] and [Zn(phen)L_2] have been obtained and characterized. The preservation of the 1,5-*O*,*S*-coordination mode of L^- in the adducts have been established on the basis of the IR and NMR data comparison.

Luminescent zinc *N*-thioacylamidophosphates can be used as new light-converting molecular devices since they (i) are air/moisture stable, (ii) show luminescent properties in the solid state, and at the same time (iii) ligands can be easily prepared from widely used amines and isothiocyanates [4,11].

Acknowledgements

We thank Dr. P. Mayer for collecting the data sets for the crystal structure determination. This work was supported by the joint program of CRDF and the Russian Ministry of Education and Science (BRHE 2004 Y2-C-07-02 and BRHE 2008 Y5-C-07-09); Russian Science Support Foundation.

Appendix A. Supplementary data

CCDC 646784–646786 contain the supplementary crystallographic data for **1f**, **1h** and **1l**, respectively. These data can be obtained free of charge via http://www.ccdc.cam.ac.uk/conts/retrieving.html, or from the Cambridge Crystallographic Data Centre, 12 Union Road, Cambridge CB2 1EZ, UK; fax: (+44) 1223-336-033; or e-mail: deposit@ccdc.cam.ac.uk. Supplementary data associated with this article can be found, in the online version, at doi:10.1016/j.poly.2008.03.005.

References

[1] (a) X.H. Bu, M.L. Tong, H.C. Chang, S. Kitagawa, S.R. Batten, Angew. Chem. Int. Ed. 43 (2004) 192;
(b) C.D. Wu, C.Z. Lu, H.H. Zhuang, J.S. Huang, J. Am. Chem. Soc. 124 (2002) 3836;
(c) X.L. Wang, C. Qin, E.B. Wang, L. Xu, Z.M. Su, C.W. Hu, Angew. Chem. Int. Ed. 43 (2004) 5036;
(d) J.S. Seo, D. Whang, H. Lee, I. Jun, J. Oh, Y.J. Jeon, K. Kim, Nature (London) 404 (2000) 982;
(e) K. Liang, H. Zheng, Y. Song, M.F. Lappert, Y. Li, X. Xin, Z. Huang, J. Chen, S. Lu, Angew. Chem. Int. Ed. 43 (2004) 5776;
(f) D. Bradshaw, T.J. Prior, E.J. Cussen, J.B. Claridge, M.J. Rosseinsky, J. Am. Chem. Soc. 126 (2004) 6106;
(g) M. Tominaga, K. Suzuki, M. Kawano, T. Kusukawa, T. Ozeki, S. Sakamoto, K. Yamaguchi, M. Fujita, Angew. Chem. Int. Ed. 43 (2004) 5621.
[2] (a) L. Han, M.C. Hong, R.H. Wang, J.H. Luo, Z.H. Lin, D.Q. Yuan, Chem. Commun. (2003) 2580;
(b) Y. Wang, J.H. Yu, M. Guo, R.R. Xu, Angew. Chem. Int. Ed. 42 (2003) 4089.
[3] (a) M. Reinel, R. Richter, R. Kirmse, Z. Anorg. Allg. Chem. 628 (2002) 41;
(b) M. Kampf, R. Richter, L. Hennig, A. Eidner, J. Baldamus, R. Kirmse, Z. Anorg. Allg. Chem. 630 (2004) 2677;
(c) M. Kampf, R. Richter, J. Griebel, A. Weller, R. Kirmse, Z. Anorg. Allg. Chem. 631 (2005) 698.
[4] F.D. Sokolov, D.A. Safin, N.G. Zabirov, V.V. Brusko, B.I. Khairutdinov, D.B. Krivolapov, I.A. Litvinov, Eur. J. Inorg. Chem. (2006) 2027.

[5] F.D. Sokolov, D.A. Safin, N.G. Zabirov, P.V. Zotov, R.A. Cherkasov, Russ. J. Gen. Chem. 12 (2005) 1919.
[6] F.D. Sokolov, V.V. Brusko, N.G. Zabirov, R.A. Cherkasov, Curr. Org. Chem. 10 (2006) 27.
[7] K.R. Koch, Coord. Chem. Rev. 216/217 (2001) 473.
[8] (a) F.D. Sokolov, N.G. Zabirov, L.N. Yamalieva, V.G. Shtyrlin, R.R. Garipov, V.V. Brusko, A.Yu. Verat, S.V. Baranov, P. Mlynarz, T. Glowiak, H. Kozlowski, Inorg. Chim. Acta. 359 (2006) 2087;
(b) F.D. Sokolov, S.V. Baranov, N.G. Zabirov, D.B. Krivolapov, I.A. Litvinov, B.I. Khairutdinov, R.A. Cherkasov, Mendeleev Commun. 17 (2007) 222;
(c) F.D. Sokolov, S.V. Baranov, D.A. Safin, F.E. Hahn, M. Kubiak, T. Pape, M.G. Babashkina, N.G. Zabirov, J. Galezowska, H. Kozlowski, R.A. Cherkasov, New J. Chem. 31 (2007) 1661.
[9] R.R. Garipov, V.G. Shtyrlin, D.A. Safin, Y.I. Zyavkina, F.D. Sokolov, A.L. Konkin, A.V. Aganov, A.V. Zakharov, Chem. Phys. 320 (2006) 59.
[10] X. Shen, X. Shi, B. Kang, Y. Liu, Y. Tong, H. Jiang, K. Chen, Polyhedron 17 (1998) 4049.
[11] D.A. Safin, Ph.D. Thesis, Kazan State University, Kazan, Russia, 2006, p. 195.
[12] L.J. Farrugia, J. Appl. Cryst. 30 (1997) 565.
[13] (a) C. Seward, J. Chan, D. Song, S.-N. Wang, Inorg. Chem. 42 (2003) 1112;
(b) Q.D. Liu, W.L. Jia, G. Wu, S.-N. Wang, Organometallics 39 (2000) 2397;
(c) W. Yang, H. Schmider, Q. Wu, Y.-S. Zhang, S.-N. Wang, Inorg. Chem. 42 (2003) 1112.
[14] (a) K.-J. Wei, Y.-S. Xie, J. Ni, M. Zhang, Q.-L. Liu, Cryst. Growth Des. 6 (2006) 1341;
(b) J. Pang, E.J.P. Marcotte, C. Seward, R.S. Brown, S.N. Wang, Angew. Chem. Int. Ed. 40 (2001) 4042.
[15] (a) L.Y. Zhang, G.F. Liu, S.L. Zheng, B.H. Ye, X.M. Zhang, X.M. Chen, Eur. J. Inorg. Chem. (2003) 2965;
(b) C. Qin, X. Wang, E. Wang, Y. Qi, H. Jin, S. Chang, L. Xu, J. Mol. Struct. 749 (2005) 138.

Available online at www.sciencedirect.com
ScienceDirect
Polyhedron 27 (2008) 2029–2030
POLYHEDRON
www.elsevier.com/locate/poly

Erratum

Erratum to "Copper(II) complexes with pyrazolyl-substituted nitronyl and imino nitroxides" [Polyhedron 27 (2008) 739–740]

Eugene V. Tretyakov, Svyatoslav E. Tolstikov, Elena V. Gorelik, Matvey V. Fedin, Galina V. Romanenko, Artem S. Bogomyakov, Victor I. Ovcharenko *

International Tomography Center, Siberian Branch, Russian Academy of Sciences, Institutskaya Str., 3a, RU-630090 Novosibirsk, Russian Federation

Received 21 January 2008; accepted 21 January 2008
Available online 10 March 2008

The authors regret that in the experimental section, everywhere where they occurred, complex $Cu_2(H_2O)_2(L^6)_2 \cdot 2DMF$ should be numbered as **3** and not **2**, and complex $Cu_2(OAc)_2(H_2O)_2\ (L^3)_2$ has to be numbered as **2** and not **3**. The same correction is needed in the column headings (Compound) of Tables 1 and 2. The correct column headings should be: Compound **1 3 2 4** (instead of "Compound **1 2 3 4**").

A revised experimental section is appended.

2.2.2. $Cu_2(H_2O)_2(L^6)_2 \cdot 2DMF$ (**3**)

A solution of $Cu(OAc)_2 \cdot H_2O$ (130 mg, 0.66 mmol) in water (2 ml) was added to a solution of nitronyl nitroxide **HL**^{2} (100 mg, 0.33 mmol) in MeOH (3 ml). The resulting solution was stored for 12 h; then the solvent was distilled off in vacuum at room temperature. The residue was crystallized as described for **1**. Compound **3** was obtained as greenish blue crystals suitable for an X-ray analysis. Yield 110 mg (77%). IR: $\tilde{\nu}_{max}$ = 481, 548, 607, 662, 798, 848, 875, 1026, 1074, 1101, 1138, 1170, 1298, 1324, 1351, 1379, 1403, 1467, 1510, 1627, 1666, 2993, 3393 cm^{-1}. Elemental *Anal.* Calc. for $C_{28}H_{44}Cu_2N_{10}O_{12}$: C, 40.1; H, 5.3; N, 16.7. Found: C, 39.9; H, 5.3; N, 16.7%. When conducted in DMF, the reaction also gave compound **3** in ~85% yield.

2.2.3. $Cu_2(OAc)_2(H_2O)_2(L^3)_2$ (**2**)

A solution of $Cu(OAc)_2 \cdot H_2O$ (80 mg, 0.39 mmol) in water (1.5 ml) was added to a solution of imino nitroxides **HL**^{3} (80 mg, 0.39 mmol) in a mixture of water (1.5 ml), MeOH (1 ml), and EtOH (1.5 ml). The resulting solution was stored for 12 h; then the solvent was distilled off in vacuum at room temperature. The residue was processed as described for **1**. Complex **2** was obtained as dark green crystals suitable for an X-ray analysis. Yield 40 mg (30%). IR: $\tilde{\nu}_{max}$ = 422, 468, 567, 611, 633, 684, 723, 795, 891, 935, 968, 1020, 1077, 1137, 1188, 1260, 1340, 1369, 1400, 1482, 1593, 1676, 2928, 2972, 3248, 3454 cm^{-1}. Elemental *Anal.* Calc. for $C_{24}H_{40}Cu_2N_8O_8$: C, 41.4; H, 5.8; N, 16.1. Found: C, 41.6; H,5.7; N, 16.1%.

DOI of original article: 10.1016/j.poly.2007.11.003
* Corresponding author. Tel.: +7 383 3331945; fax: +7 383 3331399.
E-mail address: Victor.Ovcharenko@tomo.nsc.ru (V.I. Ovcharenko).

0277-5387/$ - see front matter © 2008 Elsevier Ltd. All rights reserved.
doi:10.1016/j.poly.2008.01.011

Table 1
Crystal data and details of experiment for complexes **1**–**4**

Compound	**1**	**3**	**2**	**4**
Formula	$Cu_4(OH)_2(OAc)_4(DMF)_2(L^1)_2$	$Cu_2(H_2O)_2(L^6)_2 \cdot 2DMF$	$Cu_2(OAc)_2(H_2O)_2(L^3)_2$	$Cu_2(DMF)_2(L^7)_2$
FW	1115.04	839.81	693.70	773.80
Space group	*Pbca*	$P2_1/n$	*Pc*	$P2_1/c$
Z	4	2	2	2
a (Å)	10.936(2)	7.1873(8)	11.504(2)	10.541(2)
b (Å)	20.537(4)	22.521(3)	9.338(2)	15.485(3)
b (Å)	21.349(4)	11.278(1)	14.083(3)	10.527(2)
β (°)		97.529(2)	99.381(3)	107.21(3)
V (Å)^3	4794.6(15)	1809.9(3)	1492.6(5)	1641.3(6)
D_{calc} (g · cm^{-3})	1.545	1.541	1.543	1.566
μ (Mo Kα) (cm^{-1})	0.1824	1.248	1.484	1.360
θ (°)	1.91–23.30	1.81–23.31	1.79–29.61	2.02–23.34
I_{hkl} (collected/unique)	26404/3450	13834/2597	12953/6842	12371/2353
R_{int}	0.0388	0.0918	0.0817	0.2020
N	330	324	428	275
Goodness-of-fit (GOF)	1.296	1.023	0.901	1.204
R_1 for $I > 2\sigma_I$	0.0337	0.0499	0.0480	0.1050
wR_2	0.0960	0.1002	0.1094	0.2058
R_1 for all data	0.0415	0.0725	0.0689	0.1430
wR_2	0.1008	0.1074	0.1203	0.2240

Table 2
Selected bond lengths (Å) and angles (°) for complexes **1**–**4**

Compound	**1**		**3**	**2**		**4**
Cu–O_L	2.014(2)		1.974(3)			1.922(5)
Cu–O_{OAc}	1.940(2)	1.933(2)	1.958(3)	1.961(4)	1.971(4)	1.963(5)
	2.487(2)	1.956(2)				2.293(7)
Cu–O_{OH}	1.943(2)	1.945(2)				
		2.295(2)				
Cu–O_{DMF}	2.394(3)					
Cu–Ow			2.282(5)	2.278(5)	2.276(5)	
Cu–N_L				2.111(5)	2.088(5)	
Cu–N_{Pz}	1.944(3)	1.968(3)	1.935(4)	1.992(5)	1.952(5)	1.942(6)
			1.973(3)	2.049(5)	1.978(5)	1.955(5)
N–O	1.301(4)		1.310(4)	1.294(8)	1.247(8)	1.342(7)
	1.267(4)		1.271(4)			
∠CuO_LN	122.5(2)		124.2(3)			123.7(4)
∠CN_2-Pz	13.0(3)		7.3(3)	5.3(8)	6.8(9)	3(1)
–O···O–	6.246		3.668(5)	4.379(5)		
Cu···O–			3.426(4)			
Cu···Cu	3.3830(8)	3.1217(7) 3.1453(8)	3.919(1)	4.0490(9)		3.921(2)

Polyhedron 27 (2008) 2031–2034

Contents lists available at ScienceDirect

Polyhedron

journal homepage: www.elsevier.com/locate/poly

Synthesis, crystal structure and electrochemistry of a ruthenium complex coordinated with an ambidentate 2-mercaptopyridinato *N*-oxide ligand

Tomohiko Hamaguchi *, Yoshimasa Inoue, Kikujiro Ujimoto, Isao Ando

Department of Chemistry, Faculty of Science, Fukuoka University, 8-19-1 Nanakuma, Jonan-ku, Fukuoka 814-0180, Japan

ARTICLE INFO

Article history:
Received 5 December 2007
Accepted 16 March 2008
Available online 5 May 2008

Keywords:
Ruthenium complex
2-Mercaptopyridine *N*-oxide
Monodentate coordination

ABSTRACT

A polypyridyl ruthenium complex monodentately coordinated by 2-mercaptopyridine *N*-oxide was prepared as a candidate for showing linkage isomerisation. [Ru(bpy)(tpy)(2-OpyS)]PF_6 (bpy: 2,2′-bipyridine; tpy: 2,2′:6′,2″-terpyridine; 2-OpyS$^-$: anion of 2-mercaptopyridine *N*-oxide) was synthesised and structurally characterised. The complex contains a 2-OpyS$^-$ ligand coordinating only with the sulphur atom. Electrochemically induced linkage isomerisation was examined for this complex.

© 2008 Elsevier Ltd. All rights reserved.

1. Introduction

Linkage isomerisation is known to occur in complexes of which the metal atom is bound to an ambidentate ligand that has two or more different donor atoms [1–17]. In general, metal ions act as Lewis acids and coordination atoms of ligands serve as Lewis bases. According to the hard and soft acids and bases (HSAB) principle, soft coordination atoms preferentially bind to Ru(II) ions and hard coordination atoms bind to Ru(III) ions, because Ru(II) ions are softer than those of Ru(III). Therefore, if a ruthenium complex is designed to contain a monodentately coordinated ligand with coordination atoms of different softness (or hardness), the linkage isomerisation between Ru(II)–[soft coordination atom] and Ru(III)–[hard coordination atom] should be observed on oxidation or reduction of ruthenium. Many ruthenium–dimethylsulfoxide (dmso) complexes, which exhibit electrochemically induced linkage isomerisation, have been reported [8–17]. For example, $[Ru^{II}(NH_3)_5(dmso)]^{2+}$ [8] is one of the most well-known molecules. In this complex, the S atom of dmso coordinates to the Ru(II) and the O atom does not coordinate. After oxidation of Ru(II) to Ru(III), the complex isomerises to the other isomer in which Ru(III) is coordinated to the O atom.

In this study, a ruthenium complex was designed as a candidate for showing linkage isomerisation as follows. The anion of 2-mercaptopyridine *N*-oxide (2-OpyS$^-$) is an ambidentate ligand that has different types of coordination atoms in one molecule. So far, some studies have reported that 2-OpyS$^-$ monodentately coordinates to a metal ion [18], although complexes with an ambidentate ligand are largely unexplored [19]. Therefore, the ruthenium complex monodentated by 2-OpyS$^-$ is designed to contain 2,2′-bipyridine(bpy) and 2,2′:6′,2″-terpyridine(tpy) as ancillary ligands. We report here the synthesis, characterisation and electrochemical investigation of the ruthenium complex $[Ru^{II}(bpy)(tpy)(2\text{-}OpyS)]PF_6$ (**1**).

2. Experimental

2.1. Materials

All materials were purchased from commercial suppliers (Wako Pure Chemical Industries Ltd., Kanto Chemical Co. Inc. and Acros Organics) and were used without further purification.

2.2. Instrumentation

The crystal structure measurement was made on a Rigaku AFC-5 diffractometer with graphite-monochromated Mo Kα (λ = 0.71069 Å) radiation. The psi-scan correction was applied. The structure was solved by the direct method (SHELXS-97 [20]), and was refined by the full matrix least-square method on F^2 (SHELXL-97 [20]). Hydrogen atoms were included in the calculated positions and refined as a riding model. The ^{1}H NMR spectrum was measured on a Varian Inova 400WB NMR spectrometer at room temperature. Chemical shifts were referenced to the acetonitrile signal at δ 1.93 ppm, corresponding to TMS at δ 0.00 ppm. The absorption spectrum was measured using a SIMADZU UV-3600 UV–Vis–NIR spectrophotometer and 10-mm quartz cell at a concentration of 3.49×10^{-5} mol dm^{-3}. Cyclic voltammetry was performed on a BAS BAS100B/W using three electrode cells (glassy

* Corresponding author. Tel.: +81 92 871 6631x6213; fax: +81 92 865 6030.
E-mail address: thama@fukuoka-u.ac.jp (T. Hamaguchi).

0277-5387/$ - see front matter © 2008 Elsevier Ltd. All rights reserved.
doi:10.1016/j.poly.2008.03.013

carbon electrode as working electrode, Pt coil electrode as counter electrode and homemade Ag^+/Ag electrode as reference electrode). The medium was 0.1 mol dm^{-3} n-Bu_4NPF_6/CH_3CN. The concentration of the complex was 1×10^{-3} mol dm^{-3}. $E_{1/2}$ of the ferrocenium/ferrocene couple was 0.10 V versus Ag^+/Ag. Scan rate was 50 mV s^{-1}. C, H and N analysis was furnished by Service center of the elementary analysis of organic compound of Kyushu University. ESI-Mass spectrum was recorded on a JEOL JMS-T100CS mass spectrometer.

2.3. Synthesis

A mixture of a suspension of $[Ru(bpy)(tpy)Cl]Cl \cdot 2.5H_2O$ [21] (0.50 g, 0.82 mmol) in H_2O (30 cm^3) and a solution of $AgCF_3COO$ (2 equiv.) in H_2O (20 cm^3) was heated at 80 °C for 30 min. The precipitate was filtrated off after cooling the mixture to room temperature. 2-OpySNa (0.69 g, 4.1 mmol) was added to the filtrate, and the solution was allowed to stand for 2 days. KPF_6 (1.84 g, 10 mmol) was added to the solution, and the resulting precipitate was filtrated (0.48 g). The crude product (0.20 g) was purified by recrystallization from H_2O/acetone with a yield of 0.047 g (8.2%). *Anal.* Calc. for $C_{30}H_{23}N_6O_1S_1Ru_1P_1F_6 \cdot 0.5H_2O$: C, 46.76; H, 3.14; N, 10.91. Found: C, 46.78; H, 3.06; N, 10.96%. ESI-MS: m/z 617 (calc(M−PF_6) = 617).

Absorption data (CH_3CN) λ/nm (ε/dm^3 mol^{-1} cm^{-1}): 585sh (3670), 494 (5670), 444sh (5070), 362sh (6880), 304 (28 500), 292 (37 700), 278sh (32 800), 249 (43 100).

^1H NMR (400 MHz, CD_3CN) δ/ppm: 6.31 (d, 7.8 Hz, 1H, 2-OPyS$^-$), 6.38 (t, 7.5 Hz, 1H, 2-OPyS$^-$), 6.58 (t, 5.8 Hz, 1H, 2-OPyS$^-$), 6.94 (t, 5.7 Hz, 1H, bpy), 7.09 (t, 5.6 Hz, 2H, tpy), 7.20 (d, 5.6 Hz, 1H, bpy), 7.31 (d, 6.4 Hz, 1H, 2-OPyS$^-$), 7.69 (d, 5.0 Hz, 2H, tpy), 7.74 (m, 1 H+2H, bpy+tpy), 7.97 (t, 5.6 Hz, 1H, bpy), 8.02 (t, 8.1 Hz, 1H, tpy), 8.13 (d, 8.1 Hz, 2H, tpy), 8.25 (t, 7.9 Hz, 1H, bpy), 8.33 (d, 8.1 Hz, 1H, bpy), 8.36 (d, 8.1 Hz, 2H, tpy), 8.56 (d, 8.1 Hz, 1H, bpy), 11.33 (d, 5.8 Hz, 1H, bpy).

Crystallographic data: crystal colour black, crystal habit plate, crystal dimensions 0.50 mm × 0.50 mm × 0.08 mm, empirical formula $C_{30}H_{23}F_6N_6OPRuS$, M = 761.64, crystal system monoclinic, space group $P2_1/n$, a = 9.0777(11), b = 18.866(2), c = 16.8965(13) Å, β = 97.833(9)°, V = 2866.6(5) Å^3, Z = 4, D_{calc} = 1.765 g cm^{-3}, T = 296(2) K, parameters 415, reflections collected 6977, independent reflections 6572, reflections used 5114 for $I > 2\sigma(I)$, R_{int} = 0.0830, R_1 and wR_2 were 0.0326 and 0.0840 for $I > 2\sigma(I)$, respectively ($R_1 = \sum||F_o| - |F_c||/\Sigma|F_o|$ $wR_2 = ((\sum(w(F_o^2 - F_c^2)^2))/\sum(wF_o^4))^{0.5}$).

3. Results and discussion

3.1. Synthesis and identification

The reaction of $[Ru(bpy)(tpy)Cl]^+$ and Ag^+ produced $[Ru(bpy)(tpy)(H_2O)]^{2+}$. In the resulting complex $[Ru(bpy)(tpy)(H_2O)]^{2+}$, the Ru atom is coordinated to five inert N atoms of bpy/tpy and one labile O atom of water. Since the five positions are protected from coordination, 2-OpyS$^-$, which is a bidentate ligand, can coordinate to ruthenium through only one atom. Complex **1** was prepared by the reaction of $[Ru(bpy)(tpy)(H_2O)]^{2+}$ and excess 2-mercaptopyridine N-oxide sodium salt at room temperature. The complex cation was precipitated from the reaction mixture as its PF_6 salt. The crude product was purified as black crystals by recrystallisation from H_2O/acetone. Complex **1** is soluble in polar solvents such as CH_3CN and acetone and is insoluble in nonpolar solvents such as benzene and chloroform.

Single crystals of **1** suitable for single-crystal X-ray analysis were obtained by slow recrystallisation from a H_2O/acetone solution at room temperature. The crystal structure of **1** is shown in Fig. 1. As mentioned above, 2-OpyS$^-$ has two different types of coordination atoms in one molecule; it is interesting that the Ru atom is coordinated by either the S atom or the O atom of 2-OpyS$^-$. Fig. 1 shows that the 2-OpyS$^-$ ligand coordinates to the Ru atom through only the S atom, and this coordination environment is a reasonable example of the HSAB principle being obeyed. Each **1** molecule contains one PF_6 anion and the ruthenium is of the Ru(II) species (see ^1H NMR discussion below); therefore, the 2-OpySH ligand is deprotonated and coordinates to Ru as an anion form. The S(1)–C(26) and N(6)–O(1) bond lengths are 1.733(4) and 1.308(4) Å, respectively. These indicate that 2-OpyS$^-$ may coordinate to the Ru in the thione form rather than the thiolate form and that the negative charge of the 2-OpyS$^-$ ligand is mainly localised on the O atom [18,22,23]. Tridentated tpy coordinates in meridional fashion with the central nitrogen closest to the Ru atom, the *cis*-position of tpy is filled by the S atom of the monodentate 2-OpyS$^-$ ligand, and the remaining coordination positions are coordinated by the N atoms of bpy. This coordination environment forms a distorted octahedral structure on the Ru. Bpy plane and tpy plane are almost orthogonal (83.97(5)°); however, the angles between 2-OpyS$^-$ plane and bpy plane and between 2-OpyS$^-$ plane and tpy plane are 63.77(7)° and 70.24(6)°, respectively. The steric repulsion between 2-OpyS$^-$ and the other ligands forces 2-OpyS$^-$ into this arrangement, and therefore, the O atom is kept away from the Ru atom in the crystal.

^1H NMR spectrum of **1** in CD_3CN is a complicated spectrum, and almost all peaks are in the narrow range of δ 6 to δ 9 ppm (Fig. 1S in Supplementary material). The complex contains 18 non-equivalent pyridyl protons, which have considerably similar electronic environments. We have assigned all peaks to the individual protons of the ligands by the ^1H correlation spectroscopy (COSY) experiment; therefore, single-crystal X-ray analysis of **1** should also reveal a unique structure in CH_3CN solution. The signals for the tpy indicate that there is twofold symmetry, which suggests rotation of the 2-OpyS$^-$ around the Ru–S bond. Sharp signals in the normal region reveal that **1** is diamagnetic, i.e., the ruthenium species is Ru(II).

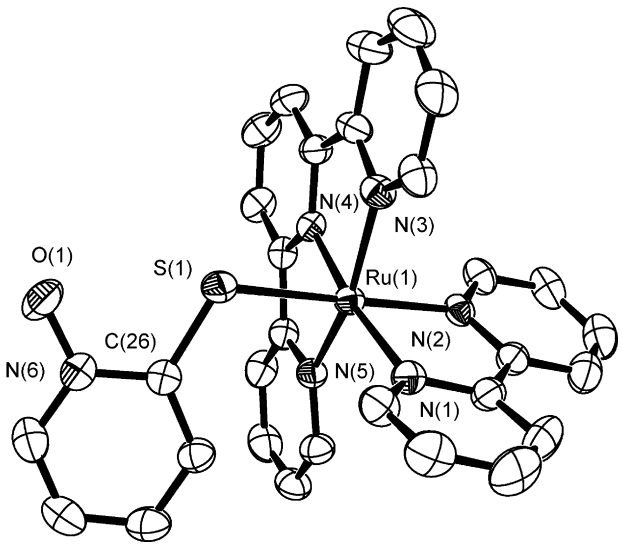

Fig. 1. Molecular structure of the complex cation of **1**. Thermal ellipsoids are drawn at the 50% probability level, and hydrogen atoms are omitted. Selected bond lengths (Å) and angles (°): Ru(1)–N(1) = 2.095(3), Ru(1)–N(2) = 2.064(3), Ru(1)–N(3) = 2.079(3), Ru(1)–N(4) = 1.961(3), Ru(1)–N(5) = 2.099(3), Ru(1)–S(1) = 2.4194(10), S(1)–C(26) = 1.733(4), N(6)–O(1) = 1.308(4), N(2)–Ru(1)–N(1) = 77.82(12), N(4)–Ru(1)–N(3) = 79.76(12), N(4)–Ru(1)–N(5) = 78.98(11), N(2)–Ru(1)–S(1) = 175.00(8), N(4)–Ru(1)–N(1) = 172.40(12) and N(3)–Ru(1)–N(5) = 158.63(12).

The absorption spectrum of **1** was measured in acetonitrile (Fig. 2S in Supplementary material). Four weak broad bands are seen in the visible region and four intense sharp bands are in the UV region. The former bands are assigned to metal-to-ligand charge transfer (MLCT), and the latter bands are assigned to a ligand centred π–π^* transition. Various MLCT and π–π^* transitions are caused by three pyridine-derivative ligands.

3.2. Electrochemical properties

One anion of 2-OpyS$^-$ contains one O and one S atom, and the S atom is softer than the O atom. Therefore, this complex might exhibit electrochemically induced linkage isomerisation of Ru(II)–S to Ru(III)–O upon oxidation, such as in $[Ru(NH_3)_5(dmso)]^{2+}$ [8] and $[Ru(bpy)(tpy)(dmso)]^{2+}$ [14]. To investigate electrochemically induced linkage isomerisation of **1**, cyclic voltammograms were obtained. For anodic scan starting at −1.50 V versus Ag^+/Ag (Fig. 2a), one reversible redox couple was observed at $E_{1/2}$ = 0.72 V versus Ag^+/Ag. A cathodic peak at E_c = −0.76 V and an anodic peak at E_a = 0.19 V versus Ag^+/Ag were also observed. After oxidising at 1.00 V for 3 min, almost the same voltammogram was observed with a cathodic scan starting at 1.00 V versus Ag^+/Ag ($E_{1/2}$ = 0.72 V, E_c = −0.71 V and E_a = 0.19 V versus Ag^+/Ag). This irreversible redox behaviour at E_c and E_a might imply that **1** showed linkage isomerisation caused by the redox of the ruthenium [5,8,15].

Cyclic voltammograms of **1** and the ligands were compared due to confirm whether the metal centre is responsible for the irreversible redox behavior. Fig. 2b is the cyclic voltammogram of 2-OpySH in 1 equiv. Et_3N/CH_3CN, where 2-OpySH is in the deprotonated form (2-OpyS$^-$). Regardless of scan direction, 2-OpyS$^-$ has approximately the same irreversible redox behavior as **1** (anodic scan: E_c = −1.38 V and E_a = 0.03 V versus Ag^+/Ag; cathodic scan:E_c = −1.37 V and E_a = −0.04 V versus Ag^+/Ag). Therefore, the ligand and not the metal centre is responsible for the irreversible redox behavior, which might imply electrochemically induced linkage isomerisation. The reversible redox couple at $E_{1/2}$ = 0.72 V versus Ag^+/Ag is associated with Ru(III/II), and this complex does not show electrochemically induced linkage isomerisation.

The short distance between the Ru and O atoms should be important for electrochemically induced linkage isomerisation from Ru(II)–S to Ru(III)–O. For example, $[Ru(bpy)(tpy)(dmso)]^{2+}$ [14], which has almost the same local coordination environment as the Ru of **1**, exhibits linkage isomerisation. The distances of Ru–S and Ru···O in $[Ru(bpy)(tpy)(dmso)]^{2+}$ are 2.282(1) and 3.204(2) Å, respectively. In the case of **1**, the Ru–S and Ru···O distances are 2.4194(10) and 5.1917(30) Å, respectively. Complex **1** might have too long Ru···O to form a Ru–O bond by comparison with Ru···O distance of $[Ru(bpy)(tpy)(dmso)]^{2+}$; however, 2-OpyS$^-$ ligand is able to rotate around the Ru–S bond (see ^{1}H NMR discussion). The rotation around Ru–S and C–S bond on the computer obtained the closest distance as ca. 3.5 Å, which seems not to be long. Therefore, isomerisation is not affected by the structure. On the other hand, Rack and co-workers mention the importance of ancillary ligands. They remark that weak-field π-basic ligands do not allow the Ru(III) centre to appear hard enough to favor the hard O-donor over the soft S-donor in [Ru(tpy)(ancillary ligand)(dmso)]$^{n+}$ [12,16,17]. Their discussion is in the case of dmso complex instead of 2-OpyS$^-$ complex; however, we think that the Ru(III) in **1** also might prefer to make Ru–S bond instead of Ru–O due to the electron density.

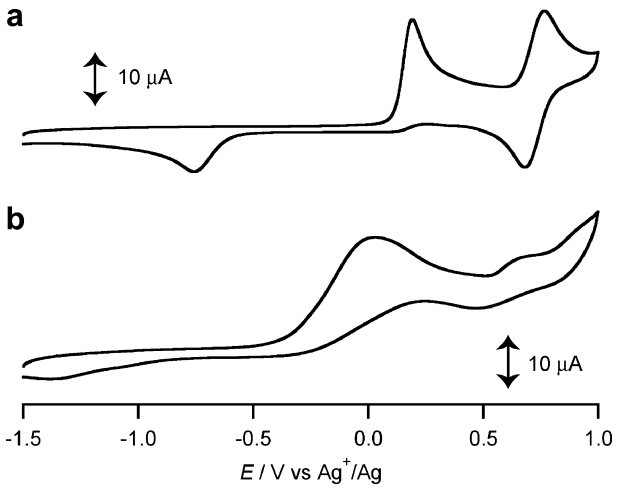

Fig. 2. Cyclic voltammograms of (a) **1** in CH_3CN and (b) 2-OpySH in 1 equiv. Et_3N/CH_3CN.

4. Conclusion

$[Ru(bpy)(tpy)(2\text{-}OpyS)]PF_6$ was prepared, crystallographically characterised and electrochemically investigated. The 2-OpyS$^-$ ligand coordinates to the Ru(II) only through the S atom in the isolated complex. To the best of our knowledge, **1** is the first structurally characterised example of a monodentate κS bound 2-OpyS$^-$ ligand in the ruthenium complex reported so far.

The 2-OpyS$^-$ ligand is also possible to coordinate to central metal with O atom; however, the complex does not show linkage isomerisation from Ru(II)–S to Ru(III)–O under the condition in this study. The reason why the complex shows no isomerisation might come from the electron density on the Ru centre. In future studies, we would investigate a family of $[Ru^{II}(ancillary\ ligand)(2\text{-}OpyS)]^{n+}$ complexes, and we will address the relationship among the electron density of the Ru, the property of ancillary ligand and electrochemically induced linkage isomerisation.

Acknowledgement

This work was supported in part by funds (No. 075001) from the Central Research Institute of Fukuoka University.

Appendix A. Supplementary data

CCDC 668962 contains the supplementary crystallographic data for **1**. These data can be obtained free of charge via http://www.ccdc.cam.ac.uk/conts/retrieving.html, or from the Cambridge Crystallographic Data Centre, 12 Union Road, Cambridge CB2 1EZ, UK; fax: (+44) 1223-336-033; or e-mail: deposit@ccdc.cam.ac.uk. CCDC contain the supplementary crystallographic data for **1**. Supplementary data associated with this article can be found, in the online version, at doi:10.1016/j.poly.2008.03.013.

References

[1] L. Cheng, I. Novozhilova, C. Kim, A. Kovalevsky, K.A. Bagley, P. Coppens, G.B. Richter-Addo, J. Am. Chem. Soc. 122 (2000) 7142.
[2] D.P. Fairlie, Y. Ilan, H. Taube, Inorg. Chem. 36 (1997) 1029.
[3] H.E. Toma, E. Giesbrecht, R.L.E. Rojas, Can. J. Chem. 61 (1983) 2520.
[4] A.Y. Lovalevsky, K.A. Bagley, P. Coppens, J. Am. Chem. Soc. 124 (2002) 9241.
[5] S. Fanni, F.M. Weldon, L. Hammarström, E. Mukhtar, W.R. Browne, T.E. Keyes, J.G. Vos, Eur. J. Inorg. Chem. (2001) 529.
[6] O. Johansson, R. Lomoth, Chem. Commun. (2005) 1578.
[7] H.E. Toma, R.C. Rocha, Croat. Chem. Acta 74 (2001) 499.
[8] A. Yeh, N. Scott, H. Taube, Inorg. Chem. 21 (1982) 2542.
[9] J.J. Rack, J.R. Winkler, H.B. Gray, J. Am. Chem. Soc. 123 (2001) 2432.
[10] C. Sens, M. Rodríguez, I. Romero, A. Llobet, T. Parella, B.P. Sullivan, J. Benet-Buchholz, Inorg. Chem. 42 (2003) 2040.
[11] A. Tomita, M. Sano, Inorg. Chem. 33 (1994) 5825.
[12] A. Tomita, M. Sano, Inorg. Chem. 39 (2000) 200.

[13] M. Sano, H. Taube, Inorg. Chem. 33 (1994) 705.
[14] D.O. Silva, H.E. Toma, Can. J. Chem. 72 (1994) 1705.
[15] J.J. Rack, A.A. Rachford, A.M. Shelker, Inorg. Chem. 42 (2003) 7357.
[16] J.J. Rack, H.B. Gray, Inorg. Chem. 38 (1999) 2.
[17] A.A. Rachford, J.L. Petersen, J.J. Rack, Inorg. Chem. 44 (2005) 8065.
[18] J.-T. Hung, S. Kumaresan, L.-C. Lin, Y.-S. Wen, L.-K. Liu, K.-L. Lu, J.R. Hwu, Organometallics 15 (1996) 5065.
[19] E.P. Kelson, P.P. Phengsy, J. Chem. Soc., Dalton Trans. (2000) 4023.
[20] G.M. Sheldrick, SHELXL-97, University of Göttingen, Germany, 1997.
[21] D.C. Ware, P.A. Lay, H. Taube, Inorg. Synth. 24 (1985) 299.
[22] W.-F. Liaw, C.-H. Hsieh, S.-M. Peng, G.-H. Lee, Inorg. Chim. Acta 332 (2002) 153.
[23] J.D. Curry, R.J. Jandacek, J. Chem. Soc., Dalton Trans. (1972) 1120.

Polyhedron 27 (2008) 2035–2042

Contents lists available at ScienceDirect

Polyhedron

journal homepage: www.elsevier.com/locate/poly

Syntheses and structural characterization of three new silver(I) coordination polymers with 1-(2-pyrazinyl)piperazine ligands

Hui-An Tsai [a,d], Mei-Shan Hu [a], Ming-Yu Teng [b], Maw-Cherng Suen [a,*], Ju-Chun Wang [c]

[a] Department of Material and Fiber, Nanya Institute of Technology, Jhongli, Taiwan, ROC
[b] Department of Chemical and Material Engineering, Nanya Institute of Technology, Jhongli, Taiwan, ROC
[c] Department of Chemistry, Soochow University, Taipei, Taiwan, ROC
[d] R&D Center for Membrance Technology, CYCU, Taiwan, ROC

ARTICLE INFO

Article history:
Received 3 January 2008
Accepted 16 March 2008
Available online 28 May 2008

Keywords:
Coordination polymer
1-(2-Pyrazinyl)piperazine
Silver salts
Self-assembly

ABSTRACT

Three novel supramolecules of the Ag(I) complexes of $[Ag_4(pyapa)_4(SO_4)_2 \cdot 6H_2O]_n$, **1**, $\{[Ag_2(pyapa)_2][ClO_4]_2\}_n$, **2** and $\{[Ag_2(pyapa)_2(H_2O)][NO_3]_2\}_n$, **3**, (pyapa = 1-(2-pyrazinyl)piperazine) have been prepared by self-assembly of Ag(I) salts with 1-(2-pyrazinyl)piperazine (pyapa) in MeOH/H_2O system. The IR, TGA and elemental analysis have been recorded and all the complexes have been structurally characterized by X-ray crystallography confirming that complexes **1**–**3** are one-dimensional coordination polymers. The pyapa ligands in complexes **1**–**3** bind soft acid Ag(I) ions through the pyrazinyl and piperazinyl groups forming the 1-D polymeric chains. The anions SO_4^{2-} in complexes **1** shows the disordered geometries and bridging the Ag(I) atoms, while the anions ClO_4^- and NO_3^- in complexes **2**–**3** are not coordinated to the Ag(I) atoms, and all of them play an important roles in linking cationic chains into 3-D supramolecular structures. Thermal gravimetric analyses (TGA) were carried out to investigate their thermal properties.

© 2008 Elsevier Ltd. All rights reserved.

1. Introduction

Recently, a great effort has been devoted to the self-assembly of organic and inorganic molecules in the solid state, because it extends the range of designing new solids with desired physical and chemical properties [1,2]. The range and variety of self-assembled inorganic structures that can be constructed relies on the suitable metal-ligand interactions and supramolecular contacts, i.e., hydrogen bondings and other weak interactions [3]. The self-assembly of supramolecular structures using metal coordination has become the focus of intense interest over the past decade [4]. This is largely due to the range of potential applications in electrical, magnetic, optical devices [5] and porous zeolite mimics [6]. The specific properties of each coordination network are directly related to its atomic structure, which is a function of both the ligand and the metal. There has been a resurgent interest on extended organic or organometallic crystals based on hydrogen bonds and metal coordination bonds [7–9].

It is, therefore, important to try to understand, and control, the interplay between the coordination characteristics of the ligands and the metals, and the ultimate shape of the self-assembled superstructure. Much study has centered upon the use of supramolecular contacts between suitable molecules to generate multidimensional arrays or networks. The design of supramolecular assemblies via ligand design, the coordination characteristics of the metal ion, and the length of the spacer has resulted in a variety of structural motifs [10]. Many topologically promising architectures have been constructed for the silver(I) ion with bidentate building blocks containing nitrogen donor. The various types of polymeric structure include 1-D, 2-D and 3-D network structures [11]. Despite some recent progress, the ability to predict and control the supramolecular assembly of molecules remains elusive, and much more work is required to understand the inter- and intra-molecular forces that determine the patterns of molecular structure and crystal packing in the solid state. So far, various ligands, such bipyridine-type and biphenyl cyanide-type ligands, have been used for supramolecular building blocks [12–14].

Various ligands have been used for supramolecular building blocks, but exploitation of the polydentate 1-(2-pyrazinyl)piperazine (pyapa) has until recently unprecedented. The ligand process two functionalities with pyrazinyl and the piperazinyl groups. The affinity of Ag^+ for N-donor ligands, especially pyrazinyl and the piperazinyl group, is well known. In this paper, we report three novel supramolecular Ag(I) complexes of $[Ag_4(pyapa)_4(SO_4)_2 \cdot 6H_2O]_n$, (pyapa = 1-(2-pyrazinyl)piperazine) **1**, $\{[Ag_2(pyapa)_2][ClO_4]_2\}_n$, **2** and $\{[Ag_2(pyapa)_2(H_2O)][NO_3]_2\}_n$, **3**.

* Corresponding author. Tel.: +886 03 4361070; fax: +886 03 4658965.
E-mail address: sun@nanya.edu.tw (M.-C. Suen).

0277-5387/$ - see front matter © 2008 Elsevier Ltd. All rights reserved.
doi:10.1016/j.poly.2008.03.015

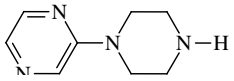

2. Experimental

2.1. General procedures

All manipulations were carried out under air. IR spectra were obtained from a Jasco FT/IR-460 plus spectrometer. Elemental analyses were obtained from a PE 2400 series II CHNS/O analyzer or a HERAEUS VaruoEL analyzer. Thermogravimetric analyses (TGA) were conducted on a SDT 2960 using a heating rate of 20 C/min in a nitrogen atmosphere.

2.2. Materials

The reagents 1-(2-pyrazinyl)piperazine (pyapa), Ag_2SO_4, $AgClO_4$ and $AgNO_3$ were purchased from Acros Co.

2.3. Preparation of complex *1*

1-(2-Pyrazinyl)piperazine (pyapa) (0.328 g, 0.20 mmol) in 5 ml EtOH was layered onto a solution of Ag_2SO_4 (0.311 g, 0.10 mmol) in 5 ml H_2O. The resulting solution was slowly diffused for several weeks to give colorless crystal. Yield: 0.0372 g, 27.0% *Anal.* Calc. for **1** ($C_{32}H_{48}Ag_4N_{16}O_{14}S_2$): C, 27.92; H, 3.51; N, 16.28. Found: C, 27.88; H, 3.51; N, 16.22%. IR (KBr disk, cm^{-1}): 3435 (w), 3205 (br), 3106 (m), 2955 (m), 2920 (m), 2487 (m), 1638 (m), 1580 (m), 1518 (m), 1490 (m), 1436 (m), 1313 (m), 1259 (m), 1201 (m), 1119 (m), 995 (m), 944 (m), 829 (m), 619 (m).

2.4. Preparation of complex *2*

Complex **2** was prepared as for **1**. Yield: 0.0416 g (28%). *Anal.* Calc. for **2** ($Ag_2C_{16}H_{24}Cl_2O_8N_8$): C, 25.86; H, 3.25: N; 15.08. Found: C, 25.82; H, 3.20; N, 15.11%. IR (KBr disk, cm^{-1}): 3436 (w), 3244 (br), 3099 (m), 2960 (m), 2840 (m), 1631 (m), 1583 (m), 1519 (m), 1486 (m), 1433 (m), 1205 (m), 1107 (m), 1090 (m), 995 (m), 937 (m), 822 (m), 626 (m).

2.5. Preparation of complex *3*

Complex **3** was prepared as for **1**. Yield: 0.0213 g (31%). *Anal.* Calc. for **3** ($Ag_2C_{16}H_{26}O_7N_{10}$): C, 28.00; H, 3.82; N, 20.41. Found: C, 28.14; H, 3.85; N, 20.36%. IR (KBr disk, cm^{-1}): 3399 (w), 3246 (br), 3108 (m), 2956 (m), 2920 (m), 2804 (m), 1652 (m), 1518 (m), 1439 (m), 1439 (m), 1366 (m), 1309 (m), 1261 (m), 1201 (m), 1176 (m), 1139 (m), 1078 (m), 1002 (m), 948 (m), 832 (m), 767 (m), 739 (m), 641 (m), 543 (m).

2.6. X-ray crystallography

The diffraction data of **1** was collected on a Bruker AXS Smart 1000 CCD diffractometer, which was equipped with graphite-monochromated Mo Kα (Kα = 0.71073 Å) radiation. Data reduction was carried by standard methods with use of well-established computational procedures [15]. Basic information pertaining to crystal parameters and structure refinement is summarized in Table 1. The structure factors were obtained after Lorentz and polarization corrections. The positions of the heavy atoms, including the silver atoms, were located by the direct method. The oxygen atoms (O(5), O(6) and O(8)) of sulfate anions in complex **1** are disordered and thus with the ratio of 0.5:0.5 occupancy were found. The remaining atoms were found in a series of alternating difference Fourier maps and least-square refinements [16]. The final residuals of the first refinement were $R_1 = 0.0418$, $wR_2 = 0.1062$. The crystallographic procedures for **2** and **3** were similar to those for **1**. Basic information pertaining to crystal parameters and structure refinement is summarized in Table 1.

2.7. Syntheses and spectroscopics studies

Complexes of $[Ag_4(pyapa)_4(SO_4)_2 \cdot 6H_2O]_n$, (pyapa=1-(2-pyrazinyl)piperazine) **1**, $\{[Ag_2(pyapa)_2][ClO_4]_2\}_n$, **2** and $\{[Ag_2(pyapa)_2(H_2O)][NO_3]_2\}_n$, **3** were prepared by reactions of Ag_2SO_4, $AgClO_4$ and $AgNO_3$ with pyapa in $MeOH/H_2O$ system. All these complexes were structurally characterized by X-ray crystallography. Crystals suitable for X-ray diffraction studies were obtained

Table 1
Crystal data for complexes **1**–**3**

Compound	**1**	**2**	**3**
Formula	$C_{32}H_{48}Ag_4N_{16}O_{14}S_2$	$C_{16}H_{24}Ag_2Cl_2N_8O_8$	$Ag_2C_{16}H_{26}O_7N_{10}$
M	1376.46	743.07	686.21
Crystal system	monoclinic	monoclinic	monoclinic
Space group	$P2_1$	$P2_1/c$	$P2_1/c$
a (Å)	12.749(2)	7.7025(11)	16.4968(15)
b (Å)	13.996(3)	37.438(5)	19.3653(18)
c (Å)	13.749(3)	17.166(2)	7.3600(7)
β (°)	108.542(4)	101.917(3)	96.066(2)
V (Å^3)	2325.9(8)	4843.4(12)	2338.1(4)
Z	2	8	4
D_{calc} (g/cm^3)	1.965	2.038	1.947
$F(000)$	1368	2944	1364
μ(Mo Kα) (mm^{-1})	1.829	1.898	1.735
λ(Mo Kα) (Å)	0.71073	0.71073	0.71073
Range (2θ) for data collection (°)	$3.12 \leqslant 2\theta \leqslant 52.34$	$3.26 \leqslant 2\theta \leqslant 52.18$	$2.48 \leqslant 2\theta \leqslant 51.98$
Goodness of fit[c]	0.925	1.204	1.344
Final R indices [$I > 2\sigma(I)$][a,b]	$R_1 = 0.0418$, $wR_2 = 0.1062$	$R_1 = 0.0753$, $wR_2 = 0.2308$	$R_1 = 0.0372$, $wR_2 = 0.0998$
R indices (all data)	$R_1 = 0.0530$, $wR_2 = 0.1146$	$R_1 = 0.1316$, $wR_2 = 0.2584$	$R_1 = 0.0500$, $wR_2 = 0.1110$
Largest difference peak and hole (e/Å^3)	0.871 and −0.948	0.906 and −1.651	0.848 and −0.582

[a] $R_1 = \Sigma||F_o| - |F_c||/\Sigma|F_o|$.
[b] $wR_2 = [\Sigma w(F_o^2 - F_c^2)^2/\Sigma w(F_o^2)^2]^{1/2}$. $w = 1/[\sigma^2(F_o^2) + (ap)^2 + (bp)]$, $p = [\max(F_o^2 \text{ or } 0) + 2(F_c^2)]/3$. $a = 0.0800$, $b = 0.0000$, **1**; $a = 0.1250$, $b = 0.0000$, **2**; $a = 0.0500$, $b = 0.0000$, **3**.
[c] Quality-of-fit = $[\Sigma w(|F_o^2| - |F_c^2|)^2/N_{observed} - N_{parameters}]^{1/2}$.

by pyapa in methanolic solution was layered onto a solution of Ag(I) salts in H_2O. The IR spectrum of the complex **1** clearly shows the bands of SO_4^{2-} anions at 1119, 995 and 687 cm^{-1}, indicating the mondendate coordination mode (C_{3v} symmetry). For **2** clearly indicated the presence of ClO_4^- bands at 1090 and 624 cm^{-1}.

2.8. Structure of complex *1*

A single crystal X-ray structural analysis of crystals of **1**, obtained by layer the pyapa methanolic solution on the top of Ag_2SO_4 aqua-solution, revealed the formation of a complex of $[Ag_4(pyapa)_4(SO_4)_2 \cdot 6H_2O]_n$. Colorless crystals of **1** conform to the space group $P2_1$ with two molecules in a unit cell Fig. 1 shows the asymmetric unit ORTEP diagrams for **1**. Selected bond distances and angles are listed in Table 2. The sulfate anion is disordered such that two different molecules, each possessing 50% occupancy, can be solved. Fig. 1a and b show the asymmetry unit ORTEP diagrams of these two disordered anions, while Fig. 1c shows their overlap and the relationship

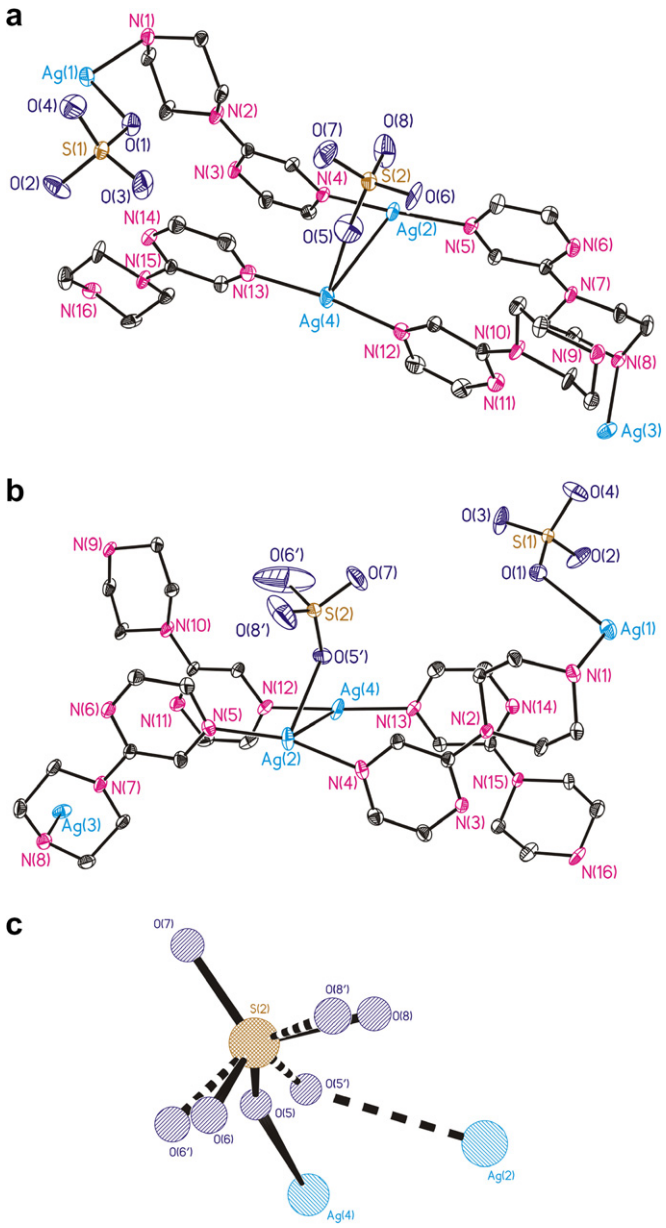

Fig. 1. An ORTEP diagrams of **1**, showing the two disordered asymmetric units, (a) and (b), and the overlap of the two sulfate anions, (c).

Table 2
Selected bond distances (Å) and angles (°) for complex **1**–**3**

Complex **1**			
Ag–N(1)	2.226(2)	Ag–N(4A)	2.299(2)
Ag–N(3B)	2.311(3)		
N(1)–Ag–N(4A)	124.46(8)	N(1)–Ag–N(3B)	140.25(9)
N(4A)–Ag–N(3B)	90.60(9)		
Complex **2**			
Ag(1)–N(1)	2.154(9)	Ag(1)–N(8A)	2.180(9)
Ag(2)–N(5)	2.110(10)	Ag(2)–N(4)	2.131(9)
Ag(3)–N(16B)	2.118(9)	Ag(3)–N(9)	2.167(10)
Ag(4)–N(13)	2.158(8)	Ag(4)–N(12)	2.186(8)
N(1)–Ag(1)–N(8A)	173.0(4)	N(5)–Ag(2)–N(4)	174.9(4)
N(16B)–Ag(3)–N(9)	176.8(5)	N(13)–Ag(4)–N(12)	177.2(3)
Complex **3**			
Ag(1)–N(1)	2.188(4)	Ag(1)–N(4A)	2.229(4)
Ag(1)–N(3B)	2.439(5)		
N(1)–Ag(1)–N(4A)	150.68(15)	N(1)–Ag(1)–N(3B)	112.92(16)
N(4A)–Ag(1)–N(3B)	92.97(15)		

Symmetry transformations used to generate equivalent atoms:
(*A*): $-x+3, -y+1, -z$; (*B*): $-x+3, y-1/2, -z+1/2$; (*C*): $-x+3, y+1/2, -z+1/2$, for **1**; (*A*): $x+1, -y-1/2, z+1/2$; (*B*): $-x+2, y+1/2, -z+1/2$; (*C*): $-x+3, -y-1, -z+1$; (*D*): $x-1, -y-1/2, z-1/2$; (*E*): $-x+2, y-1/2, -z+1/2$, for **2**; (*A*): $-x+3/2, y+1/2, -z+3/2$; (*B*): $-x+1/2, y+1/2, -z+3/2$; (*C*): $-x+1/2, y-1/2, -z+3/2$; (*D*): $-x+3/2, y-1/2, -z+3/2$, for **3**.

between the Ag(2), Ag(4) and the SO_4^{2-} anion. The asymmetry units contain four Ag atoms, two sulfate anions and four pyapa groups. All the sulfate anions in complex **1** are coordinated to the silver centers in monodentate fashion. Fig. 2a shows the coordination geometry about the Ag metal center. The Ag metal centers possess two types of geometries. The Ag(1), Ag(2) and Ag(4) centers adopt a slightly distorted triangular planar coordination geometries, while Ag(3) adopts a linear geometry. The selected bond distances and angles are listed in Table 2. The Ag(2) and Ag(4) atoms are bonded to four pyrazinyl nitrogen atoms (Ag–N = 2.133(6)–2.158(5) Å) from the four different pyapa groups and one sulfate oxygen atom (Ag–O = 2.473(3) and 2.502(2) Å). The Ag(1) bonded to two piperazinyl nitrogen atoms (Ag–N = 2.235(5) and 2.234(6) Å) and a monodentate SO_4^2 oxygen atom to complete the disorder triangular planar geometry, while Ag(3) bonded to two piperazinyl nitrogen atoms (Ag–N = 2.179(6) and 2.196(6) Å) in the linear geometry [N(8)–Ag(3)–N(16B) = 167.7(2)°]. Each Ag(I) coordinated to two pyapa ligands and each pyapa bridged two Ag(I) atoms in complex **1**. Fig. 2b and c shows the pyapa ligand bridging each Ag atoms through pyrazinyl and piperarzinyl nitrogen atoms and formed the helical chains, which the Ag(1) and Ag(2) centers forming the blue one and Ag(3) and Ag(4) centers forming the purple one. The helixes interlink each through Ag···Ag interactions (Ag···Ag = 3.0477(10) Å) and the π–π stacking between the pyrazinyl rings (3.688 and 3.798 Å). The Ag···Ag distances in the helical chains separated by the bridging pyapa are 8.836 and 8.970 Å. The dihedral angles between the two pyrazinyl rigns that coordinated to the Ag atom through the nitrogen atoms are 9.5° and 10.0°. Some few double helical motifs are related, especially if there are several kinds of donor groups in ligand molecular or with flexible ligands. For instances, the ligand 1,3-bis(4-pyridyl)propane (bpp) reacts with $AgCF_3SO_3$ afforded $\{[Ag(bpp)](CF_3SO_3)\}_n$ double helical chains which are also interlinking through Ag···Ag interactions [17] and π–π stacking [18].

Fig. 3 shows the 1-D polymeric helices interlinked each through the weak O···Ag interactions (O···Ag = 2.783–3.086 Å). In complex **1**, the 1-D helices are further linked by the anions through Ag···O interactions (O···Ag = 2.783, 2.826, 3.086 and 3.210 Å), the rare CH···Ag interactions (H···Ag = 2.988–3.348 Å, ∠C–H···Ag = 122.3–147.1°) and CH···O interactions (H···O = 2.486–2.523 Å, ∠C–H···O = 146.6–170.5°) hydrogen bonds to form the 3-D supramolecular structure, Fig. 3.

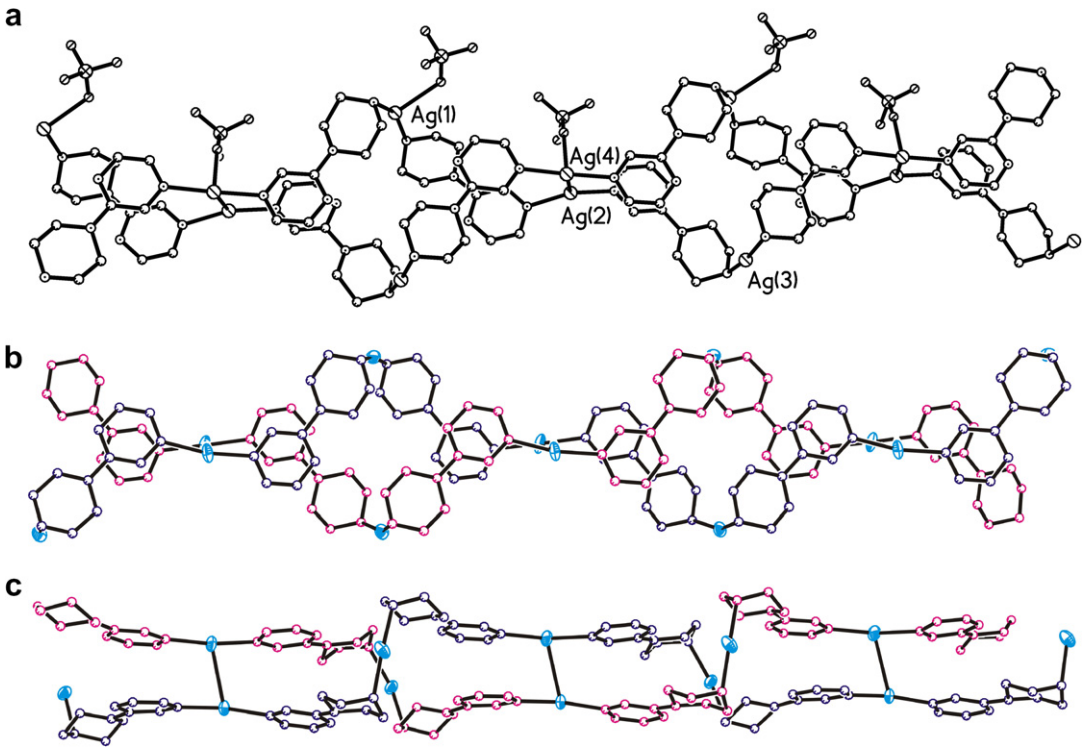

Fig. 2. (a) The structure drawing of complex **1** showing the metal center coordination location, (b) and (c) two fashions of the double helical chains.

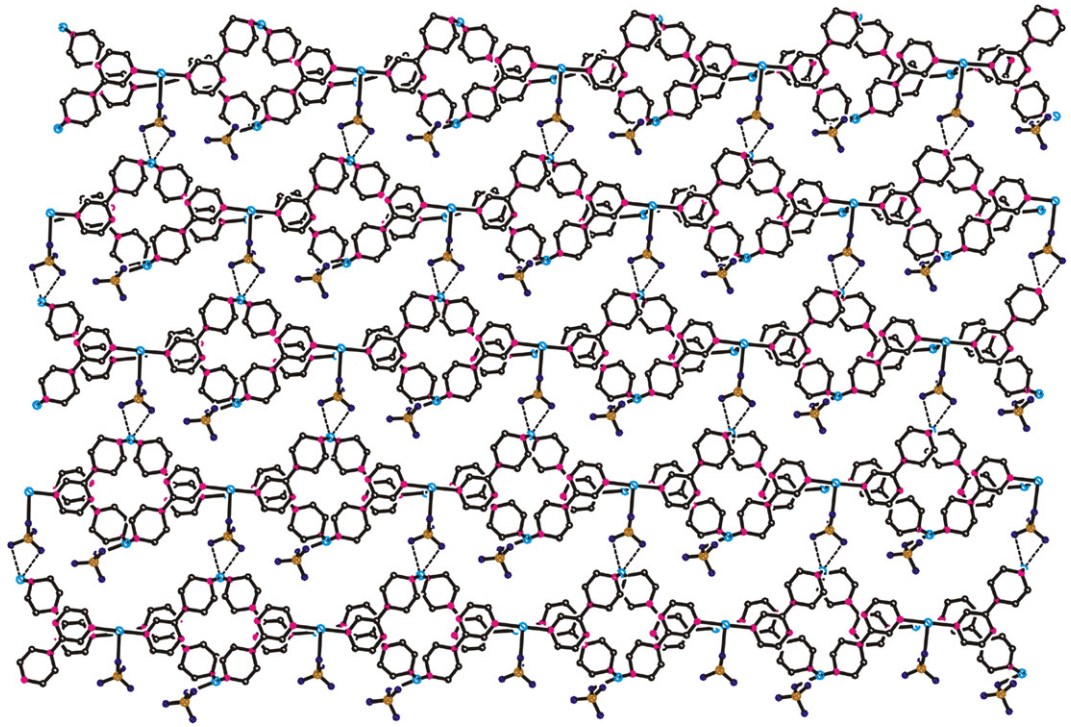

Fig. 3. The packing diagram of complex **1** shows the 2-D sheets forming by weak Ag···O interactions.

2.9. Structure of complex **2**

The crystal structure of complex **2** belongs to the space group $P2_1/c$. A representative ORTEP diagram shows the asymmetric unit of complex **2**, which containing four silver atoms, four perchlorate anions and four bidentate pyapa groups (Fig. 4a). Table 2 list the bond distances and angles around silver atoms for complex **2**. The Ag(I) atoms which are coordinated by two pyrazinyl nitrogen atoms of different pyapa ligands [Ag–N = 2.110(10)–2.186(8) Å] or two piperarzinyl nitrogen atoms of pyapa groups [Ag–N = 2.118(9)–2.180(9) Å] are linear geometries in Ag(1), Ag(2), Ag(3) and Ag(4) [∠N(1)–Ag(1)–N(8A) = 173.0(4)°, ∠N(5)–Ag(2)–N(4) = 174.9(4)°, ∠N(9)–Ag(3)–N(16B) = 176.8(5)°, ∠N(13)–Ag(4)–N(12) = 177.2(3)°]. Fig. 4b shows the silver atoms of Ag(1) and

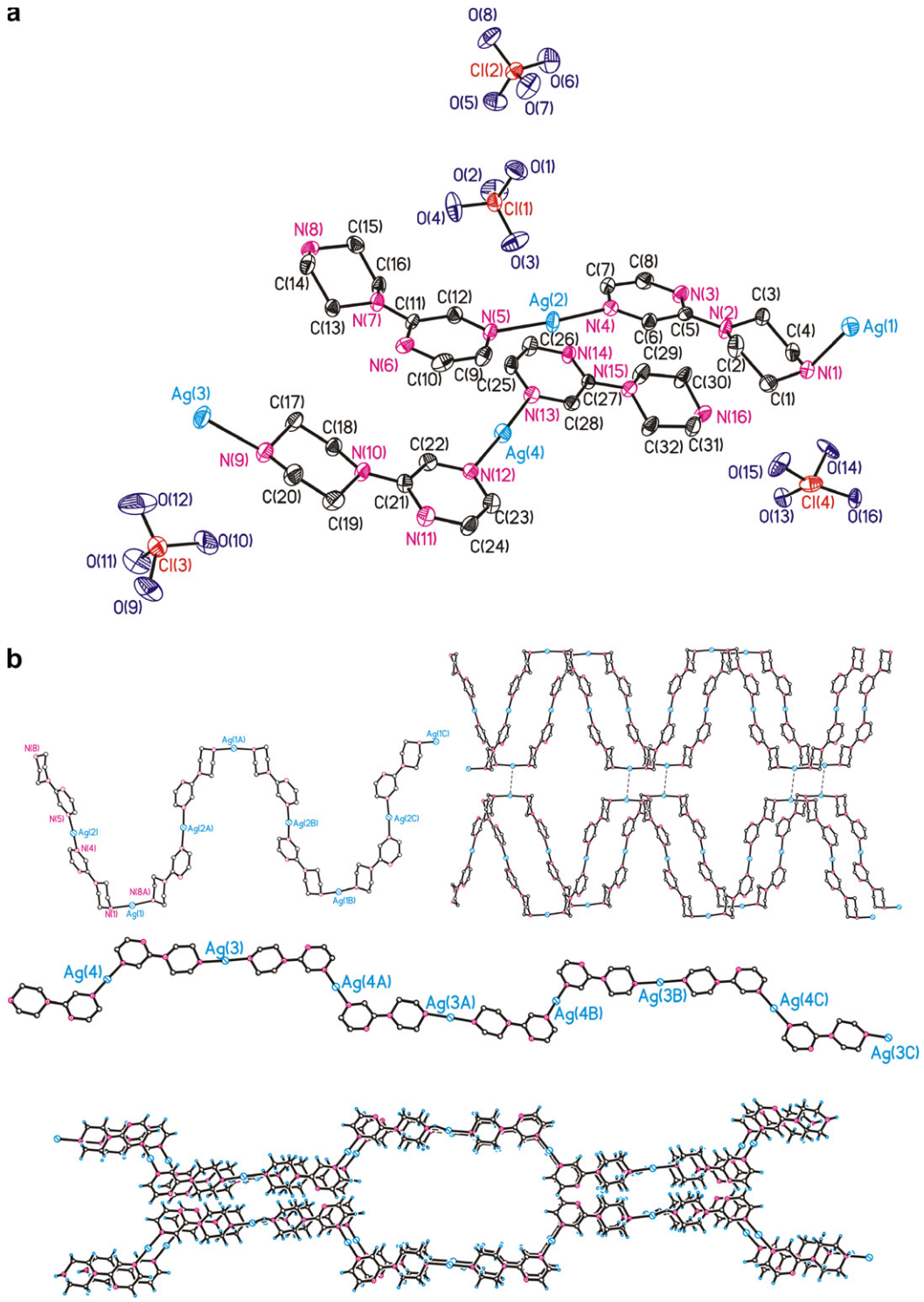

Fig. 4. (a) An asymmetry unit ORTEP drawing of **2**. (b) Two types of $[Ag(pyapa)]_n^{n+}$ cationic chains in **2**.

Ag(2) coordinated to pyapa ligands forming a zig-zag chain that is different from the chain forming by Ag(3), Ag(4) and pyapa groups. The dihedral angles between the two pyrazinyl rings that coordinated to the Ag atoms through the nitrogen atoms are almost coplanar in the degrees of 2.5° and 3.7°. The Ag···Ag distances in the zig-zag chains separated by the bridging pyapa are 9.000 Å.

The packing diagrams (Fig. 5top) show two fashions of the polymeric chains containing Ag(1) and Ag(2) or the one containing Ag(3) and Ag(4) interlink each through weak Ag···Ag interactions (Ag···Ag = 4.004 Å), while the view along the *c*-axis shows two types chains packing through series Ag···Ag (Ag···Ag = 3.892 Å) and Ag–N (Ag–N = 3.167–3.431 Å) interactions (Fig. 5bottom). When looking along the *a*-axis, complex **2** forms the 3-D open-channel supramolecular structure, which are linking by the anions and cationic chains through Ag···O, Ag···N interactions and N–H···N, CH···Ag hydrogen bonds (Ag···O = 3.275 and 3.359 Å, CH···Ag = 3.307 Å, N–H···N = 2.591 Å).

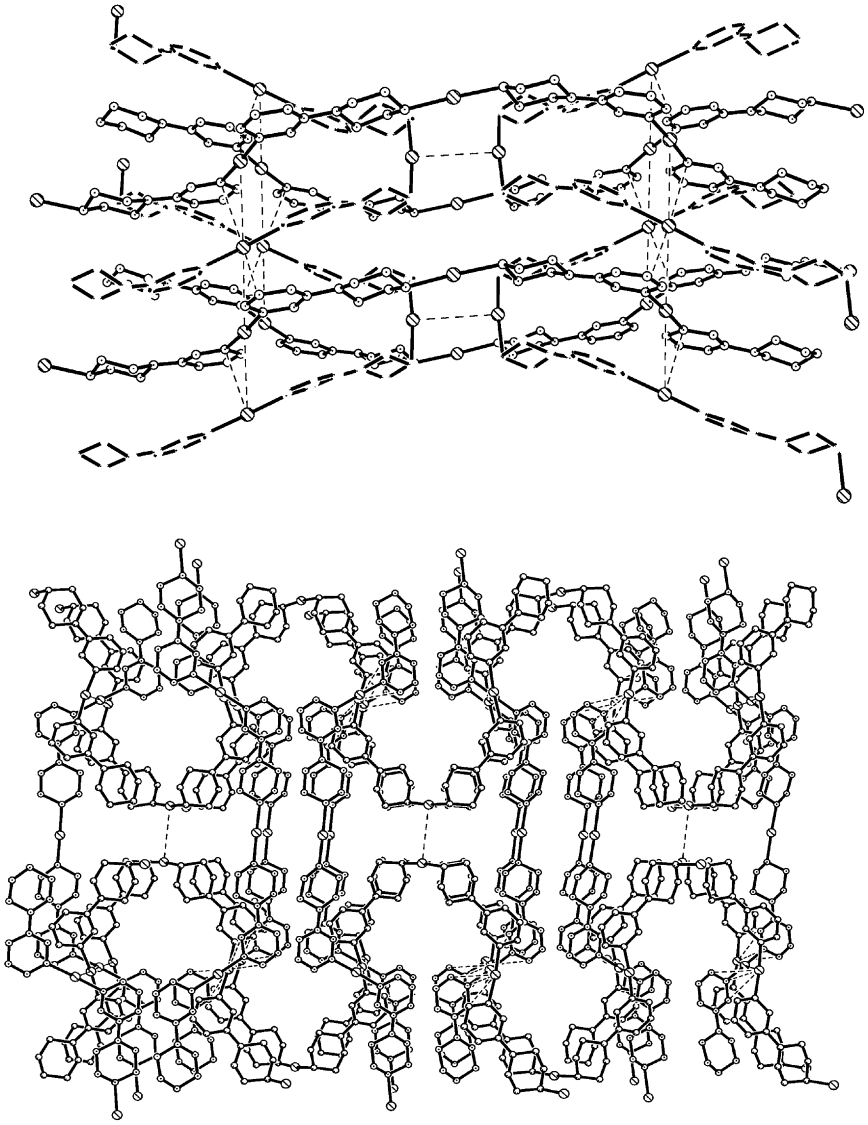

Fig. 5. Packing diagrams of **2**.

2.10. Structure of complex **3**

The structure **3** was solved in the space group $P2_1/c$. Fig. 6a shows the asymmetric unit of complex **3**, which contains two Ag(I) atom, two pyapa groups, two nitrate anions and a bonded water molecule. Fig. 6b shows the local coordination of the Ag(I) centers in complex **3** forming the zig-zag polymeric chain. Table 2 list the bond distances and angles around Ag(1) and Ag(2) for complex **3**. The Ag(1) atom bond two piperazinyl nitrogen atoms (Ag–N = 2.188(3)–2.217(3) Å) and the silver metal center adopts slightly linear geometry (N–Ag–N = 165.41(14)°), while Ag(2) atom bond two pyrazinyl nitrogen atoms (Ag–N = 2.167(4)–2.175(3) Å), one bound water molecule (Ag–O = 2.577(4) Å) and the silver metal center adopts slightly disorder T-shaped geometry [∠N(4)–Ag(2)–N(5) + ∠N(4)–Ag(2)–O(7) + ∠N(5)–Ag(2)–O(7) = 359.7°]. Each Ag(I) coordinated to two pyapa ligands and each pyapa bridged two Ag(I) atom in **3**. The dihedral angle between the two pyrazinyl rings that coordinated to the Ag atom through the nitrogen atoms is almost coplanar in the degree of 3.5°. The Ag···Ag distances in the zig-zag chains separated by the bridging pyapa are 9.124 Å.

Fig. 7a shows the cationic molecules in complex **3** linking each through the Ag···N and Ag···Ag weak interactions to form the 2-D

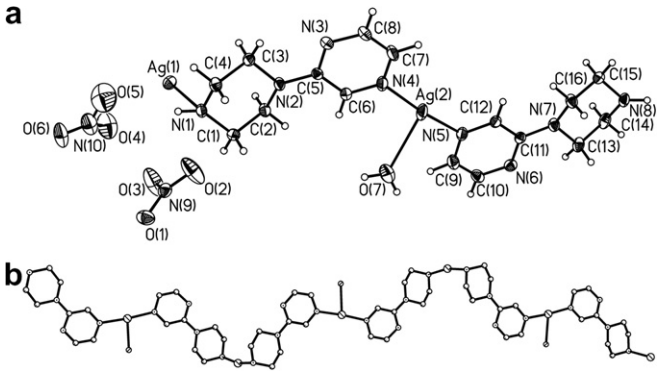

Fig. 6. (a) An ORTEP drawing of complex **3**. (b) The structure drawing of Ag(I) centers coordination location.

pleated layers. The Ag···N distances are in the range from 3.257 to 3.442 Å, and the distances of Ag···Ag between two zig-zag chains is 3.682 Å. In complex **3**, Fig. 7b, the 2-D pleated sheets are further linked by the anions and solvent molecules and through Ag···O

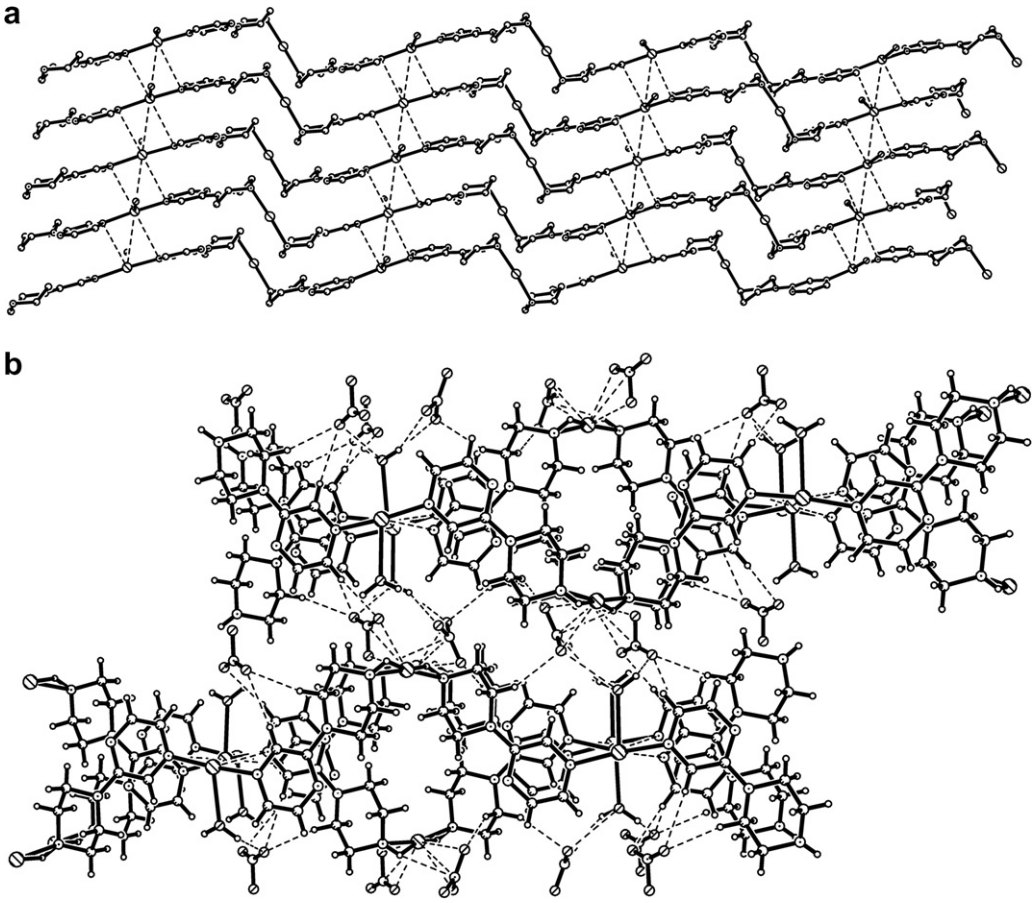

Fig. 7. (a) The 2-D sheet showing the weak Ag···Ag and Ag···N interactions among the 1-D zig-zag chains. (b) Packing diagram of **3** shows the anions and solvent molecules interlinking cationic layers through serious hydrogen bonds.

interactions, C–H···O and/or O–H···O hydrogen bonds to form 3-D supramolecular structures (Ag···O = 2.677–3.292 Å, C–H···O = 2.431–2.527 Å, ∠C–H···O = 135.4–172.5°, O–H···O = 2.159–2.536 Å, ∠O–H···O = 103.0–159.7°).

3. Thermal properties

Thermal gravimetric analyses (TGA) were carried out to examine the thermal stability of **1**–**3**. The samples were heated up in air at 1 atm pressure with the heating rate of 10 °C min^{-1}. The TGA curve shows that **1**is the first loss took place between 150 and 220 °C and was associated with the loss of the H_2O molecules (calculated 7.8%, observed 7.6%). The second loss took place between 220 and 250 °C, corresponding to the loss SO_4^{2-} anions and pyapa ligands (calculated 61.6%, observed 61.2%). The TGA for **2** showed the loss of ClO_4^- anions in range 150–220 °C (calculated 26.8%, observed 26.7%), followed by the loss of pyapa ligands (calculated 44.1%, observed 44.3%). The TGA curve shows that **3**is the first loss took place between 95 and 135 °C and was associated with the loss of the H_2O molecules (calculated 2.6%, observed 2.5%). The second loss took place between 135 and 230 °C, corresponding to the loss NO_3^- anions and pyapa ligands (calculated 56.8%, observed 57.1%).

4. Conclusions

In this study, the coordination chemistry of Ag(I) salts with 1-(2-pyrazinyl)piperazine (pyapa) was investigated. The synthesis and structures of three novel complexes $[Ag_4(pyapa)_4(SO_4)_2 \cdot 6H_2O]_n$, **1**, $\{[Ag_2(pyapa)_2][ClO_4]_2\}_n$, **2** and $\{[Ag_2(pyapa)_2(H_2O)][NO_3]_2\}_n$, **3**, have been successfully accomplished. The double helices 1-D polymeric chain structures was seen in complex **1**, and the pyapa acted as the bidentate ligand that bonded Ag(I) atoms. The helices interlinks each through strong Ag···Ag interactions and π–π stacking. In complexes **2** and **3** show the zig-zag polymeric chains, which interact through the weak Ag···O and Ag···N interactions between Ag(I) atoms and the pyrazinyl groups of pyapa ligands that formed the pleated 2-D supramolecular layers, respectively. In complexes **1**–**3**, the same ratio of Ag(I) atom to pyapa ligand is 1–1, but display the different supramolecular architectures.

Acknowledgements

We are grateful to the Nanya Institute of Technology and the National Science Council of the Republic of China for support.

Appendix A. Supplementary data

CCDC 618086, 618085 and 618084 contains the supplementary crystallographic data for **1**, **2** and **3**. These data can be obtained free of charge via http://www.ccdc.cam.ac.uk/conts/retrieving.html, or from the Cambridge Crystallographic Data Centre, 12 Union Road, Cambridge CB2 1EZ, UK; fax: (+44) 1223-336-033, or e-mail: deposit@ccdc.cam.ac.uk. Supplementary data associated with this article can be found, in the online version, at doi:10.1016/j.poly.2008.03.015.

References

[1] (a) G.R. Desiraju, Angew. Chem., Int. Ed. Engl. 34 (1995) 2311;
(b) G.R. Desiraju, Chem. Commun. (1997) 1475;
(c) J.M. Lehn, Supramolecular Chemistry, VCH, Weinheim, 1995.

[2] (a) R. Robson, B.E. Abrahams, S.R. batten, R.W. Gable, B.F. Hoskins, J. Lieu, Supramolecular Architecture, ACS Publications, Washington, DC, 1992;
(b) S.R. Batten, R. Robson, Angew. Chem., Int. Ed. 37 (1998) 1460;
(c) O.M. Yaghi, H. Li, C. Davis, D. Richardson, T.L. Groy, Acc. Chem. Res. 31 (1998) 474;
(d) H. Gudbjartson, K. Biradha, K.M. Poirier, M.J. Zaworotko, J. Am. Chem. Soc. 121 (1999) 2599;
(e) C.B. Aakeröy, K.R. Seddon, Chem. Soc. Rev. (1993) 397;
(f) M. Fujita, K. Ogura, Coord. Chem. Rev. 148 (1996) 249;
(g) S.-I. Noro, R. Kitauta, M. Kondo, S. Kitagawa, T. Ishii, H. Matauzaka, M. Yamashita, J. Am. Chem. Soc. 124 (2002) 2568;
(h) S. Kitagawa, M. Kondo, Bull. Chem. Soc. Jpn. 71 (1998) 1739.

[3] (a) R.P. Sijbesma, E.W. Meijer, Curr. Opin. Colloid Interface Sci. 4 (1999) 24;
(b) S.C. Zimmerman, P.S. Corbin, Struct. Bonding 96 (2000) 63;
(c) D.C. Sherrington, K.A. Taskinen, Chem. Soc. Rev. 30 (2001) 83;
(d) D.S. Lawrence, T. Jiang, M. Levett, Chem. Rev. 95 (1995) 2229.

[4] (a) L. Fabbrizza, A. Poggi (Eds.), Transition Metals in Supramolecular Chemistry, Kluwer Academic, The Netherlands, 1994;
(b) J.-M. Lehn (Ed.), Comprehensive Supramolecular Chemistry, Pergamon Press, Oxford, 1995;
(c) K. Biradha, M. Fujita, Adv. Supramol. Chem. 6 (2000) 1.

[5] (a) J.A. McCleverty, M.D. Ward, Acc. Chem. Res. 31 (1998) 842;
(b) C.-T. Chen, K.S. Suslick, Coord. Chem. Rev. 128 (1993) 293;
(c) D.W. Bruce, Acc. Chem. Res. 33 (2000) 831.

[6] (a) M.J. Zaworotko, Angew. Chem., Int. Ed. 39 (2000) 3052;
(b) S. Lopez, S.W. Keller, Inorg. Chem. 38 (1999) 1883. and references therein.

[7] (a) J. Konnert, D. Britton, Inorg. Chem. 5 (1966) 1193;
(b) H.-L. Hu, M.-C. Suen, C.-W. Yeh, J.-D. Chen, Polyhedron 24 (2005) 1497;
(c) M.-C. Suen, Y.-H. Wang, Y.-F. Hsu, C.-W. Yeh, J.-D. Chen, J.-C. Wang, Polyhedron 24 (2005) 2913;
(d) B.F. Hoskins, R. Robson, J. Am. Chem. Soc. 112 (1990) 1546.

[8] (a) M.C. Etter, Acc. Chem. Res. 23 (1990) 120;
(b) P.J. Hagrman, J. Zubieta, Inorg. Chem. 38 (1999) 4480;
(c) Y.-H. Wang, K.-L. Chu, H.-C. Chen, C.-W. Yeh, Z.-K. Chan, M.-C. Suen, J.-D. Chen, J.-C. Wang, CrystEngComm (2006) 84;
(d) M.-C. Suen, Y.-H. Wang, J.-C. Wang, J. Chin. Chem. Soc. 51 (2004) 43;
(e) C.-W. Yeh, Y.-S. Yen, W.-B. Lin, C.-W. Su, J.-D. Chen, J.-C. Wang, Struct. Chem. 16 (2005) 141.

[9] (a) K.J. Lin, Angew. Chem., Int. Ed. Engl. 38 (1999) 2730;
(b) M.-C. Suen, T.-C. Keng, J.-C. Wang, Polyhedron 21 (2002) 2705;
(c) H. Li, A. Laine, M. O'Keefee, O.M. Yaghi, Science 283 (1999) 145;
(d) H. Li, M. Eddaoudi, M. O'Keefee, O.M. Yaghi, Nature (London) 402 (1999) 276;
(e) H. Li, A. Laine, M. Eddaoudi, M. O'Keefee, O. M Yaghi, J. Am. Chem. Soc. 121 (1999) 6096.

[10] (a) Y. Kang, S.S. Lee, K.-M. Park, S.H. Lee, S.O. Kang, J. Ko, Inorg. Chem. 40 (2001) 1488;
(b) B.B. Amabilino, J.F. Stoddart, Chem. Rev. 95 (1995) 2725;
(c) D.M.L. Goodgame, S. Menzer, A.M. Smith, D.J. Willam, Angew. Chem., Int. Ed. Engl. 34 (1995) 574;
(d) P. Losier, M.J. Zaworotko, Angew. Chem., Int. Ed. Engl. 35 (1996) 2779.

[11] (a) A.J. Blake, N.R. Champness, P. Hubberstey, W.-S. Li, M.A. Withersby, M. Schröder, Coord. Chem. Rev. 183 (1999) 117;
(b) S. Muthu, J.H.K. Yip, J.J. Vittal, J. Chem. Soc., Dalton Trans. (2002) 4561. and references therein;
(c) A.Y. Robin, K.M. Formm, Coord. Chem. Rev. 250 (2006) 2127. and references therin.

[12] P.J. Hagrman, D. Hagrman, J. Zubieta, Angew. Chem., Int. Ed. Engl. 38 (1999) 2638. and references therein.

[13] (a) S. Batten, R. Robson, Angew. Chem., Int. Ed. Engl. 37 (1998) 1998. and references therein;
(b) Y.-B. Dong, X. Zhao, G.-X. Jin, R.-Q. Huang, M.R. Smith, Eur. J. Inorg. Chem. (2003) 4017;
(c) Y.-B. Dong, J.-P. Ma, X. Zhao, G.-X. Jin, R.-Q. Huang, M.R. Smith, Dalton Trans. (2003) 4324.

[14] (a) Y.-F. Hsu, J.-D. Chen, Eur. J. Inorg. Chem. (2004) 1488;
(b) H.-L. Hu, C.-W. Yeh, J.-D. Chen, Eur. J. Inorg. Chem. (2004) 4696. and references therein;
(c) M.-C. Suen, H.-A. Tsai, J.-C. Wang, J. Chin. Chem. Soc. 52 (2005) 1085.

[15] XSCANS, Release, 2.1, Siemens Energy & Automation, Inc., Madison, Wisconsin, USA, 1995.

[16] SHELXTL 5.10, Bruker Analytical X-ray Instruments Inc., Karlsruche, Germany, 1997.

[17] (a) F. Robinson, M.J.J. Zaworotko, Chem. Soc. Chem. Commun. (1995) 2413;
(b) M.A. Withersby, A.J. Blake, N.R. Champness, P. Hubberstey, W.-S. Li, M. Schröder, Angew. Chem., Int. Ed. Engl. 36 (1997) 2327;
(c) O.M. Yaghi, H.J. Li, Am. Chem. Soc. 118 (1996) 295;
(d) L. Carlucci, G. Ciani, P. Macchi, D.M. Proserpio, Chem. Commun. (1998) 1837;
(e) M.-L. Tong, Y.-M. Wu, H.-C. Chang, S. Kitagawa, Inorg. Chem. 41 (2002) 4846.

[18] (a) L. Carlucci, G. Ciani, D.W.V. Gundenberg, D.M. Proserpio, Inorg. Chem. 36 (1997) 3812;
(b) C. Janiak, J. Chem. Soc., Dalton Trans. (2000) 3885;
(c) S. Paliwal, S. Geib, C.S.J. Wilcox, Am. Chem. Soc. 116 (1994) 4497;
(d) A.N. Khlobystov, N.R. Champness, D.A. Lemenovskki, A.G. Majouga, N.V. Zyk, M. Schröder, Coord. Chem. Rev. 222 (2001) 155;
(e) A.J. Black, G. Baum, N.R. Champness, S.S.M. Chung, P.A. Cooke, D. Fenske, A.N. Khlobystov, D.A. Lemenovskki, W.S. Li, M. Schröder, J. Chem. Soc., Dalton Trans. (2000) 4285;
(f) M. Munakata, L.P. Wu, M. Yamamoto, T. Kuroda-Sowa, M.J. Maekawa, Am. Chem. Soc. 118 (1996) 3117;
(g) T. Sugimori, H. Masuda, N. Ohata, K. Koiwai, A. Odani, O. Yamauchi, Inorg. Chem. 36 (1997) 576.

Polyhedron 27 (2008) 2043–2048

Contents lists available at ScienceDirect

Polyhedron

journal homepage: www.elsevier.com/locate/poly

Synthesis and characterization of mononuclear and dinuclear Mn complexes with *N*,*N*′-disubstituted octaaza macrocycle

Wonchoul Park [a], Jang-Hoon Cho [b], Hong-In Lee [b], Mira Park [c], Myoung Soo Lah [c], Dongyeol Lim [a,*]

[a] Department of Chemistry, Sejong University, Seoul 143-747, South Korea
[b] Department of Chemistry, Kyungpook National University, Daegu 702-701, South Korea
[c] Department of Chemistry and Applied Chemistry, Hanyang University, Ansan, Kyunggi-do 426-791, South Korea

ARTICLE INFO

Article history:
Received 5 November 2007
Accepted 20 March 2008
Available online 12 May 2008

Keywords:
Manganese(II) complexes
Octaaza macrocycle
Crystal structures

ABSTRACT

A new 24-membered octaaza macrocyclic ligand (**L**) containing two methoxybenzyl pendant arms has been synthesized. While its complexation with $MnCl_2$ in the presence of perchlorate anion yielded a mononuclear complex, $[Mn\mathbf{L}](ClO_4)_2$, a similar reaction in the absence of perchlorate anion led to an endocyclic dinuclear complex, $[Mn_2\mathbf{L}Cl_4]$. In $[Mn\mathbf{L}](ClO_4)_2$, the Mn(II) ion was tightly surrounded by the N8-macrocyclic ligand to form a distorted bicapped octahedral geometry. In $[Mn_2\mathbf{L}Cl_4]$, the endomacrocyclic bound two manganese ions are bridged via two chloro ligands to form a bis-(μ-chloro) Mn_2Cl_2 diamond core. Each Mn(II) ion in the dinuclear complex is additionally ligated with a diaminomethyl pyridinyl nitrogen donor atom of the ligand and a terminal chloride, which leads to a distorted octahedral geometry of the N_3Cl_3 donor set. An EPR study of $[Mn\mathbf{L}](ClO_4)_2$ in DMSO or DMF showed an unprecedented Mn(II) EPR signal spreading from ~100 G over ~7000 G with ^{55}Mn nuclear hyperfine structures at 600–1800 G. For $[Mn_2\mathbf{L}Cl_4]$, a typical high-spin Mn(II) signal was observed near $g = \sim 2$ with an average ^{55}Mn nuclear hyperfine coupling constant of 91 G and small ZFS.

© 2008 Elsevier Ltd. All rights reserved.

1. Introduction

The synthesis and coordination chemistry of polyaza macrocyclic ligands bearing pendant arms has attracted much interest in the last few decades [1,2]. The incorporation of pendant arms on polyaza macrocyclic ligands can change the complexation capability of the ligands, and can increase the stability of their complexes with multiple metal ions. Among the transition metals that form complexes with polyaza macrocycles, manganese is well known to have an important role in many biological reactions [3], such as water oxidation (photosystem II) [4], decomposition of hydrogen peroxide (catalase), and dismutation of the superoxide anion radical (superoxide dismutase). Therefore, studies on manganese complexes with various geometries would expand our understanding of the coordination geometries and the mechanisms of manganese enzymes.

The octaaza macrocycle containing two pyridyl groups, specifically 3,6,9,17,20,23,29,30-octaazatricyclo[23,3,1,1]triaconta-1(29),-11,13,15,25,27-hexaene (BPBD) shown in Scheme 1, has been studied as a host for phosphate and transition metal ions [5,6]. Its Cu(II), Ni(II) and Zn(II) complexes have been prepared and the structure determined [6–8]; all of them were dinuclear and each metal ion in the complexes was coordinated to the equatorial four nitrogen atoms of the macrocycle. We have prepared a new 24-membered octaaza macrocycle that contains two methoxybenzyl substituents as pendant arms (Fig. 1). When a Mn(II) ion was complexed with the ligand, two different species were obtained, depending on conditions, one is the mononuclear Mn(II) complex in the presence of perchlorate anion and the other is a dinuclear Mn(II) endomacrocyclic complex with a bis-μ-chloro bridge in the absence of perchlorate anion. The latter structure is an attractive model for the study of the role of chloride anions in the manganese assembly found in photosynthetic water oxidation systems [9]. Here, we present the synthesis of a new ligand and its manganese complexes (Scheme 1), the solid-state characterizations of the complexes using single-crystal structure analysis, and studies on the solution characteristics using EPR spectroscopy.

2. Experimental

2.1. General procedures and methods

All reagents were obtained from commercial suppliers and used without purification unless specified otherwise. ^1H and ^{13}C NMR spectra were collected on a Bruker AVANCE II 500 spectrometer at resonance frequencies of 500.1 MHz and 125.7 MHz, respectively. The solvents used were $CDCl_3$ and D_2O. The chemical shifts (in ppm) are reported from tetramethylsilane or referenced to

* Corresponding author. Tel.: +82 2 3408 3218; fax: +82 2 462 9954.
E-mail address: dylim@sejong.ac.kr (D. Lim).

0277-5387/$ - see front matter © 2008 Elsevier Ltd. All rights reserved.
doi:10.1016/j.poly.2008.03.021

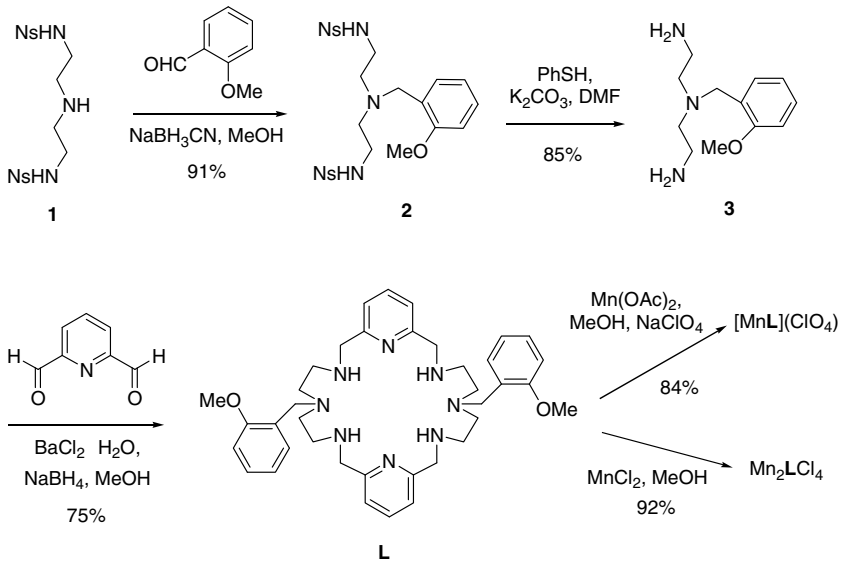

Scheme 1. Synthesis of macrocyclic ligand **L** and its two manganese complexes.

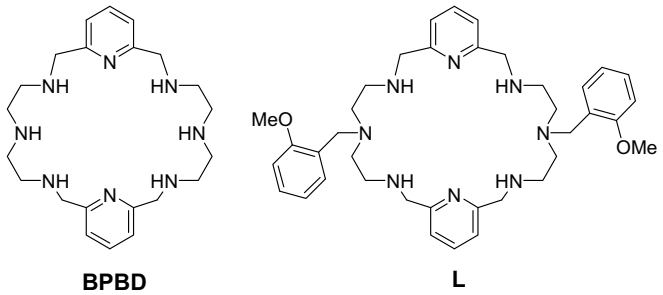

Fig. 1. Structure of *N,N′*-disubstituted octaaza macrocycle.

solvent on the δ scale. LRMS (ESI) spectra were recorded on an Agilent 1100 LC/MSD instrument. The ATR-FTIR spectra of the manganese complexes were measured from 4000 cm^{-1} to 650 cm^{-1} with a Spectrum 100 spectrometer (Perkin–Elmer).

2.2. Synthesis of the macrocycle *L*

2.2.1. 4-(2-Methoxy-benzyl)-1,7-bis(2-nitrophenylsulfonyl)-1,4,7-triazaheptane (*2*)

Compound **1** (in Scheme 1) [10] (1.0 g, 2.11 mmol) and a 2-methoxybenzaldehyde (0.35 g, 2.53 mmol) were mixed in MeOH (30 mL) at room temperature. Sodium cyanoborohydride (0.20 g, 3.17 mmol) and glacial acetic acid (0.13 g, 2.11 mmol) were added, and the mixture was stirred for 6 h at room temperature. The reaction mixture was quenched with saturated aqueous $NaHCO_3$ solution, and the product was extracted with CH_2Cl_2. The solvent was removed in vacuo, and the crude product was purified by chromatography on a silica gel column (1:2 hexane/EtOAc) to give a light yellow solid. Yield, 1.14 g (91%). ^{1}H NMR (500 MHz, $CDCl_3$); δ 7.99–7.98 (m, 2H), 7.70–7.75 (m, 2H), 7.69–7.66 (m, 4H), 7.20 (t, 1H, J = 7.8 Hz), 7.04 (d, 1H, J = 7.3 Hz), 6.88 (d, 1H, J = 8.2 Hz), 6.79 (t, 1H, J = 7.4 Hz), 3.89 (s, 4H), 3.54 (s, 2H), 3.01 (t, 4H, J = 5.7 Hz), 2.56 (t, 4H, J = 4.7 Hz); ^{13}C NMR (125.76 MHz, $CDCl_3$); δ 158.05, 148.08, 133.49, 133.43, 132.58, 131.17, 130.69, 129.25, 125.46, 125.39, 120.28, 110.93, 55.53, 54.27, 53.82, 41.43. ESI-MS $[M+H]^+$: 594.3.

2.2.2. N^1-(2-amino-ethyl)-N^1-(2-methoxy-benzyl)-ethane-1,2-diamine (*3*)

Thiophenol (0.46 g, 4.2 mmol) was added to a stirred solution of compound **2** (1.0 g, 1.68 mmol) and anhydrous potassium carbonate (0.70 g, 5.05 mmol) in dimethyl formamide (DMF). The resulting mixture was stirred for 4 h at room temperature and then the solvent was removed in vacuo. The residue was dissolved in a mixture of EtOAc (50 mL) and 1 N-HCl (20 mL). The aqueous layer was washed with EtOAc until the by-product was removed, and then basified with 2 N-KOH. The aqueous solution was extracted with CH_2Cl_2, dried over Na_2SO_4 and concentrated in vacuo to give a colorless viscous oil. Yield, 0.38 g (85%). ^{1}H NMR (500 MHz, D_2O) as a HCl salt; δ 7.35 (t, 1H, J = 7.9 Hz), 7.25 (m, 1H, J = 7.4 Hz), 7.06 (d, 1H, J = 8.3 Hz), 6.98 (t, 1H, J = 7.4 Hz), 3.81 (s, 3H), 3.59 (s, 2H), 3.07 (t, 4H, J = 5.7 Hz), 2.75 (t, 4H, J = 5.8 Hz); ^{13}C NMR (125.76 MHz, D_2O); δ 157.70, 131.91, 129.82, 125.10, 120.92, 111.82, 55.55, 51.50, 50.37, 36.90. ESI-MS $[M+H]^+$: 224.3.

2.2.3. 6,20-Bis-(2-methoxy-benzyl)-3,6,9,17,20,23,29,30-octaaza-tricyclo[23.3.1.111,15]triaconta-1(29),11,13,15(30),25,27-hexaene (*4*)

A solution of compound **3** (0.30 g, 1.34 mmol) in MeOH was added dropwise over 15 min to 2,6-diformylpyridine (0.18 g, 1.34 mmol) and $BaCl_2 \cdot 2H_2O$ (0.16 g, 0.67 mmol) in MeOH. The resulting mixture was refluxed for 4 h. After the yellow solution was allowed to cool to room temperature, solid $NaBH_4$ (0.25 g, 6.7 mmol) was added slowly and stirred for 30 min, and then the solvent was removed in vacuo. The residue was dissolved in a mixture of CH_2Cl_2 (50 mL) and 1 N-HCl (20 mL). The aqueous layer was washed with CH_2Cl_2 until the by-product was removed, and then basified with 2 N-KOH. The aqueous solution was extracted with CH_2Cl_2 and the organic layer was dried over Na_2SO_4 and concentrated. The crude product was purified by chromatography on a silica gel column (10:1 MeOH/NH_4OH) to give a light yellow viscous oil. Yield, 0.66 g (75%). ^{1}H NMR (500 MHz, D_2O) as a HCl salt: 7.88 (dt, 2H, J = 1.5 and 7.8 Hz), 7.45 (dt, 1H, J = 1.4 and 8.1 Hz), 7.39 (d, 4H, J = 7.9 Hz), 7.36 (dd, 2H, J = 1.4H and 7.4 Hz), 7.04-6.99 (m, 4H), 4.42 (s, 6H), 4.39 (s, 4H), 3.74 (s, 4H), 3.72 (m, 8H), 3.64 (m, 8H); ^{13}C NMR (125.76 MHz, D_2O): 157.95, 149.95, 139.66, 132.70, 132.62, 123.16, 121.30, 116.90, 111.75, 55.61, 53.93, 50.75, 50.04, 42.15. ESI-MS $[M+H]^+$: 653.6.

2.2.4. $[MnL](ClO_4)_2$

$Mn(OAc)_2 \cdot 4H_2O$ (28 mg, 0.16 mmol) was added to a stirred solution of macrocyclic ligand **L** (50 mg, 0.08 mmol) in MeOH (5 mL) and the resulting mixture was stirred at room temperature for 2 h. Sodium perchlorate (20 mg, 0.16 mmol) was added and the mixture was stirred for another 30 min. The crude product was dissolved in H_2O (10 mL), extracted with CH_2Cl_2, and dried over Na_2SO_4. The solvent was removed in vacuo to give a light yellow solid. Yield, 61 mg (84%). Colorless single-crystals suitable for X-ray diffraction studies were obtained by slow evaporation of CH_2Cl_2 solution of Mn complex. IR (powder, cm^{-1}): 3319 (w), 2856 (w), 1601 (m), 1583 (m), 1492 (m), 1466 (m), 1451 (m), 1248 (m), 1165 (m), 1081 (s). ESI-MS $[MnLClO_4]^+$: 806.5.

2.2.5. $[Mn_2LCl_4] \cdot CH_3OH$

Anhydrous $MnCl_2$ (38 mg, 0.3 mmol) was added to a stirred solution of macrocyclic ligand **L** (100 mg, 0.15 mmol) in MeOH (10 mL) and the resulting mixture was stirred for 1 h at room temperature. The white precipitate was collected by filtration and washed with cooled MeOH and ether, and dried in vacuo. Yield, 0.12 g (92%). Colorless single crystals suitable for X-ray diffraction studies were obtained by vapor diffusion of diethyl ether into a solution of the Mn complex in methanol. IR (powder, cm^{-1}): 3243 (w), 3221 (w), 2801 (w), 1601 (m), 1582 (m), 1494 (m), 1467 (m), 1434 (m), 1244 (m), 1152 (m). ESI-MS $[Mn_2LCl_4–MnCl_3]^+$: 742.5.

2.3. Crystallography

Crystals were coated with paratone oil to prevent loss of crystallinity on exposure to air. Data were collected at −100 °C using Mo-Kα radiation (λ = 0.71073 Å) employing a Bruker SMART CCD equipped with a graphite crystal, incident-beam monochromator. The SMART and SAINT software packages [11] were used for data collection and integration, respectively. The data were corrected for absorbance using SADABS [12] based upon Laue symmetry using equivalent reflections. Structures were solved by direct methods, and refined using full-matrix, least-squares calculations employing the SHELXTL–PLUS software package [13]. All non-hydrogen atoms were refined anisotropically. Hydrogen atoms in the crystal of $[MnL](ClO_4)_2$ were found by difference Fourier peaks, and refined isotropically, but hydrogen atoms in the crystal of $[Mn_2LCl_4] \cdot CH_3OH$ were assigned isotropic displacement coefficients U(H) = 1.2U (C, N) or 1.5U (C_{methyl}, O), and their coordinates were allowed to ride on their respective atoms. Crystal and intensity data are given in Table 1.

2.4. EPR spectroscopy

X-band (9 GHz) EPR spectra were recorded on a Jeol JES-TE300 ESR spectrometer using 100 kHz field modulation. Low-temperature spectra were obtained using a Jeol ES-DVT3 variable temperature controller for liquid nitrogen temperature and an Oxford continuous-flow cryostat ESR900 for liquid helium temperature.

3. Results and discussion

3.1. Synthesis

The synthesis of ligand **L** is described in Scheme 1. Bis-nosylated diethylenetriamine **1** was prepared as described [10], and the secondary amine was reductively alkylated with 2-methoxybenzaldehyde to give compound **2** with 91% yield in the presence of sodium cyanoborohydride. Two nosyl groups of compound **2** were removed under basic conditions in 85% yield, and then cyclized with 2,6-diformylpyridine under reducing conditions in a 2 + 2 manner, yielding the disubstituted octaaza macrocycle **L**. The ligand was complexed with Mn(II) ion under different conditions (see Section 2) to afford the two complexes $[MnL](ClO_4)_2$ and $[Mn_2LCl_4]$, respectively.

Table 1
Crystal data and structure refinement for $[MnL](ClO_4)_2$ and $[Mn_2LCl_4] \cdot CH_3OH$

	$[MnL](ClO_4)_2$	$[Mn_2LCl_4] \cdot CH_3OH$
Empirical formula	$C_{38}H_{52}Cl_2MnN_8O_{10}$	$C_{39}H_{56}Cl_4Mn_2N_8O_3$
Formula weight	906.72	936.60
Temperature (K)	173(2)	173(2)
Wavelength (Å)	0.71073	0.71073
Crystal system	monoclinic	orthorhombic
Space group	$P2_1/n$	$Pccn$
Unit cell dimensions		
a (Å)	10.4164(10)	14.3503(11)
b (Å)	21.403(2)	17.0012(12)
c (Å)	18.6642(18)	17.6197(13)
α (°)	90	90
β (°)	99.285(2)	90
γ (°)	90	90
V (Å^3)	4106.5(7)	4298.7(5)
Z	4	4
D_{calc} (Mg/m^3)	1.467	1.447
Absorption coefficient (mm^{-1})	0.519	0.883
F(000)	1900	1952
Crystal size (mm)	0.45 × 0.20 × 0.13	0.50 × 0.13 × 0.13
θ Range for data collection (°)	1.90–28.29	1.86–28.30
Reflections collected	25 579	25 691
Independent reflections [R_{int}]	9683 [0.0311]	5256 [0.0646]
Completeness to θ = 28.29° (%)	94.9	98.3
Maximum and minimum transmission	0.9356 and 0.8000	0.8938 and 0.6665
Data/restraints/parameters	9683/0/740	5256/0/267
Goodness-of-fit (GOF) on F^2	1.017	1.011
Final R [$I > 2\sigma(I)$]	R_1 = 0.0459 wR_2 = 0.1080	R_1 = 0.0413 wR_2 = 0.0941
R (all data)	R_1 = 0.0790 wR_2 = 0.1252	R_1 = 0.0827 wR_2 = 0.1127
Largest differences in peak and hole (e Å^{-3})	0.616 and −0.440	0.533 and −0.340

3.2. Description of the crystal structures

The molecular structure of $[MnL](ClO_4)_2$ is shown in Fig. 2. In the crystal structure of the complex, the Mn(II) ion is encapsulated by the N8-macrocyclic ligand, resulting in an overall distorted bicapped octahedral geometry. The planes of a typical meridional tridentate, two 2,6-diaminomethyl pyridine moiety of the ligand [N(2), N(1), and N(8) and N(6), N(5), and N(7) with Mn ion] are

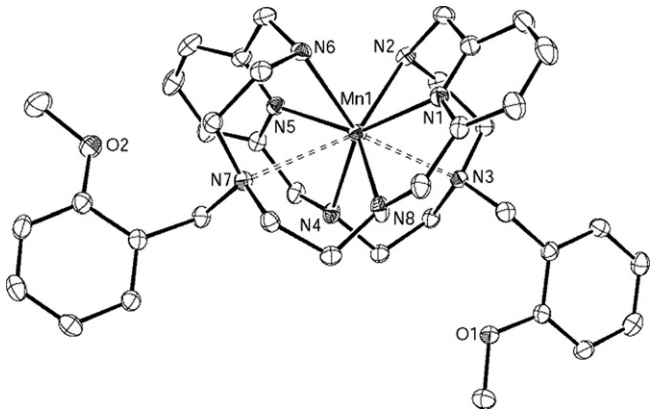

Fig. 2. ORTEP view of the cation of $[MnL](ClO_4)_2$ complex with 30% probability. Hydrogen atoms are omitted for clarity.

Table 2
Selective bond distances (Å) and angles (°) for [Mn**L**](ClO$_4$)$_2$

Mn(1)–N(1)	2.261(2)	Mn(1)–N(8)	2.340(2)
Mn(1)–N(5)	2.263(2)	Mn(1)–N(2)	2.381(2)
Mn(1)–N(4)	2.336(2)	Mn(1)–N(6)	2.411(2)
N(1)–Mn(1)–N(5)	144.61(7)	N(4)–Mn(1)–N(2)	109.97(8)
N(1)–Mn(1)–N(4)	140.55(7)	N(8)–Mn(1)–N(2)	139.83(8)
N(5)–Mn(1)–N(4)	71.79(7)	N(1)–Mn(1)–N(6)	82.05(7)
N(1)–Mn(1)–N(8)	71.78(8)	N(5)–Mn(1)–N(6)	71.63(7)
N(5)–Mn(1)–N(8)	136.46(7)	N(4)–Mn(1)–N(6)	136.38(8)
N(4)–Mn(1)–N(8)	87.50(8)	N(8)–Mn(1)–N(6)	103.33(8)
N(1)–Mn(1)–N(2)	72.22(8)	N(2)–Mn(1)–N(6)	88.71(7)
N(5)–Mn(1)–N(2)	83.71(7)		

slightly bent [i.e. the torsional angles of N(2), Mn(1), N(1), and N(8) and N(6), Mn(1), N(5), and N(7) are −161.89° and 155.80°, respectively]. The two pyridine planes are twisted about −71° and wrap round the Mn ion, and the remaining "open" spaces are capped with two weakly coordinated tertiary nitrogen atoms. The distances of Mn–N(3) and Mn–N(7) are 2.838 Å and 2.989 Å, respectively.

Selected bond distances and angles are given in Table 2. The average distance between Mn and pyridyl nitrogen atoms [N(1) and N(5)] is 2.262 Å, while that of Mn secondary amines is 2.367 Å, reflecting the stronger coordination ability of the pyridyl nitrogen. These average distances are similar to those found in other manganese complexes of acyclic ligands [14–16].

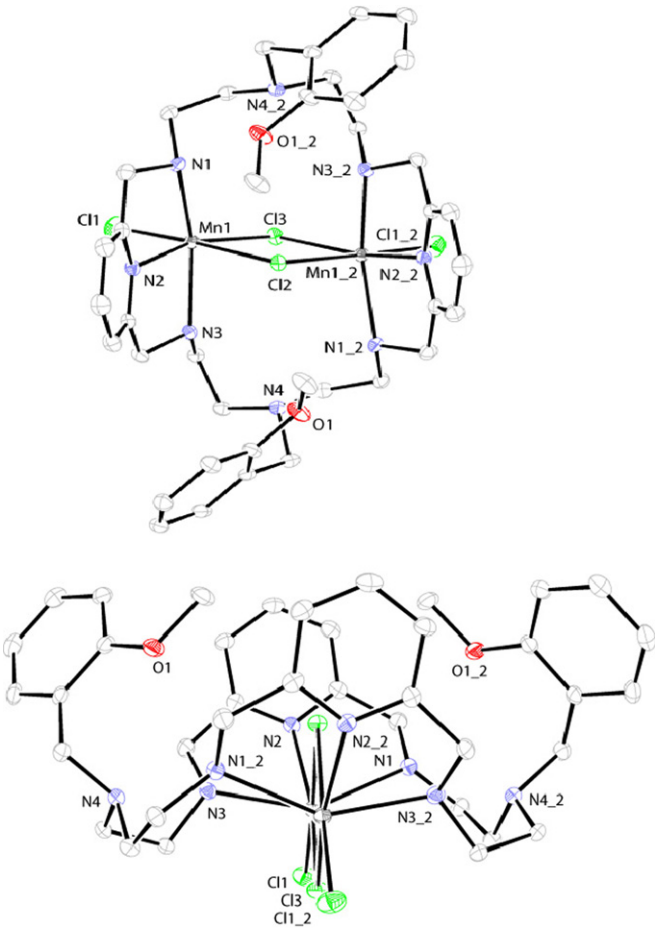

Fig. 3. ORTEP view (top and side) of [Mn$_2$**L**Cl$_4$] with 30% probability. The complex is on the crystallographic 2-fold axis. Hydrogen atoms are omitted for clarity.

The crystal structure of [Mn$_2$**L**Cl$_4$] is displayed in Fig. 3. The complex consists of two endo-encapsulated Mn(II) centers bridged by two chloro ligands, which leads to a bis-μ-chloro Mn$_2$Cl$_2$ diamond core. Each Mn(II) atom is coordinated additionally with a diaminomethyl pyridine and a terminal chloride, giving a six-coordinated N$_3$Cl$_3$ ligand donor set with distorted octahedral geometry. This type of dinuclear chloro-bridged Mn(II) compound with N/O ligands is relatively rare [17–27] and, as far as we know, this is the first example of a structurally defined Mn(II) endomacrocyclic complex with a bis-μ-chloro bridge.

The selected bond lengths and bond angles for [Mn$_2$**L**Cl$_4$] are given in Table 3. As in the mononuclear manganese complex above, the bond distances to the Mn(II) ion are shorter for the pyridyl nitrogen atoms N(2) (2.230 Å) than for the secondary nitrogen atoms N(1) (2.343 Å) and N(3) (2.296 Å). The two Mn–Cl bond distances in the Mn$_2$Cl$_2$ diamond core are slightly different (2.5261 Å and 2.6608 Å), and are longer than the terminal Mn–Cl bond distances (2.4135 Å), as expected for the chloride in bridging mode. The Mn–Mn distance is 3.886 Å, which is comparable to that found in other bis-μ-chloro-bridged Mn(II) complexes [17–27]. The bond angles in the diamond core are 82.80° [Cl(3)–Mn(1)–Cl(2)], 82.81° [Cl(3)–Mn(1)#1–Cl(2), #1: $-x+3/2$, $-y+1/2$, z], 93.82° [Mn(1)–Cl(2)–Mn(1)#1], and 100.57° [Mn(1)#1–Cl(3)–Mn(1)]. The significant difference between the two chloride-centered bridging angles (93.82° and 100.57°) may arise from the different bridging chloride environments caused by the conformational restriction on the ligand in a 2-fold symmetric environment. The structural feature of our bis-μ-chloro-bridged Mn(II) complex, in comparison to other dinuclear BPBD complexes on which no significant interaction between two metal ions is found [7,8], seems to arise from the attractive hydrophobic interaction between the pendant arm and the pyridine moiety of the ligand.

3.3. EPR spectra

Fig. 4 displays frozen-solution EPR spectra obtained from [Mn**L**](ClO$_4$)$_2$ and [Mn$_2$**L**Cl$_4$] dissolved in DMSO and DMF at 110 K. The overall shape of each spectrum is unchanged at helium temperature, but the signal intensities are increased. [Mn**L**](ClO$_4$)$_2$ exhibits an unprecedented Mn(II) EPR spectrum. The EPR signal obtained from the sample in DMSO spreads from ~100 G over ~7000 G, while that in DMF shows almost the same feature as in DMSO, with ^{55}Mn nuclear hyperfine structures at 600–1800 G.

EPR of the high-spin Mn(II) (d^5, $S = 5/2$) complex can be described by the Hamiltonian [28]:

$$\boldsymbol{H} = D\left[S_z^2 - \frac{1}{3}S(S+1)\right] + E(S_x^2 - S_y^2) + \beta \boldsymbol{B}\cdot\boldsymbol{g}\cdot\boldsymbol{S} + \boldsymbol{S}\cdot\boldsymbol{A}\cdot\boldsymbol{I}$$

Table 3
Selective bond distances (Å) and angles (°) for [Mn$_2$**L**Cl$_4$] · CH$_3$OH[a]

Mn(1)–N(2)	2.230(2)	Mn(1)–Cl(3)	2.5261(7)
Mn(1)–N(3)	2.296(2)	Mn(1)–Cl(2)	2.6608(7)
Mn(1)–N(1)	2.343(2)	Cl(2)–Mn(1)#1	2.6608(7)
Mn(1)–Cl(1)	2.4135(8)	Cl(3)–Mn(1)#1	2.5261(7)
N(2)–Mn(1)–N(3)	73.76(8)	Cl(1)–Mn(1)–Cl(3)	99.56(3)
N(2)–Mn(1)–N(1)	74.94(8)	N(2)–Mn(1)–Cl(2)	81.73(6)
N(3)–Mn(1)–N(1)	146.56(8)	N(3)–Mn(1)–Cl(2)	80.67(6)
N(2)–Mn(1)–Cl(1)	95.64(6)	N(1)–Mn(1)–Cl(2)	83.50(6)
N(3)–Mn(1)–Cl(1)	97.46(6)	Cl(1)–Mn(1)–Cl(2)	177.10(3)
N(1)–Mn(1)–Cl(1)	97.02(6)	Cl(3)–Mn(1)–Cl(2)	82.80(2)
N(2)–Mn(1)–Cl(3)	161.35(6)	Mn(1)–Cl(2)–Mn(1)#1	93.82(3)
N(3)–Mn(1)–Cl(3)	93.49(6)	Mn(1)#1–Cl(3)–Mn(1)	100.57(4)
N(1)–Mn(1)–Cl(3)	113.53(6)		

[a] Due to the C_2 symmetric nature of the complex, only half of the data is displayed. #1: $-x+3/2$, $-y+1/2$, z.

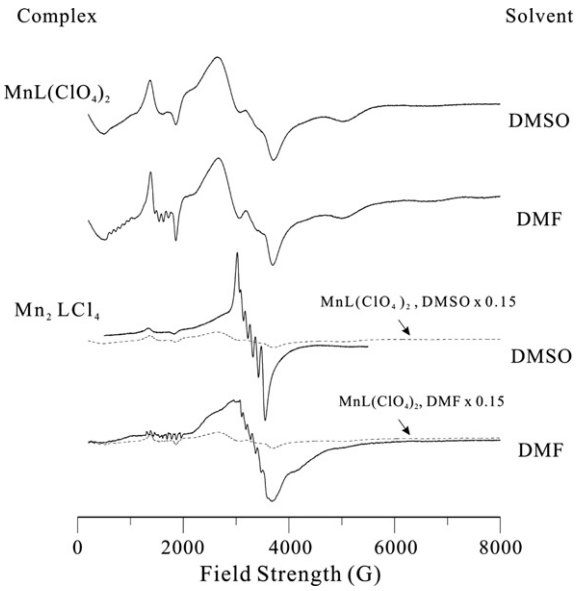

Fig. 4. EPR spectra of the complexes $[MnL](ClO_4)_2$ and $[Mn_2LCl_4]$ dissolved in DMSO and DMF. Numerically reduced $[MnL](ClO_4)_2$ EPR spectra (broken line) are inserted for comparison. *Experimental conditions*: microwave frequency, 9.221 GHz; microwave power, 1.2 mW; modulation width, 10 G for $[MnL](ClO_4)_2$ and 5 G for $[MnL](ClO_4)_2$; time constant, 0.3 s; scan time, 4 min; temperature, 110 K.

where D and E are the axial and rhombic zero-field splitting (ZFS) parameters, $\boldsymbol{B}\cdot\boldsymbol{g}\cdot\boldsymbol{S}$ represents the electron Zeeman interaction, and $\boldsymbol{S}\cdot\boldsymbol{A}\cdot\boldsymbol{I}$ is the nuclear hyperfine coupling term. High-spin Mn(II) in the octahedral field of the $^6A_{1g}$ state generally has small ZFS parameters (D and E) and its X-band EPR signal is readily interpretable. However, as revealed by the single-crystal study of the complex, where Mn–N bond lengths are in the range of 2.26–2.41 Å and N–Mn–N bond angles are 71.6–144.6°, the Mn–N coordination structure is severely distorted from the octahedral geometry, which would give rise to strong ZFS and hamper the quantitative analysis of the spectra at the X-band. The previous multifrequency EPR experiment on a high-spin Mn(II) complex with an N_6 donor set consisting of two tridentate 1,4,7-triazacyclononane ligands showed that the D value of the complex is 0.090 cm^{-1} and E/D is 0.1 [29]. The X-band spectrum of $[MnL](ClO_4)_2$ is similar to but not identical with that reported. We performed numerical simulations to fit the observed spectra using the parameters reported previously for four to six-coordinated high-spin Mn(II) complexes [30,31]. None provides a good explanation of the X-band EPR of $[MnL](ClO_4)_2$. Further investigation using high-field high-frequency EPR to elucidate the details of the electronic structure of this highly distorted $Mn(II)N_6$ compound exhibiting an unprecedented X-band EPR spectra is needed and is being planned [30].

The EPR of $[Mn_2LCl_4]$ in DMF (Fig. 4) shows a typical high-spin Mn(II) feature near $g \sim 2$ with an average ^{55}Mn nuclear hyperfine coupling constant of 91 G and small ZFS, and shows weak signals at $g = 4.91$ (1343 G) and $g = 3.60$ (1830 G). The EPR in DMF displays a richer signal from low field up to ~6000 G with some ^{55}Mn nuclear hyperfine structures. Though the crystal structure tells us that $[Mn_2LCl_4]$ has a bis-μ-Cl bridged Mn(II)Mn(II) dinuclear center, the spectra do not resemble previously reported EPR of spin-coupled Mn(II)Mn(II) complexes [32–34]. Closer examination of the spectra reveals some signal intensity that resembles the EPR features of $[MnL](ClO_4)_2$, represented by a broken line (EPR of $[MnL](ClO_4)_2 \times 0.15$), implying that the $[Mn_2LCl_4]$ solution contains the mononuclear species, $[MnL]^{2+}$. A plausible explanation can be derived from the crystal structure of $[Mn_2LCl_4]$. The Mn_2 dinuclear center of $[Mn_2LCl_4]$ is exposed to the outside of the ligand pocket along the molecular C_2 axis toward the face consisting of terminal chloride ions and one of the bridging chloride ions, whereas the Mn site of $[MnL](ClO_4)_2$ is buried inside the chelating ligand. The structural characteristics of $[Mn_2LCl_4]$ make the Mn_2 center vulnerable to attack by basic solvents, and changes the dinuclear complex to a more stable mononuclear species, $[MnL]^{2+}$. But the signal from $[MnL]^{2+}$ is not fully responsible for the observed intensity of $[Mn_2LCl_4]$ in both DMSO and DMF. The hyperfine structure near $g \sim 2$ indicates that a solvated mononuclear Mn(II) species also exists in the solution. The remaining intensities may arise from the dinuclear Mn_2 center of $[Mn_2LCl_4]$. Hence, the observed EPR spectra suggest that $[Mn_2LCl_4]$ in the solvent is in an equilibrium in the forms of $[Mn_2LCl_4]$, $[MnL]^{2+}$, and solvated mononuclear Mn(II).

4. Conclusions

The complexation of new ligand **L**, a 24-membered octaaza macrocyclic ligand containing two non-coordinating pendant arms, with Mn(II) gave a mononuclear $[MnL](ClO_4)_2$ in the presence of perchlorate ion, but an endocyclic dinuclear $[Mn_2LCl_4]$ in the absence of perchlorate ion. The crystal structure analysis of $[MnL](ClO_4)_2$ revealed that a Mn(II) ion is encapsulated with the N8-macrocyclic ligand, resulting in an overall distorted bicapped octahedral geometry. In the crystal structure of $[Mn_2LCl_4]$, an endomacrocyclic dinuclear bis-μ-Cl-bridged center was observed, where two Mn(II) ions formed a Mn_2Cl_2 diamond core with two bridging chloro ligands. Each Mn(II) ion is coordinated additionally with a diaminomethyl pyridine of the ligand and terminal chloride, giving a six-coordinated N_3Cl_3 ligand donor set with distorted octahedral geometry. An EPR study of $[MnL](ClO_4)_2$ exhibited an unprecedented Mn(II) EPR signal in DMSO and DMF, spreading from ~100 G over ~7000 G with ^{55}Mn nuclear hyperfine structures at 600–1800 G. For the $[Mn_2LCl_4]$ complex, a typical high-spin Mn(II) signal appeared near $g \sim 2$ with an average ^{55}Mn nuclear hyperfine coupling constant of 91 G and small ZFS, and weak signals were found at $g = 4.91$ (1343 G) and $g = 3.60$ (1830 G).

Acknowledgements

This work was supported by a Grant from the MarineBio21, Ministry of Maritime Affairs and Fisheries, Korea. M.S.L. acknowledges the financial support of KOSEF (R01-2005-000-10490-0). HRMS(FAB) data were obtained from the facilities of the Korea Basic Science Institute.

Appendix A. Supplementary data

CCDC 658518 and 658519 contain the supplementary crystallographic data for $[MnL](ClO_4)_2$ and $[Mn_2LCl_4]$. These data can be obtained free of charge via http://www.ccdc.cam.ac.uk/conts/retrieving.html, or from the Cambridge Crystallographic Data Centre, 12 Union Road, Cambridge CB2 1EZ, UK; fax: (+44) 1223-336-033; or e-mail: deposit@ccdc.cam.ac.uk. Supplementary data associated with this article can be found, in the online version, at doi:10.1016/j.poly.2008.03.021.

References

[1] K.E. Krakowiak, J.S. Bradshaw, D.J. Zamecka-Krakowiak, Chem. Rev. 89 (1989) 929.
[2] P.V. Bernhardt, G.A. Lawrance, Coord. Chem. Rev. 104 (1990) 297.
[3] C.F. Yocum, V.L. Pecoraro, Curr. Opin. Chem. Biol. 3 (1999) 182.
[4] S. Mukhopadhyay, S.K. Mandal, S. Bhaduri, W.H. Armstrong, Chem. Rev. 104 (2004) 3981.
[5] A. Bencini, A. Bianchi, E. Garcia-Espana, E.C. Scott, L. Morales, B. Wang, T. Deffo, F. Takusagawa, M.P. Mertes, K.B. Mertes, P. Paoletti, Bioorg. Chem. 20 (1992) 8.

[6] Q. Lu, R.I. Carroll, J.H. Reibenspies, A.E. Martell, A. Clearfield, J. Mol. Struct. 470 (1998) 121.
[7] M. del Carmen Fernández-Fernández, R. Bastida, A. Macias, P. Pérez-Lourido, L. Valencia, Polyhedron 26 (2007) 5317.
[8] J. Martínez-Sánchez, R. Bastida, A. Macías, P. Pérez-Lourido, L. Valencia, Polyhedron 25 (2006) 3495.
[9] B.C. Unni Nair, J.E. Sheats, R. Ponteciello, D. Van Engen, V. Petrouleas, G.C. Dismukes, Inorg. Chem. 28 (1989) 1582.
[10] J.-M. Siaugue, F. Segat-Dioury, I. Sylvestre, A. Favre-Réguillon, J. Foos, C. Madic, A. Guy, Tetrahedron 57 (2001) 4713.
[11] SMART and SAINT, Area Detector Software Package and SAX Area Detector Integration Program; Bruker Analytical X-ray, Madison, WI, 1997.
[12] SADABS, Area Detector Absorption Correction Program; Bruker Analytical X-ray, Madison, WI, 1997.
[13] G.M. Sheldrick, SHELXTL-PLUS, Crystal Structure Analysis Package; Bruker Analytical X-ray, Madison, WI, 1997.
[14] R. van Gorkum, J. Berding, D.M. Tooke, A.L. Spek, J. Reedijk, E. Bouwman, J. Catal. 252 (2007) 110.
[15] J.A. Lessa, A. Horn Jr., C.B. Pinheiro, L.L. Farah, M.N. Eberlin, M. Benassi, R.R. Catharino, C. Fernandes, Inorg. Chem. Commun. 10 (2007) 863.
[16] Y. Gultneh, A. Farooq, K.D. Karlin, S. Liu, J. Zubiet, Inorg. Chim. Acta 211 (1993) 171.
[17] J.-Z. Wu, E. Bouwman, A.M. Mills, A.L. Spek, J. Reedijk, Inorg. Chim. Acta 357 (2004) 2694.
[18] M.A.S. Goher, M.A.M. Abu-Youssef, F.A. Mautner, A. Popitsch, Polyhedron 12 (1993) 1751.
[19] A. Garoufis, S. Kasselouri, S. Boyatzis, C.P. Raptopoulou, Polyhedron 18 (1999) 1615.
[20] Z.M. Wang, M. Yuan, Z. He, C.-S. Liao, C.-H. Yan, J. Chin. Chem. Soc. 58 (2000) 1615.
[21] I. Romero, M.-N. Collomb, A. Deronzier, A. Llobet, E. Perret, J. Pécaut, L.L. Pape, J.-M. Latour, Eur. J. Inorg. Chem. 2001 (2001) 69.
[22] G.A. van Albada, A. Mohamadou, W.L. Driessen, R. Gelder, S. Tanase, J. Reedijk, Polyhedron 23 (2004) 2387.
[23] A. Majumder, M. Westerhausen, A.N. Kneifel, J.-P. Sutter, N. Daro, S. Mitra, Inorg. Chim. Acta 359 (2006) 3841.
[24] M. Lubben, A. Meetsma, B.L. Feringa, Inorg. Chim. Acta 230 (1995) 169.
[25] E. Sinn, J. Chem. Soc., Dalton Trans. (1976) 162.
[26] S. Bieller, M. Bolte, H.-W. Lerner, M. Wagner, Inorg. Chem. 44 (2005) 9489.
[27] I. Romero, M. Rodríguez, A. Llobet, M. Corbella, G. Fernández, M.-N. Collomb, Inorg. Chim. Acta 358 (2005) 4459.
[28] A. Abragam, B. Bleaney, Electron Paramagnetic Resonance of Transition Ions, Dover Publication Inc., New York, 1986.
[29] L.R. Gahan, V.A. Grillo, T.W. Hambley, G.R. Hanson, C.J. Hawkins, E.M. Proudfoot, B. Moubaraki, K.S. Murray, D. Wang, Inorg. Chem. 35 (1996) 1039.
[30] J. Krzystek, A. Ozarowski, J. Telser, Coord. Chem. Rev. 250 (2006) 2308.
[31] C. Mantel, C. Baffert, I. Romero, A. Deronzier, J. Pécaut, M.N. Collomb, C. Duboc, Inorg. Chem. 43 (2004) 6455.
[32] T. Howard, J. Telser, V.J. DeRose, Inorg. Chem. 39 (2000) 3379.
[33] T.M. Sossong Jr., S.V. Khangulov, R.C. Cavalli, D.R. Soprano, G.C. Dismukes, D.E. Ash, J. Biol. Inorg. Chem. 2 (1997) 433.
[34] A.P. Golombek, M.P. Hendrich, J. Magn. Res. 165 (2003) 33.

Polyhedron 27 (2008) 2049–2058

Contents lists available at ScienceDirect

Polyhedron

journal homepage: www.elsevier.com/locate/poly

Crown-templated assembling of the inorganic binuclear fluoro-containing anions in the system ZrO_2/HfO_2 (Nb_2O_5/Ta_2O_5)–HF–H_2O-azacrown ether

Marina S. Fonari [a,*], Victor Ch. Kravtsov [a], Yurii A. Simonov [a], Stepan S. Basok [b], Eduard V. Ganin [c,d], Vladimir O. Gelmboldt [d], Kinga Suwinska [e], Janusz Lipkowski [e], Olga A. Alekseeva [f], Nina G. Furmanova [f]

[a] Institute of Applied Physics, Academy of Sciences of R. Moldova, Academiei Str., 5 MD-2028 Chisinau, Republic of Moldova
[b] A.V. Bogatsky Physico-Chemical Institute, National Academy of Sciences of Ukraine, Lustdorfskaya Doroga 86, 650080 Odessa, Ukraine
[c] Odessa State Environmental University, Odessa, Ukraine
[d] Physico-Chemical Institute of Environment and Human Protection, Odessa, Ukraine
[e] Institute of Physical Chemistry Polish Academy of Sciences, Warszawa, Poland
[f] Institute of Crystallography RAS, Moscow, Russia

ARTICLE INFO

Article history:
Received 29 December 2007
Accepted 20 March 2008
Available online 9 May 2008

Keywords:
Rarely observed metal oxide fluoride anions
Aza crown ethers
Hydrogen bond
Crystal structure

ABSTRACT

The interaction of ZrO_2/HfO_2 or Nb_2O_5/Ta_2O_5 with an aqueous solution of hydrofluoric acid in the presence of aza-crown ether resulted in novel organically templated metal oxyfluorides of the compositions $[(HA15C5)_2][Ta_2F_{10}O]$ (**1**), $[(HA18C6\cdot H_2O)(A18C6\cdot H_2O)][(H_2O)Nb_2F_9O]\cdot H_2O$ (**2**), $[(HA18C6\cdot H_2O)(M_2F_{10}\cdot 2H_2O)\cdot(H_3O)\cdot H_2O]$ (**3**, **4**) and $[(H_2DA18C6)(M_2F_{10}\cdot 2H_2O)\cdot 2H_2O]$ (**5**, **6**) (M = Zr, Hf, A15C5 = aza-15-crown-5, A18C6 = aza-18-crown-6, DA18C6 = diaza-18-crown-6). Complexes **1**–**6** were identified by single crystal X-ray diffraction. In **1**, the negative charge of the $[(TaF_5)_2O]^{2-}$ centrosymmetric dianion is balanced by two azonia-15C5 cations, while in **2** the charge of asymmetric $[(H_2O)NbF_4ONbF_5]^-$ monoanion is compensated by azonia-18C6 cation. The crystal of **2** revealed an extensive hydrogen bonding between the anions, protonated and neutral macrocycles and water molecules that combine the components into 2D sheet. Complexes **3**–**4** and **5**–**6** are isostructural in pairs; in all of them the rigid 2D inorganic motif is formed through the association of the$[(M_2F_{10}\cdot 2H_2O)]^{2-}$ anions by means of OH···F hydrogen bonds. The similar 3D supramolecular architecture in **3**–**6** represents an alternation of the negatively-charged inorganic sheets and the columns of $(HA18C6)^+$ or $(DA18C6)^{2+}$ organic cations glued by oxonium cations or water molecules.

© 2008 Elsevier Ltd. All rights reserved.

1. Introduction

The successful efforts undertaken by Atwood to stabilize the Lewis acidic species by the complexation with crown ethers [1], initiated our long-standing interest to the fluoro-containing Lewis acids (BF_3, SiF_4, GeF_4, SbF_3, etc.) and the products of their transformations in aqueous solutions in the presence of crown ether macrocyclic molecules as organic-templating species. Following to Atwood and Selig [1,2], we have discovered the possibility to retain the rather unstable neutral adducts of the composition $BF_3\cdot H_2O$ [3] and $SiF_4\cdot 2H_2O$ [4] in the complexes with *classic all O-containing crown ethers* (18-crown-6, *cis–anti–cis*-dicyclohexyl-18-crown-6) stabilised by the OH···O hydrogen bonding between the intermediate water molecule and crown oxygen atoms. In the case of SbF_3 interaction with the macrocyclic molecule (18C6, B18C6, *cis*-isomers of DCH18C6, thia-[1.5]DB18C6) [5], the electronic effects are crucial, and the anhydrous adducts of the 1:1 ratio are held together through the interaction of the antimony atom lone pair with O-collective electronic system.

The interaction of the fluorosilicic acid (H_2SiF_6, FSA) solution with aza-containing macrocycles has resulted in ionic crystalline complexes of the compositions $(HA18C6\cdot H_2O)$ $[SiF_5(H_2O)]\cdot H_2O$, $(H_2DA18C6)[SiF_5(H_2O)]_2$, $(HA12C4)_2[SiF_5(H_2O)]_2\cdot 3H_2O$ [6], (A18C6, aza-18-crown-6; DA18C6, diaza-18-crown-6; A12C4, aza-12-crown-4), which have represented the structural evidence for the existence in the solid state of the $[SiF_5(H_2O)]^-$ anion, the labile product of the hydrolytic transformations of $[SiF_6]^{2-}$ anion. So far these three complexes remain the only known examples of the crystallographically proven existence of the $[SiF_5(H_2O)]^-$ anion in the solid state. The major role in stabilisation of the asymmetric and labile $[SiF_5(H_2O)]^-$ species plays the multiple H-bonding interactions between 'organic' and 'inorganic' components.

The problem of concentration and extraction of such elements as Zr, Hf, Nb, Ta encouraged us to apply the macrocyclic molecules

* Corresponding author. Tel.: +373 22 73 81 54; fax: +373 22 72 58 87.
E-mail addresses: fonari.xray@phys.asm.md (M.S. Fonari), edganin@yahoo.com (E.V. Ganin), eksvar@ukr.net (V.O. Gelmboldt), klatrat@ichf.edu.pl (K. Suwinska), furm@ns.crys.ras.ru (N.G. Furmanova)

0277-5387/$ - see front matter © 2008 Elsevier Ltd. All rights reserved.
doi:10.1016/j.poly.2008.03.023

with the aim to obtain new supramolecular complexes involving these elements in the form of neutral or anionic fluoro-containing species and crown ethers. In the previously reported system ZrO_2/HfO_2–HF–H_2O–18C6, the crystals suitable for X-ray diffraction have been obtained only for Hf, and the crystalline complex of the composition $[(18C6)(H_3O)_2(Hf_2O_{10}\cdot 2H_2O)\cdot 4H_2O]$ has been studied [7]. Although the *neutral* 18C6 molecule has been used in synthesis, the resulting supramolecular complex combines both neutral and ionic species. The $(Hf_2O_{10}\cdot 2H_2O)^{2-}$ anions form inorganic 2D sheet through the OH···F hydrogen bonds and is adjusted to the 18C6 molecules *via* oxonium clusters of the composition $(H_7O_3)^+$. The 3D supramolecular architecture represents an alternation of the inorganic sheets and columns of H-bonded crown-ethers and water molecules.

Our recent study of the systems Nb_2O_5/Ta_2O_5 (NbF_5/TaF_5)–HF–H_2O–CE for a wide range of oxygen-containing crown ethers showed that in the crystalline ionic complexes of the compositions $[CE\cdot H_3O][MF_6]$ for 18C6, B18C6, *cis–syn–cis*-DCH18C6 and diphenyl-20C6, $[(CE)_2\cdot H_7O_3][MF_6]$ for [1.5]DB18C6 [6], $[CE\cdot H_5O_2][MF_6]$ for 15C5 and tetrabenzo-30C10, $[(CE)_2\cdot H_5O_2][(CE)_2\cdot H_3O][MF_6]_2$ for B15C5 and $[(CE)_2\cdot H_3O][MF_6]$ for B12C4, the negative charge of NbF_6^-/TaF_6^- anions is balanced by the oxonium ions [8]. Thus, the general feature for these complexes is a retention of metal-containing *anionic species* by neutral O-containing crown molecules due to the acidity of the reaction medium introduced by the presence of hydrofluoric acid. We also showed that in spite of either the MF_5 pentafluorides or the corresponding M_2O_5 oxides were used as starting materials, all-O-containing CEs extract NbF_6^-/TaF_6^- hexafluoroniobate/hexafluorotantalate anions in the form of crystalline complexes.

Keeping in mind the disclosed ability of aza-containing crown ethers to extract the hydrolytically unstable species from FSA solutions [7], we have used the aza-containing crown ethers, A15C5, A18C6 and DA18C6 with the aim to extract the products of interaction of ZrO_2/HfO_2 and Nb_2O_5/Ta_2O_5 with an aqueous solution of hydrofluoric acid. Six new complexes, $[(HA15C5)_2][Ta_2F_{10}O]$ (**1**), $[(HA18C6\cdot H_2O)(A18C6\cdot H_2O)][(H_2O)\ Nb_2F_9O]\cdot H_2O$ (**2**), $[(HA18C6\cdot H_2O)(Zr_2F_{10}\cdot 2H_2O)\cdot(H_3O)\cdot H_2O]$ (**3**), $[(HA18C6\cdot H_2O)$-$(Hf_2F_{10}\cdot 2H_2O)\cdot(H_3O)\cdot H_2O]$ (**4**), $[(H_2DA18C6)(Zr_2F_{10}\cdot 2H_2O)\cdot 2H_2O]$ (**5**), $[(H_2DA18C6)(Hf_2F_{10}\cdot 2H_2O)\cdot 2H_2O]$ (**6**) were obtained and studied by single crystal X-ray diffraction.

2. Experimental

2.1. Materials and apparatus

Caution! Hydrofluoric acid is toxic and corrosive, and must be handled with extreme caution and the appropriate protective gear! If contact with the liquid or vapor occurs, proper treatment procedures should immediately be followed [9]. Crown ethers were purchased from ACROS, ZrO_2, HfO_2, Nb_2O_5 and Ta_2O_5 were purchased from Aldrich and were used without further purification. Complexes **1**–**6** were obtained by an interaction of the corresponding oxides with the 40% aqueous HF followed by treatment of the resulting solution with the corresponding crown ether and were analyzed for C, H and N in a Perkin Elmer 240 °C instrument.

2.2. Synthesis

2.2.1. $[(HA15C5)_2][Ta_2F_{10}O]$ (**1**)

Crystals of complex **1** separated in a quantitative yield, and are colorless transparent prisms, soluble in methanol, ethanol; m.p. 152–153 °C. *Anal.* Calc. for $C_{20}H_{44}F_{10}N_2O_9Ta_2$: C, 23.82; H, 4.40; F, 18.84; N, 2.78. Found: C, 23.80; H, 4.43; F, 18.86; N, 2.81%.

2.2.2. $[(HA18C6\cdot H_2O)(A18C6\cdot H_2O)][(H_2O)Nb_2F_9O]\cdot H_2O$ (**2**)

Crystals of complex **2** separated in a quantitative yield, and are colorless transparent prisms, soluble in methanol, ethanol; m.p. 115–117 °C. *Anal.* Calc. for $C_{24}H_{59}F_9N_2Nb_2O_{15}$: C, 29.64; H, 6.11; F, 17.58; N, 2.88. Found: C, 29.69; H, 6.13; F, 17.63; N, 2.84%.

2.2.3. $[(HA18C6\cdot H_2O)(Zr_2F_{10}\cdot 2H_2O)\cdot(H_3O)\cdot H_2O]$ (**3**)

Crystals of complex **3** separated in an approximately quantitative yield, and are colorless transparent prisms, soluble in methanol; m.p. ≫250 °C. *Anal.* Calc. for $C_{12}H_{37}F_{10}NO_{10}Zr_2$: C, 19.80; H, 5.12; F, 26.10; N, 1.92. Found: C, 19.7; H, 5.15; F, 26.14; N, 1.90%.

2.2.4. $[(HA18C6\cdot H_2O)(Hf_2F_{10}\cdot 2H_2O)\cdot(H_3O)\cdot H_2O]$ (**4**)

Crystals of complex **4** separated in an approximately quantitative yield, and are colorless transparent prisms, soluble in methanol; m.p. ≫250 °C. *Anal.* Calc. for $C_{12}H_{37}F_{10}Hf_2NO_{10}$: C, 15.97; H, 4.13; F, 21.05; N, 1.55. Found: C, 15.94; H, 4.15; F, 21.08; N, 1.57%.

Table 1
Crystal data and structure refinement parameters for complexes **1**–**6**

	1	**2**	**3**	**4**	**5**	**6**
Composition	$C_{20}H_{44}F_{10}N_2O_9Ta_2$	$C_{24}H_{59}F_9N_2Nb_2O_{15}$	$C_{12}H_{37}F_{10}NO_{10}Zr_2$	$C_{12}H_{37}F_{10}Hf_2NO_{10}$	$C_{12}H_{36}F_{10}N_2O_8Zr_2$	$C_{12}H_{36}F_{10}Hf_2N_2O_8$
CCDC number	671858	671860	671862	671859	671863	671861
Formula weight	1008.47	972.55	727.87	907.38	708.87	883.41
Crystal system	triclinic	orthorhombic	orthorhombic	orthorhombic	triclinic	triclinic
Space group	$P\bar{1}$	$Pna2_1$	$Pca2_1$	$Pca2_1$	$P\bar{1}$	$P\bar{1}$
a (Å)	8.995(4)	19.734(4)	15.651(3)	15.637(3)	8.9617(6)	8.915(2)
b (Å)	9.021(3)	10.303(2)	11.487(2)	11.495(2)	10.5137(7)	10.530(2)
c (Å)	11.965(5)	19.618(4)	15.923(3)	15.814(3)	14.3368(11)	14.295(3)
α (°)	86.12(3)	90.0	90.0	90.0	108.059(3)	107.94(2)
β (°)	69.26(2)	90.0	90.0	90.0	98.930(3)	98.70(2)
γ (°)	66.50(2)	90.0	90.0	90.0	96.118(5)	96.18(2)
V (Å^3)	829.6(5)	3988.7(14)	2862.7(9)	2842.5(10)	1251.38(15)	1244.9 (2)
Z	1	4	4	4	2	2
D_{calc} (Mg/m^3)	2.019	1.620	1.689	2.109	1.881	2.357
μ (mm^{-1})	6.690	0.678	0.833	7.405	0.945	8.446
F(000)	486	2000	1464	1720	712	840
Reflections collected/unique	10006/2927	37300/7821	5377/5377	3212/3212	5441/5441	5701/5701
Reflections with $I > 2\sigma(I)$	2499	7014	3386	2358	3861	5221
Goodness-of-fit	1.001	1.019	1.002	1.000	1.003	1.004
R_1, wR_2 [$I > 2\sigma(I)$]	0.0223, 0.0337	0.0329, 0.0760	0.0397, 0.0934	0.0395, 0.1024	0.0853, 0.2212	0.0565, 0.1664

Table 2
Selected bond distances (Å) and angles (°) for complexes **1**–**6**

Complex ***1***			
Ta(1)–F(2)	1.847(3)	Ta(1)–O(1M)	1.8869(7)
Ta(1)–F(4)	1.861(3)	Ta(1)–F(3)	1.898(2)
Ta(1)–F(1)	1.865(3)	Ta(1)–F(5)	1.908(2)
F(2)–Ta(1)–F(4)	175.90(12)	F(1)–Ta(1)–F(3)	174.17(10)
F(2)–Ta(1)–F(1)	89.59(15)	O(1M)–Ta(1)–F(3)	91.72(7)
F(4)–Ta(1)–F(1)	92.02(16)	F(2)–Ta(1)–F(5)	87.56(12)
F(2)–Ta(1)–O(1M)	93.76(9)	F(4)–Ta(1)–F(5)	88.71(12)
F(4)–Ta(1)–O(1M)	89.90(9)	F(1)–Ta(1)–F(5)	88.66(12)
F(1)–Ta(1)–O(1M)	93.59(9)	O(1M)–Ta(1)–F(5)	177.40(9)
F(2)–Ta(1)–F(3)	87.64(12)	F(3)–Ta(1)–F(5)	86.09(11)
F(4)–Ta(1)–F(3)	90.41(13)		
O(1)–C(1)–C(2)–N(1)	44.6(5)	C(6)–O(3)–C(7)–C(8)	−177.1(4)
C(1)–C(2)–N(1)–C(3)	−61.8(5)	O(3)–C(7)–C(8)–O(4)	66.1(5)
C(2)–N(1)–C(3)–C(4)	−178.6(3)	C(7)–C(8)–O(4)–C(9)	179.2(4)
N(1)–C(3)–C(4)–O(2)	59.2(4)	C(8)–O(4)–C(9)–C(10)	−170.1(4)
C(3)–C(4)–O(2)–C(5)	−146.1(4)	O(4)–C(9)–C(10)–O(1)	−64.0(5)
C(4)–O(2)–C(5)–C(6)	93.4(5)	C(9)–C(10)–O(1)–C(1)	136.5(4)
O(2)–C(5)–C(6)–O(3)	−63.1(5)	C(10)–O(1)–C(1)–C(2)	−77.8(5)
C(5)–C(6)–O(3)–C(7)	171.0(4)		
Complex ***2***			
Nb(1)–O(1M)	1.734(3)	Nb(2)–F(9)	1.710(3)
Nb(1)–F(1)	1.884(3)	Nb(2)–F(5)	1.890(2)
Nb(1)–F(2)	1.911(2)	Nb(2)–F(6)	1.919(2)
Nb(1)–F(4)	1.929(2)	Nb(2)–F(7)	1.919(3)
Nb(1)–F(3)	1.930(3)	Nb(2)–F(8)	1.958(2)
Nb(1)–O(1W)	2.311(3)	Nb(2)–O(1M)	2.344(3)
O(1M)–Nb(1)–F(1)	100.03(16)	F(9)–Nb(2)–F(5)	99.02(17)
O(1M)–Nb(1)–F(2)	99.66(12)	F(9)–Nb(2)–F(6)	98.80(13)
F(1)–Nb(1)–F(2)	90.31(11)	F(5)–Nb(2)–F(6)	91.66(13)
O(1M)–Nb(1)–F(4)	97.92(11)	F(9)–Nb(2)–F(7)	98.95(17)
F(1)–Nb(1)–F(4)	90.22(14)	F(5)–Nb(2)–F(7)	161.60(12)
F(2)–Nb(1)–F(4)	162.03(11)	F(6)–Nb(2)–F(7)	89.45(15)
O(1M)–Nb(1)–F(3)	98.99(16)	F(9)–Nb(2)–F(8)	96.77(13)
F(1)–Nb(1)–F(3)	160.96(11)	F(5)–Nb(2)–F(8)	88.28(14)
F(2)–Nb(1)–F(3)	87.22(13)	F(6)–Nb(2)–F(8)	164.24(10)
F(4)–Nb(1)–F(3)	86.44(15)	F(7)–Nb(2)–F(8)	85.74(15)
O(1M)–Nb(1)–O(1W)	176.82(13)	F(9)–Nb(2)–O(1M)	179.04(14)
F(1)–Nb(1)–O(1W)	79.47(12)	F(5)–Nb(2)–O(1M)	80.93(13)
F(2)–Nb(1)–O(1W)	83.49(13)	F(6)–Nb(2)–O(1M)	82.16(10)
F(4)–Nb(1)–O(1W)	78.96(12)	F(7)–Nb(2)–O(1M)	81.03(13)
F(3)–Nb(1)–O(1W)	81.50(13)	F(8)–Nb(2)–O(1M)	82.28(11)
	A	B	
O(1)–C(1)–C(2)–N(1)	67.9(5)	−41.9(11)	
C(1)–C(2)–N(1)–C(3)	−176.4(4)	−175.1(7)	
C(2)–N(1)–C(3)–C(4)	174.6(4)	171.3(7)	
N(1)–C(3)–C(4)–O(2)	−67.8(5)	49.7(10)	
C(3)–C(4)–O(2)–C(5)	176.3(4)	102.7(6)	
C(4)–O(2)–C(5)–C(6)	177.8(4)	176.6(5)	
O(2)–C(5)–C(6)–O(3)	64.2(5)	74.0(5)	
C(5)–C(6)–O(3)–C(7)	178.9(4)	−175.3(4)	
C(6)–O(3)–C(7)–C(8)	−178.3(4)	−166.3(3)	
O(3)–C(7)–C(8)–O(4)	−64.7(5)	−70.1(4)	
C(7)–C(8)–O(4)–C(9)	178.6(4)	166.1(3)	
C(8)–O(4)–C(9)–C(10)	179.5(3)	−176.9(3)	
O(4)–C(9)–C(10)–O(5)	67.3(4)	69.9(4)	
C(9)–C(10)–O(5)–C(11)	−179.9(3)	174.5(4)	
C(10)–O(5)–C(11)–C(12)	179.6(4)	−174.4(4)	
O(5)–C(11)–C(12)–O(1)	−66.4(5)	−69.7(5)	
C(11)–C(12)–O(1)–C(1)	−175.2(3)	178.5(5)	
C(12)–O(1)–C(1)–C(2)	−178.2(4)	−114.4(7)	
Complex ***3***			
Zr(1)–F(4)	1.959(7)	Zr(2)–F(6)	1.984(6)
Zr(1)–F(2)	1.968(5)	Zr(2)–F(8)	1.982(6)
Zr(1)–F(1)	1.999(6)	Zr(2)–F(7)	1.994(5)
Zr(1)–F(3)	2.033(7)	Zr(2)–F(5)	2.006(6)
Zr(1)–F(1m)	2.147(8)	Zr(2)–F(1m)	2.135(7)
Zr(1)–F(2m)	2.150(7)	Zr(2)–F(2m)	2.142(7)
Zr(1)–O(1w)	2.207(6)	Zr(2)–O(2w)	2.208(8)
Zr(1)–Zr(2)	3.6039(8)		
F(4)–Zr(1)–F(2)	174.8(3)	F(6)–Zr(2)–F(8)	176.6(3)
F(4)–Zr(1)–F(1)	91.8(3)	F(6)–Zr(2)–F(7)	87.6(3)
F(2)–Zr(1)–F(1)	91.8(3)	F(8)–Zr(2)–F(7)	90.1(3)
F(4)–Zr(1)–F(3)	89.0(3)	F(6)–Zr(2)–F(5)	93.7(3)
F(2)–Zr(1)–F(3)	90.2(3)	F(8)–Zr(2)–F(5)	89.6(3)
F(1)–Zr(1)–F(3)	144.9(3)	F(7)–Zr(2)–F(5)	143.8(3)
F(4)–Zr(1)–F(1m)	89.5(2)	F(6)–Zr(2)–F(1m)	89.7(2)
F(2)–Zr(1)–F(1m)	87.8(2)	F(8)–Zr(2)–F(1m)	90.4(2)
F(1)–Zr(1)–F(1m)	75.0(3)	F(7)–Zr(2)–F(1m)	141.10(19)
F(3)–Zr(1)–F(1m)	140.1(2)	F(5)–Zr(2)–F(1m)	75.1(2)
F(4)–Zr(1)–F(2m)	88.8(3)	F(6)–Zr(2)–F(2m)	87.3(2)
F(2)–Zr(1)–F(2m)	86.00(18)	F(8)–Zr(2)–F(2m)	89.7(2)
F(1)–Zr(1)–F(2m)	140.1(2)	F(7)–Zr(2)–F(2m)	75.6(2)
F(3)–Zr(1)–F(2m)	75.0(3)	F(5)–Zr(2)–F(2m)	140.57(18)
F(1m)–Zr(1)–F(2m)	65.2(2)	F(1M)–Zr(2)–F(2m)	65.5(2)
F(4)–Zr(1)–O(1w)	93.4(3)	F(6)–Zr(2)–O(2w)	89.7(4)
F(2)–Zr(1)–O(1w)	91.3(3)	F(8)–Zr(2)–O(2w)	92.0(3)
F(1)–Zr(1)–O(1w)	72.0(3)	F(7)–Zr(2)–O(2w)	71.8(3)
F(3)–Zr(1)–O(1w)	72.9(3)	F(5)–Zr(2)–O(2w)	72.0(2)
F(1m)–Zr(1)–O(1w)	146.9(2)	F(1m)–Zr(2)–O(2w)	147.0(2)
F(2m)–Zr(1)–O(1w)	147.8(2)	F(2m)–Zr(2)–O(2w)	147.4(2)
Zr(2)–F(1m)–Zr(1)	114.64(10)	Zr(2)–F(2m)–Zr(1)	114.20(10)
	A	B	
O(1)–C(1)–C(2)–N(1)	−72(3)	66(2)	
C(1)–C(2)–N(1)–C(3)	179(2)	−176(2)	
C(2)–N(1)–C(3)–C(4)	−173(3)	161(4)	
N(1)–C(3)–C(4)–O(2)	53(5)	−53(5)	
C(3)–C(4)–O(2)–C(5)	−166(4)	171(3)	
C(4)–O(2)–C(5)–C(6)	−170(3)	164(2)	
O(2)–C(5)–C(6)–O(3)	−63(2)	69(3)	
C(5)–C(6)–O(3)–C(7)	172(2)	−179.2(19)	
C(6)–O(3)–C(7)–C(8)	170.4(18)	174(2)	
O(3)–C(7)–C(8)–O(4)	72(3)	−43(3)	
C(7)–C(8)–O(4)–C(9)	−164(2)	156(2)	
C(8)–O(4)–C(9)–C(10)	−174(2)	166(3)	
O(4)–C(9)–C(10)–O(5)	−76(3)	64(4)	
C(9)–C(10)–O(5)–C(11)	179(3)	174(3)	
C(10)–O(5)–C(11)–C(12)	173(2)	176(3)	
O(5)–C(11)–C(12)–O(1)	69(2)	−58(3)	
C(11)–C(12)–O(1)–C(1)	−178.4(19)	−175.0(19)	
Complex ***4***			
Hf(1)–F(4)	1.939(11)	Hf(2)–F(6)	1.974(11)
Hf(1)–F(2)	1.987(9)	Hf(2)–F(8)	1.977(8)
Hf(1)–F(3)	2.003(9)	Hf(2)–F(5)	1.996(7)
Hf(1)–F(1)	2.011(10)	Hf(2)–F(7)	2.014(9)
Hf(1)–F(1m)	2.161(15)	Hf(2)–F(1m)	2.104(16)
Hf(1)–F(2m)	2.171(14)	Hf(2)–F(2m)	2.110(16)
Hf(1)–O(1w)	2.202(10)	Hf(2)–O(2w)	2.184(12)
Hf(1)–Hf(2)	3.5840(9)		
F(4)–Hf(1)–F(2)	172.5(7)	F(6)–Hf(2)–F(5)	91.5(6)
F(4)–Hf(1)–F(3)	89.8(6)	F(8)–Hf(2)–F(5)	90.2(6)
F(2)–Hf(1)–F(3)	87.4(6)	F(6)–Hf(2)–F(7)	89.2(7)
F(4)–Hf(1)–F(1)	91.5(5)	F(8)–Hf(2)–F(7)	89.9(7)
F(2)–Hf(1)–F(1)	94.6(5)	F(5)–Hf(2)–F(7)	143.0(8)
F(3)–Hf(1)–F(1)	147.6(10)	F(6)–Hf(2)–F(1m)	88.9(6)
F(4)–Hf(1)–F(1m)	88.5(5)	F(8)–Hf(2)–F(1m)	90.8(5)
F(2)–Hf(1)–F(1m)	89.0(5)	F(5)–Hf(2)–F(1m)	75.3(5)
F(3)–Hf(1)–F(1m)	138.6(6)	F(7)–Hf(2)–F(1m)	141.7(6)
F(1)–Hf(1)–F(1m)	73.7(6)	F(6)–Hf(2)–F(2m)	87.4(5)
F(4)–Hf(1)–F(2m)	87.1(5)	F(8)–Hf(2)–F(2m)	90.7(5)
F(2)–Hf(1)–F(2m)	85.4(5)	F(5)–Hf(2)–F(2m)	142.1(5)
F(3)–Hf(1)–F(2m)	73.9(6)	F(7)–Hf(2)–F(2m)	74.9(5)
F(1)–Hf(1)–F(2m)	138.5(6)	F(1m)–Hf(2)–F(2m)	66.8(4)
F(1M)–Hf(1)–F(2m)	64.7(5)	F(6)–Hf(2)–O(2w)	90.4(8)
F(4)–Hf(1)–O(1w)	95.3(8)	F(8)–Hf(2)–O(2w)	91.0(8)
F(2)–Hf(1)–O(1w)	90.7(8)	F(5)–Hf(2)–O(2w)	71.6(5)
F(3)–Hf(1)–O(1w)	74.7(7)	F(7)–Hf(2)–O(2w)	71.4(6)
F(1)–Hf(1)–O(1w)	72.9(6)	F(1m)–Hf(2)–O(2w)	146.9(4)
F(1m)–Hf(1)–O(1w)	146.5(5)	F(2m)–Hf(2)–O(2w)	146.2(4)
F(2m)–Hf(1)–O(1w)	148.5(5)	Hf(2)–F(1M)–Hf(1)	114.3(2)
F(6)–Hf(2)–F(8)	178.0(7)	Hf(2)–F(2M)–Hf(1)	113.7(3)
Complex ***5***			
Zr(1)–F(4)	1.970(6)	Zr(2)–F(8)	1.980(6)
Zr(1)–F(2)	1.990(6)	Zr(2)–F(6)	1.988(6)
Zr(1)–F(3)	2.012(5)	Zr(2)–F(7)	2.012(5)
Zr(1)–F(1)	2.029(5)	Zr(2)–F(5)	2.018(5)
Zr(1)–F(2m)	2.141(5)	Zr(2)–F(1m)	2.151(5)

(*continued on next page*)

Table 2 (*continued*)

Zr(1)–F(1m)	2.162(5)	Zr(2)–F(2m)	2.158(5)
Zr(1)–O(1w)	2.231(6)	Zr(2)–O(2w)	2.212(7)
Zr(1)–Zr(2)	3.6159(11)		
F(4)–Zr(1)–F(2)	175.4(3)	F(8)–Zr(2)–F(6)	173.6(3)
F(4)–Zr(1)–F(3)	88.4(3)	F(8)–Zr(2)–F(7)	89.3(3)
F(2)–Zr(1)–F(3)	95.2(3)	F(6)–Zr(2)–F(7)	89.8(3)
F(4)–Zr(1)–F(1)	90.4(3)	F(8)–Zr(2)–F(5)	92.4(3)
F(2)–Zr(1)–F(1)	88.4(3)	F(6)–Zr(2)–F(5)	92.1(3)
F(3)–Zr(1)–F(1)	143.1(2)	F(7)–Zr(2)–F(5)	144.2(2)
F(4)–Zr(1)–F(2m)	90.2(2)	F(8)–Zr(2)–F(1m)	87.9(3)
F(2)–Zr(1)–F(2m)	88.0(2)	F(6)–Zr(2)–F(1m)	88.8(2)
F(3)–Zr(1)–F(2m)	75.0(2)	F(7)–Zr(2)–F(1m)	141.2(2)
F(1)–Zr(1)–F(2m)	141.9(2)	F(5)–Zr(2)–F(1m)	74.7(2)
F(4)–Zr(1)–F(1m)	89.3(3)	F(8)–Zr(2)–F(2m)	88.4(3)
F(2)–Zr(1)–F(1m)	86.1(2)	F(6)–Zr(2)–F(2m)	85.3(2)
F(3)–Zr(1)–F(1m)	140.7(2)	F(7)–Zr(2)–F(2m)	75.54(19)
F(1)–Zr(1)–F(1m)	76.2(2)	F(5)–Zr(2)–F(2m)	140.3(2)
F(2m)–Zr(1)–F(1m)	65.78(18)	F(1m)–Zr(2)–F(2m)	65.68(18)
F(4)–Zr(1)–O(1w)	95.1(3)	F(8)–Zr(2)–O(2w)	93.1(3)
F(2)–Zr(1)–O(1w)	88.7(3)	F(6)–Zr(2)–O(2w)	92.6(3)
F(3)–Zr(1)–O(1w)	72.0(2)	F(7)–Zr(2)–O(2w)	71.6(2)
F(1)–Zr(1)–O(1w)	71.3(2)	F(5)–Zr(2)–O(2w)	72.6(2)
F(2m)–Zr(1)–O(1w)	146.4(2)	F(1m)–Zr(2)–O(2w)	147.2(2)
F(1m)–Zr(1)–O(1w)	147.2(2)	F(2m)–Zr(2)–O(2w)	147.1(2)
Zr(2)–F(1m)–Zr(1)	114.0(2)	Zr(2)–F(1m)–Zr(1)	114.5(2)
	A	B	
O(1)–C(1)–C(2)–N(1)	55.5(14)	69.2(15)	
C(1)–C(2)–N(1)–C(3)	54.9(14)	174.7(12)	
C(2)–N(1)–C(3)–C(4)	−171.4(10)	167.4(13)	
N(1)–C(3)–C(4)–O(2)	57.1(15)	51.7(19)	
C(3)–C(4)–O(2)–C(5)	81.3(14)	−174.7(14)	
C(4)–O(2)–C(5)–C(6)	167.7(10)	68(3)	
O(2)–C(5)–C(6)–O(1)	175.1(10)	61(3)	
C(5)–C(6)–O(1)–C(1)	177.1(10)	−178(2)	
C(6)–O(1)–C(1)–C(2)	167.0(10)	−175.4(15)	
Complex ***6***			
Hf(1)–F(4)	1.963(8)	Hf(2)–F(8)	1.967(8)
Hf(1)–F(2)	1.983(7)	Hf(2)–F(6)	1.972(8)
Hf(1)–F(3)	1.997(6)	Hf(2)–F(7)	2.003(6)
Hf(1)–F(1)	2.021(6)	Hf(2)–F(5)	2.015(6)
Hf(1)–F(2m)	2.133(5)	Hf(2)–F(2m)	2.134(5)
Hf(1)–F(1m)	2.207(5)	Hf(2)–F(1m)	2.146(5)
Hf(1)–O(1w)	2.215(7)	Hf(2)–O(2w)	2.191(7)
Hf(1)–Hf(2)	3.5970(9)		
F(4)–Hf(1)–F(2)	175.7(3)	F(8)–Hf(2)–F(6)	173.3(3)
F(4)–Hf(1)–F(3)	88.0(4)	F(8)–Hf(2)–F(7)	88.9(4)
F(2)–Hf(1)–F(3)	95.2(3)	F(6)–Hf(2)–F(7)	89.5(3)
F(4)–Hf(1)–F(1)	90.5(3)	F(8)–Hf(2)–F(5)	93.1(4)
F(2)–Hf(1)–F(1)	88.6(3)	F(6)–Hf(2)–F(5)	92.0(3)
F(3)–Hf(1)–F(1)	143.8(3)	F(7)–Hf(2)–F(5)	144.4(3)
F(4)–Hf(1)–F(2m)	90.1(3)	F(8)–Hf(2)–F(2m)	87.7(3)
F(2)–Hf(1)–F(2m)	88.0(3)	F(6)–Hf(2)–F(2m)	85.6(3)
F(3)–Hf(1)–F(2m)	75.0(2)	F(7)–Hf(2)–F(2m)	75.2(2)
F(1)–Hf(1)–F(2m)	141.2(2)	F(5)–Hf(2)–F(2m)	140.3(2)
F(4)–Hf(1)–F(1m)	90.4(3)	F(8)–Hf(2)–F(1m)	88.7(3)
F(2)–Hf(1)–F(1m)	85.3(3)	F(6)–Hf(2)–F(1m)	88.6(3)
F(3)–Hf(1)–F(1m)	141.2(2)	F(7)–Hf(2)–F(1m)	142.6(2)
F(1)–Hf(1)–F(1m)	74.9(2)	F(5)–Hf(2)–F(1m)	73.0(2)
F(2m)–Hf(1)–F(1m)	66.3(2)	F(2M)–Hf(2)–F(1m)	67.4(2)
F(4)–Hf(1)–O(1w)	95.0(4)	F(8)–Hf(2)–O(2w)	93.6(4)
F(2)–Hf(1)–O(1w)	88.7(3)	F(6)–Hf(2)–O(2w)	92.1(4)
F(3)–Hf(1)–O(1w)	72.6(3)	F(7)–Hf(2)–O(2w)	71.6(3)
F(1)–Hf(1)–O(1w)	71.5(3)	F(5)–Hf(2)–O(2w)	72.8(3)
F(2m)–Hf(1)–O(1w)	147.0(3)	F(2m)–Hf(2)–O(2w)	146.8(2)
F(1m)–Hf(1)–O(1w)	146.0(2)	F(1m)–Hf(2)–O(2w)	145.8(2)
Hf(2)–F(1m)–Hf(1)	111.5(2)	Hf(1)–F(2m)–Hf(2)	114.9(2)

2.2.5. $[(H_2DA18C6)(Zr_2F_{10}\cdot 2H_2O)\cdot 2H_2O]$ (**5**)

Crystals of complex **5** separated in an approximately quantitative yield, and are colorless transparent prisms, soluble in methanol; m.p. ≫250 °C. *Anal.* Calc. for $C_{12}H_{36}F_{10}N_2O_8Zr_2$: C, 20.33; H, 5.12; F, 26.80; N, 3.95. Found: C, 20.37; H, 5.10; F, 26.84; N, 3.98%.

2.2.6. $[(H_2DA18C6)(Hf_2F_{10}\cdot 2H_2O)\cdot 2H_2O]$ (**6**)

Crystals of complex **6** separated in an approximately quantitative yield, and are colorless transparent prisms, soluble in methanol; m.p. ≫250 °C. *Anal.* Calc. for $C_{12}H_{36}F_{10}Hf_2N_2O_8$: C, 16.32; H, 4.11; F, 21.51, N, 3.17.Found: C, 16.30; H, 4.15; F, 21.54, N, 3.15

2.3. X-ray diffraction study

The experimental data for complexes **1**, **2** were recorded on a Xcalibur S with a CCD detector (Mo Kα radiation (λ = 0.71073 Å), graphite monochromator, ω scan mode). The X-ray intensity data for complexes **3**–**6** were recorded on a Nonius CCD area detector diffractometer employing graphite monochromatized Mo Kα radiation in ϕ and ω scan mode. Final unit cell dimensions were obtained and refined on the entire data set. Integration and scaling resulted in a data set corrected for Lorentz and polarization effects using DENZO [10]. The scaling as well as the global refinement of crystal parameters were performed by SCALEPACK [10]. The absorption correction for **1**–**6** was applied using SADABS [11] The structure solution and refinement proceeded similarly using SHELX-97 program package [12] for all structures. The non-hydrogen atoms were treated anisotropically (full-matrix least-squares method on F^2). In complexes **3** and **4**, the macrocycle, water molecules and oxonium ions are disordered over two positions with equal occupancies. In **3**–**4**, the H–O atoms of the disordered water molecules and oxonium ions were not localized. N–H atoms were found from geometric considerations. The X-ray study for complexes **5**–**6** revealed their lamellar structure and the disorder due to the shift of the layers being parallel to the crystallographic plane (101). The major crystal component corresponds to 86% and 85% in the crystals of **5** and **6**, correspondingly. Two minor shifted components with the contributions of 11% and 2% for **5** and 11% and 3 % for **6** were detected. For minor components only position of inorganic anions were localized. The crown and water molecules were refined with the occupancies that correspond to the major component. In all complexes, C-bound H atoms were placed in calculated positions, with C–H distances of 0.97 Å, and were treated using a riding-model approximation, with $U_{iso}(H) = 1.2U_{eq}(C)$. In **2**, H-atoms of water molecules and NH-groups were determined from a difference Fourier map and were then allowed to refine isotropically with $U_{iso}(H) = 1.5U_{eq}(O)$ and O–H and N–H distances subjected to DFIX restraints. The X-ray data and the details of the refinement for **1**–**6** are summarized in Table 1, the selected geometric parameters are given in Table 2, the hydrogen bonding geometry is given in Table 3.

3. Results and discussion

3.1. Description of the structures

3.1.1. $[(HA15C5)_2][Ta_2F_{10}O]$ (**1**)

The ORTEP view for complex **1** is shown in Fig. 1. Compound **1** crystallises in the triclinic space group $P\bar{1}$. The formula unit comprises of the $[(TaF_5)_2O]^{2-}$ dianion which resides on an inversion center, and two azonia-15C5 monocations which compensate the negative charge and are bound with the anion *via* NH···F hydrogen bond, N(1)–H(1N1)···F(3) ($x+1$, y, z), H···F 2.07(4), N···F 2.886(4) Å, NHF angle 165(3)°. The Ta(1) atom has a distorted octahedron surrounding (Table 2) with the Ta–F distances falling in the range 1.847(3)–1.908(2) Å, the maximal deviations of the F–Ta–F bond angles from the straight and right angles being 5.83(10)° and 3.9(10)°, correspondingly, and the deviation for the O–Ta–F angle from the right angle being 3.76(8)°. The geometry of the $[(TaF_5)_2O]^{2-}$ dianion coincides with that in the structure of bis(tetraethylammonium)μ-oxo-bis(pentafluorotantalum(v)) [13]. The

Table 3
Hydrogen bond distances (Å) and angles (°) for complexes **1**, **2**, **3**, **5**

D–H···A	*d*(D–H)	*d*(H···A)	*d*(D···A)	∠(DHA)	Symmetry transformation for acceptor
Complex **1**					
N(1)–H(1)···F(3)	0.83(3)	2.07(4)	2.886(4)	165(3)	$-x+1, y, z$
N(1)–H(2)···O(4)	0.94(5)	1.94(5)	2.835(5)	159(4)	x, y, z
Complex **2**					
N(1A)–H(1A)···O(2wa)	0.90	1.93	2.785(5)	157	x, y, z
N(1A)–H(2A)···F(8)	0.90	1.96	2.804(4)	156	x, y, z
N(1B)–H(1B)···O(2wb)	0.89(2)	1.78(2)	2.663(5)	171(6)	x, y, z
O(1w)–H(1w1)···O(3w)	0.86(2)	1.84(2)	2.686(5)	171(6)	$x, y-1, z$
O(1w)–H(2w1)···F(9)	0.83(2)	1.89(3)	2.690(4)	162(5)	$x, y-1, z$
O(2wa)-H(2wa)···O(3A)	0.88(2)	2.02(2)	2.894(4)	168(6)	x, y, z
O(2wa)-H(1wa)···O(5A)	0.92(2)	2.04(2)	2.923(4)	161(5)	x, y, z
O(2wb)–H(2wb)···O(5B)	0.86(2)	1.94(3)	2.762(4)	159(6)	x, y, z
O(2wb)–H(1wb)···O(3B)	0.85(2)	2.01(3)	2.822(4)	160(6)	
O(3w)–H(1w3)···O(4A)	0.84(2)	1.96(3)	2.774(4)	162(8)	$-x+3/2, y+1/2, z+1/2$
O(3w)–H(2w3)···O(4B)	0.86(2)	2.22(2)	2.886(4)	134(3)	$-x+3/2, y-1/2, z+1/2$
Complex **3**					
O(1w)–H(1w1)···F(5)	0.94	1.63	2.567(8)	176	$-x+1/2, y, z-1/2$
O(1w)–H(2w1)···F(7)	0.93	1.65	2.584(8)	178	$-x, -y, z-1/2$
O(2w)–H(1w2)···F(1)	0.93	1.66	2.592(10)	178	$-x+1/2, y, z+1/2$
O(2w)–H(2w2)···F(3)	0.91	1.65	2.556(10)	179	$-x, -y, z+1/2$
N(1a)–H(1A1)···F(6)	0.90	2.14	2.98(2)	154	$x+1/2, -y+1, z$
N(1a)–H(1A2)···O(3w)	0.90	2.10	2.900(15)	148	x, y, z
N(1b)–H(1B1)···O(3w)	0.90	1.96	2.839(13)	164	x, y, z
N(1b)–H(1B2)···F(2)	0.90	1.99	2.888(18)	173	$x+1/2, -y+1, z$
Complex **5**					
O(1w)–H(1w)···F(1)	0.95	1.66	2.612(8)	175	$-x+1, -y+1, -z+1$
O(1w)–H(2w)···F(5)	0.95	1.64	2.590(8)	172	$x-1, y, z$
O(2w)–H(3w)···F(3)	0.94	1.64	2.576(8)	178	$x+1, y, z$
O(2w)–H(4w)···F(7)	0.98	1.66	2.620(9)	163	$-x+2, -y+1, -z$
N(1A)–H(1A1)···F(2)	0.90	1.98	2.812(12)	153	$-x+1, -y+1, -z+1$
N(1A)–H(1A2)···O(3W)	0.90	2.06	2.900(13)	153	$-x+1, -y+2, -z+1$
N(1B)–H(1B1)···O(4W)	0.90	2.48	3.037(13)	120	$-x+1, -y, -z+1$
N(1B)–H(1B2)···O(4W)	0.90	2.01	2.899(14)	169	$x, y, z+1$
O(3w)–H(1w3)···F(4)	0.92	1.91	2.759(10)	152	x, y, z
O(3w)–H(2w3)···F(8)	0.95	1.94	2.881(10)	172	x, y, z
O(4w)–H(1w4)···F(2)	0.93	1.92	2.789(9)	156	x, y, z
O(4w)–H(2w4)···F(6)	0.93	1.82	2.709(9)	159	x, y, z

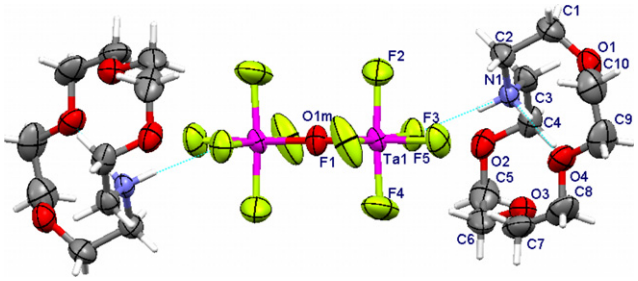

Fig. 1. ORTEP drawing of **1** with the numbering scheme and hydrogen bonding distances shown by dashed lines. Thermal ellipsoids are shown at the 50% probability level.

$(HA15C5)^+$ cation has a distorted shape fixed by the intramolecular N(1)–H(2N1)···O(4) hydrogen bond, H···O 1.94(5), N···O 2.835(5) Å, NHO angle 159(4)°. The similar macrocycle conformation (N···O 2.858 Å) was found in the structure of N-(2-methoxy-4-((4-nitrophenyl)azo)phenyl)-1,4,7,10-tetraoxa-13-azoniacyclopentadecane hexafluorophosphate [14]. It is noteworthy that **1** represents the only second after [13] known example of the organically templated tantalum oxofluoride and the first compound where the macrocycle is used in this function.

3.1.2. *[(HA18C6 · H_2O)(A18C6 · H_2O)][$(H_2O)Nb_2F_9O$] · H_2O (**2**)*

Compound **2** crystallizes in the space group $Pna2_1$. The content of the asymmetric unit is shown in Fig. 2. It comprises of $[(H_2O)NbF_4O\ NbF_5]^-$ anion, two macrocycles (designated A and B; cycle A represents monocation, cycle B represents neutral molecule) centered by two water molecules, and bridging water molecule O(3w). The X-ray data unambiguously showed that $[(H_2O)NbF_4ONbF_5]^-$ is built of $(H_2O)NbF_4O$ and $ONbF_5$ moieties joined *via* common oxygen atom. Complex **2** is the first known example of non-symmetric binuclear aqua niobium oxofluoride and only the second example after bis(ethylenediaminium) μ-oxo-bis[tetrafluorooxoniobium(V)], $(C_2H_{10}N_2)_2[(NbF_5O)_2O]$ [15] dimeric unit. The anion has an angular shape with the Nb(1)–O(1)–Nb(2) angle equal to 158.4(2)° and the Nb(1)···Nb(2) distance of 4.008 Å. The geometry of two octahedral units is rather similar: the longest Nb(1)–O(1w) distance of 2.310(3) Å corresponds to the longest Nb(2)–O(1m) distance of 2.346(3) Å in the second octahedron, while the shortest Nb(1)–O(1m) distance of 1.732(3) Å corresponds to the shortest Nb(2)–F(9) distance of 1.709(3) Å in the second octahedron, etc. The conclusions made by Poeppelmeier et al. [16] about out-of-center distortions observed in Group 5 and 6 metal oxide fluoride octahedra with the general formula of $[MO_xF_{6-x}]^{n-}$ ($x = 1$, $M = V^{5+}$, Nb^{5+}, Ta^{5+}, $n = 2$) that arise from the inherent differences between M=O and M–F bonding and allow for the strong dπ–pπ metal–oxide orbital interactions, are manifested themselves either in purely inorganic niobium oxyfluorides, e.g., Li_2NbOF_5, $Rb_5Nb_3OF_{18}$ [17] or in mixed inorganic–organic compounds, $[4\text{-apyH}]_2[Cu(4\text{-apy})_4(NbOF_5)_2]$ (4-apy = 4-aminopyridine), $Cd(3\text{-apy})_4(NbOF_5)$ (3-apy = 3-aminopyridine), $Cd(py)_4NbOF_5$ (py = pyridine) [16], $[NEt_3H][NbOF_4(H_2O)]$ [18] and can be extrapolated to the reported here new anion, $[(H_2O)NbF_4ONbF_5]^-$ (Table 3).

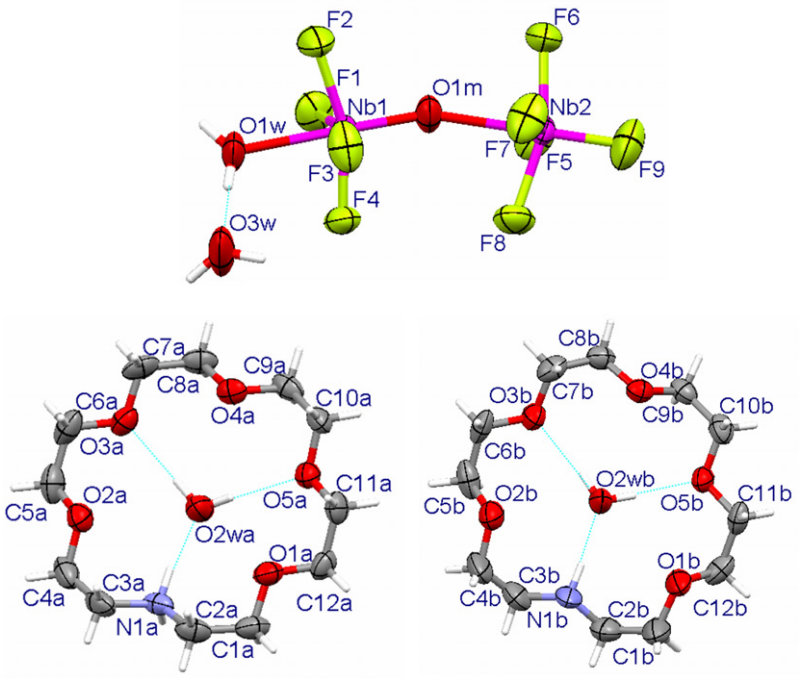

Fig. 2. ORTEP drawing of **2** with the numbering scheme and hydrogen bonding distances shown by dashed lines. Thermal ellipsoids are shown at the 50% probability level.

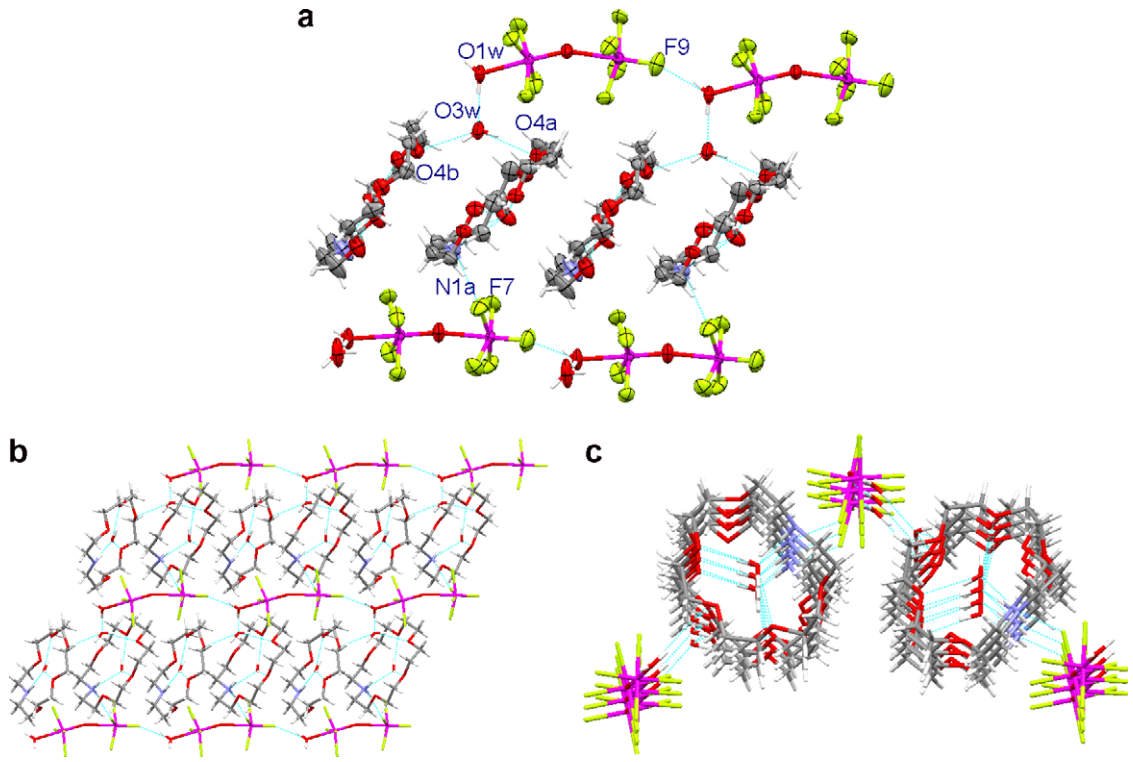

Fig. 3. View of the layer in **2**. (a) Fragment of layer with the numbering of the atoms participating in hydrogen bonding. (b) View along *a* direction. (c) View along *b* direction.

The specific feature of this anion is a *trans*-arrangement of water molecule referring to μ-oxoatom. As it is known, in the hetero-ligand metal complexes with the d^0 configuration of the central atom the mutual ligand influence is manifested in the form of *trans*-effect [19], while the relative stabilization of either *cis*- or *trans*-isomers of the complexes MF_4XO is dictated by the difference in σ- and π-donor characteristics of X and Y ligands [20]. For the oxo-bridge and water molecule arranged in the opposite points of the row of static trans-influence and being essentially different by their σ-, π-donor properties, the approaches [20] indicate the stabilization of the *trans*-form that is agreed with experimental data. It is interesting to note that in formally similar dimeric anion $[Nb_2F_8O_3]^{4-}$ [15] the double-bonded oxygen atoms are arranged in a *cis*-position to the oxo-bridge that is typical for the octahedral

fluorocomplexes of d^0-metals with multiple-bound ligands [20].

In the crystal, the anions translated along *a* direction form OH···F hydrogen bond chain (Fig. 3, Table 3). The analysis of the system of hydrogen bonding as well as the pronounced distinctions in A and B crown ethers' conformations (see Table 2) permit to conclude that in the crystal both monoprotonated and neutral forms of A18C6 co-exist. Water molecules center both macrocycles and act in a similar way, as a double H-donor towards two crown oxygen atoms and as a single H-acceptor towards nitrogen atom (Fig. 2, Table 3). In molecule A, the hydrogens of $>H_2N^+$ group are *endo*,*exo*-oriented that facilitates for the *exo*-oriented hydrogen atom its participation in $NH^+\cdots F$ hydrogen bonding with the anion. Water molecule O(3w) occupies an intermediate position between the negatively charged inorganic chain and rows of macrocyclic molecules and bridges A and B crown molecules *via* OH···O hydrogen bonds. Thus, the supramolecular architecture in **2** represents a 2D sheet built of the alternating negatively-charged inorganic chains and rows of crown molecules, where A and B macrocyclic molecules arranged in approximately parallel planes (the dihedral angle between the planes (A/B) of NO_5 atom set is equal to 13.8(1)°) alternate (Fig. 3).

3.1.3. *[(HA18C6 · H_2O)(M_2O_{10} · 2H_2O) · (H_3O) · (H_2O)] (M = Zr, Hf) (**3**, **4**)*

The system ZrO_2/HfO_2–HF–H_2O–aza18C6 resulted in two isostructural crystalline complexes of the composition [(HA18C6 · H_2O)(M_2O_{10} · 2H_2O) · (H_3O) · (H_2O)] (**3**, **4**), so the only complex **3** is further discussed. Complexes crystallize in the orthorhombic space group $Pca2_1$. The asymmetric unit for **3** is shown in Fig. 4. It comprises of the $(Zr_2F_{10} \cdot 2H_2O)^{2-}$ dianion, azonia-18C6 cation, oxonium ion, and two water molecules. In the dimeric $(Zr_2F_{10} \cdot 2H_2O)^{2-}$ anion, the coordination environment of each Zr atom represents a pentagonal bipyramid. In the equatorial plane of the anion, the bridging F(1m) and F(2m) atoms form a double bridge, with the Zr–F distances being in the range 2.135(7)–2.150(7) Å, and coordinated to Zr water molecules located along the Zr(1)···Zr(2) line, Zr···O distances being 2.207(6) and 2.208(7) Å, Zr(1)···Zr(2) separation being 3.604(1) Å. Our survey of the CSD [21] revealed no examples of such organically templated zirconate anion. The only known relative example with the same Brutto formula of the anion is a tetramethylammonium pentafluoro-zirconium monohydrate, $(C_4H_{12}N)_2(Zr_2F_{10} \cdot 2H_2O)$ [22], where the coordinated to Zr water molecules are arranged perpendicular to the Zr···Zr line.

The monoprotonated macrocyclic molecule in the complex is disordered over two positions (A and B) with equal probabilities. Similar to complex **2**, water molecule O(3w) centers the macrocyclic cation and acts as a double H-donor towards two crown oxygens and as a single H-acceptor towards *endo*-oriented H-atom of NH_2-group. It was impossible to unambiguously find the positions of hydrogen atoms in water molecule due to the severe disorder of the macrocycle and the proposition of the possible hydrogen bonding was assumed from consideration of the shortest O(3w)···N(O) crown distances which adopt the following values in two (A and B) systems: 2.91(2), 2.97(2) and 2.74(2) Å to atoms O(1A), O(3A) and O(5A), respectively and 2.86(3), 3.03(2) and 2.72(2) Å to atoms O(1B), O(2B) and O(5B), respectively.

The anions form in the crystal an inorganic layer due to OH···F hydrogen bonds between the coordinated to Zr water molecules and four equatorial fluorine atoms (Fig. 5, Table 3), in such a way, that every anion is surrounded by four closest neighbors, the association of the anions occurs *via* alternation of $R_2^2(8)$ and $R_4^4(16)$ hydrogen-bonded rings. The similar inorganic sheet is generated in structures containing $(Hf_2F_{10} \cdot 2H_2O)^{2-}$ anion, hexamethyldiammonium pentafluorohafnate tetrahydrate $(C_6N_2H_{18})[Hf_2F_{10}(H_2O)_2] \cdot 4H_2O$, tetramethylenediammonium pentafluorohafnate hexahydrate $(C_4N_2H_{14})[Hf_2F_{10}(H_2O)_2] \cdot 4H_2O$ [23] as well as in the complex $[(18C6)(H_3O)_2(Hf_2O_{10} \cdot 2H_2O) \cdot 4H_2O]$ [7].

The disorder of the macrocycle causes the disordering of the oxonium ion labelled O5o(a,b) and solvated water molecule O4w(a,b) which are bound in a slightly different mode with the macrocycle and inorganic layer (Fig. 4). The 3D supramolecular architecture in **3** is formed *via* alternation of the inorganic layers and rows of macrocyclic molecules held together via oxonium

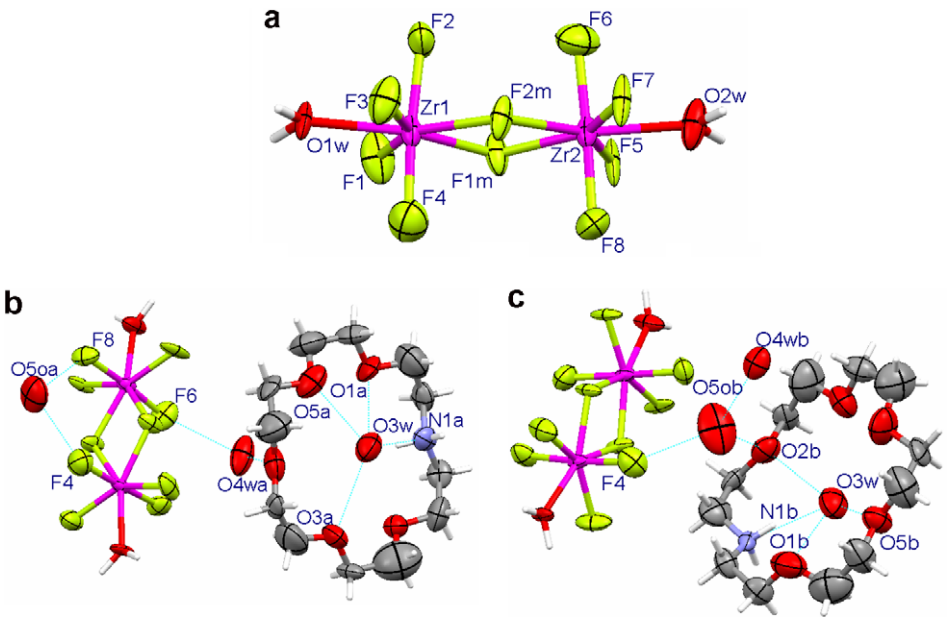

Fig. 4. ORTEP drawing of **3**. (a) View of the $(Zr_2F_{10} \cdot 2H_2O)^{2-}$ anion with the numbering scheme. (b) View of the crown molecule in position A, water molecules and oxonium ion O(5oa) that participate in hydrogen bonds in this system. (c) View of the crown molecule in position B, water molecules and oxonium ion O(5ob) that participate in hydrogen bonds in this system with partial numbering scheme. Complete numbering scheme in crown molecule is the same as in **2** (Fig. 2). Hydrogen bonding distances shown by dashed lines. Thermal ellipsoids are shown at the 50% probability level.

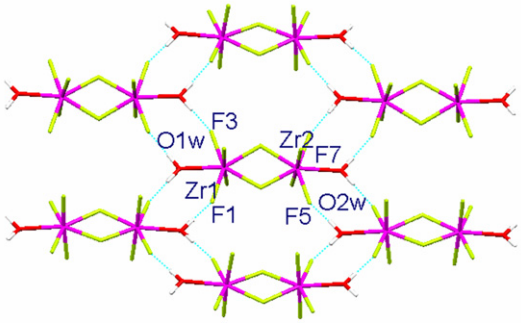

Fig. 5. Fragment of inorganic layer in **3**.

and water molecules. Besides these indirect interactions, the direct $NH^{+}\cdots F^{-}$ contacts between charged units also exist (Table 3, Fig. 6).

*3.1.4. $[(H_2DA18C6)(M_2O_{10}\cdot 2H_2O)\cdot 2H_2O]$ (M = Zr, Hf) (**5**, **6**)*

The interaction in the system ZrO_2/HfO_2–HF–H_2O–1,10-diaza18C6 resulted in two isostructural complexes $[(H_2DA18C6)(M_2O_{10}\cdot 2H_2O)\cdot 2H_2O]$ (**5**, **6**), and only complex **5** is further discussed. Complexes crystallize in the triclinic space group $P\bar{1}$. The content of the asymmetric unit is shown in Fig. 7. It comprises of the $(Zr_2F_{10}\cdot 2H_2O)^{2-}$ anion and two water molecules in general positions and two halves of two crystallographically different diazonia-18C6 cations (A and B), which reside on inversion centers. The structure of the dimeric anion is the same as in **3** and in its Hf analogue in **4** and **6**, the coordination environment of each Zr atom represents a pentagonal bipyramid (Table 2).

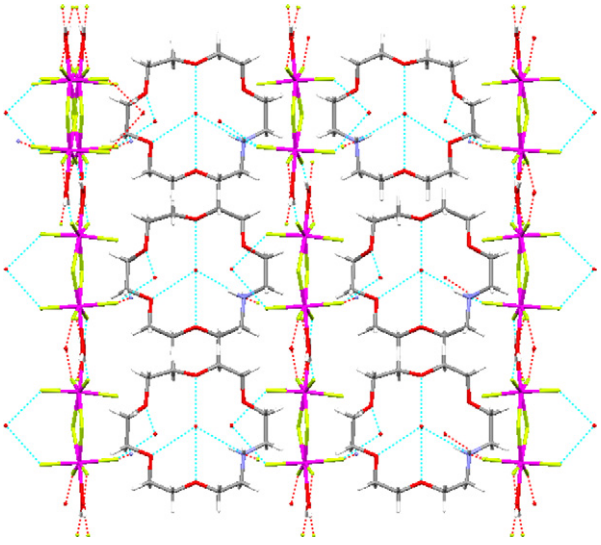

Fig. 6. Fragment of the crystal packing in **3**.

Similar to **3**, the anions in **5** formulate a rigid inorganic negatively charged 2D sheet sustained by OH···F hydrogen bonds (Table 3). Two water molecules O(3w) and O(4w) in an identical mode are bridging two pairs of the anion's axial fluorine atoms (Table 3). Further, these two water molecules in different modes act as intermediates between the inorganic anion and macrocyclic cations. Fig. 8a demonstrates interactions between the components in the complex. Water molecule O(3w) acts in a 'side' mode, and as a single H-acceptor forms N(1a)H···O(3w) hydrogen bond with the A macrocycle, while the second H-atom of the same $\geqslant NH_2^{+}$ group is involved in a single charged-assisted N(1a)H···F(2) hydrogen bond, it is a unique such contact (between the charged species) in this structure. Water molecule O(4w) is situated above the macrocyclic cation B and, acting as a double H-acceptor across the cavity, binds both protons of $\geqslant N(1b)H_2$ ammonia group. It explains, why this macrocycle does not have any direct contacts with the anionic layer. The different modes of water inclusion as well as the distinctions in the interaction with the anionic component, determine the different conformations of A and B macrocyclic cations (Fig. 7, Table 2). Nevertheless, the 3D supramolecular architecture still remains very similar to that one described for **3** (**4**) and for the aforementioned complex $[(18C6)(H_3O)_2(Hf_2O_{10}\cdot 2H_2O)\cdot 4H_2O]$ [7] (Fig. 8b) and represents the alternation of inorganic layers and rows of macrocyclic cations attached, where the A and B macrocycles alternate.

Summarizing these two sections, the following general remarks can be given. Complexes **3**–**6** have enriched a rather restricted family of the aqua, fluoro-containing zirconates [22] and hafnates [23]. For the compounds containing the anions of the similar composition $(M_2O_{10}\cdot 2H_2O)^{2-}$ (M = Zr, Hf), the different arrangement of the coordinated to the central atom water molecules is observed: they are always displayed in the equatorial plane and either lie along the M–M line (complexes **3**–**6**, $[(18C6)(H_3O)_2(Hf_2O_{10}\cdot 2H_2O)\cdot 4H_2O]$ [7]) or perpendicular to it. Besides the discussed here crown-templated complexes, the similar inorganic 2D motif also has been recorded in hexamethyldiammonium pentafluorohafnate tetrahydrate, tetramethylenediammonium pentafluorohafnate hexahydrate [23] and can be considered as a reproducible supramolecular motif. The type of bridging of axial fluorine atoms *via* coordinated or solvated water molecule or oxonium ion found in **3**–**4**, and **5**–**6**, was also registered in Refs. [22,23]. Moreover, this bridge can also represent two-membered H_5O_2 oxonium cluster as in $[(18C6)(H_3O)_2(Hf_2O_{10}\cdot 2H_2O)\cdot 4H_2O]$

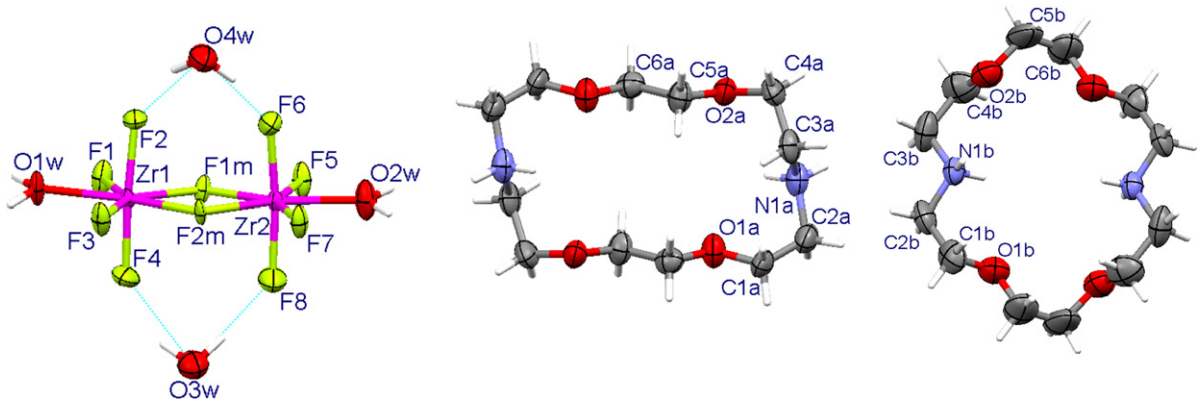

Fig. 7. ORTEP drawing of **5** with the numbering scheme and hydrogen bonding distances shown by dashed lines. Thermal ellipsoids are shown at the 50% probability level.

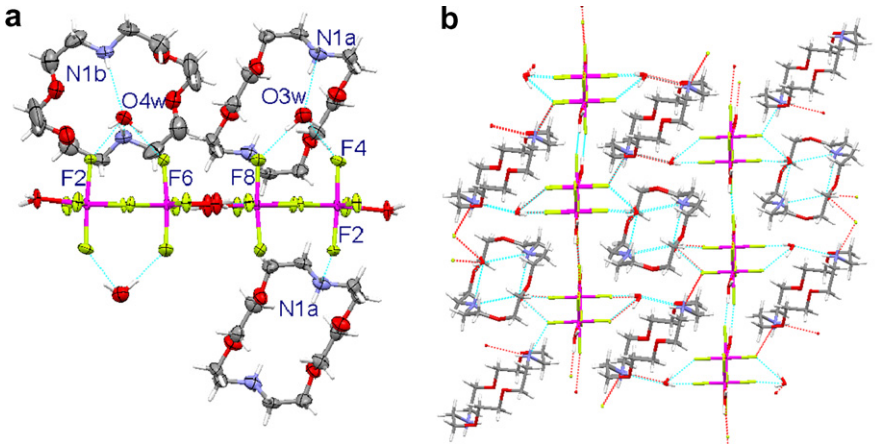

Fig. 8. Fragment of crystal packing in **5**. (a) Fragment of the structure demonstrating the interactions between the inorganic layer and macrocyclic cations, only atoms participating in hydrogen bonding are labeled. (b) 3D network in **5**.

[7] or association of water molecule and ammonium group of templated amine. For **3**–**6**, we conclude the reproduction of 3D supramolecular architecture, which represents the alternation of 2D inorganic sheets and columns of 18-membered crown ethers glued by the different number of water molecules. We also observe the gradual decrease of water content in the complexes with the increase of the positive charge of the macrocyclic cation.

4. Conclusion

The interaction of ZrO_2/HfO_2 or Nb_2O_5/Ta_2O_5 with an aqueous solution of hydrofluoric acid in the presence of aza-crown ether resulted in novel organically templated metal oxofluorides of the compositions $[(HA15C5)_2][Ta_2F_{10}O]$ (**1**), $[(HA18C6\cdot H_2O)$-$(A18C6\cdot H_2O)][(H_2O)\ Nb_2F_9O]\cdot H_2O$ (**2**), $[(HA18C6\cdot H_2O)(M_2F_{10}\cdot 2H_2O)\cdot(H_3O)\cdot H_2O]$ (**3**, **4**) and $[(H_2DA18C6)(M_2F_{10}\cdot 2H_2O)\cdot 2H_2O]$ (**5**, **6**) (M = Zr, Hf, A15C5 = aza-15-crown-5, A18C6 = aza-18-crown-6, DA18C6 = diaza-18-crown-6). The unique ability of crown macrocyclic molecules to form the complexes with novel or rarely observed anions has been demonstrated. So far **1**–**6** represent the exclusive examples of *crown-templated* mixed O,F-containing anions for Zr, Hf, Nb and Ta. The Ta complex **1** represents the second example of such organically templated anion alongside with [9] and the first example of the macrocyclic molecule used in this function. For the first time, the structural information has been obtained for the anion $[(H_2O)NbF_4ONbF_5]^-$ in the complex with macrocyclic molecule. Complex **2** represents a perspective example of the non-centrosymmetric solid with the local ordered anion, thus being crystallized in an acentric space group with an ordered inorganic unit, it might give rise to the new NLO materials. Complexes **3**–**6** give bright examples of the reproducible supramolecular motifs where the factors of domination of inorganic framework and dimensionality of crown molecule are decisive ones. We concluded, that the substitution of one or two oxygen atoms in 18C6 molecule by nitrogen atom did not crucially change the composition of the negatively-charged framework for Zr and Hf in particular and the 3D supramolecular architecture in a whole in the row 18C6–A18C6–DA18C6. The isostructural products have been obtained for Zr and Hf.

Acknowledgement

This work was supported by the Russian Foundation for Basic Research and the Academy of Sciences of R. Moldova (Project No. 06-03-90894-Mol-a).

Appendix A. Supplementary data

CCDC 671858, 671860, 671862, 671859, 671863 and 671861 contains the supplementary crystallographic data for **1**, **2**, **3**, **4**, **5** and **6**. These data can be obtained free of charge via http://www.ccdc.cam.ac.uk/conts/retrieving.html, or from the Cambridge Crystallographic Data Centre, 12 Union Road, Cambridge CB2 1EZ, UK; fax: (+44) 1223-336-033; or e-mail: deposit@ccdc.cam.ac.uk. Supplementary data associated with this article can be found, in the online version, at doi:10.1016/j.poly.2008.03.023.

References

[1] S.G. Bott, A. Alvanipour, J.L. Atwood, J. Incl. Phenom. Mol. Recog. Chem. 10 (1991) 153.
[2] H. Feinberg, I. Columbus, S. Cohen, M. Rabinovitz, H. Selig, G. Shoham, Polyhedron 12 (1993) 2913.
[3] (a) Y.A. Simonov, V.O. Gelmboldt, E.V. Ganin, A.A. Dvorkin, M.S. Fonari, L.V. Ostapchuk, J. Lipkowski, Koord. Khim. (Russ.) (Coord.Chem.) 21 (1995) 760;
(b) M.S. Fonari, Yu.A. Simonov, M.D. Mazus, E.V. Ganin, V.O. Gelmboldt, Kristallografiya (Russ.) (Crystallogr. Rep.) 42 (1997) 858.
[4] Yu.A. Simonov, Ed.V. Ganin, A.A. Dvorkin, M.S. Fonari, V.O. Gelmboldt, A.A. Ennan, Supramol. Chem. 3 (1994) 185.
[5] (a) J. Lipkowski, M.S. Fonari, V.Ch. Kravtsov, V.O. Gelmboldt, E.V. Ganin, Yu.A. Simonov, J. Chem. Cryst. 26 (1996) 823;
(b) M.S. Fonari, E.V. Ganin, V.O. Gelmboldt, J. Lipkowski, S.A. Kotlyar, G.L. Kamalov, Acta Crystallogr., Sect. 62 (2006) m1021.
[6] (a) V.O. Gelmboldt, Yu.A. Simonov, E.V. Ganin, M.S. Fonari, V.Ch. Kravtsov, A.A. Dvorkin, L.V. Ostapchuk, A.A. Ennan, Koord. Khim. 22 (1996) 21;
(b) V.O. Gelmboldt, E.V. Ganin, M.S. Fonari, Yu.A. Simonov, L.V. Koroeva, A.A. Ennan, S.S. Basok, S. Shova, H. Kählig, V.B. Arion, B.K. Keppler, Dalton Trans. 27 (2007) 2915.
[7] V.O. Gelmboldt, E.V. Ganin, L.V. Koroeva, M.S. Fonari, Yu.A. Simonov, V.Ch. Kravtsov, J. Lipkowski, Zh. Neorg. Khim. (Russ. J. Inorg. Chem.) 46 (2001) 1833.
[8] (a) M.S. Fonari, N.G. Furmanova, W.-J. Wang, E.V. Ganin, I.A. Verin, Yu.A. Simonov, V.O. Gelmboldt, Kristallografiya (Russ. Crystallogr. Rep.) 51 (2006) 856;
(b) M.S. Fonari, O.A. Alekseeva, N.G. Furmanova, K.A. Lysenko, W.-J. Wang, S.-W. Tang, E.V. Ganin, V.O. Gelmboldt, Yu.A. Simonov, Kristallografiya (Russ. Crystallogr. Rep.) 52 (2007) 271;
(c) M.S. Fonari, Yu.A. Simonov, W.-J. Wang, S.-W. Tang, E.V. Ganin, V.O. Gelmboldt, T.S. Chernaya, O.A. Alekseeva, N.G. Furmanova, Polyhedron 26 (2007) 5193;
(d) E.V. Ganin, V.O. Gelmboldt, L.V. Koroeva, M.S. Fonari, Yu.A. Simonov, J. Lipkowski, S.A. Kotlyar, G.L. Kamalov, J. Incl. Phenom. 56 (2006) 345;
(e) N.G. Furmanova, M.X. Rabadanov, T.S. Chernaya, M.S. Fonari, Yu.A. Simonov, E.V. Ganin, V.O. Gelmboldt, R.Ya. Grygorash, S.A. Kotlyar, G.L. Kamalov, Kristallografiya (Russ. Crystallogr. Rep.) 53 (2008) 273.
[9] (a) J.C. Bertolini, J. Emerg. Med. 10 (1992) 163;
(b) D. Peters, R. Miethchen, J. Fluorine Chem. 79 (1996) 161;
(c) E.B. Segal, Chem. Health Saf. 7 (2000) 18.
[10] Z. Otwinowski, W. Minor, in: C.W. Carter, R.M. Sweet (Eds.), Methods in Enzymology, Macromolecular Crystallography, Part A, vol. 276, Academic Press, London, 1996, p. 307.
[11] G.M. Sheldrick, SADABS, Bruker AXS Inc., Madison, WI, USA, 1997.

[12] G.M. Sheldrick, SHELXS 97 and SHELXL 97, Programs for Crystal Structure Solution and Refinement, University of Göttingen, Germany, 1997.
[13] J.C. Dewan, A.J. Edwards, J.Y. Calves, J.E. Guerchais, J. Chem. Soc., Dalton Trans. (1977) 978.
[14] T. Gunnlaugsson, M. Nieuwenhuyzen, L. Richard, V. Thoss, J. Chem. Soc., Perkin Trans. 2 (2002) 141.
[15] N.F. Stephens, P. Lightfoot, Acta Crystallogr., Sect. C 61 (2005) m344.
[16] (a) M.E. Welk, A.J. Norquist, F.P. Arnold, C.L. Stern, K.R. Poeppelmeier, Inorg. Chem. 41 (2002) 5119;
(b) P.A. Maggart, A.L. Kopf, C.L. Stern, K.R. Poeppelmeier, CrystEngComm 6 (2004) 451;
(c) H.K. Izumi, J.E. Kirsch, C.L. Stern, K.R. Poeppelmeier, Inorg. Chem. 44 (2005) 884;
(d) P.C.R. Guillory, J.E. Kirsch, H.K. Izumi, C.L. Stern, K.R. Poeppelmeier, Cryst. Growth Des. 6 (2) (2006) 382.
[17] (a) J. Galy, S. Andersson, J. Portier, Acta Chem. Scand. 23 (1969) 2949;
(b) A.I. Agulyanskii, V.E. Zavodnik, V.Ya. Kuznetsov, N.V. Sidorov, S.Yu. Stefanovich, D.V. Tsikaeva, V.T. Kalinnikov, Izv. Akad. Nauk SSSR Neorg. Mater. 27 (1991) 1055.
[18] N.G. Furmanova, I.A. Verin, A.N. Zozulin, E.G. Il'in, Kristallografiya 37 (1) (1992) 136.
[19] A.A. Levin, P.N. Diyachkov, Élektronnoe stroenie, struktura i prevrasenia geteroligandnyh molekul [BOOK] (1990) 256.
[20] Yu.A. Buslaev, E.G. Ilin, Interligand interactions and stereochemistry of octahedral different ligand complexes (Mezhligandnyie vzaimodeistviya I stereokhimiya oktaedricheskikh raznoligandnyx kompleksov, Russ.) Itogi nauki i tekhniki. Ser. neorgan. khimiya. T. 16. M.: VINITI, 1987. 98s.
[21] F.N. Allen, Acta Crystallogr., Sect. B 58 (2002) 380.
[22] B.V. Bukvetskii, A.V. Gerasimenko, R.L. Davidovich, M.A. Medkov, Koord. Khim. (Russ. Coord. Chem.) 11 (1985) 77.
[23] (a) A.V. Gerasimenko, R.L. Davidovich, V.V. Tkachev, S.W. Ng, Acta Crystallogr., Sect. E 62 (2006) m196;
(b) V.V. Tkachev, L.O. Atovmyan, V.B. Logvinova, R.L. Davidovich, Koord. Khim. (Russ. Coord. Chem.) 22 (1996) 234;
(c) V.V. Tkachev, L.O. Atovmyan, V.B. Logvinova, R.L. Davidovich, Koord. Khim. (Russ. Coord. Chem.) 22 (1996) 7727.

Polyhedron 27 (2008) 2059–2064

Contents lists available at ScienceDirect

Polyhedron

journal homepage: www.elsevier.com/locate/poly

Face-to-face interactions of metallic oxo-clusters: Synthesis and crystal structure of new isopolyvanadotungstate salts – $Co(H_2O)_6K_2V_2W_4O_{19}$ and $[Co(H_2O)_6]_2V_2W_4O_{19}$

Hafedh Driss [a,b,1], René Thouvenot [b,2], Mongi Debbabi [a,*]

[a] Laboratoire de Physico-Chimie des Matériaux, Ecole Nationale d'Ingénieurs de Monastir, 5019 Monastir, Tunisia
[b] Laboratoire de Chimie Inorganique et Matériaux Moléculaires (UMR CNRS 7071), Institut de Chimie Moléculaire (FR 2769), Case Courrier. 42, UPMC Univ Paris 06, 4 place Jussieu, 75005 Paris, France

ARTICLE INFO

Article history:
Received 12 February 2008
Accepted 25 March 2008
Available online 15 May 2008

Keywords:
Polyoxometalates
Hydrogen bonds
X-ray structure
Lindqvist structure

ABSTRACT

Crystals of $Co(H_2O)_6K_2V_2W_4O_{19}$ (**1**) and $[Co(H_2O)_6]_2V_2W_4O_{19}$ (**2**) were obtained from aqueous solution of $[V_2W_4O_{19}]^{4-}$ and cobalt(II) nitrate. The structure of $[V_2W_4O_{19}]^{4-}$ is that of the Lindqvist anion in which the two vanadium and four tungsten atoms are statistically distributed over the six metallic positions. The $[V_2W_4O_{19}]^{4-}$ and the $[Co(H_2O)_6]^{2+}$ octahedra are arranged alternately with their faces parallel to each other for maximal interactions (face-to-face interaction). The structure of **1** shows the presence of large mono-directional channels along *c*-axis with a quasi hexagonal section of 8.52×6.35 Å^2 which are filled by cobalt. The structure of **2** can be viewed as a pillar arrangement of $[Co(H_2O)_6]_2V_2W_4O_{19}$ units along *c*-axis.

© 2008 Elsevier Ltd. All rights reserved.

1. Introduction

Polyoxometalates represent a class of compounds that show a great variety of structural building blocks. In addition to their remarkable chemical and physical properties they have various fields of applications such as catalysis [1–4], medicine [5,6] and material science [7–9]. Vanadium–tungsten mixed isopolyanions were firstly described by Finkener [10] and Rosenheim [11], then in 1894 by Friedheim [12,13] and in 1915 by Prandtl [14]. In 1963, Chauveau and Souchay [15] confirmed the V/W = 2:4 stoichiometry and determined the pH range for the stability of this species. In 1971, Flynn and Pope [16], gave efficient methods to prepare the complexes $[V_xW_{6-x}O_{19}]^{-2-x}$ ($x = 1, 2$). IR and Raman spectroscopic studies in solution and in the solid state have shown that these anions have likely the Lindqvist structure [17,18] with respectively one and two tungsten atoms being replaced by vanadium. The stability in aqueous solution of such species depends strongly on the pH [19,20]. The high charge and large size of the isopolyanions make them nice building units for self assembly in variable clusters packing and to form various internal structures and functionalities [21]. Different modes of interactions govern ionic clusters packing, such as coordination bonds, hydrogen bonds and ionic interactions. As recently shown by Son et al. in the complex $[Al_{13}O_4(OH)_{24}(H_2O)_{12}]_2[V_2W_4O_{19}]_3(OH)_2 \cdot 27H_2O$ [22], electrostatic interactions between oppositely charged polyhedra reinforced by hydrogen bonds, result in face-to-face arrangement of these ionic clusters. The resulting species show bi-dimensional honeycomb layers of clusters. The present work constitutes a contribution to this domain by the synthesis and the structural characterization of two new salts of substituted isopolyanions $Co(H_2O)_6K_2V_2W_4O_{19}$ and $[Co(H_2O)_6]_2V_2W_4O_{19}$ which present face-to-face clusters arrangement.

2. Experimental

Reagent grade cobaltous nitrate $Co(NO_3)_2 \cdot 6H_2O$, was purchased from Acros and used as received. $K_4V_2W_4O_{19} \cdot 8H_2O$ was prepared according to the literature [16]. The IR spectra have been recorded from KBr pellets on a FT-IR Bio-Rad FTS 165 spectrometer with a resolution of 4 cm^{-1}.

2.1. Synthesis

2.1.1. Preparation of $Co(H_2O)_6K_2V_2W_4O_{19}$ (**1**)

An orange solution of divanado-tetratungstate was prepared by dissolving $K_4V_2W_4O_{19} \cdot 8H_2O$ (1 g, 0.69 mmol) in 25 mL of distilled water (pH ≈ 5). Violet solution of cobalt(II) nitrate was obtained by dissolving $Co(NO_3)_2 \cdot 6H_2O$ (0.40 g, 1.38 mmol) in 25 mL of distilled water (pH ≈ 5.4). After mixing the resulting dark orange solution (pH ≈ 5) was stirred and heated for 10 min at 50 °C then

* Corresponding author. Tel.: +216 73 501 786; fax: +216 73 501 786/500 514.
E-mail addresses: rene.thouvenot@upmc.fr (R. Thouvenot), mongi.debbabi@e-nim.rnu.tn (M. Debbabi).
[1] Fax: +216 73 500 514.
[2] Fax: +33 1 44 27 38 41.

0277-5387/$ - see front matter © 2008 Elsevier Ltd. All rights reserved.
doi:10.1016/j.poly.2008.03.020

left at room temperature until evaporation to dryness (*ca.* 1 week). The crude product was purified by crystallization: it was redissolved in a minimum amount (*ca.* 10 mL) of distilled water, then the solution was filtered by suction filtration (in glass frit No. 4) to eliminate some insoluble residues. Crystals obtained by evaporation at room temperature were collected before dryness, washed successively with water/ethanol mixture (50/50 v/v) and by diethylic ether. Yield of $Co(H_2O)_6K_2V_2W_4O_{19}$: 0.67 g, 67% based on polyoxoanion. IR (KBr pellets 300–1000 cm^{-1}): 364 (m), 368 (m), 436 (s), 455 (s), 592 (m), 596 (m), 787 (vs), 941 (s), 956 (vs), 989 (m). Well-shaped dark orange prismatic crystals suitable for X-ray data collection were obtained after slow recrystallization in distilled water.

2.1.2. Preparation of $[Co(H_2O)_6]_2V_2W_4O_{19}$ (**2**)

To 5 mL of a dark orange aqueous solution of **1** (0.5 g, 0.34 mmol, pH ≈ 5) was added 5 mL of an aqueous solution of $Co(NO_3)_2 \cdot 6H_2O$ (0.10 g, 0.34 mmol, pH ≈ 5.4). The subsequent treatment was the same as that used for **1**. Yield of $[Co(H_2O)_6]_2V_2W_4O_{19}$: 0.17 g, 34%. IR (KBr pellets 300–1000 cm^{-1}): 369 (m), 372 (m), 441 (s), 452 (s), 587 (m), 591 (m), 793 (vs), 946 (s), 962 (vs), 991 (m). After recrystallization in distilled water well-shaped orange prismatic crystals suitable for X-ray data collection were obtained.

2.2. X-ray single-crystal structure determination

An orange prismatic crystal (0.10 × 0.12 × 0.12 mm^3) of **1** was mounted on a four-circle CAD-4 Enraf Nonius diffractometer using graphite-monochromated Mo Kα radiation (0.71073 Å). Intensity data were collected at 293 K. Treatment of data and refinement of cell parameters have been performed using Express program CAD-4 [23,24]. The data reduction has been assured by the program RC93 (Watkin et al., 1994).

An orange parallelepipedic crystal (0.10 × 0.11 × 0.12 mm^3) of **2** was mounted on a Kappa-CCD Bruker AXS diffractometer using graphite-monochromated Mo Kα radiation (λ = 0.71073 Å). Data were collected at 293 K. Refinement of cell parameters has been performed by Dirax/lsq (Duisenberg and Schreurs, 1989–2000) and data reduction by EvalCCD (Duisenberg and Schreurs 1990–2000).

Table 1
Crystallographic data and refinement parameters for compounds **1** and **2**

Crystal data and refinement details	**1**	**2**
Empirical formula	$Co(H_2O)_6K_2V_2W_4O_{19}$	$[Co(H_2O)_6]_2V_2W_4O_{19}$
Formula weight	1386.64	1475.32
Crystal system	orthorhombic	trigonal
Space group	*Cmcm*	$R\bar{3}m$
a (Å)	11.645(4)	11.080(6)
b (Å)	13.242(6)	
c (Å)	15.417(6)	18.452(9)
V (Å^3)	2377.4(16)	1961.7(18)
Z	4	3
D_{calc} (g cm^{-3})	3.841	3.746
μ (Mo Kα) (mm^{-1})	21.163	19.550
θ Range (°)	2.329–26.969	2.392–39.745
Limiting indices	$0 \leqslant h \leqslant 14$, $0 \leqslant l \leqslant 16$, $0 \leqslant k \leqslant 19$	$-16 \leqslant h \leqslant 19$, $-19 \leqslant l \leqslant 19$, $0 \leqslant k \leqslant 32$
Reflection collected	1407	1396
Data completeness	99.9%	99.5%
Data used/restraints/parameters	1104/2/110	925/85/36
Goodness-of-fit on *F*	1.0541	1.0744
Final R_1, wR_2 [$I > 3\sigma(I)$]	0.0443, 0.0484	0.0397, 0.0425
Largest differential peak and hole (e Å)$^{-3}$	−1.62, 1.37	−1.93, 1.98

The positional parameters of metal and of most oxygen atoms of the clusters were obtained by direct methods and refined with full-matrix least-squares technique on *F* using SHELXS86 [25]. The crystallographic software CRYSTALS [26] was used for the refinement of the structure and the preparation of data for the publication. The structure representations were drawn with DIAMOND program [27]. The crystal data and details of data collection and refinement for crystals of **1** and **2** are summarized in Table 1.

3. Results and discussion

3.1. Synthesis

It is well known that stability of polyoxoanion in aqueous solution dramatically depends on the pH. Obtaining polyanions as crystalline material from their aqueous solution require the use of an appropriate counterion which does not strongly affect the pH. Stability range of $[V_2W_4O_{19}]^{4-}$ is $4 \leqslant pH \leqslant 7$ [20]. For the obtainment of transition metal salts of this anion it is therefore important to maintain the pH of the solution between 4 and 7 during the addition of counterion; e.g. Co^{2+} aqueous solutions (pH = 5.4) are therefore appropriate for that purpose. All attempts to obtain the all-cobalt species $[Co(H_2O)_6]_2V_2W_4O_{19}$ (**2**) directly from $K_4V_2W_4O_{19}$ and cobalt nitrate failed even with a large excess of the later. The mixed potassium cobalt salt **1** crystallizes instead from the solution. Potassium-free **2** was ultimately obtained by addition of cobalt nitrate to a solution of **1**.

3.2. Infrared spectroscopy

The infrared spectra of $K_4V_2W_4O_{19} \cdot 8H_2O$, **1** and **2** are very similar and characteristic of the substituted Lindqvist structure: the stretching modes of the M–O_t bonds appear at relatively high wavenumbers (900–1006 cm^{-1}) and those implying the bridging oxygen atoms at ca 800 cm^{-1}. Low-wavenumber bands were assigned to bending vibrations of the oxocluster (see Table 2). It should be noted that the two high frequency modes are shifted to low wavenumbers by 10–15 cm^{-1} in the cobalt-containing species (with respect to the potassium salt); such a shift has been already reported for the guanidinium salt [28] and also for Keggin derivatives [29]. This could originate from specific cation–anion interactions implying the external oxygen atoms of the polyoxometallates.

3.3. Structural analysis

3.3.1. Structural determination

Crystals of $Co(H_2O)_6K_2V_2W_4O_{19}$ (**1**) were obtained from an aqueous solution of potassium salt of $[V_2W_4O_{19}]^{4-}$ and cobalt(II) nitrate. Crystals of $[Co(H_2O)_6]_2V_2W_4O_{19}$ (**2**) were obtained from an aqueous solution of **1** and cobalt(II) nitrate.

Both compounds **1** and **2** contain $[V_2W_4O_{19}]^{4-}$ oxocluster. This anion is isostructural with $W_6O_{19}^{2-}$ [30], $Nb_6O_{19}^{8-}$ [31], $Ta_6O_{19}^{8-}$

Table 2
Selected IR data (in cm^{-1}) for compounds $K_4V_2W_4$, **1** and **2**

Assignment [18]	$K_4V_2W_4$	$Co(H_2O)_6K_2V_2W_4$	$[Co(H_2O)_6]_2V_2W_4$
ν M–O_t	1005 (m)	990 (m)	991 (m)
	970 (s)	957 (s)	962 (s)
	942 (s)	941 (s)	942 (s)
ν_{as} M–O_b	790 (vs)	787 (vs)	793 (vs)
ν_s M–O_b	590 (m)	590 (m)	591 (m)
	540 (w)		
	440 (s)	442 (s)	440 (s)
ν_{as} M–O_c	370 (m)	365 (m)	372 (m)

[32], $Mo_6O_{19}^{2-}$ [33] and has the so-called Lindqvist structure with general formula $M_6O_{19}^{n-}$. This structure is based on the arrangement of six edge-sharing octahedra with overall O_h symmetry. It contains three types of oxygen atoms: six terminal oxygen atoms O_t (M–O_t ~ 1.7 Å), twelve oxygen atoms O_b bridging two metals (M–O_b ~ 1.9Å) and one central oxygen atom O_c common to the six MO_6 octahedra (M–O_c ~ 2.3Å).

As was already observed for the guanidinium $(CN_3H_6)_4V_2W_4O_{19}$ [28] and Al_{13} [22] salts, compounds **1** and **2** exhibit a random V/W distribution over the metal sites. This orientational disorder of the $[V_2W_4O_{19}]^{4-}$ anion is a consequence of a regular distribution of the anionic charge over the external oxygen atoms. The problem of statistical disorder is frequently encountered in the structural resolutions of substituted and lacunary polyoxometalates for which it is impossible to derive specific metrical parameters [34]. Refinements of the structures were performed by forcing the vanadium and tungsten atoms to occupy the same crystallographic sites. In both cases refinement converged to statistical occupancies of 1/3 and 2/3 for V and W respectively in agreement with $[V_2W_4O_{19}]^{4-}$ formula. For both compounds the Co–O_w (O_w: water oxygen) average distance of 2.1 Å is typical for those found in related Co–O complexes as seen in Table 3. Valence sum calculations according to Brown's method using VALIST program [35] show that in both compounds **1** and **2** the oxidation state of cobalt is close to +2.

*3.3.1.1. Crystal structure description of $Co(H_2O)_6K_2V_2W_4O_{19}$ (**1**).* The asymmetric unit is composed of fifteen independent non-hydrogen atoms, corresponding to one potassium atom, one cobalt atom linked to four oxygen atoms (water oxygen) and nine atoms generating the $V_2W_4O_{19}$ anion. In $V_2W_4O_{19}$ the nine atoms are divided in two metallic atoms (M = 2/3 W and 1/3 V) and seven oxygen atoms labelled according to their position in the structure: 1 O_c, 2 O_t and 4 O_b are central, terminal and bridging oxygen atoms respectively. The reduction in the atom numbers in the asymmetric unit is due to the high symmetry of the orthorhombic system in which crystallizes the compound **1**.

The cobalt octahedra are disordered over two positions. In the asymmetric unit all representative atoms of cobalt octahedra (labelled Co13, O14, O15, O16 and O17) are located at special positions and some of them occupy partially their positions: the cobalt and two oxygen atoms (Co13, O16 and O17) occupy their positions at 50% and the two other oxygen atoms (O14 and O15) occupy fully their positions. The atomic parameters and selected bonds are reported in Tables 4 and 5. The anisotropic displacement and the full refinement data are available as supplementary materials.

The X-ray observed structure for cobalt cation is a face sharing dimeric species (Fig. 1) statistically disordered over two position with 50% occupancy of each position; this crystallographic solution is consistent with electroneutrality of the whole molecule. The refinement of the cobalt occupancy (at Wyckoff position f) without constraint reveals that its real value is 50%. The refinement converges and the thermal displacement of the oxygen atoms is considerably reduced when occupancies of the oxygen atoms located out of the shared face is reduced by half.

The structure of compound **1** can be viewed as stacking of isopolyanion layers along *c*-axis. The cohesion between these layers is ensured by electrostatic interactions between the cluster anions and the potassium atoms (Fig. 2). The potassium atoms are coordinated to four V_2W_4 units belonging to two adjacent layers. In each layer, the potassium atom is linked to one terminal oxygen of one polyanion and one bridging oxygen atom of the other, with an average distance of about 2.836 Å (Fig. 3).

Table 3
Co–O bond lengths for selected cobalt compounds

Compound	*d*(Co–O) (Å)	Reference
$Co(H_2O)_6K_2V_2W_4O_{19}$ (**1**)	1.96(2) min 2.207(16) max	This work
$[Co(H_2O)_6]_2V_2W_4O_{19}$ (**2**)	2.069(6) min 2.161(8) max	This work
$[Co(H_2O)_6](CH_3C_6H_4SO_3)_2$	2.0529(14) min 2.0810(16) max	[36]

Table 5
Selected bond distances (in Å) for $Co(H_2O)_6K_2V_2W_4O_{19}$ (**1**)

Atom–oxygen bonds	
W1≡V3–O5	2.282
–O6	1.906
–O7	1.916
–O11	1.668
W2≡V4–O5	2.294
–O7	1.913
–O8	1.939
–O9	1.896
–O10	1.677
Co13–O14	2.189
–O15	2.208
–O16	2.085
–O17	1.963
K12–O10	2.845
–O6	2.827

Table 4
Atomic parameters for $Co(H_2O)_6K_2V_2W_4O_{19}$ (**1**)

Element	Symbol	Label	Mult.	Wyckoff	*x*	*y*	*z*	Occ.
W	W1		8	f	0	0.35780(1)	0.58358(1)	0.667
V	V3		8	f	0	0.64219(1)	0.41639(1)	0.333
W	W2		16	h	0.13795(2)	0.43112(2)	0.41176(2)	0.667
V	V4		16	h	0.13796(2)	0.43118(2)	0.41173(2)	0.333
O	O5	O_c	4	b	0	0.5	0.5	1
O	O6	O_b	16	h	0.1128(7)	0.4394(6)	0.6394(5)	1
O	O7	O_b	16	h	0.1124(6)	0.3280(5)	0.4965(5)	1
O	O8	O_b	8	e	0.2271(7)	0.5	0.5	1
O	O9	O_b	8	f	0	0.3889(7)	0.3575(6)	1
O	O10	O_t	16	h	0.2398(8)	0.3788(5)	0.3493(5)	1
O	O11	O_t	8	f	0	0.2539(8)	0.6447(7)	1
K	K12		8	g	0.2772(3)	0.2007(2)	0.25	1
Co	Co13		8	f	0	0.0822(3)	0.3414(3)	0.500
O	O14	O_w	8	g	0.1277(10)	0.0239(9)	0.25	1
O	O15	O_w	4	c	0	0.2106(15)	0.25	1
O	O16	O_w	16	h	−0.1337(10)	0.1478(9)	0.4115(7)	0.500
O	O17	O_w	8	f	0	−0.0456(18)	0.4059(14)	0.500

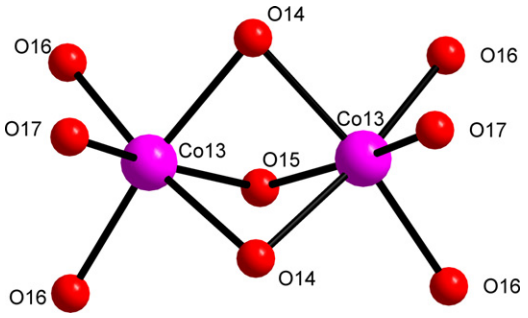

Fig. 1. Dimeric face-sharing cobalt octahedra in **1** with 50% occupancy on each position.

The resulting network generates large one-dimensional channels with cross sectional area of 8.5 × 6.3 Å^2 along *c*-axis, in which are located the cobalt octahedra $Co(H_2O)_6^{2+}$. These channels constitute ca. 70% of unit cell volume.

*3.3.1.2. Crystal structure description of $[Co(H_2O)_6]_2V_2W_4O_{19}$ (**2**).* The high symmetry of the space group $R\bar{3}m$ in which crystallizes the compound **2** reduces to eight the number of independent non-hydrogen atoms in the asymmetric unit. The polyoxoanion $V_2W_4O_{19}^{4-}$ is generated by five atoms: one metallic atom (2/3 W and 1/3 V) and four oxygen atoms (1 O_c, 2 O_b and 1 O_t). The cobalt octahedron $Co(H_2O)_6^{2+}$ is represented by cobalt and two oxygen atoms (water oxygen).

The basic motif of **2** consists of one $V_2W_4O_{19}^{4-}$ and two $Co(H_2O)_6^{2+}$ forming neutral molecules. The isopolyanion and cobalt octahedra are arranged alternately with their faces parallel to each other. Crystal structure of **2** can be described by the pillar packing of $[Co(H_2O)_6]_2V_2W_4O_{19}$ along the *c*-axis. The spacing distance between $[Co(H_2O)_6]_2V_2W_4O_{19}$ entities along *c*-axis is ca. 4 Å, (Fig. 4). Cohesion of the pillar structure is ensured by electrostatic forces and hydrogen bonds as discussed below. The atomic parameters and selected bonds are reported in Tables 6 and 7.

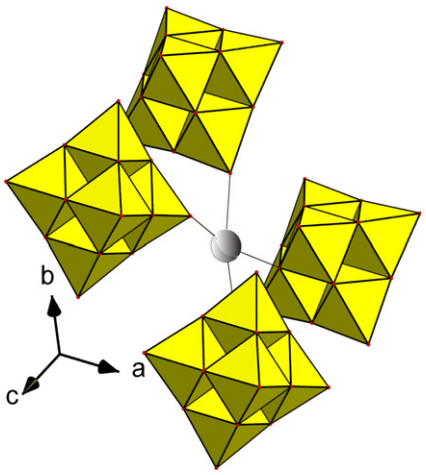

Fig. 3. Coordination of the potassium cation in **1**.

The anisotropic displacement and the full refinement data are available as supplementary materials.

3.4. Face-to-face interaction

For both compounds hydrogen bonds ensure the cohesion between $V_2W_4O_{19}^{4-}$ faces and those of $[Co(H_2O)_6]^{2+}$ octahedra. Hydrogen bond lengths O···O between the oxygen atoms of the V_2W_4 cluster, and water molecules coordinated to cobalt vary between 2.70 and 2.90 Å. The triangular contacting faces for both title compounds are nearly parallel to each other with an angular shift of 0.81° and 0.51°, respectively for **1** and **2** (Fig. 5).

4. Conclusion

The reaction of $V_2W_4O_{19}^{4-}$ with $[Co(H_2O)_6]^{2+}$ in aqueous solution at adequate pH results in complexes $Co(H_2O)_6K_2V_2W_4O_{19}$ (**1**)

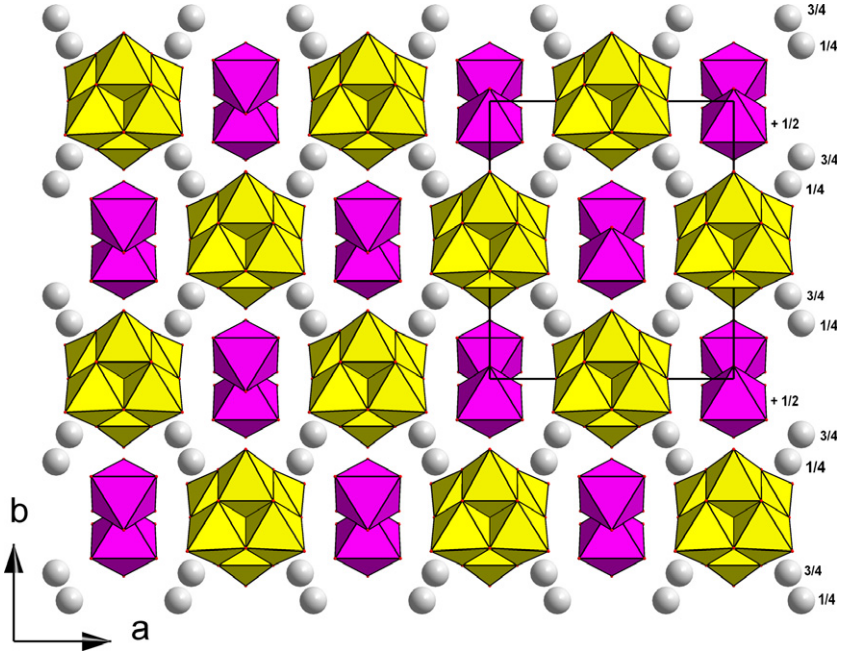

Fig. 2. Structure of **1**: view down *c*-axis. $V_2W_4O_{19}$: yellow, K: light grey and $Co(H_2O)_6$: purple. (For interpretation of the references to colour in this figure legend, the reader is referred to the web version of this article.)

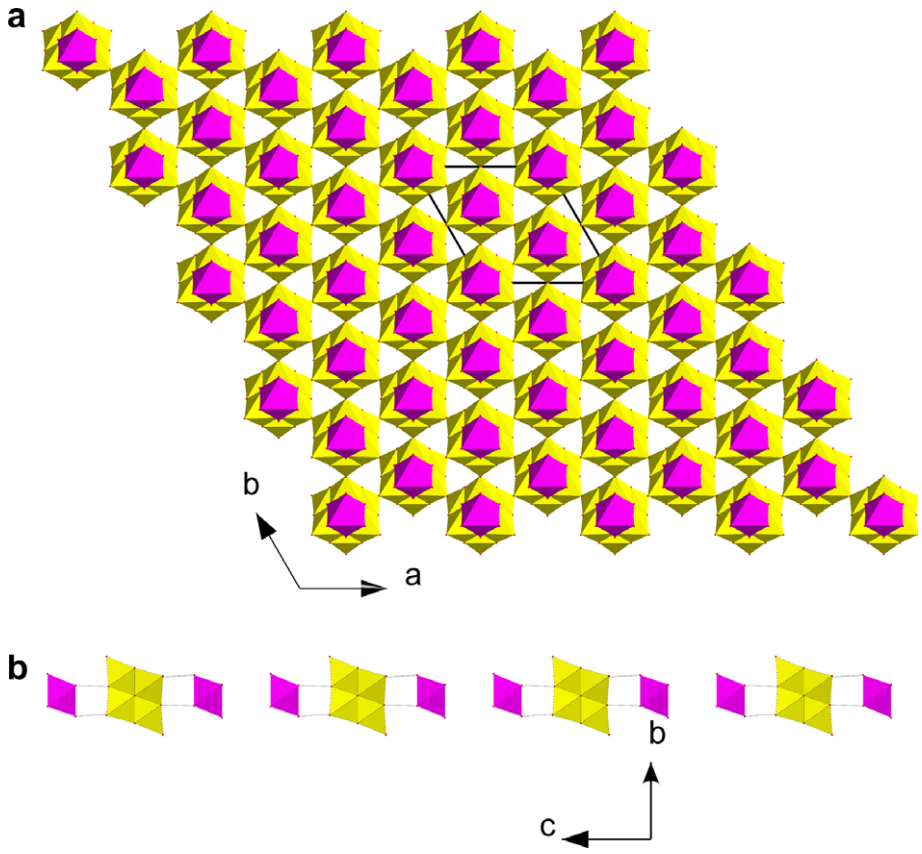

Fig. 4. Structure of **2**: (a) view down *c*-axis, (b) pillar along *c*-axis. $V_2W_4O_{19}$: yellow, $Co(H_2O)_6$: purple. (For interpretation of the references to colour in this figure legend, the reader is referred to the web version of this article.)

Table 6
Atomic parameters for $[Co(H_2O)_6]_2V_2W_4O_{19}$ (**2**)

Element	Symbol	Label	Mult.	Wyckoff	*x*	*y*	*z*	Occ.
W	W1		18	h	0.76572(4)	0.53147(4)	0.40571(4)	0.667
V	V1		18	h	0.76572(4)	0.53147(4)	0.40571(4)	0.333
O	O1	O_c	3	a	0.66670	0.33330	0.33330	1
O	O2	O_b	18	h	0.5867(3)	0.4133(3)	0.4509(2)	1
O	O3	O_b	18	f	0.66670	0.5723(4)	0.33330	1
O	O6	O_t	18	h	0.8360(3)	0.6721(6)	0.4595(3)	1
Co	Co1		6	c	1.33330	0.66670	0.33827(8)	1
O	O4	O_w	18	h	1.4226(3)	0.5774(3)	0.4011(3)	1
O	O5	O_w	18	h	1.5235(12)	0.7617(6)	0.2755(5)	1

Table 7
Selected bond distances (in Å) for $[Co(H_2O)_6]_2V_2W_4O_{19}$ (**2**)

Atom–oxygen bonds	
W1≡V1–O1	2.324
–O2	1.936
–O3	1.921
–O6	1.675
Co1–O5	2.162
–O4	2.069

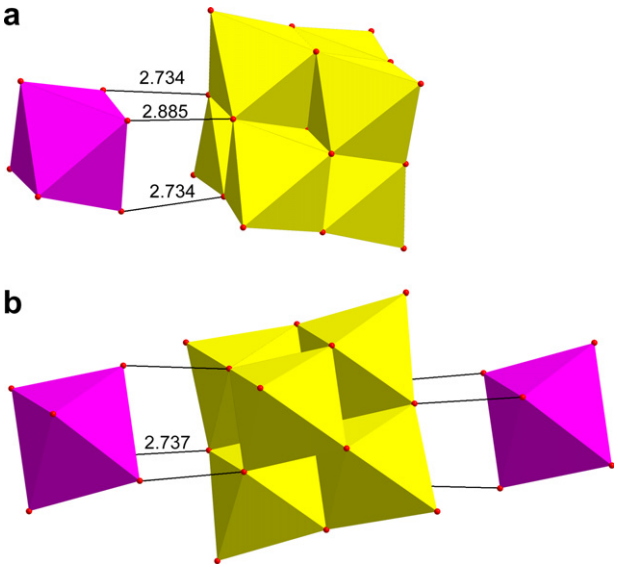

Fig. 5. Face-to-face interactions through hydrogen bonds: (a) for compound **1**, (b) for compound **2**. $V_2W_4O_{19}$: yellow, $Co(H_2O)_6$: purple. (For interpretation of the references to colour in this figure legend, the reader is referred to the web version of this article.)

and $[Co(H_2O)_6]_2V_2W_4O_{19}$ (**2**). Both compounds represent ionic species with direct interactions via hydrogen bonds and electrostatic interactions between the oxygen atoms of the isopolyanion and the hexa-aquo-cobalt(II) cation. According to the X-ray data, the clusters of $V_2W_4O_{19}^{4-}$ and $[Co(H_2O)_6]^{2+}$ octahedra are arranged alternately and have their faces parallel to each other. The structure of **1** shows a large one-dimensional channels with cross sectional area of 8.5×6.3 Å^2 along *c*-axis, in which are located the cobalt octahedra $Co(H_2O)_6^{2+}$. These channels constitute ca. 70% of unit cell volume. Structure of compound **2** represents a compact building block of pillar-shaped neutral molecules of

$[Co(H_2O)_6]_2V_2W_4O_{19}$. These structures show the influences of the local interactions such as hydrogen bonds and electrostatic interactions, on the disposition and the relative orientation of the different ionic entities constituting the crystal.

Acknowledgements

We greatly acknowledge financial support from the Direction Générale de la Recherche Scientifique et Technique (Tunisia), the Centre National de la Recherche Scientifique (France) and the Comité Mixte pour la Coopération Universitaire (CMCU program 05G1211). We are also grateful to Prof. A. Driss (Laboratoire de Cristallochimie, Faculté des Sciences de Tunis) for crystal data collection of **1** and for his assistance in structure resolution and P. Herson (Laboratoire de Chimie Inorganique et Matériaux Moléculaires, Université Pierre & Marie Curie) for data collection of **2**.

Supplementary data

Further details of the crystal structure investigations can be obtained from the Fachinformationszentrum Karlsruhe, 76344 Eggenstein-Leopoldshafen, Germany, (fax: (49) 7247-808-666; e-mail: crysdata@fiz-karlsruhe.de) on quoting the depository number CSD 418652 and 418653 for **1** and **2** respectively. Supplementary data associated with this article can be found, in the online version, at doi:10.1016/j.poly.2008.03.020.

References

[1] D.M. Gould, W.P. Griffith, M. Spiro, J. Mol. Catal. A: Chem. 175 (2001) 289.
[2] A. Yoshida, S. Hikichi, N. Mizuno, J. Organomet. Chem. 692 (2007) 455.
[3] O.A. Kholdeeva, T.A. Trubitsina, M.N. Timofeeva, G.M. Maksimov, R.I. Maksimovskaya, V.A. Rogov, J. Mol. Catal. A: Chem. 232 (2005) 173.
[4] N. Mizuno, M. Misono, Chem. Rev. 98 (1998) 199.
[5] J. Li, R. Tan, R. Li, X. Wang, E. Li, F. Zhai, S. Zhang, Inorg. Chem. Commun. 10 (2007) 216.
[6] J.T. Rhule, C.L. Hill, D.A. Judd, R.F. Schinazi, Chem. Rev. 98 (1998) 327.
[7] F. Chai, L. Wang, L. Xu, X. Wang, J. Huang, Dyes Pigments 76 (2008) 113.
[8] T. Akutagawa, D. Endo, S.-I. Noro, L. Cronin, T. Nakamura, Coord. Chem. Rev. 251 (2007) 2547.
[9] G. Yang, H. Guo, M. Wang, M. Huang, H. Chen, B. Liu, S. Dong, J. Electroanal. Chem. 600 (2007) 318.
[10] R. Finkener, Ber. Dtsch. Chem. Ges. 11 (1878) 1638.
[11] A. Rosenheim, H. Jahn, Ber. Dtsch. Chem. Ges. 26 (1893) 1191.
[12] F. Carl, Z. Anorg. Chem. 6 (1894) 11.
[13] F. Carl, Z. Anorg. Chem. 6 (1894) 27.
[14] P. Wilhelm, Z. Anorg. Allg. Chem. 92 (1915) 198.
[15] F. Chauveau, P. Souchay, Bull. Soc. Chim. (France) 3 (1963) 561.
[16] C.M. Flynn, M.T. Pope, Inorg. Chem. 10 (1971) 2524.
[17] C.M. Flynn, M.T. Pope, Inorg. Chem. 12 (1973) 1626.
[18] R. Thouvenot, Doctoral Dissertation, Université Pierre et Marie Curie, Paris, 1978.
[19] M. Dabbabi, M. Boyer, J. Inorg. Nucl. Chem. 38 (1976) 1011.
[20] C.M. Flynn Jr., M.T. Pope, Inorg. Chem. 10 (1971) 2745.
[21] M.C.K. Franca, J.G. Eon, M. Fournier, E. Payen, O. Mentre, Solid State Sci. 7 (2005) 1533.
[22] J.H. Son, Y.U. Kwon, Inorg. Chem. 43 (2004) 1929.
[23] A.J.M. Duisenberg, J. Appl. Crystallogr. 25 (1992) 92.
[24] J. Macicek, A. Yordanov, J. Appl. Crystallogr. 25 (1992) 73.
[25] G.M. Sheldrick, SHELXS86: Program for the Solution of Crystal Structure, University of Göttingen, Germany, 1986.
[26] P.W. Betteridge, J.R. Carruthers, R.I. Cooper, K. Prout, D.J. Watkin, J. Appl. Crystallogr. 36 (2003) 1487.
[27] K. Brandenburg, DIAMOND V2.0; Gerhard-Domagk-Straβe 1, 53121 Bonn, Germany, 1998.
[28] K. Nishikawa, A. Kobayashi, Y. Sasaki, Bull. Chem. Soc. Jpn. 48 (1975) 889.
[29] R.F. Klevtsova, E.N. Yurchenko, L.A. Glinskaya, L.I. Kuznetsova, L.G. Detusheva, T.P. Lazarenko, J. Struct. Chem. 32 (1992) 538.
[30] J. Fuchs, W. Freiwald, H. Hartl, Acta Crystallogr. (1978) 1764.
[31] I. Lindqvist, Ark. Kemi. 5 (1953) 247.
[32] I. Lindqvist, B. Aronsson, Ark. Kemi. 7 (1954) 49.
[33] H.R. Allcock, E.C. Bissell, E.T. Shawl, Inorg. Chem. 12 (1973) 2963.
[34] F. Bannani, H. Driss, R. Thouvenot, M. Debbabi, J. Chem. Crystallogr. 37 (2007) 37.
[35] A.S. Wills, I.D. Brown, VALIST, CEA, France, 1999.
[36] S. Cabaleiro-Martinez, J. Castro, J. Romero, J.A. Garcia-Vazquez, A. Sousa, Acta Crystallogr., Sect. C: Cryst. Struct. Commun. 56 (2000) e249.

Polyhedron 27 (2008) 2065–2068

Contents lists available at ScienceDirect

Polyhedron

journal homepage: www.elsevier.com/locate/poly

Unusual coordination geometries of silver(I) 4,5-diazafluoren-9-one complexes

A.R. Biju, M.V. Rajasekharan *

School of Chemistry, University of Hyderabad, Hyderabad 500 046, India

ARTICLE INFO

Article history:
Received 12 March 2008
Accepted 28 March 2008
Available online 10 May 2008

Keywords:
Silver
Dafone
Planar silver complex
Interpenetration
Geometry optimization

ABSTRACT

Two complexes of silver(I) with 4,5-diazafluoren-9-one (dafone) which are the first examples of Ag-dafone complexes were synthesized and structurally characterized. Crystals of $[Ag(dafone)_2]NO_3 \cdot H_2O$ (**1**) contain two strictly planar four-coordinate Ag(I) complexes. The silver coordination polyhedron in $[Ag_2(4,4'\text{-bpy})(dafone)_4]BF_4$ (**2**) is a highly distorted tetrahedron. Its crystal structure is built by a two-fold interpenetration of identical porous networks. The unusual coordination in the two compounds (planar four-coordinate d^{10} ion in **1**, chelation with two long Ag–N bonds in **2** and low bond valence sums in both complexes) is in part due to the large chelate bite of dafone, and in part due to the stacking and other intermolecular interactions influencing the coordination geometry of Ag(I). This was further probed through molecular simulation of $[Ag(N\text{–}N)_2]^+$ complexes using DFT calculations.

© 2008 Elsevier Ltd. All rights reserved.

1. Introduction

4,5-Diazafluoren-9-one (dafone) is a derivative of 1,10-phenanthroline (phen), having an exocyclic keto function [1]. Even though silver(I) complexes of other diimine ligands like 2,2′-biyridine (bpy) and phen are known [2–6], little is known about the dafone complexes. Silver, due to its d^{10} configuration has no electronically imposed preference for any particular coordination geometry. The observed stereochemistry and crystal structures are influenced by several factors like steric interactions between ligands, π–π stacking interaction between aromatic rings, Ag ... Ag interactions and counter anions [7,8]. Recent reports of silver(I) complexes of derivatives of bpy and pyridine ligands further substantiate the above factors [2,9]. Unlike phen and bpy, dafone has a large N–N bite distance (2.99 Å) enforced by the rigid five-membered centre ring, which makes it unique among the diimine ligands [10]. In order to explore the effect of the geometry of dafone on silver coordination, we have synthesized two complexes of silver(I) with dafone having nitrate and tetraflouroborate anions.

2. Experimental

2.1. Materials and physical measurements

All chemicals were of reagent grade obtained from commercial sources and were used without further purification. Dafone was prepared using a reported procedure [1]. IR spectra were recorded using KBr discs on a Jasco FT/IR 5300 spectrometer in the range 4000–400 cm^{-1}. Elemental analysis for C, H and N was performed on a Perkin–Elmer 240C elemental analyzer.

2.2. Synthesis

2.2.1. Synthesis of $[Ag(dafone)_2]NO_3 \cdot H_2O$ (*1*)

Dafone (0.181 g, 1.00 mmol) dissolved in acetonitrile (15 mL) was added to an aqueous solution (15 mL) of $AgNO_3$ (0.085 g, 0.50 mmol), with constant stirring. It was filtered and kept for crystallization at room temperature to yield yellow needle shaped crystals suitable for X-ray data collection. Yield 0.250 g, (0.453 mmol, 90%). *Anal.* Calc. for $C_{22}H_{14}AgN_5O_6$ (M.W. 552.25 g): C, 47.85; H, 2.56; N, 12.68. Found: C, 47.72; H, 2.52; N, 12.93%. Important IR absorptions (KBr disk, cm^{-1}): 3576, 3425, 3034, 1834, 1718, 1593, 1462, 1259, 916 and 758.

2.2.2. Synthesis of $[Ag_2(4,4'\text{-bipyridine})(dafone)_4](BF_4)_2$ (*2*)

4,4′-Bipyridine (0.039 g, 0.25 mmol) and dafone (0.181 g, 1.00 mmol) were dissolved in acetonitrile (20 mL) and slowly added to an acetonitrile solution (10 mL) of $AgBF_4$ (0.098 g, 0.50 mmol) while stirring. It was filtered and kept for crystallization at room temperature to yield yellow block shaped crystals. Yield 0.295 g (0.232 mmol, 93%). *Anal.* Calc. for $C_{54}H_{32}Ag_2B_2F_8N_{10}O_4$ (M.W. 1274.25 g): C, 50.90; H, 2.53; N, 10.99. Found: C, 50.84; H, 2.58; N, 10.73%. Important IR absorptions (KBr disk, cm^{-1}): 3097, 1728, 1593, 1566, 1464, 1406, 1259, 1055, and 758.

2.3. X-ray crystallography

X-ray data were collected on a Bruker SMART APEX CCD X-ray diffractometer, using graphite-monochromated Mo Kα radiation

* Corresponding author. Tel.: +91 40 23134857; fax: +91 40 23012460.
E-mail address: mvrsc@uohyd.ernet.in (M.V. Rajasekharan).

0277-5387/$ - see front matter © 2008 Elsevier Ltd. All rights reserved.
doi:10.1016/j.poly.2008.03.025

(λ = 0.71073 Å) at 298 K. Data were reduced using SAINTPLUS [11] and a multi-scan absorption correction using SADABS [12] was performed. The structures were solved by direct method using SHELXS-97 and full-matrix least-square refinement was carried out using SHELXL-97 [13]. All ring hydrogen atoms were assigned on the basis of geometrical considerations and were allowed to ride upon the respective carbon atoms. Hydrogen atoms on the water molecules were located from the difference maps and geometrical constraints were applied. Drawings were made using ORTEP3 for windows [14] and Mercury [15]. Crystallographic data are in Tables 1 and 2.

2.4. Computational details

DFT calculations were done by using B3LYP [16] exchange correlation function as implimented in the GUASSIAN-03 [17]. Ag(I) ion was described with the LANL2DZ basis set, including effective core potential, whereas 6-31G(d) basis set was used for C, N, O and H atoms.

3. Results and discussion

3.1. Structure of [Ag(dafone)$_2$]NO$_3$ · H$_2$O (**1**)

There are two crystallographically independent, but chemically similar Ag(dafone)$_2^+$ cations in the unit cell of **1** (Fig. 1). Each four-coordinate silver atom is situated on a crystallographic inversion centre. The coordination is, therefore, strictly planar even though the dafone ligands deviate slightly (4.3° Ag(1); 5.2° Ag(2)) from the AgN4 plane. There is a large asymmetry in the chelating bond distances of dafone with two short and two long bonds (2.22 and 2.69 Å for Ag(1); 2.25 and 2.65 Å for Ag(2)). Most previously reported [Ag(N–N)$_2$]$^+$ complexes are near-symmetric chelates exhibiting a flattened tetrahedral coordination with dihedral angles in the range 18–80° [2–6,18–25]. The two complex cations in **1** inter-

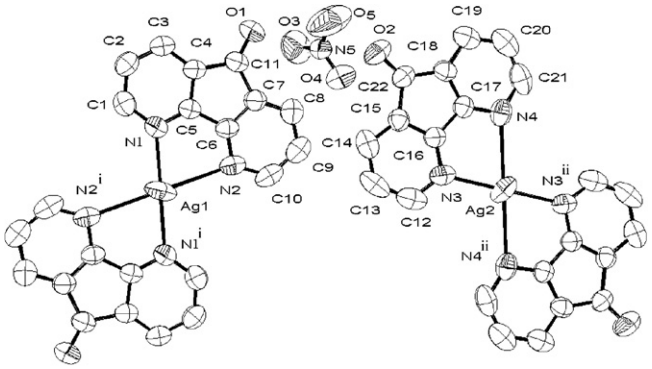

Fig. 1. ORTEP view of the two crystallographically independent complex cations and the nitrate anion of compound**1**. Atoms are represented as 50% probability ellipsoids and ring hydrogen atoms have been omitted for clarity. [Symmetry code: (i) $-x+1, -y+2, z+1$. (ii) $-x, -y, -z+1$.]

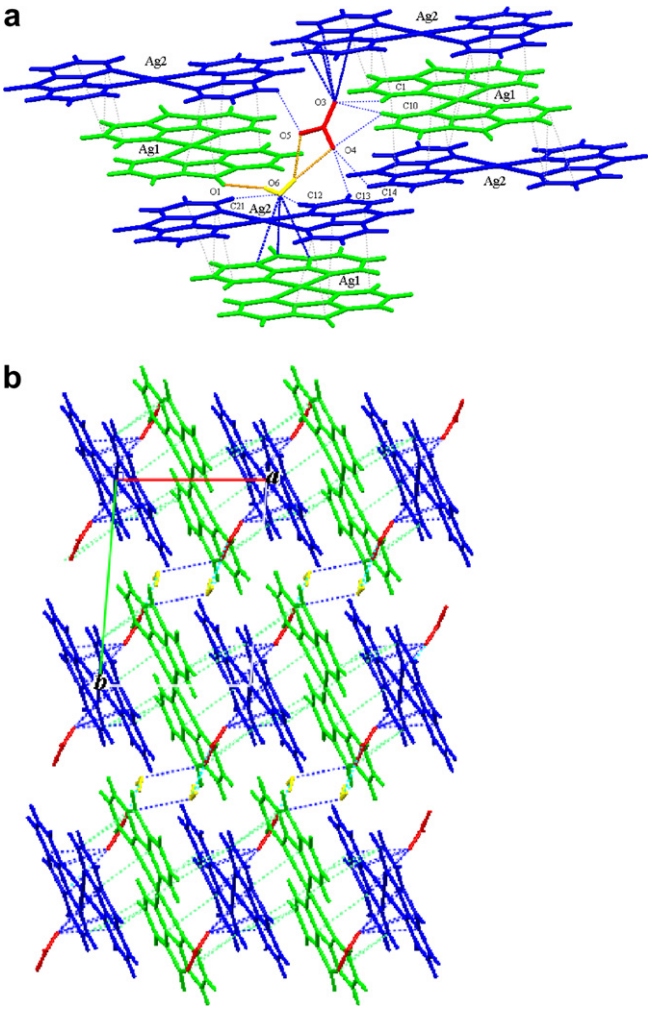

Fig. 2. (a) Weak interactions involving the complex cations, anion and lattice water in **1**. (b) A view of the crystal packing in the *ab*-plane.

Table 1
Crystal data and structure refinement for compounds **1** and **2**

	1	**2**
Formula	$C_{22}H_{14}AgN_5O_6$	$C_{54}H_{32}Ag_2B_2F_8N_{10}O_4$
Formula weight	552.25	1274.26
Crystal system	triclinic	triclinic
a (Å)	7.5988(9)	8.8909(14)
b (Å)	11.4730(13)	10.2543(17)
c (Å)	13.2265(15)	14.229(2)
α (°)	114.849(2)	91.856(2)
β (°)	90.815(2)	101.272(2)
γ (°)	93.866(2)	107.774(2)
V (Å^3)	1042.8(2)	1205.6(3)
Z	2	1
D_{calc} (g cm^{-3})	1.759	1.755
Space group	$P\bar{1}$	$P\bar{1}$
μ (mm^{-1})	1.019	0.905
Crystal size (mm)	0.40 × 0.20 × 0.06	0.32 × 0.24 × 0.14
θ Range for data collection (°)	1.70–26.05	1.47–26.07
Reflection collected, completeness (%)	10950, 99.2	12608, 99.5
Unique reflections, R_{int}, parameters	4100, 0.0213, 318	4747, 0.0175, 361
Goodness-of-fit on F^2	1.030	1.042
$R(F_o^2)$ [$I > 2\sigma(I)$]	0.0427	0.0319
$wR(F_o^2)$ [$I > 2\sigma(I)$]	0.1027	0.0839

Table 2
Selected bond lengths (Å) and angles (°)

*[Ag(dafone)$_2$]NO$_3$ · H$_2$O (**1**)*			
Ag(1)–N(1)	2.222(3)	Ag(2)–N(4)	2.650(3)
Ag(1)–N(2)	2.695(3)	N(1)–Ag(1)–(N2)	74.59(9)
Ag(2)–N(3)	2.254(3)	N(3)–Ag(2)–N(4)	75.01(9)
*[Ag$_2$(4,4′-bipyridine)(dafone)$_4$](BF$_4$)$_2$ (**2**)*			
Ag–N(1)	2.2464(19)	N(5)–Ag–N(3)	109.97(7)
Ag–N(5)	2.2433(19)	N(5)–Ag–N(4)	85.80(7)
Ag–N(3)	2.593(2)	N(1)–Ag–N(3)	92.97(7)
Ag–N(4)	2.644(2)	N(1)–Ag–N(4)	122.61(6)
N(5)–Ag–N(1)	148.87(7)	N(3)–Ag–N(4)	70.45(6)

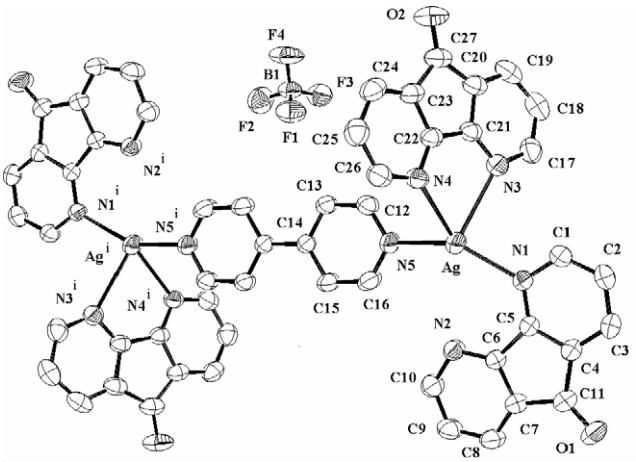

Fig. 3. ORTEP view of the dinuclear cation and anion in compound **2**. Atoms are represented as 50% probability ellipsoids and ring hydrogen atoms have been omitted for clarity. [Symmetry code: (i) $-x+1, -y+1, -z+1$.]

act through π-stacking (3.36–3.50 Å) leading to an interdigitized packing. The nitrate ion and the lattice water molecule participate in H-bonding (O–H···O, C–H···O) and O···π interactions (Fig. 2).

As early as 1986, Goodwin et al. [26] after considering electronic as well as steric factors, concluded that the flattening distortion in bis-chelate complexes of Ag(I) with hetero-aromatic ligands is imposed by π-stacking interactions in the lattice. The wide range of the observed torsion angles reveal that there is considerable plasticity in the coordination polyhedron of this class of four-coordinate Ag(I) complexes. Compound **1**, represents the extreme situation of perfect planarity. However, it should be noted that the flattening is accompanied by a highly unsymmetrical (to the extent of 15–20%) chelate bonds. Further, Ag(I) in this compound has an abnormally low bond valence sum [27] of 0.78–0.81 (expected value 1.0). Other complexes, for example $Ag(bpy)_2^+$, typically have a bond valence sum of 0.98. It appears that the relatively weak metal–ligand interaction is compensated by intermolecular interactions, especially π-stacking. The dominant role of lattice interactions in controlling the coordination geometry of Ag(I) complexes has been previously noted [28].

3.2. Structure of $[Ag_2(4,4'\text{-bipyridine})(dafone)_4](BF_4)_2$ (**2**)

The cation in **2** is dinuclear with a crystallographic inversion centre (Fig. 3). The coordination polyhedron at each silver atom is a highly distorted tetrahedron with two short (2.24 and 2.25 Å), and two long (2.59 and 2.64 Å) bonds. Of the two-coordinated dafone molecules, one forms a single short bond, while the other forms 2-weak chelating bonds. The fourth coordination position of each silver atom is occupied by a nitrogen atom of the bridging 4,4′-bipyridine. The cations are assembled into porous two-dimensional sheets by C–H···F and C–H···O interactions. However, the pores are blocked by the two-fold interpenetration of identical networks with the adjacent networks connected by π···π stacking (3.30–3.48 Å) interactions (Fig. 4). Compound **2** further illustrates the weakness of Ag-dafone interaction. The chelating dafone in this complex presents the unusual picture of two long Ag–N bonds, while the singly bonded dafone forms a normal Ag–N bond. Even in this compound, the bond valence sum is only 0.82.

3.3. Geometry optimizations

Geometry optimization using DFT for $[Ag(N\text{-}N)_2]^+$ ion, with N–N = bpy, phen, or dafone, resulted in a tetrahedral structure for all the three complexes with the following bond distances (Å) and dihedral angles (°): bpy, 2.38, 87.6; phen, 2.39, 90.0; dafone, 2.41–2.52, 89.8. The optimized bond distances for the bpy and phen complexes are within 0.14 Å of the crystallographic values (CSD REFCODE for the bpy complex MAYCIZ; for the phen complex IGULOL01). However, the dihedral angles in the crystal structures are 39.5° in both structures, corresponding to flattened tetrahedral coordination. There are also local minima in the case of dafone, within about 0.2 eV, in which the complex ion is planar or nearly planar with two short and two long bonds. However, the long

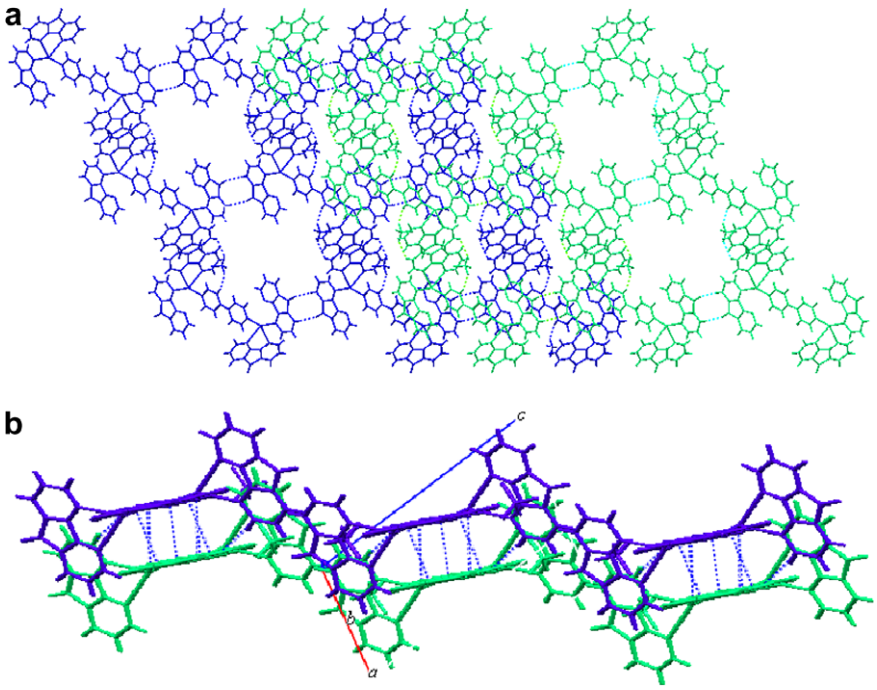

Fig. 4. (a) Two-fold interpenetrating layers of **2** viewed in the *bc*-plane. (b) Side view showing stacking interactions between the interpenetrating layers.

bonds were so long (2.8 Å) that the complex is actually two-coordinate. It may be recalled that bis-chelates with *trans*-geometry having four short bonds are not possible for these ligands due to α-hydrogen strain (bulk effect). In summary, the simulations show that the "gas-phase" ion will have a regular tetrahedral geometry for all the three ligands even though in the case of dafone the Ag–N bond distances will be considerably longer compared to bpy or phen. Therefore, the flattened structures observed in crystals must be due to lattice effects.

4. Conclusion

Like in the case of $Cu(dafone)_2X_2$ [10] complexes, dafone prefers a *trans* bis-chelate configuration with two short and two long bonds in $[Ag(dafone)_2]^+$. If it is the Jahn–Teller effect which uses the unfavorable chelate bite as a handle to distort the molecular structure in the case of Cu(II), it is the intermolecular interaction in the crystal lattice which plays this role for Ag(I). The above silver(I) complex ion is perfectly planar in the crystal though the coordination plane is far from square. A recent review [29] on "square planar" silver(I) complexes lists about 65 such complexes which form about 2% of the crystallographically characterized silver(I) complexes. Even this small number includes those whose coordination is best described as planar [2 + 2] as well as those in which a significant tetrahedral distortion and/or distant axial interactions are present. As stated in the above review, while square planar complexes will be sought after for use as four-connected nodes or secondary building blocks for the design of silver(I) coordination networks, there is no simple way to predict the precise circumstances that will lead to a square planar geometry.

Dafone forms much weaker bonds with silver compared to bpy or phen, so much so that in mixed ligand complexes it may even act as a mono-dentate ligand or as a weak chelating ligand. Even though the mono-dentate mode and the asymmetric chelating mode have been observed in many other complexes [10,30–37] with different metal ions, the weak chelate with two long bonds seen in the crystals of **2** is unusual.

Acknowledgements

We thank a referee for bringing to our notice a recent review on square planar silver(I) complexes. This work was supported by CSIR, India. A.R.B thanks UGC for a research fellowship. Infrastructure support from UGC (UPE program) and DST (X-ray diffractometer facility) is also acknowledged. The DFT calculations were performed using the CMSD facility.

Appendix A. Supplementary data

CCDC 668064 and 668065 contain the supplementary crystallographic data for **1** and **2**. These data can be obtained free of charge via http://www.ccdc.cam.ac.uk/conts/retrieving.html, or from the Cambridge Crystallographic Data Centre, 12 Union Road, Cambridge CB2 1EZ, UK; fax: (+44) 1223-336-033; or e-mail: deposit@ccdc.cam.ac.uk. Supplementary data associated with this article can be found, in the online version, at doi:10.1016/j.poly.2008.03.025.

References

[1] L.J. Henderson Jr., F.R. Fronczek, W.R. Cherry, J. Am. Chem. Soc. 106 (1984) 5876.
[2] G.A. Bowmaker, Effendy, S. Marfuah, B.W. Skelton, A.H. White, Inorg. Chim. Acta 358 (2005) 4371.
[3] P.-G. Li, Q.-L. Wang, D.-S. Li, F. Fu, G.-C. Qi, Z. Kristallogr. New Cryst. Struct. 221 (2006) 391.
[4] J.L. Atwood, M.L. Simms, D.A. Zatko, Cryst. Struct. Commun. 2 (1973) 279.
[5] M. Leschke, G. Rheinwald, H. Lang, Z. Anorg. Allg. Chem. 628 (2002) 2470.
[6] S.E. Paramonov, N.P. Kuzmina, S.I. Troyanov, Polyhedron 22 (2003) 837.
[7] S. Sailaja, M.V. Rajasekharan, Inorg. Chem. 42 (2003) 5675.
[8] S. Sailaja, M.V. Rajasekharan, Inorg. Chem. 39 (2000) 4586.
[9] E.C. Constable, C.E. Housecroft, B.M. Kariuki, C.B. Smith, Aust. J. Chem. 59 (2006) 30.
[10] S. Menon, M.V. Rajasekharan, Polyhedron 17 (1998) 2463.
[11] SAINTPLUS, Bruker AXS Inc., Madison, Wisconsin, USA, 2003.
[12] G.M. Sheldrick, SADABS, Program for Empirical Absorption Correction, University of Gottingen, Gottingen, Germany, 1996.
[13] M. Sheldrick, SHELX-97, Programs for Crystal Structure Analysis, University of Gottingen, Gottingen, Germany, 1997.
[14] L.J. Farrugia, J. Appl. Crystallogr. 30 (1997) 565.
[15] C.F. Macrae, P.R. Edgington, P. McCabe, E. Pidcock, G.P. Shields, R. Taylor, M. Towler, J. van de Streek, J. Appl. Crystallogr. 39 (2006) 453.
[16] A.D. Becke, J. Chem. Phys. 98 (1993) 5648.
[17] M.J. Frisch, G.W. Trucks, H.B. Schlegel, G.E. Scuseria, M.A. Robb, J.R.Cheeseman, J.A. Montgomery Jr., T. Vreven, K.N. Kudin, J.C. Burant, J.M. Millam, S.S. Iyengar, J. Tomasi, V. Barone, B. Mennucci, M. Cossi, G. Scalmani, N. Rega, G.A. Petersson, H. Nakatsuji, M. Hada, M. Ehara, K. Toyota, R. Fukuda, J. Hasegawa, M. Ishida, T. Nakajima, Y. Honda, O. Kitao, H. Nakai, M. Klene, X. Li, J.E. Knox, H.P. Hratchian, J.B. Cross, C. Adamo, J. Jaramillo, R. Gomperts, R.E. Stratmann, O. Yazyev, A.J. Austin, R. Cammi, C. Pomelli, J.W. Ochterski, P.Y. Ayala, K. Morokuma, G.A. Voth, P. Salvador, J.J. Dannenberg, V.G. Zakrzewski, S. Dapprich, A.D. Daniels, M.C. Strain, O. Farkas, D.K. Malick, A.D. Rabuck, K. Raghavachari, J.B. Foresman, J.V. Ortiz, Q. Cui, A.G. Baboul, S. Clifford, J. Cioslowski, B.B. Stefanov, G. Liu, A. Liashenko, P. Piskorz, I. Komaromi, R.L. Martin, D.J. Fox, T. Keith, M.A. Al-Laham, C.Y. Peng, A. Nanayakkara, M. Challacombe, P.M.W. Gill, B. Johnson, W. Chen, M.W. Wong, C. Gonzalez, J.A. Pople, GAUSSIAN 03, Revision B.05, Gaussian Inc., Pittsburgh PA, USA, 2003.
[18] M.D. Stephenson, M.J. Hardie, Cryst. Growth Des. 6 (2006) 423.
[19] P.R. Ashton, V. Balzani, A. Credi, O. Kocian, D. Pasini, L. Prodi, N. Spencer, J.F. Stoddart, M.S. Tolley, M. Venturi, A.J.P. White, D.J. Williams, Chem. Eur. J. 4 (1998) 590.
[20] A.J. Pallenberg, T.M. Marschner, D.M. Barnhart, Polyhedron 16 (1997) 2711.
[21] C. Titze, W. Kaim, S. Zalis, Inorg. Chem. 36 (1997) 2505.
[22] H.-P. Wu, C. Janiak, G. Rheinwald, H. Lang, J. Chem. Soc., Dalton Trans. (1999) 183.
[23] M. Wen, E. Kejia, M. Munakata, Y. Suenaga, T.K. Sowa, M. Maekawa, S.G. Yan, Mol. Cryst. Liq. Cryst. Sci. Technol., Sect. A 457 (2006) 203.
[24] E.C. Constable, C.E. Housecroft, M. Neuburger, I. Poleschak, M. Zehnder, Polyhedron 22 (2003) 93.
[25] M.D. Ward, S.M. Couchman, J.C. Jeffery, Acta Crystallogr. C 54 (1998) 1820.
[26] K.V. Goodwin, D.R. McMillin, W.R. Robinson, Inorg. Chem. 25 (1986) 2033.
[27] M. O'Keeffe, N.E. Brese, J. Am. Chem. Soc. 113 (1991) 3226.
[28] G. Swarnabala, M.V. Rajasekharan, Polyhedron 15 (1996) 3197.
[29] A.G. Young, L.R. Handon, Coord. Chem. Rev. (2007), doi:10.1016/j.ccr.2007.07.017.
[30] C. Balagopalakrishna, M.V. Rajasekharan, S. Bott, J.L. Atwood, B.L. Ramakrishna, Inorg. Chem. 31 (1992) 2843.
[31] Z.-L. Lu, C.-Y. Duan, Y.-P. Tian, X.-Z. You, Inorg. Chem. 35 (1996) 2253.
[32] S. Menon, M.V. Rajasekharan, Inorg. Chem. 36 (1997) 4983.
[33] P. Kulkarni, S. Padhye, E. Sinn, C.E. Anson, A.K. Powell, Inorg. Chim. Acta 332 (2002) 167.
[34] B. Li, B. Li, X. Zhu, Y. Zhang, Inorg. Chem. Commun. 6 (2003) 1304.
[35] H.-J. Yang, H.-Z. Kou, F. Gao, A.-L. Cui, R.-J. Wang, Acta Crystallogr. E60 (2004) m611.
[36] Z.-Y. Wu, D.-J. Xu, Acta Crystallogr. E60 (2004) m839.
[37] Y.-P. Li, P. Yang, Z.-X. Huang, F.-X. Xie, Acta Crystallogr. C61 (2005) m7.

Polyhedron 27 (2008) 2069–2076

Contents lists available at ScienceDirect

Polyhedron

journal homepage: www.elsevier.com/locate/poly

The structure of selected magnesium carbonate minerals – A near infrared and mid-infrared spectroscopic study

Ray L. Frost *, Silmarilly Bahfenne, Jessica Graham, B. Jagannadha Reddy

Inorganic Materials Research Program, School of Physical and Chemical Sciences, Queensland University of Technology, G.P.O. Box 2434, Brisbane, Queensland 4001, Australia

ARTICLE INFO

Article history:
Received 14 December 2007
Accepted 28 March 2008
Available online 5 May 2008

Keywords:
Artinite
Dypingite
Carbonate
NIR spectroscopy
Vibrational spectroscopy
OH-overtones
Cation substitution effects

ABSTRACT

The approach to remove green house gases by pumping liquid CO_2 several kilometres below the ground implies that many carbonate containing minerals will be formed. Among these minerals the formation of dypingite and artinite are possible; thus necessitating a study of such minerals. Two carbonate bearing minerals dypingite and artinite with a hydrotalcite related formulae have been characterised by a combination of infrared and near-infrared spectroscopy. The infrared spectra of both minerals are characterised by OH and water stretching vibrations. Both the first and second fundamental overtones of these bands are observed in the NIR spectra in the 7030–7235 cm^{-1} and 10490–10570 cm^{-1}. Intense $(CO_3)^{2-}$ symmetric and antisymmetric stretching vibrations confirm the distortion of the carbonate anion. The position of the water bending vibration indicates water is strongly hydrogen bonded to the carbonate anion in the mineral structure. Split NIR bands at around 8675 and 11100 cm^{-1} indicates that some replacement of magnesium ions by ferrous ions in the mineral structure has occurred.

© 2008 Elsevier Ltd. All rights reserved.

1. Introduction

The ability to be able to easily and readily detect minerals is of importance [1,2]. This is especially so where carbonate minerals are concerned. The technique of NIR spectroscopy does meet these requirements. What is probably not appreciated is that many carbonate containing minerals especially the secondary minerals are soluble and can translocate. The proposal to remove green house gases by pumping liquid CO_2 several kilometres below the ground requires formation of many carbonate containing minerals [3–5]. Two magnesium carbonate minerals which may form under such conditions of high CO_2 partial pressure are dypingite $Mg_5(CO_3)_4(OH)_2 \cdot 5H_2O$ [6–10] and artinite $Mg_2(CO_3)(OH)_2 \cdot 3H_2O$ [11–20].

The study of the magnesium carbonates is of extreme importance in the development of technology for the removal of green house gases. Magnesium minerals such as brucite, periclase and hydrotalcites have the potential for the sequestration of carbon dioxide. The formation and reaction pathways of hydroxy and hydrous carbonates of magnesium are essential for the understanding of this sequestration. The hydration–carbonation reaction path in the $MgO–CO_2–H_2O$ system at ambient temperature and atmospheric CO_2 is of essential significance from the standpoint of carbon balance and the removal of green house gases from the atmosphere. A better understanding of the global masses of Mg and CO_2 and the thermal stability of the hydrated carbonates of magnesium will provide fundamental knowledge of carbon dioxide removal. From a practical point of view, the exact knowledge of the reaction path in $MgO–CO_2–H_2O$ system is of great significance to the performance of brucite and related minerals for green house gas removal. The reaction path involving carbonation of brucite ($Mg(OH)_2$) is particularly complex, as Mg has a strong tendency to form a series of metastable hydrous carbonates. These metastable hydrous carbonates include hydromagnesite ($Mg_5(CO_3)_4(OH)_2 \cdot 4H_2O$, or $Mg_4(CO_3)_3(OH)_2 \cdot 3H_2O$), artinite ($Mg_2CO_3(OH)_2 \cdot 3H_2O$), nesquehonite ($MgCO_3 \cdot 3H_2O$), and lansfordite ($MgCO_3 \cdot 5H_2O$). The free energy of formation for these hydroxy and hydrous carbonates differs and their formation depends on the partial pressure of CO_2.

There are many applications of near infrared spectroscopy [21–29]. Many of these studies have been applied to minerals and soils [1,2,29–32]. One means of studying the distant planets and comets is the use of NIR spectroscopy [23,24,26,27,33–35]. Recently, Frost et al. used NIR spectroscopy to study some hydroxyl phosphated minerals [36,37] and some autunites [38,39]. The technique of NIR spectroscopy can be used at distances away from the spectrometer using a fibre optic probe and the NIR technique does have the possibility of detecting carbonate minerals. Many carbonate minerals contain both bonded water and adsorbed water; several minerals contain hydroxyl groups. NIR spectroscopy has often been referred to as 'proton' spectroscopy. This means that any mineral

* Corresponding author. Tel.: +61 7 3864 2407; fax: +61 7 3138 1804.
E-mail address: r.frost@qut.edu.au (R.L. Frost).

0277-5387/$ - see front matter © 2008 Elsevier Ltd. All rights reserved.
doi:10.1016/j.poly.2008.03.019

or compound containing protons will be able to be determined using NIR spectroscopy. Thus because of the presence of water and OH units, the hydroxyl and hydrated carbonate minerals lend themselves to analyses by NIR spectroscopy. Near-IR spectral regions may be conveniently divided into three spectral regions: (a) the high wavenumber region above 7500 cm^{-1} attributed to electronic bands, (b) between 5400 and 7500 cm^{-1} attributed to the first overtone of the fundamental hydroxyl stretching modes and (c) the 4000–5400 cm^{-1} region attributed to water combination modes [36,39–42]. This paper reports the detection of selected carbonate minerals using NIR spectroscopy with a fibre optic probe.

2. Experimental

2.1. Minerals

The following minerals were used in this research: (a) dypingite – Yoshikawaite, Shinshiro Shi, Aichi Prefecture, Japan, (b) Sample 4 dypingite – Clear Creek District, Southern San Benito County, CA, (c) Sample 3 artinite – Clear Creek District, Southern San Benito County, CA and (d) Sample 7 artinite – Higasi-Kuroda-Guchi, Inasa-Cho, Inasa-Gun, Aichi Prefecture, Japan. The phase purity of the minerals was checked by X-ray diffraction and the chemical composition by EDX measurements.

2.2. Near-infrared (NIR) spectroscopy

NIR spectra were collected on a Nicolet Nexus FT-IR spectrometer with a Nicolet Near-IR Fibreport accessory (Madison, WI). The reason for using a fibre optic probe is the ease of operation and the fact that the probe can be brought to the mineral and can be used at some distance from the spectrometer. A white light source was used, with a quartz beam splitter and TEC NIR InGaAs detector. Spectra were obtained from 13 000 to 4000 cm^{-1} (0.77–2.50 μm) by the co-addition of 256 scans at a spectral resolution of 8 cm^{-1}. A mirror velocity of 1.266 m s^{-1} was used. The spectra were transformed using the Kubelka-Munk algorithm to provide spectra for comparison with published absorption spectra. Spectral manipulations, such as baseline correction, smoothing and normalisation, were performed using the software package GRAMS (Galactic Industries Corporation, NH, USA).

2.3. Mid-IR spectroscopy

Infrared spectra were obtained using a Nicolet Nexus 870 FT-IR spectrometer with a smart endurance single bounce diamond ATR cell over the 4000–525 cm^{-1} range obtained by the co-addition of 64 scans with a resolution of 4 cm^{-1} and a mirror velocity of 0.6329 cm/s. Spectra were co-added to improve the signal to noise ratio.

Band component analysis was undertaken using the Jandel 'Peakfit' (Erkrath, Germany) software package which enabled the type of fitting function to be selected and allows specific parameters to be fixed or varied accordingly. The Lorentz–Gauss ratio was maintained at values greater than 0.7 and fitting was undertaken until reproducible results were obtained with squared correlations (r^2) greater than 0.995. Band fitting of the spectra is quite reliable providing there is some band separation or changes in

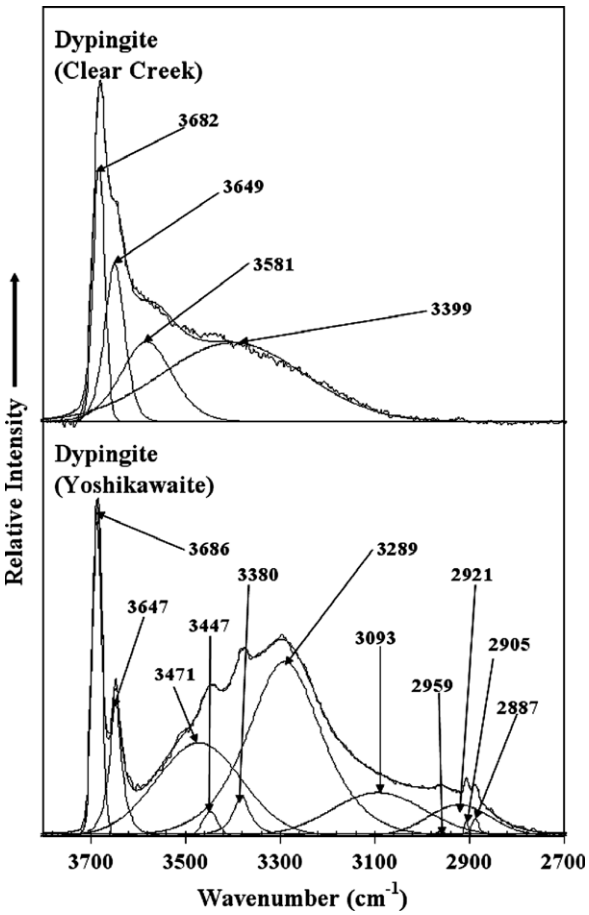

Fig. 1. Infrared spectra of artinite in the 2700–3800 cm^{-1} region.

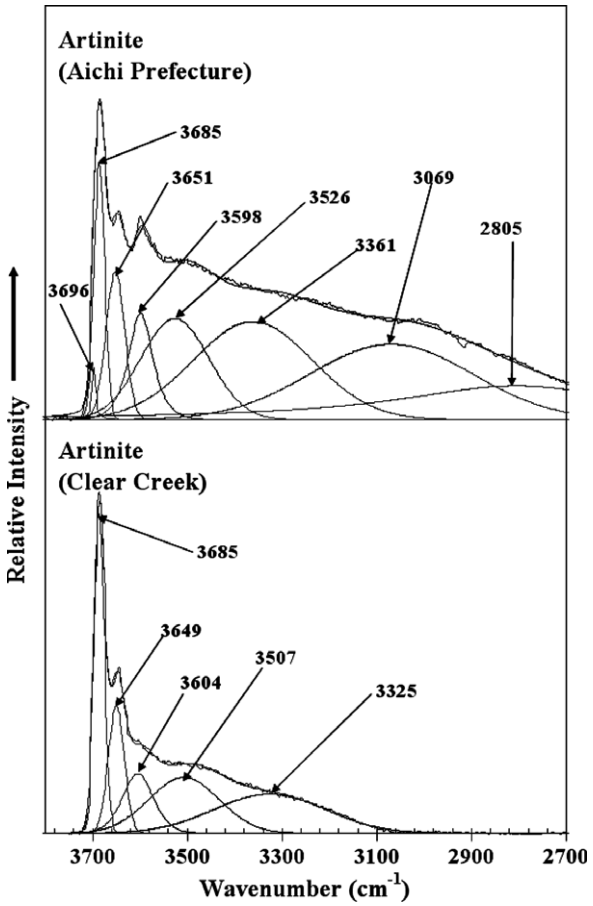

Fig. 2. Infrared spectra of dypingite in the 2700–3800 cm^{-1} region.

the spectral profile. The band intensities were calculated as a percentage of the total normalised band intensity.

3. Results and discussion

3.1. Mid-infrared spectroscopy

The infrared spectrum of dypingite and artinite are shown in Figs. 1 and 2. The results of the infrared spectral analysis are reported in Table 1. The infrared spectra of dypingite in the OH stretching region displays two features: (a) two sharp bands at 3647 and 3686 cm^{-1} and (b) a number of broad overlapping bands centred upon 3289, 3380 and 3447 cm^{-1} (Yoshikawaite). The first two bands are assigned to the hydroxyl stretching vibrations of OH units whereas the broad bands are assigned to water stretching bands. The infrared bands at 2887, 2995, 2921 and 2959 cm^{-1} in Yoshikawaite dypingite is ascribed to adsorbed organics on the surface of the dypingite. The variation in intensity of the water stretching bands shows that some variation in the formula of dypingite may occur and is a function of the water partial pressure. This variation in intensity is readily observed in Fig. 1. Such variation in intensity of the bands assigned to water stretching vibrations may be complicated by the adsorption of water on the mineral surface. The same explanation is suitable for the mineral artinite. Two sharp bands at 3649 and 3685 cm^{-1} are observed for the Clear creek artinite and three bands at 3651, 3685 and 3696 cm^{-1} for the Aichi artinite. These bands are attributed to the stretching vibrations of the OH units. The other bands in the spectra are assigned to water stretching bands.

The infrared spectra of dypingite and artinite in the 525–1625 cm^{-1} region are shown in Figs. 3 and 4 respectively. The sharp bands at 1071 (Yoshikawaite) and the shoulder at 1078 cm^{-1} (Clear Creek) are attributed to the $(CO_3)^{2-}$ carbonate symmetric stretching mode. The observation of this mode in the infrared spectra provides evidence for the distortion of the carbonate anion and consequential loss of symmetry. Such a band should be not observed in the infrared spectrum but would be intense in the Raman spectrum. The band is observed at 1076 cm^{-1} for

Table 1
Infrared spectroscopic band deconvolution of dypingite and artinite

Dypingite 1 (Yoshikawaite)			Dypingite 4 (Clear Creek)			Artinite 3 (Clear Creek)			Artinite 7 (Aichi Pref)		
Center	FWHM	%	Center	FWHM	%	Center	FWHM	%	Center	FWHM	%
									3697	9	0.3
3686	24	3.9	3682	29	6.5	3686	26	8.6	3686	27	3.5
3647	30	1.2	3649	50	7.2	3650	39	5.3	3652	47	3.6
3471	211	10.2				3604	76	5.0	3598	60	1.8
			3582	127	4.6						
						3507	175	5.1	3526	170	4.4
3447	37	0.5							3362	296	14.9
3381	42	1.1	3400	352	24.3	3326	276	11.3	3069	403	15.5
3290	182	17.7									
3093	228	5.1									
2959	21	0.1									
2922	155	2.5									
2906	9	0.1									
2888	17	0.2									
									2805	609	13.7
			2049	367	3.3						
1683	16	0.3									
									1644	75	1.1
1599	65	7.7							1578	83	3.2
1588	27	1.4	1586	159	7.4	1591	107	7.4			
1509	53	3.3	1534	22	0.5	1535	18	0.5			
1480	29	3.3									
1424	17	0.7									
1405	110	9.6	1439	49	2.1	1442	23	1.2	1439	99	3.5
1403	5.0	0.2							1382	55	1.5
1375	23	1.6									
1363	9	0.6									
						1376	181	5.7			
			1312	203	2.8				1325	67	2.8
1072	39	3.1							1260	98	0.8
			1079	39	2.9	1076	34	6.4	1084	31	1.1
1009	48	3.5							1050	50	2.4
949	59	9.2	1012	83	14.1	1017	42	9.9			
			947	87	17.5	982	43	6.3	996	64	4.9
882	12	0.2				948	57	18.0	952	76	16.8
852	10	0.1				844	32	0.2			
799	19	0.1									
756	29	0.3									
714	47	0.3							763	51	0.8
									723	18	0.1
						657	36	0.8	639	77	1.8
600	79	6.5	618	79	5.6	610	62	6.2	613	35	0.4
573	8	0.1									
									569	24	0.3
546	45	1.3	548	40	1.1	552	40	2.0	556	10	0.1
									539	18	0.3
									527	6	0.2
									525	6	0.2

artinite (Clear Creek) and 1083 cm^{-1} for the Aichi artinite. The $(CO_3)^{2-}$ symmetric stretching mode is complimented with the antisymmetric stretching modes found in the 1300–1450 cm^{-1} region where a series of overlapping bands may be observed providing a complex spectral profile. For the dypingite from Clear Creek, these $(CO_3)^{2-}$ symmetric stretching bands are observed at 1312, 1438, 1534 and 1585 cm^{-1}. These bands appear better defined for the Yoshikawaite dypingite with clearly resolved bands at 1380, 1405, 1479 and 1509 cm^{-1}. For the artinite minerals these $(CO_3)^{2-}$ antisymmetric stretching modes are observed at 1325, 1381, 1439 cm^{-1} (Aichi) and 1376, 1441, 1535 cm^{-1} (Clear Creek).

In the spectrum of the Yoshikawaite dypingite two bands are observed at 1599 and 1682 cm^{-1}. The probable assignment of these two bands is to the water HOH bending mode. The fact that two bands are observed suggests that there are two types of water present in the dypingite structure. The band at 1599 cm^{-1} is attributed to non-hydrogen bonded water and corresponds to the position of the water bending mode of water vapour. Whereas the band at 1682 cm^{-1} corresponds to water not bonded by hydrogen bridges. For artinite, two bands are observed at 1578 and 1643 cm^{-1}. This latter band shows that the water is very strongly hydrogen bonded. This band corresponds to the water stretching vibration at low wavenumber whereas the 1595 cm^{-1} band is reflected in the OH stretching region by the bands in the 3200–3450 cm^{-1} region.

Two intense infrared bands are observed at 948 and 1008 cm^{-1} (Yoshikawaite dypingite) and 947 and 1012 cm^{-1} (Clear Creek). These bands are observed at 947 and 1017 cm^{-1} for the Clear Creek sample and at 952 and 995 cm^{-1} for the Aichi mineral. One possible assignment of these bands is to the OH deformation modes of the MgOH units. For the Yoshikawaite dypingite infrared spectrum low intensity infrared bands are observed at 755 and 799 cm^{-1}. For the Aichi artinite these bands are observed at 722 and 762 cm^{-1}. These bands are assigned to the $(CO_3)^{2-}\nu_4$ bending modes. The observation of more than one band supports the concept that there are multiple $(CO_3)^{2-}$ bending modes as a result of the distortion of the $(CO_3)^{2-}$ units in the dypingite and artinite structures. For the Yoshikawaite dypingite infrared spectrum, two bands are observed at 852 and 882 cm^{-1}. These bands are assigned to the $(CO_3)^{2-}\nu_2$ bending modes. A very low intensity band is observed for the Clear Creek artinite at 844 cm^{-1} which may correspond with this assignment.

Two bands are observed at 548 and 618 cm^{-1} for the Clear Creek dypingite and at 546 and 600 cm^{-1} for the Yoshikawaite dypingite. For the clear Creek artinite the bands are observed at 552 and 610 cm^{-1} and at 568 and 638 cm^{-1} for the Aichi artinite. These bands are too low in position to be interpreted as $(CO_3)^{2-}$ bending modes. One possible assignment of these bands is to the water librational modes.

3.2. Near-infrared (NIR) spectroscopy

Spectra are divided into: (a) the spectral region between 5500 and 8000 cm^{-1}, corresponding to the first fundamental overtone of the mid-infrared OH stretching vibration; (b) the spectral region between 4000 and 5500 cm^{-1} attributed to the water OH overtones, carbonate combination bands and (c) the spectral region between 8000 and 12 000 cm^{-1} corresponding to the second

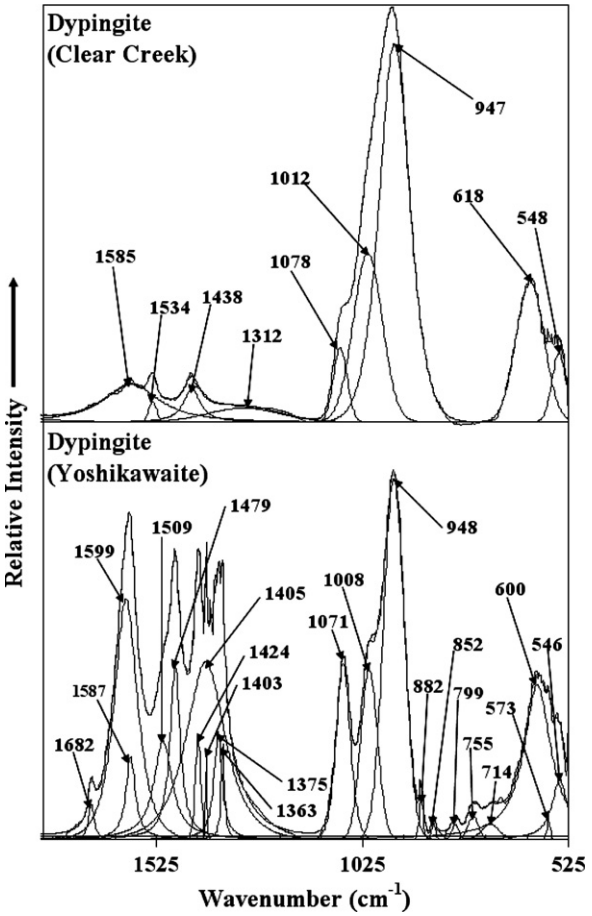

Fig. 3. The infrared spectra of dypingite in the 525–1625 cm^{-1} region.

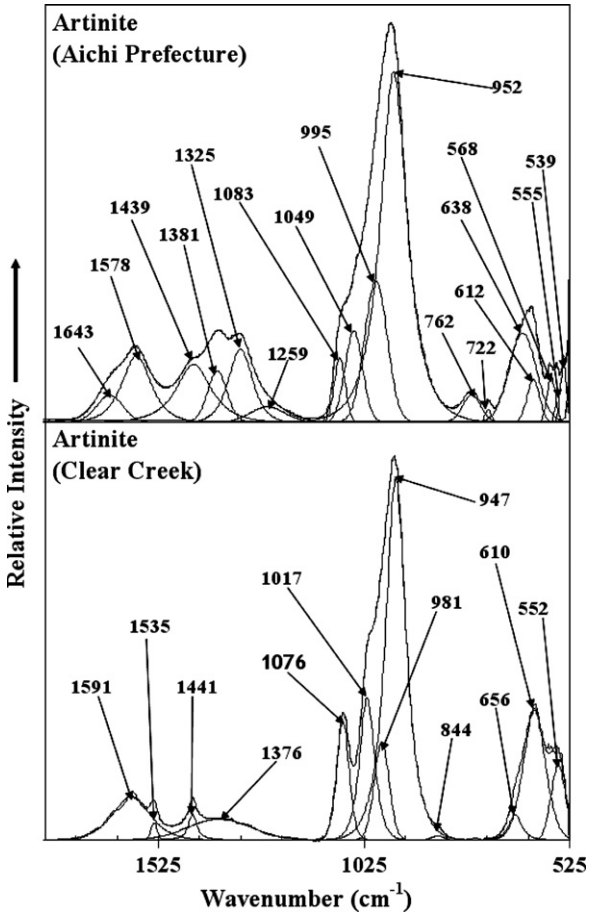

Fig. 4. The infrared spectra of artinite in the 525–1625 cm^{-1} region.

fundamental overtone of the OH stretching vibrations and also includes electronic bands resulting from transition metal ions in the structure [43–51].

The NIR spectra in the 5500–8000 cm^{-1} region of dypingite and artinite are shown in Figs. 5 and 6. The results of the NIR spectral analysis are reported in Table 2. The distinct feature of the NIR spectra of dypingite is the very sharp bands in this spectral region. For the Clear Creek dypingite a sharp intense band at 7127 cm^{-1} is observed with other lower intensity bands at 6914 and 7200 cm^{-1}. The NIR spectrum of the Yoshikawaite dypingite shows more complexity with bands at 7128, 7179, 7210 and 7237 cm^{-1}. These bands are attributed to the first fundamental overtone of the OH stretching vibrations. Similar spectra are observed for the artinite mineral samples. The Aichi artinite shows three sharp bands at 7166, 7207 and 7234 cm^{-1}. Lower intensity bands are observed at 7060, 7355 and 7760 cm^{-1}. The NIR spectrum of the Clear Creek dypingite shows broader bands with peaks at 6991, 7098, 7192 cm^{-1}. The sharp bands are the first fundamental overtone of the OH stretching bands (i.e. $2\nu_1$). It must be remembered that there are no selection rules for the NIR spectra and fundamentally all combinations of the OH stretching vibrations are allowed, i.e. Raman bands and infrared bands can combine as well as the doubling of the wavenumbers of the bands. It is probable the bands in this spectral region result from the addition or subtraction of the OH deformation mode and the doubling of the first overtone of the OH stretching vibration (i.e. $2\nu_1 \pm \delta\nu$).

The NIR spectra in the 4000–5500 cm^{-1} region for dypingite are shown in Fig. 7 and for artinite in Fig. 8. For the Clear Creek dypingite two bands are observed at 4987 and 5147 cm^{-1}; for the Yoshikawaite dypingite three bands are observed at 4732, 5052 and 5201 cm^{-1}. These bands are probably a combination of water and carbonate bands. Carbonate bands are normally found in this spectral region resulting from the doubling of the symmetric and antisymmetric carbonate stretching bands $2(\nu_1 + \nu_3)$. A number of bands are observed in the 4000–4500 cm^{-1} region. These may be simply described as combination bands resulting from combination of bands in the mid-IR spectral region. The spectrum in this spectral region of artinite shows similarity to that of dypingite; however the ratio of the intensity of the bands appears different. The Aichi artinite NIR spectrum displays bands at 4702, 4766, 5051 and 5212 cm^{-1}. The Clear Creek artinite NIR spectrum shows bands at 4747, 5035 and 5208 cm^{-1}.

For the Clear Creek dypingite, a number of bands are observed at 4109, 4233, 4300 and 4409 cm^{-1}; for the Yoshikawaite dypingite three bands are observed at 4103, 4179, 4300 and 4387 cm^{-1}. For the artinite mineral samples greater complexity in the 4000 to 4500 spectral region is observed. Prominent NIR bands are observed for the Clear Creek artinite are observed at 4300, 4386 and 4461 cm^{-1}; for Aichi artinite NIR bands are found at 4294, 4377 and 4461 cm^{-1}. Bands in this spectral region result from the combination of bands in the mid-IR spectral region.

The NIR spectra in the 8000–12000 cm^{-1} region of artinite and dypingite are shown in Figs. 9 and 10. There are two features in this spectral region that are noteworthy: firstly there are bands at around 10446 cm^{-1} for Clear Creek dypingite and 10536, 10611 and 10999 cm^{-1} for the Yoshikawaite dypingite; these bands are assigned to the second overtone of the OH stretching vibrations (i.e. $3\nu_1$ and $3\nu_3$). Secondly there is a broad feature centred upon

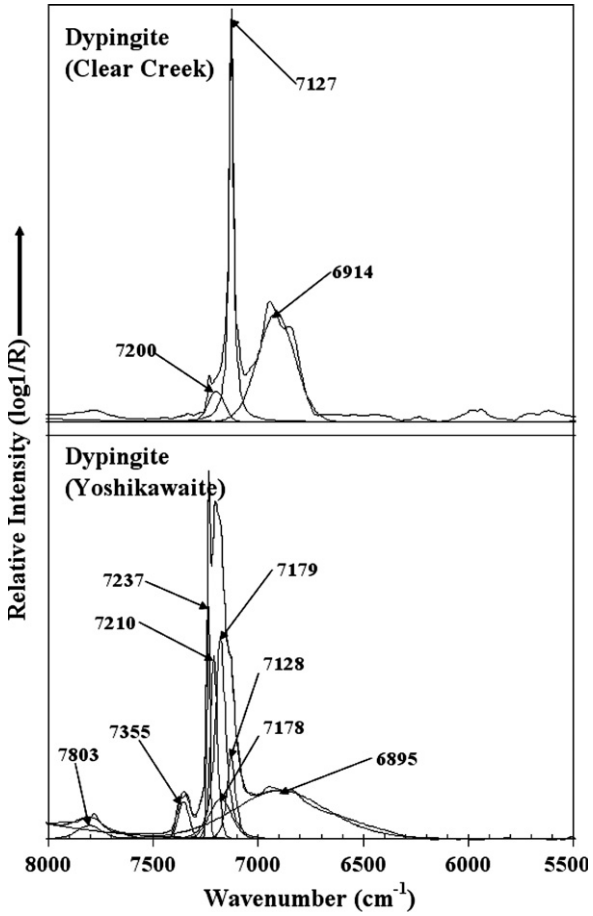

Fig. 5. Near-infrared spectra of artinite in the 5500–8000 cm^{-1} region.

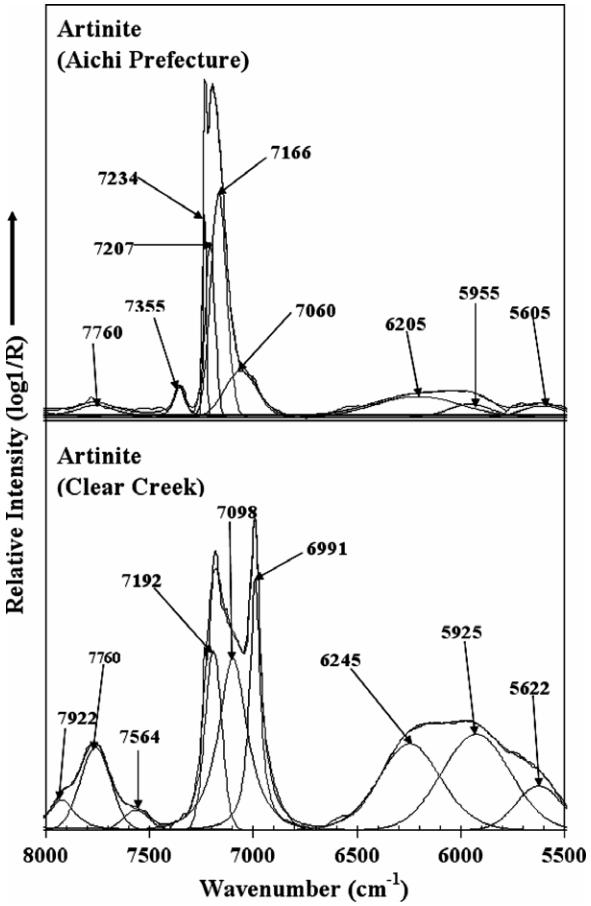

Fig. 6. Near-infrared spectra of dypingite in the 5500–8000 cm^{-1} region.

Table 2
Near-infrared spectroscopic band deconvolution of dypingite and artinite

Dypingite 1			Dypingite 4			Artinite 3			Artinite 7		
Center	FWHM	%	Center	FWHM	%	Center	FWHM	%	Center	FWHM	%
11000	837	6.4									
						11857	972	2.6			
						11075	326	1.1	11049	467	4.6
10611	19	0.1							10605	23	0.2
10536	229	1.9							10524	133	0.6
			10447	27	0.3	10332	339	11.9			
			10036	156	0.1						
									9843	546	3.5
						9028	217	3.6			
8599	1189	16.8							8604	688	14.4
						8471	193	0.8			
			8376	575	2.8	7923	147	1.8			
7804	136	0.9									
						7761	172	4.9	7760	230	1.8
						7565	143	1.0			
									7355	62	1.3
7356	60	1.0									
7237	16	1.9							7235	19	1.9
7211	38	3.6	7200	91	1.1				7208	54	4.7
						7192	95	5.9	7167	89	10.0
7180	55	6.5	7128	26	5.8						
7179	125	2.3									
7128	48	2.1									
						7098	164	11.6	7060	183	4.3
						6991	59	7.1			
6896	525	12.3	6914	207	8.6						
						6245	353	10.8	6206	489	5.1
						5925	389	12.8	5956	243	1.7
						5622	259	3.9	5606	236	1.4
5201	140	4.3				5208	142	2.4	5213	123	4.3
			5147	217	30.0						
5052	293	11.6				5035	245	9.9	5051	228	12.4
			4987	316	18.0						
						4747	230	3.9	4766	51	1.1
4733	133	4.0							4702	63	1.2
						4462	39	0.5	4461	49	1.2
4387	134	6.0	4409	91	3.8	4386	85	3.4	4377	118	4.7
4300	59	4.9	4300	47	1.3	4300	60	3.2	4295	58	8.5
4272	25	1.4									
			4233	173	7.9						
4180	150	10.2							4209	11	0.1
						4188	36	0.3	4197	19	0.3
									4171	37	0.7
						4140	21	0.2	4121	57	0.9
4103	67	1.8	4109	132	9.3						
						4084	6	0.1	4083	23	0.3
						4061	89	0.9			
						4042	18	0.2			
									4017	27	0.2
4004	337	0.0				4002	40	0.1			
			3998	139	1.8						

around 8598 and 10999 cm^{-1}. These bands are attributed to electronic bands of the ferrous ion. There is an important implication based upon this observation: namely that according to the formula no ferrous ion is in the structure dypingite $Mg_5(CO_3)_4(OH)_2 \cdot 5H_2O$ and artinite $Mg_2(CO_3)(OH)_2 \cdot 3H_2O$. The intensity of the bands suggests that a significant amount of Fe^{2+} has replaced some of the Mg^{2+} in the structure. The intensity of the bands for the Clear Creek dypingite is very low for the Fe^{2+} electronic band. The intensity is higher for the Yoshikawaite dypingite. Some replacement of the Mg^{2+} by Fe^{2+} is likely. Thus the formula is more likely to be $(Fe^{2+},Mg)_5(CO_3)_4(OH)_2 \cdot 5H_2O$. In other words the formula of artinite is more likely to be $(Fe^{2+},Mg)_2(CO_3)(OH)_2 \cdot 3H_2O$. Sharp bands for artinite are found at 10523 and 10604 cm^{-1} and are assigned to the second overtone of the OH stretching vibrations.

4. Conclusions

The concept of geosequestration involves the pumping of liquefied green house gases to significant depths below the surface of the earth. The high partial pressure of CO_2 is significant in that many different types of carbonates will be formed. Among these minerals there is the possibility of the formation of dypingite and artinite which are related at least in chemical formula to the hydrotalcite or layered double hydroxide minerals. A combination of infrared and near infrared spectroscopy has been used to characterise these two minerals and the bands related to the mineral structure. Importantly the observation of split broad bands in the 8000–12000 cm^{-1} region is evidence for the partial replacement of Mg^{2+} by Fe^{2+} in the mineral structure.

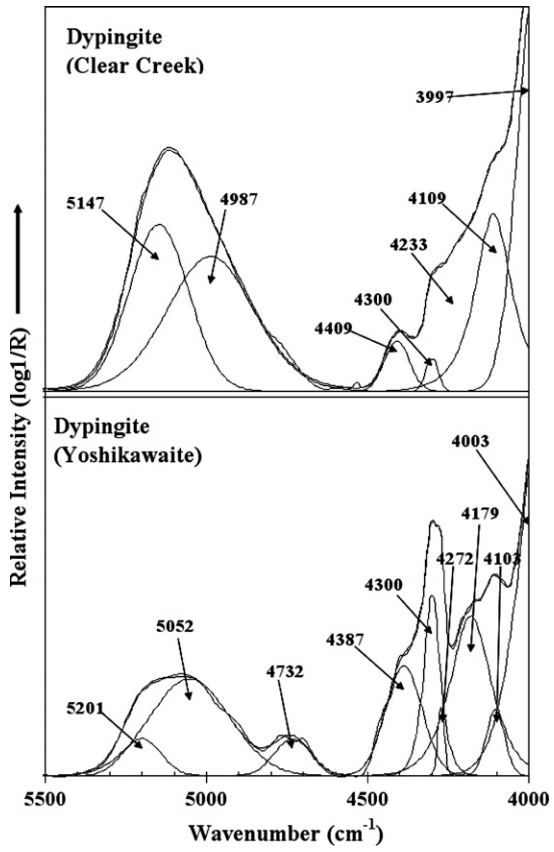

Fig. 7. Near-infrared spectra of artinite in the 4000–5500 cm^{-1} region.

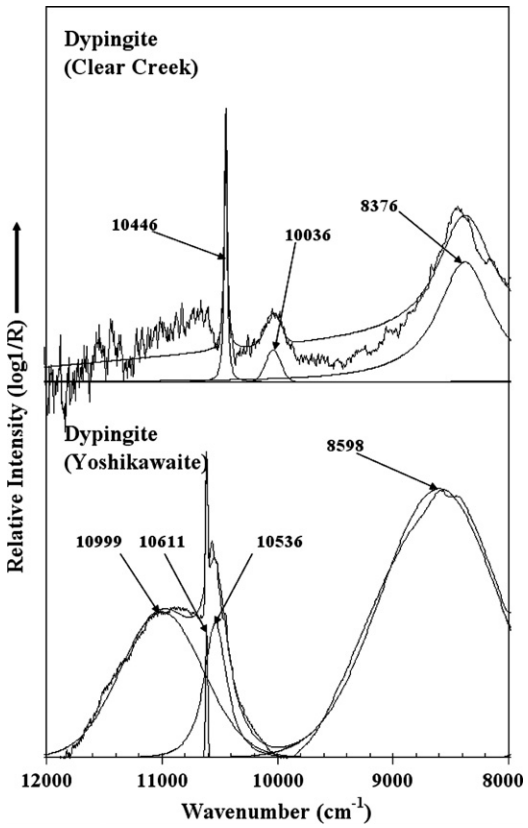

Fig. 9. Near-infrared spectra of artinite in the 8000–12 000 cm^{-1} region.

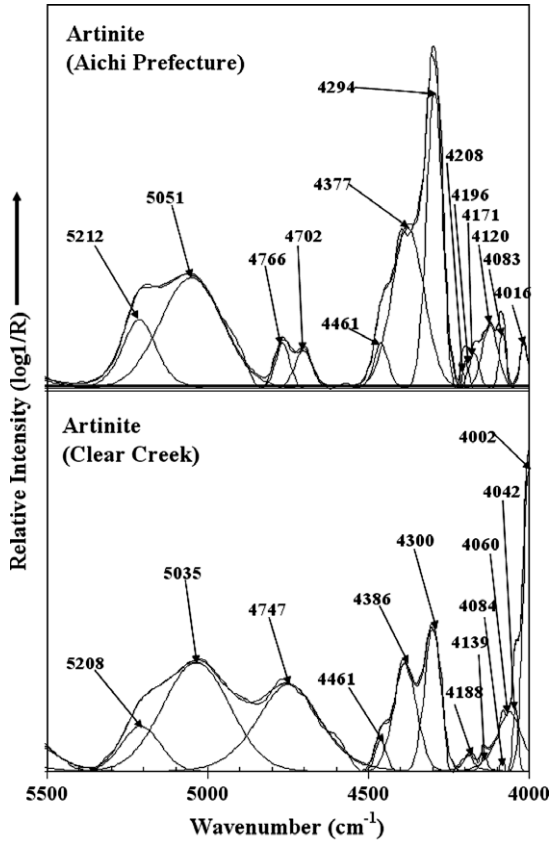

Fig. 8. Near-infrared spectra of dypingite in the 4000–5500 cm^{-1} region.

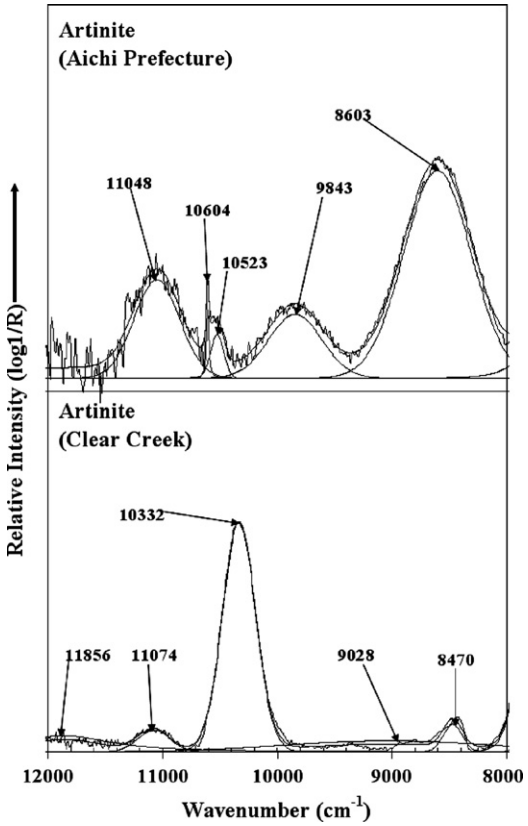

Fig. 10. Near-infrared spectra of dypingite in the 8000–12 000 cm^{-1} region.

Acknowledgements

The financial and infra-structure support of the Queensland University of Technology, Inorganic Materials Research Program is gratefully acknowledged. The Australian Research Council (ARC) is thanked for funding the instrumentation. One of the authors, B. Jagannadha Reddy is grateful to the Queensland University of Technology for the award of a Visiting Fellowship.

References

[1] G.R. Hunt, R.P. Ashley, Econ. Geol. Bull. Soc. Econ. Geol. 74 (1979) 1613.
[2] G.R. Hunt, R.C. Evarts, Geophysics 46 (1981) 316.
[3] J.W. Anthony, R.A. Bideaux, K.W. Bladh, M.C. Nichols, Handbook of Mineralogy, Mineral Data Publishing, Tuscon, AZ, USA, 2003.
[4] L.B. Railsback, Carbonate Evaporite 14 (1999) 1.
[5] S.W.M. Blake, C. Cuff, Preparation and Use of Cationic Halides, Sequestration of Carbon dioxide. Application: WO WO, Perma-Carb Pty Ltd., Australia, 2007, 66pp.
[6] P.P. Smolin, T.A. Ziborova, Dokl. Akad. Nauk SSSR 226 (1976) 923 (Mineral).
[7] G.O. Nechiporenko, G.V. Sokolova, T.A. Ziborova, G.P. Bondarenko, Mineralogic. Z. 10 (1988) 78.
[8] J.H. Canterford, G. Tsambourakis, B. Lambert, Mineral. Mag. 48 (1984) 437.
[9] P.J. Davies, B. Bubela, Chem. Geol. 12 (1973) 289.
[10] G. Raade, Am. Mineral. 55 (1970) 1457.
[11] H.G.M. Edwards, S.E.J. Villar, J. Jehlicka, T. Munshi, Spectrochim. Acta Part A 61 (2005) 2273.
[12] E. Konigsberger, L.-C. Konigsberger, H. Gamsjager, Geochim. Cosmochim. Acta 63 (1999) 3015.
[13] M. Akao, S. Iwai, Acta Crystallogr., Sect. B 33 (1977) 3951.
[14] J.R. Guenter, H.R. Oswald, J. Solid State Chem. 21 (1977) 211.
[15] K.N. Goswami, Indian J. Pure Appl. Phys. 12 (1974) 667.
[16] H. Jagodzinski, Mineral. Petrog. Mitt. 10 (1965) 297.
[17] M. deWolff, Acta Crystallogr. 5 (1952) 286.
[18] M. Fenoglio, Period. Mineral. 13 (1942) 1.
[19] L. Brugnatelli, Centr. Min. 35 (1903) 144.
[20] L. Brugnatelli, Rend. Ist. Lombardo 35 (1902) 869.
[21] F. Cariati, L. Erre, G. Micera, P. Piu, C. Gessa, Clay Clay Miner. 29 (1981) 157.
[22] C.-W. Chang, D.A. Laird, M.J. Mausbach, C.R. Hurburgh Jr., Soil Sci. Soc. Am. J. 65 (2001) 480.
[23] N. Hirao, Ganseki Kobutsu Kagaku 31 (2002) 111.
[24] N.R. Izenberg, S.L. Murchie, J.F. Bell III, L.A. McFadden, D.D. Wellnitz, B.E. Clark, M.J. Gaffey, Meteorit. Planet. Sci. 38 (2003) 1053.
[25] I.R. Lewis, N.C. Chaffin, M.E. Gunter, P.R. Griffiths, Spectrochim. Acta Part A 52 (1996) 315.
[26] L.A. McFadden, D.D. Wellnitz, M. Schnaubelt, M.J. Gaffey, J.F. Bell III, N. Izenberg, S. Murchie, C.R. Chapman, Meteorit. Planet. Sci. 36 (2001) 1711.
[27] S. Murchie, L. Kirkland, S. Erard, J. Mustard, M. Robinson, Icarus 147 (2000) 444.
[28] J.L. Post, L. Borer, Appl. Clay Sci. 16 (2000) 73.
[29] J.W. Van Groenigen, C.S. Mutters, W.R. Horwath, C. Van Kessel, Plant Soil 250 (2003) 155.
[30] R.L. Frost, J.T. Kloprogge, Z. Ding, Spectrochim. Acta Part A 58 (2002) 1657.
[31] R.L. Frost, E. Mako, J. Kristof, E. Horvath, J.T. Kloprogge, Langmuir 17 (2001) 4731.
[32] H.D. Ruan, R.L. Frost, J.T. Kloprogge, Appl. Spectrosc. 55 (2001) 190.
[33] I. Biering, K. Larsen, T. Garp, D.H. Christensen, C.B. Koch, P.W. Jensen, O.F. Nielsen, Asian Chem. Lett. 7 (2003) 99.
[34] T.H. Burbine, R.P. Binzel, Icarus 159 (2002) 468.
[35] T.J. McCoy, T.H. Burbine, L.A. McFadden, R.D. Starr, M.J. Gaffey, L.R. Nittler, L.G. Evans, N. Izenberg, P.G. Lucey, J.I. Trombka, J.F. Bell III, B.E. Clark, P.E. Clark, S.W. Squyres, C.R. Chapman, W.V. Boynton, J. Veverka, Meteorit. Planet. Sci. 36 (2001) 1661.
[36] R.L. Frost, K.L. Erickson, Spectrochim. Acta Part A 61 (2005) 51.
[37] R.L. Frost, K.L. Erickson, Spectrochim. Acta Part A 61 (2005) 45.
[38] R.L. Frost, K.L. Erickson, M.O. Adebajo, M.L. Weier, Spectrochim. Acta Part A 61 (2005) 367.
[39] R.L. Frost, K.L. Erickson, O. Carmody, M.L. Weier, Spectrochim. Acta Part A 61 (2005) 749.
[40] R.L. Frost, O. Carmody, K.L. Erickson, M.L. Weier, Spectrochim. Acta Part A 61 (2005) 1923.
[41] R.L. Frost, K.L. Erickson, Spectrochim. Acta Part A 61 (2004) 51.
[42] R.L. Frost, K.L. Erickson, Spectrochim. Acta Part A 61 (2004) 45.
[43] R.L. Frost, S.J. Palmer, B.J. Reddy, Vib. Spectrosc. 44 (2007) 154.
[44] R.L. Frost, B.J. Reddy, D.L. Wain, W.N. Martens, Spectrochim. Acta Part A 66 (2007) 1075.
[45] R.L. Frost, D.L. Wain, W.N. Martens, B.J. Reddy, Spectrochim. Acta Part A 66 (2007) 1068.
[46] S. Palmer, B.J. Reddy, R.L. Frost, Polyhedron 26 (2007) 524.
[47] B.J. Reddy, R.L. Frost, Spectrochim. Acta Part A 66 (2007) 312.
[48] B.J. Reddy, R.L. Frost, J. Near Infrared Spectrosc. 15 (2007) 115.
[49] B.J. Reddy, R.L. Frost, W.N. Martens, D.L. Wain, J.T. Kloprogge, Vib. Spectrosc. 44 (2007) 42.
[50] B.J. Reddy, R.L. Frost, M.L. Weier, W.N. Martens, J. Near Infrared Spectrosc. 14 (2006) 241.
[51] R.L. Frost, R.-A. Wills, W. Martens, M. Weier, B.J. Reddy, Spectrochim. Acta Part A 62 (2005) 42.

Polyhedron 27 (2008) 2077–2082

Contents lists available at ScienceDirect

Polyhedron

journal homepage: www.elsevier.com/locate/poly

The synthesis and characterization of new aminoadamantane derivatives of hexachloro-*cyclo*-triphosphazene

Radka Kočí Voznicová [a], Jan Taraba [a], Jiří Příhoda [a,*], Milan Alberti [b]

[a] Department of Chemistry, Faculty of Science, Masaryk University, Kotlářská 2, CZ-611 37 Brno, Czech Republic
[b] Department of Physical Electronics, Faculty of Science, Masaryk University, Kotlářská 2, CZ-611 37 Brno, Czech Republic

ARTICLE INFO

Article history:
Received 14 January 2008
Accepted 3 April 2008
Available online 12 May 2008

Keywords:
cyclo-Triphosphazene
1-Aminoadamantane
Amantadine
Memantine
Crystal and molecular structure

ABSTRACT

The reactions of hexachloro-*cyclo*-triphosphazene $P_3N_3Cl_6$ (**1**) with 1-aminoadamantane (amantadine, Ad-NH_2) and 1-amino-3,5-dimethyladamantane (memantine, Mem) were studied. New geminally substituted phosphazene derivatives, $P_3N_3Cl_4$(NH-Ad)$_2$ (**2**), $P_3N_3Cl_2$(NH-Ad)$_4$ (**3**) and $P_3N_3Cl_2$(Mem)$_4$ (**4**), were prepared. The substances **3** and **4** were fully characterized by ^{31}P NMR and IR spectroscopies and elemental analysis. Molecular and crystal structures of **2**–**4** were determined by X-ray diffraction. The compounds are triclinic, space group $P\bar{1}$. Compound **3** crystallized from dichloromethane as a solvate.

© 2008 Elsevier Ltd. All rights reserved.

1. Introduction

Phosphazenes, compounds having –P=N– group in their molecules, constitute one of the important class of compounds in the chemistry of phosphorus and nitrogen. First heterocyclic compounds of the composition $(PNCl_2)_3$ and $(PNCl_2)_4$ were isolated in the 1830s [1–3] from the reaction of PCl_5 with NH_4Cl. Since that time, a diverse class of phosphazene ring and linear species has been investigated [4–7]. Hexachloro-*cyclo*-triphosphazene, $P_3N_3Cl_6$, being easily prepared, is commonly used as a starting material for many substitutions [8].

Within the context of biological and pharmacological properties of some amido- and aminophosphazenes, nucleophilic substitutions (ammonolysis and aminolysis) belong to the two main reaction types. In the course of these reactions, a lone electron pair of the reagent nitrogen atom attacks a phosphorus atom of the phosphazene cycle, and amido- or amino-*cyclo*-triphosphazene derivatives are formed under release of HCl [2,3].

The result of the reaction of phosphazene derivative with nucleophile reagent strongly depends on reaction conditions whereas a series of various substitution derivatives can be formed [5,9–14].

The interest in these reactions does not subside even at present. Many research groups focus their effort on the study and comparison of individual reactions, collecting all possible structural and chemical data of new compounds with the aim of their practical utilization [15–17]. However, only two articles dealing with reactions of $P_3N_3Cl_6$ with cycloalkylamino substituents have been published so far [18,19]. Allcock and co-workers [18] studied the reaction of $P_3N_3Cl_6$ with 1-aminoadamantane in molar ratio 1:12 (Scheme 1). Gem-*tetrakis*(adamantanamino)dichloro-*cyclo*-triphosphazene (**3**) (in major yield) and *hexakis*(adamantanamino)-*cyclo*-triphosphazene (**5**) were prepared in this reaction, but only crystal and molecular structures of **5** were determined.

Another paper summarized results of the study of reactions of $P_3N_3Cl_6$ with some cycloalkylamines [19] where geminal tetrakis derivatives $P_3N_3Cl_2(NHR)_4$, R = $-C_6H_{11}$, $-C_5H_9$, $-C_3H_5$ were identified as major products.

It is worth mentioning that some aminoadamantane derivatives themselves are used as pharmaceuticals, such as anti-virals, anti-diabetics, anti-parkinsonians, anti-tuberculosis, and analgesics. The most important pharmacologically effective representatives based on adamantane are 1-aminoadamantane (amantadine, Ad-NH_2) and *N*-ethylaminoadamantane (rimantadine, Rim) that were tested in the treatment of viral diseases [20,21]. Amantadine can also cause palliation of Parkinsonic symptoms. 1-Amino-3,5-dimethyladamantane (memantine, Mem) improves capillary blood return of the brain and can be used in the treatment of dementia [22].

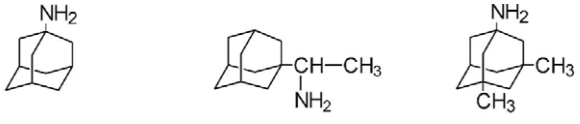

amantadine (Ad-NH_2) rimantadine (Rim) memantine (Mem)

* Corresponding author. Tel.: +420 549 496 690; fax: +420 549 492 443.
E-mail address: prihoda@chemi.muni.cz (J. Příhoda).

0277-5387/$ - see front matter © 2008 Elsevier Ltd. All rights reserved.
doi:10.1016/j.poly.2008.04.001

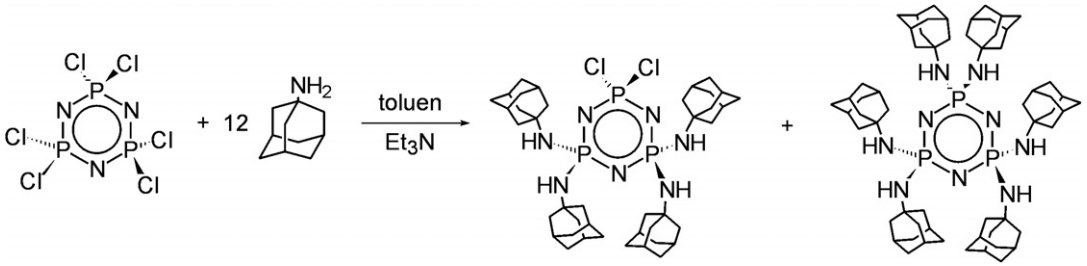

Scheme 1. Reaction of hexachloro-*cyclo*-triphosphazene with aminoadamantane (1:12) by Allcock [18].

Table 1
Amount of starting compounds and solvents used in the reactions

Synthesized compound	$P_3N_3Cl_6$ (g/mmol)	Aminoadamantane reagent (g/mmol)		Et_3N (g/mmol)	Solvent (cm^3)		Time of heating (h)
2	0.298/0.857	Ad-NH_2	1.037/6.856		diethyl ether	20	12
3	0.216/0.621	Ad-NH_2	1.127/7.452	0.754/7.452	toluene	24	48
4	0.216/0.621	Mem	1.336/7.452	0.754/7.452	toluene	24	48

We suppose that derivatives of chlorophosphazenes bearing aminoadamantane group could be very promising from the point of their biological activity and potential practical use. Therefore it is surprising that only one paper [18] deals with the reaction of chlorophosphazene with aminoadamantane derivative.

Results of our investigations of the course of reactions of hexachloro-*cyclo*-triphosphazene with amantadine and memantine are summarized in this article.

2. Experimental

2.1. Reagents and general procedures

All procedures, syntheses and sample preparations were performed using Schlenk technique under dry nitrogen atmosphere. Solvents, such as toluene, dichloromethane, diethyl ether, and *n*-hexane (all Aldrich, p.a.) were purified and dried according to procedures described by Perrin and Armarego [23]. Pure hexachloro-*cyclo*-triphosphazene (**1**) (BASF) was obtained from its mixture with octachloro-*cyclo*-tetraphosphazene by crystallization from *n*-hexane and subsequent sublimation in vacuum at 60 °C. The purity of **1** was proved by MS spectrometry and ^{31}P NMR spectroscopy.

Amantadine (Ad-NH_2) and memantine (Mem) were prepared from the corresponding hydrochlorides (Aldrich, p.a.) by neutralization with 1.5-fold excess of KOH. This procedure was carried out in a separatory funnel and "free" amantadine and memantine were extracted with three portions of dichloromethane. The organic phases were combined, dried with anhydrous $MgSO_4$, and amantadine and memantine were obtained from the filtrate by evaporation of the solvent. Their purity was proved by IR and Raman spectroscopies.

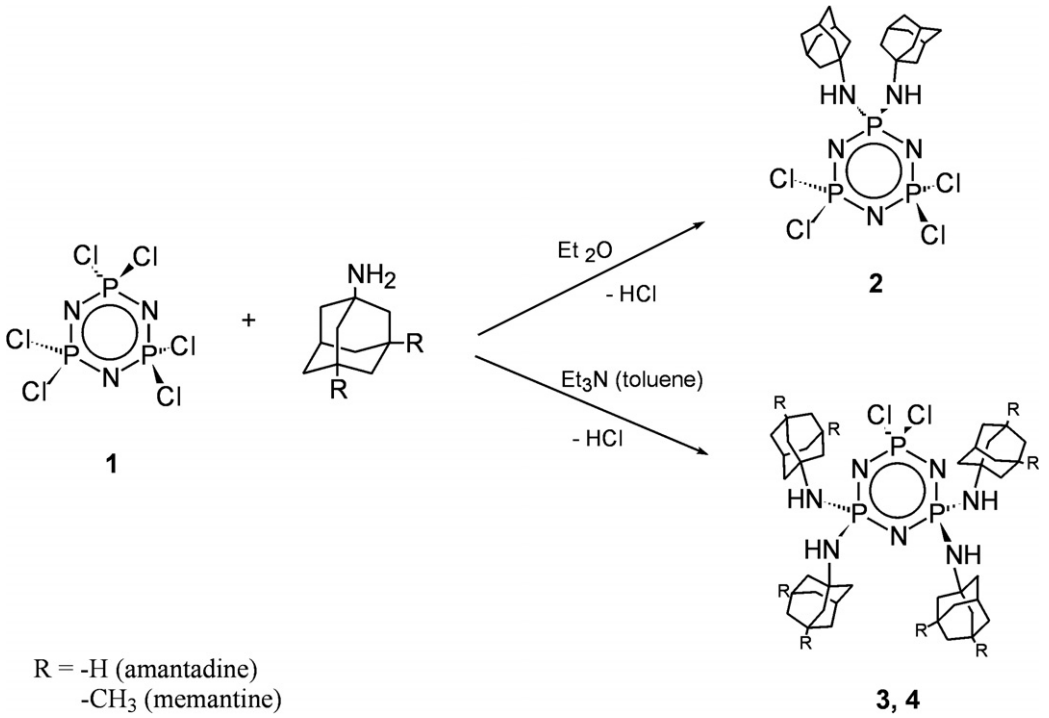

Scheme 2. Reaction of **1** with aminoadamantanes; R = –H (amantadine) or $–CH_3$ (memantine).

Triethylamine (Et_3N) was purified according to [23] and distilled before use.

2.2. Instrumentation

^{31}P NMR spectra were recorded on a 500 MHz Bruker DRX AVANCE spectrometer and were referenced to 85% H_3PO_4 (external standard). The samples were sealed in Simax® tubes (diameter 4 mm) and inserted in original Wilmad® NMR cuvettes (diameter 5 mm), the space between the two cuvettes was filled with D_2O (external lock), and samples were measured in the coaxial NMR cuvette system.

Mass spectra were measured using the MAT Trio 1000, Series II, Finnigan, excitation energy 70 eV, connected to a gas chromatograph GC 8000 with DB-5 column. The sample (1–2 μl) in a suitable solvent was injected onto the column, the temperature of the heated zone was 50–280 °C, and the heating rate 10 °C min^{-1}. Nitrogen was used as carrier-gas.

IR spectra were measured by a Bruker IFS 28 spectrometer either in KBr disks containing 1.0–1.7 mg of the sample and 100 mg KBr. Raman spectra of solid samples were measured in Raman capillaries using a Bruker IFS 55 Equinox apparatus, equipped with a FRA 106/S adapter, (Nd:YAG laser, λ = 064 nm, W = 150–400 mW).

Table 2
^{31}P NMR data for **2**–**4**

Compound	2	3	4
δ [PCl_2] (ppm)	19.0 (d)	20.0 (t)	19.9 (t)
δ [$P(NHR)_2$] (ppm)	1.7 (t)	4.1 (d)	3.8 (d)
$^2J_{P-N-P}$ (Hz)	45.6	51.5	52.6

Table 4
Selected bond lengths (Å) and angles (°)

	2	3	4
P(1)–N(1)	1.6371 (16)	1.604 (2)	1.6032 (13)
P(1)–N(3)	1.6199 (16)	1.627 (2)	1.6205 (14)
P(2)–N(1)	1.5681 (16)	1.600 (2)	1.5981 (14)
P(2)–N(2)	1.5929 (17)	1.623 (2)	1.6156 (14)
P(3)–N(2)	1.5921 (17)	1.562 (2)	1.5616 (14)
P(3)–N(3)	1.5595 (16)	1.565 (2)	1.5582 (14)
P–Cl	2.0188 (10) [a]	2.0383 (11) [a]	2.0308 (9) [a]
P–N(H)	1.6315 (17) [a]	1.6480 (20) [a]	1.6463 (16) [a]
N(H)–C	1.4905 (18) [a]	1.4858 (19) [a]	1.4835 (17) [a]
N(3)–P(1)–N(1)	112.29 (8)	114.36 (11)	114.49 (7)
N(1)–P(2)–N(2)	120.18 (9)	114.11(11)	114.48 (7)
N(2)–P(3)–N(3)	119.99 (9)	121.56 (12)	121.84 (7)
P(1)–N(1)–P(2)	122.56 (10)	126.70 (14)	126.04 (8)
P(2)–N(2)–P(3)	117.31 (10)	121.79 (14)	121.11 (9)
P(3)–N(3)–P(1)	124.04 (10)	121.30 (13)	120.94 (9)
Cl–P–Cl	99.83 (4) [a]	98.27 (5)	99.18 (5)
N(H)–P–N(H)	105.14 (9)	102.21 (11) [a]	102.47 (10) [a]
P–N(H)–C	129.02 (13) [a]	128.48 (15) [a]	128.73 (14) [a]

[a] Average.

Elemental analyses (C, H and N) were performed on a Fisons Instruments EA-1108 elemental analyzer.

Diffraction data were collected using the KUMA KM-4 κ-axis diffractometer with graphite-monochromated Mo Kα radiation (λ = 0.71069 Å) equipped with a CCD detector. All structures were solved by direct methods, and refined by full-matrix least-squares methods using anisotropic thermal parameters for the non-hydrogen atoms. The software XCALIBUR CCD system [24] was used for data collection/reduction and the SHEXTL software [25] was used for the structure solution, refinement, and drawing preparation. Thermal ellipsoids are drawn at the 50% probability level.

Table 3
Crystal data and structure refinement

Compound	2	3	4
Empirical formula	$C_{20}H_{32}C_{14}N_5P_3$	$C_{42}H_{68}C_{l6}N_7P_3$	$C_{48}H_{80}C_{l2}N_7P_3$
Formula weight	577.22	976.64	919
Temperature (K)	120		
Wavelength (Å)	0.71069		
Crystal system	triclinic	triclinic	triclinic
Space group	$P\bar{1}$	$P\bar{1}$	$P\bar{1}$
Unit cell dimensions			
a (Å)	10.793(2)	10.807(2)	14.315(3)
b (Å)	10.845(2)	13.295(3)	14.706(3)
c (Å)	12.053(2)	16.318(3)	14.729(3)
α (°)	87.85(3)	84.59(3)	64.86(3)
β (°)	70.80(3)	87.99(3)	63.29(3)
γ (°)	72.98(3)	84.69(3)	89.55(3)
Volume (Å^3)	1271.3(4)	2323.4(8)	2442.4(8)
Z	2	2	2
D_{calc} (Mg m^{-3})	1.508	1.396	1.25
Absorption coefficient (mm^{-1})	0.675	0.513	0.272
F(000)	600	1032	992
Crystal size (mm)	0.15 × 0.15 × 0.10	0.25 × 0.20 × 0.20	0.20 × 0.20 × 0.15
θ Range for data collection (°)	3.18–28.30	3.09–27.39	3.36–27.41
Limiting indices	$-13 \leqslant h \leqslant 13$, $-13 \leqslant k \leqslant 14$, $-10 \leqslant l \leqslant 15$	$-13 \leqslant h \leqslant 11$, $-16 \leqslant k \leqslant 16$, $-20 \leqslant l \leqslant 20$	$-18 \leqslant h \leqslant 18$, $-18 \leqslant k \leqslant 16$, $-17 \leqslant l \leqslant 18$
Reflections collected/unique [R_{int}]	9020/5478 [0.0266]	22279/9324 [0.0300]	15566/9731 [0.0154]
Completeness to 2θ = 25.00 (%)	96.90	99.40	97.70
Absorption correction	psi-scan	psi-scan	psi-scan
Maximum and minimum transmission	1.000 and 0.968	1.000 and 0.976	1.000 and 0.987
Refinement method	full-matrix least-squares on F^2		
Data/restrains/parameters	5478/0/297	9324/0/539	9731/0/565
Goodness-of-fit on F^2	0.981	0.956	1.087
Final R indices [$I > 2\sigma(I)$]	R_1 = 0.0328, wR_2 = 0.0857	R_1 = 0.0516, wR_2 = 0.1309	R_1 = 0.0350, wR_2 = 0.0952
R indices (all data)	R_1 = 0.0420, wR_2 = 0.0902	R_1 = 0.0724, wR_2 = 0.1427	R_1 = 0.0441, wR_2 = 0.0993
Largest difference peak and hole (e Å^{-3})	0.428 and −0.399	1.407 and −0.830	0.564 and −0.344

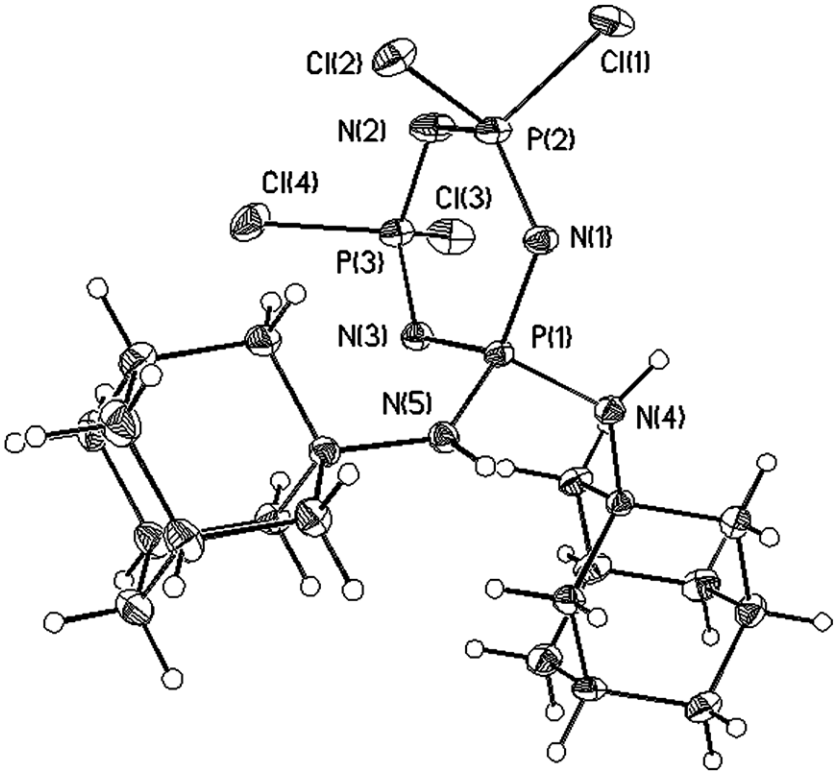

Fig. 1. The ORTEP drawing of **2**. The thermal ellipsoids of non-hydrogen atoms are drawn at 50% probability level.

Crystals of **2** for X-ray determination were obtained directly from the reaction mixture. Single crystals of **3** and **4** were grown from concentrated dichloromethane solutions at room temperature over few days.

2.3. Synthesis

The reaction of $P_3N_3Cl_6$ (**1**) with aminoadamantanes was carried out simply by mixing the solutions of **1** and aminoadamantane derivatives under permanent stirring in the corresponding molar ratios (see Table 1). The excess of Ad-NH_2 (for compound **2**) or triethylamine (for **3** and **4**) played the role of HCl acceptor. The reaction mixture was placed in a tube and heated on oil bath for several hours. The temperature of the bath depended on the boiling point of the solvent. After cooling, the amine hydrochloride was filtered off. Reaction products were obtained after partial (**2**) or complete (**3** and **4**) evaporation of the solvent. Compound **2** was isolated in the crystalline form, while **3** and **4** were obtained as white solid powders and were purified by recrystallization from toluene.

2.3.1. $P_3N_3Cl_4(NH\text{-}Ad)_2$ (**2**)

The yield of **2** was very small, only few crystals were isolated that were used for X-ray study. M.p.: ≫300 °C. $^{31}P\{^1H\}$ NMR (CH_2Cl_2): δ = 19.0 ppm (d), 1.7 ppm (t), $^2J_{P-N-P}$ = 45.6 Hz.

2.3.2. $P_3N_3Cl_2(NH\text{-}Ad)_4$ (**3**)

Yield: 0.355 g (63% with respect to **1**). M.p.: ≫300 °C. $^{31}P\{^1H\}$ NMR (CH_2Cl_2): δ = 20.0 ppm (t), 4.1 ppm (d), $^2J_{P-N-P}$ = 51.5 Hz. *Anal.* Calc. for $P_3N_3Cl_2(NH\text{-}Ad)_4$: C, 59.54; H, 8.00; N, 12.16. Found: C, 58.02; H, 7.30; N, 11.39%. IR: 450 vw, 480 w, 499 w, 549 m, 591 w, 616 sh, 767 vw, 799 w, 837 w, 876 w, 939 vw, 970 w, 1007 m, 1092 m, 1124 m, 1184 m, 1192 sh, 1221 s, 1241 sh, 1285 vw, 1308 w, 1340 w, 1357 w, 1400 w, 1453 w, 2849 m, 2895 vs, 2932 sh, 3250 vw, 3372 vw, 3407 w.

2.3.3. $P_3N_3Cl_2(Mem)_4$ (**4**)

Yield: 0.341 g (69% with respect to **1**). M.p.: 135–138 °C. $^{31}P\{^1H\}$ NMR (CH_2Cl_2): 19.9 ppm (t), 3.8 ppm (d), $^2J_{P-N-P}$ = 52.6 Hz. *Anal.* Calc. for $P_3N_3Cl_2(Mem)_4$: C, 62.73; H, 8.78; N, 10.67. Found: C, 59.21[1]; H, 8.62; N, 9.56%. IR: 447 w, 500 w, 551 m, 591 w, 621 vw, 686 vw, 757 w, 802 s, 839 sh, 868 w, 952 w, 961 sh, 983 w, 1026 s, 1042 s, 1081 vs, 1098 sh, 1142 w, 1182 vs, 1198 s, 1230 s, 1262 s, 1248 w, 1332 w, 1357 m, 1406 w, 1455 m, 2840 s, 2862 m, 2900 vs, 2918 sh, 2944 s, 3273 w, 3372 w, 3397 w.

3. Results and discussion

The formation of compounds **2**–**4** in the course of reaction between **1** and aminoadamantane derivatives is described in Scheme 2.

The $^{31}P\{^1H\}$ NMR spectra of **2**–**4** are very simple. They consist of the characteristic system of multiplets (doublet and triplet, AX_2 spin system) [18,19,26] which corresponds to the suggested structures of geminally substituted derivatives (see Table 2).

The attempt to assign some bands in IR spectra of **3** and **4** was done [27–30]. The absorption bands in region 3200–3400 cm^{-1} can be ascribed to the valence vibrations of N–H groups. Valence vibrations (υ_{as} and υ_s) of CH_x groups (x = 1–3) were found between 2849 and 2932 cm^{-1} for **3** and 2840 and 2944 cm^{-1} for **4**. Bands of deformation vibrations δ_{as} of CH_x groups (x = 1–3) occurs in region 1308–1453 cm^{-1} for **3**, between 1332 and 1455 cm^{-1} for compound **4**, respectively. Signals between 1221 and 1285 cm^{-1} (for **3**) and 1230 and 1248 cm^{-1} (for **4**) correspond to valence vibrations of "endocyclic" P–N bonds or deformation vibrations δ_s of CH_3 groups. Valence vibrations υ_s, υ_{as}, of exocylic P–N bonds, possi-

[1] In this case the lower carbon content was found. According to our experience, very stable phosphorus nitrides are formed during combustion of chlorophosphazene samples and carbon is partially absorbed in these nitrides. Therefore carbon cannot be completely determined.

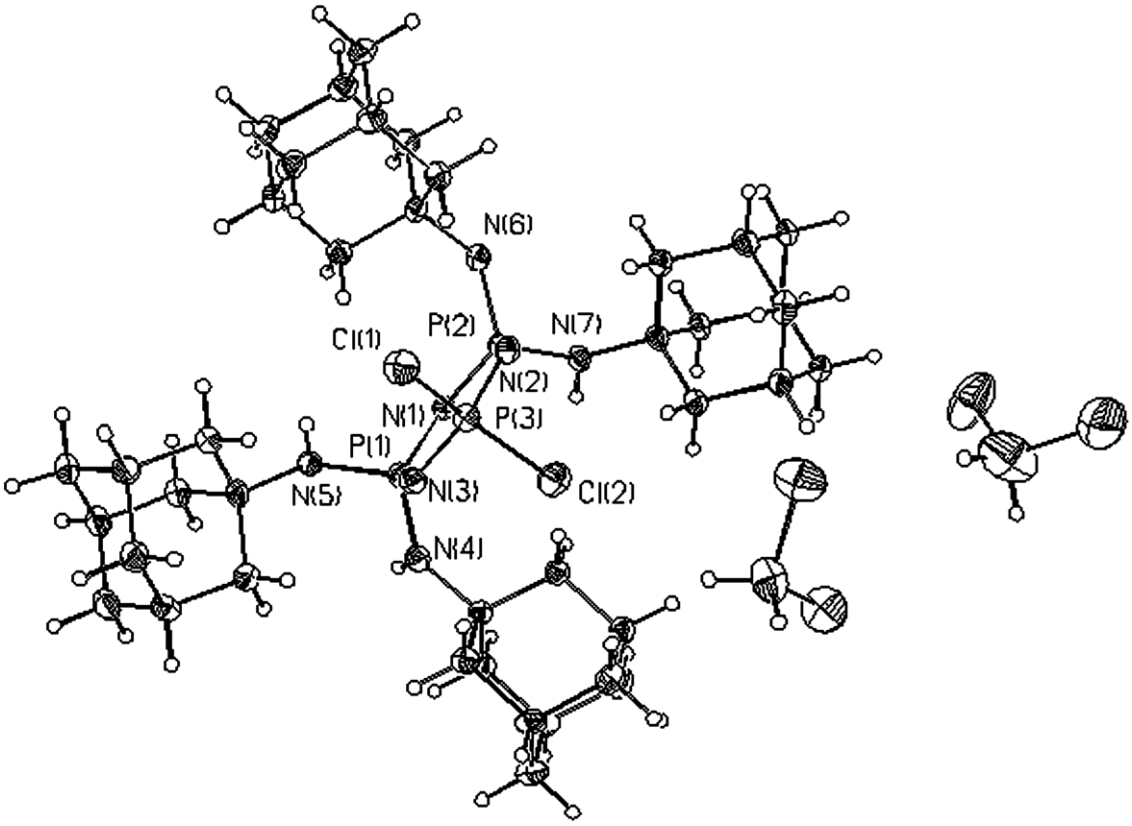

Fig. 2. The ORTEP drawing of **3**. The thermal ellipsoids of non-hydrogen atoms are drawn at 50% probability level.

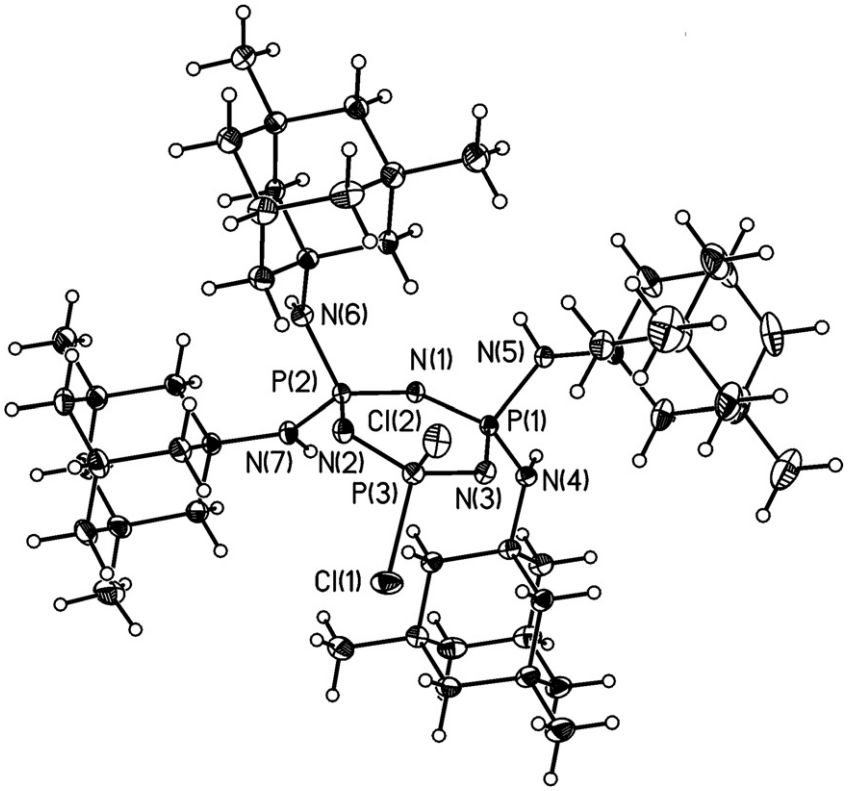

Fig. 3. The ORTEP drawing of **4**. The thermal ellipsoids of non-hydrogen atoms are drawn at 50% probability level.

Table 5
Hydrogen bonding parameters (Å, °) for compounds **2** and **4**

D–H	d(D–H)	d(H···A)	∠DHA	d(D···A)	A
Compound **2**					
N5–H11	0.652	2.604	171.55	3.251	N1 [$-x+2, -y+1, -z+1$]
Compound **4**					
N4–H1	0.810	2.501	170.37	3.302	N2 [$-x+1, -y+2, -z$]

Hydrogen bonds with H···A < r(A) + 2.000 Å and ∠DHA > 110°.

bly also υ_{as} P–N–C vibrations, were observed at wavenumbers 1124–1192 cm^{-1} for **3** and 1142–1198 for **4**. The bands of valence vibrations at 549 cm^{-1} for **3** and 551 cm^{-1} for **4** in spectrum correspond to υ_{as} vibrations of P–Cl groups.

Molecular and crystal structures of **2**–**4** were determined by using X-ray diffraction. The basic crystallographic data are given in Table 3 and selected bond lengths and angles in Table 4.

X-ray determinations proved that all three compounds are triclinic, space group $P\bar{1}$, compound **3** crystallized with two molecules of dichloromethane (Figs. 1–3).

The asymmetric unit of **2**–**4** consists of one symmetric independent molecule. All molecules lie on the common position.

Comparison of molecules **2**–**4** with **1** [31] shows a significant elongation of P–Cl bonds (2.010–2.045 in **2**–**4** to 1.985 Å in **1**) while the length of P–N(H) bond is very similar to other aminophosphazenes (1.621–1.657 Å) [19,32,33]. The substitution of chlorine atoms led to changes in P[N(H)]–N bond lengths of the phosphazene ring (1.598–1.620) when compared with other P(Cl)–N bonds (1.559–1.575 Å).

Crystal structures of **2** and **4** show relevant short contacts. Two molecules of **2** and **4** are bonded together by two N–H···N hydrogen bonds (see Table 5), while **3** contains no H-bridges probably due to the solvation effect of dichloromethane.

The six-membered phosphazene ring in **2** is not strictly planar. All N atoms are slightly distorted from the P1, P2, P3 plane (0.10–0.21 Å). Phosphazene rings of **3** and **4** are situated in a plane and distortions of N atoms are very small. The angles between the phosphazene ring (def. P1, P2, P3 plane) and the planes formed by PCl_2 or $P(NH)_2$, respectively, are in the range of 84.18–89.99°.

Acknowledgements

This work was supported by the Ministry of Education, Youth and Sports of the Czech Republic MSM0021622411. The authors express their gratitude to the Czech Grant Agency for Grant No. 203/02/0436, and Academy of Sciences of the Czech Republic KAN 101630651.

We thank our colleagues from the Faculty of Science, Palacky University, Olomouc, Czech Republic for carrying out elemental analyses.

Appendix A. Supplementary data

CCDC 652802, 652803 and 652804 contain the supplementary crystallographic data for **2**, **3** and **4**. These data can be obtained free of charge via http://www.ccdc.cam.ac.uk/conts/retrieving.html, or from the Cambridge Crystallographic Data Centre, 12 Union Road, Cambridge CB2 1EZ, UK; fax: (+44) 1223-336-033, or e-mail: deposit@ccdc.cam.ac.uk.

References

[1] H. Rose, Ann. Chem. 11 (1834) 131.
[2] J. Liebig, Ann. Chem. 11 (1834) 139.
[3] J.H. Gladstone, J.D. Holmes, J. Chem. Soc. 17 (1864) 225.
[4] H.R. Allcock, Chem. Rev. 72 (1972) 315.
[5] C.W. Allen, Chem. Rev. 91 (1991) 119.
[6] H.R. Allcock, Polyhedron 6 (1987) 119.
[7] C.W. Allen, The Chemistry of Inorganic Homo- and Heterocycles, Academic Press, London, 1987. p. 501.
[8] R. Schenk, G. Römer, Chem. Ber. B 57 (1924) 1343.
[9] R.N. Das, R.A. Shaw, B.C. Smith, M. Woods, J. Chem. Soc., Dalton Trans. (1973) 709.
[10] D.J. Lingley, R.A. Shaw, M. Woods, S.S. Krishnamurthy, Phosphorus Sulfur 4 (1978) 379.
[11] S. Das, R. Keat, R.A. Shaw, B.C. Smith, J. Chem. Soc. (1965) 5032.
[12] N.V. Mani, A.J. Wagner, Acta Crystallogr., Sect. B 27 (1971) 51.
[13] M.J. Begley, D.B. Sowerby, T.T. Bamgboye, J. Chem. Soc., Dalton Trans. (1979) 1401.
[14] W. Polder, A.J. Wagner, Cryst. Struct. Commun. 5 (1976) 253.
[15] M. Kretscham, U. Diefenbach, Z. Anorg, Allg. Chem. 624 (1998) 335.
[16] J.F. Bickley, R. Bonar-Law, G.T. Lawson, P.I. Richards, F. Rivals, A. Steiner, S. Zacchini, Dalton Trans. (2003) 1235.
[17] S.W. Barlett, S.J. Coles, D.B. Davies, M.B. Hursthouse, H. Ibisoglu, A. Kilic, R.A. Shaw, Ün Ilker, Acta Crystallogr., Sect. B 62 (2006) 321.
[18] W.E. Krause, M. Parvez, K.B. Visscher, H.R. Allcock, Inorg. Chem. 35 (1996) 6337.
[19] V. Chandrasekhar, K. Vivekanandan, S. Nagendran, T.S. Andavan, N.R. Weathers, J.C. Yarbrough, A.W. Cordes, Inorg. Chem. 37 (1998) 6192.
[20] J.S. Wishnok, J. Chem. Educ. 50 (1973) 780.
[21] W.L. Dovies, R.R. Grunnert, R.F. Haff, Science 144 (1964) 862.
[22] J. Patočka, Psychiatrie 6 (2002) 35.
[23] D.D. Perrin, W.L.F. Armagedo, Purification of Laboratory Chemicals, 3rd ed., Pergamon Press, Oxford, 1988.
[24] Oxford Diffraction Ltd., XCALIBUR CCD System, CrysAlis Software System, Version 1.168, Oxford, England, 2001.
[25] Bruker, SHELXTL, Version 5.10. Bruker AXS Inc., Madison, WI, USA, 1997.
[26] R. Keat, R.A. Shaw, M. Woods, J. Chem. Soc., Dalton Trans. (1976) 1582.
[27] H. Bürger, Organometal. Chem. Rev. A 3 (1968) 426.
[28] J.-P. Huvenne, G. Vergoten, P. Legrand, J. Mol. Struct. 63 (1980) 47.
[29] P.C. Painter, J. Zarian, M.M. Coleman, Appl. Spectrosc. 36 (3) (1982) 265.
[30] R. Voznicová, M. Alberti, J. Taraba, D. Dastych, P. Kubáček, J. Příhoda, Collect. Czech. Chem. Commun. 72 (2007) 1407.
[31] G.J. Bullen, J. Chem. Soc. A (1971) 1450.
[32] J.K. Fincham, M.B. Hursthouse, H.G. Parkes, L.S. Shaw, R.A. Shaw, Acta Crystallogr., Sect. B 42 (1986) 462.
[33] B. Tercan, T. Hokelek, S. Bilge, B. Ozguc, Z. Kilic, Acta Crystallogr., Sect. C 60 (2004) 381.

Polyhedron 27 (2008) 2083–2090

Contents lists available at ScienceDirect

Polyhedron

journal homepage: www.elsevier.com/locate/poly

A flexible bipyridyl-type linking ligand and its coordination polymers of cobalt, zinc and cadmium: $[Co(L)(NO_3)_2]$, $[Zn(L)(NO_3)_2]$, $[CdL_2(NO_3)_2]$ and $[CdL_2(NO_3)_2](C_6H_6)_2$ (L = (4-py)–CH_2–NH–$(CH_3)C_6H_3$–$C_6H_3(CH_3)$–NH–CH_2–(4-py))

Dongwon Min, Hyun Sue Huh, Soon W. Lee *

Department of Chemistry (BK21), Sungkyunkwan University, Natural Science Campus, Suwon 440-746, Republic of Korea

ARTICLE INFO

Article history:
Received 28 February 2008
Accepted 14 March 2008
Available online 16 May 2008

Keywords:
Flexible bipyridyl-type linking ligand
Coordination polymer
Reduction

ABSTRACT

A long, flexible bipyridyltype linking ligand **L** [(4py)–CH_2–NH–$(CH_3)C_6H_3$–$C_6H_3(CH_3)$–NH–CH_2–(4-py)], which possesses two terminal 4-pyridyl groups, was prepared by reducing its parent diimine ligand (4-py)–CH=N–$(CH_3)C_6H_3$–$C_6H_3(CH_3)$–N=CH–(4-py). Four novel polymeric species based on **L**, $[Co(\mathbf{L})(NO_3)_2]$ (**1**), $[Zn(\mathbf{L})(NO_3)_2]$ (**2**), $[CdL_2(NO_3)_2]$ (**3**) and $[CdL_2(NO_3)_2](C_6H_6)_2$ (**4**), could be synthesized under solvothermal conditions. Whereas polymers **1** and **2** have a 1D zigzag-chain structure, polymers **3** and **4** have a 2D network structure. The N···N separation between the two pyridyl groups in **L** (the free ligand) is 19.871(3) Å, whereas this distance varies from 11.934(4) to 16.373(8) Å in its coordination polymers.

© 2008 Elsevier Ltd. All rights reserved.

1. Introduction

Construction of coordination polymers, also called metal–organic frameworks, by combining appropriate linking ligands and transition metals is currently under intensive study due to their desirable properties applicable to magnetism, photoluminescence, catalytic properties and gas storage [1–6]. Relatively short bipyridyl-type ligands have been used extensively in preparing various metal–organic networks [7–10] as well as pure organic networks [11]. Very long linking ligands containing terminal pyridyls, however, were recently employed in preparing coordination polymers with various topologies [12–19]. We also prepared several long bipyridyl-type ligands $\mathbf{L}^1$–$\mathbf{L}^6$ (Chart 1) and their coordination polymers [20–25].

In controlling the network topologies of coordination polymers, several experimental parameters are known, including the size or polarity of the counterion [26–28], the length of the spacer [29], the pH value of the reaction solution [30], and the nature of the solvents used [31]. Furthermore, it is also known that ligands containing a flexible backbone provide conformational freedom to create greater structural diversity [31,32]. Among the ligands $\mathbf{L}^1$–$\mathbf{L}^6$, ligands $\mathbf{L}^5$ and $\mathbf{L}^6$ turned out to be flexible due to the ring flip of the intervening cyclohexyl fragment in these ligands [24]. On the other hand, ligands $\mathbf{L}^1$–$\mathbf{L}^4$ are structurally rigid because of the presence of the diimine fragments (–CH=N–) in their backbones, that is, a complete conjugated π system. Considering our previous works related to ligands $\mathbf{L}^1$–$\mathbf{L}^6$, we decided to reduce this type of ligands to enhance their structural flexibility that would lead to the creation of novel coordination polymers, which cannot be obtained from their parent diimine ligands. With this aim in mind, we reduced the diimine ligand **L′** [(4-py)–CH=N–$(CH_3)C_6H_3$–$(CH_3)C_6H_3$–N=CH–(4-py)] with sodium borohydride to produce the corresponding flexible ligand **L** [(4-py)–CH_2–NH–$(CH_3)C_6H_3$–$(CH_3)C_6H_3$–NH–CH_2–(4-py)], in which free rotations about the Ar–NH, NH–CH_2 and CH_2–(4-py) bonds may be possible. Herein we report the preparation of this flexible ligand (**L**) and its coordination polymers, $[Co(\mathbf{L})(NO_3)_2]$ (**1**), $[Zn(\mathbf{L})(NO_3)_2]$ (**2**), $[CdL_2(NO_3)_2]$ (**3**) and $[CdL_2(NO_3)_2](C_6H_6)_2$ (**4**).

2. Experimental

All the solid chemicals were purified by recrystallization, and all solvents were distilled and stored over molecular sieves. Infrared (IR) samples were prepared as KBr pellets, and their spectra were obtained in the range 400–4000 cm^{-1} on a Nicolet 320 FTIR spectrophotometer. Elemental analyses were performed with EA1110 (CE instrument, Italy) at the Korea Basic Science Institute. Thermogravimetric analysis (TGA) was conducted on a TA4000/SDT 2960 instrument at the Cooperative Center for Research Facilities (CCRF) in Sungkyunkwan University. ^1H and $^{13}C\{^1H\}$ NMR data were collected on a 500 MHz Varian Inova spectrometer.

* Corresponding author. Tel.: +82 31 290 7066; fax: +82 31 290 7075.
E-mail address: soonwlee@skku.edu (S.W. Lee).

0277-5387/$ - see front matter © 2008 Elsevier Ltd. All rights reserved.
doi:10.1016/j.poly.2008.03.024

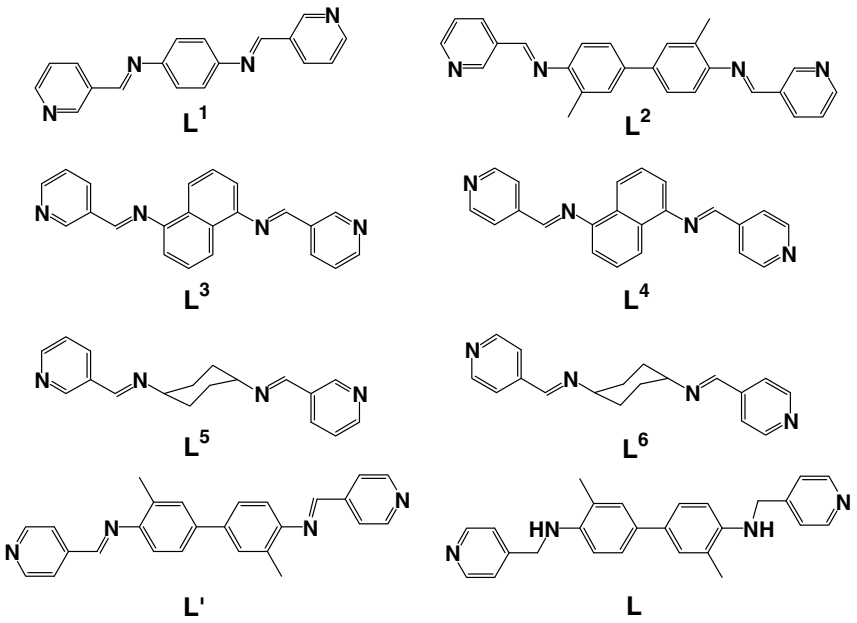

Chart 1.

2.1. Preparation of [(4-py)–CH=N–$(CH_3)C_6H_3$–$C_6H_3(CH_3)$–N=CH–(4-py)] (**L′**)

To 4-pyridine carboxaldehyde (6.30 ml, 66.8 mmol) in methanol (200 ml) was added *o*-tolidine dihydrochloride hydrate {[–$C_6H_3(CH_3)$-4-$NH_2]_2 \cdot 2HCl \cdot H_2O$, 9.52 g, 33.4 mmol)} at room temperature. After the addition of dichlomethane (400 ml) and then several drops of formic acid, the mixture was stirred at room temperature for 24 h. The solvent was removed under vacuum, and the residue was extracted with dichloromethane (500 ml), and washed with a saturated Na_2CO_3 solution (500 ml) and then with water (500 ml × 2). The organic phase was dried over $MgSO_4$ and filtered. Upon removal of the solvent, an analytically pure yellow crystalline solid was obtained in 86% yield. ^{1}H NMR (500 MHz, $CDCl_3$) δ: 8.77 (m, 4H), 8.46 (m, 2H), 7.80 (m, 2H), 7.54–7.32 (m, 4H), 7.07 (m, 2H), 2.49 (s, 6H). $^{13}C\{^1H\}$ NMR (125 MHz, $CDCl_3$) δ: 157.0, 150.8, 149.2, 143.2, 139.3, 133.5, 129.3, 125.5, 122.5, 118.0, 18.7. IR (KBr, cm^{-1}): 1622 (s), 1595 (s), 1546 (w), 1484 (w), 1414 (w), 1322 (w), 1220 (w), 1124 (s), 1059 (s), 989 (s), 822 (s), 645 (s), 556 (s), 518 (s), 486 (s). *Anal.* Calc. for $C_{26}H_{22}N_4$: C, 78.97; H, 5.68; N, 14.35. Found: C, 78.94; H, 6.07; N, 14.82%.

2.2. Preparation of [(4-py)–CH_2–NH–$(CH_3)C_6H_3$–$C_6H_3(CH_3)$–NH–CH_2–(4-py)] (**L**)

To compound **L′** (7.0 g, 17.9 mmol) in methanol (200 ml) and dichlomethane (300 ml) was added sodium borohydride (6.78 g, 179 mmol) in small portions with stirring at room temperature. The resulting mixture was stirred at room temperature for 12 h. The solvent was removed under vacuum, and the residue was extracted with dichloromethane (300 ml), and washed with water (300 ml × 3). The organic phase was dried over $MgSO_4$ and filtered, and upon removal of the solvent, an analytically pure yellow crystalline solid was obtained (6.22 g, 15.8 mmol, 88% yield). ^{1}H NMR (500 MHz, $CDCl_3$) δ: 8.58 (m, 4H), 7.34–7.21 (m, 10H), 6.47 (dd, 2H), 4.47 (s, 4H), 4.07 (br s, 2H), 2.28 (s, 6H). ^{13}C NMR (125 MHz, $CDCl_3$)δ: 150.2, 149.4, 144.2, 131.3, 128.8, 125.3, 122.6, 122.3, 110.7, 47.4, 18.0. IR (KBr, cm^{-1}): 3322 (w), 1603 (s), 1503 (s), 1470 (w), 1440 (w), 1414 (w), 1308 (s), 1254 (s), 1140 (w), 1065 (w), 992 (w), 804 (w). *Anal.* Calc. for $C_{26}H_{26}N_4$: C, 79.16; H, 6.64; N, 14.20. Found: C, 79.30; H, 6.62; N, 14.70%.

2.3. Preparation of [$Co(L)(NO_3)_2$] (**1**)

A mixture of $Co(NO_3)_2 \cdot 6H_2O$ (29.7 mg, 0.10 mmol), ligand **L** (39.4 mg, 0.1 mmol), methanol (10 ml) and benzene (3 ml) was heated in a vial at 70 °C for 3 days and then cooled to room temperature by air-cooling. The crystalline product was collected by filtration, washed with methanol, and air-dried to give violet crystals of polymer **1** (25 mg, 0.043 mmol, 43%). IR (KBr, cm^{-1}): 3427 (w), 1618 (s), 1502 (s), 1429 (w), 1382 (w), 1292 (s), 1261 (s), 1145 (w), 1018 (w), 806 (w). *Anal.* Calc. for $C_{26}H_{26}CoN_6O_6$: C, 54.18; H, 4.54; N, 14.55. Found: C, 54.06; H, 4.58; N, 14.18%.

2.4. Preparation of [$Zn(L)(NO_3)_2$] (**2**)

Polymer **2** was prepared similarly to polymer **1**. A mixture of $Zn(NO_3)_2 \cdot 6H_2O$ (29.7 mg, 0.10 mmol), ligand **L** (39.4 mg, 0.10 mmol), methanol (10 ml) and benzene (5 ml) was heated at 70 °C for 10 days. Yield: 5.1%. IR (KBr, cm^{-1}): 3426 (w), 1622 (s), 1505 (s), 1494 (s), 1432 (s), 1383 (s), 1305 (s), 1263 (s), 1146 (w), 1063 (w), 1031 (w), 805 (w). *Anal.* Calc. for $C_{26}H_{26}ZnN_6O_6$: C, 53.48; H, 4.49; N, 14.39. Found: C, 53.31; H, 4.70; N, 14.60%.

2.5. Preparation of [$CdL_2(NO_3)_2$] (**3**)

A mixture of $Cd(NO_3)_2 \cdot 4H_2O$ (30.0 mg, 0.10 mmol), ligand **L** (39.0 mg, 0.10 mmol) and methanol (10 ml) was heated in a vial at 70 °C for 3 days and then cooled to room temperature by air-cooling. The crystalline product was collected by filtration, washed with methanol, and air-dried to give yellow crystals of polymer **3** (25 mg, 0.0244 mmol, 49%). IR (KBr, cm^{-1}): 3434 (w), 3408 (w), 1611 (s), 1584 (w), 1506 (s), 1425 (s), 1383 (s), 1309 (s), 1268 (s), 1145 (w), 1102 (w), 1013 (w), 876 (w), 823 (w), 801 (w). *Anal.* Calc. for $C_{52}H_{52}CdN_{10}O_6$: C, 60.91; H, 5.11; N, 13.66. Found: C, 60.12; H, 4.98; N, 14.01%.

Table 1
X-ray data collection and structure refinement details

	L	1	2	3	4
Empirical formula	$C_{26}H_{26}N_4$	$C_{26}H_{26}CoN_6O_6$	$C_{26}H_{26}ZnN_6O_6$	$C_{52}H_{52}CdN_{10}O_6$	$C_{64}H_{64}CdN_{10}O_6$
Formula weight	394.51	577.46	583.90	1025.44	1181.65
Temperature (K)	296(2)	293(2)	293(2)	296(2)	293(2)
Crystal system	monoclinic	monoclinic	monoclinic	triclinic	monoclinic
Space group	$P2_1/c$	$C2/c$	$C2/c$	$P\bar{1}$	$P2_1/n$
a (Å)	10.9086(2)	27.619(7)	27.745(6)	9.2849(10)	12.241(3)
b (Å)	17.3633(4)	7.683(2)	7.734(2)	9.5473(9)	15.970(3)
c (Å)	11.3236(3)	12.507(4)	12.468(4)	15.163(2)	15.141(3)
α (°)				95.80(1)	
β (°)	99.822(2)	98.86(2)	99.42(2)	100.53(1)	93.80(2)
γ (°)				116.78(1)	
V (Å^3)	2113.36(8)	2622(1)	2639(1)	1153.8(2)	2953.4(9)
Z	4	4	4	1	2
D_{calc} (g cm^{-3})	1.240	1.463	1.469	1.476	1.329
μ (mm)	0.075	0.707	0.983	0.538	0.430
$F(000)$	840	1196	1208	530	1228
T_{min}		0.3995	0.6064	0.8909	0.6132
T_{max}		0.4408	0.6733	0.9788	0.6309
Number of reflections measured	16944	2353	2300	18365	5445
Number of reflections unique	5223	2301	2248	5632	5188
Number of reflections with $I > 2\sigma(I)$	1592	1882	1293	2352	3199
Number of parameters refined	375	181	181	313	345
2θ Range (°)	3.5–50	3.5–50	3.5–50	4.8–57.0	3.5–50
Maximum, in $\Delta\rho$ (e Å^{-3})	0.134	0.299	0.867	0.715	0.997
Minimum, in $\Delta\rho$ (e Å^{-3})	−0.151	−0.283	−0.801	−0.481	−0.859
Goodness-of-fit on F^2	0.762	1.038	1.082	0.976	1.039
R_1[a]	0.0482	0.0431	0.0782	0.0631	0.0749
wR_2[b]	0.0970	0.1037	0.1762	0.1429	0.1875

[a] $R_1 = \sum[|F_o| - |F_c|]/\sum|F_o|]$.
[b] $wR_2 = \sum[w(F^2_o - F^2_c)^2]/\sum[w(F^2_o)^2]^{1/2}$.

Table 2
Selected bond lengths (Å) and angles (°)

Ligand ***L***					
N2–C7	1.395(2)	N2–C6	1.438(3)	N3–C16	1.392(2)
N3–C21	1.425(3)	C7–N2–C6	120.2(2)	C16–N3–C21	121.3(2)
N2–C6–C3	110.9(2)	N3–C21–C22	111.5(2)		
Polymer ***1***					
Co1–O2	2.070(2)	Co1–O1	2.286(2)	Co1–N1	2.072(2)
N2–C7	1.395(4)	N2–C6	1.431(4)	O2–Co1–N1	113.1(1)
O2–Co1–O1	84.8(1)	N1–Co1–O1	160.6(1)	C7–N2–C6	123.6(3)
N2–C6–C3	117.5(2)				
Polymer ***2***					
Zn1–O1	2.039(7)	Zn1–N1	2.052(6)	Zn1–O3	2.492(9)
N2–C7	1.407(10)	N2–C6	1.434(12)	O1–Zn1–N1	117.1(3)
O1–Zn1–O3	54.5(3)	N1–Zn1–O3	88.7(3)	C7–N2–C6	123.2(9)
N2–C7–C8	118.7(7)				
Polymer ***3***					
Cd1–O1	2.354(5)	Cd1–N3	2.338(6)	Cd1–N1	2.345(4)
N2–C7	1.381(6)	N2–C6	1.427(6)	N3–Cd1–N1	92.1(2)
N3–Cd1–O1	83.5(2)	N1–Cd1–O1	88.1(2)	C7–N2–C6	124.1(4)
N2–C6–C3	116.2(4)				
Polymer ***4***					
Cd1–O1	2.333(9)	Cd1–N1	2.380(5)	Cd1–N4	2.364(5)
N2–C7	1.403(8)	N2–C6	1.440(9)	O1–Cd1–N4	95.8(4)
O1–Cd1–N4	84.2(4)	O1–Cd1–N1	84.8(3)	C7–N2–C6	121.3(6)
N2–C6–C3	115.3(6)				

2.6. Preparation of $[CdL_2(NO_3)_2](C_6H_6)_2$ (**4**)

Polymer **4** was prepared similarly to polymer **1**. A mixture of $Cd(NO_3)_2 \cdot 4H_2O$ (30.0 mg, 0.10 mmol), ligand **L** (39.0 mg, 0.10 mmol), methanol (10 ml) and benzene (5 ml) was heated at 70 °C for 3 days. Yield: 10%. IR (KBr, cm^{-1}): 3408 (w), 1611 (s), 1510 (s), 1424 (s), 1383 (s), 1309 (s), 1264 (s), 1218 (w), 1142 (w), 1062 (w), 1039 (w), 1014 (w), 992 (w), 803 (w), 687 (w). *Anal.* Calc. for $C_{64}H_{64}CdN_{10}O_6$: C, 65.05; H, 5.46; N, 11.85. Found: C, 64.80; H, 5.33; N, 12.01%.

2.7. X-ray structure determination

All X-ray data were collected with a Siemans P4 diffractometer (**1**, **2** and **4**) or a Bruker Smart APEX2 diffractometer (**L** and **3**) equipped with a Mo X-ray tube. No absorption corrections were made for the ligand **L**, but intensity data were empirically corrected for absorption with ψ-scan data (**1**, **2**, **4**) or SADABS (**3**) [33]. All calculations were carried out with SHELXTL programs [34]. All structures were solved by direct methods. All non-hydrogen atoms were refined anisotropically. All hydrogen atoms were generated in idealized positions and refined using the riding model.

A colorless crystal of **L** of approximate dimensions 0.18 × 0.12 × 0.10 mm^3, shaped as a block, was used for crystal and intensity data collection. A violet crystal of **1** (a block, 0.36 × 0.28 × 0.10 mm^3), a yellow crystal of **2** (a block, 0.26 × 0.24 × 0.06 mm^3), a yellow crystal of **3** (0.22 × 0.12 × 0.04 mm^3) and a yellow crystal of **4** (a block, 0.42 × 0.12 × 0.10 mm^3) were used. Details of the crystal data, intensity collection and refinement details are given in Table 1. Selected bond lengths and angles are given in Table 2.

3. Results and discussion

3.1. Synthesis

A long, flexible bis(monodentate) linking ligand $C_{26}H_{26}N_4$ (**L**), which possesses two terminal pyridyl groups with their nitrogen atoms in the 4,4′-positions, was prepared in two steps on a relatively large scale (Eq. (1)). In the first step, the diimine species [(4-py)–CH=N–$(CH_3)C_6H_3$–$C_6H_3(CH_3)$–N=CH–(4-py)] (**L′**), a positional isomer of the ligand **L**[2] (Chart 1), was prepared in 86% yield by the condensation of a diamine (*o*-tolidine dihydrochloride hydrate) and a pyridinealdehyde (4-pyridine carboxaldehyde) at room temperature. In the second step, **L′** was reduced with sodium borohydride to give [(4-py)–CH_2–NH–$(CH_3)C_6H_3$–$C_6H_3(CH_3)$–NH–CH_2–(4-py)] (**L**) in 88% yield.

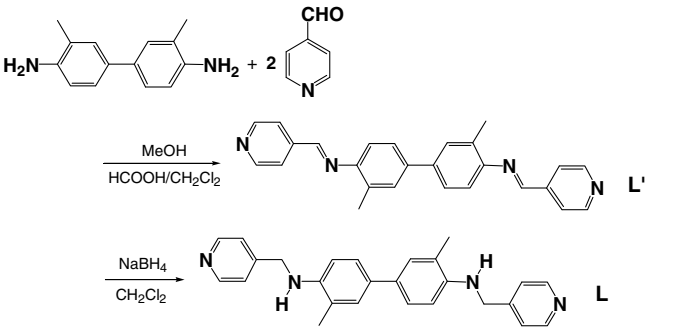

(1)

Because of the possible rotations about the Ar–NH, NH–CH_2 and CH_2–(4-py) single bonds, the ligand **L** is expected to be considerably more flexible than $\mathbf{L}^1$–$\mathbf{L}^4$ [20–23]. However, X-ray structural analysis of ligand **L** and its coordination polymers **1**–**4** revealed that this ligand exhibits only two out of several possible conformations, in which the two terminal 4-pyridyl groups (or two central methyl groups) are located on either the opposite (*Z*-mode) or the same (*U*-mode) side of the central biphenyl fragment [35]. The *Z*-mode conformer can be transformed to the *U*-mode one by rotation about the central C–C bond, and vice versa.

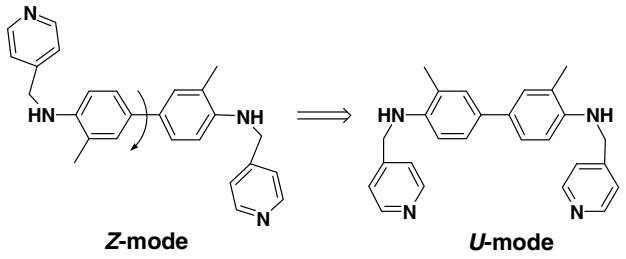

Solvothermal treatment of cobalt(II) nitrate and zinc(II) nitrate with the ligand **L** in methanol–benzene at 70 °C produced a 1D cobalt $[Co(\mathbf{L})(NO_3)_2]$ (**1**) and a 1D zinc coordination polymer $[Zn(\mathbf{L})(NO_3)_2]$ (**2**), respectively (Eqs. 2 and 3). In addition, a 2D grid cadmium polymer $[Cd\mathbf{L}_2(NO_3)_2]$ (**3**) was prepared from cadmium(II) nitrate and the ligand **L** in methanol at 70 °C (Eq. (4)). Interestingly, when the last reaction was carried out in a mixed solvent (methanol–benzene), a guest-containing cadmium polymer, $[Cd\mathbf{L}_2(NO_3]_2](C_6H_6)_2$ (**4**), was prepared (Eq. (5)).

$$Co(NO_3)_2 + \mathbf{L} \xrightarrow{MeOH/C_6H_6} [Co(\mathbf{L})(NO_3)_2]\ (\mathbf{1}) \quad (2)$$

$$Zn(NO_3)_2 + \mathbf{L} \xrightarrow{MeOH/C_6H_6} [Zn(\mathbf{L})(NO_3)_2]\ (\mathbf{2}) \quad (3)$$

$$Cd(NO_3)_2 + \mathbf{L} \xrightarrow{MeOH} [Cd\mathbf{L}_2(NO_3)_2]\ (\mathbf{3}) \quad (4)$$

$$Cd(NO_3)_2 + \mathbf{L} \xrightarrow{MeOH/C_6H_6} [Cd\mathbf{L}_2(NO_3)_2](C_6H_6)\ (\mathbf{4}) \quad (5)$$

It would be meaningful to consider the preparation of polymers **1** and **2**. Our initial goal was to prepare coordination polymers that contained guest (benzene) molecules, which might be able to act as a template to enhance the dimensionality of the target polymers. Inconsistent with our expectation, reactions only in methanol did not produce suitable crystals for X-ray diffraction. Only the reactions in the presence of benzene led to the formation of single crystalline products, which do not contain the benzene molecules. Although we do not know the exact function of benzene in our reaction system, benzene appears to have promoted the formation of good crystals. Similar observations were previously reported in the preparation of $[Cu_3(C_6H_8O_4)_3(H_2O)_2(C_6H_{11}OH)]$ [36], $[M_3(2,6\text{-}NDC)_3(bipy)_{1.5}]$ (M = Ni, Co; 2,6-NDC = 2,6-naphthalenedicarboxylate; bipy = 4,4′-bipyridyl) [37] and $[Cu(1,3\text{-}BDC)(H_2O)]\cdot 2H_2O$ (1,3-BDC = 1,3-benzenedicarboxylate) [38].

3.2. Structure

The molecular structure of **L**, with the atom-numbering scheme, is shown in Fig. 1, in which two terminal pyridyl groups are linked by a diamide moiety (–CH_2–NH–$(CH_3)C_6H_3$–$(CH_3)C_6H_3$–NH–CH_2–) and have their pyridyl nitrogen atoms at the *para* positions (4,4′). Ligand **L** has a *Z*-conformation, in which two methyl substituents are directed to opposite directions (*anti* orientation). The N···N separation between the two terminal pyridyl rings is 19.871(3) Å, and these rings are essentially parallel to each other with a dihedral angle of 3.7(2)°. The two phenyl rings in the central biphenyl fragment are significantly twisted from each other by 39.17(6)°. The N2–C6 (1.438(3) Å) and N3–C21 (1.425(3) Å) bond lengths indicate N–C single bonds.

A monomer unit of polymer **1** is shown in Fig. 2, which shows that the Co(II) metal is 6-coordinate and its coordination sphere consists of two pyridyl nitrogens and four η^2-nitrato oxygen atoms. The Co metal lies on the crystallographic C_2-axis, which explains the *Z* value of **4** rather than **8** (Table 1). The N–H hydrogen is involved in intermolecular N–H···O hydrogen bonding: N2–H2 = 0.73 Å; N2···O1 ($-x$, $y+1$, $-z+1/2$) = 2.66 Å; N2–H2···O1 = 136°. The projection of polymer **1** along the *b*-axis demonstrates its one-dimensional zigzag structure (Fig. 3). This chain is formed by the bridging **L** ligands linking Co metals in the [1 0 1] direction, with a N···N separation of 16.112(6) Å and a Co···Co separation of 19.275(4) Å. The **L** ligands adopt the *Z*-conformation, which is quite similar to that found in the molecular ladder prepared from $Cd(NO_3)_2$ and 1,4-bis(4-pyridylmethyl)benzene in a 2:3 molar ratio [39].

Polymer **2** is isostructural with polymer **1**, and its monomer unit and projection along the *b*-axis are presented in Figs. 4 and 5, respectively. The Zn metal lies on the crystallographic C_2-axis, and the nitrato ligand η^2-coordinates in an asymmetric mode (Zn1–O1 = 2.039(7) Å; Zn1–O3 = 2.492(9) Å). The N···N separation in the one-dimensional zigzag chain is 16.083(11) Å, and the Zn···Zn separation is 19.302(4) Å.

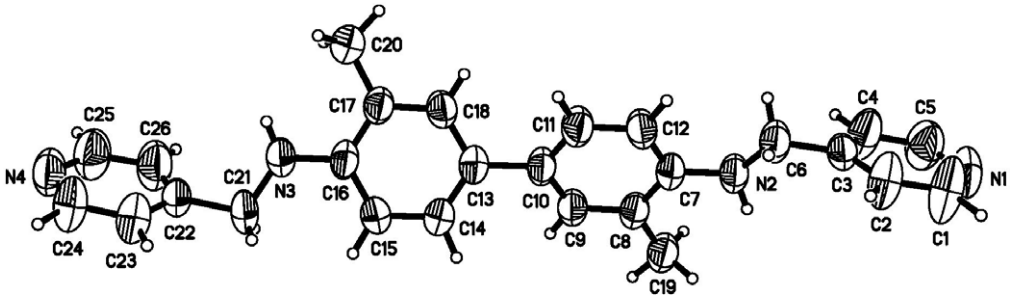

Fig. 1. ORTEP drawing of ligand **L** with 50% probability thermal ellipsoids.

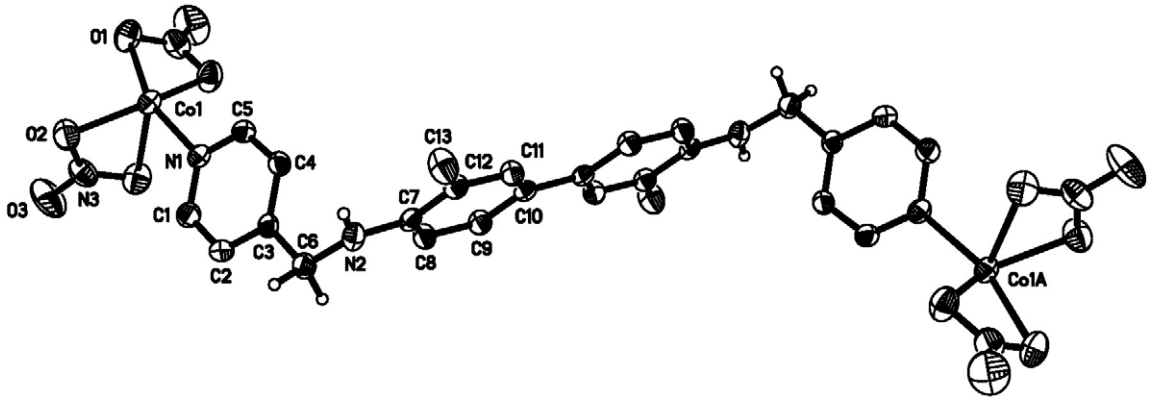

Fig. 2. Local coordination environment around the cobalt atom in polymer **1**. Unlabelled atoms are related to labelled atoms by the inversion symmetry.

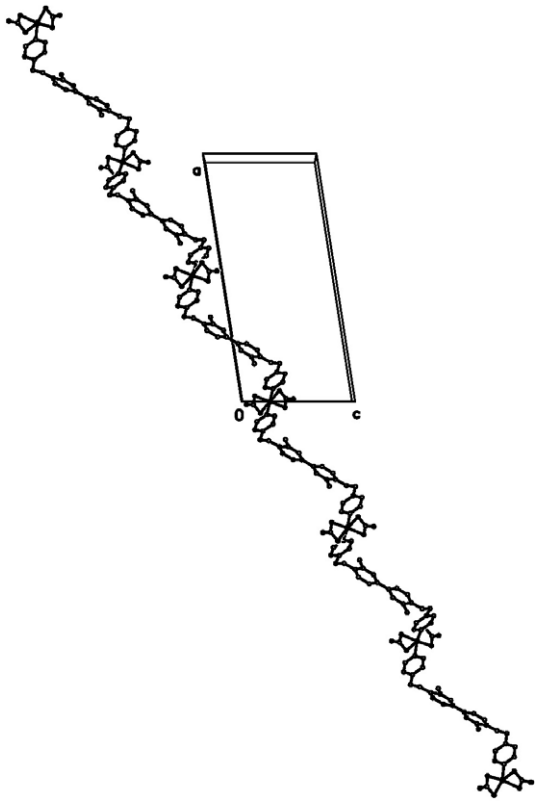

Fig. 3. Projection of polymer **1** along the *b*-axis, showing a linear zigzag chain structure.

A monomer unit of polymer **3** is given in Fig. 6, which shows that the Cd(II) metal is 6-coordinate and its coordination sphere consists of four pyridyl nitrogens and two oxygens of two η^1-NO_3 ligands. The Cd metal is located on the crystallographic inversion center. The N2–C6 and N2–C7 bond lengths are 1.427(6) and 1.381(6) Å, respectively. Fig. 7 shows a projection along the *a*-axis. Polymer **3** has a 2D structure that extends approximately in the [0 1 1] direction, and consists of layers of grids. Each grid consists of four Cd metals and four **L** ligands, forming a large 84-membered (80 ligand atoms and 4 Co metals) ring with dimensions of ca. 20.2×20.3 Å^2 (based on the Cd···Cd separations). Despite the presence of large repeating rings, polymer **3** does not exhibit the interpenetration phenomenon and does not contain guest molecules, either. In polymer **3**, the ligands have practically the same N···N separation [16.363(8) and 16.373(10) Å]. In addition, the metals also have practically the same Cd···Cd separation [20.274(3) and 20.201(3) Å].

A monomer unit of polymer **4** is shown in Fig. 8. The Cd(II) metal is 6-coordinate with a $[CdN_4O_2]$ core, and its coordination sphere consists of four pyridyl nitrogens and two oxygens of two η^1-NO_3 ligands. The N···N separation between the terminal pyridyl rings is 11.934(8) Å. The N3–H3 hydrogen is involved in intermolecular N–H···O hydrogen bonding: N3–H3 = 0.72 Å; N2···O3 $(-x+2, -y, -z+2)$ = 2.46 Å; N3–H3···O3 = 163°.

Fig. 9 shows a projection of polymer **4** approximately perpendicular to the (0 1 1) plane, which shows a 2D compact network containing benzene guest molecules. It is worth noting that all the **L** ligands in polymer **4** adopt the *U*-conformation (*syn*-orientation of pyridyl groups). This type of coordination of bipyridyl-based ligands is rather unusual and was previously reported for [Cd(3-pmpmd)$_{1.5}$(NO$_3$)$_2$] · EtOH and [Zn(3-pmpmd)$_{1.5}$(NO$_3$)$_2$] · MeOH (3-

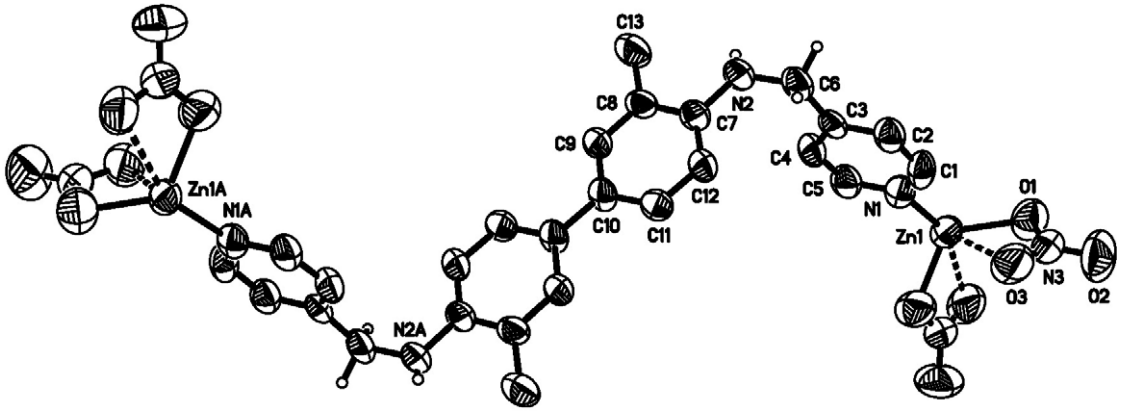

Fig. 4. ORTEP drawing of local environment of zinc in polymer **2**.

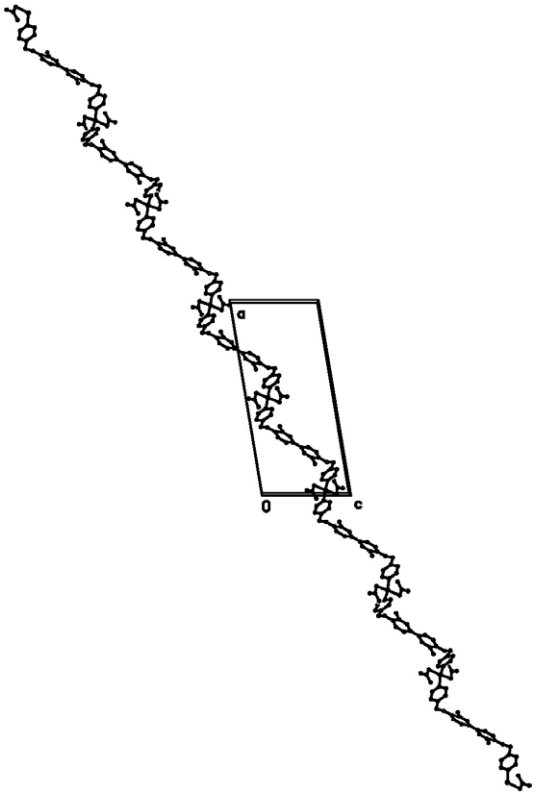

Fig. 5. Projection of polymer **2** along the *b*-axis, showing a linear zigzag chain structure.

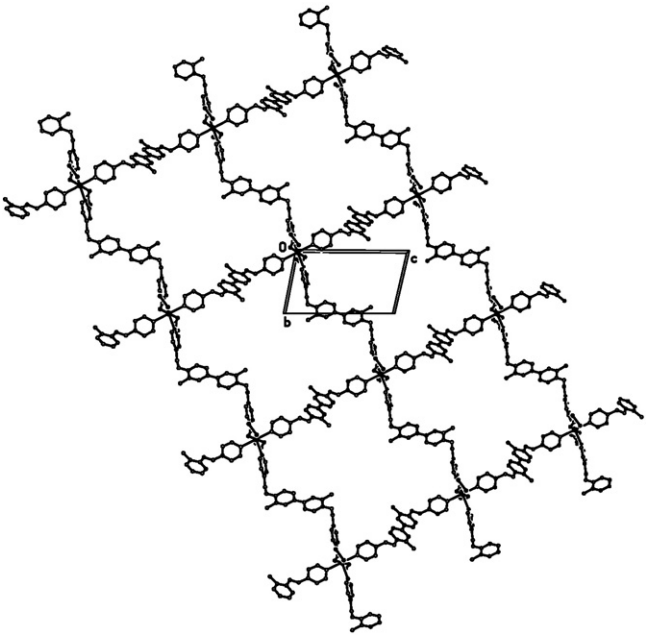

Fig. 7. Projection of polymer **3** along the *a*-axis, showing a 2D grid network.

pmpmd = *N*,*N*′-bis(3-pyridylmethyl)pyromellitic diimide) [35]. The benzene guest molecules are located inside the cavities of the 2D framework. Each cadmium metal is linked by four ligands that approximately form a square plane with 90° to one another. If the four ligands are taken as two independent sets of two ligands,

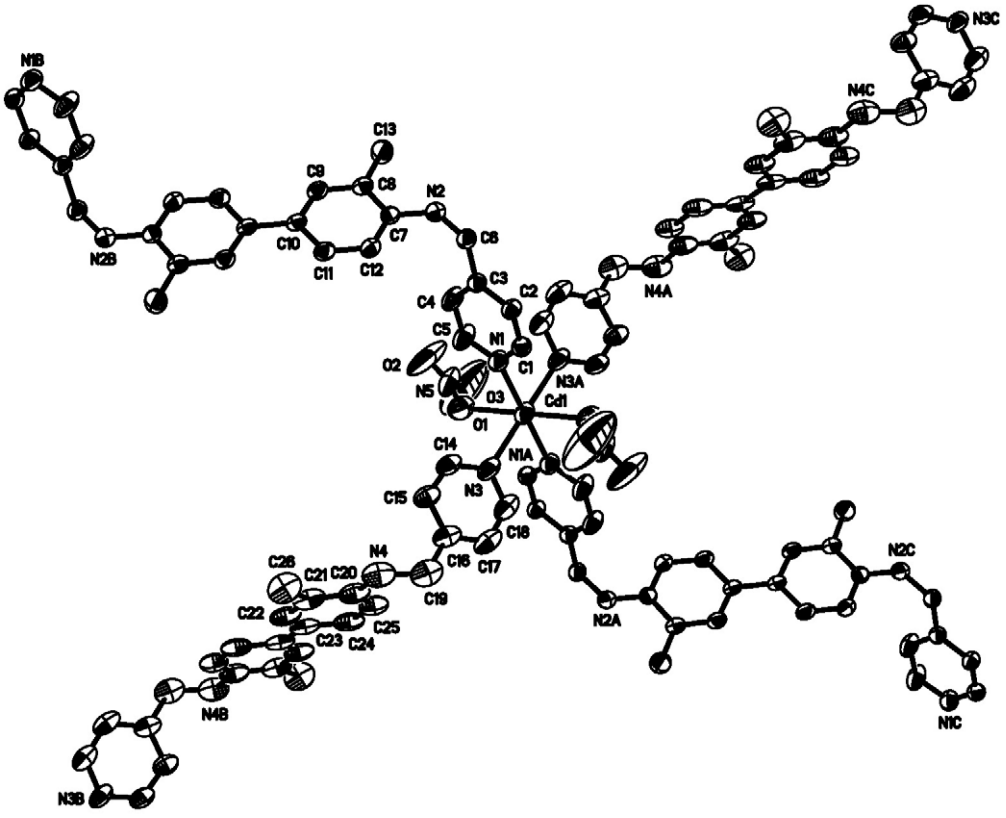

Fig. 6. Local coordination environment of cadmium in polymer **3**.

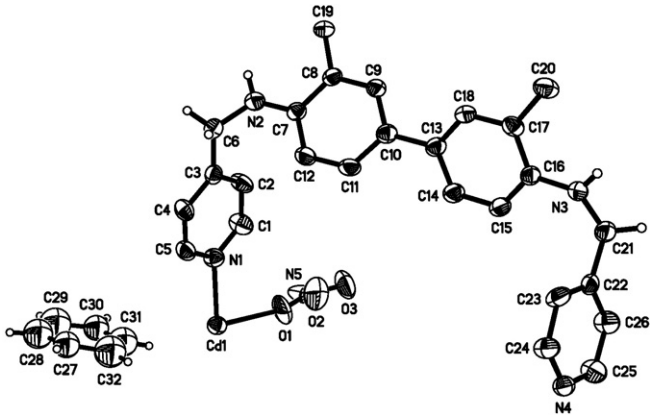

Fig. 8. Local coordination environment around the cadmium atom in polymer **4**.

Fig. 6 looks like a combination of two honeycombs (red and black), each of which is generated by each ligand set. Nevertheless, in fact, the actual unit in polymer **4** is a 84-membered ring, composed of four Cd atoms and four ligands (M_4L_4). Although polymers **3** and **4** have the same framework formula {[Cd**L**$_2$(NO_3)$_2$]}, their framework structures are essentially different, depending on the absence (**3**) or presence (**4**) of guest molecules.

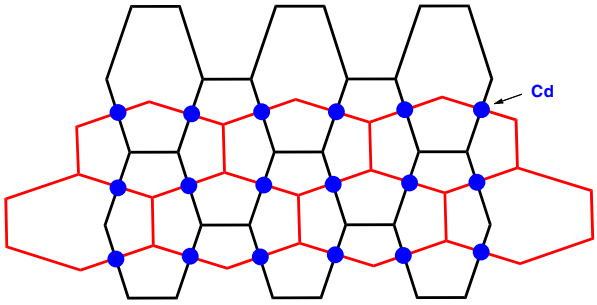

3.3. Thermogravimetric analyses

Thermogravimetric analyses (TGA) were performed on polymers **1**–**4** by heating them up to 800 °C. The framework of polymer **1** is stable up to 202 °C, above which an abrupt weight loss occurs between 202 and 275 °C, followed by another abrupt weight loss between 373 and 416 °C, which corresponds to the breakdown of its framework. Polymer **2** is stable up to 261 °C, and two subsequent weight losses occur at 261–264 and 373–449 °C. These data indicate that the thermal stability of the framework of polymer **2** is higher than that of polymer **1**. The TGA of polymer **3** displays two steps of weight loss: an abrupt weight loss at 256–523 °C and a gradual weight loss above 582 °C. The guest-containing polymer **4** exhibits a gradual weight loss (about 16%) in the range 178–215 °C, corresponding to the loss of the guest benzene molecules. The framework of polymer **4** decomposes above 273 °C. When heated at 220 °C for 2 h, polymer **4** gave its guest-free form, which is amorphous. Therefore, we gave up desorption–resorption experiments for this polymer.

4. Conclusion

In summary, we prepared a long, flexible (4,4′-bipyridyl)-type linking ligand **L** [(4-py)–CH_2–NH–(CH_3)C_6H_3–C_6H_3(CH_3)–NH–CH_2–(4-py)] by reducing its parent diimine species (4-py)–CH═N–(CH_3)C_6H_3–C_6H_3(CH_3)–N═CH–(4-py) (**L**′). Novel zinc (**1**), cobalt (**2**) and cadmium (**3** and **4**) coordination polymers were prepared from the corresponding metal nitrates and the ligand **L** under solvothermal conditions. The N···N separation between the two pyridyl groups in **L** (in the free state) is 19.871(3) Å, and this distance varies from 11.934(4) to 16.373(8) Å in the polymers **1**–**4**. In addition, **L** coordinates to the metal via its terminal pyridyl nitrogen atoms either in the *Z*-mode (in polymers **1**–**3**) or in the *U*-mode (in polymer **4**). Whereas polymers **1** and **2** have a 1D zigzag-chain structure, polymers **3** and **4** have a 2D network structure. Several conclusions may be drawn from our work: (1) Reduction of diimine with $NaBH_4$ to give its reduced form proceeds readily at room temperature in high yield. (2) Benzene promoted the formation of high-quality crystals of polymers **1** and **2**. (3) The various N···N separations and two conformation modes in

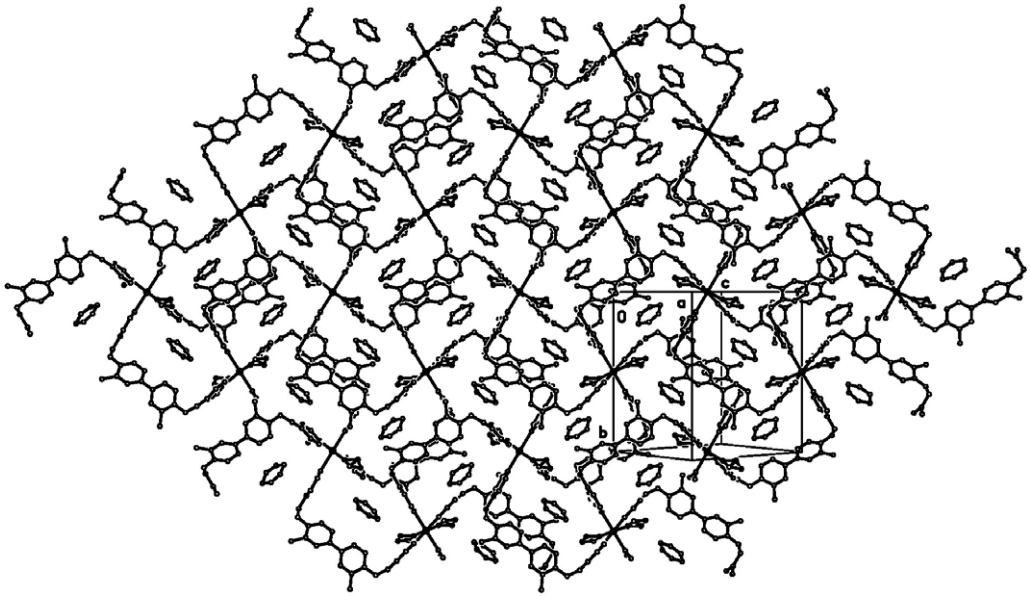

Fig. 9. Projection of polymer **4**, showing the *U*-mode of ligand **L**.

the coordination polymers indicate the high flexibility of ligand **L**. (4) The amine nitrogen atoms in **L** do not bind to the metal in all the polymers.

5. Supplementary data

CCDC 672275, 672276, 672277, 672278 and 672279 contain the supplementary crystallographic data for **L**, **1**, **2**, **3** and **4**. These data can be obtained free of charge via http://www.ccdc.cam.ac.uk/conts/retrieving.html, or from the Cambridge Crystallographic Data Centre, 12 Union Road, Cambridge CB2 1EZ,UK; fax: (+44) 1223-336-033; or e-mail: deposit@ccdc.cam.ac.uk.

References

[1] P.J. Hagrman, D. Hagrman, J. Zubieta, Angew. Chem., Int. Ed. 38 (1999) 2638.
[2] M.J. Zaworotko, B. Moulton, Chem. Rev. 101 (2001) 1629.
[3] M. Eddaoudi, D.B. Moler, H. Li, B. Chen, T.M. Reineke, M.O. Keeffe, O.M. Yaghi, Acc. Chem. Res. 34 (2001) 319.
[4] K. Nomiya, H. Yokoyama, J. Chem. Soc., Dalton Trans. (2002) 2483.
[5] A.Y. Robin, K.M. Fromm, Coord. Chem. Rev. 250 (2006) 2127.
[6] J.J. Vittal, Coord. Chem. Rev. 251 (2007) 1781.
[7] O.M. Yaghi, H. Li, C. Davis, D. Richardson, T.L. Groy, Acc. Chem. Res. 31 (1998) 474.
[8] S.R. Batten, R. Robson, Angew. Chem., Int. Ed. 37 (1998) 1460.
[9] A.J. Blake, N.R. Champness, P. Hubberstey, W.-S. Li, M.A. Withersby, M. Schröder, Coord. Chem. Rev. 183 (1999) 117.
[10] S.A. Barnett, N.R. Champness, Coord. Chem. Rev. 246 (2003) 145.
[11] M.B. Zaman, M. Tomura, Y. Yamashita, Org. Lett. 2 (2000) 273.
[12] H.-F. Zhu, L.-Y. Kong, T.-A. Okamura, J. Fan, W.-Y. Sun, N. Ueyama, Eur. J. Inorg. Chem. (2004) 1465.
[13] X.-M. Quyang, B.-L. Fei, T.-A. Okamura, H.-W. Bu, W.-Y. Sun, W.-X. Tang, N. Ueyama, Eur. J. Inorg. Chem. (2003) 618.
[14] M.B. Zaman, M.D. Smith, D.M. Curtin, H.-C. zur Loye, Inorg. Chem. 41 (2002) 4895.
[15] E. Bosch, C.L. Barnes, New J. Chem. 25 (2001) 1376.
[16] Y.-B. Dong, M.D. Smith, R.C. Layland, H.-C. zur Loye, Chem. Mater. 12 (2000) 1156.
[17] Y.-B. Dong, M.D. Smith, H.-C. zur Loye, Inorg. Chem. 39 (2000) 4927.
[18] Y.-B. Dong, M.D. Smith, H.-C. zur Loye, J. Solid State Chem. 155 (2000) 143.
[19] M.A. Withersby, A.L. Blake, N.R. Champness, P.A. Cooke, P. Hubberstey, W.-S. Li, M. Schröder, Inorg. Chem. 38 (1999) 2259.
[20] H.N. Kim, H.K. Lee, S.W. Lee, Bull. Korean Chem. Soc. 26 (2005) 6.
[21] D. Min, Y.-B. Cho, H.K. Lee, S.W. Lee, Inorg. Chim. Acta 359 (2006) 577.
[22] Y.-B. Cho, D. Min, H.K. Lee, S.W. Lee, Cryst. Growth Des. 6 (2006) 342.
[23] S.H. Kim, H.S. Huh, S.W. Lee, J. Mol. Struct. 841 (2007) 78.
[24] H.S. Huh, S.W. Lee, Inorg. Chem. Commun. 10 (2007) 1244.
[25] H.S. Huh, H.J. Yun, S.W. Lee, Inorg. Chim. Acta, doi:10.1016/j.ica.2007.10.024.
[26] M. Du, X.-H. Bu, Y.-M. Guo, H. Liu, Inorg. Chem. 41 (2002) 4904.
[27] S.M. Kil, P.S. Myunghyun, J. Am. Chem. Soc. 122 (2000) 6834.
[28] A.J. Blake, N.R. Champness, P.A. Cooke, J.E.B. Nicolson, C. Wilson, J. Chem. Soc., Dalton Trans. (2000) 3811.
[29] X.-H. Bu, W. Chen, S.-L. Lu, R.-H. Zhang, D.-Z. Liao, W.-M. Bu, M. Shionoya, F. Brisse, J. Ribas, Angew. Chem., Int. Ed. 40 (2001) 3201.
[30] M. Du, X.H. Bu, Y.M. Guo, J. Ribas, C. Diaz, Chem. Commun. (2002) 2550.
[31] J. Yang, J.-F. Ma, Y.Y. Liu, S.-L. Li, G.-L. Zheng, Eur. J. Inorg. Chem. (2005) 2174.
[32] R.-Q. Zou, C.-S. Liu, Z. Huang, T.-L. Hu, X.-H. Bu, Cryst. Growth Des. 6 (2006) 99.
[33] G.M. Sheldrick, SADABS, Program for Absorption Correction, University of Göttingen, 1996.
[34] Bruker, SHELXTL, Structure Determination Software Programs, Bruker Analytical X-ray Instruments Inc., Madison, WI, USA, 1997.
[35] X.Q. Lu, J.J. Jiang, H.-C. zur Loye, B.S. Kang, C.Y. Su, Inorg. Chem. 44 (2005) 1810.
[36] P.M. Forster, P.M. Thomas, A.K. Cheetham, Chem. Mater. 14 (2002) 17.
[37] S.W. Lee, H.J. Kim, Y.K. Lee, K. Park, J.-H. Son, Y.-U. Kwon, Inorg. Chim. Acta 353 (2003) 151.
[38] H.K. Lee, D. Min, B.-Y. Cho, S.W. Lee, Bull. Korean Chem. Soc. 25 (2004) 1955.
[39] M. Fujita, Y.J. Kwon, O. Sasaki, K. Yamaguchi, K. Ogura, J. Am. Chem. Soc. 117 (1995) 7287.

Polyhedron 27 (2008) 2091–2096

Contents lists available at ScienceDirect

Polyhedron

journal homepage: www.elsevier.com/locate/poly

Synthesis, crystal structure and biological activity of 1-(1*H*-benzoimidazol-2-yl)-ethanone thiosemicarbazone and its cobalt complex

Mehmet Poyraz [a,*], Musa Sari [b,*], Fatih Demirci [c], Muberra Kosar [c], Seref Demirayak [d], Orhan Büyükgüngör [e]

[a] *Afyon Kocatepe University, Faculty of Science and Arts, Department of Chemistry, 03200 Afyonkarahisar, Turkey*
[b] *Gazi University, Department of Physics Education, Besevler, 06500 Ankara, Turkey*
[c] *Anadolu University, Faculty of Pharmacy, Department of Pharmacognosy, 26470 Eskisehir, Turkey*
[d] *Anadolu University, Faculty of Pharmacy, Department of Pharmaceutical Chemistry, 26470 Eskisehir, Turkey*
[e] *Ondokuz Mayis University, Faculty of Science and Arts, Department of Physics, TR-55139, Turkey*

ARTICLE INFO

Article history:
Received 31 October 2007
Accepted 14 March 2008
Available online 20 May 2008

Keywords:
Ethanone
Benzimidazole
Thiosemicarbazone
Crystal structure
Antimicrobial activity
Free radical scavenging activity

ABSTRACT

1-(1*H*-Benzoimidazol-2-yl)-ethanone thiosemicarbazone (H_2L) (**1**) was obtained by the condensation reaction of 2-acetylbenzimidazole, thiosemicarbazide and acetic acid in ethanol. The novel cobalt(III) complex [Co(L)(HL)] **2** was prepared by the direct reaction of $CoCl_2 \cdot 6H_2O$ with the ligand H_2L. The reaction products were characterized by elemental analysis, thermogravimetric analysis (TGA), FT-IR and mass spectrometry for H_2L, and magnetic measurement for the Co(III) complex. The crystal and molecular structures of complex **2** and the free ligand **1** were also determined by single-crystal X-ray structure analysis. The crystal structure data suggests that in compound **2**, two ligands (H_2L) coordinate to cobalt in a N_2S tridentate fashion, giving a distorted octahedral geometry. Furthermore, compounds **1** and **2** were evaluated for their antimicrobial properties using a broth microdilution assay against various human pathogenic bacteria and the yeast *Candida tropicalis*, resulting in moderate minimum inhibitory concentrations (MIC = 0.25–1 mg/mL) when compared to standard antimicrobial agents. The free radical scavenging activity of the compounds against 1,1-diphenyl-2-picrylhydrazyl hydrate (DPPH) was also investigated.

© 2008 Elsevier Ltd. All rights reserved.

1. Introduction

The benzimidazoles are a subject of interest to medicinal chemistry because of the broad spectrum of their biological and pharmaceutical properties. Benzimidazole complexes have been previously investigated for their antifungal [1,2], antibacterial [3,4], antimicrobial [5,6], antiamoebic [7,8], antiparasitic [9] and antitumor activities [10,11]. Although many thiosemicarbazones and their transition metal ion complexes have been studied extensively, due to their wide range of biological activities [12–16], there is very limited information about the structural characterization of benzimidazole thiosemicarbazone derivatives. The pharmacological or coordinative information about imidazole thiosemicarbazone derivatives and some of their complexes are limited in the literature [17–19].

In this present study, the synthesis, structural characterization and crystal structures of the free ligand and its cobalt(III) complex is reported (to the best of our knowledge it is the first X-ray study of H_2L and one of its complexes). Furthermore, the antimicrobial and radical scavenging activity of complex **2** and the free ligand **1** against various pathogenic microorganisms and the 1,1-diphenyl-2-picrylhydrazyl hydrate (DPPH) radical were evaluated.

2. Experimental

2.1. General procedures and materials

All the chemicals used were spectroscopic and analytical grade. They were used as received from commercial sources (Sigma–Aldrich, and AlfaEaser). The IR spectra were recorded on a Perkin Elmer BX-II FT–IR spectrophotometer, using a KBr disk, in the range 4000–400 cm^{-1}. Thermogravimetric analyses were performed on a Linseis Thermowaage L81 Series thermal analysis system by heating (increases of 20 °C/min) *ca.* 8 mg of the samples under an air atmosphere in the temperature range 25–150 °C. Elemental analyses for C, N, S and H were performed on Elementar Vario III EL. Magnetic susceptibility measurements were performed on pulverised samples at room temperature on a Sherwood Magway MSB Mk1 balance.

2.2. Synthesis of the 1-(1H-benzoimidazol-2-yl)-ethanone thiosemicarbazone ligand (*1*)

A slightly modified procedure was applied to prepare the thiosemicarbazone derivative [20]. Thus, a mixture of 2-acetylbenzimidazole (5 mmol), thiosemicarbazide (5 mmol) and 1 mL acetic acid in 50 mL ethanol was refluxed for 6 h. The raw product precipitated in a cooled solution, and was then filtered and recrystallised

* Corresponding authors.
E-mail addresses: poyraz@aku.edu.tr (M. Poyraz), msari@gazi.edu.tr (M. Sari).

0277-5387/$ - see front matter © 2008 Elsevier Ltd. All rights reserved.
doi:10.1016/j.poly.2008.03.030

from ethanol (max. yield: 80%). Elemental *Anal.* Calc. for $C_{10}H_{11}N_5S \cdot H_2O \cdot C_2H_5OH$: C, 48.47; H, 6.38; N, 23.58; S, 10.76. Found: C, 47.56; H, 6.18; N, 23.94; S, 10.88%. MS (*m*/*z*, %): 233. IR (KBr, cm^{-1}): $\nu(NH_2) + \nu(NH) + \nu(OH)$ 3300–2800 (br); $\nu(C{=}N) + \delta(NH_2)$ 1629 (s); $\delta(NH)$ 1543 (s); $\nu(ring) + \delta(NCS)$ 1499 (s), 1468 (m), 1447 (m); $\nu(C{=}S) + \gamma(CH)$ 846(m); $\gamma(CH)$ 766 (m); $\delta(ring)$ 656 (s).

2.3. Synthesis of [1-(1H-benzoimidazol-2-yl)-ethanone thiosemicarbazone]$_2$ cobalt

A solution of the crystalline ligand (0.125 g, 0.538 mmol) in ethanol (40 mL) was added to a solution of $CoCl_2 \cdot 6H_2O$ (0.0635 g, 0.267 mmol) in 20 mL wet ethanol. The resulting mixture was stirred under reflux at least for 40 h. The solution was left for slow evaporation at room temperature. The resulting crystals of the complex were separated from the solution after few days (30% yield, w/w). The oxidation of Co(II) occurred during the reaction and the Co(III) complex was obtained. This was due to air oxidation during evaporation of solvent as observed in the synthesis of a similar compound in the literature [19]. Elemental *Anal.* Calc. for $C_{20}H_{19}N_{10}S_2Co \cdot H_2O$: C, 44.44; H, 3.92; N, 25.91; S, 11.86. Found: C, 44.52; H, 4.02; N, 25.48; S, 11.55%. IR (KBr, cm^{-1}): $\nu(NH_2) + \nu(NH) + \nu(OH)$ 3422m, 3305 w, 3170(m); $\nu(C{=}N) + \delta(NH_2)$ 1612 m; $\delta(NH)$ 1540 (m); $\nu(ring) + \delta(NCS)$ 1496(w), 1464(s); $\nu(C{=}S) + \gamma(CH)$ 839; $\gamma(CH)$ 744(m); $\delta(ring)$ 695 (w).

2.4. X-ray structure determinations of [$C_{12}H_{18}N_5O_2S$] (**1**) and [$C_{20}H_{21}CoN_{10}S_2$] (**2**)

Measurements of **1** and **2** were made on a Stoe IPDS II CCD X-ray diffractometer employing plane graphite Mo Kα monochromatized radiation (λ = 0.71073 Å), using the ω–2θ scan mode. Unit cell parameters were refined from the setting angles of 25 centered reflections in the range of (**1**) $2.33 \leqslant \theta \leqslant 25.00$ and (**2**) $1.69 \leqslant \theta \leqslant 25.25$. The structures were solved by direct methods and refined by full-matrix least-squares techniques on F^2 using the solution program SHELXS-97 and refined using SHELXL-97 [21]. Empirical absorption corrections were applied by the integration method via X-RED software [22]. All non-hydrogen atoms were refined with anisotropic displacement parameters and hydrogen atoms were included in their idealized positions and refined isotropically except for the water hydrogen atoms which were located from difference maps and refined with isotropic thermal parameters. The crystal data and structure refinement details for complex **1** and **2** are given in Table 1. ORTEP drawings [23] of the molecules with 40% probability displacement thermal ellipsoids and the atom labelling scheme are shown in Figs. 1 and 2, respectively.

Table 1
Crystal data and structure refinement details for compounds **1** and **2**

	1	**2**
Chemical formula	$C_{12}H_{19}N_5O_2S$	$C_{20}H_{21}CoN_{10}OS_2$
Formula weight	297.39	540.54
Temperature (K)	293(2)	293(2)
Wavelength (Å)	0.71073	0.71073
Crystal system, space group	triclinic, $P\bar{1}$	triclinic, $P\bar{1}$
Unit cell dimensions		
a (Å)	5.7106(8)	13.6655(12)
b (Å)	8.7700(13)	13.8831(13)
c (Å)	15.493(2)	16.9323(15)
α (°)	88.359(12)	89.965(7)
β (°)	83.052(12)	101.724(7)
γ (°)	85.327(12)	118.844(7)
Volume (Å^3)	767.52(19)	2733.4(5)
Z	2	4
D_{calc} (Mg m^{-3})	1.287	1.314
Absorbtion coefficient (mm^{-1})	0.220	0.812
F(000)	316	1112
Crystal size (mm)	0.240 × 0.140 × 0.100	0.350 × 0.250 × 0.140
$2\theta_{max}$ (°)	50.00	50.50
Limiting indices	$-6 \leqslant h \leqslant 6$, $-10 \leqslant k \leqslant 10$, $-18 \leqslant l \leqslant 18$	$-16 \leqslant h \leqslant 16$, $-16 \leqslant k \leqslant 16$, $-20 \leqslant l \leqslant 20$
Number of reflections used	1403	6792
Number of parameters	192	630
Final *R* indices [$I \geqslant 2\sigma(I)$]	R_1 = 0.0612, wR_2 = 0.1246	R_1 = 0.0628, wR_2 = 0.1398
Goodness-of-fit on F^2	0.968	1.035
$\Delta\rho_{min}$, $\Delta\rho_{max}$ (e Å^{-3})	−0.343, 0.383	−0.372, 0.595

2.5. Biological evaluation

2.5.1. Antimicrobial activity

A modified broth microdilution susceptibility assay was used [24,25]. Stock solutions of the test samples (2 mg/mL) were prepared in 25% (v/v) dimethylsulfoxide (DMSO, Carlo Erba), which were used as the initial concentration and later serially diluted in an equal volume of Mueller–Hinton broth (MHB, Merck, Germany) up to 0.98 μg/mL in a 96-well microtiter plate format. Microbial suspensions were grown as previously described [24], which were standardized to 10^8 CFU mL^{-1} using the McFarland No. 0.5 standard, also in MHB. Each microbial suspension (100 μL) was then added to the dilutions under sterile conditions. The last row, which contained only the dilutions of the test samples without the microorganism, was used as a negative control. To eliminate solvent effects, DMSO dilutions were considered as another control, separately. After incubation at 37 °C for 24 h the first well without turbidity was determined as the minimum inhibition concentration (MIC, mg/mL). Chloramphenicol and Ketoconazole were used as standard antimicrobials. Strain sources and activity results are given in Table 2.

2.5.2. Quantitative free radical scavenging activity using DPPH

The test substances were subjected to a quantitative UV-spectroscopic microdilution assay [26], where inhibitory concentrations (IC) were determined in comparison with standard substances. Stock solutions of each test sample were prepared to obtain a final concentration of 0.5 mg/mL in methanol, which were transferred in aliquots of 100 μL of each test solution to the first row of the 96-well plate. Ten-fold serial dilutions in an equal amount of MeOH were prepared and vortexed for 5 min. DPPH was dissolved in methanol to obtain a stock reagent solution with a final concentration of 80 μg/mL. To initiate the reaction, 100 μL of DPPH solution was added into each well and left for 30 min in the dark. Vitamin C, BHT (butylated hydroxytoluene) and quercetin were used as positive controls at the same concentration, DPPH + MeOH served as a negative control and only MeOH was used as a blank on the same test plate. The UV absorbance was read at 517 nm using a microplate spectrophotometer (BioTek, Powerwave) at room temperature. All experiments were performed on quadruplets in two different plates. The results were expressed as mean ± standard deviation (n = 8). For statistical evaluations and calculations Gen5 Data Analysis Software (BioTek) was used. The antioxidant activity was expressed as half maximal of the inhibitory concentration (IC_{50}) required to inhibit DPPH radical formation, as determined from the log-dose inhibition curve. The value was calculated using the formula $IC_{50} = [(A_0 - A_1)/A_0] \times 100$ where A_0 is the absorbance of the control and A_1 the absorbance of the test sample. Comparative results of the test samples and standards are given in Table 3.

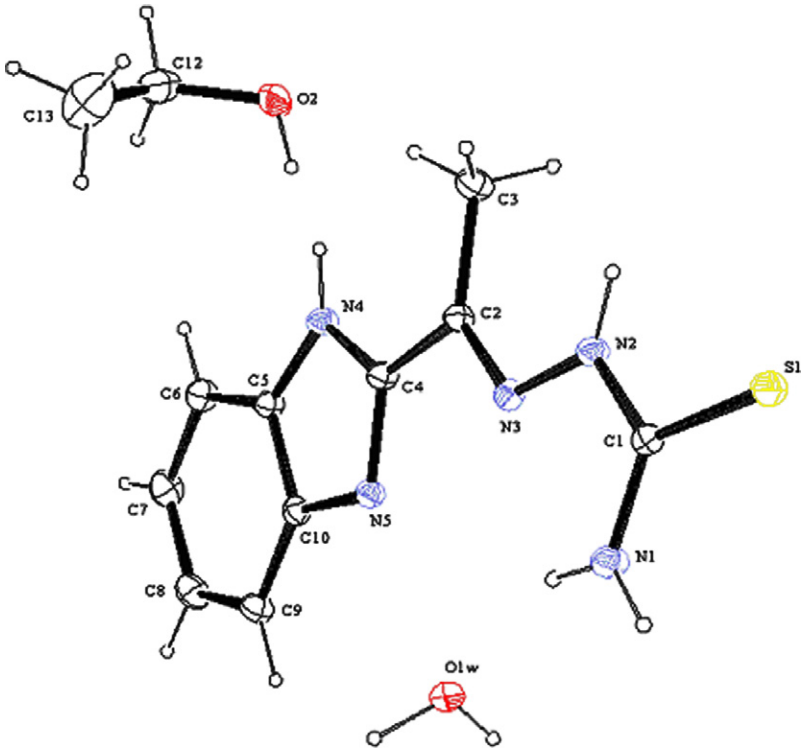

Fig. 1. The molecular structure and atomic labelling scheme of compound **1**. Displacement ellipsoids are drawn at the 40% probability level.

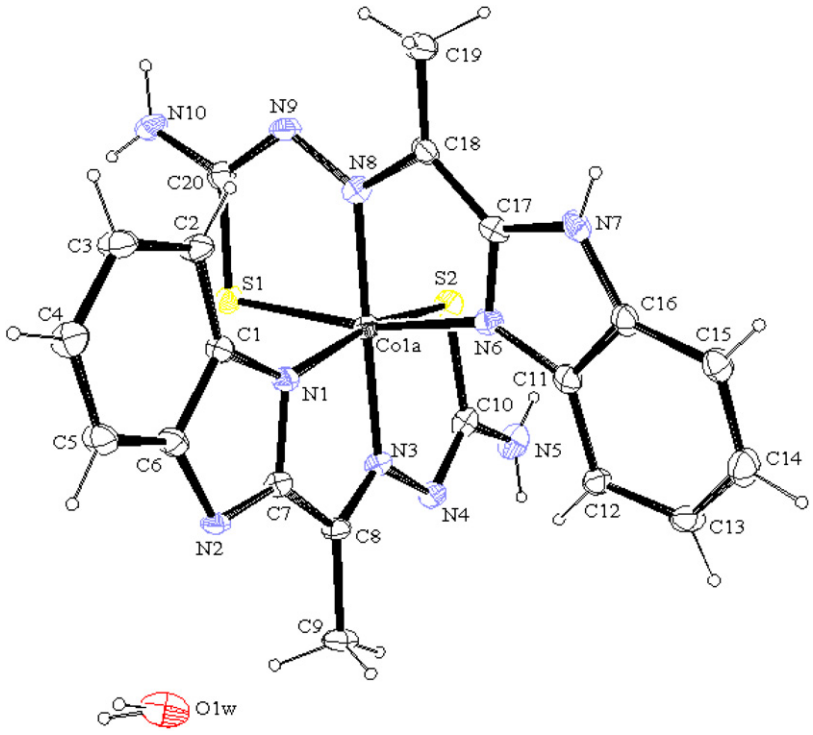

Fig. 2. The molecular structure and atomic labelling scheme of molecule A in **2**. Displacement ellipsoids are drawn at the 40% probability level. We have shown only one component for clarity.

3. Results and discussion

3.1. Description of the structures

3.1.1. Solid-state structure of [1-(1*H*-benzoimidazol-2-yl)-ethanone] (**1**)

The free ligand, 1-(1*H*-benzoimidazol-2-yl)-ethanone, crystallizes into a triclinic lattice with the space group $P\bar{1}$. The molecular structure of **1** with the atomic numbering scheme is given in Fig. 1 and selected bond distances and angles are presented in Table 4. The ligand adopts an (*E*)-configuration about the C1–N2 and C4–N4 bonds with both the azomethine nitrogen atoms. As illustrated in Fig. 1, the asymmetric unit of the free ligand consists of one molecule of ethanol and one molecule of water. The C1–S1 [1.697(4) Å], C1–N2 [1.351(5) Å], N2–N3 [1.367(4) Å] and C2–N3

Table 2
Antimicrobial activity results[a]

Microorganisms	Strain no.	1	2	Chloramphenicol	Ketoconazole
Escherichia coli	NRRL B-3008	0.25	0.5	0.0078	nt
Staphylococcus aureus	ATCC 6538	0.25	0.5	0.0019	nt
Pseudomonas aeruginosa	ATCC 27853	1	0.5	0.125	nt
Enterobacter aerogenes	NRRL 3567	0.5	0.5	0.0039	nt
Proteus vulgaris	NRRL B-123	1	0.5	0.0156	nt
Salmonella typhimurium	ATCC 13311	0.5	0.5	0.0039	nt
Bacillus cereus	NRRL B-3711	0.5	0.5	0.031	nt
Candida tropicalis	NRRL Y-12968	0.25	0.25	nt	0.25

[a] MICs are given as mg/mL, nt: not tested.

Table 3
The free radical scavenging activity results of compounds **1** and **2**

Test substance	IC_{50}: mg/mL
1	>0.500
2	>0.500
Vit C	0.008 ± 0.002
BHT	0.024 ± 0.002

Mean ± standard deviation (n = 8).

Table 4
Selected bond distances (Å) and angles (°) for compound **1**

C1–N1	1.312(6)	C4–N5	1.359(5)
C1–N2	1.351(5)	C5–N4	1.371(5)
C1–S1	1.697(4)	C10–N5	1.387(5)
C2–N3	1.286(5)	N2–N3	1.367(4)
C4–N4	1.320(5)	O2–C12	1.409(8)
N1–C1–N2	117.5(4)	N4–C4–N5	112.6(3)
N1–C1–S1	123.3(3)	C1–N2–N3	117.9(4)
N2–C1–S1	119.2(3)	C4–N4–C5	105.7(3)
N3–C2–C4	112.9(4)		

[1.286(5) Å] bond distances are comparable with those of related ligands [27–29]. The above bond distances indicate that there is some electron delocalization in the thiosemicarbazide side chain. The thiosemicarbazone skeleton comprising of atoms N3, N4, C1, S1 and N1 has a maximum deviation of 0.010 (2) Å from the mean plane. The C2–N3 bond distance [1.286(5) Å] is appreciably close to that of a C=N double bond (1.28 Å) [30], confirming the azomethine bond formation. Intermolecular N–H···O and N–H···S hydrogen bonds link the molecules, helping to stabilize the crystal structure. The parameters for the hydrogen bonding interaction in ligand **1** are as follows: H(4)···O(2) 1.94 Å, N(4)···O(2) 2.778(5) Å, N(4)–H(4)···O(2) 164°; H(2)···N(4) 2.06 Å, O(2)···N(4) 2.777(5) Å, O(2)-H(2)···N(4) 146°.

3.1.2. Solid-state structure of $[C_{20}H_{21}CoN_{10}OS_2]$ (**2**)

The crystal of **2** is triclinic and the asymmetric unit consists of two independent and similar molecules (A and B), $[C_{20}H_{21}CoN_{10}OS_2]$. The coordination environment of the cobalt atom may be considered as a distorted octahedral geometry with the thiosemicarbazone ligand (H_2L) **1** coordinated to the cobalt ion as a tridentate N_2S chelate via the four azomethinic nitrogen atoms and two thioamide sulfur atoms. Structurally there are a few significant differences between the (H_2L) (**1**) ligand and the novel cobalt(III) complex [Co(L)(HL)] (**2**). The C1–S1 bond distance has been increased from 1.697(4) Å (**1**) to [1.734(5)–1.727(6) Å] in complex (**2**). The C–S bond distances still have an intermediate value between a single (1.82 Å) and double (1.56 Å) C–S bond [29]. This is an indication that there is some electron delocalization in the thiosemicarbazide chain, but that it is independent of coordination. Selected bond distances and angles are listed in Table 5.

In the Co complex, two ligands coordinate in the expected meridional conformation via azomethinic nitrogens [N(3) and N(8)] and sulfur atoms. The *trans* angle involving the azomethinic nitrogens of the two ligands is 177.02(16)°, showing less distortion from octahedral symmetry than in $[[Ni(HAm4M)_2](ClO_4)_2 \cdot 2H_2O]$, in which this angle is 173.1(3)° [31]. The other two *trans* angles, each of which involves the terminal donors of one of the tridentate ligands are approximately 167.2°. As expected the sulfur and imine nitrogen atoms in both molecules (A and B) of the ligand are in the *cis* conformation with respect to the C20–N9 bonds [12]. The two donor nitrogen atoms, N1 and N3, in A and B also lie *cis* to each other. The oxidation state of three for cobalt is shown by its coordination bond distances Co–S and Co–$N_{azomethine}$ (Table 5), which are in the expected range ranges of 2.2278(14)–2.2305(14), 1.909(4)–1.950(4) Å, respectively, as noted for several Co(III) complexes [32–34]. The loss of the proton originally bound to N(9) produces a negative charge which is delocalized in the N8–N9–C20 system, as indicated by the bond distances and in particular S(1)–C(20) (1.735(5) Å) and C(20)–N(9) (1.323(6) Å). The other ligand, not deprotonated on N(4), is in the thione form [S(2)–C(10) 1.725(6), C(10)–N(4) 1.348(5) Å]. The coordination of the cobalt ion is not completely regular; the bond angles at the Co1A atom range from 82.55(15)° to 97.84(12)°. The two molecules of the ligand are practically planar [maximum deviations of 0.037(2) and

Table 5
Selected bond distances (Å) and angles (°) for compound **2**

Co1a–N1	1.950(4)	Co2b–N11	1.963(4)
Co1a–N3	1.909(4)	Co2b–N13	1.903(4)
Co1a–N6	1.964(4)	Co2b–N16	1.971(4)
Co1a–N8	1.913(4)	Co2b–N18	1.902(4)
Co1a–S1	2.2278(14)	Co2b–S3	2.2347(14)
Co1a–S2	2.2305(14)	Co2b–S4	2.2222(14)
S1–C20	1.735(5)	S3–C40	1.740(5)
S2–C10	1.725(6)	S4–C30	1.732(6)
N3–N4	1.378(5)	N13–N15	1.359(6)
N8–N9	1.351(5)	N18–N19	1.375(5)
N1–Co1a–N6	90.36(15)	N11–Co2b–N16	91.43(15)
N1–Co1a–S1	89.17(12)	N11–Co2b–S3	90.56(12)
N1–Co1a–S2	167.28(11)	N11–Co2b–S4	167.77(12)
N3–Co1a–N1	82.42(15)	N13–Co2b–N11	82.81(16)
N3–Co1a–N6	95.05(15)	N13–Co2b–N16	94.69(15)
N3–Co1a–N8	177.11(16)	N13–Co2b–S3	97.86(12)
N3–Co1a–S1	97.79(12)	N13–Co2b–S4	85.03(13)
N3–Co1a–S2	84.95(12)	N15–N13–Co2b	124.2(3)
N4–N3–Co1a	124.6(3)	N16–Co2b–S3	167.44(11)
N6–Co1a–S1	166.97(11)	N16–Co2b–S4	90.83(11)
N6–Co1a–S2	92.72(12)	N18–Co2b–N11	94.33(15)
N8–Co1a–N1	96.02(15)	N18–Co2b–N13	175.83(16)
N8–Co1a–N6	82.47(16)	N18–Co2b–N16	82.32(16)
N8–Co1a–S1	84.63(12)	N18–Co2b–S3	85.17(12)
N8–Co1a–S2	96.61(12)	N18–Co2b–S4	97.88(11)
N9–N8–Co1a	124.5(3)	N19–N18–Co2b	124.3(3)
S1–Co1a–S2	90.59(5)	S4–Co2b–S3	89.84(6)

−0.022(2) Å, respectively]. The angles generated at the cobalt centre by the chelating donor points (N and S) differ slightly in the two coordinating ligands. It appears that the angles at the cobalt centre in the chelate rings are controlled to some extent by the ligand geometry. The bond distances and angles around the cobalt atom are in agreement with literature values [35–37].

3.2. Spectral studies, thermogravimetric analysis (TGA), magnetic measurement

The thermal analytical data of the ligand show that when the temperature was raised up to 377 K, the weight loss was 21%, indicating loss from the crystal of one water molecule and one ethanol molecule. The thermal analytical data of the Co(III) complex show that when the temperature was raised to 377 K, the weight loss was 3.3%, indicating loss from the crystal of one water molecule. The crystalline complex lost H_2O molecules of hydration below 100 °C, and lost coordinated H_2O molecules above 100 °C. Magnetic susceptibility data indicate that the Co(III) complex is diamagnetic (at ~300 K) as expected for a spin-paired d^6 ion.

3.3. IR spectra

(i) The disappearance of the ν(NH) bands is verified in the complex which contains the ligand in its bideprotonated form. (ii) The coordination of the azomethine nitrogen atom to the metal ion is suggested by the shifting of the band of ν(C=N) at 1612 cm^{-1} to a lower wavenumber. (iii) The coordination of the sulfur atom causes, in the spectra of the complex, the shift of the band at 839 cm^{-1} to a lower frequency value. (iv) The coordination of the deprotonated imidazole nitrogen is shown by the shift of the δ(ring) in complex to higher frequency values [19].

3.4. Antimicrobial and free radical scavenging activity

A selection of human pathogenic Gram positive and Gram negative bacteria and the yeast *C. tropicalis* were interacted under in vitro conditions with the synthesized **2** (complex) and **1** (ligand). A modified broth microdilution assay [24] was used to evaluate their antimicrobial properties. Compound **1** was more effective against *E. coli* and *S. aureus* among the tested bacteria and the yeast *Candida tropicalis* when compared to the other tested compounds. Interestingly, compound **2** showed the best inhibitory activity against the yeast *C. tropicalis*, like compound **1**, with a MIC value of 0.25 mg/mL at the same level as the standard antifungal agent Ketoconazole. Overall, good to moderate inhibitions (0.25–1 mg/mL) were observed against the tested microorganisms, when compared to standard antimicrobial agents. Compounds **1** and **2** were also evaluated for their free radical scavenging activity using the DPPH radical. When compared to standard antioxidant compounds such as Vitamin C, and BHT with IC_{50} values of 0.008 and 0.020 mg/mL, respectively, both **1** and **2** displayed IC_{50} values more than 0.5 mg/mL and are rated rather inactive.

In vitro biological evaluations using standard methods may have correlations to in vivo results, which are practical and fast in obtaining bioactivity results of individual compounds. Also standard bioassay methods can produce comparable results to other similar studies. Previous antimicrobial studies [1–9] support that such complexes can exhibit remarkable biological and pharmacological effects.

4. Conclusion

To the best of our knowledge the crystal structures of compounds **1** and **2** are obtained for the first time and evaluated for their physicochemical and biological activities. Preliminary biological activity screens of the compounds showing antifungal activity suggest further evaluations of derivatives of the tested substances, also in other bioassays.

Acknowledgements

This work was partly supported by grants from Afyonkarahisar Kocatepe University, The Presidency of the Commission of Scientific Research Projects (BAPK-042.FENED.08) and Turkish State Planning Organization (DPT-2005 K-12060). In addition, the authors acknowledge and give thanks to the Faculty of Arts and Sciences, Ondokuz Mayis University, Turkey, for use of the Stoe IPDS-2 diffractometer purchased under Grant F.279 of the University Research Fund.

Appendix A. Supplementary data

CCDC 653264 and 653265 contain the supplementary crystallographic data for **1** and **2**. These data can be obtained free of charge via http://www.ccdc.cam.ac.uk/conts/retrieving.html, or from the Cambridge Crystallographic Data Center, 12 Union Road, Cambridge CB2 1EZ, UK; fax: +44 1223-336-033; or e-mail: deposit@ccdc.cam.ac.uk.

References

[1] D.A. Horton, G.T. Bourne, M.L. Smythe, Chem. Rev. 103 (2003) 893.
[2] H. Kucukbay, R. Durmaz, E. Orhan, S. Gunal, Il Farmaco 58 (2003) 431.
[3] V.K. Limesova, J. Koci, K. Waisser, J. Kaustova, Il Farmaco 57 (2002) 259.
[4] Y. He, B. Wu, J. Yang, D. Robinson, L. Risen, R. Ranken, L. Blyn, S. Sheng, E.E. Swayze, Bioorg. Med. Chem. Lett. 13 (2003) 3253.
[5] G. Ayhan, N. Altanlar, Il Farmaco 58 (2003) 1345.
[6] N.S. Pawar, D.S. Dalal, S.R. Shimpi, P.P. Mahulikar, Eur. J. Pharm. Sci. 21 (2004) 115.
[7] N. Bharti, Shailendra, M.T. Gonzalez Garza, D.E. Cruz-Vega, J. Castrogarza, K. Saleem, F. Naqvi, M.R. Maurya, A. Azam, Med. Chem. Lett. 12 (2002) 869.
[8] S. Ozden, D. Atabey, S. Yildiz, H. Goker, Bioorg. Med. Chem. 13 (2005) 1587.
[9] G. Navarrete-Vazquez, R. Cedillo, A. Hernandez-Campos, J. Yepez, F. Hernndez-Luis, J. Valldez, R. Morales, R. Cortes, M. Hernandez, R. Castillo, Bioorg. Med. Chem. Lett. 11 (2001) 187.
[10] A.A. Spasov, I.N. Yozhitsa, L.I. Bugavea, V.A. Anisimova, J. Pharm. Chem. 33 (1999) 232.
[11] T.A. Kabanos, A.D. Kersmidas, D. Mentzafos, U. Russo, A. Terzis, J.M. Tsangaris, J. Chem. Soc., Dalton Trans. (1992) 2729.
[12] M.J.M. Campbell, Coord. Chem. Rev. 15 (1975) 279.
[13] K.C. Agarwal, A.C. Sartorelli, in: G.P. Ellis, G.B. West (Eds.), Progress in Medicinal Chemistry, vol. 15, Elsevier, Amsterdam, 1978, p. 321.
[14] S.B. Padhye, G.B. Kauffman, Coord. Chem. Rev. 63 (1985) 127.
[15] D.X. West, S.B. Padhye, P.B. Sonawane, Struct. Bonding 76 (1991) 1.
[16] D.X. West, A.E. Liberta, S.B. Padhye, R.C. Chikate, P.B. Sonawane, A.S. Kumbhar, R.G. Xerande, Coord. Chem. Rev. 123 (1993) 49.
[17] D.X. West, M. Lockwood, J.N. Albert, A.E. Liberta, Spectrochim. Acta 49 (1993) 1809.
[18] J.S. Casas, A. Castineiras, M.C. Rodriguez Argüelles, A. Sanchez, J. Sordo, A. Vazquez-Lopez, E. Vazquez-Lopez, J. Chem. Soc., Dalton Trans. (2000) 2267.
[19] M.C. Rodriguez-Argüelles, E.C. Lopez-Silva, J. Sanmartin, A. Bacchi, C. Pelizzi, F. Zani, Inorg. Chim. Acta 357 (2004) 2543.
[20] B.S. Furniss, A.J. Hannaford, P.W.G. Smith, A.R. Tatchell, Vogel's Textbook of Practical Organic Chemistry, 5th ed., John Wiley and Sons Inc., New York, 1989. p. 1258.
[21] G.M. Sheldrick, SHELXS97 and SHEXL97: Program for Crystal Structure Solution and Refinement, University of Göttingen, Germany, 1997.
[22] Stoe & Cie, X-AREA (Version 1.18) and X-RED32 (Version 1.04), Stoe & Cie, Darmstadt, Germany, 2002.
[23] L.J. Farrugia, J. Appl. Crystallogr. 30 (1997) 565.
[24] G. Iscan, F. Demirci, N. Kirimer, M. Kürkcüoğlu, K.H.C. Baser, J. Agric. Food Chem. 50 (2002) 3943.
[25] E.W. Koneman, S.D. Allen, W.M. Janda, P.C. Schreckenberger, W.C. Winn, Color Atlas and Textbook of Diagnostic Microbiology, Lippincott-Raven Publishers, Philadelphia, 1997. pp. 785–856.
[26] Y. Kumarasamy, M.E. Fergusson, L. Nahar, S.D. Sarker, Pharmaceut. Biol. 40 (2002) 307.
[27] G.F. de Sousa, D.X. West, C.A. Brown, J.K. Swearingen, J. Váldez-Martinez, R.A. Toscano, S. Hernández-Ortega, M. Hörner, R.J. Bortluzzi, Polyhedron 19 (2000) 841.
[28] M. Vázquez, L. Fabrizzi, A. Taglietti, R.M. Pedrido, A.M. González-Noya, M.R. Bermejo, Angew. Chem., Int. Ed. 43 (2004) 1962.

[29] M.A. Ali, A.H. Mirza, W.B. Ejau, P.V. Bernhardt, Polyhedron 25 (2006) 3337.
[30] D.X. West, J.K. Swearingen, J. Valdéz-Martínez, S. Hernández-Ortega, A.K. El-Sawaf, F. Meurs, A. Castineiras, I. García, E. Bermejo, Polyhedron 18 (1999) 2919.
[31] I. García, E. Bermajo, A.K. El Sawaf, A. Castiñeiras, D.X. West, Polyhedron 21 (2002) 729.
[32] M. Belicchi Ferrari, G. Gasparri Fava, G. Pelosi, P. Tarasconi, Polyhedron 19 (2000) 1895.
[33] M. Belicchi Ferrari, G. Gasparri Fava, M. Lanfranchi, C. Pelizzi, P. Tarasconi, J. Chem. Soc., Dalton Trans. (1991) 1951.
[34] M. Belicchi Ferrari, G. Gasparri Fava, G. Pelosi, M.C. Rodriguez-Argüelles, P. Tarasconi, J. Chem. Soc., Dalton Trans. (1995) 3035.
[35] E.C. Moore, M.S. Zedeck, K.C. Agrawal, A.C. Sartorelli, Biochemistry 9 (1970) 4492.
[36] S. Chandra, U. Kumar, H.S. Verma, Oriental J. Chem. 19 (2003) 355.
[37] N.C. Saha, R.J. Butcher, S. Chaudhari, N. Saha, Polyhedron 22 (2003) 383.

Polyhedron 27 (2008) 2097–2104

Contents lists available at ScienceDirect

Polyhedron

journal homepage: www.elsevier.com/locate/poly

Crystal structures of two (3-hydroxy-4-nitrobenzoato) complexes of magnesium(II): Ionic entities stabilized by stacking interactions and extensive hydrogen bonding

Georges Morgant [a,*], Jean d'Angelo [a,*], Didier Desmaële [a], Emma Dichi [b], Mehrez Sghaier [b], Bernard Fraisse [c], Pascal Retailleau [d], Véronique Brumas [e], Marina M.L. Fiallo [e], Alain Tomas [f]

[a] Université Paris-Sud, Laboratoire Biocis, UMR CNRS 8076, IFR 141, Faculté de Pharmacie, 5 Rue Jean-Baptiste Clément, F-92296 Châtenay-Malabry, France
[b] Université Paris-Sud, Equipe Matériaux et Santé, EA 401, Faculté de Pharmacie, 5 Rue Jean-Baptiste Clément, F-92296 Châtenay–Malabry, France
[c] Laboratoire SPMS, UMR CNRS 8580, Ecole Centrale Paris, Grande Voie des Vignes, F-92295 Châtenay-Malabry, France
[d] Centre National de la Recherche Scientifique, Institut de Chimie des Substances Naturelles, Laboratoire de Cristallochimie, 91198 Gif-sur-Yvette, France
[e] LERISM, LU 48, Université Toulouse III Paul Sabatier, 118 Route de Narbonne, 31062 Toulouse, France
[f] Laboratoire de Cristallographie et RMN biologiques, UMR CNRS 8015, Université Paris Descartes, Faculté de pharmacie, 4 Avenue de l'Observatoire, 75005 Paris, France

ARTICLE INFO

Article history:
Received 12 February 2008
Accepted 14 March 2008
Available online 20 May 2008

This paper is dedicated to the memory of our regretted colleague, Professor John R.J. Sorenson.

Keywords:
Magnesium complexes
3-Hydroxy-4-nitrobenzoic acid
X-ray structure
Hydrogen bonding
Stacking interactions

ABSTRACT

The crystal structures of two Mg(II) complexes of 3-hydroxy-4-nitrobenzoic acid have been reported. The first complex, **2** ($C_{14}H_{20}N_2O_{16}Mg$), consists of ionic entities comprising one hexaaquamagnesium cation and two organic carboxylate anions. The second complex, **3** ($C_7H_{15}NO_{11}Mg$) consists of zwitterionic entities comprising one organic ligand per Mg atom. In both cases, the complexes are linked through an extensive hydrogen bonding network. The 3D supramolecular architectures of these complexes are also stabilized by two types of stacking interactions. An interesting interconversion between the two complexes was observed in aqueous solution.

© 2008 Elsevier Ltd. All rights reserved.

1. Introduction

Besides their relevance to solid state structures and supramolecular design [1–3], (salicylato)-metal complexes have attracted considerable attention because of their promising anti-inflammatory and anticonvulsant activities [4–10]. As part of a systematic program devoted to the study of the structure–activity relationships of (salicylato)-metal complexes, we recently reported the preparation, crystal structures and anticonvulsant activities of Zn(II) and Co(II) tetraaqua(3-nitro-4-hydroxybenzoato) complexes [11]. Interestingly, promising pharmacological responses were obtained for these complexes as anticonvulsants. An exciting feature in this series is the possibility of modifying the original structure by moving groups attached to the aromatic nucleus. Herein we report the crystal structures of two Mg(II) complexes of 3-hydroxy-4-nitrobenzoic acid, the latter corresponding to the formal permutation of the hydroxyl and nitro groups in the above ligand [11].

2. Experimental

2.1. Materials

High purity 3-hydroxy-4-nitrobenzoic acid (ligand **1** in Fig. 1) and anhydrous magnesium chloride were purchased from Acros (USA) and were used without further purification.

2.2. Physical measurements

Characterization of the complexes: Elemental analyses (C, H and N) were performed on a Perkin–Elmer 2400 analyzer. The IR spectra were recorded with a Bruker Vector 22 spectrometer. The UV spectra were recorded with a Gasco V550 spectrometer. Thermogravimetric analysis (TGA) was carried out on a TA Instruments TGA Q500 apparatus. Calibration was performed at different

* Corresponding authors. Tel.: +33 146835648 (G. Morgant), +33 146835699 (J. d'Angelo).
E-mail addresses: georges.morgant@u-psud.fr (G. Morgant), jean.dangelo@u-psud.fr (J. d'Angelo).

0277-5387/$ - see front matter © 2008 Elsevier Ltd. All rights reserved.
doi:10.1016/j.poly.2008.03.027

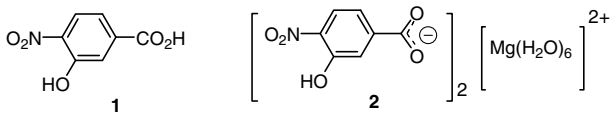

Fig. 1. Canonical representations of ligand **1** and salt $[(C_7H_4NO_5)^-]_2[Mg(H_2O)_6]^{2+}$ (**2**).

temperatures using Curie magnetic transitions for the recommended materials: alumel (163 °C), nickel (354 °C); calibration (mass) was carried out using a standard mass of 100 mg, calibration of the furnace was made between 100 and 900 °C to verify the thermocouple operation. All the experiments were performed under dry nitrogen, with a flow rate of 6×10^{-2} l min^{-1}. Analysis of the compounds out of nitrogen purging was conducted at a heating rate of 20 °C min^{-1}, in order to determine the percentage of mass loss with the best precision. A differential scanning calorimetry (DSC) experiment has been carried out with a TA Instruments Universal V4.2E apparatus under nitrogen flow. The samples were introduced in aluminum pans and covered with holed caps in order to avoid an uncontrolled variation of pressure. Calibration of the temperature was performed with indium (156.6 °C) and tin (231.9 °C) of quality 5 N at a heating rate of 10 °C min^{-1}. Impedance measurements of aqueous solutions were performed using a VoltaLab 80 (Radiometer Analytical) with a 2-pole cell with two platinum plates. The signal amplitude was 100 mV. A continuous potential of 0 mV was imposed. Measurements were obtained at 20 °C at 1 kHz frequency.

Potentiometric measurements of the ligand **1**: The experimental conditions of the reactant concentrations and pH were chosen from speciation calculations so that all species characterized from the potentiometric investigations and being of spectroscopic interest could be made successively predominant in solution. The different pH values investigated were imposed on test solutions by adding negligible volumes of concentrated NaOH or HCl. UV–Vis absorption spectra were recorded at room temperature in the 200–800 nm range using a double beam Lambda 2 Perkin–Elmer (equipped with 1 mm quartz cells). A water blank was used as a reference. The results were expressed as ε (molar absorption coefficient) with respect to the molar concentrations of the ligand.

2.3. Preparation of the complexes

2.3.1. $C_{14}H_{20}N_2O_{16}Mg$ (*2*)

The monosodium salt of ligand **1** was prepared by neutralizing **1** (0.915 g, 5 mmol) with 5 ml of 1 M NaOH. To this solution was added anhydrous $MgCl_2$ (0.238 g, 2.5 mmol) in 5 ml of water. After a few days **2** was filtered, crystallized from water and dried over magnesium sulfate. Yield: 0.903 g (73%). *Anal.* Calc. for $C_{14}H_{20}N_2O_{16}Mg$ (**2**): C, 33.86; H, 4.06; N, 5.64. Found: C, 33.25; H, 3.85; N, 5.44%. IR (neat, cm^{-1}): 3585(m), 3557(m), 3229(m), 2951(m), 1670(m), 1601(m), 1557(s), 1475(m), 1430(m), 1380(s), 1348(s), 1316(s), 1273(m), 1239(s), 1170(s), 1070(m), 957(m), 910(m), 839(s), 786(s), 750(s), 671(s), 632(s), 607(s). UV spectrum (in water): λ_{max} = 283 nm, ε = 14700; λ_{max} = 354 nm, ε = 5200. The conductance and pH of the 2×10^{-2} M solution in water were found to be 2.05×10^{-3} Ω^{-1} cm^{-1} and 4.85, respectively. TGA analysis of **2** revealed a mass loss of 21.4% on heating from 70 to 195 °C, corresponding to a loss of six water molecules (Calc. 21.8%). The DSC study of **2** revealed, as the main events, two endotherms centered at 122 and 181 °C corresponding to loss of water.

2.3.2. $C_7H_{15}NO_{11}Mg$ (*3*)

Ligand **1** (1.07 g, 5.85 mmol) and $Mg(OH)_2$ (0.450 g, 7.76 mmol) were heated under reflux in a mixture of acetone (30 mL) and water (5 mL) for 3 days. A red solid was obtained which was filtered and crystallized from water. Yield: 1.34 g (73%). *Anal.* Calc. for $C_7H_{15}NO_{11}Mg$ (**3**): C, 26.82; H, 4.82, N, 4.49. Found: C, 26.79; H, 4.82; N, 4.55%. IR (neat, cm^{-1}): 3187(m), 1665(m), 1534(s), 1441(s), 1396(s), 1329(s), 1251(s), 1218(s), 1065(s), 970(m). UV–Vis spectrum (in water): λ_{max} = 284 nm, ε = 8370; λ_{max} = 358 nm, ε = 3370; shoulder centered at ca 430 nm, ε = ca 1500. The conductance and pH of the 2×10^{-2} M solution in water were found to be 1.82×10^{-3} Ω^{-1} cm^{-1} and 6.42, respectively. TGA analysis of **3** revealed a mass loss of 33.9% on heating from 60 to 340 °C, corresponding to a loss of six water molecules (Calc. 34.4%). The DSC study of **3** revealed, as the main event, an endotherm centered at 147 °C corresponding to loss of water.

2.4. X-ray diffraction study

Diffraction data for salt **2** were collected on a Bruker-SMART three axis diffractometer equipped with a SMART 1000 CCD area detector using graphite monochromated Mo Kα X-radiation (wavelength λ = 0.71073 Å) at 100.0(1) K. The low temperature was reached by an evaporated liquid nitrogen stream over the crystal, provided by the Oxford Cryosystem device. Data collection and processing were carried out using the Bruker SMART programs [12] and empirical absorption correction was applied using the SADABS computer program [12]. The structure was solved by direct methods SIR97 [13], and refined by full-matrix least-squares based on F^2 using CRYSTALS software [14]. Structural data for complex **3** were obtained with monochromated Mo Kα radiation (λ = 0.71073 Å) on a Nonius Kappa detector at 293 K, with data collection and reduction using the HKL package [15]. The structure was solved by direct methods in the space group $P\bar{1}$ using SHELXS-97 [16] and refined by least-squares methods on F using CRYSTALS software [14]. All non-hydrogen atoms were anisotropically refined. The hydrogen atoms were located in difference Fourier maps. H atoms were refined isotropically with U_{iso} = 1.20 U_{eq}, where U_{eq} is the equivalent isotropic atomic displacement parameter of the attached atom. The

Table 1
Crystal data and structure refinement parameters for $C_{14}H_{20}N_2O_{16}Mg$ (**2**) and $C_7H_{15}NO_{11}Mg$ (**3**)

	2	**3**
Empirical formula	$C_{14}H_{20}N_2O_{16}Mg$	$C_7H_{15}NO_{11}Mg$
Molecular weight	496.62	313.51
Color	honey–colored	burgundy
Crystal system	triclinic	triclinic
Space group	$P\bar{1}$	$P\bar{1}$
a (Å)	7.091(5)	6.806(1)
b (Å)	7.177(5)	9.664(1)
c (Å)	10.243(5)	11.185(1)
α (°)	94.134(5)	72.59(5)
β (°)	103.693(5)	74.55(5)
γ (°)	103.559(5)	72.34(5)
V (Å^3)	487.8(5)	656.3(3)
Z	1	2
D_{calc} (g cm^{-3})	1.690	1.586
Absorption coefficient (mm^{-1})	0.184	0.193
$F(000)$	258	328
Crystal size (mm^3)	0.05 × 0.20 × 0.25	0.08 × 0.17 × 0.25
θ Ranges (°)	2.07 to 30.10	1.95 to 26.43
$h/k/l$	−9,9/ − 9,9/0,13	−8,8/ − 11,12/0,13
T (K)	100	293
Number of reflections collected	3667	5149
Number of reflections used $\geqslant 2\sigma(I)$	2121	1827
Parameters	151	182
$R[F]$	0.0264	0.0286
$wR[F]$	0.0312	0.0336
Goodness–of–fit on F^2	1.1222	1.1134
Residual density (e Å^{-3})	−0.36; 0.56	−0.27; 0.26
Refine ls shift/su.max	0.0054	0.00047

crystal parameters, data collection and the refinement details of compounds **2** and **3** are reported in Table 1.

3. Results and discussion

3.1. Description of the crystal structure of salt 2

Salt **2** can be represented by the general formula $[(C_7H_4NO_5)^-]_2[Mg(H_2O)_6]^{2+}$. The canonical drawing of this complex is represented in Fig. 1 and the CAMERON [17] molecular structure in Fig. 2, with the atom numbering system used in Table 2, which lists the most relevant bond distances and angles.

Compound **2** belongs to a well-documented family of ionic metal carboxylates [1,18–25]. The formula unit consists of a Mg^{++} cation located on an inversion center and two 3-hydroxy-4-nitrobenzoate anions related by symmetry. The Mg^{++} atom is octahedrally coordinated by six water molecules, with a slightly irregular geometry. The two Mg–O distances are rather similar [Mg–O(10) and Mg–O(12) are equal to 2.094 and 2.105 Å, respectively], while the third one, Mg–O(11), is much shorter (2.005 Å) (Fig. 3). These distances are comparable to those found in related compounds [26].

Regarding the ligand geometry, it is noteworthy that the $C(26)_{carboxylato}$ and $N(23)_{nitro}$ atoms deviate significantly from the aromatic mean plane [$\Delta C(26)_{carboxylato}$ and $\Delta N(23)_{nitro}$: +0.156 and +0.090 Å, respectively].

The two 3-hydroxy-4-nitrobenzoate anions are not directly coordinated to magnesium, but there are important hydrogen-bonded interconnections between the cations and anions. Thus, from a total of seven hydrogen bonds found in the asymmetric unit, four are involved in connections with the carboxylato groups: Mg–O(10)–H(101)···O(26)^{i}–C=O, Mg–O(11)–H(111)···O(26)^{iii}–C=O, Mg–O(10)–H(102)···O(27)^{iii}–C=O, Mg–O(12)–H(122)···O(27)^{v}–C=O, and two with the nitro groups: Mg–O(11)–H(112)···O(22)^{ii}–N=O, Mg–O(12)–H(121)···O(23)^{iv}–N=O. It is noteworthy that the lengths of the bridges involved in these interconnections are highly dissimilar. In this respect, the bond set connecting the carboxylato group O(26)^{iii}–C=O to the Mg atom incorporates two exceptionally short bridges: Mg–O(11) [2.005 Å, while the related Mg–O(10) and Mg–O(12) coordination distances are 2.094 and 2.105 Å, respectively] and H(111)···O(26)^{iii} [1.813 Å, while the related H(101)···O(26)^{i}, H(102)··· O(27)^{iii} and H(122)···O(27)^{v} H-bond distances are 1.906, 1.931 and 1.940 Å, respectively], making it an energetically favored pathway for the joining of the anions to the cations. On the other hand, the phenol and nitro groups found in the 3-hydroxy-4-nitrobenzoate anions of salt **2** are linked together through a conventional internal hydrogen bond: O(22)–H(22)···O(23). In sharp contrast, the *ortho*-nitrophenol moieties found in the Zn(II) and Co(II) (3-nitro-4-hydroxybenzoato) complexes take part in an original parallelogram–shaped structure consisting of alternate intra- and inter-molecular hydrogen bonds [11] (Fig. 4 and Table 3).

The individual zero-dimensional units (0D) of salt **2** are further engaged in alternate layers of $[Mg(H_2O)_6]^{2+}$ cations and stacked organic anions, resulting in 2D and 3D supramolecular architectures

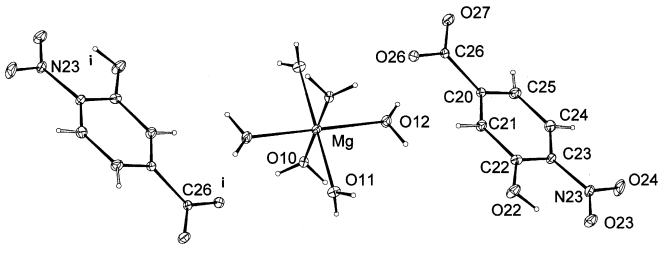

Fig. 2. Labelled CAMERON diagram of $[(C_7H_4NO_5)^-]_2[Mg(H_2O)_6]^{2+}$ (**2**). Ellipsoids are drawn at the 50% probability level. Symmetry code: i, $-x$, $-y$, $-z+2$.

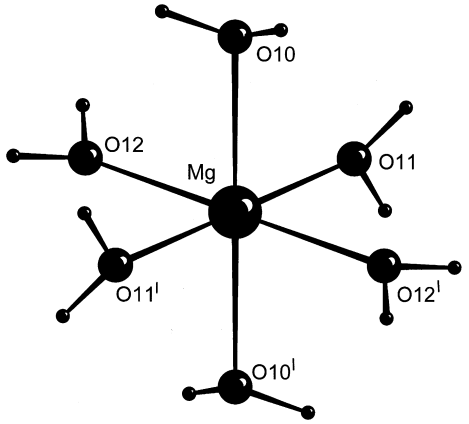

Fig. 3. Coordination octahedron around the Mg center in $[(C_7H_4NO_5)^-]_2[Mg(H_2O)_6]^{2+}$ (**2**). Symmetry code: i, $-x$, $-y$, $-z+2$.

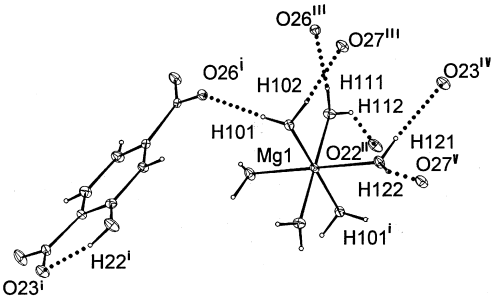

Fig. 4. Labelled diagram of $[(C_7H_4NO_5)^-]_2[Mg(H_2O)_6]^{2+}$ (**2**) showing the H-bonding associations as broken lines. Symmetry codes: i, $-x$, $-y$, $-z+2$; ii, $-x$, $-y$, $-z+1$; iii, $x-1$, y, z; iv, $-x$, $-y+1$, $-z+1$; v, $-x+1$, $-y+1$, $-z+2$. For symmetry reasons, only half of the hydrogen bonds have been represented.

Table 2
Selected bond distances (Å) and bond angles (°) for $[(C_7H_4NO_5)^-]_2[Mg(H_2O)_6]^{2+}$ (**2**)

Bond lengths		Bond angles	
Mg–O(10)	2. 094(2)	O(10)–Mg–O(11)	89.47(6)
Mg–O(11)	2.005(2)	O(10)–Mg–O(12)	88.03(7)
Mg–O(12)	2.105(2)	O(11)–Mg–O(12)	88.43(5)
O(22)–C(22)	1.350(2)	O(10)–Mg–O(12)^{i}	91.97(4)
O(23)–N(23)	1.243(2)	O(23)–N(23)–O(24)	122.67(11)
O(24)–N(23)	1.221(2)	O(26)–C(26)–O(27)	124.80(12)
O(26)–C(26)	1.272(2)		
O(27)–C(26)	1.249(2)		

Symmetry code: i, $-x$, $-y$, $-z+2$.

Table 3
H-bond donor/acceptor scheme (Å, °) for $[(C_7H_4NO_5)^-]_2[Mg(H_2O)_6]^{2+}$ (**2**)

D–H·A	*d*(D–H)	*D*(H···A)	∠(DHA)	*d*(D–A)
O(22)–H(22)···O(23)	0.848(2)	1.898(1)	142.68(4)	2.623(2)
O(10)–H(101)···O(26)^{i}	0.816(2)	1.906(1)	172.72(4)	2.717(2)
O(11)–H(112)···O(22)^{ii}	0.813(2)	2.166(1)	138.87(3)	2.829(2)
O(10)–H(102)···O(27)^{iii}	0.872(2)	1.931(1)	173.02(3)	2.798(2)
O(11)–H(111)···O(26)^{iii}	0.820(2)	1.813(1)	169.96(4)	2.625(2)
O(12)–H(121)···O(23)^{iv}	0.854(2)	2.137(1)	173.45(3)	2.987(2)
O(12)–H(122)···O(27)^{v}	0.850(2)	1.940(1)	165.08(4)	2.769(2)

Symmetry codes: i, $-x$, $-y$, $-z+2$; ii, $-x$, $-y$, $-z+1$; iii, $x-1$,y, z; iv, $-x$, $-y+1$, $-z+1$; v, $-x+1$, $-y+1$, $-z+2$.

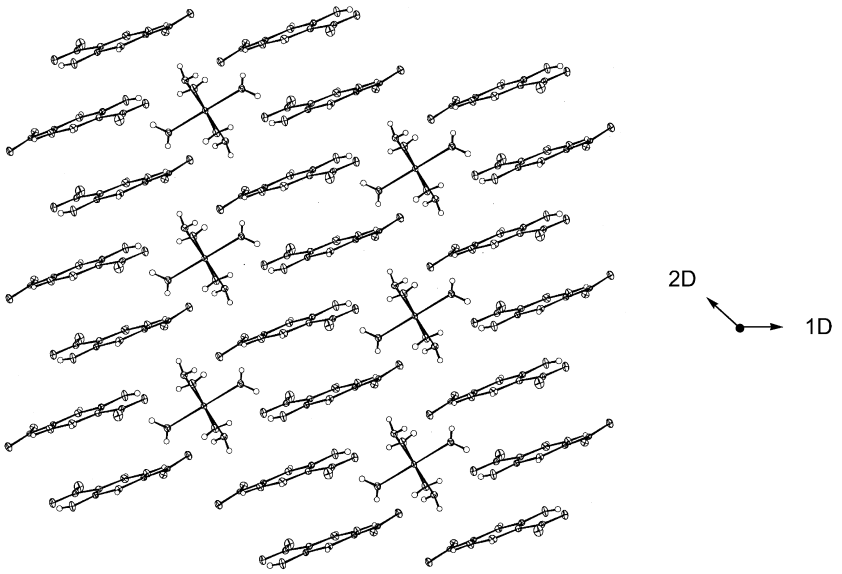

Fig. 5. 2D perspective diagram of $[(C_7H_4NO_5)^-]_2[Mg(H_2O)_6]^{2+}$ (**2**) viewing the alternate stacking of planar layers of 3-hydroxy-4-nitrobenzoate anions in between slabs of hexaaquamagnesium(II) cations. Hydrogen bonds are omitted for clarity.

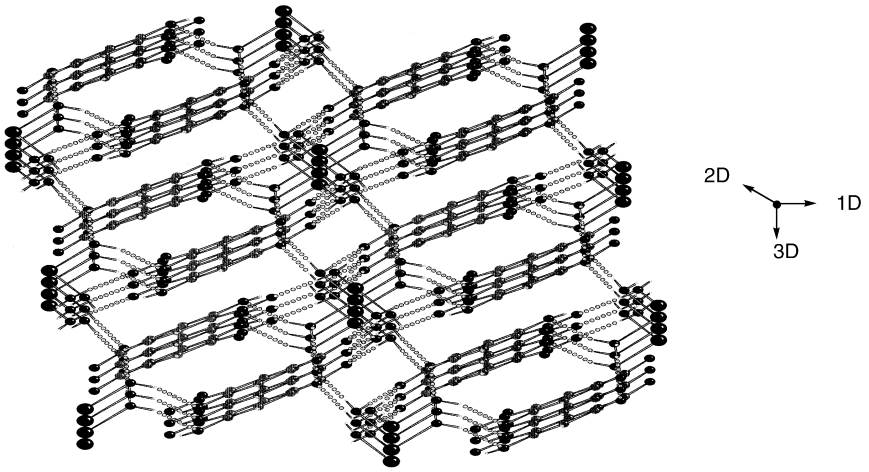

Fig. 6. Packing of $[(C_7H_4NO_5)^-]_2[Mg(H_2O)_6]^{2+}$ (**2**) showing the H-bonded 3D continuum as broken lines. Mg(II) centers are symbolized by large circles.

(Figs. 5 and 6). The most salient feature of the 3D architecture is the extensive coordination of the Mg(II) centers to the aromatic ligands through a complex hydrogen bond network. Four types of alternate channels are thus generated in the *b*-direction, the two larger ones measuring ca 3.1 × 7.7 and 3.5 × 4.0 Å^2 (Fig. 6).

The crystal packing of **2** is also governed by π–π stacking interactions involving the anionic aromatic moieties in a head-to-tail, *anti*-facial arrangement of the aromatic nuclei planes P(1) [C(20) until C(25)] and P(2) [C(20) until C(25); symmetry: $-x+1$, $-y+1$, $-z+1$]. The values of the mean interplanar spacing, the ring-centroid separation and the ring-centroid offset are, respectively, 3.534, 3.740 and 1.224 Å.

3.2. Description of the crystal structure of complex **3**

Complex **3** can be represented by the general formula $C_7H_3NO_5Mg(H_2O)_4 \cdot 2H_2O$. The canonical drawing of this complex is represented in Fig. 7 and the CAMERON [8] molecular structure in Fig. 8, with the atom numbering system used in Table 4, which lists the most relevant bond distances and angles.

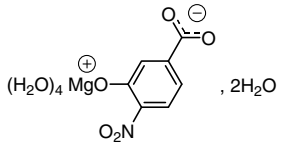

Fig. 7. Canonical representation of $C_7H_3NO_5Mg(H_2O)_4 \cdot 2H_2O$ (**3**).

The asymmetric unit of complex **3** consists of a zwitterion comprising of one organic ligand in its dianionic state and one magnesium cation. This type of structure is rather unusual [1,27–31]. One of the most salient features in **3** is the direct ligation of the magnesium cation to the phenoxo group. This can be interpreted by referring to the two acidities of ligand **1** (see Section 3.4.1). With the carboxylic acid in **1** ($pK_a = 3.11$) being ca 3×10^3 more acidic than the phenol group ($pK_a = 6.59$), the highest negative charge in the zwitterion **3** resides necessarily at the phenoxo site bonded to the Mg^{2+} cation. The Mg atom of **3** is octahedrally coordinated by four water molecules, one phenoxo group and one nitro group of

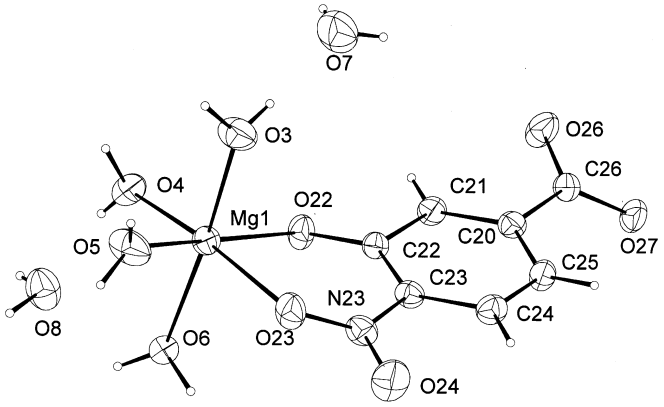

Fig. 8. Labelled CAMERON diagram of $C_7H_3NO_5Mg(H_2O)_4 \cdot 2H_2O$ (**3**). Ellipsoids are drawn at the 50% probability level.

Table 4
Selected bond distances (Å) and bond angles (°) for $C_7H_3NO_5Mg(H_2O)_4 \cdot 2H_2O$ (**3**)

Bond lengths		Bond angles	
Mg–O(3)	2.055(2)	O(4)–Mg–O(5)	97.96(9)
Mg–O(4)	2.036(2)	O(5)–Mg–O(23)	88.10(8)
Mg–O(5)	2.052(2)	O(4)–Mg–O(22)	94.96(8)
Mg–O(6)	2.071(2)	O(22)–Mg–O(23)	80.22(8)
Mg–O(22)	1.998(2)	O(3)–Mg–O(6)	171.97(6)
Mg–O(23)	2.164(2)	O(23)–N(23)–O(24)	119.10(2)
O(24)–N(23)	1.229(2)	O(22)–C(22)–C(23)	125.93(2)
O(26)–C(26)	1.258(2)	O(24)–N(23)–C(23)	120.09(2)
O(27)–C(26)	1.260(2)	O(26)–C(26)–O(27)	122.92(2)

the aromatic ligand. Two additional water molecules, although not directly coordinated with the Mg atom, are involved in an extensive H-bonding network (see below). The octahedron around the Mg atom exhibits an irregular geometry. The four Mg–O (water) distances are rather similar [2.036(2)–2.071(2) Å], while the Mg–$O(22)_{phenoxo}$ distance [1.998(2) Å] is much shorter than the Mg–$O(23)_{nitro}$ distance [2.164(2) Å] (Fig. 9).

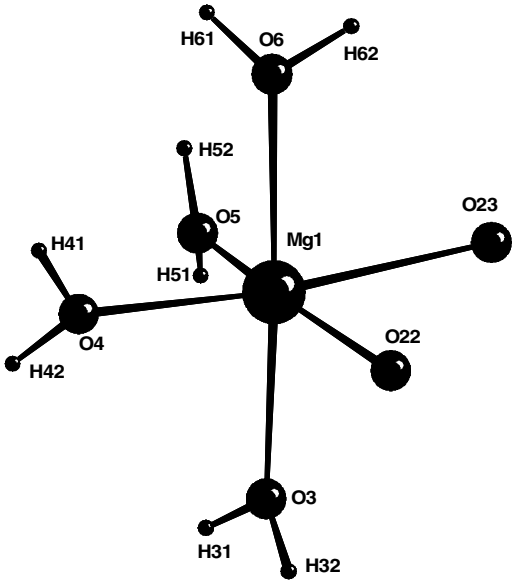

Fig. 9. Coordination octahedron around the Mg center in $C_7H_3NO_5Mg(H_2O)_4 \cdot 2H_2O$ (**3**).

Regarding the ligand geometry, it must be emphasized that the $C(26)_{carboxylato}$ atom is nearly located on the aromatic mean plane [$\Delta C(26)_{carboxylato}$: +0.004 Å], while the $N(23)_{nitro}$ and $O(22)_{phenoxo}$ atoms deviate slightly from this plane [$\Delta N(23)_{nitro}$: −0.054 Å, $\Delta O(22)_{phenoxo}$: +0.064 Å].

In other respects, it should be noted that the $O(23)_{nitro}$–Mg(1) coordination bond (length: 2.164 Å) takes part in a six-membered ring involving O(23), Mg(1), O(22), C(22), C(23) and N(23) atoms. The peculiar flattened boat-shaped conformation of this ring was highlighted through the orthogonal deviations of the ring atoms from the ring mean plane (in Å): −0.010 for ΔO(23), −0.063 for ΔMg(1), +0.119 for ΔO(22), −0.060 for ΔC(22), −0.061 for ΔC(23) and +0.075 for ΔN(23).

The carboxylate anion of complex **3** is not directly coordinated to the magnesium cation, but there are important hydrogen bonds joining the zwitterionic species. In particular, there are six interconnections between the carboxylato groups and each magnesium cation, involving either a single water molecule: O=C–$O(26)^{ii}\cdots$H(42)–O(4)–Mg, O=C–$O(27)^{iii}\cdots$H(51)–O(5)–Mg, O=C–$O(27)^{v}\cdots$H(61)–O(6)–Mg, O=C–$O(27)^{vi}\cdots$H(62)–O(6)–Mg, or two water molecules: O=C–$O(26)^{v}\cdots$H(82)–O(8)$\cdots$H(41)–O(4)–Mg, O=C–$O(26)^{vii}\cdots$H(81)–O(8)$\cdots$H(41)–O(4)–Mg (Fig. 10 and Table 5).

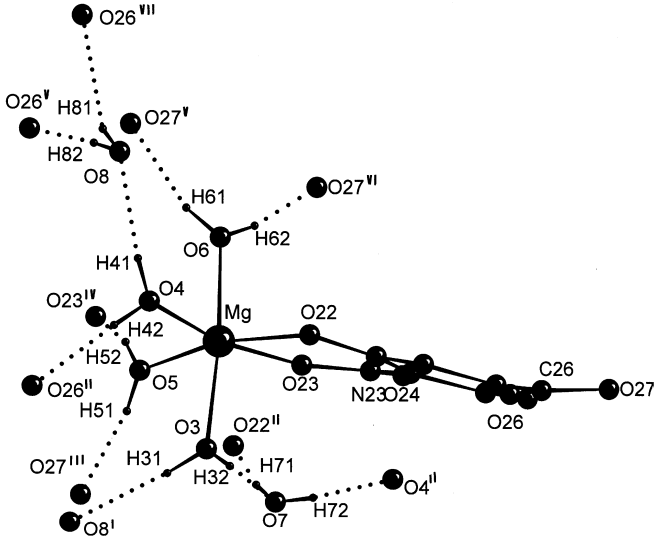

Fig. 10. Labelled diagram of $C_7H_3NO_5Mg(H_2O)_4 \cdot 2H_2O$ (**3**) showing the H-bonding associations as broken lines. Symmetry codes: i, $x+1, y, z$; ii, $-x+1, -y+1, -z+2$; iii, $x+1, y, z-1$; iv, $-x+1, -y+2, -z+1$; v, $x,y,z-1$; vi, $-x, -y+2, -z+2$, vii, $-x, -y+1, -z+2$.

Table 5
H-bond donor/acceptor scheme (Å, °) $C_7H_3NO_5Mg(H_2O)_4 \cdot 2H_2O$ (**3**)

D–H$\cdots\cdots$A	*d*(D–H)	*D*(H$\cdots$A)	∠(DHA)	*d*(D–A)
$O(3)–H(31)\cdots O(8)^{i}$	0.832(2)	1.983(2)	174.51(6)	2.813(2)
$O(3)–H(32)\cdots O(7)$	0.823(2)	1.893(2)	174.46(7)	2.713(2)
$O(4)–H(41)\cdots O(8)$	0.806(2)	1.957(2)	169.46(6)	2.755(2)
$O(4)–H(42)\cdots O(26)^{ii}$	0.816(2)	1.902(2)	173.15(6)	2.717(2)
$O(5)–H(51)\cdots O(27)^{iii}$	0.822(2)	2.036(2)	164.00(5)	2.837(2)
$O(5)–H(52)\cdots O(23)^{iv}$	0.819(2)	2.147(2)	154.65(6)	2.895(2)
$O(6)–H(61)\cdots O(27)^{v}$	0.825(2)	2.057(2)	157.92(5)	2.843(2)
$O(6)–H(62)\cdots O(27)^{vi}$	0.844(2)	1.888(2)	168.95(5)	2.728(2)
$O(7)–H(71)\cdots O(22)^{ii}$	0.836(2)	1.978(2)	167.67(6)	2.823(2)
$O(7)–H(72)\cdots O(4)^{ii}$	0.788(2)	2.312(2)	162.61(5)	3.104(2)
$O(8)–H(81)\cdots O(26)^{vii}$	0.816(2)	2.272(2)	145.61(5)	2.978(2)
$O(8)–H(82)\cdots O(26)^{v}$	0.829(2)	1.908(2)	175.57(6)	2.728(2)

Symmetry codes: i, $x+1, y, z$; ii, $-x+1, -y+1, -z+2$; iii, $x+1, y, z-1$; iv, $-x+1, -y+2, -z+1$; v, $x, y, z-1$; vi, $-x, -y+2, -z+2$, vii, $-x, -y+1, -z+2$.

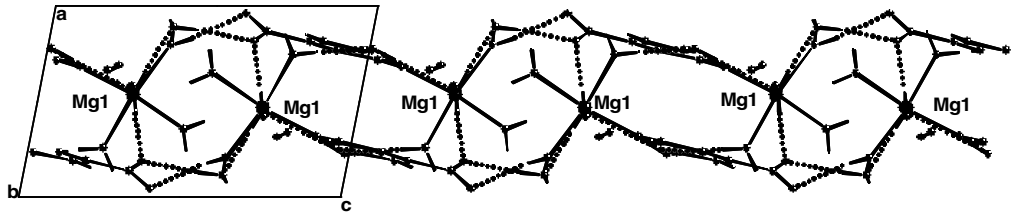

Fig. 11. Structural of part of $C_7H_3NO_5Mg(H_2O)_4 \cdot 2H_2O$ (**3**) indicating the 1D chain structure. The H-bonded continuum is symbolized as broken lines.

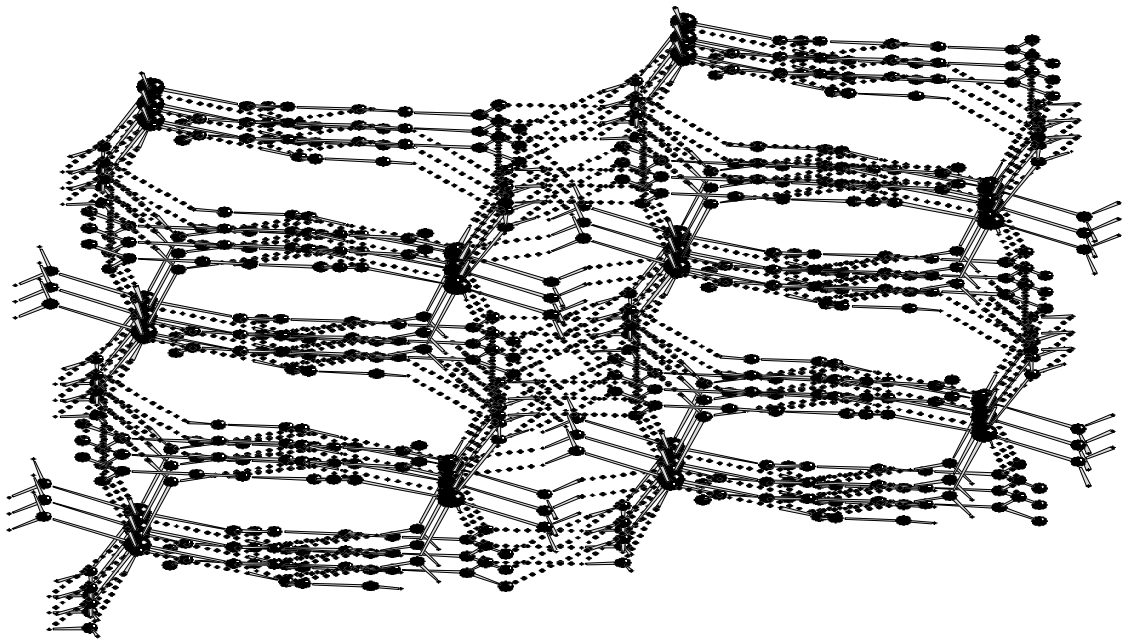

Fig. 12. Packing of $C_7H_3NO_5Mg(H_2O)_4 \cdot 2H_2O$ (**3**) showing the H-bonded 3D continuum as broken lines. Mg centers are symbolized by large circles.

The individual units of complex **3** are further engaged in a complicated hydrogen bond network, forming infinite chains along the *b*-axis (Fig. 11). These, in turn, self-assemble via hydrogen bonds, resulting in a 3D supramolecular architecture. Two types of alternate channels are thus generated in the *b*-direction, measuring ca 3.3×6.1 and 3.6×8.8 Å^2 (Fig. 12).

The crystal packing of **3** is also governed by π–π stacking interactions involving the anionic aromatic moieties. The type I-stacking involves a head-to-tail *anti*-facial arrangement of the aromatic nuclei planes P1, [P1: C(20) until C(25)] and P(2) [P2: C(20) until C(25); symmetry: $-x, -y + 2, -z + 2$] with a mean interplanar spacing of 3.345 Å. The two rings have a centroid separation of 3.534 Å, corresponding to a ring-centroid offset of 1.139 Å.

3.3. Interconversion of complexes *2* and *3* in aqueous solution

The identification of the ultimate entity that crosses the blood–brain barrier is of the highest importance for understanding the mode of action of anticonvulsant drugs of the (salicylato)-metal complexes family [32]. In this regard, the behavior of complexes **2** and **3** in aqueous solution was investigated, revealing a facile interconversion between the two compounds.

The conversion of **2** to **3** was revealed through the following water/1-octanol extraction experiment [11,33]. Salt **2** (300 mg, 6.1×10^{-4} mol) was dissolved in deionized water (30 ml). This solution was extracted with 1-octanol (30 ml) at room temperature. The extraction was repeated four times and the 1-octanol extracts combined. After removal of 1-octanol by vacuum distillation at 1 Torr, ligand **1** (71 mg), was obtained as a pale yellow solid, which was unambiguously identified by comparison with an authentic sample using R_f values in thin layer chromatography and ^{1}H NMR spectroscopy. During this experiment, the color of the aqueous phase changed from pale yellow to bright orange. Evaporation of this solution at room temperature under vacuo gave complex **3** as a microcrystalline bright red solid (174 mg, 93% yield). The above outcome can be interpreted on the basis of two-step equilibrium of salt **2** in aqueous medium, depicted in Fig. 13. The first step of this process involves the dissociation of the salt into the 3-hydroxy-4-nitrobenzoate anion and the magnesium(II) cation. These, in turn, may interconvert through proton transfer into ligand **1** and complex **3** (in which one metal atom is coordinated to one ligand molecule acting as a bidendate linker through its carboxylato and phenoxo groups). Because of its

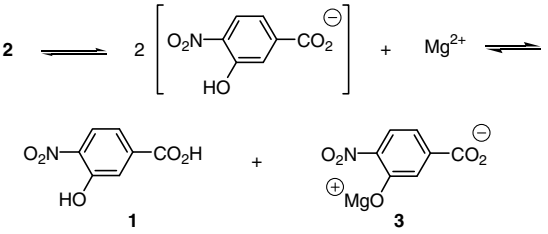

Fig. 13. Equilibrium of salt **2** in aqueous solution. The water molecules coordinated to the metal atom have been omitted for clarity.

marked lipophilicity (calculated log*P* = 1.78) [31], ligand **1** is extractable with 1-octanol (an operation that drives the equilibrium toward partners **1** and **3**), while the hydrophilic complex **3** remains in the aqueous phase.

The conversion of **3** to **2** was revealed through the following experiment. To a solution of complex **3** (0.157 g, 0.5×10^{-3} mol) in 2 ml of water was added a solution of ligand **1** (0.092 g, 0.5×10^{-3} mol) in 2 ml of ethanol at room temperature. The bright orange color of the solution changed instantaneously to pale yellow. After evaporation of the solvents, salt **2** was obtained in quantitative yield.

3.4. Potentiometric measurements of ligand *1*

Since the magnesium(II) complexes **2** and **3** correspond to ligand **1** (3-hydroxy-4-nitrobenzoic acid) in its mono– and dianionic states, respectively, the protonation constants and UV–Vis spectra of **1** as a function of the pH were determined. The distribution of species as a function of pH were also investigated, involving potentiometric measurements and simulation studies.

3.4.1. Determination of the protonation constants of *1*

The protonation constants (p*K*a) of the acidic functions of 3-hydroxy-4-nitrobenzoic acid (**1**) have been calculated. The carboxylic group (p*K*a = 3.106 ± 0.003) is more acidic than benzoic acid (4.20), in agreement with the acid-strengthening effect of the electron-withdrawing nitro group in the *para* position (3.44 for 4-nitrobenzoic acid) and of the phenol function in the *meta* position (4.08 for 3-hydroxybenzoic acid). Concerning the phenol function, the lowest value observed ($pK_a = 6.590 \pm 0.002$), compared to phenol itself (9.96), is in agreement with the electron-withdrawing effect of both the nitro (7.22 for 2-nitrophenol) and carboxylic groups.

3.4.2. UV–Vis spectra of *1* as a function of pH

In the 200–600 nm region, at high acidic pH values, 3-hydroxy-4-nitrobenzoic acid (**1**) displays three absorption bands centered at around 211, 276 and 353 nm (Fig. 14 and Table 6). These are all $\pi \rightarrow \pi^*$ transitions corresponding to $A_{1g} \rightarrow E_{1u}$ (E_1-band), $A_{1g} \rightarrow B_{1u}$ (E_2-band) and $A_{1g} \rightarrow B_{2u}$ (B–band) transitions in the benzene ring, corrected by the bathochromic shift due to the auxochromic 3,4-substituted groups [34]. The shoulder present at 244 nm could be assigned to the $n \rightarrow \pi^*$ transitions of the carboxyl function whereas the weak $n \rightarrow \pi^*$ transition of the nitro function is submerged by the E_2 band at 276 nm. As the pH is increased, the deprotonation of the carboxyl function induces a bathochromic shift in the $A_{1g} \rightarrow B_{1u}$ transition. Above pH 8.0, the deprotonation of the phenol function results in a general bathochromic shift of all the bands, being stronger for the E_1-band and the B-bands, the last one being responsible of the color change from pale yellow to bright orange. Isosbestic points are present at 199, 235, 318 and 362 nm.

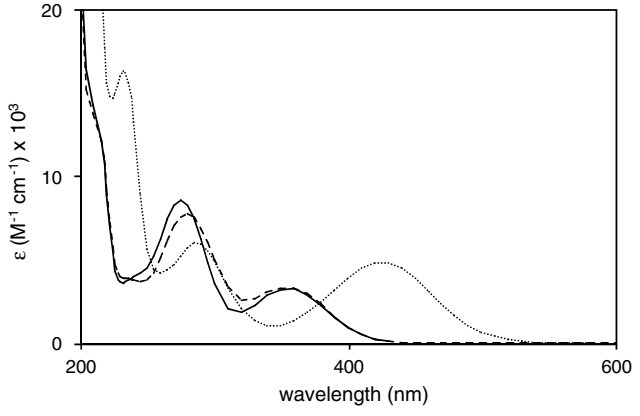

Fig. 14. UV–visible spectra of 3-hydroxy-4-nitrobenzoic acid (**1**) in aqueous solution as a function of pH: pH 2.0 (——); 4.0 (– – –); 10.2 (. . .); $[LH_2] = 1.0 \times 10^{-3}$ M, [NaCl] = 0.15 M.

Table 6
λmax and ε in the UV–Vis spectra of 3-hydroxy-4-nitrobenzoic acid (**1**) (LH_2) in aqueous solution as a function of the pH[a]

Species	pH	$\pi \rightarrow \pi^*$	$n \rightarrow \pi^*$	$\pi \rightarrow \pi^*$	$\pi \rightarrow \pi^*$
		E_1	(COOH)	E_2	B
LH_2	2.0	211 sh (14000)	244 sh (3950)	275 (8620)	356 (3300)
LHNa	4.0	211 sh (14000)	235 sh (3815)	279 (7763)	353 (3290)
LNa_2	10.2	232 (16250)	submerged	285 (6000)	422 (4845)

[a] λ_{max} in nm, ε in $M^{-1}\,cm^{-1}$.

3.4.3. Distribution of species as a function of pH

Potentiometric measurements of the system, ligand **1** and $MgCl_2$ in the presence of NaOH were first recorded according to a previously reported procedure [35,36] (data not shown). Formation constants of species were subsequently calculated by means of ESTA [37] and MINIQUAD [38] programs. Regarding the ligand **1** (LH_2)/NaOH system, increasing the pH from 1 to 8 results in the successive formation of LHNa and LNa_2 species, as expected (Fig. 15). Regarding the ligand **1** (LH_2)/$MgCl_2$/NaOH system, increasing the pH from 2 to 8 results in the successive formation of $(LH)_2Mg$ (complex **2**), LMg (complex **3**) and $Mg(OH)_2$ species (Fig. 16). It is noteworthy that the optimal pH values for the formation of Mg(II) complexes **2** and **3** (ca 4.7 and 7.0, respectively) are

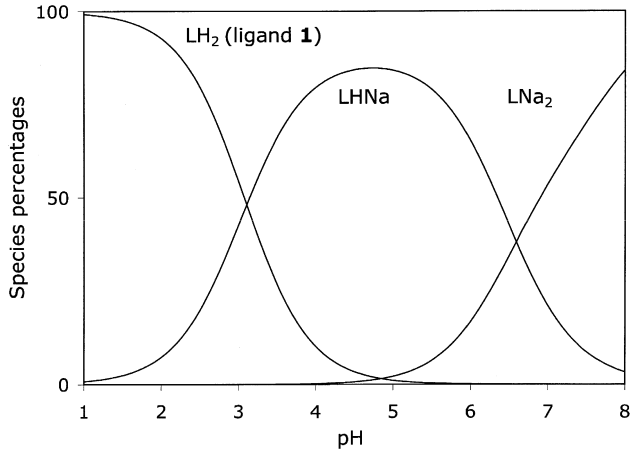

Fig. 15. Distribution of species as a function of pH in the ligand **1**/NaOH system (ligand speciation) ($[LH_2] = 10^{-3}$ M).

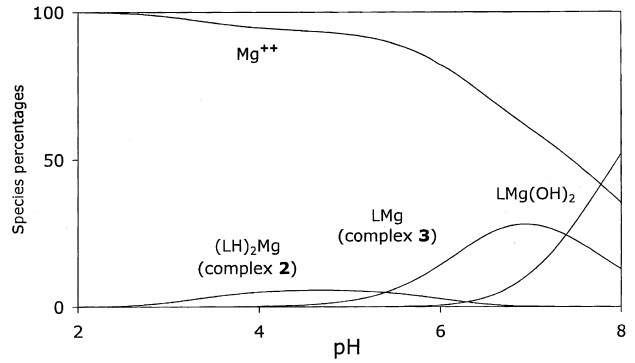

Fig. 16. Distribution of species as a function of pH in the ligand **1**/$MgCl_2$/NaOH system (metal speciation) ($[LH_2] = [MgCl_2] = 10^{-3}$ M).

close to the pH values of the 2×10^{-2} M water solutions of these complexes (4.85 and 6.42 for **2** and **3**, respectively, see Sections 2.3.1 and 2.3.2).

4. Conclusion

The crystal structures of two magnesium(II) complexes of 3-hydroxy-4-nitrobenzoic acid (**1**) have been reported. The first complex (**2**) is comprised of two organic anions and one hexaaquamagnesium cation. In these ionic entities, the anions do not coordinate directly to magnesium, but there are important hydrogen-bonded interconnections between the cations and anions. The second complex (**3**) consists of an original zwitterionic structure comprising one organic ligand in its dianionic state and one magnesium cation. One of the most salient features in this structure is the direct ligation of the magnesium to the phenoxo group. The carboxylate anion of this zwitterion is not directly coordinated to the magnesium cation, but there are important hydrogen bonds joining the zwitterionic units. The 3D supramolecular architectures of complexes **2** and **3** are also stabilized by two types of stacking interactions involving the aromatic part of ligand **1**.

An interesting interconversion between the two complexes was observed in aqueous solution, involving the addition/release of one ligand molecule. This phenomenon was supported by potentiometric measurements of ligand **1** in the presence of Na^+ and Mg^{++} cations. The distributions of species as a function of pH were also determined through simulation studies.

Appendix A. Supplementary data

CCDC 655902 and 675372 contain the supplementary crystallographic data for **2** and **3**. These data can be obtained free of charge via http://www.ccdc.cam.ac.uk/conts/retrieving.html, or from the Cambridge Crystallographic Data Centre, 12 Union Road, Cambridge CB2 1EZ, UK; fax: (+44) 1223-336-033; or e-mail: deposit@ccdc.cam.ac.uk. Supplementary data associated with this article can be found, in the online version, at doi:10.1016/j.poly.2008.03.027.

References

[1] F.D. Rochon, G. Massarweh, Inorg. Chim. Acta 304 (2000) 190.
[2] S.H. Rahaman, D. Bose, H. Chowdhury, G. Mostafa, H.-K. Fun, B.K. Ghosh, Polyhedron 24 (2005) 1837.
[3] N.E. Ghermani, G. Morgant, J. d'Angelo, D. Desmaële, B. Fraisse, F. Bonhomme, E. Dichi, M. Sghaier, Polyhedron 26 (2007) 2880.
[4] J.R.J. Sorenson, Free Radic. Biol. Med. 13 (1992) 593.
[5] G. Morgant, N. Bouhmaida, L. Balde, N.E. Ghermani, J. d'Angelo, Polyhedron 25 (2006) 2229.
[6] J.R.J. Sorenson, J. Med. Chem. 19 (1976) 135.
[7] J.R.J. Sorenson, Prog. Med. Chem. 15 (1978) 211.
[8] B. Viossat, J.-C. Daran, G. Savouret, G. Morgant, F.T. Greenaway, N.-H. Dung, V.A. Pham-Tran, J.R.J. Sorenson, J. Inorg. Biochem. 96 (2003) 375.
[9] P. Lemoine, B. Viossat, N.H. Dung, A. Tomas, G. Morgant, F.T. Greenaway, J.R.J. Sorenson, J. Inorg. Biochem. 98 (2004) 1734.
[10] B. Viossat, F.T. Greenaway, G. Morgant, J.-C. Daran, N.-H. Dung, J.R.J. Sorenson, J. Inorg. Biochem. 99 (2005) 355.
[11] J. d'Angelo, G. Morgant, N.E. Ghermani, D. Desmaële, B. Fraisse, F. Bonhomme, E. Dichi, M. Sghaier, Y. Li, Y. Journaux, J.R.J. Sorenson, Polyhedron 27 (2008) 537.
[12] ASTRO (5.00), SAINT (5.007) and SADABS (5.007), Data Collection and Processing Software for the SMART System (5.054), Siemens (BRUKER–AXS) Analytical X-ray Instruments Inc., Madison, WI, 1998.
[13] A. Altomare, M.C. Buria, M. Camalli, G.L. Cascarano, G. Giacovazzo, A. Guagliardi, A. Grazia, G. Moliterni, G. Polidori, R. Spagna, J. Appl. Crystallogr. 32 (1999) 115.
[14] D.J. Watkin, C.K Prout, J.R. Carruthers, P.W. Betteridge, R.I. Prout, CRYSTALS Issue 11, Chemical Crystallography Laboratory, University of Oxford, UK, 2001.
[15] Z. Otwinowski, W.W. Minor, Meth. Enzymol. 276 (1997) 307.
[16] G.M. Sheldrick, SHELXS-97, Program for Crystal Structure Solution, University of Göttingen, Germany, 1997.
[17] D.J. Watkin, C.K. Prout, L.J. Pearce, CAMERON, Chemical Crystallography Laboratory, University of Oxford, UK, 1996.
[18] B.J. Gunderman, S.N. Dubey, P.J. Squattrito, Acta Crystallogr. C53 (1997) 17.
[19] L. Karanović, D. Poleti, G.A. Bogdanović, A. Spasojević-de-Biré, Acta Crystallogr. C 55 (1999) 911.
[20] J.-F. Ma, J. Yang, J.-F. Liu, Acta Crystallogr. E 59 (2003) m478.
[21] J.-F. Ma, J. Yang, J.-F. Liu, Acta Crystallogr. E 59 (2003) m481.
[22] J.-F. Ma, J. Yang, J.-F. Liu, Acta Crystallogr. E 59 (2003) m483.
[23] J.-F. Ma, J. Yang, J.-F. Liu, Acta Crystallogr. E 59 (2003) m485.
[24] J.-F. Ma, J. Yang, J.-F. Liu, Acta Crystallogr. E 59 (2003) m487.
[25] J. Abdelhak, S. Namouchi Cherni, T. Jouini, Z. Kristallogr. NCS 220 (2005) 183.
[26] E.A. Kiseleva, S.I. Troyanov, Yu.M. Korenev, Russ. J. Coord. Chem. 33 (2007) 85.
[27] D. Poleti, D.R. Stojaković, B.V. Prelesnik, R.M. Herak, Acta Crystallogr. C 44 (1988) 242.
[28] D. Poleti, L. Karanović, Acta Crystallogr. C 45 (1989) 1716.
[29] A.H. Cowley, G.S. Hair, B.G. McBurnett, R.A. Jones, Chem. Commun. (1999) 437.
[30] P.J. Bailey, D. Loroño-González, P. Parsons, Chem. Commun. (2003) 1426.
[31] S. Sharif, D.R. Powell, D. Schagen, T. Steiner, M.D. Toney, E. Fogle, H.-H. Limbach, Acta Crystallogr. B 62 (2006) 480.
[32] N.J. Abbott, I.A. Romero, Mol. Med. Today (1996) 106.
[33] N. Bodor, P. Buchwald, J. Phys. Chem. B 101 (1997) 3404.
[34] R.M. Silverstein, C.G. Bassler, T.C. Morrill, Spectrometric Identification of Organic Compounds, John Wiley & Sons, New York, 1974.
[35] B. Halova-Lajoie, V. Brumas, M.M.L. Fiallo, G. Berthon, J. Inorg. Biochem. 100 (2006) 362.
[36] V. Brumas, H. Miche, M.M.L. Fiallo, J. Inorg. Biochem. 101 (2007) 565.
[37] P.M. May, K. Murray, D.R. Williams, Talanta 35 (1985) 825.
[38] A. Sabatini, A. Vacca, P. Gans, Talanta 21 (1974) 53.

Polyhedron 27 (2008) 2105–2112

Contents lists available at ScienceDirect

Polyhedron

journal homepage: www.elsevier.com/locate/poly

Influence of counter anions on structural, spectroscopic and electrochemical behaviours of copper(II) complexes of dipyrido[3,2-f: 2′,3′-h]-quinoxaline (dpq) ☆

Papu Biswas *, Supriya Dutta, Meenakshi Ghosh

Department of Inorganic Chemistry, Indian Association for the Cultivation of Science, Jadavpur, Kolkata 700 032, India

ARTICLE INFO

Article history:
Received 15 February 2008
4 April 2008
Accepted 4 April 2008
Available online 27 May 2008

Keywords:
Dipyridoquinoxaline
Copper(II) complexes
Crystal structure
Electronic spectra
Electrochemistry

ABSTRACT

A set of three copper(II) complexes, $[Cu^{II}(dpq)_2Cl_2]$ (**1**), $[\{Cu^{II}(dpq)_2(SCN)\}\{Cu^{II}(dpq)(SCN)_3\}]$ (**2**) and $[Cu^{II}(dpq)_2(N_3)](ClO_4)$ (**3**), derived from the ligand dipyrido[3,2-f: 2′,3′-h]-quinoxaline (dpq) have been reported. The molecular and the crystal structures of all the complexes have been determined by X-ray crystallography. The structural results confirm that depending on the selected anions, a great variety of geometries are observed with copper(II). The light blue compound **1** has a distorted octahedral geometry with a $[CuN_4Cl_2]$ core. Compound **2** consists of a cationic part, $\{Cu^{II}(dpq)_2(SCN)\}^+$, and an anionic part, $\{Cu^{II}(dpq)(SCN)_3\}^-$. In both the cationic and anionic part, the geometry around the copper(II) ion is distorted square pyramidal. In compound **3**, one azide anion is coordinated to the metal centre providing a distorted square pyramidal geometry. The quinoxaline ring in **1** and **2** is involved in intermolecular π–π interactions leading to the generation of a sinusoidal chain in **1** and a zigzag chain in **2**. The electronic absorption spectra and the redox behaviour of all the complexes have been studied in dimethyl sulfoxide.
© 2008 Elsevier Ltd. All rights reserved.

1. Introduction

Metal ion complexes with bidentate ligands continue to be of strong interest in many areas of chemistry. 2,2′-Bipyridine (bpy) and 1,10-phenanthroline (phen) have been extensively used as chelating ligands in both analytical and preparative coordination chemistry [1]. More recently, systematic studies of substituted bipyridines, phenanthrolines and other α-diimine derivatives have been undertaken [2–9]. Ligands based on the 2,2′-bipyridine (bpy) and 1,10-phenanthroline (phen) frameworks have played a particularly important role because of the imbedded π electron system present. Their complexes with metal ions spanning much of the periodic table have led to a wide variety of systems with interesting structural, spectroscopic, catalytic, biomimetic, DNA binding and cleavage properties [10,11]. A key feature of these six-membered heterocyclic rings is their π-electron deficiency, which make them excellent π-acceptor ligands. Consequently, they have been used to stabilize various metal complexes in lower oxidation states [12,13].

Of particular interest, copper complexes of these ligands have been studied for a variety of reasons, including intense interest in their catalytic properties in organic synthesis, control in polymerization reactions and biomimetic behaviour. These types of copper complexes have also been studied for their relevance to the active-site structures of metalloproteins [14]. The redox chemistry of copper polypyridines is of particular interest as they undergo significant changes in their coordination geometry during the redox process. The influence of the inner coordination-sphere upon the redox properties of the copper(II/I) couple has received considerable attention, being stimulated, to a large part, by the importance of this redox couple in enzymes. The ability to deliberately control the microstructure of a coordination polymer by using macroscopic principles, through dissociation/binding ligands from/to metal centres by an applied potential can have numerous material applications [15].

Phenanthroline-based ligands such as dipyrido[3,2-f: 2′,3′-h]-quinoxaline (dpq), dipyridophenazine (dppz) and 7,8-dimethylpyridophenazine (dppx) with an extended planar quinoxaline moiety, can act as good bidentate ligands as well as good binders to DNA. Several ruthenium(II) complexes, such as $[RuL_2(dpq)]^{2+}$ (L = bpy or phen), have been synthesized because they bind to DNA strongly by intercalating the aromatic dpq ligand between the base pair. Moreover, on binding to DNA they strongly luminesce to act as "light switches" [16]. More recently it has also been shown that copper(II) complexes having photoactive and DNA binding ligands cleave DNA on irradiation with red light [17]. Ternary copper(II) complexes derived from tridentate ONO and ONS ligands and the DNA binding ligand dpq cleave DNA on exposure to red light [18]. We have earlier reported the syntheses, X-ray crystal structures, spectroscopic properties and redox activities of zinc(II), copper(I), copper(II), nickel(II), cobalt(II), cobalt(III), iron(II) and

☆ Supporting information for this article is available on the WWW under http://www.elsevier.com/locate/poly or from the author.

* Corresponding author.
E-mail addresses: icpb3@iacs.res.in, biswaspapu@rediffmail.com (P. Biswas).

0277-5387/$ - see front matter © 2008 Elsevier Ltd. All rights reserved.
doi:10.1016/j.poly.2008.04.017

manganese(II) complexes of dpq [19]. In this present study, we have reported the influence of various anions such as Cl^-, SCN^- and N_3^- on the structural, spectroscopic and electrochemical properties of copper(II) complexes of the dpq ligand.

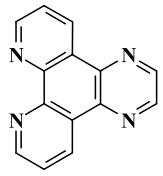

dpq

2. Experimental

2.1. Materials

All the chemicals were obtained from commercial sources and were used as received. The solvents were dried and purified according to standard methods [20]. 1,2-Diaminoethane was dried over potassium hydroxide before vacuum distillation. 1,10-Phenanthroline-5,6-dione and dipyrido[3,2-f: 2′,3′-h]-quinoxaline (dpq) were prepared according to the reported methods [19,21].

Caution: The perchlorate salts reported here are potentially explosive and should be handled with care.

2.2. Preparation of metal complexes

2.2.1. $[Cu^{II}(dpq)_2Cl_2]$ (**1**)

To a stirred suspension of dpq (0.23 g, 1 mmol) in acetonitrile (20 mL) was added an acetonitrile solution (5 mL) of $Cu(ClO_4)_2 \cdot 6H_2O$ (0.19 g, 0.5 mmol) followed by an excess NaCl solution (5 mL) in water (0.12 g, 2 mmol). The light blue crystalline product that deposited after 15 min of stirring was collected by filtration and washed with a little acetonitrile-water (1:1) mixture. The filtrate was kept for an overnight period, during which time light blue single crystals suitable for X-ray crystallography appeared. Yield: 0.15 g (50%). *Anal.* Calc. for $C_{28}H_{16}N_8Cl_2Cu$: C, 56.15; H, 2.69; N, 18.70. Found: C, 56.24; H, 2.72; N, 18.65%. UV–Vis–NIR (λ_{max}, nm/ε, $M^{-1}\,cm^{-1}$): 250(100000), 295(35000), 350(10000), 450(880), 740(125), 925(95).

2.2.2. $[\{Cu^{II}(dpq)_2(SCN)\}\{Cu^{II}(dpq)(SCN)_3\}]$ (**2**)

This compound was prepared in the same way as described for **1**, using NaSCN solution in water instead of NaCl. Yield: 0.20 g (74%). *Anal.* Calc. for $C_{46}H_{24}N_{16}S_4Cu_2$: C, 52.31; H, 2.29; N, 21.22. Found: C, 52.40; H, 2.35; N, 21.15%. IR (KBr): νSCN^- = 2098s, 2071s cm^{-1}. UV–Vis–NIR (λ_{max}, nm/ε, $M^{-1}\,cm^{-1}$): 260(120000), 300(44000), 340(13000), 405(1300), 710(140), 940(sh).

2.2.3. $[Cu^{II}(dpq)_2(N_3)](ClO_4)$ (**3**)

This compound can be obtained following the same method described above for **1** and **2** using NaN_3 solution in water. Yield: 0.60 g (75%). *Anal.* Calc. for $C_{28}H_{16}N_{11}O_4ClCu$: C, 50.23; H, 2.40; N, 23.01. Found: C, 50.30; H, 2.42; N, 22.95%. IR (KBr): ν_{as} N_3^- = 2036s, $\nu_s N_3^-$ = 1338m, $\nu_s ClO_4^-$ = 1120s, 1081s, 622m cm^{-1}. UV–Vis–NIR (λ_{max}, nm/ε, $M^{-1}\,cm^{-1}$): 260(105000), 290(33000), 340(9000), 400(2000), 680(110), 1050(sh).

2.3. Physical measurements

The C, H and N analyses were performed on a Perkin–Elmer 2400 II elemental analyzer. IR spectra were recorded using KBr disks on a Shimadzu FTIR 8400S spectrometer. The electronic absorption spectra were obtained with a Perkin–Elmer 950 UV/Vis/NIR spectrophotometer. The electrochemical measurements were carried out with a BAS 100 B electrochemistry system using a three-electrode assembly comprising a glassy carbon working electrode, Pt auxiliary electrode and an aqueous Ag/AgCl reference

Table 1
Crystallographic data and structure refinement parameters for $[Cu^{II}(dpq)_2Cl_2]$ (**1**), $[\{Cu^{II}(dpq)_2(SCN)\}\{Cu^{II}(dpq)(SCN)_3\}]$ (**2**) and $[Cu^{II}(dpq)_2(N_3)](ClO_4)$ (**3**)

	1	**2**	**3**
Empirical formula	$C_{28}H_{16}N_8Cl_2Cu$	$C_{46}H_{24}N_{16}S_4Cu_2$	$C_{28}H_{16}N_{11}O_4ClCu$
Formula weight	598.93	1056.13	669.52
Temperature (K)	293(2)	293(2)	293(2)
Crystal system	monoclinic	triclinic	triclinic
Space group	*C*2/*c*	*P*$\bar{1}$	*P*$\bar{1}$
Unit cell dimensions			
a (Å)	8.3541(5)	8.4206(9)	6.9398(3)
b (Å)	12.3685(8)	13.0030(13)	10.6756(4)
c (Å)	22.8107(14)	20.434(2)	19.0046(7)
α (°)	90.00	89.1220(10)	97.471(2)
β (°)	93.281(2)	83.2740(10)	98.806(2)
γ (°)	90.00	74.7740(10)	107.062(2)
Volume ($Å^3$)	2353.1(3)	2143.7(4)	1307.15(9)
Z	4	2	2
D_{calc} (Mg/m^3)	1.691	1.636	1.701
F(000)	1212	1068	678
Crystal size (mm)	0.06 × 0.05 × 0.02	0.20 × 0.10 × 0.05	0.20 × 0.02 × 0.01
	1	**2**	**3**
μ (mm^{-1})	1.194	1.245	1.000
θ_{min}, θ_{max}	1.79, 31.78	1.00, 25.80	1.10, 29.76
Reflections collected	21400	16528	22675
Data/restraints/parameters	4000/0/177	8134/0/705	7224/0/406
Goodness-of-fit on F^2	1.037	1.013	1.046
Final *R* indices	R_1[a] = 0.0430	R_1 = 0.0475	R_1 = 0.0535
[$I > 2\sigma(I)$]	wR_2[b] = 0.0996	wR_2 = 0.1094	wR_2 = 0.1520
R indices (all data)	R_1 = 0.0647	R_1 = 0.0804	R_1 = 0.0784
	wR_2 = 0.1093	wR_2 = 0.1333	wR_2 = 0.1684

[a] $R_1 = \sum |F_o| - |F_c| / \sum |F_o|$.
[b] $wR_2(F^2) [\sum w(F_o^2 - F_c^2)^2 / \sum w(F_o^2)^2]^{1/2}$.

electrode. The cyclic voltammetric (CV) and square wave voltammetric (SWV) measurements were carried out at 25 °C under a nitrogen atmosphere at room temperature. The solutions were 1 mmol dm^{-3} in complexes and 0.1 mol dm^{-3} in tetraethylammonium perchlorate (TEAP) as the supporting electrolyte. All CV experiments were carried out at a scan rate of 100 mV/s. The reference electrode was separated from the bulk electrolyte by a salt bridge containing the supporting electrolyte in nitromethane solution. IR compensation was made automatically during each run. Under the experimental conditions the $E_{1/2}$ values of the ferrocene/ferrocenium couple was observed at 390 mV in dimethyl sulfoxide.

2.4. Crystallography

For complexes **1**–**3** single crystals suitable for X-crystallography were obtained by slow evaporation of the filtrate of the reaction mixture. The crystals were mounted on glass fibres using perfluoropolyether oil. Intensity data were collected on a Bruker-AXS SMART APEX II diffractometer at 293(2) K using graphite-monochromated Mo Kα radiation (λ = 0.71073 Å). The data were processed with SAINT [22] and absorption corrections were made with SADABS [22]. The structures were solved by direct and Fourier methods and refined by full-matrix least-squares methods based on F^2 using SHELX-97 [23]. For the structure solutions and refinements, the SHELX-TL software package [24] was used. The non-hydrogen atoms were refined anisotropically, while the hydrogen atoms were placed at geometrically calculated positions with fixed thermal parameters. Crystal data and details of data collection are listed in Table 1.

3. Results and discussion

3.1. Synthesis

The ligand dipyrido[3,2-f: 2′,3′-h]-quinoxaline, abbreviated as dpq, has been obtained by the [1+1] cyclocondensation between 1,10-phenanthroline-5,6-dione and 1,2-diaminoethane. All the complexes **1**–**3** are obtained by the direct reaction between the ligand dpq, $Cu(ClO_4)_2 \cdot 6H_2O$ and NaX [X = Cl (**1**), SCN (**2**), N_3 (**3**)] in a 2:1:4 ratio. The single crystals were grown by slow evaporation of the filtrate after collecting the precipitated bulk compound.

3.2. Infrared spectra

The characteristic IR spectral bands for the anions of complexes **2** and **3** are given in the Section 2, while full details are given in the supplementary material. The ligand dpq has four strong bands at around 1575, 1465, 1392 and 740 cm^{-1} due to the phenanthroline moiety. In all the complexes **1**–**3**, these four characteristic bands have undergone shifts in energy. The band of dpq at 1392 cm^{-1} is split into bands at 1405 and 1385 cm^{-1} in all the compounds.

In the thiocyanate complex [{$Cu^{II}(dpq)_2(SCN)$}{$Cu^{II}(dpq)(SCN)_3$}] (**2**), in addition to the above discussed features observed for dpq, two strong sharp bands due to the thiocyanate are observed at 2098 and 2071 cm^{-1}, the positions of which are normally considered [25] to be due to terminally N-coordinated NCS^- ligands. Two bands are observed due to the thiocyanate because both the cationic and anionic parts in compound **2** possess thiocyanate ligands, which gives rise to two bands. In the azide complex [$Cu^{II}(dpq)_2(N_3)$](ClO_4) (**3**), a strong band due to the $\nu_{as}N_3^-$ vibration is observed at 2036 cm^{-1} and a medium band due to the $\nu_sN_3^-$ vibration is observed at 1338 cm^{-1}. Complex **3** also exhibits characteristic bands due to the perchlorate ion at *ca.* 1100 cm^{-1} and *ca.* 622 cm^{-1}.

3.3. Crystal structures

3.3.1. [$Cu^{II}(dpq)_2Cl_2$] (**1**)

The molecular structure of the complex [$Cu^{II}(dpq)_2Cl_2$] (**1**) is shown in Fig. 1 and the relevant bond distances and angles are given in Table 2. A two-fold axis passes mid-way through the metal-bound chloride atoms Cl(1) and Cl(1A). The coordination environment around the six-coordinated metal centre [CuN_4Cl_2] may be considered as distorted octahedral. The atoms N(2), N(2A), Cl(1) and Cl(1A) form the best plane, although the atoms N(2)/N(2A) are displaced from the mean plane by ±0.195(2) Å and Cl(1)/Cl(1A) by ±0.164(2) Å. The metal atom lies exactly on the mean plane. The nitrogen atoms N(1) and N(1A) are *trans*-axially disposed to the metal centre, the equatorial Cu–N distances [2.1731(18) Å] are somewhat longer than the axial Cu–N distances [2.0475(16) Å], while the equatorial Cu–Cl distances [2.5456(8) Å] are much longer. The *trans*-axial N(1)–Cu–N(1A) angle is 168.14(7)°, while the *trans*-equatorial N(2)–Cu–Cl(1) angle is 171.09(5)°.

Another interesting structural feature of this compound is the presence of two types of π–π interaction. First one is between the pyrazine ring C(13)C(14)N(3)C(11)C(12)N(4) and the aromatic ring C(11)C(12)C(9)C(10)C(5)C(4) [the distance between the two centroids is 3.513 Å] and second one is between two pyrazine rings of adjacent molecules [the distance between the two centroids is 3.732 Å]. These two π–π interactions give rise to a sinusoidal pattern in the molecule as shown in Fig. 2.

3.3.2. [{$Cu^{II}(dpq)_2(SCN)$}{$Cu^{II}(dpq)(SCN)_3$}] (**2**)

In complex **2**, the asymmetric unit contains one complex cation and one complex anion species *viz.* $\{Cu^{II}(dpq)_2(SCN)\}^+$ and $\{Cu^{II}(dpq)(SCN)_3\}^-$. An ORTEP projection of the cation and anion in **3** is shown in Fig. 3a and b.

In the five-coordinated copper(II) cationic part, $\{Cu^{II}(dpq)_2(SCN)\}^+$, the metal centre adopts a distorted square pyramidal geometry (Fig. 3a) with the atoms N(5)N(9)N(10)N(16) forming the basal plane, while the pyridyl nitrogen N(6) occupies the apical position. The atoms N(5), N(9), N(10) and N(16) are deviated from their least-squares plane by *ca.* ±0.152(9) Å. The copper(II) centre is displaced from the basal mean plane by 0.069 Å towards the N(6)

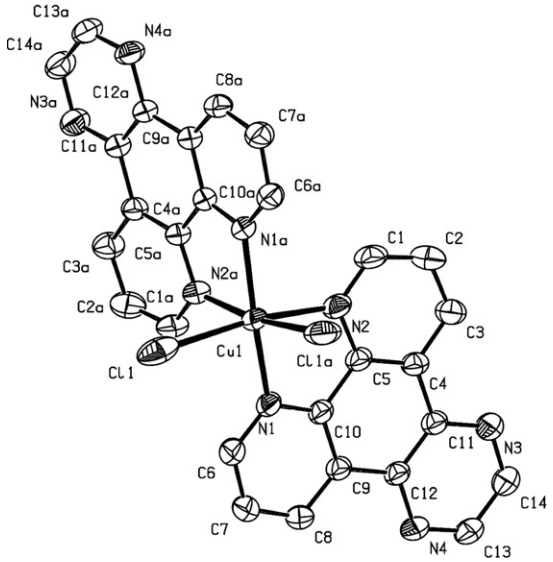

Fig. 1. An ORTEP representation of the molecule [$Cu^{II}(dpq)_2Cl_2$] (**1**) showing 50% probability displacement ellipsoids. 'A' indicates symmetry operation: (−*x*, *y*, 1/2 − *z*).

Table 2
Selective bond distances (Å) and angles (°) for compounds **1**–**3**

$[Cu^{II}(dpq)_2Cl_2]$[a] (**1**)		$[\{Cu^{II}(dpq)_2(SCN)\}\{Cu^{II}(dpq)(SCN)_3\}]$ (**2**)				$[Cu^{II}(dpq)_2(N_3)](ClO_4)$ (**3**)	
Cu(1)–N(1)	2.0475(16)	Cu(1)–N(5)	2.044(4)	Cu(2)–N(1)	2.030(4)	Cu(1)–N(1)	2.015(2)
Cu(1)–N(2)	2.1731(18)	Cu(1)–N(6)	2.266(3)	Cu(2)–N(2)	2.028(4)	Cu(1)–N(2)	2.034(3)
Cu(1)–Cl(1)	2.5456(8)	Cu(1)–N(9)	2.021(3)	Cu(2)–N(13)	2.293(4)	Cu(1)–N(5)	2.193(2)
Cu(1)–N(1A)	2.0475(16)	Cu(1)–N(10)	2.031(3)	Cu(2)–N(14)	1.939(4)	Cu(1)–N(6)	2.028(2)
Cu(1)–N(2A)	2.1731(18)	Cu(1)–N(16)	1.935(4)	Cu(2)–O(15)	1.950(4)	Cu(1)–N(9)	1.972(3)
Cu(1)–Cl(1A)	2.5456(8)						
N(1)–Cu(1)–N(2)	78.37(6)	N(5)–Cu(1)–N(6)	77.14(13)	N(1)–Cu(2)–N(2)	80.62(15)	N(1)–Cu(1)–N(2)	81.04(10)
N(1A)–Cu(1)–N(2A)	78.37(6)	N(5)–Cu(1)–N(9)	93.45(12)	N(1)–Cu(2)–N(13)	95.69(14)	N(1)–Cu(1)–N(5)	98.77(9)
N(1)–Cu(1)–N(1A)	168.14(7)	N(5)–Cu(1)–N(10)	172.56(14)	N(1)–Cu(2)–N(14)	162.94(16)	N(1)–Cu(1)–N(6)	175.49(12)
N(2)–Cu(1)–N(2A)	92.96(7)	N(5)–Cu(1)–N(16)	93.29(15)	N(1)–Cu(2)–N(15)	92.47(16)	N(1)–Cu(1)–N(9)	92.30(12)
N(1)–Cu(1)–N(2A)	93.41(6)	N(6)–Cu(1)–N(9)	90.96(13)	N(2)–Cu(2)–N(13)	89.86(14)	N(2)–Cu(1)–N(5)	96.30(10)
N(2)–Cu(1)–N(1A)	93.41(6)	N(6)–Cu(1)–N(10)	97.56(13)	N(2)–Cu(2)–N(14)	92.23(15)	N(2)–Cu(1)–N(6)	95.44(10)
N(1)–Cu(1)–Cl(1)	92.76(5)	N(6)–Cu(1)–N(16)	102.81(14)	N(2)–Cu(2)–N(15)	170.69(16)	N(2)–Cu(1)–N(9)	162.04(11)
N(2)–Cu(1)–Cl(1)	171.09(5)	N(9)–Cu(1)–N(10)	81.31(12)	N(13)–Cu(2)–O(14)	99.79(16)	N(5)–Cu(1)–N(6)	78.75(9)
N(1A)–Cu(1)–Cl(1)	94.94(3)	N(9)–Cu(1)–N(16)	165.73(14)	N(13)–Cu(2)–O(15)	97.08(16)	N(5)–Cu(1)–N(9)	101.21(11)
N(2A)–Cu(1)–Cl(1)	86.73(5)	N(10)–Cu(1)–N(16)	92.99(15)	N(14)–Cu(2)–O(15)	92.71(17)	N(6)–Cu(1)–N(9)	91.88(12)
N(1)–Cu(1)–Cl(1A)	95.25(5)						
N(2)–Cu(1)–Cl(1A)	86.73(5)						
Cl(1)–Cu(1)–Cl(1A)	94.94(3)						
N(1A)–Cu(1)–Cl(1A)	92.76(5)						
N(2A)–Cu(1)–Cl(1A)	171.09(5)						

[a] For **1** 'A' indicates: $-x, y, 1/2 - z$.

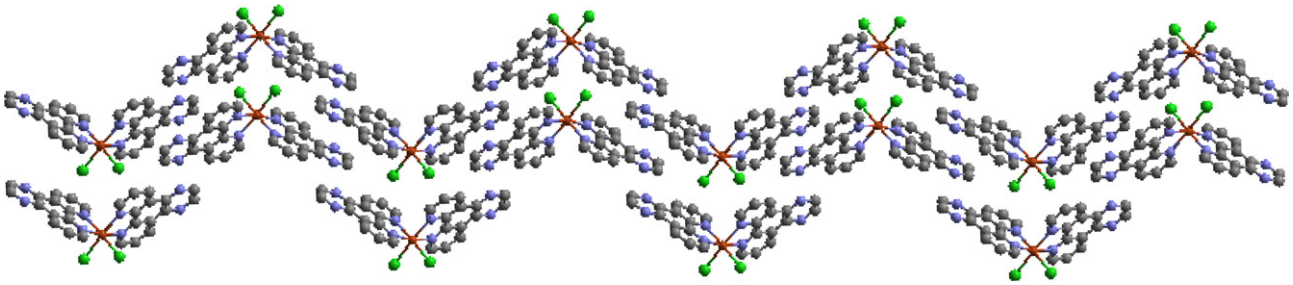

Fig. 2. Sinusoidal growth of the molecule $[Cu^{II}(dpq)_2Cl_2]$ (**1**) through π–π stacking interactions.

atom. The distortion of the geometry from a square pyramidal or trigonal bipyramidal geometry can be described in terms of the parameter τ [26] (the parameter $\tau = (\varphi_1 - \varphi_2)/60$, where φ_1 and φ_2 are the largest and second largest N–Cu–N angles; the value of $\tau = 1$ corresponds to trigonal bipyramidal and $\tau = 0$ to square pyramidal geometry, respectively), which in this case is 0.114. The three Cu(1)–N(pyridyl) distances [Cu(1-)-N(5) = 2.044(4) Å, Cu(1)–N(9) = 2.021(3) Å and Cu(1)–N(10) = 2.031(3) Å] in the basal plane are longer than Cu(1)–N(thiocyanate) distance [Cu(1)–N(16) = 1.935(4) Å]. On the other hand, the axial Cu(1)–N(pyridyl) distance [Cu(1)–N(6) = 2.266(3) Å] is significantly longer relative to the Cu(1)–N(pyridyl) distances in the basal plane.

In the five-coordinated anionic part, $\{Cu^{II}(dpq)(SCN)_3\}^-$, the metal centre $[CuN_5]$ also adopts a distorted square pyramidal geometry (Fig. 3b), which is evident from its τ value of 0.13. The donor atoms N(1), N(2), N(14) and N(15) around copper(II) form a basal plane from which the metal atom is displaced towards the apical coordination site N(13) by 0.199(3) Å. In the basal plane, the two Cu(2)–N(pyridyl) distances [Cu(2)–N(1) = 2.030(4) Å, Cu(2)–N(2) = 2.028(4) Å] are almost the same, whereas the two Cu(2)–N(thiocyanate) distances [Cu(2)–N(14) = 1.939(4) Å, Cu(2)–N(15) = 1.950(4) Å] vary to some extent. The apical Cu(2)–N(thiocyanate) distance [Cu(2)–N(13) = 2.293(4) Å] is considerably longer relative to the Cu(2)–N(thiocyanate) distances in the basal plane. The relevant bond distances and bond angles are given in Table 2.

Similar to complex **1**, complex **2** also possesses three types of extensive π–π interactions which produce a zigzag chain in the molecule, as shown in Fig. 4. The first one is between N(8)C(41)C(40)N(7)C(35)C(43) of the pyrazine ring in the cationic part with the C(31)C(30)C(29)C(28)C(35)C(43) aromatic ring of an adjacent cationic part, for which the distance between the two centroids is 3.586 Å. In the second case, the N(3)C(44)C(45)N(4)C(8)C(9) pyrazine ring of the anionic part interacts with the N(12)C(48)C(49)N(11)C(23)C(47) pyrazine ring of the adjacent cationic part [the distance between the two centroids is 3.554 Å]. This π–π interaction also exists between two adjacent anionic parts. The N(3)C(44)C(45)N(4)C(8)C(9) pyrazine ring in the anionic part is involved in a π–π interaction with the pyrazine ring of the adjacent anionic part. In this case, the distance between the two centroids is 3.822 Å.

3.3.3. $[Cu^{II}(dpq)_2(N_3)](ClO_4)$ (**3**)

The ORTEP representation of the cation $[Cu(dpq)_2(N_3)]^+$ in **3** is shown in Fig. 5 and the pertinent bond distances and angles are given in Table 2. The five-coordinated copper(II) centre $[CuN_5]$ appears to be lying between trigonal bipyramidal and square pyramidal geometries. In complex **3** $\tau = 0.224$, that is the coordination polyhedra can be considered as a distorted square pyramid. The distorted square pyramidal geometry of the copper centre is based on consideration of the N(1), N(2), N(6) and N(9) atoms forming the basal plane, which, however, are displaced from the mean plane by *ca.* ±0.164(11) Å. In this description, the metal centre is displaced from the basal plane by 0.124(2) Å towards the axial donor N(5). The distances of the copper centre from the donor atoms in the square plane are unequal; the Cu–N(1) [2.015(2) Å], Cu–N(2) [2.034(3) Å] and Cu–N(6) [2.028(2) Å] distances are considerably

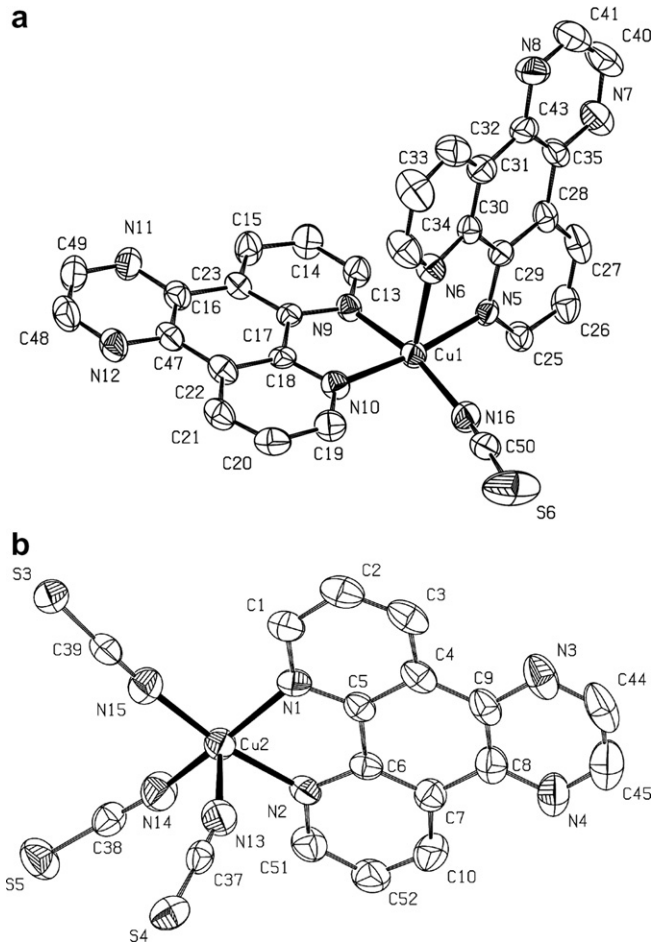

Fig. 3. (a) An ORTEP representation of the complex cation $[Cu^{II}(dpq)_2(SCN)]^+$ and (b) complex anion $[Cu^{II}(dpq)(SCN)_3]^-$ in the complex **2** showing 50% probability displacement ellipsoids.

longer than the Cu–N(9) distance [1.972(3) Å]. The axial distance Cu–N(5) [2.193(2) Å], however, is somewhat longer than the equatorial bond lengths.

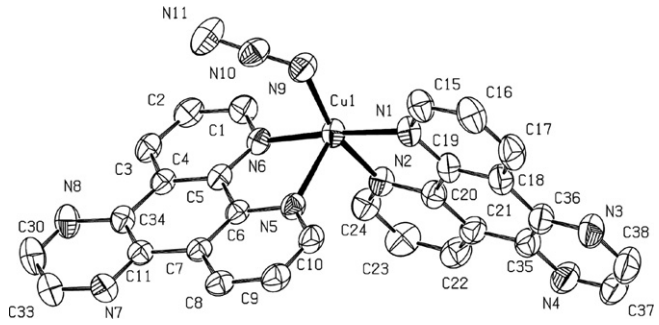

Fig. 5. An ORTEP representation of the cation of the complex $[Cu^{II}(dpq)_2N_3](ClO_4)$ (**3**) showing 50% probability displacement ellipsoids.

In the basal plane, the distances N(2)···N(6) = 3.005 Å, N(6)···N(9) = 2.875 Å and N(1)···N(9) = 2.876 Å are longer relative to N(1)···N(2) = 2.631 Å, which indicates deviations from a regular square plane. Again, considerable departure of the relevant angles in the basal plane [N(1)–Cu–N(2) = 81.04(10)°, N(1)–Cu–N(9) = 92.30(12)°, N(2)–Cu–N(6) = 95.44(10)° and N(6)–Cu–N(9) = 91.88(12)°] from the desired angle of 90° are also indicative of deviation from an ideal square pyramidal geometry.

Like compounds **1** and **2**, the N(3)C(36)C(35)N(4)C(37)C(38) pyrazine ring of compound **3** is involved in an intermolecular π–π interaction with the C(21)C(35)C(36)C(18)C(19)C(20) aromatic ring [the distance between the two centroids is 3.804 Å] of an adjacent molecule. But, unlike **1** and **2**, this π–π interaction does not give rise to any specific pattern in compound **3**. This may be due to the presence of the tetrahedral perchlorate anion, which in turn inhibits the close approach of the adjacent molecules for the strong π–π interaction required for the formation of a polymeric pattern.

3.4. Electronic spectra

The absorption spectroscopic behaviour of compounds **1**–**3** have been studied in dimethyl sulfoxide. The UV–Vis–NIR spectral data for these compounds in dimethyl sulfoxide are given in Section 2.

All of the complexes exhibit three very strong absorption bands at 250–260, 290–300 and 340–350 nm due to the ligand centred π–π* transitions.

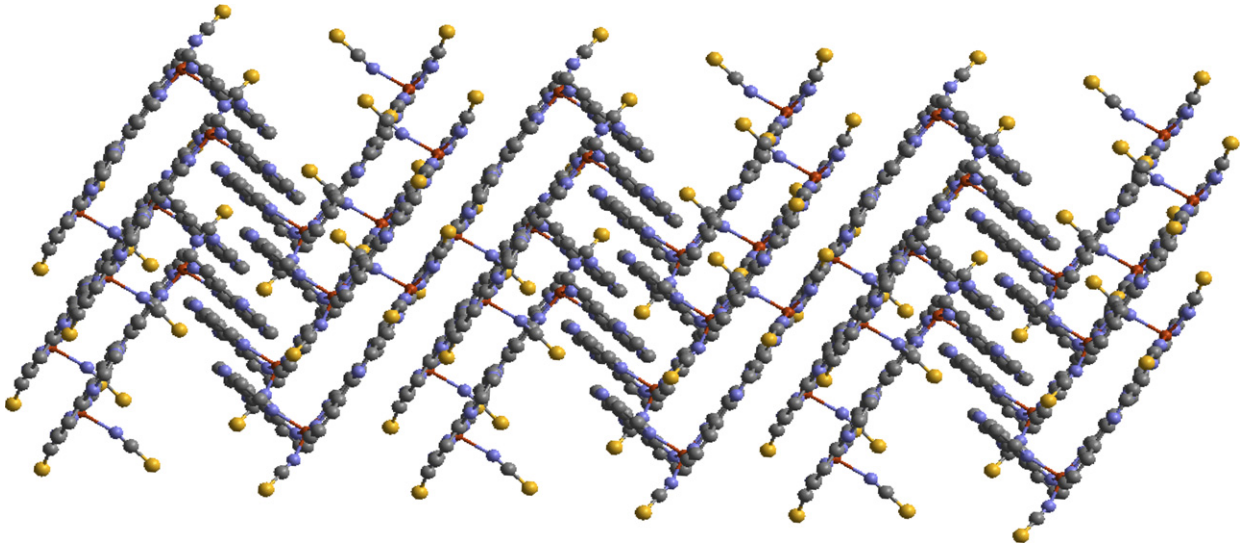

Fig. 4. Zigzag chain in the molecule $[\{Cu^{II}(dpq)_2(SCN)\}\{Cu^{II}(dpq)(SCN)_3\}]$ (**2**) through π–π stacking interactions.

The six-coordinated octahedral copper complex exhibits three bands in the visible range at 450 nm ($\varepsilon = 880\ M^{-1}\ cm^{-1}$), 740 nm ($\varepsilon = 120\ M^{-1}\ cm^{-1}$) and 925 ($\varepsilon = 95\ M^{-1}\ cm^{-1}$). The well-resolved peak at 450 nm is most likely due to a $Cl^- \rightarrow Cu^{II}$ ligand-to-metal charge transfer (LMCT) [27] transition, while the other two bands observed are due to d–d transitions.

Both compounds **2** and **3** exhibit a peak at around 400 nm and an unresolved broad band between 600 and 1300 nm. Clearly, the peak at around 400 nm in both compounds is due to a ligand-to-metal charge transfer. It is of interest to note that although for both compounds the ligand-to-metal charge transfer (LMCT) transitions $SCN^- \rightarrow Cu^{II}$ (**2**) and $N_3^- \rightarrow Cu^{II}$ (**3**) occur at almost same energy 25 000 cm^{-1}, their intensities are very different. It is documented, especially for copper(II) complexes, that a single d–d band with a high energy shoulder is indicative of a trigonal bipyramidal stereochemistry around the metal centre, while an absorption envelop with a low energy shoulder is characteristic of a square pyramidal geometry. Some pentacoordinated copper(II) complexes with two d–d bands of equal intensity appear to possess an intermediate distorted geometry [27]. The broadness of these bands with a low energy shoulder are indicative of the presence of more than two transitions at lower energies, as expected for copper(II) in a distorted square pyramidal environment. Indeed, deconvolution of the absorption spectrum of **3** in dimethyl sulfoxide by Gaussian line-shape analysis gives rise to three peaks (shown in Fig. 6), which are due to the $d_{xz}, d_{yz} \rightarrow d_{x^2-y^2}$ ($\lambda = 670$ nm, $\varepsilon = 70\ M^{-1}\ cm^{-1}$), $d_{xy} \rightarrow d_{x^2-y^2}$ ($\lambda = 705$ nm, $\varepsilon = 52\ M^{-1}\ cm^{-1}$) and $d_{z^2} \rightarrow d_{x^2-y^2}$ ($\lambda = 1060$ nm, $\varepsilon = 20\ M^{-1}\ cm^{-1}$) transitions in a descending order of energy.

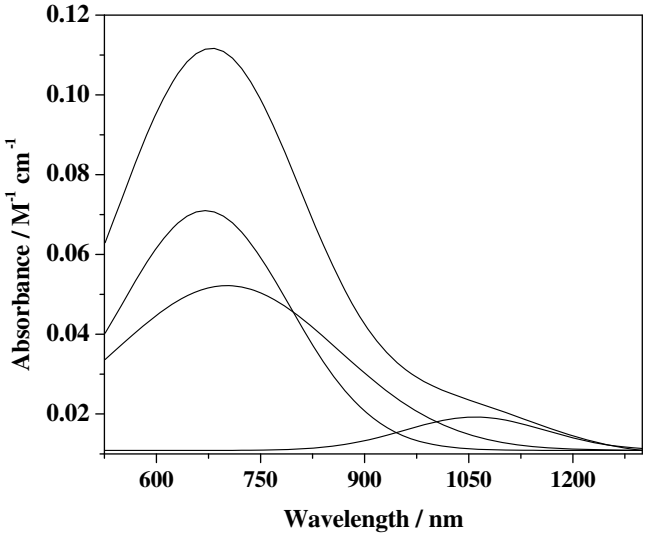

Fig. 6. Visible and near infrared absorption spectra of the complex $[Cu^{II}(dpq)_2N_3](ClO_4)$ (**3**) in dimethyl sulfoxide (10^{-3} M). The three bands below the spectrum are obtained by Gaussian line-shape analysis and added together give the experimental line.

Table 3
Electrochemical data[a] for complexes **1**–**3** in dimethyl sulfoxide

Compound	$E_{1/2}$[b] (mV)	ΔE_p[c]
$[Cu^{II}(dpq)_2Cl_2]$ (**1**)	90	75
$[\{Cu^{II}(dpq)_2(SCN)\}$	125, −1070 ($E_{p,c}$)	70
$\{Cu^{II}(dpq)(SCN)_3\}]$ (**2**)	−245 ($E_{p,a}$)	
$[Cu^{II}(dpq)_2(N_3)](ClO_4)$ (**3**)	50	120

[a] All the potentials are against the Ag/AgCl reference electrode.
[b] $E_{1/2}$ values are the average of those obtained from cyclic voltammetric and square wave voltammetric measurements, which are within ±5 mV.
[c] ΔE_p Refers to peak-to-peak separation at a scan rate of 100 mV/s.

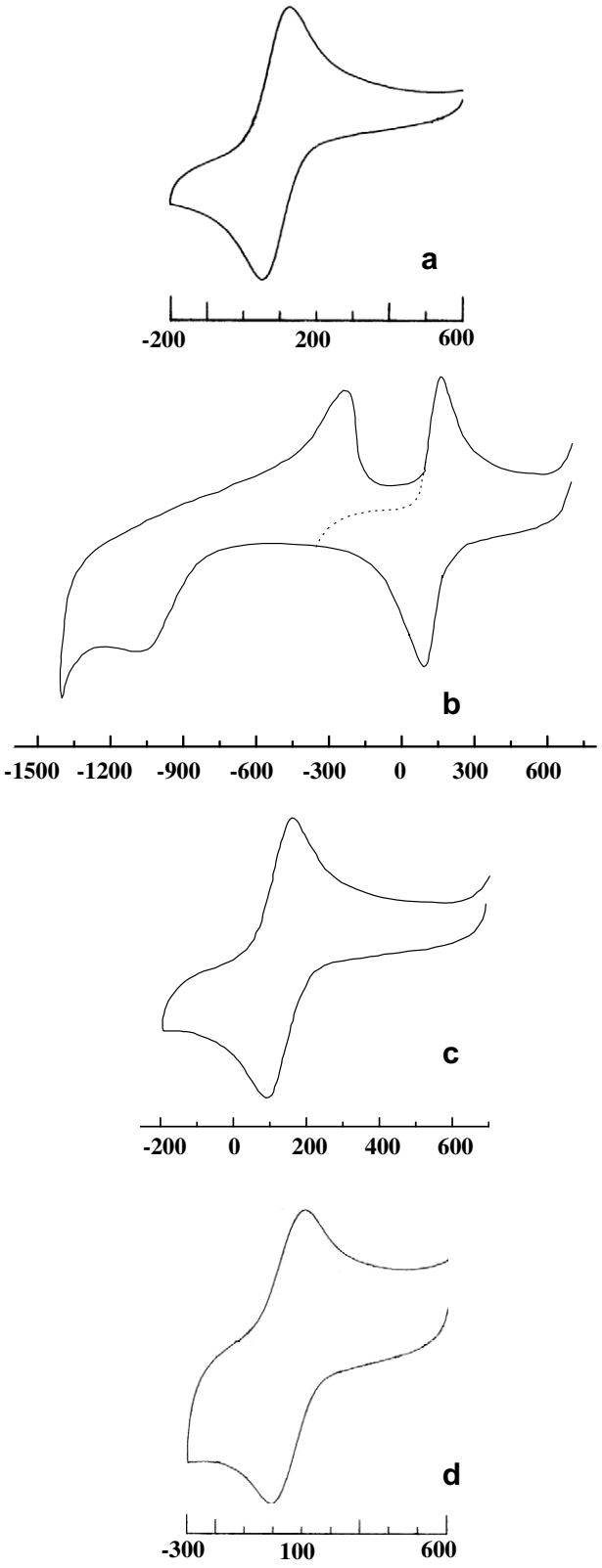

Fig. 7. Cyclic voltammograms of complexes (a) $[Cu^{II}(dpq)_2Cl_2]$ (**1**), (b) $[\{Cu^{II}(dpq)_2(SCN)\}\{Cu^{II}(dpq)(SCN)_3\}]$ (**2**) in the range 700 to −1400 mV, (c) $[\{Cu^{II}(dpq)_2(SCN)\}\{Cu^{II}(dpq)(SCN)_3\}]$ (**2**) in the range 700 to −200 mV and (d) $[Cu^{II}(dpq)_2N_3](ClO_4)$ (**3**) in dimethyl sulfoxide. Scan rate was 100 mV/s for all experiments.

3.5. Electrochemistry

The electrochemical characteristics of complexes **1**, **2** and **3** in dimethyl sulfoxide have been examined by cyclic voltammetry (cv) and square wave voltammetry (swv) and the observed redox potentials are given in Table 3.

As shown in Fig. 7a, the copper(II) complex $[Cu^{II}(dpq)_2Cl_2]$ (**1**) undergoes one electron reversible ($\Delta E_p = 75$ mV) reduction at $E_{1/2} = 90$ mV. As shown in Fig. 7b, in the potential range +700 to −1400 mV, complex **2** exhibits two cathodic responses at +90 and −1070 mV, while in the return sweep two anodic peaks are observed at −245 and +160 mV. The two cathodic peaks are evidently due to the one electron reduction processes $[Cu^{II}(dpq)_2(SCN)]^+ \rightarrow [Cu^{I}(dpq)_2(SCN)]$ (+90 mV) and $[Cu^{II}(dpq)(SCN)_3]^- \rightarrow [Cu^{I}(dpq)(SCN)_3]^{2-}$ (−1070 mV). However, the reduced species $[Cu^{I}(dpq)(SCN)_3]^{2-}$, being unstable in solution, undergoes decomposition and consequently in the return sweep the observed anodic peak at −245 is not related to the original species. To verify this, the cyclic voltammogram shown in Fig. 7c was recorded in the spectral window +700 to −200 mV. It may be noted that in this case a single reversible voltammogram with $E_{1/2} = 125$ mV and $\Delta E_p = 70$ mV is obtained with $E_{p,c} = 90$ mV and the corresponding $E_{p,a} = 160$ mV. The copper(II) complex $[Cu^{II}(dpq)_2(N_3)](ClO_4)$ (**3**) undergoes a one electron quasireversible ($\Delta E_p = 120$ mV) reduction at $E_{1/2} = 50$ mV (Fig. 7d). The variation in reduction potential of the Cu^{2+}/Cu^{+} couple for complexes **1**–**3** may be attributed to the variation of electronic contribution of the different anions over the copper centre.

4. Conclusion

Copper(II) complexes (**1**–**3**) of dipyrido[3,2-f: 2′,3′-h]-quinoxaline (dpq) have been synthesized and structurally characterized. Various spectroscopic and electrochemical properties of these compounds have been studied.

The most significant aspect of the study is the isolation and structural characterization of three copper(II) complexes of dpq. The structure determination of compound $[Cu^{II}(dpq)_2Cl_2]$ (**1**) has revealed that copper(II) has a hexacoordinated geometry and can be best described as a slightly distorted octahedral geometry with a $[CuN_4Cl_2]$ core around the copper ion. The structure determination of compound **2** has established the presence of one complex cation and one complex anion in the asymmetric unit, *viz.* $\{Cu^{II}(dpq)_2(SCN)\}^+$ and $\{Cu^{II}(dpq)(SCN)_3\}^-$. In both the cationic and anionic part, the geometry around copper(II) is distorted square pyramidal with $\tau = 0.114$ [for $\{Cu^{II}(dpq)_2(SCN)\}^+$] and $\tau = 0.13$ [for $\{Cu^{II}(dpq)(SCN)_3\}^-$]. In the crystal lattice of complexes **1** and **2**, the quinoxaline and aromatic rings of the complex unit are involved in intermolecular π–π interactions which leads to the generation of a sinusoidal chain in complex **1** and a zigzag chain in complex **2**. The compound $[Cu^{II}(dpq)_2(N_3)](ClO_4)$ (**3**) also shows a distorted square pyramidal geometry ($\tau = 0.224$) with a $[CuN_5]$ core around the copper cation. Electrochemical studies carried out for **1** and **3** in dimethyl sulfoxide show that while **1** undergoes a reversible reduction at $E_{1/2} = 90$ mV, **3** undergoes a quasireversible reduction at $E_{1/2} = 50$ mV. The electrochemical behaviour reveals that complex **2** exhibits a reversible one electron reduction at $E_{1/2} = 125$ mV and one irreversible one electron reduction at $E_{p,c} = -1070$ mV.

Acknowledgements

We are grateful to Prof. K. Nag for providing laboratory facilities and helpful discussions. P.B., S.D. and M.G. thank the C.S.I.R., Government of India for providing a research fellowship. Crystallography was performed at the DST, India-funded National Single Crystal Diffractometer Facility at the Department of Inorganic Chemistry, IACS, Kolkata.

Appendix A. Supplementary data

CCDC 677282, 677283, and 677284 contain the supplementary crystallographic data for **1**, **2** and **3**. These data can be obtained free of charge via http://www.ccdc.cam.ac.uk/conts/retrieving.html, or from the Cambridge Crystallographic Data Centre, 12 Union Road, Cambridge CB2 1EZ, UK; fax: (+44) 1223-336-033; or e-mail: deposit@ccdc.cam.ac.uk. Supplementary data associated with this article can be found, in the online version, at doi:10.1016/j.poly.2008.04.017.

References

[1] J. Reedijk, in: G. Wilkinson, R.D. Gillard, J.A. McCleverty (Eds.), Comprehensive Coordination Chemistry, vol. 2, Pergamon, Oxford, UK, 1987, p. 73.
[2] (a) L.Y. Chung, E.C. Constable, M.S. Khan, J. Lewis, Inorg. Chim. Acta 185 (1991) 93;
(b) G.R. Newkome, D.K. Kohli, F. Fronczek, J. Chem. Soc., Chem. Commun. (1980) 9;
(c) E.C. Constable, S.M. Elder, J. Healy, D.A. Tocher, J. Chem. Soc., Dalton Trans. (1990) 1669;
(d) E.C. Constable, R. Chotalia, J. Chem. Soc., Chem. Commun. (1992) 64;
(e) A.S. Abushamleh, H.A. Goodwin, Aust. J. Chem. 41 (1988) 873.
[3] (a) T. Garber, S.V. Wallendael, D.P. Rillema, M. Kirk, W.E. Hatfield, J.H. Welch, P. Singh, Inorg. Chem. 29 (1990) 2863;
(b) Y. Yao, M.W. Perkovic, D.P. Rillema, C. Woods, Inorg. Chem. 31 (1992) 3956.
[4] (a) M. Athar Masood, P.S. Zacharias, J. Chem. Soc., Dalton Trans. (1991) 111;
(b) M. Athar Masood, D.J. Hodgson, Inorg. Chem. 32 (1993) 4839.
[5] (a) P.J. Burke, K. Henrick, D.R. McMillin, Inorg. Chem. 21 (1982) 1881;
(b) R.J. Crutchley, R. Hynes, E.J. Gabe, Inorg. Chem. 29 (1990) 4921;
(c) R.N. Williams, L.D. Cola, F. Hartl, J.J. Hagref, J.N. Planeix, A.D. Cian, N.W. Hosseini, Coord. Chem. Rev. 230 (2002) 253;
(d) J. Wang, J. Reibenspies, R.J. Motekaitis, A.E. Martell, J. Chem. Soc., Dalton Trans. (1995) 1511.
[6] (a) M.T. Miller, P.K. Gantzel, T.B. Karpishin, Inorg. Chem. 38 (1999) 3414;
(b) M.T. Miller, P.K. Gantzel, T.B. Karpishin, Inorg. Chem. 38 (1999) 5246;
(c) D.H. Lee, N.N. Murthy, K.D. Karlin, Inorg. Chem. 36 (1997) 5785;
(d) N.K. Eggleston, D.R. McMillin, K.S. Koenig, A.J. Pallenberg, Inorg. Chem. 36 (1997) 172;
(e) C.T. Cunningham, J.J. Moore, K.L.H. Cunningham, P.E. Fanwick, Inorg. Chem. 39 (2000) 3638.
[7] (a) G.A.V. Albada, I. Mutikainen, O. Roubeau, U. Turpeinen, J. Reedijk, Inorg. Chim. Acta 331 (2002) 208;
(b) G.A.V. Albada, A. Mohamadou, I. Mutikainen, U. Turpeinen, J. Reedijk, Eur. J. Inorg. Chem. (2004) 3733.
[8] (a) R.D. Willett, G. Pon, C. Nagy, Inorg. Chem. 40 (2001) 4342;
(b) T. Pintauer, J. Qiu, G. Kickelbick, K. Matyjaszewski, Inorg. Chem. 40 (2001) 2818;
(c) J. Cody, J. Dennisson, J. Gilmore, D.G. VanDerveer, M.M. Henary, A. Gabrielli, C.D. Sherrill, Y. Zhang, C.-P. Pan, C. Burda, C.J. Fahrni, Inorg. Chem. 42 (2003) 4918.
[9] S. Itoh, N. Kishikawa, T. Suzuki, H.D. Takagi, J. Chem. Soc., Dalton Trans. (2005) 1066.
[10] (a) T. Otsuka, N. Takahashi, N. Fujigasaki, A. Sekine, Y. Ohashi, Y. Kaizu, Inorg. Chem. 38 (1999) 1340;
(b) T. Wada, K. Tsuge, K. Tanaka, Inorg. Chem. 39 (2000) 1340;
(c) M. Sjodin, S. Styring, B. Akermark, L. Sun, L. Hammarstrom, J. Am. Chem. Soc. 122 (2000) 3932;
(d) F.G. Gao, A.J. Bard, J. Am. Chem. Soc. 122 (2000) 7426.
[11] (a) K.E. Erkkila, D.T. Odom, J.K. Barton, Chem. Rev. 99 (1999) 2777;
(b) H.T. Chifotides, K.R. Dunbar, Acc. Chem. Res. 38 (2005) 146.
[12] D.O. Bucher, J.P. Sauvage, J.M. Kern, J. Am. Chem. Soc. 111 (1989) 7791.
[13] M. Athar Masood, R. Jagannathan, P.S. Zacharias, J. Chem. Soc., Dalton Trans. (1991) 2553.
[14] E.I. Solomon, U.N. Sundaram, T.E. Machonkin, Chem. Rev. 96 (1996) 2563.
[15] (a) E.I. Solomon, D.W. Randall, T. Glaser, Coord. Chem. Rev. 200 (2000) 595;
(b) P. Comba, R. Remenyi, Coord. Chem. Rev. 228 (2003) 9.
[16] (a) I. Greguric, J.R. Aldrich-Wright, J.G. Collins, J. Am. Chem. Soc. 119 (1997) 3621;
(b) J.G. Collins, A.D. Sleeman, J.R. Aldrich-Wright, I. Greguric, T.W. Hambley, Inorg. Chem. 37 (1998) 3133;
(c) J.G. Collins, J.R. Aldrich-Wright, I.D. Greguric, P.A. Pellegrini, Inorg. Chem. 38 (1999) 5502;
(d) P.A. Pellegrini, J.R. Aldrich-Wright, J. Chem. Soc., Dalton Trans. (1988) 2341;
(e) N. Gupta, N. Grover, G.A. Neyhart, W. Liang, P. Singh, H.H. Thorp, Angew. Chem., Int. Ed. 31 (1992) 1048;

(f) J.-G. Liu, Q.-L. Zhang, X.-F. Shi, L.-N. Ji, Inorg. Chem. 40 (2001) 5045;
(g) A. Greguric, I.D. Greguric, T.W. Hambley, J.R. Aldrich-Wright, J.G. Collins, J. Chem. Soc., Dalton Trans. (2002) 849;
(h) J.R. Aldrich-Wright, R.F. Fenton, I.D. Greguric, T.W. Hambley, P.A. Williams, J. Chem. Soc., Dalton Trans. (2002) 4666.

[17] (a) A.M. Thomas, M. Nethaji, S. Mahadevan, A.R. Chakravarty, J. Inorg. Biol. Chem. 94 (2003) 171;
(b) S. Dhar, D. Senapati, P.A.N. Reddy, P.K. Das, A.R. Chakravarty, Chem. Commun. (2003) 2452. and ref. therein.

[18] S. Dhar, M. Nethaji, A.R. Chakravarty, Inorg. Chem. 45 (2006) 11043. and ref. therein.

[19] M. Ghosh, P. Biswas, U. Flörke, Polyhedron 26 (2007) 3750.

[20] D.D. Perrin, W.L. Armarego, D.R. Perrin, Purification of Laboratory Chemicals, 2nd ed., Pergamon, Oxford, 1980.

[21] (a) M. Yamada, Y. Tanaka, Y. Yoshimoto, S. Kurda, I. Shimao, Bull. Chem. Soc. Jpn. 65 (1992) 1006;
(b) J.E. Dichson, L.A. Summers, Aust. J. Chem. 23 (1970) 1023.

[22] SAINT, version 6.02, SADABS, version 2.03, Bruker AXS Inc.; Madison, Wisconsin, 2002.

[23] G.M. Sheldrick, SHELXL-97 Program for the Refinement of Crystal Structures, University of Götingen, Götingen, Germany, 1997.

[24] SHELXTL, version 6.10; Bruker AXS Inc.; Madison, WI, 2002.

[25] K. Nakamoto, Infrared and Raman Spectra of Inorganic and Coordination Compounds, 5th ed., VCH-Wiley, New York, 1997.

[26] A.W. Addison, T.N. Rao, J. Reedijk, J. van Rijn, G.C. Vershoor, J. Chem. Soc., Dalton Trans. (1984) 1349.

[27] A.B.P. Lever, Inorganic Electronic Spectroscopy, 2nd ed., Elsevier, Amsterdam, 1984.

Polyhedron 27 (2008) 2113–2118

Contents lists available at ScienceDirect

Polyhedron

journal homepage: www.elsevier.com/locate/poly

Complexation of Curium(III) with hydroxamic acids investigated by time-resolved laser-induced fluorescence spectroscopy

M. Glorius *, H. Moll, G. Bernhard

Forschungszentrum Dresden-Rossendorf, Institute of Radiochemistry, 01314 Dresden, Germany

ARTICLE INFO

Article history:
Received 9 January 2008
Accepted 8 April 2008
Available online 22 May 2008

Keywords:
Cm(III)
Complexation
TRLFS
Hydroxamic acids

ABSTRACT

The unknown complex formation of Cm(III) with two hydroxamic acids, salicylhydroxamic (SHA) and benzohydroxamic acid (BHA) was studied by time-resolved laser-induced fluorescence spectroscopy (TRLFS). Hydroxamate containing chelating substances have the potential to enhance the solubility and mobility of metals and radionuclides by forming complexes. We explored the fluorescence properties, lifetimes and individual fluorescence emission spectra of the formed Cm(III) hydroxamate species. In both Cm(III)–hydroxamic acid systems a 1:1 and a 1:2 complex of the type $M_pL_qH_r$ could be identified from the fluorescence emission spectra having peak maxima at 600 and 609 nm, respectively. An indirect excitation mechanism of the Cm(III) fluorescence was observed in the presence of the hydroxamic acids. Consistent stability constants were determined by using either indirect or direct excitation mode of the Cm(III) fluorescence. In the Cm(III)–SHA system, the stability constants are $\log\beta_{111} = 16.52 \pm 0.14$ and $\log\beta_{121} = 24.09 \pm 0.62$. The complex formation constants of the Cm(III)–BHA species result to $\log\beta_{110} = 6.52 \pm 0.19$ and $\log\beta_{120} = 11.60 \pm 0.50$. The stability constants were compared to those of natural pyoverdins.

© 2008 Elsevier Ltd. All rights reserved.

1. Introduction

The migration and mobilization of actinides by various environmental compounds is very important for the long-term risk assessment of nuclear waste disposal sites. The influence of microbes and bioligands secreted by microbes on the mobilization of trivalent actinides is little investigated [1–4]. To understand the complex interaction processes of actinides in biological systems on a molecular level, it is necessary to explore the complexation behavior of actinides with selected bioligands of relevant functionalities as model compounds. A special group of natural bioligands with a high potential to bind actinides are siderophores of the pyoverdin-type [4–11]. Pyoverdins are secreted under iron limited conditions from *Pseudomonas* ssp., which are ubiquitous aerobic soil bacteria. The preferred binding places for metals at the pyoverdin molecule are the hydroxamic acid group at the peptide chain and the catechol functionality of the chromophor [4,5]. In this study, we simulate the hydroxamic acid function identified in pyoverdins with simple model ligands, salicylhydroxamic (SHA) and benzohydroxamic acid (BHA) (Fig. 1). Of special importance is the investigation of the interaction of bioligands with long-lived actinides like uranium and curium. In previous studies [12,13], we used UV–Vis spectroscopy and time-resolved laser-induced fluorescence spectroscopy (TRLFS) to determine the stability constants of the complex formation between uranium(VI) and hydroxamic acids. Furthermore, we determined the absorption and fluorescence properties of the formed uranium(VI) species with SHA and BHA. At present, no results are available about the complex formation of hydroxamic acids with trivalent actinides, e.g., curium(III). Recently, the complexation of ^{248}Cm(III) with pyoverdins was studied by Moll et al. in 2007 [4]. Three 1:1 complexes were identified with stability constants of $\log\beta_{121} = 32.50 \pm 0.06$, $\log\beta_{111} = 27.40 \pm 0.11$, and $\log\beta_{101} = 19.30 \pm 0.17$. These large formation constants compared to other chelating agents illustrate the unique complexation properties of hydroxamate containing pyoverdin-type siderophores.

To address the lack of studies of the complexation of aromatic hydroxamic acids with Cm(III), we thus present findings regarding the complex formation of Cm(III) with two hydroxamic acids using TRLFS. Due to the excellent fluorescence properties of Cm(III), this method enabled the working at trace Cm(III) concentrations (3×10^{-7} M). We explored the fluorescence properties, lifetimes and individual fluorescence emission spectra of the formed Cm(III) species. An indirect excitation mechanism for the Cm(III) fluorescence was observed in the presence of the hydroxamic acids. The stability constants determined either by indirect (360 nm) or direct (395 nm) excitation of the Cm(III) fluorescence were compared. The determination of stability constants by indirect fluorescence excitation is a new possibility to study and validate the complexation of fluorescent actinides with ligands. The determined stability constants of the identified complexes were compared to those of

* Corresponding author. Tel.: +49 351 260 2895; fax: +49 351 260 3553.
E-mail address: m.glorius@fzd.de (M. Glorius).

0277-5387/$ - see front matter © 2008 Elsevier Ltd. All rights reserved.
doi:10.1016/j.poly.2008.04.002

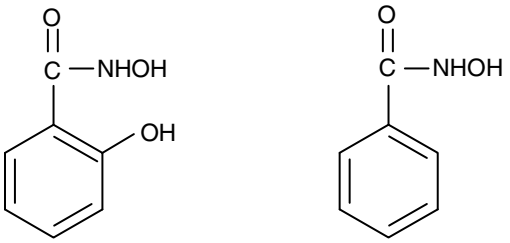

Fig. 1. Structures of the hydroxamic acids considered in this paper.

the pyoverdins [4]. The results of this study increase our understanding of the mobilization of trivalent actinides with hydroxamic acids.

2. Experimental

2.1. Solutions and reagents

A stock solution of the long-lived curium isotope ^{248}Cm ($t_{1/2} = 3.4 \times 10^5$ years) was used. The solution had the following composition: 97.3% ^{248}Cm, 2.6% ^{246}Cm, 0.04% ^{245}Cm, 0.02% ^{247}Cm, and 0.009% ^{244}Cm in 1.0 M $HClO_4$. All experiments were made in a glove box under nitrogen atmosphere at 25 °C. The sodium perchlorate, salicylhydroxamic (SHA) and benzohydroxamic (BHA) acids used were of analytical grade. Salicylhydroxamic acid was provided by Sigma–Aldrich, Germany and the other chemicals were ordered from Merck, Germany. The stock solutions of the ligands were freshly prepared for each experiment. To avoid carbonate complexation of Cm(III), carbonate free water and NaOH solution were used. The Cm(III) concentration was fixed to 3×10^{-7} M in all TRLFS measurements. The concentration of the ligands was varied between 1×10^{-5} M and 1×10^{-3} M. The pH was measured using an InLab 427 combination pH puncture electrode (Mettler-Toledo Giessen, Germany) calibrated in H^+ concentration units. The pH was changed between 2.0 and 9.0 by adding analytical grade NaOH or $HClO_4$ with an accuracy of ±0.02 units. All experiments were made in an ionic medium where the sodium concentration was kept constant at 0.1 M by adding $NaClO_4$.

In the Cm(III)–SHA system four series of experiments were made; in the first three series we investigated the complexation of Cm^{3+} and the ligand at three different ligand concentrations, 1.5×10^{-5}, 1.5×10^{-4} and 3.26×10^{-4} M, by varying the pH between 2 and 9. In the fourth run, we varied the ligand concentration between 1×10^{-5} and 1×10^{-4} M at pH 8. In the Cm(III)–BHA system three series of experiments were made with constant ligand concentrations of 1.5×10^{-4} M, 3.65×10^{-4} M and 1×10^{-3} M by varying the pH between 2 and 9.

2.2. TRLFS measurements: experimental setup

The time-resolved laser-induced fluorescence spectra were recorded at 25 ± 2 °C using a flash lamp pumped Nd:YAG-OPO laser system (Powerlite Precision II 9020 laser and Green PANTHER EX OPO from Continuum, Santa Clara, CA, USA). Further details about the laser system can be found in [4]. The system consists of an Oriel MS 257 monochromator and spectrograph with a 300 or 1200 lines mm^{-1} grating and an Andor iStar ICCD camera (Lot-Oriel Group, Darmstadt, Germany). The emission spectra were recorded in the 570–659 nm (1200 lines mm^{-1}) and 500–700 nm (300 lines mm^{-1}) ranges, respectively. The laser pulse energy was monitored using a photodiode and was between 3 and 7 mJ depending on the used excitation wavelength. A constant time window of 1 ms was applied, and two excitation wavelengths of 360 and 395 nm were used. For measuring the time-dependent emission decay, the delay time between laser pulse and camera grating was scanned with time intervals between 10 and 20 μs.

2.3. TRLFS measurements: evaluation of the fluorescence spectra

The fluorescence spectra were evaluated using the ORIGIN 7.5G (OriginLab Corporation, USA) code. The stability constants were determined using the factor analysis program SPECFIT [14]. SPECFIT calculates the complex formation constants and the single component spectra at both excitation wavelength of 395 and 360 nm based on the observed changes in the fluorescence emission spectra by varying a given physico-chemical parameter, e.g., pH or ligand concentration. We could demonstrate the successful application of SPECFIT to describe the coordination chemistry of Cm(III) in different organic systems [4,15–17]. Input parameters for the calculations with SPECFIT were the known total concentrations of Cm^{3+} and the ligand, the pH of each sample and the protonation constants of

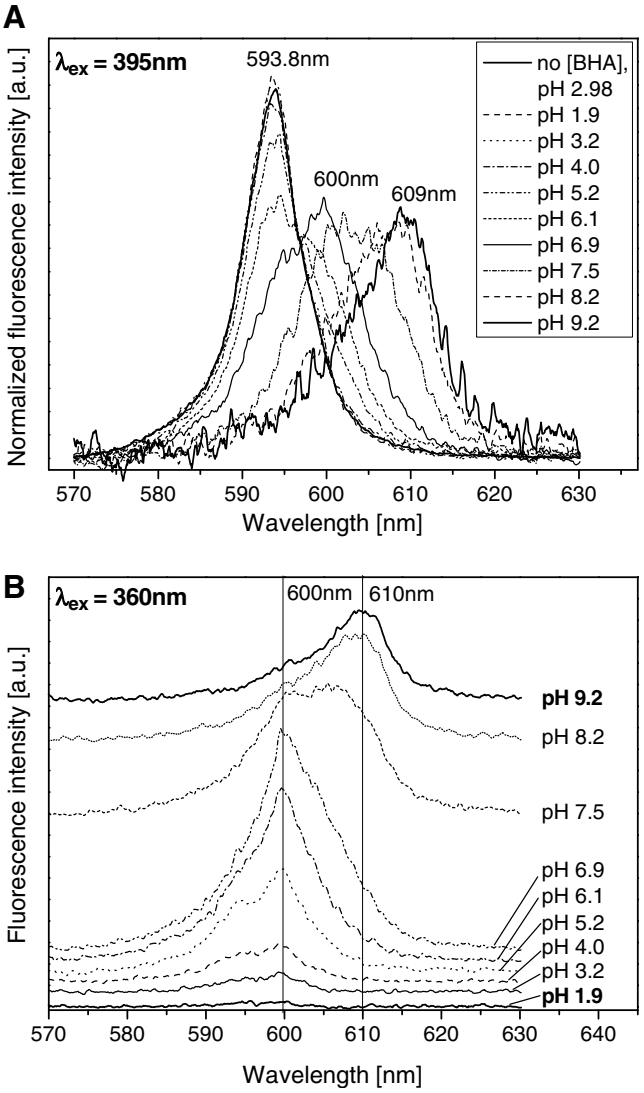

Fig. 2. Fluorescence emission spectra of 3×10^{-7} M Cm^{3+} and 1.5×10^{-4}M BHA as a function of pH at an excitation wavelength of (A) 395 nm (direct excitation mode) and (B) 360 nm (indirect excitation mode). The spectra at an excitation wavelength of 395 nm are scaled to the same peak area and the spectra at excitation wavelength of 360 nm are energy corrected.

SHA ($\log\beta_{011} = 10.05 \pm 0.03$, $\log\beta_{012} = 17.72 \pm 0.09$) and BHA ($\log\beta_{011} = 8.76 \pm 0.05$) [12]. As well, the known emission spectrum of the Cm^{3+} aquo ion was used in the SPECFIT calculations.

3. Results and discussion

3.1. Benzohydroxamic acid

The fluorescence emission spectra of 3×10^{-7} M Cm(III) with 1.5×10^{-4} M BHA in the pH range 2–9 are shown in Fig. 2. The spectra are recorded at two different excitation wavelengths. The spectra with an excitation wavelength of 395 nm are shown in Fig. 2A, the spectra with an excitation wavelength of 360 nm are summarized in Fig. 2B. The Cm^{3+} aquo ion has a characteristic fluorescence emission band maximum of 593.8 nm at an excitation wavelength of 395 nm. In Fig. 2A we observed a pronounced red shift of the emission maximum with increasing pH. This indicates the complex formation between Cm(III) and BHA. At an excitation wavelength of 360 nm (Fig. 2B) we identified an increasing fluorescence intensity and red shift of the emission maximum with increasing pH. From this we can conclude that the concentration of the Cm(III)–hydroxamate species increased with increasing pH. The complexation is accompanied by an increase of the fluorescence emission lifetime. At pH values equal to or less than 7, the fluorescence lifetime increased from 65 μs for the Cm^{3+} aquo ion to 85 μs showing monoexponential decay. At pH values greater than 8, a biexponential decay was measured with lifetimes of 75 and 150 μs. In the pH range 4–7, a second Cm(III) species besides the Cm^{3+} aquo ion with a peak maximum at 600 nm dominates more and more the sum fluorescence spectrum. Above pH 7 a third Cm(III) species appeared with a peak maximum at 609 nm. These experimental findings, the two identified peak maxima and the two identified lifetimes give clear evidence for the formation of two different Cm(III)–BHA species.

Previous studies [4,18–20] have shown that fluorescence emission of complexes between Cm(III) and organic ligands like pyoverdins and humic acids can be generated either by direct excitation of the Cm(III) fluorescence or by excitation of the ligand followed by an energy transfer from the ligand molecule to the Cm(III) ion (indirect excitation). So, the fluorescence properties of the Cm(III)–BHA complex species can be also determined by an excitation at 360 nm (spectra shown in Fig. 2B) via the discussed energy transfer from the BHA molecule to the Cm(III). A comparison of the spectra at the two excitation wavelengths in dependence of the pH is shown in Fig. 3. At an excitation wavelength of 395 nm and pH 4, the spectrum shows no influence of the beginning complex formation. In contrast to this, the spectrum measured at an excitation wavelength of 360 nm exhibits clearly a peak at 600 nm corresponding to the formation of the first complex. Also at pH 6 and 7, the formation of Cm(III)–BHA species influences strongly the measured sum fluorescence spectra using the indirect excitation mode in contrast to the spectra at 395 nm. At pH 8, where no uncomplexed Cm(III) species exist, the measured spectra exhibit the same peak maxima at both excitation wavelengths.

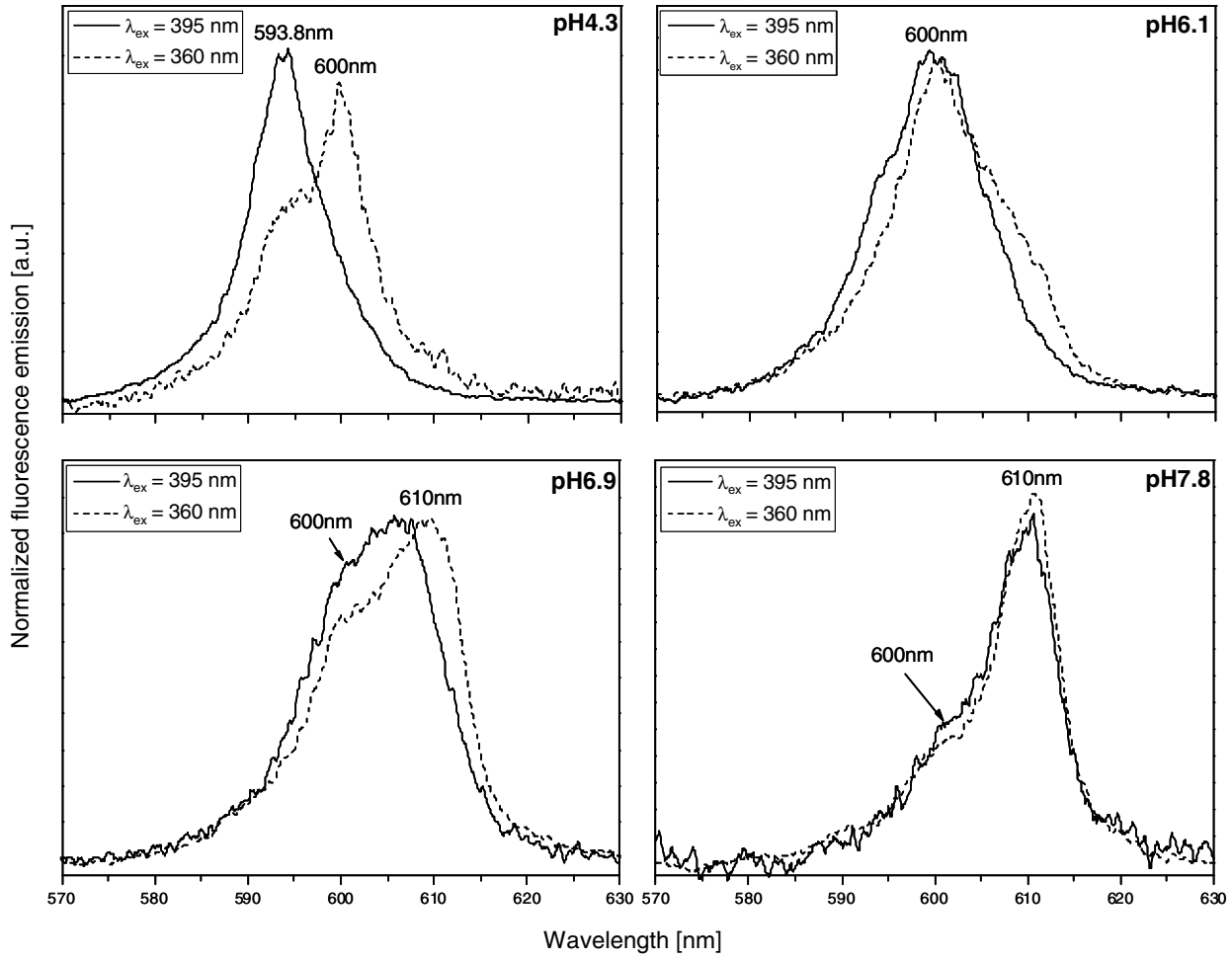

Fig. 3. Direct comparison of fluorescence emission spectra of the curium(III)–benzohydroxamate system measured at excitation wavelengths of 360 (indirect excitation mode) and 395 nm (direct excitation mode).

To describe the complex formation reactions the factor analysis program SPECFIT was used. As a result of the SPECFIT calculations, the variations observed in the fluorescence emission spectra can be described by the following equilibria:

$$Cm^{3+} + C_6H_4CONHO^- \rightleftharpoons Cm[C_6H_4CONHO]^{2+} \qquad \log\beta_{110} \qquad (1)$$

$$Cm^{3+} + 2C_6H_4CONHO^- \rightleftharpoons Cm[C_6H_4CONHO]_2^{+} \qquad \log\beta_{120} \qquad (2)$$

The stability constants were determined at both excitation wavelengths. At an excitation wavelength of 395 nm the stability constant for the 1:1 complex, $Cm[C_6H_4CONHO]^{2+}$, was determined to be $\log\beta_{110} = 6.42 \pm 0.11$ and for the 1:2 complex, $Cm[C_6H_4CONHO]_2^{+}$, $\log\beta_{120} = 11.25 \pm 0.36$ at an ionic strength of 0.1 M. The stability constants at an excitation wavelength of 360 nm are $\log\beta_{110} = 6.61 \pm 0.21$ and $\log\beta_{120} = 11.95 \pm 0.35$. The stability constants determined either by indirect (360 nm) or direct (395 nm) excitation of the Cm(III) fluorescence are consistent and show the applicability of the indirect excitation to determine complex formation equilibria. The corresponding single component spectra of the curium–benzohydroxamate species at both wavelengths are shown in Fig. 4. The emission maxima of both benzohydroxamate species are in agreement measured either with direct or indirect excitation.

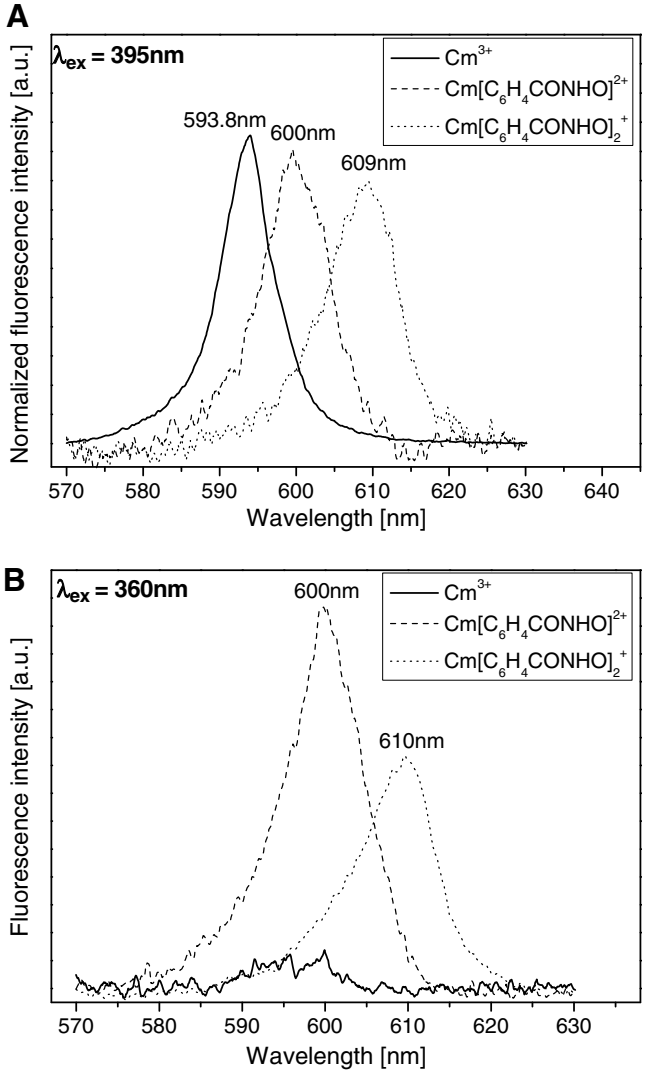

Fig. 4. Fluorescence emission spectra of the single components in the Cm^{3+}–BHA system at an excitation wavelength of (A) 395 nm and (B) 360 nm.

3.2. Salicylhydroxamic acid

The measured fluorescence emission spectra of Cm(III) with SHA in the pH range 4–8 (spectra not shown here) at an excitation wavelength of 395 nm show a red shift of the emission maxima with increasing pH from the characteristic emission maximum of Cm(III) at 593.8 nm via 600 nm to an emission maximum at 608 nm indicating the complex formation between Cm(III) and SHA. Two different Cm(III)–SHA species are formed. The first complex species appears in the pH range 4–7 with a peak maximum of 600 nm and a lifetime of 80 μs and the second species with a lifetime of 200 μs and a peak maximum of 608 nm occurs at pH values greater than 7.

The fluorescence emission spectra at both excitation wavelength of 395 and 360 nm were analyzed with the factor analysis program SPECFIT. The calculated single component spectra of the Cm(III)–SHA complex species are similar to those of the Cm–BHA system and are not shown here. The complexation reactions can be expressed as follows:

$$Cm^{3+} + OC_6H_4CONHO^{2-} + H^+ \rightleftharpoons Cm[HOC_6H_4CONHO]^{2+} \qquad \log\beta_{111} \qquad (3)$$

$$Cm^{3+} + 2OC_6H_4CONHO^{2-} + H^+ \rightleftharpoons Cm[HOC_6H_4CONHO,OC_6H_4CONHO] \qquad \log\beta_{121} \qquad (4)$$

The stability constant for the 1:1 complex, $Cm[HOC_6H_4CONHO]^{2+}$, and the 1:2 complex, $Cm[HOC_6H_4CONHO, OC_6H_4CONHO]$, are $\log\beta_{111} = 16.52 \pm 0.14$ and $\log\beta_{121} = 24.09 \pm 0.62$ at an ionic strength of 0.1 M, respectively. The 1:2 complex is a mixed complex consisting of two different deprotonated ligand molecules ($HOC_6H_4CONHO^-$ and $OC_6H_4CONHO^{2-}$) and a Cm^{3+} ion. There are evidences that the phenolic OH-group of one of the ligand molecules is deprotonated through the complexation. The longer lifetime of the 1:2 complex of SHA (200 μs) in comparison to the lifetime of the 1:2 complex of BHA (150 μs) could indicate an involvement of the phenolic OH-group during the complexation.

4. Conclusions

Table 1 gives a summary of the determined emission maxima, lifetimes and complex formation constants of the Cm(III)–hydroxamic acid complexes in comparison to those of the Cm(III)-*Pseudomona fluorescens* pyoverdin species. For a better direct comparison of the strength of the formed species the determined $\log\beta$ values were recalculated in $\log K$ values using the involved aqueous ligand species. The $\log K$ values of the 1:1 complexes of BHA and SHA show that SHA and BHA form 1:1 complexes with similar stability. In case of the 1:2 complexes BHA has a lower stability constant than SHA which indicates a stronger complex formation of Cm(III) with salicylhydroxamic acid. This is in agreement with the results obtained with uranium(VI) [12,21] and other metals like Fe(III) and Cu(II) [22–25]. The larger stability constants of SHA are probably caused by the influence of the additional phenolic OH group, which was also described by Khairy [26] and O'Brien [24]. The complex formation constants of the three Cm(III)-pyoverdin species identified by Moll et al. [4] are larger than the constants of the hydroxamic acids. One reason could be the different structure of the pyoverdins and the larger number of functional groups in these molecules. The model ligands simulate only one functional group of the pyoverdins. The functional groups in the pyoverdin molecule that participate in the metal binding are the catechol group of the chromophore and hydroxamate and α-hydroxy acid moieties at the peptide chain. The complexation of metals with the pyoverdins is influenced by all these functional groups and the structure of the molecule itself. There-

Table 1
Summary of emission maxima, lifetimes, complex stability constants log β and log K of the curium(III) complexes identified in this study in comparison to Cm(III)-*P. fluorescens* pyoverdin constants

Ligand	$M_pL_qH_r$	Complex species	Emission (nm)	Lifetime (μs)	log β	log K	Ref.
Cm^{3+}	100		593.8	68 ± 1			this work
SHA	111	$Cm[HOC_6H_4CONHO]^{2+}$	600	80 ± 5	16.52 ± 0.14	6.47[a]	this work
	121	$Cm[HOC_6H_4CONHO, OC_6H_4CONHO]$	608	200 ± 28	24.09 ± 0.62	14.04[b]	this work
BHA	110	$Cm[C_6H_4CONHO]^{2+}$	600	85 ± 8	6.52 ± 0.19	6.52	this work
	120	$Cm[C_6H_4CONHO]_2^{+}$	609	150 ± 23	11.60 ± 0.50	11.60	this work
Pyoverdin	112	CmH_2L^{+}	602.2	86 ± 2 (80%) 198 ± 10 (20%)	32.50 ± 0.06	9.83[c,e]	[4]
	111	CmHL	608.4	83 ± 2 (64%) 229 ± 5 (36%)	27.40 ± 0.11	15.20[d,e]	[4]
	110	CmL^{-}	610.8	100 ± 5 (71%) 330 ± 10 (29%)	19.30 ± 0.17	19.30[e]	[4]

[a] $Cm^{3+} + HOC_6H_4CONHO^{-} \rightleftharpoons Cm[HOC_6H_4CONHO]^{2+}$.
[b] $Cm^{3+} + HOC_6H_4CONHO^{-} + OC_6H_4CONHO^{2-} \rightleftharpoons Cm[HOC_6H_4CONHO, OC_6H_4CONHO]$.
[c] $Cm^{3+} + LH_2^{2-} \rightleftharpoons CmH_2L^{+}$.
[d] $Cm^{3+} + LH^{3-} \rightleftharpoons CmHL$.
[e] Recalculated in this study.

fore, pyoverdins form stronger complexes with Cm(III) than the model ligands with one hydroxamic acid functionality.

Fluorescence lifetime measurements were used to obtain information about the composition of the first coordination sphere of curium(III). In 1994, Kimura and Choppin [27] found a linear relationship between the lifetime and the number of water molecules in the first coordination sphere of Cm(III). The Cm^{3+} aquo ion is characterized by a measured lifetime of 68 μs, which corresponds to nine water molecules, while the value of 1370 μs measured in D_2O [28] corresponds to zero water molecules in the first coordination sphere of curium(III). In case of a complex formation of the Cm^{3+} aquo ion, the lifetimes of the Cm(III) species increase indicating the exclusion of water molecules out of the first coordination sphere. In all samples with pH values up to 5, a mono-exponential decay was measured with an averaged lifetime of 80 μs in the Cm(III)–SHA system and 85 μs in the Cm(III)–BHA system. This lifetime might correspond to the 1:1 Cm(III)–hydroxamic acid complexes. In samples with pH values above 5, a bi-exponential decay was detected with average lifetimes of 80 and 200 μs for SHA and 85 and 150 μs for BHA, respectively. The second larger lifetime could correspond to the 1:2 complexes. The average number of water molecules in the first coordination sphere calculated with the determined fluorescence lifetimes is 7.3 (SHA) and 6.8 (BHA) for the 1:1 complex and 2.4 (SHA) and 3.5 (BHA) for the 1:2 complex, respectively. During the formation of the 1:1 complex with both hydroxamic acids two water molecules are excluded out of the first coordination sphere. This is in good agreement with the complex stoichiometry found with SPECFIT in the two Cm(III)–hydroxamic acids systems. In a first assumption also caused by the lack of information regarding the structure of Cm(III)–hydroxamate compounds, we assume that the complex stoichiometry and structure of the 1:1 Cm(III)–SHA and Cm(III)–BHA complexes are similar to the U(VI)-SHA and -BHA complexes. The coordinating atoms in the complexes are the hydroxamic acid oxygens ([O,O]-mode), the other reasonable coordination mode via the phenolic oxygen and the nitrogen atom ([N,O′]-mode) could be excluded according to Ref. [29]. So, the Cm^{3+} aquo ion binds like the UO_2^{2+}-ion to the hydroxamic acids via the two hydroxamate oxgens. As a result of the formation of the 1:2 complex of Cm(III)–SHA 6–7 water molecules leave the first coordination sphere. The outcome of the SPECFIT calculation points to a five- or six- coordinated Cm(III)-atom depending if the phenolic OH-groups are involved in the complex formation or not. Six released water molecules suggest that the protonated OH-group is concerned in the complexation. In the Cm(III)–BHA system the fluorescence lifetime of the 1:2 complex suggest that five water molecules are released due to the complex formation. The bidentate coordination of two hydroxamate groups of BHA to Cm(III) would result in five remaining water molecules. The observed difference could be explained by additional interactions with the π-system of the ring. In case of the 1:1 complexes with the hydroxamic acids the relationship between the lifetime and the number of released water molecules agree well with the stoichiometry of the complexes found with SPECFIT. However, we cannot exclude quench mechanism during the complexation via the organic ligands, which might cause that the linear relationship of Kimura and Choppin would be inapplicable. On that account the fluorescence decay was used for comparison and to give evidences for the structure of the formed complexes.

To summarize we studied the until now unknown interaction of Cm(III) with hydroxamic acids using TRLFS. We determined the stability constants of the Cm(III)–SHA and Cm(III)–BHA species by direct (395 nm) and indirect (360 nm) excitation of the fluorescence. The stability constants were compared to those of natural pyoverdins. The stability constants determined by indirect excitation of the Cm(III) agree well with the constants determined by direct excitation of the Cm(III) fluorescence. Therefore, the investigation of complex formation equilibria by indirect excitation points to a new possibility to study the complex formation of fluorescent actinides with organic ligands. The results presented also in comparison with the constants of the natural pyoverdins [4], contribute to a better understanding of the speciation and mobilization of trivalent actinides by hydroxamate compounds by exploring their fluorescence properties.

Acknowledgements

This work was funded by the BMWi under Contract Number 02E9985. The authors are indebted to the US Department of Energy, Office of Basic Energy Sciences, for the use of ^{248}Cm via the transplutonium element production facilities at Oak Ridge National Laboratory; ^{248}Cm was made available as part of collaboration between FZD and the Lawrence Berkeley National Laboratory (LBNL).

References

[1] H. Moll, T. Stumpf, M. Merroun, A. Rossberg, S. Selenska-Pobell, G. Bernhard, Environ. Sci. Technol. 38 (2004) 1455.
[2] T. Ozaki, J.B. Gillow, A.J. Francis, T. Kimura, T. Ohnuki, Z. Yoshida, J. Nucl. Sci. Technol. 3 (2002) 950.
[3] T. Ozaki, T. Kimura, T. Ohnuki, A.J. Francis, Radiochim. Acta 94 (2006) 715.
[4] H. Moll, A. Johnsson, M. Schäfer, K. Pedersen, H. Budzikiewicz, G. Bernhard, BioMetals, (2007), in press, doi:10.1007/s10534-007-9111-x.

[5] A.-M. Albrecht-Gary, S. Blanc, N. Rochel, A.Z. Ocaktan, M.A. Abdallah, Inorg. Chem. 33 (1994) 6391.
[6] M. Bouby, I. Billard, H.J. Maccordick, Czech. J. Phys. 49 (1999) 769.
[7] M. Bouby, I. Billard, J. MacCordick, J. Alloy Compd. 271 (1998) 206.
[8] J.R. Brainard, B.A. Strietelmeier, P.H. Smith, P.J. Langstonunkefer, M.E. Barr, R.R. Ryan, Radiochim. Acta 58 (9) (1992) 357.
[9] N.V. Jarvis, R.D. Hancock, Inorg. Chim. Acta 182 (1991) 229.
[10] H. Moll, M. Glorius, G. Bernhard, A. Johnsson, K. Pedersen, M. Schäfer, H. Budzikiewicz, J. Geomicrobio. (2008), in press.
[11] M.P. Neu, J.H. Matonic, C.E. Ruggiero, B.L. Scott, Angew. Chem., Int. Edit. 39 (2000) 1442.
[12] M. Glorius, H. Moll, G. Bernhard, Radiochim. Acta 95 (2007) 151.
[13] M. Glorius, H. Moll, G. Bernhard, J. Radioanal. Nucl. Chem. (2007).
[14] R.A. Binstead, A.D. Zuberbühler, B. Jung, in SPECFIT Global Analysis System Version 3.0.34, 2003.
[15] H. Moll, G. Bernhard, J. Coord. Chem. 60 (2007) 1795.
[16] H. Moll, G. Bernhard, J. Radioanal. Nucl. Chem. 274 (2007) 603.
[17] H. Moll, G. Geipel, G. Bernhard, Inorg. Chim. Acta 358 (2005) 2275.
[18] M.A. Kim, P.J. Panak, D.C. Breban, A. Priemyshev, J.I. Yun, A. Mansel, J.I. Kim, Colloid Surf. A-Physicochem. Eng. Asp. 296 (2007) 206.
[19] P. Panak, R. Klenze, J.I. Kim, H. Wimmer, J. Alloy Compd. 225 (1995) 261.
[20] X.K. Wang, T. Rabung, H. Geckeis, P.J. Panak, R. Klenze, T. Fanghanel, Radiochim. Acta 92 (2004) 691.
[21] M. Glorius, H. Moll, G. Bernhard, J. Radioanal. Nucl. Chem. 277 (2008) 371.
[22] E. Farkas, E. Kozma, M. Petho, K.M. Herlihy, C. Micera, Polyhedron 17 (1998) 3331.
[23] A.W.H. Lam, W.T. Wong, S. Gao, G.H. Wen, X.X. Zhang, Eur. J. Inorg. Chem. (2003) 149.
[24] E.C. O'Brien, E. Farkas, M.J. Gil, D. Fitzgerald, A. Castineras, K.B. Nolan, J. Inorg. Biochem. 79 (2000) 47.
[25] G. Schwarzenbach, K. Schwarzenbach, Helv. Chim. Acta 46 (1963) 1390.
[26] E.M. Khairy, M.M. Shoukry, M.M. Khalil, M.M.A. Mohamed, Transit. Met. Chem. 21 (1996) 176.
[27] T. Kimura, G.R. Choppin, J. Alloy Compd. 213 (1994) 313.
[28] N.M. Edelstein, R. Klenze, T. Fanghanel, S. Hubert, Coord. Chem. Rev. 250 (2006) 948.
[29] J. Wiebke, A. Moritz, M. Glorius, H. Moll, G. Bernhard, M. Dolg, Inorg. Chem. (2008), in press, doi:10.1021/ic702162r.

Polyhedron 27 (2008) 2119–2126

Contents lists available at ScienceDirect

Polyhedron

journal homepage: www.elsevier.com/locate/poly

The first hybrid organic–inorganic frameworks based on lanthanide(III) sulfate chains, *in situ* generated oxalate and organic pillars of 1,4-piperazinediacetic acid

Juan Yang [a], Ning Lu [a], Gong Zhang [a], Lin Cheng [b], Shao-Hua Gou [a,b,*]

[a] School of Chemistry and Chemical Engineering, State Key Laboratory of Coordination Chemistry, Nanjing University, Nanjing 210093, China
[b] School of Chemistry and Chemical Engineering, Southeast University, Nanjing 211189, China

ARTICLE INFO

Article history:
Received 18 February 2008
Accepted 6 April 2008
Available online 16 May 2008

Keywords:
Hybrid organic–inorganic framework
Magnetic properties
Thermogravimetric properties

ABSTRACT

Two series of new three-dimensional (3D) hybrid organic–inorganic frameworks $[Ln_2(H_2pda)(C_2O_4)(SO_4)_2(H_2O)_2]_n$ [I, Ln = Nd (**1**), Y (**2**)] and $\{[Ln_2(H_2pda)(C_2O_4)(SO_4)_2(H_2O)_2]\cdot 2H_2O\}_n$ [II, Ln = Pr (**3**), Ce (**4**) and Eu (**5**)] (where H_2dpa = 1,4-piperazinediacetic acid) have been synthesized by the reactions of H_2pda, lanthanide oxides and H_2SO_4 under similar hydrothermal conditions. All compounds are constructed by two-dimensional hybrid organic–inorganic layers, which originate from different lanthanide(III) sulfate chains and *in situ* generated μ_4-oxalates, and organic H_2dpa pillars. The coordination modes of sulfate in I and II are, respectively, η^4,μ_3-pentadentate and η^3,μ_3-tridentate, resulting in the different inorganic $[Ln(SO_4)(H_2O)]_\infty$ chains that have not been documented so far. In I, each organic H_2dpa pillar is connected with two Ln(III) ions in a bis-monodentate fashion, while it is linked to four Ln(III) ions in a bis-bidentate *syn–anti* mode in II. Meanwhile, each Ln(III) ion in I and II is linked by one and two H2pda ligands, respectively. The observations hint that application of lanthanide(III) sulfate chains and flexible spacer pillars can self-assemble into interesting hybrid organic–inorganic framework solids. Compounds **1** and **3** are air stable and both the three-dimensional frameworks can be retained below 180 °C. The variable-temperature magnetic studies show that the χ_M values of **1** and **3** increase on the falling temperature, which may be attributed to the depopulation of Stark levels and/or intramolecular antiferromagnetic coupling between the metal centers.

© 2008 Elsevier Ltd. All rights reserved.

1. Introduction

Recent years have witnessed an explosion of great interest in hybrid organic–inorganic framework solids not only for their intriguing architectures and topologies, but also for their potential applications in optical, electrical, magnetic, and microporous materials [1–4]. A powerful strategy for constructing such organic–inorganic aggregates is directed self-assembly of designed organic ligands and inorganic skeletons. The inorganic skeletons are built up from two parts: metallic cations and oxoanions. The metal elements range from main group elements to transition metal elements. And most of "oxo-anion part" works have often been involved in tetrahedral anions as $[TO_4]$ units (T = tetrahedrally coordinated element), such as phosphates [5], germanites [6], arsenates [7], and selenites [8]. Recently, there has been growing interest in the study of open-framework architectures containing tetrahedral oxo-anions of sulfurs not only due to their versatile coordination modes such as monodentate, μ_2-, μ_3-, μ_4- and μ_5-bridges and so on, but also due that they have been known to promote a diversity of structural arrangements in inorganic solids [9]. And that the materials including metal sulfates are usually much thermally stable [10]. However, it is noted that such sulfate-based compounds reported mainly focus on the d-block transition metals. So far, there are only several examples of lanthanide sulfates [11–13] published in the CCDC [14], and most of them are based on simple lanthanide sulfates in the presence of templating amines as balance cations [12]. Hence, hybrid organic–inorganic frameworks including inorganic skeletons formed by lanthanide sulfate and bridging organic pillars have been rarely reported [13].

In the past study, rigid spacer ligands such as benzene di-, and tri-carboxylates have been successfully used to produce various extended structures with metal ions, but flexible spacer ligands turn out to be much difficult to control their conformations in the architecture of the products. Recent interest in design of polydentate flexible ligands has propagated a family of piperazine-based ligands, because the chair configuration of piperazine can reduce their coordination modes, which makes piperazine or its related species structurally or functionally directing polymeric constructions [15–19], compatible to its analogue-cyclohexane-based organic species such as 1,4-cyclohexanedicarboxylate with (*a*,*a*), (*a*,*e*) and (*e*,*e*) conformers [20]. However, most of the published

* Corresponding author. Address: School of Chemistry and Chemical Engineering, State Key Laboratory of Coordination Chemistry, Nanjing University, Nanjing 210093, China. Tel./fax: +86 025 83595068.
E-mail address: sgou@nju.edu.cn (S.-H. Gou).

0277-5387/$ - see front matter © 2008 Elsevier Ltd. All rights reserved.
doi:10.1016/j.poly.2008.04.003

piperazine-based examples are concentrated on organic phosphates [16,17] or bipyridyl substituents [18,19]. To the best of our knowledge, there has been no coordination polymers reported, being constructed by piperazine-based carboxylates [14].

Herein, based on bridging 1,4-piperazinediacetic acid and different inorganic lanthanide sulfate chains, we report two series of hybrid organic–inorganic frameworks, $[Ln_2(H_2pda)(C_2O_4)(SO_4)_2(H_2O)_2]_n$ [I, Ln = Nd (**1**), Y (**2**)] and $\{[Ln_2(H_2pda)(C_2O_4)(SO_4)_2(H_2O)_2]\cdot 2H_2O\}_n$ [II, Ln = Pr (**3**), Ce (**4**) and Eu (**5**)] (H_2dpa = 1,4-piperazinediacetic acid), which have been structurally characterized.

2. Experimental section

2.1. Materials and methods

All solvents and reagents were obtained commercially and used without further purification. Infrared (IR) spectra were recorded on a Bruker Vector 22 FT-IR spectrophotometer. C, H, N and S microanalyses were carried out with a Perkin-Elmer 1400C analyzer. Thermal analysis (TG) was performed on a TGA Q500 thermal analyzer under nitrogen atmosphere at a scan rate of 10 °C min^{-1}. Magnetic susceptibility data of powder samples were collected in the temperature range of 1.8–300 K with the use of a Quantum Design MPMS XL-7 SQUID magnetometer. $H_2pda\cdot 2H_2O$ was prepared according to the reported procedures [21] and confirmed with elemental analysis and single crystal X-ray diffraction.

2.2. Synthesis of compounds

2.2.1. Synthesis of $[Nd_2(H_2pda)(C_2O_4)(SO_4)_2(H_2O)_2]_n$ (*1*)

A mixture of $H_2pda\cdot 2HCl$ (0.019 g, 0.1 mmol), Nd_2O_3 (0.034 g, 0.1 mmol), 50% H_2SO_4 (0.1 mL), and water (6 mL) were heated in a 15-mL Teflon-lined vessel at 160 °C for 3 days, followed by slow cooling (5 °C h^{-1}) to room temperature. After filtration and washing with H_2O, pink block crystals were collected and dried in air (0.012 g, yield ca. 35% based on H_2pda). *Anal.* Calc. for $C_{10}H_{18}N_2Nd_2O_{18}S_2$: C, 14.89; H, 2.25; N, 3.47; S, 7.95. Found: C, 14.87; H, 2.29; N, 3.45; S, 7.93%. FT-IR (KBr, cm^{-1}): 3508b, 3404m, 2987w, 2785w, 2638w, 1622s, 1463m, 1376w, 1339w, 1143vs, 1106vs, 1067vs, 985m, 713w, 611m.

2.2.2. Synthesis of $[Y_2(H_2pda)(C_2O_4)(SO_4)_2(H_2O)_2]_n$ (*2*)

The reaction was carried out in a method similar to that for **1**, using Y_2O_3 (0.023 g, 0.1 mmol) instead of Nd_2O_3. After filtration and washing with H_2O, colorless block crystals were collected and dried in air (0.018 g, yield ca. 46% based on H_2pda). *Anal.* Calc. for $C_{10}H_{18}N_2O_{18}S_2Y_2$: C, 17.25; H, 2.61; N, 4.02; S, 9.21. Found: C, 17.28; H, 2.57; N, 4.00; S, 9.18%. FT-IR (KBr, cm^{-1}): 3422b, 3028 s, 3010s, 2977w, 2783w, 2636w, 1724vs, 1673s, 1468m, 1403vs, 1324w, 1146w, 1122 m, 1062m, 988m, 977m, 670m.

2.2.3. Synthesis of $[[Pr_2(H_2pda)(C_2O_4)(SO_4)_2(H_2O)_2].2H_2O]_n$ (*3*)

Compound **3** was prepared in an analogous way to that for **1**, using Pr_6O_{11} (0.036 g, 0.035 mmol) instead of Nd_2O_3. After filtration and washing with H_2O, dark-green block crystals were collected and dried in air (0.023 g, yield ca. 55% based on H_2pda). *Anal.* Calc. for $C_{10}H_{22}N_2O_{20}Pr_2S_2$: C, 14.36; H, 2.65; N, 3.35; S,

Table 2
Selected bond lengths (Å) of **1–5**

1			
Nd1–O1W	2.46(5)	Nd1–O7b	2.66(4)
Nd1–O2	2.34(5)	Nd1–O8b	2.50(5)
Nd1–O4	2.43(6)	Nd1–O3c	2.459(6)
Nd1–O5	2.47(5)	Nd1–O7h	2.48(4)
Nd1–O6	2.71(5)		
2			
Y1–O1W	2.34(3)	Y1–O7b	2.73(4)
Y1–O2	2.26(3)	Y1–O8b	2.38(4)
Y1–O4	2.35(4)	Y1–O3c	2.41(4)
Y1–O5	2.36(5)	Y1–O7h	2.37(4)
Y1–O6	2.74(5)		
3			
Pr1–O1W	2.52(3)	Pr1–O6a	2.47(3)
Pr1–O2	2.51(4)	Pr1–O4d	2.52(4)
Pr1–O3	2.46(4)	Pr1–O1h	2.41(4)
Pr1–O5	2.43(3)	Pr1–O8i	2.45(3)
4			
Ce1–O1W	2.54(5)	Ce1–O6a	2.49(5)
Ce1–O2	2.52(7)	Ce1–O4d	2.54(6)
Ce1–O3	2.48(6)	Ce1–O1h	2.44(6)
Ce1–O5	2.46(6)	Ce1–O8i	2.46(5)
5			
Eu1–O1W	2.47(7)	Eu1–O6a	2.42(7)
Eu1–O2	2.45(8)	Eu1–O4d	2.47(7)
Eu1–O3	2.41(8)	Eu1–O1h	2.32(6)
Eu1–O5	2.35(7)	Eu1–O8i	2.37(6)

Symmetry codes for **1–2**: b: $x, 1+y, z$; c: $1-x, y, 1/2-z$; h: $1/2-x, 1/2+y, 1/2-z$; g: $1/2-x, -1/2+y, 1/2-z$. For **3–5**: a: $x, -1+y, z$; d: $1-x, 2-y, 1-z$; h: $3/2-x, 3/2-y, 1-z$; i: $3/2-x, 5/2-y, 1-z$.

Table 1
Crystal data and structure refinement for **1–5**

Compound	1	2	3	4	5
Formula	$C_{10}H_{18}N_2Nd_2O_{18}S_2$	$C_{10}H_{18}N_2O_{18}S_2Y_2$	$C_{10}H_{22}N_2O_{20}Pr_2S_2$	$C_{10}H_{22}Ce_2N_2O_{20}S_2$	$C_{10}H_{22}Eu_2N_2O_{20}S_2$
FW	806.88	696.22	836.26	834.68	858.36
Space group	*C*2/*c*	*C*2/*c*	*C*2/*c*	*C*2/*c*	*C*2/*c*
a (Å)	19.702(5)	19.392(3)	19.295(3)	19.353(3)	19.143(3)
b (Å)	6.3477(2)	6.2757(9)	6.8100(9)	6.8362(1)	6.7219(1)
c (Å)	17.352(4)	16.999(2)	16.377(2)	16.400(3)	16.323(3)
α (°)	90	90	90	90	90
β (°)	109.973(4)	108.279(2)	94.369(4)	94.312(3)	94.581(4)
γ (°)	90	90	90	90	90
V (Å^3)	2039.6(9)	1964.4(5)	2145.7(5)	2163.6(6)	2093.7(6)
Z	4	4	4	4	4
D_c (g cm^{-3})	2.628	2.354	2.589	2.562	2.723
T (K)	293(2)	293(2)	293(2)	293(2)	293(2)
μ (mm^{-1})	5.337	6.193	4.788	4.452	6.244
R_1[a] ($I > 2\sigma$)	0.0419	0.0626	0.0322	0.0496	0.0529
wR_2[b] (all data)	0.0829	0.1502	0.0822	0.1067	0.0907
Goodness-of-fit	1.095	0.999	1.066	1.040	1.026

[a] $R_1 = \sum ||F_o| - |F_c|| / \sum |F_o|$.

[b] $wR_2 = \left[\frac{\sum w(F_o^2 - F_c^2)^2}{\sum w(F_o^2)^2}\right]^{1/2}$.

Table 3
Selected hydrogen bond lengths (Å) and bond angles (°) of **1**–**5** (D, donor atom; A, acceptor atom)

D–H···A	D–H (Å)	H···A (Å)	D···A (Å)	D–H···A (°)
1				
O1w–H1wa···O1i	0.97	1.85	2.70(8)	144
N1–H1a···O6b	0.91	2.09	2.96(7)	162
O1w–H1wb···O1h	0.96	2.09	2.84(7)	133
O1w–H1wb···O6h	0.96	2.48	3.10(9)	122
C2–H2a···O3n	0.97	2.27	3.18(8)	156
C3–H3a···O4n	0.97	2.45	3.36(8)	157
C3–H3b···O2	0.97	2.37	2.95(9)	118
C3–H3b···O4	0.97	2.37	3.24(8)	149
2				
O1w–H1wa···O1i	0.95	1.88	2.71(6)	144
N1–H1a···O6b	0.90	2.02	2.89(7)	161
O1w–H1wb···O1h	0.95	2.08	2.83(7)	134
O1w–H1wb···O6h	0.95	2.41	3.04(6)	123
C2–H2a···O3n	0.97	2.24	3.16(8)	158
C3–H3a···O4n	0.97	2.44	3.37(8)	160
C3–H3b···O2	0.97	2.40	2.97(7)	117
C3–H3b···O4	0.97	2.30	3.18(8)	150
3				
O1w–H1wa···O7n	0.95	1.96	2.77(5)	142
O1w–H1wb···O7	0.95	1.79	2.72(5)	163
O2w–H2wa···O2wk	0.95	2.37	2.82(7)	108
O2w–H2wa···O3k	0.95	2.31	3.8(6)	129
O2w–H2wb···O4	0.95	2.56	3.20(6)	126
O2w–H2wb···O2k	0.95	2.57	3.18(6)	122
O2w–H2wb···O5d	0.95	2.41	3.00(7)	120
C2–H2a···O4k	0.97	2.57	3.24(6)	126
C2–H2a···O8h	0.97	2.45	3.37(6)	158
C2–H2a···O7r	0.97	2.35	3.28(6)	160
C3–H3a···O3s	0.97	2.45	3.19(6)	132
C3–H3b···O4d	0.97	2.56	3.29(6)	132
4				
O1w–H1wa···O7n	0.95	1.95	2.76(8)	142
O1w–H1wb···O7	0.96	1.80	2.73(9)	163
O2w–H2wa···O2wk	0.96	2.37	2.82(1)	108
O2w–H2wa···O3k	0.96	2.33	3.03(1)	129
O2w–H2wb···O4	0.95	2.58	3.22(1)	126..
O2w–H2wb···O2k	0.95	2.58	3.18(1)	122
O2w–H2wb···O5d	0.95	2.40	2.99(1)	120
C2–H2a···O8h	0.97	2.47	3.40(1)	159
C2–H2a···O7r	0.97	2.34	3.27(1)	161
C3–H3a···O3s	0.97	2.45	3.19(1)	132
C3–H3b···O4d	0.97	2.58	3.31(1)	132
5				
O1w–H1wa···O7n	0.95	1.99	2.81(9)	143
O1w–H1wb···O7	0.94	1.79	2.71(9)	165
O2w–H2wa···O2wk	0.94	2.37	2.82(1)	109
O2w–H2wa···O3k	0.94	2.28	2.96(1)	129
O2w–H2wb···O4	0.94	2.50	3.16(1)	127
O2w–H2wb···O5d	0.94	2.38	2.98(1)	121
C2–H2a···O4k	0.97	2.55	3.22(1)	126
C2–H2a···O8h	0.97	2.43	3.35(1)	158
C2–H2a···O7r	0.97	2.36	3.29(1)	161
C3–H3a···O3s	0.97	2.45	3.18(1)	132
C3–H3b···O4d	0.97	2.57	3.29(1)	131

Symmetry codes for **1**–**2**: b: x, $1+y$, z; h: $1/2-x$, $1/2+y$, $1/2-z$; i: x, $1-y$, $-1/2+z$; *n*: $1-x$, $1-y$, $1-z$. For **3**–**5**: c: $1-x$, y, $1/2-z$; d: $1-x$, $2-y$,$1-z$; h: $3/2-x$, $3/2-y$, $1-z$; k: $1-x$, $1-y$, $1-z$; n: $3/2-x$, $-1/2+y$, $3/2-z$; r: x, $2-y$, $-1/2+z$; s: x, $1-y$, $-1/2+z$.

7.67. Found: C, 14.39; H, 2.60; N, 3.36; S, 7.63%. FT-IR (KBr, cm^{-1}): 3509m, 3393b, 2986m, 2853w, 2632w, 1622vs, 1463s, 1421s, 1375m, 1338m, 1268m, 1143vs, 1104vs, 1065vs, 984s, 950m, 757m, 712m, 610s, 584m.

*2.2.4. Synthesis of {[$Ce_2(H_2pda)(C_2O_4)(SO_4)_2(H_2O)_2] \cdot 2H_2O\}_n$ (**4**)*

Compound **4** was obtained in a way like **1**, using CeO_2 (0.034 g, 0.2 mmol) instead of Nd_2O_3. After filtration and washing with H_2O, colorless block crystals were collected and dried in air (0.018 g, yield ca. 46% based on H_2pda). *Anal.* Calc. for $C_{10}H_{22}Ce_2N_2O_{20}S_2$: C, 14.39; H, 2.66; N, 3.36; S, 7.68. Found: C, 14.36; H, 2.69; N, 3.38; S, 7.64%. FT-IR (KBr, cm^{-1}): 3447.1b, 2976w, 2786w, 2602m, 1728vs, 1467w, 1403vs, 1329m, 1296m, 1266m, 1213m, 1127m, 1079m, 990s, 758m, 669s.

*2.2.5. Synthesis of [$[Eu_2(H_2pda)(C_2O_4)(SO_4)_2(H_2O)_2] \cdot 2H_2O]_n$ (**5**)*

Compound **5** was prepared in a similar way to that for **1**, using Eu_2O_3 (0.033 g, 0.1 mmol), instead of Nd_2O_3. After filtration and washing with H_2O, colorless block crystals were collected and dried in air (0.009 g, yield ca. 21% based on H_2pda). *Anal.* Calc. for $C_{10}H_{22}Eu_2N_2O_{20}S_2$: C, 13.99; H, 2.58; N, 3.26; S, 7.47. Found: C, 14.04; H, 2.61; N, 3.27; S, 7.42%. FT-IR (KBr, cm^{-1}): 3510m, 3383b, 3015m, 1669vs, 1650vs, 1475m, 1423s, 1374w, 1336w, 1273w, 1103vs, 1037s, 976m, 962w, 837w, 719w, 704m, 668m, 605s.

2.3. X-ray crystallography

Diffraction intensities for the compounds were collected on a Bruker SMART CCD area-detector diffractometer (Mo Kα, 0.71073 Å). Absorption corrections were applied by using multi-scan program SADABS [22]. The structures were solved by direct methods and refined with full-matrix least-squares technique with the SHELXTL program package [23]. Anisotropic thermal parameters were applied to all the non-hydrogen atoms. Organic hydrogen atoms were generated geometrically (C–H 0.96 Å) and refined with isotropic temperature factors. Hydrogen atoms on oxygen and nitrogen atoms were located from difference maps and refined isotropically with geometric AFIX restraints of 0.85–0.95 Å. Crystallographic data are summarized in Table 1. Selected bond distances are listed in Table 2, and hydrogen bonding parameters are given in Table 3.

3. Results and discussion

3.1. Synthesis

The syntheses exploit hydrothermal conditions, which have been demonstrated to be particularly effective for the fabrication of interesting organic–inorganic hybrid materials. The reaction conditions employed for the preparations of **1**–**5** were relatively simple. Thus, all the compounds were prepared from mixtures of the appropriate lanthanide oxide, $H_2pda \cdot 2HCl$, 50% H_2SO_4 and H_2O at 160 °C for 3 days. After the reactions, the pH values were between 2 and 3. Surprisingly, compounds **1** and **2** have different inorganic chains of lanthanide sulfate and different frameworks from those of **3**, **4** and **5**, under the similar conditions, which may be attributed to the inherent coordination characteristic of different lanthanide cations. Meanwhile, oxalates were unexpectedly *in situ* generated as a μ_4-oxobridged ligand in these coordination polymers, which may come from the decomposition of the cayboxylic groups of the ligand in the hydrothermal synthesis with high temperature and pressure [24]. It is noted that H_2pda exists as a zwitterionic ligand in all the complexes as shown in Scheme 1. The reaction scheme is shown in Scheme 2. All the products are

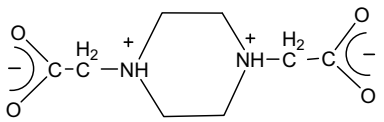

H_2pda

Scheme 1. Structural formula of H_2pda.

$$H_2pda + Ln_2O_3 + H_2SO_4 \xrightarrow{160\,^{\circ}C} [Ln_2(H_2pda)(C_2O_4)(SO_4)_2(H_2O)_2]_n \quad (Ln = Nd, Y)$$

$$H_2pda + Ln_xO_y + H_2SO_4 \xrightarrow{160\,^{\circ}C} \{[Ln_2(H_2pda)(C_2O_4)(SO_4)_2(H_2O)_2].2H_2O\}_n \quad (Ln = Pr, Ce, Eu)$$

Scheme 2. Reaction scheme.

not soluble in H_2O and common organic solvents such CH_3OH, CH_3CN, and CH_3COCH_3.

3.2. Type I structure of **1** and **2**

Single-crystal XRD study has revealed that both complexes **1** and **2** crystallize in the monoclinic system, *C*2/*c* space group. Since the crystals of **1** and **2** are isomorphous, only the structure of **1** is depicted in detail. Compound **1** is a three-dimensional framework consisting of two-dimensional hybrid organic–inorganic layers, which originate from inorganic $[Nd(SO_4)(H_2O)]\infty$ chains and *in situ* generated μ_4-oxalates, and organic H_2pda pillars. As shown in Fig. 1a, each Nd(III) ion is surrounded by nine oxygen atoms, in which five oxygen atoms are from three sulfates, two from one oxalate ($C_2O_4^{2-}$), one carboxylate oxygen atom from one H_2pda, and one from a water molecule, forming a NdO_9 polyhedron of distorted mono capped square antiprism. The average Nd–O bond distance of NdO_9 polyhedra is 2.50 Å, comparable with that in a Nd(III) compound coordinated by nine oxygen atoms from two terminal water molecules, three chelating and one monodentate sulfates (2.51 Å) [12g]. The shortest Nd–O separation is 2.34(5) Å, resulting from the Nd1–O2 bond of carboxylate, and the longest is 2.71(6) Å of Nd1–O6 from the sulfate. Other distances of Nd–O(sulfate) vary in the range of 2.48(4)–2.66(4) Å. Also, Nd–O3c and Nd–O4 bonds from oxalate are 2.46(6) and 2.43(6) Å, respectively. The distance of Nd(III) and the coordinated water is 2.46(5) Å.

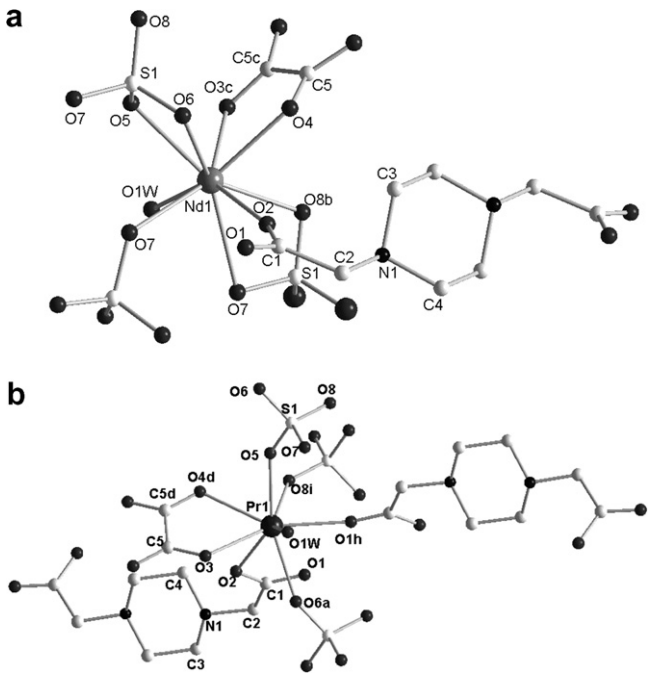

Fig. 1. Local coordination environment of compounds **1** (a) and **3** (b) with 30% thermal ellipsoids. All the hydrogen atoms are omitted for clarity. Symmetry codes for **1**, b: *x*, 1 + *y*, *z*; c: 1 − *x*, *y*, 1/2 −*z*; for **3**, a: *x*, −1 + *y*, *z*; d: 1 − *x*, 2 − *y*,1 − *z*; h: 3/2 − *x*, 3/2 − *y*, 1 − *z*.

The 3D framework can be considered as hybrid organic–inorganic layers pillared by organic H_2pda ligands. The layers consist of inorganic $[Nd(SO_4)(H_2O)]\infty$ chains running along the *b*-axis and μ_4-oxobridged $C_2O_4^{2-}$ derived from the decomposition of carboxylates. Within the chain, Nd(III) ions are arranged zigzag-like, with the shortest intrachain Nd···Nd distance of 4.77 Å, and each pair of Nd ions is bridged by a μ_2-O bridge of one SO_4^{2-} to form a $[Nd_2O]$ triangular unit. These units form the chains by sharing their two apexes (Nd^{3+} ions). Meanwhile, SO_4^{2-} anions are also in a zigzag-like arrangement complementary to the zigzag array of Nd ions, and adopt five-coordinated modes with one μ_2-O and three monodentate oxygen atoms to bridge three Nd(III) ions of an isosceles triangle in the chains (Figs. 2c and 3a). The Nd···Nd distance along the larger bottom edge of these $[Nd_3]$ triangles is 6.35 Å. This chain-like structure is different from those of reported lanthanide sulfates in the literatures [11a,12a,12b,12c,12d]. The adjacent chains are linked *via* μ_4-oxalate to form a 2D hybrid organic–inorganic layer with the shortest interchain Nd···Nd distance 6.29 Å (Fig. 3c). Finally, these 2D layers, parallel to the *ab* plane, are further pillared by organic H_2pda ligands in a bis-monodentate fashion, resulting in an interesting three-dimensional pillared-layer framework, as shown in Fig. 3d. The interlayer distance is *ca.* 8.7 Å. The H_2pda pillars also interact with the adja-

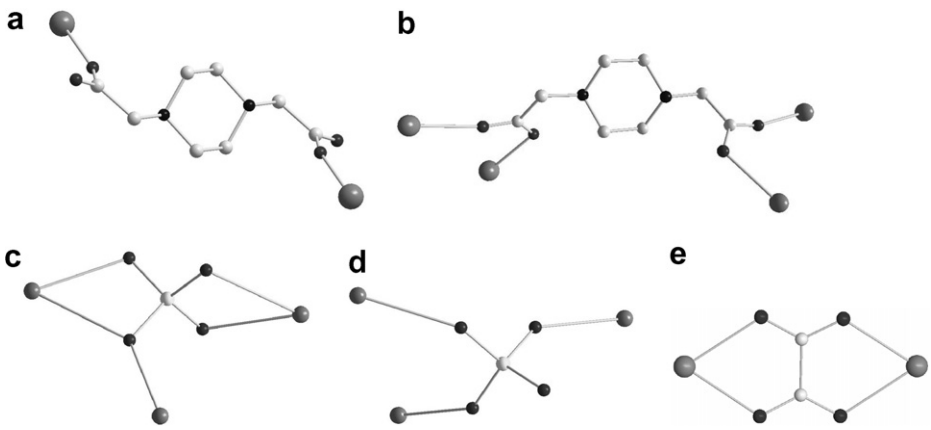

Fig. 2. Coordination modes of H_2pda, SO_4^{2-} and $C_2O_4^{2-}$ anions observed in **1**–**5**.

cent layers *via* O–H···O, N–H···O and C–H···O hydrogen bonds (Table 3), which contributes to the additional stability of the structure. The O–H···O hydrogen bonds originate from the coordinated waters from the layers and the uncoordinated carboxylate oxygens from the adjacent pillars with the O···O distances 2.70(8) and 2.84(7) Å. The N–H···O hydrogen bond comes from the protonated N atom of the pillar and the O atom of SO_4^{2-}, and the N···O distance is 2.96(7) Å. The C–H···O hydrogen bonds involve the piperazine C–H and the oxygen atoms of $C_2O_4^{2-}$, the C···O distances being 2.95(9) and 3.36(8) Å.

3.3. Type II structure of **3**, **4** and **5**

The structure of type II, represented by compound **3**, is different from those of type I, though it can also be described as a three-dimensional framework consisting of hybrid organic–inorganic layers of Pr(III), $C_2O_4^{2-}$ and SO_4^{2-}, and organic H_2pda pillar. First of all, the local coordination environment around a Ln(III) ion is significantly different. As shown in Fig. 1b, each Pr(III) ion is eight-coordinated and exhibits a distorted dodecahedral geometry with three sites occupied by three oxygen atoms of three SO_4^{2-} and two sites by $C_2O_4^{2-}$. The last sites are completed by one water molecule and one carboxylate oxygen atom from a H_2pda ligand. The Pr-O distances range from 2.41(4) to 2.52(4) Å with the average value 2.47 Å, comparable with those in Pr(III) complexes coordinated by eight oxygen atoms (2.46 and 2.49 Å) [25].

Compared with the extended inorganic moieties of type I, the inorganic parts of **3** are different from $[Ln(SO_4)(H_2O)]\infty$ chains along the *b*-axis. In the chains, each pair of Pr(III) ions is bridged by a pair of SO_4^{2-} anions to form an inorganic $[Pr_2(O–S–O)_2]$ eight-membered ring, as shown in Fig. 4a. There are two kinds of eight-membered rings in one chain, one is that the bridges

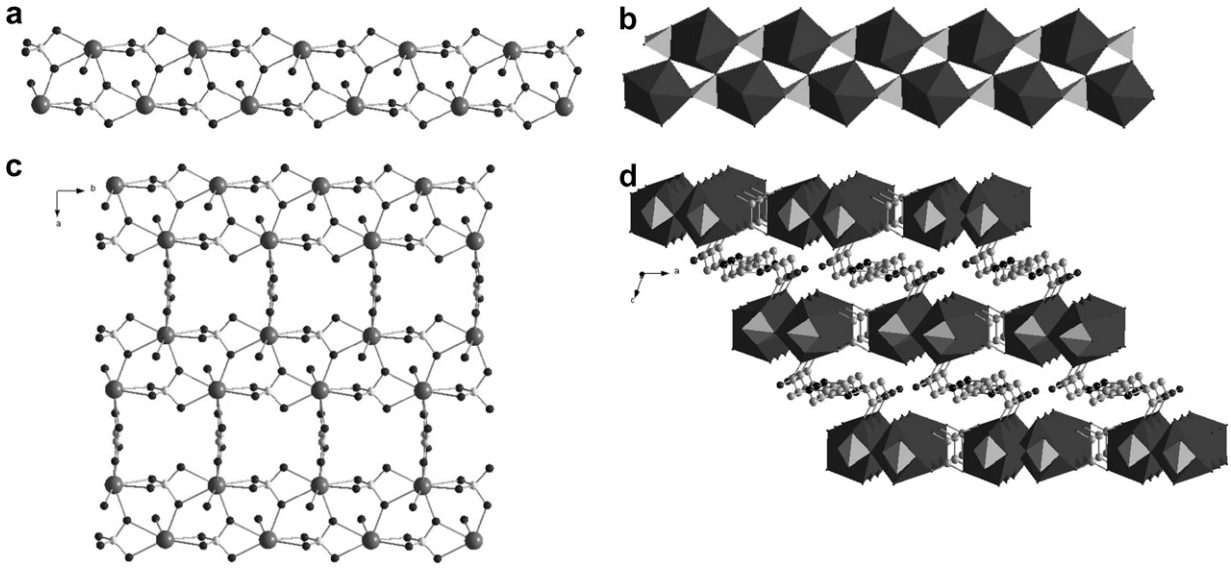

Fig. 3. Structures of 1D inorganic $[Nd(SO_4)(H_2O)]\infty$ chain (a), its polyhedral form (b, grey: SO_4 polyhedra; black: NdO_9 polyhedra), 2D hybrid organic–inorganic layer linked *via* $C_2O_4^{2-}$ anions (c), and 3D framework pillared by H_2pda (d).

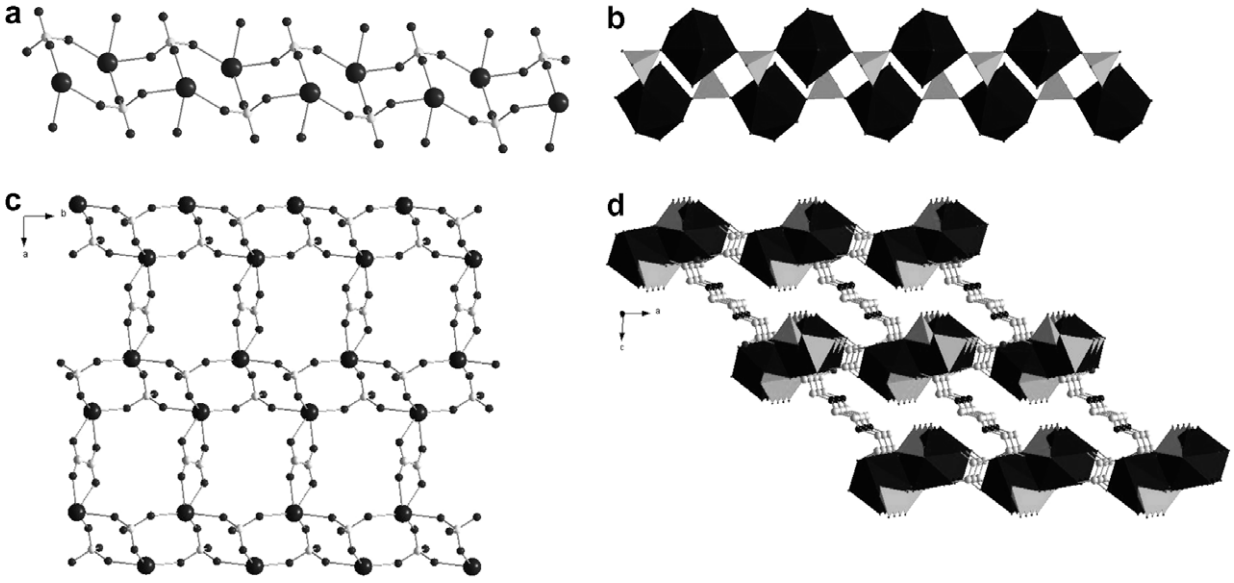

Fig. 4. Structures of 1D $[Pr(SO_4)(H_2O)]\infty$ inorganic chain (a), its polyhedral form (b, grey: SO_4 polyhedra; black: PrO_8 polyhedra), 2D hybrid organic–inorganic layer linked *via* $C_2O_4^{2-}$ anions (c), and the 3D framework pillared by H_2pda (d).

between the Pr ions are only two SO_4^{2-} anions; the other is that the bridges are two *syn–anti* carboxylates, respectively, coming from two H_2pda ligands, apart from two bridging SO_4^{2-} anions. The Pr···Pr distances in the rings are 5.66 and 4.38 Å, respectively. These two inorganic rings are alternately arranged into an inorganic $[Pr(SO_4)(H_2O)]_\infty$ chain by sharing their two apexes (Pr^{3+} ions) with the coordinated H_2O molecules. The Pr(III) ions are arranged as an unequal zigzag-like chain. Moreover, just like **1**, SO_4^{2-} anions are also in a zigzag-like arrangement and each SO_4^{2-} bridges three Ln(III) ions of an isosceles triangle in one chain with a larger Pr···Pr distance 6.81 Å (Fig. 4a). However, the sulfates in **3** adopt η^3,μ_3- tridentate coordination modes, different from those (η^4,μ_3-pentadentate coordination modes) of **1** (Figs. 2d and 4a). Meanwhile, intrachain strong hydrogen bonds are found between the coordinated water molecules and the oxygen atoms of SO_4^{2-} groups [O1w···O7n 2.77(5) and O1w···O7 2.72(5) Å] to stabilize the chain. To the best of our knowledge, such a lanthanide sulfate chain has not been reported so far [14].

The adjacent chains are linked *via* μ_4-oxalate to form a 2D hybrid organic–inorganic layer (Fig. 4c). The shortest interchain Pr···Pr distance is 6.41 Å, which is a little longer than that of **1** (6.29 Å). The 3D structure is generated by the connections of the layers *via* the H_2pda ligands, as shown in Fig. 4d. Each carboxylate of H_2pda links two Pr(III) ions from one chain in a bidentate *syn–anti* mode. Therefore, each organic pillar is connected with four Pr(III) ions from two adjacent layers (Fig. 2b). Meanwhile, each Pr(III) ion is connected by two H_2pda pillars from the above and below the layers, respectively. The 3D structure is sustained by extensive weak C–H···O hydrogen bonds, which originate from the carbon atoms of H_2pda pillars and the oxygen atoms from the SO_4^{2-} [C2···O8h 3.36(6) and C2···O7r 3.28(6) Å] and $C_2O_4^{2-}$ anions [C2···O4k 3.24(6), C3···O3s 3.19(6) and C3···O4d 3.29(6) Å] of the adjacent layers. It is noted that there are "empty" spaces in the 3D network, which are filled with dinuclear water molecules with a distance of 2.82(7) Å. These $(H_2O)_2$ clusters are stabilized in the apertures of this 3D construction by the hydrogen bonds, which involves the oxygen atom from SO_4^{2-} [O2w···O5d 3.00(7) Å] and $C_2O_4^{2-}$ anions [O2w···O3k 3.01(6) and O2w···O4 3.20(6) Å] of the $[Pr(SO_4)(H_2O)(C_2O_4)]$ layers, and the carboxylate oxygen atoms [O2w···O2k 3.18(6) Å] from the bridging H_2pda ligands.

3.4. Thermogravimetric properties

All compounds are air stable and can retain their structural integrity at room temperature for a considerable length of time. The thermogravimetric analyses of powder samples **1** and **3** were carried out from 24 to 780 °C under nitrogen atmosphere at the heating rate of 10 °C min^{-1}, as shown in Fig. 5. For compound **1**, it is stable below 180 °C, which shows that the materials including metal sulfates are rather thermally stable. An initial weight loss of 4.5% occurred between 180 and 220 °C corresponds to the removal of the coordinated water molecules (4.5% calculated). The weight loss of 50% in a range of 220–780 °C indicates the decomposition of the whole structure. The TGA curve of **3** shows a weight loss of 2.1% in the temperature range of 24–213 °C, which is in agreement with the removal of the encapsulated water molecules (4.3% calculated). The second weight loss of 4.1% between 213 and 248 °C corresponds to the removal of two coordinated water molecules per formula unit (4.3% calculated). The decomposition of the whole framework occurs from 248 to 780 °C.

3.5. Magnetic properties

The magnetic susceptibility of **1** has been measured in the temperature range of 1.8–300 K at an applied field of 2000 Oe and the plots of χ_M and $\chi_M T$ versus T are shown in Fig. 6. When the temperature decreases from 300 K, the χ_M value gradually increases from 0.005 cm^3 mol^{-1} to 0.400 cm^3 mol^{-1} at 1.8 K. Meanwhile, the $\chi_M T$ value per Nd(III) ion is 1.45 cm^3 K mol^{-1} at 300 K, which is slightly less than the theoretical value of 1.64 cm^3 K mol^{-1} for magnetically isolated Nd(III) ions, then decreases to 0.72 cm^3 K mol^{-1} at 1.8 K on falling. The variable-temperature magnetic properties of a free rare earth ion generally shows strong deviations from the Curie–Weiss law, and $\chi_M T$ decreases with the cooling temperature owing to the

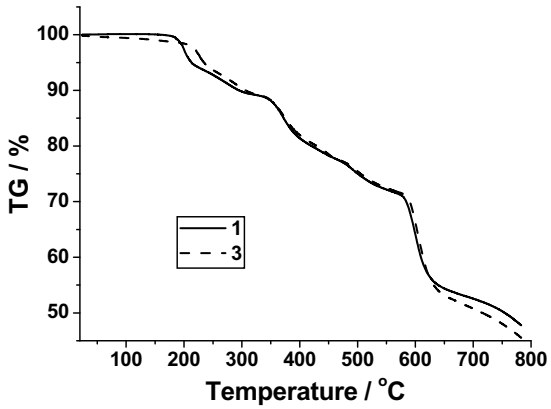

Fig. 5. TG plots for **1** and **3**.

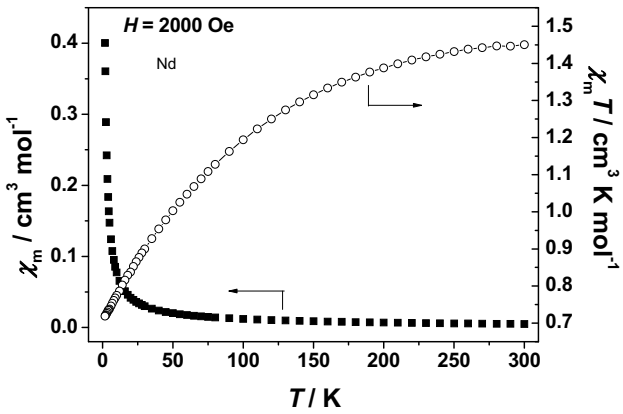

Fig. 6. Temperature dependence of χ_M (■) and $\chi_M T$ (○) for **1**.

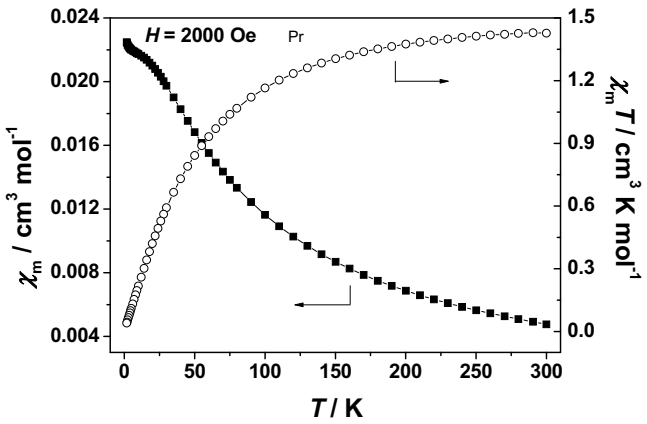

Fig. 7. Temperature dependence of χ_M (■) and $\chi_M T$ (○) for **3**.

depopulation of Stark levels [26]. Therefore, the magnetic behavior of **1** may be ascribed to intramolecular antiferromagnetic coupling between the metal centers and/or the orbital coupling contribution.

Compound **3** shows a similar profile of $\chi_M T$ in the temperature range of 1.8–300 K (Fig. 7). The $\chi_M T$ value (1.43 $cm^3\,K\,mol^{-1}$) per Pr(III) ion at 300 K is somewhat lower than that expected for an isolated Pr(III) ion (1.60 $cm^3\,K\,mol^{-1}$). On cooling, $\chi_M T$ falls to 0.04 $cm^3\,K\,mol^{-1}$ at 1.8 K, and the χ_M (0.005 $cm^3\,mol^{-1}$ at 300 K) exhibits an increase to 0.022 $cm^3\,mol^{-1}$ at 1.8 K. This may also be attributed to the depopulation of Stark levels and/or intramolecular antiferromagnetic coupling between the metal centers.

4. Conclusion

Among the two series of complexes $[Ln_2(H_2pda)(C_2O_4)(SO_4)_2(H_2O)_2]_n$ [I, Ln = Nd (**1**), Y (**2**)] and $\{[Ln_2(H_2pda)(C_2O_4)(SO_4)_2(H_2O)_2]\cdot 2H_2O\}_n$ [II, Ln = Pr (**3**), Ce (**4**) and Eu (**5**)] prepared by the solvothermal reactions of H_2pda, lanthanide oxides and H_2SO_4 under similar conditions, the structures are all based on organic H_2pda pillars and two-dimensional hybrid organic–inorganic layers, which come from different $[Ln(SO_4)(H_2O)]\infty$ chains and *in situ* generated μ_4-oxalates. Corresponding to the different coordination polyhedra of different lanthanide(III) ions, sulfate anions adopt different coordination modes in the chains, which results in the difference of inorganic $[Ln(SO_4)(H_2O)]\infty$ chains. This work demonstrates that use of lanthanide(III) sulfate chains and flexible spacer pillars can generate interesting hybrid organic–inorganic framework solids.

5. Supplementary data

CCDC 675193, 675194, 675195, 675196, 675197 contain the supplementary crystallographic data for compounds **1**, **2**, **3**, **4** and *5*. These data can be obtained free of charge via http://www.ccdc.cam.ac.uk/conts/retrieving.html, or from the Cambridge Crystallographic Data Centre, 12 Union Road, Cambridge CB2 1EZ, UK; fax: (+44) 1223-336-033; or e-mail: deposit@ccdc.cam.ac.uk.

Acknowledgement

This work was supported by the National Natural Science Foundation of China (No. 20271026).

References

[1] (a) G.R. Desiraju, Crystal Engineering: The Design of Organic Solids, Elsevier, Amsterdam, 1989;
(b) W. Jones, Organic Molecular Solids: Properties and Applications, CRC Press, New York, 1997;
(c) A.D. Bond, W. Jones, in: W. Jones, C. Rao (Eds.), Supramolecular Organization and Materials Design, Cambridge University Press, Cambridge, 2002. references therein.
[2] (a) M.J. Zaworotko, B. Moulton, Chem. Rev. 101 (2001) 1629;
(b) O.R. Evans, W.B. Lin, Acc. Chem. Rev. 35 (2002) 511;
(c) N.W. Ockwig, O. Delgado-friedrichs, M. O'keeffe, O.M. Yaghi, Acc. Chem. Res. 38 (2005) 176;
(d) J.P. Zhang, X.M. Chen, Chem. Commun. (2006) 1689. and references therein..
[3] (a) G.B. Garder, D. Venkataraman, J.S. Moore, S. Lee, Nature 374 (1995) 792;
(b) J.S. Seo, D. Whang, H. Lee, S.I. Jun, J. Oh, Y.J. Jeon, K. Kim, Nature 404 (2000) 982;
(c) M.E. Davis, Nature 417 (2002) 813;
(d) M. Eddaoudi, J. Kim, N. Rosi, D. Vodak, J. Wachter, M. O'Keeffe, O.M. Yaghi, Science 295 (2002) 469;
(e) R. Kitaura, S. Kitagawa, Y. Kubtoa, T.C. Kobayashi, K. Kindo, Y. Mita, A. Matsuo, M. Kobayashi, H.C. Chang, T.C. Ozawa, M. Suzuki, M. Sakata, M. Takata, Science 298 (2002) 2358;
(f) K. Yamamoto, Y. Sakata, Y. Nohara, Y. Takahashi, T. Tatsumi, Science 300 (2003) 470.
[4] (a) S.R. Batten, R. Robson, Angew. Chem., Int. Ed. 39 (1998) 1461;
(b) P.J. Hagrman, D. Hagrman, J. Zubieta, Angew. Chem., Int. Ed. 38 (1999) 2638;
(c) S. Batten, R. Robson, Angew. Chem., Int. Ed. 37 (1998) 1460;
(d) M. Fujita, Y.J. Kwon, S. Washizu, K. Ogura, J. Am. Chem. Soc. 116 (1994) 1151;
(e) O.R. Evans, H.L. Ngo, W.B. Lin, J. Am. Chem. Soc. 123 (2001) 10395;
(f) C.Y. Su, A.M. Goforth, M.D. Smith, P.J. Pellechia, H.C. Zur Loye, J. Am. Chem. Soc. 126 (2004) 3576;
(g) J. Dutour, G. Férey, Angew. Chem., Int. Ed. 43 (2004) 6290.
[5] (a) For examples, S. Fernandez, J.L. Mesa, J.L. Pizarro, L. Lezama, M.I. Arriortua, T. Rojo, Angew. Chem., Int. Ed. 41 (2002) 3683;
(b) J.A. Rodgers, W.T.A. Harrison, Chem. Commun. (2000) 2385;
(c) W.T.A. Harrison, M.L.F. Phillips, J. Stanchfield, T.M. Nenoff, Inorg. Chem. 40 (2001) 895;
(d) C. Qin, L. Xu, Y.G. Wei, X.L. Wang, F.Y. Li, Inorg. Chem. 42 (2003) 3107;
(e) G. Alberti, M. Bartocci, M. Santarelli, R. Vivani, Inorg. Chem. 36 (1997) 3574.
[6] L.H. Bi, U. Kortz, B. Keita, L. Nadjo, Dalton Trans. (2004) 3184.
[7] (a) E. Burkholder, S. Wright, V. Golub, C.J. O'Connor, J. Zubieta, Inorg. Chem. 42 (2003) 7460;
(b) S.T. Zheng, J. Zhang, G.Y. Yang, Solid State Sci. 7 (2005) 149;
(c) S. Drueke, K. Wieghardt, B. Nuber, J. Weiss, H.P. Fleischhauer, S. Gehring, W. Haase, J. Am. Chem. Soc. 111 (1989) 8622;
(d) R.P. Doyle, P.E. Kruger, M. Julve, F. Lloret, M. Nieuwenhuyzen, CrystEngComm 4 (2002) 13;
(e) L.H. Huang, H.M. Kao, K.H. Lii, Inorg. Chem. 41 (2002) 2936.
[8] (a) D. Udayakumar, M. Dan, C.N.R. Rao, Eur. J. Inorg. Chem. (2004) 1733;
(b) J.N. Behera, A.A. Ayi, C.N.R. Rao, Chem.Commun. (2004) 968;
(c) Y.N. Mikhailov, Y.E. Gorbunova, O.V. Shishkina, L.B. Serezhkina, V.N. Serezhkin, Russ. J. Inorg. Chem. 44 (1999) 1448;
(d) E.A. Demchenko, E.V. Mit'kovskaya, Y.N. Mikhailov, Y.E. Gorbunova, L.B. Serezhkina, V.N. Serezhkin, Russ. J. Inorg. Chem. 47 (2002) 1826.
[9] (a) For examples, L. Carlucci, G. Ciani, M. Moret, D.M. Proserpio, S. Rizzato, Angew.Chem., Int. Ed. 39 (2000) 1506;
(b) M.L. Tong, X.M. Chen, CrystEngComm 2 (2000) 1;
(c) J. Fan, B. Sui, T. Okamura, W.Y. Sun, W.X. Tang, N. Ueyama, Dalton Trans. (2002) 3868;
(d) J.H. Luo, M.C. Hong, R.H. Wang, D.Q. Yuan, R. Cao, L. Han, Y.Q. Xu, Z.Z. Lin, Eur. J. Inorg. Chem. (2003) 3623;
(e) M. Du, Y.M. Guo, S.T. Chen, X.H. Bu, S.R. Batten, J. Ribas, S. Kitagawa, Inorg.Chem. 43 (2004) 1287;
(f) B. Ding, L. Yi, Y. Wang, P. Cheng, D.Z. Liao, S.P. Yan, Z.H. Jiang, H.B. Song, H.G. Wang, Dalton Trans. (2006) 665.
[10] Y.P. Yuan, R.Y. Wang, D.Y. Kong, J.G. Mao, A. Clearfirld, J. Solid State Chem. 178 (2005) 2030.
[11] (a) M.S. Khiyalov, I.R. Amiraslanov, F.N. Musaev, K.S. Mamedov, Russ. J. Struct. Chem. 23 (1982) 119;
(b) Y.P. Yuan, J.L. Song, J.G. Mao, Inorg. Chem. Commun. 7 (2004) 24;
(c) H. Akkari, P. Benard-Rocherulle, H. Merazig, T. Roisnel, J. Rocherulle, Solid State Sci. 8 (2006) 704.
[12] (a) C. Baux, C. Daiguebonne, O. Guillou, K. Boubekeur, R. Carlier, L. Sorace, A. Caneschi, J. Alloys Comp. 344 (2002) 114;
(b) Y. Xing, Y.L. Liu, Z. Shi, H. Meng, W.Q. Pang, J. Solid State Chem. 174 (2003) 381;
(c) A.B. Ilyukhin, S.P. Petrosyants, Russ. J. Inorg. Chem. 49 (2004) 1338;
(d) S.P. Petrosyants, A.B. Ilyukhin, A.Y. Sukhorukov, Russ. Coord. Chem. 31 (2005) 576;
(e) T. Bataille, D. Louer, J. Mater. Chem. 12 (2002) 3487;
(f) Y. Xing, Z. Shi, G.H. Li, W.Q. Pang, Dalton Trans. (2003) 940;
(g) M. Dan, J.N. Behera, C.N.R. Rao, J. Mater. Chem. 14 (2004) 1257;
(h) T. Bataille, D. Louer, J. Solid State Chem. 177 (2004) 1235;
(i) Y.P. Yuan, R.Y. Wang, D.Y. Kong, J.G. Mao, A. Clearfield, J. Solid State Chem. 178 (2005) 2030.
[13] Z. He, E.Q. Gao, Z.M. Wang, C.H. Yan, M. Kurmoo, Inorg. Chem. 44 (2005) 862.
[14] Cambridge structural database, CCDC, Cambridge, Version 5.28 updates (Aug 2007).
[15] (a) B. Chiari, O. Piovesana, T. Tarantelli, P.F. Zanazzi, Inorg. Chem. 23 (1984) 3398;
(b) M. Bera, J. Ribas, W.T. Wong, D. Ray, Inorg. Chem. Commun. 7 (2004) 1242;
(c) S. Mukhopadhyay, D. Mandal, P.B. Chatterjee, C. Desplanches, J.P. Sutter, R.J. Butcher, M. Chaudhury, Inorg. Chem. 43 (2004) 8501;
(d) K.E. Vostrikova, E. Belorizky, J. Pecaut, P. Rey, Eur. J. Inorg. Chem. 1181 (1999);
(e) O.P. Mel'nik, M.G. Mys'kiv, V.N. Davydov, Russ. Coord. Chem. 29 (2003) 363;
(f) O. Schlager, K. Wieghardt, A. Rufinska, B. Nuber, Dalton Trans. (1996) 1659.
[16] (a) D.F. Sun, R. Cao, Y.C. Liang, M.C. Hong, Chem. Lett. (2002) 198;
(b) D.F. Sun, R. Cao, W.H. Bi, X.J. Li, Y.Q. Wang, M.C. Hong, Eur. J. Inorg. Chem. (2003) 38;
(c) D.F. Sun, R. Cao, W.H. Bi, X.J. Li, Y.Q. Wang, M.C. Hong, Eur. J. Inorg. Chem. (2004) 2144;
(d) J.A. Groves, P.A. Wright, P. Lightfoot, Inorg. Chem. 44 (2005) 1736;
(e) J.A. Groves, P.A. Wright, P. Lightfoot, Dalton Trans. (2005) 2007;
(f) J.A. Groves, N.F. Stephens, P.A. Wright, P. Lightfoot, Solid State Sci. 8 (2006) 397.
[17] (a) N. Choi, I. Khan, R.W. Matthews, M. McPartlin, B.P. Murphy, Polyhedron 13 (1994) 847;
(b) J.L. Song, J.G. Mao, Y.Q. Sun, A. Clearfield, Eur. J. Inorg. Chem. (2003) 4218;

(c) J.L. Song, J.G. Mao, J. Solid State Chem. 178 (2005) 3514;
(d) Z.Y. Du, S.M. Ying, J.G. Mao, J. Mol. Struct. 788 (2006) 218;
(e) Y. Wang, S.S. Bao, W. Xu, J.S. Chen, S. Gao, L.M. Zheng, J. Solid State Chem. 177 (2004) 1297.
[18] (a) R. Frohlich, M. Nieger, K. Rissanen, Polyhedron 18 (1999) 2265;
(b) D. Pocic, J.M. Planeix, N. Kyritsakas, A. Jouaiti, M.W. Hosseini, CrystEngComm 7 (2005) 624.
[19] (a) Y.Y. Niu, H.W. Hou, Y.L. Wei, Y.T. Fan, Y. Zhu, C.X. Du, X.Q. Xin, Inorg. Chem. Commun. 4 (2001) 358;
(b) H.W. Hou, Y.L. Song, Y.L. Wei, Y.T. Fan, Y. Zhu, L.K. Li, C.X. Du, Macromolecules 36 (2003) 999;
(c) H. Xu, Y.L. Song, H.W. Hou, Inorg. Chim. Acta 357 (2004) 3541;
(d) H. Xu, Y.L. Song, L.W. Mi, H.W. Hou, M.S. Tang, Y.L. Sang, Y.T. Fan, Y. Pan, Dalton Trans. (2006) 838.
[20] (a) For examples, Y.J. Kim, D.Y. Jung, Chem. Commun. (2002) 908;
(b) W.H. Bi, R. Cao, D.F. Sun, D.Q. Yuan, X. Li, Y.Q. Wang, X.J. Li, M.C. Hong, Chem. Commun. (2004) 2104;
(c) B.L. Chen, F.R. Fronczek, B.H. Courtney, F. Zapata, Crystal Growth Des. 6 (2006) 825;
(d) M. Kurmoo, H. Kumagai, M. Akita-Tanaka, K. Inoue, S. Takagi, Inorg. Chem. 45 (2006) 1627;
(e) J.X. Chen, M. Ohba, D.Y. Zhao, W. Kaneko, S. Kitagawa, Crystal Growth Des. 6 (2006) 664;
(f) Y.J. Qi, Y.H. Wang, C.W. Hu, M.H. Cao, L. Mao, E.B. Wang, Inorg. Chem. 42 (2003) 8519.
[21] I. Tímea, L. István, Synthesis 20 (2005) 3555.
[22] Sheldrick, G.M. SADABS 2.05, University of Göttingen, 2002.
[23] SHELXTL 6.10, Bruker Analytical Instrumentation, Madison, WI, USA, 2000.
[24] (a) X.J. Gu, D.F. Xue, Crystal Growth Des. 7 (2007) 1726;
(b) J.Y. Lu, J. Macias, J. Lu, J.E. Cmaidalka, Crystal Growth Des. 2 (2002) 485.
[25] (a) H. Zhang, L.Y. Duan, Y. Lan, E.B. Wang, C.W. Hu, Inorg. Chem. 4 (2003) 8053;
(b) A. Thirumurugan, S. Natarajan, Eur. J. Inorg. Chem. (2004) 762.
[26] O. Kahn, Molecular Magnetism, VCH: Weinheim, Germany, 1993.

Polyhedron 27 (2008) 2127–2130

Contents lists available at ScienceDirect

Polyhedron

journal homepage: www.elsevier.com/locate/poly

Synthesis and characterization of novel tantalum(V) complexes containing oxazoline and DMA ligation

Sajjad Mohebbi [a,*], Abdeljalil Assoud [b]

[a] Department of Chemistry, University of Kurdistan, P.O. Box 416, Sanandaj, Iran
[b] Department of Chemistry, University of Waterloo, Waterloo, Ontario, Canada

ARTICLE INFO

Article history:
Received 25 March 2008
Accepted 4 April 2008
Available online 17 May 2008

Keywords:
Tantalum(V) complexes
Oxazoline
Chelating-diamide ligand

ABSTRACT

Two six coordinate tantalum(V) oxazoline complexes, $[Ta(OX)(NMe_2)_4]$ (**1**) and $[Ta(OX)_2(NMe_2)_3]$ (**2**), formed by the reaction of $[Ta(NMe_2)_5]$ with the chelating di-nitrogen ligand 4,4-dimethyl-2-pyrrole-2-oxazoline in 1:1, 1:2 and/or 1:3 molar ratios have been investigated. The structural study of **1** and **2** by X-ray crystallography shows that they both adopt geometries best described as distorted octahedral with N–Ta–N angles of 172.6(3)° and 169.4(2)°, respectively. The nitrogen atoms of the oxazoline are bound directly to the tantalum, leading to a five-membered metallacycle in the basal plane. The N–Ta–N and Ta–N–C angles of the basal five-membered oxazoline ring are 71° and 113–117°, respectively.

© 2008 Elsevier Ltd. All rights reserved.

1. Introduction

Metal–organic complexes of early transition metals bearing nitrogen containing ligands have received increasing attention over the last couple of years [1–3]. Significant attention has been focused on metal complexes supported by cyclopentadienyl-based ligand sets [4,5], but there is also growing interest in the use of complexes with dialkoxide [6,7] or diamide ligands [8–16]. Interest in studying chelating-diamide supported Group 4 complexes is due to their easily preparation together with the fact their the steric and electronic properties can be tuned by varying the nitrogen substituents. d^0 Group 4 metal complexes (Ti, Zr, Hf) of diamide ligands show good catalytic activity for the polymerization of α-olefins [9–23]. In response to the growing interest in alternatives to classical metallocene-based catalysts, we have become interested in examining the chemistry of a relatively unexplored class of mixed amido ligands (Scheme 1).

Typically, the synthesis of these compounds is one-step process involving the reaction between $Ta(NMe_2)_5$ and oxazoline. In this paper, we describe the first six coordinate tantalum(V) complexes to contain two types of oxazoline binding by the reactions of $Ta(NMe_2)_5$ with 4,4-dimethyl-2-pyrrole-2-oxazoline (OX) in 1:1, 1:2 and 1:3 molar ratios. The molecular structure of $[Ta(OX)(NMe_2)_4]$ (**1**) and $[Ta(OX)_2(NMe_2)_3]$ (**2**) are also reported.

2. Experimental

2.1. Materials and methods

All experimental procedures were conducted under an inert atmosphere, either in a N_2 filled dry box or by using standard Schlenk techniques. Diethyl ether was distilled from sodium benzophenone ketyl; toluene, hexanes and pentane were distilled from sodium; dichloromethane was distilled from CaH_2. The distilled solvents were stored under an argon atmosphere and over 4 Å molecular sieves. All NMR solvents were degassed and stored over 4 Å molecular sieves in a N_2 filled drybox. $Ta(NMe_2)_5$ was synthesized according to the improved procedure for the preparation of homoleptic metal amide complexes reported by Jordan et al. [24]. The 4,4-dimethyl-2-pyrrole-2-oxazoline was synthesized according to previously published procedures [25,26].

^{1}H NMR spectra were measured on a Varian Gemini 200 spectrometer using sealed NMR tubes. The chemical shifts are reported in parts per million (ppm) downfield from tetramethyl-silane and referenced to residual proton peaks of the NMR solvents. Electronic Ionization Mass spectra were recorded using a Varian MAT spectrometer. *m*/*z* values were referenced to ^{35}Cl, ^{90}Zr, ^{180}Hf and ^{181}Ta. Elemental analysis was performed by a 2400 Analyzer, series II CHN/O Perkin-Elmer. X-ray diffraction data were collected using a Bruker Ax SMART 1K CCD and refined with the SHELXL and SHELXS program suite.

2.2. Synthesis of $[Ta(OX)(NMe_2)_4]$ (**1**)

To a toluene solution of $Ta(NMe_2)_5$ (0.55 g, 1.37 mmol) at room temperature (r.t.) was added a toluene solution of 4,4-dimethyl-2-pyrrole-2-oxazoline (0.2255 g, 1.37 mmol). A change of color to

* Corresponding author. Tel.: +98 871 6622127; fax: +98 871 6660075.
E-mail address: smohebbi@uok.ac.ir (S. Mohebbi).

0277-5387/$ - see front matter © 2008 Elsevier Ltd. All rights reserved.
doi:10.1016/j.poly.2008.04.004

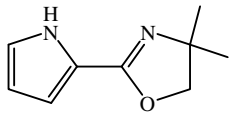

Scheme 1. 4,4-Dimethyl-2-pyrrole-2-oxazoline.

dirty yellow was observed. The mixture was stirred for 48 h at r.t. (connected to an oil bubbler to release the $HNMe_2$ produced during the reaction). After removal of the reaction solvent under reduced pressure and leaving for one week at −37 °C, bright red crystals were formed which were suitable for single-crystal X-ray diffraction. The crystals were washed with several portions of hexane to yield 0.395 g (76%) of $[Ta(OX)(NMe_2)_4]$ (**1**). Elemental analysis Calc. for $C_{17}H_{35}N_6OTa$: C, 39.23; H, 6.78; N, 16.15. Found: C, 39.28; H, 6.64; N, 16.02%. Mass Spec. Calc.: 520.2352 *m*/*e*, Found: (FAB) 639.2352 *m*/*e*.

2.3. Synthesis of $[Ta(OX)_2(NMe_2)_3]$ (**2**)

To a toluene solution of $Ta(NMe_2)_5$ (0.55 g, 1.37 mmol) at room temperature (r.t.) was added a toluene solution of 4,4-dimethyl-2-pyrrole-2-oxazoline (0.451 g, 2.74 mmol or 0.676 g, 4.11 mmol). The solution color slowly changed to yellow. The mixture was allowed to stir for 48 h at r.t. (connected to an oil bubbler to release the $HNMe_2$ produced during the reaction). After removal of the reaction solvent under reduced pressure and leaving for one week at −37 °C, bright red crystals were obtained, which were washed with several portions of hexane to yield 0.454 g (71%) of $[Ta(OX)_2(NMe_2)_3]$ (**2**). Elemental analysis Calc. for $C_{24}H_{40}N_7O_2Ta$: C, 45.07; H, 6.30; N, 15.33. Found: C, 45.20; H, 6.23; N, 15.44%. Mass Spec. Calc.: 639.2723 *m*/*e*, found: (FAB) 639.2723 *m*/*e*.

Table 1
Crystal data and structure refinement for $[Ta(OX)(NMe_2)_4]$ (**1**) and $[Ta(OX)_2(NMe_2)_3]$ (**2**)

Formula	$Ta(OX)_2(NMe_2)_3$	$Ta(OX)(NMe_2)_4$
Formula weight	639.58	520.46
Temperature (K)	203(2)	203(2)
Wavelength (Å)	0.71073	0.71073
Crystal system, space group	monoclinic, *P*2(1)/*c*	monoclinic, *P*2(1)/*c*
Unit cell dimensions		
a (Å)	13.5317(15)	16.9179(17)
b (Å)	12.8163(14)	8.7308(9)
c (Å)	15.7159(17)	16.4338(17)
α (°)	90	90
β (°)	91.222(2)	116.0190(10)
γ (°)	90	90
Volume (Å^3)	2724.9(5)	2181.4(4)
Z, D_{calc} (Mg/m^3)	4, 1.559	4, 1.585
Absorption coefficient (mm^{-1})	4.067	5.055
F(000)	1288	1040
Crystal size (mm)	0.10 × 0.5 × 0.2	0.1 × 0.1 × 0.1
θ Range for data collection (°)	1.51–28.58	1.34–28.85
Limiting indices	$-17 \leqslant h \leqslant 18$, $0 \leqslant k \leqslant 16$, $0 \leqslant l \leqslant 21$	$-22 \leqslant h \leqslant 19$, $0 \leqslant k \leqslant 11$, $0 \leqslant l \leqslant 22$
Reflections collected/unique [R_{int}]	19241/6002 [0.0484]	38892/5261 [0.0749]
Completeness to θ (%) = 28.58	86.20	92.10
Absorption correction	semi-empirical from equivalents	
Maximum and minimum transmission	1.000000 and 0.621616	1.000000 and 0.748945
Refinement method	full-matrix least-squares on F^2	
Data/restraints/parameters	6002/0/307	5261/0/226
Goodness-of-fit on F^2[a]	1.08	1.027
Final *R* indices [$I > 2\sigma(I)$]	$R_1 = 0.0516$, $wR_2 = 0.1403$	$R_1 = 0.0460$, $wR_2 = 0.0819$
R indices (all data)	$R_1 = 0.0625$, $wR_2 = 0.1488$	$R_1 = 0.0877$, $wR_2 = 0.0934$
Largest difference in peak and hole (e Å^{-3})	1.828 and −2.028	1.549 and −1.435

[a] GOF $= /[\sum w(|F_o| - /|F_c|)^2/(n - /p)]^{1/2}$; *n*, number of independent reflections; *p*, number of parameters.

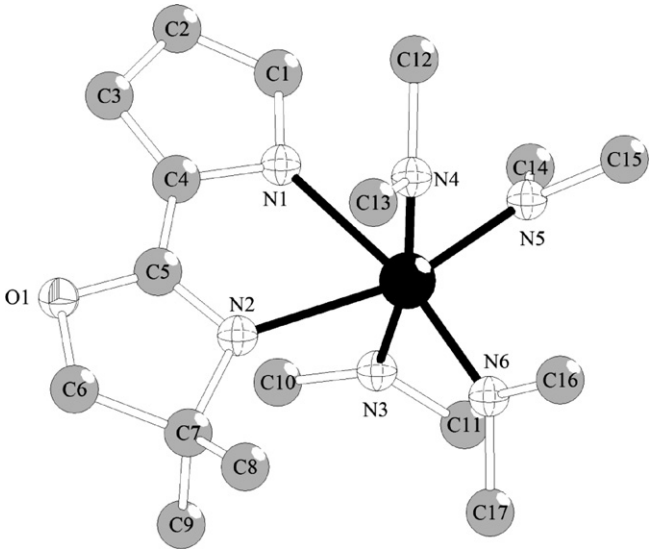

Fig. 1. Molecular structure of $[Ta(OX)(NMe_2)_4]$ (**1**) (H-atoms omitted for clarity) with selected bond distances (Å) and angles (deg); Ta–N(1) 2.272(6), Ta–N(2) 2.350(5), Ta–N(3) 2.033(6), Ta–N(4) 2.037(6), Ta–N(5) 2.002(6), Ta–N(6) 2.009(6), N(5)–Ta–N(6) 102.1(2), N(5)–Ta–N(3) 92.4(2), N(6)–Ta–N(3) 96.0(2), N(5)–Ta–N(4) 91.1(2), N(6)–Ta–N(4) 93.1(2), N(3)–Ta–N(4) 169.4(2), N(5)–Ta–N(1) 91.9(2), N(6)–Ta–N(1) 165.8(2), N(3)–Ta–N(1) 85.9(2), N(4)–Ta–N(1) 83.9(2), N(5)–Ta–N(2) 163.5(2), N(6)–Ta–N(2) 94.4(2), N(3)–Ta–N(2) 87.2(2), N(4)–Ta–N(2) 86.5(2), N(1)–Ta–N(2) 71.6(2).

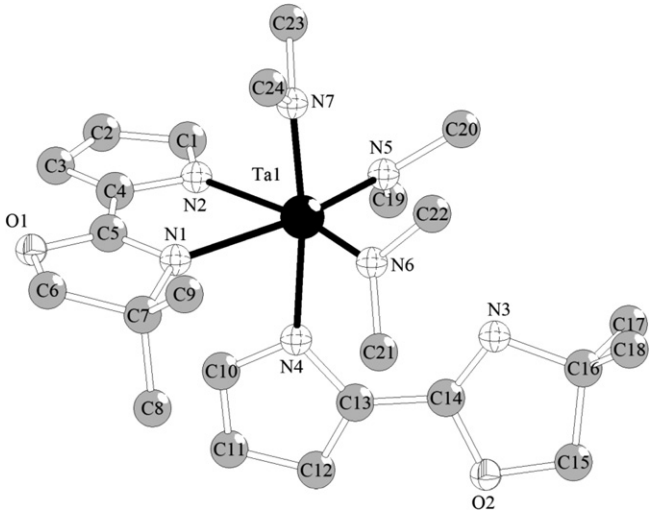

Fig. 2. Molecular structure of $[Ta(OX)_2(NMe_2)_3]$ (**2**) (H-atoms omitted for clarity) with selected bond distances (Å) and angles (deg); Ta–N(2) 2.251(6), Ta–N(1) 2.344(7), Ta–N(4) 2.249(6), Ta–N(5) 2.007(6), Ta–N(6) 2.005(6), Ta–N(7) 1.978(7), N(7)–Ta–N(6) 104.7(3), N(7)–Ta–N(5) 93.0(3), N(6)–Ta–N(5) 91.4(3), N(7)–Ta–N(4) 91.2(2), N(6)–Ta–N(4) 93.4(2), N(5)–Ta–N(4) 172.6(3), N(7)–Ta–N(2) 89.8(3), N(6)–Ta–N(2) 165.5(3), N(5)–Ta–N(2) 87.3(2), N(4)–Ta–N(2) 86.6(2), N(7)–Ta–N(1) 161.2(3), N(6)–Ta–N(1) 93.9(3), N(5)–Ta–N(1) 89.3(3), N(4)–Ta–N(1) 84.8(2), N(2)–Ta–N(1) 71.7(2).

2.4. X-ray crystal structure analysis

Single-crystal diffraction experiments were carried out at 203 K on a Bruker-AXS-SMART (CCD 1000) diffractometer with

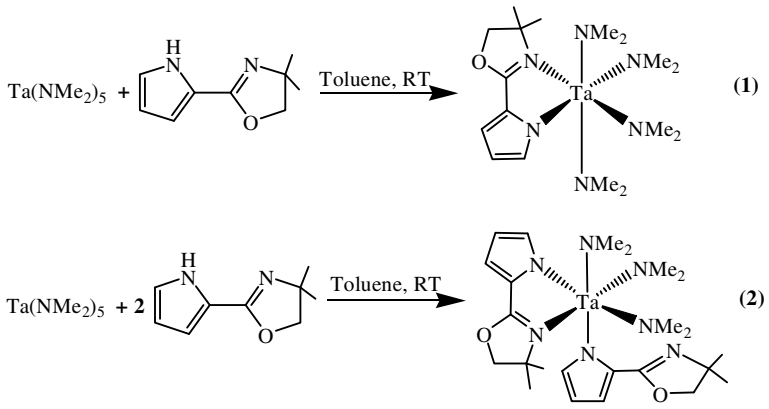

Scheme 2. Synthesis reaction map of **1** and **2**.

monochromated Mo Kα radiation (0.71073 Å). The structures were solved by direct methods and refined anisotropically with the SHELXL-97 program suite [27,28]. The crystals were mounted on capillary using inert oil and transferred immediately to the cold gas stream (203 K) of the diffractometer. Crystallographic data is presented in Table 1. The molecular structures of **1** and **2** in the solid state are shown in Figs. 1 and 2.

3. Results and discussion

Herein, we describe the synthesis and structural characterization of tetrakis(dimethylamido)(4,4-dimethyl-2-pyrrole-2-oxazoline)tantalum(V) and tris(dimethylamido)bis(4,4-dimethyl-2-pyrrole-2-oxazoline)tantalum(V). The later compound contains one anchoring oxazoline ligand and is the first complex to contain two types of oxazoline binding. The reaction of $[Ta(NMe_2)_5]$ with the chelating di-nitrogen ligand 4,4-dimethyl-2-pyrrole-2-oxazoline*(OX)* in 1:1, 1:2 and/or 1:3 molar ratios yielded the tantalum(V) oxazoline complexes $[Ta(OX)(NMe_2)_4]$ (**1**) and $[Ta(OX)_2(NMe_2)_3]$ (**2**) in high yield (71% and 76%) (Scheme 2). Their structures have been characterized by X-ray crystallography. In the 1:2 and 1:3 ratio cases, only displacement of 2 equiv. of dimethylamine occurs, yielding (**2**) while in the case of the 1:1 reaction, displacement of 1 equiv. of dimethylamine occurs, yielding $[Ta(OX)(NMe_2)_4]$ (**1**). In fact treatment of pentakis(dimethylamido)tantalum with more than 2 equiv. of 4,4-dimethyl-2-pyrrole-2-oxazoline did not lead to substitution of more dimethylamido groups, and only **2** was isolated. Similar results have reported by Darrin S. Richeson with a symmetrical chelating bidentate guanidinate anion to give $[CyNC(NMe_2)NCy]Ta(NMe_2)_4$ [29] or Charles H. Winter with the 3,5-di-*tert*-butylpyrazolato ligand to give tris(dimethylamido)bis(3,5-di-*tert*-butylpyrazolato) tantalum(V) [30]. But multiple insertion products have been observed in the analogous reactions of Me_xTaCl_{5-x}; ($x = 1,2,3$) with carbodiimides RNCNR; (R = isopropyl, cyclohexyl, *p*-tolyl) to give acetamidinate complexes $MCl_4[RN–C(Me)=NR]$, $MeMCl_3[RN–C(Me)=NR]$ and $MCl_3[RN–C(Me)=NR]_2$; M = Ta, Nb [31–33].

These observations and also the Soft Chemistry Approach [34] revealed both steric and electronic factors play a central role in determining the overall structure. In the most fascinating observation, the size and number of ligands are definitely more important than their chemical nature [34]. Another possibility for the decreased reactivity of **2** towards further insertion may arise from the increased π-donating ability of the amido group and the consequent reduction in the acidity of the Ta center. In compound **2**, the values for the Ta–NMe_2 distances are short enough to establishment this π-interaction [35] (Ta–N(5), Ta–N(6) and Ta–N(7) are 2.007, 2.005 and 1.978 Å, respectively) and the orientation of the amido groups is consistent with d–p interactions between the nitrogen p orbitals and metal d_{xy}, d_{xz}, d_{yz} orbitals of the distorted octahedral geometry.

The room temperature ^1H NMR spectrum of **1** displays two singlets at 3.10 and 3.38 ppm in a 2:2 ratio, that are assigned to the NMe_2 groups. Also two singlets at 3.14 and 3.49 ppm (1:2 integration ratio) were observed for **2**, corresponding to the NMe_2 groups, whilst three equal intensity resonances were expected. The observed equivalency of the equatorial NMe_2 groups, even at −30 °C, may imply the presence of a fast exchange process which equilibrates the NMe_2 groups on the NMR timescale.

The X-ray diffraction studies of **1** and **2** show that octahedral coordination geometries are found in the solid state with N–Ta–N angles of 172.6° and 169.4°, respectively. Molecular drawings of **1** and **2** and their selected bond lengths and angles are presented in Figs. 1 and 2. The nitrogen atoms of the oxazoline are bound directly to the tantalum center, leading to a five-membered metallacycle in the basal plan. The compound $[Ta(OX)_2(NMe_2)_3]$ (**2**) adopts a distorted octahedral geometry about the tantalum center with one bidentate oxazoline ligand occupying two equatorial sites and another oxazoline ligand anchored by an amido N-bond in an axial position. The dimethylamido ligands occupy two equatorial and one axial site. The bite angle of the ligand (N(1)–Ta–N(2): 71.68°) is smaller than that observed for other bidentate amido complexes reported in the literature, due to the five-membered chelate ring, but is bigger than that reported by D.S. Richeson for the four-membered carbodiimide-Ta chelate ring in $Ta(NMe_2)_4$-$[CyNC(NMe_2)NCy]$ (58.66°) [29].

This is an extremely tight bite angle and the tightest observed in compounds of this nature [36,37]. Related complexes display similar tight chelate angles. The reason for such a tight bite angle is unclear but it would appear to be attributable to the need for some sort of adjustment in the chelate ring shape to allow for the size of the tantalum and the high coordination number of 6 that is achieved. The Ta–N(1)–C(5) and Ta–N(2)–C(4) angles of the basal five-membered oxazoline ring are 113° and 117°, respectively. The Ta–N(1) and Ta–N(2) bond lengths of the oxazoline ligand, 2.250(6) and 2.344(7) Å, are longer than the Ta–N bond distances of the Ta–NMe_2 units (1.977(7), 2.005(6) and 2.007(6) Å). The torsion angle around N(1), N(2), N(6) and N(7) is 2.83° indicating a pseudo-octahedral geometry.

In $[Ta(OX)(NMe_2)_4]$ (**1**), the six octahedral positions are occupied by two axial dimethylamido, two equatorial dimethylamido and two N-bonded oxazoline ligands. The torsion angle of **1** around N(1), N(2), N(5) and N(5) is 1.04°, indicating an octahedral geometry. The N(1)–Ta–N(2) angle of 71.57° is almost the same as that

observed for **2**. The Ta–N(1) and Ta–N(2) bond lengths of the oxazoline ligand, 2.350(5) and 2.272(6) Å, are longer than the Ta–N bond lengths of the NMe_2 ligands (equatorial: 2.002(6), 2.009(6) Å and axial: 2.038(6), 2.033(6) Å). In both compounds **1** and **2**, the angles between the mean planes of the axial amides are nearly orthogonal, an alignment appropriate for these two amides to interact with two orthogonal tantalum d_{xz} and d_{yz} orbitals. The two equatorial amido ligands also exhibit a preferred orientation for maximum π-overlap with the remaining tantalum d_{xy} orbital, because the angles of 90° would be achieved. Opposing this orientation are the steric interactions between the axial and equatorial amido ligands and the fact that the two amido ligands are competing for donation to a single orbital.

4. Summary

In conclusion, we have demonstrated 4,4-dimethyl-2-pyrrole-2-oxazoline compounds have been successfully employed as chelating amido-imine ligands in the synthesis of the air and moisture sensitive tantalum amido complexes $[Ta(OX)(NMe_2)_4]$ (**1**) and $[Ta(OX)_2(NMe_2)_3]$ (**2**) in high yield via the amide elimination method. In addition, the first example of the reactions of tantalum pentakis amido complexes with oxazoline has been reported. Structural studies of **1** and **2** show they both adopt geometries best described as distorted octahedral with N–Ta–N angles of 169.4(2)° and 173.6(3)°, respectively. The nitrogen atoms of the oxazoline are bound directly to the tantalum center, leading to a five-membered metallacycle in the basal plan. In $[Ta(OX)(NMe_2)_4]$ (**1**), six octahedral positions are occupied with two axial dimethylamido, two equatorial dimethylamido and two N-bonded oxazoline ligands. $[Ta(OX)_2(NMe_2)_3]$ (**2**) adopts a geometry with an axial dimethylamido, two equatorial dimethylamido, an equatorial amido-imine oxazoline and finally an anchored N-bonded amido oxazoline ligand at an axial position. We have shown that the oxazoline ligand can be inserted into Ta-amido functions. The structure of complex **2** indicates some of the steric and electronic features by providing initial details on the role of the ligand. But in the case of our study it seems that steric hindrance may play a more important role in these reactions. Our future researches will be directed at clarifying these issues through manipulation of ancillary ligands.

Acknowledgement

This work was supported by the ministry of Science, Research and Technology of Iran.

Appendix A. Supplementary data

CCDC numbers 677003 and 677002 contain the supplementary crystallographic data for $[Ta(OX)(NMe_2)_4]$ (**1**) and $[Ta(OX)_2$- $(NMe_2)_3]$ (**2**), respectively. These data can be obtained free of charge via http://www.ccdc.cam.ac.uk/conts/retrieving.html, or from the Cambridge Crystallographic Data Centre, 12 Union Road, Cambridge CB2 1EZ, UK; fax: (+44) 1223-336-033; or e-mail: deposit@ccdc.cam.ac.uk. Supplementary data associated with this article can be found, in the online version, at doi:10.1016/j.poly.2008.04.004.

References

[1] Markku Talja, Mika Polamo, Polyhedron 25 (2006) 3039.
[2] A. Baunemann, D. Rische, A. Milanov, Y. Kim, M. Winter, C. Gemel, R.A. Fischer, J. Chem Soc., Dalton Trans. (2005) 3051. and references therein.
[3] C.H. Winter, Aldrichim. Acta 33 (2000) 3.
[4] H.H. Brintzinger, D. Fischer, R. Mulhaupt, B. Rieger, R.M. Waymouth, Angew. Chem., Int. Ed. Engl. 34 (1995) 1143.
[5] W.J. Kaminsky, J. Chem. Soc., Dalton Trans. (1998) 1413.
[6] A. Vanderlinden, C.J. Schaverien, N. Meijboom, C. Ganter, A.G. Orpen, J. Am. Chem. Soc. 117 (1995) 3008.
[7] S. Fokken, T.P. Spaniol, J. Okuda, F.G. Sernetz, R. Mulhaupt, Organometallics 20 (1997) 4240.
[8] K. Aoyagi, P.K. Gantzel, K. Kalai, T.D. Tilley, Organometallics 15 (1996) 923.
[9] F. Guerin, D.H. McConville, J.J. Vittal, G.A.P. Yap, Organometallics 17 (1998) 5172. and references therein.
[10] L.C. Liang, R.R. Schrock, W.M. Davis, D.H. McConville, J. Am. Chem. Soc. 122 (1999) 5797.
[11] C. Lorber, B. Donnadieu, R. Choukroun, Organometallics 19 (2000) 1963.
[12] T.H. Warren, R.R. Schrock, W.M. Davis, Organometallics 15 (1996) 562.
[13] N.A.H. Male, M. Thornton-Pett, M.J. Bochmann, J. Chem. Soc., Dalton Trans. (1997) 2487.
[14] B. Tsuie, D.C. Swenson, R.F. Jordan, J.L. Petersen, Organometallics 16 (1997) 1392.
[15] S. Pritchett, P. Gantzel, P.J. Walsh, Organometallics 16 (1997) 5130.
[16] R.R. Schrock, F. Schattenmann, M. Aizenberg, W.M. Davis, Chem. Commun. (1998) 199.
[17] K. Nomura, K. Oya, Y. Imanishi, Polymer 41 (2000) 2755.
[18] C.H. Lee, Y.H. La, W.J. Park, Organometallics 19 (2000) 344.
[19] S. Tinkler, R.J. Deeth, D.J. Duncalf, A. McCamley, Chem. Commun. (1996) 2623.
[20] J.D. Scollard, D.H. McConville, J. Am. Chem. Soc. 118 (1996) 10008.
[21] R. Vollmerhaus, P.C. Shao, N.J. Taylor, S. Collins, Organometallics 18 (1999) 2731.
[22] Y.M. Jeon, J. Heo, W.M. Lee, T.H. Chang, K. Kim, Organometallics 18 (1999) 4107.
[23] R.D.W. Kemmitt, S. Mason, M.R. Moore, J. Fawcett, D.R. Russell, J. Chem. Soc., Chem. Commun. (1990) 1535.
[24] G.M. Diamond, R.F. Jordan, J.L. Petersen, J. Am. Chem. Soc. 118 (1996) 8024.
[25] P.G. Cozzi, C. Floriani, A. Chiesivilla, C. Rizzoli, Inorg. Chem. 34 (1995) 2921.
[26] H. Brunner, B. Haßler, Z. Naturforsch. 53b (1998) 476.
[27] G.M. Sheldrick, SHELLXT [Nicolet XRD], Madison, WI, 1986.
[28] G.M. Diamond, R.F. Jordan, J.L. Petersen, Organometallics 15 (1996) 4045.
[29] M.K.T. Tin, G.P.A. Yap, D.S. Richeson, Inorg. Chem. 38 (1999) 998.
[30] I.A. Guzei, G.P.A. Yap, C.H. Winter, Inorg. Chem. 36 (1997) 1738.
[31] J.D. Wilkins, J. Organomet. Chem. 80 (1974) 349.
[32] M.G.B. Drew, J.D. Wilkins, J. Chem. Soc., Dalton Trans. (1974) 1579.
[33] M.G.B. Drew, J.D. Wilkins, J. Chem. Soc., Dalton Trans. (1975) 2611.
[34] V.G. Kessler, Chem. Commun. (2003) 1213.
[35] M.H. Chisholm, L.-S. Tan, J.C. Huffman, J. Am. Chem. Soc. 104 (1982) 4879.
[36] H.O. Davies, A.C. Jones, E.A. McKinnell, J. Raftery, C.A. Muryn, M. Afzaal, P. O'Brien, J. Mater. Chem. 16 (2006) 2226.
[37] S. Batsanov, A.V. Churakov, J.A.K. Howard, A.K. Hughes, A.L. Johnson, A.J. Kingsley, I.S. Neretin, K. Wade, J. Chem. Soc., Dalton Trans. (1999) 3867.

Polyhedron 27 (2008) 2131–2142

Contents lists available at ScienceDirect

Polyhedron

journal homepage: www.elsevier.com/locate/poly

Synthetic study of the ternary copper(II)/maleamate(-1)/1,10-phenanthroline reaction system: Mononuclear, dinuclear and polymeric complexes

Katerina N. Lazarou [a], Spyros P. Perlepes [b], Vassilis Psycharis [a], Catherine P. Raptopoulou [a,*]

[a] Institute of Materials Science, NCSR "Demokritos", 153 10 Aghia Paraskevi Attikis, Greece
[b] Department of Chemistry, University of Patras, 265 04 Patras, Greece

ARTICLE INFO

Article history:
Received 14 February 2008
Accepted 9 April 2008
Available online 22 May 2008

Keywords:
Amide methanolysis
Copper/1,10-phenanthroline complexes
Crystal structures
IR spectra
Maleamate(-1) complexes

ABSTRACT

The use of the maleamic acid (H_2L)/1,10-phenathroline "blend" in copper(II) chemistry has yielded mononuclear and dinuclear complexes, and one coordination polymer. The chemical and structural identity of the products depends on the solvent, the absence or presence of external hydroxides in the reaction mixtures, the nature of the inorganic anion present in the copper(II) starting material and the molar ratio of the reactants. The maleamato(-1) complexes $[Cu_2(HL)_3(phen)_2](NO_3)$ (**2**, **7**), $[Cu(HL)(phen)_2](OH)$ (**3**), $[Cu(HL)_2(phen)]$ (**4**) and $[Cu(HL)(NO_3)(phen)]_n$ (**8**) have been prepared and structurally characterized. The dinuclear cations **2** and **7** are structurally similar to the cation of complex $[Cu_2(HL)_3(phen)_2](ClO_4)$ (**1**) which was previously communicated. The maleamato(-1) ligand adopts a variety of coordination modes in the above complexes, ranging from the familiar *syn,syn* $\eta^1:\eta^1:\mu_2$ bridging mode and the rare monoatomic bridging ($\eta^1:\mu_2$) mode in the structures of **2** and **7**, to the terminal monodentate in the structures of **3** and **4**. Complex **8** is a 1D, zigzag coordination polymer in which the carboxylato group of the HL^- ligand is asymmetrically coordinated to two Cu^{II} ions adopting the *syn,anti* $\eta^1:\eta^1:\mu_2$ mode; the amide O atom is also coordinated, thus forming an unusual 7-membered chelating ring. The crystal structures of the complexes are stabilized by a variety of H-bonding patterns which lead to interesting supramolecular architectures. Characteristic IR bands of the complexes are discussed in terms of the known structures, and the coordination modes of the HL^- ligand.

© 2008 Elsevier Ltd. All rights reserved.

1. Introduction

There continues to be great interest by inorganic chemistry groups around the world in the synthesis and characterization of polynuclear (also known as clusters) and polymeric (also known as coordination polymers, metal–organic frameworks or organic–inorganic hybrid coordination polymers in the case where the metal–organic connectivity is interrupted by "inorganic" bridges) 3d-metal molecular complexes. Among the diverse reasons for the interest for new clusters are the search for models of metal-containing biological sites [1], and new high-spin molecules [2] and single-molecule magnets [3,4]. Coordination polymers have various applications in catalysis, electrical conductivity, magnetism, luminescence, non-linear optics, molecular electronics, medicine, sensing and zeolitic behaviour [5]. There thus continues to be a need for new synthetic methods to clusters and coordination polymers.

The success of organic chemists in establishing methods for making large, complicated molecules and organic polymers in a systematic and controlled manner is one of the great collective achievements of 20th-century science. The attitude of mind involved in such processes has become inculcated in all synthetic chemists. By comparison, transition metal chemists have made little progress in discovering general approaches to preparing compounds containing large or infinite numbers of metal centers. This is because until recently means for routine characterization of such compounds did not exist, and because the obvious biological relevance and commercial applications of large organic molecules and organic polymers were not matched by properties of polynuclear and polymeric metal complexes. The lack of control in transition metal chemistry has led to the neologism "self-assembly" being coined [6]. In the last decade, several groups have been introducing an element of design into the assembly process by choosing rigid ligands which have strong preferences for specific bonding modes and metal ions with preferred coordination geometries. This "designed assembly" approach has produced many beautiful clusters [7] and coordination polymers [8]. The structures of such compounds are moderately predictable, based on the preferred coordination geometry of the metal ion, the number of pre-organized donor sites presented by the ligand and on the limited flexibility of the ligand. Other researchers, including our group, use much less well-behaved *bridging* organic ligands for the preparation of clusters [9] and coordination polymers [10].

* Corresponding author. Tel.: +30 210 6503365; fax: +30 210 6519430.
E-mail address: craptop@ims.demokritos.gr (C.P. Raptopoulou).

0277-5387/$ - see front matter © 2008 Elsevier Ltd. All rights reserved.
doi:10.1016/j.poly.2008.04.005

Once formation of a five- or six-membered chelate ring is excluded, the coordinative flexibility of any polydentate ligand increases enormously. This flexibility in turn allows stabilization of many unpredictable structures, almost invariably incorporating further ligands such as oxide, hydroxide, alkoxides, inorganic anions or organic coligands. In the case of clusters, this approach has been termed "serendipitous assembly" [11]. The advantages of serendipidous assembly in cluster chemistry and of less-designed (or "non-programmed") assembly in the chemistry of coordination polymers are considerable. Most often designed assembly requires similar coordination at each metal site, and this restricts the number of accessible structures, e.g. to Platonic solids, rings and grids in the case of cluster chemistry. On the other hand, serendipitous or less designed assembly vastly increases the range of compounds available for study. The unusual structures of some of these compounds can lead to novel properties.

A frequently used family of organic ligands, often in combination with terminal aromatic N-donors, for the construction of clusters [12] and coordination polymers [13] consists of aliphatic α,ω-dicarboxylates, $^{-}OOC\text{-}(CH_2)_n\text{-}COO^{-}$ (**I** in Fig. 1; $n = 2,3,4\ldots$), $^{-}OOC\text{–}CH{=}CH\text{–}COO^{-}$ (**II** in Fig. 1, fumarate; **III** in Fig. 1, maleate) and $^{-}OOC\text{–}C{\equiv}C\text{–}COO^{-}$ (**IV** in Fig. 1, acetylene dicarboxylate), which are capable of bridging metal ions at various distances [14]. In contrast to the large body of knowledge in this area, *practically nothing is known about the metal complexes of the monoanionic monoamides of α,ω-dicarboxylates*, $^{-}OOC\text{–}(CH_2)_n\text{–}CONH_2$ (**V** in Fig. 1; $n = 2,3,4,\ldots$), $^{-}OOC\text{–}CH{=}CH\text{–}CONH_2$ (**VI** in Fig. 1, fumarate monoamide; **VII** in Fig. 1, maleate monoamide or maleamate) and $^{-}OOC\text{–}C{\equiv}C\text{–}CONH_2$ (**VIII** in Fig. 1, acetylene dicarboxylate monoamide). The presence of an amide functionality, instead of a carboxylate group, is expected – due to different charge (neutral versus ionic), electronic properties and hydrogen bonding effects – to alter the coordination behaviour of these ligands (and hence the identity of the resultant metal complexes) in comparison with that of aliphatic α,ω-dicarboxylates.

With the above considerations in mind, we have explored "ligand blend" reaction systems involving the succinamate(-1) ligand, $^{-}OOC\text{–}CH_2\text{–}CH_2\text{–}CONH_2$ ($n = 2$ in **V** of Fig. 1; $Hsucm^{-}$) and various aromatic *N*,*N*′-donors as a means to dinuclear and polymeric copper(II) compounds [15]. Thus, several reaction schemes involving various copper(II) sources, $Hsucm^{-}$ and 4,4′-dimethyl-2,2′-bipyridine (dmbpy) or 2,2′-bipyridine (bpy) afforded [15] the complexes $[Cu_2(Hsucm)_3(dmbpy)_2](OH)$, $[Cu_2(Hsucm)_2(dmbpy)_2(H_2O)_2](ClO_4)_2$, $[Cu_2(OH)(H_2O)(Hsucm)(bpy)_2](ClO_4)_2$ and $\{[Cu_4(Hsucm)_5(dmbpy)_4](ClO_4)_3\}_n$. The dinuclear complexes contain extremely rare cores, while the novel cationic coordination polymer consists of alternating $\{Cu_2(Hsucm)_2(dmbpy)_2\}^{2+}$ and $\{Cu_2(Hsucm)_3(dmbpy)_2\}^{+}$ dinuclear units. We also reported the *binary* 1D coordination polymers $[Ln(Hsucm)_3(H_2O)]_n$ which feature only $Hsucm^{-}$ ligands that exhibit three different coordination modes [16].

We illustrate herein how the use of the maleamate(-1) (**VII** in Fig. 1; HL^{-})/1,10-phenanthroline(phen) ligand combination in copper(II) chemistry leads to interesting mononuclear, dinuclear and polymeric complexes that contain the intact HL^{-}. The aromatic donor is necessary for the successful crystallization of the complexes (vide infra) and its use allows direct structural comparison with the complexes featuring the corresponding α,ω-dicarboxylate(-2) (**III** in Fig. 1; maleate) and the succinamate(-1) ligand, i.e., the $Cu^{II}/^{-}OOC\text{–}CH{=}CH\text{–}COO^{-}$/phen and $Cu^{II}/Hsucm^{-}$/phen complexes. The coordination chemistry of maleamic acid (H_2L) is almost unknown. The present work can be considered as continuation of our research efforts on the oxamate(-1) or its derivatives (**X** in Fig. 1) [17] and malonamate(-1) (**XI** in Fig. 1) [18] 3d-metal complexes.

The structure of the copper(II) maleamate(-1) complex $[Cu_2(HL)_3(phen)_2](ClO_4)\cdot 1.5MeCN\cdot 0.5H_2O$ (**1** $\cdot 1.5MeCN\cdot 0.5H_2O$) has been communicated by our group [19]. We also reported in the preliminary communication [19] of this work that the $Cu(ClO_4)_2\cdot 6H_2O/H_2L$/phen reaction system in MeOH, in the absence of external hydroxide ions, affords the remarkable complex $[Cu_2(L')_2(ClO_4)(phen)_2(MeOH)](ClO_4)$ (**5**) in which the maleamate(-1) ion has been transformed to the monomethyl maleate(-1) ligand L'^{-} (**IX** in Fig. 1) via a novel, metal-ion assisted/promoted process and through the formation of the HL^{-}-free coordination polymer $[Cu(ClO_4)(phen)(MeOH)_2]_n$ (**6a**); the structure of the latter was assigned on the basis of its spectral similarity with the structurally characterized 1D compound $[Cu(ClO_4)(phen)(MeCN)_2]_n(ClO_4)_n$ (**6b**) [19].

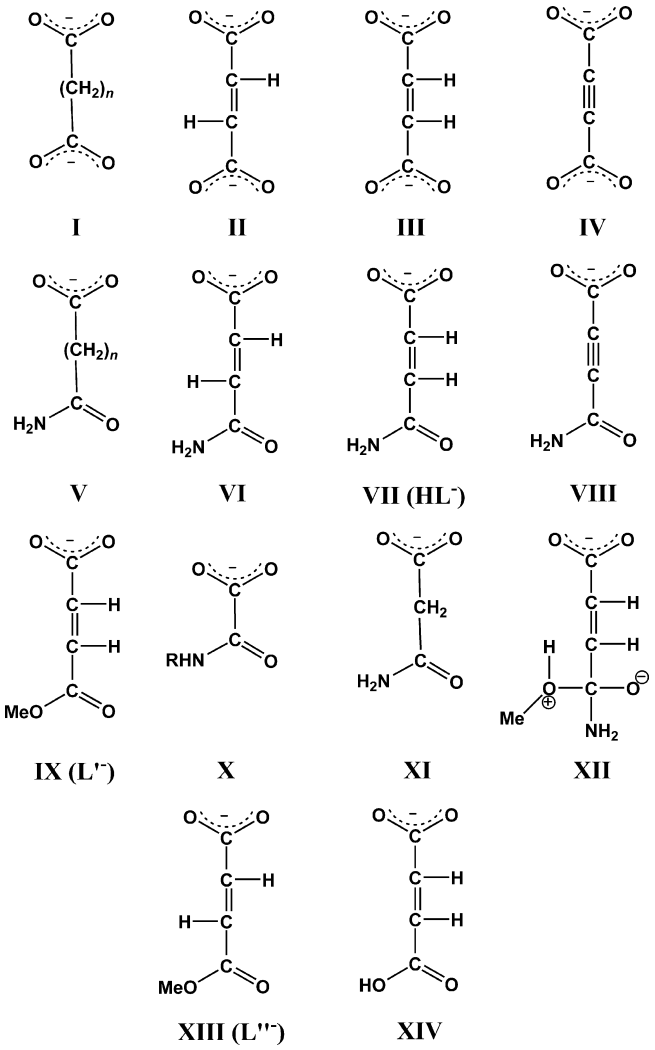

Fig. 1. Some of the dicarboxylate(-2) and amide-carboxylate(-1) ligands discussed in the text. The ligand used in this work is the maleamate(-1) ion (**VII**, HL^{-}). The succinamate(-1) ligand used in our previous studies is ligand **V** with $n = 2$ ($Hsum^{-}$). **XII** is the *possible* intermediate formed during the Cu^{II}-assisted transformation of HL^{-} to L'^{-}[19]. R = H (oxamate), Me, Et, ...

2. Experimental

2.1. General and spectroscopic measurements

All manipulations were performed under aerobic conditions using materials (reagent grade) and solvents as received. Microanalyses (C,H,N) were performed by the University of Ioannina

(Greece) Microanalytical Laboratory using an EA 1108 Carlo Erba analyzer.

IR spectra (4000–450 cm^{-1}) were recorded on a Perkin-Elmer 16 PC FT-spectrometer with samples prepared as KBr pellets.

Safety note: Perchlorate salts are potentially explosive; such compounds should be synthesized and used in small quantities, and treated with utmost care at all times.

2.2. Compound preparation

Since the detailed syntheses and full characterized data of complexes **1**, **5**, **6a** and **6b** were not reported of this work [19], we incorporate these details below.

2.2.1. $[Cu_2(HL)_3(phen)_2](ClO_4) \cdot 1.5MeCN \cdot 0.5H_2O$ (**1** $\cdot 1.5MeCN \cdot 0.5H_2O$)

A colourless aqueous solution (1.5 ml) of $LiOH \cdot H_2O$ (0.018 g, 0.44 mmol) was added to a colourless solution of H_2L (0.049 g, 0.43 mmol) in MeCN (20 ml) to give a white suspension. Solid phen $\cdot H_2O$ (0.044 g, 0.22 mmol) was then added and the resulting colourless solution was stirred for 20 min. A light blue solution of $Cu(ClO_4)_2 \cdot 6H_2O$ (0.080 g, 0.22 mmol) in MeCN (10 ml) was finally added to obtain a blue solution. X-ray quality blue prismatic crystals of the product were obtained by layering of the blue solution with a mixture of Et_2O/*n*-hexane (30 ml, 1:1 v/v). The crystals were collected by filtration under vacuum, washed with cold MeCN (5 ml), Et_2O (5 ml) and dried in air. Typical yields were in the 55–60% range. FT-IR (KBr pellet, cm^{-1}): 3422m, 3350m, 3190w, 3066w, 1692s, 1628s, 1586s, 1554s, 1520m, 1432s, 1370sh, 1304m, 1280m, 1220w, 1146sh, 1090s, 852m, 814w, 784w, 722m, 656sh, 622m. The dried solid analysed as solvent-free. *Anal.* Calc. for $C_{36}H_{28}N_7O_{13}ClCu_2$ (929.25): C, 46.53; H, 3.04; N, 10.55%. Found: C, 46.30; H, 2.92; N, 10.70%.

2.2.2. $[Cu_2(HL)_3(phen)_2](NO_3) \cdot 2.5MeCN \cdot 2H_2O$ (**2** $\cdot 2.5MeCN \cdot 2H_2O$)

A colourless aqueous solution (2 ml) of $LiOH \cdot H_2O$ (0.018 g, 0.44 mmol) was added to a solution of H_2L (0.049 g, 0.43 mmol) in MeCN (20 ml) to give a white suspension. Solid phen $\cdot H_2O$ (0.044 g, 0.22 mmol) was then added and the resulting colourless solution was stirred under heating for 20 min. A turquoise solution of $Cu(NO_3)_2 \cdot 2.5H_2O$ (0.051 g, 0.22 mmol) in MeCN (10 ml) was finally added to obtain a blue mixture, which was filtered to give a clear blue solution. X-ray quality light blue, needle-like crystals of the product formed in a closed vial after four days. The crystals were collected by filtration under vacuum, washed with Et_2O (2×2 ml) and dried in air. Typical yields were in the 55–60% range. FT-IR (KBr pellet, cm^{-1}): 3375sb, 3184mb, 3091w, 3062w, 1676m, 1643s, 1575vs, 1548sh, 1520m, 1493w, 1431s, 1383vs, 1312wb, 1225w, 1203w, 1189w, 1143w, 1107w, 1045wb, 994vw, 962wb, 902w, 873w, 850m, 823w, 739w, 720m, 673w, 650m, 630w, 476vw. The dried solid analysed as **2** $\cdot 2H_2O$. *Anal.* Calc. for $C_{36}H_{32}N_8O_{14}Cu_2$ (927.85): C, 46.60; H, 3.48; N, 12.08. Found: C, 46.47; H, 3.21; N, 12.27%.

2.2.3. $[Cu(HL)(phen)_2](OH) \cdot 0.5MeCONH_2 \cdot 0.75H_2O$ (**3** $\cdot 0.5MeCONH_2 \cdot 0.75H_2O$) and $[Cu(HL)_2(phen)]$ (**4**) in a mixture

A colourless aqueous solution (1.5 ml) of $LiOH \cdot H_2O$ (0.014 g, 0.34 mmol) was added to a solution of H_2L (0.038 g, 0.33 mmol) in MeCN (25 ml) to give a white suspension. Solid $CuCl_2 \cdot 2H_2O$ (0.038 g, 0.22 mmol) was then added to obtain a light blue slurry. A colourless solution of phen $\cdot H_2O$ (0.044 g, 0.22 mmol) in MeCN (10 ml) was added to the above light blue slurry under stirring yielding a darker light blue mixture, which was stirred for ~1 h. The final "solution" was filtered off and the light blue solution was layered with Et_2O (60 ml). X-ray quality blue prismatic and purple needle-like crystals in an approximate ratio of 1:1 formed, which were separated manually and dried in air. X-ray crystallography revealed that blue prisms correspond to complex **3** $\cdot 0.5 MeCONH_2 \cdot 0.75H_2O$ and purple needles correspond to complex **4**. FT-IR for **3** $\cdot 0.5 MeCONH_2 \cdot 0.75H_2O$ (KBr pellet, cm^{-1}): 3425sb, 3275wb, 1681m, 1628m, 1596m, 1519m, 1431s, 1384s, 1305m, 1227vw, 1146w, 1106w, 872w, 850m, 778vw, 722m, 668w, 621w, 460vw. *Anal.* Calc. for $C_{29}H_{25}N_{5.5}O_{5.25}Cu$ (598.14): C, 58.23; H, 4.22; N, 12.88. Found: C, 57.95; H, 4.03; N, 12.96%. FT-IR for **4** (KBr pellet, cm^{-1}): 3510sh, 3376mb, ~3200wb, 1676m, 1654w, 1628w, 1576s, 1521m, 1432vs, 1304m, 1202w, 1148vw, 1108vw, 874m, 850m, 821w, 718m, 668m, 652w, 608vw, 530vw, 489vw, 471vw. *Anal.* Calc. for $C_{20}H_{16}N_4O_6Cu$ (471.95): C, 50.90; H, 3.42; N, 11.87. Found: C, 50.72; H, 3.38; N, 11.99%.

2.2.4. $[Cu(HL)(phen)_2](OH) \cdot 0.5MeCONH_2 \cdot 0.75H_2O$ (**3** $\cdot 0.5MeCONH_2 \cdot 0.75H_2O$)

A colourless aqueous solution (3 ml) of $LiOH \cdot H_2O$ (0.032 g, 0.78 mmol) was added to a solution of H_2L (0.046 g, 0.40 mmol) in MeCN (25 ml) to give a white suspension. Solid $CuCl_2 \cdot 2H_2O$ (0.068 g, 0.40 mmol) was then added and the obtained light blue slurry turned into green during 45 min of stirring. A colourless solution of phen $\cdot H_2O$ (0.159 g, 0.80 mmol) in MeCN (10 ml) was then added to the above mixture, which was further stirred for 30 min. The final clear turquoise solution of the product was layered with Et_2O. Slow mixing gave X-ray quality, blue prismatic crystals, which were collected by filtration under vacuum and dried in air. Typical yields were in the 65-70% range. FT-IR spectroscopy and microanalytical data showed that the blue prismatic crystals correspond to complex **3** $\cdot 0.5MeCONH_2 \cdot 0.75H_2O$.

2.2.5. $[Cu_2(L')_2(ClO_4)(phen)_2(MeOH)](ClO_4)$ (**5**)

Solid phen $\cdot H_2O$ (0.057 g, 0.28 mmol) was dissolved in a colourless solution of H_2L (0.050 g, 0.43 mmol) in MeOH (20 ml). A blue solution of $Cu(ClO)_2 \cdot 6H_2O$ (0.107 g, 0.29 mmol) in MeOH (10 ml) was then added to obtain a turquoise solution which was layered with a mixture of Et_2O/*n*-hexane (35 ml, 1:1 v/v). Slow mixing initially gave a turquoise polycrystalline solid (**6a**). Upon storage of the closed layering tube at room temperature for one week, the polycrystalline powder was transformed into blue, X-ray quality crystals of the product. The crystals were collected by filtration under vacuum and dried in air. Typical yields were >60%. FT-IR (KBr pellet, cm^{-1}): 3461mb, 3356m, 3093wb, 2953w, 1719s, 1697m, 1644w, 1583vs, 1520m, 1495w, 1445s, 1432s, 1358w, 1346w, 1302vw, 1234s, 1174m, 1150sh, 1116vs, 1106vs, 1053sh, 930w, 875w, 846m, 825w, 774vw, 742vw, 720s, 683vw, 652w, 624s, 546vw, 458vw, 432w, 405vw. The IR spectrum of the turquoise powder (see spectrum of **6a**) is completely different compared to that of **5**. *Anal.* Calc. for $C_{35}H_{30}N_4O_{17}Cl_2Cu_2$(976.68): C, 43.04; H, 3.10; N, 5.74. Found: C, 42.98; H, 2.94; N, 5.82%.

2.2.6. $[Cu(ClO_4)(phen)(MeOH)_2]_n(ClO_4)_n$ (**6a**)

A colourless solution of phen $\cdot H_2O$ (0.170 g, 0.86 mmol) in MeOH (15 ml) was added to a light blue solution of $Cu(ClO_4)_2 \cdot 6H_2O$ (0.319 g, 0.86 mmol) in the same solvent (20 ml). The resultant blue solution was layered with Et_2O (55 ml). Slow mixing gave a turquoise polycrystalline powder, which was collected by filtration, washed with Et_2O (3×2 ml) and dried in air. The yield was ~65%. FT-IR (KBr pellet, cm^{-1}): 3440 mb, 3070vw, 1629vw, 1585m, 1521m, 1494w, 1430s, 1406w, 1388w, 1342w, 1225w, 1148m, 1088vs, 874m, 847s, 777w, 738w, 720s, 687vw, 668w, 652w, 623w. This IR spectrum is identical to that of the turquoise polycrystalline solid which was initially isolated during the preparation of **5** (paragraph 2.2.5) and very similar to the IR spectrum of **6b** (see below). *Anal.* Calc. for $C_{14}H_{16}N_2O_{10}Cl_2Cu$ (506.77): C, 33.18; H, 3.19; N, 5.53. Found: C, 32.90; H, 3.21; N, 5.68%.

*2.2.7. $[Cu(ClO_4)(phen)(MeCN)_2]_n(ClO_4)_n$ (**6b**)*

A solution of phen · H_2O (0.087 g, 0.44 mmol) in MeCN (15 ml) was added to a light blue solution of $Cu(ClO_4)_2 \cdot 6H_2O$ (0.163 g, 0.44 mmol) in the same solvent (40 ml) to give a turquoise solution. X-ray quality, turquoise crystals of the product formed by vapour diffusion of Et_2O onto the turquoise solution. The crystals were collected by filtration under vacuum, washed with cold MeCN (1 ml), Et_2O (2 ml) and dried in air. Typical yields were in the 55–60% range. FT-IR (KBr pellet, cm^{-1}): 3450mb, 3050vw, 1628w, 1608w, 1586m, 1516m, 1496w, 1349m, 1147vs, 1107vs, 1093vs, 940w, 870m, 852s, 776m, 734m, 720s, 636sh, 627s. *Anal.* Calc. for $C_{16}H_{14}N_4O_8Cl_2Cu$ (524.79): C, 36.62; H, 2.69; N, 10.68. Found: C, 36.18; H, 2.61; N, 10.83%.

*2.2.8. $[Cu_2(HL)_3(phen)_2](NO_3) \cdot MeOH \cdot H_2O$ (**7** · MeOH · H_2O)*

Solid LiOH · H_2O (0.018 g, 0.44 mmol) was added to a colourless solution of H_2L (0.049 g, 0.43 mmol) in MeOH (20 ml). The resultant solution was refluxed for 2 h and solid $Cu(NO_3)_2 \cdot 2.5\,H_2O$ (0.067 g, 0.29 mmol) was added. The colour of the solution immediately turned to light blue-turquoise. A solution of phen · H_2O (0.057 g, 0.28 mmol) in MeOH (10 ml) was then added yielding a final blue solution. X-ray quality blue prismatic crystals of the product formed by vapour diffusion of Et_2O onto the reaction solution. The crystals were collected by filtration under vacuum, washed with cold MeOH (1 ml), Et_2O (5 ml) and dried in air. Typical yields were in the 45–50 % range. FT-IR (KBr pellet, cm^{-1}): 3400mb, 3173w, 2927w, 2805w, 1678m, 1620sh, 1598vs, 1516m, 1493w, 1427m, 1384s, 1336m, 1311m, 1223w, 1203w, 1181vw, 1144w, 1106w, 1025wb, 871w, 850m, 829w, 775w, 737w, 722s, 647w, 613m, 561w, 515w, 484w, 453vw. The dried solid analysed as **7** · H_2O. *Anal.* Calc. for $C_{36}H_{30}N_8O_{13}Cu_2$ (909.83): C, 47.52; H, 3.33; N, 12.32. Found: C, 47.85; H, 3.24; N, 11.97%.

*2.2.9. $[Cu(HL)(NO_3)(phen)]_n$ (**8**)*

Solid phen · H_2O (0.057 g, 0.28 mmol) was dissolved in a colourless solution of H_2L (0.050 g, 0.43 mmol) in MeOH (20 ml). The obtained solution was mixed with a light blue solution of $Cu(NO_3)_2 \cdot 2.5\,H_2O$ (0.067 g, 0.29 mmol) in MeOH (8 ml). The final blue solution was layered with Et_2O. Slow mixing gave X-ray quality blue-turquoise crystals, which were collected by filtration under vacuum, washed with cold MeOH (1 ml), Et_2O (4 ml) and dried in air. Typical yields were >60%. FT-IR (KBr pellet, cm^{-1}): 3284mb, 3060s, 1748w, 1609s, 1588s, 1564s, 1519m, 1492m, 1456w, 1431s, 1385vs, 1344s, 1313vs, 1257m, 1225m, 1142w, 1106w, 1042w, 1001vw, 971m, 875m, 850s, 828w, 803w, 761vw, 740m, 721s, 651s, 618m, 560w, 509vw, 432m. *Anal.* Calc. for $C_{16}H_{12}N_4O_6Cu$ (419.87): C, 45.77; H, 2.89; N, 13.35. Found: C, 45.95; H, 2.85; N, 13.09 %.

2.3. Single-crystal X-ray crystallography

Details for the crystallographic characterization of **1** · 1.5MeCN · 0.5H_2O, **5** and **6b** have been reported earlier [19]. Light blue prismatic crystals of **2** · 2.5MeCN · 2H_2O (0.10 × 0.20 × 0.65 mm) were mounted in capillary. Diffraction measurements were made on a Rigaku R-AXIS SPIDER Image Plate diffractometer using graphite monochromated Cu Kα radiation at room temperature. Data collection (ω-scans) and processing (cell refinement, data reduction and empirical absorption correction) were performed using the CRYSTALCLEAR program package [20]. The crystals of **2** · 2.5MeCN · 2H_2O had poor diffraction ability, despite their sufficient size. Data were collected to $2\theta_{max} = 143.8°$ ($\sin\theta/\lambda = 0.6165$), but only the data to $2\theta_{max} = 118°$ were used, because at higher 2θ values more than half of the data collected were unobserved. Blue prismatic crystals of **3** · 0.5$MeCONH_2$ · 0.75H_2O (0.15 × 0.30 × 0.60 mm), blue-purple dichroic crystals of **4** (0.04 × 0.05 × 0.55 mm) and blue-turquoise crystals of **8** (0.20 × 0.40 × 0.85 mm) were mounted in air. Blue crystals of **7** · MeOH · H_2O (0.15 × 0.50 × 0.85 mm) were mounted in capillary. The crystals of **7** · MeOH · H_2O had poor diffraction ability (despite their sufficient size) showing large ω-widths with shoulders on each side. The data collected to only $2\theta_{max} = 29°$ were adequate to solve the structure, which is very similar to the structure of the well characterized compound **2**. Thus, we felt that the complete structural characterization was not crucial. Diffraction measurements were made on a Crystal Logic Goniometer diffractometer using graphite monochromated Mo Kα radiation for **3** · 0.5$MeCONH_2$ · 0.75H_2O, **7** · MeOH · H_2O and **8**, and on a $P2_1$ Nicolet diffractometer upgraded by Crystal Logic using graphite monochromated Cu Kα radiation for **4**. Unit cell dimensions were determined and refined by using the angular settings of 25 automatically centered reflections in the range $11° < 2\theta < 23°$ for **3** · 0.5$MeCONH_2$ · 0.75H_2O, **7** · MeOH · H_2O and **8**, and $22° < 2\theta < 54°$ for **4**. Intensity data were recorded using a θ-2θ scan. Three standard reflections monitored every 97 reflections showed less than 3% intensity fluctuation and no decay. Lorentz, polarization and psi-scan absorption corrections (for **8** only) were applied using Crystal Logic software. Important crystal data and parameters for data collection for **2** · 2.5MeCN · 2H_2O, **3** · 0.5$MeCONH_2$ · 0.75H_2O, **4** and **8** are reported in Table 1.

The structures were solved by direct methods using SHELXS-97 [21] and refined by full-matrix least-squares techniques on F^2 with SHELXL-97 [22]. Further experimental crystallographic details for **2** · 2.5MeCN · 2H_2O: $2\theta_{max} = 118°$, reflections collected/unique/used 28955/6354 [R(int) = 0.0731]/6354, 603 parameters refined, $(\Delta/\sigma)_{max} = 0.006$, $(\Delta\rho)_{max}/(\Delta\rho)_{min} = 0.586/-0.644$ e/Å^3, R_1/wR_2 (for all data) 0.1457/0.2706. All hydrogen atoms were introduced at calculated positions as riding on their bonded atoms. All non-H atoms were refined anisotropically, except those of the solvate acetonitrile molecules which were refined isotropically. No H atoms for the solvate molecules were included in the refinement. Further experimental crystallographic details for **3** · 0.5$MeCONH_2$ · 0.75H_2O: $2\theta_{max} = 50°$, reflections collected/unique/used 5490/5240 [R(int) = 0.0167]/5240, 460 parameters refined, $(\Delta/\sigma)_{max} = 0.004$, $(\Delta\rho)_{max}/(\Delta\rho)_{min} = 0.910/-0.333$ e/Å^3, R_1/wR_2 (for all data) 0.0823/0.1893. Hydrogen atoms were located by difference maps and refined isotropically. All non-H atoms were refined anisotropically, except those of the water solvate molecules which were refined isotropically. There is also a disordered, over a centre of symmetry, acetamide solvate molecule, which is the hydrolysis product of the MeCN reaction solvent. No H atoms for the solvate molecules were included in the refinement. Further experimental crystallographic details for **4**: $2\theta_{max} = 118°$, reflections collected/unique/used 2885/2641 [R(int) = 0.0281]/2641, 345 parameters refined, $(\Delta/\sigma)_{max} = 0.000$, $(\Delta\rho)_{max}/(\Delta\rho)_{min} = 0.416/-0.650$ e/Å^3, R_1/wR_2 (for all data) 0.0370/0.0968. Hydrogen atoms were located by difference maps and refined isotropically. All non-H atoms were refined anisotropically. Further experimental crystallographic details for **7** · MeOH · H_2O: $C_{37}H_{34}N_8O_{14}Cu_2$, fw = 941.81, a = 11.80(3), b = 12.21(3), c = 15.75(3) Å, $\alpha = 69.52(6)°$, $\beta = 76.47(7)°$, $\gamma = 77.21(7)°$, $V = 2042.41(2)$ Å^3, $Z = 2$, space group $P\bar{1}$, $2\theta_{max} = 29°$, reflections collected/unique/used 1640/1505 [R(int) = 0.0264]/1505, 255 parameters refined, $(\Delta/\sigma)_{max} = 0.370$, $(\Delta\rho)_{max}/(\Delta\rho)_{min} = 0.997/-1.421$ e/Å^3, R_1/wR_2 (for 1311 refs with $I > 2\sigma(I)$) 0.1566/0.4009, R_1/wR_2 (for all data) 0.1662/0.4179. Only the copper atoms were refined anisotropically, the rest were refined isotropically. No H atoms were included in the refinement. Further experimental crystallographic details for **8**: $2\theta_{max} = 50°$, reflections collected/unique/used 2851/2851 [R(int) = 0.0000]/2851, 292 parameters refined, $(\Delta/\sigma)_{max} = 0.001$, $(\Delta\rho)_{max}/(\Delta\rho)_{min} = 0.688/-0.863$ e/Å^3, R_1/wR_2 (for all data) 0.0724/0.1807. Hydrogen atoms were located

Table 1
Crystallographic data for complexes **2** · 2.5MeCN · $2H_2O$, **3** · 0.5$MeCONH_2$ · 0.75H_2O, **4** and **8**

	2 · 2.5MeCN · $2H_2O$	**3** · 0.5$MeCONH_2$ · 0.75H_2O	**4**	**8**
Formula	$C_{41}H_{39.5}Cu_2N_{10.5}O_{14}$	$C_{29}H_{25}CuN_{5.5}O_{5.25}$	$C_{20}H_{16}CuN_4O_6$	$C_{16}H_{12}CuN_4O_6$
Formula weight	1030.41	598.09	471.91	419.84
Space group	$P2_1/n$	$P\bar{1}$	$P\bar{1}$	*Pbca*
a (Å)	10.2623(2)	11.001(4)	9.860(4)	13.180(10)
b (Å)	33.1525(6)	12.404(5)	13.005(5)	9.750(10)
c (Å)	13.9424(3)	12.658(5)	7.290(3)	25.22(2)
α (°)		113.43(2)	96.68(2)	
β (°)	105.085(1)	96.260(10)	97.03(2)	
γ (°)		102.850(10)	92.94(2)	
V (Å^3)	4580.0(2)	1507.0(10)	919.4(6)	3241(5)
Z	4	2	2	8
T (°C)	20	25	25	25
Radiation	Cu Kα	Mo Kα	Cu Kα	Mo Kα
ρ_{calc} (g cm^{-3})	1.494	1.315	1.705	1.721
μ (mm^{-1})	1.810	0.771	2.131	1.393
R_1[a]	0.0777[b]	0.0629[c]	0.0361[d]	0.0579[e]
wR_2[a]	0.2111[b]	0.1723[c]	0.0957[d]	0.1639[e]

[a] $w = 1/[\sigma^2(F_o^2) + (aP)^2 + bP]$ and $P = (\max F_o^2,0) + 2F_c^2/3$, $R_1 = \sum(|F_o| - |F_c|)/\sum(|F_o|)$ and $wR_2 = \{\sum[w(F_o^2 - F_c^2)^2]/\sum[w(F_o^2)^2]\}^{1/2}$.
[b] For 3258 reflections with $I > 2\sigma(I)$.
[c] For 4232 reflections with $I > 2\sigma(I)$.
[d] For 2548 reflections with $I > 2\sigma(I)$.
[e] For 2320 reflections with $I > 2\sigma(I)$.

by difference maps and refined isotropically. All non-H atoms were refined anisotropically.

3. Results and discussion

3.1. Syntheses

Our efforts to prepare *binary* Cu^{II}/HL^- complexes were both successful and unsuccessful. The 1:2 reactions between $Cu(NO_3)_2 \cdot 2.5H_2O$ or $Cu(ClO_4)_2 \cdot 6H_2O$ and H_2L in H_2O, H_2O/MeCN or MeCN *in the absence of an external base* give polycrystalline blue solids in almost quantitative yields which have identical IR spectra. Analytical data repeatedly confirmed the empirical formula $Cu(HL)_2$ (**9**). The IR spectrum of **9** reveals the presence of coordinated amide group and bidentate carboxylate groups (vide infra). The same compound is readily isolated from the reaction of $[Cu_2(O_2CMe)_4(H_2O)_2]$ and four equivalents of H_2L in H_2O, H_2O/MeCN or MeCN. The 1:2:2 $Cu(ClO_4)_2 \cdot 6H_2O/H_2L/LiOH \cdot H_2O$ or NaOMe reaction systems in the same solvents or solvent mixtures, i.e. in the presence of an external base, lead to greenish-blue polycrystalline powders with identical IR spectra; the yields of these reactions are moderate. The same product is also isolated from MeOH or EtOH. Analytical data repeatedly confirmed the empirical formula $Cu(HL)_2 \cdot H_2O$ (**10**) for this solid. The IR study (vide infra) of this compound reveals the presence of "free", i.e. uncoordinated, amide groups and bridging carboxylate groups. Despite our numerous efforts (more than fifty samples were examined), we could not grow crystals of **9** and **10** suitable for single-crystal X-ray crystallography and thus their structures remain unknown. Based on the analytical data and IR spectra, we tentatively propose a polymeric structure for **9** with an O(amide),O(carboxylate), O′(carboxylate) bridging behaviour of HL^- resulting in six-coordinate Cu^{II} centres and a dinuclear, $[Cu_2(HL)_4(H_2O)_2]$, structure of the common paddle-wheel type for **10** with a bidentate bridging O(carboxylate), O′(carboxylate) coordination of HL^- and a five-coordinate (most probably square pyramidal) coordination geometry about the metal ions. Since compounds **9** and **10** have not been crystallographically characterized, their preparations are not given in the experimental (Section 2.2).

The synthetic investigation of the Cu^{II}/H_2L/phen reaction system leads to interesting mononuclear, dinuclear and polymeric complexes. We have studied the influence of four synthetic parameters on the chemical and structural identity of the products; these are the solvent, the absence or presence of external OH^-s in the reaction mixtures, the nature of the inorganic anion present in the copper(II) starting material and the molar ratio of the reactants.

Having obtained and identified complex **1** (see Section 2.2.1) [19], the next question addressed was whether, and in what manner, changes in the inorganic anion of the copper(II) starting material (keeping the same solvent mixture, i.e. MeCN/H_2O) might affect the product identity. The reaction of $Cu(NO_3)_2 \cdot 2.5H_2O$ with a mixture of H_2L and phen · H_2O, in the presence of LiOH · H_2O (1:2:1:2 molar ratio), in a solvent mixture comprising MeCN and H_2O (20:1 v/v) under slight heating led to a blue solution, from which were subsequently isolated light blue crystals of $[Cu_2(HL)_3(phen)_2](NO_3) \cdot 2.5MeCN \cdot 2H_2O$ (**2** · 2.5MeCN · $2H_2O$) in satisfactory yield. The molecular structures of the cations $[Cu_2(HL)_3(phen)_2]^+$ present in **1** and **2** are identical (vide infra). This, combined with the stronger coordination tendency of the NO_3^- ion (compared with that of the ClO_4^- ion) [23] indicates the great thermodynamic stability of this cation.

The use of $CuCl_2$ as starting material led to completely different chemistry. The 1:1.5:1:1.5 $CuCl_2 \cdot 2H_2O/H_2L$/phen · H_2O/LiOH · H_2O reaction mixture in MeCN/H_2O (20:1 v/v) gave a light blue solution, which upon layering with Et_2O yielded crystals that were obviously a mixture of two products. Microscopic examination showed both blue prisms and purple needles to be present in a visual ratio of roughly 1:1. Their not-too-dissimilar solubility prevented chemical separation. However, the extreme differences in colour and in crystal shape were fortuitous and allowed easy manual separation of the two materials. The prismatic and needle-like crystals were crystallographically characterized as complexes $[Cu(HL)(phen)_2](OH) \cdot 0.5MeCONH_2 \cdot 0.75H_2O$ (**3** · 0.5$MeCONH_2$ · 0.75H_2O) and $[Cu(HL)_2(phen)]$ (**4**), respectively.

With the identities of **3** and **4** established, convenient syntheses of pure materials were sought under alternative reaction conditions. Complex **3** has a Cu^{II}/HL^-/phen ratio of 1:1:2 and contains a hydroxide counterion, whereas the initial reaction solution had a Cu^{II}/HL^-/phen/OH^- ratio of 1:1.5:1:1.5. Thus, attempts to obtain pure **3** were made by adjusting the Cu^{II}/H_2L/phen/OH^- reaction ratio to 1:1:2:2. Using this modified reaction ratio, we were lucky enough to isolate the blue prisms of **3** as the only product, see paragraph 2.2.4 of Section 2. Complex **4** has a Cu^{II}/HL^-/phen ratio

of 1:2:1, whereas this ratio in the initial reaction solution was 1:1.5:1:1.5. In seeking to prepare the pure complex **4**, it was logical to carry out reactions employing the 1:2:1:2 $Cu^{II}/H_2L/phen/OH^-$ ratio. This reaction mixture in $MeCN/H_2O$ led to the isolation of *almost* pure purple needles of **4** in good yields (typically higher than 50%). However, careful examination of the purple material revealed trace amounts of blue microcrystals and/or specks which were shown to be complex **3** by IR spectroscopy. Thus, the manual separation of purple crystals from their above described mixture with **3** remains the only source of **4** to date for further measurements. It is likely that every reaction solution contains a mixture of $[Cu(HL)(phen)_2]^+$(the cation of **3**) and $[Cu(HL)_2(phen)]$ (**4**) in equilibrium, with factors such relative solubility, hydroxide concentration, lattice energy and crystallization kinetics, amongst others, determine the identity of the isolated products.

Somewhat to our surprise, the crystal structure of **3** contains lattice acetamide ($MeCONH_2$) molecules. The $MeCONH_2$ molecule is the hydrolysis product of the MeCN solvent, which is favoured in the presence of the metal ion [24]. The initial formed hydroxyimine, MeC(=NH)OH, tautomerizes to the amide, the hydrolysis in this particular case not proceeding to the formation of $MeCO_2H$ or $MeCO_2^-$. The formation of $MeCONH_2$ in an MeCN-containing reaction mixture and its incorporation in a complex (albeit as a ligand) were recently observed during the preparation of the cluster $[Fe_6(\mu_3\text{-}O)_2(O_2CPh)_{10}(salox)_2(MeCONH_2)_2] \cdot 6MeCN$ [25], where $salox^{2-}$ is the salicylaldehyde oximate(-2) ligand.

Having confirmed [19] that the $HL^- \rightarrow L'^-$ transformation takes place in OH^--free methanolic reaction mixtures (see also preparation of complex **5** in Section 2.2.5), the next question addressed was whether, and in what manner, addition of external base might affect the product identity. The 1:2:1:2 $Cu(ClO_4)_2 \cdot 6H_2O/H_2L/phen \cdot H_2O/LiOH \cdot H_2O$ reaction mixture in MeOH led to a pale blue solution, which upon layering with Et_2O or Et_2O/*n*-hexane gave a turquoise polycrystalline solid (**11**) in high yield (~70%). Analytical data are consistent with the empirical formula $Cu(HL)_{1.5}(phen)\text{-}(ClO_4)_{0.5} \cdot xMeOH$ ($x = 0.5$–1.0), while its IR spectrum indicates the presence of ionic perchlorates. Based on the structure of **7** · MeOH · H_2O (vide infra), we believe that **11** is a dinuclear complex possessing the cation $[Cu_2(HL)_3(phen)_2]^+$ with a molecular structure akin to the structures of the cations that are present in **1**, **2** and **7**. Seeking for the structural characterization of a product from the $Cu^{II}/H_2L/phen/OH^-$ reaction system in MeOH, we carried out an analogous reaction using $Cu(NO_3)_2 \cdot 2.5H_2O$ as starting material. We were lucky to easily crystallize and roughly solve the structure of $[Cu_2(HL)_3(phen)_2](NO_3) \cdot MeOH \cdot H_2O$ (**7** · MeOH · H_2O); as mentioned in Section 2.3, the quality of the structure is not particularly good, but we were able to reveal the gross structural features of this compound. Thus, the presence of external OH^-s in MeOH does *not* favour the formation of a Cu^{II}/L'^-/phen complex.

We came across complex $[Cu(HL)(NO_3)(phen)]_n$ (**8**) when we tried to prepare the nitrate analogue of complex $[Cu_2(L')_2(ClO_4)\text{-}(phen)_2(MeOH)](ClO_4)$ (**5**) [19]. Our desire was to investigate whether the nature of the inorganic anion plays any role in the $HL^- \rightarrow L'^-$ transformation. These at first glance trivial efforts led to an interesting coordination polymer. The reaction explored was that between $Cu(NO_3)_2 \cdot 2.5H_2O$, one and a half equivalents of H_2L and one equivalent of phen · H_2O in MeOH *in the absence* of external OH^-s. The blue solution obtained was layered with Et_2O to give blue-turquoise, X-ray quality crystals of **8** in higher than 60% yield. If the layering tube remains undisturbed for 4–5 days, few (3–4) small dark blue crystals of the known [26] 1D coordination polymer $[Cu(NO_3)_2(phen)]_n$ (**12**) appear; the identity of **12** was confirmed by single-crystal, X-ray crystallography, because we had not suspected that this compound does not contain HL^- or L'^- (we neglected to look carefully at the IR spectrum!). With the identities of **8** and **12** established, a convenient preparative route for the former was sought by increasing the H_2L/Cu^{II} ratio from 1.5:1 to 3:1. Our attempts were in vain because we could not avoid the *slow* precipitation of a small amount of **12**. However, taking advantage of the different rate of crystallization, we could obtain an analytically pure batch of crystals of **8** which were used for further characterization; for this reason, the slow appearance of few small, dark blue crystals of **12** is not mentioned in Section 2.2.9.

We were disappointed at not observing the Cu^{II}-assisted/promoted $HL^- \rightarrow L'^-$ transformation [19] during the investigation of the $Cu(NO_3)_2 \cdot 2.5H_2O/H_2L/phen$ reaction system in MeOH. The obvious, initial conclusion was that this transformation is anion-dependent and it is not favoured in the presence of NO_3^- ions! However, prolonged storage (e.g. for 45 days) of $Cu(NO_3)_2 \cdot 2.5H_2O/H_2L/phen \cdot H_2O$ (1:1:1) reaction mixtures in MeOH or EtOH in closed flasks or layering tubes (with Et_2O) leads to solids with no reproducible analytical data, but with IR spectra that exhibit a strong band at 1720 cm^{-1} attributable to the $\nu(C{=}O)_{ester}$ vibration. Experimental work at the time of submission of this work has allowed access to complex $[Cu(L'')_2(NO_3)(phen)_2(EtOH)](NO_3)$, where L''^- is the monoethyl maleate(-1) ligand. Further synthetic studies on the general $CuX_2/H_2L/phen$ reaction system in alcohols (ROH) are in progress; we have been investigating the effects of the nature of X^-, the nature of R, the reactants' concentration and the crystallization rate on the chemical and structural identity of the products.

3.2. Description of structures

The crystallographically established coordination modes of HL^- in complexes **2**–**4**, **7** and **8** are shown in Fig. 2. Aspects of the molecular and crystal structures of representative complexes are presented in Figs. 3–10, while selected interatomic distances and angles are listed in Tables 2–4.

The molecular structures of the dinuclear cations that are present in complexes **1** · 1.5MeCN · $0.5H_2O$, **2** · 2.5MeCN · $2H_2O$ and

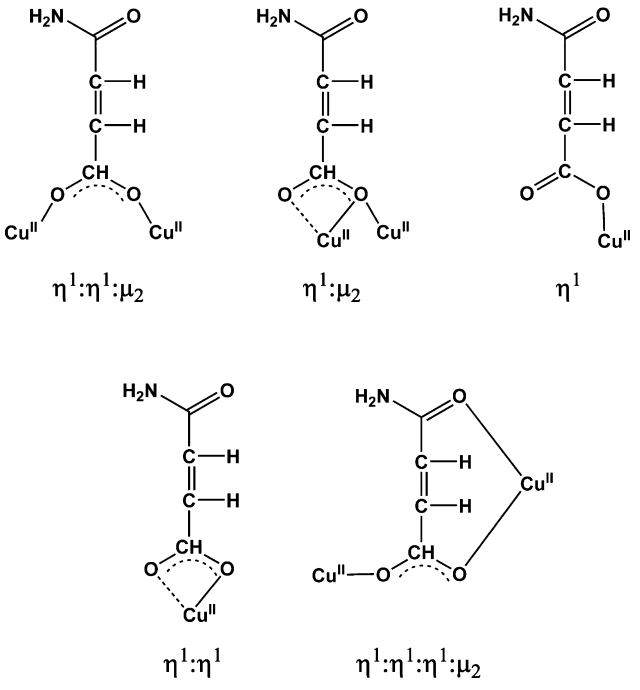

Fig. 2. The crystallographically established coordination modes of the maleamate-(-1) (HL^-) ligand in the copper(II) complexes **2**–**4**, **7** and **8**.

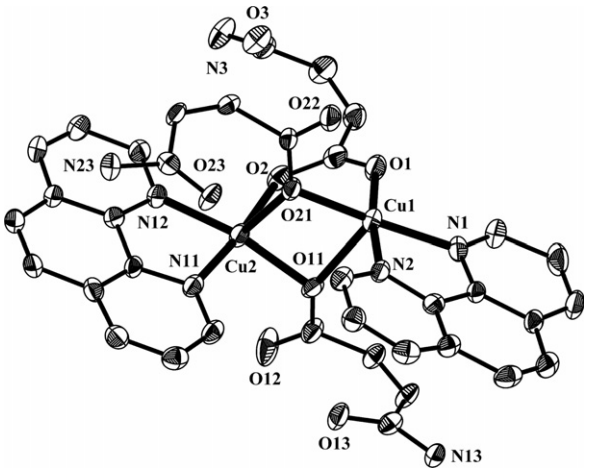

Fig. 3. Partially labeled ORTEP plot of the cation of **2** · 2.5MeCN · $2H_2O$ with ellipsoids drawn at the 30% probability level. H atoms have been omitted for clarity.

7 · MeOH · H_2O are very similar. We give below a comparative structural description for the cations of **1** (Fig. S1) [19] and **2** (Fig. 3, Table 2). The structure of the cation in both complexes consists of two Cu^{II} ions bridged by the carboxylate groups of the three HL^- ligands; one carboxylate group is in the familiar $\eta^1{:}\eta^1{:}\mu_2$ mode and the other two in the relatively rare monoatomic bridging mode ($\eta^1{:}\mu_2$), see Fig. 2. A chelating phen molecule completes five-coordination at each metal center. The neutral primary amide groups of the HL^- ligands remain uncoordinated. As is sometimes [27] (but not always [28]) observed for monoatomic bridging carboxylate groups, there is evidence for weak interactions between the metal ions and the "free" carboxylate oxygen atoms. For example, the Cu(1)···O(22) and Cu(2)···O(12) distances in **2** are only 2.989(5) and 2.882(5) Å, respectively. The coordination geometry about each metal ion in both complexes is well described as square pyramidal with the bridging carboxylate oxygen atoms occupying the apical positions for the two Cu^{II} centers; for example, atoms O(11) and O(21) occupy the apical positions for Cu(1) and Cu(2), respectively. Analysis of the shape-determining angles using the

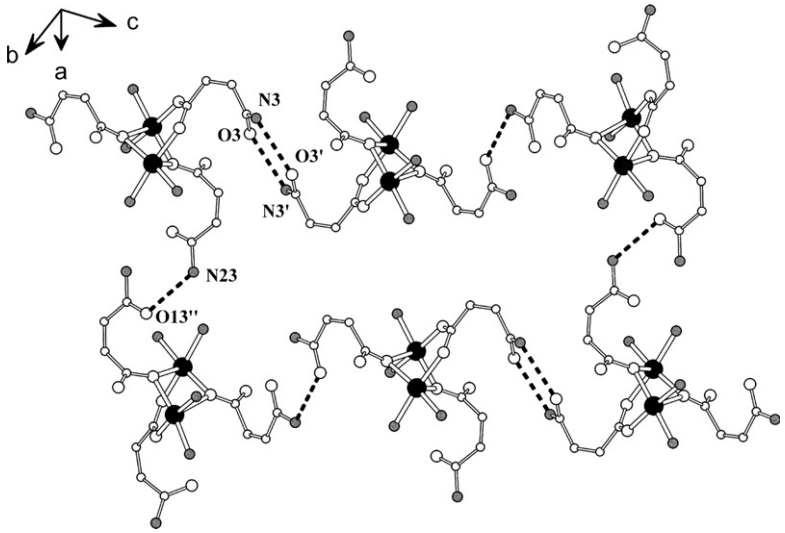

Fig. 4. Partially labelled portion of the supramolecular structure of **2** · 2.5MeCN · $2H_2O$ showing one loop of six H-bonded $[Cu_2(HL)_3(phen)_2]^+$ cations. Colour code: Cu, black; O, large white; N, grey; C, small white; H bonds, dashed lines. Only the N atoms of the phen ligands are shown.

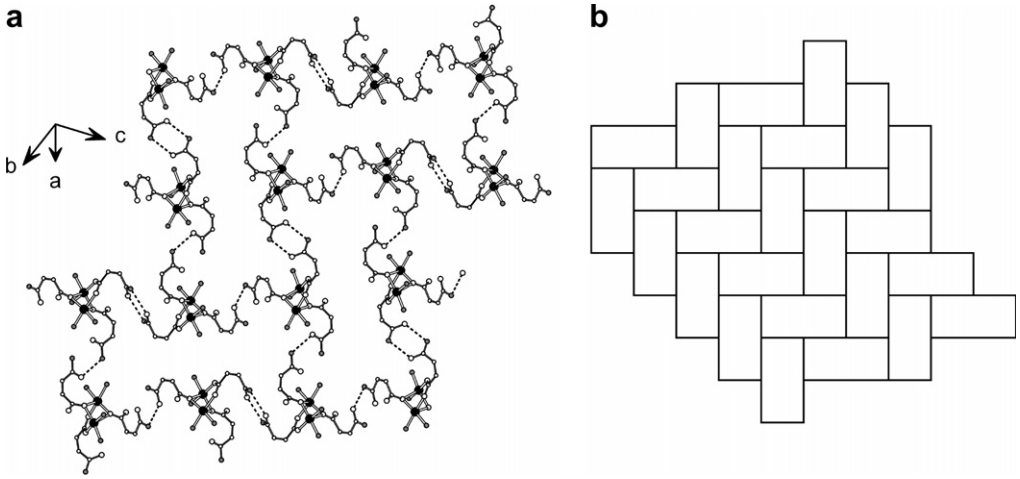

Fig. 5. (a) A part of one layer in the supramolecular structure of **2** · 2.5MeCN · $2H_2O$. Colour code as in Fig. 4. The dashed lines represent H bonds. Only the N atoms of the phen ligands are shown. (b) Schematic drawing showing the pattern of the H-bonded loops.

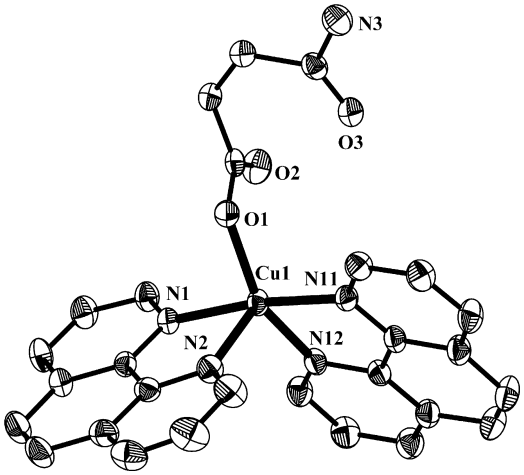

Fig. 6. Partially labeled ORTEP plot of the cation of **3** · 0.5MeCONH$_2$ · 0.75H$_2$O with ellipsoids drawn at the 30% probability level. H atoms have been omitted for clarity.

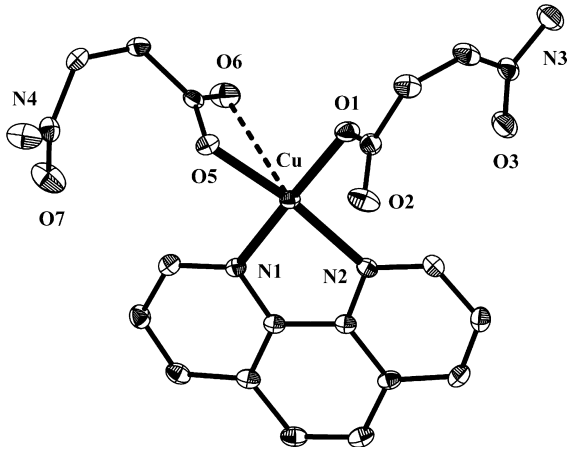

Fig. 7. Partially labelled ORTEP plot of **4** with ellipsoids drawn at the 30% probability level. The dashed line indicates a weak bonding interaction. H atoms have been omitted for clarity.

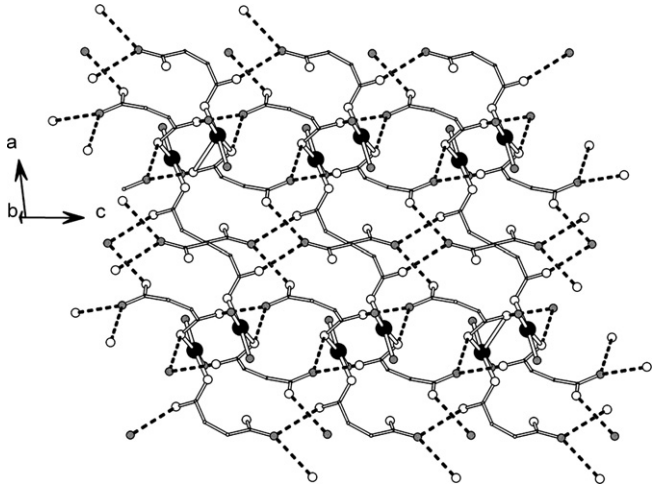

Fig. 8. A part of the 3D H-bonded network that stabilizes the crystal structure of **4**. Colour code as in Figs. 4 and 5. The dashed lines represent H bonds. Only the N atoms of the phen ligands are shown.

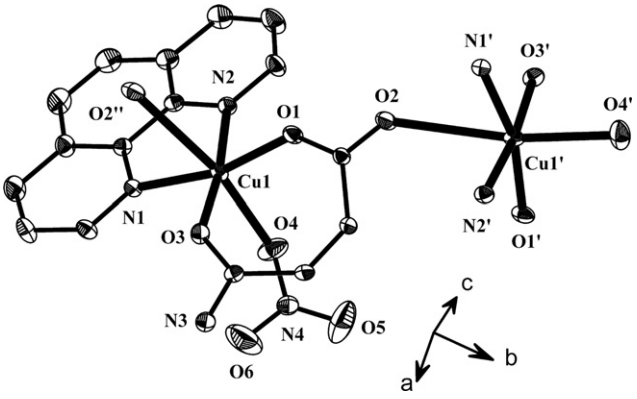

Fig. 9. Partially labelled ORTEP plot of a very small fragment of one chain of complex **8** with ellipsoids drawn at the 30% probability level. H atoms have been omitted for clarity. *Symmetry codes*: (′) $1-x$, $0.5+y$, $1.5-z$; (″) $1-x$, $-0.5+y$, $1.5-z$.

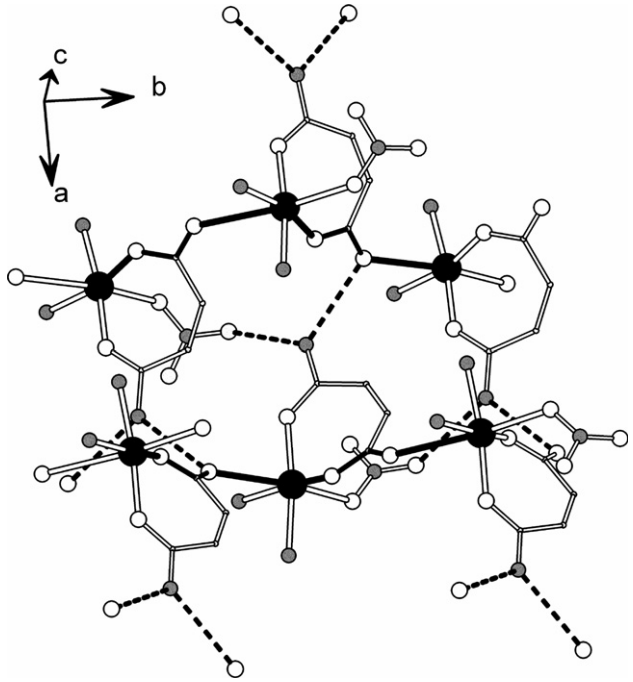

Fig. 10. A plot of the 2D H-bonded network in the crystal structure of **8**. Colour code as in Figs. 4, 5 and 8. The dashed lines represent H bonds along the chains. Only the N atoms of the phen ligands are shown.

approach of Reedijk, Addison and co-workers [29] yields trigonality index, τ, values of 0.025 and 0.042 for Cu(1) and Cu(2), respectively, in **1**, and 0.033 and 0.106 for Cu(1) and Cu(2), respectively, in **2** ($\tau = 0$ and 1 for perfect *sp* and *tbp* geometries, respectively). As expected, the axial bonds are the longest. For **1**, the dihedral angle between the two least-squares basal planes is 21.5°, and the angle between the two phen planes is 23.2°. The corresponding angles for **2** are 17.8° and 9.0°, respectively.

In the crystal structure of **2**, the cations are associated through two N(3)···O(3) ($2-x$, $-y$, $2-z$), as well as through N(23)···O(13) ($0.5+x$, $0.5-y$, $0.5+z$) H bonds forming loops of six H-bonded cations (Fig. 4, Table S1); the loops are adjacent to each other, thus creating layers that extend parallel to the (101) plane (Fig. 5).

Complexes **1**, **2** and **7** are new welcome additions in the very small family of complexes containing the extremely rare $\{Cu^{II,II}_2(\eta^1{:}\mu_2\text{-}O_2CR)_2(\eta^1{:}\eta^1{:}\mu_2\text{-}O_2CR)\}^+$ core [15,30], where RCO_2^-

Table 2
Selected interatomic distances (Å) and angles(°) for complex **2** · 2.5MeCN · $2H_2O$

Distances			
Cu(1)–O(1)	1.924(6)	Cu(2)–O(11)	1.957(4)
Cu(1)–O(21)	1.935(4)	Cu(2)–N(11)	1.958(6)
Cu(1)–N(2)	1.967(6)	Cu(2)–N(12)	1.998(6)
Cu(1)–N(1)	1.989(6)	Cu(2)–O(21)	2.286(5)
Cu(1)–O(11)	2.301(5)	Cu(1)···Cu(2)	3.163(2)
Cu(2)–O(2)	1.955(5)		
Angles			
O(1)–Cu(1)–O(21)	91.1(2)	O(2)–Cu(2)–N(11)	174.2(2)
O(21)–Cu(1)–N(2)	94.8(2)	O(11)–Cu(2)–N(11)	94.8(2)
O(1)–Cu(1)–N(1)	91.5(3)	O(2)–Cu(2)–N(12)	92.6(3)
O(21)–Cu(1)–N(1)	174.4(2)	O(11)–Cu(2)–N(12)	167.8(2)
N(2)–Cu(1)–N(1)	82.3(3)	N(11)–Cu(2)–N(12)	82.4(3)
O(1)–Cu(1)–O(11)	88.1(2)	O(2)–Cu(2)–O(21)	88.3(2)
O(21)–Cu(1)–O(11)	80.9(2)	O(11)–Cu(2)–O(21)	80.8(2)
N(2)–Cu(1)–O(11)	97.6(2)	N(11)–Cu(2)–O(21)	90.7(2)
N(1)–Cu(1)–O(11)	104.2(2)	N(12)–Cu(2)–O(21)	111.0(2)
O(2)–Cu(2)–O(11)	90.7(2)		

is a simple carboxylate (R = H, Me, Ph, ..., i.e. R is a non-coordinating group).

The structure of **3** · $0.5MeCONH_2$ · $0.75H_2O$ consists of the mononuclear cation $[Cu(HL)(phen)_2]^+$ (Fig. 6, Table 3), a hydroxide counteranion, and acetamide and water solvate molecules; the latter three will not be further discussed. The coordination sphere of the complex cation consists of four N atoms belonging to the two chelating phen molecules and one carboxylate oxygen from the terminal monodentate (η^1, Fig. 2) HL^- ligand. The metal coordination geometry may be described as distorted square pyramidal with the N(2) atom occupying the apical position at Cu(1). As a result, the Cu(1)–N(2) bond length (2.198(4) Å) is longer than the Cu(1)–N(1,11,12) bond distances (1.995(3)–2.057(4) Å). The τ value is 0.31 and thus the geometry about the metal ion is significantly distorted. The cations of **3** are held together through two N(3)···O(3) ($-x$, $1-y$, $1-z$) H bonds to form dimers, dimensions being N(3)···O(3) = 2.992 Å, HN(3A)···O(3) = 2.072 Å and N(3)–HN(3A)···O(3) = 168.0° (Table S2). The intermolecular distance of 2.896 Å between the hydroxide O atom and the carboxylato oxygen atom O(1) is a strong evidence of the presence of a H bond between the two atoms.

Complex **3** joins a family of structurally characterized complexes of the general formula $[Cu(O_2CR)(phen)_2]^+$ [31], where R is a non-coordinating group; however, in most of these complexes the carboxylate group of RCO_2^- is chelating, notable exceptions being complexes $[Cu(O_2CMe)(phen)_2](BF_4)$ [31e], $[Cu(O_2CMe)(phen)_2](O_2CMe)\cdot A$ [31f], where A is the neutral lattice molecule 2-(ethylthio)-4-oxopteridine, and $[Cu(HCO_2)(phen)_2](BF_4)$ [31g].

The structure of **4** (Fig. 7, Table 3) consists of mononuclear $[Cu(HL)_2(phen)]$ molecules. Two carboxylate oxygen atoms from the two terminal monodentate HL^- ligands (η^1, Fig. 2) and two phen nitrogen atoms create the coordination environment around the Cu^{II} atom. The metal coordination geometry is well described as square planar, the two *trans* coordination angles being 171.9(1)° (O(5)–Cu–N(2)) and 173.9(1)° (O(1)–Cu–N(1)). The carboxylato group of one HL^- ligand can be alternatively considered as asymmetric chelating (η^1:η^1, Fig. 2) as evidenced by the Cu–O distances of 1.947(2) (Cu–O(5)) and 2.805(2) (Cu–O(6)) Å; on the other hand, the carboxylato group of the second HL^- ligand is undoubtedly considered as monodentate due to the large Cu–O(2) distance of 3.050(2) Å. Adopting this alternative description of the carboxylate coordination mode, the metal coordination geometry may be described as distorted square pyramidal with the weakly bonding O(6) atom occupying the apical position at Cu; this view is emphasized in Fig. 7. The primary amide groups of the two HL^- ligands remain uncoordinated in **4**; instead, both participate in hydrogen bonding interactions that lead to the formation of a 3D framework (Fig. 8, Table S2).

Complex **4** is only the second structurally characterized example of a mononuclear complex with the formula $[Cu(RCO_2)_2(phen)]$, the first being the bis(3-methylbenzoato-O,O′)(phenanthroline-N,N′)copper(II) [32]; however, in the latter both carboxylate groups are chelating resulting in a six-coordinate species. It should be mentioned at this point that two other, mononuclear copper(II) complexes containing two (monodentate) carboxylate ligands and one phen ligand have been crystallographically characterized. These are $[Cu(Cl_3CCO_2)_2(phen)(H_2O)]$ [33a] and $[Cu(O_2CPh)_2(phen)(H_2O)]$ [33b]; both contain one aquo ligand resulting in a true 5-coordination at the metal centre.

Complex **8** in a 1D coordination polymer comprising neutral $[Cu(HL)(NO_3)(phen)]_n$ chains (Fig. 9, Table 4). The carboxylato group of the HL^- ligand is asymmetrically coordinated to two neighbouring Cu^{II} ions adopting the *syn,anti* η^1:η^1:μ_2 mode, thus promising the formation of zigzag chains which extend parallel to the (1 0 0) plane. Two carboxylate oxygen atoms (from different HL^- ligands), two N atoms from the phen ligand, one oxygen atom (O(4)) from the monodentate nitrato group and the amide oxygen (O(3)) of HL^- create a distorted octahedral environment around the Cu^{II} centre. The Jahn–Teller sites are atoms O(4) and the carboxylate oxygen atom O(2″) ($1-x$, $-0.5+y$, $1.5-z$); the Cu(1)–O(4) and Cu(1)–O(2) ($1-x$, $-0.5+y$, $1.5-z$) distances are 2.398(5) and 2.751(5) Å, respectively. As a result of the orientation of the Jahn–Teller axis, the two $Cu–O_{carboxylato}$ bond lengths differ about

Table 3
Selected interatomic distances (Å) and angles (°) for complexes **3** · $0.5MeCONH_2$ · $0.75H_2O$ and **4**

3 · $0.5MeCONH_2$ · $0.75H_2O$		**4**	
Distances			
Cu(1)–O(1)	1.985(3)	Cu–O(1)	1.937(2)
Cu(1)–N(11)	1.995(3)	Cu–O(5)	1.947(2)
Cu(1)–N(1)	2.006(3)	Cu–N(2)	2.006(2)
Cu(1)–N(12)	2.057(4)	Cu–N(1)	2.018(2)
Cu(1)–N(2)	2.198(4)	Cu···O(6)	2.805(4)
Angles			
O(1)–Cu(1)–N(11)	92.6(1)	O(1)–Cu–O(5)	89.23(8)
O(1)–Cu(1)–N(1)	93.3(1)	O(1)–Cu–N(2)	96.10(8)
N(11)–Cu(1)–N(1)	171.7(1)	O(5)–Cu–N(2)	171.92(8)
O(1)–Cu(1)–N(12)	153.1(1)	O(1)–Cu–N(1)	173.87(8)
N(11)–Cu(1)–N(12)	81.8(1)	O(5)–Cu–N(1)	93.58(8)
N(1)–Cu(1)–N(12)	95.5(1)	N(2)–Cu–N(1)	81.71(8)
O(1)–Cu(1)–N(2)	97.8(1)		
N(11)–Cu(1)–N(2)	93.3(2)		
N(1)–Cu(1)–N(2)	80.1(1)		
N(12)–Cu(1)–N(2)	108.8(2)		

Table 4
Selected interatomic distances (Å) and angles (°) for the cationic chain of complex **8**

Distances			
Cu(1)···Cu(1′)	6.644(1)	Cu(1)–N(2)	2.015(4)
sCu(1)–O(1)	1.919(4)	Cu(1)–O(4)	2.398(5)
Cu(1)–O(3)	1.934(4)	Cu(1)–O(2″)	2.751(5)
Cu(1)–N(1)	2.012(4)		
Angles			
O(1)–Cu(1)–O(3)	95.1(2)	N(1)–Cu(1)–O(4)	91.9(2)
O(1)–Cu(1)–N(1)	165.3(2)	N(2)–Cu(1)–O(4)	88.7(2)
O(3)–Cu(1)–N(1)	92.4(2)	O(2″)–Cu(1)–O(1)	92.8(1)
O(1)–Cu(1)–N(2)	89.7(2)	O(2″)–Cu(1)–N(2)	89.2(1)
O(3)–Cu(1)–N(2)	173.0(2)	O(2″)–Cu(1)–O(3)	85.5(1)
N(1)–Cu(1)–N(2)	81.9(2)	O(2″)–Cu(1)–N(1)	75.2(1)
O(1)–Cu(1)–O(4)	99.9(2)	O(2″)–Cu(1)–O(4)	167.1(2)
O(3)–Cu(1)–O(4)	95.5(2)		

Symmetry codes: (′) $1-x$, $0.5+y$, $1.5-z$; (″) $1-x$, $-0.5+y$, $1.5-z$.

0.8 Å (Cu(1)–O(1) 1.919(4) Å, Cu(1)–O(2″) 2.751(5) Å); this significant difference is reflected on the C–O carboxylate bond distances which also differ (C–O(1) 1.270(6) Å, C–O(2) 1.231(6) Å). The maleamate(-1) ligand adopts the η^1:η^1: η^1:μ_2 coordination mode (Fig. 2) in **8** and this is the first case in which amide coordination of HL^- is realized; **8** is the first example of a polymeric metal complex involving the HL^- ligand. Of remarkable interest is the formation of the 7-membered $CuO_{amide}C{=}C{-}CO_{carboxylate}$ chelating ring.

There are two H bonding interactions in the crystal lattice of **8**, which result in the formation of a 2D network that extends parallel to the (0 0 1) plane, see Fig. 10. Their dimensions are: N(3)···O(5) $(1.5-x,\ -0.5+y,\ z)$ = 2.927 Å, HN(3A)···O(5) = 2.077 Å, N(3)–HN(3A)···O(5) = 151.5° and N(3)···O(2) $(0.5+x,\ y,\ 1.5-z)$ = 2.896 Å, HN(3B)···O(2) = 2.149 Å, N(3)–HN(3B)···O(2) = 159.2°.

If we ignore the preliminary communication of this work [19], complexes **1**, **2**, **3**, **4**, **7** and **8** are the first structurally characterized maleamate complexes of *any* metal. However, it should be mentioned at this point that few metal complexes of N-substituted maleamate ligands have been structurally characterized [34]. These are $[Bu^n{}_3Sn^{IV}(L1)]_n$[34a], where $L1^-$ is the N-(1-naphthyl)maleamato(-1) ligand, and $[Mo^{II}(\eta^3\text{-}C_3H_4\text{-Me-2})(L2)(CO)_2\text{-}(phen)]$ [34b], where $L2^-$ is the N-(*p*-tolyl)maleamato(-1) ligand. $L1^-$ behaves as an $O_{carboxylate}$, O_{amide} bidentate bridging ligand leading to polymeric chains, while $L2^-$ acts as a terminal $O_{carboxylate}$ monodentate ligand. The Mo^{II} complex was prepared from the reaction of $[Mo^{II}(\eta^3\text{-}C_3H_4\text{-Me-2})\{NH(p\text{- tolyl})(CO)_2(phen)\}]$ with maleic anhydride in THF and the $L2^-$ ligand resulted from the coupling between maleic anhydride and the coordinated amido group of the starting material.

3.3. IR spectra

Complexes **2**–**4** and **7**–**11** were characterized by IR spectroscopy. Complexes **2**, **3**, **7**, **10** and **11** exhibit a variable intensity, very broad band above 3100 cm^{-1}, assignable to ν(OH) vibrations of coordinated or/and lattice MeOH/H_2O [10a], and to $\nu(OH)_{hydroxo}$ mode (only in **3**). The broadness and relatively low frequency of this band are both indicative of H bonding.

Absorptions of free phen in the 1600–1400 cm^{-1} region, attributed to ring stretching vibrations, shift to higher frequencies upon chelation in **2**–**8** and **11**. The 854 and 738 cm^{-1} bands of free phen, assigned to out-of-plane C–H deformations, shift to lower frequencies, sometimes with splitting of the former [35].

In the spectrum of **11**, the strong band at around 1090 cm^{-1} and the medium band at 620–625 cm^{-1} are attributed to the $\nu_3(F_2)$ and $\nu_4(F_2)$ modes (ν_d(ClO) and δ_d(OClO), respectively) of the uncoordinated T_d perchlorate ions, respectively [36a].

The IR spectra of **2** and **7** are indicative of the presence of ionic nitrates; their – crystallographically established – existence is deduced from the appearance of the $\nu_3(E')$ ν_d(NO) mode of the D_{3h} ionic nitrate at ~1385 cm^{-1} [36a]. The IR spectrum of **8** in KBr (Section 2.2.9) exhibits the strong $\nu_3(E')$ band at 1385 cm^{-1}; it is thus indicative of the presence of ionic nitrates, although the structure of the complex (Section 3.2) revealed no NO_3^- counterions! This suggest [36b] that a certain amount of nitrato ligands are replaced by bromides (thus generating ionic nitrates) in the KBr matrix. It is well known that pressing a pellet affects the nitrate coordination [36b,36c], and this consequently affects the nitrate vibrations [36b,36c,36d]. In the Nujol and hexachlorobutadiene mull spectra of **8** (not cited in Section 2.2.9), the bands at 1455 and 1320 cm^{-1} are assigned to the $\nu_5(B_2)$ ($\nu_a(NO_2)$) and $\nu_1(A_1)$ ($\nu_s(NO_2)$) stretching modes (under C_{2v} symmetry), respectively, of the nitrato ligand [36a]; their separation is small (135 cm^{-1}) in accordance with the monodentate character of the nitrate group [36a].

The spectra of **2**–**4** and **7**–**11** exhibit the typical bands of the primary amide and carboxylate groups [37]. Tentative IR assignments of few diagnostic bands attributed to these groups are given in Table 5. The assignments have been given in comparison with the data obtained for sodium maleamate (Na(HL)), assumed to contain a "free" carboxylate group [37b], oxamato(-1) (**X** in Fig. 1; R = H) [17b], malonamato(-1) (**V** in Fig. 1; n = 1) [18] and succinamato-(-1) (**V** in Fig. 1; n = 2) [15,16] metal complexes, and taking into account literature reports [37]. As a general remark, we must emphasize that some of the vibrational modes shown in Table 5 are strongly coupled and thus the proposed assignments must be regarded as approximate descriptions of the vibrations. The typical bands of the neutral amide group ($\nu_{as}(NH_2)$, $\nu_s(NH_2)$, $\delta(NH_2)$, ν(CN)) in the spectra of **2**–**4**, **7**, **10** and **11** are situated at approximately the same wavenumbers to those in the spectrum of Na(HL), confirming (**2**–**4**, **7**) or suggesting (**10**, **11**) the non-participation of the amide group in coordination. In the spectrum of **8**, the ν(CN) mode shifts to higher frequencies compared to Na(HL), whereas the $\nu(C{=}O)_{amide}$ band shows a frequency decrease. These shifts confirm the amide-O coordination [16,18]. Upon coordination via oxygen, the positively charged Cu^{II} ion stabilizes the negative charge on the O atom; the amide function now occurs in its polar resonance form and thus the double bond character of the CN bond increases (hence the shift of ν(CN) to higher wavenumbers), while the double bond character of the CO bond decreases (hence the shift of ν(CO) to lower wavenumbers). For **9**, only the $\nu(C{=}O)_{amide}$ band shows a frequency decrease. The difference $\Delta(\Delta = \nu_{as}(CO_2)-\nu_s(CO_2))$ for **3** is more than that of Na(HL), as expected for the crystallographically confirmed monodentate mode of the carboxylate

Table 5
Diagnostic amide and carboxylate IR bands (cm^{-1}) and their tentative assignments for sodium maleamate[a] and complexes **2**–**4** and **7**–**11**

Compound[b]	$\nu_{as}(NH_2)$[c]	$\nu_s(NH_2)$[c]	$\nu(C{=}O)_{amide}$	$\delta(NH_2)$	ν(C=C)	$\nu_{as}(CO_2)$[e]	ν(CN)[e]	$\nu_s(CO_2)$[e]
Na(HL)	3385sb	3160mb	1677s	1636m[d]	1636m[d]	1576s	1449s	1407m
2	3375sb	3184mb	1676m	1643s[d]	1643s[d]	1575vs, 1548s	1431s[d]	1431s[d]
3	3425sb	3275wb	1681m	1628m[d]	1628m[d]	1596m	1431s	1384s
4	3376mb	~3200wb	1676m	1654w	1628w	1576s	1432vs[d]	1432vs[d]
7	3400mb	3173w	1678m	1620sh[d]	1620sh[d]	1598vs, 1560m	1427m[c]	1427m[c]
8	3284mb[d]	3284mb[d]	1609s[d]	1588m	1609s[d]	1564s	1492m	1431s
9	3542m	3398m	1654m	1624m[d]	1624m[d]	1578m	1442s	1424m
10	3434mb	3188mb	1674m	1646m	1608s	1586s	1450m	1426m
11	3355sb	3185mb	1688s	1629m	1615sh	1585s, 1551s	1433s[d]	1433s[d]

Abbreviations: b, broad; m, medium; s, strong; sh, shoulder; v, very; w, weak.

[a] Prepared from the 1:1 reaction between H_2L and NaOH in EtOH, followed by precipitation with Et_2O.

[b] Solvate molecules have not been included

[c] For the solvent (coordinated, lattice) – containing complexes, these bands are components of the ν(OH) manifold.

[d] Overlapping bands.

[e] These vibrations may include an aromatic stretching character in **2**–**4**, **7**, **8** and **11**.

ligation [37b]. Owing to the presence (confirmed for **2**, **7** and proposed for **11**) of two different types of carboxylate bridges in the complexes containing the cation $[Cu_2(LH)_3(phen)_2]^+$, two $\nu_{as}(CO_2)$ bands are observed [15]. The difference Δ for **8**, **9** and **10** is less than that of Na(HL), as expected for the crystallographically confirmed (**8**) or suggested (**9**, **10**) bidentate bridging mode of the carboxylate ligation [37b].

4. Concluding comments and perspectives

The initial use of the HL^-/phen "ligand blend" in Cu(II) chemistry has yielded complexes (**3**, **4**, **8**) or a group of complexes (**1** [19], **2**, **7**), each of which promises to be a new family of copper(II) compounds. The dinuclear complexes **1**, **2** and **7** have bridging units that rarely appear in $Cu^{II,II}_2$ chemistry, while **8** is an interesting 1D polymer where polymerization is solely achieved by the carboxylate group of the HL^- ligand. Complexes **3** and **4** are new members in the $[Cu(RCO_2)(N,N'\text{-donor})_2]^+$ and $[Cu(RCO_2)_2(N,N'\text{-donor})]$ families of complexes, respectively. The structural diversity of the maleamato(-1) complexes described stems in part from the ability of HL^- to exhibit a variety of distinct coordination modes; no less than five ligation modes were observed in complexes **2**–**4**, **7** and **8**. We do believe that HL^- is also capable of acting as μ_3 and μ_4 ligand, thus increasing the possibilities for polynuclear complex and/or coordination polymer formation. Preliminary results in our group indicate that "fine-tuning" of the synthetic and crystallization conditions can bring remarkable changes in the ligation modes of HL^-, and in the structures of the resulting metal complexes.

The structural chemistry of the Cu^{II}/ HL^-/phen system, as detailed in the above discussion for **2**–**4**, **7** and **8**, does not show similarities to that of the $Cu^{II}/^-OOC–CH{=}CH–COO^-$/phen system [38,39], due to the different nature (charge, donor groups) of HL^- and the maleate(-2) (**III** in Fig. 1) or fumarate(-2) (**II** in Fig. 1) ligands. Even the hydrogenmaleate(-1) ion, $Hmal^-$ (**XIV**, Fig. 1), which can be considered as a "structural analogue" of HL^-, forms the complex $[Cu(Hmal)(phen)(H_2O)_2]^+(Hmal^-)$ [40], which is different from the mononuclear complexes **3** and **4**. A direct comparison of the chemistry of the $Cu^{II}/HL^-/N,N'$-donor system with that of the $Cu^{II}/^-OOC–CH_2–CH_2–CONH_2$ (**V** with $n = 2$ in Fig. 1; Hsucm)/N,N′-donor system is not feasible, because phen has not yet been used in the latter. However, complexes $[Cu_2(Hsucm)_3(dmbpy)_2](OH)$ [15], **2** and **7** have structurally similar cations, the only difference being the different nature of the aromatic bidentate N,N′-chelate (dmbpy = 4,4′-dimethyl-2,2′-bipyridine). It should be mentioned that no transformation of the amide group to the methyl ester group was observed during the investigation of the Cu^{II}/Hsucm$^-$/bpy or dmbpy system in MeOH [15].

Complexes of other 3d- or 4f-metal ions with the HL^-/phen ligand combination are not known to date, and it is currently not evident whether the chemical identity and structure of such compounds, and the $HL^-\rightarrow L'^-$ transformation [19] are dependent on the particular nature of the metal ion. It is also clear that the metal ion/LH^- chemistry warrants expansion to other bidentate and *tridentate* aromatic N-heterocycles. We are studying these matters. In the preliminary communication of this work [19], we have reported that the tridentate chelating ligand 2,6-bis(pyrazol-1-yl)pyridine(bppy) gives complexes $[Cu_2(HL)_2(bppy)_2](ClO_4)_2$ and $[Cu_2(L')_2(bppy)_2](ClO_4)_2$ in MeCN and MeOH, respectively.

Acknowledgement

S.P.P. thanks the Research Committee of the University of Patras for support (K. Caratheodory Program No. 03016).

Appendix A. Supplementary data

CCDC 678054, 678055, 678056 and 678056 contain the supplementary crystallographic data for $\mathbf{2}\cdot 2.5MeCN\cdot 2H_2O$, $\mathbf{3}\cdot 0.5MeCONH_2\cdot 0.75H_2O$, **4** and **8**. These data can be obtained free of charge via http://www.ccdc.cam.ac.uk/conts/retrieving.html, or from the Cambridge Crystallographic Data Centre, 12 Union Road, Cambridge CB2 1EZ, UK; fax: (+44) 1223-336-033; or e-mail: deposit@ccdc.cam.ac.uk. Supplementary data associated with this article can be found, in the online version, at doi:10.1016/j.poly.2008.04.005.

References

[1] (a) For example, see: B. Xu, N.D. Chasten, J. Biol. Chem. 266 (1991) 19965;
(b) T.G. Carrell, A.M. Tyryshkin, G.C. Dismukes, J. Biol. Inorg. Chem. 7 (2002) 2;
(c) A. Mishra, W. Wernsdorfer, K.A. Abboud, G. Christou, Chem. Commun. (2005) 54.
[2] (a) A.M. Ako, I.J. Hewitt, V. Mereacre, R. Clérac, W. Wernsdorfer, C.E. Anson, A.K. Powell, Angew. Chem., Int. Ed. 45 (2006) 4926;;
(b) Th. C. Stamatatos, K.A. Abboud, W. Wernsdorfer, G. Christou, Angew. Chem., Int. Ed. 46 (2007) 884.
[3] (a) For excellent reviews, see: G. Christou, D. Gatteschi, D.N. Hendrickson, R. Sessoli, MRS Bull. 25 (2000) 66;
(b) D. Gatteschi, R. Sessoli, Angew. Chem., Int. Ed. 42 (2003) 268;
(c) R. Bircher, G. Chaboussant, C. Dobe, H.U. Güdel, S.I. Ochsenbein, A. Sieber, O. Waldman, Adv. Funct. Mater. 16 (2006) 209;
(d) G. Aromi, E.K. Brechin, Struct. Bonding 122 (2006) 1.
[4] (a) Representative work with the participation of our group: Th. C. Stamatatos, D. Foguet-Albiol, S.-C. Lee, C.C. Stoumpos, C.P. Raptopoulou, A. Terzis, W. Wernsdorfer, S.O. Hill, S.P. Perlepes, G. Christou, J. Am. Chem. Soc. 129 (2007) 9484;
(b) C.J. Milios, C.P. Raptopoulou, A. Terzis, F. Lloret, R. Vicente, S.P. Perlepes, A. Escuer, Angew. Chem., Int. Ed. 43 (2004) 210.
[5] (a) For interesting reviews concerning the chemistry and applications of coordination polymers, see: C. Janiak, Dalton Trans. (2003) 2781. Dalton Perspective;
(b) S.R. Batten, R. Robson, Angew. Chem., Int. Ed. Engl. 37 (1998) 1460;
(c) M. Munakata, L.P. Wu, T. Kuroda-Sowa, Adv. Inorg. Chem. 46 (1999) 173;
(d) S.R. Batten, Curr. Opin. Solid State Mater. Sci. 5 (2001) 107;
(e) S. Kitagawa, S. Noro, in: J.A. McCleverty, T.J. Meyer (Eds.), Comprehensive Coordination Chemistry II, vol. 7, Elsevier, Amsterdam, 2004, pp. 231–261;
(f) A.Y. Robin, K.M. Fromm, Coord. Chem. Rev. 250 (2006) 2127;
(g) Y. Zhou, M. Hong, X. Wu, Chem. Commun. (2006) 135. feature article;
(h) C. Coulon, H. Miyasaka, R. Clérac, Struct. Bonding 122 (2006) 163;
(i) D.-K. Bucar, G.S. Papaefstathiou, T.D. Hamilton, Q.L. Chu, I.G. Georgiev, L.R. MacGillivray, Eur. J. Inorg. Chem. (2007) 4559. microreview;
(j) J.L.C. Rowsell, O.M. Yaghi, Micropor. Mesopor. Mater. 73 (2004) 3.
[6] R.E.P. Winpenny, in: J.P. Sauvage (Ed.), Transition Metals in Supramolecular Chemistry, vol. 5, Wiley, Chichester, 1999, pp. 193–223.
[7] (a) P.N.W. Baxter, J.-M. Lehn, J. Fisher, M.-T. Youinou, Angew. Chem., Int. Ed. Engl. 33 (1994) 2284;
(b) M. Fujita, K. Umemoto, M. Yoshizawa, N. Fujita, T. Kusukawa, K. Biradha, Chem. Commun. (2001) 509.
[8] (a) M. Eddaoudi, D.B. Moler, H. Li, B. Chen, T.M. Reineke, M. O'Keeffe, O.M. Yaghi, Acc. Chem. Res. 34 (2001) 319;
(b) O.M. Yaghi, M. O'Keeffe, N.W. Ockwig, H.K. Chae, M. Eddaoudi, J. Kim, Nature 423 (2003) 705;
(c) G.S. Papaefstathiou, L.R. MacGillivray, Coord. Chem. Rev. 246 (2003) 169;
(d) S. Kitagawa, R. Kitaura, S.-i. Noro, Angew. Chem., Int. Ed. 43 (2004) 2334;
(e) M.J. Rosseinsky, Micropor. Mesopor. Mater. 73 (2004) 15.
[9] (a) Representative work from our group: Th. C. Stamatatos, A.K. Boudalis, K.V. Pringouri, C.P. Raptopoulou, A. Terzis, J. Wolowska, E.J.L. McInnes, S.P. Perlepes, Eur. J. Inorg. Chem. (2007) 5098;
(b) C. Papatriantafyllopoulou, G. Aromi, A.J. Tasiopoulos, V. Nastopoulos, C.P. Raptopoulou, S.J. Teat, A. Escuer, S.P. Perlepes, Eur. J. Inorg. Chem. (2007) 2761;
(c) C. P Raptopoulou, Y. Sanakis, A.K. Boudalis, V. Psycharis, Polyhedron 24 (2005) 711;
(d) C.P. Raptopoulou, A.K. Boudalis, Y. Sanakis, V. Psycharis, J.M. Clemente-Juan, M. Fardis, G. Diamantopoulos, G. Papavassiliou, Inorg. Chem. 45 (2006) 2317.
[10] (a) Representative work from our group: C. Papatriantafyllopoulou, C.P. Raptopoulou, A. Terzis, J.F. Janssens, E. Manessi-Zoupa, S.P. Perlepes, J.C. Plakatouras, Polyhedron 26 (2007) 4053;
(b) C.J. Milios, G.S. Papaefstathiou, C.P. Raptopoulou, A. Terzis, S.P. Perlepes, Bioinorg. Chem. Appl. (2007). [Article id 28508];
(c) K. Skorda, Th. C. Stamatatos, A.P. Vafiadis, A.T. Lithoxoidou, A. Terzis, S.P. Perlepes, J. Mrozinski, C.P. Raptopoulou, J.C. Plakatouras, E.G. Bakal bassis, Inorg. Chim. Acta 358 (2005) 565;
(d) G.S. Papaefstathiou, R. Vicente, C.P. Raptopoulou, A. Terzis, A. Escuer, S.P. Perlepes, Eur. J. Inorg. Chem. (2002) 2488.

[11] For an excellent provocative account, see: R.E.P. Winpenny, J. Chem. Soc. Dalton Trans. (2002) 1. Dalton Perspective.
[12] (a) For example, see: D. Ghoshal, T.K. Maji, G. Mostafa, S. Sain, T.-H. Lu, J. Ribas, E. Zangrando, N.R. Chaudhuri, Dalton Trans. (2004) 1687;
(b) M.-X. Li, G.-Y. Xie, S.-L. Jin, Y.-D. Gu, M.-Q. Chen, J. Liu, Z. Xu, X.-Z. You, Polyhedron 15 (1996) 535.
[13] (a) For example, see: M. McCann, M.T. Casey, M. Devereux, M. Curran, G. Ferguson, Polyhedron 16 (1997) 2547;
(b) S. Dalai, P.S. Mukherjee, G. Rogez, T. Mallah, M.G.B. Drew, N.R. Chaudhuri, Eur. J. Inorg. Chem. (2002) 3292;
(c) S. Konsar, P.S. Mukherjee, E. Zangrando, F. Lloret, N.R. Chaudhuri, Angew. Chem., Int. Ed. (2002) 1561.
[14] (a) C. Pettinari, F. Marchetti, A. Drozdov, in: J.A. McCleverty, T.J. Meyer (Eds.), Comprehensive Coordination Chemistry II, vol. 1, Elsevier, Amsterdam, 2004, pp. 240–246;
(b) N. Guillou, C. Livage, G. Férey, Eur. J. Inorg. Chem. (2006) 4963 (microreview).
[15] I. Chadjistamatis, A. Terzis, C.P. Raptopoulou, S.P. Perlepes, Inorg. Chem. Commun. 6 (2003) 1365.
[16] A. Messimeri, V. Nastopoulos, A. Terzis, C.P. Raptopoulou, C. Papadimitriou, S.P. Perlepes, Inorg. Chem. Commun. 8 (2005) 578.
[17] (a) For example, see: G.S. Papaefstathiou, A. Peeters, A.T.H. Lenstra, H.O. Desseyn, S.P. Perlepes, J. Mol. Struct. 559 (2001) 167;
(b) C. Vansant, H.O. Desseyn, S.P. Perlepes, Trans. Met. Chem. 20 (1995) 454.
[18] C. Vascant, H.O. Desseyn, V. Tangoulis, C.P. Raptopoulou, A. Terzis, S.P. Perlepes, Polyhedron 14 (1995) 2115.
[19] K.N. Lazarou, I. Chadjistamatis, V. Psycharis, S.P. Perlepes, C.P. Raptopoulou, Inorg. Chem. Commun. 10 (2007) 318.
[20] Rigaku/MSC, CRYSTALCLEAR, Rigauk/MSC Inc., The Woodlands, TX, USA, 2005.
[21] G.M. Sheldrick, SHELXS-97, Structure Solving Program, University of Göttingen, Germany, 1997.
[22] G.M. Sheldrick, SHELXL-97, Program for the Refinement of Crystal Structures from Diffraction Data, University of Göttingen, 1997.
[23] F.A. Cotton, G. Wilkinson, C.A. Murillo, M. Bochmann, Advanced Inorganic Chemistry, 6th ed., Wiley, New York, 1999. p. 489..
[24] E.C. Constable, Metals and Ligand Reactivity, VCH, Weinheim, 1996. pp. 46–56, 65–72..
[25] C.P. Raptopoulou, A.K. Boudalis, Y. Sanakis, V. Psycharis, J.M. Clemente-Juan, M. Fardis, G. Diamantopoulos, G. Papavassiliou, Inorg. Chem. 45 (2006) 2317.
[26] D.L. McFadden, A.T. McPhail, J. Chem. Soc., Dalton Trans. (1975) 1993.
[27] G. Christou, S.P. Perlepes, E. Libby, K. Folting, J.C. Huffman, R.J. Webb, D.N. Hendrickson, Inorg. Chem. 29 (1990) 3657.
[28] J.-P. Costes, F. Dahan, J.-P. Laurent, Inorg. Chem. 24 (1985) 1018.
[29] A.W. Addison, T.N. Rao, J. Reedijk, J. Rijn, G.C. Verschoor, J. Chem. Soc., Dalton Trans. (1984) 1349.
[30] (a) H. Matsushima, M. Koikawa, N. Nakashima, T. Tokii, Chem. Lett. (1995) 869;
(b) X.-Y. Le, X.-H. Zhou, K.-B. Yu, L.-N. Ji, Chin. J. Chem. 18 (2000) 638.
[31] (a) C.J. Simmons, N.W. Alcock, K. Seff, W. Fitzgerald, B.J. Hathayaw, Acta Crystallogr., Sect. B 41 (1985) 42;
(b) C.J. Simmons, K. Seff, F. Clifford, B.J. Hathayaw, Acta Crystallogr., Sect. C 39 (1983) 1360;
(c) W. Fitzgerald, B. Hathayaw, C.J. Simmons, J. Chem. Soc., Dalton Trans. (1985) 141;
(d) C. Escobar, O. Wittke, Acta Crystallogr., Sect. C 39 (1983) 1643;
(e) W. Fitzgerald, B. Hathaway, Acta Crystallogr., Sect. C 40 (1984) 243;
(f) J. Perkinson, S. Brodie, K. Yoon, K. Mosny, P.J. Carroll, T.V. Morgan, S.J.N. Burgmayer, Inorg. Chem. 30 (1991) 719;
(g) J.-Z. Cui, Y.-J. Yi, H. Zhang, H.-L. Gao, H.-T. Wang, Acta Crystallogr., Sect. E 63 (2007) m587.
[32] T.-G. Xu, D.-J. Xu, Acta Crystallogr., Sect. E 60 (2004) m1650.
[33] (a) P. Yin, M.-L. Hu, Q. Miao, Acta Crystallogr., Sect. E 61 (2005) m1854;
(b) L. Tian, X.-Y. Long, Jiegou Huaxue (Chin. J. Struct. Chem.) 19 (2000) 363.
[34] (a) M. Parvez, S. Ali, S. Ahmad, M.H. Bhatti, M. Mazhar, Acta Crystallogr., Sect. C 58 (2002) m334;
(b) D. Morales, J. Pérez, L. Riera, V. Riera, D. Miguel, M.E.G. Mosquera, S. García-Granda, Chem. Eur. J. 9 (2003) 4132.
[35] M.D. Grillone, F. Benetollo, G. Bombieri, Polyhedron 10 (1991) 2171.
[36] (a) K. Nakamoto, Infrared and Raman Spectra of Inorganic and Coordination Compounds, fourth ed., Wiley, New York, 1986. pp.121–125, 130–141, 251, 253–257.;
(b) G.J. Kleywegt, W.G.R. Wiesmeijer, G.J. Van Driel, W.L. Driessen, J. Reedijk, J.H. Noordik, J. Chem. Soc., Dalton Trans. (1985) 2177;
(c) E. Diamantopoulou, Th.F. Zafiropoulos, S.P. Perlepes, C.P. Raptopoulou, A. Terzis, Polyhedron 13 (1994) 1593;
(d) E. Katsoulakou, V. Bekiari, C.P. Raptopoulou, A. Terzis, P. Lianos, E. Manessi-Zoupa, S.P. Perlepes, Spectrochim. Acta Part A 61 (2005) 1627.
[37] (a) H.O. Desseyn, in: S. Patai (Ed.), The Chemistry of Acid Derivatives, vol. 2, Wiley, New York, 1992, pp. 271–303;
(b) G.B. Deacon, R.J. Phillips, Coord. Chem. Rev. 33 (1980) 227.
[38] Z. Li, D. Xu, J. Wu, M.Y. Chiang, J. Coord. Chem. 55 (2002) 1397.
[39] Y.Y. Wang, X. Wang, Q.Z. Shi, Y.C. Gao, Trans. Met. Chem. 27 (2002) 481.
[40] Y.-Q. Zheng, Z.-P. Kong, J.-L. Lin, J. Coord. Chem. 55 (2002) 1233.

Polyhedron 27 (2008) 2143–2150

Contents lists available at ScienceDirect

Polyhedron

journal homepage: www.elsevier.com/locate/poly

Dimeric *versus* monomeric nickel(II) complexes with tetraorganodichalcogenoimidodiphosphinato ligands: Crystal structures of $Ni_2[(OPPh_2)_2N]_4 \cdot CH_2Cl_2$, $Ni[(OPPh_2)_2N]_2(DMF)_2 \cdot 2H_2O$ and $[KNi[(SPPh_2)\{OP(OEt)_2\}N]_3]_2$

Alexandra Cristurean [a], Sevil Irisli [b,1], Dragos Marginean [a], Ciprian Rat [a], Anca Silvestru [a,*]

[a] Faculty of Chemistry and Chemical Engineering, "Babes-Bolyai" University, RO-400028 Cluj-Napoca, Romania
[b] Chemistry Department, Faculty of Science, Ege University, 35100 Bomova-Izmir, Turkey

ARTICLE INFO

Article history:
Received 11 October 2007
Accepted 9 April 2008
Available online 24 May 2008

Keywords:
Nickel complexes
Tetraorganodichalcogenoimido-diphosphinato ligands
Crystal and molecular structure

ABSTRACT

Nickel(II) complexes of the type $Ni[(XPR_2)(YPR'_2)N]_2$ [X = S (**1**) or O (**2**), Y = O, R = Ph, R′ = OEt] and $Ni_2[(OPPh_2)_2N]_4$ (**3**) were prepared by reacting either anhydrous $NiCl_2$ or $NiCl_2 \cdot 6H_2O$ with the potassium salt of the appropriate tetraorganodichalcogenoimidodiphosphinic acid, in 1:2 molar ratio. Recrystallization of **3** from dimethylformamide resulted in $Ni[(OPPh_2)_2N]_2(DMF)$ (**4**). Reaction between $NiCl_2$ and $K[(SPPh_2)\{OP(OEt)_2\}N]$ in an 1:3 molar ratio resulted in the ionic species $KNi[(SPPh_2)\{OP(OEt)_2\}N]_3$ (**5**). Compounds **1**–**5** were characterized by IR, electronic spectroscopy and mass spectrometry. The molecular structures of $\mathbf{3} \cdot CH_2Cl_2$, $\mathbf{4} \cdot 2H_2O$ and **5** were determined by single-crystal X-ray diffraction. A dimeric structure was found in case of complex $\mathbf{3} \cdot CH_2Cl_2$, with both monometallic biconnective and homobimetallic triconnective $[(OPPh_2)_2N]^-$ units, while an octahedral environment around nickel was established in the monomeric complex $\mathbf{4} \cdot 2H_2O$ by monometallic biconnective $[(OPPh_2)_2N]^-$ and DMF ligands, respectively. The crystal of the ionic species **5** contains discrete tetranuclear units in which the phosphorus ligands act heterobimetallic, either (*O*,*O*,*S*)-triconnective or (*S*,*O*,*O*,O_{Et})-tetraconnective, and (*N*,*O*,*O*,*S*)-heterotrimetallic tetraconnective, resulting in an octahedral environment around nickel and a square-pyramidal one around potassium, respectively. Powder X-ray diffraction studies on **5** are in agreement with the single-crystal investigation.

© 2008 Elsevier Ltd. All rights reserved.

1. Introduction

Metal complexes of tetraorganodichalcogenoimidodiphosphinato ligands, $[(XPR_2)(YPR'_2)N]^-$, attracted an increased interest for many years, due to their properties and potential applications as catalysts in organic synthesis, components in optical or electronic devices and sensors, NMR shift reagents, as well as derivatives with biological activity. Inorganic and organometallic derivatives either of Main Group [1] or transition metal complexes [2] were previously described. Several nickel(II) complexes of type $Ni[(XPR_2)(YPR'_2)N]_2$ were reported so far. For compounds containing the same chalcogen atoms, *e.g.* $Ni[(SPR_2)_2N]_2$ (R = Me [3,4], Ph [5,6]) and $Ni[(SePPh_2)_2N]_2$ [7], monomeric structures with a tetrahedral NiE_4 core (E = S, Se) were found by single-crystal X-ray diffraction, while in the case of the derivative $Ni[(SPMe_2)(SPPh_2)N]_2$ [5] a square-planar NiS_4 core was observed. The monothio derivatives $Ni[(OPPh_2)(SPR_2)N]_2$ (R = Me, Ph) are also monomeric, with chelating monometallic biconnective ligands, resulting in tetrahedral NiO_2S_2 cores [8]. For the dioxo derivative $Ni[(OPPh_2)_2N]_2$, a dimeric structure was previously proposed in benzene solution according to the molecular mass measurements [9].

Here we report on the synthesis and spectroscopic characterization of the new derivatives $Ni[(SPPh_2)\{OP(OEt)_2\}N]_2$ (**1**) and $Ni[(OPPh_2)\{OP(OEt)_2\}N]_2$ (**2**), the ionic species $KNi[(SPPh_2)\{OP(OEt)_2\}N]_3$ (**5**) as well as the adduct $Ni[(OPPh_2)_2N]_2(DMF)_2 \cdot 2H_2O$ ($\mathbf{4} \cdot 2H_2O$). The crystal and molecular structure of the dimeric $Ni_2[(OPPh_2)_2N]_4 \cdot CH_2Cl_2$ ($\mathbf{3} \cdot CH_2Cl_2$), its adduct $\mathbf{4} \cdot 2H_2O$ and the ionic derivative **5** are also discussed.

2. Experimental

The organophosphorus ligands were prepared according to literature methods: $K[(SPPh_2)\{OP(OEt)_2\}N]$, $K[(OPPh_2)\{OP(OEt)_2\}N]$

* Corresponding author. Tel.: +40 264 593833; fax: +40 264 590818.
E-mail addresses: sevil.irisli@ege.edu.tr (S. Irisli), ancas@chem.ubbcluj.ro (A. Silvestru).
[1] Tel.: +90 232 3884000.

0277-5387/$ - see front matter © 2008 Elsevier Ltd. All rights reserved.
doi:10.1016/j.poly.2008.04.006

[10]. K[(OPPh$_2$)$_2$N] was obtained by stirring the free acid with KOBu^t in diethyl ether. NiCl$_2$ was dehydrated by keeping NiCl$_2 \cdot 6H_2O$ for two weeks in the oven at 120 °C and subsequently stored under argon. Solvents were dried (THF on potassium, EtOH and MeOH on magnesium and CH_2Cl_2 on $CaCl_2$) and distilled under argon prior to be used. IR spectra were recorded in the range 4000–400 cm^{-1} in KBr pellets on a Jasco FT/IR-615 equipment, while the electronic spectra were recorded on a Jasco V-550 spectrometer. Mass spectra were recorded on a FINNIGAN MAT 8200 (CI), a FINNIGAN MAT 8222 (FAB) and a Bruker Esquire LC instrument (ESI), respectively. Magnetic moments were determined on a Sherwood MSB AUTO instrument and elemental analysis were performed on a VarioEL analyzer. The experimental powder diffraction pattern was obtained with a Shimadzu XRD-6000 diffractometer using a Cu Kα X-ray radiation, while the simulated X-ray powder diffraction pattern was obtained with the MERCURY CSD 2.0 program [11].

2.1. Preparation of bis[P,P-diethoxi-P′,P′-diphenyl-P′-thioimidodiphosphinato]nickel, Ni[(SPPh$_2$){OP(OEt)$_2$}N]$_2$ (**1**)

A mixture of K[(SPPh$_2$){OP(OEt)$_2$}N] (0.511 g, 1.25 mmol) and NiCl$_2$ (0.148 g, 0.62 mmol) was stirred for 8 h in a mixture of THF (40 ml) and ethanol (10 ml) at reflux. The solvent was removed in vacuum and the solid was treated with CH_2Cl_2. KCl was filtered off and the solution was concentrated in vacuum. A yellow-brown solid product was isolated. Yield: 0.39 g (78%), M.p. 99 °C. *Anal.* Calc. for $C_{32}H_{40}N_2O_6P_4S_2Ni$: C, 48.33; H, 5.03; N, 3.52. Found: C, 47.98; H, 5.16; N, 3.48%. IR (cm^{-1}): 1255vs [ν_{as}(P$_2$N)], 1105s [ν(PO)], 1043vs, br [ν(POC)], 596s [ν(PS)]. λ_{max} (cm^{-1}), CH_2Cl_2 (blue): 14620, 16129, 17921, 21209; THF (yellow): 12048, 22026. CI$_{neg}$ MS (*m*/*z*, %): 794 (85) [M$^-$], 368 (100) [{(SPPh$_2$){OP(OEt)$_2$}N}$^-$], 336 (38) [{(PPh$_2$){OP(OEt)$_2$}N}$^-$]. μ = 1.88 BM.

2.2. Preparation of bis[P,P-diethoxi-P′,P′-diphenyl-imidodiphosphinato]nickel, Ni[(OPPh$_2$){OP(OEt)$_2$}N]$_2$ (**2**)

A mixture of K[(OPPh$_2$){OP(OEt)$_2$}N] (0.720 g, 1.84 mmol) and NiCl$_2$ (0.119 g, 0.92 mmol) was stirred for 8 h in a mixture of THF (40 ml) and ethanol (10 ml) at reflux, under argon atmosphere. The solvent was removed in vacuum and the solid was treated with CH_2Cl_2. KCl was filtered off and the solution was concentrated in vacuum. A pale yellow solid product was isolated. Yield: 0.63 g (90%), M.p. 108–110 °C. *Anal.* Calc. for $C_{32}H_{40}N_2O_8P_4Ni$: C, 50.36; H, 5.25; N, 3.67. Found: C, 5.31; H, 5.17; N 3.52%. IR (cm^{-1}): 1261vs [ν_{as}(P$_2$N)], 1103vs [ν(PO)], 1041vs, 1028vs [ν(POC)]. λ_{max} (cm^{-1}), CH_2Cl_2 (blue): 14652, 16181, 18099, 21276; THF (yellow): 12706, 22321. CI$_{neg}$ MS (*m*/*z*, %): 762 (92) [M$^-$], 352 (100) [{(OPPh$_2$){OP(OEt)$_2$}N}$^-$], 336 (23) [{(PPh$_2$){OP(OEt)$_2$}N}$^-$]. μ = 2.19 BM.

2.3. Preparation of tetrakis[tetraphenylimidodiphosphinato]dinickel, Ni$_2$[(OPPh$_2$)$_2$N]$_4$ (**3**) and bis(dimethylformamide)bis(tetraphenyl-imidodiphosphinato)nickel, Ni[(OPPh$_2$)$_2$N]$_2$(DMF)$_2$ (**4**)

A solution of NiCl$_2 \cdot 6H_2O$ (0.24 g, 1.0 mmol) in methanol (15 ml) was added to a solution of K[(OPPh$_2$)$_2$N] (0.88 g, 2.0 mmol) in methanol (15 ml). The reaction mixture was stirred at room temperature for 12 h. The solvent was removed in vacuum and the solid was extracted with benzene (20 ml). The benzene solution was concentrated in vacuum to ca. 10 ml and layered with hexane. Yellow crystals of **3** were isolated by filtration. Yield 0.80 g (86%), M.p. 290 °C. *Anal.* Calc. for $C_{48}H_{40}N_2O_4P_4Ni$: C, 64.66; H, 4.53; N, 3.14. Found: C, 64.58; H, 4.37; N, 3.16%. IR (cm^{-1}): 1232vs [ν_{as}(P$_2$N)], 1136vs [ν(PO)], 1097vs [ν(PO)]. λ_{max} (cm^{-1}), CH_2Cl_2 (yellow): 11904, 18182, 22727; THF (yellow): 12670, 23614. CI$_{neg}$ MS (*m*/*z*, %): 890 (100) [Ni{(OPPh$_2$)$_2$N}$_2^-$], 416 (7) [{(OPPh$_2$)$_2$N}$^-$], 216 (5) [{(OPPh$_2$)N}$^-$]. FAB + MS (*m*/*z*, %): 1783 (15) [{Ni$_2$[(OPPh$_2$)$_2$N]$_4$ + 2H}$^+$], 1366 (38) [{Ni$_2$-[(OPPh$_2$)$_2$N]$_3$ + 2H}$^+$], 891 (100) [{Ni[(OPPh$_2$)$_2$N]$_2$ + H}$^+$]. μ = 3.26 BM.

Compound **3** was dissolved at room temperature in dimethylformamide. The yellow solution was concentrated in vacuum. Yellow-green crystals of **4** quantitatively formed at −5 °C. M.p. 115 °C (dec.). *Anal.* Calc. for $C_{54}H_{54}N_4O_6P_4Ni$: C, 62.52; H, 5.21; N, 5.40. Found: C, 62.83; H, 5.32; N, 5.28%. IR (cm^{-1}): 1643vs [ν(CO)], 1230vs, br [ν_{as}(P$_2$N)], 1130vs [ν(PO)], 1105vs [ν(PO)]. λ_{max} (cm^{-1}), CH_2Cl_2 (yellow): 11904, 14706, 18248, 22727; THF (yellow): 12658, 23809. CI$_{neg}$ MS (*m*/*z*, %): 890 (100) [{Ni-[(OPPh$_2$)$_2$N]$_2$}$^-$], 416 (7) [{(OPPh$_2$)$_2$N}$^-$], 216 (5) [{(OPPh$_2$)N}$^-$]. μ = 3.10 BM.

2.4. Preparation of potassium [tris{P,P-diethoxi-P′,P′-diphenyl-P′-thioimidodiphosphinato}nickel], KNi[(SPPh$_2$){OP(OEt)$_2$}N]$_3$ (**5**)

(a) A mixture of K[(SPPh$_2$){OP(OEt)$_2$}N] (0.766 g, 1.86 mmol) and NiCl$_2$ (0.148 g, 0.62 mmol) was stirred for 16 h in methanol (40 ml) at room temperature. The solvent was removed in vacuum and the solid was treated with CH_2Cl_2. KCl was filtered off and the solvent was removed in vacuum, resulting in a yellow-brown solid product. Yield: 0.58 g (77%). M.p. 118–119 °C. *Anal.* Calc. for $C_{48}H_{60}N_3O_9P_6$ S_3KNi: C, 47.94; H, 4.99; N, 3.50. Found: C, 48.21; H, 4.82; N, 3.24%.

(b) Alternatively, **5** was obtained by stirring a 1:1 mixture of **1** (0.794 g, 1 mmol) and K[(SPPh$_2$){OP(OEt)$_2$}N] (0.407 g, 1 mmol) in methanol (50 ml) at room temperature, for 24 h. The solvent was removed in vacuum from the blue-green solution, resulting quantitatively in a yellow-brown solid. M.p. 118–119 °C. *Anal.* Calc. for $C_{48}H_{60}N_3O_9S_3P_6KNi$: C, 47.94; H, 4.99; N, 3.50. Found: C, 47.82; H, 4.92; N, 3.53%. IR (cm^{-1}): 1261vs [ν_{as}(P$_2$N)], 1103s [ν(PO)], 1033vs, br [ν(POC)], 590s [ν(PS)]. λ_{max} (cm^{-1}), CH_2Cl_2 (blue): 14652, 16168, 17746, 21459; THF (yellow): 12053, 22321. CI$_{neg}$ MS (*m*/*z*, %): 794 (78) [M-K[(SPPh$_2$){OP(OEt)$_2$}N]$^-$], 407 (5) [K[(SPPh$_2$){OP(OEt)$_2$}N]$^-$] 368 (100) [{(SPPh$_2$){OP(OEt)$_2$}N}$^-$], 336 (38) [{(PPh$_2$){OP(OEt)$_2$}N}$^-$], ESI− (*m*/*z*, %): 1166 (100), [Ni[(SPPh$_2$){OP(OEt)$_2$}N]$_3^-$], 833 (82) [K$_2$Ni[(SPPh$_2$){OP(OEt)$_2$}-N]$_2^-$], 407 (35) [K[(SPPh$_2$){OP(OEt)$_2$}N]$^-$]. μ = 3.36 BM.

2.5. Crystal structure determinations

Block crystals of Ni$_2$[(OPPh$_2$)$_2$N]$_4 \cdot CH_2Cl_2$ (**3** $\cdot CH_2Cl_2$) (yellow), Ni[(OPPh$_2$)$_2$N]$_2$(DMF)$_2 \cdot 2H_2O$ (**4** $\cdot 2H_2O$) (yellow-green) and KNi[(SPPh$_2$){OP(OEt)$_2$}N]$_3$ (**5**) (yellow-brown) were attached with epoxy glue on cryoloops. The data were collected at room temperature on a Bruker SMART APEX CCD diffractometer using graphite-monochromated Mo Kα radiation (λ = 0.71073 Å). The details of the crystal structure determination and refinement are given in Table 1.

The structures were refined with anisotropic thermal parameters. The hydrogen atoms were refined with a riding model and a mutual isotropic thermal parameter. For structure solving and refinement the software package SHELX-97 was used [12]. The drawings were created with the DIAMOND program [13].

3. Results and discussion

The title nickel(II) complexes were obtained by salt metathesis reactions between anhydrous NiCl$_2$ or NiCl$_2 \cdot 6H_2O$ and the potassium salt of the corresponding tetraorganodichalcogenoimidodiphosphinic acid, according to the following equations:

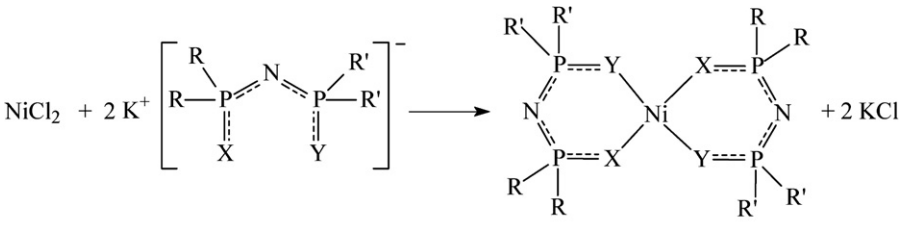

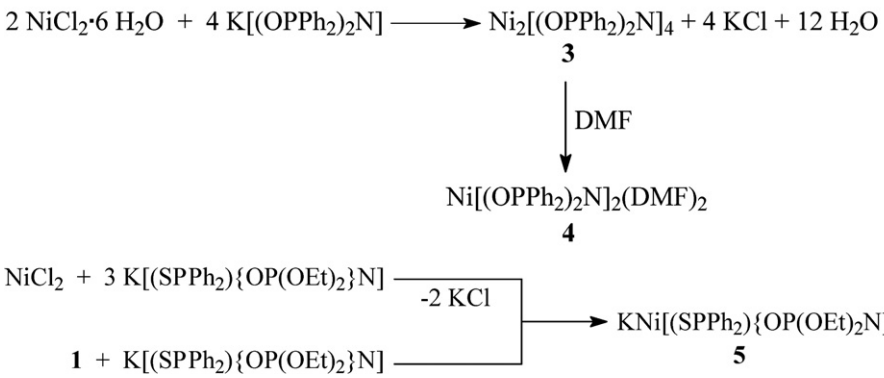

The reactions between $K[(XPR_2)(YPR'_2)N]_2$ and nickel dichloride were performed using either dehydrated $NiCl_2$ or $NiCl_2 \cdot 6H_2O$ in a tetrahydrofurane/ethanol mixture (**1** and **2**), or methanol as solvent (**3** and **5**), respectively. The use of anhydrous $NiCl_2$ and argon atmosphere resulted in a considerable increase in the yields of compounds **1** and **2**. The formation of the ionic species **5** through both methods of preparation was confirmed by powder X-ray diffraction studies. The experimental spectrum is in a good agreement with the simulated one based on the single-crystal X-ray diffraction data (Fig. 1).

All isolated compounds are stable as solids in open atmosphere for weeks. They are paramagnetic in solid state. Attempts to characterize these compounds as $CDCl_3$ solutions by NMR spectroscopy failed suggesting their paramagnetic nature in solution too.

The CI_{neg} mass spectra of compounds **1** and **2** show the molecular ion with high intensity (85% for **1** and 92% for **2**, respectively). In case of compounds **3** and **4** the $[Ni\{(Ph_2PO)_2N\}_2]^-$ ion appeared with 100% intensity in CI_{neg} mass spectra. The dimeric species **3** was confirmed by FAB mass spectroscopy, while the formation of **5** was revealed by ESI mass spectra.

Table 1
Crystal data and structure refinement for $Ni_2[(OPPh_2)_2N]_4 \cdot CH_2Cl_2$ (**3** $\cdot CH_2Cl_2$), $Ni[(OPPh_2)_2N]_2(DMF)_2 \cdot 2H_2O$ (**4** $\cdot 2H_2O$) and $KNi[(SPPh_2)\{OP(OEt)_2\}N]_3$ (**5**)

	3 $\cdot CH_2Cl_2$	**4** $\cdot 2H_2O$	**5**
Molecular formula	$C_{97}H_{82}Cl_2N_4Ni_2O_8P_8$	$C_{54}H_{58}N_4NiO_8P_4$	$C_{96}H_{116}K_2N_6Ni_2O_{18}P_{12}S_6$
M	1867.75	1073.61	2401.60
Temperature (K)	293(2)	297(2)	297(2)
Crystal size (mm)	0.30 × 0.28 × 0.21	0.60 × 0.55 × 0.44	0.35 × 0.29 × 0.23
Crystal system	Monoclinic	Monoclinic	Orthorhombic
Space group	*P*2(1)/*n*	*P*2(1)/*n*	*Pbca*
Radiation	Mo Kα, 0.71073 Å	Mo Kα, 0.71073 Å	Mo Kα, 0.71073 Å
Unit cell dimension			
a (Å)	16.433(3)	9.4672(15)	24.9858(10)
b (Å)	21.222(3)	20.951(3)	17.6058(7)
c (Å)	26.375(4)	13.363(2)	25.8683(10)
α (°)	90	90	90
β (°)	104.266(3)	94.442(3)	90
γ (°)	90	90	90
V (Å^3)	8915(2)	2642.6(7)	11379.3(8)
Z	4	2	4
D_{calc} (g cm^{-3})	1.392	1.349	1.402
F_{000}	3864	1124	4992
μ(Mo Kα) (mm^{-1})	0.686	0.545	0.746
θ Range for data collections (°)	1.25–26.37	1.81–26.37	1.62–25.00
Reflections collected	71288	20850	79397
Independent reflections [R_{int}]	18241 [0.0465]	5387 [0.0362]	10020 [0.1005]
Maximum and minimum transmissions	0.87 and 0.803	0.7954 and 0.7356	0.8471 and 0.7802
Refinement method		Full-matrix least-squares on F^2	
Data/restraints/parameters	18241/0/1095	5387/0/332	10020/0/646
Goodness-of-fit on F^2	1.210	1.220	1.243
	R_1 = 0.0709	R_1 = 0.0503	R_1 = 0.1129
	wR_2 = 0.1472	wR_2 = 0.1088	wR_2 = 0.2344
R indicies (all data)	R_1 = 0.0832	R_1 = 0.0530	R_1 = 0.1317
	wR_2 = 0.1528	wR_2 = 0.1101	wR_2 = 0.2444
Largest difference peak and hole (e Å^{-3})	0.629 and −0.761	0.449 and −0.440	0.798 and −1.458

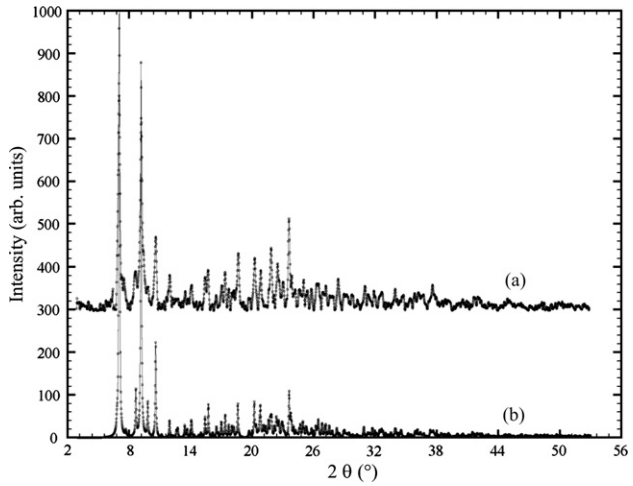

Fig. 1. (a) Experimental powder diffraction pattern and (b) the simulated X-ray powder diffraction spectrum obtained from the single-crytal cif file of **5**.

Strong infrared absorptions were observed for all complexes in the region 1260–1230, 1140–1100, 1050–1030 and about 600 cm^{-1} and they were assigned to $\nu_{as}(P_2N)$, $\nu(PO)$, $\nu(POC)$ and $\nu(PS)$ stretching vibrations, respectively, by comparison with the IR spectra of the free acids and their alkali metal salts [1,10,14], thus suggesting the coordination of the ligand units through both chalcogen atoms. For the adduct **4** the coordination of the DMF molecules to the metal atom is reflected in a shift of the C=O vibration from 1675 cm^{-1} in the free DMF to 1643 cm^{-1} in the adduct spectrum.

All derivatives are well soluble in CH_2Cl_2, resulting in blue-green (**1**, **2** and **5**) or yellow (**3** and **4**) solutions, respectively. The solutions of all compounds in coordinating solvents, *i.e.* tetrahydrofurane or methanol, are yellow. The electronic spectra of compounds **1**, **2** and **5** exhibit four absorption maxima in CH_2Cl_2 solutions, around 21 000, 18 000, 16 000 and 14 600 cm^{-1}, assignable to tetracoordinate species [5,8]. According to the magnetic moments (about 2.0 BM) found for compounds **1** and **2** in solid state, the formation of a mixture of tetrahedral and square-planar species might be suggested [15]. It can be mentioned here that the crystal of the related copper(II) complex, $Cu[(OPPh_2)(SPPh_2)N]_2$, was reported to contain both tetrahedral and square-planar isomers [16].

For the derivative **3** in CH_2Cl_2 solution the observed absorptions (22 727, 18 182 and 11 904 cm^{-1}) are similar to those reported previously for the dimeric $Ni_2[(OPPh_2)_2N]_4$ species in benzene solution [9], while in case of its adduct with dimethylformamide (**4**) a fourth absorption appeared around 14 700 cm^{-1}. This behavior might be consistent with a mixture of octahedral and pentacoordinate species in solution. The magnetic moments recorded in solid state for compounds **3**–**5** (3.26, 3.10 and 3.36 BM, respectively) are consistent with paramagnetic species with two unpaired electrons. In THF all compounds gave strong absorptions in the region 22 000–24 000 cm^{-1} accompanied by weaker absorptions in the region 12 000–13 000 cm^{-1}.

*3.1. Crystal and molecular structure of $Ni_2[(OPPh_2)_2N]_4 \cdot CH_2Cl_2$ (**3** $\cdot CH_2Cl_2$) and $Ni[(OPPh_2)_2N]_2(DMF)_2 \cdot 2H_2O$ (**4** $\cdot 2H_2O$)*

Single crystals of $Ni_2[(OPPh_2)_2N]_4 \cdot CH_2Cl_2$ (**3** $\cdot CH_2Cl_2$), suitable for X-ray diffraction studies, were obtained from CH_2Cl_2/*n*-hexane (1:4, v:v).

The crystal of **3** consists of distinct dinuclear units separated by normal van der Waals distances between heavy atoms. An ORTEP-like view with the atoms numbering scheme is given in Fig. 2. Selected bond lengths and angles are listed in Table 2.

Three of the phosphorus ligands act as homobimetallic triconnective units, bridging the two metal centers, while the fourth one acts monometallic biconnective. The result is a fused polycyclic system formed by three six-membered NiO_2P_2N rings and three non-planar four-membered Ni_2O_2 rings [dihedral angles:

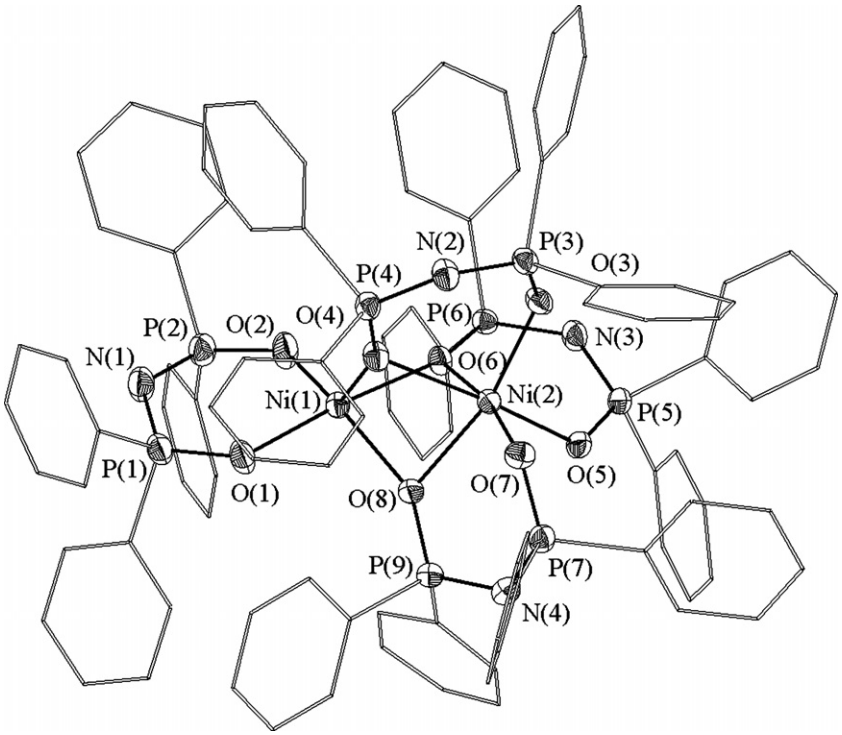

Fig. 2. ORTEP plot of the dinuclear unit in the crystal of **3** $\cdot CH_2Cl_2$. The atoms are drawn with 40% probability ellipsoids. Hydrogen atoms and CH_2Cl_2 are omitted.

Table 2
Selected interatomic distances (Å) and angles (°) in $Ni_2[(OPPh_2)_2N]_4 \cdot CH_2Cl_2$ ($\mathbf{3} \cdot CH_2Cl_2$)

Ni(1)–O(1)	1.982(3)	Ni(2)–O(3)	1.997(2)
Ni(1)–O(2)	1.970(3)	Ni(2)–O(4)	2.208(2)
Ni(1)–O(4)	2.031(2)	Ni(2)–O(5)	2.011(2)
Ni(1)–O(6)	2.052(2)	Ni(2)–O(6)	2.086(2)
Ni(1)–O(8)	2.062(2)	Ni(2)–O(7)	2.020(2)
		Ni(2)–O(8)	2.131(2)
P(1)–O(1)	1.513(3)	P(5)–O(5)	1.499(2)
P(1)–N(1)	1.589(3)	P(5)–N(3)	1.592(3)
P(2)–N(1)	1.583(4)	P(6)–N(3)	1.578(3)
P(2)–O(2)	1.512(3)	P(6)–O(6)	1.520(2)
P(3)–O(3)	1.505(2)	P(7)–O(7)	1.506(3)
P(3)–N(2)	1.589(3)	P(7)–N(4)	1.589(3)
P(4)–N(2)	1.579(3)	P(8)–N(4)	1.570(3)
P(4)–O(4)	1.524(2)	P(8)–O(8)	1.517(2)
O(1)–Ni(1)–O(6)	174.99(11)	O(3)–Ni(2)–O(8)	165.77(10)
O(2)–Ni(1)–O(8)	149.00(11)	O(4)–Ni(2)–O(5)	165.54(10)
		O(6)–Ni(2)–O(7)	169.25(10)
O(4)–Ni(1)–O(1)	102.09(11)	O(3)–Ni(2)–O(4)	90.97(9)
O(4)–Ni(1)–O(2)	125.46(11)	O(3)–Ni(2)–O(5)	95.50(10)
O(4)–Ni(1)–O(6)	80.30(10)	O(3)–Ni(2)–O(6)	93.23(10)
O(4)–Ni(1)–O(8)	81.52(10)	O(3)–Ni(2)–O(7)	96.41(10)
O(1)–Ni(1)–O(2)	93.23(11)	O(8)–Ni(2)–O(4)	76.02(9)
O(2)–Ni(1)–O(6)	88.86(10)	O(8)–Ni(2)–O(5)	95.95(10)
O(6)–Ni(1)–O(8)	80.49(9)	O(8)–Ni(2)–O(6)	78.14(9)
O(8)–Ni(1)–O(1)	95.45(10)	O(8)–Ni(2)–O(7)	91.46(10)
		O(4)–Ni(2)–O(6)	75.57(9)
		O(6)–Ni(2)–O(5)	91.13(10)
		O(5)–Ni(2)–O(7)	92.67(10)
		O(7)–Ni(2)–O(4)	99.45(10)
Ni(1)–O(1)–P(1)	131.79(17)	Ni(2)–O(5)–P(5)	122.77(14)
O(1)–P(1)–N(1)	116.97(17)	O(5)–P(5)–N(3)	118.92(15)
P(1)–N(1)–P(2)	124.2(2)	P(5)–N(3)–P(6)	126.88(19)
O(2)–P(2)–N(1)	116.40(17)	O(6)–P(6)–N(3)	116.00(15)
Ni(1)–O(2)–P(2)	132.17(16)	Ni(2)–O(6)–P(6)	124.13(14)
		Ni(1)–O(6)–P(6)	148.47(15)
Ni(2)–O(3)–P(3)	121.25(14)	Ni(2)–O(7)–P(7)	120.27(14)
O(3)–P(3)–N(2)	118.34(15)	O(7)–P(7)–N(4)	117.67(15)
P(3)–N(2)–P(4)	128.3(2)	P(8)–N(4)–P(7)	126.5(2)
O(4)–P(4)–N(2)	115.59(15)	O(8)–P(8)–N(4)	115.77(15)
Ni(2)–O(4)–P(4)	121.08(13)	Ni(2)–O(8)–P(8)	122.06(13)
Ni(1)–O(4)–P(4)	153.97(16)	Ni(1)–O(8)–P(8)	152.09(15)
Ni(1)–O(4)–Ni(2)	84.57(9)	Ni(1)–O(8)–Ni(2)	85.83(9)
Ni(1)–O(6)–Ni(2)	87.24(9)		

O(4)Ni(1)O(6)/O(4)Ni(2)O(6) 54.6°; O(4)Ni(1)O(8)/O(4)Ni(2)O(8) 57.8°; O(4)Ni(1)O(8)/O(4)Ni(2)O(8) 54.2°]. The two nickel atoms are in different environments: Ni(1) has a distorted square-pyramidal coordination geometry, with O(4) atom in apical position and the nickel atom out of the best O(1)O(2)O(6)O(8) plane (0.29 Å), while Ni(2) has a distorted octahedral geometry being surrounded by six oxygen atoms. The Ni_2O_8 core may be considered as resulted from a $Ni(1)O_5$ square pyramid and a $Ni(2)O_6$ octahedron, with a common trigonal face described by the O(4), O(6) and O(8) atoms (Fig. 3). The two nickel atoms are brought very close each other, at a distance less than the sum of their van der Waals radii [Ni(1)···Ni(2) 2.8552(8) Å *versus* $\sum_{vdW}$(Ni, Ni) 3.20 Å [17]. This compound displays a different structure compared with the related dimeric manganese(II) derivative, $[Mn\{(OPPh_2)_2N\}_2]_2$, where both metal centers have the same coordination geometry, *i.e.* trigonal bipyramidal, with two of the imidodiphosphinato ligands acting as monometallic biconnective units, with a *cis* orientation with respect to the four-membered Mn_2O_2 ring; the other two phosphorus ligands are homobimetallic triconnective, the result being a fused tricyclic $Mn_2O_4P_4N_2$ system [18].

The nickel–oxygen distances are different. The shorter bonds [Ni(1)–O(1) 1.982(3), Ni(1)–O(2) 1.970(3) Å] are established by

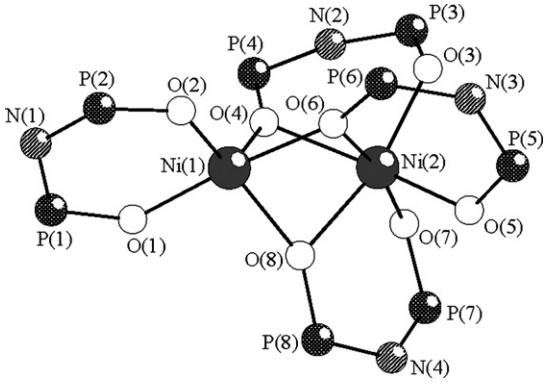

Fig. 3. View of the $Ni_2O_8P_8N_4$ core in the crystal of $\mathbf{3} \cdot CH_2Cl_2$.

the isobidentate, monometallic biconnective ligand which coordinate the Ni(1) atom. They are considerably shorter than the corresponding metal–oxygen bonds in the adduct $\mathbf{4} \cdot 2H_2O$ in which the phosphorus ligands exhibit an anisobidentate, monometallic biconnective pattern [Ni(1)–O(1) 2.1133(17), Ni(1)–O(2) 2.0542(17) Å]. The bridging Ni–O–Ni systems are not symmetric (Table 2), with Ni(1)–O distances shorter than Ni(2)–O distances. The remaining, terminal, Ni(2)–oxygen bond distances are of intermediate magnitude between the bridging metal–oxygen and Ni(1)–O bonds established by the monometallic biconnective ligand, respectively.

The phosphorus–nitrogen [1.570(3)–1.592(3) Å] and phosphorus–oxygen [1.499(2)–1.524(2) Å] distances are intermediate between single and double bonds [cf. $Ph_2P(=S)–N=P(–SMe)Ph_2$ [19]: P=N 1.562(2) Å, P–N 1.610(2) Å, $Ph_2P(O)OH$ [20]: P=O 1.486(6) Å, P–O 1.526(6) Å], thus suggesting some delocalization of the π electrons. However the resulting NiO_2P_2N rings are not planar. All ligands acting as homobimetallic triconnective units establish six-membered NiO_2P_2N rings which exhibit distorted boat conformation, with Ni(2) and nitrogen atoms in apices. The fourth six-membered NiO_2P_2N ring, established by the monometallic biconnective ligand, has an envelope conformation, folded on the imaginary P(1)···P(2) axis, with the nitrogen atom −0.31 Å out of the almost planar NiO_2P_2 skeleton.

Recrystallization of **3** from dimethylformamide led to isolation of the adduct $Ni[(OPPh_2)_2N]_2(DMF)_2 \cdot 2H_2O$ ($\mathbf{4} \cdot 2H_2O$). Its crystal consists of discrete molecules with Ni atom as inversion center, separated by normal van der Waals distances. An ORTEP-like view with the atoms numbering scheme is given in Fig. 4 and selected bond lengths and angles are listed in Table 3.

The two imidodiphosphinato ligands act as monometallic biconnective units, chelating the metal center through both oxygen atoms. This results in a *spiro*-bicyclic system with Ni as *spiro* atom, occupying an inversion center. The NiO_4 system is planar, with different Ni–O distances [Ni–O(1) 2.1134(16) Å, Ni–O(2) 2.0541(16) Å]. The six-membered NiO_2P_2N rings are of boat conformations [with Ni(1) and nitrogen atoms in apices] and folded along the imaginary O(1)···O(2a) and O(1a)···O(2) axis [dihedral angle of 16.4° between the best P_2O_2 and NiO_4 planes] on opposite sides of the planar NiO_4 core [deviations from NiO_4 plane: P(1) −0.462, P(2a) −0.385, N(1a) −0.703 Å, and P(1a) 0.462, P(2) 0.385, N(1) 0.703 Å, respectively]. The phosphorus–oxygen [P(1)–O(1) 1.5106(18), P(2)–O(2) 1.5088(17) Å] and phosphorus–nitrogen [P(1)–N(1a) 1.593(2), P(2)–N(1) 1.582(2) Å] distances, respectively, are equivalent and intermediate between single P–E and double P=E (E = O, N) bonds. The two dimethylformamide groups complete the axial position of the octahedral environment around the metal center and the $Ni–O_{DMF}$ bond lengths are intermediate between the short and the long metal–oxygen bonds established by

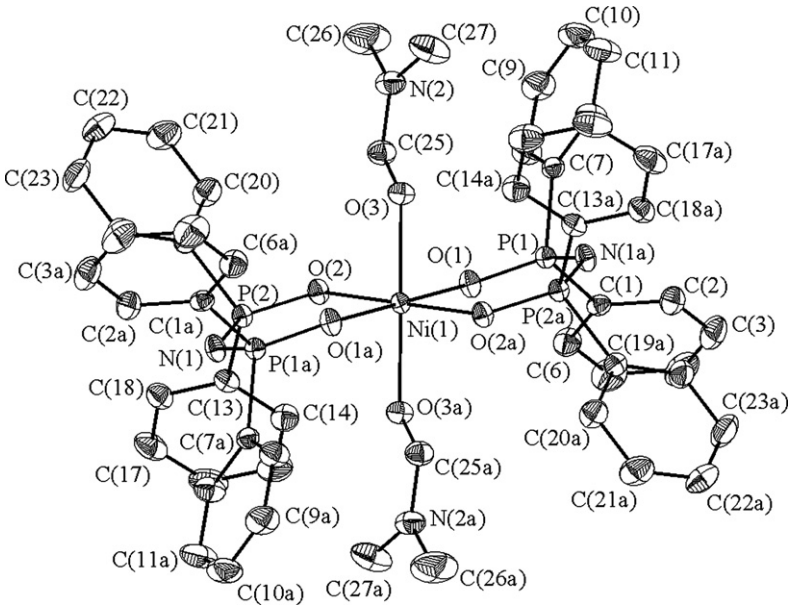

Fig. 4. ORTEP plot at 30% probability and the atom numbering scheme for **4** · $2H_2O$. The hydrogen atoms are omitted.

Table 3
Selected interatomic distances (Å) and angles (°) in $Ni[(OPPh_2)_2N]_2(DMF)_2 \cdot 2H_2O$ (**4** · $2H_2O$)

Ni(1)–O(1)	2.1133(17)	Ni(1)–O(2)	2.0542(17)
Ni(1)–O(3)	2.0921(19)		
P(1)–O(1)	1.5106(18)	P(2)–O(2)	1.5088(17)
P(1)–N(1a)	1.593(2)	P(2)–N(1)	1.582(2)
O(1)–Ni(1)–O(1a)	180.00	O(2)–Ni(1)–O(2a)	180.00
O(3)–Ni(1)–O(3a)	180.00		
O(3)–Ni(1)–O(1)	87.25(7)	O(3)–Ni(1)–O(2)	90.36(7)
O(3)–Ni(1)–O(1a)	92.75(7)	O(3)–Ni(1)–O(2a)	89.64(7)
O(1)–Ni(1)–O(2)	87.57(7)	O(1)–Ni(1)–O(2a)	92.43(7)
Ni(1)–O(1)–P(1)	127.49(10)	Ni(1)–O(2)–P(2)	129.92(10)
O(1)–P(1)–N(1a)	118.84(10)	O(2)–P(2)–N(1)	118.66(10)
P(1)–N(1a)–P(2a)	127.92(13)		

Symmetry equivalent positions ($2 - x$, $-y$, $-z$) are given by "a".

a phosphorus ligand unit. The distortion of the octahedral NiO_6 core is reflected in the difference between the *endo* and *exo* cyclic O–Ni–O bond angles in the equatorial plane [O(1)–Ni(1)–O(2a) (*endo*) 92.43(7)°, O(1)–Ni(1)–O(2) (*exo*) 87.57(7)°].

3.2. Crystal and molecular structure of $[KNi[(SPPh_2)\{OP(OEt)_2\}N]_3]_2$ (**5**)

Yellow-brown crystals of (**5**) were grown from a CH_2Cl_2/*n*-hexane (1:4, v:v) mixture.

Compound **5** displays a tetranuclear structure and its ORTEP-like diagram with the atom numbering scheme is depicted in Fig. 5. Selected bond distances and angles are given in Table 4.

The phosphorus ligands exhibit different bridging patterns. They are coordinated to the nickel center through the sulfur atoms

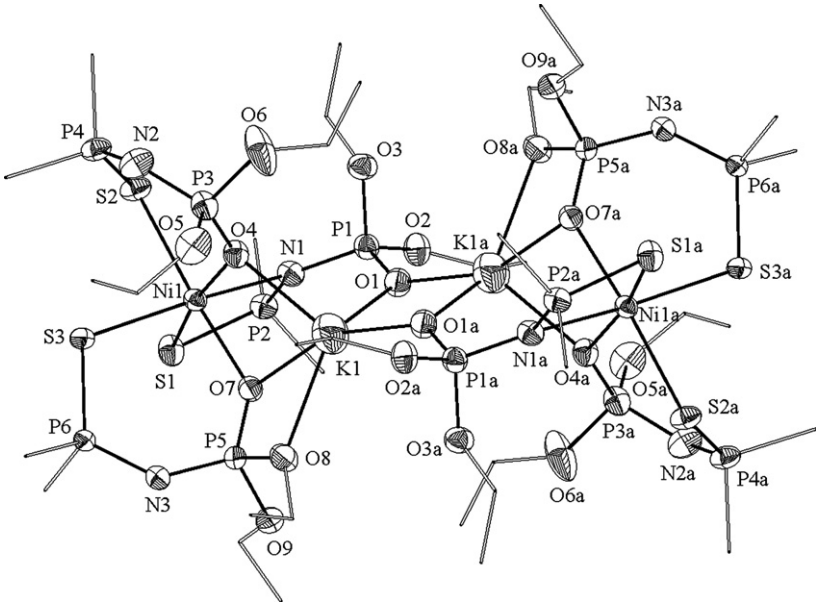

Fig. 5. ORTEP plot of the dimer unit in the crystal of **5**. The atoms are drawn with 30% probability ellipsoids. For clarity, only *ipso* carbons of the phenyl groups are shown and the hydrogen atoms are omitted.

Table 4
Selected interatomic distances (Å) and angles (°) in $KNi[(SPPh_2)\{OP(OEt)_2\}N]_3$ (**5**)

Ni(1)–O(4)	2.094(5)	K(1)–O(1)	2.362(6)
Ni(1)–O(7)	2.086(5)	K(1)–O(1a)	2.346(6)
Ni(1)–S(1)	2.464(2)	K(1)–O(4)	2.387(6)
Ni(1)–S(2)	2.477(2)	K(1)–O(7)	2.419(6)
Ni(1)–S(3)	2.422(2)	K(1)–O(8)	2.540(6)
Ni(1)–N(1)	2.238(6)		
P(1)–O(1)	1.480(6)	P(2)–S(1)	1.984(3)
P(1)–N(1)	1.610(7)	P(2)–N(1)	1.611(6)
P(1)–O(2)	1.583(6)		
P(1)–O(3)	1.568(6)		
P(3)–O(4)	1.489(6)	P(4)–S(2)	1.999(3)
P(3)–N(2)	1.551(8)	P(4)–N(2)	1.587(8)
P(3)–O(5)	1.577(7)		
P(3)–O(6)	1.565(7)		
P(5)–O(7)	1.485(5)	P(6)–S(3)	1.984(3)
P(5)–N(3)	1.565(6)	P(6)–N(3)	1.601(6)
P(5)–O(8)	1.591(6)		
P(5)–O(9)	1.574(6)		
O(4)–Ni(1)–S(1)	168.64(16)	O(7)–Ni(1)–S(2)	175.70(15)
N(1)–Ni(1)–S(3)	167.52(17)		
O(4)–Ni(1)–O(7)	84.2(2)	S(1)–Ni(1)–O(7)	92.89(15)
O(4)–Ni(1)–N(1)	93.5(2)	S(1)–Ni(1)–N(1)	75.30(17)
O(4)–Ni(1)–S(2)	91.86(16)	S(1)–Ni(1)–S(2)	90.67(8)
O(4)–Ni(1)–S(3)	98.94(16)	S(1)–Ni(1)–S(3)	92.25(8)
O(7)–Ni(1)–N(1)	86.4(2)	S(2)–Ni(1)–S(3)	87.03(7)
N(1)–Ni(1)–S(2)	92.18(18)	O(7)–Ni(1)–S(3)	95.24(15)
K(1)–O(1)–P(1)	123.7(3)	K(1a)–O(1)–P(1)	141.4(3)
O(1)–P(1)–N(1)	117.6(3)	K(1)–O(1)–K(1a)	87.9(2)
P(1)–N(1)–P(2)	133.0(4)		
S(1)–P(2)–N(1)	105.9(2)	Ni(1)–N(1)–P(1)	128.3(3)
Ni(1)–S(1)–P(2)	81.27(9)	Ni(1)–N(1)–P(2)	97.4(3)
Ni(1)–O(4)–P(3)	132.2(3)	Ni(1)–O(7)–P(5)	138.2(3)
O(4)–P(3)–N(2)	119.9(4)	O(7)–P(5)–N(3)	120.3(3)
P(3)–N(2)–P(4)	132.9(5)	P(5)–N(3)–P(6)	130.2(4)
S(2)–P(4)–N(2)	118.6(3)	S(3)–P(6)–N(3)	120.0(2)
Ni(1)–S(2)–P(4)	105.68(10)	Ni(1)–S(3)–P(6)	110.61(10)
K(1)–O(4)–P(3)	124.1(3)	K(1)–O(7)–P(5)	103.1(3)
K(1)–O(8)–P(5)	95.0(3)		
Ni(1)–O(4)–K(1)	100.1(2)	Ni(1)–O(7)–K(1)	99.3(2)
O(1)–K(1)–O(4)	90.2(2)	O(4)–K(1)–O(7)	71.32(19)
O(1)–K(1)–O(7)	92.3(2)	O(4)–K(1)–O(8)	110.8(2)
O(1)–K(1)–O(8)	132.2(3)	O(4)–K(1)–O(1a)	130.0(2)
O(1)–K(1)–O(1a)	92.1(2)		
O(7)–K(1)–O(8)	58.24(18)	O(8)–K(1)–O(81a)	104.0(2)
O(7)–K(1)–O(1a)	158.2(2)		

Symmetry equivalent positions ($-x$, $-y$, $1-z$) are given by "a".

which describe a triangular face of the distorted octahedral environment. The oxygen atoms of the SPNPO skeletons are involved in bridges between metal centers, *i.e.* O(4) and O(7) atoms bridge the metal atoms of a $KNi[(SPPh_2)\{OP(OEt)_2\}N]_3$ unit, while O(1) atom is involved in a bridge between the two potassium atoms of the $[KNi[(SPPh_2)\{OP(OEt)_2\}N]_3]_2$ dimer. The N(1) atom completes the octahedral coordination of the nickel atom ($NiNO_2S_3$ core), while the coordination sphere around the potassium atom is completed by an oxygen atom from an ethoxy group belonging to the $KNi[(SPPh_2)\{OP(OEt)_2\}N]_3$ unit [K(1)–O(8) 2.540(6) Å]. Thus phosphorus ligands can be described as (*O*,*O*,*S*)-heterobimetallic triconnective, (*S*,*O*,*O*,O_{Et})-heterobimetallic tetraconnective and (*N*,*O*,*O*,*S*)-heterotrimetallic tetraconnective, respectively. As far very few examples of complexes are known in which the nitrogen atom of the imidodiphosphinato ligand is involved in interaction with the metal center, *i.e.* *S*,*N*-monometallic biconnective in $Pd[(SPR_2)\{OP(OPh)_2\}N]_2$ (R = Ph, Pr^i) [21], *O*,*N*-monometallic biconnective in the dimeric $[PhHg\{OP(OPh)_2\}_2N]_2$ [22] and *X*,*X*,*N*-monometallic triconnective coordination in $[2\text{-}(Me_2NCH_2)C_6H_4]BiCl[(XPPh_2)_2N]$ (X = S, Se) [23]. As result of the coordination patterns of the phosphorus ligands different metalocycles are formed. The six-membered Ni(1)S(2)P(4)N(2)P(3)O(4) and Ni(1)S(3)P(6)N(3)P(5)O(7) chelate rings have twisted boat or chair conformations, with Ni(1)/N(2) and Ni(1)/N(3) atoms, respectively, in apices. The K_2O_2 ring is planar, while the $NiKO_2$ ring is folded [dihedral angle O(4)Ni(1)O(7)/O(4)K(1)O(7) 22.1°]. The dihedral angle between the K_2O_2 ring and the KO_2 fragment of the $NiKO_2$ is 88.6°.

The Ni–chalcogen distances are similar for the three ligand units. The Ni–S bond lengths [Ni(1)–S(1) 2.464(2), Ni(1)–S(2) 2.477(2), Ni(1)–S(3) 2.422(2) Å] are longer than in other Ni(II) thioato derivatives, *i.e.* the tetrahedral $Ni[(OPPh_2)(SPR_2)N]_2$ [2.306(4)/2.305(4) Å, R = Me; 2.306(4)/2.286(4) Å, R = Ph] [8] or $Ni[(SPPh_2)_2N]_2$ [2.281(2)–2.316(2) Å] [5] and the square-planar $Ni[(SPMe_2)(SPPh_2)N]_2$ [2.231(1)/2.247(1) Å] [5], $Ni_3S_2(S_2COR)_2(dppe)$ [2.170(1)–2.235(1) Å, R = Me; 2.151(4)–2.247(6) Å, R = Et] or $Ni(S_2CO)(dppe)$ [2.1853(8)–2.1970(8) Å] [24] complexes. The Ni–O distances [Ni(1)–O(4) 2.094(5), Ni(1)–O(7) 2.086(5) Å] are similar to those found in compounds **3** · CH_2Cl_2 and **4** · $2H_2O$, but slightly longer in comparison with the values found in $Ni[(OPPh_2)(SPR_2)N]_2$ [1.950(7)/1.959(7) Å, R = Me; 1.950(8)/1.956(7) Å, R = Ph] [8]. Significant differences were observed in case of the K–O distances [range 2.346(6)–2.540(6) Å]. The shortest bonds correspond to the K–O–K bridge [K(1)–O(1) 2.362(6), K(1)–O(1a) 2.346(6) Å], while the longest one corresponds to the K–O_{Et} interaction [K(1)–O(8) 2.540(6) Å]. It can be mentioned that only one OEt group is involved in interaction to each potassium center.

The phosphorus–nitrogen and phosphorus–chalcogen distances suggest that the monothioimidodiphosphinato ligands are primarily coordinated to nickel through sulfur. The phosphorus–sulfur [P(2)–S(1) 1.984(3), P(4)–S(2) 1.999(3) and P(6)–S(3) 1.984(3) Å] and terminal phosphorus–oxygen [P(1)–O(1) 1.480(6), P(3)–O(4) 1.489(6) and P(5)–O(7) 1.485(5) Å] bond lengths are equivalent in all three ligand units. Their magnitude is intermediate between single P–S and the double P=S bonds [cf. $Ph_2P(=S)\text{–}N=P(\text{–}SMe)Ph_2$ [19]: P–S 2.071(1) and P=S 1.954(1) Å] and consistent with double P=O bonds, respectively [cf. $Ph_2P(O)OH$ [20]: P=O 1.486(6) Å, P–O 1.526(6) Å].

Acknowledgements

This work was supported by the National University Research Council of Romania (CNCSIS Grant: A-358/2006). S.I. is grateful for financial support in form of the Scientific and Technical Research Council of Turkey (TUBITAK) - NATO B2 fellowship.

Appendix A. Supplementary data

CCDC 612983, 612984 and 626929 contain the supplementary crystallographic data for **3** · CH_2Cl_2, **4** · $2H_2O$ and **5**. These data can be obtained free of charge via http://www.ccdc.cam.ac.uk/conts/retrieving.html, or from the Cambridge Crystallographic Data Centre, 12 Union Road, Cambridge CB2 1EZ, UK; fax: (+44) 1223-336-033, or e-mail: deposit@ccdc.cam.ac.uk. Supplementary data associated with this article can be found, in the online version, at doi:10.1016/j.poly.2008.04.006.

References

[1] C. Silvestru, J.E. Drake, Coord. Chem. Rev. 223 (2001) 117.
[2] J.D. Woollins, J. Chem. Soc., Dalton. Trans. (1996) 2893.
[3] M.R. Churchill, J. Cooke, J.P. Fennessey, J. Wormald, Inorg. Chem. 10 (1971) 1031.

[4] M.R. Churchill, J. Cooke, J. Wormald, A. Davison, E.S. Switkes, J. Am. Chem. Soc. 91 (1969) 6518.
[5] R. Roesler, C. Silvestru, G. Espinoza-Perez, I. Haiduc, R. Cea-Olivares, Inorg. Chim. Acta 241 (1996) 47.
[6] P. Bhattacharyya, J. Novosad, J. Phillips, A.M.Z. Slawin, D.J. Williams, J.D. Woollins, J. Chem. Soc., Dalton Trans. (1995) 1607.
[7] C. Papadimitriou, P. Veltsistas, J. Novosad, R. Cea-Olivares, A. Toscano, P. Garcia y Garcia, M. Lopez-Cardosa, A.M.Z. Slawin, J.D. Woollins, Polyhedron 16 (1997) 2727.
[8] A. Silvestru, D. Balc, R. Roesler, J.E. Drake, I. Haiduc, Inorg. Chim. Acta 305 (2000) 106.
[9] A. Davison, E.S. Switkes, Inorg. Chem. 10 (1971) 837.
[10] G. Balazs, J.E. Drake, C. Silvestru, I. Haiduc, Inorg. Chim. Acta 287 (1999) 61.
[11] Mecury: visualization and analysis of crystal structures C.F. Macrae et al., J. Appl. Crystallogr. 39 (3) (2006) 453.
[12] G.M. Sheldrik, SHELX-97, Universität Göttingen, Germany, 1997.
[13] DIAMOND—Visual Crystal Structure Information System, Crystal Impact, Bonn, Germany, 2001.
[14] I. Ghesner, C. Palotas, A. Silvestru, C. Silvestru, J.E. Drake, Polyhedron 20 (2001) 1101.
[15] A. Deeg, W. Kuchen, D. Langsch, D. Mootz, W. Peters, H. Wunderlich, Z. Anorg, Allg. Chem. 606 (1991) 119.
[16] A. Silvestru, A. Rotar, J.E. Drake, M.B. Hursthouse, M.E. Light, S.I. Farcas, R. Rösler, C. Silvestru, Can. J. Chem. 79 (2001) 983.
[17] J. Huheey, E. Keiter, R. Keiter, Anorganische Chemie. Prinzipien von Struktur und Reaktivitaet, 2. Auflage, Walter de Gruyter, Berlin, 1995, p. 335.
[18] I. Szekely, C. Silvestru, J.E. Drake, G. Balazs, S.I. Farcas, I. Haiduc, Inorg. Chim. Acta 299 (2000) 247.
[19] I. Ghesner, A. Soran, C. Silvestru, J.E. Drake, Polyhedron 22 (2003) 3395.
[20] D. Fenske, R. Mattes, J. Loens, K.-F. Tebbe, Chem. Ber. 106 (1973) 1139.
[21] M. Necas, M.R. St J. Foreman, J. Marek, J.D. Woollins, J. Novosad, New J. Chem. 25 (2001) 1256.
[22] H. Richter, E. Fluck, H. Riffel, H. Hess, Z. Anorg. Allg. Chem. 491 (1982) 266.
[23] L. Balazs, O. Stanga, H.J. Breunig, C. Silvestru, Dalton Trans. (2003) 2237.
[24] I. Haiduc, R.F. Semeniuc, M. Campian, V.Ch. Kravtsov, Y.A. Simonov, J. Lipkowski, Polyhedron 22 (2003) 2895.

Polyhedron 27 (2008) 2151–2156

Contents lists available at ScienceDirect

Polyhedron

journal homepage: www.elsevier.com/locate/poly

Kinetics and mechanism of the oxidation of tris(1,10-phenanthroline)iron(II) by peroxomonosulphate (oxone) ion

Manu Mehrotra, Raj N. Mehrotra *

Department of Chemistry, JNV University, Jodhpur 342 005, Rajasthan, India

ARTICLE INFO

Article history:
Received 18 March 2008
Accepted 15 April 2008
Available online 27 May 2008

Keywords:
Kinetics
Mechanism
Redox reactions
Peroxomonosulphate
Oxidation of tris(1,10-phenanthroline)iron(II)

ABSTRACT

The oxidation of tris(1,10-phenanthroline)Fe(II) with peroxomonosulphate (oxone) ion is first order with respect to both the substrate and the oxidant. The rate is accelerated by the alkali metal ion and the plot of k_0 against $[M^+]$ indicates that a part of the rate is independent of [alkali metal ion] where k_0 is the true rate constant for the reaction and is equal to $k_{obs} - k_h$. The rate constant k_h refers to the hydrolysis of $[Fe(phen)_3]^{2+}$ ion. It is explained by assuming the formation of an ion pair between M^+ and SO_5^{2-} ions whereas a similar ion pair between M^+ and HSO_5^- ions is not favoured in view of the slope value of the Davies plot for the effect of ionic strength which has a slope of −2.02. There is spectral evidence for the formation of an intermediate and accordingly the intermediates $[Fe(phen)_3\cdots HSO_5]^+$ and $[Fe(phen)_3\cdots M\cdots SO_5]^+$ are assumed to be formed in the proposed mechanism where M^+ ion acts as a bridge. The disproportionation of the intermediates is considered to be rate determining. The H^+ ions retard the rate and the plot of $k_0[H^+]$ against $[H^+]$ has an intercept on the rate ordinate.

© 2008 Elsevier Ltd. All rights reserved.

1. Introduction

The salts of two peroxoacids of sulphur, peroxomono and peroxodisulphuric acid, are strong oxidants. The peroxodisulphate ($S_2O_8^{2-}$) ion is one of the most powerful and useful oxidant with E° = 2.01 V [1]. Despite the high oxidation potential, several oxidation reactions do not proceed at a convenient rate at ambient temperature because the activation energy of the rate limiting homolysis of $S_2O_8^{2-}$ to $SO_4^{-\cdot}$ is approximately 125 kJ mol^{-1} [2] and such reactions were catalysed either by Ag^+ or Cu^{2+} ions. Ag^{2+} ion is usually considered as the active oxidant in Ag^+ catalysed reactions though in certain cases Ag^{3+} is the reactive entity. A large number of oxidations of both inorganic and organic substrates by $S_2O_8^{2-}$ ion have been extensively studied in the past and the subject was of such great interest that a number of reviews were published [3–7].

Peroxodisulphate salts, $K_2S_2O_8$, $(NH_4)_2S_2O_8$ or $Na_2S_2O_8$, are available in pure state whereas potassium salt of peroxomonosulphuric acid is obtained as a mixture of $KHSO_5 \cdot K_2SO_4 \cdot KHSO_4$. The triple salt, $2KHSO_5–KHSO_4–K_2SO_4$, is commercially known as oxone which is a monosubstituted derivative of H_2O_2. Thus it is thermodynamically more powerful as an oxidant than H_2O_2 and kinetically more reactive. These properties make HSO_5^- a potentially important strong oxidant which was first described in the oxidation reactions [8,9] and some of the later studies include the oxidations of aldehydes [10], $[(NH_3)_5CoS_2O_3]^+$ [11], amino acids [12], sulphide ion [13], tris (2,2′-bipyridyl) Ru(II) [14], Ti(III), Fe(II) and α-oxygen substituted radicals [15], NO_2^- ion [16], *para*-substituted anilines [17], aminobenzoic acids [18], Co^{2+} ion in presence of molybdate ion [19] and that of $[Co(II)W_{12}O_{40}]^{6-}$ [20].

Therefore it was considered timely to study the oxidation of tris(1,10-phenanthroline)Fe(II), hereafter referred to as $[Fe(phen)_3]^{2+}$ ion because its oxidation by 6-molybedocobaltate(III) ion had been investigated earlier in this laboratory [21]. It was noted that the optical density of the $[Fe(phen)_3]^{2+}$ solution in sulphuric acid decreased with time. Therefore, the rates of hydrolysis (k_h) were also studied. The true rate constant (k_0) for different reaction mixtures was calculated by subtracting the rate of hydrolysis (k_h) from the k_{obs} values or $k_0 = k_{obs} - k_h$.

2. Experimental

2.1. Materials

The peroxomonosulphate (oxone) solutions were freshly prepared by weighing of the sample (Dupont). The solution was standardised as described below.

An accurately weighed sample of oxone (0.3–0.4 g) is dissolved in 50 ml of decinormal oxalic acid solution in a glass stoppered conical flask. To this solution was added a Ag_2SO_4 solution prepared by dissolving 0.2 g of the sample in 20 ml of 10% sulphuric acid. The mixture was heated on a water bath until no more CO_2 was evolved. The mixture was diluted to about 100 ml with water

* Corresponding author. Tel.: +91 2912721478.
E-mail address: mehrotra_rn@yahoo.co.in (R.N. Mehrotra).

0277-5387/$ - see front matter © 2008 Elsevier Ltd. All rights reserved.
doi:10.1016/j.poly.2008.04.011

at 40 °C. The excess oxalic acid left in the mixture was titrated with a standard decinormal permanganate solution. The exact molecular weight of the sample was thus determined.

The few crystals of potassium permanganate (E. Merck, GR) are dissolved in hot distilled water that had been previously degassed with pure nitrogen gas. The solution, left overnight, is filtered and the concentration is checked by measuring its absorbance at 525 nm (ε_{525} = 2400) [22].

A standard solution of oxalic acid (E. Merck, GR) is prepared by accurate weighing of the sample.

The preparation of tris(phenanthroline)iron(II) complex is carried out in aqueous solution by mixing ferrous ammonium sulphate (Qualigens, AR) and 1,10-phenanthroline (phen) (E. Merck). The concentration of 1,10-phenanthroline is slightly more than three times the concentration of ferrous ammonium sulphate so that the ligand completely complexes the Fe(II). The purity of the prepared complex is verified by spectrophotometry. The complex shows a maximum absorbance at 510 nm with ε_{510} = 10990 ± 10 against a literature value = 11 000 $dm^3\ mol^{-1}\ cm^{-1}$ [23]. Solutions older than 48 h are discarded.

The tris(phenanthroline)iron(III) complex is prepared by oxidising tris(phenanthroline)iron(II) complex in sulphuric acid by lead oxide [24,25] and the blue solution so obtained is filtered through a sintered G4 crucible.

Sodium hydrogen sulphate solution is prepared by half neutralisation of a standard solution of sulphuric acid (Basynth, AR) with a calculated volume of a solution of sodium hydroxide (E. Merck, GR). The solution so prepared is checked again with titrating it against a standard solution of sodium hydroxide.

The solutions of LiCl (Sigma, LR), NaCl (Sarabhai M, GR), KCl (Ranbaxy, AR) and CsCl (Sigma, LR) are prepared by the direct weighing of the samples.

2.2. Spectral measurements

A HP 8452 UV–Vis spectrophotometer with a 2 nm band width and an integration time of 1 s is used to measure the spectra of the non-reacting solutions at room temperature.[1] The method adopted for recording the spectra of the reaction mixtures is described below.

The solutions of desired concentrations of oxone and $[Fe(phen)_3]^{2+}$ at appropriate $[H^+]$ are taken in test tubes, which are immersed in melting ice taken in a beaker and allowed to stand for sufficient time to attain the thermal equilibrium. The melted water is drained out from time to time. The idea is to slow down the rate of the reaction to an extent that would permit the recording of the meaningful spectra for qualitative analysis only because the temperature and the time taken in mixing and recording the spectra are not precisely and uniformly maintained. These solutions are quickly mixed to give reaction mixtures which are immediately transferred to silica cell which is returned to its compartment and the spectra are recorded immediately.

2.3. Spectral studies at different $[HSO_5^-]$ ion

The optical densities of the reaction mixtures, $10^5[Fe(phen)_3^{2+}]$ = 3.0, $[H^+]$ = 0.005 and $1.0 \leqslant 10^4[HSO_5^-] \leqslant 10.0$ mol dm^{-3} are measured under the experimental conditions described above (these spectra are available as Supplemental data). It is noted that the optical density of the reaction mixtures increased with the increase in $[HSO_5^-]$ though the wavelength of maximum absorbance of $[Fe(phen)_3]^{2+}$ ion is not changed.

2.4. Spectral studies at different $[H^+]$ ion

In another series of experiments the optical density of the reaction mixtures, $10^5[Fe(phen)_3^{2+}]$ = 3.0 and $10^4[HSO_5^-]$ = 5.0 mol dm^{-3} at $0.001 \leqslant [H^+] \leqslant 0.1$ mol dm^{-3} are measured. It is noted that the optical density did not show any change with the increase in $[H^+]$ suggesting that H^+ ion has no effect on the species formed by mixing of $[Fe(phen)_3]^{2+}$ and HSO_5^- ions.

2.5. Rate measurement

The oxidation of $[Fe(phen)_3]^{2+}$ is studied in sulphuric acid (0.05 mol dm^{-3}) at constant ionic strength (μ = 1 mol dm^{-3}, $NaHSO_4$) under pseudo first-order conditions. i.e., [oxone] ≫ $[Fe(phen)_3^{2+}]$ ion. The progress of the reaction is followed at 510 nm using a Spectrochem MKII colorimeter [26]. The pseudo first-order rate k_{obs} is calculated by plotting the log (optical density) against time, Fig. 1, which are drawn using EXCEL program which provides the least square values of the slopes and intercepts of the plots. The pseudo first-order rate constant k_{obs} is calculated from the slopes of the plots in Fig. 1. The plots were linear for 60–70% of the reaction. The reproducibility of the pseudo first-order rate was within 3–5%.

In addition to the above the rate of hydrolysis (k_h) of $[Fe(phen)_3]^{2+}$ ion is also estimated for a given condition of concentrations of H^+ ion, ionic strengths and temperatures used in the kinetics runs of the main reaction. The same set up was used except that HSO_5^- ion was not added to the kinetic run. The k_h is obtained from the slope of the linear plots such as shown in Fig. 1. The estimated k_h is subtracted from k_{obs} to have the true value of the pseudo first-order rate constant k_0 which are reported in the tables.

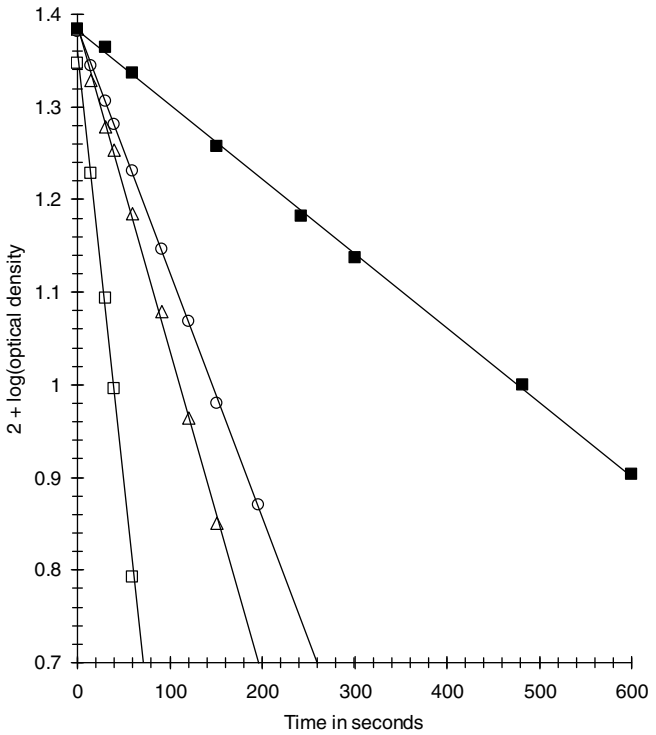

Fig. 1. The usual first-order plots of the log (optical density) against time with the initial $10^5[Fe(phen)_3^{2+}]$ = 2.0, and $[HSO_5^-]$ = 0.1, $[H^+]$ = 0.05, μ = 1.0 and 40 °C (□); $[HSO_5^-]$ = 0.05, $[H^+]$ = 0.05, μ = 0.9 and 40 °C (△); $[HSO_5^-]$ = 0.07, $[H^+]$ = 0.05, μ = 1.0 and 35 °C (○); $[HSO_5^-]$ = 0.01, $[H^+]$ = 0.15, μ = 3.1 mol dm^{-3} and 40 °C (■).

[1] The instrument could not be used for the kinetics study since it had no facility for thermostating the solutions at the desired temperature.

Table 1
Study of the stoichiometry of the reaction between HSO_5^- and $[Fe(phen)_3]^{2+}$ ions

S. no.	$10^4[Fe(phen)_3^{2+}]$ initial mol dm^{-3}	$10^4[HSO_5^-]$ initial mol dm^{-3}	$10^4[Fe(phen)_3^{2+}]$ final mol dm^{-3}	$\frac{\Delta[Fe(phen)_3^{2+}]}{\Delta[HSO_5^-]}$
1	3.13	1.16	0.84	1.97
2	5.07	2.22	0.61	2.01
3	11.1	5.08	0.88	2.01
4	17.4	7.58	2.54	1.96
5	34.3	15.0	4.47	1.99
6	31.5	15.0	1.62	1.99

Average $\Delta[Fe(phen)_3^{2+}]/\Delta[HSO_5^-] = 1.99 \pm 0.02$.

2.6. Stoichiometry

The stoichiometry of the reaction between $[HSO_5^-]$ and $[Fe(phen)_3]^{2+}$ is studied using reaction mixtures having different concentration ratios of the reagents but $[Fe(phen)_3^{2+}]$ ion is always present in excess. The unreacted $[Fe(phen)_3^{2+}]$ is estimated at 510 nm at the completion of the reaction. The oxidation products, $[Fe(phen)_3]^{3+}$ and SO_4^{2-} do not interfere in the study. The experimental results are given in Table 1. Thus the stoichiometry of the reaction is expressed by Eq. (1).

$$2[Fe(phen)_3]^{2+} + HSO_5^- + H^+ \rightarrow 2[Fe(phen)_3]^{3+} + SO_4^{2-} + H_2O \quad (1)$$

2.7. Characterisation of the oxidation product

That $[Fe(phen)_3]^{3+}$ is the oxidation product of $[Fe(phen)_3]^{2+}$, Eq. (1), is confirmed by comparing the spectra of an authentically prepared solution of $[Fe(phen)_3]^{3+}$ and that obtained from the spent reaction mixture each of which has a λ_{max} at 603 nm confirming that $[Fe(phen)_3]^{3+}$ is the oxidation product of $[Fe(phen)_3]^{2+}$.

2.8. Test for free radical

The solution of oxone and $[Fe(phen)_3]^{2+}$ are degassed by N_2 and 5 ml of distilled acrylonitrile is added to each solution, which remained clear over few minutes before these are mixed to initiate the reaction. The reaction mixture remained clear over a period of time. However, a negative test does not necessarily negates the formation of a free radical in the reaction; this is likely to be the case if the lower valent metal ion is oxidised at a rate much faster than the rate of initiation of the polymerisation of the monomer.

3. Results

The first-order dependence of the reaction on $[Fe(phen)_3]^{2+}$ is confirmed by the invariance of k_0 values, $10^3 k_0 = 3.42 \pm .02$ (s^{-1}), for several reactions with initial $0.025 \leqslant 10^4[Fe(phen)_3]^{2+} \leqslant 4.0$ mol dm^{-3} at the constant concentrations of the other reagents. The effect of the initial $[HSO_5^-]$ on the k_0, Table 2, resulted in the linear plots, Fig. 2, of k_0 against $[HSO_5^-]$ that passed through the origin indicating that the reaction is first order with respect to the $[HSO_5^-]$. The dependence of rate constants, k_0, on $0.005 \leqslant [H^+] \leqslant 0.50$ mol dm^{-3} at ionic strength = 3.1 mol dm^{-3}, Table 3, indicated that the k_0 decreased with the increase in $[H^+]$. The linear plot between $k_0[H^+]$ and $[H^+]$ with an intercept on the rate ordinate is shown in Fig. 3 Therefore the empirical rate law of the reaction is given by the Eq. (2).

$$\frac{-d[Fe(phen)_3^{2+}]}{dt} = \frac{(a[H^+] + b)[HSO_5^-][Fe(phen)_3^{2+}]}{[H^+]} \quad (2)$$

Table 2
Dependence of k_0 ($=k_{obs} - k_h$) on $[HSO_5^-]$ at different temperatures $10_5[Fe(phen_3)^{2+}] = 2.0$, $[H^+] = 0.05$ and $[\mu] = 1.0$ mol dm^{-3}

$[HSO_5^-]$ (mol dm^{-3})	$10^4 k_0$ (s^{-1})				
	32 °C	35 °C	38 °C	41 °C	44 °C
0.001	0.01	0.04	0.10	0.70	2.70
0.004	0.64	0.67	0.87	2.30	3.70
0.007	3.38	3.50	3.97	5.50	7.20
0.010	5.19	5.48	7.54	10.4	13.2
0.03	19.1	25.3	32.4	34.1	49.3
0.05	32.1	45.4	54.3	70.9	94.2
0.07	46.6	56.6	82.7	98.7	123
0.10	69.8	88.5	114	143	183

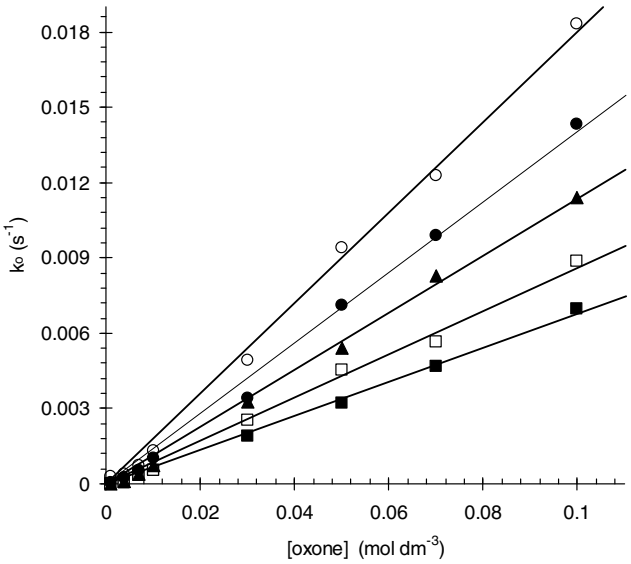

Fig. 2. The linear plots, that pass through the origin, of k_0 (s^{-1}) against $[HSO_5^-]$ at temperatures 32 °C (■), 35 °C (□), 38 °C (▲), 41 °C (●) and 44 °C (○).

Table 3
Dependence of k_0 on $[H^+]$ at 40 °C $10^5[Fe(phen)_3^{2+}] = 2.0$, $[HSO_5^-] = 0.010$ and $[I] = 3.10$ mol dm^{-3}

$[H^+]$ (mol dm^{-3})	0.005	0.02	0.035	0.05	0.10	0.15	0.20	0.25	0.35	0.45	0.50
$10^3 k_0$ (s^{-1})	2.36	1.35	1.31	1.29	1.18	1.05	1.03	1.01	0.98	0.94	0.93

The effect of the alkali chlorides (MCl) ($M^+ = Li^+$, Na^+, K^+ and Cs^+) on the reaction rate is studied to find out if the rates in presence of M^+ ions follow the same pattern as reported in the oxidations of Cl^- and Br^- ions [27], and I^- ion [28] by HSO_5^- ion. The rate increased in the order $I^- > Br^- > Cl^-$ indicating that the rate increases in the direction of increasing polarisability of these halide ions [28]. A perusal of the results, Table 4 indicates that the k_0 for the same $[Cl^-]$ ion increases in the order $Cs^+ > K^+ > Na^+ > Li^+$ that paralleled their polarisability. The almost same intercept on the rate ordinate of the linear plots between k_0 (s^{-1}) and $[M^+]$, Fig. 4, indicate that the rate of the reaction is almost the same in the absence of the alkali metal ions. The linear plot between (k_0 – intercept)/$[M^+]$ (=slope of the plots) and respective polarisability, Fig. 5, values of which are taken from the literature [29] indicates that the rate accelerated by the alkali metal ions is linearly correlated with the polarisability of the alkali metal ion.

The effect of the ionic strength on the rate of the reaction is investigated with $NaHSO_4$, which does not chemically participate in the reaction. The results, Table 5, indicated that the k_0 value decreased with the increase in $[NaHSO_4]$. The linear plot of log k_0 against $\{\sqrt{\mu}/(1 + \sqrt{\mu}) - 0.01\mu\}$, Fig. 6, is consistent with the Davies

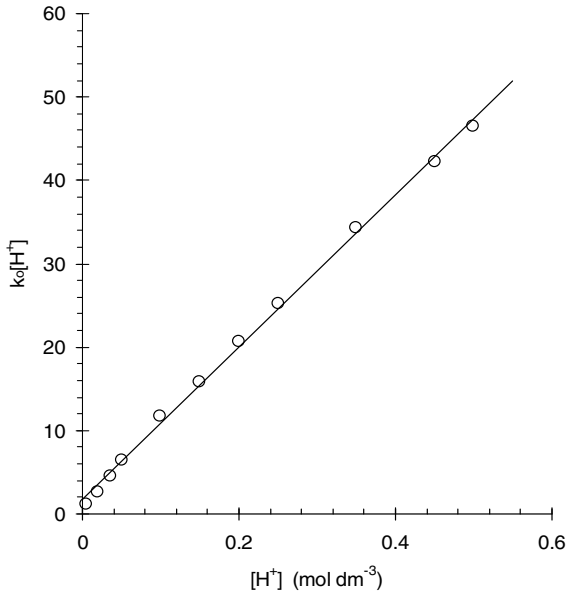

Fig. 3. The linear plot of $k_0[H^+]$ against $[H^+]$ with an intercept on the rate ordinate at 40 °C.

Table 4
Dependence of k_0 on [alkali chloride] at 40 °C $10^5[Fe(phen)_3]^{2+}$ = 2.0, $[HSO_5^-] = 0.01$, $[H^+]$ = 0.05 mol dm^{-3}

10^3k_0 (s^{-1})				
[MCl] (mol dm^{-3}), M^+=	Li^+	Na^+	K^+	Cs^+
0.01	2.32	2.34	2.38	2.83
0.02	2.74	2.90	2.84	3.87
0.04	3.58	3.62	3.88	4.34
0.06	4.43	4.74	4.92	5.88
0.08	5.26	5.26	5.96	7.20
0.10	6.10	6.75	7.10	8.83
0.14	7.78	7.83	9.08	11.3
0.17	9.05	9.79	10.6	13.2
0.20	10.3	10.9	12.2	15.6

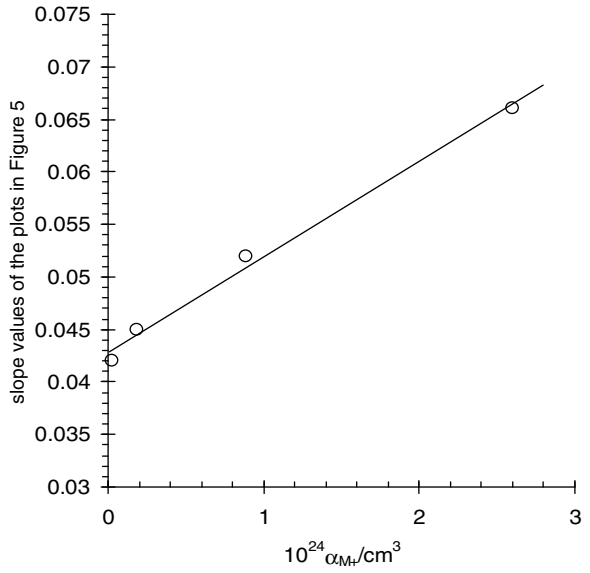

Fig. 5. The linear plot of the slope values of the plots in Fig. 5 against α_{M+}.

Table 5
Dependence of k_0 on the ionic strength of the reaction mixture at 40 °C $10^5[Fe(phen)_3]^{2+}$ = 2.0, $[HSO_5^-] = 0.050$, $[H^+]$ = 0.05 mol dm^{-3}

[μ] (mol dm^{-3})	0.7	0.8	0.9	1.0	1.2	1.3	1.4	1.5	1.7	1.8
10^3k_0 (s^{-1})	8.82	8.02	7.22	7.15	6.60	6.05	5.93	5.81	5.52	5.30

equation [30] with the slope equal to −2.02 indicating that the reacting ions have opposite charges and one of these ions has a charge of two.

4. Mechanism and discussion

The oxidation of $[Fe(phen)_3]^{2+}$ by $[HSO_5]^-$ is a first-order reaction both in $[HSO_5^-]$ and $[Fe(phen)_3^{2+}]$. The first indication that

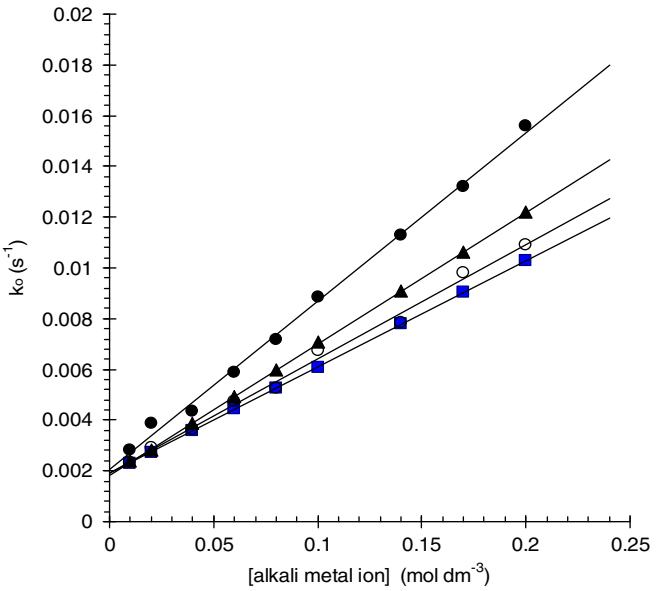

Fig. 4. The linear plot, that has an intercept on the rate ordinate, of k_0 (s^{-1}) against $[M^+]$ at 40 °C where $M^+ = Li^+$ (■), Na^+ (○), K^+ (▲) and Cs^+ (●).

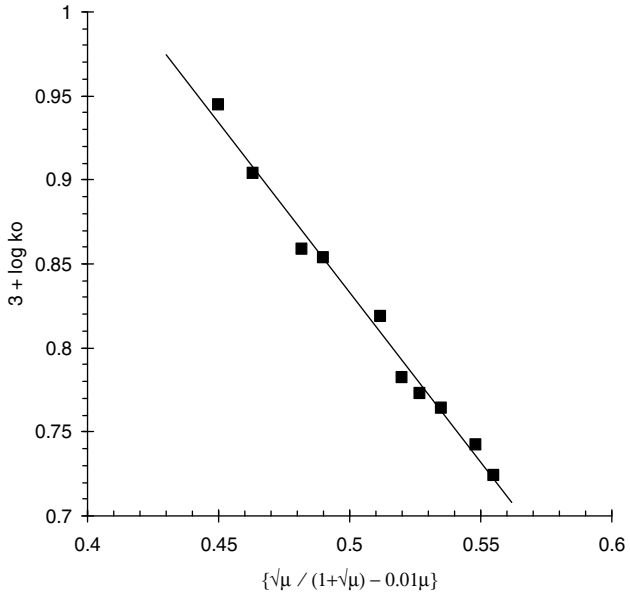

Fig. 6. The linear plot of log k_0 against $\{\sqrt{\mu}/(1+\sqrt{\mu}) - 0.01\sqrt{\mu}\}$. The slope of the plot is −2.02.

the pseudo first-order rate k_{obs}, calculated from the slopes of the linear plots of log(optical densities of the unreacted $[Fe(phen)_3]^{2+}$ solutions) against time, is not the true rate constant for the reaction is provided by the linear plot of k_{obs} against $[HSO_5^-]$ having intercepts on the rate ordinate and the fact that the k_{obs} is almost independent of $[H^+]$. The hydrolysis of $[Fe(phen)_3]^{2+}$ ion is indicated by the decrease in the optical density of sulphuric acid solution of $[Fe(phen)_3]^{2+}$ with time. Therefore, the rate constants (k_h) for the hydrolysis of $[Fe(phen)_3]^{2+}$ were measured under the identical conditions. The true rate constant, k_0, for the reaction is thus equal to ($k_{obs} - k_h$). The k_0 thus obtained is found to be dependent on $[H^+]$.

The electronic structure of peroxomonosulphuric acid is such that one of its proton is similar to that present in sulphuric acid and the other proton resembles that present in H_2O_2. Hence, peroxomonosulphuric acid is considered a strong acid which is fully ionized and its Lewis base $[HSO_5^-]$ is a weak acid with a K_a value = 4×10^{-10} mol dm^{-3} [31].

The formation of a weak intermediate, $[Fe(phen)_3 \cdots HSO_5]^+$ is indicated by the spectral study of the reaction mixtures, which has been discussed in the earlier part of the paper. It may be noted that a similar intermediate is proposed in the oxidation of SCN^- by $[Fe(phen)_3]^{3+}$ ion [32]. Since $[Fe(phen)_3]^{2+}$ is substitution inert, therefore an outer-sphere intermediate is most likely.

The role of alkali metal ions M^+ (=Li^+, Na^+, K^+ and Cs^+) has been discussed previously [33] and therefore a detailed discussion is avoided. The order of the retardation of the rate parallels the ionic size of the strongly hydrated alkali metal ions $Li^+ > Na^+ > K^+ > Cs^+$ [34] therefore the hydrated alkali metal ions are involved in the reaction. The linear plot of $k_{obs}/[M^+]$ against $\propto_{M+}$, Fig. 5, is suggestive of the role of alkali metal ions as a bridge between $[Fe(phen)_3]^{2+}$ and the reactive SO_5^{2-} ion species. A large sized alkali metal ion associated with high value of polarisability is likely to be more effective as a bridge. The greater polarisability of the larger cations [35], and the polarisability of the organic ligand acting as a bridge in the electron transfer between metal ions are reported [36]. The nature of the bridge is most likely to be $[Fe(phen)_3]^{2+} \cdots M^+ \cdots SO_5^{2-}$ where M^+ ion is part of the ion pair with SO_5^{2-} ion. The k_0, which is accelerated by M^+, has two components one of which is independent of $[M^+]$. It indicated that there are two reaction paths one of which involves M^+ ions.

In view of the stoichiometry of the reaction and the above discussion the following reactions are considered to constitute the most probable mechanism of the reaction:

$$HSO_5^- \overset{K_a}{\rightleftharpoons} H^+ + SO_5^{2-} \quad (3)$$

$$SO_5^{2-} + M^+ \overset{K_m}{\rightleftharpoons} MSO_5^- \quad (4)$$

$$[Fe(phen)_3]^{2+} + HSO_5^- \overset{K_1}{\rightleftharpoons} [Fe(phen)_3 \cdots HSO_5]^+ \quad (5)$$

$$[Fe(phen)_3]^{2+} + MSO_5^- \overset{K_2}{\rightleftharpoons} [Fe(phen)_3 \cdots M \cdots SO_5]^+ \quad (6)$$

$$[Fe(phen)_3 \cdots HSO_5]^+ \overset{k_1}{\rightarrow} [Fe(phen)_3]^{3+} + HSO_5^{2-} \quad (7)$$

$$[Fe(phen)_3 \cdots M \cdots SO_5]^+ \overset{k_2}{\rightarrow} [Fe(phen)_3]^{3+} + MSO_5^{2-} \quad (8)$$

$$H^+ + HSO_5^{2-} + [Fe(phen)_3]^{2+} \overset{fast}{\rightarrow} SO_4^{2-} + H_2O + [Fe(phen)_3]^{3+} \quad (9)$$

$$2H^+ + MSO_5^{2-} + [Fe(phen)_3]^{2+} \overset{fast}{\rightarrow} MSO_4^- + H_2O + [Fe(phen)_3]^{3+} \quad (10)$$

Since HSO_5^- is a derivative of H_2O_2, therefore HSO_5^- may act both as one and two electron accepting oxidant. In view of the stoichiometry and the fact that $[Fe(phen)_3]^{2+}$ is one electron donor the behaviour of HSO_5^- behaving as a one electron accepting oxidant in rate limiting steps (7) and (8) and the following fast reactions (9) and (10) is justified. In view of a single electron transfer the formation of the free radical is expected but the same was not detected probably for the reason that the rates of the reactions (9) and (10) far exceed the rate of initiation of the polymerisation of the monomer and there are several examples in the literature where free radical could not be detected for a single electron transfer.

The rate of disappearance of $[Fe(phen)_3]^{2+}$ in terms of the reactions (3)–(8) is deduced as given below:

$$\frac{-d[Fe(phen)_3{}^{2+}]}{dt} = 2(k_1K_1 + \frac{k_2K_2K_mK_a[M^+]}{[H^+]})[Fe(phen)_3{}^{2+}][HSO_5^-] \quad (11)$$

From the consideration of the equilibrium (3) and (4), and that of (5) and (6) it can be shown that $K_a + K_mK_a[M^+]$, and $K_1[HSO_5^-][H^+] + K_2K_a[HSO_5^-]$ are negligible in comparison to $[H^+]$. Therefore it is assumed that $[HSO_5^-] = [S^{VIII}]_0$ and $[Fe(phen)_3{}^{2+}] = [Fe^{II}(phen)_3]_0$ where $[X]_0$ denote the analytical concentrations of the related species. The Eq. (10) is therefore replaced by the Eq. (12) where k_0 as defined above is equal to $k_{obs} - k_h$.

$$\frac{-d[Fe^{II}(phen)_3]}{dt[Fe^{II}(phen)_3]_0} = k_0 = \frac{2(k_1K_1[H^+] + k_2K_2K_mK_a[M^+])[S^{VIII}]_0}{[H^+]} \quad (12)$$

Eq. (12) is consistent with the linear plots of k_0 against $[HSO_5^-]$ passing through the origin, Fig. 2, and is also consistent with the linear plots of $k_0[H^+]$ against $[H^+]$, Fig. 3, and the linear plots k_0 against $[M^+]$, Fig. 4, having an intercept on the rate ordinate.

An explanation is needed for not considering the equilibrium $HSO_5^- + M^+$ $HMSO_5$ in the mechanism. Such an equilibrium is not considered because the formation the intermediate complex of MSO_5 with $[Fe(phen)_3]^{2+}$, if considered, would have been inconsistent with the slope value −2.02 of the Davies plot in Fig. 6 which suggests that the reactants are oppositely charged and that one of the reactants has two charges which is consistent with the equilibrium (4).

Acknowledgements

The financial grants from UGC (F.12-59/1997) and (F.12-147/2001) are acknowledged with thanks. Thanks are also due to the Department of Science and Technology (DST) for sanctioning the grant (2/17/83/STP-III) for purchase of the stopped flow instrument. Thanks are also due to Kriti Mehrotra, my grand daughter, at Cornell University, in helping with certain references.

Appendix A. Supplementary data

The measured optical densities of the reaction mixtures, $10^5[Fe(phen)_3{}^{2+}] = 3.0$, $[H^+] = 0.005$ and $10.0 \leqslant 10^4[HSO_5^-] \geqslant 1.0$ mol dm^{-3} are available in the figure form. Supplementary data associated with this article can be found, in the online version, at doi:10.1016/j.poly.2008.04.011.

References

[1] W.M. Latimer, The Oxidation States of the Elements and their Potential in Aqueous Solutions, Prentice-Hall, New York, 1952. p. 78.
[2] J.M. Anderson, J.K. Kochi, J. Am. Chem. Soc. 92 (1970) 1651.
[3] D.A. House, Chem. Rev. 62 (1962) 185.
[4] W.K. Wilmarth, A. Haim, in: J.O. Edward (Ed.), Peroxide Reaction Mechanism, Interscience, New York, 1962, p. 175.
[5] E.J. Behrman, J.E. McIssac, Annual Reports on Mechanisms of Reactions of Sulphur Compounds, Intra-Science Research Foundation, Santa Monica, USA, vol. 2, 1968, p. 235.
[6] I.R. Wilson, in: C.H. Bamford, C.F.H. Tipper (Eds.), Comprehensive Chemical Kinetics, vol. 6, Elsevier, New York, 1972, p. 340.
[7] G.J. Buist, in: C.H. Banford, C.F.H. Tipper (Eds.), Comprehensive Chemical Kinetics, vol. 6, Elsevier, New York, 1972, p. 456.
[8] M. Anbar, H. Taube, J. Am. Chem. Soc. 76 (1954) 6243.
[9] F. Secco, M. Venturini, J. Chem. Soc., Dalton Trans. (1976) 1410.

[10] M.S. Ramchandran, T.S. Vivekanandam, V. Arunachalam, Bull. Chem. Soc. Jpn. 59 (1986) 1549.
[11] R.J. Balahura, M.D. Johnson, Inorg. Chem. 27 (1988) 3104.
[12] M.S. Ramachandran, T.S. Vivekanandam, N. Paul, D. Singh, Indian J. Chem., Sect. A 27 (1988) 498.
[13] E.A. Betterton, M.R. Hoffmann, Environ. Sci. Technol. 24 (1990) 1819.
[14] L. Venkatasubramaniam, P. Dharmalingam, P. Maruthamuthu, Int. J. Chem. Kinetics 22 (1990) 69.
[15] B.C. Gilbert, J.K. Stell, J. Chem. Soc., Perkin Trans. 2 (1991) 1105.
[16] M. Spiro, Electrochem. Acta 24 (1979) 313.
[17] A.A. Jameel, P. Maruthamuthu, J. Indian Chem. Soc. 75 (1998) 368.
[18] R.S. Panda, S.C. Pradhan, J. Indian Chem. Soc. 77 (2000) 315.
[19] A.L. Nolan, R.C. Burns, G.A. Lawrance, J. Chem. Soc., Dalton Trans. (1996) 2629.
[20] A.L. Nolan, R.C. Burns, G.A. Lawrance, J. Chem. Soc., Dalton Trans. (1998) 3041.
[21] B. Goyal, M. Mehrotra, A. Prakash, Raj N. Mehrotra, Indian J. Chem., Sect. A 40 (2001) 965.
[22] R. Stewart, Oxidations by permanganate, in: K.B. Wiberg (Ed.), Oxidation in Organic Chemistry, Academic Press, New York, 1965, p. 14.
[23] M. Kimura, G. Wada, Inorg. Chem. 17 (1978) 2239.
[24] E.I. Heiba, R.M. Dessau, J. Am. Chem. Soc. 93 (1971) 524.
[25] M. Kimura, Y. Kaneko, J. Chem. Soc., Dalton Trans. (1982) 423.
[26] V. Soni, R.S. Sindal, Raj N. Mehrotra, Polyhedron 24 (2005) 1167.
[27] D.H. Fortnum, C.J. Battaglia, S.R. Cohen, J.O. Edwards, J. Am. Chem. Soc. 82 (1960) 778.
[28] F. Secco, M. Venturini, J. Chem. Soc., Dalton Trans. (1976) 1410.
[29] C.N. Rao, Hand Book of Chemistry and Physics (1967) 234.
[30] C.W. Davies, Ion Association, Butterworths, London, 1962. p. 39.
[31] D.L. Ball, J.O. Edwards, J. Am. Chem. Soc. 78 (1956) 1125.
[32] F.T. Tang, P.M. Henry, Can. J. Chem. 53 (1975) 3319.
[33] M. Mehrotra, V. Soni, Raj N. Mehrotra, Polyhedrron 27 (2008) 609.
[34] K.H. Stern, E.S. Amis, Chem. Rev. 59 (1959) 1.
[35] J.A.A. Ketelaar, Chemical Constitution, Elsevier, 1958. p. 91.
[36] J.K. Halpern, L.E. Orgel, Discuss. Faraday Soc. 29 (1960) 32.

Polyhedron 27 (2008) 2157–2166

Contents lists available at ScienceDirect

Polyhedron

journal homepage: www.elsevier.com/locate/poly

Synthesis, characterization and crystal structure of binuclear diorganotin(IV) complexes derived from hexadentate diacylhydrazone ligands

Han-dong Yin *, Ji-chun Cui, Yan-ling Qiao

Department of Chemistry, Liaocheng University, Liaocheng 252059, China

ARTICLE INFO

Article history:
Received 18 February 2008
Accepted 6 April 2008
Available online 24 May 2008

Keywords:
Diorganotin(IV)
Diacylhydrazone
Synthesis
Crystal structure

ABSTRACT

Six new diorganotin(IV) complexes of the type $(R_2Sn)_2L$ (L = L1 R = Me **1**, *n*Bu **2**; L = L2 R = Me **3**, *n*Bu **4**; L = L3 R = Me **5**, *n*Bu **6**) have been obtained by the reaction of new hexadentate diacylhydrazone ligands H_4L1 [bis(2-hydroxybenzaldehyde)terephthalohydrazone], H_4L2 [bis(2-hydroxy-3-methoxybenzaldehyde)terephthalohydrazone] or H_4L3 [bis(2-hydroxy-1-naphthaldehyde)terephthalohydrazone] with diorganotin(IV) dichloride in the presence of sodium ethoxide. All the diacylhydrazones and the complexes were characterized by elemental analysis, IR and NMR spectra. Complexes **2**, **4**, **5** and **6** were also characterized by X-ray crystallography diffraction analysis which revealed that the complexes have similar structures containing binuclear diorganotin(IV) skeletons. Furthermore weak but significant intermolecular Sn···O bonds, hydrogen bonds, C–H···π stacking or π···π stacking lead to aggregation and assembly of these complexes into 1D, 2D or 3D supramolecular frameworks.

© 2008 Elsevier Ltd. All rights reserved.

1. Introduction

Organotin complexes have been the subject of interest for some time because of their biological and commercial applications [1–6]. In recent years, organotin(IV) complexes with Schiff bases have received increasing attention owing to their antitumor activities and potential applications in biotechnology [7–13]. Acylhydrazones, as one kind of Schiff base, and their metal complexes have been widely studied due to their versatile applications in the fields of analytical, medicinal chemistry and biotechnology [14–21]. These ligands, owing to their facile keto–enol tautomerization and the availability of several potential donor sites, can coordinate with metals. So acylhydrazone organotin(IV) complexes were of interest for structural reasons. The crystal structures of some diorganotin(IV) complexes with the ONO tridentate ligands salicylaldehyde arylhydrazones have been studied [22,23], and we have recently reported some organotin(IV) complexes with *o*-hydroxyarylaldehyde arylhydrazones and pyruvic acid arylhydrazones [24–29]. Usually, tin atoms in complexes derived from ONO tridentate ligands are penta-coordinate with a trigonal bipyramidal (TBP) geometry [23,28,29]. In tin derivatives with a TBP geometry, the metal center can act as a Lewis acid, whose coordination number can be increased by addition of molecules having electron donating atoms [24–26,28], changing the geometry to distorted octahedral or pentagonal bipyramidal. The supramolecular structures of the Schiff base complexes [30] and organotin(IV) complexes [31,32] have been discussed.

However, organotin(IV) complexes with diacylhydrazone have been less widely studied [33,34]. As part of our investigation dealing with the study of diorganotin(IV) species derived from Schiff base ligands, we report herein the synthesis and structural analysis of six new derivatives containing hexadentate diacylhydrazones ligands. The ligands are derived from terephthalohydrazide and three different *o*-hydroxyarylaldehydes, and contain a double set of ONO donor atoms (Scheme 1), thus allowing for the preparation of dinuclear metal complexes. Similar ligands have been reported [35] with a double set of NNO donor atoms.

2. Experimental

2.1. Materials and measurements

All reagents were commercially available, and were used without further purification. Terephthalohydrazide was prepared by the reaction of dimethyl terephthalate with hydrazine hydrate in ethanol and recrystallized from a large amount of water as colourless needles according to the published methods [36]. IR spectra were recorded with a Nicolet-460 spectrophotometer, as KBr discs. ^1H, ^{13}C and ^{119}Sn NMR spectra were recorded with a Varian Mercury Plus 400 spectrometer. The chemical shifts are reported in ppm with respect to the references and are stated relative to the inner reference tetramethylsilane for ^1H and ^{13}C NMR spectroscopy, and to the external reference tetramethyltin for ^{119}Sn NMR

* Corresponding author. Tel./fax: +86 6358239121.
E-mail address: handongyin@lcu.edu.cn (H.-d. Yin).

0277-5387/$ - see front matter © 2008 Elsevier Ltd. All rights reserved.
doi:10.1016/j.poly.2008.04.013

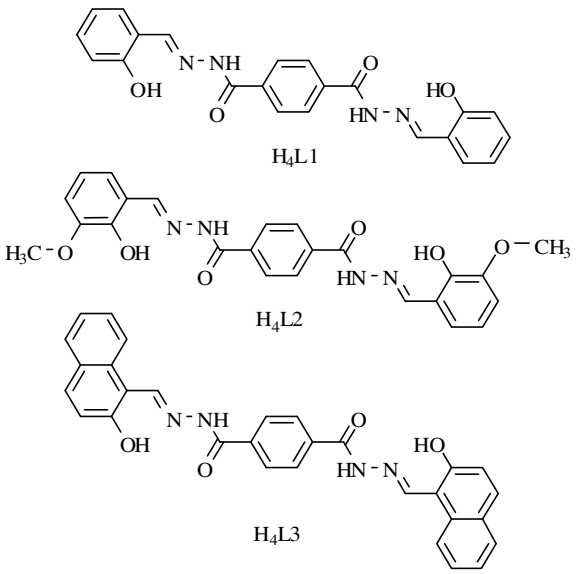

Scheme 1.

spectroscopy. Elemental analyses were performed with a PE-2400II elemental analyzer.

2.2. Synthesis of diacylhydrazones H_4L1, H_4L2 and H_4L3

2.2.1. Bis(2-hydroxybenzaldehyde)terephthalohydrazone (H_4L1)

A mixture of terephthalohydrazide (0.970 g, 5.0 mmol) and 2-hydroxybenzaldehyde (1.830 g, 15.0 mmol) was refluxed in acetic acid for 2 h. The yellow solid formed was filtered off, washed with water and ethanol in turn and dried in vacuum. Yield 1.569 g (78%). *Anal.* Calc. for $C_{22}H_{18}N_4O_4$ (402.40): C, 65.66; H, 4.51; N, 13.92. Found: C, 65.59; H, 4.54; N 14.01%. IR (KBr, cm^{-1}): 3415 (s, N–H), 3252 (s, O–H), 1675 (s, C=O), 1620 (m, C=N). ^1H NMR (400 MHz, DMSO-d_6, 25 °C): 12.22 (s, 2H, OH), 11.22 (s, 2H, NH), 8.69 (s, 2H, CH), 8.10 (s, 4H, ArH), 7.59 (d, J = 7.6 Hz, 2H, ArH), 7.33 (t, J = 7.2 Hz, 2H, ArH), 6.91–7.00 (m, 4H, ArH).

2.2.2. Bis(2-hydroxy-3-methoxybenzaldehyde)terephthalohydrazone (H_4L2)

A similar procedure to the synthesis of H_4L1 was carried out using 2-hydroxy-3-methoxybenzaldehyde in place of 2-hydroxybenzaldehyde. Yield 1.829 g (79%). *Anal.* Calc. for $C_{24}H_{22}N_4O_6$ (462.45): C, 62.33; H, 4.79; N, 12.12. Found: C, 62.43; H 4.70; N, 12.23%. IR (KBr, cm^{-1}): 3421 (s, N–H), 3260 (m, O–H), 1678 (s, C=O), 1626 (m, C=N). ^1H NMR (400 MHz, DMSO-d_6, 25 °C): 12.17 (s, 2H, OH), 11.79 (s, 2H, NH), 8.65 (s, 2H, CH), 8.11 (s, 4H, ArH), 6.85–7.10 (m, 6H, ArH), 3.89 (s, 6H, CH_3).

2.2.3. Bis(2-hydroxy-1-naphthaldehyde)terephthalohydrazone (H_4L3)

A similar procedure to the synthesis of H_4L1 was carried out using 2-hydroxy-1-naphthaldehyde in place of 2-hydroxybenzaldehyde. Yield 2.034 g (81%). *Anal.* Calc. for $C_{30}H_{22}N_4O_4$ (502.52): C, 71.70; H, 4.41; N, 11.15. Found: C, 71.58; H, 4.47; N, 11.23%. IR (KBr, cm^{-1}): 3426 (s, N–H), 3259 (s, O–H), 1675 (s, C=O), 1622 (m, C=N). ^1H NMR (400 MHz, DMSO-d_6, 25 °C): 12.84 (s, 2H, OH), 12.29 (s, 2H, NH), 9.57 (s, 2H, CH), 8.20 (d, J = 8.0 Hz, 2H, Np), 8.15 (s, 4H, ArH), 8.01 (d, J = 8.8 Hz, 2H, Np), 7.88 (d, J = 8.0 Hz, 2H, Np), 7.59 (t, J = 7.6 Hz, 2H, Np), 7.40 (t, J = 7.6 Hz, 2H, Np), 7.21 (d, J = 8.8 Hz, 2H, Np).

2.3. Synthesis of complexes **1**–**6**

2.3.1. $[(CH_3)_2Sn]_2L1$ (**1**)

The ligand H_4L1 (0.201 g, 0.5 mmol) was added in a mixture of ethanol and benzene (V/V: 1/1) (30 ml) to sodium ethoxide

Table 1
Crystal data and structure refinement details for complexes **2**, **4**, **5** and **6**

Complex	**2**	**4**	**5**	**6**
Empirical formula	$C_{38}H_{50}N_4O_4Sn_2$	$C_{40}H_{54}N_4O_6Sn_2$	$C_{34}H_{30}N_4O_4Sn_2$	$C_{46}H_{54}N_4O_4Sn_2$
Formula weight	864.20	924.25	796.00	964.31
Crystal system	monoclinic	triclinic	monoclinic	triclinic
Space group	$P2(1)/c$	$P\bar{1}$	$P2(1)/c$	$P\bar{1}$
a (Å)	10.554(3)	11.7355(14)	9.2391(11)	9.472(3)
b (Å)	10.437(3)	11.9163(18)	21.053(3)	10.073(3)
c (Å)	17.700(5)	17.683(2)	8.171(2)	12.007(3)
α (°)	90	104.604(3)	90	94.507(3)
β (°)	92.035(3).	105.327(3)	96.642(2)	97.135(3)
γ (°)	90	97.306(2)	90	104.975(3)
Volume (Å^3)	1948.6(9)	2257.5(5)	1578.8(5)	1090.7(5)
Z	2	2	2	1
D_{calc} (g cm^{-3})	1.473	1.360	1.674	1.468
Absorption coefficient	1.324	1.151	1.626	1.191
F(000)	876	940	788	490
Crystal size (mm)	0.45 × 0.27 × 0.23	0.30 × 0.21 × 0.15	0.43 × 0.24 × 0.11	0.56 × 0.41 × 0.29
θ Range for data collection (°)	2.27–25.01	2.29–25.01	1.93–25.00	1.72–25.01
Limiting indices	$-12 \leqslant h \leqslant 12$, $-9 \leqslant k \leqslant 12$, $-21 \leqslant l \leqslant 21$	$-13 \leqslant h \leqslant 13$, $-14 \leqslant k \leqslant 11$, $-17 \leqslant l \leqslant 21$	$-10 \leqslant h \leqslant 9$, $-19 \leqslant k \leqslant 25$, $-9 \leqslant l \leqslant 9$	$-11 \leqslant h \leqslant 11$, $-11 \leqslant k \leqslant 11$, $-11 \leqslant l \leqslant 14$
Reflections collected/unique (R_{int})	9852/3436 (0.0579)	11164/7649 (0.0444)	7969/2737 (0.0358)	5596/3732 (0.0227)
Completeness to θ = 25.01 (%)	99.8	96.3	98.3	97.2
Maximum and minimum transmission	0.7505 and 0.5873	0.8463 and 0.7241	0.8414 and 0.5414	0.7239 and 0.5552
Data/restraints/parameters	3436/0/219	7649/0/469	2737/0/199	3732/75/255
Goodness-of-fit on F^2	1.002	1.000	1.003	1.003
Final R indices [$I > 2\sigma(I)$]	R_1 = 0.0415, wR_2 = 0.1001	R_1 = 0.0680, wR_2 = 0.1758	R_1 = 0.0411, wR_2 = 0.0884	R_1 = 0.0463, wR_2 = 0.1179
R indices (all data)	R_1 = 0.0785, wR_2 = 0.1313	R_1 = 0.1388, wR_2 = 0.2372	R_1 = 0.0607, wR_2 = 0.0982	R_1 = 0.0630, wR_2 = 0.1379
Largest difference in peak and hole (e Å^{-3})	0.702 and −0.423	1.104 and −1.033	0.506 and −0.420	1.437 and −0.549

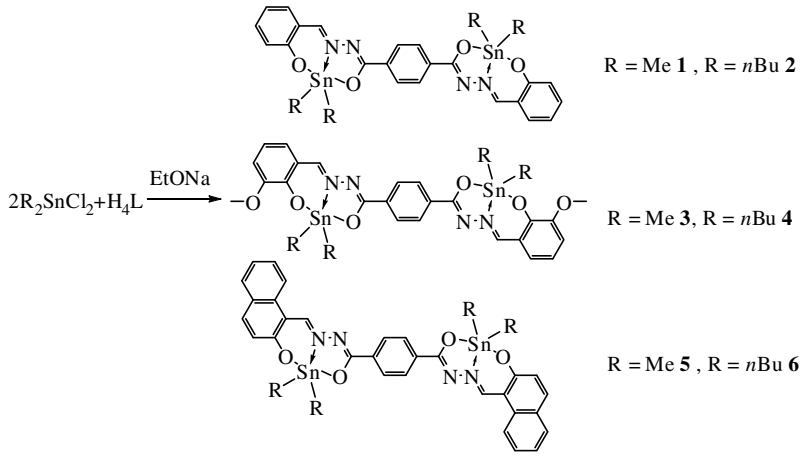

Scheme 2. Synthesis of the dinuclear diorganotin(IV) complexes **1**–**6**.

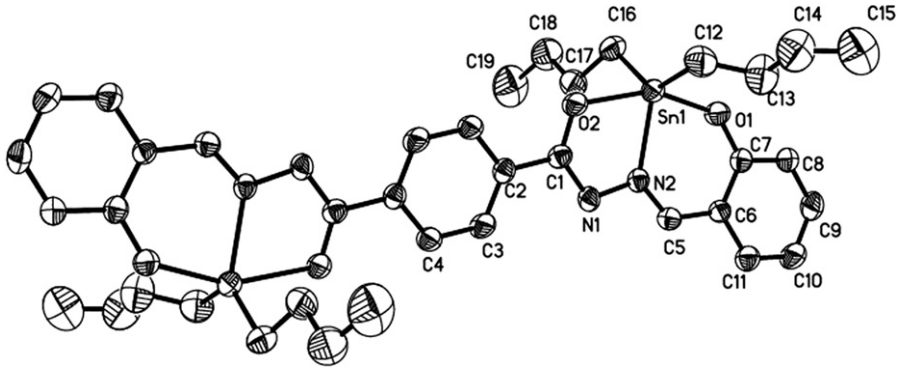

Fig. 1. The molecular structure of complex **2**.

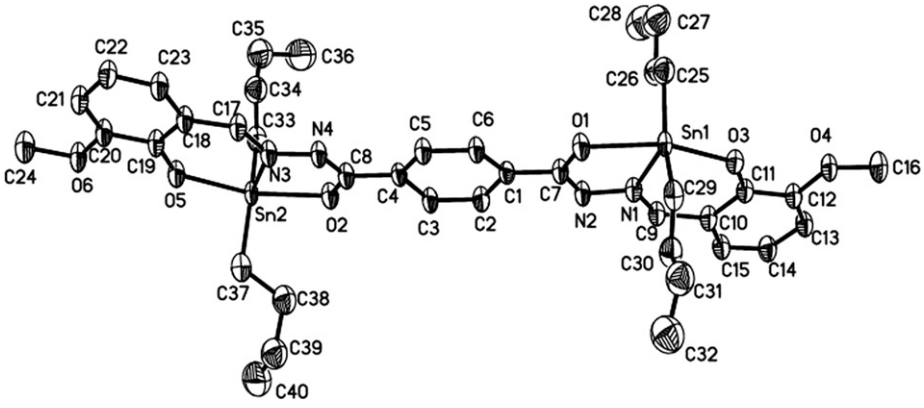

Fig. 2. The molecular structure of complex **4**.

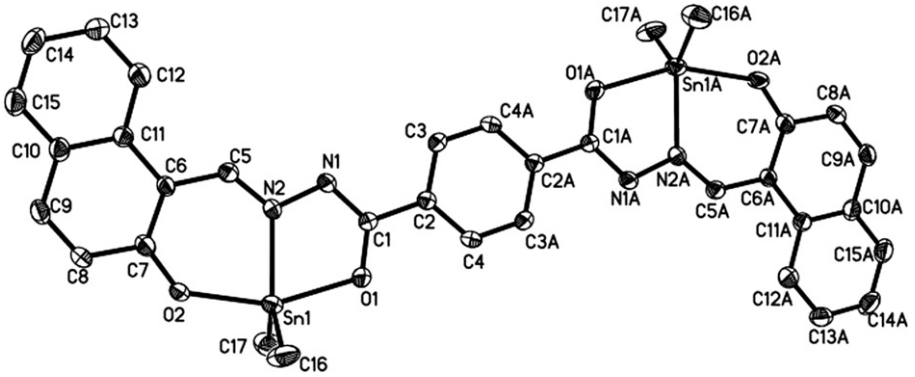

Fig. 3. The molecular structure of complex **5**.

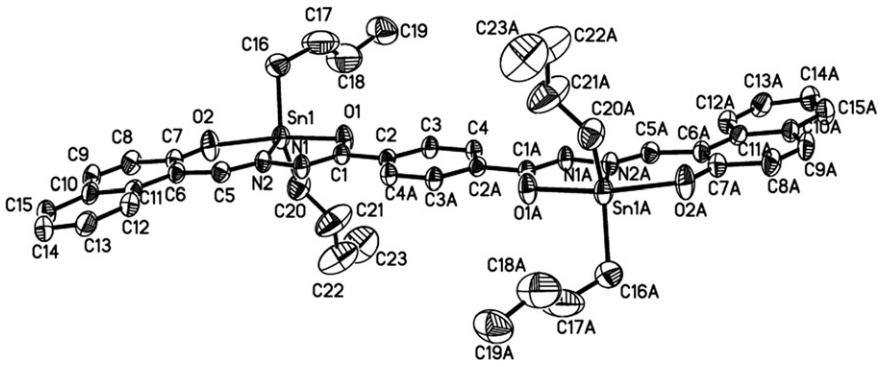

Fig. 4. The molecular structure of complex **6**.

(0.136 g, 2.0 mmol), and the mixture was stirred for 0.5 h. $(CH_3)_2SnCl_2$ (0.220 g, 1.0 mmol) was then added, stirring for 6 h under reflux. After cooling down to room temperature, the solution was filtered and evaporated to dryness, the solid was then recrystallized from dichloromethane–ethanol. *Anal.* Calc. for $C_{26}H_{26}N_4O_4Sn_2$ (695.93): C, 44.87; H, 3.76; N, 8.05. Found: C, 44.78; H, 3.73; N, 8.16%. IR (KBr, cm^{-1}): 1607 (s, C=N), 1592 (m, C=N–N=C), 572 (m, Sn–O), 481 (w, Sn–N). ^1H NMR (400 MHz, $CDCl_3$, 25 °C): 8.75 (s, 2H, CH), 8.11 (s, 4H, ArH), 7.34 (d, J = 6.8 Hz, 2H, ArH), 7.20 (d, J = 7.2 Hz, 2H, ArH), 6.70–6.80 (m, 4H), 0.86 (s, 12H, $SnCH_3$). ^{13}C NMR (100 MHz, $CDCl_3$, 25 °C): 169.25, 167.11, 161.71, 135.75, 135.43, 134.39, 127.28, 121.51, 116.91, 116.71, 1.40. ^{119}Sn NMR (149 MHz, $CDCl_3$, 25 °C): −149.82.

2.3.2. $[(C_4H_9)_2Sn]_2L1$ (**2**)

A similar procedure to the synthesis of **1** was carried out using $(C_4H_9)_2SnCl_2$ in place of $(CH_3)_2SnCl_2$. *Anal.* Calc. for $C_{38}H_{50}N_4O_4Sn_2$ (864.25): C, 52.81; H, 5.83; N, 6.48. Found: C, 52.89; H, 5.90; N, 6.40%. IR (KBr, cm^{-1}): 1605 (s, C=N), 1591 (m, C=N–N=C), 570 (m, Sn–O), 478 (w, Sn–N). ^1H NMR (400 MHz, $CDCl_3$, 25 °C): 8.77 (s, 2H, CH), 8.12 (s, 4H, ArH), 7.33 (d, J = 6.8 Hz, 2H, ArH), 7.19 (d, J = 7.2 Hz, 2H, ArH), 6.72–6.81 (m, 4H, ArH), 1.55–1.81 (m, 16H, Sn–CH_2CH_2–), 1.36 (m, 8H, –CH_2–Me), 0.86 (t, J = 7.2 Hz, 12H, –CH_3). ^{13}C NMR (100 MHz, $CDCl_3$, 25 °C): 169.05, 167.03, 161.64, 135.69, 135.29, 134.27, 127.46, 121.66, 117.03, 116.79, 26.86, 26.47, 22.29, 13.60. ^{119}Sn NMR (149 MHz, $CDCl_3$, 25 °C): −187.41.

2.3.3. $[(CH_3)_2Sn]_2L2$ (**3**)

A similar procedure to the synthesis of **1** was carried out using H_4L2 in place of H_4L1. *Anal.* Calc. for $C_{28}H_{30}N_4O_6Sn_2$ (755.98): C, 44.48; H, 4.00; N, 7.41. Found: C, 44.72; H, 3.98; N, 7.52%. IR (KBr, cm^{-1}): 1610 (s, C=N), 1595 (m, C=N–N=C), 572 (m, Sn–O), 480 (w, Sn–N). ^1H NMR (400 MHz, $CDCl_3$, 25 °C): 8.85 (s, 2H, CH), 8.16 (s, 4H, ArH), 7.01 (d, J = 7.2 Hz, 2H, ArH), 6.78 (d, J = 6.8 Hz, 2H, ArH), 6.61 (t, J = 7.6 Hz, 2H, ArH), 3.89 (s, 6H, OCH_3), 0.84 (s, 12H, $SnCH_3$). ^{13}C NMR (100 MHz, $CDCl_3$, 25 °C): 169.14, 161.78, 157.86, 135.90, 127.45, 125.85, 116.58, 116.11, 115.88, 56.36, 1.33. ^{119}Sn NMR (149 MHz, $CDCl_3$, 25 °C): −148.76.

2.3.4. $[(C_4H_9)_2Sn]_2L2$ (**4**)

A similar procedure to the synthesis of **1** was carried out using $(C_4H_9)_2SnCl_2$ and H_4L2 in place of $(CH_3)_2SnCl_2$ and H_4L1. *Anal.* Calc. for $C_{40}H_{54}N_4O_6Sn_2$ (924.30): C, 51.98; H, 5.89; N, 6.06. Found: C, 51.89; H, 5.79; N, 6.17%. IR (KBr, cm^{-1}): 1601 (s, C=N), 1599 (m, C=N–N=C), 578 (m, Sn–O), 481 (w, Sn–N). ^1H NMR (400 MHz, $CDCl_3$, 25 °C): 8.77 (s, 2H, CH), 8.13 (s, 4H, ArH), 6.93 (d, J = 7.2 Hz, 2H, ArH), 6.82 (d, J = 6.8 Hz, 2H, ArH), 6.67 (t, J = 7.6 Hz, 2H, ArH), 3.86 (s, 6H, OCH_3) 1.54–1.67 (m, 16H, Sn–CH_2CH_2–), 1.35 (m, 8H, –CH_2–Me), 0.84 (t, J = 7.2 Hz, 12H, –CH_3). ^{13}C NMR (100 MHz, $CDCl_3$, 25 °C): 169.07, 161.69, 157.72, 135.72, 127.47, 125.89, 116.64, 116.15, 115.87, 56.31, 26.86, 26.43, 22.82, 13.57. ^{119}Sn NMR (149 MHz, CDCl3, 25 °C): −186.36.

Table 2
Selected bond lengths (Å) and bond angles (°) of complexes **2**, **4**, **5** and **6**

Complex ***2***			
Sn(1)–O(1)	2.079(4)	Sn(1)–C(16)	2.113(6)
Sn(1)–C(12)	2.126(7)	Sn(1)–O(2)	2.162(4)
Sn(1)–N(2)	2.174(5)	N(1)–C(1)	1.313(7)
O(2)–C(1)	1.281(6)	N(2)–C(5)	1.288(7)
O(1)–Sn(1)–C(16)	93.4(2)	O(1)–Sn(1)–C(12)	99.7(3)
C(16)–Sn(1)–C(12)	131.8(3)	O(1)–Sn(1)–O(2)	154.9(2)
C(16)–Sn(1)–O(2)	92.5(2)	C(12)–Sn(1)–O(2)	94.5(3)
O(1)–Sn(1)–N(2)	83.1(2)	C(16)–Sn(1)–N(2)	116.5(2)
C(12)–Sn(1)–N(2)	111.1(3)	O(2)–Sn(1)–N(2)	72.4 (2)
Complex ***4***			
Sn(1)–C(29)	2.088(1)	Sn(1)–C(25)	2.123(1)
Sn(1)–O(3)	2.167(7)	Sn(1)–N(1)	2.198(9)
Sn(1)–O(1)	2.206(7)	Sn(2)–C(33)	2.106(1)
Sn(2)–C(37)	2.116(1)	Sn(2)–O(5)	2.166(7)
Sn(2)–O(2)	2.180(7)	Sn(2)–N(3)	2.219(9)
N(1)–C(9)	1.288(1)	O(2)–C(8)	1.293(1)
N(2)–C(7)	1.277(1)	N(3)–C(17)	1.282(1)
O(1)–C(7)	1.263(1)	N(4)–C(8)	1.307(1)
C(29)–Sn(1)–C(25)	151.6(5)	C(29)–Sn(1)–O(3)	97.0(4)
C(25)–Sn(1)–O(3)	92.3(4)	C(29)–Sn(1)–N(1)	104.1(5)
C(25)–Sn(1)–N(1)	103.7(4)	O(3)–Sn(1)–N(1)	82.3(3)
C(29)–Sn(1)–O(1)	90.6(4)	C(25)–Sn(1)–O(1)	93.1(4)
O(3)–Sn(1)–O(1)	153.1(3)	N(1)–Sn(1)–O(1)	70.8(3)
C(33)–Sn(2)–C(37)	152.5(5)	C(33)–Sn(2)–O(5)	93.5(4)
C(37)–Sn(2)–O(5)	92.6(4)	C(33)–Sn(2)–O(2)	92.7(4)
C(37)–Sn(2)–O(2)	93.5(4)	O(5)–Sn(2)–O(2)	153.9(3)
C(33)–Sn(2)–N(3)	102.3(4)	C(37)–Sn(2)–N(3)	105.1(4)
O(5)–Sn(2)–N(3)	82.2(3)	O(2)–Sn(2)–N(3)	71.7(3)
Complex ***5***			
Sn(1)–O(2)	2.088(4)	Sn(1)–C(16)	2.099(6)
Sn(1)–C(17)	2.110(6)	Sn(1)–O(1)	2.117(4)
Sn(1)–N(2)	2.154(4)	N(1)–C(1)	1.297(6)
O(1)–C(1)	1.297(6)	N(2)–C(5)	1.290(6)
O(2)–Sn(1)–C(16)	95.0(2)	O(2)–Sn(1)–C(17)	96.8(2)
C(16)–Sn(1)–C(17)	121.5(3)	O(2)–Sn(1)–O(1)	155.4(2)
C(16)–Sn(1)–O(1)	95.3(2)	C(17)–Sn(1)–O(1)	96.7(2)
O(2)–Sn(1)–N(2)	82.0(1)	C(16)–Sn(1)–N(2)	116.7(2)
C(17)–Sn(1)–N(2)	121.6(2)	O(1)–Sn(1)–N(2)	73.4(1)
Complex ***6***			
Sn(1)–O(2)	2.091(4)	Sn(1)–C(20)	2.108(8)
Sn(1)–O(1)	2.127(4)	Sn(1)–C(16)	2.130(8)
Sn(1)–N(2)	2.152(5)	N(1)–C(1)	1.298(7)
O(1)–C(1)	1.297(7)	N(2)–C(5)	1.303(7)
O(2)–Sn(1)–C(20)	94.4(3)	O(2)–Sn(1)–O(1)	155.3(2)
C(20)–Sn(1)–O(1)	96.7(2)	O(2)–Sn(1)–C(16)	93.2(3)
C(20)–Sn(1)–C(16)	126.8(3)	O(1)–Sn(1)–C(16)	97.7(3)
O(2)–Sn(1)–N(2)	82.2(2)	C(20)–Sn(1)–N(2)	117.2(3)
O(1)–Sn(1)–N(2)	73.2(2)	C(16)–Sn(1)–N(2)	116.0(3)

*2.3.5. $[(CH_3)_2Sn]_2L3$ (**5**)*

A similar procedure to the synthesis of **1** was carried out using H_4L3 in place of H_4L1. *Anal.* Calc. for $C_{34}H_{30}N_4O_4Sn_2$ (796.05): C, 51.30; H, 3.80; N, 7.04. Found: C, 51.41; H, 3.89; N, 6.96%. IR (KBr, cm^{-1}): 1603 (s, C=N), 1587 (m, C=N–N=C), 566 (m, Sn–O), 472 (w, Sn–N). ^1H NMR (400 MHz, $CDCl_3$, 25 °C): 9.73 (s, 2H, CH), 8.16 (s, 4H, ArH), 8.09 (d, J = 8.4 Hz, 2H, Np), 7.78 (d, J = 9.2 Hz, 2H, Np), 7.71 (d, J = 8.0 Hz, 2H, Np), 7.54 (t, J = 7.2 Hz, 2H, Np), 7.33 (t, J = 7.6 Hz, 2H, Np), 6.94 (d, J = 9.2 Hz, 2H, Np), 0.88 (s, 12H, $SnCH_3$). ^{13}C NMR (100 MHz, $CDCl_3$, 25 °C): 168.88, 167.72, 157.34, 136.83, 135.56, 133.68, 129.17, 128.12, 127.35, 127.22, 124.25, 123.17, 119.16, 107.13, 1.35. ^{119}Sn NMR (149 MHz, $CDCl_3$, 25 °C): −151.20.

*2.3.6. $[(C_4H_9)_2Sn]_2L3$ (**6**)*

A similar procedure to the synthesis of **1** was carried out using $(C_4H_9)_2SnCl_2$ and H_4L3in place of $(CH_3)_2SnCl_2$ and H_4L1. *Anal.* Calc. for $C_{46}H_{54}N_4O_4Sn_2$ (964.37): C, 57.29; H, 5.64; N, 5.81. Found: C, 57.18; H, 5.59; N, 5.92%. IR (KBr, cm^{-1}): 1606 (s, C=N), 1585 (m, C=N–N=C), 564 (m, Sn–O), 470 (w, Sn–N). ^1H NMR (400 MHz, $CDCl_3$, 25 °C): 9.78 (s, 2H, CH), 8.18 (s, 4H, ArH), 8.15 (d, J = 8.4 Hz, 2H, Np), 7.77 (d, J = 9.2 Hz, 2H, Np), 7.65 (d, J = 8.0 Hz, 2H, Np), 7.54 (t, J = 7.6 Hz, 2H, Np), 7.29 (t, J = 7.6 Hz, 2H, Np), 6.96 (d, J = 9.2 Hz, 2H, Np), 1.51–1.71 (m, 16H, $Sn–CH_2CH_2–$), 1.36 (m, 8H, $–CH_2–Me$), 0.87 (t, J = 6.8 Hz, 12H, $–CH_3$). ^{13}C NMR (100 MHz, $CDCl_3$, 25 °C): 169.46, 168.01, 157.12, 136.68, 135.67, 133.81, 129.16, 128.04, 127.36, 127.14, 124.37, 123.01, 119.16, 107.08, 26.86, 26.46, 22.07, 13.60. ^{119}Sn NMR (149 MHz, $CDCl_3$, 25 °C): −188.78.

2.4. X-ray crystallography

Crystals were mounted in Lindemann capillaries under nitrogen. All X-ray crystallographic data were collected on a Bruker SMART CCD 1000 diffractometer with graphite monochromated Mo Kα radiation (λ = 0.71073 Å) at 298(2) K. A semi-empirical absorption correction was applied to the data. The structures were solved by direct methods using SHELXS-97 and refined against F^2 by full-matrix least squares using SHELXL-97. Hydrogen atoms were placed in calculated positions. Crystal data and experimental details of the structure determinations are list in Table 1.

3. Results and discussion

3.1. Synthesis of the diorganotin(IV) complexes

The hexadentate ligands H_4L1, H_4L2 and, H_4L3 were obtained from the reaction of terephthalohydrazide with 2-hydroxybenzaldehyde, 2-hydroxy-3-methoxybenzaldehyde and 2-hydroxy-1-naphthaldehyde, respectively. The dinuclear tin complexes **1**–**6**

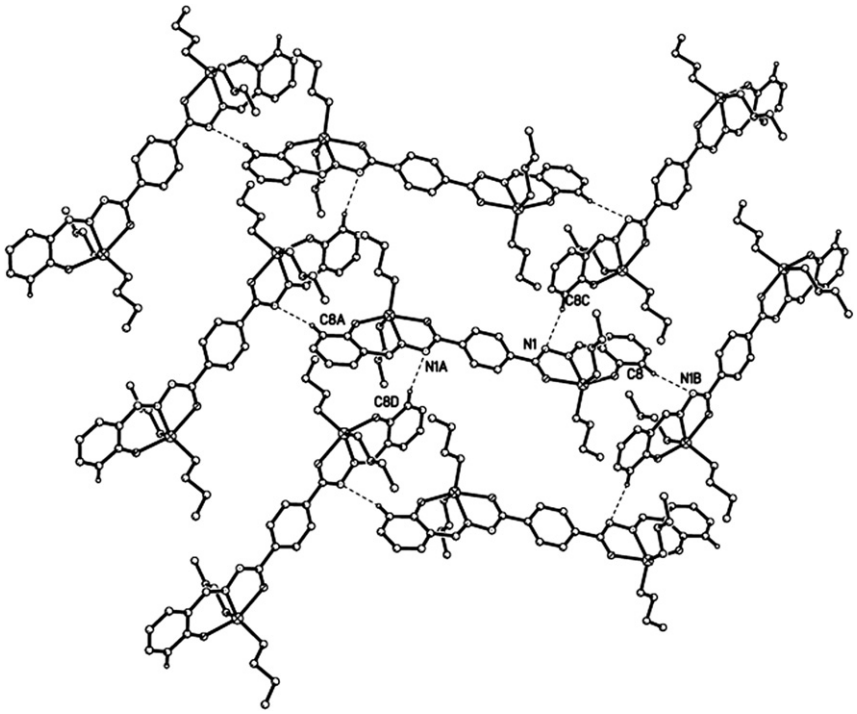

Fig. 5. Supramolecular structure of complex **2** showing the 2D framework *via* intermolecular C–H···N hydrogen bonds.

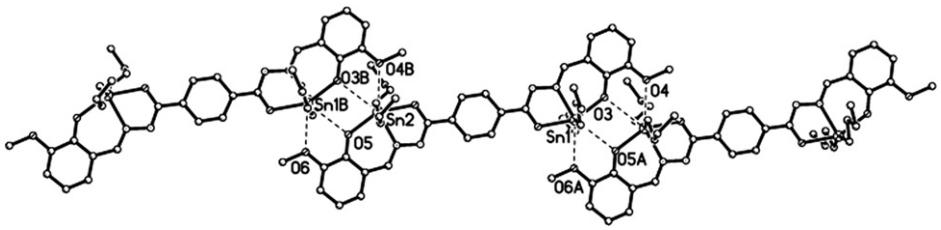

Fig. 6. The 1D chain linkage from intermolecular Sn···O interactions of complex **4**.

were prepared by reaction of one equivalent of the ligands with two equivalents of the corresponding diorganotin(IV) dichloride. Sodium ethoxide was used as a base for the deprotonation of the ligand as described in the preparative part (Scheme 2). Complexes **1**–**6** are solid, with an intense orange colour, and are soluble in polar organic solvents and stable under atmospheric conditions. The solids were recrystallized from dichloromethane–ethanol and orange single crystals were formed by slow evaporation at room temperature for **2**, **4**, **5** and **6**.

3.2. IR spectra

In the IR spectra of the ligands, the stretching vibration bands of N–H, O–H and C=O appear at 3415–3426, 3250–3260 and 1670–1678 cm^{-1}, respectively, and these bands disappear from the spectra of complexes **1**–**6**. The disappearance of ν_{O-H} shows the deprotonation of the –OH group and its subsequent coordination to the central tin atom. The disappearance of $\nu_{C=O}$ unambiguously confirms that the ligand coordinates with the tin in the enol form. The $\nu_{C=N}$ band of the ligands at 1620–1626 cm^{-1} shifts to 1611–1603 cm^{-1} in the spectra of the complexes **1**–**6**, suggesting coordination of the imine nitrogen to the tin moiety [24,25,27]. The characteristic absorptions at 1599–1585 cm^{-1} in the spectra of these complexes indicate the presence of a C=N–N=C group [23,25–27]. Two new bands at 578–564 and 470–481 cm^{-1} are characteristic of Sn–O and Sn–N absorptions, respectively [27].

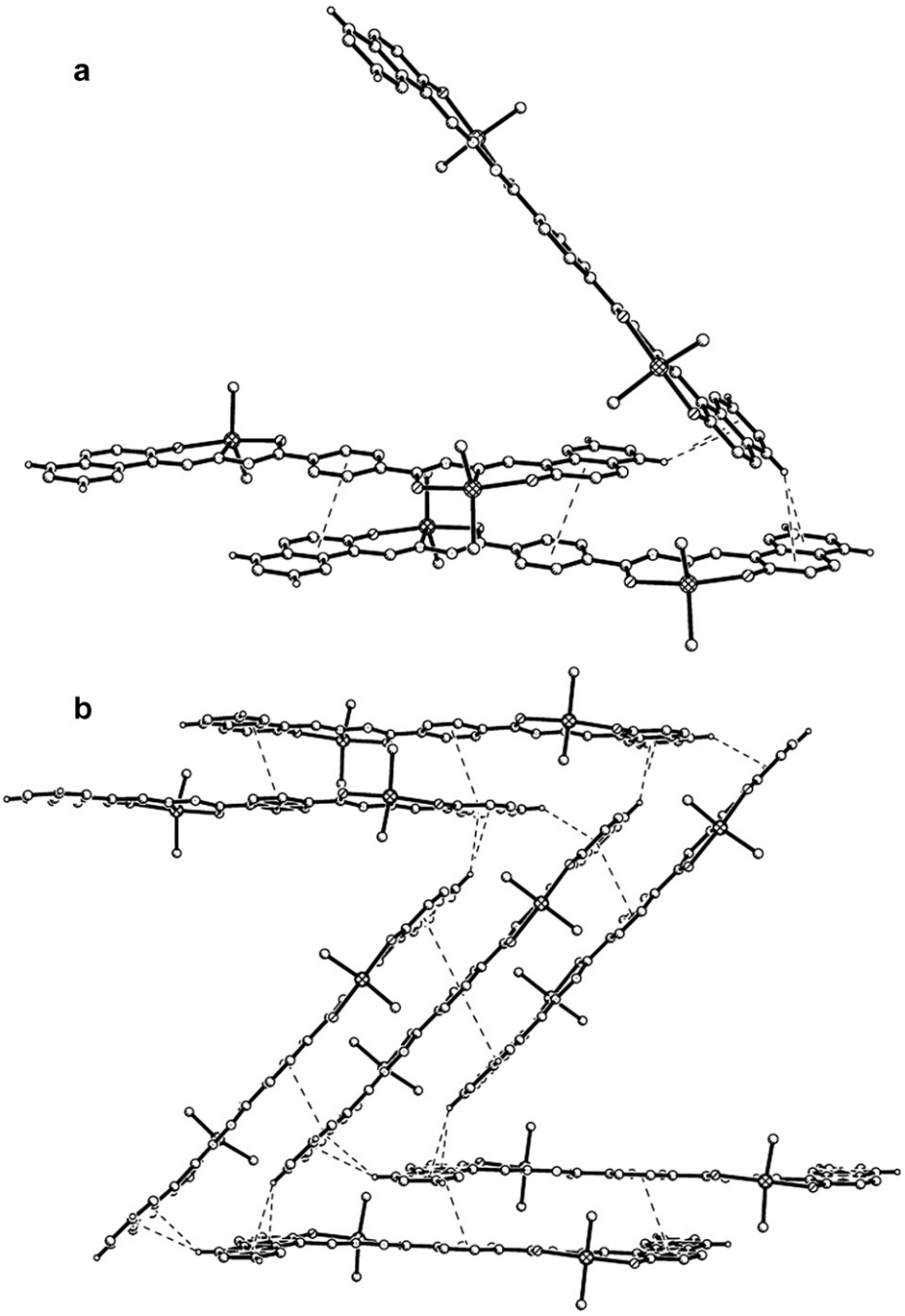

Fig. 7. Supramolecular structure of complex **5**, (a) showing C–H···π stacking and π···π stacking interactions and (b) showing the 2D framework via intermolecular C–H···π stacking and π···π stacking interactions.

3.3. NMR spectra

In the ^{1}H NMR spectra of the free ligands, the single resonance of the proton (–NHN=) is observed at 11.22, 11.79 and 12.29 ppm, respectively, and it is absent in the spectra of the complexes, thus indicating deprotonation of the –NHN= group and confirming that the ligand coordinates to the tin in the enol form. In the ^{1}H NMR spectra of complexes **1**–**6** there is no signal resonance for Ar–OH, which strongly suggests that the phenolic oxygen atoms participate in coordination to the tin atom. The ^{119}Sn NMR spectra of complexes **1**–**6** show only one signal at −149.82, −187.41, −148.76, −186.36, −154.20 and −188.78 ppm, respectively. According to the literature reported [37–39], the coordinated number of the tin atoms are all five-coordinate. The conclusions are supported by the results of the X-ray diffraction studies of complexes **2**, **4**, **5** and **6**, which suggests that the intermolecular Sn···O interaction of **4** probably does not survive in solution.

3.4. Description of structures *2*, *4*, *5* and *6*

The molecular structures of **2**, **4**, **5** and **6** are given in Figs. 1–4, respectively, and selected bond lengths and bond angles are given in Table 2. From the structures we can see that the complexes show similar structures, containing binuclear diorganotin(IV) skeletons showing a trans conformation (centrosymmetry). The alkyl side chains of complex **6**, however, are disordered. In all the complexes, each of the two tin atoms has a coordination number of five, resulting from the bonding to phenolate-O, imine-N and deprotonated amide-O atoms of the moieties of H_4L1, H_4L2 or H_4L3, which are hexadentate ligands that function as tetrabasic in the enol form, and two carbon atoms from the organic tin substituents. The distortion from the perfect trigonal bipyramidal geometry is mainly due to the rigidity of the chelate rings and the large covalent radius of the tin(IV) atoms. As observed in similar complexes, the oxygen atoms are in axial positions; the

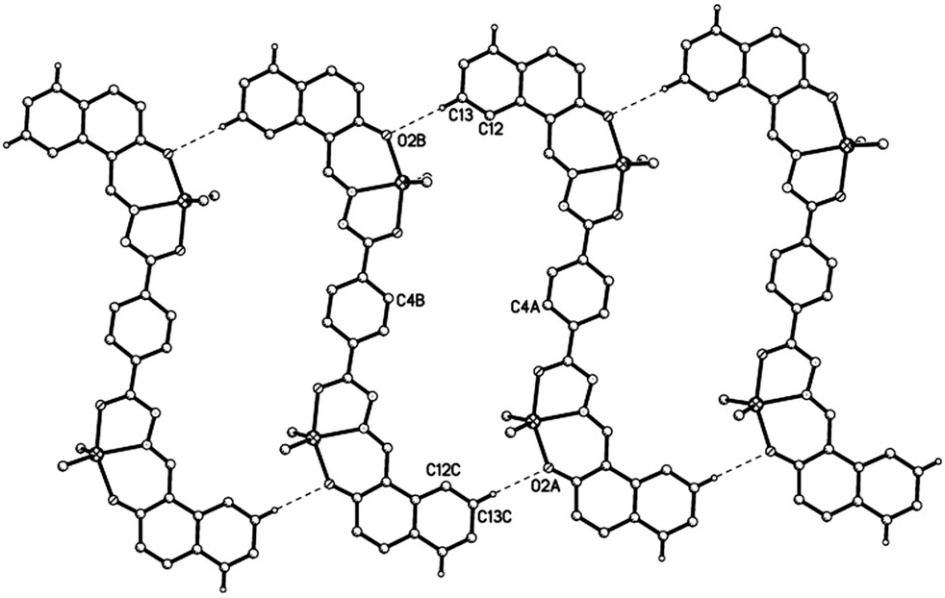

Fig. 8. Supramolecular structure of complex **5**, showing the 1D chain *via* intermolecular C–H···O hydrogen bonds.

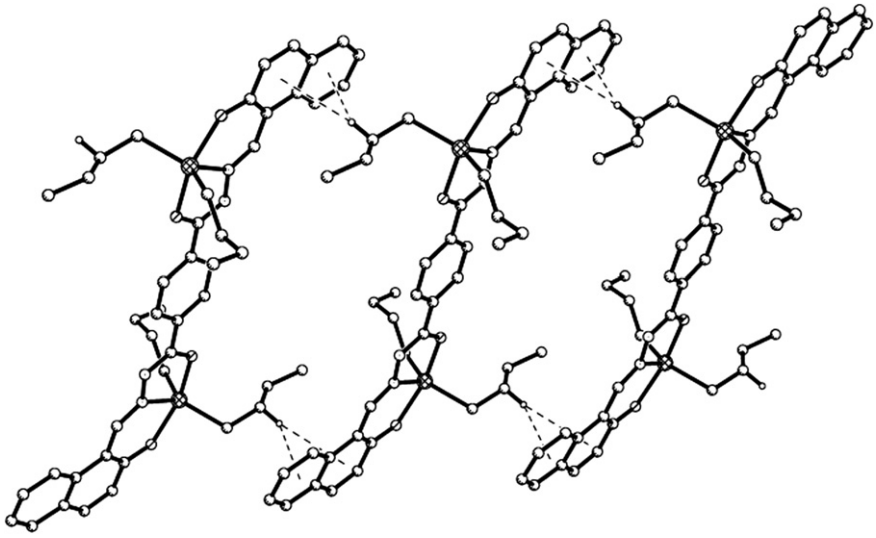

Fig. 9. The 1D chain linked by intermolecular C–H···π interactions of complex **6**.

nitrogen atom forms a coordination bond with the tin atom and it is found in an equatorial position, as well as the two organic substituents. There are five and six membered Sn–N–N–C–O and Sn–N–C–C–C–O rings imposing the constraints.

The C–O and C–N bond lengths in the amide functionality of the complexes are within 1.263(12)–1.297(7) and 1.277(13)–1.313(7) Å, respectively. These values are consistent with the enolate form of the amide functionality [27,40]. The Sn–N distances 2.174(5) Å for **2**, 2.198(9) and 2.219(9) Å for **4**, 2.154(4) Å for **5**, 2.152(5) Å for **6**] are greater than the sum of the non-polar covalent radii, 2.15 Å, but are considerably shorter than the sum of the Van der Waals radii (3.75 Å) and should be considered as bonding interactions, indicating strong tin–nitrogen interactions, and they lie in the range 2.140(6)–2.327(2) Å which has been reported for Sn–N bond lengths [25–29,33,34]. The Sn–O(amide) bond lengths [between 2.117(4) and 2.206(7) Å] and the Sn–O(phenolate) bond lengths [between 2.079(4) and 2.169(5) Å] are in excellent agreement with other previously known acylhydrazone diorganotin(IV) complexes in the literatures [25–29,33,34]. The Sn–O(amide) bond length is longer than the Sn–O(phenolate) in the same complex. The O–Sn–O bond angles [154.9(2)° for **2**, 153.1(3)° and 153.9(3)° for **4**, 155.4(2)° for **5**, 155. 3(2)° for **6**] are deviate from the linear angle 180°. The Sn–C bond lengths fall in a narrow range from 2.082(12) to 2.130(8) Å for complexes **2**, **4**, **5** and **6**, typical for organotin(IV) derivatives. The related C–Sn–C angles [131.8(3)° for **2**, 151.6(5)° and 152.5(5)° for **4**, 121.5(3)° for **5**, 126.8(3)° for **6**] are deviated from 120°.

Further analysis of the supramolecular structures of complexes **2**, **4**, **5** and **6** shows that they are different from each other. The supramolecular structure of complex **2** is shown in Fig. 5, showing a 2D framework with C–H···N hydrogen bonding interactions. It can be seen that each discrete molecule links with another four monomers through the same four intermolecular C(8)–H(8)···N(1) hydrogen bonds, and a 42-membered macrocycle is formed by the four such hydrogen bonds. The H(8)···N(1), C(8)···N(1) distances and the C(8)–H(8)···N(1) angle are 2.569 Å, 3.476 Å and 164.87°, respectively, which is similar to that reported in the literature [41].

The salient feature of the supramolecular structure of complex **4** is a 1D polymer linkage made up from weak interactions of Sn···O bonds. As shown in Fig. 6, there are four Sn···O bonds forming a head-to-tail arrangement. The distances of the Sn···O bonds (Sn(1)···O(5A) = 2.971 Å, Sn(1)···O(6A) = 2.824 Å, Sn(2)···O(3B) = 2.984 Å, Sn(2)···O(4B) = 2.829 Å) are considerably longer than the normal Sn–O covalent bond, but they are much shorter than the van der Waals radii of Sn and O (3.68 Å), which is reasonable as an intermolecular interaction according to literature reports [42]. Due to the Sn···O intermolecular interactions, the tin atoms adopt a distorted pentagonal bipyramidal geometry in the solid state, which is not observed in solution. The C–Sn–C bond angles have values of 151.6(5)° and 152.5(5)°, larger than 131.8(3)° for **2**, 121.5(3)° for **5** and 126.8(3)° for **6**, allowing for the Sn···O intermolecular interactions.

The supramolecular structure of complex **5** is dominated by intermolecular C–H···π, π···π stacking interactions and C–H···O hydrogen bonds. An intermolecular edge-to-face C–H···π stacking interaction has been identified between the C(15) atom and the naphthalene nucleus [H(15)···Cg(2) = 3.084 Å], as shown in Fig. 7a. This can be considered as a pair of bifurcated intermolecular C–H···π interactions (Table S1), which is similar to another organotin complex that has been reported [43], forming a head-to-tail zigzag 2D network (Fig. 7b). There is also π···π stacking interactions between the ring (C2–C4, C2A–C4A) and the ring (C6–C10) found in the structure (Fig. 7a), the distance between the ring centroids is 3.634 Å and the dihedral angle of the two rings is 20.61°. As shown in Fig. 8, a 34-membered macrocycle is formed by two intermolecular C–H···O [C(13)···O(2B) = 3.517 Å, H(13)···O(2B) = 2.588 Å, C(13)–H(13)···O(2B) = 177.67°] hydrogen bonds between two discrete molecules, and the size of the macrocycle channel is 15.633 × 6.690 Å (transannular C12···C12C and C4A···C4B). A one-dimensional polymeric chain structure along the a axis is linked by the C–H···O hydrogen bonds with a head-to-tail arrangement. Furthermore this zigzag 2D network is associated with adjacent layers by intermolecular C–H···O hydrogen bonds, forming a 3D framework.

In Fig. 9 the supramolecular structure of complex **6** exhibits a 1D chain structure *via* intermolecular point-to-face C–H···π stacking interactions. The C–H···π interaction is identified between C17 and the naphthalene nucleus. This can be considered as a pair of bifurcated intermolecular C–H···π interactions too (Table S1), the closest contact of 2.849 Å is H(17A)···C(11). The C–H···π interaction is similar to that in **5**, but the difference is that the C–H of **6** comes from the aryl group of the ligand and the C–H of **5** is the butyl group of the diorganotin moiety. These weak but significant stacking interactions stabilize the crystal structures.

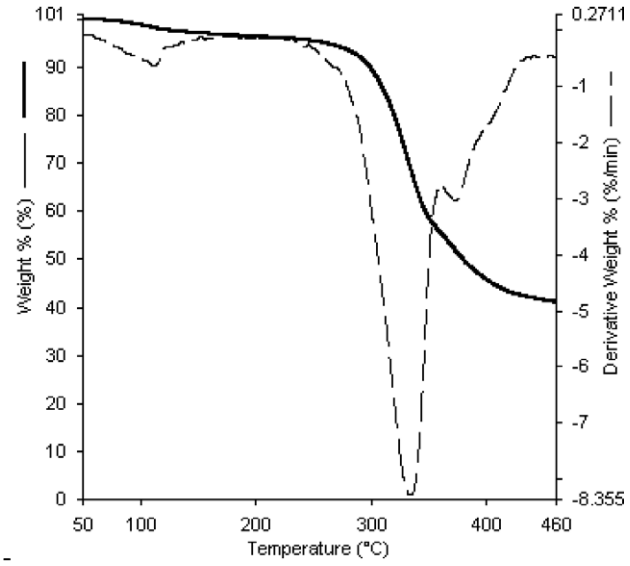

Fig. 10. TGA curve of complex **2**.

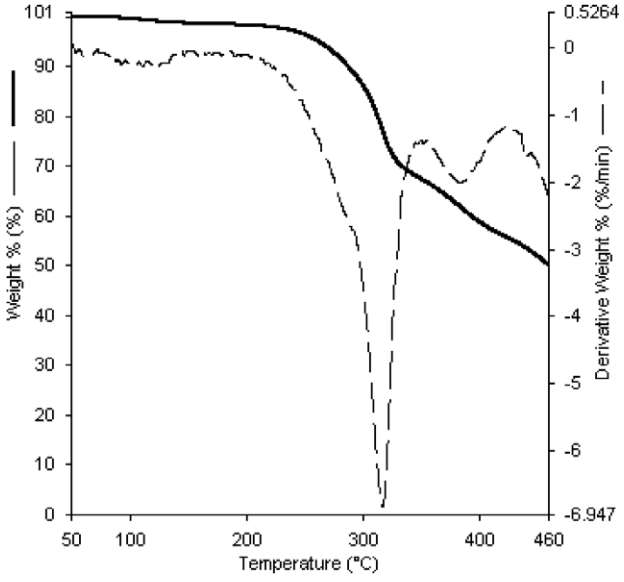

Fig. 11. TGA curve of complex **4**.

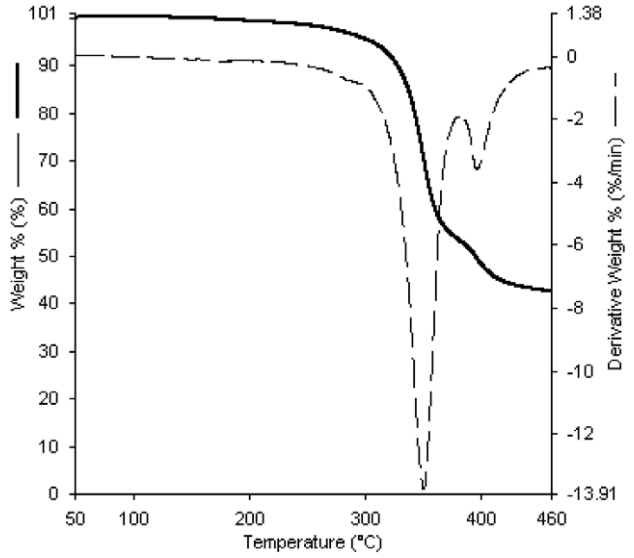

Fig. 12. TGA curve of complex **5**.

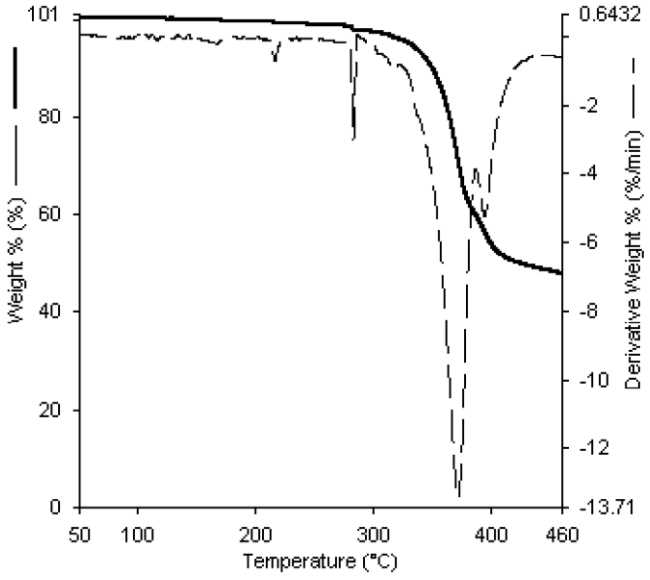

Fig. 13. TGA curve of complex **6**.

3.5. Thermogravimetric analysis

To study the stability of complexes **2**, **4**, **5** and **6**, thermogravimetric analysis (TGA) was performed in the temperature range 50–500 °C under a N_2 atmosphere. The TGA curves of complexes **2**, **4**, **5** and **6** exhibit one continuous weight loss stage in the range 250–400 °C (Figs. 10–13). In general, complexes **2**, **4**, **5** and **6** exhibit good thermal stability [44,45].

4. Conclusions

The molecular structures of four new diorganotin(IV) complexes have been reported. Although the *o*-hydroxyarylaldehyde terephthalohydrazone ligands have the same coordination capacity function as a rigid bridging tetrabasic hexadentate moiety binding two tin atoms through ONO donor atoms, and both tin atoms are in a trigonal bipyramidal environment, different intermolecular interactions which lead to aggregation and assembly of these complexes into 1D, 2D or 3D supramolecular frameworks are observed in the solid state. This can be attributed to different aryl groups of the hydrazones and alkyl groups of the diorganotin units.

Acknowledgements

We acknowledge the financial support of the Natural Science Foundation of China (No. 20771053) and the Shangdong Province Science Foundation (No. 2005ZX09).

Appendix A. Supplementary data

CCDC 660815, 660814, 660817 and 660816 contain the supplementary crystallographic data for complexes **2**, **4**, **5** and **6**. These data can be obtained free of charge via http://www.ccdc.cam.ac.uk/conts/retrieving.html, or from the Cambridge Crystallographic Data Centre, 12 Union Road, Cambridge CB2 1EZ, UK; fax: (+44) 1223-336-033; or e-mail: deposit@ccdc.cam.ac.uk. Supplementary data associated with this article can be found, in the online version, at doi:10.1016/j.poly.2008.04.013.

References

[1] Y. Arakawa, in: P.J. Smith (Ed.), Chemistry of Tin, Blackie Academic and Professional, London, 1998.
[2] Y. Hori, T. Hagiwara, Int. J. Biol. Macromol. 25 (1999) 237.
[3] A. Orita, K. Sakamoto, Y. Hamada, A. Mitsutome, J. Otera, Tetrahedron 55 (1999) 2899.
[4] J. Otera, Chem. Rev. 93 (1993) 1449.
[5] S. Durand, K. Sakamoto, T. Fukuyama, A. Orita, J. Otera, A. Duthie, D. Dakternieks, M. Schulte, K. Jurkschat, Organometallics 19 (2000) 3220.
[6] A. Orita, Y. Hamada, T. Nakano, S. Toyoshima, J. Otera, Chem. Eur. J. 7 (2001) 3321.
[7] R.S. Collinson, D.E. Ferton, Coord. Chem. Rev. 148 (1996) 19.
[8] P. Yang, M. Guo, Coord. Chem. Rev. 185 (1999) 189.
[9] M. Gielen, Metal-Based Drugs 1 (1994) 213.
[10] M. Nath, S. Pokharia, R. Yadav, Coord. Chem. Rev. 215 (2001) 99.
[11] A.J. Crowe, P.J. Smith, C.J. Cardin, H.E. Parge, F.E. Smith, Cancer Lett. 24 (1984) 45.
[12] V.I. Bregadze, S.A. Glazun, P.V. Petrovakii, Z.A. Starikova, V.Y. Rochev, H. Dalil, M. Biesemans, R. Willem, M. Gielen, D.D. Vos, Appl. Organomet. Chem. 17 (2003) 453.
[13] L. Pellerito, L. Nagy, Coord. Chem. Rev. 224 (2002) 111.
[14] H. Adams, D.E. Fenton, G. Minardi, E. Mura, M. Angelo, Inorg. Chem. Commun. 3 (2000) 24.
[15] Z.Y. Yang, R.D. Yang, F.S. Li, K.B. Yu, Polyhedron 19 (2000) 2599.
[16] M.L. Vitolo, J. Webb, J. Inorg. Biochem. 20 (1984) 255.
[17] E. Baker, M.L. Vitolo, J. Webb, Biochim. Pharmacol. 34 (1985) 3011.
[18] G. Tamasi, L. Chiasserini, L. Savini, A. Sega, R. Cini, J. Inorg. Biochem. 99 (2005) 1347.
[19] C.M. Armstrong, P.V. Bernhardt, P. Chin, D.R. Richardson, Eur. J. Inorg. Chem. (2003) 1145.
[20] P.V. Bernhardt, P. Chin, P.C. Sharpe, D.R. Richardson, J. Chem. Soc., Dalton Trans. 30 (2007) 3232.
[21] P. Melnyk, V. Leroux, C. Sergheraerta, P. Grellier, Bioorg. Med. Chem. Lett. 16 (2006) 31.
[22] M.F. Iskander, L. Labib, M.M.Z. Nour El-Din, M. Tawfik, Polyhedron 8 (1989) 2755.
[23] D.K. Dey, B. Samanta, A. Lycka, L. Dahlenburg, Z. Naturforsch. 58b (2003) 336.
[24] H.D. Yin, S.W. Cheng, Inorg. Chim. Acta 359 (2006) 3330.
[25] H.D. Yin, M. Hong, H.L. Xu, Z.J. Gao, G. Li, D.Q. Wang, Eur. J. Inorg. Chem. (2005) 4572.
[26] H.D. Yin, M. Hong, Q.B. Wang, S.C. Xue, D.Q. Wang, J. Organomet. Chem. 690 (2005) 1669.
[27] H.D. Yin, M. Hong, G. Li, D.Q. Wang, J. Organomet. Chem. 690 (2005) 3714.
[28] H.D. Yin, S.W. Cheng, J. Organomet. Chem. 691 (2006) 3103.
[29] H.D. Yin, S.W. Cheng, L.W. Li, D.Q. Wang, Inorg. Chim. Acta 360 (2007) 2215.
[30] J. Lewiński, J. Zachara, I. Justyniak, M. Dranka, Coord. Chem. Rev. 249 (2005) 1185.
[31] V. Chandrasekhar, S. Nagendran, S. Bansal, A. Wallace Cordes, A. Vij, Organometallics 21 (2002) 3297.
[32] C.L. Ma, J.S. Sun, R.F. Zhang, D.Q. Wang, J. Organomet. Chem. 692 (2007) 4029.
[33] A. Bacchi, A. Bonardi, M. Carcelli, P. Mazza, P. Pelagatti, C. Pelizzi, G. Pelizzi, C. Solinas, F. Zani, J. Inorg. Biochem. 69 (1998) 101.
[34] M.P. Degaonkar, V.G. Puranik, S.S. Tavale, S. Gopinathan, C. Gopinathan, Bull. Chem. Soc. Jpn. 67 (1994) 1797.
[35] Z. He, C. He, Z.M. Wang, E.Q. Gao, Y. Liu, C.H. Yan, J. Chem. Soc., Dalton Trans. 4 (2004) 502.

[36] D.Q. Long, S.S. Chen, H. Chen, Chin. J. Synth. Chem. 14 (2006) 69.
[37] J. Holecek, M. Nadvornik, K. Handlir, A. Lycka, J. Organomet. Chem. 315 (1986) 299.
[38] D. Dakternieks, A. Duthie, D.R. Smyth, C.P.D. Stapleton, E.R.T. Tiekink, Organometallics 22 (2003) 4599.
[39] F.P. Pruchnik, M. Banbula, Z. Ciunik, M. Latocha, B. Skop, T. Wilczok, Inorg. Chim. Acta 356 (2003) 62.
[40] S. Das, G.P. Muthukumaragopal, S.N. Pal, S. Pal, New J. Chem. 27 (2003) 1102.
[41] S. Das, S. Pal, J. Mol. Struct. 753 (2005) 68.
[42] V. Barba, E. Vega, R. Luna, H. Höpfl, H.I. Beltrán, L.S. Zamudio-Rivera, J. Organomet. Chem. 692 (2007) 731.
[43] C.L. Ma, Y.W. Han, R.F. Zhang, Inorg. Chim. Acta 360 (2007) 2439.
[44] C.L. Ma, G.R. Tian, R.F. Zhang, Inorg. Chem. Commun. 9 (2006) 882.
[45] C.L. Ma, M.Q. Yang, R.F. Zhang, J.K. Li, Inorg. Chem. Commun. 10 (2007) 1330.

Polyhedron 27 (2008) 2167–2174

Contents lists available at ScienceDirect

Polyhedron

journal homepage: www.elsevier.com/locate/poly

Metallosupramolecular silver and mercury complexes constructed from two bis[4-(3-pyridyl)pyrimidinylthiomethyl]benzenes: Effect of positional isomerism of ligands and metal ions

Hua-Ze Dong [b], Hai-Bin Zhu [a], Xia Liu [b], Shao-Hua Gou [a,b,*]

[a] School of Chemistry and Chemical Engineering, Southeast University, Nanjing 211189, China
[b] State Key Laboratory of Coordination Chemistry, Nanjing University, Nanjing 210093, China

ARTICLE INFO

Article history:
Received 21 February 2008
Accepted 8 April 2008
Available online 24 May 2008

Keywords:
Metallosupramolecule
Positional isomerism
Single-handed helix
Structure elucidation

ABSTRACT

$[Ag_2L^2(NO_3)_2]_n$ (**1**), $[HgL_{0.5}{}^2OAc_2]_n$ (**2**), $[HgL^2I_2]_n$ (**3**), $[Ag_3L_2{}^3(NO_3)_3]^n$ (**4**) and $[HgL^3I_2]_n$ (**5**) were assembled by the reactions of L^2 and L^3 (L^2 = 1,2-bis[4-(3-pyridyl)pyrimidinylthiomethyl]benzene, L^3 = 1,3-bis[4-(3-pyridyl)pyrimidinylthiomethyl]benzene) with $AgNO_3$, $Hg(OAc)_2$ and HgI_2. The structural motifs of these complexes are multiform, from 3D interpenetrating networks and corrugated 2D networks to a 1D single stranded helix.It is found that conformation changes of the ligands after interaction with the metal salts occur due to positional isomerism of the xylyl groups and the effect of the metal ions.

© 2008 Elsevier Ltd. All rights reserved.

1. Introduction

Remarkable attention has been paid to the rational design and assembly of new coordination polymers and metal–organic frameworks with heterocyclic thiolates or thioethers in recent years for their fascinating structural topologies and potential uses as functional materials [1–6]. Within these molecules, not only N atoms from heterocyclic donors, but S atoms of thioether spacers are capable of binding metal ions, with a preference for d^{10} metal ions such as Cu(I) and Ag(I) ions, to form discrete and polymeric structures with 1D, 2D and 3D motifs. The generation of coordination architectures depends on the combination of factors including the geometric sphere of the inorganic metal ions and the geometry of the organic spacers, as well as counteranions and solvent effects.

In our previous work, we reported a flexible dithioether ligand, L^1 (shown in Scheme 1), which was treated with mercurous salts to yield discrete macrocyclic complexes or 1D polymers [7]. Since the ligand contains multiple metal binding sites, including pyridyl and pyrimidinyl donor sets, it is compatible with the coordination geometric requirement of specific metal centers to form multi-stranded arrays. The ligand also contains an alkyl chain that is liable to generate flexibility and to produce unpredictable structures, and so it is very difficult for us to modulate the frameworks to get the physical and chemical properties as desired. In our continuing study, we rectified the ligand by substituting xylyl groups for alkyl moieties to offer sufficient rigidity to impose a given stereochemistry at the metal centers. Herein reported are metallosupramolecular silver and mercury complexes produced by two new ligands L^2 and L^3, as shown in Scheme 1.

2. Experimental

2.1. Materials and physical measurements

All the commercially available chemicals were of reagent grade and were used as received without further purification. Analyses for carbon, hydrogen and nitrogen were performed on a Perkin–Elmer 1400C analyzer. Infrared spectra (4000–400 cm^{-1}) were measured with a Bruker Vector 22 FT-IR spectrophotometer on KBr disks. Electrospray ionization (ESI) mass spectra were recorded on a Finnigan MAT SSQ 710 mass spectrometer in a scan range of 100–1200 amu. ^1H NMR spectroscopic measurements were performed on a Bruker AM-500 NMR spectrometer, using TMS ($SiMe_4$) as an internal reference at room temperature. Thermogravimetric analysis (TGA) measurements were performed on a TGA Q500 thermal analyzer in flowing N_2 with a heating rate of 20 °C min^{-1}.

2.2. Syntheses of L^2 and L^3

Both L^2 and L^3 were made by a similar method as follows. To a solution of 4-(pyridin-3-yl) pyrimidine-2-thiol (1.89 g, 10 mmol)

* Corresponding author. Address: School of Chemistry and Chemical Engineering, Southeast University, Nanjing 211189, China. Tel.: +86 25 83272381; fax: +86 25 83595068.
E-mail address: sgou@seu.edu.cn (S.-H. Gou).

0277-5387/$ - see front matter © 2008 Elsevier Ltd. All rights reserved.
doi:10.1016/j.poly.2008.04.016

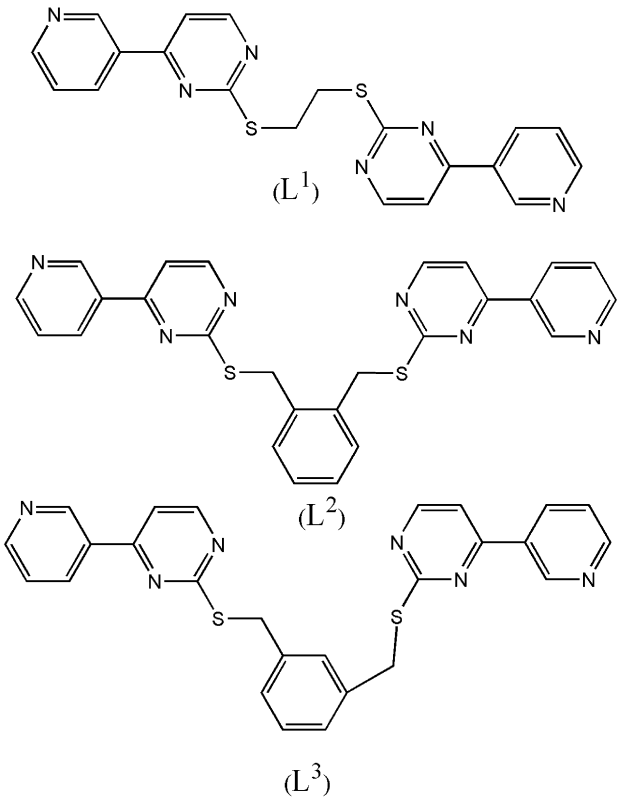

Scheme 1.

and sodium hydroxide (0.40 g, 10 mmol) in dry ethanol (150 mL), 1,2-bis(bromomethyl)benzene or 1,3-bis(bromomethyl)benzene (1.32 g, 5 mmol) in $CHCl_3$ (10 mL) was added. The mixture was stirred and refluxed for 6 h. After cooling, yellow precipitates were filtered, washed with water and ethanol, and dried in vacuum. For L^2: yield 74.6%, M.p.: 167–168 °C. *Anal.* Calc. for $C_{26}H_{20}N_6S_2$: C, 64.98; H, 4.19; N, 17.49. Found: C, 64.94; H, 4.17; N, 17.53%. IR (KBr, cm^{-1}): 1586 (w), 1578 (s), 1559 (vs), 1537 (s), 1478 (w), 1428 (m), 1399 (s), 1346 (s), 1328 (m), 1200 (m), 1180 (m), 1103 (w), 1023 (w), 828 (w), 810 (m), 703 (m). ESI-MS: 982.7 ($[2L^2+Na]^+$, 100%); 503.2 ($[L^2+Na]^+$, 20%); 481.3 ($[L^2+H]^+$, 10%). ^1H NMR (δ, 500 MHz, $CDCl_3$): 9.18 (s, 2H, pyridyl-H), 8.71 (d, 2H, pyrimidinyl-H), 8.54 (d, 2H, pyridyl-H), 8.35 (d, 2H, pyridyl-H), 7.53 (t, 2H, pyridyl-H), 7.42 (t, 2H, aryl-H), 7.33 (d, 2H, pyrimidinyl-H), 7.26 (d, 2H, aryl-H), 4.73 (s, 4H, methylene-H). Single crystals of L^2 suitable for X-ray diffraction were grown from a methanol solution by slow evaporation in air at room temperature.

For L^3: M.p.: 109–110 °C. *Anal.* Calc. for $C_{26}H_{20}N_6S_2$: C, 64.98; H, 4.19; N, 17.49. Found: C, 64.97; H, 4.23; N, 17.46%. IR (KBr, cm^{-1}): 1590 (w), 1556 (s), 1537 (s), 1479 (w), 1423 (m), 1398 (s), 1347 (s), 1322 (m), 1200 (s), 1178 (m), 1021 (w), 828 (w), 804 (m), 701 (m). ESI-MS: 503.17 ($[L^3+Na]^+$, 100%); 481.3 ($[L^3+H]^+$, 95%). ^1H NMR (δ, 500 MHz, $CDCl_3$): 9.25 (s, 2H, pyridyl-H), 8.75 (d, 2H, pyrimidinyl-H), 8.61 (d, 2H, pyridyl-H), 8.37 (d, 2H, pyridyl-H), 7.47 (t, 2H, pyridyl-H), 7.40 (d, 2H, pyrimidinyl-H), 7.37 (d, 2H, aryl-H), 7.26 (t, 2H, aryl-H), 4.49 (s, 4H, methylene-H). Single crystals of L^3 suitable for X-ray diffraction were obtained in a similar way to that of L^2.

2.3. Preparation of the metal complexes

2.3.1. $[Ag_2L^2(NO_3)_2]_n$ (**1**)

To a suspension of L^2 (24.0 mg, 0.05 mmol) in chloroform (5 mL) in a tube, a solution of $AgNO_3$ (8.5 mg, 0.05 mmol) in acetonitrile (5 mL) was very slowly added dropwise. Crystal products formed after ten days in the dark (yield: 40%). *Anal.* Calc. for $C_{26}H_{20}N_8O_6S_2Ag_2$: C, 38.07; H, 2.46; N, 13.66. Found: C, 38.11; H, 2.43; N, 13.63%. IR (KBr, cm^{-1}): 1597 (w), 1569 (s), 1542 (m), 1480 (w), 1404 (m), 1384 (vs), 1348 (s), 1326 (s), 1292 (m), 1206 (m), 1181 (w), 1027 (w), 817 (w), 723 (w), 698 (w).

2.3.2. $[HgL_{0.5}{}^2OAc_2]_n$ (**2**)

Compound **2** was prepared by adding a methanol (50 mL) solution of the ligand (0.48 g, 1.0 mmol) to a methanol (30 mL) solution of $Hg(OAc)_2$ (0.32 g, 1.0 mmol). The resulting colorless solution was stirred and refluxed for 3 hours, then it was filtered after cooling. Colorless diamond-shaped crystals of **2** were obtained (yield: 63%). *Anal.* Calc. for $C_{17}H_{16}N_3O_4SHg$: C, 36.53; H, 2.88; N, 7.52. Found: C, 36.57; H, 2.84; N, 7.50%. IR (KBr, cm^{-1}): 1561 (s), 1542 (s), 1480 (w), 1432 (m), 1412 (m), 1341 (m), 1325 (m), 1202 (w), 1191 (w), 1048 (w), 1024 (w), 817(w), 723 (w), 699 (w).

2.3.3. $[HgL^2I_2]_n$ (**3**)

A solution of HgI_2 (0.45 g, 1.0 mmol) in methanol (40 mL) was added to a stirred solution of L^2 (0.48 g, 1.0 mmol) in 20 mL of

Table 1
Crystal data and details of the structure determination for L^2, L^3 and complexes **1–5**

Complex	L^2	**1**	**2**	**3**
Empirical formula	$C_{26}H_{20}N_6S_2$	$C_{26}H_{20}N_8O_6S_2Ag_2$	$C_{17}H_{16}N_3O_4SHg$	$C_{26}H_{20}I_2N_6S_2Hg$
Formula weight	480.62	820.36	558.98	935.00
Crystal system	*Pbca*	$P2_1/n$	$C2/c$	$P2_1$
Space group	orthorhombic	monoclinic	monoclinic	monoclinic
a (Å)	12.390(3)	11.7922(12)	26.622(3)	7.0561(8)
b (Å)	13.739(4)	17.7635(18)	7.4956(8)	18.544(2)
c (Å)	27.407(7)	13.1806(14)	20.561(2)	10.9438(13)
α (°)	90	90	90	90
β (°)	90	95.546(2)	118.530(2)	101.060(2)
γ (°)	90	90	90	90
V (Å^3)	4666(2)	2748.0(5)	3604.7(7)	1405.4(3)
Z	8	4	8	2
D_{calc} (g cm^{-3})	1.369	1.983	2.060	2.210
μ (mm^{-1})	0.256	1.637	8.683	7.849
F(000)	2000	1624	2136	872
Reflections collected/ unique (R_{int})	21826/4106 (0.096)	14604/5402 (0.043)	9282/3543 (0.044)	7577/4997 (0.053)
Parameters	307	397	237	334
Final R [$I > 2\sigma(I)$]	$R_1 = 0.0711$ $wR_2 = 0.1319$	$R_1 = 0.054$, $wR_2 = 0.0858$	$R_1 = 0.0463$ $wR_2 = 0.0948$	$R_1 = 0.0521$, $wR_2 = 0.1066$
Goodness-of-fit	1.06	1.05	1.04	0.98

Complex	L^3	**4**	**5**
Empirical formula	$C_{26}H_{20}N_6S_2$	$C_{52}H_{40}N_{15}O_9S_4Ag_3$	$C_{26}H_{20}I_2N_6S_2Hg$
Formula weight	480.62	1470.88	935.00
Crystal system	$P\bar{1}$	*Pnn2*	$P\bar{1}$
Space group	triclinic	orthorhombic	triclinic
a (Å)	11.262(7)	23.458(4)	8.5040(9)
b (Å)	13.299(8)	7.5546(14)	12.4424(14)
c (Å)	16.278(10)	16.518(3)	14.0037(15)
α (°)	84.557(10)	90	111.023(2)
β (°)	78.935(10)	90	92.892(2)
γ (°)	72.936(11)	90	96.700(2)
V (Å^3)	2285(2)	2927.3(9)	1366.8(3)
Z	4	2	2
D_{calc} (g cm^{-3})	1.397	1.669	2.272
μ (mm^{-1})	0.261	1.204	8.070
F(000)	1000	1468	872
Reflections collected/ unique (R_{int})	11255/7883 (0.040)	14764/5739 (0.094)	9291/4631 (0.040)
Parameters	613	353	334
Final R [$I > 2\sigma(I)$]	$R_1 = 0.0662$, $wR_2 = 0.1863$	$R_1 = 0.0699$, $wR_2 = 0.1480$	$R_1 = 0.0748$, $wR_2 = 0.2373$
Goodness-of-fit	0.92	1.04	1.02

methanol. White precipitates formed immediately, which were filtered out and dried under vacuum (yield: 71%). Colorless single crystals of **3** were obtained from the filtrate. *Anal.* Calc. for $C_{26}H_{20}I_2N_6S_2Hg$: C, 33.40; H, 2.16; N, 8.99. Found: C, 33.42; H, 2.14; N, 8.95%. IR (KBr, cm^{-1}): 1596 (w), 1555 (s), 1541 (s), 1480 (w), 1425 (m), 1407 (m), 1344 (s), 1326 (m), 1300 (w), 1198 (m), 1173 (m), 1040 (w), 811 (m), 723 (w), 698 (m).

2.3.4. $[Ag_3L_2^3(NO_3)_3]^n$ (**4**)

A similar method to **1** was adopted. Yield, 30%. *Anal.* Calc. for $C_{52}H_{40}N_{15}O_9S_4Ag_3$: C, 42.46; H, 2.74; N, 14.28. Found: C, 48.42; H, 2.83; N, 14.23%. IR (KBr, cm^{-1}): 1602 (w), 1564 (s), 1540 (m), 1484 (w), 1402 (s), 1383 (s), 1358 (s), 1325 (s), 1303 (m), 1206 (m), 1181 (w), 1027 (w), 810 (w), 725 (w), 694 (w).

2.3.5. $[HgL^3I_2]_n$ (**5**)

An analogous way to **3** was used. *Anal.* Calc. for $C_{26}H_{20}I_2N_6S_2Hg$: C, 33.40; H, 2.16; N, 8.99. Found: C, 33.38; H, 2.24; N, 8.98%. IR (KBr, cm^{-1}): 1590 (w), 1561 (s), 1542 (s), 1484 (w), 1405 (m), 1346 (s), 1327 (m), 1302 (w), 1195 (m), 1176 (m), 1041 (w), 809 (m), 721 (w), 695 (m).

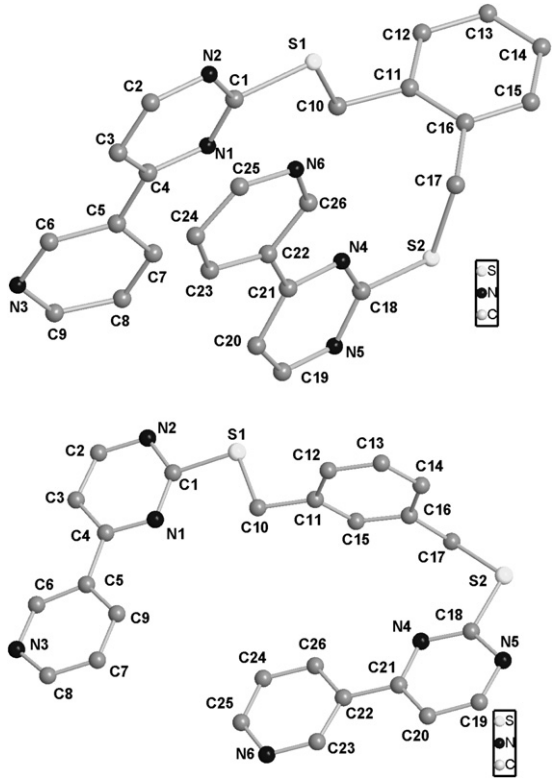

Fig. 1. Perspective views of L^2 (top) and L^3 (bottom) with the atom-numbering scheme, hydrogen atoms are omitted for clarity.

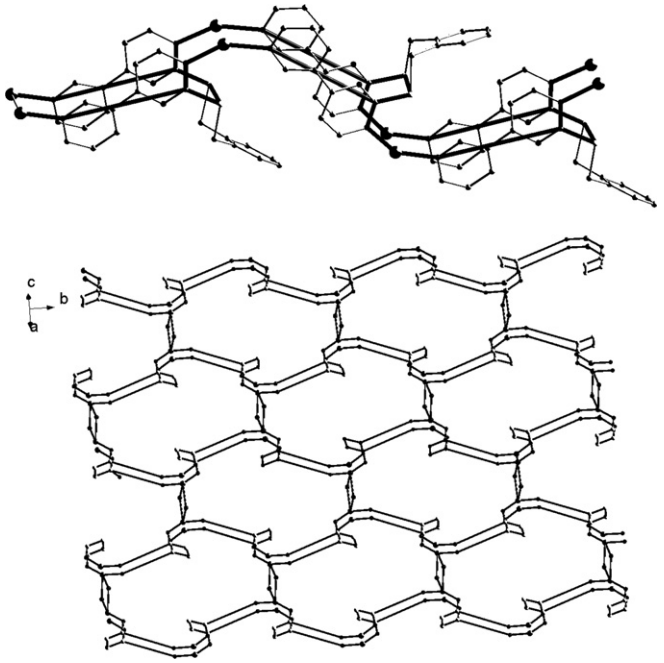

Fig. 2b. Top: L^2 can be abstracted as a chair-shaped motif in black color; bottom: 2D supramolecular network in **1**, tapes are linked by nitrate anions as black dots.

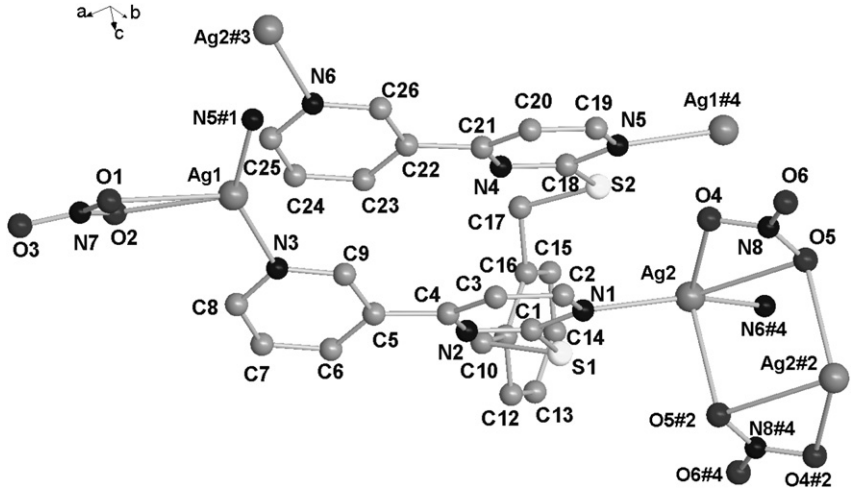

Fig. 2a. Molecular structure of **1**, hydrogen atoms are omitted for clarity. Selected bonds length (Å) and angles (°): Ag1–O1, 2.598(4); Ag1–O2, 2.617(5); Ag1–N3, 2.198(5); Ag1–N5#1, 2.197(6); Ag2–O4, 2.490(5); Ag2–N1, 2.248(5); Ag2–O5, 2.868; Ag2–N6#5, 2.216(5); Ag2–O5#2, 2.574(4); O1–Ag1–O2, 47.44(15); O1–Ag1–N3, 124.70(16); O1–Ag1–N5#1, 86.36(17); O2–Ag1–N3, 88.58(17); O2–Ag1–N5#1, 124.10(19); N3–Ag1–N5#1, 146.81(19); O4–Ag2–N1, 87.05(17); O4–Ag2–N6#5, 122.15(19); O4–Ag2–O5#2, 102.58(13); N1–Ag2–N6#5, 149.3(2); O5#2–Ag2–N1, 87.95(16); O5#2–Ag2–N6#5, 94.01(19). Symmetry codes: #1, 0.5 − *x*, −0.5 + *y*, 1.5 − *z*; #2, −*x*, 1 − *y*, 2 − *z*; #3, 0.5 − *x*, −0.5 + *y*, 1.5 − *z*; #4, 0.5 − *x*, 0.5 + *y*, 1.5 − *z*.

2.4. Crystallographic analyses

Diffraction data for L^2, L^3 and complexes **1**–**5** were measured on a Bruker SMART 1K CCD diffractometer [8] at 291 K using graphite monochromated Mo Kα radiation (λ = 0.71073 Å). Lorentz polarization and absorption corrections were applied. The structures were solved by direct methods and refined with the full-matrix least-squares technique using SHELXTL version 5.1 [9]. Anisotropic thermal parameters were assigned to all non-hydrogen atoms. The hydrogen atoms were geometrically fixed and allowed to ride on the attached atoms. The Flack parameters of complexes **3** and **4** are 0.023(8) and 0.01(5). A summary of the crystal data and refinement results are listed in Table 1.

3. Results and discussion

3.1. Description of the crystal structures of L^2 and L^3

The molecular structures of L^2 and L^3 with the atom-numbering scheme are shown in Fig. 1. The two ligands crystallize in different space groups, *Pbca* (L^2) and $P\bar{1}$ (L^3), with different crystallographic symmetry. Due to the $-SCH_2-$ spacer, L^2 adopts a *cis* conformation with two arms on the same side of the central phenyl ring. It is noted that the pyridyl ring and the pyrimidinyl ring in each arm are not coplanar, their dihedral angles in the two arms are 8.4° and 15.9°, respectively. Similar to L^2, the arms of L^3 are also close and the dihedral angles between the heterocyclic rings are 2.2° and 16.8°, respectively.

3.2. $[Ag_2L^2(NO_3)_2]_n$ (**1**)

X-ray crystallographic analysis reveals that **1** crystallizes in the monoclinic system, $P2_1/n$ space group. As shown in Fig. 2a, there are two types of silver ions (named Ag1 and Ag2) in the crystal structure. Ag1 is coordinated by two N atoms and two O atoms in a distorted square planar geometry, in which the two N atoms (N3, N5#) are from different heterocycles of distinct ligands, and the two O donors (O1, O2) are from one nitrate anion. Ag2 adopts a distorted square pyramid configuration composed of two N donors and three O donors. The two nitrogen atoms (N1, N6#), from different ligands, and two oxygen atoms (O4, O5), from one nitrate anion, are placed in the equatorial plane, while the O5#2 atom from another nitrate anion is located in the axial position. Two neighboring Ag2 centers (Ag2 and Ag2#2), linked by O–O bridges of two nitrate anions, form a four-membered centrosymmetric dinuclear cyclic unit with an Ag–Ag distance of 4.149 Å. This distance is a little longer than the van der Waals contact distance for Ag–Ag (3.40 Å) [10]. In **1**, the Ag–O bond lengths are between 2.490(5) and 2.868 Å, while the Ag–N bond lengths vary from 2.197(6) to 2.248(5) Å, which are all in the range for normal values [3].

Similar to the structure of the free ligand, each L^2 ligand adopts a close *cis* conformation with two heterocyclic arms on the same side. L^2 presents a tetradentate-bridging mode. Due to the spacial

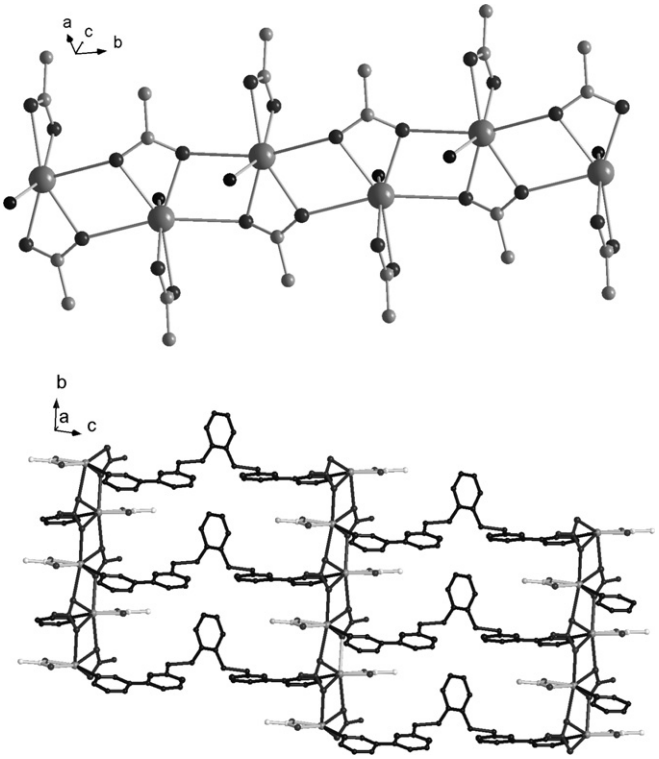

Fig. 3b. Top: view of the Hg–O tape; bottom: 2D network in **2**, tapes are linked by ligands in the *bc* plane.

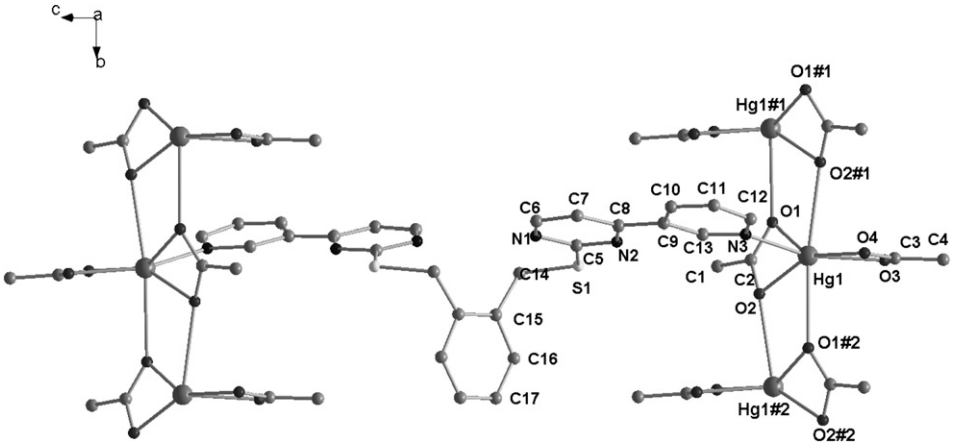

Fig. 3a. Molecular structure of complex **2**, hydrogen atoms are omitted for clarity. Selected bonds length (Å) and angles (°): Hg1–O1, 2.507(6); Hg1–O2, 2.329(6); Hg1–O3, 2.237(5); Hg1–O4, 2.495(6); Hg1–N3, 2.256(8); Hg1–O2#1, 2.738(5); Hg1–O1#2, 2.780(6); O3–Hg1–N3, 149.8(3); O1#2–Hg1–N3, 97.2(2); O2#1–Hg1–N3, 80.0(2); O4–Hg1–N3, 96.8(3); O2–Hg1–N3, 88.9(2); O1–Hg1–N3, 90.2(2); O2#1–Hg1–O3, 86.04(19); O1#2–Hg1–O3, 88.13(19); O1–Hg1–O3, 110.6(2); O2–Hg1–O3, 120.9(2); Hg1–O1–Hg1#1, 102.8(2); Hg1–O2–Hg1#2, 109.1(2). Symmetry code: #1, 0.5 − *x*, −0.5 + *y*, 0.5 − *z*; #2, 0.5 − *x*, 0.5 + *y*, 0.5 − *z*; #3, 1 − *x*, *y*, 1.5 − *z*; #4, 0.5 + *x*, −0.5 + *y*, 1 + *z*; #5, 0.5 + *x*, 0.5 + *y*, 1 + *z*.

hindrance with silver ions induced by the two arms in the *cis* position, only four N atoms of the heterocycles link four metal atoms to generate infinite 1D tapes, in which two pyrimidinyl planes of one ligand are almost parallel to each other, with a small dihedral angle of 1.7°, as are two pyridyl rings, with a dihedral angle of 2.9°. It is observed that some NO_3^- anions preferentially bridge the 1D tape structures via Ag2–O5 contacts to generate a 2D network (Fig. 2b).

3.3. $[HgL_{0.5}{}^2OAc_2]_n$ (**2**)

A single crystal XRD study has revealed that $[HgL_{0.5}{}^2OAc_2]_n$ (**2**) crystallizes in the *C*2/*c* space group. One symmetric unit of **2** contains one ligand, two metal atoms and four-coordinated acetate anions. As depicted in Fig. 3a, the metal ion lies in a seven-coordinated environment with a HgN_2O_5 unit. Each metal ion is chelated by two bidentate acetates through their O atoms, forming two four-membered metallocycles. Furthermore the chelating O atoms of one acetato ligand also link the neighboring Hg ions to yield 1D infinite ladders with a Hg–Hg distance of 4.134 Å (Fig. 3b, top), which run parallel to the *b* axis. These isolated ladders are interlaced into a corrugated plane through N atoms of pyridyl rings from L^2 (shown in Fig. 3b, bottom).

Different from **1**, L^2 in **2** adopts a *trans* conformation, opening its two heterocyclic arms which are on the opposite side of the central phenyl ring, and the ligand acts as a terminal pyridine group to weave the ladders. The pyrimidinyl and pyridyl rings are almost parallel each other with a dihedral angle of 2.1°, and the dihedral angle between the heterocyclic plane and the phenyl plane is 80.1° (see Figs. 4a and 4b).

3.4. $[HgL^2I_2]_n$ (**3**)

By replacing $Hg(OAc)_2$ with HgI_2 in the reaction with L^2, $[HgL^2I_2]_n$ (**3**) was obtained, which crystallizes in the monoclinic system, $P2_1$ space group. The structure of **3** consists of one-dimensional neutral chains where the Hg(II) ion is coordinated by two iodide anions and two pyridine nitrogen atoms of different ligands. In this case, the geometric sphere around each metal atom is tetrahedral, but slightly distorted.

Both Hg–N and Hg–I distances in **3** are in the range of those found in the other complexes [11]. It is noted that the pyrimidinyl ring and the pyridyl ring of L^2 are obviously not coplanar, the dihedral angle between the two heterocyclic rings is ca. 24.4°. In the solid state, the adjacent zigzag chains are stacked through C7–H···N5 hydrogen bonding (d_{C7-N5} = 3.436(19) Å; ∠C7–H···N5 = 147.00°, symmetry code: $1-x$, $-1/2+y$, $1-z$) to form corrugated 2D planes.

In the crystal packing of **3**, L^2 takes a *N*,*N*′-bidentate bridging pattern. Meanwhile, the ligand adopts a *trans* conformation with its arms on opposite sides of the central phenyl ring and outspreading to link two metal ions by using the N atoms of the pyridyl rings.

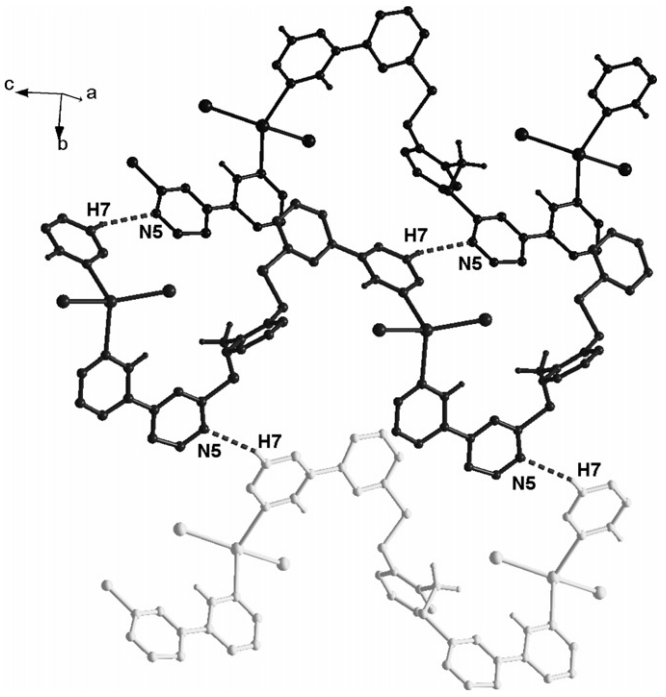

Fig. 4b. 2D supramolecular network in **3**. Interchain hydrogen bonding interactions are represented as dashed lines.

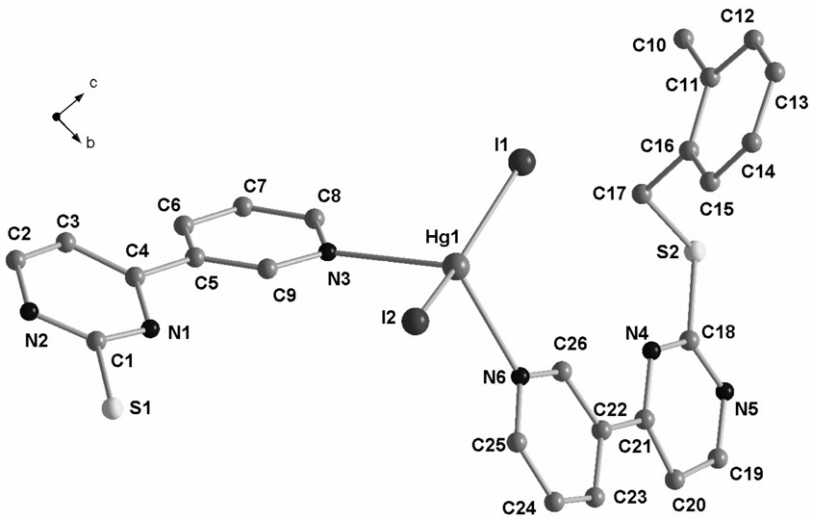

Fig. 4a. Molecular structure of **3** showing the numbering scheme, hydrogen atoms are omitted for clarity. Selected bonds length (Å) and angles (°): Hg1–I1, 2.6362(12); Hg1–I2, 2.6514(11); Hg1–N3, 2.487(11); Hg1–N6, 2.440(10); I1–Hg1–I2, 149.88(4); I1–Hg1–N3, 98.7(3); I1–Hg1–N6, 100.5(3); I2–Hg1–N3, 95.7(3); I2–Hg1–N6, 97.6(3); N3–Hg1–N6, 113.8(4).

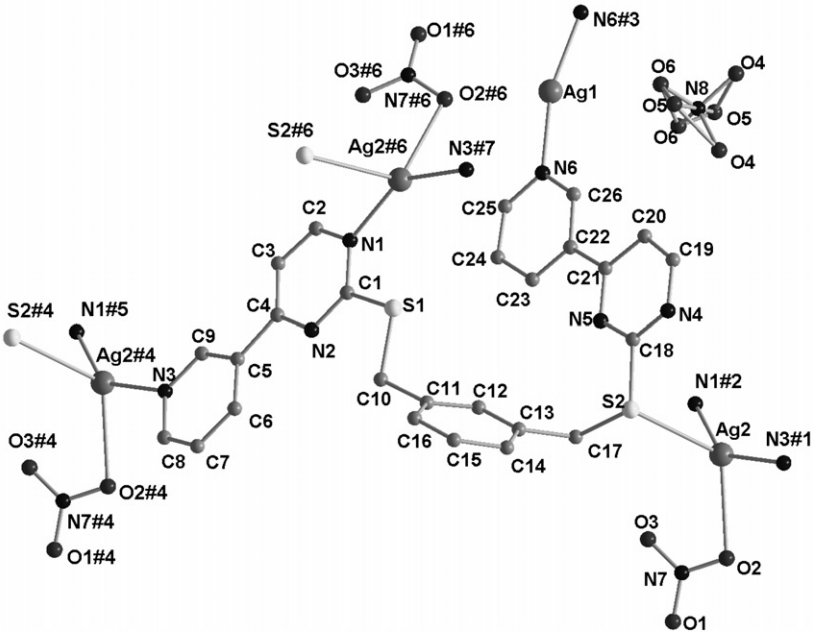

Fig. 5a. Coordination pattern of **4** showing the numbering scheme, hydrogen atoms are omitted for clarity. Selected bonds length (Å) and angles (°): Ag1–N6, 2.122(9); Ag1–N6#3, 2.122(9); Ag2–O2, 2.553(12); Ag2–N1#2, 2.226(8); Ag2–N3#1, 2.234(9); Ag2–S2, 2.930(4); N6–Ag1–N6#, 163.9(4); S2–Ag2–O2, 116.7(3); S2–Ag2–N3#1, 99.3(3); S2–Ag2–N1#2, 89.3(2); O2–Ag2–N3#1, 85.5(3); O2–Ag2–N1#2, 121.4(3); N1#2–Ag2–N3#1, 144.3(3). Symmetry codes: #1, *x*, *y*, −1 + *z*; #2, 0.5 − *x*, 0.5 + *y*, −0.5 + *z*; #3, 1 − *x*, 2 − *y*, *z*; #4, *x*, *y*, 1 + *z*; #5, 0.5 − *x*, 0.5 + *y*, 0.5 + *z*; #6, 0.5 − *x*, −0.5 + *y*, 0.5 + *z*; #7, 0.5 − *x*, −0.5 + *y*, −0.5 + *z*.

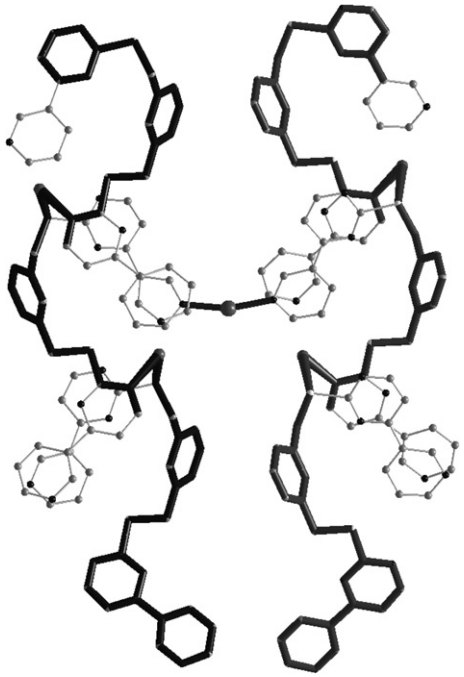

Fig. 5b. Perspective view of the helixes held by a silver atom.

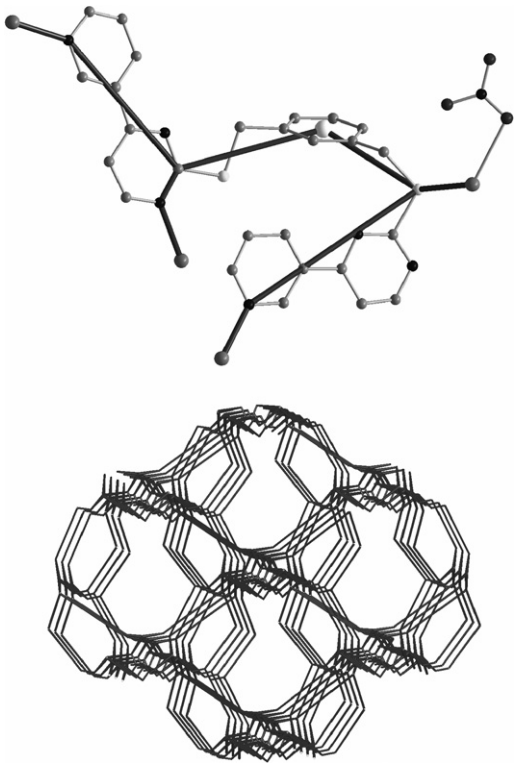

Fig. 5c. Top: the ligand can be abstracted as a kangaroo-shaped motif in black color; bottom: 3D network of **4**.

3.5. $[Ag_3L_2^3(NO_3)_3]^n$ (**4**)

Compound **4** crystallizes in the orthorhombic system of a non-centrosymmetric space group, *Pnn*2. The asymmetric unit is composed of three Ag ions, two independent L^3 ligands, two-coordinated nitrate anions and a free nitrate counteranion.

There are also two types of coordination modes for the metal atoms. Ag1 is coordinated by two pyridyl N atoms from different ligands in a slightly distorted linear geometry with a N–Ag–N bond angle of 163.9° and a Ag–N bond distance of 2.122(9) Å, similar to those found in the other two-coordinated Ag complexes [2,3]. Ag2 is tetra-coordinated in a distorted tetrahedral fashion (AgN_2OS) and bound by one S atom, two different N atoms from two ligands and one O donor from a nitrate anion.

Owing to the spacial hindrance induced by two arms in *meta* positions, each L^3 in **4** acts as a tetradentate ligand, in which a sulfur atom and three nitrogen atoms from different heterocycle groups are bound to four Ag atoms in four different directions (Fig. 5a). It is noteworthy that the S atom and the pyrimidinyl N atom from one arm are not coordinated to silver ions at the same time. Two kinds of modes of the nitrate anions are present, in which one is free and the other is moored to the four-coordinated Ag(I) center. Additionally, two arms attached to the central benzene ring adopt an ajar conformation, and the dihedral angles between each of the pyrimidinyl rings and the central benzene ring are 73.1° and 69.6°, while the angles between the pyrimidinyl rings and the pyridine rings are 7.5° and 6.2°, respectively. Furthermore, silver atoms with tetradentate patterns are bridged by L^3 to form a single chiral helical chain with a separation of 18.164(2) Å, then two adjacent single stranded helical chains with opposite chirality are connected by silver atoms with a bidentate pattern (shown in Fig. 5b).

As far as we know, such a structure is unprecedented for Ag(I) complexes with thioether ligands, although the silver–thioether system has been well investigated [2–5]. Interestingly, the ligand acts as a μ_4-bridge to link four silver ions, forming a kangaroo-shaped motif, and the framework can be assigned as an interpenetrating network (Fig. 5c).

3.6. $[HgL^3I_2]_n$ (**5**)

By replacing L^2 with L^3 in the reaction with HgI_2, $[HgL^3I_2]_n$ (**5**) was obtained. Differently from **3**, **5** crystallizes in the triclinic system, $P\bar{1}$ space group. The crystallographic analysis of **5** revealed that its structure is a one-dimensional polymeric helix consisting of $[HgL^3I_2]$ units (Fig. 6a). Each mercury atom, coordinated by two iodide anions and two pyridine nitrogen atoms of different ligands, is located in a slightly distorted tetrahedral geometric sphere.

Hg–N and Hg–I distances in **5** are almost equivalent and also in the range of those found in other complexes [11]. It is observed that the two dihedral angles between the pyrimidinyl ring and the pyridyl ring in L^3 are distinct, one is nearly coplanar with a small dihedral angle of 6.2°, and the other is ca. 26.4°. In comparison, the dihedral angle between two pyridyl rings coordinated to the mercury atom is 61.7° in **3**, while it is 81.4° in **5**.

Each L^3 in **5** takes an ajar configuration and acts as a *N,N′*-bidentate ligand to link mercury atoms to form a single stranded helix with a period of 8.504 Å. Furthermore, as shown in Fig. 6b, effective $\pi\cdots\pi$ stacking is observed between the adjacent helical chains with opposite chirality, and the centroid–centroid distance is 3.699 Å.

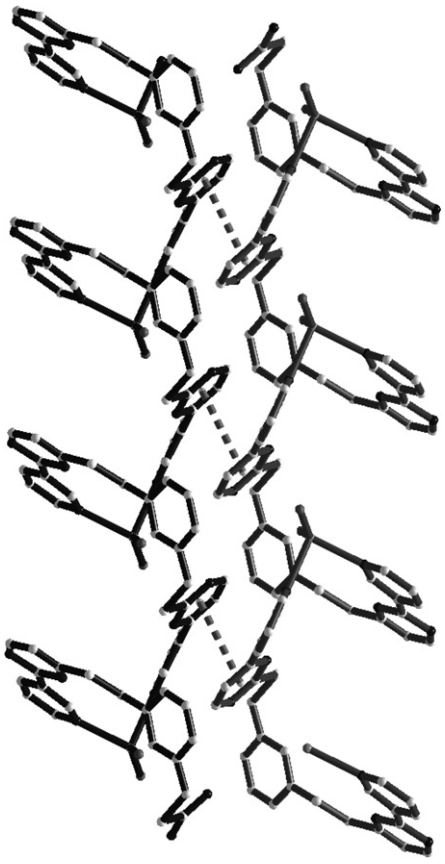

Fig. 6b. Perspective view of the helixes held by $\pi\cdots\pi$ stacking interactions.

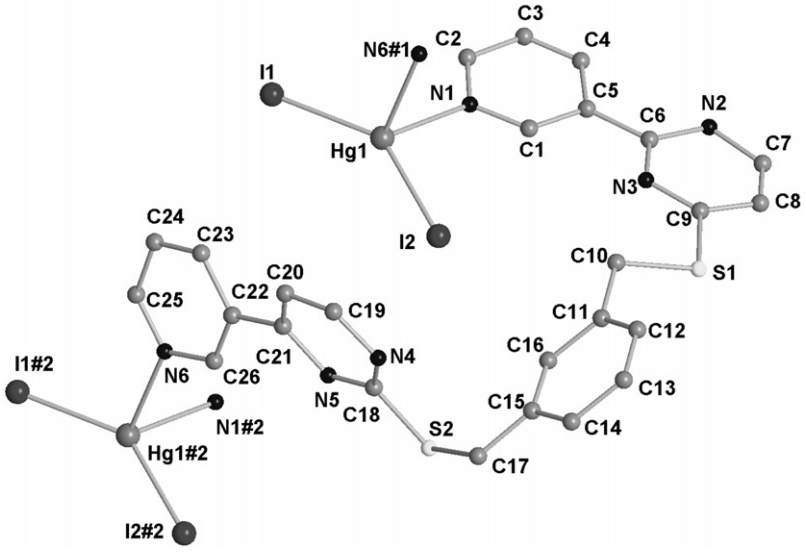

Fig. 6a. Molecular structure of **5** showing the numbering scheme, hydrogen atoms are omitted for clarity. Selected bonds length (Å) and angles (°): Hg1–I1, 2.492(2); Hg1–I2, 2.469(2); Hg1–N1, 2.435(14); Hg1–N6#1, 2.409(12); I1–Hg1–I2, 142.71(7); I1–Hg1–N1, 113.4(4); I1–Hg1–N6#1, 100.7(3); I2–Hg1–N1, 96.5(4); I2–Hg1–N6#1, 102.2(3); N1–Hg1–N6#1, 88.1(5). Symmetry codes: #1, $-1+x, y, z$; #2, $1+x, y, z$.

Additionally, there also are C–H···I hydrogen bonding interactions (d_{C19-I2} = 3.731(15) Å; ∠C19–H···I 2 = 155.0°; d_{C25-I1} = 3.562(17) Å; ∠C25–H···I1 = 129.00°, symmetry code: $-x$, $2-y$, $-z$; $1-x$, $3-y$, $1-z$) that form a 3D network.

In complex **1**, L^2 takes a tetradentate-bridging pattern through the nitrogen atoms from heterocycles to connect four silver ions and adopts a close *cis* configuration with respect to the xylyl group. While in **4**, L^3 adopts an ajar conformation with respect to the xylyl group and a tetradentate-bridging mode through the nitrogen atoms and sulfur atom to connect four silver ions. Owing to the positional isomerism of the two arms in L^2 and L^3, complex **1** packs into a centrosymmetric space group $P2_1/n$, while complex **4** packs into a noncentrosymmetric space group *Pnn*2, which includes single stranded helical chains. In **3**, L^2 adopts an open *trans* conformation with respect to the xylyl group and takes a *N*,*N*′-bidentate bridging pattern to connect the mercury atoms and form zig-zag chains. While in **5**, L^3 adopts an ajar conformation and the *N*,*N*′-bidentate bridging pattern to connect the mercury atoms, forming helixes with a similar reason as above. All these reveal that the positional isomerism of two arms in both L^2 and L^3 play an important role in the formation of the above compounds. As for **4** and **5**, both of them contain stranded helical chains, but the chirality was not present in complexes due to the interactions between opposite chiral chains.

Additionally, in complexes **1** and **2** counteranions also act as bridging ligands to chelate metal ions to form corrugated 2D planes.

4. Conclusion

In this study, five novel complexes with different architectures, $[Ag_2L^2(NO_3)_2]_n$ (**1**), $[Hg_2L^2(OAc)_4]_n$ (**2**), $[HgL^2I_2]_n$ (**3**), $[Ag_3L_2{}^3(NO_3)_3]^n$ (**4**) and $[HgL^3I_2]_n$ (**5**) were constructed from L^2 and L^3. In **1**–**3**, L^2 adopts different coordination modes and forms quite different coordination architectures. However, in the structures of **4** and **5**, L^3 takes an ajar configuration to construct more complicated networks than the other examples. Compared with those complexes [7] resulting from L^1, the present study demonstrates that the nature of positional isomerism and sufficient rigidity of the ligand in addition to the geometric needs of the metal atoms and the effect of the anions play an important role in the crystal packing of MOFs.

5. Supplementary data

CCDC 676723, 676724, 676725, 676726 676727, 676728 and 676729 contain the supplementary crystallographic data for two ligands and **1**, **2**, **3** , **4** and **5**. These data can be obtained free of charge via http://www.ccdc.cam.ac.uk/conts/retrieving.html, or from the Cambridge Crystallographic Data Centre, 12 Union Road, Cambridge CB2 1EZ, UK; fax: (+44) 1223-336-033, or e-mail: deposit@ccdc.cam.ac.uk.

Acknowledgements

We acknowledge the National Natural Science Foundation of China (Project No. 20271026) for financial support of this work.

References

[1] (a) C.M. Hartshorn, P.J. Steel, J. Chem. Soc., Dalton. Trans. (1998) 3935;
(b) D.A. McMorran, C.M. Hartshorn, P.J. Steel, Polyhedron 23 (2004) 055;
(c) M. Eddaoudi, D.B. Moler, H.L. Li, B.L. Chen, T.M. Reineke, M. O'Keeffe, O.M. Yaghi, Acc. Chem. Res. 34 (2001) 319;
(d) O.M. Yaghi, M. O'Keeffe, N.W. Ockwig, H.K. Chae, M. Edaoudi, J. Kim, Nature 423 (2003) 705;
(e) A.R. Millward, O.M. Yaghi, J. Am. Chem. Soc. 127 (2005) 17998;
(f) S.S. Kaye, A. Dailly, O.M. Yaghi, J.R. Long, J. Am. Chem. Soc. 129 (2007) 14176;
(g) H. Furukawa, J. Kim, K.E. Plass, O.M. Yaghi, J. Am. Chem. Soc. 128 (2006) 8398;
(h) M.W. Hosseini, Acc. Chem. Res. 38 (2005) 313;
(i) D. Salazar-Mendoza, S.A. Baudron, M.W. Hosseini, Inorg. Chem. 47 (2008) 766;
(j) S. Kitagawa, R. Kitaura, S. Noro, Angew. Chem., Int. Ed. 43 (2004) 2334;
(k) S.R. Batten, R. Robson, Angew. Chem., Int. Ed. 37 (1998) 1460;
(l) L. Kovbasyuk, M. Hoppe, H. Pritzkow, R. Krämer, Eur. J. Inorg. Chem. 5 (2001) 1353;
(m) Z. Atherton, D.M.L. Goodgame, S. Menzer, D.J. Williams, Polyhedron 18 (1999) 273;
(n) A.M.W. Cargill Thompson, I. Blandford, H. Redfearn, J.C. Jeffery, M.D. Ward, J. Chem. Soc., Dalton Trans. (1997) 2661.
[2] (a) Y. Zheng, J.R. Li, M. Du, R.Q. Zou, X.H. Bu, Cryst. Growth Des. 5 (2005) 215;
(b) Y.B. Xie, C. Zhang, J.R. Li, X.H. Bu, J. Chem. Soc., Dalton Trans. (2004) 562;
(c) Y. Zheng, M. Du, J.R. Li, R.H. Zhang, X.H. Bu, J. Chem. Soc., Dalton Trans. (2003) 1509;
(d) X.H. Bu, Y.B. Xie, J.R. Li, R.H. Zhang, Inorg. Chem. 42 (2003) 7422;
(e) R.F. Song, Y.B. Xie, J.R. Li, X.H. Bu, J. Chem. Soc., Dalton Trans. (2003) 4742;
(f) R.F. Song, Y.B. Xie, X.H. Bu, J. Mol. Struct. 657 (2003) 311.
[3] (a) L. Han, B.L. Wu, Y.Q. Xu, M.Y. Wu, Y.Q. Gong, B.Y. Lou, B.Q. Chen, M.C. Hong, Inorg. Chim. Acta 358 (2005) 2005;
(b) L. Han, M.C. Hong, R.H. Wang, B.L. Wu, Y. Xu, B.Y. Lou, Z.Z. Lin, Chem. Commun. (2004) 2578;
(c) M.C. Hong, Y.J. Zhao, W.P. Su, R. Cao, M. Fujita, Z.Y. Zhou, J. Am. Chem. Soc. 122 (2000) 4819;
(d) W.P. Su, M.C. Hong, J.B. Weng, R. Cao, S.F. Lu, Angew. Chem., Int. Ed. 39 (2000) 2911;
(e) W.P. Su, R. Cao, M.C. Hong, W.T. Wong, J.X. Lu, Inorg. Chem. Commun. 2 (1999) 241;
(f) M.C. Hong, W.P. Su, R. Cao, M. Fujita, J.X. Lu, Chem. Eur. J. 6 (2000) 427;
(g) R.H. Wang, M.C. Hong, W.P. Su, Y.C. Liang, R. Cao, Y.J. Zhao, J.B. Weng, Polyhedron 20 (2001) 3165;
(h) R.H. Wang, M.C. Hong, W.P. Su, Y.C. Liang, R. Cao, Y.J. Zhao, J.B. Weng, Inorg. Chim. Acta 323 (2001) 139;
(i) R.H. Wang, M.C. Hong, R. Cao, Y.J. Zhao, J.B. Weng, Aust. J. Chem. 56 (2003) 1167.
[4] C. L Chen, C.Y. Su, Y.P. Cai, H.X. Zhang, A.W. Xu, B.S. Kang, H.C. Loye, Inorg. Chem. 42 (2003) 3738.
[5] (a) P.J. Caradoc-Davies, L.R. Hanton, J. Chem. Soc., Dalton Trans. (2003) 1754;
(b) P.J. Caradoc-Davies, L.R. Hanton, Chem. Commun. (2001) 1098;
(c) P.J. Caradoc-Davies, L.R. Hanton, W.J. Henderson, Chem. Soc., Dalton Trans. (2001) 2749;
(d) P.J. Caradoc-Davies, L.R. Hanton, K. Lee, Chem. Commun. (2000) 783;
(e) L.R. Hanton, K. Lee, J. Chem. Soc., Dalton Trans. (2000) 1161.
[6] (a) R. Peng, D. Li, T. Wu, X.P. Zhou, S.W. Ng, Inorg. Chem. 45 (2006) 4035;
(b) D. Li, W.J. Shi, L. Hou, Inorg. Chem. 44 (2005) 3907;
(c) R. Peng, T. Wu, D. Li, CrystEngCommun. 7 (2005) 595.
[7] H.Z. Dong, J. Yang, X. Liu, S.H. Gou, Inorg. Chem., doi:10.1021/ic702157r.
[8] SMART and SAINT. Area Detector Control and Integration Software, Siemens Analytical X-Ray Systems Inc., Madison, WI, 1996.
[9] G.M. Sheldrick, SHELXTL V5.1 Software Reference Manual, Bruker AXS Inc., Madison, WI, 1997.
[10] (a) Y. Du, S.R. Wlison, P. Zhang, K. Hirsch, J.S. Moore, J. Chem. Educ. 74 (1997) 915;
(b) S. Ganguly, S. Chattopadhyay, C. Sinha, A. Chakravorty, Inorg. Chem. 39 (2000) 2954.
[11] (a) C.Y. Su, A.M. Goforth, M.D. Smith, H.C.Z. Loye, Inorg. Chem. 42 (2003) 5685;
(b) T.J. Burchell, D.J. Eisler, R.J. Puddephatt, Inorg. Chem. 43 (2004) 5550.

Polyhedron 27 (2008) 2175–2185

Contents lists available at ScienceDirect

Polyhedron

journal homepage: www.elsevier.com/locate/poly

Copper(I/II) and cobalt(II) coordination chemistry of relevance to controlled radical polymerization processes

Ulrich Baisch, Rinaldo Poli *

Laboratoire de Chimie de Coordination, 205, route de Narbonne, F-31077 Toulouse Cedex 4, France

ARTICLE INFO

Article history:
Received 30 January 2008
Accepted 14 March 2008
Available online 15 May 2008

Keywords:
Coordination chemistry
Cobalt
Copper
Me_6TREN ligand
Controlled radical polymerization

ABSTRACT

The reaction of various alkyl halides (1-bromoethylbenzene, BEB; 1-chloroethylbenzene, CEB; methyl iodide; 1-bromoethylacetate, BEA; and ethyl-2-bromopropionate, EBP) with CuBr/L (L = bipy, Me_6TREN) has been investigated in the presence of $[Co(acac)_2]$ or $[Co(acac)_2]$/py, with the goal of generating radicals by halogen atom transfer to Cu^I for subsequence trapping by Co^{II} and generation of an alkylcobalt(III) product. No evidence for the formation of the target product has been obtained. The various reactions, carried out under different conditions, have led to the crystallization of the following compounds: $\{[Cu(bipy)_2Br]^+\}_2\{[Cu_2Br_4]^{2-}\}$ (**1**); $[Cu(Me_6TREN)Br]Br$; $[Cu(Me_6TREN)Br_{0.37}Cl_{0.63}]Br$ (**2**); *trans*-$[Co(acac)_2(THF)_2]$ (**3**); $[Co(Me_6TREN)Br]Br$ (**4**); $[Cu(Me_7TREN)I]\{[Cu_2I_2(Br_{0.628}I_{0.372})_2]_{0.9}[I]_{0.2}\}$ (**5**); $[C_6H_8N]_2[CoI_4]$ (**6**); $[Co(acac)_3]$; and $[Co(acac)_2(THF)_2CoBr_2]$ (**7**). The structures of **1**–**7** have been determined by single-crystal X-ray diffraction.

© 2008 Elsevier Ltd. All rights reserved.

1. Introduction

Controlled radical polymerization (CRP) is the fastest developing field in modern polymer chemistry [1]. The scope and flexibility of this technique to access polymers with well-defined structure, chain length, and composition is unmatched by any other polymerization method. Although non-metal-based methods are also known, the coordination and organometallic chemistry of the transition metals involving one-electron processes (homolytic bond cleavage, atom transfer reactions) has been shown to be of fundamental importance in CRP [2].

There are three ways in which a transition metal complex can mediate CRP, all based on one-electron processes: (i) reversible halogen atom transfer to a reduced metal catalyst, termed atom transfer radical polymerization (ATRP) [3,4]; (ii) homolytic cleavage of metal–carbon bonds, termed organometallic radical polymerization (OMRP) [5,6]; and (iii) degenerative transfer (DT), involving a rapid associative exchange between the active and dormant chains on a transition metal complex [7,8]. Our group investigates the intimate details of coordination chemistry related to transition metal mediated CRP. We have developed a family of compounds capable of simultaneous control by ATRP and OMRP [9–11], rationalized the effect of certain Lewis acid promoters [12,13] and explained the reason for the observation of low initiator efficiencies under certain conditions [14]. The possible interplay of various one-electron processes in CRP has been recently outlined in a review [2].

Of current interest is the unique ability of compound $Co(acac)_2$ to mediate the CRP of vinyl acetate (VAc), a challenging monomer for which previous attempts by ATRP and OMRP methods had failed. This compound was recently reported to provide excellent control by a proposed OMRP mechanism for a bulk polymerization (*i.e.* without solvent or additives) [15,16], but our studies have in fact demonstrated its action through a DT mechanism under these conditions, though the mechanism switches to OMRP in the presence of neutral donors [17]. The reasons for this behavior are summarized in Scheme 1. Whereas the Co–C bond in the organometallic dormant chain is not weak enough to afford a significant free radical concentration in the absence of ligand, stabilization of the Co^{II} radical trap by further coordination of L to give 6-coordinate $[Co(acac)_2L_2]$ shifts the radical formation equilibrium and allows the CRP to be sustained by the OMRP mechanism. The 6-coordinate, L-bonded Co^{III} dormant chain cannot undergo DT because it is coordinatively saturated, whereas the 5-coordinate ligand-free chain, $[(acac)_2Co\text{-}(m)_xR]$, is able to promote DT. In a more recent contribution, we have carried out computational investigations on the nature of the Co^{III} chain-end [18]. However, no simple alkylcobalt(III) compound that could represent a model of the OMRP dormant chain or DT transfer agent has so far been isolated and characterized with the acetylacetonate ligand environment, $[RCo(acac)_2]$ or $[RCo(acac)_2L]$. This is in contrast with other alkylcobalt(III) species, containing for instance a porphyrin ligand environment [19–21].

* Corresponding author. Tel.: +33 05 61 33 31 85; fax: +33 05 61 55 30 03.
E-mail address: rinaldo.poli@lcc-toulouse.fr (R. Poli).

0277-5387/$ - see front matter © 2008 Elsevier Ltd. All rights reserved.
doi:10.1016/j.poly.2008.03.022

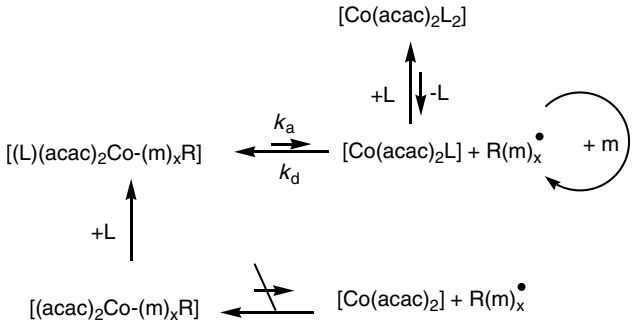

Scheme 1. Influence of ligand coordination to the mechanism of $[Co(acac)_2]$-mediated CPR of VAc.

We have therefore set out to prepare one such compound. This particular synthetic target does not appear straightforward. With supporting ligands such as porphyrin of Schiff bases, organylcobalt(III) products are easily accessed by first reducing $Co^{II}L$ to $[Co^{I}L]^-$, followed by reaction with an alkyl halide [19,20,22]. The hard acac ligand, however, does not provide sufficient stability to the putative $[Co(acac)_2]^-$ anion. A few derivatives have also been prepared by alkylation of halocobalt(III) reagents [23]. However, $[Co^{III}(acac)_2Y]$ (Y = halogen) are non-existing compounds. A final method leading to organylcobalt(III) compounds is one-electron oxidative addition of alkyl halides to Co^{II} reagents [23], see Scheme 2, a drawback being that half of the Co^{II} reagent is sacrificed for making the Co^{III}–Y by-product.

However, we find that no reaction takes place between $[Co(acac)_2]$ and BEB, which is a quite active alkyl halide (weak C–Y bonds). The reason for this lack of reactivity may be thermodynamic: cobalt prefers to remain in the +II oxidation state with hard ligands such as acac, and the co-product $[Co(acac)_2Y]$ (which is non-existent as already mentioned) does not provide sufficient thermodynamic help to achieve the oxidative addition process. A possible key to alleviate this problem is therefore to use a stronger halogen acceptor. We have considered the use of the Cu^{I} system CuBr/L (L = N-based ligand such as hexamethyl-tris(aminoethyl)amine (Me_6TREN) or 2,2′-bipyridine (bipy)). It has already been reported that CuBr/L systems abstract efficiency halide radicals from alkyl halides, forming the related Cu^{II} products [24–27], while Cu^{I} does not have sufficient affinity for carbon-based radicals [28]. Indeed, this is the basis for the high efficiency of this family of Cu^{I} systems as ATRP catalysts [3]. Some of these complexes, especially the *in situ* made [(Me_6TREN)CuBr], are very rapid under very mild conditions (room temperature or below) [29]. In this manner, we were hoping that alkyl radicals could be efficiently trapped by $[Co(acac)_2]$. Scheme 3 shows the reaction pathway envisaged for this transformation, which might be carried out in the presence of an additional monodentate ligand L, such as pyridine. Indeed, the organylcobalt(III) product should be stabilized by addition of a neutral ligand, with formation of a 6-coordinate $[Co(R)(acac)_2(L)]$ complex, because low-spin Co^{III} is known to strongly prefer an octahedral coordination environment.

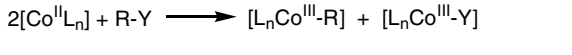

Scheme 2. Generation of R–Co^{III} products by one-electron oxidative addition or R–Y to Co^{II} precursors.

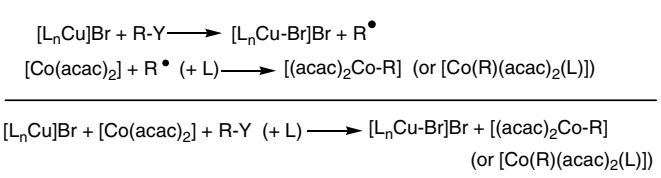

Scheme 3. Possible reaction pathway for alkyl halides in the presence of [{Me_6-TREN}Cu]Br and $[Co(acac)_2]$.

In this contribution, we present the results of synthetic efforts along these lines. Unfortunately, we have not attained our desired goal, because many side reactions take place as will be discussed in detail in the next section. However, the isolated and characterized compounds present some novelty in $Cu^{I/II}$ and Co^{II} coordination chemistry and may therefore represent useful reference for future work in CRP by the use of these metal systems.

2. Results and discussion

2.1. Reaction of $[Cu(bipy)_2]Br$ and 1-bromoethylbenzene

We started our studies with the CuBr/bipy system, since the ligand is easily available. This is known to form the salt-like compound $[Cu(bipy)_2]^+Br^-$ in solution [30]. However, this compound is not one of the fastest activators for ATRP (*i.e.* capable of generating free radicals from an alkyl halide at a high rate under mild conditions) [29]. The rate of radical generation depends on the C–Y bond strength of the halide compound used [31], therefore we restricted our studies with this copper complex to the relatively active initiator 1-bromoethylbenzene (BEB). The reaction was carried out in MeOH at room temperature, leading to the immediate formation of a red precipitate after the addition of CuBr, signaling the formation of a Cu(II) product. This compound was crystallized and characterized by X-ray diffraction.

The X-ray determination revealed the formation of the mixed valence Cu(I)/Cu(II) salt $\{[Cu(bipy)_2Br]^+\}_2\{[Cu_2Br_4]^{2-}\}$ (**1**) (Fig. 1). Selected bond lengths and distances are shown in Table 1. The structure of **1** features a centrosymmetric $[Cu_2Br_6]^{2-}$ ion, which sits on two-fold axis, and two symmetry-related $[Cu(bipy)_2Br]^+$ cations. The Cu(II) cation is in a distorted trigonal bipyramidal coordination, with axial Cu–N bonds of 1.981(2) and 1.987(2) Å while longer Cu–N bonds of 2.070(2) and 2.083(3) Å occur in the equatorial positions as well as the Cu–Br bond with 2.4936(9) Å. The monovalent Cu2 site adopts a trigonal planar $CuBr_3$ coordination, with Cu2–Br2 (bridging) bonds of 2.4689(10) Å and Cu2–Br3 (terminal) bonds of 2.3215(12) Å. The structure of the cation has already been reported in the simpler $[Cu(bipy)_2Br]Br$ salt [32], as well as with other anions [33–36] and the $[Cu_2Br_6]^{2-}$ dianion has also been crystallographically characterized in other compounds [37–45]. All bond distances are in good agreement with those reported in the above cited structures.

The formation of this compound can be understood on the basis of bromine atom transfer from BEB to $[Cu(bipy)_2]^+$ to generate the Cu^{II} cation $[Cu(bipy)_2Br]^+$, while the Br^- ion is trapped by additional CuBr to yield the Cu^{I} dianion $[Cu_2Br_4]^{2-}$. Thus, not all CuBr has reacted with bipy, or perhaps bipy coordination is reversible and these particular crystallization conditions favor the precipitation of this ion combination. Other mixed-valence Cu^{I}/Cu^{II} salts have previously been obtained, for instance $[Cu^{II}(dNpby)_2Br]^+$-$[Cu^{I}Br_2]^-$ where dNpby = 4,4′-di(5-nonyl)-2,2′-bipyridine [46], but the anion is a linear mononuclear [Br–Cu–Br]$^-$ complex in this compound. It seems that small subtleties tip the choice of the Cu^{I} anion for a mononuclear ($[CuBr_2]^-$) or dinuclear ($[Cu_2Br_4]^{2-}$) form.

The formation of compound **1** suggests that $CH_3(Ph)CH$ radicals are being produced, therefore this reaction was repeated in the presence of $[Co(acac)_2]$. However, the course of the reaction did not change and there was no spectroscopic evidence for the formation of an alkylcobalt(III) derivative. It is possible that the Co–$CH(CH_3)Ph$ bond is too weak to be formed in an irreversible fashion

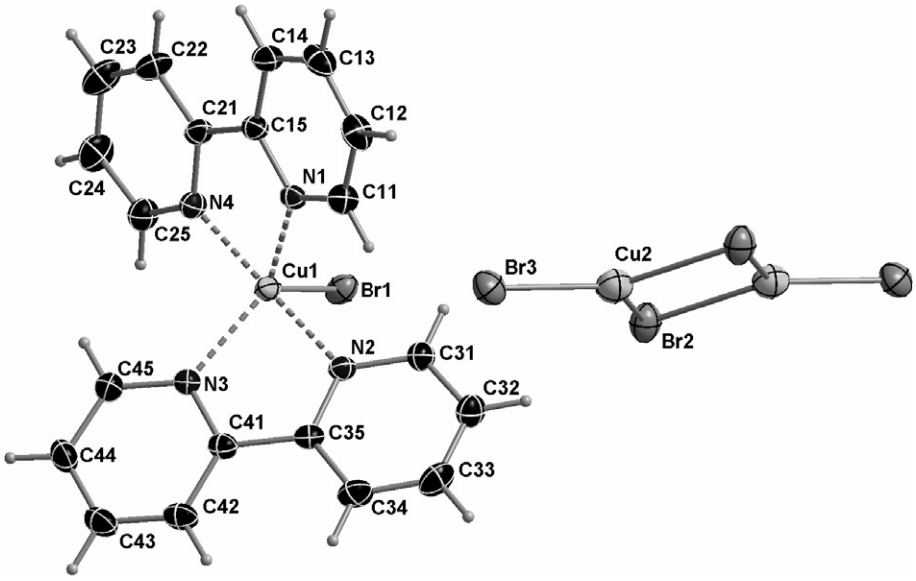

Fig. 1. Molecular structure of **1** at 180 K (50% probability ellipsoids).

Table 1
Selected bond distances (Å) and angles (°) for $[Cu(bipy)_2Br]_2[Cu_2Br_4]$ (**1**)[a]

Cu1–N2	1.981(2)	N4–Cu1–N1	80.29(9)	$Br2^i$–Cu2–$Cu2^i$	55.64(3)
Cu1–N4	1.987(2)	N2–Cu1–N3	80.01(10)	Br2–Cu2–$Cu2^i$	53.27(3)
Cu1–N1	2.070(2)	N4–Cu1–N3	100.68(10)	$Cu2^i$–Br2–Cu2	71.09(4)
Cu1–N3	2.083(3)	N1–Cu1–N3	123.74(9)	C11–N1–Cu1	128.16(19)
Cu1–Br1	2.4936(9)	N2–Cu1–Br1	92.16(7)	C15–N1–Cu1	113.28(18)
Cu2–$Cu2^i$	2.8295(16)	N4–Cu1–Br1	90.86(8)	C35–N2–Cu1	116.64(19)
Cu2–Br3	2.3215(12)	N1–Cu1–Br1	117.65(7)	C31–N2–Cu1	123.69(19)
Cu2–$Br2^i$	2.3973(8)	N3–Cu1–Br1	118.57(7)	C45–N3–Cu1	128.89(19)
$Cu2^i$–Br2	2.3972(8)	Br3–Cu2–$Br2^i$	127.39(3)	C41–N3–Cu1	112.92(19)
Cu2–Br2	2.4689(10)	Br3–Cu2–Br2	123.70(4)	C25–N4–Cu1	124.6(2)
N2–Cu1–N4	176.1(1)	$Br2^i$–Cu2–Br2	108.91(4)	C21–N4–Cu1	116.07(18)
N2–Cu1–N1	96.12(9)	Br3–Cu2–$Cu2^i$	176.96(3)		

[a] (i): $3-x, -y, 2-z$.

at room temperature. Therefore, we have tried to generate these radicals at lower temperatures with a more active Cu complex.

2.2. Reaction of CuBr(Me_6TREN) and 1-bromoethylbenzene or 1-chloroethylbenzene

Me_6TREN, in combination with CuBr, provides one of the fastest initiating systems in copper mediated CRP. In order to insure sufficient solubility of all materials at low temperature, we switched solvent to THF. As already described [47], complexes $[Cu(Me_6TREN)X]$ (X = Cl, Br, I) that form by combination of CuX and Me_6TREN are not stable at room temperature, yielding fast disproportionation into Cu^0 and $[Cu^{II}(Me_6TREN)X]X$ and are also quite sensitive to aerial oxidation. This has been confirmed in our study: the disproportionation can be easily observed by the development of a green color, characteristic of the Cu^{II} system, from the colorless solution of the Cu^I complex. At lower temperatures and under strict exclusion of air and moisture the solution remains colorless.

Addition of BEB (1 equiv.) and $[Co(acac)_2]$ led to the isolation of light green single-crystals, which were identified as the already reported [48] $[Cu(Me_6TREN)Br]Br$. The same reaction was worked out using 1-chloroethylbenzene (CEB) instead of BEB, with similar results. Single-crystal structure determination of the green crystals revealed the formation of $[Cu(Me_6TREN)Br_{0.37}Cl_{0.63}]Br$ (**2**). Selected bond lengths and angles for compound **2** are shown in Table 2 and the molecular structure is shown in Fig. 2. This structure is isomorphous with that of the all-Br analogue. The only difference is a compositional Cl/Br disorder in the Cu-bonded position, but not in the free anion. This selectivity is probably related to the lower solubility of the bromide salt, joint with the lower activation barrier for nucleation and crystal growth relative to the barrier for Cl/Br exchange between the coordinated and free position. The Cu atom adopts a trigonal bipyramidal coordination geometry, with the axial Cu–N1 and Cu–Cl/Br bonds coinciding with the crystallographic three-fold axis. The axial Cu–N bond is significantly shorter than the equatorial one. Because of the mixed Cl/Br position, the Cu–Cl/Br distance does not carry any chemical meaning. As expected, it is shorter compared to the Cu–Br bond in the all-Br analogue (2.393(3) Å) [48] while it is longer than the Cu–Cl distance in $[Cu(Me_6TREN)Cl]^+$ (2.234(2) Å) [47]. The trigonal bipyramidal environment is only slightly distorted with N1–Cu–N2 angles of 84.19(9)° and N2–Cu–$N2^i$ angles of 118.99(3)°.

The formation of these Cu^{II} complexes confirms the fast and effective oxidation of Cu^I by halogen atom transfer from the organic halide molecule, therefore implying the formation of $CH_3(Ph)CH$ radicals in solution. The above reactions yielded a pink/red THF solution as the mother solution of the isolated crystals. There was no indications from spectroscopic analyses that the formation of an alkylcobalt(III) compound had taken place, while attempts to crystallize the pink/red component soluble in THF were not successful. We conclude that, even at lower temperatures, the Co^{III}–$CH(CH_3)Ph$ bond is probably too weak to withstand reversible

Table 2
Selected bond distances (Å) and angles (°) of $[Cu(Me_6TREN)Br_{0.37}Cl_{0.63}]Br$ (**2**)[a]

Cu1–N1	2.062(6)	N1–Cu1–Cl1|Br1	180.00(8)	C1–N1–C1^{i}	109.9(2)
Cu1–N2	2.149(3)	N2–Cu1–Cl1|Br1	95.81(9)	C2–N2–Cu1	104.5(2)
Cu1–Cl1|Br1	2.3170(14)	N1–Cu1–N2	84.19(9)	C3–N2–Cu1	114.7(2)
N1–C1	1.493(4)	N2–Cu1–N2^{i}	118.99(3)	C4–N2–Cu1	111.7(2)
N2–C2	1.477(5)	N1–C1–C2	110.1(3)	C3–N2–C2	109.5(3)
N2–C3	1.476(5)	N2–C2–C1	109.5(3)	C4–N2–C3	107.0(3)
N2–C4	1.472(5)	C1–N1–Cu1	109.0(2)	C4–N2–C2	109.4(3)

[a] (i): 0.5 + *y*, 0.5 − *z*, 1 − *x*.

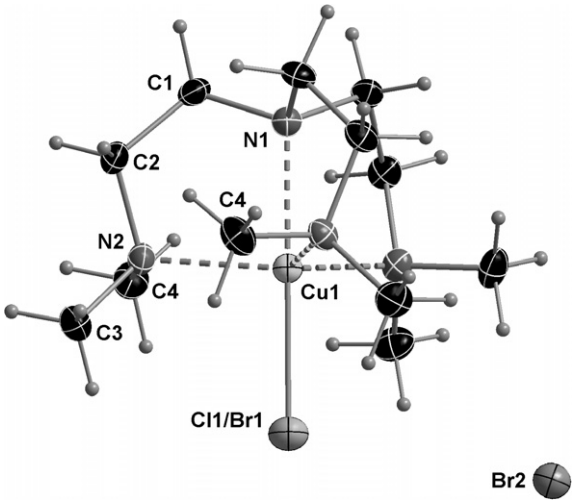

Fig. 2. Molecular structure of **2** at 180 K (50% probability ellipsoids).

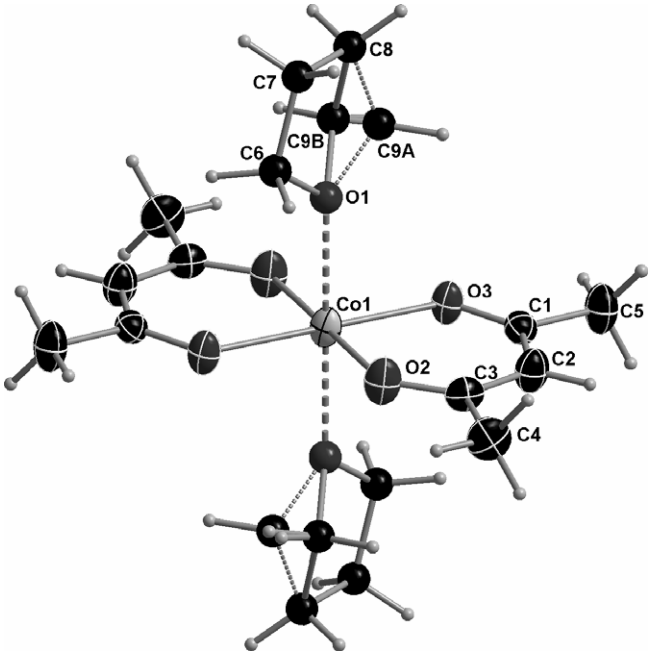

Fig. 3. Molecular structure of **7** at 160 K (50% probability ellipsoids).

homolytic rupture and ultimately leads to decomposition with formation of the typical radical decomposition products (coupling to $PhCH(CH_3)CH(CH_3)Ph$ and disproportionation to ethylbenzene and styrene).

2.3. Reaction of CuBr(Me$_6$TREN) and ethyl-2-bromopropionate

Using this organic halide, no apparent reaction occurred at low temperature, indicating that the C–Br bond is less susceptible to atom transfer than that of BEB. Warming the solution to room temperature led to the development of a green color, which yielded crystals of $Co(acac)_3$. When the same reaction was repeated and maintained at low temperature for an extended period, red crystals were isolated, corresponding to the THF solvate complex $[Co(acac)_2(THF)_2]$ (**3**).

Compound **3** is only stable at low temperature and decomposes by solvent loss upon standing for longer than 5 min under mineral oil at ambient temperature. The Co^{II} ion has an octahedral coordination with the two acac ligands in equatorial positions and THF in the axial positions. A two-fold axis is situated in the metal center of the molecule (Fig. 3). Many X-ray structures of *trans*-$[Co(acac)_2(L)_2]$ derivatives have been previously published (L = py, H_2O, CH_3OH, imidazole, etc.) [49–54], but that with THF had not yet been reported. The THF molecules show disorder with half of the molecules oriented into two different envelope conformations. Selected bond distances and angles are shown in Table 3. The Co–O(acac) bond lengths are in good agreement with those reported for the above mentioned other solvent adducts, as well as with those of solvent-free $[Co(acac)_2]$ [51,55], where in fact the coordination environment is pseudo-octahedral due to skewed stacking with neighboring molecules. The Co–O(THF) distances are significantly longer than the Co–O(acac) bonds. This result is quite logical considering that a neutral solvent molecule should be more weakly bonded to the metal center compared to the anionic acac ligand.

Table 3
Selected bond distances (Å) and angles (°) of $[Co(acac)_2THF_2]$ (**3**)[a]

Co1–O1	2.163(2)	O2–Co1–O2^{i}	180.00(14)	O2–Co1–O1^{i}	89.4(1)
Co1–O2	2.012(2)	O2–Co1–O3^{i}	90.38(9)	O2^{i}–Co1–O1^{i}	90.6(1)
Co1–O3	2.025(2)	O2^{i}–Co1–O3^{i}	89.62(9)	O3^{i}–Co1–O1^{i}	90.16(9)
O1–C6	1.414(4)	O2–Co1–O3	89.62(9)	O3–Co1–O1^{i}	89.84(9)
O1–C9A	1.452(14)	O2^{i}–Co1–O3	90.38(9)	C6–O1–Co1	126.4(2)
O1–C9B	1.440(14)	O2–Co1–O1	90.6(1)	C9B–O1–Co1	120.1(6)
O2–C3	1.253(4)	O2^{i}–Co1–O1	89.4(1)	C9A–O1–Co1	122.5(6)
O3–C1	1.258(3)	O3^{i}–Co1–O1	89.84(9)	C3–O2–Co1	126.5(2)
		O3–Co1–O1	90.16(9)	C1–O3–Co1	125.58(19)

[a] (i): −*i*, −*y*, 1 − *z*.

The isolation of compound **3** is not to be considered surprising, since the solution contains $[Co(acac)_2]$ in THF, thus the bis-adduct is certainly present, at least in equilibrium amounts, especially at low temperatures. The recovery of **3** gives no indication as to whether or not the Cu^{I} reagent has abstracted a halogen atom.

2.4. Reaction of CuBr(Me$_6$TREN) and methyl iodide

We have next turned our attention to an alkyl halide that would yield a stronger Co–C bond. The homolytic bond dissociation energy of R–X bonds for a variety of R groups and for X = Cl, Br, I has been the subject of a computational study [18]. Methyl is the alkyl group at the top of the list. Although not yet supported by

an extensive computational investigation on an homologous series of organometallic compounds, it may be anticipated that the strength of M–R bonds should roughly parallel that of R–X bonds, thus the $(acac)_2Co–CH_3$ bond is expected to have a reasonable strength. Indeed, recent calculations have shown that $(acac)_2Co–R$ bonds with $R = CH_3(X)CH$ ($X = CH_3O$, CH_3COO and CH_3OOC) are weaker than with $R = CH_3$ [18]. On the other hand, the strength of CH_3-X increases in the order X = I < Br < Cl. Thus, MeCl should be difficult to activate. We have chosen to work with CH_3I, also in consideration of the fact that this compound is a volatile liquid and therefore easier to handle. Several reactions were carried out at different temperatures and with different order of reagent addition, but no alkylcobalt(III) compound was crystallized under any circumstances. The products that were crystallized are summarized in Scheme 4.

2.5. Structure of [{Me_6TREN}CoBr]Br (**4**)

The violet crystals of **4** reveal a trigonal bipyramidal coordination geometry around the Co^{II} center with axial Co–N and Co–Br bonds and three equatorial Co–N bonds. The most important distances and angles are listed in Table 4, whereas the molecular structure is shown in Fig. 4. This structure is already reported in the literature, but based on data collected at room temperature and much less precisely determined [56]. The structure is also isomorphours with those of **2** and the all-Br analogue, [Cu(Me_6-TREN)Br]Br, discussed above. As expected, all distances are slightly longer in **3** than in the Cu analogue, because of the slightly larger ionic radius of Co^{II}.

Table 4
Selected bond distances (Å) and angles (°) of [Co(Me_6TREN)Br]Br (**4**)[a]

Co1–N1	2.137(2)	N1–Co1–Br2	98.83(6)	C3–N2–Co1	108.15(17)
Co1–N2	2.215(4)	N2–Co1–Br2	180.00(6)	N1–C2–C3	110.2(2)
Co1–Br2	2.4471(7)	N1–Co1–N1^{i}	117.69(3)	N2–C3–C2	110.1(2)
N1–C1	1.488(4)	N1–Co1–N2	81.17(6)	C1–N1–C4	106.9(2)
N1–C2	1.484(3)	C1–N1–Co1	113.21(17)	C2–N1–C1	109.4(2)
N1–C4	1.491(3)	C2–N1–Co1	107.67(17)	C2–N1–C4	109.6(2)
N2–C3	1.484(3)	C4–N1–Co1	109.91(16)	C3–N2–C3^{i}	110.76(16)

[a] (i): 0.5 − *z*, 1 − *x*, −0.5 + *y*.

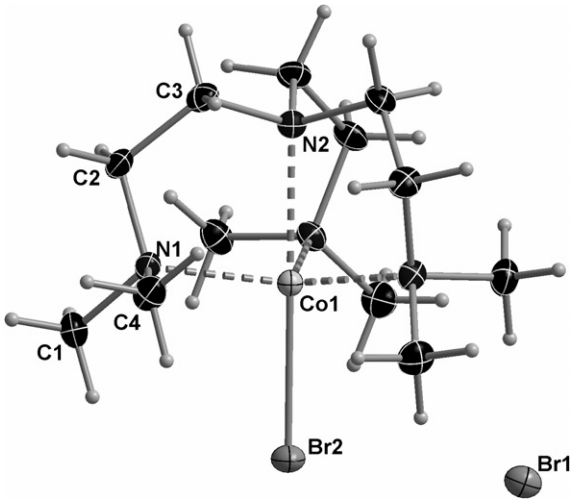

Fig. 4. Molecular structure of **4** at 150 K (50% probability ellipsoids).

2.6. [{Me_7TREN}CuI]$_2$[$Cu_{1.80}Br_{1.13}I_{2.67}$] (**5**)

This structure features ordered $[Cu(Me_7TREN)I]^+$ ions in the cationic sites, whereas the anionic sites are occupied by a compositional disorder of $[Cu_2I_2(I/Br)_2]^{2-}$ and free I^- ions. There are two cations per each anionic site, with one full cation and half the dianion in the asymmetric unit around an inversion center. Overall, all Cu species are in the oxidation state I, explaining the almost

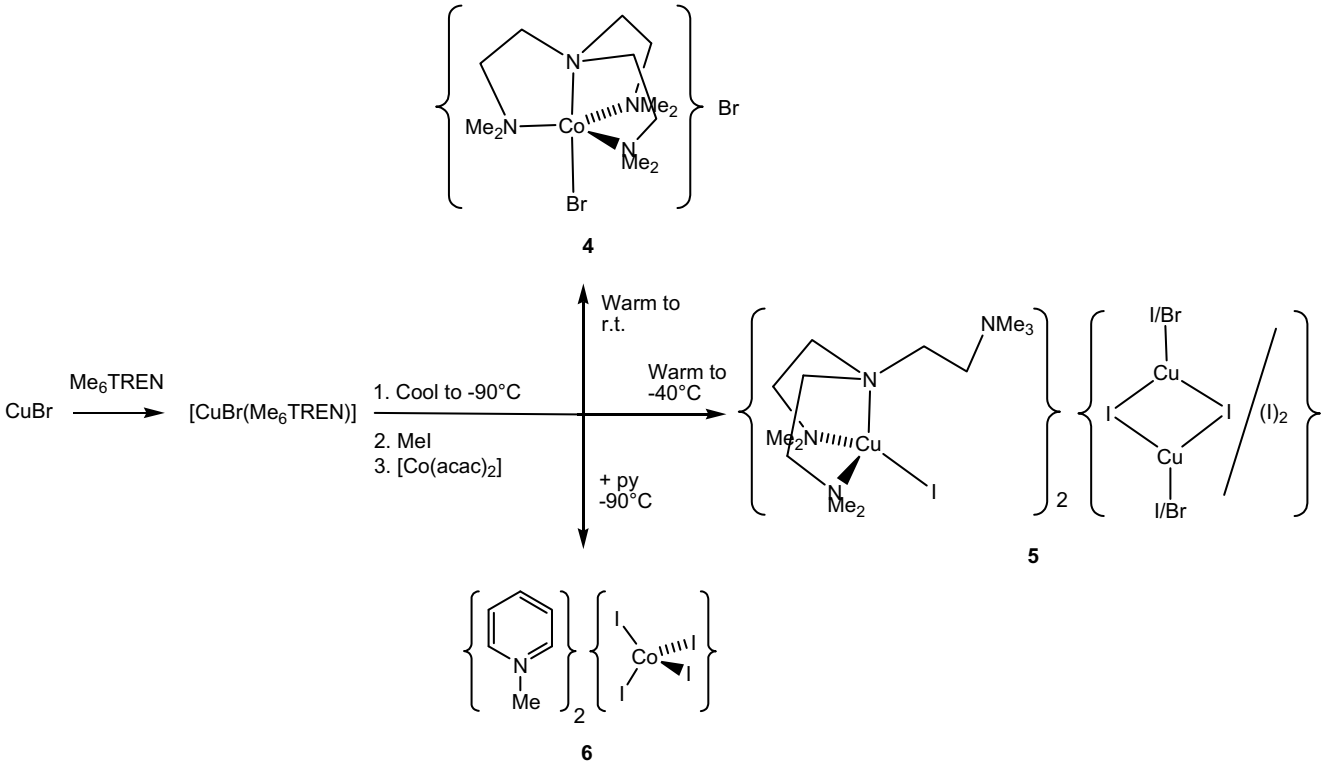

Scheme 4. Products generated by the reaction of $[Co(acac)_2]$ with MeI in the presence of [Cu(Me_6TREN)Br].

colorless aspect of the crystals. Fig. 5 shows a representation of the molecule with the dinuclear Cu^{I} dianion. Whereas the I3 site is fully occupied, the Cu2 and Br2/I2 sites refine with 90% occupancy. Moreover, the terminal halide position is a compositional disorder of atoms Br2 and I2 in a 62.8:37.2 ratio. Thus, the structure may be described as $[Cu(Me_7TREN)I]\{[Cu_2I_2(Br_{0.628}I_{0.372})_2]_{0.9}\ [I]_{0.2}\}$, with 90% of the molecules having the disordered $[Cu_2I_2(Br_{0.628}I_{0.372})_2]^{2-}$ ion and 10% having two I^- ions. This kind of crystallographic defect is well known for its ability to change the color of a correct structure significantly [57]. Selected distances and angles for this compound are listed in Table 5.

The Cu(I) cation is better described as a distorted trigonal pyramid than as a tetrahedron, with the Cu1–N3, Cu1–N2 and Cu1–I1 bonds being close to a trigonal planar arrangement with angles close to 120° (sum of the three angles = 353.8°), while a longer Cu1–N1 bond is located on the apex of the pyramid. This distortion is caused by the tridentate nature of the N_3 ligand, forcing the *cis*–N–Cu–N angles to be significantly smaller than the ideal tetrahedral value (N2–Cu1–N1: 84.3(4)°; N1–Cu1–N3: 83.7(4)°). Other cations with the same CuN_3I coordination environment around 4-coordinate Cu^{I} and with similar open tridentate N_3 ligands show the same distortion [58–62], while complexes with three monodentate N-donors or with symmetric *cyclo*-N_3 ligands adopt a more regular tetrahedral geometry [39,63–69]. The Cu2 site is in a trigonal planar coordination, like the $[Cu_2Br_4]^{2-}$ ion of compound **1**. A number of structures containing the $[Cu_2I_4]^{2-}$ ion have been previously reported [63–66], but no related structure with a compositional Br/I disorder has been described so far, to the best of our knowledge. The localization of the disorder in the terminal position suggests that the softer iodide anion has a stronger preference for the bridging site.

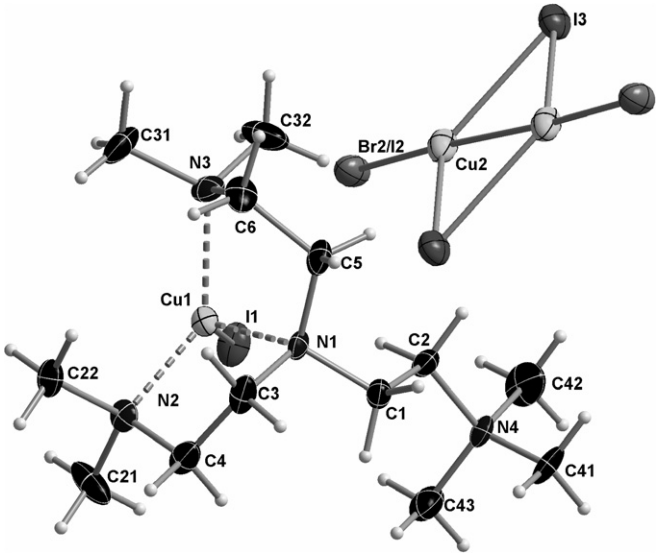

Fig. 5. Molecular structure of **5** at 160 K (50% probability ellipsoids).

2.7. $[C_5H_5NMe]_2[CoI_4]$ (**6**)

When the reaction was carried out as outlined above at −90 °C, except that pyridine was added in the hope of stabilizing an alkylcobalt(III) product in the form of a 6-coordinate complex, methylation of pyridine took place, as shown by the X-ray structure of a new compound with the composition $[C_6H_8N]_2[CoI_4]$ (**6**). A view of the molecule is shown in Fig. 6. The entire molecule, which is composed by two *N*-methylpyridinium cations and by a tetrahedral $[CoI_4]^{2-}$ dianion, is contained in the asymmetric unit. Selected bond lengths and distances are listed in Table 6. The geometry around Co^{II} is very close to ideal tetrahedral, with all I–Co–I angles laying between 107.3° and 112.8°. The Co–I bond distances of 2.583–2.608 Å coincide very well with those found in other compounds containing the same dianion [70–73].

The nature of the identified compounds resulting from this reaction (Scheme 4) brings us to the following conclusions. First, it is quite surprising to see how readily the acac ligand is displaced from Co^{II}, in spite of the chelate effect associated with this ligand. Two of the characterized compounds feature the Co^{II} ion surrounded by other ligands, in the 5-coordinate $[Co(Me_6TREN)Br]^+$ cation and in the 4-coordinate $[CoI_4]^{2-}$ dianion. Second, the electrophilic reactivity of MeI prevails on the homolytic rupture of the C–I bond and yields methylation of the Me_6TREN and py ligands, affording products that contain the $(Me_7TREN)^+$ and $(C_5H_5NMe)^+$ ions. One curious observation is that compound **4** contains only bromide and no iodide, including as free anion, even though it is obtained under very similar conditions as compound **5** where plenty of iodide enters the coordination sphere of the metal in both cation and anion.

2.8. Reaction of $CuBr(Me_6TREN)$ and 1-bromoethylacetate

Until now, we have found that the $CH_3(Ph)CH$ radicals are too stabilized to afford sufficiently strong R–Co^{III} bonds, whereas MeI, which should lead in principle to a stable Me–Co^{III} derivative, prefers to yield complex products of nucleophilic substitution at carbon and subsequent halide and neutral ligand exchange processes between copper and cobalt. In light of these results, our last attempt involved a halide molecule that is precursor of a radical of intermediate strength: $CH_3(CH_3COO)CH$. Indeed, the $[Co(acac)_2]$ complex controls the VAc polymerization by reversibly trapping the PVAc growing chain, $R_0\{CH_2CH(OOCCH_3)\}_nCH_2(CH_3COO)CH$, forming a Co^{III}-capped dormant chain as represented in Scheme 5 (R_0 = radical derived from the initiator) [15,17]. Another indication that the above-mentioned radical should lead to a stable adduct is

Table 5
Selected bond distances (Å) and angles (°) of $[Cu(Me_7TREN)I]_2[Cu_{1.8}Br_{1.13}I_{2.67}]$ (**5**)[a]

Cu1–N3	2.123(9)	N3–Cu1–N2	119.9(4)	$I3^i$–Cu2–$Cu2^i$	58.99(7)
Cu1–N2	2.131(9)	N3–Cu1–N1	83.7(4)	Cu2–I3–$Cu2^i$	61.80(7)
Cu1–N1	2.270(9)	N2–Cu1–N1	84.3(4)	C1–N1–Cu1	119.1(7)
Cu1–I1	2.5034(16)	N3–Cu1–I1	116.6(3)	C5–N1–Cu1	105.3(7)
Cu2–Br2/I2	2.432(2)	N2–Cu1–I1	117.3(3)	C3–N1–Cu1	102.2(7)
Cu2–I3	2.535(2)	N1–Cu1–I1	127.4(2)	C21–N2–Cu1	112.5(7)
Cu2–$I3^i$	2.541(2)	Br2/I2–Cu2–I3	120.69(8)	C22–N2–Cu1	114.4(7)
Cu2–$Cu2^i$	2.607(4)	Br2/I2–Cu2–$I3^i$	121.01(8)	C4–N2–Cu1	103.4(7)
I3–$Cu2^i$	2.541(2)	I3–Cu2–$I3^i$	118.20(7)	C31–N3–Cu1	114.0(8)
		Br2/I2–Cu2–$Cu2^i$	176.96(12)	C6–N3–Cu1	105.0(7)
		I3–Cu2–$Cu2^i$	59.21(7)	C32–N3–Cu1	108.4(7)

[a] (i): $-x, -2-y, 1-z$.

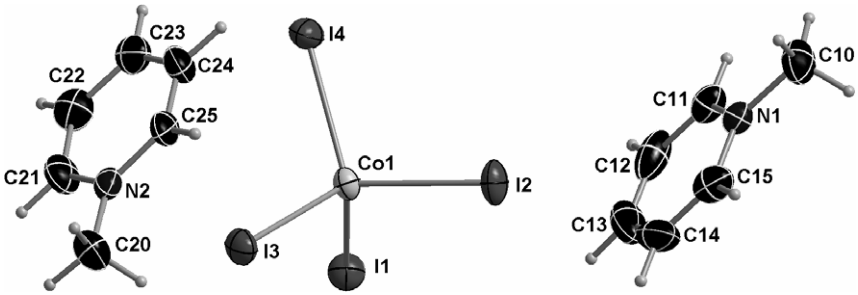

Fig. 6. Molecular structure of **6** at 180 K (50% probability ellipsoids).

Table 6
Selected bond distances (Å) and angles (°) of $[C_6H_8N]_2[CoI_4]$ (**6**)

Co1–I1	2.6084(8)	I1–Co1–I2	108.64(3)	C10–N1–C11	119.6(5)
Co1–I2	2.6030(8)	I1–Co1–I3	107.40(3)	C10–N1–C15	120.6(5)
Co1–I3	2.5828(7)	I1–Co1–I4	112.10(3)	C11–N1–C15	119.8(5)
Co1–I4	2.5943(8)	I2–Co1–I3	112.80(3)	C20–N2–C21	120.5(5)
N1–C10	1.477(7)	I2–Co1–I4	107.29(3)	C20–N2–C25	119.1(5)
N2–C20	1.463(7)	I3–Co1–I4	108.68(3)	C21–N2–C25	120.2(5)
N1–C11	1.344(6)			N1–C11–C12	120.8(6)
N1–C15	1.339(7)			N1–C15–C14	120.7(6)
N2–C21	1.336(7)			N2–C21–C22	120.6(5)
N2–C25	1.333(6)			N2–C25–C24	120.6(5)

Ref. [18].

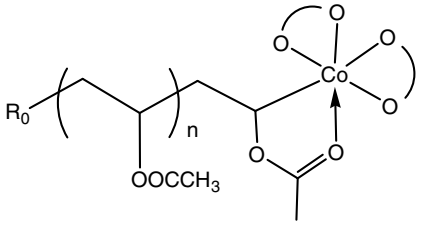

Scheme 5. Proposed structure of the dormant chain for the $[Co(acac)_2]$-controlled polymerization of VAc.

the recent isolation of a mixture of cobalt-capped short oligomers by thermally decomposing the mild radical initiator V-70 in the presence of VAc and a large excess of $[Co(acac)_2]$. The product was assigned the structure shown in Scheme 5, where $R_0 = (CH_3)_2(CH_3O)CCH_2C(CN)(CH_3)$, with an average n value of ca. 3 [18], on the basis of NMR and IR spectroscopy and derivatizations. The chelating mode indicated in Scheme 5 for the Co-bonded monomer unit is suggested by a DFT calculation on the model $[Co(acac)_2\{CH(OOCCH_3)CH_3\}]$ system and by the known preference of Co^{III} for an octahedral coordination. Thus, we have chosen compound $CH_3(CH_3COO)CHBr$ (1-bromoethylacetate, BEA) as halide precursor. Bromine rather than iodine was selected as halogen atom in order to disfavor the reactivity towards nucleophilic attack. Also, in order to minimize nucleophilic substitution problems, pyridine was not used in these reactions.

Using this organic halide, no apparent reaction occurred at low temperature, whereas only compound $Co(acac)_3$ was identified amongst the product obtained after warming the solution to room temperature, as already observed for the reaction with BEP. If the reaction solution was not allowed to warm up but rather kept at −80 °C, the formation of blue crystals was observed over a period of 10 days. This product was identified as a new binuclear Co(II) complex $[Co(acac)_2(THF)_2CoBr_2]$ (**7**). The molecular structure of this compound is depicted in Fig. 7 and selected bond lengths and distances are listed in Table 7. The corresponding dichloride compound, $[Co(acac)_2(THF)_2CoCl_2]$, displaying the same coordination geometry, has previously been described [74]. The molecule is composed of two bivalent Co atoms, connected to each other by two bridging oxygen atoms O11 and O22. Atom Co1 adopts an octahedral coordination mode, with two chelating acetylacetonate ligands and two *trans* THF molecules, whereas Co2 has a tetrahedral coordination environment, defined by the bridging atoms O11 and O22 of two different acetylacetonate ligands and two Br atoms. Due to the bridging oxygen atoms O11 an O22 which impose a small O11–Co2–O22 angle, the angle Br–Co–Br is widened relative to the tetrahedral value. The Co1–O bonds to the non-bridging atoms O12 and O21 are shorter than those to the bridging ones. The Co2–O bonds are even shorter, as expected from the lower coordination. All bond distances and angles involving the O atoms correspond very closely to those reported for the chloride analogue [74]. The Co–Br bonds agree well with values reported in the literature for other tetrahedrally coordinated Co^{II} bromides.

Compound **7** forms under similar operating conditions that led to the isolation of **3** by using the reagent BEP. Both products are coordination compounds of Co^{II}. However, whereas compound **3** may be obtained by direct interaction of $[Co(acac)_2]$ and the solvent, without the intervention of the halide reagent, the incorporation of bromine atoms in compound **7** requires the intervention of

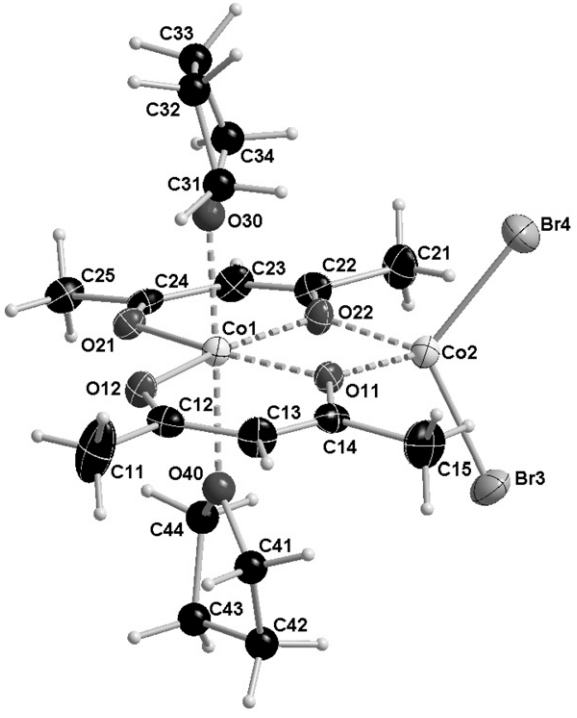

Fig. 7. Molecular structure of **7** at 180 K (50% probability ellipsoids).

Table 7
Selected bond distances (Å) and angles (°) of $[Co(acac)_2(THF)_2CoBr_2]$ (**7**)

Co1–O11	2.082(5)	O11–Co1–O12	87.5(2)	O11–Co2–Br4	112.49(16)
Co1–O12	2.022(5)	O11–Co1–O21	166.1(2)	O22–Co2–Br3	111.26(17)
Co1–O21	2.008(5)	O11–Co1–O30	92.9(2)	O22–Co2–Br4	115.54(17)
Co1–O22	2.082(5)	O11–Co1–O40	89.3(2)	Br3–Co2–Br4	118.69(6)
Co1–O30	2.145(5)	O12–Co1–O21	106.1(2)	Co1–O11–C14	127.4(5)
Co1–O40	2.146(6)	O12–Co1–O22	166.1(2)	Co1–O12–C12	128.9(5)
Co2–O11	2.027(5)	O12–Co1–O30	89.8(2)	Co1–O21–C24	129.0(5)
Co2–O22	1.998(6)	O12–Co1–O40	90.1(2)	Co1–O22–C22	128.9(5)
Co2–Br4	2.3559(15)	O21–Co1–O22	87.8(2)	Co1–O30–C31	125.3(5)
Co2–Br3	2.3666(14)	O21–Co1–O30	89.7(2)	Co1–O30–C34	124.7(5)
		O21–Co1–O40	88.2(2)	Co1–O40–C44	125.5(5)
Co1–O11–Co2	99.1(2)	O22–Co1–O30	89.6(2)	Co1–O40–C41	126.7(5)
Co1–O22–Co2	100.0(2)	O22–Co1–O40	91.0(2)	Co2–O11–C14	131.8(5)
O11–Co1–O22	78.7(2)	O30–Co1–O40	177.8(2)	Co2–O22–C22	130.6(5)
O11–Co2–O22	82.0(2)	O11–Co2–Br3	111.20(16)		

Refs. [17,18].

the BEA reagent, therefore giving indirect evidence of the production of $CH_3(CH_3COO)CH$ radicals. Recall that no disproportionation occurs for [Cu(Me$_6$TREN)Br] when this is kept at low temperatures. The formation of compound **7** may be envisaged as follows. Bromine atom transfer to [CuBr(Me$_6$TREN)] affords $[Cu(Me_6TREN)Br]^+Br^-$ and $CH_3(CH_3COO)CH$. Ligand exchange between $[Co(acac)_2]$ and the bromide ion generates "Co(acac)Br", which may dimerize and undergo ligand redistribution, to yield **7** with the help of further coordination of two THF molecules. According to our previous findings [17,18], the $CH_3(CH_3COO)CH$ radicals should be efficiently trapped by $[Co(acac)_2]$. However, our best efforts to identify an organometallic species by ^{1}H NMR in the mother solution of the crystals have not met with success. We cannot exclude that such a species is formed, but we do not have any evidence to support this possibility at the moment.

3. Conclusion

$[Co(acac)_2]$ has so far resisted the synthesis of a simple alkyl derivative, $[RCo^{III}(acac)_2]$ or $[RCo^{III}(acac)_2(L)]$. All attempts made in our laboratory and reported herein have resulted in side reactions that reveal the limitations of this synthetic strategy and the challenge of this synthetic target: the R–Co^{III} is weak for the unreactive radicals, namely those that can be generated most easily; R–X precursors with reactive radicals engage more readily in other reaction pathways (nucleophilic halide displacement by neutral ligands) whereas the simple one-electron oxidative addition is thermodynamically unfavorable. However, we still believe that it may be possible, given an appropriate method of rapidly generating a large amount of reactive radicals under very mild conditions, to synthesize a sufficiently stable organylcobalt(III) complex supported by two acetylacetonate groups, which would represent a model for the chain end in the dormant form of PVAc grown by $[Co(acac)_2]$-mediated CRP.

4. Experimental

4.1. General

All manipulations were carried out under strict oxygen-free and dry argon atmosphere. Reaction vessels were flame-dried under vacuum before use and standard Schlenk techniques were used to carry out all reactions. Toluene and THF were purified by distillation under argon after drying over sodium/benzophenone ketyl. *n*-Pentane and CH_2Cl_2 were dried respectively over $LiAlH_4$ and P_4O_{10} and then freshly distilled under argon prior to use. MeI, ethyl-2-bromoproprionate (EBP), 1-bromoethylbenzene (BEB), and 1-chloroethylbenzene (CEB) were dried over molecular sieve and distilled under reduced pressure before use. Me$_6$TREN [75] and 1-bromoethylacetate (BEA) [76,77] were synthesized according to the literature methods. $[Co(acac)_2]$ was purchased from Alfa Aesar and sublimed under reduced pressure and filled into glass ampoules under argon atmosphere. CuBr (99.9%) was purchased from Alfa Aesar. All other reagents used were of commercially available reagent-grade quality and were used without further purification.

4.2. Syntheses

4.2.1. Formation of compound $\{[Cu(bipy)_2Br]^+\}_2\{[Cu_2Br_4]^{2-}\}$ (**1**)

A Schlenk tube equipped with a magnetic stirrer was charged with 2 mL of freshly distilled methanol, 0.043 g 2,2′-bipyridine (0.272 mmol), and 35 μL BEB (0.262 mmol). CuBr (0.019 g; 0.13 mmol) was added subsequently at room temperature, leading to an immediate color change to intense brown–red. Stirring overnight yielded a red precipitate, which was isolated and dissolved in acetone. Single-crystals of **1** were produced upon storing the solution at 4 °C for 2 days.

4.2.2. Formation of [Cu(Me$_6$TREN)Br]Br

CuBr (0.05 g, 0.35 mmol) was placed into a Schlenk tube equipped with a magnetic stirrer and 3 mL of freshly distilled toluene was added. Three freeze–pump–thaw cycles guaranteed an oxygen-free atmosphere. One hundred and twenty-four microliters Me$_6$TREN (0.52 mmol) were added at room temperature and the mixture was stirred until a colorless solution was obtained. The solution was then cooled to −90 °C using acetone and liquid nitrogen. Subsequently, BEB (71 μL, 0.052 mmol) was added and the solution was stirred for another 30 min. In a separate Schlenk tube $[Co(acac)_2]$ (0.09 g, 0.35 mmol) was dissolved in 2 mL of THF and the solution was cooled to −90 °C. Three freeze–pump–thaw procedures guaranteed an oxygen-free atmosphere. While cooling down, the violet $[Co(acac)_2]$ solution became red. Then, the $[Co(acac)_2]$ solution was added to the other solution at −90 °C using a cannula and the reaction was stirred for another 2 h and then placed in a −20 °C freezer. Crystallization took place in 3 days. The crystalline green solid was redissolved in CH_2Cl_2 and crystallized placing the solution again into the freezer (−20 °C). Suitable light green single-crystals were obtained, which were identified as the already reported [48] [Cu(Me$_6$TREN)Br]Br by comparison of the unit cell parameters.

4.2.3. Formation of compound [Cu(Me$_6$TREN) $Br_{0.37}Cl_{0.63}$]Br (**2**)

CuBr (0.134 g, 0.93 mmol) was placed into a Schlenk tube equipped with a magnetic stirrer and 3 mL of freshly distilled

Table 8
Crystallographic data for all compounds

Compound	1	2	3	4	5	6	7
Empirical formula	$C_{20}H_{16}Br_3Cu_2N_4$	$C_{12}H_{30}Br_{1.37}Cl_{0.63}CuN_4$	$C_{18}H_{30}CoO_6$	$C_{12}H_{30}Br_2CoN_4$	$C_{26}H_{66}Br_{1.13}Cu_{3.80}I_{4.67}N_8$	$C_{18}H_{30}Br_2Co_2O_6$	$C_{18}H_{30}Br_2Co_2O_6$
Formula mass (g mol^{-1})	679.18	425.53	401.35	449.15	1415.17	754.80	620.10
Temperature T (K)	180	180	160	150	160	180	180
Wavelength λ (Å)	0.71073 (Mo Kα)						
Crystal system	triclinic	cubic	monoclinic	cubic	triclinic	orthorhombic	orthorhombic
Space group	$P\bar{1}$	$P2_1/3$	$C2/c$	$P2_1/3$	$P\bar{1}$	$C2/c$	$P2_12_12_1$
a (Å)	8.7884(18)	11.9666(6)	15.485(2)	12.0768(3)	8.2697(10)	28.376(4)	9.5934(7)
b (Å)	11.449(2)		11.1151(14)		8.5175(10)	9.2662(9)	14.5601(11)
c (Å)	12.346(3)		12.9790(13)		18.607(2)	16.5472(14)	17.1601(13)
α (°)	64.95(3)				77.337(10)		
β (°)	84.89(3)		116.091(10)		86.862(15)	109.953(9)	
γ (°)	77.64(3)				66.140(11)		
Cell volume (Å^3)	1099.3(5)	1713.61(15)	2006.3(4)	1761.39(8)	1168.6(3)	4089.7(8)	2396.9(3)
Formula units/cell Z	2	4	4	4	1	8	4
ρ_{calc} (g cm^{-3})	2.052	1.649	1.329	1.694	2.011	2.452	1.718
μ (mm^{-1})	7.401	4.551	0.883	5.506	5.783	6.869	4.746
F(000)	654	870	852	908	675	2728	1240
Crystal size (mm)	0.38 × 0.29 × 0.24	0.34 × 0.31 × 0.30	0.24 × 0.12 × 0.09	0.29 × 0.26 × 0.25	0.81 × 0.47 × 0.40	0.19 × 0.18 × 0.04	0.12 × 0.11 × 0.06
Diffractometer device	oxford-diffraction XCALIBUR						
Scan type	omega scan						
2θ range (°)	3.43–32.11	2.41–27.45	2.51–25.00	2.92–32.04	2.67–27.50	2.62–32.02	2.76–27.50
Reflections connected	11900	14609	5996	19109	10011	15764	18634
Unique reflections (R_{int})	6967 (0.0230)	1314 (0.0417)	1774 (0.0332)	2007 (0.0263)	5337 (0.0697)	6264 (0.0336)	5518 (0.0722)
Reflections with $F_0^2 \geqslant 2\sigma$ (F_0^2)	5230	1253	1275	1890	1854	3471	3311
Completeness to θ (%)	90.5 (32.11°)	100 (27.45°)	99.9 (25.00°)	98.4 (32.04°)	99.6 (27.5°)	87.9 (32.02°)	99.8 (27.50°)
Absorption correction	semiempirical						
Minimum and maximum transmission	0.086 and 0.1708	0.189 and 0.257	0.7871 and 0.9200	0.1961 and 0.2500	0.5411 and 0.7952	0.3384 and 0.7900	0.6085 and 0.7741
Refinement method	full-matrix least squares on F^2						
Data/restrains/parameters	6967/0/262	1314/0/60	1774/0/125	2007/0/59	5337/0/201	6264/0/173	5518/0/254
Goodness-of-fit (GOF) on F^2	1.067	1.315	1.038	1.374	0.781	0.901	0.922
R_1 [$I > 2\sigma(I)$]	0.0366	0.0307	0.0379	0.0253	0.0446	0.0267	0.0392
wR_2	0.0850	0.0861	0.1117	0.0626	0.0925	0.0677	0.0763
Absolute structure parameter		-0.05(2)		0.008(14)			
Maximum, minimum residual density (e Å^{-3})	1.043, −0.960	1.618, −0.487	0.465, −0.302	2.746, −0.695	1.429, −0.975	0.983, −1.121	0.830, −0.947

THF was added. Three freeze–pump–thaw cycles guaranteed an oxygen-free atmosphere. Me_6TREN (220 μL, 0.93 mmol) was added at room temperature and the mixture was stirred until a colorless solution was obtained. The solution was then cooled down to −90 °C using acetone and liquid nitrogen. Subsequently, CEB (97 μL, 0.93 mmol) was added and the solution was stirred for another 30 min. In a separate Schlenk tube $[Co(acac)_2]$ (0.09 g, 0.35 mmol) was dissolved in 2 mL of THF and the solution was cooled to −90 °C. Three freeze–pump–thaw procedures guaranteed an oxygen-free atmosphere. While cooling down, the violet $[Co(acac)_2]$ solution became red. Then, the $[Co(acac)_2]$ solution was slowly added to the other solution at −90 °C using a cannula and the reaction was stirred for another 7 h. Crystallization took place after addition of 0.5 mL *n*-pentane and yielded tetrahedral shaped dark green single-crystals of **2**.

4.2.4. Reaction of CuBr, Me_6TREN, $[Co(acac)_2]$ and EBP. Formation of compound $[Co(acac)_3]$

$[\{Me_6TREN\}CuBr]$ was prepared freshly at −90 °C in THF by addition of Me_6TREN (139 μL, 0.6 mmol) to a mixture of CuBr (0.086 g, 0.6 mmol) in 3 mL THF. Addition of equimolar amounts of $[Co(acac)_2]$ (0.152 g), EBP (0.072 mL) and acetonitrile (0.060 mL) took place subsequently. After addition of $[Co(acac)_2]$ the solution turned red and after addition of EBP no change of color was observed. The solution was warmed up slowly to room temperature, leading to a green solution. This was evaporated to dryness and the residue was redissolved in acetone. The solution was placed into the fridge at 4 °C and dark green crystals were obtained after 2 weeks. X-ray diffraction experiments identified this compound as $[Co(acac)_3]$ by comparison of the unit cell parameters with those already available in the literature [78,79].

*4.2.5. Formation of compound $[Co(acac)_2(THF)_2]$ (**3**)*

$[\{Me_6TREN\}CuBr]$ was prepared freshly at −90 °C in THF by addition of Me_6TREN (90 μL, 0.35 mmol) to a mixture of CuBr (0.050 g, 0.35 mmol) in 3 mL THF. In a separate Schlenk tube $[Co(acac)_2]$ (0.100 g, 0.39 mmol) was dissolved in 3 mL of THF and EBP (0.038 mL, 0.35 mmol) was added dropwise to the pink solution. The two solutions were combined at −80 °C using a cannula. The resulting intense red solution was kept stirring for 3 h and than stored at −80 °C. After 1 week a blue solution had formed and red crystals of **3** had formed at the bottom of the Schlenk tube.

*4.2.6. Formation of compound $[\{Me_6TREN\}CoBr]Br$ (**4**)*

CuBr (0.066 g, 0.46 mmol) was placed in a Schlenk tube equipped with a magnetic stirrer and 2 mL of freshly distilled THF was added. Three freeze–pump–thaw cycles guaranteed an oxygen-free atmosphere. Me_6TREN (107 μL, 0.46 mmol) was added at room temperature and the mixture was stirred until a colorless solution was obtained. The solution was then cooled down to −90 °C. Subsequently, methyl iodide (62 μL, 0.46 mmol) and immediately afterwards $[Co(acac)_2]$ (0.118 g, 0.46 mmol) were added to the solution. Warming up the reaction mixture to room temperature led to a brown solution over a large amount of amorphous white precipitate. The solid was separated and washed with a mixture of toluene/acetone. All toluene/acetone fractions were united and left standing on a vibration-free place. After 1 week both a white precipitate and violet crystals had formed at the bottom of the Schlenk tube. The crystals were separated and redissolved in CH_2Cl_2. Cooling the solution to 4 °C yielded tetrahedral shaped violet crystals of compound **4**.

*4.2.7. Formation of compound $[\{Me_7TREN\}CuI]_2[Cu_{1.80}Br_{1.13}I_{2.67}]$ (**5**)*

CuBr (0.1 g, 0.70 mmol) was placed into a Schlenk tube equipped with a magnetic stirrer and 3 mL of freshly distilled THF was added. Three freeze–pump–thaw cycles guaranteed an oxygen-free atmosphere. Me_6TREN (165 μL, 0.70 mmol) was added at room temperature and the mixture was stirred until a colorless solution was obtained. The solution was then cooled to −90 °C. Subsequently, methyl iodide (100 μL, 1.2 mmol) and immediately afterwards $[Co(acac)_2]$ (0.02 g, 0.08 mmol) were added to the solution. Warming up the reaction mixture to −40 °C led to a green solution over a colorless precipitate. The solution was separated from the solid and evaporated to dryness under reduced pressure. The solid was dissolved in dry acetone, yielding a green solution. Addition of *n*-pentane and crystallization at −80 °C with pentane layered on top of the CH_2Cl_2 solution yielded almost colorless (slightly greenish) air and moisture sensitive crystals of compound **5** at the bottom of the Schlenk tube.

*4.2.8. Formation of compound $[C_5H_5NMe]_2[CoI_4]$ (**6**)*

CuBr (0.021 g, 0.15 mmol) was placed in a Schlenk tube equipped with a magnetic stirrer and 3 mL of freshly distilled THF was added. Three freeze–pump–thaw cycles guaranteed an oxygen-free atmosphere. Me_6TREN (35 μL, 0.15 mmol) was added at room temperature and the mixture was stirred until a colorless solution was obtained. The solution was then cooled to -90 °C. $[Co(acac)_2]$ (0.080 g, 0.31 mmol) was added and dissolved, followed by methyl iodide (39 μL, 0.62 mmol) and pyridine (25 μL, 0.31 mmol). Storing the resulting red solution at −80 °C for 1 week yielded green plate-like crystals of compound **6**.

*4.2.9. Formation of compound $[Co(acac)_2(THF)_2CoBr_2]$ (**7**)*

$[\{Me_6TREN\}CuBr]$ was prepared freshly at −90 °C in THF by addition of Me_6TREN (135 μL, 0.58 mmol) to a mixture of CuBr (0.080 g, 0.56 mmol) in 3 mL THF. In a separate Schlenk tube $[Co(acac)_2]$ (0.150 g, 0.58 mmol) was dissolved in 2 mL of THF. Equimolar amounts of BEA (0.072 mL) and acetonitrile (0.060 mL) were subsequently added. The two solutions were combined at −80 °C using a cannula. The resulting brown–red solution was stirred for 3 h and than stored at −80 °C. After 5 weeks, blue crystals of compound **7** had formed on the bottom of the Schlenk tube.

4.2.10. X-ray structural studies

A single-crystal of each compound was mounted under inert perfluoropolyether on the tip of a cactus spike and cooled immediately in the cryostream of an Oxford-Diffraction XCALIBUR CCD diffractometer. The structures were solved by direct methods (SHELXS-97 [80]) and refined by least-square procedures on F^2 using SHELXL-97 [81]. All H atoms attached to carbon atoms were introduced in ideal positions and treated as riding models. Absolute structures were confirmed by the refinement of Flack's enantiopole parameter [82] and by careful examination of the sensitive reflections. Crystal data and refinement parameters are shown in Table 8.

5. Supplementary data

CCDC 674118, 674119, 674120, 674121, 674122, 674123 and 674124 contain the supplementary crystallographic data for **1**, **2**, **3**, **4**, **5**, **6** and **7**. These data can be obtained free of charge via http://www.ccdc.cam.ac.uk/conts/retrieving.html, or from the Cambridge Crystallographic Data Centre, 12 Union Road, Cambridge CB2 1EZ, UK; fax: (+44) 1223-336-033; or e-mail: deposit@ccdc.cam.ac.uk.

Acknowledgement

We thank the "Agence National de la Recherche" (Contract No. NT05-2_42140) for support of this work.

References

[1] K. Matyjaszewski, Y. Gnanou, L. Leibler (Eds.), Macromolecular Engineering: Precise Synthesis, Materials Properties, Applications, 2007.
[2] R. Poli, Angew. Chem., Int. Ed. Engl. 45 (2006) 5058.
[3] K. Matyjaszewski, J.H. Xia, Chem. Rev. 101 (2001) 2921.
[4] M. Kamigaito, T. Ando, M. Sawamoto, Chem. Rev. 101 (2001) 3689.
[5] B.B. Wayland, G. Poszmik, S. Mukerjee, J. Am. Chem. Soc. 116 (1994) 7943.
[6] B.B. Wayland, S. Mukerjee, G. Poszmik, D.C. Woska, L. Basickes, A.A. Gridnev, M. Fryd, S.D. Ittel, ACS Symp. Ser. 685 (1998) 305.
[7] B.B. Wayland, X.-F. Fu, Z. Lu, M. Fryd, Polymer Preprints 230th ACS National Meeting, August 28 to September 1, 2005, Washington, DC.
[8] B.B. Wayland, C.-H. Peng, X. Fu, Z. Lu, M. Fryd, Macromolecules 39 (2006) 8219.
[9] E. Le Grognec, J. Claverie, R. Poli, J. Am. Chem. Soc. 123 (2001) 9513.
[10] F. Stoffelbach, R. Poli, P. Richard, J. Organometal. Chem. 663 (2002) 269.
[11] F. Stoffelbach, D.M. Haddleton, R. Poli, Eur. Polym. J. 39 (2003) 2099.
[12] F. Stoffelbach, R. Poli, Chem. Commun. (2004) 2666.
[13] R. Poli, F. Stoffelbach, S. Maria, J. Mata, Chem. Eur. J. 11 (2005) 2537.
[14] F. Stoffelbach, R. Poli, S. Maria, P. Richard, J. Organomet. Chem 692 (2007) 3133.
[15] A. Debuigne, J.R. Caille, R. Jérôme, Angew. Chem., Int. Ed. Eng. 44 (2005) 1101.
[16] A. Debuigne, J.-R. Caille, R. Jérôme, Macromolecules 38 (2005) 5452.
[17] S. Maria, H. Kaneyoshi, K. Matyjaszewski, R. Poli, Chem. Eur. J. 13 (2007) 2480.
[18] A. Debuigne, Y. Champouret, R. Jérôme, R. Poli, C. Detrembleur, Chem. Eur. J. 14 (2008) 4046.
[19] H. Ogoshi, E. Watanabe, N. Koketsu, Z. Yoshida, Bull. Chem. Soc. Jpn. 49 (1976) 2529.
[20] M. Perree-Fauvet, A. Gaudemer, P. Boucly, J. Devynck, J. Organomet. Chem. 120 (1976) 439.
[21] M.K. Geno, J. Halpern, J. Am. Chem. Soc. 109 (1987) 1238.
[22] E.G. Samsel, J.K. Kochi, J. Am. Chem. Soc. 108 (1986) 4790.
[23] D. Dodd, M.D. Johnson, J. Organomet. Chem. 52 (1973) 1.
[24] K. Matyjaszewski, H.-J. Paik, P. Zhou, S.J. Diamanti, Macromolecules 34 (2001) 5125.
[25] A.K. Nanda, K. Matyjaszewski, Macromolecules 36 (2003) 8222.
[26] A.K. Nanda, K. Matyjaszewski, Macromolecules 36 (2003) 599.
[27] A.K. Nanda, K. Matyjaszewski, Macromolecules 36 (2003) 1487.
[28] K. Matyjaszewski, B.E. Woodworth, Macromolecules 31 (1998) 4718.
[29] T. Pintauer, W. Braunecker, E. Collange, R. Poli, K. Matyjaszewski, Macromolecules 37 (2004) 2679.
[30] K. Matyjaszewski, T.E. Patten, J. Xia, J. Am. Chem. Soc. 119 (1997) 674.
[31] M.B. Gillies, K. Matyjaszewski, P.-O. Norrby, T. Pintauer, R. Poli, P. Richard, Macromolecules 36 (2003) 8551.
[32] M.A. Khan, D.G. Tuck, Acta Crystallogr., Sect. B B37 (1981) 1409.
[33] C. O'sullivan, G. Murphy, B. Murphy, B. Hathaway, J. Chem. Soc., Dalton Trans. (1999) 1835.
[34] B.J. Hathaway, A. Murphy, Acta Crystallogr., Sect. B B36 (1980) 295.
[35] R.P. Hammond, M. Cavaluzzi, R.C. Haushalter, J.A. Zubieta, Inorg. Chem. 38 (1999) 1288.
[36] J.L. Song, J.G. Mao, H.Y. Zeng, Z.C. Dong, Eur. J. Inorg. Chem. (2004) 538.
[37] R.P. Shibaeva, V.F. Kaminskii, N.D. Kushch, A.V. Zvarykina, E.B. Yagubskii, Dokl. Akad. Nauk. SSSR 251 (1980) 162.
[38] M. Asplund, S. Jagner, Acta Chem. Scand., Ser. A A38 (1984) 135.
[39] A.J. Canty, L.M. Engelhardt, P.C. Healy, J.D. Kildea, N.J. Minchin, A.H. White, Aust. J. Chem. 40 (1987) 1881.
[40] S. Andersson, S. Jagner, Acta Chem. Scand., Ser. A A41 (1987) 230.
[41] H. Adams, G. Candeland, J.D. Crane, D.E. Fenton, A.J. Smith, Chem. Commun. (1990) 93.
[42] D.G. Lonnon, D.C. Craig, S.B. Colbran, Inorg. Chem. Commun. 5 (2002) 958.
[43] D.G. Lonnon, D.C. Craig, S.B. Colbran, P.V. Bernhardt, J. Chem. Soc., Dalton Trans. (2004) 778.
[44] X.F. Huang, Y.M. Song, X.S. Wang, J. Pang, J.L. Zuo, R.G. Xiong, J. Organomet. Chem. 691 (2006) 1065.
[45] B. Le Gall, F. Conan, N. Cosquer, J.-M. Kerbaol, M.M. Kubicki, E. Vigier, Y. Le Mest, J. Sala Pala, Inorg. Chim. Acta 324 (2001) 300.
[46] G. Kickelbick, T. Pintauer, K. Matyjaszewski, New J. Chem. 26 (2002) 462.
[47] M. Becker, F.W. Heinemann, S. Schindler, Chem. Eur. J. 5 (1999) 3124.
[48] M. Di Vaira, P.L. Orioli, Acta Crystallogr. B 24 (1968) 595.
[49] P. Werndrup, V.G. Kessler, J. Chem. Soc., Dalton Trans. (2001) 574.
[50] M. Doering, W. Ludwig, E. Uhlig, S. Wocadlo, U. Mueller, Z. Anorg. Allg. Chem. 611 (1992) 61.
[51] F.A. Cotton, R.C. Elder, Inorg. Chem. 5 (1966) 423.
[52] R.C. Elder, Inorg. Chem. 7 (1968) 1117.
[53] G.J. Bullen, Acta Crystallogr. 12 (1959) 703.
[54] J. Burgess, J. Fawcett, D.R. Russell, S.R. Gilani, Acta Crystallogr., Sect. C: Cryst. Struct. Commun. C56 (2000) 649.
[55] F.A. Cotton, R.C. Elder, Inorg. Chem. 4 (1965) 1145.
[56] M. Di Vaira, P. Orioli, Inorg. Chem. 6 (1967) 955.
[57] W. Kleber, H.-J. Bautsch, Einführung in die Kristallographie, Verl. Technik, Berlin, 1998.
[58] Y.C.M. Pennings, W.L. Driessen, J. Reedijk, Acta Crystallogr., Sect. C: Cryst. Struct. Commun. 44 (1988) 2095.
[59] D.W. Min, Y.K. Do, Chem. Lett. (1994) 1989.
[60] Y. Byun, D. Min, J. Do, H. Yun, Y. Do, Inorg. Chem. 35 (1996) 3981.
[61] D. Walther, K. Hamza, H. Gorls, W. Imhof, Z. Anorg. Allg. Chem. 623 (1997) 1135.
[62] M.A. Halcrow, C.A. Kilner, Acta Crystallogr., Sect. C: Cryst. Struct. Commun. 58 (2002) m424.
[63] M. Asplund, S. Jagner, M. Nilsson, Acta Chem. Scand., Ser. A 36 (1982) 751.
[64] M. Asplund, S. Jagner, Acta Chem. Scand., Ser. A 38 (1984) 297.
[65] M. Asplund, S. Jagner, Acta Chem., Scand. Ser. A 38 (1984) 411.
[66] A. Basu, S. Bhaduri, N.Y. Sapre, P.G. Jones, Chem. Commun. (1987) 1724.
[67] S. Bhaduri, N.Y. Sapre, P.G. Jones, J. Chem. Soc., Dalton Trans. (1991) 2539.
[68] G.Z. Hu, E.M. Holt, Acta Crystallogr. Sect., C: Cryst. Struct. Commun. 50 (1994) 1576.
[69] D.W. Allen, J.P.L. Mifflin, S. Coles, Chem. Commun. (1998) 2115.
[70] M.R. Pressprich, R.D. Willett, Acta Crystallogr., Sect. C: Cryst. Struct. Commun. C47 (1991) 1188.
[71] N.E. Kuz'mina, K.K. Palkina, E.V. Savinkina, D.A. Biryukov, I.A. Kozlova, Zh. Neorg. Khim. 46 (2001) 1324.
[72] G.J. Leigh, J.R. Sanders, P.B. Hitchcock, J.S. Fernandes, M. Togrou, Inorg. Chim. Acta 330 (2002) 197.
[73] G.M. Espallargas, L. Brammer, P. Sherwood, Angew. Chem., Int. Ed. Engl. 45 (2006) 435.
[74] M. Doring, H. Gorls, E. Uhlig, K. Brodersen, L. Dahlenburg, A. Wolski, Z. Anorg. Allg. Chem. 614 (1992) 65.
[75] S. Strandman, P. Pulkkinen, H. Tenhu, J. Polym. Sci., Polym. Chem. 43 (2005) 3349.
[76] L.H. Ulich, R. Adams, J. Am. Chem. Soc. 43 (1921) 660.
[77] S.H. Cho, G.D. Choi, G.H. Lee, Y.S. Yoon, (CJ Corp., S. Korea). Application: KR, 2002.
[78] P.K. Hon, C.E. Pfluger, J. Coord. Chem. 3 (1973) 67.
[79] G.J. Kruger, E.C. Reynhardt, Acta Crystallogr. B 30 (1974) 822.
[80] G.M. Sheldrick, SHELXS-97. Program for Crystal Structure solution, University of Göttingen, Göttingen, Germany, 1997.
[81] G.M. Sheldrick, SHELXL-97. Program for Crystal Structure refinement, University of Göttingen, Göttingen, Germany, 1997.
[82] H.D. Flack, G. Bernardinelli, Acta Crystallogr., Sect. A: Found. Cryst. 55 (pt.5) (1999) 908.

Polyhedron 27 (2008) 2186–2192

Contents lists available at ScienceDirect

Polyhedron

journal homepage: www.elsevier.com/locate/poly

Synthesis and characterization of new soluble phthalocyanines containing macrocycle units

Beytullah Ertem [a,*], Ahmet Bilgin [b], Halit Kantekin [a], Yaşar Gök [c]

[a] Department of Chemistry, Karadeniz Technical University, 61080 Trabzon, Turkey
[b] Department of Science Education, Kocaeli University, 41380 Kocaeli, Turkey
[c] Department of Chemistry, Pamukkale University, Kınıklı Campus, 20070 Kınıklı/Denizli, Turkey

ARTICLE INFO

Article history:
Received 23 January 2008
Accepted 12 March 2008
Available online 6 May 2008

Keywords:
Heterocrowns
Soluble phthalocyanines
Metallophthalocyanines
Extraction

ABSTRACT

A soluble metal-free phthalocyanine **5** and its metal complexes (Zn, Ni, Co and Cu) **6**, **7**, **8** and **9** containing eight 16-membered tetrathiamonoaza macrocycles on peripheral substituent positions have been synthesized. The metal-free phthalocyanine **5** was synthesized from 4,5-*bis*{[2-(1,4,10,13-tetrathia-7-azacyclohexadecan-7-yl)ethyl]oxy}phthalonitrile **4**. The metal complexes **6**, **7** and **8** were prepared by a tetramerization reaction of the phthalonitrile derivative **4** with appropriate materials. Copper(II) phthalocyanine **9** was prepared by the reaction of 4,5-*bis*{[2-(1,4,10,13-tetrathia-7-azacyclohexadecan-7-yl)ethyl]oxy}-1,2-dibromobenzene **3** with excess CuCN and dry quinoline. Liquid–liquid extraction of several heavy metal ions such as Ag^+, Hg^{2+}, Pb^{2+}, Cd^{2+}, Cu^{2+} and Zn^{2+} with compound **5** was also tested using picrate as the anion of the ion pair. The extraction avidity of **5** for Ag^+ was found to be highest in the liquid–liquid phase extraction experiments. The new compounds were characterized by a combination of elemental analysis, UV–Vis, FT-IR, NMR and mass spectral data.

© 2008 Elsevier Ltd. All rights reserved.

1. Introduction

Supramolecular materials can be designed and created from simple molecular building blocks by self-assembly and self-organization using non-covalent interactions [1]. Phthalocyanines [2] have been employed extensively as subunits for the construction of functional materials since they exhibit special optical and electronic properties and self-organizing abilities to form columnar mesophases, Langmuir–Blodgett (LB) multilayers and aggregates in solution, or in the solid state [3]. The main forces that drive these self-assembly processes are the π–π stacking interactions between the aromatic rings. The introduction of either or both long aliphatic hydrocarbon chains or/and macrocyclic substituents at the periphery of the rigid phthalocyanine core can improve the organization properties of these molecules by exploiting either their mesogenic behavior [4] or the ability of their macrocyclic subunits to form complexes with different ions [5,6]. By contrast, hydrogen-bonding interactions have hardly been employed at all to self-assemble phthalocyanine molecules [7].

The solubility and ion-binding ability of phthalocyanines containing homo- and hetero-crowns are receiving considerable attention in view of their effect on the aggregation of the molecules [5,6]. It has been demonstrated that phthalocyanines substituted with four 15-crown–5 analogs are capable forming ion channels that allow the migration of alkali or alkaline earth ions [8]. Phthalocyanines with long alkyl or alkoxy groups as well as with crown ethers are also reported to form a new type of liquid crystals, namely the discotic mesophase [9].

Alkyl substitution increases the solubility of phthalocyanines, and the effect of bulky substituents is shown to be higher than that of smaller ones, e.g. methyl [10]. Substitution of a phthalocyanine with eight ethoxy hetero-crown moieties, therefore, is expected to enhance the solubility and improve the intermolecular stacking. In this work we report the synthesis and properties of new heterocrowns and their phthalocyanines with eight ethoxy-tetrathiamonoaza macrocycles. In addition, the extraction capability of assorted heavy metal ions with the metal-free phthalocyanine **5** is tested.

2. Experimental

2.1. Materials

Starting reagents were either purchased from Aldrich or, unless noted otherwise, prepared in the manner described in previous papers. We prepared 1,7,10,14-tetrathia-4-azacyclohexadecane (**2**) [11] and 1,2-bis(2-iodoethoxy)-4,5-dibromobenzene (**1**) [12] using literature procedures. All reactions were performed under an argon atmosphere using standard Schlenk techniques. Pentan-1-ol was distilled from sodium. All other reagents and solvents were of

* Corresponding author. Tel.: +90 462 377 3651; fax: +90 462 325 3196.
E-mail address: bertem@ktu.edu.tr (B. Ertem).

0277-5387/$ - see front matter © 2008 Elsevier Ltd. All rights reserved.
doi:10.1016/j.poly.2008.03.017

reagent grade quality from commercial suppliers and were dried before use as described in the literature [13]. Silica gel (70–230 mesh) and Merck 90 active neutral alumina were used in the separation and purification of compounds by column chromatography with the indicated eluents.

2.2. Measurements

Melting points were determined with an electrothermal apparatus and were uncorrected. Routine ^{1}H, ^{13}C NMR and IR spectra were recorded on a Varian XL-200 spectrometer and a Perkin–Elmer Spectrum One spectrometer with the samples in KBr pellets, respectively. UV–Vis spectra were recorded on a model Shimadzu 1601 UV–Vis spectrometer using cells of 10 mm pathlength at room temperature. Mass spectra were measured on Micromass Quatro LC/ULTIMA LC–MS/MS spectrometers. The elemental analyses of the compounds were determined on a CHNS-932 LECO instrument. The metal contents of the metallophthalocyanine were determined with a Unicam 929 AA spectrophotometer in solutions prepared by decomposition of the metallophthalocyanines in conc. sulfuric acid and conc. nitric acid solution followed by digestion in conc. hydrochloric acid solution and deionized water.

2.3. Synthesis

2.3.1. Synthesis of 4,5-bis{[2-(1,4,10,13-tetrathia-7-azacyclohexadecan-7-yl)ethyl]oxy}-1,2-dibromobenzene (**3**)

Compound **2** (5.96 g, 20 mmol) was dissolved in 300 mL of dry acetonitrile containing anhydrous Cs_2CO_3 (9.78 g, 30 mmol) and anhydrous NaI (0.45 g, 3 mmol), and purged under an argon atmosphere in a 1000 mL three necked round-bottomed flask. Initially the mixture was stirred at 50 °C for 1 h and afterwards a solution of **1** (7.2 g, 12.5 mmol, 25% excess) in 100 mL of dry acetonitrile was added dropwise over a period of 3 h, at the same temperature. The reaction mixture was refluxed at 100 °C under argon for 6 days and monitored by TLC using [chloroform:petroleum ether:methanol (6:3:1)]. The reaction mixture was cooled to room temperature, filtered and the solvent was removed by evaporation. The residue was dissolved in 150 mL of dichloromethane and extracted with (2×10 mL) water. The combined organic extract was dried over $MgSO_4$ and then filtered and evaporated to dryness. The crude product was purified by column chromatography on silica gel [chloroform:petroleum ether:methanol (6:3:1)] to give the dibromo derivative **3**. Yield: 6.3 g (69%), m.p. = 238–240 °C. *Anal.* Calc. for $C_{32}H_{54}Br_2N_2O_2S_8$ (915.08): C, 42.00; H, 5.95; N, 3.06; S, 28.03. Found: C, 41.68; H, 6.61; N, 2.81; S, 28.26%. IR (KBr): υ_{max} (cm^{-1}) = 3056 (C–H aromatic), 2977–2870 (CH_2), 1592–1581 (aromatic C=C), 1498 (C–H), 1234 (Ar–O–C), 645 (C–Br). ^{1}H NMR (ppm, $CDCl_3$): δ = 6.84 (s, 2H, ArH), 4.14 (t, 4H, $ArOCH_2$), 3.06–2.92 (m, 12H, NCH_2), 2.85–2.74 (m, 32H, CH_2SCH_2), 2.07–1.93 (m, 4H, CH_2–C*H*$_2$–CH_2). ^{13}C NMR (ppm, $CDCl_3$): δ = 148.3 (ArCO), 120.1 (ArCH), 114.2 (ArC–Br), 71.2 ($ArOCH_2$), 54.3 (CH_2NCH_2), 50.2 (NCH_2CH_2O–Ar), 33.1–32.9 (–N–CH_2–*C*H$_2$–S–*C*H$_2$–), 31.5–31.1 (–S–CH_2–*C*H$_2$–S–*C*H$_2$–), 29.4 (CH_2–*C*H$_2$–CH_2). MS (ES positive) *m*/*z*: 915.1 $[M]^+$.

2.3.2. Synthesis of 4,5-bis{[2-(1,4,10,13-tetrathia-7-azacyclohexadecan-7-yl)ethyl]oxy}phthalonitrile (**4**)

Compound **3** (7.00 g, 7.65 mmol), CuCN (2.05 g, 23 mmol), 30 mL of dry DMF and three drops of pyridine were placed in a Schlenk tube under argon and gently heated, then subsequently heated to 165 °C. The reaction was monitored by TLC using chloroform: petroleum ether (7:3). The reaction mixture was kept at this temperature for 24 h, after which the solution was cooled to room temperature. After adding 200 mL of NH_3 (25%) into the reaction mixture, oxygen gas was passed through the solution for 48 h. Then it was washed with water until the filtrate was neutral, and dried *in vacuo*. The crude product was placed in a Soxhlet extractor and extracted with chloroform for 3 days. The extract was evaporated to dryness under reduced pressure and dissolved in 25 mL of dry methanol and then placed inside the refrigerator at −18 °C for several hours. Light brown crystals were filtered off and dried *in vacuo*. Yield: 2.72 g (44%), m.p. = 226–227 °C. *Anal.* Calc. $C_{34}H_{54}N_4O_2S_8$ (807.31): C, 50.58; H, 6.74; N, 6.94; S, 31.77; Found: C, 50.93; H, 6.41; N, 7.23; S, 31.60%. IR (KBr): υ_{max} (cm^{-1}) = 3049 (C–H aromatic), 2920–2849 (CH_2), 2234 (C≡N), 1596–1506 (aromatic C=C), 1255 (Ar–O–C), 1100, 960, 750, 685. ^{1}H NMR (ppm, $CDCl_3$): δ = 7.78 (s, 2H, ArH), 4.25 (t, 4H, $ArOCH_2$), 3.14–2.87 (m, 12H, NCH_2), 2.82–2.78 (m, 32H, CH_2SCH_2), 2.10–1.96 (m, 4H, CH_2–C*H*$_2$–CH_2). ^{13}C NMR (ppm, $CDCl_3$): δ = 151.8 (ArCO), 118.4 (ArCH), 114.9 (C≡N), 109.6 (ArC), 71.9 ($ArOCH_2$), 53.6 (CH_2NCH_2), 51.4 (NCH_2CH_2O–Ar), 32.7–32.4 (–N–CH_2–*C*H$_2$–S–*C*H$_2$–), 31.3–30.9 (–S–CH_2–*C*H$_2$–S–*C*H$_2$–), 28.7 (CH_2–*C*H$_2$–CH_2). MS (ES positive) *m*/*z*: 807.4 $[M]^+$.

2.3.3. Synthesis of the metal-free phthalocyanine (**5**)

Compound **4** (1.91 g, 2.37 mmol), 2.5 mL of dry pentan-1-ol and 3–5 drops of 1,8-diazabicyclo[5.4.0]undec-7-ene (DBU) were placed in a Schlenk tube under an argon atmosphere. The reaction mixture was heated gently to 90 °C for 1 h and then it was heated and stirred at 150 °C for 24 h. After cooling to room temperature, 10 mL of methanol/diethyl ether (1:1, v/v) was added and stirred for 45 min. The dark green metal-free phthalocyanine derivative was filtered off, washed with diethyl ether and dried *in vacuo*. Yield: 0.936 g (49%), m.p. > 300 °C. *Anal.* Calc. $C_{136}H_{218}N_{16}O_8S_{32}$ (3231.25): C, 50.55; H, 6.80; N, 6.94; S, 31.75. Found: C, 50.87; H, 6.47; N, 6.65; S, 31.98%. IR (KBr): υ_{max} (cm^{-1}) = 3394 (N–H), 3066 (Ar–H), 2917–2849 (CH_2), 1634 (C=N), 1595–1569 (C=C), 1268, 1250 (Ar–O), 1030 (N–H), 960, 853, 757, 687. ^{1}H NMR (ppm, DMSO-d_6): δ = 8.17 (s, 8H, ArH), 4.10 (t, 16H, $ArOCH_2$), 3.02–2.93 (m, 48H, NCH_2), 2.90–2.69 (m, 128H, CH_2SCH_2), 1.98–1.67 (m, 16H, CH_2–C*H*$_2$–CH_2), −3.96 (br, 2H, N–H). ^{13}C NMR (ppm, DMSO-d_6): δ = 152.4 (C=N), 150.3 (ArCO), 119.1 (ArCH), 106.8 (ArC), 70.3 ($ArOCH_2$), 52.3 (CH_2NCH_2), 50.8 (NCH_2CH_2O–Ar), 32.3–31.9 (–N–CH_2–*C*H$_2$–S–*C*H$_2$–), 30.7–30.4 (–S–CH_2–*C*H$_2$–S–*C*H$_2$–), 28.2 (CH_2–*C*H$_2$–CH_2). UV/Vis ($CHCl_3$) λ_{max} ($\log\varepsilon$) = 712 (4.82), 672 (4.70), 649 (4.45), 611 (3.78), 369 (4.63), 332 (4.75). MS (ES positive) *m*/*z*: 3231.4 $[M]^+$.

2.3.4. Synthesis of phthalocyaninato zinc(II) (**6**)

Compound **4** (0.81 g, 1 mmol), $Zn(OAc)_2 \cdot 2H_2O$ (55 mg, 0.25 mmol) and 1.5 mL of dry quinoline were placed into a well-stoppered Schlenk tube under an argon atmosphere. The reaction mixture was heated at 210 °C for 8 h. After cooling to room temperature, the dark green reaction mixture was diluted and the product was precipitated by adding 10 mL of ethanol. The resulting green precipitate was filtered off, washed with EtOH, H_2O and diethyl ether separately and dried *in vacuo*. Yield: 0.512 g (62%), m.p. > 300 °C. *Anal.* Calc. $C_{136}H_{216}N_{16}O_8S_{32}Zn$ (3294.61): C, 49.58; H, 6.61; N, 6.80; S, 31.15; Zn, 1.98. Found C, 49.89; H, 6.33; N, 6.51; S, 31.77; Zn, 1.72%. IR (KBr): υ_{max} (cm^{-1}) = 3032 (Ar–H), 2925–2857 (CH_2), 1618 (C=N), 1596–1555 (C=C), 1445 (C–H), 1380, 1224–1201 (Ar–O–C), 1121, 1048–1017 (CH_2–O), 946, 658. ^{1}H NMR (ppm, DMSO-d_6): δ = 7.97 (s, 8H, ArH), 4.16 (t, 16H, Ar-OCH_2), 3.15–2.89 (m, 48H, NCH_2), 2.86–2.68 (m, 128H, CH_2SCH_2), 2.06–1.73 (m, 16H, $CH_2CH_2CH_2$). UV/Vis (pyridine) λ_{max} ($\log\varepsilon$) = 694 (4.66), 652 (4.28), 624 (4.03), 366 (4.57), 325 (4.67), 292 (4.75). MS (ES positive) *m*/*z*: 3295.8 $[M+1]^+$.

2.3.5. Synthesis of phthalocyaninato nickel(II) (**7**)

A mixture of compound **4** (0.81 g, 1 mmol), $Ni(OAc)_2 \cdot 4H_2O$ (75 mg, 0.30 mmol) and DBU (152 mg, 1 mmol) was refluxed under

an argon atmosphere in pentan-1-ol (20 mL) for 24 h. The cooled suspension was poured into MeOH (60 mL) and the precipitate was centrifuged, washed with EtOAc, EtOH, H_2O and diethyl ether, and dried *in vacuo*. Further purification was carried out using column chromatography, silica gel, $CHCl_3$/MeOH, (9:1 v/v). Yield: 0.60 g (73%), m.p. > 300 °C. *Anal.* Calc. for $C_{136}H_{216}N_{16}O_8S_{32}Ni$ (3282.74): C, 49.68; H, 6.62; N, 6.82; S, 31.20; Ni, 1.79. Found: C, 49.87; H, 6.45; N, 6.58; S, 31.49; Ni, 1.93%. IR (KBr): υ_{max} (cm^{-1}) = 3045 (Ar–H), 2960–2870 (CH_2), 1624 (C=N), 1598–1560 (C=C), 1450 (C–H), 1374, 1220–1205 (Ar–O–C), 1100–1030 (CH_2–O), 958, 662. ^1H NMR (ppm, DMSO-d_6): δ = 7.93 (s, 8H, ArH), 4.10 (t, 16H, $ArOCH_2$), 3.20–2.93 (m, 48H, NCH_2), 2.82–2.64 (m, 128H, CH_2SCH_2), 2.03–1.78 (m, 16 H, $CH_2CH_2CH_2$). UV/Vis (pyridine) λ_{max} ($\log\varepsilon$)=695 (4.77), 640 (4.02), 606 (3.88), 369 (4.41), 322 (4.84). MS (ES positive) *m*/*z*: 3284.1 $[M+1]^+$.

2.3.6. Synthesis of phthalocyaninato cobalt(II) (**8**)

A mixture of compound **4** (0.81 g, 1 mmol), urea (105.6 mg, 1.76 mmol), $Co(OAc)_2 \cdot 4H_2O$ (75 mg, 0.30 mmol), a catalytic amount of $(NH_4)_2MoO_4$ (40 mg) and quinoline (2 mL) was kept at 200–210 °C under an argon atmosphere for 6 h. The cooled mixture was poured into CH_3CN (40 mL) and the precipitate was filtered off after 1 h of stirring. The crude product was washed sequentially with EtOAc, EtOH, H_2O and acetone, and dried *in vacuo*. The cobalt(II) phthalocyanine was purified by column chromatography, neutral alumina, $CHCl_3$/MeOH, (100:1 v/v). Yield: 0.39 g (47%), m.p. > 300 °C. *Anal.* Calc. for $C_{136}H_{216}N_{16}O_8S_{32}Co$ (3288.17): C, 49.68; H, 6.62; N, 6.82; S, 31.20; Co, 1.79. Found: C, 49.46; H, 6.79; N, 7.07; S, 31.46; Co, 1.58%. IR (KBr): υ_{max} (cm^{-1}) = 3050 (Ar–H), 2975–2889 (CH_2), 1625 (C=N), 1600–1575 (C=C), 1440 (C–H), 1365, 1234–1228 (Ar–O–C), 1120–1025 (CH_2–O), 950, 656. ^1H NMR (ppm, DMSO-d_6): δ = 7.96 (s, 8H, ArH), 4.12 (t, 16H, $ArOCH_2$), 3.15–2.90 (m, 48H, NCH_2), 2.87–2.69 (m, 128H, CH_2SCH_2), 2.09–1.82 (m, 16 H, $CH_2CH_2CH_2$). UV/Vis (pyridine) λ_{max} ($\log\varepsilon$) = 692 (4.66), 645 (3.93), 607 (3.86), 372 (4.62), 313 (4.80). MS (ES positive) *m*/*z*: 3289.1 $[M+1]^+$, 3288.2 $[M]^+$.

2.3.7. Synthesis of phthalocyaninato copper(II) (**9**)

A mixture of **3** (0.915 g, 1 mmol), CuCN (0.269 g, 3 mmol) and dry quinoline (2.5 mL) was heated under argon at 215 °C for 24 h. At the end of this period, the mixture was cooled to room temperature and 30 mL of ethanol was added to this mixture, and filtered, washed with ethanol and diethyl ether to remove any unreacted organic residue. The crude product was heated and stirred with a solution of 0.5 M NaCN in a mixture of 75 mL of water:ethanol (1:3) for 3 h and filtered off, then washed with hot water, ethanol and diethyl ether. The dark green solid was chromatographed on neutral alumina using chloroform:methanol (100:1) as the eluent. The extract was evaporated to dryness and dried *in vacuo*. Yield: 0.272 g (33%), m.p. > 300 °C. *Anal.* Calc. $C_{136}H_{216}N_{16}O_8S_{32}Cu$ (3292.78): C, 49.61; H, 6.61; N, 6.81; S, 31.16; Cu, 1.93. Found: C, 49.28; H, 6.35; N, 7.08; S, 31.70; Cu, 1.69%. IR (KBr): υ_{max} (cm^{-1}) = 3043 (Ar–H), 2923–2850 (CH_2), 1620 (C=N), 1590–1502 (C=C), 1425 (C–H), 1357, 1293 (Ar–O–C), 1122 (C–O–C), 960, 645. UV/Vis (pyridine) λ_{max} ($\log\varepsilon$) = 687 (4.73), 642 (4.06), 611 (3.93), 364 (4.59), 315 (4.75). MS (ES positive) *m*/*z*: 3293.9 $[M+1]^+$.

2.3.8. Measurement of the heavy metal-binding properties of (5)

The extraction properties of **5** were investigated under liquid–liquid phase and neutral conditions using heavy metal picrates (Ag^+, Hg^{2+}, Pb^{2+}, Cd^{2+}, Cu^{2+}, Zn^{2+}) as substrates and measuring by UV–Vis spectra the amounts of metal picrate in the aqueous phase before and after treatment with compound **5**. The heavy metal picrates were prepared from a mixture of the metal nitrates and picric acid in deionized water. We also prepared 2×10^{-3} M solutions of compound **5** in chloroform. Then equal volumes of both the metal picrate solutions and compound solution were added into plastic bottles, closed and then mechanically shaken for 5 h by a shaker at 25 ± 1 °C. Finally we took the aqueous phase and measured the absorbance at the maximum wavelength of each metal picrate solution. For each combination of host and metal picrate, the picrate extraction was conducted on three different samples and the average value of percent picrate extracted, with a standard deviation, was calculated. The picrate extraction results are presented in Table 1. In the absence of host, a blank experiment, no metal ion picrate extraction was detected. The extractability was determined based on the absorbance of the picrate ion in the aqueous solutions. The extractability was calculated by using the equation below:

$$E(\%) = [(A_{before} - A_{after})/A_{before}] \times 100$$

where A_{before} is the absorbance in the absence of ligand and A_{after} denotes the absorbance in the aqueous solution phase after extraction.

Table 1
Heavy metal picrate extractions from aqueous solutions into chloroform by using **5**[a]

Metal ion	Extractability of the metal-free phthalocyanine **5** (%)[b]	λ_{max} (nm) of metal picrate
Ag^+	93.2 ± 0.1	354
Hg^{2+}	64.7 ± 0.1	358
Pb^{2+}	48.4 ± 0.1	360
Cd^{2+}	70.5 ± 0.1	362
Cu^{2+}	43.6 ± 0.1	352
Zn^{2+}	37.3 ± 0.1	347

[a] Temperature 25 ± 1 °C; aqueous phase (10 mL), [picrate] = 2.0×10^{-3} M; organic phase (chloroform, 10 mL), [extractant] = 2.0×10^{-3} M.
[b] Average and standard deviation for three independent measurements.

3. Result and discussion

The synthetic routes to **3**–**9** are exhibited in Schemes 1 and 2. We report here the synthesis and structural properties of a series of novel metal-free and metallophthalocyanines. The dibromo derivative **3** was obtained by a substitution reaction of compound **2** and 1,2-bis(2-iodoethoxy)-4,5-dibromobenzene **1** in the presence of anhydrous Cs_2CO_3 and anhydrous NaI in dry acetonitrile at reflux temperature for 6 days under argon. The crude product was purified by column chromatography on silica gel, chloroform:petroleum ether:methanol (6:3:1) to give **3** in 69% yield. In the ^1H NMR spectrum of **3**, the signals corresponding to the N–H protons in the precursor compound **2** disappeared after the macrocyclization reaction. The resonance peaks are in good agreement with the proposed structure in the ^1H NMR spectrum of **3**, being at δ = 4.14, 3.06–2.92 and 2.85–2.74 ppm corresponding to Ar–O–CH_2, N–CH_2 and CH_2–S–CH_2 groups respectively. In the ^{13}C NMR spectrum, the existence of new carbon resonances at δ = 148.3, 120.1 and 114.2 ppm are also in good accord with the proposed structure. Further, the infrared data of **3** give sufficient support for the desired product formation. In the IR spectrum of compound **3**, the presence of characteristic vibrations belonging to (=CH aromatic ring), (aliphatic CH_2) and (C–Br) were observed at 3056, 2977–2870 and 645 cm^{-1}, respectively. The LC/ES mass spectrum of **3**, which shows a molecular ion peak at *m*/*z* = 915.1 $[M]^+$, confirms the proposed formula.

Substitution of the bromo groups in **3** by cyanide in a Rosenmund-von Braun reaction using three equivalents of CuCN [14], affords the corresponding phthalonitrile **4** in 44% yield after purification by column chromatography on silica gel with chloroform:petroleum ether: (7:3) solvent mixture. The critical point in this route is to isolate the dicyano derivative, which was

accomplished by keeping the concentration of the reactants sufficiently low and by making use of a moderately high boiling point solvent to avoid the formation of copper phthalocyanine [15]. In the IR spectrum of **3**, the signal at 645 cm^{-1} that was for the C–Br bond vanished and a new peak arose in the IR spectrum of **4** at 2234 cm^{-1}, which was attributed to the dicyano groups. The rest of the spectrum is closely similar to that of the precursor dibromo derivative, including the characteristic vibrations of **3**. The ^1H NMR spectrum of **4** was recorded after dissolution in $CDCl_3$ at room temperature, and exhibited the expected signals indicating the integrity of **4** in that solvent. The spectrum was almost identical with that of **3**, as expected. In the proton-decoupled ^{13}C NMR spectrum of compound **4**, the presence

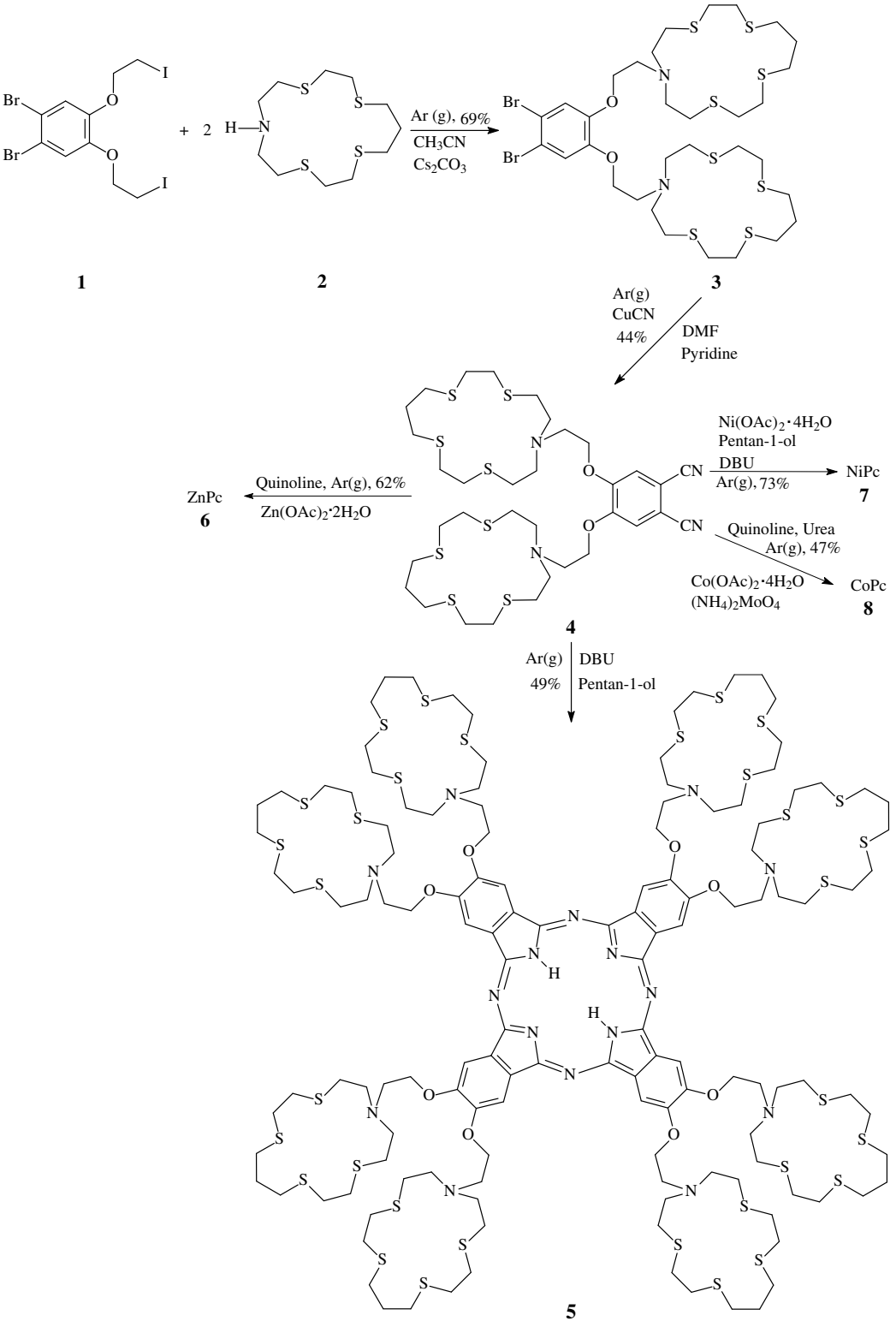

Scheme 1. Synthesis of metal-free and metallo (Zn, Ni, Co) phthalocyanines.

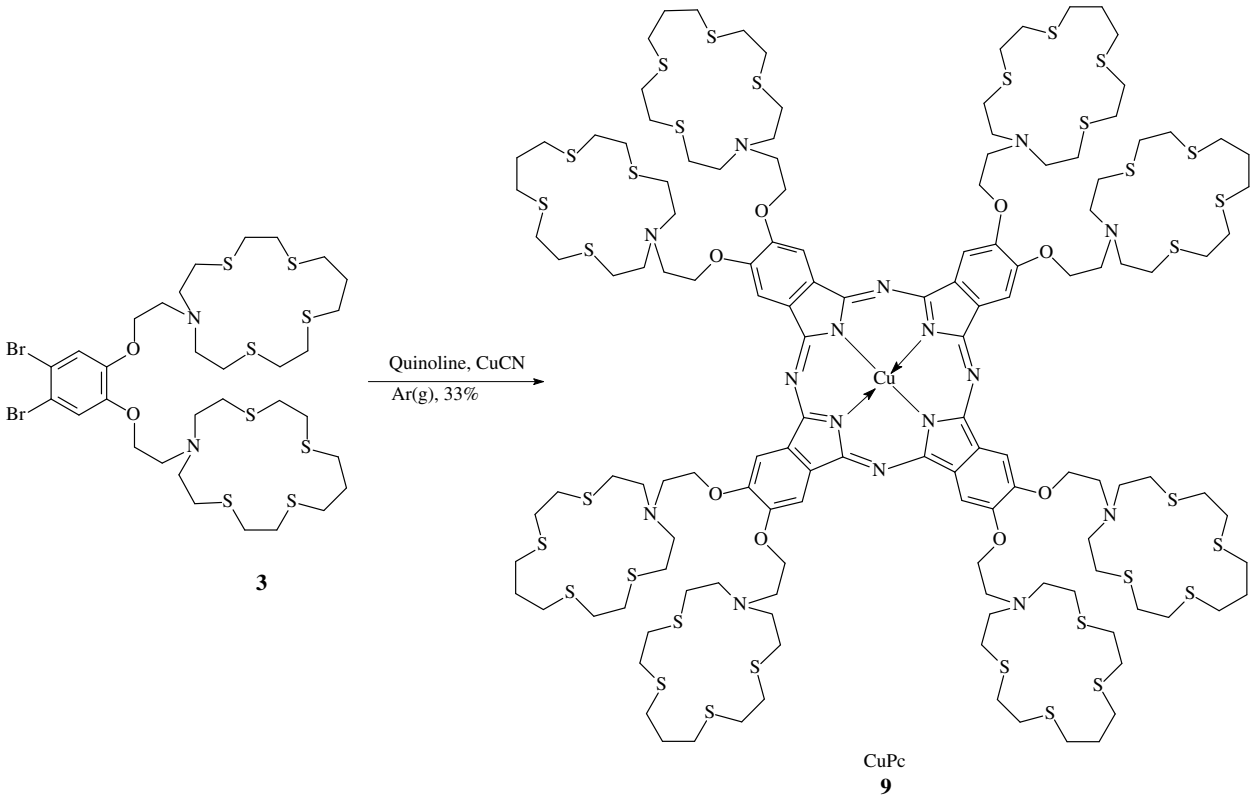

Scheme 2. Synthesis of copper phthalocyanine.

of a signal at δ = 114.9 ppm, attributable to C≡N groups, indicates that the conversion has occurred. Compound **4** displayed the expected molecular ion peak in its mass spectrum at m/z = 807.4 $[M]^+$.

The self-condensation of the dicyano compound **4** in a high-boiling solvent, such as dry pentan-1-ol, in the presence of a few drops of 1,8-diazabicyclo[5.4.0]undec-7-ene (DBU) as a strong base at reflux temperature under a dry argon atmosphere afforded the metal-free phthalocyanine **5** in 49% yield as a dark green solid. A diagnostic feature of the formation of **5** from **4** is the disappearance of the sharp vibration of the dicyano groups at 2234 cm^{-1} of the reactant. The stretching vibrations at 3394 cm^{-1} for **5** can be attributed to the N–H bond of the inner core of the metal-free phthalocyanine. A ^1H NMR investigation of compound **5** provided the characteristic chemical shifts for the expected structure. The inner core protons of compound **5** could also be observed at δ = - 3.96 ppm as a broad signal. In the ^{13}C NMR spectrum of this compound, all the signals are identical to those of the precursor dicyano derivative **4** except for the dicyano carbon atoms. The peak related to C≡N groups in the ^{13}C NMR spectrum of **4** vanished in the case of the metal-free phthalocyanine **5**. Other peaks in the ^{13}C NMR spectrum resembled those of the precursor compound **4**. The molecular ion of **5** was observed at m/z = 3231.4 $[M]^+$ and was in accord with the suggested structure.

Metallophthalocyanines **6**, **7** and **8** have been prepared from the dicyano derivative **4** and the appropriate metal salts in the required solvents and catalysts under an argon atmosphere in yields of 62%, 73% and 47%, respectively. A comparison of the IR spectra obtained for **4** and **6**, **7** and **8** confirmed the conversion of the C≡N groups into the characteristic skeleton of phthalocyanine. In this case, the C≡N band at 2234 cm^{-1} of compound **4** disappeared and C=N stretching vibrations of the inner core of the metallophthalocyanines **6**, **7** and **8** appeared at 1618, 1624, 1625 cm^{-1}, respectively. In the ^{13}C NMR spectrum of compound **4**, the presence of a signal at δ = 114.9 ppm, attributable to the C≡N groups, vanished in the case of complexes **6**, **7** and **8**. The ^{13}C NMR and ^1H NMR spectra of **6**, **7** and **8** were almost identical with that of the metal-free phthalocyanine **5**. The elemental analyses and LC/ES mass spectral data of all the metallophthalocyanines (**6**–**8**) were consistent with the proposed structures. The molecular ion clusters $[M+1]^+$ for metallophthalocyanines **6**, **7** and **8**, at 3295.8, 3284.1, and 3289.1, respectively, were found by the ES/MS technique, together with some reasonable fragment ions.

Copper(II) phthalocyanine **9** has been synthesized directly from the dibromo derivative **3** and CuCN in a high boiling solvent such as quinoline. The crude product was washed several times with ethanol to remove the unreacted starting material and was subsequently treated with a solution of NaCN to separate the excess CuCN. The yield of the crude product was only moderate (33%), and the purification steps were tedious and required a final chromatography on neutral alumina using chloroform:methanol (100:1) as the eluent. A comparison of the IR spectra obtained on **3** and **9** confirmed the conversion of the bromo groups into the characteristic skeleton of phthalocyanine. In this case, the C–Br band at 645 cm^{-1} disappeared and C=N stretching vibrations at 1620 cm^{-1} appeared. The mass spectrum of **9** was measured by the LC/ES MS technique and the complex displayed a peak corresponding to $[M+1]^+$ at m/z = 3293.9. Elemental analysis data were also in good accord with the proposed formula.

The electronic absorption spectrum of the metal-free phthalocyanine **5** in chloroform at room temperature is shown in Fig. 1. It displayed a split Q-band as expected and there are two strong bands in the Soret region [16]. The split Q-band, characteristic of metal-free phthalocyanines, is observed for **5** at λ_{max} = 712 and 672 nm with a shoulder at 649 nm, indicating monomeric species; monomeric species with D_{2h} symmetry shows two intense absorptions at around 700 nm [17]. Such split Q-band absorptions in

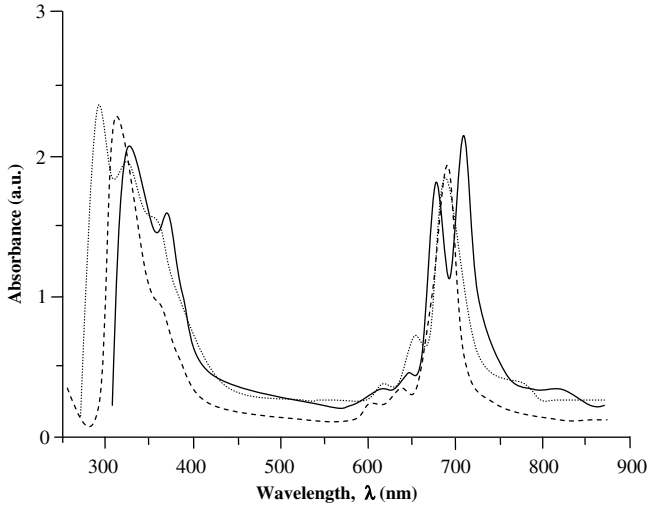

Fig. 1. Electronic absorption spectra of **5** (—) (3.50×10^{-5} M) in $CHCl_3$, **6** (···) (3.50×10^{-5} M) and **7** (---) (3.50×10^{-5} M) in pyridine.

chloroform are due to the $\pi \rightarrow \pi^*$ transition of this fully conjugated 18 π electron system [17d,18]. The zinc(II) **6**, nickel(II) **7**, cobalt(II) **8** and copper(II) **9** phthalocyanine complexes showed the expected absorptions (Figs. 1 and 2), with the main peaks of the Q- and B-bands appearing at λ_{max} = 694, 695, 692, 687 nm and 292, 322, 313, 315 nm, respectively. This result is typical of metal complexes of substituted and unsubstituted metallophthalocyanines with D_{4h} symmetry [5b,10], where a single band of high intensity in the visible region is observed. Upon dilution (*ca.* 3.5×10^{-5} M) the absorption spectra of these compounds displayed significant changes in band positions and molar absorptivities [19]. Increasing the concentration (1×10^{-4} M to 3.5×10^{-5} M) led to aggregation, which is easily monitored by the position of the Q-band, which shifted to shorter wavelengths and showed a decrease in the molar absorption coefficient.

3.1. Solvent extraction of heavy metal cations

Polythioether crowns are well-known to bind soft cations [20] while oxygen-containing crowns are ideally suited for the ligation of hard cations [21]. The heavy metal ion-binding property of compound **5**, having tetrathia-monoaza-16-crown-5 units, was estimated by solvent extraction of heavy metal picrates from the aqueous to an organic phase (Table 1). As can be seen in Table 1, the highest extraction avidity of **5** was determined as 93.2% for Ag^+. As expected, the obtained extraction values for Ag^+, Cd^{2+}, Hg^{2+} and Pb^{2+} were high. This is because sulfur containing ligands are especially appropriate for complexation with heavy metal cations such as Ag^+, Cd^{2+} and Hg^{2+} due to the softness of sulfur [20] and the size match between the cation and host cavity [22]. On the other hand, the metal-free phthalocyanine core has to be taken into consideration for the extraction process. There are many articles on the metal extraction properties of metal-free phthalocyanines [23] and the highest extraction affinity was determined for Ag^+. Although the extraction studies were not conducted under the same conditions, the extraction avidity of **5** in the case of Ag^+, Cd^{2+} and Hg^{2+} cations are somewhat higher than those of previously studied polymeric phthalocyanines which have acyclic polythio ether moieties [24]. The higher extraction avidity might be due to the macrocyclic effect. In the case of Cu(II) and Zn(II), the size of the 16-membered macrocyclic cavity of **5** is too large to accommodate the metal ion, which leads to the poorer extraction of these metals with this reagent.

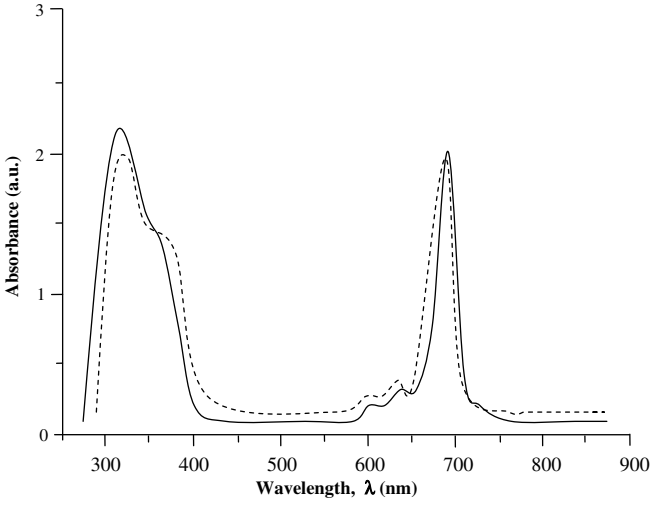

Fig. 2. Electronic absorption spectra of **8** (—) (3.50×10^{-5} M) and **9** (---) (3.50×10^{-5} M) in pyridine.

4. Conclusion

In this work, we describe the synthetic procedure and characterization of new soluble phthalocyanines substituted with eight tetrathiamonoaza macrocycles through ethoxy bridges. In addition, the heavy metal cation-binding property of **5** was evaluated using a solvent extraction technique and compared to our earlier works. The extractants from our earlier works in the case of Ag^+, Cd^{2+} and Hg^{2+} cations have lower cation-binding capacities than that in this work. Picrate was used as the counter anion. The cation-binding avidity of **5** for Ag^+, amongst the heavy metals, was found to be the highest.

Acknowledgements

Financial support from The Scientific & Technical Research Council of Turkey (TUBITAK), Project Number: TBAG-2453(104T065) (Ankara, Turkey) and the Research Fund of Karadeniz Technical University, Project Number: 2002.111.2.8 (Trabzon/Turkey) is gratefully acknowledged.

References

[1] (a) J.-M. Lehn, Supramolecular Chemistry, VCH, Weinheim, 1995;
(b) M.C.T. Fyfe, J.F. Stoddart, Acc. Chem. Res. 30 (1997) 393;
(c) J. Simon, J.-J. André, A. Skoulios, Nouv. J. Chim. 10 (1986) 295;
(d) J. Sly, P. Kasák, E.G. Nadal, C. Rovira, L. Górriz, P. Thordarson, D.B. Amabilino, A.E. Rowan, R.J.M. Nolte, J. Chem. Soc., Chem. Commun. (2005) 1255.
[2] (a) K.M. Kadish, K.M. Smith, R. Guilard (Eds.), The Porphyrin Handbook, vols. 15–20, Academic Press, New York, 2003;
(b) C.C. Leznoff, A.B.P. Lever (Eds.), Phthalocyanines: Properties and Applications, vols. 1–4, VCH Publishers Inc., New York, 1989–1996.
[3] (a) C.F. van Nostrum, Adv. Mater. 8 (1996) 1027;
(b) J.A.A.W. Elemans, R. van Hameren, R.J.M. Nolte, A.E. Rowan, Adv. Mater. 18 (2006) 1251.
[4] (a) C. Piechocki, J. Simon, A. Skoulios, D. Guillon, P. Weber, J. Am. Chem. Soc. 104 (1982) 5245;
(b) R.J.M. Nolte, Liq. Crystallogr. 33 (2006) 1373;
(c) J.F. van der Pol, E. Neeleman, J.W. Zwikker, R.J.M. Nolte, W. Drenth, J. Aerts, R. Visser, S.J. Picken, Liq. Crystallogr. 33 (2006) 1378;
(d) M. Durmuş, S. Yeşilot, V. Ahsen, New J. Chem. 30 (2006) 675.
[5] (a) V. Ahsen, E. Yılmazer, M. Ertaş, Ö. Bekâroğlu, J. Chem. Soc., Dalton Trans. (1988) 401;
(b) O.E. Sielcken, M.M. van Tilborg, M.F.M. Roks, R. Hendriks, W. Drenth, R.J.M. Nolte, J. Am. Chem. Soc. 109 (1987) 4261.
[6] (a) S. Sarıgül, Ö. Bekâroğlu, Chem. Ber. 122 (1989) 291;
(b) T. Topuance, V. Ahsen, J. Simon, J. Am. Chem. Soc. 116 (1994) 5352;
(c) N. Kobayashi, M. Togashi, T. Osa, K. Ishii, S. Yamauchi, H. Hino, J. Am. Chem. Soc. 118 (1996) 1073;
(d) A. Bilgin, Ç. Yağcı, A. Mendi, U. Yıldız, Polyhedron 26 (2007) 617.

[7] J.A. Duro, G. de la Torre, T. Torres, Tetrahedron Lett. 36 (1995) 8079.
[8] C. Sirlin, L. Bosio, J. Simon, V. Ahsen, E. Yılmazer, Ö. Bekâroğlu, Chem. Phys. Lett. 139 (1987) 362.
[9] (a) M. Hanack, A. Beck, H. Lehmann, Synthesis (1987) 703;
(b) C.F. van Nostrum, R.J.M. Nolte, J. Chem. Soc., Chem. Commun. (1996) 2365.
[10] (a) A. Bilgin, B. Ertem, Y. Gök, Eur. J. Inorg. Chem. (2007) 1703;
(b) E.A. Cuellar, T.J. Marks, Inorg. Chem. 20 (1981) 3766.
[11] L.G.A. van de Water, F. ten Hoonte, W.L. Driessen, J. Reedijk, D.C. Sherrington, Inorg. Chim. Acta 303 (2000) 77.
[12] S.Z. Yıldız, Y. Gök, New J. Chem. 22 (1998) 1365.
[13] D.D. Perin, W.L.F. Armarego, Purification of Laboratory Chemicals, 2nd ed., Pergamon Press, Oxford, 1989.
[14] G. Ellis, T. Romney-Alexander, Chem. Rev. 87 (1987) 779.
[15] M. Hanack, J. Metz, G. Pawlowski, Chem. Ber. 115 (1982) 2836.
[16] K. Kasuga, T. Idehara, M. Handa, K. Isa, Inorg. Chim. Acta 196 (1992) 127.
[17] (a) N. Kobayashi, A.B.P. Lever, J. Am. Chem. Soc. 109 (1987) 7433;
(b) J.C. Swarts, E.H.G. Langner, N. Krokeide-Hove, M.J. Cook, J. Mater. Chem. 11 (2001) 434;
(c) A.W. Snow, J.S. Shirk, R.G.S. Pong, J. Porphyrins Phthalocyanines 4 (2000) 518;
(d) A.G. Gürek, Ö. Bekâroğlu, J. Chem. Soc., Dalton Trans. (1994) 1419.
[18] W. Kroenke, M.E. Kenney, Inorg. Chem. 6 (1964) 1587.
[19] Y. Gök, H. Kantekin, A. Bilgin, D. Mendil, İ. Değirmencioğlu, J. Chem. Soc., Chem. Commun. (2001) 285.
[20] (a) K. Saito, Y. Masuda, E. Sekido, Anal. Chim. Acta. 151 (1984) 447;
(b) A.J. Blake, M. Schröder, Adv. Inorg. Chem. 35 (1990) 1;
(c) S.R. Cooper, S.C. Rawle, Crown Thioether Chemistry; Structure and Bonding, vol. 72, Springer-Verlag, Berlin, 1990. p. 1;
(d) I. Vujasinovic, J. Veljkovic, K.M. Maerski, J. Org. Chem. 69 (2004) 8550.
[21] L.F. Lindoy, The Chemistry of Macrocyclic Ligand Complexes, Cambridge University Press, Cambridge, U.K., 1989. p. 90.
[22] J.W. Steed, J.L. Atwood, Supramolecular Chemistry, Wiley, Chichester, 2000.
[23] Y.A. Zolotov, Macrocyclic Compounds in Analytic Chemistry, John Wiley & Sons Inc., New York, 1997. p. 149.
[24] (a) A. Bilgin, Ç. Yağcı, U. Yıldız, Macromol. Chem. Phys. 206 (2005) 2257;
(b) A. Bilgin, A. Mendi, U. Yıldız, Polymer 26 (2006) 8462.

Polyhedron 27 (2008) 2193–2201

Contents lists available at ScienceDirect

Polyhedron

journal homepage: www.elsevier.com/locate/poly

Synthesis, structure and solution chemistry of a family of dinuclear hydrazonato-vanadium(V) complexes with $[OV(\mu\text{-}O)VO]^{4+}$ core

Bipul Mondal [a], Tarun Ghosh [a], Manas Sutradhar [b], Gurunath Mukherjee [b], Michael G.B. Drew [c], Tapas Ghosh [a,*]

[a] Department of Chemistry, Ramakrishna Mission Vivekananda Centenary College, Rahara, Kolkata 700 118, India
[b] Department of Chemistry, University College of Science, 92, Acharya Prafulla Chandra Road, Kolkata 700 009, India
[c] Department of Chemistry, The University of Reading, P.O. Box 224, Whiteknights, Reading RG6 6AD, UK

ARTICLE INFO

Article history:
Received 4 March 2008
Accepted 25 March 2008
Available online 6 May 2008

Keywords:
Oxo-bridged oxovanadium(V) complexes
Dioxovanadium(V) complexes
Hydrazone complexes
Crystal structure
Solution chemistry
Hammett plots

ABSTRACT

Dinuclear trioxidic $[\{VOL\}_2\mu\text{-}O]$ (**1**–**4**) complexes were synthesized from the reaction of $[V^{IV}O(acac)_2]$ with an equimolar amount of H_2L [H_2L is the general abbreviation of hydrazone ligands (H_2L^{1-4}) derived from the condensation of benzoyl hydrazine with either 2-hydroxyacetophenone or its *para* substituted derivatives] in acetone or CH_2Cl_2 or acetonitrile. These $V_2O_3L_2$ complexes were also obtained from the reaction of $VOSO_4$ with H_2L in the presence of two equivalents sodium acetate in aqueous-methanolic (50% V/V) medium and also from the decomposition of $[V^{IV}O(L)(bipy/phen)]$ complexes in CH_2Cl_2 solution. Black monoclinic crystals of **2** and **4** with *C*2/*c* space group were obtained from the reaction of $[V^{IV}O(acac)_2]$, respectively, with H_2L^2 and H_2L^4 in acetone in which the respective ligands are bonded meridionally to vanadium in their fully deprotonated enol forms. The V–O bond lengths follow the order: V–O(oxo) < V–O(oxo-bridged) < V–O(phenolate) < V–O(enolate). Complexes (**1**–**4**) are diamagnetic exhibiting LMCT transition band near 380 nm in CH_2Cl_2 solution and they are electroactive displaying a quasi-reversible reduction peak in the 0.14–0.30 V *versus* SCE region. The λ_{max} and the reduction peak potential (E_p^c) values show linear relationships with the Hammett constant (σ) of the substituents in the hydrazone ligands.

These dinuclear complexes are converted to the corresponding mononuclear *cis* dioxo complexes $K(H_2O)^+[V^VO_2(L)]^-$ (**5**–**8**) and mixed-ligand $[V^VO(L)(hq)]$ complexes on reaction, respectively, with two equivalents KOH in methanol and two equivalents 8-hydroxyquinoline (Hhq) in $CHCl_3$. Ascorbic acid reduces the dioxovanadium(V) complexes reversibly under aerobic condition.

© 2008 Elsevier Ltd. All rights reserved.

1. Introduction

Vanadium is an interesting transition metal which has the ability to exist in a wide range of oxidation states starting from −III to +V, of which the states III, IV and V are biologically important [1]. Vanadium easily switches between the oxidation states IV and V and the stabilization of either of these two states under aerobic condition depends upon the basicity of the coordinated ligand and also on the pH of the reaction medium. Of these three, the +V state has received considerable attention probably due to its two important properties: (i) it can exist in three motifs viz., mononuclear VO^{3+} and VO_2^+ motifs and dinuclear $V_2O_3^{4+}$ motif and (ii) it has the ability to exist in either five or six coordinated environment. These motifs are stable in solution around the physiological pH (~7) only when the metal is coordinated with sufficiently strong ligand for preventing the precipitation of hydroxides. A systematic study regarding the exclusive formation of any one of these three motifs with O,N-donor ligands [as V(V) due to its hard acidic nature, has strong affinity towards hard basic O,N-donor ligands] and their interconversion is an important area of contemporary research. Hydrazone ligands derived from the condensation of benzoyl hydrazine with aromatic 2-hydroxycarbonyl compounds are important tridentate O,N-donor ligands containing two intermediate basic phenolic and amide groups and one neutral imine moiety. This work was motivated by four objectives: (i) to synthesize the complexes containing $V_2O_3^{4+}$ core with a family of abovementioned hydrazone ligands, (ii) to rationalize the various synthetic routes for the formation of such type of complexes with these hydrazone ligands, (iii) to examine the feasibility of conversion of these dinuclear complexes into the mononuclear complexes with VO^{3+} and VO_2^+ motifs and (iv) to study the effect of *para* substituents in the hydrazone ligands on the electronic property of vanadium in these dinuclear complexes. With this background,

* Corresponding author. Tel.: +91 03 3256 85674; fax: +91 03 3235 19755.
E-mail address: ictg_64@yahoo.co.in (T. Ghosh).

0277-5387/$ - see front matter © 2008 Elsevier Ltd. All rights reserved.
doi:10.1016/j.poly.2008.03.018

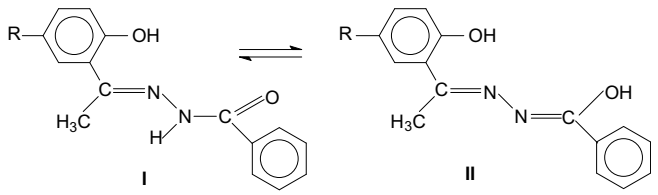

H_2L	R
H_2L^1	H
H_2L^2	CH_3
H_2L^3	OCH_3
H_2L^4	Cl

Scheme 1.

herein we have used four tridentate dibasic hydrazone ligands (H_2L^{1-4}, general abbreviation H_2L; the two H's representing the dissociable phenolic and amide protons) derived from the condensation of benzoyl hydrazine with 2-hydroxyacetophenone and its *para* substituted derivatives (Scheme 1). Stable structurally characterized oxo-bridge divanadium(V) complexes are not numerous [2–12] and particularly with hydrazone ligands are very rare [10–12]. The study of the chemistry of such type of dinuclear vanadium(V) complexes is important in connection with its catalytic [13–17] and medicinal [18–21] activities.

2. Experimental

2.1. Materials

$VOSO_4 \cdot 5H_2O$, acetyl acetone (Hacac) (CDH, India), benzoyl hydrazine, 2-hydroxyacetophenone and its *para* substituted derivatives (Aldrich, USA) were used as obtained. Hydrazone ligands (H_2L^{1-4}) [22] (Scheme 1) and $[V^{IV}O(acac)_2]$ [23] were prepared following the methods reported in the literature. Other chemicals and solvents were of analytical reagent grade and used without further purification.

2.2. Synthesis of the complexes $[V_2O_3(L)_2]$ (**1**–**4**)

All the four dinuclear complexes **1**–**4** were synthesized by a simple general method using either $[VO(acac)_2]$ or $VOSO_4 \cdot 5H_2O$ or $[V^{IV}O(L)(bipy/phen)]$ [24] as the starting material.

2.2.1. $[V_2O_3(L^1)_2]$ (**1**)

2.2.1.1. Method 1. To a filtered solution of H_2L^1 (0.254 g, 1 mmol) in acetone (20 cm^3) was added with stirring an acetone (15 cm^3) solution of $[VO(acac)_2]$ (0.265 g, 1 mmol) and the resulting reaction mixture was heated under reflux for 2 h. The reaction mixture was then kept for slow evaporation at room temperature. Black crystals of **1**, obtained after 3 days were collected by filtration after washing with acetone and dried over silica gel. Yield: 0.29 g (88.7%). *Anal.* Calc. for $C_{30}H_{24}N_4O_7V_2$ (654.43): C, 55.01; H, 3.67; N, 8.56. Found: C, 54.85; H, 3.95; N, 8.42%. Selected IR data (cm^{-1}): ν = 1592 (s, C=$N_{azomethine}$); 1302 (s, C–$O_{enolate}$); 1073 (m, N–N); 998 (s, V=O); 874 [s, V–(μ-O)–V]. ^1H NMR (300 MHz; $CDCl_3$): δ = 2.26 (s, 3H, 3 × 8-H); 7.04 (t, J = 7.3 Hz, 2H, 12-H and 14-H); 7.15–7.20 (m, 1H, 5-H); 7.30 (dd, J = 7.1 and 0.7 Hz, 1H, 3-H); 7.32–7.35 (m, 1H, 13-H); 7.37 (ddd, J = 7.1, 7.0 and 0.6 Hz, 1H, 4-H); 7.65 (dd, J = 7.4 and 0.7 Hz, 2H, 11-H and 15-H); 7.69 (dd, J = 7.3 and 0.6 Hz, 1H, 6-H) ppm.

Dark brown compound of **1** in the powder form was obtained on replacing acetone by acetonitrile or CH_2Cl_2 as the reaction medium.

2.2.1.2. Method 2. To a warm aqueous-methanolic solution (20 cm^3, 1:4 V/V) of H_2L^1 (0.254 g, 1 mmol) and sodium acetate trihydrate (0.272 g, 2 mmol) was added aqueous solution (10 cm^3) of $VOSO_4 \cdot 5H_2O$ (0.253 g, 1 mmol). The reaction mixture was stirred for 3 h at ~ 60 °C. A dark brown compound (0.25 g, 76.45%) (which was found to be identical in all respect with **1**, characterized by elemental analysis and also by various spectroscopic methods) thus obtained was filtered, washed with water, aqueous-methanol and then dried over silica gel (fused).

2.2.1.3. Method 3. Orange-red $[V^{IV}O(L^1)(bipy)]$ (0.10 g, 0. 21 mmol) complex was dissolved in wet dichloromethane (30 cm^3) and kept at room temperature. After 5 days black microcrystalline compound of **1** (0.061 g, 88.40%) were obtained. The compound was characterized by elemental analysis and also by various spectroscopic methods.

2.2.2. $[V_2O_3(L^2)_2]$ (**2**)

Complex **2** was prepared analogously to **1**, replacing H_2L^1 by H_2L^2 as black crystals (suitable for X-ray diffraction study). Yield: 0.29 g (85.04%). *Anal.* Calc. for $C_{32}H_{28}N_4O_7V_2$ (682.46): C, 56.27; H, 4.10; N 8.21. Found: C, 55.95; H, 4.21; N, 8.12%. Selected IR data (cm^{-1}): ν = 1590 (s, C=$N_{azomethine}$); 1294 (s, C–$O_{enolate}$); 1076 (m, N–N); 992 (s, V=O); 884 [s, V–(μ-O)–V]. ^1H NMR (300 MHz; $CDCl_3$): δ = 2.26 (s, 3H, 3 × 8-H); 2.45 (s, 3H, 3 × 16-H); 7.05 (t, J = 7.3 Hz, 2H, 12-H and 14-H); 7.24 (d, J = 8.0 Hz, 1H, 3-H); 7.31 (dt, J = 7.3 and 0.8 Hz, 1H, 13-H); 7.49 (dd, J = 8.0 and 1.0 Hz, 1H, 4-H); 7.51 (d, J = 1.0, 1H, 6-H), 7.64 (dd, J = 7.3 and 0.8 Hz, 2H, 11-H and 15-H) ppm.

2.2.3. $[V_2O_3(L^3)_2]$ (**3**)

Complex **3** was also prepared analogously to **1**, replacing H_2L^1 by H_2L^3. Yield: 0.31 g (86.83%). *Anal.* Calc. for $C_{32}H_{28}N_4O_9V_2$ (714.48): C, 53.75; H, 3.92; N, 7.84. Found: C, 53.54; H, 4.08; N, 7.77%. Selected IR data (cm^{-1}): ν = 1588 (s, C=$N_{azomethine}$); 1286 (s, C–$O_{enolate}$); 1068 (m, N–N); 993 (s, V=O); 877 [s, V–(μ-O)–V]. ^1H NMR (300 MHz; $CDCl_3$): δ = 2.26 (s, 3H, 3 × 8-H); 3.90 (s, 3H, 5-OCH_3); 7.07 (t, J = 7.3 Hz, 2H, 12-H and 14-H); 7.18 (d, J = 0.8 Hz, 1H, 6-H); 7.26 (dd, J = 7.6 and 0.8 Hz, 1H, 4-H); 7.29 (d, J = 7.6 Hz, 1H, 3-H); 7.33 (dt, J = 7.3 and 0.8 Hz, 1H, 13-H); 7.65 (dd, J = 7.6 and 0.8 Hz, 2H, 11-H and 15-H) ppm.

2.2.4. $[V_2O_3(L^4)_2]$ (**4**)

Complex **4** was also prepared similarly to **1**, replacing H_2L^1 by H_2L^4. Yield: 0.30 g (91.29%). *Anal.* Calc. for $C_{30}H_{22}Cl_2N_4O_7V_2$ (723.29): C, 49.77; H, 3.04; N, 7.74. Found: C, 49.56; H, 3.16; N, 7.70%. Selected IR data (cm^{-1}): ν = 1589 (s, C=$N_{azomethine}$); 1278 (s, C–$O_{enolate}$); 1094 (m, N–N); 1003 (s, V=O); 878 [s, V–(μ-O)–V]. ^1H NMR (300 MHz; $CDCl_3$): δ = 2.24 (s, 3H, 3 × 8-H); 7.10 (t, J = 7.3 Hz, 2H, 12-H and 14-H); 7.31 (d, J = 8.8 Hz, 1H, 3-H); 7.33 (dt, J = 7.3 and 0.7 Hz, 1H, 13-H); 7.62 (dd, J = 8.8 and 2.0 Hz, 1H, 4-H); 7.64 (dd, J = 7.3 and 0.7 Hz, 2H, 11-H and 15-H); 7.70 (d, J = 2.0 Hz, 1H, 6-H) ppm.

2.3. Conversion of $[V_2O_3(L)_2]$ complexes to $K(H_2O)^+[VO_2(L)]^-$ complexes

2.3.1. Conversion of $[V_2O_3(L^1)_2]$ (**1**) to $K(H_2O)^+[VO_2(L^1)]^-$ (**5**)

To a methanolic solution (25 cm^3) of KOH (0.02 g, ~0.3 mmol) was added $[V_2O_3(L^1)_2]$ (0.10 g, 0.15 mmol) and the reaction mixture was stirred for 4 h at ~60 °C. An intense yellow solution was obtained which was kept for slow evaporation at room temperature. A yellow microcrystalline product of **5**, obtained after 5 days, was filtered, washed with methanol and dried over silica gel. Yield: 0.10 g (83.33%). *Anal.* Calc. for $C_{15}H_{14}N_2O_5KV$ (392.33): C, 45.88; H,

3.57; N, 7.14. Found: C, 45.52; H, 3.78; N, 7.06%. Selected IR data (cm^{-1}): ν = 1594 (s, C=$N_{azomethine}$); 1240 (s, C–$O_{enolate}$); 1030 (m, N–N); 876, 945 (s, sym and antisym VO_2^+); 3435 (m, H_2O). Λ_M (DMF) = 65 Ω^{-1} cm^2 mol^{-1}. ^1H NMR (300 MHz; DMSO-d_6): δ = 2.81 (s, 3H, 3 × 8-H); 6.77 (t, J = 7.7, 2H, 12-H and 14-H); 7.26 (dt, J = 7.7 and 1.7, 1H, 13-H); 7.38–7.41 (m, 1H, 5-H); 7.42–7.44 (m, 1H, 3-H); 7.69 (dd, J = 7.4 and 1.3, 1H, 6-H); 7.70–7.72 (m, 1H, 4-H); 8.00 (dd, J = 7.7 and 1.7, 2H, 11-H and 15-H) ppm. UV/Vis (CH_3OH): λ_{max} (ε, dm^3 mol^{-1} cm^{-1}) = 376 nm (7056), 309 nm (12 190).

*2.3.2. Conversion of $[V_2O_3(L^2)_2]$ (**2**) complex to $K(H_2O)^+[VO_2(L^2)]^-$ (**6**)*

Complex **6** was prepared analogously to **5**, replacing $[V_2O_3(L^1)_2]$ by $[V_2O_3(L^2)_2]$. Yield: 0.090 g (75.0%). *Anal.* Calc. for $C_{16}H_{16}N_2O_5KV$ (406.35): C, 47.25; H, 3.94; N, 6.89. Found: C, 46.95; H, 4.12; N, 6.78%. Selected IR data (cm^{-1}): ν = 1592 (s, C=$N_{azomethine}$); 1245 (s, C–$O_{enolate}$); 1030 (m, N–N); 905, 933 (s, sym and antisym VO_2^+); 3431 (m, H_2O). Λ_M (DMF) = 64 Ω^{-1} cm^2 mol^{-1}. ^1H NMR (300 MHz; DMSO-d_6): δ = 2.25 (s, 3H, 3 × 16-H); 2.80 (s, 3H, 3 × 8-H); 6.66 (d, J = 8.4 Hz, 1H, 3-H); 7.08 (dd, J = 8.4 and 1.0 Hz, 1H, 4-H); 7.36-7.39 (m, 2H, 12-H and 14-H); 7.40–7.43 (m, 1H, 13-H); 7.50 (d, J = 1.0 Hz, 1H, 6-H); 8.00 (dd, J = 7.9 and 2.2 Hz, 2H, 11-H and 15-H) ppm. UV/Vis (CH_3OH): λ_{max} (ε, dm^3 mol^{-1} cm^{-1}) = 385 nm (6705), 310 nm (13 490).

*2.3.3. Conversion of $[V_2O_3(L^3)_2]$ (**3**) complex to $K(H_2O)^+[VO_2(L^3)]^-$ (**7**)*

Complex **7** was also prepared analogously to **5**, replacing $[V_2O_3(L^1)_2]$ by $[V_2O_3(L^3)_2]$. Yield: 0.10 g (84.75%). *Anal.* Calc. for $C_{16}H_{16}N_2O_6KV$ (422.35): C, 45.46; H, 3.79; N, 6.63. Found: C, 45.14; H, 3.98; N, 6.52%. Selected IR data (cm^{-1}): ν = 1590 (s, C=$N_{azomethine}$); 1213 (s, C–$O_{enolate}$); 1027 (m, N–N); 905, 915 (s, sym and antisym VO_2^+); 3421 (H_2O). Λ_M (DMF) = 63 Ω^{-1} cm^2 mol^{-1}. ^1H NMR (300 MHz; DMSO-d_6): δ = 2.81 (s, 3H, 3 × 8-H); 3.73 (s, 3H, 3 × 5-OCH_3); 6.70 (d, J = 8.9 Hz, 1H, 3-H); 6.94 (dd, J = 8.9 and 1.9 Hz, 1H, 4-H); 7.16-7.20 (m, 1H, 13-H); 7.33–7.41 (m, 2H, 12-H and 14-H); 7.43 (d, J = 1.9 Hz, 1H, 6-H); 8.02 (dd, J = 7.8 and 1.8 Hz, 2H, 11-H and 15-H) ppm. UV/Vis (CH_3OH): λ_{max} (ε, dm^3 mol^{-1} cm^{-1}) = 400 nm (1046), 311 nm (2405).

*2.3.4. Conversion of $[V_2O_3(L^4)_2]$ (**4**) complex to $K(H_2O)^+[VO_2(L^4)]^-$ (**8**)*

Complex **8** was also prepared analogously to **5**, replacing $[V_2O_3(L^1)_2]$ by $[V_2O_3(L^4)_2]$. Yield: 0.11 g (93.22%). *Anal.* Calc. for $C_{15}H_{13}N_2O_5ClKV$ (426.77): C, 42.18; H, 3.05; N, 6.56. Found: C, 41.92; H, 3.17; N, 6.47%. Selected IR data (cm^{-1}): ν = 1595 (s, C=$N_{azomethine}$); 1240 (s, C–$O_{enolate}$); 1029 (m, N–N); 904, 945 (s, sym and antisym VO_2^+); 3450 (m, H_2O). Λ_M (DMF) = 57 Ω^{-1} cm^2 mol^{-1}. ^1H NMR (300 MHz; DMSO-d_6): δ = 2.81 (s, 3H, 3 × 8-H); 6.78 (d, J = 8.8 Hz, 1H, 3-H); 7.26 (dd, J = 8.8 and 2.6 Hz, 1H, 4-H); 7.39–7.42 (m, 2H, 12-H and 14-H); 7.44–7.48 (m, 1H, 13-H); 7.70 (d, J = 2.6, 1H, 6-H); 8.02 (dd, J = 7.8 and 1.8 Hz, 2H, 11-H and 15-H) ppm. UV/Vis (CH_3OH): λ_{max} (ε, dm^3 mol^{-1} cm^{-1}) = 386 nm (8620), 308 nm (14 630).

2.4. Conversion of $[V_2O_3(L)_2]$ complexes to [VO(L)(hq)] complexes

2.4.1. Conversion of $[V_2O_3(L^1)_2]$ complex to $[VO(L^1)(hq)]$ complex

$CHCl_3$ solution (10 cm^3) of 8-hydroxyquinoline (Hhq) (0.025 g, 0.17 mmol) was added to a solution of $[V_2O_3(L^1)_2]$ (0.05 g, 0.075 mmol) in $CHCl_3$ (20 cm^3). The yellow colour of the solution was changed gradually to violet. The mixture was stirred for 8 h and the intense violet solution was filtered and the filtrate was left to evaporate slowly in the air. Shiny black crystalline product (0.065 g, 91.55%) obtained after 6 days was collected by filtration after washing with $CHCl_3$ and then dried over silica gel, which was found to be identical in all respects with the compound $[VO(L^1)(hq)]$, which we have already prepared by different method and published very recently [22].

Other mixed-ligand complexes of this type with the H_2L^{2-4} ligands were also obtained similarly by the reaction of Hhq with the respective $[V_2O_3(L)_2]$ complex.

2.5. Physical measurements

Elemental analyses were performed on a Perkin–Elmer 2400 CHNS/O analyzer. Electronic spectra (in CH_2Cl_2 of $[\{VO(L)\}_2\mu$-O] and [VO(L)(hq)] complexes and in CH_3OH of dioxovanadium(V) complexes) were recorded on a Hitachi U-3501 spectrophotometer and IR spectra (as KBr pellets) were taken on a Perkin–Elmer 782 spectrophotometer. The ^1H NMR spectra were recorded either in $CDCl_3$ [of **1**–**4** complexes] or in DMSO-d_6 [of **5**–**8** complexes] on a Bruker AM 300L (300 MHz) superconducting FT NMR spectrophotometer. Conductivity measurements of complexes **5**–**8** were performed at 298 K in DMF solution with the Systronics 304 digital conductivity meter. Electrochemical measurements were performed at 298 K in CH_2Cl_2 solution of complexes **1**–**4** and in DMSO solution of complexes **5**–**8** for *ca.* 10^{-3} M using Et_4NClO_4 as supporting electrolyte under a dry N_2 atmosphere on a PC controlled PAR model 273 A electrochemistry system. A Pt disk, a Pt wire auxiliary electrode and an aqueous saturated calomel electrode (SCE) were used in a three-electrode configuration. All the potential values reported here are uncorrected for junction contribution. The ferrocene/ferrocinium (Fc/Fc^+) couple was used as the internal standard.

2.6. Crystallographic data collection and refinement

For **2**, data were measured with Mo Kα radiation at 298 K using the MAR research Image Plate System. Suitable single crystals were positioned at 70 mm from the Image Plate. A total of 95 frames were measured at 2° intervals with a counting time of 2 min. Data analyses were carried out with the XDS program [25]. The structures were solved using direct methods with the SHELXS-97 program [26]. Absorption corrections were carried out using the DIFABS program [27]. For complex **4**, data were measured with Mo Kα radiation at 150 K using the Oxford Diffraction X-calibur system. The crystal was mounted at 50 mm from the CCD. A total of 321 frames were measured with a counting time of 10 s. Data analysis was carried out with CRYSALIS [28] and absorption correction was carried out with the ABSPACK program [29]. For the two structures, the non-hydrogen atoms were refined with anisotropic thermal parameters. The hydrogen atoms bonded to carbon were included in

Table 1
Crystal data and structure determination summary of **2** and **4**

	2	**4**
Empirical formula	$C_{32}H_{28}N_4O_7V_2$	$C_{30}H_{22}Cl_2N_4O_7V_2$
Formula weight	682.46	723.29
Crystal colour	black	black
Crystal system	monoclinic	monoclinic
Space group	*C*2/*c*	*C*2/*c*
a (Å)	21.09(2)	20.7868(15)
b (Å)	14.793(17)	15.032(11)
c (Å)	20.89(2)	20.593(3)
β (°)	109.500(10)	111.659(11)
V (Å^3)	6144(12)	5980.5(11)
Z	8	8
ρ_{calc} (g cm^{-3})	1.476	1.607
μ (mm^{-1})	0.663	0.859
F(000)	2800	2928
Data/restrains/parameters	5865/0/412	6667/0/409
Goodness-of-fit on F^2	0.698	1.124
R indices [$I > 2\sigma(I_0)$] *R*1, *wR*2	0.0565, 0.1380	0.0822, 0.2320
R indices (all data): *R*1, *wR*2	0.1108, 0.1470	0.1128, 0.2438

geometric positions and given thermal parameters equivalent to 1.2 times those of the atom to which they were attached. The structures were refined on F^2 using SHELXL-97 program [26] and molecular graphics were computed using PLATON [30]. All crystallographic data are summarized in Table 1.

3. Results and discussion

3.1. Synthesis of dinuclear $[V_2O_3(L)_2]$ complexes and their conversion into their mononuclear analogues

$[V_2O_3(L)_2]$ (**1–4**) complexes were prepared by various synthetic routes starting from different VO^{2+} precursor, viz., $VOSO_4$, $[V^{IV}O(acac)_2]$ and $[V^{IV}O(L)(bipy/phen)]$ complexes. Reaction of equimolar amounts of $VOSO_4$ with the respective H_2L (where H_2L is the general abbreviation of H_2L^{1-4}) in presence of two equivalents sodium acetate in aqueous-methanolic (50% V/V) medium in air afforded the $[V_2O_3(L)_2]$ complex in good yield as dark brown powdered material, while, the black crystalline $[V_2O_3(L)_2]$ complexes were obtained by the reaction of $[VO(acac)_2]$ with equimolar amount of H_2L in refluxing acetone. Such complexes were further obtained on replacing acetone by acetonitrile or CH_2Cl_2 and also from the decomposition of the mixed-ligand $[V^{IV}O(L)(bipy/phen)]$ complexes (which were prepared by the reported method [24]) in CH_2Cl_2 solution. The oxidizing agent is most likely the aerial dioxygen and all the stated reactions can be represented by the following equations:

$$2V^{IV}OSO_4 + 2H_2L + 4CH_3COONa + 1/2O_2 \rightarrow [\{V^{V}O(L)\}_2\mu\text{-}O] + 2Na_2SO_4 + 4CH_3COOH \quad (1)$$

$$2[V^{IV}O(acac)_2] + 2H_2L + 1/2O_2 \rightarrow [\{V^{V}O(L)\}_2\mu\text{-}O] + 4Hacac \quad (2)$$

$$2[V^{IV}O(L)(bipy/phen)] + 1/2O_2 \rightarrow [\{V^{V}O(L)\}_2\mu\text{-}O] + 2bipy/phen \quad (3)$$

where Hacac, bipy and phen are, respectively, acetyl acetone, 2,2′-bipyridine and 1,10-phenanthroline.

These dinuclear oxovanadium(V) complexes can easily be converted to either dioxovanadium(V) complexes **5–8** or mixed-ligand complexes of the type $[V^{V}O(L)(hq)]$ (which we have already synthesized by different method and reported very recently [22]) on reaction, respectively, with two equivalents KOH in methanol and two equivalents 8-hydroxyquinoline (Hhq) in $CHCl_3$. Eqs (4) and (5) represent the above-mentioned reactions.

$$[\{V^{V}O(L)\}_2\mu\text{-}O] + 2KOH + H_2O \rightarrow 2K(H_2O)^{+}[VO_2(L)]^{-} \quad (4)$$

$$[\{V^{V}O(L)\}_2\mu\text{-}O] + 2Hhq \rightarrow 2[V^{V}O(L)(hq)] + H_2O \quad (5)$$

Complexes **1–4** are freely soluble in CH_2Cl_2, $CHCl_3$ but sparingly soluble in CH_3OH, C_2H_5OH etc. while complexes **5–8** are freely soluble in CH_3OH, DMSO, DMF but sparingly soluble in CH_3CN and insoluble in CH_2Cl_2. In spite of our best efforts, none of the dioxovanadium(V) complexes **5–8**, afforded single crystals suitable for structure determination by X-ray crystallography. Among the four $[V^{IV}O(L)(bipy)]$ and four $[V^{IV}O(L)(phen)]$ complexes, only the $[V^{IV}O(L^4)(bipy)]$ complex on decomposition in CH_2Cl_2–C_6H_6 solution yielded the crystals [31] of $[V_2O_3(L^4)_2]$ containing benzene molecules as solvent of crystallization. The analytical and spectroscopic data of the present $[V^{V}O(L)(hq)]$ complexes are identical in all respects to our earlier report [22]. Scheme 2 represents all the above-mentioned reactions.

3.2. IR spectra of the complexes

The IR spectral data of all the complexes are given in Section 2. Disappearance of two ligand bands in the regions 1646–1651 cm^{-1} and 2924-2989 cm^{-1} due to (C=O) and (NH) stretches [22],

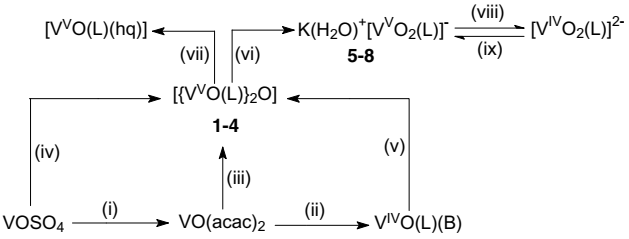

Scheme 2. (i) Acetyl acetone (Hacac) + two equivalents CH_3COONa in water; (ii) H_2L + bipy or phen (B) in 1:1 molar ratio in methanol; (iii) one equivalent H_2L in acetone or dichloromethane or acetonitrile; (iv) H_2L + two equivalents CH_3COONa in methanol–water (50% V/V); (v) CH_2Cl_2; (vi) two equivalents KOH in methanol; (vii) two equivalents 8-hydroxyquinoline (Hhq) in $CHCl_3$; (viii) ascorbic acid (in excess) in methanol; (ix) air.

respectively, indicates the enolisation of the amide functionality and subsequent metal coordination through deprotonation. The enolisation is further supported by the appearance of a new band near 1278–1302 cm^{-1} region in complexes **1–4** and near 1213–1245 cm^{-1} region in complexes **5–8**, attributed to (C–O) (enolate) stretching. The characteristic (N–N) stretching band for the dimeric complexes appears in the 1068–1094 cm^{-1} region while that for dioxo complexes is observed in the 1027–1030 cm^{-1} region. These bands are appreciably in the higher energy region compared to the corresponding free ligands due to diminished repulsion between the lone pairs of adjacent nitrogen atoms, indicating the coordination of one of the two nitrogen lone pairs [32–34]. The coordination of the phenolic oxygen to the vanadium with deprotonation is confirmed from the disappearance of the ligand band in the region 3215–3240 cm^{-1} due to (O–H) (phenolic) stretching and the appearance of a new strong band in the 1349–1363 cm^{-1} attributed to (C–O) (phenoate) stretching [22,35,36]. Thus, all the four hydrazone ligands acting as tridentate dibasic ONO donors in all these complexes. In the IR spectra of complexes **5–8**, the strong sharp band appeared in the region 3421–3450 cm^{-1} may be assigned to H_2O molecule.

Two sharp bands, one near 1000 cm^{-1} and other near 880 cm^{-1} exhibited by the dinuclear complexes **1–4**, have been attributed to (V=O) and [V–(μ-O)–V] stretches, respectively [6,10,11]. The *cis* dioxo nature of complexes **5–8**, was confirmed from the appearance of two sharp bands in the 876–905 cm^{-1} and 915–945 cm^{-1} regions which are assigned to symmetric and antisymmetric stretching of the VO_2^{+} motifs [6,33,34,36–38]. Such (V=O) stretching values are in favour of the pentacoordinated environment [6,10,11,33,34,36–38] around the metal center in all the **1–8** complexes.

3.3. Structure of **2** and **4**

The structure of **4** is isomorphous with **2** with the chlorine atoms replacing the methyl groups in the *para* position with respect to phenolic OH in the aryloxy ring of the ligands and they belong to the monoclinic crystal system with *C*2/*c* space group. Molecular view of **2** and **4** are given in Figs. 1 and 2, respectively. The selected bond parameters are given in Table 2. Two structurally very similar but crystallographically distinct respective $[V_2O_3(L)_2]$ molecules are present in both the crystal lattices of **2** and **4** with the bridging oxygen lying on a crystallographic 2-fold axis such that the two halves of each of the two molecules are crystallographically equivalent. The coordination sphere of the vanadium is of the VO_4N type and the coordination geometry at the metal center can best be fitted to a distorted square pyramid with oxo oxygen O(1) at the apex. The phenolate O(2), the enolate O(3), the imine nitrogen N(1) atoms of the fully deprotonated $(L^2)^{2-}$ and $(L^4)^{2-}$ ligands in their enol forms and the bridging oxygen O(4)

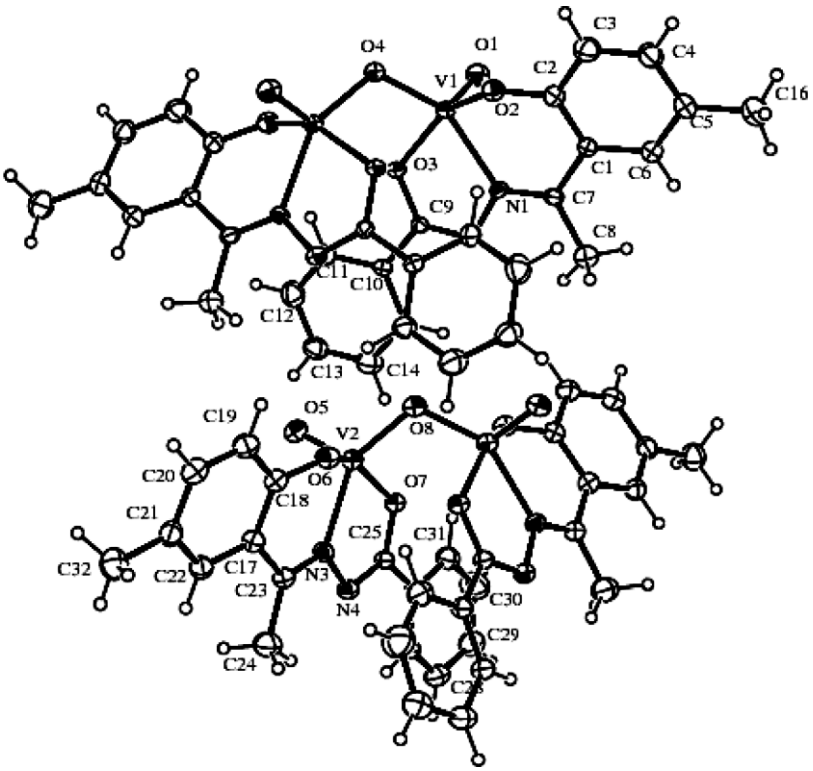

Fig. 1. Molecular structure of complex **2** with thermal ellipsoids drawn at 50% probability level.

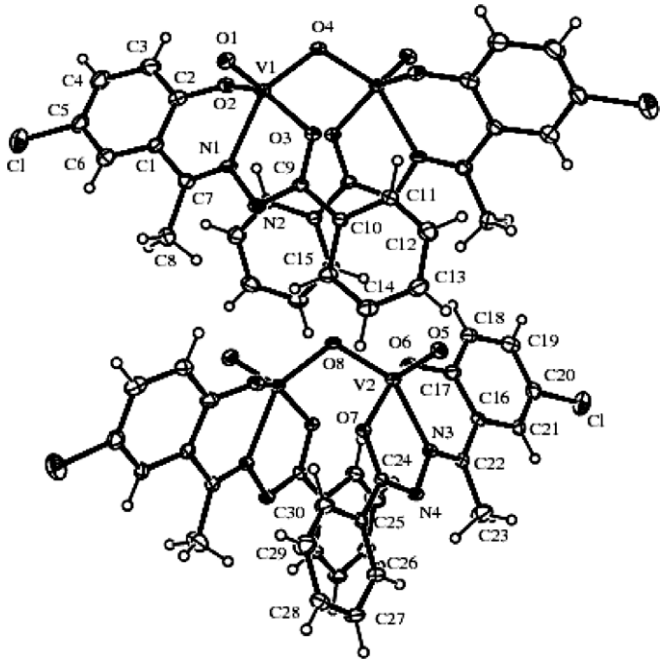

Fig. 2. Molecular structure of complex **4** with thermal ellipsoids drawn at 50% probability level.

atoms constitute the tetragonal plane from which the vanadium atom is displaced by 0.527 Å in one molecule and by 0.539 Å in the other molecule of **2** (these values are 0.534 and 0.525 Å for **4**) towards the terminal O(1) and O(5) atoms respectively. The average O(axial)–V–O/N(basal) angle is ~104°, which is only slightly different from the average angle of 102° for a square pyramidal complex (C_{4v}) as explained by Muetterties and Guggenberger [39]. The τ parameter [40] (equal to $\Delta/60°$, where Δ is the difference between the largest and next-to-largest ligand–metal–ligand angles) is also another useful geometrical discriminator ($\Delta = 0$, $\tau = 0$ for idealized square pyramid). The τ value is 0.039 and 0.004, respectively, for V(1) and V(2) centers for **2** while for **4** it is, respectively, 0.074 and 0.018, indicating very slight distortion from the perfect square pyramidal structure. These also indicate that the extent of distortion is different for each of the vanadium centers even within the same structure.

The dihedral angles between the two symmetry related pyramid bases V(1) and V(1)$1, V(2) and V(2)$1 ($1 = symmetry element $1 - x$, y, $0.5 - z$) in **2** are 62.19° and 59.25°, respectively (which are, respectively, 61.36° and 58.7° in **4**). The two terminal oxygen atoms O(1) and O(1) are mutually *trans* lying on opposite sides of the V–O–V plane and the distance of each oxygen atom from the plane is 0.875 Å and 0.889 Å in **2** while it is 0.860 Å and 0.874 Å in **4**. The O(1)–V(1)–V(1)$1–O(1)$1 and O(5)–V(2)–V(2)$1–O(5)$1 torsion angles are 134.99° and 133.95° in **2** while this angles are, respectively, 133.92° and 134.21° in **4**. The V=O^t (t = terminal) [1.584(4)–1.589(3) Å], V–O^b (b = bridging) [1.784(3)–1.801(2) Å] distances, the other bond lengths and bond angles are very similar to the reported analogous hydrazone complexes [10–12]. The O–C, N–C and N–N distances are consistent with the enolate forms of the corresponding ligands. An examination of the bond length parameters reveals a general order: V–O^t < V–O^b < V–O^p (p = phenolic) < V–O^e (e = enolic), which can be explained on the basis of basicity of donor atoms and their π-bonding ability. The V–O–V angles are very similar and are close to 113°, which is consistent with the reported values of analogous hydrazone complexes [10–12]. The non-bonded V–V distances are 2.988(4) Å and 2.976(3) Å in **2** [2.989(2) Å and 2.967(2) Å in **4**], which are also very similar to those of other reported hydrazone complexes [10–12].

Table 2
Selected bond distances (Å) and angles (°) for complexes **2** and **4**

	2	4
V(1)–O(1)	1.589(3)	1.584(4)
V(1)–O(2)	1.817(3)	1.800(4)
V(1)–O(3)	1.933(3)	1.935(3)
V(1)–O(4)	1.785(3)	1.799(2)
V(1)–N(1)	2.096(4)	2.096(4)
V(1)–V(1)	2.988(4)$1	2.9885(18)$1
V(2)–O(5)	1.586(3)	1.584(3)
V(2)–O(6)	1.827(3)	1.813(4)
V(2)–O(7)	1.948(3)	1.953(4)
V(2)–O(8)	1.784(3)	1.801(2)
V(2)–N(3)	2.102(4)	2.113(4)
V(2)–V(2)	2.976(3)$1	2.9667(17)$1
O(1)–V(1)–O(2)	103.82(15)	104.11(15)
O(1)–V(1)–O(3)	103.89(15)	105.10(17)
O(1)–V(1)–O(4)	108.63(15)	108.58(16)
O(1)–V(1)–N(1)	99.23(15)	99.18(19)
O(1)–V(1)–V(1)$1	133.59(12)	134.20(13)
O(2)–V(1)–O(3)	147.07(12)	145.60(16)
O(2)–V(1)–N(1)	83.05(12)	82.94(12)
O(2)–V(1)–V(1)$1	108.79(9)	107.66(14)
O(3)–V(1)–N(1)	75.26(12)	74.86(13)
O(3)–V(1)–V(1)$1	61.85(7)	62.01(11)
O(4)–V(1)–O(2)	101.78(9)	100.57(13)
O(4)–V(1)–O(3)	85.81(12)	86.95(13)
O(4)–V(1)–N(1)	149.42(12)	150.03(17)
O(4)–V(1)–V(1)$1	33.19(10)	33.83(11)
N(1)–V(1)–V(1)$1	116.50(9)	116.58(11)
V(1)–O(4)–V(1)$1	113.6(2)	112.3(2)
O(5)–V(2)–O(6)	103.51(16)	102.26(18)
O(5)–V(2)–O(7)	102.79(15)	104.32(17)
O(5)–V(2)–O(8)	109.10(15)	107.99(17)
O(5)–V(2)–N(3)	100.80(15)	100.25(16)
O(5)–V(2)–V(2)$1	133.81(11)	133.92(15)
O(6)–V(2)–O(7)	147.70(12)	148.04(15)
O(6)–V(2)–N(3)	82.17(13)	83.01(17)
O(6)–V(2)–V(2)$1	109.82(12)	110.40(12)
O(7)–V(2)–N(3)	74.77(13)	75.11(16)
O(7)–V(2)–V(2)$1	62.05(9)	60.85(9)
O(8)–V(2)–O(6)	102.50(11)	102.42(11)
O(8)–V(2)–O(7)	86.14(13)	85.92(13)
O(8)–V(2)–N(3)	147.46(13)	149.15(13)
O(8)–V(2)–V(2)$1	33.45(16)	34.56(11)
N(3)–V(2)–V(2)$1	114.42(9)	114.92(11)
V(2)–O(8)–V(2)$1	113. 1(2)	110.9(2)

$1 = Symmetry element $1 - x, y, 0.5 - z$.

3.4. Proton NMR spectra of the complexes

We are considering the ^{1}H NMR spectra of complexes **1**–**4** and **5**–**8** taken, respectively, in $CDCl_3$ and DMSO-d_6 solution and their spectral data are presented in the experimental section. The coordination modes of the ligands in the complexes were confirmed by comparing the ^{1}H NMR spectra of the complexes with the respective ligands. The DMSO-d_6 solution of the ligands exhibits signals at $\delta \sim 11.00$ ppm and $\delta \sim 13.00$ ppm which are attributed respectively to NH and OH protons [22]. These signals are absent in all these complexes suggesting their tautomerisation of the keto form into enol form and subsequent coordination of the enolic and phenolic oxygens through deprotonation.

In the ^{1}H NMR spectra of **1**–**4**, the methyl protons H(8) appear as a singlet at δ2.24–δ2.26 ppm region. The methyl protons H(16) in **2** also appear as a singlet at δ2.45 ppm and the singlet at δ3.90 ppm in **3** is attributed to methoxy H(5-OCH_3) protons. The aromatic protons appear in the δ7.04–δ7.70 ppm region. The significant downfield shift (~0.3 ppm) of the methyl protons H(8) (appearing at δ2.81 ppm in complexes **5**–**8**) indicating the coordination of azomethine (C═N) nitrogen to the metal. Singlets at δ2.25 ppm and δ3.73 ppm in **6** and **7** are attributed, respectively, to methyl H(16) and methoxy H(5-OCH_3) protons. In these dioxovanadium(V) complexes, the aromatic protons appear in the δ6.66–δ8.02 ppm region. The disappearance of signal corresponding to H_2O protons in these complexes is probably due to exchange with the solvent. The ^{1}H NMR spectral data of the mixed-ligand [VO(L)(hq)] complexes are identical with the reported values which are described in our earlier paper [22].

3.5. Conductivity of the dioxovanadium(V) complexes

The conductivity of the dioxovanadium(V) complexes **5**–**8** were measured in *N*,*N*-dimethylformamide (DMF) solution at 298 K with a view to examine their electrolytic nature and their molar conductance values have been found to be in the 57–65 Ω^{-1} cm^2 mol^{-1} region, indicating their 1:1 electrolytic [41] nature thus, supporting their molecular formulae.

Based on the results of above studies, it is reasonable to assume the gross structures **III** and **IV**, respectively, for the complexes **1**–**4** and **5**–**8** (Scheme 3).

3.6. Electronic spectra of the complexes

All the complexes are diamagnetic indicating the +V oxidation state of the metal with a 3d^0 configuration and consequently no d–d transition band is expected in their electronic spectra. The electronic spectra of **1**–**4** complexes and [VO(L)(hq)] complexes were recorded in CH_2Cl_2 solution while that of **5**–**8** complexes were recorded in CH_3OH in the 300–800 nm regions. The electronic spectral data of **1**-**4** are listed in Table 3 while those of **5**–**8** are described in Section 2. All these complexes exhibit very intense transitions; the lowest energy band near 380 nm is assigned to ligand-to-metal charge transfer (LMCT) transition. The ligand char-

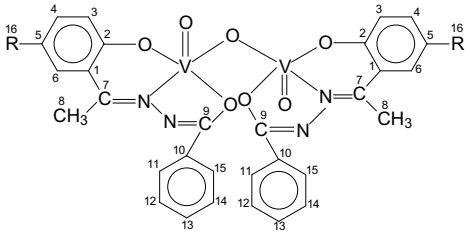

R	Complex
H	**1**
CH_3	**2**
OCH_3	**3**
Cl	**4**

III

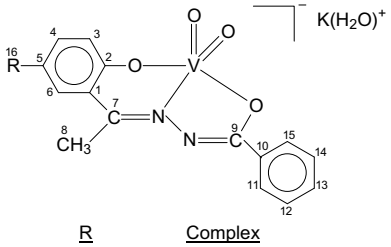

R	Complex
H	**5**
CH_3	**6**
OCH_3	**7**
Cl	**8**

IV

Scheme 3.

Table 3
Electronic spectral[a] and electrochemical[a,b] data of the complexes **1–4** at 298 K

Compound	UV–Vis	Electrochemical parameters		
	λ_{max}, nm (ε, dm^3 mol^{-1} cm^{-1})	E_p^c (V)	E_p^a (V)	$E_{1/2}$[c] (V) (ΔE_p (mV)
$[V_2O_3(L^1)_2]$ (**1**)	382 (15377); 320 (32877)	+0.21	+0.29	+0.25 (80)
$[V_2O_3(L^2)_2]$ (**2**)	376 (15992); 320 (36106)	+0.16	+0.25	+0.21 (90)
$[V_2O_3(L^3)_2]$ (**3**)	374 (23059); 326 (37093)	+0.15	+0.27	+0.21 (120)
$[V_2O_3(L^4)_2]$ (**4**)	388 (13520); 326 (31003)	+0.24	+0.36	+0.30 (120)

ΔE_p = difference of cathodic and anodic peak potential values.
[a] In CH_2Cl_2.
[b] At a Pt disk electrode; supporting electrolyte: Et_4NClO_4 (TEAP, 0.1 M), scan rate 50 mV s^{-1}, reference electrode SCE, solute concentration $\sim 10^{-3}$ M.
[c] $E_{1/2}$ is calculated as the average of anodic (E_p^a) and cathodic (E_p^c) peak potential values.

acteristic $\pi \rightarrow \pi^*$ transition band of the azomethine group appeared near 320 nm for **1–4** complexes and near 310 nm for **5–8** complexes. An examination of the λ_{max} (for LMCT transition) values of **1–4** complexes indicates that an electron donating group (viz., CH_3 and OCH_3) at the *para* position with respect to phenolic OH group in the aryloxy ring, decreases the λ_{max} value, while, an electron withdrawing group (e.g., Cl) increases it, which is expected from the ligands' basicity point of view. But such a trend is not observed for the dioxo complexes **5–8**, probably due to the accumulation of negative charge on the vanadium, which eliminates the relatively small substituent effect inhibiting us to examine the substituent effect on the electronic property of vanadium in these dioxovanadium(V) complexes.

3.7. Electrochemistry of the complexes

Complexes **1–4** exhibit a quasi-reversible reduction peak ($E_{1/2}$) in CH_2Cl_2 solution (Fig. 3) near +0.25 V *versus* SCE due to VO^{3+}/VO^{2+} couple. The appearance of the single reduction peak suggests the identical electronic environment at both the two vanadium centers. However, the electrochemical study of complexes **5–8** in DMSO solution indicated that they are not electro-active in the voltage range −1.0 to 1.0 V. A scrutiny of the redox potential data (Table 3) indicates a similar trend in the reduction peak potential ($E^c{}_p$) values for complex **1–4** like their electronic spectra, it decreases with the increase of electron donating property of the substituent at the *para* position as in the case of **2** and **3** in comparison to the unsubstituted species (viz., **1**) and the opposite is true for the presence of an electron withdrawing group (viz., **4**).

3.8. Influence of ligand substituents on the electronic aspects of the complexes

Four hydrazone ligands H_2L^{1-4} with three substituents of different Hammett parameter (σ) values [H (σ = 0.00), CH_3 (σ = −0.17), OCH_3 (σ = −0.27) and Cl (σ = +0.23)] [42] in the aryloxy ring of the hydrazone ligands have been used in this work with a view to study their effect on the electronic property of the vanadium in these dinuclear complexes. We have already stated that in the complexes **2** and **3** with electron donating substituents, a decrease in λ_{max} value (for the LMCT transition) and reduction peak potential (E_p^c) value was observed compared to complex **1** and for complex **4** with an electron withdrawing substituent, the opposite is true. To find out the quantitative relation of λ_{max} and E_p^c values with σ, the respective values are plotted which give the following linear relations, equations (6) and (7) (Figs. 4 and 5).

$$\text{UV—Vis}: \ \lambda_{max}\ (\text{nm}) = 381.51 + 28.82 \times \sigma \quad (6)$$

$$\text{CV}: \ E_p^c\ (\text{V}) = 0.20 + 0.19 \times \sigma \quad (7)$$

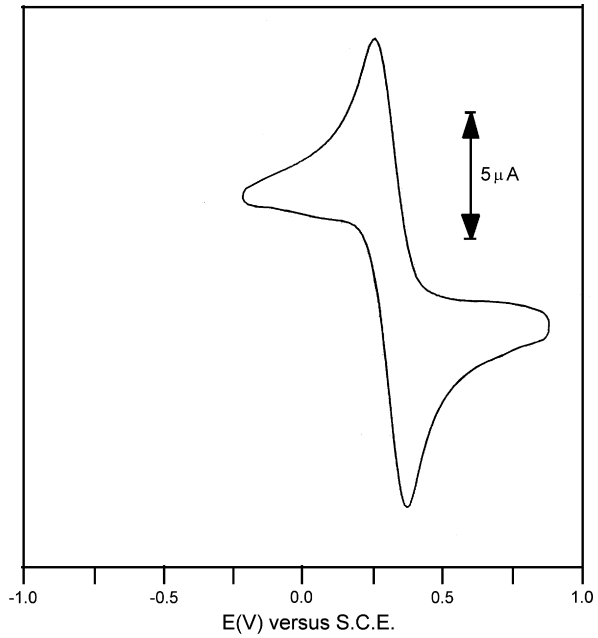

Fig. 3. Cyclic voltammogram of complex **4** in CH_2Cl_2 solution.

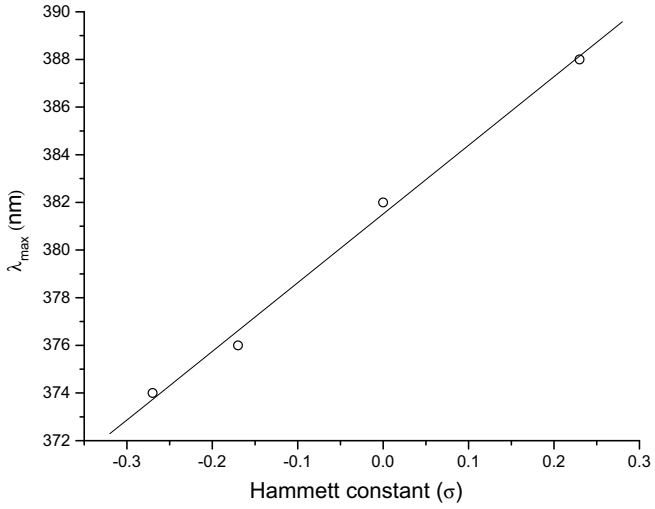

Fig. 4. Plot of λ_{max} *vs.* Hammett constant (σ) of complexes **1–4**.

These correlations have *r* values of ∼1.0 and 0.98, respectively and the estimated error in $d\lambda_{max}/d\sigma$ and $dE_p^c/d\sigma$ value is, respectively, 1.57 and 0.025. The estimated error in the intercept of Figs. 4 and 5 is, respectively, 0.31 and 0.005. These two relations indicate that the dependence of the λ_{max} value on the substituent (i.e., $d\lambda_{max}/d\sigma$) is 28.82 nm and that of E_p^c value (i.e., $dE_p{}^c/d\sigma$) is 0.19 V.

By the elimination of σ from the above two linear equations (6) and (7), one can obtain the following Eq. (8), a relation between λ_{max} and E_p^c parameters:

$$\lambda_{max}\ (\text{nm}) = 351.25 + 151.68 \times E_p^c \quad (8)$$

Almost identical relation, equation (9) is obtained with *r* value ∼0.99 when λ_{max} values are plotted against the respective E_p^c values (Fig. 6).

$$\lambda_{max} = 351.85 + 148.15 \times E_p^c \quad (9)$$

All these relations demonstrate the sensitivity of the vanadium electron density on σ of the R substituent in these dinuclear complexes.

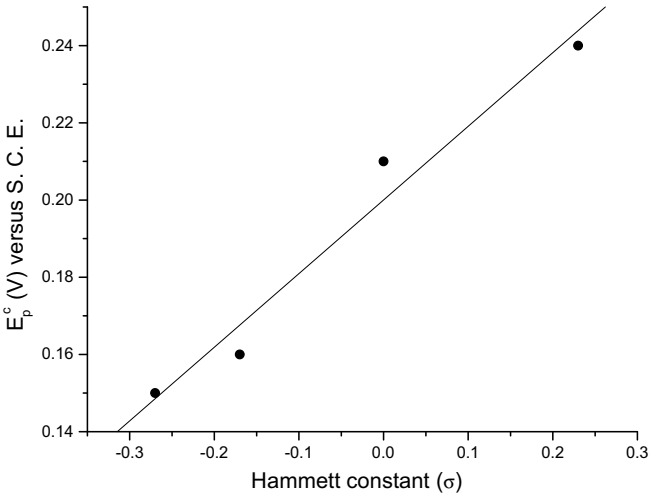

Fig. 5. Plot of E_p^c *vs.* Hammett constant (σ) of complexes **1**–**4**.

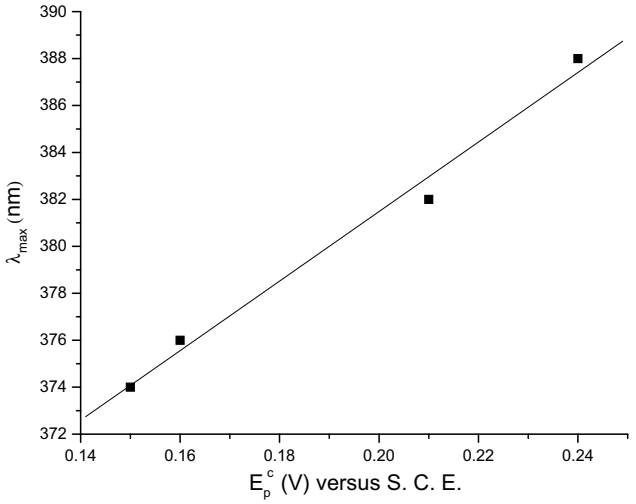

Fig. 6. Plot of λ_{max} *vs.* E_p^c of complexes **1**–**4**.

3.9. Reaction of $K(H_2O)^+[VO_2(L)]^-$ (**5**–**8**) complexes with ascorbic acid

The reaction of $K(H_2O)^+[VO_2(L)]^-$ complexes with ascorbic acid was monitored spectrophotometrically. In each case after the addition of reducing agent (*ca.* 10 times than of the complex) a new band in the visible region near 675 nm ($\varepsilon \sim 250\ dm^3\ mol^{-1}\ cm^{-1}$) (Table 4, Fig. 7) was detected which is assigned to a d–d transition of the resulting V^{IV} species [43,44]. After keeping the solution for sometime, the intensity of the new band decreases gradually and finally the initial spectrum was obtained in a time interval ~12 h. These observations strongly suggest that during the reaction with ascorbic acid, the $K(H_2O)^+[VO_2(L)]^-$ complexes are reduced by it to form the corresponding V^{IV} complex presumably of the type $[V^{IV}O_2(L)]^{2-}$. The reappearance of an almost identical original spectrum (before reduction) after ~12 h indicates that the ligand remained coordinated to the vanadium in the reduced V^{IV} species and these reduced species are not stable under this environment.

Table 4
Electronic spectral (400-800 nm) data of the complexes **5**–**8** in presence of excess (~10 times) ascorbic acid in methanol at 298 K

Compound	λ_{max}, nm (ε, $dm^3\ mol^{-1}\ cm^{-1}$)
$K(H_2O)^+[VO_2(L^1)]^-$ (**5**)	674 (226)
$K(H_2O)^+[VO_2(L^2)]^-$ (**6**)	677 (258)
$K(H_2O)^+[VO_2(L^3)]^-$ (**7**)	678 (262)
$K(H_2O)^+[VO_2(L^1)]^-$ (**8**)	674 (244)

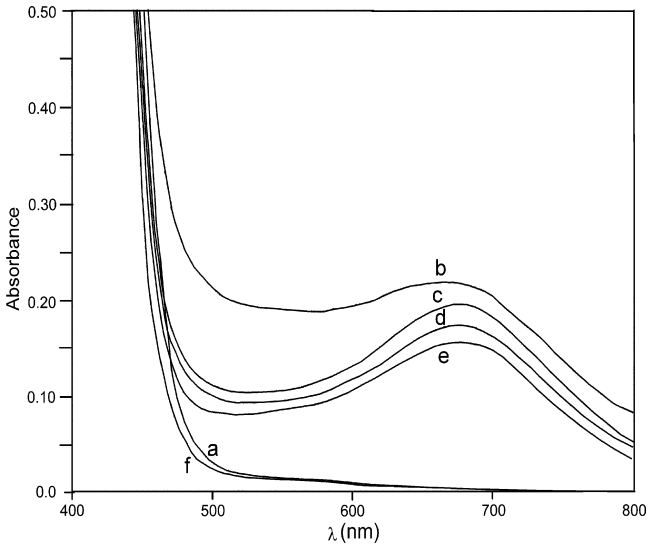

Fig. 7. Electronic spectra (400–800 nm) of a 7.973×10^{-4} mol dm^{-3} methanol solution of complex **2**: (a) before the addition of ascorbic acid, (b) immediately after the addition of ascorbic acid, (c) 10 min after the addition of ascorbic acid, (d) 30 min after the addition of ascorbic acid, (e) 60 min after the addition of ascorbic acid and (f) 720 min after the addition of ascorbic acid. The amount of ascorbic acid was about 10 times than that of the concentration of the complex.

4. Conclusion

Hydrazone complexes **1**–**4** containing $V_2O_3^{4+}$ motif can be synthesized following various synthetic routes starting from different VO^{2+} precursors and these hydrazone ligands are very suitable for the stabilization of this motif. The formation of these dinuclear complexes from the decomposition of mixed-ligand $[V^{IV}O(L)(bipy/phen)]$ complexes in CH_2Cl_2 solution indicates that these ligands have strong tendency for the stabilization of vanadium in its highest (+V) oxidation state. These dinuclear complexes can be converted to the complexes with VO_2^+ motif simply by increasing the pH (~11) of the solution (with the addition of KOH) and to the complexes with VO^{3+} motif by adding a monobasic bidentate strong chelating ligand (viz., Hhq). This study also indicates that the substituents(R) have significant effect on controlling the spectroscopic and electro-chemical properties of vanadium in these oxo-bridged dinuclear complexes. The dioxovanadium(V) complexes are reduced reversibly by the ascorbic acid under aerobic condition which is biologically important particularly in relation to insulin enhancing activity.

Acknowledgements

Our sincere thanks are due to the University Grants Commission (New Delhi, India) for financial assistance. We are grateful to our College authorities for providing research facilities. We are also grateful to Dr. S. Chattopadhyay, Department of Inorganic Chemistry, University of Kalyani, Kalyani, India for electrochemical measurements. We thank EPSRC and the University of Reading, UK for funds for the Image Plate System.

Appendix A. Supplementary data

CCDC 654298 and 654300 contain the supplementary crystallographic data for **2** and **4**. These data can be obtained free of charge via http://www.ccdc.cam.ac.uk/conts/retrieving.html, or from the Cambridge Crystallographic Data Centre, 12 Union Road, Cambridge CB2 1EZ, UK; fax: (+44) 1223-336-033, or e-mail: deposit@ccdc.cam.ac.uk. Supplementary data associated with this article can be found, in the online version, at doi:10.1016/j.poly.2008.03.018.

References

[1] D. Rehder, Inorg. Chem. Commun. 6 (2003) 604.
[2] S. Yamada, C. Katayama, J. Tanaka, M. Tanaka, Inorg. Chem. 23 (1984) 253.
[3] K. Nakajima, M. Kojima, K. Toriumi, K. Saito, J. Fujita, Bull. Chem. Soc. Jpn. 62 (1989) 760.
[4] U. Casellato, P.A. Vigato, R. Graziani, M. Vidali, F. Milani, M.M. Musiani, Inorg. Chim. Acta 61 (1982) 121.
[5] A.A. Diamantis, J.M. Frederiksen, Md.A. Salam, M.R. Snow, E.R.T. Tiekink, Aust. J. Chem. 39 (1986) 1081.
[6] S. Dutta, P. Basu, A. Chakravorty, Inorg. Chem. 32 (1993) 5343.
[7] J. Chakravarty, S. Dutta, A. Chakravorty, J. Chem. Soc., Dalton Trans. (1993) 2857.
[8] H. Schmidt, M. Bashirpoor, D. Rehder, J. Chem. Soc., Dalton Trans. (1996) 3865.
[9] C. Grüning, H. Schmidt, D. Rehder, Inorg. Chem. Commun. 2 (1999) 57.
[10] N.R. Sangeetha, S. Pal, Bull. Chem. Soc. Jpn. 73 (2000) 357.
[11] R. Dinda, P. Sengupta, S. Ghosh, T.C.W. Mak, Inorg. Chem. 41 (2002) 1684.
[12] A. Sundheim, R. Mattes, Z. Naturforsch. 48B (1993) 1848.
[13] R.R. Eady, Coord. Chem. Rev. 237 (2003) 23 and references therein.
[14] (a) D. Rehder, G. Santoni, G.M. Licini, C. Schulzke, B. Meier, Coord. Chem. Rev. 237 (2003) 53;
(b) J.N. Carter-Frankline, J.D. Parrish, R.A. Tchirret-Guth, R.D. Little, A. Butler, J. Am. Chem. Soc. 125 (2003) 3688.
[15] P.J. Stankicwicz, A.S. Tracey, D.C. Crans, in: H. Sigel, A. Sigel (Eds.), Vanadium and its Role in Life, Metal Ions in Biological Systems, vol. 31, Marcel Dekker, New York, 1995 (Chapter 9).
[16] (a) F. Wolf, C. Lorber, R. Choukroun, B. Donnadieu, Inorg. Chem. 42 (2003) 7839;
(b) C. Lorber, R. Choukroun, B. Donnadieu, Inorg. Chem. 42 (2003) 673;
(c) H. Hagen, J. Boersma, G. van Koten, Chem. Soc. Rev. 31 (2002) 357;
(d) S. Gambarotta, Coord. Chem. Rev. 237 (2003) 229.
[17] (a) H.B. ten Brink, H.E. Schoemaker, R. Wever, Eur. J. Biochem. 268 (2001) 132;
(b) T.S. Smith, V.L. Pecoraro, Inorg. Chem. 41 (2002) 6754.
[18] A. Evangelou, Crit. Rev. Oncol. Hematol. 42 (2002) 249.
[19] (a) S.A. Dikanov, B.D. Liboiron, C. Orvig, J. Am. Chem. Soc. 124 (2002) 2969;
(b) D.C. Crans, L. Yang, J.A. Alfano, L.H. Chi, W. Jin, M. Mahroof-Tahir, K. Robbins, M.M. Toloue, L.K. Chan, A.J. Plante, R.Z. Grayson, G.R. Willsky, Coord. Chem. Rev. 237 (2003) 13.
[20] A. Butler, J.V. Walker, Chem. Rev. 93 (1993) 1937.
[21] M.J.M. Campbell, Coord. Chem. Rev. 15 (1975) 279.
[22] T. Ghosh, B. Mondal, T. Ghosh, M. Sutradhar, G. Mukherjee, M.G.B. Drew, Inorg. Chim. Acta 360 (2007) 1753.
[23] R.A. Rowe, M.M. Jones, Inorg. Synth. 5 (1957) 113.
[24] T. Ghosh, B. Mondal, J. Chem. Res. (2007) 407.
[25] W. Kabsch, J. Appl. Crystallogr. 21 (1988) 916.
[26] G.M. Sheldrick, SHELX-97 Program for Crystallography Refinement, University of Gottingen, Germany, 1997.
[27] N. Walker, D. Stuart, Acta Crystallogr., Sect. A 39 (1983) 158.
[28] CRYSALIS Program, Oxford Diffraction Ltd., 2005.
[29] ABSPACK Program, Oxford Diffraction Ltd., 2005.
[30] A.L. Spek, PLATON-94 Program, Utrecht University, The Netherlands, 2004.
[31] T. Ghosh, B. Mondal, R. Banerjee, Unpublished results.
[32] S. Perlepes, D. Nicholls, M.R. Harrison, Inorg. Chim. Acta 102 (1985) 137.
[33] M.R. Maurya, S. Khurana, W. Zhang, D. Rehder, J. Chem. Soc., Dalton Trans. (2002) 3015.
[34] M.R. Maurya, S. Agarwal, C. Bader, M. Ebel, D. Rehder, J. Chem. Soc., Dalton Trans. (2005) 537.
[35] T. Ghosh, S. Bhattacharya, A. Das, G. Mukherjee, M.G.B. Drew, Inorg. Chim. Acta 358 (2005) 989.
[36] V. Vergopoulos, W. Priebsch, M. Fritzsche, D. Rehder, Inorg. Chem. 32 (1993) 1844.
[37] G. Asgedom, A. Sreedhara, J. Kivikoski, J. Valkonen, E. Kolehmainen, C.P. Rao, Inorg. Chem. 35 (1996) 5674.
[38] M. Sutradhar, G. Mukherjee, M.G.B. Drew, S. Ghosh, Inorg. Chem. 45 (2006) 5150.
[39] E.L. Muetterties, L.J. Guggenberger, J. Am. Chem. Soc. 96 (1974) 1748.
[40] A.W. Addison, T.N. Rao, J. Reedjik, J. van Rijn, G.C. Verschoor, J. Chem. Soc., Dalton Trans. (1984) 1349.
[41] W.J. Geary, Coord. Chem. Rev. 7 (1971) 81.
[42] L.P. Hammett, Physical Organic Chemistry, 2nd ed., McGraw-Hill, New York, 1970.
[43] T. Ghosh, Transit. Met. Chem. 31 (2006) 560.
[44] P. Noblía, E.J. Baran, L. Otero, P. Draper, H. Cerecetto, M. González, O.E. Piro, E.E. Castellano, T. Inohara, Y. Adachi, H. Sakurai, D. Gambino, Eur. J. Inorg. Chem. (2004) 322.

Polyhedron 27 (2008) 2202–2208

Contents lists available at ScienceDirect

Polyhedron

journal homepage: www.elsevier.com/locate/poly

Synthesis, structures and photophysical properties of polynuclear copper(I) iodide complexes containing phosphine and 4,4′-bipyridine ligands

Xin Gan [a], Wen-Fu Fu [a,c,*], Yong-Yue Lin [b], Mei Yuan [c], Chi-Ming Che [b,*], Shao-Ming Chi [a], Hui-Fang Jie Li [a], Jian-Hua Chen [a], Yong Chen [c], Zhong-Yong Zhou [d]

[a] College of Chemistry and Chemical Engineering, Yunnan Normal University, Kunming 650092, PR China
[b] Department of Chemistry, HKU-CAS Joint Laboratory on New Materials, The University of Hong Kong, Pokfulam Road, Hong Kong SAR, PR China
[c] Technical Institute of Physics and Chemistry, Chinese Academy of Sciences, Peking 100080, PR China
[d] Department of Applied Biology and Chemical Technology, The Hong Kong Polytechnic University, Hong Hum, Hong Kong SAR, PR China

ARTICLE INFO

Article history:
Received 14 October 2007
Accepted 22 March 2008
Available online 20 May 2008

Keywords:
Copper(I) iodide
Mixed ligands
Polynuclear complexes
Crystal structures
Photochemical studies

ABSTRACT

The highly luminescent polynuclear Cu^{I} iodide complexes, $[(Cu_2I_2)(4,4'\text{-bipy})(PCy_3)_2]_2 \cdot 4H_2O$ (**1**), $[(Cu_2I_2)(4,4'\text{-bipy})(PCy_3)_2]_\infty$ (**2**), $[(Cu_2I_2)(4,4'\text{-bipy})(dcpm)]_\infty$ (**3**) and $[(Cu_2I_2)(4,4'\text{-bipy})(dppm)]_\infty$ (**4**), were prepared by reacting CuI with tricyclohexylphosphine (PCy_3), bis(dicyclohexylphosphino)methane (dcpm) or bis(diphenylphosphino)methane (dppm) and 4,4′-bipyridine (4,4′-bipy), and their structures were determined by X-ray crystal analysis. The reported complexes $[CuClPCy_3]_2$ (**5**) and $[CuIPCy_3]_2$ (**6**) were also prepared for comparison. In solid state, complexes **1**–**6** display intense long-lived phosphorescence with λ_{max} at 605, 565, 640, 570, 430 and 450 nm at room temperature, and the solid-state emission quantum yields are 0.11, 0.20, 0.29, 0.35, 0.67 and 0.83, respectively. The relatively high-energy emissions of **5** and **6** are attributed to arising from metal-centered MC ($3d \rightarrow 4s, 4p$) excited state, while the low-energy emissions of **1**–**4** are assigned to a metal-to-ligand charge transfer ($d \rightarrow \pi^*$ MLCT) excited state.

© 2008 Elsevier Ltd. All rights reserved.

1. Introduction

Copper(I) complexes of polypyridyl ligands, such as $[Cu(diimine)_2]^+$, have been extensively studied for their potential applications in photocatalysis, molecular electronics and materials science [1–4]. The structures of polynuclear Cu^{I} complexes formed by the reaction of CuX and phosphine or bulky nitrogen organic base have been described previously [5–11]. All these complexes contain μ_2 or μ_3-bridging X atoms, and their structures are dependent upon the phosphine or nitrogen donor auxiliary ligands. The complexes $[CuXPCy_3]_2$ (X = Cl, I) are neutral dimeric species, they have been structurally characterized but no photophysical properties have been reported [12]. Recent studies showed that polynuclear Cu^{I} complexes containing halide and phosphine ligands have intriguing structures and rich photoluminescent properties [13–15]. Examples of these copper(I) complexes having Cu centers arranged in a tetrahedron with the tetrahedral faces capped by halides are known [16]. There are also examples of polymeric copper(I) complexes having a "stairstep" configuration [17]. In the case of $[(CuI)_4(dcpm)_2]$, the peripheral dcpm and iodide ligands bridge each edge of the Cu_4 plane to form a $Cu_4P_4I_2$ core [18]. In general, polynuclear Cu^{I} complexes with phosphine and halide ligands have multiple emissive excited states, which were assigned to the excited state with either metal-to-ligand charge-transfer MLCT or ligand-to-metal charge-transfer XMCT, or a mixture of halide-to-copper and metal-centered MC charge-transfer parentage [19]. Ford and Vogler had reported detailed studies on the photophysical properties of the tetranuclear cubane CuX clusters with dpmp (dpmp = 2-(diphenylmethyl)pyridine) and Py (Py = pyridine) ligands [20]. The relatively higher energy emissions for the complexes $Cu_4X_4L_4$ at 440–500 nm were attributed to coming from halide-to-ligand charge-transfer XLCT excited states, whereas the longer wavelength emissions at 570–630 nm were assigned to originate from excited states with mixed XMCT and MC orbital parentages [21]. In this work, we report the structures and spectroscopic properties of the polynuclear Cu^{I} complexes, $[(Cu_2I_2)(4,4'\text{-bipy})(PCy_3)_2]_2 \cdot 4H_2O$ (**1**), $[(Cu_2I_2)(4,4'\text{-bipy})(PCy_3)_2]_\infty$ (**2**), $[(Cu_2I_2)(4,4'\text{-bipy})(dcpm)]_\infty$ (**3**) and $[(Cu_2I_2)(4,4'\text{-bipy})(dppm)]_\infty$ (**4**). The photophysical properties of the reported complexes $[CuClPCy_3]_2$ (**5**) and $[CuIPCy_3]_2$ (**6**) were also examined for comparison purpose, but their syntheses and crystal structures would not be described in this paper [12].

* Corresponding authors. Address: College of Chemistry and Chemical Engineering, Yunnan Normal University, Kunming 650092, PR China.
E-mail addresses: wf_fu@yahoo.com.cn (W.-F. Fu), cmche@hku.hk (C.-M. Che).

0277-5387/$ - see front matter © 2008 Elsevier Ltd. All rights reserved.
doi:10.1016/j.poly.2008.03.026

2. Experimental

The CuX (Aldrich), 4,4′-bipyridine (Aldrich), PCy_3 (Strem), dcpm (Strem) and dppm (Aldrich) were used as received. Solvents (HPLC grade) used in the spectroscopic procedure were dried over suitable reagents and distilled under an argon atmosphere immediately prior to use.

2.1. Preparation of $[(Cu_2I_2)(4,4'\text{-bipy})(PCy_3)_2]_2$ (**1**) and $[(Cu_2I_2)(4,4'\text{-bipy})(PCy_3)_2]_\infty$ (**2**)

To a suspending solution of CuI (0.095 g, 0.5 mmol) in dichloromethane (15 mL) was added solid 4,4′-bipyridine (0.039 g, 0.25 mmol). The mixture was stirred for 4 h, and then PCy_3 (0.14 g, 0.5 mmol) in dichloromethane (5 mL) was added to the yellow suspending solution. The mixture became red immediately and the yellow suspension dissolved gradually. The resulting solution was stirred for another 2 h and then filtered. The reaction mixture was concentrated in vacuum and the crude product was recrystallized from CH_2Cl_2/diethyl ether to give the orange crystals of complex **1**. 0.173 g (63%). ^{31}P NMR ($CDCl_3$): δ 51.5. *Anal.* Calc. $C_{92}H_{148}N_4P_4Cu_4I_4$ (powders): C, 50.33; H, 6.80; N, 2.55. Found: C, 50.28; H, 6.91; N, 2.59%. If the preparation of complex **1** was processed by refluxing in dichloromethane, complex **2** were obtained. 0.195 g (71%). ^{31}P NMR ($CDCl_3$): δ 51.7. *Anal.* Calc. $(C_{46}H_{74}N_2P_2Cu_2I_2)_\infty$: C, 50.33; H, 6.80; N, 2.55. Found: C, 50.42; H, 6.71; N, 2.61%.

2.2. Preparation of $[(Cu_2I_2)(4,4'\text{-bipy})(dcpm)]_\infty$ (**3**) and $[(Cu_2I_2)(4,4'\text{-bipy})(dppm)]_\infty$ (**4**)

Complex **3** was synthesized by adding excess 4,4′-bipyridine (0.078 g, 0.5 mmol) to a suspending solution of CuI (0.095 g, 0.5 mmol) in dichloromethane (20 mL). The mixture was stirred for 2 h, and dcpm (0.102 g, 0.25 mmol) in dichloromethane (5 mL) was then added to the yellow suspending solution. The mixture became red gradually. The product was separated by filtration, and the crude product was recrystallized from CH_2Cl_2/$CHCl_3$/diethyl ether to give the red crystals. 0.137 g (58%). ^{31}P NMR ($CDCl_3$): δ −2.8. *Anal.* Calc. $(C_{35}H_{54}N_2P_2Cu_2I_2)_\infty$: C, 44.45; H, 5.76; N, 2.96. Found: C, 44.51; H, 5.73; N, 3.05%. The orange crystals of complex **4** were prepared following the same procedure as **3** except that dppm was used. 0.154 g (67%). ^{31}P NMR ($CDCl_3$): δ −20.8. *Anal.* Calc. $(C_{35}H_{30}N_2P_2Cu_2I_2)_\infty$: C, 45.62; H, 3.28; N, 3.04. Found: C, 45.54; H, 3.36; N, 3.14%.

2.3. Calculation details

All calculations were carried out at the GAUSSIAN 03 package in Virtual Laboratory for Computational Chemistry, CNIC, CAS at the B3LYP level [22,23]. The basis sets which contained in G03 library used for C, P, N and H atoms was 6-31G(d) while effective core potentials with a LanL2DZ basis set of G03 were employed for transition metals. The 6-311G (d) basis set for I, Cl was downloaded from the EMSL basis set library [24]. The contour plots of MOs were obtained with the Gauss View 3.07 program.

2.4. Instrumentation and physical measurements

Electronic absorption spectra were recorded at ambient temperature with a HP8453 UV–Vis spectrophotometer. Crystals of suitable size were mounted either on glass fibres or in capillary tubes. X-ray data were collected either on an MAR PSD for **1**, a Rigaku Saturn for **2**, or a Bruker SMART diffractometer for **3** and **4**. Intensity data were collected by ω-2θ scans technique. The images were interpreted and integrated using program of DENZO [25]. The structures were solved by Direct method (SIR92) or Patterson method (PATTY) and expanded by Fourier method [26]. Structural refinement on F or F^2 by full-matrix least square analysis was performed using the SHELXL 97 program [27]. The ORTEP drawings of the structures were displayed with hydrogen atoms omitted for clarity. The unweighted and weighted agreement factors (R_f, R_w) and the goodness of fit are calculated. Crystal data and details on data collection and refinement are summarized in Table 1.

Corrected emission spectra were obtained on a Spex Fluorolog-2 Model F III A1 fluorescence spectrofluorometer adapted to a right-angle configuration. Filters of suitable bandpass were used to cut off the second harmonic of the monochromatic excitation light source and stray light. Solutions for emission measurements were degassed by at least four freeze–pump–thaw cycles. Low-temperature (77 K) emission spectra for glass- and solid-state samples were recorded for 5-mm diameter quartz tubes which were

Table 1
Selected crystallographic and data collection parameters for complexes **1**–**4**

Complex	**1**	**2**	**3**	**4**
Formula	$C_{92}H_{156}N_4P_4Cu_4I_4O_4$	$C_{46}H_{74}N_2P_2Cu_2I_2$	$C_{70}H_{108}Cu_4I_4N_4P_4$	$C_{70}H_{60}Cu_4I_4N_4P_4$
M	2267.97	1097.89	1891.24	1842.97
T (K)	301	113	294(2)	294(2)
Crystal system	triclinic	triclinic	orthorhombic	orthorhombic
Space group	$P\bar{1}$	$P\bar{1}$	$Pbn2_1$	$Pna2_1$
a (Å)	10.267(2)	9.992(2)	17.413(5)	23.859(4)
b (Å)	15.135(5)	13.992(3)	19.386(5)	18.306(3)
c (Å)	18.274(3)	17.802(4)	23.367(6)	17.338(3)
α (°)	73.34(2)	79.044(6)	90	90
β (°)	74.83(2)	87.595(6)	90	90
γ (°)	86.16(2)	83.709(4)	90	90
V (Å^3)	2625.5(10)	2428.2(9)	7888(4)	7573(2)
Z	1	2	4	4
D_{calc} (g cm^{-3})	1.434	1.502	1.593	1.613
Crystal size (mm)	0.20 × 0.10 × 0.07	0.18 × 0.16 × 0.10	0.20 × 0.18 × 0.14	0.20 × 0.18 × 0.14
F(000)	1156	1116	3776	3568
Index range (h, k, l)	0, 12; −18, 18; −20, 21	−13, 13; −19, 19; −24, 24	−22, 20; −21, 25; −30, 29	−35, 21; −23, 23; −22, 22
$2\theta_{max}$ (°)	51	58.14	55.2	55.2
Number of unique reflection	8344	12418	17280	16788
R_f	0.051	0.034	0.0536	0.0612
R_w	0.065	0.0852	0.0928	0.1544
Goodness-of-fit	1.87	1.035	0.998	1.010
Residual electron density (e Å^{-3})	1.01, −0.89	0.855, −1.988	0.92, −0.82	0.939, −0.886

placed inside a liquid nitrogen bath contained in a quartz optical Dewa flask.

Measurement of emission quantum yields of powdered samples involves determining the diffuse reflectance of complexes **1**–**6** relative to KBr at the excitation wavelength [28]. The measured results were corrected according to the relative response of the detector as a function of wavelength. Emission lifetimes of solid or solution samples were performed with a Quanta Ray DCR-3 Nd-YAG laser with pulse-width of 8 ns and excitation wavelength of 266 nm (fourth harmonic). Emission signals were collected at right angles to the excitation pulse by a Hamamatsu R928 photomultiplier tube and recorded on a Tektronix model 2430 digital oscilloscope.

3. Results and discussion

3.1. Description of the structures

The photophysical properties of CuX complexes with phosphine and/or bulky nitrogen organic base ligands have received considerable interest over the past decades. The complexes $[(Cu_2I_2)(4,4'\text{-bipy})(PCy_3)_2]_2 \cdot 4H_2O$ (**1**) and $[(Cu_2I_2)(4,4'\text{-bipy})(PCy_3)_2]_\infty$ (**2**) were both obtained by reacting CuI with tricyclohexylphosphine and 4,4′-bipyridine in stoichiometric ratio of 1:1:0.5 in dichloromethane solutions. When the reaction was conducted at room temperature, **1** was isolated with two water molecules of crystallization. In contrast, the 1-D complex **2** was obtained from the reaction in refluxing dichloromethane solution. Their structures have been determined by X-ray crystal analysis. Perspective views of the molecules are depicted in Figs. 1 and 2, and their bond lengths and angles are given in Table 2. The asymmetric unit of complex **1** consists of half the molecule and the whole molecule is generated by inversion, as shown in Fig. 1. Complex **1** contains a 22-membered ring, and can be viewed as two $[CuIPCy_3]_2$ fragments connected by two bridging 4,4′-bipyridine ligands. In contrast, **2** consists of $[(Cu_2I_2)(PCy_3)_2]$ subunits bridged by 4,4′-bipyridine ligands into an infinite chain, being similar to that of $[(Cu_2I_2)(4,4'\text{-bipy})(PPh_3)_2]_\infty$ [29]. The Cu atoms of **1** and **2** have a distorted tetrahedral configuration. The distortion from tetrahedral geometry is evidenced by the wider P–Cu–N angle (123.2(2)°) and the narrower I–Cu–N (101.6(2)°), I–Cu–I (103.17(4)°) ones for **1**, and P–Cu–N (119.40(7)°), I–Cu–N (102.03(7)°) and I–Cu–I (105.14 (2)°) ones for **2**. Both complexes exhibit symmetric CuI_2Cu core. The average Cu–I bond lengths of 2.727 Å for **1**, and 2.680 Å for **2** are slightly longer than those of 2.573 Å in **6**. The average Cu–I–Cu angles in both **1** (72.48°) and **2** (77.00°) are slightly larger than that of **6** (70.97°). Complex **1** has a Cu···Cu distance of 3.224(2) Å, whereas different Cu···Cu distances of 3.267(0) and 3.404(1) Å are found in **2**. We note that the two pyridyl rings of 4,4′-bipyridine in **2** are twisted with a dihedral angle of 27.6°, while the 4,4′-bipyridine in **1** is almost coplanar.

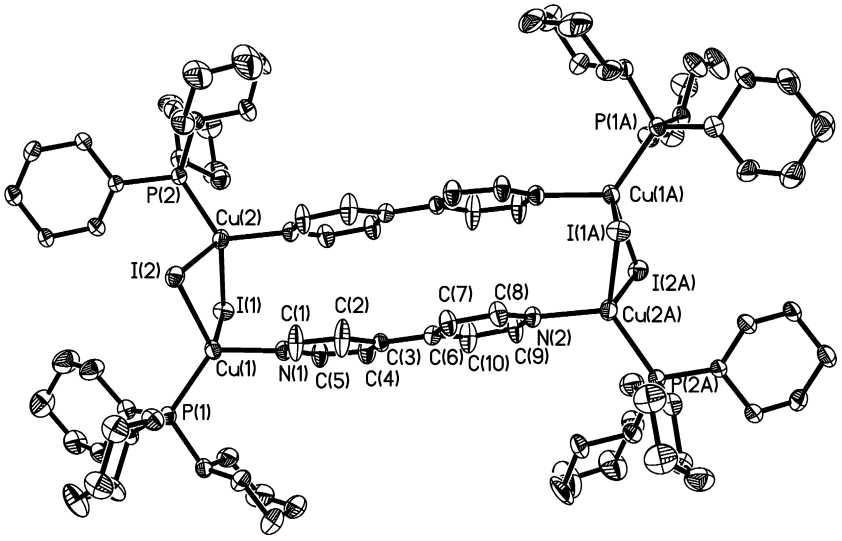

Fig. 1. Perspective view of $[(Cu_2I_2)(4,4'\text{-bipy})(PCy_3)_2]_2$ (30% probability ellipsoids).

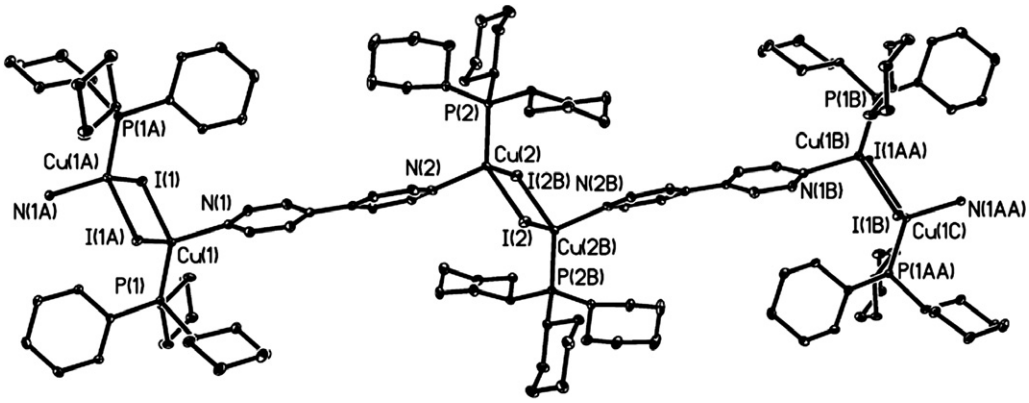

Fig. 2. Perspective view of $[(Cu_2I_2)(4,4'\text{-bipy})(PCy_3)_2]_\infty$ (30% probability ellipsoids).

Table 2
Selected bond lengths and bond angles of **1**–**4**

Complex ***1***			
Cu(1)–I(1)	2.778(1)	Cu(2)–I(1)	2.722(1)
Cu(1)–P(1)	2.237(2)	Cu(1)–N(1)	2.079(7)
Cu(1)–I(1)–Cu(2)	71.77(4)	I(1)–Cu(1)–I(2)	103.17(4)
I(1)–Cu(1)–N(1)	101.6(2)	I(1)–Cu(1)–P(1)	108.66 (7)
Complex ***2***	#1 $-x, -y, -z+2$	#2 $-x+2, -y, -z+1$	
Cu(1)–I(1)	2.6613(6)	Cu(1)–I(1)#1	2.7119(7)
Cu(1)–P(1)	2.2285(9)	Cu(1)–N(1)	2.054(2)
Cu(2)–I(2)#2	2.6442(7)	Cu(2)–I(2)	2.6993(6)
Cu(2)–P(2)	2.2287(9)	Cu(2)–N(2)	2.058(2)
N(1)–Cu(1)–P(1)	119.40(7)	I(1)–Cu(1)–I(1)#1	105.14(2)
N(1)–Cu(1)–I(1)#1	102.96(7)	P(1)–Cu(1)–I(1)#1	107.64(2)
I(1)–Cu(1)–N(1)	102.03(7)	I(1)–Cu(1)–P(1)	117.93(7)
N(2)–Cu(2)–P(2)	114.09(7)	N(2)–Cu(2)–I(2)#2	109.93(7)
P(2)–Cu(2)–I(2)#2	111.02(2)	N(2)–Cu(2)–I(2)	98.35(7)
P(2)–Cu(2)–I(2)	121.19(3)	I(2)#2–Cu(2)–I(2)	100.87(2)
Cu(1)–I(1)–Cu(1)#1	74.860(16)	Cu(2)#2–I(2)–Cu(2)	79.13(2)
Complex ***3***			
Cu(1)···Cu(2)	2.7110(9)	Cu(3)···Cu(4)	2.7240(9)
Cu(1)–I(1)	2.6917(9)	Cu(1)–I(2)	2.761(1)
Cu(1)–P(1)	2.203(1)	Cu(1)–N(1)	2.044(3)
Cu(1)–I(1)–Cu(2)	60.45(2)	N(1)–Cu(1)–I(1)	100.99(7)
N(1)–Cu(1)–P(1)	123.37(8)	N(1)–Cu(1)–Cu(2)	141.31(8)
P(1)–Cu(1)–Cu(2)	95.31(3)	I(1)–Cu(1)–Cu(2)	59.82(3)
Cu(2)–Cu(1)–I(2)	60.59(3)	P(1)–Cu(1)–I(1)	112.89(3)
Complex ***4***			
Cu(1)···Cu(2)	2.7827(7)	Cu(3)···Cu(4)	2.7706(7)
I(1)–Cu(1)	2.5971(6)	I(2)–Cu(1)	2.7490(6)
Cu(1)–N(1)	2.042(3)	Cu(1)–P(1)	2.226(1)
Cu(1)–I(1)–Cu(2)	61.18 (2)	N(1)–Cu(1)–P(1)	114.16(8)
N(1)–Cu(1)–I(1)	106.29(7)	P(1)–Cu(1)–I(1)	118.24(3)
I(1)–Cu(1)–I(2)	105.37(2)	I(1)–Cu(1)–Cu(2)	63.96(2)

The preparation of $[(Cu_2I_2)(4,4'\text{-bipy})(dcpm)]_\infty$ (**3**) and $[(Cu_2I_2)(4,4'\text{-bipy})(dppm)]_\infty$ (**4**) are similar to that of **1** except that the PCy_3 ligand is replaced by bridging dcpm or dppm ligand. Perspective views of **3** and **4** are depicted in Figs. 3 and 4, respectively. Selected bond lengths and angles of the complexes are listed in Table 2. The structures of **3** and **4** consist of 1-D [–Cu(P^P) $(\mu_2\text{-I})_2$Cu(4,4′-bipy–)] zig-zag chains. The [–Cu(P^P)$(\mu_2\text{-I})_2$Cu(4,4′-bipy–)] unit as the building block contains two 6-membered rings with bridging biphosphine and iodide lignds, and a distorted square –Cu$(\mu_2\text{-I})_2$Cu– unit with torsion angles being 36.25(2)° and 41.75(2)° in **3** and **4**, respectively (Fig. 4). In contrast, for **4** there are two crystallographically non-equivalent chains. The Cu···Cu distances in **3** (2.7110 Å) and **4** (2.7706 Å) are slightly shorter than that in **6** (2.8925 Å), while the Cu–I–Cu bond angles are 59.91(2)° for **3** and 61.41(2)° for **4**. The coordination geometry of the Cu^I center in **4** is much close to tetrahedron with bond angles varying from 104.91(7)° to 114.16(8)°, whereas those angles of **3** vary from 100.99(7)° to 123.37(8)°. The two pyridyl rings of bridging 4,4′-bipy ligand are twisted with dihedral angles being 29.3(4)° and 26.3(4)° for **3** and **4**, respectively.

3.2. Electronic absorption spectra

The UV–Vis absorption spectral data for **1**–**6** in acetonitrile or dichloromethane solutions are summarized in Table 3 and the absorption spectra are depicted in Fig. 5. For **5** and **6**, the electronic absorption spectra in dichloromethane show high-energy absorption peaks at 233 nm with tails extending to ca. 320 nm. A definitive assignment of the UV absorption is difficult due to the strong absorption of the ligands. However, density functional theory (DFT) calculation showed HOMO–LUMO gaps are 223.5 and 235.7 nm for **5** and **6**, respectively. This is consistent with the experimental results described as MC (metal-centered) transition (Fig. 6). The DFT investigations of complexes **2**–**4** containing bipy ligand show that the character of the HOMO is dominated by metal orbitals with iodide contribution, whereas the LUMO is mainly localized on the pyridyl rings and displays π^* character (Fig. 6). The energy gaps were calculated for **2**–**4**, being 337, 392 and 397 nm, respectively. The calculated wavelength nicely correlates with the presence of the broad absorption bands measured at 350–390 nm in dichloromethane solutions of **1**–**4**. Thereby, the low-energy absorptions are assigned to a MLCT ($Cu^I \rightarrow$ 4,4′-bipyridine) transition.

Complexes **5** and **6** have vacant coordination site at Cu^I, allowing for substrate-binding reactions. As depicted in Fig. 5, the absorption bands of **5** and **6** in acetonitrile solutions are red-shifted from 260 and 270 nm in dichloromethane to 275 and 286 nm, respectively, indicating the coordination of CH_3CN to Cu^I centers. Furthermore, this absorption band around 360 nm of **1** and **2** in dichloromethane is not present in acetonitrile solutions (**3** and **4** being sparely soluble). Indeed, the similarity of the absorption spectra for complexes **1**, **2**, **5** and **6** in acetonitrile solutions suggests that the substitution of 4,4′-bipyridine by CH_3CN solvent molecule occurs in the case of **1** and **2**.

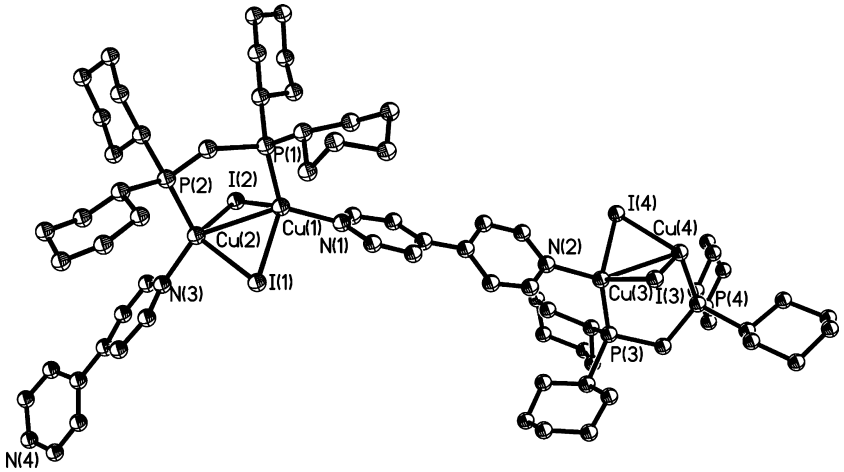

Fig. 3. Perspective view of $[(Cu_2I_2)(4,4'\text{-bipy})(dcpm)]_\infty$ (30% probability ellipsoids).

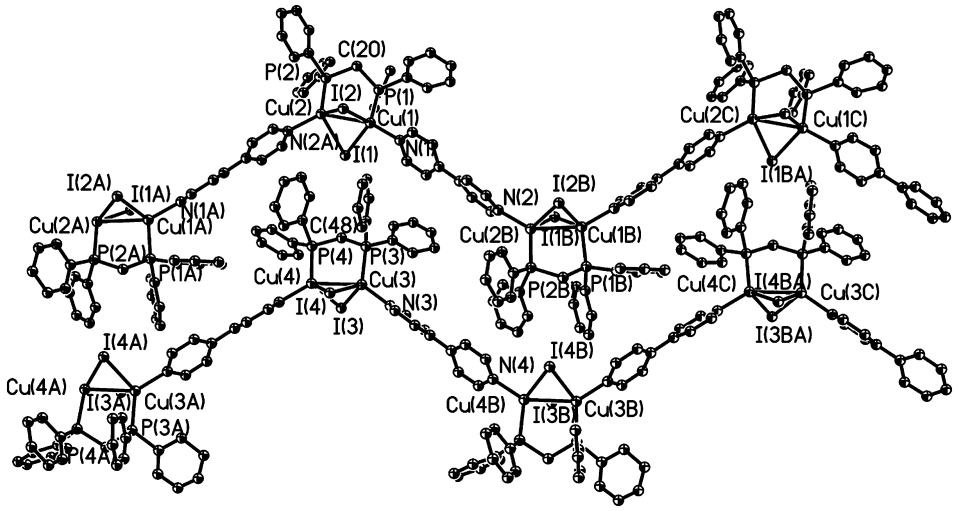

Fig. 4. Perspective view of $[(Cu_2I_2)(4,4'\text{-bipy})(dppm)]_\infty$ (30% probability ellipsoids).

3.3. Emission spectra

Upon excitation at 330 nm, **1**–**6** exhibit intense photoluminescence with λ_{max} at 605, 565, 640, 570, 430 and 450 nm and the measured emission quantum yields are 0.11, 0.20, 0.29, 0.35, 0.67 and 0.83 in the solid state at room temperature, respectively (Figs. 7 and 8). The high solid-state emission quantum yields of **5** and **6** suggest that the $[CuXPCy_3]_2$ solids can be useful as blue light emitting materials. The spectral data are summarized in Table 3. The emissions have lifetimes on the microsecond timescale, implying that these emissions originate from triplet excited state. We propose that the relative high-energy emissions for **5** and **6** originate from metal-centered 3d → (4s, 4p) triple excited state, and the low-energy emissions for **1**, **2**, **3** and **4** are from the triplet-parentage MLCT excited state, assignment of the latter is based on the results of DFT calculations and the fact that the emission maxima for **1**–**4** are red-shifted from that of **6** [30].

The solid state of complexes **1** and **2** at 77 K exhibits intense luminescences at 640 and 580 nm which are ascribed to phosphorescence derived from the ^{3}MLCT state. Whereas complex **6** displays two intense emission bands centered at 455 and 395 nm in solid state at 77 K, which are similar to the solid emissions of the reported $[(CuI)_4(pyridine)_4]$, $[(CuI)_3(dcpm)_2]$, and $[(CuI)_4(dcpm)_2]$ complexes at 77 K [18,31]. In butyronitrile glassy solution at 77 K, both of **5** and **6** exhibit two emission bands at 400, 480 nm and 390, 480 nm, respectively. The low-energy emission centered at 480 nm is tentatively attributed to solvent exciplex formation. All complexes are non-emissive in dichoromethane or acetonitrile solutions.

Table 3
Spectroscopic and photophysical properties of complexes **1**–**6**

complex	Medium (T/K)	λ_{abs} (nm) (ε [dm^3 mol^{-1} cm^{-1}])	λ_{em} (nm)/ι (μs)	ϕ_{em}
1	CH_2Cl_2 (298)	232 (80 492), 269 (sh) (18 933), 363 (sh) (2077)	Non-emissive	
	CH_3CN (298)	242 (93 620), 267 (sh) (15 769)	Non-emissive	
	Glass (77)[a]		545/41.8	
	Solid (298)		605/1.8	0.11
	Solid (77)		640/3.8	
2	CH_2Cl_2 (298)	232 (51 287), 267 (sh) (13 238), 355 (sh) (2755)	Non-emissive	
	CH_3CN (298)	244 (55 100), 270 (sh) (6230)	Non-emissive	
	Glass (77)[a]		550/50.1	
	Solid (298)		565/2.2	0.20
	Solid (77)		580/81.1	
3	CH_2Cl_2 (298)	236 (21 458), 385 (sh) (1196)	Non-emissive	
	Solid (298)		640/1.3	0.29
4	CH_2Cl_2 (298)	270 (sh) (13 502), 365 (321)	Non-emissive	
	Solid (298)		570/2.6	0.35
5	CH_2Cl_2 (298)	234 (13 403), 260 (sh) (270)	Non-emissive	
	CH_3CN (298)	226 (19 822), 275 (sh) (849)	Non-emissive	
	Glass (77)[a]		400/22.8, 480 (sh)/53.2	
	Solid (298)		430/37.3	0.67
	Solid (77)		430/57.4	
6	CH_2Cl_2 (298)	233 (17 063), 270 (sh) (2053)	Non-emissive	
	CH_3CN (298)	244 (31 288), 286 (sh) (571)	Non-emissive	
	Glass (77)[a]		390/55.7, 480/86.0	
	Solid (298)		450/3.9	0.83
	Solid (77)		395/7.8, 455/4.8	

[a] Solvent: butyronitrile; sh = shoulder.

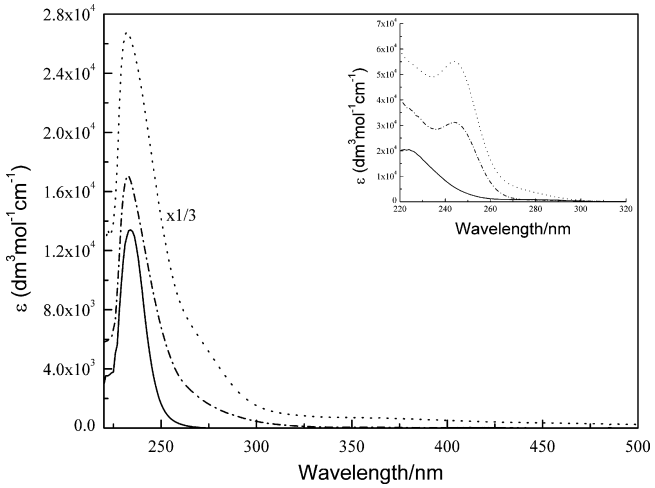

Fig. 5. UV–Vis spectra of $[(Cu_2I_2)(4,4'\text{-bipy})(PCy_3)_2]_2$ (dot line), $[CuClPCy_3]_2$ (solid line) and $[CuIPCy_3]_2$ (dashed dot line) in dichloromethane solution at room temperature. Inset: complexes $[(Cu_2I_2)(4,4'\text{-bipy})(PCy_3)_2]_\infty$ (dot line) **5** (solid line) and **6** (dashed dot line) in acetonitrile.

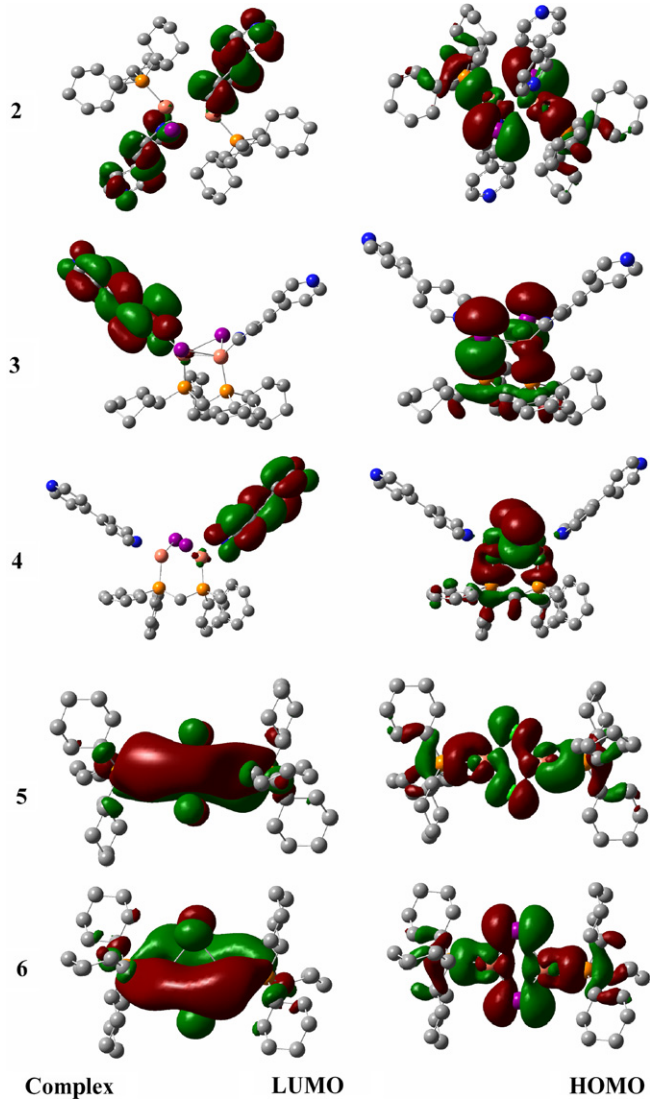

Fig. 6. Plots of the relevant HOMOs and LUMOs for complexes **2**–**6**.

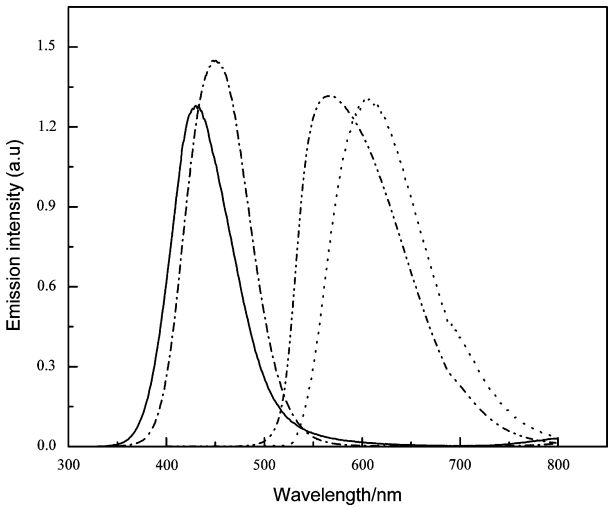

Fig. 7. Room-temperature solid-state emission spectra of $[(Cu_2I_2)(4,4'\text{-bipy})(PCy_3)_2]_2$ (dot line), $[(Cu_2I_2)(4,4'\text{-bipy})(PCy_3)_2]_\infty$ (dashed dot dot line), $[CuClPCy_3]_2$ (solid line) and $[CuIPCy_3]_2$ (dashed dot line) with excitation at 330 nm.

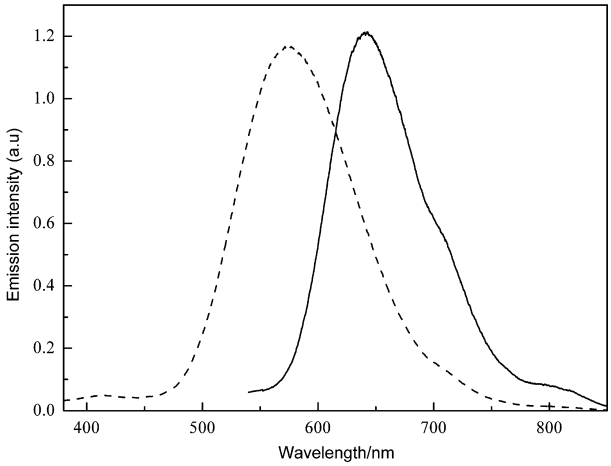

Fig. 8. Room-temperature solid-state emission spectra of $[(Cu_2I_2)(4,4'\text{-bipy})(dcpm)]_\infty$ (solid line) and $[(Cu_2I_2)(4,4'\text{-bipy})(dppm)]_\infty$ (**4**) (dashed line) with excitation at 330 nm.

4. Conclusion

In this work, we obtained four new polynuclear Cu^I complexes by reacting CuI with 4,4′-bipyridine and tricyclohexylphosphine, bis(dicyclohexylphosphino)methane or bis(diphenylphosphino)-methane. Their crystal structures and photophysical properties have been examined. Also, we have examined the spectroscopic properties of the related $[CuClPCy_3]_2$ and $[CuIPCy_3]_2$ complexes. All of the complexes exhibit intense phosphorescent emissions with λ_{em} varying 430–640 nm in solid state at room temperature. These emissions were attributed to arising from metal-centered MC (3d → 4s, 4p) excited state for **5** and **6**, and a triplet-parentage MLCT (Cu^I → 4,4′-bipyridine) excited state for **1**–**4**. The successful preparation of these Cu^I complexes with relatively high emission quantum yields in solid state provides great potential for light emitting materials.

Acknowledgement

The work was supported by the National Basic Research Program of China (973 program 2005CCA06800, 2007CB613304), the

National Natural Science Foundation of China (NSFC Grant No. 20761006, 20671094, 90610034). We thank the foundation (50418010) for NSFC/RGC Joint Research.

Appendix A. Supplementary material

CCDC 639946, 639947, 639948 and 639949 contain the crystallographic data for (**1**), (**2**), (**3**) and (**4**). These data can be obtained free of charge via http://www.ccdc.cam.ac.uk/conts/retrieving.html, or from the Cambridge Crystallographic Data Center, 12 Union Road, Cambridge CB2 1EZ, UK; fax: (+44) 1223-336-033; or e-mail: deposit@ccdc.cam.ac.uk. Supplementary data associated with this article can be found, in the online version, at doi:10.1016/j.poly.2008.03.026.

References

[1] D.R. McMillin, K.M. McNett, Chem. Rev. 98 (1998) 1201.
[2] M. Ruthkosky, C.A. Kelly, F.N. Castellano, G.J. Meyer, Coord. Chem. Rev. 171 (1998) 309.
[3] J.R. Nitschke, Angew. Chem., Int. Ed. 43 (2004).
[4] M.T. Miller, P.K. Gantzel, T.B. Karpishin, J. Am. Chem. Soc. 121 (1999) 4292.
[5] I. Jeb, P. Taborsky, J. Pospíšil, C. Näther, Dalton Trans. (2007) 2263.
[6] J. Díez, M.P. Gamasa, J. Gimeno, A. Aguirre, S. García-Granda, J. Holubova, L.R. Falvello, Organometallics 18 (1999) 662.
[7] R. Wolf, E. Hey-Hawkins, Angew. Chem., Int. Ed. 44 (2005) 6241.
[8] G. Kickelbick, U. Reinöhl, T.S. Ertel, A. Weber, H. Bertagnolli, K. Matyjaszewski, Inorg. Chem. 40 (2001) 6.
[9] A. Tsuboyama, K. Kuge, M. Turugori, S. Okada, M. Hoshino, K. Ueno, Inorg. Chem. 46 (2007) 1992.
[10] T.H. Kim, Y.W. Shin, J.S. Kim, S.S. Lee, J. Kim, Inorg. Chem. Commun. 10 (2007) 717.
[11] H. Araki, K. Tsuge, Y. Sasaki, S. Ishizaka, N. Kitamura, Inorg. Chem. 44 (2005) 9667.
[12] (a) M.R. Churchill, F.J. Rotella, Inorg. Chem. 18 (1979) 166;
(b) G.L. Soloveichik, O. Eisenstein, J.T. Poulton, W.E. Streib, J.C. Huffman, K.G. Caulton, Inorg. Chem. 31 (1992) 3306.
[13] Z. Mao, H.Y. Chao, Z. Hui, C.M. Che, W.F. Fu, K.K. Cheung, N.Y. Zhu, Chem. Eur. J. 9 (2003) 2885.
[14] V.W.W. Yam, W.K.M. Fung, K.K. Cheung, Angew. Chem., Int. Ed. 35 (1996) 1100.
[15] X.Y. Liu, F. Mota, P. Alemany, J.J. Novoa, S. Alvarez, Chem. Commun. (1998) 1149.
[16] L.M. Engelhardt, P.C. Healy, J.D. Kildea, A.H. White, Aust. J. Chem. 42 (1989) 107.
[17] N.S. Persky, J.M. Chow, K.A. Poschmann, N.N. Lacuesta, S.L. Stoll, S.G. Bott, S. Obrey, Inorg. Chem. 40 (2001) 29.
[18] W.F. Fu, X. Gan, C.M. Che, Q.Y. Cao, Z.Y. Zhu, N.Y. Zhu, Chem. Eur. J. 10 (2004) 2228.
[19] J.A. Simon, W.E. Palke, P.C. Ford, Inorg. Chem. 35 (1996) 6413.
[20] A. Vogler, H. Kunkely, J. Am. Chem. Soc. 108 (1986) 7211.
[21] C.K. Ryu, M. Vitale, P.C. Ford, Inorg. Chem. 32 (1993) 869.
[22] M.J. Frisch, G.W. Trucks, H.B. Schlegel, et al. GAUSSIAN 03, Revision C.02 Gaussian Inc., Wallingford CT, 2004.
[23] C. Lee, W. Yang, R.G. Parr, Phys. Rev. B 37 (1988) 785.
[24] EMSL basis set library available at <http://www.emsl.pnl.gov/forms/basisform.html>.
[25] DENZO: In "The HKL Manual – A description of programs DENZ O, XDISPLAYF, and SCALEPACK" written by D. Gewirth with the cooperation of the program authors Z. Otwinowski and W. Minor (1995), Yale University, New Haven, USA.
[26] (a) SIR 92 D. Harker, J.S. Kasper, Acta Crystallogr. 1 (1948) 70;
(b) PATTY: P.T. Beurskens, G. Admiraal, G. Beurskens, W.P. Bosman, S. Garcia-Granda, R.O. Gould, J.M.M. Smits, C. Smykalla. The DIRDIF Program System, Technical Report of the Crystallography Laboratory, University of Nijmegen, The Netherlands, 1992.
[27] G.M. Sheldrick, SHELXS-97 and SHELXL-97, Programs for the Solution and Refinement of Crystal Structures, University of Göttingen, Germany, 1997.
[28] M.S. Wrighton, D.S. Ginley, D.L. Morse, J. Phys. Chem. 78 (1974) 2229.
[29] R.Z. Li, D. Li, X.C. Huang, Z.Y. Qi, X.M. Chen, Inorg. Chem. Commun. 6 (2003) 1017.
[30] P. Pallavicini, M. Boiocchi, G. Dacarro, C. Mangano, New J. Chem. 31 (2007) 927.
[31] K.R. Kyle, C.K. Ryu, J.A. DiBenedetto, P.C. Ford, J. Am. Chem. Soc. 113 (1991) 2954.

Polyhedron 27 (2008) 2209–2215

Contents lists available at ScienceDirect

Polyhedron

journal homepage: www.elsevier.com/locate/poly

Synthesis, structure and reactivity of *azosalophen* complexes of palladium

Poulami Pattanayak [a], Jahar Lal Pratihar [a], Debprasad Patra [a], Vedavati G. Puranik [b], Surajit Chattopadhyay [a,*]

[a] Department of Chemistry, University of Kalyani, Kalyani, West Bengal 741 235, India
[b] Center for Materials Characterization, National Chemical Laboratory, Pune 411 008, India

ARTICLE INFO

Article history:
Received 6 March 2008
Accepted 14 March 2008
Available online 19 May 2008

Keywords:
Orthopalladation
Oxygen insertion
2-(arylazo)-1-*N*-salicylidene phenylamine
Azosalophen complex

ABSTRACT

The ligands 2-(arylazo)-1-*N*-salicylidene phenylamine, H_2L_{sal}, (where H represents the dissociable protons upon complexation) afford stable orthopalladated complexes, $[(L_{sal})Pd]$, upon treatment with $Na_2[PdCl_4]$. The dinegative anionic $(L_{sal})^{2-}$ ligands bind Pd(II) in a tetradentate (C, N, N, O) fashion with a distorted square planar geometry. The newly synthesized palladium complexes underwent oxygen insertion into the Pd–C bond with *m*CPBA (*m*-chloroperbenzoic acid) or TBHP (terbutylhydroperoxide)/$[VO(acac)_2]$ leading to the formation of stable *azosalophen* complexes of Pd(II) with the (O, N, N, O) coordination mode of the oxygenated ligand.

© 2008 Elsevier Ltd. All rights reserved.

1. Introduction

The synthesis of target molecules via metal assisted routes is an important area of current chemical research [1]. Interest in the chemistry of transition metal complexes incorporating the *salen* type of ligands, **1**, has accelerated research in this area during the last few years due to the discovery of their catalytic properties – towards alkene epoxidation in particular [2].

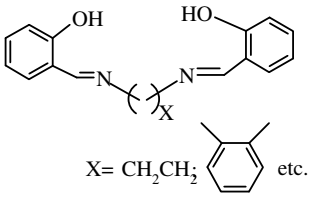

1

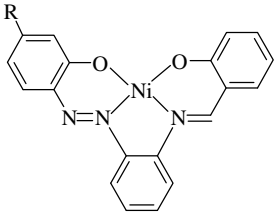

2

Studies on tuning the catalytic activity of such complexes by modifying the ligand backbone are under progress. As a consequence, developments in the area of asymmetric epoxidation of unfunctionalised alkenes are remarkable [3]. Recently, we have reported the synthesis and properties of Ni(II) complexes incorporating new *azosalophen* ligands, **2** [4]. Although the *azosalophen* ligands are analogous to *salen*-like ligand systems in terms of coordination mode, there are significant differences in the characteristics of the donor atoms. The Ni(II)-*azosalophen* complexes could be prepared via orthonickelation followed by O-insertion into the Ni-C(aryl) bond with peroxo oxygen donors [4]. As described earlier, issues relating to O-insertion with peroxo reagents needed to be studied more extensively [4]. The inquisitiveness to such issues and our desire to prepare *azosalophen* complexes of a heavier congener of the group 10 elements (*i.e.* Pd(II)) prompted us to carry out this work.

Herein we report the synthesis and structure of new orthopalladated complexes of tetradentate (C, N, N, O) azo-aldimine ligands and the reactions of the newly synthesized Pd-C (aryl) bonded compounds with peroxo reagents, *viz.* *m*CPBA and TBHP, to obtain Pd(II) analogues of **2**.

2. Results and discussion

2.1. Syntheses and characterization of cyclopalladated $[(L_{sal})Pd]$ complexes

The reaction of H_2L_{sal}, **3**, with sodium tetrachloropalladate, $Na_2[PdCl_4]$, in warm methanol afforded the orthopalladated complexes $[(L_{sal})Pd]$, **4** (Eq. (1)). The analytical and spectroscopic data matched well with the formulation. The structure was confirmed by X-ray studies on $[(L^3{}_{sal})\ Pd]$ (see below) as a representative example.

* Corresponding author. Tel.: +91 9830141198; fax: +91 33 25828282.
E-mail address: scha8@rediffmail.com (S. Chattopadhyay).

0277-5387/$ - see front matter © 2008 Elsevier Ltd. All rights reserved.
doi:10.1016/j.poly.2008.03.028

eqn (1)

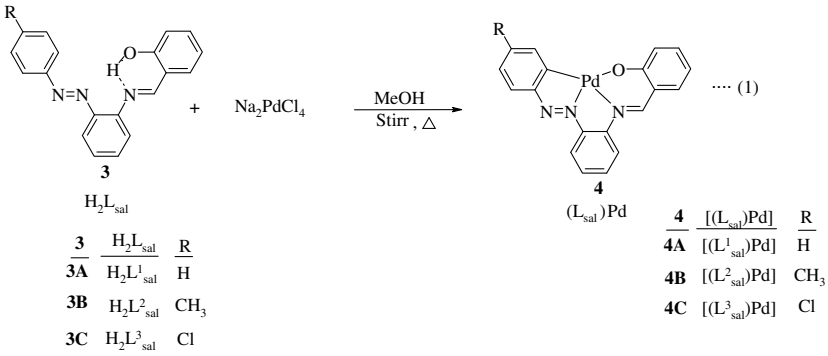

H_2L_{sal}

3	H_2L_{sal}	R
3A	$H_2L^1_{sal}$	H
3B	$H_2L^2_{sal}$	CH_3
3C	$H_2L^3_{sal}$	Cl

4	[(L_{sal})Pd]	R
4A	[(L^1_{sal})Pd]	H
4B	[(L^2_{sal})Pd]	CH_3
4C	[(L^3_{sal})Pd]	Cl

The *bi*- and *tri*-dentate azo and imine ligands [5–7] have been demonstrated to form orthopalladated complexes, as given in Chart 1 (**5**–**9**). The complexes of type **9** are good examples where orthopalladation occurs in tridentate azo–imine ligand systems [5d]. It is worthwhile to mention, in this context, that [(L_{sal})Pd], **4**, are a type of orthopalladated complex incorporating tetradentate azo–imine ligands and the coordination mode (C, N, N, O) is also new.

The orange–brown solutions of the [(L_{sal})Pd] complexes in dichloromethane (CH_2Cl_2) display characteristic UV–Vis spectra with several structured absorption bands within the region 300–500 nm for MLCT transitions. A representative UV–Vis spectrum of [(L^2_{sal})Pd], **4B**, is shown in Fig. 1. The spectral data are collected in Section 3 and the spectra of the other complexes are given in Figs. S1–S3 (supplementary).

The $\nu_{C=N}$ and $\nu_{N=N}$ bands of the [(L_{sal})Pd] complexes are shifted to lower wavenumbers (~1605 and ~1430 cm^{-1}, respectively) than those of the ligands (~1615 and ~1452 cm^{-1}, respectively), consistent with the coordination of the aldimine (N=CH) and azo (N=N) nitrogens [4]. The IR spectral data of all the [(L_{sal})Pd] complexes are collected in Section 3 and the spectra are given in Figs. S4–S6.

The atom numbering scheme for the ^1H NMR spectral analysis is given in Fig. 3 (see below). The ^1H NMR spectra show that the aldimino proton (N=CH) of the [(L_{sal})Pd] complexes shifts marginally upfield (δ 8.43–8.57) relative to the ligands (~δ8.62) [4]. The –OH signal of the free ligands (~δ13.60) [4] is absent in the palladium complexes indicating deprotonation of the phenolic groups and their coordination to the metal as phenoxide. Twelve aromatic protons of [(L^1_{sal})Pd] (**4A**) appear within the δ 6.57–7.85 range. The ^1H NMR spectrum of [(L^2_{sal})Pd] (**4B**), and [(L^3_{sal})Pd] (**4C**), are less complicated in the aromatic region. The disappearance of two doublet resonances for 3, 5-H and 2, 6-H of the $H_2L^2_{sal}$ and $H_2L^3_{sal}$ ligands in **4B** and **4C** were

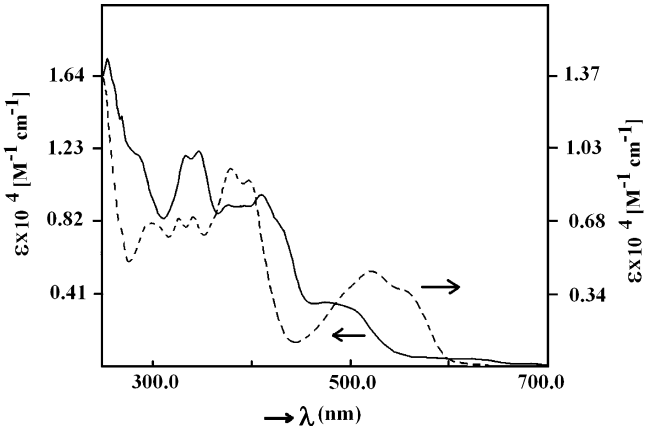

Fig. 1. UV–Vis spectra of **4B** (—) and **10B** (- - -). The arrows indicate the scales of the corresponding spectra.

attributed to the metallation at the ortho carbon of the pendant aryl ring. Unfortunately the singlet for 3H did not separate from the other aromatic proton resonances in the spectra of **4B** and **4C**. The ^1H NMR spectra of [(L_{sal})Pd] are given in Figs. S7–S9 and data are collected in Section 3.

The electrospray mass spectrum (HRMS-QTOF) in CH_2Cl_2 solution (positive mode) was recorded for [(L^3_{sal})Pd], **4C**, as a representative example (Fig. 2). The mass spectrum is consistent with the composition and molecular mass. The major envelope could be simulated satisfactorily (Fig. 2b) on the basis of the formula $C_{19}H_{12}N_3PdOCl$.

Unequivocal characterization of the orthometallated complexes, [(L_{sal})Pd], was performed by X-ray analysis of [(L^3_{sal})Pd]

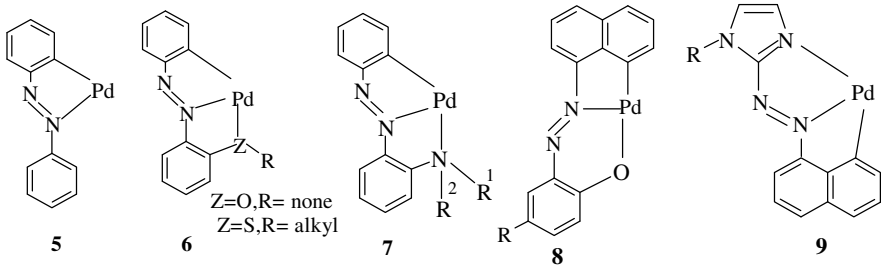

Chart 1.

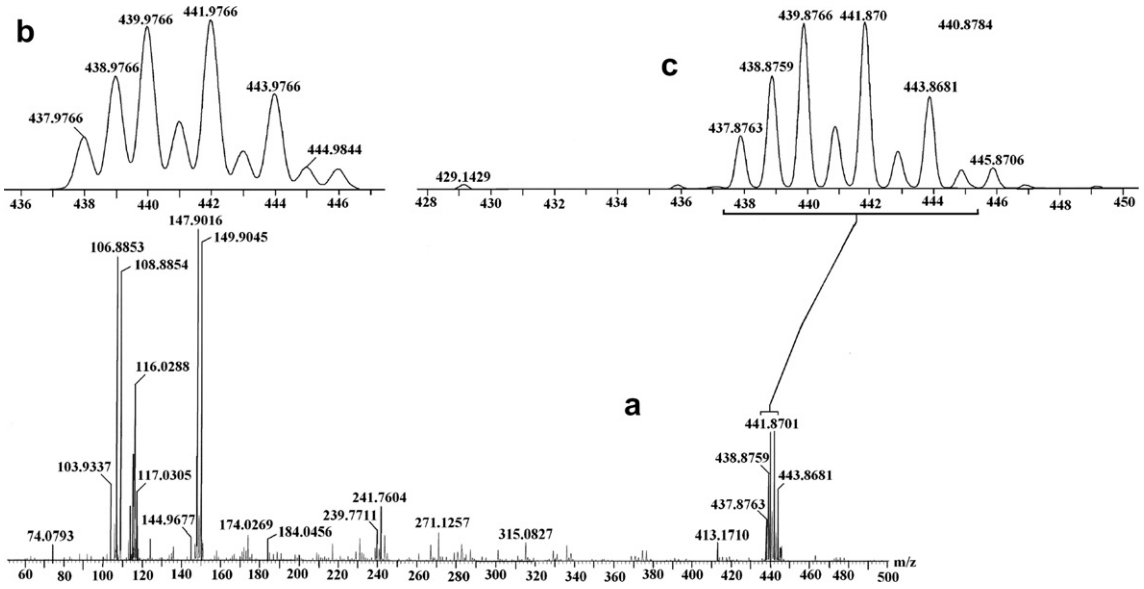

Fig. 2. (a) Electrospray mass spectrum (positive mode) of [(L^3_{sal})Pd] in CH_3CN. (b) Simulated spectrum of [(L^3_{sal})Pd]. (c) Enlarged view of the major envelope of the original spectrum.

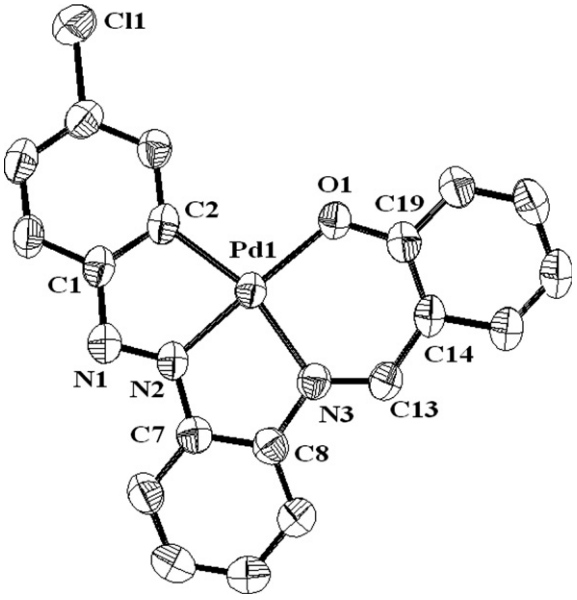

Fig. 3. Perspective view of the molecular structure of [(L^3_{sal})Pd] with the atom numbering scheme. The hydrogen atoms have been omitted for clarity.

Table 1
Selected bond distances (Å) and angles (°) for Compound **4C**

Distances			
Pd(1)–O(1)	1.995(3)	N(3)–C(8)	1.424(5)
Pd(1)–N(3)	2.023(3)	N(3)–C(13)	1.300(5)
Pd(1)–N(2)	1.922(4)	C(7)–C(8)	1.401(5)
Pd(1)–C(2)	2.002(4)	C(1)–C(2)	1.409(7)
O(1)–C(19)	1.320(5)	C(14)–C(19)	1.425(5)
N(1)–N(2)	1.269(5)	C(13)–C(14)	1.434(5)
N(1)–C(1)	1.401(5)		
Angles			
N(2)–N(1)–C(1)	109.1(4)	Pd(1)–N(3)–C(8)	111.4(3)
O(1)–Pd(1)–N(3)	95.09(13)	N(2)–Pd(1)–C(2)	102.79(16)
O(1)–Pd(1)–C(2)	102.79(16)	N(2)–Pd(1)–N(3)	82.74(14)
N(1)–N(2)–C(7)	121.2(3)	N(3)–Pd(1)–C(2)	161.85(17)
N(2)–Pd(1)–N(3)	82.74(14)	Pd(1)–N(3)–C(8)	111.4(3)

(**4C**). Fig. 3 shows the perspective view of the molecular structure. Table 1 contains selected bond distances and angles. The dinegative anion $(L^3_{sal})^{2-}$ binds the Pd(II) centre in a distorted square planar geometry.

The Pd(C, N, N, O) coordination sphere of the [(L^3_{sal})Pd] molecule is planar with a maximum deviation of 0.08 Å from the least square plane. The planar molecules in the asymmetric unit are held as weak staggered dimers with Pd–Pd distances of 3.197 Å, as shown in Fig. 4.

The dimers are arranged in a stair-like manner where the inter dimer Pd–Pd distance is 6.296 Å. Pd–C 2.002(4) Å and Pd–O 1.995(3) Å distances are within the normal range [5a,7]. Between the Pd–N(azo) and Pd–N(imine) distances, the former is shorter due to either stronger π-backbonding or a stronger *trans* influence of carbon [8,9c] compared to the phenoxide oxygen.

2.2. Syntheses and characterization of [(OL_{sal})Pd] from [(L_{sal})Pd]

The new oxygenated complexes, [(OL_{sal})Pd] (**10**), were prepared by the highly selective metaloxylation [10] of [(L_{sal})Pd] with

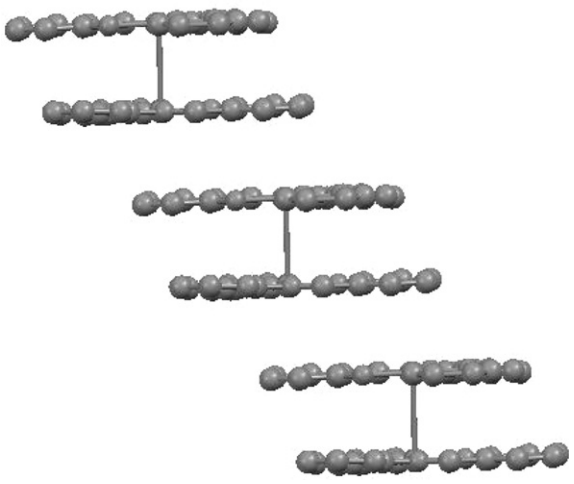

Fig. 4. Packing of [(L^3_{sal})Pd] showing the stair-like arrangement of planar molecules. The line between a pair indicates the weak Pd···Pd interaction at a distance of 3.206 Å

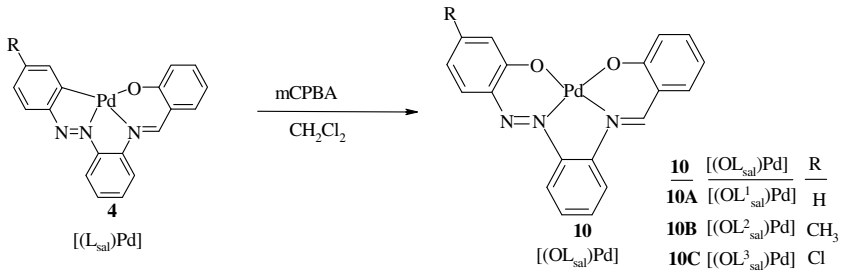

Scheme 1.

*m*CPBA. The oxygen insertion into the Pd–C bond of [(L$_{sal}$)Pd] occurred upon treatment with *m*CPBA in dichloromethane solvent at room temperature to afford diamagnetic and electro neutral Pd(II) complexes, [(OL$_{sal}$)Pd] (Scheme 1). The formation of the [(OL$_{sal}$)Pd] complexes from [(L$_{sal}$)Pd], was monitored spectrophotometrically up to the extent of ~75% conversion. Nevertheless, after every reaction, the pure [(OL$_{sal}$)Pd] complex was isolated in ~50% yield on employing a conventional purification procedure on a silica gel preparative TLC plate. Although the large difference between the spectrophotometric and isolated yields could not be accounted for, it was believed that a transformation on the silica gel TLC plate may be one of the reasons, since the pure products separated well leaving unidentified materials at the bottom of the plate.

The metaloxylated complexes, [(OL$_{sal}$)Pd], displayed two characteristic low energy overlapping absorptions near 560 and 520 nm in contrast to the parent orthopalladated complexes. Representative spectra of [(OL$^2_{sal}$)Pd] and [(L$^2_{sal}$)Pd] are given in Fig. 1 for comparison. There are six MLCT absorptions for [(OL$_{sal}$)Pd] in the 300–560 nm range. UV–Vis spectral data are collected in Section 3 and the spectra are given in Figs. S10 – S12.

The $\nu_{C=N}$ and $\nu_{N=N}$ stretches for the [(OL$_{sal}$)Pd] complexes appear in the ranges 1605–1607 cm^{-1} and 1430–1445 cm^{-1}, indicating the coordination of the azo (N=N) and aldimine (N=CH) nitrogen donors [4]. The IR spectra are given in Figs. S13–S15 and the spectral data are collected in Section 3.

The ^{1}H NMR spectra of the [(OL$_{sal}$)Pd] complexes feature the aldimine (N=CH) proton resonance near δ 8.60, indicating the intactness of the azo-methine function upon treatment with *m*CPBA. The spectral patterns for the aromatic protons of [(OL$_{sal}$)Pd] are similar to the parent [(L$_{sal}$)Pd] complexes, but there are expected mismatches in the chemical shifts. The singlet for 3-H separated well in the case of [(OL$^2_{sal}$)Pd] indicating substitution at C3. The ^{1}H NMR spectral features for the aromatic protons of all the complexes are consistent with their formulation and structures. Data are collected in Section 3 and the ^{1}H NMR spectra are given in Figs. S16–S18.

The electrospray mass spectrum in CH_2Cl_2 solution (positive mode) has been recorded for [(OL$^3_{sal}$)Pd] as a representative example. The mass spectrum is consistent with the composition and molecular mass. The major envelope could be simulated satisfactorily on the basis of the formula $C_{19}H_{13}N_3PdO_2Cl$ (Fig. 5).

The difference of 16 units between the masses of [(L$^3_{sal}$)Pd] and [(OL$^3_{sal}$Pd)] justified the O-insertion into the Pd–C bond.

Reaction of (L$_{sal}$)Pd (**4**) with *t*-butylhydroperoxide (TBHP) in protic (^{t}BuOH) or aprotic (CH_2Cl_2) solvents did not afford the metaloxylated complexes, [(OL$_{sal}$)Pd] (**10**), whereas in the presence of a catalytic amount of [VO(acac)$_2$] the metaloxylation reaction occurred in both CH_2Cl_2 or ^{t}BuOH solvents. Thus the oxygen transfer process has been assumed to take place via an *in situ* formation of a vanadium-peroxo species. The oxygen insertions into the Pd–C bond with *m*CPBA for orthopalladated complexes incorporating

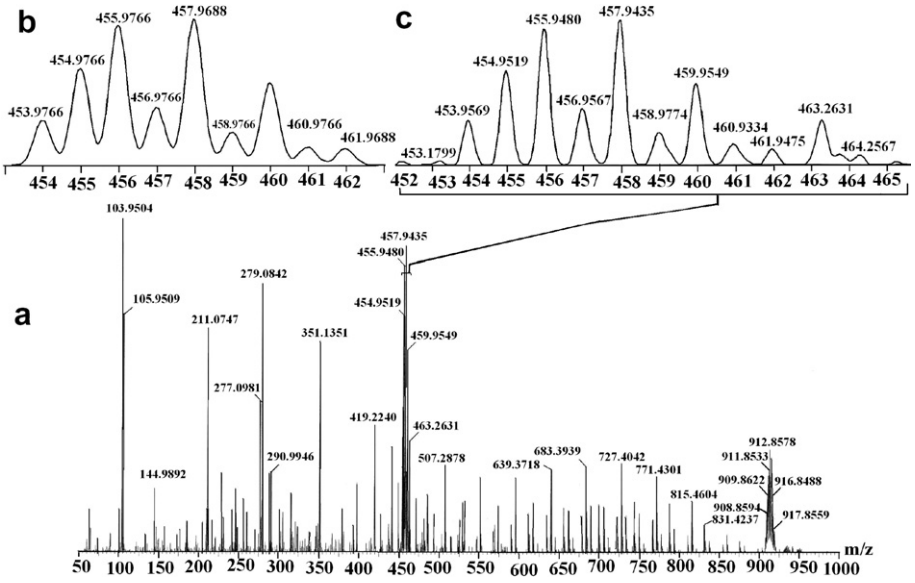

Fig. 5. (a) Electrospray mass spectrum (positive mode) of [(OL$^3_{sal}$)Pd] in CH_3CN. (b) Simulated spectrum of [(OL$^3_{sal}$)Pd]. (c) Enlarged view of the major envelope of the original spectrum.

azobenzene and related ligands were reported earlier [10]. TBHP induced oxygen insertion is hitherto unknown for such complexes.

3. Experimental

3.1. Materials

The solvents used in the reactions were of reagent grade obtained from E. Merck, Kolkata, India and were purified and dried by reported procedures [11]. Palladium chloride was purchased from Arora Matthey (India). H_2O_2 (6%, 50% in aqueous solution) was purchased from E. Merck, Kolkata, India. *m*CPBA (~70%) (the activity of *m*CPBA was determined iodometrically before use and it was 47.5%) and TBHP (~70%) were obtained from Aldrich, USA and used as received. Disodium tetrachloropalladate was prepared by a reported procedure [12]. 2-(Arylazo) aniline was prepared according to the procedure described earlier [12].

3.2. Syntheses of the complexes [(L_{sal})Pd] (**4**)

The complexes [(L^1_{sal})Pd], [(L^2_{sal})Pd] and [(L^3_{sal})Pd] (**4A**, **4B** and **4C**) were prepared by a similar procedure. The details for the preparation of **4A** are given below.

3.2.1. [(L^1_{sal})Pd] (**4A**)

A solution of $H_2L^1_{sal}$ (104 mg, 0.346 mmol) in 10 mL ethanol was added to a solution of Na_2PdCl_4 (100 mg, 0.346 mmol) in 20 mL ethanol. The mixture was stirred for 12 h. The brown solid precipitate was separated by filtration and purified by preparative silica gel G TLC with binder. The eluent was benzene. Upon evaporation of the solvent, the brown solid of pure **4A** was obtained (83 mg, 60% yield). IR (KBr, cm^{-1}): ν(C=N) 1605, ν(N=N) 1375. ^{1}H NMR ($CDCl_3$, 500 MHz): δ 6.56 (t, 1H), 7.03 (t, 1H), 7.14 (t, 1H), 7.22 (d, 2H), 7.32 (t, 2H), 7.47–7.42 (m, 2H), 7.62 (d, 1H), 7.77 (d, 1H), 7.85 (d, 1H), 8.55 (s, 1H). Electronic spectrum (λ_{max}/nm (ε/dm^2 mol^{-1}) in CH_2Cl_2 solution): 500^{sh}, 496 (1910), 475 (2090), 427 (4990), 407 (6260), 372 (6530), 341 (8510), 332 (8690), 255 (12980). *Anal.* Calc. for $C_{19}H_{13}N_3OPd$: C, 56.29; H, 3.20; N, 10.37. Found: C, 56.33; H, 3.18; N, 10.40%.

3.2.2. [(L^2_{sal})Pd] (**4B**)

This complex was prepared following a similar procedure as described for **4A** using the ligand $H_2L^2_{sal}$ in place of $H_2L^1_{sal}$ (59 mg, 57% yield). IR (KBr, cm^{-1}): ν(C=N) 1606, ν(N=N) 1378. ^{1}H NMR ($CDCl_3$, 500 MHz): δ = 2.37 (s, 3H), 6.57 (t, 1H), 6.95 (d, 1H), 7.04 (d, 1H), 7.20–7.23 (m, 3H), 7.31 (t, 1H), 7.44 (t, 1H), 7.61 (d, 1H), 7.65 (d, 1H), 7.83 (d, 1H), 8.50 (s, 1H). Electronic spectrum (λ_{max}/nm (ε/dm^2 mol^{-1}) in CH_2Cl_2 solution): 500^{sh}, 490 (4150), 475 (4400), 430 (9640), 410 (11930), 377 (11200), 347 (15050), 334 (14712), 255 (17000). *Anal.* Calc. for $C_{20}H_{15}N_3OPd$: C, 57.23; H, 3.57; N, 10.02. Found: C, 57.30; H, 3.60; N, 10.08%.

3.2.3. [(L^3_{sal})Pd] (**4C**)

This complex was prepared following a similar procedure as described for **4A** using the ligand $H_2L^3_{sal}$ in place of $H_2L^1_{sal}$ (75 mg, 50% yield). IR (KBr, cm^{-1}): $\nu_{C=N}$ 1605, $\nu_{N=N}$ 1376. ^{1}H NMR ($CDCl_3$, 500 MHz): δ = 6.58 (t, 1H), 7.00 (d, 1H), 7.11(d, 1H), 7.12 (d, 1H), 7.18- 7.23 (m, 2H), 7.30–7.36 (m, 1H), 7.47 (t, 1H), 7.59 (d, 1H), 7.65 (d, 1H), 7.80 (d, 1H), 8.48 (s, 1H). Electronic spectrum (λ_{max}/nm (ε/dm^2 mol^{-1}) in CH_2Cl_2 solution): 500^{sh}, 496 (5100), 471 (5813), 429 (10610), 402 (12750), 379 (16060), 344 (19120), 331 (19460), 255 (28880). ESI-MS: *m*/*z* 440. *Anal.* Calc. for $C_{19}H_{12}N_3PdOCl$: C, 51.81; H, 2.72; N, 9.54. Found: C, 51.90; H, 2.78; N, 9.50%.

3.3. Syntheses of the complexes [(OL_{sal})Pd] (**10**)

All the [(OL_{sal})Pd] complexes (**10**) were prepared by a similar procedure. The details for the preparation of **10A** are given below.

3.3.1. [(OL^1_{sal})Pd] (**10A**)

A solution of (72 mg, 0.412 mmol) *m*CPBA was added dropwise to a stirred solution of **4A** (50 mg, 0.123 mmol) in 25 mL dichloromethane. Immediately, the color of the solution began to change from brown to pink. The stirring was continued for 30 min. Evaporation of the solvent under vaccuo afforded a pink solid mass. The solid mass thus obtained was washed thrice with diethyl ether, taking 5 mL for each wash. The product was then purified by preparative TLC using benzene as the eluent. The pink band was collected (57 mg, 55% yield). IR (KBr, cm^{-1}): ν(C=N) 1605, ν(N=N) 1377. ^{1}H NMR ($CDCl_3$, 500 MHz): δ = 6.67 (t, 1H), 6.83 (t, 1H), 7.32 (t, 1H), 7.36–7.43 (m, 4H), 7.46–7.49 (m, 1H), 7.84–7.86 (m, 2H), 8.31 (d, 1H), 8.57 (s, 1H). Electronic spectrum (λ_{max}/nm (ε/dm^2 mol^{-1}) in CH_2Cl_2 solution): 560 (6250), 526 (7800), 390^{sh}, 374 (16470), 343 (13600), 326 (13790), 300 (14260). *Anal.* Calc. for $C_{19}H_{13}N_3PdO_2$: C, 54.15; H, 3.08; N, 9.97. Found: C, 54.19; H, 3.10; N, 10.00%.

3.3.2. [(OL^2_{sal})Pd] (**10B**)

Complex **10B** was prepared using **4B** in place of **4A** by a similar procedure as described for **10A** (49 mg, 60% yield). IR (KBr, cm^{-1}): ν(C=N) 1606, ν(N=N) 1378. ^{1}H NMR ($CDCl_3$, 500 MHz): δ = 2.46 (s, 3H), 6.68 (t, 2H), 7.18 (s, 1H); 7.24 (d, 1H), 7.32 (t, 1H), 7.38-7.43 (m, 3H), 7.72 (d, 1H), 7.84 (d, 1H), 8.30 (d, 1H), 8.59 (s, 1H). Electronic spectrum (λ_{max}/nm (ε/dm^2 mol^{-1}) in CH_2Cl_2 solution): 554 (3400), 522 (13300), 398 (26500), 379 (28150), 341 (21030), 327 (20570), 298 (20460). *Anal.* Calc. for $C_{20}H_{15}N_3PdO_2$: C, 55.17; H, 3.44; N, 9.65. Found: C, 55.20; H, 3.40; N, 9.68%.

3.3.3. [(OL^3_{sal})Pd] (**10C**)

This complex was prepared following a similar procedure as described for **10A** using **4C** in place of **4A** (52 mg, 50% yield). IR (KBr, cm^{-1}): ν(C=N) 1605, ν(N=N) 1376. ^{1}H NMR ($CDCl_3$, 500 MHz): δ = 6.70 (t, 1H), 6.83 (d, 1H), 7.36 (t, 1H), 7.41–7.43 (m, 2H), 7.44–7.48 (m, 2H), 7.80 (d, 1H), 7.85 (d, 1H), 8.30 (d, 1H), 8.57 (s, 1H). Electronic spectrum (λ_{max}/nm (ε/dm^2 mol^{-1}) in CH_2Cl_2 solution): 562 (6150), 518 (10120), 398^{sh}, 341 (19340), 326 (17100), 300 (17510). ESI-MS: *m*/*z*, 456. *Anal.* Calc. for $C_{19}H_{12}N_3PdO_2Cl$: C, 50.00; H, 2.63; N, 9.21. Found: C, 50.12; H, 2.60; N, 9.16%.

3.4. Physical measurements

Electronic spectra were recorded on a Shimadzu UV-2401 PC spectrophotometer. IR spectra were taken on a Perkin–Elmer L120-00A FT IR spectrophotometer (4000–225 cm^{-1}) in KBr pellets. C, H, N analyses were performed on a Perkin–Elmer 240C elemental analyzer. NMR spectra were drawn on a Brucker Avance RPX 500 MHz spectrometer in $CDCl_3$ using TMS as the internal standard. ESI mass spectra were recorded on a micro mass Q-TOF mass spectrometer (Serial No. YA 263).

3.5. Crystallography

Crystals of [(L^3_{sal})Pd] were grown by slow evaporation of dicholoromethane solution at 298 K. Data were collected on a Brucker smart CCD diffractometer using Mo-Kα monochromator (λ = 0.71043 Å). Structure solutions were performed using the SHELX-97 PC version program. The full-matrix least square and anisotropic refinements were performed on all the atoms. Hydrogen atoms were included at calculated positions. The data collection parameters and relevant crystal data are collected in Table 2.

Table 2
Crystallographic data for complex **4C**

Chemical formula	$C_{19}H_{12}ClN_3OPd$
Formula weight	440.19
Crystal system	triclinic
Space group	$P\bar{1}$
a (Å)	7.5450(16)
b (Å)	12.390(3)
c (Å)	18.383(4)
α (°)	79.352(3)
β (°)	81.081(3)
γ (°)	74.006(3)
λ (Å)	0.71073
V (Å^3)	1613.6(6)
Z	4
Temperature (K)	293
ρ (Mg/m^3)	1.812
μ (mm^{-1})	1.328
R (all data)	0.0465
wR_2 [$I > 2\sigma(I)$]	0.1144
Goodness-of-fit	1.16

4. Conclusion

Synthesis of *metalloazosalophen* of Pd(II) could be carried out via orthopalladation followed by O-insertion. TBHP or *m*CPBA have been used for O-insertion. Although TBHP alone was unsuitable, in the presence of $[VO(acac)_2]$ the O-insertion occurred. Nevertheless, the oxygenated complex $[(OL_{sal})Pd]$ could not be demetallated using conventional techniques to obtain the free azosalophen, H_2OL_{sal}, ligand.

Acknowledgements

We are thankful to the DST (New Delhi) for funding under the SERC scheme. The necessary laboratory and infrastructural facilities are provided by the Dept. of Chemistry, University of Kalyani. The support of DST under the FIST program and DRS-SAP to the Department of Chemistry, University of Kalyani are acknowledged.

Appendix A. Supplementary data

CCDC 659270 contain the supplementary crystallographic data for **4C**. These data can be obtained free of charge via http://www.ccdc.cam.ac.uk/conts/retrieving.html, or from the Cambridge Crystallographic Data Centre, 12 Union Road, Cambridge CB2 1EZ, UK; fax: (+44) 1223-336-033; or e-mail: deposit@ccdc.cam.ac.uk. Supplementary data associated with this article can be found, in the online version, at doi:10.1016/j.poly.2008.03.028.

References

[1] (a) M. Ryang, Y. Sawa, S.N. Somasundaram, S. Murai, S. Tsutsumi, J. Organomet. Chem. 46 (1972) 375;
(b) P. DeShong, D.R. Sidler, P.J. Rybczynski, G.A. Slough, A.L. Rheinghold, J. Am. Chem. Soc. 110 (1988) 2575;
(c) R. Streubel, H. Wilkens, F. Ruthe, P.G. Jones, Organometallics 25 (2006) 4830;
(d) J. Ruiz, V. Riera, M. Vivanco, Organometallics 8 (1989) 967;
(e) K. Ogata, J. Seta, K. Sugawara, N. Tsutsumi, Y. Yamamoto, K. Kuge, K. Tatsumi, Inorg. Chim. Acta. 359 (2006) 1549;
(f) I. Ojima, Transition metal compounds in organic synthesis 1, in: R. Crabtree (Ed.), Comprehensive Organometallic Chemistry, Yale University, New Haven, CT, USA. and M. Mingos, 3rd ed., vol. 10, Application II, Oxford University, Oxford, UK, Elsevier, 2006.;
(g) T. Hiyama, Transition metal compounds in organic synthesis 2, in: in: R. Crabtree (Ed.), Comprehensive Organometallic Chemistry, Yale University, New Haven, CT, USA. and M. Mingos, 3rd ed., vol. 12, Application III, Oxford University, Oxford, UK, Elsevier, 2006.
[2] (a) E.G. Samsel, K. Srinivasan, J.K. Kochi, J. Am. Chem. Soc. 107 (1985) 7606;
(b) K. Srinivasan, P. Michaud, J.K. Kochi, J. Am. Chem. Soc. 108 (1986) 2309;
(c) R.A. Sheldon, J.K. Kochi, Metal-Catalyzed Oxidation of Organic Compounds, Academic, New York, 1981;
(d) K. Srinivasan, P. Michaud, J.K. Kochi, J. Am. Chem. Soc. 108 (1986) 2309;
(e) E.G. Samsel, K. Srinivasan, J.K. Kochi, J. Am. Chem. Soc. 107 (1985) 7606;
(f) K. Srinivasan, P. Michaud, J.K. Kochi, J. Am. Chem. Soc. 108 (1986) 2309;
(g) T.S. Siddall, N. Miyaura, J.C. Huffman, J.K. Kochi, J. Chem. Soc., Chem. Commun. (1983) 1185;
(h) K. Srinivasan, J.K. Kochi, Inorg. Chem. 24 (1985) 4671;
(i) K. Srinivasan, P. Michaud, J.K. Kochi, J. Am. Chem. Soc. 108 (1986) 2309;
(j) K. Srinivasan, S. Perrier, J.K. Kochi, J. Mol. Catal. 36 (1986) 297.
[3] (a) R. Irie, Y. Ito, T. Katsuki, Synlett (1991) 265;
(b) N.S. Finney, P.J. Pospisil, S. Chang, M. Palucki, R.G. Konsler, K.B. Hansen, E.N. Jacobsen, Angew. Chem., Int. Ed. Engl. 36 (1997) 1720;
(c) H. Sasaki, R. Irie, T. Hamada, K. Suzuki, T. Katsuki, Tetrahedron 50 (1994) 11827;
(d) C. Kokubo, T. Katsuki, Tetrahedron 52 (1996) 13895;
(e) K. Ito, T. Katsuki, Tetrahedron Lett. 34 (1993) 2661;
(f) K. Ito, T. Katsuki, Chem. Lett. (1994) 1857;
(g) K. Miura, T. Katsuki, Synlett (1999) 783;
(h) T. Hashihayata, Y. Ito, T. Katsuki, Tetrahedron 53 (1997) 9541;
(i) T. Hashihayata, Y. Ito, T. Katsuki, Synlett (1996) 1079;
(j) W. Zhang, J.L. Loebach, S.R. Wilson, E.N. Jacobsen, J. Am. Chem. Soc. 112 (1990) 2801;
(k) R. Irie, K. Noda, Y. Ito, N. Matsumoto, T. Katsuki, Tetrahedron Lett. 31 (1990) 7345;
(l) E.N. Jacobsen, A. Pfaltz, H. Yamamoto (Eds.), Comprehensive Asymmetric Catalysis, vol. 1–3, Springer, Berlin, 1999;
(m) M.S. Sigman, P. Vachal, E.N. Jacobsen, Angew. Chem., Int. Ed. Engl. 39 (2000) 1279;
(n) J.M. Keith, J.F. Larrow, E.N. Jacobsen, Adv. Synth. Catal. 1 (2001) 5;
(o) E.N. Jacobsen, in: E.N. Jacobsen, A. Pfaltz, H. Yamamoto (Eds.), Comprehensive Asymmetric Catalysis, vol. 2, Springer, Berlin, 1999, p. 649;
(p) M. Palucki, N.S. Finney, P.J. Pospisil, M.L. Güler, T. Ishida, E.N. Jacobsen, J. Am. Chem. Soc. 120 (1998) 948;
(q) N. S Finney, P.J. Pospisil, S. Chang, M. Palucki, R.G. Konsler, K.B. Hansen, E.N. Jacobsen, Angew. Chem., Int. Ed. Engl. 36 (1997) 1720;
(r) E.N. Jacobsen, W. Zhang, A.R. Muci, J.R. Ecker, L. Deng, J. Am. Chem. Soc. 113 (1991) 7063;
(s) E.N. Jacobsen, W. Zhang, J. Org. Chem. 56 (1991) 2296;
(t) Y. Yamashita, T. Katsuki, Synlett (1995) 829;
(u) T. Katsuki, K.B. Sharpless, J. Am. Chem. Soc. 102 (1980) 5974;
(v) W. Zhang, J.L. Loebach, S.R. Wilson, E.N. Jacobsen, J. Am. Chem. Soc. 112 (1990) 2801;
(w) E.J. Allain, L.P. Hager, L. Deng, E.N. Jacobsen, J. Am. Chem. Soc. 115 (1993) 4415;
(x) M. Palucki, P.J. Pospisil, W. Zhang, E.N. Jacobsen, J. Am. Chem. Soc. 116 (1994) 9333;
(y) K. Noda, N. Hosoya, R. Irie, Y. Yamashita, T. Katsuki, Tetrahedron 50 (1994) 9609;
(z) T. Katsuki, K.B. Sharpless, J. Am. Chem. Soc. 102 (1980) 5974.
[4] P. Pattanayak, J.L. Pratihar, D. Patra, A. Burrows, M. Mohan, S. Chattopadhyay, Eur. J. Inorg. Chem. (2007) 4263.
[5] (a) D.N. Neogi, A.N. Biswas, P. Das, R. Bhawmick, P. Bandyopadhyay, Inorg. Chim. Acta 360 (2007) 2181;
(b) D.N. Neogi, A.N. Biswas, P. Das, P. Bandyopadhyay, Polyhedron 25 (2006) 2149;
(c) R. Bhawmick, P. Bandyopadhyay, Polyhedron 15 (1996) 2923;
(d) J. Dinda, D. Das, P.K. Santra, C. Sinha, L.R. Falvello, J. Organomet. Chem. 629 (2001) 28.
[6] (a) A.C. Cope, R.W. Siekman, J. Am. Chem. Soc. 87 (1965) 3272;
(b) I. Omae, Chem. Rev. 79 (1979) 287.
[7] (a) S. Chattopadhyay, C. Sinha, P. Basu, A. Chakravorty, Organometallics 10 (1991) 135;
(b) S. Chattopadhyay, C. Sinha, P. Basu, A. Chakravorty, J. Organomet. Chem. 414 (1991) 427;
(c) C. Sinha, D. Bandyopadhyay, A. Chakravorty, Inorg. Chem. 27 (1988) 173;
(d) J. Pratihar, N. Maiti, P. Pattanayak, S. Chattopadhyay, Polyhedron 24 (2005) 953;
(e) S. Chattopadhyay, C. Sinha, S.B. Choudhury, A. Chakravorty, J. Organomet. Chem. 427 (1992) 11;
(f) C.K. Pal, S. Chattopadhyay, C. Sinha, A. Chakravorty, J. Organomet. Chem. 439 (1992) 91;
(g) T.K. Bag, T.K. Misra, C. Sinha, Polyhedron 24 (1998) 4109.
[8] A.H. Velders, H. Kooijman, A.L. Spek, J.G. Haasnoot, D. de Vos, J. Reedijk, Inorg. Chem. 39 (2000) 2966.
[9] (a) J.L. Pratihar, N. Maiti, S. Chattopadhyay, Inorg. Chem. 44 (2005) 6111;
(b) J. Pratihar, D. Patra, S. Chattopadhyay, J. Organomet. Chem. 690 (2005) 4816;
(c) D. Patra, J.I. Pratihar, B. Shee, P. Pattanayak, S. Chattopadhyay, Polyhedron 25 (2006) 2637.
[10] (a) A.K. Mahapatra, D. Bandyopadhyay, P. Bandyopadhyay, A. Chakravorty, Inorg. Chem. 25 (1986) 2214;
(b) A.K. Mahapatra, D. Bandyopadhyay, P. Bandyopadhyay, A. Chakravorty, J. Chem. Soc., Chem. Commun. (1984) 999;

(c) C. Sinha, D. Bandyopadhyay, A. Chakravorty, Inorg. Chem. 27 (1988) 1173;
(d) A.J. Canty, M.C. Denney, W.B. Sketlton, A.H. White, Organometallics 23 (2004) 1122;
(e) A.J. Canty, M.C. Denney, G. van Koten, A.H. White, Organometallics 23 (2004) 5432;
(f) P.L. Alsters, H.T. Teunissen, J. Boersma, A.L. Spek, G. van Koten, Organometallics 12 (1993) 4691.

[11] (a) P. Chattopadhyay, M.K. Nayak, S.P. Bhattacharya, C. Sinha, Polyhedron 16 (1997) 1291;
(a) F. Basuli, P. Chattopadhyay, C. Sinha, Polyhedron 15 (1996) 2439.
[12] (a) N. Maiti, S. Pal, S. Chattopadhyay, Inorg. Chem. 40 (2001) 2204;
(b) N. Maiti, B.K. Dirghangi, S. Chattopadhyay, Polyhedron 22 (2003) 3109;
(c) N. Maiti, S. Pal, S. Chattopadhyay, Indian J. Chem. 42A (2003) 2327.

Polyhedron 27 (2008) 2216–2220

Contents lists available at ScienceDirect

Polyhedron

journal homepage: www.elsevier.com/locate/poly

A novel bismercury(II) complex of bidentate N^{21},N^{22}-bridged porphyrin: [((benzamido-κ*N*)phenylmercury-κ*Hg*–N^{21},N^{22})-*meso*-tetraphenylporphyrinato-N^{23},N^{24}]phenylmercury(II) toluene solvate

Kwan-Tin Chen [a], Fuh-An Yang [a], Jyh-Horung Chen [a,*], Shin-Shin Wang [b], Jo-Yu Tung [c,*]

[a] Department of Chemistry, National Chung-Hsing University, Taichung 40227, Taiwan
[b] Material and Chemical Research Laboratories, Hsin-Chu 300, Taiwan
[c] Department of Occupational Safety and Health, Chung Hwai University of Medical Technology, Tainan 713, Taiwan

ARTICLE INFO

Article history:
Received 14 March 2008
Accepted 27 March 2008
Available online 19 May 2008

Keywords:
Mercury porphyrin
X-ray diffraction
Mercury NMR
Bismercury

ABSTRACT

Reaction of PhHgOAc with *N*-NHCOC$_6$H$_5$–Htpp gave a bismercury(II) complex [((benzamido-κ*N*)phenylmercury-κ*Hg*–N^{21},N^{22})-*meso*-tetraphenylporphyrinato-N^{23},N^{24}]phenylmercury(II) toluene solvate [Hg(Ph)(N^{21},N^{22}–(Ph)–Hg–N(COPh)tpp · C$_6$H$_5$CH$_3$; **3** · C$_6$H$_5$CH$_3$] with Hg(1)–N(5) as N^{21},N^{22}-bridged atoms. The crystal structure of **3** · C$_6$H$_5$CH$_3$ was determined. The Hg(1)···Hg(2) distance is 3.611(7) Å. Hence, no metallophilic Hg(II)···Hg(II) interaction is present. **3** in CDCl$_3$ was characterized by ^{1}H, ^{13}C, and ^{199}Hg NMR. The ^{199}Hg NMR spectrum for **3** in CDCl$_3$ solution 20 °C clearly reveals that there are two different Hg nuclei, i.e. Hg(1) and Hg(2) and this NMR data provides an evidence that **3** remains as a bismercury species in CDCl$_3$ solution. The ^{199}Hg NMR spectrum for a 0.2 M solution of **3** in CDCl$_3$ at 20 °C is observed at −1088 ppm for Hg(2) nucleus with ^3J(Hg–H) = 188 Hz and an effective coordination number of five and at −1119 ppm for Hg(1) nucleus with ^3J(Hg–H) = 177 Hz and an effective coordination number of four. The proton and ^{199}Hg NMR spectra clearly show ^3J(Hg–H) coupling and these NMR data indicate no ligand exchange for **3** in CDCl$_3$.

© 2008 Elsevier Ltd. All rights reserved.

1. Introduction

Pd complexes of N^{21},N^{22}-bridged porphyrins with a one-carbon (methano) bridge were isolated by Callot and co-workers [1]. Setsune et al. have shown that N^{21},N^{22}-etheno bridged porphyrin serves as a bidentate nitrogen base ligand for stable coordination to palladium for complexes [(1,2-diphenyletheno-N^{21},N^{22})-*meso*-tetraphenylporphyrinato-N^{23},N^{24}](η^3-allyl)palladium(II) chloride (**1a**) [2] and Pd^{II}(C(O)Me)(Cl)(N^{21},N^{22}-(PhC═CPh)(TPP)) (**1b**) [3], and to rhodium for complexes [N^{21},N^{22}-(PhC═CPh)(TPP)]Rh^I(COD)-ClO$_4$ (**2a**) (where COD = η^4-1,5-cyclooctadienyl) and [N^{21},N^{22}-(PhC═CPh)(TPP)]Rh^I(CO)$_2$ClO$_4$ (**2b**) (Chart 1) [4].

Organopalladium complexes **1a** and **1b** with bidentate nitrogen base ligands have recently been recognized as useful in enantioselective organic transformations and polymerization reactions [2]. Organomercury(II) compounds of the type PhHg$^+$ has received growing attention mainly related to the search for toxicological compounds and versatile reagents in controlled transmetallation reactions [5]. In view of the rich photochemistry and electrochemistry of porphyrins, it is of great interest to generate organomercury complex of porphyrin. A thorough review of the literature shows that there is no prior report on phenylmercury(II) with free base *N*-NHCOC$_6$H$_5$–Htpp [6]. The coordination chemistry of phenylmercury(II) explored with anions derived from base *N*-NHCOC$_6$H$_5$–Htpp reveal the formation of the phenylmercury(II) complex of [((benzamido-κ*N*)phenylmercury-κ*Hg*–N^{21},N^{22})-*meso*-tetraphenylporphyrinato-N^{23},N^{24}]phenylmercury(II) toluene solvate [Hg(Ph)(N^{21},N^{22}–(Ph)–Hg–N(COPh)tpp · C$_6$H$_5$CH$_3$; **3** · C$_6$H$_5$-CH$_3$]. Compound **3** · C$_6$H$_5$CH$_3$ is a new class of bismercury porphyrin complex with Hg(1)–N(5) ligand bidentately coordinated to N^{21},N^{22}-porphyrin and with Hg(2) as metal bridge (Fig. 1). We report here on the synthesis, ^{1}H, ^{13}C and ^{199}Hg NMR spectroscopic characterization of this novel bidentate porphyrin **3** as well as the crystal structure of it.

2. Experimental

2.1. [Hg(Ph)(N^{21},N^{22}–(Ph)–Hg–N(COPh)tpp · C$_6$H$_5$CH$_3$; **3** · C$_6$H$_5$CH$_3$]

A mixture of PhHgOAc (0.07 g, 2.1 × 10^{-4} mol, 98% from Acros) and *N*-NHCOC$_6$H$_5$–Htpp (0.073 g, 1.0 × 10^{-4} mol) in pyridine (10 cm^3) was stirred at 100 °C for 3 h [6]. After concentrating, the residue was dissolved in a suitable amount of toluene, dried over anhydrous Na$_2$SO$_4$ and filtered. The filtrate was concentrated and recrystallized from toluene–hexane [1:3 (v/v)] yielding blue solid

* Corresponding authors.
E-mail address: JyhHChen@dragon.nchu.edu.tw (J.-H. Chen).

0277-5387/$ - see front matter © 2008 Elsevier Ltd. All rights reserved.
doi:10.1016/j.poly.2008.03.029

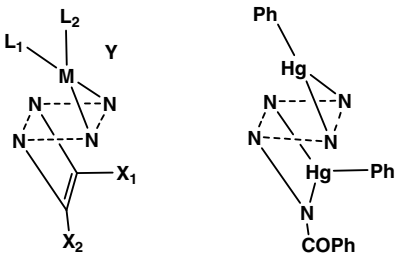

(1a, 1b)
(2a, 2b)

(3)

(1a) M = Pd(II), L_1 = π-(allyl), L_2 = empty, X_1 = X_2 = Ph, Y = Cl^-

(1b) M = Pd(II), L_1 = $COCH_3$, L_2 = Cl, X_1 = X_2 = Ph, Y = empty

(2a) M = Rh(I), L_1 = L_2 = COD , X_1 = X_2 = Ph, Y = ClO_4^-

(2b) M = Rh(I), L_1 = CO, L_2 = CO , X_1 = X_2 = Ph, Y = ClO_4^-

(3) M = Hg(II), L_1 = Ph, L_2 = empty, X_1 = Ph, X_2 = COPh

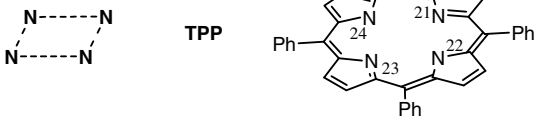

Chart 1.

of **3** (0.08 g, 7×10^{-5} mol, 70%) which was again dissolved in toluene and layered with hexane to get blue crystals for single crystal X-ray analysis. ^{1}H NMR (299.95 MHz, $CDCl_3$, 20 °C): δ 8.95 [d, $H_β$ (2, 13), ^3J(H–H) = 4.2 Hz]; 8.77 [d, $H_β$ (3, 12), ^3J(H–H) = 4.2 Hz]; 8.47 [s, $H_β$ (7, 8)]; 7.07 [s, $H_β$ (17, 18)]; 8.49 [s, *o*′-H(38, 40) and *o*′-H(34, 44)]; 8.17 [s, *o*-H(26, 32)]; 8.02 [s, *o*-H(22, 28)]; 7.89-7.73 (m, *m*, *p*-H); 6.61 [t, Hg(1)–Ph–H_4 or H(55), ^3J(H–H) = 7.5 Hz]; 6.49 [t, Hg(1)–Ph–$H_{3,5}$ or H(54, 56), ^3J(H–H) = 7.5 Hz]; 6.39 [t, BA–Ph–H_4 or H(49), ^3J(H–H) = 7.5 Hz], where BA = benzamido group; 6.18 [t, BA–Ph–$H_{3,5}$ or H(48, 50), ^3J(H–H) = 8.1 Hz]; 6.07 [t, Hg(2)–Ph–H_4 or H(61), ^3J(H–H) = 7.5 Hz]; 5.84 [t, Hg(2)–Ph–$H_{3,5}$ or H(60, 62), ^3J(H–H) = 7.8 Hz and ^4J(Hg–H) = 54 Hz]; 5.03 [d, BA–Ph–$H_{2,6}$ or H(47, 51), ^3J(H–H) = 8.4 Hz]; 4.23 [d, Hg(1)–Ph–$H_{2,6}$ or H(53, 57), ^3J(H–H) = 7.8 Hz and ^3J(Hg–H) = 186 Hz]; 3.18 [d, Hg(2)–Ph–$H_{2,6}$ or H(59, 63), ^3J(H–H) = 7.8 Hz and ^3J(Hg–H) = 198 Hz]. ^{199}Hg NMR (107.24 MHz, $CDCl_3$, 20 °C): δ −1088 [t, Hg(2), ^3J(Hg–H) = 188 Hz]; −1119 [t, Hg(1), ^3J(Hg–H) = 177 Hz]. MS (FAB): M^+ 1287 (calcd for $C_{63}H_{43}Hg_2N_5O$: 1287). UV–Vis spectrum, λ(nm) [$\varepsilon \times 10^{-3}$ (M^{-1} cm^{-1})] in CH_2Cl_2: 448 (213), 462 (48.1), 620 (25.3).

2.2. Spectroscopy

Proton and ^{13}C NMR spectra in $CDCl_3$ (99.8% from Aldrich) were recorded at 299.95 (or 599.94) and 150.87 MHz, respectively, on Varian VXR-300 (or Varian Unity Inova-600) spectrometers locked on deuterated solvent, and referenced to the solvent peak. Proton NMR spectrum is relative to $CDCl_3$ at 7.24. ^{199}Hg NMR spectrum in $CDCl_3$ was obtained at 107.24 MHz at 20 °C on a Bruker DMX-600 spectrometer locked on deuterated solvent. Chemical shifts of ^{199}Hg NMR spectrum were measured relative to an external reference of 0.5 M phenylmercury(II) acetate in DMSO-d_6 (−1439.5 ppm) but reported relative to dimethylmercury (0.0 ppm). HMQC (heteronuclear multiple quantum coherence) was used to correlate protons and carbon through one-bond coupling and HMBC (heteronuclear multiple bond coherence) for two- and three-bond proton–carbon coupling. Nuclear Overhauser effect (NOE) difference and ^{1}H–^{1}H COSY spectra were employed to determine the ^{1}H–^{1}H proximity through space over a distance of up to about 4 Å.

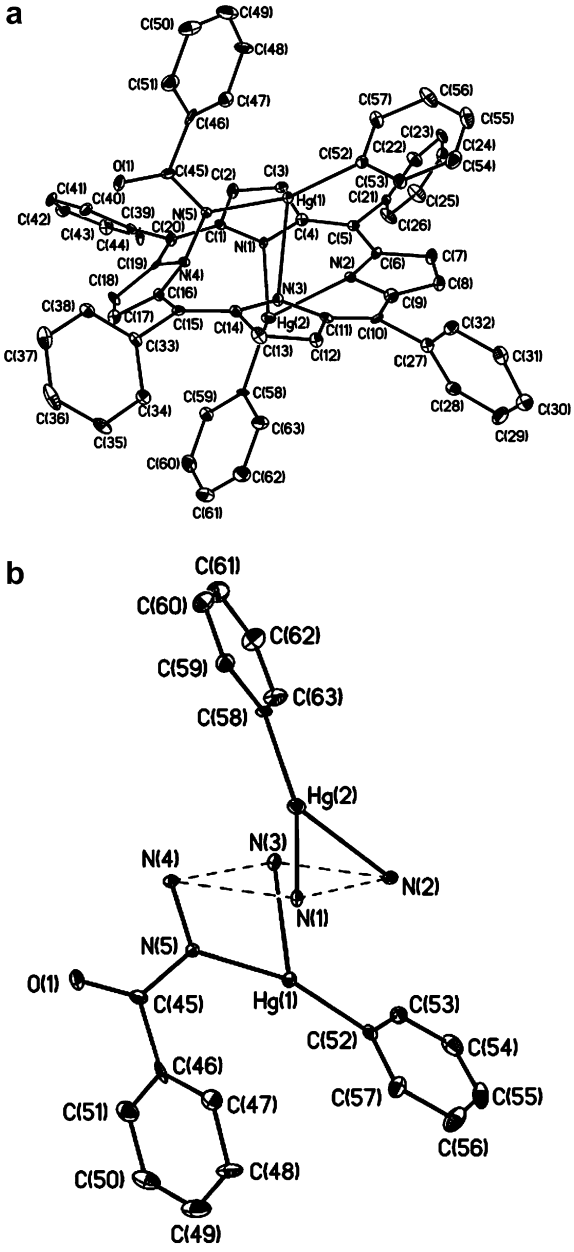

Fig. 1. (a) Molecular configuration and atom-labeling scheme for **3** · $C_6H_5CH_3$, with ellipsoids drawn at 30% probability. Hydrogen atoms and solvent $C_6H_5CH_3$ are omitted for clarity. (b) Diagram of two planes of Hg coordination [i.e., plane of Hg(2), N(1), N(2) and plane of Hg(1), N(3), N(4), N(5)] and the porphyrin 4N mean plane of **3**.

The positive ion fast atom bombardment mass spectrum (FAB MS) was obtained in a nitrobenzyl alcohol (NBA) matrix using a JEOL JMS–SX/SX 102A mass spectrometer. UV–Vis spectra were recorded at 20 °C on a HITACHI U–3210 spectrophotometer.

2.3. Crystallography

Table 1 presents the crystal data for **3** · $C_6H_5CH_3$. Measurements were taken on a BRUKER SMART APEXCCD area detector diffractometer using monochromatized Mo Kα radiation (λ = 0.71073 Å). Multi-scan absorption corrections were made for **3** · $C_6H_5CH_3$. The structure was solved by direct methods (SHELXTL-97) [7] and re-

Table 1
Crystal data for **3** · $C_6H_5CH_3$

Empirical formula	$C_{70}H_{51}Hg_2N_5O$ (**3** · $C_6H_5CH_3$)
Formula weight	1379.34
Space group	$P\bar{1}$
Crystal system	triclinic
a (Å)	10.9541(5)
b (Å)	12.1645(5)
c (Å)	20.6548(9)
α (°)	80.535(1)
β (°)	87.235(1)
γ (°)	86.234(1)
V (Å^3)	2707.0(2)
Z	2
F(000)	1348
D_{calc} (g cm^{-3})	1.692
μ (mm)	5.716
Goodness-of-fit	1.139
Crystal size (mm^3)	0.30 × 0.20 × 0.05
θ_{min}, θ_{max} (°)	2.41, 25.1
T (K)	150(2)
Number of reflections measured	9528
Number of reflections observed	7901 ($I > 2\sigma(I)$)
R [$I > 2\sigma(I)$][a]	0.0567
wR[b]	0.1168

[a] $R_1 = [\sum||F_o| - |F_c||/\sum|F_o|]$.
[b] $wR_2 = \{\sum[w(F_o^2 - F_c^2)^2]/\sum[w(F_o^2)^2]\}^{1/2}$.

Table 2
Selected bond distances (Å) and angles (°) for compound **3** · $C_6H_5CH_3$

3 · $C_6H_5CH_3$			
Hg(1)–N(5)	2.096(7)	Hg(2)–N(1)	2.226(7)
Hg(1)–N(3)	2.693(7)	Hg(2)–N(2)	2.425(7)
Hg(1)···N(2)	2.852(7)	Hg(2)···N(3)	2.831(7)
Hg(1)–C(52)	2.056(9)	Hg(2)···N(4)	2.826(7)
Hg(1)···Hg(2)	3.611(7)	Hg(2)–C(58)	2.061(8)
C(52)–Hg(1)–N(3)	114.0(3)	C(58)–Hg(2)–N(1)	153.4(3)
C(52)–Hg(1)–N(5)	164.6(3)	C(58)–Hg(2)–N(2)	129.2(3)
N(3)–Hg(1)–N(5)	79.0(2)	N(1)–Hg(2)–N(2)	77.0(2)

fined by the full-matrix least-squares method. The three atoms [i.e., C(9), C(30), and C(42)] were refined with isotropic displacement parameters. All non-hydrogen atoms, except the three atoms [i.e., C(9), C(30), and C(42)] atoms, were refined with anisotropic thermal parameters, whereas all hydrogen atoms were placed in calculated positions and refined with a riding model. Table 2 lists selected bond distances and angles for **3** · $C_6H_5CH_3$.

3. Results and discussion

3.1. Molecular structure of **3** · $C_6H_5CH_3$

The molecular framework is depicted in Fig. 1a for **3** · $C_6H_5CH_3$. The covalent bond of Hg(2)–C(58) = 2.061(8) Å and Hg(1)–C(52) = 2.056(9) Å in **3** are smaller than the sum of the covalent radii of Hg and C (2.26 Å) [8,9]. The mercury nitrogen bond distances [Hg(2)–N(1) = 2.226(7), Hg(2)–N(2) = 2.425(7) and Hg(1)–N(3) = 2.693(7), Hg(1)–N(5) = 2.096(7) Å] in **3**, are well below the upper limit of a typical Hg–N covalent bond [2.75(2) Å] [8,9]. Hence, C(58), N(1) and N(2) are bonded covalently to Hg(2) atom in **3**. In a similar way, the Hg(1) is tri-coordinated with two nitrogen atoms [i.e., N(3) and N(5)] of the porphyrin and one carbon atom [i.e. C(52)] of phenyl group in **3**. We adopt the plane of four pyrrole nitrogen atoms [i.e., N(1), N(2), N(3), and N(4)] as a reference plane 4N for **3** · $C_6H_5CH_3$. Because of the larger size of Hg^{2+} [$\gamma(Hg^{2+})$ = 0.83 Å with coordination number (CN) = 3] [10], Hg(2) lies 1.47 Å above the 4N plane in **3** · $C_6H_5CH_3$, compared to Hg(1) which lies 2.07 Å below the plane in the same complex (Fig. S1 in Supplementary material). The separation between atoms Hg(1) and Hg(2) is 3.611 Å, which is larger than the sum of van der Waals radii of two Hg(II), 3.50(7) Å [9]. Hence, no metallophilic Hg(II)···Hg(II) interaction in **3** · $C_6H_5CH_3$ may be anticipated.

The mercury coordination sphere can be categorized in terms of their primary (or characteristic) and effective coordination [11,12]. The Hg(2)···N(3) = 2.831 Å, and Hg(2)···N(4) = 2.826 Å around the Hg(2) atom and Hg(1)···N(2) = 2.852 Å around the Hg(1) atom in **3** are longer than 2.75(2) Å but are significantly smaller than the sum of the van der Waals radii of Hg and N(3.28 Å). These three longer Hg···N contacts are described as weak (secondary) bonds. The effective coordination around Hg(2) in **3** may be construed as an expansion of the secondary valency of mercury from three to five {3 +2[N(3), N(4)]}. In a similar fashion, the effective coordination around Hg(1) in **3** is expanded from three to four {3 +1[N(2)]}.

In the X-ray structure of **3** · $C_6H_5CH_3$ shown in Fig. 1a and b, the N(1) N(2) Hg(2) is canted by 54.2° (or 46.1°) from the mean 4N porphyrin plane [or from the porphyrin plane defined by four *meso* carbons, C(5), C(10), C(15), and C(20)]. The angle (46.1°) is smaller than those of the corresponding canted angles of 53–63° in compounds **1a**, **1b** and **2a**, **2b** [13]. The Hg(1) N(3) N(4) N(5) plane is tilted from the 4N plane by 59.7°. The porphyrin macrocycle is indeed distorted because of the presence of the $NCOC_6H_5$ group in **3** · $C_6H_5CH_3$. Thus, N(4) pyrrole rings bearing the $NCOC_6H_5$ group in **3** · $C_6H_5CH_3$ deviate most from the 4N plane and are oriented separately with a dihedral angle of 40.9°, whereas small angles of 25.2°, 14.4° and 1.5° occur with N(1), N(2), and N(3) pyrroles for **3** · $C_6H_5CH_3$. Such a large deviation from planarity for the N(4) pyrrole is also reflected by observing a 15-16 ppm upfield shift in the ^{13}C NMR spectrum of C_β (17, 18) at 117.6 ppm compared to 133.6 ppm for C_β (7, 8), 132.9 ppm for C_β (3, 12), and 132.5 ppm for C_β (2, 13) (Table S1 in the Supplementary material). The dihedral angles between the mean plane of the skeleton (4N) and the plane of the phenyl groups are 68.6° [C(24)], 59.2° [C(30)], 50.8° [C(36)], and 28.8° [C(42)] for **3** · $C_6H_5CH_3$. Likewise, the dihedral angles between the mean plane of the 4N and the plane of the phenyl group coordinated to the Hg atom are 139.3° [C(55)], and 118.2° [C(61)] for **3** · $C_6H_5CH_3$. The Hg(1) atom may be described as transoid relative to carbonyl oxygen [i.e. O(1)] of the benzamido (BA) group.

3.2. ^1H, ^{13}C NMR spectra for **3** in $CDCl_3$

Complex **3** was characterized by ^1H and ^{13}C NMR spectra. Compound **3** remains the same as bismerury complex, but became more symmetrical than that of its solid state, due to some conformational changes in the solution state, with a mirror plane running through the N(2)–Hg(1)–Hg(2)–N(4) unit. There are four distinct β-pyrrole protons H_β, four β-pyrrole carbons C_β, four α-pyrrole carbons C_α, two different *meso* carbons C_{meso} and two phenyl-C_1 carbons for **3** (Table S1 in Supplementary material). The ^1H NMR spectra for a 0.02 M solution of **3** in $CDCl_3$ showed these four different types of H_β at 20 °C (Fig. S2 in Supplementary material). The doublet at 8.95 ppm is assigned to H_β (2, 13) with ^3J(H–H) = 4.8 Hz and the other doublet at 8.77 ppm is due to H_β (3, 12) with ^3J(H–H) = 4.2 Hz. The singlet at 8.47 ppm is due to H_β (7, 8) and the other singlet at 7.07 ppm is due to H_β (17, 18). The rotation of the phenyl group along C_1–C_{meso} [C(10)–C(27) or C(5)–C(21)] bond is slow at 20 °C. This slow rotation is evidenced by the two broad singlets at 8.17 and 8.02 ppm due to *ortho*-protons *o*-H(26,32) and *o*-H (22,28), respectively (Fig. S2 in Supplementary material). However, the rotation of the phenyl group along C(15)–C(33) [or C(20)–C(39)] bond for **3** at 20 °C is situated at the fast exchange region. In this fast exchange region, the ^1H NMR of phenyl group *ortho*-protons *o*-H (38,40) and *o*-H (34,44)

of **3** in $CDCl_3$ (or CD_2Cl_2) observed as broad singlet at 8.49 ppm at 20 °C. (Fig. S2 in Supplementary material). From our previous work we knew that the rate of intramolecular exchange of the *ortho*-protons for **3** should be slow at −50 °C in $CDCl_3$ (or at −90 °C in CD_2Cl_2) and should appear as two sets of doublets at −50 °C (or −90 °C): one doublet is assigned to *ortho*-protons *o*-H (38,40) and the other doublet is due to *ortho*-protons *o*-H (34,44) as for compounds Tl(tpp-*N*-O)(OAc) [14] and Cd(N–NHCO-2-C_4H_3O-tpp)(OAc) [15]. However, the solubility of **3** in $CDCl_3$ (or CD_2Cl_2) became worse as the temperature was decreased (at −50 °C in $CDCl_3$ or at −90 °C in CD_2Cl_2). Hence, the ^{1}H resonance for the *ortho*-protons *o*-H (38,40) and *o*-H (34,44) observed as broad singlet at 8.49 ppm at 20 °C. The benzamido group (BA), Hg(2)–Ph, Hg(1)–Ph protons in **3** are sitting at the region where a strong ring current effect of the bidentate porphyrin would be induced. Hence, all BA, Hg(2)–Ph, Hg(1)–Ph protons are shifted upfield compared to their counterparts on free BA–Ph, Hg(2)–Ph, and Hg(1)–Ph. On the basis of the ring model [16], as the distance between the geometrical center (C_t) of the 4N plane and axial protons gets smaller, the shielding effect becomes larger. The average distance between $C_t\cdots$Hg(2)–Ph–$H_{2,6}$, $C_t\cdots$Hg(2)–Ph–$H_{3,5}$ and $C_t\cdots$Hg(2)–Ph–H_4 increases from 4.026, 6.056 to 6.868 Å. Likewise, the average distance between $C_t\cdots$Hg(1)–Ph–$H_{2,6}$, $C_t\cdots$Hg(1)–Ph–$H_{3,5}$ and $C_t\cdots$Hg(1)–Ph–H_4 increases from 4.480, 6.492 to 7.250 Å. The fact that all three distances between $C_t\cdots$Hg(2)–Ph are shorter than those of $C_t\cdots$Hg(1)–Ph indicates that ring current effect in Hg(2)–Ph protons would be larger and in turn the ^{1}H upfield shifts for Hg(2)–Ph protons would be still higher. This observation is corroborated by the doublet at 3.18 ppm with satellites of ^3J(Hg–H) = 198 Hz for Hg(2)–Ph–$H_{2,6}$ and the doublet at 4.23 ppm with ^3J(Hg–H) = 186 Hz for the Hg(1)–Ph–$H_{2,6}$, the triplet at 5.84 ppm with well-resolved ^4J(Hg–H) of 54 Hz for the Hg(2)–Ph–$H_{3,5}$ and the triplet at 6.49 ppm with ^4J(Hg–H) = 48 Hz [1] for Hg(1)–Ph–$H_{3,5}$, the triplet at 6.07 ppm for Hg(2)–Ph–H_4 and the triplet at 6.61 ppm for Hg(1)–Ph–H_4 (Fig. 2a). Coupling of ^{199}Hg to both the *ortho* phenyl protons and *meta* phenyl protons of $HgPh^+$ in **3** was apparent. These coupling satellites had the same multiplicity as the parent resonance and appeared to be approximately one-fifth the size of the main resonance consistent with the 16.8% natural abundance of ^{199}Hg. The ^{1}H NMR also revealed that the aromatic protons of the BA–Ph group in **3** appear as two triplet at 6.39 ppm (BA–Ph–H_4) with ^3J(H–H) = 7.5 Hz and at 6.18 ppm (BA–Ph–$H_{3,5}$) with ^3J(H–H) = 8.1 Hz and a doublet at 5.03 ppm (BA–Ph–$H_{2,6}$) with ^3J(H–H) = 8.4 Hz (Fig. 2a). This observation is consistent with the fact that the average distance between $C_t\cdots$BA–Ph–$H_{2,6}$, and $C_t\cdots$BA–Ph–$H_{3,5}$, and $C_t\cdots$BA–Ph–H_4 increases from 4.906, 6.706 to 7.425 Å. X-ray diffraction analysis unambiguously confirms that **3** is a bismercury complex. In addition, FAB MS indicates that molecular ion (M^+) of **3** is 1287. This further supports that **3** is a bismercury species in the solid phase. The strong diamagnetic shielding observed for all six resonances of the Hg(2)–Ph and the Hg(1)–Ph protons within **3** in the ^{1}H NMR spectrum suggests that **3** remains in a dinuclear mercury(II) complex in the solution phase.

3.3. ^{199}Hg NMR spectrum for **3** in $CDCl_3$

We have obtained ^{199}Hg NMR data on **3** in $CDCl_3$ at 20 °C to minimize solvent, solvolysis, and temperature effects [17]. The ^{199}Hg NMR spectrum for a 0.2 M solution of **3** in $CDCl_3$ shows two different types of Hg at 20 °C (Fig. 2b). The triplet at −1088 ppm is assigned as Hg(2) with ^3J(Hg–H) = 188 Hz and the other triplet at −1119 ppm is due to Hg(1) with ^3J(Hg–H) = 177 Hz. The ratio of Hg(2)/Hg(1) species obtained via integration of the two ^{199}Hg NMR peaks is nearly 1:1. This ^{199}Hg NMR data provides a second evidence that **3** remains as a bismercury species in $CDCl_3$ solution. The ^3J(Hg–H) of 198 Hz (or 186 Hz) for the Hg(2)–Ph–$H_{2,6}$ [or Hg(1)–Ph–$H_{2,6}$] protons was observed by ^{1}H NMR and was ~10 Hz larger than that of 188 Hz (or 177 Hz) for the same Hg(2)–Ph–$H_{2,6}$ [or Hg(1)–Ph–$H_{2,6}$] with mercury nucleus being measured by ^{199}Hg NMR (Table 3). Similar results with Δ^3J(Hg–H) = 14.7 Hz were obtained for the Hg(1)–Ph–$H_{2,6}$ protons of HgPh(4-NCH_3NCTPP) (Table 3) [18]. The chemical shift anisotropy (CSA) relaxation mechanism is a dominant contribution to ^{199}Hg spin–lattice relaxation in **3** [19]. The high field NMR spectroscopy, at 14.1 T [ν_0(Hg) = 107.24 MHz], may lead to very rapid relaxation. In the case of spin–spin coupling this can cause line broadening for neighboring nuclei or even ^{199}Hg–H decoupling [20–22]. This rapid relaxation explained that ^3J(Hg–H) coupling constants for **3** obtained from proton spectra are larger than those from mercury spectra. The difference is about 10 Hz (or 5%) shown in Table 3. The proton and ^{199}Hg NMR spectra clearly show

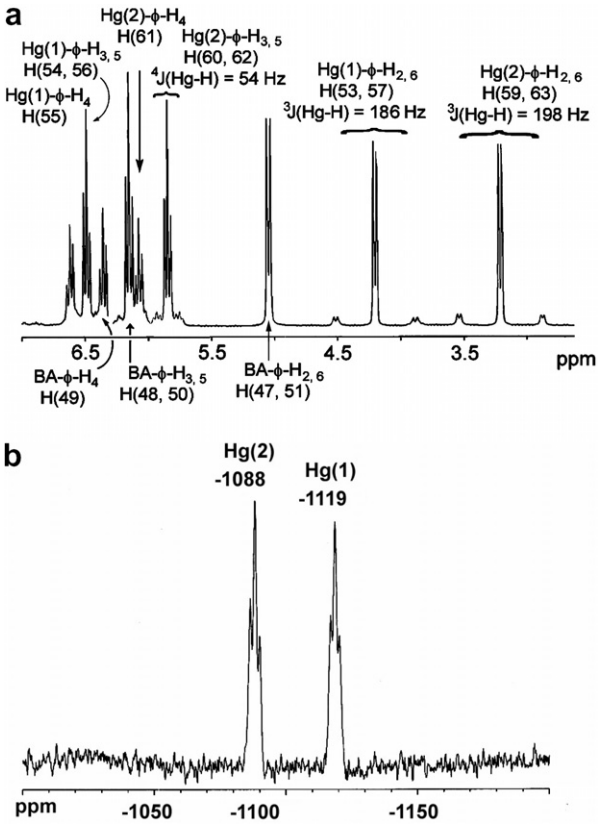

Fig. 2. (a) ^{1}H NMR spectrum at 299.95 MHz for a 0.02 M solution of **3** in $CDCl_3$ at 20 °C, showing Hg(1)–Ph, Hg(2)–Ph and BA protons, where BA = benzamido group, ϕ = Ph. (b) The ^{199}Hg NMR spectra at 107.24 MHz for a 0.2 M solution of **3** in $CDCl_3$ at 20 °C.

Table 3
Comparison of ^3J(Hg–H) (Hz) coupling constants for the Hg-Ph–$H_{2,6}$ protons via ^{1}H and ^{199}Hg NMR spectra for **3** in $CDCl_3$ and HgPh(4-NCH_3NCTPP) in CD_2Cl_2 at 20 °C

Compounds	^3J(Hg–H) [^{1}H]	^3J(Hg–H) [^{199}Hg]	Δ^3J(Hg–H)[a]
Complex **3**			
Hg(1)–Ph–$H_{2,6}$	186	177	9
Hg(2)–Ph–$H_{2,6}$	198	188	10
HgPh(4-NCH_3NCTPP) [16]:Hg(1)–Ph–$H_{2,6}$	186.7	172	14.7

[a] Δ^3J(Hg–H) = ^3J(Hg–H) [^{1}H] − ^3J(Hg–H) [^{199}Hg].

[1] ^4J(Hg–H) = 48 Hz for Hg(1)–Ph–$H_{3,5}$ of **3** was observed at 599.94 MHz in $CDCl_3$ at 20 °C.

^3J(Hg–H) coupling. The presence of the mercury–proton coupling is an important indicator of no ligand exchange in **3** [17].

Heteronuclear coupling constants for ^{199}Hg in alkyl mecurials have been determined to decrease in the order $^1J \gg {}^3J > {}^2J > {}^4J$ [21,22]. This order explains that the coupling constant of ^3J(Hg–H) = 193 ± 5 Hz (or 182 ± 5) for the Hg(2)–Ph–$H_{2,6}$ protons [or Hg(1)–Ph–$H_{2,6}$] of **3** is larger than that of ^4J(Hg–H) = 54 Hz (or 48 Hz) for Hg(2)–Ph–$H_{3,5}$ [or Hg(1)–Ph–$H_{3,5}$] protons. Changes in the coupling could possibly come from a Karplus-type relationship [24,25], but the variations in the number of bonds to the $HgPh^+$ unit could also be a critical factor. It is known in the case of ^{199}Hg NMR spectroscopy that an increasing coordination number generally lowers the chemical shift [23]. This fact explained that the ^{199}Hg signal of the Hg(2) nucleus with an effective coordination number of five lies downfield by 31 ppm from that of the Hg(1) nucleus with a smaller effective coordination number of four. Additionally, this also results in an increased effective nuclear charge for the mercury nucleus Hg(2), i.e., Z_{eff} [Hg(2)], and an increased s character of the hybrid orbital for Hg(2) in the three and four-bond couplings to the protons [26]. Therefore coupling constants of ^3J(Hg–H) and ^4J(Hg–H) from Hg(2) are larger than those couplings from Hg(1), respectively.

4. Conclusions

This paper describes synthesis, X-ray, multinuclear NMR and MS characterization of a single bis(mercury(II)) complex of *N*-substituted tetraphenylporphyrin, namely, **3**. The two Hg atoms are in different environments. The two different Hg environments are clearly seen in the ^{199}Hg NMR spectrum as well as some interesting Hg–H couplings.

Acknowledgements

The financial support from the National Science Council of the R.O.C. under Grant NSC 95-2113-M-005-014-MY3 is gratefully acknowledged.

Appendix A. Supplementary data

CCDC 638203 contains the supplementary crystallographic data for **3** · $C_6H_5CH_3$. These data can be obtained free of charge via http://www.ccdc.cam.ac.uk/conts/retrieving.html, or from the Cambridge Crystallographic Data Centre, 12 Union Road, Cambridge CB2 1EZ, UK; fax: (+44) 1223-336-033; or e-mail: deposit@ccdc.cam.ac.uk.

References

[1] H.J. Callot, J. Fisher, R. Weiss, J. Am. Chem. Soc. 104 (1982) 1272.
[2] Y. Takao, T. Takeda, J. Watanabe, J. Setsune, Organometallics 22 (2003) 233.
[3] J. Setsune, T. Yamauchi, S. Tanikawa, Y. Hirose, J. Watanabe, Organometallics 23 (2004) 6058.
[4] J. Setsune, T. Yamauchi, S. Tanikawa, Chem. Lett. (2002) 188.
[5] A. Spencer, in: G. Winkinson, R. Gillard, J.A. McCleverty (Eds.), Comprehensive Organometallic Chemistry, vol. 6, Pergamon Press, Oxford, 1987, p. 1026.
[6] F.A. Yang, J.H. Chen, H.Y. Hsieh, S. Elango, L.P. Hwang, Inorg. Chem. 42 (2003) 4603.
[7] G.M. Sheldrick, SHELXL 97, Program for the Refinement of Crystal Structure from Diffraction Data, University of Gottingen, Gottingen, Germany, 1997.
[8] M.C. Wang, L.S. Sue, B.C. Liau, B.T. Ko, S. Elango, J.H. Chen, Inorg. Chem. 40 (2001) 6064.
[9] S. Das, C.H. Hung, S. Goswami, Inorg. Chem. 42 (2003) 8592.
[10] J.E. Huheey, E.A. Keiter, R.L. Keiter, Inorganic Chemistry, 4th ed., Harper Collins College Publishers, New York, 1993. pp. 114–292.
[11] D. Grdenic, Quart. Rev. 19 (1965) 303.
[12] D. Matkovic-Calogovic, N. Davidovic, Z. Popovic, Z. Zugaj, Acta Crystallogr. C54 (1998) 1766.
[13] J. Setsune, J. Synth. Org. Chem. Jpn. 62 (2004) 1227.
[14] F.A. Yang, K.Y. Cho, J.H. Chen, S.S. Wang, J.Y. Tung, H.Y. Hsieh, F.L. Liao, G.H. Lee, L.P. Hwang, S. Elango, Polyhedron 25 (2006) 2207.
[15] J.Y. Tung, J.H. Chen, Polyhedron 26 (2007) 589.
[16] C.E. Johnson Jr., F.A. Bovey, J. Chem. Phys. 29 (1958) 1012.
[17] M.L. Helm, G.P. Helton, D.G. VanDerveer, G.J. Grant, Inorg. Chem. 44 (2005) 5696.
[18] K.T. Chen, F.A. Yang, J.H. Chen, S.S. Wang, J.Y. Tungs, personal communication.
[19] D.G. Gillies, L.P. Blaauw, G.R. Hays, R. Huis, D.H. Clague, J. Magn. Reson. 42 (1981) 420.
[20] P. Ghosh, P.J. Desrosiers, G. Parkin, J. Am. Chem. Soc. 120 (1998) 10416.
[21] R.J. Benn, H. Gunther, A. Maercker, V. Menger, P. Schmitt, Angew. Chem., Int. Ed. Engl. 21 (1982) 295.
[22] F. Brady, R.W. Matthews, M.J. Forster, D.G. Gillies, J. Chem. Soc., Chem. Commun. (1981) 911.
[23] B. Wrackmeyer, R. Contreres, Annu. Rep. NMR Spectrosc. 24 (1992) 267.
[24] D.C. Bebout, J.F. Bush II, K.K. Crahan, M.E. Kastner, D.A. Parrish, Inorg. Chem. 37 (1998) 4641.
[25] R.P. Blake, B. Lee, M.F. Summers, J.B. Park, Z.H. Zhou, M.W.W. Adams, New J. Chem. 18 (1994) 387.
[26] R.K. Harris, Nuclear Magnetic Resonance Spectroscopy, Longman, Harlow, 1986. p. 225.

Polyhedron 27 (2008) 2221–2225

Contents lists available at ScienceDirect

Polyhedron

journal homepage: www.elsevier.com/locate/poly

Ni(II) complexes of 4′-(2-pyridyl)-2,2′:6′,2″-terpyridine: Structure of mono- and bis-chelates containing anion···π interactions

Sumanta Kumar Padhi, Rojalin Sahu, Vadivelu Manivannan *

Department of Chemistry, Indian Institute of Technology Guwahati, Guwahati 781 039, Assam, India

ARTICLE INFO

Article history:
Received 22 March 2008
Accepted 4 April 2008
Available online 24 May 2008

Keywords:
Ni(II) complexes
Terpyridine
Optical spectra
Magnetism
Crystal structure
Anion···π interaction
Water dimer

ABSTRACT

The mono- and bis-Ni(II) chelates of 4′-(2-pyridyl)-2,2′:6′,2″-terpyridine (**L**) having the molecular formula $[[Ni(\mathbf{L})(H_2O)_3](NO_3)_2]_3[Ni(\mathbf{L})(NO_3)(H_2O)_2](NO_3)\cdot 5H_2O$ (**1**) and $[Ni(\mathbf{L})_2](PF_6)_2\cdot 2H_2O$ (**2**), respectively, are synthesized. The structural, optical and magnetic characteristics are determined. The asymmetric unit of (**1**) contains three $[Ni(\mathbf{L})(H_2O)_3]^{2+}$ (**1a**) and one $[Ni(\mathbf{L})(NO_3)(H_2O)_2]^{+}$ (**1b**) species along with five water molecules and seven nitrate ions. In both **1a** and **1b**, the bivalent nickel has pseudo-octahedral *mer*-N_3O_3 and in **2**, *mer*-N_3N_3 environments. The molecular packing reveals the presence of water–nitrate ion network, $(NO_3^-)\cdots\pi$ interaction in **1** and F···π interaction in **2** and water dimer in both. Both **1** and **2** exhibits d–d transitions in visible and intra-ligand charge transfer (ILCT) in UV regions. The emission spectra are of $\pi \rightarrow \pi^*$ character for $\lambda_{ex} = 345$ nm.

© 2008 Elsevier Ltd. All rights reserved.

1. Introduction

Polydentate ligands containing N-donor heterocyclic rings have covered extra dimension in the realms of coordination chemistry. The transition metal complexes of polypyridines have wide range of utilities as in the field of photochemistry [1], biological activities [2], enantioselective synthesis [3] and supramolecular chemistry [4]. The immobilization of terpyridine ligands onto poly(ethylene glycol)–polystyrene beads results in flexible and highly accessible metal grafting resins [5]. Bivalent nickel complexes of terpyridine and its 4′-(phenyl) derivatives containing mono- and bis-chelates are reported over the years [6,7].

Water plays a crucial role in many biological and chemical processes. Solid-state structural studies that describe water clusters, chains, and sheets in various crystalline solids are another important area of intensive research [8]. The formation and structure of co-crystals are of interest to the pharmaceutical industry as well [9].

This work stems from our interest in the coordination chemistry of 4′-(2-pyridyl)-2,2′:6′,2″-terpyridine (**L**) [10] and is studied by other groups as well [11]. Herein, we report the synthesis, characterization and structure of mono- and bis-Ni(II) chelates of **L** that contain water–nitrate ion network, anion···π interaction and water dimer.

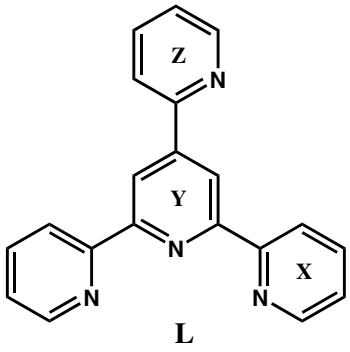

L

2. Experimental

2.1. Instrumentation and materials

A Perkin–Elmer Spectrum One spectrometer for FT-IR spectra (4000–250 cm^{-1}), Cary Eclipse EL05033882 for fluorescence, Perkin–Elmer Lambda 25 spectrometer for UV–Vis spectra and a Lakshore VSM Setup for room temperature magnetic data were used for performing the relevant measurements.

X-ray crystallographic data were collected using Bruker SMART APEX-CCD diffractometer with Mo Kα radiation ($\lambda = 0.71073$ Å). The intensity data were corrected for Lorentz and polarization

* Corresponding author. Tel.: +91 361 258 2306; fax: +91 361 258 2349.
E-mail address: mani@iitg.ernet.in (V. Manivannan).

0277-5387/$ - see front matter © 2008 Elsevier Ltd. All rights reserved.
doi:10.1016/j.poly.2008.04.008

effects and empirical absorption corrections was applied using SAINT program [12,13]. All the structures were solved by direct methods using SHELXS-97 [14]. The Friedel opposites were merged (*R*(int) and *R*(sigma) values, respectively, for **1** are 0.0000 and 0.0017; for **2** are 0.0000 and 0.0024) and the data were used for further refinements. Non-hydrogen atoms located from the difference Fourier maps were refined anisotropically by full-matrix least-squares on F^2, using SHELXL-97 [14]. All hydrogen atoms were included in the calculated positions (except H2C, H5C, H14C, H36C, H37B and H37C, which were generated from FMAP for **1**) and refined isotropically using a riding model.

2-Acetylpyridine, 2-picolylamine, KPF_6 (Aldrich, USA), $Ni(NO_3)_2 \cdot 6H_2O$ (Merck India Ltd.), and solvents were used as received without further purification. 4′-(2-pyridyl)-2,2′:6′,2″-terpyridine, **L**, was prepared using the reported procedure [10b].

2.2. Synthesis of the complexes

2.2.1. $[[Ni(\mathbf{L})(H_2O)_3][(NO_3)_2]_3[Ni(\mathbf{L})(NO_3)(H_2O)_2](NO_3) \cdot 5H_2O$ (**1**)

To 41 mg (0.13 mmol) of 4′-(2-pyridyl)-2,2′:6′,2″-terpyridine (**L**) dissolved in 20 mL of methanol, a methanolic solution (10 mL) of 115 mg (0.395 mmol) $Ni(NO_3)_2 \cdot 6H_2O$ was added and stirred for 1 h. After a week, pale green crystals deposited were collected after washing with ice-cold methanol. Yield: 37 mg (50% based on **L**). IR (KBr), cm^{-1}: 1614 (C=N_{py}), 1558, 1384 (NO_3). *Anal.* Calc. for $C_{80}H_{88}N_{24}O_{40}Ni_4$: C, 42.46; H, 3.89; N, 14.86. Found: C, 42.62; H, 3.96; N, 14.71%. During the crystallization, small amounts of reddish-brown crystals of composition $[Ni(\mathbf{L})_2](NO_3)_2$ were also isolated.

2.2.2. $[Ni(\mathbf{L})_2](PF_6)_2 \cdot 2H_2O$ (**2**)

To 30 mg (0.10 mmol) of $Ni(NO_3)_2 \cdot 6H_2O$ dissolved in 50 mL of methanol, 63 mg (0.21 mmol) of 4′-(2-pyridyl)-2,2′:6′,2″-terpyridine and then an aqueous solution of 50 mg (0.27 mmol) of KPF_6 were added with stirring. The reaction mixture was stirred for another 4 h and left undisturbed. Block like reddish-brown crystals of **2** were obtained after a week. Yield: 62 mg (60%). IR (KBr), cm^{-1}: 1614 (C=N_{py}), 1603 (C=N_{py}), 1573, 1557, 842 (P–F). *Anal.* Calc. for $C_{40}H_{32}F_{12}N_8O_2P_2Ni$: C, 47.74; H, 3.18; N, 11.14. Found: C, 47.81; H, 3.23; N, 11.05%.

3. Results and discussion

3.1. Optical spectra and magnetism

The UV–Vis spectrum of **1** and **2** in methanol (Fig. S1), exhibits d–d transitions in visible and intra-ligand charge transfer (ILCT) in UV regions [15]. The λ_{max} and their molar extinction coefficient values obtained after fitting to Gaussian are listed in Table 1. Both the complexes display the typical transitions, $^3A_{2g} \rightarrow {}^3T_{2g}$ at a lower and $^3A_{2g} \rightarrow {}^3T_{1g}(P)$ at the higher energies. The energy of the $^3A_{2g} \rightarrow {}^3T_{2g}$ transition, follow the trend **2** > **1** in accordance with strong field nature of **L** compared to H_2O/NO_3^-, while that of the $^3A_{2g} \rightarrow {}^3T_{1g}(P)$ remain invariant. But the transition $^3A_{2g} \rightarrow {}^3T_{1g}(F)$ was not observed which may be obscured by the intra-ligand bands. In case of **1** and **2** a sharp spin forbidden transition observed having their maxima at 770 and 750 nm, respectively. The intra-ligand charge transfer transitions are of $\pi \rightarrow \pi^*$ and $n \rightarrow \pi^*$ (from 4′-(2-pyridyl)) in origin.

Table 1
UV–Vis data[a]

Complex	λ_{max}, nm (ε, M^{-1} cm^{-1})	
	d–d transition	ILCT
1	890 (14), 770 (1.5), 570 (15)	344 (8770), 330 (10065), 296 (15665), 288 (28665), 265 (37045)
2	800 (18), 750 (1), 570 (13)	347 (12010), 330 (14630), 358 (15250), 300 (19170), 288 (36880)

[a] In methanol.

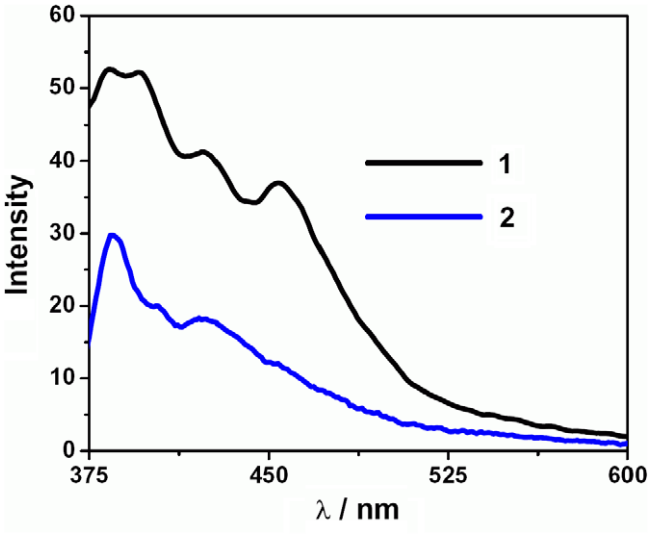

Fig. 1. Emission spectra of **1** and **2**.

The emission spectra of **1** and **2** in acetonitrile, exhibit $\pi \rightarrow \pi^*$ character (Fig. 1) and indicates that the emission is from a significantly intra-ligand $\pi \rightarrow \pi^*$ state [16]. The envelope of the vibronic structure has a 'domed' shape and the energy spacing within the transition is of the order 8.5×10^4 cm^{-1}. This is a typical signature of Frank–Condon envelope type $\pi \rightarrow \pi^*$ emission in polypyridine complexes [16]. The structured bands with vibronic components at 384, 397, 423 and 454 nm (for **1**) and at 385, 403, 423 and 455 nm (for **2**) are observed for λ_{ex} = 345 nm.

The μ_{eff} values calculated from the least square fitting of the initial magnetization curve ($\chi = M/H$) for **1** and **2** are, respectively, 2.97 and 3.66 BM. The value is slightly higher than the $\mu_{s.o.}$ value for **1**, and is largely higher for **2**. Complex **2** exhibits a distinct hysteresis loop having the coercivity loss is 186 G [17].

3.2. Molecular structures

The molecular structures of $[[Ni(\mathbf{L})(H_2O)_3](NO_3)_2]_3[Ni(\mathbf{L})(NO_3)(H_2O)_2]NO_3 \cdot 5H_2O$ (**1**) and $[Ni(\mathbf{L})_2](PF_6)_2 \cdot 2H_2O$ (**2**) were determined by X-ray crystallography. The crystallographic data and refinement parameters are summarized in Table 2 and selected bond parameters are listed in Table 3, Table S1.

The asymmetric unit of **1** contains three dicationic $[Ni(\mathbf{L})(H_2O)_3]^{2+}$ (**1a**) species and a monocationic $[Ni(\mathbf{L})(NO_3)(H_2O)_2]^+$ (**1b**) unit along with five water molecules. Overall, seven nitrate ions are present in the outer sphere to balance the cationic charge. The bond parameters in the three identical **1a** are comparable with each other. A perspective view of one of the **1a** and the **1b** are shown in Fig. 2.

In both **1a** and **1b**, the bivalent nickel is hexa-coordinated and has a distorted octahedral geometry having a *mer*-N_3O_3 environment. The three nitrogen atoms of **L** occupy sites in the equatorial plane and the fourth equatorial site is occupied by the oxygen atom of a water molecule in **1a** and a monodentate nitrate ion in **1b**. The two axial sites are occupied by two water molecules in both the species. In general, the Ni–$N_{(Y)}$ distances are shorter by 0.124(1) Å than Ni–$N_{(X)}$ and a similar trend is reported in the monochelates of terpyridine and its 4′-(phenyl) derivatives [6]. This is

Table 2
Crystallographic data and refinement parameters

	1	2
Empirical formula	$C_{80}H_{88}N_{24}O_{40}Ni_4$	$C_{80}H_{64}F_{24}N_{16}O_4P_4Ni_2$
CCDC number	648157	648158
Formula weight	2260.49	2010.72
Temperature (K)	296(2)	296(2)
Wavelength (Å)	0.71073	0.71073
Crystal system	triclinic	triclinic
Space group	$P\bar{1}$	$P\bar{1}$
a (Å)	15.965(1)	16.405(1)
b (Å)	17.020(1)	16.461(1)
c (Å)	19.960(1)	17.587(1)
α (°)	97.940(2)	94.215(2)
β (°)	110.611(2)	99.433(2)
γ (°)	106.047(2)	113.753(2)
V (Å^3)	4708.6(4)	4236.6(3)
Z	2	2
D_{calc} (g cm^{-3})	1.594	1.578
μ (mm^{-1})	0.893	0.634
Goodness-of-fit[a] on F^2	1.050	1.044
R [$I > 2\sigma(I)$]	$R_1 = 0.0293$[b], $wR_2 = 0.0712$[c]	$R_1 = 0.0762$[b], $wR_2 = 0.2053$[c]
R indices (all data)	$R_1 = 0.0293$[b], $wR_2 = 0.0713$[c]	$R_1 = 0.0762$[b], $wR_2 = 0.2053$[c]

[a] GOF = $[\sum[w(F_o^2 - F_c^2)^2]/M - N]^{1/2}$ (M = number of reflections, N = number of parameters refined).
[b] $R_1 = \sum||F_o| - |F_c||/\sum|F_o|$.
[c] $wR_2 = [\sum[w(F_o^2 - F_c^2)^2]/\sum[w(F_o^2)^2]]$.

observed in transition metal complexes of terpyridine and substituted terpyridines is due to a more efficient overlap of metal t_{2g} orbitals with the π^* orbitals of the central pyridyl ring. Within the **1b** units, the Ni–$O_{(ax)}$ distances are longer by 0.049(1) Å than that of the Ni–$O_{(eq)}$ distances. In **1a** and **1b**, the intersection of the planes of NiN_3 and NiO_3 deviate from a right angle by 0–4°. The bond angles subtended at the metal center is suggestive of a distorted octahedral geometry. The distortion around the chelating ligand **L** is more severe as is evident from the *cis*-angles lying in the range 77–79°, while the *trans*-angles are in the range 155–158°. The **Z** rings of **L** deviate from planarity with respect to **Y** ring by about 5–12(1)°.

Table 3
Selected bond distances (Å)

1a		1b		2	
Ni1–N1	2.115(1)	Ni4–N13	2.144(1)	Ni1–N1	2.118(3)
Ni1–N2	1.988(1)	Ni4–N14	1.993(1)	Ni1–N2	2.005(3)
Ni1–N3	2.093(1)	Ni4–N15	2.114(1)	Ni1–N3	2.117(3)
Ni1–O1	2.097(1)	Ni4–O10	2.068(1)	Ni1–N5	2.123(3)
Ni1–O2	2.067(1)	Ni4–O11	2.107(1)	Ni1–N6	1.989(3)
Ni1–O3	2.024(1)	Ni4–O12	2.069(1)	Ni1–N7	2.121(3)

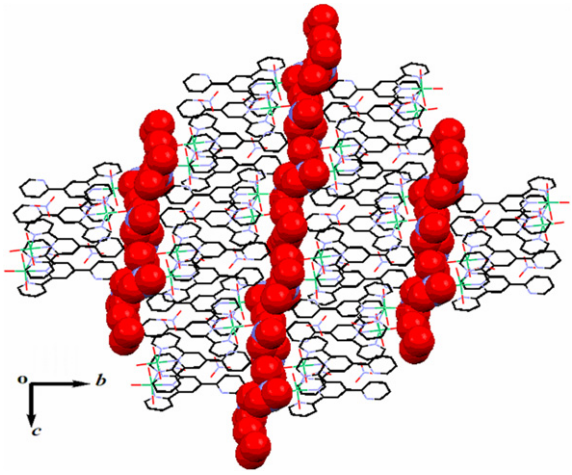

Fig. 3. Molecular packing of **1**.

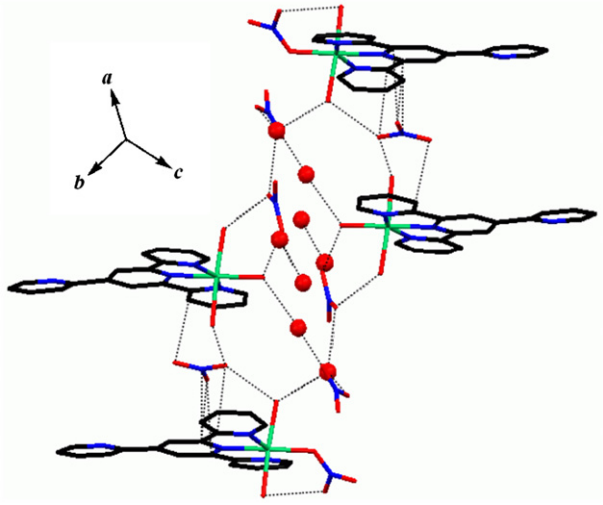

Fig. 4. Water–nitrate ions network and nitrate ion in π–π interaction.

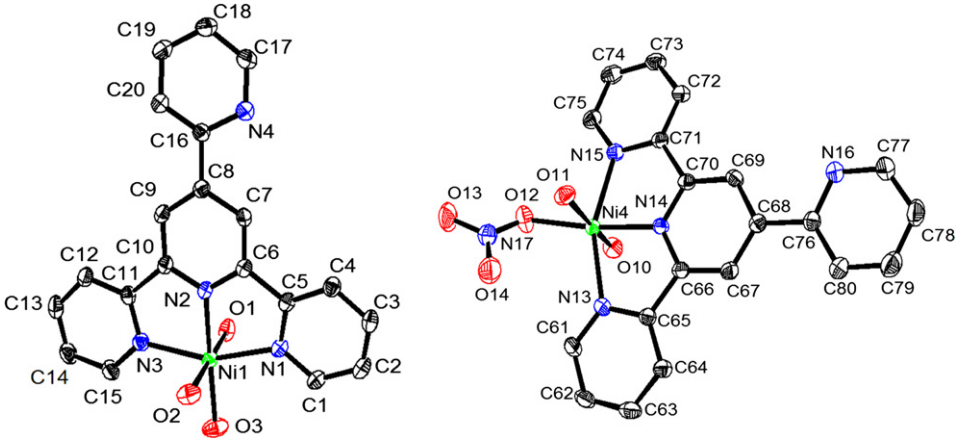

Fig. 2. ORTEP (30% probability and hydrogen atoms are omitted for clarity) of **1a** and **1b**.

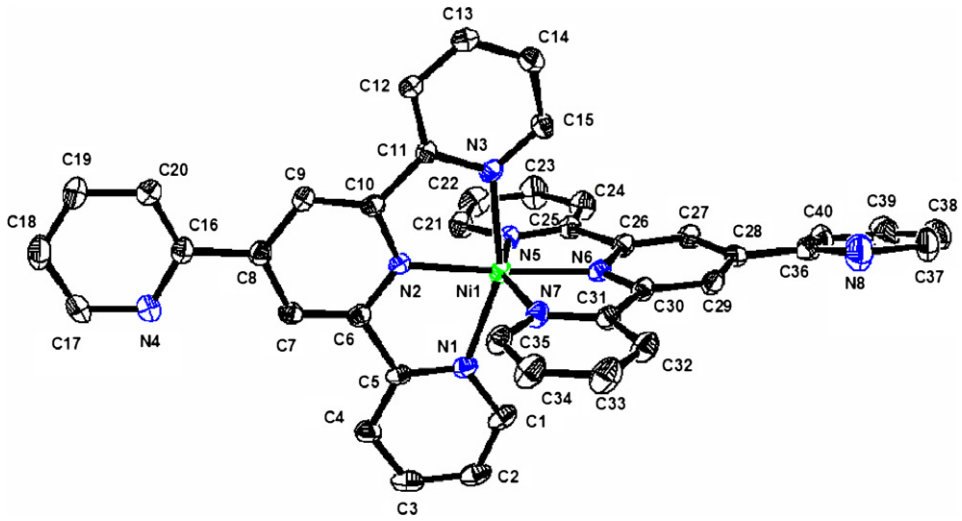

Fig. 5. ORTEP (30% probability and hydrogen atoms are omitted for clarity) of $[Ni(\mathbf{L})_2]^{2+}$ ion in **2**.

The molecular packing of **1** on viewing down the *a*-axis is shown in Fig. 3 and contains bands of **1a** and **1b**, juxtaposed with each other exposing the coordinated water and the nitrate for interlinking. The bands also incorporate four of nitrate ions and among them two are held by π–π stacking (with aromatic rings) [18] as well as hydrogen bonding interactions and the other two are by hydrogen bonding interactions only. These bands are interlinked by layers of five water molecules and the three nitrate ions through hydrogen bonds, leading the network structure. The network consists of centrosymmetric half-units containing crown-shaped $H_2O\cdots H_2O\cdots NO_3\cdots H_2O$–Ni1– $H_2O\cdots NO_3\cdots H_2O$ and chair form of $H_2O\cdots NO_3\cdots H_2O\cdots H_2O\cdots NO_3\cdots H_2O\cdots NO_3\cdots H_2O$ links (Fig. 4). Other notable feature is the presence of a water dimer O36···O40 (2.795(1) Å). The relevant non-bonded interactions are listed in Table S2.

Complex **2** crystallized in a triclinic space group $P\bar{1}$ and the asymmetric unit contains two $[Ni(\mathbf{L})_2]^{2+}$ species and four PF_6^- anions along with four water molecules. The bond parameters in both of the $[Ni(\mathbf{L})_2]^{2+}$ units are within comparable limits. A perspective view of one of the $[Ni(\mathbf{L})_2]^{2+}$ ion is shown in Fig. 5. The bivalent nickel atom is coordinated by six nitrogen atoms of two **L** ligands in a distorted octahedral fashion. The distortion around the nickel atom is evident from the *cis*- and *trans*-angles ranges of 77–78° and about 155°, respectively, within the **L**. The two NiN_3 planes intersect by 88°. As noted in **1**, the Ni–$N_{(Y)}$ distances in **2** are shorter than those of Ni–$N_{(X)}$ by about 0.121(1) Å and a similar trend is observed in the Ni(II) bischelates of terpyridine and its 4′-(phenyl) analog [7]. The **Z** rings of **L** deviate widely from planarity with respect to **Y** ring as inferred from the torsional angle range 2–31°.

The packing diagram of **2** depicting the presence of F···π interactions [19] with the aromatic ring is shown in Fig. 6. These non-bonded contacts lie in the narrow range 3.08(1)–3.12(1) Å. The PF_6^- anions also form C–H···F hydrogen bonds and the H···F non-bonded distances are included in Table S2. In addition, C–H···O and C–H···N interactions and the presence of a water dimer, O1···O2 having a distance of 2.622(1) Å are significant to note.

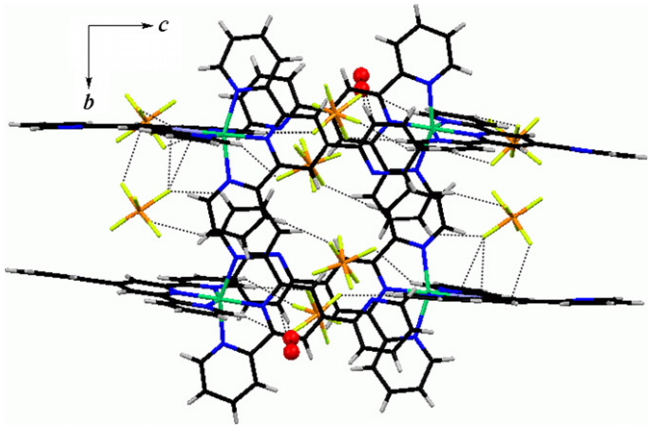

Fig. 6. Packing diagram of **2**.

4. Conclusion

The mono- and bis-nickel(II) chelates of 4′-(2-pyridyl)-2,2′:6′,2″-terpyridine were synthesized. Their electronic spectra reveal that the energy of the $^3A_{2g} \rightarrow {}^3T_{2g}$ transition, follow the trend **2** > **1** and that of the $^3A_{2g} \rightarrow {}^3T_{1g}(P)$ remain invariant. The complexes exhibit $\pi \rightarrow \pi^*$ type emission and behave as two-electron paramagnets. Structural studies shows the presence of a water dimer (in both) as well as $(NO_3^-)\cdots\pi$ and F···π interactions, in **1** and **2**, respectively. In **1**, water–nitrate ion network having crown and chair forms are present.

Acknowledgements

We are grateful to Council of Scientific and Industrial Research, New Delhi for financial grant and to the Department of Science and Technology, New Delhi for establishing single crystal X-ray diffractometer facility under FIST scheme. The authors are thankful to CIF, IIT Guwhati for the VSM facility and Babulal Das for X-ray data.

Appendix A. Supplementary data

CCDC 648157 and 648158 contain the supplementary crystallographic data for this paper. These data can be obtained free of charge via http://www.ccdc.cam.ac.uk/conts/retrieving.html, or from the Cambridge Crystallographic Data Centre, 12 Union Road, Cambridge CB2 1EZ, UK; fax: (+44) 1223-336-033, or e-mail: deposit@ccdc.cam.ac.uk. Supplementary data associated with this

article can be found, in the online version, at doi:10.1016/j.poly.2008.04.008.

References

[1] (a) J.-P. Sauvage, J.-P. Collin, J.-C. Chambron, S. Guillerez, C. Coudret, V. Balzani, F. Barigelletti, L. De Cola, L. Flamigni, Chem. Rev. 94 (1994) 993;
(b) V. Balzani, F. Scandola, in: J.S. Connolly (Ed.), Photochemical Conversion and Storage of Solar Energy, Academic Press, New York, 1981, p. 97;
(c) J.H. Alstrum-Acevedo, M.K. Brennaman, T.J. Meyer, Inorg. Chem. 44 (2005) 6802;
(d) G.J. Meyer, Inorg. Chem. 44 (2005) 6852.

[2] (a) S. Bonse, J.M. Richards, S.A. Ross, G. Lowe, R.L. Krauth-Siegel, J. Med. Chem. 43 (2000) 4812;
(b) K. Jennette, S.J. Lippard, G. Vassiliades, W. Bauer, Proc. Natl. Acad. Sci. USA 71 (1974) 3839.

[3] (a) G. Chelucci, Synth. Commun. 23 (1993) 1897;
(b) J. Uenishi, K. Nishiwaki, S. Hata, K. Nakamura, Tetrahedron Lett. 35 (1994) 7973;
(c) G. Chelucci, M.A. Cabras, A. Saba, J. Mol. Catal. A 95 (1995) L7.

[4] (a) G.F. Swiegers, T.J. Malefetse, Chem. Rev. 100 (2000) 3483;
(b) H. Hofmeier, U.S. Schubert, Chem. Soc. Rev. 33 (2004) 373.

[5] (a) S. Schmatloch, A.M.J. van den Berg, A.S. Alexeev, H. Hofmeier, U.S. Schubert, Macromolecules 36 (2003) 9943;
(b) U.S. Schubert, A. Alexeev, P.R. Andres, Macromol. Mater. Eng. 288 (2003) 852.

[6] (a) N. Baidya, M. Olmstead, P.K. Mascharak, Inorg. Chem. 30 (1991) 929;
(b) Y.D.M. Champouret, J.-D. Maŕechal, I. Dadhiwala, J. Fawcett, D. Palmer, K. Singh, G.A. Solan, Dalton Trans. (2006) 2350;
(c) R. Cortes, M.I. Arriortua, T. Rojo, X. Solanst, D. Beltran, Polyhedron 5 (1986) 1987;
(d) M.L. Calatayud, J. Sletten, M. Julve, I. Castro, J. Mol. Struct. 741 (2005) 121;
(e) E.C. Constable, D. Phillips, P.R. Raithby, Inorg. Chem. Commun. 5 (2002) 519;
(f) R. Baggio, M.T. Garland, M. Perec, Inorg. Chim. Acta 310 (2000) 103.

[7] (a) B.J. Childs, D.C. Craig, M.L. Scudder, H.A. Goodwin, Aust. J. Chem. 52 (1999) 673;
(b) A.T. Baker, D.C. Craig, A.D. Rae, Aust. J. Chem. 48 (1995) 1373;
(c) R. Cortes, L. Lezama, J.I.R. Larramendi, M. Insausti, J.V. Folgado, G. Madariagab, T. Rojo, J. Chem. Soc., Dalton Trans. (1994) 2573;
(d) G.U. Priimov, P. Moore, P.K. Maritim, P.K. Butalanyi, N.W. Alcock, J. Chem. Soc., Dalton Trans. (2000) 445;
(e) C. Alonso, L. Ballester, A. Gutiérrez, M.F. Perpiñán, A.E. Sánchez, M.T. Azcondo, Eur. J. Inorg. Chem. (2005) 486;
(f) E.C. Constable, J. Lewis, M.C. Liptrot, P.R. Raithby, Inorg. Chim. Acta I78 (1990) 47.

[8] J.P. Bouquiere, J.L. Finney, M.S. Lehmann, P.F. Lindley, H.F.J. Savage, Acta Crystallogr., Sect. B 49 (1993) 79.

[9] (a) J. Bernstein, Polymorphism in Molecular Crystals, Clarendon Press, Oxford, 2002;
(b) R. Hilfiker, Polymorphism: In the Pharmaceutical Industry, Wiley–VCH, Weinheim, 2006;
(c) M. Zaworotko, J. Pharm. Pharmacol. 58 (2006) A91;
(d) G.P. Stahly, Cryst. Growth Des. 7 (2007) 1007.

[10] (a) S.K. Padhi, D. Saha, R. Sahu, J. Subramanian, V. Manivannan, Polyhedron 27 (2008) 1714;
(b) S.K. Padhi, V. Manivannan, Inorg. Chem. 45 (2006) 7994.

[11] (a) J.E. Beves, E.L. Dunphy, E.C. Constable, C.E. Housecroft, C.J. Kepert, M. Neuburger, D.J. Price, S. Schaffner, Dalton Trans. (2008) 386;
(b) W.-J. Shi, L. Hou, D. Li, Y-G. Yin, Inorg. Chim. Acta 360 (2007) 588;
(c) H. Feng, X.-P. Zhou, T. Wu, D. Li, Y.-G. Yin, S.W. Ng, Inorg. Chim. Acta 359 (2006) 4027;
(d) K.J. Arm, W. Leslie, J.A. Gareth Williams, Inorg. Chim. Acta 359 (2006) 1222;
(e) L. Hou, D. Li, W.-J. Shi, Y-G. Yin, S.W. Ng, Inorg. Chem. 44 (2005) 7825.

[12] G.M. Sheldrick, SADABS, University of Göttingen, Göttingen, Germany, 1996.

[13] SMART and SAINT, Siemens Analytical X-ray Instruments Inc., Madison, WI, 1996.

[14] G.M. Sheldrick, SHELXS-97 and SHELXL-97, University of Göttingen, Göttingen, Germany, 1997.

[15] A.B.P. Lever, Inorganic Electronic Spectroscopy, Elsevier, Amsterdam, 1986.

[16] (a) J.S. Field, R.J. Haines, L.P. Ledwaba Jr., R. McGuire, O.Q. Murno, M.R. Low, D.R. McMillin, Dalton Trans. (2007) 192;
(b) J.J. Moore, J.J. Nash, P.E. Fanwick, D.R. McMillin, Inorg. Chem. 41 (2001) 6387;
(c) H. Yersin, D. Donges, Top. Curr. Chem. (2001) 81;
(d) M.K. DeArmond, J.E. Hills, J. Chem. Phys. 54 (1971) 2247.

[17] (a) C.J. O'Connor, Prog. Inorg. Chem. 29 (1982) 203;
(b) O. Kahn, Molecular Magnetism, Wiley–VCH, 1993;
(c) M.A. Halcrow, Polyhedron 26 (2007) 3523.

[18] B.R. Manzano, F.A. Jalon, I.M. Ortiz, M.L. Soriano, F. Gomez de la Torre, J. Elguero, M.A. Maestro, K. Mereiter, T.D.W. Claridge, Inorg. Chem. 47 (2008) 413.

[19] M. Zaccheddu, C. Filippi, F. Buda, J. Phys. Chem. A 112 (2008) 1627.

Polyhedron 27 (2008) 2226–2230

Contents lists available at ScienceDirect

Polyhedron

journal homepage: www.elsevier.com/locate/poly

A ^{11}B NMR study of zwitterionic and cationic monoborate complexes with cationic 1,2-diol ligands

Michael A. Beckett [a,*], Catherine C. Bland [a], K. Sukumar Varma [b]

[a] School of Chemistry, Bangor University, Bangor, Gwynedd LL57 2UW, UK
[b] Pilkington Building Products R and D, European Technical Centre, Lathom, Lancashire L40 5UF, UK

ARTICLE INFO

Article history:
Received 3 January 2008
Accepted 9 April 2008
Available online 19 May 2008

Keywords:
Cationic monoborate complexes
Zwitterionic monoborate complexes
^{11}B NMR
Cationic 1,2-diol ligands

ABSTRACT

The interaction of $B(OH)_3$ with $[R_3N\{CH_2CH(OH)CH_2OH\}]$ [OH] (R_3 = Me_3, Me_2Et, $MeEt_2$, Me_2Bz, $Me_2\{CH_2CH_2OH\}$) in a 1:2, 1:1, and 5:1 ratio in aqueous solution has been studied by ^{11}B NMR spectroscopy and the equilibrium species present have been identified. The cationic bischelate $[R_3N\{CH_2CH(O)CH_2O\}_2B]^+$ dominates the 2:1 ratio solutions, zwitterionic monochelate species, $[R_3N\{CH_2CH(O)CH_2O\}B(OH)_2]$, dominate the 1:1 solutions and the pentaborate anion, $[B_5O_6(OH)_4]^-$, dominates the 1:5 solutions. Borate solutions derived from $[NMe_4][OH]$ and $[Me_3NCH_2CH_2OH][OH]$ have also been studied by ^{11}B NMR. Spectra of these borate solutions are essentially the same as those observed for borate solutions with alkali metal cations, and structure directing effects (towards the anion) are not observed in borate systems.

© 2008 Elsevier Ltd. All rights reserved.

1. Introduction

Boric acid is well known to form anionic four-coordinate tetrahedral complexes with bidentate chelating ligands (Eqs. (1) and (2)) [1]. Ligands studied include those derived from polyols, 1,2-diols, 1,3-diols, benzene-1,2-diols, and α-hydroxycarboxylic acids [2–6]. Borate complexes of this type have found use in the synthesis, separation and identification of both synthetic and naturally occurring polyol derivatives [1,7]. These reactions also form the basis of a volumetric analytical method for $B(OH)_3$ where the H_3O^+ ions that are liberated by the presence of excess polyol (usually mannitol or sorbitol) may be titrated with NaOH(aq) [8].

$$B(OH)_3 + HOCR_2CR_2OH \rightarrow [(HO)_2B(OCR_2CR_2O)]^- + H_3O^+ \quad (1)$$

$$B(OH)_3 + 2HOCR_2CR_2OH \rightarrow [B(OCR_2CR_2O)_2]^- + 2H_2O + H_3O^+ \quad (2)$$

^{11}B NMR is a convenient method for studying borate speciation in aqueous solution in the presence of diols since characteristic chemical shifts are observed for the different species present [9–14]. We have recently become interested in cationic 1,2-diols, derived from substituted ammonium cations, as potentially chelating ligands and report here their interactions with $B(OH)_3$ which result in the formation of new zwitterionic and cationic monoborate complexes.

2. Experimental

2.1. General

Reagents were purchased from Aldrich Chemical Co. and Lancaster Synthesis Ltd. and were used without further purification. Solvents were standard reagent grade and were used as supplied unless otherwise stated. Multi-element solution NMR spectra were recorded at room temperature (298 K) on a Bruker Avance 500 (11.7 T) spectrometer operating at 500 MHz for ^{1}H, 125 MHz for ^{13}C–{^{1}H}, and 160 MHz for ^{11}B–{^{1}H} and referenced to $(CH_3)_4Si$ or $BF_3 \cdot OEt_2$. Chemical shifts (δ) are reported in ppm, and J coupling in Hz. Mass spectrometry data were obtained by direct infusion (DI) of the samples using a Bruker microTOF spectrometer in electrospray ionisation (ESI) mode. MS samples were dissolved in H_2O or MeOH prior to analysis. Elemental analyses (C, H, N) were performed on a Carlo Erba EA-110E analyser, using helium as the carrier gas.

2.2. Preparation of tetraorganoammonium hydroxides

The general method is given for **1**[OH] which is a slightly modified version of a literature method [15]. Spectroscopic and analytical data are given for all compounds **1**–**7**[OH].

2.2.1. $[Me]_3NCH_2CH(OH)CH_2OH]OH$ (*1*[OH])

Ethanolic trimethylamine solution (23.80 ml, 100 mmol, *ca.* 4.2 M) was cooled on an ice bath. 2,3-Epoxy-1-propanol (8.00 ml, 120 mmol) was added slowly via syringe to the amine over 10 min, while maintaining the solution temperature between 15

* Corresponding author.
E-mail address: m.a.beckett@bangor.ac.uk (M.A. Beckett).

0277-5387/$ - see front matter © 2008 Elsevier Ltd. All rights reserved.
doi:10.1016/j.poly.2008.04.007

and 25 °C. After 30 min, H_2O (10 ml) was added, causing an exothermic reaction. After reducing the temperature to 25 °C, H_2O (10 ml) was added and the reaction mixture was stirred overnight. The unreacted glycidol was extracted using $CHCl_3$ (4 × 40 ml), and the aqueous phase was reduced in volume on the rotary evaporator to a yellow solution (28.13 g). An aliquot of the solution (1.00 ml) was titrated against HCl (2.00 M) in order to determine the hydroxide concentration, using universal indicator solution to identify the neutral end point. [OH^-] = 3.50 M. Yield = 89%. NMR: (500 MHz, D_2O) δ_H = 2.98 s (9H), 3.04 dd (1H), 3.21 dd (1H), 3.35 dd (2H), 3.94 m (1H); (125 MHz, D_2O) δ_C = 54.0, 64.9, 67.3, 70.3. MS (DI/ESI): $^{12}C_6{}^1H_{16}{}^{14}N^{16}O_2$ calc. 134.1176 *m*/*z*; obs. 134.1159 *m*/*z*.

2.2.2. [$Me_2EtNCH_2CH(OH)CH_2OH$]OH (**2**[OH])

Yield = 77%. NMR: (500 MHz, D_2O) δ_H = 1.08 t, (3H), 2.84 s (6H), 3.15–3.29 m (6H), 3.86 s (1H); (63 MHz, D_2O) δ_C = 10.2, 53.3, 53.5, 63.7, 67.5, 69.6, 70.0. MS (DI/ESI): $^{12}C_7{}^1H_{18}{}^{14}N^{16}O_2$ calc. 148.1332 *m*/*z*; obs. 148.1306, 222.1676 *m*/*z*.

2.2.3. [$Me_2(CH_2CH_2OH)NCH_2CH(OH)CH_2OH$]OH (**3**[OH])

Yield = 77% (lit. [15] 76%). NMR: (500 MHz, D_2O) δ_H = 2.72 s (6H), 2.89–3.13 m (6H), 3.47 s (2H), 3.80 s (1H); (125 MHz, D_2O) δ_C = 52.0, 52.2, 55.1, 64.4, 66.3, 66.8, 68.2. MS (DI/ESI): $^{12}C_7{}^1H_{18}{}^{14}N^{16}O_3$ calc. 164.1332 *m*/*z*; obs. 164.1432, 238.1777, 312.2130 *m*/*z*.

2.2.4. [$Et_2MeNCH_2CH(OH)CH_2OH$]OH (**4**[OH])

Yield = 66%. NMR: (500 MHz, D_2O) δ_H = 1.21 t (6H), 2.95 s (3H), 3.14 dd (1H), 3.26 m (1H), 3.32–3.51 m (6H), 4.05 m (1H); (125 MHz, D_2O) δ_C = 7.2, 47.9, 57.2, 57.6, 64.6, 66.5, 70.5. MS (DI/ESI): $^{12}C_8{}^1H_{20}{}^{14}N^{16}O_2$ calc. 162.1489 *m*/*z*; obs. 162.1503, 236.1834, 310.2184 *m*/*z*.

2.2.5. [$Me_2BzNCH_2CH(OH)CH_2OH$]OH (**5**[OH])

Yield = 61%. NMR: (500 MHz, D_2O) δ_H = 2.93 s (3H), 2.96 s (3H), 3.32 d (2H), 3.44 m, (2H), 4.16 m (1H), 4.42 m (2H), 7.42 m (5H); (63 MHz, D_2O) δ_C = 52.7, 53.3, 67.3, 69.5, 70.6, 72.1, 129.8, 131.8, 133.4, 135.8. MS (DI/ESI): $^{12}C_{12}{}^1H_{20}{}^{14}N^{16}O_2$ calc. 210.1489 *m*/*z*; obs. 210.1483 *m*/*z*.

2.2.6. [$Me_2N(CH_2CH(OH)CH_2OH)_2$]OH (**6**[OH])

Yield = 65%. NMR: (500 MHz, D_2O) δ_H = 3.13 s (3H), 3.16 s, (3H), 3.30–3.57 m (8H), 4.03 dt, (1H), 4.16 dt (1H); (63 MHz, D_2O) δ_C = 55.2, 56.0, 66.8, 67.2, 68.7, 69.2, 70.5, 70.9. MS (DI/ESI): $^{12}C_8{}^1H_{20}{}^{14}N^{16}O_4$ calc. 194.1387 *m*/*z*; obs. 194.1365, 268.1764 *m*/*z*.

2.2.7. Attempted preparation of [$Et_3NCH_2CH(OH)CH_2OH$]OH (**7**[OH])

NMR: (500 MHz, D_2O) δ_H = 1.05 d (9H), 2.81 s (18H) 2.91 q (3H), 3.06–3.28 m (23H), 3.52 s (2H), 3.82 t (2H), 3.98 s (1H); (125 MHz, D_2O) δ_C = 7.5, 50.6, 50.8, 61.0, 62.7, 64.8, 66.9, 67.4, 67.8, 70.4, 72.3, 74.3. MS (DI/ESI): $^{12}C_9{}^1H_{22}{}^{14}N^{16}O_2$ calc. 176.1645 *m*/*z*; obs. 176.1649, 250.1984, 324.2331, 398.2680, 472.3009 *m*/*z*.

2.3. Preparation of tetraorganoammonium borate solutions

The tetraorganoammonium borate solutions were prepared in three sets with cation:boron ratios of 2:1, 1:1 and 1:5. In general, the required molar ratio of $B(OH)_3$ was dissolved in the tetraalkylammonium hydroxide solution (molarity as determined above) although in some cases this process was facilitated by additional H_2O solvent and gentle heating. This is described in detail for the 2:1 **1**[OH]:$B(OH)_3$ solution: an aqueous solution of **1**[OH] (3.1651 g, 3.50 M, 10.0 mmol) was placed in a narrow high-sided vial. $B(OH)_3$ (0.3051 g, 5.00 mmol) was added and the mixture stirred overnight to yield a transparent yellow solution. The resulting solution was ~1.8 M in [B]. ^{11}B NMR data for this and the other solutions arising from **1**–**6**[OH] and $B(OH)_3$ are given in Table 1. 1:1 and 1:5 [NMe_4][OH]:$B(OH)_3$ solutions and 1:1 and 1:5 [$Me_3NCH_2CH_2OH$][OH]:$B(OH)_3$ solutions were prepared in a similar manner to yield 2.0, 5.6, 2.0, and 6.8 M total [B], respectively. ^{11}B NMR (160 MHz, D_2O) data for these 4 solutions (in the same order) are δ_B = 2.4 (100%) $[B(OH)_4]^-$; δ_B = 1.1 (18%) $[B_5O_6(OH)_4]^-$, 13.0 $[B_3O_3(OH)_4]^-$ (33%), 18.6 (49%) $B(OH)_3$; δ_B = 2.0 (100%) $[B(OH)_4]^-$; and δ_B = 1.1 (15%) $[B_5O_6(OH)_4]^-$, 13.7 $[B_3O_3(OH)_4]^-$ (53%), 18.7 (32%) $B(OH)_3$.

Table 1

Cation	~Total [B]/M	B speciation (integration, % of total ^{11}B signal)				
		Bis[a] chelate	Mono[b] chelate	$[B(OH)_4]^-$[c]	$B(OH)_3$[d]	$[B_5O_6(OH)_4]^-$[e]
(a) [$R_3N\{CH_2CH(OH)CH_2OH\}$][OH]:$B(OH)_3$ = 2:1						
1	1.8	64	35	1		<1
2	0.9	65	34	1		<1
3	1.3	64	34	2		
4	1.6	77	23			
5	1.0	63	32	5		<1
6	1.8	90	10			
(b) [$R_3N\{CH_2CH(OH)CH_2OH\}$][OH]:$B(OH)_3$ = 1:1						
1	3.0	31	69			
2	2.0	29	71			
3	2.7	25	60	15		
4	2.5	32	64	3		1
5	2.0	35	63	<1		2
6	3.5	82	18			
(c) [$R_3N\{CH_2CH(OH)CH_2OH\}$][OH]:$B(OH)_3$ = 1:5						
1	6.3	4	6		74	16
2	4.7	6	9		71	14
3	5.8	3	4		75	18
4	6.1	12	6		65	17
5	5.0	3	5		79	13
6	9.4	23	15		52	10

[a] Neutral zwitterionic monochelate complex, [$R_3N\{CH_2CH(O)CH_2O\}B(OH)_2$], with δ ^{11}B ~ 6.0 ppm.
[b] Cationic bischelate complex, [$R_3N\{CH_2CH(O)CH_2O\}_2B$]$^+$, with $\delta^{11}B$ ~ 10.0 ppm.
[c] More correctly, $[B(OH)_3/[B(OH)_4]^-$ equilibrium fast exchange, $\delta^{11}B$ ~ 2.0 ppm.
[d] More correctly, $[B(OH)_3/[B(OH)_4]^-$ equilibrium fast exchange, $\delta^{11}B$ ~ 19.0 ppm.
[e] $\delta^{11}B$ ~ 1.0 ppm. This signal is attributed to the four-coordinate *spiro* B centre of the pentaborate anion. The four three-coordinate B centres of the pentaborate anion are very broad and difficult to detect above background noise by ^{11}B NMR [18].

2.4. Preparation of tetraorganoammonium chlorides, **1**,**2**,**4**–**7**[Cl]

The general method is described below for **1**[Cl]. Yields, analytical data and spectroscopic data are reported for compounds **2**,**4**–**7**[Cl].

2.4.1. [$Me_3NCH_2CH(OH)CH_2OH$]Cl (**1**[Cl])

Ethanolic trimethylamine solution (23.80 g, 100 mmol, *ca.* 4.2 M) was cooled on an ice bath. 3-Chloro-1,2-propanediol (8.40 ml, 100 mmol) was added slowly via syringe to the amine, followed by methanol (60 ml). The mixture was heated to reflux (*ca.* 60 °C) overnight, and the solvent was removed by rotary evaporation to give a crude yellow oil. Small portions of the oil were washed with a large excess of acetone to afford a fine white hygroscopic powder (9.42 g, 56%). NMR: (500 MHz, D_2O) δ_H = 3.19 s (9H), 3.39 dd (1H), 3.43 dd (1H), 3.56 d (2H), 4.25 m (1H); (125 MHz, D_2O) δ_C = 54.2, 63.6, 66.4, 68.2. EA: Calc. for $C_6H_{16}ClNO_2$: C, 42.5; H, 9.5; N, 8.3. Found: C, 42.0; H, 9.7; N, 8.2%. MS (DI/ESI): $^{12}C_6{}^1H_{16}{}^{14}N^{16}O_2$ calc. 134.1176 *m*/*z*; obs. 134.1138 *m*/*z*.

2.4.2. [$Me_2EtNCH_2CH(OH)CH_2OH$]Cl (**2**[Cl])

Colourless oil (87%). NMR: (500 MHz, D_2O) δ_H = 1.41 t (3H), 3.18 s (6H), 3.42–3.61 m (6H), 4.23 m (1H); (63 MHz, D_2O) δ_C = 9.5, 52.7,

52.9, 63.0, 66.0, 67.8, 68.4. EA: Calc. for $C_7H_{18}ClNO_2$: C, 45.8; H, 9.9; N, 7.6. Found: C, 44.3; H, 10.0; N, 7.1%. MS (DI/ESI): $^{12}C_7{}^1H_{18}{}^{14}N^{16}O_2$ calc. 148.1332 *m/z*; obs. 148.1313 *m/z*.

*2.4.3. [$Et_2MeNCH_2CH(OH)CH_2OH$]Cl (**4**[Cl])*

White hygroscopic powder (52%). NMR: (500 MHz, D_2O) δ_H = 1.43 t (6H), 2.99 s (3H), 3.29 d (2H), 3.38 m (4H), 3.47 dd (1H), 3.49 dd (1H), 4.16 p (1H); (63 MHz, D_2O) δ_C = 9.9, 50.6, 60.1, 60.5, 65.1, 66.4, 68.6. EA: Calc. for $C_8H_{20}ClNO_2$: C, 48.6; H, 10.2; N, 7.1. Found: C, 47.1; H, 10.1; N, 6.7%. MS (DI/ESI): $^{12}C_8{}^1H_{20}{}^{14}N^{16}O_2$ calc. 162.1489 *m/z*; obs. 162.1473 *m/z*.

*2.4.4. [$Me_2BzNCH_2CH(OH)CH_2OH$]Cl (**5**[Cl])*

White hygroscopic powder (16.53 g, 67%). NMR: (500 MHz, D_2O) δ_H = 3.05 s (3H), 3.08 s (3H), 3.38 m (2H), 3.51 d (2H), 4.31 m (1H), 4.54 s (2H), 7.50 m (5H); (63 MHz, D_2O) δ_C = 53.0, 53.5, 66.4, 68.7, 68.8, 72.3, 129.7, 131.8, 133.5, 135.8. EA: Calc. for $C_{12}H_{20}ClNO_2$: C, 58.6; H, 8.2; N, 5.7. Found: C, 58.8; H, 8.6; N, 5.9%. MS (DI/ESI): $^{12}C_{12}{}^1H_{20}{}^{14}N^{16}O_2$ calc. 210.1489 *m/z*; obs. 210.1496 *m/z*.

*2.4.5. [$Me_2N(CH_2CH(OH)CH_2OH)_2$]Cl (**6**[OH])*

Colourless oil (99%). NMR: (500 MHz, D_2O) δ_H = 3.20 d (3H), 3.22 s (3H), 3.44–3.49 m (4H), 3.52 d (2H), 3.53 d (2H), 4.24 m (2H); (125 MHz, D_2O) δ_C = 52.7, 53.0, 63.7, 66.2, 67.2, 67.5. EA: Calc. for $C_8H_{20}ClNO_4$: C, 41.8; H, 8.8; N, 6.1. Found: C, 38.7; H, 8.9; N, 5.9%. MS (DI/ESI): $^{12}C_8{}^1H_{20}{}^{14}N^{16}O_4$ calc. 194.1387 *m/z*; obs. 194.1389 *m/z*.

*2.4.6. [$Et_3NCH_2CH(OH)CH_2OH$]Cl (**7**[Cl])*

White hygroscopic powder (61%). NMR: (500 MHz, D_2O) δ_H = 1.23 t (9H) CH_3 ^3J 7.3, 3.24 dd (1H) CH_2 ^2J 14.8 ^3J 1.3, 3.28 dd (1H) CH_2 ^2J 14.8 ^3J 1.6, 3.32 dq (3H) CH_3CH_2 ^2J 14.5 ^3J 7.3, 3.39 dq (3H) CH_3CH_2 ^2J 14.5 ^3J 7.3, 3.49 dd (1H) CH_2OH ^2J 11.7 ^3J 6.0, 3.54 dd (1H) CH_2OH ^2J 11.7 ^3J 5.7,4.14 dt (1H) $CHOH$ ^3J 5.7 ^3J 6.0 ^3J 1.3 ^3J 1.6; (125 MHz, D_2O) δ_C = 6.8 CH_3, 53.7 CH_3CH_2N, 58.8 CH_2N, 63.7 $CHOH$, 65.7 CH_2OH. EA: Calc. for $C_9H_{22}ClNO_2$: C, 51.0; H, 10.5; N, 6.6. Found: C, 48.3; H, 9.8; N, 6.3%. MS (DI/ESI): $^{12}Cg138_9{}^1H_{22}{}^{14}$ $N^{16}O_2$ Calc. 176.1645 *m/z*; obs. 176.1629 *m/z*.

2.5. Reaction of tetraorganoammonium chlorides with sodium borate in MeOH/H_2O

The general method is given for **2**[Cl]. Spectroscopic and analytical data are given for all reactions involving **2**,**4**–**7**[OH] with $Na[B(OH)_4]$. **2**[Cl] (1.25 g, 6.8 mmol), dissolved in MeOH (15 ml), was added to H_2O (5 ml) containing NaOH (0.28 g, 6.8 mmol) and $B(OH)_3$ (0.42 g, 6.8 mmol). This resulted in an exothermic reaction, and the mixture was left to stir overnight. The solvent was removed (rotary evaporator) to yield a sticky white solid. NMR: (160 MHz, D_2O) δ_B = 10.4 (8%), 6.2 (51%), 4.7 (41%). This solid was extracted into MeOH, and the soluble fraction afforded a white solid, upon solvent evaporation. NMR: (160MHz, D_2O) δ_B = 10.4 (91%), 6.1, (9%). **4**[Cl] gave δ_B = 10.5 (11%), 6.1 (55%), 4.4 (34%); and then 10.4 (9%), 6.2 (91%). **5**[Cl] gave δ_B = 10.5 (7%), 6.2 (52%), 4.4 (41%); and then 10.4 (8%), 6.2 (56%), 3.2 (36%). **6**[Cl] gave δ_B = 10.5 (39%), 6.2 (61%); and then 10.5 (23%), 6.2 (77%). **7**[Cl] gave δ_B = 10.4 (3%), 6.2 (38%), 3.4 (59%); and then 10.4 (17%), 6.2 (49%), 3.3 (34%).

3. Results and discussion

In order to investigate the reactions of diol-functionalised tetraorganoammmonium cations with $B(OH)_3$ it was first necessary to prepare the cations in aqueous solutions with hydroxide counterions. The following cations, which contain increasing chain length and steric bulk about the N centre, were selected as suitable target compounds: $[R_3N\{CH_2CH(OH)CH_2OH\}][OH]$, where R_3 = Me_3 (**1**), Me_2Et (**2**), $Me_2\{CH_2CH_2OH\}$ (**3**), $MeEt_2$ (**4**), Me_2Bz (**5**), $Me_2\{CH_2CH(OH)CH_2OH\}$ (**6**), Et_3 (**7**). Compounds **3**[OH] and **6**[OH] also had additional OH functionalities. Lovett has published a method for the preparation of **3**[OH] [15] involving quarternisation of a tertiary amine by ring opening of 2,3-epoxy-1-propanol in the presence of H_2O and this method was attempted for the syntheses of **1**–**7**[OH] (Eq. (3)). All reactions, with the exception of that intended to produce **7**[OH], gave the desired products in relatively good yields (61–89%). ^1H and ^{13}C spectra of the resulting solutions (except **7**[OH]), although complicated by the chiral and prochiral centres on the cations, were consistent with the expected structures. The ^{13}C spectrum for "**7**[OH]" indicated that oligomerisation of the glycidol had occurred (δ_C 66.9–74.2 and δ_H 3.0–3.3 ppm) and signals attributable to unreacted Et_3N were also detected. This suggests that steric hindrance about the nitrogen atom prevented rapid quarternisation by the epoxide. Accurate mass spectrometry data (DI/ESI) confirmed that the desired cations had been formed in all reactions. Aqueous solutions of **2**[OH], **3**[OH], **4**[OH] and **6**[OH] also showed weak signals at *m/z* values corresponding to ions with masses that were multiples of 74 *m/z* greater than those of the target cations. 74 *m/z* corresponds to a 'ring-opened glycidol' unit and therefore suggests that oligomerisaton of the epoxide did occur to a small extent, as a competing reaction, under these experimental conditions. In contrast, and consistent with NMR data, the accurate mass spectrometry data for solution "**7**[OH]" demonstrated that the extent of oligomerisation was so great that this was the dominant reaction process. Solution **7**[OH] was therefore not used for further studies. With the exception of **3**[OH] [15] all other compounds are previously unreported.

$$R_3N + CH_2(O)CHCH_2OH + H_2O \rightarrow [R_3N\{CH_2CH(OH)CH_2OH\}][OH] \quad (3)$$

$$R_3N + ClCH_2CH(OH)CH_2OH \rightarrow [R_3N\{CH_2CH(OH)CH_2OH\}][Cl] \quad (4)$$

Chloride salts of the same series of diol-functionalised tetraorganoammonium cations were also prepared, **1**,**2**,**4**–**7**[Cl]. These chlorides, obtained as white hygroscopic solids or colourless oils, were isolated in good yields (56–99%) by the quaternisation reaction (Eq. (4)). The hygroscopic nature of these materials made it difficult to obtain reliable elemental analysis data, although 'close fits' are reported in Section 2. Surprisingly, only compounds **1**[Cl] and **4**[Cl] have had characterisation data previously reported [16,17]. ^1H and ^{13}C spectra were consistent with the structures. The ^1H spectrum of **7**[Cl] was particularly well resolved and a complete assignment of the observed coupling patterns is given in the experimental characterisation data. Accurate mass spectrometry data (DI/ESI) confirmed that the desired cations had been obtained in all cases.

The interaction of **1**–**6**[OH] with $B(OH)_3$ in aqueous solution in molar ratios 2:1, 1:1, and 1:5 were examined by ^{11}B NMR spectroscopy, and results are presented in Table 1. A representative ^{11}B spectrum for the solution obtained from **1**[OH] and $B(OH)_3$ in a 2:1 ratio is shown in Fig. 1, where the presence of 2 major high frequency signals and 2 very minor low frequency signals can clearly be seen. Formation of the neutral zwitterionic monoborate and cationic monoborate complexes are shown in Eqs. (5) and (6). The resonance signals at 10.0, 6.1, 1.8, and 0.96 may be assigned [11,14] to the (α,β)(α,β)-bischelate complex cation, $[R_3N\{CH_2CH(O)CH_2O\}_2B]^+$, Fig. 2(ii), the neutral (α,β)-monochelate zwitterionic complex, $[R_3N\{CH_2CH(O)CH_2O\}B(OH)_2]$, Fig. 2(i), the orthoborate ion, $[B(OH)_4]^-$, and the four-coordinate B atom of the pentaborate anion, $[B_5O_6(OH)_4]^-$, respectively.

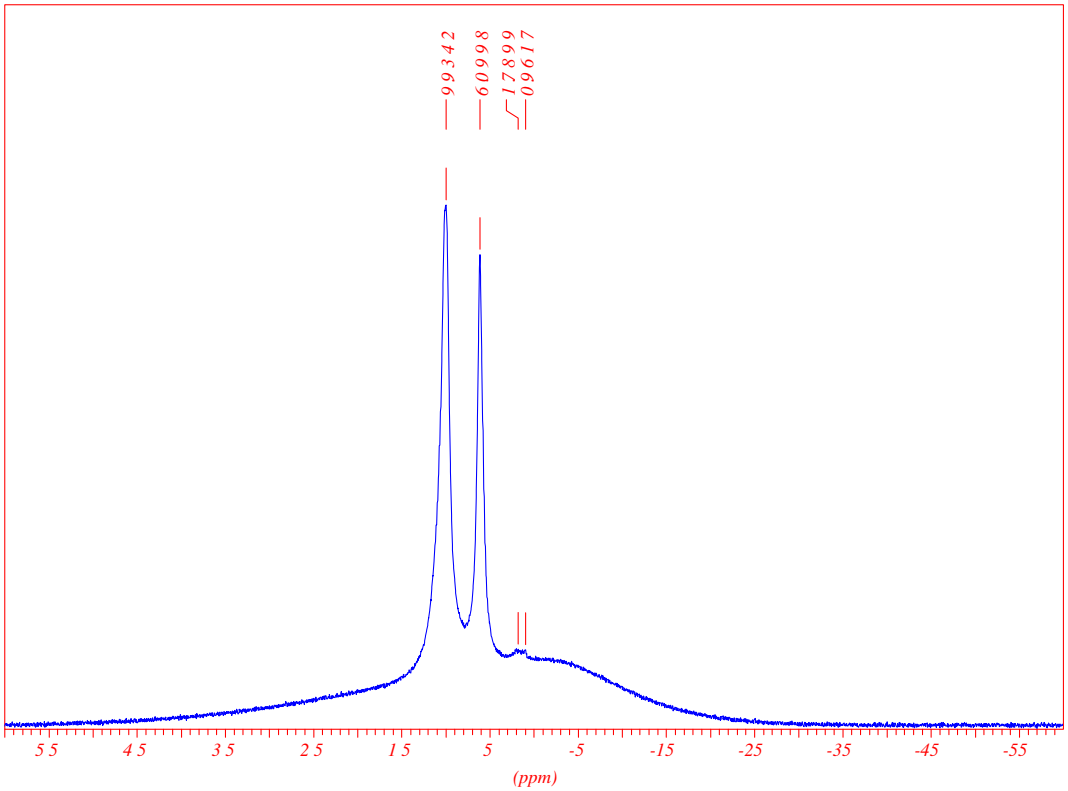

Fig. 1. Representative ^{11}B spectrum of a solution obtained from **1**[OH]:$B(OH)_3$ 2:1 in aqueous solution ([B] ~ 1.8 M).

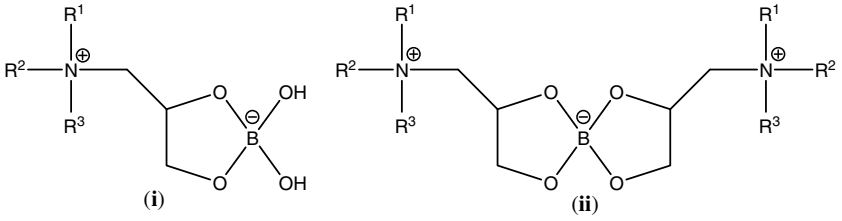

Fig. 2. Structural formula of the tetrahedral (i) zwitterionic and (ii) cationic monoborates.

The data reported for compounds **1**–**5**[OH] with $B(OH)_3$ in a 2:1 ratio in Table 1 demonstrate that bischelate cationic monoborate species are the major species present in solution, accounting for ~67% of the total B present. This result is not unsurprising considering the molar ratios, but that ~33% of the total B is present as the neutral zwitterionic monochelate species is perhaps unexpected. Presumably the neutral zwitterionic species are stabilised by Coulombic interactions, and such effects destabilise the bischelate cationic complex. The identity of the substituent groups at N^+ has very little influence on the equilibrium concentrations of the species observed. In particular, **3**[OH], with the 2-hydroxyethyl substituent on N^+, did not show any differing behaviour, indicating that this 'isolated' hydroxy group was not interacting with the B centre. The reaction of **6**[OH] with $B(OH)_3$ in a 2:1 ratio led to the formation of a cationic complex borate complex in a far higher proportion compared with that observed for **1**–**5**[OH]. Although **6**[OH] has two potential bidendate sites per N^+, the cation was still not observed exclusively.

$$[R_3N\{CH_2CH(OH)CH_2OH\}][OH] + B(OH)_3 \rightarrow [R_3N\{CH_2CH(O)CH_2O\}B(OH)_2] + 2H_2O \quad (5)$$

$$[R_3N\{CH_2CH(OH)CH_2OH\}][OH] + [R_3N\{CH_2CH(O)CH_2O\}B(OH)_2] \rightarrow [R_3N\{CH_2CH(O)CH_2O\}_2B][OH] + 2H_2O \quad (6)$$

The interaction of **1**–**5**[OH] with $B(OH)_3$ in a 1:1 ratio (Table 1) showed identical species present to those observed in the 2:1 ratio but their relative amounts were different. The neutral zwitterionic monoborate was now the dominant species (~65% of total B), but the cationic bischelate was still observed in significant quantities (~30%). **6**[OH], with the 2 diol substituents on N^+, gave a cationic complex in preference to the zwitterionic complex.

The spectra obtained for **1**–**5**[OH] with $B(OH)_3$ in a 1:5 ratio were fundamentally different from those with lower $B(OH)_3$ ratios (Table 1). Now the major species present were the pentaborate anion $[B_5O_6(OH)_4]^-$ and unreacted $B(OH)_3$, and the B atoms are approximately equally divided between these two species. At first sight this appears contrary to the integration values of ~18% and ~70%, respectively. However, the four three-coordinate centres of the pentaborate anion have never been observed and are believed to be so broad that they are effectively lost in the baseline and therefore may be considered as NMR silent [18]. Since there must be four such three-coordinate centres associated with each four-coordinate B atom, their presence, although not seen, must be taken into account when noting the location of the B atoms. The zwitterionic and cationic monoborate species are also present in theses samples, in small and approximately equal amounts, and comprise ~5–10% of total B. The reaction of **6**[OH] with $B(OH)_3$

at 1:5 again gave a solution with a higher proportion of zwitterionic and cationic species (~30% of total B) with the remaining total B split almost equally between the $B(OH)_3$ and $[B_5O_6(OH)_4]^-$.

In order to further extend the above study we investigated the reactions of $[Me_4N][OH]$ with $B(OH)_3$ and $[Me_3NCH_2OH][OH]$ with $B(OH)_3$ in 1:1 and 1:5 ratios. These cations have a strong structure directing effect in related silicate systems [19] where the octameric cubic $[Si_8O_{20}]^{8-}$ type structures are observed in preference to the normal equilibrium mixtures of Q^n species, which are favoured when alkali metal cations are present. The resulting solutions gave ^{11}B spectra which were similar to those described by Salentine [20] for aqueous solutions containing metal borates and 'synthetic' alkali metal borates prepared from corresponding ratios of alkali metal hydroxides and $B(OH)_3$, and contain $[B_5O_6(OH)_4]^-$, $[B_3O_3(OH)_4]^-$ and $B(OH)_3$. Our TMA and choline borate solutions were more concentrated than those described by Salentine and accordingly have more of the boron present as triborate anions rather than boric acid. Therefore there is very little or no structure directing effect, in relation to borate anion speciation, associated with these cations in aqueous solution. A comparison of sodium, TMA and choline borate solutions with the borate solutions prepared using **1**–**5**[OH] (Table 1) can also be made: the $[B_3O_3(OH)_4]^-$ anion does not occur in the presence of **1**–**5**[OH], and chelated monoborates are formed in preference to this anion.

Having shown by ^{11}B NMR the existence in aqueous solution of the neutral zwitterionic and cationic monoborate species, our attention was subsequently drawn to trying to isolate and then purify these species. Attempts to isolate the zwitterionic species by extraction into polar non-aqueous solvents were unsuccessful and our focus shifted to trying to obtain these neutral species in non-aqueous solvents. The reaction of the tetraorganoamomonium chlorides, **1**,**2**,**4**–**7**[Cl] with $B(OH)_3$ in a 1:1 molar ratio in MeOH solution was attempted but the three-coordinate B centres were unreactive towards ester formation [9,10]. A variation of this procedure involved the interaction of methanolic solutions of **2**,**4**–**7**[Cl] with 1 equiv. of $Na[B(OH)_4]$ (dissolved in the minimum amount of H_2O); the aim here was to eliminate NaCl and form the neutral zwitterionic monoborate (Eq. (7)).

$$[R_3N\{CH_2CH(OH)CH_2OH\}][Cl] + Na[B(OH)_4] \rightarrow NaCl + [R_3N\{CH_2CH(O)CH_2O\}B(OH)_2] + 2H_2O \quad (7)$$

NMR analysis of these solutions confirmed that they contained the desired zwitterionic monoborate as the major component (41–61%) in all cases, but that there were still significant amounts of the cationic (8–39%) and uncomplexed $B(OH)_3/B(OH)_4$ species present. Removal of solvent and extraction of the residues with MeOH yielded soluble fractions which contained predominantly zwitterionic monoborates; thus the proportion of B contained in the zwitterionic complexes derived from **2**[Cl] and **4**[Cl] was increased to 91%. Extraction with other polar solvents was attempted but were not as effective in 'purifying' the zwitterionic monoborates. However, it was never possible to isolate pure samples of the zwitterionic monoborates as the cationic monoborates were slightly soluble in MeOH. This was evidenced by their characteristic ^{11}B chemical shift and qualitative tests for $Cl^-(AgNO_3)$.

4. Conclusion

The interaction of $B(OH)_3$ with a number of cationic 1,2-diol moieties derived from substituted tetraorganoammonium cations $[R_3N\{CH_2CH(OH)CH_2OH\}]^+$ (with $[OH]^-$ or $[Cl]^-$ counterions) at B:N ratios of 2:1, 1:1 and 1:5 have been investigated by ^{11}B NMR spectroscopy. Complex equilibria appear to operate in all cases but cationic bischelate species, $[R_3N\{CH_2CH(O)CH_2O\}_2B]^+$, dominate in the 2:1 ratio solutions, zwitterionic monochelate species, $[R_3N\{CH_2CH(O)CH_2O\}B(OH)_2]$, dominate in the 1:1 solutions, and the pentaborate anion, $[B_5O_6(OH)_4]^-$, dominates in the 1:5 solutions. The ^{11}B NMR spectra of borate solutions derived from $[NMe_4][OH]$ and $[Me_3NCH_2CH_2OH][OH]$ are essentially the same as those observed for borate solutions with alkali metal cations, and structure directing effects (towards the anion) are not observed in these borate systems.

Acknowledgements

We thank Pilkington Plc and the EPSRC for financial support.

References

[1] J. Emri, B. Gyori, in: G. Wilkinson, R.D. Gillard, J.A. McCleverty (Eds.), Comprehensive Coordination Chemistry, vol. 3, Pergamon Press, 1987 (Chapter 24, 81, and references cited therein).
[2] J. Boeseken, N. Vermass, J. Phys. Chem. 35 (1931) 1477.
[3] L. Babcock, R. Pizer, Inorg. Chem. 22 (1983) 174.
[4] J.P. Lorand, J.O. Edwards, J. Org. Chem. 24 (1959) 769.
[5] R.P. Oertel, Inorg. Chem. 11 (1972) 544.
[6] K. Yoshino, M. Kotaka, M. Okamoto, H. Kakihana, Bull. Chem. Soc. Jpn. 52 (1979) 3005.
[7] W. Kliegel, Bor in biologie, medizin und pharmazie, Springer, Berlin, 1980.
[8] J. Bassett, R.C. Denny, G.H. Jeffery, J. Mehnham, in: Vogels Textbook of Quantitative Inorganic Analysis, 4th ed., Longman, London and New York, 1978, p. 311.
[9] J.G. Dawber, D.H. Matusin, J. Chem. Soc., Faraday Trans. 1 78 (1982) 2521.
[10] J.G. Dawber, G.E. Hardy, J. Chem. Soc., Faraday Trans. 1 80 (1984) 2467.
[11] J.G. Dawber, S.I.E. Green, J. Chem. Soc., Faraday Trans. 1 82 (1986) 3407.
[12] J.G. Dawber, J. Chem. Soc., Faraday Trans. 1 83 (1987) 771.
[13] J.G. Dawber, S.I.E. Green, J.C. Dawber, S. Gabrail, J. Chem. Soc., Faraday Trans. 1 84 (1988) 41.
[14] Y. Miyazaki, K. Yoshimura, Y. Miura, H. Sakashita, K. Ishimaru, Polyhedron 22 (2003) 909.
[15] E.G. Lovett, J. Org. Chem. 56 (1991) 2755.
[16] V. Meyer, Chem. Ber. 2 (1869) 187.
[17] A.W. Moyer, V. Du Vigneaud, J. Biol. Chem. 143 (1942) 373.
[18] R.K. Momii, N.H. Nachtrieb, Inorg. Chem. 6 (1967) 1189.
[19] D. Hoebbel, G. Garzo, G. Engelhardt, A. Vargha, Anorg. Allg. Chem. 494 (1982) 31.
[20] C.G. Salentine, Inorg. Chem. 22 (1983) 3920.

Polyhedron 27 (2008) 2231

Contents lists available at ScienceDirect

Polyhedron

journal homepage: www.elsevier.com/locate/poly

Erratum

Erratum to "Synthesis and characterization of some novel cadmium(II) complexes with 3-hydroxypicolinic acid (3-OHpicH): Crystal and molecular structures of $[CdI(3\text{-}OHpic)(3\text{-}OHpicH)(H_2O)]_2$, $[Cd(3\text{-}OHpic)_2(H_2O)_2]$ and $[Cd(3\text{-}OHpic)_2]_n$" [Polyhedron 27 (2008) 1479–1488]

Boris-Marko Kukovec [a], Zora Popović [a,*], Gordana Pavlović [b], Marijana Vinković [c], Dražen Vikić-Topić [c]

[a] Laboratory of General and Inorganic Chemistry, Department of Chemistry, Faculty of Science, University of Zagreb, Horvatovac 102a, HR-10000 Zagreb, Croatia
[b] Laboratory of General Chemistry, Department of Applied Chemistry, Faculty of Textile Technology, University of Zagreb, Prilaz baruna Filipovića 28a, HR-10000 Zagreb, Croatia
[c] NMR Centre, Ruđer Bošković Institute, Bijenička cesta 54, HR-10000 Zagreb, Croatia

The authors would like to replace Table 3 on page 1486 with this one due to the several mistakes.

Table 3
Selected bond distances (Å) and angles (°) for $[CdI(3\text{-}OHpic)(3\text{-}OHpicH)(H_2O)]_2$ (**1**), $[Cd(3\text{-}OHpic)_2(H_2O)_2]$ (**2**) and $[Cd(3\text{-}OHpic)_2]_n$ (**3**)

1		**2**		**3**	
Bond distances					
Cd1–N1	2.348(3)	Cd1–N1	2.299(1)	Cd1–N1	2.285(7)
Cd1–O1	2.327(2)	Cd1–O1	2.301(1)	Cd1–N2	2.290(7)
Cd1–O7	2.305(3)	Cd1–O4	2.309(1)	Cd1–O1	2.510(8)
Cd1–O4	2.339(2)			Cd1–O1^{iii}	2.340(8)
Cd1–I1^{i}	2.922(1)			Cd1–O4	2.486(8)
Cd1–I1	2.947(1)			Cd1–O4^{iii}	2.344(9)
Bond angles					
O4–Cd1–N1	174.4(1)	N1–Cd1–N1^{ii}	180.0(1)	N1–Cd1–N2	105.5(3)
O1–Cd1–I1^{i}	165.4(1)	O1–Cd1–O1^{ii}	180.0(1)	O1–Cd1–O1^{iii}	155.3(2)
O7–Cd1–I1	172.0(1)	O4–Cd1–O4^{ii}	180.0(1)	O4–Cd1–O4^{iii}	157.0(2)
O1–Cd1–N1	71.5(1)	N1–Cd1–O1	73.3(1)	N1–Cd1–O1	65.0(6)
O1–Cd1–O4	106.9(1)	N1–Cd1–O1^{ii}	106.7(1)	N2–Cd1–O4	63.0(5)
O7–Cd1–O1	85.8(1)	N1–Cd1–O4	85.6(1)	N1–Cd1–O1^{iii}	132.8(6)
O7–Cd1–O4	81.9(1)	N1–Cd1–O4^{ii}	94.4(1)	N2–Cd1–O1^{iii}	93.2(5)
O7–Cd1–N1	92.6(1)	O1–Cd1–O4	91.3(1)	N1–Cd1–O4^{iii}	88.8(5)
O7–Cd1–I1^{i}	93.4(1)	O1–Cd1–O4^{ii}	88.7(1)	N2–Cd1–O4^{iii}	132.8(6)
O4–Cd1–I1^{i}	87.4(1)			O1^{iii}–Cd1–O4^{iii}	49.3(2)
N1–Cd1–I1^{i}	94.0(1)			N1–Cd1–O4	103.4(5)
O1–Cd1–I1	90.0(1)			O1–Cd1–O4^{iii}	123.6(2)
O4–Cd1–I1	92.9(1)			N2–Cd1–O1	97.7(5)
N1–Cd1–I1	92.4(1)			O4–Cd1–O1^{iii}	128.6(2)
I1–Cd1–I1^{i}	92.4(1)			O4–Cd1–O1	46.1(2)

Symmetry code: (i) $1-x, -y, 2-z$; (ii) $-x, -y, 1-z$; (iii) $1/2-x, y-1/2, 2-z$.

DOI of original article: 10.1016/j.poly.2008.01.021
* Corresponding author. Tel.: +385 1 4606354; fax: +385 1 4606341.
E-mail address: zpopovic@chem.pmf.hr (Z. Popović).

0277-5387/$ - see front matter © 2008 Elsevier Ltd. All rights reserved.
doi:10.1016/j.poly.2008.03.014

Polyhedron 27 (2008) 2233–2242

Contents lists available at ScienceDirect

Polyhedron

journal homepage: www.elsevier.com/locate/poly

Novel supramolecular network in tri- and mono-nuclear oxovanadium(V)-salicyl-hydroximate: Synthesis, structure and catalytic oxidation of hydrocarbons using H_2O_2 as terminal oxidant

Tapan K. Si [a], Santu Chakraborty [b], Alok K. Mukherjee [b], Michael G.B. Drew [c], Ramgopal Bhattacharyya [a,*]

[a] Department of Chemistry, Jadavpur University, Kolkata 700 032, India
[b] Department of Physics, Jadavpur University, Kolkata 700 032, India
[c] School of Chemistry, University of Reading, P.O. Box 224, Whiteknight, Reading, RG6 6AD, UK

ARTICLE INFO

Article history:
Received 20 January 2008
Accepted 31 March 2008
Available online 24 June 2008

Keywords:
Vanadium(V) complexes
Salicylhydroximates
Supramolecular structure
Hydrocarbon oxidation
Hydrogen peroxide

ABSTRACT

Two oxovanadium(V) salicylhydroximate complexes, $[VO(SHA)(H_2O)]\cdot 1.58H_2O$ (**1**) and $[V_3O_3(CSHA)_3(H_2O)_3]\cdot 3CH_3COCH_3$ (**2**) have been synthesized by reaction of VO_4^{3-} with *N*-salicyl hydroxamic acid ($SHAH_3$) and *N*-(5-chlorosalicyl) hydroxamic acid ($CSHAH_3$), respectively, in methanol medium. Compound **1** on reaction with pyridine 2,6-dicarboxylic acid ($PyDCH_2$) yields mononuclear complex $[VO(SHAH_2)(PyDC)]$ (**3**). Treatment of compound **3** with hydrogen peroxide at low pH (2-3) and low temperature (0–5 °C) yields a stable oxoperoxovanadium(V) complex $H[VO(O_2)(PyDC)(H_2O)]\cdot 2.5H_2O$ (**4**). All four complexes (**1**–**4**) have been characterized by spectroscopic (IR, UV–Vis, ^{51}V NMR) and single crystal X-ray analyses. Intermolecular hydrogen bonds link complex **1** into hexanuclear clusters consisting of six $\{VNO_5\}$ octahedra surrounded by twelve $\{VNO_5\}$ octahedra to form an annular ring. While the molecular packing in **2** generates a two-dimensional framework hydrogen bonds involving the solvent acetone molecules, the mononuclear complexes **3** and **4** exhibit three-dimensional supramolecular architecture. The compounds **1** and **2** behave as good catalysts for oxygenation of benzylic, aromatic, carbocyclic and aliphatic hydrocarbons to their corresponding hydroxylated and oxygenated products using H_2O_2 as terminal oxidant; the process affords very good yield and turnover number. The catalysis work shows that cyclohexane is a very easily oxidizable substrate giving the highest turnover number (TON) while *n*-hexane and *n*-heptane show limited yield, longer time involvement and lesser TON than other hydrocarbons.
© 2008 Elsevier Ltd. All rights reserved.

1. Introduction

Activation of C–H bond is one of the challenging problems in homogeneous catalysis research since it involves conversion of crude oil and natural gas constituents into oxygenated derivatives such as alcohols or carbonyl compounds. In this respect dioxygen and hydrogen peroxide are two most useful oxidants from economic and environmental standpoints [1–3]. Interest in oxovanadium(V) chemistry has recently been accelerated due to high potentiality of dioxygen activation along with the ability of oxo-peroxo vanadium(V) species to function as important intermediates in the in vivo enzymatic processes [4–7]. Also synthetic oxoperxovanadium(V) complexes are known to exhibit stoichiometric and in some cases catalytic oxidation of various organic substrates to their oxidized products [8–10]. Mimoun et al. [11] reported oxovanadium(V) peroxo complexes of the types $[VO(O_2)(O–N)(L)]$ and $[VO(O_2)(O–N)_2]^-$, where L = solvent molecule; O–NH = pyridine 2-carboxylic acid and pyrazine 2-carboxylic acid and the complexes were shown to be good oxidizing agents for the stoichiometric hydroxylation of aromatic hydrocarbons. The first catalytic hydrocarbon oxidation using oxovanadium(V) compounds was furnished by Shul'pin et al. [12] using the Mimoun type compounds [11]. Using those catalysts Shul'pin et al. [13] also succeeded in the oxidation of methane to methanol, formaldehyde or formic acid with tertiary butyl hydroperoxides (TBHP) as oxidant [14]. Remias et al. [8] reported oxidation of benzene and cyclohexane using $[V(acac)_3]$, $[VO(acac)_2]$ and $[VO(O_2)(2\text{-picolinate})(H_2O)_2]$ as catalysts and H_2O_2 as oxidant. We described [15] the synthesis and crystal structure of a hydroxamato[1] complex, namely $[VO(BPHA)_2(Cl)]$; (BPHAH = *N*-benzoyl *N*-phenyl hydroxamic acid [16]) which was shown to act as catalyst for the oxidation of wide variety of hydrocarbons. Besides, being good analytical reagents [17,18] and having siderophoric role, the hydroxamic acids are also important for numerous biological functions [19]. In this paper, we report the

* Corresponding author. Tel.: +91 (33)2414 6193; fax: +91 (33)2414 6584.
E-mail address: argibhatta@yahoo.co.in (R. Bhattacharyya).

[1] Fisher et al. (D.C. Fisher, S.J. Barclay-Peet, C.A. Balfe, K.N. Raymond, Inorg. Chem. 28 (1989) 4399, isolated and structurally characterized a couple of hydroximato (derived from primary hydroxamic acid where one of the hydroxylamine protons is substituted) complexes but erratically described as hydroxamato complexes.

0277-5387/$ - see front matter © 2008 Elsevier Ltd. All rights reserved.
doi:10.1016/j.poly.2008.03.031

synthesis, spectroscopic and structural characterization of salicylhydroximato-oxovanadium(V) complexes, $[VO(SHA)(H_2O)] \cdot 1.58H_2O$ (**1**) and $[V_3O_3(CSHA)_3(H_2O)_3] \cdot 3CH_3COCH_3$ (**2**) ($SHAH_3$ = *N*-salicyl hydroxamic acid and $CSHAH_3$ = *N*-(5-chlorosalicyl) hydroxamic acid along with their catalytic properties in functionalization of hydrocarbons. This work also reports the synthesis and structural characterization of two mononuclear oxovanadium(V) complexes, $[VO(SHAH_2)(PyDC)]$ (**3**) and the other is a peroxovanadium(V) complex $H[VO(O_2)(PyDC)(H_2O)] \cdot 2.5H_2O$ (**4**), [20]. Complex **3** is obtained by reaction of complex **1** with $PyDCH_2$ and is the second example of an oxovanadium(V) complex containing uninegetive bidentate (O,O donor) salicylhydroximate ligands [21,22] whereas complex **4** is obtained by the reaction of **3** with hydrogen peroxide. Notably, oxoperoxovanadium(V) complexes with $PyDC^{2-}$ ligand [23] exhibits poor catalytic properties in the oxidation of hydrocarbons due to their unusual stability.

2. Experimental

2.1. Physical measurements

The IR spectra were recorded as KBr pallets on a Nicolet 520 FTIR spectrometer and Electronic spectra on a Hitachi U-3410 UV–Vis–NIR spectrophotometer. ^1H NMR spectra was measured in $CDCl_3$ on a Bruker AM 360 (300 MHz) FT NMR spectrometer using TMS as an internal standard. The 51 V NMR was recorded in CD_3CN on a GEOL 400 MHz NMR spectrometer and a systronics (India) model 335 digital conductivity bridges where a bottle type cell was used to determine the molar conductance values of the isolated complexes at 25 °C using a thermostatic arrangement. The magnetic susceptibilities at 298 K were obtained by the Gouy method using $Hg[Co(NCS)_4]$ as a standard. Elemental analyses were performed with the help of a Perkin–Elmer 240C elemental analyzer. GLC measurements were done in an Agilent model 6890N gas chromatograph using HP-1 and INNOWAX capillary column in FID mode with dinitrogen as carrier gas.

2.2. Materials

Ammonium metavanadate and hydroxylamine hydrochloride were of extrapure variety and obtained from Sisco Research Laboratory (India). Methyl Salicylate was obtained from S.D. Fine-Chem. Ltd (India). 5-Chloro salicylic acid and 2,6-pyridine dicarboxylic acid ($PyDCH_2$) were obtained from Aldrich Chemicals. Potassium hydroxide pellets and methanol (G.R.) were the products of E. Merck (India) and were directly used. Ethanol (95%) was obtained from Bengal Chemical and Pharmaceutical Works (Calcutta), and was lime distilled before use. All other chemicals needed were obtained from E. Merck (India). *N*-Salicyl hydroxamic acid ($SHAH_3$) and *N*-(5-chloro salicyl) hydroxamic acid ($CSHAH_3$) were synthesized following the literature method [16]. Acetonitrile, dichloromethane and acetone were further purified by the literature method [24] for physico-chemical studies. Iolar II grade dioxygen, dihydrogen, zero air, and dinitrogen gas used for chromatographic analysis were obtained from Indian Refrigeration Stores, Calcutta. Cyclohexane and ethylbenzene were obtained from S.D. Fine-Chem. Ltd (India) while cyclohexanol, cyclohexanone, tetralin and tetralone were obtained from Sisco Research Laboratory, India (extrapure AR grade). Toluene, benzene, *n*-hexane, *n*-heptane and *n*-pentane, diphenylmethane, *n*-heptanol, *n*-hexanol, *n*-pentanol, benzaldehyde and phenol were obtained from E. Merck (India) (G.R grade). Triply distilled (all glass) water was used whenever necessary. All the solvents used for chromatographic analysis were either of HPLC, spectroscopic, or GR grade and in all cases their purity was confirmed by GC analysis before use.

2.3. Preparation of the complexes

2.3.1. $[VO(H_2O)(SHA)] \cdot 1.58H_2O$ (**1**) and $[V_3O_3(H_2O)_3(CSHA)_3] \cdot 3CH_3COCH_3$ (**2**)

NH_4VO_3 (0.586 g, 5 mmol) was dissolved in 15 mL of distilled water by stirring at 40–55 °C. The pH of the solution was adjusted at 3–4 by adding 4(M) HCl. $SHAH_3$ (0.76 g, 5 mM; 0.94 g $CSHAH_3$ for compound **2**) was dissolved in minimum volume of methanol (ca.15 mL) and the resulting solution was added to vanadate solution, with stirring (15 min) when the solution becomes deep blue which was kept at room temperature. After 2–3 days, deep blue cubes separated. The crystals were collected (for **1**), washed off with distilled water and dried in vacuo. Yield: 1.05 g (77.5%). *Anal.* Calc. for $C_7H_6NO_{6.58}V$: C, 32.25; H, 2.32; N, 5.41; V, 19.60. Found: C, 32.03; H, 2.43; N, 5.10; V, 19.15%. IR (KBr disc, cm^{-1}): 3441(broad), 1626(w), 1598(s): ν(C=O), 1566(w), 1468(s), 1365(s), 1240(m), 1157(w), 1108(w), 1044(w), 971(s): ν(V=O), 757(m), 678(m), 644(m), 582(w), 508(w), 451(w). ^{51}V NMR (105.03 MHz, CD_3CN, 296 K): δ ppm, −236.58. UV–Vis, λ_{max} nm (ε $M^{-1}cm^{-1}$): 625(18380), 493(sh), 294(34690), 247(sh). The crude compound (**2**) was recrystallized by slow diffusion of acetone solution of the compound in light petroleum (40–60 °C). Yield: 1.2 g (73%). *Anal.* Calc. for $C_{30}H_{33}Cl_3N_3O_{18}V_3$: C, 36.6; H, 3.38; N, 4.27; Cl, 10.83; V, 15.56. Found: C, 36.47; H, 3.40; N, 4.16; Cl, 11.42; V, 15.13%. IR (KBr disc, cm^{-1}): 3367(broad), 1627(w), 1596(s): ν(C=O), 1556(w), 1500(s), 1458(s), 1429(m), 1334(s), 1294(m), 1230(m), 1161(w), 1122(w), 1051(w), 977(s) and 962(s): ν(V=O), 894(w), 862(w), 825(m), 763(w), 739(s), 669(w), 626(m), 601(w), 541(w), 499(w), 455(w), 375(w). UV–Vis λ_{max} nm (ε M^{-1} cm^{-1}): 629(14360), 488(sh), 292(27300), 239(35700).

2.3.2. $[VO(SHAH_2)(PyDC)]$ (**3**)

Complex **1**, 0.403 g (0.5 mmol) was dissolved in methanol (25 mL) and 10 mL aqueous solution of $PyDCH_2$ (0.250 g, 1.5 mmol) was mixed with stirring. After 30 min a deep purple solid was separated. The crude solid was filtered off, washed with water and dried in vacuo. Yield: 0.362 g (62%). Good crystals were obtained by slow diffusion of acetone solution of the complex in light petroleum (40–60 °C). *Anal.* Calc. for $C_{14}H_9N_2O_8V$: C, 43.75; H, 2.34; N, 7.29; V, 13.28. Found: C, 43.15; H, 2.35; N, 6.99; V, 12.92%. IR (KBr disc, cm^{-1}) 3103(m), 2879(w), 1684(s): ν(C=O), 1606(m), 1527(m), 1469(w), 1425(w), 1332(s), 1290(w), 1240(m), 1176(w), 1147(w), 1140(w), 1085(w), 979(s): ν(V=O), 919(m), 842(w), 755(m), 682(w), 669(w), 605(w), 449(w), 387(w). ^{51}V NMR (105.03 MHz, CD_3CN, 296 K): δ ppm, −423.80. UV–Vis λ_{max} nm (ε M^{-1} cm^{-1}): 478(8000); 289(6100); 243(18000).

2.3.3. $H[VO(O_2)(PyDC)(H_2O)] \cdot 2.5H_2O$ (**4**)

Compound **3** (0.401 g, 1.05 mmol) was treated with 30% aqueous H_2O_2 (1 ml, 12.5 mmol) by maintaining the pH of the solution at 2–3 with 4(M) HCl at 0–5 °C. The solution became orange red and was allowed stand in the deep freeze. After 15 days, orange red crystals separated. *Anal.* Calc. for $C_7H_{11}NO_{10.5}V$: C, 25.60; H, 3.34; N, 4.26; V, 15.54. Found: C, 25.27; H, 3.27; N, 4.13; V, 14.98 IR (KBr disc, cm^{-1}): 3209(broad), 3089(w), 2846(w), 1645(s): ν(C=O), 1437(m), 1380(s), 1273(w), 1188(m), 1151(w), 1081(m), 1037(w), 974(s): ν(V=O), 925(s): ν[O–O], 858(w), 837(w), 777(m), 750(m), 682(m), 605(w), 569(m), 451(w). UV–Vis λ_{max} nm (ε M^{-1} cm^{-1}): 427(2700), 270(26500).

2.4. X-ray structure analyses for complexes **1**, **2**, **3** and **4**

Intensity data of complexes were recorded on a Bruker SMART CCD area detector (for **1** and **3**) and an Oxford diffraction X-Calibur CCD system (for **2** and **4**) using graphite monochromated Mo Kα radiation (λ = 0.71073 Å). Data analyses were carried out with the

SMART [25] and CRYSALIS [26] programs. The data were corrected for absorption effects using the programs SADABS [27] for **1** and **3** and ABSPACK [28] for **2** and **4**. The structures were solved using direct methods with the SHELX-97 program [29]. In **1**, O8 atom of solvent water molecule was disordered over two positions with occupancy 0.5 and O6 atom of another solvent water molecule was partially occupied (occupancy 0.25). The hydrogen atoms on water molecule, bonded to V atom in **1**, **2** and **4**, were located from difference Fourier maps. The hydrogen atoms (excluding that on the disordered O atom) were included in geometrical positions and assigned fixed isotropic thermal parameters. The non-hydrogen atoms were refined with anisotropic thermal parameters. Relevant crystal data and refinement results for complexes **1**–**4** are given in Table 1.

2.5. Experimental procedure of catalytic hydrocarbons oxidation

The experimental procedure for the catalytic hydrocarbon oxidation reaction involving a wide variety of substrates is described as follows: an acetonitrile solution (10 cm^3) containing a given substrate (5 mmol), oxovadium(V) catalyst (0.05–0.005 mmol) and 30% H_2O_2 (25 mmol) in a high-pressure reactor (100 mL capacity Parr type hydrogenation apparatus) at 60–80 °C was stirred for definite period as shown in Table 7. When required, an aliquot (0.1 mL) of the reaction solution was withdrawn with the help of long needle syringe and was subjected to multiple ether extractions and 1 μL concentrated ether extract was injected to the GC port with the help of 10 μL syringe. The retention times of the peaks were compared with those of commercial standards and the unknown peaks were characterized by GC–MS analysis. In some cases nitrobenzene was used as the internal standard for the calculation of GC yield. The isolated yield in some cases is obtained by multiple ether extractions of the reaction solution after the reaction is over followed by evaporation of ether and acetonitrile by distillation at a mildly reduced pressure (using water aspirator). Isolated yields are however not included in the Table 8. Parr type apparatus was used for the convenience of the physico-chemical studies but it is not absolutely necessary for laboratory as well as industry.

3. Results and discussions

3.1. General characterization, IR and electronic spectroscopy

The compound **1**–**3** are non electrolytes in acetonitrile but **4** (which is freely soluble in water but not in acetonitrile) in aqueous solution exhibits a molar conductance value of 120 Ω^{-1} cm^2 mol^{-1}. This value is much lower for a free H_3O^+ as anticipated for an anionic complex with the structure $H[VO(O_2)(PyDC)(H_2O)] \cdot 2.5H_2O$ confirmed by analytical, spectroscopic and X-ray crystallographic methods. However a $\sqrt{c}$ versus Λ_M plot (Λ_M = molar conductance) of the said aqueous solution shows an asymptotic nature of curve (Fig. S.1) which indicates the existence of protons in undissociated form in one of the carboxylic acid group of coordinated $PyDC^{2-}$ ligand in aqueous solution [30]. All the compounds are diamagnetic at 298 K. As recorded in Section 2, the ν(V=O) vibration in **1**–**4** appears at 971, 977, 979 and 974 cm^{-1}, respectively, indicating that the ligand effect on ν(V=O) varies in the order **3** > **2** > **4** > **1**. The ν(C=O) bands for $SHAH_3$ and $CSHAH_3$ ligands are observed at 1620 and 1625 cm^{-1}, respectively. On complexation these ν(C=O) are shifted to lower wave numbers and appear almost in the same region for both the cases (see experimental section). In $PyDCH_2$, the ν(C=O) vibration occurs at 1705 cm^{-1} but in case of **3** which contains two types of C=O groups, one for the coordinated $SHAH_2^-$ and the other for $PyDC^{2-}$, respectively, appear at 1606 and 1684 cm^{-1}. In compound **4** the ν(C=O) of coordinated $PyDC^{2-}$ appears at 1647 cm^{-1}. In the case of coordinated $PyDC^{2-}$ ligand, the ν(C=O) appearing at ca. 40 cm^{-1} lower wave number region due to lower dative O → C π overlap. The ν(O–O) absorption band in **4** appears at 925 cm^{-1}.

In the complex **1** a new electronic spectral band appears at λ_{max} = 625 nm (ε = 18 375 M^{-1} cm^{-1}) along with a shoulder at 493 nm. These bands can be ascribed to the LMCT transitions in

Table 1
Crystal data and structure refinement parameters for complexes **1**, **2**, **3** and **4**, respectively

	1	**2**	**3**	**4**
Empirical formula	$C_7H_6NO_{6.58}V$	$C_{30}H_{33}Cl_3N_3O_{18}V_3$	$C_{14}H_9N_2O_8V$	$C_7H_{11}NO_{10.5}V$
M_r	260.40	982.76	384.17	328.11
T (K)	293(2)	150(2)	293(2)	150(2)
λ (Å)	0.71073	0.71073	0.71073	0.71073
Crystal system	trigonal	triclinic	monoclinic	monoclinic
Space group	$R-3c$	$P\bar{1}$	$P2_1/c$	$C2/c$
Unit cell dimensions				
a (Å)	14.111(2)	10.478(2)	8.102(1)	11.397(1)
b (Å)	14.111(2)	11.294(2)	12.018(2)	25.581(3)
c (Å)	50.570(11)	18.005(3)	14.957(3)	8.402(2)
α (°)	90.00	96.38(1)	90.00	90.00
β (°)	90.00	105.74(1)	96.66(1)	97.31(1)
γ (°)	120.00	95.77(1)	90.00	90.00
V (Å^3), Z	8720(3), 36	2019.1(5), 2	1446.6(4), 4	2429.7(7), 8
D_{calc} (g cm^{-3})	1.785	1.616	1.764	1.794
μ (mm^{-1})	1.039	0.955	0.737	0.872
F(000)	4704	996	776	1336
Crystal size (mm)	0.25 × 0.25 × 0.25	0.30 × 0.12 × 0.12	0.26 × 0.22 × 0.18	0.25 × 0.13 × 0.13
θ Range for data collection (°)	2.32–28.34	2.55–30.00	2.18–28.36	2.96–25.00
Reflections collected	18 674	11 313	9577	6322
Independent reflections (R_{int})	2429 (0.0762)	3723 (0.0669)	3562 (0.0558)	2129 (0.0159)
Completeness to $\theta = \theta_{max}$ (%)	99.9	95.9	98.8	99.3
Refinement method	full matrix-least squares on F^2			
Data/restraints/parameters	2429/2/147	11 313/36/532	3562/0/ 226	2129/9/203
Goodness-of-fit on F^2	1.286	0.752	1.083	1.049
Final R indices [$I > 2\sigma(I)$]	R_1 = 0.0682	R_1 = 0.0584	R_1 = 0.0599	R_1 = 0.0389
	wR_2 = 0.1660	wR_2 = 0.1204	wR_2 = 0.1138	wR_2 = 0.1237
R indices (all data)	R_1 = 0.0911	R_1 = 0.1326	R_1 = 0.0876	R_1 = 0.0484
	wR_2 = 0.1757	wR_2 = 0.1301	wR_2 = 0.1450	wR_2 = 0.1280
Largest difference in peak and hole (e Å^{-3})	1.521 and −0.790	0.644 and −0.621	0.723 and −0.785	0.326 and −0.552

the trinuclear deep blue compound (acidified VO_4^{3-} is light yellow and the $SHAH_3$ ligand is colourless). Two other low wave length bands are due to intra-ligand transitions and a drastic change in values is due to the fact that in one mole of complex there occurs three moles of ligand. The spectrum of trinuclear deep blue complex **2** ($CSHAH_3$ ligand is also colorless) exhibits similar band sequences as **1** (see Section 2). The slight difference of the actual position of bands between **1** and **2** is due to the presence of chlorine substituent in $CSHAH_3$ ligand. The electronic spectrum of compound **3** which contains both the $SHAH_2^-$ and $PyDC^{2-}$ ligands shows one new (which does not occur in ligand spectra) band at λ_{max} = 478 nm (ε = 8000 M^{-1} cm^{-1}) assignable to the LMCT transition in the reddish mononuclear compound **3** where $PyDC^{2-}$ (($PyDCH_2$ is colourless) coordinates via two oxygen atoms and one nitrogen atom and $SHAH_2^-$ ligand coordinates via two oxygen atoms (see Fig. 6) In orange red **4** the band at λ_{max} = 427 nm; (ε = 2700 M^{-1} cm^{-1}) is due to LMCT transition of $O_2^{2-} \rightarrow$ Vanadium(V).

3.2. Molecular structures

The asymmetric unit of **1** consists of one-third of the trinuclear vanadium salicylhydroximate cluster (Fig. 1), one aqua ligand coordinating to the metal center and solvent water molecules (one lying on the threefold axis, one disordered over two sites with occupancy 0.5 each, and the remaining one with occupancy value 0.25), while that in **2** comprises of a trinuclear vanadium chlorosalicylhydroximate (Fig. 2) with three solvent acetone molecules. The vanadium ions in **1** and **2** are in +5 oxidation state as VO^{3+} unit and related by a threefold axis. The three oxygen and one nitrogen atoms of triply deprotonated ligands, SHA^{3-} (in **1**) and $CSHA^{3-}$ (in **2**) are bound to vanadium, an individual ligand, however donates two hetero-atoms (O,N) to one vanadium atom while the remaining two oxygen atoms of the ligand bind to the adjacent vanadium atom. One oxo and one aqua ligands complete the hexa-coordination of each metal center. The bonding sequence repeats within the cluster forming a nine-membered $V_3N_3O_3$ ring with the vanadium atoms exhibiting distorted octahedral geometries. The phenolate O, aqua O and two hydroximate O, N atoms define the equatorial plane around each vanadium atom while the carboxyl and the oxo O atoms occupy the axial sites; the displacements of metal ions from the corresponding equatorial planes are 0.230(1) Å in **1** and 0.019(1)–0.235(1) Å in **2**. The vanadium-oxo bond lengths in **1** [1.597(3) Å] and **2** [1.580(3)–1.601(3) Å] (Tables 2 and 3) are similar to that reported for analogous structures [31,32]. The V–N [2.030(3) Å in **1** and 2.019(3)–2.037(3) Å in **2**] and V–O [1.851(3) Å in **1** and 1.852(3)–1.861(3) Å in **2**] bond lengths to the hydroximate ligands correspond to the bond distances in oxovanadium(V) hydroximate compounds that have been structurally characterized [33,34]. The V–O(aqua) bond distances in **1** [2.080(3) Å] and **2** [2.049(3)–2.070(3) Å] lie within the range 2.008(2) Å reported for $V–OH_2$(*cis*) and $V–OH_2$(*trans*) distances in aqua oxovanadium(V) complexes [35,36]. The lengthening of V–O (carbonyl) distances [2.136(3) Å in **1** and 2.129(3)–2.150(3) Å in **2**] compared to V–O (phenolic) bond lengths [1.868(3) Å in **1** and 1.862(2)–1.898(3) Å in **2**] in the complexes is due to *trans* influence of the oxo-ligand [37]. The V–V distances in **1** and **2** lie in the range 4.636–4.665 Å.

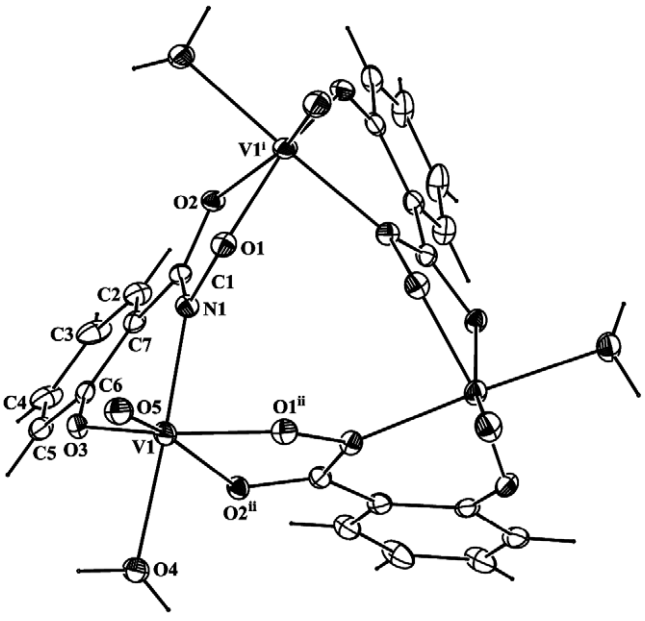

Fig. 1. A view of molecule **1** with atom numbering scheme (lattice held H_2O molecules are omitted for the sake of clarity) (symmetry codes: (i) $-y+1, x-y+1, z$; (ii) $-x+y, -x+1, z$).

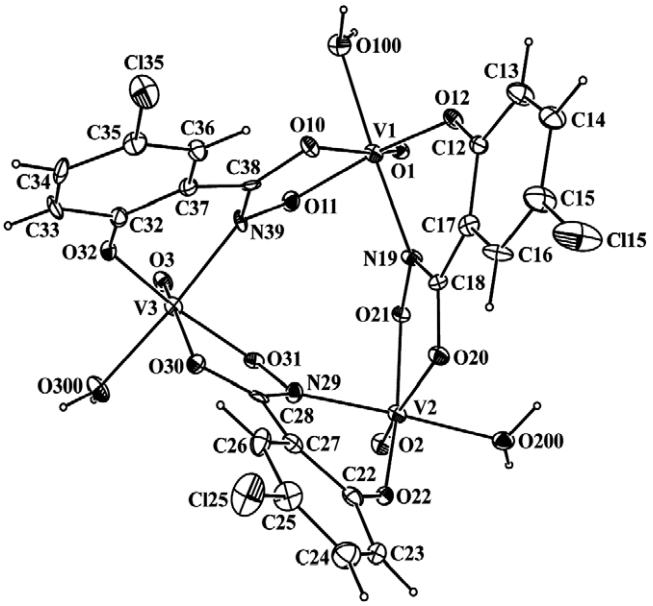

Fig. 2. A view of molecule **2** with atom numbering scheme (lattice held CH_3COCH_3 molecules are omitted for the sake of clarity).

The coordination geometry around the metal center in mononuclear complex **3** (Fig. 3) can be described as distorted octahedral, while that in **4** (Fig. 4) is distorted pentagonal bipyramidal with the oxo O [O(5) in **3** and O(300) in **4**] and carboxyl O [O(2) in **3** or aqua O(400) in **4**] atoms occupying the apical sites. In **3** and **4**, the V–O bond distances *trans* to the oxo ligand are elongated [V(1)–O(2) 2.126(3) in **3**, V(1)–O(400) 2.237(2) in **4**] compared to V–O (equatorial) bond lengths (Tables 4 and 5). Other V–O and V–N bond distances in **3** and **4** (Tables 4 and 5) are comparable to the corresponding values reported for monomeric oxovanadium(V) complexes [38,39]. The two essentially planar

Table 2
Selected bond lengths (Å) and bond angles (°) for **1**

V(1)–N(1)	2.030(3)	O(1)–V(1)–O(5)	95.27(15)
V(1)–O(1)	1.851(3)	O(1)–V(1)–N(1)	85.60(13)
V(1)–O(2)	2.136(3)	N(1)–V(1)–O(3)	82.76(13)
V(1)–O(3)	1.868(3)	O(3)–V(1)–O(4)	90.39(14)
V(1)–O(4)	2.080(3)	O(4)–V(1)–O(1)	99.10(14)
V(1)–O(5)	1.597(3)	O(4)–V(1)–O(2)	79.95(12)

Table 3
Selected bond lengths (Å) and angles (°) for **2**

V(1)–O(1)	1.580(3)	O(1)–V(1)–O(11)	94.01(14)
V(1)–O(12)	1.898(3)	O(1)–V(1)–O(12)	104.87(14)
V(1)–O(10)	2.150(3)	O(1)–V(1)–O(10)	165.34(13)
V(1)–O(11)	1.852(3)	O(10)–V(1)–N(19)	91.65(12)
V(1)–O(100)	2.049(3)	O(100)–V(1)–N(19)	167.78(13)
V(1)–N(19)	2.032(3)	O(2)–V(2)–N(29)	96.63(15)
V(2)–O(2)	1.601(3)	O(2)–V(2)–O(21)	95.27(13)
V(2)–O(20)	2.129(3)	O(2)–V(2)–O(22)	107.53(14)
V(2)–O(21)	1.861(3)	O(21)–V(2)–N(29)	86.13(13)
V(2)–(O22)	1.862(2)	O(200)–V(2)–N(29)	169.99(13)
V(2)–(O200)	2.064(3)	O(3)–V(3)–O(32)	107.65(14)
V(2)–N(29)	2.019(3)	O(3)–V(3)—N(39)	96.78(14)
V(3)–O(3)	1.592(3)	O(32)–V(3)–N(39)	81.89(13)
V(3)–O(30)	2.146(3)	O(300)–V(3)–N(39)	170.27(13)
V(3)–O(31)	1.857(3)	V(3)–O(300)	2.070(3)
V(3)–O(32)	1.869(3)	V(3)–N(39)	2.037(3)

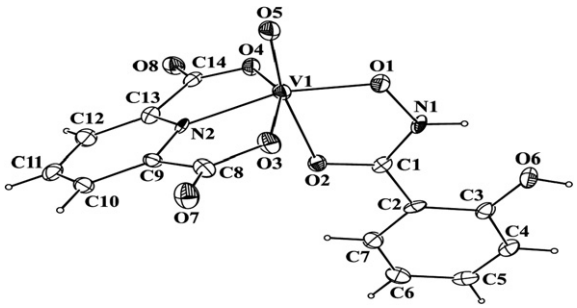

Fig. 3. A molecular view of **3** with atom numbering scheme.

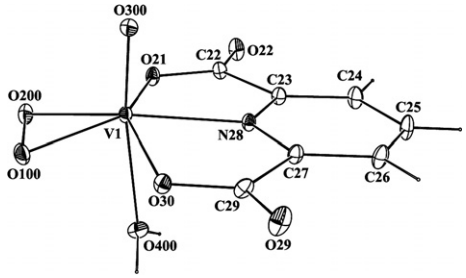

Fig. 4. A view of molecule **4** with atom numbering scheme (lattice held H_2O molecules are omitted for the sake of clarity).

2,6-pyridine dicarboxylate and *N*-salicylhydroximate ligands in **3** are nearly orthogonal to each other; the dihedral angle between the least-squares planes through the ligand atoms is 83.6°(1).

The trinuclear complex molecules in **1** are linked by intermolecular O–H···O hydrogen bonds (Table 6) forming a hexamolecular cluster (Fig. 5). Each hexamolecular cluster consists of six VNO_5 octahedra surrounded by twelve VNO_5 octahedra forming an annular ring with the inner and outer diameters 11.4 and 19.7 Å, respectively. The solvent H_2O molecules lie within the inner core of the ring. The hexamolecular clusters in **1** are interpenetrated forming a novel three-dimensional framework structure (Fig. 6).

In complex **2**, a pair of intermolecular O(300)–H(6)···O(2) hydrogen bonds (Table 6) connects two complex molecules forming a centrosymmetric $R_2^2(14)$ dimeric ring centered at (1/2,1/2,0). The linking of dimeric rings via intermolecular O(300)–H(5)···O(12) hydrogen bonds in **2** produces an infinite one-dimensional chain propagating along the [100] direction. Additional reinforcement within the polymeric chain is provided by the solvent

Table 4
Selected bond lengths (Å) and angles (°) for **3**

V(1)–O(1)	1.850(3)	O(1)–V(1)–O(2)	76.13(11)
V(1)–O(2)	2.126(3)	O(3)–V(1)–N(2)	75.44(13)
V(1)–O(3)	1.956(3)	O(4)–V(1)–N(2)	75.75(12)
V(1)–O(4)	1.979(3)	O(1)–V(1)–N(2)	161.52(13)
V(1)–O(5)	1.591(3)	O(2)–V(1)–O(5)	168.62(13)
V(1)–N(2)	2.052(3)	O(3)–V(1)–O(4)	150.59(12)

Table 5
Selected bond lengths (Å) and bond angles (°) for **4**

V(1)–O(300)	1.592(2)	O(300)–V(1)–O(100)	102.45(10)
V(1)–O(100)	1.871(2)	O(300)–V(1)–O(21)	95.96(9)
V(1)–O(200)	1.875(2)	N(28)–V(1)–O(400)	79.73(9)
V(1)–O(21)	2.054(2)	O(200)–V(1)–O(21)	81.30(9)
V(1)–O(30)	2.070(2)	O(100)–V(1)–O(400)	84.23(9)
V(1)–N(28)	2.090(2)	O(100)–V(1)–O(30)	81.73(9)
O(100)–O(200)	1.432(3)	O(100)–V(1)–O(200)	44.96(10)

Table 6
Selected hydrogen bonds for complexes **1**, **2** and **3**, respectively

D–H···A	D–H	H···A	D···A	D–H···A
Complex ***1***				
O(4)–H(4B)···O2^{i}	0.86(5)	1.98(5)	2.825(5)	168(4)
Complex ***2***				
O(100)–H(1)···O(74)	0.86(4)	1.85(4)	2.712(5)	176(5)
O(200)–H(3)···O(94)	0.89(2)	1.76(3)	2.637(5)	167(3)
O(200)–H(4)···O(84)	0.84(4)	1.95(4)	2.779(4)	172(4)
O(100)–H(2)···O(84)^{ii}	0.85(3)	1.84(3)	2.681(4)	176(6)
O(300)–H(5)···O(12)^{iii}	0.86(4)	1.94(4)	2.760(4)	158(4)
O(300)–H(6)···O(2)^{iv}	0.85(3)	1.88(2)	2.722(4)	170(5)
C(83)–H(83B)···N(29)^{v}	0.96(3)	2.40(3)	3.342(6)	168(3)
Complex ***3***				
N(1)–H(1)···O(8)^{vi}	0.86(1)	2.12(1)	2.796(4)	135(1)
O(6)–H(6A)···O(7)^{vii}	0.82(1)	1.97(1)	2.726(4)	154(1)
C(10)–H(10)···O(5)^{viii}	0.93(1)	2.58(1)	3.338(5)	139(1)
$C_g(5)$–$C_g(5)^{ix}$			3.779(3)	

Symmetry codes: (i) $y-2/3, x-1/3, -z+1/6$; (ii) $-x, 1-y, 2-z$; (iii) $1+x, y, z$; (iv) $1-x, 1-y, 2-z$; (v) $x, -1+y, z$; (vi) $-x+1, y+1/2, -z+1/2$; (vii) $x-1, -y+1/2, z-1/2$; (viii) $-x+2, -y, -z+1/2$; (ix) $1-x, -y, -z$. $C_g(5)$ is the centriod of the ring C(2)–C(7).

acetone molecules through O(200)–H(4)···O(84) and O(100)–H(2)···O(84) intermolecular hydrogen bonds. The remaining C–H···N hydrogen bonds involving solvent acetone molecules join the parallel [100] chains along the [010] direction to generate a two-dimensional network in **2** (Fig. 7).

The intermolecular aggregation in **3** is determined by a combination of O–H···O, N–H···O, C–H···O hydrogen bonds and π–π stacking interactions (Table 6). Intermolecular O(6)–H(6A)···O(7) and N(1)–H(1)···O(8) hydrogen bonds link the molecules into two-dimensional net of $R_4^4(34)$ ring. Finally, the interlinking of two-dimensional nets by C(10)–H(10)···O(5) hydrogen bond forms a three-dimensional supramolecular framework in **3**. The molecular packing in **3** is such that the π–π stacking interactions between the phenyl rings (C2–C7) of adjacent molecules are optimized. The phenyl rings (C2–C7) of molecule at (x,y,z) and $(1-x,-y,-z)$ are strictly parallel, with an interplanar spacing of 3.34 Å, ring centriod separation of 3.778 Å, corresponding to a ring offset of 1.76 Å.

The crystal packing in **4** exhibits several intermolecular O–H···O and C–H···O hydrogen bonds (Table 7). The pairs of C–H···O hydrogen bonds, C(24)–H(24)···O(29) and C(26)–H(26)···O(22), connect molecules of **4** into infinite one-dimensional chain

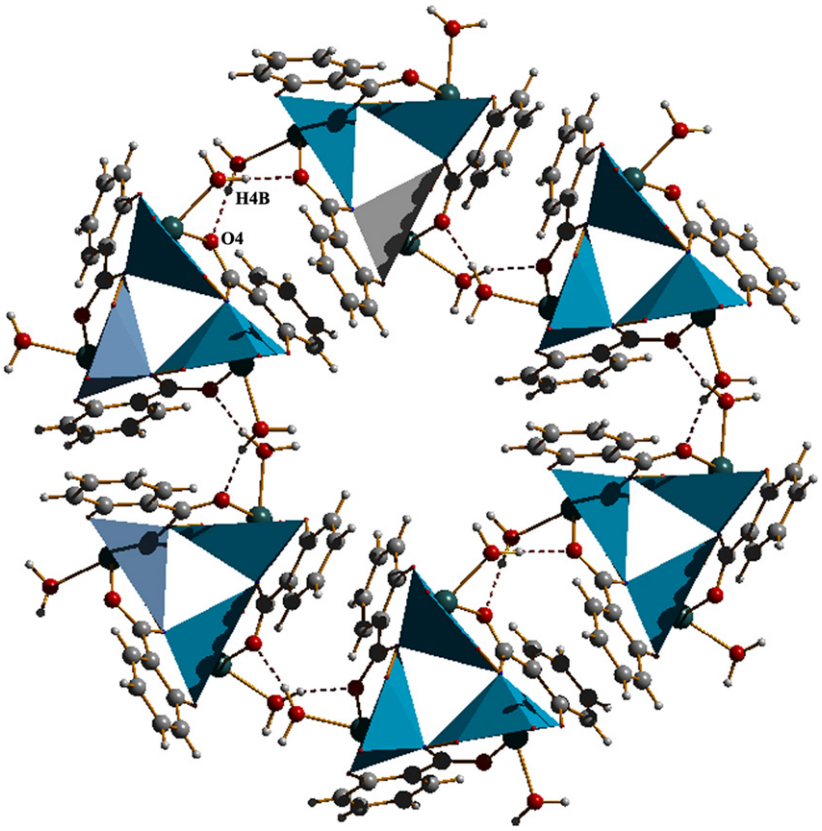

Fig. 5. The molecular packing of **1** showing the formation of hexamolecular cluster.

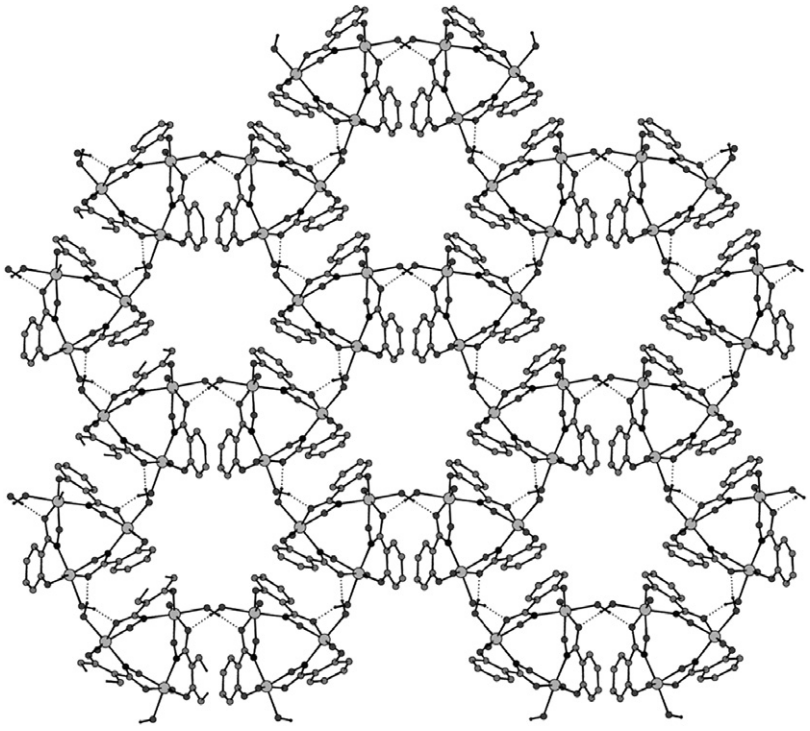

Fig. 6. Three-dimensional supramolecular network formed by interpenetrating hexamolecular rings in **1**.

propagating along the [101] direction through the formation of $R_2^2(10)$ rings. Inter-linking of parallel chains via O(400)–H(401)···O(22) hydrogen bonds generates two-dimensional molecular sheets, which are further connected by intermolecular O–H···O hydrogen bonds involving the lattice water molecules to form a three-dimensional supramolecular framework in **4**.

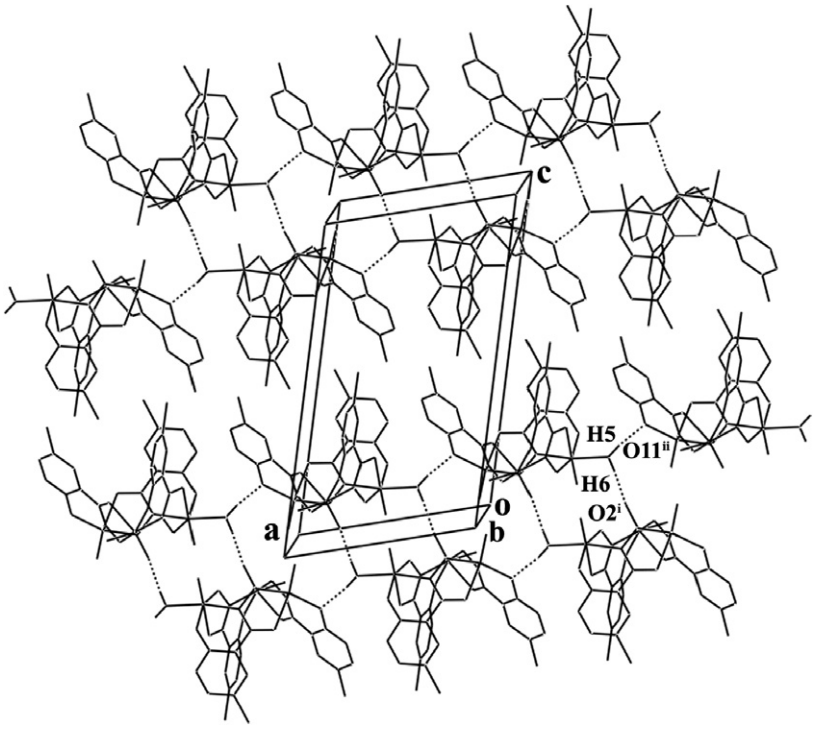

Fig. 7. Two-dimensional supramolecular network in **2** (symmetry codes: (i) $1-x, 1-y, 2-z$; (ii) $1+x, y, z$).

Table 7
Selected intermolecular contacts for **4**

D–H···A	D–H	H···A	D···A	D–H···A
C(24)–H(24)···O(29)^{i}	0.93(1)	2.41(1)	3.234(4)	147(1)
C(26)–H(26)···O(22)^{ii}	0.93(1)	2.42(1)	3.239(4)	147(1)
O(400)–H(401)···O(22)^{iii}	0.84(3)	1.90(3)	2.729(3)	169(3)
O(400)–H(402)···O(1)^{iv}	0.85(3)	1.90(3)	2.726(4)	163(3)
O(1)–H(101)···O(29)^{v}	0.86(3)	1.89(3)	2.745(3)	178(3)
O(1)–H(102)···O(100)^{v}	0.86(2)	2.39(2)	3.103(3)	141(3)

Symmetry codes: (i) $x-1/2, -y+1/2, z-1/2$; (ii) $x+1/2, -y+1/2, z+1/2$; (iii) $-x+1, y, -z+1/2$; (iv) $x, y, z+1$; (v) $x, -y+1, z-1/2$.

3.3. ^{51}V NMR spectroscopy

The ^{51}V NMR spectra for the complexes **1** and **3** at temperature 296 K in CD_3CN solvent exhibited a single peak namely, at −236.58 ppm for **1** and −423.80 ppm for **2** signifying a single species in solution in both the cases. The upfield shifting on going from **1** to **3** indicates that the nucleus of **3** is more shielded than that of **1** (by 187.2 ppm). This is due to the transformation of trinuclear complex **1** containing only bridging SHA^{3-} ligands to a mononuclear mixed ligand ($PyDC^{2-}$ and $SHAH_2^{-}$) complex **2**, in which one of the ligands, namely SHA^{3-} captures two protons [40] and also a new ONO ligand is incorporated which shields the vanadium nucleus more effectively.

3.4. Catalytic properties of the complexes

Complexes **1** and **2** posses efficient catalytic properties in the oxidation/functionalization of aromatic, carbocyclic and aliphatic hydrocarbons to their phenolic, alcoholic and carbonyl functions as shown in the Table 8, where **1** is shown as a representative catalyst. The catalytic efficiency of the two oxovanadium(V) complexes **1** and **2** for hydrocarbon oxidation are very much comparable (shown in Table 9) indicating that the electron withdrawing chlorine substituent in **2** has little resultant effect in the catalytic oxidation reaction. Compound **3** is not a good catalyst. The Table 8 exhibits that the catalytic potentiality of **1** is quite satisfactory without the uses of any additives or co-catalysts compared to other oxovanadium(V) catalysts reported earlier [8–10]. However product selectivity obtained are not very good excepting in a few cases, namely, benzene, diphenylmethane and toluene (up to 10 h). After 10 h toluene starts affording other products (see Table 8) but in benzene and diphenylmethane the selectivity is maintained until the completion of the reaction when almost quantitative conversion of substrate to products occurs (for details see S1). It has been observed that some products are selectively obtained at a short reaction time but if the reaction is allowed to proceed for a longer period other products appear. Interesting examples are shown by tetralin and cyclohexane substrates (for explanation see S2). Another interesting example is provided by the conversion of ethyl benzene to 1-phenyl ethanol vis-a-vis acetophenone. It is observed that the 1-phenyl ethanol (24%) is obtained at a higher proportion than acetophenone (19.5%) upto a reaction period of 12 h and then acetophenone production started increasing at the cost of 1-phenyl ethanol (Fig S2; see also Table 8). 2-pentanone (39.4%) and 2-pentanol (24.6%) and 2-pentanoic acid (9.2%) are obtained as the main products from n-pentane functionalization. 2-Hexanone (33.4%), 1-hexanol (18.46%), 2-hexanol (12%) and hexanoic acid (5%) are obtained as the principal products from *n*-hexane. The substrate *n*-heptane affords mainly 2-heptanone (31.8%), 1-heptanol (22.6%) and 2-heptanol (11.8%).

3.5. Probable mechanism of catalytic oxidation of hydrocarbons

The catalytic reaction mixture contains the hydrocarbon substrate, H_2O_2 and the trinuclear complex **1** as catalyst which is converted to a new intermediate peroxo species $[V^{V}O(O_2)(SHAH_2)(H_2O)]$ (**A**) by reacting with H_2O_2 (see Scheme 1). This in situ generated peroxo species **A** oxidizes the C–H bond of the substrate (hydrocarbons) leading to the oxygenated products via the forma-

Table 8
Catalytic oxidation of aromatic, carbocyclic and aliphatic hydrocarbons using **1** as catalyst and H_2O_2 as terminal oxidant

Hydrocarbons (5 mmol) $\xrightarrow[25\ \text{mmol}\ H_2O_2/CH_3CN/80\ ^\circ C]{0.05-0.005\ \text{mmol}[V_2O_3(SHA)_3(H_2O)_3]\ (\mathbf{1})}$ Oxygenated organic products

Entry	Substrate	Product/s	Time (h)	% Conversion	[a]GC yield (%)	[b]% Selectivity/proporation	[c]TON
1			24	90	90	100	360
2			10	38	38	100	76
2a		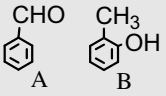 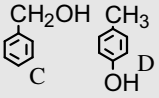	30	86	85	A-53 B-15 C-19.5 D-8.8	172
3		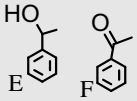	30	92	92	E-14.5 F-79.5	368
4		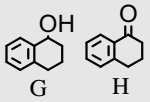	30	89	89	G-7 H-93	356
5			30	90	90	100	360
6		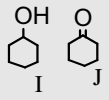	10	98	98	I-58 J-42	980
7		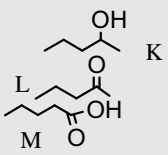	30	78	76	K-32 L-50 M-12	156
8		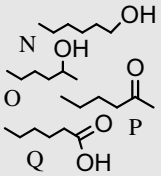	30	72	71	N-26 O-17 P-47 Q-7	72

Table 8 (*continued*)

Entry	Substrate	Product/s	Time (h)	% Conversion	[a]GC yield (%)	[b]% Selectivity/proporation	[c]TON
9		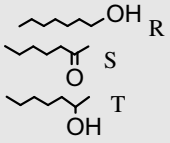	30	69	67	R-33 S-46 T-15	69

[a] The detailed calculation of GC yield is given as supporting information.
[b] %Selectivity is a spectacular in the given time frame.
[c] T.O.N = ratio of moles of products obtained to the moles of catalyst used. The mole ratios of the catalyst to the substrate are as follows: 1:400 (for entries 1, 3, 4 and 5), 200 (for entries 2, 2a and 7), 1000 (for entry 6) and 100 (for entries 8 and 9).

Table 9
Comparative catalytic efficiency of compound **1** and **2** in the case of some representative hydrocarbons oxidation

Entry	Catalyst	Oxidation of benzene (t = 15 h)		Oxidation of cyclohexanol (t = 10)	
		GC yield (%)	TON	GC yield (%)	TON
1	$[V_3O_3(SHA)_3(H_2O)_3]$ (**1**)	55	550	98	980
2	$[V_3O_3(CSHA)_3(H_2O)_3]$ (**2**)	48	480	84	840

In both the cases, the substrate: catalyst ratio is 1000:1 and concentration of H_2O_2 is 25 mmol.

tion of two intermediates $[V^{IV}O(OOH)(SHAH_2)(H_2O)]$ (**B**) and $[V^{V}O_2(SHAH_2)(H_2O)]$ (**C**). The intermediate **C** then reacts with H_2O_2 to form **A**. All the above observations suggest a sequence of reaction steps as is shown in the Scheme 1 using cyclohexane as representative substrate. That the invocation of radical mechanism is necessary, is confirmed by the acceleration of the rate of reaction when the experiment is conducted by the irradiation of a tungsten lamp as well as by adding traces of azoisobutyronitrile (AIBN) and decelaration of the same by using benzoquinone during the course of reaction. Surprisingly, in an earlier report [15] we failed to notice the effect of AIBN and benzoquinone.

4. Conclusions

V_2O_5 and the allied vanadium compounds were long known to have industrial uses as substrate oxidation catalyst operating via heterogeneous mode. But solid vanadium compounds acts as irritants to the conjunctive and respiratory tract. Consequently the

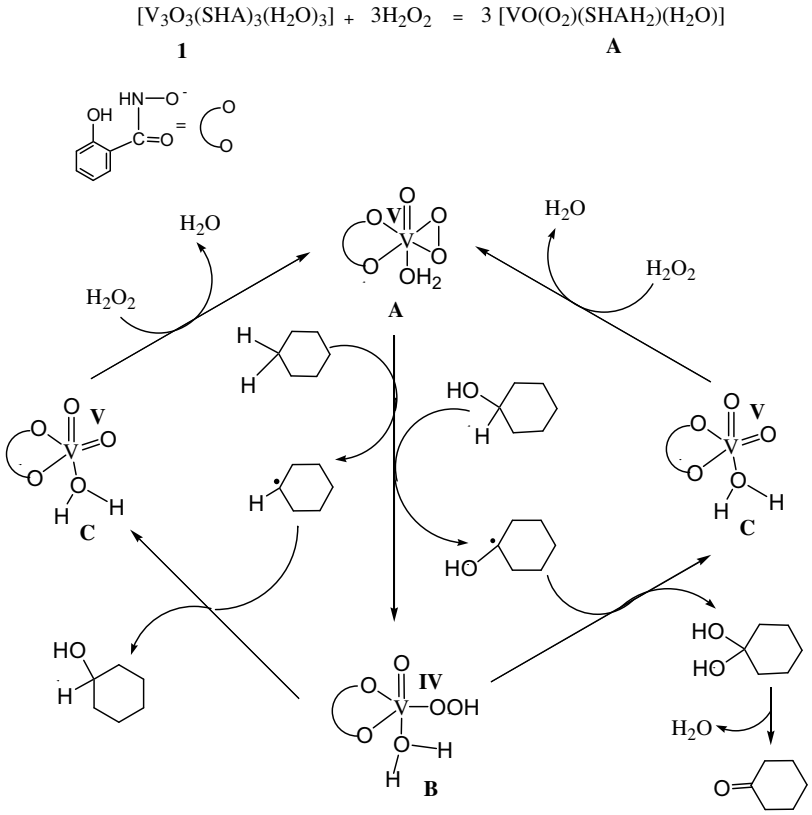

Scheme 1. Probable mechanism of the catalytic oxidation of hydrocarbons (cyclohexane as representative substrate) using compound **1** as catalysts in presence of H_2O_2.

inhalation of catalyst dust is extremely unpleasant and should be avoided. The homogeneous oxidation of organic compounds by vanadium complexes as catalyst becomes very much effective in presence of H_2O_2 or dioxygen as terminal oxidant instead of *tert*-butyl hydroperoxide (TBHP). We have observed that TBHP as terminal oxidant behaves as far less selective in hydrocarbon oxidation using **1** and **2** as catalyst. Moreover, TBHP is not at all an environment friendly oxidant specially at temperature above 50–60 °C and even if operated at a lower temperature waste disposal problem arises. If the experiment is conducted at higher temperature, CO and CO_2 are evolved via the decomposition of TBHP.

Acknowledgements

Financial assistance from U.G.C and D.S.T New Delhi is acknowledged. T.K.S and S.C. thank University Grant Commission for fellowship. We thank D.S.T for funding Agilent 6890N Gas Chromatograph with dual detector facilities.

Appendix A. Supplementary data

CCDC 675168, 655780, 655781 and 655778 contain the supplementary crystallographic data for **1**, **2**, **3** and **4**. These data can be obtained free of charge via http://www.ccdc.cam.ac.uk/conts/retrieving.html, or from the Cambridge Crystallographic Data Centre, 12 Union Road, Cambridge CB2 1EZ, UK; fax: (+44) 1223-336-033; or e-mail: deposit@ccdc.cam.ac.uk. The supplementary data also contains GC yield calculation method, text S.1, S.2 and figures (Figs. S.1 and S.2). Supplementary data associated with this article can be found, in the online version, at doi:10.1016/j.poly.2008.03.031.

References

[1] G.B. Shul'pin, Organic Reactions Catalysed by Metal Complexes, Nauka, Moscow, 1988 (in Russian).
[2] A.E. Shilov, G.B. Shul'pin, Russ. Chem. Rev. 59 (1990) 853.
[3] S.T. Oyama, J.W. Hightower (Eds.), Catalytic Selective Oxidation, American Chemical Society, Washington, 1993.
[4] H. Vilter, Vanadium dependent haloperoxidases, in: H. Sigel, A. Sigel (Eds.), Metal Ions in Biological Systems: Vanadium and Its Role in Life, vol. 31, Marcel Dekker, New York, 1995.
[5] D. Rehder, G. Santoni, G.M. Licini, V. Schuzke, B. Meier, Coord. Chem. Rev. 237 (2003) 53.
[6] R.A. Carter-Franklin, R.D. Little, A. Butler, J. Am. Chem. Soc. 125 (2003) 3688.
[7] K.H. Thompson, J.H. Mcweill, C. Orvig, Chem. Rev. 99 (1999) 2561.
[8] J.E. Remias, J.A. Pavlosky, A. Sen, J. Mol. Catal. A: Chem. 203 (2003) 179.
[9] E. Battistel, R. Tassinari, M. Fornaroli, L. Bonoldi, J. Mol. Catal. A: Chem. 202 (2003) 107.
[10] S. Mohebbi, A.H. Sererstini, Trans. Met. Chem. 32 (2006) 749.
[11] H. Mimoun, L. Saussine, E. doire, M. Postel, J. Fischer, R. Weiss, J. Am. Chem. Soc. 105 (1983) 3101.
[12] G.B. Shul'pin, D. Attanasio, L. Suber, J. Catal. 142 (1993) 147.
[13] G.V. Nizova, G. Sűss-Fink, G.B. Shul'pin, Chem. Commun. (1997) 397.
[14] M. Lin, A. Sen, J. Am. Chem. Soc. 114 (1992) 7307. obtained better turnover numbers in the oxidation of ethane to acetic and formic acid.
[15] T.K. Si, K. Chowdhury, M. Mukherjee, D.C. Bera, R. Bhattacharyya, J. Mol. Catal. A: Chem. 219 (2004) 241.
[16] An alternative nomenclature of *N*-benzoyl *N*-phenyl hydroxylamine (A.K. Majumdar, in: R. Belcher, A. Frieser (Eds.), *N*-Benzoylphenylhydroxylamine and Its Analouges, Pergamon Press, Braunschweig, 1971 and references cited therein) is no longer used.
[17] J.B. Neilands, Struct. Bond. (Berlin) 58 (1984) 1.
[18] C.J. Marmion, K.B. Nolan, Royal College of Surgeons in Ireland, Research by Department/Chemistry and Physics. <http://www.resi.ie/>.
[19] K.N. Raymond, C.J. Carrano, Acc. Chem. Res. 12 (1979) 183.
[20] The ammonium salt of this compound is however structurally characterized. See the reference R.E. Drew, F.W.B. Einstein, Inorg. Chem. 12 (1973) 829.
[21] V.L. Pecoraro, Inorg. Chim. Acta 155 (1989) 171.
[22] D.C. Crans, J.J. Smee, E. Gaidamauskas, L. Yang, Chem. Rev. 104 (2004) 849.
[23] A.G.J. Ligtenberg, R. Hage, B.L. Feringa, Coord. Chem. Rev. 237 (2003) 89.
[24] A.I. Vogel, in: B.S. Furniss, A.J. Hannaford, P.W.J. Smith, A.R. Tatchell (Eds.), Text Book of Practical Organic Chemistry, 5th ed., Longman, UK, 1989, p. 399.
[25] SMART (Version 5.624) Bruker AXS Inc., Madison, Wisconsin, USA, 2000.
[26] CRYSALIS, Oxford Diffraction Ltd., Version 1, 2005.
[27] SADABS (Version 2.03), Bruker AXS Inc., Madison, WI, USA.
[28] ABSPACK, Oxford Diffraction Ltd., 2005.
[29] G.M. Sheldrick, SHELX-97: Program for Crystal Structures Solution, University of Göttingen, Germany, 1997.
[30] P. Buglyo', D.C. Crans, E.M. Nagy, R.L. Lindo, L. Yang, J.J. Smee, W. Jin, L.-H. Chi, M.E. Godzala, G.R. Willsky, Inorg. Chem. 44 (2005) 5416.
[31] A.D. Keramidas, S. Miller, O.P. Anderson, D.C. Crans, J. Am. Chem. Soc. 119 (1997) 8901.
[32] Y. Jin, H.-I. Lee, M. Pyo, M.S. Lah, Dalton Trans. (2005) 797.
[33] D.C. Fisher, S.J. Barclay-Peet, C.A. Balfe, K.N. Raymond, Inorg. Chem. 28 (1989) 4399.
[34] D. Rehder, C. Schulzke, H. Dua, C. Meinke, J. Hanss, M. Epple, J. Inorg. Biochem. 80 (2000) 115.
[35] S. Nica, A. Pohlmann, W. Plass, Eur. J. Inorg. Chem. (2005) 2032.
[36] K.I. Smith, L.L. Borer, M.M. Olmstead, Inorg. Chem. 42 (2003) 7410.
[37] M.R. Maurya, S. Agarwal, M. Ehel, D. Rehder, J. Chem. Soc., Dalton Trans. (2005) 537.
[38] D. Neculai, A.M. Neculai, H.W. Roesky, R.H. Irmer, B. Walfort, D. Stalke, Dalton Trans. (2003) 2831.
[39] J. Gatjens, B.N. Meier, T. Kiss, E.M. Nagy, P. Buglyo, H. Sakurai, K. Kawabe, D. Rehder, Chem. Eur. J. 9 (2003) 4924.
[40] M. Časný, D. Rehder, Dalton Trans. (2004) 639.

Polyhedron 27 (2008) 2243–2250

Contents lists available at ScienceDirect

Polyhedron

journal homepage: www.elsevier.com/locate/poly

Unusual coordination in a silver thionate complex. Synthesis, structural characterization and theoretical calculations of dinuclear and polynuclear silver(I) thiosaccharinates with pyridine and 1,10-phenanthroline

Mariana Dennehy [a], Ricardo M. Ferullo [a], Oscar V. Quinzani [a,*], Sandra D. Mandolesi [a], Norberto Castellani [b], Michael Jennings [c]

[a] Departamento de Química, Universidad Nacional del Sur, Avda. Alem 1253, B8000CPB Bahía Blanca, Argentina
[b] Departamento de Física, Universidad Nacional del Sur, Avda. Alem 1253, B8000CPB Bahía Blanca, Argentina
[c] X-ray Structures Western, Chemistry Department, University of Western Ontario, London, Ontario, Canada N6A 5B7

ARTICLE INFO

Article history:
Received 20 November 2007
Accepted 11 April 2008
Available online 2 June 2008

Keywords:
Silver
Thiones
X-ray structures
DFT calculations
Pyridine
Phenanthroline

ABSTRACT

Treatment of $Ag_6(tsac)_6$ (tsac = thiosaccharinate anion) with pyridine (py) and 1,10-phenanthroline (*o*-phen) each affords two novel silver(I)-thiosaccharinate complexes: dinuclear $[Ag_2(tsac)_2py]$ (**1**) and polynuclear $[Ag(tsac)(o\text{-phen})]_n$ (**2**). Both crystal structures have been determined by X-ray diffraction and spectroscopic structural analysis (IR and Raman, UV–Vis, ^1H and ^{13}C NMR) have also been made for both compounds. Thermal stability analysis (TGA and DTA) of complex **1** are used to confirm the strength of the pyridine coordination to the silver ion. The molecular structure of complex **1** shows some astonishing characteristics. The two silver atoms are in different environments: one of them is surrounded by two S atoms, while the other completes its coordination sphere by three N atoms, two from the thiosaccharinate anions and the third from a pyridine molecule. The short Ag(1)–Ag(2) contact distance, 2.9681(8) Å, indicates an interaction between the two silver metal atoms exists. Complex **2** shows a thiosaccharinate molecule bridging two silver atoms through the exocyclic S atom while the *o*-phenanthroline ligand is coordinated as a bidentate *N,N* chelate, forming a polynuclear chain. Quantum chemical calculations confirm the argentophilic character of the Ag–Ag interaction in complex **1**, and its structure and vibrational assignments were correlated and confirmed theoretically.

© 2008 Elsevier Ltd. All rights reserved.

1. Introduction

The use of silver(I) coordination compounds as building blocks for the construction of dimeric, polymeric or supramolecular structures is a continuous growing research field [1–4]. Interesting applications in photographic industry [5,6], medicine [7,8], luminescent [9] and magnetic [10] devices, have been investigated for such new substances. The flexibility of silver(I) ions to adopt different coordination geometries, such as linear, bent, T-shaped, trigonal planar, or tetrahedral, contributes to the existence of a great variety of coordination architectures [4]. Also, the tendency of silver(I) ions to aggregate themselves, reported as "argentophilicity", can control the shape of their coordination spheres in the solid state structures [11–14]. The argentophilic interaction has been calculated as weaker than the closed shell interactions of the other coinage metals [15–18], but the results are still controversial [14,19,20]. The argentophilicity of silver(I) ions has been demonstrated in a number of substances with ligand unsupported Ag(I)–Ag(I) short interactions [11–14] and more examples exist of ligand supported arrangements [8,21–23].

In the chemistry of silver carboxylates many examples of polymeric structures based on dimeric "$Ag_2(RCOO)_2$" building blocks have been reported (see Scheme 1I) [21,23]. In many of those complexes the intra-annular Ag–Ag distances fall in the range between 2.8 and 3.0 Å, very close to the 2.88 Å interatomic distance in metallic silver [24]. Also, very short distances have been reported for bis(3-hydroxy-4-phenyl-2,2,3-trimethylcyclohexane-carboxilato)disilver(I) (2.778(5) Å) [25] and silver-1,2-benzenedicarboxylate-monomethyl ester (2.7529(16) Å) [5]. The thioamidate functional group from deprotonated cyclic thioamides can also form similar dimeric silver complexes with short Ag–Ag distances [6,26]. Two different coordination arrangements are possible, one with a trans; *head-to-tail*, and another with a trans; *head-to-head* orientation of the bridges (Scheme 1-IIa and IIb, respectively) [24].

* Corresponding author. Tel.: +54 291 4595159; fax: +54 291 4595160.
E-mail address: quinzani@criba.edu.ar (O.V. Quinzani).

0277-5387/$ - see front matter © 2008 Elsevier Ltd. All rights reserved.
doi:10.1016/j.poly.2008.04.012

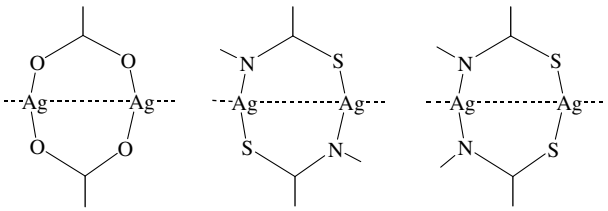

Scheme 1. Disilver(I) arrangements with bridging carboxylates (I) or thionates (II).

As far as we know, there are a few examples of silver(I) thionates (cyclic thioamidates) with the anions acting as μ_2-S,N bridges [6,26]. These complexes preferentially adopt the μ_2-S and μ_3-S,N coordination forms [28–30]. Recently we reported a new Ag(tsac) complex (tsac: thiosaccharinate anion) with a very uncommon polymeric structure built by dinuclear units, $[Ag_2(tsac)_2]_n$, with a short Ag–Ag distance of 2.9194(4) Å [26]. The dimers shown a trans; *head-to-tail* disposition.

Despite the great number of metal-thionate complexes reported in the last decades, which have been the subject of several reviews [27,31–34], the silver-thionate chemistry has been developed very recently. Most of the compounds reported have been binary silver thionates, with a dominance of tetra- or hexanuclear molecular structures [30], or silver-thionate-phosphane ternary complexes, ranging from mononuclear to very complex polynuclear structures [35–38]. There are almost no reports of ternary complexes of Ag(I)-thionates with nitrogenated bases as secondary ligands, in contrast to the broad field developed about the silver salts of less coordinating anions [39,40]. The number of atoms bonded to the silver cations is strongly dependent on the nature of the ligands and on the stoichiometry of the forming reaction. In the coordination chemistry of coinage (I) metals, metal–nitrogen containing ligand complexes are often used as building blocks [2,13,41], Recently we prepared the dinuclear $[Ag_2(tsac)_2(2,2'\text{-bipy})_2]$ complex, which shows a very short Ag–Ag bond distance of 2.7884(12) Å, one of the shortest distances reported for a dinuclear silver(I) complex [37].

Knowing the versatility of the thiosaccharinate ligand to coordinate metals in different forms, such as monocoordination through the exocyclic S atom (S_{exo}), S,N-chelating, S^2-bridging, S,N-bridging, or S^2,N-bridging [26,30,37,38,42–44], we decided to further explore the chemistry of silver thiosaccharinate with pyridine based nitrogenated compounds, with the aim to modulate the Ag(I)–tsac interaction. Silver(I)–pyridine complexes have been know for a long time, and they can show different metal to ligand molar relations [39,40,45]. In this work we report the structural and spectroscopic characterization of two new ternary silver thiosaccharinate complexes with pyridine and 1,10-phenanthroline. The results at DFT and MP2 (DFT: density functional theory; MP2: second order Moller–Plesset theory) levels of the new pyridine complex is also reported.

2. Experimental

2.1. General remarks

All chemicals were of analytical reagent grade and used as purchased. The solvents used were of analytical reagent grade and dried by commonly used techniques [46]. Solid thiosaccharin (Htsac) in its α-form was prepared following the technique published by Schibye et al. [47] and characterized by melting point and IR spectroscopy [48]. The elemental analysis of C, N, H and S were performed with a Carlo Erba EA1108 instrument at INQUIMAE (FCEyN, UBA, Argentina) and were found to be in good agreement with the calculated values. The IR spectra of the substances were recorded as KBr pellets in the 4000–400 cm^{-1} range on a Nicolet Nexus FTIR spectrometer. The Raman dispersion spectra of the solid substances in the region between 3500 and 100 cm^{-1} were obtained with a FRA 106 accessory mounted on a Bruker IFS 66 FTIR instrument, employing the 1064 nm line from a Nd-YAG laser. The UV–Vis spectra of the solids (dispersed in KBr) were registered using a Cecil 2021 spectrophotometer. The ^1H and ^{13}C NMR spectra of the compounds in DMSO-d_6 solutions, at 300 K, were recorded using a multi-nuclear Bruker ARX-300 instrument. The chemical shift data were measured employing the replacement methods and are reported relative to TMS. The use of PPh_3 for increasing the solubility of Ag complexes has been well established, and used before by ourselves and by other authors [30,49]. Thermal decomposition of the $[Ag_2(tsac)_2py]$ sample was evaluated simultaneously by thermogravimetric and differential thermal analyses (TGA/DTA) carried out in a Rigaku TAS 1000 equipment, under nitrogen flow, with Al_2O_3 powder as a reference sample. The heating rate was kept constant at 5 K min^{-1}. The sample was heated from room temperature (294 K) to 723 K.

2.2. Synthesis of [pyridine-bis{μ_2-S:N-(1,1-dioxide-1,2-benzoisothiazol-3-thionato-κ^2S:N^3)-silver(I)}] $[Ag_2(tsac)_2(py)]$ (**1**)

The complex was obtained by adding a solution of Htsac (0.010 g/0.050 mmol) in 3 mL of MeCN to a solution of $AgNO_3$ (0.0085 g/0.050 mmol) in 2 mL of pyridine. In the resulting clear solution, a pale yellow precipitate slowly appeared. The precipitate was filtered and washed with diethyl ether. Yield: 42%. *Anal.* Calc. for $C_{19}H_{13}Ag_2N_3O_4S_4$: C, 33.0; H, 1.9; N, 6.1; S, 18.6. Found: C, 32.9; H, 2.2; N, 6.1; S, 18.5%. ^1H NMR (DMSO-d_6, δ in ppm): 8.09–8.02 (m,2 H), 7.97–7.88 (m, 2H), 7.88–7.77 (m, 5H), 7.77–7.65 (m, 4H); ^{13}C NMR (DMSO-d_6, δ in ppm): δ 187.9, 150.0, 138.51, 136.52, 133.79, 132.85, 131.86, 125.58, 124.29, 120.60.

The same compound was also obtained by adding solid Ag(tsac) (0.012 g/0.039 mmol) to 2 mL of pyridine. The yellow solution formed produced crystals by slow diffusion of diethyl ether. Pale, yellow rods, both air and light stable and suitable for X-ray diffraction analysis were obtained.

It is important to point out the large excess of pyridine used in both synthesis.

2.3. Synthesis of poly[(1,10-phenanthroline-κ^2N:N)-μ_2-S-(1,1-dioxide-1,2-benzoisothiazol-3-thionato)silver(I)] $[Ag(tsac)(o\text{-phen})]_n$ (**2**)

A yellow solution of Ag(tsac) (0.012 g, 0.040 mmol) was obtained by dissolution in a PPh_3 solution (0.010 g, 0.040 mmol) in acetonitrile (MeCN) (5 mL) under mechanical stirring, at room temperature. Slow addition of an 1,10-phenanthroline (*o*-phen) solution (5 mL) in MeCN (0.007 g, 0.04 mmol) gave a pale yellow microcrystalline solid (Ag/tsac/*o*-phenanthroline molar ratio: 1:1:1). The solid was collected by filtration and washed with small amounts of diethyl ether. The compound was air and light-stable. Yield: 60%. *Anal.* Calc. for $C_{19}H_{12}AgN_3O_2S_2$: C, 46.9; N, 8.6; H, 2.5; S, 13.2. Found: C, 46.8; N, 8.6; H, 2.6; S, 13.2%. ^1H NMR ($CDCl_3$, δ in ppm): 9.44–9.22 (m, 2H), 8.48–8.27 (m, 2H), 8.14–7.79 (m, 1H), 7.84–7.77 (m, 2H), 7.75–7.68 (m, 1H), 7.65–7.38 (m, 4H).

Despite the low solubility of the complex in all common organic solvents, saturated solutions of the complex in MeCN were allowed to slowly evaporate at room temperature, and 24 h later yellow single crystals suitable for X-ray diffraction were formed.

The same compound was prepared by addition of $AgNO_3$ (0.0080 g, 0.050 mmol), to a MeCN solution (8 mL) of *o*-phen (0.0090 g, 0.050 mmol). A white solid then appeared. The addition

of Htsac (0.010 g, 0.050 mmol) with mechanical stirring turned the precipitate to a pale yellow microcrystalline solid in less than 10 min.

By reaction of *o*-phen (0.0090 g, 0.050 mmol) with Ag(tsac) (0.012 g, 0.040 mmol) in dimethylsulfoxide (DMSO) (2.0 mL), the same microcrystalline precipitate was obtained.

2.4. Crystal structures

For both complexes, data was collected on a Nonius Kappa-CCD area detector diffractometer with COLLECT (Nonius B.V., 1997–2002). The unit cell parameters were calculated and refined from the full data set. Crystal cell refinement and data reduction were carried out using HKL2000 DENZO-SMN (Otwinowski & Minor, 1997). The absorption correction was applied using HKL2000 DENZO-SMN (SCALEPACK). The SHELXTL/PC V6.14 for Windows NT (Sheldrick, G.M., 2001) [50] suite of programs was used to solve the structure by Patterson methods for **1** and direct methods for **2**. Subsequent difference Fourier syntheses allowed the remaining atoms to be located. Data for complex **1** were collected at 298 K and at 150 K for complex **2**. The crystal data and refinement parameters for the two structures are listed in Table 1. Interatomic distances and angles are listed in Tables 2 and 3. Complex **1** was located on a symmetry element so only half of the molecule was resolved and refined. Complex **2** was refined as a single species but the extended structure was a linear polymer. All of the non-hydrogen atoms were refined with anisotropic thermal parameters. The hydrogen atom positions were calculated geometrically and were included as riding on their respective carbon atoms.

2.5. Theoretical calculations

In order to save computational costs, density functional theory (DFT) quantum-mechanical calculations were done to optimize the geometry of complex **1**. The gradient corrected Becke's three parameters hybrid exchange function in combination with the correlation function of Lee, Yang and Parr (B3LYP) as implemented in the software package GAUSSIAN 03 [51] were used. Geometry optimization procedures were started from the experimental crystallographic data of $[Ag_2(tsac)_2py]$ employing the 6-31G** basis sets for C, H, S, N and O atoms. For silver atoms, the LANL2DZ effective core potentials and valence basis set were used. For complex **1**, the nature of Ag–Ag interaction was studied by analyzing their MO's within the Moller–Plesset perturbation (MP2) formalism. When using MP2 method, both LANL2DZ and LANL2DZ with f functions were used. Besides, a vibrational analysis was performed at B3LYP level of calculations.

The atomic charges were computed according to the NBO (natural bond orbital) population analysis which is based on quantum perturbation theory [52].

Table 1
Crystal data and structure refinement for $[Ag_2(tsac)_2(py)]$ (**1**), and $[Ag(tsac)(o\text{-phen})]_n$ (**2**)

	$[Ag_2(tsac)_2(py)]$	$[Ag(tsac)(o\text{-phen})]_n$
Empirical formula	$C_{19}H_{13}Ag_2N_3O_4S_4$	$C_{19}H_{12}AgN_3O_2S_2$
Formula weight	691.30	486.31
Temperature (K)	298(2)	150(2)
Wavelength (Å)	0.71073	0.71073
Crystal system	monoclinic	monoclinic
Space group	*C*2/*c*	*P*21/*c*
Unit cell dimensions		
a (Å)	20.2059(9)	9.1630(4)
b (Å)	12.8104(7)	24.7850(9)
c (Å)	8.3868(3)	7.9115(3)
α (°)	90	90
β (°)	108.747(3)	101.374(2)
γ (°)	90	90
V (Å^3)	2055.71(16)	1761.45(12)
Z	4	4
D_{calc} (Mg/m^3)	2.234	1.834
Absorption coefficient (mm^{-1})	2.347	1.402
F(000)	1352	968
Crystal size (mm)	0.30 × 0.25 × 0.20	0.47 × 0.08 × 0.05
θ Range for data collection (°)	2.91–25.03	2.75–26.37
Index ranges	$-23 \leqslant h \leqslant 24$, $-15 \leqslant k \leqslant 13$, $-9 \leqslant l \leqslant 9$	$-11 \leqslant h \leqslant 11$, $-30 \leqslant k \leqslant 29$, $-9 \leqslant l \leqslant 9$
Reflections collected	11864	19749
Independent reflections (R_{int})	1807 (0.068)	3592 (0.066)
Completeness to θ (%)	25.03° (99.9)	26.37° (99.6)
Absorption correction	semi-empirical from equivalents	semi-empirical from equivalents
Maximum and minimum transmission	0.6511 and 0.5394	0.9332 and 0.5556
Refinement method	full-matrix least-squares on F^2	full-matrix least-squares on F^2
Data/restraints/parameters	1807/0/148	3592/0/244
Goodness-of-fit on F^2	1.023	1.037
Final *R* indices [$I > 2\sigma(I)$]	$R_1 = 0.0322$, $wR_2 = 0.0732$	$R_1 = 0.0323$, $wR_2 = 0.0656$
R indices (all data)	$R_1 = 0.0467$, $wR_2 = 0.0778$	$R_1 = 0.0516$, $wR_2 = 0.0705$
Extinction coefficient	0.0044(2)	
Largest difference in peak and hole (e Å^{-3})	0.716 and −0.719	0.459 and −0.631

3. Results and discussion

3.1. Crystal structures

3.1.1. $[Ag_2(tsac)_2(py)]$ (**1**)

The solid state structure of complex **1** consists of dinuclear units of $[Ag_2(tsac)_2(py)]$. Fig. 1 shows a plot of its structure. The symmetric structure is fairly uncommon showing Ag atoms in two different environments and thiosaccharinate anions in a trans; *head-to-head* disposition. One Ag atom is in a planar arrangement bound to three atoms in a T-shaped structure, two exocyclic sulfur atoms

Table 2
Bond lengths (Å) and angles (°) for $[Ag_2(tsac)_2(py)]$ (**1**)

Bond lengths	Experimental	Calculated[a]	Angles	Experimental	Calculated[a]
Ag(1)–S(1)	2.3875(11)	2.4513	S(1)–Ag(1)–S(1)#1	172.17(6)	172.42
Ag(1)–S(1)#1	2.3875(11)	2.4516	S(1)–Ag(1)–Ag(2)	93.92(3)	93.79
Ag(1)–Ag(2)	2.9681(8)	3.0526	S(1)#1–Ag(1)–Ag(2)	93.92(3)	93.77
Ag(2)–N(3)#1	2.302(3)	2.3086	N(3)#1–Ag(2)–N(3)	156.72(18)	154.09
Ag(2)–N(3)	2.302(3)	2.3107	N(3)–Ag(2)–N(21)	101.64(9)	102.89
Ag(2)–N(21)	2.352(5)	2.4263	N(21)–Ag(2)–Ag(1)	180.00(1)	178.26
S(1)–C(2)	1.694(4)	1.7110	C(2)–S(1)–Ag(1)	106.33(15)	104.50
C(2)–N(3)	1.318(5)	1.3227	N(3)–C(2)–S(1)	125.5(3)	126.62

Symmetry transformations used to generate equivalent atoms: #1, $-x+1, y, -z+3/2$.
[a] Calculated using DFT theory: Basis set: 6-31G* (H, C, N, O, P, S)/LANL2DZ (Ag).

Table 3
Bond lengths (Å) and angles (°) for $[Ag(tsac)(phen)]_n$ (**2**)

Distances	Experimental	Angles	Experimental
Ag–N(22)	2.324(3)	N(22)–Ag–N(11)	71.66(9)
Ag–N(11)	2.364(3)	N(22)–Ag–S(1)#1	146.35(7)
Ag–S(1)#1	2.4312(8)	N(11)–Ag–S(1)#1	131.98(7)
Ag–S(1)	2.7488(8)	N(22)–Ag–S(1)	102.04(6)
S(1)–C(2)	1.701(3)	N(11)–Ag–S(1)	89.23(6)
S(1)–Ag#2	2.4311(8)	S(1)#1–Ag–S(1)	101.78(3)
C(2)–N(3)	1.318(4)	C(2)–S(1)–Ag#2	97.90(11)
C(2)–C(10)	1.503(4)	C(2)–S(1)–Ag	97.92(10)
N(3)–S(4)	1.641(3)	Ag#2–S(1)–Ag	110.03(3)
S(4)–O(41)	1.434(2)		

Symmetry transformations used to generate equivalent atoms: #1, $x,-y+1/2, z-1/2$; #2, $x,-y+1/2,z+1/2$.

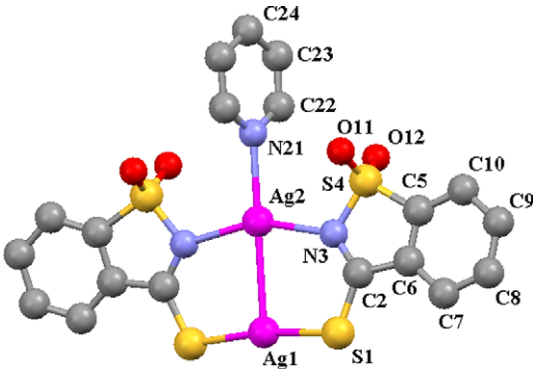

Fig. 1. Molecular structure of $[Ag_2(tsac)_2py]$ (**1**) with 50% probability ellipsoids. H atoms have been omitted for clarity.

of thiosaccharinate anions (S_{exo}) and the other Ag atom. The second Ag atom is in a square-planar arrangement bound to the silver atom and three nitrogen atoms, two of them belonging to the endocyclic N atoms (N_{endo}) of thiosaccharinate anions and the other to the pyridine molecule. The Ag–Ag distance in this complex is 2.9681(8) Å, between the 2.88 Å assigned for metal–metal distance [24] and the sum of van-der-Waals radii of 3.44 Å [53], revealing a real metal–metal interaction. This intermetallic interaction is forced by the bridges of the tsac anions, as was confirmed from the theoretical calculations. As was already mentioned there are many examples of silver dimeric complexes in the literature, but as far as we know, none of them show this arrangement, which has three identical atoms surrounding one silver center and two different atoms around the second metal center. As examples of similar structures shown in the literature, Xu and Sang have reported the synthesis of [catena-(bis(μ_2-2,2′-bi-imidazole)-(μ_2-oxalato)-di-silver)] a complex which has two silver atoms, one of which is bonded to one O and two N atoms, and the other one is bonded to two nitrogen from the imidazol molecule (Scheme 2a) [54]. In this compound the silver–silver distance is 2.9331(17) Å. Nomiya et al. have synthesized catena-[(μ_3-(*R*)-2-pyrrolidone-5-carboxylato)-(μ_2-(*R*)-2-pyrrolidone-5-carboxylato)-di-silver(I)], where the two silver atoms are bonded to two and three oxygen atoms, respectively (Scheme 2b). The silver–silver distance in this compound is 2.899(2) Å, close to that of metallic silver [55].

The Ag–S distance (2.3875(11) Å) in complex **1** is the shortest that we have found in the different Ag-thiosaccharinates crystallized to date (between 2.4875 and 2.748 Å) [30,36,37]. The Ag–N_{endo} distance is 2.302(3) Å and the Ag–N_{py} distance is 2.352(5) Å, both in the order expected for such bonds [37,39]. The donor capacity of the thiosaccharinates coordinated through both the S_{exo} and the N_{endo}, are enough to fill the requirements of the coordination

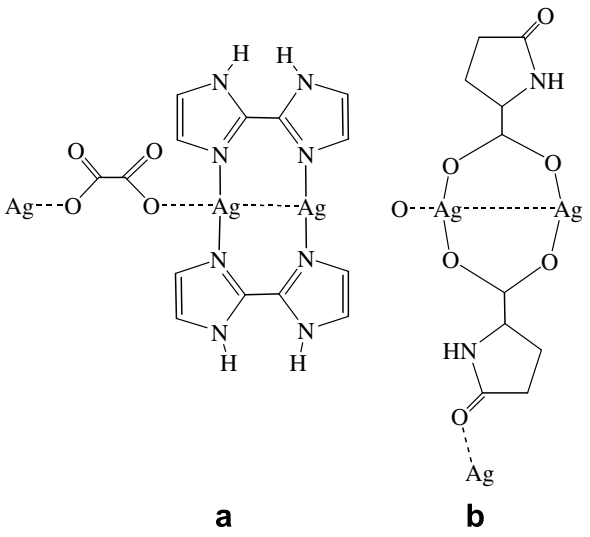

Scheme 2. Disilver(I) complexes with asymmetric four/three coordination spheres from [54,55].

sphere of both silver centers. Some reported polynuclear Ag(I)–pyridine complexes with different counter anions also show Ag–Ag bond lengths of 2.96–3.00 Å [13]. The alignment of the pyridine with the two silver atoms (N(21)–Ag–Ag angle of 180°) introduces symmetry on complex **1**. The thiosaccharinate anions are almost planar and they are twisted from each other by only 6.6°, making them almost coplanar.

So far, we have crystallized only one other silver-thiosaccharinate coordinated to the metal center through a S,N-bridging coordination mode, the complex $[Ag_2(tsac)_2]_n$ [26]. As was already pointed out in this case each silver center is coordinated to the *exo*-sulfur and the *endo*-nitrogen of two different thiosaccharinates, in a dinuclear *head-to-tail* arrangement.

3.1.2. $[Ag(tsac)(o\text{-}phen)]_n$ (**2**)

Complex **2** was very well defined and was bound to adjacent molecules to ultimately form a linear chain of alternating Ag and

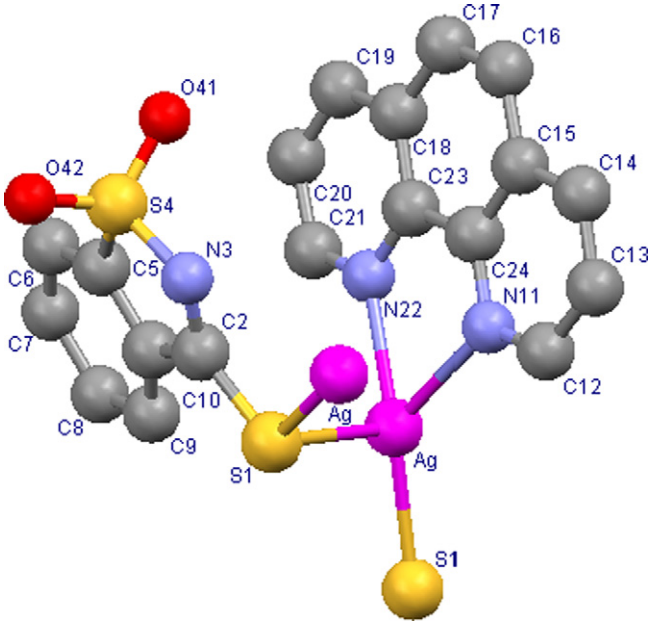

Fig. 2. Molecular structure of $[Ag(tsac)(phen)]_n$ (**2**) with 50% probability ellipsoids. H atoms have been omitted for clarity.

S atoms. Fig. 2 shows a plot of the structure. The silver atom is coordinated to the two N atoms of a 1,10-phenanthroline ligand and two S_{exo} atoms in a trigonal bipyramidal environment with one of the apical atoms missing. The structure strongly resembles that of the dimer $[Ag_2(tsac)_2(2,2'\text{-bipy})_2]$ in the way it is coordinated to the thiosaccharinate anion and to the second ligand [37]. However, in complex **2** there is an open chain perhaps because of the steric demands of the bulky 1,10-phenanthroline. The thiosaccharinate anion is coordinated in a μ_2-S bridging mode via the S_{exo} atom. The Ag–S bond distances (2.4312(8) and 2.7488(8) Å) and the Ag–N_{phen} bond lengths (2.324(3) and 2.364(3) Å) are in the order expected from other silver(I) complexes [33,39,56]. These latter distances are quite similar to the bond distances of Ag—$N_{2-2'bipy}$ in $[Ag_2(tsac)_2(2,2'\text{-bipy})_2]$ (2.327(5) and 2.356(5) Å). The C–S_{exo} bond distance is 1.701(3) Å, longer than the thiocarbonylic bond in complex **1** (1.694(4) Å). The Ag···Ag distance of 4.248 Å is greater than the sum of the van-der-Waals radii of two silver(I) atoms and no metal–metal interaction exist in complex **2** [53].

3.2. FTIR, Raman and UV–Vis spectra

The vibrational spectra of **1** and **2**, both compounds dispersed in KBr discs, are consistent with the X-ray structures. They show all the bands required by the presence of the thiosaccharinate anion and those bands due to the coligands. A selection of the characteristic bands and their assignments are listed in Table 4.

The most interesting bands to be observed in these complexes are those related to the five membered ring of the thiosaccharinate anions, located between 1500 and 400 cm^{-1}, and the low energy metal–ligands vibrations. The thione benzenic ring vibrational bands show no significant differences after coordination. The bands attributable to the N–H bond vibrations, ν(NH) and δ(NH), which in the free ligand appear at 3341 and 1376 cm^{-1}, respectively [30], are absent in the spectra of both complexes. Since there are also no bands between 3000 and 2550 cm^{-1} (the ν-(SH) absorption region) we conclude that the ligand is in the deprotonated form in both complexes. In complexes **1** and **2** the bands corresponding to the stretching motion of the reinforced C–N bonds appear at higher wavenumbers compared to the values found for the "free" thiosaccharinate in bis(triphenylphosphine) iminium thiosaccharinate, while those due to the stretching of the weakened C–S bonds move to lower frequencies (for PNP(tsac) ν(CN): 1365, and $\nu(CS_{exo})$: 1010 cm^{-1}) [57]. These observations confirm the presence of tightly bonded thiosaccharinate ligands. Complex **2** shows the same thiosaccharinate coordination mode (μ_2-S) as $[Ag_2(tsac)_2(2,2'\text{-bipy})_2]$, but the asymmetry of the bridge in complex **2** shifts the ν(CN) and $\nu(CS_{exo})$ vibrations of $[Ag_2(tsac)_2(2,2'\text{-bipy})_2]$ (1411 and 997 cm^{-1}, respectively) [37], to slightly higher frequencies. In the $[Ag_2(tsac)_2(py)]$ complex the thiosaccharinate anions are coordinated to the silver centers through a different coordination mode: μ-S,N, and the positions of the bands due to the thiosaccharinate movements discussed above are shifted (1409 and 1008 cm^{-1}), showing changes in the bond orders of the thioamidate functional groups upon relocalization of the negative charge.

For complex **1**, some characteristic vibrational bands (1594, 1441, 1217, 1071, 702 and 440 cm^{-1}) corresponding to stretching motions of the pyridine ring have been observed [58]. The vibrational bands of the 1,10-phenanthroline ligand in complex **2** remain virtually unaffected after complexation [59]. The metal–ligand stretching vibrations were assigned to the Raman bands appearing at 303 (sym-S_{exo}–Ag–S_{exo}), 180 (sym-N_{endo}–Ag–N_{endo}), and 132 cm^{-1} (Ag–N_{py}), taking into account the DFT theoretical structural calculations performed over the complex (see below).

The UV–Vis spectra of **1** and **2** as solid complexes dispersed in KBr disks yield results similar to each other. They show a weak broad band at 330 and 348 nm, respectively, due to the $\pi \rightarrow \pi^*$ transition of the C–S_{exo} bond expected for thiosaccharin and other thiones [60]. Other intense bands in the range 200–230 and 270 nm were assigned to the $\pi \rightarrow \pi^*$ transitions of the benzene rings [61].

Table 4
FTIR and Raman spectral bands (cm^{-1}) and intensities of PNP(tsac) $[Ag_2(tsac)_2py]$ (**1**) and $[Ag(tsac)(o\text{-phen})]_n$ (**2**)

PNP(tsac)[a]		$[Ag_2(tsac)_2py]$				$[Ag(tsac)(o\text{-phen})]_n$		Assignments[b]
IR[c]	Raman	IR		Raman		IR	Raman	
		Observed	Calc.[d] (int)	Observed	Calc. (int)			
		1594m	1657 (10)					ν_σ(CN) py
1365s	1366w	1409m	1447 (100)	1386vs	1446 (100)	1427m		ν(CN) $\delta(\phi$S)
[e]		1319s	1318 (71)			1303vs	1296w	νas(SO_2)
1147vs	1147m	1168vs	1139 (92)	1154vs	1164 (20)	1154vs	1151m	νs(SO_2)
1116vs		1157w	1134 (1)	1131w	1139 (5)	1123w		νs(SO_2)$\delta(\phi$CN)
1010s	1010w	1008m	1021 (30)	1013w	1031 (7)	1002m	1000vw	ν(CS) δ(CNS)
826s	825w	797s	756 (9)			816m		ν(NS) δ(CCC)
		702m	704 (12)					γ(CH) py
589m	588vw	587m	581 (15)					γ(SO_2)
551vs	550vw	555m	549 (14)	556w	548 (1)	553m	553vw	δ(SO_2)δ(CS)
	517vw	533m	532 (19)	538w	533 (6)	541m	520w	δ_ω(SO_2)
		439vw	431 (6)					γ(CCC) py
	373s			368vs	354 (13)		369m	ν(NSϕ)
				303vw	299 (4)		308w	νs(AgS)
	266m			266w	256 (4)		269vw	δ(iso)
				257w	247 (6)		246vw	δ(iso)
				180w	170 (1)			νs(AgN)
							157m	νs(AgNo-phen)
				132w	131 (1)			νs(AgNpy)
					118 (2)			γ(AgNpy)
					86 (0.22)			νs(AgAg)

[a] Ref. 54; PNP: bis(triphenylphosphine)iminium cation.
[b] ν: stretching, δ: in plane bending, γ: out of plane bending, ϕ: bencenic ring, as: asymmetric, s: symmetric, iso: isoindolic ring.
[c] vs: very strong, s: strong, m: medium, w: weak, vw: very weak.
[d] Calculated using DFT theory: Basis set: 6-31G** (H, C, N, O, P, S)/LANL2DZ (Ag).
[e] Overlapped with a strong PNP band.

3.3. ^{1}H and ^{13}C NMR spectra

The room temperature ^{1}H and ^{13}C NMR spectra of saturated solutions of complex **1** and **2** in DMSO-d_6, were obtained and the chemical displacements compared with the "free" thiosaccharinate ligand data [54] and also to the "free" pyridine and 1,10-phenanthroline molecules [62].

In accord with the vibrational spectra discussed above, the ^{1}H NMR spectra of the complexes contain neither the signal of the SH proton, appearing at 6.42 ppm in the spectrum of the free thiosaccharin, nor the signal due to the possible NH proton at around 9 ppm, indicating the presence of only deprotonated thiosaccharinate ligands in both compounds. The ^{1}H NMR signals of the tsac anions and the pyridine ligand lie superimposed in the same spectral region and cannot be assigned clearly. The ^{13}C NMR spectrum of complex **1** shows the signals of a coordinated pyridine moiety (150.01 (*o*-C), 139.51 (*p*-C) and 125.58 (*m*-C) ppm) (for free pyridine: 149.9, 135. 9, and 123.8 ppm, respectively [62]). One signal, appearing at 187.09 ppm (C2 atom) belongs to an anion coordinated through the exocyclic sulfur atom [38]. The other six signals of the tsac anions have been observed and assigned. Some other weak signals in the region between 138 and 120 ppm suggest that the structure of complex **1** partially breaks down in the DMSO-d_6 solution.

The ^{1}H NMR spectrum of complex **2** shows the signals of a coordinated 1,10-phenanthroline molecule, 9.44–9.22 (α-H), and 8.48–8.27 (β-H) ppm (for free *o*-phen: 9.11 and 7.79, respectively [62]) and the rest of the multiplets are due to the thiosaccharinate and to the other two phenanthroline hydrogens. The ^{13}C NMR spectra obtained for complex **2** were of poor quality due to the low solubility of the substance preventing any assignment of the observed signals.

3.4. Thermogravimetric analysis (TGA) and differential thermal analysis (DTA) of complex *1*

The thermogravimetric analysis of $[Ag_2(tsac)_2py]$ show a first step of weight loss of 10.85% of the initial mass, from 203 to 231 °C, with a corresponding endothermic peak in the DTA curve with a minimum at 222 °C. The calculated weight loss for one pyridine molecule was of 11.43%. These results indicate that the pyridine molecule is tightly bonded to one of the silver(I) centers of the molecule [63]. The end of the pyridine mass loss was partially superimposed with a second complex and continuous exothermic mass loss, not completed within the temperature range of the study, corresponding to the first part of the degradation of the thiosaccharinate ligands [44].

3.5. Quantum chemical calculations

In order to understand the curious structure of complex **1** and the metal–metal interaction from a theoretical point of view, quantum chemical investigations have been carried out, in a first stage, using the DFT formalism [64]. The geometric structure was optimized and the vibrational spectrum was predicted. The results obtained are a good reproduction of the experimentally observed structural parameters (see Table 2). It has been demonstrated for this type of substances that the B3LYP method (with the selected basis sets) yields good agreements with the experimental geometries, overestimating sometimes the bond distances in metal dimers [14,20,45,65]. As can be seen from Table 2, the calculated Ag–Ag distance is slightly larger than the experimental one. In calculations of neutral metal–metal interactions, it is generally accepted that the DFT formalism can reproduce reasonably well several experimental properties [20,66].

A complete MO analysis of complex **1** was performed at both DFT and MP2 approaches. The existence of MO's with high Ag–Ag bond character was similarly observed for both methods. Following the conclusions of other authors that MP2 formalism can be a better method to analyze metal–metal interactions [14,17,20], we will discuss the results obtained with the MP2 perturbation approach. For time computing convenience, the geometry obtained at B3LYP level was taken and a single point MP2 calculation was carried out. Those results showed that complex **1** has 141 occupied MOs. The use of two different basis sets (LANL2DZ and LANL2DZ with f diffuse functions) gave no significant differences in the shape and composition of the MOs. Here, only the results obtained using the LANL2DZ basis set have been presented. The HOMO (−9.09 eV) and LUMO (+0.95 eV) orbitals are both of π character. The first is localized basically over pyridine atoms and the second is primarily over the tsac anions. The Ag–Ag interaction was studied by analyzing the nature of all the MOs. It was observed that MOs HOMO-29, HOMO-30 and HOMO-34 show Ag–Ag bonding character. They are located at −14.56, −14.56 and −14.77 eV, respectively (Figs. 3–5). Along the Ag–Ag contact, the HOMO-30 is a σ-bond with 21% of Ag contribution. The HOMO-34 is also a σ-bond with 22% of Ag contribution and 9% of S(1) and S(1′). The HOMO-29 has a π-type character with a similar contribution of Ag atoms (23%).

As can be expected, several MOs have bonding character over the bridges Ag(1)–S–C–N–Ag(2), expressing the existence of tight bonds between the tsac anions and the Ag(I) centers.

According to the NBO analysis at MP2 level (calculations from B3LYP and MP2 methods yielded similar results, showing the same trend), the atomic positive net charge of Ag(2) is greater than that of Ag(1) (+0.89 and +0.69 e, respectively). On the other hand, the calculated net charges for N(3), S(1) and N(21) are −1.00, −0.36 and −0.65 e, respectively. When the NBO analysis was done on free pyridine and on the same dinuclear structure optimized without the pyridine molecule (*head-to-head* orientation), only the net charges for Ag(2) and N(21) decrease (+0.84 e) and increase (−0.51 e), respectively, showing that the Ag(2) center is harder when it has the pyridine ligand. The total energy of complex **1** is 0.55 eV more stable than the free pyridine plus the dinuclear structure optimized without the pyridine molecule, in agreement with the experimental observations of the existence of a tightly bonded pyridine molecule. The total energy of the dimeric unit was calculated also for the *head-to-tail* orientation observed for the

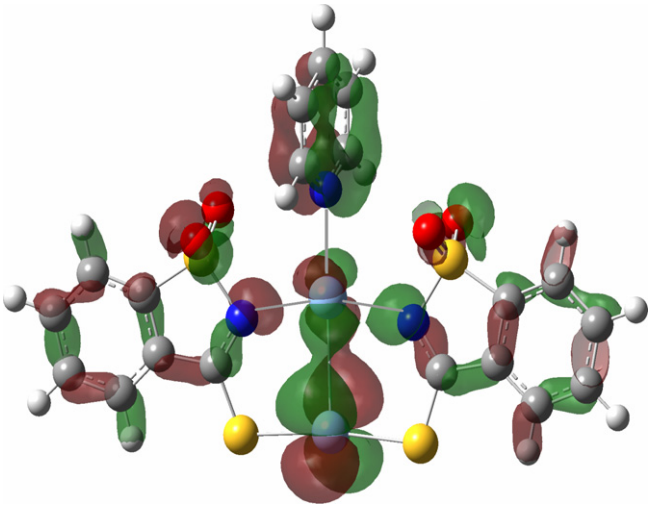

Fig. 3. Plot of HOMO-29 of complex **1** showing Ag–Ag interaction.

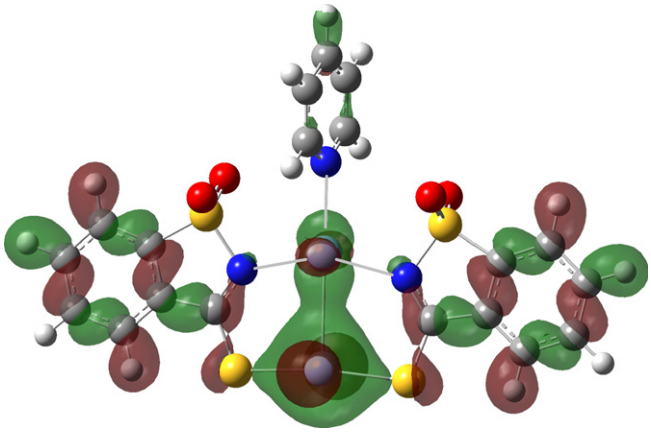

Fig. 4. Plot of HOMO-30 of complex **1** showing Ag–Ag interaction.

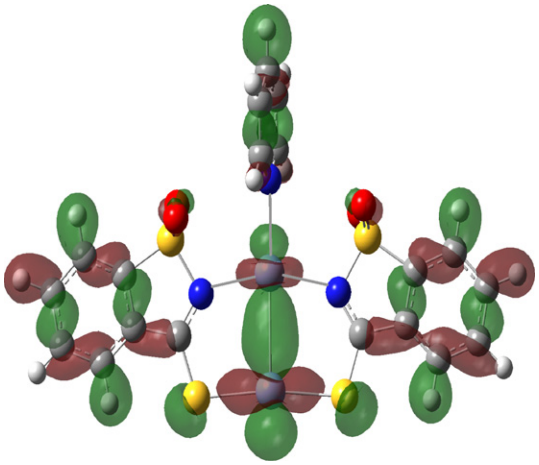

Fig. 5. Plot of HOMO-34 of complex **1** showing Ag–Ag and Ag–S interaction.

$[Ag_2(tsac)_2]_n$ complex, resulting in 0.11 eV more stable than for the *head-to-head* orientation [67].

The theoretical vibrational analysis performed with the optimized geometry of complex **1** at the DFT level yields vibrational spectra in good agreement with the experimental spectra. Considering an ideal C_{2v} symmetry point group for the complex $[Ag_2(tsac)_2py]$, the calculated 129 normal modes of vibration transform as 43 A1 + 20 A2 + 28 B1 + 38 B2. Some of the symmetric A1 vibrations are expected and observed with medium to high intensity in the Raman spectra of the substance as well as some of the B1 and B2 vibrational modes in the IR spectra. A selection of those molecular movements and their tentative assignments are shown in Table 4. The calculated wavenumbers for the stretching of the $Ag–N_{py}$ bond is between that predicted by Wu et al. for a py-Ag^+ fragment (184.6 cm^{-1}) and a py-Ag_2 fragment (106.8 cm^{-1}) in accord with the calculated positive net charges for the Ag centers [58]. Wu et al. also predicted the stretching of the Ag–Ag bond for a py-Ag_2 fragment (192.1 cm^{-1}), with an optimized Ag–Ag bond length of 2.616 Å. Our calculated stretching energy of the metal dimer in complex **1**, with a longer Ag–Ag optimized distance (3.0525 Å) and, thus, a lower calculated frequency, could not be confirmed experimentally, because it was outside of the range of confidence for our Raman spectra.

We tried to simulate the structure of complex **2** using the same type of calculation used for complex **1**, building short oligomeric structures with different kind of terminal molecules. However, owing to the polymeric nature of this structure, all the attempts to obtain reasonably good optimized geometries were unsuccessful.

4. Conclusions

Two new ternary silver(I) complexes are described, in which the metal atoms are coordinated by thiosaccharinate anions and by two other ligands: pyridine and 1,10-phenanthroline. One of the complexes, $[Ag_2(tsac)_2py]$, is particularly curious because of the two different environments that surround the metal centers. The other complex $[Ag(tsac)(o\text{-phen})]_n$, containing a bulky ligand, yields a polymeric chain, with the thiosaccharinates anions acting as bridging ligands between two metallic centers in a μ_2-S mode. The 1,10-phenanthroline chelates as expected in a η^2-N–N manner. The theoretical calculations performed corroborate that even if it is "ligand assisted", an argentophilic interaction is present in complex **1**.

Acknowledgements

We gratefully acknowledge the support of this project (Project M24/Q025) by SGCyT-UNS. We also want to thank Dr. J.A. Güida for recording the Raman spectra and Dra. M.R. Prat for helping us to record the TGA/DTA curves of one of the complexes studied in this work.

Appendix A. Supplementary data

CCDC 667712 and 667713 contain the supplementary crystallographic data for $Ag_2(tsac)_2py$ (**1**) and $[Ag(tsac)(o\text{-phen})]_n$ (**2**). These data can be obtained free of charge via http://www.ccdc.cam.ac.uk/conts/retrieving.html, or from the Cambridge Crystallographic Data Centre, 12 Union Road, Cambridge CB2 1EZ, UK; fax: (+44) 1223-336-033; or e-mail: deposit@ccdc.cam.ac.uk. Complete tables of experimental (**1** and **2**) and calculated (**1**) vibrational data, and of calculated structural parameters (**1**) can be obtained from authors upon request. Supplementary data associated with this article can be found, in the online version, at doi:10.1016/j.poly.2008.04.012.

References

[1] M. Munakata, L.P. Wu, G.L. Ning, Coord. Chem. Rev. 198 (2000) 171.
[2] A.N. Khlobystov, A.J. Blake, N.R. Champness, D.A. Lemenovskii, A.G. Majouga, N.V. Zyk, M. Schröder, Coord. Chem. Rev. 222 (2001) 155.
[3] S.-L. Zheng, M.-L. Tong, X.-M. Chen, Coord. Chem. Rev. 246 (2003) 185.
[4] C.-L. Chen, B.-S. Kang, C.-Y. Su, Aust. J. Chem. 59 (2006) 3.
[5] D.R. Whitcomb, M. Rajeswaran, Polyhedron 25 (2006) 1747.
[6] D.R. Whitcomb, M. Rajeswaran, J. Coord. Chem. 59 (2006) 1253.
[7] G. Manzoni de Oliveira, L.R. Zoclo Gris, L. de Lourenço Marques, E. Schulz Lang, Z. Anorg. Allg. Chem. 633 (2007) 610.
[8] S. Abuskhuna, J. Briody, M. McCann, M. Devereux, K. Kavanagh, J. Barreira Fontecha, V. McKee, Polyhedron 23 (2004) 1249.
[9] Y.-B. Dong, P. Wang, R.-Q. Huang, M.D. Smith, Inorg. Chem. 43 (2004) 4727.
[10] P. Lin, R.A. Henderson, R.W. Harrington, W. Clegg, C.-D. Wu, X.-T. Wu, Inorg. Chem. 43 (2004) 181.
[11] A.A. Mohamed, L.M. Pérez, J.P. Fackler Jr., Inorg. Chim. Acta 358 (2005) 1657.
[12] X-L. Liu, G.-C. Guo, M.-L. Fu, X.-H. Liu, M.-S. Wang, J.-S. Huang, Inorg. Chem. 45 (2006) 3679.
[13] C.Y. Chen, J.Y. Zeng, H.M. Lee, Inorg. Chem. 360 (2007) 21.
[14] L. Ray, M.M. Shaikh, P. Ghosh, Inorg. Chem. 47 (2008) 230.
[15] E.J. Fernández, J.M. López-de-Luzuriaga, M. Monge, M.A. Rodríguez, O. Crespo, M.C. Gimeno, A. Laguna, P.G. Jones, Inorg. Chem. 37 (1998) 6002.
[16] R. Pyykkö, Chem. Rev. 97 (1997) 597.
[17] R. Pyykkö, Angew. Chem., Int. Ed. 116 (2004) 4512.
[18] R. Pyykkö, Inorg. Chim. Acta 358 (2005) 4113.
[19] L. Mangko, M. Schweizer, G. Rauhut, M. Schütz, H. Werner, Phys. Chem. Chem. Phys. 4 (2002) 1006.
[20] E. O'Grady, N. Kaltsoyannis, Phys. Chem. Chem. Phys. 6 (2004) 680.
[21] D.R. Whitcomb, M. Rajeswaran, Inorg. Chim. Acta 361 (2008) 1357.
[22] C.-M. Che, S.-W. Lai, Coord. Chem. Rev. 249 (2005) 1296.
[23] X.-M. Chen, T.C.W. Mak, J. Chem. Soc., Dalton Trans. (1991) 1219.

[24] N.B.N. Greenwood, A. Earnshaw, Chemistry of the Elements, Pergamon, Oxford, 1989. p. 1368.
[25] P. Coggon, A.T. McPhail, J. Chem. Soc., Chem. Commun. (1972) 91.
[26] M. Dennehy, O.V. Quinzani, R.A. Burrow, Acta Crystallogr., Sect. C 63 (2007) m395.
[27] E.S. Raper, Coord. Chem. Rev. 165 (1997) 475.
[28] W. Su, M. Hong, J. Weng, Y. Liang, Y. Zhai, R. Cao, Z. Zhou, A.S.C. Chan, Inorg. Chim. Acta 331 (2002) 8.
[29] A. Castiñeiras, I. García-Santos, S. Dehnen, P. Sevillano, Polyhedron 25 (2006) 3653.
[30] M. Dennehy, G.P. Tellería, S.H. Tarulli, O.V. Quinzani, S.D. Mandolesi, J.A. Güida, G.A. Echeverría, O.E. Piro, E.E. Castellano, Inorg. Chim. Acta 360 (2007) 3169.
[31] E.S. Raper, Coord. Chem. Rev. 129 (1994) 91.
[32] E.S. Raper, Coord. Chem. Rev. 153 (1996) 199.
[33] J.A. García-Vázquez, J. Romero, A. Souza, Coord. Chem. Rev. 193–195 (1999) 691.
[34] P.D. Akrivos, Coord. Chem. Rev. 210–213 (2001) 181.
[35] P. Aslanidis, S. Divanidis, P.J. Cox, P. Karagiannidis, Polyhedron 24 (2005) 853.
[36] Y. Zhao, M. Hong, Y. Liang, W. Su, R. Cao, Z. Zhou, A. Chan, Polyhedron 20 (2001) 2619.
[37] M. Dennehy, O.V. Quinzani, M. Jennings, J. Mol. Struct. 841 (2007) 110.
[38] M. Dennehy, S.D. Mandolesi, O.V. Quinzani, M. Jennings, Z. Anorg. Allg. Chem. 633 (2007) 2746.
[39] Effendy, F. Marchetti, C. Pettinari, R. Pettinari, M. Ricciutelli, B.W. Skelton, A.H. White, Inorg. Chem. 43 (2004) 2157.
[40] G. Bowmaker, Effendy, K.C. Lim, B.W. Skelton, D. Sukarianingsih, A. White, Inorg. Chim. Acta 358 (2005) 4342.
[41] A.J. Blake, N.R. Champness, P. Hubberstey, W.-S. Li, M.A. Withersby, M. Schröder, Coord. Chem. Rev. 183 (1999) 117.
[42] S.H. Tarulli, O.V. Quinzani, O.E. Piro, E.J. Baran, J. Mol. Struct. 656 (2003) 161.
[43] S.H. Tarulli, O.V. Quinzani, O.E. Piro, E.E. Castellano, E.J. Baran, J. Mol. Struct. 797 (2006) 56.
[44] D.R. Pérez, S.H. Tarulli, O.V. Quinzani, J. Dristas, R. Faccio, L. Suescun, A. Mombrú, Z. Anorg. Allg. Chem. 633 (2007) 1066.
[45] D.Y. Wu, M. Hayashi, Y.J. Shiu, K.K. Liang, C.H. Chang, Y.L. Yeh, S.H. Lin, J. Phys. Chem. A 107 (2003) 9658.
[46] A. Vogel, Textbook of Practical Organic Chemistry, Longman Group Limited, London, 1978.
[47] S. Schibye, R.S. Pedersen, S.O. Lawesson, Bull. Soc. Chim. Belges 87 (1978) 229.
[48] O. Grupče, M. Penavić, G. Jovanovski, J. Chem. Crystallogr. 24 (1994) 581.
[49] C. Lopez, J.P. Fackler, R. Staples, S. Wang, R. Winpenny, Croat. Chem. Acta 68 (1995) 793.
[50] G.M. Sheldrick, SHELXTL-01, Programs for Crystal Structural Analysis, University of Göttingen, Germany, 2001.
[51] M.J. Frisch et al., GAUSSIAN 03, Revision C.02, Gaussian, Inc., Wallingford, CT, 2004.
[52] A.E. Reed, L.A. Curtiss, F. Weinhold, Chem. Rev. 88 (1988) 899.
[53] A. Bondi, J. Phys. Chem. 68 (1964) 441.
[54] R.-L. Sang, L. Xu, Eur. J. Inorg. Chem. (2006) 1260.
[55] K. Nomiya, S. Takahashi, R. Noguchi, J. Chem. Soc., Dalton Trans. (2000) 4369.
[56] J. Onuegbu, R.J. Butcher, C. Hosten, U.C. Udeochu, O. Bakare, Acta Crystallogr., Sect. E 63 (2007) m2309.
[57] M. Dennehy, O.V. Quinzani, S.D. Mandolesi, J.A. Güida, G.A. Echeverría, O.E. Piro, Monatsh. Chem. 138 (2007) 669.
[58] D.Y. Wu, B. Ren, Y.-X. Jiang, X. Xu, Z.-K. Tian, J. Phys. Chem. A 106 (2003) 9042.
[59] M.M. Campos-Vallette, R.E. Clavijo, F. Mendizabal, W. Zamudio, R. Baraona, G. Diaz, Vib. Spectrosc. 12 (1996) 37.
[60] M. Petiau, J. Fabian, J. Mol. Struct., Theochem 538 (2001) 253.
[61] C. Kutal, Coord. Chem. Rev. 99 (1990) 213.
[62] L. Pazderski, J. Tousek, J. Sitkowski, L. Kozerski, R. Marek, E. Szlyk, Magn. Reson. Chem. 45 (2007) 24.
[63] O.V. Quinzani, S.H. Tarulli, C. Marcos, S. García Granda, E.J. Baran, Z. Anorg. Allg. Chem. 625 (1999) 1848.
[64] R.G. Parr, W. Yang, Density Functional Theory of Atoms and Molecules, Oxford University Press, New York, 1988.
[65] J. El-Bahraoni, J. Molina-Molina, D. Portal-Olea, J. Phys. Chem. A 102 (1998) 2443.
[66] N.E. Schultz, Y. Zhao, D.G. Truhlar, J. Phys. Chem. A 109 (2005) 4388.
[67] Unpublished results.

Polyhedron 27 (2008) 2251–2258

Contents lists available at ScienceDirect

Polyhedron

journal homepage: www.elsevier.com/locate/poly

The influence of substituents at the C^2 carbon of thiosemicarbazones on bonding and nuclearity of silver(I) complexes

Tarlok S. Lobana [a,*], Sonia Khanna [a], Geeta Hundal [a], Ben-Jie Liaw [b], Chen W. Liu [b]

[a] Department of Chemistry, Guru Nanak Dev University, Amritsar 143 005, India
[b] Department of Chemistry, National Dong Hwa University, Hualien 974, Taiwan

ARTICLE INFO

Article history:
Received 25 January 2008
Accepted 14 April 2008
Available online 4 June 2008

Keywords:
Silver(I)
Tetrahedral complexes
Thiosemicarbazones
Sulfur-bridged dinuclear complexes

ABSTRACT

Several thiosemicarbazones of the type ($R^1R^2C^2{=}N^3{-}N^2H{-}C(=S)N^1H_2$) were reacted with silver salts, yielding a variety of complexes with different ligand coordination modes, nuclearities and stoichiometries. Reaction of silver(I) chloride with 2-benzoylpyridine thiosemicarbazone, HL^1, has formed a sulfur-bridged dimer, $[Ag_2Cl_2(\mu\text{-}S\text{–}HL^1)_2(PPh_3)_2]$ **2**, while a similar reaction with 2-acetylpyridine thiosemicarbazone, HL^2, has formed a mononuclear complex $\{AgCl(\eta^1\text{-}S\text{–}HL^2)_2(PPh_3)\}$ **1**, with an unusual Ag:ligand:PPh_3 stoichiometry of 1:2:1. Reaction of silver(I) nitrate/acetate with benzophenone thiosemicarbazone, HL^3, and acetone thiosemicarbazone, HL^4, have yielded mononuclear complexes, $[Ag(ONO_2)(\eta^1\text{-}S\text{–}HL^3)(PPh_3)_2]$ **3**, and $[Ag(N^3,S\text{–}HL^4)(PPh_3)_2]X$ (X=NO_3 **4**, CH_3COO **5**). In complexes **1** and **3** and in dimeric complex **2**, the ligands exhibit the usual η^1-S-bonding and μ-S-bridging coordination commonly observed for thiosemicarbazone ligands with tetrahedral coinage metal ions. In complexes **4** and **5**, however, weak binding properties of nitrate or acetate anions to silver favored N^3,S-chelation with the methyl substituents at the C^2 carbon of the thiosemicarbazones.

© 2008 Elsevier Ltd. All rights reserved.

1. Introduction

Thiosemicarbazones, an important class of N–S donor ligands, have displayed variable bonding properties in their complexes and have shown use in a variety of different applications [1–7]. Among coinage metals, copper in its divalent state has been intensively investigated [8,9c], while reports on the chemistry of Cu^I, Ag^I, Au^I are limited [9]. Recently, from our lab, several Cu^I halide complexes of thiosemicarbazones with triphenylphosphine coligands have been reported [10]. In a recent study of Ag^I–thiosemicarbazone complexes, it was observed that thiosemicarbazone ligands with alkyl or aryl rings at the C^2 carbon have formed halogen bridged dimers, $[Ag_2(\mu\text{-}X)_2(Htsc)_2(PPh_3)_2]$ {R^1 = Ph, R^2 = H, X = Br; R^1 = R^2 = Me, X = Br; R^1 = Ph, R^2 = Me, X = Cl, Br, see Chart 1 for substitution patterns of the thiosemicarbazones}, but with five membered rings such as pyrrole or thiophene, only sulfur-bridged dimers $[Ag_2X_2(\mu\text{-}S\text{–}Htsc)_2(PPh_3)_2]$ {R^1 = pyrrole, R^2 = H, X = Br; R^1 = thiophene, R^2 = H, X = Cl} were isolated [11]. For R^1 = pyridine, R^2 = H, only monomer complexes $[AgX(\eta^1\text{-}S\text{–}Htsc)(PPh_3)_2]$ (X = Cl, Br, I) were isolated [11].

The interest into the chemistry of thiosemicarbazone also pertains to their utility in the biosciences as anticancer, antibacterial and antifungal agents and in the analytical field as ion sensors [5–7]. For example, thiosemicarbazone derivatives of copper(II) – especially with pyridyl substituents at the C^2 carbon have proved to be more effective as anticancer or antimicrobial agents than the ligand by itself, probably due to the increased lipophilicity of the complexes as compared to the free ligand alone [8], and the complexes have also shown promising results in vivo. In view of the still limited investigations into the chemistry of silver(I) thiosemicarbazones as described above, we thus intended to investigate the coordination chemistry of particularly pyridyl based thiosemicarbazones with silver(I). In the present paper, we investigate the influence of different combinations of pyridyl, phenyl and methyl substituents at the C^2 carbon of thiosemicarbazones on the bonding patterns and the nuclearity of complexes with silver(I) halides and psuedohalides (Chart 1).

2. Experimental

2.1. Materials and techniques

Silver(I) nitrate, silver(I) acetate, sodium chloride, sodium bromide and triphenylphosphine were procured from Aldrich Chemicals Ltd. and used as received. Silver(I) halides (X = Cl, Br) were freshly prepared by reacting silver(I) nitrate with sodium chloride or bromide in methanol. 2-Benzoylpyridine thiosemicarbazone (HL^1), 2-acetylpyridine thiosemicarbazone (HL^2), benzophenone thiosemicarbazone (HL^3) and acetone thiosemicarbazone (HL^4)

* Corresponding author. Tel.: +91 183 22 57604; fax: +91 183 22 58820.
E-mail address: tarlokslobana@yahoo.co.in (T.S. Lobana).

0277-5387/$ - see front matter © 2008 Elsevier Ltd. All rights reserved.
doi:10.1016/j.poly.2008.04.027

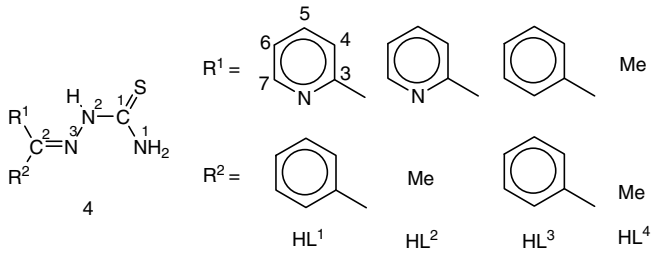

HL[1] = 2-benzoylpyridine thiosemicarbazone
HL[2] = 2-acetylpyridine thiosemicarbazone
HL[3] = benzophenone thiosemicarbazone
HL[4] = acetone thiosemicarbazone

Chart 1.

were prepared using the literature methods [10a,12]. C, H and N analyses were obtained with a Thermoelectron FLASHEA1112 CHNS analyzer. Infrared spectra were recorded from KBr pellets in the range 4000–200 cm^{-1} on a Pye–Unicam SP-3-300 spectrophotometer. Melting points were determined with a electrically heated Gallenkamp apparatus. ^1H NMR were recorded on a JEOL AL-300 FT spectrometer operating at a frequency of 300 MHz using $CDCl_3$ as the solvent with TMS as the internal standard. ^{31}P NMR spectra were recorded on a Bruker ACP-300 spectrometer operating at a frequency of 121.5 MHz with H_3PO_4 as the external standard with $\delta = 0$.

2.2. Synthesis of the complexes

2.2.1. $[AgCl(\eta^1\text{-}S\text{–}HL^2)_2(PPh_3)]$ (**1**)

To AgCl (0.025 g, 0.17 mmol) suspended in acetonitrile (15 mL) was added ligand HL^2 (0.034 g, 0.17 mmol), and stirring was continued for 24 h. To the white solid formed was added solid PPh_3 (0.046 g, 0.17 mmol), which partially cleared the solution. Addition of another mole of PPh_3(0.046 g, 0.17 mmol) resulted in the formation of a clear solution, which was filtered and kept for crystallization. Slow evaporation yielded crystals of $[AgCl(HL^2)_2(PPh_3)]$ (**1**) along with that of the known $[AgCl(PPh_3)]_4$ cubane (50%) which were manually separated (**1** white, 37 %, m.p. 190–192 °C). *Anal.* Calc. for $C_{34}H_{35}AgClN_8PS$: C, 51.38; H, 4.41; N, 14.10. Found: C, 51.66; H, 4.89; N, 14.25%. Main IR peaks (KBr, cm^{-1}): ν(N–H) 3542s, 3427s, 3412m, 3280b (–NH_2–), 3153m (–NH–); ν(C=N) + δNH_2 + ν(C=C) 1585s, 1550s, 1521s; ν(C=S) 770s, 836s; ν(C–N) 1050s; ν(P–C_{Ph}) 1095s. The complex is soluble in $CHCl_3$ and partially in CH_3CN.

2.2.2. $[Ag_2Cl_2(\mu\text{-}S\text{–}HL^1)_2(PPh_3)_2]$ (**2**)

Compound **2** was prepared in a similar fashion as compound **1**. (Yellow, 57 %, m.p. 183–185 °C). *Anal.* Calc. for $C_{62}H_{54}Ag_2Cl_2N_8P_2S_2$: C, 56.20; H, 4.08; N, 8.46. Found: C, 56.60; H, 4.29; N, 8.93%. Main IR peaks (KBr, cm^{-1}): ν(N–H) 3417s, 3217s (–NH_2–); ν(N–H) 3170 cm^{-1}; ν(C=N) + δNH_2 + ν(C=C) 1604s, 1602s, 1477s; ν(C=S) 816s, 895s; ν(C–N) 995s; ν(P–C_{Ph}) 1096s. The complex is soluble in $CHCl_3$ and partially in CH_3CN.

2.2.3. $[Ag(ONO_2)(\eta^1\text{-}S\text{–}HL^3)(PPh_3)_2]$ (**3**)

To $AgNO_3$ (0.025 g, 15 mmol) in CH_3CN (15 mL) was added PPh_3 (0.076 g, 30 mmol) and stirring was continued at a temperature of 50–60 °C for 2 h. The solid ligand HL^3 was added (0.037 g, 15 mmol) to the clear hot solution, and stirring was continued for another 30 min after switching off heating. The resulting clear solution was filtered and kept for crystallization to form light yellow colored crystals. The complex is highly soluble in $CHCl_3$. (Yellow, 69%, m.p. 185–187 °C). *Anal.* Calc. for $C_{50}H_{43}AgN_4O_3P_2S$: C, 63.17; H, 4.53; N, 5.90. Found: C, 63.03; H, 4.64; N, 6.23%. Main IR peaks (KBr, cm^{-1}): ν(N–H) 3458s, 3321s (–NH_2–), 3141m (–NH–); ν(NO) 1434s, 1471s, 1369b; ν(C=N) + δNH_2 + ν(C=C) 1608s, 1565s, 1500s; ν(C=S) 823s (thioamide moiety); ν(C–N) 1184m, 1064s; ν(P–C_{Ph}) 1094s. The complex is soluble in $CHCl_3$ and partially in CH_3CN.

2.2.4. $[Ag(N^3,S\text{–}HL^4)(PPh_3)_2](NO_3)$ (**4**)

To $AgNO_3$ (0.025 g, 0.15 mmol) in CH_3CN (15 mL) was added HL^4 (0.020 g, 15 mmol) and stirring was continued for 2 h. To the white solid formed was added PPh_3 (0.039 g, 0.15 mmol), which partially cleared the solution. Addition of another mole of PPh_3 (0.039 g, 0.15 mmol) resulted in the formation of a clear solution, which was filtered and kept for crystallization. The complex is soluble in $CHCl_3$. (White, 65%, m.p. 154–156 °C). *Anal.* Calc. for $C_{40}H_{39}AgN_4O_3P_2S$: C, 58.14; H, 4.72; N, 6.78. Found: C, 58.42; H, 3.98; N, 6.81% Main IR peaks (KBr, cm^{-1}): ν(N–H) 3375s, 3325m (–NH_2–), 3186m (–NH–); ν(NO) 1359s, 1301b; ν(C=N) + δNH_2 + ν(C=C) 1645b, 1562s; ν(C=S) 823s (thioamide moiety); ν(C–N) 1041s, 1068s; ν(P–C_{Ph}) 1095s. The complex is soluble in $CHCl_3$ and partially in CH_3CN.

2.2.5. $[Ag(N^3,S\text{–}HL^4)(PPh_3)_2](CH_3COO)$ (**5**)

To $Ag(OOCCH_3)$ (0.025 g, 0.15 mmol) in acetone (15 mL) was added HL^4 (0.020 g, 0.15 mmol) and stirring was continued for 2 h. To the white solid formed, was added PPh_3 (0.039 g, 0.15 mmol), which partially cleared the solution. Addition of another mole of PPh_3 (0.039 g, 0.15 mmol) resulted in the formation of a clear solution, which was filtered and kept for crystallization. The complex is soluble in $CHCl_3$. Crystals were grown from an acetone solution at room temperature. (White, 69%, m.p. 150–152 °C). *Anal.* Calc. for $C_{42}H_{42}AgN_3O_2P_2S$: C, 61.26; H, 5.11; N, 5.43. Found: C, 61.62; H, 5.55; N, 5.43%. Main IR bands (KBr, cm^{-1}): ν(N–H) 3285b (–NH_2–), 3130m (–NH–); $\nu(C\text{–}O)_{as}$ 1670b, 1585s; $\nu(C\text{–}O)_{sym}$ 1404b; ν(C=N) + δNH_2 + ν(C=C) 1564s, 1477m; ν(C=S) 837s (thioamide moiety); ν(C–N) 1152s, 997s; ν(P–C_{Ph}) 1093s. The complex is soluble in $CHCl_3$ and CH_3CN.

3. X-ray crystallography

A suitable crystal of complex **1** was mounted on Bruker AXS SMART APEX CCD diffractometer and likewise crystals of **4** and **5** were mounted on a Bruker APEX II diffractometer with graphite monochromatised Mo Kα radiation ($\lambda = 0.71073$ Å). The unit cell dimensions and intensity data were measured at 100(2) K for **1** and at 273(2) K for **4** and **5**. Data were reduced and corrected for absorption using SMART and SAINT (**1**) [13a] or XCAD-49 (**4** and **5**). The structures were solved by direct methods and refined by full matrix least squares based on F^2 with anisotropic thermal parameters for non-hydrogen atoms using SHELXTL (structure solution, refinement and some molecular graphics). All non-hydrogen atoms were refined anisotropically. All hydrogen atoms were placed in calculated positions and were refined with an isotropic displacement parameter 1.5 (methyl) or 1.2 times (all others) that of the adjacent carbon or oxygen atom.

Suitable light yellow crystals of complexes **2** and **3** were mounted on a Siemens P4 diffractometer and data were collected using a scanning mode with graphite monochromatised Mo Kα radiation ($\lambda = 0.71069$ Å). Unit cell dimensions and data were collected at 295(2) K. Cell parameters were refined using 25 reflections in the θ range of 1.70–29.96° using XSCANS [13b]. The data were corrected for Lorentz and polarization effects and a psi-scan absorption correction was also applied. The structures were solved

Table 1
Crystallographic data for complexes **1**–**5**

	1	2	3	4	5
Empirical formula	$C_{34}H_{35}AgClN_8PS$	$C_{62}H_{54}Ag_2Cl_2N_8P_2S_2$	$C_{50}H_{43}AgN_4O_3P_2S$	$C_{40}H_{39}AgN_4O_3P_2S$	$C_{42}H_{42}AgN_3O_2P_2S$
M.wt.	794.11	1323.83	949.75	825.62	822.66
Crystal color	colorless	yellow	pale yellow	colorless	colorless
Crystal system	triclinic	triclinic	triclinic	monoclinic	monoclinic
Space group	$P\bar{1}$	$P\bar{1}$	$P\bar{1}$	$P2_1/c$	$P2_1/c$
a (Å)	8.0367(5)	11.804(2)	9.658(5)	12.9850(7)	13.078(2)
b (Å)	10.7546(7)	12.208(2)	9.938(5)	11.2547(6)	11.407(2)
c (Å)	21.1659(14)	12.969(2)	24.028(5)	26.6850(14)	26.611(5)
V (Å^3)	1780.3(2)	1494.6(4)	2250.4(17)	3870.5(4)	3948.5(12)
α (°)	78.391(1)	116.91(1)	89.430(5)	90	90
β (°)	83.457(1)	92.23(1)	87.890(5)	97.025(2)	95.965(3)
γ (°)	88.772(1)	112.04(1)	77.540(5)	90	90
Z	2	1	2	4	4
D_{calc} (Mg m^{-3})	1.481	1.471	1.402	1.417	1.384
μ(Mo Kα) (mm^{-1})	0.840	0.914	0.612	0.700	0.683
Reflections collected	18428	5451	9454	59092	51544
Unique reflections (R_{int})	8804 (0.0355)	5183 (0.0230)	8491 (0.0460)	9659 (0.0957)	9456 (0.0204)
Final R indices					
[$I \geqslant 2\sigma I$], R_1 and wR_2	0.0427, 0.1013	0.0319, 0.0852	0.0364, 0.0949	0.0450, 0.1057	0.0341, 0.0913

by direct methods and refined by Full-matrix least-squares refinement techniques on F^2 using SIR-92 and SHELXL-97 [13c]. All non-hydrogen atoms were refined anisotropically. All hydrogen atoms were attached geometrically riding on their respective carrier atoms with Uiso being 1.5, 1.2 and 1.2 times the Uiso of their carrier methyl, methylene and aromatic carbon atoms, respectively. Scattering factors from the International Tables for X-ray crystallography were used [13d]. Data reduction, structure solution, refinement and drawing of molecular graphics were performed using SHELXTL-PC [13e] and WINGX [13f]. Table 1 gives crystal data for complexes.

4. Results and discussion

4.1. Synthesis

Several thiosemicarbazones of the type ($R^1R^2C^2$=N–NH–C(=S)N^1H_2) were reacted with a selection of silver salts (see Chart 1 for the substitution patterns of the ligands). Addition of triphenylphosphine to the reaction mixtures yielded a variety of complexes with different ligand coordination modes, nuclearities and stoichiometries. An overview of reaction conditions and products formed is given in Scheme 1.

Silver(I) chloride suspended in acetonitrile slowly reacted with HL^2 (R^1 = py and R^2 = Me) over a period of 24 h and formed white insoluble solid and the addition of two moles of triphenylphosphine completely dissolved the solid. The clear solution on slow evaporation at room temperature yielded crystals of tetrahedral complex [AgCl(HL^2)$_2$(PPh_3)] **1**, with an unusual stoichiometry (Ag:Htsc:PPh_3: 1:2:1) along with crystals of the known cubane complex, [AgCl(PPh_3)]$_4$ [14]. Complex **1** differs from the known tetrahedral monomers such as [AgCl(η^1-S–Hpytsc)(PPh_3)$_2$] **6** (Hpytsc = pyridine-2-carbaldehyde thiosemicarbazone) [11]. Reaction of silver(I) chloride with HL^1ligand (R^1 = py and R^2 = Ph) did not form the similar complex, rather a sulfur-bridged dimer, [Ag_2Cl_2(μ-S–HL^1)$_2$(PPh_3)$_2$] **2** along with the known cubane complex [AgCl(PPh_3)]$_4$ were formed. Thus the formation of **2** is analogous to the more general trend of formation of the sulphur-bridged dimers, [Ag_2X_2(μ-S–Htsc)$_2$(PPh_3)$_2$], {R^1 = pyrrole, R^2 = H, X = Br; R^1 = thiophene, R^2 = H, X = Cl}, reported in the literature [11]. It is pointed

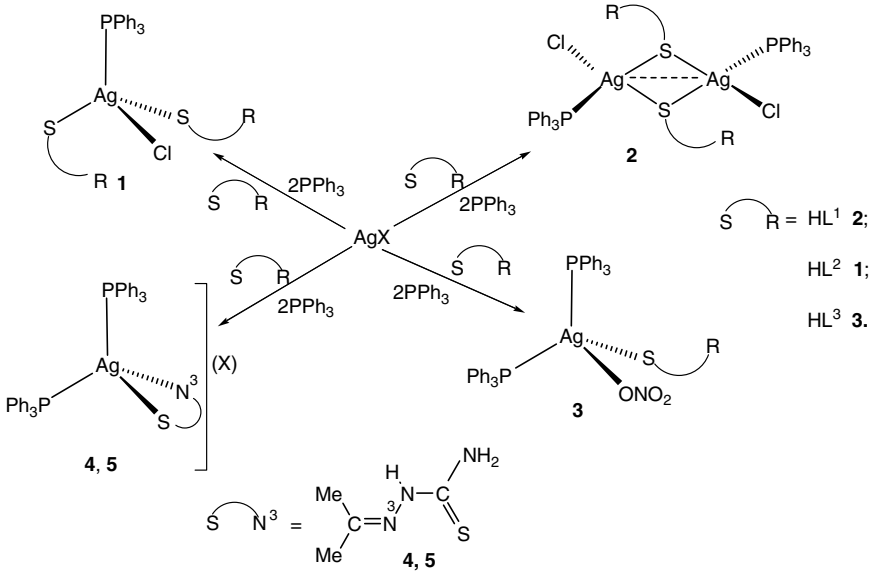

Scheme 1.

out here that only 1:1:2 (Ag:Htsc:PPh_3) molar ratio yielded the crystalline products **1** and **2**, and stoichiometry of these complexes is controlled by the nature of the substituents at C^2 carbon. Thus the substitution of the hydrogen atom at the C^2 carbon by a methyl group (sp3 carbon) was able to prevent the binding of a second PPh_3 ligand to the Ag^I center in case of **1.** Introduction of a similarly bulky phenyl substituent at C^2 also did prevent the addition of two phosphine ligands and no tetrahedral monomeric complex either similar to **1** or **6** was formed, and instead yielded a sulfur-bridged dimer, $[Ag_2Cl_2(\mu\text{-}S\text{–}HL^1)_2(PPh_3)_2]$ **2.** Reaction of HL^1 or HL^2 with silver(I) nitrate/acetate led to decomposition and no product could be identified.

Reaction of silver(I) nitrate or acetate with HL^4 ($R^1 = R^2 = Me$) yielded insoluble solids which were reacted with two moles of phosphine ligands and clear solutions formed on slow evaporation at room temperature yielded $[Ag(N^3,S\text{–}HL^4)(PPh_3)_2](NO_3)$ **4** and $[Ag(N^3,S\text{–}HL^4)(PPh_3)_2](CH_3COO)$ **5**, with an N^3, S-chelation mode (Scheme 1). Similar bonding was also observed in one mononuclear tetrahedral complex, $[Cu(HL^4)_2](Cl)$ [9a]. Thus with the methyl substituents at C^2 carbon and with the weak binding to silver by the nitrate or acetate anions vis-à-vis halide ions, HL^4ligand changes conformation from E-mode to Z-mode for chelation to the metal center.

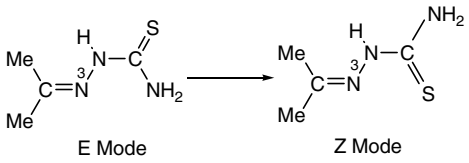

This behaviour of HL^4 is different from that with silver(I) bromide which yielded bromo-bridged dimer $[Ag_2(\mu\text{-}Br)_2(HL^4)_2(PPh_3)_2]$ [11]. Silver(I) nitrate did not react with the ligand HL^3($R^1 = R^2 = Ph$). Thus silver(I) nitrate was first reacted with triphenylphosphine and to the clear solution was added the HL^3 ligand. Slow evaporation of the solution yielded crystals of $[Ag(ONO_2)(\eta^1\text{-}S\text{–}HL^3)(PPh_3)_2]$ **3**. Formation of **3** is analogous to the reaction of copper(I) halides with HL^3, wherein analogous tetrahedral $[CuX(\eta^1\text{-}S\text{–}HL^3)(PPh_3)_2]$ (X = Cl, Br) complexes were obtained [10a]. HL^3 did not react with silver(I) chloride neither directly or nor via reaction of $[AgCl(PPh_3)]_4$ with HL^3. Thus the behaviour of HL^3 and HL^4 is clearly different, and the nature of the substituents (Ph, Ph, **3** versus Me, Me, **4**, **5**) appears to control the final products.

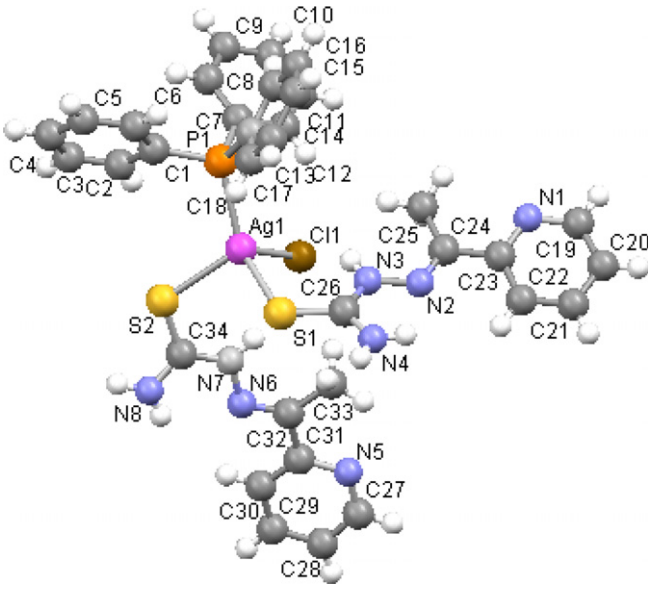

Fig. 1. Molecular structure of complex **1**.

4.2. Structures of complexes

The complexes were analyzed using single crystal X-ray diffraction. Complexes **1** and **2** crystallized in triclinic crystal system while complexes **3**–**5** crystallized in monoclinic system. Complex **2** is dinuclear while other complexes (**1**, **3**–**5**) are mononuclear. Table 2 shows important bond parameters and coordination modes of thiosemicarbazone ligands.

Silver(I) is coordinated by two sulfur atoms, one phosphorus and one chlorine atoms in mononuclear complex $[AgCl(\eta^1\text{-}S\text{–}HL^2)_2(PPh_3)]$ **1**(Fig. 1). The uncommon stoichiometry of this complex results in a slight deviation of both bond angles and distances relative to the commonly known tetrahedral Ag(I) complexes, such

Table 2
A comparison of important bond distances (Å) and bond angles (°) for complexes **1**–**5** with other related complexes

Complex no.	X, (mode)	Ag–S	Ag–X (Ag–P)	P–Ag–P	P–Ag–X	S–Ag–X	P–Ag–S
1	Cl (η^1-S)	2.5330(7), 2.6113(7)	2.6509(7) (2.4178(8))		109.63(2)	101.35(2), 101.01(2)	129.88(3), 112.35(2)
3	O (η^1-S)	2.5627(13)	2.557(3) (2.4689(13), 2.4956(10))	122.86(3)	93.80(8), 108.10(7)	97.62(7)	128.37(4), 100.80(3)
4	N^3 (N^3,S)	2.5723(10)	2.484(3) (2.4416(9), 2.4625(10))	129.95(3)	109.06(8), 111.98(7)	73.31(7)	113.43(3), 104.76(4)
5	N^3 (N^3,S)	2.5618(7)	2.4642(18) (2.4625(7), 2.4800(7))	128.155 (19)	110.88(5), 111.25(5)	74.07(4)	105.40(2), 114.13(2)
6 [11]	Cl (η^1-S)	2.6284(7)	2.6448(7) (2.4409(7), 2.4879(7))	120.03(2)	101.98(2), 109.26(2)	102.72(2)	102.97(2), 117.54(2)
		Ag–S	Ag–X (Ag–P)	Ag–S–Ag, S–Ag–S	P–Ag–X (S–Ag–X)	P–Ag–S	Ag···Ag
2	Cl (μ-S)	2.6772(10) 2.6715(10)	2.4839(10) (2.4318(10))	88.98(3), 91.02(3)	127.16(4), 107.21(4) (104.12(3))	102.48(3) 117.08(3)	3.748(4)
7 [11]	Br, (μ-S)	2.6070(9) 2.6851(9)	2.6857(4) (2.4394(9))	82.96(2), 97.04(2)	113.66(2), 111.31(2) (113.66(2))	114.88(3) 112.60(3)	3.5057(0)
8 [11]	Cl, (μ-S)	2.611(2) 2.876(2)	2.520(2) (2.428(18))	68.33(6), 111.67(6)	124.85(6), 106.53(6) (93.97(3))	113.45(6) 104.36(6)	3.0902(15)

$[AgCl(\eta^1\text{-}S\text{–}Hpytsc)(PPh_3)_2]$ (**6**) (Hpytsc = pyridine-2-carbaldehyde thiosemicarbazone), $[Ag_2Br_2(\mu\text{-}S\text{–}Hptsc)_2(PPh_3)_2]$ (**7**) (Hptsc = pyrrole-2-carbaldehyde thiosemicarbazone), $[Ag_2Cl_2(\mu\text{-}S\text{–}Httsc)_2(PPh_3)_2]$ (**8**) (Httsc = thiophene-2-carbaldehyde thiosemicarbazone) [11].

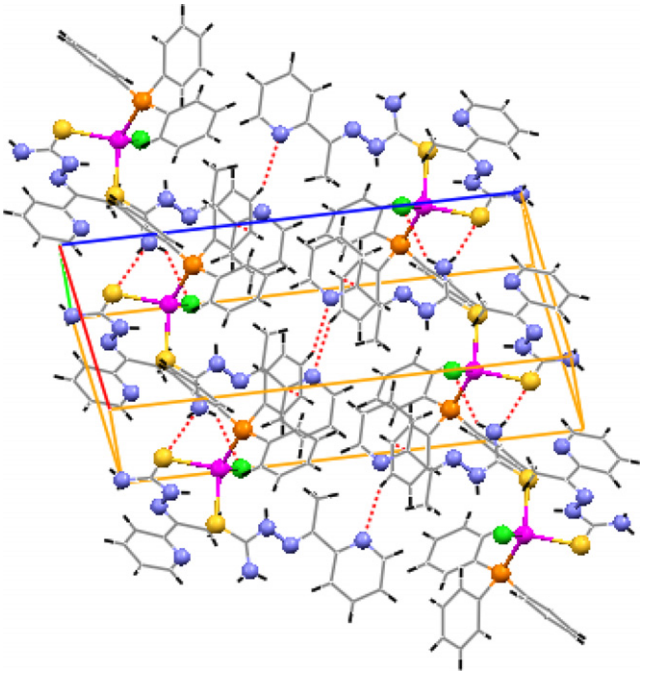

Fig. 2. Packing diagram of complex **1**.

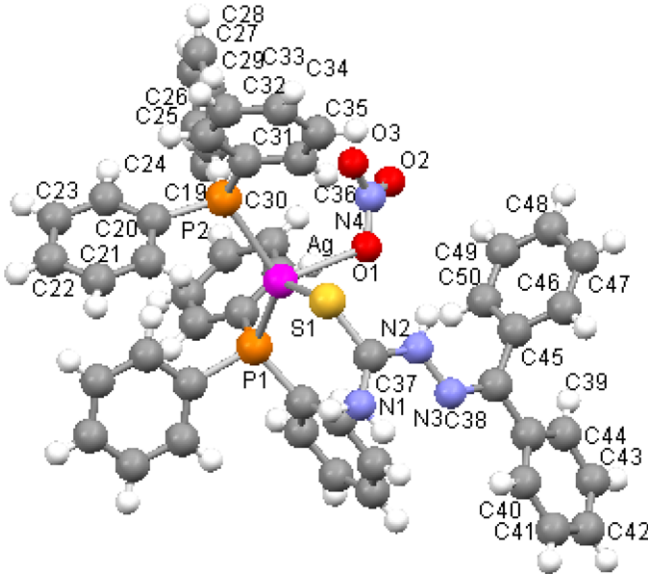

Fig. 3. Molecular structure of complex **3**. (Hydrogen atoms have been omitted for clarity.)

as [AgCl(η^1-S–Hpytsc)(PPh_3)$_2$] **6** (Hpytsc = pyridine-2-carbaldehyde thiosemicarbazone) [11]. The packing of complex **1** shows intermolecular $N^1H\cdots Cl$ and N^1–$H\cdots S$ hydrogen bonds forming 1D polymeric chains, which are further interlinked via intermolecular C–$H_{Ph-P}\cdots N^4_{(py)}$ hydrogen bonds to form a 2D structure (Fig. 2). Molecular structure of complex [Ag(ONO_2)(η^1-S–HL^3)(PPh_3)$_2$] **3** is similar to that of related tetrahedral complex **6**, except for the presence of the O-bonded nitrate group in lieu of the chlorine atom (Fig. 3). The presence of the weakly coordinating nitrate group significantly alter the bond angles and distances of **3** relative to those of **6** [11]. The packing diagram of **3** shows the presence of intermolecular $-HN^1H\cdots O$ type of hydrogen bonds between amino and nitrate groups resulting in a 1D linear chain parallel to the *a* axis. The linear chains are further extended into a 2D network by means of $CH_{Ph}\cdots S$ and $CH_{Ph}\cdots O_{NO3}$ interactions involving phenyl rings of PPh_3 (Figs. 4a and 4b).

The thiosemicarbazone ligand is N^3, S-chelated in complex [Ag(N^3,S–HL^4)(PPh_3)$_2$](NO_3) **4** (Fig. 5). The cation is linked to nitrate via its C–$H_{(methyl)}\cdots O$, N^2-$H\cdots O$ and N^1–$H\cdots O$ hydrogen bonds. Two units of **4** combine via second N^1–$H\cdots O$ hydrogen bonds forming a dimer (Fig. 6). The bonding and packing pattern of [Ag(N^3,S–HL^4)(PPh_3)$_2$](CH_3COO)] **5** is similar to **4**.

Finally the dinuclear complex [Ag_2Cl_2(μ-S–HL^1)$_2$(PPh_3)$_2$] **2** is sulfur bridged and its central $Ag_2(\mu\text{-}S)_2Ag$ core forms a parallelogram. Each silver atom is further coordinated to a terminal chlorine and one P atom of PPh_3 (Fig. 7). The bond parameters and core angles are comparable to other sulfur-bridged dimers reported in the literature (Table 2) [11]. Complex **2** shows the presence of intramolecular $-HN^1H\cdots Cl$ and $N^2H\cdots N^4$ hydrogen bonds and two dimeric molecules are further linked via short $CH\cdots Cl$ contacts involving phenyl rings of PPh_3 resulting in 1D polymeric chain. The chain is extended in 2D via intermolecular $CH\cdots\pi$ interactions (Fig. 8).

5. IR and NMR spectral studies

IR spectroscopy of all complexes confirmed the presence of the individual ligands and counterions via their ν(N–H), ν(C–N), ν(C=C), ν(C=N), and ν(N–O), ν(P–C) vibrational modes. The ν(C=S) thioamide bands are located at 770–837 cm^{-1}, which suggests (in agreement with the X-ray data) a significant weakening of the C=S double bond in all complexes. The ^{1}H NMR spectra of complexes **1**–**4** reveal the presence of -N^2H, -N^1H_2, methyl and ring proton signals generally at low field relative to their corresponding free ligands (Table 3). The ^{31}P NMR spectra of tetrahedral complexes**1**, **3**–**5** showed coordination shifts ($\delta_{complex} - \delta_{ligand}$) comparable to the literature reports on tetrahedral silver(I)–thiosemicarbazone complexes [11]. An additional band at δ 30.81 ppm in **3** reveals the formation of another species, probably a sulfur-bridged dimer in the solution state.

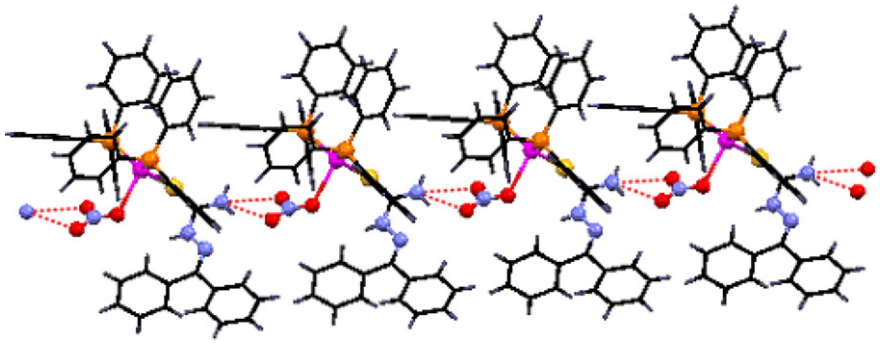

Fig. 4a. Formation of a 1D linear chain due to amine N1 and NO_3^- hydrogen bonding interactions parallel to *a* axis.

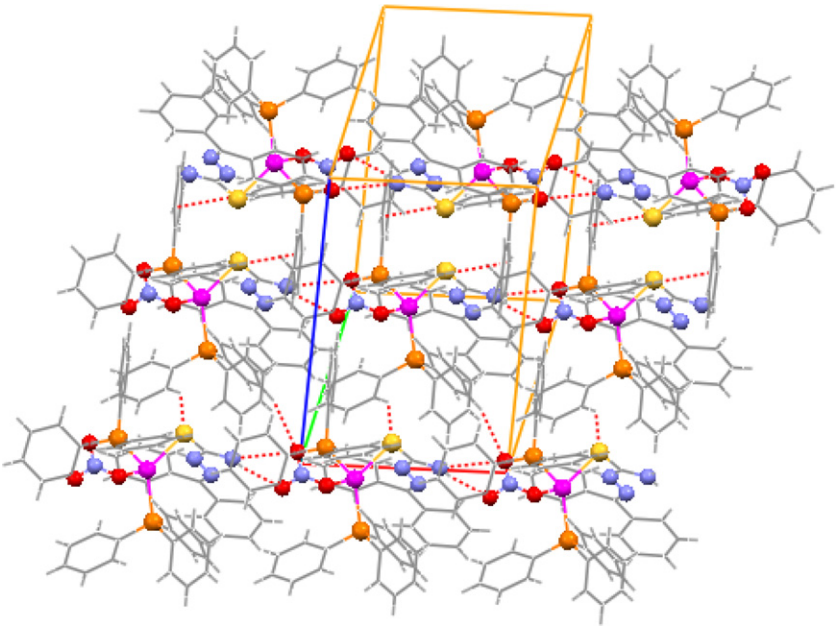

Fig. 4b. Formation of a 2D network in the *ab* plane of complex **3**.

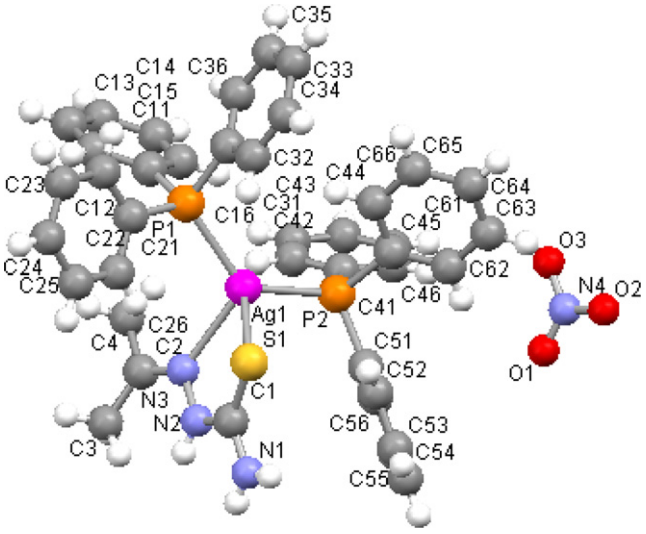

Fig. 5. Molecular structure of complex **4** (complex **5** has a similar structure).

6. Conclusion

The substituents at C^2 carbon appear to control the stoichiometry, nuclearity and dentacy of thiosemicarbazone complexes of silver(I) salts. For R^1 = pyridyl and R^2 = H, only tetrahedral monomers, $[AgCl(\eta^1\text{-S–Hpytsc})(PPh_3)_2]$ (X = Cl **6**) were formed [11]. The substitution of the hydrogen atom at the C^2 carbon by a methyl group (sp^3 carbon) (R^1 = pyridyl and R^2 = Me) was able to prevent the binding of a second PPh_3 ligand to the Ag^Icenter in case of **1** and formed complex $[AgCl(HL^2)_2(PPh_3)]$ **1**, with an unusual stoichiometry (1:2:1: Ag:Htsc:PPh_3). Introduction of a similarily bulky phenyl substituent at C^2 also did prevent the addition of two phosphine ligands, and presumably formed three coordinate species, $\{AgCl(HL^1)(PPh_3)\}$ which dimerised to yield a sulfur-bridged dinuclear complex, $[Ag_2Cl_2(\mu\text{-S–}HL^1)_2(PPh_3)_2]$ **2**, and no tetrahedral monomeric complex either similar to **1** or **6** was formed. The presence of both the methyl groups at C^2 carbon ($R^1 = R^2$ = Me, HL^4) favored N^3, S-chelation in **4** and **5**, and this property of HL^4 is supported by chelation in $[Cu(HL^4)_2]Cl$ reported in the literature [9a]. Also when the anion is more tightly bonded to the metal cen-

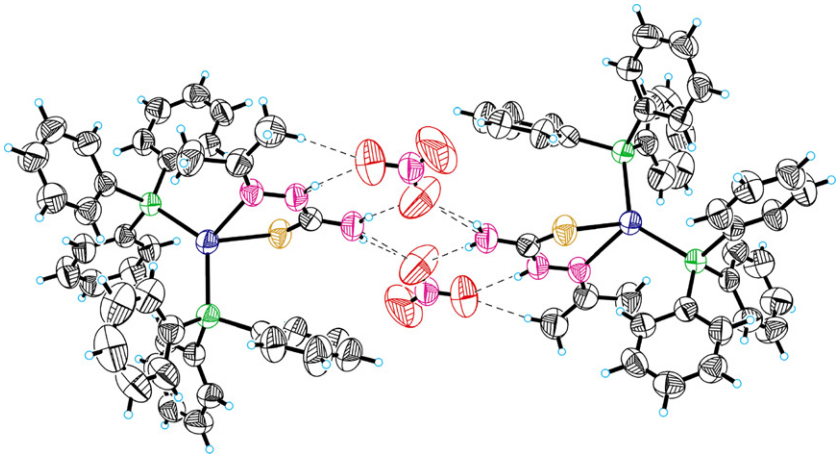

Fig. 6. Packing diagram of complex **4**.

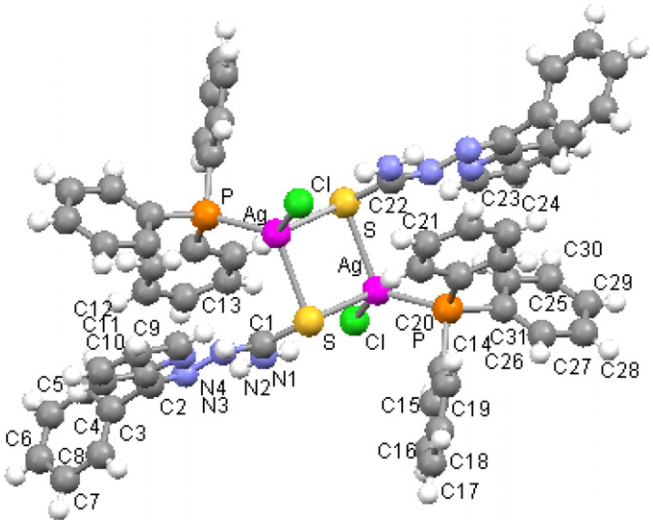

Fig. 7. Molecular structure of complex **2**.

ter as in silver(I) bromide, this ligand yielded a bromo-bridged dimer, $[Ag_2(\mu\text{-}Br)_2(\eta^1\text{-}S\text{–}HL^4)_2(PPh_3)_2]$ [11]. With both phenyl groups at C^2 carbon ($R^1 = R^2 =$ Ph, HL^3), only tetrahedral complexes of more common stoichiometry, $[Ag(ONO_2)(\eta^1\text{-}S\text{–}HL^3)(PPh_3)_2]$ **3** or $[CuCl(\eta^1\text{-}S\text{–}HL^3)(PPh_3)_2]$ [10a] are formed.

In short stoichiometry, dentacy and nuclearity of coinage metal complexes with thiosemicarbazones is influenced by the substituents at C^2 carbon, and also by the nature of the anion/metal. The chelation by neutral thiosemicarbazones is limited and apart from three examples discussed in this paper, there are only two more examples of chelation by neutral thiosemicarbazones [11,15].

Acknowledgements

Financial assistance from CSIR, New Delhi (F.No.9/254(159)/2005-EMR-I) and research facilities to one of us (Sonia) by the university are gratefully acknowledged. The authors thank Matthias Zeller of Youngstown State University, USA for his useful suggestions and in X-ray crystallography.

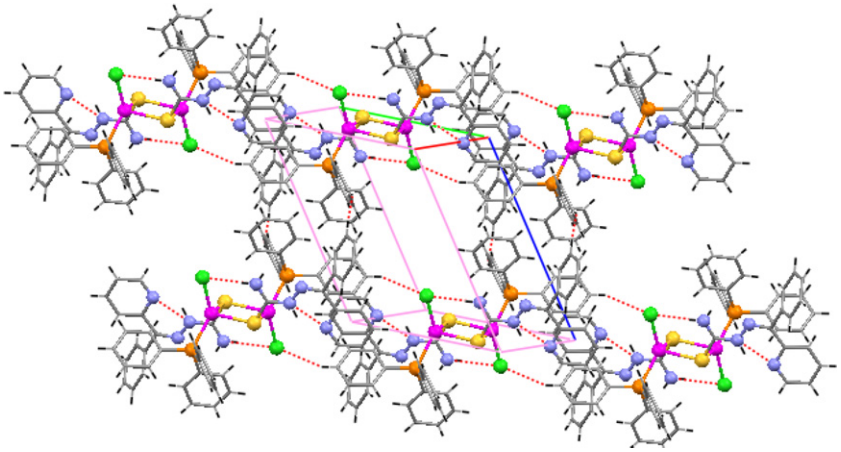

Fig. 8. Packing diagram of complex **2**.

Table 3
NMR data (δ, ppm) for complexes **1**–**5**

Compound	^{1}H NMR				^{31}P ($\Delta\delta$)
	$-N^2H$	$-N^1H_2$	CH_3	Ligand protons	
$[AgCl(\eta^1\text{-}S\text{–}HL^2)_2(PPh_3)]$ **1**	14.79b	9.24b	2.49s, 2.14s	8.76d, 8.61d (C^7H); 7.57d, 7.95d (C^4H); 7.72–7.75m ($C^{5,6}H$); 7.30–7.44m (Ph + N^1H_2)	6.55 (11.2)
$[Ag_2Cl_2(\mu\text{-}S\text{–}HL^1)_2(PPh_3)_2]$ **2**	14.07s	9.52s, 7.67b,		8.83d (C^7H); 7.81td (C^6H); 7.30–7.61m (Ph + $C^{4,5}H$)	11.21 (15.9)
$[Ag(ONO_2)(\eta^1\text{-}S\text{–}HL^3)(PPh_3)_2]$ **3**	9.20s	8.55sb		7.27–7.70m (Ph + N^1H_2)	30.81 (35.51) 2.74 (7.44)
$[Ag(N^3,S\text{–}HL^4)(PPh_3)_2](NO_3)$ **4**	11.64s		1.98s, 1.91s	7.25–7.43m (Ph + N^1H_2)	8.8 (13.5)
$[Ag(N^3,S\text{–}HL^4)(PPh_3)_2](CH_3COO)$ **5**[a]			2.17s, 2.01s	7.27–7.70m (Ph + N^1H_2)	7.3 (12.0)
HL^1	13.86s	8.56s		8.23d (C^7H); 7.77td (C^6H); 7.30–7.56m (N^1H_2 + Ph + C^5H); 7.31d (C^4H)	
HL^2	14.7s	8.86sb	2.44s, 2.40s	8.77d, 8.62d (C^7H); 7.97d, 7.54d (C^4H); 7.55–7.92m (N^1H_2 + $C^{5,6}H$)	
HL^3	8.68s	7.81s, 7.45s		7.27–7.61m (Ph)	
HL^4	8.44s	7.27s, 6.19sb	2.02s, 1.91s		

[a] It did not show this $-N^2H$ signal probably due to its exchange with the acetate anion in solution.

Appendix A. Supplementary data

CCDC 673439, 666768, 658221, 673440 and 673441 contain the supplementary crystallographic data for **1**, **2**, **3** and **4**. These data can be obtained free of charge via http://www.ccdc.cam.ac.uk/conts/retrieving.html, or from the Cambridge Crystallographic Data Centre, 12 Union Road, Cambridge CB2 1EZ, UK; fax: (+44) 1223-336-033; or e-mail: deposit@ccdc.cam.ac.uk. See supplementary for bond parameters, X-ray figures and packing diagrams of various complexes. Supplementary data associated with this article can be found, in the online version, at doi:10.1016/j.poly.2008.04.027.

References

[1] (a) D.X. West, S.B. Padhye, P.B. Sonaware, Struct. Bond. (Berlin) 76 (1991) 4;
(b) J.-M. Yang, W.-M. Ma, B.-H. Chen, G.-S. Huang, Y.-X. Ma, Acta Crystallogr., Sect. E 60 (2004) m852;
(c) D.X. West, A.E. Liberta, S.B. Padhye, R.C. Chilate, P.B. Sonaware, A.S. Kumbhar, R.G. Yerande, Coord. Chem. Rev. 123 (1993) 49;
(d) J.S. Casas, M.S. Garcia-Tasende, J. Sordo, Coord. Chem. Rev. 209 (2000) 197.

[2] (a) D. Kovala-Demertzi, M.A. Demertzis, J.R. Miller, C.S. Prampton, J.P. Jasinski, D.X. West, J. Inorg. Biochem. 92 (2002) 137;
(b) P.N. Yadav, M.A. Demertzis, D. Kovala-Demertzi, S. Skoulika, D.X. West, Inorg. Chim. Acta 349 (2003) 30;
(c) G.F. de Sousa, V.M. Deflon, E. Niquet, J. Mol. Struct. 587 (2004) 17;
(d) T.S. Lobana, A. Sanchez, J.S. Casas, A. Castineiras, J. Sordo, M.S. Garcia-Tasende, Polyhedron 17 (1998) 3701.

[3] (a) R. Carballo, A. Castineiras, T. Perez, Z. Naturforsch., B. 56 (2001) 881;
(b) R. Carballo, J.S. Casas, E. Garcia-Martinez, G.P. Gabian, A. Sanchez, J. Sordo, E.M. Vazquez-Lopez, J.C. Garcia-Monteagudo, J.C.U. Abram, J. Organomet. Chem. 658 (2002) 1;
(c) J.S. Casas, M.V. Castano, A. Sanchez, J. Sordo, Polyhedron 21 (2002) 1651.

[4] (a) I. Paul, F. Basuli, T.C.W. Mak, S. Bhattacharya, Angew. Chem., Int. Ed. 40 (2001) 2923;
(b) D. Kovala- Demertzi, M.A. Demertzis, J.R. Miller, C.S. Prampton, J.P. Jasinski, D.X. West, J. Inorg. Biochem. 92 (2002) 137.

[5] (a) M.B. Ferrari, G.G. Fava, G. Pelosi, P. Tarasconi, Polyhedron 19 (2000) 1895;
(b) D.X. West, Y. Yang, T.L. Klein, K.I. Goldberg, A.E. Liberta, J. Valdes-Martinez, R.A. Toscano, Polyhedron 14 (1995) 1681.

[6] (a) J. Garcia-Tojal, A. Garcia-Orad, J.L. Serra, J.L. Pizarro, L. Lezama, M.I. Arriourtua, T. Rojo, J. Inorg. Biochem. 78 (1999) 45;
(b) A. Perez-Robolledo, J.D. Ayala, G.M. de Lema, N. Marchini, G. Bombieri, C.L. Zani, E.M. Souza-Fagundes, H. Beraldo, Eur. J. Med. Chem. 40 (2005) 467;
(c) M.B. Ferrari, F. Bisceglie, G.G. Fava, G. Pelosi, P. Tarasconi, R. Albertini, S. Pinelli, J. Inorg. Biochem. 89 (2002) 36.

[7] (a) M.B. Ferrari, G.G. Fava, P. Tarasconi, R. Albertini, S. Pinelli, R. Starcich, J. Inorg. Biochem. 53 (1994) 13;
(b) M.B. Ferrari, F. Bisceglie, C. Casoli, S. Durot, I. Morgenstern-Badarau, G. Pelosi, E. Pilotti, S. Pinelli, P. Tarasconi, J. Med. Chem. 48 (2005) 1671;
(c) A.D. Naik, P.A.N. Reddy, M. Nethaji, A.R. Chakravarty, Inorg. Chim. Acta 349 (2003) 149.

[8] (a) D.X. West, S.B. Padhye, P.B. Sonaware, Struct. Bond. (Berlin) 76 (1991) 4;
(b) D.X. West, A.E. Liberta, S.B. Padhye, R.C. Chilate, P.B. Sonaware, A.S. Kumbhar, R.G. Yerande, Coord. Chem. Rev. 123 (1993) 49;
(c) D.X. West, J.S. Ives, J. Krejci, M.M. Salberg, T.L. Zumbahlen, G.A. Bain, A.E. Liberta, J. Valdes-Martinez, S. Hernadez-Ortiz, R.A. Toscano, Polyhedron 14 (1995) 2189;
(d) M. Joseph, M. Kuriakose, M.R.P. Kurup, E. Suresh, A. Kishore, S.G. Bhat, Polyhedron 25 (2006) 61;
(e) M.A. Ali, A.H. Mirza, A.M.S. Hossssian, M. Nazimuddin, Polyhedron 20 (2001) 1045.

[9] (a) S. Lhuachan, S. Siripaisarnpipat, N. Chaichat, Eur. J. Inorg. Chem. (2003) 263;
(b) L.A. Ashfield, A.R. Cowley, J.R. Dilworth, P.S. Donnely, Inorg. Chem. 43 (2004) 4121;
(c) T.S. Lobana, Rekha, R.J. Butcher, Transition Met. Chem. 29 (2004) 291. and references therein.

[10] (a) T.S. Lobana, S. Khanna, R.J. Butcher, A.D. Hunter, M. Zeller, Polyhedron 25 (2006) 2755;
(b) T.S. Lobana, Rekha, R.J. Butcher, A. Castineiras, E. Bermejo, P.V. Bharatam, Inorg. Chem. 45 (2006) 1535;
(c) T.S. Lobana, S. Khanna, R.J. Butcher, A.D. Hunter, M. Zeller, Inorg. Chem. 46 (2007) 5826;
(d) T.S. Lobana, S. Khanna, R.J. Butcher, Z. Anorg. Allg. Chem. 633 (2007) 1820;
(e) T.S. Lobana, Rekha, B.S. Sidhu, A. Castineiras, E. Bermejo, T. Nishioka, J. Coord. Chem. 58 (2005) 803.

[11] T.S. Lobana, S. Khanna, R. Sharma, G. Hundal, R. Sultana, M. Chaudhary, R.J. Butcher, A. Castineiras, Cryst. Growth Des. 8 (2008) 1203.

[12] T.S. Lobana, A. Sanchez, J.S. Casas, A. Castineiras, J. Sordo, M.S. Garcia-Tasende, E.M. Vazquez-Lopez, J. Chem. Soc., Dalton Trans. (1997) 4289.

[13] (a) Bruker, SMART, SAINT and XREP, Area Detector Control, and Data Integration and Reduction Software, Bruker Analytical X-ray Instruments, Inc., Madison, Wisconsin, USA, 1995.;
(b) XSCANS, Siemens Analytical X-ray Instruments Inc., Madison, WI, USA, 1994.;
(c) G.M. Sheldrick, SHELXL-97, Program for Refinement of Crystal Structures, University of Gottingen, Gottingen, Germany, 1997;
(d) International Tables for X-ray Crystallography, vol. C, Kluwer, Dordrecht, The Netherlands, 1995;
(e) G.M. Sheldrick, SHELXTL-PC, Release 5.03, Siemens Analytical X-ray Instruments Inc., Madison, WI, USA, 1995;
(f) G.X. Win, L.J.J. Farrugia, Appl. Crystallogr. 32 (1999) 837.

[14] B.-K. Teo, J.C. Calabrese, Inorg. Chem. 15 (1976) 2467.

[15] Tarlok S. Lobana, Poonam Kumari, Ray J. Butcher, Inorg. Chem. Commun. 11 (2008) 11.

Polyhedron 27 (2008) 2259–2264

Contents lists available at ScienceDirect

Polyhedron

journal homepage: www.elsevier.com/locate/poly

Displacement of neutral nitrogen donors by chloride in $[Pt(SNS)(R\text{-}py)](ClO_4)_2$ (SNS = 2,6-bis(methylthiomethyl)pyridine; R-py = pyridines): A reactivity comparison between *meta*- and *para*-substituted pyridines

Bruno Pitteri *, Marco Bortoluzzi

Dipartimento di Chimica, Università Cà Foscari di Venezia, Calle Larga S. Marta 2137, 30123 Venezia, Italy

ARTICLE INFO

Article history:
Received 28 March 2008
Accepted 15 April 2008
Available online 2 June 2008

Keywords:
Platinum
Kinetics
Pyridines
Reaction mechanisms
Chelate ligands

ABSTRACT

The kinetics of the process $[Pt(SNS)(R\text{-}py)]^{2+} + Cl^- \rightarrow [Pt(SNS)Cl]^+ + R\text{-}py$ {SNS = 2,6-bis(methylsulfanylmethyl)pyridine; R-py = *meta*- or *para*-substituted pyridines covering a wide range of basicity} were studied in methanol at 25 °C. The reactions obey the usual two-term rate law observed in the substitution reactions of square-planar d^8 complexes. The plots of $\log k_2$ {k_2 = second-order rate constants} against the pK_a of the heterocycles conjugate acids highlighted a different sensitivity of the two groups of N-donors to changes in basicity, the*para*-substituted pyridines (4R-py) showing a weaker dependence on pK_a than the *meta*-substituted (3R-py). The results have been explained on the basis of a π-acidity difference between 3R-py and 4R-py which influences the reaction ground state.

© 2008 Elsevier Ltd. All rights reserved.

1. Introduction

In several studies regarding the relationship between the basicity of N-donor heterocycles such as pyridines, thiazoles, imidazoles and oxazoles and their nucleophilic behavior towards planar tetra-coordinated Pt(II) complexes we reported kinetic and equilibrium data concerning the reversible displacement of chloride from some Pt(II) derivatives containing polydentate ligands, e.g., $[Pt(SS)Cl_2]$ [1], $[Pt(SNS)Cl]^+$ [2,3], $[Pt(NSN)Cl]^+$ [4], $[Pt(terpy)Cl]^+$ [5,6], $[Pt(NN)Cl_2]$ [7], $[Pt(bpma)Cl]^+$ [8] {SS = 1,2-bis(phenylsulfanyl)ethane; SNS = 2,6-bis(methylsulfanylmethyl)pyridine; NSN = bis(2-pyridylmethyl)sulfide; terpy = 2,2′:6′,2″-terpyridine; NN = biacethylbis(*N*-methyl-*N*-phenyl)oxazone, bpma = bis(2-pyridylmethyl)amine}. In all the cases, the substitution reactions take place with an associative mechanism, where the rate constants for the forward and reverse reactions obey the general relationship $k_{obs} = k_1 + k_2[\text{nucleophile}]$, which is usual for nucleophilic substitution on planar four-coordinate d^8 metal complexes [9]. The k_1 term is the first-order rate constant for the nucleophilic attack on the substrate by the solvent, whereas k_2 is the second-order rate constant for the nucleophilic attack on the substrate by the nucleophile.

The k_2 constants are remarkably influenced by the nature of the considered nitrogen donors and in both the forward and reverse reactions a linear free-energy relationship, $\log k_2 = \alpha pK_a + \text{constant}$, exists between the rate constant and the basicity of the ligands, represented by the pK_a values of their conjugate acids. Steric retardation is always observed for heterocycles containing one or two *ortho* groups (usually called hindered bases in these types of reactions) and these effects are in many cases about additive. Moreover, it was observed that the reactivity of the N-donors not only depends upon their basicity, but also upon the ligand nature in the order six-membered heterocycles > five-membered heterocycles and this different behavior was mainly attributed to different interactions of the two groups of ligands with the metal fragment in the ground state.

In some of the previously cited kinetic studies [5,8] *meta*-substituted pyridines (3R-py) were also considered and their reactivity appeared similar to that of *para*-substituted pyridines (4R-py), but during our last work on square-planar d^8 metal complexes, regarding the reaction $AuCl_3(R\text{-}py) + Cl^- \rightarrow AuCl_4^- + R\text{-}py$ {R-py = 3R-py and 4R-py}, we found kinetic data not completely comparable for the two groups of pyridines[10], the *meta*-substituted resulting slightly less reactive than the *para*-substituted of comparable pK_a. In order to determine if this difference in reactivity also exists in Pt(II) complexes, the kinetics of displacement of *meta*- and *para*-substituted pyridines by chloride from $[Pt(SNS)(R\text{-}py)]^{2+}$ substrates in methanol are here reported.

* Corresponding author. Tel.: +39 412348558; fax: +39 412348517.
E-mail address: pitteri@unive.it (B. Pitteri).

0277-5387/$ - see front matter © 2008 Elsevier Ltd. All rights reserved.
doi:10.1016/j.poly.2008.04.031

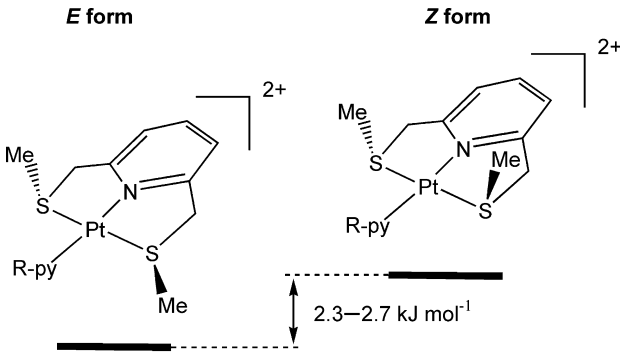

Fig. 1. $[Pt(SNS)(R\text{-}py)](ClO_4)_2$ *entgegen* (*E*) and *zusammen* (*Z*) forms.

2. Results and discussion

2.1. Synthesis and characterization of the complexes

All the complexes $[Pt(SNS)(R\text{-}py)](ClO_4)_2$ {SNS = 2,6-bis(methylsulfanylmethyl)pyridine; R-py = 4-methoxypyridine (4-MeO-py), 4-chloropyridine (4-Cl-py), pyridine (py), 4-methylpyridine (4-Me-py), 4-aminopyridine (4-NH_2-py), 3-methoxypyridine (3-MeO-py), 3-methylpyridine (3-Me-py), 3-chloropyridine (3-Cl-py), 3-iodopyridine (3-I-py), 3-fluoropyridine (3-F-py), 3-phenylpyridine (3-Ph-py), 3-hydroxymethylpyridine (3-CH_2OH-py)} were obtained in pure form following the same reaction pathway, i.e., by reacting the chloro-precursor $[Pt(SNS)Cl](ClO_4)$ [11] with a stoichiometric amount of the appropriate N-donor heterocycle in hot water and subsequently adding an excess of lithium perchlorate as precipitating agent.

Elemental analyses (C, H, N) of the synthesized products are in good agreement with the proposed formulations. All the complexes are soluble in polar organic solvents such as dimethylformamide, where they behave as 2:1 electrolytes [12]. As already reported for $[Pt(SNS)(py)](ClO_4)_2$ [13], ^1H NMR spectra show that all the $[Pt(SNS)(R\text{-}py)](ClO_4)_2$ complexes exist in solution in two chemically non-equivalent isomeric forms depending on the relative position of the S-bonded methyl groups respect to the coordinating plane (see Section 3, Table 4 for NMR characterizations details). In particular, the two S–CH_3 can mutually be in *entgegen* (*E* form) or *zusammen* (*Z* form) position, as depicted in Fig. 1. The *E* isomer is a mixture of two chemically and magnetically equivalent enantiomers.

The Pt–S bonds are strongly enough to make the interconversion process slow on NMR timescale at room temperature, therefore the *E* and *Z* forms of $[Pt(SNS)(R\text{-}py)](ClO_4)_2$ can be easily observed in the ^1H NMR spectra. The *E*/*Z* ratio, determined from NMR signals integration, is about 2.5–3/1, corresponding to a Gibbs energy difference between the *Z* and the *E* forms in the range 2.3–2.7 kJ mol^{-1}. As example, in Fig. 2 are reported the sulfur-bonded methyl signals of the two chemically non-equivalent forms of $[Pt(SNS)(py)](ClO_4)_2$.

2.2. Substitution reactions

When a solution of the $[Pt(SNS)(R\text{-}py)](ClO_4)_2$ substrate was allowed to react with an appropriate excess of chloride in methanol, repetitive scanning of the spectrum in the region 220–380 nm showed that the reaction evolves with time in a first-order fashion leading to the substitution of the neutral base by a chloride ion. The presence of well maintained isosbestic points and the comparison of the final spectrum with that of original samples of the substitution products at the same concentration clearly indicate a single reaction stage. Even if, as described above, the $[Pt(SNS)(R\text{-}py)](ClO_4)_2$ derivatives exist in two isomeric forms, all kinetic runs are strictly monoexponential and subsequent changes have never been observed. This probably means that the equilibrium ratio of the *E* and *Z* forms is maintained throughout the substitution reactions and the interconversion is fast relative to the substitution rate, therefore what is measured is a weighted average of the reactivity of the two forms.

The kinetics were studied at constant ionic strength (I = 0.1 mol dm^{-3}, $[NBu^n_4]ClO_4$), primary salt effects being present in a reaction involving charged reagents. The reactions were studied in the presence of 0.01 mol dm^{-3} $HClO_4$. Preliminary experiments showed that, at constant chloride concentration, the rate of reaction was not dependent on the concentration of acid over the range 0.002–0.02 mol dm^{-3}. The acid serves to protonate the released N-donor ligand and force the reaction to completion.

For a better comparison of a possible reactivity difference between *meta*- and *para*-substituted pyridines we have again exam-

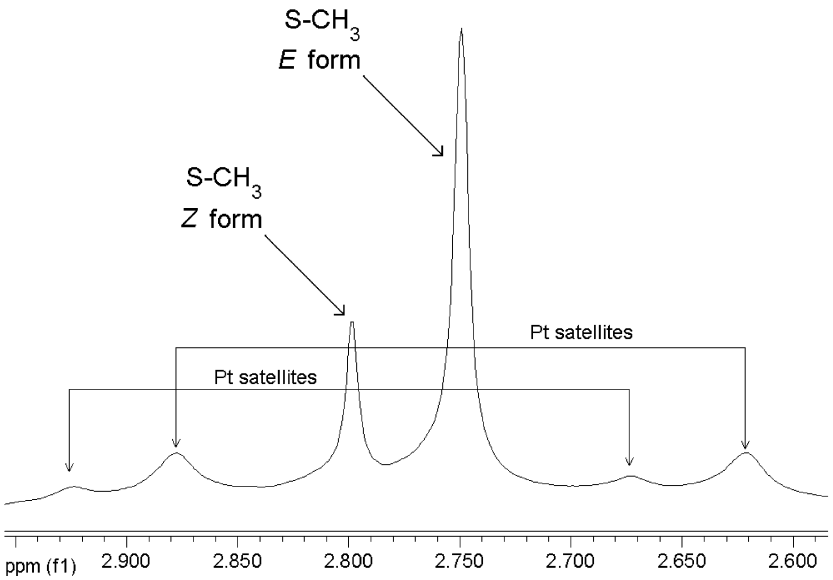

Fig. 2. Sulfur-bonded methyl groups ^1H NMR signals of $[Pt(SNS)(py)](ClO_4)_2$.

Table 1
First order rate constants, k_{obs}, for the reaction $[Pt(SNS)(R\text{-}py)]^{2+} + Cl^- \rightarrow [Pt(SNS)Cl]^+ + R\text{-}py$ in methanol at 25 °C; I = 0.1 mol dm^{-3}, $[NBu^n_4]ClO_4$, 0.01 mol dm^{-3} $HClO_4$

R-py	[Cl]/mol dm^{-3}	$10^3 k_{obs}$/s^{-1}	R-py	[Cl$^-$]/mol dm^{-3}	$10^3 k_{obs}$/s^{-1}
4-Me-py	0.005	0.065 ± 0.003	3-MeO-py	0.005	0.105 ± 0.002
	0.01	0.129 ± 0.004		0.01	0.247 ± 0.007
	0.02	0.259 ± 0.002		0.02	0.451 ± 0.009
	0.03	0.381 ± 0.004		0.03	0.712 ± 0.004
	0.04	0.521 ± 0.004		0.04	0.913 ± 0.002
	0.05	0.642 ± 0.001		0.05	1.173 ± 0.003
4-MeO-py	0.005	0.043 ± 0.002	3-I-py	0.005	0.876 ± 0.001
	0.01	0.089 ± 0.006		0.01	1.681 ± 0.002
	0.02	0.174 ± 0.003		0.02	3.324 ± 0.007
	0.03	0.262 ± 0.003		0.03	5.336 ± 0.006
	0.04	0.360 ± 0.001		0.04	6.848 ± 0.002
	0.05	0.432 ± 0.007		0.05	8.760 ± 0.004
4-Cl-py	0.005	0.531 ± 0.008	3-Ph-py	0.005	0.143 ± 0.004
	0.01	1.186 ± 0.003		0.01	0.258 ± 0.006
	0.02	2.103 ± 0.004		0.02	0.517 ± 0.001
	0.03	3.404 ± 0.002		0.03	0.815 ± 0.005
	0.04	4.306 ± 0.006		0.04	1.083 ± 0.008
	0.05	5.607 ± 0.009		0.05	1.341 ± 0.003
py	0.005	0.121 ± 0.006	3-F-py	0.005	1.094 ± 0.003
	0.01	0.243 ± 0.004		0.01	2.258 ± 0.006
	0.02	0.518 ± 0.002		0.02	4.257 ± 0.002
	0.03	0.755 ± 0.006		0.03	6.785 ± 0.002
	0.04	0.977 ± 0.009		0.04	8.903 ± 0.007
	0.05	1.286 ± 0.003		0.05	12.025 ± 0.004
4-NH_2-py	0.03	0.018 ± 0.003	3-Me-py	0.005	0.055 ± 0.007
	0.07	0.047 ± 0.003		0.01	0.108 ± 0.003
	0.1	0.064 ± 0.003		0.02	0.236 ± 0.002
				0.03	0.349 ± 0.009
3-Cl-py	0.005	1.212 ± 0.002		0.04	0.442 ± 0.004
	0.01	2.404 ± 0.007		0.05	0.576 ± 0.005
	0.02	4.807 ± 0.004			
	0.03	7.711 ± 0.004	3-CH_2OH-py	0.005	0.099 ± 0.004
	0.04	10.016 ± 0.005		0.01	0.190 ± 0.005
	0.05	12.820 ± 0.007		0.02	0.374 ± 0.004
				0.03	0.612 ± 0.009
				0.04	0.772 ± 0.001
				0.05	0.998 ± 0.006

The indicated errors were obtained from the non linear least-squares fit of experimental data to $D_t = D_\infty + (D_0 - D_\infty)\exp(-k_{obs}t)$ {D_0 = absorbance after mixing the reactants, D_∞ = absorbance at completion of reaction}.

ined some of the reactions in Ref. [2], in the same experimental conditions, increasing the number of N-donors. The rate constants were determined in the usual way from the change in absorbance as a function of time at a convenient wavelength (260 nm) and the observed rate constants, k_{obs}, collected in Table 1, obey the general relationship $k_{obs} = k_1 + k_2[Cl^-]$ [9], which is usual for nucleophilic substitutions on square-planar platinum complexes. The k_1 terms, referring to the pathway in which the rate determining step is the nucleophilic attack of the solvent, followed by the rapid entry of chloride into the solvento complex [14], are usually quite small and give a negligible contribution to the whole process. The k_2 terms are the second-order rate constants for the direct attack of Cl^- at the substrate and are summarized in Table 2 together with the pK_a values of the heterocycles conjugated acids $[H(R\text{-}py)]^+$ taken from Refs. [15–17].

As depicted in Fig. 3, both for 4R-py (□ in Fig. 3) and 3R-py (■ in Fig. 3) a linear relationship between $\log k_2$ and the corresponding pK_a values exists, but the gradient values (α) for the two groups of ligands are meaningfully different, being $\alpha = -0.419 \pm 0.006$ for the *para*-substituted pyridines and $\alpha = -0.516 \pm 0.006$ for the *meta*-substituted. This means that a different sensitivity of the two groups of N-donors to changes in basicity exists, the 3R-pyridines showings a weaker dependence on the conjugate acid pK_a than the 4R-pyridines. As already observed in a previous work on Au(III) complexes [10], the chemical behavior of the non-substituted pyridine (py) in its displacement by chloride from the metal center is comparable to that of the *para*-substituted pyridines.

Table 2
Second order rate constants, k_2, and pK_a of $[H(R\text{-}py)]^+$ for the reaction $[Pt(SNS)(R\text{-}py)]^{2+} + Cl^- \rightarrow [Pt(SNS)Cl]^{2+} + R\text{-}py$ in methanol at 25 °C; I = 0.1 mol dm^{-3}, $[NBu^n_4]ClO_4$, 0.01 mol dm^{-3} $HClO_4$

R-py	k_2/dm^3 mol s^{-1}	pK_a of $[H(R\text{-}py)]^+$
4-MeO-py	0.00876 ± 0.0001	6.47
4-Cl-py	0.111 ± 0.003	3.84
4-Me-py	0.0129 ± 0.0001	6.03
4-NH_2-py	0.00066 ± 0.00004	9.12
py	0.0254 ± 0.0006	5.25
3-MeO-py	0.0234 ± 0.0001	4.91
3-Me-py	0.0114 ± 0.0002	5.52
3-Cl-py	0.258 ± 0.004	2.84
3-I-py	0.175 ± 0.003	3.25
3-F-py	0.238 ± 0.008	2.97
3-Ph-py	0.0270 ± 0.0003	4.80
3-CH_2OH-py	0.0199 ± 0.0004	5.00

pK_a values were taken from Refs. [15–17].

This result can not be in any way ascribed to different steric effects in the ground or in the transition state between the two groups of heterocycles, this demonstrated by the behavior of ligands having very similar pK_a values but quite different bulks, such as 3-phenylpyridine and 3-methoxypyridine. Therefore, the differ-

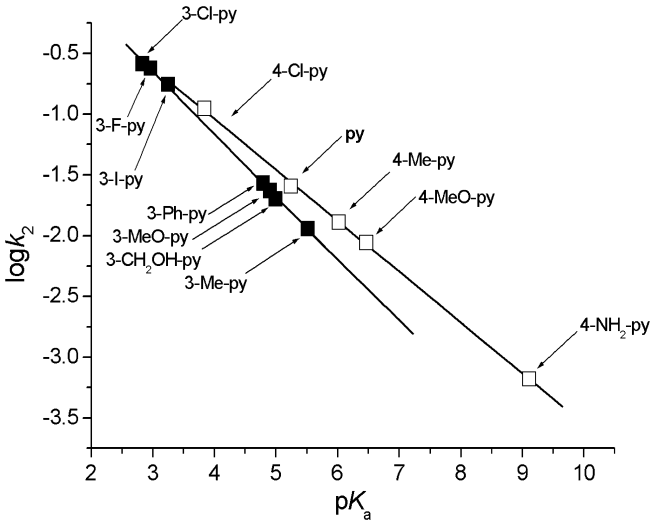

Fig. 3. Plots of $\log k_2$ for the reaction $[Pt(SNS)(R\text{-}py)]^{2+} + Cl^- \rightarrow [Pt(SNS)Cl]^{2+} + R\text{-}py$ against pK_a of $[H(R\text{-}py)]^+$. □ = pyridine and *para*-substituted pyridines, ■ = *meta*-substituted pyridines.

ent trends of *meta*- and *para*-substituted pyridines must have an electronic origin.

For the entry of pyridines on $[Pt(SNS)Cl](ClO_4)$, in the same experimental conditions, a free-energy relationship between $\log k_2$ and pK_a was found [2], with $\alpha = 0.15$. The parameter α is a measure of the ability of a substrate to discriminate among isosteric nitrogen donors and can be assumed to be a relative measure of its electrophilicity. The asynchronous substitution, characteristic of planar tetra-coordinate Pt(II) complexes, offers the opportunity to describe separately the energetic contributions of bond formation and bond rupture to the free energy of activation[14]. As already discussed [1,2] the relatively large dependence of reactivity upon the basicity of the nitrogen donors in the reverse as compared to the forward reactions allows us to postulate an associative asynchronous displacement mechanism with a transition state in which the nitrogen ligand is partially bonded to the metal, and the Pt–Cl bond is almost completely formed, as depicted in Fig. 4. Therefore, the different interaction with the Pt(II) fragment of *meta*- and *para*-substituted pyridines should not greatly affect the reaction transition state $[Pt(SNS)Cl(R\text{-}py)]^{\ddagger\oplus}$.

For these reasons it seems reasonable to conclude that the lower reactivity towards displacement of 3R-pyridines on growing the conjugate acid pK_a values could be mainly ascribed to an increasing stability of the corresponding $[Pt(SNS)(3R\text{-}py)]^{2+}$ ground state

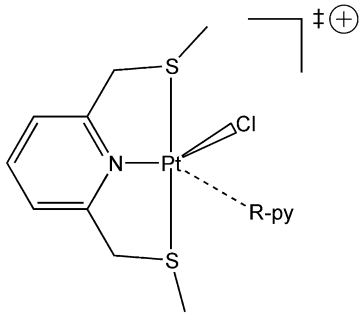

Fig. 4. Transition state geometry for the reaction $[Pt(SNS)(R\text{-}py)]^{2+} + Cl^- \rightarrow [Pt(SNS)Cl]^+ + R\text{-}py$.

complexes and a consequent growth of the ground state – transition state energy barrier, as illustrated in Fig. 5.

By admitting that the pK_a values could be used as a relative measure of pyridines σ-donor character, the enforcement of the Pt–N bond in the $[Pt(SNS)(3R\text{-}py)]^{2+}$ derivatives, compared to the corresponding 4R-py complexes, can be tentatively ascribed to a stronger π-acceptor character of *meta*-substituted pyridines respect to that of *para*-substituted, once bonded to the [Pt(SNS)] fragment. On growing the Pt ⇐ N σ-donor contribution by increasing the N-donor conjugated acid pK_a value, the Pt ⇒ N π-back-donation will be also enforced, the σ-donation increasing the electron density on the metal center. The synergy of the two bond contributions, if a more efficient metal-to-ligand back-donation in the case of $[Pt(SNS)(3R\text{-}py)]^{2+}$ complexes is admitted, is therefore able to explain the experimentally observed reactivity difference of the two groups of heterocycles towards their displacement from Pt(II) metal center and why this difference grows on increasing the conjugated acids pK_a.

When the same substitution reaction was studied for the gold(III) complexes $AuCl_3(R\text{-}py)$, the *meta*-substituted pyridines were found to be less reactive than the *para*-substituted independently from the pK_a [10]. This difference between $[Pt(SNS)(R\text{-}py)]^{2+}$ and $AuCl_3(R\text{-}py)$ complexes towards pyridine displacement can be due to the different electron density existing between the metal centers of the [Pt(SNS)] and $[AuCl_3]$ fragments. The [Pt(SNS)] fragment is positively doubly-charged and Pt is bonded to two π-acid sulfur atoms, while the $[AuCl_3]$ fragment is neutral and the chloro-ligands are σ- and π-donors. This means that in the described cases the platinum center is less electron rich than the gold one, therefore the more efficient metal-to-ligand back-donation of the *meta*-substituted pyridines is observable only when strongly σ-donor heterocycles, having high pK_a values, are coordinated to platinum.

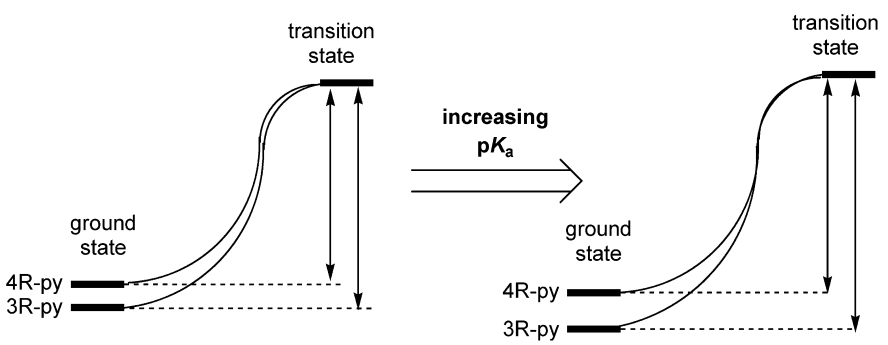

Fig. 5. $[Pt(SNS)(R\text{-}py)]^{2+} + Cl^- \rightarrow [Pt(SNS)Cl]^+ + R\text{-}py$ reaction energy barrier in the case of *meta*- and *para*-substituted pyridines considering different pK_a values.

3. Experimental

3.1. Materials

Pure reagent grade tetrabutylammonium perchlorate $[NBu^n_4]ClO_4$ and lithium chloride LiCl (Aldrich) were dried over P_2O_5 in a vacuum desiccator and used without further purifications. Pyridines were best-quality Aldrich products, distilled or re-crystallized before use if necessary. Anhydrous methanol was obtained by distillation over Mg wires, but traces of water did not appear to have any appreciable effect upon the reactions. Dimethylformamide (DMF) was distilled at reduced pressure before use. Deuterated nitromethane was purchased from Aldrich. 2,6-Bis(methylsulfanylmethyl)pyridine (SNS) was prepared by reacting 2,6-bis(chloromethyl)pyridine and

Table 3
Analytical data (calculated values in parentheses)

Complex	Analysis (%)		
	C	H	N
$[Pt(SNS)(4\text{-Me-py})](ClO_4)_2$	26.1 (26.3)	2.49 (2.94)	4.16 (4.08)
$[Pt(SNS)(py)](ClO_4)_2$	25.1 (25.0)	2.63 (2.70)	4.09 (4.16)
$[Pt(SNS)(4\text{-Cl-py})](ClO_4)_2$	23.8 (23.8)	2.27 (2.42)	3.78 (3.96)
$[Pt(SNS)(3\text{-Cl-py})](ClO_4)_2$	23.6 (23.8)	2.38 (2.42)	3.91 (3.96)
$[Pt(SNS)(4\text{-MeO-py})](ClO_4)_2$	24.5 (24.4)	2.82 (2.93)	4.23 (4.07)
$[Pt(SNS)(3\text{-MeO-py})](ClO_4)_2$	24.4 (24.4)	2.74 (2.93)	4.21 (4.07)
$[Pt(SNS)(3\text{-Me-py})](ClO_4)_2$	26.5 (26.3)	2.78 (2.94)	4.02 (4.08)
$[Pt(SNS)(3\text{-F-py})](ClO_4)_2$	24.2 (24.4)	2.34 (2.48)	4.21 (4.06)
$1[Pt(SNS)(3\text{-I-py})](ClO_4)_2$	21.0 (21.1)	2.17 (2.15)	3.61 (3.51)
$[Pt(SNS)(3\text{-}CH_2OH\text{-py})](ClO_4)_2$	25.5 (25.7)	2.22 (2.17)	4.08 (3.99)
$[Pt(SNS)(4\text{-}NH_2\text{-py})](ClO_4)_2$	24.7 (24.5)	2.71 (2.79)	6.02 (6.11)
$[Pt(SNS)(3\text{-Ph-py})](ClO_4)_2$	32.0 (32.1)	2.73 (2.96)	3.61 (3.74)

Table 4
^1H NMR spectroscopic data for the $[Pt(SNS)(R\text{-py})](ClO_4)_2$ complexes

R-py	^1H NMR (CD_3NO_2, 25 °C)
3-MeO-py	δ = 8.72 (d, $^4J_{H,H}$ = 2.6 Hz, $^3J_{Pt,H}$ = 40.9 Hz, 1H, *py-H*$_2^E$), 8.67 (d, $^4J_{H,H}$ = 2.5 Hz, 0.3H, *py-H*$_2^Z$), 8.59 (d, $^3J_{H,H}$ = 5.3 Hz, $^3J_{Pt,H}$ = 36.7 Hz, 1.3H, *py-H*$_6^E$ + *py-H*$_6^Z$), 8.30 (t, $^3J_{H,H}$ = 8.0 Hz, 1.3H, *SNS-py-H*$_4^E$ + *SNS-py-H*$_4^Z$), 7.88 (d, $^3J_{H,H}$ = 8.0 Hz, 2H, *SNS-py-H*$_{3-5}^E$), 7.86 (d, $^3J_{H,H}$ = 8.0 Hz, 0.6H, *SNS-py-H*$_{3-5}^Z$), 7.80–7.59 (m, 2.6H, *py-H*$_{4-5}^E$ + *py-H*$_{4-5}^Z$), 5.22, 4.88 (AB spin system, $^2J_{H,H}$ = 17.5 Hz, $^3J_{Pt,HB}$ = 50.3 Hz, 4H, *S–CH*$_2^E$), 5.22, 5.01 (AB spin system, $^2J_{H,H}$ = 16.9 Hz, 1.2H, *S–CH*$_2^Z$), 4.02 (s, 0.9H, *OCH*$_3^Z$); 4.01 (s, 3H, *OCH*$_3^E$), 2.80 (s, $^3J_{Pt,H}$ = 50.1 Hz, 1.8H, *SCH*$_3^Z$), 2.75 (s, $^3J_{Pt,H}$ = 51.3 Hz, 6H, *SCH*$_3^E$) ppm. *E*/*Z* ratio = 3/1
3-Ph-py	δ = 9.30 (d, $^4J_{H,H}$ = 2.0 Hz, $^3J_{Pt,H}$ = 37.7 Hz, 1H, *py-H*$_2^E$), 9.27 (d, $^4J_{H,H}$ = 2.0 Hz, 0.3H, *py-H*$_2^Z$), 8.98 (d, $^3J_{H,H}$ = 5.4 Hz, $^3J_{Pt,H}$ = 33.0 Hz, 1H, *py-H*$_6^E$), 8.95 (d, $^3J_{H,H}$ = 5.4 Hz, 0.3H, *py-H*$_6^Z$), 8.44 (m, 0.3H,*py-H*$_4^Z$), 8.42 (dd, $^3J_{H,H}$ = 8.2 Hz, $^4J_{H,H}$ = 2.0 Hz, 1H, *py-H*$_4^E$), 8.32 (t, $^3J_{H,H}$ = 8.2 Hz, 1.3H,*SNS-py-H*$_4^E$ + *SNS-py-H*$_4^Z$), 7.89 (d, $^3J_{H,H}$ = 8.2 Hz, 2H, *SNS-py-H*$_{3-5}^E$), 7.86 (d, $^3J_{H,H}$ = 8.0 Hz, 0.6H, *SNS-py-H*$_{3-5}^Z$), 7.85–7.56 (m, 7.8H, *Ph*^{E} + *Ph*^{Z} + *py-H*$_5^E$ + *py-H*$_5^Z$), 5.24, 4.89 (AB spin system, $^2J_{H,H}$ = 17.2 Hz, $^3J_{Pt,HB}$ = 51.2 Hz, 4H, *S-CH*$_2^E$), 5.24, 5.03 (AB spin system, $^2J_{H,H}$ = 16.8 Hz, 1.2H, *S-CH*$_2^Z$), 2.84 (s, $^3J_{Pt,H}$ = 49.9 Hz, 1.8H, *SCH*$_3^Z$), 2.77 (s, $^3J_{Pt,H}$ = 51.3 Hz, 6H, *S-CH*$_3^E$) ppm. *E*/*Z* ratio = 3/1
3-I-py	δ = 9.34 (d, $^4J_{H,H}$ = 1.8 Hz, $^3J_{Pt,H}$ = 38.8 Hz, 1H, *py-H*$_2^E$), 9.31 (d, $^4J_{H,H}$ = 1.8 Hz, 0.3H, *py-H*$_2^Z$), 9.04 (dd, $^3J_{H,H}$ = 5.9 Hz,$^4J_{H,H}$ = 1.1 Hz, $^3J_{Pt,H}$ = 37.0 Hz, 1H, *py-H*$_6^E$), 8.99 (dd, $^3J_{H,H}$ = 5.9 Hz, $^4J_{H,H}$ = 1.1 Hz, 0.3H, *py-H*$_6^Z$), 8.50 (ddd, $^3J_{H,H}$ = 8.2 Hz, $^4J_{H,H}$ = 1.8 Hz, $^4J_{H,H}$ = 1.1 Hz, 1.3H, *py-H*$_4^E$ + *py-H*$_4^Z$), 8.31 (t, $^3J_{H,H}$ = 8.2 Hz, 1.3H,*SNS-py-H*$_4^E$ + *SNS-py-H*$_4^Z$), 7.89 (d, $^3J_{H,H}$ = 8.2 Hz, 2H, *SNS-py-H*$_{3-5}^E$), 7.86 (d, $^3J_{H,H}$ = 8.2 Hz, 0.6H, *SNS-py-H*$_{3-5}^Z$), 7.55 (dd, $^3J_{H,H}$ = 8.2 Hz, $^3J_{H,H}$ = 5.9 Hz, 1.3H, *py-H*$_5^E$ + *py-H*$_5^Z$), 5.22, 4.87 (AB spin system, $^2J_{H,H}$ = 17.5 Hz, $^3J_{Pt,HB}$ = 51.1 Hz, 4H, *S-CH*$_2^E$), 5.22, 5.01 (AB spin system, $^2J_{H,H}$ = 16.8 Hz, 1.2H, *S-CH*$_2^Z$), 2.80 (s, $^3J_{Pt,H}$ = 49.0 Hz, 1.8H, *SCH*$_3^Z$), 2.74 (s, $^3J_{Pt,H}$ = 50.8 Hz, 6H, *S-CH*$_3^E$) ppm. *E*/*Z* ratio = 3/1
3-Me-py	δ = 8.87 (s, $^3J_{Pt,H}$ = 37.7 Hz, 1H, *py-H*$_2^E$), 8.84 (s, 0.4H, *py-H*$_2^Z$), 8.79 (d, $^3J_{H,H}$ = 5.8 Hz, $^3J_{Pt,H}$ = 37.0 Hz, 1H, *py-H*$_6^E$), 8.76 (d, $^3J_{H,H}$ = 5.8 Hz, 0.4H, *py-H*$_6^Z$), 8.30 (t, $^3J_{H,H}$ = 7.9 Hz, 1.4H,*SNS-py-H*$_4^E$ + *SNS-py-H*$_4^Z$), 8.01 (d, $^3J_{H,H}$ = 8.1 Hz, 1.4H, *py-H*$_4^E$ + *py-H*$_4^Z$), 7.89 (d, $^3J_{H,H}$ = 7.9 Hz, 2H, *SNS-py-H*$_{3-5}^E$), 7.86 (d, $^3J_{H,H}$ = 7.9 Hz, 0.8H, *SNS-py-H*$_{3-5}^Z$), 7.62 (dd, $^3J_{H,H}$ = 8.1 Hz, $^3J_{H,H}$ = 5.8 Hz, 1.4H, *py-H*$_5^E$ + *py-H*$_5^Z$), 5.22, 4.88 (AB spin system, $^2J_{H,H}$ = 17.9 Hz, $^3J_{Pt,HB}$ = 50.8 Hz, 4H, *S-CH*$_2^E$), 5.22, 5.01 (AB spin system, $^2J_{H,H}$ = 16.9 Hz, 1.6H, *S-CH*$_2^Z$), 2.79 (s, $^3J_{Pt,H}$ = 50.0 Hz, 2.4H, *SCH*$_3^Z$), 2.74 (s, $^3J_{Pt,H}$ = 51.2 Hz, 6H, *SCH*$_3^E$), 2.48 (s, 4.2H, *CH*$_3^E$ + *CH*$_3^Z$) ppm. *E*/*Z* ratio = 2.5/1
3-F-py	δ = 9.04 (dd, d, $^4J_{H,H}$ = 2.7 Hz, $^3J_{F,H}$ = 3.1 Hz, $^3J_{Pt,H}$ = 43.1 Hz, 1H, *py-H*$_2^E$), 9.00 (dd, d, $^4J_{H,H}$ = 2.7 Hz, $^3J_{F,H}$ = 3.1 Hz, 0.3H, *py-H*$_2^Z$), 8.93 (d, $^3J_{H,H}$ = 5.4 Hz, $^3J_{Pt,H}$ = 35.0 Hz, 1H, *py-H*$_6^E$), 8.90 (d, $^3J_{H,H}$ = 5.4 Hz, 0.3H, *py-H*$_6^Z$), 8.31 (t, $^3J_{H,H}$ = 8.1 Hz, 1.3H,*SNS-py-H*$_4^E$ + *SNS-py-H*$_4^Z$), 8.12–7.96 (m, 1.3H, *py-H*$_4^E$ + *py-H*$_4^Z$), 7.90 (d, $^3J_{H,H}$ = 8.1 Hz, 2H, *SNS-py-H*$_{3-5}^E$), 7.86 (d, $^3J_{H,H}$ = 8.1 Hz, 0.6H, *SNS-py-H*$_{3-5}^Z$), 7.83–7.78 (m, 1.3H, *py-H*$_5^E$ + *py-H*$_5^Z$), 5.22, 4.88 (AB spin system, $^2J_{H,H}$ = 17.5 Hz, $^3J_{Pt,HB}$ = 51.6 Hz, 4H, *S-CH*$_2^E$), 5.21, 5.02 (AB spin system, $^2J_{H,H}$ = 16.9 Hz, 1.2H, *S-CH*$_2^Z$), 2.81 (s, $^3J_{Pt,H}$ = 49.3 Hz, 1.8H, *SCH*$_3^Z$), 2.75 (s, $^3J_{Pt,H}$ = 50.0 Hz, 6H, *SCH*$_3^E$) ppm. *E*/*Z* ratio = 3/1
3-Cl-py	δ = 9.14 (d, $^4J_{H,H}$ = 2.3 Hz, $^3J_{Pt,H}$ = 39.7 Hz, 1H, *py-H*$_2^E$), 9.10 (d, $^4J_{H,H}$ = 2.3 Hz, 0.4H, *py-H*$_2^Z$), 9.01 (dd, $^3J_{H,H}$ = 6.0 Hz,$^4J_{H,H}$ = 1.1 Hz, $^3J_{Pt,H}$ = 35.8 Hz, 1H, *py-H*$_6^E$), 8.97 (dd, $^3J_{H,H}$ = 6.0 Hz, $^4J_{H,H}$ = 1.1 Hz, 0.4H, *py-H*$_6^Z$), 8.31 (t, $^3J_{H,H}$ = 8.1 Hz, 1.4H,*SNS-py-H*$_4^E$ + *SNS-py-H*$_4^Z$), 8.21 (ddd, $^3J_{H,H}$ = 8.5 Hz, $^4J_{H,H}$ = 2.3 Hz, $^4J_{H,H}$ = 1.1 Hz, 1.4H, *py-H*$_4^E$ + *py-H*$_4^Z$), 7.89 (d, $^3J_{H,H}$ = 8.1 Hz, 2H, *SNS-py-H*$_{3-5}^E$), 7.86 (d, $^3J_{H,H}$ = 8.1 Hz, 0.8H, *SNS-py-H*$_{3-5}^Z$), 7.76 (dd, $^3J_{H,H}$ = 8.5 Hz, $^3J_{H,H}$ = 6.0 Hz, 1.4H, *py-H*$_5^E$ + *py-H*$_5^Z$), 5.23, 4.87 (AB spin system, $^2J_{H,H}$ = 17.7 Hz, $^3J_{Pt,HB}$ = 52.0 Hz, 4H, *S-CH*$_2^E$), 5.22, 5.01 (AB spin system, $^2J_{H,H}$ = 17.1 Hz, 1.6H, *S-CH*$_2^Z$), 2.81 (s, $^3J_{Pt,H}$ = 50.4 Hz, 2.4H, *SCH*$_3^Z$), 2.74 (s, $^3J_{Pt,H}$ = 50.4 Hz, 6H, *S-CH*$_3^E$) ppm. *E*/*Z* ratio = 2.5/1
3-CH_2OH-py	δ = 9.00 (s, $^3J_{Pt,H}$ = 38.2 Hz, 1H, *py-H*$_2^E$), 8.98 (s, 0.4H, *py-H*$_2^Z$), 8.89 (d, $^3J_{H,H}$ = 5.5 Hz, $^3J_{Pt,H}$ = 36.0 Hz, 1H, *py-H*$_6^E$), 8.86 (d, $^3J_{H,H}$ = 5.5 Hz, 0.4H, *py-H*$_6^Z$), 8.31 (t, $^3J_{H,H}$ = 8.1 Hz, 1.4H,*SNS-py-H*$_4^E$ + *SNS-py-H*$_4^Z$), 8.14 (d, $^3J_{H,H}$ = 7.9 Hz, 1.4H, *py-H*$_4^E$ + *py-H*$_4^Z$), 7.89 (d, $^3J_{H,H}$ = 8.1 Hz, 2H, *SNS-py-H*$_{3-5}^E$), 7.86 (d, $^3J_{H,H}$ = 8.1 Hz, 0.8H, *SNS-py-H*$_{3-5}^Z$), 7.72 (dd, $^3J_{H,H}$ = 7.9 Hz, $^3J_{H,H}$ = 5.5 Hz, 1.4H, *py-H*$_5^E$ + *py-H*$_5^Z$), 5.24, 4.89 (AB spin system, $^2J_{H,H}$ = 18.2 Hz, $^3J_{Pt,HB}$ = 49.6 Hz, 4H, *S-CH*$_2^E$), 5.23, 5.02 (AB spin system, $^2J_{H,H}$ = 16.9 Hz, 1.6H, *S-CH*$_2^Z$), 4.84 (s, 2.8H, *CH*$_2O^E$ + *CH*$_2O^Z$), 2.81 (s, $^3J_{Pt,H}$ = 50.5 Hz, 2.4H, *SCH*$_3^Z$), 2.76 (s, $^3J_{Pt,H}$ = 50.5 Hz, 6H, *S-CH*$_3^E$) ppm. *E*/*Z* ratio = 2.5/1
4-Cl-py	δ = 8.96, 7.80 (AA′BB′ spin system, $^3J_{AB} = {}^3J'_{A'B} =$ 7.0 Hz, $^4J_{AA'}$ = 1.0 Hz, $^4J_{BB'}$ = 4.0 Hz, $^3J_{Pt,HA} = {}^3J_{Pt,HA'}$ = 36.9 Hz, 4H, *A*,*A*′ = *py-H*$_{2-6}^E$, B, B′ = *py* − *H* $^E_{3-5}$), 8.93, 7.83 (AA′BB′ spin system, $^3J_{AB} = {}^3J'_{A'B}$ = 7.0 Hz, $^4J_{AA'}$ = 1.0 Hz, $^4J_{BB'}$ = 4.0 Hz, 1.2H, *A*,*A*′ = *py-H*$_{2-6}^Z$, *B*,*B*′ = *py-H*$_{3-5}^Z$), 8.31 (t, $^3J_{H,H}$ = 8.1 Hz, 1.3H,*SNS-py-H*$_4^E$ + *SNS-py-H*$_4^Z$), 7.89 (d, $^3J_{H,H}$ = 8.1 Hz, 2H, *SNS-py-H*$_{3-5}^E$), 7.86 (d, $^3J_{H,H}$ = 8.1 Hz, 0.6H, *SNS-py-H*$_{3-5}^Z$), 5.21, 4.87 (AB spin system, $^2J_{H,H}$ = 17.6 Hz, $^3J_{Pt,HB}$ = 51.4 Hz, 4H, *S-CH*$_2^E$), 5.21, 5.01 (AB spin system, $^2J_{H,H}$ = 16.7 Hz, 1.2H, *S-CH*$_2^Z$), 2.80 (s, $^3J_{Pt,H}$ = 51.4 Hz, 1.8H, *SCH*$_3^Z$), 2.74 (s, $^3J_{Pt,H}$ = 50.5 Hz, 6H, *S-CH*$_3^E$) ppm. *E*/*Z* ratio = 3/1
4-MeO-py	δ = 8.75, 7.24 (AA′BB′ spin system, $^3J_{AB} = {}^3J'_{A'B}$ = 7.0 Hz, $^4J_{AA'}$ = 1.0 Hz, $^4J_{BB'}$ = 4.0 Hz, $^3J_{Pt,HA} = {}^3J_{Pt,HA'}$ = 37.3 Hz, 4H, *A*,*A*′ = *py-H*$_{2-6}^E$, *B*,*B*′ = *py-H*$_{3-5}^E$), 8.71, 7.27 (AA′BB′ spin system, $^3J_{AB} = {}^3J'_{A'B}$ = 7.0 Hz, $^4J_{AA'}$ = 1.0 Hz, $^4J_{BB'}$ = 4.0 Hz, 1.6H, *A*,*A*′ = *py-H*$_{2-6}^Z$, *B*,*B*′ = *py-H*$_{3-5}^Z$), 8.29 (t, $^3J_{H,H}$ = 7.9 Hz, 1.4H, *SNS-py-H*$_4^E$ + *SNS-py-H*$_4^Z$), 7.88 (d, $^3J_{H,H}$ = 7.9 Hz, 2H, *SNS-py-H*$_{3-5}^E$), 7.85 (d, $^3J_{H,H}$ = 7.9 Hz, 0.8H, *SNS-py-H*$_{3-5}^Z$), 5.20, 4.87 (AB spin system, $^2J_{H,H}$ = 18.0 Hz, $^3J_{Pt,HB}$ = 49.6 Hz, 4H, *S-CH*$_2^E$), 5.20, 5.00 (AB spin system, $^2J_{H,H}$ = 17.1 Hz, 1.6H, *S-CH*$_2^Z$), 4.07 (s, 1.2H, *OCH*$_3^Z$), 4.06 (s, 3H, *OCH*$_3^E$), 2.79 (s, $^3J_{Pt,H}$ = 50.0 Hz, 2.4H, *SCH*$_3^Z$), 2.74 (s, $^3J_{Pt,H}$ = 50.5 Hz, 6H, *S-CH*$_3^E$) ppm. *E*/*Z* ratio = 2.5/1
4-Me-py	δ = 8.80, 7.57 (AA′BB′ spin system, $^3J_{AB} = {}^3J'_{A'B}$ = 7.0 Hz, $^4J_{BB'}$ = 4.3 Hz, $^3J_{Pt,HA} = {}^3J_{Pt,HA'}$ = 36.9 Hz, 4H, *A*,*A*′ = *py-H*$_{2-6}^E$, *B*,*B*′=*py-H*$_{3-5}^E$), 8.77, 7.60 (AA′BB′ spin system, $^3J_{AB} = {}^3J'_{A'B}$ = 7.0 Hz, $^4J_{BB'}$ = 4.3 Hz, 1.6H, *A*,*A*′ = *py-H*$_{2-6}^Z$, *B*,*B*′= *py-H*$_{3-5}^Z$), 8.30 (t, $^3J_{H,H}$ = 8.0 Hz, 1.4H,*SNS-py-H*$_4^E$ + *SNS-py-H*$_4^Z$), 7.89 (d, $^3J_{H,H}$ = 8.0 Hz, 2H, *SNS-py-H*$_{3-5}^E$), 7.86 (d, $^3J_{H,H}$ = 7.9 Hz, 0.8H, *SNS-py-H*$_{3-5}^Z$), 5.21, 4.87 (AB spin system, $^2J_{H,H}$ = 17.2 Hz, $^3J_{Pt,HB}$ = 49.2 Hz, 4H, *S-CH*$_2^E$), 5.21, 5.01 (AB spin system, $^2J_{H,H}$ = 17.0 Hz, 1.6H, *S–CH*$_2^Z$), 2.79 (s, $^3J_{Pt,H}$ = 51.2 Hz, 2.4H, *SCH*$_3^Z$), 2.74 (s, $^3J_{Pt,H}$ = 51.6 Hz, 6H, *S-CH*$_3^E$), 2.58 (s, 1.2H, *CH*$_3^Z$), 2.57 (s, 3H, *CH*$_3^E$) ppm. *E*/*Z* ratio = 2.5/1
4-NH_2-py	δ = 8.43–8.13 (m, 4.2H, *py-H*$_{2-6}^E$ + *py-H*$_{2-6}^Z$ + *SNS-py-H*$_4^E$ + *SNS-py-H*$_4^Z$), 7.85 (d, $^3J_{H,H}$ = 8.0 Hz, 2H, *SNS-py-H*$_{3-5}^E$), 7.83 (d, $^3J_{H,H}$ = 8.0 Hz, 0.8H, *SNS-py-H*$_{3-5}^Z$), 6.85 (m, 0.8H, *py-H*$_{3-5}^Z$), 6.81 (m, $^3J_{H3,H2} = {}^3J_{H5,H6}$ = 7.4 Hz, $^4J_{H3,H5}$ = 4.3 Hz, 2H,*py-H*$_{3-5}^E$), 5.79 (s, br, 2.8H, *NH*$_2^E$ + *NH*$_2^Z$), 5.18, 4.98 (AB spin system, $^2J_{H,H}$ = 17.0 Hz, 1.6H, *S-CH*$_2^Z$), 5.16, 4.86 (AB spin system, $^2J_{H,H}$ = 17.8 Hz,$^3J_{Pt,HB}$ = 48.8 Hz, 4H, *S-CH*$_2^E$), 2.80 (s, $^3J_{Pt,H}$ = 50.8 Hz, 2.4H, *SCH*$_3^Z$), 2.74 (s, $^3J_{Pt,H}$ = 51.8 Hz, 6H, *S-CH*$_3^E$) ppm. *E*/*Z* ratio = 2.5/1
py	δ = 9.00 (dd, $^3J_{H,H}$ = 5.3 Hz, $^4J_{H,H}$ = 1.4 Hz, $^3J_{Pt,H}$ = 37.4 Hz, 2H,*py-H*$_{2-6}^E$), 8.97 (dd, $^3J_{H,H}$ = 5.3 Hz, $^4J_{H,H}$ = 1.4 Hz, 0.8H,*py-H*$_{2-6}^Z$), 8.31 (t, $^3J_{H,H}$ = 8.0 Hz, 1.4H,*SNS-py-H*$_4^E$ + *SNS-py-H*$_4^Z$), 8.2 (tt, $^3J_{H,H}$ = 7.8 Hz, $^4J_{H,H}$ = 1.4 Hz, 1.4H, *py-H*$_4^E$ + *py-H*$_4^Z$), 7.89 (d, $^3J_{H,H}$ = 8.0 Hz, 2H, *SNS-py-H*$_{3-5}^E$), 7.86 (d, $^3J_{H,H}$ = 8.0 Hz, 0.8H, *SNS-py-H*$_{3-5}^Z$), 7.76 (dt, $^3J_{H,H}$ = 5.3 Hz, $^3J_{H,H}$ = 7.8 Hz, 2.8H,*py-H*$_{3-5}^E$ + *py-H*$_{3-5}^Z$), 5.22, 4.88 (AB spin system, $^2J_{H,H}$ = 17.1 Hz, $^3J_{Pt,HB}$ = 51.4 Hz, 4H, *S-CH*$_2^E$), 5.22, 5.02 (AB spin system, $^2J_{H,H}$ = 16.9 Hz, 1.6H, *S-CH*$_2^Z$), 2.80 (s, $^3J_{Pt,H}$ = 50.2 Hz, 2.4H, *SCH*$_3^Z$), 2.75 (s, $^3J_{Pt,H}$ = 51.0 Hz, 6H, *S-CH*$_3^E$) ppm. *E*/*Z* ratio = 2.5/1

sodium methanthiolate following a published procedure [2,18]. The chloro-precursor [Pt(SNS)Cl](ClO_4) was obtained by reacting *cis*/*trans*-[$PtCl_2(SMe_2)_2$] and SNS according to a reported method [11] and its purity was confirmed by ^{1}H NMR spectroscopy and elemental analysis.

3.2. Kinetics

Electronic spectra and kinetic measurements were obtained on a Perkin–Elmer Lambda 15 spectrophotometer. The reactions were initiated by adding a 0.0151 mol dm^{-3} DMF solution (20 μl) of the substrate complex, [Pt(SNS)(R-py)]$^{2+}$, to a solution (3 cm^3) of the chloride ion in methanol, previously brought to the reaction temperature (25 °C) in a thermostatic cell in the spectrophotometer. The concentration of the entering group was always larger enough to provide pseudo-first-order conditions. After preliminary repetitive scan experiments in the range 240–360 nm to search for isosbestic points and spectral changes, the kinetics were studied by measuring the changing absorbance at suitable wavelength (260 nm) as a function of time. Pseudo-first-order rate constants (k_{obs}, s^{-1}) were obtained either from the gradients of plots of $\log(D_t - D_\infty)$ versus time or from a non-linear least-square fit of experimental data to $D_t = D_\infty + (D_0 - D_\infty)\exp(-k_{obs}t)$ with D_0, D_∞ and k_{obs} as the parameters to be optimized (D_0 = absorbance after mixing of reactants, D_∞ = absorbance at completion of reaction). Second order rate constants k_2 (dm^3 mol s^{-1}) were determined by linear regression of k_{obs} values versus chloride concentration. The k_{obs} and k_2 values are reported in Tables 1 and 2, respectively.

3.3. Preparation of the complexes

All the complexes [Pt(SNS)(R-py)](ClO_4)$_2$ {R-py = 4-methoxypyridine (4-MeO-py), 4-chloropyridine (4-Cl-py), pyridine (py), 4-methylpyridine (4-Me-py), 4-aminopyridine (4-NH_2-py), 3-methoxypyridine (3-MeO-py), 3-methylpyridine (3-Me-py), 3-chloropyridine (3-Cl-py), 3-iodopyridine (3-I-py), 3-fluoropyridine (3-F-py), 3-phenylpyridine (3-Ph-py), 3-hydroxymethylpyridine (3-CH_2OH-py)} were prepared by the following general method: [Pt(SNS)Cl](ClO_4) (0.264 g, 0.5 mmol) was dissolved in hot water (60–70 °C) (30 ml) and a stoichiometric amount of the nitrogen-donor base, dissolved in water (2–3 ml), was added drop by drop under stirring. After 10 min of reaction, addition of an excess of solid $LiClO_4$ (0.106 g, 1.0 mmol) and slow cooling of the solution at room temperature resulted in the formation of the crystalline product, which was filtered off, washed twice with methanol (2–4 ml) and dried *in vacuo* over P_2O_5.

3.4. Complexes characterization

^{1}H NMR spectra were taken in CD_3NO_2 at 25 °C on a Bruker Avance 300 or a Bruker AC 200 spectrometers. Chemical shifts were referenced internally to the non-deuterated solvent resonances and are quoted relative to tetramethylsilane (δ = 0 ppm). Very near resonances were sometimes resolved by applying a sine-bell apodization. COSY, NOESY and homonuclear decoupling experiments were performed to improve the characterizations of the complexes. The SWAN-MR and MESTRE-C software packages were used for NMR spectroscopic data treatment and spin systems simulation [19]. The conductivity of 1×10^{-3} mol dm^{-3} solutions of the complexes in DMF at 25 °C was measured with a Radiometer CDM 83 instrument. Elemental analyses were performed by the Microanalytical Laboratory of Faculty of Pharmaceutical Sciences of the University of Padua. Analytical and ^{1}H NMR spectra are collected in Tables 3 and 4, respectively. Hydrogen atoms are numerated following the common conventions for the considered heterocycles. *E* and *Z* suffixes are used to indicate the isomeric forms having the S-bonded methyl groups mutually in *entgegen* or *zusammen* position.

Acknowledgment

The financial support of Ca' Foscari University of Venice is gratefully acknowledged.

References

[1] M. Bellicini, L. Cattalini, G. Marangoni, B. Pitteri, J. Chem. Soc., Dalton Trans. (1994) 805.
[2] B. Pitteri, G. Marangoni, L. Cattalini, J. Chem. Soc., Dalton Trans. (1994) 3539.
[3] M. Bonivento, L. Cattalini, G. Marangoni, B. Pitteri, T. Bobbo, Trans. Met. Chem. 22 (1997) 46.
[4] B. Pitteri, G. Marangoni, L. Cattalini, Polyhedron 14 (1995) 2331.
[5] B. Pitteri, G. Marangoni, F. Visentin, L. Cattalini, T. Bobbo, Polyhedron 17 (1998) 475.
[6] B. Pitteri, M. Bortoluzzi, Polyhedron 25 (2006) 2698.
[7] G. Annibale, L. Cattalini, L. Maresca, G. Michelon, G. Natile, Inorg. Chim. Acta 10 (1974) 21.
[8] B. Pitteri, G. Marangoni, L. Cattalini, F. Visentin, V. Bertolasi, P. Gilli, Polyhedron 20 (2001) 869.
[9] F. Basolo, R.G. Pearson, Mechanisms in Inorganic Reactions, 2nd ed., Wiley, New York, 1967.
[10] B. Pitteri, M. Bortoluzzi, Eur. J. Inorg. Chem. (2007) 5138.
[11] G. Annibale, M. Bortoluzzi, G. Marangoni, B. Pitteri, Trans. Met. Chem. 30 (2005) 748.
[12] W.J. Geary, Coordin. Chem. Rev. 7 (1971) 81.
[13] B. Pitteri, M. Bortoluzzi, G. Marangoni, Trans. Met. Chem. 30 (2005) 1008.
[14] M.L. Tobe, in: G. Wilkinson, R.D. McCleverty (Eds.), Comprehensive Coordination Chemistry, vol. I, Pergamon, Oxford, 1987.
[15] D.D. Perrin, Dissociation Constants of Organic Bases in Aqueous Solutions, Butterworth, London, 1965.
[16] R.M. Smith, A.E. Martell, Critical Stability Constants, 2nd ed., vol. 2, Plenum Press, New York, 1990.
[17] H.K. Hall, J. Phys. Chem. 60 (1956) 63.
[18] B. Pitteri, L. Canovese, G. Chessa, G. Marangoni, P. Uguagliati, Polyhedron 11 (1991) 2363.
[19] (a) G. Balacco, J. Chem. Inf. Comput. Sci. 34 (1994) 1235;
(b) J.C Cobas Gòmez, F.J. Sardina Lòpez, *MestRe-C*, Universidad de Santiago de Compostela, Spain.

Polyhedron 27 (2008) 2265–2270

Contents lists available at ScienceDirect

Polyhedron

journal homepage: www.elsevier.com/locate/poly

Iron(III) complexes of the tris-(3-aminopropyl) derivative of a 14-membered tetraazamacrocycle: Potentiometric, spectroscopic and electrochemical studies

Krassimira P. Guerra [a], Rita Delgado [a,b,*]

[a] Instituto de Tecnologia Química e Biológica, UNL, Apartado 127, 2781-901 Oeiras, Portugal
[b] Instituto Superior Técnico, Departamento de Química, Av. Rovisco Pais, 1049-001 Lisboa, Portugal

ARTICLE INFO

Article history:
Received 25 January 2008
Accepted 17 April 2008
Available online 4 June 2008

Keywords:
Macrocycle
Iron(III) mono- and dinuclear complexes
Stability constants
Electrochemistry

ABSTRACT

The properties of the iron(III) complexes of the ditopic macrocyclic ligand with three aminopropyl pendant arms, L^1 = 3,7,11-tris-(3-aminopropyl)-3,7,11,17-tetraazabicyclo[11.3.1]heptadeca-1(17),13,15-triene were investigated in aqueous solution. Potentiometric studies indicated the presence of mononuclear $[FeH_hL^1]^{h+3}$ (h = 0–3), and dinuclear $[Fe_2L^1]^{6+}$, $[Fe_2L^1(OH)]^{5+}$ and $[Fe_2L^1(OH)_2]^{4+}$ complexes, and their stability constants were determined at 298.2 K and ionic strength 0.10 mol dm^{-3} in KNO_3. The log$K$ values of mononuclear protonated species indicated the consecutive deprotonation of the aminopropyl arms, suggesting the nitrogen donor atoms from the macrocycle as the preferred coordination environment for the first metal centre, and the amines from the pendant arms for the second one. The dinuclear complex is formed at about 85% of the total amount of the metal ion for 2:1 Fe:L^1 ratio solutions at pH 4.0–4.5. The log$K$ values of the deprotonation of dinuclear hydrolysed species are consistent with the presence of two water molecules directly bound to the metal centres. Spectroscopic UV–Vis and IR data for 2:1 Fe^{3+}:L^1 ratio samples confirmed the existence of dinuclear and hydroxo dinuclear species. EPR spectra of these solutions were interpreted by an equilibrium of two high-spin d^5 state of iron(III) species with different rhombic E/D distortions. Electrochemical studies also established the formation of mono- and dinuclear complexes, showing irreversible redox behaviour. The two metal centres on the dinuclear complexes have only weak interactions.

© 2008 Elsevier Ltd. All rights reserved.

1. Introduction

The iron(II/III) centres of nonheme-iron enzymes exhibit exceptional spectroscopic and electrochemical properties which give useful data for the comprehension of the catalytic and biological behaviour of these enzymes [1]. On the other hand, a significant number of synthetic models that replicate on some aspects of nonheme-iron enzyme active sites were produced based in macrocyclic polyamines [2] or tripodal multidentate ligands containing pyridine, amine and carboxamato units [3–5] or aliphatic and aromatic amines including nitrogen heterocyclic groups such as imidazol [6,7]. They form Fe(III) peroxo-species and some of them are able to duplicate the DNA cleavage action of bleomycin [8,9]. High-valent (Fe^{4+} or Fe^{5+})-oxo species, quoted as intermediate species in the reaction of nonheme iron enzymes with O_2, were created by photolysis of iron(III) complexes of an azide (N_3) derivative of macrocylic ligands such as tacn or cyclam [10,11] (see in Scheme 1 the structure of ligands). Reviews describing successes and challenges of models for nonheme iron dioxygen-activating enzymes were recently published [12,13]. The wide range of information on structural, spectroscopic and reaction mechanisms contributed to the better understanding of biological systems. This knowledge is also used to create new catalysts, in dioxygen green chemistry of varied organic reactions [1,4,9,12,13] and in medicine. For instance, the Fe^{2+}/Fe^{3+} complexes of *N*,*N*′,*N*″-tris(2-pyridylmethyl)-*cis*,*cis*-1,3,5-triaminocyclohexane display cytotoxicity toward cultured bladder cancer cells [14].

Functionalized derivatives of tetraazamacrocyclic ligands are able to coordinate ferric ion with strong binding ability and adopting various conformations of similar energy [15]. The dichloro iron(III) tetrafluoroborate complex of a 14-membered tetraazamacrocycle containing pyridine (L^2) was found to catalyse the decomposition of H_2O_2 in water up to pH 4.6, showing catalase-like or (and) peroxidise-like activities [16] and its X-ray crystal structure was determined [17]. The stability constants of Fe(III) complexes of acetate derivatives of 14- and 12-membered tetraazamacrocycles containing pyridine, L^3 and L^4, respectively, were determined and spectroscopic studies revealed that the metal centre is coordinated to the macrocyclic nitrogen atoms and one or two oxygen atoms from the pendant arms [18,19].

In the present work we decided to study the ferric complexes of a tetraazamacrocycle functionalized with aminopropyl pendant

* Corresponding author. Address: Instituto de Tecnologia Química e Biológica, UNL, Apartado 127, 2781-901 Oeiras, Portugal. Tel.: +351 214 46 97 37/8; fax: +351 214 41 12 77.
E-mail address: delgado@itqb.unl.pt (R. Delgado).

0277-5387/$ - see front matter © 2008 Elsevier Ltd. All rights reserved.
doi:10.1016/j.poly.2008.04.030

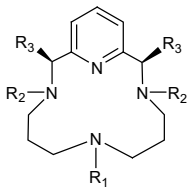

L¹ $R_1 = R_2 = (CH_2)_3NH_2$; R_3 = H

L² $R_1 = R_2$ = H; $R_3 = CH_3$

L³ $R_1 = CH_3$; $R_2 = CH_2CO_2H$; R_3 = H

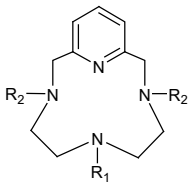

L⁴ $R_1 = R_2 = CH_2CO_2H$

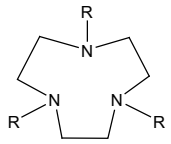

tacn, R = CH_3

triazacyclononane, R = H

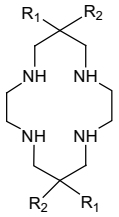

cyclam, $R_1 = R_2$ = H

diammac, $R_1 = CH_3$; $R_2 = NH_2$

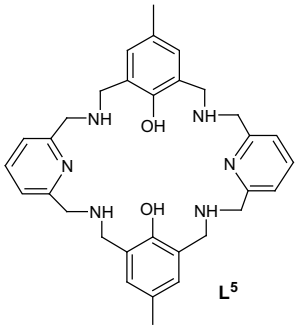

L⁵

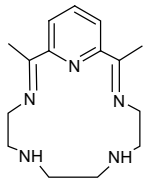

L⁶

Scheme 1.

arms, L^1 (3,7,11-tris-(3-aminopropyl)-3,7,11,17-tetraaza-bicyclo-[11.3.1]heptadeca-1(17),13,15-triene), taking into account that L^1 may exhibit specific and unpredicted coordination behaviour with some transition metal ions [20]. Mono- and dinuclear complexes are formed in water and they showed good solubility in this solvent. Potentiometric, spectroscopic and electrochemical studies in aqueous solution were carried out, revealing that the presence of soft nitrogen donor atoms in the ligand led to interesting and not expected behaviour.

2. Results and discussion

2.1. Stability constants

The complexation behaviour of L^1 with Fe^{3+} ion was studied by potentiometric method in aqueous solution, at 298.2 K and ionic strength 0.10 mol dm^{-3} in KNO_3. The stability constants determined are listed in Table 1, and the protonation constants also compiled were previously determined [20]. The final model obtained comprises titrations of different metal to ligand ratios, from 0.5:1 to 2:1. Precipitation limited the pH range studied, which was of about 7 for the 2:1 and 7.5 for the 0.5:1.

Mononuclear $[FeH_hL^1]^{h+3}$ ($h = 0$–3) and dinuclear $[Fe_2L^1]^{6+}$, $[Fe_2L^1(OH)]^{5+}$ and $[Fe_2L^1(OH)_2]^{4+}$ species were found at the studied pH range. The species distribution curves for the iron(III) complexes of L^1 at 1:1 and 2:1 ratios, obtained with the Hyss program [21], are shown in Fig. 1. The dinuclear complex exists even for the 1:1 stoichiometry while the $[FeL^1]^{3+}$ complex is only formed upon pH 6 and it is found in insignificant amounts at 2:1 ratio. Three mononuclear protonated species were formed at lower pH, simultaneously with the $[Fe_2L^1]^{6+}$, corresponding to the successive deprotonation of the ammonium groups of the arms. The $[Fe_2L^1]^{6+}$ species was formed at about 85% of the total amount of the metal ion at pH 4 for the 2:1 ratio (Fig. 1b). Upon this pH value two water molecules, directly bounded to the metal ion, start to deprotonate, forming the $[Fe_2L^1(OH)]^{5+}$ and $[Fe_2L^1(OH)_2]^{4+}$ species. At pH about 5 precipitation occurred probably resulting from dimerization of the dihydroxo species [22]. Indeed, the values of $\log K_{Fe_2L^1(OH)} = 5.95$ and $\log K_{Fe_2L^1(OH)_2} = 7.6$ suggest that the water molecules are strongly bound to the metal centres. Values of the same order were also found for the *N,N′*-bis(2-methylpyridyl) ethylenediamine ($\log K_{Fe_2L(OH)} = 5.7$ and $\log K_{Fe_2L(OH)_2} = 6.2$) [23] and the 24-membered of the hexaazadiphenol macrocyclic ligand (L^5) ($\log K_{Fe_2L^5(OH)} = 2.92$ and $\log K_{Fe_2L^5(OH)_2} = 7.34$) [24].

The $\log K_{FeL^1} = 25.95$ and $\log K_{Fe_2L^1} = 12.07$ are very high values for a ligand only containing amine donors, or when compared with the corresponding values of other derivatives of the parent tetraazamacrocycles with pyridine unit [18,19]. Then the first value was confirmed by a competition reaction using dtpa (diethylenetriamino-pentaethanoic acid) as the second ligand [18]. The second ligand need to be capable to compete with L^1 for iron(III) and to be a compound for which the protonation and the stability constants with Fe^{3+} are well known, as it is the case of dtpa [25]. The high stability constant values of L^1 with iron(III) can be partly explained by the large overall basicity of the aminopropyl arms of L^1 [26] and(or) special accommodation of the metal centre into the structure

Table 1
Protonation constants of L^1 and its stability constants with Fe^{3+}

Equilibrium reaction[a]	$\log \beta_{H_hL_1}$	Equilibrium reaction[a]	$\log K_{H_hL_1}$
$L^1 + H^+ \rightleftarrows (HL^1)^+$	10.74	$L^1 + H^+ \rightleftarrows (HL^1)^+$	10.74
$L^1 + 2H^+ \rightleftarrows (H_2L^1)^{2+}$	20.82	$(HL^1)^+ + H^+ \rightleftarrows (H_2L^1)^{2+}$	10.08
$L^1 + 3H^+ \rightleftarrows (H_3L^1)^{3+}$	30.31	$(H_2L^1)^2 + H^+ \rightleftarrows (H_3L^1)^{3+}$	9.49
$L^1 + 4H^+ \rightleftarrows (H_4L^1)^{4+}$	38.07	$(H_3L^1)^{3+} + H^+ \rightleftarrows (H_4L^1)^{4+}$	7.76
$L^1 + 5H^+ \rightleftarrows (H_5L^1)^{5+}$	43.64	$(H_4L^1)^{4+} + H^+ \rightleftarrows (H_5L^1)^{5+}$	5.57
$L^1 + 6H^+ \rightleftarrows (H_6L^1)^{6+}$	47.16	$(H_5L^1)^{5+} + H^+ \rightleftarrows (H_6L^1)^{6+}$	3.52
	$\log \beta_{M_mH_hL_1}$		$\log K_{M_mH_hL_1}$
$Fe^{3+} + L^1 \rightleftarrows [FeL^1]^{3+}$	25.95(6)	$Fe^{3+} + L^1 \rightleftarrows [FeL^1]^{3+}$	25.95
$Fe^{3+} + H^+ + L^1 \rightleftarrows [FeHL^1]^{4+}$	33.48(4)	$[FeL^1]^{3+} + H^+ \rightleftarrows [FeHL^1]^{4+}$	7.53
$Fe^{3+} + 2H^+ + L^1 \rightleftarrows [FeH_2L^1]^{5+}$	39.09(6)	$[FeHL^1]^{4+} + H^+ \rightleftarrows [FeH_2L^1]^{5+}$	5.61
$Fe^{3+} + 3H^+ + L^1 \rightleftarrows [FeH_3L^1]^{6+}$	43.88(9)	$[FeH_2L^1]^{5+} + H^+ \rightleftarrows [FeH_3L^1]^{6+}$	4.79
$2Fe^{3+} + L^1 \rightleftarrows [Fe_2L^1]^{6+}$	38.02(4)	$[FeL^1]^{3+} + Fe^{3+} \rightleftarrows [Fe_2L^1]^{6+}$	12.07
$2Fe^{3+} + L^1 + H_2O \rightleftarrows [Fe_2L^1(OH)]^{5+} + H^+$	32.07(8)	$[Fe_2L^1(OH)]^{5+} + H^+ \rightleftarrows [Fe_2L^1]^{6+} + H_2O$	5.95
$2Fe^{3+} + L^1 + 2H_2O \rightleftarrows [Fe_2L^1(OH)_2]^{4+} + 2H^+$	24.5(1)	$[Fe_2L^1(OH)_2]^{4+} + H^+ \rightleftarrows [Fe_2L^1(OH)]^{5+} + H_2O$	7.6

$T = 298.2$ K and $I = 0.1$ mol dm^{-3} in KNO_3.

[a] Water molecules directly bound to the metal centres were omitted, because it is impossible by these studies to define the number of them.

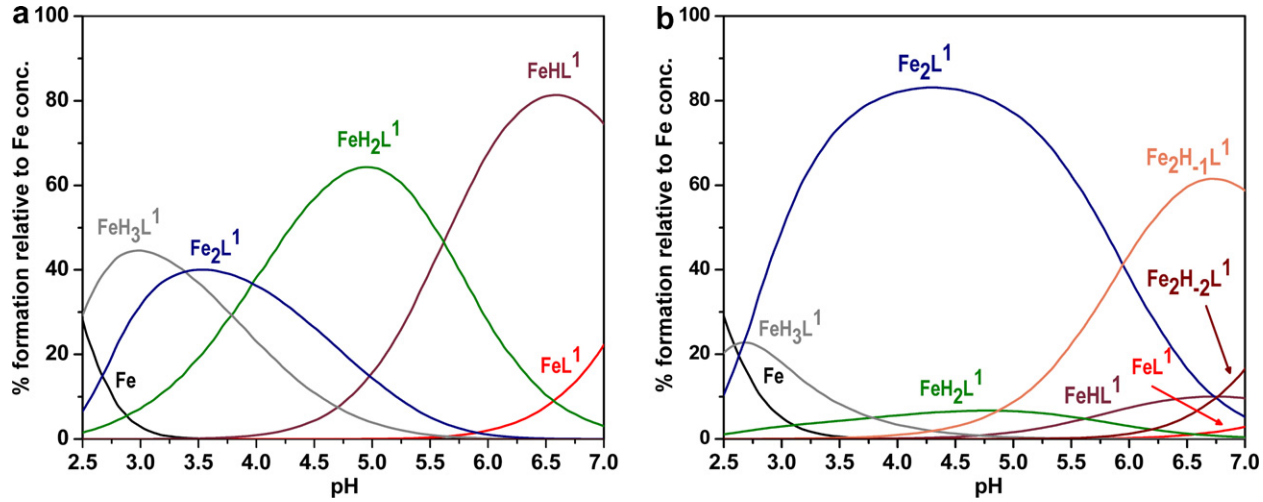

Fig. 1. Species distribution curves of iron(III) complexes of L^1: (a) $C_{Fe} = C_{L^1} = 0.001$ mol dm^{-3}; (b) $C_{Fe} = 2C_{L^1} = 0.001$ mol dm^{-3}. The charges of the species are omitted.

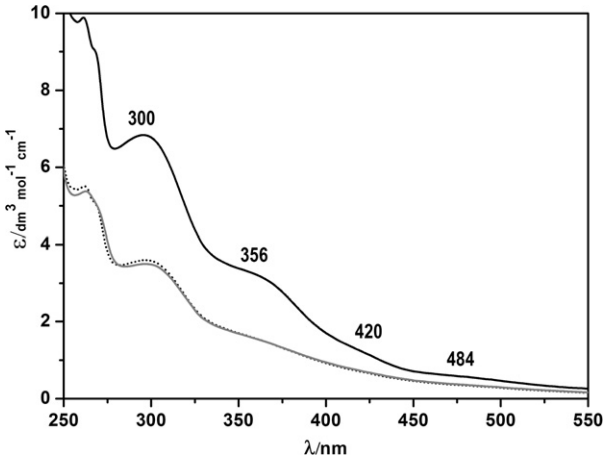

Fig. 2. UV–Vis spectra of 1:1 Fe^{3+}:L^1 ratio aqueous solutions ($C_{L^1} = 3.4 \times 10^{-4}$ mol dm^{-3}, pH 3.4, grey line and 7.4, short dot line) and 2:1 Fe^{3+}:L^1 ratio, ($C_{L^1} = 1.88 \times 10^{-4}$ mol dm^{-3}, pH 5.0, black solid line), at $T = 298$ K.

of L^1. The values of the three protonated species suggest the successive deprotonation of the aminopropyl arms. Upon coordination of the first metal ion by the donor atoms of the macrocycle, the second metal ion should coordinate to the arms. Both centres need additional water molecules to complete the corresponding coordination spheres.

The iron(III) ion usually bind strongly to "hard" donor atoms, such as oxygen atoms, and the amine ligands tend to prefer the iron(II) ion. However, the aminopropyl arms of predominantly donor character are likely to provide an electron-rich coordination environment for the metal centre imposing virtually no steric constraints. Additionally, the flexibility of the arms assists the metal centre to achieve the preferential octahedral geometry, and the relatively large distances between the two coordination sites also favours the dinuclear complex formation.

2.2. UV–Vis spectroscopic measurements

The UV–Vis spectral data of aqueous solutions of the iron(III) complexes of L^1 at 1:1 and 2:1 ratios and different pH values were recorded, see Fig. 2. All the spectra show very intense bands at 262–284 nm (with several shoulders), at 296–302 nm and shoulders at 420–422 nm. The former ones should be attributed to intra-ligand charge transfer bands, and the last ones were assigned to LMCT bands [6,27]. The electronic spectra as expected for a d^5 metal ion give no structural information because the strong charge-transfer absorptions overlap the weak forbidden d–d transitions.

The strong absorptions at 360–420 nm region have been tentatively ascribed to oxygen–iron(III) charge transfer bands [27] as found in natural proteins, such as oxohemerythrin [28,29], and synthetic oxo-bridged diiron complexes of ligands containing nitrogen donor atoms [6,30–32]. The bands at 440–510 nm have been assigned to mixed LMCT and near-UV oxygen to Fe charge transfer bands due to their unusual intensity [27,32].

Table 2
Rhombic distortions (E/D) and effective g-values expected from the high-spin species of the dinuclear iron(III) complex of L^1[a]

E/D	Doublet	g_1	g_2	g_3
$E/D \approx 0.173$	$\|\pm5/2\rangle$	9.93	0.18	0.22
	$\|\pm3/2\rangle$	<u>5.24</u>	3.08	3.43
	$\|\pm1/2\rangle$	1.31	<u>8.90</u>	2.35

[a] The values observed in the experimental spectra are underlined.

2.3. EPR spectroscopic studies

The spectrum of the 2:1 Fe(III)/L^1 ratio solution and pH about 5, for which the dinuclear ferric complex of L^1 was presented at about 85% in relation to total Fe(III) ion (Fig. 1b) at $T = 11.5$ and 98 K exhibits signals at $g \approx 8.90$, 5.24, 4.29 and large signal at $g \approx 2$. The resonances at lower field were ascribed to high-spin d^5 iron(III) species with different rhombic E/D distortions. The signal at $g \approx 2$ might be attributed to possible intermolecular interactions. No changes on resonances from the middle $|\pm3/2\rangle$ ($g \approx 5.24$) and the ground $|\pm1/2\rangle$ ($g \approx 8.90$) Kramer's doublets were observed from 11.5 to 98 K and very small differences were found on the relative intensity of the signals suggesting a low D value.

The well resolved signal at $g \approx 4.29$ is typical of the transition between the middle Kramer's doublet of other isomer of rhombic distorted iron(III) ion in high–spin state with $E/D = 1/3$. Using the spin-hamiltonian formalism for high-spin ferric iron [33], the low-field resonances at 8.90 and 5.24 can be assigned to another species with rhombic (E/D) distortion ≈0.173. The effective g-values expected for each Kramer's doublet are indicated in the Table 2.

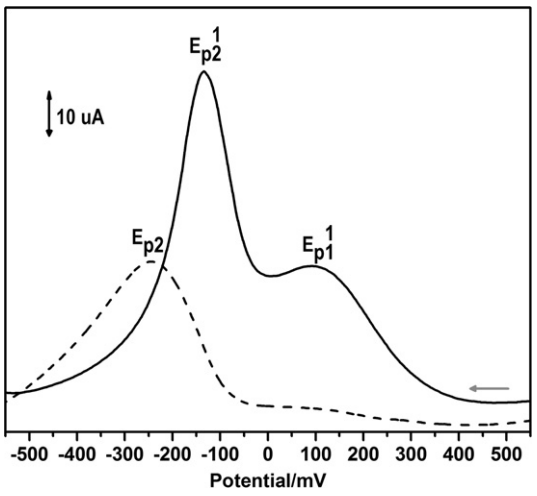

Fig. 3. Square-wave voltammetry profiles of Fe^{3+}/L^1 solutions at 1:1 ratio (dashed line), and 2:1 ratio (solid line) at pH 4.5. $C_{L^1} = 2.0 \times 10^{-3}$ mol dm^{-3} in 0.2 mol dm^{-3} KNO_3, potential vs. Ag/AgCl, glassy carbon working electrode, SW frequency 15 Hz, amplitude 25 mV and step height 4 mV.

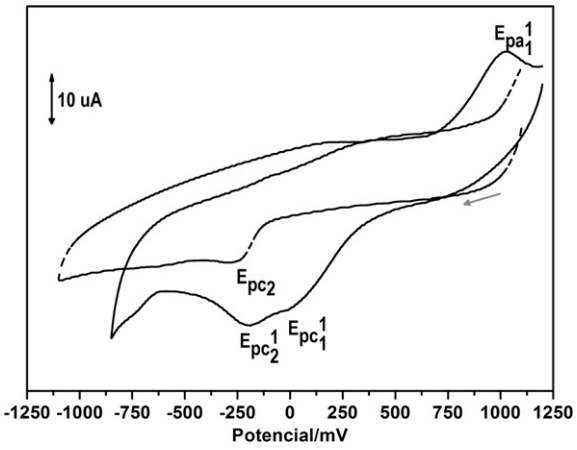

Fig. 4. Cyclic voltammetry profiles of Fe^{3+}/L^1 solutions at 1:1 (dashed line), and 2:1 ratios (solid line), at pH 4.5. $C_{L^1} = 2.0 \times 10^{-3}$ and 4.0×10^{-3} mol dm^{-3} in 0.2 and 0.4 mol dm^{-3} KNO_3, using glassy carbon working electrode at potential scan rate 0.1 V/s^{-1}, potential vs. Ag/AgCl.

2.4. IR spectroscopy

The IR spectrum of 2:1 Fe(III)/L^1 ratio solid sample in KBr showed bands at 3450 cm^{-1} (broad band) characteristic to the OH stretching modes of lattice water and intramolecular OH hydrogen bonds, 1380 cm^{-1} associated with tertiary aromatic amine vibrations and 1640 cm^{-1} due to the N–H bent vibrations characteristic for primary amines. The weak sharp asymmetric vibration band at 804 cm^{-1}, can be attributed to the metal–oxygen–metal asymmetric stretch vibrations [27,34], observed also for other hydroxo-bridged complexes of nitrogen donor ligands: linear [6,30] and macrocyclic ligands, such as 1,4,7-triazacyclononane [31] and L^6 [35]. The bands at 1030–1100 cm^{-1} region were only observed for the dinuclear ferric complex.

2.5. Electrochemical studies

The square wave voltammetry (SWV) profiles of iron(III)/L^1 solutions at 1:1 and 2:1 ratios, scanned at the potential window +1100/−1100 mV, were shown in Fig. 3, and the cyclic voltammograms (CV) of these solutions, recorded at the potential range of +1100 to −1100 and +1200 to −850 mV, respectively, are shown in Fig. 4. The 1:1 ratio solution showed one main peak, and a slightly amount of another species, suggesting that the main process corresponds to the reduction of the mononuclear complex, as indicated by the distribution diagram of Fig. 1a. The SWV profile of this species exhibits the reduction wave at $E_p = -240$ mV (peak E_{p2} in Fig. 3), and the oxidation wave was not observed. In the same experimental conditions, two peaks were observed (E_{p1}^1 and E_{p2}^1) for the 2:1 ratio solution at pH 4.5, at the value where 85% of dinuclear complex was formed relative to total metal concentration, see Fig. 1b. The process corresponding to the reaction $(Fe^{3+/3+})_2L^1 + e \rightleftarrows (Fe^{3+}/Fe^{2+})L^1$ was represented by the peak E_{p1}^1 and occurred at +95 mV (data from SWV). This peak is well defined at slow scan rate (25 mV/s^{-1}). To the peak at $E_{p2}^1 = -136$ mV corresponds the second redox process $(Fe^{3+}/Fe^{2+})L^{1+} + e \rightleftarrows (Fe^{2+}/Fe^{2+})L^1$. Only one anodic peak at $E_{pa1}^1 = +1010$ mV (Fig. 4) was observed at the sweep rate of 0.050–0.500 V/s. The reduction peak at about −750 mV can be attributed to a very small amount of $Fe(NO_3)_3$ in solution.

The electrochemical reactions in both cases are irreversible [36], the charge transfer is extremely slow and only one of the heterogeneous reactions on the electrode surface, the reduction, was measurable. Therefore, the concentrations of both redox species are controlled by the charge transfer reaction and are far from the thermodynamic equilibrium. The cathodic process occurred but the formed Fe^{2+} species was removed from the electrode surface due to reactions with oxygen (or other fast chemical transformation) in aqueous medium and thus no oxidation trace was observed.

The lack of solubility of the complexes in solvents other than water did not allow the study in a medium without presence of oxygen. Similar behaviour was found for the ferric mononuclear complexes of ligands with mixed nitrogen and oxygen donor atoms such as (2-hydroxybenzyl)(2-pyridylmethyl)-amine [11] and *N*,*N*′-bis(2-pyridylmethyl)-3-aminoacetate [37].

The E_{p2} value (see Fig. 3) may corresponded to the reduction of the iron(III) coordinated to the amines of the macrocyclic ring. In fact this value appears between the E_{pc} values for the Fe^{3+} complex of *N*,*N*′-bis(2-pyridylmethyl)-3-aminoacetate of −51 mV [37] and that for the Fe^{3+} complex of the N_6-macrocycle, diammac, of −350 mV [38] both values versus Ag/AgCl.

The value of E_{p2}^1 (data from SWV) is comparable to the value of the mononuclear complex, suggesting that the reduction processes occurs with the iron(III) in identical environments. The shift of this peak of 88 mV to more anodic potential in the dinuclear complex when compared to the equivalent reduction of the mononuclear complex was explained by the decrease of stabilization of the first centre imposed by the presence of the second iron(III) in the arms. As well known, the reduction potential is dependent not only of the type and number of donor atoms that can modify the Lewis acid–base character of the iron(III) core [39,40], but also of the strain of the ligand upon coordination. The different electrochemical data for both centres suggest that the two iron(III) centres have different coordination environments. The cathodic shift of the two individual reduction processes in the dinuclear complex of $\Delta E_p = E_{p2}^1 - E_{p1}^1 = 231$ mV is indicative of the weak interaction between both centres [41,42].

On the other hand, the irreversibility of the redox processes indicates that the species formed are not stable and suggests a mechanism involving other chemical steps, namely structural or conformational reorganization and/or disproportionation, as observed on other diiron complexes of nitrogen donor atoms ligands [43–45]. However, the differences on the electrochemical behaviour of the two studied complexes with the splitting and shifts of the redox potentials was explained by a weak electronic interference between the two metal centres on the dinuclear species.

3. Conclusions

The potentiometric studies of the complexation behaviour of L^1 with iron(III) ion have established the formation of mono- and dinuclear complexes in solution. Dinuclear hydroxo-complexes are formed upon pH 4. The dinuclear complex was formed even for the 1:1 stoichiometry simultaneously with mononuclear protonated species formed by the consecutive deprotonation of the ammonium groups of the arms. The ML^1 species is formed upon pH of about 6, and appears in insignificant amounts at 2:1 ratio. The thermodynamic stability constants of the mono- and dinuclear complexes were determined in the 2–7 pH range. The constant values for the deprotonation equilibria of the protonated mononuclear species are consistent with the consecutive deprotonation of the ammonium groups of the pendant arms, suggesting the macrocyclic nitrogen donor atoms as the preferred coordination sites of the first metal centre, and the aminopropyl arms for the second one. The low pH values at which the two dinuclear hydroxo-species are formed suggest that the water molecules are strongly bound to the metal centres.

The spectroscopic UV–Vis and IR data confirmed the existence of mono-, dinuclear and hydroxo-dinuclear complexes. The EPR spectral data of 2:1 ratio solution pointed to the presence of two high-spin d^5 state iron(III) species in different rhombic E/D distortion. The electrochemical studies were also consistent with the formation of mono- and dinuclear complexes with similar irreversible redox behaviour. The electrochemical properties of the two types of complexes are different, as expected, due to the different environment of both metal centres in the dinuclear complex, and the weak interaction between them.

In conclusion, our results support the formation of the dinuclear complex having the two metal centres coordinated in the two different sites of the ditopic macrocyclic ligand. Water molecules and counterions complete the metal coordination spheres. The formed dihydrolysed species precipitate below neutral pH, probably due to dimerization or polymerization, which precluded their characterization in solution at pH values higher than 5.5.

4. Experimental

4.1. Ligands and reagents

The parent macrocycle, 3,7,11,17-tetraazabicyclo[11.3.1]heptadeca-1(17),13,15-triene and its 3,7,11-tris(3-aminopropyl) derivative L^1 were synthesized by previously published methods [20]. All the chemicals were of reagent grade and used as supplied without further purification. The organic solvents were purified by standard methods [46]. The reference used for the ^1H NMR measurements in D_2O was 3-(trimethylsilyl)-propanoic acid-d_4-sodium salt and in $CDCl_3$ the solvent itself.

4.2. Potentiometric measurements

4.2.1. Preparation of solutions

The $Fe(NO_3)_3$ solutions were prepared at about 0.02 mol dm^{-3} from the analytical grade salt with demineralised water (from a Millipore/Milli-Q system). The solutions were standardized by titration with Na_2H_2edta [47] and were kept in excess of nitric acid to prevent the hydrolysis. The carbonate free solutions of the titrant, KOH, were prepared as described [20]. For the back titrations a 0.100 mol dm^{-3} solution of HNO_3 was used.

4.2.2. Equipment and work conditions

The equipment used was described previously [20]. The temperature was kept at 298.2 ± 0.1 K and atmospheric CO_2 was excluded from the cell during the titration by passing purified nitrogen across the top of the experimental solution in the reaction cell. The ionic strength of the solutions was kept at 0.10 mol dm^{-3} with KNO_3.

4.2.3. Measurements

The $[H^+]$ of the solutions was determined by the measurement of the electromotive force of the cell, $E = E^{'\circ} + Q\log[H^+] + E_j$. $E^{'\circ}$, Q, E_j, $K_w = ([H^+][OH])$ were obtained as described previously [20]. The value of K_w was found equal to $10^{-13.80}$ mol^2 dm^{-6}.

The potentiometric equilibrium measurements were carried out using 20.00 cm^3 of $\cong 2.50 \times 10^{-3}$ mol dm^{-3} ligand solution diluted to a final volume of 30.00 cm^3 in the presence of iron ion for the following C_{Fe}:C_{L1} ratios: 0.5:1, 0.7:1, 0.9:1, 1:1 at 2–7.5 pH range, and 1.5:1 and 2:1 at 2–6.5 pH range. Minimum of two replicate measurements were taken. The pH range taken for the studies was limited due to precipitation. Back-titration curves with standard HNO_3 were also performed when the equilibrium of the formed species was slow to attain.

4.2.4. Calculation of equilibrium constants

Stability constants of the various species formed in solution were obtained from the experimental data (potentiometric titrations) using the HYPERQUAD program [48]. The initial computations were obtained in the form of overall stability constants, $\beta_{M_mH_hL_1} = [M_mH_hL_1]/\{[M]^m[H]^h[L]^1\}$. Mononuclear ML, MH_hL (h = 1–3) and dinuclear $[M_2L]$, $[M_2H_{-1}L]$, $[M_2(H_{-1})_2L]$ species were found for iron(III) metal complexes of the studied ligand, being $\beta_{M_2H_{-1}L} = \beta_{M_2L(OH)} \times K_w$ and $\beta_{M_2(H_{-1})_2L} = \beta_{M_2L(OH)_2} \times (K_w)^2$.

The species proposed in a particular model were those that can be justified by the principles of co-ordination chemistry. The errors quoted are the standard deviations of the overall stability constants given directly by the program for the input data, which include all the experimental points of all titration curves used. The stability constants were obtained from about 220 experimental points and five titration curves.

4.3. Spectroscopic studies

Electronic spectra of the complexes in water were recorded with a UNICAM model UV-4 (in the UV–Vis range) or with a Shimadzu model UV-3100 (in the NIR range) spectrophotometers with solutions of 5×10^{-5} to 3.4×10^{-4} mol dm^{-3} at pH 3.4 and 7.4 for the iron(III) to ligand 1:1 ratio and 6×10^{-5}–1.9×10^{-4} mol dm^{-3} for the iron(III) to ligand 2:1 ratio at pH 4.9. EPR spectroscopic measurements of the dinuclear iron(III) complex was recorded with a Bruker ESP 380 spectrometer equipped with continuous-flow cryostats for liquid helium or liquid nitrogen, operating at X-band at 11.4 and 95 K. The complex was prepared at 2×10^{-3} mol dm^{-3} DMSO/H_2O (1:1, v/v) solutions with the metal to ligand ratio 2:1 at pH 5. IR spectra were recorded from KBr pellets of solid sample of iron(III) to ligand 2:1 ratio complex on a UNICAM Mattson 7000 spectrometer and from 2×10^{-3} mol dm^{-3} solution of iron(III) to ligand 2:1 ratio on a Bruker IFS 66/S spectrometer, using the OPUS program, version 5.5.

4.4. Electrochemical measurement

A BAS CV-50 W Voltammetric Analyzer connected to BAS/Windows data acquisition software was used for the electrochemical measurements. The cyclic voltammetry experiments were performed in a glass cell MF-1082 from BAS in a C-2 cell roofed in a Faraday cage, at 298.2 ± 0.1 K under a purified nitrogen atmosphere. The glassy carbon electrode was employed together with a reference Ag/AgCl (MF-2079 from BAS) electrode and 7.5 cm platinum coil ware (MW-2079 from BAS) with a gold plated connector

as a auxiliary electrode. The working electrode was electro-cleaned by multi cycle scanning in the electrode supporting solution, after polishing with alumina 0.3 μm, cleaned with water and sonicated before using, according with standard procedures [49]. The electrochemical reversibility of the glassy carbon electrode was tested by the simple one electron redox couple of 0.4 mol dm^{-3} aqueous solution of potassium ferricyanide $[Fe(CN)_6]^{3-}$, performed at various scan rate between 2 and 100 mV/s [50]. The applied aqueous solutions of the studied complexes were prepared in concentration 2.0–4.0 $\times 10^{-3}$ mol dm^{-3} in KNO_3 0.4 mol dm^{-3} as a supporting electrolyte, at the metal to ligand 1:1 and 2:1 ratios, which were purged by N_2 for 15 min before applying the voltage. The indicated species are predominant at the quoted pH range, based on the corresponding Hyss speciation curves [21].

Acknowledgements

The authors acknowledge Helena Carapuça, from Universidade de Aveiro, the help on the electrochemical measurements and the fruitful discussions of the results. The authors also thank Manuela Pereira for the acquisition of EPR spectra. K.P. Guerra acknowledges FCT for a grant (SFRH/BD/6492/2001).

References

[1] E.I. Solomon, T.C. Brunold, M.I. Davis, J.N. Kemsley, S-K. Lee, N. Lehnert, F. Neese, A.J. Skulan, Y.-S. Yang, J. Zhou, Chem. Rev. 100 (2000) 235.
[2] K. Wieghardt, I. Tolksdorf, W. Herrmman, Inorg. Chem. 24 (1985) 1230.
[3] V. Balland, F. Banse, E. Anoxalabéhére-Mallart, M. Chiladi, T.A. Mattioli, C. Philouze, G. Blondin, J.-J. Girerd, Inorg. Chem. 42 (2003) 2470.
[4] G. Roelfes, V. Vrajmasu, K. Chen, R.Y.N. Ho, J.-U. Rodhe, C. Zondervan, R.M. la Crois, E.P. Schudde, M. Lutz, A.L. Spek, R. Hage, B.L. Feringa, E. Münck, L. Que Jr., Inorg. Chem. 42 (2003) 2639.
[5] J.M. Rowland, M. Olmstead, P.K. Mascharak, Inorg. Chem. 40 (2001) 2810.
[6] P. Gómez-Romero, E.H. Witten, W.M. Reiff, G. Backes, J. Sanders-Loehr, G.B. Jameson, J. Am. Chem. Soc. 111 (1989) 9039.
[7] R. Viswanatan, M. Palaniandavar, T. Balasubramanian, P.T. Muthiah, J. Chem. Soc., Dalton Trans. (1996) 2519.
[8] R.M. Burger, Chem. Rev. 98 (1998) 1151.
[9] M.S. Costas, M.P. Mehn, M.P. Jensen, L. Que Jr., Chem. Rev. 104 (2004) 939.
[10] T. Jüstel, M. Müller, T. Weyhermüller, C. Kressl, E. Bill, P. Hildebrandt, M. Lengen, M. Grodzicki, A.X. Trautwein, B. Nuber, K. Wieghardt, Chem. Eur. J. 5 (1999) 793.
[11] K. Meyer, E. Bill, B. Mienert, T. Weyhermüller, K. Wieghardt, J. Am. Chem. Soc. 121 (1999) 4859.
[12] S.V. Kryatov, E.V. Rybak-Akimova, S. Schindler, Chem. Rev. 105 (2005) 2175.
[13] E.Y. Tshuva, S.J. Lippard, Chem. Rev. 104 (2004) 987.
[14] B.T. Green, J. Thorburn, M.C. Willingham, A. Thorburn, R.P. Planalp, M.W. Brechbiel, J.J. Gee, J. Wilkinson IV, F.M. Torti, S.V. Torti, J. Biol. Inorg. Chem. 277 (2002) 25568.
[15] R.D. Hancock, A.E. Martell, Chem. Rev. 89 (1989) 1875.
[16] A.C. Melnyk, N.K. Kildahl, A.R. Rendina, D.H. Busch, J. Am. Chem. Soc. 101 (1979) 3232.
[17] C.J. Cairns, R.A. Heckman, A.C. Melnyk, W.M. Davis, D.H. Busch, J. Chem. Soc., Dalton Trans. (1987) 2505.
[18] J. Costa, R. Delgado, M.C. Figueira, R.T. Henriques, M. Teixeira, J. Chem. Soc., Dalton Trans. (1997) 65.
[19] R. Delgado, S. Quintino, M. Teixeira, A. Zhang, J. Chem. Soc., Dalton Trans. (1996) 55.
[20] K.P. Guerra, R. Delgado, M.G.B. Drew, V. Félix, Dalton Trans. (2006) 4124.
[21] L. Alderighi, P. Gans, A. Ienco, D. Peters, A. Sabatini, A. Vacca, Coord. Chem. Rev. 184 (1999) 311.
[22] G. McLendon, R.J. Motekaitis, A.E. Martell, Inorg. Chem. 15 (1976) 2306.
[23] M. Branca, B. Pispisa, C. Aurisicchio, J. Chem. Soc., Dalton Trans. (1976) 1543.
[24] Z. Wang, A.E. Martell, R.J. Motekaitis, J. Reibenspies, J. Chem. Soc., Dalton Trans. (1999) 2441.
[25] R. Delgado, M.C. Figueira, S. Quintino, Talanta 45 (1997) 451.
[26] M.P. Byfield, M.S.A. Hamza, J.M. Pratt, J. Chem. Soc., Dalton Trans. (1993) 1641.
[27] D.M. Kurtz Jr., Chem. Rev. 90 (1990) 585.
[28] R.C. Reem, J.M. McCormick, D.E. Richardson, F.J. Devlin, P.J. Stephens, R.R.L. Musselman, E.I. Solomon, J. Am. Chem. Soc. 111 (1989) 4688.
[29] M. McCormick, R.C. Reem, E.I. Solomon, J. Am. Chem. Soc. 113 (1991) 9066.
[30] A. Hazell, K.B. Jensen, C.J. McKenzie, H. Toftlund, Inorg. Chem. 33 (1994) 3127.
[31] A. Spool, I.D. Williams, S.J. Lippard, Inorg. Chem. 24 (1985) 2156.
[32] J. Sanders-Loehr, W.D. Wheeler, A.K. Shiemke, B.A. Averill, T.M. Loehr, J. Am. Chem. Soc. 111 (1989) 8084.
[33] W.R. Hagen, in: R. Cammack, A.G. Sykes (Eds.), Advances in Inorganic Chemistry, vol. 38, 1992, p. 165.
[34] G. Socrates, Infrared an Raman Characteristic Group Frequencies, 3rd ed., J. Wiley & Sons Ltd, West Sussex, England, 2001. p. 95.
[35] S.M. Nelson, D.H. Busch, Inorg. Chem. 8 (1969) 1859.
[36] R. Greef, R. Peat, L.M. Peter, D. Pletcher, J. Robinson, Instrumental Methods in Electrochemistry, Ellis Horwood Ltd, Sussex, England, 1985.
[37] M.C. Rodriguez, F. Lambert, I. Morgenstern-Badarau, M. Cesario, J. Guilhem, B. Keita, L. Nadjo, Inorg. Chem. 36 (1997) 3525.
[38] P.V. Bernhardt, P. Comba, T.W. Hambley, G.A. Lawrance, Inorg. Chem. 30 (1991) 942.
[39] N.M.F. Carvalho, O.A.C. Antunes, A. Horn Jr., Dalton Trans. (2007) 1023.
[40] R.C. Holz, T.E. Elgren, L.L. Pearce, J.H. Zhang, C.J. O'Connor, L. Que Jr., Inorg. Chem. 32 (1993) 5844.
[41] M. Ghiladi, K.B. Jensen, J. Jiang, C.J. McKenzie, S. Mørup, I. Søtofte, J. Ulstrup, J. Chem. Soc., Dalton Trans. (1999) 2675.
[42] A.S. Borovik, V. Papaefthymiou, L.F. Taylor, O.P. Anderson, L. Que Jr., J. Am. Chem. Soc. 111 (1989) 6183.
[43] J. Mukherjee, V. Balamurugan, R. Gupta, R. Mukherjee, J. Chem. Soc., Dalton Trans. (2003) 3686.
[44] L. Nivorozhkin, E. Anoxalabéhére-Mallart, P. Mialane, R. Davydov, J. Guilhem, M. Cesario, J.-P. Audière, J.-J. Girerd, S. Styring, L. Schussler, J.-L. Seris, Inorg. Chem. 36 (1997) 846.
[45] S. Wang, Q. Luo, X. Wang, L. Wang, K. Yu, J. Chem. Soc., Dalton Trans. (1995) 2045.
[46] D.D. Perrin, W.L.F. Armarego, Purification of Laboratory Chemicals, 3rd ed., Pergamon, Oxford, 1988.
[47] G. Schwarzenbach, W. Flaschka, Complexometric Titrations, Methuen & Co, London, 1969.
[48] P. Gans, A. Sabatini, A. Vacca, Talanta 43 (1996) 1739.
[49] L.J. Kepley, A.J. Bard, Anal. Chem. 60 (1988) 1459.
[50] H.E. Zittel, F.J. Miller, Anal. Chem. 37 (1965) 200.

Polyhedron 27 (2008) 2271–2276

Contents lists available at ScienceDirect

Polyhedron

journal homepage: www.elsevier.com/locate/poly

Nickel(II) complexes with *N*-(thio)phosphorylthioureas AdNHC(S)NHP(X)(O*i*Pr)$_2$: Versatile coordination of phosphoryl (X = O) and thiophosphoryl (X = S) derivatives

Damir A. Safin [a,c,*], Felix D. Sokolov [a], Łukasz Szyrwiel [b], Maria G. Babashkina [a], Timur R. Gimadiev [a], F. Ekkehardt Hahn [c], Henryk Kozlowski [b], Dmitriy B. Krivolapov [d], Igor A. Litvinov [d]

[a] *A. M. Butlerov Chemistry Institute, Kazan State University, Kremlevskaya Street 18, 420008 Kazan, Russian Federation*
[b] *Faculty of Chemistry, University of Wroclaw, F. Joliot-Curie Street 14, 50383 Wroclaw, Poland*
[c] *Institut für Anorganische und Analytische Chemie, Westfälische Wilhelms-Universität Münster, Corrensstrasse 36, D-48149 Münster, Germany*
[d] *A. E. Arbuzov Institute of Organic and Physical Chemistry, Arbuzov Street 8, 420088 Kazan, Russian Federation*

ARTICLE INFO

Article history:
Received 19 March 2008
Accepted 4 April 2008
Available online 5 June 2008

Keywords:
Chelate
Hydrogen bond
Nickel complexes
Crystal structures
N-(Thio)phosphorylthiourea

ABSTRACT

The reaction of the potassium salts of *N*-(thio)phosphorylated thioureas of the common formula AdN(H)C(S)N(H)P(X)(O*i*Pr)$_2$ (X = O, **HL^{I}**; X = S, **HL^{II}**) with the Ni(II) cation in aqueous EtOH leads to [**Ni(L^{I,II})$_2$**] chelate complexes. The molecular structures of the thioureas **HL^{I,II}** and the complexes [**Ni(L^{I}-*N*,*S*)$_2$**] and [**Ni(L^{II}-*S*,*S*′)$_2$**] were elucidated by single crystal X-ray diffraction analysis, IR, ^{1}H and ^{31}P NMR spectroscopy and microanalysis. In the complex [**Ni(L^{I})$_2$**], the metal center is found to be in a square-planar N_2S_2 environment formed by the C=S sulfur atoms and the P–N nitrogen atoms of two deprotonated **L^{I}** ligands. The ligands are in a *trans* configuration. The Ni(II) atom in complex [**Ni(L^{II})$_2$**], with the deprotonated thiourea **L^{II}**, is coordinated in a square-planar fashion by the C=S and P=S sulfur atoms of two anionic ligands. The ligands are in a *cis* configuration.

© 2008 Elsevier Ltd. All rights reserved.

1. Introduction

Competitive coordination of polydentate ligands has been of interest over the last four decades [1]. The Hard Soft Acid Base (HSAB) principle has been used to explain the coordination versatility of metal cations with donor centers of polyfunctional ligands [1a]. However, the HSAB principle is not enough if the ligand contains several hard or soft coordination atoms contesting for a place in the coordination environment of a metal cation. The influence of different steric factors, additional intra- and intermolecular bonding (e.g. hydrogen bonds), the electron effects of substituents and many other factors must be taken into account.

We recently published data illustrating the influence of intramolecular hydrogen bonds on the 1,3-*N*,*S*- and 1,5-*O*,*S*-coordination of *N*-phosphoryl-*N*′-(R)-thioureas RNHC(S)NHP(O)(O*i*Pr)$_2$ (**HL**) (R = Ph [2]; R = *p*-MeOC$_6$H$_4$, *p*-BrC$_6$H$_4$, *t*-Bu, *c*-Hex [3]) with Ni(II). It was established that intramolecular hydrogen bonds N–H···O=P are a necessary condition for the 1,3-*N*,*S*-isomer stabilization in square-planar complexes of Ni(II). The destabilization of Ni(II) complexes and a change of the coordination mode from the 1,3-*N*,*S*- to the 1,5-*O*,*S*-isomer chelates takes place when H-bonding in the coordinated anionic ligands **L** is not possible (R = Et$_2$N, morpholine-*N*-yl). Thus, intramolecular hydrogen bonding realized outside the coordination sphere of the metal cation is the reason for the dramatic changes of such important parameters as bite angle and the ligand's field strength.

Herein we present the structure of two new thioureas of the common formula AdNHC(S)NHP(X)(O*i*Pr)$_2$ and their complexing properties towards the nickel(II) cation. Comparative analysis on the coordination mode of the phosphorylated (X = O) and thiophosphorylated (X = S) derivatives have been performed.

2. Experimental

2.1. Synthesis of HL^{I} and HL^{II}

A solution of 1.510 g (10 mmol) 1-adamantylamine in anhydrous CH_2Cl_2 (15 mL) was treated, whilst vigorously stirring, with a solution of 2.676 g (12 mmol) of (*i*PrO)$_2$P(O)NCS or 2.868 g (12 mmol) of (*i*PrO)$_2$P(S)NCS in anhydrous CH_2Cl_2 (10 mL). The mixture was stirred for an additional 30 min to complete the reaction. The solvent was removed in a vacuum, and the product was purified by crystallization from dichloromethane by *n*-hexane.

* Corresponding author. Address: A. M. Butlerov Chemistry Institute, Kazan State University, Kremlevskaya Street 18, 420008 Kazan, Russian Federation. Tel.: +7843 231 53 97; fax: +7843 254 37 34.
E-mail address: damir.safin@ksu.ru (D.A. Safin).

0277-5387/$ - see front matter © 2008 Elsevier Ltd. All rights reserved.
doi:10.1016/j.poly.2008.04.014

***HL*^{I}**. Yield: 3.590 g (96%). M.p. 137 °C. ^{1}H NMR (d_6-acetone): δ 1.33 (d, $^{3}J_{H,H}$ = 6.2 Hz, 12H, CH_3), 1.63–1.78 (m, 6H, C^4H_2), 2.00–2.12 (m, 3H, C^3H), 2.27 (d, $^{3}J_{H,H}$ = 2.7 Hz, 6H, C^2H_2), 4.67 (d sept, $^{3}J_{POCH}$ = 7.4 Hz, $^{3}J_{H,H}$ = 6.2 Hz, 2H, OCH), 7.85 (d, $^{2}J_{PNH}$ = 7.4 Hz, 1H, P(O)NH), 9.05 (s, 1H, NH) ppm. ^{31}P NMR (d_6-acetone): δ −0.8 (t, $^{2}J_{PNH}$ = $^{3}J_{POCH}$ = 7.5 Hz) ppm. IR (KBr): ν 1006 (POC), 1241 (P═O), 1525 (S═C–N), 3123, 3291 (NH) cm^{-1}. *Anal.* Calc. for $C_{17}H_{31}N_2O_3PS$ (374.48): C, 54.52; H, 8.34; N, 7.48. Found: C, 54.56; H, 8.28; N, 7.55%.

***HL*^{II}**. Yield: 2.847 g (73%). M.p. 107 °C. ^{1}H NMR ($CDCl_3$): δ 1.34 (d, $^{3}J_{H,H}$ = 6.2 Hz, 12H, CH_3), 1.68 (br. s, 6H, C^4H_2), 2.11 (br. s, 3H, C^3H), 2.23 (br. s, 6H, C^2H_2), 4.77 (d sept, $^{3}J_{POCH}$ = 10.7 Hz, $^{3}J_{H,H}$ = 6.2 Hz, 2H, OCH), 6.51 (br. s, 1H, P(S)NH), 7.73 (s, 1H, NH) ppm. ^{31}P NMR ($CDCl_3$): δ 53.4 (t, $^{2}J_{PNH}$ = $^{3}J_{POCH}$ = 10.5 Hz) ppm. IR (Nujol): ν 643 (P═S), 1000 (POC), 1557 (S═C–N), 3103, 3382 (NH) cm^{-1}. *Anal.* Calc. for $C_{17}H_{31}N_2O_2PS_2$ (390.54): C, 54.28; H, 8.00; N, 7.17. Found: C, 54.35; H, 8.06; N, 7.09%.

2.2. Synthesis of [*Ni*(*L*^{I})$_2$] and [*Ni*(*L*^{II})$_2$]

A suspension of 1.112 g **HL^{I}** or 1.170 g **HL^{II}** (3 mmol) in aqueous EtOH (10 mL) was mixed with an aqueous EtOH solution of potassium hydroxide (0.185 g, 3.3 mmol). An aqueous EtOH (10 mL) solution of 0.245 g $NiCl_2$ (1.9 mmol) was added dropwise under vigorous stirring to the resulting potassium salt. The mixture was stirred at room temperature for a further 3 h and left overnight. The resulting complex was extracted with dichloromethane, washed with water and dried with anhydrous $MgSO_4$. The solvent was then removed in vacuo. Violet [**Ni**(**L^{I}**)$_2$] and dark blue [**Ni**(**L^{II}**)$_2$] crystals were isolated from dichloromethane by *n*-hexane. All yields are given with respect to the ligand.

[***Ni*(*L*^{I})$_2$**]. Yield: 0.640 g (53%). M.p. 146 °C. ^{1}H NMR ($CDCl_3$): δ 1.34 (d, $^{3}J_{H,H}$ = 5.9 Hz, 24H, CH_3), 1.64 (s, 18H, C^4H_2 + C^3H), 2.07 (s, 12H, C^2H_2), 4.62 (d sept, $^{3}J_{POCH}$ = 7.2 Hz, $^{3}J_{H,H}$ = 6.0 Hz, 4H, OCH), 8.51 (s, 2H, NH) ppm. ^{31}P NMR ($CDCl_3$): δ 0.9 (t, $^{3}J_{POCH}$ = 7.3 Hz) ppm. IR (KBr): ν 997 (POC), 1198 (P═O), 1549 (SCN), 3147 (NH) cm^{-1}. *Anal.* Calc. for $C_{34}H_{60}N_4NiO_6P_2S_2$ (805.63): C, 50.69; H, 7.51; N, 6.95. Found: C, 50.76; H, 7.44; N, 6.88%.

[***Ni*(*L*^{II})$_2$**]. Yield: 0.804 g (64%). M.p. 170 °C. ^{1}H NMR ($CDCl_3$): δ 1.12–2.36 (m, 57H, CH_3 + C^2H_2 + C^3H + C^4H_2), 4.66 (br. s, 2H, OCH), 4.96 (br. s, 2H, OCH), 5.70 (d, $^{4}J_{HNCNP}$ = 5.5 Hz, 1H, NH), 9.10 (s, 1H, NH) ppm. ^{31}P NMR ($CDCl_3$): δ 51.9 (6.69 P), 53.8 (6.18 P), 55.1 (1.12 P), 58.6 (1 P) ppm. IR (Nujol): ν 606 (P═S), 989 (POC), 1508 (SCN), 3409 (NH) cm^{-1}. *Anal.* Calc. for $C_{34}H_{60}N_4NiO_4P_2S_4$ (837.77): C, 48.74; H, 7.22; N, 6.69. Found: C, 48.65; H, 7.28; N, 6.76%.

2.3. Physical measurements

NMR spectra of **HL^{I}** and [**Ni**(**L^{I}**)$_2$] were recorded on a Bruker AC 200 spectrometer using Me_4Si as an internal standard. IR spectra were recorded using a Bruker Vektor 22. Elemental analyses were performed on a Vario EL III CHNS elemental analyzer at the IAAC, University Münster, Germany. NMR spectra of **HL^{II}** and [**Ni**(**L^{II}**)$_2$] were recorded on a Varian Unity-300 NMR spectrometer using Me_4Si as an internal standard. IR spectra were recorded using a Specord M-80. Elemental analyses were performed on a Perkin–Elmer CHN elemental analyzer.

2.4. Crystal structure determination and refinement

The X-ray data for **HL^{I}** and [**Ni**(**L^{I}**)$_2$] were collected at −173 °C using a KM4CCD diffractometer and graphite-monochromated Mo Kα radiation. The images were indexed, integrated and scaled using the KUMA data reduction package [4]. The structures were solved by a direct method using SHELX97 [5] and refined by the full-matrix least-squares method on all F^2 data [6]. Non-hydrogen atoms were included in the refinement, with anisotropic displacement parameters. The hydrogen atoms were positioned geometrically and refined isotropically. The hydrogen atoms of the NH groups were included from $\Delta\rho$ maps and refined isotropically. All calculations were preformed using the WINGX program [7]. The X-ray diffraction data for **HL^{II}** and [**Ni**(**L^{II}**)$_2$] were collected at 20 °C using Bruker Kappa Apex2 (graphite-monochromator Cu Kα radiation for **HL^{II}**) and Bruker Smart Apex2 (graphite-monochromator Mo Kα radiation for [**Ni**(**L^{II}**)$_2$]) diffractometers. The images were indexed, integrated and scaled using the APEX2 data reduction package [8]. All raw data were corrected for absorption using the SADABS program [9]. The structures were solved by a direct method using the SIR [10] program and the refinement was carried out with SHELXL [11] using anisotropic thermal parameters for all non-hydrogen atoms. Hydrogen atoms were added to the structural models in calculated positions and were refined as rigid atoms. Hydrogen atoms of the NH groups for **HL^{II}** were included from $\Delta\rho$ maps and refined isotropically. All figures were made using the program PLATON [12].

***HL*^{I}**. $C_{17}H_{31}N_2O_3PS$, M_r = 374.48 g mol^{-1}, monoclinic, space group $P2(1)/c$, a = 13.150(4), b = 10.988(3), c = 13.550(4) Å, β = 105.02(3)°, V = 1891.0(10) Å^3, Z = 4, ρ = 1.315 g cm^{-3}, μ(Mo Kα) = 0.274 mm^{-1}, reflections: 15447 collected, 4440 unique, R_{int} = 0.082, R_1(all) = 0.0387, wR_2(all) = 0.0955.

***HL*^{II}**. $C_{17}H_{31}N_2O_2PS_2$, M_r = 390.55 g mol^{-1}, monoclinic, space group $C2/c$, a = 24.8344(7), b = 8.2279(2), c = 22.7318(6) Å, β = 116.6650(10)°, V = 4150.9(2) Å^3, Z = 8, ρ = 1.250 g cm^{-3}, μ(Cu Kα) = 3.146 mm^{-1}, reflections: 19257 collected, 3091 unique, R_{int} = 0.038, R_1(all) = 0.0351, wR_2(all) = 0.0987.

[Ni*(*L*^{I})$_2$*]. $C_{34}H_{60}N_4NiO_6P_2S_2$, M_r = 805.63 g mol^{-1}, monoclinic, space group $P2(1)/c$, a = 11.784(3), b = 29.4758(1), c = 11.2908(10) Å, β = 91.0200°, V = 3921.2(11) Å^3, Z = 4, ρ = 1.365 g cm^{-3}, μ(Mo Kα) = 0.730 mm^{-1}, reflections: 26880 collected, 9265 unique, R_{int} = 0.063, R_1(all) = 0.0398, wR_2(all) = 0.0887.

[Ni*(*L*^{II})$_2$*]. $C_{34}H_{60}N_4NiO_4P_2S_4$, M_r = 837.77 g mol^{-1}, monoclinic, space group $C2/c$, a = 24.040(8), b = 11.681(4), c = 15.330(6) Å, β = 106.634(6)°, V = 4125(3) Å^3, Z = 4, ρ = 1.349 g cm^{-3}, μ(Mo Kα) = 0.791 mm^{-1}, reflections: 9206 collected, 3453 unique, R_{int} = 0.049, R_1(all) = 0.0432, wR_2(all) = 0.0979.

3. Results and discussion

3.1. Synthesis

The thioureas **HL^{I}** and **HL^{II}** were prepared by the addition reaction of 1-adamantylamine to isothiocyanates of diisopropylphosphoric (iPrO)$_2$P(O)NCS and diisopropylthiophosphoric (iPrO)$_2$P(S)NCS acids, respectively. The complexes [**Ni**(**L^{I}**)$_2$] and [**Ni**(**L^{II}**)$_2$] were prepared by the following procedure: the ligand was converted to the potassium salt and followed by interaction with nickel(II) chloride (Scheme 1). The obtained compounds are crystalline solids and are soluble in most polar solvents. According to the elemental analysis, they have a ratio Ni:**L^{I,II}** of 1:2.

According to the X-ray diffraction analysis, IR, ^{1}H and ^{31}P NMR spectroscopy data, the metal center in complex [**Ni**(**L^{I}**)$_2$] is found in a square-planar N_2S_2 environment formed by the C═S sulfur atoms and the P–N nitrogen atoms. On the contrary, 1,5-*S*,*S*′-coordination of the Ni^{II} atom was found in the crystal of the [**Ni**(**L^{II}**)$_2$] complex.

3.2. IR and NMR spectroscopy

The IR spectra of **HL^{I}** and **HL^{II}** contain two absorption bands for the NH groups in the given areas: 3291–3382 (the narrow band)

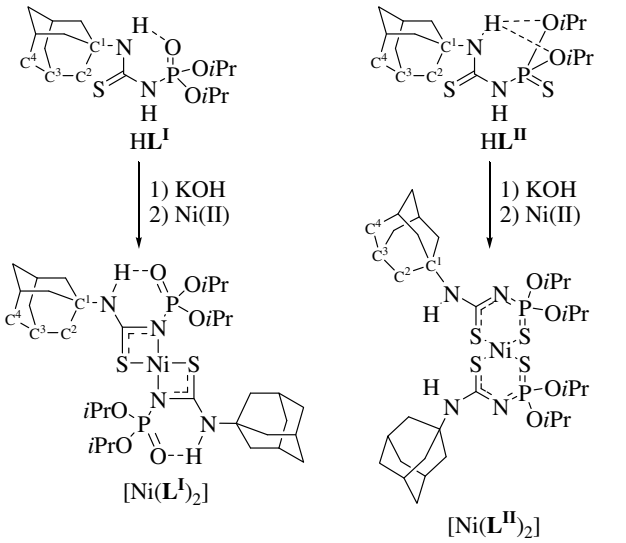

Scheme 1. Preparation of the complexes $[Ni(L^{I,II})_2]$.

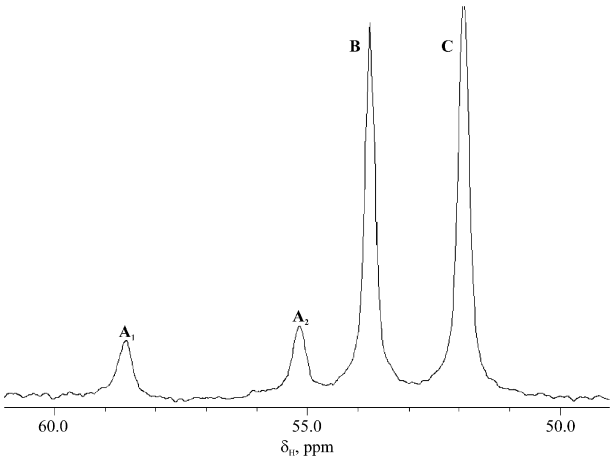

Fig. 1. ^{31}P NMR spectrum of the complex $[Ni(L^{II})_2]$.

and 3103–3123 (the wide intensive band) cm^{-1}. The bands in the low frequency region show the formation of hydrogen bonds in the solid state. The bands for the S═C–N group are at 1525–1557 cm^{-1} in the IR spectra of the obtained thioureas [13]. The absorption band of the P═S group of HL^{II} is observed in the characteristic area at 643 cm^{-1}. The IR spectrum of HL^{I} contains a strong band at 1241 cm^{-1} because of the P═O group. Presence of a wide absorption band of the POC fragments in HL^{I} and HL^{II} in the area 1000–1006 cm^{-1} also unequivocally confirms the presence of the substituted phosphoric fragment [13].

There is only a triplet signal at −0.8 and 53.4 ppm in the ^{31}P NMR spectra of HL^{I} and HL^{II}, respectively. The signal at −0.8 ppm is in the region that is characteristic for neutral *N*-phosphorylated thioureas, whereas the signal at 53.4 ppm corresponds to *N*-thiophosphorylated thioureas [14,15].

In the ^{1}H NMR spectra of HL^{I} and HL^{II} the adamantyl proton signals are at 1.63–2.27 ppm. The spectra of both ligands contain a set of signals for the *i*PrO protons: a doublet for the CH_3 protons at 1.33–1.34 ppm and a doublet of septets for the CH proton in the area 4.67–4.77 ppm. The signals at 7.85 and 6.51 ppm correspond to the P(O)NH and P(S)NH protons, respectively, in HL^{I} and HL^{II}. The main difference involves the signals at 9.05 ppm in the spectrum of the ligand HL^{I} and at 7.73 ppm for HL^{II}, corresponding to the AdNH hydrogen.

The IR and NMR spectra of the thiourea HL^{I} clearly show the presence of the strong intramolecular N–H···O═P hydrogen bonds both in the solid state and in solution [2,3,13]. The AdNH proton signal in the ^{1}H NMR spectrum of HL^{I} is low-field shifted because of the strong intramolecular N–H···O═P hydrogen bond which remains in the d_6-acetone solution.

The IR spectrum of the complex $[Ni(L^{II})_2]$ in Nujol contains an absorption band for the P═S group of the anionic form of L^{II}, which is shifted by 37 cm^{-1} to a lower frequency relative to the band of the parent ligand HL^{II}. This confirms its participation in chelate formation. The absorption band of the P═O group of L^{I} in complex $[Ni(L^{I})_2]$ is also shifted to a lower frequency relative to the band of the ligand HL^{I}, and the shift is 43 cm^{-1}. This value is the biggest among the obtained 1,3-*N*,*S*-chelates [2,3], but it is definitely smaller than those for the corresponding 1,5-*O*,*S*-isomers. The low frequency shift of the P═O group band reaches 80–100 cm^{-1} for the 1,5-*O*,*S*-chelates of similar ligands [2,3,16].

There is only the NH group absorption band in the IR spectra of complexes $[Ni(L^{I})_2]$ and $[Ni(L^{II})_2]$, at 3147 and 3409 cm^{-1}, respectively. The NH absorption band in the IR spectrum of the complex $[Ni(L^{I})_2]$ is practically in the same region as it was for the parent ligand. This, together with the small shift of the P═O group absorption band relative to the band of the ligand HL^{I}, indicates the preservation of the intramolecular N–H···O═P hydrogen bond on complex formation. A similar outcome was observed for the Ni(II) complexes with the common formula $Ni[RNHC(S)NP(O)(OiPr)_2]_2$ (R = Ph [2]; R = *p*-$MeOC_6H_4$, *p*-BrC_6H_4, *t*-Bu, *c*-Hex [3]). On the other hand, for $[Ni(L^{II})_2]$ the frequency of the NH group band is characteristic for 1,5-*O*,*S*- and 1,5-*S*,*S*′-chelates, showing the absence of intramolecular H-bonding [2,3,16,17].

In the IR spectra of the complexes $[Ni(L^{I})_2]$ and $[Ni(L^{II})_2]$ there is an intense absorption band at 1508–1549 cm^{-1} corresponding to the conjugated SCN fragment. This fact also confirms the complexes formation. In addition there is a wide intensive band for the POC group at 989–997 cm^{-1}. It confirms the preservation of the structure of the ligands in the obtained complexes.

The ^{31}P NMR spectrum of complex $[Ni(L^{I})_2]$ in $CDCl_3$ contains a single triplet signal at 0.9 ppm. which differs by a negligible margin from the signal of the parent ligand (−0.8 ppm). This confirms the non-participation of the oxygen atom of the P═O group in complex formation [2,3].

The ^{31}P NMR spectrum of $[Ni(L^{II})_2]$ is more complicated. There are four broadened singlet signals at 51.9, 53.8, 55.1 and 58.6 ppm which were denoted by A_1, A_2, **B** and **C** (Fig. 1). However, only a signal at 50.8 ppm is observed in the MAS NMR $^{31}P–\{^{1}H\}$ spectrum of the polycrystals of $[Ni(L^{II})_2]$.[1] According to the X-Ray data this signal corresponds to the *cis*-isomer.

Quite a similar pattern was found in the ^{31}P NMR spectra of the 1,5-*S*,*S*′-chelates of the formulas $Ni[PhNHC(S)NP(S)(OiPr)_2]_2$ and $Ni[tBuNHC(S)NP(S)(OiPr)_2]_2$ [17]. On the basis of this comparision, the three signal groups (A_1 + A_2, **B** and **C**) can be related respectively to the three following diamagnetic square-planar isomers, with different dispositions and conformations of two ligands. The further investigation of the structure and properties of the obtained compounds in solution is in progress.

The ^{1}H NMR spectrum of the complex $[Ni(L^{I})_2]$ contains a single set of signals for the $(iPrO)_2P(O)$ and Ad protons. The adamantyl proton signals are at 1.64–2.07 ppm. The isopropyl group is shown as a doublet for the CH_3 protons at 1.34 ppm and a doublet of septets for the CH proton at 4.62 ppm. The signal for the NHP(O) group proton is absent in the ^{1}H NMR spectrum. This confirms the presence of the anionic form of HL^{I} in the structure of the complex

[1] The detailed research of the MAS NMR $^{31}P–\{^{1}H\}$ spectra of the obtained chelates is in progress. The results will be published separately.

[**Ni(L^{I})$_2$**]. The broadened singlet signal at 8.51 ppm corresponds to the AdNH proton and is in the low-field region that is characteristic for Ni(II) complexes containing an intramolecular N–H···O=P hydrogen bond with [RNHC(S)NP(O)(O*i*Pr)$_2$]$^-$ anions [3,17].

The ^{1}H NMR spectrum of the complex [**Ni(L^{II})$_2$**] contains a double set of signals for the (*i*PrO)$_2$P(S) and Ad protons. The ratio of integrated intensities is practically equal to 1:1 and they correspond to the dominant forms **B** and **C** in solution. The signals in the area 1.12–2.36 ppm correspond to the protons of the Ad and CH_3 groups. There are two broadened singlet signals of the OCH protons at 4.66 and 4.96 ppm, and two signals of the protons of the NH group at 5.70 and 9.10 ppm.

The high-field resonance of the NH proton clearly shows a splitting due to the $^4J_{PNCNH}$ (5.5 Hz) spin–spin interaction. This was previously reported for the other 1,5-*O*,*S*- and 1,5-*S*,*S*′-chelates of *N*-(thio)phosphorylthioureas [16] and was attributed to the fact that the P–N–C–N–H chain matches the so-called *W*-criterion.

It should be noted that no such splitting is observed for the free ligands **HL^{I,II}**, other *N*-(thio)phosphorylthioureas or for the 1,3-*N*,*S*-chelates.

3.3. Crystal structures

The crystal structures of **HL^{I}** and **HL^{II}** are shown in Figs. 2 and 3, and selected values of bond lengths, bond angles are listed in Tables 1 and 2, respectively. In both ligands the NC(S)N fragment is almost planar, due to the conjugation between the nitrogen lone pairs and the double C=S bond. The phosphorus atoms are in a typical tetrahedral O_2XN environment (X = O, **HL^{I}**, X = S, **HL^{II}**). The P–N–C–N fragments are in the *syn*-conformation, and the torsion angles are as follows: −10.3(2)° **HL^{I}** and −4.6(3)° for **HL^{II}**. In the ligand **HL^{I}**, the oxygen atom of the P=O group and the sulfur atom of the C=S group are in an *anti* conformation, whereas in the ligand **HL^{II}** both sulfur atoms are located in a *syn* disposition.

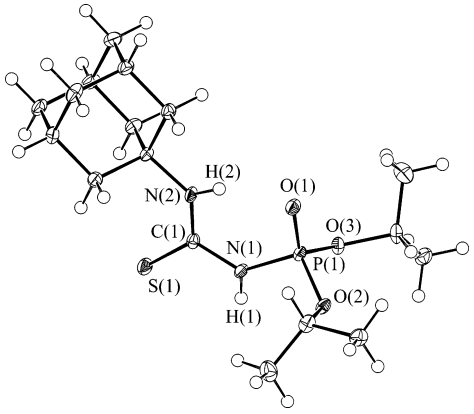

Fig. 2. Molecular structure of **HL^{I}**. Thermal ellipsoids are drawn at 50% probability.

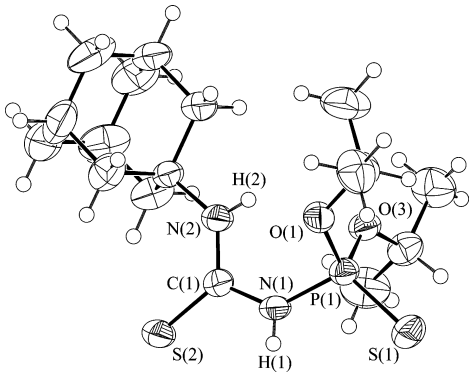

Fig. 3. Molecular structure of **HL^{II}**. Thermal ellipsoids are drawn at 50% probability.

Table 1
Selected bond lengths (Å) and bond angles (°) for **HL^{I}**

Bond lengths			
P(1)–O(1)	1.4751(13)	N(1)–C(1)	1.405(2)
P(1)–O(2)	1.5603(13)	N(2)–C(1)	1.327(2)
P(1)–O(3)	1.5669(13)	N(2)–C(2)	1.489(2)
P(1)–N(1)	1.670(2)	S(1)–C(1)	1.677(2)
Bond angles			
O(1)–P(1)–O(2)	117.36(7)	O(3)–P(1)–N(1)	106.63(7)
O(2)–P(1)–O(3)	102.00(7)	S(1)–C(1)–N(2)	126.64(13)
O(1)–P(1)–O(3)	115.49(7)	S(1)–C(1)–N(1)	117.94(13)
O(1)–P(1)–N(1)	111.43(8)	P(1)–N(1)–C(1)	130.14(13)
O(2)–P(1)–N(1)	102.56(7)	N(1)–C(1)–N(2)	115.4(2)

Table 2
Selected bond lengths (Å) and bond angles (°) for **HL^{II}**

Bond lengths			
P(1)–S(1)	1.9120(8)	N(1)–C(1)	1.390(3)
P(1)–O(1)	1.575(2)	N(2)–C(1)	1.331(3)
P(1)–O(2)	1.5811(14)	S(2)–C(1)	1.663(3)
P(1)–N(1)	1.659(2)		
Bond angles			
S(1)–P(1)–O(1)	118.63(6)	S(1)–P(1)–N(1)	112.77(7)
S(1)–P(1)–O(2)	115.85(6)	S(2)–C(1)–N(1)	119.2(2)
O(1)–P(1)–O(2)	99.36(8)	S(2)–C(1)–N(2)	125.6(2)
O(1)–P(1)–N(1)	101.20(9)	P(1)–N(1)–C(1)	130.9(2)
O(2)–P(1)–N(1)	107.14(9)	N(1)–C(1)–N(2)	115.3(2)

The *W*-criterion in the structure of complex [**Ni(L^{II})$_2$**] is realized with an *anti*-orientation of the N–C–N–H moiety (Scheme 1), because of the sterically demanding adamantyl substituents. The contribution of the observed splitting to the presence of $^4J_{PNCNH}$ spin-spin coupling was unambiguously confirmed by recording ^{1}H NMR spectra with ^{31}P decoupling.

In the crystals of the thioureas **HL^{I}** and **HL^{II}** intramolecular hydrogen bonds were found. Their parameters are presented in Table 3. In the ligand **HL^{I}** the hydrogen bond is of the N–H···O=P(intra) type, between the hydrogen atom of the AdNH group and the oxygen atom of the P=O group, whereas the thiophosphorylated analogue **HL^{II}** contains intramolecular bifurcated H-bonds between the AdNH proton and the oxygen atoms of both O*i*Pr groups. The ligand **HL^{II}** is the first example among thiophosphorylthioureas of the common formula RNHC(S)NHP(S)(O*i*Pr)$_2$ that contains an intramolecular bifurcated hydrogen bond.

In the crystal structures of the ligands **HL^{I}** and **HL^{II}** there are also intermolecular hydrogen bonds (Table 3). In the thiourea **HL^{I}** the H-bond is of the N–H···O=P(inter) type between the hydrogen atom of the PNH group of one molecule and the oxygen atom of the P=O

Table 3
Parameters of hydrogen bonds for **HL^{I}**, **HL^{II}** and [**Ni(L^{I})$_2$**] [bond lengths (Å) and bond angles (°)]

	N–H···O	*d*(H···O)	*D*(N···O)	∠(NHO)
HL^{I}	N(2)–H(2)···O(1) [intra]	1.97(2)	2.770(2)	152(2)
	N(1)–H(1)···O(1)′ [inter][a]	2.41(2)	3.194(2)	173(2)
HL^{II}	N(2)–H(2)···O(1) [intra]	2.35(3)	2.978(3)	136(2)
	N(2)–H(2)···O(2) [intra]	2.49(3)	3.038(3)	127(2)
	N(1)–H(1)···S(2)′ [inter][b]	2.66(2)	3.377(2)	163(2)
[**Ni(L^{I})$_2$**]	N(2)–H(2)···O(1)	2.06(2)	2.784(2)	151(2)
	N(2A)–H(2A)···O(1A)	2.06(2)	2.764(2)	149(2)

[a] (1 − *x*; −1/2 + *y*; 1/2 − *z*).
[b] (1/2 − *x*; 5/2 − *y*; 1 − *z*).

group of another one. As a result of the intermolecular hydrogen bonds, polymeric chains are formed along the 0*b* axis. The ligand **HL^{II}** contains intermolecular H-bonds of the N–H···S=C(inter) type, with the formation of a centrosymmetric dimer.

Figs. 4 and 5 show the structures of the complexes [**Ni**(**L^{I}**)$_2$] and [**Ni**(**L^{II}**)$_2$], respectively, and selected values of bond lengths, bond angles are given in Tables 4 and 5. According to the single crystal X-ray data these complexes are of a [**Ni**(**L**)$_2$] structure.

Complex [**Ni**(**L^{I}**)$_2$] (Fig. 4) is built in a centrosymmetric manner. The Ni(II) cation is coordinated in a square-planar fashion with the ligands arranged in a *trans* configuration. The four-membered Ni–S–C–N metallocycles are flat. The values of the two intracyclic S–Ni–N angles in the four-membered rings fall in the range 74–75°. The values of the intercyclic S–Ni–N angles are in the region 104–107° (Table 4). The C–S and C–N bonds of the chelate cycles in complex [**Ni**(**L^{I}**)$_2$] are lengthening whereas the P–N ones are shorten relative to those in the parent ligand. The length of the P=O bonds are practically the same as was found for **HL^{I}**. Thus, the C–S and P–N bond lengths indicate that these bonds are best described as single bonds, while the P=O group represents the double bond [18].

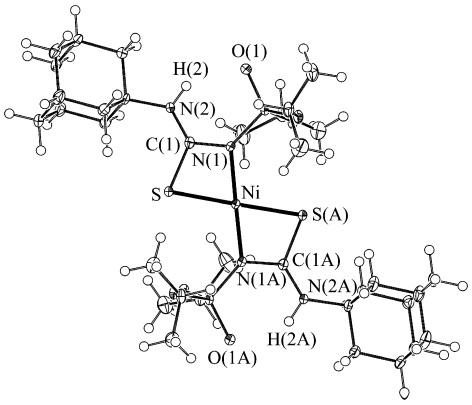

Fig. 4. Molecular structure of [**Ni**(**L^{I}**)$_2$]. Thermal ellipsoids are drawn at 50% probability.

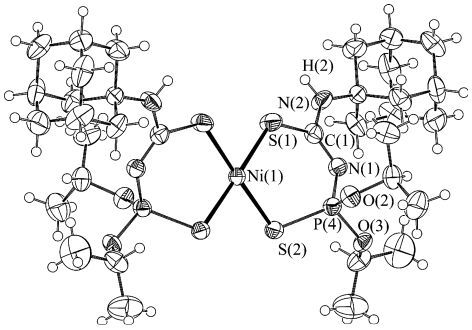

Fig. 5. Molecular structure of [**Ni**(**L^{II}**)$_2$]. Thermal ellipsoids are drawn at 50% probability.

Table 4
Selected bond lengths (Å) and bond angles (°) for [**Ni**(**L^{I}**)$_2$]

Bond lengths			
Ni–S	2.2298(8)	N(2A)–C(1A)	1.317(3)
Ni–S(A)	2.2177(8)	P(1)–N(1)	1.652(2)
Ni–N(1)	1.892(2)	P(1A)–N(1A)	1.653(2)
Ni–N(1A)	1.899(2)	P(1)–O(1)	1.474(2)
S–C(1)	1.738(2)	P(1A)–O(1A)	1.475(2)
S(A)–C(1A)	1.734(2)	P(1)–O(2)	1.568(2)
N(1)–C(1)	1.349(2)	P(1A)–O(2A)	1.565(2)
N(1A)–C(1A)	1.354(2)	P(1)–O(3)	1.571(2)
N(2)–C(1)	1.317(3)	P(1A)–O(3A)	1.5778(14)
Bond angles			
S–Ni–S(A)	176.65(2)	Ni–S(A)–C(1A)	77.86(7)
N(1)–Ni–N(1A)	179.02(7)	Ni–N(1)–P(1)	131.38(9)
S–Ni–N(1)	74.33(5)	Ni–N(1A)–P(1A)	132.31(9)
S(A)–Ni–N(1A)	74.54(5)	O(1)–P(1)–N(1)	111.95(8)
S–Ni–N(1A)	106.64(5)	O(1A)–P(1A)–N(1A)	111.65(8)
S(A)–Ni–N(1)	104.50(5)	S–C(1)–N(2)	127.9(2)
Ni–S–C(1)	77.50(7)	S(A)–C(1A)–N(2[a])	127.4(2)

Table 5
Selected bond lengths (Å) and bond angles (°) for [**Ni**(**L^{II}**)$_2$]

Bond lengths			
Ni(1)–S(2)	2.2043(14)	N(1)–C(1)	1.301(4)
Ni(1)–S(1)	2.2172(13)	P(1)–O(1)	1.570(2)
S(2)–C(1)	1.758(4)	P(1)–O(2)	1.571(3)
S(1)–P(1)	1.982(2)	N(2)–C(1)	1.349(5)
P(1)–N(1)	1.603(3)		
Bond angles			
S(1)–Ni(1)–S(2)	177.53(4)	Ni(1)–S(2)–C(1)	118.24(12)
S(1)–Ni(1)–S(1a)	80.80(4)	Ni(1)–S(1)–P(1)	104.09(5)
S(1)–Ni(1)–S(2a)	99.73(4)	S(2)–C(1)–N(2)	111.5(3)
S(2)–Ni(1)–S(2a)	79.85(4)	S(1)–P(1)–N(1)	116.56(12)
P(4)–N(1)–C(1)	122.7(2)		

In the investigated compound [**Ni**(**L^{I}**)$_2$], the AdNH hydrogen atoms are engaged in intramolecular hydrogen bonds of the AdN–H···O=P type (Table 3). Due to their formation, a flat *syn, syn* conformation of the N–C–N–P–O moieties is observed.

X-Ray structural analysis of complex [**Ni**(**L^{II}**)$_2$] shows that the nickel atom is positioned in the symmetry center of a distorted square-planar arrangement, with a *cis*-configuration of the deprotonated ligands **L^{II}** (Fig. 5). Complex [**Ni**(**L^{II}**)$_2$] is the first example of a Ni(II) cationic complex with RC(S)NHP(S)(O*i*Pr)$_2$ ligands in a *cis* configuration investigated by X-ray analysis.

The six-membered metallocycle Ni(1)–S(2)–C(1)–N(1)–P(1)–S(1) has the form of an asymmetric boat; the P(1)–N(1)–C(1)–S(2) fragment is essentially planar. The exocyclic N(2) atom is located practically in the base plane of the heterocycle. The values of the two intracyclic S–Ni–S angles in the six-membered rings are 99.73(4)°. The values of the intercyclic S–Ni–S angles are in the region 79–81° (Table 5). There are no inter- or intramolecular hydrogen bonds in the crystal structure of the complex [**Ni**(**L^{II}**)$_2$].

The Ni(1)–S(1) and Ni(1)–S(2) distances of 2.2172(13) and 2.2043(14) Å, respectively, are close, suggesting electron density delocalization between the S(1) and S(2) atoms of the ligand. The C(1)–S(2) bond length [1.758(4) Å] also indicates such a delocalization; this distance differs significantly from the C=S double bond length in thioureas and the C–S single bond length in sulfides [18].

4. Conclusions

The data presented show that in the ligands **HL^{I,II}** the structure in the solid state and the type of coordination with a Ni(II) cation are determined by the nature of the atom X.

The ligand **HL^{I}** (X = O) contains an intramolecular hydrogen bond between the AdNH proton and the oxygen atom of the P=O group, whereas in the thiourea **HL^{II}** (X = S) bifurcated H-bonding takes place between the AdNH proton and two oxygen atoms of the *i*PrO groups.

The central cation in the complex [**Ni**(**L^{II}**)$_2$] is coordinated in the 1,5-*S*,*S*′-fashion. The square-planar $NiS_2S'_2$ core is stabilized by a π-dative interaction with the sulfur atoms. According to the X-ray data, the two anionic **L^{II}** ligands in the crystal are in a *cis* configuration in spite of the presence of the bulk adamantyl substituents.

There is competition between the two coordination modes, 1,5-*O*,*S*′- versus 1,3-*N*,*S*-, in the complex [**Ni**($\mathbf{L^I}$)$_2$]. The 1,5-*O*,*S*′-mode is obviously the most favorable for steric reasons, due to the formation of the unstrained six-membered cycle. However, we have established that the Ni(II) cation is in a N_2S_2 environment. There are three reasons for its stabilization: (1) the strong (~20–25 kJ/mol) [2,3] intramolecular hydrogen bond which blocks the phosphoryl group; (2) the stronger p-π conjugation in the thioamide moiety in comparison with the SCNPO backbone; and (3) the stronger ligand field provided by the 1,3-*N*,*S*-coordinated thiourea.

Acknowledgements

This work was supported by the joint program of CRDF and the Russian Ministry of Education and Science (BRHE 2008 Y5-C-07-09); the joint program of DAAD "Michail-Lomonosov" and the Russian Ministry of Education and Science (Forschungsstipendien 2006/2007); Russian Science Support Foundation.

Appendix A. Supplementary data

CCDC 668040, 665136, 668044 and 665137 contain the supplementary crystallographic data for H$\mathbf{L^I}$, H$\mathbf{L^{II}}$, [Ni($\mathbf{L^I}$)$_2$] and [Ni($\mathbf{L^{II}}$)$_2$]. These data can be obtained free of charge via http://www.ccdc.cam.ac.uk/conts/retrieving.html, or from the Cambridge Crystallographic Data Centre, 12 Union Road, Cambridge CB2 1EZ, UK; fax: (+44) 1223-336-033; or e-mail: deposit@ccdc.cam.ac.uk. Supplementary data associated with this article can be found, in the online version, at doi:10.1016/j.poly.2008.04.014.

References

[1] (a) A.D. Garnovskii, D.A. Garnovskii, I.S. Vasilchenko, A.S. Burlov, A.P. Sadimenko, I.D. Sadekov, Russ. Chem. Rev. 66 (1997) 389;
(b) L.M. Blanco, A.D. Garnovskii, D.A. Garnovskii, B.I. Kharisov, M.A. Mendez-Rojas, I.S. Vasilchenko, in: A.D. Garnovskii, B.I. Kharisov (Eds.), Synthetic Coordination and Organometallic Chemistry, Marcel Dekker, New York–Basel, 2003.
[2] F.D. Sokolov, N.G. Zabirov, L.N. Yamalieva, V.G. Shtyrlin, R.R. Garipov, V.V. Brusko, A.Yu. Verat, S.V. Baranov, P. Mlynarz, T. Glowiak, H. Kozlowski, Inorg. Chim. Acta 359 (2006) 2087.
[3] F.D. Sokolov, S.V. Baranov, D.A. Safin, F.E. Hahn, M. Kubiak, T. Pape, M.G. Babashkina, N.G. Zabirov, J. Galezowska, H. Kozlowski, R.A. Cherkasov, New J. Chem. 31 (2007) 1661.
[4] Oxford Diffraction Poland Sp., CCD data collection and reduction GUI, Version 1.173.13 beta (release 14.11.2003), Copyright 1995–2003.
[5] G.M. Sheldrick, SHELXS-97, Program for the Solution of Crystal Structures, University of Goettingen, Germany, 1997.
[6] G.M. Sheldrick, SHELXL-97, Program for the Refinement of Crystal Structures, University of Goettingen, Germany, 1997.
[7] L.J. Farrugia, J. Appl. Crystallogr. 32 (1999) 837.
[8] APEX2 (Version 2.1), SAINTPLUS, Data Reduction and Correction Program (Version 7.31A), Bruker Advanced X-ray Solutions, BrukerAXS Inc., Madison, WI, USA, 2006.
[9] G.M. Sheldrik, SADABS, Program for Empirical X-ray Absorption Correction, Bruker-Nonis, 1990–2004.
[10] A. Altomare, G. Cascarano, C. Giacovazzo, D. Viterbo, Acta Crystallogr., Sect. A. 47 (1991) 744.
[11] G.M. Sheldrick, SHELXL-97-2 Program for Crystal Structure Refinement, University of Goettingen, Germany, 1997.
[12] A.L. Spek, Acta Crystallogr., Sect. A 46 (1990) 34.
[13] E.G. Yarkova, N.R. Safiullina, I.G. Chistyakova, N.G. Zabirov, F.M. Shamsevaleev, R.A. Cherkasov, Zh. Obshch. Khim. 60 (1990) 1790.
[14] N.G. Zabirov, V.V. Brusko, S.V. Kashevarov, F.D. Sokolov, V.A. Sherbakova, A.Yu. Verat, R.A. Cherkasov, Russ. J. Gen. Chem. 70 (2000) 1214.
[15] M.G. Zimin, R.M. Kamalov, R.A. Cherkasov, A.N. Pudovik, Phosphorus and Sulfur 13 (1982) 371.
[16] V.V. Brusko, A.I. Rakhmatullin, V.G. Shtyrlin, D.B. Krivolapov, I.A. Litvinov, N.G. Zabirov, Polyhedron 25 (2006) 1433.
[17] (a) A.Y. Verat, F.D. Sokolov, N.G. Zabirov, M.G. Babashkina, D.B. Krivolapov, V.V. Brusko, I.A. Litvinov, Inorg. Chim. Acta 359 (2006) 475;
(b) D.A. Safin, M.G. Babashkina, F.D. Sokolov, N.G. Zabirov, J. Galezowska, H. Kozlowski, Polyhedron 26 (2007) 1113;
(c) V.V. Brusko, A.I. Rakhmatullin, N.G. Zabirov, Russ. J. Gen. Chem. 70 (2000) 1603;
(d) F.D. Sokolov, D.A. Safin, N.G. Zabirov, P.V. Zotov, R.A. Cherkasov, Russ. J. Gen. Chem. 12 (2005) 1919.
[18] F.H. Allen, O. Kennard, D.G. Watson, L. Brammer, A.G. Orpen, R. Taylor, J. Chem. Soc., Perkin Trans. 2 (12) (1987) S1.

Polyhedron 27 (2008) 2277–2284

Contents lists available at ScienceDirect

Polyhedron

journal homepage: www.elsevier.com/locate/poly

Reactivity of benzil bis(4-methyl-3-thiosemicarbazone) with cadmium nitrate. Crystal structure of $[Cd(LMe_2H_4)(NO_3)_2][Cd(LMe_2H_4)(NO_3)(H_2O)]NO_3 \cdot H_2O$

David G. Calatayud, Elena López-Torres *, M. Antonia Mendiola

Departamento de Química Inorgánica, c/ Francisco Tomás y Valiente, 7, Universidad Autónoma de Madrid, Cantoblanco, 28049 Madrid, Spain

ARTICLE INFO

Article history:
Received 11 March 2008
Accepted 9 April 2008
Available online 9 June 2008

Keywords:
Bis(thiosemicarbazone) ligands
Cadmium(II) complexes
X-ray diffraction

ABSTRACT

The reaction between cadmium nitrate dihydrate and benzil bis(4-methyl-3-thiosemicarbazone), LMe_2H_4, depends on the working conditions. In methanol the reaction gives the novel complex $[Cd(LMe_2H_4)(NO_3)_2][Cd(LMe_2H_4)(NO_3)(H_2O)]NO_3 \cdot H_2O$ (**1**). Its crystal structure shows the presence of two cadmium atoms with different coordination numbers, seven and eight, and the ligands acting as N_2S_2 neutral molecules. One cadmium has the coordination sphere completed by a bidentate nitrato group and a water molecule, whereas the other one is bonded to two bidentate nitrato groups. Both molecules are joined to one nitrate ion and to an additional water molecule by hydrogen bonds. In the presence of lithium hydroxide, the reaction leads to a binuclear complex with the ligand doubly deprotonated $[Cd(LMe_2H_2)]_2$ (**2**). The complexes were characterized by elemental analysis, mass spectrometry, ^{13}C and ^{113}Cd CP/MAS NMR and, in the case of complex **1**, by X-ray diffraction.

© 2008 Elsevier Ltd. All rights reserved.

1. Introduction

In recent years, the heavy element cadmium has received increased attention due to its impact on plants and toxicity to humans, as well as for the luminescent properties of its complexes [1–6]. Cadmium is an extremely toxic element that is naturally present in the environment and also as a result of human activities. Its toxicity derives from the fact that it is rapidly localized intracellularly, mainly in the liver, and then is bound to metallothionein forming a complex that is slowly transferred to the bloodstream to be deposited in the kidneys. Therefore, it is an interesting area of research to get compounds which are able to form stable complexes with cadmium, because they could be employed as detoxificating agents. For this purpose thiosemicarbazone ligands could be very appropriate as both the ligands and their complexes have shown a wide range of pharmacological properties [7–9]. In particular, cadmium and mercury complexes of the related ligand benzil bis(thiosemicarbazone) have antimicrobial and antifungal activity [10], so it could be expected that these cadmium derivatives also possess some activity and studies are underway.

The coordination number of six for Cd(II) ions is well documented [11–13], but seven-coordinate complexes are scarce [14–17], and they are rarely found together in one compound [18]. An eight-coordinate structure is usually formed with species having larger ion radius, such as lanthanides and third row transition metals, and it is relatively unusual for the Cd(II) ion [19]. As far as we know, there are only two complexes containing simultaneously both seven- and eight-coordinate cadmium(II), a cluster and a complex with the ligand acting as bridge [20,21]. On the other hand, there are only two seven-coordinate cadmium(II) complexes of thiosemicarbazones that have been structurally characterized, one with a tridentate ligand and another containing 2,6-diacetylpyridine bis(^2N-methylthiosemicarbazone) [17,21]. Benzil bis(4-methyl-3-thiosemicarbazone) LMe_2H_4 (see Scheme 1) has four donor atoms that can lead to a tetradentate coordination mode, so there are at least two sites available on the Cd(II) ion for the NO_3^- coordination. This ligand has shown versatile behaviour with $PbPh_2Cl_2$, depending on the pH it acts as a monodeprotonated or dideprotonated ligand, it also acts as a bridge through a sulfur atom [22].

Following our systematic study on the coordination chemistry of thiosemicarbazone ligands with toxic metals [22], here we report the synthesis and structural characterization of two new cadmium coordination compounds derived from benzil bis(4-methyl-3-thiosemicarbazone). Complex **1** is obtained in methanol and it contains two different types of Cd(II) ions. The Cd(1) atom is seven-coordinate by two nitrogen and two sulfur atoms from the ligand and three oxygen from a bidentate nitrato ligand and one water molecule, but in the Cd(2) coordination sphere the water molecule is replaced by an additional bidentate nitrato group. Both units are linked to a nitrate ion and a water molecule by hydrogen bonds. Complex **2** is synthesised in the presence of lithium hydroxide, so the ligand is doubly deprotonated and the cadmium(II) atom could be penta-coordinate in a binuclear structure. To the best of our knowledge, here we report the first thiosemicarbazone

* Corresponding author.
E-mail address: elena.lopez@uam.es (E. López-Torres).

0277-5387/$ - see front matter © 2008 Elsevier Ltd. All rights reserved.
doi:10.1016/j.poly.2008.04.036

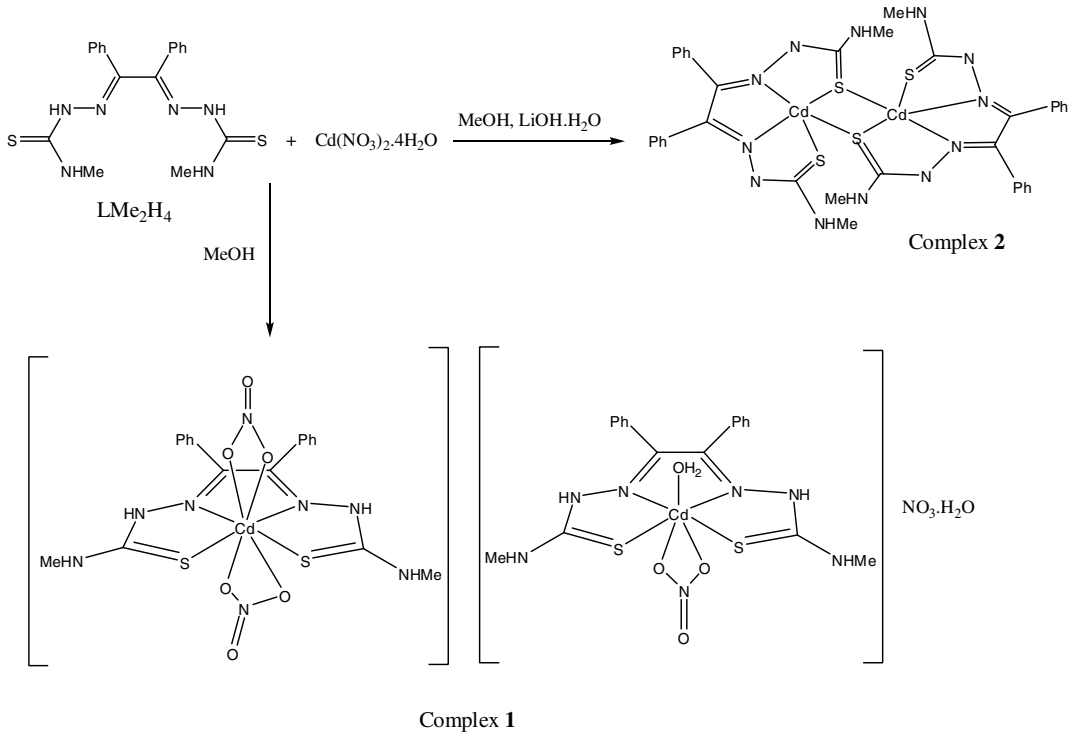

Scheme 1. A drawing showing the working conditions and the complexes obtained.

complex with eight-coordinate Cd(II). Moreover, it also is the first compound in which two cadmium ions are present with seven and eight coordination spheres in two independent units.

2. Experimental

2.1. Materials and methods

4-Methyl-3-thiosemicarbazide, 1,2-diphenylethanedione and cadmium nitrate tetrahydrate were used as received. Microanalyses were carried out using a Perkin–Elmer 2400 II CHNS/O Elemental Analyser. IR spectra in the 4000–400 cm^{-1} range were recorded as KBr pellets on a Jasco FT/IR-410 spectrophotometer. Fast atom bombardment mass spectra were recorded on a VG Auto Spec instrument using Cs as the fast atom and *m*-nitrobenzylalcohol (*m*NBA) as the matrix. ^{13}C NMR spectra were recorded on a Bruker AMX-300 spectrometer using methanol-d_4 and DMSO-d_6 as solvents and TMS as an internal reference. ^{113}Cd NMR spectra were recorded in the same spectrometer using methanol-d_4 or DMSO-d_6 as solvents and using absolutes as references, the chemical shifts are reported relative to $Cd(ClO_4)_2$ 0.1 M. ^{13}C CP/MAS NMR spectra were recorded at 298 K in a Bruker AV400WB spectrometer equipped with a 4 mm MAS-NMR probe (magic-angle spinning) and obtained using a cross-polarization pulse sequence. For the recorded spectra a contact time of 4 ms was used and recycle delays of 4 s were used. Chemical shifts are reported relative to TMS, using the CH group of adamantano as a secondary reference (29.5 ppm). ^{113}Cd CP/MAS NMR spectra were also recorded in the same spectrometer and the chemical shifts are reported relative to $Cd(ClO_4)_2$ 0.1 M, using $Cd(NO_3)_2 \cdot 4H_2O$ as secondary reference (−100 ppm).

2.2. Synthesis of benzil bis(4-methyl-3-thiosemicarbazone), LMe_2H_4

This molecule was synthesised as reported earlier [23]. Selected spectroscopic data: ^{13}C NMR (DMSO-d_6, 300 MHz, 25 °C): δ/ppm 178.6 (CS), 140.4 (CN), 133.2, 130.3, 129.1, 126.8 (Ph), 31.5 (CH_3). ^{13}C CP/MAS NMR (300 MHz, 25 °C): δ/ppm 177.2 (CS), 139.8 (CN), 130.6, 128.1, 124.7 (Ph), 32.1 (CH_3). FTIR (KBr, cm^{-1}): 3420, 3386, 3342, 3330, 3210, 3151 (s) [ν(NH)], 1608 (w) [ν(CN)], 1581 (s) [$\delta(NH_2)$] and 848 (w) [ν(CS)].

2.3. Synthesis of $[Cd(LMe_2H_4)(NO_3)_2][Cd(LMe_2H_4)(NO_3)(H_2O)]NO_3 \cdot H_2O$ (**1**)

Cadmium nitrate tetrahydrate (0.12 g, 0.39 mmol) dissolved in methanol (15 mL) was added to a LMe_2H_4 (0.15, 0.39 mmol) solution in methanol (15 mL). The mixture was stirred under reflux for 6 h. The solution was concentrated whereby a solid precipitated, which was filtered off, washed with methanol and dried in vacuo. M.p.: 187 °C. The compound was isolated as a yellow solid (0.16 g, 64%). Suitable crystals for X-ray analysis were obtained by slow evaporation of the mother liquor. M.p.: 187 °C. *Anal.* Calc. for $C_{36}H_{42}N_{16}O_{14}S_4Cd_2$ (1275.9): C, 33.88; H, 3.32; N, 17.57; S, 10.03. Found: C, 33.75; H, 3.44; N, 17.16; S, 10.19%. ^{13}C NMR (300 MHz, methanol-d_4): δ/ppm 181.0 (CS), 148.8 (CN), 131.9, 130.9, 130.7, 130.3, 130.1, 129.8, 129.5, 129.2, 128.1, 128.0 (Ph), 32.1 (CH_3). ^{113}Cd NMR (300 MHz, methanol-d_4): δ/ppm 167.3 ^{13}C CP/MAS NMR (300 MHz): δ/ppm 180.2 (CS), 148.1, 147.0 (CN), 134.1, 131.9, 130.8, 129.0, 128.1, 127.1 125.8 (Ph), 35.3, 31.4 (CH_3). ^{113}Cd CP/MAS NMR (300 MHz): δ/ppm 186.3, 144.3. MS (FAB^+): *m/z* 496.8 ($[Cd(LMe_2H_3)]^+$, 100%). FTIR (KBr, cm^{-1}) 3446, 3344, 3222 (m) [ν(NH)], 1617 (w) [ν(CN)], 1574 (s) [δ(NCS)], 1384 (s) [ν(NO)], 819 (w) [ν(CS)].

2.4. Synthesis of $[Cd(LMe_2H_4)]_2$ (**2**)

The reaction was carried out as described previously, but in the presence of $LiOH \cdot H_2O$ (0.04 g, 0.79 mmol). Complex **2** was isolated as an orange solid (0.17 g, 88%), washed with methanol and dried in vacuo. M.p.: 247 °C. *Anal.* Calc. for $C_{36}H_{36}N_{12}S_4Cd_2$ (988.8): C, 43.68; H, 3.67; N, 16.98; S, 12.96. Found: C, 43.52; H, 3.65; N, 16.84; S, 12.87%. ^{113}Cd NMR (300 MHz, DCM + $CDCl_3$): δ/ppm 410.4. ^{13}C CP/MAS NMR (300 MHz): δ/ppm 178.7, 162.5, 158.7

Table 1
Crystal data and structure refinement for $[Cd(LMe_2H_4)(NO_3)_2][Cd(LMe_2H_4)(NO_3)(H_2O)]NO_3 \cdot H_2O$ (**1**)

Empirical formula	$C_{36}H_{42}Cd_2N_{16}O_{14}S_4$
Formula weight	1275.90
Temperature (K)	100(2)
Wavelength (Å)	1.54178
Crystal system	triclinic
Space group	$P\bar{1}$
Unit cell dimensions	
a (Å)	9.396(4)
b (Å)	12.069(5)
c (Å)	23.862(11)
α (°)	83.65(3)
β (°)	86.63(3)
γ (°)	68.10(2)
Volume (Å^3)	2495.0(19)
Z	2
D_{calc} (Mg/m^3)	1.698
Absorption coefficient (mm^{-1})	9.072
$F(000)$	1284
Crystal size (mm)	0.14 × 0.12 × 0.06
θ Range for data collection (°)	1.86–66.67
Index ranges	$-11 \leqslant h \leqslant 11$, $-14 \leqslant k \leqslant 14$, $-28 \leqslant l \leqslant 28$
Reflections collected	19983
Independent reflections [R_{int}]	8342 [0.0427]
Completeness to theta = 66.67° (%)	94.4
Absorption correction	semi-empirical from equivalents
Refinement method	full-matrix least-squares on F^2
Data/restraints/parameters	8342/0/661
Goodness-of-fit on F^2	1.028
Final R indices $I > 2\sigma(I)$	$R_1 = 0.0371$, $wR_2 = 0.0960$
R indices (all data)	$R_1 = 0.0447$, $wR_2 = 0.1020$
Largest difference in peak and hole (e Å^{-3})	0.862 and −0.760

(CS), 146.0 (CN), 137.5, 135.5, 132.8, 130.4, 128.9, 127.0 (Ph), 29.9 (CH_3). ^{113}Cd CP/MAS NMR (300 MHz): δ/ppm 425.4. MS (FAB$^+$): m/z 990.8 ($[M+1]^+$, 31%), 496.9 ($[CdLMe_2H_3]^+$, 100%). FTIR (KBr, cm^{-1}) 3415, 3370 (s) [ν(NH)], 1618, 1600 (w) [ν(CN)], 1561 (s) [δ(NCS)], 836 (w) [ν(CS)].

2.5. X-ray crystallography

Data for **1** (see Table 1) were collected at 100 K with a Bruker SMART 6K CCD area-detector three-circle diffractometer with a MAC Science Co., Ltd. Rotating Anode (Cu Kα radiation, λ = 1.54178 Å) generator. The unit cell parameters were obtained by full-matrix least-squares refinements of 8342 independent reflections. The structures were solved by direct methods (SHELXS-97), completed with difference Fourier syntheses, and refined with full-matrix least squares using SHELXL-97 minimizing $\omega(F_o^2 - F_c^2)^2$. Weighted R factors (R_w) and all goodness-of-fit S are based on F^2; conventional R factors (R) are based on F, giving $R_1 = 0.0371$, $wR_2 = 0.0960$ using 19983 reflections with $I > 2\sigma(I)$ [24,25]. All non-hydrogen atoms were refined with anisotropic displacement parameters. All scattering factors and anomalous dispersions factors are contained in the SHELXTL 6.10 program library. All the hydrogen atoms were included in geometric positions except those of the water molecule, which were located by difference maps and refined isotropically.

3. Results and discussion

3.1. Synthesis

The reaction between LMe_2H_4 and cadmium nitrate depends on the presence of a basic medium (Scheme 1). The reaction carried out in methanol gives a crystalline solid (**1**), which analytical data agree with a 1:1 cadmium:ligand ratio, confirmed by its FAB mass spectrum (Fig. 1a), and the presence of two nitrate groups and one water molecule. However, the reaction in the presence of lithium hydroxide yields complex (**2**), which analytical data are in agreement with a 1:1 ratio and the absence of nitrate groups. The FAB mass spectrum (Fig. 1b) shows a peak at 494.9 corresponding to $[Cd(LMe_2H_3)]^+$ and another one at 990.8, relatively intense, corresponding to $[Cd_2(LMe_2H_2)_2+1]^+$, suggesting a binuclear structure for this complex.

3.2. Spectroscopic studies

The shifts observed in the ν(CN) and ν(CS) bands in the IR spectra of both complexes are in accordance with the ligand being bonded to the cadmium through the imine nitrogen and the sulfur atoms, acting as a tetradentate chelate in both complexes. Moreover, the IR spectrum of **1** shows a sharp and strong band at 1385 cm^{-1} corresponding to ν(N–O) of the NO_3^- group. Several bands in the ν(N–H) and δ(N–H) regions are observed, which agrees with the ligand being in the neutral form. By contrast, the spectrum of **2** only shows two bands in the amine tension region and the absence of any band assignable to the nitrate group.

Complex **2** is sparingly soluble in all common solvents and its ^{1}H and ^{13}C NMR spectra are useless, indicating the decomposition. Therefore ^{13}C and ^{113}Cd CP/MAS of both complexes were measured for comparison. The ^{13}C CP/MAS NMR spectrum of **1** shows one signal corresponding to the thioamide carbon atom, two to the imine, three to the methine carbon and seven corresponding to the aromatic carbon atoms. By contrast, the spectrum of complex **2** shows three signals corresponding to the thioamide group, one to the imine and the methine carbons and six to the aromatic carbon atoms. These differences can be explained due to the presence of ligands with a different behaviour in each complexes: in complex **1** the two ligands act in the same way, but there are a slight differences in the bonds lengths and angles; in complex **2** at least one sulfur atom is bonded to two cadmiums, acting as a bridge as observed in the organolead(IV) derivative and in the binuclear cadmium complex obtained from benzil bis(thiosemicarbazone) [22,26].

It is well known that the ^{113}Cd chemical shift is very sensitive to changes in the coordination number of cadmium as well as to the nature of the bonding, so it is a useful tool to determine the environment of this metal in a complex. Replacement of sulfur by nitrogen and oxygen atoms tends to give greater shielding [27–30] and a decrease in the coordination number tends to give greater deshielding [31,32]. ^{113}Cd CP/MAS NMR spectrum of complex **1** shows two signals at 186.3 and 144.3 ppm, whereas complex **2** only shows a signal at 425.4 ppm. These data are consistent with two cadmium atoms with different environments in complex **1** and only one kind of geometry around the metal ion in complex **2**. The values of the chemical shifts agree with the presence of seven and eight-coordinate cadmium atoms, with several oxygen atoms in the coordination sphere of both Cd(II) centres in complex **1**, while a lower coordination number and the absence of oxygen atoms is suggested for complex **2** [11,13]. The ^{113}Cd NMR spectrum of **1** in methanol only exhibits one signal at 167.3 ppm, which is almost the average between the solid state signals, indicating partial substitution of the nitrato ligands and/or the water molecule by solvent molecules, giving the same coordination sphere. The ^{113}Cd NMR spectrum of complex **2** in DCM shows the signal has been slightly displaced to 410 ppm, which indicates that the coordination sphere remains in this solvent and it is in the range expected for S_3N_2 coordination.

3.3. Crystal structure of $[Cd(LMe_2H_4)(NO_3)_2][Cd(LMe_2H_4)(NO_3)(H_2O)]NO_3 \cdot H_2O$ (**1**)

The X-ray structural analysis of complex **1** revealed the presence of two units, each containing one cadmium atom and one li-

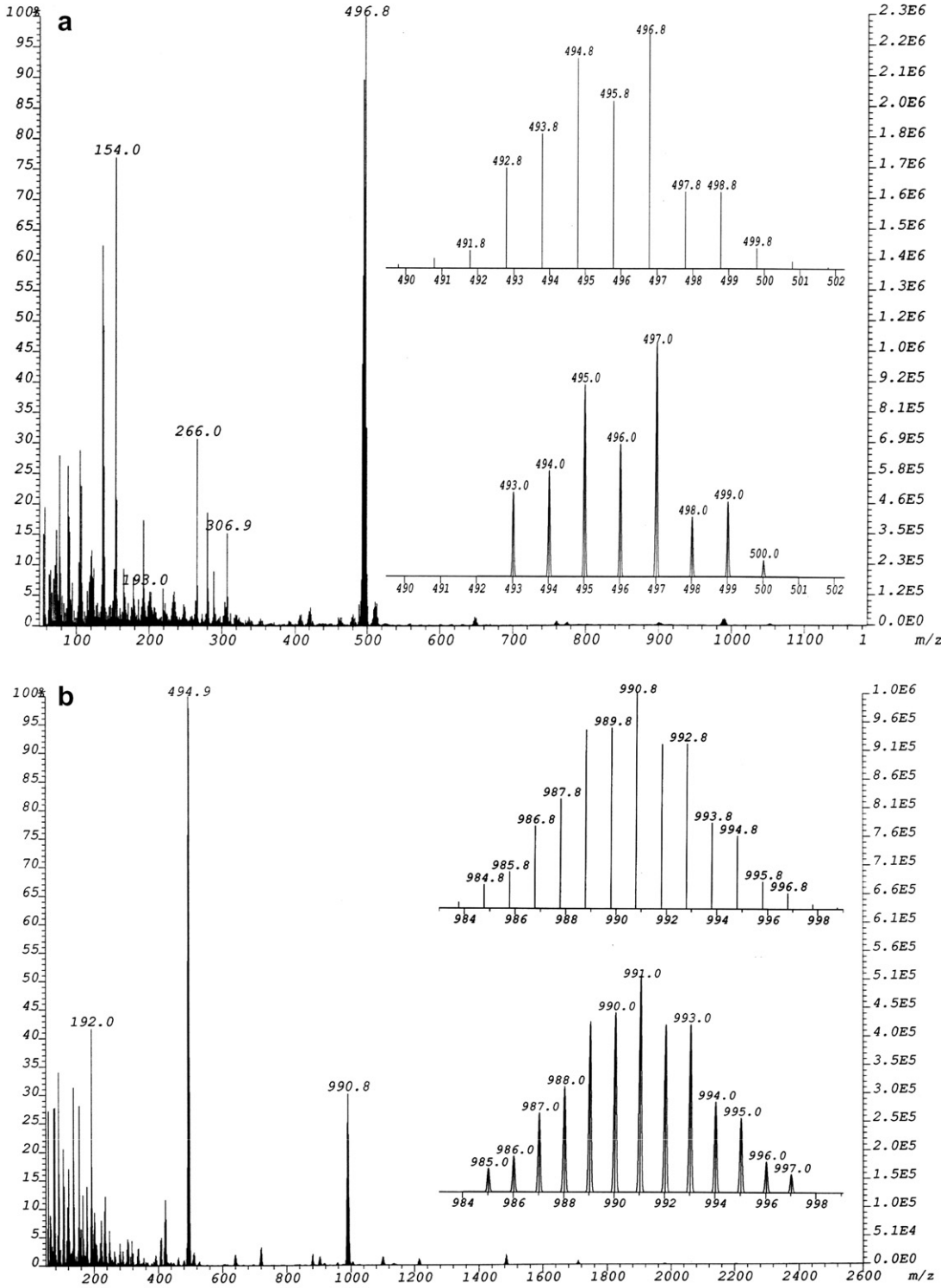

Fig. 1. (a) FAB mass spectrum of complex **1** (theoretical and experimental isotope distribution in the inset); (b) FAB mass spectrum of complex **2** (theoretical and experimental isotope distribution in the inset).

gand, with one nitrate group and a water molecule linking them (Fig. 2). The two Cd(II) ions have different coordination environments with the ligand acting, as it could be expected for this compound, as a N_2S_2 chelate and where the coordination spheres are completed by oxygen atoms. The $N_2S_2O_3$ coordination environment of the seven-coordinate Cd(1) (Fig. 3) is made up of the imine nitrogen and the sulfur atoms of the two arms of LMe_2H_4, one oxygen from a water molecule and two oxygens from a bidentate nitrato anion. The environment of the eight-coordinate Cd(2) is similar (Fig. 4), the difference being that the water molecule has been substituted by another nitrato ligand coordinated in a bidentate fashion.

The hepta-coordinate cadmium has a geometry based on a capped distorted octahedron, with the water molecule and the nit-

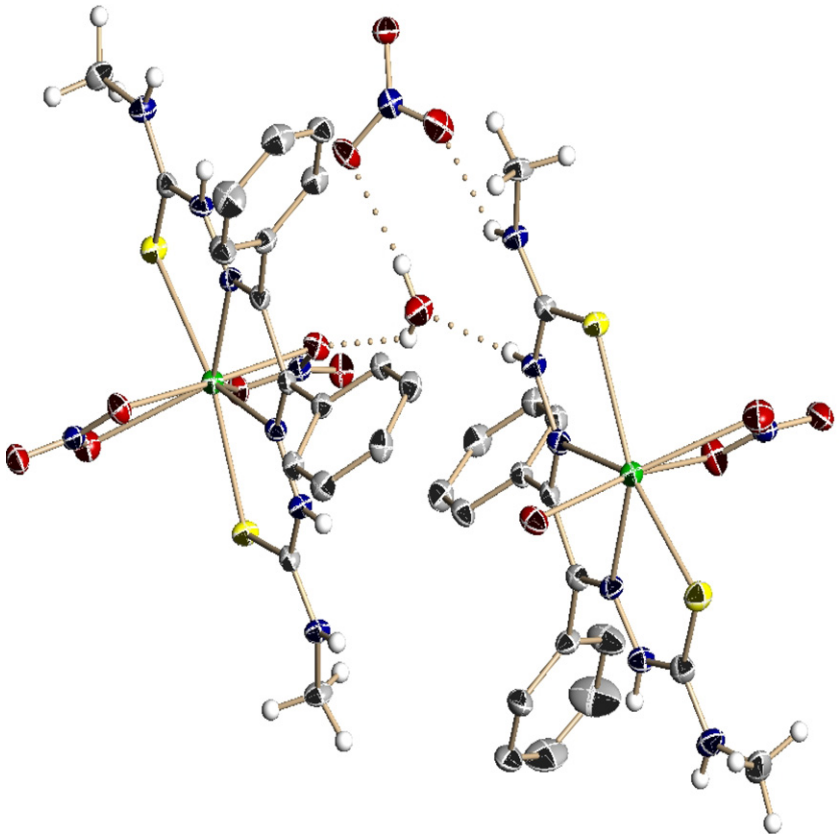

Fig. 2. The crystal structure of **1** at 50% probability including the intermolecular hydrogen bonds.

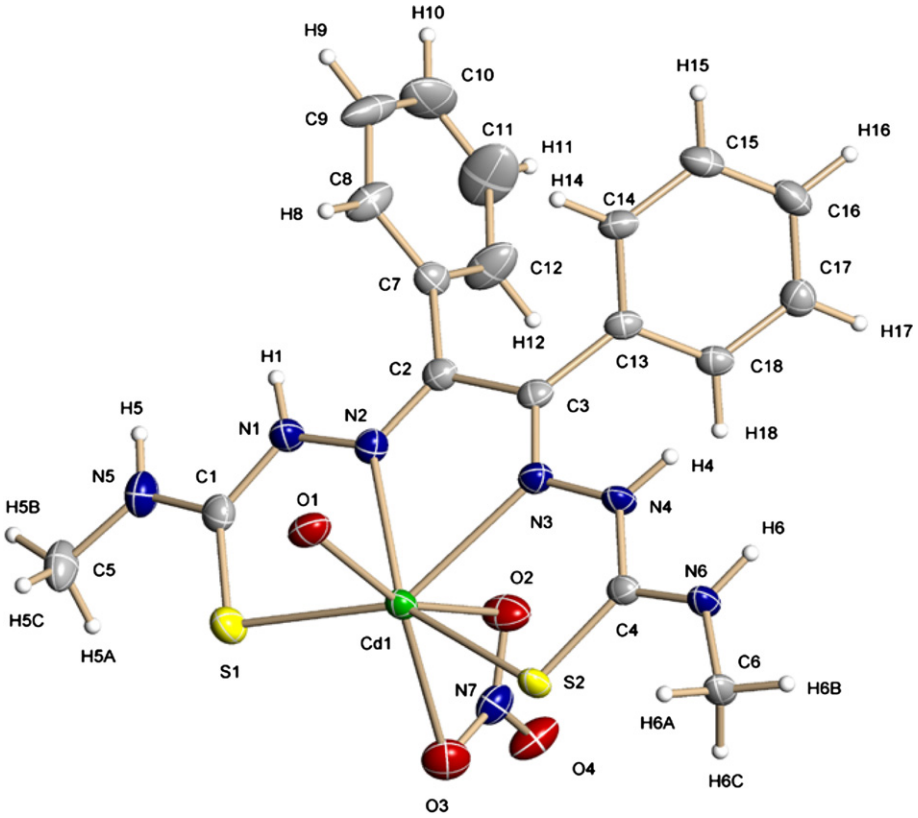

Fig. 3. The molecular structure of the complex cation in **1** with ellipsoids at 50%.

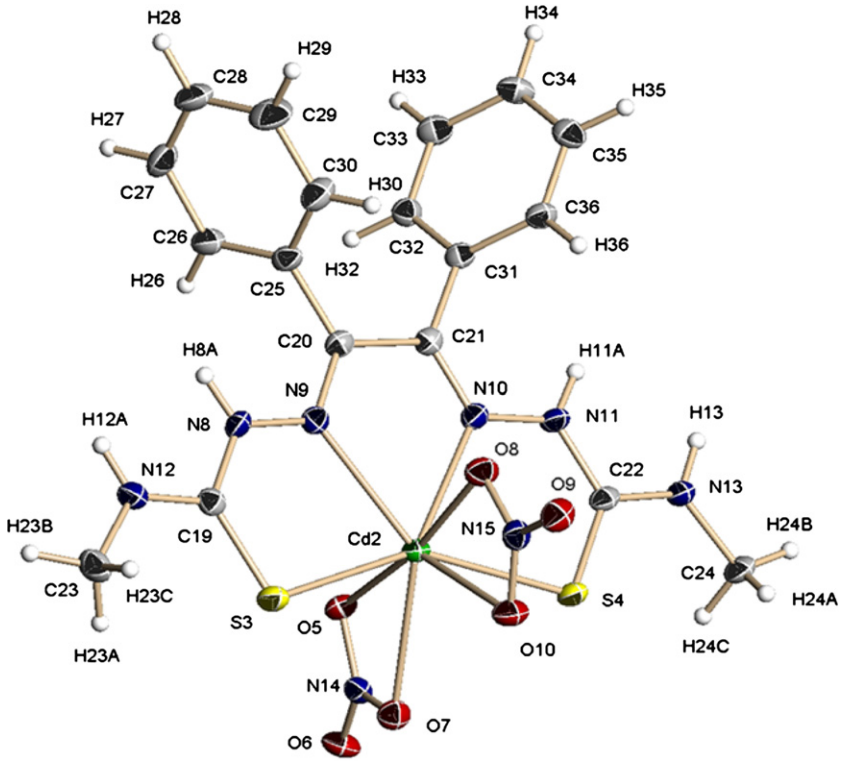

Fig. 4. The molecular structure of the neutral unit in **1** with ellipsoids at 50%.

rato group located above and under the tetradentate ligand, which is virtually planar (Fig. 3). The angle of 173.35° formed by the N atom of the bidentate nitrato group, the Cd atom and the water molecule is very close to that expected for a *trans* disposition. The Cd(1)–OH_2 bond length [2.320(3) Å] (see Table 2) is in the range observed in other Cd(II) complexes that contain nitrato ions and water molecules in their coordination sphere [20]. The Cd–O distances from the bidentate nitrato group, at 2.484(3) and 2.647(3) Å, fall within the range observed for Cd(II) compounds containing bidentate nitrato ligands and show a significant asymmetry $\delta = 0.16$ Å, which is of the same order as those observed in other cadmium complexes [14].

Cd(2) is eight-coordinate, with two nitrogen and two sulfur atoms from the benzil bis(thiosemicarbazone) ligand and four oxygen atoms from two bidentate nitrato ions (Fig. 4), which is not a common coordination number for Cd(II). The arrangement of the eight atoms around the Cd(II) centre corresponds to a distorted dodecahedron, with the angle between the N_2S_2Cd and O_4Cd planes very close to 90°. The Cd–O distances show two asymmetrically bidentate nitrato ligands with short Cd–O distances of 2.425(3) and 2.393(3) Å, and longer ones of 2.598(3) and 2.698(3) Å [33,34].

The presence of two distances for Cd–N and Cd–S bonds in each unit agrees with the distorted geometry. The Cd–N distances are not identical in both units, but they are in the range expected for a cadmium imine bond. The average bond lengths of Cd–S bonds in the seven and eight-coordinate structures are 2.583 and 2.609 Å, respectively, the difference of which arises from the increase in coordination number of the cadmium(II) ion in this complex. Similar variations are observed for the Cd–N distances.

The pseudomacrocyclic coordination mode of the ligand affords three five-member chelate rings. The bis(thiosemicarbazone) cores can be considered planar with a maximum deviation from the

Table 2
Selected bond and lengths (Å) and angles (°) for complex **1**

Cd(1)–O(1)	2.320(3)	Cd(2)–O(7)	2.598(3)
Cd(1)–N(2)	2.429(3)	Cd(2)–S(4)	2.6070(15)
Cd(1)–N(3)	2.438(3)	Cd(2)–S(3)	2.6110(14)
Cd(1)–O(2)	2.484(3)	Cd(2)–O(10)	2.698(3)
Cd(1)–S(2)	2.5753(14)	S(1)–C(1)	1.690(4)
Cd(1)–S(1)	2.5912(14)	S(2)–C(4)	1.699(4)
Cd(1)–O(3)	2.647(3)	C(1)–N(1)	1.367(5)
Cd(2)–O(8)	2.393(3)	C(2)–N(2)	1.297(5)
Cd(2)–O(5)	2.425(3)	C(3)–N(3)	1.295(5)
Cd(2)–N(9)	2.439(3)	C(4)–N(4)	1.368(5)
Cd(2)–N(10)	2.457(3)		
O(1)–Cd(1)–N(2)	84.65(10)	O(8)–Cd(2)–N(10)	79.49(9)
O(1)–Cd(1)–N(3)	88.09(10)	O(5)–Cd(2)–N(10)	93.36(9)
N(2)–Cd(1)–N(3)	65.50(10)	N(9)–Cd(2)–N(10)	65.13(10)
O(1)–Cd(1)–O(2)	157.43(10)	O(8)–Cd(2)–O(7)	138.40(8)
N(2)–Cd(1)–O(2)	74.24(10)	O(5)–Cd(2)–O(7)	50.78(8)
N(3)–Cd(1)–O(2)	76.07(10)	N(9)–Cd(2)–O(7)	134.52(9)
O(1)–Cd(1)–S(2)	92.81(8)	N(10)–Cd(2)–O(7)	132.63(9)
N(2)–Cd(1)–S(2)	138.92(8)	O(8)–Cd(2)–S(4)	96.55(8)
N(3)–Cd(1)–S(2)	73.45(8)	O(5)–Cd(2)–S(4)	86.78(7)
O(2)–Cd(1)–S(2)	97.83(8)	N(9)–Cd(2)–S(4)	138.07(7)
O(1)–Cd(1)–S(1)	88.53(8)	N(10)–Cd(2)–S(4)	72.99(7)
N(2)–Cd(1)–S(1)	73.75(8)	O(7)–Cd(2)–S(4)	74.94(7)
N(3)–Cd(1)–S(1)	139.25(8)	O(8)–Cd(2)–S(3)	91.53(7)
O(2)–Cd(1)–S(1)	93.06(8)	O(5)–Cd(2)–S(3)	90.04(7)
S(2)–Cd(1)–S(1)	147.29(3)	N(9)–Cd(2)–S(3)	73.39(8)
O(1)–Cd(1)–O(3)	151.97(9)	N(10)–Cd(2)–S(3)	138.50(7)
N(2)–Cd(1)–O(3)	115.23(10)	O(7)–Cd(2)–S(3)	78.85(7)
N(3)–Cd(1)–O(3)	117.52(10)	S(4)–Cd(2)–S(3)	148.50(3)
O(2)–Cd(1)–O(3)	49.62(9)	O(8)–Cd(2)–O(10)	49.98(8)
S(2)–Cd(1)–O(3)	84.60(8)	O(5)–Cd(2)–O(10)	139.23(8)
S(1)–Cd(1)–O(3)	79.23(8)	N(9)–Cd(2)–O(10)	121.93(9)
O(8)–Cd(2)–O(5)	170.79(8)	N(10)–Cd(2)–O(10)	118.26(9)
O(8)–Cd(2)–N(9)	78.20(10)	O(7)–Cd(2)–O(10)	88.50(8)
O(5)–Cd(2)–N(9)	93.58(9)	S(4)–Cd(2)–O(10)	79.53(7)
S(3)–Cd(2)–(10)	82.66(7)		

Table 3
Intermolecular hydrogen bonds (Å, °) in complex **1**

D–H···A	*d*(D–H)	*d*(H···A)	*d*(D···A)	<(DHA)
O(14)–H(14B)···O(5)	0.73(6)	2.35(5)	2.929(4)	136(5)
O(14)–H(14A)···O(12)	0.82(6)	2.14(6)	2.961(5)	173(6)
N(13)–H(13)···N(16)#1	0.88	2.58	3.427(4)	161.2
N(13)–H(13)···O(12)#1	0.88	1.97	2.833(4)	167.3
N(12)–H(12A)···O(9)#2	0.88	2.23	2.995(4)	145.7
N(11)–H(11A)···O(11)#1	0.88	2.14	2.926(4)	147.9
N(8)–H(8A)···O(9)#2	0.88	2.24	3.028(4)	148.4
N(6)–H(6)···O(13)	0.88	2.20	2.882(4)	133.5
N(5)–H(5)···O(4)#3	0.88	2.21	2.989(5)	147.5
N(4)–H(4)···O(14)	0.88	2.09	2.877(4)	148.4
N(1)–H(1)···O(4)#3	0.88	2.21	2.976(4)	144.6

Symmetry transformations used to generate equivalent atoms: #1 $x+1, y, z$; #2 $-x+1, -y+1, -z+1$; #3 $-x+2, -y+2, -z$.

main plane of 0.0760 Å for C(3) in the seven-coordinate unit and a 0.0616 Å deviation for the N(9) atom in the eight-coordinate one. In accordance with the symmetry of the ligand, the bond distances and angles in both thiosemicarbazone moieties in both units are very similar. The bond lengths agree well with an imine–thione form of the ligand, but with considerable electronic delocalisation through the thiosemicarbazone backbone. Thus, the thione bond distances of ca. 1.69 Å are intermediate between a theoretical C–S single and double bond (1.82 and 1.56 Å, respectively) as occurs with the N–N– bonds (ca. 1.35 vs. 1.44 Å calculated for a single N–N) and the three C–N bonds of each 4-methyl-3-thiosemicarbazone branch.

The two units are connected through hydrogen bonds involving the amino groups, the non-coordinated nitrate ion and the crystallization water molecule (Fig. 2). Finally, the molecules are held together in the crystal packing through an extended network of intermolecular hydrogen bonds involving the same groups (see Table 3).

4. Conclusions

The importance of the working conditions in the structure of coordination complexes from a bis(thiosemicarbazone) is reflected in the complexes obtained by the reaction of cadmium nitrate and benzil bis(4-methyl-3-thiosemicarbazone). Complex **1** is obtained in methanol and it contains two different types of Cd(II) ions. The Cd(1) atom is seven-coordinate by two nitrogen and two sulfur atoms from the ligand and three oxygens from a bidentate nitrato ligand and one water molecule, but the Cd(2) coordination sphere expands to eight by the exchange of the water molecule by an additional bidentate nitrato group. Both units are linked to a nitrate ion and a water molecule by hydrogen bonds. Complex **2** is synthesised in the presence of lithium hydroxide, so the ligand is doubly deprotonated and the cadmium(II) atom could be pentacoordinate in a binuclear structure. To the best of our knowledge, complex **1** is the first thiosemicarbazone complex containing eight-coordinate Cd(II). Moreover, it also is the first example in which two cadmium ions show seven and eight coordination in two independent units within the same crystal.

Acknowledgements

We thank César J. Pastor and Manuela E. Medina of "Servicio Interdepartamental de Investigación de la Universidad Autónoma de Madrid"(SIDI) (Spain). We also thank DGICYT for financial support (Project CT2005-07788/BQU) and Universidad Autónoma de Madrid for a grant to David G. Calatayud.

Appendix A. Supplementary data

CCDC 670708 contains the supplementary crystallographic data for **1**. These data can be obtained free of charge via http://www.ccdc.cam.ac.uk/conts/retrieving.html, or from the Cambridge Crystallographic Data Centre, 12 Union Road, Cambridge CB2 1EZ, UK; fax: (+44) 1223-336-033; or e-mail: deposit@ccdc.cam.ac.uk. Supplementary data associated with this article can be found, in the online version, at doi:10.1016/j.poly.2008.04.036.

References

[1] J.E. Fegusson, The Heavy Elements: Chemistry Environmental Impact and Health Effects, Pergamon Press, Oxford, 1990.
[2] G. Parkin, Chem. Rev. 104 (2004) 699.
[3] Y.Q. Huang, B. Ding, H.B. Song, B. Zhao, P. Ren, P. Cheng, H.G. Wang, D.Z. Liao, S.P. Yan, Chem. Commun. (2006) 4906.
[4] L. Yi, B. Ding, B. Zhao, P. Cheng, D.Z. Liao, S.P. Yan, Z.H. Jiang, Inorg. Chem. 43 (2004) 33.
[5] L. Yi, B. Ding, B. Zhao, P. Cheng, D.Z. Liao, S.P. Yan, Z.H. Jiang, H.B. Song, H.G. Wang, J. Chem. Soc., Dalton Trans. (2006) 665.
[6] M. Kadarkaraisamy, A.G. Sykes, Polyhedron 26 (2007) 1323.
[7] D. Sriram, P. Yogeeswari, R. Thirumurugan, R.K. Pavana, J. Med. Chem. 49 (2006) 3448.
[8] H. Beraldo, D. Cambino, Mini-Rev. Med. Chem. 4 (2004) 31.
[9] N.C. Kasuga, K. Onodera, S. Nakano, K. Hayashi, K. Nomiya, J. Inorg. Biochem. 100 (2006) 1176.
[10] F. Zani, D.G. Calatayud, E. López-Torres, M.A. Mendiola, J.R. Procopio, EUROBIC 8 Conference Book, Aveiro, Portugal, 2006, p. 153, ISBN: 989-20-0305-5.
[11] E. Bermejo, A. Castiñeiras, L.M. Fostiak, I. García Santos, J.K. Swearingen, D.X. West, Polyhedron 23 (2004) 2303.
[12] E. López-Torres, M.A. Mendiola, J. Rodríguez-Procopio, M.T. Sevilla, E. Colacio, J.M. Moreno, I. Sobrados, Inorg. Chim. Acta 323 (2001) 130.
[13] M.R. Bermejo, A.M. González-Noya, M. Martínez-Calvo, R. Pedrido, M. Maneiro, M.I. Fernández, E. Gómez-Fórneas, Z. Anorg, Allg. Chem. 633 (2007) 1911.
[14] A. Tamayo, E. Oliveira, B. Covelo, J. Casabó, L. Escrische, C. Lodeiro, Z. Anorg, Allg. Chem. 633 (2007) 1809.
[15] J. Granifo, M.T. Garland, R. Baggio, Inorg. Chem. Commun. 7 (2004) 77.
[16] M.A. Ali, A.H. Mirza, W.B. Ejau, P.V. Bernhardt, Polyhedron 25 (2006) 3337.
[17] J. Chakraborty, B. Samanta, G. Pilet, S. Mitra, Inorg. Chem. Commun. 10 (2007) 40.
[18] H-S. Wang, W. Shi, J. Xia, H.-B. Song, H.-G. Wang, P. Cheng, Inorg. Chem. Commun. 10 (2007) 856.
[19] D.B. Cordes, L.R. Hanton, Inorg. Chem. Commun. 8 (2005) 967.
[20] G. Anantharaman, M.G. Walawalkar, R. Murugaved, B. Gäbor, R. Herbst-Irmer, M. Baldus, B. Angerstein, H.W. Roesky, Angew. Chem., Int. Ed. 42 (2003) 4482.
[21] J.S. Casas, A.E. Castellano, M.S. García-Tasende, A. Sánchez, J. Sordo, J. Zukerman-Schpector, Z. Anorg. Allg. Chem. 523 (1997) 825.
[22] D.G. Calatayud, E. López-Torres, M.A. Mendiola, Inorg. Chem. 46 (2007) 10434. and refs therein.
[23] D.G. Calatayud, F.J. Escolar, E. López-Torres, M.A. Mendiola, Helv. Chim. Acta 90 (2007) 2201.
[24] G.M. Sheldrick, Acta Crystallogr., Sect. A 46 (1990) 467.
[25] G.M. Sheldrick, SHELXL-97, Program for Crystal Structure Refinement, Universität Göttingen, Göttingen, Germany, 1997.
[26] E. López-Torres, M.A. Mendiola, C.J. Pastor, B. Souto Pérez, Inorg. Chem. 43 (2004) 5222.
[27] P.S. Marchetti, S. Bank, T.W. Bell, M.A. Kennedy, P.D. Ellis, J. Am. Chem. Soc. 111 (1989) 2063.

[28] M.F. Summers, Coord. Chem. Rev. 86 (1988) 43.
[29] R. Pedrido, M.R. Bermejo, M.J. Romero, M. Vázquez, A.M. González-Moya, M. Maneiro, M.J. Rodríguez, M.I. Fernández, J. Chem. Soc., Dalton Trans. (2005) 572.
[30] R. Pedrido, M.J. Romero, M.R. Bermejo, A.M. González-Moya, I. García-Lema, G. Zaragoza, Chem. Eur. J. 14 (2008) 500.
[31] D.L. Reger, S.M. Meyers, S.S. Mason, A.L. Rheingold, B.S. Haggerty, P.D. Ellis, Inorg. Chem. 34 (1995) 4996.
[32] M.L. Helm, L.L. Hill, J.P. Lee, D.G. Van Derveer, G.J. Grant, J. Chem. Soc., Dalton Trans. (2006) 3534.
[33] S.A. Barnett, A.J. Blake, N.R. Champness, C. Wilson, J. Chem. Soc., Dalton Trans. (2005) 3852.
[34] E.R. Acuña-Cueva, R. Faure, N.A. Illán-Cabeza, S.B. Jiménez-Pulido, M.N. Moreno-Carretero, M. Quirós-Olozábal, Inorg. Chim. Acta 342 (2003) 209.

Polyhedron 27 (2008) 2285–2290

Contents lists available at ScienceDirect

Polyhedron

journal homepage: www.elsevier.com/locate/poly

β-Tetra-brominated *meso*-tetraphenylporphyrin: A conformational study and application to the Mn-porphyrin catalyzed epoxidation of olefins with tetrabutylammonium oxone

Saeed Rayati [a,*], Saeed Zakavi [b,*], Somayeh H. Motlagh [a], Vahid Noroozi [a], Maryam Razmjoo [a], Andrzej Wojtczak [c], Anna Kozakiewicz [c]

[a] Department of Chemistry, Faculty of Science, Zanjan University, P.O. Box 45195-313 Zanjan, Iran
[b] Department of Chemistry, Institute for Advanced Studies in Basic Sciences, 45195-1159 Gava-Zang, Zanjan, Iran
[c] Faculty of chemistry, N. Copernicus University, Gagarnia 7, 87-100 Torun, Poland

ARTICLE INFO

Article history:
Received 16 February 2008
Accepted 18 April 2008
Available online 3 June 2008

Keywords:
β-Tetra-brominated
meso-tetraphenylporphyrin
Epoxidation
Shift of the Q(0,0) and Soret bands
Catalyst

ABSTRACT

X-ray crystallographic studies have shown that the free base β-tetra-brominated *meso*-tetraphenylporphyrin (H_2TPPBr_4) has a slightly ruffled structure with the dihedral angles of 70.1–79.2° between the phenyl groups and the porphyrin mean plane. The N(pyrrole)–N(pyrrolenine) distance is very similar to that of the standard planar porphyrins. The decreased N–H bond length of H_2TPPBr_4 with respect to that of *meso*-tetraphenylporphyrin (H_2TPP) seems to be due to the weaker intramolecular hydrogen bond of the former relative to the latter caused by the electron-withdrawing effects of the β-bromine substituents. The large red shifts of the Soret and Q(0,0) bands of H_2TPPBr_4 in comparison with those of H_2TPP, in spite of the nearly planar porphyrin core of the compound, also may be explained on the basis of the electron-withdrawing effects of the bromine atoms. Oxidation of styrene, the *para*-substituted derivatives and cyclooctene with tetrabutylammonium oxone in the presence of catalytic amounts of β-tetra-brominated *meso*-tetraphenylporphyrinatomanganese(III) acetate immediately gives the epoxide as the sole product. Terminal double bonds and unconjugated ones are less reactive than the conjugated double bonds and show lower selectivities. Catalytic activity of the electron-deficient Mn(H_2TPPBr_4)OAc dramatically depends on the Co-catalytic activity of the nitrogen donors as the axial base. The best axial bases are the nitrogenous donors with mixed σ- and π-donor ability to the metal centre.

© 2008 Elsevier Ltd. All rights reserved.

1. Introduction

Synthetic metalloporphyrins of Fe(III), Mn(III), Cr(III), and Ru(II), (III), (VI), especially with porphyrins bearing aryl-groups at *meso*-positions, have been used in a variety of oxidation reactions, with the intention of developing biomimetic catalysts which show regio-, stereo-, shape-, and enantioselectivity with a high efficiency under mild conditions. Iron and manganese porphyrins are the most often used metalloporphyrins in the oxidation reactions, and the catalytic activity of chromium porphyrins is much inferior to those of iron-, manganese-, and ruthenium porphyrins. Metalloporphyrins are effective catalysts for the selective oxidation of hydrocarbons and other organic compounds under mild conditions. As a consequence considerable effort has been devoted to investigating the effects of variables, such as the composition of the porphyrin, the oxidant, the solvent, and the substrate [1–7].

Metalloporphyrin halogenated on the periphery of the porphyrin ring or containing halogenated substituents attached to the porphyrin ring have been shown to be particularly efficient for both epoxidation and hydroxylation reactions [6–14]. Such porphyrins are also more resistant to degradation via free-radical attack than those containing electron-donating substituents [1].

The origin of the red shifts seen in the optical spectra of non-planar porphyrins has recently generated considerable debate in the literature [15]. The introduction of four bromine atoms at the β-positions of *meso*-tetraphenylporphyrin (H_2TPP) is accompanied by electronic and structural changes in the porphyrin core.

In the present work, the conformational changes of porphyrin core upon the substitution of four bromine atoms at β-positions of H_2TPP and the shift of the Soret and Q-bands of the porphyrin have been studied. The efficacy of β-tetra-brominated *meso*-tetraphenylporphyrinatomanganese(III) acetate, Mn($TPPBr_4$)OAc in the epoxidation of olefins with tetrabutylammonium oxone (TBAO) is reported.

* Corresponding authors. Tel.: +98 241 5152578; fax: +98 241 2283203 (S. Rayati).
E-mail addresses: srayati@mail.znu.ac.ir, srayati@yahoo.com (S. Rayati).

0277-5387/$ - see front matter © 2008 Elsevier Ltd. All rights reserved.
doi:10.1016/j.poly.2008.04.019

2. Experimental

2.1. Instruments and reagents

^{1}H and ^{13}C NMR spectra were obtained in $CDCl_3$ solutions with a Bruker FT-NMR 250 (250 MHz) spectrophotometer. The residual $CHCl_3$ in conventional 99.8 at.% $CDCl_3$ gives a signal at $\delta = 7.26$ ppm, which was used for calibration of the chemical shift scale. A double beam spectrophotometer (Shimadzu, UV-240) was used for the UV–Vis absorption determination. The reaction products of oxidation were determined and analyzed by HP Agilent 6890 gas chromatograph equipped with a HP-5 capillary column (phenyl methyl siloxane 30 m × 320 μm × 0.25 μm) and flame-ionization detector.

The free base tetraphenylporphyrin was prepared and purified as reported previously [16]. Nitrogenous bases were purchased from Merck or Fluka. BzImH was recrystallized before use. n-Bu_4NHSO_5 was prepared as reported previously [17].

2.2. Bromination of H_2TPP

H_2TPPBr_4 (Fig. 1) was prepared according to the literature [18]. H_2TPP[1] (300 mg, 0.49 mmol) was dissolved in $CHCl_3$ (80 ml). To this solution, freshly recrystallised NBS (360 mg, 1.96 mmol) was added (recrystallised from hot water and dried at 80 °C under vacuum). The reaction mixture was stirred for 24 h and then $CHCl_3$ was evaporated to dryness. The residue was washed with methanol (2 × 20 ml) to remove any soluble succinimide impurities. The product, H_2TPPBr_4 was recrystallised from $CHCl_3$/n-hexane (3:1, v/v) and dried under vacuum. UV–Vis (CH_2Cl_2): λ_{max} (nm): 434.5, 533, 683. ^{1}H NMR ($CDCl_3$, 250 MHz): δ (ppm) 8.69 (s, 4H, β pyrrole), 8.16–8.19 (m, 8, o-phenyl), 7.7–7.9 (m, 12, m- and p- phenyl).

2.3. Metalation of H_2TPPBr_4

$Mn(TPPBr_4)OAc$ was prepared and purified according to the previously reported method [19]. H_2TPPBr_4 (110 mg, 0.13 mmol) was dissolved in minimum amount of methanol and then 30 ml chloroform was added. $Mn(OAc)_2 \cdot 4H_2O$ (250 mg, 1.04 mmol) was added to the reaction mixture and refluxed for a period of 2 h. UV–Vis (CH_2Cl_2): λ_{max} (nm): 379.5, 483.5, 590.

2.4. General oxidation procedure

Stock solution of the catalyst (0.003 M) and nitrogenous bases (0.5 M) (except BzImH (0.0625 M)) were prepared in CH_2Cl_2. In a 10 ml round-bottom flask the reagents were added in the following order: alkene (0.25 mmol), catalyst (0.003 mmol, 1.0 ml), nitrogenous bases (0.03 mmol, 60 μl). Tetrabutylammonium oxone (0.5 mmol, 0.206 g) was then added to the reaction solutions at 25 °C. The mixture was stirred thoroughly for 2 min at ambient temperature. Formation of epoxide was detected by GC analysis.

2.5. X-ray crystallography

The dark brown 0.26 × 0.16 × 0.05 mm single crystal was used in the diffraction experiment. The structural analysis revealed multiple bromination sites of the porphyrin system. Two of these sites occur in the same pyrrole ring at C7 and C8. They were refined as fully occupied (Br2 and Br3) although their relatively high atomic displacement parameters suggest the occupancy slightly lower than 100%. The third site at C2 (Br1) appeared in the second pyrrole ring on the final electron density maps. The occupancy of 10% was assumed, based on the observed height of the electron density peak. That reflects the statistical disorder accounting for bromination of one out of ten molecules at Br1 position. Consequently, the statistical level of the ring bromination is 4.2 per a porphyrin ring. For the Br1 bromination site, the presence of hydrogen atom with 90% occupancy was assumed to complete the model of the structure.

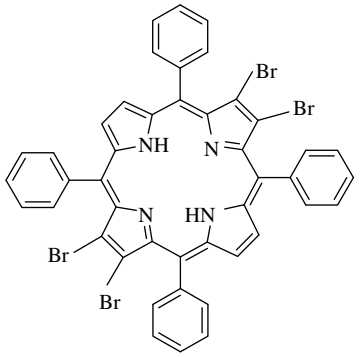

Fig. 1. H_2TPPBr_4.

The X-ray data were collected with an Oxford Sapphire CCD diffractometer using Mo Kα radiation $\lambda = 0.71073$ Å, at 293(2) K, by ω–2θ method. The space group $P2(1)/n$ was determined based on the systematic absences. The numerical absorption correction was applied [20] with the maximum and minimum transmissions of 0.8167 and 0.3711. The structure was solved by direct methods and refined with the full-matrix least-squares method on F^2 with the use of SHELX-97 program package [21]. Positions of hydrogen atoms bound to carbon were calculated from geometry, while the position of hydrogen atom bound to nitrogen was determined from the electron density map.

The data collection and refinement processes are summarized in Table 1.

3. Results and discussion

The similar crystal structure of H_2TPPBr_4 has been reported by Zou et al. [22], but revealed different cell parameters, although the same space group symmetry was reported. The differences might be attributed to the different crystallization conditions. Crystals of H_2TPPBr_4 reported here have been obtained from the $CHCl_3$/n-hexane (3:1, v/v) solution, while Zou et al. [22] obtained crystals by layering a solution of H_2TPPBr_4 in $CHC1_3$ with petroleum/piperidine (333–363 K). Also, the structure of H_2tppBr_4 reported here has an additional bromination site with 10% occupancy at C2 position.

3.1. Conformational studies

X-ray crystallographic studies show that the porphyrin ring system is slightly folded (Fig. 2), with the dihedral angles between the N1–N2–N1 [$-x+1$, $-y+1$, $-z$]–N2[$-x+1$, $-y+1$, $-z$] best plane and the pyrrole ring planes being 10.0(8)° and 3.4(8)° for N1–C1–C2–C3–C4 and N2–C6–C7–C9–C9 rings, respectively. The porphyrin system is slightly more ruffled than that reported previously [22], with the dihedral angle between two pyrrole rings of 7.5(9)°, larger than the corresponding angle of 4.8(5)° in the other structure. That might be caused by the partially occupied bromination site at Cβ (C2 position). Small change in the porphyrin geometry results in the similar N1···N1[$-x+1$, $-y+1$, $-z$] and N2···N2[$-x$;+1, $-y+1$, $-z$] distances across the ring system 4.142 (18) and 4.157

[1] According to the comment, the sentence "H_2TPPBr_4 (Fig. 1) was prepared according to the method reported by Bhyrappa et al. [18]" has been changed to "H_2TPPBr_4 (Fig. 1) was prepared according to the literature [18]". If you mean that the procedure following the above sentence should be omitted, please feel free to do that.

Table 1
Crystal data and structure refinement for H_2TPPBr_4

Compound	H_2TPPBr_4
Formula	$C_{44}H_{25.90}Br_{4.10}N_4$
Formula weight	938.22
T (K)	293 (2)
Wavelength (Å)	0.71073
Crystal system	monoclinic
Space group	$P21/n$
Unit cell dimensions	
a, Å	14.0564(11)
b, Å	6.7168(5)
c, Å	19.1835(16)
β (°)	100.342(7)
V, Å^3	1781.8(2)
Z	2
D_{calc} (Mg/m^3)	1.749
Absorption coefficient (mm^{-1})	4.670
F(000)	923
Crystal size (mm)	0.26 × 0.16 × 0.05
θ range for data collection (°)	2.95–25.00
Index ranges	$-16 \leqslant h \leqslant 16$, $-7 \leqslant k \leqslant 6$, $-22 \leqslant l \leqslant 22$,
Reflections collected/unique	11584/3114 [$R_{(int)}$ = 0.0883]
Completeness to 2θ = 25.00 (%)	91.1
Maximum and minimum transmission	0.8167 and 0.3711
Refinement method	full-matrix LS on F^2
Data/restraints/parameters	3114/42/240
Goodness-of-fit on F^2	1.390
Final R indices [$I > 2\sigma(I)$]	R_1 = 0.1282, wR_2 = 0.3661
R indices (all data)	R_1 = 0.1644, wR_2 = 0.3903
Largest difference in peak and hole (e Å^{-3})	1.154 and −1.958

[a] $R_1 = \sum||F_0| - |F_c||/\sum|F_0|$.
[b] $wR_2 = [\sum w(F_0^2 - F_c^2)^2/\sum(w|F_0|^2)^2]^{1/2}$.

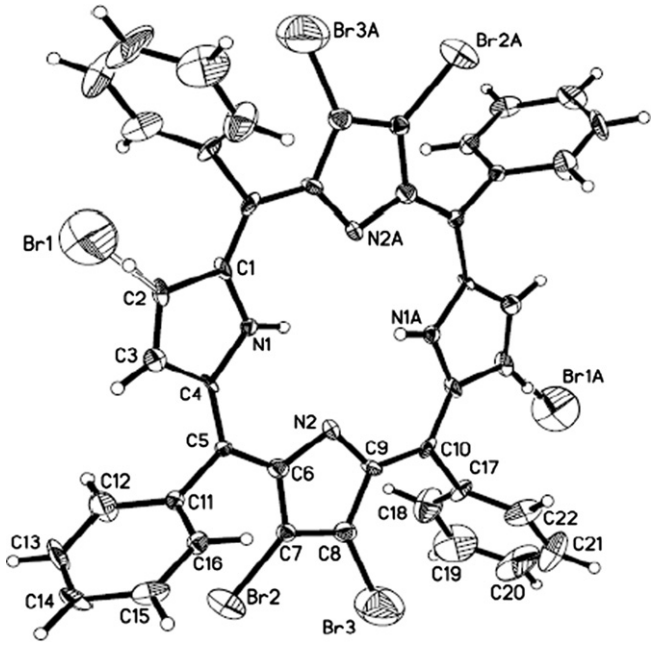

Fig. 2. View of the molecular structure of H_2TPPBr_4 in the crystal.

(18) Å, respectively. The corresponding distances in the more flat structure [22] are 4.21(2) and 4.10(2) Å. The phenyl rings are tilted relative to the pyrrole rings. The dihedral angles between C11–C16 phenyl and N1–C4 and N2–C9 pyrroles being 79.2(4)° and 76.5(4)°, respectively, while for C17–C22 phenyl the corresponding values are 76.4(5)° and 70.1(5)°. In a ruffled conformation the *meso* carbons are alternately above and below the porphyrin mean plane while the core nitrogens are in the plane. Furthermore, all of the atoms along a given edge of the porphyrin macrocycle (C_β–C_α–C_{meso}–C_α–C_β) will be on the same side of the porphyrin mean plane. The transition from edge to edge is accompanied with a transition of the atom positions from one side of the porphyrin mean plane to the other. A point of comparison to be made here is that in the ruffled conformation β carbons of the same pyrrolic subunit will be on opposite sides of the porphyrin mean plane while in the saddled conformation β carbons of the same pyrrolic subunit will be on the same side of the porphyrin mean plane. When the porphyrin is substituted with bulky substitutents on adjacent β and *meso* carbons there is an additional steric strain between those substituents. It has been shown that the bulkier the nature of the substituents, the more non-planar the porphyrin macrocycle will be. It seems that in the case of H_2TPPBr_4, partial ruffling of porphyrin core as well as the decreased co-planarity of phenyl substituents with the porphyrin mean plane would provide relief of steric strain. Angles of 60–85° between the phenyl and porphyrin mean planes were found in solids, and angles of about 40° has been calculated by Wolberg for H_2TPP in solution [23]. The dihedral angle between the phenyl substituents and porphyrin mean plane in H_2TPP and $H_2TPPBr_4$are 60–85° and 70.1–79.2°, respectively.

The N–H bond of H_2TPPBr_4 is shorter than that of H_2TPP [24,25] (Table 2) which may be explained on the basis of the weaker N–H–N hydrogen bond of former relative to that of the latter. The length of NH bond of free base porphyrins is very sensitive to the N–H–N hydrogen bond strength [26]. It has been shown that intramolecular hydrogen bonding in porphyrins can be strongly enhanced by a specific type of non-planar distortion (ruffling) of porphyrin core. Although, the bromination of porphyrin core leads to an increase in the polarity of N–H bond, but it decreases the electron densities at the pyrrolenine nitrogen atoms. Therefore, the N–H–N intramolecular hydrogen bond of electron-deficient porphyrins is expected to be weaker than that of electron rich ones [27]. However, the slight ruffling of porphyrin core of H_2TPPBr_4 seems to have little or no effect on the strength of hydrogen bond; the average N(pyrrole)–N(pyrrolenine) distance (Table 2) of H_2TPPBr_4 is 2.93 Å which is very similar to that of standard planar porphyrins and H_2TPP [26].

3.2. UV–Vis spectra of H_2TPPBr_4

UV–Vis spectra of H_2TPPBr_4 is given in Table 3. The Soret and Q-bands of H_2TPPBr_4 are red shifted with respect to that of H_2TPP (Table 2). Large shifts of the Soret and Q(0,0) bands of porphyrin

Table 2
Average bond lengths (in Å) and bond angles for H_2TPPBr_4 and H_2TPP determined by the X-ray crystallographic analysis

	H_2TPPBr_4	H_2TPP[a]
N–H	0.732	0.93 (1.006)[b]
N–C_α	1.390(13)[c], 1.371(15)[d]	1.369
C_α–C_β	1.427(15)[c], 1.453(15)[d]	1.442
C_β–C_β	1.317(18)[c], 1.365(16)[d]	1.356
C_α –C_{meso}	1.399(8)[c], 1.385(16)[d]	1.400
C_α-N–C_α	110.5(9)[c], 106.8(9)[d]	107.7
N–C_α–C_β	104.9(9)[c], 109.9(10)[d]	108.8
N–C_α–C_{meso}	126.8(10)[c], 124.9(10)[d]	126.1
C_α–C_β–C_β	109.8(11)[c], 106.7(10)[d]	107.4
C_α–C_{meso}–C_α	124.0(10)	125.6
C_{meso}–C_α–C_β	121.2(10)[c], 125.0(10)[d]	125.0
N(pyrrole)–N(pyrrolenine)	2.91–2.95	2.91–2.92

[a] See Ref. [24].
[b] See Ref. [25].
[c] Partially brominated.
[d] Dibrominated pyrrole ring.

Table 3
The Soret and Q(0,0) bands of H_2TPPBr_4 in comparison with the bands of H_2TPP

Porphyrin	Soret band λ (nm)	Q(0,0) band λ (nm)
H_2TPP	416	649
H_2TPPBr_4	438	685
$\Delta\nu$ (cm^{-1})[a]	1207.4	809.8

[a] $\Delta\nu = 10^7(1/\lambda_1 - 1/\lambda_2)$.

have been usually attributed to the out-of-plane deformations of the macrocycle and/or the enhanced co-planarity of phenyl groups with the porphyrin mean plane and/or the inductive effects of substituents at *meso* and β-positions [15,28–30]. Due to the slight folding of porphyrin core of H_2TPPBr_4 and the dihedral angles of 70-79 degrees between the phenyl substituents and the mean plane, the large red shifts of the bands of H_2TPPBr_4 relative to those of H_2TPP seems to be due to the electron-withdrawing effects of four bromine atoms. The a_{2u} to the e_g transition is responsible for the Q(0,0) band. The a_{2u} electron densities are largest on the methane carbons and pyrrole nitrogens [31,32]. Accordingly, the substitution of for bromine atoms at β-positions seems to have little or no effect on the energy level of this orbital. But the e_g electron densities are largest on the β, *meso* and α positions. Thus, the energy level of the e_g orbitals may be influenced by the electron-withdrawing effects of the bromine atoms. It is proposed that the observed red shift of the Q(0,0) band of H_2TPPBr_4 relative to the band of H_2TPP is due to the stabilization of the eg orbitals, resulted in by the inductive effects of the bromine substituents, rather than the destabilization of the a_{2u} one. the Soret band is due to the a_{1u} to e_g transition. For the a_{1u} orbitals the electron densities are largest on the pyrrole carbon atoms and the methane bridges lie on nodal planes [31,32]. Therefore, the energy level of the a_{1u} orbital may also be influenced by the electronic effects of the bromine atoms. However, the red shift of the Soret band which is larger than that of the Q(0,0) band (Table 3), may be attributed to the decreased a_{1u}–e_g gaps, resulted in by the stabilization of the e_g orbitals and the destabilization of the a_{1u} orbital.

3.3. Catalytic alkene epoxidation by $MnTPPBr_4(OAC)/Im/n\text{-}Bu_4HSO_5$ system

Oxidation of cyclooctene with TBAO in the presence of catalytic amounts of $MnTPPBr_4(OAc)$ leads to cyclooctene oxide as the sole product (Table 4). Styrene, α-methylstyrene and *para*-substituted styrenes are 100% converted within 2 min with 100% selectivity for epoxide products except for α-methylstyrene which gives 25% acetophenone as the by-product. Electron-donating (entries 3 and 4) as well as electron-deficient substituents (entry 2) on the *para* position of the aryl ring of styrene were compatible with the reaction conditions, and gave the corresponding epoxide. With the exception of cyclooctene, terminal double bonds and unconjugated ones (Table 4, entries 7, 9 and 10) are less reactive than the conjugated double bonds and show lower selectivities. Much reactivity and high selectivity observed in the case of conjugated double bonds in comparison with terminal double bonds and unconjugated ones seems to be due to the π-electron donation effects of aryl-groups to the double bond. The double bond may be cosidered as a nucleophile in the oxidation reaction.

Epoxidation of terminal alkene (oct-1-ene) and norbornene proceedes in moderate yield (51% and 24%, respectively). Alkenes with potential π-donor aryl substituents (entries 1–5), were generally more reactive than cyclohexene, cyclooctene, and 1-octene (entyies 6–8).

It has been observed that $MnTPPBr_4(OAc)$ (95% yield of epoxide) is more efficient than MnTPP(OAc) (80% yield of epoxide) in the epoxidation of cyclooctene with TBAO. This observation may be due to the enhanced electrophilic character of the possible high valent manganese oxo [33] of [$MnTPPBr_4$] with respect to that of [MnTPP] and the stability of $MnTPPBr_4$ relative to MnTPP against the degradation with oxidant.

Table 4
Epoxidation of alkenes with $n\text{-}Bu_4HSO_5$ catalyzed by $MntppBr_4(OAC)$ in the presence of Im[a]

Entry	Alkene	Conversion %	Epoxide	Selectivity %
1	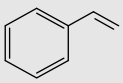	100	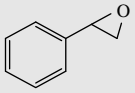	100
2	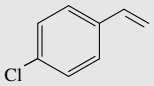	100	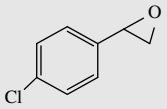	100
3	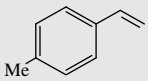	100	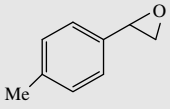	100
4	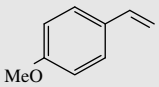	100	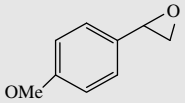	100
5	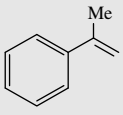	100	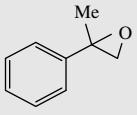	75[b]
6		95	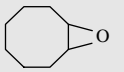	100
7		92	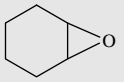	83
8	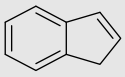	97	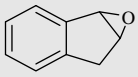	100
9		51	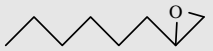	35
10	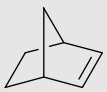	24	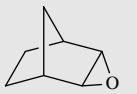	100

[a] The molar ratio for alkene:oxidant:Im:catalyst is 167:83:10:1.
[b] Acetophenone is the by-product.

3.4. Axial base effects

The results of epoxidation of cyclooctene by $n\text{-}Bu_4NHSO_5$ in the presence of different nitrogen donors as co-catalysts, under similar conditions, are given in Table 5. Although, the co-catalytic activity of the stronger donor bases is greater than that of others, but there is no correlation between the co-catalytic activity of the nitrogenous donors and the pK_a of the corresponding BH^+. The basicity of nitrogenous donors is defined relative to a bare or solvated pure σ-acceptor, i.e. proton, while the co-catalytic activity is defined on the basis of σ- or/and π- donation to a metal centre. Consequently, factors such as the steric hindrance around the metal centre and the extent of π-interaction between the axial base and the metal centre should also be considered.

Table 5
Co-catalytic activity for different nitrogen donors[a]

Entry	Nitrogen donor	pK_a (BH^+)	$MnTPPBr_4$
1	piperidine	11.123	57
2	Et_2NH	11.02	55
3	Et_3N	10.75	53
4	ImH	6.953	95
5	1-MeImH	7.86	87
6	BzImH	5.532	93
7	Py	5.25	81
8	2-MePy	5.97	43
9	3-MePy	5.52	86
10	4-MePy	6.02	90
11	3-CNPy	1.78	26
12	4-CNPy	1.86	17
13	none		9

[a] The molar ratio for alkene:oxidant:nitrogen donor:catalyst is 167:83:10:1.

The best co-catalytic activity has been observed in the case of imidazole that is the smallest axial base among the nitrogenous donors of the Table 5. While, the introduction of π-electron-withdrawing substituents at different positions of pyridine (entries 11 and 12) dramatically decreases the activity of pyridine as a nitrogen donor, substitution of methyl at 4-position of pyridine leads to only a 10 percents increase in the yield of the epoxidation of cyclooctene. It seems that the activity of nitrogen donors is strongly depends on the π-donor ability of axial base. In accordance with the explanation, co-activity of benzimidazole (entry 6) is almost equal to that of imidazole (entry 4), although the size of the former is much larger than that of the latter. It is also observed that simple amines (entries 1, 2, 3) which may be considered as pure σ-donors, are less effective than those with both σ- and π-donor abilities.

3.5. The effect of co-catalyst/catalyst ratio

The interaction of catalyst with nitrogen donors (D) can lead to the formation of both catalytically active 1:1 $DMnTPPBr_4$ and catalytically inactive 2:1 $D_2MnTPPBr_4$. Co-catalytic activity of imidazole as a function of different co-catalyst/catalyst ratio are presented in Fig. 3. An increase in Im/Mn-porphyrin molar ratio up to 10 remarkably improved the rate of conversion of cyclooctene epoxidation. However, its co-catalytic activity decreased at co-catalyst/catalyst ratio $\lesssim 50$.

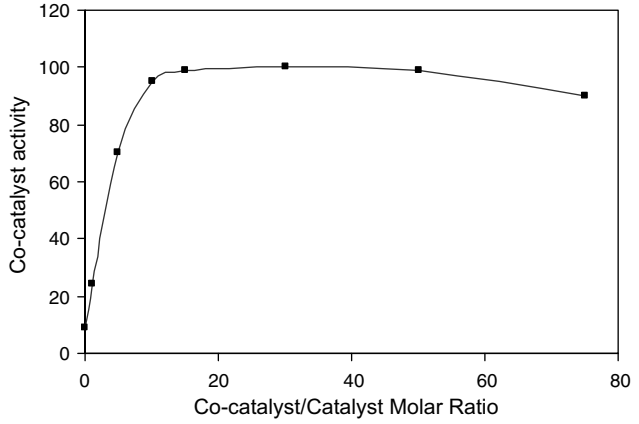

Fig. 3. Co-catalyst activity of imidazole as a function of different co-catalyst/catalyst ratio.

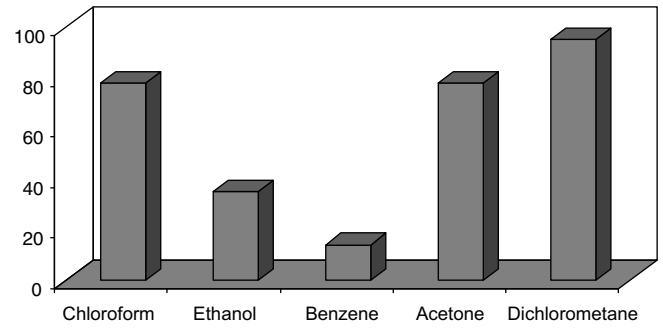

Fig. 4. Effect of the type of solvent on the conversion of cyclooctene to cyclooctene oxide at room temperature.

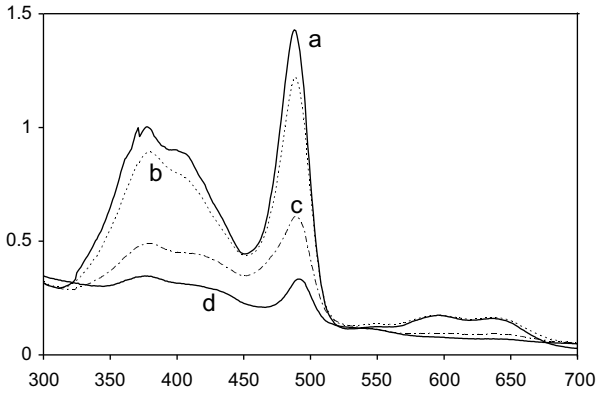

Fig. 5. UV–Vis spectra of a solution of $Mn(TPPBr_4)OAc$ in CH_2Cl_2 (a), in the presence of imidazole (b), in the presence of imidazole/TBAO and cyclooctene (c) and in the presence of imidazole/TBAO (d), at room temperature after 1 min.

3.6. Solvent effect in the epoxidation reactions with n-Bu_4HSO_5

The influence of the solvent nature in the catalytic epoxidation of cyclooctene by $MnTPPBr_4$/Im/n-Bu_4HSO_5 system, were examined. Inspection of results in Fig. 4 shows that CH_2Cl_2 is the best solvent because of high solubility of all starting materials.

3.7. Stability of the catalyst against the degradation with oxidant

It has been shown that catalyst stability is a major factor contributing to apparent catalyst ability [34]. It is observed that destruction of metalloporphyrin in the absence of olefin is faster than the time that cyclooctene was used (Fig. 5).

4. Conclusions

In spite of the nearly planar structure of H_2TPPBr_4, the Soret and Q(0,0) bands of the β-brominated porphyrin are red shifted with respect to those of H_2TPP which is probably due to the electron-withdrawing effects of four bromine atoms. $Mn(TPPBr_4)OAc$/TBAO/Imidazole is an efficient catalytic system for the selective epoxidation of conjugated double bonds. The enhanced stability of $Mn(TPPBr_4)OAc$ relative to Mn(TPP)OAc against degradation with the oxidant and higher yields of epoxide make this electron-deficient Mn-porphyrin more efficient than Mn(TPP)OAc in the epoxidation of olefins.

Acknowledgements

We gratefully acknowledge practical support of this study by Zanjan University, Institute for Advanced Studies in Basic Sciences and N. Copernicus University.

Appendix A. Supplementary data

CCDC 675329 contains the supplementary crystallographic data for the titled porphyrin. These data can be obtained free of charge via http://www.ccdc.cam.ac.uk/conts/retrieving.html, or from the Cambridge Crystallographic Data Center, 12 Union Road, Cambridge CB2 1EZ, UK; fax: +44 1223-336-033; or e-mail: deposit@ccdc.cam.ac.uk. Supplementary data associated with this article can be found, in the online version, at doi:10.1016/j.poly.2008.04.019.

References

[1] R.A. Sheldon, Metalloporphyrins in Catalytic Oxidations, Marcel Dekker, New York, 1994.
[2] F. Montanari, L. Casella, Metalloporphyrins Catalyzed Oxidations, Kluwer Academic Publishers, Boston, MA, 1994.
[3] W. Nam, S.Y. Oh, Y.J. Sun, J. Kim, W.K. Kim, S.K. Woo, W. Shin, J. Org. Chem. 68 (2003) 7903.
[4] D. Mansuy, Pure Appl. Chem. 59 (1987) 759.
[5] S. Funyu, T. Isobe, S. Takagi, D.A. Tryk, H. Inoue, J. Am. Chem. Soc. 125 (2003) 5734.
[6] N.A. Stephenson, A.T. Bell, J. Am. Chem. Soc. 127 (2005) 8635.
[7] Z. Gross, L. Simkhovich, Tetrahedron Lett. 39 (1998) 8171.
[8] Q.H. Xia, H.Q. Ge, C.P. Ye, Z.-M. Liu, K.X. Su, Chem. Rev. 105 (2005) 1603.
[9] W. Nam, S.Y. Oh, M.H. Lim, M.H. Choi, S.Y. Han, G.J. Jhon, Chem. Commun. (2000) 1787.
[10] T.G. Traylor, C. Kim, W.P. Fann, C.L. Perrin, Tetrahedron 54 (1998) 1787.
[11] Z. Li, C.G. Xia, C.Z. Xu, Tetrahedron Lett. 44 (2003) 9229.
[12] J. Rosenthal, B.J. Pistorio, L.L. Chng, D.G. Nocera, J. Org. Chem. 70 (2005) 1885.
[13] K.T. Moore, I.T. Horvath, M.J. Therien, Inorg. Chem. 39 (2000) 3125.
[14] J.P. Collman, H.T. Fish, P.S. Wagenknecht, D.A. Tyvoll, L.L. Chng, T.A. Eberspacher, J.I. Brauman, J.W. Bacon, L.H. Pignolet, Inorg. Chem. 35 (1996) 6746.
[15] R.E. Haddad, S. Gazeau, J. Pe' caut, J.-C. Marchon, C.J. Medforth, J.A. Shelnutt, J. Am. Chem. Soc. 125 (2003) 1253.
[16] A.D. Adler, F.R. Longo, J.D. Finarelli, J. Goldmacher, J. Asour, L. Korsakoff, J. Org. Chem. 32 (1967) 476.
[17] D. Mohajer, A. Rezaeifard, Tetrahedron Lett. 43 (2002) 1881.
[18] P.K. Kumar, P. Bhyrappa, B. Varghese, Tetrahedron Lett. 44 (2003) 4849.
[19] E. Nascimento, G. Silva, F.A. Caetano, M.A.M. Fernandez, D.C. Silva, M.E.M.D. Carvalho, J.M. Pernaut, J.S. Reboucas, Y.M. Idemori, J. Inorg. Biochem. 99 (2005) 1193.
[20] CRYSALIS CCD171 and RED171 package of programs, Oxford Diffraction, 2000.
[21] G.M. Sheldrick, SHELXS97 and SHELXL97, University of Göttingen, Germany, 1997.
[22] J.-Z. Zou, Z. Xu, M. Li, X.Z. You, Acta Crystallogr. C 51 (1995) 760.
[23] A. Wolberg, J. Mol. Struct. 21 (1974) 61.
[24] S.J. Silvers, A. Tulinsky, J. Am. Chem. Soc. 89 (1967) 3331.
[25] A. Rosa, G. Ricciardi, E.J. Baerends, A. Romeo, L.M. Scolaro, J. Phys. Chem. A 107 (2003) 11468.
[26] M.S. Somma, C.J. Medforth, N.Y. Nelson, M. Olmstead, R.G. Khoury, K.M. Smith, Chem. Commun. (1999) 1221.
[27] K.F. Purcell, J.C. Kotz, Inorganic Chemistry, Saunders, Philadelphia, 1977. p. 190.
[28] M. Meot-Ner, A.D. Adler, J. Am. Chem. Soc. 97 (1975) 5107.
[29] S.G. Dimagno, A.K. Wertsching, C.R. Ross, J. Am. Chem. Soc. 117 (1995) 8279.
[30] S. Zakavi, N.G. Gharab, Polyhedron 26 (2007) 2425.
[31] M. Gouterman, J. Chem. Phys. 30 (1959) 1139.
[32] M. Gouterman, J. Mol. Spectrosc. 6 (1961) 138.
[33] D. Mohajer, L. Sadeghian, J. Mol. Catal. A: Chem. 272 (2007) 191.
[34] I.D. Cunningham, T.N. Danks, J.N. Hay, I.S. Gunathilagan, C. Janczak, J. Mol. Catal. A: Chem. 185 (2002) 25.

Polyhedron 27 (2008) 2291–2300

Contents lists available at ScienceDirect

Polyhedron

journal homepage: www.elsevier.com/locate/poly

Effect of pendant arm position and length on the structure and properties of nickel aromatic dicarboxylate coordination polymers incorporating a kinked organodiimine

Maxwell A. Braverman [a], Richard J. Staples [a], Ronald M. Supkowski [b], Robert L. LaDuca [a,*]

[a] Lyman Briggs College and Department of Chemistry, E-30 Holmes Hall, Michigan State University, East Lansing, MI 48825, USA
[b] Department of Chemistry and Physics, King's College, Wilkes-Barre, PA 18711, USA

ARTICLE INFO

Article history:
Received 20 January 2008
Accepted 21 April 2008
Available online 4 June 2008

Keywords:
Coordination polymer
Nickel
Phenylenediacetate
Homophthalate
Dipyridylamine
Crystal structure
Thermogravimetric analysis
Antiferromagnetism

ABSTRACT

Hydrothermal synthesis has afforded three nickel coordination polymers incorporating both aromatic dicarboxylates and the kinked and hydrogen bonding capable organodiimine 4,4′-dipyridylamine (dpa). These were characterized by single-crystal X-ray diffraction, infrared spectroscopy, and thermogravimetric analysis. $[Ni(1,2\text{-phda})(dpa)(H_2O)]_n$ (1,2-phda = 1,2-phenylenediacetate, **1**) displays (4,4) rhomboid grid-like 2D layers that aggregate into 3D through O–H···O hydrogen bonding. Shortening one of the pendant arms of the dicarboxylate ligand resulted in a shift to (6,3) herringbone style 2D coordination layer motifs in $\{[Ni(hmph)(dpa)] \cdot 1.33H_2O\}_n$ (hmph = homophthalate, **2**), which stack in an AA′B pattern. $[Ni(1,3\text{-phda})(dpa)(\mu\text{-}H_2O)_{0.5}]_n$ (1,3-phda = 1,3-phenylenediacetate, **3**) manifests a canted primitive cubic type coordination polymer lattice constructed from dinuclear $\{Ni_2(\mu\text{-}H_2O)\}$ kernels linked into 3D through tethering 1,3-phda and dpa ligands. Analysis of the variable temperature magnetic susceptibility of **3** indicated the presence of antiferromagnetic superexchange within its dinuclear units ($g = 2.290(2)$, $J = -4.21(2)\ cm^{-1}$).

© 2008 Elsevier Ltd. All rights reserved.

1. Introduction

Coordination polymer solids generated from divalent metal ions and dicarboxylate tethering ligands have attracted significant interest not only for their aesthetically appealing structures, but also for their promise in diverse technological applications such as gas storage [1], small molecule shape-selectivity [2], ion-exchange [3], catalysis [4], and optical devices [5]. A wide range of structural patterns occurs in these systems, based on the disposition of the donor groups within the dicarboxylate moieties, coordination geometry preferences of the specific metal ions used, and an array of available binding and bridging modes achievable with these ligands. While the predominant synthetic effort has focused on aromatic dicarboxylate tethers such as isophthalate and terephthalate, aliphatic α,ω-dicarboxylate ligands have also proven useful in the construction of new coordination polymer topologies due to their ability to adopt energetically similar but different conformations [6]. However, coordination polymers constructed from dicarboxylate tethers containing both aromatic rigidity and aliphatic pendant arm flexibility, for example phenylenediacetate isomers, are less common [7].

More recently, several researchers have augmented the structural complexity and functional utility of dicarboxylate-containing inorganic/organic hybrid materials by employing neutral organodiimine co-ligands such as the rigid-rod 4,4′-bipyridine (4,4′-bpy). These dipodal nitrogen bases can link metal cations through their distal pyridyl nitrogen donor atoms, supplementing the covalent connectivity provided by the metal/dicarboxylate backbone to produce structurally interesting solids with promising properties [8–11]. Several members of this dual-ligand class of coordination polymers with d^{10} ions exhibit luminescent properties [9]; one especially intriguing solid, the interpenetrated 3D material $[Zn(terephthalate)(4,4'\text{-bpy})_{0.5}]$, can serve as a stationary phase for the chromatographic separation of linear and branched alkanes [11]. The conformational flexibility of α,ω-dicarboxylate ligands can also facilitate reversible crystal-to-crystal structural reorganizations upon removal/re-addition of guest species within dual-ligand coordination polymers [12].

Recently our group has been investigating the synthesis and characterization of metal/dicarboxylate coordination polymers containing the organodiimine 4,4′-dipyridylamine (dpa) as a neutral co-ligand. Unlike the more commonly employed 4,4′-bpy, dpa has a kinked disposition of its terminal nitrogen donor atoms in addition to hydrogen bonding donating capability at its central amine. We have shown that both covalent and supramolecular interactions provided by the dpa ligand can synergistically act in

* Corresponding author. Tel.: +1 5174322268.
E-mail address: laduca@msu.edu (R.L. LaDuca).

0277-5387/$ - see front matter © 2008 Elsevier Ltd. All rights reserved.
doi:10.1016/j.poly.2008.04.038

structure-direction during self-assembly, to produce structural patterns different from those within similar coordination polymers based on 4,4′-bpy [12–15]. For example, $[Ni(adipate)(dpa)(H_2O)]_n$ exhibited the first-ever example of 3-fold interpenetration within the PtS structure type [12], and $\{[Ni(dpa)_2(succinate)_{0.5}]Cl\}_n$ manifested an unprecedented 5-connected self-penetrated network with a "regular" 6^{10} topology [13]. The combination of zinc salts with phenylenediacetate isomers and dpa resulted in luminescent coordination polymers with differing two-dimensional (2D) and three-dimensional (3D) structural morphologies, depending on the position of the pendant acetate arms within the dicarboxylate moieties [14].

Herein we report the successful extension of this previous work into a nickel-based system, with the synthesis and structural characterization of three new coordination polymers with differing morphologies, constructed from both dpa and aromatic dicarboxylates with one or more flexible pendant arms: $[Ni(1,2\text{-phda})(dpa)(H_2O)]_n$ (**1**; 1,2-phda = 1,2-phenylenediacetate), $\{[Ni(hmph)(dpa)] \cdot 1.33H_2O\}_n$ (**2**; hmph = homophthalate), and $[Ni(1,3\text{-phda})(dpa)(\mu\text{-}H_2O)_{0.5}]_n$ (**3**; 1,3-phda = 1,3-phenylenediacetate). Thermal properties of these new coordination polymers are also reported herein, along with a variable temperature magnetic susceptibility study for **3**.

2. Experimental

2.1. General considerations

$NiCl_2 \cdot 6H_2O$ (Fisher) and all dicarboxylic acids (Aldrich) were obtained commercially. The organodiimine 4,4′-dipyridylamine (dpa) was prepared via a published procedure [15]. Water was deionized above 3 MΩ in-house. Thermogravimetric analysis was performed on a TA Instruments TGA 2050 Thermogravimetric Analyzer with a heating rate of 10 °C/min up to 900 °C. Elemental Analysis was carried out using a Perkin Elmer 2400 Series II CHNS/O Analyzer. IR spectra were recorded on powdered samples on a Perkin Elmer Spectrum One instrument. Powder X-ray diffraction patterns were obtained via θ–2θ scans performed on a Rigaku Rotaflex instrument. Variable temperature magnetic susceptibility data (2–300 K) were collected on a Quantum Design MPMS SQUID magnetometer at an applied field of 0.1 T. After each temperature change the sample was kept at the new temperature for 5 min before magnetization measurement to ensure thermal equilibrium. The susceptibility data were corrected for diamagnetism using Pascal's constants.

2.2. Preparation of $[Ni(1,2\text{-phda})(dpa)(H_2O)]_n$ (**1**)

$NiCl_2 \cdot 6H_2O$ (0.088 g, 0.37 mmol), dpa (0.127 g, 0.74 mmol) and 1,2-phenylenediacetic acid (0.072 g, 0.37 mmol) were added to 10 mL of distilled H_2O in a 23 mL Teflon-lined Parr acid digestion bomb. The bomb was sealed, heated to 120 °C for 48 h, and then gradually cooled to ambient temperature. Green blocks of **1** (0.050 g, 31% yield based on Ni) were obtained after filtration, washing with distilled water and acetone, and drying in air. Crystals of **1** were stable indefinitely in air. *Anal.* Calc. for $C_{20}H_{19}N_3NiO_5$**1**: C, 54.59; H, 4.35; N, 9.55. Found: C, 53.99; H, 4.46; N, 9.54%. IR (cm^{-1}): 3285 w br, 1589 s, 1547 w, 1515 s, 1437 w, 1408 m, 1366 s, 1337 m, 1289 w, 1213 m, 1149 w, 1014 m, 939 w, 903 w, 850 w, 831 w, 812 s, 779 w, 716 s, 695 m, 650 m.

2.3. Preparation of $\{[Ni(hmph)(dpa)] \cdot 1.33H_2O\}_n$ (**2**)

$NiCl_2 \cdot 2H_2O$ (0.088 g, 0.37 mmol), homophthalic acid (0.067 g, 0.37 mmol), dpa (0.127 g, 0.74 mmol), and 0.25 mL 1.0 M NaOH solution were placed into 10 g (555 mmol) distilled H_2O in a 23 mL Teflon-lined Parr acid digestion bomb (1:1:2: 1500 mol ratio). The bomb was sealed and heated at 120 °C for 48 h, whereupon

Table 1
Crystal and structure refinement parameters for **1**–**3**

	1	**2**	**3**
Empirical formula	$C_{40}H_{38}N_6Ni_2O_{10}$	$C_{19}H_{19.667}N_3NiO_{5.333}$	$C_{20}H_{18}N_3NiO_{4.5}$
Formula weight	880.18	434.09	431.08
Collection T (K)	293	173	173
λ (Å)	0.71073	0.71073	0.71073
Color and habit	green block	green block	green block
Crystal size (mm)	0.45 × 0.40 × 0.40	0.31 × 0.28 × 0.20	0.30 × 0.12 × 0.10
Crystal system	monoclinic	monoclinic	monoclinic
Space group	$P2_1/n$	$P2_1/c$	$I2/a$
a (Å)	17.076(3)	14.9502(3)	17.416(6)
b (Å)	10.987(2)	21.5180(4)	11.810(3)
c (Å)	21.522(4)	18.4272(3)	21.913(7)
β (°)	108.635(2)	103.5970(10)	99.654(3)
V (Å^3)	3826.1(13)	5761.86(18)	4443.1(19)
Z	4	12	8
D_{calc} (g cm^{-3})	1.528	1.492	1.289
μ (mm^{-1})	1.052	1.048	0.903
Minimum/maximum transmission	0.843	0.765	0.897
hkl ranges	$-22 \leqslant h \leqslant 22$, $-14 \leqslant k \leqslant 13$, $-27 \leqslant l \leqslant 26$	$-19 \leqslant h \leqslant 19$, $-26 \leqslant k \leqslant 28$, $-23 \leqslant l \leqslant 24$	$-20 \leqslant h \leqslant 20$, $-14 \leqslant k \leqslant 14$, $-26 \leqslant l \leqslant 26$
Total reflections	41 023	141 018	20 942
Unique reflections	8714	13 593	3911
R_{int}	0.0204	0.0687	0.0916
Parameters/restraints	541/8	796/12	300/7
R_1 (all data)[a]	0.1013	0.1223	
R_1 ($I > 2\sigma(I)$)[a]	0.0384	0.0488	0.0810
wR_2 (all data)[b]	0.1134	0.1404	0.2720
wR_2 ($I > 2\sigma(I)$)[b]	0.1070	0.1171	0.2446
Maximum/minimum residual (e$^-$/Å^3)	0.764/−0.457	1.298/−0.705	1.181/−0.461
Goodness-of-fit	1.049	1.022	1.057

[a] $R_1 = \sum||F_o| - |F_c||/\sum|F_o|$. [b] $wR_2 = \{\sum[w(F_o^2 - F_c^2)^2]/\sum[wF_o^2]^2\}^{1/2}$.

it was cooled slowly in air to 25 °C. Small green crystals of **2** (0.146 g, 91% yield based on Ni) were isolated after washing with distilled water. *Anal.* Calc. for $C_{19}H_{19.667}N_3NiO_{5.333}$ (**2**): C, 52.57; H, 4.57; N, 9.68. Found; C, 52.11; H, 4.43; N, 9.39%. IR (cm^{-1}): 3450 w br, 3012 w, 1637 w, 1598 s, 1548 w, 1522 s, 1491 m, 1444 w, 1421 m, 1401 s, 1359 s, 1292 w, 1208 m, 1090 w, 1057 w, 1022 m, 943 w, 908 w, 872 m, 852 w, 834 w, 812 s, 724 s, 695 m, 677 m, 661 w.

2.4. Preparation of [Ni(1,3-phda)(dpa)(μ-H_2O)$_{0.5}$]$_n$ (**3**)

$NiCl_2 \cdot 6H_2O$ (0.088 g, 0.37 mmol), dpa (0.127 g, 0.74 mmol) and 1,2-phenylenediacetic acid (0.072 g, 0.37 mmol) were added to 10 mL of distilled H_2O in a 23 mL Teflon-lined Parr acid digestion bomb. The bomb was sealed, heated to 120 °C for 48 h, and then gradually cooled to ambient temperature. Green blocks of **3** (0.100 g, 63% yield based on Ni) were obtained after filtration, washing with distilled water and acetone, and drying in air. Crystals of **3** were stable indefinitely in air. *Anal.* Calc. for $C_{20}H_{18}N_3NiO_{4.5}$ **3**: C, 55.73; H, 4.21; N, 9.75. Found: C, 55.48; H, 4.02; N, 9.48%. IR (cm^{-1}): 2910 w br, 1744 w, 1590 s, 1513 m, 1486 m, 1440 w, 1385 s, 1340 m, 1266 w, 1210 m, 1060 w, 1017 s, 905 w, 843 w, 822 s, 712 s, 680 w, 657 m.

3. X-ray crystallography

Single crystals of all materials were subjected to single-crystal X-ray diffraction using a Bruker-AXS SMART 1k (**1**, **3**) or APEX II CCD (**2**) instrument. Reflection data were acquired using graphite-monochromated Mo Kα radiation ($\lambda = 0.71073$ Å). The data were integrated via SAINT [16]. Lorentz and polarization effect and empirical absorption corrections were applied with SADABS [17]. The structures were solved using direct methods and refined on F^2 using SHELXTL [18]. All non-hydrogen atoms were refined anisotropically. Hydrogen atoms bound to carbon atoms were placed in calculated positions and refined isotropically with a riding model. The hydrogen atoms bound to the central nitrogen of the dpa moieties and all aqua ligands were found via Fourier difference maps, restrained at fixed positions, and then refined isotropically with thermal parameters 1.2 times the average U_{ij} values of the atoms to which they are bound. Hydrogen atoms could not be located for the disordered water molecule of crystallization within the structure of **2**. The aromatic rings within the 1,3-phda ligands in **3** exhibited disorder over three sets of positions, which were modeled as a 50:25:25 ratio. Relevant crystallographic data for **1**–**3** are listed in Table 1.

Table 2
Selected bond distance (Å) and angle (°) data for **1**

Ni1–O3	2.0218(17)	O3–Ni1–O9	95.70(8)
Ni1–O9	2.0471(19)	O3–Ni1–N4$^{\#1}$	89.04(7)
Ni1–N4$^{\#1}$	2.0732(18)	O9–Ni1–N4$^{\#1}$	93.41(8)
Ni1–O5	2.1022(17)	O3–Ni1–O5	163.10(7)
Ni1–N6	2.1053(18)	O9–Ni1–O5	101.20(8)
Ni1–O6	2.2343(17)	N4$^{\#1}$–Ni1–O5	89.85(7)
Ni2–O8$^{\#2}$	2.008(2)	O3–Ni1–N6	85.44(7)
Ni2–O10	2.0213(19)	O9–Ni1–N6	92.61(8)
Ni2–N3$^{\#3}$	2.1041(19)	N4$^{\#1}$–Ni1–N6	172.20(7)
Ni2–N1	2.1310(19)	O5–Ni1–N6	93.84(7)
Ni2–O1	2.1608(18)	O3–Ni1–O6	102.39(7)
Ni2–O2	2.1954(17)	O9–Ni1–O6	161.91(8)
O1–C28	1.260(3)	N4$^{\#1}$–Ni1–O6	87.00(7)
O2–C28	1.263(3)	O5–Ni1–O6	60.71(6)
O3–C30	1.255(3)	N6–Ni1–O6	88.81(7)
O4–C30	1.237(4)	O8$^{\#2}$–Ni2–O10	102.59(9)
O5–C38	1.262(3)	O8$^{\#2}$–Ni2–N3$^{\#3}$	84.61(8)
O6–C38	1.261(3)	O10–Ni2–N3$^{\#3}$	92.41(8)
O7–C40	1.236(6)	O8$^{\#2}$–Ni2–N1	89.83(8)
O8–C40	1.229(5)	O10–Ni2–N1	94.60(8)
		N3$^{\#3}$–Ni2–N1	171.86(8)
		O8$^{\#2}$–Ni2–O1	163.20(9)
		O10–Ni2–O1	94.15(7)
		N3$^{\#3}$–Ni2–O1	93.41(7)
		N1–Ni2–O1	90.20(7)
		O8$^{\#2}$–Ni2–O2	102.78(8)
		O10–Ni2–O2	154.23(8)
		N3$^{\#3}$–Ni2–O2	85.54(7)
		N1–Ni2–O2	89.92(7)
		O1–Ni2–O2	60.42(6)

Symmetry transformations to generate equivalent atoms: #1 $x - 1/2$, $-y + 3/2$, $z - 1/2$; #2 $x + 1$, y, z; #3 $x + 1/2$, $-y + 3/2$, $z + 1/2$.

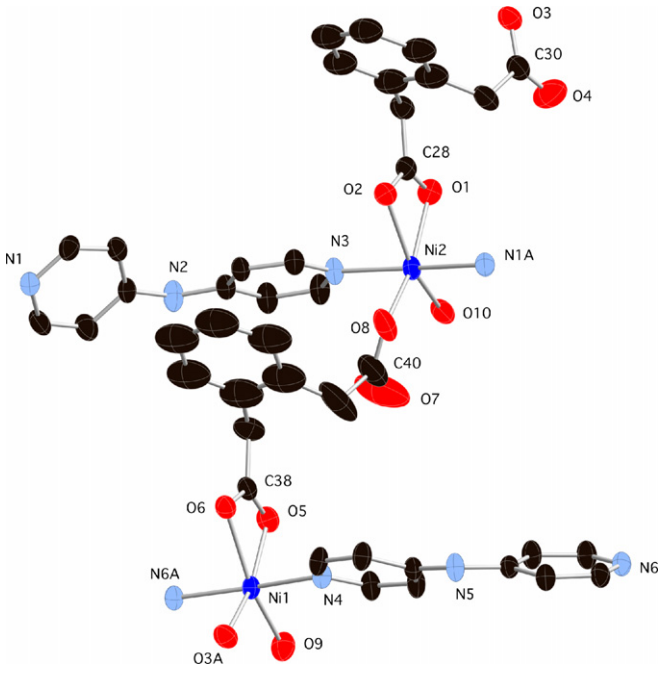

Fig. 1. Coordination environment of **1** with thermal ellipsoids drawn at 50% probability and partial atom numbering scheme. Hydrogen atoms have been omitted for clarity. Atoms labelled with an "A" designation are generated by crystallographic symmetry.

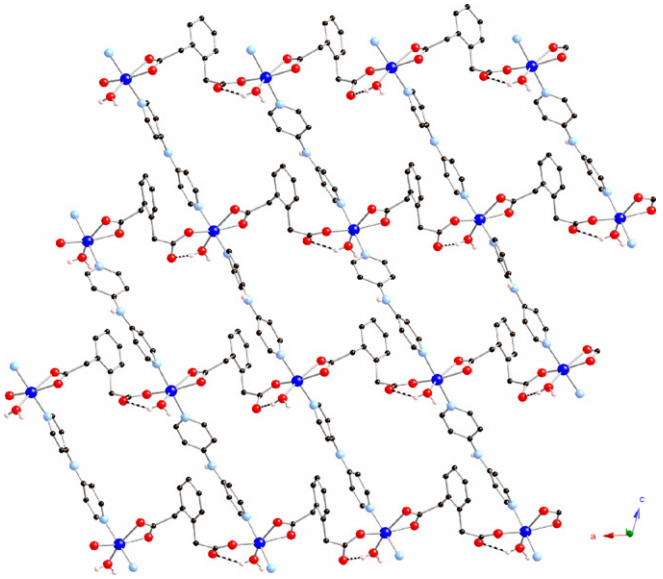

Fig. 2. Face-on view of the [Ni(1,2-phda)(dpa)(H_2O)]$_n$ 2D (4,4)-grid layer in **1**. Intralayer hydrogen bonding is shown as dashed lines.

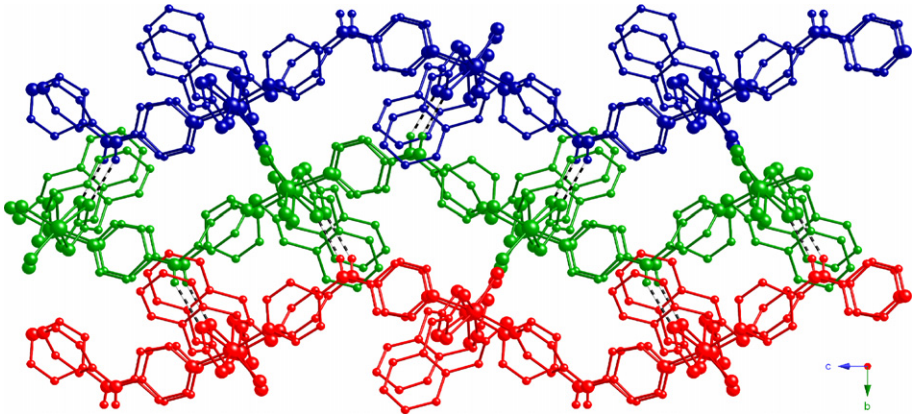

Fig. 3. Stacking of $[Ni(1,2\text{-phda})(dpa)(H_2O)]_n$ layers in **1** along the *b* crystal direction in an ABA pattern by interlayer hydrogen bonding (shown as dashed lines).

4. Results and discussion

4.1. Synthesis and spectral characterization

The coordination polymers **1**–**3** were prepared cleanly under hydrothermal conditions via combination of nickel chloride, dpa, and the requisite dicarboxylic acid. The infrared spectra of **1**–**3** were consistent with their structures as determined by X-ray diffraction (*vide infra*). Sharp, medium intensity bands in the range of ~1600 cm^{-1} to ~1200 cm^{-1} were ascribed to stretching modes of the pyridyl rings of the dpa moieties [19]. Features corresponding to pyridyl ring puckering mechanisms were evident in the region between 820 cm^{-1} and 600 cm^{-1}. Asymmetric and symmetric C–O stretching modes of the carboxylate moieties were evidenced by very strong, slightly broadened bands at ~1590 cm^{-1} and ~1370 cm^{-1}. Broad bands in the region of ~3400 cm^{-1} to ~3000 cm^{-1} in all cases represent N–H stretching modes within the dpa ligands and O–H stretching modes within ligated or unligated water molecules. The broadness of these latter spectral features is caused by significant hydrogen bonding pathways within **1**–**3**. Phase purity was verified with powder XRD by comparison with powder patterns predicted from the single-crystal structures.

4.2. Structural description of $[Ni(1,2\text{-phda})(dpa)(H_2O)]_n$ (*1*)

As revealed by single-crystal X-ray diffraction, the asymmetric unit (Fig. 1) of compound **1** contains two crystallographically distinct nickel atoms (Ni1, Ni2), two 1,2-phda dianions (*phda-A*, C21–C30/O1–O4; *phda-B*, C31–C40/O5–O8), two dpa ligands (*dpa-A*, C1–C10/N1–N3; *dpa-B*, C11–C20/N4–N6), and two ligated water molecules (O9, O10). Both crystallographically distinct Ni atoms display a distorted octahedral $[NiO_4N_2]$ coordination geometry, where the two *trans*-disposed nitrogen donor atoms belong to *dpa-A* and *dpa-B* ligands, respectively. The equatorial plane of each coordination octahedron is occupied by two oxygen atoms from a chelating carboxylate terminus of a 1,2-phda ligand, one oxygen atom from a monodentate carboxylate group of a crystallographically distinct 1,2-phda ligand, and an aqua ligand. Bond lengths and angles about the nickel atoms are consistent with the chelation-imposed distorted octahedral coordination geometry (Table 2).

Extension of the structure through the exobidentate chelating/monodentate 1,2-phda ligands results in a one-dimensional (1D) $[Ni(1,2\text{-phda})(H_2O)]_n$ chain motif that propagates along the *a* crystal direction. Within the $[Ni(1,2\text{-phda})(H_2O)]_n$ chain Ni1 and Ni2

Table 3
Hydrogen bonding distance (Å) and angle (°) data for **1**–**3**

D–H···A	*d*(H···A)	∠DHA	*d*(D···A)	Symmetry transformation for A
Complex ***1***				
O9–H9A···O4	1.833(19)	160(3)	2.641(3)	
O9–H9B···O1	2.247(18)	165(3)	3.043(3)	$-x+1, -y+2, -z$
O10–H10A···O5	1.931(17)	173(3)	2.771(2)	$-x+1, -y+2, -z$
O10–H10B···O7	2.24(3)	129(3)	2.819(4)	$-x+1, -y+2, -z$
O10–H10B···O7	2.18(2)	137(3)	2.824(4)	$x+1, y, z$
N2–H2N···O6	2.36(2)	147(3)	3.133(3)	$-x+1, -y+1, -z$
N5–H5N···O2	2.195(19)	161(3)	3.018(3)	$-x+3/2, y+1/2, -z+1/2$
Complex ***2***				
O1W–H1WA···O3	2.13	179.2	2.983(4)	
O1W–H1WB···O10	1.91	157.4	2.723(4)	
O2W–H2WB···O7	2.00(3)	161(6)	2.857(5)	$x+1, y, z$
O3W–H3WB···O6	3.01(6)	89(4)	3.115(5)	$-x+1, -y+1, z$
N2–H2N···O11	1.987(18)	172(3)	2.857(3)	$x, -y+3/2, z-1/2$
N5–H5N···O4	1.949(18)	172(3)	2.827(3)	
N8–H8N···O5	1.954(18)	170(3)	2.849(3)	
Complex ***3***				
O1–H1A···O5	1.79(4)	151(8)	2.573(7)	$-x+1/2, y, -z+1$
N2–H2N···O3	1.97(3)	171(8)	2.848(8)	$x-1/2, -y+1, z$

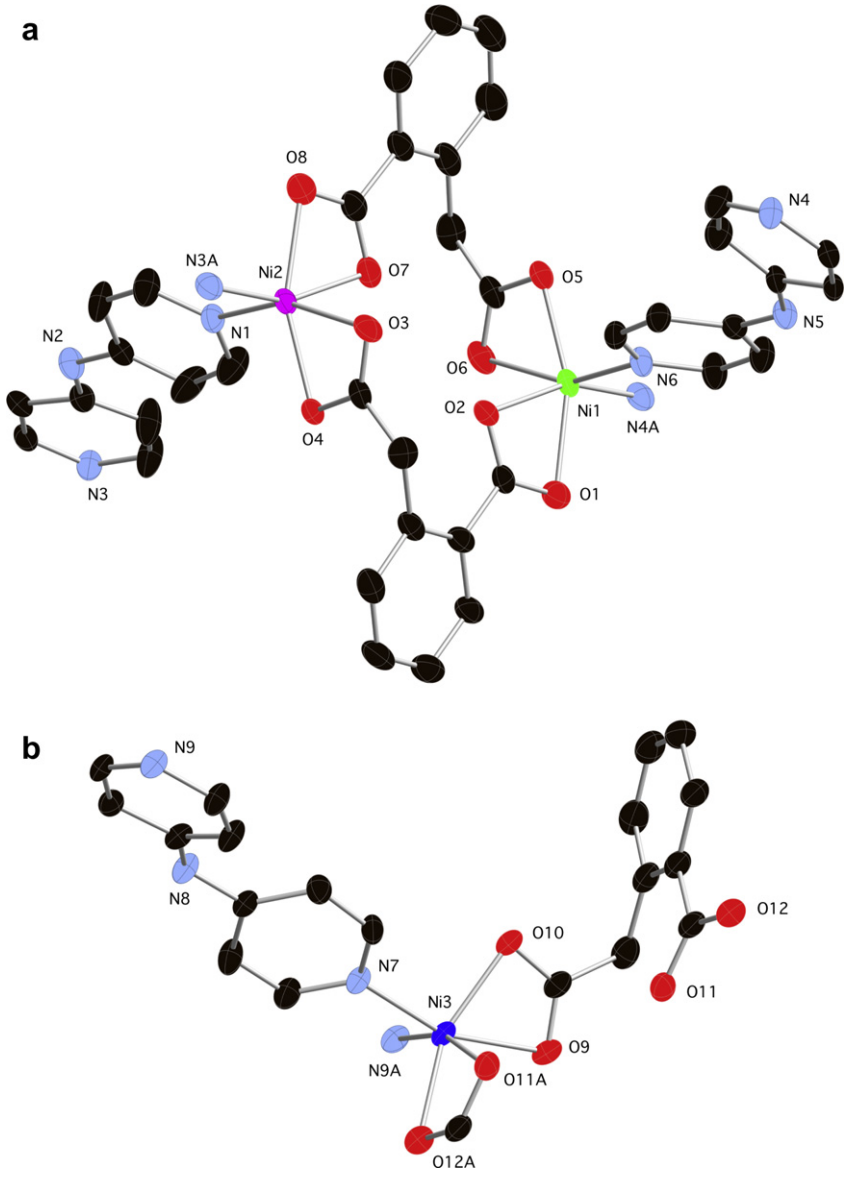

Fig. 4. Coordination environments of **2** with thermal ellipsoids shown at 50% probability and partial atom numbering scheme (top, Ni1 and Ni2 and attached ligands; bottom, Ni3 and attached ligands). Hydrogen atoms and water molecules of crystallization have been omitted for clarity. Atoms labelled with an "A" designation are generated by crystallographic symmetry.

centers are linked through *phda-A* and *phda-B* ligands in an alternating pattern, with Ni···Ni distances toggling between 8.112 Å and 8.976 Å, respectively. The varying Ni···Ni distances are promoted by the conformational flexibility of the pendant arms of the 1,2-phda ligands, despite the identical carboxylate binding modes. The carboxylate termini of *phda-A* are twisted by ~60° and ~70° relative to the ligand's aromatic ring plane, while the related carboxylate torsions for *phda-B* are ~40° and ~57°, thus allowing a greater distance span across the ligated pendant arms of *phda-B*. Covalent bonding within the $[Ni(1,2\text{-phda})(H_2O)]_n$ chains is supplemented by hydrogen bonding donation by the aqua ligands to unligated oxygen atoms from the monodentate carboxylate groups of the 1,2-phda ligands.

Adjacent $[Ni(1,2\text{-phda})(H_2O)]_n$ chain subunits are subsequently conjoined into a two-dimensional (2D) $[Ni(1,2\text{-phda})(dpa)(H_2O)]_n$ (4,4) rhomboid grid coordination polymer layer (Fig. 2) by exobidentate dpa ligands; the layer motif runs parallel to the *ac* crystal plane. Ni1 centers are linked by *dpa-B* ligands, fostering a Ni1···Ni1 contact distance of 11.525 Å; the pyridyl rings within *dpa-B* are twisted by 28.1° with respect to each other. Similarly, Ni2 atoms are strutted by *dpa-A* ligands with a Ni2···Ni2 contact distance of 11.548 Å. The inter-ring torsion within *dpa-A* is slightly larger, at 32.7°.

Due to the conformation-imposed varying tether lengths, two different grid sizes are observed within the $[Ni(1,2\text{-phda})(dpa)(H_2O)]_n$ layers. The grid spaces bracketed by the shorter *phda-A* tethers measure 11.067 × 16.595 Å, as determined by through-space Ni···Ni distances, with Ni···Ni···Ni angles of 66.0° and 114.2°. The more pinched grid spaces, delineated by the longer *phda-B* tethers, measure 10.766 × 17.646 Å, with Ni···Ni···Ni angles of 61.8° and 118.0°. Neighboring $[Ni(1,2\text{-phda})(dpa)(H_2O)]_n$ layers stack in an ABA pattern along the *b* crystal direction, primarily through interlayer hydrogen bonding between the central amine units of the dpa ligands and oxygen atoms belonging to chelating carboxylate moieties within 1,2-phda ligands (Fig. 3). Hydrogen bonding parameters for **1** are given in Table 3. The 2D non-interpenetrated layered structure of **1** is dramatically different from its related zinc congener, $\{[Zn(1,2\text{-phda})(dpa)] \cdot H_2O\}_n$, which

Table 4
Selected bond distance (Å) and angle (°) data for **2**

Ni1–N4	2.039(2)	O5–Ni1–O6	61.58(8)
Ni1–O5	2.048(2)	N6–Ni1–O6	156.58(9)
Ni1–N6$^{\#1}$	2.057(2)	O1–Ni1–O6	105.72(8)
Ni1–O1	2.093(2)	O2–Ni1–O6	90.18(8)
Ni1–O2	2.113(2)	N3$^{\#2}$–Ni2–N1	96.57(10)
Ni1–O6	2.215(2)	N3$^{\#2}$–Ni2–O4	100.50(9)
Ni2–N3$^{\#2}$	2.034(2)	N1–Ni2–O4	97.10(9)
Ni2–N1	2.039(2)	N3$^{\#2}$–Ni2–O7	95.27(9)
Ni2–O4	2.089(2)	N1–Ni2–O7	95.73(9)
Ni2–O7	2.103(2)	O4–Ni2–O7	158.34(8)
Ni2–O8	2.104(2)	N3$^{\#2}$–Ni2–O8	157.06(10)
Ni2–O3	2.193(2)	N1–Ni2–O8	91.29(9)
Ni3–N9$^{\#1}$	2.039(2)	O4–Ni2–O8	99.85(8)
Ni3–N7	2.044(2)	O7–Ni2–O8	62.42(8)
Ni3–O11$^{\#3}$	2.089(2)	N3$^{\#2}$–Ni2–O3	89.76(9)
Ni3–O10	2.098(2)	N1–Ni2–O3	158.20(9)
Ni3–O9	2.115(2)	O4–Ni2–O3	61.18(8)
Ni3–O12$^{\#3}$	2.137(2)	O7–Ni2–O3	104.46(8)
		O8–Ni2–O3	90.85(8)
N4–Ni1–O5	98.52(9)	N9$^{\#1}$–Ni3–N7	95.30(10)
N4–Ni1–N6$^{\#1}$	99.51(10)	N9$^{\#1}$–Ni3–O11$^{\#3}$	97.84(9)
O5–Ni1–N6$^{\#1}$	95.30(9)	N7–Ni3–O11$^{\#3}$	96.51(9)
N4–Ni1–O1	95.90(9)	N9$^{\#1}$–Ni3–O10	98.01(9)
O5–Ni1–O1	160.34(8)	N7–Ni3–O10	99.24(9)
N6$^{\#1}$–Ni1–O1	95.42(9)	O11$^{\#3}$–Ni3–O10	156.46(8)
N4–Ni1–O2	157.12(9)	N9$^{\#1}$–Ni3–O9	91.59(9)
O5–Ni1–O2	100.85(8)	N7–Ni3–O9	161.13(9)
N6–Ni1–O2$^{\#1}$	90.72(9)	O11$^{\#3}$–Ni3–O9	99.93(8)
O1–Ni1–O2	62.59(8)	O10–Ni3–O9	62.34(8)
N4–Ni1–O6	88.42(9)	N9$^{\#1}$–Ni3–O12$^{\#3}$	160.09(9)
		N7–Ni3–O12$^{\#3}$	88.12(9)
		O11$^{\#3}$–Ni3–O12$^{\#3}$	62.26(8)
		O10–Ni3–O12$^{\#3}$	100.79(8)
		O9–Ni3–O12$^{\#3}$	91.36(8)

Symmetry transformations to generate equivalent atoms: #1 x, $-y+1/2$, $z+1/2$; #2 x, $-y+3/2$, $z+1/2$; #3 $-x$, $-y+1$, $-z+1$.

possesses a 4-fold interpenetrated $SrAl_2$(sra) lattice [14]. The octahedral coordination preference of the nickel ions in **1**, at the expense of tetrahedral coordination in the zinc analogue, is a plausible rationalization for this significant structural change.

4.3. Structural description of $\{[Ni(hmph)(dpa)] \cdot 1.33H_2O\}_n$ (**2**)

The large asymmetric unit of compound **2** (Fig. 4a and b) consists of three crystallographically unique nickel atoms (Ni1–Ni3), hmph dianions (*hmph-A*, O1–O4; *hmph-B*, O5–O8; *hmph-C*, O9–O12) and dpa ligands (*dpa-A*, N1–N3; *dpa-B*, N4–N6; *dpa-C*, N7–N9), along with four water molecules of crystallization. All nickel atoms adopt a $[NiO_4N_2]$ distorted octahedral geometry, with *cis*-disposed nitrogen donors from two different, yet crystallographically identical, dpa ligands. The remaining four coordination sites are taken up by oxygen atoms from chelating carboxylate groups from crystallographically distinct *hmph-A* and *hmph-B* ligands for Ni1 and Ni2, and from a pair of crystallographically identical *hmph-C* ligands for Ni3. Bond lengths and angles about Ni1, Ni2, and Ni3 are similar, and are stated in Table 4.

By means of two bisbridging bischelating hmph ligands (*hmph-A* and *hmph-B*), Ni1 and Ni2 are joined into a binuclear kernel with a Ni···Ni distance of 5.590 Å. In turn, Ni1 atoms are linked through tethering *dpa-B* ligands (with an inter-ring torsion of 23.5°), providing a Ni···Ni distance equal to 11.633 Å. Ni2 atoms conjoin to other Ni2 atoms through *dpa-C* (inter-ring torsion = 18.1°) with a slightly shorter Ni···Ni through-ligand distance of 11.591 Å. Therefore each Ni1 is connected to two other Ni1 atoms and one Ni2 atom, while Ni2 is connected to two other Ni2 atoms and one Ni atom, constructing a 3-connected 2D $[Ni(hmph)(dpa)]_n$ coordination polymer layer motif (Layer A, Fig. 5a). Considering the

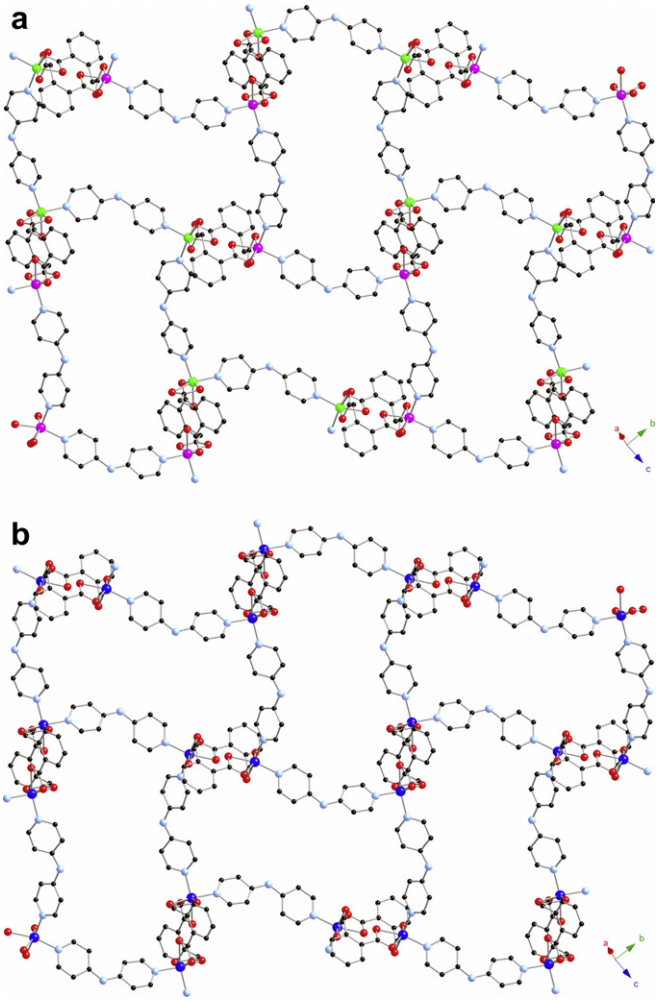

Fig. 5. Layers A (top) and B (bottom) in **2**, viewed individually slightly offset from the *a* crystal direction.

hmph-A and *hmph-B* linkages as a single connector between Ni1 and Ni2 atoms allows the visualization of the coordination polymer layer as a (6,3) herringbone pattern.

A very similar 2D $[Ni(hmph)(dpa)]_n$ (6,3) herringbone pattern is formed by linkage of Ni3 atoms to three other Ni3 atoms, through two *dpa-A* ligands (inter-ring torsion = 27.2°) and two *hmph-C* ligands (Layer B, Fig. 5b). The through-dpa Ni3···Ni3 distances within the layer are all identical, at 11.578 Å; while the through-space Ni3···Ni3 distances bracketed by the crystallographically identical *hmph-C* tethers are 5.584 Å. Both layer A and layer B motifs are situated parallel to the *bc* crystal plane.

It is likely that the subtle conformational variances between the dpa and hmph ligands result in the presence of two crystallographically distinct layers within the structure of **2**; the layers should be considered conformers as opposed to true supramolecular isomers. The different Ni···Ni through-space distances across the six-membered circuits within each layer type may also reflect these variances. Ni···Ni through-space distances within layer *A* measure 15.85, 18.31, and 22.14 Å, allowing accommodation of water molecule dimers (O1W···O3W) and isolated water molecules of crystallization (O4W). On the other hand, only isolated water molecules of crystallization (O2W) are present within layer B, where the Ni···Ni through-space distances measure 16.57, 18.25, and 21.61 Å.

The $[Ni(hmph)(dpa)]_n$ (6,3) layer motifs stack along the *a* crystal direction in a repeating AA′B pattern (Fig. 6), where layers A and A′

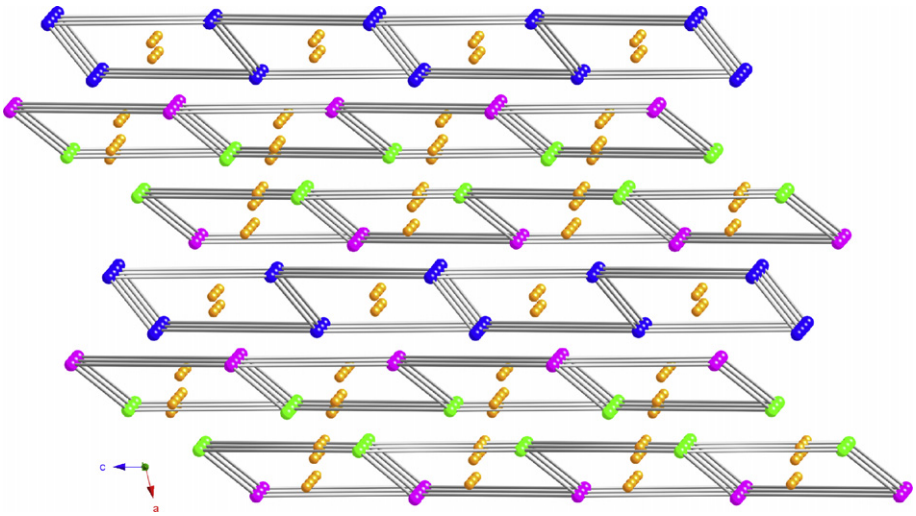

Fig. 6. AA′B layer stacking pattern within **2**. Water molecules of crystallization can be seen as spheres within the layers.

are related by crystallographic inversion. The pattern repeat distance of 14.950 Å defines the *a* lattice parameter. Interlayer supramolecular connectivity is fostered by the central amine units of the dpa ligands, which engage in hydrogen bonding to chelating carboxylate oxygen atoms at the longer pendant arm of the hmph ligands that project into the incipient voids within the (6,3) layers. Metrical parameters for the hydrogen bonding patterns in **2** are given above in Table 3.

4.4. Structural description of $[Ni(1,3\text{-phda})(dpa)(\mu\text{-}H_2O)_{0.5}]_n$ (**3**)

The asymmetric unit of compound **3** (Fig. 7) contains a single divalent nickel atom, one 1,3-phda dianion, one entire dpa molecule, and a ligated water molecule located on a crystallographic 2-fold axis. As is the case for **2**, the nickel atom possesses a distorted $[NiO_4N_2]$ octahedral coordination environment with a *cis* orientation of its nitrogen donors, which belong to two different dpa ligands. Bond lengths and angles about the nickel atom are standard for octahedral coordination (Table 5). Three of the oxygen donors belong to three different 1,3-phda ligands, while the remaining coordination site is occupied by an aqua ligand. Each 1,3-phda ligand serves as an exotridentate linker, connecting two nickel atoms at one carboxylate terminus in a bisbridging binding mode with a third nickel atom via the other carboxylate locus in a monodentate binding mode.

The aqua ligand serves to bridge two Ni atoms in a μ_2-fashion; both Ni atoms are in turn also bridged by two carboxylate termini from two different 1,3-phda ligands to a triply bridged binuclear unit (Fig. 8). These have a Ni···Ni distance of 3.603 Å, with the two bridging carboxylate groups situated 88.13° apart. Individual binuclear units are connected into a 1D $[Ni_2(1,3\text{-phda})_2(\mu\text{-}H_2O)]_n$ chain motif, coursing along the *a* crystal direction, by means of the monodentate carboxylate termini of the 1,3-phda ligands (Fig. 9). The Ni···Ni contact distance through the full extent of the 1,3-phda dianionic tethers is 8.881 Å.

Adjacent $[Ni_2(1,3\text{-phda})_2(\mu\text{-}H_2O)]_n$ chains are conjoined in the *b* and *c* crystal directions by dpa ligands to construct the 3D coordination polymer network of **3**. The dpa ligands contain an inter-ring

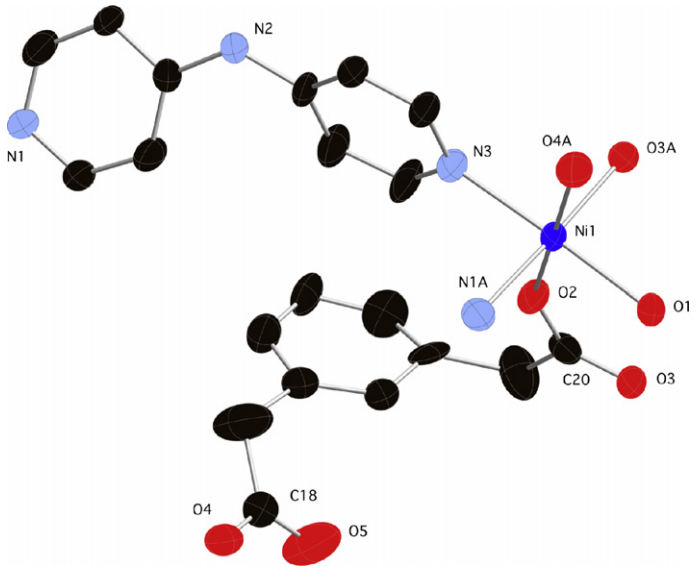

Fig. 7. Coordination environment of **3** with thermal ellipsoids shown at 50% probability and partial atom numbering scheme. Atoms labelled with an "A" designation are generated by crystallographic symmetry.

Table 5
Selected bond distance (Å) and angle (°) data for **3**

Ni1–O2$^{\#1}$	2.061(5)	O2$^{\#1}$–Ni1–O1	91.22(19)
Ni1–O4	2.067(5)	O4–Ni1–O1	90.7(2)
Ni1–O3	2.069(5)	O3–Ni1–O1	92.29(18)
Ni1–N1	2.094(6)	N1–Ni1–O1	90.1(2)
Ni1–O1	2.094(4)	O2$^{\#1}$–Ni1–N3$^{\#2}$	89.4(2)
Ni1–N3$^{\#2}$	2.108(6)	O4–Ni1–N3$^{\#2}$	88.8(2)
O2$^{\#1}$–Ni1–O4	176.1(2)	O3–Ni1–N3$^{\#2}$	90.0(2)
O2$^{\#1}$–Ni1–O3	88.2(2)	N1–Ni1–N3$^{\#2}$	87.6(3)
O4–Ni1–O3	88.3(2)	O1–Ni1–N3$^{\#2}$	177.6(2)
O2$^{\#1}$–Ni1–N1	91.6(2)	Ni1–O1–Ni1$^{\#1}$	118.7(3)
O4–Ni1–N1	91.7(2)	O3–Ni1–N1	177.7(2)

Symmetry transformations to generate equivalent atoms: #1 $-x+1/2, y, -z+1$; #2 $-x, y+1/2, -z+1/2$.

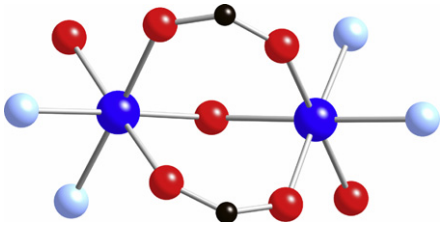

Fig. 8. Triply bridged {$Ni_2(\mu\text{-}H_2O)$} binuclear unit in **3**, with complete coordination spheres shown.

torsion of 41.3°, which fosters a Ni···Ni distance of 11.337 Å. Alternatively, the structure of **3** may be visualized as $[Ni_2(\mu\text{-}H_2O)(dpa)_2]_n^{4n+}$ cationic layers buttressed via 1,3-phda ligands. Treating the centroids of the {$Ni_2(\mu\text{-}H_2O)$} kernels as the connecting nodes allows the coordination polymer connectivity of **3** to be considered as a 6-connected canted primitive cubic (pcu) lattice with $4^{12}6^3$ topology (Fig. 10). The 3D covalent connectivity of **3** is supplemented by hydrogen bonding patterns mediated by the bridging water molecules and the central amine groups of the dpa ligands (see Table 3 for more detail).

4.5. Variable temperature magnetism of 3

To probe possible spin communication across its binuclear subunits, a sample of **3** was subjected to variable temperature magnetic study. The $\chi_m T$ product at 300 K was 1.09 cm^3 K mol^{-1} Ni, slightly higher than expected for an uncoupled Ni^{2+} $S=1$ ion (1.00 cm^3 K mol^{-1}), perhaps indicative of some crystal field anisotropy. The value of $\chi_m T$ decreased slowly below 50 K, reaching 1.00 cm^3 K mol^{-1}; the decrease was significantly more rapid below this temperature, reaching 0.00796 cm^3 K mol^{-1} at 2 K. Decreasing $\chi_m T$ product values in systems with dimeric {Ni_2} kernels can be ascribed either to antiferromagnetic superexchange through bridging ligands, or zero field splitting due to anisotropy.

The magnetic data was fit to Eq. (1), derived for a Heisenberg dimer of $S=1$ spins [20], and a temperature independent magnetism term was included (Fig. 11). The variables have their usual magnetochemical meanings. Best fit parameters were $g=2.290(2)$, $J=-4.21(2)\ cm^{-1}$, $\chi_{TI}=-6.2\times10^{-4}\ cm^3\ mol^{-1}$ with $R=1.48\times10^{-3}=\{\sum[(\chi_m T)_{obs}-(\chi_m T)_{calc}]^2\}^{1/2}$. The negative value of J corroborates the presence of antiferromagnetic coupling through the bridging carboxylate and aqua ligands in **3**. However, this value should be construed as an upper limit due to the likely presence of cooperative effects due to zero-field splitting (D parameter).

$$\chi_m T=\left(\frac{Ng^2\beta^2}{k}\right)\left[\frac{e^x+5e^{3x}}{1+3e^x+5e^{3x}}\right]+\chi_{TI}T \qquad (1)$$

where $x=J/kT$.

Given the substantially longer Ni···Ni distances in **1** and **2**, the magnetic behavior of these materials is expected to be dominated by zero-field splitting. As such, they were not subjected to variable temperature magnetic study.

4.6. Thermal analysis of 1–3

Thermogravimetric analysis was performed on samples of compounds **1**–**3** to investigate their robustness and decomposition pathways. Compound **1** manifested minimal mass loss until ~150 °C, whereupon dehydration commenced. This process was complete by ~240 °C, with the mass loss of 5.1% roughly consistent with elimination of one equivalent of water per nickel atom (4.1% calc.). The thermogram then exhibited a plateau until ~300 °C, at which temperature the organic components of the coordination polymer were ejected. The final mass remnant of 14.3% at 900 °C roughly matches with the deposition of Ni metal (13.3% calc.). Compound **2** underwent dehydration between 25 °C and 330 °C, with an observed mass loss of 5.2% (5.5% calc. for complete loss of water molecules of crystallization). At this latter temperature combustion of the organic ligands occurred. The final mass remnant of 17.6% represents the production of NiO (17.2% predicted). Compound **3** released its bridging water molecules between 25 °C and ~250 °C (3.0% mass loss, 2.1% predicted). Removal of the organic components took place between ~275 °C and ~600 °C, likely depositing NiO (17.2% mass loss observed, 17.7% calc.). TGA traces for **1**–**3** are depicted in Figs. S1–S3.

5. Conclusions

Variance of pendant arm length and position within aromatic dicarboxylate ligands has allowed access to a diversity of two-

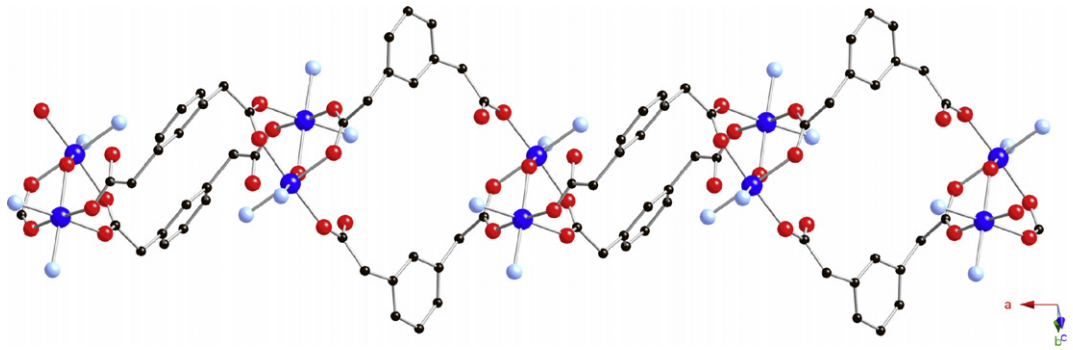

Fig. 9. $[Ni_2(1,3\text{-phda})_2(\mu\text{-}H_2O)]_n$ 1D chain motif in **3**.

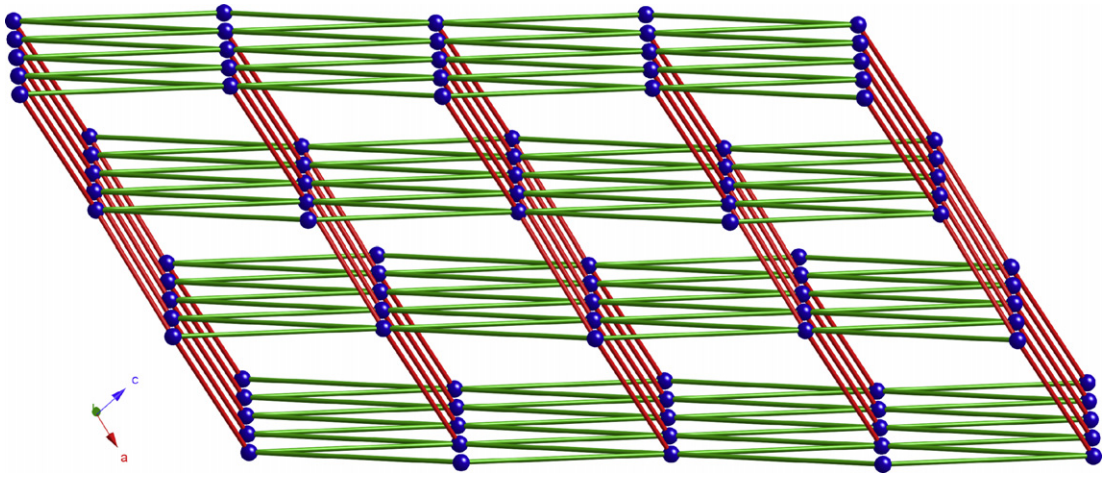

Fig. 10. Framework view of the canted primitive cubic 3D structure pattern in **3**. The $\{Ni_2(\mu\text{-}H_2O)\}$ binuclear units are represented as spheres, with organic ligands shown as solid rods. The 1,3-phda ligands connect the binuclear units along the *a* crystal direction.

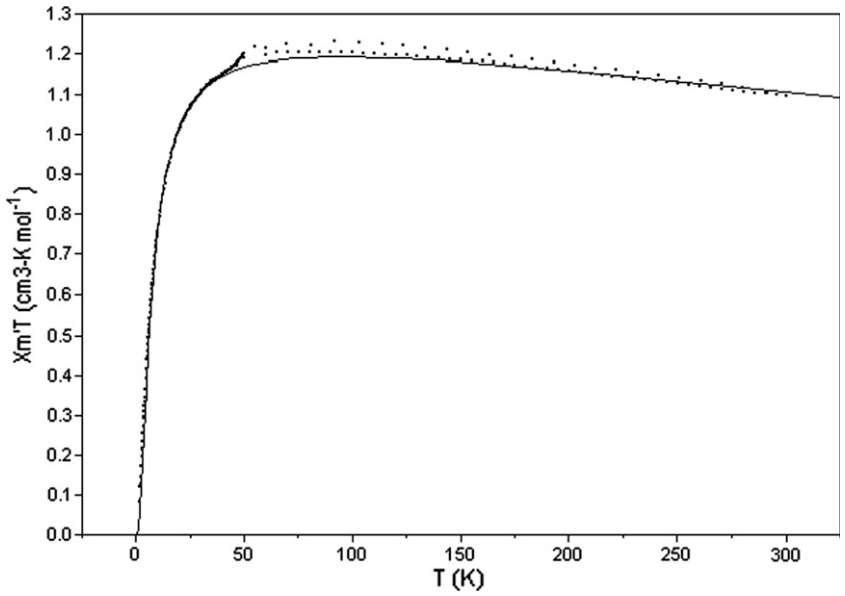

Fig. 11. $\chi_m T$ vs. T plot for **3**. The solid line indicates the best fit to Eq. (1) in the text.

and three-dimensional nickel coordination polymer structure types in a co-ligand system with the kinked and hydrogen bonding donating organodiimine dpa. The *ortho* disposition of acetate groups within 1,2-phda results in a "standard" rhomboid grid 2D coordination polymer morphology in **1**, albeit with slightly different grid apertures imparted by the conformational flexibility of the dpa ligands and the pendant arms of the dicarboxylate ligands. Shortening one of the pendant arms by one methylene unit did not change the overall coordination polymer dimensionality, but did adjust the layer morphology into a herringbone pattern and also altered the stacking pattern of the layered motifs. Use of the 1,3-phda ligand, which possesses a *meta* disposition of acetate pendant arms and a wider separation between its carboxylate termini, appeared to promote the formation of antiferromagnetically coupled triply bridged dinuclear units which conjoined into a 3D coordination polymer with a canted primitive cubic structure type. In all cases, the supramolecular hydrogen bonding pathways provided by the dpa ligand serve an important ancillary structure-directing role. Additional coordination polymers incorporating the dpa ligand have been recently prepared in our laboratory; reports concerning their structures and physicochemical properties will ensue in due course.

Acknowledgements

The authors gratefully acknowledge Michigan State University for financial support of this work. M.A.B. acknowledges the MSU Quality Fund Undergraduate Research Program for financial support. We thank Dr. Rui Huang for elemental analysis and Mr. Hayed D. Salaame for experimental assistance. SDG.

Appendix A. Supplementary data

CCDC 674722, 674723 and 674724 contain the supplementary crystallographic data for **1**, **2** and **3**. These data can be obtained free of charge via http://www.ccdc.cam.ac.uk/conts/retrieving.html, or from the Cambridge Crystallographic Data Centre, 12 Union Road, Cambridge CB2 1EZ, UK; fax: (+44) 1223-336-033; or e-mail:

deposit@ccdc.cam.ac.uk. TGA traces for **1**, **2** and **3** are also available via the Web edition of this journal. Supplementary data associated with this article can be found, in the online version, at doi:10.1016/j.poly.2008.04.038.

References

[1] (a) For example: J.L.C. Roswell, O.M. Yaghi, Angew. Chem., Int. Ed. Engl. 44 (2005) 4670;
(b) M. Kondo, T. Okubo, A. Asami, S.-I. Noro, T. Yoshitomi, S. Kitagawa, T. Ishii, H. Matsuzaka, Angew. Chem., Int. Ed. Engl. 38 (1999) 140;
(c) A.C. Sudik, A.R. Millward, N.W. Ockwig, A.P. Cote, J. Kim, O.M. Yaghi, J. Am. Chem. Soc. 127 (2005) 7110.

[2] (a) For example: J.S. Seo, D. Whang, H. Lee, S.I. Jun, J. Oh, Y.J. Jeon, K. Kim, Nature 404 (2000) 982;
(b) A. Cingolani, S. Galli, N. Masciocchi, L. Pandolfo, C. Pettinari, A. Sironi, J. Am. Chem. Soc. 127 (2005) 6144.

[3] (a) For example: Q.-R. Fang, G.-S. Zhu, M. Xue, J.-Y. Sun, S.-L. Qiu, Dalton Trans. (2006) 2399;
(b) X.-M. Zhang, M.-L. Tong, H.K. Lee, X.-M. Chen, J. Solid State Chem. (2001) 118;
(c) O.M. Yaghi, H. Li, T.L. Groy, Inorg. Chem. 36 (1997) 4292.

[4] (a) For example: S.G. Baca, M.T. Reetz, R. Goddard, I.G. Filippova, Y.A. Simonov, M. Gdaniec, N. Gerbeleu, Polyhedron 25 (2006) 1215;
(b) H. Han, S. Zhang, H. Hou, Y. Fan, Y. Zhu, Eur. J. Inorg. Chem. 8 (2006) 1594;
(c) W. Mori, S. Takamizawa, C.N. Kato, T. Ohmura, T. Sato, Micropor. Mesopor. Mater. 73 (2004) 15.

[5] (a) For example: S. Zang, Y. Su, Y. Li, Z. Ni, Q. Meng, Inorg. Chem. 45 (2006) 174;
(b) L. Wang, M. Yang, G. Li, Z. Shi, S. Feng, Inorg. Chem. 45 (2006) 2474;
(c) S. Wang, Y. Hou, E. Wang, Y. Li, L. Xu, J. Peng, S. Liu, C. Hu, New J. Chem. 27 (2003) 1144.

[6] (a) For example: D. Ghoshal, A.K. Ghosh, G. Mostafa, J. Ribas, N.R. Chaudhuri, Inorg. Chim. Acta 360 (2007) 1771;
(b) C. Livage, C. Egger, M. Nogues, G. Ferey, Compt. Rend. Acad. Sci. Ser. Chem. 4 (2001) 221.

[7] (a) L. Pan, K.M. Adams, H.E. Hernandez, X. Wang, C. Zheng, Y. Hattari, K. Kaneko, J. Am. Chem. Soc. 125 (2003) 3062;
(b) Y.-F. Zhou, R.-H. Wang, B.-L. Wu, R. Cao, M.-L. Hong, J. Mol. Struct. 697 (2004) 73;
(c) J. Zhou, C. Sun, J. Linpei, J. Mol. Struct. 832 (2007) 55;
(d) Y. Yang, M.-H. Zheng, S.H. Zhang, H. Liang, Acta Crystallogr., Sect. E 63 (2007) m2392.

[8] (a) W.-G. Lu, C.-Y. Su, T.-B. Lu, L. Jiang, J.-M. Chen, J. Am. Chem. Soc. 128 (2006) 34;
(b) S. Horike, R. Matsuda, S. Kitagawa, Stud. Surface Sci. Cat. 156 (2005) 725;
(c) C. Qin, X.-L. Wang, Y.-G. Li, E.-B. Wang, Z.-M. Su, L. Xu, R. Clerac, Dalton Trans. (2005) 2609;
(d) Y.-Q. Zheng, E.-R. Ying, Polyhedron 24 (2005) 397;
(e) S.K. Ghosh, J. Ribas, P.K. Bharadwaj, Cryst. Growth Des. 5 (2005) 623;
(f) X.-Z. Sun, Y.-F. Sun, B.-H. Ye, X.-M. Chen, Inorg. Chem. Commun. 6 (2003) 1412.

[9] L. Xu, G.-C. Guo, B. Liu, M.-S. Wang, J.-S. Huang, Inorg. Chem. Commun. 7 (2004) 1145.

[10] H.-P. Jia, W. Li, Z.-F. Ju, J. Zhang, Eur. J. Inorg. Chem. (2006) 4264.

[11] B. Chen, C. Liang, J. Yang, D.S. Contreras, Y.L. Clancy, E.B. Lobkovsky, O.M. Yaghi, S. Dai, Angew. Chem., Int. Ed. 45 (2006) 1390.

[12] M.R. Montney, S. Mallika Krishnan, R.M. Supkowski, R.L. LaDuca, Inorg. Chem. 46 (2007) 7362.

[13] M.R. Montney, S. Mallika Krishnan, N.M. Patel, R.M. Supkowski, R.L. LaDuca, Cryst. Growth Des. 7 (2007) 1145.

[14] M.A. Braverman, R.L. LaDuca, Cryst. Growth Des. 7 (2007) 2343.

[15] P.J. Zapf, R.L. LaDuca, R.S. Rarig, K.M. Johnson, J. Zubieta, Inorg. Chem. 37 (1998) 3411.

[16] SAINT, Software for Data Extraction and Reduction, Version 6.02, Bruker AXS, Inc., Madison, WI, 2002.

[17] SADABS, Software for Empirical Absorption Correction, Version 2.03, Bruker AXS, Inc., Madison, WI, 2002.

[18] G.M. Sheldrick, SHELXTL, Program for Crystal Structure Refinement, University of Gottingen, Gottingen, Germany, 1997.

[19] M. Kurmoo, C. Estournes, Y. Oka, H. Kumagai, K. Inoue, Inorg. Chem. 44 (2005) 217.

[20] O. Khan, Molecular Magnetism, VCH Publishers, New York, 1993.

Polyhedron 27 (2008) 2301–2308

Contents lists available at ScienceDirect

Polyhedron

journal homepage: www.elsevier.com/locate/poly

Co(II), Ni(II) and Cu(II) complexes of new [1+1] and [2+2] macrocyclic ligands derived from 1,4-bis(2′-formylphenyl)-1,4-dioxabutane and *cis*-1,2-diaminocyclohexane

M[a] del Carmen Fernández-Fernández [a], Rufina Bastida de la Calle [a,*], Alejandro Macías [a], Laura Valencia Matarranz [b,*], Paulo Pérez-Lourido [b]

[a] Departamento de Química Inorgánica, Universidad de Santiago de Compostela, Avda. de las Ciencias s/n, 15782 Santiago de Compostela, La Coruña, Spain
[b] Departamento de Química Inorgánica, Facultad de Química, Universidade de Vigo, 36310 Vigo, Pontevedra, Spain

ARTICLE INFO

Article history:
Received 25 October 2007
Accepted 22 April 2008
Available online 12 June 2008

Keywords:
Transition metal complex
Oxaaza macrocyclic ligand
X-ray structure

ABSTRACT

Two new macrocyclic ligands, L^1 (14-membered N_2O_2) and L^2 (28-membered N_4O_4) from [1+1] and [2+2] condensation, respectively, have been obtained in a one-pot synthesis starting from 1,4-bis(2′-formylphenyl)-1,4-dioxabutane and *cis*-1,2-diaminocyclohexane.

Both ligands were synthesized in the same pot reaction in satisfactory yield and purity. The use of a washing and recrystallization processes allowed the separation of each macrocyclic ligand.

No metal complexes were isolated with the small L^1 macrocycle. However, metal complexes with the 28-membered macrocycle L^2, using hydrated nitrate and perchlorate salts of transition Co(II), Ni(II) and Cu(II) metal ions, have been synthesized and characterized by microanalysis, LSI mass spectrometry, IR, UV–Vis spectroscopy, magnetic studies and conductivity measurements.Crystal structures of L^1, as well as $[Co(HL^2)(NO_3)_2(CH_3CN)]$ $(NO_3)\cdot 2CH_3CN$, $[NiL^2(NO_3)](NO_3)\cdot 2H_2O\cdot CH_3CN$ and $[Cu_2L^2(NO_3)_4]\cdot 4CH_3CN$ complexes, have been determined. The X-ray studies show the presence of a hexacoordinated mononuclear exomacrocyclic complex for Co(II), whilst in the dinuclear Cu(II) complex both copper atoms are exocyclically coordinated by the nitrogen atoms from the ligand in a square planar environment. The crystal structure of $[NiL^2(NO_3)](NO_3)\cdot 2H_2O\cdot CH_3CN$ shows a mononuclear endomacrocyclic complex with the metal ion in a distorted octahedral environment.

© 2008 Elsevier Ltd. All rights reserved.

1. Introduction

The complexation properties of oxaazamacrocycles have been extensively studied in the last decades [1–8]. The cavity size, the rigidity and the donor type of the macrocycle is important in governing the host–guest interactions and the selectivity of metal ions [9,10].

The formation of multimetallic transition metal complexes offers an important route for the construction of new types of magnetic materials [11–14], development of catalytic reagents [15–18] models of metalloenzymes [19–21] and the construction of metallosupramolecular architectures [22,23].

One strategy for the synthesis of multimetallic complexes includes the use of large macrocycles, which allow accommodation of two or more metal ions. They can be used to hold the metal centers at a fixed distance, and the fact that metal ions can be precisely positioned within the macrocyclic entity provides then interesting properties [24,25].

During the last years our research group has been investigating structure–function relationships in the complexation behavior of transitional and post-transitional metal ions with mixed donor atoms macrocyclic ligands [26–29].

In previously works Lindoy and co-workers reported that with the oxaazamacrocycle ligand L^A (Fig. 1), the 1:1 metal:ligand complexes in solution and in solid state were observed [30–34], but they have no evidence for the formation of 2:1 metal:ligand species with L^B in solution or in the solid state, and only mononuclear complexes were obtained [35].

In this paper, we report the synthesis and characterization of two macrocyclic systems: the [1+1] 14-membered N_2O_2 macrocycle, L^1, and the analogue [2+2] 28-membered N_4O_4 macrocycle, L^2 (Fig. 1), which present cyclohexyl rings between amine groups instead of ethylenic chains in the case of the L^A and L^B mentioned above. We also report a study of the complexation capability towards Co(II), Ni(II) and Cu(II) transition metal ions. We have seen that no metal complexes were able to be isolate with L^1 but the formation of dinuclear species was confirmed with L^2.

* Corresponding authors. Tel.: +34 986 812607; fax: +34 986 813798 (L.V. Matarranz); tel.: +34 981 591076; fax: +34 981 597525 (R.B. de la Calle).
E-mail addresses: qibastid@usc.es (R.B. de la Calle), qilaura@uvigo.es (L.V. Matarranz).

0277-5387/$ - see front matter © 2008 Elsevier Ltd. All rights reserved.
doi:10.1016/j.poly.2008.04.043

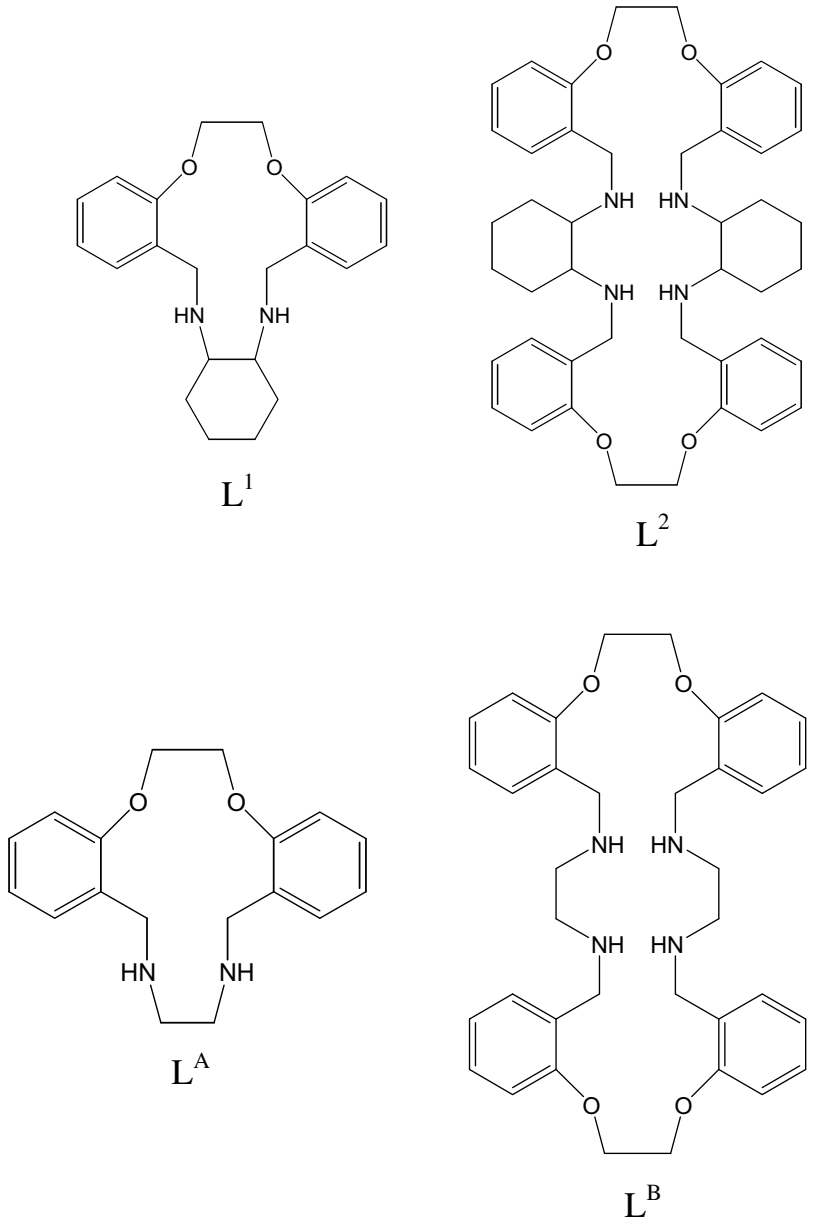

Fig. 1. L^1 and L^2 macrocyclic ligands.

The X-ray crystal structure of the ligand L^1 and the crystal structures of the Co(II), Ni(II) and Cu(II) nitrate complexes with L^2 are reported.

2. Experimental

2.1. Chemicals and starting materials

1,4-bis(2′-formylphenyl)-1,4-dioxabutane was synthesized as described [36], *cis*-1,2-diaminocyclohexane and metal salts were commercial products (from Alfa and Aldrich) and were used without further purifications. Solvents were of reagent grade and were purified by the usual methods. *Caution*: Although no problems were encountered during the course of this work, perchlorate salts must be handled with care due to their potentially explosive nature.

2.2. Synthesis of the ligands

1,4-Bis(2-formylphenyl)-1,4-dioxabutane (2 mmol, 0.54 g) was dissolved in methanol (75 mL) under reflux and a solution of *cis*-1,2-diaminocyclohexane (2 mmol, 0.4 g) in methanol (30 mL) was added. The solution was refluxed for 4 h and stands to cool. $NaBH_4$ (20 mmol, 0.76 g) were added slowly. The solution was evaporated to dryness. The residue was then extracted with water–chloroform. The organic layer was dried over $MgSO_4$ filtered off and evaporated to dryness to yield a yellow oil. Ethyl ether was added and the resultant white solid was filtered off and recrystallized in acetonitrile giving the ligand L^1 as a white crystalline solid. The solution was concentrated to dryness and the white solid taken up in acetone, filtered off and the filtrate was concentrated to dryness and the resultant solid was dissolved in acetonitrile. After three days, the solution was filtered off and the filtrate reduced to dryness and characterized as L^2.

L^1: *Anal. Calc. for $C_{22}H_{28}N_2O_2$: C, 74.9; H, 8.0; N, 7.9. Found: C, 74.8; H, 8.0; N, 7.9%. Yield: 30%. IR (KBr, cm^{-1}): 1600, 1490, 1452 [ν(C=C)],* 1058 [ν(C–O–C)]. LSI-MS (*m/z*): 353 $[L^1+H]^+$. Colour: white.

L^2: *Anal. Calc. for $C_{44}H_{56}N_4O_4$: C, 74.9; H, 8.0; N, 7.9. Found: C, 74.8; H, 8.0; N, 7.8%. Yield: 42%. IR (KBr, cm^{-1}): 1600, 1490, 1452 [ν(C=C)],* 1058 [ν(C–O–C)]. LSI-MS (*m/z*): 705 $[L^2+H]^+$. Colour: white.

2.3. Synthesis of metal complexes

To a methanolic solution (10 mL) of L^2 (0.1 mmol, 0.0704 g) was added a solution of the appropriate metal salt (0.15 mmol) in methanol (10 mL) and the solution was heated at reflux for 3 h and stand to cool. The solution was concentrated until *ca.* 10 mL. The product obtained was filtered off and dried under vacuum. The complexes were found to be air-stable and soluble in acetonitrile, dimethyl sulfoxide and dimethyl formamide and are, in general, insoluble in water, absolute ethanol, methanol, diethyl ether, chloroform, dichloromethane and acetone.

2.3.1. $[Co_2L^2](ClO_4)_4 \cdot 2CH_3CN$

Anal. Calc.: C, 44.3; H, 4.6; N, 6.5. Found: C, 44.9; H, 4.6; N, 6.2%. Yield: 48%. IR (KBr, cm^{-1}): 1453, 1493, 1602 [ν(C=C)$_{ar}$], 625, 1100 [$\nu(ClO_4^-)$]. LSI-MS (*m/z*): 805 $[L^2(ClO_4)]^+$, 705 $[L^2+H]^+$. Λ_M/Ω^{-1} cm^2 mol^{-1} (in CH_3CN): 415 (4:1). Colour: red.

2.3.2. $[Co_2L^2](NO_3)_4 \cdot 2CH_3CN$

Anal. Calc.: C, 50.1; H, 5.2; N, 12.2. Found: C, 50.9; H, 5.1; N, 11.6%. Yield: 43%. IR (KBr, cm^{-1}): 1453, 1493, 1602 [ν(C=C)$_{ar}$], 755, 839, 1064, 1240, 1384 [$\nu(NO_3^-)$]. LSI-MS (*m/z*): 825 $[CoL^2(NO_3)]^+$, 705 $[L^2+H]^+$. Λ_M/Ω^{-1} cm^2 mol^{-1} (in CH_3CN): 318 (2:1). Colour: pink.

2.3.3. $[Ni_2L^2](ClO_4)_4 \cdot 3CH_3CN$

Anal. Calc.: C, 44.8; H, 4.7; N, 7.3. Found: C, 44.2; H, 5.1; N, 7.6%. Yield: 65%. IR (KBr, cm^{-1}): 1454, 1490, 1602 [ν(C=C)$_{ar}$], 624, 1103 [$\nu(ClO_4^-)$]. LSI-MS (*m/z*): 861 $[NiL^2(ClO_4)]^+$, 762 $[NiL^2]^+$. Λ_M/Ω^{-1} cm^2 mol^{-1} (in CH_3CN): 420 (4:1). Colour: green.

2.3.4. $[NiL^2](NO_3)_2$

Anal. Calc.: C, 59.5; H, 6.4; N, 9.5. Found: C, 59.9; H, 6.1; N, 9.6%. Yield: 32% IR (KBr, cm^{-1}): 1452, 1490, 1601 [ν(C=C)$_{ar}$], 756, 1086, 1239, 1384 [$\nu(NO_3^-)$]. LSI-MS (*m/z*): 824 $[NiL^2(NO_3)]^+$, 761 $[NiL^2]^+$. Λ_M/Ω^{-1} cm^2 mol^{-1} (in CH_3CN): 127 (1:1). Colour: blue.

2.3.5. $[Cu_2L^2](NO_3)_4$

Anal. Calc.: C, 49.0; H, 5.0; N, 10.4. Found: C, 48.8; H, 5.3; N, 10.5%. Yield: 42%. IR (KBr, cm^{-1}): 1453, 1492, 1602 [ν(C=C)$_{ar}$], 753, 1058, 1238, 1384 [$\nu(NO_3^-)$]. LSI-MS (*m/z*): 766 $[CuL^2]^+$, 705 $[L^2+H]^+$. Λ_M/Ω^{-1} cm^2 mol^{-1} (in CH_3CN): 308 (2:1). Colour: blue.

2.4. Physical measurements

Elemental analyses were performed in a Carlo-Erba EA microanalyser. Infra-red spectra were recorded as KBr discs on a Bruker IFS-66V spectrophotometer. LSI-MS were recorded using a Micromass Autospec spectrometer with 3-nitrobenzyl alcohol as the matrix. Conductivity measurements were carried out in 10^{-3} mol dm^{-3} acetonitrile solutions at 20 °C using a WTW LF3 conductivimeter. ^{1}H, ^{13}C, DEPT 135 and HMQC ^{1}H-^{13}C NMR spectra were recorded on a Bruker 500 MHz, and $CDCl_3$ was used as solvent. Solid state electronic spectra were recorded on a Hitachi 4-3200 spectrophotometer using $MgCO_3$ as reference. Magnetic studies were determined at r.t. on a vibration sample

Table 1
Crystal data and structure refinement for L^1, $[Co(HL^2)(NO_3)_2(CH_3CN)](NO_3) \cdot 2CH_3CN$, $[NiL^2(NO_3)](NO_3) \cdot 2H_2O \cdot CH_3CN$ and $[Cu_2L^2(NO_3)_4] \cdot 4CH_3CN$

	L^1	$[CoHL^2(NO_3)_2(CH_3CN)](NO_3) \cdot 2CH_3CN$	$[NiL^2(NO_3)](NO_3) \cdot 2H_2O \cdot CH_3CN$	$[Cu_2L^2(NO_3)_4] \cdot 4CH_3CN$
Empirical formula	$C_{22}H_{28}N_2O_2$	$C_{50}H_{66}N_{10}O_{13}Co$	$C_{46}H_{63}N_7O_{11}Ni$	$C_{52}H_{68}Cu_2N_{12}O_{16}$
Formula weight	352.47	1074.06	948.74	1244.26
Temperature (K)	293(2)	120(2)	293(2)	120(2)
Wavelength (Å)	0.71073	0.71073	0.71073	0.71073
Crystal system	monoclinic	triclinic	monoclinic	monoclinic
Space group	*P*21/*n*	*P*$\bar{1}$	*P*21/*c*	*C*2/*c*
Unit cell dimensions				
a (Å)	10.872(2)	12.1289(19)	13.327(3)	24.193(6)
b (Å)	9.137(2)	13.566(2)	26.182(5)	11.219(3)
c (Å)	19.053(4)	18.015(3)	14.987(3)	21.384(5)
α (°)		83.411(2)		
β (°)	100.435(4)	78.737(2)	108.482(3)	92.800(5)
γ (°)		66.905(2)		
Volume (Å^3)	1861.4(7)	2671.7(7)	4959.3(18)	5797(2)
Z	4	2	4	4
D_{calc} (Mg/m^3)	1.258	1.335	1.271	1.426
Absorption coefficient (mm^{-1})	0.081	0.393	0.454	0.811
Crystal size (mm)	0.64 × 0.32 × 0.30	0.52 × 0.46 × 0.27	0.60 × 0.47 × 0.38	0.47 × 0.29 × 0.10
θ Range for data collection (°)	2.01–26.42	1.63–28.33	1.95–26.73	1.91° and 27.88°
Index ranges	$-13 \leqslant h \leqslant 13$, $0 \leqslant k \leqslant 11$, $0 \leqslant l \leqslant 23$	$-15 \leqslant h \leqslant 16$, $-17 \leqslant k \leqslant 17$, $0 \leqslant l \leqslant 24$	$-16 \leqslant h \leqslant 15$, $0 \leqslant k \leqslant 33$, $0 \leqslant l \leqslant 18$	$-31 \leqslant h \leqslant 31$, $0 \leqslant k \leqslant 14$, $0 \leqslant l \leqslant 28$
Reflections collected	15809	33554	82773	51293
Independent reflections (R_{int})	3826 (0.0381)	12668 (0.0287)	10519 (0.0536)	6910 (0.0555)
Completeness to θ	99.9% (26.42°)	95.1% (268.33°)	100% (26.73°)	99.7% (27.88°)
Absorption correction	SADABS	SADABS	SADABS	SADABS
Maximum and minimum transmission	0.9762 and 0.9503	0.9014 and 0.8219	0.8463 and 0.7722	
Refinement method	full-matrix least-squares on F^2	full-matrix least-squares on F^2	full-matrix least-squares on F^2	full-matrix least-squares on F^2
Data/restraints/parameters	3826/0/243	12668/0/690	10519/24/642	6910/0/380
Goodness-of-fit on F^2	1.034	1.089	1.122	1.112
Final *R* indices [$I > 2\sigma(I)$]	R_1 = 0.0414, wR_2 = 0.1026	R_1 = 0.0349, wR_2 = 0.0859	R_1 = 0.0809, wR_2 = 0.2611	R_1 = 0.0385, wR_2 = 0.1023
R indices (all data)	R_1 = 0.0643, wR_2 = 0.1117	R_1 = 0.0490, wR_2 = 0.0909	R_1 = 0.0983, wR_2 = 0.2773	R_1 = 00560, wR_2 = 0.1093
Largest difference in peak and hole (e Å^{-3})	0.274 and −0.209	0.343 and −0.281	2.831 and −0.823	0.418 and −0.355

magnetometer (VSM) Digital Measurement System 1660 with a magnetic field of 5000 G.

2.5. X-ray data collection, structure determination, and refinement

The crystals were obtained by slow recrystallization of the compounds from acetonitrile. The details of the X-ray crystal data, and the structure solution and refinement are given in Table 1. Measurements were made on a Bruker SMART CCD 1000 area diffractometer. All data were corrected for Lorentz and polarization effects. Empirical absorption corrections were also applied for all the crystal structures obtained [37]. Complex scattering factors were taken from the program package SHELXTL [38]. The structures were solved by direct methods which revealed the position of all non-hydrogen atoms. All the structures were refined on F^2 by a full-matrix least-squares procedure using anisotropic displacement parameters for all non-hydrogen atoms. The hydrogen atoms were located in their calculated positions and refined using a riding model.

3. Results and discussion

L^1 and L^2 ligands were each readily obtained in a one-pot synthesis from commercial reagents in satisfactory yield and purity without the need for column chromatography. The direct reaction of 1,4-bis(2′-formylphenyl)-1,4-dioxabutane and *cis*-1,2-diaminocyclohexane in methanol under reflux followed by an *in situ* reduction with $NaBH_4$ gave an air-stable pale yellow solid characterized as a mixture of the ligands L^1 and L^2, as was evidenced by mass spectrometry. Through studies employing the pure L^1 product, the pure L^2 product and known mixtures of both, we have shown that mass spectrometry can be employed to give an indication of purity. The use of a washing and recrystallization processes allowed the separate isolation of each macrocycle. By slow crystallization of the mixture in acetonitrile, a white crystalline compound was obtained after two days. The crystalline precipitate was filtered off and characterized as pure L^1 ligand. The solution was concentrated by rotary evaporation and a white powder was obtained, which was characterized as the L^2 ligand with a little impurity of L^1. The solid was taken up in acetone, filtered off, and the filtrate was reduced to dryness. The solid was again dissolved in acetonitrile and after three days the solution was filtered off, reduced to dryness, and the white powder obtained was characterized as pure L^2 ligand.

Crystals suitable for X-ray diffraction of L^1 were obtained from the acetonitrile solution. Crystal data and structure refinement are given in Table 1. Molecular structure and bond lengths (Å) are given in Fig. 2. The structure belongs to $P21/n$ monoclinic space group. Bond distances and angles are all within the normal ranges. The structure shows that the molecule is slightly folded with a dihedral angle between the plane containing the aromatic rings of 79.65°; the cyclohexane ring shows a chair conformation. The presence of the cyclohexane and the two aromatic rings introduce a high rigidity in the small [1+1] macrocycle L^1, but beforehand the arrangement of the donor atoms seems to be adequate for complexation. The rms value of the four donor atoms in the molecule is 0.23.

No inter- or intramolecular π,π-stacking interactions are present in the structure.

L^1 and L^2 ligands were also characterized by elemental analysis, LSI-MS, IR, ^1H and ^{13}C NMR spectroscopy. LSI mass spectrometry provided evidence for the sole presence of L^1 (*m/z* 353, assignable to $[L^1+H]^+$), or L^2 (*m/z* 705, assignable to $[L^2+H]^+$).

The IR spectra (KBr disc) of both ligands show no bands corresponding to carbonyl or primary amine groups, further confirming that cyclization took place. Also no imine bands appear in the spectra. A broad band centered at 3423 cm^{-1} present in the spectra, attributable to the presence of solvent molecules, hides the secondary amine bands of the ligands. Two intense bands at 1600, 1490 and 1452 cm^{-1} attributable to the ν(C=C) of the aromatic rings of the molecules are also observed.

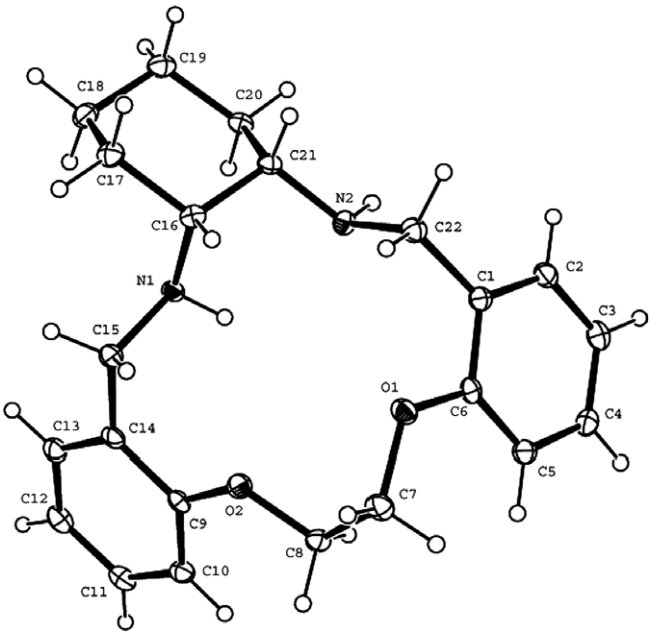

Fig. 2. Crystal structure of **L**[1] and bond lengths (Å): C(1)–C(2) 1.386(2); C(1)–C(6) 1.405(2); C(1)–C(22) 1.505(2); C(2)–C(3) 1.383(2); C(3)–C(4) 1.379(2); C(4)–C(5) 1.387(2); C(5)–C(6) 1.384(2); C(6)–O(1) 1.3721(18); C(7)–O(1) 1.4310(18); C(7)–C(8) 1.498(2); C(8)–O(2) 1.4258(18); C(9)–O(2) 1.3628(18); C(9)–C(10) 1.390(2); C(9)–C(14) 1.400(2); C(10)–C(11) 1.389(2); C(11)–C(12) 1.379(2); C(12)–C(13) 1.386(2); C(13)–C(14) 1.381(2); C(14)–C(15) 1.506(2); C(15)–N(1) 1.4583(19); C(16)–N(1) 1.4671(19); C(16)–C(17) 1.528(2); C(16)–C(21) 1.536(2); C(17)–C(18) 1.518(2); C(18)–C(19) 1.521(2); C(19)–C(20) 1.520(2); C(20)–C(21) 1.520(2); C(21)–N(2) 1.4716(19); C(22)–N(2) 1.4665(19).

The ^1H and ^{13}C NMR spectra of the ligands L^1 and L^2 (Table 2) have been recorded using deuterated chloroform as solvent, and confirm the integrity of the ligands and their stability in solution. The NMR spectra of the ligands are completely similar, and assignment of the proton signals was based upon standard 2D homonuclear (COSY) and $^1H/^{13}C$ heteronuclear spectra (HMQC). The aromatic region of the ^1H NMR spectrum shows two multiplets belonging to the phenyl groups; the ethylenic protons signal appears as a singlet at δ 4.2 ppm. The benzyl protons appear as a multiplet at δ 3.6 ppm, probably due to the rigidity incorporated to the macrocyclic framework by the cyclohexane groups. The peaks belonging to the cyclohexane protons appear between δ 2.5 and 1.15 ppm.

Attempts to isolate metal complexes with L^1 were unsuccessful and the free ligand was always recovered from the reaction.

Transitional Co(II), Ni(II) and Cu(II) metal complexes of L^2 were synthesized by reaction of the ligand and the appropriate metal salt in refluxing acetonitrile. The complexes were synthesized as described in Section 2 and, in general, the reactions gave in general good yields of analytically pure products. Complexes were characterized by elemental analysis, LSI mass spectrometry, IR and UV–Vis spectroscopy, magnetic and conductivity measurements.

3.1. Crystal structures

By slow recrystallization of the dinuclear compound $[Co_2L^2](NO_3)_4 \cdot 2CH_3CN$ in acetonitrile, crystals of $[Co(HL^2)(NO_3)_2(CH_3CN)](NO_3) \cdot 2CH_3CN$ were obtained. The crystal structure was

Table 2
Data and assignation of ^1H and ^{13}C NMR spectra of L^1 and L^2 in $CDCl_3$

^1H		^{13}C	
Assignment	δ (ppm)	Assignment	δ (ppm)
H_{1eq}, H_{2eq}	1.15 (m, 4H or 8H)		
H_{1ax}	1.63 (m, 2H or 4H)	C_1	27.65
H_{2ax}	1.51 (m, 2H or 4H)	C_2	22.36
H_3	4.20 (s, 4H or 8H)	C_3	66.46
H_4–H_7	7.30–6.70 (m, 4H or 8H)	C_4–C_7	130–111
		C_8	120.59
		C_9	156.70
H_{10}	3.60 (m, 4H or 8H)	C_{10}	45.92
H_{11}	2.50 (s, 2H or 4H)	C_{11}	54.85
–NH	1.90 (b, 2H or 4H)		

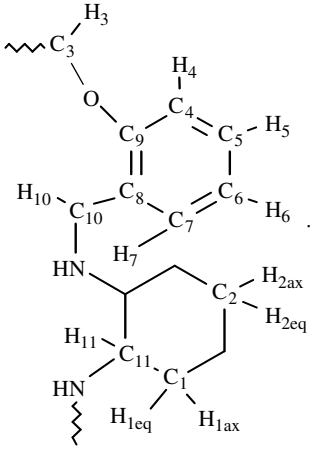

studied by X-ray diffraction and the molecular structure of the complex is shown in Fig. 3 together with the atomic numbering scheme adopted and selected bond distances (Å) and angles (°). Crystal data and structure refinement are given in Table 1.

The crystal structure is consistent with the cation complex $[Co(HL^2)(NO_3)_2(CH_3CN)]^+$, and a well separated nitrate ion and two acetonitrile molecules.

The structure of $Co(HL^2)(NO_3)_2(CH_3CN)]^+$ shows the presence of a Co(II) mononuclear complex, where the metal ion is exomacrocyclicly coordinated by two nitrogen atoms from one diaminocyclohexane fragment, one oxygen atom from a monodentate nitrate ion, two oxygen atoms from a bidentate nitrate ion and the nitrogen atom from an acetonitrile molecule. The Co(II) ion presents a six coordination number in a $\{N_3O_3\}$ core with a distorted octahedral environment. The equatorial plane can be described by one nitrogen donor atom from the ligand, N(3), and the three oxygen atoms from the nitrate groups [N(3)–O(4N)–O(3N)–O(1N), rms 0.0825]. The axial axis is determined by the nitrogen donor atom from the ligand N(4), and the nitrogen atom from the acetonitrile molecule N(3S). All the bond lengths between the metal ions and the donor atoms are quite similar. The monodentate nitrate group provides the shortest bond distance to the ion [Co(1)–O(4N), 2.026(10) Å], whilst the main distortion from a regular octahedral geometry is attributable to the small bite of the bidentate nitrate ligand [O(1N)–Co(1)–O(3N), 58.97(4)°]. The average value of the Co–N bond length is 2.15 Å, which is similar to that found in other macrocyclic nitrate complexes of octahedral Co(II) [39]. The ether oxygen atoms are not coordinated to the metal ion.

The hydrogen atoms belonging to the amine groups of the ligand have been encountered, and the structure shows that the ligand molecule is protonated in one of the free secondary amine groups. An extra nitrate ion is present in the structure to ensure the electric neutrality of the lattice. Thus, starting from the dinuclear compound $[Co_2L^2](NO_3)_4 \cdot 2CH_3CN$, the protonation of the

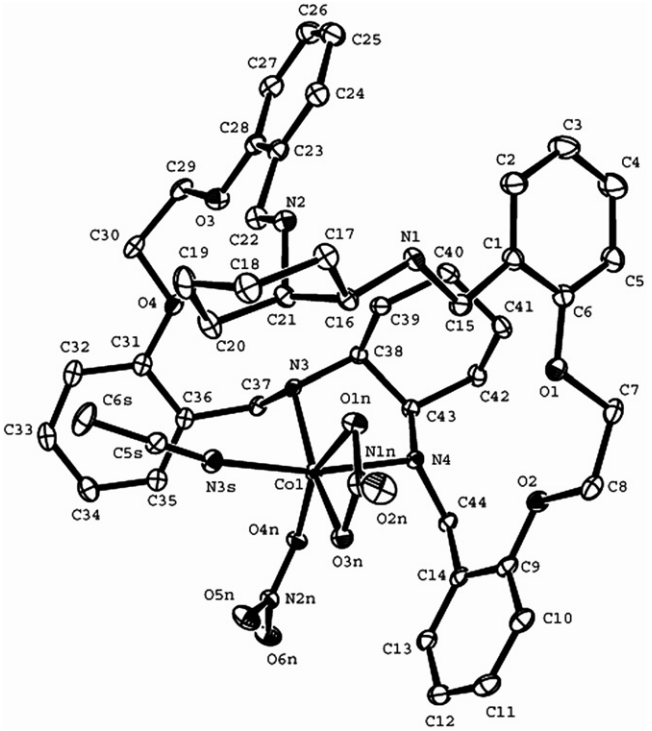

Fig. 3. Crystal structure of $[Co(HL^2)(NO_3)_2\ (CH_3CN)](NO_3) \cdot 2CH_3CN$; Selected bond lengths (Å) and angles (°): N(3)–Co(1) 2.1490(12); N(3S)–Co(1) 2.1148(13); N(4)–Co(1) 2.1574(12); O(1N)–Co(1) 2.1811(11); O(3N)–Co(1) 2.1907(11); O(4N)–Co(1) 2.0269(10); O(4N)–Co(1)–N(3S) 101.14(5); O(4N)–Co(1)–N(3) 93.06(4); N(3S)–Co(1)–N(3) 89.06(5); O(4N)–Co(1)–N(4) 87.48(4); N(3S)–Co(1)–N(4) 168.00(5); N(3)–Co(1)–N(4) 82.10(4); O(4N)–Co(1)–O(1N) 160.74(4); N(3S)–Co(1)–O(1N) 87.57(5); N(3)–Co(1)–O(1N) 104.33(4); N(4)–Co(1)–O(1N) 86.78(4); O(4N)–Co(1)–O(3N) 103.76(4); N(3S)–Co(1)–O(3N) 88.20(4); N(3)–Co(1)–O(3N) 163.18(4); N(4)–Co(1)–O(3N) 97.92(4); O(1N)–Co(1)–O(3N) 58.97(4).

ligand and a demetalation reaction of one of the Co(II) metal ions took place (a precipitate, probably due to hydroxyl species was also observed). The configuration of the coordinated amine groups N(3) and N(4) is R,S (or S,R), as both isomers are present in the structure.

The dihedral angle between the plane containing the aromatic rings C1–C6 and C9–C14 is 87.70°, and 80.17° between C23–C28 and C31–C36.

Some intra and intermolecular interactions through hydrogen bonds are present in the crystal lattice: [N1–H1N···N2 = 2.614 Å, 127.61°], [N3–H4N···O4 = 2.963Å, 126.94°], [N4–H5N···O2 = 2.948 Å, 124.20°], [N1–H2N···O9N_$1 = 2.804 Å, 155.46°], [N1–H2N···O7N_$1 = 3.085 Å, 143.04°], [N2–H3N···O8N_$2 = 3.568 Å, 155.20°], [N2–H3N···O9N_$2 = 3.064 Å, 152.31°]. $1 = x, $+y$, $+z + 1$, $2 = $-x + 1$, $-y + 1$, $-z + 1$.

The complex $[NiL^2(NO_3)](NO_3) \cdot 2H_2O.CH_3CN$ was obtained by recrystallization of the complex $[NiL^2](NO_3)_2$ from acetonitrile. The molecular structure together with selected bond lengths (Å) and angles (°) are given in Fig. 4. The crystal data and structure refinement are given in Table 1.

The X-ray crystal structure shows a mononuclear endomacrocyclic cation complex of type $[NiL^2(NO_3)]^+$. A free nitrate ion, two water and one acetonitrile molecules are also present in the crystal lattice. The metal center presents a six-coordinate $\{N_4O_2\}$ core in a distorted octahedral geometry. The Ni^{2+} ion is situated in the cavity of the macrocycle and it is bonded to the four nitrogen atoms from the macrocyclic backbone and two oxygen atoms from a bidentate nitrate group. The ether oxygen atoms from the ligand are not coordinated to the metal. The main distortion from a regular octahedral geometry can be attributed again to the small bite of the bidentate nitrate group [O(2N)–Ni(1)–O(1N), 60.70(11)°]. The

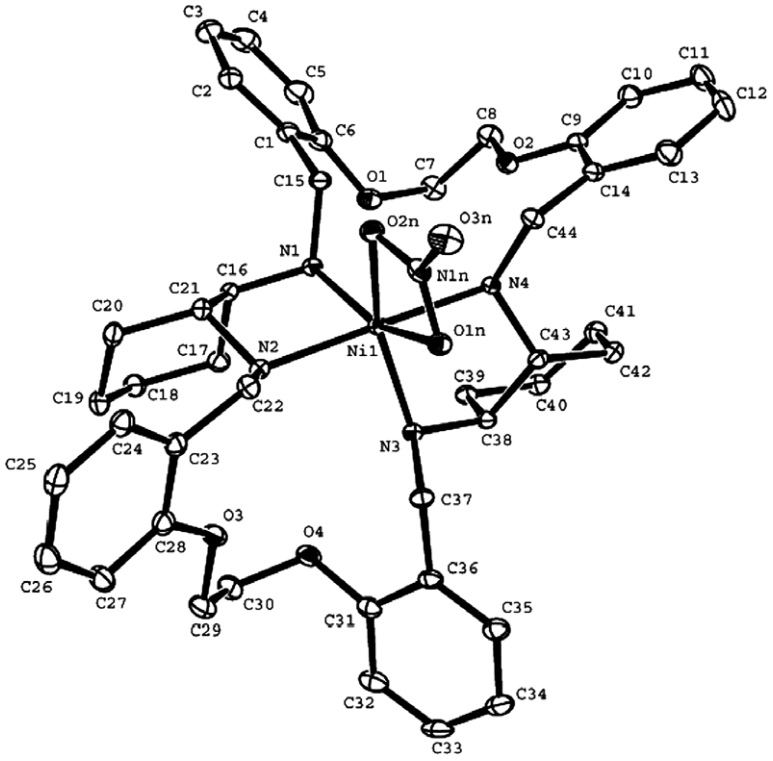

Fig. 4. Crystal structure of $[NiL^2(NO_3)](NO_3) \cdot 2H_2O \cdot CH_3CN$; Selected bond lengths (Å) and angles (°): Ni(1)–N(3) 2.075(3); Ni(1)–N(1) 2.079(3); Ni(1)–O(2N) 2.124(3); Ni(1)–O(1N) 2.150(3); Ni(1)–N(2) 2.153(3); Ni(1)–N(4) 2.184(3); N(3)–Ni(1)–N(1) 107.89(14); N(3)–Ni(1)–O(2N) 155.86(13); N(1)–Ni(1)–O(2N) 96.15(12); N(3)–Ni(1)–O(1N) 95.23(12); N(1)–Ni(1)–O(1N) 156.83(13); O(2N)–Ni(1)–O(1N) 60.70(11); N(3)–Ni(1)–N(2) 94.58(13); N(1)–Ni(1)–N(2) 82.75(13); O(2N)–Ni(1)–N(2) 90.49(12); O(1N)–Ni(1)–N(2) 97.21(12); N(3)–Ni(1)–N(4) 82.94(12); N(1)–Ni(1)–N(4) 94.32(13); O(2N)–Ni(1)–N(4) 93.32(12); O(1N)–Ni(1)–N(4) 86.87(12); N(2)–Ni(1)–N(4) 175.43(13).

structure is similar to that obtained by Lindoy and co-workers with L^B $[NiL^B(NCS)_2]$ [35], which presents two *cis* thiocyanate ions instead of a nitrate group, with the metal also in an octahedral geometry.

The Ni–N distances are lightly shorter in $[NiL^2(NO_3)]^+$ (the average value being 2.128 Å) than in $[NiL^B(NCS)_2]$ (average value of 2.149 Å). The longer distance corresponds to Ni(1)–N(4), 2.184(3) Å. The average value of the Ni–O bond length is 2.138 Å, which is similar to that found in other macrocyclic nitrate complexes of octahedral Ni(II) [40,41].

The equatorial plane can be described by the nitrogen donor atoms N(1) and N(3) from the ligand and both oxygen atoms from the nitrate group O(1N) and O(2N). [N(1)–N(3)–O(1N)–O(2N), rms 0.0071]. The axial axis is occupied by the nitrogen donor atom N(2) and N(4) from the ligand [N(2)–Ni(1)–N(4), 175.43(13)°].

The configuration of the coordinated amine groups N(1), N(2), N(3) and N(4) is *S*,*R*,*S*, R (or *R*,*S*,*R*,*S*), as both isomers are present in the structure.

The dihedral angles between the planes containing the aromatic rings are 70.67° between C1–C6 and C9–C14 and 72.83° between C23–C28 and C31–C36.

Some intramolecular interactions through hydrogen bonds have been found: [N1–H1C···O1 = 2.837 Å, 125.25°], [N2–H2C···O3 = 2.825 Å, 126.58°], [N3–H3C···O4 = 2.845 Å, 128.76°], [N4–H4C···O2 = 2.873 Å, 134.82°]. Also hydrogen bond interactions occur between the water molecules and the nitrate ions and acetonitrile molecules.

The crystal structure shows that the free nitrate group is disordered with an occupancy of ca. 50% in each site.

Crystals suitable for X-ray diffraction belonging to the compound $[Cu_2L^2(NO_3)_4] \cdot 4CH_3CN$ were obtained by slow recrystallization of the complex $[Cu_2L^2](NO_3)_4$ in acetonitrile. The molecular structure of the complex together with selected bond lengths (Å) and angles (°) are given in Fig. 5. Crystal data and structure refinement are given in Table 1.

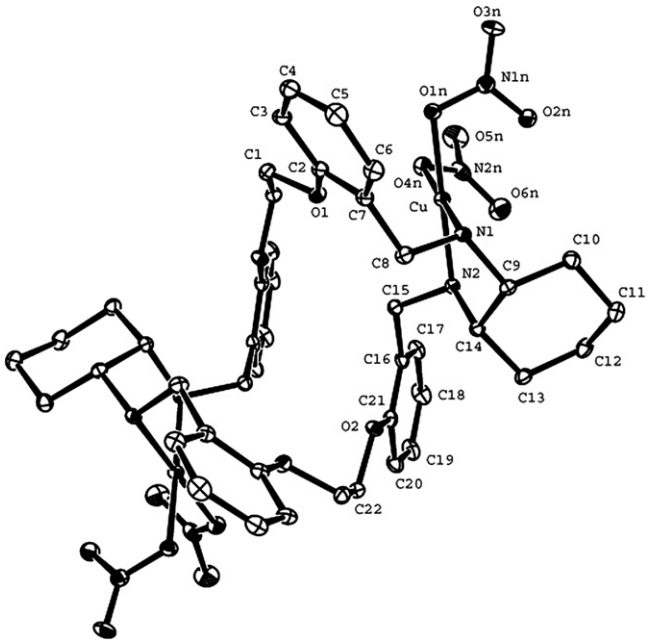

Fig. 5. Crystal structure of $[Cu_2L^2(NO_3)_4] \cdot 4CH_3CN$; Selected bond lengths (Å) and angles (°): Cu–O(4N) 1.9692(15); Cu–N(1) 1.9757(18); Cu–O(1N) 1.9905(15); Cu–N(2) 2.0135(18); O(4N)–Cu–N(1) 179.78(8); O(4N)–Cu–O(1N) 86.73(6); N(1)–Cu–O(1N) 93.40(7); O(4N)–Cu–N(2) 95.45(7); N(1)–Cu–N(2) 84.43(7), O(1N)–Cu–N(2) 177.82(6).

As has been shown previously in the coordination behavior of other oxaaza macrocyclic ligands towards Cu(II) ions, the metal

ion is coordinated mainly with the N donor atoms. [7,31] In this case, the structural analysis shows a dinuclear exomacrocyclic complex where each Cu(II) ion is in a $\{N_2O_2\}$ coordination environment. Both Cu(II) ions are out of the macrocyclic cavity, coordinated by two contiguous amine nitrogen atoms from one aminocyclohexane fragment, and the coordination environment is completed by two monodentate nitrate groups. The geometry around each Cu(II) ion can be described as quite regular square planar. The four donor atoms are practically in a plane (rms 0.0023) and the distance between the Cu(II) and the plane is 0.0008 Å. The bond distances from the donor atoms to the Cu(II) ion are similar, and the shortest one belongs to one monodentate nitrate group [Cu–O(4N), 1.9692 Å]. The configuration of the amine groups N(1) and N(2) is *R*,*S* (or *S*,*R*).

Again, the ether oxygen atoms from the ligand do not participate in coordination. The Cu^{2+} ions are displaced out of the macrocyclic cavity and there is no interaction between them [Cu···Cu_$1, 8.36 Å].

The macrocycle is folded and the aromatic rings are stacked in pairs. Analysis of the intramolecular ring–ring interactions reveals a slipped π,π-interaction between the aromatic rings C16–C21 and C16_$1-C21_$1 of the molecule (Symmetry operation $-x, y, z + 1/2$) [42]. The distance between centroids (D_{c-c}) has a value of 4.05 Å and the dihedral angle between the planes containing these aromatic rings is 11.98°. The dihedral angle between the planes containing the aromatic rings C2–C7 and C2_$1–C7_$1 is 33.6°, and the average distance between the planes is 3.6 Å.

Two intramolecular interactions through hydrogen bonds were found in the crystal structure: [N1–H1N···N2S = 3.107 Å, 175.1°], [N2–H2N···O6N = 2.879 Å, 136.4°].

3.2. Spectroscopic and magnetic studies

The IR spectra of the L^2 complexes show similar features. The ν(C=C) bands of the aromatic rings are generally shifted to higher wavenumbers than in the free ligand, suggesting the coordination to the metal ions [43,44].

An intensive broad band centered about 3440 cm^{-1} in the IR spectra of the complexes due to the presence of solvent molecules is present in all spectra.

In the IR spectra of the nitrate complexes, the region associated with the NO stretches show bands that clearly identify these species as containing coordinate nitrate groups. A band at 1380 cm^{-1}, associated with the presence of ionic nitrate, is also present.

The IR spectra of the perchlorate complexes feature absorptions attributable to ionic perchlorate at 1100 and 626 cm^{-1}, indicating that these groups are not coordinated to the metal centers [45,46].

The results of LSI-MS of the complexes provide important evidence of the formation of the complexes as they feature peaks attributable in all cases to the species $[ML^2X]^+$ and $[ML^2]^+$ (M = Co, Ni, Cu; X = NO_3^-, ClO_4^-).

Molar conductivity data were measured at room temperature using acetonitrile as solvent (10^{-3} M solutions of the complexes). The molar conductivity values obtained lie in the range previously observed for 4:1 electrolytes for the dinuclear perchlorate complexes, indicating the low coordination capability of the perchlorate groups. For the nitrate complexes, the values lie within the range of 2:1 electrolytes for the dinuclear complexes, and 1:1 for the mononuclear $[NiL^2](NO_3)_2$ complex, showing the coordination of some of these groups to the metal in solution [47].

The reflectance spectrum of $[Co_2L^2](ClO_4)_4 \cdot 2CH_3$[CN and $Co_2L^2](NO_3)_4 \cdot 2CH_3CN$ complexes shows three d–d transition bands at *ca.* 8976 (ν_1), 18248 (ν_2) and 22831 cm^{-1} (ν_3) which are probably due to the $^4T_{2g} \leftarrow {}^4T_{1g}$, $^4A_{2g} \leftarrow {}^4T_{1g}$ and $^4T_{1g}(P) \leftarrow {}^4T_{1g}$ transitions, respectively, according to a distorted octahedral high-spin Co(II) complexes [48].

The reflectance spectra of the nickel complexes $[Ni_2L^2](ClO_4)_4 \cdot 3CH_3CN$ and $[NiL^2](NO_3)_2$ show three bands at *ca.* 9980 (ν_1), 16502 (ν_2) and 28571 cm^{-1} (ν_3). These bands are attributable to the $^3T_{2g} \leftarrow {}^3A_{2g}$, $^3T_{1g}(F) \leftarrow {}^3A_{2g}$ and $^3T_{1g}(P) \leftarrow {}^3A_{2g}$ transitions, respectively, and are indicative of octahedral Ni(II) compounds. One absorption band at *ca.* 12658 cm^{-1} present also in the spectra, is probably due to the spin forbidden transition $^1Eg \leftarrow {}^3A_{2g}$, usually observed for Ni(II) complexes [49,50].

The UV–Vis spectrum of $[Cu_2L^2](NO_3)_4$ show a broad band between 14837 and 18248 cm^{-1}, typical of square planar Cu(II) complexes [51].

The value of the room temperature magnetic moments (by metal atom) of the compounds $[Co_2L^2](ClO_4)_4 \cdot 2CH_3CN$ (3.6 BM), $[Co_2L^2](NO_3)_4 \cdot 2CH_3CN$ (3.9 BM), $[Ni_2L^2](ClO_4)_4 \cdot 3CH_3CN$ (2.8 BM) and $[NiL^2](NO_3)_2$ (2.9 BM) lies in the range usually observed for high-spin octahedral Co(II), and octahedral Ni(II) complexes, respectively [52]. The magnetic moment of $[Cu_2L^2](NO_3)_4$ (1.9 BM) lie in the range observed for Cu(II) complexes.

4. Conclusion

Two new macrocyclic ligands, the14-membered N_2O_2 macrocycle L^1, and the analogue [2+2] 28-membered N_4O_4 macrocycle L^2, have been obtained in a one-pot synthesis in satisfactory yield and purity, and we also report the study of the complexation capability towards to nitrate and perchlorate salts of Co(II), Ni(II) and Cu(II) transitional metal ions. We have seen that no metal complexes were possible to isolate with L^1 but the formation of dinuclear species were confirmed with L^2.

The crystal structure of L^1 as well as of the $[Co(HL^2)(NO_3)_2(CH_3CN)](NO_3)$. $2CH_3CN$, $[NiL^2(NO_3)](NO_3) \cdot 2H_2O \cdot CH_3CN$ and $[Cu_2L^2(NO_3)_4].4CH_3CN$ complexes have been determined. In all cases the ligand is bounded to the metal ions by the nitrogen donor set of the ligand, remaining the ether oxygen atoms without participating in the coordination sphere in accordance with Pearson's *hard–soft* acid base principle. The Co(II) and the Ni(II) nitrate complexes present a mononuclear exomacrocyclic and endomacrocyclic structure, respectively, with the metal ion in an octahedral environment. The Cu(II) complex is dinuclear and the two copper atoms are exocyclically coordinated in a square planar environment.

Acknowledgements

We thank Xunta de Galicia (PGIDT01PXI20901PR) for financial support. Intensity measurements were performed at the Unidade de Raios X. RIAIDT, University of Santiago de Compostela, Spain.

Appendix A. Supplementary data

CCDC 650077, 650078, 650079 and 650080 contain the supplementary crystallographic data for L^1, $[Co(HL^2)(NO_3)_2(CH_3CN)](NO_3) \cdot 2CH_3CN$, $[NiL^2(NO_3)](NO_3) \cdot 2H_2O \cdot CH_3CN$ and $[Cu_2L^2(NO_3)_4] \cdot 4CH_3CN$. These data can be obtained free of charge via http://www.ccdc.cam.ac.uk/conts/retrieving.html, or from the Cambridge Crystallographic Data Centre, 12 Union Road, Cambridge CB2 1EZ, UK; fax: (+44) 1223-336-033; or e-mail: deposit@ccdc.cam.ac.uk. Supplementary data associated with this article can be found, in the online version, at doi:10.1016/j.poly.2008.04.043.

References

[1] J.D. Chartres, L.F. Lindoy, G.V. Meehan, Coord. Chem. Rev. 249 (2001) 216.
[2] S.K. Menon, S.K. Jogani, Y.K. Agrawal, Rev. Anal. Chem. 19 (2000) 361.

[3] C. Bazzicalupi, A. Bencini, A. Bianchi, C. Duce, P. Fornasari, C. Giorgi, P. Paoletti, R. Pardini, M.R. Tine, B. Valtancoli, J. Chem. Soc., Dalton Trans. (2004) 463.
[4] N.A. Bailey, D.E. Fenton, D.J. Winter, J. Chem. Soc., Dalton Trans. (1990) 15.
[5] K.R. Adam, L.F. Lindoy, R.J. Smith, J. Chem. Soc., Chem. Commun. (1979) 812.
[6] G. Anderegg, A. Ekstrom, L.F. Lindoy, R.J. Smith, J. Am. Chem. Soc. (1980) 2670.
[7] K.R. Adam, L.F. Lindoy, H.C. Lip, J.H. Rea, B.W. Skelton, A.H. White, J. Chem. Soc., Dalton Trans. (1981) 74.
[8] H.J. Goodwin, K. Henrick, L.F. Lindoy, M. McPartlin, P. Tasker, Inorg. Chem. 21 (1982) 3261.
[9] L.F. Lindoy, The Chemistry of Macrocyclic Ligands Complexes, Cambridge University Press, Cambridge, UK, 1989.
[10] J.- M.J.-M. Lehn, Supramolecular Chemistry, VCH, Weinheim, 1995.
[11] M. Zhao, C. Stern, A.G.M. Barrett, B.M. Hoffman, Angew. Chem., Int. Ed. 42 (2003) 462.
[12] H. Zheng, W. Zhe-Ming, G. Song, Y. Chun-Hua, Inorg. Chem. 45 (2006) 6694.
[13] J.S. Miller, A.J. Epstein, Angew. Chem., Int. Ed. 33 (1994) 385.
[14] J.S. Miller, A.J. Epstein, Angew. Chem., Int. Ed. 33 (1994) 385.
[15] V.B. Romakh, B. Therrien, G. Labat, H.S. Evans, G.B. Shul'pin, G. Suess-Fink, Inorg. Chim. Acta 359 (2006) 3297.
[16] M. Costas, C. Anda, A. Llobet, T. Parella, H.S. Evans, E. Pinilla, Eur. J. Inorg. Chem. 4 (2004) 857.
[17] R. Delgado, M.F. Cabral, R. Castanheira, A. Zhang, R. Herrmann, Polyhedron 21 (2002) 2265.
[18] C. Fraser, L. Johnston, A.L. Rheingold, B.S. Haggerty, G.K. Williams, J. Whelan, B. Bosnich, Inorg. Chem. 31 (1992) 1835.
[19] J. Costamagna, G. Ferraudi, B. Matsuhiro, M. Campos-Vallette, J. Canales, M. Villagran, J. Vargas, M.J. Aguirre, Coord. Chem. Rev. 196 (2000) 125.
[20] E.T. Papish, M.T. Taylor, F.E. Jernigan, M.J. Rodig, R.R. Shawhan, G.P. Yap, F.A. Jove, Inorg. Chem. 45 (2006) 2242.
[21] A.M. Barrios, S.J. Lippard, Inorg. Chem. 40 (2001) 1060.
[22] G. Seeber, B.M. Kariuki, L. Cronin, Chem. Commun. (2002) 2912.
[23] M. Ruben, J. Rojo, F.J. Romero-Salguero, L.H. Uppadine, J.-M. Lehn, Angew. Chem., Int. Ed. 43 (2004) 3662.
[24] S.M. Nelson, Inorg. Chim. Acta 62 (1982) 39.
[25] D.F. Fenton, U. Casellato, P.A. Vigato, M. Vitali, Inorg. Chim. Acta 62 (1982) 62, 5.
[26] H. Adams, R. Bastida, D.E. Fenton, A. Macias, S.E. Spey, L. Valencia, J. Chem. Soc., Dalton Trans. 23 (1999) 4131.
[27] H. Adams, R. Bastida, D.E. Fenton, A. Macias, S.E. Spey, L. Valencia, Inorg. Chem. Commun. 2 (1999) 513.
[28] A. Freiria, R. Bastida, M. del C. Fernandez-Fernandez, A. Macias, L. Valencia, M. Vicente, Inorg. Chem. 44 (2005) 930.
[29] M. Vicente, R. Bastida, C. Lodeiro, A. Macias, A.J. Parola, L. Valencia, S.E. Spey, Inorg. Chem. 42 (2003) 6768.
[30] L.G. Armstrong, P.G. Grimsley, L.F. Lindoy, H.C. Lip, V.A. Norris, R.J. Smith, Inorg. Chem. 17 (1978) 2350.
[31] K.R. Adam, G. Anderegg, L.F. Lindoy, H.C. Lip, M. McPartlin, J.H. Rea, R.J. Smith, P.A. Tasker, Inorg. Chem. 19 (1980) 2956.
[32] L.F. Lindoy, H.C. Lip, J.H. Rea, R.J. Smith, K. Henrick, M. McPartlin, P.A. Tasker, Inorg. Chem. 19 (1980) 3360.
[33] K. Henrick, L.F. Lindoy, M. McPartlin, P.A. Tasker, M.P. Wood, J. Am. Chem. Soc. 106 (1984) 1641.
[34] K.R. Adam, A.J. Leong, L.F. Lindoy, J. Chem. Soc., Dalton Trans. (1988) 1733.
[35] K.R. Adam, G. Anderegg, K. Henrick, A.J. Leong, L.F. Lindoy, H.C. Lip, M. McPartlin, R.J. Smith, P.A. Tasker, Inorg. Chem. 20 (1981) 4048.
[36] L.G. Armstrong, L.F. Lindoy, Inorg. Chem. 14 (1975) 1322.
[37] G.M. Sheldrick, SADABS, Program for Empirical Absorption Correction of Area Detector Data, University of Göttingen, Germany, 1996.
[38] SHELXTL version, An Integrated System for Solving and Refining Crystal Structures from Diffraction Data (Revision 5.1), Bruker AXS Ltd, Madison, WI, USA.
[39] L. Valencia, H. Adams, R. Bastida, A. De Blas, D.E. Fenton, A. Macías, A. Rodríguez, T. Rodríguez-Blas, Inorg. Chim. Acta 234 (2000) 300.
[40] K.R. Kenneth, G. Anderegg, K. Henrick, A.J. Leong, L.F. Lindoy, H.C. Lip, M. McPartlin, R.J. Smith, P.A. Tasker, Inorg. Chem. 20 (1981) 4048.
[41] J. Martínez, R. Bastida, A. Macías, L. Valencia, M. Vicente, Z. Anorg. Allg. Chem. 631 (2005) 2046.
[42] C. Janiak, J. Chem. Soc., Dalton Trans. (2000) 3885.
[43] N.S. Gill, R.H. Nuttall, D.E. Scaife, D.W. Sharp, J. Inorg. Nucl. Chem. 18 (1961) 79.
[44] S. Aime, M. Botta, U. Casellato, S. Tamburini, P.A. Vigato, Inorg. Chem. 34 (1995) 5825.
[45] M.R. Rosenthal, J. Chem. Educ. 50 (1973) 331.
[46] A.J. Hathaway, A.E. Underhill, J. Chem. Soc., Dalton Trans. (1961) 3091.
[47] W.J. Geary, Coord. Chem. Rev. 7 (1971) 81.
[48] A.B.P. Lever, Inorganic Electronic Spectroscopy, 2nd ed., Elsevier, Amsterdam, 1984.
[49] W.J. Eilbeck, F. Holmes, A.E. Underhill, J. Chem. Soc. (A) 5 (1967) 757.
[50] J. Reedijk, T.M. Mulder, J.A. Smit, Inorg. Chim. Acta 13 (1975) 219.
[51] A.B.P. Lever, Inorganic Electronic Spectroscopy, 2nd ed., Elsevier, Amsterdam, 1984.
[52] B.N. Figgis, Introduction to Ligand Fields, Interscience, New York, 1967.

Polyhedron 27 (2008) 2309–2314

Contents lists available at ScienceDirect

Polyhedron

journal homepage: www.elsevier.com/locate/poly

Mercury(II) complex of inverted *N*-methylated porphyrin: HgPh(2-NCH$_3$NCTPP)

Cheng Chun Peng [a], Fuh-An Yang [a], Jyh-Horung Chen [a,*], Shin-Shin Wang [b], Jo-Yu Tung [c,*]

[a] *Department of Chemistry, National Chung-Hsing University, Taichung 40227, Taiwan*
[b] *Material Chemical Laboratories, Hsin-Chu 300, Taiwan*
[c] *Department of Occupational Safety and Health, Chung Hwai University of Medical Technology, Tainan 717, Taiwan*

ARTICLE INFO

Article history:
Received 6 March 2008
Accepted 23 April 2008
Available online 5 June 2008

Keywords:
Mercury
X-ray diffraction
N-inverted *N*-methylated porphyrin
^{1}H relaxation

ABSTRACT

The reaction of PhHgOAc with 2-NCH$_3$NCTPPH (**2**) gave a mercury(II) complex of (phenylato)(2-*N*-methyl-5,10,15,20-tetraphenyl-21-carbaporphyrinato-*N*,*N*′,*N*″)-mercury(II), [HgPh(2-NCH$_3$NCTPP); **7**]; the coordination sphere around Hg(1) in **7** was a four-coordinate derivative with a seesaw geometry and dipole–dipole (DD) interaction governed the longitudinal relaxation rate for Hg(1)–Ph–H$_{2,6}$ protons of **7** in CDCl$_3$ (0.01 M) at 599.95 MHz.

© 2008 Elsevier Ltd. All rights reserved.

1. Introduction

Latos-Grazynski and coworkers first reported the synthesis of 2-*N*-methyl-5,10,15,20-tetraphenyl-21-carbaporphyrin, 2-NCH$_3$NCTPPH (**2**) [or 2-NCH$_3$CTPPH] [1]. Recently, Ziegler et al. reported an improved methodology for the *N*-alkylation of the porphyrin isomer *N*-confused porphyrin [2]. The combination of polar solvent and the use of Cs_2CO_3 base affords externally modified products in high yield without separation difficulties eliminating the use of large excess of alkylating reagent. In this paper, we focus on *N*-methylated N-confused porphyrin. Hence the choice of the references is restricted to *N*-methylated *N*-confused porphyrin. Compound **2** in this work was prepared in the way as described by Ziegler group using CH_3I and *p*-xylene in 48.6% yield [2] (Scheme 1). Unlike the NH tautomerism exists in NCTPPH$_2$ (**1**), the free base **2** has only one stable form. Thus, a placement of a metal ion of interest with a diamagnetic property and with I = 1/2 in a core of *N*-methylated carbaporphyrin provides a promising route to reveal the coordination modes of 2-NCH$_3$NCTPP$^-$. Hitherto, 2-NRNCTPPH (R = CH_2COOEt, CH_2CH_2Br) has been shown to coordinate metals in the core forming metal square-planar complexes possessing a carbon–metal bond (Chart 1a) for Co(II) (I = 7/2) in Co(NCTPP-CH_2COOEt)py (**3**) [2], Ni(II) (I = 3/2) in [2-(2′-CH_2CH_2Br)NCTPP]Ni^{II} (**4**) [3] and κ^3-fashion coordination type complex with Re(I) (I = 5/2) in Re (NMeNCTPP)(CO)$_3$ (**5**) [4] and with Fe(II) (I = 1/2) in (MeCTPPH)Fe^{II}Br (**6**) [5] (Chart 1b). The phenylmercury(II) cation which binds to a variety of ligand sites ranging from N, O and C atoms, serves as a good probe ion as it is unifunctional, affording complexes with a well-defined stereochemistry [6]. The coordination chemistry of phenylmercury(II) explored with anions derived from base **2** reveals the formation of the phenylmercury(II) complex of (phenylato)(2-*N*-methyl-5,10,15,20-tetraphenyl-21-carbaporphyrinato-*N*,*N*′,*N*″)-mercury(II), [HgPh(2-NCH$_3$NCTPP); **7**]. Here we described the synthesis, X-ray structure determination and spectroscopic characterization of **7**. Our understanding is that such structure-spectroscopic correlations will provide valuable info for further development of the coordination modes in inverted *N*-methylated metal porphyrin complex for metal with I = 1/2. To the best of our knowledge, compound **7** represents the first stable, diamagnetic and monomeric mercury(II) complex in *N*-confused porphyrin derivative with the HgPh$^+$ moiety and I = 1/2. In order to explain the discrepancy of Hg–H coupling constant between the proton spectra and the mercury spectra (the difference is about 8%), we discuss the relaxation effects (T_1) for the Hg(1)–Ph–H$_{2,6}$ protons of **7** in CDCl$_3$. We report herein the measurements of T_1 (^{1}H) as a function of temperature for Hg(1)–Ph–H$_{2,6}$ protons of **7** by considering the relaxation pathways with the relative roles of dipolar coupling and chemical shift anisotropy, respectively.

2. Experimental

2.1. NCH$_3$NCTPP (**2**)

Heating a solution of NCTPPH$_2$ (0.5 g, 0.81 mmol) and CH_3I (0.3 mL, 2.1 mmol) in dry *p*-xylene (10 mL) in the presence of dry Cs_2CO_3 (0.5 g, 1.5 mmol) for 2 h followed by filtration, afforded the crude product. Elution with EtOAc–CH_2Cl_2 [1:4 (v/v)] as green band on silica gel (70–230 mesh, 60 g) and removal of the solvent

* Corresponding authors.
E-mail address: JyhHChen@dragon.nchu.edu.tw (J.-H. Chen).

0277-5387/$ - see front matter © 2008 Elsevier Ltd. All rights reserved.
doi:10.1016/j.poly.2008.04.033

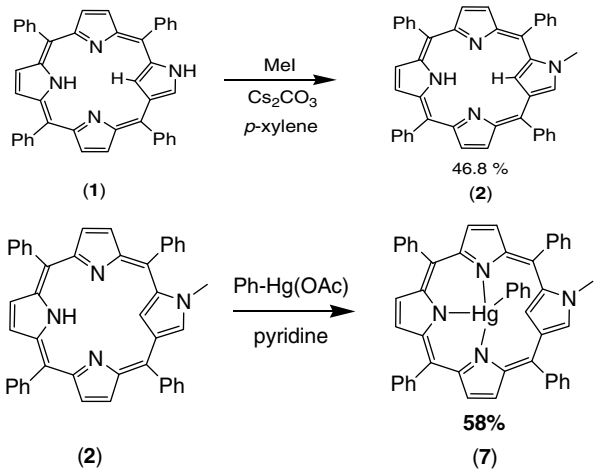

Scheme 1.

and recrystallization from CH_2Cl_2–MeOH [1:2 (v/v)] gave the blue solids of **2** (0.3 g, 0.47 mmol, 48.6%).

2.2. HgPh(NCH$_3$NCTPP) [or HgPh(NCTPP-CH$_3$)] (7)

A mixture of PhHgOAc (40 mg, 0.12 mmol) and 2-NCH_3 NCTPPH (63 mg, 0.1 mmol) in pyridine (5 cm^3) was stirred at 60 °C for 2 h. After concentrating, the residue was dissolved in a suitable amount of toluene, dried over anhydrous Na_2SO_4 and filtered. The filtrate was concentrated and recrystallized from CH_2Cl_2–hexane [1:1 (v/v)] yielding blue solids of **7** (53 mg, 0.058 mmol, 58%) which was again dissolved in $CHCl_3$ and layered with hexane to get blue crystals for single crystal X-ray analysis. ^{1}HNMR (599.95 MHz, CD_2Cl_2, 20 °C): δ 8.16 [d, H_β(7), ^3J(H–H) = 4.8 Hz]; 8.06 [d, H_β(18), ^3J(H–H) = 4.8 Hz]; 7.84 [d, ^3J(H–H) = 5.1 Hz] and 7.83 [d, ^3J(H–H) = 5.1 Hz] for H_β(12) and H_β(13); 7.75 [d, H_β(8), ^3J(H–H) = 4.2 Hz]; 7.72 [d, H_β(17), ^3J(H–H) = 4.8 Hz]; Inverted *N*-methylate pyrrole ring: 2.79 [s, N-CH_3], −0.08 [d, C(2)-H, ^4J(H–H) = 1.5 Hz], 6.09 [d, C(3)–H, ^4J(H–H) = 1.5 Hz]. Hg–Ph (where Hg–Ph = the phenyl group (Ph) coordinated to Hg atom): 4.58 [d, Hg(1)–Ph–$H_{2,6}$, ^3J(H–H) = 7.8 Hz and ^3J(Hg–H) = 186.7 Hz], 6.25 [t, Hg(1)–Ph–$H_{3,5}$, ^3J(H–H) = 7.5 Hz and ^4J(Hg–H) = 48 Hz], 6.36 [t, Hg(1)–Ph–H_4, ^3J(H–H) = 7.2 Hz]. Ph: 7.99 [d, Ph–$H_{2,6}$(28, 38), ^3J(H–H) = 6.6 Hz], 7.96 [s, Ph–$H_{2,6}$(22)], 7.95 [s, Ph–$H_{2,6}$(26)], 7.89 [bs, Ph–$H_{2,6}$(32, 34)], 7.69-7.59 [m, Ph–$H_{3,5}$ and Ph–H_4]. ^{13}CNMR(150.87 MHz, $CDCl_3$, 20 °C): δ 162.0 (s) and 153.8 (s) for C_α(16, 19); 161.8 (s) and 152.0 (s) for C_α(6, 9); 157.1 (s) and 156.4 (s) for C_α(11, 14); 137.0 [s, C_{meso}(5, 20)]; 126.8 [s, C_{meso}(10, 15)]; 134.2 [s, C_β(7)]; 133.8 [s, C_β(18)], 132.6(s) and 132.2 (s) for C_β(12, 13); 131.8 [s, C_β(17)]; 131.1 [s, C_β(8)]; 148.4 [s, Hg(1)–Ph–C_1 or C(46)]; 135.3 [s, Hg(1)–Ph–$C_{2,6}$ or C(47, 51)]; 126.2 [s, Hg(1)–Ph–$C_{3,5}$ or C(48, 50)]; 125.3 [s, Hg(1)–Ph–C_4 or C(49)]; 38.3 [s, N-CH_3 or C(45)]; 131.1 [s, C(1)]; 96.6 [s, C(2)]; 129.8 [s, C(3)]; 125.1 [s, C(4)]; 136.1 [s, Ph–$C_{2,6}$ or C(22, 26)]; 134.4 [s, Ph–$C_{2,6}$ or C(28, 38)]; 133.8 [s, Ph–$C_{2,6}$ or C(32, 34)]; 128.4(s), 128.35(s), 128.1(s), 127.4(s), 127.17(s), and 127.16(s) for Ph–$C_{3,5}$ and Ph–C_4; 142.94(s), 142.87(s), 141.3(s) and 140.7(s) for Ph–C_1 [or C(21), C(27), C(33), C(39)]. ^{199}Hg NMR (107.24 MHz, $CDCl_3$, 20 °C): δ −1037 [t, Hg(1), ^3J(Hg–H) = 172 Hz]. UV–Vis spectrum, λ (nm) [$\varepsilon \times 10^{-3}$ (M^{-1} cm^{-1})] in CH_2Cl_2: 451 (129.0), 476 (165.2), 660 (17.7), 715 (21.2). MS (FAB): M^+ 906 (Calc. for $C_{51}H_{36}Hg_1N_4$: 906).

Table 1
Crystal data for **7** · 0.5 C_6H_{14} · $CHCl_3$ · CH_2Cl_2 · H_2O

Compound	**7** · 0.5C_6H_{14} · $CHCl_3$ · CH_2Cl_2 · H_2O
Empirical formula	$C_{51}H_{36}Hg_1N_4$ (0.5C_6H_{14} · $CHCl_3$ · CH_2Cl_2 · H_2O)
Formula weight	1161.75
Space group	$P2_1/c$
Crystal system	monoclinic
a (Å)	14.202(7)
b (Å)	26.025(12)
C (Å)	15.254(7)
α (°)	90
β (°)	116.924(6)
γ (°)	90
V (Å^3)	5027(4)
Z	4
F(000)	2304
D_{Calc} (g cm^{-3})	1.535
μ(Mo Kα) (mm^{-1})	3.371
S	0.958
Crystal size (mm)	0.15 x 0.11 x 0.08
θ (°)	1.56 to 28.41
T (K)	273(2)
Number of reflections measured	12638
Number of reflections observed	6493
R_1[a] (%)	7.44
wR_2[b] (%)	15.43

[a] $R_1 = [\sum||F_o| - |F_c||/\sum|F_o|]$.
[b] $wR_2 = \{\sum[w(F_o^2 - F_c^2)^2]/\sum[w(F_o^2)^2]\}^{1/2}$.

2.3. Spectroscopy

Proton spectrum in CD_2Cl_2 (or $CDCl_3$) were recorded at 599.94 MHz on Varian Unity Inova-600 spectrometers locked on deuterated solvent, and referenced to the solvent peak. Proton NMR spectrum is relative to CD_2Cl_2 at 5.3 ppm ($CDCl_3$ at 7.24 ppm). ^{199}Hg NMR was obtained at 107.24 MHz on a Bruker DMX-600 spectrometer locked on deuterated solvent. Chemical shifts of ^{199}Hg were measured relative to an external reference of

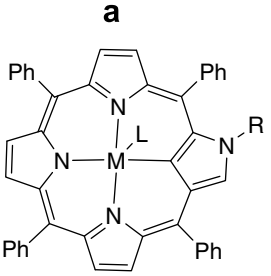

(**3**) M = Co(II) , R = CH_2COOEt , L = pyridine
(**4**) M = Ni(II) , R = CH_2CH_2Br , L = empty

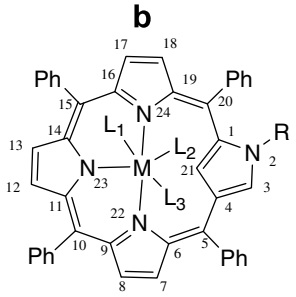

(**5**) M = Re(I) , R = CH_3 , L_1=L_2=L_3 = CO
(**6**) M=Fe(II), R=CH_3, L_1=Br, L_2=L_3=empty
(**7**) M=Hg(II), R=CH_3, L_1=Ph, L_2=L_3=empty

Chart 1.

Table 2
Selected bond distances (Å) and angles (°) for compound **7** · $0.5C_6H_{14}$ · $CHCl_3$ · CH_2Cl_2 · H_2O

7 · $0.5C_6H_{14}$ · $CHCl_3$ · CH_2Cl_2 · H_2O			
Bond lengths (Å)			
Hg(1)–N(1)	2.581(8)	Hg(1)–N(2)	2.130(7)
Hg(1)–N(3)	2.607(8)	Hg(1)–C(46)	2.058(9)
Hg(1)···C(2)	3.057(7)	Hg(1)···H(2A)	2.821(7)
Bond angles (°)			
C(46)–Hg(1)–N(1)	107.8(3)	C(46)–Hg(1)–N(2)	171.3(3)
C(46)–Hg(1)–N(3)	107.5(3)	N(1)–Hg(1)–N(2)	77.3(3)
N(1)–Hg(1)–N(3)	108.5(2)	N(2)–Hg(1)–N(3)	76.8(3)
Hg(1)···H(2A)···C(2)	95.7(3)		

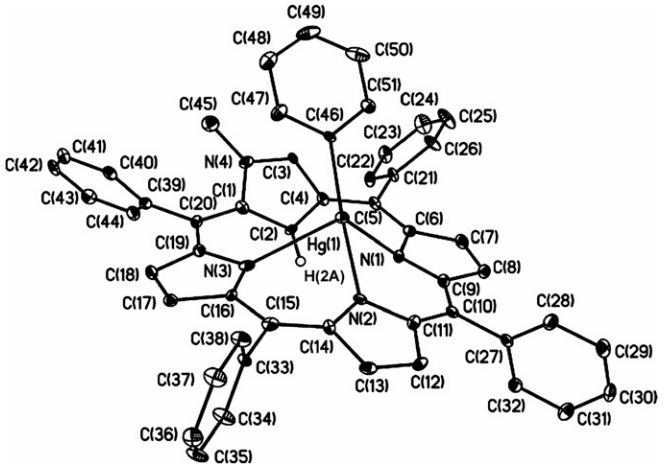

Fig. 1. Molecular configuration and atom-labeling scheme for **7** · 0.5 C_6H_{14} · $CHCl_3$ · CH_2Cl_2 · H_2O, with ellipsoids drawn at 30% probability. Hydrogen atoms and solvents (0.5 C_6H_{14}, $CHCl_3$, CH_2Cl_2 and H_2O) are omitted for clarity.

0.5 M phenylmercury(II) acetate in DMSO-d_6 (−1439.5 ppm) but reported relative to dimethylmercury (0.0 ppm). HMQC (heteronuclear multiple quantum coherence) was used to correlate protons and carbon through one-bond coupling and HMBC (heteronuclear multiple bond coherence) for two- and three-bond proton–carbon coupling. Nuclear Overhauser effect (NOE) difference spectroscopy was employed to determine the ^1H–^1H proximity through space over a distance of up to about 4 Å.

The positive ion fast atom bombardment mass spectrum (FAB MS) was obtained in a nitrobenzyl alcohol (NBA) matrix using a JEOL JMS-SX/SX 102 A mass spectrometer. UV–Vis spectra were recorded at 20 °C on a HITACHI U-3210 spectrophotometer.

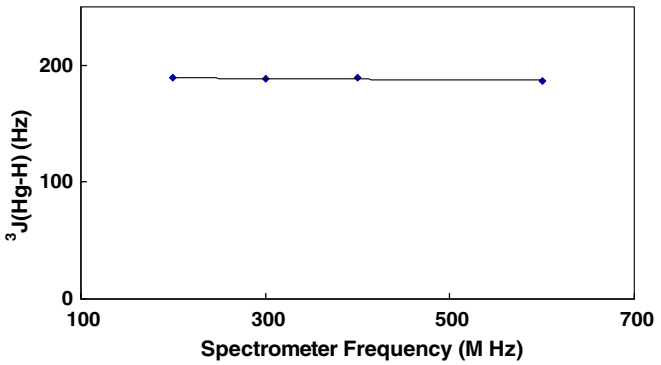

Fig. 3. Frequency (or field) dependence of ^3J(Hg–H) coupling constants for Hg(1)–Ph–$H_{2,6}$ of **7** in $CDCl_3$ (0.01 M) at 20 °C.

2.4. Crystallography

Table 1 presents the crystal data as well as other information for **7** · $0.5C_6H_{14}$ · $CHCl_3$ · CH_2Cl_2 · H_2O. Measurement was taken on a Bruker AXS SMART-1000 diffractometer using monochromatized Mo Kα radiation (λ = 0.71073 Å). Empirical absorption correction was made for **7** · 0.5 C_6H_{14} · $CHCl_3$ · CH_2Cl_2 · H_2O. The structure was solved by direct methods (SHELXTL-97) [7] and refined by the full-matrix least-squares method. One equivalent of CH_2Cl_2 solvent in **7** · $0.5C_6H_{14}$ · $CHCl_3$ · CH_2Cl_2 · H_2O is disordered with an occupancy factor of 0.57 [or 0.6] for Cl(4′) [or Cl(5)] and 0.43 [or 0.4] for Cl(4) [or Cl(5′)], respectively. All non-hydrogen atoms were refined with anisotropic thermal parameters, whereas all hydrogen atoms were placed in calculated positions and refined with a riding model. Table 2 lists selected bond distances and angles for **7** · $0.5C_6H_{14}$ · $CHCl_3$ · CH_2Cl_2 · H_2O.

3. Results and discussion

3.1. Molecular structure of 7

Using the d^{10} metal mercury(II), new mononuclear mercury **7** complex was synthesized. The synthetic strategy is outlined in Scheme 1.

During the metallation of free base **2** with PhHg(OAc) (Scheme 1), the soft acid Hg^{2+} prefers to retain one phenyl ligand (soft base)

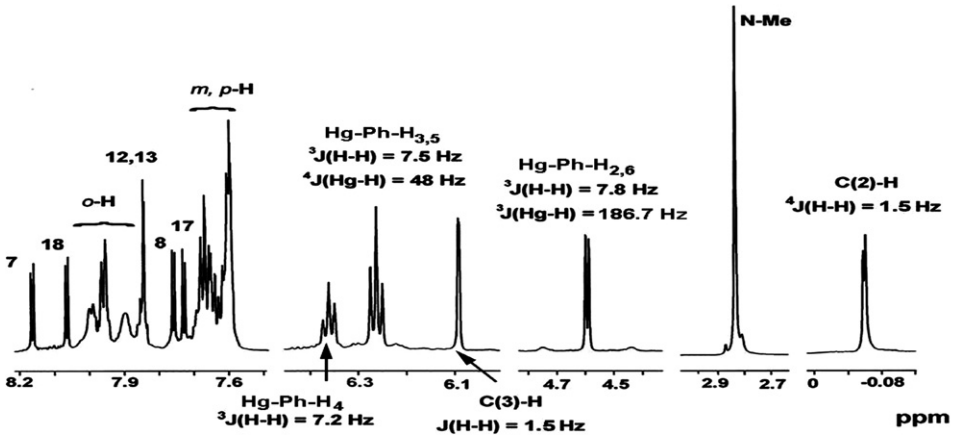

Fig. 2. ^1H NMR spectra at 599.94 MHz for a 0.01 M solution of **7** in CD_2Cl_2 at 20 °C.

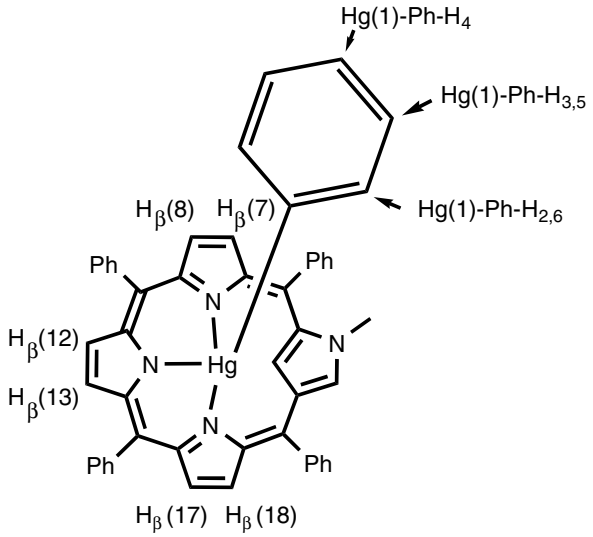

(7)

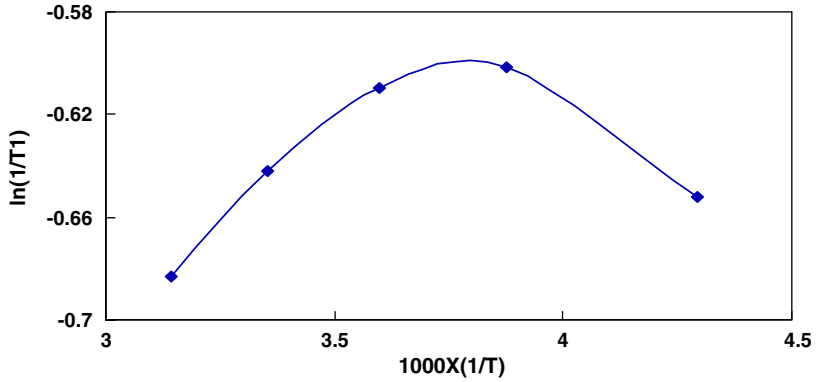

Fig. 4. Temperature dependence of ^{1}H spin-lattice relaxation rate for Hg(1)–Ph–$H_{2,6}$ of **7** in $CDCl_3$ (0.01 M) at 599.95 MHz.

and coordinates to the N [i.e., N(2)] of **2** to form a four-coordinate complex **7** with a seesaw geometry and the angle of N(2)–Hg(1)–C(46) in **7** is 171.3(3)° (Table 2).

The molecular structural information of **7** was elucidated by X-ray crystallographic analysis (Fig. 1 and Tables 1 and 2). In **7**, tripyrran (or tri-pyrrole) moiety coordinated to the metal center in κ^3-fashion and the mercury metal further has one phenyl ligand. The rest pyrrole ring was tilted from the porphyrin mean plane, consisting of $C_{20}N_4$ atoms, at 26.5° for **7**, so as to avoid steric repulsion. The metal–ligand bond distances and the angles are summarized in Table 2. The covalent bond of Hg(1)–C(46) = 2.058 (9) Å in **7** is smaller than the sum of the covalent radii of Hg and C (2.26 Å). The mercury nitrogen bond distances [Hg(1)–N(1) = 2.581(8), Hg(1)–N(2) = 2.130(7), and Hg(1)–N(3) = 2.607(8) Å] in **7** are well below the upper limit of a typical Hg–N covalent bond [2.75(2) Å] [8]. The C(2) is no longer bonded to Hg(1) in **7** as indicated by their longer internuclear distances, 3.057(7) Å for Hg(1)···C(2) in **7**. Hence, C(46), N(1), N(2), and N(3) are bonded covalently to the Hg(1) atom in **7** and the Hg(1)···C(2) and Hg(1)···H(2A) distances are 3.057(7) and 2.821(7) Å. These values are in the similar magnitude as compared to the van der Waals contact (3.15–3.20 Å for Hg···C and 2.70–2.95 Å for Hg ···H) [9]. Thus, these two distances do not support the formation of a weak agostic bond for Hg(1)···H(2A). The value of 95.7(3)° for Hg(1)–H(2A)–C(2) angle is well outside the reported range for a "truly agostic" type of bond. Furthermore, the satellite doublet signals with J(Hg–H) coupling for the resonance of C(2)–H was not observed. Thus the overall Hg(II) complex of **7** is not a side-on η^1-coordination type complex [10]. Since the three remaining nitrogen atoms and the Ph group are linked to the Hg(II) cation, the structure of **7** in inverted *N*-methylated porphyrin is similar to that

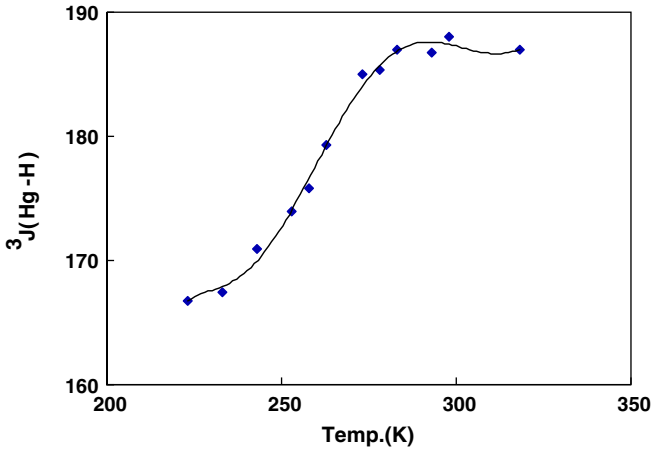

Fig. 5. Temperature dependence of observed ^{3}J(Hg–H) coupling constant for Hg(1)–Ph–$H_{2,6}$ of **7** in $CDCl_3$ (0.01 M) at 599.95 MHz.

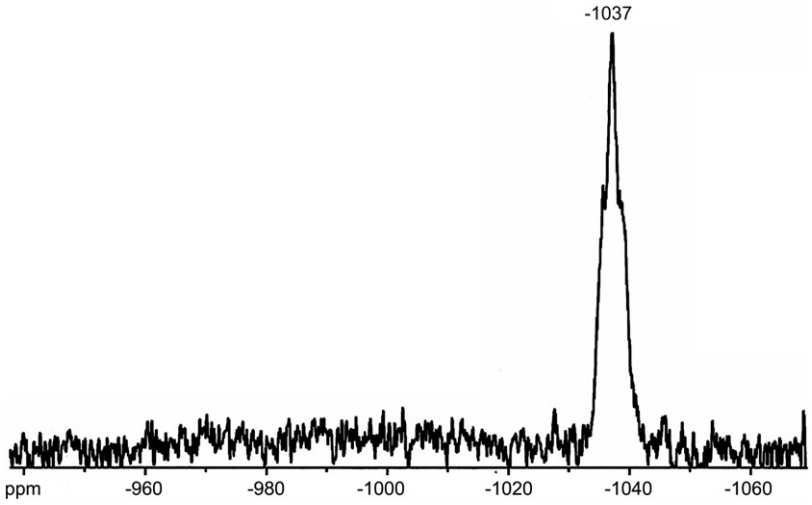

Fig. 6. ^{199}Hg NMR spectra at 107.24 MHz for a 0.2 M solution of **7** in $CDCl_3$ at 20 °C.

of HgPh(*N*-NHCO-2-C_4H_3S-TPP) (**8**) in the normal porphyrin derivatives with one inner nitrogen atom of the porphyrin being functionalized [6].

3.2. ^{1}H NMR for 7 in CD_2Cl_2

Complex **7** was characterized by ^{1}H, ^{13}C and ^{199}Hg NMR spectra. In solution, the molecule has effective C_s symmetry with a mirror plane running through the Hg(1)–C(22)–N(2)–C(2) unit for **7**. As a result, the ^{1}H NMR spectrum will exhibit six pyrrole resonances [H_β(7), H_β(18), H_β(12), H_β(13), H_β(8), H_β(17)] for **7** (Fig. 2). The ^{1}H NMR indicates that the aromatic protons of Hg(1)–Ph in **7** appears as a doublet at 4.58 ppm with a coupled satellites ^3J(Hg–H) of 186.7 Hz for Hg(1)–Ph–$H_{2,6}$, a triplet at 6.25 ppm with ^4J(Hg–H) of 48 Hz for the Hg(1)–Ph–$H_{3,5}$, and a triplet at 6.36 ppm for Hg(1)–Ph–H_4 of **7** in CD_2Cl_2 at 20 °C (Fig. 2). The methyl of **7** gives the resonance at 2.79 ppm (CD_2Cl_2, 293 K) strongly upfield of the signal that free base 2-NCH_3NCTPPH exhibits (3.31 ppm). The outer C(3)–H proton (δ = 6.09 ppm) is scalar coupled [^4J(H–H) = 1.5 Hz] to inner C(2)–H proton (δ = −0.08 ppm) (Fig. 2). Non-equivalence of the two sides of the macrocycle will cause each phenyl ring to have two distinct *ortho* resonances with one set of *ortho* protons *o*-H(28, 38), *o*-H(32, 34), for phenyl C(30) and C(36) and the other set of *ortho* protons *o*′-H(22,44), *o*′-H(26,40), for phenyl C(24) and C(42), unless the rotation around the C_{meso}–C_1 [C(10)–C(27), C(15)–C(33) or C(5)–C(21), C(20)–C(39)] bond is sufficiently fast in **7** (Fig. 2).

$(T_1)^{-1} = R_1$ is in general a sum of four contributions;

$(T_1)_{obs}^{-1} = (T_1)_{SR}^{-1} + (T_1)_{DD}^{-1} + (T_1)_{CSA}^{-1} + (T_1)_{SC}^{-1}$ corresponding to relaxation arising from the spin–rotation interaction, nuclear dipole–dipole coupling, chemical shift anisotropy, and scalar coupling [11]. $(T_1)_{CSA}^{-1}$ and $(T_1)_{SC}^{-1}$ are field dependent contributions which vary, respectively, as H_0^2 and H_0^{-2}(H_0 is the external field strength) [11]. The apparent coupling constant ^3J(Hg–H) for Hg(1)–Ph–$H_{2,6}$ of **7** in $CDCl_3$ at 20 °C is independent of the magnetic field strength implicating that chemical shift anisotropy (CSA) and scalar coupling (SC) are not the sources of the ^{1}H relaxation in the extreme narrowing conditions (Fig. 3). The temperature dependence of $(T_1)^{-1}$ for Hg(1)–Ph–$H_{2,6}$ in $CDCl_3$ at 599.95 MHz (Fig. 4) indicates the substantial contribution from dipole–dipole (DD) interaction in the −40 °C to +45 °C temperature range. This DD interaction is due to the coupling between [Hg(1)–Ph–$H_{2,6}$] protons and [Hg(1)] metal. In addition to the above magnetic field independence of the coupling constants, strong temperature dependence is observed. Specifically, the ^3J(Hg–H) coupling constants are maximum close at room temperature as illustrated in Fig. 5. Since the dipole–dipole interactions (DD) are the major contributors to the ^{1}H T_1 relaxation, these interactions indicate that the increase of temperature [12] leads to reduced T_1^{-1} (^{1}H) for Hg(1)–Ph–$H_{2,6}$ through a decrease of rotational correlation time (τ_c) during the fast motion regime. This decrease in T_1 relaxation rate explains that ^3J(Hg–H) increases from 166.7 to 186.7 Hz when temperature is increased from −50 °C to 20 °C (Fig. 5).

3.3. ^{199}Hg NMR for 7 in $CDCl_3$

The ^{199}Hg spectra at 20 °C shows a triplet signal at −1037 ppm with ^3J(Hg–H) = 172 Hz for a 0.2 M solution of **7** in $CDCl_3$, which is near to −1074 ppm, the position of the Hg(2) signal observed for a 0.05 M solution of [$(HgPh)_2$(*N*-*p*-$NSO_2C_6H_4{}^t$Bu-TPP); **9**] in $CDCl_3$, (Fig. 6) [6]. Hence the signal at δ −1037 ppm of **7** is due to Hg(1) nucleus with a coordination number of four. The chemical shift anisotropy (CSA) relaxation mechanism is a dominant contribution to ^{199}Hg spin-lattice relaxation in **7** [13]. The high field NMR spectroscopy, at 14.1 T [ν_o(Hg) = 107.24 MHz], may lead to very rapid relaxation. In the case of spin–spin coupling this can cause line broadening for neighboring nuclei or even ^{199}Hg–H decoupling [12,14,15]. This rapid relaxation of **7** obtained from its proton spectra in $CDCl_3$ at 20 °C (^3J(Hg–H) of 186.7 Hz for the Hg(1)–Ph–$H_{2,6}$ protons) is larger than that of mercury spectra (172 Hz), which gives the difference of about 15 Hz (8%).

4. Conclusions

The metal complex **7** bearing κ^3-porphyrin ligand with coordination environment [*N*,*N*, *N*, *C*(axial)] was synthesized. Compound **7** has been characterized by X-ray crystallography and NMR. Longitudinal relaxation rate composed of dipolar contribution for the Hg(1)–Ph–$H_{2,6}$ of **7** in 0.01 M solution was discussed.

Appendix A. Supplementary data

CCDC 674872 contains the supplementary crystallographic data for **7**. These data can be obtained free of charge via http://www.ccdc.cam.ac.uk/conts/retrieving.html, or from the Cambridge Crystallographic Data Centre, 12 Union Road, Cambridge CB2 1EZ, UK; fax: (+44) 1223-336-033 or e-mail: deposit@ccdc.cam.ac.uk.

Acknowledgement

The financial support from the National Science Council of the R.O.C. under Grant NSC 95-2113-M-005-014-MY3 is gratefully acknowledged.

References

[1] P.J. Chmielewski, L. Latos-Grazynski, J. Chem. Soc. Perkin Trans. 2 (1995) 503.
[2] W. Qu, T. Ding, A. Cetin, J.D. Harvey, M.J. Taschner, C.J. Ziegler, J. Org. Chem. 71 (2006) 811.
[3] I. Schmidt, P.J. Chmielewski, Z. Ciunik, J. Org. Chem. 67 (2002) 8917.
[4] M. Toganoh, H. Furuta, Chem. Lett. 34 (2005) 1034.
[5] K. Rachlewicz, D. Gorzelanczyk, L. Latos-Grazynski, Inorg. Chem. 45 (2006) 9742.
[6] H.Y. Hsieh, C.W. Cheng, F.A. Yang, J.H. Chen, Y.T. Tung, S.S. Wang, L.P. Hwang, Polyhedron 26 (2007) 4915.
[7] G.M. Sheldrick, SHELXL-97 Program for the Refinement of Crystal Structure from Diffraction Data, University of Gottingen, Gottingen, Berlin, 1997.
[8] M.C. Wang, L.S. Sue, B.C. Liau, B.T. Ko, S. Elango, J.H. Chen, Inorg. Chem. 40 (2001) 6064.
[9] J.E. Huheey, E.A. Keiter, R.L. Keiter, Inorganic Chemistry, 4th ed., Harper Collins. College Publishers, New York, 1993, pp. 114, 292.
[10] H. Furuta, T. Morimoto, A. Osuka, Inorg. Chem. 43 (2004) 1618.
[11] R.M. Hawk, R.R. Sharp, J. Chem. Phys. 60 (1974) 1522.
[12] P. Ghosh, P.J. Desrosiers, G. Parkin, J. Am. Chem. Soc. 120 (1998) 10416.
[13] D.G. Gillies, L.P. Blaauw, G.R. Hays, R. Huis, D.H. Clague, J. Magn. Reson. 42 (1981) 420.
[14] R.J. Benn, H. Gunther, A. Maercker, V. Menger, P. Schmitt, Angew. Chem., Int. Ed. Engl. 21 (1982) 295.
[15] F. Brady, R.W. Matthews, M.J. Forster, D.G. Gillies, J. Chem. Soc., Chem. Commun. (1981) 911.

Polyhedron 27 (2008) 2315–2326

Contents lists available at ScienceDirect

Polyhedron

journal homepage: www.elsevier.com/locate/poly

A systematic investigation of the $CuCl_2/H_2mal/phen$ reaction system (H_2mal = malonic acid): Solution and solid state studies of its products

Catherine Gkioni [a], Athanassios K. Boudalis [a], Yiannis Sanakis [a], Leondios Leondiadis [b], Vassilis Psycharis [a], Catherine P. Raptopoulou [a,*]

[a] Institute of Materials Science, NCSR "Demokritos", 15310 Aghia Paraskevi, Athens, Greece
[b] Institute of Radioisotopes-Radiodiagnostic Products, NCSR "Demokritos", 15310 Aghia Paraskevi, Athens, Greece

ARTICLE INFO

Article history:
Received 7 March 2008
Accepted 23 April 2008
Available online 12 June 2008

Keywords:
Copper(II) complexes
Malonato complexes
1,10-Phenanthroline
Mass spectrometry
Dynamic combinatorial chemistry

ABSTRACT

The systematic investigation of the parameter space of the $CuCl_2/H_2mal/phen$ reaction system in MeOH resulted in the isolation of seven different complexes either as mixtures or in pure form, six of which have been structurally characterized. The molar ratios of the reactants and the crystallization methods have been systematically varied, leading to the isolation of compounds $[Cu(H_2O)(phen)(mal)]$ (**1**), $[Cu(MeOH)(phen)(mal)]$ (**2**), $[Cu_2Li_2Cl_2(phen)_2(mal)_2(MeOH)_4]$ (**3**), $[Cu_2(phen)_4(mal)][CuCl(phen)(mal)](OH)$ (**4**), $[CuCl(phen)_2]Cl$ (**5**), and $[CuCl(phen)(mal)][CuCl(phen)_2][Cu(phen)_2(Hmal)]Cl$ (**6**). The coordination versatility of the malonato ligand has been confirmed by the presence of three different coordination modes and its two deprotonation states in compounds **1**–**6**. Solution studies on methanolic solutions of **2**–**4** and **6** by mass spectrometry revealed the absence of parent ion peak and the presence of fragment ions of low relative abundance not previously found in their crystal structure, thus indicating decomposition and rearrangement/reorganization of the complexes in solution and confirming the dynamic character of their solutions. Compounds **3** and **4** have been also studied in the solid state by EPR spectroscopy and magnetic measurements.

© 2008 Elsevier Ltd. All rights reserved.

1. Introduction

The coordination chemistry of the aliphatic α-ω dicarboxylates of the general formula $^-OOC–(CH_2)_n–COO^-$ has been widely investigated because it has found to exhibit a high coordination versatility. This is mainly due to (i) the presence of two carboxylato groups, (ii) the conformational freedom of the carbon skeleton (for $n \geqslant 1$), giving rise to various relative orientation of the two carboxylato moieties, (iii) the possibility to obtain mono- or di-anionic forms, (iv) the probability of triply coordinated oxygen atoms, and (v) the possibility to form secondary building blocks [1]. Thus, while oxalates ($n = 0$, H_2ox), act as rigid bridging ligands, giving rise to structures with dimensionalities ranging from zero to three [2], with the 2D honeycomb structure being the predominant one [3], the malonato ion ($n = 1$, H_2mal), offers the additional advantage of the relative location of the two carboxylato groups in the 1,3 positions supporting simultaneous chelating bidentate and various carboxylato-bridging coordination modes, thus leading to structures with variable architectures [4]. When combined with other bridging and/or chelating ligands, the malonato ion has afforded mononuclear, dinuclear, trinuclear, tetranuclear as well as 1D, 2D and 3D structures [5–11].

One of our areas of interest lies in the field of structure/properties relationship. For that purpose we have been embarked on the systematic exploration of the parameter space of reaction systems involving first-row transition-metal ions and various ligands, by varying several "degrees of freedom", like ligand substituents [12], solvent [13], crystallization method [14], as well as reactivity of metal clusters [15]. The isolation of one – or more – products from these systems in a pure form is also of prime importance, since a parallel area of interest is the physical study of these products in the solid state. The coordination versatility of the malonato ligand and its substituted derivatives, which can lead to novel metal ion topologies and cluster nuclearities bearing interesting physical properties, has prompted us to investigate their coordination chemistry. We have previously reported our results concerning the copper(II) coordination chemistry of methyl-malonic acid ($HOOC–CH(CH_3)–COOH$) in the presence of 1,10-phen and 2,2′-bpy [16]. Herein we present a systematic investigation of the parameter space of the $CuCl_2/H_2mal/phen$ reaction system in MeOH, and we examine the products that result from variations of two "degrees of freedom", i.e. the reaction mixture stoichiometry and the crystallization method (Table 1). Apart from crystallographic studies of products that result as single-crystals, we

* Corresponding author. Tel.: +30 210 6503365; fax: +30 210 6519430.
E-mail address: craptop@ims.demokritos.gr (C.P. Raptopoulou).

0277-5387/$ - see front matter © 2008 Elsevier Ltd. All rights reserved.
doi:10.1016/j.poly.2008.04.044

Table 1
The crystallographically characterized products from the $CuCl_2/H_2mal/phen$ reaction system in MeOH

Complex	Formula
1	$[Cu(H_2O)(phen)(mal)] \cdot H_2O$
2	$[Cu(MeOH)(phen)(mal)]$
3	$[Cu_2Li_2Cl_2(phen)_2(mal)_2(MeOH)_4]$
4	$[Cu_2(phen)_4(mal)][CuCl(phen)(mal)](OH) \cdot 4.4(MeOH) \cdot 0.4(H_2O)$
5	$[CuCl(phen)_2]Cl \cdot MeOH$
6	$[CuCl(phen)(mal)][CuCl(phen)_2][Cu(phen)_2(Hmal)]Cl \cdot 2MeOH \cdot 2H_2O$

conduct solution studies of some of the isolated products by means of mass spectrometry.

2. Experimental

2.1. General and spectroscopic measurements

All manipulations were performed under aerobic conditions using materials as received (Aldrich Co.). All chemicals and solvents were of reagent grade. Elemental analysis for C, H, and N was performed on a Perkin Elmer 2400/II automatic analyzer. IR spectra were recorded from KBr pellets in the range 4000–400 cm^{-1} on a Bruker Equinox 55/S FT-IR spectrophotometer. Electron-spray ionization mass spectra of **2**–**4** and **6** were recorded on an AQA Navigator, Finnigan mass spectrometer. Test solutions in 50% aqueous methanol were infused into the electrospray interface at a flow rate of 0.1 mL min^{-1}, using a Harvant Syringe pump. Negative or positive ion ESI spectra were acquired by adjusting the needle and cone voltages accordingly. Hot nitrogen gas (Dominic-Hunter UHPLCMS-10) was used for desolvation at 170 °C. Variable-temperature magnetic susceptibility measurements were carried out on polycrystalline samples of **3** and **4** in the 5.0–300 K temperature range using a Quantum Design MPMS SQUID magnetometer under a magnetic field of 1 T. Diamagnetic corrections for the complexes were estimated from Pascal's constants. The magnetic susceptibility has been computed by exact calculation of the energy levels associated with the spin Hamiltonian, through diagonalization of the full matrix with a general-symmetry program [17]. Least-squares fittings were accomplished with an adapted version of the function-minimization program MINUIT [18]. The error factor R is defined as $R = \sum \frac{(\chi_{exp} - \chi_{calc})^2}{N\chi^2_{exp}}$, where N is the number of experimental points. X-band EPR spectra were recorded on a Bruker ER 200D EPR spectrometer equipped with an Oxford Instruments ESR900 cryostat, a Bruker NMR Gaussmeter and an Anritsu microwave frequency counter.

2.2. Compound preparation

2.2.1. $[Cu(H_2O)(phen)(mal)] \cdot H_2O$ (**1** $\cdot H_2O$)

Solid phen $\cdot H_2O$ (0.099 g, 0.50 mmol) and $CuCl_2 \cdot 6H_2O$ (0.085 g, 0.50 mmol) were added to a refluxing solution of H_2mal (0.052 g, 0.50 mmol) and LiOH $\cdot H_2O$ (0.042 g, 1.0 mmol) in methanol (20 mL). The colour of the solution immediately turned to sky-blue and the reflux continued for 15 min, during which time no noticeable colour change or solid precipitation was observed. Slow evaporation of the sky-blue solution afforded large X-ray quality blue prismatic crystals of **1** after 4 days (yield: 0.013 g, 7.14%). The crystals were collected by filtration and dried *in vacuo*. The resulting powder was analyzed as solvent-free. *Anal.* Calc. for $C_{15}H_{12}CuN_2O_5$: C, 49.52; H, 3.32; N, 7.70. Found: C, 49.37; H, 3.34; N, 7.66%. FT-IR (KBr discs, cm^{-1}): 3480(m), 3050(s), 2980(sh), 2910(sh), 1590(vs), 1520(vs), 1495(sh), 1428(s), 1380(vs), 1340(s), 1282(s), 1224(m), 1209(m), 1143(m), 1110(m), 1050(m), 1033(m), 980(m), 955(m), 855(vs), 792(w), 778(m), 725(vs), 645(m), 430(m).

2.2.2. [Cu(MeOH)(phen)(mal)] (**2**)

2.2.2.1. Method A. A procedure same as for the synthesis of **1** was followed and X-ray quality blue prismatic crystals of **2** were obtained by layering of Et_2O (2:1 v/v) to the sky-blue reaction solution (yield: 0.015 g, 7.94%). The crystals were collected by filtration and dried *in vacuo*. *Anal.* Calc. for $C_{16}H_{14}CuN_2O_5$: C, 50.86; H, 3.73; N, 7.41. Found: C, 50.70; H, 3.71; N, 7.38%. FT-IR (KBr discs, cm^{-1}): 3490(s), 3407(vs), 3279(s), 3050(s), 2980(sh), 2910(sh), 1592(vs), 1520(vs), 1494(sh), 1428(s), 1381(vs), 1364(sh), 1343(s), 1282(s), 1224(m), 1209(m), 1144(m), 1108(m), 1049(m), 1033(m), 981(m), 955(m), 855(vs), 792(w), 779(m), 725(vs), 647(m), 430(m).

2.2.2.2. Method B. Solid phen $\cdot H_2O$ (0.049 g, 0.25 mmol) and $CuCl_2 \cdot 6H_2O$ (0.043 g, 0.25 mmol) were added to a refluxing solution of H_2mal (0.052 g, 0.50 mmol) and LiOH $\cdot H_2O$ (0.042 g, 1.0 mmol) in methanol (20 mL). The colour of the solution immediately turned to sky-blue and the reflux continued for 15 min, during which time no noticeable colour change or solid precipitation was observed. X-ray quality blue prismatic crystals of **2** were obtained either by layering or by vapour diffusion of Et_2O (2:1 v/v) to the reaction mixture. The identity of the products in each case was established by unit cell determination [a = 7.074(9), b = 11.84(2), c = 18.38(2) Å, β = 95.35(4)°, V = 1533(6) $Å^3$ (crystals from vapour diffusion) and a = 7.09(2), b = 11.86(3), c = 18.40(4) Å, β = 95.51 (3)°, V = 1540(10) $Å^3$ (crystals from layering), see Table 2].

2.2.3. $[Cu_2Li_2Cl_2(phen)_2(mal)_2(MeOH)_4]$ (**3**)

2.2.3.1. Method A. A procedure same as for the synthesis of **1** was followed, and X-ray quality light-blue crystals of **3** (yield: 0.015 g, 3.32%), along with large blue prismatic crystals of **2**, were obtained by vapour diffusion of Et_2O (2:1 v/v) to the sky-blue reaction solution. The crystals were separated manually and dried *in vacuo*. *Anal.* Calc. for $C_{34}H_{36}Cl_2Cu_2Li_2N_4O_{12}$: C, 45.15; H, 4.01; N, 6.19. Found: C, 45.01; H, 3.99; N, 6.17%. FT-IR (KBr discs, cm^{-1}): 3426(vs), 3066(sh), 1618(vs), 1518(s), 1489(m), 1421(vs), 1342(sh), 1331(s), 1312(sh), 1272(sh), 1252(sh), 1217(m), 1198(w), 1165(m), 1140(s), 1105(m), 1050(w), 1035(w), 1002(w), 970(s), 947(m), 874(m), 852(vs), 837(m), 785(m), 725(vs), 649(w), 577(s), 493(w), 472(w), 430(w).

2.2.3.2. Method B. Solid phen $\cdot H_2O$ (0.099 g, 0.50 mmol) and $CuCl_2 \cdot 6H_2O$ (0.128 g, 0.75 mmol) were added to a refluxing solution of H_2mal (0.052 g, 0.50 mmol) and LiOH $\cdot H_2O$ (0.042 g, 1.0 mmol) in methanol (20 mL). The colour of the solution immediately turned to sky-blue and the reflux continued for 15 min, during which time no noticeable colour change or solid precipitation was observed. X-ray quality light-blue prismatic crystals of **3**, along with small portions of a green powder, were obtained either by layering or by vapour diffusion of Et_2O (2:1 v/v) to the reaction mixture. The identity of the product was established by unit cell determination (a = 8.40(1), b = 8.75(2), c = 14.32(2) Å, α = 84.10 (4)°, β = 76.65(4)°, γ = 69.93(4)°, V = 962(6) $Å^3$, see Table 2).

2.2.4. $[Cu_2(phen)_4(mal)][CuCl(phen)(mal)](OH) \cdot 4.4(MeOH) \cdot 0.4(H_2O)$ (**4** $\cdot 4.4MeOH \cdot 0.4H_2O$)

2.2.4.1. Method A. Solid phen $\cdot H_2O$ (0.099 g, 0.50 mmol) and $CuCl_2 \cdot 6H_2O$ (0.043 g, 0.25 mmol) were added to a refluxing solution of H_2mal (0.052 g, 0.50 mmol) and LiOH $\cdot H_2O$ (0.042 g, 1.0 mmol) in methanol (20 mL). The colour of the solution immediately turned to sky-blue and the reflux continued for 15 min, during which time a white precipitate was formed and removed by filtration. X-ray quality blue-turquoise crystals of **4** were obtained by slow vapour diffusion of Et_2O (2:1 v/v) to the sky-blue reaction solution (yield: 0.049 g, 14.47%). The same reaction mixture when layered with Et_2O (2:1 v/v) leads to the formation of a mixture of **2**

and **3**. The crystals of **4** were collected by filtration and dried *in vacuo*. The resulting powder was analyzed as solvent-free. *Anal.* Calc. for $C_{66}H_{51}ClCu_3N_{10}O_9$: C, 58.54; H, 3.80; N, 10.34. Found: C, 58.36; H, 3.81; N, 10.31%. FT-IR (KBr discs, cm^{-1}): 3406(vs), 3053 (m), 1582(vs), 1518(vs), 1494(w), 1427(vs), 1355(m), 1341(m), 1247(w), 1224(w), 1144(w), 1105(w), 959(w), 938(w), 851(vs), 779(w), 723(vs), 648(m), 428(w).

2.2.4.2. Method B. Solid phen · H_2O (0.099 g, 0.50 mmol) and $CuCl_2 \cdot 6H_2O$ (0.043 g, 0.25 mmol) were added to a refluxing solution of H_2mal (0.026 g, 0.25 mmol) and LiOH · H_2O (0.021 g, 0.50 mmol) in methanol (20 mL). The colour of the solution immediately turned to sky-blue and the reflux continued for 15 min, during which time no noticeable colour change or solid precipitation was observed. X-ray quality blue-turquoise crystals of **4** were obtained by layering of Et_2O (2:1 v/v) to the reaction mixture. The identity of the crystals was established by FT-IR spectroscopy.

2.2.4.3. Method C. Solid phen · H_2O (0.165 g, 0.83 mmol) and $CuCl_2 \cdot 6H_2O$ (0.085 g, 0.50 mmol) were added to a refluxing solution of H_2mal (0.034 g, 0.33 mmol) and LiOH · H_2O (0.028 g, 0.66 mmol) in methanol (20 mL). The colour of the solution immediately turned to sky-blue and the reflux continued for 15 min, during which time no noticeable colour change or solid precipitation was observed. X-ray quality blue-turquoise crystals of **4**, along with blue prismatic crystals of **2**, light-blue prismatic crystals of **3**, green prismatic crystals of **5** and green needle-like crystals of **7**, were obtained by vapour diffusion of Et_2O (2:1 v/v) to the sky-blue reaction mixture. The crystals were separated manually and they were identified by FT-IR spectroscopy.

*2.2.5. [CuCl(phen)$_2$]Cl · MeOH (**5** · MeOH)*

A procedure as for the synthesis of **4** was followed (Method A), the only difference being the rapid rate of vapour diffusion of Et_2O to the sky-blue reaction mixture. As a result a mixture of large X-ray quality green prismatic crystals of **5**, blue-turquoise crystals and light-green needle-like crystals was formed which were separated manually. The blue-turquoise crystals and the light-green needles were identified by FT-IR spectroscopy as **4** and as a copper phenanthrolinato complex (**7**), respectively. Compounds **5** and **7** present similar infrared spectra (see below) and presumably they have analogous molecular structures with different unit cell parameters and/or solvate molecules. The crystals of **5** were separated manually and were dried *in vacuo*. The resulting powder was analyzed as solvent-free. *Anal.* Calc. for $C_{24}H_{16}Cl_2Cu_2N_4$: C, 51.62; H, 2.89; N, 10.03. Found: C, 51.46; H, 2.88; N, 9.99%. FT-IR (KBr discs, cm^{-1}) for **5**: 3521(m), 3364(m), 2987(m), 1625(m), 1605(m), 1583(m), 1518(vs), 1494(m), 1427(vs), 1339(m), 1309(w), 1227 (m), 1209(w), 1144(m), 1105(m), 1034(w), 956(vw), 911(vw), 869(sh), 856(vs), 782(m), 723(vs), 649(m), 614(m), 588(m), 428 (m). FT-IR (KBr discs, cm^{-1}) for **7**: 3416(vs), 3051(w), 2921(w), 1626(m), 1605(w), 1584(m), 1518(s), 1494(w), 1427(vs), 1339(w), 1308(w), 1225(w), 1144(m), 1105(m), 869(sh), 852(vs), 780(m), 723(vs), 648(w), 429(w).

*2.2.6.[CuCl(phen)(mal)][CuCl(phen)$_2$][Cu(phen)$_2$(Hmal)]Cl · 2MeOH · 2H$_2$O (**6** · 2MeOH · 2H$_2$O)*

2.2.6.1. Method A. Solid phen · H_2O (0.099 g, 0.50 mmol) and $CuCl_2 \cdot 6H_2O$ (0.043 g, 0.25 mmol) were added to a refluxing solution of H_2mal (0.026 g, 0.25 mmol) and LiOH · H_2O (0.021 g, 0.50 mmol) in methanol (20 mL). The colour of the solution immediately turned to sky-blue and the reflux continued for 15 min, during which time no noticeable colour change or solid precipitation was observed. X-ray quality blue-turquoise crystals of **6** were obtained by slow vapour diffusion of Et_2O (2:1 v/v) to the sky-blue reaction solution (yield: 0.020 g, 5.70%), along with large green crystals and light green needle-like crystals which were identified as **5** and **7**, respectively, by FT-IR spectroscopy. The crystals of **6** were separated manually and dried *in vacuo*. The resulting powder was analyzed as solvent-free. *Anal.* Calc. for $C_{66}H_{45}Cl_3Cu_3N_{10}O_8$: C, 56.50; H, 3.23; N, 9.98. Found: C, 56.33; H, 3.24; N, 9.95%. FT-IR (KBr discs, cm^{-1}): 3347(s), 3058(m), 2930(sh), 2817(w), 1714(s), 1605(vs), 1583(sh), 1518(vs), 1493(m), 1428(vs), 1372(m), 1340 (m), 1274(m), 1255(w), 1225(w), 1208(w), 1152(m), 1106(m), 1030(m), 999(vw), 970(w), 938(w), 912(w), 869(sh), 851(vs), 779 (w), 724(vs), 672(w), 648(m), 582(w), 507(w), 474(w), 429(m).

2.2.6.2. Method B. The procedure was the same as above but 0.25 mmol of LiOH · H_2O were used instead. Layer or slow vapour diffusion of Et_2O (2:1 v/v) to the sky-blue solution afforded blue-turquoise crystals of **6** whose identity was confirmed by unit cell determination. (a = 14.05(1), b = 15.18(2), c = 17.22(2) Å, α = 68.28(3)°, β = 74.44(3)°, γ = 72.89(3)°, V = 3209(9) Å^3, see below, X-ray crystallography).

2.3. Single-crystal X-ray crystallography

Blue prismatic crystals of **1** (0.10 × 0.30 × 0.70 mm) and **2** (0.30 × 0.40 × 0.70 mm) were mounted in air. A light-blue prismatic crystal of **3** (0.30 × 0.40 × 0.70 mm), a blue-turquoise crystal of **4** (0.15 × 0.50 × 0.70 mm), a green crystal of **5** (0.15 × 0.30 × 0.55 mm) and a blue-turquoise crystal of **6** (0.15 × 0.30 × 0.60 mm) were mounted in capillaries. Diffraction measurements were made on a Crystal Logic Dual Goniometer diffractometer using graphite monochromated Mo radiation (for **1**–**3**, **5** and **6**) and on a $P2_1$ Nicolet diffractometer upgraded by Crystal Logic using graphite monochromated Cu radiation (for **4**). Important crystal data and parameters for data collection for **2**–**4** are reported in Table 2. Unit cell dimensions were determined and refined by using the angular settings of 25 automatically centered reflections in the range $11° < 2\theta < 23°$ (for **1**–**3**, **5** and **6**) and in the range $22° < 2\theta < 54°$ (for **4**). Three standard reflections monitored every 97 reflections showed less than 3% intensity fluctuation and no decay. Lorentz, polarization and psi-scan absorption corrections (for **4** only) were applied using Crystal Logic software. The structures were solved by direct methods using SHELXS-97 [19] and refined by full matrix least-squares techniques on F^2 with SHELXL-97 [20]. For compounds **1**, **5** and **6** only preliminary crystallographic determination was performed. The molecular structures of **1** and **5** are known, although in different space groups, but their characterization was crucial from the chemical point of view in terms of the species isolated from the reaction mixture examined. Thus we felt that the complete structural characterization of **1** and **5** would not add any further potential to our investigation. On the other hand, the crystals of the new compound **6** were of poor quality showing large ω-widths with shoulders on one side, a fact that is also reflected to the quality of the crystallographic data (see below), while our repeating efforts to improve the quality of the crystals of **6** were unsuccessful. Even so, the structural characterization of **6** was valuable, since complex **6** constitutes the only isolated species containing the $Hmal^-$ anion; an observation very helpful for the interpretation of the Mass Spectra (see below). Further experimental crystallographic details for **1** · H_2O: $C_{15}H_{15}CuN_2O_6$; f_w = 382.83; space group triclinic $P\bar{1}$; a = 8.093(6) Å, b = 11.017(8) Å, c = 17.66 (1) Å, α = 88.39(3)°, β = 79.82(3)°, γ = 74.94(2)°, V = 1503.18 Å^3, Z = 4; ρ_{calc} = 1.692 g cm^{-3}; μ(Mo Kα) = 1.49 mm^{-1}; T = 25 °C; $2\theta_{max}$ = 34°; scan speed 4.0°/min; scan range 1.6 + $\alpha_1\alpha_2$ separation; reflections collected/unique/used, 1949/1754 [R_{int} = 0.0091]/1754; 273 parameters refined; $(\Delta/\sigma)_{max}$ = 0.004; $(\Delta\rho)_{max}/(\Delta\rho)_{min}$ = 0.506/−0.294 e/Å^3; R_1/wR_2 for 1670 reflections with $I > 2\sigma(I)$, (for all data), 0.0497/0.1306, (0.0522/0.1363). Only the metal and the coordinated atoms

Table 2
Crystallographic data for complexes **2**–**4** · 4.4MeOH · 0.4H_2O

	2	**3**	**4** · 4.4MeOH · 0.4H_2O
Formula	$C_{16}H_{14}CuN_2O_5$	$C_{34}H_{36}Cl_2Cu_2Li_2N_4O_{12}$	$C_{70.4}H_{63.4}ClCu_3N_{10}O_{13.8}$
Fw	377.83	904.52	1496.38
Space group	$P2_1/c$	$P\bar{1}$	$P2_1/n$
T (°C)	298	298	298
λ (Å)	Mo Kα (0.71073)	Mo Kα (0.71073)	Cu Kα (1.5418)
a (Å)	7.061(3)	8.372(2)	16.409(8)
b (Å)	11.817(4)	8.696(7)	21.970(13)
c (Å)	18.345(7)	14.265(9)	20.793(11)
α (°)		84.15(3)	
β (°)	95.45(2)	76.60(2)	110.97(2)
γ (°)		69.93(3)	
V (Å^3)	1523.78	948.6(1)	6999.52(6)
Z	4	1	4
ρ_{calc} (g cm^{-3})	1.647	1.583	1.420
μ (Mo Kα) (mm^{-1})	1.46	1.328	1.997
R_1[a]	0.0328[b]	0.0360[c]	0.0651[d]
wR_2[a]	0.0866[b]	0.0963[c]	0.1714[d]

[a] $w = 1/[\sigma^2(F_o^2) + (aP)^2 + bP]$ and $P = (\max)(F_o^2,0) + (2F_c^2)/3$. $R_1 = \sum(|F_o| - |F_c|)/\sum(|F_o|)$ and $wR_2 = \{\sum[w(F_o^2 - F_c^2)^2]/\sum[w(F_o^2)^2]\}^{1/2}$.
[b] For 2401 reflections with $I > 2\sigma(I)$.
[c] For 3139 reflections with $I > 2\sigma(I)$.
[d] For 7283 reflections with $I > 2\sigma(I)$.

were refined anisotropically, the rest were refined isotropically. No H-atoms were included in the refinement. Further experimental crystallographic details for **2**: $2\theta_{max} = 50°$, scan speed 4.5°/min; scan range 1.6 + $\alpha_1\alpha_2$ separation; reflections collected/unique/used, 2910/2680 [$R_{int} = 0.0278$]/2680; 273 parameters refined; $(\Delta/\sigma)_{max} = 0.006$; $(\Delta\rho)_{max}/(\Delta\rho)_{min} = 0.255/-0.610$ e/Å^3; R_1/wR_2 (for all data), 0.0380/0.0906. Hydrogen atoms were located by difference maps and were refined isotropically. All non-H atoms were refined anisotropically. Further experimental crystallographic details for **3**: $2\theta_{max} = 50°$, scan speed 4.0°/min; scan range 1.6 + $\alpha_1\alpha_2$ separation; reflections collected/unique/used, 3586/3336 [$R_{int} = 0.0092$]/3336; 303 parameters refined; $(\Delta/\sigma)_{max} = 0.004$; $(\Delta\rho)_{max}/(\Delta\rho)_{min} = 0.727/-1.029$ e/Å^3; R/R_w (for all data), 0.0376/0.0981. Hydrogen atoms were located by difference maps and were refined isotropically, except those of the methyl groups which were introduced at calculated positions as riding on bonded atoms. All non-H atoms were refined anisotropically. Further experimental crystallographic details for **4**: $2\theta_{max} = 116.5°$, scan speed 1.5°/min; scan range 2.45 + $\alpha_1\alpha_2$ separation; reflections collected/unique/used, 9984/9675 [$R_{int} = 0.0302$]/9675; 903 parameters refined; $(\Delta/\sigma)_{max} = 0.006$; $(\Delta\rho)_{max}/(\Delta\rho)_{min} = 0.575/-0.517$ e/Å^3; R_1/wR_2 (for all data), 0.0845/0.1931. Hydrogen atoms were introduced at calculated positions as riding on bonded atoms. All non-H atoms were refined anisotropically, except of the methanol and water solvate molecules which were refined isotropically with fixed occupation factors. Further experimental crystallographic details for **5** · MeOH: $C_{25}H_{20}Cl_2CuN_4O$; $f_w = 526.89$; space group monoclinic $P2_1/n$; $a = 14.476(8)$ Å, $b = 10.648(6)$ Å, $c = 15.062(7)$ Å, $\beta = 100.19(2)°$, $V = 2285(3)$ Å^3, $Z = 4$. Further experimental crystallographic details for **6** · 2MeOH · 2H_2O: $C_{68}H_{57}Cl_3Cu_3N_{10}O_{12}$; $f_w = 1503.21$; space group triclinic $P\bar{1}$; $a = 13.99(2)$ Å, $b = 15.24(2)$ Å, $c = 17.09(2)$ Å, $\alpha = 69.09(3)°$, $\beta = 74.53(4)°$, $\gamma = 73.04(4)°$, $V = 3202(9)$ Å^3, $Z = 2$; $\rho_{calc} = 1.560$ g cm^{-3}; μ(Mo Kα) = 1.186 mm^{-1}; $T = 25$ °C; $2\theta_{max} = 38.5°$; scan speed 2.0°/min; scan range 1.6 + $\alpha_1\alpha_2$separation; reflections collected/unique/used, 5415/5125 [$R_{int} = 0.0171$]/5415; 632 parameters refined; $(\Delta/\sigma)_{max} = 0.001$; $(\Delta\rho)_{max}/(\Delta\rho)_{min} = 3.501/-2.772$ e/Å^3; R_1/wR_2 for 3914 reflections with $I > 2\sigma(I)$, (for all data), 0.0949/0.2392, (0.1206/0.2657). All non-H atoms were refined anisotropically, except of the solvate molecules and those of the [Cu(phen)$_2$(Hmal)]$^+$ cation which were refined isotropically (only the copper ion was refined anisotropically). No H-atoms were included in the refinement.

3. Results and discussion

3.1. Syntheses

In order to explore the parameter space of the $CuCl_2$/H_2mal/phen reaction system in methanol, we first employed the 1:1:1 molar ratio reaction in the presence of stoichiometric amounts of LiOH · H_2O to ensure deprotonation of the malonic acid. Three species have been isolated from the same sky-blue reaction mixture depending on the crystallization method employed: (i) slow evaporation afforded the mononuclear complex [Cu(H_2O)(phen)(mal)] (**1**), (ii) layering of Et_2O afforded the analogous mononuclear complex [Cu(MeOH)(phen)(mal)] (**2**) (see Section 2, Method A), and (iii) vapour diffusion of Et_2O led to the heterometallic tetranuclear complex [$Cu_2Li_2Cl_2$(phen)$_2$(mal)$_2$(MeOH)$_4$] (**3**) (see Section 2, Method A). The 1:1:1 stoichiometry initially employed in the Cu^{II}/H_2mal/phen reaction system is reflected to the stoichiometry of the three products. A summary of the reactions employed and the complexes isolated is depicted in Scheme 1.

To further explore the parameter space of the above reaction system we varied the molar ratios of the reactants, first by systematically increasing each one's molar ratio, leaving at the same time all other parameters unchanged. Thus, the 1.5:1:1 respective molar ratio led to the isolation of complex **3** regardless of the crystallization method (see Section 2, Method B) along with small portions of green powder which is probably a copper(II) phenanthrolinato complex (based on its colour). The excess of the Cu^{II} ions in the reaction mixture is not reflected to the Cu^{II}/H_2mal/phen stoichiometry in **3**, but it promoted the isolation of a non-malonato complex (green powder). The 1:2:1 respective molar ratio led to **2** regardless of the crystallization method (see Section 2, Method B). Thus, excess of H_2mal in the reaction mixture afforded exclusively **2** without 'pushing' the equilibrium to the isolation of other complexes from the reaction mixture. On the contrary, the 1:1:2 Cu^{II}/H_2mal/phen molar ratio reaction afforded several products depending on the crystallization method: (i) layering of Et_2O to the sky-blue solution afforded compound [Cu_2(phen)$_4$(mal)]-[CuCl(phen)(mal)](OH) (**4**) (see Section 2, Method B), and (ii) vapour diffusion of Et_2O to the same reaction mixture afforded a mixture of [CuCl(phen)$_2$]Cl (**5**), [CuCl(phen)(mal)][CuCl(phen)$_2$][Cu(phen)$_2$-(Hmal)]Cl (**6**) (see Section 2, Method A), and light-green microcrystalline needles (**7**) showing superimposable IR spectra with **5**. Thus,

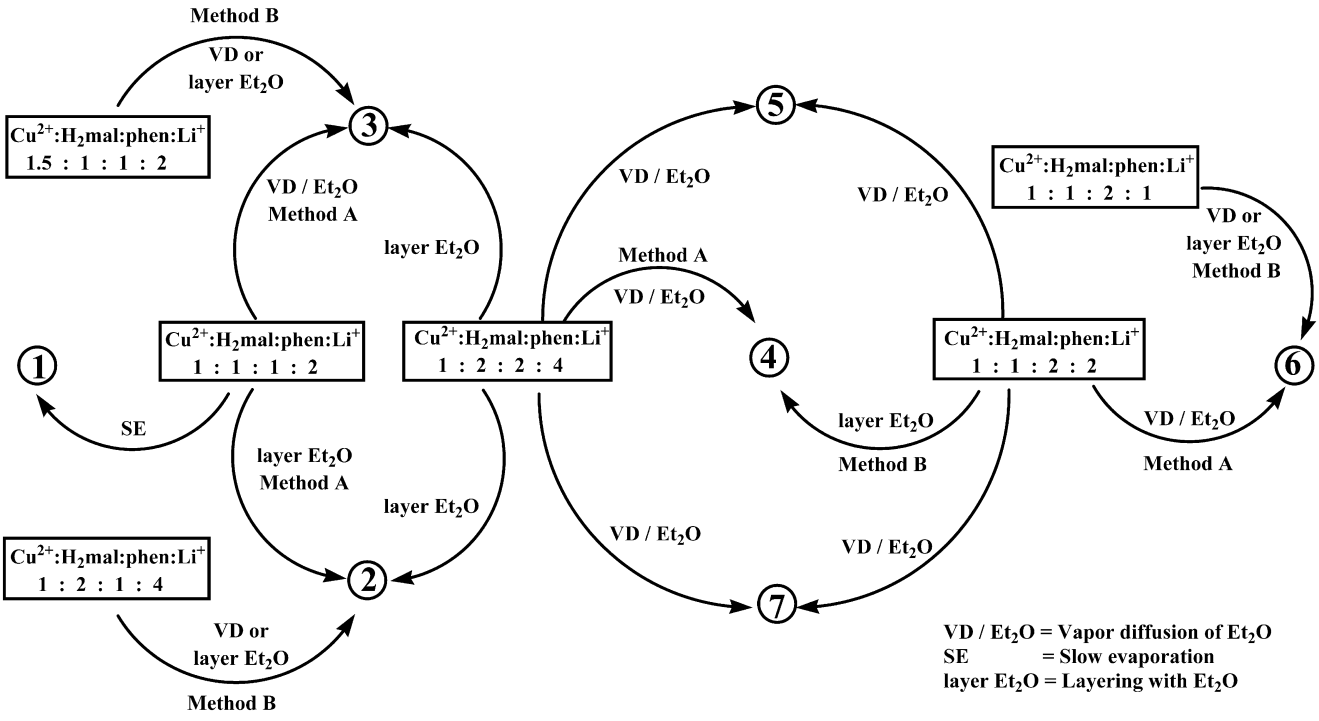

Scheme 1. Diagram of the reaction pathways, showing the various combinations of stoichiometries and crystallization methods, and the products obtained by each. The 1.5:1:2.5:2 system leads to **2**–**5** and **7**, and is not shown for simplicity.

from a chemical point of view, we conclude that complexes **5** and **7** are identical, although they present different crystal structure parameters. The excess of phen in the reaction mixture seems as the most determinant factor since it 'pushes' the equilibrium to the isolation of phen-rich complexes (see molecular structures of **4**, **5** and **6**).

In a next step, we varied the molar ratios of the reactants by simultaneously increasing the H_2mal and phen, leaving at the same time all other parameters unchanged. Thus, the 1:2:2 respective molar ratio led to the isolation of different mixtures of products depending on the crystallization method: (i) layering of Et_2O afforded a mixture of **2** and **3**, (ii) slow vapour diffusion of Et_2O afforded exclusively compound **4**, and (iii) rapid vapour diffusion of Et_2O afforded a mixture of **4**, **5** and **7**. As in the previous case, the excess of phen, rather than the excess of H_2mal, plays the predominant role since it facilitates the isolation of phen-rich complexes (see molecular structures of **4**, and **5).**

Similarly, we increased the molar ratios of Cu^{II} and phen with respect to H_2mal using the 1.5:1:2.5 Cu^{II}/H_2mal/phen molar ratio (not shown in Scheme 1), based on the stoichiometry of **4** (see synthesis of **4**, method C). By keeping the same reaction conditions (i.e. respective H_2mal/LiOH · H_2O molar ratio, solvent, crystallization method) that led to the isolation of **4**, we have simultaneously isolated compounds **2**–**5** and **7**. The simultaneous excess of Cu^{II} (previously leading to the isolation of **3** and probably **7**) and phen (previously leading to the isolation of **4**, **5**, **7**) in the reaction mixture is in agreement with the isolation of a mixture of complexes.

In all cases above, the 1:2 H_2mal/LiOH · H_2O molar ratio was used to ensure the full deprotonation of H_2mal. This is in agreement with the presence of the mal^{2-} anion in the crystal structures of compounds **1**–**4**, whereas the presence of $Hmal^-$ in the $[Cu(phen)_2(Hmal)]^+$ species found in **6** was not anticipated. We have thus wondered whether the isolation of a compound containing exclusively the $Hmal^-$ anion would be possible, and we have employed the 1:1 H_2mal/LiOH · H_2O molar ratio while keeping the overall Cu^{II}/H_2mal/phen molar ratio to 1:1:2 (see Section 2, Method B). However, regardless of the crystallization method, the only product isolated was compound **6**, leading us to conclude that both mal^{2-} and $Hmal^-$ anions coexist in the reaction mixtures and their subsequent coordination is impeded by complicated and yet unknown reaction mechanisms and conditions.

Conclusively, our results from the investigation of the parameter space of the $CuCl_2/H_2$mal/phen reaction system in MeOH can be summarized as follows: (i) the reaction mixtures examined have afforded seven different products either in pure form or as mixtures; (ii) the complexes have been isolated based on their different solubilities; (iii) the excess of Cu^{II} in the reaction mixture leads to the isolation of **3** and probably **5** or **7** as green powder; (iv) the excess of H_2mal in the reaction mixture leads to the isolation of pure **2** despite the 1:1:1 stoichiometry found in its molecular structure; (v) the excess of phen seems to play the predominant role leading to the isolation of the phen-rich complexes **4**, **5**, **6** and **7** along with the equimolar complexes **2** and **3**; (vi) each of the 1:1:1, 1:1:2, 1:2:2 and 1.5:1:2.5 Cu^{II}/H_2mal/phen reaction mixtures has afforded several products, some of which resulted from two different mixtures, and some of which were afforded by only one (Scheme 1); and (vii) other species coexisting in the reaction mixture cannot be excluded. Thus, we may conclude that each of these mixtures behaves like a Dynamic Combinatorial Library (DCL), containing many different species in equilibrium. These species can be selectively isolated, by means of crystallization in different solvent systems. It is also of interest, that these DCLs exhibit overlaps, as many isolated species are common to more than one of those DCLs.

The fact that solutions of transition-metal ions and one or more ligands form complicated mixtures of products in equilibrium, due to the labile nature of the metal–ligand and other non-covalent bonds that may eventually form (H-bonds, π–π stacking, etc.) is not new, and this is one of the attributes that make this chemistry so difficult to control. From this multitude of products in equilibrium it is often possible to isolate one or more products by their selective precipitation and subsequent crystallization, although it

still remains a challenge to isolate different species from a DCL, and more so to structurally characterize them [21]. In other cases, structures were not available [22], or of marginal quality [23], but the products were identified spectroscopically. In most cases, the molecular recognition of the DCL member with small molecules or ions has been served as the selection process. Very elegant examples of this work include metallosupramolecular tetrahedral [24], cubes and open books [25], tetra-, hexa- and octanuclear ferric wheels [26], linear and circular helicates [27], tetra- and hexanuclear helicates [28], bowls and capsules [29], porphyrin cages [30], tetrahedra and helicates [31], various metallacryptates [32] and Borromean Rings and Solomon Knots [33] which have been identified as members of DCLs, and in some cases isolated.

The particularity of the present system is that the isolation of specific species is not based on supramolecular recognition, but on their solubility in a given solvent system. What is also noteworthy is that a large number of such species has been structurally characterized.

3.2. Description of structures

The crystallographic characterization of **1** and **2** revealed the presence of mononuclear species [Cu(L)(phen)(mal)] (L = H_2O (**1**), MeOH (**2**)). The structure of **1** has been reported previously [5a]. An ORTEP plot of **2** is given in Fig. 1, selected bond distances and angles for both structures are given as Supplementary data (Table S1). The coordination geometry around the Cu^{II} ion in both **1** and **2** is square-pyramidal; the basal positions are occupied by the nitrogen atoms of the phen and the oxygen atoms (O(1) and O(3)) of the bidentate chelating mal^{2-} ligand, whereas the apical position is occupied by the monodentate ligand. In the structure of **2**, two centrosymmetrically related mononuclear species are hydrogen bonded and form dimers [Om(1)···O(4) ($-x$, $-y$, $1-z$) = 2.813 Å, HOm(1)···O(4) = 2.221 Å, Om(1)–HOm(1)···O(4) = 166.6°] (Fig. S1).

An ORTEP plot of the structure of **3** is given in Fig. 2, selected bond distances and angles are listed in Table S2. The structure of **3** consists of neutral heterometallic tetranuclear $Cu^{II}_2Li^{I}_2$ units held together by two bidentate [chelating] + bis(unidentate) mal^{2-} ligands (Scheme 2). The coordination geometry around the two Cu^{II} ions is square-pyramidal, (τ = 0.19). The basal positions of the square pyramid are occupied by the nitrogen atoms of the phen and the oxygen atoms O(1) and O(3) of the mal^{2-} ligand. The apical position is occupied by a chloride atom at 2.502(2) Å. The Cu–N and Cu–O bond lengths are *ca.* 2.02 and 1.95 Å, respectively. The coordination

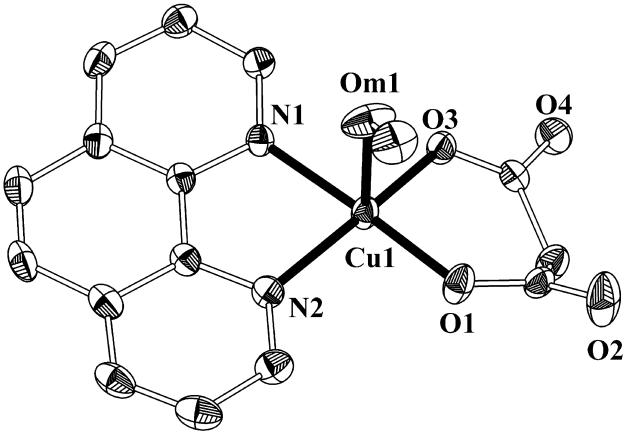

Fig. 1. Partially labeled ORTEP plot of **2** with ellipsoids drawn at the 30% probability level (Hydrogen atoms have been omitted for clarity).

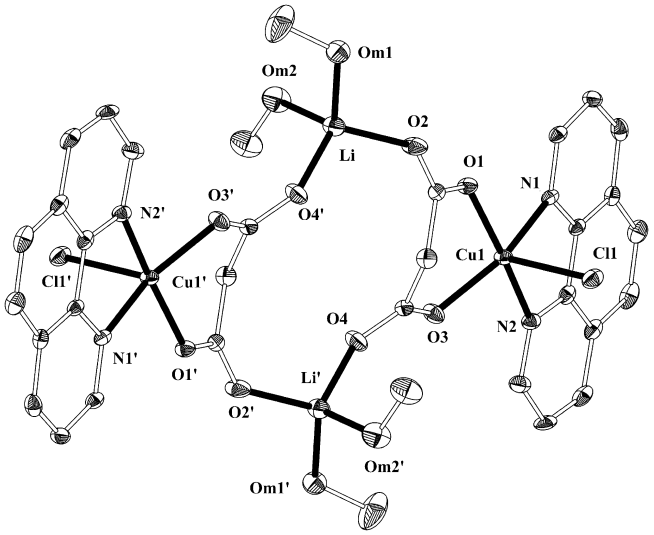

Fig. 2. Partially labeled ORTEP plot of **3** with ellipsoids drawn at the 30% probability level (Hydrogen atoms have been omitted for clarity). Primed atoms are generated by symmetry ($' = -x, -y, 1-z$).

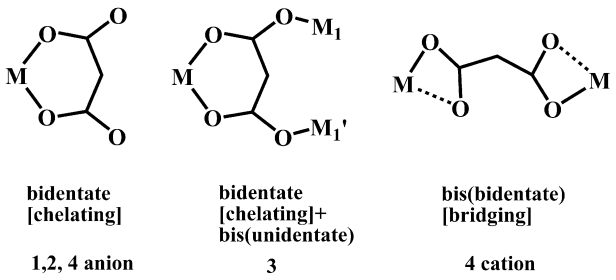

Scheme 2. The coordination modes of the malonato ligand in **1**–**4**.

geometry around the two Li^{I} ions is tetrahedral comprised by two oxygen atoms O(2) and O(4′) belonging to two centrosymmetrically related mal^{2-} ligands and two coordinated methanol molecules. The bond distances around Li^{I} range from 1.901(5) to 1.956(5) Å. The neutral heterometallic tetranuclear molecules of **3** are hydrogen bonded [Om(1)···O(4) ($-1+x$, y, z) = 2.831 Å, HOm(1)···O(4) = 2.240 Å, Om(1)–HOm(1)···O(4) = 156.7°; Om(2)···Cl(1) (x, $-1+y$, z) = 3.058 Å, HOm(2)···Cl(1) = 2.327 Å, Om(2)–HOm(2)···Cl(1) = 163.1°] and form layers that extend parallel to the *ab* plane (Fig. S2).

The molecular structure of **4** consists of the complex cation $[Cu_2(phen)_4(mal)]^{2+}$, the complex anion $[CuCl(phen)(mal)]^{-}$, one hydroxide anion, as well as methanol and water solvate molecules. An ORTEP plot of the complex cation and anion is given in Fig. 3, and selected bond distances and angles are listed in Table S3. Each Cu^{II} ion in the cation of **4** presents an O_2N_4 distorted octahedral coordination geometry comprised by the nitrogen atoms of two phen molecules and two carboxylato oxygen atoms of the mal^{2-} ligand. Each carboxylato group of the mal^{2-} ligand is asymmetrically coordinated to the Cu^{II} ions (Cu(1)–O(1) = 1.955(5), Cu(1)–O(2) = 2.884(5), Cu(2)–O(3) = 1.970(6), Cu(2)–O(4) = 2.770(6) Å), presenting the novel bis(bidentate) [bridging] coordination mode (Scheme 2). The Cu–N bond distances fall in the range 1.990(7)–2.207(10) Å. The coordination geometry around the Cu^{II} ion in the anion of **4** is square-pyramidal (τ = 0.16) comprised of the nitrogen atoms of the phen and the oxygen atoms of the bidentate chelating mal^{2-} ligand (Scheme 2) in the basal positions and a chloride atom at the apex at 2.567(6) Å. The Cu–N and Cu–O bond distances are *ca.* 2.02 and 1.92 Å, respectively. The overall coordination environment around

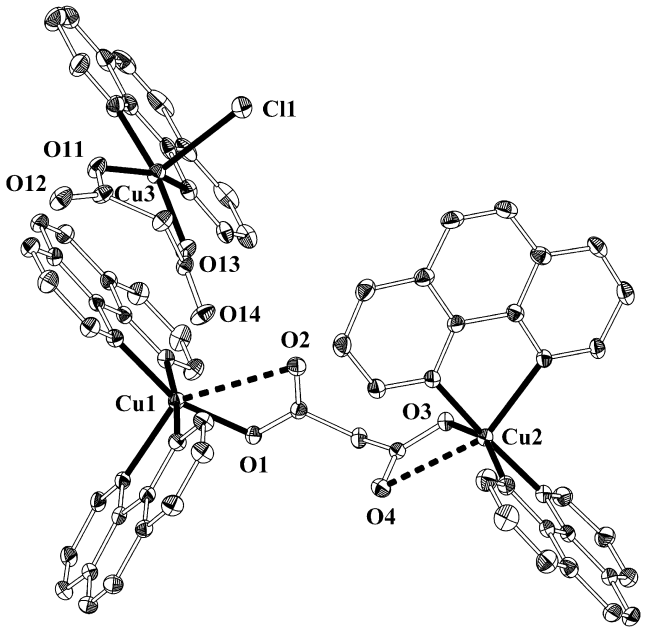

Fig. 3. Partially labeled ORTEP plot of the cation and anion of **4** with ellipsoids drawn at the 30% probability level (hydrogen atoms have been omitted for clarity).

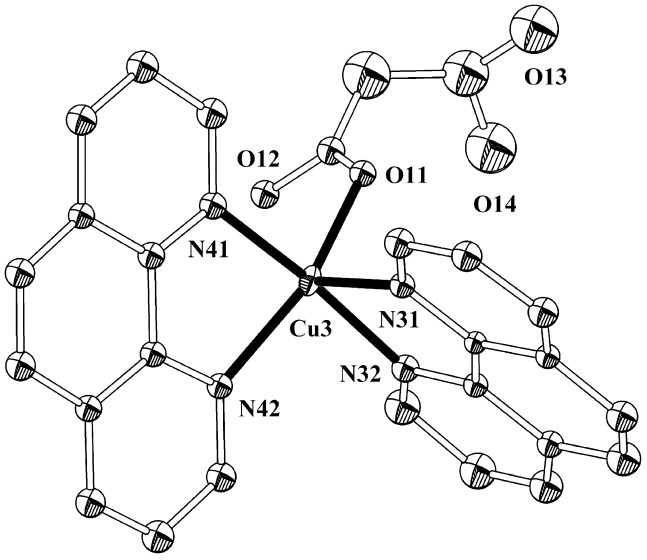

Fig. 4. Partially labelled ORTEP plot of the new cationic species $[Cu(phen)_2(Hmal)]^+$ found in the structure of **6** with ellipsoids drawn at the 30% probability level (hydrogen atoms have been omitted for clarity).

Cu(3) is quite similar to that found around Cu(1) and its centrosymmetric equivalent in the structure of **3**.

The structural characterization of **5** revealed the presence of $[CuCl(phen)_2]Cl$, whose structure has been previously reported [34]. The coordination geometry around the Cu^{II} ion is distorted trigonal bipyramidal ($\tau = 0.58$) comprised of two phen ligands and a chloride atom.

The structural characterization of **6** revealed the presence of three mononuclear species, the cation $[CuCl(phen)_2]^+$ also found in **5**, the anion $[CuCl(phen)(mal)]^-$ also found in **4**, and the new cationic species $[Cu(phen)_2(Hmal)]^+$ whose structure is shown in Fig. 4. Selected bond distances and angles are given as Supplementary data (Table S4). The coordination geometry around the Cu^{II} ion in $[Cu(phen)_2(Hmal)]^+$ resembles that of Cu(1) and Cu(2) in the cation of **4**. Two phen molecules and an oxygen atom from the $Hmal^-$ ligand are coordinated to the metal in a square-pyramidal geometry ($\tau = 0.17$). Three nitrogen atoms and the unidentate $Hmal^-$ ligand occupy the basal positions of the square pyramid, whereas the forth nitrogen atom is directed at the apex. The presence of the monoanion $Hmal^-$ has not been encountered in the other structurally characterized species isolated from this reaction system. The Cu–N bond lengths fall in the range 1.988(11)–2.177(11) Å, the Cu(3)–O(11) bond distance is 2.035(2) Å whereas O(12) is 2.980 Å away of the metal ion.

3.3. Mass spectrometry

For the elucidation of the solution chemistry of the system, the complexes that could be obtained in pure form were studied. Mass spectra of complexes **2**–**4** and **6** recorded in 50% aqueous methanolic solutions are given in Figs. 5–8, respectively. Characteristic peaks and their interpretation are listed in Table 3 and summarized in Scheme 3. The main characteristic of all spectra is the absence of the parent ion peak leading to the conclusion that all complexes spontaneously decompose in solution, thus the peaks observed correspond to various molecular fragments, some of which are common in all spectra. In the spectra of **2**–**4** and **6** the basic peak (with relative abundance 100%) appears at $M/z \sim 302$

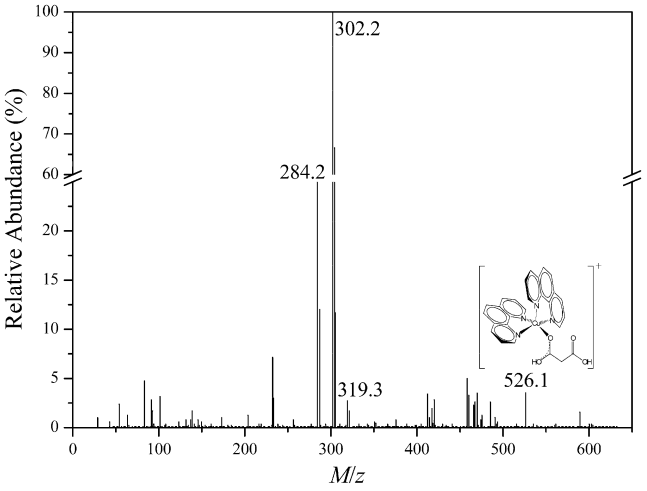

Fig. 5. Mass spectra from methanolic solutions of **2.**

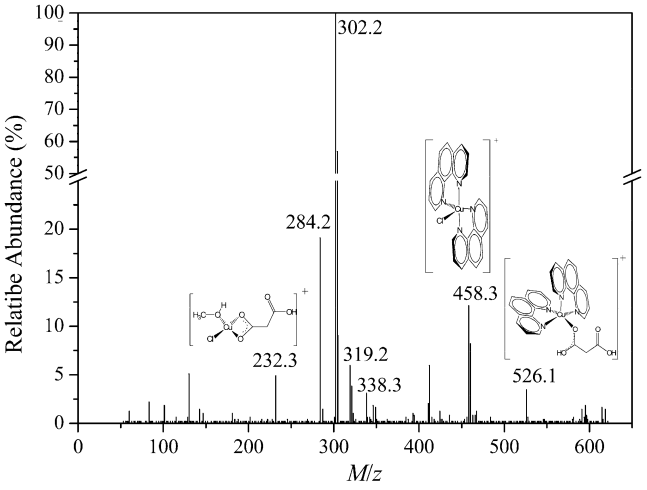

Fig. 6. Mass spectra from methanolic solutions of **3**.

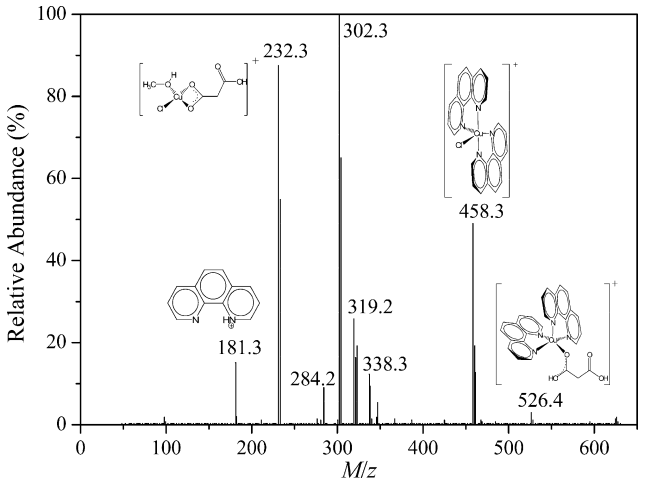

Fig. 7. Mass spectra from methanolic solutions of **4**.

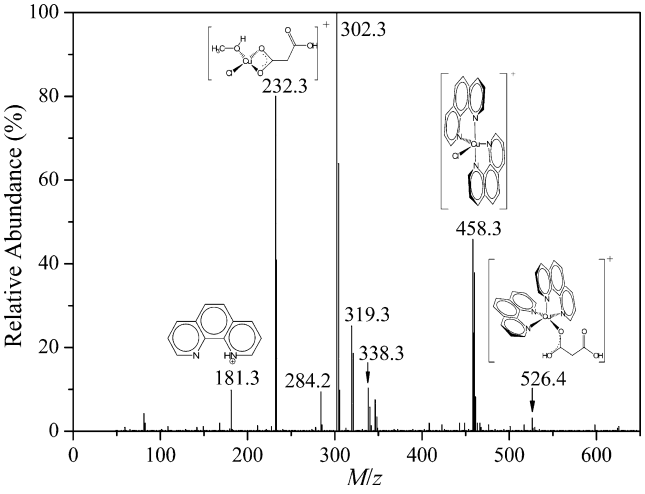

Fig. 8. Mass spectra from methanolic solutions of **6**.

Table 3
Mass spectra from 50% aqueous methanolic solutions of compounds **2**–**4** and **6**

Fragment (calc. *M*/*z*)	**2** Obs. *M*/*z*(%)	**3** Obs. *M*/*z* (%)	**4** Obs. *M*/*z* (%)	**6** Obs. *M*/*z* (%)
$[Cu(phen)_2(malH)]^+$ (526.5)	526.1 (3.5)	526.1 (3.5)	526.4 (3)	526.4 (3)
$[CuCl(phen)_2]^+$ (459)		458.3 (12)	458.3 (45)	458.3 (45)
$[CuCl(phen)(CH_3COOH)]^+$ (339)		338.3 (3)	338.3 (8)	338.3 (10)
$[Cu(OH)(phen)(CH_3COOH)]^+$ (319.5)	319.3 (3)	319.2 (5)	319.2 (25)	319.3 (25)
$[Cu(phen)(CH_3COOH)]^+$	302.2 (100)	302.2 (100)	302.3 (100)	302.3 (100)
Abstraction of OH^- from $[Cu(phen)(CH_3COO)]^+$ (284.5)	284.2 (25)	284.2 (20)	284.2 (10)	284.2 (10)
$[CuCl(MeOH)(malH)]^+$ (235)		232.3 (5)	232.3 (85)	232.3 (80)
$[phenH]^+$ (181)			181.3 (15)	181.3 (12)

and it is attributed to the molecular fragment $[Cu(phen)(CH_3COO)]^+$ (theoretical $M/z = 302.5$) generated by decarboxylation of the malonato ligand. Further abstraction of OH^- from the above fragment, also common during the decomposition of organic acids, is recorded at 284.2 in the spectra of the four complexes. In the spectra of $[Cu_2Li_2Cl_2(phen)_2(mal)_2(MeOH)_4]$ (**3**) the peak at $M/z = 458.3$ is assigned to the fragment $[CuCl(phen)_2]^+$ (theoretical $M/z = 459$). In the spectra of $[Cu_2(phen)_4(mal)][CuCl(phen)(mal)](OH)$ (**4**) the two peaks at M/z 458.3 and 232.4 are assigned to the cationic fragments $[CuCl(phen)_2]^+$ (theoretical $M/z = 459$) and $[CuCl(MeOH)(Hmal)]^+$ (theoretical $M/z = 233$). A peak at $M/z = 181.3$ with relative abundance 15% corresponds to the cation $[phenH]^+$ (theoretical $M/z = 181$). Finally, in the spectra of $[CuCl(phen)(mal)][CuCl(phen)_2][Cu(phen)_2(malH)]Cl$ (**6**), a set of peaks at 232.3 and 319.3 with relative abundance 80% and 25%, respectively, are assigned to the cationic fragment $[CuCl(MeOH)(Hmal)]^+$ (theoretical $M/z = 233$) as in the case of **4**, and to $[Cu(OH)(phen)(CH_3COO)]^+$ (theoretical $M/z = 319.5$). The peak at $M/z = 458.3$ with relative abundance 45% is attributed to the presence of the cationic fragment $[CuCl(phen)_2]^+$, one of the cations found in the crystal structure of **6**, as well as in the structure of **5**. The molecular ion of $[phenH]^+$ also appears in the spectra of **6** at $M/z = 181.3$.

Another common feature in the mass spectra of the four complexes is the presence of peaks with relative abundance less than 15% at $M/z \sim 526$ and ~ 338. In particular, the peak at $M/z \sim 526$ corresponds well to the theoretical value of 526.5 calculated for the cationic species $[Cu(phen)_2(Hmal)]^+$, one of the cations found in the crystal structure of **6**. The peak at $M/z \sim 338$, may be attributed to the cation $[CuCl(phen)(CH_3COOH)]^+$ with theoretical M/z value 339.

Careful inspection of the mass spectra leads to the following conclusions: (i) the cationic fragment $[Cu(phen)_2(Hmal)]^+$ present in the methanolic solutions of the four compounds is present in the solid state only in **6**; (ii) the cationic fragment $[CuCl(phen)_2]^+$ present in the methanolic solutions of **3**, **4** and **6** is present in the solid state in **5** and **6**; (iii) the cationic fragment $[Cu(phen)(CH_3COO)]^+$ in the methanolic solutions of the four compounds originates from the species $[CuX(phen)(mal)]^z$, which in the solid state are present in **2** ($z = 0$, X = MeOH) and in **4** and **6** ($z = -1$, X = Cl); and (iv) the cationic fragment $[CuCl(phen)(CH_3COOH)]^+$ in the methanolic solutions of **3**, **4** and **6** originates from the anionic species $[CuCl(phen)(mal)]^-$ which in the solid state is present in **4** and **6**. Thus the methanolic solutions of **2**–**4** and **6** contain fragments of the complexes that have been previously isolated from the various $CuCl_2/H_2mal/phen$ reaction systems, and the most important is that these fragments are not present in the solid state structure of the complex under examination. It is thus evident that compounds **2**–**4** and **6** decompose in solution followed by rearrangement/reorganization to species isolated in complexes **1**–**6**, confirming the dynamic character of the system. Thus mass spectrometry supports indirectly our consideration that the various $CuCl_2/H_2mal/phen$ reaction mixtures examined constitute a set of overlapping Dynamic Combinatorial Libraries whose members are complexes of the various ligands to the metal ions in solution.

3.4. Magnetic susceptibility studies

Complexes **3** and **4** were chosen for a magnetic study since their structures suggested the possibility of magnetic exchange. The $\chi_M T$ products for **3** and **4** at 300 K are 0.77 and 1.41 $cm^3\,mol^{-1}\,K$ (Fig. 9). These are close to the values expected for two and three non-interacting $S = 1/2$ spins (0.83 and 1.24 $cm^3\,mol^{-1}\,K$, respectively, $g = 2.1$). For **3**, the slightly lower value than theoretically predicted indicates antiferromagnetic interactions. This is confirmed by the drop of $\chi_M T$ upon cooling, which is more abrupt below 50 K, falling to 0.75 $cm^3\,mol^{-1}\,K$ at 5 K. For **4**, on the other hand, $\chi_M T$ increases upon cooling to a broad maximum of

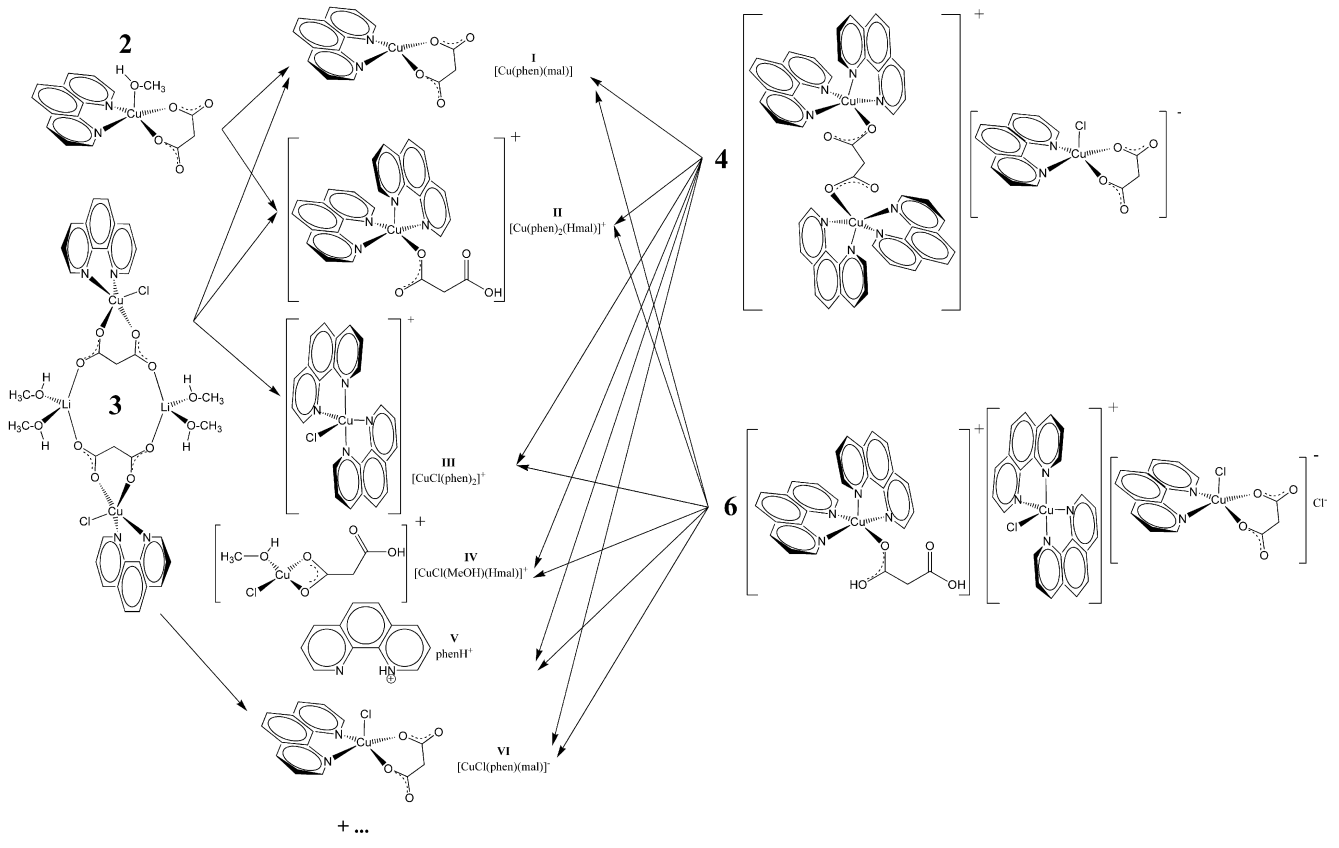

Scheme 3. Species that form upon dissolution of **2**–**4** and **6** in MeOH. Species **II**–**V** are directly observed by ESI-MS data, while the presence of **I** and **VI** is inferred by the presence of the decarboxylated fragments $[Cu(phen)(CH_3COO)]^+$ and $[CuCl(phen)(CH_3COOH)]^+$, respectively. Dissolved species, present in certain complexes (e.g. **II** in **6**) may have formed from transformation of complexes that did not initially contain them in the solid state (e.g. **II** from **2**), confirming the dynamic character of the reaction system.

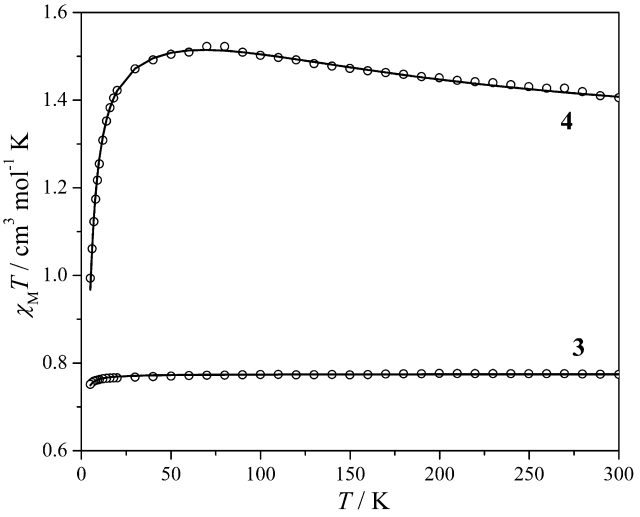

Fig. 9. χ_M vs. T and $\chi_M T$ vs. T experimental data for complexes **3** and **4**, and theoretical curves based on the Hamiltonians of Eqs. (1) and (2), respectively.

1.51 $cm^3\ mol^{-1}$ K at ~70 K, before falling abruptly to a value of 0.99 $cm^3\ mol^{-1}$ K at 5 K. This overall behaviour indicates the interplay of ferro- and antiferromagnetic interactions.

The close Cu···Cu distances between neighboring molecules (8.4–8.7 Å), which are comparable to the intramolecular intermetallic separation (9.818 Å), suggest the possible existence of both intra- and intermolecular magnetic interactions. However, in order not to overparametrize our problem, a simple dimer model was considered for the interpretation of the magnetic susceptibility data of **3**. The corresponding Hamiltonian was

$$\hat{H} = -2J\hat{\mathbf{S}}_1\hat{\mathbf{S}}_2 \quad (1)$$

Fitting of the data according to this model yielded best-fit parameters $J = -0.19\ cm^{-1}$, $g = 2.032$ with $R = 3.9 \times 10^{-6}$. This very weak coupling agrees with the structural parameters of **3**, in which Cu(1) and Cu(1′) are separated by a distance of ~9.82 Å, and magnetic exchange must be transmitted through a series of seven diamagnetic atoms.

For the interpretation of the magnetic susceptibility data of **4**, certain assumptions were made. Given its structure, a relatively strong interaction was expected between Cu(1) and Cu(2) via the malonato bridge. Initial attempts to fit the data considering only this interaction failed to reproduce the data. Thus, it was considered that Cu(3) might also be involved in magnetic exchange. Inspection of the molecular structure of **4**, led us to assume that Cu(3) should mainly interact with Cu(1) through a π–π stacking interaction. Thus, inclusion of a second exchange coupling brought about a remarkable improvement to the fits. The Hamiltonian used was

$$\hat{H} = -2(J_1\hat{\mathbf{S}}_1\hat{\mathbf{S}}_2 + J_2\hat{\mathbf{S}}_1\hat{\mathbf{S}}_3) \quad (2)$$

Fitting according to that model yielded best-fit parameters $J_1 = 80.0\ cm^{-1}$, $J_2 = -3.4\ cm^{-1}$, $g = 2.136$ with $R = 3.7 \times 10^{-5}$. J_1 corresponds to the magnetic exchange mediated through the malonato bridge, which is expected to be stronger than the one mediated through the π–π interaction and more ferromagnetic, given the propensity of malonates to promote ferromagnetic couplings in various coordination modes [35].

Another point of interest concerns the malonato-mediated exchange coupling, which is strongly ferromagnetic. Qualitatively we could rationalize this by the relatively large intermetallic separation, in combination with the fact that the malonato bridge is coordinated to the equatorial positions of the copper atoms. Due to the first situation, the direct orbital overlap of the copper atoms is expected to be negligible, thus suppressing the antiferromagnetic component of the magnetic exchange. Due to the second situation, the malonate occupies the magnetic orbitals of the copper atoms (mainly of $d_{x^2-y^2}$ character), thus strong interactions can be expected, which should be of ferromagnetic character. We should stress, however, that complex **4** is the first copper(II) complex to our knowledge to exhibit the *syn–syn* bridging mode of the malonate through two different carboxylate functions. Thus, it is not a simple task to propose a mechanism for the magnetic exchange, and theoretical studies should be pursued toward that direction. These, however, are beyond the scope of this work.

3.5. EPR spectroscopy

X-band EPR spectra from powdered samples of **3** and **4** were recorded in the 4.2–300 K temperature range. For both complexes no significant variation with temperature was observed. The 4.2 K spectra are shown in Fig. 10. Evident is the lack of hyperfine splitting features as is frequently observed in concentrated solid samples of Cu^{II} complexes where exchange interactions are present [36].

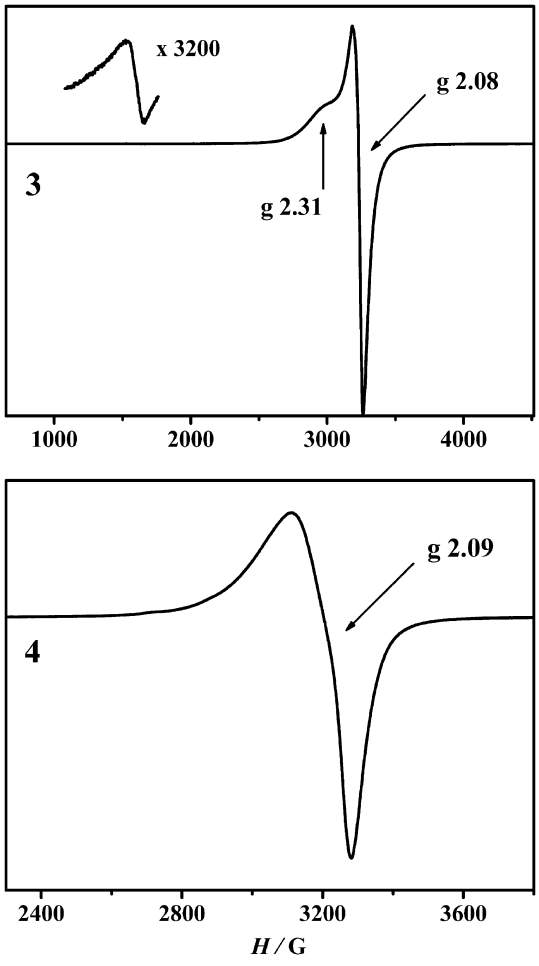

Fig. 10. X-band EPR spectra from powdered samples of **3** and **4** at 4.2 K. *EPR conditions*: **3**: microwave power, 0.13 mW; mod. ampl., 0.5 Gpp ($\Delta m_S = \pm 1$ transitions); microwave power, 2.2 mW; mod. ampl., 10 Gpp (half field transition). The half-field transition signal has been multiplied by the indicated factor; the different recording conditions have been considered. Compound **4**: microwave power 0.13 mW; mod. ampl., 1.0 Gpp. Microwave frequency (9.42 GHz).

For **3** the spectrum consists of a relatively broad absorption at $g \sim 2.31$ and a narrower derivative feature at $g \sim 2.08$. Present also is a much weaker signal at ~1600 G. From the crystal structure of **3**, the closest intramolecular Cu···Cu distance within the heterometallic tetranuclear unit is ~9.8 Å, whereas hydrogen bonding interactions lead to the formation of layers extending parallel to the *ab* plane (Fig. S2). The intermolecular Cu···Cu distances within these layers range from *ca.* 8.3 to 14.5 Å. The magnetic measurements discussed above indicate small intramolecular exchange interactions. Weak dipolar intra- or intermolecular interactions, may affect the EPR spectra. The weak feature at ~1600 G is consistent with the so-called half-field transition ($\Delta m_S = \pm 2$) arising from such dipolar interactions [37]. If we approximate the present situation with a dimeric model, the relative intensity between the weak feature at ~1600 G ($\Delta m_S = \pm 2$ transition) and the much stronger signal in the $g = 2.31$–2.07 region ($\Delta m_S = \pm 1$ transitions) may be used in order to estimate the Cu···Cu distances [37]. We find that this ratio is consistent with Cu···Cu distances of the order of 8–9 Å, in reasonable agreement with the crystallographic data.

The EPR spectrum from a powdered sample of **4** consists of a broad asymmetric signal in the 3000 G region, with a zero cross point at $g \sim 2.09$ (Fig. 10). No other signals are observed in spectra recorded in various temperatures. The magnetic susceptibility measurements for **4** were modeled with an exchange coupled trimer yielding an $S = 3/2$ ground state. The temperature behaviour of the spectra indicates that the individual spin states cannot be discriminated. The apparent anisotropy of the spectrum is lower than this anticipated for an isolated Cu^{II} ion in a square-pyramidal geometry. Such a behaviour is observed in concentrated solid state Cu^{II} complexes in the presence of misalignment of the local molecular axes of the copper ions [36]. Misalignment for the three copper ions is indicated from the crystal structure of **4** (Fig. 3).

4. Summary and conclusions

The investigation of the $CuCl_2/H_2mal$/phen reaction system (H_2mal = malonic acid) in MeOH led to the isolation of an unexpectedly large number of products. Indeed, seven complexes have been isolated, six of which have been structurally characterized, i.e. complexes $[Cu(H_2O)(phen)(mal)]$ (**1**), $[Cu(MeOH)(phen)(mal)]$ (**2**), $[Cu_2Li_2Cl_2(phen)_2(mal)_2(MeOH)_4]$ (**3**), $[Cu_2(phen)_4(mal)][CuCl(phen)(mal)](OH)$ (**4**), $[CuCl(phen)_2]Cl$ (**5**), and $[CuCl(phen)(mal)][CuCl(phen)_2][Cu(phen)_2(Hmal)]Cl$ (**6**). Complex **7** was identified as analogous to **5** based on their superimposable IR spectra. The large variety of accessible complexes initially obtained, prompted us to study this system in greater depth and in a systematic manner.

Thus, variation of the molar ratios and the crystallization methods employed, afforded compounds **1**–**7** either in pure form or as mixtures, indicating that all these species (and probably other, more soluble ones) exist in equilibrium in the reaction solution. Initial attempts to isolate those complexes by employing stoichiometric reactions, resulted in various mixtures of **1**–**7** rather than pure products. However, careful choice of stoichiometries and crystallization conditions allowed us to obtain pure products in most cases (**1**–**4**, **6**). The observation that several species are present in equilibrium in solution, in ratios depending on the starting materials stoichiometries, led us to conclude that, in effect, these reaction systems constitute a set of overlapping Dynamic Combinatorial Libraries. Indeed, due to the labile nature of the metal–ligand coordination bonds, complexes **1**–**7** should coexist in various ratios in the reaction mixtures, through a constant formation–decomposition process.

However, we wished to corroborate this conclusion through an independent experimental technique. Mass-spectrometric studies would be ideally suited to study the chemical equilibrium in this reaction system, and were therefore undertaken. Mass spectra recorded on solutions of pure **2**–**4** and **6** in 50% aqueous MeOH revealed the absence of the parent ion peaks along with the presence of fragments previously observed in the crystal structures of **1**–**6**. The most important feature observed in the mass spectra of pure **2**, **3**, **4** and **6** is the presence of fragments not present in the crystal structure of the corresponding complex. Thus, a conclusion that can be safely drawn is that each of the complexes decomposes upon dissolution to yield a dynamic mixture of species, although a full identification of the species present in solution does not seem a tractable task. The existence of such equilibria is a characteristic trait of a DCL.

Concluding, we may note that several examples of DCLs based on transition-metal complexes have been previously reported. However, what is unprecedented in this case is that the "selection" step employed to separate the DCL members, is based on their solubility and crystallization properties, and not on supramolecular recognition. Also noteworthy is the number of DCL members identified, characterized and isolated: *seven* DCL members were identified, *six* of them were structurally characterized and *five* of them were isolated in pure form. Following these synthetic and spectroscopic studies in solution, physical studies in the solid state, i.e. magnetic and EPR studies of **3** and **4**, were carried out in order to complete the investigation of the system.

Appendix A. Supplementary data

CCDC 644552, 644553, 644554, 644555, 644556 and 644557 contain the supplementary crystallographic data for **1**, **2**, **3**, **4**, **5** and **6**. These data can be obtained free of charge via http://www.ccdc.cam.ac.uk/conts/retrieving.html, or from the Cambridge Crystallographic Data Centre, 12 Union Road, Cambridge CB2 1EZ, UK; fax: (+44) 1223-336-033; or e-mail: deposit@ccdc.cam.ac.uk. Tables S1–S4 contain selected bond distances and angles for compounds **1**–**4** and **6**, respectively. Figs. S1 and S2 show the lattice structures of **2** and **3**, respectively, due to hydrogen bonding interactions. Supplementary data associated with this article can be found, in the online version, at doi:10.1016/j.poly.2008.04.044.

References

[1] See for example: C.N.R. Rao, S. Natarajan, R. Vaidhyanathan, Angew. Chem., Int. Ed. 43 (2004) 1466.

[2] (a) T.R. Felthouse, E.J. Laskowski, D.N. Hendrickson, Inorg. Chem. 16 (1977) 1077;
(b) H.K. Fun, S.S. Raj, X. Fang, L.M. Zheng, X.Q. Xin, Acta Crystallogr., Sect. C 55 (1999) 903;
(c) B. Modec, J.V. Brencic, D. Dolenc, J. Zubieta, J. Chem. Soc., Dalton Trans. (2002) 4582;
(d) A. Escuer, R. Vicente, X. Solans, M. Font-Bardia, Inorg. Chem. 33 (1994) 6007;
(e) M.R. Sundberg, R. Kivekas, J.K. Koskimies, J. Chem. Soc., Chem. Commun. (1991) 526;
(f) S. Kitagawa, T. Okubo, S. Kawata, M. Kondo, M. Katada, H. Kobayashi, Inorg. Chem. 34 (1995) 4790. and references cited therein;
(g) G.D. Munno, R. Ruiz, F. Lloret, J. Faus, R. Sessoli, M. Julve, Inorg. Chem. 34 (1995) 408;
(h) S. Decurtins, H.W. Schmalle, R. Pellaux, A. Hauser, M.E. von Arx, P. Fischer, Synth. Met. 85 (1997) 1689.

[3] (a) R.P. Farrell, T.W. Hambley, P.A. Lay, Inorg. Chem. 34 (1995) 757;
(b) L. Soto, J. Garcia, E. Escriva, J.P. Legros, J.-P. Tuchagues, F. Dahan, A. Fuertes, Inorg. Chem. 28 (1989) 3378;
(c) R. Pellaux, H.W. Schmalle, S. Decurtins, P. Fischer, F. Fauth, B. Ouladdiaf, T. Hauss, Physica B 234 (1997) 783;
(d) R. Pellaux, H.W. Schmalle, S. Decurtins, R. Huber, P. Fischer, B. Ouladdiaf, T. Hauss, S. Decurtins, Inorg. Chem. 36 (1997) 2301;
(e) Y.H. Kiang, S. Lee, Z. Xu, W. Choe, G.B. Gardner, Adv. Mater. 12 (2000) 767;
(f) G.B. Gardner, D. Venkataraman, J.S. Moore, S. Lee, Nature 374 (1995) 792.

[4] (a) Y. Rodríguez-Martín, J. Sanchiz, C. Ruiz-Pérez, F. Lloret, M. Julve, Cryst. Eng. Commun. 4 (2002) 631;
(b) C. Ruiz-Pérez, M. Hernández-Molina, J. Sanchiz, T. López, F. Lloret, M. Julve, Inorg. Chim. Acta 298 (2000) 245;
(c) D. Ghosal, T.K. Maji, T. Mallah, T.-H. Lu, G. Mostafa, N.R. Chaudhuri, Inorg. Chim. Acta 358 (2005) 1027;
(d) C. Ruiz-Pérez, J. Sanchiz, M. Hernández-Molina, F. Lloret, M. Julve, Inorg. Chim. Acta 298 (2000) 202;
(e) Y.-Q. Zheng, H.-Z. Xie, J. Coord. Chem. 57 (2004) 1537;
(f) S.F. Saadeh, K.L. Trojan, J.W. Kampf, W.E. Hatfield, V.L. Pecoraro, Inorg. Chem. 37 (1993) 3034.

[5] (a) W.-L. Kwik, K.-P. Ang, H.S.-O. Chan, V. Chebolu, S.A. Koch, J. Chem. Soc., Dalton Trans. (1986) 2519;
(b) L. Gasque, R. Moreno-Esparza, E. Mollins, J. Briansó-Penalva, L. Rutz-Ramírez, G. Medina-Dickinson, Acta Crystallogr., Sect. C 55 (1999) 158;
(c) E. Suresh, M.M. Bhadbhade, Acta Crystallogr., Sect. C 53 (1997) 193.

[6] (a) S. Sain, T.K. Maji, G. Mostafa, T.-H. Lu, N.R. Chaudhuri, Inorg. Chim. Acta 351 (2003) 12;
(b) Y. Rodríguez-Martín, J. Sanchiz, C. Ruiz-Pérez, F. Lloret, M. Julve, Inorg. Chim. Acta 326 (2001) 20.

[7] Q.-Z. Zhang, C.-Z. Lu, W.-B. Yang, J. Coord. Chem. 58 (2005) 1759.

[8] Y. Rodríguez-Martín, M. Hernández-Molina, F.S. Delgado, J. Pasán, C. Ruiz-Pérez, J. Sanchiz, F. Lloret, M. Julve, Cryst. Eng. Commun. 4 (2002) 440.

[9] C. Ruiz-Pérez, M. Hernández-Molina, P. Lorenzo-Luis, F. Lloret, J. Cano, M. Julve, Inorg. Chem. 39 (2000) 3845.

[10] Y. Rodríguez-Martín, C. Ruiz-Pérez, J. Sanchiz, F. Lloret, M. Julve, Inorg. Chim. Acta 318 (2001) 159.

[11] (a) H.-Y. Bie, J.-H. Yu, K. Zhao, J. Lu, L.-M. Duan, J.-Q. Xu, J. Mol. Struct. 741 (2005) 77;
(b) S. Sain, T.K. Maji, G. Mostafa, T.-H. Lu, N.R. Chaudhuri, New J. Chem. 27 (2003) 185;
(c) F.S. Delgado, J. Sanchiz, C. Ruiz-Pérez, F. Lloret, M. Julve, Inorg. Chem. 42 (2003) 5938;
(d) T.-F. Liu, H.L. Sun, S. Gao, S.-W. Zhang, T.C. Lau, Inorg. Chem. 42 (2003) 4792;
(e) X. Zhang, C. Lu, Q. Zhang, S. Lu, W. Yang, J. Liu, H. Zhuang, Eur. J. Inorg. Chem. (2003) 1181.

[12] For a comprehensive review of our work see: A.K. Boudalis, Y. Sanakis, C.P. Raptopoulou, V. Psycharis, A. Terzis, Polyhedron 25 (2006) 1391. and Refs. [7–10] therein.

[13] (a) C.P. Raptopoulou, A.K. Boudalis, Y. Sanakis, V. Psycharis, Polyhedron 24 (2005) 711;
(b) C.P. Raptopoulou, A.K. Boudalis, Y. Sanakis, V. Psycharis, J.M. Clemente-Juan, M. Fardis, G. Diamantopoulos, G. Papavassiliou, Inorg. Chem. 45 (2006) 2317.

[14] A.K. Boudalis, V. Nastopoulos, A. Terzis, C.P. Raptopoulou, S.P. Perlepes, Z. Naturforsch. 56b (2001) 122.

[15] A.K. Boudalis, B. Donnadieu, V. Nastopoulos, J.M. Clemente-Juan, A. Mari, Y. Sanakis, J.-P. Tuchagues, S.P. Perlepes, Angew. Chem., Int. Ed. 43 (2004) 2266.

[16] C. Gkioni, A.K. Boudalis, Y. Sanakis, C.P. Raptopoulou, Polyhedron 26 (2007) 2536.

[17] (a) J. Aussoleil, P. Cassoux, P. de Loth, J-P.J.-P. Tuchagues, Inorg. Chem. 28 (1989) 3051;
(b) J.M. Clemente-Juan, C. Mackiewicz, M. Verelst, F. Dahan, A. Bousseksou, Y. Sanakis, J.-P. Tuchagues, Inorg. Chem. 41 (2002) 1478.

[18] F. James, M. Roos, Comput. Phys. Commun. 10 (1975) 345.

[19] G.M. Sheldrick, SHELXS-97: Structure Solving Program, University of Göttingen, Germany, 1997.

[20] G.M. Sheldrick, SHELXL-97: Crystal Structure Refinement, University of Göttingen, Germany, 1997.

[21] M. Albrecht, I. Janser, J. Runsink, G. Raabe, P. Weis, R. Fröchlich, Angew. Chem., Int. Ed. 43 (2004) 6662.

[22] (a) D. Schultz, J.R. Nitschke, Proc. Natl. Acad. USA 102 (2005) 11191;
(b) S. Hiraoka, M. Fujita, J. Am. Chem. Soc. 121 (1999) 10239;
(c) D. Schultz, J.R. Nitschke, Angew. Chem., Int. Ed. 45 (2006) 2453.

[23] J.R. Nitschke, J.M. Lehn, Proc. Natl. Acad. USA 100 (2003) 11970.

[24] M. Albrecht, I. Janser, S. Burk, P. Weis, Dalton Trans. (2006) 2875.

[25] S.P. Argent, H. Adams, L.P. Harding, M.D. Ward, Dalton Trans. (2006) 542.

[26] R.W. Saalfrank, I. Bernt, E. Uller, F. Hampel, Angew. Chem., Int. Ed. Engl. 36 (1997) 2482.

[27] (a) B. Hasenknopf, J.-M. Lehn, N. Boumedience, E. Leize, A. Van Dorselaer, Angew. Chem., Int. Ed. 37 (1998) 3265;
(b) G. Baum, E.C. Constable, D. Fenske, C.E. Housecroft, T. Kulke, Chem. Commun. (1999) 195;
(c) F. Tuna, J. Hambling, A. Jackson, G. Clarkson, N.W. Alcock, M.J. Hannon, Dalton Trans. (2003) 2141.

[28] B. Hasenknopf, J.-M. Lehn, N. Boumediene, A. Dupont-Gervais, A. Van Dorsselaer, B. Kneisel, D. Fenske, J. Am. Chem. Soc. 119 (1997) 10956.

[29] S.J. Park, D.M. Shin, S. Sakamoto, K. Yamaguchi, Y.K. Chung, M.S. Lah, J.-I. Hong, Chem. Eur. J. 11 (2005) 235.

[30] (a) E. Stultz, Y.-F. Ng, S.M. Scott, J.K.M. Sanders, Chem. Commun. (2002) 524;
(b) E. Stultz, S.M. Scott, A.D. Bond, S.J. Teat, J.K.M. Sanders, Chem. Eur. J. 9 (2003) 6039.

[31] M. Scherer, D.N. Caulder, D.W. Johnson, K.N. Raymond, Angew. Chem., Int. Ed. 38 (1999) 1588.

[32] (a) M. Albrecht, O. Blau, R. Fröhlich, Chem. Eur. J. 5 (1999) 48;
(b) M. Albrecht, O. Blau, R. Fröhlich, Proc. Natl. Acad. USA 99 (2002) 4867.
[33] C.D. Pentecost, K.S. Chichak, A.J. Peters, G.W.V. Cave, S.J. Cantrill, J.F. Stoddart, Angew. Chem., Int. Ed. 46 (2007) 218.
[34] L. Lu, S. Qin, P. Yang, M. Zhu, Acta Crystallogr., Sect. E 60 (2004) m574.
[35] C. Ruiz-Pérez, Y. Rodríguez-Martín, M. Hernández-Molina, F.S. Delgado, J. Pasán, J. Sanchiz, F. Lloret, M. Julve, Polyhedron 22 (2003) 2111.
[36] B.J. Hathaway, D.E. Billing, Coord. Chem. Rev. 5 (1970) 143.
[37] A. Bencini, D. Gatteschi, EPR of Exchange Coupled Systems, Springer Verlag, Berlin, Heidelberg, 1990.

Polyhedron 27 (2008) 2327–2336

Contents lists available at ScienceDirect

Polyhedron

journal homepage: www.elsevier.com/locate/poly

Controlled assembly of zero-, one- and two-dimensional metal-organic frameworks involving in situ ligand synthesis under different reaction pH

Guang-Xiang Liu *, Rong-Yi Huang, Heng Xu, Xue-Jun Kong, Liang-Fang Huang, Kun Zhu, Xiao-Ming Ren

Anhui Key Laboratory of Functional Coordination Compounds, School of Chemistry and Chemical Engineering, Anqing Normal University, Anqing 246003, PR China

ARTICLE INFO

Article history:
Received 2 February 2008
Accepted 15 April 2008
Available online 12 June 2008

Keywords:
Coordination polymers
In situ synthesis
Carboxylate ligand
Cadmium(II)
Photoluminescence property

ABSTRACT

Five cadmium(II) metal-organic frameworks, namely $[Cd(BIPA)(daf)(H_2O)_3]\cdot 2H_2O$ (**1**), $Cd_2(BDC)_2(pdon)_2(H_2O)_2$ (**2**), Cd(BIPA)(pdon) (**3**), Cd(BIPA)(daf) (**4**) and $[Cd_2(BIPA)_2(pdon)_2]\cdot H_2O$ (**5**) (H_2BIPA = 5-bromoisophthalic acid, H_2BDC = terephthalic acid, pdon = 1,10-phenanthroline-5,6-dione, daf = 4,5-diaza-fluoren-9-one), have been constructed from cadmium(II) salts with multi-carboxylate ligands and pdon ligands under different reaction pH. The framework structures of these polymeric complexes have been determined by the X-ray single crystal diffraction technique. The differences of the five metal-organic frameworks demonstrate that the reaction pH has an important effect on the structure of these complexes. The thermal analyses of these five complexes have been measured and discussed. Additionally, four complexes show strong fluorescence in the solid state at room temperature.

© 2008 Elsevier Ltd. All rights reserved.

1. Introduction

The rational design and synthesis of metal-organic frameworks have been of increasing interest recently in materials science and chemical research since they may provide a new strategy for achieving solid functional materials with potential applications in the areas of catalysis, gas storage, magnetism and optics [1,2]. Consequently, a series of metal-organic frameworks with various structural motifs including honeycomb, brick wall, bilayer, ladder, herringbone, diamondoid and rectangular grid, have been deliberately designed and synthesized. Being an important subclass of metal-organic polymers, d^{10} metal complexes have been found to exhibit intriguing structures and photoluminescent properties [3]. A series of d^{10} metal-organic frameworks with bridging carboxyate ligands and phenanthroline-like terminal chelating ligands have been described recently [4]. So far, many efforts in this field have focused on the influence of ligand spacers of flexible bridging ligands on framework formation of their coordination polymers [5]. However, studies on the effects of the reaction pH on framework formation of complexes have rarely been reported [6].

Additionally, recent studies have revealed that crystal growth under hydrothermal conditions occasionally involves in situ ligand synthesis, which not only provides a powerful synthesis method for organic ligands that are difficult to synthesize but also represents a potential new direction for novel inorganic–organic hybrid network construction through crystal engineering [7,8]. Examples of in situ ligand syntheses under hydrothermal conditions include hydrolysis of –CN and –COOR groups [7], hydroxylation [8] and carbon–carbon bond formation by reductive coupling or oxidative coupling [9].

Taking into account the factors mentioned above, we have paid considerable interest to the reactions of various metal salts with multi-carboxylate ligands and the influence of the reaction pH on the structure of the resultant complexes, and we have found that the reaction pH is one of the key factors in the formation of the coordination architectures [10]. As an extension of our previous work, we are paying attention to 1,10-phenanthroline-5,6-dione (pdon) because of its peculiar reactivity (Scheme 1) in organic chemistry [11]. Two nucleophilic centers (nitrogen and oxygen lone pairs) are contained in the quinone-like pdon molecule, with all the non-hydrogen atoms being sp^2-hybridized. The presence of two electronegative heteroatoms not only creates basic properties in the Lewis sense but also, because of conjugation, makes it possible to alter the electron density in different parts of the molecule. As a result, a dramatic change in reactivity can occur, which is not observed in the case of the corresponding aromatic homocyclic analogue, phenanthrenequinone. Herein we report on five new coordination polymers, namely $[Cd(BIPA)(daf)(H_2O)_3]\cdot 2H_2O$ (**1**), $Cd_2(BDC)_2(pdon)_2(H_2O)_2$ (**2**), Cd(BIPA)(pdon) (**3**), Cd(BIPA)(daf) (**4**) and $[Cd_2(BIPA)_2(pdon)_2]\cdot H_2O$ (**5**), obtained by the reaction of cadmium(II) salts with multi-carboxylate ligands and pdon ligands under different reaction pH, which involve in situ synthesis of 4,5-diaza-fluoren-9-one (daf) from pdon.

* Corresponding author. Tel./fax: +86 556 5500090.
E-mail address: liugx@live.com (G.-X. Liu).

0277-5387/$ - see front matter © 2008 Elsevier Ltd. All rights reserved.
doi:10.1016/j.poly.2008.04.035

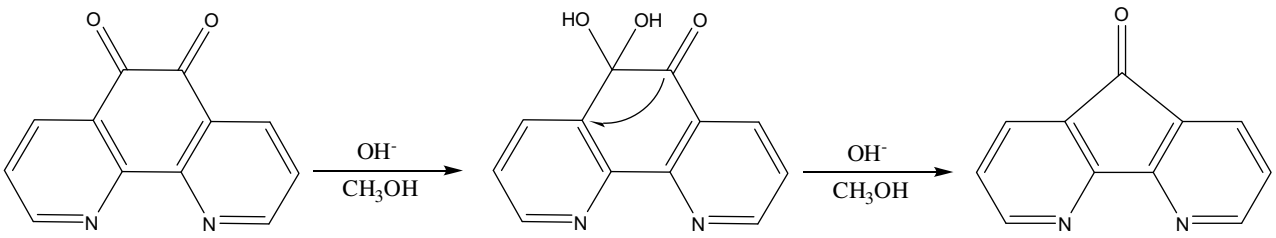

Scheme 1. Schematic representation of the possible transformation mechanism of pdon to daf.

2. Experimental

2.1. Materials and methods

All commercially available chemicals and solvents were of reagent grade and were used as received without further purification. 1,10-Phenanthroline-5,6-dione (pdon) was synthesized following the published procedure [12]. Elemental analyses for C, H and N were performed on a Perkin–Elmer 240C Elemental Analyzer at the Analysis Center of Nanjing University. FT-IR spectra were recorded in the range 400–4000 cm^{-1} on a Bruker Vector22 FT-IR spectrophotometer as KBr pellets. The luminescent spectra for the powdered solid samples were recorded at room temperature on an Aminco Bowman Series 2 spectrofluorometer with a Xenon arc lamp as the light source. In the measurements of emission and excitation spectra the pass width was 5.0 nm. All the measurements were carried out under the same experimental conditions. TG analyses were performed on a Perkin–Elmer TGA7 instrument in flowing N_2 with a heating rate of 20 °C min^{-1}.

2.2. Synthesis of the complexes

2.2.1. Synthesis of $[Cd(BIPA)(daf)(H_2O)_3] \cdot 2H_2O$ (**1**)

A mixture containing $Cd(NO_3)_2 \cdot 4H_2O$ (30.8 mg, 0.1 mmol), pdon (21.0 mg, 0.1 mmol), H_2BIPA (16.6 mg, 0.1 mmol), NaOH (16.0 mg, 0.4 mmol), 5 ml H_2O and 5 ml CH_3OH (the pH value was 9) was heated at 160 °C for 3 days in a 25 ml Teflon lined stainless steel vessel under autogenous pressure. After the reaction mixture was slowly cooled down to room temperature, yellow platelet crystals were produced in a yield of 54%. *Anal.* Calc. for $C_{19}H_{19}N_2BrO_{10}Cd$: C, 36.36; H, 3.05; N, 4.46. Found: C, 36.33; H, 3.04; N, 4.44%. IR (KBr pellet, cm^{-1}): 3397 (br), 3057 (w), 1607 (s), 1582 (s), 1434 (m), 1376 (s), 1307 (m), 1183 (m), 1034 (w), 939 (w), 834 (m), 772 (m), 688 (m), 565 (m), 437 (m).

2.2.2. Synthesis of $Cd_2(BDC)_2(pdon)_2(H_2O)_2$ (**2**)

A mixture containing $Cd(NO_3)_2 \cdot 4H_2O$ (30.8 mg, 0.1 mmol), pdon (21.0 mg, 0.1 mmol), H_2BDC (16.6 mg, 0.1 mmol), NaOH (8.0 mg, 0.2 mmol) and 10 ml H_2O (the pH value was 7) was heated at 160 °C for 3 days in a 25 ml Teflon lined stainless steel vessel under autogenous pressure. After the reaction mixture was slowly cooled down to room temperature, yellow platelet crystals were produced in a yield of 58%. *Anal.* Calc. for $C_{40}H_{24}N_4O_{14}Cd_2$: C, 47.59; H, 2.40; N, 5.55. Found: C, 47.61; H, 2.43; N, 5.57%. IR (KBr pellet, cm^{-1}): 3431 (br), 3053 (m), 2358 (w), 1663 (s), 1610 (s), 1576 (s), 1516 (m), 1496 (w), 1442 (m), 1404 (s), 1354 (s), 1311 (s), 1284 (s), 1226 (w), 1144 (w), 1125 (m), 1104 (w), 1047 (w), 1031 (w), 936 (w), 918 (w), 866 (w), 846 (s), 818 (w), 771 (s), 725 (s), 715 (m), 696 (m), 641 (w), 610 (w), 564 (w), 438 (w).

2.2.3. Synthesis of Cd(BIPA)(pdon) (**3**)

An identical procedure to **2** was followed to prepare **3** except that H_2BDC was replaced by H_2BIPA, and the pH value was adjusted to 7 with NaOH, yield 64%. *Anal.* Calc. for $C_{20}H_9BrN_2O_6Cd$:

Table 1
Crystallographic data for complexes **1**–**5**

Compound	**1**	**2**	**3**	**4**	**5**
Empirical formula	$C_{19}H_{19}N_2BrO_{10}Cd$	$C_{40}H_{24}N_4O_{14}Cd_2$	$C_{20}H_9BrN_2O_6Cd$	$C_{19}H_9BrN_2O_5Cd$	$C_{40}H_{20}Br_2N_4O_{13}Cd_2$
Formula weight	627.67	1009.43	565.60	537.59	1149.22
Crystal system	triclinic	monoclinic	monoclinic	monoclinic	orthorhombic
Space group	*P*-1	$P2_1/c$	$P2_1/c$	$P2_1/c$	*Pbcn*
a (Å)	6.9994(17)	10.7507(8)	13.9849(19)	14.131(3)	14.0658(14)
b (Å)	10.781(3)	14.5947(11)	7.8845(11)	8.0869(15)	9.5474(10)
c (Å)	15.018(4)	24.4109(18)	16.731(2)	16.515(3)	28.168(3)
α (°)	93.050(3)	90	90	90	90
β (°)	94.117(3)	98.4480(10)	100.079(2)	114.070(2)	90
γ (°)	101.272(3)	90	90	90	90
V (Å^3)	1105.9(5)	3788.6(5)	1816.4(4)	1723.2(5)	3782.7(7)
Z	2	4	4	4	4
T (K)	293(2)	293(2)	293(2)	293(2)	293(2)
D_{calcl} (g cm^{-3})	1.885	1.770	2.068	2.072	2.018
μ (mm^{-1})	2.853	1.200	3.446	3.623	3.313
F(000)	620	2000	1096	1040	2232
$2\theta_{max}$ (°)	25.05	25.00	25.05	25.05	25.04
Data collected	5238	18651	8630	8164	17591
Independent data	3760	6657	3208	3031	3306
R_{int}	0.0356	0.0828	0.0197	0.0255	0.1156
Data/restraints/parameters	3760/2/306	6657/4/541	3208/0/271	3031/0/253	3306/0/280
Goodness-of-fit	1.014	0.934	1.003	1.003	1.002
R_1 [$I > 2\sigma(I)$][a]	0.0585	0.0541	0.0238	0.0245	0.0337
wR_2 [$I > 2\sigma(I)$][b]	0.1569	0.1215	0.0651	0.0656	0.0659

[a] $R_1 = \sum||F_o| - |F_c||/\sum|F_o|$.
[b] $wR_2 = |\sum w(|F_o|^2 - |F_c|^2)|/\sum|w(F_o)^2|^{1/2}$, $w = 1/[\sigma^2(F_o^2) + (aP)^2 + bP]$. $P = (F_o^2 + 2F_c^2)/3$.

C, 42.47; H, 1.60; N, 4.95. Found: C, 42.51; H, 1.63; N, 4.98%. IR (KBr pellet, cm^{-1}): 3422 (br), 1609 (vs), 1566 (s), 1489 (w), 1478 (w), 1438 (m), 1397 (m), 1375 (s), 1282 (w), 1151 (w), 1125 (w), 932 (w), 771 (s), 738 (m), 696 (m), 524 (m), 435 (m).

2.2.4. Synthesis of Cd(BIPA)(daf) (4)

The preparation of **4** was similar to that described for **1** except that the pH of the solution of H_2BIPA was adjusted to 8 rather than 9, yield: 51%. *Anal.* Calc. for $C_{19}H_9BrN_2O_5Cd$: C, 42.45; H, 1.69; N, 5.21. Found: C, 42.48; H, 1.67; N, 5.19%. IR (KBr pellet, cm^{-1}): 3436 (br), 3051 (m), 2361 (w), 1657 (s), 1608 (s), 1576 (s), 1519 (m), 1485 (w), 1444 (m), 1403 (s), 1371 (s), 1321 (s), 1286 (s), 1233 (w), 1121 (w), 1109 (w), 1045 (w), 1033 (w), 935 (w), 921 (w), 867 (w), 839 (s), 821 (w), 773 (s), 722 (s), 691 (m), 646 (w), 608 (w), 562 (w).

2.2.5. Synthesis of $[Cd_2(BIPA)_2(pdon)_2]\cdot H_2O$ (5)

A mixture containing $Cd(NO_3)_2\cdot 4H_2O$ (30.8 mg, 0.1 mmol), pdon (21.0 mg, 0.1 mmol), H_2BIPA (24.5 mg, 0.2 mmol), NaOH (6.0 mg, 0.15 mmol) and 10 ml H_2O (the pH value was 6) was heated at 180 °C for 3 days in a 25 ml Teflon lined stainless steel vessel under autogenous pressure. After the reaction mixture was slowly cooled down to room temperature, yellow pillar crystals were produced in a yield of 71%. *Anal.* Calc. for $C_{40}H_{20}Br_2N_4O_{13}Cd_2$: C, 41.80; H, 1.75; N, 4.86. Found: C, 41.82; H, 1.77; N, 4.83%. IR (KBr pellet, cm^{-1}): 3455 (br), 3056 (m), 2357 (w), 1667 (s), 1608 (s), 1574 (s), 1513 (m), 1495 (w), 1439 (m), 1405 (s), 1356 (s), 1314 (s), 1286 (s), 1227 (w), 1147 (w), 1123 (m), 1107 (w), 1043 (w), 1032 (w), 935 (w), 919 (w), 864 (w), 843 (s), 821 (w), 768 (s), 723 (s), 719 (m), 694 (m), 637 (w), 607 (w), 562 (w), 441 (w).

Table 2
Selected bond lengths (Å) and angles (°) for complex **1**

Cd(1)–O(2W)	2.294(4)	Cd(1)–O(1)	2.467(4)
Cd(1)–O(1W)	2.345(4)	Cd(1)–N(1)	2.467(4)
Cd(1)–O(2)	2.350(4)	Cd(1)–N(2)	2.515(5)
Cd(1)–O(3W)	2.361(4)		
O(2W)–Cd(1)–O(1W)	175(1)	O(1W)–Cd(1)–N(1)	95(1)
O(2W)–Cd(1)–O(2)	93(1)	O(2)–Cd(1)–N(1)	155(1)
O(1W)–Cd(1)–O(2)	89(1)	O(3W)–Cd(1)–N(1)	74(1)
O(2W)–Cd(1)–O(3W)	98(1)	O(1)–Cd(1)–N(1)	149(1)
O(1W)–Cd(1)–O(3W)	85(1)	O(2W)–Cd(1)–N(2)	93(1)
O(2)–Cd(1)–O(3W)	81(1)	O(1W)–Cd(1)–N(2)	82(1)
O(2W)–Cd(1)–O(1)	89(1)	O(2)–Cd(1)–N(2)	132(1)
O(1W)–Cd(1)–O(1)	90(1)	O(3W)–Cd(1)–N(2)	142(1)
O(2)–Cd(1)–O(1)	54(1)	O(1)–Cd(1)–N(2)	79(1)
O(3W)–Cd(1)–O(1)	135(1)	N(1)–Cd(1)–N(2)	72(1)
O(2W)–Cd(1)–N(1)	82(1)		

Table 3
Selected bond lengths (Å) and angles (°) for complex **2**

Cd(1)–O(1)	2.163(6)	Cd(2)–O(2W)	2.243(6)
Cd(1)–O(1W)	2.221(6)	Cd(2)–O(8)#1	2.337(6)
Cd(1)–N(1)	2.328(7)	Cd(2)–N(3)	2.345(7)
Cd(1)–O(6)	2.327(6)	Cd(2)–N(4)	2.355(8)
Cd(1)–N(2)	2.397(6)	Cd(2)–O(7)#1	2.398(5)
Cd(1)–O(5)	2.398(5)	Cd(2)–C(40)#1	2.734(8)
Cd(2)–O(4)	2.204(5)		
O(1)–Cd(1)–O(1W)	91.2(2)	O(4)–Cd(2)–N(3)	155.1(3)
O(1)–Cd(1)–N(1)	87.6(2)	O(2W)–Cd(2)–N(3)	89.9(2)
O(1W)–Cd(1)–N(1)	114.8(2)	O(8)#1–Cd(2)–N(3)	95.8(2)
O(1)–Cd(1)–O(6)	96.3(2)	O(4)–Cd(2)–N(4)	90.8(2)
O(1W)–Cd(1)–O(6)	149.9(2)	O(2W)–Cd(2)–N(4)	124.0(2)
N(1)–Cd(1)–O(6)	94.7(2)	O(8)#1–Cd(2)–N(4)	90.1(2)
O(1)–Cd(1)–N(2)	158.1(2)	N(3)–Cd(2)–N(4)	69.7(3)
O(1W)–Cd(1)–N(2)	94.8(2)	O(4)–Cd(2)–O(7)#1	115.9(2)
N(1)–Cd(1)–N(2)	70.7(2)	O(2W)–Cd(2)–O(7)#1	91.3(2)
O(6)–Cd(1)–N(2)	89.1(2)	O(8)#1–Cd(2)–O(7)#1	54.5(2)
O(1)–Cd(1)–O(5)	110.1(2)	N(3)–Cd(2)–O(7)#1	89.0(2)
O(1W)–Cd(1)–O(5)	94.9(2)	N(4)–Cd(2)–O(7)#1	137.2(2)
N(1)–Cd(1)–O(5)	145.4(2)	O(4)–Cd(2)–C(40)#1	111.0(2)
O(6)–Cd(1)–O(5)	55(1)	O(2W)–Cd(2)–C(40)#1	118.8(2)
N(2)–Cd(1)–O(5)	90.4(2)	O(8)#1–Cd(2)–C(40)#1	26.9(2)
O(4)–Cd(2)–O(2W)	88.4(2)	N(3)–Cd(2)–C(40)#1	91.4(2)
O(4)–Cd(2)–O(8)#1	99.7(2)	N(4)–Cd(2)–C(40)#1	113.5(2)
O(2W)–Cd(2)–O(8)#1	145.0(2)		

Symmetry transformations used to generate equivalent atoms: #1 $x+1, y-1, z$; #2 $x-1, y+1, z$.

2.3. X-ray crystallography

The crystallographic data collections for complexes**1**–**5** were carried out on a Bruker Smart Apex II CCD with graphite-monochromated Mo Kα radiation ($\lambda = 0.71073$ Å) at 293(2) K using the ω-scan technique. The data were integrated using the SAINT program, which also corrected the intensities for Lorentz and polarization effects [13]. An empirical absorption correction was applied using the SADABS program [14]. The structures were solved by direct methods using the program SHELXS-97 and all non-hydrogen atoms were refined anisotropically on F^2 by the full-matrix least-squares technique using the SHELXL-97 crystallographic software package [15,16]. The hydrogen atoms of water molecules were located from difference Fourier maps and the other hydrogen atoms were generated geometrically. All calculations were performed on a personal computer with the SHELXL-97 crystallographic software package. The details of the crystal parameters, data collection and refinement for four complexes are summarized in Table 1. Selected bond lengths and angles with their estimated standard deviations for **1**, **2**, **4** and **5** are shown in Tables 2–5, respectively.

3. Results and discussion

3.1. Crystal structures of complexes 1–5

3.1.1. $[Cd(BIPA)(daf)(H_2O)_3]\cdot 2H_2O$ (1)

X-ray single-crystal structural analysis revealed that complex **1** crystallizes in the triclinic space group $P\bar{1}$ and that the pdon ligand

Table 4
Selected bond lengths (Å) and angles (°) for complex **4**

Cd(1)–O(1)	2.222(2)	Cd(1)–N(2)	2.378(3)
Cd(1)–O(3)#1	2.228(2)	Cd(1)–N(1)	2.477(3)
Cd(1)–O(2)#2	2.298(2)		
O(1)–Cd(1)–O(3)#1	89.71(9)	O(2)#2–Cd(1)–N(2)	107.41(8)
O(1)–Cd(1)–O(2)#2	101.12(8)	O(1)–Cd(1)–N(1)	108.39(8)
O(3)#1–Cd(1)–O(2)#2	84.55(8)	O(3)#1–Cd(1)–N(1)	161.06(9)
O(1)–Cd(1)–N(2)	151.48(9)	O(2)#2–Cd(1)–N(1)	86.46(8)
O(3)#1–Cd(1)–N(2)	92.88(9)	N(2)–Cd(1)–N(1)	73.99(9)

Symmetry transformations used to generate equivalent atoms: #1 $-x+1, y-1/2, -z+3/2$; #2 $-x+1, -y+1, -z+1$.

Table 5
Selected bond lengths (Å) and angles (°) for complex **5**

Cd(1)–O(4)#1	2.185(3)	Cd(1)–N(1)	2.322(3)
Cd(1)–O(3)#2	2.254(2)	Cd(1)–N(2)	2.352(2)
Cd(1)–O(2)	2.257(2)	Cd(1)–O(1)	2.561(2)
O(4)#1–Cd(1)–O(3)#2	96.7(1)	O(2)–Cd(1)–N(2)	176.30(9)
O(4)#1–Cd(1)–O(2)	83.94(9)	N(1)–Cd(1)–N(2)	70.64(9)
O(3)#2–Cd(1)–O(2)	92.90(9)	O(4)#1–Cd(1)–O(1)	137.21(9)
O(4)#1–Cd(1)–N(1)	114.3 (1)	O(3)#2–Cd(1)–O(1)	88.90(9)
O(3)#2–Cd(1)–N(1)	142.81(9)	O(2)–Cd(1)–O(1)	53.36(8)
O(2)–Cd(1)–N(1)	109.69(9)	N(1)–Cd(1)–O(1)	82.16(8)
O(4)#1–Cd(1)–N(2)	92.6(1)	N(2)–Cd(1)–O(1)	130.05(9)
O(3)#2–Cd(1)–N(2)	88.70(9)		

Symmetry transformations used to generate equivalent atoms: #1 $x-1/2, y-1/2, -z+1/2$; #2 $-x+2, y, -z+1/2$.

was transformed in situ into daf during the hydrothermal process. The asymmetric unit in **1** consists of one Cd(II) atom, one BIPA ligand, three coordinated water molecules and two lattice water molecules. Each Cd(II) atom is seven-coordinated with a distorted pentagonal bipyramidal geometry, being coordinated by two nitrogen atoms of one daf in a chelate mode, two oxygen atoms of one carboxylate group and three aqua ligands. Two nitrogen atoms (N1, N2) and three oxygen atoms (O1, O2, O3W) lie in the equatorial plane, while the other two other aqua ligands occupy the apical positions, as shown in Fig. 1a. The coordination bond lengths and angles around the Cd(II) centre are in the range 2.294(4)–2.515(5) Å and 54.08(14)–175.65(13)°, respectively, as listed in Table 2.

The coordination modes of BIPA and BDC in this work are summarized in Scheme 2. As can be seen in Scheme 2a, one carboxylate group adopts a bidentate chelating mode and the other carboxylate group remains depronated and does not take part in the coordination. As a result complex **1** is a zero-dimensional complex and is further linked into a 1D chain structure through π···π interactions (Fig. 2b).

In the packing structure of **1**, as shown in Fig. 1c, the 1D chains are firstly linked into a 2D layer by O–H···O hydrogen bonds between the oxygen atoms of the coordinated water molecules (O2W and O3W) and the carboxylate group from adjacent chains, with O···O distances ranging from 2.744(6) to 2.874(6) Å (Table S1). Then the 2D layers are further connected through O–H···O hydrogen bonds between the oxygen atoms of the coordinated water molecules (O1W and O2W) and the oxygen atoms of the lattice water molecules (O4W and O5W) with O···O distances of 2.744(6) and 2.756(3) Å (Fig. 1c, Table S1).

Although pdon was used as the original organic reagent in the preparation of **1**, the daf ligand was unexpectedly found in the final

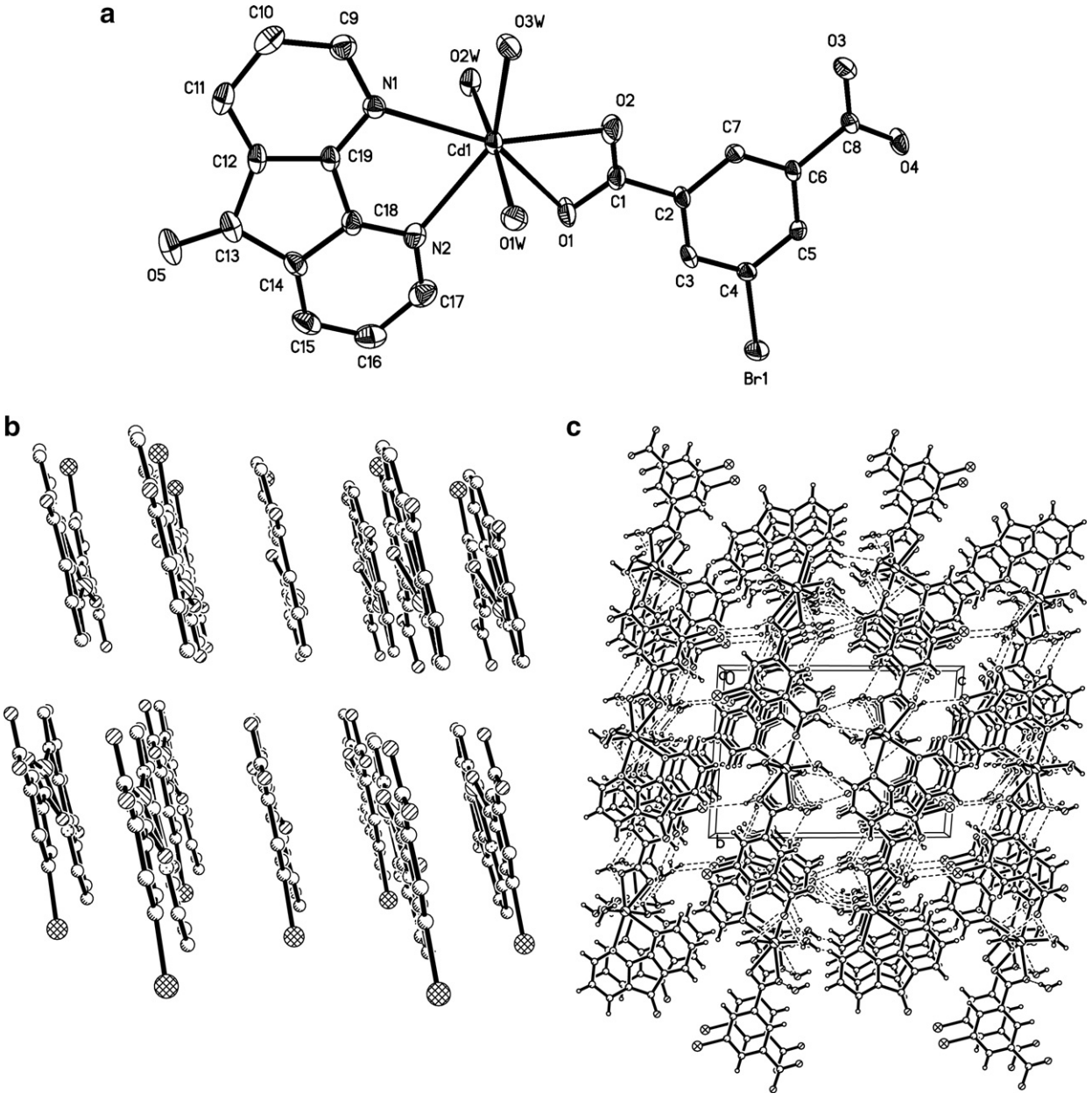

Fig. 1. (a) Coordination environment of the Cd(II) atom in complex **1** with the ellipsoids drawn at the 30% probability level, hydrogen atoms and water molecules are omitted for clarity. (b) Side view of **1** showing the 1D chain structure through π···π interactions (the coordinated water molecules and lattice water molecules are omitted for clarity). (c) Projection of the structure of **1** along *a*-axis (dotted lines represent hydrogen-bonding).

products, which indicates an in situ transformation of pdon into daf during the course of the hydrothermal treatment. As shown in the literature [8] on ligand reactions under hydrothermal conditions in the presence of metal ions, the ligation of the metal ion will cause some decrease of electron density on the aromatic ring of the organic ligand, and hence promote nucleophilic attack by water molecules or hydroxy groups. In this case, it seems most probable that the hydroxy groups act effectively as nucleophiles, attacking the carbonyl carbon atoms of pdon. As a result, the hydration of the carbonyl groups of pdon furnishes an intermediate diol or even a double diol. When the sp^2 carbonyl carbon atoms become sp^3-hybridized, the carbon–carbon bond is then cleaved, probably because of the crowding, resulting in the formation of daf. The formation mechanism of daf in **1** shows some similarity to that of dimethyl 2,2′-bipyridine-3,3′-dicarboxylate in a previously reported pure organic reaction [11b]. Although the exact mechanism of ligand transformation has not yet been proved, slow hydrolysis of the carbonyl groups ensures that an excess of NaOH remains in solution, thereby promoting the formation of less soluble polymeric networks. Equally important, the in situ slow daf formation also ensures the growth of large single crystals that are suitable for X-ray structure determination.

3.1.2. $Cd_2(BDC)_2(pdon)_2(H_2O)_2$ (**2**)

Single-crystal X-ray diffraction analysis revealed that complex **2** is a 1D zigzag coordination polymer. The asymmetric unit of **2** contains two cadmium atoms, two BDC ligands, two pdon ligands and two coordinated water molecules. As illustrated in Fig. 2a, the two Cd atoms are both six-coordinated by three oxygen atoms from two different BDC ligands, two nitrogen atoms from one pdon molecule and one oxygen atom from a coordination water molecule to give a distorted octahedral geometry. The Cd–O bond lengths fall in the range 2.163(6)–2.398(5) Å and the Cd–N bond lengths fall in the range 2.328(7)–2.397(6) Å (Table 3), which are in good agreement with those found in other Cd-containing coordination frameworks [17]. The BDC^{2-} ligands acts as a bidentate bridging ligand, but the coordination modes of the carboxyl groups are different, one adopt a bis(bidentate) chelating mode, while the other adopts a bis(monodentate) mode (Scheme 2d and e). Each BDC ligand bridges two cadmium atoms to form a 1D zigzag infinite chain (Fig. 2b) with Cd···Cd distances of 11.551 and 11.191 Å. The 1D zigzag chains form a 2D undulating network due to hydrogen-bonding interactions between the coordinated water molecule and the carboxylate group (Table S1). Adjacent 2D networks are ultimately extended into a 3D supramolecular structure through π–π stacking interactions with a centroid-to-centroid distance of 3.775(3) Å between pdon ligands (Fig. 2c).

3.1.3. Cd(BIPA)(pdon) (**3**) and Cd(BIPA)(daf) (**4**)

The results of X-ray crystallographic analysis revealed that complexes **3** and **4** crystallize in the same monoclinic $P2_1/c$ space group with similar cell parameters (Table 1), which indicate that they are isomorphous and isostructural. Thus, as a typical example, only the structure of **4** is described here in detail. The asymmetric unit of **4** consists of one Cd(II) atom, one BIPA ligand and one daf ligand. The Cd(II) atom is in a square-pyramidal coordinated geometry with three oxygen atoms and two nitrogen atoms. Two oxygen atoms (Cd1–O1 = 2.222(2) Å, Cd1–O2 = 2.298(2) Å) from two carboxylate groups of the BIPA ligands and two nitrogen atoms (Cd1–N1 = 2.477(3) Å, Cd1–N2 = 2.378(3) Å) from one def ligands are ligated to the Cd(II) ion in the quasi-plane, with another oxygen atom belonging to the third BIPA ligand (Cd1–O3 = 2.228(2) Å) being located in the axial position (Table 4), as displayed in Fig. 3a.

Different from that of complex **1**, each BIPA ligand acts as a tri-connector linking three Cd(II) atoms in complex **4** (Scheme 2c), one of carboxylate groups is connected with one Cd(II) atom through a monodentate O atom, while the other bonds with two Cd(II) atoms, consequently resulting in the formation of a 2D layer (Fig. 3b). The 2D layer is developed in an undulated bilayer pattern parallel to the *bc*-plane. By treating the Cd(II) atom as a single node and connecting the nodes according to the connectivity defined by the geometrical centers of the benzene rings of the BIPA ligands, a distorted 2D (4.8^2) network (denoted the feb net) [18] sustained by 3-connected nodes is then yielded, as illustrated in Fig. 3c. The van de Waals interactions extend the 2D layer into a 3D supramolecular net.

3.1.4. $[Cd_2(BIPA)_2(pdon)_2] \cdot H_2O$ (**5**)

In order to further investigate the pH influence on the formation and structure of the complex, the pH value of the ligand solution was carefully adjusted to 6.0, while the other experimental conditions remained the same as those used for the preparation of **3**. As a result, complex **5** was obtained with an entirely different structure. The asymmetric unit of complex **5** contains one Cd ion, one

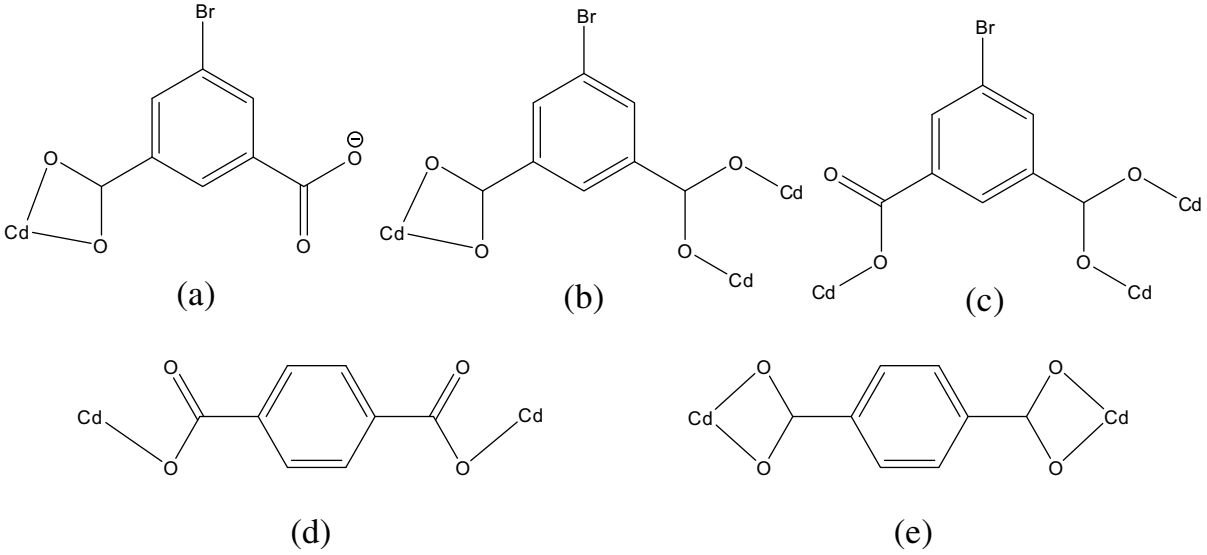

Scheme 2. Coordination modes of the BIPA and BDC ligands in complexes **1**–**5**.

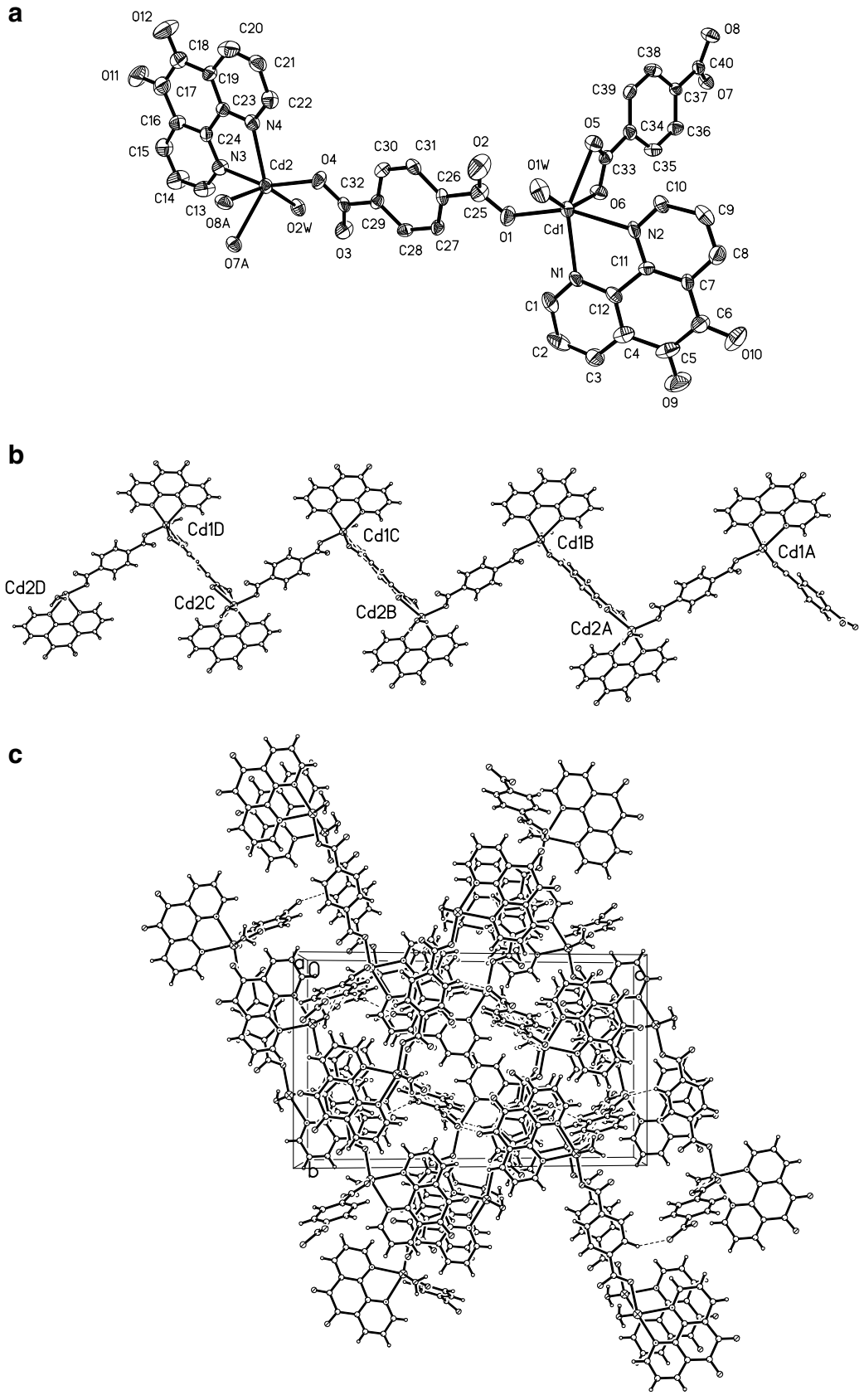

Fig. 2. (a) Coordination environment of the Cd(II) atom in complex **2** with the ellipsoids drawn at the 30% probability level, hydrogen atoms are omitted for clarity. (b) One-dimensional zigzag chain structure of complex **2**. (c) Projection of the structure of **2** along *a*-axis (dotted lines represent hydrogen-bonding).

pdon ligand, one BIPA ligand and half of the lattice water molecule. As shown in Fig. 4a, the Cd atom shows a distorted-octahedral geometry, being chelated by two N atoms from one pdon ligand. The remaining four coordination sites are occupied by four oxygen

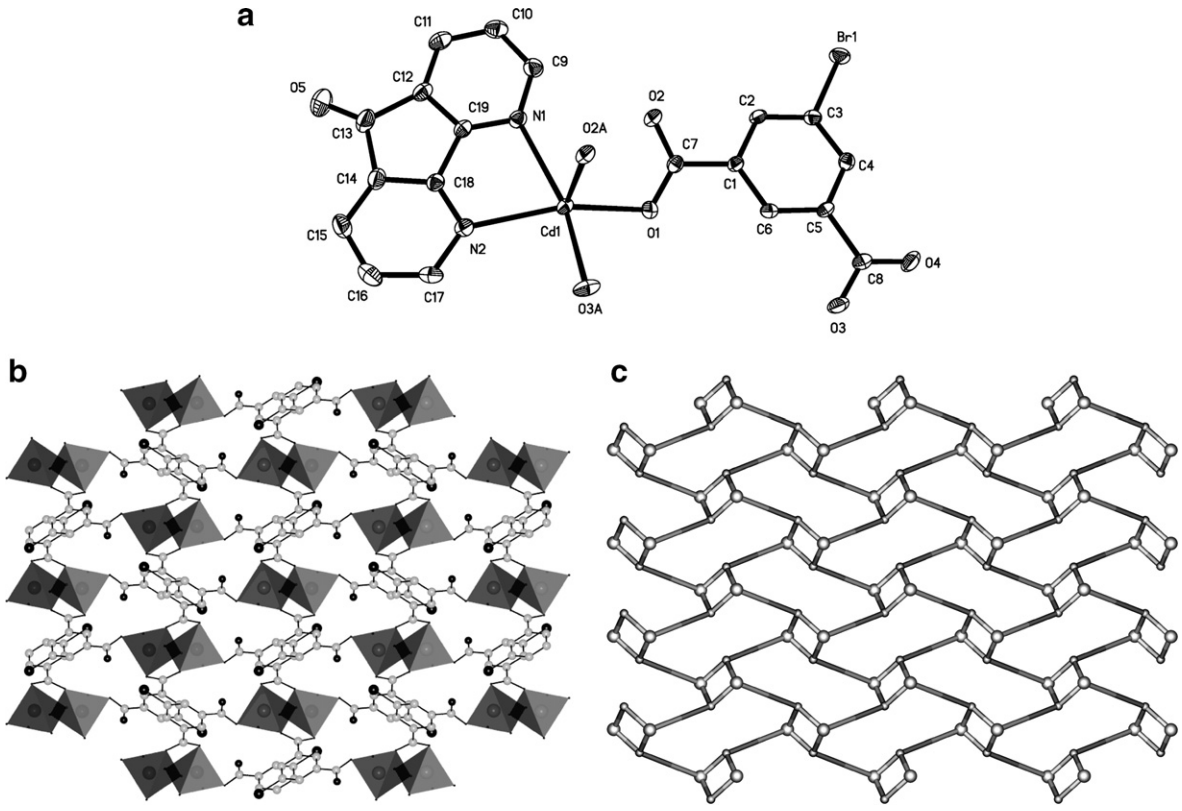

Fig. 3. (a) Coordination environment of the Cd(II) atom in complex **4** with the ellipsoids drawn at the 30% probability level, hydrogen atoms are omitted for clarity. (b) 2D layer structure of complex **4** along the *a*-axis. (c) Projection of the structure of **4** showing the (4.8^2) net based on Cd atoms and BIPA ligands.

atoms from three BIPA ligands. The Cd–O bond lengths are in the range 2.185(3)–2.561(2) Å and the Cd–N bond lengths are 2.322(3) and 2.352(2) Å (Table 5). In complex **5**, the BIPA ligands adopt a coordination mode different from those in complexes **1**, **3** and **4**: it acts as a tri-connector to link three Cd atoms through one bis-monodentate carboxylic O atom from one carboxylate group and a bidentate carboxylic O atom from the other carboxylate group, as depicted in Scheme 2b.

As shown in Fig. 4b, the bidentate carboxylic group links two Cd atoms in a *syn-anti* fashion to form a one-dimensional zigzag chain structure with a Cd···Cd separation of 5.135(3) Å, in which the distances are in the normal range compared with those reported (4.972–5.256 Å) in the literature [19]. The 1D Cd(CO_2) chains are further bridged into a two-dimensional undulating bilayer structure through the other carboxylate group. Interestingly, when viewed along the *b*-axis, the two-dimensional layer contains rectangular windows with dimensions of ca. 4.974×5.535 Å^2 that are occupied by pdon ligands and the lattice water molecules. By treating the Cd(II) atom as a single node and connecting the nodes according to the connectivity defined by the geometrical centers of the benzene rings of the BIPA ligands, a distorted 2D (4.10^2) network (denote the KIb net) [20] sustained by three-connected nodes is then yielded, as illustrated in Fig. 4c. The van de Waals interactions extend the 2D layer into a 3D supramolecular framework.

3.2. Effect of synthetic conditions on the structures of the complexes

It has been reported that synthetic conditions, such as pH value, reaction temperature, solvent, etc., are the key factors in assembling MOFs. As to the synthesis of **1**, **3** and **4**, all the reaction conditions are the same except for the difference of the reaction pH. As a result, complex **1**, obtained at a relatively high pH value, is a 0D structure with the Cd(II) center bonded by three water molecules, and it is accompanied by an in situ reaction. While in **4**, obtained at a slightly lower pH than **1**, a more complicated 2D network was generated, also accompanied by an in situ reaction. However for **3**, obtained at a pH close to 7, its framework is similar to that of **4**, but the in situ reaction did not happen in the absence of alkali. Therefore, a rough conclusion could be made that the pdon ligand can be converted into the daf ligand in the presence of alkali, which is in agreement with the previous reports [21].

In addition, it might be ascribed to the fact that the carboxylate ligands were deprotonated before the in situ reaction by a comparison of **3** and **4**. From the points discussed above, it is suggested that the increase of reaction pH may result in a different connectivity of the carboxylate ligand, controlling the in situ reaction and further fabricating a more complicated structure.

3.3. Properties

3.3.1. Luminescent properties

Inorganic–organic hybrid coordination complexes, especially with d^{10} metal centers, have been investigated for fluorescence properties owing to their potential applications as luminescent materials, such as light-emitting diodes (LEDs) [22]. Therefore, in the present study, the photoluminescence properties of **2**–**5** as well as free H_2BIPA and the H_2BDC ligand were investigated in the solid state at room temperature. As shown in Fig. 5, there are two intense emission peaks at 413 and 435 nm (λ_{ex} = 310 nm) for **2**, 421 and 442 nm (λ_{ex} = 330 nm) for **3**, 422 and 450 nm (λ_{ex} = 334 nm) for **5**. For excitation wavelengths between 280 and 480 nm, there is no obvious emission observed for free H_2BIPA and H_2BDC under the same experimental conditions, while it is reported that free pdon shows fluorescence emission in the solid state. The emission bands for phen are at 371 and 395 nm (λex = 290 nm) [23], and compared with the pdon ligand a clear

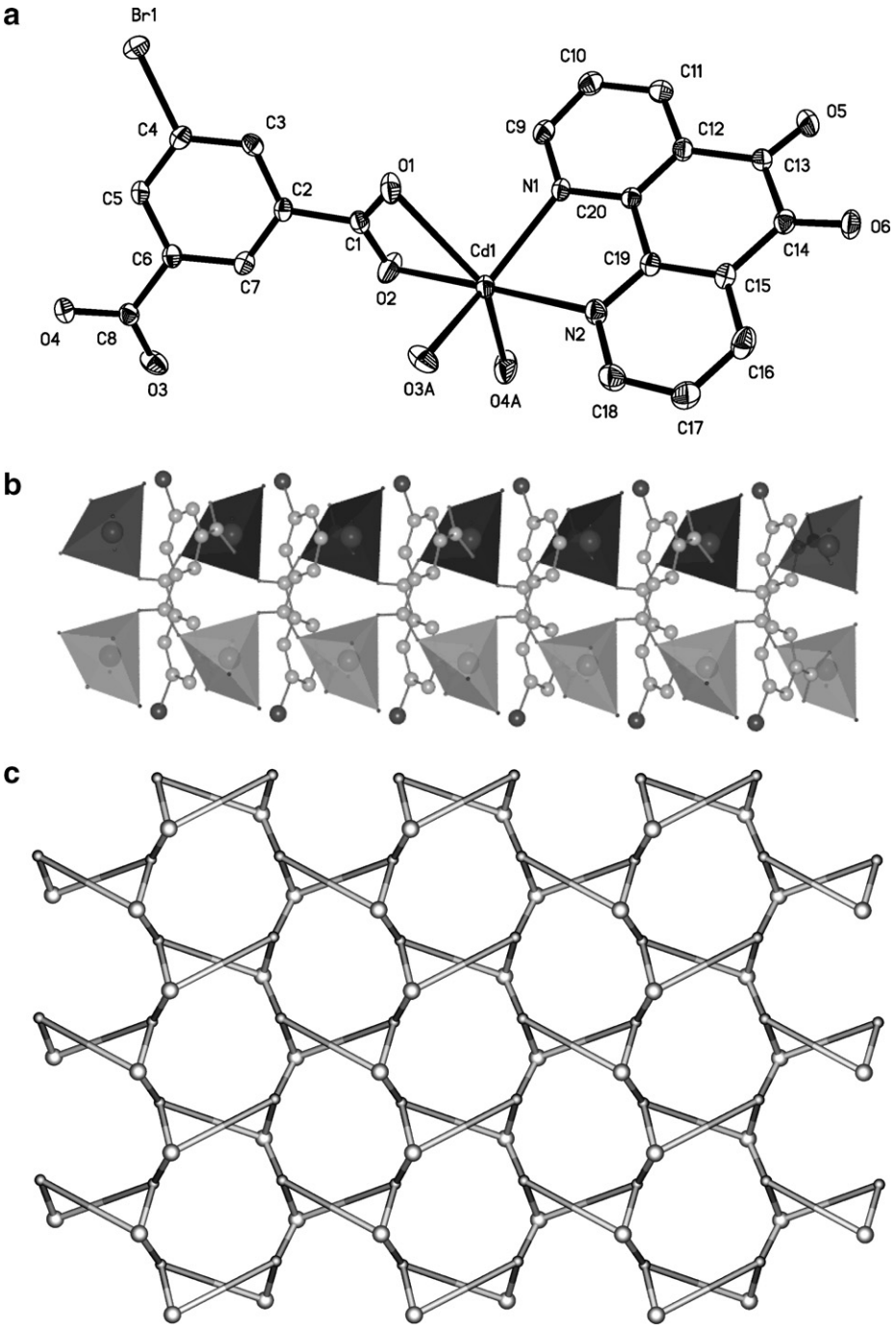

Fig. 4. (a) Coordination environment of the Cd(II) atom in complex **5** with the ellipsoids drawn at the 30% probability level, hydrogen atoms are omitted for clarity. (b) Bilayer structure of complex **5** along the *a*-axis. (c) Projection of the structure of **5** showing the (4×10^2) net based on Cd atoms and BIPA ligands.

red shift occurs in **2**, **3** and **5**, which might also be attributed to a ligand-to-metal charge transfer (LMCT) transition [24]. There is only a intense emission peak at 406 nm for **4**, which means a red shift of ca. 40 nm relative to that of the free daf (λ_{max} = 375 nm) [25]. We tentatively assign it to a LMCT transition [26].

3.3.2. Thermal properties

Thermal gravimetric analyses (TGA) were carried out to examine the thermal stabilities of **1**–**5**. The results show that complexes **1**–**5** are very stable in air at ambient temperature, which make them potential candidates for practical applications. The samples were heated up in air at 1 atm pressure with a heating rate of 20 °C min^{-1}, as shown in Fig. 6. The TGA curve shows that**1** is stable up to 96 °C. A weight loss of 5.6% occurred in the temperature range 96–128 °C, presumably due to the removal of two lattice water molecules (calcd. 5.7%). A total weight loss of 8.4% occurred in the temperature range 136–200 °C, mainly corresponding to the removal of the one coordinated water molecule per formula unit (calcd. 8.6%). Another weight loss of 65.7% occurred in the temperature range 300–465 °C, corresponding to the removal of one BIPA ligand and one pdon ligand per formula unit (calcd. 66.2%), no weight losses were observed up to 800 °C, indicating the complete deposition of the complex with the formation of CdO as the final product. The TGA curve of **2** shows that the first weight loss of 3.4% between 110 and 160 °C corresponds to the loss of the two coordinated water molecule per formula unit (calcd. 3.56%), then

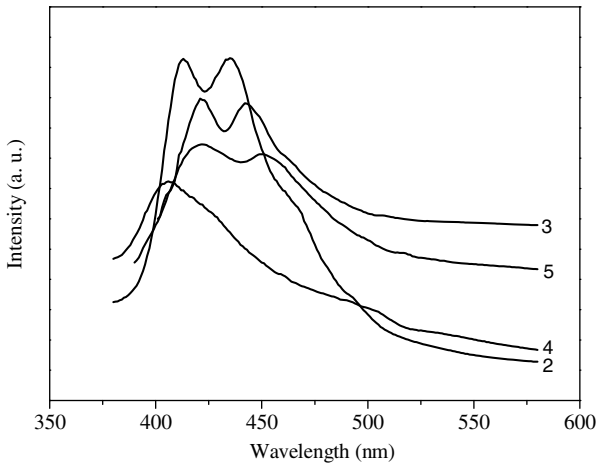

Fig. 5. The emission spectra of **2**–**5** in the solid state at room temperature.

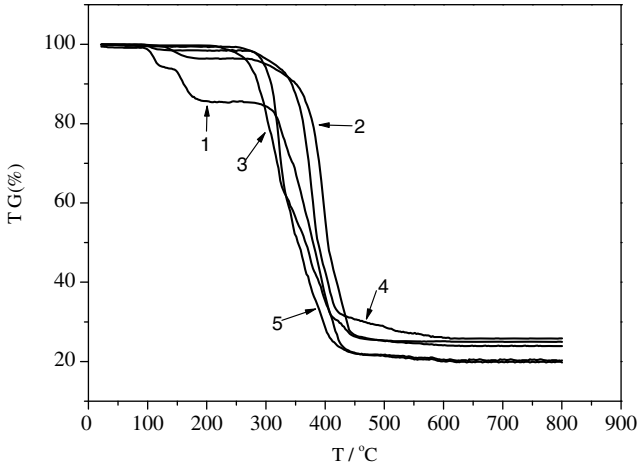

Fig. 6. TG curve of complexes **1**–**5**.

it was stable up to 290 °C. The framework collapsed in the temperature range 290–800 °C before the final formation of a metal oxide. The TGA curve shows that **3** and **4** are stable up to 300 °C. The framework collapsed in the temperature range 300–800 °C, suggesting that the organic ligands decompose slowly over a wide temperature range. The TGA curve of **5** shows that the first weight loss of 1.51% between 90 and 136 °C corresponds to the loss of the one lattice water molecules (calcd. 1.57%), and then it is stable up to 280 °C. The framework collapsed in the temperature range 280–800 °C, before the final formation of a metal oxide.

4. Conclusion

In summary, we have synthesized five novel metal-organic frameworks based on multi-carboxylate ligands and a chelate ligand by hydrothermal reactions. The successful syntheses of the five complexes indicate that it is promising to build up unusual architectures via a different reaction pH, thus opening up a new field in the preparation of metal coordination polymers with potential luminescent properties.

5. Supplementary data

CCDC 675859, 666353, 675860, 675861 and 675862 contain the supplementary crystallographic data for **1**, **2**, **3**, **4** and **5**. These data can be obtained free of charge via http://www.ccdc.cam.ac.uk/conts/retrieving.html, or from the Cambridge Crystallographic Data Centre, 12 Union Road, Cambridge CB2 1EZ, UK; fax: (+44) 1223-336-033; or e-mail: deposit@ccdc.cam.ac.uk.

Acknowledgements

This work was supported by the National Natural Science Foundation of China (No. 20731004) and the Natural Science Foundation of Education Commission of Anhui Province, China (Nos. KJ2007B092, KJ2008B004).

References

[1] (a) J.L.C. Rowsell, O.M. Yaghi, Angew. Chem., Int. Ed. 46 (2005) 4670;
(b) N.L. Rosi, J. Eckert, M. Eddaoudi, D.T. Vodak, J. Kim, M. O'Keeffe, O.M. Yaghi, Science 300 (2003) 1127;
(c) S. Kitagawa, R. Kitaura, S. Noro, Angew. Chem., Int. Ed. 43 (2004) 2334;
(d) O.M. Yaghi, M. O'Keeffe, N.W. Ockwing, H.K. Chae, M. Eddaoudi, J. Kim, Nature 423 (2003) 705;
(e) C. Janiak, J. Chem. Soc., Dalton Trans. (2003) 2781;
(f) M.E. Davis, Nature 417 (2002) 813;
(g) O.R. Evans, W. Lin, Acc. Chem. Res. 35 (2002) 511;
(h) M. Eddaoudi, D.B. Moler, H. Li, B. Chen, T. Reineke, M. O'Keeffe, O.M. Yaghi, Acc. Chem. Res. 34 (2001) 319;
(i) D. Maspoch, D.R. Molinaa, J. Veciana, Chem. Soc. Rev. 36 (2007) 770.
[2] (a) S.L. Zheng, M.L. Tong, X.M. Chen, Coord. Chem. Rev. 246 (2003) 185;
(b) S.R. Batten, K.S. Murray, Coord. Chem. Rev. 246 (2003) 103;
(c) L. Carlucci, G. Ciani, D.M. Proserpio, Coord. Chem. Rev. 246 (2003) 247;
(d) A.J. Blake, N.R. Champness, P. Hubberstey, W.S. Li, M.A. Withersby, M. Schröder, Coord. Chem. Rev. 183 (1999) 117;
(e) N.R. Champness, J. Chem. Soc., Dalton Trans. (2006) 877;
(f) A.Y. Robin, K.M. Fromm, Coord. Chem. Rev. 250 (2006) 2127;
(g) C. Kepert, Chem. Commun. (2006) 695.
[3] (a) V.W.W. Yam, K.K.W. Lo, Chem. Soc. Rev. 28 (1999) 323;
(b) Y. Ma, H.Y. Chao, Y. Wu, S.T. Lee, W.Y. Yu, C.M. Che, Chem. Commun. (1998) 2491.
[4] (a) W.H. Bi, R. Cao, D.F. Sun, D.Q. Yuan, X. Li, Y.Q. Wang, X.J. Li, M.C. Hong, Chem. Commun. (2004) 2104;
(b) A. Thirumurugan, C.N.R. Rao, J. Mater. Chem. 15 (2005) 3852;
(c) X.L. Wang, H.Y. Lin, T.L. Hu, J.L. Tian, X.H. Bu, J. Mol. Struct. 798 (2006) 34;
(d) Y.S. Song, B. Yan, Z.X. Chen, J. Solid State Chem. 179 (2006) 4037;
(e) X.L. Wang, Y.F. Bi, H.Y. Lin, G.C. Liu, Cryst. Growth Des. 7 (2007) 1086.
[5] (a) S.Q. Zang, Y. Su, Y.Z. Li, Z.P. Ni, H.Z. Zhu, Q.J. Meng, Inorg. Chem. 45 (2006) 3855;
(b) D.R. Xiao, E.B. Wang, H.Y. An, Y. Li, Z.M. Su, C.Y. Sun, Chem. Eur. J. 12 (2006) 6528.
[6] L.Y. Zhang, G.F. Liu, S.L. Zheng, B.H. Ye, X.M. Zhang, X.M. Chen, Eur. J. Inorg. Chem. (2003) 2965.
[7] (a) W.-B. Lin, O.R. Evans, R.-G. Xiong, Z.-Y. Wang, J. Am. Chem. Soc. 120 (1998) 13272;
(b) W.-B. Lin, Z.-Y. Wang, L. Ma, J. Am. Chem. Soc. 121 (1999) 11249;
(c) O.R. Evans, W.-B. Lin, Chem. Mater. 13 (2001) 3009;
(d) O.R. Evans, W.-B. Lin, Chem. Mater. 13 (2001) 2705.
[8] (a) X.-M. Zhang, M.-L. Tong, X.-M. Chen, Angew. Chem., Int. Ed. 41 (2002) 1029;
(b) X.-M. Zhang, M.-L. Tong, M.-L. Gong, H.-K. Lee, L. Luo, K.-F. Li, Y.-X. Tong, X.-M. Chen, Chem. Eur. J. 8 (2002) 3187;
(c) J. Tao, Y. Zhang, M.-L. Tong, X.-M. Chen, T. Yuen, C.L. Lin, X.-Y. Huang, J. Li, Chem. Commun. (2002) 1342.
[9] (a) R. Evans, W. Lin, Cryst. Growth Des. 1 (2001) 9;
(b) R.-G. Xiong, J. Zhang, Z.-F. Chen, X.-Z. You, C.-M. Che, H.-K. Fun, J. Chem. Soc., Dalton Trans. (2001) 780.
[10] Q. Chu, G.X. Liu, T.-a. Okamura, Y.Q. Huang, W.Y. Sun, N. Ueyama, Polyhedron 27 (2008) 812.
[11] (a) F. Calderazzo, F. Marchetti, G. Pampaloni, V. Passarelli, J. Chem. Soc., Dalton Trans. (1999) 4389;
(b) W.Z. Antkowiak, A. Sobczak, Tetrahedron 57 (2001) 2799.
[12] C. Hiort, P. Lincoln, B. Nordén, J. Am. Chem. Soc. 115 (1993) 3448.
[13] SAINT, Version 6.02a, Bruker AXS Inc., Madison, W1, 2002.
[14] G.M. Sheldrick, SADABS, Program for Bruker Area Detector Absorption Correction, University of Göttingen, Göttingen, Germany, 1997.
[15] G.M. Sheldrick, SHELXS-97, Program for Crystal Structure Solution, University of Göttingen, Göttingen, Germany, 1997.
[16] G.M. Sheldrick, SHELXL-97, Program for Crystal Structure Refinement, University of Göttingen, Göttingen, Germany, 1997.
[17] (a) S.Q. Xia, S.M. Hu, J.C. Dai, X.T. Wu, J.J. Zhang, Z.Y. Fu, W.X. Du, Inorg. Chem. Commun. 7 (2004) 51;
(b) X.J. Zhang, Y.P. Tian, S.L. Li, M.H. Jiang, A. Usman, S. Chantrapromma, H.K. Fun, Polyhedron 22 (2003) 397;
(c) L.Y. Zhang, G.F. Liu, S.L. Zheng, B.H. Ye, X.M. Zhang, X.M. Chen, Eur. J. Inorg. Chem. (2003) 2965.

[18] M. O'Keeffe, B.G. Hyde, Crystal Structures I. Patterns and Symmetry, VCH, Washington, DC, 1996.
[19] (a) M. Eddaoudi, J. Kim, N. Rosi, D. Vodak, J. Wachter, M. O'Keefe, O.M. Yaghi, Science 295 (2002) 469;
(b) N. Stock, T. Bein, Angew. Chem., Int. Ed. 43 (2004) 749;
(c) L. Pan, T. Frydel, M.B. Sander, X. Huang, J. Li, Inorg. Chem. 40 (2001) 1271.
[20] (a) O.D. Friedrichs, M. O'Keeffe, O.M. Yaghi, Acta Crystallogr. A59 (2003) 22;
(b) E. Koch, W. Fischer, Z. Kristallogr. 148 (1978) 107.
[21] X.M. Zhang, H.S. Wu, X.M. Chen, Eur. J. Inorg. Chem. (2003) 2959.
[22] (a) U.H.F. Bunz, Chem. Rev. 100 (2000) 1605;
(b) W. Wang, H. Schmider, Q. Wu, Y.S. Zhang, S. Wang, Inorg. Chem. 39 (2000) 2397;
(c) Y.B. Chen, J. Zhang, J.K. Cheng, Y. Kang, Z.J. Li, Y.G. Yao, Inorg. Chem. Commun. 7 (2004) 1139.
[23] X. Shi, G.S. Zhu, Q.R. Fang, G. Wu, G. Tian, R.W. Wang, D.L. Zhang, M. Xue, S.L. Qiu, Eur. J. Inorg. Chem. (2004) 185.
[24] (a) J. Tao, Y. Zhang, M.L. Tong, X.M. Chen, T. Yuan, C.L. Lin, X.Y. Huang, J. Li, Chem. Commun. (2002) 1342;
(b) X.L. Wang, C. Qin, E.B. Wang, Y.G. Li, N. Hao, C.W. Hu, L. Xu, Inorg. Chem. 43 (2004) 1850;
(c) S.L. Zheng, J.H. Yang, X.L. Yu, X.M. Chen, W.T. Wong, Inorg. Chem. 43 (2004) 830.
[25] L.J. Henderson, F.R. Fronczek, W.R. Cherry, J. Am. Chem. Soc. 106 (1984) 5876.
[26] (a) P. Kulkarni, S. Padhye, E. Sinn, Inorg. Chim. Acta 321 (2001) 193;
(b) Y.X. Wang, W.J. Perez, G.Y. Zheng, P.D. Rillema, Inorg. Chem. 37 (1998) 2051;
(c) Y.X. Wang, W.J. Perez, G.Y. Zheng, P.D. Rillema, Inorg. Chem. 37 (1998) 2227.

Polyhedron 27 (2008) 2337–2340

Contents lists available at ScienceDirect

Polyhedron

journal homepage: www.elsevier.com/locate/poly

Synthesis and characterization of low valent vanadium thiolate complexes

Andrew D. Sutton, James C. Fettinger, Brian D. Rekken, Philip P. Power *

Department of Chemistry, One Shields Avenue, University of California, Davis, CA 95616, USA

ARTICLE INFO

Article history:
Received 14 January 2008
Accepted 30 April 2008
Available online 10 June 2008

Keywords:
Vanadium
Thiolate
Terphenyl

ABSTRACT

The reaction of the bulky lithium terphenyl thiolate LiSAr′ (Ar′ = C_6H_3-2,6-(C_6H_3-2,6-Pr^i_2)$_2$) with $VI_2(THF)_2$ in THF resulted in the formation of two new V(II) and V(III) thiolate complexes. The addition of one equivalent of LiSAr′ to $VI_2(THF)_4$ led to the isolation of the dimeric V(II) species {V(μ-SAr′)I}$_2$ (**2**); a rare example of a structurally characterized V(II) thiolate. The thiolate ligands bridge the two vanadium centers, which are also bonded to a terminal iodide. In addition, there is an η^6-interaction between a flanking aryl ring from a terphenyl substituent with each metal. The attempted preparation of the vanadium dithiolate V(SAr′)$_2$ by reaction of $VI_2(THF)_2$ with two equivalents of LiSAr′ led to disproportionation which resulted in the isolation of the V(III) product V(SAr′)$_2$I (**3**) in which the vanadium center is coordinated by two sulfurs, an iodine, and a weaker interaction to a flanking aryl ring of the terphenyl group.
© 2008 Elsevier Ltd. All rights reserved.

1. Introduction

Transition metal thiolate and related derivatives [1–4] have been extensively studied because of their relevance for biological systems [5,6]. In many instances, they can serve as structural models for active sites in numerous metal–sulfur proteins such as ferredoxins [7,8] or nitrogenases [9–11], which feature cysteine residues as ligands [6]. However, the preparation of the simplest neutral homoleptic transition metal thiolates has often been difficult because of extensive M-(μ-SR)-M thiolate bridging which results in the formation of intractable oligomers or polymers. The use of sufficiently bulky ligands [12,13] such as –SC_6H_2-2,4,6-Bu^t_3 (–SMes*) [14,15] and –SC_6H_2-2,4,6-Ph_3 [16] mitigates extensive bridging interactions so that low coordinate species, exemplified by the dimeric transition metal complexes [{M(SMes*)$_2$}$_2$] (M = Mn, Fe, Co) [15] and [{Fe(SC_6H_2-2,4,6-Ph_3)$_2$}$_2$] [16], can be obtained. In a more recent development, the use of the very hindered thiolate derivative, –SAr* (Ar* = C_6H_3-2,6-(C_6H_2-2,4,6-Pr^i_3)$_2$) has led to the isolation of a series of soluble, monomeric first row transition metal(II) dithiolates M(SAr*)$_2$ (M = Cr, Mn, Fe, Co, Ni and Zn) in which the metals are nominally two-coordinate [17]. These complexes exhibit linear (or nearly linear) S–M–S units with varying degrees of weak interaction between the metal center and the flanking aryl rings of the terphenyl ligands. We wished to extend these results to vanadium via the synthesis and characterization of low valent vanadium thiolates of formula V(SAr)$_2$ (Ar = bulky terphenyl). Vanadium thiolates have been studied because of their potential relevance to the function of vanadium nitrogenase enzymes [18–20]. Vanadium nitrogenases, although less well understood than their molybdenum analogues [6–10,21], are believed to have a similar coordination environment to Mo in Mo-based nitrogenases, with low oxidation state (II–IV) oxidation states [11,18–20] wherein the metal is coordinated to several sulfur atoms. We now report on our initial investigations which have resulted in the synthesis of two low coordinate V(II) and V(III) thiolate complexes.

2. Experimental

2.1. General procedures

All manipulations were carried out with use of modified Schlenk techniques under an argon atmosphere or in a Vacuum Atmospheres HE-43 drybox. All solvents were dried by the method of Grubbs and degassed three times (freeze–thaw) prior to use, $VI_2(THF)_4$ was synthesized according to the literature procedure [22]. ^{1}H NMR spectra were recorded on a Varian 300 MHz instrument and referenced to the residual protio benzene in the C_6D_6 solvent. Melting points were recorded in glass capillaries sealed under N_2 or Ar and are uncorrected. UV–Vis data were recorded on a Hitachi-1200 spectrometer. Solution magnetic moment measurements were carried out by the method of Evans as a solution in C_6D_6 [23].

2.2. Ar′SH (*1*)

The terphenyl thiol Ar′SH was synthesized in an analogous manner to that described for the related thiol HSC_6H_3-2,6(C_6H_2-2,4,6-Pr^i_3)$_2$ [24]. Yield: 72%, m.p. 165–168 °C. ^{1}H NMR (C_6D_6, 400 MHz, 25 °C): δ 1.11 (d, $^3J_{HH}$ = 6.8 Hz 12 H, *o*-CH(CH_3)$_2$), 1.32 (d, $^3J_{HH}$ = 6.8 Hz, 12H, *o*-CH(CH_3)$_2$), 2.83 (sept,

* Corresponding author.
E-mail address: pppower@ucdavis.edu (P.P. Power).

0277-5387/$ - see front matter © 2008 Elsevier Ltd. All rights reserved.
doi:10.1016/j.poly.2008.04.039

$^3J_{HH}$ = 6.9 Hz, 4H, *o*-C*H*(CH$_3$)$_2$), 3.08 (S, 1H, –SH), 6.96 (1H *p*-C$_6$H$_3$), 7.21 (d, $^3J_{HH}$ = 7.6 Hz, 2H, *m*-C$_6$H$_3$-2, 6-Pr$_2^i$), 7.31 (d, $^3J_{HH}$ = 7.6 Hz, 2H, *p*-C$_6$H$_3$-2, 6-Pr$_2^i$. ^{13}C{^{1}H} NMR (C$_6$D$_6$, 100.59 MHz): δ 24.00, δ 24.92 (*o*-CH(*C*H$_3$)$_2$), 31.14 (*o*-*C*H(CH$_3$)$_2$), 123.67 (*m*-C$_6$H$_3$-2, 6-Pr$_2^i$), 124.36 (*i*-C$_6$H$_3$), 129.20 (*p*-C$_6$H$_3$-2, 6-Pr$_2^i$, 129.9 (*m*-C$_6$H$_3$), 135.61 (*i*-C$_6$H$_3$-2, 6-Pr$_2^i$), 138.00 (*p*-C$_6$H$_3$) 138.68 (*o*-C$_6$H$_3$-2, 6-Pr$_2^i$), 147.26 (*o*-C$_6$H$_3$).

2.3. [V(μ-SAr′)I]$_2$ (**2**)

(LiSAr′)$_2$ (generated in solution from 0.872 g, 2.0 mmol and LiBu^n (1.6 M in hexanes, 1.25 mL)), in THF (25 mL), was added dropwise to a stirred suspension of VI$_2$(THF)$_4$ (1.186 g, 2.0 mmol) in THF (25 mL) cooled to *ca.* 0 °C. The resulting dark, brown-red solution was stirred overnight while it was allowed to warm to room temperature. The solvent was removed under reduced pressure and the resulting dark red solid was extracted with hexane (30 mL) and filtered. The volume of the filtrate was reduced to *ca.* 5 mL under reduced pressure to afford dark red, X-ray quality crystals of **2** after storage for 3 days at *ca.* −20 °C. Yield: 0.768 g (63%) m.p. = 230 °C (dec). ^{1}H NMR (400 MHz, C$_6$D$_6$, 25 °C): δ = 7.1 (br, s), 6.9 (br, s), 3.7 (br, s), 2.7 (br, m), 1.3 (br, d), 1.0 (br, d). UV/Vis (hexanes; λ_{max}, nm (ε, mol^{-1} L cm^{-1})): 282 (7300), 384 (2500), 466 (2000). μ_{eff} = 3.61 μ_B/vanadium.

2.4. [V(SAr′)$_2$I] (**3**)

A THF (40 mL) solution of (LiSAr′)$_2$ (1.744 g, 4.0 mmol) in THF (50 mL) was added dropwise to a stirred suspension of VI$_2$(THF)$_4$ (1.186 g, 2.0 mmol) in THF (25 mL) with cooling in an ice bath. The resulting dark green solution was allowed to warm to room temperature and stirred overnight. The solvent was removed under reduced pressure and resulting dark green solid was extracted with hexane (40 mL) and filtered. The volume of the solution was reduced to *ca.* 10 mL which afforded green, X-ray quality crystals of **3** after 7 days at *ca.* 7 °C. Yield 0.552 g (23%) m.p. = 174–178 °C (dec). ^{1}H NMR (300 MHz, C$_6$D$_6$, 25 °C): δ = 7.10 (br, d), 2.95 (br, s), 1.21 (br, s), 1.05 (br, s). UV/Vis (hexanes; λ_{max}, nm (ε, mol^{-1} L cm^{-1})): 328 (3050), 390 (2000), 440 (1400), 638 (1600). μ_{eff} = 2.64 μ_B/vanadium.

2.5. X-ray data collection

X-ray quality crystals of **2** or **3** were removed from the Schlenk tube and immediately covered with a layer of hydrocarbon oil. A suitable crystal was selected, attached to a glass fiber, and placed in the cold temperature stream as previously described [25]. The data were collected near 90 K using a Bruker APEX (**2**) or a SMART 1000 (**3**) diffractometer and Mo Kα (λ = 0.71073 Å) radiation. Absorption corrections were applied using SADABS [26]. The structures were solved by use of direct methods in SHELXS [27] and refined by the full-matrix least-squares procedure in SHELXL. All non hydrogen atoms were refined anisotropically, while hydrogens were placed at calculated positions and included in the refinement by using a riding model. Some details of the data collection and refinement are given in Table 1. Further details are in the supplementary material.

Table 1
Selected crystallographic data and collection parameters for **2** and **3**

	2	**3**
Formula	$C_{60}H_{74}S_2V_2I_2$	$C_{71}H_{98}IOS_2V$
f_w	1214.99	1209.45
Color, habit	red, plate	green, rod
Crystal system	monoclinic	monoclinic
Space group	$P2_1/c$	$P2_1/n$
a (Å)	13.086(1)	13.4040(5)
b (Å)	13.278(1)	34.915(1)
c (Å)	16.507(2)	13.8562(5)
α (°)	90	90
β (°)	105.170(2)	92.949(1)
γ (°)	90	90
V (Å^3)	2768(4)	6476.1(4)
Z	2	4
d_{calc} (Mg/m^3)	1.458	1.240
θ Range (°)	2.00–27.50	1.17–25.25
μ (mm^{-1})	1.565	0.735
Number of observed ($I > 2\sigma(I)$) data	4435	7976
R_1 (observed data)	0.0422	0.0487
wR_2 (all data)	0.0897	0.1384

3. Results and discussion

The use of sterically encumbering ligands has played a key role in the stabilization of low coordinate (coordination number $\leqslant$3) compounds throughout the periodic table [28]. Early work focused on bulky ligands attached via a second row element C, N, or O in alkyl, aryl, amido, alkoxo on aryloxo ligands. The application of ligands based on elements from the third or later rows, involving for example, silyl, phosphido, or thiolate ligands, was a later development for a number of reasons that included synthetic and steric considerations as well as weaker metal–ligand bonding [28]. Although there is now a vast chemistry of transition metal thiolates, the fact that the sulfur can carry only one organic substituent has limited their application in the stabilization of low coordination numbers. We have recently used the very large terphenyl thiolate ligand −SC$_6$H$_3$-2, 6(C$_6$H$_2$-2, 4, 6-Pr$_3^i$)$_2$ (–SAr*) [24] to synthesize a series of divalent transition metal complexes (M(SAr*)$_2$ (M = Cr, Mn, Fe, Co)) [17] and their zinc analogue Zn(SAr*)$_2$. These feature linear or almost linear metal coordination for Cr, Mn, Co, Ni and Zn whereas Fe(SAr*)$_2$ displays a bent (S–Fe–S = 151.48(2)°) geometry and an apparent tendency to rearrange to a sandwich structure involving metal–aryl ring coordination [17]. A feature of the complexes is that, with the exception of the unique iron derivative, all the secondary metal–ligand interactions (mainly to *ipso*-carbons from a flanking aryl ring of the terphenyl ligand) are weak and exceed 2.5 Å, with the longest being observed for Mn(SAr*)$_2$ (Mn–S=2.951(2) Å). Such distances exceed those in the corresponding η^5 or η^6-bonded metal arene complexes by a significant margin. For example, the Cr–C interaction is 2.502(2) Å in Cr(SAr*)$_2$ whereas in Cr(η^5-C$_5$H$_5$)$_2$ the Cr–C distance is 2.142(3) Å and the Cr–centroid distance is 1.61 Å [29]. The above findings encouraged us to extend the approach to vanadium and it was hoped that the employment of a bulky terphenyl thiolate ligand would allow us to obtain the first example of a two-coordinate V(II) species.

The reaction of VI$_2$(THF)$_4$ with one or two equivalents of LiSAr* did not afford readily characterizable products. We turned instead to the related –SAr′ ligand which has similar steric properties to –SAr* and can be synthesized by a similar route. It differs from Ar* only in the absence of *para*-Pr^i substituents from the flanking aryl rings. The addition of one equivalent of LiSAr′ to a suspension of VI$_2$(THF)$_4$ in THF at 0 °C (Eq. (1)) afforded a dark red-brown solution from which deep red crystals of **2** could be isolated in

$$2VI_2(THF)_4 + 2LiSAr' \xrightarrow{0\ ^\circ C, THF} [V(\mu\text{-}SAr')I]_2 + 2LiI \quad (1)$$

63% yield. These were characterized by UV–Vis spectroscopy, magnetic studies and X-ray crystallography. The results of the diffraction study of **2** are illustrated in Fig. 1. It represents a very rare example of a structurally characterized vanadium (II) thiolate [4,30–33]. It is dimeric and the metals are linked by thiolate bridges to form a V$_2$S$_2$ core structure. Each vanadium is also coordinated to a terminal iodide. The V$_2$S$_2$ core is characterized by an inversion center with internal S–V–S and V–S–V angles of 100.86(4)° and

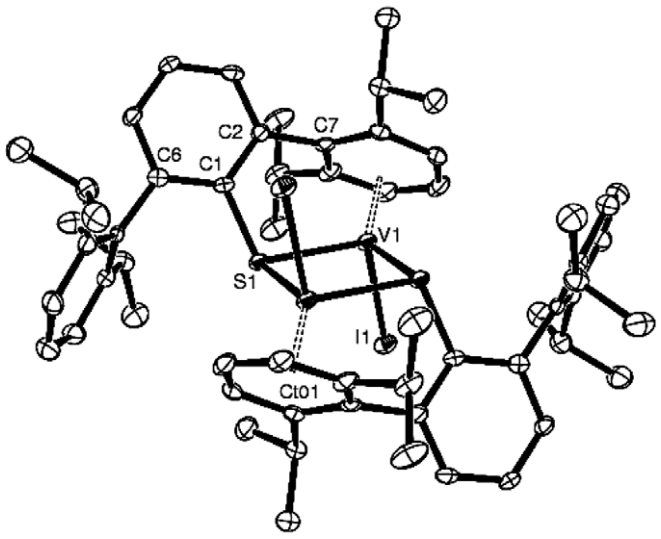

Fig. 1. Thermal ellipsoid (30%) plot of $[V(\mu\text{-}SAr')I]_2$ (**2**) ($Ar' = C_6H_3\text{-}2,6\text{-}(C_6H_3\text{-}2,6\text{-}Pr^i_2)_2$). Hydrogen atoms are not shown.

79.14(4)°, respectively. The V–I bonds subtend an angle of 100.37(3)° with respect to the V_2S_2 plane. In addition there is an η^6-interaction between a flanking aryl ring of the terphenyl ligand and each vanadium center. This interaction is relatively short (V(1)–Ct = 1.909(2) Å, Ct = centroid) and is comparable to that observed in vanadocene (1.917 (2) Å) [30] (1.962 Å), but marginally longer than that in $V(\eta^5\text{-}C_5Me_5)_2$ (1.873(2) Å) [31]. The data thus indicate the presence of a relatively strong vanadium–aryl ring interaction in **2**. This is also supported by the difference in the average C–C bond lengths in the interacting (1.415 Å avg.) and non interacting (1.401 Å avg.) aryl ring. The V–S bond lengths are 2.395(1) and 2.412(1) Å. These may be compared with the V(II)–S distances in $[V(Spy)_2(TMEDA)]$ (Spy = pyridine-2-thiolate, TMEDA = tetramethylethylenediamine; V–S = 2.252(2) and 2.547(2) Å) [33], $[V(Spy)_3]^-$ (V–S = 2.545 Å (avg.)) [31] and in $[V(SC_6H_3\text{-}2,6\text{-}Cl_2)_2(TMEDA)]$ (V–S = 2.464(2) and 2.468(2) Å) [34]. The metal centers in these complexes are six-coordinate or quasi six-coordinate, and, if the V–aryl interaction in **2** is viewed as occupying three coordination sites, the metal center in **2** may also be regarded as having six-coordination. In view of this, the V–S bond lengths in **2** may be regarded as being somewhat shorter than expected especially since the thiolate groups are bridging. It may be that the presence of a halogen ligand in **2**, which increases the positive charge on the metal, may cause the shorter V–S bond. The V–I bond length in **2** (2.7228(8) Å) is a little shorter than that in vanadium (II) complexes $[VI_2(depe)_2]$ (depe = bis(diethylphosphino)ethane) [22,30] (2.779(2) Å), $[VI_2(THF)([9]aneS_3)]$[35] ([9]aneS$_3$ = 1,4,7-trithiacyclononane) (2.787(2) and 2.798(3) Å) and *cis*-$VI_2(DME)_2$ [36] (2.811(2) and 2.805(2) Å) (see Tables 2 and 3)

The addition of freshly prepared Ar′SLi to $VI_2(THF)_4$ suspended in THF in a 2:1 ratio results in the formation of the monomeric vanadium (III) thiolate $[V(SAr')_2I]$ **3**, which presumably arises via a disproportionation process. Each vanadium center is coordinated to a terminal iodide and two thiolate ligands. However, the coordination geometry of the (see Fig. 2)

Table 2
Selected bond lengths (Å) and angles (°) for **2**

V(1)–I(1)	2.7228(8)	S(1)–V(1)–S(1)#1	100.86(4)
V(1)–Ct01	1.909(2)	S(1)–V(1)–I(1)	96.84(3)
V(1)–S(1)	2.396(1)	S(1)#1–V(1)–I(1)	96.33(3)
V(1)–S(1)#1	2.413(1)	V(1)–S(1)–V(1)#1	79.14(4)
S(1)–C(1)	1.793(4)	V(1)–C(1)–S(1)	104.44(1)
V(1)–V(1)#	3.063(1)		

Table 3
Selected bond lengths (Å) and angles (°) for **3**

V(1)–I(1)	2.6659(8)	S(1)–V(1)–S(2)	108.85(5)
V(1)–Ct	1.972(3)	S(1)–V(1)–I(1)	90.10(4)
V(1)–S(1)	2.292(1)	S(2)–V(1)–I(1)	96.77(4)
V(1)–S(2)	2.284(1)	C(1)–S(1)–V(1)	106.8(2)
S(1)–C(1)	1.771(4)	C(31)–S(2)–V(1)	119.3(2)
S(2)–C(31)	1.786(4)		

$$VI_2(THF)_4 + 2LiSAr' \xrightarrow{0\ ^\circ C,THF} [V(SAr')_2I] + 2LiI + V(I) \quad (2)$$

VS_2I array is pyramidal ($\sum$ °V = 295.72(5)) rather than planar and there is an η^6-interaction involving the flanking aryl ring of the terphenyl substituent and the vanadium center. The V–(Ct) distance (1.972(3) Å) is significantly longer than it is in **2**, however. This is especially noteworthy in view of the fact that effective ionic radius of six-coordinate V^{3+} (0.64 Å) is smaller that of V^{2+} (0.79 Å) [37] which may lead to an expectation for a shorter V^{3+}-centroid contact. On the other hand, the higher electron deficiency and reduced crowding of the metal center in **2** may account for the shorter V(II)–centroid distance. Nonetheless, inspection of the bond distances in the interacting and non interacting aryl rings of the S(I) ligand shows the average C–C distance in the former 1.405 Å are longer than those in the latter consistent with a weakening of the CC-bonding. The V–S–C angle for the interacting terphenyl V(I)–S(I)–C(1) = 106.8(2)° is ca. 12.5° narrower than the 119.3(2) observed for the thiolate ligand. The difference in the V^{n+} effective ionic radii is indeed reflected in the V–S bond lengths, 2.292(1) and 2.284(1) Å, which are over 0.1 Å shorter than those in **2**. The V–S distances are also shorter than those in $[V(tipt)_3(THF)_2]$ (tipt = 2,4,6-tri-isoproplbenzenethiolate) [38] (2.308(1), 2.334(1), 2.320(1) Å) or the 2.364 Å in $[V(SNC_9H_6)_3]$ [32]. The V–I distance 2.6659(8) Å is also shorter in **3**, but the shortening is not as great as it is for the V–S bonds. It may be compared with the V–I distance in $[VI(Ind)_2]$ (2.794(1) Å) [39].

The magnetic moments of the two compounds were measured in C_6D_6 by the Evans' method. These measurements afforded magnetic moments consistent with d^3 (**1**, μ_{eff} = 3.67μ_B per vanadium) and d^2 (**2**, μ_{eff} = 2.64μ_B) electron configurations. Both values indicate that there is little orbital contribution to the magnetic moment and that there is little coupling between the vanadiums in **2** (V–V = 3.063(1) Å). The presence of unpaired electrons gave rise to

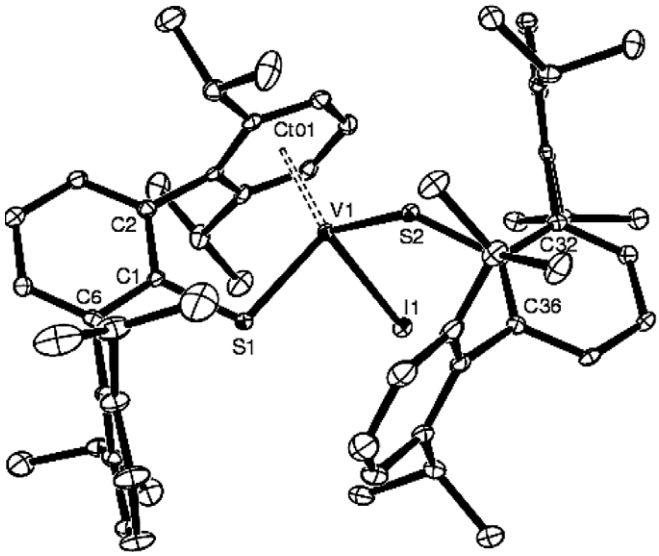

Fig. 2. Thermal ellipsoid (30%) plot of $V(SAr')_2I \cdot hexane \cdot THF$ (**2** · hexane · THF) ($Ar' = C_6H_3\text{-}2,6\text{-}(C_6H_3\text{-}2,6\text{-}Pr^i_2)_2$). Hydrogen atoms and solvent molecules are not shown.

broad and largely featureless paramagnetically shifted ^{1}H NMR spectra for both **2** and **3**.

4. Conclusions

The synthesis of **2** and **3** demonstrates the ability of bulky terphenyl thiolates to stabilize early transition metal complexes in low oxidation states. Nonetheless, a vanadium dithiolate V(SAr′), analogous to those reported for $M(SAr^{*})_2$ (M = Cr, Mn, Fe, Co, Ni, Zn), could not be isolated by a similar synthetic route due to a disproportionation reaction. However, the isolation of the iodide **2** in good yield may prove to be a useful reagent for further synthesis and the study of additional reactivity. For example, it may be useful as a precursor for the construction of V–V bonds via reductive coupling. In addition, two-coordinate V(II) may yet be obtainable from **2** with use of another less reducing coligand. Attempts to isolate such complexes are in hand.

Acknowledgements

We would like to thank Dr. Eric Rivard for assistance in the magnetic measurements and useful discussions, and the Petroleum Research Fund administered by the American Chemical Society and the National Science Foundation.

Supplementary data

CCDC 671397 and 671398 contain the supplementary crystallographic data for **2** and **3**. These data can be obtained free of charge via http://www.ccdc.cam.ac.uk/conts/retrieving.html, or from the Cambridge Crystallographic Data Centre, 12 Union Road, Cambridge CB2 1EZ, UK; fax: (+44) 1223-336-033; or e-mail: deposit@ccdc.cam.ac.uk.

References

[1] I.G. Dance, Polyhedron 5 (1986) 1037.
[2] B. Krebs, G. Henkel, Angew. Chem., Int. Ed. 30 (1991) 768.
[3] B.-S. Kang, M.-C. Hong, T. Wen, H.Q. Liu, J.-X. Lu, J. Cluster Sci. 6 (1995) 379.
[4] D.W. Stephan, T.T. Nadasdi, Coord. Chem. Rev. 147 (1996) 147.
[5] See for example selected articles in Chem. Rev. 104 (2004) 2.
[6] S.J. Lippard, J.M. Berg, Principles of Bioinorganic Chemistry, University Science Books, 1994.
[7] R.H. Holm, Compr. Coord. Chem. II 8 (2004) 61.
[8] H. Bernert, R.H. Holm, I.E. Munck, Science 277 (1997) 653.
[9] B.K. Burgess, D.J. Love, Chem. Rev. 96 (1996) 2983.
[10] J.B. Howard, D.C. Rees, Chem. Rev. 96 (1996) 2965.
[11] R.R. Eady, Coord. Chem. Rev. 237 (2003) 23.
[12] J.R. Dilworth, J. Hu, Adv. Inorg. Chem. 33 (1994) 411.
[13] K. Ruhlandt-Senge, Commun. Inorg. Chem. 19 (1997) 351.
[14] R. Rundel, Chem. Ber. 101 (1968) 2956.
[15] P.P. Power, S.C. Shoner, Angew. Chem., Int. Ed. 30 (1991) 330.
[16] K. Ruhlandt-Senge, P.P. Power, Bull. Chem. Soc. Fr. 129 (1993) 594.
[17] T. Nguyen, A. Panda, M.M. Olmstead, A.F. Richards, M. Stender, M. Brynda, P.P. Power, J. Am. Chem. Soc. 127 (2005) 8545.
[18] D. Rehder, S. Jantzen, in: J.O. Nriagu (Ed.), Structure Function and Models of Biogenic Vanadium Compounds, Wiley, New York, 1998, p. 251.
[19] D. Rehder, Coord. Chem. Rev. 182 (1999) 297.
[20] H. Nekola, D. Wang, J. Gruning, A. Gatzens, A. Behrens, D. Rehder, Inorg. Chem. 41 (2002) 2379.
[21] O. Einsle, F.A. Tezcan, S.L.A. Andrade, M. Benedikt-Schmidt, M. Yoshida, J.B. Howard, D.C. Rees, Science 297 (2002) 1696.
[22] P.B. Hitchcock, D.L. Hughes, G.J. Leigh, J.R. Saunders, J. de Souza, C.J. McGarry, L.F. Larkworthy, Dalton Trans. (1994) 3683.
[23] (a) D.F. Evans, J. Chem. Soc. 1959 (2003) 5;
(b) K. Sun, J. Magn. Reson. 82 (1989) 169.
[24] M. Niemeyer, P.P. Power, Inorg. Chem. 35 (1996) 7264.
[25] H. Hope, in: A.L. Wayda, M.Y. Darensbourg (Eds.), Experimental Organometallic Chemstry, ACS Symposium Series, vol. 357, American Chemical Society, Washington, DC, 1987 (Chapter 10).
[26] SADABS: Area-detection Absorption Correction: Bruker AXS Inc., Madison, WI, 1996.
[27] SHELXS and SHELXL PC: version 5.03; Bruker AXS Inc., Madison, WI, 1994.
[28] P.P. Power, J. Organomet. Chem. 689 (2004) 3904.
[29] E. Keulen, F. Jellinek, J. Organomet. Chem. 5 (1966) 490.
[30] R.D. Rogers, J.L. Atwood, D. Foust, M.D. Rausch, J. Cryst. Mol. Struct. 11 (1981) 183.
[31] S. Gambarotta, C. Floriani, A. Chiesi-Villa, C. Guastini, Inorg. Chem. 23 (1984) 1739.
[32] G. Henkel, B. Krebs, W. Schmidt, Angew. Chem., Int. Ed. 31 (1992) 1366.
[33] J.G. Reynolds, S.C. Sendlinger, A.M. Murray, J.C. Huffman, G. Christou, Angew. Chem., Int. Ed. 31 (1992) 1253.
[34] J.A. Davis, C.P. Davie, D.B. Sable, W.H. Armstrong, Chem. Commun. (1998) 1649.
[35] S.L. Davis, M.C. Durrant, D.L. Hughes, C. Le Floch, S.J.A. Pope, G. Reid, R.L. Richards, J.R. Saunders, Dalton Trans. (1998) 2191.
[36] F. Calderazzo, G.E. Benedetto, G. Papaloni, C.M. Mossmer, J. Strähle, K. Wurst, J. Organomet. Chem. 451 (1993) 73.
[37] R.D. Shannon, Acta. Cystallogr., Sect. A 32 (1976) 751.
[38] C.R. Randall, W.H. Armstrong, Chem. Commun. (1988) 986.
[39] J.R. Bocarsly, C. Floriani, C. Chiesi-Villa, C. Guastini, Inorg. Chem. 26 (1987) 1871.

Polyhedron 27 (2008) 2341–2348

Contents lists available at ScienceDirect

Polyhedron

journal homepage: www.elsevier.com/locate/poly

A pyrazine-bridged linear pentanuclear copper(II) complex and related tri- and dinuclear complexes showing various coordination structures and magnetic couplings

Nobumasa Koyama [a], Takayuki Ishida [a,b,*], Takashi Nogami [a], Tamizo Kogane [a,*]

[a] Department of Applied Physics and Chemistry, The University of Electro-Communications, Chofu, Tokyo 182-8585, Japan
[b] Course of Coherent Optical Science, The University of Electro-Communications, Chofu, Tokyo 182-8585, Japan

ARTICLE INFO

Article history:
Received 15 March 2008
Accepted 21 April 2008
Available online 19 June 2008

Keywords:
Pyrazine
Copper(II) ion
Molecule-based magnetic materials
Supramolecular chemistry
Magnetic property

ABSTRACT

Sterically bulky pyrazines have been successfully utilized for the preparation of discrete oligo-nuclear TBP (trigonal bipyramidal), SqP (square pyramidal), and Oh (octahedral) copper(II) complexes. We have synthesized a unique linear pentanuclear complex [{Cu(hfac)$_2$}$_5$(μ-2-butyl-3-methylpyrazine)$_4$]. The two terminal copper(II) ions have a SqP structure while the three inner ions have an Oh one. The solvent molecule was incorporated in the clearance of the lattice. From another reaction under harsh conditions, we separated [{Cu(hfac)$_2$}$_3$(μ-2-butyl-3-methylpyrazine)$_2$], which can be regarded as the central moiety of the pentanuclear one. We also prepared a dinuclear complex [{Cu(hfac)$_2$}$_2$(μ-tetramethylpyrazine)], in which the pyrazine nitrogen atoms were located at TBP equatorial positions. Single-crystal EPR measurements supported its compressed TBP structure. The exchange coupling was antiferromagnetic with $J_{TBP-TBP}/k_B = -3.6$ K. The linear trinuclear [{Cu(hfac)$_2$}$_3$(μ-2,3,5-trimethylpyrazine)$_2$], having two TBP Cu ions with an intervening Oh Cu ion, showed very weak antiferromagnetic coupling. DFT calculations on these compounds indicated that the σ-type orbital overlap between the Cu and N atoms is essential for superexchange interactions.

© 2008 Elsevier Ltd. All rights reserved.

1. Introduction

A wide variety of complexes have been developed in which π-conjugated *N*-donor ligands are used for rigid building blocks and controllable superexchange couplers [1]. Pyrimidines and pyrazines have a highly directive nature of the nitrogen lone pairs and have attracted much attention in the construction of supramolecular structures such as porous materials [2] and molecular grids [3]. These diazaaromatic rings have characteristic σ/π-electron systems providing magnetic exchange pathways, and especially the pyrimidine skeleton has been utilized as a ferromagnetic coupler as expected from its spin-polarization mechanism [4]. However, the role of couplers has proved to depend on the coordination structures and the σ/π nature of the transition-metal spins [5,6]. On the other hand, pyrazines mostly work as an antiferromagnetic coupler [7–9]. For convenience of discussion, the bridging geometries of the pyrazine (pyz) systems are classified into three types (Chart 1) for copper(II) complexes ($3d^9$; $S_{Cu} = 1/2$). Only a few examples showing ferromagnetic coupling are known, which has been explained in terms of orbital orthogonality in the equatorial–axial (eq–ax) combination of the two nitrogen lone pairs [10,11].

The ax–ax type is less important for magnetochemistry, since these magnetic couplings are very small; for example, one-dimensional (1-D) [Cu(hfac)$_2$(μ-pyz)]$_n$ (Hhfac stands for 1,1,1,5,5,5-hexafluoropentane-2,4-dione) showed $J/k_B = -0.03$ K [12,13], where the spin Hamiltonian is defined as $-2J\Sigma S_i \cdot S_j$. We also systematically prepared 1-D [Cu(hfac)$_2$(μ-L)]$_n$ (L = substituted pyrazines) and revealed that they exhibited practically negligible antiferromagnetic interactions [14].

The magneto-structural relation has been discussed on the octahedral (Oh) Cu ion whose magnetic orbital is well defined as $3d_{x^2-y^2}$ located on a coordination basal (i.e., eq) plane. Studies on the magnetic coupling across diazaaromatic rings between trigonal bipyramidal (TBP) Cu ions are relatively rare [9,15], whilst those of oxo-, halo- and cyano-bridged TBP compounds are more often found in the literature [16]. In the present work, we have synthesized and characterized a simple dinuclear complex containing two TBP Cu ions with a pyz bridge, which can be regarded as a successful example of the application of steric hindrance from substituents on a pyz ring. Discrete oligo-nuclear complexes have

* Corresponding authors. Address: Department of Applied Physics and Chemistry, The University of Electro-Communications, Chofu, Tokyo 182-8585, Japan. Tel.: +81 42 443 5490; fax: +81 42 443 5501 (T. Ishida).
E-mail address: ishi@pc.uec.ac.jp (T. Ishida).

0277-5387/$ - see front matter © 2008 Elsevier Ltd. All rights reserved.
doi:10.1016/j.poly.2008.04.040

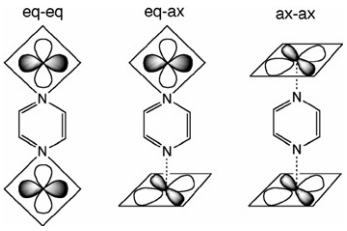

Chart 1. Coordination geometry of Cu-μ-pyz-Cu systems.

various coordination spheres at the terminal Cu ions, and accordingly they can provide us good examples for the study on the magneto-structural relationship.

In addition, we have characterized a very unique linear-arrayed pentanuclear copper(II) complex where the two terminal Cu ions possess a square pyramidal (SqP) coordination sphere. We can compare the magnetic couplings between the Oh–SqP and Oh–TBP interactions. The lobe direction of the magnetic orbital can be confirmed from theoretical calculations, and the magnetic coupling mechanism will be explained in connection with the above classification.

2. Results

2.1. Preparation and spectral characterization

Complexation of anhydrous $[Cu(hfac)_2]$ and 2-butyl-3-methylpyrazine (bmpyz) afforded a novel linear pentanuclear complex $[\{Cu(hfac)_2\}_5(\mu\text{-bmpyz})_4]$ (**1**). The preparation was highly reproducible as indicated by the same product being obtained from complexations in various solvents such as pentane, hexane, octane and cyclohexane. In spite of the ample reproducibility of the pentanuclearity, we also found that thermal degradation of the reaction mixture, after prolonged refluxing conditions for example, gave a trinuclear compound $[\{Cu(hfac)_2\}_3(\mu\text{-bmpyz})_2]$ (**2**). Compound **2** was usually contaminated with **1** and could not be obtained in a pure form, as indicated by the elemental analysis (see Section 5).

Complexation of $[Cu(hfac)_2]$ with tetramethylpyrazine (tmpyz) gave a 2:1 compound, $[\{Cu(hfac)_2\}_2(\mu\text{-tmpyz})]$ (**3**). For comparison, we investigated the known linear trinuclear complex $[\{Cu(hfac)_2\}_3(\mu\text{-trpyz})_2]$ (**4**; trpyz stands for 2,3,5-trimethylpyrazine), in which the central Cu ion has an Oh structure while two outer Cu ions have a TBP structure [17].

One of the authors (T.K.) has been reported that IR spectroscopy is a versatile tool for structural determination of various compounds obtained from $[Cu(hfac)_2]$ [14,17,18]. In the simple complex **3**, split ν(C–O) bands were observed at 1653 and 1645 cm^{-1}, which are assigned to the stretching vibrations of carbonyls in the chelated hfac ligands with short and long C–O distances, respectively. The splitting arises from non-equivalent C–O bonds in each hfac chelate ring (for the molecular structure, see Chart 2). Similarly, split ν(C–O) bands were observed for the hfac chelate rings around the five-coordinated Cu ion of **4**. The IR spectrum of **4** has three bands at 1658, 1644 and 1639 cm^{-1} in the C–O stretching region [17]. As compared with the spectrum of **3**, the split bands (1658 and 1644 cm^{-1}) may be assigned to the vibrations of the hfac ligands around the five-coordinated Cu ion with a TBP structure, the rest (1639 cm^{-1}) around the six-coordinated Cu ion with an Oh structure.

On the other hand, no split was observed for the hfac ring deformation band at 675 cm^{-1} for **3**, indicating that the two chelated hfac ligands are equivalent. *N*-Ax square-pyramidal (SqP) structures showed no split in the ν(C–O) and hfac ring deformation bands [12,18c], while the *N*-eq SqP structure shows both split bands. From the analysis of the ν(C–O) and hfac ring deformation bands, the *N*-eq TBP structures of **3** and **4** can be characterized as an *N*-ax or *N*-eq SqP type.

The IR spectrum of **1** was somewhat complicated, indicating the presence of various types of hfac chelate rings. Weak and strong ν(C–O) bands were observed at 1657 and 1641 cm^{-1}, respectively. Strong and weak hfac ring deformation bands were also observed at 679 and 670 cm^{-1}, respectively. We can point out that both weak bands arise from one of the non-equivalent hfac chelate rings around the five-coordinated Cu ion, namely an *N*-eq SqP structure. On the other hand, both strong bands are assigned to the stretching vibrations of carbonyls in the hfac chelated rings and hfac ones around the six-coordinated Cu ion having an elongated Oh geometry [12,14].

2.2. Molecular structures

Fig. 1 shows the molecular structure of **1** in the crystal of **1** · (octane). The terminal Cu ions (Cu1 and Cu1*) have an *N*-eq SqP structure. The ax Cu1–O4 bond length (2.150(4) Å) is longer than the eq ones (1.940(3)–2.029(4) Å). The angular structural index parameter τ [19] and its modified parameter χ [20] have been defined for the five-coordination geometry. The τ and χ values for Cu1 in **1** are 0.18 and 0.23, respectively. These values are close to zero, the value for an ideal SqP structure. The inner Cu ions (Cu2, Cu3 and Cu2*) have an elongated Oh geometry. Owing to steric reasons, all of the nitrogen atoms occupy the ax positions. The Cu–N distances are considerably long (2.442(5)–2.513(4) Å), and are comparable with those of the 1-D $[Cu(hfac)_2(\mu\text{-L})]_n$ (L = substituted pyrazines) [14]. The two bmpyz ligands around Cu3 are arranged in a head-to-head fashion, but those around Cu2 are in a head-to-tail fashion. The intramolecular Cu1···Cu2 and Cu2···Cu3 distances are 7.2473(10) and 7.5574(8) Å, respectively.

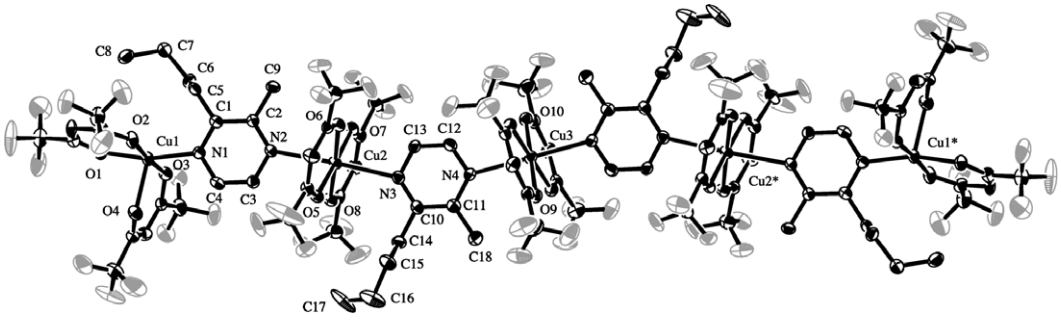

Fig. 1. Ortep drawing of $[\{Cu(hfac)_2\}_5(\mu\text{-bmpyz})_4]$ (**1**) in the crystal of **1** · (octane). Thermal ellipsoids are drawn at the 50% probability level. Hydrogen atoms are omitted. Symmetry operation code of * is $-x, -y+2, -z$. Selected bond lengths: Cu1–N1, 2.029(4); Cu2–N2, 2.513(4); Cu2–N3, 2.485(4); Cu3–N4, 2.442(5) Å. Only the major conformation is shown for the disordered terminal methyl group (C17).

The N4···N3–Cu2 angle (164.0(2)°) is considerably bent from an ideal axial array, which would relieve the steric congestion nearby and enable Cu2 to form an Oh structure. On the other hand, the environment around N1–Cu1 is still highly crowded, leading to a penta-coordination SqP structure at Cu1, and the chain growth is limited accordingly. Note that the N2–Cu2 distance is longer than the other ax N3–Cu2 and N4–Cu3 distances, being consistent with a possible mechanism of the formation of **2**; N2–Cu2 bond cleavage may easily occur in the thermal degradation reaction of **1**, leading to a decrease of the steric repulsion between the large butyl group (C14–C15–C16–C17) and the hfac ligands coordinated to Cu2.

The crystal of **1** has a large void volume where the solvent molecules are incorporated. We can find relatively large thermal ellipsoids at the butyl groups, such as C14–C15–C16–C17. The terminal methyl group (C17) is disordered into two conformational positions with an occupancy ratio of 0.668(17):0.332(17). The molecular packing seems to be still loose around in that area.

The crystal structure analysis as well as elemental analysis on **1** indicate that the solvent molecule is incorporated with a molar ratio of 1:1 when pentane, hexane and octane are used as solvents, and two solvent molecules are present when **1** is crystallized from cyclohexane (Fig. 2). Severe disorder of the solvent molecules was found for **1** · (pentane) and **1** · (hexane). The cell parameters are quite similar to each other in the triclinic $P\bar{1}$ space group and the molecular skeletons of **1** are practically identical among the various solvated crystals, regardless of the solvent used. The rigid rod-like structure of **1** seems to have a strong self-assembly character and constructs a tough host network.

The single-crystal X-ray diffraction study revealed that **2** approximately corresponds to the central Cu_3 portion of **1**. There are two crystallographically independent molecules in a unit cell, which are quite similar to each other. One molecule is shown in Fig. 3. Each molecule has an inversion center at the central Cu ion. The butyl groups exhibit some disorder with respect to the zig-zag conformation. All of the nitrogen atoms are located at ax positions. The outer $Cu(hfac)_2$ moieties are slightly pyramidalized. The Cu1 ion is located above the basal O1–O2–O3–O4 plane by 0.211(2) Å. This distance is close to the values of similar *N*-ax SqP copper(II) compounds (0.228(3) Å for $[\{Cu(hfac)_2\}_3(\mu\text{-}5\text{-}pym)_2]$ [17] and 0.24 Å for $[\{Cu(hfac)_2\}_2(\mu\text{-}pyz)]$ [12]), but is slightly longer than those of *N*-eq SqP copper(II) compounds (0.167(2) Å at the terminal copper ion in **1** and 0.157(2) Å in $[Cu(hfac)_2(5\text{-}Hmpz)]$ [18c] for example). However, the Cu1–N1 distance (2.333(3) Å) is considerably longer than the values for the corresponding bond in $[\{Cu(hfac)_2\}_2(\mu\text{-}pyz)]$ (2.250(17) Å) [12] and

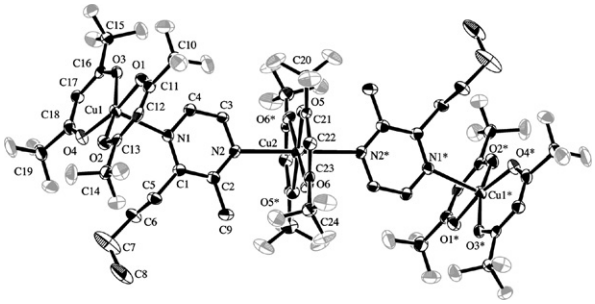

Fig. 3. Ortep drawing of $[\{Cu(hfac)_2\}_3(\mu\text{-}bmpyz)_2]$ (**2**). Thermal ellipsoids are drawn at the 50% probability level. Hydrogen atoms are omitted. Symmetry operation code of * is $-x+1, -y, -z+1$. Selected bond lengths: Cu1–N1, 2.333(3); Cu2–N2, 2.463(4), Cu1–O1, 1.943(3); Cu1–O2, 1.940(3); Cu1–O3, 1.950(3); Cu1–O4, 1.940(3); Cu2–O5, 1.955(3); Cu2–O6, 1.968(3) Å. Only the major conformation is shown for the disordered terminal methyl group (C8).

$[\{Cu(hfac)_2\}_3(\mu\text{-}5\text{-}pym)_2]$ (2.282(5) Å) [17], owing to the bulky butyl group.

The single-crystal X-ray diffraction study revealed that **3** crystallized in the orthorhombic *Fddd* space group. Fig. 4 shows the molecular structure of **3**. A quarter of the structure is a crystallographically independent unit. The Cu1–N1–O2–$O2^{\#}$ atoms of **3** form a strict plane because of the crystal symmetry. The ax Cu1–O1 (1.919(2) Å) distance is somewhat shorter than the eq Cu1–O2 and Cu1–N1 distances. The coordination geometry of the Cu ion belongs to a compressed *N*-eq TBP type. The τ and χ values are 0.67 and 0.71, respectively. Although these values are appreciably smaller than unity for an ideal TBP structure, they belong to the TBP category [19,20]. The O2–Cu1–N1 and $O2^{\#}$–Cu1–N1 bond angles (136.81(6)°) are considerably larger than the ideal trigonal angle of 120°. The resultant O2–Cu1–$O2^{\#}$ angle is only 86.37(9)°. The slightly small index values are attributed to such angular deviations, which arise from substantial steric interactions from the methyl groups in tmpyz. The two Cu ions are separated by 6.8542(8) Å in the molecule.

The crystal structure of **4** was determined at 90 K (not shown; Chart 2 for the molecular structure), though the determination at room temperature has already been reported [17]. The coordination geometry around the terminal Cu ions is similar to that of Cu1 in **3**. The Cu1–N1 distance in **3** (2.066(3) Å) is slightly longer than that of the corresponding bond in **4** (2.023(2) Å). The central Cu ion in **4** has an elongated Oh structure, the hfac oxygen atoms being coordinated at the eq positions. Owing to the partially relief of the steric hindrance, six-coordination is allowed, but the ax

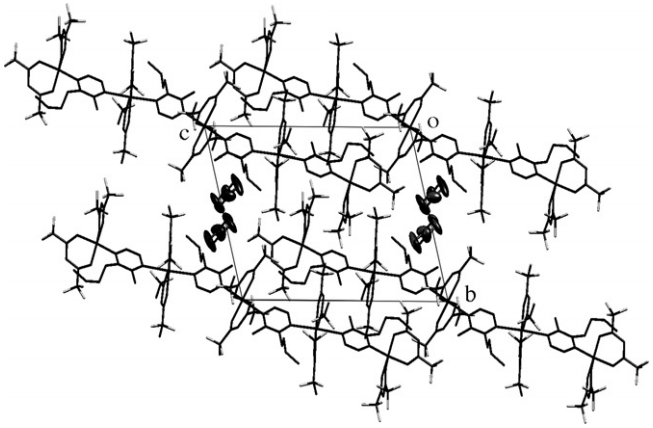

Fig. 2. Molecular arrangement of $[\{Cu(hfac)_2\}_5(\mu\text{-}bmpyz)_4]$ (**1**) and the cyclohexane molecules in the crystal of **1** · $(cyclohexane)_2$. Thermal ellipsoids of the cyclohexane molecules are drawn at the 50% probability level. Hydrogen atoms are omitted.

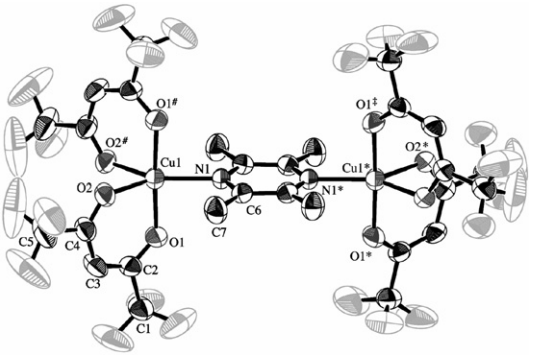

Fig. 4. Ortep drawing of $[\{Cu(hfac)_2\}_2(\mu\text{-}tmpyz)]$ (**3**) with thermal ellipsoids at the 50% probability level. Hydrogen atoms are omitted. Symmetry operation codes are: #: $1/4-x, 1/4-y, z$; *: $x, 1/4-y, 1/4-z$; ‡: $1/4-x, y, 1/4-z$. Selected bond lengths (Å) and angles (°): Cu1–O1, 1.919(2); Cu1–O2, 2.101(2); Cu1–N1, 2.066(3); O1–Cu1–O2, 90.65(10); O1–Cu1–N1, 88.43(6); N1–Cu1–O2, 136.81(6).

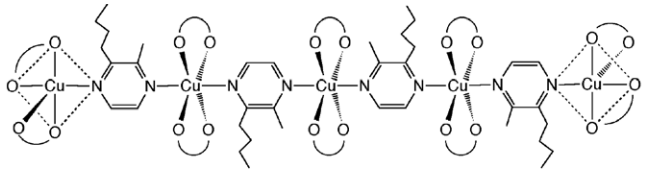

[Cu(hfac)$_2$-bmpyz-Cu(hfac)$_2$-bmpyz-Cu(hfac)$_2$-bmpyz-Cu(hfac)$_2$-bmpyz-Cu(hfac)$_2$]

(**1**)

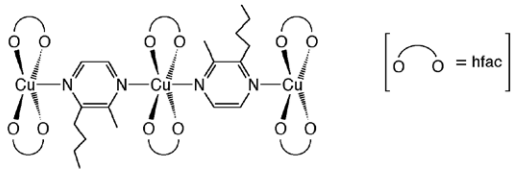

[Cu(hfac)$_2$-bmpyz-Cu(hfac)$_2$-bmpyz-Cu(hfac)$_2$] (**2**)

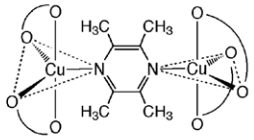

[Cu(hfac)$_2$-tmpyz-Cu(hfac)$_2$] (**3**)

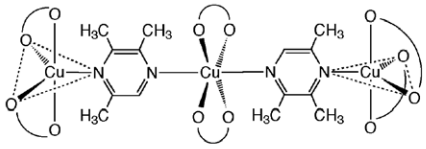

[Cu(hfac)$_2$-trpyz-Cu(hfac)$_2$-trpyz-Cu(hfac)$_2$] (**4**)

Chart 2. Molecular structures of **1**–**4**.

bonds (2.443(2) Å) are elongated like the quinoxaline- and phenazine-bridged Oh copper(II) chain compounds [14]. The coordinating ability of the 1-nitrogen atom in tmpyz and trpyz seems to be stronger than the 1-nitrogen atom in 2,6-dimethylpyrazine, because the latter occupied an Oh–ax position with a quite long Cu–N bond (2.606(2) Å) [14]. The intramolecular Cu···Cu separation is 7.1845(3) Å.

The τ and χ values for the TBP Cu ion in **4** were found to be 0.71 and 0.73, respectively, at room temperature. However, they became somewhat smaller, 0.66 and 0.68, respectively, at 90 K. This finding means that the distortion proceeds from TBP to SqP at low temperature.

2.3. EPR spectra

We measured the EPR spectra of **3** to confirm the TBP structure of the copper(II) ion. Thanks to the orthorhombic lattice of the crystal of **3**, we could easily determined $g_{//}$ as a g factor when a magnetic field was applied along the crystallographic a axis, while $g_{\perp}$ was obtained when a field was applied on the bc plane. At room temperature we observed a single line in the $\Delta m_S = \pm 1$ region using a single crystal of **3** by means of X-band EPR spectroscopy. We determined anisotropic g factors as $g_a = 2.083$, $g_b = 2.245$ and $g_c = 2.138$ (Fig. 5). These values fell in the typical ranges of g factors found in room-temperature data of compressed TBP copper(II) complexes [21]. The finding of $2 \leqslant g_{//} < g_{\perp}$, known as the "inverse" trend, indicates the d_{z^2} magnetic state of the copper(II) ion [21,22]. In addition, a forbidden transition of $\Delta m_S = \pm 2$ was also observed almost isotropically at $g \approx 4.25$, which can be assigned to the triplet state in a thermal equilibrium.

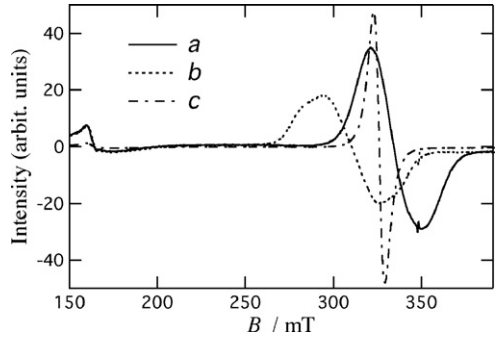

Fig. 5. X-Band EPR spectra of **3**. Symbols a, b and c denote the measurements with applied fields parallel to the crystallographic a, b and c axes, respectively.

The dominant TBP character in **3** could finally be confirmed by the fact that the magnetic orbital corresponds to $3d_{z^2}$ from a calculational study (see below).

2.4. Magnetic properties

We measured the magnetic susceptibilities of **1** · (octane), **3** and **4** on a SQUID magnetometer. Compound **4** is known, but its magnetic properties have not been reported to date [17]. Compound **2** could not be obtained as a pure form. All of the nitrogen atoms are located at ax positions in **2**, and accordingly we can expect that the magnetic couplings in **2** are negligible [12–14].

Fig. 6a shows the $\chi_m T$ product plotted against T for the three specimens below 100 K. The $\chi_m T$ value of **1** · (octane) was practically constant, with a value of 2.23 cm^3 K mol^{-1}. We estimated $|J|/k_B < 0.1$ K (antiferromagnetic) between any neighboring copper ions with $g_{avg} = 2.173(2)$ (the exchange parameter is defined as $-2J$). The small interaction in **1** is confirmed from the magnetization curve; that is the data measured at 1.8 and 4.5 K almost followed the theoretical Brillouin function (Fig. 6b). Similar magnetic measurements and analysis on other solvated specimens gave almost identical results.

On the other hand, **3** exhibited obvious magnetic coupling. The $\chi_m T$ value of **3** monotonically decreased upon cooling, indicating the presence of an antiferromagnetic interaction. The observed interaction is attributed to the through-bond Cu(TBP)-μ-tmpyz-Cu(TBP) superexchange. We applied the spin Hamiltonian, $H = -2J_{TBP-TBP} S_1 \cdot S_2$; i.e., the molar magnetic susceptibility can be written as the Bleaney–Bowers equation [23]. The optimized parameters are: $J_{TBP-TBP}/k_B = -3.583(6)$ K with $\chi_{TIP} = 0.001289(5)$ cm^3 mol^{-1} and $g = 2.2531(9)$, where χ_{TIP} stands for the temperature-independent paramagnetic susceptibility. The calculated curve is superposed in Fig. 6a, and the fit was satisfactory. The antiferromagnetic interaction in **3** was confirmed in the magnetization curve (Fig. 6b). The magnetization data measured at 1.8 K fell appreciably below the theoretical Brillouin function with $S = 1/2$. The S-shape curve is attributed to a spin reorientation from a singlet to a triplet state. The Zeeman energy ($g\mu_B H$) obtained from the magnitude of the field (ca. 3 T at 1.8 K) at which the magnetization starts to upsurge can be converted to the thermal energy ($k_B T$) at 4.5 K. The $|J_{TBP-TBP}|$ value agrees well with this estimation. At higher temperatures the S-shape became ambiguous, indicating the thermal population of the triplet state.

The $\chi_m T$ value of **4** only slightly decreased upon cooling, clearly indicating a structure-dependence of magnetic coupling; i.e., the superexchange interaction $|J_{TBP-Oh}|$ along the Cu(TPB)-μ-trpyz-Cu(Oh) skeleton in **4** is much smaller than $|J_{TBP-TBP}|$ across tmpyz in **3**. We determined the exchange parameter from the doublet–quartet model [24] based on the spin Hamiltonian $H = -2J_{TBP-Oh}(S_1 \cdot S_2 + S_2 \cdot S_3)$, to give $J_{TBP-Oh}/k_B = -0.121(4)$ K with $\chi_{TIP} = 0.000458(7)$ cm^3 mol^{-1} and $g_{avg} = 2.2272(8)$. The small interaction in **4** is also indicated from the magnetization curve (Fig. 6b).

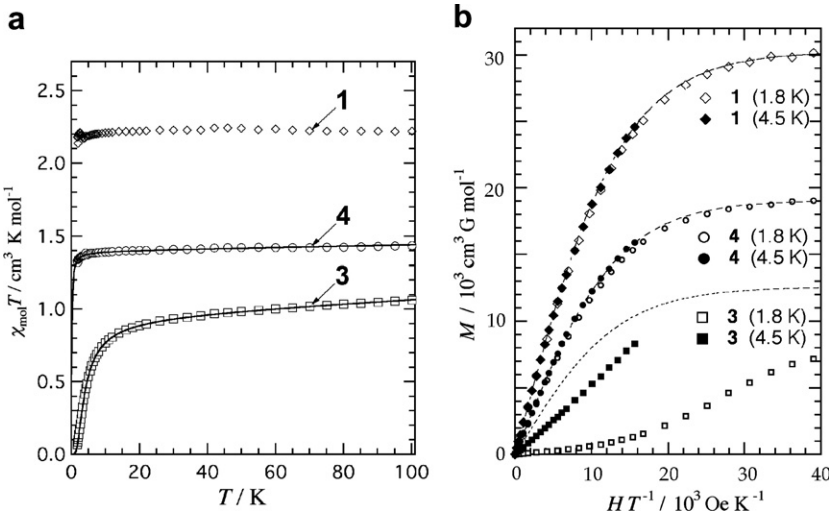

Fig. 6. (a) Temperature dependence of the product $\chi_{mol}T$ for **1** · (octane), **3** and **4** measured at 5000 Oe. The solid lines represent the best fit curves. See the text for the parameters. (b) Magnetization curves for **1** · (octane), **3** and **4** measured at 1.8 and 4.5 K. Dotted lines represent calculated curves for non-interacting Cu_5, Cu_3 and Cu_2 spins based on the $S = 1/2$ Brillouin function.

2.5. DFT calculation

A $3d_{z^2}$ or $3d_{x^2-y^2}$ character is crucial for the Cu-Cu magnetic coupling and may be predicted from the geometry and crystal-field theory. However, a theoretical calculation would be a more reliable way to determine the direction of the magnetic orbitals as well as the ground spin states. We performed a UB3LYP/6-31G(d,p) calculation using the structural parameters given from the crystallographic study.

A dinuclear model [{Cu(hfac)$_2$}$_2$(μ-bmpyz)$_2$] as a terminal dinuclear moiety of **1** was examined to explain part of the magnetic properties of **1**. We can reduce the calculation cost, assuming that the inner Cu-Cu interactions are disregarded. We found that the converged self-consistent-field (SCF) energies of [{Cu(hfac)$_2$}$_2$(μ-bmpyz)$_2$] were −7964.55583715 and −7964.55583691 a.u. for the singlet and triplet states, respectively, where the SCF convergence criterion was set to 10^{-9} a.u. The ground low-spin state was indicated. The exchange coupling parameter J was calculated to be −0.038 K from $\Delta E_{ST} = -2.4 \times 10^{-7}$ a.u. The spin density surface is drawn in Fig. 7a, clearly representing the singly-occupied molecular orbitals (SOMOs) carrying a $3d_{x^2-y^2}$ character both at the SqP and Oh Cu ions as usual. The present ΔE_{ST} seems close to the limit of the accuracy of such MO calculations. However the ground state prediction was reproducible when other basis sets were applied, such as Lanl2dz.

The converged SCF energies of **3** were −7464.54993268 and −7464.54992288 a.u. for the singlet and triplet states, respectively. A ground low-spin state was indicated. The exchange coupling parameter J was calculated to be −1.6 K from $\Delta E_{ST} = -9.8 \times 10^{-6}$ a.u. The spin density surface is drawn in Fig. 7b, clearly representing the SOMOs carrying a $3d_{z^2}$ character at the TBP Cu ions, being consistent with the EPR result. The N lone pair at the TBP eq position appreciably contributes to the SOMO.

We applied a dinuclear model in **4**, namely [{Cu(hfac)$_2$}$_2$(μ-trpyz)$_2$], to a similar calculation (Fig. 7c). We obtained the converged SCF energies of −7806.71550428 and −7806.71550348 a.u. for the singlet and triplet states, respectively. The low-spin state is favored, and therefore the whole molecule of **4** would also favor a low spin (doublet) state at the ground state owing to antiferromagnetic interaction on both sides. The exchange coupling parameter J was calculated to be −0.13 K from $\Delta E_{ST} = -8.0 \times 10^{-7}$ a.u. In sharp contrast to the TBP Cu ions, the Oh Cu ion has a magnetic orbital solely on the eq plane as clarified from the absence of the spin distribution onto the pyrazine bridge.

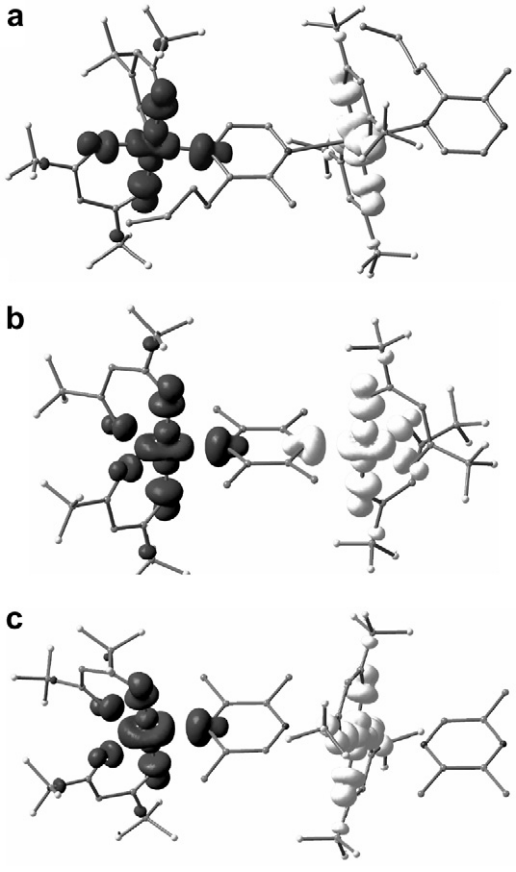

Fig. 7. Spin density surfaces of the singlet states of (a) the dinuclear model [{Cu(hfac)$_2$}$_2$(μ-bmpyz)$_2$] in **1**, (b) [{Cu(hfac)$_2$}$_2$(μ-tmpyz)$_2$] (**3**) and (c) the dinuclear moiety [{Cu(hfac)$_2$}$_2$(μ-trpyz)$_2$] in **4**. Dark grey: positive spin; light grey: negative spin. Hydrogen atoms are omitted.

The exchange interaction parameters were well reproduced as follows: $|J_{SqP-Oh}|/k_B < 0.1$ K versus −0.038 K (calc.) for **1**, $J_{TBP-TBP}/k_B = -3.6$ K versus −1.6 K (calc.) for **3** and $J_{TBP-Oh}/k_B =$

−0.12 K versus −0.13 K (calc.) for **4**. These satisfactory results support the reliability of the magnetic orbital pictures. The magnetic coupling depends on the presence or absence of the interaction between the Cu dσ and N lone pair orbitals, as Fig. 7 clearly illustrates.

3. Discussion

Somewhat large *J* values (−30.5 and −44 K) were observed for the dicopper complexes containing the sterically hindered tetra(2-pyridyl)pyrazine [25]. When the large displacement of the metal from the pyz plane causes the orbital overlap between the Cu $3d_{x^2-y^2}$ and N $2p_z$ orbitals, the pyz π-pathway would be operative and strengthens the antiferromagnetic interaction [26] as expected from the spin polarization scheme [4]. In the present study, **3** belongs to the eq–eq category, where the Cu ions have a TBP structure. The magneto-structure relation exploited on Oh Cu complexes basically holds for complexes containing TBP Cu ions, since the magnetic orbital is distributed at the eq positions as well as the ax positions of the TBP coordination sphere. The magnitude of the *J* value (−3.6 K) seems quite usual among the eq–eq pyz-bridged complexes [7,8]. The observed coupling can be attributed to the intrinsic σ-type exchange pathway, thanks to the strict orthogonal arrangement between the Cu e_g and N $2p_z$ orbitals.

Haddad et al. reported that the pyz nitrogen atom was located at a TBP ax position in $[\{Cu(tren)_2\}_2(\mu\text{-pyz})](ClO_4)_2$ (tren stands for tris(2-aminoethyl)amine) [9]. The exchange interaction was −4.6 K [9], which is slightly larger than that of **3**, despite of the longer ax Cu–N distance. The reason apparently resides in the character of the lobe direction of the magnetic $3d_{z^2}$ orbital.

To our knowledge, there have been two reports on ferromagnetic compounds belonging to the eq–ax category of pyz-bridged Oh Cu complexes [10,11]. The orthogonality between the Cu $3d_{x^2-y^2}$ and N $2p_z$ orbitals is essential, which is supported by an extended superexchange mechanism, originally proposed for M–X–M systems by Anderson [27], Goodenough [28] and Kanamori [29,30]. Fig. 8a shows a possible MO diagram explaining the role of the ferromagnetic couplers. When the energy gap Δ is sufficiently small, the electron configuration is regulated by Hund's rule. We can draw practically the same diagrams including two $3d_{x^2-y^2}$ orbitals for Oh(eq)-Oh(ax) and SqP(eq)-Oh(ax) dinuclear complexes as well as $3d_{z^2}$ and $3d_{x^2-y^2}$ orbitals for TBP(eq)-Oh(ax) dinuclear complexes.

In the present study, although the dinuclear portions of **1** and **4** belong to the eq–ax category, we could not observe ferromagnetic coupling. A reason for this may be attributed to the broken orthogonality, which is indicated by the N1···N2–Cu2 angles of 168.0(2)° for **1** and the corresponding angle (N2···N1–Cu1) of 168.76(12)° for **4**.

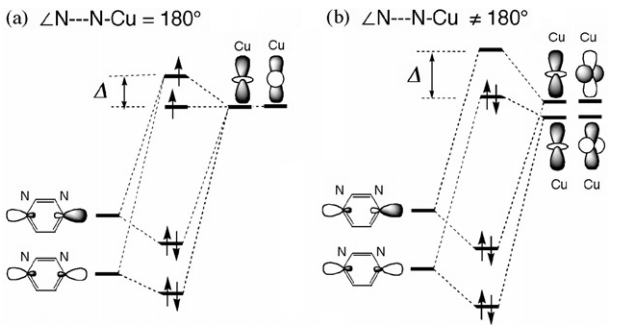

Fig. 8. Orbital interaction diagram between the pyz N lone pairs and two Cu magnetic orbitals (a) with a linear N···N–Cu geometry and (b) with a non-linear N···N–Cu geometry.

Fig. 8b depicts the antiferromagnetic couplings from the MO theory. The energy gap Δ becomes wide owing to the increase of the orbital overlaps, leading to the preference of the ground low-spin state.

4. Conclusions

Sterically bulky pyrazines are successfully utilized for the preparation of discrete oligo-nuclear TBP, SqP and Oh Cu complexes, in contrast to the previous report on the infinite Oh Cu chains involving less bulky pyrazine bridges [14]. We have characterized the unique linear pentanuclear complex (**1**). Although several branched pentanuclear copper(II) complexes are known [31], to the best of our knowledge, the present compound is the first self-assembled linear pentanuclear copper(II) complex without preorganization of bridging ligands. We synthesized a dinuclear copper(II) complex (**3**) in which the N atoms are located at an eq site at each TBP Cu ion. The magneto-structure relation exploited on Oh Cu complexes basically holds for complexes containing TBP Cu ions as well as SqP ions, since the magnetic orbital is confirmed to be present at the eq positions of the TBP and SqP coordination spheres. Appreciable magnetic coupling was found for **3**, which belongs to the eq–eq category. The σ-pathway is essential for the superexchange mechanism, and the magnitude of *J* was precisely evaluated.

5. Experimental

5.1. Materials

Bis(1,1,1,5,5,5-hexafluoropentane-2,4-dionato)copper(II) was purified by the reported method [32]. 2-Butyl-3-methylpyrazine (Tokyo Chemical Industry Co.), tetramethylpyrazine and 2,3,5-trimethylpyrazine (Aldrich Chemical Co.) were used without further purification.

5.1.1. Preparation of *1*

The complex $[Cu(hfac)_2]$ (273 mg, 0.57 mmol) was dissolved in octane (30 cm^3) with 2-butyl-3-methylpyrazine (68.8 mg, 0.46 mmol). The solution was refluxed for 1 h. After the solvent was evaporated at room temperature, green crystals were formed. They were filtered and then washed with a small amount of chilled octane. The yield was 35% as **1** · (octane). Mp. 85 - 87°C. The crystals were suitable for elemental analysis, X-ray diffraction study and magnetic measurements without further purification. The elemental analysis (C, H, N) of the products was carried out on a Fisons EA-1108 by the usual combustion method. *Anal.* Calc. for $C_{94}H_{84}Cu_5F_{60}N_8O_{20}$: C, 36.38; H, 2.73; N, 3.61. Found: C, 36.13; H, 2.65; N, 3.67%. IR spectra were recorded on a Horiba TF-720 Fourier transform infrared spectrophotometer. IR (KBr disk) *ν*(C–O) 1657 and 1641, ring def. 679 and 670, $\delta_s CF_3$ 596 and 580 cm^{-1}.

5.1.2. Preparation of *2*

The complex $[Cu(hfac)_2]$ (258 mg, 0.54 mmol) was dissolved in octane (8 cm^3) with 2-butyl-3-methylpyrazine (66 mg, 0.44 mmol). The solution was refluxed for 2.5 h. After the solvent was evaporated at room temperature, green crystals were formed. The yield was 34% as **2**. Mp. 79–83°C. The elemental analysis indicated the presence of a small amount of **1** · (octane) as an impurity. *Anal.* Calc. for $\{C_{48}H_{34}Cu_3F_{36}N_4O_{12}\}_{0.8}\{C_{94}H_{84}Cu_5F_{60}N_8O_{20}\}_{0.2}$ (i.e., $\mathbf{2}_{0.8}(\mathbf{1} \cdot (\text{octane}))_{0.2}$): C, 34.22; H, 2.21; N, 3.35. Found: C, 34.09; H, 2.51; N, 3.62%. IR (KBr disk) *ν*(C–O) 1641, ring def. 680, $\delta_s CF_3$ 597 cm^{-1}.

5.1.3. Preparation of *3*

The complex $[Cu(hfac)_2]$ (97 mg, 0.20 mmol) was dissolved in pentane (10 cm^3) with half a molar quantity of tetramethylpyr-

azine (14 mg, 0.10 mmol). The solution was refluxed for 1 h. After the solvent was evaporated at room temperature, green crystals were formed. They were filtered, washed with a small amount of chilled pentane and dried *in vacuo*. The yield was 62%. Mp. 116–118 °C. The crystals were suitable for elemental analysis, X-ray diffraction study and magnetic measurements without further purification. *Anal.* Calc. for $C_{28}H_{16}Cu_2F_{24}N_2O_8$: C, 30.81; H, 1.48; N, 2.57. Found: C, 31.03; H, 1.72; N, 2.56%. The formula of **3** was also confirmed by Electro-spray-ionization time-of-flight mass spectroscopy (ESI-MS), which was recorded on a JEOL JMS-T100LC mass spectrometer, using methanol as a solvent. Calc. for **3**: m/z 1089.9, found: m/z 1113.6 ($M + Na^+$). IR (KBr disk) ν(C–O) 1653 and 1645, ring def. 675, $\delta_s CF_3$ 596 and 586 cm^{-1}.

5.1.4. Preparation of 4

Compound **4** (mp. 105–107°C) was prepared by the reported method [17].

5.2. X-ray crystallographic analysis

X-ray diffraction data of **1**–**4** were collected on a Rigaku *R*-axis RAPID diffractometer with graphite monochromated Mo Kα radiation ($\lambda = 0.71069$ Å). The structures were directly solved by the heavy-atom method and expanded using Fourier techniques in the CRYSTALSTRUCTURE program package [33]. A numerical absorption correction was used. All of the hydrogen atoms were located at calculated positions and the parameters were refined as "riding". The thermal displacement parameters of the non-hydrogen atoms were refined anisotropically. Full-matrix least-squares methods were applied using all of the unique reflection data. The crystal structure of **4** was also determined, which is practically the same as that of the previous report [17] and the refinement was improved because of the lower temperature. Selected crystallographic data are listed in Table 1.

The cell parameters of the solvated complexes from **1** are listed below. **1** · (pentane): $a = 11.660(10)$, $b = 13.919(13)$, $c = 19.545(19)$ Å, $\alpha = 102.26(8)$, $\beta = 98.52(7)$, $\gamma = 101.50(7)°$, $V = 2977(5)$ Å^3. **1** · (hexane): $a = 11.678(5)$, $b = 13.821(5)$, $c = 19.601(10)$ Å, $\alpha = 101.42(4)$, $\beta = 98.62(4)$, $\gamma = 102.00(4)°$, $V = 2972(2)$ Å^3. The molecular skeletons of **1** were confirmed, though the solvent molecules were highly disordered.

5.3. Magnetic measurements

Magnetic properties of polycrystalline specimens of **1**, **3** and **4** were measured on a Quantum Design MPMS SQUID magnetometer equipped with a 7 T coil in a temperature range 1.8–300 K. The magnetic responses were corrected with diamagnetic blank data of the sample holder measured separately. The diamagnetic contribution of the sample itself was estimated from Pascal's constants.

5.4. EPR measurements

EPR spectra of **3** were recorded on a Bruker ESP300E X-band (9.7 GHz) spectrometer. A single crystal sample was mounted on a quartz sample tube with a slight amount of Apiezon H grease and the crystal axis was carefully oriented under a microscope. The crystal planes were defined with Miller indexes by means of X-ray diffraction, and the crystallographic axes could be assigned on a single crystal.

5.5. DFT calculation

Molecular orbital calculations were performed on the GAUSSIAN 03 program [34]. We applied unrestricted density functional (DFT) UB3LYP methods with the Becke exchange functional [35] and the Lee–Yang–Parr correlation functional [36]. The 6-31G(d,p) basis set was chosen. The convergence criterion for the energy was set at 10^{-9} a.u. The structural parameters of **1**, **3** and **4** were given from the crystallographic data. The energies of the triplet and broken-symmetry singlet states were calculated, and the exchange parameter J was derived by the expression $2J = E_{BS} - E_T$ [37].

6. Supplementary data

CCDC 662859, 662860, 662861, 631791 and 631792 contains the supplementary crystallographic data for **1** · (octane), **1** · (cyclohexane)$_2$, **2**, **3** and **4**. These data can be obtained free of charge via http://www.ccdc.cam.ac.uk/conts/retrieving.html, or from the Cambridge Crystallographic Data Centre, 12 Union Road, Cambridge CB2 1EZ, UK; fax: (+44) 1223-336-033; or e-mail: deposit@ccdc.cam.ac.uk.

Table 1
Selected crystallographic data for **1** · (octane), **1** · (cyclohexane)$_2$, **2**, **3** and **4**

Compounds	**1** · (octane)	**1** · (cyclohexane)$_2$	**2**	**3**	**4**
Formula	$C_{94}H_{84}Cu_5F_{60}N_8O_{20}$	$C_{98}H_{90}Cu_5F_{60}N_8O_{20}$	$C_{48}H_{34}Cu_3F_{36}N_4O_{12}$	$C_{28}H_{16}Cu_2F_{24}N_2O_8$	$C_{44}H_{26}Cu_3F_{36}N_4O_{12}$
Formula weight	3103.37	3157.46	1733.40	1091.50	1677.29
Habit	green block	green block	green block	green block	green block
Dimension (mm^3)	0.9 × 0.9 × 0.5	0.8 × 0.7 × 0.4	0.8 × 0.7 × 0.5	0.72 × 0.40 × 0.38	0.80 × 0.51 × 0.45
T (K)	105	100	101	293	90
Crystal system	triclinic	triclinic	triclinic	orthorhombic	triclinic
Space group	$P\bar{1}$	$P\bar{1}$	$P\bar{1}$	*Fddd*	$P\bar{1}$
a (Å)	11.655(6)	11.6583(15)	9.4791(15)	12.619(6)	8.8148(5)
b (Å)	14.062(6)	14.2928(19)	16.919(2)	20.790(14)	8.8744(4)
c (Å)	19.630(9)	19.785(3)	20.000(3)	30.237(14)	19.1601(8)
α (°)	102.68(3)	103.242(3)	83.754(5)	90	83.823(3)
β (°)	98.16(4)	97.891(3)	88.617(4)	90	82.549(3)
γ (°)	102.09(4)	101.659(4)	89.665(2)	90	81.624(2)
V (Å^3)	3009(2)	3084.0(7)	3187.5(8)	7933(7)	1464.29(12)
Z	1	1	2	8	1
D_{calc} (g cm^{-3})	1.712	1.700	1.806	1.828	1.902
Unique data	12810	13045	14442	2281	6694
μ(Mo Kα) (mm^{-1})	1.028	1.004	1.157	1.233	1.255
R_{int}	0.058	0.052	0.080	0.071	0.055
$R(F)$[a] ($I > 2\sigma(I)$)	0.0601	0.0597	0.0629	0.0447	0.0410
$R_w(F^2)$[b] (all data)	0.0759	0.0682	0.0893	0.0585	0.0738

[a] $R = \sum||F_o| - |F_c||/\sum|F_o|$.
[b] $R_w = [\sum w(F_o^2 - F_c^2)^2/\sum w(F_o^2)^2]^{1/2}$.

Acknowledgements

This work was supported by Grants-in-Aid for Scientific Research (Nos. 17550166 and 19550135) from the Ministry of Education, Culture, Sports, Science and Technology, Japan.

References

[1] O. Kahn, Molecular Magnetism, VCH, New York, 1993.
[2] (a) S. Kitagawa, R. Kitaura, S. Noro, Angew. Chem., Int. Ed. 43 (2004) 2334;
(b) J.A.R. Navarro, E. Barea, M.A. Galindo, J.M. Salas, M.A. Romero, M. Quiros, N. Masciocchi, S. Galli, A. Sironi, B. Lippert, J. Solid State Chem. 178 (2005) 2436.
[3] (a) M. Ruben, J. Rojo, F.J. Romero-Salquero, L.H. Uppadine, J.-M. Lehn, Angew. Chem., Int. Ed. 43 (2004) 3644;
(b) J.-M. Lehn, Supramolecular Chemistry. Concept and Perspectives, VCH, Weinheim, Germany, 1995. Chapter 9.
[4] (a) H. Iwamura, Adv. Phys. Org. Chem. 26 (1990) 179;
(b) A. Rajca, Chem. Rev. 94 (1994) 871.
[5] (a) T. Ishida, S. -i. Mitsubori, T. Nogami, N. Takeda, M. Ishikawa, H. Iwamura, Inorg. Chem. 40 (2001) 7059;
(b) T. Ishida, T. Kawakami, S.-i. Mitsubori, T. Nogami, K. Yamaguchi, H. Iwamura, J. Chem. Soc., Dalton Trans. (2002) 3177;
(c) T. Ishida, S.-i. Mitsubori, N. Takeda, M. Ishikawa, H. Iwamura, T. Nogami, Synth. Met. 71 (1995) 1791;
(d) M. Yasui, Y. Ishikawa, N. Akiyama, T. Ishida, T. Nogami, F. Iwasaki, Acta Crystallogr., Sect. B 57 (2001) 288;
(e) T. Kusaka, T. Ishida, D. Hashizume, F. Iwasaki, T. Nogami, Chem. Lett. (2000) 1146;
(f) K. Nakayama, T. Ishida, R. Takayama, D. Hashizume, M. Yasui, F. Iwasaki, T. Nogami, Chem. Lett. (1998) 497.
[6] (a) T. Ezuhara, K. Endo, K. Matsuda, Y. Aoyama, New J. Chem. 24 (2000) 609;
(b) L.C. Tabares, J.A.R. Navarro, J.M. Salas, M. Willermann, Inorg. Chim. Acta 318 (2001) 2001;
(c) R. Feyerherm, J. Magn. Magn. Mater. 256 (2003) 328.
[7] (a) H.W. Richardson, W.E. Hatfield, J. Am. Chem. Soc. 98 (1976) 835;
(b) G. Mennenga, L.J. de Jongh, W.J. Huiskamp, J. Reedijk, J. Magn. Magn. Mater. 44 (1984) 89;
(c) P.R. Hammar, M.B. Stone, D.H. Reich, C. Broholm, P.J. Gibson, M.M. Turnbull, C.P. Landee, M. Oshikawa, Phys. Rev. B 59 (1999) 1008.
[8] (a) J. Darriet, M.S. Haddad, E.N. Duesler, D.N. Hendrickson, Inorg. Chem. 18 (1979) 2679;
(b) T. Okubo, M. Kondo, S. Kitagawa, Synth. Met. 85 (1997) 1661;
(c) G.W. Inman Jr., W. Hatfield, Inorg. Chem. 11 (1972) 3085;
(d) J.S. Haynes, S.J. Rettig, J.R. Sams, J. Trotter, R.C. Thompson, Inorg. Chem. 27 (1988) 1237;
(e) S. Amaral, W.E. Jensen, C.P. Lande, M.M. Turnbull, F.M. Woodward, Polyhedron 20 (2001) 1317;
(f) F.F. Awwadi, C.P. Landee, M.M. Turnbull, B. Twamley, B.M. Wells, Polyhedron 24 (2005) 2153.
[9] M.S. Haddad, D.N. Hendrickson, J.P. Cannady, R.S. Drago, D.S. Bieksza, J. Am. Chem. Soc. 101 (1979) 898.
[10] C.J. O'Connor, C.L. Klein, R.J. Majeste, L.M. Trefonas, Inorg. Chem. 21 (1982) 64.
[11] G. Beobide, O. Castillo, A. Luque, U. García-Couceiro, J.P. Carcía-Terán, P. Román, Inorg. Chem. 45 (2006) 5367.
[12] R.C.E. Belford, D.E. Fenton, M.R. Truter, J. Chem. Soc., Dalton Trans. (1974) 17.
[13] M. Nakagawa, Y. Ishikawa, T. Kogane, T. Ishida, M. Yasui, F. Iwasaki, T. Nogami, Mol. Cryst. Liq. Cryst. 286 (1996) 29.
[14] T. Kogane, N. Koyama, T. Ishida, T. Nogami, Polyhedron 26 (2007) 1811.
[15] (a) J.-L. Pierre, P. Chautemps, S. Refaif, C. Beguin, A. El Marzouki, G. Serratrice, E. Saint-Aman, P. Rey, J. Am. Chem. Soc. 117 (1995) 1965;
(b) H. Ohtsu, Y. Shimazaki, A. Odani, O. Yamauchi, W. Mori, S. Itoh, S. Fukuzumi, J. Am. Chem. Soc. 122 (2000) 5733;
(c) J. Suárez-Varela, E. Colacio, A. Romerosa, J.C. Avilarosón, M.A. Hidalgo, J. Romero, Inorg. Chim. Acta 217 (1994) 39;
(d) H. Oshio, U. Nagashima, Inorg. Chem. 29 (1990) 3321;
(e) V. Tudor, V. Kravtsov, M. Julve, F. Lloret, Y.A. Simonov, J. Lipkowski, V. Buculei, M. Andruh, Polyhedron 20 (2001) 3033.
[16] (a) H. Grove, J. Sletten, M. Julve, F. Lloret, J. Chem. Soc., Dalton Trans. (2001) 2487;
(b) C. Fernandes, A. Neves, A.J. Bortoluzzi, A.S. Mangrich, E. Rentschler, B. Szpoganicz, E. Schwingel, Inorg. Chim. Acta 320 (2001) 12;
(c) R.J. Parker, L. Spiccia, B. Moubaraki, K.S. Murray, B.W. Skelton, A.H. White, Inorg. Chim. Acta 300–302 (2000) 922;
(d) X.-H. Bu, M. Du, Z.-L. Shang, R.-H. Zhang, D.-Z. Liao, M. Shionoya, T. Clifford, Inorg. Chem. 39 (2000) 4190.
[17] T. Kogane, K. Kobayashi, M. Ishii, R. Hirota, M. Nakahara, J. Chem. Soc., Dalton Trans. (1994) 13.
[18] (a) T. Kogane, M. Ishii, K. Harada, R. Hirota, M. Nakahara, Bull. Chem. Soc. Jpn. 62 (1989) 2524;
(b) T. Kogane, M. Ishii, K. Harada, R. Hirota, M. Nakahara, Bull. Chem. Soc. Jpn. 63 (1990) 1005;
(c) T. Kogane, K. Kobayashi, M. Ishii, R. Hirota, M. Nakahara, Chem. Lett. (1991) 419;
(d) T. Kogane, K. Harada, R. Hirota, A. Urushiyama, Polyhedron 15 (1996) 4093.
[19] A.W. Addison, T.N. Rao, J. Reedjik, J. van Rijin, C.G. Verschoor, J. Chem. Soc., Dalton Trans. (1984) 1349.
[20] T. Konno, K. Tokuda, J. Sakurai, K.-i. Okamoto, Bull. Chem. Soc. Jpn. 73 (2000) 2767.
[21] (a) N. Wei, N.N. Murthy, K.D. Karlin, Inorg. Chem. 33 (1994) 6093;
(b) A.W. Addison, H.M. Hendriks, J. Reedijk, L. Thompson, Inorg. Chem. 20 (1983) 103.
[22] (a) B.J. Hathaway, D.E. Billing, Coord. Chem. Rev. 5 (1970) 143;
(b) A. Bencini, I. Bertini, D. Gatteschi, A. Scozzafava, Inorg. Chem. 17 (1978) 3194;
(c) D. Reinen, C. Friebel, Inorg. Chem. 23 (1984) 791.
[23] B. Bleaney, K.D. Bowers, Proc. R. Soc. London A 214 (1952) 451.
[24] R.W. Jotham, S.F. Kettle, J.A. Marks, J. Chem. Soc., Faraday Trans. 2 (1976) 125.
[25] (a) E. Burkholder, V. Golub, C.J. O'Connor, J. Zubieta, Inorg. Chem. 42 (2003) 6729;
(b) M. Craf, H. Stoeckli-Evans, A. Escuer, R. Vicente, Inorg. Chim. Acta 257 (1997) 89.
[26] G. Beobide, O. Castillo, U. García-Couceiro, J.P. García-Terán, A. Luque, M. Martínez-Ripoll, P. Román, Eur. J. Inorg. Chem. (2005) 2586.
[27] P.W. Anderson, Phys. Rev. 115 (1959) 2.
[28] J.B. Goodenough, Phys. Rev. 100 (1955) 564.
[29] J. Kanamori, J. Phys. Chem. Solids 10 (1959) 87.
[30] H. Oshio, M. Nakano, Chem. Eur. J. 11 (2005) 5178.
[31] (a) P. Gamez, P. de Hoog, O. Roubeau, M. Lutz, W.L. Driessen, A.L. Spek, J. Reedijk, Chem. Commun. (2002) 1499;
(b) P. Klüfers, T. Kunte, Z. Anorg. Allg. Chem. 630 (2004) 553;
(c) E. Farkas, D. Bátka, E. Csapó, P. Buglyó, W. Haase, D. Sanna, Polyhedron 26 (2007) 543.
[32] J.A. Bertrand, R.I. Kaplan, Inorg. Chem. 5 (1966) 489.
[33] CRYSTALSTRUCTURE, version 3.8, Rigaku/MSC, The Woodlands, TX 77381, USA, 2003.
[34] M.J. Frisch, G.W. Trucks, H.B. Schlegel, G.E. Scuseria, M.A. Robb, J.R. Cheeseman, J.A. Montgomery Jr., T. Vreven, K.N. Kudin, J.C. Burant, J.M. Millam, S.S. Iyengar, J. Tomasi, V. Barone, B. Mennucci, M. Cossi, G. Scalmani, N. Rega, G.A. Petersson, H. Nakatsuji, M. Hada, M. Ehara, K. Toyota, R. Fukuda, J. Hasegawa, M. Ishida, T. Nakajima, Y. Honda, O. Kitao, H. Nakai, M. Klene, X. Li, J.E. Knox, H.P. Hratchian, J.B. Cross, C. Adamo, J. Jaramillo, R. Gomperts, R.E. Stratmann, O. Yazyev, A.J. Austin, R. Cammi, C. Pomelli, J.W. Ochterski, P.Y. Ayala, K. Morokuma, G.A. Voth, P. Salvador, J.J. Dannenberg, V.G. Zakrzewski, S. Dapprich, A.D. Daniels, M.C. Strain, O. Farkas, D.K. Malick, A.D. Rabuck, K. Raghavachari, J.B. Foresman, J.V. Ortiz, Q. Cui, A.G. Baboul, S. Clifford, J. Cioslowski, B.B. Stefanov, G. Liu, A. Liashenko, P. Piskorz, I. Komaromi, R.L. Martin, D.J. Fox, T. Keith, M.A. Al-Laham, C.Y. Peng, A. Nanayakkara, M. Challacombe, P.M.W. Gill, B. Johnson, W. Chen, M.W. Wong, C. Gonzalez, J.A. Pople, GAUSSIAN 03, Revision C.02, Gaussian, Inc., Wallingford, CT, 2004.
[35] A.D. Becke, J. Chem. Phys. 98 (1993) 5648.
[36] C. Lee, W. Yang, R.G. Parr, Phys. Rev. B 37 (1998) 785.
[37] E. Ruiz, J. Cano, S. Alvarez, P. Alemany, J. Comp. Chem. 20 (1999) 1391.

Polyhedron 27 (2008) 2349–2356

Contents lists available at ScienceDirect

Polyhedron

journal homepage: www.elsevier.com/locate/poly

Copper(II)–lanthanide(III) 15-metallacrown-5 complexes based on pyrazinohydroxamic acid as new multiple-binding pentagonal platforms with Lewis amphoteric nature

Evgen V. Govor [a], Andrey B. Lysenko [a,*], Alexander N. Chernega [b], Judith A.K. Howard [c], Andriy A. Mokhir [d], Joachim Sieler [e], Konstantin V. Domasevitch [a,*]

[a] Inorganic Chemistry Department, Kiev University, Volodimirska Street 64, Kiev 01033, Ukraine
[b] Institute of Organic Chemistry, Murmanskaya Street 5, Kiev-94 02094, Ukraine
[c] Department of Chemistry, University of Durham, Durham DH1 3LE, UK
[d] Anorganisch-Chemisches Institut, Universität Heidelberg, Im Neuenheimer Feld 270, 69120 Heidelberg, Germany
[e] Institut für Anorganische Chemie, Universität Leipzig, Linnéstraße 3, D-04103 Leipzig, Germany

ARTICLE INFO

Article history:
Received 29 January 2008
Accepted 27 April 2008
Available online 8 June 2008

Keywords:
Metallacrowns
Pyrazinohydroxamic acid
Heterobimetallic complexes
Coordination polymers
Crystal structures

ABSTRACT

Reaction of copper(II) acetate, lanthanium(III) or gadolinium(III) nitrate (1/5 equiv.) with pyrazinohydroxamic acid (H_2Pyzha) in DMF led to a series of new heterobimetallic 15-metallacrown-5 complexes. In a MeOH/H_2O solution the complexes exist as molecular unassociated metallacrowns. In solid state their structures are more complicated as it has been confirmed by X-ray analysis: discrete molecular metallacrowns $[Gd(NO_3)_2\{Cu(pyzha)\}_5(DMF)_4(NO_3)] \cdot 0.5C_6H_6 \cdot H_2O$ (**1**), $[Gd(NO_3)_2\{Cu(pyzha)\}_5(DMF)_5](NO_3) \cdot 1.5DMF \cdot 0.5H_2O$ (**2**), $[La(NO_3)_2\{Cu(pyzha)\}_5(DMF)_5]NO_3 \cdot 1.5DMF \cdot 2C_6H_6$ (**3**) are solvates, whereas compound $[\{La(NO_3)_2\{Cu(pyzha)\}_5(DMF)_5\}_2(\mu^2\text{-}NO_3)](NO_3) \cdot 3DMF$ (**4**) is a dimer, where μ-bridged nitrate links two copper centres of the adjacent metallamacrocycles. Complex $[Gd(NO_3)_2\{Cu(pyzha)\}_5(DMF)_2(H_2O)(NO_3)] \cdot CH_2Cl_2 \cdot DMF$ (**5**) self-associates into a polymer chain by means of one pyrazine moiety and the copper ring atom. Reaction of the molecular metallacrowns with excess of inorganic salts $CdBr_2$ or $Cu(OAc)_2$ proceeds as anion methathesis process affording heteroanionic metallacrowns: molecular $[Gd(NO_3)_2\{Cu(pyzha)\}_5(DMF)_5]$ $[Gd(NO_3)_2\{Cu(pyzha)\}_5(DMF)_4(H_2O)][CdBr_4] \cdot 1.5DMF$ (**6**), and 3D hydrogen bonded polymer $[La(\mu^2\text{-}OAc)(H_2O)_3\{Cu(pyzha)\}_5(H_2O)_4(NO_3)](NO_3) \cdot 4H_2O$ (**7**).

© 2008 Elsevier Ltd. All rights reserved.

1. Introduction

Heterometallic lanthanide/metal multinuclear complexes containing multiple-binding sites represent attractive examples of acceptor (Lewis acid) systems for selective interaction with neutral guest molecules and anions. They are used as catalysts [1–3], chemical sensors [4], contrast reagents for magnetic resonance imaging (Gd(III) chelates [5,6]), and in preparation of unique magnetic materials [7–22]. Molecular design of such receptors with further controllable integration into frameworks is an interesting perspective. These frameworks may be used as sophisticated materials with many potential applications. In particular, the lanthanide encapsulated 15-metallacrown-5 complexes (15-MC-5), discovered by Pecoraro and co-workers [6,23–32], provide a sufficient number of coordination sites situated in close proximity to bind substrates and, thus, they could be regarded as a multiple Lewis acid moiety. These metallamacrocycles could be designed rationally from simple inorganic salts and available organic precursors, such as picoline or isoquinoline hydroxamic acids and related non-planar α-amino hydroxamic acids. Such organic ligands may form two fused five-membered metalochelate rings, therefore they yield planar pseudo-pentagonal core of 15-MC-5. Only few examples of extended structural motifs of the metallacrowns have been realized through either bridging anions [6,26,27] or ligand periphery functionality, e.g., carbonyl oxygen atoms [26,29,31,32]. In this context, the employing the pyrazine moieties, *via* introducing pyrazinohydroxamic acid into 15-MC-5 core, offers essential advantages versus, for instance, pyridine heterocycle because in this case five additional σ-donor groups are introduced into the metallacrown periphery (Scheme 1). Such a ligand modification opens a possibility towards controllable association of the metallamacrocycles into the framework exploiting its Lewis amphoteric nature: either donor activity of five exterior nitrogen/oxygen atoms to coordinate bridging metal ions or alternative acceptor properties of the metallacrown metal centres for binding bridging anions.

In this paper, we describe synthesis, solution behaviour, reactivity towards typical inorganic salts ($CdBr_2$ or $Cu(OAc)_2$) and solid

* Corresponding authors.
E-mail address: dk@univ.kiev.ua (K.V. Domasevitch).

0277-5387/$ - see front matter © 2008 Elsevier Ltd. All rights reserved.
doi:10.1016/j.poly.2008.04.042

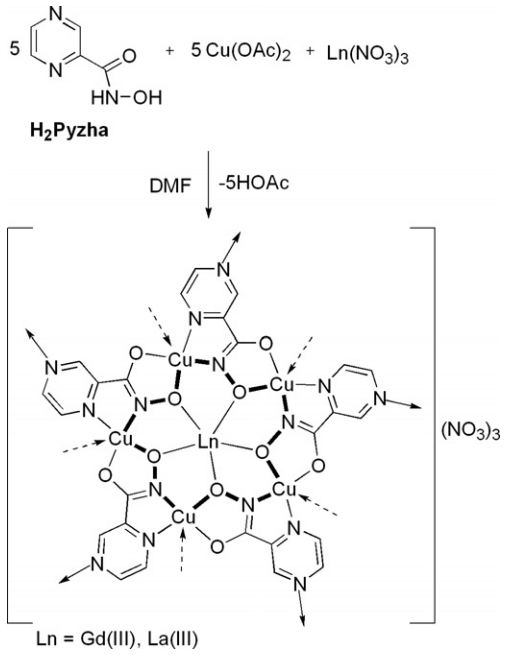

Scheme 1.

state structures of new Gd(III) and La(III) encapsulated 15-MC-5 complexes based on pyrazinohydroxamate ligand. The differentiation of ionic radii between the encapsulated La(III) and Gd(III) could be rationally utilized as an important tool to control bowl-shape distortion of the MC platform from the planar geometry.

2. Results and discussion

Pyrazinohydroxamic acid reacts readily with a mixture of Cu(II) and Ln(III) salts (Ln = Gd(III), La(III)), generating heterobimetallic metallamacrocyclic core, 15-metallacrown-5 complex. A one-step reaction is carried out in DMF solution and affords the desired product in expected high yield ranging from 50% to 70%. In contrast to previous studies describing the general method for preparation of the 15-MC-5 complexes [30], we have used a higher concentration of lanthanide(III) salt (16 mM), hydroxamic acid and copper(II) acetate (80 mM) in the reaction solution (see Section 4).

First, we examined the solution behaviour of the pyrazinohydroxamate metallacrowns by electrospray mass spectrometry (ESI-MS$^+$). These spectra demonstrated the following features: in water–methanol solution the corresponding peaks of molecular ions $Ln(NO_3)_2[15\text{-}MC_{Cu(II)N(pyzha)}\text{-}5]^+$, $Ln(NO_3)[15\text{-}MC_{Cu(II)N(pyzha)}\text{-}5]^{2+}$, $Ln[15\text{-}MC_{Cu(II)N(pyzha)}\text{-}5]^{3+}$ (Ln = Gd, La) remained intact and were found at 1288.9 *m*/*z*, 610.7 and 386.5 for Gd(III) complexes and at 1269.3, 601.2, 308.2 for the La(III)-encapsulated complexes, respectively. These data reflect the similarity in a solution behaviour between the prepared pyrazinometallacrowns and picolinato-metallacrowns described by Pecoraro and co-workers [6].

As previously shown [26], two faces of the 15-MC-5 pentagonal platform could be discriminated by distribution of axially bound molecules. This situation, in case of the 15-MC-5 pyrazinohydroxamates, induces chirality within the molecular macrocyclic structure generating a pair of enantiomers: anticlockwise (A) with the cyclic Cu–N–O orientation and clockwise (C) with the opposite Cu–N–O orientation (Scheme 2).

In the solid state these features have been confirmed by X-ray analysis. The crystal structures of molecular compounds $[Gd(NO_3)_2\{Cu(pyzha)\}_5(DMF)_4(NO_3)] \cdot 0.5C_6H_6 \cdot H_2O$ (**1**), $[Gd(NO_3)_2\{Cu(pyzha)\}_5(DMF)_5](NO_3) \cdot 1.5DMF \cdot 0.5H_2O$ (**2**) and $[La(NO_3)_2\{Cu(pyzha)\}_5(DMF)_5]NO_3 \cdot 1.5DMF \cdot 2C_6H_6$ (**3**) reveal a racemic mixture of the both enantiomers consisting of a typical metallacrown core (Figs. 1, 2 and Tables 1, 2). Either of the five pyrazinohydroxamic ligands is twice deprotonated and forms two fused five-membered metalochelates with the two ring-forming Cu(II) atoms. For the closely related complexes **1** and **2**, the effective agreement between the cavity radius of the macrocycle (1.12 Å) and the ionic radius of nine-coordinate gadolinium ion (1.12 Å [21]) affords perfect location of the lanthanide in the center of the metallacrown with the negligible displacement from the least-square plane of five hydroxamate oxygen atoms (±0.02 Å). The coordination sphere of the Gd(III) ion is completed by five equatorial oxygen atoms of hydroxamates (Gd–O 2.39–2.46 Å) and two axial bidentate nitrate groups, which are symmetrically bound to the metal center above and below the MC plane (Gd–O 2.44–2.53 Å). The similar coordination was previously described for the Eu(III)/Cu(II) picolinehydroxamate 15-MC-5 complex [6]. The coordinated DMF molecules occupy the apical positions of the square-pyramidal Cu(II) atoms from one side of the metallacrowns, forming a complete coordination shell. Note that metallacrown-face discrimination phenomenon towards the bound solvent molecules results in a non-planar distortion of the 15-MC-5 core and, therefore, a cone-shaped geometry of the metallamacrocycle. The deviation from planarity is evidenced by displacements of the cavity centre of the metallacrown from the least-square plane of the five peripheral pyrazine nitrogens. Presumably, such a distortion effect is dependent upon the number of coordinated molecules, their molecular size and distribution on either metallacrown platform.

In neutral complex **1**, four DMF molecules and one nitrate, which are bound to the Cu(II) ring atoms from the convex side, fill up less space above the metallacrown plane than five coordinated DMF molecules in complex **2**. This affords notable difference in the deviation value of Gd(III) atom, centered in the cavity, from the best plane of the five exterior nitrogen atoms (0.80 and 1.00 Å for **1** and **2**, respectively).

Unlike the gadolinium complexes, the significantly smaller MC cavity size versus ionic radius of La(III) ion (1.22 Å for nine-coordinate

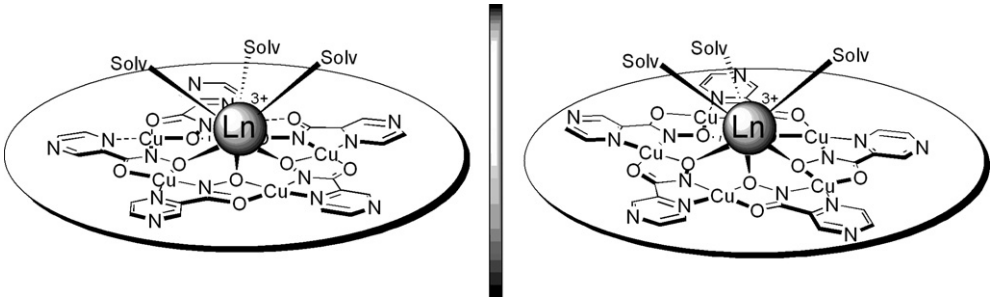

Scheme 2.

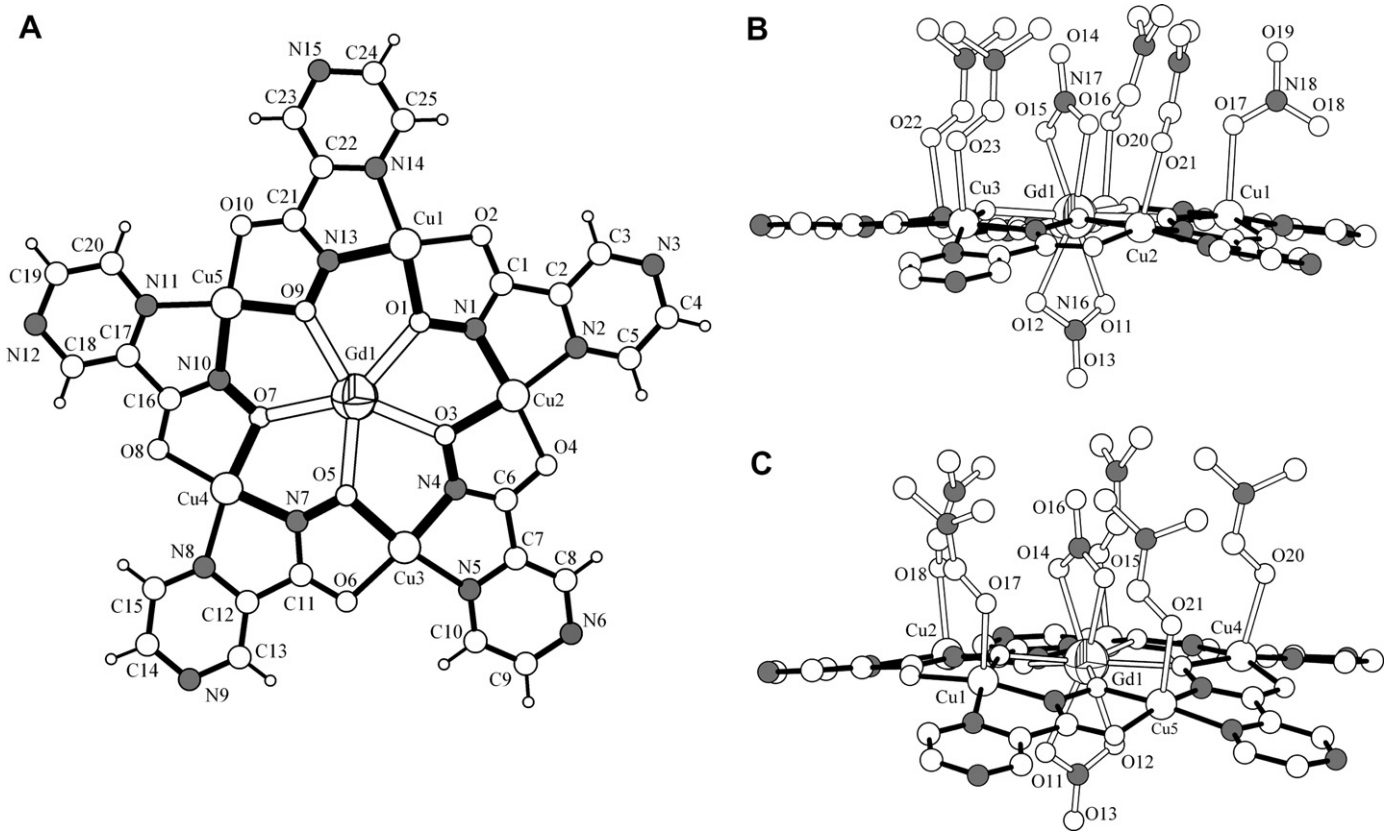

Fig. 1. Molecular structure of Gd(III) encapsulated 15-MC-5 complexes: (A) top view of $[Gd(NO_3)_2\{Cu(pyzha)\}_5(DMF)_4(NO_3)] \cdot 0.5C_6H_6 \cdot H_2O$ **1** (a ring based on the –Cu–N–O– unit is outlined in bold); (B) side view of complex **1**; (C) side view of complex cation $[Gd(NO_3)_2\{Cu(pyzha)\}_5(DMF)_5]^+$ of metallacrown **2**. (Unbound solvent molecules or/and nitrate anions located in the lattice are not shown.)

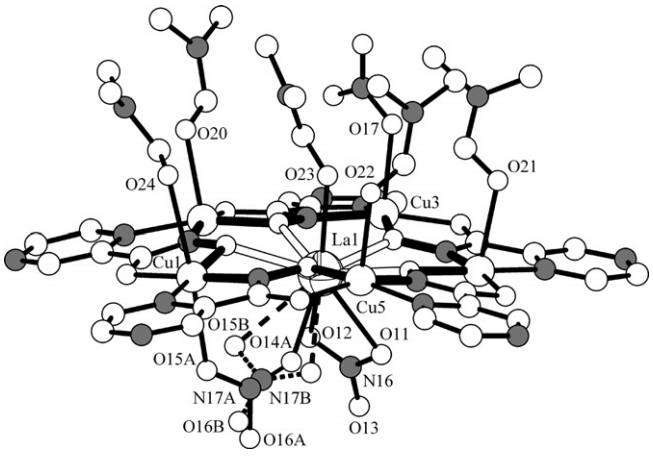

Fig. 2. Side view of the La(III) encapsulated cation $[La(NO_3)_2\{Cu(pyzha)\}_5(DMF)_5]^+$ of metallacrown **3** (one of disordered nitrate anion is shown as a dash line), (La(1)–O(23) 2.52 Å, La(1)–O(12) 2.62 Å, La(1)–O(11) 2.71 Å, Cu(3)–O(17) 2.31 Å); the third nitrate, unbound DMF and benzene molecules are present in the crystal lattice (not shown).

ion) in metallacrown **3** (Fig. 2) results, similarly to a lanthanide porphyrin, in a half-sandwich-type complex, where the encapsulated La(III) centre lies ~0.62 Å above the plane of the macrocycle. The cone-shape metallacrown platform binds five DMF molecules and monodentate nitrate from the convex side, whereas the opposite side is occupied by two nitrate anions coordinated to La(III). Such a distribution of the bound molecules and anions leads to less deviation from planarity (~0.73 Å) of the whole metallacrown platform unlike those observed for complexes **1** and **2**. The nitrate groups coordinated to La(III) demonstrate different binding modes: one NO_3-group is bound in a bidentate chelate fashion, while the other is crystallographically disordered between two positions displaying different chemical roles, such as chelating-bidentate (La(1)–O(14B) 2.72 and La(1)–O15(B) 2.85 Å) and a bridging-bidentate mode between the lanthanide atom and the Cu(1) atom.

The crystal packing behavior of the metallacrowns **1**–**3**, possessing a distinct bowl-shape geometry and large surface area (~215 $Å^2$), offers the opportunity to form intermolecular cavities, which are perfectly suitable to accommodate unbound solvent guests (e.g., DMF, H_2O, benzene) (Fig. 3). The tight packing of the metallamacrocycles also achieved through intermolecular π–π stacking interaction (~3.20 Å).

The La(III) encapsulated complex **4** has a molecular dimeric structure (Fig. 4A). An enantiomeric pair of metallacrowns are linked by a bidentate nitrate anion, which bridges two copper centres from the convex faces of adjacent metallacrowns. Additionally, the convex side is occupied by five DMF molecules, which complete the coordination environment of square pyramidal Cu(II) (Cu–I 2.27–2.34 Å) as well as the deca-coordinated La(III) ion (La(1)–O(17) 2.55 Å), while the concave side contains two bidentate nitrates which are symmetrically bound to the La(III) ion. The crystal packing of such a dimer affords formation of the cages which are filled by uncoordinated DMF molecules (Fig. 4B).

The Lewis amphoteric nature of the synthesized complexes may be the driver to its spontaneous assembly to form the extended network. In the crystal structure of metallacrown **5**, the adjacent enantiomers $[Gd(NO_3)_2\{Cu(pyzha)\}_5(DMF)_2(H_2O)(NO_3)]$ are linked to each other through one of the five peripheral pyrazine nitrogens

Table 1
Crystal data and structure refinement for 15-metallacrown-5 complexes **1**–**7**

	1	2	3	4	5	6	7
Formula	$C_{37}H_{43}Cu_5GdN_{22}O_{23}\cdot 0.5C_6H_6\cdot H_2O$	$C_{40}H_{50}Cu_5GdN_{23}O_{24}\cdot 1.5C_3H_7NO\cdot 0.5H_2O$	$C_{40}H_{50}Cu_5LaN_{23}O_{24}\cdot 1.5C_3H_7NO\cdot 2C_6H_6$	$C_{83}H_{107}Cu_{10}La_2N_{47}O_{49}\cdot 3C_3H_7NO$	$C_{31}H_{31}Cu_5GdN_{20}O_{22}\cdot C_3H_7NO\cdot CH_2Cl_2$	$C_{77}H_{95}Br_4CdCu_{10}Gd_2N_{43}O_{42}\cdot 1.5C_3H_7NO$	$C_{27}H_{32}Cu_5LaN_{17}O_{25}\cdot 4H_2O$
M	1695.95	1830.63	1959.50	3679.66	1668.73	3786.54	1523.37
T (K)	173	173	173	173	173	223	203
Crystal system	triclinic	triclinic	triclinic	triclinic	monoclinic	triclinic	triclinic
Space group	$P\bar{1}$	$P\bar{1}$	$P\bar{1}$	$P\bar{1}$	$P2_1/c$	$P\bar{1}$	$P\bar{1}$
Z	2	2	2	1	4	2	2
a (Å)	12.4159(4)	11.2347(5)	11.9831(5)	11.8137(4)	14.996(3)	13.034(2)	11.5490(4)
b (Å)	15.1935(5)	12.9575(6)	15.8282(7)	15.8137(5)	18.118(4)	22.424(4)	12.9166(4)
c (Å)	16.7702(5)	23.958(1)	20.9019(9)	18.3528(6)	23.820(5)	25.236(5)	18.7124(7)
α (°)	71.792(1)	98.130(2)	91.224(1)	93.319(1)	90.00	108.553(8)	107.835(1)
β (°)	83.787(2)	92.764(1)	92.635(2)	98.063(2)	99.70(3)	90.379(7)	93.561(1)
γ (°)	77.448(1)	92.135(2)	99.412(2)	102.671(1)	90.00	92.590(7)	113.503(2)
V (Å^3)	2930.5(2)	3445.2(3)	3905.3(3)	3298.1(2)	6379(2)	6984(2)	2381.9(2)
D_{calcd} (g cm^{-3})	1.922	1.765	1.666	1.853	1.737	1.801	2.124
μ(Mo Kα) (mm^{-1})	2.996	2.559	1.962	2.317	2.831	3.805	3.183
θ_{max} (°)	25.68	26.37	26.73	25.68	25.68	26.37	28.70
Measured reflections	25948	18744	35534	28943	44466	87073	92994
Unique reflections	11064	13776	16394	12415	12021	28010	12203
Parameters	836	921	1041	914	347	1632	705
R_1, wR_2 $I > 2\sigma(I)$	0.060, 0.108	0.063, 0.167	0.095, 0.188	0.087, 0.166	0.092, 0.223	0.056, 0.134	0.033, 0.086
R_1, wR_2 (all data)	0.112, 0.119	0.089, 0.176	0.147, 0.200	0.151, 0.189	0.153, 0.245	0.109, 0.146	0.046, 0.090

Table 2
Selected bond distances (Å) for 15-metallacrown-5 complexes **1**–**7**

15-MC-5	1	2	3	4	5	6	7
Ln–O (oxime)	2.412(5)–2.454(5)	2.388(5)–2.460(5)	2.523(6)–2.574(6)	2.511(7)–2.625(8)	2.392(8)–2.469(10)	2.393(5)–2.466(8)	2.527(2)–2.567(2)
Ln–O (NO_3^-, chelate–bidentate)	2.444(7)–2.519(7)	2.459(6)–2.533(6)	2.624(8)–2.710(8) 2.724(17), 2.845(17)	2.674(8)–2.763(7)	2.470(10)–2.539(10)	2.466(8)–2.547(9)	
Ln–O (nitrate or acetate bridge)			2.493(13)				2.453(2)
Ln–O (DMF)			2.524(8)	2.550(8)			
La–O (H_2O)							2.547(2)–2.698(2)
Cu–N (oxime)	1.899(6)–1.928(6)	1.899(7)–1.942(6)	1.917(8)–1.949(8)	1.915(9)–1.932(9)	1.916(10)–1.948(11)	1.890(6)–1.927(6)	1.912(2)–1.941(2)
Cu–N (pyrazine)	1.994(6)–2.030(7)	2.003(6)–2.023(7)	2.006(8)–2.032(9)	2.004(10)–2.057(9)	2.005(11)–2.032(10)	2.000(6)–2.062(7)	2.003(2)–2.042(2)
Cu–O (nitrate)	2.311(7)	–	2.311(7)	2.400(19), 2.454(22)	2.245(10)	–	2.771(4)
Cu–O (DMF)	2.271(7)–2.322(6)	2.196(6)–2.271(6)	2.306(9)–2.353(7)	2.271(8)–2.338(11)	2.229(19), 2.259(11)	2.241(7)–2.344(7)	
Cu–O (water)					2.483(23)	2.322(9)	2.347(7)–2.539(4)
N–O (hydroxamate)	1.371(8)–1.390(7)	1.381(8)–1.404(8)	1.361(9)–1.389(11)	1.381(11)–1.402(11)	1.356(14)–1.386(12)	1.358(8)–1.412(7)	1.370(3)–1.386(3)
C–O (carboxyl)	1.288(9)–1.311(8)	1.268(10)–1.321(9)	1.288(13)–1.305(11)	1.279(13)–1.298(13)	1.280(14)–1.339(16)	1.269(10)–1.299(10)	1.270(4)–1.312(3)
Ln–O (oxime plane)	0.02	0.01	0.62	0.66	0.04	0.02, 0.03	0.71
Ln–N (exterior pyrazine plane)	0.80	1.00	0.11	0.54	0.86	1.07, 1.20	0.94

(donor) and the Cu(II) ring atom (acceptor) (Cu(2)–N(12), x, 0.5 − y, 0.5 + z, 2.36 Å) giving the achiral polymer chain (Fig. 5). Two bidentate nitrate anions are symmetrically bound to the encapsulated nine-coordinated Gd(III) ion (Gd–O 2.47–2.54 Å) on either side of the metallacrown ring while the third nitrate anion is bound to a copper(II) ion (Cu(1)–O(17) 2.25 Å), maintaining the charge balance. The axial positions in coordination environment of the other Cu(II) ions are completed by DMF (Cu–O 2.23, 2.26 Å) and water molecule (Cu(4)–O(21) 2.48 Å). The cone-shape distortion of the macrocycle (~0.85 Å) is close to that for molecular complex **1**. There are CH_2Cl_2 and DMF molecules that are present in the crystal lattice. This structure demonstrates that bound molecules (anions) in the coordination shell of the metallamacrocycle could be effectively exchanged by even weak σ-donor ligands, e.g., pyrazine.

We assumed that integration of the molecular metallacrowns into frameworks could be a versatile process utilizing a step-by-

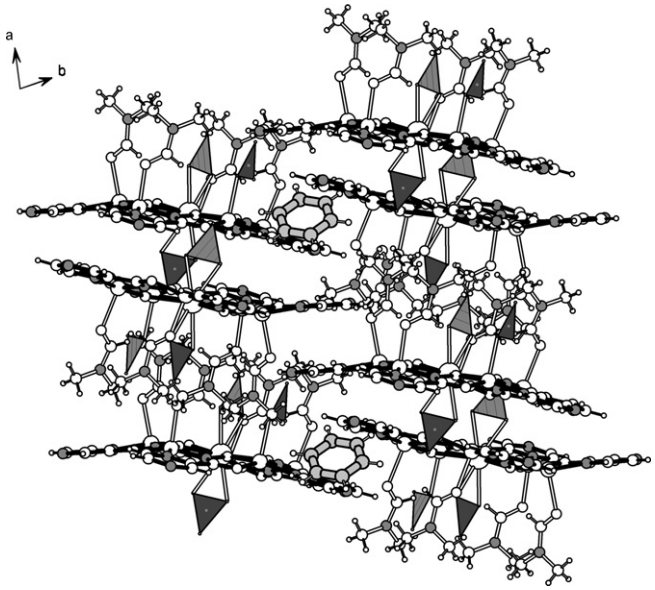

Fig. 3. Crystal packing view of molecular metallacrowns **1** illustrating the accommodation of benzene molecules (side view).

step approach, where the metallamacrocycle behaves as a ligand towards inorganic salts. However, the interaction between the Gd/Cu metallacrowns, generated *in situ*, and a five-fold molar equivalent excess of $CdBr_2$ followed by crystallization affords anion methathesis reaction prior to formation of coordination framework polymer. The crystal structure of molecular compound $[Gd(NO_3)_2\{Cu(pyzha)\}_5(DMF)_5][Gd(NO_3)_2\{Cu(pyzha)\}_5(DMF)_4(H_2O)]\ [CdBr_4] \cdot 1.5DMF$ (**6**) consists of two kinds of discrete metallacrown cations, uncoordinated $CdBr_4^{2-}$ dianion and DMF molecules. The complex cations differ from each other by coordinated solvent shell. In the crystal lattice they both are stacked together in a concave/concave packing mode to form a pocket of 3×4 Å suitable for incorporating a DMF molecule (Fig. 6A and B). The packing motif is supported by shorted contacts between the negatively charged oxygen atom of the bidentate nitrate and the carbon atoms of pyrazine ($-x$, $1-y$, $-z$: O–C 2.99–3.14 Å). The remaining space within the lattice is occupied by additional uncoordinated DMF molecules, which are directed towards the metallacrown rings giving a short interaction of O22–C5B 3.10 Å ($-x$, $2-y$, $1-z$). Such features in the packing behaviour increase a bowl-shape geometry of the metallacrown cations (1.07 and 1.20 Å for $[Gd(NO_3)_2\{Cu(pyzha)\}_5(DMF)_5]^+$ and $[Gd(NO_3)_2\{Cu(pyzha)\}_5(DMF)_4(H_2O)]^+$, respectively).

Another situation was observed in crystal structure of $[La(\mu^2\text{-}OAc)(H_2O)_3\{Cu(pyzha)\}_5(H_2O)_4(NO_3)](NO_3) \cdot 4H_2O$ (**7**) (Fig. 7). The acetate-anion, which is more nucleophilic than the nitrate, and water molecules effectively substitute the nitrates and DMF in the coordination sphere of encapsulated La(III) and ring-forming Cu(II) atoms. The nine-coordinated La(III) ion sits 0.71 Å above the convex side of the metallacrown plane towards the bound acetate. The latter, in a similar bridging coordination mode of nitrate in structure **3**, behaves an as intramolecular bridge between La(III) and one of the copper centres (La(1)–O(11) 2.45 and Cu(5)–O(12) 2.23 Å). The nine-coordinated environment of La(III) is completed in the axial positions by water molecules (La–O 2.64, 2.70 Å), two of which occupy the convex face of the metallacrown, while the other is located on the opposite side (La–O13 2.55 Å). The other, axial ligands (H_2O and NO_3) bound to the Cu(II) ring atoms, are distributed between both faces of the metallacrown. The coordinated anions and aqua molecules form complicated intra- and intermolecular hydrogen bonding interactions shown in Fig. 7A, affording the first formation of a hydrogen bonded centrosymmetrical metallacrown dimer (O(13)···O(8), $2-x$, $2-y$, $2-z$ 2.743(3), ∠O13–H2W···O8 159°). These two metallacrowns are tightly stacked together (~3.36 Å) leading to almost flat geometry of the macrocycle with minimal distortion from planarity ~0.23 Å. In the crystal lattice, the intermolecular hydrogen bonding interactions define the integration of the metallacrown dimers into the 3D network. Such bonding involves the uncoordinated periphery pyrazine moieties on one hand and coordinated to Cu(II) centres aqua ligands on the other (N6···O17, $2-x$, $1-y$, $1-z$, 2.900(4), ∠O17–H7W···N6 160°; O29···N3, $1-x$, $2-y$, $1-z$, 2.881(5), ∠O29–H19W···N3 163°) as well as interactions between two types of nitrate anions and water molecules.

3. Conclusion

We have introduced a series of Cu(II)–Ln(III) 15-metallacrown-5 based on pyrazinohydroxamic acid as a new multiple-binding platform bearing Lewis amphoteric properties. These complexes have discrete molecular 15-MC-5 core, which could be either dimerized in solid state by means of bridging nitrate anion or self-assembled into the extended framework through periphery pyrazine nitrogen atoms and copper centres. Reaction of molecular metallacrowns with excess of $CdBr_2$ or $Cu(OAc)_2$ proceeds as an anion methathesis process affording heteroanionic metallacrowns.

4. Experimental

4.1. Reagents and general procedures

Compound H_2Pyzha [33] was prepared according to the literature procedures. All chemicals were reagent grade and used without further purification. The hydrate stoicheometry of gadolinium nitrate used $Gd(NO_3)_3 \cdot xH_2O$ ($x = 5.44$) was established by complexonometry.

4.2. Spectroscopy and analytical characterizations

The solution speciation of the planar 15-MC-5 structures was investigated by mass spectrometry using Q-Tof Ultima ESI mass spectrometer (Macromass/Waters). Samples were injected at 5 μL/min rate using a syringe pump. Positive ions were detected. IR spectra were recorded with a UR-10 spectrometer (4000–400 cm^{-1}).

Elemental analyses (C, H and N) were performed with a Perkin–Elmer 2400 analyzer.

4.3. Preparation of metallacrowns

The synthesis of **1**–**5** was essentially the same. In a typical procedure, a 5.25 mL DMF solution of $Cu(OAc)_2 \cdot H_2O$ (99.8 mg, 0.500 mmol) and $La(NO_3)_3 \cdot 6H_2O$ or $Gd(NO_3)_3 \cdot xH_2O$ ($x = 5.44$) (0.100 mmol) was mixed with a 1 mL DMF solution of H_2Pyzha (69.6 mg, 0.500 mmol). It immediately caused change in color from blue to intensive dark green. The resultant solution was stirred at rt for 1 h followed by vapor diffusion technique: diffusion of ether–benzene solution (1:1) gave compounds $[Gd(NO_3)_2\{Cu(pyzha)\}_5(DMF)_4(NO_3)] \cdot 0.5C_6H_6 \cdot H_2O$ (**1**), $[La(NO_3)_2\{Cu(pyzha)\}_5(DMF)_5]NO_3 \cdot 1.5DMF \cdot 2C_6H_6$ (**3**), diffusion of Et_2O resulted in $[Gd(NO_3)_2\{Cu(pyzha)\}_5(DMF)_5](NO_3) \cdot 1.5DMF \cdot 0.5H_2O$ (**2**), $[\{La(NO_3)_2\{Cu(pyzha)\}_5(DMF)_5\}_2(\mu^2\text{-}NO_3)](NO_3) \cdot 3DMF$ (**4**); Et_2O/CH_2Cl_2 (1:1) yielded $[Gd(NO_3)_2\{Cu(pyzha)\}_5(DMF)_2(H_2O)(NO_3)] \cdot CH_2Cl_2 \cdot DMF$ (**5**).

Synthesis of heteroanionic metallacrowns $[Gd(NO_3)_2\{Cu(pyzha)\}_5(DMF)_5][Gd(NO_3)_2\{Cu(pyzha)\}_5(DMF)_4(H_2O)][CdBr_4] \cdot 1.5DMF$

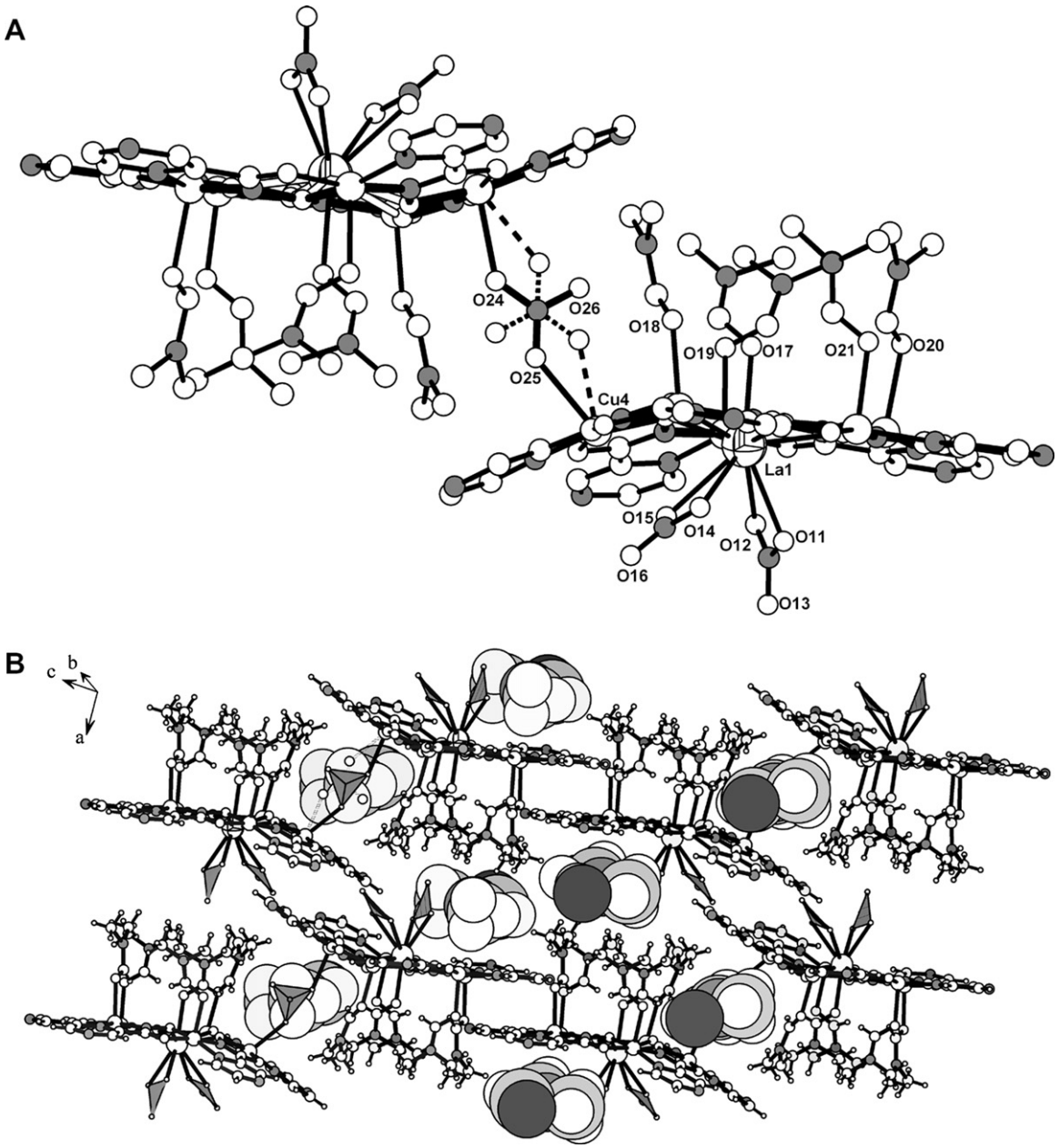

Fig. 4. (A) Side view of metallacrown $[\{La(NO_3)_2\{Cu(pyzha)\}_5(DMF)_5\}_2(\mu^2\text{-}NO_3)](NO_3)\cdot 3DMF$ (**4**), (Cu(4)–O(25) (x, y, z) 2.45 Å, Cu(4)–O(24) ($1-x$, $1-y$, $2-z$) 2.40 Å, La(1)–O(11) 2.68 Å, La(1)–O(12) 2.67 Å, La(1)–O(14) 2.76 Å, La(1)–O(15) 2.71, Å) (one of the disordered bridging nitrate is shown as a dash line); (B) crystal packing side view of **4** illustrating the accommodation of the unbound DMF molecules.

(**6**), and $[La(\mu^2\text{-}OAc)(H_2O)_3\{Cu(pyzha)\}_5(H_2O)_4(NO_3)](NO_3)\cdot 4H_2O$ (**7**).

A 5.25 mL DMF solution of $Cu(OAc)_2\cdot H_2O$ (99.8 mg, 0.500 mmol), $Gd(NO_3)_3\cdot xH_2O$ ($x = 5.44$) (44.1 mg, 0.100 mmol) was mixed with a 1 mL DMF solution of H_2Pyzha (69.6 mg, 0.500 mmol). The resulted solution was stirred at rt for 1 h and then $CdBr_2\cdot 4H_2O$ (86.1 mg, 2.50 mmol) was added. The resultant solution was stirred for another hour and then filtered off. The desired dark green crystals of complex **6** were grown at rt for a few weeks.

A 5.25 mL DMF–H_2O solution of $Cu(OAc)_2\cdot H_2O$ (99.8 mg, 0.500 mmol), $La(NO_3)_3\cdot 6H_2O$ (43.3 mg, 0.100 mmol) was mixed with a 1 mL DMF solution of H_2Pyzha (69.6 mg, 0.500 mmol). The resulted solution was stirred at rt for 1 h and then Cu powder (15.9 mg, 0.250 mmol) was added. The mixture was stirred at 75 °C for ~8 h, then a vapor diffusion with ether yielded the desired complex $[La(\mu^2\text{-}OAc)(H_2O)_3\{Cu(pyzha)\}_5(H_2O)_4(NO_3)](NO_3)\cdot 4H_2O$ (**7**).

Analytical data for the synthesized complexes:

(**1**) *Anal.* Calc. for $C_{40}H_{48}Cu_5GdN_{22}O_{24}$: C, 28.33; H, 2.85; N, 18.17. Found: C, 28.01; H, 2.91; 17.98%.

(**2**) *Anal.* Calc. for $C_{44.5}H_{61.5}Cu_5GdN_{24.5}O_{26}$: C, 29.20; H, 3.39; Gd, N, 18.75. Found: C, 28.87; H, 3.43; N, 18.61%.

(**3**) *Anal.* Calc. for $C_{56.5}H_{72.5}Cu_5LaN_{24.5}O_{25.5}$: C, 34.63; H, 3.73; N, 17.51. Found: C, 34.33; H, 3.85; N, 17.32%.

(**4**) *Anal.* Calc. for $C_{92}H_{128}Cu_{10}La_2N_{50}O_{52}$: C, 30.03; H, 3.51; N, 19.03. Found: C, 29.82; H, 3.65; N, 18.77%.

(**6**) *Anal.* Calc. for $C_{81.5}H_{105.5}Br_4CdCu_{10}Gd_2N_{44.5}O_{43.5}$: C, 25.85; H, 2.81; N, 16.46. Found: C, 25.49; H, 2.97; N, 16.13%.

(**7**) *Anal.* Calc. for $C_{27}H_{40}Cu_5LaN_{17}O_{29}$: C, 21.29; H, 2.65; N, 15.63. Found: C, 21.00; H, 2.74; N, 15.41%.

Since fast loss of the solvent molecules (CH_2Cl_2), the analytical data for complex **5** were not performed.

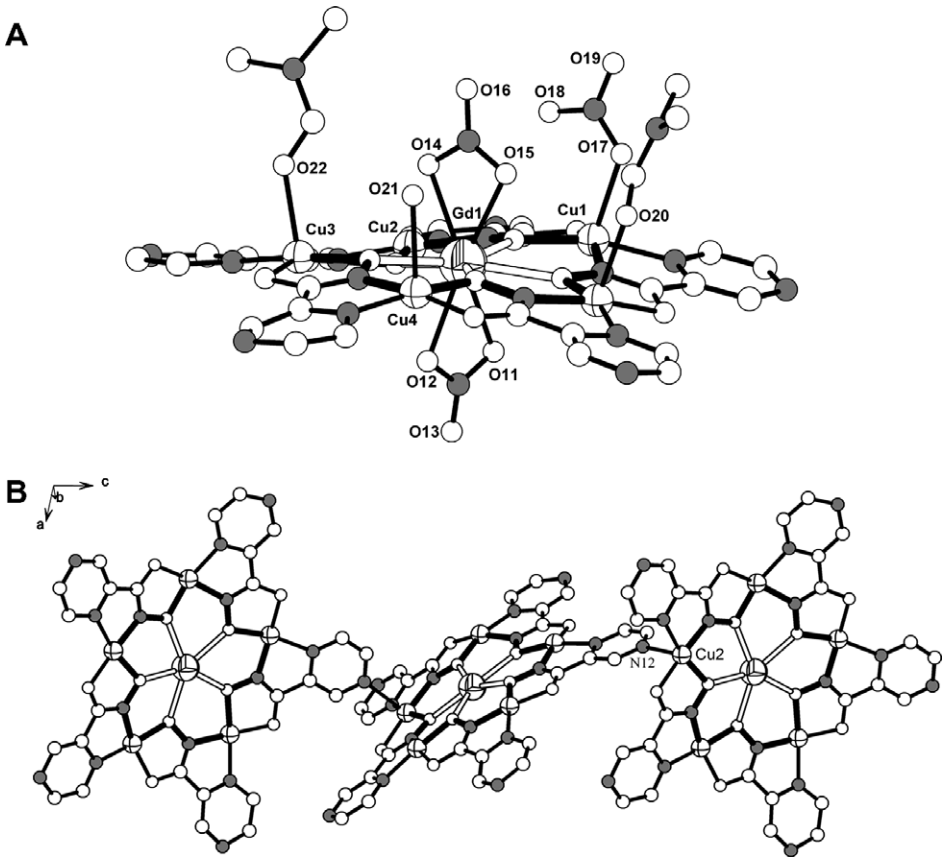

Fig. 5. (A) Side view of molecular structure of metallacrown $[Gd(NO_3)_2\{Cu(pyzha)\}_5(DMF)_2(H_2O)(NO_3)] \cdot CH_2Cl_2 \cdot DMF$, **5**; (B) formation of achiral polymer chain through self-assembling of the metallacrown complexes.

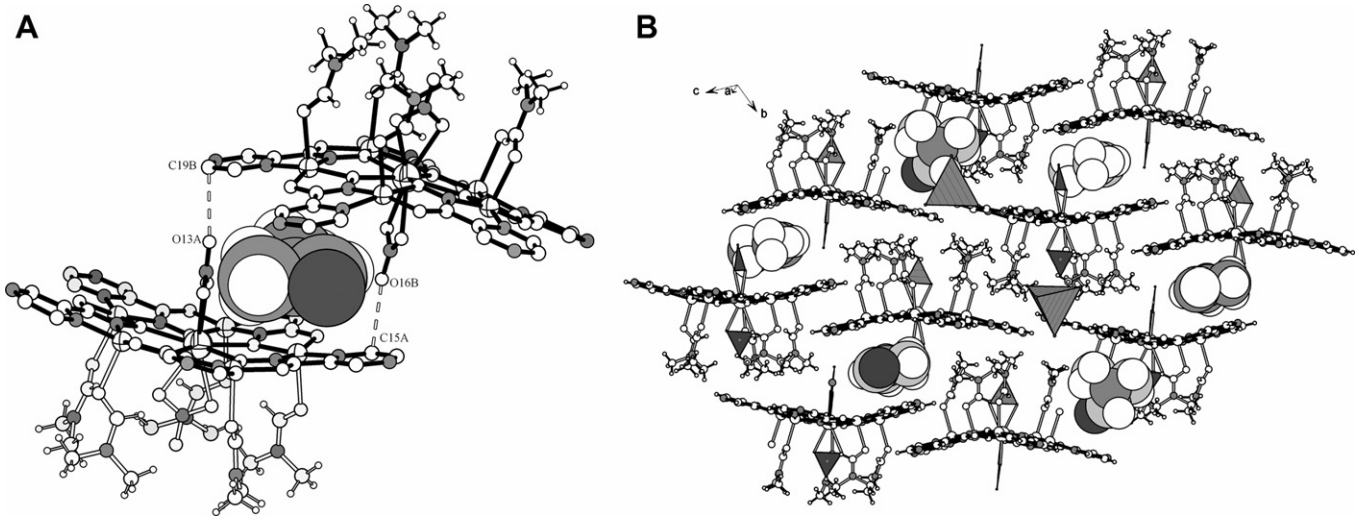

Fig. 6. (A) A concave/concave packing of two metallacrown cations $[Gd(NO_3)_2\{Cu(pyzha)\}_5(DMF)_5]^+$ and $[Gd(NO_3)_2\{Cu(pyzha)\}_5(DMF)_4(H_2O)]^+$ (**6**) affords encapsulation of DMF molecule ($-x$, $1-y$, $-z$: C15A–O16B 3.00, O13A–C19B 2.99, O13A–C20B 3.01, O16B–C14A 3.14 Å); (B) crystal packing side view of **6** demonstrating the accommodation of the unbound DMF molecules within the lattice.

The typical IR absorption bands (KBr, cm^{-1}) observed for the complexes: 3030 m, 1650 m, 1600 s, 1580 s, 1520 w, 1470 m, 1380 s, 1190 m, 1150 w, 1070 s, 960 s, 860 w, 750 m, 690 w, 570 m.

4.4. Crystal structure determinations

Crystallographic measurements were made using a Bruker SMART CCD area-detector diffractometer (graphite monochromated Mo Kα radiation, $\lambda = 0.71073$ Å; empirical absorption correction using SADABS). The structures were solved by direct methods using the program SHELXS-97 [34]. The refinement and all further calculations were carried out using SHELXL-97 [34]. The non-H atoms were refined anisotropically, using weighted full-matrix least-squares of F^2 (Table 1). CH hydrogen atoms were placed in calculated positions with their isotropic U values set to be 1.2 (CH) or 1.5 (CH_3) times greater then U_{eq} of the corresponding carbon atom.

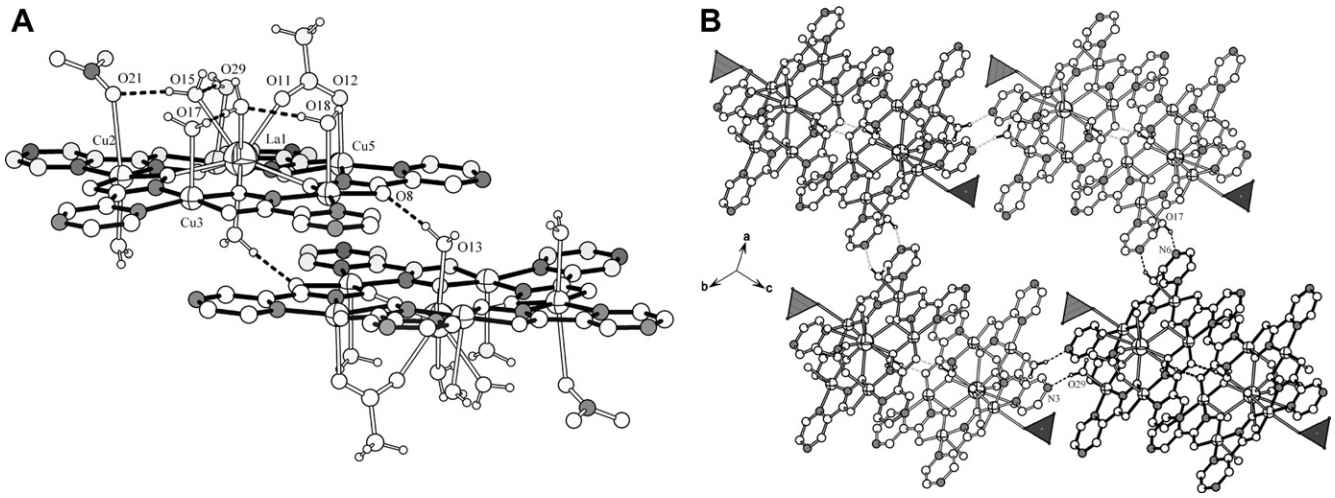

Fig. 7. (A) Side view of centrosymmetrical hydrogen bonded molecular dimer $[La(\mu^2\text{-}OAc)(H_2O)_3\{Cu(pyzha)\}_5(H_2O)_4(NO_3)](NO_3)\cdot 4H_2O$, **7**; (B) the hydrogen bonded metallacrown dimers are integrated in crystal lattice by means of a number of intermolecular hydrogen bondings involving uncoordinated nitrate anions and aqua ligands. The lattice water molecules and the third nitrate are not shown.

Some of the structures exhibit typical disorder for solvent of crystallization molecules as well as high thermal motion for outer methyl groups of coordinated DMF molecules. For structure **6**, the corresponding carbon atoms as well as the atoms of non-coordinated DMF were refinded with isotropic displacement parameters. These DMF solvent molecules were refined with fixed standard geometry parameters. In structure **5**, non-coordinated molecules of DMF and CH_2Cl_2 were badly disordered and the remaining electron density was modelled using squeeze [35], only the heavy Gd and Cu atoms were refined anisotropically for the sake of overall convergence and the hydrogen atoms of the water molecule were not included. The squeeze routine was also successfully used for modelling of electron density corresponding to a non-coordinated disordered NO_3^- anion in **4**. In this structure, the nitrogen atom of NO_3^- group resides on a centre of inversion and hence three oxygen atoms were equally disordered. It was possible to refine the atoms anisotropically without restraints in geometry. Very high anisotropy of thermal motion for Cu(1) atom in structure **3** was indicative of the disorder and two equal contributions (separated by 0.54 Å above and below the molecular plane) were refined anisotropically. Structure **7** shows equal disorder for one coordinated water molecule and non-coordinated NO_3^- anion. The hydrogen atoms of disordered water molecule were not added, while for the rest of water molecules the hydrogen atoms were located and then fixed with standard OH separations (0.85 Å). Graphical visualisation of the structures was made using program DIAMOND [36].

Appendix A. Supplementary material

CCDC 629079, 629080, 629081, 629082, 629083, 629084 and 629085 contain the supplementary crystallographic data for **1**, **2**, **3**, **4**, **5**, **6** and **7**. These data can be obtained free of charge via http://www.ccdc.cam.ac.uk/conts/retrieving.html, or from the Cambridge Crystallographic Data Centre, 12 Union Road, Cambridge CB2 1EZ, UK; fax: (+44) 1223-336-033; or e-mail:deposit@ccdc.cam.ac.uk. Supplementary data associated with this article can be found, in the online version, at doi:10.1016/j.poly.2008.04.042.

References

[1] H.C. Aspinall, Chem. Rev. 102 (2002) 1807.
[2] M. Shibasaki, N. Yoshikawa, Chem. Rev. 102 (2002) 2187.
[3] J. Inanaga, H. Furuno, T. Hayano, Chem. Rev. 102 (2002) 2211.
[4] Y. Matuura, S. Matsushima, M. Sakamoto, Y. Sadaoka, J. Mater. Chem. 3 (1993) 767.
[5] P. Caravan, J.J. Ellison, T.J. McMurry, R.B. Lauffer, Chem. Rev. 99 (1999) 2293.
[6] A.J. Stemmler, J.W. Kampf, M. L Kirk, B.H. Atasi, V.L. Pecoraro, Inorg. Chem. 38 (1999) 2807.
[7] A. Bencini, C. Benelli, A. Caneschi, R.L. Carlin, A. Die, D. Gatteschi, J. Am. Chem. Soc. 107 (1985) 8128.
[8] H.O. Stumpf, L. Ouahab, Y. Pei, P. Bergerat, O. Kahn, J. Am. Chem. Soc. 116 (1994) 3866.
[9] J.-P. Costes, F. Dahan, A. Dupuis, J.-P. Laurent, Inorg. Chem. 36 (1997) 3429.
[10] E. Coronada, C.-J. Gomez-Garcıa, Chem. Rev. 98 (1998) 273.
[11] J. Liu, E.A. Meyers, J.A. Cowan, S.G. Shore, Chem. Commun. (1998) 2043.
[12] S. Decurtins, M. Gross, H.W. Schmalle, S. Ferlay, Inorg. Chem. 37 (1998) 2443.
[13] D.M.J. Doble, C.H. Benison, A.J. Blake, D. Fenske, M.S. Jackson, R.D. Kay, W.-S. Li, M. Schröder, Angew. Chem. Int. Ed. 38 (1999) 1915.
[14] B.-Q. Ma, S. Gao, G. Su, G.-X. Xu, Angew. Chem. Int. Ed. 40 (2001) 434.
[15] J.-P. Costes, J.M. Clemente-Juan, F. Dahan, F. Dumestre, J.-P. Tuchagues, Inorg. Chem. 41 (2002) 2886.
[16] J.-P. Costes, F. Dahan, F. Dumestre, J.M. Clemente-Juan, J. Garcia-Tojal, J.-P. Tuchagues, Dalton Trans. (2003) 464.
[17] T. Shiga, M. Ohba, H. Ohkawa, Inorg. Chem. 43 (2004) 4435.
[18] R. Koner, H.-H. Lin, H.-H. Wei, S. Mohanta, Inorg. Chem. 44 (2005) 3524.
[19] F. He, M.-L. Tong, X. Ming Chen, Inorg. Chem. 44 (2005) 8285.
[20] J.-C.G. Bünzli, C. Piguet, Chem. Rev. 102 (2002) 1897.
[21] C. Benelli, D. Gatteschi, Chem. Rev. 102 (2002) 2369.
[22] Y. Zhou, M. Hong, X. Wu, Chem. Commun. (2006) 135.
[23] D.P. Kessissiglou, J.W. Kampf, V.L. Pecoraro, Polyhedron 13 (1994) 1379.
[24] A.J. Stemmler, J.W. Kampf, V.L. Pecoraro, Angew. Chem. 35 (1996) 2841.
[25] V.L. Pecoraro, A.J. Stemmler, B.R. Gibney, J.J. Bodwin, H. Wang, J.W. Kampf, A. Barwinski, Progress in Inorganic Chemistry, John Wiley & Sons Inc., 1997.
[26] V.L. Pecoraro, J.J. Bodwin, A.D. Cutland, J. Solid State Chem. 152 (2000) 68.
[27] J.J. Bodwin, V.L. Pecoraro, Inorg. Chem. 39 (2000) 3434.
[28] A.D. Cutland, J.A. Halfen, J.W. Kampf, V.L. Pecoraro, J. Am. Chem. Soc. 123 (2001) 6211.
[29] A.D. Cutland-Van Noord, J.W. Kampf, V.L. Pecoraro, Angew. Chem. 41 (2002) 4668.
[30] A.J. Stemmler, V.L. Pecoraro, Inorg. Synth. 33 (2002) 67.
[31] C.M. Zaleski, E.C. Depperman, J.W. Kampf, M.L. Kirk, Vincent L. Pecoraro, Inorg. Chem. 45 (2006) 10022.
[32] G. Mezei, C.M. Zaleski, V.L. Pecoraro, Chem. Rev. 107 (2007) 4933.
[33] S. Kushner, H. Dalalian, J.L. Sanjurjo, F.L. Bach, S.R. Safir Jr., V.K. Smith, J.H. Williams Jr., J. Am. Chem. Soc. (1952) 3617.
[34] G.M. Sheldrick, SHELXS-97 & SHELXL-97, Computer Programs for the Solution and Refinement of X-ray Crystal Structures, University of Göttingen, Göttingen, Germany, 1997.
[35] A.L. Spek, J. Appl. Crystallogr. 36 (2003) 7.
[36] K. Brandenburg, DIAMOND 2.1c, Crystal Impact GbR, Bonn, 1999.

Polyhedron 27 (2008) 2357–2364

Contents lists available at ScienceDirect

Polyhedron

journal homepage: www.elsevier.com/locate/poly

A series of three-dimensional coordination polymers with general formula $[\{Ln(H_2O)_n\}\{Re_6Te_8(CN)_6\}] \cdot xH_2O$ (Ln = Eu, Gd, Tb, Dy, Ho, Er, Tm, Yb; n = 3, 4, x = 0, 2.5)

Maria S. Tarasenko [a], Nikolay G. Naumov [b,*], Dmitry Yu. Naumov [a], Sung-Jin Kim [b,*], Vladimir E. Fedorov [a]

[a] Nikolaev Institute of Inorganic Chemistry, Siberian Branch of Russian Academy of Sciences, 3 Ak. Lavrentiev Ave., Novosibirsk 630090, Russia
[b] Department of Chemistry and Nano Sciences, Ewha Womans University, Seoul 120-750, Republic of Korea

ARTICLE INFO

Article history:
Received 18 December 2007
Accepted 29 April 2008
Available online 4 July 2008

Keywords:
Rhenium
Octahedral cluster
Cyanide
Lanthanides
Coordination framework

ABSTRACT

A series of new compounds containing rare earth cations (Eu to Yb) and paramagnetic cluster anion $[Re_6Te_8(CN)_6]^{3-}$ was prepared and investigated. The X-ray structural analyses have revealed that the compounds $[\{Ln(H_2O)_4\}\{Re_6Te_8(CN)_6\}] \cdot 2.5H_2O$; Ln = Eu (**1**), Tb (**3**), Dy (**4**), Ho (**5**), Er (**6**), Tm (**7**), $[\{Gd(H_2O)_3\}\{Re_6Te_8(CN)_6\}] \cdot 2.5H_2O$ (**2**) and $[\{Yb(H_2O)_4\}\{Re_6Te_8(CN)_6\}]$ (**8**) are three-dimensional polymers based on Re–CN–Ln interactions. Measurements of magnetic susceptibility for **2** and **5** showed that effective magnetic moment (at 300 K) was 8.13 μ_B for compound **2** and 10.79 μ_B for compound **5** with weak antiferromagnetic ordering appeared at low temperatures.

© 2008 Elsevier Ltd. All rights reserved.

1. Introduction

The chemistry of rhenium octahedral cluster cyanides $[Re_6Q_8(CN)_6]^{4-/3-}$, Q = S, Se, Te (Fig. 1) is in a stage of rapid investigation in past decade [1–19]. Ability of cyanogroups coordinated to rhenium to act as bridging ligands allowed to use these anions as building blocks for construction of coordination polymers based on strong covalent Re–C≡N–M bridges. To date, numerous polymeric coordination compounds were obtained with transition and post transition metals. With few exceptions [4,6,17] 3d transition metals in these polymers have octahedral environment. The type of structure depends mainly on a number of bridged cyanogroups of cluster anion as well as a number of cyanide ligands in coordination environment of cation.

The crystallochemistry of rare earth metals differs from that of 3d transition metals due to increased ionic radii, larger coordination numbers and stereochemical flexibility of ligand environment. Compounds $[Ln(H_2O)_3Re_6Te_8(CN)_6] \cdot nH_2O$ (Ln = La, Nd) obtained by reaction of $K_4Re_6Te_8(CN)_6$ with $LnCl_3 \cdot nH_2O$ in hydrothermal conditions [13] contained lanthanide atoms having tricapped trigonal prismatic environment. They are coordinated by six nitrogen atoms of CN groups of different cluster anions and three water molecules. In the recent work [20] it was shown that the interaction of heavy Ln^{3+} cations (Ln = Tb–Lu) with $[Re_6Se_8(CN)_6]^{3-}$ complex anion lead to formation of another family of polymer based on lanthanide cations and rhenium cluster complexes with general formula $Ln(H_2O)_3[Re_6Se_8(CN)_6] \cdot 3.5H_2O$. In these compounds each lanthanide is surrounded by five cyanogroups and three water molecules that resulted in formation of unusual framework with (5,5) connectivity according to notation given in [21]. It was shown that for heavy Ln^{3+} cations (Ln = Tb–Lu) structure of forming polymer is intact to nature of lanthanide.

In present work we report the synthesis and crystal structures of new compounds built from rare earth cations Ln^{3+} (Ln = Eu–Yb) and $[Re_6Te_8(CN)_6]^{3-}$ cluster anion obtained by reaction in aqueous solution. These compounds are described with general formula $[\{Ln(H_2O)_n\}\{Re_6Te_8(CN)_6\}] \cdot xH_2O$ (n = 3, 4; x = 0, 2.5) and characterized by extended three-dimensional framework based on strong covalent Re–CN–Ln interactions. The compounds **1**, **3**–**6** ($[\{Ln(H_2O)_4\}\{Re_6Te_8(CN)_6\}] \cdot 2.5H_2O$) were isostructural while the compounds $[\{Gd(H_2O)_3\}\{Re_6Te_8(CN)_6\}] \cdot 2.5H_2O$ (**2**), $[\{Tm(H_2O)_4\}\{Re_6Te_8(CN)_6\}] \cdot 2.5H_2O$ (**7**) and $[\{Yb(H_2O)_4\}\{Re_6Te_8(CN)_6\}]$ (**8**) were crystallized in different structure types.

2. Experimental

2.1. General

$Cs_4Re_6Te_8(CN)_6 \cdot 2H_2O$ was prepared from polymeric Re_6Te_{15} as described elsewhere [12]. All other reagents were used as

* Corresponding authors. Tel.: +7 383 3309253; fax: +7 383 3309489 (N.G. Naumov); tel.: +82 02 3277 2350; fax: +82 02 3277 3419 (S.J. Kim).
E-mail addresses: naumov@che.nsk.su (N.G. Naumov), sjkim@ewha.ac.kr (S.-J. Kim).

0277-5387/$ - see front matter © 2008 Elsevier Ltd. All rights reserved.
doi:10.1016/j.poly.2008.04.054

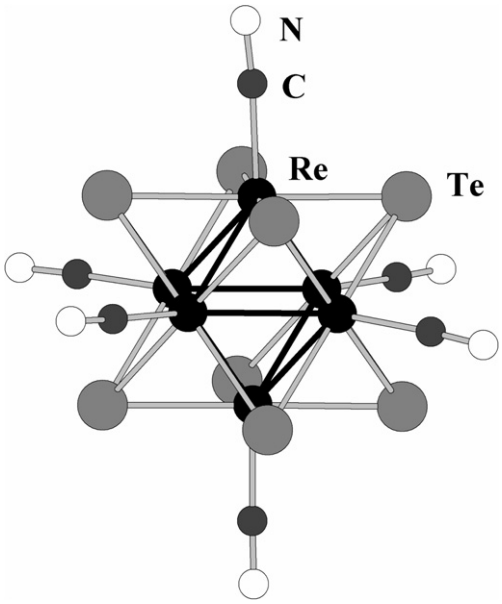

Fig. 1. Structure of cluster anion $[Re_6Te_8(CN)_6]^{3-}$.

purchased. Infrared spectra were measured in KBr disks with Scimitar FTS 2000 spectrometer in the range 4000–375 cm^{-1}. Individuality of crystalline powder samples was confirmed by X-ray powder diffractometry on Philips APD 1700 diffractometer. Magnetic measurements were performed in applied magnetic field of 5 kOe within the temperature range 4–300 K using a Quantum Design MPMS-5 SQUID magnetometer. Diamagnetic corrections were estimated from Pascal tables. Analyses were performed on a Thermo Jarrell Ash Atomscan 25 with the use of standards purchased from GFS Chemicals, Inc. (Re, Te) and Aldrich Chemical Company (Co, Ni, Zn). Energy Dispersive Spectrometry (EDS) analyses, using an Oxford LINK ISIS spectrometer implanted on a scanning electron microscope JEOL JSM 6400 (standards were taken from the apparatus standard library), were performed on several selected single-crystals from the preparation.

2.2. Syntheses

2.2.1. Preparation of $[\{Eu(H_2O)_4\}\{Re_6Te_8(CN)_6\}] \cdot 2.5H_2O$ (**1**)

$Cs_4Re_6Te_8(CN)_6 \cdot 2H_2O$ 57.2 mg (0.02 mmol) was dissolved in 6 mL of water, then $EuCl_3 \cdot 6H_2O$ 14.6 mg (0.04 mmol) in 2 mL of water and 0.1 mL of concentrated HCl were added. After three days dark brown crystals of **1** were filtered and washed with small amount of water. Yield: 32.5 mg (62.9%). *Anal.* Calc. for $C_6H_{13}EuN_6O_{6,5}Re_6Te_8$: C, 2.81; H, 0.51; N, 3.28. Found: C, 2.7; H, 0.45; N, 3.2%. Heavy atoms ratio by EDS (normalized to Re_6): Eu:Re:Te = 0.95:6.0:7.9. IR: ν_{OH} 3431–3417 cm^{-1} (band); δ_{HOH} 1625–1610 cm^{-1} (band); ν_{CN} 2092 cm^{-1}; ν_{ReC} 472 cm^{-1}; δ_{ReCN} 403 cm^{-1}.

2.2.2. Preparation of $[\{Gd(H_2O)_3\}\{Re_6Te_8(CN)_6\}] \cdot 2.5H_2O$ (**2**)

Compound was prepared using the same method. The $GdCl_3 \cdot 6H_2O$ (14.9 mg, 0.04 mmol) was used instead of $EuCl_3 \cdot 6H_2O$. Yield: 46.11 mg (90.4%). *Anal.* Calc. for $C_6H_{13}GdN_6O_{6,5}Re_6Te_8$: C, 2.81; H, 0.51; N, 3.27. Found: C, 2.9; H, 0.45; N, 3.4%. Heavy atoms ratio by EDS (normalized to Re_6): Gd:Re:Te = 1.0:6.0:8.1. IR: ν_{OH} 3589–3404 cm^{-1} (band); δ_{HOH} 1603 cm^{-1}; ν_{CN} 2104, 2117 cm^{-1}; ν_{ReC} 474 cm^{-1}; δ_{ReCN} 401 cm^{-1}.

2.2.3. Preparation of $[\{Tb(H_2O)_4\}\{Re_6Te_8(CN)_6\}] \cdot 2.5H_2O$ (**3**)

Compound was prepared using the same method. The $TbCl_3 \cdot 6H_2O$ (14.9 mg, 0.04 mmol) was used instead of $EuCl_3 \cdot 6H_2O$. Yield: 39.2 mg (76.3%). *Anal.* Calc. for $C_6H_{13}TbN_6O_{6,5}Re_6Te_8$: C, 2.80; H, 0.51; N, 3.27. Found: C, 2.7; H, 0.55; N, 3.1%. Heavy atoms ratio by EDS (normalized to Re_6): Tb:Re:Te = 1.1:6.0:8.0. IR: ν_{OH} 3433 cm^{-1}; δ_{HOH} 1610 cm^{-1}; ν_{CN} 2094 cm^{-1}; ν_{ReC} 470 cm^{-1}; δ_{ReCN} 403 cm^{-1}.

2.2.4. Preparation of $[\{Dy(H_2O)_4\}\{Re_6Te_8(CN)_6\}] \cdot 2.5H_2O$ (**4**)

Compound was prepared using the same method. The $DyCl_3 \cdot 6H_2O$ (15.1 mg, 0.04 mmol) was used instead of $EuCl_3 \cdot 6H_2O$. Yield: 37.7 mg (59.3%). *Anal.* Calc. for $C_6H_{13}DyN_6O_{6,5}Re_6Te_8$: C, 2.80; H, 0.51; N, 3.27%. Found: C, 2.8; H, 0.47; N, 3.3%. Heavy atoms ratio by EDS (normalized to Re_6): Dy:Re:Te = 1.09:6.0:8.0. IR: ν_{OH} 3433 cm^{-1}; δ_{HOH} 1626 cm^{-1}; ν_{CN} 2096, 2083 cm^{-1}; ν_{ReC} 487, 471 cm^{-1}; δ_{ReCN} 403 cm^{-1}.

2.2.5. Preparation of $[\{Ho(H_2O)_4\}\{Re_6Te_8(CN)_6\}] \cdot 2.5H_2O$ (**5**)

Compound was prepared using the same method. The $HoCl_3 \cdot 6H_2O$ (15.2 mg, 0.04 mmol) was used instead of $EuCl_3 \cdot 6H_2O$. Yield: 20 mg (31.3%). *Anal.* Calc. for $C_6H_{13}HoN_6O_{6,5}Re_6Te_8$: C, 2.80; H, 0.51; N, 3.26. Found: C, 2.8; H, 0.53; N, 3.1%. Heavy atoms ratio by EDS (normalized to Re_6): Ho:Re:Te = 1.1:6.0:8.1. IR: ν_{OH} 3593–3425 cm^{-1} (br.); δ_{HOH} 1603 cm^{-1}; ν_{CN} 2100, 2085 (w.) cm^{-1}; ν_{ReC} 474 cm^{-1}; δ_{ReCN} 403 cm^{-1}.

2.2.6. Preparation of $[\{Er(H_2O)_4\}\{Re_6Te_8(CN)_6\}] \cdot 2.5H_2O$ (**6**)

Compound was prepared using the same method. The $ErCl_3 \cdot 6H_2O$ (15.3 mg, 0.04 mmol) was used instead of $EuCl_3 \cdot 6H_2O$. Yield: 33.6 mg (53.3%). *Anal.* Calc. for $C_6H_{13}ErN_6O_{6,5}Re_6Te_8$: C, 2.79; H, 0.51; N, 3.26. Found: C, 2.7; H, 0.55; N, 3.2%. Heavy atoms ratio by EDS (normalized to Re_6): Er:Re:Te = 1.0:6.0:8.1. IR: ν_{OH} 3435 cm^{-1}; δ_{HOH} 1630 cm^{-1}; ν_{CN} 2100, 2085 cm^{-1}; ν_{ReC} 492, 476 cm^{-1}; δ_{ReCN} 403 cm^{-1}.

2.2.7. Preparation of $[\{Tm(H_2O)_4\}\{Re_6Te_8(CN)_6\}] \cdot 2.5H_2O$ (**7**)

Compound was prepared using the same method. The $TmCl_3 \cdot 6H_2O$ (15.3 mg, 0.04 mmol) was used instead of $EuCl_3 \cdot 6H_2O$. Yield: 48.8 mg (77.3%). *Anal.* Calc. for $C_6H_{13}TmN_6O_{6,5}Re_6Te_8$: C, 2.79; H, 0.51; N, 3.26. Found: C, 2.9; H, 0.45; N, 3.3%. Heavy atoms ratio by EDS (normalized to Re_6): Tm:Re:Te = 0.95:6.0:8.0. IR: ν_{OH} 3431 cm^{-1}; δ_{HOH} 1616 cm^{-1}; ν_{CN} 2102, 2088 (w.) cm^{-1}; ν_{ReC} 478 cm^{-1}; δ_{ReCN} 406 cm^{-1}.

2.2.8. Preparation of $[\{Yb(H_2O)_4\}\{Re_6Te_8(CN)_6\}]$ (**8**)

Compound was prepared using the same method. The $YbCl_3 \cdot 6H_2O$ (14.5 mg, 0.04 mmol) was used instead of $EuCl_3 \cdot 6H_2O$. Yield: 22.9 mg (45.1%). *Anal.* Calc. for $C_6H_8YbN_6O_4Re_6Te_8$: C, 2.84; H, 0.32; N, 3.31. Found: C, 2.8; H, 0.3; N, 3.2%. Heavy atoms ratio by EDS (normalized to Re_6): Gd:Re:Te = 1.0:6.0:7.9. IR: ν_{OH} 3439 cm^{-1}; δ_{HOH} 1626 cm^{-1}; ν_{CN} 2104, 2089 cm^{-1}; ν_{ReC} 497, 480 cm^{-1}; δ_{ReCN} 403 cm^{-1}.

2.2.9. X-ray structural studies

The structures of **1**–**8** were solved by single-crystal X-ray diffraction analysis. A suitable single-crystals were taken from bulk samples and were mounted on Bruker Nonius X8 Apex 4K CCD diffractometer fitted with graphite monochromated Mo Kα radiation (λ = 0.71073 Å). The data were collected at 150 K for all structures by standard technique [22]. Absorption corrections were made empirically using SADABS program [23]. Structures were solved by direct methods and refined by full-matrix least-squares method using SHELXTL program set [24]. Crystal data and details of the final refinement are given in Table 1.

Structures **2** and **7** were ordered while in structures **1**, **3**–**6** and **8** a disorder of Ln atoms and coordinated water molecules was found.

Table 1
Crystal data and structure refinement for **1–8**

	1	2	3	4	5	6	7	8
Empirical formula	$C_6H_{13}EuN_6O_{6.5}Re_6Te_8$	$C_6H_{11}GdN_6O_{5.5}Re_6Te_8$	$C_6H_{13}N_6O_{6.5}Re_6TbTe_8$	$C_6H_{13}DyN_6O_{6.5}Re_6Te_8$	$C_6H_{13}HoN_6O_{6.5}Re_6Te_8$	$C_6H_{13}ErN_6O_{6.5}Re_6Te_8$	$C_6H_{13}N_6O_{6.5}Re_6Te_8Tm$	$C_6H_8N_6O_4Re_6Te_8Yb$
Formula weight	2563.18	2550.46	2570.14	2573.72	2576.15	2578.48	2580.15	2539.25
Crystal system	monoclinic	triclinic	monoclinic	monoclinic	monoclinic	monoclinic	monoclinic	monoclinic
Space group, *Z*	*P2/n*, 4	*P*1, 2	*P2/n*, 4	*P2/n*, 4	*P2/n*, 4	*P2/n*, 4	*P2/c*, 8	*C2/m*, 2
a (Å)	14.6465(5)	9.2420(6)	14.5846(4)	14.6284(6)	14.6097(8)	14.5746(5)	18.2109(8)	13.4602(7)
b (Å)	13.2886(5)	12.2519(9)	13.2465(4)	13.2384(5)	13.2178(7)	13.1811(4)	13.1454(6)	13.2803(8)
c (Å)	17.7214(6)	14.4835(9)	17.6890(5)	17.7792(8)	17.7623(11)	17.7093(5)	26.622(1)	9.2638(5)
α (°)		94.953(2)						
β (°)	112.2030(10)	103.207(2)	112.0200(10)	112.2590(10)	112.259(2)	112.1770(10)	102.028(1)	102.839(2)
γ (°)		97.462(2)						
V (Å^3)	3193.39(19)	1571.62(18)	3168.13(16)	3186.5(2)	3174.4(3)	3150.44(17)	6233.1(5)	1614.55(16)
D_x (g/cm^3)	5.331	5.390	5.388	5.365	5.390	5.436	5.499	5.223
μ (mm^{-1})	31.776	32.394	32.282	32.222	32.483	32.883	33.394	32.368
Crystal size (mm)	0.22 × 0.10 × 0.08	0.08 × 0.06 × 0.05	0.22 × 0.06 × 0.04	0.20 × 0.10 × 0.08	0.12 × 0.06 × 0.02	0.22 × 0.06 × 0.04	0.06 × 0.04 × 0.04	0.13 × 0.05 × 0.03
2*θ* Range (°)	1.54–32.58	1.69–32.58	1.55–29.57	1.54–32.58	1.98–28.28	1.55–29.57	1.14–29.57	2.18–28.28
Reflections collected	32803	16017	27528	32628	22728	24249	46532	5933
Unique (R_{int})	11519 (0.0335)	10694 (0.0236)	8909 (0.0378)	11578 (0.0457)	7855 (0.0457)	8849 (0.0451)	17446 (0.0480)	2055 (0.0234)
T_{min}:T_{max}	0.1854:0.0542	0.2392:0.3485	0.3583:0.0532	0.1825:0.0599	0.5627:0.1119	0.3530:0.0520	0.3485:0.2392	0.3801:0.1555
R_1/wR_2 [$I > 2\sigma(I)$]	0.0522/0.1030	0.0550/0.1465	0.0360/0.0759	0.0751/0.1594	0.0607/0.1352	0.0665/0.1461	0.0401/0.0726	0.0485/0.1528
R_1/wR_2 (all data)	0.0630/0.1058	0.0800/0.1585	0.0572/0.0831	0.0930/0.1649	0.0880/0.1439	0.0846/0.1523	0.0896/0.0839	0.0628/0.1636
Goodness-of-fit	1.201	1.039	1.031	1.137	1.066	1.128	0.934	1.097

On the first stage of refinement of structure **1** europium atom located in general 4e Wickoff position had unusual atomic displacement parameters (principal mean square atomic displacements were about 0.1290 0.0100 0.0059). In addition coordination environment of lanthanide contained 11 ligands (nitrogen from clusters and oxygen atoms) with non-reliable distances to lanthanide cation (from 2.1 to 2.7 Å). Then Eu atom was split in two positions with s.o.f equal to 50% and refined anisotropically. On the last stage s.o.f. of Eu1 and Eu2 atoms were refined in assumption that the sum of occupancies was restricted to a fully occupied 4e position. Atoms of N1, N2, N4, N6 and O1 are common to two positions of europium atoms and are fully occupied. Occupancies for other oxygen atoms completing coordination environment of Eu1 (O11, O12 and O13) and Eu2 (O21, O22 and O23) were fixed to the value of corresponding lanthanide atom. The same procedure was applied for compounds **3–6**. Models of disorder for compound **6** are given in Fig. 2.

In the structure of **8** Yb atom occupies special 4h Wickoff positions located near inversion center with the distance between symmetry generated atoms 1.781 Å and its s.o.f. was set to 0.5. Occupancy factors of oxygen atoms O1 and O2 linked to Yb1 atom were assumed as 0.5 according to s.o.f. of Yb. Hydrogen atoms of the water molecules were not located.

3. Results and discussion

3.1. The crystal structures

All structures contain cluster anion complexes $[Re_6Te_8(CN)_6]^{3-}$. Structure of octahedral cyano-telluride rhenium cluster in oxidized state was described previously [25] and depicted in Fig. 1. Interatomic distances in anions for **1–8** are listed in Table 2. These distances are consistent with those found in other compounds with this anion [13,18,25]. Comparison of data for compounds **1–8** shows no dependence of nature of lanthanide cations on interatomic distances in $[Re_6Te_8(CN)_6]^{3-}$ cluster anion.

3.2. Structures of *1*, *3–6*

The compounds **1**, **3–6** crystallize in *P2/n* space group and are isostructural. Details of structure of Er (**6**) compound are shown in Figs. 2, 3 and Figs. S1a, S1b. In this structure Er atoms occupy two neighbor positions with close occupancies (0.46(2) for Er1 and 0.54(2) for Er2).

Four nitrogen atoms of cyanogroups of different cluster anions (N1, N2, N4, N6) and one oxygen atom of water molecule (O1) are common for two positions of erbium atoms (Fig. 2). Additionally each Er atom is coordinated by three half occupied oxygen

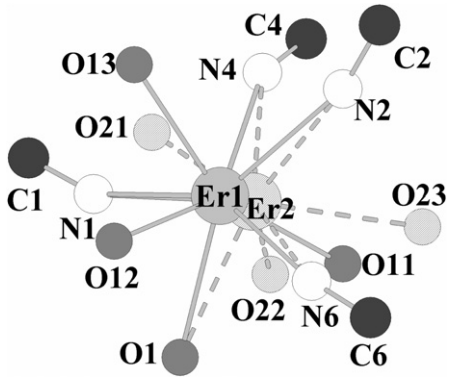

Fig. 2. Coordination environment of Er(III) in compound **6**.

Table 2
Selected distances (Å) of cluster anion for **1–8**

Distances	1	2	3	4
Re–Re	2.6723(6)–2.6949(6) mean 2.685(7)	2.6715(7)–2.6874(7) mean 2.681(4)	2.6748(5)–2.6959(5) mean 2.685(6)	2.6735(10)–2.6954(10) mean 2.684(6)
Re–Te	2.6834(9)–2.7081(9) mean 2.694(7)	2.6791(10)–2.7051(10) mean 2.695(6)	2.6826(8)–2.7084(8) mean 2.694(7)	2.6820(14)–2.7065(14) mean 2.694(7)
Re–C	2.06(1)–2.10(1) mean 2.08(2)	2.07(1)–2.10(1) mean 2.08(1)	2.06(1)–2.10(1) mean 2.08(1)	2.06(2)–2.11(2) mean 2.08(2)
C–N	1.15(2)–1.19(2) mean 1.16(2)	1.13(2)–1.17(2) mean 1.15(1)	1.15(1)–1.17(1) mean 1.16(1)	1.15(3)–1.20(3) mean 1.17(2)
	5	**6**	**7**	**8**
Re–Re	2.6735(11)–2.6959(11) mean 2.685(6)	2.6723(10)–2.6948(11) mean 2.684(7)	2.6657(7)–2.7015(7) mean 2.685(10)	2.6670(11)–2.6778(8) mean 2.670(5)
Re–Te	2.6820(16)–2.7060(15) mean 2.694(7)	2.6788(15)–2.7070(16) mean 2.693(7)	2.6698(9)–2.7130(9) mean 2.694(8)	2.6899(11)–2.7050(11) mean 2.697(5)
Re–C	2.06(2)–2.11(2) mean 2.08(2)	2.04(2)–2.10(2) mean 2.08(2)	2.06(1)–2.11(1) mean 2.08(1)	2.07(2), 2.12(2)
C–N	1.12(3)–1.18(3) mean 1.14(2)	1.14(3)–1.21(3) mean 1.17(3)	1.13(1)–1.19(2) mean 1.16(2)	1.08(3), 1.14(3)

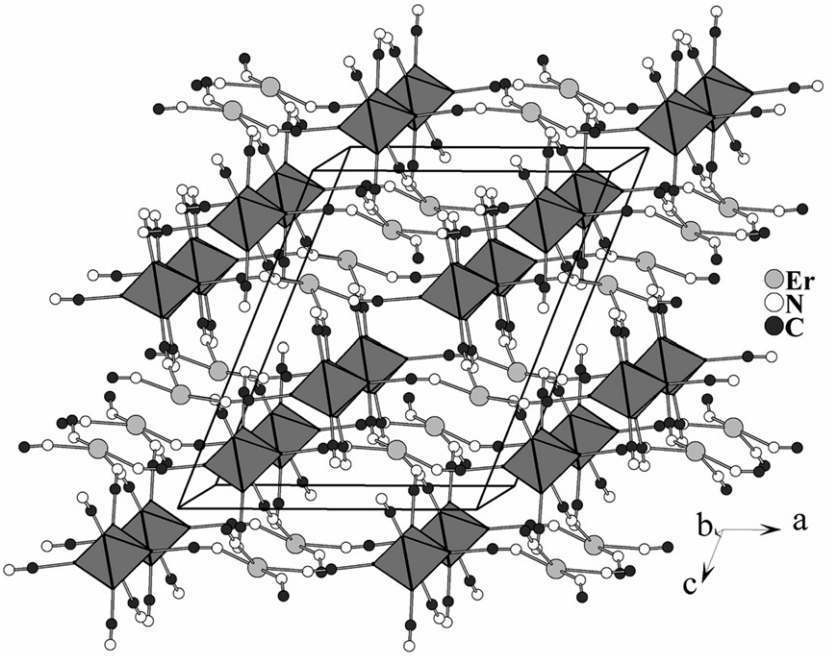

Fig. 3. View of framework in structure of $[\{Er(H_2O)_4\}\{Re_6Te_8(CN)_6\}] \cdot 2.5H_2O$ (**6**). Te, Er2 and O atoms are omitted for clarity. Clusters Re_6 are shown as polyhedral.

atoms (O11, O12 and O13 for Er1 and O21, O22 and O23 for Er2) that complete coordination sphere of Er to distorted tetragonal antiprism (Figs. S1a, S1b). Interatomic distances in coordination environment of Ln as well as Ln(1)–Ln(2) distances are listed in Table 3. Ln–O and Ln–N(CN) distances have typical values lying within 2.3–2.5 Å (see for example [26] – Eu, [27] – Tb, [28] – Dy, [29] – Ho, Er, Gd, [20] – Tb – Yb).

Each cluster anion is bridged with four cations of lanthanide by cyanogroups. Coordination environment of Ln(III) contains four nitrogen atoms that leads to formation of three-dimensional framework with (4,4) connectivity according to notation given in [21]. Two *trans*-cyanogroups of cluster complex remain uncoordinated. Coordination environment of Ln(III) contains four nitrogen atoms and therefore form 3D network (Fig. 3). Additionally structures contain four positions of solvate water molecules (O1w, O2w, O3w and O4w) forming six hydrogen bonds to coordinated water molecule (O–O distances are within 2.69–2.99 Å) and to nitrogen atoms (N–O distances are within 2.67–2.85 Å).

The distances in lanthanide environment (Ln–N(CN) and Ln–O(H_2O)) are gradually decreased in the series **1**, **3**–**6** with the increase of atomic number of Ln according to lanthanide contraction.

3.3. Structure of *2*

The compound **2** is crystallizing in $P\bar{1}$ space group. The coordination polyhedron of Gd(III) is distorted tetragonal antiprism (Fig. 4). Coordination environment consists of three water molecules (O1, O2, O3) and five nitrogen atoms (N1, N2, N3, N4, N5) of different cluster anions. Ln–O and Ln–N(CN) distances have typical values lying within 2.3–2.5 Å.

Table 3
Selected distances (Å) of cationic environment for **1–8**

Distances	**1**	**2**	**3**	**4**
Ln(1)–N(CN)	2.40(1)–2.56(1) mean 2.47(7)	2.46(1)–2.48(1) mean 2.46(1)	2.36(1)–2.51(1) mean 2.44(6)	2.33(2)–2.48(2) mean 2.42(7)
Ln(2)–N(CN)	2.37(1)–2.52(1) mean 2.46(6)	– –	2.33(1)–2.55(1) mean 2.44(9)	2.39(2)–2.54(2) mean 2.42(9)
Ln(1)–O(H_2O)	2.40(2)–2.46(2) mean 2.42(3)	2.41(1)–2.42(1) mean 2.42(1)	2.37(1)–2.48(1) mean 2.42(4)	2.34(4)–2.44(4) mean 2.38(5)
Ln(2)–O(H_2O)	2.34(3)–2.45(4) mean 2.38(5)	– –	2.22(3)–2.43(2) mean 2.34(9)	2.36(3)–2.44(3) mean 2.41(4)
Ln(1)–Ln(2)	0.480(3)	–	0.534(1)	0.550(2)
	5	**6**	**7**	**8**
Ln(1)–N(CN)	2.34(2)–2.56(2) mean 2.42(9)	2.29(2)–2.535(18) mean 2.39(10)	2.40(1)–2.41(1) mean 2.40(1)	2.43(2), 2.52(2) –
Ln(2)–N(CN)	2.35(2)–2.50(2) mean 2.43(6)	2.39(2)–2.49(2) mean 2.41(7)	2.36(1)–2.41(1) mean 2.39(2)	– –
Ln(1)–O(H_2O)	2.15(3)–2.47(3) mean 2.35(12)	2.26(3)–2.40(2) mean 2.36(7)	2.30(1)–2.47(1) mean 2.37(8)	2.37(5), 2.63(5) –
Ln(2)–O(H_2O)	2.37(2)–2.40(3) mean 2.39(2)	2.28(5)–2.34(3) mean 2.32(3)	2.31(1)–2.42(1) mean 2.37(6)	– –
Ln(1)–Ln(2)	0.550(2)	0.552(2)	–	1.768(3)

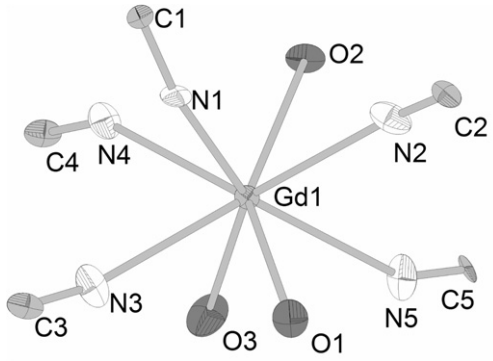

Fig. 4. Coordination environment of Gd(III) in compound **2**. Displacement ellipsoids are drawn at the 50% probability level.

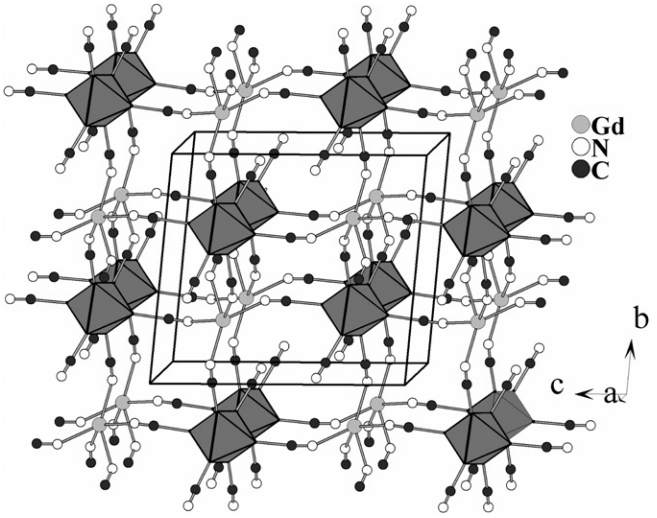

Fig. 5. View of framework in structure of $[\{Gd(H_2O)_3\}\{Re_6Te_8(CN)_6\}] \cdot 2.5H_2O$ (**2**). Te and O atoms are omitted for clarity. Clusters Re_6 are shown as polyhedral.

Each cluster anion connects with five cations of gadolinium and each cation of gadolinium is coordinated by five nitrogen atoms of cluster complexes, that leads to formation of three-dimensional network with (5,5) connectivity (Fig. 5). Additionally structure **2** contains three solvate water molecules (O1w–O3w) forming three hydrogen bonds to coordinated water molecules (O–O distances are 2.81, 2.85 Å) and to nitrogen atoms (N–O distance is 2.69 Å). Distance between uncoordinated atom of nitrogen and Gd(III) is 4.563(18) Å.

3.4. Structure of **7**

The compound **7** is crystallizing in *P*2/*c* space group. The structure of **7** contains two crystallographically independent cluster anions (Re11–Re16 and Re21–Re26) and two independent Tm atoms (Tm11 and Tm21). Coordination environment of each Tm atoms are formed by four nitrogen atoms from different cyanoclusters and four oxygen atoms (N11, N12, N23, N26, O11, O12, O13, O14 for Tm11 and N14, N16, N21, N25, O21, O22, O23, O24 for Tm21) and can be described as distorted tetragonal antiprism (Figs. S2a and S2b). Distances Tm–O and Tm–N are lying within 2.3–2.5 Å and are listed in Table 3. Each cluster anion is linked by cyanogroups to four Tm cations that leads to formation of three-dimensional framework with (4,4) connectivity (Fig. 6). Two *trans*-cyanogroups of each cluster complex remain uncoordinated. Additionally structure **7** contains five solvate water molecules (O1w–O5w) forming seven hydrogen bonds to coordinated water molecules (O–O distances are 2.65–2.87 Å) and to nitrogen atoms (N–O distances are 2.76–3.03 Å).

3.5. Structure of ***8***

The compound **8** is crystallizing in *C*2/*m* space group. Details of structure compound are shown in Fig. 7. In this compound ytterbium cation is located in two close positions generated by mirror plane. Two nitrogen atoms of cyanogroups of different cluster anions (N2, N2′) are common for these two positions of ytterbium atoms (Fig. 8). Additionally each Yb atom is coordinated by two nitrogen atoms (N1, N1′) of different cluster anions and four half occupied oxygen atoms (O1, O1′, O2, O2′) that

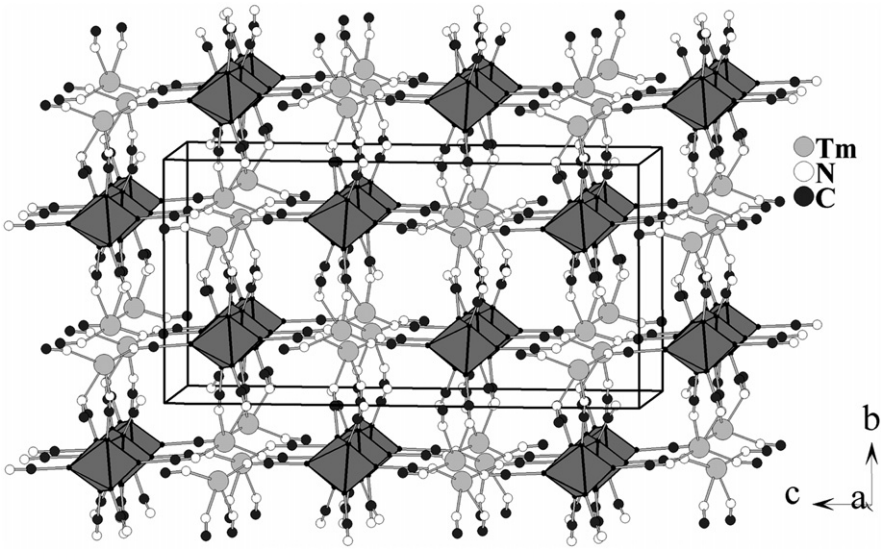

Fig. 6. View of framework in structure of $[\{Tm(H_2O)_4\}\{Re_6Te_8(CN)_6\}] \cdot 2.5H_2O$ (**7**). Te and O atoms are omitted for clarity. Clusters Re_6 are shown as polyhedral.

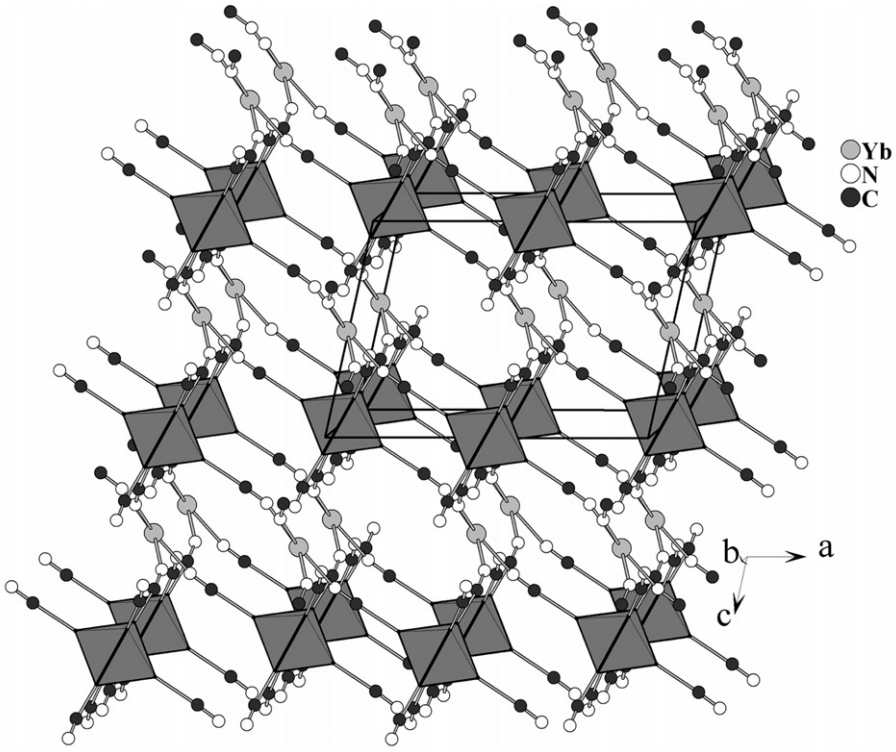

Fig. 7. View of framework in structure of $[\{Yb(H_2O)_4\}\{Re_6Te_8(CN)_6\}]$ (**8**). Te and O atoms are omitted for clarity. Clusters Re_6 are shown as polyhedral.

complete coordination sphere of Yb to distorted tetragonal antiprism (Fig. S3). Interatomic distances in coordination environment of Ln and Ln(1)–Ln′(1) distances are listed in Table 3. Ln–O(H_2O) and Ln–N(CN) distances have typical values lying within 2.3–2.6 Å [29].

4. Discussion

4.1. Synthesis

All compounds **1**–**8** were obtained by interaction of aqueous solutions of $Cs_4Re_6Te_8(CN)_6$ with $LnCl_3 \cdot nH_2O$ in acidic media. Mixture of these solutions were stable in oxygen-free atmosphere and no crystals were formed within a week. Exposure of reaction mixture on air resulted in slow one-electron oxidation of $[Re_6Te_8(CN)_6]^{4-}$ anion to paramagnetic $[Re_6Te_8(CN)_6]^{3-}$ by oxygen. It was found [3] that tellurium anion $[Re_6Te_8(CN)_6]^{4-}$ undergoes one-electron oxidation in electrochemical cell at 0.53 V. Chemical oxidation of $[Re_6Te_8(CN)_6]^{4-}$ by bromine [25] or iodine [30] was also reported. The process of oxidation of anion can be easily monitored by change of colour of solution from dark orange to dark brown and this process is followed by precipitation of black prism of compounds **1**–**8**. The precipitation of cluster polymers upon oxidation of tellurium cluster anion in solution was found also in

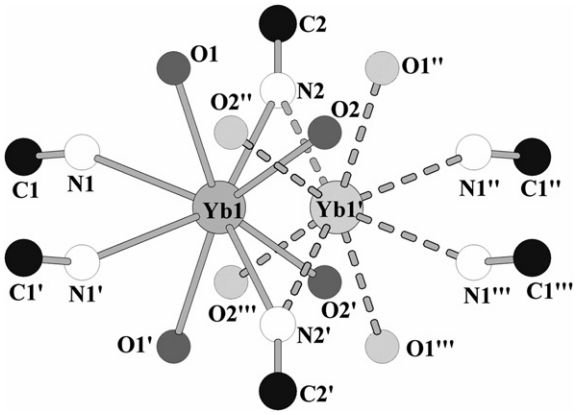

Fig. 8. Coordination environment of Yb(III) in compound **8**.

hydrothermal conditions [13] as well as for selenium cluster anion in acid solution [20].

The crystals **1**–**8** were rather stable under mother liquor while exposure on air resulted in partial dehydration of compounds and in loss of crystallinity of samples.

4.2. Structures

X-ray structural analysis revealed that all studied structures are coordination polymers with Re–CN–Ln bridges. Comparison of the structures**1**–**8** showed that despite of relatively small distinctions in atomic radii of lanthanides Eu–Yb in series of compounds **1**–**8** four types of structures are realized.

Structures **1**, **3**–**6** are isostructural and can be roughly described as primitive cubic packing of anions (Fig. S4). Distances between centers of cluster anions vary 9.1–9.54 Å (for Er structure). Cations of Ln occupy two close positions near center of cube formed by anions. The Ln1–Ln2 distance increases slightly from Eu compound (0.479 Å) to Er one (0.551 Å). The framework of these compounds has (4,4) connectivity.

Structure of compound **7** (Tm) has similar connectivity (4,4) of framework and is closely related to above structures. Unit cell volume is doubled and thulium atoms occupy two ordered positions in neighbor cubes. The application of cell vector transformation **a**′ = **2c**, **b**′ = **b**, **c**′ = **a** to compound **7** leads to structural model similar to that found in compound **1.** Structure of **8** has reduced unit cell compared to **1** with retention of packing motif. In the unit cell ytterbium atoms are disordered over two symmetry generated positions with Yb–Yb separation about 1.77 Å.

It should be noted that compounds $[\{Ln(H_2O)_3\}\{Re_6Te_8(CN)_6\}]\cdot 4H_2O$ (**9**) with large lanthanides, Ln = La, Nd [13] crystallized in another structure with six cyano-bridges Re–CN–Ln per cluster.

The diversity of structural types formed in systems Ln–$[Re_6Te_8(CN)_6]^{3-}$ is quite surprising, because inorganic lanthanides often adopt one or two structural types for all series of lanthanides [31]. Related compounds based on selenocyanide cluster anion $[Re_6Se_8(CN)_6]^{3-}$, namely $[\{Ln(H_2O)_3\}\{Re_6Se_8(CN)_6\}]\cdot 3.5H_2O$, were isostructural for heavy lanthanides Ln = Tb–Lu [20]. Such distinctions may be explained of different sizes of $[Re_6Te_8(CN)_6]^{3-}$ and $[Re_6Se_8(CN)_6]^{3-}$. Increased size of tellurium anion compared to selenium one leads to increased voids between anions and hence several possible positions for lanthanide cations. That also may stimulate structural disorder of cations between close positions.

To best our knowledge topology of reported compounds **1**, **3**–**7** with (4,4) connectivity framework have never occurred in cyanometallate polymers, while compound **2** with (5,5) framework has only one topologic equivalent to $(H_3O)\{Ce(H_2O)_4[W(CN)_8]\}\cdot 2H_2O$ [32].

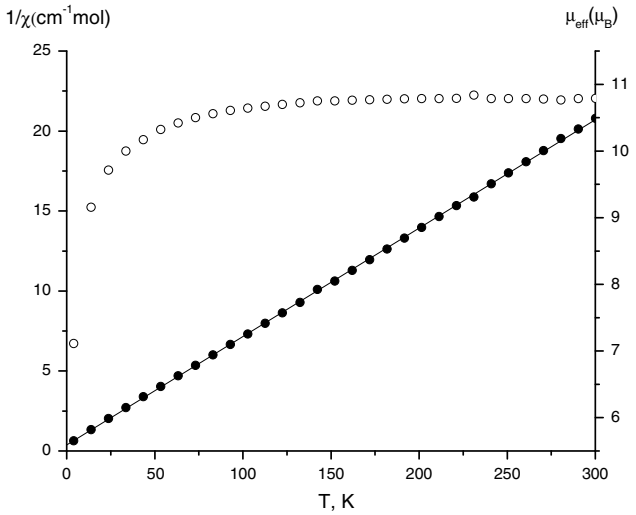

Fig. 9. The temperature dependence of effective magnetic moment (μ_{eff}) and reciprocal magnetic susceptibility ($1/\chi$) for **5**.

4.3. Magnetic properties

The measurement of the temperature dependence of the magnetic susceptibility for polycrystalline samples **2** and **5** showed that these compounds are paramagnetic over the temperature range (4–300 K). Effective magnetic moment for compound **2** at 300 K is 8.13 μ_B. This value is in a good agreement with μ_{eff} = 8.14 μ_B calculated for two non-interacting magnetic centers: Gd^{3+} ($\mu_{eff} = [g_J^2 J(J+1)]^{1/2}$ μ_B = 7.9 μ_B) and paramagnetic anion $[Re_6Te_8(CN)_6]^{3-}$ (μ_{eff} = 1.96 μ_B [33]). Temperature dependence for magnetic susceptibility for **2** follows to Curie–Weiss law $\chi = \frac{N\beta^2\mu_{eff}^2}{3k(T-\theta)} = 8.275/(T-1.95)$. Effective magnetic moment for compound **5** at 300 K is 10.79 μ_B. This value is in a good agreement with μ_{eff} = 10.78 μ_B, calculated for two weakly interacting magnetic centers: Ho^{3+} ($\mu_{eff} = [g_J^2 J(J+1)]^{1/2}$ μ_B = 10.61 μ_B) and paramagnetic anion $[Re_6Te_8(CN)_6]^{3-}$ (μ_{eff} = 1.96 μ_B [33]). Temperature dependence for magnetic susceptibility for **5** follows to Curie–Weiss law $\chi = \frac{N\beta^2\mu_{eff}^2}{3k(T-\theta)} = 14.76/(T+5.5)$ (Fig. 9).

Acknowledgements

This work was supported by the SRC program of the Korea Science and Engineering Foundation (KOSEF) through the Center for Intelligent Nano-Bio Materials at Ewha Womans University (Grant R11-2005-008-03001-0) Rosnauka (2006-Pи-19.0/001/650, Contract No. 02.442.117414) and Russian Foundation of Basic Research (grants 08-03-90413 and 06-03-89503).

Appendix A. Supplementary data

Figs. S1–S3 showing coordination environment of rare earth cations in structures **6**–**8**. Figs. S4–S8 showing primitive cubic packing of anions in the structures. Further details of the crystal structure investigations of **1**–**8** can be obtained from the Fachinformationszentrum Karlsruhe, 76344 Eggenstein-Leopoldshafen, Germany, (fax: (49) 7247-808-666; e-mail: crysdata@fiz.karlsruhe.de) on quoting the depository number CSD 418866–418873. Copies of this information may be obtained free of charge. Supplementary data associated with this article can be found, in the online version, at doi:10.1016/j.poly.2008.04.054.

References

[1] Y.V. Mironov, A.V. Virovets, V.E. Fedorov, N.V. Podberezskaya, O.V. Shishkin, Y.T. Struchkov, Polyhedron 14 (1995) 3171.
[2] N.G. Naumov, A.V. Virovets, M.N. Sokolov, S.B. Artemkina, V.E. Fedorov, Angew. Chem., Int. Ed. 37 (1998) 1943.
[3] T. Yoshimura, S. Ishizaka, Y. Sasaki, H.B. Kim, N. Kitamura, N.G. Naumov, M.N. Sokolov, V.E. Fedorov, Chem. Lett. (1999) 1121.
[4] N.G. Naumov, A.V. Virovets, V.E. Fedorov, Inorg. Chem. Commun. 3 (2000) 71.
[5] N.G. Naumov, D.V. Soldatov, J.A. Ripmeester, S.B. Artemkina, V.E. Fedorov, Chem. Commun. (2001) 571.
[6] S.B. Artemkina, N.G. Naumov, A.V. Virovets, O. Oeckler, A. Simon, S.B. Erenburg, N.V. Bausk, V.E. Fedorov, Eur. J. Inorg. Chem. (2002) 1198.
[7] Y. Kim, S.M. Park, W. Nam, S.J. Kim, Chem. Commun. (2001) 1470.
[8] Y. Kim, S.M. Park, S.J. Kim, Inorg. Chem. Commun. 5 (2002) 592.
[9] S.M. Park, Y. Kim, S.J. Kim, Eur. J. Inorg. Chem. (2003) 4117.
[10] Y. Kim, S. Kim, S.J. Kim, M.K. Lee, M. Kim, H. Lee, C.S. Chin, Chem. Commun. (2004) 1692.
[11] N.G. Naumov, M.S. Tarasenko, A.V. Virovets, Y. Kim, S.J. Kim, V.E. Fedorov, Eur.J. Inorg. Chem. (2006) 298.
[12] H. Imoto, N.G. Naumov, A.V. Virovets, T. Saito, V.E. Fedorov, J. Struct. Chem. (Engl. Trans.) 39 (1998) 720.
[13] S.B. Artemkina, N.G. Naumov, A.V. Virovets, V.E. Fedorov, Eur. J. Inorg. Chem. (2005) 142.
[14] Y.V. Mironov, N.G. Naumov, K.A. Brylev, O.A. Efremova, V.E. Fedorov, K. Hegetschweiler, Angew. Chem., Int. Ed. 43 (2004) 1297.
[15] N.G. Naumov, S.B. Artemkina, A.V. Virovets, V.E. Fedorov, J. Solid State Chem. 153 (2000) 195.
[16] N.G. Naumov, A.V. Virovets, V.E. Fedorov, J. Struct. Chem. (Engl. Trans.) 41 (2000) 499.
[17] L.G. Beauvais, M.P. Shores, J.R. Long, Chem. Mater. 10 (1998) 3783.
[18] M.P. Shores, L.G. Beauvais, J.R. Long, J. Am. Chem. Soc. 121 (1999) 775.
[19] E.G. Tulsky, N.R.M. Crawford, S.A. Baudron, P. Batail, J.R. Long, J. Am. Chem. Soc. 125 (2003) 15543.
[20] M.S. Tarasenko, N.G. Naumov, A.V. Virovets, D.Y. Naumov, N.V. Kurat'eva, Y.V. Mironov, V.N. Ikorskii, V.E. Fedorov, J. Struct. Chem. (Engl. Trans.) 46 (2005) S134.
[21] M. O'Keeffe, M. Eddaoudi, H.L. Li, T. Reineke, O.M. Yaghi, J. Solid State Chem. 152 (2000) 3.
[22] Bruker AXS Inc., APEX2 (Version 1.08), SAINT (Version 7.03), Bruker advanced X-ray solutions, Madison, Wisconsin, USA, 2004.
[23] Bruker AXS Inc., SADABS (Version 2.11), Bruker advanced X-ray solutions, Madison, Wisconsin, USA, 2004.
[24] Bruker AXS Inc., SHELXTL (Version 6.12), Bruker advanced X-ray solutions, Madison, Wisconsin, USA, 2004.
[25] N.G. Naumov, E.V. Ostanina, A.V. Virovets, M. Schmidtman, A. Muller, V.E. Fedorov, Russ. Chem. Bull. 51 (2002) 866.
[26] J.R. Li, L.Z. Cai, R.Q. Zou, G.W. Zhou, G.C. Guo, X.H. Bu, J.S. Huang, Acta Crystallogr., Sect. E 58 (2002) M686.
[27] Q.H. Zhao, Q.H. Wang, R.B. Fang, Transition Met. Chem. 29 (2004) 144.
[28] X.R. Sun, Z.D. Chen, F. Yan, S. Gao, K.K. Cheung, C.M. Che, X.X. Zhang, J. Clust. Sci. 13 (2002) 103.
[29] V.P. Fedin, I.V. Kalinina, A.V. Virovets, D. Fenske, Russ. Chem. Bull. 52 (2003) 126.
[30] M.V. Bennett, L.G. Beauvais, M.P. Shores, J.R. Long, J. Am. Chem. Soc. 123 (2001) 8022.
[31] M.S. Wickleder, Chem. Rev. 102 (2002) 2011.
[32] I.V. Saramaga, V.M. Davidov, D.I. Semenishin, V.V. Dovgei, Ukr. Khim. Zhurn. (Russ. Ed.) 67 (2001) 14.
[33] T.V. Larina, V.N. Ikorskii, N.T. Vasenin, V.F. Anufrienko, N.G. Naumov, E.V. Ostanina, V.E. Fedorov, Russ. J. Coord. Chem. 28 (2002) 554.

Polyhedron 27 (2008) 2365–2371

Contents lists available at ScienceDirect

Polyhedron

journal homepage: www.elsevier.com/locate/poly

Quinoxaline sensitised lanthanide ion luminescence: Syntheses, spectroscopy and X-ray crystal structure of Na{1,4,7-tris[(*N*-diethyl)carbamoylmethyl]-1,4,7, 10-tetraazacyclododecane-10-(2-methylquinoxaline)}I_3 C_7H_8

Michael Andrews [a], Rebecca H. Laye [b], Lindsay P. Harding [c], Simon J.A. Pope [a,*]

[a] School of Chemistry, Main Building, Cardiff University, Museum Avenue, Cardiff CF10 3AT, United Kingdom
[b] Department of Chemistry, The University of Sheffield, Dainton Building, Brook Hill, Sheffield S3 7HF, United Kingdom
[c] School of Biological and Chemical Sciences, University of Huddersfield, Queen Street, Huddersfield HD1 3DH, United Kingdom

ARTICLE INFO

Article history:
Received 10 January 2008
Accepted 1 April 2008
Available online 29 May 2008

Keywords:
Lanthanide complex
Luminescence
pH response

ABSTRACT

The synthesis of a quinoxaline-appended aza-macrocyclic ligand together with corresponding Ln^{III} complexes are described. The luminescence properties of the complexes show that the quinoxaline unit sensitises both visible (Eu^{III}) and near-IR (Nd^{III} and Yb^{III}) emitting lanthanide ions. UV–Vis absorption and time-resolved photophysical studies together with X-ray structural data suggest that as well as contributing chromophorically, the quinoxaline moiety generally participates in the first coordination sphere of Ln^{III}. The luminescent pH response of the Eu^{III} complex is also reported. The form of the steady state spectrum changes profoundly in the pH range 2–12, implying a change in the coordination environment, which was confirmed with time-resolved lifetime measurements that suggest an increase in europium inner sphere hydration at acidic pH.

© 2008 Elsevier Ltd. All rights reserved.

1. Introduction

The use and potential application of lanthanide ion complexes to a variety of bio-imaging modalities has driven significant progress and diversity in the design of such compounds [1]. This rapid development has advanced the discipline with respect to lanthanide-based responsive probes for, amongst others, Zn^{II} [2], Cu^{II} [3], alkali metals [4], pH [5], pO_2 [6], halide ions [7], and various anionic residues [8]. The nature of the response is clearly dependent on the lanthanide in question. Gd^{III}-based probes are attractive in MRI applications and rely upon control of the hydration sphere and therefore overall relaxivity of the Gd^{III} complex [9]. Notable examples include MRI probes for esterase activity [10] where the inner sphere hydration of the Gd^{III} centre is enhanced upon esterase exposure and Ca^{II} response [11]. However, the design of luminescent lanthanide-based probes requires an alternative set of criteria. Although high-denticity ligands are a prerequisite (stability in aqueous environments is clearly preferential for biological applications) the incorporation and photophysical compatibility of the photoactive components is essential. Lanthanide luminescence arises from f–f transitions and therefore requires the use of a sensitising chromophore. In turn, the choice of chromophore is determined, to a certain extent, by the lanthanide to be sensitised. The generally accepted and most common mechanism for lanthanide sensitisation proceeds *via* a chromophore-localised triplet state [12]. Therefore for the visibly emitting lanthanides such as Eu^{III} and Tb^{III} the choice of chromophore is far more limited than for near-IR emitting lanthanides such as Nd^{III}, Er^{III} and Yb^{III}. However, consideration of the optical properties of biological tissue and particularly autofluorescence in fluorescence microscopy, are also key in the choice of chromophore [13]. Consequently, luminescent lanthanide complexes which allow long wavelength sensitisation are extremely attractive. The successful choices of antennae for use with millisecond lifetime emitters like Eu^{III} and Tb^{III} are too numerous to cover here, but notable examples are heterocyclic species such as xanthone derivatives [14], and entities like acridone [15]. Such aromatic species absorb in the low energy portion of the UV region whilst maintaining sensitising capabilities for Eu^{III} and Tb^{III}. Although autofluorescence can be circumvented by utilising time-gating techniques, depth of tissue penetration can still be problematic and this has led to the exploitation of near-IR fluorophores for enhanced fluorescence imaging [13]. Lanthanides of relevance to this area are predominantly Yb^{III} and Nd^{III} whilst Er^{III} generally possesses poor or non-emissivity in protic media with only rare exceptions [16]. For such ions, with energetically lower lying excited states, the variety of sensitising chromophore can be greatly expanded. As well as heterocyclic species, d-metal chromophoric entities derived from Ru^{II} (diimine and tetracyano varieties) [17], Re^{I} and Os^{II} [18] moieties (which utilise

* Corresponding author. Tel.: +44 0 29 20879316; fax: +44 0 29 20874030.
E-mail address: popesj@cardiff.ac.uk (S.J.A. Pope).

0277-5387/$ - see front matter © 2008 Elsevier Ltd. All rights reserved.
doi:10.1016/j.poly.2008.04.010

triplet MLCT donor states) to Ir^{III} [19], Cr^{III} [20], Pt^{II} [21], and even Tb^{III} ions [22] all of which have been shown to facilitate sensitised f–f emission.

In this paper we describe the use of quinoxaline as a sensitising chromophore for both visible and near-IR emitting lanthanide ions. The study reports synthetic routes to the ligand and its corresponding Ln^{III} complexes together with the spectroscopic and photophysical attributes of the complexes, concluding with a description of the luminescent pH response of the Eu^{III} complex.

2. Results and discussion

2.1. Synthesis of the ligand and complexes

Our synthetic methodology relied upon coupling 2-bromomethylquinoxaline with a 1,4,7-functionalised tetraaza macrocycle. Initially the macrocyclic precursor of choice was 1,4,7-tris(*tert*-butoxycarbonylmethyl)-1,4,7,10-tetraazacyclododecane, which has been successfully employed to access a large range of functionalised DO3A-derived macrocyclic ligands. However, in this case we found that the deprotection step (trifluoroacetic acid, dichloromethane) associated with the conversion of the ^{t}Bu-ester to the carboxylic acid induced cleavage of the methyl-quinoxaline from the cyclen framework as evidenced by mass spectrometry and ^{1}H NMR. Therefore our attention turned to amide-functionalised macrocyclic derivatives where there is no need for a deprotection step. In particular we selected the diethylamido version since we anticipate exploiting the inherent amphiphilicity of the resultant complexes in future applied work (Scheme 1).

IR vibrational spectra were obtained on solid samples utilising an ATR-equipped IR spectrometer. **2** displayed vibrational frequencies consistent with the presence of appropriate organic functional groups, in particular the amide stretch, ν(C=O), at 1703 cm^{-1}. For the complexes the amide stretch is diagnostic of coordination and was observed at *ca.* 1600 cm^{-1}, the low energy shift indicative of a weakening of the carbonyl bond due to lanthanide coordination. Additionally the spectra for the complexes also confirmed the presence of the relevant counter ions, for example a strong ν(S=O) stretch was noted at 1027 cm^{-1} corresponding to the triflate anion. Mass spectra of the complexes were recorded and for each sample showed a cluster of peaks associated with the loss of one counter anion, yielding the monocation, $\{M \cdot 2X\}^+$ with appropriate isotopic distributions in each case. Additional peaks at lower *m*/*z* were assigned according to the expected sequential loss of counter ions.

The absorption properties of the ligand were investigated. The spectrum of **2** in acetonitrile displayed a well-resolved transition at 294 nm with a weaker feature at 357 nm. These are assigned to π–π^* (with the possibility of some n–π^* contribution particularly in the lower energy band) transitions. The corresponding lanthanide complexes showed one dominant transition at approximately 320 nm (π–π^*) with a much weaker shoulder on the red-edge of this transition.

3. Single crystal X-ray structural determination of Na{1,4,7-tris[(*N*-diethyl)carbamoylmethyl]-1,4,7,10-tetraazacyclododecane-10-(2-methylquinoxaline)}I_3 C_7H_8

A highly concentrated toluene solution of the ligand was stored at −20 °C for 2 weeks after which time crystalline material started to form. A brown, block-like crystal with dimensions of 0.35 × 0.03 × 0.02 mm was subjected to single crystal X-ray diffraction analysis. The study confirmed the integrity of the proposed ligand framework as the sodium salt, with two unique whole molecules in the asymmetric cell together with two solvent (toluene) molecules and two counter ions (I_3^-). The chemical formula of the crystal is $C_{42}H_{67}N_9NaO_3$ I_3 C_7H_8. Diffraction data were collected on a Nonius Kappa CCD 4-circle diffractometer controlled using KAPPACCD Server Software [23] and collect [24] and using graphite-monochromated Mo Kα radiation (k = 0.71073 Å) at 150(3) K. Final cell refinement and data reduction were carried out using DENZO and SCALEPACK from the HLKF suite of programmes [25]. An absorption correction was applied by the multiscan method using the SORTVA program. The theta range for data collection was 1.15–27.08 ° with 20579 independent reflections and completeness to 27.08° of 94.4%. The structure was refined on F_0^2 using all data with final R indices [$I > 2\sigma(I)$] of R_1 = 0.0839 and wR_2 = 0.2065. The crystal system is triclinic with a $P\bar{1}$ space group and the unit cell itself possesses dimensions a = 12.562(3) Å, b = 18.648(4) Å and c = 22.955(5) with α = 99.34(3)°, β = 103.65(3)° and γ = 103.09(3)°. The unit cell has a volume of 4955.6(17) $Å^3$ and Z = 4 giving a density of 1.946 mm^{-1}. Selected bond lengths and bond angles reported in Table 1. As represented in Fig. 1 the structure reveals an encapsulated sodium ion coordinated by three amide oxygens, four macrocyclic nitrogens and the N(5) quinoxaline nitrogen. There are no other solvent molecules associated with the coordination sphere of the sodium ion. The charge is balanced by the I_3^- counterion, presumably liberated by the use of KI in the synthesis of **2**. Although solid state the structure solution of Na{1,4,7-tris[(*N*-diethyl)carbamoylmethyl]-1,4,7,10-tetraazacyclododecane-10-(2-methylquinoxaline)}I_3 is informative since it suggests that a lanthanide complex of the ligand would probably favour a coordination environment where the quinoxaline chromophore participates in the first coordination sphere, despite the relatively bulky ethyl groups of the amide arms. The ionic radius of an 8-coordinate sodium ion is 1.32 Å and therefore larger than that of the trivalent lanthanides Nd^{III}, Eu^{III} and Yb^{III} with 1.12, 1.09 and 1.01 Å, respectively [26]. Despite this we have found sodium complexes of these types of ligands to be useful predictors of the corresponding lanthanide coordination environment [2d]. This is of particular

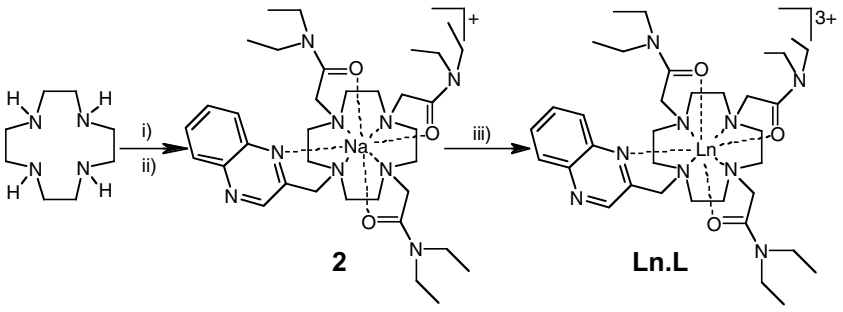

Scheme 1. Syntheses of the ligand (**2**) and its complexes (**Ln · L**): (i) 3 equiv. *N*-diethyl-2-chloroacetamide, $NaHCO_3$, MeCN; (ii) 1 equiv. 2-bromomethylquinoxaline, KI, $NaHCO_3$, MeCN, 60 °C, 24 h; (iii) $Ln(OTf)_3$ or $Ln(NO_3)_3$, MeOH, 50 °C, 24 h.

Table 1
Selected bond lengths (Å) and bond angles (°) for Na{1,4,7-tris[(*N*-diethyl)carbamoylmethyl]-1,4,7,10-tetraazacyclododecane-10-(2-methylquinoxaline)}I_3 C_7H_8

Bond lengths (Å)			
Na(1)–O(1)	2.551(12)	Na(2)–O(4)	2.543(11)
Na(1)–O(2)	2.421(11)	Na(2)–O(5)	2.406(11)
Na(1)–N(1)	2.564(13)	Na(2)–O(6)	2.542(11)
Na(1)–N(2)	2.585(13)	Na(2)–N(10)	2.599(13)
Na(1)–N(3)	2.583(13)	Na(2)–N(11)	2.595(12)
Na(1)–O(3)	2.617(11)	Na(2)–N(12)	2.635(11)
Na(1)–N(4)	2.663(13)	Na(2)–N(13)	2.552(12)
Na(1)–N(5)	2.659(13)	Na(2)–N(14)	2.692(12)
Na(1)–C(25)	3.084(17)	Na(2)–C(66)	3.071(15)
I(1)–I(2)	2.901(2)	I(4)–I(5)	2.923(2)
I(1)–I(3)	2.929(2)	I(4)–I(6)	2.935(2)
Bond angles (°)			
O(2)–Na(1)–O(1)	81.3(4)	O(5)–Na(2)–O(6)	81.1(3)
O(2)–Na(1)–N(1)	157.3(4)	O(5)–Na(2)–O(4)	79.0(3)
O(1)–Na(1)–N(1)	85.4(4)	O(6)–Na(2)–O(4)	133.6(4)
O(2)–Na(1)–N(3)	65.5(4)	O(5)–Na(2)–N(13)	84.5(3)
O(1)–Na(1)–N(3)	125.2(4)	O(6)–Na(2)–N(13)	64.5(3)
N(1)–Na(1)–N(3)	108.9(4)	O(4)–Na(2)–N(13)	151.9(4)
O(2)–Na(1)–N(2)	85.3(4)	O(5)–Na(2)–N(11)	123.7(4)
O(1)–Na(1)–N(2)	64.3(4)	O(6)–Na(2)–N(11)	154.5(4)
N(1)–Na(1)–N(2)	72.4(4)	O(4)–Na(2)–N(11)	63.9(4)
N(3)–Na(1)–N(2)	70.4(4)	N(13)–Na(2)–N(11)	108.9(4)
O(2)–Na(1)–O(3)	79.4(4)	O(5)–Na(2)–N(10)	156.2(4)
O(1)–Na(1)–O(3)	136.9(4)	O(6)–Na(2)–N(10)	84.8(4)
N(1)–Na(1)–O(3)	122.3(4)	O(4)–Na(2)–N(10)	124.2(4)
N(3)–Na(1)–O(3)	79.8(4)	N(13)–Na(2)–N(10)	72.0(3)
N(2)–Na(1)–O(3)	150.0(4)	N(11)–Na(2)–N(10)	69.9(4)
O(2)–Na(1)–N(5)	127.6(4)	O(5)–Na(2)–N(12)	65.2(3)
O(1)–Na(1)–N(5)	75.6(4)	O(6)–Na(2)–N(12)	124.9(3)
N(1)–Na(1)–N(5)	65.5(4)	O(4)–Na(2)–N(12)	82.7(4)
N(3)–Na(1)–N(5)	158.9(4)	N(13)–Na(2)–N(12)	69.8(4)
N(2)–Na(1)–N(5)	123.1(4)	N(11)–Na(2)–N(12)	69.3(3)
O(3)–Na(1)–N(5)	86.4(4)	N(10)–Na(2)–N(12)	108.9(4)
O(2)–Na(1)–N(4)	123.5(4)	O(5)–Na(2)–N(14)	127.0(4)
O(1)–Na(1)–N(4)	154.6(4)	O(6)–Na(2)–N(14)	74.2(3)
N(1)–Na(1)–N(4)	69.5(4)	O(4)–Na(2)–N(14)	85.3(4)
N(3)–Na(1)–N(4)	69.0(4)	N(13)–Na(2)–N(14)	122.6(4)
N(2)–Na(1)–N(4)	109.0(4)	N(11)–Na(2)–N(14)	91.8(4)
O(3)–Na(1)–N(4)	61.1(3)	N(10)–Na(2)–N(14)	66.1(4)
N(5)–Na(1)–N(4)	90.4(4)	N(12)–Na(2)–N(14)	160.7(4)
I(2)–I(1)–I(3)	177.93(5)	I(5)–I(4)–I(6)	178.82(5)

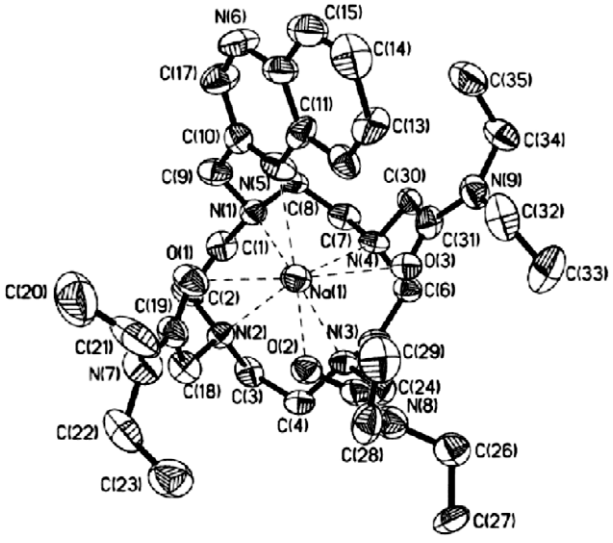

Fig. 1. Structural representation of Na{1,4,7-tris[(*N*-diethyl)carbamoylmethyl]-1,4,7,10-tetraazacyclododecane-10-(2-methylquinoxaline)}I_3 C_7H_8 with 50% probability ellipsoids (counter ion and solvent of crystallisation omitted for clarity).

use when interpreting the luminescence behaviour of the lanthanide complexes.

3.1. Photophysical studies

The lanthanide complexes **Ln · L** were synthesised to investigate the suitability of the quinoxaline chromophore to sensitise both visibly (Eu^{III}) and near-IR emissive (Nd^{III} and Yb^{III}) lanthanide ions. As discussed earlier the quinoxaline unit absorbs reasonably at *ca.* 355 nm, but due to its coordinative ability and thus proximate positioning, should promote efficient energy transfer upon sensitisation. Firstly the fluorescent properties of the non-lanthanide precursor were assessed. In aerated aqueous solution the precursor complex **2** is fluorescent upon irradiation at 300–360 nm. The broad, structureless emission is centred on 415 nm. Unfortunately, room temperature measurements conducted on a de-aerated solution did not allow the triplet state of the quinoxaline component to be obtained.

For the complexes **Ln · L** each gave emission spectra characteristic of the coordinated ion and are consistent with inclusion in the binding site. The use of chromophoric *'antennae'* to sensitise lanthanide ions is a well-established methodology for circumventing the inherently poor molar extinction coefficients associated with f–f transitions [1c]. However, for the visibly emitting ions such as Eu^{III} careful choice of the chromophore is required. Lowering the energy of excitation is an attractive proposition with regard not only to the energetic efficiency of the system, but also the avoidance of UV light which can cause autofluorescence in applied studies such as fluorescence microscopy [1]. In this study the coordinating quinoxaline chromophore can be sensitised at wavelengths of 320–390 nm (Fig. 2).

Time-resolved measurements were obtained on either H_2O/D_2O or $MeOH/CD_3OD$ solutions of the complexes (Table 2). The wavelengths of excitation for each system were indirect irradiation (λ_{ex} = 355 nm) for Nd^{III} and Yb^{III} and both direct and indirect irradiation for Eu^{III} (λ_{ex} = 396 and 355 nm, respectively). In each case the decay profile was analysed as a single exponential component indicative of a single coordinated lanthanide environment, except where discussed.

Fig. 2 shows the steady state fluorescence emission spectrum of **Eu · L** in methanol and highlights two key features: the tail of the residual emission of the quinoxaline chromophore and the well-resolved line-like emission bands from the emissive $^5D_0$ state of the Eu^{III} ion. The transitions associated with Eu^{III} appear at λ_{em} = 579, 592, 616, 651, 688 and 699 nm following excitation at 320–380 nm, thus confirming that the quinoxaline chromophoric unit sensitises Eu^{III}. The excitation spectrum (Fig. 2, left) confirms sensitisation *via* the quinoxaline chromophore with features at 325 nm and 355–390 nm attributed to the ligand. The luminescence lifetimes in H_2O and D_2O are reasonably typical of amide-derived ligands and overall nine-coordinate Eu^{III} complexes.

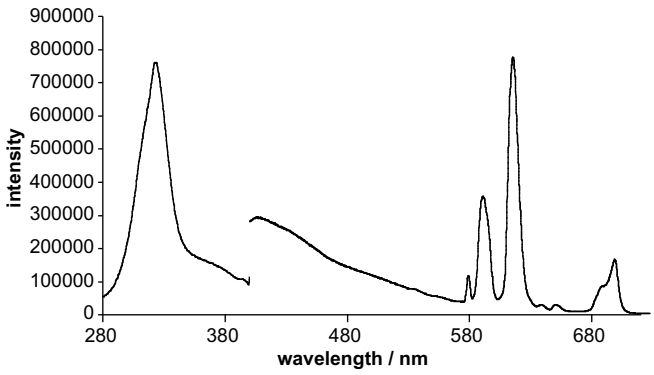

Fig. 2. Excitation (left, λ_{em} = 615 nm) and emission (right, λ_{ex} = 320 nm, not time-gated) spectra of **Eu · L** in methanol solution.

Table 2
Luminescence lifetimes of the complexes

Complex	τ_H (μs)	τ_D (μs)	q
Nd · L[a]	0.186	0.399	0.4
Eu · L[b]	551	1250	0.9
Yb · L[a]	0.904	1.370	0.7

[a] Measurements obtained in MeOH and CD_3OD using λ_{ex} = 355 nm.
[b] Measurements obtained in H_2O and D_2O using λ_{ex} = 355 or 396 nm. Lifetimes are associated with a ±10% error.

Application of the lifetimes to the determination of the inner sphere solvation of Eu^{III} was undertaken using the relation $q = 1.25[(k_{H_2O} - k_{D_2O}) - 0.25]$ [27]. In the case of **Eu · L** this yielded q = 0.9, corresponding to one inner sphere solvent molecule, which is consistent with an eight-coordinate binding mode of the ligand and therefore probably suggests that the quinoxaline unit participates in binding to Eu^{III} even in the presence of a coordinating polar solvent such as water.

For the near-IR emitting species **Nd · L** and **Yb · L** an excitation wavelength of 355 nm was employed. The Nd^{III}complex displayed near-IR emission dominated by a peak at 1058 nm ($^4F_{3/2} \rightarrow {}^4F_{11/2}$) (note: utilising a longpass filter prevented the observation of the higher energy $^4F_{3/2} \rightarrow {}^4F_{9/2}$ transition). The lifetimes of the transition were recorded as 186 and 399 ns in MeOH and CD_3OD (Fig. 3), respectively. These values were also obtained when using a detection wavelength of 1340 nm corresponding to the much weaker $^4I_{13/2}$ transition. Such lifetimes are reasonably consistent with the proposed coordination environment of Nd^{III}, but the abundance of proximate C–H oscillators may well quench the emission and lifetimes to some degree. Application of the equation for the inner sphere hydration of Nd^{III} $[q = 290(k_{MeOH} - k_{CD_3OD}) - 0.4]$ also adds credence to our assertion that the quinoxaline chromophore participates in the coordination sphere since using this relationship gives q = 0.4. However, the application of such an approach to Nd^{III} should be treated with care since the inherent errors associated with q in this case are much higher [27]. The steady state emission spectrum of **Yb · L** in CD_3OD (Fig. 4) revealed a spectral profile common for Yb^{III} with a peak at 972 nm ($^2F_{5/2} \rightarrow {}^4F_{7/2}$)together with a broadened shoulder to low energy beyond 1000 nm. The latter feature is frequently assigned to vibronic components within the transition although in this case no fine structure was observed. The time-resolved studies for **Yb · L** were less clear cut with the decay in methanol fitting well to a single exponential giving a lifetime of 904 ns, whereas in CD_3OD the decay was best fitted to two components of 1.37 (87%, and used in Table 2) and 2.59 μs (13%). Using the dominant component equates to q = 0.7 whilst the lesser results in q = 1.4. It is reasonable that the two forms of the complex exist in non-deuterated methanol as well, but possess very similar lifetimes that are difficult to differentiate statistically. However, given that the wavelength of absorption (λ_{max} = 319 nm) of the quinoxaline chromophore is not as red-shifted as for the other lanthanide complexes it may be that in coordinating solvent the quinoxaline is more weakly bound to Yb^{III} and resolved on the timescale of the lifetime measurements. What is clear however is that the quinoxaline unit sensitises ytterbium and in the case of a coordinated chromophore it is important to consider a Dexter mechanism for energy transfer. Consequently, in the case of **Yb · L**, it is also possible that energy transfer proceeds *via* electron exchange and the formation of an Yb^{II} intermediate (*i.e.* LMCT) [28].

We are also interested in designing responsive complexes for use as chemosensors. In particular utilising the emissive properties of Eu^{III} which possess structured emission in the visible region through deactivation of the $^5D_0$ excited state to the ground states of ^7F_J (J = 0,1,2,3,4). The relative intensity of the J = 2 state is known to be hypersensitive and can thus be exploited in the design of responsive complexes. We have been developing such an approach for use in the detection of metal ions in physiologically modelled aqueous environments whereby binding of the analyte modulates the degree of hydration of the Eu^{III} ion. Our interest in exploiting the coordinating quinoxaline for such applications is described below with respect to pH response in aqueous solution.

The pH dependent luminescence properties were investigated since the nitrogen heteroatoms in the quinoxaline chromophore should be liable to protonation in acidic media. As noted earlier the Eu^{III} complex should be a particularly interesting complex to study in this regard since the J = 2 state is known to be hypersensitive and the emission profile, in general, sensitive to changes in both the coordination geometry and nature of the donor atoms within the coordination sphere [1c,2d,5]. Thus, the pH dependence was assessed in H_2O. Our investigations show that **Eu · L** is very sensitive to changes in pH in the range 2–11. At pH/pD 2 the analysis of the decay profiles suggest that **Eu · L** possesses q = 2.2 obtained from lifetimes of 0.35 and 1.24 ms in H_2O and D_2O respectively. This change in innersphere hydration is ascribed to

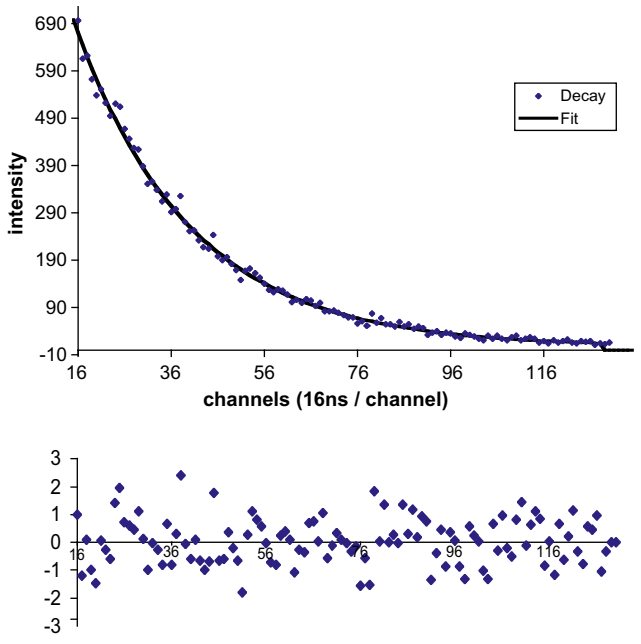

Fig. 3. Above: Fitted single-exponential decay for the complex **Nd · L** in CD_3OD obtained with λ_{ex} = 355 nm and λ_{em} = 1055 nm. Below: associated residuals.

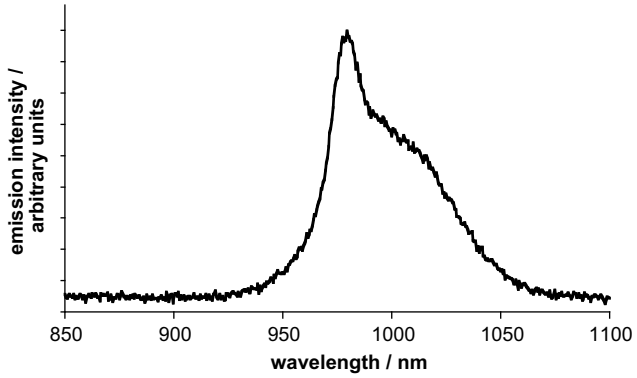

Fig. 4. Steady state emission spectrum for **Yb · L** in CD_3OD solution (λ_{ex} = 355 nm).

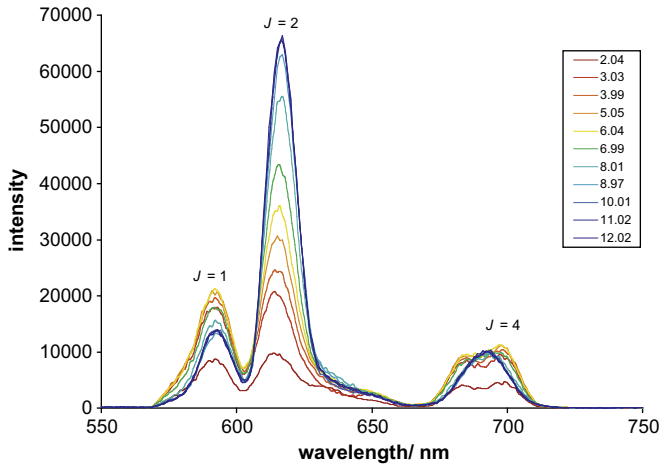

Fig. 5. Steady state spectra showing the changes in the Eu^{III} emission between pH 12.0 and 2.0.

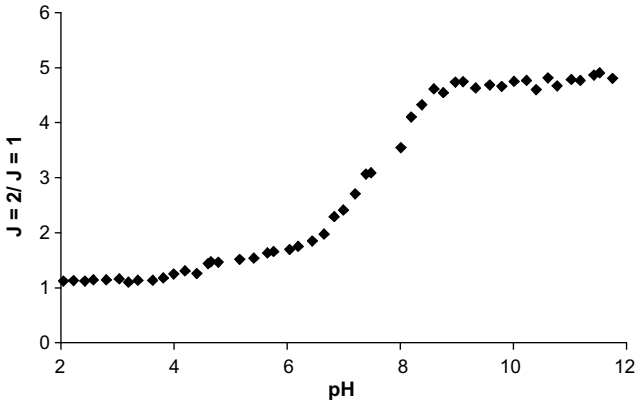

Fig. 6. Graph demonstrating the $J = 1$ and 2 ratiometric pH response of the Eu^{III} complex.

the quinoxaline becoming uncoordinated from the Eu^{III} centre, presumably as a consequence of protonation. Fig. 5 shows the changes in emissive spectral form associated with the various pH regimes. In basic conditions the $J = 4$ transition appears as a broad single peak at 692 nm, but as the pH decreases this is resolved into two separate peaks at 684 and 699 nm. As the pH decreases from pH 7 to pH 3 the intensity of the $J = 1$ transition increases to a broad maximum, before decreasing slightly, while the intensity of the $J = 2$ transition increases throughout the pH range. The result of these differing intensities is that the ratio of $J = 1$ to $J = 2$ changes significantly in the biorelevant region of pH 6–9 (Fig. 6). Such a ratiometric change is advantageous in responsive probes as it allows a modulation in emission to be attributed to a change in microenvironment rather than variable probe concentration, which fluorescence intensity alone cannot distinguish.

4. Conclusions

This study shows that the simple quinoxaline moiety is a useful chromophore for sensitising a range of visible and near-IR emitting lanthanide ions. It facilitates relatively longwave irradiation (300–350 nm) and is thus a useful consideration in the future design of lanthanide-based probes aimed at fluorescence applications. When combined with the unique luminescence properties of Eu^{III} this work demonstrates that the emission properties of the resultant complex, **Eu** · **L**, are highly sensitive to different pH regimes, in particular those of physiological relevance (pH 6–8.5). Towards acidic pH this appears to be a consequence of protonation of the quinoxaline unit and a consequential increase in the inner sphere hydration of Eu^{III}.

5. Experimental

5.1. Materials and procedures

Although all new compounds are air stable both in the solid state and solution, the complexes appear to be mildly hygroscopic. Luminescence pH titrations were carried out in a background of constant ionic strength ($I = 0.1$ NaCl, 295 K). Solutions were made basic by addition of 1 M NaOH and titrated to acidic pH using small aliquots of (1–30 μL) of 1 M, 0.1 M or 0.01 M HCl solution in accordance with related studies [5]. In order to avoid any errors due to dilution, HCl solutions contained the same concentration of {Eu · L}$(OTf)_3$ as the sample. Luminescence spectra were recorded every 0.25 pH with $\lambda_{ex} = 320$ nm.

5.2. General physical measurements

All photophysical data were obtained on a JobinYvon–Horiba Fluorolog spectrometer fitted with a JY TBX picosecond photodetection module and a Hamamatsu R5509-73 detector (cooled to −80 °C using a C9940 housing). The pulsed laser source was a Continuum Minilite Nd:YAG configured for 355 nm output. Lifetimes were obtained using the JY–Horiba FluorHub single photon counting module. IR spectra were recorded on a Varian 7000 FT-IR. Mass spectra were obtained using a Bruker MicroTOF LC.

5.3. Syntheses of ligands and complexes

5.3.1. 1,4,7-Tris[(N-diethyl)carbamoylmethyl]-1,4,7,10-tetraazacyclododecane [29]

A mixture of 1 equiv. cyclen (0.25 g, 1.45 mmol), 3 equiv. $NaHCO_3$ (0.37 g, 4.35 mmol) and a catalytic amount of KI were stirred in acetonitrile (50 ml) under nitrogen and cooled to 0 °C. A solution of 3 equiv. *N*-diethyl-2-chloroacetamide (0.65 g, 4.35 mmol) in acetonitrile (20 ml) was added dropwise over 30 min. The mixture was allowed to warm to room temperature and stirred for a further 72 h. The solvents were removed *in vacuo* and the crude reaction mix was purified by recrystallisation with diethyl ether followed by recrystallisation from hot toluene to give the pure product as a brown oil. Yield: 0.429, 52%. ^{1}H NMR (400 MHz, $CDCl_3$, 300 K): $\delta_H = 9.96$ (1H, br s, N*H*), 3.52 (2H, s, COCH_2), 3.45 (4H, s, COCH_2), 3.27 (8H, q, $^3J_{HH} = 7.2$ Hz, CH_2CH$_3$), 3.18 (4H, q, $^3J_{HH} = 7.1$ Hz, CH_2CH$_3$), 3.04 (4H, d, ring CH_2), 3.02 (4H, s, ring CH_2), 2.81 (8H, s, ring CH_2), 1.10 (6H, t, $^3J_{HH} = 7.1$ Hz, CH$_2$CH_3) and 1.02 (12H, t, $^3J_{HH} = 7.1$ Hz, CH$_2$CH_3). ES$^+$ MS (MeCN): found m/z 512. $\{M+H\}^+$ requires m/z 512.

5.3.2. {1,4,7-Tris[(N-diethyl)carbamoylmethyl]-1,4,7,10-tetraazacyclododecane-10-(2-methylquinoxaline)} · NaCl (**2**)

One equivalents of 2-bromomethyl quinoxaline (0.035 g, 0.157 mmol) was added to a stirred solution of 1 equiv. of the cyclen triamide (0.08 g, 0.157 mmol) in dry acetonitrile (20 ml) and heated to 60 °C under nitrogen. After 1 h 1.1 equiv. $NaHCO_3$ (0.0145 g, 0.168 mmol) and a catalytic amount of KI were added and the reaction was stirred for a further 18 h. The reaction mixture was filtered, the solvent was removed *in vacuo* and the crude reaction mixture was purified by recrystallisation from hot toluene to give the pure product as a yellow-brown solid, isolated as the

sodium chloride salt. Yield: 0.047 g, 42%. ^{1}H NMR (400 MHz, $CDCl_3$, 300 K): δ_H = 8.85 (1H, s, aromatic), 8.00 (2H, m, aromatic), 7.63 (1H, m, aromatic), 7.56 (1H, m, aromatic), 3.42 (8H, br m, CH_2CO and –CH_2–quin), 3.20 (8H, m, CH_2CH_3), 2.97 (8H, br s), 2.73 (4H, m, CH_2CH_3), 2.1–2.7 (8H, br m), 1.11 (12H, m, CH_2CH_3) and 0.83 (6H, t, $^3J_{HH}$ = 6.4 Hz, CH_2CH_3) ppm. $^{13}C\{^1H\}$ NMR ($CDCl_3$, 300K): δ_C 13.1, 14.5, 14.8, 40.9, 41.5, 41.6, 55.3, 56.1, 129.5, 129.8, 129.9, 130.0, 146.5, 169.3, 170.5 ppm. IR ν_{max}(ATR, solid): 1703, 1588, 1503, 1458, 1372, 1290, 1267, 1202, 1107, 1015, 881, 838, 791, 748 cm^{-1}. ES$^+$ MS: found m/z 654. {M+H−NaCl}$^+$ requires m/z 654.

5.4. General method for lanthanide complexation

The lanthanide complexes were prepared by stirring the ligand with 1 equiv. of $Ln(OTf)_3$or $Yb(NO_3)_3$ in MeOH (approx. 15 ml) for approximately 24 h at 50 °C. The reaction was followed by TLC (MeOH:DCM 1:9) and judged to be complete when free ligand was no longer observed on the TLC plate. The resulting mixture was concentrated and the desired product precipitated from solution upon addition of diethyl ether. The complexes were obtained as light brown solids in >90% yield.

5.4.1. {Eu · L}(OTf)$_3$

ES$^+$ MS (MeCN): found m/z 1104. {M−OTf}$^+$$C_{37}H_{59}EuF_6N_9O_9S_2$ requires m/z 1104. IR ν_{max}(ATR, solid): 1600, 1458, 1250, 1155, 1079, 1028, 954, 918, 636 cm^{-1}. UV–Vis λ_{max} (ε/mol^{-1} dm^3 cm^{-1}): 238 (14942), 324 (3718) nm.

5.4.2. {Nd · L}(OTf)$_3$

ES$^+$ MS (MeCN): found m/z 1095. {M−OTf}$^+$$C_{37}H_{59}F_6N_9NdO_9S_2$ requires m/z 1095. IR ν_{max}(ATR, solid): 1598, 1482, 1445, 1256, 1160, 1078, 1027, 954, 918, 793, 636 cm^{-1}. UV–Vis λ_{max} (ε/mol^{-1} dm^3 cm^{-1}): 241 (12377), 323 (4725) nm.

5.4.3. {Yb · L}(NO$_3$)$_3$

ES$^+$ MS (MeCN): found m/z 1013, 991 and 951. {M}$^+$ $C_{35}H_{59}N_{12}O_{12}Yb$ requires m/z 1013, {M−NO_3+MeCN}$^+$$C_{37}H_{62}$-$N_{12}O_9Yb$ requires m/z 992, {M−NO_3}$^+$$C_{35}H_{59}N_{11}O_9Yb$ requires m/z 951. IR (ν_{max})(ATR, solid): 1605, 1404, 1295, 1260, 1075, 1023, 952, 793, 636 cm^{-1}. UV–Vis λ_{max}(ε/mol^{-1} dm^3 cm^{-1}): 219 (18785), 319 (2503) nm.

5.5. Structure analysis and refinement

The structure was solved by direct methods using SHELXS-97 and was completed by iterative cycles of ΔF-syntheses and full-matrix least squares refinement. All non-H atoms were refined anisotropically and difference Fourier syntheses were employed in positioning idealised hydrogen atoms and were allowed to ride on their parent C-atoms. All refinements were against F^2 and used SHELX-97 [30].

Acknowledgements

The EPSRC are thanked for support (EP/E048390/1) together with the Universities of Sheffield, Huddersfield and Cardiff.

Appendix A. Supplementary data

CCDC 668789 contains the supplementary crystallographic data for this paper. These data can be obtained free of charge via http://www.ccdc.cam.ac.uk/conts/retrieving.html, or from the Cambridge Crystallographic Data Centre, 12 Union Road, Cambridge CB2 1EZ, UK; fax: (+44) 1223-336-033; or e-mail: deposit@ccdc.cam.ac.uk. Supplementary data associated with this article can be found, in the online version, at doi:10.1016/j.poly.2008.04.010.

References

[1] (a) S. Pandya, J. Yu, D. Parker, Dalton Trans. (2006) 2757;
(b) T. Gunnlaugsson, F. Stomeo, Org. Biomol. Chem. 5 (2007) 1999;
(c) J.-C.G. Bünzli, C. Piguet, Chem. Soc. Rev. 34 (2005) 1048;
(d) T. Gunnlaugsson, J.P. Leonard, Chem. Commun. (2005) 3114;
(e) A.-S. Chauvin, C. Vandevyer, S. Comby, J.-C.G. Bünzli, Chem. Commun. (2007) 1716;
(f) D. Parker, R. Pal, Chem. Commun. (2007) 474;
(g) R.J. Aarons, J.K. Notta, M.M. Meloni, R. Vidyasagar, J. Narvainen, S. Allan, N. Spencer, R.A. Kauppinen, J.S. Snaith, S. Faulkner, Chem. Commun. (2006) 909.
[2] (a) O. Reany, T. Gunnlaugsson, D. Parker, Chem. Commun. (2000) 473;
(b) O. Reany, T. Gunnlaugsson, D. Parker, J. Chem. Soc., Perkin Trans. 2 (2000) 1819;
(c) K. Hanaoka, K. Kikuchi, H. Kojima, Y. Urano, T. Nagano, J. Am. Chem. Soc. 126 (2004) 12470;
(d) S.J.A. Pope, R.H. Laye, Dalton Trans. (2006) 3108.
[3] T. Gunnlaugsson, J.P. Leonard, K. Senchal, A.J. Harte, Chem. Commun. (2004) 782.
[4] (a) T. Gunnlaugsson, J.P. Leonard, Dalton Trans. (2005) 3204;
(b) J.B. Coldwell, C.E. Felton, L.P. Harding, R. Moon, S.J.A. Pope, C.R. Rice, Chem. Commun. (2006) 5048.
[5] (a) M.P. Lowe, D. Parker, O. Reany, S. Aime, M. Botta, G. Castellano, E. Gianolio, R. Pagliarin, J. Am. Chem. Soc. 123 (2001) 7601;
(b) T. Gunnlaugsson, J.P. Leonard, K. Senechal, A.J. Harte, J. Am. Chem. Soc. 125 (2003) 12063.
[6] D. Parker, J.A.G. Williams, Chem. Commun. (1998) 245.
[7] R.K. Mahajan, I. Kaur, R. Kaur, S. Uchida, A. Onbimaru, S. Shinoda, H. Tsukube, Chem. Commun. (2003) 2238.
[8] (a) J.I. Bruce, R.S. Dickins, L.J. Glovenlock, T. Gunnlaugsson, S. Lopinski, M.P. Lowe, D. Parker, R.D. Peacock, J.J.B. Perry, S. Aime, M. Botta, J. Am. Chem. Soc. 122 (2000) 9674;
(b) A.J. Harte, P. Jensen, S.E. Plush, P.E. Kruger, T. Gunnlaugsson, Inorg. Chem. 45 (2006) 9465;
(c) J.P. Leonard, C.M.G. dos Santos, S.E. Plush, T. McCabe, T. Gunnlaugsson, Chem. Commun. (2007) 129;
(d) S.J.A. Pope, B.P. Burton-Pye, R. Berridge, T. Khan, P.J. Skabara, S. Faulkner, Dalton Trans. (2006) 2907.
[9] P. Caravan, Chem. Soc. Rev. 35 (2005) 512.
[10] M. Giardiello, M.P. Lowe, M. Botta, Chem. Commun. (2007) 4044.
[11] (a) For example: W. Li, S. Fraser, T. Meade, J. Am. Chem. Soc. 121 (1999) 1413;
(b) W. Li, G. Parigi, M. Fragai, C. Luchinat, T.J. Meade, Inorg. Chem. 41 (2002) 4018.
[12] (a) S. Faulkner, J.L. Matthews, in: M.D. Ward (Ed.), Comprehensive Coordination Chemistry, Applications of Coordination Complexes, 2nd ed., vol. 9, Elsevier, Amsterdam, 2003;
(b) D. Parker, Coord. Chem. Rev. 205 (2000) 109.
[13] S. Faulkner, S.J.A. Pope, B.P. Burton-Pye, Appl. Spectrosc. Rev. 40 (2005) 1.
[14] (a) J. Yu, D. Parker, R. Pal, R.A. Poole, M.J. Cann, J. Am. Chem. Soc. 128 (2006) 2294;
(b) C.P. Montgomery, D. Parker, L. Lamarque, Chem. Commun. (2007) 3841.
[15] A. Dadbhoy, S. Faulkner, P.G. Sammes, J. Chem. Soc., Perkin Trans. 2 (2002) 348.
[16] S.J.A. Pope, Polyhedron 26 (2007) 4818.
[17] (a) S.I. Klink, H. Keizer, F.C.J.M. van Veggel, Angew. Chem., Int. Ed. 39 (2000) 4319;
(b) M.D. Ward, Coord. Chem. Rev. 251 (2007) 1663;
(c) J.-M. Herrera, S.J.A. Pope, A.J.H.M. Meijer, T.L. Easun, H. Adams, W.Z. Alsindi, X.-Z. Sun, M.W. George, S. Faulkner, M.D. Ward, J. Am. Chem. Soc. 128 (2007) 11491;
(d) K. Senechal-David, S.J.A. Pope, S. Quinn, S. Faulkner, T. Gunnlaugsson, Inorg. Chem. 45 (2006) 10040.
[18] (a) S.J.A. Pope, B.J. Coe, S. Faulkner, R.H. Laye, Dalton Trans. (2005) 1482;
(b) S.J.A. Pope, B.J. Coe, S. Faulkner, Chem. Commun. (2004) 1550;
(c) S.J.A. Pope, B.J. Coe, S. Faulkner, E.V. Bichenkova, X. Yu, K.T. Douglas, J. Am. Chem. Soc. 126 (2004) 9490.
[19] P. Coppo, M. Duati, V.N. Kozhevnikov, J.W. Hofstraat, L. DeCola, Angew. Chem., Int. Ed. 44 (2005) 1806.
[20] D. Imbert, M. Cantuel, J.-C.G. Bunzli, C. Berardinelli, C. Piguet, J. Am. Chem. Soc. 125 (2003) 15698.
[21] (a) N. Shavaleev, L.P. Moorcraft, S.J.A. Pope, Z.R. Bell, S. Faulkner, M.D. Ward, Chem. Eur. J. 8 (2003) 5283;
(b) T.K. Ronson, T. Lazarides, H. Adams, S.J.A. Pope, D. Sykes, S. Faulkner, S.J. Coles, M.B. Hursthouse, W. Clegg, R.W. Harrington, M.D. Ward, Chem. Eur. J. 12 (2006) 9299.
[22] S. Faulkner, S.J.A. Pope, J. Am. Chem. Soc. 125 (2003) 10526.
[23] KAPPACCD Server Software: Windows 3.11 Version, B.V. Nonius, Delft, The Netherlands, 1997.
[24] COLLECT, B.V. Nonius Delft, The Netherlands, 1998.
[25] HKL DENZO HKL SCALEPACK: Z. Otwinowski, W. Minor, Methods in enzymology, in: C.W. Carter Jr., R.M. Sweet (Eds.), Macromolecular Crystallography, Part A, vol. 276, Academic Press, New York, 1997, p. 307.
[26] R.D. Shannon, Acta Crystallogr., Sect. A 32 (1976) 751.

[27] A. Beeby, B.P. Burton-Pye, S. Faulkner, G.R. Motson, J.C. Jeffery, J.A. McCleverty, M.D. Ward, Dalton. Trans. (2002) 1923.
[28] W.D. Horrocks, J.P. Bolender, W.D. Smith, R.M. Supkowski, J. Am. Chem. Soc. 119 (1997) 5972.
[29] During the course of this work this compound was isolated using an alternative approach: K. Nwe, J.P. Richard, J.R. Morrow, Dalton Trans. (2007) 5171.
[30] SHELXL-PC Package, Bruker Analytical X-ray Systems, Madison, WI, 1998.

Polyhedron 27 (2008) 2372–2378

Contents lists available at ScienceDirect

Polyhedron

journal homepage: www.elsevier.com/locate/poly

A new [Ni^{II}_4] distorted cubane assembly on four solvent derived μ_3-OMe corners: Solvent dependent formation and cleavage of exogenous bridges

Debashree Mandal [a], Chang Seop Hong [b], Hyoung Chan Kim [c], Hoong-Kun Fun [d], Debashis Ray [a,*]

[a] Department of Chemistry, Indian Institute of Technology, Kharagpur 721 302, India
[b] Department of Chemistry and Center for Electro- and Photo-Responsive Molecules, Korea University, Seoul 136-701, Republic of Korea
[c] Systems Research Team, Research & Development Division, Nuclear Fusion Research Center, Daejeon 305-333, Republic of Korea
[d] X-ray Crystallography Unit, School of Physics, Universiti Sains Malaysia, 11800 Minden, Penang, Malaysia

ARTICLE INFO

Article history:
Received 4 April 2008
Accepted 10 April 2008
Available online 2 June 2008

Keywords:
Tetranuclear
μ_3-Methanolate
8-Quinolinolate
Glycinol coordination
Bridge cleavage

ABSTRACT

A new Ni_4 distorted cubane complex [$Ni_4(\mu_3\text{-}OMe)_4Q_4(MeOH)_4$] (**1**) (where Q^- is the anion of 8-quinolinol) is obtained from the reaction of NaQ with $Ni(OAc)_2 \cdot 4H_2O$ in refluxing MeOH *via* solvent derived μ_3-OMe assisted self-assembly of four nickel(II) centres. The periphery of [$Ni_4(OMe)_4$] cubane is covered by four Q^- and four MeOH molecules. This methanol specific reaction is not supported in solvent glycinol (Hgl; $NH_2(CH_2)_2OH$), an amine substituted ethanol, producing monomeric [$NiQ_2(Hgl)_2$] $\cdot 2H_2O$ (**2** $\cdot 2H_2O$) instead and is able to cleave **1** to yield **2** $\cdot 2H_2O$. The cryomagnetic susceptibility data of powdered **1** can be modeled by a two *J* equation yielding $J_1 = -1.8(1)\ cm^{-1}$, $J_2 = 3.9(1)\ cm^{-1}$ and $g = 2.24$.

© 2008 Elsevier Ltd. All rights reserved.

1. Introduction

Interest in synthesis and characterization of high-nuclearity transition metal complexes has grown considerably in recent years, particularly due to their relevance to multi-electron transfer centers in biology [1] and magnetostructural research [2]. Donor groups from both endo- and exogenous ligands can initiate the nucleation of self-assembly processes during the multinuclear complex formation [2,3]. Several single atom bridging groups (X) such as MeO^-, HO^-, RO^-, PhO^- or N_3^- in different bridging modes play key roles in [Ni_4] complex geometry, for example star-shaped A [4], defective dicubane B [5], or distorted cubane C [6,7] (Scheme 1). Within these structures, reports on exogenous μ_3-OMe [8] supported cubane complexes having peripheral bidentate ligands are scarce.

The ligand 8-quinolinol (HQ) and its derivatives have been known as a potent analytical reagents for more than a century and showed renewed interest in recent time for novel electron transport and emissive behavior when coordinated to Al^{3+} as novel organic light-emitting device (OLED) fabrication material [9]. Attachment of conjugated fluorophores to this family of ligands lead metal ion coordination dependent changes in fluorescence pattern for sensor development [10]. Recently Winpenny et al. have shown that reactions of HMQ (2-methyl 8-quinolinol) with [$M_2(H_2O)(Piv)_4(HPiv)_4$] (M = Ni, Co) [11] in acetone yield four O,O′ face-diagonal bridged [$M_4(Piv)_4(MQ)_4$] (Piv = $(CH_3)_3CCO_2$) (Scheme 2, left) [12].

Another closely related ligand Hhmp (2-hydroxymethylpyridine) has shown to provide [Ni(hmp)(MeOH)Cl]$_4$ (Scheme 2, right) from the μ_3 corner supports [2c]. In this paper we report the synthesis and characterization of [$Ni_4(\mu_3\text{-}OMe)_4Q_4(MeOH)_4$] (**1**) on four solvent derived exogenous μ_3-methoxide cube corners showing different mode of binding of peripheral N,O donor ligands (Scheme 2, top). In **1** the key role of solvent derived methoxo bridges was identified following the same synthesis in glycinol (Hgl) as reaction solvent yielding [$NiQ_2(Hgl)_2$] $\cdot 2H_2O$ (**2** $\cdot 2H_2O$) quantitatively. This synthetic result may be considered novel since glycinol based Schiff bases are known to support tetranuclear Ni^{II} complexes by providing four μ_3-ethoxide imine supports [13]. Complex **2** $\cdot 2H_2O$ can also be obtained *via* the methoxo bridge cleavage reaction of **1** is refluxing glycinol for half an hour. The contrasting role of glycinol as a solvent and a component of Schiff base can be indicated (Scheme S1). The biology the resting state of acireductone dioxygenase [14] and *Escherichia coli* glyoxalase I (GlxI) [15] responsible for detoxification of cytotoxic pyruvaldehyde exhibit octahedral O/N coordination around mononuclear Ni(II) centres. We herein describe the synthesis, crystal structure and low temperature magnetic characterization of a new tetranuclear Ni^{II} complex and its solvent-triggered descend to an octahedral mononuclear Ni^{II} complex.

* Corresponding author. Fax: +91 3222 255303/82252.
E-mail address: dray@chem.iitkgp.ernet.in (D. Ray).

0277-5387/$ - see front matter © 2008 Elsevier Ltd. All rights reserved.
doi:10.1016/j.poly.2008.04.023

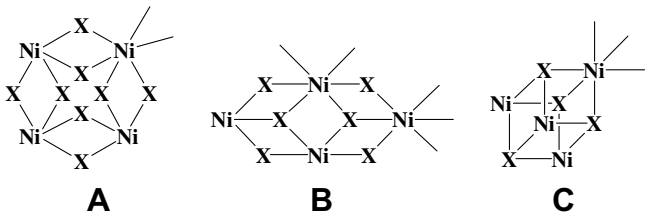

Scheme 1.

2. Experimental

2.1. Materials and instrumentation

All preparations and manipulations were performed under aerobic conditions using chemicals as received. The chemicals used were obtained from the following sources: 8-quinolinol from S.D. Fine Chem, India. Nickel acetate tetrahydrate was obtained from Fluka AG, Switzerland. All other chemicals and solvents were reagent grade materials and were used as received without further purification. Microanalyses (C, H and N) were performed using a Perkin–Elmer 240C elemental analyzer. IR spectra in 200–4000 cm^{-1} range were obtained on a Perkin–Elmer RX1 FT-IR spectrometer prepared as KBr pellets. Electronic spectra in 190–3200 nm range were recorded on a Shimadzu 1601 UV–Vis–NIR spectrophotometer using 1 cm quartz cells. Solution electrical conductivity was measured using a Unitech type UI31C digital conductivity meter with a solute concentration of 10^{-3} M. Powder X-ray diffraction in the powder sample have been measured using X pert pro, Philips, The Netherlands. The room temperature magnetic susceptibilities in the solid-state were measured using a home built Gouy balance fitted with a Polytronic d.c. power supply. The experimental magnetic susceptibilities were corrected for the diamagnetism using Pascal's constants. Variable temperature magnetic measurements were carried out on polycrystalline samples (ca. 30 mg) using a Quantum Design MPMS-7 SQUID magnetometer operating at a constant magnetic field of 1 T between 1.8 and 300 K. The experimental magnetic moment was corrected for the diamagnetic contribution from the sample holder and the diamagnetic response from the sample, which was evaluated from Pascal's constants.

CAUTION!! Perchlorate salts are potentially explosive and should be handled in very small quantities.

2.2. Synthesis

2.2.1. NaQ

Solutions of HQ (4.0 g, 27.5 mmol) in MeCN (80 ml) and NaOH (1.1022 g, 27.5 mmol) in MeOH (30 ml) were combined, and the mixture was heated to reflux for 15 min. The resultant yellow solution was then concentrated in vacuum until crystals began forming. Storage of the solution at 0 °C for 24 h afforded white needles, which were filtered off and washed with cold MeOH. Further concentration of the filtrate and washings and storage at 0 °C gave a second crop of crystals; total yield 80%. The white crystalline product becomes yellow on drying. IR (KBr, cm^{-1}): 3230 (br), 3043 (m), 1561 (s), 1493 (s), 1459 (s), 1421 (m), 1373 (m), 1361 (s), 1314 (s) 1277 (m), 1096 (s), 1064 (m), 894 (m), 822 (s), 792 (s), 752 (s), 714 (m), 650 (m).

2.2.2. $[Ni_4(\mu_3\text{-}OMe)_4Q_4(MeOH)_4]$ (**1**)

A mixture of $Ni(O_2CCH_3)\cdot 4H_2O$ (0.3017 g, 1.2 mmol), NaOH (0.048 g, 1.2 mmol), and NaQ (0.2 g. 1.2 mmol) in MeOH (50 ml) was refluxed for 30 min, affording a yellow-green precipitate, which was filtered off and washed with MeOH. Single crystals of **1** were obtained by the slow evaporation of a dichloromethane solution of compound layered with methanol in 1:1 (v/v) ratio. The isolated crystals are of X-ray quality but lose solvent when removed from the mother liquor. The powdered sample was finally dried in vacuum over P_4O_{10}. Yield: 1.16 g (90%). *Anal.* Calc. for $C_{44}H_{52}N_4O_{12}Ni_4$ (1063.74): C, 49.67; H, 4.88; N, 5.26; Ni, 22.09. Found: C, 49.9; H, 4.84; N, 5.24; Ni, 22.03%. IR (KBr, cm^{-1}): 3195 (br), 3042 (m), 1601 (m), 1577 (s), 1498 (s), 1465 (s), 1323 (m), 1282 (m), 1034 (s), 820 (s), 786 (m), 735 (m), 643 (m), 504 (m). Molar conductance, Λ_M: (DMF solution) 17.0 Ω^{-1} cm^2 mol^{-1}. UV–vis spectra [Λ_{max}, nm (ε, l mol^{-1} cm^{-1})]: (DMF solution) 628 (157), 395 (2388), 372 (5407), 271 (12297).

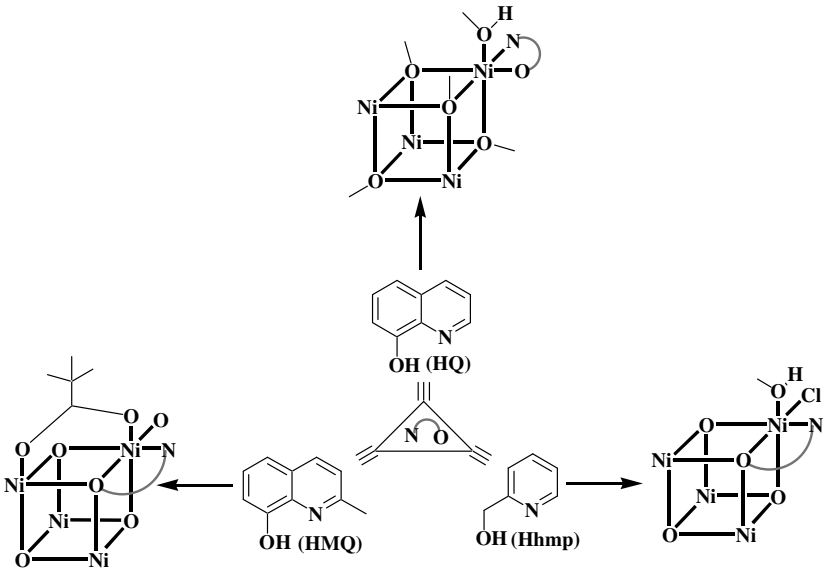

Scheme 2.

2.2.3. $[NiQ_2(Hgl)_2] \cdot 2H_2O$ ($\mathbf{2} \cdot 2H_2O$)

A mixture of $Ni(O_2CMe) \cdot 4H_2O$ (0.301 g, 1.2 mmol), NaOH (0.048 g, 1.2 mmol), and NaQ (0.2 g. 1.2 mmol) in glycinol (100 ml) was refluxed for 30 min, affording green block crystals by evaporation of solvent after 3 weeks. The powdered compound was finally dried in vacuum over P_4O_{10}. Yield: 0.31 g (45%). *Anal.* Calc. for $C_{22}H_{30}N_4O_6Ni$ (504.878): C, 52.33; H, 5.94; N, 11.09; Ni, 11.62. Found: C, 51.9; H, 5.23; N, 11.05; Ni, 11.18%. IR (KBr, cm^{-1}): 3313 (m), 2940 (m), 1598 (m), 1567 (s), 1495 (s), 1462 (s), 1369 (m), 1314 (s), 1217 (s), 1109 (s), 1028 (sb), 821(s), 780 (m), 748 (m), 498 (m). Molar conductance, Λ_M: (DMF solution) 35 Ω^{-1} cm^2 mol^{-1}. UV–vis spectra [Λ_{max}, nm (ε, 1 mol^{-1} cm^{-1})]: (DMF solution) 578 (268), 410 (27352), 335 (98818), 271 (16749).

2.2.4. Solvent driven transformation of **1** to $\mathbf{2} \cdot 2H_2O$

Complex **1** (0.5 g, 0.47 mmol) was refluxed in glycinol (10 ml) for half an hour and the resulting brownish green solution kept for solvent evaporation. After 30 days green colored block crystals was subsequently obtained from the reaction mixture in 43% yield (0.2 g). The formation of $\mathbf{2} \cdot 2H_2O$ was confirmed by elemental analysis and X-ray structure determination.

2.3. X-ray crystallography

The green block single crystals of complexes $[Ni_4(\mu_3\text{-}OMe)_4Q_4(MeOH)_4]$ (**1**) and $[NiQ_2(Hgl)_2] \cdot 2H_2O$ ($\mathbf{2} \cdot 2H_2O$) are suitable for the X-ray analysis. Complex **1** was grown by the slow evaporation of dichloromethane with methanol in 1:1 (v/v) ratio afforded large green crystals of the complex and green crystal of $\mathbf{2} \cdot 2H_2O$ was grown by the slow evaporation of the reaction mixture. The intensity data for single crystal of compound **1** and $\mathbf{2} \cdot 2H_2O$ were collected on a Bruker APEX-II CCD diffractometer with Mo Kα radiation (λ = 0.71073 Å) and an Oxford Cyrosystem Cobra low-temperature attachment. The structures were solved by direct methods (SIR97 [16]) and refined using full-matrix least-squares with all non-hydrogen atoms anisotropically and hydrogens included on calculated positions, riding on their carrier atoms. All calculations were performed using SHELXL-97 [17] and PARST [18] implemented in WINGX [19] system of programme.

3. Results and discussion

3.1. Syntheses, reactivity and spectroscopic characterizations

Using bidentate N,O donor ligand quinonemonoximate we reported a family of distorted $[Ni_4]$ cubane complexes in 1998 [20]. This was the first example of use of oxime based N,O donor ligands for the isolation of tetranuclear nickel(II) complexes. In 2003 Winpenny et al. used another N,O donor ligand 8-hydroxy quinolidine (HMQ, Scheme 2) and showed its reactions with $[M_2(H_2O)(Piv)_4(HPiv)_4]$ (M = Co, Ni) in acetone to provide ligandμ_3-phenolate end supported novel M_4 cubanes [12]. 2-Hydroxymethylpyridine (Hhmp) in deprotonated form provides one more example of {N,O} donor ligand coordinated $[Ni_4]$ cubane $[Ni(hmp)(MeOH)(Cl)]_4$ having μ_3 supports from hmp^- ligands. In this background we explored the latest example of N,O donor ligand HQ (Scheme 2) in this sequel. The synthesis of $[Ni_4(\mu_3\text{-}OMe)_4Q_4(MeOH)_4]$ (**1**) was achieved via the reaction of $Ni(OAc)_2 \cdot 4H_2O$, sodium 8-quinolinolate (NaQ) and NaOH in 1:1:1 molar ratio in MeOH medium at room temperature under reflux for 0.5 h. Green microcrystalline product was subsequently obtained from the reaction mixture in 90% yield.

The elemental analysis, solution electrical conductivity and room temperature magnetic susceptibility data are consistent with the molecular formula $[Ni_4(\mu_3\text{-}OMe)_4Q_4(MeOH)_4]$ for **1**. If the same reaction is carried out in MeCN we get the reported mononuclear species $NiQ_2(HQ)$ [21]. In the above reaction replacement of MeOH solvent by $NH_2CH_2CH_2OH$ (Hgl; glycinol) produced $[NiQ_2(Hgl)_2] \cdot 2H_2O$ ($\mathbf{2} \cdot 2H_2O$) thus identifying the important role of the solvent (Scheme S1). Dark green micro crystals of $\mathbf{2} \cdot 2H_2O$ in 45% yield were subsequently obtained after solvent evaporation.

The crucial role of the MeOH solvent was further verified by observing a solvent driven bridge cleavage of **1**. Reaction of **1** with glycinol in refluxing condition for 0.5 h leads to a brownish green solution, which on keeping undisturbed for 30 days yields green block crystals of $\mathbf{2} \cdot 2H_2O$ in 43% yield. Elemental analysis, solution molar electrical conductivity, room temperature magnetic susceptibility and molecular structure determination by X-ray crystallography confirm the formation of $\mathbf{2} \cdot 2H_2O$.

3.2. Infrared spectroscopy

The FTIR spectral data for the complexes **1** and $\mathbf{2} \cdot 2H_2O$ are given in the experimental section. The complexes **1** and $\mathbf{2} \cdot 2H_2O$ show strong absorption bands at 1577 and 1567 cm^{-1} respectively due to C=C and C=N vibrations [22] of the ligand Q^- (the value for free NaQ is 1561 cm^{-1}). The peaks for ring vibrations are obtained at 786 and 780 cm^{-1}, respectively for complexes **1** and $\mathbf{2} \cdot 2H_2O$. Broad medium bands centred at 3195 and 3313 cm^{-1} are observed corresponding to ν(OH) stretching vibrations of the coordinated methanol and lattice water molecules in **1** and $\mathbf{2} \cdot 2H_2O$, respectively.

3.3. Description of structures

3.3.1. $[Ni_4(\mu_3\text{-}OMe)_4Q_4(MeOH)_4]$ (**1**)

Compound is soluble in chlorinated solvents, and layering of a solution of **1** in dichloromethane with methanol in 1:1 (v/v) ratio afforded large yellow-green crystals suitable for X-ray structure determination. Compound **1** crystallizes in tetragonal $I4_1/a$ space group and its labeled ORTEP is shown in Fig. 1. Crystallographic data for **1** and $\mathbf{2} \cdot 2H_2O$ are given in Table 1. The bond distances and angles for the **1** and $\mathbf{2} \cdot 2H_2O$ are given in Table 2.

The structure of **1** incorporate a distorted $[Ni_4(\mu_3\text{-}O)_4]$ cubane core, where the μ_3-O bridges are derived from methanol molecules [23]. The peripheral coordinations around each distorted octahedral (inset of Fig. 1) Ni^{II} ion is completed by four terminal MeOH ligands, which participate in intramolecular hydrogen-bonding interactions (O···O distance: 2.74 Å) with the phenolate type O atoms of the Q^- ligands, across four of the six faces of the Ni_4 cubane. As a result, these four faces exhibit shorter Ni···Ni separation (3.07 Å), longer O···O distance of 2.74 Å, smaller Ni–O–Ni angles (95.9° (3) and 96.3° (3)), and smaller Ni–O–O–Ni dihedral angle (166°). The other two faces that are not engaged in hydrogen-bonding interactions show shorter O···O distance of 2.65 Å [6], longer Ni···Ni separations of 3.16 Å, greater Ni–O–Ni [11] angle (100.0° (3)), and greater Ni–O–O–Ni dihedral angle (176°). This has the effect of lowering the effective symmetry of the $[Ni_4(OMe)_4]^{4+}$ unit from T_d to D_{2d} [8]. The molecular flat surface of each Q^- ligand is coplanar with the Ni_2O_2 faces involved in hydrogen-bonding interactions (dihedral angle is 8.05°). In addition, **1** appears to possess a slight tetragonal compression within the octahedral NO_5 coordination environment along the O–Ni–O axis made from the O atoms of phenolate group of Q^- and bridging MeO^- ligand, with Ni–O bonds on this vector of 2.05–2.07 Å versus 2.07–2.09 Å for the in plane Ni–O and Ni–N bonds. These Ni–O bond lengths lie well within the range of reported values for the corresponding lengths in other Ni_4 clusters [8]. The individual Ni_4 molecules are well separated with neighboring intermolecular Ni···Ni separations of 6.39 and 7.29 Å. In addition, there are no obvious intercubane hydrogen bonds. Along crystallographic '*b*'

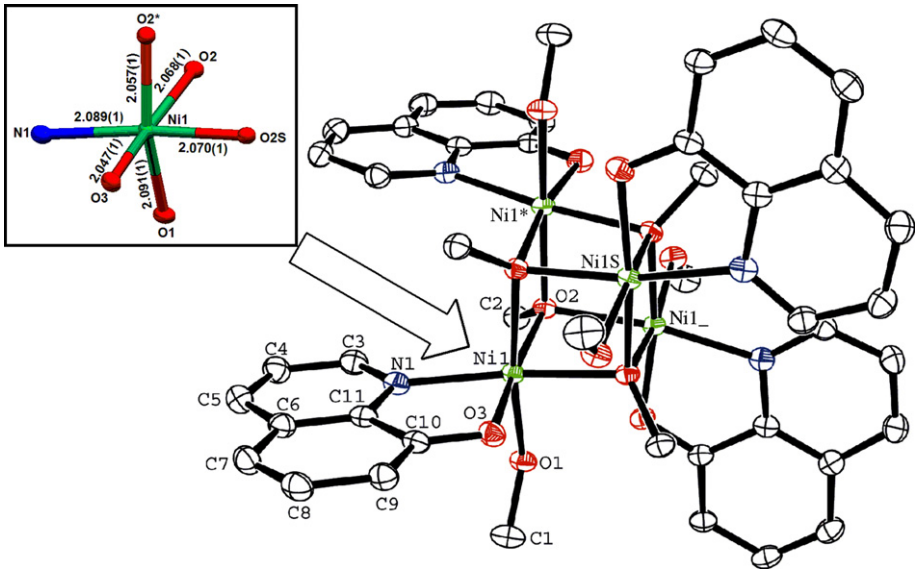

Fig. 1. ORTEP [19] representation of $[Ni_4(\mu_3\text{-}OMe)_4Q_4(MeOH)_4]$ (**1**) showing the thermal ellipsoids at 30% probability level. Hydrogen atoms are omitted for clarity. Symmetry code: (*) $-x+1, -y+3/2, z+0$ (S) $y-1/4, -x+5/4, -z+1/4$ (_) $-y+5/4, x+1/4, -z+1/4$.

Table 1
Crystallographic data for compounds **1** and **2** · $2H_2O$

Compound	**1**	**2** · $2H_2O$
Formula	$C_{44}H_{52}N_4O_{12}Ni_4$	$C_{22}H_{30}N_4O_6Ni$
M	1063.74	504.878
Space group	$I4_1/a$	$P\bar{1}$
Crystal system	tetragonal	triclinic
a (Å)	14.2808(1)	7.7967(2)
b (Å)	14.2808(1)	9.7962(3)
c (Å)	22.3766(4)	16.1736(4)
α (°)	90	74.885(1)
β (°)	90	88.375(1)
γ (°)	90	83.769(1)
U (Å^3)	4563.51(9)	1185.53(6)
Z	4	2
T (K)	100(2)	100(2)
D_{calc} (g cm^{-3})	1.548	1.387
$F(000)$	2208	512
μ(Mo Kα) (cm^{-1})	1.691	0.862
Measured reflections	119222	27907
Crystal size (mm)	0.43 × 0.38 × 0.34	0.44 × 0.60 × 0.41
R_{int}	0.0437	0.0213
hkl ranges	−24, 25; − 25, 25; − 40, 40	−11, 11; − 14, 14; − 24, 24
θ_{min}–θ_{max} (°)	0.999–39.76	0.981–32.50
$R(F^2)$ (observed reflections)	0.0327	0.0468
$wR(F^2)$ (all reflections)	0.0793	0.1266
Goodness of fit	1.054	1.105
$\Delta\rho_{max}$; $\Delta\rho_{min}$ (e Å^{-3})	1.409; −0.457	1.208; −0.707

$R_1 = \sum(||F_o| - |F_c||)/\sum|F_o|$. $wR_2 = [\sum w(|F_o| - |F_c|)^2/\sum w(F_o)^2]^{1/2}$.
$w = 0.75/(\sigma^2(F_o) + 0.0010F_o^2)$.

axis the complex **1** is packed nicely in a pair wise arrangement of well separated tetramers (Fig. S1a) and whereas an interpenetrating net-like arrangement is observed along '*c*' axis (Fig. S1b). Several other $[Ni_4]$ complexes are known with similar cubane structures engaged in intermolecular hydrogen-bonding interactions [6d,6e,6h]. In a space-fill model the D_{2d} symmetry of the complex **1** is shown with four different colors for each of the repeating unit (Fig. S2). The five-membered chelate rings from capping ligands exert a tetragonal compression around the Ni coordination sites of complex **1**.

3.3.2. $[NiQ_2(Hgl)_2] \cdot 2H_2O$ (**2**)

Complex **2** · $2H_2O$ crystallizes in triclinic $P\bar{1}$ space group. The solid-state structure of **2** · $2H_2O$ (Fig. 2) identifies the ctc (*cis–trans–cis*; N^{py}, O^{ph}, N^{am}) isomer and contains discrete mononuclear complex of Ni^{II} with amine end coordinated dangling glycinols in N_4O_2 environment and different from the NO_5 environment in **1**.

Such amine end coordinations are important and shown to be photolabile and useful for amino acid photodelivery [24]. The bis-chelated nickel(II) centre prefers to bind the neutral nitrogen ends of glycinol in comparison to the hydroxy ends as seen earlier in $[Ni(NH_3CH_2CH_2OH)_2(H_2O)_4](SO_4)_2$ [25]. We were unable to replace coordinated MeOH molecules in **1** by glycinol in OH coordination mode. The distorted octahedral N_4O_2 coordination environment around Ni^{II} shows (inset of Fig. 2) tetragonal compression originating from five-membered chelation of ligands along the O–Ni–O vector involving the phenolate O atoms of Q^- ligands, with Ni–O bonds on this vector of 2.05(1)–2.07(1) Å versus 2.09(1)–2.13(1) Å for the in plane Ni–N bonds. The average Ni–O and Ni–N distances are slightly longer than those in $[Ni_4]$ complex. A columnar packing of complex **2** is observed along crystallographic '*b*'-axis (Fig. S3). The most interesting feature of this structure is the formation of an intramolecularly hydrogen bonded tetrameric water cluster from lattice water molecules present in the crystals of **2** · $2H_2O$. The four water molecules of crystallization, two from each monomer, show intricate H-bonding network within the intermolecular space forming a dimer of Ni^{II} neutral monomers [26]. Out of these only O(1W) show full occupancy and O(2W) is disordered with partial occupancies 0.5, 0.3 and 0.2 on O(2aW), O(2bW) and O(2cW). The monomers are linked together through six self complementary H-bonds as established between phenolate oxygen O(1) with water O(1W), O(1W) and O(2aW*) and O(3) of pendant alcohol and O2aW, having O(1)···O(1W), O(1W)···O(2aW*)and O(3)···O(2aW) distances of 2.66, 2.84 and 2.82 Å, respectively (Fig. S4). The relevant hydrogen bonded O···O separations are given in Table 3.

Water hydrogen atoms could not be located in the crystal structure [27]. The involvement of the hydroxy ends of coordinated glycinol molecules in H-bonding interactions with lattice water molecules prevent deprotonation and made them unavailable for metal ion coordination. The individual mononuclear Ni complexes are well separated with intermolecular Ni···Ni separations of 7.80–9.80 Å.

3.4. Magnetic behavior

The magnetic data for **1** were measured at 1 T in the temperature range of 1.8–300 K and plotted in the form of $\chi_M T$ versus T

Table 2
Selected bond lengths (Å) and bond angles (°) of complex **1** and **2** · $2H_2O$

Bond lengths of **1**			
Ni(1)–O(3)	2.0476(8)	Ni(1)–O(2)	2.0687 (7)
Ni(1)–N(1)	2.089(1)	Ni(1)–O(1)	2.0913(8)
Ni(1)–O(2*)	2.0576(7)	Ni(1)–O(2S)	2.0702(8)
O(2*)···O(2S)	2.739	O(2)···O(2*)	2.648
Ni(1*)···Ni(1)	3.163	Ni(1*)···Ni(1S)	3.074
Bond angles of **1**			
O(3)–Ni(1)–O(2)	170.50(3)	O(3)–Ni(1)–O(2*)	93.31(3)
O(2*)–Ni(1)–O(2)	79.83(3)	O(3)–Ni(1)–O(2S)	89.82(3)
O(2*)–Ni(1)–O(2S)	83.15(3)	O(2)–Ni(1)–O(2S)	82.87(3)
O(3)–Ni(1)–N(1)	80.28(4)	O(2S)–Ni(1)–N(1)	97.56(3)
O(2)–Ni(1)–N(1)	107.00(3)	O(2S)–Ni(1)–N(1)	170.09(3)
O(3)–Ni(1)–O(1)	99.44(3)	O(2*)–Ni(1)–O(1)	166.32(3)
O(2)–Ni(1)–O(1)	86.92(3)	O(2S)–Ni(1)–O(1)	91.90(3)
N(1)–Ni(1)–O(1)	89.52(4)	C(1)–O(1)–Ni(1)	126.88(8)
Ni(1*)–O(2*)–Ni(1S)	95.92(3)	Ni(1*)–O(2)–Ni(1_)	96.27(3)
Ni(1*)–O(2*)–Ni(1)	100.08(3)	O(2*)–Ni(1*)– O(2S)	82.87(3)
O(2*)–Ni(1S)– O(2S)	83.15(3)	O(2*)–Ni(1*)– O(2)	79.83(3)
Ni(1*)–O(2*)–O(2S)–Ni(1S)	166.49	Ni(1*)–O(2*)–O(2)–Ni(1)	176.03
Bond lengths of **2** · $2H_2O$			
Ni(1)–O(1)	2.048(1)	Ni(1)–O(2)	2.069(1)
Ni(1)–N(2)	2.094(1)	Ni(1)–N(1)	2.101(1)
Ni(1)–N(4)	2.116(1)	Ni(1)–N(3)	2.134(1)
Bond angles of **2** · $2H_2O$			
O(1)–Ni(1)–O(2)	170.52(5)	O(1)–Ni(1)–N(2)	92.44(6)
O(2)–Ni(1)–N(2)	80.06(5)	O(1)–Ni(1)–N(1)	80.42(5)
O(2)–Ni(1)–N(1)	93.60(5)	N(2)–Ni(1)–N(1)	89.36(5)
O(1)–Ni(1)–N(4)	90.72(7)	O(2)–Ni(1)–N(4)	95.55(7)
N(2)–Ni(1)–N(4)	93.84(6)	N(1)–Ni(1)–N(4)	170.71(7)
O(1)–Ni(1)–N(3)	96.17(6)	O(2)–Ni(1)–N(3)	91.15(6)
N(2)–Ni(1)–N(3)	171.12(6)	N(1)–Ni(1)–N(3)	89.97(6)
N(4)–Ni(1)–N(3)	88.19(7)	C(2)–O(1)–Ni(1)	113.49(1)

Symmetry code: (*) $-x+1, -y+3/2, z+0$; (S) $y-1/4, -x+5/4, -z+1/4$; (_) $-y+5/4, x+1/4, -z+1/4$.

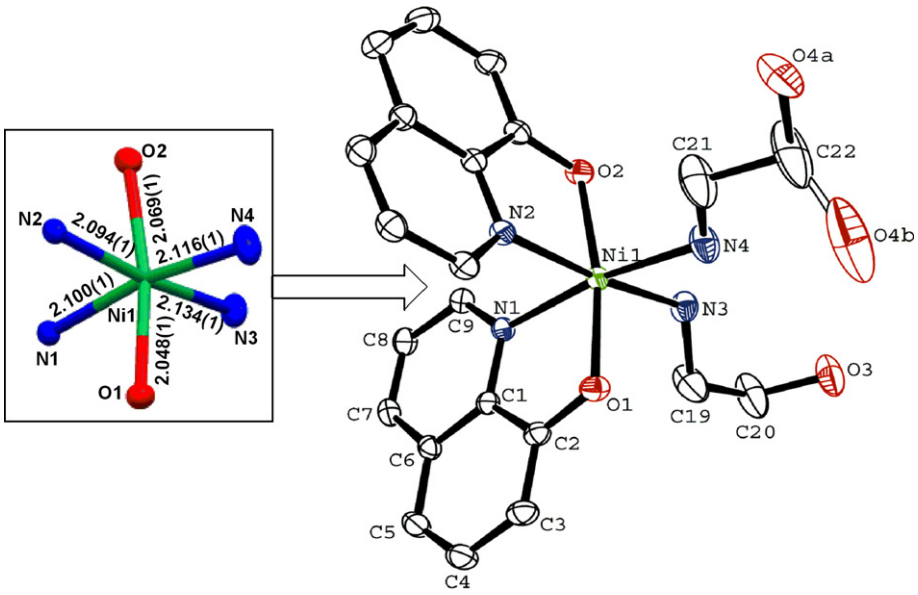

Fig. 2. ORTEP [19] representation of $[NiQ_2(Hgl)_2]$ showing the thermal ellipsoids at 30% probability level. Hydrogen atoms are omitted for clarity.

(Fig. 3). At 300 K, the $\chi_M T$ value of 5.22 $cm^3\ K\ mol^{-1}$ is larger than the spin-only one (5.02 $cm^3\ K\ mol^{-1}$) expected for non-interacting four Ni^{II} spins with $g = 2.24$, indicating that dominant ferromagnetic interactions are present. As temperature is lowered, $\chi_M T$ increases gradually, reaching a maximum of 9.15 $cm^3\ K\ mol^{-1}$ at 15 K and then decreases drastically. The magnetic pathways are shown in Scheme 3; the J_1 and J_2 stand for the longer Ni···Ni (3.163 Å) and the shorter routes (3.074 Å), respectively. From the structural data, the J_1 pathway involves the greater Ni–O–Ni angle (100.0°) and greater Ni–O–O–Ni dihedral angle (176°), whereas the J_2 route consists of the smaller Ni–O–Ni angles (95.9° and 96.3°) and smaller Ni–O–O–Ni dihedral angle (166°). It is known that the exchange interactions between Ni(II) centers in the Ni_4 cubane structures are governed by the Ni–O–Ni angle and Ni–O–O–Ni dihedral angle [28]. The ferromagnetic to antiferromagnetic transition takes place when the Ni–O–Ni angle and Ni–O–O–Ni dihedral

Table 3
O···O hydrogen bond lengths (Å) in hydrogen bonded nickel(II) dimer complex (**2** · $2H_2O$) (see Fig. 3)

O(1)···O(1W)	2.657	O(1W)···O(2aW*)	2.838
O(3)···O(2aW)	2.825	O(1W*)···O(2cW)	2.851
O(4B)···O(2cW)	3.033	O(2cW)···O(2cW*)	2.646
O(2cW)···O(2aW)	2.416	O(4B)···O(2aW*)	2.111

Symmetry code: (*) $1-x, -1-y, -1-z$.

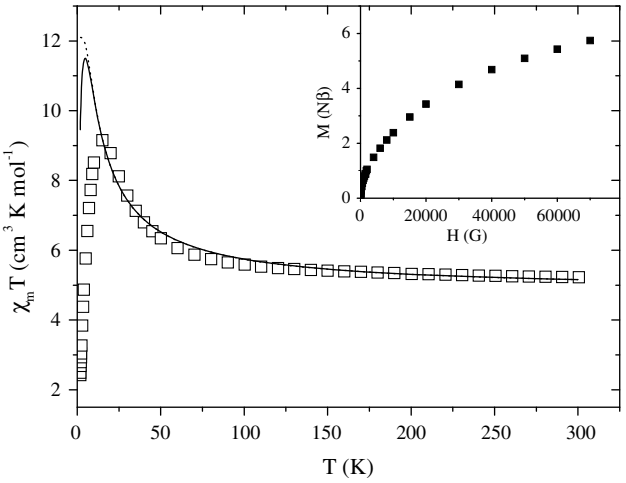

Fig. 3. Plot of $\chi_M T$ vs. T of **1** at 1 T. The dotted and solid lines are the simulated results from isotropic and anisotropic magnetic models, respectively. The inset shows the field dependence of the magnetization at 1.8 K.

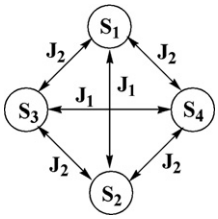

Scheme 3.

angle pass through about 98° and 170°, respectively [28]. Accordingly, it would be reasonably assigned that J_1 mediates an antiferromagnetic coupling and J_2 transmits a ferromagnetic coupling. The spin Hamiltonian used to fit the data is $H = -2J_1(S_1 \cdot S_2 + S_3 \cdot S_4) - 2J_2(S_1 \cdot S_3 + S_1 \cdot S_4 + S_2 \cdot S_3 + S_2 \cdot S_4)$. The data above 7 K was fitted employing the analytical expression of a tetranuclear Ni_4 cubane system under consideration of a molecular field approximation (zJ'). A best fit affords $g = 2.24(1)$, $J_1 = -1.8(1)\ cm^{-1}$, and $J_2 = 3.9(1)\ cm^{-1}$, and $zJ' = 0.39(1)\ cm^{-1}$. The obtained results are similar to those of other Ni_4 spin clusters [6d,6h,28]. The M(H) data at 1.8 K, shown in the inset of Fig. 3, are not saturated even at 7 T.

4. Conclusions

In summary, simultaneous bridging and five-membered chelation of solvent derived MeO^- in μ_3 mode and the bidentate ligand, Q^-, leads to the formation of a distorted $[Ni_4(MeO)_4]$ cubane exhibiting two different types of Ni_2O_2 faces having Ni···Ni separations of 3.07 and 3.16 Å, respectively. The coupling between adjacent Ni ions is moderately antiferromagnetic for longer separation and the shorter separation feature a weak ferromagnetic super-exchange. The role of solvent for tetranuclear assembly has been justified when the synthesis is repeated in solvent glycinol in place of MeOH and the studying the reactivity of glycinol toward **1** which culminates in bridge cleavage and generation of $[NiQ_2(Hgl)_2] \cdot 2H_2O$.

Acknowledgements

D. M. acknowledges the Council of Scientific and Industrial Research, New Delhi, India for her research fellowship. C. S. H. acknowledges the financial support from the Korean Government (MOEHRD, Basic Research Promotion Fund) (KRF-2005-070-C00068). H.C.K. and H-K.F. acknowledge the financial supports from the Korean Government and the Government of Malaysia.

Appendix A. Supplementary data

CCDC 616819 and 616817 contain the supplementary crystallographic data for compounds **1** and **2** · $2H_2O$. These data can be obtained free of charge via http://www.ccdc.cam.ac.uk/conts/retrieving.html, or from the Cambridge Crystallographic Data Centre, 12 Union Road, Cambridge CB2 1EZ, UK; fax: (+44) 1223-336-033; or e-mail: deposit@ccdc.cam.ac.uk. Supplementary data associated with this article can be found, in the online version, at doi:10.1016/j.poly.2008.04.023.

References

[1] (a) K. Alcantara, B. Munge, Z. Pendon, H.A. Frank, J.F. Rusling, J. Am. Chem. Soc. 128 (2006) 14930;
(b) K.N. Ferreira, T.M. Iverson, K. Maghlaoui, J. Barber, S. Iwata, Science 303 (2004) 1831;
(c) Z. Liu, H. Yan, K. Wang, T. Kuang, T. Zhang, L. Gui, X. An, W. Chang, Nature (London) 428 (2004) 287;
(d) B. Loll, J. Kern, W. Saenger, A. Zouni, J. Biesiadka, Nature (London) 438 (2004) 1040;
(e) A. Zouni, H.-T. Witt, J. Keru, P. Fromme, N. Krauss, W. Saenger, P. Orth, Nature (London) 409 (2001) 739.
[2] (a) M. Manoli, A. Prescimone, R. Bagai, A. Mishra, M. Murugesu, S. Parsons, W. Wernsdorfer, G. Christou, E.K. Brechin, Inorg. Chem. 46 (2007) 6968;
(b) T. Shiga, H. Oshio, Sci. Tech. Adv. Mater. 6 (2005) 565;
(c) E.-C. Yang, W. Wernsdorfer, L.N. Zakharov, Y. Karaki, A. Yamaguchi, R.M. Isidro, G.-D. Lu, S.A. Wilson, A.L. Rheingold, H. Ishimoto, D.N. Hendrickson, Inorg. Chem. 45 (2006) 529;
(d) C.G. Efthymiou, C.P. Raptopoulou, A. Terzis, R. Boča, M. Korabic, J. Mrozinski, S.P. Perlepes, E.G. Bakalbassis, Eur. J. Inorg. Chem. (2006) 2236.
[3] T.A. Hudson, K.J. Berry, B. Moubaraki, K.S. Murray, R. Robson, Inorg. Chem. 45 (2006) 3549.
[4] (a) D. Mandal, V. Bertolasi, G. Aromí, D. Ray, Dalton. Trans. 20 (2007) 1989;
(b) J. Ribas, M. Monfort, R. Costa, X. Solans, Inorg. Chem. 32 (1993) 695.
[5] P. King, R. Clérac, W. Wernsdorfer, C.E. Anson, A.K. Powell, Dalton Trans. (2004) 2670.
[6] (a) X.-Y. Song, Y.-H. Xu, L.-C. Li, D.-Z. Liao, Z.-H. Jiang, Inorg. Chim. Acta 360 (2007) 2039;
(b) J.P. Wikstrom, A.Y. Nazarenko, W.M. Reiff, E.V. Rybak-Akimova, Inorg. Chim. Acta 360 (2007) 3733;
(c) C. Papatriantafyllopoulou, C.G. Efthymiou, C.P. Raptopoulou, R. Vicente, E. Manessi-Zoupa, V. Psycharis, A. Escuer, S.P. Perlepes, J. Mol. Struct. 829 (2007) 176;
(d) A. Sieber, C. Boskovic, R. Bircher, O. Waldmann, S.T. Ochsenbein, G. Chaboussant, H.U. Güdel, N. Kirchner, J.V. Slageren, W. Wernsdorfer, A. Neels, H. Stoeckli-Evans, S. Janssen, F. Juranyi, H. Mutka, Inorg. Chem. 44 (2005) 4315;
(e) M. Moragues-Canovas, M. Helliwell, L. Ricard, E. Riviere, W. Wernsdorfer, E. Brechin, T. Mallah, Eur. J. Inorg. Chem. (2004) 2219;
(f) S. Mukherjee, T. Weyhermüller, E. Bothe, K. Wieghardt, P. Chaudhuri, Eur. J. Inorg. Chem. (2003) 863;
(g) J.M. Clemente-Juan, B. Chansou, B. Donnadieu, J.P. Tuchagues, Inorg. Chem. 39 (2000) 5515;
(h) A. Escuer, M. Font-Bardia, S.B. Kumar, X. Solans, R. Vicente, Polyhedron 18 (1999) 909;
(i) M.S. El Fallah, E. Rentschler, A. Caneschi, D. Gatteschi, Inorg. Chim. Acta 247 (1996) 231;
(j) K.S. Murray, Adv. Inorg. Chem. 43 (1995) 261.
[7] (a) Y.-M. Li, Y.-M. Zhang, R.-B. Fu, S.-C. Xiang, T.-L. Sheng, D.-Q. Yuan, X.-H. Huang, X.-T. Wu, Polyhedron 25 (2006) 1618;
(b) E.-C. Yang, W. Wernsdorfer, S. Hill, R.S. Edwards, M. Nakano, S. Maccagnano, L.N. Zakharov, A.L. Rheingold, G. Christou, D.N. Hendrickson, Polyhedron 22 (2003) 1727.

[8] (a) M. Halcrow, J.S. Sun, J.C. Huffman, G. Christou, Inorg. Chem. 34 (1995) 4167;
(b) M.A. Halcrow, J.C. Huffman, G. Christou, Angew. Chem., Int. Ed. 34 (1995) 889.
[9] C. Pérez-Bolívar, V.A. Montes, J.P. Anzenbacher, Inorg. Chem. 45 (2006) 9610.
[10] M.A. Palacios, Z. Wang, V.A. Montes, G.V. Zyryanov, B.J. Hausch, K. Jursíková Jr., P. Anzenbacher, Chem. Commun. (2007) 3708.
[11] G. Aromí, A.S. Batsanov, P. Christian, M. Helliwell, A. Parkin, S. Parsons, A.A. Smith, G.A. Timco, R.E.P. Winpenny, Chem. Eur. J. 9 (2003) 5142.
[12] G. Aromí, A.S. Batsanov, P. Christian, M. Helliwell, O. Roubeau, G.A. Timco, R.E.P. Winpenny, Dalton Trans. (2003) 4466.
[13] (a) C. Boskovic, E. Rusanov, H. Stoeckli-Evans, H.U. Güdel, Inorg. Chem. Commun. 5 (2002) 881;
(b) R. Basler, C. Boskovic, G. Chaboussant, H.U. Güdel, M. Murrie, S.T. Ochsenbein, A. Sieber, Chem. Phys. Chem. 4 (2003) 910.
[14] (a) E. Szajna-Fuller, K. Rudzka, A.M. Arif, L.M. Berreau, Inorg. Chem. 46 (2007) 5499;
(b) E. Szajna-Fuller, K. Rudzka, A.M. Arif, L.M. Berreau, Inorg. Chem. 46 (2007) 5486.
[15] G. Davidson, S.L. Clugston, J.F. Honek, M.J. Maroney, Inorg. Chem. 39 (2000) 2962.
[16] A. Altomare, M.C. Burla, M. Camalli, G.L. Cascarano, C. Giacovazzo, A. Guagliardi, A.G. Moliterni, G. Polidori, R. Spagna, SIR97, J. Appl. Crystallogr. 32 (1999) 115.
[17] G.M. Sheldrick, SHELX-97, Program for Crystal Structure Refinement, University of Gottingen, Germany, 1997.
[18] M. Nardelli, J. Appl. Crystallogr. 28 (1995) 659.
[19] (a) L.J. Farrugia, J. Appl. Crystallogr. 32 (1999) 837;
(b) M.N. Burnett, C.K. Johnson, ORTEP III, Report ORNL-6895, Oak Ridge National Laboratory, Oak Ridge, TN, 1996.
[20] U. Mukhopadhyay, D. Ray, Indian J. Chem. 37A (1998) 191.
[21] A. Yuchi, K. Imai, H. Wada, M. Shiro, G. Nakagawa, Bull. Chem. Soc. Jpn. 59 (1986) 3847.
[22] R.J. Magee, L. Gordon, Talanta 10 (1963) 851.
[23] (a) D. Mandal, D. Ray, Inorg. Chem. Commun. 10 (2007) 1202;
(b) A.R. Paital, M. Sarkar, M. Mikuriya, D. Ray, Eur. J. Inorg. Chem. (2007) 4762.
[24] M. Salierno, C. Fameli, R. Etchenique, Eur. J. Inorg. Chem. (2008) ASAP.
[25] P. Naumov, V. Jordanovska, M.G.B. Drew, S.W. Ng, Solid State Sci. 4 (2002) 455.
[26] A.R. Paital, W.T. Wong, G. Aromí, D. Ray, Inorg. Chem. 46 (2007) 5727.
[27] V. Shivaiah, T. Chatterjee, K. Srinivasu, S.K. Das, Eur. J. Inorg. Chem. (2007) 231.
[28] J.J. Borrás-Almenar, J.M. Clemente-Juan, E. Coronado, B.S. Tsukerblat, J. Comput. Chem. 22 (2001) 985.

Polyhedron 27 (2008) 2379–2385

Contents lists available at ScienceDirect

Polyhedron

journal homepage: www.elsevier.com/locate/poly

Ring opening complexation of nickel(II) and copper(II) by 2-phenyl-2-(2-pyridyl)imidazolidine: Synthesis, spectra and X-ray crystal structures

Sanaa M. Emam [a,1], Patrick McArdle [a,*], James McManus [b], Mary Mahon [b]

[a] Chemistry Department, National University of Ireland, Galway, Ireland
[b] Chemistry Department, University of Bath, UK

ARTICLE INFO

Article history:
Received 7 February 2008
Accepted 10 April 2008
Available online 4 June 2008

Keywords:
Schiff base
Azide
X-ray crystal structure
DFT calculations
Nickel(II)
Copper(II) complexes

ABSTRACT

The cyclic structure of 2-phenyl-2-(2-pyridyl)imidazolidine (**1**) derived from the condensation of 1,2-diaminoethane and 2-benzoylpyridine has been confirmed by X-ray crystallography. Reaction of (**1**) with salts of nickel(II) and copper(II) leads to metal induced ring opening and the formation of complexes containing the tridentate ligand (L). The formulae of the complexes derived from NiX_2 and CuX_2 are $[NiL_2]X_2$ and $[CuLY]X_2$ (X=ClO_4^-, Y = H_2O, CH_3CN and N_3^-). Crystal structures were obtained for (**1**), $[NiL_2][ClO_4]_2$, $[CuL(CH_3CN)][ClO_4]_2$, $[CuL(H_2O)][NO_3]_2$ and $[CuLN_3][ClO_4]$.

© 2008 Elsevier Ltd. All rights reserved.

1. Introduction

Schiff base ligands have played an important role in our understanding of the coordination chemistry of transition metal ions and Schiff base complexes have a broad range of applications including, enzyme inhibition [1], anti-microbial action [2] and catalytic activity when encapsulated in zeolite Y [3]. In this paper, the imidazoline (**1**), the result of a disfavoured 5-*Endo-Trig* cyclization [4], is reacted with nickel and copper salts to yield tridentate complexes. The structures of the complexes which could be crystallized and analysed by X-ray diffraction are discussed. Prompted by reports of the use of DFT calculations in modeling nickel and copper complexes, with similar and greater complexity than those described here [5,6], it has been found that while calculations for the nickel system reproduced the details of the crystallographic results the copper results were less satisfactory.

2. Experimental

2.1. Chemicals and materials

2-Benzoylpyridine and 1,2-diaminoethane (from Sigma–Aldrich and BDH) were used without further purification. Sodium azide (Sigma–Aldrich), $Ni(ClO_4)_2 6H_2O$ (Sigma–Aldrich), $Cu(ClO_4)_2 6H_2O$ (Aldrich), $Ni(NO_3)_2 6H_2O$ (Merck) and $Cu(NO_3)_2 4H_2O$ (Riedel de-Haen) were used as received. All other chemicals and solvents were AR grade and used as received. Ethanol was dried prior to use.

2.2. Instrumentation

Elemental analyses (carbon, hydrogen and nitrogen) were carried out on a Perkin–Elmer 240 CHN elemental analyzer. IR spectra were measured on a Perkin–Elmer Spectrum One Diamond-ATR-FT-IR instrument spectrometer, UV–Vis spectra were recorded using a Varian Cary 50 spectrometer using 1 cm quartz cuvettes. ^1H and ^{13}C NMR spectra were recorded on a JEOL ECX-400 NMR spectrometer at room temperature with tetramethylsilane as internal reference. Magnetic moments were measured on a Sherwood Scientific magnetic susceptibility balance at room temperature. The diamagnetic corrections were calculated by using Pascal's constants and $Hg[Co(SCN)_4]$ was used as a calibrant. Molar conductivities were measured using freshly prepared 10^{-3} M solutions in nitromethane, acetonitrile and dimethylformamide at

* Corresponding author.
E-mail address: p.mcardle@nuigalway.ie (P. McArdle).
[1] Permanent address: Chemistry Department, Faculty of Science, El-Menoufia University, Shebin El-Kom, Egypt.

0277-5387/$ - see front matter © 2008 Elsevier Ltd. All rights reserved.
doi:10.1016/j.poly.2008.04.028

room temperature, using a Jenway 4310 conductivity meter and the cell constant was calibrated with 0.01 M KCl solution. Melting points were measured using a Gallenkamp melting point apparatus.

2.3. Synthesis of 2-phenyl-2-(2-pyridyl)imidazolidine (**1**)

The ligand 2-phenyl-2-(2-pyridyl) imidazolidine was prepared using a slight variation of the procedure reported in the literature [7]. An anhydrous ethanol solution (15 cm^3) of 2-benzoylpyridine (8.0 g, 0.04 mol), was treated dropwise with 1,2-diaminoethane (2.62 g, 0.05 mol) in the same solvent (5.0 cm^3) with constant stirring and the mixture was then heated under reflux for 16 h. The yellow solution was concentrated under reduced pressure, cooled and the formed faint yellow precipitate filtered. The product was re-crystallized from *n*-hexane giving almost colourless crystals, melting point is (83–85 °C). *Anal.* Calc. for $C_{14}H_{15}N_3L$: C, 74.63; H, 6.7; N, 18.67. Found: C, 74.81; H, 6.47; N, 18.46%. IR (Diamond ATR cm^{-1}): υ(N–H) 3320, 3247 (broad); υ(C=N) 1620, 1538, 1567, υ(C=C) 1490 1448, 1425. ^1H NMR data in $CDCl_3$ at 298 K: δ (ppm): 8.73 d(1) (H_6); 8.5 t(1) (H_4); 7.95 m(1) (H_5); 7.69 d(1) (H_3); 7.57–7.42 m(5) (H_{13}–H_{17}); 3.05 m(2) (H_{10}); 2.99 m(2) (H11); 2.82 br(2) (H 7, 9).^{13}C NMR in $CDCl_3$: δ (ppm): 163.3 (C-2); 150.2 (C6); 144.2 (C12); 136.7 (C4); 128.28 (C14, 16); 127.1 (C13, 17); 122.1 (C15); 85.9 (C8); 46.3(C10,11); UV–Vis (CH_3CN): λ_{max} 290, 275 and 252 nm.

2.4. Preparation of metal complexes, L= (**1**)

2.4.1. [Ni(L)$_2$][ClO$_4$]$_2$ (**2**)

To a stirred solution of (**1**) (1.0 g, 0.004 mol) in acetonitrile (7 cm^3), a solution of $Ni(ClO_4)_2 \cdot 6H_2O$ (1.6 g, 0.004 mol) in the same solvent (7 cm^3) was added dropwise with constant stirring. The solution colour changed from yellow to a dark red. The reaction mixture was stirred at room temperature for 3 h and left to stand overnight. Evaporation of the solvent left a toffee like residue. This was dissolved in warm methanol from which red crystals were obtained. *Anal.* Calc. for $C_{28}H_{30}N_6Cl_{I2}NiO_8$ (**2**): C, 47.48; H, 4.23; N, 11.86. Found: C, 47.49; H, 4.07; N, 12.21%. Λ_M (Ω^{-1} cm^2 mol^{-1}) in CH_3CN and CH_3NO_2: 275 and 156. IR (Diamond ATR cm^{-1}): υ(N–H) 3342, 3293 (broad, m); 1646 υ(C=N); 1595, 1580 υ(C=C), υ(C=N)$_{py}$, δ(N–H), υ(ClO_4) 1070; UV–Vis (CH_3CN; λ_{max}):784, 531, 464 nm. μ_{eff} (BM): 3.34.

The red crystals were re-crystallized from a chloroform methanol mixture to give a second crop of red crystals of formula $C_{28}H_{30}N_6Cl_{I2}NiO_8 \cdot CHCl_3$ which were suitable for crystallography.

2.4.2. [Ni(L)(N$_3$)$_2$DMF] (**3**)

The ligand (**1**) (1.0 g, 0.004 mol) was dissolved in absolute ethanol (5 cm^3) and a solution of $Ni(ClO_4)_2 6H_2O$ (1.6 g, 0.004 mol) in ethanol (7 cm^3) was added drop-wise with constant stirring. The yellow colour of the solution changed to a dark red with the formation of a semi-solid mass. Rapid stirring for one hour led to the formation of a solid which was treated with a hot methanolic solution (15 cm^3) of NaN_3 (1.2 g, 0.016 mol). The reaction mixture was stirred for 4 h and a buff precipitate formed. This was left to stand for 24 h and then stirred for 2 h, filtered and the filtrate was dissolved in hot acetonitrile filtered concentrated and allowed to cool to room temperature yielding yellowish brown micro crystals. These crystals were dissolved in DMF and re-crystallized by vapour diffusion of diethyl ether from an adjacent container. This afforded dark brown crystals (melting point 195 °C) which were not suitable for crystallography. *Anal.* Calc. for $C_{17}H_{22}N_{10}ONi$: C, 46.28; H, 5.02; N, 31.75. Found: C, 45.35; H, 4.08; N, 33.91%. Λ_M (S cm^2 mol^{-1}) in DMF: 23.0. IR (cm^{-1}): υ(N–H) 3312, 3247, 3153; υ(N_3) 2020; υ(C=N) 1650; υ(C=C), υ(C=N)$_{py}$, δ(N–H), 1589, 1570. UV–Vis (DMF. λ_{max}): 690, 522, 463 nm. μ_{eff} (BM): 3.30.

2.4.3. [Cu(L)(CH$_3$CN)][ClO$_4$]$_2$ (**4**)

To a stirred solution of (**1**) (1.0 g, 0.004 mol) in absolute ethanol (6 cm^3), a solution of $Cu(ClO_4)_2 \cdot 6H_2O$ (1.6 g, 0.004 mol) in acetonitrile (3 cm^3) was added dropwise with constant stirring. The colour changed from yellow to green and then to blue as the copper perchlorate solution was added. The reaction mixture was stirred for 5 h at room temperature and a blue precipitate formed. It was isolated by filtration, washed with a mixture of ethanol and acetonitrile and dried under vacuum. Crystals grown from acetone solution were of poor quality however crystallization from a mixture of acetonitrile and ethanol afforded a blue needles of suitable quality for X-ray crystallography. Melting point 200 °C. *Anal.* Calc. for $C_{16}H_{18}N_4O_8Cl_2Cu$: C, 36.34; H, 3.34; N, 10.59. Found: C,36.11; H, 3.19; N, 10.59%. Λ_M (S cm^2 mol^{-1} in CH_3CN) and CH_3NO_2: 270 and 133. IR (cm^{-1}): υ(N–H) 3300, 3255, 3158; υ(C=N) 1636; υ(C=C), υ(C=N)$_{py}$, δ(N–H) 1598, 1580; υ(ClO_4) 1053. UV–Vis (CH_3CN; λ_{max}): 606, 412 nm. μ_{eff} (BM): 1.75.

2.4.4. [CuL(N$_3$)][NO$_3$] (**5**)

An ethanolic solution (12 cm^3) of $Cu(NO_3)_2 6H_2O$ (2.2 g, 0.01 mol) was added dropwise to ethanolic solution (10 cm^3) of (**1**) (1.0 g, 0.0044 mol) with continuous stirring. The reaction mixture was stirred for one hour and the solution changed colour to a greenish-blue. To this NaN_3 (1.2 g, 0.02 mol) in hot methanol (15 cm^3) was added slowly with constant stirring. The colour changed immediately and a brown precipitate formed. The reaction mixture was stirred for 3 h. at room temperature, the precipitate was filtered, washed with few drops of ethanol and dried under vacuum. This precipitate was disgraded (as it proved to be a mixture). The green filtrate was concentrated using a rotary evaporator and kept at 4 °C in a fridge for several weeks. Unusual dark green spherical pseudo-crystals (unsuitable for crystallography) were isolated, washed with few drops of ethanol and dried under vacuum. Melting point 115 °C. *Anal.* Calc. for $C_{14}H_{15}N_7O_3Cu$: C, 42.8; H, 3.84; N, 24.96. Found: C, 42.32; H, 3.10; N, 25.09%. Λ_M (S cm^2 mol^{-1}) in CH_3CN and CH_3NO_2: 128 and 68. IR (cm^{-1}): υ(N–H) 3292, 3244, 151; υ(N_3) 2042; υ(C=N) 1660, 1636; υ(C=C), υ(C=N)$_{py}$, δ(N–H) 1594, υ(NO_3) 1411. UV–Vis (CH_3CN; λ_{max}): 614, 518 nm. μ_{eff} (BM): 1.74.

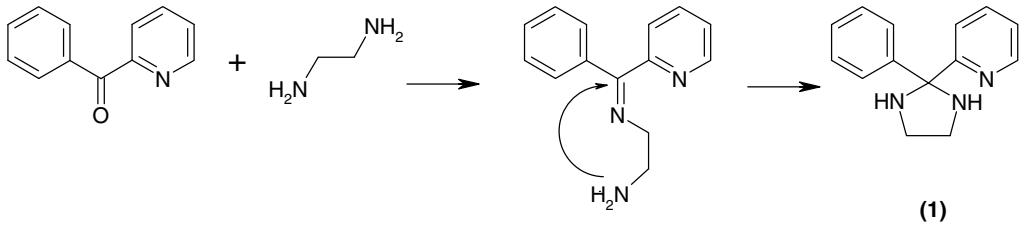

(1)

Scheme 1.

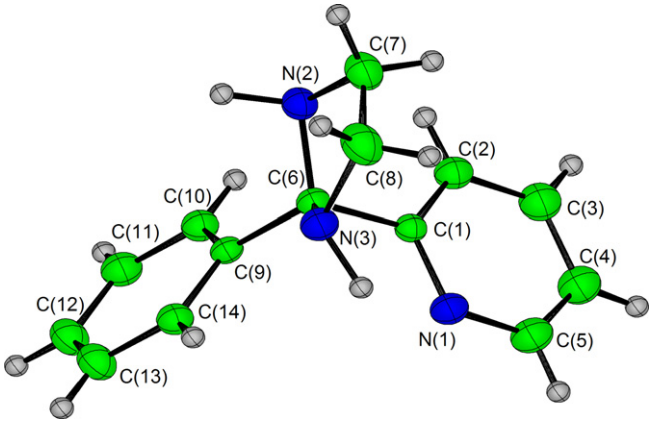

Fig. 1. ORTEX diagram of $C_{14}H_{15}N_3$, L (**1**) with 40% probability ellipsoids.

2.4.5. $[CuL(H_2O)][NO_3]_2$ (**6**)

The filtrate remaining after the filtration of (**5**) was left to stand at room temperature for several weeks and a precipitate formed. This was isolated by filtration, and washed with few drops of ethanol and crystallized from methanol solution and dark blue crystals were grown by slow vapour diffusion of diethyl ether from an adjacent container which were suitable for X-ray crystallography. Melting point 135 °C. *Anal.* Calc. for $C_{14}H_{17}N_5O_7Cu$ (**6**): C, 39.03; H, 3.97; N, 16.25. Found: C, 38.49; H, 4.01; N, 15.23%. Λ_M ($S\,cm^2\,mol^{-1}$) in CH_3CN and CH_3NO_2: 141 and 50. IR (cm^{-1}): υ(O–H) 3400–2327; υ(N–H) 3293, 3240,3135; υ(C=N) 1645; 1597, 1585; $\upsilon(NO_3)$ 1411. UV–Vis (CH_3CN; λ_{max}): 648, 516 nm. μ_{eff} (BM): 1.76.

2.4.6. $[CuL(N_3)][ClO_4]$ (**7**)

A blue methanolic solution (7 cm^3) of $Cu(ClO_4)_2 \cdot 6H_2O$ (1.6 g, 0.004 mol) was added dropwise to a methanolic solution (7 cm^3) of **L** (0.5 g, 0.002 mol) with continuous stirring. The mixture was stirred for 20 min and then NaN_3 (0.6 g, 0.01 mol) in aqueous methanol (10 cm^3, 1:1) was added slowly with a constant stirring. The blue colour of the reaction mixture changed to dark brown with the formation of green precipitate. This was filtered off washed with methanol and dried. It was re-crystallized from hot acetonitrile to give blue crystals which were suitable for crystallography. Its melting point is 175 °C. *Anal.* Calc. for $C_{14}H_{15}N_6O_4ClCu$ (**7**): C, 39.07; H, 3.51; N, 39.53. Found: C,39.27; H, 2.99; N, 19.45%. (Λ_M $S\,cm^2\,mol^{-1}$) in CH_3CN CH_3NO2: 153 and 104. IR (cm^{-1}): υ(N–H) 3317, 3264, 3148; υ(C=N) 1649; 1598, 1585; $\upsilon(ClO_4)$ 1096. UV–Vis (CH_3CN; λ_{max}): 611, 513 nm. μ_{eff} (BM): 1.80.

2.4.7. $[Cu_2(L)_2(Pyz)][ClO_4]_4\ CH_3CN \cdot (H_2O)_{0.5}$ (**8**)

To a solution of (**1**) (1.0 g, 0.004 mol) in C_2H_5OH (10 cm^3) was added solution of $Cu(ClO_4)_26H_2O$ (3.3 g, 0.004 mol) in water (5 cm^3). The solution colour changed from yellow to blue and the reaction mixture was then stirred for 30 min. at room temperature. To this pyrazine (1.4 g, 0.02 mol) in water (5 cm^3) was added slowly with constant stirring. After stirring at room temperature for 5 h the solution was allowed to stand and a precipitate was filtered, washed with ethanol and dried under vacuum over P_2O_5. It was crystallized from a mixture of CH_3CN and CH_3OH (1:3) by slow vapour diffusion of diethyl ether from an adjacent container giving dark violet crystals which were not suitable for X-ray crystallography. Melting point 140 °C. *Anal.* Calc. for $C_{34}H_{38}N_9O_{16.5}Cl_4Cu_2$ (**8**): C, 36.93; H, 3.46; N, 11.49. Found (>250 °C): C, 37.12; H, 3.36, N, 10.54%. Λ_M ($S\,cm^2\,mol^{-1}$) in CH_3CN: 507. IR (cm^{-1}): υ(O–H) 3567, 3407; υ(N–H) 3316, 3260, 3140; υ(C=N) 1649; υ(C=C), $\upsilon(C{=}N)_{py}$

Table 1
Crystal data and structure refinement parameters

Compound	(**1**)	(**2**)	(**4**)	(**6**)	(**7**)
Empirical formula	$C_{14}H_{15}N_3$	$C_{29}H_{31}Cl_5N_6NiO_8$	$C_{16}H_{18}Cl_2CuN_4O_8$	$C_{14}H_{17}CuN_5O_7$	$C_{14}H_{15}ClCuN_6O_4$
Formula weight	225.29	827.56	528.78	430.87	430.31
Temperature (K)	298(2)	298(2)	150(2)	298(2)	150(2)
Wavelength (Å)	0.71069	0.71069	0.71073	0.71069	0.71073
Crystal system	monoclinic	monoclinic	orthorhombic	monoclinic	monoclinic
Space group	*C*2/c	*P*21/*c*	*Pbca*	*P*21/*c*	*C*2/*c*
Unit cell dimensions					
a (Å)	16.690(2)	15.097(2)	7.14000(10)	8.486(2)	24.6030(8)
b (Å)	5.796(1)	25.636(3)	22.8780(2)	23.617(3)	8.2460(3)
c (Å)	24.465(3)	18.197(2) $\gamma = 90°$	25.5040(3)	8.7509(9)	17.1500(7)
β (°)	95.25(2)	90.74(2)		92.130(10)	106.7130(10)
Volume ($Å^3$)	2356.7(6)	7042.1(15)	4166.05(8)	1752.6(5)	3332.4(2)
Z	8	8	8	4	8
Density (calculated) (Mg/m^3)	1.270	1.561	1.686	1.633	1.715
Absorption coefficient (mm^{-1})	0.078	0.987	1.358	1.296	1.507
F(000)	960	3392	2152	884	1752
Crystal size (mm)	0.55 × 0.42 × 0.26	0.47 × 0.38 × 0.21	0.40 × 0.20 × 0.10	0.47 × 0.41 × 0.26	0.10 × 0.05 × 0.05
θ Range for data collection (°)	1.67–20.34	1.57–20.52	3.56–27.46	1.72–20.43	4.98–27.47
Index ranges	$-16 \leqslant h \leqslant 15$; $-5 \leqslant k <= 5$; $-23 \leqslant l \leqslant 23$	$-14 \leqslant h \leqslant 14$; $-23 \leqslant k <= 24$; $-17 \leqslant l \leqslant 17$	$-9 \leqslant h \leqslant 9$; $-29 \leqslant k \leqslant 29$; $-33 \leqslant l \leqslant 33$	$-7 \leqslant h <= 7$; $-22 \leqslant k \leqslant 22$; $-8 \leqslant l \leqslant 8$	$-31 \leqslant h <= 31$; $-8 \leqslant k \leqslant 10$; $-22 \leqslant l \leqslant 21$
Reflections collected	4312	22 309	58 203	6763	11 733
Independent reflections [*R*(int)]	1137 [0.0361]	6869 [0.0367]	4751 [0.0732]	1639 [0.0528]	3679 [0.0781]
Reflections observed (>2σ)	1091	6306	3514	1566	2583
Data completeness	0.977	0.972	0.997	0.941	0.964
Absorption correction	none	none	none	none	none
Data/restraints/parameters	1137/0/157	6869/0/883	4751/2/307	1639/0/245	3679/2/243
Goodness-of-fit on F^2	1.066	1.036	1.028	1.094	1.022
Final *R* indices [$I > 2\sigma(I)$]	$R_1 = 0.0363$ $wR_2 = 0.1029$	$R_1 = 0.0656$ $wR_2 = 0.1743$	$R_1 = 0.0377$ $wR_2 = 0.0846$	$R_1 = 0.0467$ $wR_2 = 0.1247$	$R_1 = 0.0437$ $wR_2 = 0.0843$
R indices (all data)	$R_1 = 0.0387$ $wR_2 = 0.1046$	$R_1 = 0.0706$ $wR_2 = 0.1786$	$R_1 = 0.0619$ $wR_2 = 0.0948$	$R_1 = 0.0523$ $wR_2 = 0.1410$	$R_1 = 0.0784$ $wR_2 = 0.0987$
Largest difference peak and hole (e $Å^{-3}$)	0.130 and −0.136	1.158 and −0.811	0.419 and −0.457	0.781 and −0.474	0.365 and −0.467

Table 2
Selected bond lengths (Å) and angles (°) for (**1**)

N(2)–C(6)	1.466(3)	N(2)–C(7)	1.468(3)
N(3)–C(8)	1.465(3)	N(3)–C(6)	1.480(2)
C(6)–C(9)	1.520(3)	C(1)–C(6)	1.540(3)
C(6)–C(9)	1.520(3)	C(7)–C(8)	1.510(3)
C(1)–C(6)–C(9)	107.5(2)	C(6)–N(3)–C(8)	106.1(2)
C(6)–N(2)–C(7)	103.3(2)	N(2)–C(7)–C(8)	105.8(2)
N(3)–C(8)–C(7)	105.9(2)	C(1)–C(6)–N(2)	109.6(2)

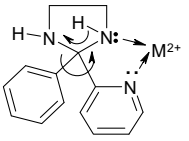

Fig. 2. Metal induced ring opening of the imadazoline.

δ(N–H) 1600, 1567; $\upsilon(ClO_4)$ 1095, 1043. UV–Vis (CH_3CN; λ_{max}): 650, 512 nm. μ_{eff} (BM): 1.09.

2.5. Crystallography

Reflection data were collected either on a Marresearch image plate system or on a Nonius kappa CCD system. Data reduction were carried out using the XDS and DENZO/SCALEPACK packages. respectively [8] The structures was solved by direct methods, SHELXS-97, and refined by full matrix least squares using SHELXL-97 [9,10]. SHELX operations were automated using ORTEX which was also used to obtain the drawings [11]. Hydrogen atoms were included in calculated positions with thermal parameters 30% larger than the atom to which they were attached. The non-hydrogen atoms were refined anisotropically. All calculations were performed on a Pentium PC.

2.6. Calculations

DFT calculations were carried out using PC-GAMESS [12] which was driven by the molecular modeling software within the OSCAIL package [13].

3. Results and discussion

3.1. Structure of the ligand

The condensation of 2-benzoyl pyridine and 1,2-diaminoethane has been reported and the structure of the product assigned as 2-

Table 3
Selected bond lengths (Å) and angles (°) for (**2**)

Ni(1)–N(1)	2.121(5)	Ni(1)–N(2)	1.996(5)
Ni(1)–N(3)	2.103(5)	Ni(1)–N(4)	2.112(5)
Ni(1)–N(5)	2.016(5)	Ni(1)–N(6)	2.093(5)
Ni(2)–N(7)	2.121(5)	Ni(2)–N(8)	1.998(5)
Ni(2)–N(9)	2.095(5)	Ni(2)–N(10)	2.115(5)
Ni(2)–N(11)	2.017(5)	Ni(2)–N(12)	2.088(5)
N(1)–Ni(1)–N(2)	81.4(2)	N(1)–Ni(1)–N(3)	158.4(2)
N(1)–Ni(1)–N(4)	92.1(2)	N(1)–Ni(1)–N(5)	100.7(2)
N(1)–Ni(1)–N(6)	89.5(2)	N(7)–Ni(2)–N(8)	80.5(2)
N(7)–Ni(2)–N(9)	158.3(2)	N(7)–Ni(2)–N(10)	90.7(2)
N(7)–Ni(2)–N(11)	101.6(2)	N(7)–Ni(2)–N(12)	91.0(2)

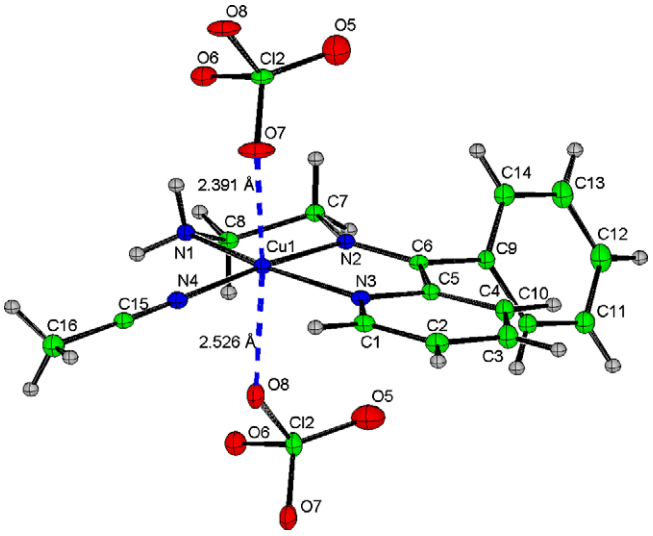

Fig. 4. ORTEX diagram of $[CuL(CH_3CN)][ClO_4]_2$ (**4**), with 40% probability ellipsoids.

Table 4
Selected bond lengths (Å) and angles (°) for (**4**)

Cu(1)–N(1)	2.008(2)	Cu(1)–N(2)	1.957(2)
Cu(1)–N(3)	1.996(2)	Cu(1)–N(4)	1.983(2)
Cu(1)–O(7)	2.391(2)	N(1)–Cu(1)–N(2)	83.51(9)
N(1)–Cu(1)–N(3)	163.95(9)	N(1)–Cu(1)–N(4)	96.37(9)
N(2)–Cu(1)–N(3)	80.77(8)	N(2)–Cu(1)–N(4)	174.70(8)
N(3)–Cu(1)–N(4)	98.98(8)	N(1)–Cu(1)–O(7)	92.15(8)
N(2)–Cu(1)–O(7)	97.87(9)	N(3)–Cu(1)–O(7)	93.20(8)
N(4)–Cu(1)–O(7)	87.43(9)		

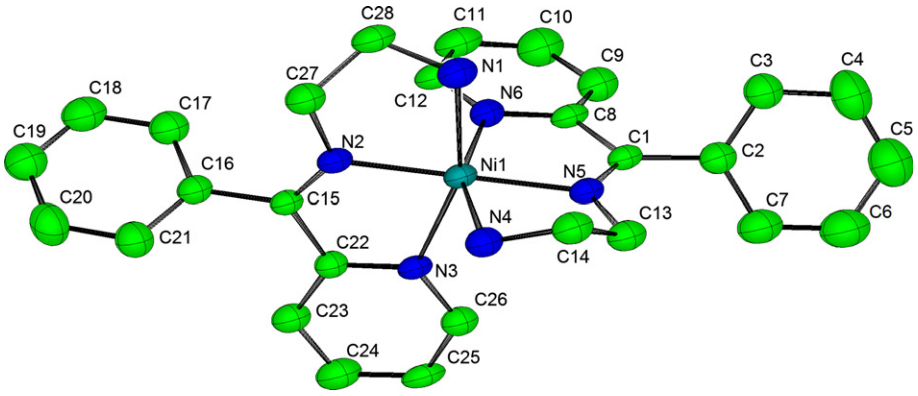

Fig. 3. ORTEX diagram of the cation of $[NiL_2][ClO_4]_2$ (**2**) with 40% probability ellipsoids and hydrogen atoms omitted for clarity.

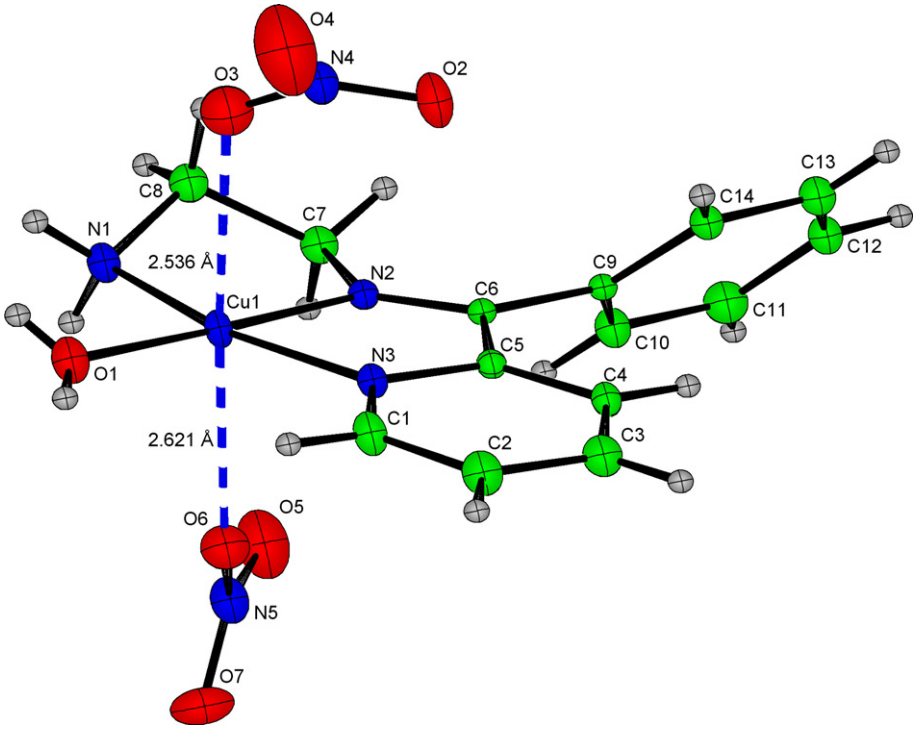

Fig. 5. ORTEX diagram of the cation of $[Cu(L)(H_2O)][(NO_3)_2]$ (**6**), with 40% probability ellipsoids.

Table 5
Selected bond lengths (Å) and angles (°) for (**6**)

Cu(1)–O(1)	1.942(5)	Cu(1)–N(2)	1.948(5)
Cu(1)–N(1)	1.994(5)	Cu(1)–N(3)	2.003(5)
Cu(1)–O(3)	2.621(6)	Cu(1)–O(6)	2.536(5)
N(1)–Cu(1)–N(2)	84.2(2)	N(1)–Cu(1)–N(3)	164.9(2)
N(2)–Cu(1)–N(3)	80.8(2)	O(1)–Cu(1)–N(1)	93.9(2)
O(1)–Cu(1)–N(2)	178.0(2)	O(1)–Cu(1)–N(3)	101.1(2)
O(3)–Cu(1)–O(6)	173.6(2)		

phenyl-2-(2-pyridyl)imidazolidine, (**1**), using ^{1}H and ^{13}C NMR. It is reasonable to suggest that the reaction proceeds *via* initial formation of the imine and subsequent cyclization as shown in Scheme 1.

Since this is an example of an unfavorable 5-*Endo-Trig* cyclization [4], the crystal structure was determined to confirm the NMR assignment. The X-ray structure of (**1**) is shown in Fig. 1.

Table 6
Selected bond lengths (Å) and angles (°) for (**7**)

Cu(1)–N(4)	1.946(3)	Cu(1)–N(2)	1.950(3)
Cu(1)–N(3)	2.010(3)	Cu(1)–N(1)	2.033(3)
N(1)–C(8)	1.494(4)	N(2)–C(6)	1.279(4)
N(2)–C(7)	1.466(4)	N(3)–C(1)	1.333(4)
N(3)–C(5)	1.364(4)	N(4)–N(5)	1.204(4)
N(5)–N(6)	1.162(4)	C(1)–C(2)	1.381(5)
C(2)–C(3)	1.382(5)	C(3)–C(4)	1.398(5)
C(4)–C(5)	1.384(5)	C(5)–C(6)	1.498(4)
C(6)–C(9)	1.491(4)	C(7)–C(8)	1.522(5)
N(4)–Cu(1)–N(2)	173.0(1)	N(4)–Cu(1)–N(3)	94.9(1)
N(2)–Cu(1)–N(3)	80.5(1)	N(4)–Cu(1)–N(1)	101.8(1)
N(2)–Cu(1)–N(1)	83.7(1)	N(3)–Cu(1)–N(1)	161.1(1)
C(8)–N(1)–Cu(1)	107.2(2)	C(6)–N(2)–C(7)	126.9(3)
C(6)–N(2)–Cu(1)	118.8(2)	C(7)–N(2)–Cu(1)	114.3(2)
C(1)–N(3)–C(5)	118.6(3)	C(1)–N(3)–Cu(1)	127.9(2)
C(5)–N(3)–Cu(1)	113.4(2)	N(5)–N(4)–Cu(1)	126.0(2)
N(6)–N(5)–N(4)	176.6(3)	N(3)–C(1)–C(2)	122.3(3)

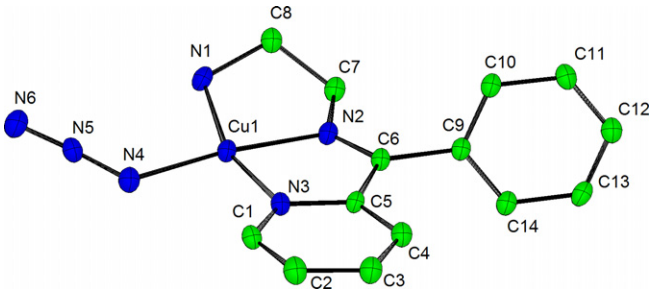

Fig. 6. ORTEX diagram of the cation of $[Cu(L)N_3][ClO_4]$ (**7**), with 40% probability ellipsoids and hydrogen atoms omitted for clarity.

Crystal data are given in Table 1 and selected bond lengths and angles are given in Table 2.

DFT calculations on (**1**) using B3LYP functionals at the 6-31G* level suggest that in the gas phase the cyclic structure is more stable than the open imine form by 13.1 kJ mol^{-1}. Thus the unfavourable 5-*Endo-Trig* cyclization may in part be possible in this case due to the higher stability of the cyclic form. If solvent effects are ignored, and if equilibrium was possible, this energy difference translates to an equilibrium concentration of the cyclic form that is approximately 5×10^3 times greater than the imine form. There is spectroscopic and kinetic evidence that the imine form may have appreciably higher concentrations in polar solvents [14]. There are many well established examples of 5-*Endo-Trig* cyclizations in the literature [15,16].

3.2. Ring opening complexation

When (**1**) was reacted with Cu(II) and Ni(II) salts no complexes containing the cyclic structure were observed. In every case where crystal structures were obtained only the open form was observed in the complexes. This reaction is probably an example of a cationic

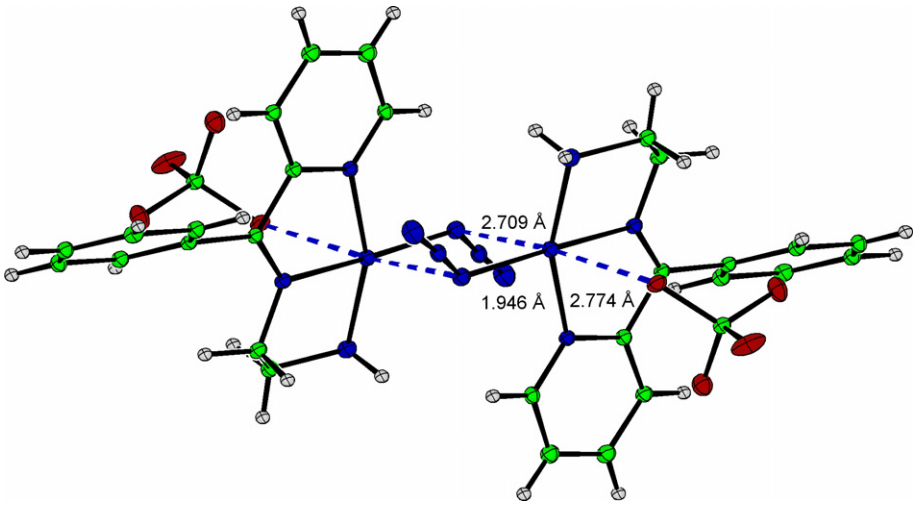

Fig. 7. ORTEX diagram of showing the weak interactions in the crystal structure of (**7**).

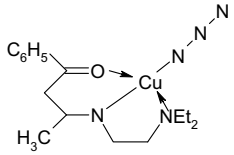

Fig. 8. Structure of (**8**).

metal induced ring opening reaction. A possible mechanism is illustrated in Fig. 2.

This mechanism is related to that proposed for the Fe(III) catalysed opening of an imidazolidine ring in the presence of alcohols [17].

3.3. Reaction of (*1*) with nickel perchlorate (*2*)

Reaction of (**1**) with nickel perchlorate led to the isolation of a red solid. It was characterized by elemental analysis, IR and ^{1}H and ^{13}C NMR. Crystals grown from a chloroform/methanol mixture were suitable for X-ray crystallography. The structure of a cation from the crystal structure of (**2**) is shown in Fig. 3. Crystal data are given in Table 1 and selected bond lengths and angles are given in Table 3. There are two almost identical formula units in the crystallographic asymmetric unit. Each of the ligands in the cation is tridentate with and the overall geometry is close to octahedral. Thus within each asymmetric unit there are four examples of nickel ligand binding moeties. The nickel–nitrogen distances in all cases are in order of increasing length; imine, pyridine and primary amine. For example in Fig. 3 the Ni(1)–N(2), Ni(1)–N(3) and Ni(1)–N(1) are 1.996(5), 2.103(5) and 2.121(5) Å.

To see if this order of bond lengths was due to crystal packing or a genuine property of the complex the structure of the cation was optimized using DFT calculations using B3LYP functionals at the 6-31G* level [12]. The results while giving slightly longer distances nevertheless gave the same order of bond lengths; N-i-N(2) 2.040, Ni–N(3) 2.115 and Ni–(N1) 2.183 Å. The bonding to nickel on the part of the unsaturated nitrogens is clearly stronger than that of the primary nitrogen. It is possible that a small amount of strain in the chelate rings is the cause of the shortest Ni–N bond being to the middle nitrogen. The observed magnetic moment of 3.34 μB is higher that the spin-only value for two unpaired electrons of 2.83 μB however it is within the observed range for octahedral nickel(II) complexes [18,19].

3.4. Reaction of (*2*) with sodium azide

When complex (**2**) was reacted with sodium azide a product of formula $[Ni(L)(N_3)_2(DMF)]$ (**3**) was isolated. Single crystals suitable for X-ray crystallography could not be obtained. This formula is assigned on the basis of elemental analysis, spectroscopic, magnetic and conductivity data. In the IR spectrum bands due to azide, DMF and the Schiff base were all observed. The observed conductivity is an order of magnitude lower than that observed for (**2**) in agreement with its covalent formulation.

3.5. Reaction of (*1*) with copper nitrate and acetonitrile in methanol

Treatment of a solution of (**1**) in methanol with copper perchlorate gave a blue solution from which after addition of acetonitrile blue crystals of formula $[CuL(CH_3CN)][ClO_4]_2$ (**4**) were obtained. The structure of a cation from (**4**) and its contacts to one of the perchlorate anions is shown in Fig. 4, crystal data are in Table 1 and selected bond distances and angles are given in Table 4. The geometry about copper is tetragonally distorted octahedral with metal nitrogen distances within the square plane close to 2.0 Å and longer contacts to the oxygen atoms of symmetry related perchlorate anions of 2.391(2) and 2.526(2) Å, respectively. The metal nitrogen bond lengths within the salicylaldimine ligand show the same order observed in the nickel complex (**2**) above.

3.6. Reaction of (*1*) with copper nitrate and sodium azide in ethanol

An ethanolic solution of copper nitrate was reacted with (**1**) and sodium azide. On standing for some time tiny green spheres grew from solution. These spheres did not diffract X-rays and they had the properties of a glass. The formula $[CuLN_3][NO_3]$ (**5**) was assigned to this solid on the basis of analytical and spectroscopic data. Attempts to grow crystals from the filtrate of this reaction led to the isolation of crystals of $[Cu(L)(H_2O)][(NO_3)_2]$ (**6**), in which water had replaced the azide anion. The structure of the cation from (**6**) is shown in Fig. 5, crystal data are given in Table 1 and selected bond lengths and angles are given in Table 5. The geometry about the copper is tetragonally distorted octahedral with longer contacts to nitrate oxygens. The coordinated water molecule is involved in strong hydrogen bond contacts to nitrate ions, O···O distances of 2.739(7) and 2.763(7) Å to O6 and O3, respectively, and there are contacts from nitrate O7 to N1 of 3.078(7) Å which extend the hydrogen bond network throughout the lattice.

When weak interactions are included the stereochemistry of the copper(II) ion is often difficult to describe due to the distortions resulting from the Jahn–Teller effect. In an extensive review of this area using structure correlation analysis Murphy and Hathaway have analysed the range of observed structures and the crystal structure of (**5**) lies well within that range [20]. Attempts were made to model the strongly bonded square planar portion of the structure using the DFT calculation methods that had been successfully applied to the nickel complex above. In the crystal structure of (**6**) the copper and the three nitrogen atoms are essentially planar, with a maximum deviation from least squares plane of 0.02 Å. The oxygen atom is just 0.10 Å above this plane. In the DFT optimised structure the maximum deviation from the plane defined by the copper and the three nitrogens is 0.18 Å and the oxygen is 1.12 Å out of that plane. Attempts to model the complete $[Cu(L)(H_2O)][(NO_3)_2]$ unit were even less successful. The B3LYP functional appears to be able to model Cu(II) when the relative geometry of the ligating atoms is restrained to some extent [5,6]. A recent review of DFT functionals has suggested that B3LYP has some serious shortcomings and perhaps more advanced functionals are required for the Cu(II) complexes described here [21].

3.7. Reaction of (*1*) with copper perchlorate and sodium azide in methanol

When the reaction above was repeated using copper perchlorate in methanol solution it was possible to isolate good quality crystals of the copper azide $[Cu(L)N_3][ClO_4]$ (**7**). Crystal data are given in Table 1 and selected bond lengths and angles are in Table 6. The crystal structure of the cation from this salt without the weaker interactions which complete the tetragonally distorted octahedral geometry is shown in Fig. 6.

The geometry about the copper is close to square-planar with N2 showing the greatest deviation from the best plane through the four nitrogens of 0.15 Å and the copper is 0.04 Å out of the plane. The tetragonally distorted octahedral geometry about copper is achieved by the addition of two weak interactions involving highly asymmetric bridging on the part of the azide ligands, 1.946(3) and 2.709(3) and a weak interaction involving a perchlorate anion, 2.774(3) Å (Fig. 7).

There are many reported structures of azide complexes in which the azide ligand is seen to span the range from mono-dentate through semi-bridging to symmetrical bridging. Structure (**7**) is close to mono-dentate. The energy difference between mono-dentate and bridging structures is however small and less than typical lattice energies. This point is clearly evident in the recently reported structure of complex (**8**), depicted in Fig. 8, which Sarker et al. have described [22,23]. In the reported crystal structure both symmetrically bridged μ-azido and mono-dentate square-planar geometries are present in the same asymmetric unit.

4. Conclusion

2-Phenyl-2-(2-pyridyl)imidazolidine reacts with Ni(II) and Cu(II) salts to give stable complexes containing the tridentate open form of the ligand. Combined structural and theoretical calculations show that DFT calculations using the B3LYP functionals at the 6-31G* level reproduce the geometry of the Ni(II) complexes but are less successful in modelling the Cu(II) complexes.

Appendix A. Supplementary data

CCDC 677183, 677184, 677185, 677186 and 677187 contain the supplementary crystallographic data for **1**, **2**, **4**, **6** and **7**. These data can be obtained free of charge via http://www.ccdc.cam.ac.uk/conts/retrieving.html, or from the Cambridge Crystallographic Data Centre, 12 Union Road, Cambridge CB2 1EZ, UK; fax: (+44) 1223-336-033, or e-mail: deposit@ccdc.cam.ac.uk. Supplementary data associated with this article can be found, in the online version, at doi:10.1016/j.poly.2008.04.028.

References

[1] D. Shi, Z. You, C. Xu, Q. Zhang, H. Zhu, Inorg. Chem. Commun. 10 (2007) 404.
[2] C.M. Sharaby, Spectrochim. Acta A 66 (2007) 127.
[3] C. Jin, W. Fan, Y. Jia, B. Fan, J. Ma, R. Li, J. Mol. Cat. A: Chem. 249 (2006) 23.
[4] J.E. Baldwin, J. Chem. Soc., Chem. Commun. (1976) 734.
[5] V. Ruangpornvisuti, Struct. Chem. 18 (2007) 977.
[6] S. Ritimukta, S.I. Gorelsky, L. Basumallick, H.J. Hwang, R.C. Pratt, T.D.P. Stack, Y. Lu, K.O. Hodgson, B. Hedman, E.I. Solomon, J. Am. Chem. Soc. 130 (2008) 3866.
[7] H. Sharghi, H. Naeimi, Synlett 12 (1998) 1343.
[8] (a) XDS, W. Kabasch, J. Appl. Crystallogr. 21 (1988) 916;
(b) Denzo/Scalepack, Z. Otwinowski, W. Minor, International Tables for Crystallography, vol. F, Springer, 2001.
[9] G.M. Sheldrick, Acta Crystallogr., Sect. A 46 (1990) 467.
[10] G.M. Sheldrick, SHELXL-97 A Computer Program for Crystal Structure Determination, University of Gottingen, 1997.
[11] P. McArdle, J. Appl. Crystallogr. 28 (1995) 65.
[12] PC GAMESS program provided by A.A. Granovsky, PC GAMESS version 7.1.5, <http://classic.chem.msu.su/gran/gamess/index.html>.
[13] P. McArdle, K. Gilligan, D. Cunningham, R. Dark, M. Mahon, CrystEngComm 6 (2004) 303.
[14] J. McManus, M.J. Hynes, unpublished observations.
[15] A. Ishita, O. Tamura, Tetrahedron Lett. 43 (2002) 473.
[16] T. Yamazaki', S. Hiraoka, J. Sakamoto, T. Kitazume, J. Fluorine Chem. 101 (2000) 309.
[17] V.M. Ugalde-Saldivar, H. Hopfl, N. Farfan, A.R. Toscano, M.E. Sosa-Torres, Inorg. Chim. Acta 358 (2005) 3545.
[18] C.E. Housecroft, A.G. Sharpe, Inorganic Chemistry, 3rd ed., Pearson, Harlow, 2008, p. 672.
[19] F.A. Cotton, G. Wilkinson, C.A. Murillo, M. Bochmann, Advanced Inorganic Chemistry, 6th ed., Wiley, New York, 1999. p. 839.
[20] B. Murphy, B. Hathaway, Coord. Chem. Rev. 243 (2003) 237.
[21] Y. Zhao, D.G. Truhlar, Acc. Chem. Res. 41 (2008) 157.
[22] B. Sarkar, M.S. Ray, M.G.B. Drew, C. Lu, A. Ghosh, J. Coord.Chem. 60 (2007) 2165.
[23] F.H. Allen, Acta Crystallogr., Sect. B 58 (2002) 380.

Polyhedron 27 (2008) 2386–2394

Contents lists available at ScienceDirect

Polyhedron

journal homepage: www.elsevier.com/locate/poly

Deamination process in the formation of a copper(II) complex with glutamic acid and a new ligand derived from guanidinoacetic acid: Synthesis, characterization, and molecular modeling studies

Jussara Lopes de Miranda [a,*], Jackeline da Silva Coelho [a,b], Luiza Cristina de Moura [a], Marcelo Hawrylak Herbst [c], Bruno Araújo Cautiero Horta [b], Ricardo Bicca de Alencastro [b], Magaly Girão Albuquerque [b]

[a] Departamento de Química Inorgânica, Instituto de Química, Universidade Federal do Rio de Janeiro, 21949-900, Rio de Janeiro, RJ, Brazil
[b] Departamento de Química Orgânica, Instituto de Química, Universidade Federal do Rio de Janeiro, 21949-900, Rio de Janeiro, RJ, Brazil
[c] Departamento de Física dos Sólidos, Instituto de Física, Universidade Federal do Rio de Janeiro, 21949-900, Rio de Janeiro, RJ, Brazil

ARTICLE INFO

Article history:
Received 9 November 2007
Accepted 11 April 2008
Available online 13 June 2008

Keywords:
Copper(II) complex
Guanidinoacetic acid
Glutamic acid
Deamination

ABSTRACT

A deamination process was observed after copper(II) complexation reaction with guanidinoacetic (Gaa) and glutamic acids (Glu), forming the binuclear copper(II) complex $K_2Cu_2C_{16}H_{23}N_7O_{12} \cdot 1/2H_2O$ (**1**), which was characterized by elemental analysis (CHN), spectroscopy methods (IR and EPR), powder X-ray diffraction, thermogravimetric analysis (TGA), and mass spectrometry. A new ligand, namely biguanide-1,5-diethanoate (Bge) ($C_6H_9N_5O_4$), was formed during complexation, probably due to the reaction between two Gaa species and the consequent release of a significant amount of ammonia, thus, characterizing the deamination process. In complex **1**, Bge behaved as a tetradentated ligand, using its oxygen and nitrogen atoms as coordinating sites to both Cu(II) ions. In addition, Glu has coordinated to Cu(II) through its α-N and O atoms. Theoretical calculations of the *cis–cis*, *cis–trans*, and *trans–trans* isomers of **1**, considering three prototropic forms of the Bge ligand, were carried out using semi-empirical quantum mechanics (PM3/*d*). DFT (B3LYP and B3P86) calculations of complex **1**, in which a hydrogen atom replaced the side chain of Glu, were also carried out using the 6-31G(d) basis set and the LanL2DZ effective core potential for the transition metal. Based on experimental and theoretical data, we concluded that the *trans–trans* isomer of the binuclear copper(II) complex **1** should be the most stable, although the occurrence of other isomers, even if in minor quantities, should not be disregarded.

© 2008 Elsevier Ltd. All rights reserved.

1. Introduction

Deamination and deimination reactions play important biological roles due to the anti-cancer and anti-viral potential use of the enzymes that catalyze them. One example is the transcription-coupled mutagenesis that is induced by the activation-induced deaminase (AID), which deaminates C and U in DNA [1,2]. Another example is arginine deiminase (ADI), which is mainly found in prokaryotes, and which catalyzes the deimination of the guanidino group of L-arginine producing ammonia [1,2]. ADI has also been found in a primitive eukaryote, *Giardia intestinalis*, which is one of the most commonly transmitted intestinal pathogens [1,2]. ADI has been considered a potential anti-cancer agent due to its cell proliferation inhibitory activity, and its *in vivo* anti-tumor activity has been reported [3,4]. Another example is peptidylarginine-deiminase (PAD), which has been described primarily in mammalians, and is responsible for the guanidino group deimination of the carboxy-terminal arginine residues of various peptides to produce ammonia [5,6]. It is interesting to note that mammalian PAD's are metalloenzymes [7].

Due to fact that there are several examples of deamination reactions involving the guanidino group of arginine, we began to investigate these processes with the guanidino group of guanidinoacetic acid (Gaa) (Fig. 1). Although Gaa is a non-essential amino acid, it is the immediate precursor of creatine, formed, mainly in the kidneys, by the reaction between arginine and glycine [8]. The biological functions in which Gaa takes part in or is involved in are of great diversity. Besides being considered as an endogenous convulsant [9,10], it has already been used as a more sensitive marker for renal dysfunction [11]. Gaa is also involved in insulin regulation [11], cholesterol production [12] and hepatic encephalopathy [13]. The increase of Gaa concentration in the brain is responsible for epileptic seizures [14]. Recently, Gaa quantification in plasma and urine has turned out to be very important, since it can be used as a diagnosis tool for the guanidinomethlytransferase deficiency

* Corresponding author. Tel.: +55 21 2562 7552.
E-mail address: jussara@iq.ufrj.br (J.L. de Miranda).

0277-5387/$ - see front matter © 2008 Elsevier Ltd. All rights reserved.
doi:10.1016/j.poly.2008.04.024

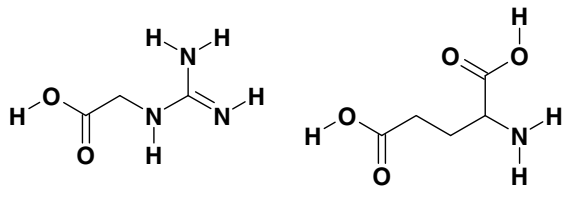

Fig. 1. Chemical structures of the neutral forms of guanidinoacetic acid (Gaa) and glutamic acid (Glu).

[15–19]. In addition, it has been observed that after cisplatin administration on the urinary tract of neoplasic patients, Gaa concentration decreased significantly [20].

Besides Gaa (Fig. 1), another amino acid, glutamic acid (Glu) (Fig. 1), is also present in the system that we are investigating. Glu was chosen because we were interested on the influence of the possible guanidino-carboxylate interactions in the deamination reactions. These guanidino-interactions are known to be highly specific due to the double hydrogen bonds formation pattern [21], and they are present in some important recognition sites, e.g. in Cu, Zn-superoxide dismutase [22], in carboxypeptidase [23], and between the human immunodeficiency virus and the host cell wall receptor [25].

Since several biological deamination reactions are metal dependent, we have chosen copper(II) ion not only due to its important role in a number of enzymatic reactions in the organism [26], specially those involving the guanidino group [22,23], but also to its well known template function in coordination reactions. Moreover, previous work has already been done in aqueous solution with Gaa, Glu and Cu(II), in the study of guanidino-carboxylate interactions in copper(II) ternary complexes with both of these amino acids [22]. The predominant complex species in specific pH ranges are already known, and so is the mechanism of competition between Gaa and Glu.

Several Gaa complexes have already been synthesized with different metal ions, such as Cr(III), Co(II), Ni(II), Cu(II) and Zn(II) [27]. In one of the copper complexes – $Cu_2(GAA)_4(NO_3)_2$ (tetrakis(μ-guanidinoacetic acid-κ2O:O′)bis[(nitrate-κO)copper(II)]), Gaa coordinates only through the two oxygen atoms of the carboxylate groups in a bridged way [28]. However, in another copper(II) complex, synthesized in different conditions, a new derivative of Gaa was formed, the Oag ligand, N^1-carboxylate-methylguanidinooxidoacetate, which formed the complex $[Cu_2(Oag)(Gaa)H_2O]NO_3 \cdot 2H_2O$ [29]. A mechanism of formation of Oag, based on EPR and potentiometric analyses, has been proposed [30].

In this work, we focused our attention in the synthesis and structural elucidation of **1** ($K_2Cu_2C_{16}H_{23}N_7O_{12} \cdot 1/2H_2O$), a binuclear copper(II) complex formed from Gaa, Glu, and Cu(II). The complexation reaction was accomplished with a deamination process, producing a new ligand, biguanide-1,5-diethanoate (Bge) ($C_6H_9N_5O_4$). The synthesized Cu(II) complex **1** , $K_2Cu_2(Bge)(Glu)_2 \cdot 1/2H_2O$, was characterized by elemental analysis (CHN), spectroscopy methods (IR and EPR), powder X-ray diffraction, thermogravimetric analysis (TGA), and mass spectrometry. In addition, the possible geometric isomers and prototropic forms of **1** have been investigated by theoretical methods. The new ligand Bge has been also isolated and analyzed by ^{1}H NMR and ^{13}C NMR.

2. Experimental

2.1. Materials and methods

All reagents were of pure grade and were used without further purification.

2.2. Synthesis of $K_2Cu_2(Bge)(Glu)_2 \cdot 1/2H_2O$ (**1**)

An aqueous solution of glutamic acid (1 mmol/L, 0.14714 g, Aldrich) was added to an aqueous solution of Gaa (1 mmol/L, 0.11712 g, Aldrich). $Cu(NO_3)_2 \cdot 3H_2O$ (0.2446 g, Merck) was slowly added to the resultant mixture, under permanent stirring at 60 °C, and the solution was refluxed at 60 °C for 2 h. After that, an aqueous solution of KOH (0.3 mol/L, Merck) was slowly added until the solution reached pH 6–7, the range value observed in previous potentiometric studies [22], in which the ternary complex among Cu(II), Gaa and Glu was predominant. After that, the mixture was refluxed at 60 °C for 24 h, and by reduction of the solvent volume, a blue precipitate was formed. The blue precipitate was thoroughly washed with water and acetone. The yield was 40% and its melting point was 219–220 °C. Elemental analysis (CHN) was conducted according to standard micro analytical procedures (CHN Perkin–Elmer Analyzer). *Anal.* Calc. for $K_2Cu_2C_{16}H_{23}N_7O_{12}.1/2H_2O$: C, 26.15%; H, 3.36%; N, 13.35%. Found: C, 25.92%; H, 3.17%; N, 13.64% (M.M. = 719 Da).

2.3. Spectroscopy methods

Infrared (IR) spectroscopy analyses were performed in a Nicolet 760-FT-IR spectrometer, using KBr pellets in the 4000–500 cm^{-1} range and polyethylene nujol films in the 600–100 cm^{-1} range, with gain 2, strong apodization, aperture 30, resolution 4.0 and number of scan superior to 100.

Electron paramagnetic resonance (EPR) spectra were recorded at room temperature and at 77 K on a Bruker ESP 380 FT-CW spectrometer, operating in X-band (9.5 GHz) and 100 kHz field modulation, using quartz tubes and a cylindrical resonant cavity. The modulation amplitude was 5.0 Gauss and microwave power was 2.21×10^2 mW. Measurements of *g*-factors were done against DPPH standard (g = 2.0037).

2.4. Powder X-ray diffraction

Powder X-ray diffraction data were obtained with an X-ray diffractometer using Cu Kα radiation. Samples were spread out on glass and scanned at 20 min^{-1}. The beam voltage and beam current were 35 kV and 14 mA, respectively.

2.5. Thermogravimetric analysis

Thermogravimetric analysis (TGA) was done in a Perkin–Elmer TGA 7 thermogravimetric balance in nitrogen atmosphere, in a 25–900 °C temperature range and a step range of 5–10 °C.

2.6. Mass spectrometric analysis

The mass spectrometric analysis was done in a $_{252}$Cf PDMS (Plasma Desorption Mass Spectrum) mass spectrometer. A suspension of complex **1** in ethanol has been prepared for this analysis.

2.7. Isolation and NMR analysis of the new ligand Bge from the complex $K_2Cu_2(Bge)(Glu)_2 \cdot 1/2H_2O$ (**1**)

The ligand Bge has been isolated from complex **1** in order to be analyzed separately. First, a 1:1 nitric acid:water solution was added to 0.478 g of complex **1** until total solubilization. Three mL of water were added to the resultant solution which pH was 1. This latter solution has been eluted in a 20 cm × 1.2 cm height × diameter column packed with a cationic Rhome and Haas resin. The time of the elution was 30 min.

The resultant light brown solution has been analyzed by ^{1}H NMR and ^{13}CNMR. The ^{1}H and ^{13}C NMR experiments were carried

out on a Bruker DRX-400 (9.4T) spectrometer operating at Larmor frequencies of 400.13 and 100.61 MHz, respectively, using a 5.0 mm probe head in D_2O/H_2O solution. The ^1H NMR spectrum was recorded with water suppression using 3-9-19 pulse sequence with gradients [31–33]. The ^{13}C NMR spectra were recorded using a single pulse acquisition with small pulse angle ($\pi/2$) and a recycle delay of 0.3 s. The ^{13}C and ^1H NMR spectra were referenced relatively to TSS.

2.8. Theoretical methods

Graphical manipulations and semi-empirical quantum mechanics calculations were carried out using the Spartan'04 Windows (version 1.0.1) molecular modeling package (Wave function, Inc., Irvine, CA) [34]. Geometry optimizations and heats of formation were calculated using the Parametric Method 3 (PM3) Hamiltonian that is parameterized for copper atom among others transition-metal elements. All calculations were performed in vacuum without any kind of geometric restrictions.

We have performed energy minimizations on the three possible geometric isomers of complex **1**, namely, *cis–cis* (*cc*), *cis–trans* (*ct*), and *trans–trans* (*tt*) (Fig. 2A). In addition, it was also considered the tautomerism involving the biguanide group of the Bge ligand of **1**, since we cannot establish a definitive position of the hydrogen atom. Therefore, we have investigated the stability of the three possible prototropic forms of **1**, namely tautomers A, B, and C (see Fig. 2B), for each isomer. Fig. 2B shows the three prototropic forms (A, B, and C) of the *cis–cis* isomer. Moreover, each prototropic form B could also have two spatial isomers, since one nitrogen atom is a tetrahedral stereocenter, which means that the absolute configuration of this atom could be *R* or *S*.

Regarding the overall charge of complex **1**, we have calculated three species, namely the dianionic form ($Cu_2C_{16}H_{23}N_7O_{12}$, total charge = −2), and two neutral forms, in which in the former the negative charge of each carboxylate group was neutralized with a proton ($Cu_2C_{16}H_{25}N_7O_{12}$, total charge = 0) and in the latter, with a sodium cation ($Na_2Cu_2C_{16}H_{23}N_7O_{12}$, total charge = 0), since potassium is not parameterized in the PM3 method.

In addition, we have performed DFT calculations for complex **1**, replacing the side chain of Glu by a hydrogen atom in order to reduce computer time. We have carried out the DFT calculations using B3LYP and B3P86 functionals [35]. The 6-31G(d) basis set was applied for all atoms except for the copper atom, for which was chosen the LanL2DZ effective core potential [36]. All geometries were fully optimized using the GAUSSIAN 98 program [37].

3. Results and discussion

3.1. IR spectroscopic analysis

The relevant infrared data are presented in Table 1. The two bands at 3545 and 3438 cm^{-1} are due to the stretching modes of O–H of lattice water. The H_2O bending mode was observed at 1630 cm^{-1}. The rocking and wagging bands of water occurred in 708 and 572 cm^{-1}. The shift observed for water bands are due to extensive hydrogen bonding [38].

In addition, several other bands, related to stretching N–H modes of amines were observed in the same range. The spectrum shows a greater number of νN–H bands in **1** as compared to the original amino acids, Glu and Gaa. The bands at 3390 and 3309 cm^{-1}, as well as at 3335 and 3289 cm^{-1} can be attributed to the two pairs of asymmetric and symmetric stretching of N–H of primary amines [39,40]. Since the first pair of bands is shifted in relation to the correspondent Gaa ones (at 3384 and 3303 cm^{-1}) [27], they should be attributed to the biguanide-1,5-diethanoate (Bge) ligand. Another band at 3134 cm^{-1} can be also related to the primary νN–H, although, in this case, it is closer to the correspondent Glu band, which occurs at 3132 cm^{-1} [41]. The significant increase in the number of primary N–H stretching modes is in agreement with the proposed structure, considering that all of these bands except the last one (which is related to the Glu fragment) could be related to the primary amines in the intermediary chain formed by the new ligand, Bge. The bands at 3237 and 3250 cm^{-1} were neither present in the Gaa nor in the Glu spectra, and could be attributed to the νN–H of the secondary amine, present in the Bge spectrum.

The band at 1668 cm^{-1} is characteristic of the νC=N from the guanidino group [27], and indicates that this group is still present and is not directly involved in the coordination to Cu(II). This is in agreement with the Bge structure that includes a guanidino group in its central moiety. The non-participation of the terminal

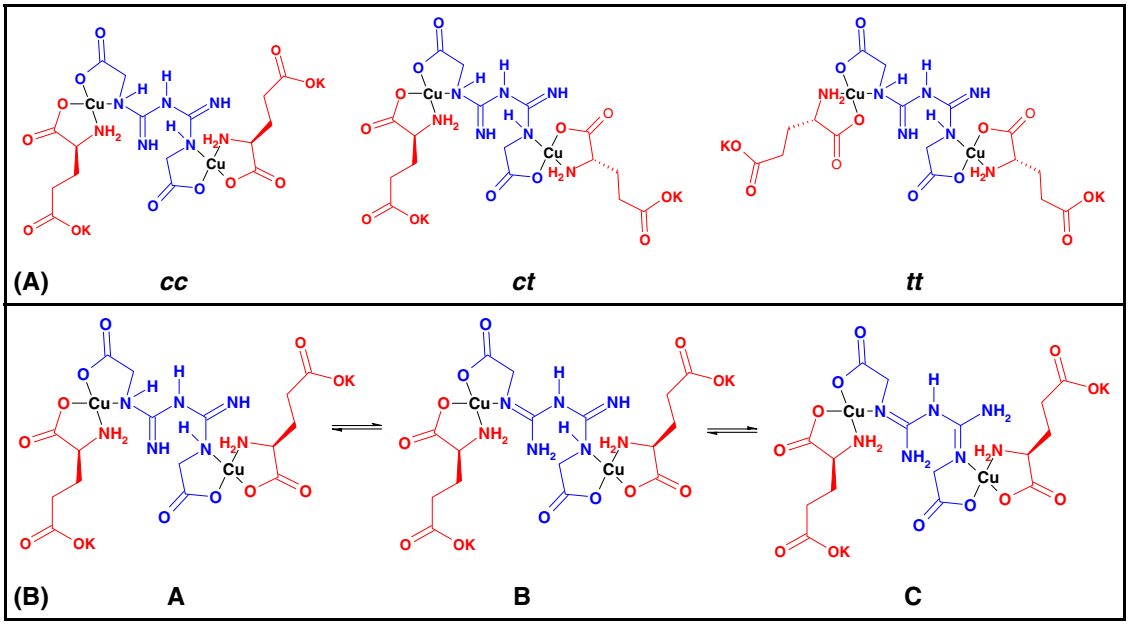

Fig. 2. Schematic representation of the three geometric isomers of complex **1** and their three possible prototropic forms. (A) Geometric isomers *cis–cis* (*cc*), *cis–trans* (*ct*), and *trans–trans* (*tt*) of **1**. (B) Prototropic forms (tautomers) A, B, and C of the *cis–cis* isomer of complex **1**.

Table 1
Principal infrared data of Gaa, Glu, and $K_2[Cu_2(Bge)(Glu)_2]$

Gaa[a]	Glu[b]	$K_2[Cu_2(Bge)(Glu)_2]$	Attempted assignments
Wave number (cm^{-1})			
		3558/3438	νO–H (H_2O)
3386	3132	3434, 3390	νNH
3303	3073	3309	νNH
		3335, 3289	νNH
3173		3134	νNH
		3237, 3250	νsecNH
1672/1668		1668	νC=N (guanidino)
1625/1583	1647/1631	1624, 1583	νa CO_2^- + δ NH_3^+
		1560	νa CO_2^- (non-coordinated)
	1512	1511	δ NH_3^+
1411	1419	1405, 1385	νs CO_2^-
		1394	νs CO_2^- ((non-coordinated)
		444	νa M–N
		412	νs M–N
		352	νa M–O
		336	νs M–O

[a] Ref. [27].
[b] Ref. [39].

nitrogen atoms of the guanidino group in the coordination was also observed in other copper(II) complexes of Gaa previously synthesized by our group [27,28].

The IR spectrum shows that the carboxylate asymmetric (1609, 1583 cm^{-1}) and symmetric stretching (1405, 1385 cm^{-1}) modes, both related to coordinated carboxylate groups, are shifted due to the metal coordination. On the other hand, the bands at 1560 and 1394 cm^{-1} should be related to the terminal ionic carboxylate groups since the difference between them ($\Delta\nu$ = 166 cm^{-1}) is similar to the one observed for the ionic acetate group [38]. The amino group deformation bands that are observed at 1624 cm^{-1} probably couple with the carboxylate stretching modes.

Therefore, the fact that significant shifts are observed in the normal amino and carboxylate group frequencies prompted us to assume that the nitrogen and oxygen atoms from these groups should be involved in coordination. Consequently, there are two possible geometric isomers for each copper coordination center, i.e., *cis* and *trans*, whereas for the whole complex involving two copper sites, there are three possibilities, the *cis–cis*, the *cis–trans*, and the *trans–trans* isomers. Since in the 500–100 cm^{-1} range the bands relative to two νCu–N and two νCu–O vibrations were observed at 444, 412, 352 and 336 cm^{-1} respectively, a C_2 symmetry could be proposed for the complex **1**. Considering the whole complex, the only isomer that presents geometry closer to a C_2 symmetry is the *trans–trans*, even though we cannot disregard the presence of the other isomers. In addition, some skeletal modes of Glu were observed in 419 and 400 cm^{-1}, but the characteristic skeletal modes of Gaa (436 and 319 cm^{-1}) were absent. This can be easily understood since the Glu chain was not changed in the complex **1**, while Gaa suffered severe modifications.

3.2. EPR spectroscopic analysis

The electron paramagnetic resonance spectrum of complex **1** indicated the presence of a square-planar copper(II) environment. Comparisons were done between EPR data from the complex **1** and the paddlewheel complex $Cu_2(Gaa)_4(NO_3)_2$ [28]. The solid powdered compounds were analyzed by EPR, but their spectra consist of unresolved broad lines, characteristic of large line widths with respect to the value of the hyperfine coupling constant *A*. The estimated isotropic $\langle g \rangle$ values of the mentioned complexes were the same and equal to 2.13, which corroborates the square-planar geometry for each site, typical of Cu(II) coordination to amino acids such as aspartic acid [42,43].

3.3. Powder X-ray analysis

The powder X-ray diffractogram of **1** as well as of $Cu(Glu)_2$ [44] are shown in Fig. 3. They are similar, with the exception of one special peak. This can be explained by the similarity of the coordination sites of both complexes (α-N and O atoms). However, the bridged ligand Bge can somehow affect the packing of the layers and account for this difference.

3.4. Thermogravimetric analysis

Complex **1** presents a-two-step weight loss process and it is stable up to 219 °C. From 30 to 120 °C, only the crystallization water was lost (1%). The first and most important step of mass loss (Fig. 4a) was between 219 and 260 °C that corresponds to the decarboxylation of the compound relative to the loss of five carboxylate groups (29%). The second step of weight loss (Fig. 4b), from 260 to 600 °C corresponds to the degradation of the decarboxylated fragment of **1**, forming a residue that may be relative to K_2O + 2 CuO.

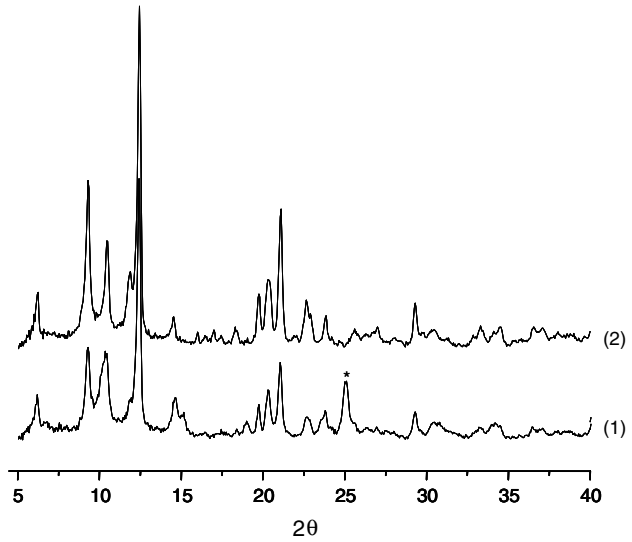

Fig. 3. Powder X-ray diffractograms of complexes $Cu_2Bge(Glu)_2$ (**1**) and $Cu(Glu)_2$ (**2**) (Kα Co and $5° \leqslant 2\theta \geqslant 40°$). The asterisk is related to Bge structural modification in the whole complex.

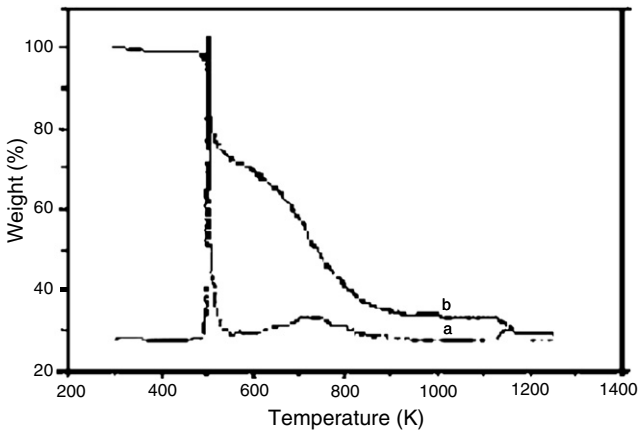

Fig. 4. Thermogravimetric analysis of complex $K_2[Cu_2(Bge)(Glu)_2]$.

3.5. Mass spectrometry analysis

The positive mass spectrum of **1** (Fig. 5) presents the fragmentation pattern analogous to other copper complexes with amino acids, such as Gly, Tyr, Glu and Arg [45]. The single and intense peak at 220 is related to H_3L (L = Bge), while the peak at 289 may be related to H_7LCu, with all the amino, imino and carboxylate groups protonated with the exception of one carboxylate group involved in the copper coordination. The peaks with higher mass are related to species involving both L (Bge) and Glu. The peak at 499 is attributed to Cu_2H_5LGlu, the one at 497 to $Cu_2H_3LH_2Glu$ and the one at 554 to $Cu_2H_3LH_2Glu_2$ with loss of the two most external carboxylate groups.

3.6. Analysis of the eluted solution from the isolated ligand Bge

The ^1H NMR spectrum of the eluted solution of complex **1**, $K_2Cu_2(Bge)(Glu)_2 \cdot 1/2H_2O$, is shown in Fig. 6. Although Cu(II) ion has been removed from the elution, in addition to Bge ligand, glutamic acid is also present in this solution. We did not attempt to remove it by derivatization due to possible interference in Bge characterization.

Table 2 shows the assignments of the chemical shifts in ppm related to Bge and Glu from the eluted solution, and also to Gaa from the literature [46]. Since the experiments were recorded in H_2O/D_2O, the exchange of the NH protons occurred as it is already expected. Ethanol hydrogen peaks are also present as a triplet at 1.16 ppm and a quartet at 3.64 ppm. Five peaks should be related to Glu: a triplet at 4.18 ppm for Hα, a multiplet at 2.26 ppm for Hβ, a triplet at 2.67 for Hγ and a broad peak at 8.22 ppm for the amino-H. Those assignments are in good agreement with the literature data considering the difference in pH value [47].

Bge presents three peaks (Table 2). The doublet at 4.13 ppm should be related to Ha from Bge (at pH 1) since the analogous hydrogen atom in Gaa, which is Ha, is at 3.73 ppm (at pH 3). The peak at 7.37 ppm (1H) should be relative to Hb, which corresponds to Hb signal (6.65 ppm) in Gaa structure. The peak at 8.22 ppm is very broad and should be attributed to both Hc and Hd from Bge and the amino group from Glu, which is in agreement with the calculated integration value of eight protons. The correspondent Hc in Gaa is at 7.12 ppm. Comparing the structures of Bge and Gaa, it can be easily observed that the hydrogen atoms are more deshielded in Bge, due to the presence of two carboxylic groups in addition to the resonance π bonds.

^{13}C NMR spectrum is shown in Fig. 7. In Table 3 the ^{13}C chemical shifts from Bge and Glu are shown. Analogous to ^1H NMR, in addition to the chemical shifts relative to carbon atoms from Bge, there are also other ones due to carbon atoms from Glu. Ethanol peaks are also present as a triplet at 57.79 ppm and a quartet at 18.13 ppm. As Glu is present in the eluted solution at pH 1, we can attribute the peaks comparing with its data at pH 3.34 in the literature, which was the closest pH value available [47]. Therefore, the peaks at 175.98 and 171.07 ppm should be related to C1 and C5, respectively (177.83 and 174.45 ppm [47]) , at 52.15 ppm to C2, 29.27 to C3 and 24.58 ppm to C4 (54.78, 30.94 and 26.39 ppm lit.).

Bge should present three peaks in the ^{13}C NMR spectrum (Fig. 7) due to its symmetric structure, which results in three equivalent carbon atoms. Actually, there are three peaks in its ^{13}C NMR spectrum (Table 3). The carboxylic carbon atoms C1 in Bge should be equivalent and assigned as 171.88 ppm, which is characteristic to carboxylic chemical shift. The peaks at 157.06 and at 42.56 ppm should be relative to C3 and C2, according to their positions.

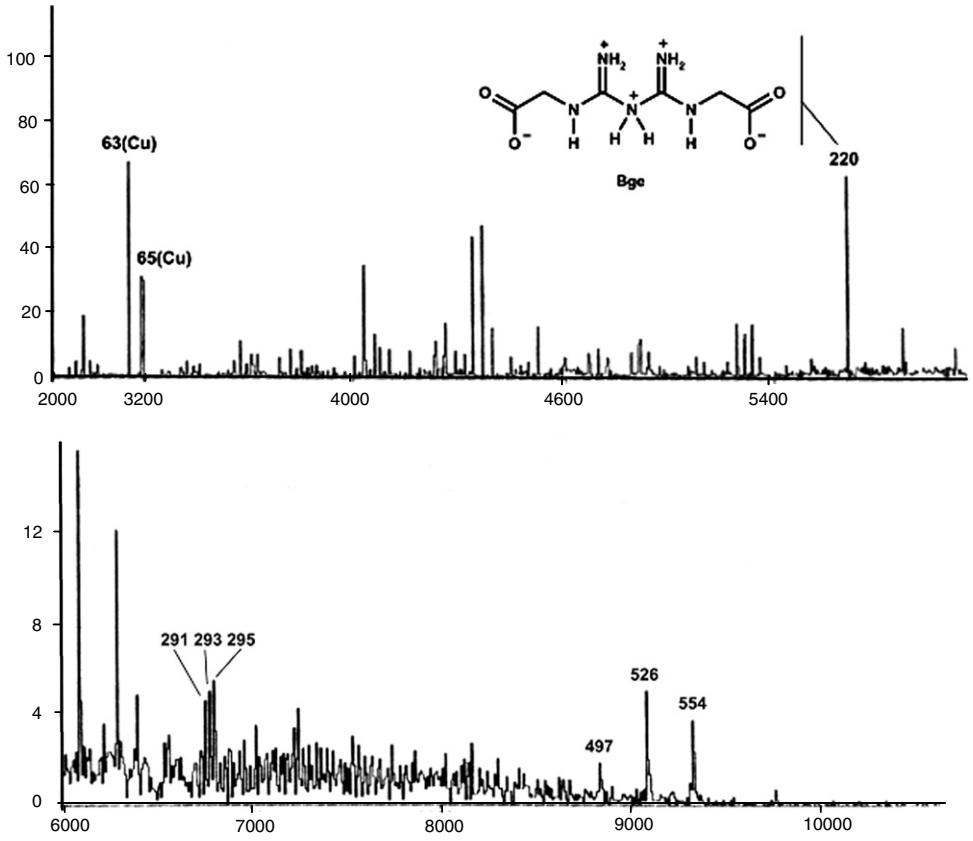

Fig. 5. Positive mass spectrum of the complex $K_2[Cu_2(Bge)(Glu)_2]$.

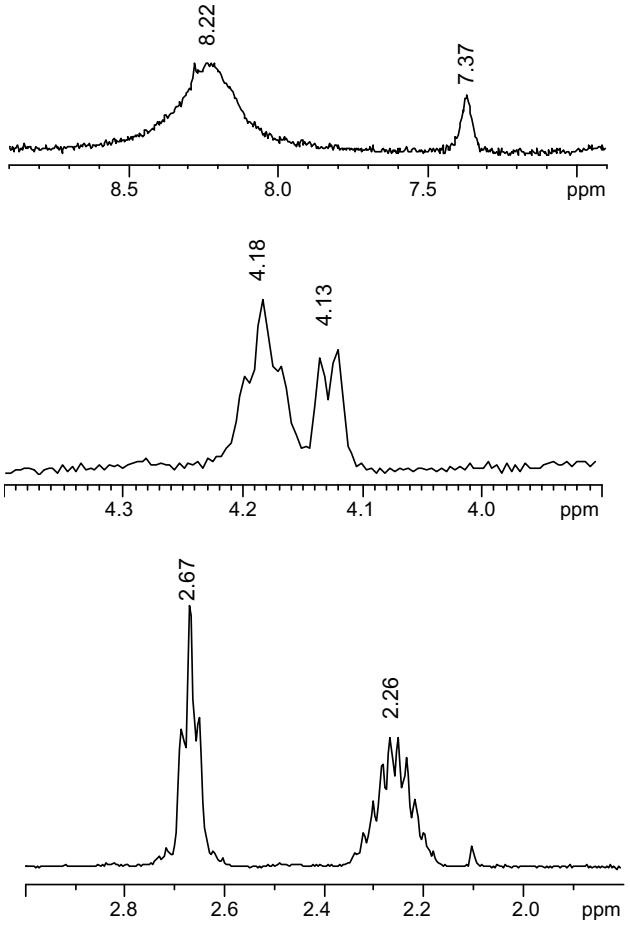

Fig. 6. ^{1}H NMR of the eluted solution of complex **1**.

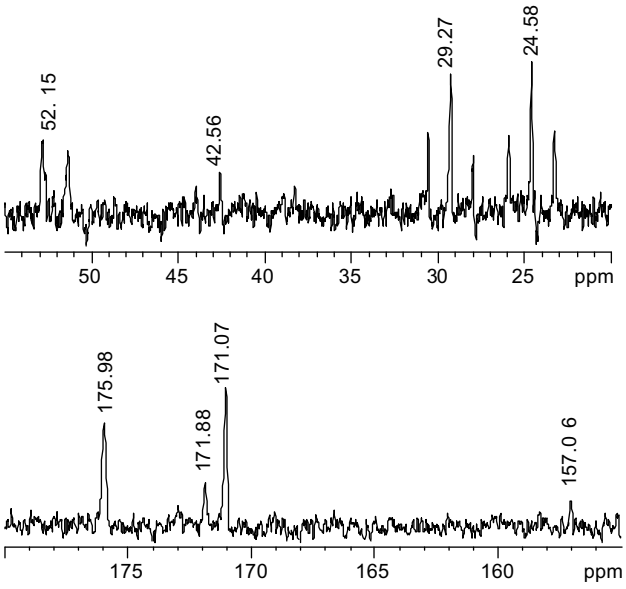

Fig. 7. ^{13}C NMR of the eluted solution from complex **1**.

Table 2
^{1}H NMR chemical shifts (δ) and assignments of the eluted solution of complex **1** and Gaa

Structures	δ (ppm)	Assignment
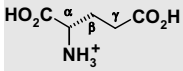	2.26 (m) 2.67 (t) 4.18 (t) 8.22 (br)	Hβ (Glu) Hγ (Glu) Hα (Glu) H–NH_3 + (Glu)
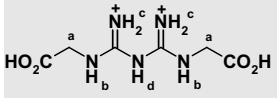	4.13 (d) 7.37 (s) 8.22 (br)	Ha (Bge) Hb (Bge) Hc/Hd (Bge)
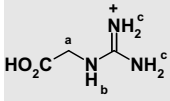	3.73 (d)[a] 6.65 (s)[a] 7.12 (br)[a]	Ha (Gaa) Hb (Gaa) Hc (Gaa)

s, singlet; d, doublet; t, triplet; m, multiplet; br, broad.
[a] Ref. [46].

Table 3
^{13}C NMR chemical shifts (δ) and assignments of the eluted solution of complex **1**

Structures	δ (ppm)	Assignment
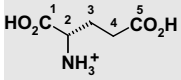	175.98 171.07 24.58 (t) 29.27 (t) 52.15 (d)	C1 (Glu) C5 (Glu) C4 (Glu) C3 (Glu) C2 (Glu)
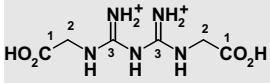	171.88 157.06 42.56	C1 (Bge) C3 (Bge) C2 (Bge)

3.7. Proposal of a mechanistic scheme for the new ligand formation (Bge)

Since a new ligand, i.e. biguanide-1,5-diethanoate (Bge), has been formed during the complexation reaction, probably due to the reaction between the guanidino groups of two Gaa moieties, we now propose a mechanism for its formation. This proposal is in line with the already proposed mechanism for transamidination on the copper(II) Gaa complex [30], and takes into account the quantification of ammonia in the final solution obtained during synthesis of **1** that characterizes the deamination process. We have found a significant amount of ammonia, which, however, could not be related to the total ammonia content due to possible losses during the synthetic process.

Fig. 8 shows the proposed mechanistic scheme for the new ligand formation (Bge) in the $K_2[Cu_2(Bge)(Glu)_2]$ complex, where R (Fig. 8) replaces the lateral chain of Glu (i.e. R = $CH_2CH_2CO_2^-$) for the sake of simplicity. Moreover, the copper ion was already considered complexed with Gaa and Glu, i.e. forming the Glu–Cu(II)–Gaa complex, and probably it may play a template effect in the catalytic process, because the direct reaction between the two amino acids (i.e. Gaa and Glu) without the metal participation does not take place. In the proposed mechanism, the first step describes a nucleophilic attack of a guanidino group of the first Glu–Cu(II)–Gaa specie on another guanidino group of the second Glu–Cu(II)–Gaa specie. The second step is an internal proton transfer (p.t.) probably mediated by a solvent water molecule involving two steps, and the third step corresponds to the ammonia elimination to form the new ligand (Bge), which makes a bridge between the two Glu moieties. The final complex, i.e. Glu–Cu(II)–Bge–Cu(II)–Glu, is shown as a zwitterion (Fig. 8). This kind of condensation, a transamination reaction in which ammonia is evolved, is known and it was observed in polycondensation reactions performed with hexamethylenediamine and dicyandiamide to give polyhexamethylene biguanidine [45].

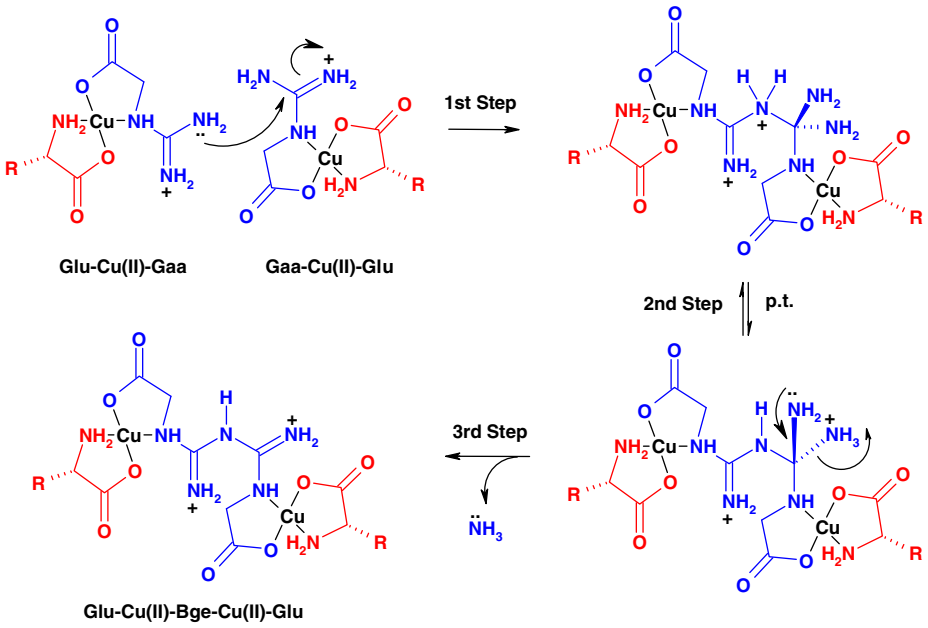

Fig. 8. Proposed mechanistic scheme of the new ligand (Bge) formation in the $K_2[Cu_2(Bge)(Glu)_2]$ complex from the reaction between two Glu–Cu(II)–Gaa species ($R = CH_2CH_2CO_2^-$).

3.8. Theoretical results

The prototropic form A (Fig. 2B) of complex **1** was not stable, regardless if we considered the dianion or the neutral forms and the *cis–cis*, *cis–trans* or *trans–trans* isomers. All tentative calculations of prototropic form A did not converge or resulted in a different final system in which one or more covalent bonds were broken, and hydrogen atom migrations were observed. Therefore, Table 4 shows only the PM3/*d* heats of formation (ΔH_f) values for the prototropic forms B and C of the dianionic and the neutral (X = H or Na) states of complex **1** considering *cis* and *trans* isomers.

Our calculations showed that the model complexes using the prototropic form B of the dianionic states of complex **1** in which at least one Cu(II) coordination center is *trans* are more stable than the *cis–cis* isomer by at least 100 kcal/mol (Table 4). However, when one considers the prototropic form C, this difference falls to about 10 kcal/mol. Overall, the *cis–trans* and *trans–trans* isomers of the prototropic form C of complex **1** are the most stable among the dianionic states. Fig. 9 shows the *trans–trans* isomer, the most stable anionic isomer of **1**. The same tendency described above for the stability of the *cis–cis* and *trans–trans* isomers was also observed in the prototropic forms B and C of the neutral states (X = H) of complex **1**.

Table 4
Codes used to identify the calculated isomers, prototropic forms, ionization states o complex **1**, and the heat of formation (ΔH_f) values of the dianionic and neutral (H and Na) prototropic forms (B and C) of complex **1** calculated by PM3/*d* (Spartan)

PF[a]	X[b]	TC[c]	*cis–cis*[d]	ΔH_f[e]	*cis–trans*[d]	ΔH_f[e]	*trans–trans*[d]	ΔH_f[e]
A[f]		−2	*cc*-1A (−2)		*ct*-1A (−2)		*tt*-1A (−2)	
B		−2	cc^R-1B (−2)	−603.96	c^Rt-1B (−2)	−732.54	t^Rt-1B (−2)	−732.81
B		−2	cc^S-1B (−2)	−565.91	c^St-1B (−2)	−700.64	t^St-1B (−2)	−732.86
B		−2			ct^R-1B (−2)	−732.26		
B		−2			ct^S-1B (−2)	−764.60		
C		−2	*cc*-1C (−2)	−766.62	*ct*-1C (−2)	**−776.06**	*tt*-1C (−2)	**−776.68**
A[f]	H	0	*cc*-1A (H)		*ct*-1A (H)		*tt*-1A (H)	
B	H	0	cc^R-1B (H)	−604.81	c^Rt-1B (H)	−670.97	t^Rt-1B (H)	−671.63
B	H	0	cc^S-1B (H)	−600.00	c^St-1B (H)	−615.26	t^St-1B (H)	−676.18
B	H	0			ct^R-1B (H)	−703.76		
B	H	0			ct^S-1B (H)	−704.92		
C	H	0	*cc*-1C (H)	−703.37	*ct*-1C (H)	**−706.15**	*tt*-1C (H)	**−707.70**
A[f]	Na	0	*cc*-1A (Na)		*ct*-1A (Na)		*tt*-1A (Na)	
B	Na	0	cc^R-1B (Na)	−735.80	c^Rt-1B (Na)	−723.07	t^Rt-1B (Na)	−746.24
B	Na	0	cc^S-1B (Na)	−700.00	c^St-1B (Na)	−740.80	t^St-1B (Na)	−760.21
B	Na	0			ct^R-1B (Na)	−798.78		
B	Na	0			ct^S-1B (Na)	−788.10		
C	Na	0	*cc*-1C (Na)	−762.05	*ct*-1C (Na)	**−838.96**	*tt*-1C (Na)	**−854.40**

[a] PF means the prototropic form A, B and C of complex **1** (see Fig. 2).
[b] X means the element in the general formulae $X_2[Cu_2(BGE)(Glu)_2]$ of the modeled complex.
[c] TC means the total charge of the modeled complex.
[d] Possible geometric isomers of the modeled complex, where *c* and *t* means *cis* and *trans* geometric isomer, respectively, and ^{R} and ^{S} means *R* and *S* absolute configuration, respectively, of the tetrahedral nitrogen atom (stereocenter).
[e] ΔH_f means heat of formation in kcal/mol.
[f] None final stable structure was obtained starting from A prototropic form.

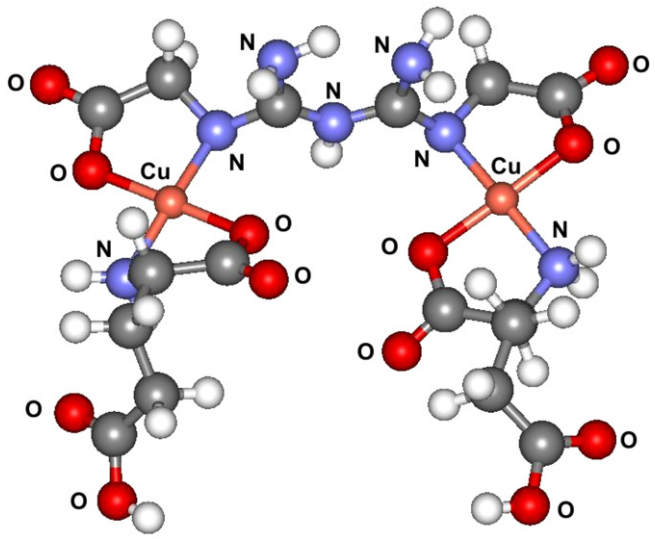

Fig. 9. The ball and stick representation of the prototropic form C of the neutral *trans–trans*, *tt*-1C (H) (Table 1), isomer of complex **1** calculated by PM3/*d* method.

Considering the prototropic form B of the neutral states (X = Na) of complex **1**, the optimized complexes *cis–trans*^{R} and *cis–trans*^{S} are more stable than the other isomers by about 30 kcal/mol (Table 4). However, for the prototropic form C, the complexes in which at least one Cu(II) coordination center is *trans* are more stable than the *cis–cis* isomer by at least 80 kcal/mol. Overall, the prototropic forms C *trans–trans* and*cis–trans* are more stable than the prototropic forms B by at least 40 kcal/mol (Table 4).

The results obtained by the PM3/*d* method (Table 2) for the dianionic and neutral prototropic forms (B and C) of complex **1** pointed to the *trans–trans* isomer as the most stable structure. This is consistent with our infrared data, since its geometry has a C_2 symmetry.

These results are in agreement with DFT theoretical calculations of the *cis–trans*-isomerization reaction of a bis(glycinato)copper(II) complex in which a reaction barrier (*cis–trans*) of about 7.9 kcal/mol was found for a ring-twisting mechanism [48]. They are also in accordance with experimental results in which the isomerization was only observed in the *cis–trans* direction [49].

Table 5 shows some selected geometric parameters of the metal coordination center of the *trans*-Cu(II)$(Gln)_2$ structure as determined by X-ray diffraction [50]. The calculated (PM3/*d*) gas phase geometric parameters of the most stable structure of **1** in the neutral form (X = H), the *trans–trans* prototropic form C. They are also in good agreement with the corresponding experimental values. The O–Cu–O and N–Cu–N angles are very close to 180°, according with the EPR data.

Although semi empirical calculations provided valuable information for the present systems at low computational cost, we decided to perform geometry optimizations using more accurate methods. We performed DFT calculations on simpler models of the geometrical isomers of complex **1**, making a substitution on the final carbon chain of Glu by hydrogen atoms. The *trans–trans* was the most stable structure, favored by more than 20 kcal/mol in comparison to the *cis–trans* and by around 50 kcal/mol in comparison to the *cis–cis* on both levels of theory used (B3LYP/6-31G* and B3P86/6-31G*). The *trans–trans* structure showed similar C_2

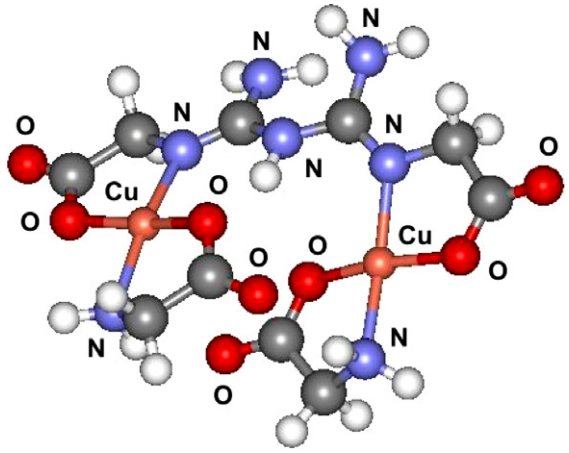

Fig. 10. The ball and stick representation of the prototropic form C of the *trans–trans* isomer of complex **1**, replacing the α-carbon substituent of Glu by a hydrogen atom, calculated by DFT method.

Table 5
Selected bond lengths (Å) and bond angles (°) for *trans*-Cu(II)$(Gln)_2$ and complex **1** (*trans–trans*-1C, X = H)

trans-Cu(II)$(Gln)_2$ (Experimental solid state)[a]				*tt*-1C (H) structure of complex **1** calculated by PM3/*d* (gas phase)[b]							
Bond lengths											
CuN^1	1.994	CuN^2	1.955	Cu^1N^1	1.868	Cu^1N^2	1.876	Cu^2N^3	1.866	Cu^2N^4	1.874
CuO^1	1.931	CuO^2	1.964	Cu^1O^1	1.835	Cu^1O^2	1.839	Cu^2O^3	1.832	Cu^2O^4	1.849
Bond angles											
N^1CuO^1	84.2	N^2CuO^2	84.0	$N^1Cu^1O^1$	92.74	$N^2Cu^1O^2$	93.77	$N^3Cu^2O^3$	91.63	$N^4Cu^2O^4$	91.09
N^1CuO^2	94.8	N^2CuO^1	96.8	$N^1Cu^1O^2$	85.59	$N^2Cu^1O^2$	87.93	$N^3Cu^2O^4$	89.59	$N^4Cu^2O^3$	87.89
N^1CuN^2	174.5			$N^1Cu^1N^2$	177.59			$N^3Cu^2N^4$	173.68		
O^1CuO^2	178.5			$O^1Cu^1O^2$	178.19			$O^3Cu^2O^4$	177.83		

[a] Ref. [50].
[b] This work.

symmetry (Fig. 10), which is in agreement with the experimental results.

4. Conclusions

We have synthesized a complex involving the guanidinoacetic acid, glutamic acid and copper(II) ion via a deamination reaction between these two amino acids and a consequent formation of an adduct between them that is the new ligand, biguanide-1,5-diethanoate (Bge). The infrared spectroscopy, X-ray diffraction, electronic paramagnetic resonance, thermogravimetric analysis and mass spectrum data have characterized the formation of the complex $K_2[Cu_2(Bge)(Glu)_2]$ (**1**), where two copper sites are coordinated by a bridged Bge in addition of the α-*N*,*O*-glutamic acid coordination. The possibility of different isomers of **1** led us to perform semi-empirical and also *ab initio* calculations. Among the *cis–cis*, *cis–trans* and *trans–trans* isomers, the latter showed the greater stabilization from the modeling studies. This is in agreement with the spectroscopic data, especially from infrared data, since the symmetry of the *trans–trans* isomer is close to a C_2 point group, which presents four infrared active bands, two νCu–O and two νCu–N, all of them observed in the complex spectrum.

Considering the *trans–trans* isomer of **1**, it is interesting to notice that guanidino–carboxylate interactions, which play important biological role, are possible to occur between the non-carboxylate group of Glu and the guanidino group of the neighbor complex, making specific recognizing sites.

The isolation and ^{1}H NMR and ^{13}C NMR analysis of Bge showed a good agreement with the expected results comparing with the Gaa NMR analysis.

Finally, the formation of Bge *in vitro*, catalyzed by copper, an important metal site of several enzymes, may represent an alternative route of synthesis of biomolecules. Since the deamination and deimination processes are involved in anti-viral and anti-cancer diseases, this kind of reaction between two amino acids that are present in our organism may contribute to the understanding of the biological role of these two species.

Acknowledgements

The authors thank the Brazilian agencies "Coordenação de Aperfeiçoamento de Pessoal de Nível Superior" (CAPES), "Conselho Nacional de Desenvolvimento Científico e Tecnológico" (CNPq), "Fundação Carlos Chagas Filho de Amparo à Pesquisa do Estado do Rio de Janeiro" (FAPERJ) and "Fundação José Bonifácio" (FUJB) from "Universidade Federal do Rio de Janeiro" (UFRJ) for their support. They also thank the van Der Graaf Laboratory, from Physics Department of "Pontíficia Universidade Católica do Rio de Janeiro" for the mass spectrometry analysis. SDBSWeb: http://riodb01.ibase.aist.go.jp/sdbs/ (National Institute of Advanced Industrial Science and Technology, accessed in august 2007).

References

[1] L.A. Knodler, E.O. Sekyere, T.S. Stewart, P.J. Schofield, M.R. Edwards, J. Biol. Chem. 273 (8) (1998) 4470.
[2] E.D. Larson, N. Maizels, Genome Biol. 5 (2004) 211.
[3] H. Gong, F. Zolzer, G. von Recklinghausen, J. Rossler, S. Breit, W. Havers, T. Fotsis, L. Schweigerer, Biochem. Biophys. Res. Commun. 261 (1) (1999) 10.
[4] W.T. McGraw, J. Potempa, D. Farley, J. Travis, Infect. Immun. 67 (7) (1999) 3248.
[5] L.J. Shen, K. Beloussow, W.-C. Shen, Cancer Lett. 231 (1) (2006) 30–35.
[6] H. Shirai, T.L. Blundell, K. Mizuguchi, Trends Biochem. Sci. 26 (2001) 465.
[7] E.R. Vossenaar, A.J.W. Zendman, W.J. van Venrooij, et al., Bioessays 25 (2003) 1106.
[8] J.F. Pilsum, R.P. Martin, E. Kito, J. Biol. Chem. 222 (1956) 225.
[9] T. Itoh, K. Yufu, R. Edamatsu, H. Yatsuka, A. Mori, in: P.P. De Deyn, P.B. Marescau, V. Stalon, I.A. Qureshi (Eds.), Guanidino Compounds in Biology and Medicine, John Libbey & Company Ltd., London, 1992, pp. 419–424.
[10] M. Ishizaki, H. Kitamura, Y. Taguma, K. Aoyagi, M. Narita, in: P.P. Deyn, B. Marescau, V. Stalon, I.A. Qureshi (Eds.), Guanidino Compounds in Biology and Medicine, John Libbey & Company Ltd., 1992, pp. 275–280.
[11] M. Kuroda, Nephron 65 (1993) 605.
[12] K. Sugyiama, A. Ohishi, H. Syiu, H. Takeuchi, J. Nutr. Sci. Vitaminol. 35 (1989) 623.
[13] P.P. De Deyn, B. Marescau, R. D'Hooge, I. Possemiers, J. Nagler, C.H. Mahler, Neurochem. Int. 27 (1995) 227.
[14] A. Mori, M. Kohno, T. Masumizu, Y. Noda, L. Packer, Biochem. Mol. Biol. Int. 40 (1996) 135.
[15] A. Schulze, T. Hess, R. Wevers, E. Mayatepek, P. Bachert, B. Marescau, M.V. Knopp, P.P. Deyn, H.J. Bremer, D. Rating, J. Pediatr. 131 (1997) 626.
[16] A. Shulze, Mol. Cell Biochem. 244 (1–2) (2003) 143.
[17] V. Leuzzi, M.C. Bianchi, M. Tosetti, C. Carducci, C.A. Cerquiglini, G. Cioni, I. Antonozzi, Neurology 55 (2000) 1407.
[18] S. Stöckler, U. Holzbach, F. Hanefeld, I. Marquardt, G. Helms, M. Requart, et al., Pediatr. Res. 36 (3) (1994) 409.
[19] A.I. Zugno, F.M. Stefanello, E.L. Streck, T. Calcagnotto, C.M.D. Wannmacher, M. Wajner, A.T.S. Wyse, Int. J. Devl. Neurosci. 21 (2003) 183.
[20] M. Yasuda, K. Sugahara, J. Zhang, T. Shuin, H. Kodama, Physiol. Chem. Phys. Med. NMR 32 (2000) 119.
[21] J.L. Miranda, J. Felcman, Polyhedron 22 (2003) 225. and references herein.
[22] J. Verhelst, J. Berwaerts, B. Marescau, R. Abs, H. Neels, C. Mahler, Metab. Clin. Exp. 46 (1997) 1063.
[23] J.A. Tainer, E.D. Getzoff, J.S. Richard, D.C. Richardson, Nature 306 (1983) 284.
[25] R. Wyatt, J. Sodoroski, Science 280 (1998) 284.
[26] J.J.R. Fraústo da Silva, R.J.P. Williams, The Biological Chemistry of the Elements – The Inorganic Chemistry of Life, Clarendon Press, Oxford, 1994. p. 338.
[27] J. Felcman, J.L. Miranda, Synth. React. Inorg. Met.-Org. Chem. 31 (2001) 873.
[28] J.L. Miranda, J. Felcman, J.L. Wardell, J.M.S. Skakle, Acta Crystallogr., Sect. C 58 (2002) M471.
[29] J. Felcman, R.A. Howie, J.L. Miranda, J.M.S. Skakle, J.L. Wardell, Acta Crystallogr., Sect. C 59 (2003) m103.
[30] J.L. Miranda, J. Felcman, O. Versiane, M.H. Herbst, Inorg. Chem. Commun. 7 (2004) 1198.
[31] M. Piotto, V. Saudek, V. Sklenar, J. Biomol. NMR 2 (1992) 661.
[32] V. Sklenar, M. Piotto, R. Leppik, V. Saudek, J. Magn. Reson. Ser. A 102 (1993) 241.
[33] T.R. Cundari, J. Deng, J. Chem. Inf. Comput. Sci. 39 (1999) 376.
[34] Axel D. Becke, J. Chem. Phys. 104 (1996) 1040.
[35] P.J. Hay, W.R. Wadt, J. Chem. Phys. 82 (1985) 270.
[36] M.J. Frisch, G.W. Trucks, H.B. Schlegel, G.E. Scuseria, M.A. Robb, J.R. Cheeseman, V.G. Zakrzewski, J.A. Montgomery, Jr., R.E. Stratmann, J.C. Burant, S. Dapprich, J.M. Millam, A.D. Daniels, K.N. Kudin, M.C. Strain, O. Farkas, J. Tomasi, V. Barone, M. Cossi, R. Cammi, B. Mennucci, C. Pomelli, C. Adamo, S. Clifford, J. Ochterski, G.A. Petersson, P.Y. Ayala, Q. Cui, K. Morokuma, D.K. Malick, A.D. Rabuck, K. Raghavachari, J.B. Foresman, J. Cioslowski, J.V. Ortiz, A.G. Baboul, B.B. Stefanov, G. Liu, A. Liashenko, P. Piskorz, I. Komaromi, R. Gomperts, R.L. Martin, D.J. Fox, T. Keith, M.A. Al-Laham, C.Y. Peng, A. Nanayakkara, C. Gonzalez, M. Challacombe, P.M.W. Gill, B. Johnson, W. Chen, M.W. Wong, J.L. Andres, C. Gonzalez, M. Head-Gordon, E.S. Replogle, J.A. Pople, GAUSSIAN 98, Revision A.7, Gaussian, Inc., Pittsburgh, PA, 1998.
[37] K. Nakamoto, Infrared and Raman Spectra of Inorganic and Coordination Compounds – Part B: Applications in Coordination, Organometallic, and Bioinorganic Chemistry, 5th ed., John Wilwy & Sons, Inc., New York, 1997.
[38] L.J. Bellamy, R.L. Williams, Spectrochim. Acta 9 (1957) 341.
[39] F.J. Ramírez, J.T. López Navarrete, Spectrochim. Acta 51 (1995) 293.
[40] T. Lu, X. Li, Z. Mão, W. Qiu, L. Ji, K. Yu, Polyhedron 17 (1998) 75.
[41] L. Antolini, G. Marcotrigiano, l. Menabue, G.C. Pellacani, M. Saladini, Inorg. Chem. 21 (1982) 2263.
[42] C. Gramaccioli, R.E. Marsh, Acta Crystallogr. 283 (1966) 594.
[43] M. Nizutani, N. Maejima, K. Jitsukawa, H. Masuda, H. Einaga, Inorg. Chim. Acta (1998) 105.
[44] H. Lavanant, Y. Hoppilliard, J. Mass Spectrom. 32 (1997) 1037.
[45] Y. Zhang, J. Jiang, Y. Chen, Polymer 40 (1999) 6189.
[46] S.C. Pereira, J.L. Miranda, Dissertation Thesis, Estudo da Formação de Complexos de Paládio(II) de Importância Biológica Envolvendo os Aminoácidos: Ácidos Guanidoacético, Glutâmico e Aspártico, Universidade Federal do Rio de Janeiro, 2003, p. 56.
[47] SDBSWeb: http://riodb01.ibase.aist.go.jp/sdbs/ (National Institute of Advanced Industrial Science and Technology, accessed in august 2007).
[48] C.S. Tautermann, J. Sabolovic', A.F. Voegele, K.R. Liedl, J. Phys. Chem. B 108 (2004) 2098.
[49] B.W. Delf, R.D. Gillard, P. O'Brien, J. Chem. Soc., Dalton Trans. 8 (1979) 1301.
[50] P. Deschamps, N. Zerrouk, I. Nicolis, T. Martens, E. Curis, M.F. Charlot, J.J. Girerd, T. Prange, S. Benazeth, J.C. Chaumeil, A. Tomas, Inorg. Chim. Acta 353 (2003) 22.

Polyhedron 27 (2008) 2395–2401

Contents lists available at ScienceDirect

Polyhedron

journal homepage: www.elsevier.com/locate/poly

A pyrazolyl-terminated 2,2′:6′,2″-terpyridine ligand: Iron(II), ruthenium(II) and palladium(II) complexes of 4′-(3,5-dimethylpyrazol-1-yl)-2,2′:6′,2″-terpyridine

Jonathon E. Beves, Edwin C. Constable *, Catherine E. Housecroft *, Markus Neuburger, Silvia Schaffner

Department of Chemistry, University of Basel, Spitalstrasse 51, CH-4056 Basel, Switzerland

ARTICLE INFO

Article history:
Received 7 February 2008
Accepted 11 April 2008
Available online 2 June 2008

This paper is dedicated to the memory of Dr. Alan G. Sharpe, a respected colleague, friend and chemical educator.

Keywords:
2,2′:6′,2″-Terpyridine
Heterocyclic
Coordination
Iron
Ruthenium
Palladium

ABSTRACT

The preparation of 4′-(3,5-dimethylpyrazol-1-yl)-2,2′:6′,2″-terpyridine (**2**) under acidic conditions results in the formation of the salts $[H_2\mathbf{2}][MeOSO_3]_2$ and $[H_2\mathbf{2}][EtOSO_3]_2$, treatment of which with base leads to neutral **2**. The structure of $[H_2\mathbf{2}][EtOSO_3]_2 \cdot H_2O$ has been established by single crystal X-ray diffraction. The complexes $[Fe(\mathbf{2})_2][PF_6]_2$ and $[Ru(\mathbf{2})_2][PF_6]_2$ have been prepared and characterized, and the single crystal structure determination of $[Ru(\mathbf{2})_2][PF_6]_2$ is reported; $[Fe(\mathbf{2})_2][PF_6]_2$ is isostructural with $[Ru(\mathbf{2})_2][PF_6]_2$. Treatment of $[Fe(\mathbf{2})_2]^{2+}$ with $PdCl_2$ produces $[Pd(\mathbf{2})Cl]^+$, isolated and structurally characterized as the hexafluoridophosphate salt, illustrating that metal exchange within the tpy-binding domain occurs in preference to palladium(II) coordination by the *N*-donor atom of the pendant 3,5-dimethylpyrazol-1-yl unit in **2**. $[Pd(\mathbf{2})Cl]^{2+}$ can also be prepared from $PdCl_2$ and $[H_2\mathbf{2}][MeOSO_3]_2$ in refluxing methanol.

© 2008 Elsevier Ltd. All rights reserved.

1. Introduction

The coordination chemistries of ligands based upon 2,6-di(pyrazol-1-yl)pyridine, 6-(pyrazol-1y-l)-2,2′-bipyridine and 6,6′-di(pyrazol-1-yl)-2,2′-bipyridine are now well established, the coordination domain of 2,6-di(pyrazol-1-yl)pyridine being analogous to that of 2,2′:6′,2″-terpyridine [1,2]. In contrast, ligands in which one or more pyrazol-1-yl substituents are directly linked to 2,2′:6′,2″-terpyridine remain unexplored, although a report of a 2,2′:6′,2″-terpyridine bearing a pendant tris(pyrazol-1-yl) functionality has appeared [3]. We considered it worthwhile to explore synthetic routes to 4′-(pyrazol-1-yl)-2,2′:6′,2″-terpyridine ligands and to investigate their coordination chemistry. We are currently interested in using homoleptic metal complexes with pendant coordination domains (e.g. $[M(\mathbf{1})_2]^{2+}$ where **1** = 4′-(4-pyridyl)-2,2′:6′,2″-terpyridine) as building blocks in the formation of coordination polymers [4–7]. The replacement of the pendant 4-pyridyl units in $[M(\mathbf{1})_2]^{2+}$ by pyrazol-1-yl or substituted pyrazol-1-yl units should generate a complex which may be viewed as an expanded bis(pyrazolyl)methane ligand, in much the same way as we consider $[M(\mathbf{1})_2]^{2+}$ to be an expanded 4,4′-bipyridine [4–10]. Altering the position of the *N*-donor atom in the pendant pyridine rings [11,12] does not preclude the corresponding homoleptic complex from functioning as an expanded bipyridine ligand [13]. However, we appreciated that the basicity of the pyrazolyl *N*-donors may prove to be too low to facilitate coordination to metal ions. With the ligands 2,6-di(pyrazol-1-yl)pyridine, 6-(pyrazol-1yl)-2,2′-bipyridine and 6,6′-di(pyrazol-1-yl)-2,2′-bipyridine, the chelate effect provides critical additional stability. The pK_a value of pyrazolium (2.52) indicates that pyrazole is a weaker base than imidazole (pK_a of imidazolium, 7.1), but complexes of 1-phenylimidazole, which is sterically analogous to ligand **2**, are well-known.

We report here the synthesis of the 4′-(3,5-dimethylpyrazol-1-yl)-2,2′:6′,2″-terpyridine-1,1″-diium ion $[H_2\mathbf{2}]^{2+}$, its deprotonation to form **2**, and the formation of iron(II), ruthenium(II) and palladium(II) complexes containing ligand **2**.

2. Experimental

2.1. General

^1H and ^{13}C NMR spectra were recorded on a Bruker Avance DRX 500 or 400 spectrometer; the numbering scheme adopted for ligand **2** is shown in Scheme 1. Chemical shifts for ^1H and ^{13}C NMR spectra are referenced to residual solvent peaks with respect to TMS = δ 0 ppm. Electrospray (ES) mass spectra were recorded using a Finnigan MAT LCQ mass spectrometer. Electronic absorption spectra were recorded on a Varian-Cary 5000 spectrophotometer. Electrochemical measurements were performed with an Eco

* Corresponding authors. Fax: +41 61 267 1018.
E-mail address: catherine.housecroft@unibas.ch (C.E. Housecroft).

0277-5387/$ - see front matter © 2008 Elsevier Ltd. All rights reserved.
doi:10.1016/j.poly.2008.04.022

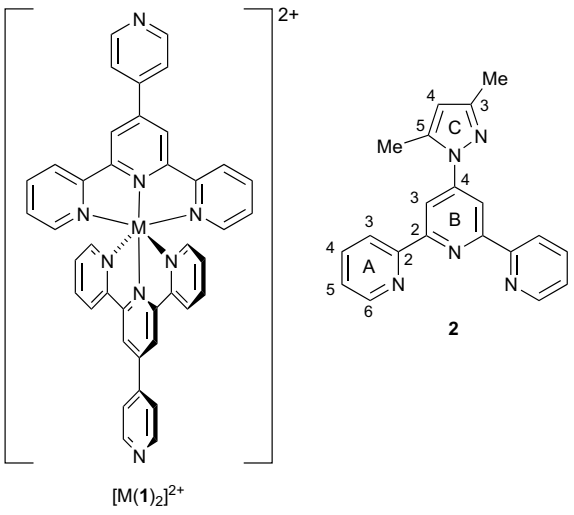

Scheme 1. Structures of $[M(\mathbf{1})_2]^{2+}$ (**1** = 4′-(4-pyridyl)-2,2′:6′,2″-terpyridine) and ligand **2** with the labelling scheme used for NMR spectroscopic assignments.

Chemie Autolab PGSTAT 20 system using glassy carbon working and platinum auxiliary electrodes with a silver wire as pseudo-reference electrode; purified MeCN was used as solvent and 0.1 M $[^nBu_4N][PF_6]$ as supporting electrolyte; ferrocene was added at the end of each experiment as an internal reference. Reactions were carried out under argon. All solvents were dried and distilled before use.

4′-Hydrazino-2,2′:6′,2″-terpyridine was prepared according to the literature procedure [14–16].

2.2. $[H_2\mathbf{2}][EtOSO_3]_2$

Pentane-2,4-dione (0.10 g, 1.0 mmol) was added to a solution of 4′-hydrazino-2,2′:6′-2″-terpyridine (0.11 g, 0.42 mmol) in EtOH (15 cm^3) and the mixture heated. Two drops of concentrated H_2SO_4 were added to the colourless solution causing the immediate formation of a milky, pale yellow suspension which dissolved on heating. The mixture was heated at reflux for 3 h and then cooled to room temperature. Et_2O was added carefully until the first sign of the formation of a precipitate was observed. The solution was then left to stand at −18°C. The fine white needles of $[H_2\mathbf{2}][EtOSO_3]_2$ which formed were collected by filtration and washed with chilled EtOH and Et_2O. $[H_2\mathbf{2}][EtOSO_3]_2$: 0.22 g, 0.38 mmol, 92%. ^{1}H NMR (500 MHz, DMSO-d_6) δ/ppm 8.88 (m, 4H, $H^{A6,A3}$), 8.71 (s, 2H, H^{B3}), 8.32 (t, J 7.3 Hz, 2H, H^{A4}), 7.78 (dd, J 6.0, 5.5 Hz, 2H, H^{A5}), 6.29 (s, 1H, H^{C4}), 3.74 (q, J 8.0 Hz, 4H, CH_2^{anion}), 2.62 (s, 3H, Me^{C5}), 2.27 (s, 3H, Me^{C3}), 1.11 (t, J 8.0 Hz, 6H, CH_3^{anion}). $^{13}C\{^1H\}$ NMR (125 MHz, DMSO-d_6) δ/ppm 154.0 (C^{B2}), 151.8 (C^{A2}), 150.5 (C^{C3}), 148.9 (C^{B4}), 147.5 (C^{A6}), 141.0 (C^{A4}), 140.8 (C^{C5}), 126.0 (C^{A5}), 122.7 (C^{A3}), 114.1 (C^{B3}), 110.2 (C^{C4}), 13.4 ($C^{Me(C5)}$), 13.3 ($C^{Me(C3)}$). ES MS m/z 328 $[H\mathbf{2}]^+$. *Anal.* Calc. for $[H_2\mathbf{2}][EtOSO_3]_2 \cdot 0.3H_2O$ requires: C, 49.23; H, 5.11; N, 11.96. Found: C, 48.94; H, 5.18; N, 12.27%.

2.3. $[H_2\mathbf{2}][MeOSO_3]_2$

Pentane-2,4-dione (0.090 g, 0.90 mmol) was added to a solution of 4′-hydrazino-2,2′:6′,2″-terpyridine (0.20 g, 0.76 mmol) in hot MeOH. Two drops of concentrated H_2SO_4 were added to the colourless solution causing the immediate formation of a milky, pale yellow suspension. The reaction mixture was heated at reflux for 2 h, after which time the precipitate had completely dissolved. After a further 3 h at reflux, the solution was cooled to room temperature and Et_2O was added carefully until the first sign of a precipitate was observed. The solution was left standing overnight at −18 °C. $[H_2\mathbf{2}][MeOSO_3]_2$ precipitated as an off-white microcrystalline solid which was collected by filtration and washed with cold EtOH. $[H_2\mathbf{2}][MeOSO_3]_2$ (0.20 g, 0.36 mmol, 47%): ^{1}H NMR (500 MHz, DMSO-d_6) δ/ppm 8.85 (d, 2H, J 5.0 Hz, H^{A6}), 8.83 (d, J 8.1 Hz, 2H, H^{A3}), 8.71 (s, 2H, H^{B3}), 8.25 (td, J 8.0, 1.3 Hz, 2H, H^{A4}), 7.72 (dd, J 6.7, 5.6 Hz, 2H, H^{A5}), 6.29 (s, 1H, H^{C4}), 3.37 (s, 3H, CH_3^{anion}), 2.62 (s, 3H, H^{C5}), 2.27 (s, 3H, H^{C3}). $^{13}C\{^1H\}$ NMR (125 MHz, DMSO-d_6) δ/ppm 154.6 (C^{B2}), 152.5 (C^{A2}), 150.4 (C^{C3}), 148.7 (C^{B4}), 148.0 (C^{A6}), 140.8 (C^{C5}), 139.9 (C^{A4}), 125.7 (C^{A5}), 122.2 (C^{A3}), 113.6 (C^{B3}), 110.2 (C^{C4}), 13.4 ($C^{Me(C5,C3)}$). ES MS m/z 328 $[H\mathbf{2}]^+$, 677 $[2(\mathbf{2}) + Na]^+$. *Anal.* Calc. for $[H_2\mathbf{2}][MeOSO_3]_2$ requires: C, 42.92; H, 4.09; N, 11.37. Found: C, 42.89; H, 4.02; N, 11.62%.

2.4. 4′-(3,5-Dimethylpyrazol-1-yl)-2,2′:6′,2″-terpyridine, **2**

$[H_2\mathbf{2}][EtOSO_3]_2$ (100 mg, 0.17 mmol) was dissolved in H_2O (10 cm^3) and an aqueous solution of NaOH (0.5 M) was added dropwise until a white precipitate resulted. Collection of the sticky solid was difficult. It was extracted into CH_2Cl_2 and the solvent removed to give neutral **2** (15 mg, 0.046 mmol, 27%). ^{1}H NMR (400 MHz, $CDCl_3$) δ/ppm 8.69 (ddd, J 4.8, 1.8, 1.0 Hz, 2H, H^{A6}), 8.66 (s, 2H, H^{B3}), 8.63 (dt, J 8.0, 1.0 Hz, 2H, H^{A3}), 7.84 (dt, J 7.6, 1.5 Hz, 2H, H^{A4}), 7.32 (ddd, J 7.6, 4.8, 1.6 Hz, 2H, H^{A5}), 6.06 (s, 1H, H^{C4}), 2.63 (s, 3H, Me^{C5}), 2.32 (s, 3H, Me^{C3}). $^{13}C\{^1H\}$ NMR (125 MHz, $CDCl_3$) δ/ppm 157.0 (C^{B2}), 155.7 (C^{A2}), 150.5 (C^{C3}), 149.3 (C^{A6}), 149.0 (C^{B4}), 140.2 (C^{C5}), 136.9 (C^{A4}), 124.1 (C^{A5}), 121.3 (C^{A3}), 114.5 (C^{B3}), 109.1 (C^{C4}), 13.7 ($C^{Me(C3)}$), 13.5 ($C^{Me(C5)}$). ^{1}H NMR (500 MHz, DMSO-d_6) δ/ppm 8.75 (ddd, J 4.6, 1.4, 0.8 Hz, 2H, H^{A6}), 8.67 (s, 2H, H^{B3}), 8.66 (d, J 7.1 Hz, 2H, H^{A3}), 8.03 (td, J 7.8, 1.8 Hz, 2H, H^{A4}), 7.53 (ddd, J 7.4, 4.8, 0.9 Hz, 2H, H^{A5}), 6.24 (s, 1H, H^{C4}), 2.59 (s, 3H, Me^{C5}), 2.26 (s, 3H, Me^{C3}). $^{13}C\{^1H\}$ NMR (125 MHz, DMSO-d_6) δ/ppm 156.4 (C^{B2}), 154.5 (C^{A2}), 150.0 (C^{C3}), 148.4 (C^{B4}), 149.4 (C^{A6}), 140.5 (C^{C5}), 137.5 (C^{A4}), 124.8 (C^{A5}), 121.0 (C^{A3}), 112.3 (C^{B3}), 110.0 (C^{C4}), 13.5 ($C^{Me(C5)}$), 13.4 ($C^{Me(C3)}$). ES-MS m/z 328 $[\mathbf{2}+H]^+$. *Anal.* Calc. for $C_{20}H_{17}N_5$ requires: C, 73.37; H, 5.23; N, 21.39. Found: C, 73.34; H, 5.29; N, 21.30%.

2.5. $[Fe(\mathbf{2})_2][PF_6]_2$

$[H_2\mathbf{2}][EtOSO_3]_2$ (19 mg, 0.033 mmol) and $FeCl_2 \cdot 4H_2O$ (4.0 mg, 0.020 mmol) were dissolved in MeOH (10 cm^3) and stirred at room temperature for 2 h. Excess aqueous NH_4PF_6 was added to precipitate the purple complex which was collected on Celite, washed with H_2O, EtOH and Et_2O, and redissolved in MeCN. Removal of the solvent gave $[Fe(\mathbf{2})_2][PF_6]_2$ as a purple solid (15 mg, 0.015 mmol, 78%). ^{1}H NMR (500 MHz, CD_3CN) δ/ppm 9.04 (s, 4H, H^{B3}), 8.53 (d, J 8.0 Hz, 4H, H^{A3}), 7.90 (td, J 7.9, 1.4 Hz, 4H, H^{A4}), 7.25 (d, J 5.5 Hz, 4H, H^{A6}), 7.10 (ddd, J 7.0, 5.7, 1.2 Hz, 4H, H^{A5}), 6.43 (s, 2H, H^{C4}), 2.90 (s, 6H, Me^{C5}), 2.44 (s, 6H, Me^{C3}). $^{13}C\{^1H\}$ NMR (125 MHz, CD_3CN) δ/ppm 161.7 (C^{B2}), 158.6 (C^{A2}), 154.4 (C^{A6}), 153.3 (C^{C3}), 149.6 (C^{B4}), 142.9 (C^{C5}), 139.7 (C^{A4}), 128.5 (C^{A5}), 125.1 (C^{A3}), 117.3 (C^{B3}), 112.0 (C^{C4}), 13.9 ($C^{Me(C3)}$), 13.8 ($C^{Me(C5)}$). ES-MS m/z 855 $[M-PF_6]^+$, 355 $[M-2PF_6]^{2+}$. UV–VIS (MeCN, 8.80×10^{-6} mol dm^{-3}) λ/nm 565 (ε/dm^3 mol^{-1} cm^{-1} 14600), 502 (sh, 5900), 317 (39000), 307 (38000), 284 (46200), 241 (23700). *Anal.* Calc. for $C_{40}H_{34}F_{12}FeN_{10}P_2 \cdot 1.5CH_3OH \cdot H_2O$ requires: C, 46.73; H, 3.97; N, 13.11. Found: C, 47.09; H, 3.61; N, 12.79%. $E°$/V versus Fc/Fc^+: +0.75, −1.44 and −1.66 V (all reversible).

2.6. $[Ru(\mathbf{2})_2][PF_6]_2$

$RuCl_3 \cdot 3H_2O$ (9.0 mg, 0.035 mmol), and $[H_2\mathbf{2}][EtOSO_3]_2$ (20 mg, 0.035 mmol) were suspended in ethane-1,2-diol (2 cm^3) and the

reaction mixture was heated in a microwave oven (800 W, 2 min). A second equivalent of $[H_2\mathbf{2}][EtOSO_3]_2$ (20 mg, 0.035 mmol) was added with one drop of *N*-ethylmorpholine and the solution was again heated in the microwave oven (800 W, 2 min) to give a deep red solution which was cooled to room temperature. It was then poured into water (50 cm^3) containing an excess of NH_4PF_6 to precipitate the hexafluoridophosphate salt of the product. The resulting red-orange precipitate was collected on Celite and washed well with H_2O, EtOH and Et_2O. The solid was dissolved in MeCN and the solvent removed to give the crude product (35 mg, 0.033 mmol, 96%, approximately 95% pure by ^1H NMR spectroscopy). This was purified by column chromatography (SiO_2, MeCN:H_2O:saturated aqueous KNO_3 7:2:2). The central portion of the main red fraction was collected, excess NH_4PF_6 was added and the volume reduced leading to the precipitation of the pure product as a dark red microcrystalline solid (26 mg, 0.025 mmol, 72%). ^1H NMR (500 MHz, CD_3CN) δ/ppm 8.86 (s, 4H, H^{B3}), 8.55 (dt, *J* 8.0, 1.0 Hz, 4H, H^{A3}), 7.94 (td, *J* 8.0, 1.3 Hz, 4H, H^{A4}), 7.49 (dt, *J* 5.6, 1.0 Hz, 4H, H^{A6}), 7.20 (ddd, *J* 7.0, 5.6, 1.3 Hz, 4H, H^{A5}), 6.37 (s, 2H, H^{C4}), 2.81 (s, 6H, Me^{C5}), 2.42 (s, 6H, Me^{C3}). $^{13}C\{^1H\}$ NMR (125 MHz, CD_3CN) δ/ppm 158.8 (C^{A2}), 156.7 (C^{B2}), 153.7 (C^{A6}), 153.0 (C^{C3}), 147.6 (C^{B4}), 142.5 (C^{C5}), 139.1 (C^{A4}), 128.7 (C^{A5}), 125.7 (C^{A3}), 117.7 (C^{B3}), 111.4 (C^{C4}), 13.8 ($C^{Me(C3)}$), 13.5 ($C^{Me(C5)}$). ES-MS *m*/*z* 901 $[M-PF_6]^+$, 378 $[M-2PF_6]^{2+}$. UV–Vis (MeCN, 1.51×10^{-5} mol dm^{-3}) λ/nm 489 (ε/ $dm^3\,mol^{-1}\,cm^{-1}$ 23 200), 307 (65 100), 284 (59 400), 241 (28 000). *Anal.* Calc. for $C_{40}H_{34}F_{12}N_{10}P_2Ru$ requires: C, 45.94; H, 3.28; N, 13.39. Found: C, 45.80; H, 3.26; N, 13.40%. E°/V versus Fc/Fc^+: +0.93, −1.52 and −1.73 V (all reversible).

2.7. [Pd(**2**)Cl][PF_6]: method 1

$[H_2\mathbf{2}][MeOSO_3]_2$ (0.035 g, 0.063 mmol) and $PdCl_2$ (0.012 g, 0.068 mmol) were dissolved in MeOH (10 cm^3) and the solution was heated at reflux for 18 h, during which time a cream precipitate formed. The reaction mixture was cooled to room temperature, filtered and the solid product washed with EtOH, $CHCl_3$ and Et_2O. The solid was dissolved in hot water and excess solid NH_4PF_6 was added to precipitate the hexafluoridophosphate salt which was collected and recrystallised from MeCN/H_2O. [Pd(**2**)Cl][PF_6] was isolated as a pale yellow solid (0.017 g, 0.027 mmol, 40%). ^1H NMR (500 MHz, DMSO-d_6) δ/ppm 8.82 (d, *J* 7.8 Hz, 2H, H^{A3}), 8.79 (dd, *J* 5.6, 1.0 Hz, 2H, H^{A6}), 8.69 (s, 2H, H^{B3}), 8.48 (td, *J* 7.9, 1.3 Hz, 2H, H^{A4}), 7.93 (ddd, *J* 6.9, 5.6, 0.9 Hz, 2H, H^{A5}), 6.41 (s, 1H, H^{C4}), 2.66 (s, 3H, Me^{C5}), 2.30 (s, 3H, Me^{C3}). Low solubility prevented ^{13}C NMR spectroscopic data from being recorded. ES MS *m*/*z* 469 $[M-PF_6]^+$. *Anal.* Calc. for $C_{20}H_{17}ClF_6N_5PPd\cdot0.5H_2O$ requires: C, 38.59; H, 2.92; N, 11.26. Found: C, 38.59; H, 3.11; N, 10.90%.

2.8. [Pd(**2**)Cl][PF_6]: method 2 (see text)

$[Fe(\mathbf{2})_2][PF_6]_2$ (0.070 g, 0.068 mmol), $PdCl_2$ (0.012 g, 0.068 mmol) and K_2CO_3 (0.10 g, 0.73 mmol) were dissolved in MeCN (30 cm^3). The solution was stirred overnight at room temperature and filtered to remove a small amount of pale yellow precipitate, assumed to be $PdCl_2$. Aqueous NH_4PF_6 was added and the resulting precipitate was collected and washed with H_2O, EtOH and Et_2O. The ^1H NMR spectrum of a CD_3CN solution of the precipitate indicated the presence of $[Fe(\mathbf{2})_2][PF_6]_2$ and [Pd(**2**)Cl][PF_6]. Slow evaporation of the CD_3CN solution gave X-ray quality crystals of [Pd(**2**)Cl][PF_6].

2.9. Crystal structure determinations

Data for $[H_2\mathbf{2}][EtOSO_3]_2\cdot H_2O$, $[Ru(\mathbf{2})_2][PF_6]_2$, [Pd(**2**)Cl][$PF_6$] and $[Fe(\mathbf{2})_2][PF_6]_2$ (see electronic supplementary data) were collected on an Enraf Nonius Kappa CCD instrument; data reduction, solution and refinement used the programs COLLECT [17], SIR92 [18], DENZO/SCALEPACK [19] and CRYSTALS [20]. Structures have been analysed using MERCURY v. 1.4.2 [21].

2.10. Crystal data for $[H_2\mathbf{2}][EtOSO_3]_2\cdot H_2O$

$C_{24}H_{31}N_5O_9S_2$, M = 597.67, triclinic, space group $P\bar{1}$, a = 7.7597(1), b = 12.6160(2), c = 15.1917(3) Å, α = 107.2079(9)°, β = 102.5902(9)°, γ = 102.9589(9)°, U = 1318.31(4) $Å^3$, Z = 2, D_{calc} = 1.506 Mg m^{-3}, μ(Mo Kα) = 0.265 mm^{-1}, T = 173 K, 6280 reflections collected. Refinement of 4355 reflections (361 parameters) with $I > 3\sigma(I)$ converged at final R_1 = 0.0386 (R_1 all data = 0.0577), wR_2 = 0.0448 (wR_2 all data = 0.0599), goodness-of-fit = 1.046.

2.11. $[Ru(\mathbf{2})_2][PF_6]_2$

$C_{40}H_{34}F_{12}N_{10}P_2Ru$, M = 1045.77, monoclinic, space group $P2_1$, a = 9.3368(3), b = 13.0679(4), c = 17.5480(6) Å, β = 103.341(2)°, U = 2083.3(1) $Å^3$, Z = 2, D_{calc} = 1.667 Mg m^{-3}, μ(Mo Kα) = 0.553 mm^{-1}, T = 173 K, 9271 reflections collected. Refinement of 7592 reflections (587 parameters) with $I > 3\sigma(I)$ converged at final R_1 = 0.0440 (R_1 all data = 0.0576), wR_2 = 0.0402 (wR_2 all data = 0.0453), goodness-of-fit = 1.080.

2.12. [Pd(**2**)Cl][PF_6]

$C_{20}H_{17}ClF_6N_5PPd$, M = 614.20, triclinic, space group $P\bar{1}$, a = 8.3796(2), b = 10.8068(2), c = 13.2536(3) Å, α = 99.108(1)°, β = 103.461(1)°, γ = 110.1509(9)°, U = 1057.73(4) $Å^3$, Z = 2, D_{calc} = 1.928 Mg m^{-3}, μ(Mo Kα) = 1.153 mm^{-1}, T = 173 K, 6172 reflections collected. Refinement of 4716 reflections (361 parameters) with $I > 3\sigma(I)$ converged at final R_1 = 0.0308 (R_1 all data = 0.0441), wR_2 = 0.0337 (wR_2 all data = 0.0435), goodness-of-fit = 1.148.

3. Results and discussion

The strategy for the preparation of ligand **2** was the cyclization reaction of pentane-2,4-dione with 4′-hydrazino-2,2′:6′,2″-terpyridine [14–16]. Such cyclizations are well documented for the syntheses of a range of pyrazoles, both in solution and over heterogeneous catalysts [22–24]. The conditions shown in Scheme 2 are similar to those reported recently for the synthesis of 1,3,5-trisubstituted pyrazoles [25]. Treatment of 4′-hydrazino-2,2′:6′,2″-terpyridine with pentane-2,4-dione in methanol in the presence of concentrated H_2SO_4, followed by cooling, resulted in the formation of an off-white crystalline solid. An analogous reaction in ethanol proceeded in a similar manner also to give a white solid. Both products proved to be poorly soluble in common organic solvents, and their solution ^1H NMR spectra were not well resolved. Elemental analysis indicated that methyl or ethyl sulfate salts of the diprotonated ligand $[H_2\mathbf{2}]^{2+}$ had been formed, and this was confirmed by a single crystal X-ray diffraction study. X-ray

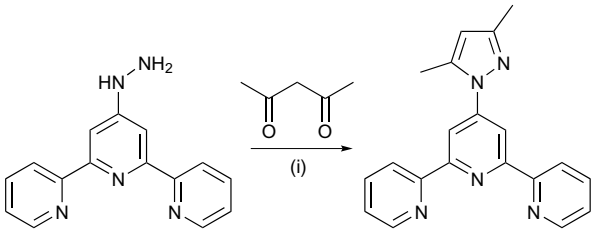

Scheme 2. Synthetic route to ligand **2**: (i) MeOH or EtOH at reflux, conc. H_2SO_4 catalyst.

quality crystals of $[H_2\mathbf{2}][EtOSO_3]_2 \cdot H_2O$ were grown by slow evaporation of an ethanol/water (1:1) solution of $[H_2\mathbf{2}][EtOSO_3]_2$. The H atoms bonded to the nitrogen atoms and the two protons of the water molecule were localized in the difference map, but were included in the refinement as fixed contributions riding on either N or O atoms. The diprotonated state of the ligand was consistent with the presence of two ethyl sulfate ions in the asymmetric unit, and is also consistent with the observation of a *cis*,*cis*-conformation for the tpy unit. Free tpy ligands typically adopt a *trans*,*trans*-conformation to minimize nitrogen lone pair–lone pair interactions. Monoprotonated ligands, $[Htpy]^+$, adopt a *cis*,*trans*-conformation as a result of a hydrogen-bonded N–H···N interaction [26–28]. Typically, in $[H_2tpy]^{2+}$, the two outer pyridine rings are protonated and hydrogen-bonded interactions involving the central pyridine *N*-atom, in addition to an acceptor atom in a solvent molecule or anion, result in a *cis*,*cis*-conformation [28–33]. In $[H_2\mathbf{2}][EtOSO_3]_2 \cdot H_2O$, the $[H_2\mathbf{2}]^{2+}$ ion is hydrogen-bonded to atom O4 of one ethyl sulfate ion as illustrated in Fig. 1 (N1···O1 = 2.757(2) Å, N1–H1···O1 = 159°, N1···N2 = 2.630(2) Å, N1–H1···N2 = 101°, N3···O1 = 2.752(2) Å, N3–H1···O1 = 156°, N3···N2 = 2.644(2) Å, N3–H1···N2 = 106°). The tpy unit deviates slightly from a planar conformation (angles between the least squares planes of the rings containing atoms N1 and N2, and N2 and N3 are 16.02(9)° and 10.37(9)°, respectively). The bond parameters within the tpy domain are unexceptional. The pyrazolyl ring is twisted out of the plane of the pyridine ring to which it is bonded, with an angle between the least squares planes of 24.2(1)°.

Hydrogen-bonded pairs of cations and anions stack with alternating pyrazolyl rings and pyridine rings contain N1; the inter-ring separation is 3.7 Å (Fig. 2). Each remaining $[EtOSO_3]^-$ anion is hydrogen bonded to a water molecule (O9···O7 = 2.864(2) Å, O9–H4···O7 = 175°). A weaker hydrogen bond links each water molecule to a cation-associated ethyl sulfate anion (O9···O2 = 3.089(2) Å, O9–H3···O2 = 156°).

Solutions of $[H_2\mathbf{2}][EtOSO_3]_2$ in DMSO-d_6 were monitored by ^{1}H NMR spectroscopy, and the appearance of a new set of ethyl signals corresponding to ethanol (quartet at δ 3.44 ppm and triplet at δ 1.06 ppm) grew in at the expense of those arising from the ethyl sulfate anions. This observation was consistent with the hydrolysis of the ethyl sulfate ion by residual water in the solvent [34], giving rise to the sulfate or hydrogen sulfate salt of $[H_2\mathbf{2}]^{2+}$. This salt was not isolated.

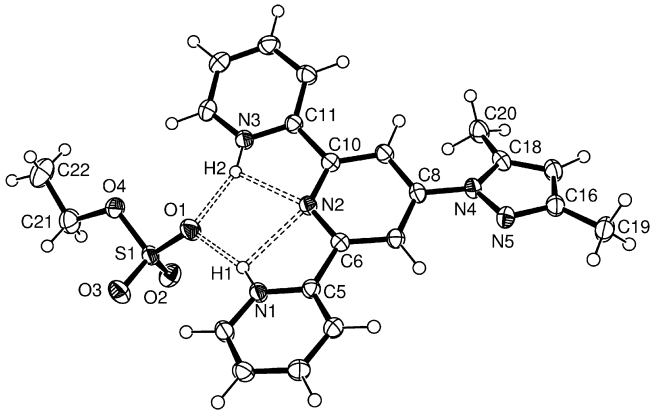

Fig. 1. The molecular structure of the $[H_2\mathbf{2}]^{2+}$ cation and the ethyl sulfate anion to which it is hydrogen-bonded in $[H_2\mathbf{2}][EtOSO_3]$textsubscript2 · H_2O; thermal ellipsoids are plotted at the 50% probability level. Selected bond parameters: N4–N5 = 1.382(2), N4–C8 = 1.404(2), N5–C16 = 1.326(2), N4–C18 = 1.379(2), C16–C17 = 1.417(3), C17–C18 = 1.361(3), S1–O1 = 1.461(1), S1–O2 = 1.442(2), S1–O3 = 1.437(1), S1–O4 = 1.588(1) Å; N4–C8–C7 = 119.5(2)°, N4–C8–C9 = 121.1(2)°, N5–N4–C18 = 111.7(1)°, N4–N5–C16 = 104.7(2)°.

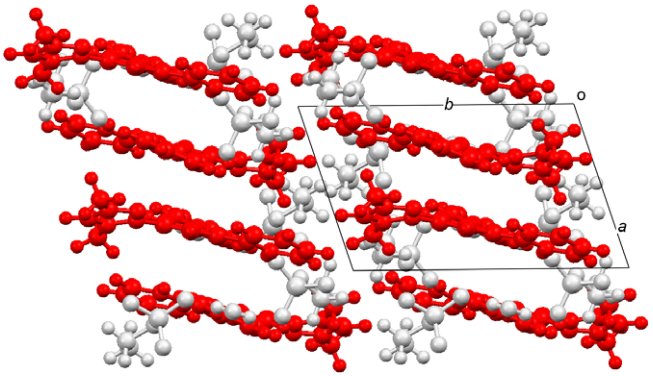

Fig. 2. Part of the packing in $[H_2\mathbf{2}][EtOSO_3]_2 \cdot H_2O$ (viewed down the *c* axis), showing stacking of cations. The $[EtOSO_3]^-$ anions and water molecules are shown in pale grey.

The methyl sulfate salt $[H_2\mathbf{2}][MeOSO_3]_2$ exhibited the same NMR spectroscopic signature to its ethyl analogue, with a singlet at δ 3.37 ppm for the methyl group replacing the triplet (δ 1.11 ppm) and quartet (δ3.74 ppm) assigned to the ethyl group in $[H_2\mathbf{2}][EtOSO_3]_2$. The isolation of ethyl or methyl sulfate salts of complexes from media in which esterification of sulfate or sulfuric acid [34] has precedent, although examples appear to be rare [35–37]. The fact that the ^{1}H and ^{13}C NMR spectroscopic signatures of $[H_2\mathbf{2}]^{2+}$ in both alkyl sulfate salts are virtually identical confirms a common protonation state of the tpy unit.

Addition of solid K_2CO_3 to an NMR sample of $[H_2\mathbf{2}][EtOSO_3]_2$ or $[H_2\mathbf{2}][MeOSO_3]_2$ resulted in a shift of the signals for the tpy protons and formation of neutral ligand **2**. Spectroscopic signals were assigned by COSY, NOESY, HMQC and HMBC techniques. The signals for protons H^{A3} and H^{A6} (see Scheme 1) overlap in the spectrum of $[H_2\mathbf{2}][EtOSO_3]_2$, appearing (in DMSO-$d_6$) as a poorly resolved multiplet centred at δ 8.88 ppm. The signals are slightly better separated in the spectrum of $[H_2\mathbf{2}][MeOSO_3]_2$. In the ^{1}H NMR spectrum of **2**, resonances for H^{A3} and H^{A6} are well separated (δ 8.63 and 8.69 ppm, respectively in $CDCl_3$ and δ 8.66 and 8.75 ppm in DMSO-d_6). The signals assigned to H^{A4} and H^{A5} shift to lower frequency on going from $[H_2\mathbf{2}]^{2+}$ to **2**, (for $[H_2\mathbf{2}][MeOSO_3]_2$ to **2** in DMSO-d_6, δ 8.25–8.03 ppm for H^{A4}, and δ 7.72–7.53 ppm for H^{A5}). In contrast, a comparison of the ^{1}H NMR spectra of $[H_2\mathbf{2}]^{2+}$ and **2** (DMSO-d_6 solutions) shows that the chemical shifts of signals assigned to protons which are remote from the site of ligand protonation vary little between the two species. There is, however, a significant solvent dependence, with signals shifting between 0.01 and 0.21 ppm on changing from a DMSO-d_6 to $CDCl_3$ solution of **2** (see Section 2). The signals for the pyrazolyl methyl groups were distinguished by the appearance in the NOESY spectrum of a cross peak between H^{B3} and H^{C5}.

On a preparative scale, the conversion of $[H_2\mathbf{2}][EtOSO_3]_2$ or $[H_2\mathbf{2}][MeOSO_3]_2$ to **2** was carried out by neutralization of an aqueous solution of $[H_2\mathbf{2}][EtOSO_3]_2$ or $[H_2\mathbf{2}][MeOSO_3]_2$ with aqueous NaOH. The resulting white precipitate was collected, dissolved in CH_2Cl_2 followed by the removal of solvent. Alternatively, solid K_2CO_3 was added to an aqueous solution of $[H_2\mathbf{2}][EtOSO_3]_2$ or $[H_2\mathbf{2}][MeOSO_3]_2$, and the resulting suspension was extracted into CH_2Cl_2. The yield of **2** (which is not particularly soluble in water) by either method is typically $\leqslant$30%. This low yield prompted us to investigate whether complex formation could be carried out using the alkyl sulfate salts instead of neutral **2**. As described below, this is indeed the case and avoids loss of material during deprotonation and ligand purification.

Ligand **2** has two potential coordination domains: the tpy and pyrazolyl *N*-donor sites. $[H_2\mathbf{2}][EtOSO_3]_2$ reacts with iron(II) at room

temperature to give a complex, the purple colour of which is characteristic of the $\{Fe(tpy)_2\}^{2+}$ chromophore. The product was isolated as the hexafluoridophosphate salt $[Fe(\mathbf{2})_2][PF_6]_2$, and its electrospray mass spectrum showed peak envelopes at m/z 855 and 355 (base peak) corresponding to $[M-PF_6]^+$ and $[M-2PF_6]^{2+}$, respectively, with isotope patterns that matched those simulated. The ^{1}H NMR spectrum of a CD_3CN solution of $[Fe(\mathbf{2})_2][PF_6]_2$ exhibited the characteristic pattern of signals for a coordinated tpy domain. In particular, the resonance for H^{A6} appears at δ 7.25 ppm, i.e. at significantly lower frequency than in the free ligand, while coordination to the metal centre causes the signal for H^{B3} to move to noticeably higher frequency (δ 9.04 ppm).

Treatment of $RuCl_3 \cdot 3H_2O$ with an equivalent of $[H_2\mathbf{2}][EtOSO_3]_2$ produces $[Ru(\mathbf{2})Cl_3]$ which reacts with a second equivalent of $[H_2\mathbf{2}][EtOSO_3]_2$ in the presence of *N*-ethylmorpholine to give $[Ru(\mathbf{2})_2]^{2+}$, isolated as the hexafluoridophosphate salt. The electrospray mass spectrum of the complex is in accord with a formulation of $[Ru(\mathbf{2})_2][PF_6]_2$, with the highest mass peak appearing at m/z 901 (assigned to $[M-PF_6]^+$) and the base peak at m/z 378 (assigned to $[M-2PF_6]^{2+}$). The isotope distributions agreed with those simulated for these ions. The ^{1}H NMR spectrum of a CD_3CN solution of $[Ru(\mathbf{2})_2][PF_6]_2$ confirmed that the tpy domain was coordinated to the ruthenium(II) centre.

The structure of the $[Ru(\mathbf{2})_2]^{2+}$ cation was confirmed by an X-ray diffraction study of $[Ru(\mathbf{2})_2][PF_6]_2$, suitable crystals being grown by slow evaporation of a CH_3CN/H_2O solution of $[Ru(\mathbf{2})_2][PF_6]_2$. The structure of the complex cation is shown in Fig. 3. The coordination environment around the ruthenium(II) centre is as expected, with the central Ru–N bond being shorter than the two outer bonds to each ligand (caption to Fig. 3). Each pyrazolyl ring is twisted with respect to the pyridine ring to which it is bonded (angles between the least squares planes for the rings containing N2 and N7, and N5 and N9 are 20.0(3)° and 36.2(3)°, respectively). The packing of cations in the solid state is supported by weak C–H(methyl)···π(pyridine) interactions. Each pyrazolyl methyl group containing atom C36 sits directly over a tpy pyridine ring containing atom N1 of the adjacent cation (Fig. 4); the distance from C36 to the centroid of the pyridine ring is 3.35 Å, which is relatively short for this type of intermolecular contact [40]. These interactions lead to the formation of loosely held chains which run parallel to the crystallographic *b* axis. Extensive interactions between aromatic C–H hydrogen atoms and the F atoms of the $[PF_6]^-$ ions also contribute towards the solid state packing. The $\{Ru(tpy)_2\}$ units are held significantly away from one another, preventing them from engaging in face-to-face or edge-to-face π-interactions [41,42]. Crystalline $[Fe(\mathbf{2})_2][PF_6]_2$ is isostructural with $[Ru(\mathbf{2})_2][PF_6]_2$ (see electronic supplementary material).

The electronic absorption spectra of acetonitrile solutions of $[Fe(\mathbf{2})_2][PF_6]_2$ and $[Ru(\mathbf{2})_2][PF_6]_2$ show MLCT bands at 565 and 489 nm, respectively. Both absorptions are shifted to lower energy compared to the MLCT absorptions for the parent $[Fe(tpy)_2]^{2+}$ (551 nm) and $[Ru(tpy)_2]^{2+}$ (475 nm) [38], but are similar to the corresponding absorptions for homoleptic complexes of iron(II) and ruthenium(II) containing 4′-(*n*-pyridyl)-2,2′:6′,2″-terpyridine (n = 2, 3 or 4) ligands [38,39]. This indicates that the introduction of the 4′-pyridyl or 4′-pyrazolyl substituents results in a lowering of the ligand π^* orbitals to a similar extent. The electronic spectra of $[Fe(\mathbf{2})_2][PF_6]_2$ and $[Ru(\mathbf{2})_2][PF_6]_2$ also exhibit a series of higher energy absorptions arising from ligand-centred $\pi^* \leftarrow \pi$ and $\pi^* \leftarrow$ n transitions. The MLCT bands of $[Fe(\mathbf{1})_2]^{2+}$ and $[Ru(\mathbf{1})_2]^{2+}$, and of the analogous complexes containing 2- and 3-pyridyl substituents, are sensitive to protonation at the pendant *N*-atom [12,38,39]. For example, red-orange $[Ru(\mathbf{1})_2]^{2+}$ (λ_{max} = 488 nm) turns pink when fully protonated (for $[Ru(H\mathbf{1})_2]^{4+}$, λ_{max} = 502 nm). The addition of an excess of trifluoroacetic acid to an acetonitrile solution of $[Ru(\mathbf{2})_2][PF_6]_2$ resulted in no shift in the position of the MLCT band, indicating that no protonation of the free nitrogen atoms on the pendant pyrazolyl substituents occurred. A similar experiment with $[Fe(\mathbf{2})_2][PF_6]_2$ also indicated that no protonation occurred; in the presence of a large excess of trifluoroacetic acid, the complex decomposed. Acetonitrile solutions of $[Ru(\mathbf{2})_2][PF_6]_2$, and solutions to which trifluoroacetic acid has been added, are non-luminescent.

Both the ruthenium and iron complexes $[M(\mathbf{2})_2]^{2+}$ are electrochemically active and each exhibits a number of reversible or quasi-reversible redox processes (Figs. S2 and S3). The M(II)/(MIII) redox processes are observed as fully reversible waves in the cyclic voltammogram (MeCN, $[Bu_4N][PF_6]$ supporting electrolyte, referenced to internal Fc/Fc^+) at +0.75 and +0.93 V for the iron and ruthenium species, respectively. These are very slightly shifted to more positive potential than the corresponding $[M(tpy)_2]^{2+}$ complexes (Ru, +0.88 V [43], Fe, +0.74 V) [38]. The iron complex also exhibits fully reversible one-electron reductions at −1.44 and

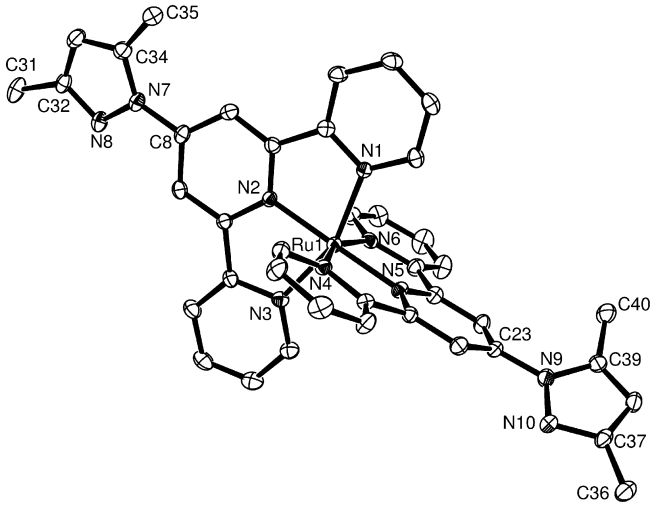

Fig. 3. Molecular structure of the $[Ru(2)_2]^{2+}$ cation in $[Ru(2)_2][PF_6]_2$ with thermal ellipsoids plotted at the 30% probability level; hydrogen atoms are omitted. Selected bond distances and angles: Ru1–N1 = 2.058(4), Ru1–N2 = 1.979(4), Ru1–N3 = 2.058(5), Ru1–N4 = 2.060(4), Ru1–N5 = 1.976(4), Ru1–N6 = 2.070(5), N7–N8 = 1.384(7), N9–N10 = 1.376(7), N7–C8 = 1.417(7), N9–C23 = 1.416(6), N7–C34 = 1.392(8), N9–C39 = 1.389(7) Å; N1–Ru1–N2 = 79.4(2)°, N2–Ru1–N3 = 78.8(2)°, N4–Ru1–N5 = 79.3(2)°, N5–Ru1–N6 = 78.7(2)°, N8–N7–C34 = 111.4(4)°, N10–N9–C39 = 111.9(4)°.

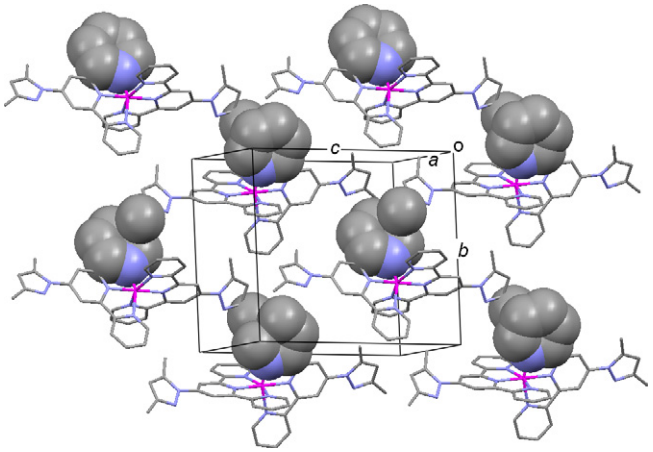

Fig. 4. Close contacts between pyridine π-systems and pyrazolyl Me substituents (shown in spacefilling representation) in the solid state structure of $[Ru(\mathbf{2})_2][PF_6]_2$. Anions and hydrogen atoms are omitted from the figure.

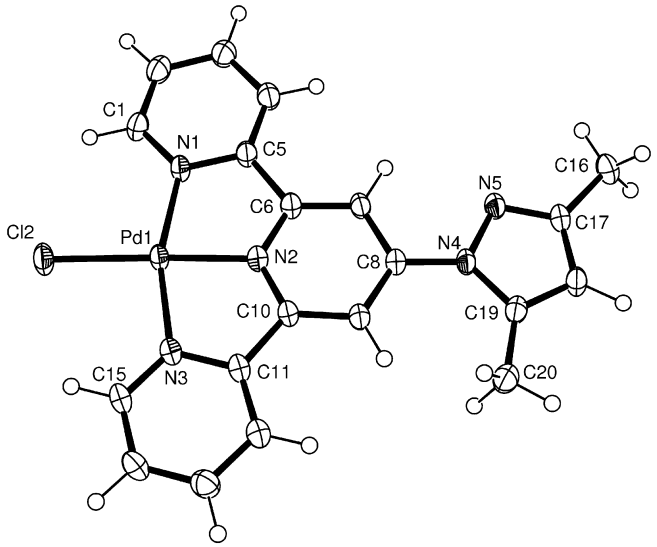

Fig. 5. Molecular structure of the $[Pd(\mathbf{2})Cl]^+$ cation in $[Pd(\mathbf{2})Cl][PF_6]$ with thermal ellipsoids plotted at the 50% probability level. Selected bond parameters: Pd1–Cl2 = 2.2932(6), Pd1–N1 = 2.030(2), Pd1–N2 = 1.941(2), Pd1–N3 = 2.021(2), N4–C8 = 1.388(3), N4–N5 = 1.381(3) Å; Cl2–Pd1–N1 = 100.13(6)°, Cl2–Pd1–N3 = 98.17(6)°, N1–Pd1–N2 = 80.73(8)°, N2–Pd1–N3 = 80.93(8)°.

−1.66 V, while the ruthenium compound shows reversible one electron-processes at −1.52 and −1.73 V. These correspond well to the ligand reduction in $[Fe(tpy)_2]^{2+}$ (−1.64 and −1.82 V) [38] and $[Ru(tpy)_2]^{2+}$ (−1.67 and −1.92 V) [38] with the shift to more positive potential of ~20 mV being attributed to the extended conjugation. In each case, there are additional quasi-reversible processes in the region of −2.3 V.

The homoleptic iron(II) and ruthenium(II) complexes each possess free *N*-donor coordination sites on the pendant pyrazolyl substituents. It is therefore of interest to investigate their use as building blocks in the formation of coordination polymers. As a preliminary experiment, we chose to investigate the reaction of $[Fe(\mathbf{2})_2][PF_6]_2$ with $PdCl_2$. An acetonitrile solution of these compounds with K_2CO_3 were stirred at room temperature overnight. The ^1H NMR spectrum of a CH_3CN solution of product precipitated as the hexafluoridophosphate salts showed the presence of $[Fe(\mathbf{2})_2][PF_6]_2$ and $[Pd(\mathbf{2})Cl][PF_6]$. X-ray quality crystals of $[Pd(\mathbf{2})Cl][PF_6]$ grew from the NMR solution (see below). No polymeric material was obtained from the reaction. $[Pd(\mathbf{2})Cl][PF_6]$ may also be prepared by treating $PdCl_2$ with $[H_2\mathbf{2}][MeOSO_3]_2$ in refluxing methanol. After the addition of NH_4PF_6, $[Pd(\mathbf{2})Cl][PF_6]$ was isolated in 40% yield. The base peak in the electrospray mass spectrum of the product appeared at *m*/*z* 469 with an isotopic distribution that was consistent with the $[Pd(\mathbf{2})Cl]^+$ ion. The palladium(II) complex is poorly soluble in most organic solvents. A ^1H

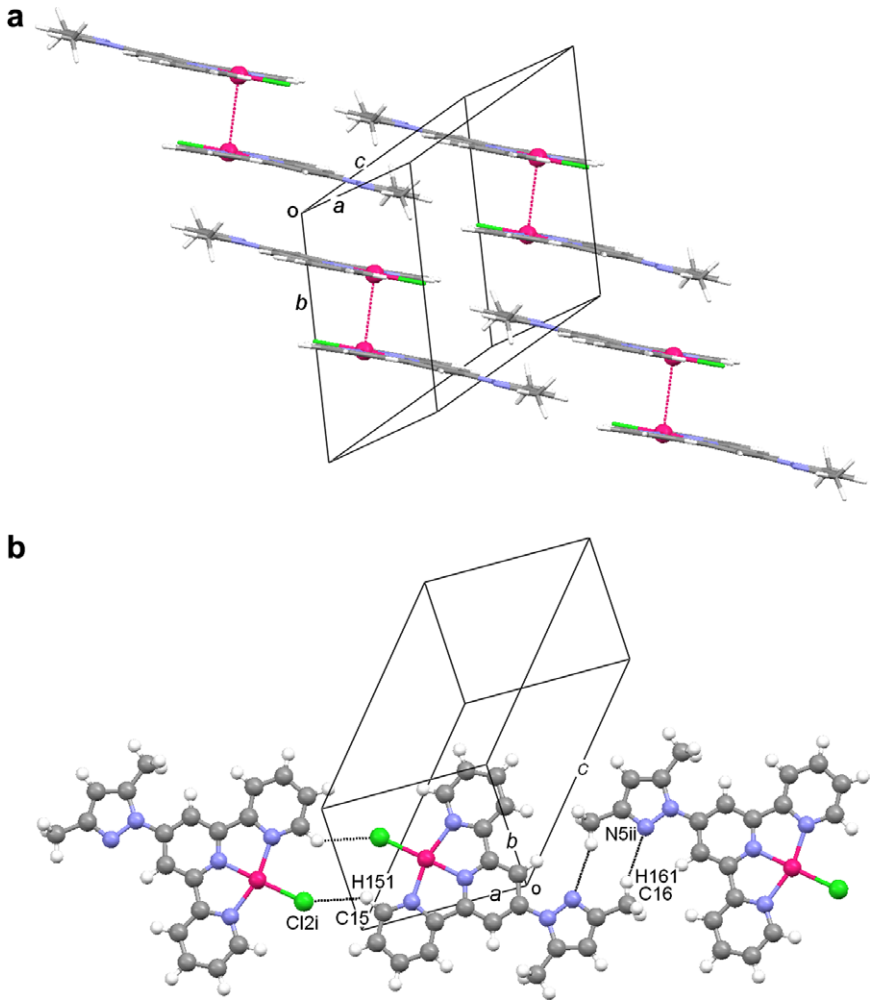

Fig. 6. (a) The assembly of step-like stacks of $[Pd(2)Cl]^+$ cations in $[Pd(2)Cl][PF_6]$. (b) Hydrogen-bonded interactions between stacks (symmetry codes: i = 2 − *x*, 1 − *y*, −*z*; ii = −1 − *x*, −*y*, −*z*).

NMR spectrum was obtained in DMSO-d_6 solution and was assigned by routine 1D and 2D-techniques. The signals for each of the tpy protons shifts to higher frequency, H^{A4} and H^{A5} being the most affected: $\Delta(\delta_{complex} - \delta_{free\ ligand}) = 0.45$ ppm for H^{A4} and 0.40 ppm for H^{A5} (both ligand and complex in DMSO-d_6). The resonances for the pyrazolyl ring proton, H^{C4}, and the methyl groups also show small shifts to higher frequency.

The structure of [Pd(**2**)Cl][PF_6] was confirmed by a single crystal X-ray diffraction study, and the molecular structure of the [Pd(**2**)Cl]$^+$ cation is depicted in Fig. 5. The palladium(II) centre is in a square planar environment, and bond parameters for the coordination sphere are as expected. Compared to the free protonated ligand [H_2**2**]$^{2+}$ in [H_2**2**][$EtOSO_3$]$_2 \cdot H_2O$, and the coordinated ligands in [Fe(**2**)$_2$]$^{2+}$ and [Ru(**2**)$_2$]$^{2+}$, the structure of the metal-bound ligand [Pd(**2**)Cl]$^+$ is noteworthy for the coplanarity of the central pyridine and the pendant pyrazolyl rings. The angle between the least squares planes of these rings is 1.0(2)°. The origin of this feature can be traced to the stacking of cations in the solid state. Fig. 6a illustrates that cations pair up by virtue of a short Pd···Pd contact of 3.3218(4) Å, and then these dimers assemble into step-like stacks, supported by aromatic π-interactions. The latter occur between sets of three heterocycles, viz. a pyridine ring containing N1 in sandwiched between a pyrazolyl ring and a pyridine ring containing N3, with inter-ring separations of ≈3.4 Å. Additional hydrogen-bond operate between the stacks, in the self-complementary pairs of interactions shown in Fig. 6b (C15H151···Cl2i = 2.78 Å, C15···Cl2i = 3.562(3) Å, C15H151···Cl2i = 135°; C16H161···N5ii = 2.61 Å, C16···N5ii = 3.566(3) Å, C16H161···N5ii = 160°). We recently reported the structure of [Pd(**1**)Cl]Cl · $3H_2O$ · DMF[44] in which the [Pd(**1**)Cl]$^+$ cations assemble into columns supported by ···Pd···Pd···Pd··· stacks. In this report, we discussed the structural classes of complexes containing {Pd(tpy)} or {Pt(tpy)} units, viz. those with ···M···M···M··· stacks and those with dimeric units.[1] The hexafluoridophosphate anions are disordered and have been modelled with each F atom disordered over two sites having fractional occupancies of 0.28 and 0.72.

4. Conclusions

In this paper, we have described the acid catalysed condensation of 4′-hydrazino-2,2′:6′,2″-terpyridine with pentane-2,4-dione to give alkyl sulfate salts of [H_2**2**]$^{2+}$. The conjugate base 4′-(3,5-dimethylpyrazol-1-yl)-2,2′:6′,2″-terpyridine, **2**, can be isolated by treatment of [H_2**2**][$ROSO_3$]$_2$ (R = Me or Et) with base, but for the synthesis of metal complexes containing ligand **2**, it is more convenient to use [H_2**2**][$ROSO_3$]$_2$ as the precursor. The complexes [Fe(**2**)$_2$]$^{2+}$, [Ru(**2**)$_2$]$^{2+}$ and [Pd(**2**)Cl]$^+$ have been prepared and characterized.

Acknowledgements

We thank the Swiss National Science Foundation and the University of Basel for financial support. Emma L. Dunphy is thanked for assistance with the electrochemical measurements.

Appendix A. Supplementary data

CCDC 666818, 666821, 666819 and 666820 contain the supplementary crystallographic data for [H_2**2**][$EtOSO_3$]$_2 \cdot H_2O$, [Ru(**2**)$_2$][PF_6]$_2$, [Fe(**2**)$_2$][PF_6]$_2$ and [Pd(**2**)Cl][PF_6]. These data can be obtained free of charge via http://www.ccdc.cam.ac.uk/conts/retrieving.html, or from the Cambridge Crystallographic Data Centre, 12 Union Road, Cambridge CB2 1EZ, UK; fax: (+44) 1223-336-033; or e-mail: deposit@ccdc.cam.ac.uk. Supplementary data associated with this article can be found, in the online version, at doi:10.1016/j.poly.2008.04.022.

References

[1] M.A. Halcrow, Coord. Chem. Rev. 249 (2005) 2880.
[2] C. Pettinari, C. Santini, in: J.A. McCleverty, T.J. Meyer (Eds.), Comprehensive Coordination Chemistry II, vol. 1, Elsevier, Oxford, 2004, p. 159.
[3] R. Zibaseresht, R.M. Hartshorn, Dalton Trans. (2005) 3898.
[4] J. Beves, E.C. Constable, C.E. Housecroft, C.J. Kepert, D.J. Price, CrystEngComm 9 (2007) 456.
[5] J.E. Beves, E.C. Constable, C.E. Housecroft, C.J. Kepert, M. Neuburger, D.J. Price, S. Schaffner, CrystEngComm 9 (2007) 1073.
[6] J.E. Beves, E.C. Constable, C.E. Housecroft, M. Neuburger, S. Schaffner, CrystEngComm 10 (in press), doi:10.1039/b713001e.
[7] J.E. Beves, D.J. Bray, J.K. Clegg, E.C. Constable, C.E. Housecroft, K.A. Jolliffe, C.J. Kepert, L.F. Lindoy, M. Neuburger, D.J. Price, S. Schaffner, F. Schaper, Inorg. Chim. Acta (in press), doi:10.1016/j.ica.2007.10.040.
[8] E.C. Constable, Coord. Chem. Rev. 252 (2008) 842.
[9] E.C. Constable, E.L. Dunphy, C.E. Housecroft, M. Neuburger, S. Schaffner, F. Schaper, S.R. Batten, Dalton Trans. (2007) 4323.
[10] E.C. Constable, C.E. Housecroft, M. Neuburger, S. Schaffner, F. Schaper, Inorg. Chem. Commun. 9 (2006) 616.
[11] E.C. Constable, C.E. Housecroft, M. Neuburger, S. Schaffner, F. Schaper, Inorg. Chem. Commun. 9 (2006) 433.
[12] J.E. Beves, E.C. Constable, E.L. Dunphy, C.E. Housecroft, C.J. Kepert, M. Neuburger, D.J. Price, S. Schaffner, Dalton Trans. (2008) 386.
[13] C.M. Ollagnier, D. Nolan, C.M. Fitchett, S.M. Draper, Inorg. Chem. Commun. 10 (2007) 1045.
[14] G. Lowe, A.S. Droz, T. Vilaiven, G.W. Weaver, L. Tweedale, J.M. Pratt, P. Rock, V. Yardley, S.L. Croft, J. Med. Chem. 42 (1999) 999.
[15] G. Lowe, A.S. Droz, J.J. Park, G.W. Weaver, Bioorg. Chem. 27 (1999) 477.
[16] Z. Zhou, G.H. Sarova, S. Zhang, Z. Ou, F.T. Tat, K.M. Kadish, L. Echegoyen, D.M. Guldi, D.I. Schuster, S.R. Wilson, Chem. Eur. J. 12 (2006) 4241.
[17] COLLECT Software, Nonius BV, 1997–2001.
[18] A. Altomare, G. Cascarano, G. Giacovazzo, A. Guagliardi, M.C. Burla, G. Polidori, M. Camalli, J. Appl. Cryst. 27 (1994) 435.
[19] Z. Otwinowski, W. Minor, in: C.W. Carter Jr., R.M. Sweet (Eds.), Methods in Enzymology, vol. 276, Academic Press, New York, 1997, p. 307.
[20] P.W. Betteridge, J.R. Carruthers, R.I. Cooper, K. Prout, D.J. Watkin, J. Appl. Cryst. 36 (2003) 1487.
[21] I.J. Bruno, J.C. Cole, P.R. Edgington, M.K. Kessler, C.F. Macrae, P. McCabe, J. Pearson, R. Taylor, Acta Crystallogr., Sect. B 58 (2002) 389.
[22] J. Elguero, in: A.R. Katritzky, C.W. Rees (Eds.), Comprehensive Heterocyclic Chemistry, vol. 5, Pergamon Press, Oxford, 1984, p. 167.
[23] F. Texier-Boullet, B. Klein, J. Hamelin, Synthesis (1986) 409.
[24] R. Sreekumar, R. Padmakumar, Synth. Commun. 28 (1998) 1661.
[25] Y. Han, H.V. Huynh, Chem. Commun. (2007) 1089.
[26] A. Kochel, Acta Crystallogr., Sect. E 62 (2006) m37.
[27] A.A. Hergold-Brundic, Z. Popovic, D. Matkovic-Calogovic, Acta Crystallogr., Sect. C 52 (1996) 3154.
[28] M.G.B. Drew, M.J. Hudson, P.B. Iveson, M.L. Russell, J.-O. Liljenzin, M. Skålberg, L. Spjuth, C. Madic, J. Chem. Soc., Dalton Trans. (1998) 2973.
[29] C.J. Kepert, B.W. Skelton, A.H. White, Aust. J. Chem. 47 (1994) 391.
[30] C. Berthon, M.S. Grigoriev, Acta Crystallogr., Sect. E 61 (2005) o1216.
[31] I.A. Charushnikova, C. Den Auwer, Koord. Khim. 30 (2004) 546.
[32] K.N. Robertson, P.K. Bakshi, S.D. Lantos, T.S. Cameron, O. Knop, Can. J. Chem. 76 (1998) 583.
[33] M.G.B. Drew, P.B. Iveson, M.J. Hudson, J.-O. Liljenzin, L. Spjuth, P.-Y. Cordier, Å. Enarsson, C. Hill, C. Madic, J. Chem. Soc., Dalton Trans. (2000) 821.
[34] S. Coffey (Ed.), Rodd's Chemistry of Carbon Compounds, Part B, 2nd ed., vol. I, Elsevier, Amsterdam, 1965, pp. 68–71.
[35] A.J. Blake, P. Hubberstey, U. Suksangpanya, C.L. Wilson, J. Chem. Soc., Dalton Trans. (2000) 3873.
[36] Y.N. Belokon, P. Carta, A.V. Gutnov, V. Maleev, M.A. Moskalenko, L.V. Yashkina, N.S. Ikonnikov, N.V. Voskoboev, V.N. Khrustalev, M. North, Helv. Chim. Acta 85 (2002) 3301.
[37] J.R. Deschamps, D.A. Knight, E.R. Goldman, J.B. Delehanty, E.L. Chang, Acta Crystallogr., Sect. E 59 (2003) m916.
[38] E.C. Constable, A.M.W. Cargill Thompson, J. Chem. Soc., Dalton Trans. (1994) 1409.
[39] E.C. Constable, C.E. Housecroft, A. Cargill Thompson, P. Passaniti, S. Silvi, M. Maestri, A. Credi, Inorg. Chim. Acta 360 (2007) 1102.
[40] G.R. Desiraju, T. Steiner, The Weak Hydrogen Bond, Oxford University Press, Oxford, 1999. pp. 123–164.
[41] J. McMurtrie, I. Dance, CrystEngComm 7 (2005) 216.
[42] J. McMurtrie, I. Dance, CrystEngComm 7 (2005) 230.
[43] E.C. Constable, E. Figgemeier, C.E. Housecroft, J. Olsson, Y.C. Zimmermann, Dalton Trans. (2004) 1918.
[44] J.E. Beves, E.C. Constable, C.E. Housecroft, M. Neuburger, S. Schaffner, Inorg. Chem. Commun. 10 (2007) 1185.

[1] See references cited in Ref. [44].

Polyhedron 27 (2008) 2402–2408

Contents lists available at ScienceDirect

Polyhedron

journal homepage: www.elsevier.com/locate/poly

Syntheses, crystal structures and magnetic behaviors of three Mn^{II}-terephthalate coordination polymers containing terminal ligands

Xiao-Ming Lu [a,*], Pei-Zhou Li [a], Xiu-Teng Wang [b], Song Gao [b], Xiao-Jun Wang [a], Shuo Wang [a], Yu-Heng Deng [a], Yong-Jun Zhang [a], Lei Zhou [c]

[a] Department of Chemistry, Capital Normal University, Beijing 100037, PR China
[b] College of Chemistry and Molecular Engineering, Peking University, Beijing 100871, PR China
[c] Institute of Chemical Defence, Beijing 102205, PR China

ARTICLE INFO

Article history:
Received 24 February 2008
Accepted 6 April 2008
Available online 2 June 2008

Keywords:
Coordination polymer
Manganese complex
Terephthalic ligand
Magnetic property

ABSTRACT

Three Mn^{II}-terephthalate coordination polymers, $\{Mn^{II}(tp)(bpy)(H_2O)\}_n$ (**1**), $\{Mn^{II}_3(tp)_{6/2}(bpy)_2\cdot(dmf)\}_n$ (**2**) and $\{Mn^{II}(tp)(phen)\}_n$ (**3**) (tp = terephthalic dianion, bpy = 2,2′-bipyridine, phen = 1,10-phenanthroline) have been synthesized and characterized by single crystal X-ray diffraction studies and low temperature (2–300 K) magnetic measurements. The structure analysis of **1**–**3** show that they all are coordination polymers composed of Mn atoms as nodes and terephthalate dianions as spacers. Interestingly, compound **1** consists of 1D infinite zigzag chains, while compound **2** consists of 2D sheets and compound **3** has a 3D framework structure. The study of the temperature dependent magnetic susceptibilities revealed that all of the polymers show antiferromagnetism.

© 2008 Elsevier Ltd. All rights reserved.

1. Introduction

The design and construction of multi-dimensional functional metal-organic coordination polymers with metal ions as nodes and bridging ligands as spacers have attracted much attention from chemists in recent years [1–3]. This has arisen not only for their various intriguing topological structures, but also for their unexpected properties for potential practical applications in material chemistry, such as heterogeneous catalysis, gas sorption, storage and separations, molecular recognition, non-linear optics, luminescent and magnetic properties [4–6].

Selection of the appropriate multidentate ligand to link paramagnetic metal ions is a powerful way for the building of polyfunctional coordination polymers. As a multidentate ligand, terephthalic acid (H_2tp) and its dianion have been used in synthetic systems, not only because they can act as short bridges via one carboxylic group or long bridges via the benzene ring, leading to abundant varieties of multi-dimensional coordination polymers with various kinds of topology, but also terephthalic acid, as an example of a benzenedicarboxylic acid, has a rigid aromatic unit as a spacer which can make give rise to very special systems that can have interesting electronic and magnetic interactions between the metal ions in the network through possible conjugative interactions (shown in Scheme 1) [7,8]. On the other hand, the terminal ligands play an important role in the structures and properties of the coordination polymers [9].

Herein, we report the synthesis, crystal structure and magnetic properties of three manganese coordination polymers, $\{Mn^{II}(tp)(bpy)(H_2O)\}_n$ (**1**), $\{Mn^{II}_3(tp)_{6/2}(bpy)_2\cdot(dmf)\}_n$ (**2**) and $\{Mn^{II}(tp)(phen)\}_n$ (**3**) (tp = terephthalic dianion, bpy = 2,2′-bipyridine, phen = 1,10-phenanthroline, dmf = *N*,*N*-dimethylformamide), with the terephthalic dianion acting as a bridging ligand and 2,2′-bipyridine (in **1** and **2**) and 1,10-phenanthroline (in **3**) as terminal ligands.

2. Experimental

2.1. Materials and general methods

All reagents for the syntheses and analyses were obtained commercially, were of analytical grade and were used without further purification, and all manipulations were carried out in the laboratory atmosphere. Elemental analyses (C, H and N) were performed on a Perkin–Elmer 240C elemental analyzer. Infrared spectra were recorded as KBr pellets on a Bruker EQUIN0X 55 IR spectrometer. Magnetic measurements were carried out with polycrystalline samples on a Quantum Design MPMS XL-5 SQUID magnetometer. The diamagnetic corrections were evaluated from Pascal's constants.

* Corresponding author.
E-mail address: xiaoming-lu@163.com (X.-M. Lu).

0277-5387/$ - see front matter © 2008 Elsevier Ltd. All rights reserved.
doi:10.1016/j.poly.2008.04.029

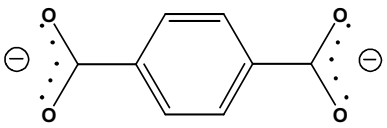

Scheme 1.

2.2. Syntheses of complexes *1* and *3*

2.2.1. $\{Mn^{II}(tp)(bpy)(H_2O)\}_n$ (*1*)

A mixture of $Mn(OAc)_2 \cdot 4H_2O$ (0.169 g, 1 mmol) in water (10 ml) and terephthalic acid (0.166 g, 1 mmol) in NaOH (80 mg, 2 mmol) aqueous solution (10 ml) were stirred at room temperature for about 12 h. Yellow crystals of compound **1** were obtained by diffusion of a 10 ml ethanol solution of 2,2′-bipyridine (0.156 g, 1 mmol) and the filtrate of the mixed solution after about 1 week (yield: about 32% based on Mn). *Anal.* Calc. for $\{Mn^{II}(tp)(bpy)(H_2O)\}_n$ (**1**): C, 54.98; H, 3.59; N, 7.12. Found: C, 55.01; H, 3.62; N, 7.16%. IR (KBr, cm^{-1}): 1576.53 s, 1475.14 m, 1438.82 s, 1378.05 s, 1151.97 m, 1058.54 w, 1018.48 m, 866.10 w, 805.18 m, 760.16 s, 736.45 m, 649.63 m, 524.31 m.

2.2.2. $\{Mn^{II}_3(tp)_{6/2}(bpy)_2 \cdot (dmf)\}_n$ (*2*)

A solution of $MnCl_2$ (0.136 g, 1 mmol) in 10 ml of water was added to a solution of terephthalic acid (0.249 g, 1.5 mmol) and 2,2′-bipyridine (0.156 g, 1 mmol) in DMF (10 ml), stirring for about 2 h at room temperature. Then the resulting solution was transferred into a Teflon-Steel autoclave inside a programmable electric furnace reactor. The mixed-solvo-thermal reaction lasted for about 3 days at about 423.15 K, and then the mixture was cooled to room temperature naturally. Yellow single crystals were obtained (yield = about 78% based on Mn). *Anal.* Calc. for $\{Mn^{II}_3(tp)_{6/2}(bpy)_2 \cdot (dmf)\}_n$ (**2**): C, 54.14; H, 3.38; N, 6.72. Found: C, 54.28; H, 3.51; N, 6.83%. IR (KBr, cm^{-1}): 1576.76 s, 1474.78 m, 1439.04 s, 1380.86 s, 1313.63 m, 1151.88 m, 1095.69 w, 1058.42 w, 1018.52 m, 971.55 w, 803.94 m, 760.23 s, 668.17 w, 649.94 m, 628.01 w, 524.9 m.

Table 1
Crystallographic data and structure refinement summary for complexes **1**–**3**

	1	2	3
Formula	$C_{18}H_{14}MnN_2O_5$	$C_{47}H_{35}Mn_3N_5O_{13}$	$C_{20}H_{12}MnN_2O_4$
Mr	393.25	1042.62	399.26
Temperature (K)	290(2)	290(2)	290(2)
Wavelength (Å)	0.71073	0.71073	0.71073
Crystal system	monoclinic	monoclinic	monoclinic
Space group	*P*2(1)/*n*	*C*2/*c*	*C*2/*c*
a (Å)	9.8665(3)	18.4033(2)	17.4786(11)
b (Å)	16.3330(6)	25.7135(3)	10.3332(6)
c (Å)	11.3035(4)	9.90320(10)	9.3359(6)
β (°)	111.6760(10)	91.4350(10)	96.173(3)
V (Å^3)	1692.75(10)	4684.86(9)	1676.38(18)
Z	4	4	4
D_{calc} (g cm^{-3})	1.543	1.478	1.582
Crystal size (mm)	0.30 × 0.24 × 0.16	0.32 × 0.24 × 0.20	0.26 × 0.24 × 0.20
Theta range (°)	2.31 to 28.33	2.21 to 28.28	2.29 to 28.28
Reflections collected/ unique	16733/4190	21921/5786	8019/2086
R_{int}	0.0292	0.0203	0.0274
Completeness to theta	99.5% (28.33)	99.5% (28.28)	99.6% (28.28)
Data/restraints/ parameters	4190/0/240	5786/0/325	2086/0/124
Refinement method	full-matrix least-squares on F^2	full-matrix least-squares on F^2	full-matrix least-squares on F^2
Goodness-of-fit on F^2	1.056	1.030	1.037
Final R_1 and wR_2 indices	R_1 = 0.0317, wR_2 = 0.0868	R_1 = 0.0323, wR_2 = 0.0949	R_1 = 0.0296, wR_2 = 0.0895
R_1 and wR_2 indices (all data)	R_1 = 0.0468, wR_2 = 0.0918	R_1 = 0.0398, wR_2 = 0.0991	R_1 = 0.0379, wR_2 = 0.0924
Min, Max peaks (*e* Å^{-3})	0.321 and −0.244	0.504 and −0.431	0.308 and −0.261

Table 2
Selected bond lengths (Å) and angles (°) for complex **1**

Mn(1)–O(1)	2.2709(11)	Mn(1)–N(1)	2.2615(14)
Mn(1)–O(2)	2.2854(11)	Mn(1)–N(2)	2.2391(14)
Mn(1)–O(3)#1	2.0985(11)	Mn(1)–O(5)	2.1625(12)
O(1)–Mn(1)–O(2)	57.30(4)	N(1)–Mn(1)–O(2)	95.66(5)
O(1)–Mn(1)–O(3)#1	97.98(5)	N(1)–Mn(1)–O(1)	94.23(5)
O(1)–Mn(1)–O(5)	146.97(5)	N(2)–Mn(1)–O(1)	88.78(5)
O(3)#1–Mn(1)–O(2)	105.69(5)	N(2)–Mn(1)–O(2)	143.80(5)
O(3)#1–Mn(1)–O(5)	86.90(5)	N(2)–Mn(1)–N(1)	72.73(5)
O(3)#1–Mn(1)–N(2)	90.01(5)	O(5)–Mn(1)–O(2)	89.86(5)
O(3)#1–Mn(1)–N(1)	158.63(5)	O(5)–Mn(1)–N(1)	92.37(5)
O(5)–Mn(1)–N(2)	124.01(5)		

Symmetry transformations used to generate equivalent atoms: #1 $x - 1/2$, $-y + 1/2$, $z + 1/2$; #2 $x + 1/2$, $-y + 1/2$, $z - 1/2$.

Table 3
Selected bond lengths (Å) and angles (°) for complex **2**

Mn(1)–O(2)	2.1323(11)	O(1)–C(11)	1.266(2)
Mn(1)–O(4)	2.2104(10)	O(2)–C(11)	1.240(2)
Mn(1)–O(6)	2.1094(12)	O(4)–C(15)	1.288(2)
Mn(2)–O(1)	2.1162(11)	O(3)–C(15)	1.242(2)
Mn(2)–O(4)	2.2057(11)	O(5)–C(19)	1.257(2)
Mn(2)–O(5)	2.0912(11)	C(19)–O(6)	1.243(2)
Mn(2)–N(1)	2.2534(14)	C(23)–O(7)	1.73(3)
Mn(2)–N(2)	2.2959(15)	O(4)–Mn(2)–N(2)	87.53(5)
O(2)#1–Mn(1)–O(2)	180.00(5)	N(1)–Mn(2)–N(2)	71.70(5)
O(4)–Mn(1)–O(4)#1	180.0	C(1)–N(1)–Mn(2)	123.09(12)
O(6)#1–Mn(1)–O(6)	180.00(6)	C(5)–N(1)–Mn(2)	118.52(12)
O(6)–Mn(1)–O(2)	93.64(6)	C(19)–O(5)–Mn(2)	121.26(10)
O(2)–Mn(1)–O(4)	88.08(4)	C(10)–N(2)–Mn(2)	123.69(13)
O(6)–Mn(1)–O(4)	89.58(5)	C(6)–N(2)–Mn(2)	117.11(12)
O(5)–Mn(2)–O(1)	101.82(5)	C(11)–O(1)–Mn(2)	126.39(10)
O(5)–Mn(2)–O(4)	109.14(4)	C(11)–O(2)–Mn(1)	140.47(12)
O(1)–Mn(2)–O(4)	93.89(4)	O(2)–C(11)–O(1)	125.66(15)
C(19)–O(6)–Mn(1)	148.96(12)	C(15)–O(4)–Mn(2)	95.04(9)
O(5)–Mn(2)–N(1)	88.34(5)	C(15)–O(4)–Mn(1)	128.26(10)
O(1)–Mn(2)–N(1)	105.10(5)	Mn(2)–O(4)–Mn(1)	105.74(4)
O(4)–Mn(2)–N(1)	151.12(5)	O(3)–C(15)–O(4)	120.69(15)
O(5)–Mn(2)–N(2)	159.42(5)	O(6)–C(19)–O(5)	125.12(15)
O(1)–Mn(2)–N(2)	88.58(5)		

Symmetry transformations used to generate equivalent atoms: #1 $-x + 1/2$, $-y + 1/2$, $-z + 1$; #2 $-x$, y, $-z + 3/2$; #3 $-x + 1/2$, $-y + 1/2$, $-z$; #4 $-x + 1$, y, $-z + 3/2$.

Table 4
Selected bond lengths (Å) and angles (°) for complex **3**

Mn(1)–O(1)	2.1387(8)	O(2)–C(7)	1.2506(12)
Mn(1)–O(2)#1	2.1183(8)	N(1)–C(1)	1.3273(14)
Mn(1)–N(1)	2.3499(9)	N(1)–C(6)	1.3554(13)
O(1)–C(7)	1.2519(13)		
O(2)#4–Mn(1)–O(2)#1	99.63(4)	C(7)–O(1)–Mn(1)	145.24(7)
O(2)#1–Mn(1)–O(1)	98.24(3)	C(7)–O(2)–Mn(1)#1	144.24(7)
O(2)#4–Mn(1)–O(1)	85.32(3)	C(1)–N(1)–Mn(1)	125.84(7)
O(1)#2–Mn(1)–O(1)	174.51(4)	C(6)–N(1)–Mn(1)	116.60(6)
N(1)#2–Mn(1)–N(1)	70.88(4)	O(2)–C(7)–O(1)	126.41(9)
O(2)#4–Mn(1)–N(1)	94.83(3)	O(1)#2–Mn(1)–N(1)	89.93(3)
O(2)#1–Mn(1)–N(1)	165.28(3)	O(1)–Mn(1)–N(1)	85.59(3)

Symmetry transformations used to generate equivalent atoms: #1 $-x$, $-y + 1$, $-z + 1$; #2 $-x$, y, $-z + 3/2$; #3 $-x + 1/2$, $-y + 1/2$, $-z + 1$; #4 x, $-y + 1$, $z + 1/2$.

2.2.3. $\{Mn^{II}(tp)(phen)\}_n$ (**3**)

A solution of $MnCl_2$ (0.136 g, 1 mmol) in 10 ml of water was added to a solution of terephthalic acid (0.249 g, 1.5 mmol) and 1,10-phenanthroline (0.198 g, 1 mmol) in DMF (10 ml), stirring for about 2 h at room temperature. Then the resulting solution was transferred into a Teflon-Steel autoclave inside a programmable electric furnace reactor. The mixed-solvo-thermal reaction lasted for about 3 days at about 423.15 K, and then the mixture was cooled to room temperature naturally. Yellow single crystals were obtained (yield = about 82% based on Mn). *Anal.* Calc. for $\{Mn^{II}(tp)(phen)\}_n$ (**3**): C, 60.17; H, 3.01; N, 7.01. Found: C, 60.31; H, 3.19; N, 7.12%. IR (KBr, cm^{-1}): 1598.26 s, 1514.15 m, 1495.77 w, 1425.86 m, 1387.00 s, 1100.70 w, 1046.49 w, 1024.00 w, 890.79 w, 863.80 w, 846.12 m, 807.17 m, 770.50 w, 750.31 s, 729.00 m, 633.97 w, 505.50 m.

2.3. Crystallographic data collection and refinement

X-ray diffraction measurements were performed on a Bruker SMART diffractometer equipped with a CCD area detector with graphite-monochromated Mo Kα radiation (Kα = 0.71073 Å) at about 290(2) K. The reflections were successfully indexed by an automated indexing routine built in the SMART program [10]. The solutions were solved by direct methods and refined by full-matrix least-squares calculations on F^2 with SHELX-97 [11]. All non-hydrogen atoms were refined anisotropically. All hydrogen atoms were located in the calculated positions using the riding model. Crystallographic data and refinement details for the structural analyses of all the complexes are summarized in Table 1, and selected bond lengths and angles with their estimated standard deviations for complexes **1**–**3** in are in Tables 2–4, respectively.

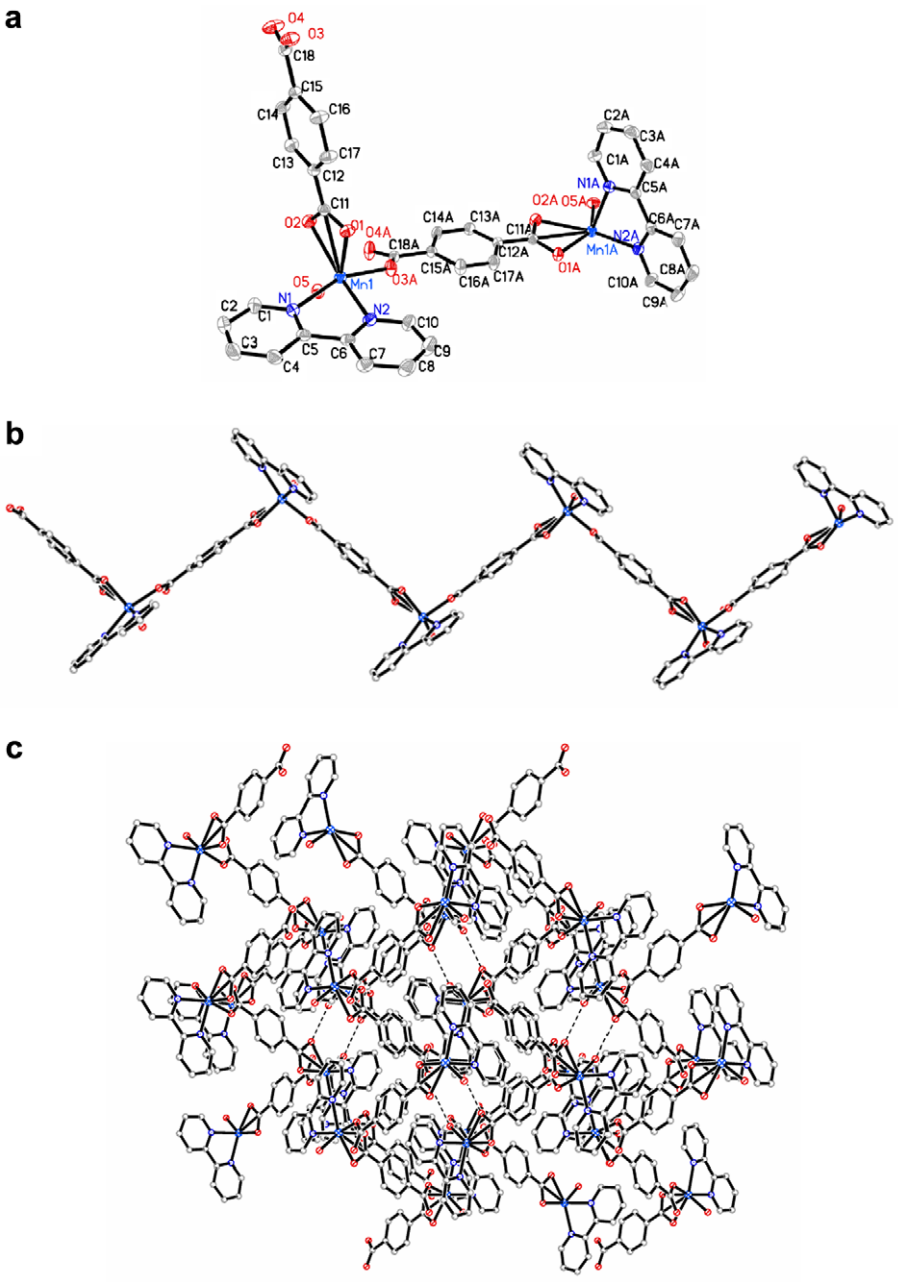

Fig. 1. (a) Perspective view of the asymmetry unit of **1**; (b) perspective view of the zigzag one-dimensional chain of **1**; (c) crystal packing diagram of **1** along the *c* axis, showing the hydrogen-bond interactions between the one-dimensional chains.

3. Results and discussion

3.1. Description of the crystal structures of complexes **1**–**3**

3.1.1. $\{Mn^{II}(tp)(bpy)(H_2O)\}_n$ (**1**)

X-ray single crystal structure determination reveals that complex **1** is a neutral one-dimensional infinite zigzag coordination chain. Each Mn^{II} center coordinates to two N donors of one 2,2′-bipyridine, three oxygen atoms belonging to two different carboxyl groups of two different terephthalic acid molecules and one water molecule, forming a distorted octahedral geometry as shown in Fig. 1a. Then, two neighboring Mn^{II} centers are connected by a terephthalic dianion which acts as a long bridge through the benzene ring as shown in Scheme 1. The 2,2′-bipyridine molecule acts as a terminal ligand which prevents the chain from growing in a straight forward direction, and making it into a zigzag chain. (Fig. 1b). Selected bond lengths and angles are listed in Table 2.

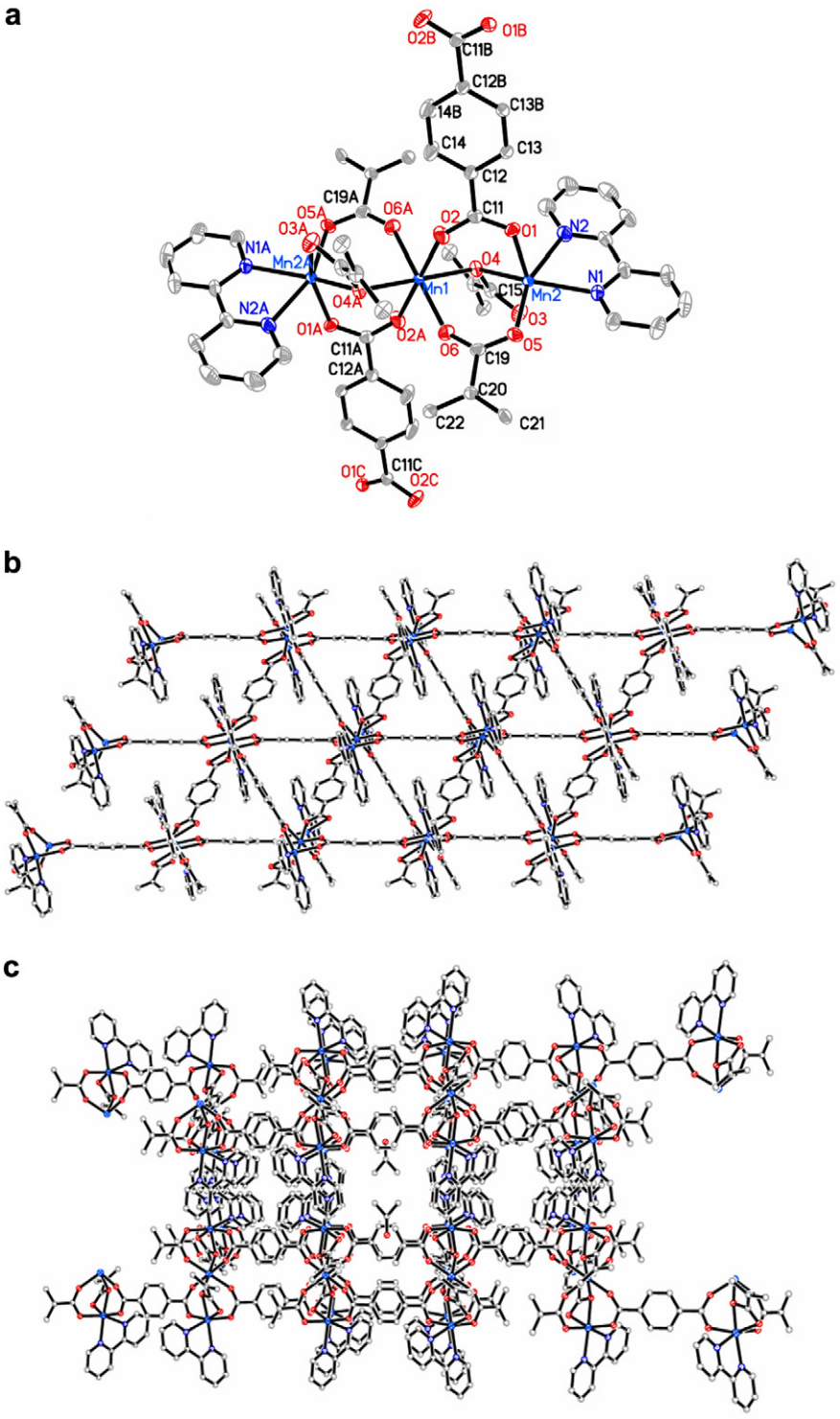

Fig. 2. (a) Perspective view of the trinuclear node of **2**; (b) perspective view of the two-dimensional sheet of **2**, viewing along the *b* axis; (c) crystal packing diagram of **2** along the *c* axis, showing the $\pi\cdots\pi$ stacking interaction between two sheets.

Analysis of the crystal packing of **1** in the unit cell indicates that there is one type of independent inner-chain O–H···O hydrogen bond and one kind of independent inter-chain O–H···O hydrogen bond (Table 3). The former is formed by the O–H group of the coordinated water molecule with the uncoordinated oxygen atom of the neighboring carboxyl groups of the terephthalic dianion in an asymmetric unit with a D···A distance of 2.6749(18) Å and an O–H–O angle of 147.1°. The inter-chain O–H···O hydrogen bonds are formed by the O–H group of the coordinated water molecule in one coordination chain with one of the coordinated oxygen atoms of the carboxyl groups of the terephthalic dianion in the adjacent coordination chain, with a D···A distance of 2.7111(17) Å and an O–H–O angle of 165(3)°.

3.1.2. $\{Mn^{II}_3(tp)_{6/2}(bpy)_2 \cdot (dmf)\}_n$ (**2**)

The crystal structure analysis shows that complex **2** adopts a 2D framework. The 2D skeleton is formed by Mn ions as nodes and tp dianions as spacers, through coordination bonds. At each node there are three Mn^{II} atoms that are in a linear arrangement with Mn···Mn distances of 3.266 Å (Fig. 2a), all of which have a distorted octahedral geometry and two adjacent octahedrons share a triangular face. The middle Mn^{II} atom is coordinated by six oxygen atoms (Mn–O = 2.038(3)–2.254(3) Å) belonging to six different tp carboxylate groups, while each of the two terminal Mn^{II} atoms is coordinated by four oxygen atoms (Mn–O = 2.038(3)–2.254(3) Å) belonging to four different tp carboxylate groups and two nitrogen atoms (Mn–N = 2.038(3)–2.254(3) Å) of one chelating 2,2′-bipyridine ligand.

Each three Mn^{II}-atoms-cluster node is bridged by six tp ligands in six directions in the 0 1 0 plane with two 2,2′-bipyridine ligands upon and down the plane, respectively, and the angles between the two directions are nearly 60° (Fig. 2b). Every three nodes are connected by three tp ligands along the 1 0 0, 1 0 1 and 2 0 1 planes to form an equilateral triangle. Then the remarkable two-dimensional

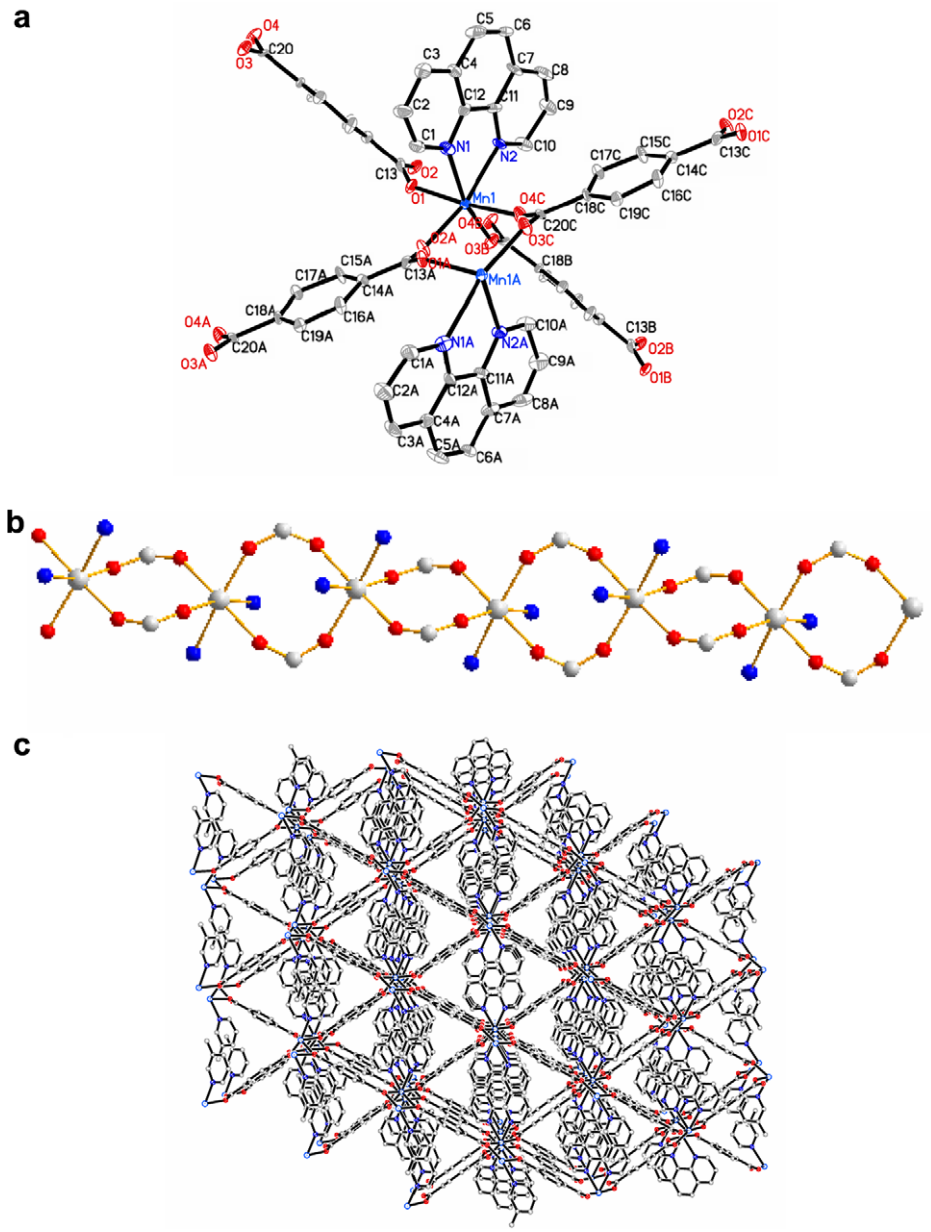

Fig. 3. (a) Perspective view of the asymmetry unit of **3**; (b) perspective view of the one-dimensional $\{Mn\}_n$ chain of **3**; (c) perspective view of the three-dimensional framework of **3** along the *c* axis.

sheets are formed by the equilateral triangle arrays (Fig. 2b). The distance between two adjacent 2,2′-bipyridine ligands of two neighboring sheets is 3.446 Å, which is within the range of $\pi\cdots\pi$ stacking interactions, 3.3–3.7 Å. The $\pi\cdots\pi$ stacking interactions between the two sheets connects the sheets into a 3D coordination polymer (Fig. 2c), the interspace of which is filled by isolated DMF molecules.

3.1.3. $\{Mn^{II}(tp)(phen)\}_n$ (3)

The crystal structure analysis shows that there is one terephthalic ligand, one 1,10-phenanthroline ligand and one Mn^{II} atom in each asymmetric unit of complex **3**, which build up a three-dimensional structural framework. Each Mn^{II} atom has a distorted octahedral geometry, being coordinated to four oxygen atoms (Mn–O = 2.106(2)–2.145(2) Å) belonging to four different carboxyl groups of four different terephthalic dianions, and two nitrogen atoms of one phen molecule (Mn–N = 2.323(2)–2.368(2) Å) (Fig. 3a).

The bidentate carboxylate groups, in pairs, belong to two different terephthalic dianions and, acting as short bridges, bridge two neighboring Mn atoms to form an eight-membered ring in a chair configuration. One of the two Mn atoms and another neighboring Mn atom are bridged by two other bidentate carboxylate groups in a pair to form another eight-membered ring plane. The two planes cross with angles of nearly 60°, and each two crossed eight-membered rings alternatively bridge the neighboring Mn atoms to form 1D $[Mn_2(CO_2)_2(phen)_2]_n$ chains with Mn···Mn distances of 4.7894 Å (Fig. 3b). Then the terephthalic dianions, acting as long bridges via the benzene ring in the directions of the two basal eight-membered ring planes, link $[Mn_2(CO_2)_2(phen)_2]_n$ chains to form the 3D structure of **3** and 1D channels along the 1D $[Mn_2(CO_2)_2(phen)_2]_n$ chains.

The 1D channels along the 1D $[Mn_2(CO_2)_2(phen)_2]_n$ chains in **3** are filled with coordinated 1,10-phenanthroline molecules. It should be pointed out that the mean distance of two neighboring face-to-face stacked 1,10-phenanthroline molecules is about 3.629 Å, which is within the range of $\pi\cdots\pi$ stacking interactions, 3.3–3.7 Å.

3.2. Magnetic properties

The variation of the molar magnetic susceptibilities χ_M was investigated for compounds **1**–**3** in the temperature range 2–300 K at a field of 1000 Oe. The study of the temperature dependent magnetic susceptibilities revealed that all the compounds show antiferromagnetic behaviour.

The thermal variation of χ_M^{-1} and $\chi_M T$ of **1** are displayed in Fig. 4a. According to the χ_M^{-1}–T curve, the magnetic behavior of **1** follows the Curie–Weiss law $\chi_M = C/(T-\theta)$ with a Curie constant C value of 4.14 $cm^3\,K\,mol^{-1}$ and a Weiss temperature θ of −0.70 K. The value of $\chi_M T$ at 300 K is 4.64 $cm^3\,K\,mol^{-1}$ per Mn^{II}, which is slightly above the expected value for the $S = 5/2$ spin-only ground state per couple of uncorrelated Mn^{II} centers (4.35 $cm^3\,K\,mol^{-1}$). This value decreases smoothly to close to 3.35 $cm^3\,K\,mol^{-1}$ at 2 K. Such magnetic behavior is typical for an antiferromagnetic coupling between the Mn^{II} ions in the chain. The magnetic susceptibility of **1** has been fitted to the Fisher model [12] of the isotropic Heisenberg antiferromagnet, and later modified by Wagner and Friedberg [13] for a Mn^{2+} system of spin 5/2, which is

$$\chi = \frac{NS(S+1)}{3kT}g^2\beta^2\frac{1-u(K)}{1+u(K)} \qquad (1)$$

where $u(K)$ is $1/K - \coth(K)$, $K = 2JS(S+1)/kT$, $g = 2$, $S = 5/2$ for Mn(II) and N, β, K, g and T have their usual meanings. Due to the interaction between adjacent chains, the fit function can be modified to include the inter-chain coupling [14]. The function, therefore, is

$$\chi_M = \frac{\chi}{1-(2zJ'/Ng^2\beta^2)\chi} \qquad (2)$$

where J' is the inter-chain exchange coupling constant and z is the number of the nearest neighbor chains. The best fitting for the data in the range of 2–300 K gives $J = -0.035$ cm^{-1}, $zJ' = +0.028$ cm^{-1} and $g = 2.00$, with $R = 4.2\times10^{-6}$, $\left[R = \left[\sum(\chi_{obs}-\chi_{calc})^2/\sum(\chi_{obs})^2\right]\right]$.

According to the χ_M^{-1}–T curve, the magnetic susceptibility data for **2** also fit well to the Curie–Weiss law in the range 2–300 K and give a Curie constant C value of 10.8 $cm^3\,K\,mol^{-1}$ and a Weiss temperature θ of −1.81 K. The value of $\chi_M T$ at 300 K is 10.85 $cm^3\,K\,mol^{-1}$ per tri-Mn^{II} unit. These value decreases smoothly to close to 7.83 $cm^3\,K\,mol^{-1}$ at 2 K. Such magnetic behavior shows antiferromagnetic couplings between the Mn^{II} ions.

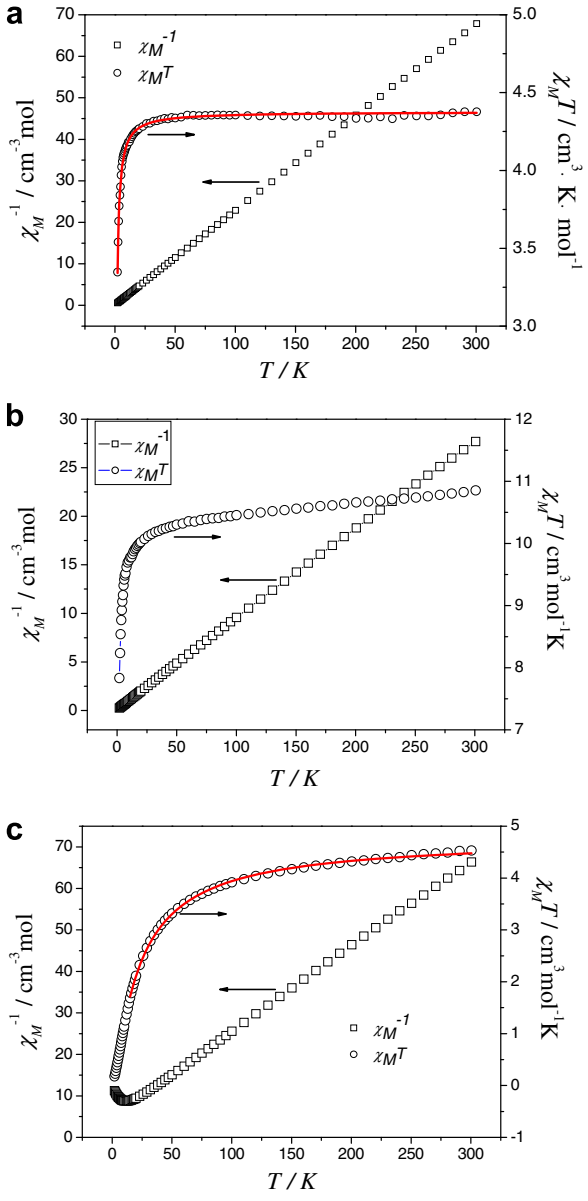

Fig. 4. (a) The thermal variation of χ_M^{-1} and $\chi_M T$ of **1**; (b) the thermal variation of χ_M^{-1} and $\chi_M T$ of **2**; (c) the thermal variation of χ_M^{-1} and $\chi_M T$ of **3**.

The magnetic susceptibility data for **3** also follows the Curie–Weiss law in the range 12–300 K ($C = 5.10\ cm^3\ K\ mol^{-1}$, $\theta = -34.4$ K). At 300 K, the $\chi_M T$ value of **3** is $4.53\ cm^3\ K\ mol^{-1}$, which is slightly above the expected value for $S = 5/2$ of a spin-only ground state per couple of uncorrelated Mn^{II} centers ($4.35\ cm^3\ K\ mol^{-1}$). This value decreases smoothly to close to $0.18\ cm^3\ K\ mol^{-1}$ at 2 K. The decrease of $\chi_M T$ is attributed to antiferromagnetic interactions between the Mn^{II} ions. As mentioned above, the 3D structure of **3** can be viewed as $[Mn_2(CO_2)_2(phen)_2]_n$ chains linked by a long bridge, the terephthalic dianions. So we can evaluate the value of the couplings via the Fisher model as in the case of **1**, where zJ' is the inter-chain interactions of the neighboring $[Mn_2(CO_2)_2(phen)_2]_n$ chains. The best fitting for the data in the range 15–300 K gives $J = -0.53\ cm^{-1}$, $zJ' = -0.69\ cm^{-1}$ and $g = 2.09$, with $R = 3.2 \times 10^{-5}$, $\left[R = \left[\sum(\chi_{obs} - \chi_{calc})^2 / \sum(\chi_{obs})^2\right]\right]$.

Comparing the magnetic properties of **1**–**3**, especially the Weiss constants (−0.70, −1.81 and −34.4 K, respectively), it is obvious that the antiferromagnetic coupling in **1** and**2** is much weaker than that in **3**, which mainly results from the difference between their structures. Compound **1** can be viewed as having isolated Mn^{II} nucleii and **2** can be viewed as isolated trinuclear Mn^{II} clusters separated by the terephthalate ligands, which act as long bridges via the benzene ring, while compound **3** can be regarded as infinite 1D Mn^{II} chains linked by short three-atom O–C–O bridges.

4. Conclusion

Three Mn^{II}-terephthalate coordination polymers have been synthesized with different terminal ligands, and the crystal structure analyses show that the compounds are in the form of 1D infinite chains or 2D sheets with 2,2′-bipyridine as a terminal ligand, while the compound with 1,10-phenanthroline as a terminal ligand has a 3D framework. Despite the different structures, a magnetic investigation indicates that all three coordination polymers show antiferromagnetism. Further works are focused on investigation of the influence of other multidentate ligands and terminal ligands to the structures and properties of the coordination polymers.

Acknowledgements

We gratefully acknowledge the Beijing Natural Science Foundation (No. 2052007) for the fund support of this research, and Dr. Charles F. Campana from Bruker AXS Inc. for the refinement of structure **2**.

Appendix A. Supplementary data

CCDC 641261, 642728 and 644541 contain the supplementary crystallographic data for **1**, **2** and **3**. These data can be obtained free of charge via http://www.ccdc.cam.ac.uk/conts/retrieving.html, or from the Cambridge Crystallographic Data Centre, 12 Union Road, Cambridge CB2 1EZ, UK; fax: (+44) 1223-336-033; or e-mail: deposit@ccdc.cam.ac.uk. Supplementary data associated with this article can be found, in the online version, at doi:10.1016/j.poly.2008.04.029.

References

[1] (a) O.M. Yaghi, M. O'Keeffe, N.W. Ockwig, H.K. Chae, M. Eddaoudi, J. Kim, Nature 423 (2003) 705;
(b) H. Li, A. Laine, M. O'Keeffe, O.M. Yaghi, Science 283 (1999) 1145.
[2] S. Kitagawa, R. Kitaura, S.-I. Noro, Angew. Chem., Int. Ed. 43 (2004) 2334.
[3] S.Y. Yu, Z.X. Zhang, E.C.-C. Cheng, Y.Z. Li, V.W.-W. Yam, H.P. Huang, R. Zhang, J. Am. Chem. Soc. 127 (2005) 17994.
[4] J.L.C. Rowsell, E.C. Spencer, J. Eckert, J.A.K. Howard, O.M. Yaghi, Science 309 (2005) 1350.
[5] (a) P.Z. Li, X.M. Lu, B. Liu, S. Wang, X.J. Zhang, Inorg. Chem. 46 (2007) 5823;
(b) X.M. Lu, B. Liu, S. Wang, Y. Deng, Inorg. Chem. Commun. 9 (2006) 403.
[6] Y. Liu, G. Li, X. Li, Y. Cui, Angew. Chem. Int. Ed. 46 (2007) 6301.
[7] W. Chen, J.Y. Wang, C. Chen, Q. Yue, H.M. Yuan, J.S. Chen, S.N. Wang, Inorg. Chem. 42 (2003) 944.
[8] C. Serre, F. Millange, C. Thouvenot, M. Noguès, G. Marsolier, D. Louër, G. Férey, J. Am. Chem. Soc. 124 (2002) 13519.
[9] B. Zhai, W.Z. Shen, X.Y. Chen, H.B. Song, W. Shi, P. Cheng, Inorg. Chem. Commun. 9 (2006) 1293.
[10] Bruker AXS, SAINT Software Reference Manual, Madison, WI, 1998.
[11] G.M. Sheldrick, SHELXTL NT Version 5.1, Program for Solution and Refinement of Crystal Structures, University of Göttingen, Germany, 1997.
[12] M.E. Fisher, Am. J. Phys. 32 (1963) 343.
[13] G.R. Wagner, S.A. Friedberg, Phys. Lett. 9 (1964) 11.
[14] J.N. McElearney, S. Merchant, R.L. Carlin, Inorg. Chem. 12 (1973) 906.

Polyhedron 27 (2008) 2409–2415

Contents lists available at ScienceDirect

Polyhedron

journal homepage: www.elsevier.com/locate/poly

Two new end-on azido bridged dinuclear copper(II) and cobalt(III) complexes derived from the (*E*)-*N*′-((pyridin-2-yl)methylene) acetohydrazide Schiff base ligand: Characterisation, crystal structures and magnetic study

Aurkie Ray [a], Sambuddha Banerjee [a], Ray. J. Butcher [b], Cédric Desplanches [c], Samiran Mitra [a,*]

[a] Department of Chemistry, Jadavpur University, Kolkata 700 032, West Bengal, India
[b] Department of Chemistry, Howard University, 2400 Sixth Street, NW Washington, DC 20059, USA
[c] ICMCB, CNRS, Université Bordeaux 1, 87, Avenue du Dr. A. Schweitzer, 33608 Pessac Cedex, France

ARTICLE INFO

Article history:
Received 14 January 2008
Accepted 16 April 2008
Available online 2 June 2008

Keywords:
Copper(II)
Cobalt(III)
Dinuclear complexes
Acetic hydrazide
Schiff bases

ABSTRACT

Metal complexes of Schiff bases derived from an aromatic hydrazide are well characterised and have been reported several times. Single crystal structures of metal hydrazone complexes derived from an aliphatic hydrazide are very rare and still remain unexplored. In this paper we report two new end-on azido bridged dinuclear copper(II) and cobalt(III) hydrazone complexes derived from an aliphatic hydrazide. The Schiff base [**LH** = $CH_3C(O)NHN{=}CHC_5H_4N$] has resulted from the condensation of acetic hydrazide and pyridine-2-carboxaldehyde. The ligand and the complexes $[Cu_2(L)_2(\mu_{1,1}\text{-}N_3)_2]$ (**1**) and $[Co_2(L)_2(\mu_{1,1}\text{-}N_3)_2(N_3)_2]$ (**2**) are characterised by elemental analysis, IR and UV–Vis spectral studies and in addition mass spectroscopy has been also carried out for **LH**. The structures of **1** and **2** have been established by X-ray crystallography. Variable temperature magnetic susceptibility measurement studies of **1** indicate the $\chi_M T$ values remain constant in the whole range of temperature 10 to 300 K at a value close of 0.75 $cm^3\,K\,mol^{-1}$, which is in good agreement with the one expected for two uncoupled copper(II) centers.

© 2008 Elsevier Ltd. All rights reserved.

1. Introduction

Synthesising dinuclear complexes using tridentate Schiff bases and bridging ligands have been carried out by many authors [1]. Coordination sites of metal ions which prefer square pyramidal geometry are blocked by such tridentate Schiff base ligands and to saturate the coordination number of the metal ion a bridging ligand (e.g. N_3, NCO, NCS, NCSe) is used to synthesise such dinuclear complexes [2–5]. Aroylhydrazones of pyridine-2-carboxaldehyde act as a potentially tridentate blocking ligand and can coordinate a given metal ion via the pyridine-N, the imine–N and the amide–O centres. Moreover, these ligands exhibit keto–enol tautomerism and can coordinate metal ions in neutral and monoanionic forms [6]. Metal complexes of aromatic hydrazide and aroylhydrazones have been synthesised earlier by Mitra and his group [7] and recently pseudohalide bridged dinuclear and polynuclear metal complexes of (*E*)-*N*′-((pyridin-2-yl)methylene)benzohydrazide have been reported by his research group [8]. Although metal complexes of aromatic hydrazones have been thoroughly explored, metal complexes of aliphatic hydrazones are yet to be explored. In order to exploit the bridging abilities of the pseudohalides several pseudohalide bridged Schiff base metal complexes of different nuclearities have been synthesised [9–11]. Such complexes especially dinuclear and polynuclear have drawn attention of many authors as they show significant structural variations and can act as potent magnetic materials. Magnetic interactions between the metal centers of such complexes can be tuned by skillful control of the chain length and the byte angle of the bridging ligands and in this respect the azide ion plays a significant role. The different types of binding modes of azide ion are shown in Fig. 1. The end-to-end or 1,3-coordination mode of N_3^- results in antiferromagnetic coupling between the metal centres but if the bond angle in M-$\mu_{1,3}$-N_3–M is very large then the sign of the coupling may be reversed [12–15]. In contrast the end-on or 1,1-coordination mode produces ferromagnetic coupling but the ferromagnetic ordering between the metal centres is reduced if the bridging byte angle exceeds 108° [16]. Dinuclear copper(II) complexes with such azide bridges have been extensively studied as they show interesting structural, magnetic, catalytic, and electron transfer properties [17–20]. Even though azide ion acts as an inhibitor of metalloprotein activities [21–23] such dinuclear azido bridged copper(II) complexes have been studied extensively [23] as dinuclear and trinuclear metallo species can act as models for active sites of metallo proteins [21a,21b,24–27].

* Corresponding author. Tel.: +91 033 2414 6666x2505; fax: +91 033 2414 6414.
E-mail address: smitra_2002@yahoo.com (S. Mitra).

0277-5387/$ - see front matter © 2008 Elsevier Ltd. All rights reserved.
doi:10.1016/j.poly.2008.04.018

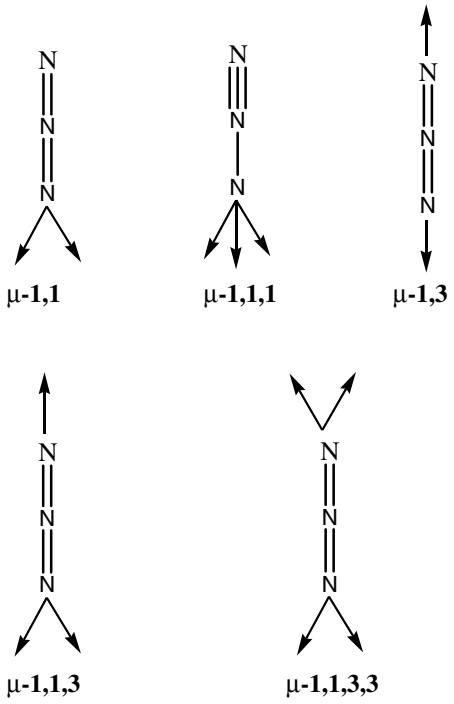

Fig. 1. Different types of binding modes of azide ion.

As an extension of the earlier work, we report two new end-on azido bridged hydrazone metal complexes $[Cu_2(L)_2(\mu_{1,1}\text{-}N_3)_2]$ (**1**) and $[Co_2(L)_2(\mu_{1,1}\text{-}N_3)_2(N_3)_2]$ (**2**) where [**LH** = $CH_3C(O)NHN{=}CHC_5H_4N$] obtained from condensation of acetic hydrazide and pyridine-2-carboxaldehyde. Aromatic hydrazides have been used so far for the preparation of Schiff bases but here we have especially chosen an aliphatic hydrazide and have condensed it with pyridine-2-carboxaldehyde to prepare the Schiff base ligand (**LH**) and have successfully synthesised two new complexes of copper(II) and cobalt(III) where N_3^- anion have bridged the respective metal centres in its end-on 1,1-coordination mode. To the best of our knowledge metal complexes of aliphatic hydrazones are rare in the literature and our group is the first to synthesise and characterise metal complexes of the (*E*)-*N*′-((pyridin-2-yl)methylene) acetohydrazide Schiff base ligand. Low temperature magnetic studies have been carried out on 1 in order to see the extent of variation caused by replacing the aromatic ring with a methyl group in the Schiff base ligand **LH**. Other routine studies have also been carried out on both the complexes and have been described.

2. Experimental

2.1. Materials

All chemicals and solvents used for the syntheses were of analytical grade. Acetichydrazide, pyridine-2-carboxaldehyde (Fluka), sodium azide (Aldrich) were used as received. Copper perchlorate hexahydrate and cobalt perchlorate hexahydrate were prepared by treatment of copper carbonate and cobalt carbonate (E. Merck, India), respectively, with 60% aqueous perchloric acid (E. Merck, India) followed by slow evaporation on a steam bath. It was then filtered through a fine glass frit and preserved in a desiccator.

2.2. Syntheses

Caution! Perchlorate salts are potentially explosive and should be used in small quantity and with much care.

2.2.1. Synthesis of the Schiff base ligand

*2.2.1.1. $[CH_3C(O)NHN{=}CHC_5H_4N]$ (**LH**).* The ligand **LH** was prepared by the condensation of acetichydrazide (0.74 g, 10 mmol) with pyridine-2-carboxaldehyde (0.95 ml, 10 mmol) in presence of glacial acetic acid (0.6 ml, 10 mmol) in methanol medium. On refluxing the methanolic solution for 5 h a pale yellow colouration was observed. The colour indicated the formation of the Schiff base ligand **LH**. The resulting light yellow liquid was used without further purification. The scheme of synthesis and the keto–enol tautomerisation of the ligand **LH** is shown in Fig. 2.

2.2.2. Syntheses of the complexes

*2.2.2.1. $[Cu_2(L)_2(\mu_{1,1}\text{-}N_3)_2]$ (**1**).* To a 20 ml methanolic solution of copper perchlorate hexahydrate (0.370 g, 1 mmol), methanolic solution of the hydrazone ligand (**LH**) (1 mmol) was added dropwise while the mixture was stirred. It was then followed by the addition of sodium azide (0.065 g, 1 mmol) in minimum volume of water–methanol mixture. The mixture was stirred for 2 h at room temperature and then filtered. The filtrate was kept at refrigerator temperature yielding bluish green, plate shaped crystals suitable for X-ray diffraction after a week. Bluish green crystals were isolated by filtration and air-dried. *Anal.* Calc. for $[C_8H_8N_6O\text{-}Cu]$: C, 35.85; H, 2.98; N, 31.37. Found: C, 35.95; H, 3.01; N, 31.41%.

2.2.3. $[Co_2(L)_2(\mu_{1,1}\text{-}N_3)_2(N_3)_2]$ (**2**)

To a 20 ml methanolic solution of cobalt perchlorate hexahydrate (0.365 g, 1 mmol), methanolic solution of the hydrazone ligand (**LH**) (1 mmol) was added dropwise and stirred. Sodium azide (0.130 g, 2 mmol) in minimum volume of water–methanol mixture was added to the mixture and was stirred for 3 h at 40 °C. While stirring the colour of the solution changed from red to dark brown. The brown solution was kept at refrigerator temperature yielding dark green, needle shaped crystals suitable for X-ray diffraction after a week. Crystals were isolated by filtration and were air-dried. *Anal.* Calc. for $[C_8H_8N_9OCo]$: C, 31.45; H, 2.62; N, 41.28. Found: C, 31.48; H, 2.69; N, 41.31%.

2.3. Physical measurements

Elemental analyses were carried out using a Perkin–Elmer 2400 II elemental analyser. The infrared spectra were recorded on a Perkin–Elmer RX 1 FT-IR spectrophotometer with a KBr disc. The electronic spectra were recorded, in acetonitrile, on a Perkin–Elmer Lambda 40 (UV–Vis) spectrophotometer. Electrochemical measurements were performed on a VersaStat–PotentioStat II cyclic voltammeter using HPLC grade acetonitrile solution as solvent and tetrabutylammonium perchlorate was used as supporting electrolyte at a scan rate 0.05 V/s. Platinum and saturated calomel electrode (SCE) were the working and the reference electrodes in the process, respectively. Mass spectra of the ligand (**LH**) was recorded by Qtof Micro YA mass spectrophotometer. Variable-temperature magnetic susceptibility measurements were carried out with a Quantum Design MPMS-5S SQUID magnetometer under an applied magnetic field of 5000 Oe. Diamagnetic corrections were estimated from Pascal tables and magnetic data were corrected for diamagnetic contributions of the sample holder. The temperature dependence of the molar magnetic susceptibility, χ_M, was measured on a polycrystalline sample in the temperature range 4–300 K.

2.4. X-ray crystallography

The X-ray diffraction experiments were carried out at 203 K on a bluish green plate shaped single crystal (0.42 mm × 0.38 mm × 0.05 mm) of **1** and a dark green needle shaped single crystal (0.42 mm × 0.18 mm × 0.16 mm) of **2**. The single crystals of **1**

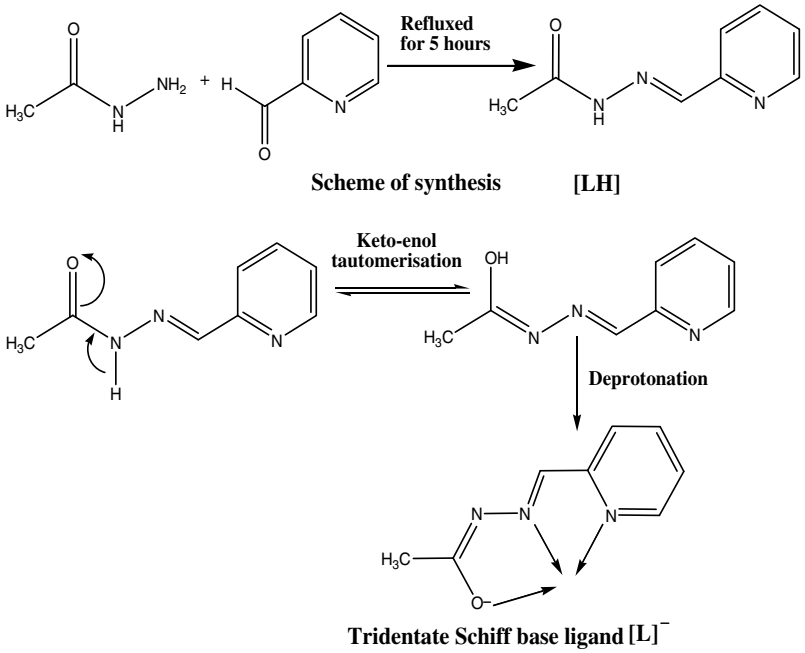

Fig. 2. Scheme of synthesis and keto–enol tautomerisation of [**LH**].

and **2** were mounted on the tip of a glass fibre and was exposed to a graphite monochromatised Mo $K\alpha$ radiation ($\lambda = 0.71073$ Å) emerging from a fine-focus sealed tube. The intensity data collection was performed with Oxford Diffraction Gemini R-Ruby diffractometer using multi scan technique. Data collection and cell refinement were performed using CRYSALISPRO software [28]. The structures of the two complexes were solved by direct method procedures in SHELXS and refined by full-matrix least-squares methods in SHELXL [29]. The calculations were carried out with the WINGX package program [30] running on a PC. Carbon-bonded hydrogen atoms were included in idealised positions and set to ride on the parent atoms. Selected crystallographic data, experimental conditions and some important features of the structural refinements of both the complexes are summarised in the Table 1.

Table 1
Crystallographic and refinement data for **1** and **2**

Complex	**1**	**2**
Chemical formula	$C_{16}H_{16}Cu_2N_{12}O_2$	$C_{16}H_{16}Co_2N_{18}O_2$
Formula weight	535.49	610.33
Crystal system	triclinic	monoclinic
Space group	$P\bar{1}$	$P1\ 21/c\ 1$
Z	1	2
a (Å)	6.8349(10)	7.7698(3)
b (Å)	8.666(3)	10.3053(6)
c (Å)	9.903(3)	14.7711(4)
α (°)	111.70(3)	90°
β (°)	109.114(18)	93.923(3)
γ (°)	95.758(19)	90
V (Å^3)	498.3(2)	1179.95(9)
Temperature (K)	203	203
Density (Mg/m^3)	1.784	1.718
Absorption coefficient (mm^{-1})	2.178	1.463
$F(000)$	270	616
Crystal size (mm)	0.42 × 0.38 × 0.05	0.42 × 0.18 × 0.16
θ Range for data collection (°)	4.63–32.53	4.60–32.64
Reflections collected	8068	11518
Independent reflections, (R_{int})	3302, 0.0274	3897, 0.0828
Number of 'observed' reflections	2459	1616
Goodness-of-fit, S	1.043	0.881
Final R indices [$I > 2\sigma(I)$]	$R_1 = 0.0301$ $wR_2 = 0.0639$	$R_1 = 0.0497$ $wR_2 = 0.0786$
R indices (all data)	$R_1 = 0.0493$ $wR_2 = 0.0725$	$R_1 = 0.1640$ $wR_2 = 0.1073$
Largest difference in peak and hole (e Å^{-3})	0.505 and −0.335	0.762 and −0.434

3. Results and discussion

The formation of the new Schiff base ligand (*E*)-*N*′-((pyridin-2-yl)methylene) acetohydrazide (**LH**) has been supported by infrared and mass spectroscopy. IR bands obtained at 1666 cm^{-1} clearly indicate the presence of an imine functionality which must have resulted due to the condensation of acetic hydrazide with pyridine-2-carboxaldehyde. IR bands at 3339 and 3302 cm^{-1} for the asymmetric and symmetric –NH_2 stretching were not observed which indicate that the primary amine functionality of acetic hydrazide has successfully condensed with the carbonyl functionality of pyridine-2-carboxaldehyde.

The mass spectrum also ensures the formation of the Schiff base ligand (**LH**). The mass spectrum of the ligand (**LH**) shows peak at m/e 186 which is attributed to the molecular ion peak $[C_8H_9N_3O\text{-}Na]^+$. In the mass spectrum the highest intensity peak was obtained at m/e 186 (100%) may be assigned to the neural hydrazone ligand **LH** bound to one sodium ion to generate molecular ion. Hence it is assertive from the mass spectrum that the proper condensation of the acetic hydrazide and pyridine-2-carboxaldehyde has resulted the Schiff base ligand (**LH**).

The most conclusive evidence which supports the condensation of acetic hydrazide with pyridine-2-carboxaldehyde is the single crystal X-ray study of **1** and **2** which clearly indicate the coordination of the deprotonated tridentate hydrazone ligand ($\mathbf{L}^-$) to the respective metal centres.

3.1. Infrared spectra

The IR spectra of **1** and **2** were analysed in comparison with that of the free ligand (**LH**) in the region 4000–250 cm^{-1}. The IR spectrum of the hydrazone ligand contains a strong C–O absorption band at 1651 cm^{-1} and a N–H absorption band at 3186 cm^{-1}. Both of these bands disappear on complexation, and a new C–O absorp-

tion band appears at 1086 and 1084 cm^{-1} in the two complexes, indicating that the hydrazone ligands have undergone deprotonation on complexation. These data give evidences for the coordination of the deprotonated Schiff base ligand to the respective metal ions [Cu(II) and Co(III)] via two nitrogen atoms and one oxygen atom. The infrared spectra of **1** and **2** display IR absorption bands at 1617, and 1605 cm^{-1} which can be assigned to the C=N stretching frequencies of the deprotonated coordinated ligand, whereas for the free ligand (**LH**) the same bands are observed at 1666 cm^{-1}, respectively. The shift of these bands on complexation towards lower wave number indicates coordination of the imine nitrogen to the metal center [31]. In the spectra of complexes strong, well resolved sharp bands at 2053 cm^{-1} and a bifurcated peak at 2076 and 2014 cm^{-1} were obtained for **1** and **2**, respectively, which are assigned to $\upsilon_{N=N}$ of the azide (N_3) group coordinated to two different metal centers, respectively. The ligand coordination to the metal center is substantiated by two bands appearing for each complex, at 414, 318 (**1**) and 421, 310 (**2**) cm^{-1} attributable to υ_{M-N} and υ_{M-O}, respectively, where M = Cu(II) for **1** and M = Co(III) for **2**. The low energy pyridine ring in-plane and out-of-plane vibrations observed in the spectrum of **LH** at 611 and 412 cm^{-1} but for the complexes are shifted to higher frequencies at 632, 640 cm^{-1} and 420, 428 cm^{-1} for **1** and **2**, respectively, which is a good indication of the coordination of the heterocyclic nitrogen to the metal centers [32].

3.2. Electronic spectra

The electronic spectral data for the complexes in acetonitrile are in good agreement with their geometries. The UV absorption bands exhibit a charge transfer transition (CT) in the range 360–390 nm for **1** and may be assigned to the ligand-to-metal charge transfer transition. The spectrum of **1** displays a broad band at 650 nm which is consistent with the expected five-coordinate geometry for copper(II) complex. For **2**, containing distorted octahedral cobalt(III) centers, the band at 570 nm appeared due to $^1A_{1g} \rightarrow {}^1T_{1g}$ transition. The higher energy band $^1A_{1g} \rightarrow {}^1T_{2g}$ was obscured by ligand to metal charge transfer bands obtained in the broad range 410–375 nm.

3.3. Cyclic voltammetry

Electrochemical properties of **1** and **2** were studied in HPLC grade acetonitrile medium with tetrabutylammonium perchlorate as supporting electrolyte at a scan rate 50 mV s^{-1}. Peaks corresponding to the potentials +1.0 V and −0.41 V were obtained for **1**. Anodic response obtained near +1.0 V (versus SCE) is believed to be due to $Cu^{II} \rightarrow Cu^{III}$ oxidation; the oxidized complex is too reactive to survive for the cathodic scan. The complex displays an irreversible reduction at −0.41 V (versus SCE) corresponding to the $Cu^{II} \rightarrow Cu^{I}$ reduction couple. The voltammogram of **2** shows peak at −0.15 V (versus SCE) which can be attributed for the reduction of cobalt(III) to cobalt(II). Another peak obtained at 0.12 V (versus SCE) is assigned to the oxidation of cobalt(II) to cobalt(III). This process is completely irreversible, characterised by a peak to peak separation (ΔE_p) of 270 mV, which remains unchanged upon changing the scan rate. There is also an inequality in the anodic peak current (i_{pa}) and the cathodic peak current (i_{pc}) of **2**, as expected for an irreversible electron transfer process.

3.4. Description of the crystal structures

3.4.1. $[Cu_2(L)_2(\mu_{1,1}\text{-}N_3)_2]$ (**1**)

An ORTEP diagram of **1** with atom numbering scheme is shown in Fig. 3. The bond dimensions about the copper centers for **1** are listed in Table 2. Crystal structure of the di-$\mu_{1,1}$-azido bridged dinuclear copper(II) complex **1**, have been compared with respect to the earlier reported dichloro and diacetato bridged copper(II) complexes $[Cu_2(\mu\text{-}Cl)_2(pabh)_2]$ (**A**), $[Cu_2(\mu\text{-}O_2CCH_3)_2(pabh)_2]$ (**B**), $[Cu_2(\mu\text{-}O_2CCH_3)_2(pamh)_2]$ (**C**) derived from two different NNO donor aroylhydrazones of pyridine-2-carboxaldehyde (pabh and pamh) [1d]. The structural study reveals that like **A**, **B** and **C**; **1** is

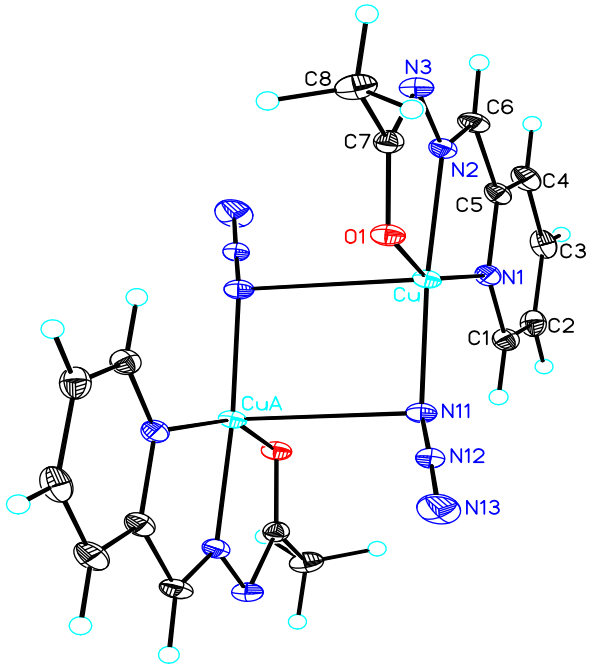

Fig. 3. ORTEP diagram of **1** with atom labeling scheme.

Table 2
Molecular dimensions (bond lengths in Å and angles in °) about the copper and cobalt centres in **1** and **2**

1		**2**	
Bond lengths (Å)			
Cu–N(2)	1.9266(16)	Co–N(2)	1.837(3)
Cu–N(11)	1.9459(16)	Co–O(1)	1.915(2)
Cu–O(1)	1.9640(17)	Co–N(1)	1.928(3)
Cu–N(1)	2.0418(19)	Co–N(121)	1.934(3)
Cu–N(11)A	2.4433(16)	Co–N(111)A	1.976(3)
N(11)–CuA	2.4433(16)	Co–N(111)	1.982(3)
		N(111)–CoA	1.976(3)
Bond angles (°)			
N(2)–Cu–N(11)	176.41(6)	N(2)–Co–O(1)	82.22(11)
N(2)–Cu-O(1)	79.79(7)	N(2)–Co–N(111)A	172.50(11)
N(11)–Cu-O(1)	101.06(7)	O(1)–Co–N(111)A	96.88(10)
N(2)–Cu–N(1)	80.30(7)	N(1)–Co–N(111)A	96.77(12)
N(11)–Cu–N(1)	98.40(7)	N(121)–Co–N(111)A	92.79(12)
O(1)–Cu–N(1)	158.92(6)	N(2)–Co–N(111)	92.91(11)
N(2)–Cu–N(11)A	96.19(6)	O(1)–Co–N(111)	88.35(10)
N(11)–Cu–N(11)A	87.13(6)	N(1)–Co–N(111)	93.16(10)
O(1)–Cu–N(11)A	99.55(6)	N(121)–Co–N(111)	171.43(11)
N(1)–Cu–N(11)A	89.40(6)	N(111)A–Co–N(111)	79.61(11)
N(12)–N(11)–Cu	124.82(14)	N(112)–N(111)–Co	120.5(2)
N(12)–N(11)–CuA	112.27(12)	CoA–N(111)–Co	100.39(11)
Cu–N(11)–CuA	92.87(6)	N(122)–N(121)–Co	118.2(2)
		N(2)–Co–N(1)	84.12(12)
		O(1)–Co–N(1)	166.32(12)
		N(2)–Co–N(121)	94.63(13)
		O(1)–Co–N(121)	88.65(11)
		N(1)–Co–N(121)	91.66(11)

Symmetry transformations used to generate equivalent atoms: A $-x+1, -y+2, -z+2$ for **1**. Symmetry transformations used to generate equivalent atoms: A $-x+1, -y+1, -z$ for **2**.

Table 3
Hydrogen bonding parameters for **1** and **2**

Complex	D—H···A	*d*(D–H) Å	*d*(H···A) Å	*d*(D···A) Å	∠(DHA)°
1	C(6)–H(6A)···N(13)#2	0.94	2.60	3.483(3)	155.6
2	C(4)–H(4A)···N(121)	0.94	2.57	3.447(5)	155.00

Symmetry transformations used to generate equivalent atoms for **1**: #2 $x+1$, y, $z+1$.

also a centrosymmetric dimer in which the copper centers are five-coordinate, bonded to three coordinating N_2O atoms from the planar ligand $\mathbf{L}^-$ and nitrogen atoms from two bridging azide anions. In **1** the chelate bite angles in the five-membered rings formed by the amide–O and the imine–N, and the pyridine-N and the imine–N are 79.78 and 80.31, respectively, and are very close to that of the earlier reported chloro and acetato species. The N–N (1.383 Å), C–N (1.276 Å) and C–O (1.964 Å) distances of the coordinated ligand $\mathbf{L}^-$ are consistent with the coordinated pabh and pamh in **A**, **B** and **C** which suggest that the hydrazone ligand have coordinated copper(II) ions in its deprotonated form. Each of the two azide anions in **1** bridges the copper(II) centers in an *end-on* fashion and this leads to a relatively smaller Cu—Cu (3.199 Å) separation in comparison to that of dichloro (3.3918 Å) and diacetato (3.273 Å) bridged copper(II) dinuclear species **A**, **B**, **C**. In **1** the azide ion bridges in an asymmetric (basal–apical) fashion so that the Cu–N bond lengths are significantly different ($\Delta d = 0.498$ Å) and the Cu–N(11)–Cu(A) bridge angle (92.87(6)°) is greater than that of Cu–Cl–Cu bridge angle in **A** (86.89(3)°) but smaller than the Cu–O–Cu bridge angle in **B** and **C** (101.4(2)°). The di-$\mu_{1,1}$-azido bridging nitrogen atoms are in a planar Cu_2N_2 ring about a crystallographic inversion centre. The azide ions are nearly linear with N–N–N angle of 175.9(2)°. The geometry of the copper(II) centers are very close to square pyramidal with $\tau = 0.291$, [$\tau = |\beta - \alpha|/60°$], where β and α are the two largest angles around the central atom; $\tau = 0$ and 1 for the perfect square pyramidal and trigonal bipyramidal geometries, respectively [33]. The square base of each of the copper(II) centers is formed by pyridyl and imine nitrogen atoms, an enolate oxygen of the Schiff base ligand ($\mathbf{L}^-$) and one bridging azide nitrogen atom. The copper(II) atoms in **1** suffer a relatively lesser displacement of 0.093 Å from the square base towards the apical bridging azide ions than that of **A**, **B** and **C**. There is only one type of N–H hydrogen bonding interaction present in **1** and is given in Table 3. In a dinuclear unit of **1** two H(6A) atoms of the two-coordinated Schiff base ligands and the two N(13) atoms of the two *end-on* coordinated azide ions participate in intermolecular H-bonding with N(13) and H(6A) atoms, respectively, of the two adjacently placed dinuclear units to form an infinite 1D polymeric chain. The 1D polymeric chain structure of **1** generated by intermolecular H-bonding interactions is shown in Fig. 4.

3.4.2. $[Co_2(L)_2(\mu_{1,1}\text{-}N_3)_2(N_3)_2]$ (**2**)

An ORTEP diagram of **2** with atom numbering scheme is given in Fig. 5 and the bond dimensions about the cobalt centers are listed in Table 2. The centrosymmetric dimer **2** differs in its coordination environment from that of **1**. Unlike the copper complex, the two cobalt(III) centers in **2** are six-coordinated. The structural study reveals that in **2** both the cobalt(III) centers are in a distorted octahedral environment which has resulted from the coordination of the polydentate N_2O donor ligand ($\mathbf{L}^-$) and three azide ions which make the chromophore a heteroatomic specie. The equatorial sites of each cobalt(III) centers in **2** are occupied by two nitrogen atoms, one enolate oxygen of the Schiff base ligand ($\mathbf{L}^-$) and one azide ion coordinated in an *end-on* fashion thereby connecting the two cobalt(III) centers. The two axial sites of the each distorted octahedral cobalt(III) centers are occupied by two other azide ions of which one shows an *end-on* bridging mode and connects the two adjacent cobalt(III) centers while the other one is in a terminal site. In the dinuclear complex two azide ions bridge in an asymmetric (basal–apical) fashion and the other two occupy terminal positions. The two $\mu_{1,1}$-bridging azide ions and the two terminally coordinated azide ions in **2** are almost linear with N–N–N angles of 177.0(4)° and 177.2(4)°, respectively. The two cobalt(III) centers are shifted from the equatorial base plane towards the axially coordinated terminal azide ions by 0.063 Å and the Co(III)···Co(III) separation in **2** is 3.041 Å. The oxidation state of the two cobalt centers in the complex is 3+ instead of 2+ which is mainly attributed to the coordination of the two terminal azide ions to the respective metal centers in the complex. Although there is only one type of N–H hydrogen bonding interaction present in **2** but weak interactions led an increase in dimensionality of **2** with respect to **1**. In the dinuclear unit of **2** two H(4A) atoms of the two coordinated Schiff base ligands and the two N(121) atoms of the two terminally coor-

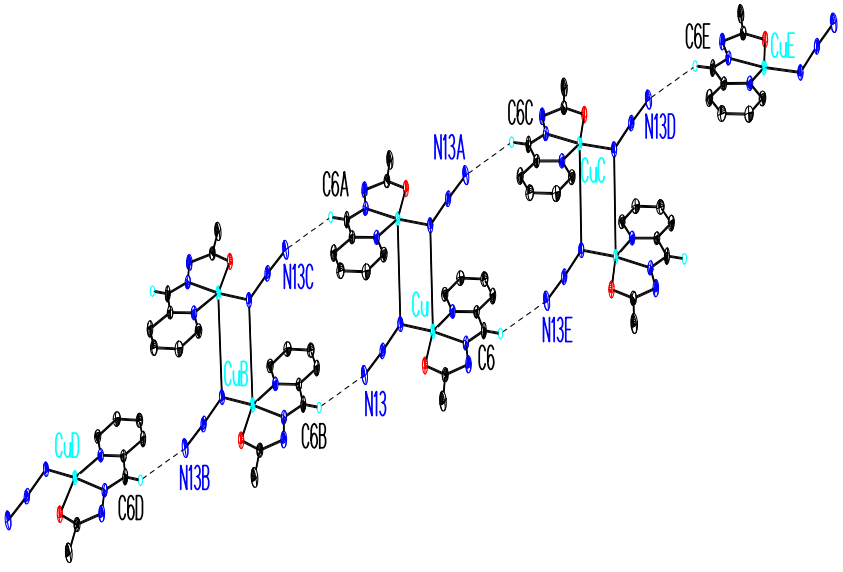

Fig. 4. Intermolecular H-bonding interactions generating 1D polymeric chain of **1**.

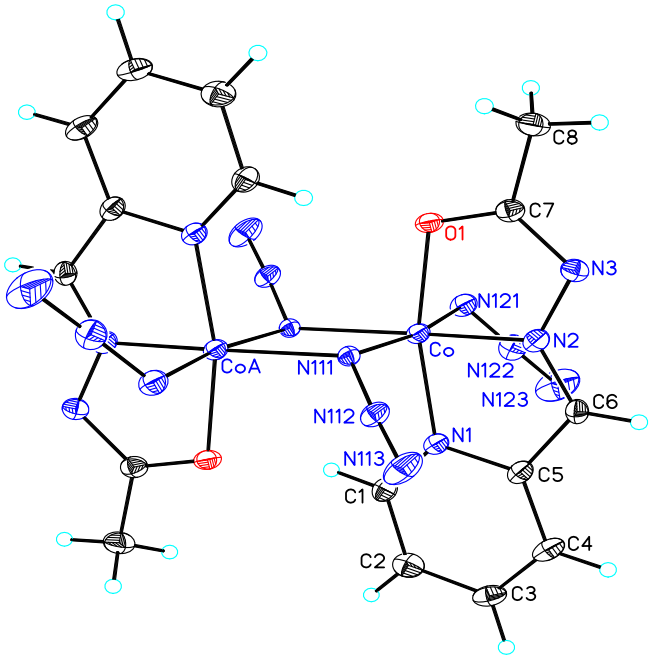

Fig. 5. ORTEP diagram of **2** with atom labeling scheme.

dinated azide ions participate in intermolecular H-bonding with H(4A) and N(121) atoms, respectively, of the other two dinuclear units to form 2D grid like structure. In the unit cell of the complex four such dinuclear units of **2** are interconnected to each other by intermolecular H-bonding to form a single grid. The intermolecular hydrogen bonding interactions is clearly indicated in the packing diagram of the complex shown in Fig. 6 and the H-bonding parameters is given in Table 3.

3.5. Magnetic study

For **1** low temperature magnetic study was performed to see the extent of interaction between two copper(II) centers through two *end-on* bridged azido ligands. In **1** the two azido ions coordinate two copper(II) centers in a basal–apical mode, i.e. each of the N atoms of the two azido-ligand connects the two copper(II) centers by binding first copper center at its apical site and the second copper center at its equatorial site, respectively. The two magnetic orbital on the copper atoms are $d_{x^2-y^2}$ (the *x* and *y* axes being defined by the short equatorial bonds). Thus the coupling is expected to be very weak. So it is well expected that there will be no direct overlap between the magnetic orbitals through the azido bridges. Thus it can be predicted that such overlap will result to a very weak coupling. The experimentally observed result of **1** is quite consistent with the theoretical explanation as the $\chi_M T$ values recorded by SQUID remains constant in the whole range of temperature 10–300 K at a value close of 0.75 $cm^3\,K\,mol^{-1}$ and is in good agreement with the one expected for two uncoupled spins 1/2. For **2** low temperature magnetic study was not performed as the complex is a dinuclear cobalt(III) species and all cobalt (III) compounds are low-spin and thus diamagnetic in nature.

4. Conclusion

This paper contributes a new class of hydrazone metal complexes which is derived from an aliphatic hydrazide. We have shown that the H-bonding interactions in both the complexes have increased the dimensionality of **1** and **2**. In **1** the dinuclear units are inter connected by H-bonding interactions to produce a 1D polymeric chain whereas in **2** it generated a 2D polymer where four such dinuclear units are inter connected to produce a grid like structure. The synthesis and characterisation of the hydrazone ligand (**LH**) and its complexes **1** and **2**, will help us and others to ex-

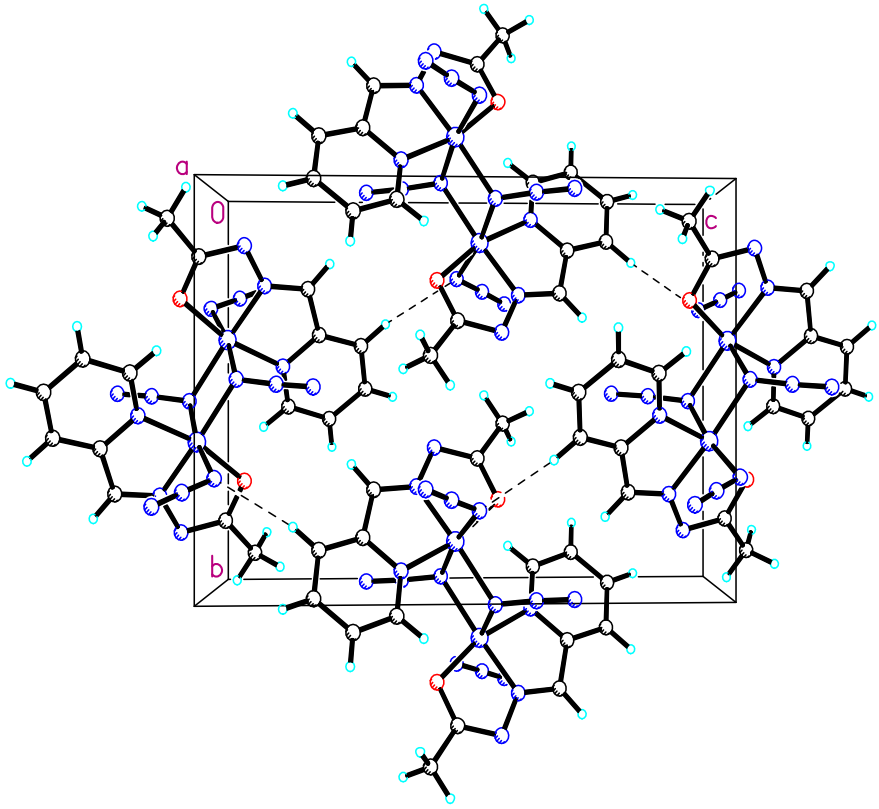

Fig. 6. Unit cell packing diagram showing intermolecular H-bonding of **2**.

plore the biological activities related to such aliphatic metal hydrazone complexes which still remain unexplored. The further extensions of this work lies in obtaining multinuclear complexes of other transition metals and to study the biological activities of such complexes.

Acknowledgements

A. Ray is thankful to the Department of Science and Technology, New Delhi, Govt. of India, for financial support and S. Banerjee acknowledges the financial assistance obtained from Defence Research and Development Organisation, New Delhi, Govt. of India. The authors also acknowledge the financial help obtained from All India Council for Technical Education, New Delhi, Govt. of India. R.J. Butcher wishes to acknowledge the NSF-MRI program for funding to obtain the diffractometer (CHE-0619278).

Appendix A. Supplementary data

CCDC 649737 and 649738 contain the supplementary crystallographic data for **1** and **2**. These data can be obtained free of charge via http://www.ccdc.cam.ac.uk/conts/retrieving.html, or from the Cambridge Crystallographic Data Centre, 12 Union Road, Cambridge CB2 1EZ, UK; fax: (+44) 1223-336-033; or e-mail: deposit@ccdc.cam.ac.uk. Supplementary data associated with this article can be found, in the online version, at doi:10.1016/j.poly.2008.04.018.

References

[1] (a) R. Karmakar, C.R. Choudhury, D.L. Hughes, G.P.A. Yap, M.S. El Fallah, C. Desplanches, J.-P. Sutter, S. Mitra, Inorg. Chim. Acta 359 (2006) 1184;
(b) C. Adhikary, D. Mal, K.-I. Okamoto, S. Chaudhuri, S. Koner, Polyhedron 25 (2006) 2191;
(c) S. Banerjee, M.G.B. Drew, C.-Z. Lu, J. Tercero, C. Diaz, A. Ghosh, Eur. J. Inorg. Chem. (2005) 2376;
(d) N.R. Sangeetha, S. Pal, Polyhedron 19 (2000) 1593.
[2] (a) J. Ribas, M. Monfort, I. Resino, X. Solans, P. Rabu, F. Maingot, M. Drillan, Angew. Chem., Int. Ed. Engl. 35 (1996) 2520;
(b) G. De Munno, M. Julve, G. Viau, F. Lloret, J. Faus, D. Viterbo, Angew. Chem., Int. Ed. Engl. 35 (1996) 1807.
[3] (a) E.A. Mauro, I.S. Klein, A.C. Saldana, D. Simone, J. Zukerman- Schpector, E.E. Castellano, Polyhedron 9 (1990) 2937;
(b) R. Vicente, A. Escuer, E. Penalba, X. Solans, M. Font-Bardia, J. Chem. Soc., Dalton Trans. (1994) 3005.
[4] (a) M. Monfort, J. Ribas, X. Solans, Inorg. Chem. 33 (1994) 4271;
(b) R. Vicente, A. Escuer, J. Ribas, X. Solans, J. Chem. Soc., Dalton Trans. (1994) 259.
[5] (a) J. Ribas, C. Diaz, X. Solans, M. Font-Bardia, J. Chem. Soc., Dalton Trans. (1997) 35;
(b) J. Ribas, C. Diaz, R. Costa, X. Tercero, X. Solans, M. Font-Bardia, Inorg. Chem. 37 (1998) 233.
[6] (a) S. Seth, S. Chakraborty, Acta Crystallogr. C40 (1984) 1530;
(b) G.F. de Sousa, C.A.L. Filgueiras, A. Abras, S.S. Al-Juaid, P.B. Hitchcock, J.F. Nixon, Inorg. Chim. Acta 218 (1994) 139.
[7] (a) B. Samanta, J. Chakraborty, D.K. Dey, V. Gramlich, S. Mitra, Struct. Chem. 18 (2007) 287;
(b) B. Samanta, J. Chakraborty, S. Shit, S.R. Batten, P. Jensen, J.D. Masuda, S. Mitra, Inorg. Chim. Acta 360 (2007) 2471;
(c) S. Sen, C.R. Choudhury, P. Talukder, S. Mitra, M. Westerhausen, A.N. Kneifel, C. Desplanches, N. Daro, J.-P. Sutter, Polyhedron 25 (2006) 1271.
[8] S. Sen, S. Mitra, D.L. Hughes, G. Rosair, C. Desplanches, Polyhedron 26 (2007) 1740.
[9] S.K. Dey, N. Mondal, M.S. El Fallah, R. Vicente, A. Escuer, X. Solans, M.F. Bardía, T. Matsushita, V. Gramlich, S. Mitra, Inorg. Chem. 43 (2004) 2427.
[10] P. Talukder, A. Dutta, S. Mitra, G. Rosair, M.S. El Fallah, J. Ribas, Dalton Trans. (2004) 4161.
[11] N.K. Karan, S. Mitra, T. Matsushita, V. Gramlich, G. Rosair, Inorg. Chim. Acta 332 (2002) 87.
[12] (a) R. Cortes, T.I. Ruiz de Larramendi, L. Lezama, T. Rojo, K. Urtiaga, M.I. Arriortua, J. Chem. Soc., Dalton Trans. (1992) 2723;
(b) M.I. Arriortua, R. Cortes, L. Lezama, T. Rojo, X. Solans, M. Font-Bardía, Inorg. Chim. Acta 174 (1990) 263.
[13] M.I. Arriortua, R. Cortes, J.L. Mesa, L. Lezama, T. Rojo, G. Villenueve, Transition Met. Chem. 13 (1988) 371.
[14] (a) M.D. Duggan, D.N. Hendrickson, Inorg. Chem. 13 (1974) 2929;
(b) T. Rojo, R. Cortes, L. Lezama, I.M. Arriortua, G. Villenueve, J. Chem. Soc., Dalton Trans. (1991) 1779.
[15] (a) C.G. Pierpont, D.N. Hendrickson, D.M. Duggan, F. Wagner, E.K. Barefield, R.L. Martin, Inorg. Chem. 14 (1975) 604;
(b) P. Chaudhuri, M. Gottmann, D. Ventur, K. Wieghardt, B. Nuber, J. Weiss, J. Chem. Soc., Chem. Commun. (1985) 1618;
(c) J. Ribas, A. Escuer, M. Monfort, R. Vicente, R. Cortés, L. Lezama, T. Rojo, Coord. Chem. Rev. 193 (1999) 1027;
(d) A.P. Ginsberg, R.W. Brookes, R.C. Sherwood, Inorg. Chem. 11 (1972) 2884.
[16] E. Ruiz, J. Cano, S. Alvarez, P. Alemany, J. Am. Chem. Soc. 43 (1998) 120.
[17] D.J. Hodgson, Prog. Inorg. Chem. 19 (1975) 182.
[18] O. Kahn, Angew. Chem., Int. Ed. Engl. 24 (1985) 834.
[19] P.A. Vigato, T. Samburini, D.E. Fenton, Coord. Chem. Rev. 106 (1990) 25.
[20] E. Spodin, J. Manzur, Coord. Chem. Rev. 119 (1992) 171.
[21] (a) E.I. Solomon, U.M. Sundaram, T.E. Machonkin, Chem. Rev. 96 (1996) 2563;
(b) N. Kitajima, Y. Moro-oka, Chem. Rev. 94 (1994) 737;
(c) K.A. Magnus, H. Ton-That, J.E. Carpenter, Chem. Rev. 94 (1994) 727.
[22] K.D. Karlin, Z. Tyekler (Eds.), Bioinorganic Chemistry of Copper, Chapman & Hall, New York, 1993.
[23] (a) T.G. Spiro, Copper Proteins, Wiley, New York, 1981;
(b) B. Reinhammer, Copper Proteins and Copper Enzymes, vol. 3, CRC, Boca Raton, FL, 1984;
(c) E.I. Solomon, M.J. Baldwin, M.D. Lowery, Chem. Rev. 92 (1992) 521;
(d) E.I. Solomon, in: L. Que (Ed.), Metal Clusters in Proteins, American Chemical Society, Washington, DC, 1988, p. 116;
(e) M. Tré- molières, J.G. Bieth, Phytochemistry 23 (1984) 501;
(f) A. Rompel, H. Fisher, K. Büldt-Karentzopoulos, D. Miewes, F. Zippel, H.F. Nolting, C. Hermes, B. Krebs, H. Witzel, J. Inorg. Biochem. 59 (1995) 715.
[24] (a) J.L. Cole, P.A. Clark, E.I. Solomon, J. Am. Chem. Soc. 112 (1990) 9534;
(b) J.L. Cole, L. Avigliano, L. Morpurgo, E.I. Solomon, J. Am. Chem. Soc. 113 (1991) 9080.
[25] E. Bouwman, W.L. Driessen, J. Reedijk, Coord. Chem. Rev. 104 (1990) 143.
[26] K.D. Karlin, Z. Tyeklár, Adv. Inorg. Biochem. 9 (1994) 123.
[27] W.B. Tolman, Acc. Chem. Res. 30 (1997) 227.
[28] CRYSALIS PRO, Crysalis Software system, Oxford Diffraction Ltd., Abingdon, UK, 2007.
[29] G.M. Sheldrick, Acta Cryst. A64 (2008) 112.
[30] L.J. Farrugia, J. Appl. Cryst. 32 (1999) 837.
[31] R.T. Conley, Infrared Spectroscopy, Allyn & Bacon, Boston, 1966.
[32] K. Nakamoto, Infrared and Raman Spectra of Inorganic and Coordination Compounds, vol. 23, Wiley, New York, 1997.
[33] A.W. Addison, T.N. Rao, J. Reedijk, J. van Rijn, G.C. Verschoor, J. Chem. Soc., Dalton Trans. (1984) 1349.

Polyhedron 27 (2008) 2416–2420

Contents lists available at ScienceDirect

Polyhedron

journal homepage: www.elsevier.com/locate/poly

Sitting-atop complex formation of free base *meso*-tetraarylporphyrins with zirconium(IV) chloride

Hossein Dehghani *, Majid Payam, Mohammad Reza Mansournia

Department of Chemistry, Faculty of Science, University of Kashan, Kashan 87317-51167, Islamic Republic of Iran

ARTICLE INFO

Article history:
Received 27 November 2007
Accepted 9 April 2008
Available online 2 June 2008

Keywords:
Porphyrin
Sitting-atop complex
Zirconium tetrachloride
SAT complex

ABSTRACT

We have succeeded in the preparation and spectroscopic characterization of sitting-atop (SAT) complexes of *meso*-tetraarylporphyrins (H_2t(X)pp) with zirconium(IV) chloride under mild conditions and at room temperature, where two pyrrolenine nitrogens in the SAT complexes, [(H_2t(X)pp)$ZrCl_4$], coordinate to a zirconium atom and two protons still remain on the pyrrole nitrogens. UV–Vis and NMR (^{1}H and ^{13}C) spectral data show that the porphyrin core of the SAT complexes is distorted and two pyrrolenine nitrogen atoms of the porphyrin act as electron donors to the zirconium atom of $ZrCl_4$.

© 2008 Elsevier Ltd. All rights reserved.

1. Introduction

Porphyrin complexes are one of the most important class of compounds in biochemistry, due to their central role in photosynthesis, oxygen transport and biological redox processes [1–5]. Fleischer and Wang studied the reaction of protoporphyrin IX derivatives with several metal ions in chloroform and observed the formation of reaction intermediates, which were called sitting-atop (SAT) complexes [6]. Such structures are formed each time during the incorporation of the metal centers, when in the stable intermediates two pyrrolic protons still remain on the porphyrins. Several sitting-atop complexes of naturally occurring and synthesis porphyrins including platinum (II), copper (II), and rhodium (I) have been reported [7–9]. Recently, Ryde and Shen performed a quantum mechanical study of SAT complexes of Mg^{2+}, Fe^{2+} and Cu^{2+} with porphyrin in water and acetonitrile solutions [10]. It was suggested that there are a large number of possible structures for the SAT complex, with 1–5 solvent molecules, one or two metal ions, and *cis* or *trans* protonation of the porphyrin ring [11]. More clear evidence for the sitting-atop complex was spectrophotometrically observed during the reaction of *meso*-tetraphenylporphyrin (H_2tpp) with the copper (II) ion in acetonitrile [12]. The basicity of acetonitrile is very weak, and therefore the pyrrole protons of H_2tpp are not easily released, even after forming the intermediate with the copper (II) ion without additional proton acceptors. This acid–base property of the solvent is responsible for the stability of the sitting-atop intermediate. But, Tsai et al. [13] working on the same reaction, reported that in a less basic solvent (chloroform) and tetra-*p*-tolylporphyrin (H_2t(4-Me)pp), only the metallated porphyrin and diprotonated free base were observed (Eq. (1)).

$$2(H_2t(4\text{-Me})pp) + M^{2+} \rightarrow M(t(4\text{-Me})pp) + H_4t(4\text{-Me})pp^{2+} \qquad (1)$$

Newly, Reed et al. studied the treatment of a metalloporphyrin with a strong acid by the microscopic reverse reaction [14]. They observed no SAT complex as an intermediate, and suggested that Funahashi et al. might have misinterpreted a mixture of M(por) and H_4(por)$^{2+}$ as SAT complexes. The similarity of the spectral data for SAT complexes and the related diprotonated species cause their characterization to be difficult and lead to a challenge in the majority of cases.

We have recently reported that the reaction of *meso*-tetraarylporphyrins with $SbCl_3$ and $BiCl_3$ acceptors produced dimer molecular complexes, [(H_2t(X)pp)MCl_3]$_2$ (M = Sb, Bi). In these complexes, the porphyrin core was distorted and acted as an electron donor to the central atom of the acceptors by the pyrrolenine nitrogens, and so two pyrrolic protons still remained on the porphyrin. The structure of the dimer molecular complexes was similar to SAT complexes. This article presents the synthesis and characterization of SAT complexes of *meso*-tetraarylporphyrins (Fig. 1) with zirconium(IV). The selection of zirconium with a high oxidation number, suitable solvent and mild conditions are the reasons that we successfully prepared the stable SAT complexes as solids. The reaction did not progress to the metallation of the porphyin and remained in the intermediate step (SAT complex). Therefore, we

* Corresponding author. Tel.: +98 0361 5555333; fax: +98 0361 5552935.
E-mail address: Dehghani@kashanu.ac.ir (H. Dehghani).

0277-5387/$ - see front matter © 2008 Elsevier Ltd. All rights reserved.
doi:10.1016/j.poly.2008.04.020

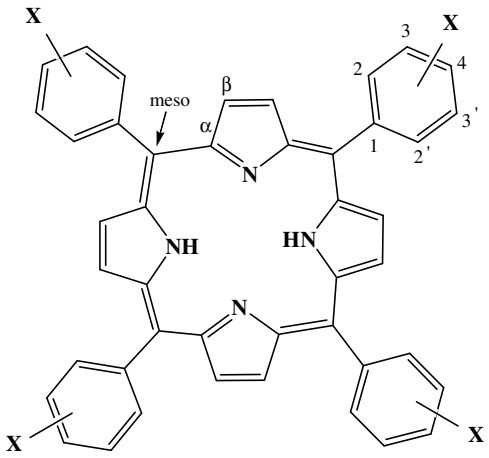

Fig. 1. *Meso*-tetraarylporphyrins, $H_2t(X)pp$.

synthesized SAT complexes containing zirconium ([$(H_2t(X)pp)$-$ZrCl_4$]) and no diprotonated or metalloporphyrin species in our reaction system.

2. Experimental

2.1. Materials

Benzaldehyde, the substituted benzaldehydes (2-Me, 3-Me, 4-Me, 2-OMe, 3-OMe, 4-OMe and 4-Cl) and $ZrCl_4$ were obtained from Merck and were used as received. All other solvents for the synthesis of the porphyrins and related SAT complexes were obtained from Merck and Fluka, and were used without further purification. Chloroform (Merck) was dried over anhydrous calcium chloride for 3 days. Pyrrole (Merck) was distilled before use. The substituted *meso*-tetraarylporphyrins and H_2tpp were prepared by the literature methods [17]. Alumina and hydrochloric acid were purchased from Merck and were used as received.

2.2. Physical measurements

The NMR spectra (^1H and ^{13}C) were recorded on a Bruker 500 Ultrashield spectrometer in $CDCl_3$. To obtain good integration results (in ^1H NMR), the concentration of the SAT complexes was 0.006 M. The residual $CHCl_3$ in the conventional 99.8% atom $CDCl_3$ gives a signal at $\delta = 7.26$ ppm, which was used for calibration of the chemical shift scale. The electronic absorption spectra were recorded in chloroform solutions on an ATI UNICAM-UV/Vis Vision SOFTWARE V-2011, spectrophotometer. The cell had an optical path length of 1 cm. FT-IR spectra were recorded on a Magna 550 Nicolet spectrometer using KBr pellets. The percentages of zirconium in the SAT complexes were obtained on a flame atomic absorption spectroscopy Model 2380 Perkin–Elmer spectrometer. The molar conductance of the SAT complexes and the diprotonated species of the porphyrins was measured on a METROHM 644 conductometer.

For the quantitative analysis of Zr and Cl in the [$(H_2t(X)pp)ZrCl_4$] SAT complexes, 0.05 mmol of each SAT complex was dissolved in 20 ml chloroform and then decomposed by adding 15 ml of double distilled water to the solution. $ZrCl_4$ hydrolyzed in water and the porphyrin remained in the organic solvent. The two phases were then separated by a decanter. The percentages of chloride and zirconium ions in the SAT complexes were determined by the mercury thiocyanato method [18] and flame atomic absorption technique, respectively.

2.3. Preparations

2.3.1. [$(H_2t(4\text{-}OMe)pp)ZrCl_4$]

Equimolar quantities (0.5 mmol) of $H_2t(4\text{-}OMe)pp$ and $ZrCl_4$ (in 2–3 ml of chloroform) were ground together in a mortar at ambient temperature for 20–30 min. The completion of the complexation was determined by UV–Vis spectroscopy. The porphyrin was completely converted to the related SAT complex and the mixture had no absorption band due to the free base porphyrin. The green related SAT complex was dried in a vacuum oven for 12 h at 50 °C. *Anal.* Calc. for $C_{48}H_{38}N_4O_4ZrCl_4$: C, 59.6; H, 4.0; N, 5.8; Cl, 14.6; Zr, 9.4. Found: C, 58.7; H, 3.9; N, 5.6; Cl, 14.2; Zr, 9.1%. ^1H NMR ($CDCl_3$): δ 0.55 (s, 2H, NH), δ 4.17 (s, 12H, OCH_3), δ 8.52–8.54 (d, 8H, 2, 2′), δ 7.52–7.55 (d, 8H, 3, 3′), δ 8.48 (s, 8H, β). IR (KBr): υ_{NH} ($\sim$3320 cm^{-1}).

2.3.2. [$(H_2t(4\text{-}Me)pp)ZrCl_4$]

This SAT complex was synthesized by the method described above. *Anal.* Calc. for $C_{48}H_{38}N_4ZrCl_4$: C, 63.8; H, 4.2; N, 6.2; Cl, 15.7; Zr, 10.1. Found: C, 63.3; H, 4.0; N, 6.1; Cl, 15.2; Zr, 9.8%. ^1H NMR ($CDCl_3$): δ 0.25 (s, 2H, NH), δ 2.83 (s, 12H, CH_3), δ 8.48–8.50 (d, 8H, 2, 2′), δ 7.80–7.82 (d, 8H, 3, 3′), δ 8.54 (s, 8H, β). IR (KBr): υ_{NH} ($\sim$3320 cm^{-1}).

2.3.3. [$(H_2tpp)ZrCl_4$]

This complex was synthesized by the method used for the [$(H_2t(4\text{-}OMe)pp)ZrCl_4$] complex. *Anal.* Calc. for $C_{44}H_{30}N_4ZrCl_4$: C, 62.3; H, 3.6; N, 6.6; Cl, 16.7; Zr, 10.7. Found: C, 61.8; H, 3.5; N, 6.5; Cl, 16.2; Zr, 10.5%. ^1H NMR ($CDCl_3$): δ 0.29 (s, 2H, NH), δ 8.59–8.62 (d, 8H, 2, 2′), δ 8.00–8.03 (t, 8H, 3, 3′), δ 7.96–7.97 (d, 4H, 4), δ 8.58 (s, 8H, β). IR (KBr): υ_{NH} ($\sim$3320 cm^{-1}).

2.3.4. [$(H_2t(3\text{-}Me)pp)ZrCl_4$]

This complex was synthesized by the method used for the [$(H_2t(4\text{-}OMe)pp)ZrCl_4$] complex. *Anal.* Calc. for $C_{48}H_{38}N_4ZrCl_4$: C, 63.8; H, 4.2; N, 6.2; Cl, 15.7; Zr, 10.1. Found: C, 62.6; H, 4.1; N, 6.1; Cl, 15.5; Zr, 9.9%. ^1H NMR ($CDCl_3$): δ 0.25 (s, 2H, NH), δ 2.83 (s, 12H, CH_3), δ 8.40–8.42 (br., 8H, 2, 2′), δ 7.89–7.92 (t, 4H, 3), δ 7.76–7.78 (d, 4H, 4), δ 8.57 (s, 8H, β). IR (KBr): υ_{NH} ($\sim$3320 cm^{-1}).

2.3.5. [$(H_2t(3\text{-}OMe)pp)ZrCl_4$]

This complex was synthesized by the method used for the [$(H_2t(4\text{-}OMe)pp)ZrCl_4$] complex. *Anal.* Calc. for $C_{48}H_{38}N_4O_4ZrCl_4$: C, 59.6; H, 4.0; N, 5.8; Cl, 14.6; Zr, 9.4. Found: C, 58.8; H, 3.9; N, 5.7; Cl, 14.5; Zr, 9.2 %. ^1H NMR ($CDCl_3$): δ 0.25 (s, 2H, NH), δ 4.16 (s, 12H, OCH_3), δ 8.17 (d, 4H, 2), δ 8.18 (t, 4H, 2′), δ 7.89–7.92 (t, 4H, 3), δ 7.49–7.52 (d, 4H, 4), δ 8.63 (s, 8H, β). IR (KBr): υ_{NH} ($\sim$3320 cm^{-1}).

2.3.6. [$(H_2t(4\text{-}Cl)pp)ZrCl_4$]

This complex was synthesized by the method used for the [$(H_2t(4\text{-}OMe)pp)ZrCl_4$] complex. *Anal.* Calc. for $C_{44}H_{26}N_4ZrCl_8$: C, 53.6; H, 2.7; N, 5.7; Cl, 28.8; Zr, 9.2. Found: C, 52.9; H, 2.6; N, 5.6; Cl, 28.4; Zr, 9.0 %. ^1H NMR ($CDCl_3$): δ 0.44 (s, 2H, NH), δ 8.51–8.53 (d, 8H, 2, 2′), δ 8.00–8.02 (d, 8H, 2, 2′), δ 8.57 (s, 8H, β). IR (KBr): υ_{NH} ($\sim$3320 cm^{-1}).

2.3.7. [$(H_2t(2\text{-}Me)pp)ZrCl_4$]

0.5 mmol of $H_2t(2\text{-}Me)pp$ and 0.6 mmol $ZrCl_4$ in 2–3 ml hot chloroform were ground together in a mortar for 30 min at room temperature affording the green SAT complex. The grinding was continued until the complexation was complete, which was determined by the disappearance of the Soret band of the porphyrin in the UV–Vis spectrum. The solvent was evaporated, and the excess $ZrCl_4$ was removed by washing the residue with dry diethylether. The produced SAT complex was dried in a vacuum oven for 12 h

at 50 °C, and was consistent with *Anal.* Calc. for $C_{48}H_{38}N_4ZrCl_4$: C, 63.8; H, 4.2; N, 6.2; Cl, 15.7; Zr, 10.1. Found: C, 63.1; H, 4.2; N, 6.1; Cl, 15.4; Zr, 9.9%. ^{1}H NMR ($CDCl_3$): δ 0.20 (s, 1H, NH), δ 0.23 (s, 1H, NH), δ 2.12 (s, 3H, CH_3), δ 2.14 (s, 3H, CH_3), δ 2.23 (s, 3H, CH_3), δ 2.26 (s, 3H, CH_3), δ 8.25–8.27 (d, 1H, 2), δ 8.30–8.32 (d, 1H, 2), δ 8.36–8.38 (d, 1H, 2), δ 8.39–8.41 (d, 1H, 2), δ 7.69–7.75 (br, 8H, 3, 3′), δ 7.80–7.82 (t, 4H, 4), δ 8.45 (s, 4H, β), δ 8.47 (s, 4H, β). IR (KBr): υ_{NH} (~3320 cm^{-1}).

2.3.8. [(H_2t(2-OMe)pp)$ZrCl_4$]

This complex was synthesized by the method used for [(H_2t(2-Me)pp)$ZrCl_4$]. *Anal.* Calc. for $C_{48}H_{38}N_4O_4ZrCl_4$: C, 59.6; H, 4.0; N, 5.8; Cl, 14.6; Zr, 9.4. Found: C, 58.8; H, 3.8; N, 5.7; Cl, 14.3; Zr, 9.0%. ^{1}H NMR ($CDCl_3$): δ 0.26 (s, 1H, NH), δ 0.29 (s, 1H, NH), δ 3.72 (6H, OCH_3), δ 3.79 (6H, OCH_3), δ 8.21–8.22 (d, 2H, 2), δ 8.29–8.31 (d, 2H, 2), δ 7.85–7.88 (t, 4H, 3), δ 7.45–7.48 (t, 4H, 3′), δ 7.40–7.43 (t, 4H, 4), δ 8.43 (s, 4H, β), δ 8.45 (s, 4H, β). IR (KBr): υ_{NH} (~3320 cm^{-1}).

2.3.9. [H_4tpp]Cl_2

To a H_2tpp solution (in chloroform) was added excess hydrochloric acid. Evaporation of the solvent produced the diprotonated porphyrin species as a green solid. ^{1}H NMR ($CDCl_3$): δ 0.31 (s, 2H, NH), δ 8.62–8.64 (d, 8H, 2, 2′), δ 7.96–8.05 (t, 8H, 3, 3′), δ 7.96–7.97 (d, 4H, 4), δ 8.60 (s, 8H, β).

3. Results and discussion

The ^{1}H NMR spectrum of the [(H_2tpp)$ZrCl_4$] SAT complex showed four signals for NH (one signal), β-pyrrole (one signal) and phenyl ring protons (two signals). This spectrum was similar to the ^{1}H NMR spectrum of H_4tpp^{2+} (Fig. 2), but was completely different from the related metalloporphyrin spectrum. The ^{1}H NMR spectrum of the [$ZrCl_2$(tpp)] metalloporphyrin shows four signals at δ 9.11 (s, pyrrole H), 8.42 (s, 4 o-H), 8.08 (t, 4 p-H) and 7.84 (s, 12H) [19]. Further, for this compound there is no signal related to NH protons, Table 1. SAT complexation of the *meso*-tetraarylporphyrins with $ZrCl_4$, similar to the molecular complexation of *meso*-tetraarylporphyrins by $SbCl_3$ [15], $BiCl_3$ [16], SO_2 [20], DDQ [21], TCNE [22] and SiR_3Cl [23], caused downfield shifts for N–H and aryl ring proton signals, and an upfield shift of the β-hydrogens (Fig. 2 and Table 1). The shifts of the internal N–H and β-protons are related to the ring current in both *meso*-teraarylporphyrins and the SAT complexes. The effect of the ring current is lost in the SAT complexed porphyrins with $ZrCl_4$. This is because of the geometric distortion of the porphyrin macrocycle which produces a positive electric charge in the porphyrin core. The downfield shifts of the aryl ring hydrogens can be related to a direct increase in the ring current of aryl groups produced by an extension of the aryl π-system [21,22]. The *ortho*-substituent porphyrins have four atropisomers. The ^{1}H NMR spectral data indicates that the four atropisomers of the *ortho*-substituent porphyrins are bonded differently to $ZrCl_4$. The ^{1}H NMR titration of H_2tpp with $ZrCl_4$ (1:0.5, 1:0.75, 1:1, 1:2 and 1:excess) in $CDCl_3$ showed that the molar ratio of the reactants in the SAT complexes is 1:1. An amount of $ZrCl_4$ less than that of H_2tpp leads to a superimposition of the spectra for the porphyrin and the related SAT complex. Addition of an excess amount of $ZrCl_4$ beyond a 1:1 mole ratio caused no changes in the spectra of [(H_2t(X)pp)$ZrCl_4$].

The ^{13}C NMR spectrum of H_2tpp gives rise to six sharp signals (120.5 (C_{meso}), 127.1 ($C_{3'}$), 128.1 ($C_{4'}$), 131.5 (C_β), 135.0 ($C_{2'}$) and 142.6 ($C_{1'}$) ppm) and a very broad signal (145 ppm) for the α-carbons, whereas the ^{13}C NMR spectrum of [(H_2tpp)$ZrCl_4$] showed seven signals (123.8 (C_{meso}), 129.3 ($C_{3'}$), 129.5($C_{4'}$), 131.1 (C_β), 140.2 ($C_{2'}$), 141.1 ($C_{1'}$) and 147.2 (C_α) ppm). The formation of the SAT

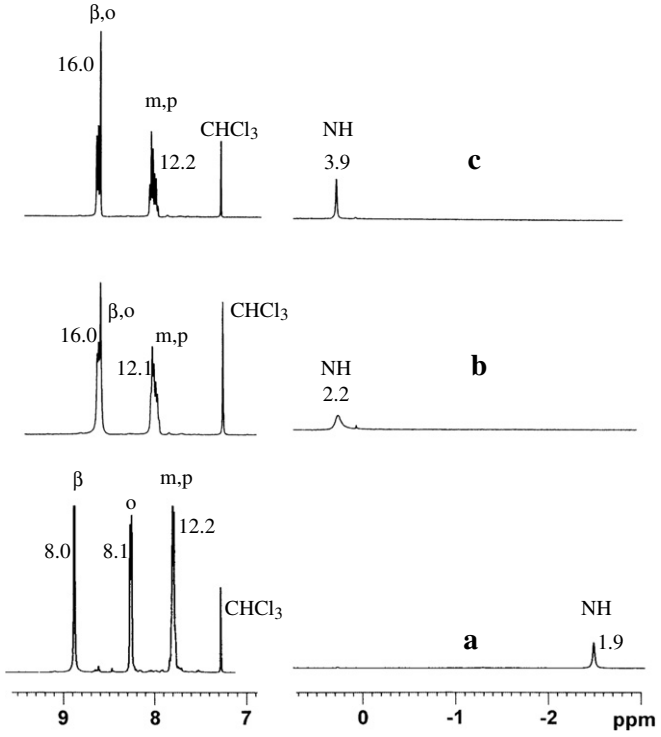

Fig. 2. ^{1}H NMR spectra of (a) H_2tpp, (b) [(H_2tpp)$ZrCl_4$] and (c) [H_4tpp]Cl_2.

Table 1
^{1}H NMR spectral data of different *meso*-tetraarylporphyrins and [H_2t(X)pp$ZrCl_4$] SAT complexes

Compounds	N–H	H_β
H_2tpp	−2.76	8.85
[(H_2tpp)$ZrCl_4$]	0.29	8.58
$\Delta\delta_1$	3.05	−0.27
$[H_4tpp]^{2+} \cdot 2Cl^-$	0.31	8.60
$\Delta\delta_2$	3.07	−0.25
[$ZrCl_2$(tpp)]		9.11
$\Delta\delta_3$		0.26
H_2t(4-Me)pp	−2.77	8.85
[(H_2t(4-Me)pp)$ZrCl_4$]	0.25	8.54
$\Delta\delta_1$	3.02	−0.31
H_2t(4-Cl)pp	−2.75	8.84
[(H_2t(4-Cl)pp)$ZrCl_4$]	0.58	8.60
$\Delta\delta_1$	3.33	−0.24
H_2t(4-OMe)pp	−2.75	8.86
[(H_2t(4-OMe)pp)$ZrCl_4$]	0.55	8.48
$\Delta\delta_1$	3.30	−0.38
H_2t(3-Me)pp	−2.75	8.88
[(H_2t(3-Me)pp)$ZrCl_4$]	0.25	8.57
$\Delta\delta_1$	3.00	−0.31
H_2t(3-OMe)pp	−2.75	8.90
[(H_2t(3-OMe)pp)$ZrCl_4$]	0.25	8.63
$\Delta\delta_1$	3.00	−0.27
H_2t(2-Me)pp	−2.64	8.67
[(H_2t(2-Me)pp)$ZrCl_4$]	0.23	8.45
$\Delta\delta_1$	2.87	−0.22
H_2t(2-OMe)pp	−2.61	8.77
[(H_2t(2-OMe)pp)$ZrCl_4$]	0.29	8.43
$\Delta\delta_1$	2.90	−0.34

$\Delta\delta_1$: Chemical shifts of the proton signals for the porphyrins upon SAT complexation.
$\Delta\delta_2$: Chemical shifts of the proton signals for the H_2tpp upon diprotonation with HCl.
$\Delta\delta_3$: Chemical shifts of the proton signals for the H_2tpp upon metallation ([$ZrCl_2$(tpp)]).

complexes sharpens the α-signals in the ^{13}C NMR spectra of the porphyrins and leads to small shifts in the other lines. These changes are quite similar to those in the molecular complexation of *meso*-tetraarylporphyrin with the acceptors $SbCl_3$, $BiCl_3$, DDQ, TCNE and SO_2 or upon diprotonation [15,16,20–23], though in the diacid species the signals due to C_α, C_β and $C_{2,2'}$ are sharper (Fig. 3). These differences are because of lower symmetry for the SAT complexes relative to the diprotonated porphyrins.

The UV–Vis spectra of the various substituted *meso*-tetraarylporphyrins contain five absorption bands in the 415–655 nm region, that upon SAT complexation with $ZrCl_4$ are shifted to the red and appear as two new bands in the 445–690 nm region (Fig. 4a, b and Table 2). The Soret band is observed in the 442–455 nm region and one weaker band appears in the 645–689 nm region. For an example, the UV–Vis spectrum of $[(H_2tpp)ZrCl_4]$ is shown in Fig. 4b. This spectrum is similar to H_4tpp^{2+} (Fig. 4c), whereas it is completely different from the $[ZrCl_2(tpp)]$ metalloporphyrin, Table 2. $[(H_2tpp)ZrCl_4]$ has two absorption bands at 446.2 and 662.4 nm, but $[ZrCl_2(tpp)]$ has five absorption bands at 398, 418, 502, 540 and 574 nm [19]. These red shifts indicate that there is an out-of-plane distortion of the porphyrin core and a strong interaction between the aryl rings and the porphyrin π-system [15,16,20–23]. ^1H NMR and UV–Vis spectral shifts upon SAT complexation of different *meso*-tetraarylporphyrins with $ZrCl_4$ indicate that the π-resonance is more important than the σ-induction effects and so, the trend in electron donating ability for the substituted *meso*-tetraarylporphyrins is *para* > *meta* > *ortho* (Tables 1 and 2). This trend is corresponded to lower steric hindrance from the ortho compared to para substituents.

^1H and ^{13}C NMR, and UV–Vis correspondences between the spectral data of the molecular complexes of *meso*-tetraarylporphyrins with $SbCl_3$ and $BiCl_3$ acceptors and the $[(H_2t(X)pp)ZrCl_4]$ SAT complexes proposed a similar structure for the porphyrin core in all of the species, with non-coplanar pyrrole rings tilted alternately up and down. In this conformation the lone pairs of two pyrrolenine nitrogens act as the electron donors to one zirconium atom of $ZrCl_4$, above or below the mean plane of the porphyrin (Fig. 5).

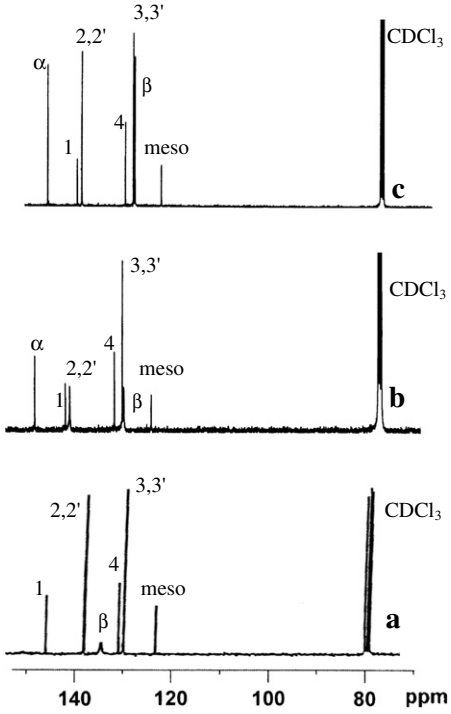

Fig. 3. ^{13}C NMR spectra of (a) H_2tpp, (b) $[(H_2tpp)ZrCl_4]$ and (c) $[H_4tpp]Cl_2$.

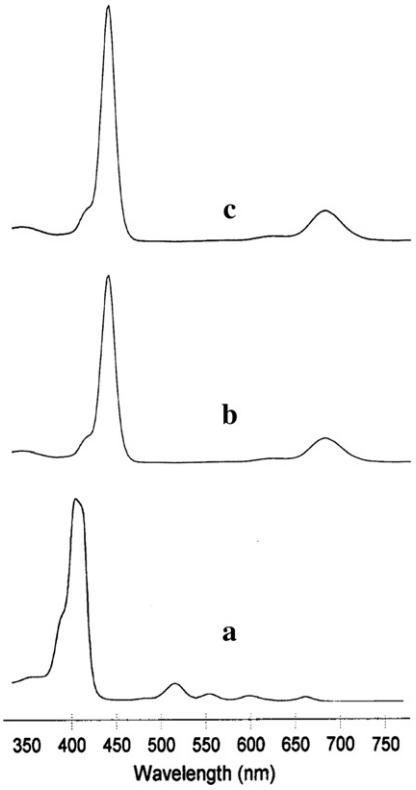

Fig. 4. UV–Vis spectra of (a) H_2tpp, (b) $[(H_2tpp)ZrCl_4]$ and (c) $[H_4tpp]Cl_2$.

Table 2
UV–Vis spectral results of the different *meso*-tetraarylporphyrins and $[H_2t(X)ppZrCl_4]$ SAT complexes in $CHCl_3$

Compounds	λ_{max} (nm)	
H_2tpp	416.7(S), 516.8, 551.5, 592.0, 648.0	
$[(H_2tpp)ZrCl_4]$	446.2	662.4
$\Delta\lambda_1$ [a]	29.5	14.4
$[H_4tpp]^{2+} \cdot 2Cl^-$	444.5(S)	659.9
$\Delta\lambda_2$ [b]	27.8	11.9
$[ZrCl_2(tpp)]$ [c]	398.0, 418.0 (S), 502.0, 540.0, 574.0	
$\Delta\lambda_3$	1.3	
$H_2t(4\text{-Me})pp$	418.3(S), 518.4, 554.0, 593.0, 649.0	
$[(H_2t(4\text{-Me})pp)ZrCl_4]$	448.0(S)	666.4
$\Delta\lambda_1$ [a]	29.7	17.4
$H_2t(4\text{-Cl})pp$	418.2(S), 517.4, 551.0, 592.1, 649.2	
$[(H_2t(4\text{-Cl})pp)ZrCl_4]$	448.0(S)	664.3
$\Delta\lambda_1$ [a]	29.8	15.1
$H_2t(4\text{-OMe})pp$	419.5(S), 520.5, 557.1, 596.0, 653.0	
$[(H_2t(4\text{-OMe})pp)ZrCl_4]$	454.5(S)	688.3
$\Delta\lambda_1$ [a]	35.0	35.3
$H_2t(3\text{-Me})pp$	418.2(S), 517.5, 550.6, 590.0, 647.2	
$[(H_2t(3\text{-Me})pp)ZrCl_4]$	446.3(S)	662.5
$\Delta\lambda_1$ [a]	28.1	15.3
$H_2t(3\text{-OMe})pp$	418.9(S), 517.0, 550.3, 590.3, 646.6	
$[(H_2t(3\text{-OMe})pp)ZrCl_4]$	450.0(S)	660.6
$\Delta\lambda_1$ [a]	31.1	14.0
$H_2t(2\text{-Me})pp$	418.1(S), 514.3, 550.1, 590.5, 646.5	
$[(H_2t(2\text{-Me})pp)ZrCl_4]$	442.3(S)	652.0
$\Delta\lambda_1$ [a]	24.2	5.5
$H_2t(2\text{-OMe})pp$	418.3(S), 514.4, 548.2, 590.1, 647.3	
$[(H_2t(2\text{-OMe})pp)ZrCl_4]$	452.5(S)	656.4
$\Delta\lambda_1$ [a]	34.2	9.1

(S): Soret band.
[a] $\Delta\lambda_1$: Red shifts for the bands of the porphyrins upon SAT complexation.
[b] $\Delta\lambda_2$: Red shifts for the bands of the porphyrins upon diprotonation with HCl.
[c] $\Delta\lambda_3$: Red shifts for the bands of the porphyrins upon metallation ($[ZrCl_2(tpp)]$).

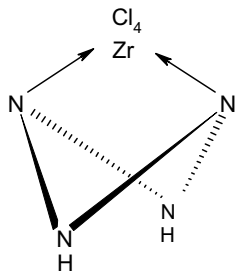

Fig. 5. Only the tetrahedrally tilted pyrrolenine nitrogens of the porphyrin core are shown. Two pyrrolenine nitrogen atoms of the porphyrin act as electron donors to a zirconium atom and the molecule of $ZrCl_4$ is located on one side of the porphyrin plane.

The position of the pyrrolic NHs (trans) in the proposed structure is similar to those in free base *meso*-tetraarylporphyrins. Zirconium(IV) chloride has one chlorine atom more than antimony(III) chloride and bismuth(III) chloride and also the formal positive charge of the central atom in zirconium(IV) chloride is more than that of antimony(III) chloride and bismuth(III) chloride. These two factors increase respectively the steric hindrance and electron accepting capability for zirconium(IV) chloride compared to $SbCl_3$ and $BiCl_3$. The steric hindrance of the four chlorine atoms in $ZrCl_4$ causes more stability of the monomer form than the dimer form in the synthesized SAT complexes.

The IR (400–4000 cm^{-1}) spectra of the free base *meso*-tetraarylporphyrins show the N–H stretching band at 3320 cm^{-1} [24], which upon SAT complexation with $ZrCl_4$ is not considerable changed. The existence of the NH band shows that the metallation of the porphyrins does not occur in our reaction system. Furthermore, this subject is proved by the presence of two NH protons in the ^1H NMR spectra of the SAT complexes.

The ^1H and ^{13}C NMR, and UV–Vis spectra of the SAT complexes of *meso*-tetraarylporphyrins with $ZrCl_4$ were similar to those of the related diprotonated species [25], but the signals of the ^1H and ^{13}C NMR (the signals of C_α, C_β and $C_{2'}$) spectra for the SAT complexes were broader than those of the diprotonated species (Fig. 2b and c, Fig. 3b and c). The broadening can be related to a lower symmetry for the SAT complexes than the diprotonated porphyrins (Fig. 5). On the other hand, the molar conductivity data for the SAT complexes and the related diprotonated species were completely different. For example, the molar conductances of the $[(H_2tpp)ZrCl_4]$ SAT complex (in nitromethane) and $[H_4tpp]Cl_2$ (in methanol) are 10.7 and 213.3 $\Omega^{-1}\,cm^2\,mol^{-1}$, respectively [26]. These results show that the SAT complexes are not electrolytes whereas the diprotonated porphyrins are 1:2 electrolytes. Consequently, the remarkable spectral correspondence between the SAT complexes and the diprotonated species suggest only an analogous tilted porphyrin core structure in these species.

The metalloporphyrin of $[ZrCl_2(tpp)]$ was synthesized by the reaction of $ZrCl_4(THF)_2$ and the dilithium salt of *meso*-tetraphenylporphyrin at reflux conditions (in toluene solvent) under an inert atmosphere [19], whereas the SAT complexes in this study are synthesized in chloroform under mild conditions. There are some other evidences that they are differed two species. The ^1H NMR spectrum of the metalloporphyrin ($[ZrCl_2(tpp)]$) shows four protons signals and its UV–Vis spectrum shows four absorption bands [19]. The corresponding spectral data for $[ZrCl_2(tpp)]$ are completely different from the related SAT complex ($[(H_2tpp)ZrCl_4]$), Tables 1 and 2. On the other hand, the chloroform solutions of the SAT complexes ($[H_2t(X)ppZrCl_4]$) rapidly decomposes to the related porphyrins by addition of natural alumina, whilst $[ZrCl_2(tpp)]$ is purified by an alumina column [19]. It is interesting that the SAT complexes decompose to the related porphyrins in the presence of donor solvents such as DMSO, but the metalloporphyrins are completely stable in these solvents. Further, in Eq. (1), the mole ratio of metal:porphyrin is 1:2 whereas it was 1:1 for our reaction system. Consequently, the synthesized complexes in this work are completely different from the known compounds of diprotonated porphyrins or related metalloporphyrins.

4. Conclusion

The *meso*-tetraarylporphyrins $H_2t(X)pp$ react with zirconium(IV) chloride to form highly stable SAT complexes (for example, $[H_2t(4\text{-}OCH_3)ppZrCl_4]$ is completely stable up to 170 °C). Selection of suitable conditions for the reaction system enabled the successful preparation of the SAT complexes as solids. NMR and UV–Vis spectral data show that the distorted porphyrin core of the SAT complexes is similar to porphyrin diacids [25] and molecular complexes of *meso*-tetraarylporphyrins with various acceptors [15,16,20–23]. In these SAT complexes, two nitrogen atoms of pyrrolenine on one side of the porphyrin plane act as electron donors to a zirconium atom of $ZrCl_4$ and two protons still remain on the pyrrole nitrogens.

Acknowledgements

This work was partly supported by the Kashan University Research Council.

References

[1] C.K. Mathews, K.E. Holde, K.G. Ahern, Biochemistry, Addison Wesley Longman, San Francisco, 2000.
[2] R.H. Garrett, C.M. Grisham, Biochemistry, Saunders College Publishing, 1999.
[3] G. Knör, A. Strasser, Inorg. Chem. Commun. 9 (2005) 471.
[4] M.D. Lim, I.M. Lorkovic, P.C. Ford, J. Inorg. Biochem. 99 (2005) 151.
[5] G.G. Martirosyan, A.S. Azizyan, T.S. Kurtikyan, P.C. Ford, Chem. Commun. (2004) 1488.
[6] E.B. Fleischer, J.H. Wang, J. Am. Chem. Soc. 82 (1960) 3498.
[7] J.P. Macquet, T. Theophahanides, Can. J. Chem. 51 (1973) 219.
[8] K. Letts, R.A. Mackay, Inorg. Chem. 14 (1975) 2993.
[9] E.B. Fleischer, F. Dioxn, Bioinorg. Chem. (7) (1977) 129.
[10] Y. Shen, U. Ryde, Inorg. Biochem. 98 (2004) 878.
[11] Y. Hsiao, U. Ryde, Inorg. Chim. Acta 359 (2006) 1081.
[12] Y. Inada, Y. Sugimoto, Y. Nakano, Y. Itoh, S. Funahashi, Inorg. Chem. 37 (1998) 5519.
[13] C.H. Tsai, J.Y. Tung, J.H. Chen, F.L. Liao, S.L. Wang, S.S. Wang, L.P. Hwang, C.B. Chen, Polyhedron 19 (2000) 633.
[14] J.L. Garate-Morales, F.S. Tham, C.A. Reed, Inorg. Chem. 46 (2007) 1514.
[15] H. Dehghani, A.R. Ansari Sardrood, Polyhedron 26 (2007) 4263.
[16] H. Dehghani, A.R. Ansari Sardrood, Bull. Chem. Soc. Jpn. 80 (2007) 518.
[17] (a) A.M.d'A. Rocha Gonsalves, J.M.T.B. Varejao, M.M. Pereira, J. Heterocycl. Chem. 28 (1991) 635;
(b) A.D. Adler, F.R. Longo, J.H. Finarelli, J. Goldmacher, J. Assour, L. Korsakoff, J. Org. Chem. 32 (1967) 476.
[18] J. Mendham, R.C. Denney, J.D. Barnes, M.J.K. Thomas, Vogel's Textbook of Quantitative Chemical Analysis, 6th ed., John Wiley & Sons, Inc., New York, 2000 (Chapter 17).
[19] H. Kim, D. Whang, K. Kim, Y. Do, Inorg. Chem. 32 (1993) 360.
[20] H. Dehghani, F. Fathi, Dyes Pigments 77 (2008) 323.
[21] D. Mohajer, H. Dehghani, J. Chem. Soc., Perkin Trans. 2 (2000) 199.
[22] D. Mohajer, H. Dehghani, Bull. Chem. Soc. Jpn. 73 (2000) 1477.
[23] D. Mohajer, S. Rayati, New J. Chem. 27 (2003) 242.
[24] H.H. Limbach, J. Henning, J. Stulz, J. Chem. Phys. 78 (1983) 5432.
[25] (a) E.C.A. Ojadi, R.I. Walter, H. Linschitz, J. Phys. Chem. 97 (1993) 13308;
(b) M. Meot-Ner, A.D. Adler, J. Am. Chem. Soc. 97 (1975) 5107;
(c) A. Stone, E.B. Fleischer, J. Am. Chem. Soc. 90 (1968) 2735.
[26] W.J. Geary, Coord. Chem. Rev. 7 (1971) 81.

Polyhedron 27 (2008) 2421–2425

Contents lists available at ScienceDirect

Polyhedron

journal homepage: www.elsevier.com/locate/poly

Cyrhetrenylimines and cyrhetrenylamines: Synthesis, characterization and X-ray crystal structure

Rodrigo Arancibia [a], Fernando Godoy [a], Gonzalo E. Buono-Core [a], A. Hugo Klahn [a,*], Enrique Gutierrez-Puebla [b], Angeles Monge [b]

[a] Instituto de Quimica, Pontificia Universidad Catolica de Valparaíso, Casilla 4059, Valparaíso, Chile
[b] Instituto de Ciencias de Materiales de Madrid, Consejo Superior de Investigaciones Cientificas, Sor Juana Inés de la Cruz 3, 28049 Madrid, Spain

ARTICLE INFO

Article history:
Received 27 December 2007
Accepted 21 April 2008
Available online 2 June 2008

Keywords:
Cyrhetrenyl Schiff bases
Reduction
Cyrhetrenylamines
X-ray characterization

ABSTRACT

Cyrhetrenyl Schiff base derivatives of the form (η^5-C_5H_4CH=NAr)$Re(CO)_3$, [Ar = Ph (**1a**) C_6H_4OMe-*p* (**1b**) and $C_6H_4NO_2$-*p* (**1c**)] have been prepared from cyrhetrenylcarbaldehyde and the corresponding aromatic amines. ^1H and ^{13}C NMR indicates that these compounds have the *anti*-(*E*) conformation in solution and the X-ray crystal structure of **1b** confirms that it also adopts the *anti*-(*E*) form in the solid state. Further reaction of cyrhetrenylaldimines **1** with sodium borohydride in methanol produces quantitatively, the corresponding amine derivatives (η^5-$C_5H_4CH_2$–NHAr)$Re(CO)_3$ [Ar = Ph (**2a**) C_6H_4OMe-*p* (**2b**) and $C_6H_4NO_2$-*p* (**2c**)]. All these cyrhetrenylamines were characterized by IR, ^1H and ^{13}C NMR, MS. Additionally, **2b** has been characterized structurally.

© 2008 Elsevier Ltd. All rights reserved.

1. Introduction

Ferrocenylimines (η^5-C_5H_5)Fe(η^5–C_5H_4CR=NAr) and ferrocenylamines (η^5-C_5H_5)Fe(η^5-$C_5H_4CHRNHAr$), R = H, Me, Ph; and Ar = a variety of substituted phenyl, have attracted a great deal of attention in the past two decade due to their wide application in molecular materials [1], bioorganometallic chemistry [2] and as ligands capable of coordinating transition metal ions giving complexes with potential applications in catalysis [3]. The above situation contrasts with the smaller number of analogous compounds bearing the cyrhetrenyl group (η^5-C_5H_4)$Re(CO)_3$, described in the literature. To our best knowledge the only known cyrhetrenylimine (η^5-C_5H_4CH=NPh)$Re(CO)_3$, was briefly described by Kolobova et al. [4,5]. More recently, complexes of these type have been used *in situ*, as intermediates for the preparation of some biological compounds containing the (η^5-C_5H_4)$Re(CO)_3$ group (see below) but details of their isolation and characterization remain unknown [6]. On the other hand, reduction of ferrocenylimines with sodium borohydride or lithium aluminium hydride has been shown to be an efficient procedure for the preparation of (*N*-aryl)-amino methylferrocenes. A similar approach have been used by Jaouen to prepare poly(amidoamine) dendrimers tethered with cyclopentadienyl rhenium tricarbonyl [6]. As part of our interest in comparing the properties of the cyrhetrenyl substituted systems with the well known analogous ferrocenyl [7], in this paper we would like to report the synthesis and characterization of the cyrhetrenylimine (Schiff base) complexes (η^5-C_5H_4CH=NAr)$Re(CO)_3$, and the cyrhetrenyl-amine derivatives (η^5-$C_5H_4CH_2$–NHAr)$Re(CO)_3$. The imine and amine complexes derived from *p*-anisidine were also studied X-ray crystallography.

2. Results and discussion

2.1. Cyrhetrenylimine complexes (η^5-C_5H_4CH=NAr)$Re(CO)_3$ (**1**)

The Schiff bases (η^5-C_5H_4CH=NAr)$Re(CO)_3$, Ar = Ph (**1a**) C_6H_4OMe-*p* (**1b**) and $C_6H_4NO_2$-*p* (**1c**) were synthesized following the same procedure to that described for analogous ferrocenylimines derivatives [8], that is by condensation of the corresponding aniline with formylcyrhetrene (η^5-C_5H_4COH)$Re(CO)_3$ [9] (Scheme 1).

The procedure consists of the reaction of equimolar amounts of formylcyrhetrene and the aromatic amine in refluxing toluene. A Dean–Stark apparatus was used to remove the toluene–water azeotrope formed during the reaction formation of **1c**. In all cases the products were isolated as white crystalline solids after crystallization from CH_2Cl_2-hexane mixture (1:5).

The IR spectra of these compounds showed the expected value of the $\nu_{C=N}$ stretch in the range 1625–1643 cm^{-1}, in CH_2Cl_2 solution. This absorption bands as well as the ν_{CO} of the carbonyls bound to rhenium are shifted to lower wavenumber when compared to the precursor formylcyrhetrene [9]. Similar $\nu_{C=N}$ frequency shifts have been reported for Schiff bases derived from

* Corresponding author. Tel.: +56 32 2273174; fax: +56 32 2273422.
E-mail address: hklahn@ucv.cl (A. Hugo Klahn).

0277-5387/$ - see front matter © 2008 Elsevier Ltd. All rights reserved.
doi:10.1016/j.poly.2008.04.021

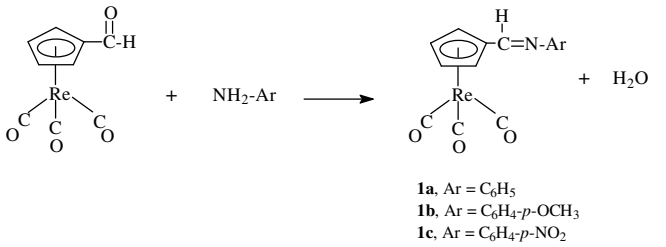

Scheme 1.

formylferrocene [8]. Each of **1a–c** showed a strong molecular ion and fragments corresponding to the successive lost of three CO, in their mass spectra.

The ^{1}H NMR spectra showed a singlet at about δ 8.0 due to the iminic proton and two apparent triplets between 5.42 and 6.07 ppm. The latter are ascribed to the monosubstituted cyclopentadienyl ring. In addition, resonances for the hydrogen atoms of the aryl ring and the methoxy substituent were also observed. ^{13}C NMR data were also in accordance with the existence of a single compound. Despite the fact that these type of compounds could adopt two different forms (*E*- or *Z*-) [1b,3c,10] their ^{1}H and ^{13}C NMR spectra, which agreed with those reported for related ferrocenyl Schiff bases [1b,3c,10], revealed that only one isomer (*E*-form) was present in solution. Further proof was provided by an X-ray crystal structure determination of **1b** (see below). The most important feature of these spectra is the presence of a low field resonance (δ 152–158) assigned to the iminyl carbon. This resonance occurs at almost the same δ as those reported for the ferrocene analogues [1,3c,10] and is indicative of some degree of conjugation of the C_5H_4 ring and the –HC=N entity.

With the aim to compare structural parameters of these compounds with the crystallographic data reported for several ferrocenylimines [1a,8c,10,11], we undertook a crystallographic study of complex **1b**. The structure of **1b** is shown in Fig. 1. Table 1 reports the crystal structure and refinement data and Table 2 shows selected bond lengths and angles. The structure confirms the *E* configuration assigned tentatively by NMR. Taking into account the internal and exocyclic C–C distances of the cyclopentadienyl ring and the classification done for substituted ferrocene derivatives [1a,10], a fulvenoid type of structure can be considered for **1b**, since it possesses alternated two short and three long C–C distances (C(2)–C(3) 1.403 Å; C(4)–C(5) 1.402 Å; C(1)–C(2) 1.446 Å; C(1)–C(5) 1.412 Å and C(3)–C(4) 1.433 Å), and the exocyclic C(1)–C(9) of 1.456 Å. Additional support for this assignment is to be found in the C=N bond length (1.265 Å), which is within the range to those measured in several ferrocenyl Schiff bases [1a,8c,10,11], and the C_5H_4CH=N part of the molecule are practically flat, the maxima deviation from the least-squares plane formed by the atoms of the C_5 ring and C(9), N(1) and C(10) atoms is only 0.1 Å. This is in agreement with the suggestion that some delocalization of electron density is found over the C_5H_4CH=N moiety. On the other hand, within the cyrhetrenyl group, the average Re–C(O) distance and the Re–C–O angle are concordant with related tricarbonyl cyclopentadienyl rhenium(I) complexes [7].

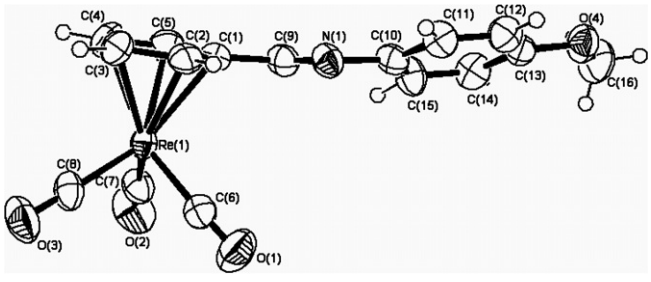

Fig. 1. Molecular structure of cyrhetrenylimine **1b**.

Table 1
Crystal data and structure refinement for **1b** and **2b**

Compound	**1b**	**2b**
Empirical Formula	$C_{16}H_{12}NO_4Re$	$C_{16}H_{14}NO_4Re$
Formula weight	468.47	470.47
Temperature (K)	295(2)	295(2)
wavelength (Å)	0.71073	0.71073
Crystal system	monoclinic	triclinic
Space group	$P2(1)/n$	$P\bar{1}$
Unit cell dimensions		
a (Å)	11.2762(5)	7.4071(5)
b (Å)	8.3746(4)	7.9042(6)
c (Å)	16.1881(7)	13.8307(10)
α (°)	90	89.3360(10)
β (°)	93.2030(10)	86.6540(10)
γ (°)	90	78.6150(10)
Volume (Å^3)	1526.31(12)	792.46(10)
Z	4	2
D_{calc} (g/cm^3)	2.039	1.967
Absorption coefficient (mm^{-1})	7.978	7.683
$F(000)$	888	446
Crystal size (mm)	0.30 × 0.20 × 0.20	0.30 × 0.20 × 0.20
θ Range for data collection (°)	2.15–29.05	2.63–29.16
Index ranges	$-15 \leqslant h \leqslant 15$, $-11 \leqslant k \leqslant 11$, $-20 \leqslant l \leqslant 21$	$-9 \leqslant h \leqslant 9$, $-10 \leqslant k \leqslant 10$, $-18 \leqslant l \leqslant 18$
Reflections collected	13557	7576
Independent reflections (R_{int})	3786 (0.0377)	3776 (0.0269)
Completeness to theta = 29.05° (%)	92.7	88.6
Absorption correction	empirical	empirical
Refinement method	full-matrix least-squares on F^2	full-matrix least-squares on F^2
Data/restraints/parameters	3786/0/236	3776/0/251
Goodness-of-fit on F^2	1.127	1.053
Final R indices [$I > 2\sigma(I)$]	R_1 = 0.0373, wR_2 = 0.0622	R_1 = 0.0262, wR_2 = 0.0585
R indices (all data)	R_1 = 0.0550, wR_2 = 0.0659	R_1 = 0.0314, wR_2 = 0.0600
Largest difference in peak and hole (e Å^{-3})	0.983 and −1.233	0.769 and −0.905

2.2. Cyrhetrenylamine complexes (η^5-$C_5H_4CH_2NHAr$)$Re(CO)_3$ (**2**)

These compounds were prepared according to the general procedure described for most ferrocenylamines [3f,11] that is, by direct reduction of the corresponding cyrhetrenyl imine complex **1** with $NaBH_4$ in anhydrous methanol, at room temperature (Scheme 2).

Table 2
Select bond lengths (Å), bond angles and dihedral angles (°) for **1b** and **2b**

Compound	**1b**	**2b**
Bond lengths (Å)		
C(1)–C(9)	1.456(7)	1.511(5)
C(9)–N(1)	1.265(7)	1.454(5)
N(1)–C(10)	1.414(6)	1.414(5)
Cp(centroid)–Re(1)	1.961(6)	1.949(5)
Re–C(CO) av.	1.923	1.904
Bond angles (°)		
N(1)–C(9)–C(1)	121.8(5)	113.1(3)
C(9)–N(1)–C(10)	119.5(5)	119.9(3)
C(13)–O(4)–C(16)	116.3(5)	117.3(4)
OC–Re–CO av.	89.57	90.18

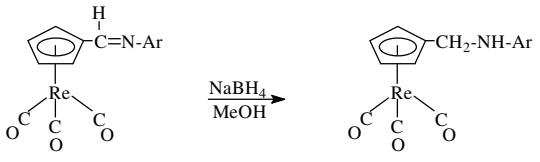

2a, Ar = C_6H_5
2b, Ar = C_6H_4-*p*-OCH_3
2c, Ar = C_6H_4-*p*-NO_2

Scheme 2.

The products were purified by column chromatography and isolated in quantitative yields as white solids. The IR spectra, in CH_2Cl_2 solution, showed as expected, the presence of two ν_{CO} bands, which are slightly shifted to lower wavenumber compared to their parent complexes **1**. In addition to the resonances of the cyclopentadienyl and aryl groups, in all cases the ^{1}H NMR spectra, in C_6D_6 solution, clearly showed at $\delta \sim 3.4$, a doublet and a broad singlet for the CH_2 and NH groups, respectively. These assignments were confirmed by ^{1}H–^{1}H NMR COSY.

The main feature of the ^{13}C NMR spectrum of each compound, in $CDCl_3$ solution, is a resonance at about 41 ppm which has been assigned to the CH_2 group on the basis of the reported chemical shifts for the methylene group in analogous ferrocenylamines [12,13]. The resonances of CO groups (Re–CO) occurred to similar chemical shift to others tricarbonyl cyclopententadienyl functionalized complexes [7,9].

The mass spectra of **2a–c** exhibited the molecular ion, and the successive loss of three CO ligands. In all cases, the most intense peak corresponds to the elimination of the amine fragment (NHAr) to give cyrhetrenylmetylene cation (*m*/*z* 349, 100%). This fragmentation is similar to that observed for the complex (η^5-$C_5H_4CH_2NHC_6H_5$)Fe(η^5-C_5H_5) [12,13].

The elementals analyses are in a good agreement with the proposed structures.

The molecular structure of amine **2b** (Fig. 2) shows no significant differences in bond lengths and angles (Table 1) when compared to the structure of the ferrocene related compounds [12–14]. The torsion angle C(10)–N–C(9)–C(1) of 59.0° indicates a Syn-Clinal arrangement of the substituents at the N–C(9) bond. The angle 81.6° between the planes of the Cp ring with the aromatic ring is almost orthogonal. On the other hand, the rhenium-ring centroid distance 1.949 (5) Å, the average Re–C(O) distance and the Re–C–O angles are concordant with the corresponding values reported for substituted-cyclopentadienyl tricarbonyl rhenium(I) complexes [7,15].

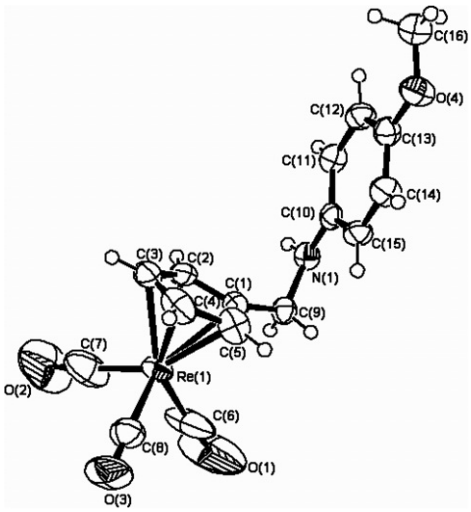

Fig. 2. Molecular structure of cyrhetrenylamine **2b**.

3. Experimental

(η^5-C_5H_4CHO)$Re(CO)_3$ was prepared according to the literature method [9]. Anilines and $NaBH_4$ were obtained commercially (Aldrich). All the solvents were purified according standard methods prior to use. Infrared spectra were recorded in solution (NaCl cell) on a Perkin–Elmer FT-1605 spectrophotometer, and the ^{1}H and ^{13}C NMR spectra were measured on a Bruker AVANCE 400 spectrometer. ^{1}H NMR chemical shifts were referenced using the chemicals shifts of residual solvent resonances, and ^{13}C chemical shifts to solvent peaks. Mass spectra were obtained on a Thermo-Finnigan MAT 900XP, at the Facultad de Ciencias Químicas y Farmacéuticas, Universidad de Chile.

3.1. (η^5-C_5H_4CH=NC_6H_5)$Re(CO)_3$ (**1a**)

To a solution of (η^5-C_5H_4CHO)$Re(CO)_3$ (50.0 mg, 0.138 mmol) in toluene (15 mL) was added 1.25 mL (0.138 mmol) of a 0.110 M aniline solution in toluene. The mixture was refluxed for 15 h. After this time, an IR spectrum of the solution showed the complete disappearance of the cyrhetrenylcarboxaldehyde complex (2033s; 1940s and 1694 cm^{-1}) and the presence of the new CO absorptions due to **1a**. The solvent was pumped off and the solid crystallized from CH_2Cl_2/hexane at −18 °C to give white crystals of **1a** (yield: 58.0 mg, 0.132 mmol, 95.7%). IR (CH_2Cl_2, cm^{-1}) 2026s, (νCO); 1934s, (νCO); 1630w, (νC=N). ^{1}H NMR ($CDCl_3$) δ: 5.44 (t, *J* = 2.4 Hz, 2H,C_5H_4); 6.00 (t, *J* = 2.4 Hz, 2H, C_5H_5); 7.09 (m, 2H, C_6H_5); 7.23 (t, *J* = 7.4, 1H, C_6H_5); 7.37 (t, *J* = 7.8, 2H, C_6H_5); 8.07 (s, 1H, C*H*=N). ^{13}C NMR ($CDCl_3$) δ: 84.9 (C_5H_4); 86.0 (C_5H_4); 99.5 (s, C_{ipso}, C_5H_4); 120.6 (s, C_6H_4); 126.3 (s, C_6H_4); 129.2 (s, C_6H_4); 151.0 (s, C_6H_4); 152.1 (*C*H=N); 192.7 (*C*O). Mass spectrum (based on ^{187}Re) *m*/*z* 439 [M$^+$], 411 [M$^+$−CO], 383 [M$^+$−2CO], 355 [M$^+$−3CO]. *Anal.* Calc. for $C_{15}H_{10}O_3NRe$: C, 41.09; H, 2.28. Found: C, 42.02; H, 2.31%.

3.2. (η^5-C_5H_4CH=$NC_6H_4OCH_3$-*p*)$Re(CO)_3$ (**1b**)

To a solution of (η^5-C_5H_4CHO)$Re(CO)_3$ 50.0 mg (0.138 mmol) in toluene (10 mL) was added *p*-anisidine 17.0 mg (0.138 mmol). The mixture was refluxed under nitrogen atmosphere for 5 h. After this time, the solution changed color from yellow to brown. The IR spectrum showed the complete disappearance of the starting complex and three new absorption bands. The solvent was removed under vacuum and a gray oil was obtained. Crystallization from CH_2Cl_2/hexane (1:5) at −18 °C to give off-white microcrystals of **1b** (Yield: 61 mg, 0.130 mmol, 94.4%). IR (CH_2Cl_2, cm^{-1}): 2026s, (νCO), 1932s, (νCO), 1627w, (νC=N). ^{1}H NMR ($CDCl_3$): δ: 3.81 (s, 3H, O*CH*$_3$); 5.42 (t, *J* = 2.4 Hz, 2H, C_5H_4); 5.96 (t, *J* = 2.4 Hz, 2H, C_5H_4); 6.90 (pseudo-dt, 2H, C_6H_4); 7.11 (pseudo-dt, 2H, C_6H_4); 8.08 (s,1H, C*H*=N). ^{13}C NMR ($CDCl_3$): δ: 55.5 (s, OCH_3); 84.8 (C_5H_4); 85.7 (C_5H_4); 100.2 (s, C_5H_4); 114.4 (s, C_6H_4); 122.0 (s, C_6H_4); 143.8 (s, C_6H_4); 150.0 (s, C_6H_4); 158.54 (*C*H=N), 192.86 (*C*O). Mass spectrum (based on ^{187}Re) *m*/*z*: 469 [M$^+$], 441 [M$^+$−CO], 413 [M$^+$−2CO], 385 [M$^+$−3CO]. *Anal.* Calc. for $C_{16}H_{12}O_4NRe$: C, 41.02; H, 2.58. Found: C, 42.13; H, 2.64%.

3.3. (η^5-C_5H_4CH=$NC_6H_4NO_2$-*p*)$Re(CO)_3$ (**1c**)

The synthesis of the complex **1c** was carried out in a similar manner to that described for complex **1b** using (η^5-C_5H_4CHO)$Re(CO)_3$ (50.0 mg, 0.138 mmol) and *p*-nitroaniline (19.0 mg, 0.138 mmol) but refluxing for 48 h using a Dean–Stark apparatus. **1c** was

obtained as white-yellow crystals (Yield: 61, 0.126 mmol, mg, 91.3%). IR (CH_2Cl_2, cm^{-1}) 2028s (νCO), 1936s (νCO), 1625w (νC=N). ^1H NMR ($CDCl_3$) δ: 5.49 (t, J = 2.0 Hz, 2H,C_5H_4), 6.03 (t, J = 2.0 Hz, 2H, C_5H_4), 7.13 (pseudo-dt, 2H, C_6H_4); 8.08 (s, 1H, CH=N); 8.24 (pseudo-dt, 2H, C_6H_4); ^{13}C NMR ($CDCl_3$): δ 85.4 (C_5H_4); 86.8 (C_5H_4); 97.5 (s, C_5H_4); 111.3 (s, C_6H_4); 121.1 (s, C_6H_4); 125.0 (s, C_6H_4); 126.3 (s, C_6H_4); 156.7 (CH=N), 192.86 (CO). Mass spectrum (based on ^{187}Re) m/z: 484 [M^+], 456 [M^+−CO], 428 [M^+−2CO], 400 [M^+−3CO]. *Anal.* Calc. for $C_{15}H_9O_5N_2Re$: C, 37.19; H, 1.86. Found: C, 37.79; H, 1.97%.

3.4. (η^5-$C_5H_4CH_2NHC_6H_5$)Re(CO)$_3$ (**2a**)

Complex **1a** (50.0 mg, 0.114 mmol) was dissolved in anhydrous methanol (10 ml) followed by addition an excess of solid $NaBH_4$ (16.0 mg, 0.423 mmol). The mixture was stirred under nitrogen atmosphere for 2 h. After this time, the IR spectrum showed the complete disappearance of the imine complex **1a**, and the presence of two new absorption bands shifted to low energy (2020, 1924 cm^{-1}). The white solid obtained after evaporation of methanol was chromatographed on a silica gel column; elution with CH_2Cl_2 moved the amine complex. The complex **2a** was isolated quantitatively as white solid, after crystallization from CH_2Cl_2/hexane (1:5) at −18 °C. (Yield: 50.0 mg, 0.114, 100%). IR (CH_2Cl_2, νCO, cm^{-1}): 2024s, 1929s. ^1H NMR ($CDCl_3$) δ: 4.14 (s, 2H, CH_2); 5.28 (t, J = 2.4 Hz, 2H, C_5H_4); 5.43 (t, J = 2.4 Hz, 2H, C_5H_4); 6.66 (d, J = 7.8 Hz, 2H, C_6H_5); 6.78 (d, J = 7.3 Hz, 1H, C_6H_5); 7.22 (pseudo-dt, 2H, C_6H_5). ^1H NMR (C_6D_6) δ: 3.19 (s, broad, 1H, NH); 3.48 (d, J = 6.6 Hz, 2H, CH_2); 4.38 (pseudo- t, 2H, C_5H_4); 4.58 (pseudo-t, 2H, C_5H_4); 6.37 (d, J = 7.7 Hz, 2H, C_6H_5); 6.79 (d, J = 7.3 Hz, 1H, C_6H_5); 7.15 (t, J = 7.7 Hz, 2H, C_6H_5). ^{13}C NMR ($CDCl_3$) δ: 41.4 (s, CH_2); 83.5 (s, C_5H_4); 83.7 (s, C_5H_4); 108.7 (s, C_5H_4); 113.1 (s, C_6H_5); 118.5 (s, C_6H_5); 129.5 (s, C_6H_5); 147.3 (s, C_6H_5); 193.9 (CO). Mass spectrum (based on ^{187}Re) m/z: 441 [M^+]; 413 [M^+−CO]; 385 [M^+−2CO]; 357 [M^+−3CO]; 349 [M^+−NHC_6H_5]. *Anal.* Calc. for $C_{15}H_{12}O_3NRe$: C, 40.81; H, 2.72. Found: C, 40.94; H, 2.86%.

3.5. (η^5-$C_5H_4CH_2NHC_6H_4OCH_3$-p)Re(CO)$_3$ (**2b**)

Complex **2b** was obtained following the same procedure described for **2a**. It was isolated as white crystals. (Yield: 50.0 mg, 0.106 mmol, 100%). IR (CH_2Cl_2, νCO, cm^{-1}): 2022 s, 1926 s. ^1H NMR ($CDCl_3$): δ 3.76 (s, 3H, OCH_3); 4.08 (s, 2H, CH_2); 5.27 (t, J = 2.4 Hz, 2H, C_5H_4); 5.41 (t, J = 2.4 Hz, 2H, C_5H_4); 6.63 (pseudo-dt, 2H, C_6H_4); 6.80 (pseudo-dt, 2H, C_6H_4). ^1H NMR (C_6D_6): δ 2.98 (s, broad, 1H, NH); 3.44 (s, 3H, OCH_3); 3.50 (d, J = 6.6 Hz, 2H, CH_2); 4.35 (t, J = 2.0 Hz, 2H, C_5H_4); 4.66 (t, J = 2.0 Hz, 2H, C_5H_4); 6.36 (pseudo-dt, 2H, C_6H_4); 6.81 (pseudo-dt, 2H, C_6H_4). ^{13}C NMR ($CDCl_3$) δ: 42.5(CH_2); 55.6 (s, OCH_3); 83.5 (s, C_5H_4); 83.6 (s, C_5H_4); 108.8 (s, C_5H_4); 114.7 (s, C_6H_4); 115.5 (s, C_6H_4); 141.3 (s, C_6H_4); 152.9 (s, C_6H_4); 193.94(CO). Mass spectrum (based on ^{187}Re) m/z: 471 [M^+]; 443 [M^+−CO]; 415 [M^+−2CO]; 387 [M^+−3CO]; 349 [M^+−NHC_6H_4-p-OCH_3]. *Anal.* Calc. for $C_{16}H_{14}O_4NRe$: C, 40.85; H, 3.00. Found: C, 40.98; H, 3.05%.

3.6. (η^5-$C_5H_4CH_2NHC_6H_4NO_2$-p)Re(CO)$_3$ (**2c**)

Complex **2b** was obtained following the same procedure described for **2a**. It was isolated as white crystals. (Yield: 50.0 mg, 0.103 mmol, 100%). IR (CH_2Cl_2, νCO, cm^{-1}): 2024 s, 1929 s. ^1H NMR ($CDCl_3$) δ: 4.24 (d, J = 5.9 Hz, 2H, CH_2); 4.54 (pseudo-t, 1H, NH); 5.33 (t, J = 2.4 Hz, 2H, C_5H_4); 5.43 (t, J = 2.4 Hz, 2H, C_5H_4); 6.63 (pseudo-dt, 2H, C_6H_4); 8.13 (pseudo-dt, 2H, C_6H_4). ^1H NMR (C_6D_6) δ: 3.21 (d, J = 6.1 Hz, 2H, CH_2); 3.48 (pseudo-t, 1H, NH); 4.37 (pseudo-t, 2H, C_5H_4); 4.48 (pseudo-t, 2H, C_5H_4); 5.80 (d, J = 9.0 Hz, 2H, C_6H_4); 8.04 (d,J = 9.0 Hz, 2H, C_6H_4). ^{13}C NMR ($CDCl_3$): δ 40.7 (s, CH_2); 83.7 (s, C_5H_4); 84.1 (s, C_5H_4); 106.2 (s, C_5H_4); 111.4 (s, C_6H_4); 126.4 (s, C_6H_4); 139.1 (s, C_6H_4); 152.2 (s, C_6H_4); 193.4 (s, CO). Mass spectrum (based on ^{187}Re) m/z: 486 [M^+]; 458 [M^+−CO]; 430 [M^+−2CO]; 402 [M^+−3CO]; 349 [M^+−NHC_6H_4-p-NO_2]. *Anal.* Calc. for $C_{15}H_{11}O_5N_2Re$: C, 37.04; H, 2.26. Found: C, 37.61; H, 2.37%.

4. Crystal structure determination

A summary of the fundamental crystal and refinement data for **1a** and **1b** are given in Table 1. Crystals of **1b** and **2b** were mounted on a Brucker-Siemens Smart CCD diffractometer equipped with a normal focus, 2.4 kW sealed tube X-ray source (Molybdenum radiation, λ = 0.71073 Å) operating at 50 kV and 20 mA. Data were collected over a hemisphere of the reciprocal space by a combination of three frame sets. The cell parameters were determined and refined by least-squares fit of all reflection collected. Each frame exposure time was of 20 s. covering 0.3° in ω. The crystal to detector distance was 5.08 cm. The first 100 frames were recollected at the end of the data collection to monitor crystal decay. Empirical absorption corrections were made using SADABS program [16]. The structure solution by direct methods, Fourier methods, and full matrix least-square refinement was carried out using SHELXTL [17] minimizing $w(F_o^2 - F_c^2)^2$. Hydrogen atoms have been located y refined isotropically except the hydrogen atoms of the methyl group of the compound **1b**. Weighted R factors (Rw) and all goodness of fit$S$ are based on F^2, conventional R factors (R) are based on F.

Acknowledgements

A.H.K. acknowledges FONDECYT (Project 1060487) and D.I. Pontificia Universidad Catolica de Valparaiso. R.A. acknowledges MECESUP and FONDECYT for a Doctoral scholarship. We also appreciate the financial support of MECESUP (Project UCH 0116) for a MS instrument. The loan of NH_4ReO_4 from MOLYMET – Chile is also much appreciated.

Appendix A. Supplementary data

CCDC 668276 and 668277 contain the supplementary crystallographic data for **1b** and **2b**. These data can be obtained free of charge via http://www.ccdc.cam.ac.uk/conts/retrieving.html, or from the Cambridge Crystallographic Data Centre, 12 Union Road, Cambridge CB2 1EZ, UK; fax: (+44) 1223-336-033; or e-mail: deposit@ccdc.cam.ac.uk. Supplementary data associated with this article can be found, in the online version, at doi:10.1016/j.poly.2008.04.021.

References

[1] (a) A. Houlton, N. Jasim, R.M.G. Roberts, J. Silver, D. Cunningham, P. McArdle, T. Higgins, J. Chem. Soc., Dalton Trans. (1992) 2235;
(b) Z. Akhter, A. Nigar, M.Y. Razzaq, H.M. Siddiqi, J. Organomet. Chem. 692 (2007) 3542.
[2] (a) M. Salmain, in: G. Jaouen (Ed.), Biorganometallics: Biomolecules Labeling Medicine, Willey-VCH, 2006, p. 181 (Chapter 6);
(b) I. Lavastre, J. Besancon, P. Brssier, C. Moise, Appl. Organomet. Chem. 5 (1991) 143;
(c) Z.H. Chohan, K.M. Khan, C.T. Supuran, Appl. Organomet. Chem. 18 (2004) 305;
(d) Z.-F. Chen, H.-L. Zou, H. Liang, R.-X. Yuan, Y. Zhang, Appl. Organomet. Chem. 18 (2004) 438.
[3] (a) R.C.J. Atkinson, K. Gerry, V.C. Gibson, N.J. Long, E.L. Marshall, L.J. West, Organometallics 26 (2007) 316;
(b) R. Bosque, C. Lopez, J. Sales, X. Solans, J. Organomet. Chem. 483 (1994) 61;
(c) M.M. Abd-Elzaher, J. Chin. Chem. Soc. 51 (2004) 499;
(d) J.M. Vila, E. Gayoso, T. Pereira, M. Mariño, J. Martinez, J.J. Fernandez, A. Fernandez, M. Lopez-Torres, J. Organomet. Chem. 637 (2001) 577;
(e) H.-X. Wang, R.-Q. Gao, X.-L. Yang, H.-F. Wu, F.-Y. Geng, R. Jin, Polyhedron 26 (2007) 1037;
(f) H.-X. Wang, Y.-J. Li, R. Jin, J.-R. Niu, H.-F. Wu, H.-Ch. Zhou, J. Xu, R.-Q. Gao, F.-Y. Geng, J. Organomet. Chem. 691 (2006) 987.

[4] N.E. Kolobova, Z.P. Valueva, Izv. Akad. Nauk SSSR, Ser. Khim. (1980) 2387.
[5] N.E. Kolobova, Z.P. Valueva, S.M. Ya, Bull. SSSR Acad. Sci., Div. Chem. 29 (1981) 1701.
[6] J.-M. Heldt, N. Fischer-Durand, M. Salmain, A. Vessires, G. Jaouen, J. Organomet. Chem. 689 (2004) 4775.
[7] T. Cautivo, F. Godoy, A.H. Klahn, G.E. Bouno-Core, D. Sierra, M. Fuentealba, M.T. Garland, Inorg. Chem. Commun. 10 (2007) 1031.
[8] (a) C. Lopez, J. Sales, X. Solans, R. Zquiak, J. Chem. Soc., Dalton Trans. (1992) 2321;
(b) R. Bosque, C. Lopez, J. Sales, X. Solans, M. Font-Bardia, J. Chem. Soc., Dalton Trans. (1994) 735;
(c) C. Lopez, R. Bosque, S. Perez, A. Roig, E. Molins, X. Solans, M. Font-Bardia, J. Organomet. Chem. 691 (2006) 475.
[9] S.S. Jones, M.D. Rausch, T. Biitterwolf, J. Organomet. Chem. 396 (1990) 279.
[10] J. Silver, J.R. Miller, A. Houlton, M.T. Ahmet, J. Chem. Soc., Dalton Trans. (1994) 3355.
[11] V. Kovac, A. Visnjevac, V. Rapic, B. Kojic-Prodic, J. Mol. Struct. 687 (2004) 107.
[12] P. Stepnicka, T. Base, I. Cisarova, J. Kubista, S. Vyskocil, M. Sticha, Collect. Czech. Chem. Commun. 68 (2003) 1206.
[13] T. Base, I. Cisarova, P. Stepnicka, Inorg. Chem. Commun. 5 (2002) 46.
[14] A. Hess, O. Brosch, T. Weyhermüller, N. Metzler-Notle, J. Organomet. Chem. 589 (1999) 75.
[15] P.J. Fitzpatrick, Y. Le Page, I.A. Butler, Acta Crystallogr., Sect. B 37 (1981) 1052.
[16] G.M. Sheldrick, SADABS, Program for Absorption Corrections Using Bruker CCD Data, University of Göttingen, Germany, 2001.
[17] SHELXTL 6.14; Bruker AXS, Inc., Madison, WI, USA, 2000–2003.

Polyhedron 27 (2008) 2426–2430

Contents lists available at ScienceDirect

Polyhedron

journal homepage: www.elsevier.com/locate/poly

The first heterometallic Cu(II)/Cr(III) complex with an open-chain Schiff-base ligand self-assembled from copper powder, Reineckes salt, ethylendiamine and acetone

Vitalina M. Nikitina [a], Oksana V. Nesterova [a,*], Vladimir N. Kokozay [a], Evgeny A. Goreshnik [b], Julia Jezierska [c]

[a] Department of Inorganic Chemistry, National Taras Shevchenko University, Volodymyrska Str. 64, Kyiv 01033, Ukraine
[b] Department of Inorganic Chemistry and Technology, Jožef Stefan Institute, Jamova Str. 39, 1000 Ljubljana, Slovenia
[c] Faculty of Chemistry, University of Wroclaw, 14 Joliot-Curie Str., 50-383 Wroclaw, Poland

ARTICLE INFO

Article history:
Received 3 April 2008
Accepted 11 April 2008
Available online 8 June 2008

Keywords:
Heterometallic complexes
Reineckes anion
Copper(II)
Schiff-base ligand
H-bonds

ABSTRACT

A novel supramolecular assembly $[\{Cu(enac)\}_2Cr(NCS)_4(NH_3)_2][Cr(NCS)_4(NH_3)_2]_3 \cdot 4(CH_3)_2CO$ (enac = 4,6,6-trimethyl-3,7-diazanon-3-ene-1,9-diamine), the first example of a Cu/Cr heterometallic compound containing a Schiff-base ligand such as enac, and an anion of Reineckes salt, $Cr(NCS)_4(NH_3)_2^-$, as a building block, was obtained by the self-assembly reaction of copper powder and Reineckes salt in an acetone/methanol (1:4) solution of ethylenediamine in the open air. An X-ray study shows that the complex includes a trinuclear Cu_2Cr cation, constructed from two $Cu(enac)^{2+}$ moieties and a *trans*-$[Cr(NCS)_4(NH_3)_2]^-$ block as a two-linking bridging ligand. The metal–metal separations within the cation are Cu···Cr = 6.393(31) Å and Cu···Cu = 12.786(63) Å. The supramolecular architecture of the complex involves two types of H-bonded chains, the first chain is generated by trinuclear cations $[\{Cu(enac)\}_2Cr(NCS)_4(NH_3)_2]^{2+}$, $[Cr(NCS)_4(NH_3)_2]^-$ anions and $(CH_3)_2CO$ molecules, while the second by crystallographically different anions of Reineckes salt and $(CH_3)_2CO$. Variable-temperature (1.8–300 K) magnetic susceptibilities show a slight change of the μ_B value at low temperature, indicative of weak antiferromagnetic interactions ($J_{CuCr} = -0.9\ cm^{-1}$) between the paramagnetic centers.

© 2008 Elsevier Ltd. All rights reserved.

1. Introduction

The design of heterometallic complexes with macrocyclic and open-chain ligands, as well as the elaboration of synthetic procedures is of current importance owing to the role which such systems play in biochemical processes, material science, catalysis, etc. [1]. One of the appealing approaches for the synthesis of coordination compounds with Schiff-base ligands is the method discovered by N.F. Curtis, which is based on the reaction of the metal complexes containing a primary amine group with aliphatic carbonyl compounds [2]. As a result, a large number of homometallic complexes with such Schiff-base ligands have been described [3–6], but the number of examples of heterometallic compounds with such ligands is still limited [7–12]. It is obvious that the simultaneous presence of two dissimilar metal centers could lead to fascinating architectures and intriguing properties, such as magnetic, catalytic, electrochemical or optical [13–16]. A popular and successful two-step approach for the preparation of heterometallic systems is the metalloligand strategy, based on the interaction between the preformed complex with free chelating sites, used as the ligand, and a complex with labile ligands playing the role of the metal [17].

It was proved that an efficient route to the preparation of novel heterometallic complexes, which eliminates the separate step of building block construction, is the direct synthesis of coordination compounds. The method is based on the self-assembly of building blocks generated *in situ* from a zerovalent metal ($M^0_{(A)}$) and an oxide or salt of the second metal ($M_{(B)}O$ or $M_{(B)}X_2$) in the same reaction vessel (L = amine or amino alcohol; Solv = non-aqueous solvent) [18–23]:

$$M^0_{(A)} - M_{(B)}O/M_{(B)}X_2 - L - NH_4X - Solv \qquad \text{(Strategy 1)}$$

Previously, it has been reported that the combination of the Curtis template reaction with the direct synthesis approach opens up new possibilities in generating heterometallic complexes with open-chain Schiff-base ligands [7–9]:

$$M^0_{(A)} - M^0_{(B)}/M_{(B)}O - L/L \cdot 2HX - NH_4X - (CH_3)_2CO - Solv \qquad \text{(Strategy 2)}$$

In the present article, we propose to combine the second strategy with the metalloligand approach and to use Reineckes salt as the source of the second metal:

$$Cu^0 - NH_4[Cr(NCS)_4(NH_3)_2]\text{-en-}(CH_3)_2CO - Solv$$

* Corresponding author.
E-mail address: nesterova@univ.kiev.ua (O.V. Nesterova).

0277-5387/$ - see front matter © 2008 Elsevier Ltd. All rights reserved.
doi:10.1016/j.poly.2008.04.032

The ability of the Cu(II) ion to exhibit different preferences in geometry and coordination number, as well as the ability of the $[Cr(NCS)_4(NH_3)_2]^-$ anion to reveal a bridging function and participate in hydrogen-bonding could lead to structural diversity and more complicated physico-chemical properties of the formed heterometallic complexes. According to the Cambridge Structural Database [24,25], examples of thiocyanato-bridged Cu(II)/Cr(III) compounds are quite limited and only one Cu(II)/Cr(III) complex based on the anion of Reineckes salt has been crystallographically characterized to date [26].

Herein, we report the synthesis, crystal structure, spectroscopic and magnetic properties of the novel complex $[\{Cu(enac)\}_2Cr(NCS)_4(NH_3)_2][Cr(NCS)_4(NH_3)_2]_3 \cdot 4(CH_3)_2CO$, which, to the best of our knowledge, represents the first example of a Cu/Cr heterometallic compound based on the anion of Reineckes salt, $Cr(NCS)_4(NH_3)_2^-$, and contains the Schiff-base ligand enac (4,6,6-trimethyl-1,9-diamino-3,7-diazanon-3-ene), in the $Cu(enac)^{2+}$ moiety.

2. Experimental

2.1. General

All chemicals were of reagent grade and were used as received. All experiments were carried out in air. Elemental analyses were performed by atomic absorption spectroscopy for copper and spectrophotometrically for chromium (as the chromate at $\lambda = 370$ nm) in the Department of Chemistry, National Taras Shevchenko University of Kyiv and with a vario EL III Universal CHNOS Elemental Analyzer (for C, H, N, S) in the Faculty of Chemistry, University of Wroclaw.

2.2. Synthesis of $[\{Cu(enac)\}_2Cr(NCS)_4(NH_3)_2][Cr(NCS)_4(NH_3)_2]_3 \cdot 4(CH_3)_2CO$

Copper powder (0.08 g, 1.26 mmol), $NH_4[Cr(NCS)_4(NH_3)_2] \cdot H_2O$ (0.89 g, 2.51 mmol), CH_3OH (20 ml), acetone (5 ml) and ethylenediamine (0.17 ml, 2.54 mmol) were heated to 50–60 °C and magnetically stirred until total dissolution of the copper was observed (10 min). The resulting solution was slowly evaporated at room temperature until dark-violet crystals suitable for crystallographic study were formed. The crystals were filtered off and dried in vacuo at room temperature. Yield: 0.90 g, 70%. *Anal.* Calc. for $C_{48}H_{96}N_{32}S_{16}O_4Cr_4Cu_2$ ($M_r = 2033.79$): C, 28.35; H, 4.76; N, 22.04; S, 25.23; Cr, 10.23; Cu, 6.25. Found: C, 28.0; H, 4.5; N, 22.3; S, 25.0; Cr, 10.6; Cu, 6.3%. IR (KBr, cm^{-1}): 3315(w), 3240(w), 3170(w), 2970(w), 2100(vs), 1685(s), 1655(s), 1610(s), 1460(m), 1420(m), 1360(m), 1310(w), 1260(s), 1230(m), 1200(w), 1110(m), 1060(m), 1040(w), 985(w), 830(w). The compound is soluble in CH_3CN, dmso and dmf.

2.3. Physical measurements

Infrared spectra were recorded as KBr discs on a UR-10 spectrophotometer in the 4000–400 cm^{-1} region using conventional techniques. UV/Vis spectra were recorded on a Perkin–Elmer Lambda 900 spectrophotometer using the diffuse-reflectance technique. The EPR spectra were recorded on a Bruker ESP 300E (Bruker, Germany) spectrometer operating at X-band and equipped with a Bruker NMR gaussmeter ER 035M and a Hewlett–Packard microwave frequency counter HP 5350B. Magnetic susceptibility data of a powdered sample were measured with a SQUID magnetometer (Quantum Design MPMSXL-5) over the temperature range 1.8–300 K at the magnetic induction of 0.5 T. The corrections for diamagnetism of the constituent atoms were calculated from Pascal's constants [27].

2.4. X-ray structure determination

$C_{48}H_{96}N_{32}S_{16}O_4Cr_4Cu_2$ (formula weight = 2033.79), 200 K, triclinic, $P\bar{1}$, $a = 11.7882(6)$, $b = 12.3534(5)$, $c = 16.4188(8)$ Å, $\alpha = 77.791(9)°$, $\beta = 83.418(9)°$, $\gamma = 80.610(9)°$, $V = 2297.6(2)$ Å^3, $Z = 1$, $D_{calc} = 1.470$ g/cm^3, 10557 reflections measured ($\Theta_{max} = 29.40$), 9269 unique ($R_{int} = 0.0252$) and of these 3871 had $F > 4\sigma(F)$ and were considered to be observed.

Data were collected on a Rigaku AFC7 diffractometer equipped with a Mercury CCD area detector using graphite monochromated Mo Kα radiation at 200 K. The data were corrected for Lorentz and polarization effects. A multi-scan absorption correction was applied to all data sets. The structure was solved by direct methods using the SIR-92 [28] program implemented in the program package TEXSAN [29] and refined with SHELX-97 [30] software (program packages TEXSAN and WINGX) [31]. Positions of the hydrogen atoms were located from the difference map of electron density and refined by the "riding" model with $U_{iso} = nU_{eq}$ of the non-hydrogen atom bonded to the H atom ($n = 1.5$ for methyl and 1.2 for other H atoms). Full-matrix least-squared refinement against F^2 in anisotropic approximation for non-hydrogen atoms (total 484 parameters) was converged to $R_1 = 0.0868$ ($wR_2 = 0.2383$, $S = 1.071$).

3. Results and discussion

3.1. Synthesis and spectroscopic characterization

The reaction of copper powder and Reineckes salt in an acetone/CH_3OH (1:4) solution of ethylenediamine, using a molar ratio of $Cu:NH_4[Cr(NCS)_4(NH_3)_2]:en$ of 1:2:2, gave a heterometallic compound with an open-chain aliphatic Schiff-base ligand (enac).

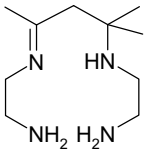

enac

The interaction proceeds in the following way:

$$2Cu^0 + 4NH_4[Cr(NCS)_4(NH_3)_2] + 4en + 8(CH_3)_2CO + O_2 \rightarrow [\{Cu(enac)\}_2Cr(NCS)_4(NH_3)_2][Cr(NCS)_4(NH_3)_2]_3 \cdot 4(CH_3)_2CO + 4NH_3 + 6H_2O$$

Noticeably, the compound could be also obtained using a molar ratio of $Cu:NH_4[Cr(NCS)_4(NH_3)_2]:en$ of 4:1:8 in the presence of ammonium thiocyanate, but in this case the homometallic complex $Cu(enac)(NCS)_2$ was formed as a byproduct.

The IR spectrum of the compound confirmed that the enac ligand is present. Its characteristic peaks at 3315 and 3240, 3170, 2970, 1685, 1610, 1060 and 985 cm^{-1}, can be easily identified as $\nu(NH_2)$, $\nu(N–H)$, $\nu(C–H)$, $\nu(C{=}N)$, $\delta(NH_2)$, $\nu(C–N)$ and $\nu(C–C)$, respectively. The presence of acetone molecules is supported by a strong $\nu(C{=}O)$ absorption peak at 1655 cm^{-1}, corresponding to the carbonyl groups involved in hydrogen bonding [32]. The intense absorption bands in the spectrum attributed to $\nu(C{\equiv}N)$ suggest the presence of bridging (2150 cm^{-1}) and terminal N-bonded thiocyanate groups (2090 cm^{-1}); the latter groups can be also recognized by the weak band at 840 cm^{-1} corresponding to the $\nu(CS)$ vibration.

The solid-state diffuse reflectance spectrum shows a broad band with a maximum at 515 nm, which probably results from overlap-

ping of d–d transitions for the octahedrally distorted Cu(II) and Cr(III) complexes [33]. Moreover, the spectrum displays a ligand-to-metal charge transfer transition at ca. 300 nm.

3.2. Description of the structure

The structure of the compound consists of a trinuclear cation $[\{Cu(enac)\}_2Cr(NCS)_4(NH_3)_2]^{3+}$, uncoordinated $[Cr(NCS)_4(NH_3)_2]^-$ anions of the Reineckes salt and acetone molecules. The Cu_2Cr cation (Fig. 1) is composed of two $Cu(enac)^{2+}$ moieties linked by a *trans*-$[Cr(NCS)_4(NH_3)_2]^-$ anion. The copper(II) center is included in a distorted square pyramidal CuN_4S chromophore. The equatorial Cu(II) positions are occupied by four nitrogen atoms of the enac ligand, with Cu–N distances in the range 1.978(11)–2.019(10) Å, with slightly shorter bond lengths to the imine nitrogen than to the secondary amine nitrogen (Table 1), which is usually observed for complexes with similar ligands [34,6]. The axial Cu–S distance has a value of 2.808(13) Å, which is close to those found in other copper(II) complexes with the sulfur atom at the apical position [35–40], indicating a *semi*-coordination character of this bond. The compound contains four crystallographically independent chromium(III) atoms. All of them are located in a distorted octahedral environment with a N_6 donor set, formed by two NH_3 molecules at the axial positions and four NCS groups in the equatorial plane. The Cr–N_{NCS} bond lengths lie within a short range [1.981(11)–2.006(11) Å], with no difference between the terminal and bridging character of the NCS groups. The terminal thiocyanate groups are almost linear [with N–C–S angles ranging from 176.7(8)° to 179.7(8)°], but the bridging NCS group shows a slight distortion from linearity, with a N–C–S angle of 175.9(8)°. The last one connects the Cu(1) and Cr(2) atoms into a trinuclear cation with a Cu(1)···Cr(2) separation of 6.39(3) Å, Cu(1)–S(4)–C(13) angle of 110.6(3)° and Cr(2)–N(6)–C(13) angle of 170.8(7)°. The Cu and Cr atom arrangement in the cation is almost linear with a Cu(1)–Cr(2)–Cu(1) angle of 179.99(1)°.

The structure is assisted by N–H···O hydrogen bonds between hydrogen atoms of the NH_3 molecules of the anions of Reineckes salt and oxygen atoms of acetone molecules (Table 2), which results in the formation of two types of supramolecular chain. The first type is generated by trinuclear $[\{Cu(enac)\}_2Cr(2)(NCS)_4(NH_3)_2]^{3+}$ cations, $[Cr(4)(NCS)_4(NH_3)_2]^-$ anions and acetone molecules (Fig. 2a), and the second one is formed by the crystallographically different anions $[Cr(1)(NCS)_4(NH_3)_2]^-$ and $[Cr(3)(NCS)_4(NH_3)_2]^-$, and acetone molecules. It is noteworthy that the weak S···S interactions of 3.693(14) Å link the second type chains into a supramolecular sheet (Fig. 2b). Finally, the structure of the complex can be best described as supramolecular assembly, where different types of H-bonded chains are arranged alternately (Fig. 3).

3.3. EPR and magnetic properties

The EPR spectra at 295 and 77 K of a polycrystalline sample of the compound exhibit an almost isotropic and very broad line

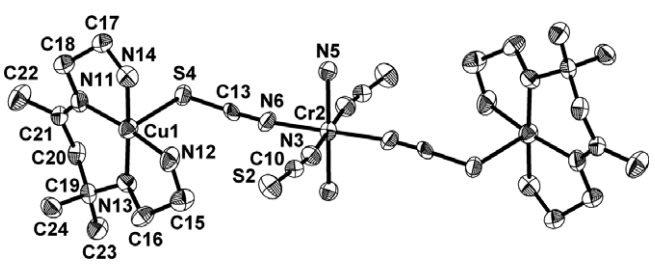

Fig. 1. A view of the trinuclear Cu_2Cr cation with the atom numbering scheme. Atom displacement ellipsoids are shown at the 50% probability level. The hydrogen atoms are omitted for clarity.

Table 1
Selected geometrical parameters (distances/Å and angles/°)

Cu(1)–N(11)	1.978(11)	Cr(2)–N(3)	1.993(12)
Cu(1)–N(12)	2.013(12)	Cr(2)–N(5)	2.063(8)
Cu(1)–N(13)	2.019(10)	Cr(2)–N(6)	1.998(9)
Cu(1)–N(14)	1.993(11)	Cr(3)–N(1)	2.005(8)
Cu(1)–S(4)^{i}	2.808(13)	Cr(3)–N(2)	1.981(11)
Cr(1)–N(4)	1.983(11)	Cr(3)–N(8)	2.07(1)
Cr(1)–N(7)	2.063(13)	Cr(4)–N(9)	2.070(14)
Cr(1)–N(32)	2.011(12)	Cr(4)–N(10)	2.006(11)
		Cr(4)–N(31)	1.994(11)
N(11)–Cu(1)–N(12)	169.4(3)	N(3)–Cr(2)–N(6)^{iii}	89.1(3)
N(11)–Cu(1)–N(13)	95.7(3)	N(5)–Cr(2)–N(5)^{iii}	180.0(3)
N(11)–Cu(1)–N(14)	84.1(3)	N(5)–Cr(2)–N(6)	93.2(3)
N(11)–Cu(1)–S(4)^{i}	89.4(2)	N(5)–Cr(2)–N(6)^{iii}	86.8(3)
N(12)–Cu(1)–N(13)	86.0(3)	N(6)–Cr(2)–N(6)^{iii}	180.0(3)
N(12)–Cu(1)–N(14)	93.6(3)	N(1)–Cr(3)–N(1)^{iv}	180.0(3)
N(12)–Cu(1)–S(4)^{i}	101.2(2)	N(1)–Cr(3)–N(2)	87.3(3)
N(13)–Cu(1)–N(14)	176.7(3)	N(1)–Cr(3)–N(2)^{iv}	92.7(3)
N(13)–Cu(1)–S(4)^{i}	87.8(2)	N(1)–Cr(3)–N(8)	91.6(3)
N(14)–Cu(1)–S(4)^{i}	95.5(2)	N(1)–Cr(3)–N(8)^{iv}	88.4(3)
N(4)–Cr(1)–N(4)^{ii}	180.0(3)	N(2)–Cr(3)–N(2)^{iv}	180.0(3)
N(4)–Cr(1)–N(7)	89.0(3)	N(2)–Cr(3)–N(8)	89.7(3)
N(4)–Cr(1)–N(7)^{ii}	91.0(3)	N(2)–Cr(3)–N(8)^{iv}	90.3(3)
N(4)–Cr(1)–N(32)	91.0(3)	N(8)–Cr(3)–N(8)^{iv}	180.0(3)
N(4)–Cr(1)–N(32)^{ii}	89.0(3)	N(9)–Cr(4)–N(9)^{v}	180.0(3)
N(7)–Cr(1)–N(7)^{ii}	180.0(3)	N(9)–Cr(4)–N(10)	88.8(3)
N(7)–Cr(1)–N(32)	89.2(3)	N(9)–Cr(4)–N(10)^{v}	91.3(3)
N(7)–Cr(1)–N(32)^{ii}	90.8(3)	N(9)–Cr(4)–N(31)	90.6(3)
N(32)–Cr(1)–N(32)^{ii}	180.0(3)	N(9)–Cr(4)–N(31)^{v}	89.4(3)
N(3)–Cr(2)–N(3)^{iii}	180.0(3)	N(10)–Cr(4)–N(10)^{v}	180.0(3)
N(3)–Cr(2)–N(5)	89.9(3)	N(10)–Cr(4)–N(31)	88.2 (3)
N(3)–Cr(2)–N(5)^{iii}	90.1(3)	N(10)–Cr(4)–N(31)^{v}	91.8(3)
N(3)–Cr(2)–N(6)	90.9(3)	N(31)–Cr(4)–N(31)^{v}	180.0(3)

Symmetry transformation used to generate equivalent atoms: (i) ⟨1 − *x*, 2 − *y*, −*z*⟩; (ii) ⟨−x, 2 − y, 1 − z⟩; (iii) ⟨−*x*, 2 − *y*, −*z*⟩; (iv) ⟨1 − *x*, 1 − *y*, 1 − *z*⟩; (v) ⟨1 − *x*, 1 − *y*, 2 − *z*⟩.

Table 2
Hydrogen bonding interactions (distances in Å and angles in °)

D–H···A	D–H	H···A	D···A	D–H···A
N(7)–H(42)···O(1)	0.965(9)	2.118(9)	3.016(15)	154.2(5)
N(8)–H(39)···O(1)^{iv}	0.953(8)	2.240(14)	3.099(19)	149.4(5)
N(5)^{x}–H(38)···O(26)^{vii}	0.910(8)	2.199(13)	3.091(19)	166.7(5)
N(9)–H(37)···O(26)	0.887(8)	2.303(11)	3.099(15)	149.2(5)

Symmetry codes: (iv) ⟨1 − *x*, 1 − *y*, 1 − *z*⟩; (vii) ⟨*x*, 1 + *y*, −1 + *z*⟩; (x) ⟨1 + *x*, *y*, *z*⟩.

around $g = 2$, which seems to be caused by resonance transitions between the electronic levels split by a small zero-field splitting parameter D (according to the Spin Hamiltonian due to at least $S = 3/2$). It suggests a rather high symmetry of the Cr(III) coordination. The lack of anisotropy and a g value of about 2 indicates that the EPR signal due to the Cu(II) center is overlapped by the spectrum of the Cr(III) center.

The results of magnetic susceptibility measurements are plotted as the effective magnetic moment (μ_{eff}) versus temperature in Fig. 4. The complex shows a room-temperature magnetic moment of 8.02 μ_B, which is very close to the calculated value of 8.01 μ_B for the non-interaction of two Cu(II) and four Cr(III) ions, where the constituent metals have typical μ_{eff} values of 1.8 and 3.8 μ_B, respectively. The good linear dependence of the reciprocal magnetic susceptibility in the whole temperature range gives the Curie–Weiss constants $\Theta = -2.03$ K and $C = 8.10$ $cm^3mol^{-1}K^{-1}$, which point to a weak antiferromagnetic behavior (Fig. 4, inset).

According to the crystal structure investigations, the compound contains a trinuclear CuCrCu cation and three isolated Reineckes anions per molar unit. Thus, the molar magnetic susceptibility can be described as follows:

$$\chi = \chi^c + 3\chi^a,$$

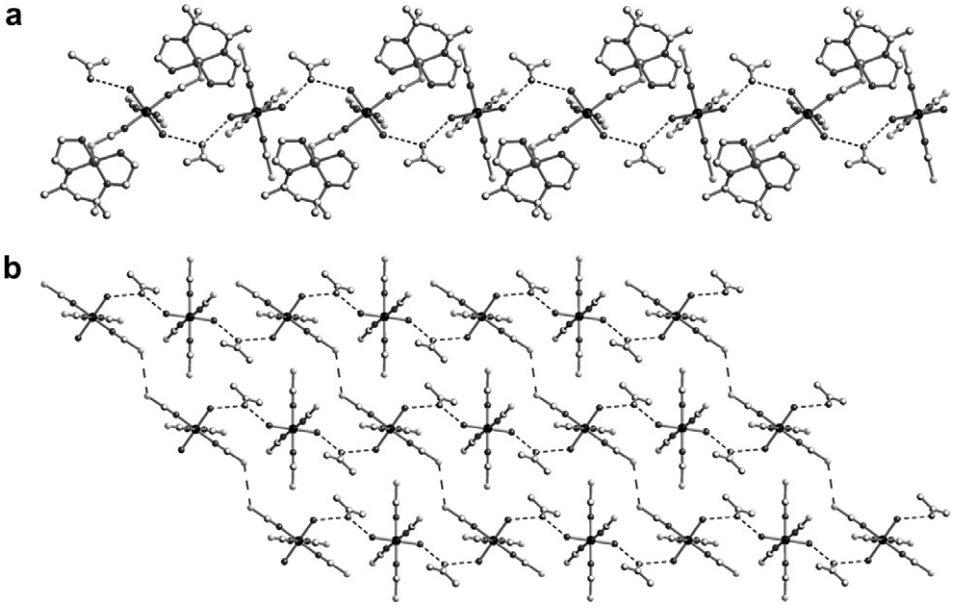

Fig. 2. Fragments of the supramolecular chain (a) and sheet (b) in the structure. The hydrogen atoms are omitted for clarity.

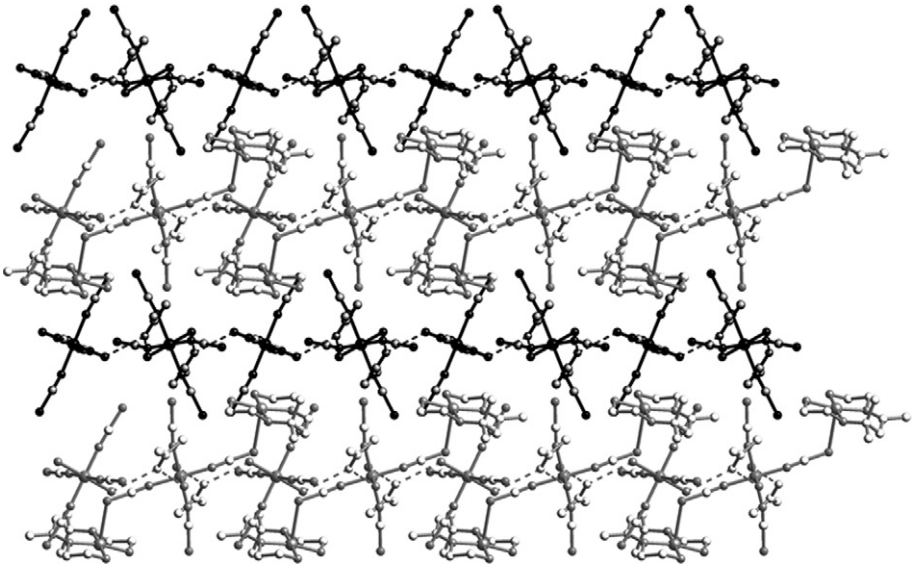

Fig. 3. Packing diagram of the complex projected onto the *ac* plane showing the alternating arrangement of two types of H-bonded chains. The hydrogen atoms are omitted for clarity.

where χ^c is the magnetic susceptibility of the trinuclear cation $[\{Cu(enac)\}_2Cr(NCS)_4(NH_3)_2]^{3+}$ and χ^a is the magnetic susceptibility of the $[Cr(NCS)_4(NH_3)_2]^-$ anion. Considering the exchange interaction between the Cu(II) ions to be very small due to the large Cu···Cu separation of 12.786(63) Å, its contribution may be neglected and the molar magnetic susceptibility of the trinuclear cation can be described by the spin-Hamiltonian $H = -2JS_{Cr}(S_{Cu1} + S_{Cu2})$ [41–43]:

$$\chi^c = \frac{Ng^2_{CuCrCu}\beta^2}{k(T-\Theta)} \times \frac{A}{B},$$
$$A = 35 + 10\exp(-5X) + \exp(-8X) + 10\exp(-3X), \quad (1)$$
$$B = 3 + 2\exp(-5X) + \exp(-8X) + 2\exp(-3X),$$

where $X = J/kT$ and all other symbols have their usual meaning. The χ^a term was evaluated for a Cr(III) ion in a tetragonally distorted octahedral environment with g_{Cr} and D variables [44]. The best fit of the experimental data was obtained with $J = -0.9\ cm^{-1}$, $\Theta = -2.9$ K, $g_{Cr} = 1.94$, $|D| = 4.4\ cm^{-1}$ and $R = 1.6 \times 10^{-4}$, where R is the agreement factor defined as $\sum[(\chi T)_{obs} - (\chi T)_{calcd}]^2 / \sum[(\chi T)_{obs}]^2$. The g_{CuCrCu} value was fixed at the 2.05 level. The zero-field splitting value (D) is somewhat greater than expected for an almost regular octahedral coordination geometry of Cr(III) in a Reineckes anion (less than $1\ cm^{-1}$ [45–47]). The likely reason for this is that the long-range interaction between the copper and chromium cations in the lattice is not completely negligible. However, implementation of the mean field model [44] did not improve the results. Also, if one considers the different ligand field strength of the NCS^- and NH_3 ligands, the environment of the Cr(III) anion could be described as tetragonally distorted. This is partially confirmed by a recent magnetic investigation of $[Cu(en)_2Cr(NCS)_4(NH_3)_2](OAc)$ (with a ligand

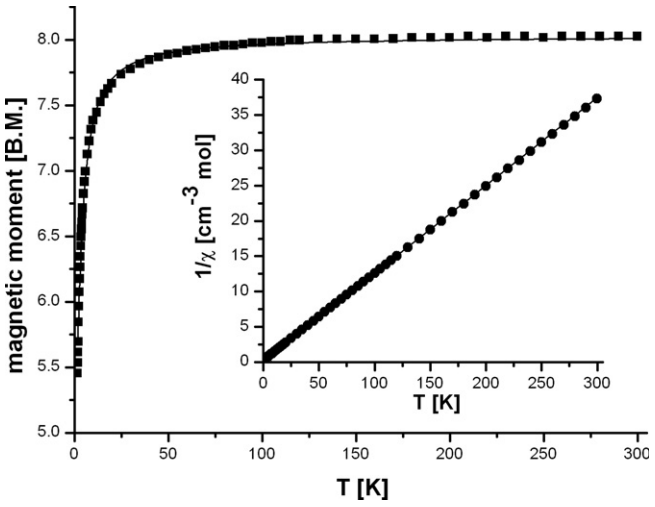

Fig. 4. Temperature dependence of experimental (■) and calculated (solid line) effective magnetic moments for the compound. The inset shows the reciprocal magnetic susceptibility (●) and the Curie–Weiss fit (solid line) as a function of temperature.

field strength and symmetry in the cation close to that reported here), which revealed a $|D|$ value of 1.9 cm^{-1} [48].

4. Conclusion

The presented work describes the synthesis of the first Cu(II)/Cr(III) complex with an open-chain Schiff-base ligand, enac, using a one-step self-assembly process from copper powder and Reinecke's salt in an acetone/methanol solution of ethylenediamine in the open air. The structure of the compound is assisted by N–H···O hydrogen bonds that link together trinuclear Cu_2Cr cations, anions of Reinecke's salt and uncoordinated $(CH_3)_2CO$ molecules forming two types of H-bonded chains. Variable-temperature magnetic susceptibility measurements show a very weak antiferromagnetic interaction between the paramagnetic centers. It is clear that such an approach is an effective and easy pathway for the synthesis of various heterometallic assemblies with open-chain Schiff-base ligands, and further investigations are underway.

Acknowledgements

This work was supported in part by the Fundamental Researches State Fund of Ukraine (Project 14.3/005). We thank Dr. Dmytro S. Nesterov for the interpretation of the data of the magnetic investigations and for helpful discussions.

Appendix A. Supplementary data

CCDC 676227 contains the supplementary crystallographic data for this paper. These data can be obtained free of charge via http://www.ccdc.cam.ac.uk/conts/retrieving.html, or from the Cambridge Crystallographic Data Centre, 12 Union Road, Cambridge CB2 1EZ, UK; fax: (+44) 1223-336-033; or e-mail: deposit@ccdc.cam.ac.uk. Supplementary data associated with this article can be found, in the online version, at doi:10.1016/j.poly.2008.04.032.

References

[1] P.A. Vigato, S. Tamburini, Coord. Chem. Rev. 248 (2004) 1717.
[2] N.F. Curtis, Coord. Chem. Rev. 3 (1968) 3.
[3] G. Mendoza-Díaz, L. Ruiz-Ramírez, R. Moreno-Esparza, Polyhedron 19 (2000) 2149.
[4] C. Zimmermann, F.W. Heinemann, A. Grohmann, Eur. J. Inorg. Chem. (2001) 547.
[5] N.F. Curtis, H.K.J. Powell, H. Puschmann, C.E.F. Rickard, J.M. Waters, Inorg. Chim. Acta 355 (2003) 25.
[6] N.F. Curtis, K. Flood, W.T. Robinson, Polyhedron 25 (2006) 1579.
[7] D.V. Shevchenko, S.R. Petrusenko, V.N. Kokozay, I. Svoboda, J. Kožišek, Inorg. Chem. Commun. 8 (2005) 665.
[8] D.V. Shevchenko, S.R. Petrusenko, V.N. Kokozay, M.V. Zhigalko, R.I. Zubatyuk, O.V. Shishkin, B.W. Skelton, P.R. Raithby, Inorg. Chim. Acta 358 (2005) 3889.
[9] D.V. Shevchenko, S.R. Petrusenko, V.N. Kokozay, B.W. Skelton, J. Coord. Chem. 57 (2004) 1287.
[10] A. Tomkiewicz, J. Mroziński, I. Brüdgam, H. Hartl, Eur. J. Inorg. Chem. (2005) 1787.
[11] N.F. Curtis, R. Pawley, W.T. Robinson, Polyhedron 26 (2007) 3003.
[12] A. Bieńko, J. Kłak, J. Mroziński, S. Domagała, B. Korybut-Daszkiewicz, K. Woźniak, Polyhedron 26 (2007) 5030.
[13] H. Zheng, W.-H. Leung, W. Tan, D. Long, W. Ji, J. Chen, F. Xin, X. Xin, J. Chem. Soc., Dalton Trans. (2000) 2145.
[14] E. Colacio, M. Ghazi, H. Stoeckli-Evans, F. Lloret, J.M. Moreno, C. Pérez, Inorg. Chem. 40 (2001) 4876.
[15] G. Marinescu, D. Visinescu, A. Cucos, M. Andruh, Y. Journaux, V. Kravtsov, Y.A. Simonov, J. Lipkowski, Eur. J. Inorg. Chem. (2004) 2914.
[16] M. Jurić, P. Planinić, N. Brničević, D. Milić, D. Matković-Čalogović, D. Pajić, K. Zadro, Eur. J. Inorg. Chem. (2006) 2701.
[17] G. Denti, S. Serroni, S. Campagna, A. Juris, M. Ciano, V. Balzani, in: A.F. Williams, C. Floriani, A.E. Merbach (Eds.), Perspectives in Coordination Chemistry, VCH, Basel, Switzerland, 1992.
[18] V.G. Makhankova, O.Yu. Vassileva, V.N. Kokozay, B.W. Skelton, L. Sorace, D. Gateschi, J. Chem. Soc., Dalton Trans. (2002) 4253.
[19] O.V. Pryma, S.R. Petrusenko, V.N. Kokozay, B.W. Skelton, O.V. Shishkin, T.S. Teplytska, Eur. J. Inorg. Chem. (2003) 1426.
[20] O.V. Nesterova, A.V. Lipetskaya, S.R. Petrusenko, V.N. Kokozay, B.W. Skelton, J. Jezierska, Polyhedron 24 (2005) 1425.
[21] E.A. Buvaylo, V.N. Kokozay, O.Yu. Vassileva, B.W. Skelton, J. Jezierska, L.C. Brunel, A. Ozarowski, Chem. Commun. (2005) 4976.
[22] D.S. Nesterov, V.N. Kokozay, B.W. Skelton, J. Jezierska, A. Ozarowski, J. Chem. Soc., Dalton Trans. (2007) 558.
[23] O.V. Nesterova, S.R. Petrusenko, V.N. Kokozay, B.W. Skelton, J. Jezierska, W. Linert, A. Ozarowski, J. Chem. Soc., Dalton Trans. (2008) 1431.
[24] Cambridge Structural Database (CSD), version 5.27, January 2006.
[25] F.H. Allen, Acta Crystallogr., Sect. B 58 (2002) 380.
[26] K.-L. Zhang, W. Chen, Y. Xu, Z. Wang, Z.J. Zhong, X.-Z. You, Polyhedron 20 (2001) 2033.
[27] E. König, Magnetic Properties of Coordination and Organometallic Transition Metal Complexes, Springer, Berlin, 1966.
[28] A. Altomare, G. Cascarano, C. Giacovazzo, A. Guagliardi, J. Appl. Crystallogr. 26 (1993) 343.
[29] Molecular Structure Corporation, TEXSAN for Windows, Single Crystal Structure Analysis Software, Version 1.06, MSC, 9009 New Trails Drive, The Woodlands, TX 77381, USA, 1997–1999.
[30] G.M. Sheldrick, SHELX-97, University of Göttingen, Germany, 1997.
[31] L.J. Farrugia, J. Appl. Cryst. 32 (1999) 837.
[32] K. Nakamoto, Infrared and Raman Spectra of Inorganic and Coordination Compounds, 4th ed., Wiley, New York, 1986.
[33] A.B.P. Lever, Inorganic Electronic Spectroscopy, 2nd ed., Elsevier Science, Amsterdam, Oxford, New York, Tokyo, 1984.
[34] N.F. Curtis, H. Puschmann, Polyhedron 25 (2006) 1204.
[35] M.A. Porai-Koshits, Zh. Struct. Khim. 4 (1963) 584.
[36] B.W. Brown, E.C. Lingafetter, Acta Crystallogr., Sect. B 17 (1964) 254.
[37] J. Ribas, C. Diaz, X. Solans, M. Font-Bardia, Inorg. Chim. Acta 231 (1995) 229.
[38] M. Kabešová, R. Boča, M. Melník, D. Valigura, M. Dunaj-Jurko, Coord. Chem. Rev. 140 (1995) 115.
[39] K. Vicent, A. Escuer, E. Peñalba, X. Solans, M. Font-Bardía, Inorg. Chim. Acta 255 (1997) 7.
[40] S. Ferlay, G. Francese, H.W. Schmalle, S. Decurtins, Inorg. Chim. Acta 286 (1999) 108.
[41] N. Matsumoto, K. Inoue, H. Okawa, S. Kida, Chem. Lett. (1989) 1251.
[42] J.Z. Zhuong, N. Matsumoto, H. Okawa, S. Kida, Inorg. Chem. 30 (1991) 436.
[43] D.J. Fu, J. Chen, X.S. Tan, L.J. Liang, S.W. Zhang, P.J. Zheng, W.X. Tang, Inorg. Chem. 36 (1997) 220.
[44] O. Kahn, Molecular Magnetism, VCH, New York, 1993.
[45] M.C. Muñoz, M. Julve, F. Lloret, J. Faus, M. Andruh, J. Chem. Soc., Dalton Trans. (1998) 3125.
[46] J. van Slageren, R. Sessoli, D. Gatteschi, A.A. Smith, M. Helliwell, R.E.P. Winpenny, A. Cornia, A.-L. Barra, A.G.M. Jansen, E. Rentschler, G.A. Timco, Chem. Eur. J. 8 (2002) 277.
[47] M. Shanmugam, L.P. Engelhardt, F.K. Larsen, M. Luban, E.J.L. McInnes, C.A. Muryn, J. Overgaard, E. Rentschler, G.A. Timco, R.E.P. Winpenny, Chem. Eur. J. 12 (2006) 8267.
[48] V.M. Nikitina, O.V. Nesterova, V.N. Kokozay, E.A. Goreshnik, C.J. Gómez Garcíia, Unpublished results.

Polyhedron 27 (2008) 2431–2435

Contents lists available at ScienceDirect

Polyhedron

journal homepage: www.elsevier.com/locate/poly

Synthesis and spectral properties of novel *seco*-porphyrazines with eight 4-biphenyl groups

Ergün Gonca [a,*], Ümmü Gülsüm Baklacı [a], Hatice Akın Dinçer [b]

[a] Department of Chemistry, Fatih University, TR34500 B.Cekmece, Istanbul, Turkey
[b] Department of Chemistry, Technical University of Istanbul, TR34469 Maslak, Istanbul, Turkey

ARTICLE INFO

Article history:
Received 21 March 2008
Accepted 21 April 2008
Available online 4 June 2008

Keywords:
4-Biphenyl
seco-Porphyrazine
Porphyrazine
Maleonitrile
Zinc
Cobalt

ABSTRACT

Magnesium porphyrazinate substituted with eight 4-biphenyl groups on the periphery positions has been synthesized for the first time from cyclotetramerization of 1,2-bis(4-biphenyl)maleonitrile in the presence of magnesium butanolate. Its demetalation by treatment with trifluoroacetic acid, resulted in a partially oxidized product, namely, octakis(4-biphenyl)-2-*seco*-porphyrazine-2,3-dione. Further reaction of this product with copper(II) acetate, zinc(II) acetate and cobalt(II) acetate has led to the metallo derivatives, [octakis(4-biphenyl)-2-*seco*-2,3-dioxoporphyrazinato] M(II) (M = Cu, Zn, Co). These novel compounds have been characterized by elemental analysis, together with FT-IR, ^{1}H NMR, UV–Vis and mass spectral data.

© 2008 Elsevier Ltd. All rights reserved.

1. Introduction

Peripherally functionalized porphyrazines (tetraazaporphyrins) and related macrocycles, modified by the attachment of peripheral substituents, have found wide applications in many areas such as chemical sensor, optic data collection, catalysis, electron transfer, liquid crystal, electrophotography, laser technology, photodynamic therapy of tumors, pigments as well as and dyes in advanced materials [1–5]. In contrast, the structurally related porphyrazines have been less well studied. However, due to the easy and multi- purpose synthetic route for the preparation of porphyrazines, namely the metal-templated cyclization of the maleonitrile precursors, these macrocyclic compounds are now subject to enhanced interest [6–10]. The porphyrazine macrocycles afford a skilful platform to build up detailed molecular superstructures and this property coupled with a full and well-improved synthetic chemistry has surpassed to the synthesis of different catalytically essential metallo porphyrazines and original model compounds of various functions [11,12].

For many years, aromatic compounds based on biphenyls were overemphasized as the most important core unit for liquid crystals, partly because of their easier synthesis and partly because the link between highly polarizable π-electron systems and mesogenity.

During the last two decades, we have been deeply interested in the preparation of novel porphyrazine and phthalocyanine derivatives. Among these are phthalocyanines which are fused to, or attached through bridges to macrocyclic structures [13] and porphyrazines with peripheral functional groups such as quaternizable amino groups [14], crown ethers [15], ferrocenes [16], triphenylphosphine [17], 4-*tert*-buthylphenylthio [18] and tosylaminoethylthio [19] can be cited.

Recently, we have synthesized porphyrazines with bulky electron rich substituents such as 1-naphthylmethylthio, 9-anthracenylmethylthio units [20,21]. We have also synthesized novel *seco*-porphyrazines substituted with 1-naphthyl, *p*-tolyl, *o*-tolyl groups on the peripheral positions [22,23] as encountered by Barrett, Hoffman and coworkers, with peripheral amino derivatives [24].

In this study, we report novel soluble porphyrazines with eight 4-biphenyl substituents appending to the periphery positions. Magnesium porphyrazinate substituted with eight 4-biphenyl groups on the periphery positions has been synthesized for the first time from the cyclotetramerization of 1,2-bis(4-biphenyl)maleonitrile in the presence of magnesium butanolate. Its demetalation by treatment with trifluoroacetic acid, resulted in a partially oxidized product, namely, octakis(4-biphenyl)-2-*seco*-porphyrazine-2,3-dione. Further reaction of this product with copper(II) acetate, zinc(II) acetate and cobalt(II) acetate has led to the metallo derivatives, [octakis(4-biphenyl)-2-*seco*-2,3-dioxoporphyrazinato] M(II) (M = Cu, Zn, Co). These novel compounds have been characterized by elemental analysis, together with FT-IR, ^{1}H NMR, UV–Vis and mass spectral data.

* Corresponding author. Tel.: +90 212 866 33 00; fax: +90 212 866 34 02.
E-mail address: egonca@fatih.edu.tr (E. Gonca).

0277-5387/$ - see front matter © 2008 Elsevier Ltd. All rights reserved.
doi:10.1016/j.poly.2008.04.025

2. Experimental

IR spectra were recorded on a Perkin–Elmer Spectrum One FT-IR (ATR sampling accessory) spectrophotometer, electronic spectra on a Unicam UV2 spectrophotometer. Elemental analyses were recorded on a Thermo Finnigan Flash EA 1112 instrument at the Instrumental Analysis Laboratory of TUBITAK Marmara Research Center. Proton NMR spectra were recorded on a Varian INOVA 500 MHz spectrometer using TMS and d-chloroform as the reference and solvent, respectively. Mass spectra were recorded on a Bruker Daltonics MicrOTOF LC–MS using the electrospray ionisation (ESI) method. The instrument was operated in positive ion mode. All starting materials were purchased from major suppliers and used without any further purification. The homogeneity of the products was tested in each step by TLC.

(4-Biphenyl)acetonitrile (**1**) was prepared according to the previously reported procedure [25].

2.1. Synthesis of 1,2-bis(4-biphenyl)maleonitrile (*2*)

A slurry of 4-biphenylacetonitrile (1.0 g, 5.2 mmol) and iodine (1.313 g, 5.200 mmol) in 1:1 Et_2O–MeOH (20 ml) was allowed to reflux under nitrogen for 1 h. The solution was cooled to room temperature, and sodium methoxide (2.2 equiv., 2.0 M, 5.7 ml) in methanol was added drop by drop (over a period of 30 min) into the reaction medium under a nitrogen atmosphere. The reaction mixture was stirred for another 3 h. During this time, more and more precipitation was formed in the solution. The solution was filtered at room temperature and the solid product was washed with water. The product was yellow colored and was very soluble in chloroform, dichloromethane and acetone, but insoluble in *n*-hexane. Yield was 0.316 g (32%). FT-IR, $\nu_{max}/(cm^{-1})$: 3070–3030 (CH, aromatic), 2218 (C≡N), 1604 (C=C, aromatic), 1486, 1405, 1209, 1140, 1005, 845, 766, 724, 691. ^{1}H NMR (d-chloroform 500 MHz): δ, ppm 7.99–7.93 (m, 4H, Ar-H), 7.80–7.75 (m, 4H, Ar-H), 7.68–7.26 (m, 10H, Ar-H). MS (ESI): (*m*/*z*): 382.2 $[M]^+$.

2.2. [2,3,7,8,12,13,17,18-Octakis(4-biphenyl)porphyrazinato]Mg(II) (*3a*)

Mg turnings (24.3 mg, 1.00 mmol) and a small I_2 crystal were refluxed in *n*-BuOH (20 ml) for about 8 h to obtain $Mg(BuO)_2$. 1,2-Bis(4-biphenyl)maleonitrile (**2**) (765 mg, 2.00 mmol) was added to this solution and the mixture was refluxed for about 8 h. The dark green product was filtered, washed with ethanol and water and dried in a vacuum. The crude product was dissolved in $CHCl_3$ and filtered. The $CHCl_3$ solution was dried over anhydrous Na_2SO_4. When the solvent was evaporated, a dark green product was obtained. Finally, pure porphyrazine was obtained by chromatography on silica gel using methanol/chloroform (1:50) mixture as eluent. The product was soluble in chloroform, dichloromethane, acetone and toluene, but insoluble in *n*-hexane. Yield: 326 mg (42%). FT-IR, $\nu_{max}/(cm^{-1})$: 3075–3025 (CH, aromatic), 1602 (C=C, aromatic), 1484, 1404, 1208, 1139, 1004, 843, 763, 722, 689. ^{1}H NMR (d-chloroform 500 MHz): δ, ppm 7.97–7.75 (m, 4H, Ar-H), 7.67–7.26 (m, 5H, Ar-H). MS (ESI): (*m*/*z*): 1554.7 $[M]^+$.

2.3. [2,3,7,8,12,13,17,18-Octakis(4-biphenyl)-2-seco-porphyrazine-2,3-dione] (*3b*)

Compound **3a** (155 mg, 0.100 mmol) was dissolved in the minimum amount of trifluoroacetic acid (~4 ml) and stirred for 5 h at room temperature. When the reaction mixture was added to ice drop by drop and neutralized with 25% ammonia solution, precipitation occurred and it was filtered. The precipitate was extracted into the chloroform and the chloroform solution was extracted with water twice. After drying over anhydrous Na_2SO_4, the solvent was evaporated to obtain the green colored metal-free porphyrazine. The crude product was purified by chromatography on silica gel using methanol/chloroform (1:50) mixture as the eluent. Yield: 100 mg (64%). FT-IR, $\nu_{max}/(cm^{-1})$: 3339 (N–H), 3072–3035 (CH, aromatic), 1721 (C=O), 1615 (C=C, aromatic), 1475, 1400, 1212, 1128, 1012, 838, 765, 718, 680. ^{1}H NMR (d-chloroform 500 MHz): 7.91–7.70 (m, 4H, Ar-H), 7.61–7.22 (m, 5H, Ar-H), −0.95 (br s, 2H, NH). MS (ESI): (*m*/*z*): 1563.2 $[M]^+$.

2.4. General procedure for metallo seco-porphyrazines (*3c–3e*)

Compound **3b** (156 mg, 0.100 mmol) in $CHCl_3$(10 ml) was stirred with the metal salt [$Cu(OAc)_2$(182 mg, 1.00 mmol), $Zn(OAc)_2$ (183 mg, 1.00 mmol) or $Co(OAc)_2$ (177 mg, 1.00 mmol)] in ethanol (15 ml) and refluxed under nitrogen for about 4 h. Then, the precipitate composed of the crude product and the excess metal salt were filtered. The precipitate was treated with $CHCl_3$ and the insoluble metal salts were removed by filtration. The filtrate was reduced to the minimum volume under reduced pressure and then added into *n*-hexane (100 ml) drop by drop to realize the precipitation. Finally, pure porphyrazine derivatives were obtained by chromatography on silica gel using methanol/chloroform (1:20) mixture as the eluent.

2.4.1. [2,3,7,8,12,13,17,18-Octakis(4-biphenyl)-2-seco-2,3-dioxoporphyrazinato] Cu(II) (*3c*)

Yield: 72 mg (44%). FT-IR, $\nu_{max}/(cm^{-1})$: 3075–3030 (CH, aromatic), 1718 (C=O), 1622 (C=C, aromatic), 1445, 1410, 1215, 1133, 1018, 868, 753, 715, 688. MS (ESI): (*m*/*z*): 1625.8 $[M]^+$.

2.4.2. [2,3,7,8,12,13,17,18-Octakis(4-biphenyl)-2-seco-2,3-dioxoporphyrazinato] Zn(II) (*3d*)

Yield: 78 mg (48%). FT-IR, $\nu_{max}/(cm^{-1})$: 3055–3025 (CH, aromatic), 1722 (C=O), 1652 (C=C, aromatic), 1440, 1248, 1118, 1023, 848, 752, 724, 685. ^{1}H NMR (d-chloroform 500 MHz): 7.92–7.81 (m, 4H, aromatic H), 7.65–7.24 (m, 5H, Ar-H). MS (ESI): (*m*/*z*): 1627.6 $[M]^+$.

2.4.3. [2,3,7,8,12,13,17,18-Octakis(4-biphenyl)-2-seco-2,3-dioxoporphyrazinato] Co(II) (*3e*)

Yield: 62 mg (38%). FT-IR, $\nu_{max}/(cm^{-1})$: 3065–3020 (CH, aromatic), 1723 (C=O), 1625 (C=C, aromatic), 1476, 1408, 1215, 1146, 1009, 879, 758, 725, 684. MS (ESI): (*m*/*z*): 1620.3 $[M]^+$.

3. Results and discussion

The starting point for these novel porphyrazine structures with eight 4-biphenyl groups bound to the periphery is 1,2-bis(4-biphenyl)maleonitrile (**2**) which was obtained from (4-biphenyl)acetonitrile (**1**) and I_2. The yellow colored product (**2**) was obtained in yield 32%. The conversion of **2** into **3a** was achieved by the template effect of magnesium butanolate (Scheme 1). The cyclotetramerization gave the dark green colored **3a** (Fig. 1) in yield 42%. It

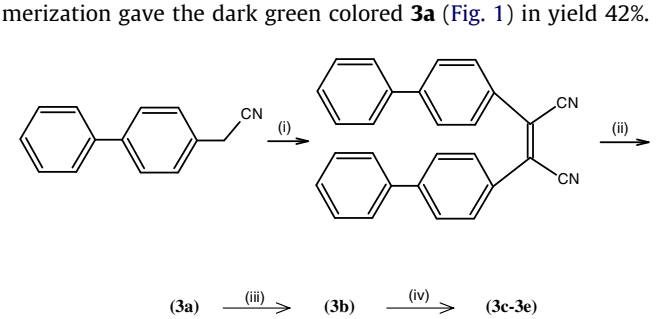

Scheme 1. (i) Et_2O–MeOH, I_2; (ii) Mg turnings, I_2, *n*-BuOH; (iii) CF_3CO_2H; (iv) EtOH and $Cu(OAc)_2$, $Zn(OAc)_2$, or $Co(OAc)_2$.

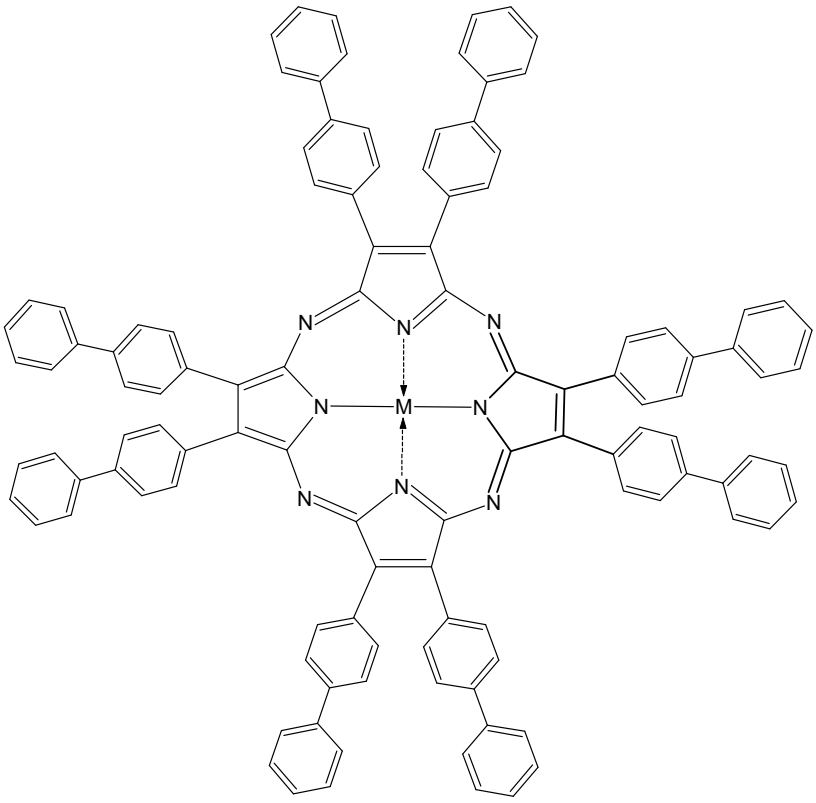

M= Mg (**3a**)

Fig. 1. [2,3,7,8,12,13,17,18-octakis(4-biphenyl)porfirazinato] Mg(II).

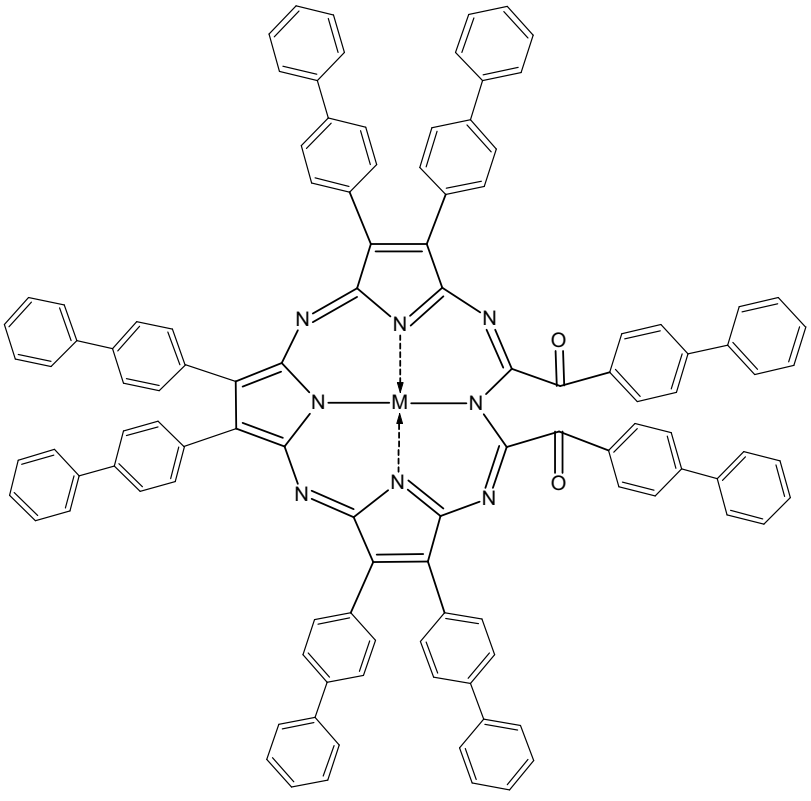

M= 2H (**3b**); Cu (**3c**); Zn (**3d**); Co (**3e**)

Fig. 2. [2,3,7,8,12,13,17,18-octakis(4-biphenyl)-2-*seco*-porphyrazine-2,3-dione] and metal derivatives {M=2H, Cu(II), Zn(II) or Co(II)}.

was soluble in chloroform, dichloromethane, acetone and toluene, but insoluble in apolar hydrocarbon solvents such as *n*-hexane.

In the conversion of **3a** into **3b** (Fig. 2) by treatment with relatively strong acids (e.g. trifluoroacetic acid), a *seco*-porphyrazine type macrocycle in which one of the four pyrrole rings has been oxidized has been the main product. Sterical tension due to the presence of eight bulky 4-biphenyl units around the core might be the main reason for the cleavage of one of the pyrrol rings. 4-biphenyl units are not comparable with dimethylamino groups [24,26,27], but are comparable with naphthyl groups as electron donors to the 18-π electron system of the inner core [26]. In the present case, the tendency of 4-biphenyl substituted porphyrazine to oxidize to the *seco*-porphyrazine derivative should be higher than dimethylamino substituted ones because the reactions were carried under inert atmospheres during these experiments, but still no product corresponding to the metal-free derivative of **3a** could be isolated. The mass spectral results have clearly indicated the change of the structure from magnesium porphyrazinate (**3a**) to the demetalated *seco*-porphyrazine (**3b**) (Figs. 3 and 4). In addition to the mass spectral results, the intense C=O absorption peak clearly differentiates oxidized products from the symmetrically octakis(4-biphenyl) substituted magnesium porphyrazinate. The metalation reactions of the demetalated *seco*-porpyrazine (**3b**) with metal salts gave the metalated species (**3c**–**e**) (Scheme 1).

All new compounds were identified through several spectroscopic techniques such as ^{1}H NMR, FT-IR, UV–Vis, mass and elemental analysis. The spectroscopic data of desired products were in accordance with the assigned structures.

Elemental analyses correspond closely with the values calculated for (**2**, **3a**–**e**) (Table 1).

In the FT-IR spectrum of **2**, the stretching vibration of C≡N peak is observed at 2218 cm^{-1}, the aromatic C–H peaks are around 3030–3070 cm^{-1} and the aromatic C=C peak is at 1604 cm^{-1}. These values comply with those reported in the literature for similar compounds [20–23]. After the conversion of dinitrile derivative (**2**) to porphyrazine (**3a**), the sharp C≡N vibration around 2218 cm^{-1} disappeared. The N–H stretching absorption of the inner core of the metal-free porphyrazine (**3b**) was observed around 3339 cm^{-1}. Furthermore, during acid-mediated demetalation of the magnesium porphyrazine (**3a**), peripheral oxidation of one pyrrole ring was confirmed with an intense absorption around 1718–1723 cm^{-1} [24,27]. The FT-IR spectra of all porphyrazines derivatives (**3a**–**e**) showed that the aromatic C–H peaks are around 3020–3075 cm^{-1} [18,20–23], indicating the presence of 4-biphenyl substituents as well as the *seco*-porphyrazine derivatives.

The N–H protons of the metal-free porphyrazine (**3b**) were also identified in the ^{1}H NMR spectra with the broad peak at $\delta = -0.95$ ppm, presenting the typical shielding of inner core protons, which is a common feature of the ^{1}H NMR spectra of metal-free porphyrazines [15,16,20,27]. In the ^{1}H NMR spectra of diamagnetic

Table 1
Elemental analyses results of the porphyrazines[a]

Compound	C	H	N
2	87.77 (87.93)	4.66 (4.74)	7.45 (7.32)
3a	86.39 (86.56)	4.54 (4.67)	7.33 (7.21)
3b	86.15 (86.02)	4.41 (4.55)	7.29 (7.17)
3c	82.64 (82.76)	4.59 (4.46)	6.78 (6.89)
3d	82.78 (82.67)	4.39 (4.46)	6.98 (6.89)
3e	82.89 (83.00)	4.59 (4.48)	6.79 (6.91)

[a] Required values are given in parentheses.

Table 2
UV–Vis data for the porphyrazines in chloroform

Compound	λ/nm (log ε/dm^3 mol^{-1} cm^{-1})		
3a	380 (4.86)	652 (4.64)	
3b	368 (4.77)	650 (4.41)	712 (4.49)
3c	348 (4.82)	658 (4.58)	
3d	356 (4.80)	654 (4.60)	
3e	352 (4.84)	656 (4.56)	

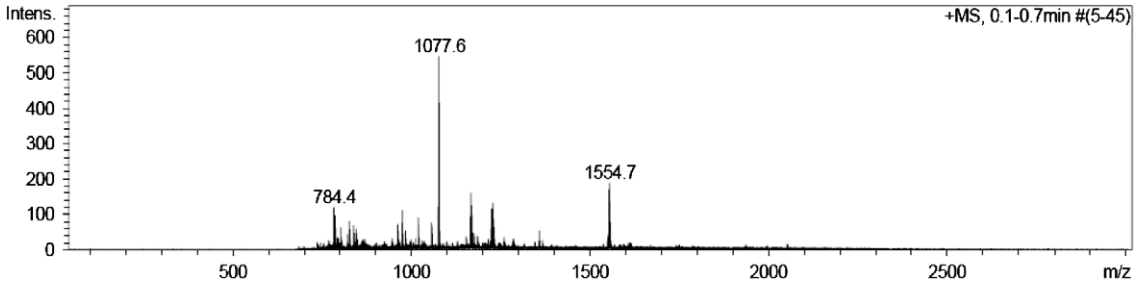

Fig. 3. Mass spectrum of **3a**.

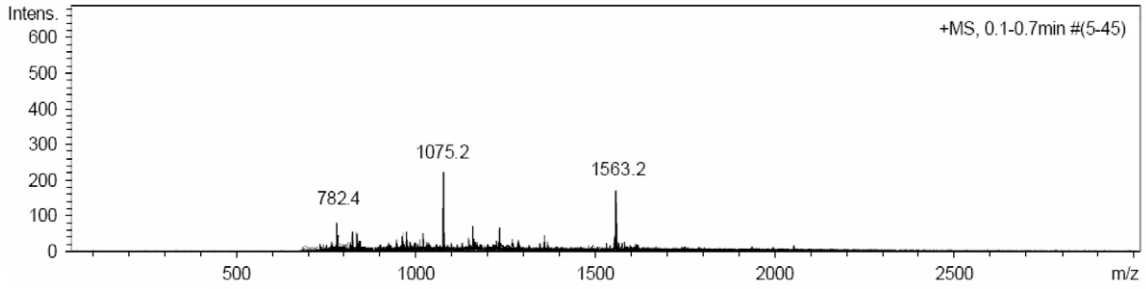

Fig. 4. Mass spectrum of **3b**.

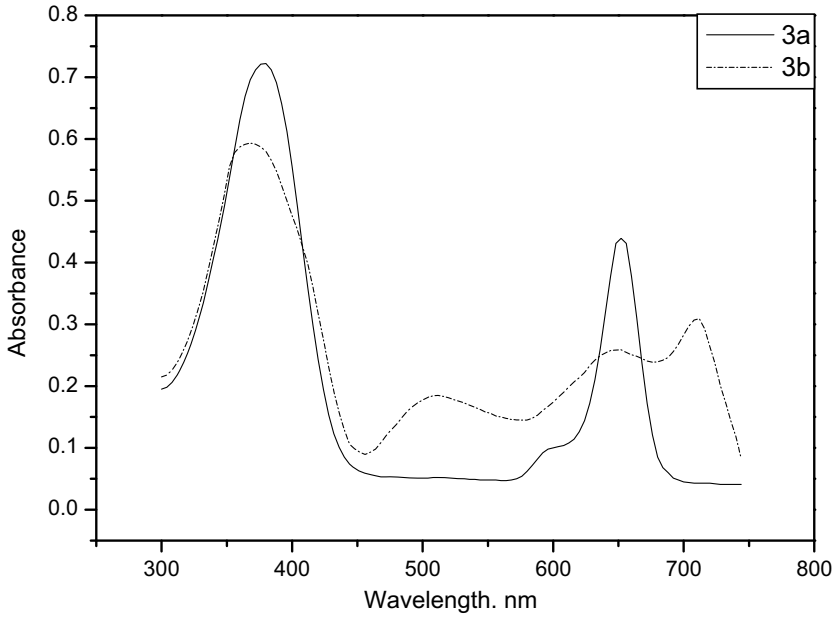

Fig. 5. UV–Vis spectra of **3a** and **3b** in chloroform.

porphyrazines **3a**, **3b** and **3d**, only one chemical shift is clearly seen: a multiplet around 7–8 ppm corresponding to the phenyl protons [20–23].

Electronic spectra are especially useful to identify the structure of the porphyrazines (**3a**–**e**). UV–Vis spectra of porphyrazine core are dominated by two intense bands, the Q band around 652 nm and the B band in the near UV region around 380 nm, both correlated to $\pi \rightarrow \pi^*$ transitions [28,29]. The presence of an electron-donating group on the periphery causes a bathochromic shift on Q bands. The UV–Vis spectra of porphyrazines (**3a**, **3c**–**e** in $CHCl_3$) prepared in the present study exhibited intense single Q band absorption of the $\pi \rightarrow \pi^*$ transitions around 652–658 nm and B bands in the near UV region around 348-380 nm (Table 2). As a consequence of the lowering of the symmetry of porphyrazine core, the electronic absorption spectrum of the *seco*-porphyrazine (**3b**) displays a split in the Q band at 650 and 712 nm. UV–Vis spectra of **3a** and **3b** in chloroform are shown in Fig. 5. An absorbance versus concentration study indicated that due to the bulky 4-biphenyl substituents, no aggregation occurred either for **3a**, **3b**.

4. Conclusion

In conclusion, we have described the synthesis and the spectral characterization of novel *seco*-porphyrazines surrounded with eight 4-biphenyl groups on the periphery. The steric requirements of these groups should be the reasons leading to oxidized *seco*-porphyrazines.

Acknowledgement

This work was supported by the Research Fund of the TÜBİTAK under the Project Number 106T499.

References

[1] J.A. McCleverty, T.J. Meyer (Eds.), Comprehensive Coordination Chemistry II, vol. 9, Elsevier Pergamon, Amsterdam, 2004.
[2] N. Kobayashi, Coord. Chem. Rev. 99 (2001) 219.
[3] N.B. McKeown, Adv. Mater. 11 (1999) 67.
[4] E.A. Luk'yanets, Mol. Mater. 1 (1992) 209.
[5] K.W. Poon, W. Liu, P.K. Chan, Q. Yang, T.W.D. Chan, T.C.W. Mak, D.K.P. Ng, J. Org. Chem. 66 (2001) 1553.
[6] N. Kobayashi, K.M. Kadish, K.M. Smith, The Porphyrin Handbook, vol. 2, Academic Press, New York, 2000. p. 301.
[7] B.D. Berezin, Coordination Compounds of Porphyrazines and Phthalocyanines, Wiley, Chichester, 1976.
[8] C.C. Leznoff, A.B.P. Lever, Phthalocyanines Properties and Applications, vol. 1-4, VCH, Weinheim, 1989.
[9] E.A. Ough, K.A.M. Creber, M.J. Stillman, Inorg. Chim. Acta (1996) 361.
[10] N. Kobayashi, C.C. Leznof, A.B.P. Lever (Eds.), Phthalocyanines: Properties and Application, vol. 2, VCH, New York, 1993.
[11] G.B. James, F.S. Molinaro, J.A. Ibers, J.P. Collman, J.I. Brauman, E. Rose, K.S. Suslick, J. Am. Chem. Soc. 102 (1980) 3224.
[12] J.P. Collman, R.R. Gagne, C.A. Reed, W.T. Robinson, G.A. Rodley, Proc. Natl. Acad. Sci. USA 71 (1974) 1326.
[13] M. Koçak, A. Gürek, A. Gül, Ö. Bekaroğlu, Chem. Berl. 127 (1994) 355.
[14] M. Polat, A. Gül, Dyes Pigments 45 (2000) 195.
[15] Ö. Sağlam, A. Gül, Polyhedron 20 (2001) 269.
[16] H. Akkuş, A. Gül, Transition Met. Chem. 26 (2001) 689.
[17] E. Gonca, A. Gül, Inorg. Chem. Commun. 8 (2005) 343.
[18] B. Keskin, Y. Köseoğlu, U. Avcıata, A. Gül, Polyhedron 27 (2008) 1155.
[19] R.Z. Uslu, A. Gül, C.R. Acad. Sci. Paris Ser. II C: Chim. 3 (2000) 643.
[20] E. Gonca, Y. Köseoğlu, B. Aktaş, A. Gül, Polyhedron 23 (2004) 1845.
[21] E. Gonca, Transition Met. Chem., in press, doi:10.1007/s11243-008-9078-7.
[22] A. Nazlı, E. Gonca, A. Gül, J. Porphyr. Phthalocya. 10 (2006) 996.
[23] E. Gonca, Ü. G. Baklacı, H.A. Dinçer (submitted for publication).
[24] A.G. Montalban, S.J. Lange, L.S. Beall, N.S. Mani, D.J. Williams, A.J.P. White, A.G.M. Barrett, B.M. Hoffman, J. Org. Chem. 62 (1997) 9284.
[25] S.P. Birkeland, G.H. Daub, F.N. Hayes, D.G. Ott, J. Org. Chem. 26 (1961) 2662.
[26] A.G. Montalban, S.M. Baum, A.G.M. Barrett, B.M. Hoffman, Dalton Trans. (2003) 2093.
[27] H. Nie, C.L. Stern, A.G.M. Barrett, B.M. Hoffman, Chem. Commun. (1999) 703.
[28] C.F. van Nostrum, R.J.M. Nolte, Chem. Commun. (1996) 2385.
[29] A.E. Pullen, C. Faulmann, P. Cassoux, Eur. J. Inorg. Chem. (1999) 269.

Polyhedron 27 (2008) 2436–2446

Contents lists available at ScienceDirect

Polyhedron

journal homepage: www.elsevier.com/locate/poly

3-(Aryl)-2-sulfanylpropenoates of mercury(II) and phenylmercury(II)

José S. Casas [a], Alfonso Castiñeiras [a], María D. Couce [b], Manuel García-Vega [a], Manuel Rosende [a], Agustín Sánchez [a], José Sordo [a,*], José M. Varela [a], Ezequiel M. Vázquez López [b]

[a] Departamento de Química Inorgánica, Facultade de Farmacia, Universidade de Santiago de Compostela, 15782 Santiago de Compostela, Galicia, Spain
[b] Departamento de Química Inorgánica, Facultade de Química, Edificio de Ciencias Experimentais, Universidade de Vigo, 36310 Vigo, Galicia, Spain

ARTICLE INFO

Article history:
Received 10 January 2008
Accepted 23 April 2008
Available online 6 June 2008

Keywords:
Sulfanylpropenoato
Mercury(II)
IR
Phenylmercury(II)
NMR
Crystal structure

ABSTRACT

Compounds $[HQ]_2[Hg(L)_2]$ and [HQ][PhHg(L)] [where HQ = diisopropylammonium cation; L = pspa, fspa, tspa, where p = 3-(phenyl), f = 3-(2-furyl), t = 3-(2-thienyl), and spa = 2-sulfanylpropenoato] have been prepared by the reaction of mercury(II) acetate or phenylmercury(II) acetate with the corresponding acid in the presence of diisopropylamine in ethanol. The compounds have been characterized by elemental analysis, FAB mass spectrometry and IR and NMR (^1H, ^{13}C) spectroscopy. The crystal structures of the $[HQ]_2[Hg(L)_2]$ compounds show the presence of diisopropylammonium cations and $[Hg(L)_2]^{2-}$ anions. In each anion the Hg atom is in an HgO_2S_2 environment and this can be described as *nido*-tbp. The crystal structures of the [HQ][PhHg(L)] compounds show the presence of diisopropylammonium cations and $[PhHg(L)]^-$ anions in which the Hg atom adopts an HgCOS distorted T-environment. The NMR data suggest that the coordination mode of the ligand L^{2-} determined by X-ray diffractometry in the solid remains in solution.
© 2008 Elsevier Ltd. All rights reserved.

1. Introduction

The useful properties of mercury and its compounds has as a counterpart in their toxic effects. This metal is widespread today and is emitted as a vapour into the atmosphere from both natural and anthropogenic sources. This vapour is slowly converted to Hg(II) by oxidative process and the mercury returns to the earth in rainwater [1]. Hg(II) has an extremely high affinity for compounds that contain sulfhydryl groups and in the blood and tissues of humans it is bound to these groups of cysteine-containing peptides and proteins. Often very stable forms include linear complexes with two sulfur ligands; however, the Hg–S bonds are labile and for higher coordination numbers the structures are flexible, often with distorted trigonal or tetrahedral coordination geometries [1,2].

The methylmercury(II) cation is formed in the environment in biotic processes by microbial metabolization and in abiotic processes by chemical reactions that do not involve living organisms. In marine sediments or at the bottom of lakes methylmercury(II) is concentrated in plankton and progresses up the food chain as it is readily absorbed and accumulated by living organisms.

The methylmercury and phenylmercury(II) cations also have a high affinity for the S-donor atoms present in proteins, peptides and amino acids. However, the behaviour as a toxic agent is different; methylmercury is neurotoxic, whereas the phenyl derivative shows toxic effects as Hg(II). These facts are consistent with the easier breakdown of the Hg–C bond in the phenyl derivative [1–3].

The breakdown of this bond once the R–Hg fragment is S-bonded is activated by the donating ability of other donor atoms that are able to provide an additional interaction to the Hg–S bond. For the organomercurial lyase enzymes that are able to degrade methylmercury, the influence of additional S-donor atoms from cysteine [4] or O-donor atoms from either a phenolic group [5] or a carboxylate group [6] have been postulated.

As alternatives to the classical chelating agents dimercaptosuccinic acid (DMSA) and dimercaptopropanesulfonic acid (DMPS) [7], the 3-(aryl)-2-sulfanylpropenoic acids (where aryl = phenyl, 2-furyl) were tested [8,9] as chelating agents against mercury intoxication through mobilization of the metal by complex formation. As these complexes have not been studied we selected these two ligands [H_2L, Scheme 1], along with the 2-thienyl derivative for comparative purposes, and reacted them with Hg(II) in order to prepare and structurally characterize the respective complexes.

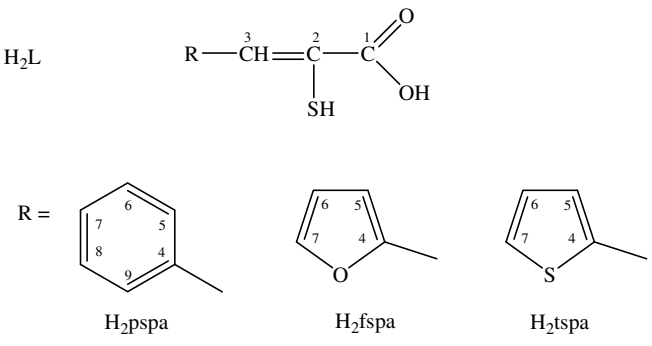

H_2pspa H_2fspa H_2tspa

* Corresponding author. Tel.: +34 981528074; fax: +34 981547102.
E-mail address: qijsordo@usc.es (J. Sordo).

0277-5387/$ - see front matter © 2008 Elsevier Ltd. All rights reserved.
doi:10.1016/j.poly.2008.04.034

This structural study is relevant because, although there are previous results on S-donor ligands coordinated to Hg(II) and carboxylate "inorganic" complexes, to the best of our knowledge Hg(II) complexes with an S_2O_2 kernel either do not contain or contain only weakly coordinated carboxylates [10]. The contrasting chelating ability of this class of ligand [11,12] should enable the preparation and study of this kernel.

In addition, in the case of phenylmercury(II), an HgCSO kernel with S,O-donor bidentate chelate ligands was not found in the literature [13] or in a search of the CSD database [14] and could contribute to our understanding of Hg–C bond cleavage. As a result, we also prepared and characterized the corresponding phenylmercury(II) complexes with these ligands.

The work described here involves the synthesis and characterization of compounds of the type $[HQ]_2[Hg(L)_2]$, in which the Hg atom has an HgO_2S_2 coordination kernel, and compounds of the type [HQ][PhHg(L)], in which an HgCSO kernel was identified and characterized by X-ray diffraction.

2. Experimental

2.1. Material and methods

The 3-(aryl)-2-sulfanylpropenoic acids H_2pspa, H_2fspa and H_2tspa were prepared by condensation of the appropriate aldehyde with rhodanine, subsequent hydrolysis in an alkaline medium and acidification with HCl [15,16]. Mercury(II) acetate, phenylmercury(II) acetate and diisopropylamine (Merck) were used as supplied. Elemental analyses were performed with a Carlo-Erba 1108 microanalyser. Melting points were determined with a Büchi apparatus and are uncorrected. IR spectra (KBr pellets or Nujol mulls) were recorded on a Bruker IFS66V FT-IR spectrophotometer and are reported in Section 2.2. ^{1}H and ^{13}C NMR spectra were recorded in dmso-d_6 or $CDCl_3$ at room temperature on Bruker AMX 300 and AMX 500 spectrometers operating at 300.14 or 500.14 (^{1}H) and 75.46 or 125.76 MHz (^{13}C), using 5 mm o.d. tubes; chemical shifts are reported relative to TMS using the solvent signal (δ^1H = 2.50 ppm; δ^{13}C = 39.50 ppm) as reference. ^{199}Hg NMR were recorded in dmso-d_6 and, in some cases, $CDCl_3$ (concentration ranging from 10^{-2} to 2.6×10^{-2} M) at room temperature on a Bruker AMX 500 spectrometer operating at 89.47 MHz. Chemical shifts are reported relative to pure dimethylmercury(II) as secondary standard. Mass spectra were recorded on a Kratos MS50TC spectrometer connected to a DS90 system and operating in FAB conditions (Xe, 8 eV) using as liquid matrix 3-nitrobenzyl alcohol.

2.2. Synthesis

2.2.1. Compounds of the type $[HQ]_2[Hg(L)_2]$

These compounds were prepared by reacting diisopropylamine, the appropriate H_2L acid and $Hg(OAc)_2$ in ethanol in a 2:2:1 molar ratio. The solid formed after agitation of the reaction mixture at room temperature was filtered off and vacuum dried.

2.2.2. $[HQ]_2[Hg(pspa)_2]$ (**1**)

H_2pspa (0.90 g, 0.005 mmol), $Hg(OAc)_2$ (0.80 g, 0.0025 mmol), diisopropylamine (0.51 g, 0.005 mmol), ethanol (50 mL), grey solid, yield: 73.6%, M.p.: 163 °C. *Anal.* Calc. for $C_{30}H_{44}N_2O_4S_2Hg$: C, 47.3; H, 5.8; N, 3.7; S, 8.4. Found: C, 47.3; H, 5.9; N, 3.6; S, 8.9%. IR (cm^{-1}): $\nu_a(CO_2^-)$ 1547s; $\nu_s(CO_2^-)$ 1343vs; $\delta(NH_2^+)$ 1618s. ^{1}H NMR (dmso-d_6, ppm): δ C(3)H 7.73 (s, 2), CH_3 1.18, NH_2^+ 8.85. ^{13}C NMR (dmso, ppm): δ C(1) 170.7, C(2) 135.9, C(3) 131.2, CH 46.0, CH_3 18.7. ^{199}Hg NMR (dmso-d_6, ppm): δ −784.7. FAB peaks at m/z (%) = 662.2 (1.20) ([HQ][Hg(pspa)$_2$] + 2H); 102.1 (100) (HQ). Recrystallization from an ethanol–dmso mixture gave crystals suitable for an X-ray study.

2.2.3. $[HQ]_2[Hg(fspa)_2]$ (**2**)

H_2fspa (0.90 g, 0.0053 mmol), $Hg(OAc)_2$ (0.45 g, 0.0026 mmol), diisopropylamine (0.54 g, 0.0053 mmol), ethanol (50 mL), yellow solid, yield: 48.2%, M.p.: 172 °C. *Anal.* Calc. for $C_{26}H_{40}N_2O_6S_2Hg$: C, 42.1; H, 5.4; N, 3.8; S, 8.2. Found: C, 42.2; H, 5.7; N, 3.2; S, 8.6%. IR (cm^{-1}): $\nu_a(CO_2^-)$ 1543s; $\nu_s(CO_2^-)$ 1344vs; $\delta(NH_2^+)$ 1620s. ^{1}H NMR (dmso-d_6, ppm): δ C(3)H 7.61 (s, 2), CH 3.27 (q, 4), CH_3 1.17 (d, 24). ^{13}C NMR (dmso-d_6, ppm): δ C(1) 169.9, C(2) 135.9, C(3) 141.4, CH 45.9, CH_3 18.70. ^{199}Hg NMR (dmso-d_6, ppm): δ −780.7. ^{199}Hg NMR ($CDCl_3$, ppm): δ −853. FAB peaks at m/z (%) = 642.2 (0.96) ([HQ][Hg(fspa)$_2$] + 2H); 102.1 (100.00) (HQ). Crystals suitable for an X-ray study were obtained from the mother liquor.

2.2.4. $[HQ]_2[Hg(tspa)_2]$ (**3**)

H_2tspa (0.90 g, 0.0048 mmol), $Hg(OAc)_2$ (0.77 g, 0.0024 mmol), diisopropylamine (0.49 g, 0.0048 mmol), ethanol (50 mL), white solid, yield: 68.7%, M.p.: 168 °C. *Anal.* Calc. for $C_{26}H_{40}N_2O_4S_4Hg$: C, 40.4; H, 5.2; N, 3.6; S, 16.6. Found: C, 39.8; H, 5.1; N, 3.3; S, 16.1%. IR (cm^{-1}): $\nu_a(CO_2^-)$ 1548s; $\nu_s(CO_2^-)$ 1335vs; $\delta(NH_2^+)$ 1612m. ^{1}H NMR (dmso-d_6, ppm): δ C(3)H 7.97 (s, 2), CH 3.27 (q, 4), CH_3 1.16 (d, 24), NH_2^+ 8.96 (s, br, 4). ^{13}C NMR (dmso-d_6, ppm): δ C(1) 170.2, C(2) 134.5, C(3) 124.6, CH 45.9, CH_3 18.7. ^{199}Hg NMR (dmso-d_6, ppm): δ –810.2. FAB peaks at m/z (%) = 673.1 (0.82) ([HQ][Hg(tspa)$_2$] + H); 102.1 (100) (HQ). Crystals suitable for an X-ray study were obtained by recrystallization from a dmso/dmf mixture.

2.2.5. Compounds of the type [HQ][PhHg(L)]

These compounds were prepared by reacting the appropriate sulfanylpropenoic acid, diisopropylamine and PhHg(OAc) in ethanol in a 1:1:1 molar ratio. The solid formed after agitation of the mixture at room temperature was filtered off and vacuum dried.

2.2.6. [HQ][PhHg(pspa)] (**4**)

H_2pspa (0.90 g, 0.005 mmol), PhHg(OAc) (1.69 g, 0.005 mmol), diisopropylamine (0.51 g, 0.005 mmol), ethanol (50 mL), white solid, yield: 69.7%, M.p.: 183 °C. *Anal.* Calc. for $C_{21}H_{27}NO_2SHg$: C, 45.2; H, 4.9; N, 2.5; S, 5.7. Found: C, 45.0; H, 4.8; N, 2.7; S, 5.8%. IR (cm^{-1}): $\nu_a(CO_2^-)$ 1553s; $\nu_s(CO_2^-)$ 1340vs; $\delta(NH_2^+)$ 1618m. ^{1}H NMR (dmso-d_6, ppm): δ C(3)H 7.66 (s, 1), CH 3.30 (q, 4), CH_3 1.19 (d, 24), NH_2^+ 8.55 (s,br, 1). ^{13}C NMR (dmso-d_6, ppm): δ C(1) 171.5, C(2) 137.9, C(3) 131.0, CH 46.0, CH_3 18.9. ^{199}Hg NMR (dmso-d_6, ppm): δ −755.4. ^{199}Hg NMR ($CDCl_3$, ppm): δ −820.9. FAB peaks at m/z (%) = 558.10 (1.44) ([HQ][PhHg(pspa)] + H); 457.98 (1.68) ([PhHg(pspa)] + H); 102.09 (100.00) (HQ). Crystals suitable for an X-ray study were obtained from the mother liquor.

2.2.7. [HQ][PhHg(fspa)] (**5**)

H_2fspa (0.90 g, 0.0053 mmol), PhHg(OAc) (1.79 g, 0.0053 mmol), diisopropylamine (0.54 g, 0.0053 mmol), ethanol (50 mL), white solid, yield: 76.6%, M.p.: 172 °C. *Anal.* Calc. for $C_{19}H_{25}NO_3SHg$: C, 41.6; H, 4.6; N, 2.6; S, 5.8. Found: C, 41.8; H, 4.6; N, 2.4; S, 5.4%. IR (cm^{-1}): $\nu_a(CO_2^-)$ 1546 m; $\nu_s(CO_2^-)$ 1334vs; $\delta(NH_2^+)$ 1620m. ^{1}H NMR (dmso-d_6, ppm): δ C(3)H 7.56 (s, 1), CH 3.30, CH_3 1.16 (d, 12), NH_2^+ 8.68 (s,br). ^{13}C NMR (dmso-d_6, ppm): δ C(1) 170.9, C(2) 141.4, C(3) 137.5, CH 46.0, CH_3 18.8. ^{199}Hg NMR (dmso-d_6, ppm): δ −776.1. ($CDCl_3$, ppm): δ −861.5. FAB peaks at m/z (%) = 549.07 (1.31) ([HQ][PhHg(fspa)]); 447.94 (2.50) ([PhHg(fspa)] + H); 102.09 (100.00) (HQ). Crystals suitable for an X-ray study were obtained from the mother liquor.

2.2.8. [HQ][PhHg(tspa)] (6)

H_2tspa (0.90 g, 0.0048 mmol), PhHg(OAc) (1.63 g, 0.0048 mmol), diisopropylamine (0.49 g, 0.0048 mmol), ethanol (50 mL), white solid, yield: 78.7%, M.p.: 184 °C. *Anal.* Calc. for $C_{19}H_{25}NO_2S_2Hg$: C, 40.5; H, 4.4; N, 2.4; S, 11.4. Found: C, 40.3; H, 4.0; N, 2.3; S, 11.0%. IR (cm^{-1}): $\nu_a(CO_2^-)$ 1552s; $\nu_s(CO_2^-)$ 1335vs; $\delta(NH_2^+)$ 1617m. ^1H NMR (dmso-d_6, ppm): δ C(3)H 7.97 (s, 1), CH 3.30 (q, 2), CH_3 1.20 (d, 12), NH_2^+ 8.84 (s, br). ^{13}C NMR (dmso-d_6, ppm): δ C(1) 171.38, C(2) 134.9, C(3) 126.2, CH 45.9, CH_3 18.7. ^{199}Hg NMR (dmso-d_6, ppm): δ −788.8. ^{199}Hg NMR ($CDCl_3$, ppm): δ −839.4. FAB peaks at m/z(%) = 565.06 (1.98) ([HQ][PhHg(tspa)]); 463.93 (3.21) ([PhHg(tspa)] + H); 102.09 (100.00) (HQ). Crystals suitable for an X-ray study were obtained from the mother liquor.

2.3. X-ray studies

Single crystals were mounted on glass fibres in Bruker Smart 1000 CCD (**1**–**3**) or Enraf-Nonius MACH3 (**4**–**6**) automatic diffractometers. Data were collected at 293 K using Mo Kα radiation (λ = 0.71073 Å). The crystal data, experimental details and refinement results are summarized in Table 1.

Corrections for Lorentz effects, polarization [17] and multi-scan (SADABS) [18] for **1**–**3** or semi-empirical (ψ scan) [19,20] for **4**–**6** absorption were carried out. The structures of **1**–**4** were solved using direct methods but by the heavy atom Patterson method in **5** and **6** [21]. In the refinement the non-H atoms were treated anisotropically [21]. The H atoms were localized from difference Fourier maps and refined as riders (N–H 0.90, C–H 0.93–0.98 Å) [21], except in **1** and **3** where the atomic position and isotropic temperature factor were also refined.

The scattering factors were taken from *International Tables for Crystallography* [22]. The main calculations were performed with SHELXL-97 [21] and PLATON [20] and figures were plotted with ZORTEP [23] and MERCURY [24].

3. Results and discussion

3.1. Compounds of the type $[HQ]_2[Hg(L)_2]$

The reaction of diisopropylamine, the corresponding H_2L acid and $Hg(OAc)_2$ in ethanol in a 2:2:1 molar ratio gave rise to solids with this composition. In all the cases the FAB spectra show peaks for the protonated $[HQ][Hg(L)_2]$ species. The compounds are soluble in dmso and dmf but insoluble or sparingly soluble in water, ethanol, acetone, chloroform and acetonitrile.

Table 1
Crystal structure and refinement data for $[HQ]_2[Hg(pspa)_2]$ (**1**), $[HQ]_2[Hg(fspa)_2]$ (**2**), $[HQ]_2[Hg(tspa)_2]$ (**3**), [HQ][PhHg(pspa)] (**4**), $[HQ_2[PhHg(fspa)]$ (**5**) and [HQ][PhHg(tspa)] (**6**)

Compound	$[HQ]_2[Hg(pspa)_2]$ (1)	$[HQ]_2[Hg(fspa)_2]$ (2)	$[HQ]_2[Hg(tspa)_2]$ (3)	[HQ][PhHg(pspa)] (4)	[HQ][PhHg(fspa)] (5)	[HQ][PhHg(tspa)] (6)
Empirical formula	$C_{30}H_{44}N_2O_4S_2Hg$	$C_{26}H_{40}N_2O_6S_2Hg$	$C_{26}H_{40}N_2O_4S_4Hg$	$C_{21}H_{27}NO_2SHg$	$C_{19}H_{25}NO_3SHg$	$C_{19}H_{25}NO_2S_2Hg$
Formula weight	761.38	741.31	773.43	558.09	548.05	564.11
Temperature (K)	293(2)	293(2)	293(2)	293(2)	293(2)	293(2)
Wavelength (Å)	0.71073	0.71073	0.71073	0.71073	0.71073	0.71073
Crystal system, space group	monoclinic, *P*2(1)/*n*	triclinic, $P\bar{1}$	monoclinic, *P*2(1)/*c*	monoclinic, *P*2(1)/*c*	orthorhombic, *Pbca*	monoclinic, *P*2(1)/*c*
Unit cell dimensions						
a (Å)	14.3539(11)	13.9291(9)	14.079(4)	8.659(2)	11.122(2)	8.300(2)
b (Å)	15.9545(13)	14.712(1)	15.321(4)	22.182(4)	17.062(4)	22.25(4)
c (Å)	15.6774(12)	18.109(1)	16.238(5)	11.092(4)	21.505(4)	11.164(2)
α (°)		92.665(1)				
β (°)	111.280(2)	111.939(1)	112.574(5)	94.80(2)	94.33(2)	94.33(2)
γ (°)		110.151(1)				
V (Å^3)	3345.5(5)	3165.5(3)	3234.2(16)	2123.0(8)	4080.6(14)	2056.1(8)
Z, D_{calc} (Mg/m^3)	4, 1.512	4, 1.555	4, 1.588	4, 1.746	8, 1.784	4, 1.822
Absorption coefficient (mm^{-1})	4.759	5.032	5.049	7.362	7.662	7.701
F (000)	1528	1480	1544	1088	2128	1096
Crystal size (mm)	0.22 × 0.21 × 0.15	0.04 × 0.15 × 0.08	0.14 × 0.15 × 0.24	0.35 × 0.30 × 0.15	0.35 × 0.25 × 0.15	0.40 × 0.30 × 0.25
Θ Range for data collection (°)	1.65–28.05	1.64–28.01	1.90–27.88	2.36–27.97	2.38–27.97	3.07–27.98
Index ranges	$-15 \leqslant h \leqslant 18$, $-19 \leqslant k \leqslant 20$, $-19 \leqslant l \leqslant 20$	$-14 \leqslant h \leqslant 18$, $-19 \leqslant k \leqslant 19$, $-23 \leqslant l \leqslant 23$	$-18 \leqslant h \leqslant 18$, $-20 \leqslant k \leqslant 20$, $-21 \leqslant l \leqslant 21$	$-11 \leqslant h \leqslant 0$, $-29 \leqslant k \leqslant 0$, $-14 \leqslant l \leqslant 14$	$-0 \leqslant h \leqslant 14$, $-22 \leqslant k \leqslant 0$, $-0 \leqslant l \leqslant 28$	$-10 \leqslant h \leqslant 10$, $-29 \leqslant k \leqslant 0$, $-14 \leqslant l \leqslant 0$
Reflections collected/ unique [R_{int}]	18 192/7388 [0.0664]	18 142/12 632 [0.0488]	24 213/7415 [0.0982]	5444/5123 [0.0479]	4909/4908 [1.0764]	1575/4936 [0.0506]
Completeness to theta	91.0% (θ = 28.05)	82.4% (θ = 28.01°)	96.1% (θ = 27.88)	97.5% (θ = 27.9)	90.3% (θ = 27.97)	97.5% (θ = 27.98)
Absorption correction	multiscan	semi-empirical from equivalents	semi-empirical from equivalents	semi-empirical from equivalents	psi scan	psi scan
Maximum and minimum transmission	1.000 and 0.486	1.000 and 0.479	1.000 and 0.644	0.971 and 0.486	0.968 and 0.515	0.982 and 0.546
Refinement method	full-matrix least-squares on F^2	full-matrix least-squares on F^2	full-matrix least-squares on F^2	full-matrix least-squares on F^2	full-matrix least-squares on F^2	full-matrix least-squares on F^2
Data/parameters	7388/0/364	12632/683	7415/346	5123/239	4908/230	4936/230
Goodness-of-fit on F^2	0.704	0.567	1.012	1.018	0–955	0.955
Final *R* indices [$I > 2\sigma(I)$]	R_1 = 0.0390, wR_2 = 0.0460	R_1 = 0.0467, wR_2 = 0.1038	R_1 = 0.0740, wR_2 = 0.1195	R_1 = 0.0450, wR_2 = 0.1018	R_1 = 0.0457, wR_2 = 0.0892	R_1 = 0.0466 wR_2 = 0.0792
R indices (all data)	R_1 = 0.1404 wR_2 = 0.0570	R_1 = 0.1193, wR_2 = 0.1327	R_1 = 0.1661, wR_2 = 0.1431	R_1 = 0.1653, wR_2 = 0.1337	R_1 = 0.2123, wR_2 = 0.1317	R_1 = 0.1737, wR_2 = 0.1043
Largest difference in peak and hole (e A^{-3})	0.868 and −0.679	1.290 and −1.098	2.096 and −1.014	1.098 and −1.359	0.866 and −1.206	1.536 and −0.852

*3.1.1. Description of the structures of $[HQ]_2[Hg(pspa)_2]$ (**1**), $[HQ]_2[Hg(fspa)_2]$ (**2**) and $[HQ]_2[Hg(tspa)_2]$ (**3**)*

Crystals suitable for X-ray study were obtained for compounds derived from H_2pspa, H_2fspa and H_2tspa. As the structures have significant similarities they are discussed together.

In all cases the crystals contain diisopropylammonium cations and anions of the type $[Hg(L)_2]^{2-}$, where L ($pspa^{2-}$, $fspa^{2-}$ and $tpsa^{2-}$) behaves as a bidentate chelate ligand bonded to Hg through an O atom of the carboxylate group and the S atom of the deprotonated SH group. The numbering scheme for the $[Hg(L)_2]^{2-}$ anions is shown in Fig. 1 and selected values for the bond distances (Å) and angles (°) are given in Tables 2 and 3.

The Hg atom in all the anions is tetracoordinated in an HgO_2S_2 environment, with slightly different parameters in molecules A and B for $[Hg(fspa)_2]^{2-}$ (Table 3). The Hg–S bond distances range from 2.333(2) Å for $[Hg(pspa)_2]^{2-}$ to 2.349(3) Å for $[Hg(tspa)_2]^{2-}$. These values are slightly shorter than those found in Hg(II) compounds with *S,S′*-bidentate ligands [25] to give an HgS_4 environment and are in the range found for linear S–Hg–S bis-thiolato complexes of Hg(II) [26]; the Hg–O bond distances range from 2.499(7) Å in $[Hg(tspa)_2]^{-}$ to 2.553(4) Å in $[Hg(pspa)_2]^{2-}$.

As far as the angles around the metal are concerned, the value for the bite angle of the ligand, which ranges from 77.56(17)° for $[Hg(fspa)_2]^{2-}$ to 80.04(15)° for $[Hg(tspa)_2]^{2-}$, is lower; the largest value is found for the S–Hg–S angle, which ranges from 168.03(9)° in $[Hg(tspa)_2]^{2-}$ to 171.83(8)° in the fspa derivative.

In order to investigate the influence that a possible Hg–S interaction between neighbouring molecules has on the S–Hg–S angle

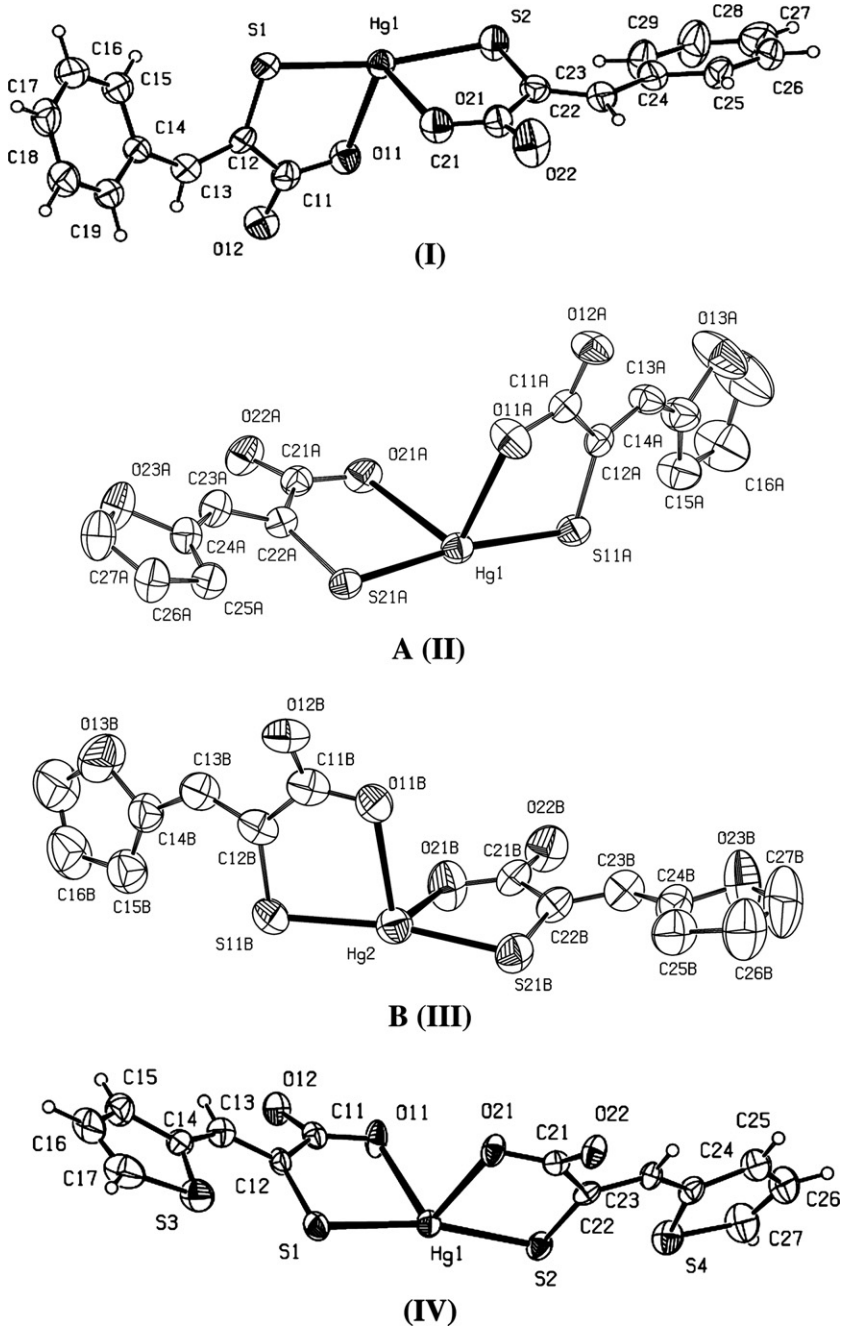

Fig. 1. ORTEP drawing showing the structures of the $[Hg(pspa)_2]^{2-}$ (I), the two molecules A(II) and B(III) of the $[Hg(fspa)_2]^{2-}$ and $[Hg(tspa)_2]^{2-}$ (IV) anions with the numbering scheme. The ellipsoids are drawn at the 30% probability level.

Table 2
Selected bond lengths (Å) and angles (°) in $[HQ]_2[Hg(pspa)_2]$ (**1**) and $[HQ]_2[Hg(tspa)_2]$ (**3**)

	$[HQ]_2[Hg(pspa)_2]$[a] (**1**)	$[HQ]_2[Hg(tspa)_2]$ (**3**)
(a) *Hg environment*		
Hg(1)–O(11)	2.510(4)	2.499(7)
Hg(1)–O(21)	2.553(4)	2.518(6)
Hg(1)–S(1)#1	3.427(2)	
Hg(1)–S(1)	2.346(2)	2.349(3)
Hg(1)–S(2)	2.333(2)	2.346(3)
O(11)–Hg(1)–S(1)	78.26(10)	79.35(16)
O(11)–Hg(1)–S(2)	110.53(11)	109.19(15)
S(1)–Hg(1)–S(2)	169.93(6)	168.03(9)
S(1)#1–Hg(1)–S(2)	79.45(5)	
S(1)#1–Hg(1)–S(1)	96.76(4)	
O(21)–Hg(1)–S(1)	106.62(11)	106.71(16)
O(21)–Hg(1)–S(2)	77.77(11)	80.04(15)
O(11)–Hg(1)–O(21)	96.95(14)	102.9(2)
O(11)–Hg(1)–S(1)#1	85.83(9)	
O(21)–Hg(1)–S(1)#1	156.55(11)	
(b) *Ligand*		
S(1)–C(12)	1.746(6)	1.747(10)
O(11)–C(11)	1.258(6)	1.223(10)
O(12)–C(11)	1.255(6)	1.259(11)
S(2)–C(22)		1.750(9)
O(21)–C(21)		1.269(10)
O(22)–C(21)		1.244(10)
O(12)–C(11)–O(11)	123.3(7)	126.1(9)
O(12)–C(11)–C(12)	118.4(6)	117.0(8)
O(11)–C(11)–C(12)	118.3(6)	116.8(9)
C(13)–C(12)–S(1)	121.1(5)	120.8(7)
C(11)–C(12)–S(1)	121.6(5)	121.5(7)
O(22)–C(21)–O(21)		123.2(8)
O(22)–C(21)–C(22)		118.4(9)
O(21)–C(21)–C(22)		118.4(8)
C(23)–C(22)–S(2)		122.0(7)
C(21)–C(22)–S(2)		120.9(7)

[a] *Symmetry operations*: #1 $-x, -y, -z$.

Table 3
Selected bond lengths (Å) and angles (°) in $[HQ]_2[Hg(fspa)_2]$ (**2**)

(a) *Hg environment*			
Hg(1)–O(11A)	2.550(7)	Hg(1)–S(11A)	2.337(3)
Hg(1)–O(21A)	2.536(6)	Hg(1)–S(21A)	2.334(3)
Hg(2)–O(11B)	2.549(6)	Hg(2)–S(11B)	2.347(2)
Hg(2)–O(21B)	2.540(6)	Hg(2)–S(21B)	2.336(2)
O(11A)–Hg(1)–S(11A)	77.56(17)	O(11A)–Hg(1)–S(21A)	108.03(17)
O(21A)–Hg(1)–S(11A)	106.95(18)	O(21A)–Hg(1)–S(21A)	78.54(18)
S(11A)–Hg(1)–S(21A)	171.83(8)	O(11A)–Hg(1)–O(21A)	98.0(2)
O(11B)–Hg(2)–S(11B)	79.15(16)	O(11B)–Hg(2)–S(21B)	107.19(16)
O(21B)–Hg(2)–S(11B)	107.86(16)	O(21B)–Hg(2)–S(21B)	78.09(16)
S(11B)–Hg(2)–S(21B)	170.90(8)	O(11B)–Hg(2)–O(21B)	98.3(2)
(b) *Ligand*			
S(11A)–C(12A)	1.766(9)	S(21A)–C(22A)	1.752(9)
S(11B)–C(12B)	1.750(9)	S(21B)–C(22B)	1.758(9)
O(11A)–C(11A)	1.246(11)	O(21A)–C(21A)	1.245(11)
O(11B)–C(11B)	1.282(11)	O(21B)–C(21B)	1.261(10)
O(12A)–C(11A)	1.227(11)	O(22A)–C(21A)	1.224(11)
O(12B)–C(11B)	1.269(10)	O(22B)–C(21B)	1.231(10)
O(12A)–C(11A)–O(11A)	124.7(9)	O(21A)–C(21A)–O(22A)	123.0(10)
O(12B)–C(11B)–O(11B)	122.8(9)	O(21B)–C(21B)–O(22B)	123.3(8)
O(12A)–C(11A)–C(12A)	117.5(10)	O(21A)–C(21A)–C(22A)	117.6(9)
O(12B)–C(11B)–C(12B)	119.5(9)	O(21B)–C(21B)–C(22B)	117.7(8)
O(11A)–C(11A)–C(12A)	117.7(9)	O(22A)–C(21A)–C(22A)	119.4(10)
O(11B)–C(11B)–C(12B)	117.6(8)	O(22B)–C(21B)–C(22B)	118.9(9)
C(13A)–C(12A)–S(11A)	120.7(7)	C(23A)–C(22A)–S(21A)	120.9(7)
C(13B)–C(12B)–S(11B)	120.5(7)	C(23B)–C(22B)–S(21B)	120.6(7)
C(11A)–C(12A)–S(11A)	121.3(8)	C(21A)–C(22A)–S(21A)	122.7(7)
C(11B)–C(12B)–S(11B)	122.9(7)	C(21B)–C(22B)–S(21B)	122.6(7)
C(13A)–C(14A)–O(13A)	114.1(10)	C(23A)–C(24A)–O(23A)	113.4(9)
C(13B)–C(14B)–O(13B)	113.8(9)	C(23B)–C(24B)–O(23B)	112.4(9)

of the Hg kernel, we analysed these distances. Only in the pspa derivative **1** were interactions found that could be considered significant [Hg–S(1)#1 = 3.4272(16) Å]. In the other two cases the intermolecular Hg–S bond distances are greater than 4 Å. At this point we must underline the variability in the sum of the van der Waals radii for Hg and S (on using the value reported by Bondi [27] we obtained a value of 3.3 Å for the sum of the two radii, which was revised to 3.7 Å [13] or to 4.016 Å on using the van der Waals radii reported by Batsanov [28]). However, the influence of this intermolecular interaction on the bond distances and angles of the Hg kernel does not seem to be significant.

The intermolecular interaction is also absent in $[Hg(Htsal)_2]$ [10] and $[Hg(Htsal)_2] \cdot$ 1,4-dioxane [29] (H_2tsal = thiosalicylic acid). The former compound, which cocrystallizes with $[Hg_2(tsal)_2(PPh_3)_2]$, has parameters [Hg–S: 2.3444(12), 2.3392(12) Å; Hg–O: 2.641(3), 2.682(3) Å; S–Hg–S: 170.12(4)°] close to those found in this work, although the Hg–O bond distances are longer and the S–Hg–S angle slightly wider. Other examples in the literature include the 2,2,6, 6-tetramethyl-3,5-heptanedione [30], the 2-dimethylamino-3-4-dioxo-cyclobut-1-en-thiolate [26] and the *N*-(piperidylthiocarbonylcarbonyl)benzamide [31] mercury(II) complexes and these also have, as in the case of the thiosalicylic acid, wider S–Hg–S bond angles than those found in this work.

For the Hg atom in the thiosalicylic acid derivative Henderson and Nicholson [10], taking into account the large tetrahedral distortion in the kernel, proposed a *nido*-trigonal bipyramidal coordination geometry or even an S–Hg–S linear geometry with a weak Hg···O interaction. The compounds described in this work have a shorter Hg–O bond distance than that found in the thiosalicylic acid derivative, making the *nido*-tbp geometry the more appropriate description.

The planarity of the L^{2-} fragment is different in the three structures. In $[Hg(pspa)_2]^{2-}$ the angle between the idealized plane of the chelate ring and that of the C(14)–C(19) phenyl ring is 22.6° and this value is 12.26° for the other L fragment. Equivalent angles are 12.68° and 10.46° in molecule A and 21.68° and 5.58° in molecule B for the fspa derivative and 10.61° and 15.52° in $[HQ]_2[Hg(tspa)_2]$, although there is a lack of planarity in the chelate ring in the latter compound (rms [Hg(1)/S(1)/O(11)/C(11)/C(12)] = 0.0917° and rms [Hg(1)/S(2)/O(21)/C(21)/C(22)] = 0.0970°).

The diisopropylammonium cation in each of the three structures has parameters that are comparable with other previously described examples [32,33].

Table 4
Structural parameters (Å, °) describing intermolecular hydrogen bonding in the complexes $[HQ]_2[Hg(L)_2]$[a]

	D–H	H···A	D···A	D–H···A
$[HQ]_2[Hg(pspa)_2]$				
N(1)–H(1A)···O(12)#1	0.91(5)	1.82(5)	2.722(6)	170(5)°
N(1)–H(1B)···O(21)	1.09(5)	1.67(5)	2.761(6)	176(4)°
N(2)–H(2A)···O(11)#1	0.87(5)	2.00(5)	2.806(6)	155(5)°
N(2)–H(2B)···O(22)	0.97(5)	1.72(5)	2.692(6)	175(5)
$[HQ]_2[Hg(fspa)_2]$				
N(11)–H(11A)···O(12B)#2	0.90	1.82	2.708(9)	169.6°
N(11)–H(11B)···O(11B)	0.90	1.89	2.777(9)	166.2°
N(41)–H(41A)···O(21B)	0.90	1.84	2.719(9)	163.8°
N(41)–H(41B)···O(12A)#4	0.90	1.94	2.827(9)	168.4°
N(21)–H(21A)···O(22B)	0.90	1.95	2.831(9)	166.2°
N(21)–H(21B)···O(11A)#5	0.90	1.88	2.761(9)	165.3°
N(31)–H(31A)···O(22A)	0.90	1.84	2.737(9)	172.1°
N(31)–H(31B)···O(21A)#3	0.90	1.89	2.776(9)	167.3°
$[HQ]_2[Hg(tspa)_2]$				
N(1)–H(11A)···O(22)#6	0.92(9)	1.84(9)	2.738(10)	164(8)°
N(1)–H(11B)···O(11)	0.90(9)	1.93(9)	2.807(10)	162(8)°
N(2)–H(21A)···O(21)#7	1.01(9)	1.79(9)	2.769(10)	163(7)°
N(2)–H(21B)···O(12)	0.81(9)	2.00(9)	2.801(10)	170(9)°

[a] *Symmetry code*: #1 $x + 1/2, -y + 1/2, z + 1/2$; #2 $-x + 2, -y + 1, -z + 1$; #3 $-x + 2, -y + 2, -z + 1$; #4 $x - 1, y - 1, z$; #5 $x, y - 1, z$; #6 $-x, y + 1/2, -z + 1/2$; #7 $x, -y + 1/2, z + 1/2$.

The $[Hg(L)]^{2-}$ anions and the $[HQ]^{+}$ cations are hydrogen bonded through the NH_2 group of the cation and the O atoms of the carboxylate group. The metric parameters for these bonds are included in Table 4. In the three structures the $[HQ]^{+}$ cation bridges two dianionic $[Hg(L)]^{2-}$ units but the final arrangement is different.

In $[HQ]_2[Hg(pspa)_2]$, two $[HQ]^{+}$ units establish a double-bridge between two $[Hg(pspa)_2]^{2-}$ anions to afford zig-zag chains (Fig. 2a) parallel to the crystallographic direction {1 1 2}. These chains are schematically represented in Fig. 2b using a rod as a symbol for the anion and a left/right arrow as a symbol for the cation. The chains are packed in the crystallographic *c*-axis, as shown in Fig. 2c, in which the hydrogen bond and the weak Hg···S interaction are underlined.

The same interaction in $[HQ]_2[Hg(fspa)_2]$ generates rack-chains running parallel to the crystallographic *b*-axis (Fig. 3) and these are also represented using the same symbols.

In contrast to the above situation, 2D molecular association is observed in the thiophene derivative. The crystal structure may be described in terms of the formation of the unit shown in Fig. 4a by bridge of four $[HQ]^{+}$ units between four $[Hg(tspa)_2]^{2-}$ units. The cyclic unit is associated with another of these units through interactions analogous to those described above (Fig. 4b). The resulting sheet is parallel to the crystallographic *bc*-plane.

3.1.2. Spectroscopy

The IR spectra of the $[HQ]_2[Hg(L)_2]$ complexes do not show a ν(SH) band, which is located near 2550 cm^{-1} in the spectra of the free ligands. Furthermore, the vibrations of the CO_2H group [ν(C=O) = 1670, 1665 and 1673 cm^{-1} for H_2pspa, H_2fspa and H_2tspa are replaced by bands typical of a carboxylate group with [$\nu_{as}(CO_2^-)$] observed between 1548 and 1543 cm^{-1} and [$\nu_{sym}(CO_2^-)$] between 1344 and 1335 cm^{-1}. As in other compounds in which the HQ cation is hydrogen bonded [12,34] to the carboxylate group the $\Delta\nu$ ($=\nu_{as}CO_2^- - \nu_{sym}CO_2^-$) parameter has values smaller than those found for a monodentate carboxylate group [35], which was attributed [34] to the effect of the N–H···O hydrogen bond on the structural parameters of the carboxylate group. A strong band at around 1610 cm^{-1} in all the spectra was assigned [36] to the $\delta(NH_2)$ vibration of the diisopropylammonium cation.

The ^{1}H NMR spectra of the complexes in all cases show the typical signals of the diisopropylammonium cation and the absence of signals attibutable to SH and COOH groups is consistent with bideprotonation of the ligand. These spectra show, in general, a shift of the C(3)–H signal to higher field on complexation, which suggests the persistence of the Hg–S bond in solution.

The persistence of the S-coordination is confirmed [37,38] by the shift of the C(3) signal in the ^{13}C NMR spectra. In these spectra the C(1) signals are in positions close to those found [34,39,40] for compounds with a monodentate coordinated carboxylate group, thus suggesting the persistence in solution of the coordination mode found in the solid state.

The ^{199}Hg NMR spectra show only a signal located between −780.7 and −810.2 ppm, indicating the presence of only one type

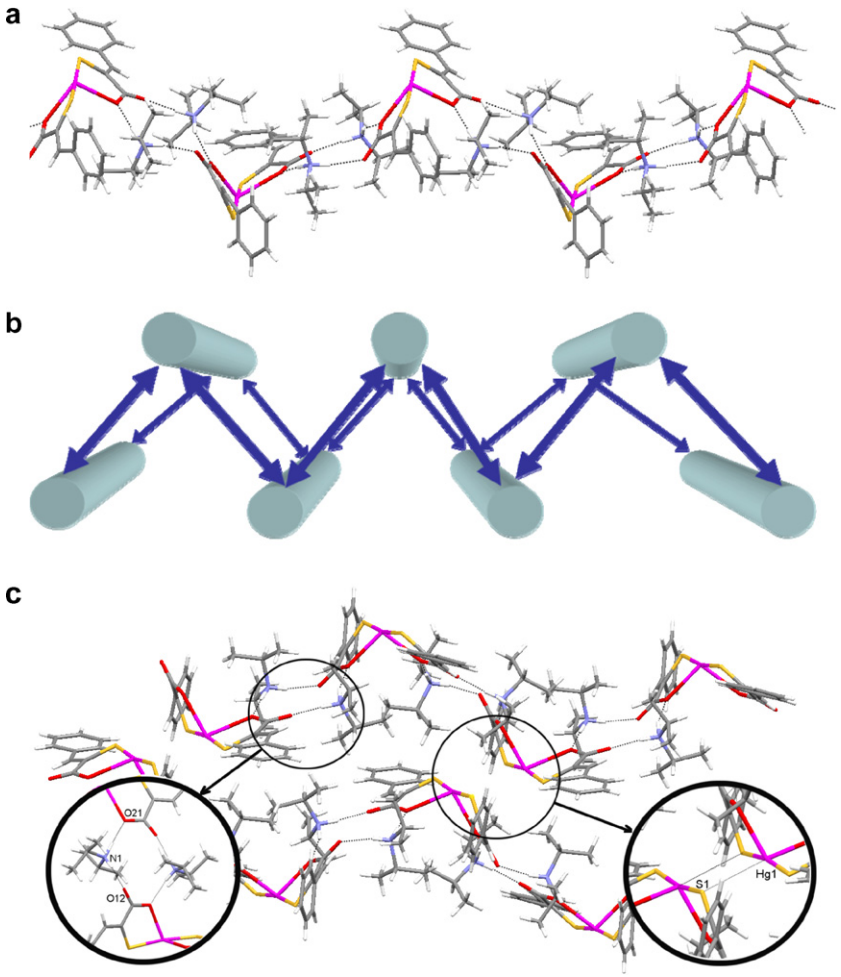

Fig. 2. (a) A view of the polymeric structure of $[HQ]_2[Hg(pspa)_2]$ (**1**) and (b) a schematic view of the structure; and (c) details of the hydrogen bonding and Hg···S intermolecular interactions.

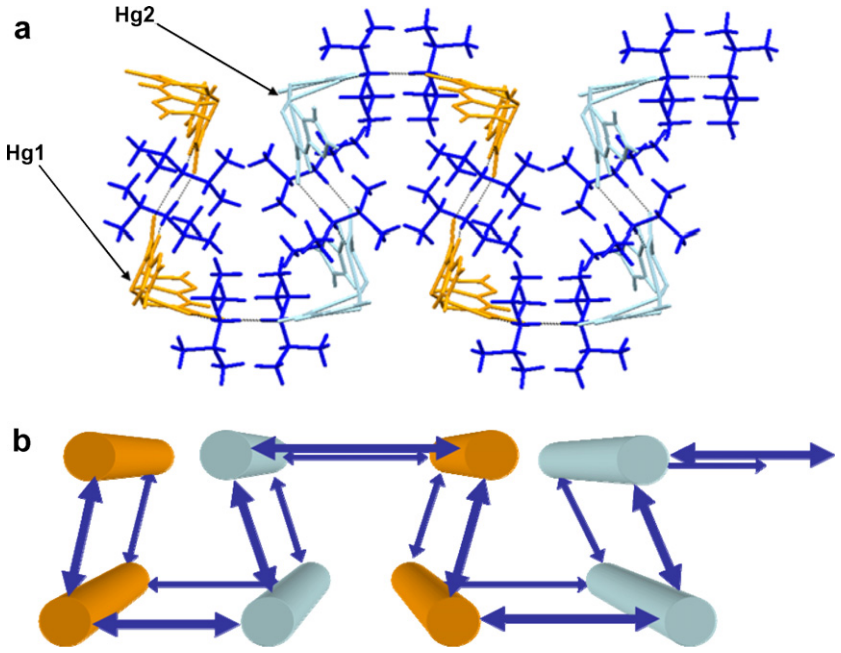

Fig. 3. (a) A view of the polymeric structure of $[HQ]_2[Hg(fspa)_2]$ (**2**) and (b) a schematic view of the structure.

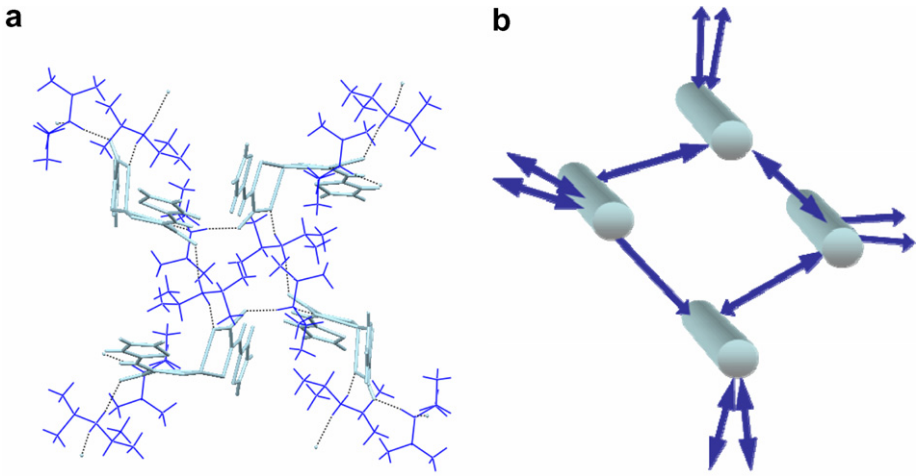

Fig. 4. (a) A partial view of the polymeric structure of $[HQ]_2[Hg(tspa)_2]$ (**3**) and (b) a schematic view of the structure.

of chemical environment for Hg(II). The position of the signal is close to the positions found for other four-coordinated Hg(II) complexes that have the HgS_2N_2 kernel [41]. In the case of **2** the spectrum was recorded in dmso/dmso-d_6 (−780.7 ppm) and in $CDCl_3$ (−853.0 ppm). The difference in the positions of the signal in these spectra is within the accepted range [42] for the influence of the solvent, suggesting the same chemical environment for the metal in both solvents, thus excluding dmso coordination. The additional coordination of these solvent molecules would increase the coordination number and should move the δ (^{199}Hg) signal to higher frequencies [41].

3.2. Compounds of the type [HQ][PhHg(L)]

Reaction of diisopropylamine, the corresponding sulfanylpropenoic acid and PhHg(OAc) in ethanol in a 1:1:1 molar ratio gave solids with this composition. The FAB mass spectra show peaks for the [HQ][HgPh(L)] molecular ion.

3.2.1. Description of the structures of [HQ][PhHg(pspa)] (*4*), [HQ][PhHg(fspa)] (*5*) and [HQ][PhHg(tspa)] (*6*)

Single crystals suitable for X-ray studies were obtained for the three phenyl mercury complexes. The similarity between the structures, indeed the structures of **4** and **6** are isotypic, again means that these compounds will be discussed together. The three crystals contain diisopropylammonium cations and $[HgPh(L)]^-$ anions that interact through hydrogen bonds. The numbering scheme for each compound is shown in Fig. 5 and selected bond distances (Å) and angles (°) are listed in Table 5.

In each anion the ligand is S,O-bidentate chelate to give a HgCOS kernel. It should be noted that such an example in which O and S atoms from the same ligand has not been found previously [13,14] for phenylmercury(II) derivatives. In this kernel the metal adopts a significantly distorted T-environment. In this environment the Hg–C bond distance is about 2.065 Å, which is normal for phenylmercury(II) derivatives [13] and the Hg–O and Hg–S

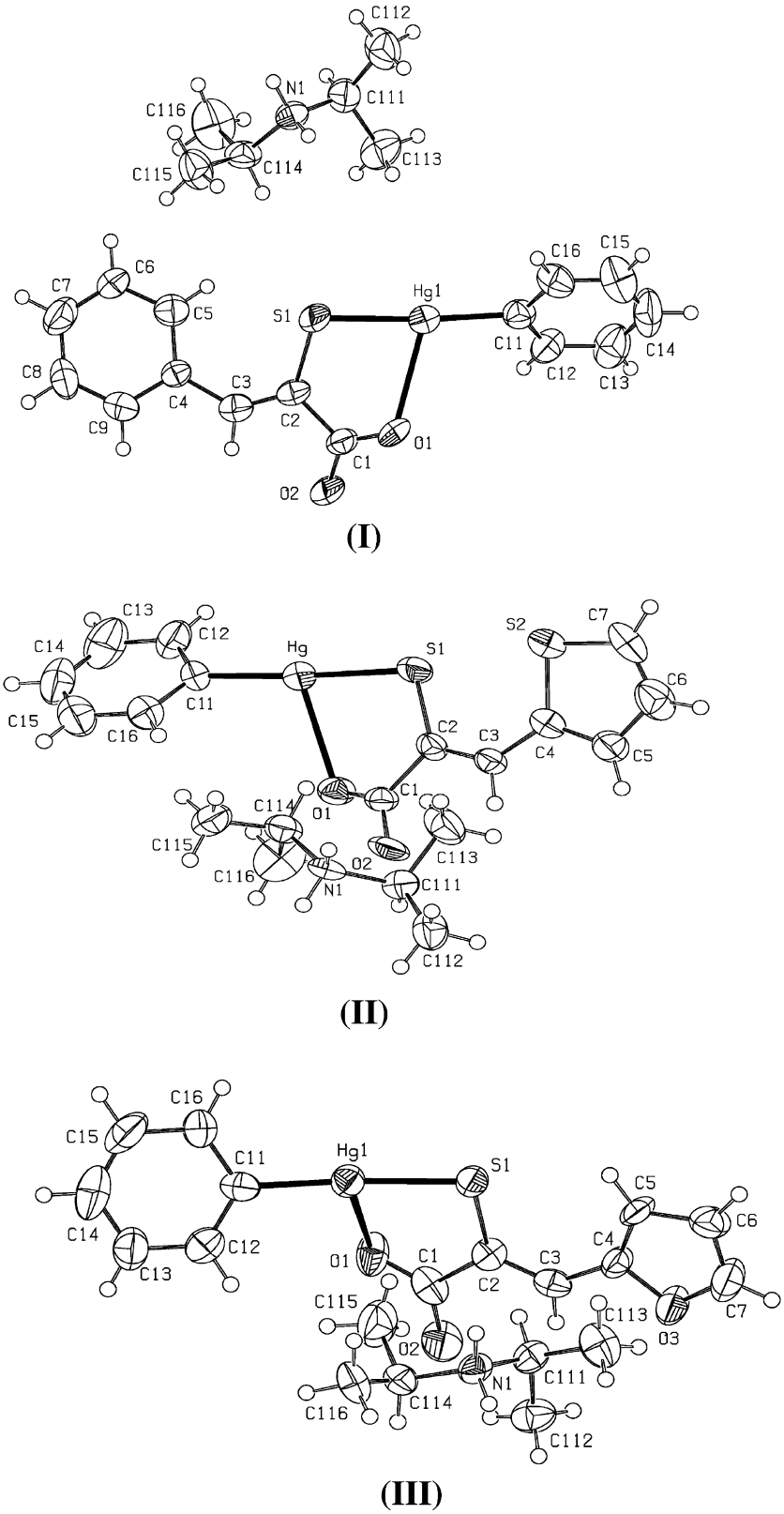

Fig. 5. ORTEP drawing showing the structures of [HQ][PhHg(pspa)] (**4**) (I), [HQ][PhHg(fspa)] (**5**) (II) and [HQ][PhHg(tspa)] (**6**) (III) with the numbering scheme. The ellipsoids are drawn at the 30% probability level.

bond distances are close to 2.565 and 2.355 Å, respectively. The values for the O–Hg–S, C–Hg–O and C–Hg–S angles are about 76.50°, 106.0° and 174.0°, respectively. The sum of these angles is close to 360° in the three anions.

For other kernels values for the Hg–S bond distance between 2.357(3) and 2.405(1) Å were previously described for $PhHg^+$ compounds with thiosemicarbazones [43] and ligands containing P–S bonds [44] and values larger than 2.370 Å have also been described

Table 5
Selected bond lengths (Å) and angles (°) in [HQ][PhHg(pspa)] (**4**), [HQ][PhHg(fspa)] (**5**) and [HQ][PhHg(tspa)] (**6**)

	HQ][PhHg(pspa)][a] (**4**)	[HQ][PhHg(fspa)] (**5**)	[HQ][PhHg(tspa)][b] (**6**)
(a) *Hg environment*			
Hg(1)–O(1)	2.560(6)	2.566(7)	2.570(6)
Hg(1)–S(1)	2.360(3)	2.353(3)	2.354(2)
Hg(1)–C(11)	2.060(10)	2.060(11)	2.075(8)
Hg(1)–S(1)#1	3.381(3)[a]	3.316(3)[b]	3.593(3)[a]
O(1)–Hg(1)–S(1)	76.04(16)	76.49(18)	77.23(14)
O(1)–Hg(1)–S(1)#1	93.73(17)[a]	97.96(19)[b]	93.82(14)[a]
S(1)–Hg(1)–S(1)#1	89.04(9)[a]	88.83(9)[b]	91.90(9)[a]
C(11)–Hg(1)–S(1)	173.7(3)	174.3(3)	175.0(3)
C(11)–Hg(1)–S(1)#1	95.6(3)[a]	96.3(3)[b]	91.4(3)[a]
C(11)–Hg(1)–O(1)	107.9(3)	105.2(3)	106.3(3)
(b) *Ligand*			
S(1)–C(2)	1.767(9)	1.765(10)	1.759(8)
O(1)–C(1)	1.259(11)	1.260(13)	1.261(9)
O(2)–C(1)	1.241(11)	1.243(13)	1.231(9)
O(2)–C(1)–O(1)	123.6(9)	124.8(10)	123.9(8)
O(2)–C(1)–C(2)	117.3(9)	116.4(11)	117.5(8)
O(1)–C(1)–C(2)	119.1(8)	118.8(10)	118.6(7)
C(3)–C(2)–S(1)	122.9(7)	122.6(8)	121.6(6)
C(1)–C(2)–S(1)	119.6(7)	119.3(8)	121.1(6)

[a] *Symmetry operation*: #1 $-x+1, -y+1, -z+1$.
[b] *Symmetry operation*: #1 $-x+1, -y+1, -\mathbf{z}$.

[45–49]. The values found for the Hg–O bonds can be considered [50] typical of relatively strong bonds.

These structures can be related with that of [HgPh(S_2COEt)] [51], in which an S-donor atom is coordinated to a $PhHg^+$ fragment to give a practically linear C–Hg–S [176.1 (4)°] environment, and with that of [HgPh(pmbp)] (pmbp = 1-phenyl-3-methyl-4-benzoylpyrazol-5-onato] [50] where the pmbp ligand has two O-donor atoms, both coordinated to the Hg atom to give an $HgCO_2$ environment reminiscent of the HgCOS present in this case. The structural parameters for the latter compound [Hg–O(1): 2.585(9) Å; Hg–O(2): 2.087(7) Å; Hg–C: 2.040(11) Å; C–Hg–O(1): 112.1(4)°; C–Hg–O(2): 168.6(3)°; O(1)–Hg–O(2): 78.3(3)°] have some similarities with these structures if the O(2) atom, trans to C but closest to the Hg atom, is replaced by the S atom of the sulfanylpropenoic fragment; the bite of the ligand is also similar.

Table 6
Structural parameters (Å, °) describing intermolecular hydrogen bonding in the complexes [HQ][HgPh(L)][a]

	D–H	H···A	D···A	D–H···A
[HQ][PhHg(pspa)]				
N(1)–H(1A)···O(1)#1	0.90	1.95	2.833(10)	167.1
N(1)–H(1B)···O(2)	0.90	1.84	2.730(9)	169.1
[HQ][PhHg(fspa)]				
N(1)–H(1A)···O(1)#2	0.90	1.98	2.855(11)	164.9
N(1)–H(1B)···O(2)	0.90	1.81	2.703(10)	169.7
[HQ][PhHg(tspa)]				
N(1)–H(1A)···O(1) #1	0.90	1.93	2.809(9)	165.8
N(1)–H(1B)···O(2)	0.90	1.84	2.734(8)	169.1

[a] *Symmetry code*: #1 = $-x+1, -y+1, -z$; #2 = $-x, -y+1, -z$.

The parameters for the diisopropylammonium cation are unremarkable and close to those previously described.

In the three crystals there are weak interactions, which are weaker in the tspa derivative, and these are depicted in the structures of the pspa and fspa derivatives shown in Fig. 6. Similar interactions in methylmercury xanthates of the type MeHgS(S)COR (R = Et, ^{i}Pr, CH_2Ph) [45] lead to supramolecular structures, but in this case such interactions could be hindered by the hydrogen bonds that exist between the diisopropylammonium cations and the corresponding anions. The parameters for these bonds, which involve the NH_2 group and the carboxylate group, are listed in Table 6.

As observed in the complexes $[HQ]_2[Hg(L)_2]$, the $[HQ]^+$ units establish two hydrogen bonds with two molecules of $[HgPh(L)]^-$

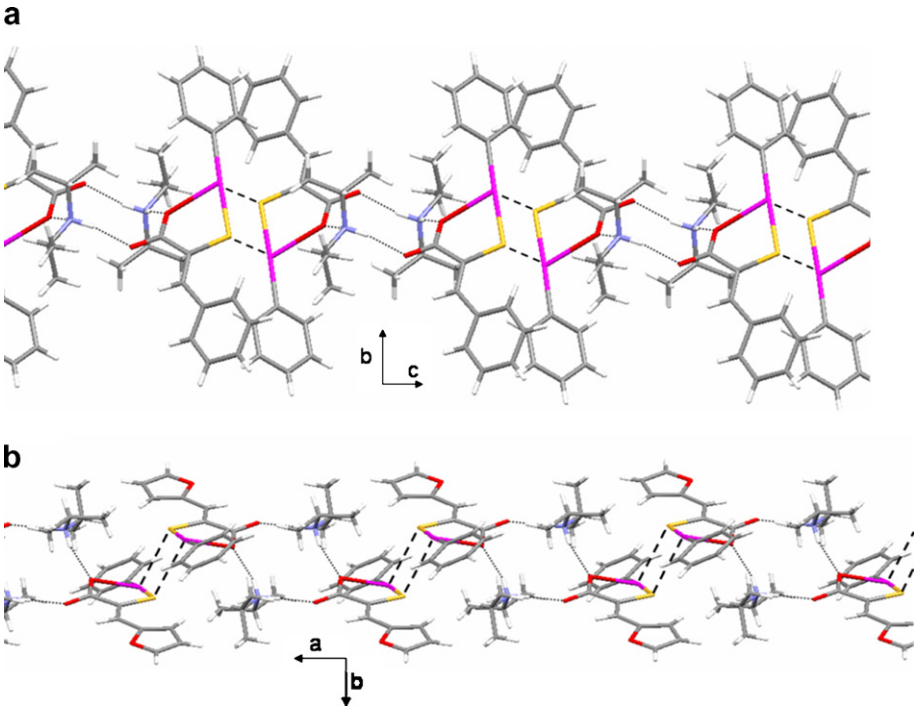

Fig. 6. The polymeric structures of: (a) [HQ][PhHg(pspa)] (**4**) and (b) [HQ][PhHg(fspa)] (**5**).

to afford centrosymmetric dimers. These units are now associated in chains running parallel to crystallographic *c* (compounds **4** and **6**) or *a* (compound **5**) axes (see Fig. 6) through the previously described weak intermolecular Hg–S interaction (Table 5).

3.2.2. Spectroscopy

As for $[HQ]_2[Hg(L)]$, the IR spectra of **4**, **5** and **6** do not show the ν(SH) band and the vibrations of the CO_2H group are replaced by bands typical of the carboxylate group. The $\Delta\nu[\nu_a(CO_2^-)-\nu_s(CO_2^-)]$ values are again typical of a monodentate carboxylate group involved in N–H···O hydrogen bonds.

The ^{1}H NMR spectra show the typical bands of the diisopropylammonium cation, lacking signals attributable to SH and COOH. Furthermore, the spectra show a shift of the C(3)–H signal to higher field on complexation, suggesting the persistence of the Hg–S bond in solution. The position of the C(3) signals in each of the ^{13}C NMR spectra of the complexes again supports S-coordination and the position of the C(1) signal suggests that the carboxylate group remains coordinated in solution. Thus, as in the $[HQ]_2[Hg(L)_2]$ complexes, the ligand remains S,O-coordinated in solution.

The ^{199}Hg NMR spectra of the three complexes show only one signal each. In $CDCl_3$ the signals for **4**, **5** and **6** are at −820.9, −861.5 and −839.4 ppm, respectively, and in dmso the signals range between −755.4 and −788.8 ppm.

The position of the signal in the spectra in chloroform is close to those found for thiosemicarbazonates of phenylmercury(II) in which the metal is tricoordinated [43]. Once again, the difference between the value in $CDCl_3$ and dmso-d_6 suggest that this latter solvent does not increase the coordination number of the metal in comparison to that found in the solid state.

4. Conclusion

In summary, two types of complexes $[HQ]_2[Hg(L)_2]$ and [HQ][PhHg(L)] where HQ is diisopropylammonium and L a bideprotonated 3-(aryl)-2-sulfanylpropenoic acid have been synthesized and characterized.

Among the $[HQ]_2[Hg(L)_2]$ complexes this study has led to the structural characterization of the unusual HgO_2S_2 kernel built on the basis of S,O-bidentate donor ligands. The chelating ability of the corresponding 3-(phenyl)- and 3-(2-furyl)-2-sulfanylpropenoic acids previously used as chelating agents against mercury intoxication is thus confirmed. This S,O-coordination mode was recently described for the widely used chelating agent DMSA, which contains SH and COOH groups, against the diorganotin(IV) fragment [52]. However, X-ray absorption spectroscopy and DFT calculations [7] suggest the presence of metallated species mainly supported by Hg–S bonds in the case of mercury.

The same coordination mode was found for the ligands in the [HQ][PhHg(L)] complexes and this enabled us to determine the structural parameters of the CHgSO kernel, which has been identified previously for S,O-bidentate chelate ligands.

Both types of complex show different supramolecular structures based on N–H···O hydrogen bonds, with weak Hg···S interactions also present in some cases.

Acknowledgement

This work was supported by the Ministerio de Educación y Ciencia, Spain, under project BQU2002-04524-C02-01.

Appendix A. Supplementary data

CCDC 667931, 667932, 667933, 667934, 667935 and 667936 contain the supplementary crystallographic data for **1**, **2**, **3**, **4**, **5** and **6**. These data can be obtained free of charge via www.ccdc.cam.ac.uk/conts/retrieving.html, or from the Cambridge Crystallographic Data Centre, 12 Union Road, Cambridge CB2 1EZ, UK; fax: +44 1223 336 033; or e-mail: deposit@ccdc.cam.ac.uk. Supplementary data associated with this article can be found, in the online version, at doi:10.1016/j.poly.2008.04.034.

References

[1] T.W. Clarkson, L. Magos, Crit. Rev. Toxicol. 36 (2006) 609.
[2] R.E. Hoffmeyer, S.P. Singh, C.J. Donan, A.R.S. Ross, R.J. Hughes, I.P. Pickering, G.N. George, Chem. Res. Toxicol. 19 (2006) 753.
[3] (a) J.P.K. Rooney, Toxicology 234 (2007) 145. and references therein;
(b) J.P.K. Rooney, Toxicology 238 (2007) 216.
[4] J.G. Melnick, G. Parkin, Science 317 (2007) 225.
[5] K.E. Pitts, A.O. Summers, Biochemistry 41 (2002) 10287.
[6] E. Gopinath, T.C. Bruice, J. Am. Chem. Soc. 109 (1987) 7903.
[7] N.G. Geoge, R.C. Price, J. Gailer, G.A. Buttigieg, M. Bonner Denton, H.H. Harris, J.J. Pickering, Chem. Res. Toxicol. 17 (2004) 999.
[8] D.N. Kachru, S. Khandelwal, B.L. Sharma, S.K. Tandon, Pharm. Toxicol. 64 (1989) 182.
[9] S. Khandelwal, D.N. Kachru, S.K. Tandon, Biochem. Int. 16 (1988) 869.
[10] W. Henderson, B.K. Nicholson, Inorg. Chim. Acta 357 (2004) 2231.
[11] J. Wagner, P. Vitali, J. Schorm, E. Giroux, Can. J. Chem. 55 (1977) 4028.
[12] E. Barreiro, J.S. Casas, M.D. Couce, A. Sánchez, R. Seoane, J. Sordo, J.M. Varela, E.M. Vázquez-López, Dalton Trans. (2007) 3074.
[13] J.S. Casas, M.S. García-Tasende, J. Sordo, Coord. Chem. Rev. 193–195 (1999) 283.
[14] F.H. Allen, Acta Crystallogr., Sect. B 58 (2002) 380.
[15] C. Gränacher, Helv. Chim. Acta 5 (1922) 610.
[16] E. Campaigne, R.E. Cline, J. Org. Chem. 21 (1956) 32.
[17] (a) Bruker Analytical Instrumentation, SAINT: SAX Area Detector Integration, 1996.;
(b) Enraf-Nonius, CAD-4 Express Software. Version 5.1. Enraf-Nonius, Delft, The Netherlands, 1995; A.L. Spek, HELENA. A Program for data reduction of CAD4 data. University of Utrecht, The Netherlands, 1997.
[18] G.M. Sheldrick, SADABS, Version 2.03, University of Göttingen, Germany, 2002.
[19] A.C.T. North, D.C. Phillips, F.S. Mathews, Acta Crystallogr., Sect. A 24 (1968) 351.
[20] A.L. Spek Platon, A Multipurpose Crystallographic Tool, University of Utrecht, The Netherlands, 1997.
[21] G.M. Sheldrick, SHELXS97 and SHELXL97, Programs for the Refinement of Crystal Structures, University of Göttingen, Germany, 1997.
[22] International Tables for X-ray Crystallography, vol. C, Kluwer Academic Publishers, Dordrecht, The Netherlands, 1995.
[23] L. Zsolnai, ZORTEP. A Program for the Presentation of THERMAL Ellipsoids, University of Heidelberg, Germany, 1997.
[24] MERCURY 1.2. A Program crystal structure visualisation and exploration. The Cambridge Crystallographic Data Centre. Cambridge. UK, <http://www.ccdc.cam.ac.uk/products/csd_system/mercury/>.
[25] J.S. Casas, M.S. García-Tasende, A. Sánchez, J. Sordo, E.M. Vázquez-López, Inorg. Chim. Acta 256 (1997) 211.
[26] U. Heinl, P. Heinse, R. Fröhlich, R. Mattes, Z. Anorg. Allg. 628 (2002) 770.
[27] J.E. Huheey, E.A. Keiter, R.L. Keiter, Inorganic Chemistry, 4th ed., Harper Collins College Publishers, New York, 1993.
[28] S.S. Batsanov, J. Mol. Struct. (Theochem) 468 (1999) 151.
[29] B.M. Al-Saadi, M. Sandström, Acta. Chem. Scand. 36 (1982) 509.
[30] (a) W. Depmeier, K. Dietrich, K. König, H. Musso, W. Weiss, J. Organomet. Chem. 314 (1986) C1;
(b) K. Dietrich, K. König, G. Mattern, H. Musso, Chem. Ber. 121 (1988) 1277.
[31] Z. Weiqun, Y. Wen, Q. Lihua, Z. Yong, Y. Zhengfeng, J. Mol. Struct. 749 (2005) 89.
[32] S.W. Ng, Acta Crystallogr. E 59 (2003) 1028.
[33] G.J. Reiß, Acta Crystallogr. E 58 (2002) m47.
[34] J.S. Casas, A. Castiñeiras, M.D. Couce, M.L. Jorge, U. Russo, A. Sánchez, R. Seoane, J. Sordo, J.M. Varela, Appl. Organomet. Chem. 14 (2000) 421.
[35] K. Nakamoto, Infrared and Raman Spectra of Inorganic and Coordination Compounds, 5th ed., John Wiley, New York, 1997. p. 60, part B.
[36] N.B. Colthup, L.H. Daly, S.E. Wiberley, Introduction to Infrared and Raman Spectroscopy, 3rd ed., Academic Press Inc., San Diego, 1990. p. 344.
[37] E. Barreiro, J.S. Casas, M.D. Couce, A. Sánchez, J. Sordo, J.M. Varela, E.M. Vázquez-López, Dalton Trans. (2003) 4754.
[38] J.S. Casas, A. Castiñeiras, M.D. Couce, N. Playá, U. Russo, A. Sánchez, J. Sordo, J.M. Varela, J. Chem. Soc., Dalton Trans. (1998) 1513.
[39] K. Gajda-Schrantz, L. Nagy, E. Kuzmann, A. Vertes, J. Holecek, A. Lycka, J. Chem. Soc., Dalton Trans. (1997) 2201.
[40] J. Holecek, A. Lycka, M. Nadvornik, K. Handlir, Collect. Czech. Chem. Commun. 56 (1991) 1908.
[41] U. Abram, A. Castiñeiras, J. García-Santos, R. Rodríguez-Riobó, Eur. J. Inorg. Chem. (2006) 3079.
[42] R.K. Harris, B.E. Mann, NMR and the Periodic Table, Academic Press, London, 1978. p. 270.
[43] T.S. Lobana, A. Sánchez, J.S. Casas, A. Castiñeiras, J. Sordo, M.S. García-Tasende, E.M. Vázquez-López, J. Chem. Soc., Dalton Trans. (1997) 4289.

[44] O. Bumbu, A. Silvestru, C. Silvestru, J.E. Drake, M.B. Hursthouse, M.E. Light, J. Organomet. Chem. 687 (2003) 118.
[45] J.S. Casas, E.E. Castellano, J. Ellena, I. Haiduc, A. Sánchez, R.F. Semeniuc, J. Sordo, Inorg. Chim. Acta 329 (2002) 71.
[46] T.S. Lobana, A. Sánchez, J.S. Casas, A. Castiñeiras, J. Sordo, M.S. García-Tasende, Main Group Met. Chem. 24 (2001) 61.
[47] A. Castiñeiras, W. Hiller, J. Strähle, J. Bravo, J.S. Casas, M. Gayoso, J. Sordo, J. Chem. Soc., Dalton Trans. (1986) 1945.
[48] J. Zukerman-Schpector, E.M. Vázquez-López, A. Sánchez, J.S. Casas, J. Sordo, J. Organomet. Chem. 405 (1991) 67.
[49] E.R.T. Tiekink, J. Organomet. Chem. 322 (1987) 1.
[50] M.F. Mahon, K.C. Molloy, B.A. Omotowa, M.A. Mesubi, J. Organomet. Chem. 525 (1996) 239.
[51] E.R.T. Tiekink, Acta Crystallogr., Sect. C 50 (1994) 861–862.
[52] Ch. Ma, Q. Zhang, Eur. J. Inorg. Chem. (2006) 3244.

Polyhedron 27 (2008) 2447–2451

Contents lists available at ScienceDirect

Polyhedron

journal homepage: www.elsevier.com/locate/poly

Nickel(II) complexes of tetradentate NSNO pyridylthioazophenol ligands: Synthesis, characterization and crystal structure

Pulak K. Dhara [a], Sandipan Sarkar [a], Michael G.B. Drew [b], Munirathinam Nethaji [c], Pabitra Chattopadhyay [a,*]

[a] Department of Chemistry, Burdwan University, Golapbag, Burdwan 713 104, India
[b] Department of Chemistry, Reading University, Reading RG 66AD, Berks, England, United Kingdom
[c] Department of Inorganic and Physical Chemistry, Indian Institute of Science, Bangalore 560 012, India

ARTICLE INFO

Article history:
Received 11 March 2007
Accepted 12 April 2008
Available online 4 June 2008

Keywords:
Nickel(II) complex
Chloro-bridge
Pyridylthioazophenol ligands
Crystal structure

ABSTRACT

Two sets of nickel(II) complexes of a series of tetradentate NSNO ligands were synthesized and isolated in their pure form. All these complexes, formulated as $[Ni(L)Cl]_2$ and $[Ni(L)(N_3)]_2$ [HL = pyridylthioazophenols], were characterized using physicochemical and spectroscopic tools. The solid-state structures of two complexes (**1a** and **2a**) were established by X-ray crystallography. The geometry about the nickel ion of the complexes is octahedral and the complexes are dimeric in nature. In **1**, two Ni(II) ions are bridged by two Cl^- anions while in **2** they are bridged by two azide ions in a μ-1,1-bridging fashion.

© 2008 Elsevier Ltd. All rights reserved.

1. Introduction

Considerable attention has been directed towards the synthesis of nickel(II) complexes in recent years. The potential role played by nickel ions, being present in the active sites of a large number of metalloproteins, has stimulated efforts to design new ligands and characterize of nickel complexes as models for providing better understanding of biological systems and for assisting in the development of new homogeneous catalysts for selective oxidation [1]. The investigation of the magnetic properties of binuclear nickel(II) complexes and correlating them with structures are important in the field of molecular magnetism. A common strategy is to prepare such complexes using a multidentate ligand along with judicial choice of a bridging ligand. The azide ligand in such complexes can act as either end-on [2–5] or end-to-end [6] bridges. The most important aspect of these bridged complexes is the variety of their magnetic exchange interactions. The end-on bridging mode of the azide ligand and the chloride ion exerts ferromagnetic exchange interactions [7–11].

As part of our continuing study on new N,S-donor polydentate ligands [12,13], and also considering the above and the fact that complexes containing N,S-donor sets are of biological relevance due to the discovery of the occurrence of similar donor environments in several bioactive molecules [14], we report here an account on the structural chemistry of two series of nickel(II) complexes having tetradentate pyridylthioazophenolate ligands (HL) (Fig. 1) along with chloride (**1**) and azide (**2**) as bridging ligands. The complexes **1** are hexacoordinated dimer complexes with a chloro-bridge, while the complexes **2** are dimers through end-on azide bridging. The single crystal X-ray structures of **1a** and **2a** are also discussed.

2. Experimental

2.1. Materials and physical measurements

All the reagents were obtained from commercial sources and were used without further purification. The pyridylthioazophenolate ligands were synthesized following the reported procedure [12].

IR spectra were obtained on a JASCO FT-IR model 420 using KBr disks and UV–Vis spectra on a JASCO UV–Vis/NIR model V-570. Microanalyses were performed with the use of a Perkin Elmer 2400 CHN elemental analyzer and nickel analyses were carried out by a gravimetric method [15]. Molar conductances (Λ_M) were measured in a systronics conductivity meter 306 model using $\sim 10^{-3}$ M solutions in MeOH. Magnetic moments (μ, BM) were obtained on a vibrating sample magnetometer PAR 155 model.

2.2. Synthesis of $[Ni(L)Cl]_2$

The preparation follows a common procedure. To a methanolic solution (15 mL) of HL1 (0.335 g, 1.0 mmol), nickel chloride hexahydrate solution (1.0 mmol) was added dropwise and the resulting solution was stirred for a period of 6 h. The solution was dried at

* Corresponding author. Tel.: +91 342 2558554x424; fax: +91 342 2530452.
E-mail address: pabitracc@yahoo.com (P. Chattopadhyay).

0277-5387/$ - see front matter © 2008 Elsevier Ltd. All rights reserved.
doi:10.1016/j.poly.2008.04.026

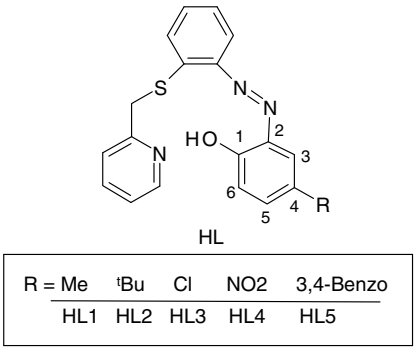

Fig. 1. The pyridylthioazophenols used as chelators.

ambient temperature. The product was collected by washing with cold MeOH–H_2O and dried. The pure crystallized product was obtained from methanol–dichloromethane. Yield 80–85%.

2.3. Synthesis of $[Ni(L)(N_3)]_2$

The preparation follows a common procedure. To a methanolic solution (15 mL) of HL1 (0.335 g, 1.0 mmol), nickel nitrate hexahydrate solution (1.0 mmol) was added dropwise and the resulting solution stirred for a period of 1 h. To this solution an aqueous solution of sodium azide (1.0 mmol) was added and stirring was continued for another 3 h. The volume of the solution was reduced at room temperature by slow evaporation. The product was collected by washing with cold MeOH–H_2O, and dried. The pure crystallized product was obtained from methanol. Yield 80–85%.

2.4. X-ray crystal structure analysis

Single crystals of **1a** suitable for X-ray work were grown by slow evaporation of a solution of complex **1a** in acetonitrile:benzene (1:1), while **2a** was grown by slow evaporation of a solution of complex **2a** in methanol:acetonitrile (2:1) at 298 K. Data of **1a** were measured with Mo Kα radiation using the MARresearch Image Plate System. Data analysis was carried out with the XDS program [16a] to provide 5133 independent reflections. The structure was solved using direct methods with the SHELX 86 program [16b]. The hydrogen atoms bonded to carbon were included in geometric positions and given thermal parameters equivalent to 1.2 times those of the atom to which they were attached. The structure was refined on F^2 using SHELXL [16c] to $R = 0.0951$, $wR_2 = 0.1945$ for 2736 reflections with $I > 2\sigma(I)$, having goodness of fit value of 1.033.

A suitable single crystal of complex **2a** was mounted on a Bruker SMART CCD diffractometer equipped with graphite monochromated Mo Kα ($\lambda = 0.71073$ Å) radiation. The intensity data were corrected for Lorentz and polarization effects. A total 14227 (unique data = 6911; $R_{int} = 0.036$) reflections were measured and 5482 reflections were observed applying the condition $I > 2\sigma(I)$. The structure was solved by Patterson syntheses and followed by successive Fourier and difference Fourier syntheses. Full matrix least squares refinements on F^2 were carried out using SHELXL-97 with anisotropic displacement parameters for all non-hydrogen atoms in all cases. The refinement converged to residual indices $R = 0.056$; $wR_2 = 0.1528$ with $I > 2\sigma(I)$. Complex neutral atom scattering factors [17a] were used throughout. All calculations were carried out using SHELXS 93 [17b], SHELXL 97 [17c], PLATON 99 [17d] and ORTEP3 [17e] programs.

Table 2
UV–Vis spectral data of nickel(II) complexes (**1**) and (**2**)

Compound	λ, nm (ε, dm^3 mol^{-1} cm^{-1})
1a	212 (57036), 236 (sh, 30605), 344 (23329), 530 (13513)
1b	211 (56086), 234 (sh, 30449), 343 (23260), 528 (13486)
1c	212 (56965), 235 (sh 30508), 342 (23289), 528 (13398)
1d	210 (56976), 232 (sh, 29896), 340 (22864), 525 (12213)
1e	214 (55905), 240 (sh, 32739), 334 (20543), 530 (14205)
2a	216 (45685), 242 (sh, 11132), 346 (8451), 530 (6324)
2b	214 (45785), 240 (sh, 11076), 342 (8265), 527 (6116)
2c	214 (45590), 239 (sh, 11097), 344 (8388), 530 (6224)
2d	212 (44986), 237 (sh, 10935), 341 (8378), 525 (6311)
2e	215 (45612), 240 (sh, 11101), 343 (8395), 531 (6289)

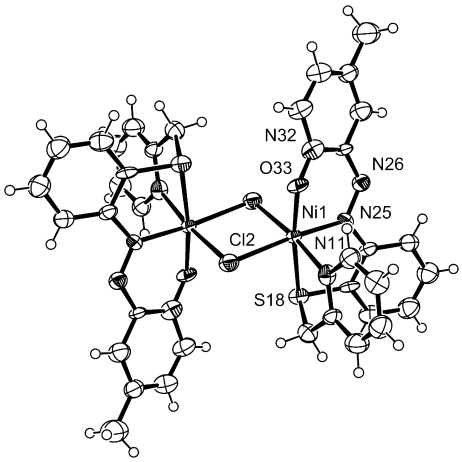

Fig. 2. An ORTEP view of the complex $[Ni_2(L1)_2Cl_2]$ with thermal ellipsoids at the 50% probability level and the atom numbering scheme.

Table 1
Microanalytical and magnetic moment (at 297 K) data of **1** and **2**

Compound	Found (calc.) %				Magnetic moment (μ) [per Ni(II) ion] BM
	C	H	N	Ni	
$[Ni(L1)Cl]_2$ (**1a**)	52.69 (53.24)	3.62 (3.73)	9.88 (9.80)	13.39 (13.70)	1.99
$[Ni(L2)Cl]_2$ (**1b**)	55.89 (56.14)	4.67 (4.54)	8.71 (8.93)	12.21 (12.48)	1.96
$[Ni(L3)Cl]_2$ (**1c**)	47.91 (48.14)	2.81 (2.89)	9.21 (9.36)	13.22 (13.08)	2.04
$[Ni(L4)Cl]_2$ (**1d**)	47.11 (47.03)	2.74 (2.83)	11.99 (12.19)	12.65 (12.78)	2.09
$[Ni(L5)Cl]_2$ (**1e**)	56.76 (56.87)	3.48 (3.44)	8.98 (9.07)	12.76 (12.64)	2.01
$[Ni(L1)(N_3)]_2$ (**2a**)	52.54 (52.45)	3.61 (3.68)	19.05 (19.32)	13.35 (13.50)	2.06
$[Ni(L2)(N_3)]_2$ (**2b**)	55.19 (55.38)	4.71 (4.61)	17.42 (17.62)	11.99 (12.12)	2.09
$[Ni(L3)(N_3)]_2$ (**2c**)	47.21 (47.45)	2.76 (2.85)	18.33 (18.45)	12.73 (12.89)	2.13
$[Ni(L4)(N_3)]_2$ (**2d**)	46.29 (46.38)	2.71 (2.79)	21.18 (21.04)	12.47 (12.60)	2.17
$[Ni(L5)(N_3)]_2$ (**2e**)	56.19 (56.08)	3.42 (3.39)	17.77 (17.84)	12.31 (12.47)	2.11

3. Results and discussion

3.1. Syntheses

The ligands, having NSNO donor centres, act as tetradentate monobasic chelators in complexation with nickel(II) in both series of complexes. Complexes (**1**) of these ligands were obtained by their reaction with equimolar amounts of nickel(II)chloride salts in methanol. Complexes (**2**) were isolated by adding aqueous sodium azide solution to the reddish coloured reaction mixture of nickel nitrate and the pyridylthioazophenolate at ambient temperature. All the complexes are soluble in common organic solvents except in ether and hexane. The conductivity measurements of the complexes **1** and **2** in methanol suggest that they exist as non-electrolytes. The magnetic moment studies at room temperature show that the complexes of both series (**1** and **2**) are paramagnetic in nature.

The IR spectra of all the complexes (**1** and **2**) show no characteristic IR bands around 3300 cm^{-1} for O–H of the H-bonded phenolic-OH of the ligand systems. This indicates coordination of the oxygen to the metal centre [12]. The $\nu_{N=N}$ mode of the free ligand (1495–1505 cm^{-1}) is shifted to lower wavenumbers ($\Delta \sim 20$–30 cm^{-1}) in the complexes, suggesting coordination of the metal ions to the azo function. The $\nu_{N=N}$ band is observed at 1465–1478 cm^{-1} for all the complexes. In addition to this, ν_{C-S} at 790 cm^{-1} for the ligands shifts to 760 cm^{-1} for the complexes **2**, and they also display a new strong stretching band at 2063 cm^{-1} which suggests the existence of end-on bridging modes in **2** [18].

The solution electronic spectra of the complexes in methanol were obtained at room temperature and the data are tabulated in Table 2. The bands lower than 400 nm are due to intramolecular $\pi \rightarrow \pi^*$ and $n \rightarrow \pi^*$ transitions for the aromatic ring. The absorption band at *ca.* 530 nm is assigned to the phenolate-O → Ni(II) charge transfer (LMCT) [19]. In octahedral nickel(II) complexes, three spin allowed transitions are expected from the energy level diagram for d^8 ions due to $^3A_{2g} \rightarrow {}^3T_{1g}$ (P), $^3A_{2g} \rightarrow {}^3T_{1g}$ (F), $^3A_{2g} \rightarrow {}^3T_{2g}$ transitions, which are observed at low to high wavelengths, respectively [20]. The transitions due to $^3A_{2g} \rightarrow {}^3T_{1g}$ (P) and $^3A_{2g} \rightarrow {}^3T_{1g}$ (F) are probably within the peaks at *ca.* 345 nm and *ca.* 530 nm, respectively. However, the intensity of the peak at around 854 nm observed in **1** due to the $^3A_{2g} \rightarrow {}^3T_{2g}$ transition is very low while in **2** a band in this region is not obtained.

3.2. Crystal structures of the Ni(II) complexes *1a* and *2a*

Perspective drawings of **1a** and **2a** with the atomic-numbering scheme are shown in Figs. 2 and 3, respectively. The crystallographic data and selected bond distances and angles are listed in Tables 3 and 4. Both crystals are of the triclinic system.

In **1a**, the two nickel(II) ions are bridged by two chloride ions in a μ-(1,1) fashion to form a Ni(II)–Ni(II) dinuclear entity in the solid state. Here each Ni(II) is octahedrally coordinated with two chloride, one pyridinic-N and one azo-N in a plane, along with thioether-S and phenolic-O in the axial positions. The molecule has a centre of symmetry and the bridging parallelogram is constructed

Table 3
Summarized crystallographic data for **1a** and **2a**

	1a	2a
Empirical formula	$C_{38}H_{32}Cl_2N_6Ni_2O_2S_2$	$C_{38}H_{32}N_{12}Ni_2O_2S_2 \cdot 0.5H_2O$
Formula weight	856.42	878.28
Crystal system	triclinic	triclinic
Space group	$P\bar{1}$	$P\bar{1}$
a (Å)	9.852(12)	11.647(2)
b (Å)	9.948(12)	12.441(2)
c (Å)	10.907(12)	15.278(3)
α (°)	103.389(10)	94.715(3)
β (°)	112.871(10)	94.194(3)
γ (°)	95.060(10)	116.023(3)
Volume (Å^3)	939.0(19)	1968.0(6)
$\rho_{calc.}$ (g/cm^3)	1.523	1.499
Z	1	2
Radiation_wavelength λ (Å)	0.71073	0.71073
$F(000)$	442	916
Temperature (K)	293(2)	293(2)
θ Range (°)	2.54 to 25.72	1.84 to 25.10
μ(Mo Kα) (mm^{-1})	1.301	1.117
Total reflections	3227	6911
Reflections above background	2735	5482
R_1	0.0951	0.0557
wR_2	0.1945	0.1528

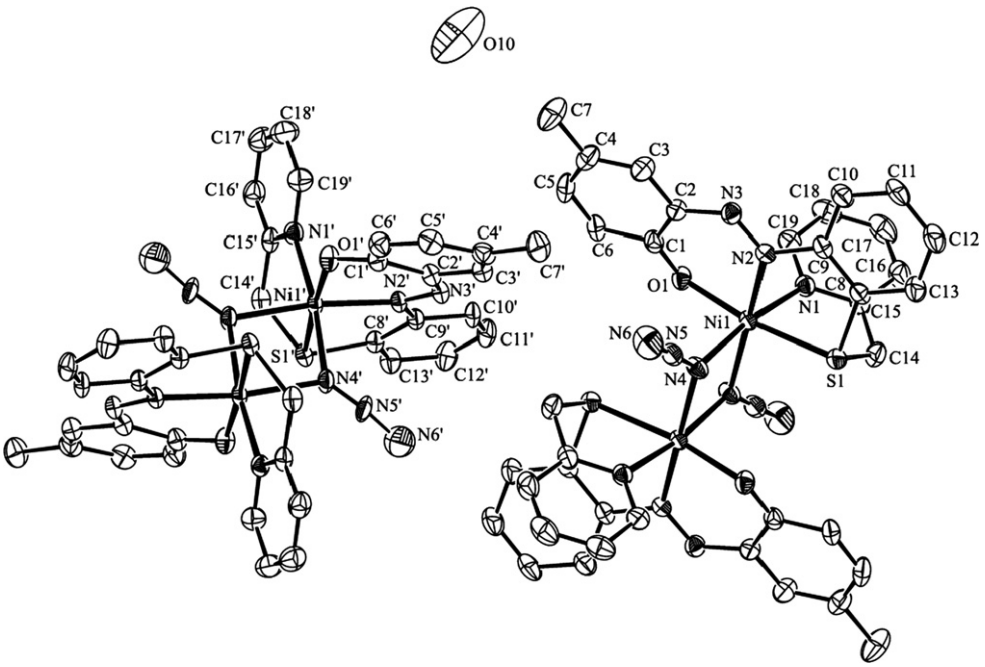

Fig. 3. An ORTEP diagram of the complex $[Ni_2(L1)_2(N_3)_2] \cdot H_2O$ (**2a**) with thermal ellipsoids at the 50% probability level (for clarity hydrogen atoms are excluded).

Table 4
Selected bond distances (Å) and bond angles (°) for **1a** and **2a**

1a			
Ni1–O33	1.946(5)	N11–Ni1–Cl2$1	172.3(2)
Ni1–N25	2.001(7)	O33–Ni1–S18	172.4(2)
Ni1–N11	2.039(7)	Cl2$1–Ni1–S18	91.6(1)
Ni1–Cl2$1	2.431(3)	N25–Ni1–S18	82.6(2)
Ni1–S18	2.431(3)	N11–Ni1–S18	81.6(2)
Ni1–Cl2	2.455(3)	O33–Ni1–Cl2	94.9(2)
O33–Ni1–N25	90.4(3)	N25–Ni1–Cl2	174.6(2)
O33–Ni1–N11	95.7(3)	N11–Ni1–Cl2	87.4(2)
N25–Ni1–N11	91.3(3)	Cl2–Ni1–Cl2$1	89.2(1)
O33–Ni1–Cl2$1	91.5(2)	S18–Ni1–Cl2	92.1(1)
N25–Ni1–Cl2$1	91.5(2)		
2a			
Molecule 1		Molecule 2	
Ni1–O1	1.971(3)	Ni1′–O1′	1.972(3)
Ni1–S1	2.405(1)	Ni1′–S1′	2.386(1)
Ni1–N1	2.115(4)	Ni1′–N1′	2.077(3)
Ni1–N2	2.026(3)	Ni1′–N2′	2.017(3)
Ni1–N4	2.096(3)	Ni1′–N4′	2.083(3)
Ni1–N4$2	2.115(4)	Ni1′–N4′$3	2.108(4)
O1–Ni1–N2	88.82(13)	O1′–Ni1′–N2′	90.22(13)
O1–Ni1–N4	92.69(14)	O1′–Ni1′–N4′	93.47(14)
N2–Ni1–N4	176.23(14)	N2′–Ni1′–N4′	172.43(14)
O1–Ni1–N1	93.06(14)	O1′–Ni1′–N1′	94.57(13)
N4–Ni1–N1	93.51(14)	N1′–Ni1′–N4′	91.76(14)
O1–Ni1–N4$2	92.42(14)	O1′–Ni1′–N4′$3	90.89(15)
N2–Ni1–N4$2	97.14(14)	N2′–Ni1′–N4′$3	91.28(13)
N4–Ni1–N4$2	79.36(15)	N4′–Ni1′–N4′$3	82.06(15)
N1–Ni1–N4$2	171.20(14)	N1′–Ni1′–N4′$3	172.27(14)
O1–Ni1–S1	171.62(9)	O1′–Ni1′–S1′	175.08(9)
N2–Ni1–S1	84.08(10)	N2′–Ni1′–S1′	85.66(10)
N4–Ni1–S1	94.67(11)	N4′–Ni1′–S1′	90.94(12)
N1–Ni1–S1	82.49(11)	N1′–Ni1′–S1′	83.54(11)
N4$2–Ni1–S1	92.89(11)	N4′$3–Ni1′–S1′	91.88(12)

Symmetry elements, $1: $1 - x, 2 - y, 1 - z$; $2: $-x, 1 - y, 1 - z$ and $3: $2 - x, -y, -z$.

by $Ni_2N_2Cl_2$ motifs with two unequal bond distances Ni1–Cl2 [2.430(3) Å] and Ni1–Cl2 [2.455(3) Å] and which are longer than that of normal Ni–Cl bond [2.270 Å] [9,10]. The bridging angles are Ni1–Cl–Ni1, 90.85(2)° and Cl2–Ni1–Cl2, 89.15(10)°, with a non-bonding Ni–Ni distance of 3.48 Å. The bridging angle Ni–Cl–Ni is shorter than other reported chloro-bridged Ni(II) complexes [9–11]. The bond Ni1–N25 (azo) [2.000(7) Å] is little bit shorter than Ni1–N11(pyridinic) [2.038(8) Å], though the two nitrogen donors are not the same.

There are two independent centrosymmetric dimers and one water molecule in the solid-state structure of **2a**. The two dimers have similar geometries. In every dimer unit, two nickel(II) ions are octahedrally coordinated with two azide-N, one pyridinic-N and one azo-N in a plane along with thioether-S and phenolic-O in the axial positions. The dimer has a centre of symmetry and the bridging parallelogram is constructed by $Ni_2N_2\{N(azido)\}_2$ motifs. The bridging angles are Ni(1)–N(4)–Ni(1)$2 100.6(1)° and N(4)–Ni(1)–N(4)$2 79.4(1)° in one molecule, with equivalent angles of 97.9(1) and 82.1(1)° in the second molecule, with Ni–Ni distances of 3.16 and 3.24 Å. The azide (N_3) bridges two nickel centres in a μ-(1,1) fashion, as predicted from the IR study. The two Ni(1)–N(4) (azide) bridging bond lengths are 2.096(3) and 2.115(4) Å in one molecule and 2.083(3) and 2.108(4) Å in the other, values which are similar to those found for Ni(1)–N(1) (pyridinic) [2.115(4), 2.077(3) Å] but longer than Ni(1)–N(2) (azo) [2.026(3), 2.017(3) Å].

3.3. Magnetic behaviour

Magnetic susceptibility data (Table 1) for **1** and **2** are in the range 1.96–2.09 BM and 2.06–2.17 BM per Ni(II) ion, respectively. These values are relatively low compared with other Ni(II) (d^8) complexes. This may be due to a ferromagnetic interaction which results from the closeness of the bridging angles to 90° (Ni1–Cl–Ni1, 90.85(2)° and Cl2–Ni1–Cl2, 89.15(10)°) and relies on quasi-orthogonal magnetic orbitals [10,11d,11e]. The bridging angle (Ni1–Cl–Ni1) is very close to 90° which is the prime factor and is a favourable condition for good ferromagnetic coupling due to the interaction between two d^8 ions in an octahedral environment having M–X–M bridging than the otherwise much weaker interactions for such halogen-bridged systems.

4. Supplementary data

CCDC 609504 and 609505 contain the supplementary crystallographic data for **1** and **2**. These data can be obtained free of charge via http://www.ccdc.cam.ac.uk/conts/retrieving.html, or from the Cambridge Crystallographic Data Centre, 12 Union Road, Cambridge CB2 1EZ, UK; fax: (+44) 1223-336-033; or e-mail: deposit@ccdc.cam.ac.uk.

Acknowledgements

Financial support from Council of Scientific and Industrial Research (CSIR), New Delhi, India is gratefully acknowledged. M.G.B. Drew thanks EPSRC and the University of Reading for funds for the Image Plate system.

References

[1] (a) M.J. Maroney, in: R.B. King (Ed.), Encyclopedia of Inorganic Chemistry, Wiley, Sussex, England, 1994, p. 2412;
(b) J.R. Lancaster Jr., The Biochemistry of Nickel, VCH, New York, 1988;
(c) J.A. Kovacs, in: L. Marzilli, G.L. Eichhorn (Eds.), Advance in Inorganic Biochemistry, vol. 9, Elsevier, New York, 1993. ch.5;
(d) R.M. Buonomo, I. Font, M.J. Maguire, J.H. Reibenspies, T. Tuntulani, M.Y. Darensbourg, J. Am. Chem. Soc. 117 (1995) 963.
[2] (a) M.G. Barandika, R. Cortes, L. Lezama, M.K. Urtiaga, M.I. Arriortua, T. Rojo, J. Chem. Soc., Dalton Trans. (1999) 2971;
(b) M.I. Arriortua, R. Cortes, L. Lezama, T. Rojo, X. Solans, M. Font-Bardia, Inorg. Chim. Acta 174 (1990) 263.
[3] (a) A. Escuer, R. Vicente, X. Solans, Inorg. Chem. 34 (1995) 1793;
(b) A. Escuer, R. Vicente, J. Ribas, J. Magn. Magn. Mater. 110 (1992) 181.
[4] (a) A. Escuer, R. Vicente, M.S. El Fallah, X. Solans, M. Font-Bardia, Inorg. Chim. Acta 247 (1996) 85;
(b) R. Cortes, J.I. Ruiz de Larramendi, L. Lezama, T. Rojo, K. Urtiaga, M.I. Arriortua, J. Chem. Soc., Dalton Trans. (1992) 2723.
[5] (a) J. Ribas, M. Monfort, C. Diaz, C. Bartos, X. Solans, Inorg. Chem. 33 (1994) 484;
(b) R. Vicente, A. Escuer, J. Ribas, M.S. El Fallah, X. Solans, M. Font-Bardia, Inorg. Chem. 32 (1993) 1920.
[6] (a) A. Escuer, R. Vicente, M.S. El Fallah, X. Solans, M. Font-Bardia, Inorg. Chim. Acta 278 (1998) 43;
(b) A. Escuer, I. Castro, F. Mautner, M.S. El Fallah, R. Vicente, X. Solans, Inorg. Chim. Acta 247 (1996) 85;
(c) J. Ribas, M. Monfort, B.K. Ghosh, R. Cortes, X. Solans, M. Font-Bardia, Inorg. Chem. 35 (1996) 864;
(d) J. Ribas, M. Monfort, C. Diaz, C. Bartos, X. Solans, Inorg. Chem. 32 (1993) 3557;
(e) C.G. Pierpont, D.N. Hedrickson, D.M. Duggana, F. Wagner, E.K. Barefield, Inorg. Chem. 14 (1975) 604;
(f) P. Chaudhuri, M. Guttman, D. Ventur, K. Weighardt, B. Nuber, J. Weiss, J. Chem. Soc., Chem. Commun. 1 (1985) 1618.
[7] J. Ribas, A. Escuer, M. Monfot, R. Vicente, R. Cortes, L. Lezama, T. Rojo, Coord. Chem. Rev. 193 (1999) 102.
[8] (a) F.F. de Biani, E. Ruiz, J. Cano, J.J. Novoa, S. Alvarej, Inorg. Chem. 39 (2000) 3221;
(b) E. Ruiz, J. Cano, S. Alvarej, P. Alemany, J. Am. Chem. Soc. 120 (1998) 11122;
(c) M.A. Aebersold, B. Gillon, O. Plantevin, L. Pardi, O. Kahn, P. Bergerat, I. Von. Seggern, F. Tuezek, L. Ohrstrom, A. Grand, E. Lelievri-Berna, J. Am. Chem. Soc. 120 (1998) 5238;
(d) L.K. Thompson, S.S. Tandon, M.E. Manuel, Inorg. Chem. 34 (1995) 2356;
(e) M.F. Charjot, O. Kahm, M. Chaillet, C. Larrieu, J. Am. Chem. Soc. 108 (1986) 2574.
[9] Q.X. Li, Q.H. Luo, Y.Z. Li, C.Y. Duan, O.Y. Tu, Inorg. Chim. Acta 358 (2005) 504.
[10] (a) P.W. Anderson, Phys. Rev. 115 (1959) 2;
(b) G.T. Rado, H. Suhl (Eds.), Magnetism, vol. 1, Academic Press, New York, 1963 (Chapter 2);
(c) J.B. Goodenough, Phys. Rev. 100 (1955) 564;
(d) J.B. Goodenough, J. Phys. Chem. Solids 6 (1958) 287;
(e) J. Kanamori, J. Phys. Chem. Solids 10 (1959) 87.

[11] (a) Z.H. Zhang, X.H. Bu, Z.A. Zhu, Z.H. Jiang, Y.T. Chen, Trans. Met. Chem. 21 (1996) 235;
(b) C.P. Landee, R.D. Willett, Inorg. Chem. 20 (1981) 2521;
(c) K.O. Joung, C.J. O'Connor, E. Sinn, R.L. Carlin, Inorg. Chem. 18 (1979) 804;
(d) Y. Journaux, O. Kahn, J. Chem. Soc., Dalton Trans. (1979) 1575;
(e) A.P. Ginsberg, R.L. Martin, R.W. Brookes, R.C. Sherwood, Inorg. Chem. 11 (1972) 2884.
[12] (a) P.K. Dhara S. Pramanik, T.H. Lu, M.G.B. Drew, P. Chattopadhyay, Polyhedron 23 (2004) 2457;
(b) P.K. Dhara, S. Pramanik, T.H. Lu, P. Chattopadhyay, J. Coord. Chem. 58 (2005) 985;
(c) P.K. Dhara, M.G.B. Drew, P. Chattopadhyay, Polyhedron 25 (2006) 1945;
(d) P.K. Dhara, M.G.B. Drew, P. Chattopadhyay, Trans. Met. Chem. 31 (2006) 740;
(e) P.K. Dhara, M.G.B. Drew, P. Chattopadhyay, J. Coord. Chem 60 (2007) 627.
[13] P.K. Dhara, B. Das, J.M. Lo, P. Chattopadhyay, Appl. Radiat. Isot. 62 (2005) 729.
[14] (a) R.L. Richard, Coord. Chem. Rev. 154 (1996) 83;
(b) R.P. Happe, W. Roseboom, A.J. Pierik, S.P. Albracht, K.A. Bagley, Nature 385 (1997) 126;
(c) A. Volveda, E. Gracin, C. Piras, A.L. Delacey, V.M. Fernandez, E.C. Hatchikian, M. Frey, J.C. Fontecilla-Camps, J. Am. Chem. Soc. 118 (1996) 12989;
(d) A. Volveda, M.H. Charon, C. Piras, E.C. Hatchikian, M. Frey, J.C. Fontecilla-Camps, Nature 373 (1995) 580;
(e) R. Cammack, Nature 373 (1995) 556.
[15] A.I. Vogel, A Text Book of Quantitative Inorganic Analysis, ELBS & Longmans, London, 1962.
[16] (a) W. Kabsch, J. Appl. Crystallogr. 21 (1988) 916;
(b) G.M. Sheldrick, Acta Crystallogr., Sect. A 46 (1990) 467;
(c) G.M. Sheldrick, SHELXL, Program for Crystal Structure Refinement, University of Gottingen, 1993.
[17] (a) A.J.C. Wilson, International Tables for X-ray Crystallography, vol. C, Kluwer, Dordrecht, 1992 (Tables 4.2.6.8 and 6.1.1.4.).;
(b) G.M. Sheldrick, SHELXS 97, Program for the Solution of Crystal Structure, University of Gottingen, 1997.;
(c) G.M. Sheldrick, SHELXL 97, Program for the Solution of Crystal Structure, University of Gottingen, Germany, 1997.;
(d) A.L. Spek, PLATON, Molecular Geometry Program, University of Utrecht, The Netherlands, 1999.;
(e) L.J. Farrugia, J. Appl. Crystallogr. 30 (1997) 565.
[18] K. Nakamoto, Infrared Spectra of Inorganic and Coordination compounds, Wiley, New York, 1997.
[19] (a) E. Berti, A. Caneschi, C. Daiguebonne, P. Dapporto, M. Formica, V. Fusi, L. Giorgi, A. Guerri, M. Micheloni, P. Paoli, R. Pontellini, P. Rossi, Inorg. Chem. 42 (2003) 348;
(b) Y. Shimazaki, S. Huth, S. Hirota, O. Yamauchi, Bull. Chem. Soc. Jpn. 73 (2000) 1187.
[20] F.A. Cotton, G. Wilkinson, C.A. Murillo, M. Bochmann, Advanced Inorganic Chemistry, 6th ed., John Wiley and Sons, New York, 1999.

Polyhedron 27 (2008) 2452–2458

Contents lists available at ScienceDirect

Polyhedron

journal homepage: www.elsevier.com/locate/poly

Cadmium–halide and mixed cadmium–halide–dicyanamide polymers mediated by ancillary 2-aminoalkyl-pyridine ligands: Synthesis, X-ray single crystal structures and luminescence property

Tanmay Chattopadhyay [a], Arpita Banerjee [a], Kazi Sabnam Banu [a], Eringathodi Suresh [b,*], Munirathinam Netahji [c], Giovanni Birarda [d], Ennio Zangrando [d,*], Debasis Das [a,*]

[a] Department of Chemistry, University of Calcutta, 92, A.P.C. Road, Kolkata 700 009, India
[b] Analytical Science Discipline, Central Salt and Marine Chemicals Research Institute, G.B. Marg, Bhavnagar 364 002, India
[c] Department of Inorganic and Physical Chemistry, Indian Institute of Science, Bangalore 560 012, India
[d] Dipartimento di Scienze Chimiche, University of Trieste, Via L. Giorgieri 1, 34127 Trieste, Italy

ARTICLE INFO

Article history:
Received 7 April 2008
Accepted 25 April 2008
Available online 14 June 2008

Keywords:
Mixed halide–dicyanamide polymers
Crystal structures
Luminescence property

ABSTRACT

A series of mixed halide–dicyanamide and halide complexes of cadmium(II) mediated by 2-aminoalkyl-pyridine ligands [2-aminomethylpyridine (ampy) and 2-aminoethylpyridine (aepy)] have been synthesized. Five of them, $[CdCl(dca)(aepy)]_n$ (**1**), $[CdBr(dca)(ampy)]_n$ (**2**), $[CdCl(dca)(ampy)]_n$ (**3**) (dca = dicyanamide); $[CdI_2(aepy)]_n$ (**4**), and $[CdI_2(ampy)]_n$ (**5**), (dca = dicyanamide) have been characterized by X-ray single crystal structure analysis. The structural determination shows that the compounds are 1D coordination polymers, with the exception of **3** that gives origin to a 2D sheet-like network. The ampy and aepy ligands (also with the occurrence of dca anions in **1**–**3**) reveal to be useful ancillary fragments for the construction of unprecedented Cd–halide polymeric species. The crystal packing shows that the dimensionality of all compounds is enlarged to 2D, and 3D in the case of complex **3**, through π–π interactions occurring between the pyridine rings. All the species exhibit interesting luminescence property in solution as well in solid state which is originated from ligand-centered π–π^* transitions. The fluorescence band maxima and fluorescence efficiency (in methanol) are found to be dependent not only on the pyridine ligand but also on the type of halide, and the co-ligand. Solid state luminescent study implies that π–π interactions occurring between pyridine rings are also important in controlling the fluorescence intensity. Amongst the synthesized complexes reported, complex **5** exhibits the highest fluorescence efficiency in methanol.

© 2008 Elsevier Ltd. All rights reserved.

1. Introduction

Cadmium(II) based metal–organic coordination networks (MOCNs) that extend "infinitely" into one, two or three dimensions (1D, 2D and 3D, respectively), *via* more or less covalent metal–ligand bonding, have been the subject of great interest in recent years owing to their potential application in catalysis, optical properties evolution, clathration, *etc.* [1–5]. The special behavior of cadmium(II) lies on its d^{10} configuration and softness which permit a wide variety of geometries and coordination numbers. Coordination polymers of cadmium(II) have been exploited by using organic ligands as well as coordinating anions (*e.g.*, Cl^-, Br^-, I^-, SCN^-, N^{3-}, $SeCN^-$, $N(CN)_2^-$) [6–20], which are an integral part of the resulting polyhedra. The ligands, as well as the anions, are observed to control the structural diversity and stereochemistry of the cadmium(II) centre and consequently the physical and chemical properties of the species. In presence of pyridine-type ligands coordination polymers of cadmium(II) are observed to exhibit interesting luminescence property and many of such species have been investigated in order to explore the possibility of their application in sensor technology and electroluminescent devices [21–37]. Pyridine and its derivatives are generally non luminescent but their coordination polymers, especially with Cd(II), may exhibit luminescence properties. Moreover, these species possess the ability of affecting the emission wavelength of organic materials upon metal coordination. To the best of our knowledge no investigation has been carried out to rationalize the role of halides and dicyanamide on the structure and luminescence properties of Cd(II)(2-aminoalkyl-pyridine) systems. Thus we report herein the synthesis and characterization of a series of mixed halide–dicyanamide and of halide complexes of cadmium(II) mediated by 2-aminoalkyl-pyridine ligands [2-amino-

* Corresponding authors. Tel.: +91 33 24837031 (D. Das).
E-mail address: dasdebasis2001@yahoo.com (D. Das).

0277-5387/$ - see front matter © 2008 Elsevier Ltd. All rights reserved.
doi:10.1016/j.poly.2008.04.047

methylpyridine (ampy) and 2-aminoethylpyridine (aepy)], with the aim to investigate systematically the role of the halide, dicyanamide and organic ligands having different chelating ring. The latter molecules intervene on the structural motif topology of the coordination polymers, as well as on the luminescence property that was investigated in solution as well as in the solid state.

2. Experimental

2.1. Materials

High purity (2-aminomethyl)pyridine (ampy) and 2-(aminoethyl)pyridine (aepy) were purchased from Fluka and Lancaster Chemical Company Inc., respectively. Cadmium(II) chloride, cadmium(II) bromide tetrahydrate and cadmium(II) iodide were purchased from Aldrich Chemical Company Inc. and used as received. Sodium dicyanamide was purchased from Fluka. All other chemicals were of AR grade.

2.2. Physical measurements

Elemental analyses (carbon, hydrogen and nitrogen) were performed using a Perkin–Elmer 240C elemental analyzer and cadmium (II) content was estimated gravimetrically. Infrared spectra were recorded on KBr disks (400–4000 cm^{-1}) with a Perkin–Elmer RXI FTIR spectrophotometer. UV–Vis spectra were measured on a Hitachi U-3501 spectrophotometer. Fluorescence spectra of the complexes were recorded in solid powder state with a Perkin–Elmer model LS 55 Luminescence spectrometer. The fluorescence spectra of ligands and the complexes are also recorded in solution using methanol as a solvent.

2.3. Synthesis of the complexes

2.3.1. $[CdCl(dca)(aepy)]_n$ (**1**)

A methanolic solution (5 mL) of aepy (0.122 g, 1 mmol) was slowly poured drop wise into a hot methanolic solution (10 mL) of cadmium(II) chloride (0.183 g, 1 mmol). Sodium dicyanamide (0.178 g, 2 mmol) dissolve in water (1 mL) added dropwise to it. The resultant mixture was stirred for 2 h and filtered. The filtrate was kept in $CaCl_2$ containing desiccator. The colorless single crystals suitable for X-ray analysis were obtained from the filtrate after few weeks. Yield 75%. *Anal. Calc. for $C_9H_{10}CdClN_5$: C, 32.13; H, 2.97; N, 20.83. Found: C, 32.12; H, 2.96; N, 20.82%. IR data:* ν = 3281 (s), 3171 (m), 2938 (m), 2884 (w), 2270 (m), 2209 (w), 2151 (s), 1606 (s), 1483 (w), 1442 (s) cm^{-1}.

2.3.2. $[CdBr(dca)(ampy)]_n$ (**2**)

It was synthesized by adopting the same procedure as in case of **1** using cadmium(II) bromide tetrahydrate and ampy (0.108 g, 1 mmol) replacing aepy. The yellow-colored single crystals suitable for X-ray analysis were obtained from the filtrate after few weeks. Yield 76%. *Anal. Calc. for $C_8H_8CdBrN_5$: C, 26.19; H, 2.18; N, 19.09. Found: C, 26.15; H, 2.16; N, 19.08%. IR data:* ν = 3337 (w), 3274 (m), 2925 (w), 2288 (m), 2231 (w), 2158 (s), 1598 (s), 1482 (w), 1436 (s) cm^{-1}.

2.3.3. $[CdCl(dca)(ampy)]_n$ (**3**)

It was synthesized following the same procedure as in case of **1** using ampy ligand (0.108 g, 1 mmol) instead of aepy. The colorless single crystals suitable for X-ray analysis were obtained from the filtrate after few weeks. Yield 78%. *Anal. Calc. for $C_8H_8CdClN_5$: C, 29.80; H, 2.48; N, 21.73. Found: C, 29.81; H, 2.46; N, 21.74%. IR data:* ν = 3358 (m), 3300 (w), 2932 (w), 2277 (m), 2233 (w), 2160 (s), 1598 (s), 1482 (w), 1433 (m) cm^{-1}.

2.3.4. $[CdI_2(aepy)]_n$ (**4**)

It was synthesised following the same procedure as in case of **1** using cadmium(II) iodide (0.366 g, 1 mmol) instead of cadmium(II) chloride. However dca was not incorporated in the crystal structure. The yellowed-colored single crystals suitable for X-ray analysis were obtained from the filtrate after few days. Yield 97%. *Anal. Calc. for $C_7H_{10}CdI_2N_2$; C, 17.20; H, 2.05; N, 5.73. Found: C, 17.19; H, 2.04; N, 5.73%. IR data:* ν = 3298 (s), 3234 (m), 2923 (m), 2877 (m), 1598 (s), 1566 (s), 1480 (s), 1436 (s) cm^{-1}.

2.3.5. $[CdI_2(ampy)]_n$ (**5**)

It was synthesised following the same procedure as in case of **4** using ampy (0.108 g, 1 mmol) instead of aepy. Here also dca was not incorporated in the crystal. The yellowed-colored single crystals suitable for X-ray analysis were obtained from the filtrate after few days. Yield 95%. *Anal. Calc. for $C_6H_8CdI_2N_2$: C, 15.17; H, 1.68; N, 5.90. Found: C, 15.16; H, 1.67; N, 5.91%. IR data:* ν = 3295 (s), 3242 (m), 2922 (m), 2870 (w), 1600 (s), 1566 (s), 1479 (s), 1434 (s) cm^{-1}.

2.3.6. $[CdBr(dca)(aepy)]_n$ (**6**)

It was synthesised by adopting the same procedure as in case of **1** using cadmium(II) bromide tetrahydrate (0.344 g, 1 mmol), instead of cadmium(II) chloride. The yellow-colored crystalline solid were obtained from the filtrate after few weeks. Yield 86%. *Anal. Calc. for $C_9H_{10}CdBrN_5$: C, 28.39; H, 2.63; N, 18.40. Found: C, 28.37; H, 2.61; N, 18.38%. IR data:* ν = 3335 (w), 3275 (w), 2943 (w), 2885 (w), 2291 (m), 2234 (w), 2159 (s), 1601 (s), 1482 (w), 1443 (s) cm^{-1}.

2.3.7. $[CdCl_2(ampy)]_n$ (**7**)

A methanolic solution (5 mL) of ampy (0.122 g, 1 mmol) was poured slowly dropwise into a hot methanolic solution (10 mL) of cadmium(II) chloride(0.183 g, 1 mmol). The resultant mixture was stirred for 2 h and filtered. The filtrate was kept in $CaCl_2$ containing desiccator. The colorless solid was obtained from the filtrate after few days. Yield 75%. *Anal. Calc. for $C_6H_8CdCl_2N_2$: C, 24.70; H, 2.74; N, 9.60. Found: C, 24.68; H, 2.73; N, 9.59%. IR data:* ν = 3305 (s), 3265 (m), 2925 (m), 2874 (w), 1685 (s), 1600 (s), 1472 (s), 1431 (s) cm^{-1}.

2.3.8. $[CdBr_2(ampy)]_n$ (**8**)

This was synthesised by adopting the same procedure as in case of **7** using cadmium(II) bromide tetrahydrate (0.344 g, 1 mmol), instead of cadmium(II) chloride. The light yellow solid was obtained from the filtrate after few days. Yield 78%. *Anal. Calc. for $C_6H_8CdBr_2N_2$: C, 18.93; H, 2.10; N, 7.36. Found: C, 18.96; H, 2.13; N, 7.38%. IR data:* ν = 3298 (s), 3256 (m), 2921 (m), 2870 (w), 1667 (s), 1596 (s), 1476 (m), 1435 (s) cm^{-1}.

2.4. X-ray data collection and structure determination

Diffraction data for the structures **1**–**5** were carried out on Bruker Smart Apex CCD diffractometer with Mo Kα radiation (λ = 0.71073 Å) by using ω–ϕ scan method. Cell refinement, indexing and scaling of the data sets were carried out using Bruker SMART and Bruker SAINT programs [38]. All the structures were solved by direct methods and Fourier analyses [39] and refined by the full-matrix least-squares method based on F^2 with all observed reflections [39]. All the calculations were performed using the WinGX System, Ver 1.64.05 [40]. Crystallographic data are given in Table 1.

3. Results and discussion

In order to synthesize the desired mixed halide–dicyanamide Cd(II) compounds containing 2-aminomethylpyridine (ampy) or

Table 1
Crystallographic data and details of structure refinements for complexes **1–5**

	1	2	3	4	5
Empirical formula	$C_9H_{10}CdClN_5$	$C_8H_8BrCdN_5$	$C_8H_8CdClN_5$	$C_7H_{10}CdI_2N_2$	$C_6H_8CdI_2N_2$
Formula weight	336.07	366.50	322.05	488.37	474.34
Crystal system	orthorhombic	triclinic	monoclinic	monoclinic	monoclinic
Space group	*Pbca*	$P\bar{1}$	$C2/c$	$P2_1/c$	$P2_1/n$
a (Å)	7.404(2)	7.522(2)	14.755(5)	14.854(3)	8.035(3)
b (Å)	15.985(3)	7.673(2)	12.565(4)	10.015(3)	6.683(3)
c (Å)	20.202(4)	10.612(3)	14.245(5)	7.720(2)	19.877(8)
α (°)		71.98(2)			
β (°)		82.08(2)	119.630(5)	92.73(2)	100.536(7)
γ (°)		83.14(2)			
Volume (Å^3)	2391.0(9)	575.0(3)	2295.6(13)	1147.1(5)	1049.4(8)
Z	8	2	8	4	4
D_{calc} (g cm^{-3})	1.867	2.117	1.864	2.828	3.002
μ Mo Kα, (mm^{-1})	2.030	5.348	2.109	7.241	7.911
$F(000)$	1312	348	1248	880	848
θ_{max} (°)	28.27	28.19	28.09	28.30	25.00
Reflections collected	13080	4867	6469	6395	4495
Unique reflections	2856	2582	2605	2615	1829
R_{int}	0.0349	0.0231	0.0327	0.0254	0.0533
Observed $I > 2\sigma(I)$	2490	2174	2383	2364	1709
Parameters	145	136	137	109	101
Goodness of fit (F^2)	1.069	1.047	1.081	1.109	1.123
R_1 ($I > 2\sigma(I)$)[a]	0.0281	0.0335	0.0365	0.0302	0.0683
wR_2[a]	0.0715	0.0896	0.1012	0.0738	0.1848
$\Delta\rho$ (e/Å^3)[b]	0.675, −0.710	0.995, −0.473	1.000, −1.241	1.045, −1.478	2.874, −4.116

[a] $R_1 = \sum||F_o| - |F_c||/\sum|F_o|$, $wR_2 = [\sum w(F^2_o - F^2_c)^2/\sum w(F^2_o)^2]^{1/2}$.
[b] The high residuals for **5** (close to iodine atoms) is due to the low crystal quality.

2-aminoethylpyridine (aepy) ligands, the Cd(II)X_2, Na(dca) and 2-aminoalkyl-pyridine ratio was maintained 1:2:1 in all cases. On the other hand, for cadmium–halide-2-aminoalkyl-pyridine compounds, the Cd(II)X_2 and 2-aminoalkyl-pyridine ligand ratio was kept just 1:1. The solvent used in all cases was methanol. Any attempt to synthesize the $[Cd(aepy)X_2]_n$ (X = Cl and Br) and $[CdI_2(ampy/aepy)(dca)]_n$ complexes failed. Since Cd(II) is a soft centre, having an inherent tendency to bind with soft anion like I^- more preferably than with hard nitrogen donor site of dca, this may represent the reason of our failure in synthesizing the $[CdI_2(ampy/aepy)(dca)]_n$ species. However, we are not convinced why $[Cd(aepy)X_2]_n$ (X = Cl and Br) did not form under the indicated reaction conditions and our efforts to synthesize these species are still underway.

3.1. Crystal structure description of complexes *1* and *2*

The crystallographic investigation of compounds **1** and **2** reveals topologically similar 1D polymers with a stair like fashion, built up by -Cd(aepy)-dca- (**1**) and -Cd(ampy)-dca- (**2**) chains, having collinear metal ions, connected by pairs of bridging halides that model the rungs (Figs. 1 and 2). The metal exhibits a distorted octahedral coordination geometry (Table 2), being chelated by the aminopyridine ligand, and in *cis* position the nitrogen donors from two different dca and two halides. The distortions of bond angles from the ideal geometry are greater in the case of **2** for the strained conformation held on chelation by the ampy ligand (chelating N(1)–Cd–N(2) angles of 85.76(8) and 72.29(12)°, respectively in **1** and **2**). All the coordination Cd–N bond distances, as well as the Cd–Cl ones, in **1** are close comparable. The correspondent figures in **2** manifest peculiar differences, the Cd–N(dca) bond lengths being slightly different, 2.317(3) and 2.356(4) Å, and the two Cd–Br bonds diverge by about 0.22 Å (2.9194(9) versus 2.696(1) Å). The metal–metal separation spanned by the *dca* anion in **1** and **2** is 7.404(2) and 7.522(2) Å, respectively, correspondent to the length of the crystallographic *a*-axis, that through the halide anions is 3.889(1) and 4.074(1) Å, respectively, in accord with the larger ionic radius for the bromide. The ampy and aepy ligands protrude

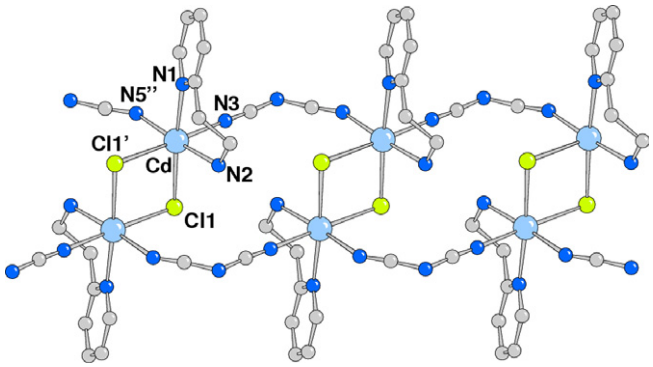

Fig. 1. Perspective view of the 1D chain of **1** developed along axis *a*.

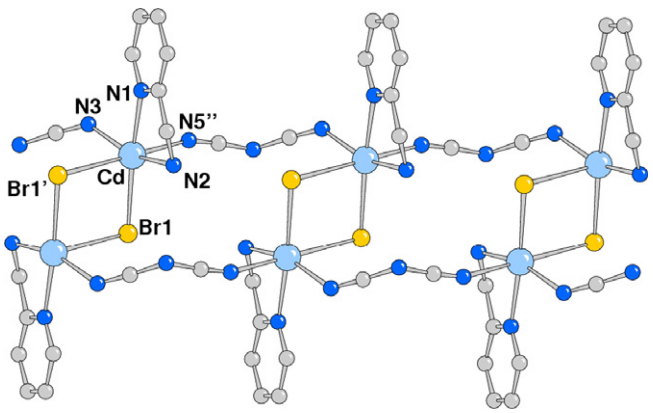

Fig. 2. Polymeric chain of **2** developed along axis *a*.

Table 2
Selected bond lengths (Å) and bond angles (°) of $[CdCl(dca)(aepy)]_n$ (**1**), $[CdBr(dca)(ampy)]_n$ (**2**), and $[CdCl(dca)(ampy)]_n$ (**3**)

	1, X = Cl	**2**, X = Br	**3**, X = Cl
Cd–N(1)	2.339(2)	2.332(3)	2.321(3)
Cd–N(2)	2.335(2)	2.341(4)	2.340(4)
Cd–N(3)	2.339(2)	2.317(3)	2.403(4)
Cd–N(5″)	2.332(2)	2.356(4)	2.272(4)
Cd–X(1)	2.6332(7)	2.696(1)	2.559(1)
Cd–X(1′)	2.6926(8)	2.9194(9)	2.740(1)
N(1)–Cd–N(2)	85.76(8)	72.29(12)	73.16(12)
N(1)–Cd–N(3)	87.36(8)	88.89(13)	82.17(13)
N(1)–Cd–N(5″)	91.87(8)	89.02(12)	161.85(14)
N(1)–Cd–X(1)	174.50(5)	173.81(8)	96.53(9)
N(1)–Cd–X(1′)	95.25(5)	93.81(8)	97.08(8)
N(2)–Cd–N(3)	91.31(10)	160.78(13)	89.05(14)
N(2)–Cd–N(5″)	176.60(10)	94.57(14)	90.58(14)
N(2)–Cd–X(1)	88.84(7)	101.59(9)	168.32(8)
N(2)–Cd–X(1′)	94.42(8)	90.26(10)	89.60(10)
N(3)–Cd–N(5″)	86.14(8)	88.80(14)	89.71(15)
N(3)–Cd–X(1)	91.73(6)	97.28(10)	95.06(11)
N(3)–Cd–X(1′)	173.86(6)	87.09(9)	178.60(10)
N(5″)–Cd–X(1)	93.48(7)	90.58(10)	100.35(12)
N(5″)–Cd–X(1′)	88.22(6)	174.97(10)	90.67(12)
X(1)–Cd–X(1′)	86.19(2)	87.06(3)	86.20(4)
Cd–X(1)–Cd′	93.81(2)	92.94(3)	93.80(4)
C–N(3)–Cd	175.2(2)	129.2(3)	145.4(4)
C–N(5″)–Cd	136.4(2)	160.0(4)	156.2(4)

Symmetry codes: (′) $-x+1, -y, -z+1$, (″) $x-1, y, z$ (**1**); (′) $x-1, y, z$, (″) $-x+1, -y+1, -z$ (**2**); (′) $-x, -y+1, -z$, (″) $x-1/2, -y+1/2, z-1/2$ (**5**).

from the chains and the packing evidences adjacent polymers linked by π–π interactions with a zip arrangement to give origin to 2D layered structure. The centroid-to-centroid distance is 3.834 Å (**1**) and 3.769 and 4.002 Å (**2**).

3.2. Crystal structure description of complex *3*

The substitution of bromide in **2** with chloride led to a complex having the same stoichiometry $[CdCl(dca)(ampy)]_n$ (**3**), but a different dimensionality. The cadmium ion shows a distorted octahedral coordination sphere (ORTEP drawing, Fig. 3) with significantly different Cd–Cl and Cd–N(dca) distances, being 2.559(1), 2.740(1) Å, and 2.272(4), 2.403(4) Å, respectively. Moreover, the Cd coordination sphere has a different configuration with respect to that observed in the bromide derivative **2**, being the ampy amine nitrogen N(2) located *trans* to a chloride, the pyridine N(1) *trans* to a dca nitrile group (Fig. 3). It is worth of note the almost comparable coordination C≡N–Cd bond angles, of 145.4(4)° and 156.2(4)° (Δ = 11°), with respect to the two values measured in the 1D polymers of **1** and **2**, that differ by 30–40° (Table 1). The polymer results a tessellated 2D undulated layered arrangement of 4,4-net topology with centro-symmetric $Cd(Cl)_2Cd$ units, defining the nodes (separated by 9.627 Å), bridged by the dca anions (Fig. 4). The pyridine rings, which protrude from the layers (Fig. 4b), interact through π–π interactions (the centroid-to-centroid distance is 3.622 Å) giving origin to a 3D arrangement.

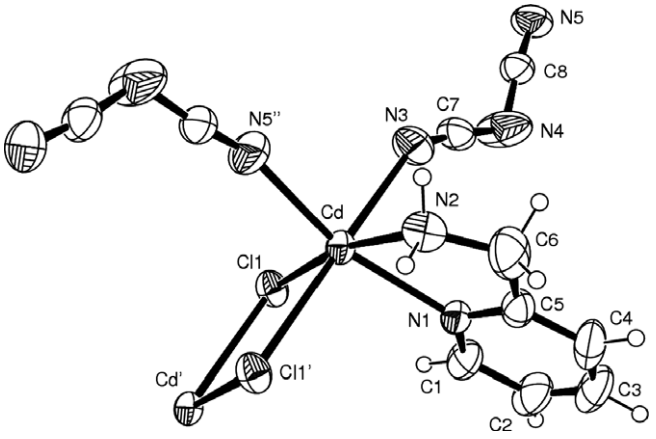

Fig. 3. Coordination sphere of Cd ion in compound **3** (ORTEP drawing, 40% probability ellipsoids).

3.3. Crystal structure description of complexes *4* and *5*

The labeled diagram of the polymeric compounds **4** and **5** are shown in Figs. 5 and 6, respectively, and a selection of bond lengths and angles is reported in Table 3. The structure of **4** consists of neutral zigzag chains, formed of Cd(aepy) units linked by double iodide bridges, which extend along the *a*-direction. The *cis*-octahedral sphere of Cd(II) shows significant distortions from the ideal values. The Cd–N distances are 2.355(4) and 2.261(4) Å, being longer that of the pyridine nitrogen donor, while the Cd–I ones fall in a range from 2.7891(7) to 3.2288(8) Å. The metal–metal distance along the chain is 4.342(1) Å and the Cd–Cd-Cd sequence form an angle of 125.48°. The Cd–I–Cd bridging angles are 87.309(12)° and 93.459(14)°. The following topology is well documented among structurally Cd–halide polymers, similar for example to the derivatives obtaining substituting aepy ligands with ethylene-1,2-diol [14] or by glycine [18,19]. The chains are associated into layers through π–π interactions occurring between py rings with a centroid-to-centroid distance of 4.195 Å. The polymeric chain of complex **5** comprises of Cd square pyramidal units being the metal chelated by the ampy ligand and by two iodide I(1) and I(2), the latter being at the apical position of the preceding metal coordination sphere. The Cd–N distances are 2.361(9) and 2.341(12) Å, the former referring to the pyridine donor, while the Cd–I(1) and the Cd–I(2) ones are 2.8234(15) and 2.9108(15) Å, being the shorter

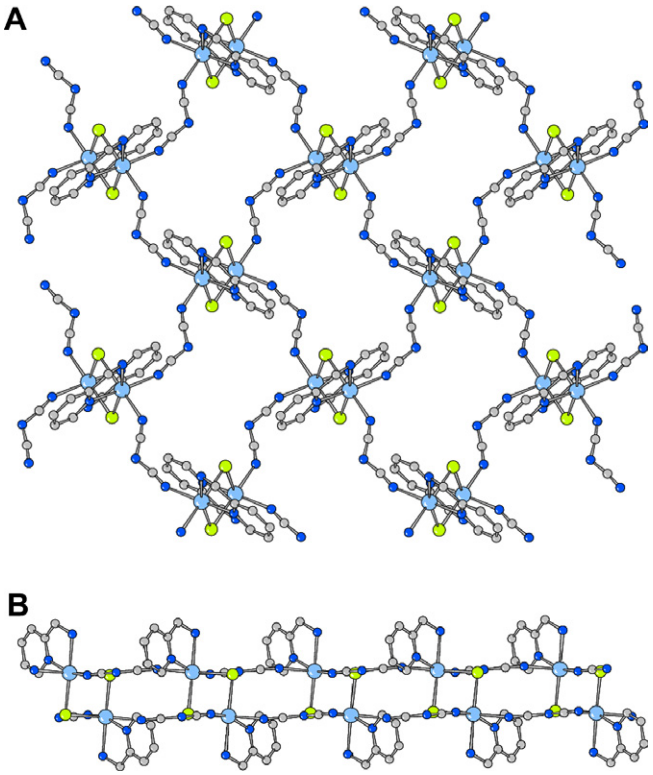

Fig. 4. 2D polymeric network of **3** view down *a*- and *b*-axis respectively.

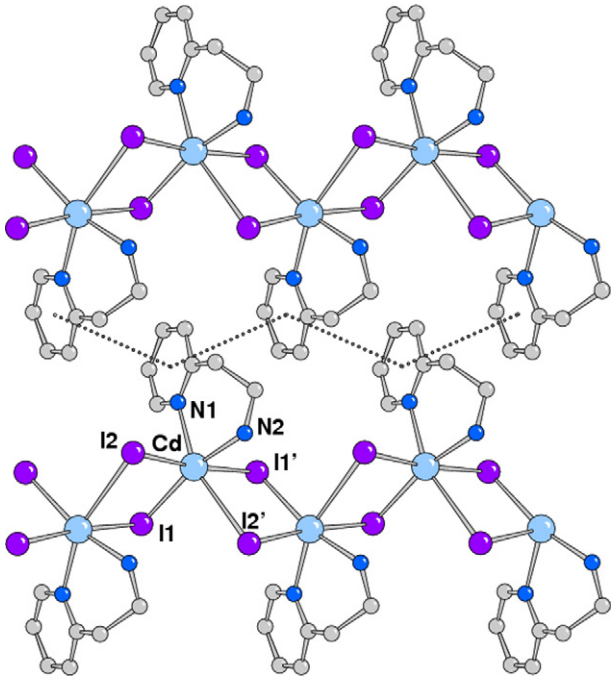

Fig. 5. Polymeric coordination chain of **4** developed along axis *c* zipped by π–π interactions occurring between py rings.

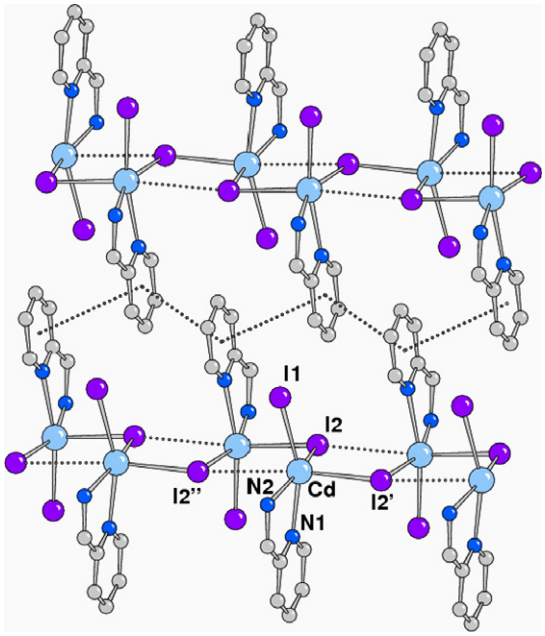

Fig. 6. Polymeric coordination chain of **5** developed along axis *b*. The dotted lines between Cd and iodo ligands indicate long distances of 3.7 Å.

that of the monodentate iodo ligand, and the apical Cd–I(2′) is slightly longer, of 2.9669(18) Å. The small bite angle N(1)–Cd–N(2) of 72.2(4)°, and the N(1)–Cd–I(1), N(2)–Cd–I(2) angles of ca. 159°, are indicative of the severe distortions inside the coordination geometry about Cd(II), which is considerably displaced from the pyramid basal plane towards the apical I(2′) by ca. 0.38 Å. In the ribbon-like polymer the Cd–I(2″) distance (indicated by the dotted line, Fig. 6) is rather long (3.730(2) Å), although shorter than the sum of Van-der Waals atom radii. The separation between Cd ions bridged by I(2) is 4.463(1) Å (slightly longer than that measured in **4**), to which corresponds a Cd–I(2)–Cd angle of 98.81(3)°. The Cd–Cd-Cd angle along the polymer is 96.94(1)°. The dimensionality is augmented through π–π interactions occurring between py rings of adjacent chains. The alternating centroid-to-centroid distances are 3.870 and 4.060 Å. However, as apparent from Fig. 6 (as well as observed for **4,** Fig. 5), the py rings are not located face-to-face and the slippage is likely to induce a weak interaction.

Table 3
Selected bond lengths (Å) and bond angles (°) of $[CdI_2(aepy)]_n$ (**4**) and $[CdI_2(ampy)]_n$ (**5**)

	(**4**)	(**5**)
Cd–N(1)	2.355(4)	2.361(9)
Cd–N(2)	2.261(4)	2.341(12)
Cd–I(1)	2.7891(7)	2.8234(14)
Cd–I(2)	3.0587(9)	2.9108(15)
Cd–I(2′)	3.2288(8)	2.9669(18)
Cd–I(1′)	3.1640(9)	–
N(1)–Cd–N(2)	87.70(13)	72.2(4)
N(1)–Cd–I(1)	104.00(10)	159.9(2)
N(1)–Cd–I(2)	93.69(9)	93.2(2)
N(1)–Cd–I(2′)	159.46(9)	94.8(2)
N(1)–Cd–I(1′)	81.33(9)	–
N(2)–Cd–I(1)	167.53(9)	93.7(3)
N(2)–Cd–I(2)	89.53(9)	159.1(3)
N(2)–Cd–I(2′)	77.48(9)	99.8(3)
N(2)–Cd–I(1′)	88.10(10)	–
I(1)–Cd–I(2)	93.94(2)	96.07(4)
I(1)–Cd–I(2′)	90.11(2)	101.87(4)
I(1)–Cd–I(1′)	89.413(19)	–
I(2)–Cd–I(2′)	100.244(18)	96.25(3)
I(2)–Cd–I(1′)	174.557(14)	–
I(2′)–Cd–I(1′)	84.019(16)	–
Cd–I(1)–Cd″	93.458(19)	–
Cd–I(2)–Cd″	87.312(17)	98.81(3)

Symmetry codes: (′) *x*, $-y+1/2$, $z-1/2$, (″) *x*, $-y+1/2$, $z+1/2$ (**4**); (′) $-x+1/2$, $y-1/2$, $-z+1/2$, (″) $-x+1/2$, $y+1/2$, $-z+1/2$ (**5**).

3.4. Absorption and fluorescence properties

In methanol, the ligands ampy and aepy show their absorption band at ~335 and ~350 nm, respectively, simply corresponding to the aromatic pyridine moiety absorption. Usually this absorption is assigned to the n–π* type of transition of pyridine aromatic ring. Excitation of free ligands at 335 and 350 nm does not show any emission band. According to Khasa's rule, n–π* type of transition does not show fluorescence and can afford, at low temperature, phosphorescence instead. Secondly, the free rotation of amino group, single bonded to the pyridine ring, leads to energy dissipation through non-radiative channels. The absorption spectra of complexes either with ampy or aepy ligand show band maxima similarly to that observed for the free ligand (broad band centered at ~350 nm). Although free ligands, dca and CdX_2 (X = Cl^-, Br^- and I^-) are not luminescent, interestingly all the cadmium coordination complexes containing the py-ligands show intense fluorescence band upon excitation at the ligand's absorption band in solution (methanol) as well as in solid state. The appearance of fluorescence upon complex formation could be inferred to MO structure change in the complex compared to that of free ligand, the HOMO–LUMO n–π* type of forbidden transition in free ligand changes to π–π* type of HOMO–LUMO transition in the metal complex. Therefore, upon complexation the non-fluorescent free ligand favors fluorescence characteristic of the simple coordinated aromatic chromophore. In addition, the freely rotating amino group is constrained by the cyclic ring formation and the non-radiative channel through free rotation path results inhibited. Hence, all complexes show characteristics fluorescence. Figs. 7A and 7B represent the lumines-

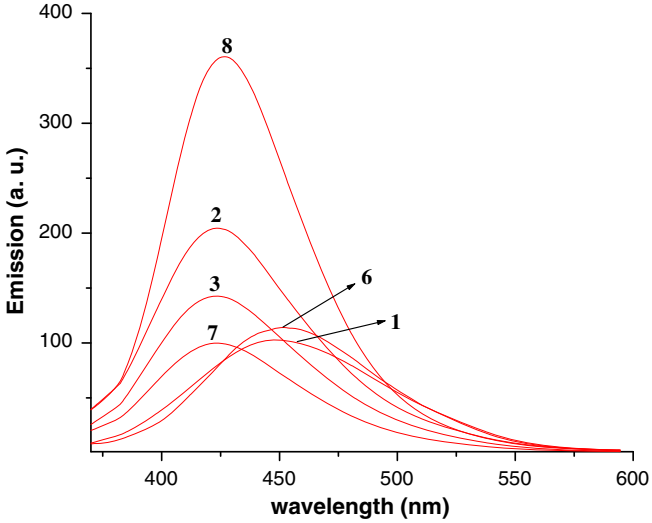

Fig. 7A. Emission spectra of **1–3** and **6–8** in methanol at room temperature.

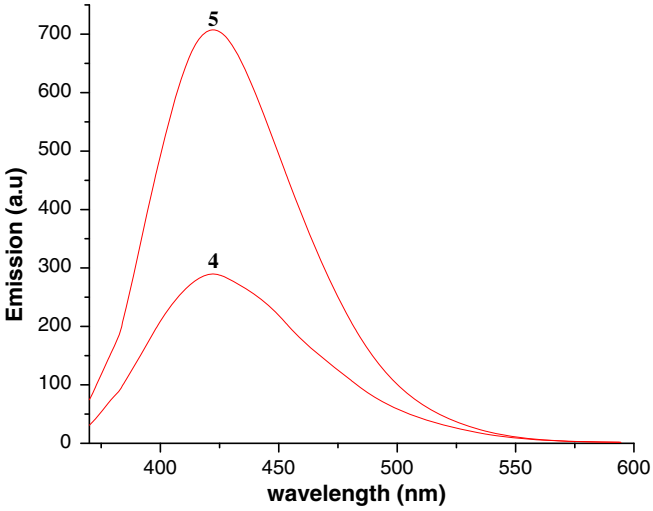

Fig. 7B. Emission spectra of **4** and **5** in methanol at room temperature.

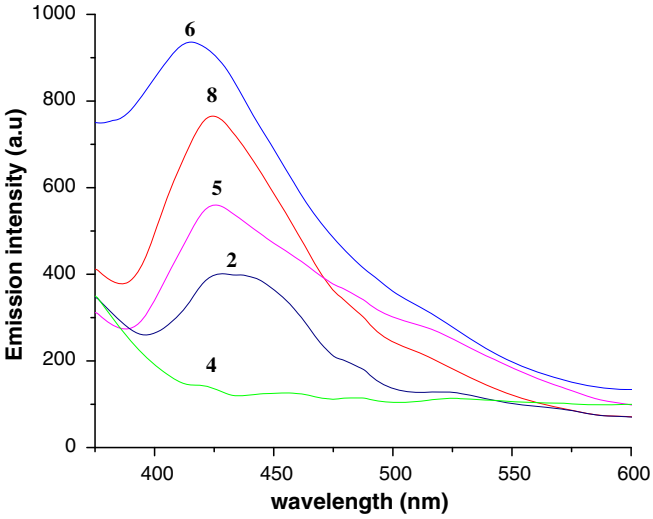

Fig. 8A. Emission spectra of **2, 4–6** and **8** in solid state at room temperature.

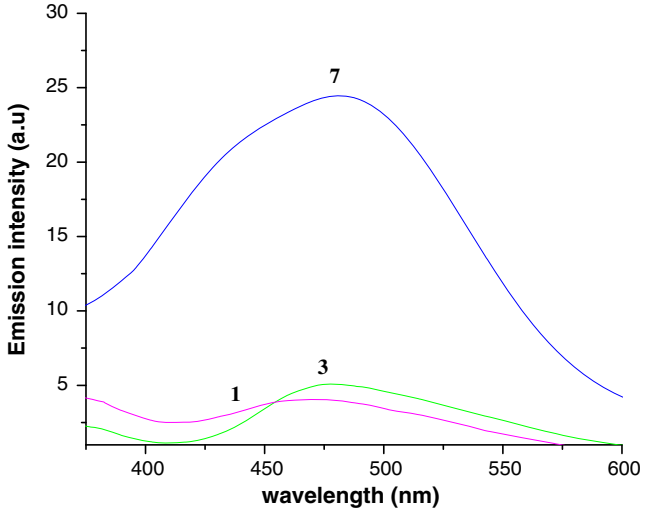

Fig. 8B. Emission spectra of **1**, **3** and **7** in solid state at room temperature.

cence spectra of complexes **1**–**8** in methanol and Figs. 8A and 8B depicted the same in the solid state. Structural investigation indicates the presence of effective π–π stacking amongst the pyridine ligands and the shortest π–π interaction is observed in complex **3** (3.622 Å) and the largest in **4** (4.195 Å). Usually π–π stacking can form H-aggregate (parallel type) or J-aggregate (ladder type) structures in the complexes, where the former generally gives rise to characteristic fluorescence. The π–π type H-aggregates, observed in our complexes; favor the intense fluorescence in them.

3.4.1. Effect of halides

One of the most significant observations in the present fluorescence study is the extraordinary high fluorescence efficiency exhibited by "iodo" ampy complex **5** in methanol (Fig. 7A; Table 4). The role of halides on the fluorescence efficiency of Cd–pyridine system under identical condition (entry complex **5**, **7** and **8**) is observed to follow the trend $I^- \gg Br^- \gg Cl^-$.

3.4.2. Effect of pyridine ligands and co-ligand, dca

The fluorescence band maxima as well as fluorescence efficiency are found to be dependent on the nature of the pyridine ligands. The present study shows that in the solid state complex with "ampy" (a ligand that forms a five-membered chelate) exhibits a red shift of the emission band in comparison with the correspondent "aepy" (a ligand that forms a six-membered chelate) complex (complex **1** & **3** and **2** & **6**). This indicates a stabilization of the energy level in the "ampy" complex more significant than in "aepy" complex. However, just opposite effect is noticed in methanol medium, i.e., complexes with "aepy" show red shifting. The effect of the co-ligand, dca is not very straight forward on

Table 4
Emission data for complexes **1–8** at room temperature in methanol and in the solid state

Complex	Emission λ_{max} (nm)		Quantum yield (φ_f) in methanol
	Solid	Methanol	
$[CdCl(dca)(aepy)]_n$ (**1**)	470	449	0.092
$[CdBr(dca)(ampy)]_n$ (**2**)	434	425	0.113
$[CdCl(dca)(ampy)]_n$ (**3**)	476	421	0.091
$[CdI_2(aepy)]_n$ (**4**)	Broad spectrum	422	0.161
$[CdI_2(ampy)]_n$ (**5**)	424	424	0.445
$[CdBr(dca)(aepy)]_n$ (**6**)	416	456	0.086
$[CdCl_2(ampy)]_n$ (**7**)	482	422	0.049
$[CdBr_2(ampy)]_n$ (**8**)	425	419	0.228

the fluorescence properties of the complexes. In absence of dca red shifting in solid state is observed when we compare complexes **3** and **7**, whereas, if we compare **2** and **8**, in presence of dca red shifting is noticed. Thus it is very difficult to rationalize the role of bridging co-ligand, dca on the fluorescence properties of Cd–pyridine system.

4. Conclusion

Cadmium (II) coordination polymers built up by halide have been widely reported, and the majority with bridging chloride [15]. However, the present compounds **1** and **2** are examples of an unprecedented topology. Conversely, Cd coordination polymers with Br [16–19] and I [20] are less common and only a few examples have been structurally characterized. As a comparison, the polymer reported by Wilkins et al. [20] is similar to compound **4** with cadmium centers bridged by pair of iodide atoms, but the metals are alternatively four- and six-coordinated (two dmso, O molecules are axially bound in the latter case). Thus the aminopyridine chelating molecule represents an ancillary ligand playing a key role in the construction of the present polymers. From our study it may be inferred that the luminescent property of coordination polymers of Cd(II)-pyridine system is largely controlled not only by pyridine ligand but also by the nature of the halide, and even by the co-ligand, dicyanamide. Further study is required to assess the luminescence phenomena in these types of complexes.

Supplementary data

CCDC 668324, 668325, 668326, 668327 and 668328 contain the supplementary crystallographic data for this paper. These data can be obtained free of charge via http://www.ccdc.cam.ac.uk/conts/retrieving.html, or from the Cambridge Crystallographic Data Centre, 12 Union Road, Cambridge CB2 1EZ, UK; fax: (+44) 1223-336-033; or e-mail: deposit@ccdc.cam.ac.uk.

Acknowledgements

The authors are thankful to Dr. Nikhil Guchhait of University College of Science and Technology, Kolkata, India for scientific discussions on fluorescence study. The authors wish to thank the Council of Scientific and Industrial Research, New Delhi (Project No. 01(1871)/03/EMR-II dated 17/03/2003) for financial support.

References

[1] Y.B. Dong, R.C. Layland, M.D. Smith, N.G. Pschirer, U.H.F. Bunz, H.C.Z. Loye, Inorg. Chem. 38 (1999) 3056.
[2] B.F. Abrahams, M.J. Hardie, B.F. Hoskins, R. Robson, E.E. Sutherland, J. Chem. Soc., Chem. Commun. (1994) 1049.
[3] T. Soma, H. Yuge, T. Iwamoto, Angew. Chem., Int. Ed. Engl. 33 (1994) 665.
[4] M. Fujita, Y.J. Kwon, M. Miyazawa, K. Ogura, J. Chem. Soc., Chem Commun. (1994) 1977.
[5] A. Mondal, G. Mostafa, A. Ghosh, I.R. Laskar, N. Ray Chaudhuri, J. Chem. Soc., Dalton Trans. (1999) 9.
[6] G. Ciani, M. Moret, A. Sironi, S. Bruni, F. Pozzi, A. Manfredini, L. Menabue, G.C. Pellacani, Inorg. Chim. Acta 158 (1989) 9.
[7] F. Cariati, G. Ciani, L. Menabue, G.C. Pellacani, G. Rassu, A. Sironi, Inorg. Chem. 22 (1983) 1897.
[8] R.D. Bailey, W.T. Pennington, Polyhedron 16 (1997) 417.
[9] H. Strasdeit, W. Saak, S. Pohl, W.L. Driessen, J. Reedijk, Inorg. Chem. 27 (1988) 1557.
[10] M. Nieuwenhuyzen, W.T. Robinson, C.J. Wilkins, Polyhedron 10 (1991) 2111.
[11] N. Mondal, M.K. Saha, S. Mitra, V. Gramlich, J. Chem. Soc., Dalton Trans. (2000) 3218.
[12] P.M. Secondo, J.M. Land, R.G. Baughman, H.L. Collier, Inorg. Chim. Acta 309 (2000) 3.
[13] H. Zhang, D.E. Zelmon, G.E. Price, B.K. Teo, Inorg. Chem. 39 (2000) 1868.
[14] F.A. Schroder, J.W. Bats, H. Fuess, E.-J. Zehnder, Anorg. Allg. Chem. 499 (1983) 181.
[15] F.H. Allen, O. Kennard, R. Taylor, Acc. Chem. Res. 16 (1983) 146.
[16] H. Ishihara, V.G. Krishnan, Shi-qi. Dou, H. Weiss, Z. Naturforsch., A: Phys. Sci. 49 (1994) 213.
[17] G. Aguirre-Zamalloa, G. Madariaga, M. Couzi, T. Breczewski, Acta Crystallogr., Sect.B 49 (1993) 691.
[18] M. Dan, C.N.R. Rao, Chem. -Eur. J. 11 (2005) 7102.
[19] R.D. Rogers, A.H. Bond, S. Aguinaga, J. Crystallogr. Spectrosc. Res. 23 (1993) 857.
[20] M. Nieuwenhuyzen, Huo.Huo Wen, C.J. Wilkins, Z. Anorg. Allg. Chem. 615 (1992) 143.
[21] C. Janiak, Dalton Trans. (2003) 2781.
[22] C. Janiak, Angew. Chem., Int. Ed. 36 (1997) 1431.
[23] S.-Q. Xia, S.-M. Hu, J.-C. Dai, X.-T. Wu, J.-J. Zhang, Z.-Y. Fu, W.-X. Du, Inorg. Chem. Commun. 7 (2004) 51.
[24] X.-J. Liu, Q.-R. Fang, G.-S. Zhu, M. Xue, X. Shi, G. Wu, G. Tian, S.-L. Qiu, L. Fang, Inorg. Chem. Commun. 7 (2004) 31.
[25] V.W.W. Yam, Y.L. Pui, K.M.C. Wong, K.K. Cheung, Chem. Commun. (2000) 1751.
[26] W.Y. Wong, K.Y. Tsang, K.H. Tam, G.L. Lu, C. Sun, J. Organomet. Chem. 601 (2000) 237.
[27] K.S. Anjali, Y.L. Pui, V.W.W. Yam, J.J. Vittal, Inorg. Chim. Acta 319 (2001) 57.
[28] H. Zhu, M. Ströbele, Z. Yu, Z. Wang, H.J. Meyer, X. You, Inorg. Chem. Commun. 4 (2001) 577.
[29] Y. Kang, C. Seward, D. Song, S. Wang, Inorg. Chem. 42 (2003) 2789.
[30] V.W.W. Yam, Y.L. Pui, K.K. Cheung, New J. Chem. 23 (1999) 1163.
[31] R.R.-Q. Fan, D.D.-S. Zhu, Y. Mu, G.G.-H. Li, Y.Y.-L. Yang, Q. Su, S.S.-H. Feng, Eur. J. Inorg. Chem. (2004) 4891.
[32] B. Ding, L. Yi, Y. Wang, P. Cheng, D.-Z. Liao, S.-P. Yan, Z.-H. Jiang, H.-B. Song, H.-G. Wang, Dalton Trans. (2006) 665.
[33] J. Zhang, Y.-R. Xie, Q. Ye, R.-G. Xiong, Z. Xue, X.-Z. You, Euro. J. Inorg. Chem. (2003) 2572.
[34] Q-Y.Q.-Y. Liu, Y.-L. Wang, L. Xu, Eur. J. Inorg. Chem. (2006) 4843.
[35] N. Kundu, D. Mandal, M. Chaudhury, E.R.T. Tiekink, Appl. Organometal. Chem. 19 (2005) 1268.
[36] M. Du, X.-J. Jiang, X.-J. Zhao, H. Cai, J. Ribas, Eur. J. Inorg. Chem. (2006) 1245.
[37] X. Li, R. Cao, W. Bi, D. Yuan, D. Sun, Eur. J. Inorg. Chem. (2005) 3156.
[38] Bruker, SMART, SAINT, Software Reference Manual Bruker AXS Inc., Madison, WI, USA, 2000.
[39] G.M. Sheldrick, SHELX97, Programs for Crystal Structure Analysis (Release 97-2), University of Göttingen, Germany, 1998.
[40] L.J. Farrugia, J. Appl. Crystallogr. 32 (1999) 837.

Polyhedron 27 (2008) 2459–2463

Contents lists available at ScienceDirect

Polyhedron

journal homepage: www.elsevier.com/locate/poly

Synthesis, structure and magnetic properties of unsymmetrical dodecanuclear Mn–Ln clusters

Valeriu Mereacre [a,b,*], Denis Prodius [a], Ayuk M. Ako [b], Narpinder Kaur [c], Janusz Lipkowski [d], Charles Simmons [e], Naresh Dalal [c], Ion Geru [a], Christopher E. Anson [b], Annie K. Powell [b], Constantin Turta [a,*]

[a] Institute of Chemistry, Academy of Sciences of Moldova, Chisinau, Academy Street 3, MD-2028, Moldova
[b] Institut für Anorganische Chemie der Universität Karlsruhe, D-76128 Karlsruhe, Germany
[c] Department of Chemistry and Biochemistry, and National High Magnetic Field Laboratory, Florida State University, Tallahassee, FL 32306, USA
[d] Institute of Physical Chemistry, Polish Academy of Sciences, 01-224 Warsaw, Poland
[e] University of Hawaii at Hilo, Natural Sciences Division, Hilo, HI 96720-4091, USA

ARTICLE INFO

Article history:
Received 28 March 2008
Accepted 25 April 2008
Available online 7 June 2008

Keywords:
Lanthanide–manganese compounds
Benzoic acid
Magnetic properties

ABSTRACT

Reaction of manganese acetate and lanthanide nitrates in the presence of excess of PhCOOH affords highly asymmetric dodecanuclear mixed-metal $[Mn_{10}Ln_2(OH)(O)_8(PhCOOH)(PhCOO)_{19}]$ (Ln = Pr^{III} (**1**), Nd^{III} (**2**)) clusters. The similar reaction, but with only 2 equiv. of PhCOOH resulted in the compounds with higher nuclearity $[Mn_{11}Eu_4(O)_8(OH)_8(PhCOO)_{18}(NO_3)_2(H_2O)_6]NO_3 \cdot 4CH_3CN$ (**3**). Variable-temperature solid-state magnetic susceptibility of **1** and **2** in the temperature range 1.8–300 K were carried out, and for both complexes antiferromagnetic exchange interactions between the metal centers were observed, giving an estimated $S = 17/2$ ground state. AC magnetic susceptibility data have revealed out-of-phase signals, which suggest that these complexes exhibit a slow relaxation of magnetization as observed in single-molecule magnets.

© 2008 Elsevier Ltd. All rights reserved.

1. Introduction

The efforts to produce large clusters with high-spin ground states and unusual magnetic properties have become of primary importance since the discovery of single-molecule magnets (SMMs) [1]. Currently, researchers are interested in synthesizing clusters with characteristic features that may increase the temperature at which the magnetization becomes blocked and the molecules exhibit magnetic hysteresis. Previously, the search for SMMs was based primarily on the use of 3d metals ions [2–5]. However, increasingly, other metal ions that exhibit high spin and single-ion anisotropy are being employed. Along these lines, lanthanide-containing molecules with strong spin-orbit interactions are very good candidates for SMM behaviour. Recently, the first SMMs containing mixed Mn^{III} (or Fe^{III}) and f-metals with different cores: Mn_6Dy_6 [6], $Mn_{11}Dy_4$ [7a], $Mn_{11}Gd_2$ [7b], Mn_5Ln_4 [7c], Mn_2Dy_2 [8], Fe_2Dy_2[9] and Fe_2Ho_2[9] were synthesized. All of them displayed frequency-dependent out-of-phase ac signals and for some of them magnetization hysteresis loops were reported [7–9]. As an extension of our previous work on Fe^{III} and Ln^{III} chemistry [10] we have now included Mn ions, in the quest to synthesize large Mn–Ln clusters examples of which are still limited in the literature.

In this paper we propose a simple and efficient procedure towards the isolation of high-nuclearity heterometallic complexes using simple manganese salts as a source of Mn^{III} ions: $[Mn_{10}Pr_2(OH)(O)_8(PhCOOH)(PhCOO)_{19}] \cdot 11CH_3CN$ (**1** · $11CH_3CN$), and $[Mn_{10}Nd_2(OH)(O)_8(PhCOOH)(PhCOO)_{19}]$ (**2**). Compounds **1** and **2** were obtained from the reaction of $Mn(CH_3COO)_2 \cdot 4H_2O$, with $Ln(NO_3)_3 \cdot 6H_2O$ (Ln = Pr^{III}, Nd^{III}) in the presence of excess of PhCOOH in yields of 64% and 60%, respectively. The similar reaction, but with only 2 equiv. of PhCOOH resulted in the compound $[Mn_{11}Eu_4(O)_8(OH)_8(PhCOO)_{18}(NO_3)_2(H_2O)_6]NO_3 \cdot 4CH_3CN$ (**3** · $4CH_3CN$) with the structure similar to $Mn_{11}Dy_4$ [7a].

2. Experimental

2.1. General considerations

All the reactions were carried out under aerobic conditions. Starting materials were obtained from commercial sources and used without further purification. Elemental analyses for C, H and N were carried out at the Institute for Inorganic Chemistry at the University of Karlsruhe.

* Corresponding authors. Address: Institute of Chemistry, Academy of Sciences of Moldova, Chisinau, Academy Street 3, MD-2028, Moldova. Tel.: +373 22 739722; fax: +373 22 739954 (V. Mereacre), tel.: +373 22 739755; fax: +373 22 739954 (C. Turta).
E-mail addresses: mereacre@mail.md (V. Mereacre), cturta@cc.acad.md (C. Turta).

0277-5387/$ - see front matter © 2008 Elsevier Ltd. All rights reserved.
doi:10.1016/j.poly.2008.04.037

2.2. Preparations

2.2.1. $[Mn_{10}Pr_2(OH)(O)_8(PhCOOH)(PhCOO)_{19}]$ (**1**) and $Mn_{10}Nd_2(OH)(O)_8(PhCOOH)(PhCOO)_{19}]$ (**2**)

Heating $Mn(CH_3COO)_2 \cdot 4H_2O$ (0.11 g, 0.45 mmol) with $Pr(NO_3)_3 \cdot 6H_2O$ or $Nd(NO_3)_3 \cdot 6H_2O$ (0.20 g, 0.45 mmol), with excess of PhCOOH (1.00 g, 8.20 mmol) in toluene (10 ml) under reflux for 20 min followed by cooling, evaporation at room temperature until dryness and recrystallizing from 10 ml of acetonitrile affords after 1 day a dark brown crystalline product, **1**, in 64% yield (**2**, in 60%). Elemental *Anal.* Calc. for $C_{140}H_{102}Mn_{10}O_{49}Pr_2$, **1** (dried): C, 49.46; H, 3.02. Found: C, 49.33; H, 2.87%. Elemental *Anal.* Calc. for $C_{140}H_{102}Mn_{10}O_{49}Nd_2$, **2** (dried): C, 49.36; H, 3.01. Found: C, 49.53; H, 2.81%.

2.2.2. $[Mn_{11}Eu_4(O)_8(OH)_8(PhCOO)_{18}(NO_3)_2(H_2O)_6]NO_3 \cdot 4CH_3CN$ (**3**)

This compound was synthesized using similar reaction, but with only 2 equiv. of PhCOOH. Yield: 60%. Elemental *Anal.* Calc. for $C_{126}H_{110}Mn_{11}N_3O_{67}Eu_4$, **3** (dried): C, 38.31; H, 2.80; N, 1.06. Found: C, 38.82; H, 2.56; N, 1.32%.

2.3. Physical measurements

The magnetic susceptibility measurements were obtained with the use of a Quantum Design SQUID magnetometer MPMS-XL. This magnetometer works between 1.8 and 400 K for dc applied fields ranging from −7 to 7 T. Measurements were performed on finely ground polycrystalline samples. *M* versus *H* measurements has been performed at 100 K to check for the presence of ferromagnetic impurities that has been found systematically absent. ac susceptibility measurements have been measured with an oscillating ac field of 3 Oe and ac frequencies ranging from 200 to 1500 Hz. The magnetic data were corrected for the sample holder and the diamagnetic contributions.

2.4. Crystal structure determination

X-ray data were collected for dry crystals of complexes **1** and **2**. In order to ensure that the space group and unit cell of compounds **1** and **2** were correct and to have better diffraction, new crystals were grown for **1** and a further unit cell was collected for crystals separated directly from mother-liquor, which gave slightly inflated cell dimensions to the first collection [a = 42.0114(7), b = 42.0114(7), c = 17.8066(6) Å, V = 31427.9(13) Å^3]. Diffraction intensity data for the new complex **1** were collected at 100 K on a Bruker SMART Apex CCD diffractometer using graphite-monochromated Mo Kα radiation. Complex **1** co-crystallizes with 11 acetonitrile solvate molecules.

X-ray data for complex **2** were collected with a Nonius Kappa CCD diffractometer using graphite-monochromated Mo radiation at 100 K. Some of phenyl rings show pronounced, partial disordering. Three of them were split into two orientations each and refined as rigid rings of idealized geometry. The resulting site occupation factors are between 40% and 60%. The temperature factors of the ring carbon atoms were kept constant at the arbitrarily set value U(iso) = 0.04. In final refinement cycles a maximum of about 2 e/Å^3 has been found and interpreted as a hydration water molecule of partial occupancy. The corresponding s.o.f. value refined to about 20% in the final cycles. All hydrogen atoms were put in calculated positions and included in final refinement as 'riding' on corresponding carbon atoms, with temperature factors set as 1.2 times U(iso) of the corresponding carbons.

X-ray crystallographic measurements for **3** were performed at 100 K using the same diffractometer as for **2**. Crystallographic data and refinement details are summarized in Table 1.

The unit cell determination confirmed that isomorphous with **1** and **2** compounds could be synthesized using salts of Sm^{III} and Eu^{III}. Attempts, to obtain crystals using salts of lanthanides from Gd^{III} to Lu^{III}, were unsuccessful.

3. Results and discussion

3.1. Structural analysis

The molecular structure of **1** and **2** were confirmed by single-crystal X-ray diffraction [11,12]. The compound **1** (Fig. 1) consists of two Pr^{III} ions, one coordinated by two O^{2-}, one OH^- ions and six benzoate O's (ninefold coordinate), the other by eight O^{2-}, one OH^- ions and one benzoate oxygen (tenfold coordinate); the mean Pr^{III}–O bond lengths are 2.54 and 2.58 Å, respectively. (Adopting $d[Pr^{III}–O] < 2.7$ Å as criterion for coordination). The 10 Mn^{III} coordination spheres are tetragonally elongated octahedral.

Table 1
Summary of crystal data and refinement details for compounds **1**, **2** and **3**

	1	**2**	**3**
Formula	$C_{162}H_{135}Mn_{10}N_{11}O_{49}Pr_2$	$C_{140}H_{102}O_{49}Mn_{10}Nd_2$	$C_{134}H_{122}Eu_4Mn_{11}N_7O_{67}$
Formula weight	3851.02	3406.11	4114.55
Wavelength (Å)	0.71073	0.71073	0.71073
T (K)	100	100	100
Crystal system	tetragonal	tetragonal	monoclinic
Space group	$P42/n$	$P42/n$	$C2/c$
a (Å)	42.0114(7)	40.6760(8)	32.2880(12)
b (Å)	42.0114(7)	40.6760(8)	28.8190(14)
c (Å)	17.8066(6)	17.7620(8)	18.2330(13)
α (°)	90.00	90.00	90.000(3)
β (°)	90.00	90.00	108.855(3)
γ (°)	90.00	90.00	90.000(3)
V (Å^3)	31427.9(13)	29388(15)	16055.5(15)
Z	8	8	8
$\rho_{(calcd)}$ (mg/m^3)	1.624	1.541	1.692
μ_{Mo} (mm^{-1})	1.470	1.603	2.460
θ Range (°)	1.24–28.24	1.25–23.95	2.62–23.26
Number of reflections measured	36242	20967	11491
Number of unique reflections [$R_{(int)}$]	28354 [0.0536]	13658 [0.0741]	9304 [0.0661]
Number of refined parameters	1952	1765	940
Goodness-of-fit for F^2	1.044	0.896	0.974
R	0.0360	0.0349	0.0499
wR	0.0886	0.0715	0.1488
Largest residuals (e Å^{-3})	+0.92/−0.52	+0.56/−0.44	+1.87/−1.96

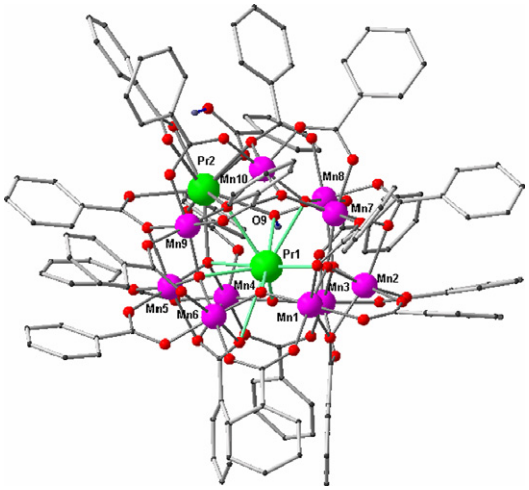

Fig. 1. Structure of the complex $[Mn_{10}Pr_2(OH)(O)_8(PhCOOH)(PhCOO)_{19}]$ (**1**); Pr (green), Mn (pink), C (black), and O (red). H atoms and solvent molecules have been omitted for clarity. (For interpretation of the references to colour in this figure legend, the reader is referred to the web version of this article.)

The Jahn–Teller radii, $R_{JT} = [\sum(R_i - \langle R\rangle)^2]^{1/2}$, vary between 0.29 and 0.66 Å, indicating differing degrees of distortion of the MnO_6 coordination spheres. Complex **2** is isomorphous with **1**. Hence, the structure of **1** is described in detail as representative for both compounds.

The central core of the complex **1** can best be described as a combination of distorted hexagonal pyramid (Mn_6Pr (Mn1, Mn2, Mn3, Mn4, Mn5, Mn6, Pr1)) (Fig. 2) and distorted tetragonal pyramid (Mn_4Pr (Mn7, Mn8, Mn9, Mn10, Pr2)) (Fig. 3) connected through six μ_4-O^{2-}, one μ_3-OH^- and six benzoates with different types of coordination of carboxylic groups. The six manganese atoms of the hexagon are not in a plane. The hexagon has a twist-boat conformation (Fig. 2, bottom) similar to cyclohexane. The Pr1 atom coordinates with ten Mn^{III} atoms through six μ_4-O^{2-}, two μ_3-O^{2-}, one μ_3-OH^- bridges and one μ-O of one carboxylate group. Thus, the coordination polyhedron may be best described as a distorted hexagonal bipyramid (capped from one side by one atom and from another part by a triangular cupola) (Fig. 2, top). The second Pr^{III} atom (Pr2) is nine-coordinated and situated in one corner of distorted tetragonal pyramid (Fig. 3) and interacts with one Pr^{III} and five Mn^{III} atoms through two μ_4-O^2, one μ_3-OH^-, two μ^3:η^2:η^1 and one μ:η^1:η^1(COO^-) bridges, with its geometry completed by one chelating $PhCOO^-$ anion and one monocoordinated PhCOOH molecule. The coordination polyhedron may be represented as a distorted, tricapped trigonal prism. The various bridging modes (μ^3:η^2:η^1, μ^4:η^2:η^2, μ^3:η^3:η^1, etc.) of the carboxylic groups give rise to the low symmetry of the structure.

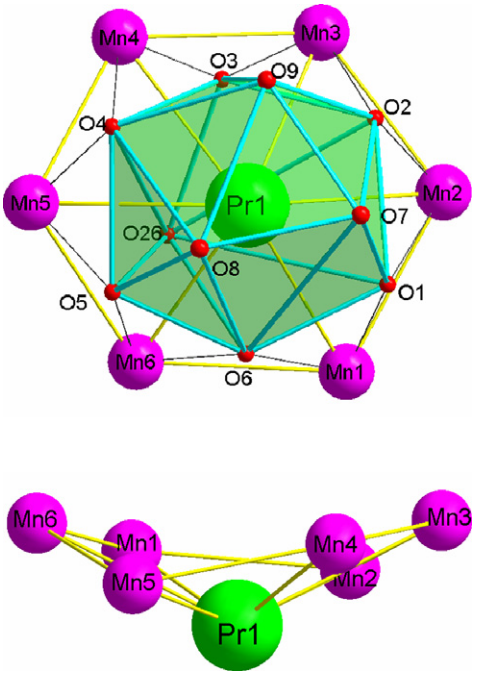

Fig. 2. The symmetry of environment (top) and twist-boat conformation (bottom) of Pr1 ion in compound **1**.

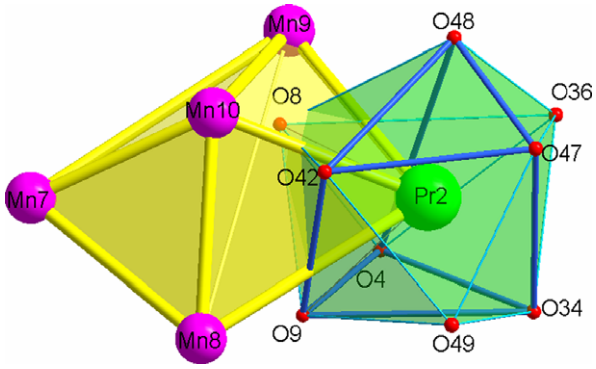

Fig. 3. Structure of pentanuclear unit (tetragonal pyramid $\{Mn_4Pr\}$) in **1** showing also the coordination environment of the Pr2 center.

The similar reaction as for **1** and **2**, but with 0.45 mmol of $Eu(NO_3)_3 \cdot 6H_2O$ and 0.90 mmol of benzoic acid resulted in the similar with $[Mn_{11}Dy_4(O)_8(OH)_6(PhCOO)_{16}(NO_3)_5(H_2O)_3] \cdot 15CH_3CN$ structure [7a] compound, the difference being only in number of nitrate groups and missing of methoxy groups: $[Mn_{11}Eu_4(O)_8(OH)_8(PhCOO)_{18}(NO_3)_2(H_2O)_6]NO_3 \cdot 4CH_3CN$ (**3**) (Fig. 4). In case of published $\{Mn_{11}Dy_4\}$ structure the O10w and O11w atoms correspond to one chelating NO_3^- group and O12 – to μ-OMe^- ion. In the structure of compound (**3**) the O10w and O11w atoms correspond to two water molecules and O12 – to OH^- anion. The charge of the whole molecule is balanced by two monodentate $C_6H_5COO^-$ anions coordinated to Eu2 and Eu2a, and one free NO_3^- anion.

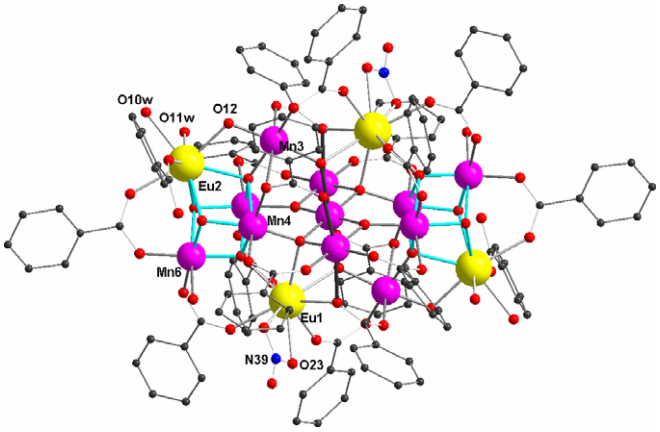

Fig. 4. Molecular structure of complex $[Mn_{11}Eu_4(O)_8(OH)_8(PhCOO)_{18}(NO_3)_2(H_2O)_6]NO_3 \cdot 4CH_3CN$ (**3**); Eu atoms are shown in yellow, Mn atoms in pink, C atoms in black and O atoms in red. H atoms are not shown. (For interpretation of the references to colour in this figure legend, the reader is referred to the web version of this article.)

3.2. Magnetic properties of **1** and **2**

Solid-state dc magnetic susceptibility (χ_M) data for compound **1** were collected in the 1.8–300 K temperature range in a 0.01 T field. The room temperature $\chi_M T$ value (Fig. 5) of 33.37 $cm^3\ mol^{-1}$ K is close to that expected for 10 Mn^{III} ($S = 2$, $g = 2$) and two Pr^{III} ($S = 1$, $L = 5$, $^3H_4$) non-interacting ions (33.20 $cm^3\ mol^{-1}$ K). Upon decreasing the temperature it remains almost constant until at about 75.50 K, when it decreases to a small plateau near 26.50 $cm^3\ mol^{-1}$ K in the approximate range 10–20 K, followed by a sharp drop down to a value 22.06 $cm^3\ mol^{-1}$ K at 1.8 K. This behaviour indicates the presence of predominantly antiferromagnetic interactions within the cluster, reaching a non-diamagnetic ground state with a relatively high spin number.

Solid-state dc magnetic susceptibility (χ_M) data for compound **2**show a similar behaviour, although the room temperature $\chi_M T$ value, 32.92 $cm^3\ mol^{-1}$ K, is less than the value expected for 10 Mn^{III} ($S = 2$, $g = 2$) and two Nd^{III} ($S = 3/2$, $L = 6$, $^4I_{9/2}$) non-interacting ions of 33.27 $cm^3\ mol^{-1}$ K and remains almost constant until around 51.50 K when it decreases sharply down to a value of 22.61 $cm^3\ mol^{-1}$ K at 1.8 K (Fig. 5).

As compounds **1** and **2** have such high $\chi_M T$ values at low temperatures and contain a large number of anisotropic paramagnetic metal ions, we can view these two compounds as potential materials with unusual magnetic properties. In order to assess whether these molecules exhibit a slow relaxation of magnetization ac magnetic susceptibility measurements were performed. The measurements were carried out in the 1.8–10 K range under 3.5 G ac field oscillating at 200–1500 Hz. In the absence of external magnetic field complex **2** showed a weak signal with a low ratio χ'/χ'' frequency- dependent out-of-phase signal (Fig. 6), which could be the tail of a peak lying at a temperature below 1.8 K. It is however difficult to conclude if **2** is a SMM based on measurements down to 1.8 K, the limit of our instrument. Very low temperature studies would therefore be necessary. Studies along these lines and on other Ln-derivatives are the objective of future work.

We have tried to estimate the appreciative spin state using of the following Hamiltonian which allows fitting of the magnetization data for compound **2** with the ANISOFIT 2.0 program [13] implemented on the MATLAB platform and Brillion function [14]:

$$H = DS_z^2 + E(S_x^2 + S_y^2) + g_{iso}\beta SB,$$

where the β is the Bohr magneton and g, D, E, S, and B represent the Lande' g factor, the axial and rhombic zero-field splitting parameters, and the spin and magnetic field vectors, respectively. A comparison between experimental data, fitting data and simulation data by Brillion function is given in Fig. 7. The results show that the spin state can by estimated at 8.5 ± 1. The exact evaluation of

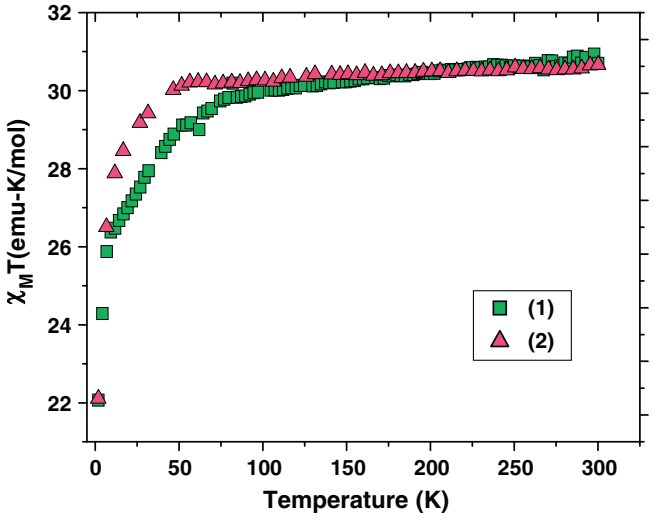

Fig. 5. $\chi_M T$ vs. T plot for complex **1** and **2** in a 100 G (0.01 T) applied dc field.

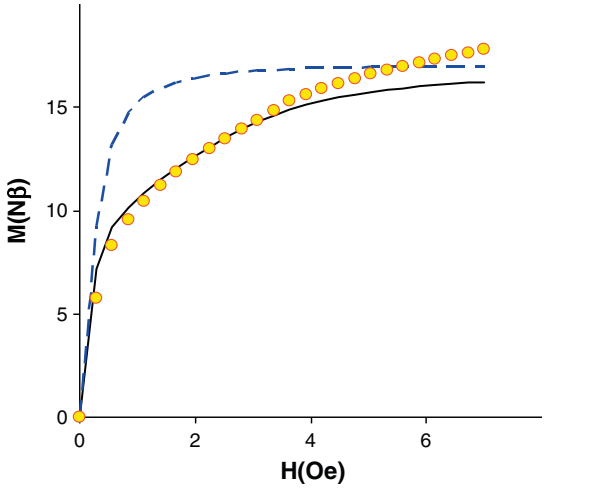

Fig. 7. Plot of magnetization at 1.8 K for compound **2** fitted by ANISOFIT 2.0 [13] program ($S = 8.5$, $g = 1.96$, $D = -0.23$ cm^{-1} $E = 0.002$) (solid line); and simulation by Brillion function ($S = 8.5$, $g = 2.0$) (dotted line).

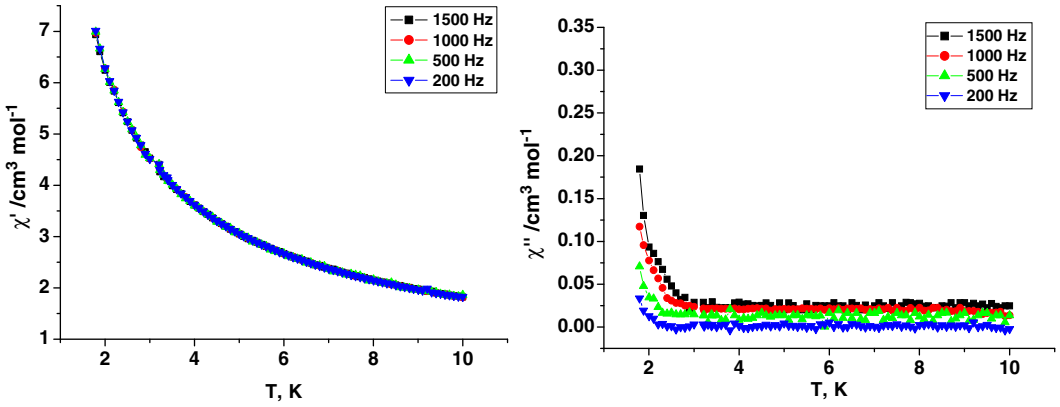

Fig. 6. Plots of the in-phase (χ') and the out-of-phase (χ''_M) ac susceptibility data for **2** under a zero static magnetic field and with different oscillating frequencies.

spin state is not possible due to spin orbital contribution from two Nd ions. The spin orbital contribution of two Nd ions was included in the approximate range of spin state ±1.

The magnetic data presented above suggest that predominantly antiferromagnetic exchange interactions are present within both types of clusters. The high nuclearity and presence of strong spin–orbit coupling effects in the **1** and **2** derivatives makes the fitting of the data to obtain Mn^{III}–Mn^{III}, Mn^{III}–Ln^{III} and Ln^{III}–Ln^{III} exchange parameters a largely unachieved task.

4. Conclusions

A convenient one step route for the synthesis of Mn–Ln polynuclear complexes is demonstrated. It is based on simple reaction between manganese acetate, lanthanide nitrates and benzoic acid. Other remarkable features of this method are successful isolation of target compounds by specific choice of benzoic acid concentration and appreciable yields and significant short reactions times. This opens a wide possibility for molecular construction of transition metal–lanthanide complexes with different nuclearity. Further experiments are underway to design such systems with other lanthanides and other carboxylate ligands, in view of enhancing SMM property.

5. Supplementary data

CCDC 666378, 666379 and 682544 contain the supplementary crystallographic data for **1**, **2** and **3**. These data can be obtained free of charge via http://www.ccdc.cam.ac.uk/conts/retrieving.html, or from the Cambridge Crystallographic Data Centre, 12 Union Road, Cambridge CB2 1EZ, UK; fax: (+44) 1223-336-033; or e-mail: deposit@ccdc.cam.ac.uk.

Acknowledgements

V.M. thanks the AvH Foundation. The research described in this publication was also made possible by Awards BGPIII MOB2-3058-CS-03, BGPIII MOP2-3061-CS-03, MTFP-017/05-FOA (D.P.) (MRDA-CRDF), and INTAS No. 05-1000008-7834.

References

[1] (a) R. Sessoli, H.-L. Tsai, A.R. Schake, S. Wang, J.B. Vincent, K. Folting, D. Gatteschi, G. Christou, D.N. Hendrickson, J. Am. Chem. Soc. 115 (1993) 1804;
(b) R. Sessoli, D. Gatteschi, A. Ganeschi, M.A. Novak, Nature 365 (1993) 141.
[2] (a) G. Christou, D. Gatteschi, D.N. Hendrickson, R. Sessoli, MRS Bull. 25 (2000) 66;
(b) J.P. Price, S.R. Batten, B. Moubaraki, K.S. Murray, Chem. Commun. (2002) 762;
(c) E.C. Saoudo, W. Wernsdorfer, K.A. Abboud, G. Christou, Inorg. Chem. 43 (2004) 4137;
(d) N.E. Chakov, W. Wernsdorfer, K.A. Abboud, G. Christou, Inorg. Chem. 43 (2004) 5919;
(e) C.J. Milios, C.P. Raptopoulou, A. Terzis, F. Lloret, R. Vicente, S.P. Perlepes, A. Escuer, Angew. Chem., Int. Ed. 43 (2004) 210;
(f) E. Coronado, A. Forment-Aliaga, A. Gaita- Arino, C. Gimenez-Saiz, F.M. Romero, W. Wernsdorfer, Angew. Chem., Int. Ed. 45 (2004) 6152;
(g) A.K. Boudalis, B. Donnadieu, V. Nastopoulos, J.M. Clemente-Juan, A. Mari, Y. Sanakis, J.-P. Tuchagues, S.P. Perlepes, Angew. Chem., Int. Ed. 43 (2004) 2266;
(h) S. Maheswaran, G. Chastanet, S.J. Teat, T. Mallah, R. Sessoli, W. Wernsdorfer, R.E.P. Winpenny, Angew. Chem., Int. Ed. 44 (2005) 5044.
[3] (a) C. Delfs, D. Gatteschi, L. Pardi, R. Sessoli, K. Wieghardt, D. Hanke, Inorg. Chem. 32 (1993) 3099;
(b) D. Gatteschi, R. Sessoli, A. Cornia, Chem. Commun. (2000) 725;
(c) J.C. Goodwin, R. Sessoli, D. Gatteschi, W. Wernsdorfer, A.K. Powell, S.L. Heath, J. Chem. Soc., Dalton Trans. (2000) 1835;
(d) C. Benelli, J. Cano, Y. Journaux, R. Sessoli, G.A. Solan, R.E.P. Winpenny, Inorg. Chem. 40 (2001) 188.
[4] (a) A.K. Boudalis, C.P. Raptopoulou, B. Abarca, R. Ballesteros, M. Chadlaoui, J.-P. Tuchagues, A. Terzis, Angew. Chem., Int. Ed. 45 (2006) 432;
(b) M. Nakano, G.-E. Matsubayashi, M. Takaki, C.K. Tatsuo, K. Amaya, J. Yoo, G. Christou, D.N. Hendrickson, Mol. Cryst. Liq. Cryst. Sci. Technol., Sect. A 376 (2002) 405;
(c) S.T. Ochsenbein, M. Murrie, E. Rusanov, H. Stoeckli-Evans, C. Sekine, H.U. Güdel, Inorg. Chem. 41 (2002) 5133.
[5] (a) E.-C. Yang, D.N. Hendrickson, W. Wernsdorfer, M. Nakano, L.N. Zakharov, R.D. Sommer, A.L. Rheingold, M. Ledezma-Gairaud, G. Christou, J. Appl. Phys. 91 (2002) 7382;
(b) M. Murrie, S.J. Teat, H. Stoeckli-Evans, H.U. Güdel, Angew. Chem., Int. Ed. 42 (2003) 4653.
[6] C. Zaleski, E. Depperman, J. Kampf, M. Kirk, V. Pecoraro, Angew. Chem., Int. Ed. 43 (2004) 3912.
[7] (a) A. Mishra, W. Wernsdorfer, K. Abboud, G. Christou, J. Am. Chem. Soc. 126 (2004) 15648;
(b) V. Mereacre, Ako M. Ayuk, R. Clérac, W. Wernsdorfer, G. Filoti, J. Bartolomé, C. Anson, A. Powel, J. Am. Chem. Soc. 129 (2007) 9248;
(c) V. Mereacre, M. Ayuk Ako, R. Clérac, W. Wernsdorfer, I. Hewitt, C. Anson, A. Powell, Chem. Eur. J. 14 (2008) 3577.
[8] A. Mishra, W. Wernsdorfer, S. Parson, G. Christou, E. Brechin, Chem. Commun. (2005) 2086.
[9] M. Murugesu, A. Mishra, W. Wernsdorfer, K. Abboud, G. Christou, Polyhedron 26 (2006) 613.
[10] C. Turta, D. Prodius, V. Mereacre, S. Shova, M. Gdaniec, Yu. Simonov, V. Kuncser, G. Filoti, A. Caneschi, L. Sorace, Inorg. Chem. Commun. 7 (2004) 576.
[11] G.M. Sheldrick, SHELX86, Acta Crystallogr. 46A (1990) 467.
[12] G.M. Sheldrick, SHELXL-97, University of Göttingen: Göttingen, Germany, 1997.
[13] (a) M.P. Shores, J.J. Sokol, J.R. Long, J. Am. Chem. Soc. 124 (2002) 2279;
(b) A. Bencini, D. Gatteschi, Electron Paramagnetic Resonance of Exchange-Coupled Systems, Springer-Verlag, New York, 1990. Section 2.5 and Appendix A, and references therein;
(c) L. Jiang, H.J. Choi, X.-L. Feng, T.-B. Lu, J.R. Long, Inorg. Chem. 46 (2007) 2181;
(d) C.-I. Yang, G. Chung, T.-S. Kuo, M. Shieh, H.-L. Tsai, Chem. Lett. 35 (2006) 724;
(e) J. Kim, S. Han, J.M. Lim, K.-Y. Choi, H. Nojiri, B.J. Suh, Inorg. Chim. Acta 360 (2007) 2647.
[14] O. Kahn, Molecular Magnetism, VCH Publishers, Inc., New York, Weinheim, Cambridge, 1993.

Polyhedron 27 (2008) 2464–2470

Contents lists available at ScienceDirect

Polyhedron

journal homepage: www.elsevier.com/locate/poly

Rhenium(IV)–copper(II) heterobimetallic complexes: Synthesis, crystal structure and magnetic properties

Alina Bieńko [a], Julia Kłak [a], Jerzy Mroziński [a,*], Rafał Kruszyński [b], Dariusz C. Bieńko [c], Roman Boča [d]

[a] Faculty of Chemistry, University of Wrocław, F.Joliot-Curie 14, 50-383 Wrocław, Poland
[b] Department of X-ray Crystallography and Crystal Chemistry, Institute of General and Ecological Chemistry Technical University Lodz, Zeromskiego 116, 90-924 Lodz, Poland
[c] Faculty of Chemistry, Wroclaw University of Technology, Smoluchowskiego 23, 50-37 Wroclaw, Poland
[d] Institute of Inorganic Chemistry, Slovak Technical University, SK 812 37 Bratislava, Slovakia

ARTICLE INFO

Article history:
Received 15 January 2008
Accepted 12 April 2008
Available online 23 June 2008

Keywords:
Chain structure
Chloro-bridged Re(IV) complexes
Macrocyclic complexes
Exchange interaction
Zero-field splitting

ABSTRACT

Two Re(IV)–Cu(II) heterometallic complexes $\{(CuL_\alpha)[ReCl_4(ox)]\}_n$ (where L_α = *N-meso*-5,12-Me_2-7,14-Et_2-[14]-4,11-dieneN$_4$), **1**, and $(CuL_\beta)[ReCl_4(ox)]$ (L_β = *N-rac*-5,12-Me_2-7,14-Et_2-[14]-4,11-dieneN$_4$*N-rac*-5,12-Me_2-7,14-Et_2-[14]-4,11-dieneN$_4$), **2**, were synthesized. The $[CuL^{2+}]$ macrocyclic cation is coordinated from above and below by $[ReCl_4(ox)]^{2-}$ units through the chloro-ligands and creates a chloro-bridged heterometallic Re^{IV}–Cu^{II} one-dimensional zig-zag chain. Compound **2** can be viewed as a heterobimetallic dinuclear unit, in which the Re(IV)-Cu(II) centers are linked by an oxalato bridge.The magnetic behavior of **1** and **2** has been investigated over the temperature range 1.8–300 K. Compound **1** behaves like a ferrimagnetic {Re(IV)–Cu(II)} bimetallic, one-dimensional chain with intrachain antiferromagnetic coupling.Compound **2** shows a weak antiferromagnetic interaction within the [Re(IV)–Cu(II)] unit along with a strong single-ion anisotropy,D(Re) = −63 cm^{-1}.

© 2008 Elsevier Ltd. All rights reserved.

1. Introduction

The search for new synthetic routes leading to polymetallic complexes is of current interest in modern inorganic chemistry [1]. One of the strategies to design polynuclear species is based on metals and organic building blocks. The building block approach was particularly developed in order to obtain heterometallic complexes with interesting magnetic, optical or electronic properties. It consists of the use of anionic complexes with potentially bridging ligands, which may interact with wide variety of assembling cations [2].

We are currently developing a synthetic approach aimed at obtaining polymetallic complexes by using the $[ReCl_4ox]^{2-}$ ion as a building block and macrocyclic-copper(II) ions as a cationic species.

Square-planar macrocyclic complexes of Cu(II) and Ni(II) with two free coordination sites at the metal atom are very attractive species in designing heterometallic complexes. Access to the metal ion is very easy when there are no substituents on the macrocyclic ring (like in the case of $[Cu(cyclam)]^{2+}$) presenting steric hindrance [3]. This situation changes with the size and character of the substituents. The position of the substituents around the equatorial nitrogen atoms of the ligands and the *N*-configuration of the macrocyclic ring influences the coordination mode of the polymetallic complexes, for instance, a simple dimeric form $(CuL)[Co(NCS)_4]$ [4], a trimeric unit $[NiL]_2[Mn(NCS)_4](ClO_4)_2 \cdot H_2O$ [5] or a chain structure $[CuL_\beta][ReCl_4(ox)]$ DMF [6].

Rhenium(IV), as a $5d^3$ ion, usually forms octahedral compounds; numerous types of hexachloro-, hexabromo- and hexaiodorhenate complexes have been throughly studied previously [7–9]. The substitution of two chloro-ligands for an oxalate group in the rhenium(IV) coordination sphere allows the synthesis of new heterodinuclear {Re(IV)–Cu(II)} complexes. The oxalate dianion is a common ligand which usually adopts a bidentate coordination mode when acting as a bridge between two metals. In fact, the coordination mode of the rhenium(IV) precursor, $[ReCl_4ox]^{2-}$ changes with the nature of the co-ligands in the coordination sphere of Cu(II), being monodentate in $[Cu(bpy)_2ReCl_4(ox)]$ and very asymmetric-bidentate in $[Cu(terpy)_2ReCl_4(ox)(H_2O)]$ [10]. The coupling between Re(IV) and Cu(II) can be of ferro- or antiferromagnetic nature; however, it is very weak in all cases because of the long Cu–O bonds and the bite angle of the oxalate ligand. Stronger coupling can be obtained when the ligand is coordinated in a symmetric-bidentate mode with two short Cu–O bonds.

In this paper, we present the synthesis, crystal structure and magnetic data over the temperature range 1.8–300 K for a coordination-unsaturated complex of copper(II) (Scheme 1) as well as of simple $[ReCl_4ox]^{2-}$ ions. It was also interesting to verify whether the geometry around the metallic centers and the electron spin

* Corresponding author. Fax: +48 713757307.
E-mail address: jmroz@wchuwr.chem.uni.wroc.pl (J. Mroziński).

0277-5387/$ - see front matter © 2008 Elsevier Ltd. All rights reserved.
doi:10.1016/j.poly.2008.04.056

density exert an influence on the crystalline structure as well as on the magnetic properties.

2. Experimental

2.1. Materials

All materials used in this work were of reagent grade purity and were used as commercially obtained. The $[CuL](ClO_4)_2$ was prepared as previously reported [11].

2.2. Synthesis of the complexes

Both complexes were prepared by similar methods. A solution of $[CuL](ClO_4)_2$ (81.44 mg, 0.15 mmol) in CH_3CN (10 cm^3) was added dropwise to a solution containing $[Bu_4N]_2[ReCl_4(ox)]$ (135.14 mg, 0.15 mmol) in the same solvent. The mixture was subsequently stirred. After a few days, a dark-pink crystalline solid was formed by slow evaporation from the violet solution. It was filtered and washed using diethyl ether (10 cm^3, twice). Yield: 108.30 mg (95%). Red, rectangular prism-shaped crystals of $\{(CuL_\alpha)[ReCl_4(ox)]\}_n$ (**1**), suitable for X-ray diffraction studies, were obtained by slow evaporation of a solution of all the reagents in CH_3CN–DMF (1:1) at room temperature. *Anal.* Calc. for $C_{18}H_{32}Cl_4CuN_4O_4Re$ (760.02): C, 28.41; H, 4.49; N, 7.35; Cl, 18.61. Found for isomer α: C, 28.50; H, 3.76; N, 7.09; Cl, 18.78%; found for isomer β: C, 28.43; H, 4.56; N, 7.20; Cl, 18.70%. The copper and rhenium contents were determined by the ICP method: calc. Re, 24.40, Cu, 8.34; found for isomer α: Re, 23.84, Cu, 7.98%; found for isomer β: Re, 24.83, Cu, 8.10%.

The purity of the compounds was confirmed by IR spectra. The infrared spectrum for each complex exhibits bands at 1725vs, 1700vs, 1666m, 1319s and 800s cm^{-1} for **1** and 1718m, 1663s, 1375m and 800m for **2**, which are associated with the oxalato ligand. Complex **1** has a single medium intensity absorption band at approximately 970 cm^{-1}, whereas in complex **2** this band is split into a doublet at 980 and 1010 cm^{-1}.

UV–Vis [λ in nm (ε)]: complex **1**: 1261, 1088, 1069, 712, 660, 493, 370, 262; complex **2**: 1268, 1089, 1071, 718, 670, 497, 258.

2.3. Magnetic measurements

Magnetic measurements were performed using a Quantum Design SQUID-based MPMSXL-5-type magnetometer in the temperature range T = 1.8–300 K. The SQUID magnetometer was calibrated with a palladium rod sample (Materials Research Corporation, measured purity 99.9985%). Measurements were made at a magnetic field of B = 0.5 T. Corrections based on subtracting the sample-holder signal were made and a contribution to the underlying diamagnetism was estimated from Pascal constants [12].

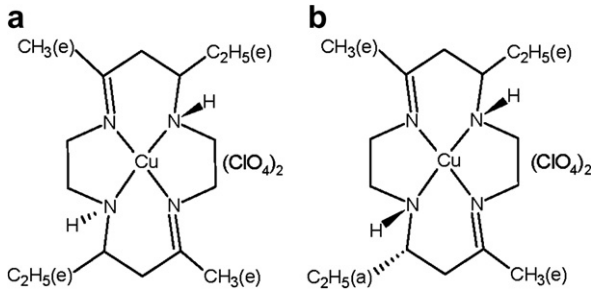

Scheme 1. Schematic view of the macrocyclic-copper(II) complexes: (a) $[CuL_\alpha](ClO_4)_2$, (b) $[CuL_\beta](ClO_4)_2$.

2.4. X-ray crystallographic study

A red rectangular prism-shaped crystal was mounted on a KM-4-CCD automatic diffractometer equipped with a CCD detector, and was used for data collection. X-ray intensity data were collected with graphite monochromated Mo Kα radiation (λ = 0.71073 Å) at a temperature of 291.0(3) K, with the ω scan mode. The exposure time was 31 s and reflections inside the Ewald sphere were collected up to $2\theta = 50°$. The unit cell parameters were determined from 9999 strongest reflections. Examination of reflections on six reference frames monitored after each 10 frames measured showed 0.3% loss of the intensity. During the data reduction above, a decay correction coefficient was taken into account. Lorentz, polarization, and numerical absorption [13] corrections were applied. The structure was solved by the partial structure expansion procedure. All the non-hydrogen atoms were refined anisotropically using the full-matrix, least-squares technique on F^2. All the hydrogen atoms were found from difference Fourier synthesis after four cycles of anisotropic refinement, and refined as "riding" on the adjacent atom with geometric idealization after each cycle of refinement and individual isotropic displacement factors equal to 1.2 times the value of the equivalent displacement factor of the parent non-methyl atom and 1.5 times of parent methyl group carbon atom. The methyl groups were allowed to rotate about their local threefold axis. The SHELXS97 [14], SHELXL97 [15] and SHELXTL [16] programs were used for all the calculations. Atomic scattering factors were those incorporated in the computer programs.

3. Results and discussion

3.1. Structural description

Details concerning the crystal data and refinement are given in Table 1. A perspective view of the structure of compound **1** occupying the asymmetric unit of the unit cell, together with the atom numbering scheme, is shown in Fig. 1. The methyl group indicated by the C(7) atom is disordered over two positions with 54:46 participation of the domains. The asymmetric unit includes a half of two macrocycles and a $ReO_4C_2Cl_2$ molecule. The copper atoms lie on inversion centers (special positions *b* and *e* of $P\bar{1}$ space group at 0, 0, 0.5 and 0.5, 0.5, 0, respectively [17]) and remaining atoms lie in general positions. The copper atoms are six coordinated by four macrocyclic nitrogen atoms and two rhenium bonded chlorine atoms.

The coordination polyhedra of the copper atoms can be described as almost ideal tetragonal bipyramid (the CuN_4moiety is planar by symmetry) with chlorine atoms in axial positions. Adopting a slightly disordered tetragonal bipyramid coordination, the rhenium atom is six coordinated by four chlorine atoms and two oxygen atoms of two carboxylic groups of oxalate substituents. The bridging chlorine atoms are located on opposite sides of the rhenium atom. The Cu–Cl distances (Table 2) are distinctly larger than the most common value of 2.293 Å, but lie in the typical range, 2.1–3.1 Å, observed for copper coordination compounds. The macrocycles conformations can be described as sc^-, sc^+, ap^-, ac^-, sc^-, ap^+, ap^+, sc^+, sc^-, ap^+, ac^+, sc^+, ap^-, ap^- and sc^+, sp^-, ap^+, ac^+, ac^+, ap^-, ac^+, sc^-, sp^+, ap^-, ac^-, ac^-, ap^+, ac^-, respectively, for the ligands bonded to the Cu(1) and Cu(2) atoms. The inversion center on the copper atoms expands the molecules to a one-dimensional zig-zag coordination polymer along the [11-1] crystallographic axis (Fig. 2).

In the structure medium strength N–H···Cl hydrogen bonds can be found (Table 3) [18], providing additional stabilization to the polymer chain. Additionally, a couple of weak C–H···O and C–H···Cl hydrogen bonds can be found in the structure (Fig. 3,

Table 1
Crystal data and structure refinement for the compound {[CuL][$ReCl_4$(ox)]}

Empirical formula	$C_{18}H_{32}Cl_4CuN_4O_4Re$
Formula weight	760.02
Temperature (K)	291.0(3)
Wavelength (Å)	λ(Mo Kα) = 0.71073
Crystal system	triclinic
Space group	$P\bar{1}$
Unit cell dimensions	
a (Å)	8.1239(6)
b (Å)	10.8056(5)
c (Å)	16.1670(9)
α (°)	73.098(5)
β (°)	83.298(5)
γ (°)	78.010(5)
Volume (Å^3)	1325.86(14)
Z	2
D_{calc} (Mg/m^3)	1.904
Absorption coefficient (mm^{-1})	5.797
F(000)	744
Crystal size (mm)	0.273 × 0.241 × 0.187
θ Range for data collection	2.64–25.00
Index ranges	$-9 \leqslant h \leqslant 8$, $-12 \leqslant k \leqslant 12$, $-19 \leqslant l \leqslant 16$
Reflections collected/unique (R_{int})	14296/4657 (0.0180)
Completeness to 2θ = 25.11° (%)	99.5
Refinement method	full-matrix least-squares on F^2
Maximum and minimum transmission	0.330 and 0.219
Data/restraints/parameters	4657/0/309
Goodness-of-fit on F^2	1.074
Final R indices [$I > 2\sigma(I)$]	R_1 = 0.0212, wR_2 = 0.0529
R indices (all data)	R_1 = 0.0248, wR_2 = 0.0548
Largest difference in peak and hole (e Å^{-3})	1.094 and −1.600

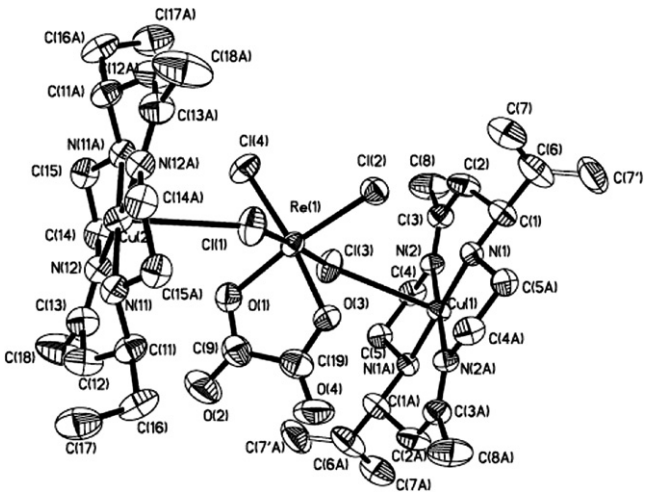

Fig. 1. The molecular conformation of the compound {[CuL][$ReCl_4$(ox)]} with the atom numbering, plotted with 50% probability displacement ellipsoids. The hydrogen atoms are omitted for clarity. The symmetry generated atoms are indicated by the "A" letter added after the atom number. The disordered methyl group is indicated by hollow connections.

Table 2) [19]. The shortest Cu(1)···Re(1) distances are 4.7177(3) Å and they exists in the polymer chain, a longer distance of 7.3517(5) Å occurs between polymer chains. These distances for the Cu(2)···Re(1) atoms are 4.6840(3) and 7.2964(6) Å, respectively.

3.2. Magnetic properties

In this section, the magnetic properties of compounds **1** and **2** are presented together with the analysis of the magnetic exchange interaction. Finally, an analysis of exchange pathways in **1** will be enlightened through spin density calculations using the DFT methodology.

Table 2
Selected structural data for {[CuLα][$ReCl_4$(ox)]} compound

Re(1)–O(1)	2.019(2)
Re(1)–O(3)	2.024(2)
Re(1)–Cl(4)	2.3388(9)
Re(1)–Cl(2)	2.3405(9)
Re(1)–Cl(3)	2.3498(9)
Re(1)–Cl(1)	2.3616(9)
O(1)–C(9)	1.309(5)
O(2)–C(9)	1.200(5)
C(9)–C(19)	1.554(6)
C(19)–O(4)	1.200(5)
C(19)–O(3)	1.310(5)
Cu(1)–N(2)	1.997(2)
Cu(1)–N(1)	2.001(3)
Cu(2)–N(12)	1.988(3)
Cu(2)–N(11)	2.013(3)
Cu(1)–Cl(3)	2.9912(9)
Cu(2)–Cl(1)	2.9767(9)
O(1)–Re(1)–O(3)	80.09(11)
O(1)–Re(1)–Cl(4)	92.89(8)
O(3)–Re(1)–Cl(4)	172.98(7)
O(1)–Re(1)–Cl(2)	173.05(7)
O(3)–Re(1)–Cl(2)	92.96(7)
Cl(4)–Re(1)–Cl(2)	94.06(4)
O(1)–Re(1)–Cl(3)	88.93(8)
O(3)–Re(1)–Cl(3)	87.86(8)
Cl(4)–Re(1)–Cl(3)	91.92(3)
Cl(2)–Re(1)–Cl(3)	90.65(3)
O(1)–Re(1)–Cl(1)	89.30(8)
O(3)–Re(1)–Cl(1)	88.79(8)
Cl(4)–Re(1)–Cl(1)	91.26(3)
Cl(2)–Re(1)–Cl(1)	90.73(3)
Cl(3)–Re(1)–Cl(1)	176.44(3)
C (9)–O(1)–Re(1)	116.6(2)
O(2)–C(9)–O(1)	124.5(4)
O(2)–C(9)–C(19)	122.4(4)
O(1)–C(9)–C(19)	113.2(3)
O(4)–C(19)–O(3)	123.0(4)
O(4)–C(19)–C(9)	123.1(4)
O(3)–C(19)–C(9)	113.9(3)
C(19)–O(3)–Re(1)	115.8(2)
N(2)#1–Cu(1)–N(2)	180.0
N(2)#1–Cu(1)–N(1)#1	94.89(11)
N(2)–Cu(1)–N(1)#1	85.11(11)
N(2)–Cu(1)–N(1)	94.89(11)
N(1)#1–Cu(1)–N(1)	180.0
N(12)#2–Cu(2)–N(12)	180.0
N(12)–Cu(2)–N(11)	94.45(12)
N(12)–Cu(2)–N(11)#2	85.55(12)
N(11)–Cu(2)–N(11)#2	180.0
Cl(3)–Cu(1)–Cl(3)#1	180.00
Cl(3)–Cu(1)–N(1)	88.69(8)
Cl(3)–Cu(1)–N(2)	82.38 (8)
Cl(1)–Cu(2)–Cl(1)#2	180.00
Cl(1)–Cu(2)–N(11)	92.67(8)
Cl(1)–Cu(2)–N(12)	98.69(8)

Distances in Å, angles in °. [Symmetry transformations used to generate equivalent atoms: #1: $-x+1$, $-y+1$, $-z$; #2: $-x$, $-y$, $-z+1$.]

The magnetic susceptibility of complexes **1** and **2** is presented in terms of the product function $\chi_{mol}T$ in Fig. 4 between 1.8 and 300 K. The data for $[Bu_4N]_2[ReCl_4(ox)]$ is also included for comparison.

Complex **1** shows a typical 1D ferrimagnetic behavior. At room temperature $\chi_{mol}T$ = 2.09 cm^3 mol^{-1} K (μ_{eff} = 4.10 μ_B) and this value is expected for a magnetically non-interacting {Cu(II)–Re(IV)} entity with local spins S(Cu) = 1/2 and S(Re) = 3/2 (2.25 cm^3 mol^{-1} K, g = 2.0). As the temperature is lowered, the value of $\chi_{mol}T$ smoothly decreases and reaches a minimum at T = 25.0 K ($\chi_{mol}T$ = 1.72 cm^3 K mol^{-1}) corresponding to a short-range order state where the two uncoupled spins of the adjacent ions {Cu(II)–Re(IV)} exist. Below

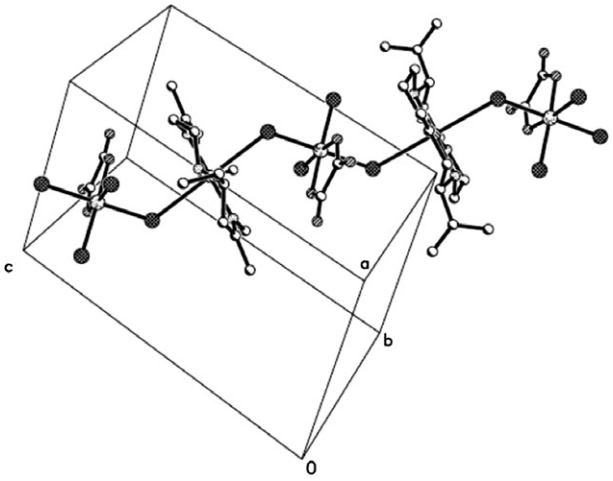

Fig. 2. The coordination polymer.

Table 3
Hydrogen bonds for {[CuL$_\alpha$][ReCl$_4$(ox)]} compound

D–H···A	*d*(D–H)	*d*(H···A)	*d*(D···A)	∠(DHA)
N(1)–H(1N)···Cl(2)	0.93	2.47	3.383(3)	165.8
N(11)–H(11N)···Cl(4)#l	0.74	2.81	3.514(3)	161.0
C(2)–H(2B)···O(4)#2	0.97	2.46	3.385(5)	159.4
C(4)–H(4A)···O(3)#3	0.97	2.57	3.380(4)	140.5
C(7)–H(7B)···Cl(2)	0.96	2.72	3.568(9)	148.3
C(8)–H(8B)···O(4)#3	0.96	2.59	3.348(7)	136.0

Distances in Å, angles in °. [Symmetry transformations used to generate equivalent atoms: #1: $-x$, $-y$, $-z+$l; #2: x, $y+$l, z; #3: $-x+$l, $-y+$l, $-z$.]

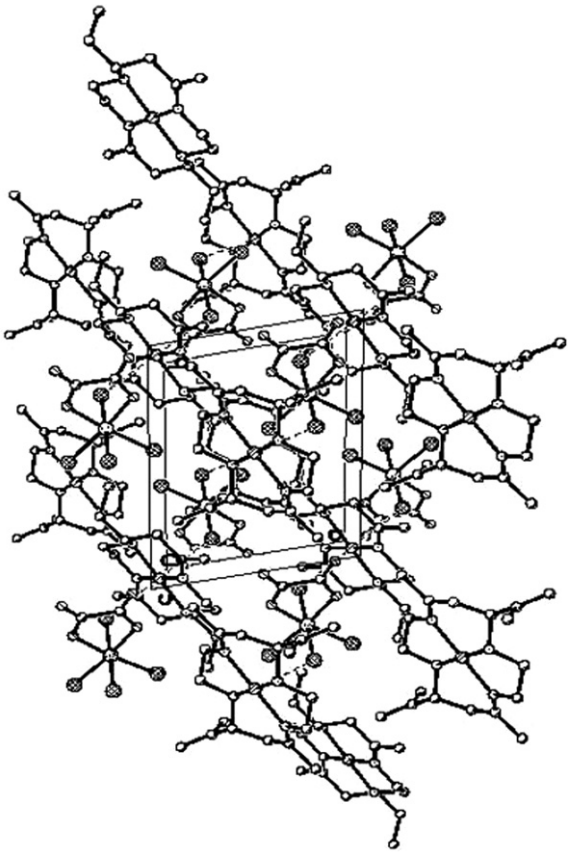

Fig. 3. Unit cell of **1** (H atoms of the macrocycle have been omitted for clarity).

this temperature the $\chi_{mol}T$ value increases and reaches a maximum at 7.0 K ($\chi_{mol}T$ = 1.87 cm^3 K mol^{-1}). Finally, it decreases abruptly between 7.0 and 1.72 K (see inset in Fig. 4). For $\chi_{mol}T$ values below the minimum, a ferrimagnetic ordering [20] in the chain exists. At very low temperatures an additional exchange interaction between the spins of the nearest neighboring chains causes the transition to a three-dimensional magnetic system.

The molar magnetic susceptibility of **1** shows an increase on cooling down to T = 5 K, where it passes through a maximum (Fig. 4, inset). The values of C and Θ determined from the relation $1/\chi_{mol} = f(T)$ over the 50–300 K range of temperatures are equal to C = 2.22 cm^3 mol^{-1} and Θ = −19.4 K, respectively. The negative value of the Weiss constant indicates an antiferromagnetic coupling.

In order to interpret the susceptibility data quantitatively, we approached it using a one-dimensional model in which the magnetic susceptibility in the high-temperature region of the examined compound may be described by two terms. The first contribution comes from the $^4A_{2g}$ term of the Re(IV) ions (with zero-field splitting), the second from the $^2T_{2g}$ term of the Cu(II) ions modified by a factor predicted from the Ising model of the magnetic exchange interactions and different local g values (g_{Cu} and g_{Re}) [14,15]. The relevant spin Hamiltonian is defined by the following equation (1) [21,22]:

$$\hat{H} = \sum_i \{ -J\hat{S}^z_{2i-1}\hat{S}^z_{2i} - j\hat{S}^z_{2i}\hat{S}^z_{2i+1} + 2D[(\hat{S}^z_{2i})^2 - 5/4] + \mu_B g_{Cu,\parallel} B_z \hat{S}^z_{2i-1} + \mu_B g_{Re,\parallel} B_z \hat{S}^z_{2i} + \mu_B g_{Cu,\perp}(B_x \hat{S}^x_{2i-1} + B_y \hat{S}^y_{2i-1}) + \mu_B g_{Re,\perp}(B_x \hat{S}^x_{2i} + B_y \hat{S}^y_{2i}) \} \quad (1)$$

where the total spins $S_{2i} = S_{Re}$ and $S_{2i-1} = S_{Cu}$; J is the isotropic exchange-coupling parameter between the Re(IV) and Cu(II) magnetic centers mediated by the chloro-donor; j is the exchange-coupling parameter through the oxalate oxygen atom, 2D is the energy gap between the ±3/2 and ±1/2 Kramers doublets of the Re(IV) center.

The least squares fit of the experimental data by this expression was limited to the range 20.0–300 K and leads to the following results: $2D$ = 126 cm^{-1}, g_{av}(Re) = 1.89, g_{av}(Cu) = 2.20 and J = −18.1 cm^{-1}, j = −0.72 cm^{-1}. The discrepancy factor, defined as $\lfloor R = \sum(\chi_{exp}T - \chi_{calc}T)^2 / \sum(\chi_{exp}T)^2 \rfloor$, is 2.05 × 10^{-5}. The calculated curve matches the magnetic data very well. It deserves to be noted that the 2D value is greater than that found for [Bu$_4$N]$_2$ReCl$_4$(ox) (2D = 53 cm^{-1}) [9]. These relatively large values of the D parameter for third-row transition metal ions reflect the large value of the spin–orbit splitting parameter ($\lambda \sim 1100$ cm^{-1} for the isolated Re(IV) ion).

The variation of the molar magnetization M_{mol} versus B at T = 2.0 K (Fig. 4, right), i.e. below the magnetic ordering, clearly supports the occurrence of spontaneous magnetic moments in complex **1**. As the magnetic field increases, the *M versus B* curve is linear up to 0.1 T, and then shows a sinusoidal variation before reaching saturation at a value of M_{sat} = 2.11 μ_B per rhenium–copper pair [20]. In such a case the ground state equals S_{max} = 1/2 + 3/2 = 2 and the magnetization (per {Cu–Re} unit) should saturate to the value of M_{sat} = 4.0 μ_B. The obtained value is substantially smaller and it evidences a sizable zero-field splitting for Re(IV) along with the antiferromagnetic exchange coupling between the Re(IV)···Cu(II) ions. For the compound [Bu$_4$N]$_2$ReCl$_4$(ox) the saturation magnetization adopts a value of M_{sat} = 1.60 μ_B (per Re atom).

At the first sight, the efficiency of the intrachain exchange pathways in complex **1** to mediate magnetic interactions is quite surprising. The literature data [6,10,23] reported a detailed description of the magnetic behaviour of heteropolynuclear complexes containing the [ReCl$_4$(ox)]$^{2-}$ ion as a building block. These compounds exhibit different coordination modes depending on the M(II) 3d metal ion and auxiliary ligand used to complete the coordination sphere: isolated dinuclear units in [ReCl$_4$(μ-ox)Mn(dmphen)$_2$] · CH$_3$CN [23]

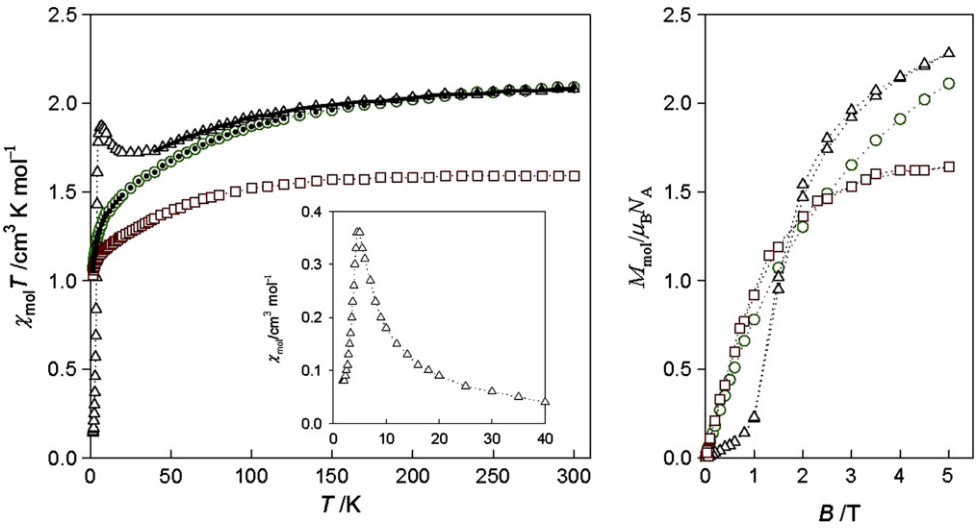

Fig. 4. Magnetic functions: (Δ, **1**) {[CuL_α][$ReCl_4$(ox)]}, (○, **2**) [CuL_β][$ReCl_4$(ox)] and (□) [Bu_4N]$_2$[$ReCl_4$(ox)]. Solid line – calculated curve. Left – temperature dependence of the product function; right – molar magnetization. Inset – the magnetic susceptibility for **1**.

and infinite chains in [CuL_β][$ReCl_4$(ox)] · DMF (L_β = *N-dl*-5,7,7,12, 14,14-hexamethyl-1,4,8,11 tetraazacyclotetradeca-4,11-diene) [6]. However in all of these cases the Re(IV) ion and M(II) metal ion are bridged by the oxalato ligand. Complex **1** is the first example in which a chloro-bridge between Re(IV) and Cu(II) exists. The crystal structure shows that the macrocyclic ligand, with a Cu(II) magnetic center, is linked by a chloro-bridge to the Re(IV) unit and thus generates a chloro-bridged bimetallic zig-zag chain.

A possible mechanism for the one-dimensional ordering in the complex under study can be understood through orbital symmetry considerations. The magnitude of the interaction is due to the overlap of the magnetic orbital on either side of the bridge. Tetrahedral distortion of the copper environment is the apparent cause for the four short equatorial bonds to N(4), N(8), N(11) and N(15), which ensure the delocalization of the unpaired electron of the d_{z^2} magnetic orbital within the equatorial plane and disrupt the orthogonality between this orbital and the d_{xy} orbital of Re(IV) through the chloro ligand. The chloro ligand between the Re(1)–Cu(1) pair causes a poor overlap, resulting in the antiferromagnetic coupling $J = -18.1$ cm^{-1}. Halide bridges have been observed in other copper complexes, but most of these have at least two bridges with angular Cu–halide–Cu bonds. The greater bond lengths of the copper atom to the axial donor will cause a negligible magnetic interaction through this pathway. The Cu–Cl bond distance in the present structure (2.97 Å) is distinctly larger than the most common value of 2.293 Å. On the other hand, there are no relatively efficient interchain exchange pathways possible. As follows from the section of the structure, the shortest Cu(1)···Re(1) distance of 4.7177(3) Å exists inside the polymer chain; the second shortest contact is as long as 7.3517(5) Å and it occurs between chains. Their counterparts for the Cu(2)···Re(1) atoms are 4.6840(3) and 7.2964(6) Å, respectively. This might provide an interchain exchange pathway, for example through the oxalate ion. Three unpaired electrons of Re(IV) are described by π-type orbitals, which have a lower efficiency in mediating exchange coupling than σ orbitals. However, the great diffuse character of the 5d type orbitals of the rhenium atom as well as its high oxidation state lead to significantly greater electronic delocalization.

To confirm this hypothesis DFT calculations were carried out. The computed spin densities are given in Table 4 (the atom numbering of the real structure of **1** has been kept). It deserves to be noted that the net spin density on a particular atomic orbital or atom is the result of two mechanisms: spin delocalization and spin polarization. As we can see in Table 4 there are only positive values of the spin densities in the examined compound, which allows us to suggest that the spin delocalization mechanism predominates and it is responsible for the great spin density on the ligand atoms. This result suggests that in complex **1** there are two magnetic exchange pathways: one (the intrachain magnetic exchange interaction between Re(IV) and Cu(II) paramagnetic centers through the chloro bridges) being much greater that the other (the interchain magnetic exchange interaction through the oxalato ligand).

Table 4
DFT-calculation atomic spin densities for **1**

Atom	Spin density	Atom	Spin density
Re(1)	3.6399	Cl(l)	0.07254
O(1)	0.0185	Cl(2)	0.0426
O(2)	0.0357	Cl(3)	0.0725
O(3)	0.0185	Cl(4)	0.0256
O(4)	0.0357	C(l)	0.0082
Cu(1)	0.3171	C(2)	0.0082

Complex **2** exhibits different magnetic properties. The product function at room temperature adopts the value of $\chi_{mol}T = 2.10$ cm^3 mol^{-1} K, which is expected for uncoupled Re(IV) and Cu(II) units. The product function smoothly decreases over a wide temperature range and then more rapidly drops down at the lowest temperature (Fig. 5). The slight decrease of $\chi_{mol}T$ can be due to the 2zero-field splitting of Re(IV) ions and to intramolecular exchange interactions between Re(IV)···Cu(II) ions.

Discussion of the magnetic properties of complex **2** requires some consideration of its structure, which is unknown because it was not possible to obtain suitable crystals for an X-ray diffraction study. Taking into account the coordination modes of the oxalato bridge, i.e. bidentate as in [CuL_β][$ReCl_4$(ox)] · DMF (L_β = *N-dl*-5,7,7,12,14,14-hexamethyl-1,4,8,11 tetraazacyclotetradeca-4,11-diene) [6] or monodentate as in [Cu(bipy)$_2$$ReCl_4$(ox)] [10], we can imagine the structure of **2** as a dinuclear complex with a single magnetic coupling parameter *J*.

The macrocyclic complex cations $[CuL_\alpha]^{2+}$ and $[CuL_\beta]^{2+}$ used in the synthesis occur in the form of two isomers, differing in the configuration of the donor nitrogen atoms. The differences in the crystalline structure of complex **1** compared to complex **2** have a significant influence on its magnetic properties. Both macrocyclic $[CuL]^{2+}$ ions have the same configuration of the carbon atoms

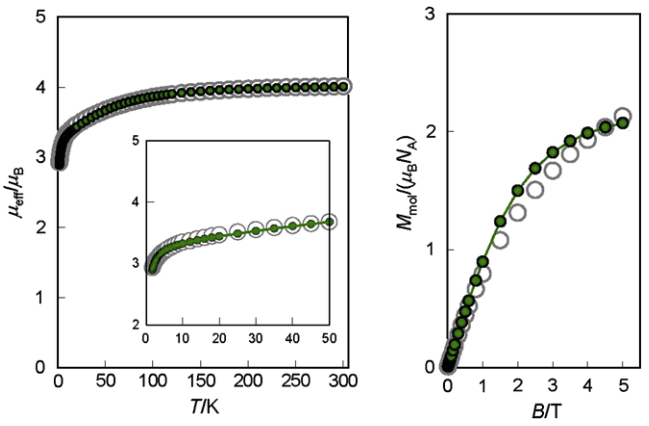

Fig. 5. Experimental (open symbols) and calculated (filled) magnetic data for **2**.

substituted with ethyl groups (*C-meso*). Complex **1** adopts the N–meso-*C-meso* configuration; thus, both ethyl groups take an equatorial position and the central ion is accessible for the bridging ligands from both sides, due to which it forms a linear polymer with the $[ReCl_4ox]^{2-}$ anion.

The inversion of configuration of one asymmetric nitrogen atom causes a partial conversion of the macrocyclic ring conformation, which is accompanied by the inversion of the conformation of the 7-ethyl group from equatorial into axial. The peripheral axial ethyl group blocks one of the axial sites in the isomeric cation (*N-rac–C-meso*). Therefore, the central copper(II) ion is able to coordinate to only one $[ReCl_4ox]^{2-}$ anion and forms the dinuclear complex **2**, bridging by only one oxygen. In fact, the presence of CH_3CN (the solvent used in this synthesis) can be ruled out by the IR spectrum and the elemental analysis. A very similar situation was observed in the previously studied compounds of the general formula (CuL)[$Co(NCS)_4$] with the same macrocyclic isomers (the crystal structures of both isomers were published elsewhere [4]). Based on these considerations, the proposed structure of **2** is shown in Scheme 2.

The magnetic properties of **2** were modelled with the spin Hamiltonian:

$$\hat{H} = -J(\vec{S}_{Re} \cdot \vec{S}_{Cu}) + \mu_B \vec{B} \cdot (g_{Re}\vec{S}_{Re} + g_{Cu}\vec{S}_{Cu}) + D_{Re}(\hat{S}^2_{Re,z} - \vec{S}^2_{Re,z}/3) \quad (2)$$

where the symbols adopt their usual meaning. The magnetic field in the Zeeman term has been applied along the molecular *z*- and *x*-axis and then the corresponding susceptibility and magnetization were averaged. The parameter set to be optimized is *J*, $g_{Re}(z)$, $g_{Re}(x)$ and g_{Cu}(iso). The axial zero-field splitting parameter for the Re(IV) ion has been recovered from the constraint offered by the spin Hamiltonian formalism [24]:

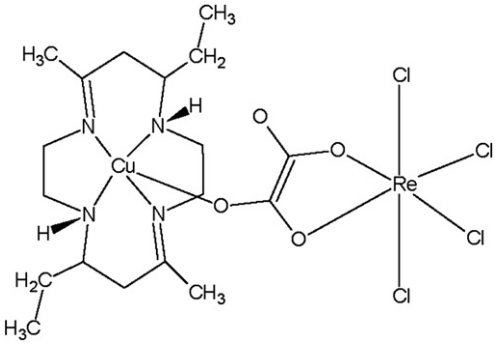

Scheme 2. Proposed dinuclear structure of $[L_\beta Cu(\mu\text{-ox})ReCl_4]$, **2**.

$$D = \lambda(g_z - g_x)/2 \quad (3)$$

with the single-ion spin–orbit splitting parameter $\lambda = 1000\ cm^{-1}$. The matrix elements of the spin Hamiltonian matrix (8×8) have been evaluated in the uncoupled basis set of spin functions, which does not suffer any constraint to magnetic parameters (like the strong-exchange limit) [25]. Indeed, the fitted *J*-value is much lower than the single-ion anisotropy *D*(Re) and the final set of parameters is $J = -0.71\ cm^{-1}$, $g_{Re}(z) = 1.687$, $g_{Re}(x) = 1.813$, g_{Cu}(iso) = 2.470 and $D(Re) = -62.7\ cm^{-1}$. The susceptibility set is recovered perfectly ($R(\chi) = 0.015$) and the magnetization set (with a simple *z*/*x*-average) is satisfactory ($R(M) = 0.078$), as displayed in Fig. 5.

It seems interesting to compare the magnetic behavior of complexes **1** and **2** with that obtained for $[CuL_\beta][ReCl_4(ox)] \cdot DMF$ (L_β = *N-dl*-5,7,7,12,14,14-hexamethyl-1,4,8,11 tetraazacyclotetradeca-4,11-diene) [6]. The partial conversion of the macrocyclic ring conformation in complexes **1** and **2** is caused by an increase of the size of the substituent in the macrocyclic ring (from methyl to ethyl group). As a consequence, the ethyl groups block the possibility of connecting Re(IV) and Cu(II) centers by the oxalato bridge as in the case of the previously reported complexes $[CuL_\beta][ReCl_4(ox)] \cdot DMF$ (L_β = *N-dl*-5,7,7,12,14,14-hexamethyl-1,4,8,11tetraazacyclotetradeca-4,11-diene) and $[(CuL\alpha)_2Cl][ReCl_4(ox)]Cl$ ($L\alpha$ = *N-dl*-5,7,7,12,12,14-hexamethyl-1,4,8,11-tetraazacyclotetradeca-4,14-diene) [6]. Replacement of the methyl group in the macrocycle coordination sphere by a more bulky ethyl group causes steric hindrance, preventing the coordination to the metal ion. However the stronger antiferromagnetic interaction has been registered in the case of the chlorine-bridge complex.

4. Conclusion

Only a few bimetallic {Re(IV)Cu(II)} chain compounds have been reported so far. In these complexes the metal ions were connected by an oxalato bridge [6,10,23]. Our results show that it is possible to synthesize a new chloro-bridged heterometallic {Re(IV)Cu(II)} chain possessing a one-dimensional zig-zag structure by using $[ReCl_4(ox)]^{2-}$ anions as components that bridge macrocyclic $[CuL]^{2+}$ cations. The magnitude of the magnetic coupling between Re(IV) and Cu(II) in this class of compounds can be tuned by changing the coordination geometry around the copper(II) ions. This coordination depends on the position of the ethyl groups around the equatorial nitrogen atoms of the ligands. In the case of **1**, a 1D ferrimagnetic chain compound was obtained. Each $[ReCl_4(ox)]^{2-}$ ion is bound by two Cu–Cl bonds to two macrocyclic fragments. The magnetic measurements indicate antiferromagnetic interactions between the Re(IV) and Cu(II) metal ions within the chains. In the case of **2**, the $[CuL_\beta]^{2+}$ ion brings about the possibility for monodentate coordination of the oxalato ligand. On the basis of literature data [4,8,9], magnetic measurements and elemental analysis, this compound can be viewed as a bimetallic Re(IV)–Cu(II) unit. Replacement of the methyl group in the macrocycle coordination sphere by a larger ethyl group influences the magnitude of the magnetic exchange interaction. The analysis of these results suggest that a stronger magnetic interaction could be obtained if the rhenium(IV) ions were coordinated by other first-row transition metal macrocycles.

5 Supplementary data

CCDC 637068 contains the supplementary crystallographic data for this paper. These data can be obtained free of charge via http://www.ccdc.cam.ac.uk/conts/retrieving.html, or from the Cambridge Crystallographic Data Centre, 12 Union Road, Cambridge CB2 1EZ, UK; fax: (+44) 1223-336-033; or e-mail: deposit@ccdc.cam.ac.uk.

Acknowledgements

This work was supported by the EC 6th FP, NoE "MAGMANet" and by the Polish Ministry of Science and Higher Education Grant No. 1T09A12430. The crystallographic part was financed by funds allocated by the Ministry of Science and Higher Education to the Institute of General and Ecological Chemistry, Technical University of Lodź. Thanks are expressed also to Slovak Grant Agencies (VEGA-1/0213/08, and COST-0006-06). The theoretical calculations were supported by a grant from the Wroclaw University of Technology. The Wroclaw centre for Networking and Supercomputing and the Poznan Supercomputer and Networking center are acknowledged for generous computer time.

References

[1] O. Kahn, Adv. Inorg. Chem. 43 (1995) 179.
[2] M. Pascu, F. Lioret, N. Avarvari, M. Julve, M. Andruh, Inorg. Chem. 43 (2004) 5189.
[3] G. Francese, S. Ferlay, H.W. Schmalle, S. Decurtins, New J. Chem. (1999) 267.
[4] A. Skorupa, B. Korybut-Daszkiewicz, J. Mroziński, Inorg. Chim. Acta (2001) 1.
[5] A. Bieńko, J. Kłak, J. Mroziński, R. Boča, I. Brüdgam, H. Hartl, J. Chem. Soc., Dalton Trans. (2007) 2681.
[6] A. Tomkiewicz, J. Mrozinski, I. Brüdgam, H. Hartl, Eur. J. Inorg. Chem. (2005) 1787.
[7] A. Tomkiewicz, A. Zygmunt, J. Mrozinski, J. Mol. Struct. 644 (2003) 97.
[8] A. Tomkiewicz, F. Villain, J. Mrozinski, J. Mol. Struct. 555 (2000) 383.
[9] A. Tomkiewicz, T.J. Bartczak, R. Kruszynski, J. Mrozinski, J. Mol. Struct. 595 (2001) 225.
[10] R. Chiozzone, R. González, C. Kremer, G. De Munno, J. Cano, F. Lloret, M. Julve, J. Faus, Inorg. Chem. 38 (1999) 4745.
[11] R.A. Koliński, B. Korybut-Daszkiewicz, Inorg. Chim. Acta 14 (1975) 237.
[12] E.A. Boudreaux, L.N. Mulay, Theory and Applications of Molecular Paramagnetism, Wiley Interscience, New York, 1976.
[13] X-RED. Version 1.18. STOE & Cie GmbH, Darmstadt, Germany, 1999.
[14] G.M. Sheldrick, Acta Crystallogr., Sect. A 46 (1990) 467.
[15] G.M. Sheldrick, SHELXL97. Program for the Solution and Refinement of Crystal Structures, University of Göttingen, Germany, 1997.
[16] G.M. Sheldrick, SHELXTL: Release 4.1 for Siemens Crystallographic Research Systems, 1990.
[17] T. Hahn (Ed.), International Tables for Crystallography Volume A, D. Reidel Publishing Company, Dordrecht, Holland, 1983.
[18] G.A. Jeffrey, W. Saenger, Hydrogen Bonding in Biological Structures, Springer, Verlag, 1994.
[19] G.R. Desiraju, T. Steiner, The Weak Hydrogen Bond in Structural Chemistry and Biology, Oxford University Press, 1999.
[20] O. Kahn, Molecular Magnetism, VCH, New York, 1993.
[21] H.O. Stumpf, Y. Pei, L. Ouahab, F. Le Berre, E. Codjovi, O. Kahn, Inorg. Chem. 32 (1993) 5687.
[22] B. Bleaney, K.D. Bowers, Proc. Roy. Soc. Ser. A 214 (1952) 451.
[23] R. Chiozzone, R. González, C. Kremer, G. De Munno, D. Armentano, F. Lloret, M. Julve, J. Faus, Inorg. Chem. 42 (2003) 1064.
[24] R. Boča, Struct. Bonding 117 (2006) 1.
[25] R. Boča, Theoretical Foundations of Molecular Magnetism, Elsevier, Amsterdam, 1999.

Polyhedron 27 (2008) 2471–2477

Contents lists available at ScienceDirect

Polyhedron

journal homepage: www.elsevier.com/locate/poly

A new coordination mode of pyrazine-2,3-dicarboxylic acid and its first monodentate complexes: Syntheses, spectral, thermal and structural characterization of $[Cu(pzdca)(H_2O)(en)_2] \cdot H_2O$ and $[Cu(pzdca)(H_2O)(dmpen)_2]$

Okan Zafer Yeşilel [a,*], Aylin Mutlu [a], Orhan Büyükgüngör [b]

[a] Department of Chemistry, Faculty of Arts and Sciences, Eskişehir Osmangazi University, 26480 Eskişehir, Turkey
[b] Department of Physics, Faculty of Arts and Sciences, Ondokuz Mayis University, 55139 Kurupelit, Samsun, Turkey

ARTICLE INFO

Article history:
Received 28 February 2008
Accepted 18 April 2008
Available online 18 June 2008

Keywords:
New coordination mode
Pyrazine-2,3-dicarboxylate complex
Pyrazine-2,3-dicarboxylic acid
Ethylenediamine complex
2,2-Dimethylpropane-1,3-diamine complex

ABSTRACT

The novel aquabis(ethylenediamine)pyrazine-2,3-dicarboxylatocopper(II) hydrate, $[Cu(pzdca)(H_2O)(en)_2] \cdot H_2O$ (**1**) and aquabis(2,2-dimethylpropane-1,3-diamine)pyrazine-2,3-dicarboxylatocopper(II) complex, $[Cu(pzdca)(H_2O)(dmpen)_2]$ (**2**), (H_2pzdca = pyrazine-2,3-dicarboxylic acid, en = ethylenediamine and dmpen = 2,2-dimethylpropane-1,3-diamine), with a new coordination mode of pyrazine-2,3-dicarboxylic acid, have been prepared and characterized by elemental analyses, IR spectroscopy, thermal analyses and single crystal X-ray diffraction. Both complexes crystallize in the triclinic system, space group $P\bar{1}$ and in which the Cu(II) ions exhibit a distorted octahedral coordination by a monodentate pzdca dianion, two bidentate en or dmpen ligands and one aqua ligand. The thermal decomposition of the complexes has been predicted with the help of thermal analyses (TG, DTG and DTA).

© 2008 Elsevier Ltd. All rights reserved.

1. Introduction

Pyrazine-2,3-dicarboxylic acid (H_2pzdca) and its anions have been of interest in coordination and supramolecular chemistry and they generally tend to react with metal salts to yield insoluble polynuclear materials. The deprotonated pzdca anions ($Hpzdca^-$ and $pzdca^{2-}$) behave as polyfunctional ligands and they are well known to act as bridging ligands in metal complexes [1–17]. The pzdca anion coordinates to metal ions via its two carboxyl groups and two nitrogen atoms of the pyrazine ring. Various possible coordination modes for the pzdca ligand, such as bidentate [18–22], bis(bidentate) bridge (μ_2) [1–4], tridentate bridge (μ_2) [5–10], tetradentate bridge μ_2 [12], μ_3 [6,11,13–16] and μ_4 [6], and bis(monodentate) bridge (μ_2) [5] have been reported. The pzdca ligand is mainly coordinated via the carboxylate oxygen, nitrogen atom and O atom of a neighboring carboxyl group, acting as a tridentate bridge [5–10]. Furthermore mixed chelating-bridging modes have also been observed [17,23]. In the complex $\{[Ph_3Sn(pzdca)\text{-}SnPh_3]_2(H_2O)\}$ [5], the pzdca ligand acts as a bridge between the tin ions, its coordination sites being the oxygen atoms of the carboxylate groups, as a bis(monodentate) ligand. In the $\{[Mn(pzdca)(H_2O)_2] \cdot 2H_2O\}_n$ [13] and $[Cd(pzdca)(phen)] \cdot H_2O$ [6] polynuclear complexes, the pzdca ligand exhibits the μ_3 coordination mode by means of a bidentate O atom of a carboxyl group, the N atom of pyrazine and as a bis(monodentate) O atom of the neighboring carboxyl group, while in the $[Cd_2(pzdca)_2(4,4'\text{-bipy})(H_2O)_2]$ polynuclear complex, the pzdca ligand is coordinated to three Cd(II) ions through two O atoms and one N atom [6]. The pzdca ligand adopts a bidentate coordination to one Cd(II) ion and one μ_2-bridging oxygen atom coordinates to the other two Cd(II) ions. Up until now, although the literature lists many reports on the coordinating presence of the pzdca ligand, the monodentate coordination mode for a pyrazine-2,3-dicarboxylic acid complex was not known.

Here we report the syntheses, spectral, thermal properties and X-ray structures of the mononuclear $[Cu(pzdca)(H_2O)(en)_2] \cdot H_2O$ (**1**) and $[Cu(pzdca)(H_2O)(dmpen)_2]$ (**2**) complexes, with a new coordination mode of the pyrazine-2,3-dicarboxylate ligand.

2. Experimental

2.1. Preparation of the complexes

A solution of pyrazine-2,3-dicarboxylic acid (0.84 g, 5 mmol) in water (20 mL) was added dropwise with stirring to a solution of $Cu(CH_3COO)_2 \cdot H_2O$ (1 g, 5 mmol) in water (20 mL). The mixture was stirred for 4 h at 50 °C and then en (0.61 g, 10 mmol) or dmpen (1.02 g, 10 mmol) in acetonitrile–water (1:1, 25 ml) was added, and the resulting solution was stirred for 2 h at 50 °C and then cooled to room temperature. The crystals formed were filtered, washed with water and then dried in air. *Anal.* Calc. for $C_{10}H_{22}N_6O_6Cu$: C, 31.13; H, 5.75; N, 21.78. Found: C, 31.63; H,

* Corresponding author.
E-mail address: yesilel@ogu.edu.tr (O.Z. Yeşilel).

0277-5387/$ - see front matter © 2008 Elsevier Ltd. All rights reserved.
doi:10.1016/j.poly.2008.04.046

5.45; N, 22.02%. *Anal.* Calc. for $C_{16}H_{32}N_6O_5Cu$: C, 42.52; H, 7.14; N, 18.59. Found: C, 42.51; H, 7.14; N, 19.10%.

2.2. Materials and measurements

All chemicals used were of reagent grade and were commercially purchased. IR spectra were obtained with a Bruker Tensor 27 FT-IR spectrometer using KBr pellets in the 4000–400 cm^{-1} range. Elemental analyses for C, H and N were carried out at the TÜBİTAK Marmara Research Centre. Magnetic susceptibility measurements at room temperature were performed using a Sherwood Scientific MXI model Gouy magnetic balance. The UV–Vis spectra were obtained for aqueous solutions of the complexes (10^{-3} M) with a Shimadzu UV-3150 spectrometer in the range 900–190 nm. A Perkin Elmer Diamond TG/DTA thermal analyzer was used to record simultaneous TG, DTG and DTA curves in static air atmosphere at a heating rate of 10 K min^{-1} in the temperature range 30–600 °C using platinum crucibles.

2.3. Crystallographic analyses

Diffraction experiments were carried out at 296 K on a Stoe IPDS diffractometer. The structure was solved by direct methods using the program SHELXS 97 [26]. All non-hydrogen atoms were refined anisotropically by full-matrix least-squares methods [26]. The relevant crystal data and experimental conditions along with the final parameters are summarized in Table 1. Selected bond lengths, bond angles and the hydrogen bonds are listed in Tables 2–4, respectively. Data collection: X-AREA, cell refinement: X-AREA, data reduction on: X-RED [27]; program used to refine structure: SHELXL 97 [26]; molecular graphics: ORTEP-3 for Windows [28]; software used to prepare material for publication: WinGX [29].

3. Results and discussion

3.1. UV–Vis spectra and magnetic susceptibilities

The electronic spectra of the mononuclear complexes **1** and **2** in water exhibit absorption bands centered at 551 (ε = 116 L mol^{-1} cm^{-1}) and 589 nm (ε = 103 L mol^{-1} cm^{-1}), respectively, due to d–d transitions. These values were assigned to $^2B_{1g} \rightarrow {}^2E_g$, $^2B_{1g} \rightarrow {}^2B_{2g}$ and $^2B_{1g} \rightarrow {}^2A_{1g}$, which lie within one broad envelope. The Δ_o values for the complexes were calculated as 18149 and 16978 cm^{-1}, respectively. The Δ_o value of **1** is higher than complex **2** due to en being a stronger field ligand than the dmpen ligand.

Comparing the spectral data of complexes **1** and **2** reveals that while the observed λ_{max} values change in methanol, acetonitrile

Table 1
The details of crystals and experimental data for **1** and **2**

Empirical formula	$C_{10}H_{22}N_6O_6Cu$	$C_{16}H_{32}N_6O_5Cu$
Formula weight	385.88	452.02
Temperature (K)	296	296
Wavelength (Å)	0.71073	0.71073
Crystal system	triclinic	triclinic
Space group	$P\bar{1}$	$P\bar{1}$
Unit cell dimensions		
a (Å)	7.3943 (5)	10.181 (1)
b (Å)	10.6715 (7)	10.823 (1)
c (Å)	10.6823 (7)	10.745 (1)
α (°)	71.328 (5)	69.353 (8)
β (°)	84.772 (5)	88.318 (9)
γ (°)	77.403 (5)	71.090 (8)
V (Å^3)	779.13 (9)	1043.3 (2)
Z	2	2
μ (mm^{-1})	1.44	1.09
D_{calc} (Mg m^{-3})	1.645	1.439
θ Range (°)	2.01–27.41	2.36–27.87
Measured reflections	13706	10203
Independent reflections	3236	4330
Absorption correction	integration	
Refinement method	full-matrix least-squares on F^2	
Final R indices [$I > 2\sigma(I)$]	R_{int} = 0.036	R_{int} = 0.052
$R[F^2 > 2\sigma(F^2)]$	0.025	0.041
$wR(F^2)$	0.065	0.103
Goodness-of-fit on F^2	1.06	1.03
Largest difference peak and hole (e Å^{-3})	0.36 and −0.34	0.88 and −0.64

Table 2
Selected bond distances (Å) in **1** and **2**

Complex **1**		Complex **2**	
N1–Cu1	1.993 (2)	N1–Cu1	2.019 (2)
N2–Cu1	2.014 (2)	N2–Cu1	2.043 (2)
N3–Cu1	2.004 (2)	N3–Cu1	2.012 (2)
N4–Cu1	2.021 (2)	N4–Cu1	2.046 (2)
O1–Cu1	2.727 (2)	O1–Cu1	2.379 (2)
O2–Cu1	2.403 (2)	O2–Cu1	2.810 (2)

Table 3
Selected bond angles (°) in **1** and **2**

Complex **1**		Complex **2**	
N1–Cu1–N3	173.27 (6)	N3–Cu1–N1	169.70 (8)
N1–Cu1–N2	85.10 (6)	N3–Cu1–N2	91.37 (8)
N3–Cu1–N2	93.76 (6)	N1–Cu1–N2	88.98 (8)
N1–Cu1–N4	95.85 (6)	N3–Cu1–N4	90.26 (8)
N3–Cu1–N4	84.96 (6)	N1–Cu1–N4	87.74 (9)
N2–Cu1–N4	177.06 (6)	N2–Cu1–N4	170.42 (8)
N1–Cu1–O2	95.69 (6)	N3–Cu1–O1	90.45 (8)
N3–Cu1–O2	90.90 (6)	N1–Cu1–O1	99.79 (9)
N2–Cu1–O2	88.34 (5)	N2–Cu1–O1	94.48 (9)
N4–Cu1–O2	94.33 (5)	N4–Cu1–O1	94.95 (9)

Table 4
Hydrogen bonding interactions for **1** and **2** (Å, °)

D–H···A	*d*(D–H)	*d*(H···A)	*d*(D···A)	∠(DHA)
Complex **1**				
N1–H6A···O3	0.90	2.36	3.069 (2)	136
N1–H6B···O4^{i}	0.90	2.02	2.914 (2)	171
N2–H5A···N6^{ii}	0.90	2.38	3.111 (2)	138
N2–H5B···O2^{iii}	0.90	2.31	3.127 (2)	151
N3–H4A···O2^{iii}	0.90	2.34	3.151 (2)	149
N3–H4B···N5^{iii}	0.90	2.51	3.083 (2)	122
N3–H4B···O1	0.90	2.63	3.098 (2)	113
N4–H3A···O5^{i}	0.90	2.43	3.183 (2)	141
N4–H3A···O3^{i}	0.90	2.46	3.200 (2)	139
N4–H3B···O6^{iv}	0.90	2.43	3.146 (2)	136
N4–H3B···O3	0.90	2.54	3.172 (2)	128
O1–H5C···O5^{i}	0.83 (2)	1.92 (2)	2.750 (1)	177 (3)
O1–H5D···O4^{ii}	0.82 (2)	2.03 (2)	2.850 (2)	179 (3)
O6–H6C···O4^{ii}	0.83 (2)	2.16 (2)	2.976 (2)	167 (3)
O6–H6D···O5^{v}	0.85 (2)	2.12 (2)	2.942 (2)	163 (3)
Complex **2**				
N1–H1C···O4^{i}	0.90	2.02	2.913 (3)	175
N1–H1D···O3	0.90	2.14	2.937 (3)	148
N2–H2A···O2^{ii}	0.90	2.21	3.084 (3)	163
N2–H2B···O5^{iii}	0.90	2.48	3.330 (3)	158
N2–H2B···N6^{iii}	0.90	2.53	3.227 (3)	135
N3–H3C···N5^{ii}	0.90	2.16	3.056 (3)	171
N3–H3D···O2	0.90	2.34	2.942 (2)	124
N4–H4E···O4^{i}	0.90	2.42	3.278 (3)	159
N4–H4E···O3^{i}	0.90	2.57	3.200 (3)	127
O1–H1E···O5^{iii}	0.75 (4)	2.03 (4)	2.781 (4)	177 (4)
O1–H1F···O5^{i}	0.86 (5)	1.93 (5)	2.771 (4)	166 (4)

Symmetry codes for complex **1**: (i) $-x+1, -y+1, -z+2$; (ii) $x, y-1, z$; (iii) $-x+1, -y+1, -z+1$; (iv) $x, y+1, z$; (v) $x-1, y-1, z$.
Symmetry codes for complex **2**: (i) $-x+1, -y+1, -z$; (ii) $-x+1, -y+1, -z+1$; (iii) $x, y+1, z$.

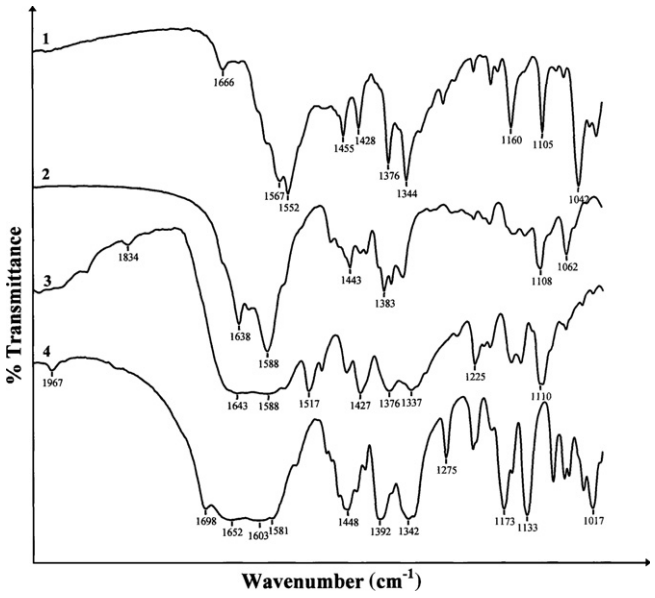

Fig. 1. A comparison of the IR spectra of Cu(II)-pzdca complexes; (**1**) [Cu(pzdca)$(H_2O)(en)_2]\cdot H_2O$, *monodentate*, (**2**) [Cu(pzdca)$(H_2O)(dmpen)_2$], *monodentate,* (**3**) [Cu(pzdca)$(phen)_2]\cdot 5.5H_2O$, *bidentate* and (**4**) [$Cu_2(pzdca)_2(dmen)_2]\cdot 6H_2O$, tridenate bridge [22].

and chloroform solvents, the absorption intensities remain almost unvaried in complexes **1** and **2**. A shoulder peak appears in the methanol spectra at 385 and 387 nm wavelengths, respectively, and is probably due to a charge-transfer.

The magnetic susceptibilities of [Cu(pzdca)$(H_2O)(en)_2]\cdot H_2O$ (**1**) and [Cu(pzdc)$(H_2O)(dmpen)_2$] (**2**) measured at room temperature show that the magnetic moment values μ_{eff} of 1.43 and 1.54 BM, respectively, are slightly smaller than the expected value (1.73 BM).

3.2. IR spectra

The IR spectra of the complexes show a broad band at 3478 cm^{-1} for **1** and 3411 cm^{-1} for **2** due to the ν(OH) vibrations of water molecules. The bands at 3336–3219 cm^{-1} for **1** and 3270–3212 cm^{-1} for **2** are attributed to the $\nu(NH_2)$ vibrations of the en and dmpen ligands, respectively. The weak band range of 3055–2895 cm^{-1} for **1** and 2954–2865 cm^{-1} for **2** can be assigned to ν(CH) vibrations. Strong absorption bands in the ranges 1753–1690 and 1396–1357 cm^{-1} correspond to the asymmetric and symmetric ν(COO) vibrations of the free H_2pzdca ligand. After coordination to the Cu(II) ions, these bands shift to lower wavenumbers and are observed in the ranges 1650–1583 and 1387–1333 cm^{-1} for **1** and 1638–1588 and 1383–1350 cm^{-1} for **2**. The differences between the asymmetric and symmetric stretches of the carboxylate groups of the two complexes, $\Delta\nu = 256$ and 247 cm^{-1}, respectively, suggest a monodentate binding of the carboxylate group to the copper(II) ions [30]. The weak bands between 450 and 613 cm^{-1} are due to Cu–N and Cu–O stretching vibrations.

The carboxyl groups of the ring appear as three main peaks at 1753, 1715 and 1690 cm^{-1} in the free 2,3-pyrazinedicarboxylic acid. Band splitting and shifts of the stretching vibrations of the carboxyl group were observed in the IR spectra of the Cu(II)-pzdca complexes, in which pzdca exhibits a different coordination mode. Therefore, the IR spectra of 2,3-pyrazinedicarboxylic acid and the Cu(II)-pzdca complexes provide important evidence for the coordination of the pzdca ligand to the copper(II) ions. The IR spectra of Cu(II)-pzdca complexes are given in Fig. 1, in which the ligand shows monodentate, bidentate and tridentate bridge coordination modes for comparison.

3.3. Thermal analyses

3.3.1. $[Cu(pzdca)(H_2O)(en)_2]\cdot H_2O$

This complex exhibits five decomposition stages (Fig. 2). In the first stage, endothermic removal of the crystal water molecule occurs in the 73–93 °C range (DTA_{max} = 91 °C, found 4.90%, calc. 4.66%). The second stage, 94–121 °C range, is related to the loss of aqua and 0.5 mol of en ligands (DTA_{max} = 114 °C, found 12.09%, calc. 12.45%). In the temperature range 122–207 °C, the third and fourth stages of the complex are related to the successive decomposition of 1 mol of en ligands, by giving an endothermic contribution (DTA_{max} = 155 and 204 °C, found 16.09%, calc. 15.57%). In the

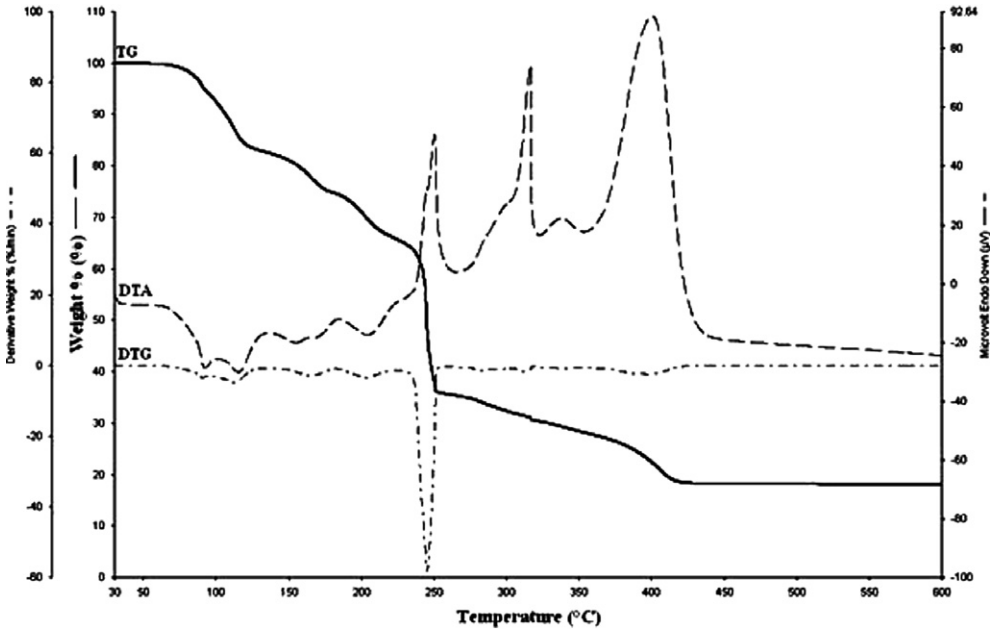

Fig. 2. TG, DTG and DTA curves of **1**.

following stage, the remaining 0.5 mol en ligand and 2 mol CO_2 are released, giving an exothermic effect (DTA_{max} = 251 °C, found 30.98%, calc. 30.59%). The Cu(II) complex shows an exothermic effect at about 317 °C that can be assigned to a phase transition. In the last stage, the remaining organic part is abruptly burnt (DTA_{max} = 400 °C), leading finally to CuO (found 81.78%, calc. 79.39%).

3.3.2. $[Cu(pzdca)(H_2O)(dmpen)_2]$

The thermal decomposition behavior of this complex was followed up to 600 °C in static air atmosphere (Fig. 3). The first stage related to the endothermic removal of the aqua ligand in the 100–154 °C temperature range (DTG_{max} = 150 °C, found 4.07%, calc. 3.98%). The second stage corresponds to the loss of dmpen and pzdca in the 193–307 °C temperature range, giving both an exothermic and endothermic effect (DTA_{max} = 221 and 225 °C), simultaneously. In the last strong exothermic stage, the remaining organic part is abruptly burnt (DTA_{max} = 456 °C). The final decomposition product, CuO, was identified by IR spectroscopy (found 82.58%, calc. 82.40%).

3.4. Crystal structures of the complexes

3.4.1. $[Cu(pzdca)(H_2O)(en)_2] \cdot H_2O$ (1)

Details of the crystal structures are given in Table 1. The crystal structure of **1**, together with the atom labelling, is shown in Fig. 4. The complex is described as a distorted octahedron and the Cu(II) ion is coordinated by two neutral en, one monodentate pzdca and one aqua ligand. The en ligand acts as a bidentate donor through the terminal nitrogen atoms creating a five membered chelate ring [Cu1–N1 = 1.993 (2), Cu1–N2 = 2.014 (2), Cu1–N3 = 2.004 (2) and Cu1–N4 = 2.021 (2) Å] (Table 2). Pzdca coordinated to the copper (II) ions through the carboxylate oxygen atom as a monodentate ligand [Cu1–O2 = 2.403 (2) Å]. To the best of our knowledge, this coordination mode has never been observed in the previously reported complexes of pyrazine-2,3-dicarboxylic acid. The Cu(1)–$O(2)_{pzdca}$ bond distance is similar to the corresponding values found in $[Cd(pzdca)(phen)] \cdot H_2O$ [2.310(2) Å] [6] and $[Cu_2(pzdca)_2(L)(H_2O)_2] \cdot 12H_2O$ [2.552(4) Å] [9], however it is somewhat shorter than that in $[Cu_2(pzdca)_2(H_2O)_2(dmen)_2] \cdot 6H_2O$ [2.887(2) Å] [22]. The distorted octahedral geometry is completed one aqua ligand [Cu1–O1 = 2.727 (2) Å]. The four nitrogen atoms from the en ligands comprise the equatorial plane and one oxygen atom of the pzdca ligand and one oxygen atom from the aqua ligand occupy axial positions [O1–Cu1–O2 = 169.61°].

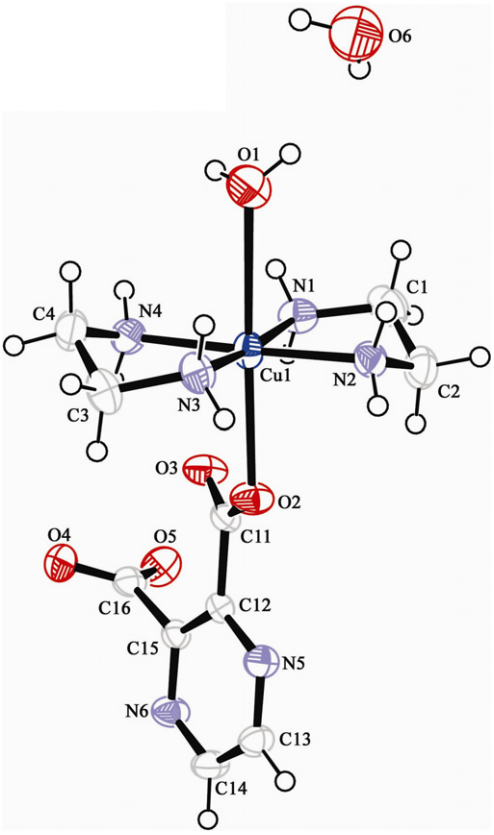

Fig. 4. Ortep III view of **1** with the atom numbering scheme.

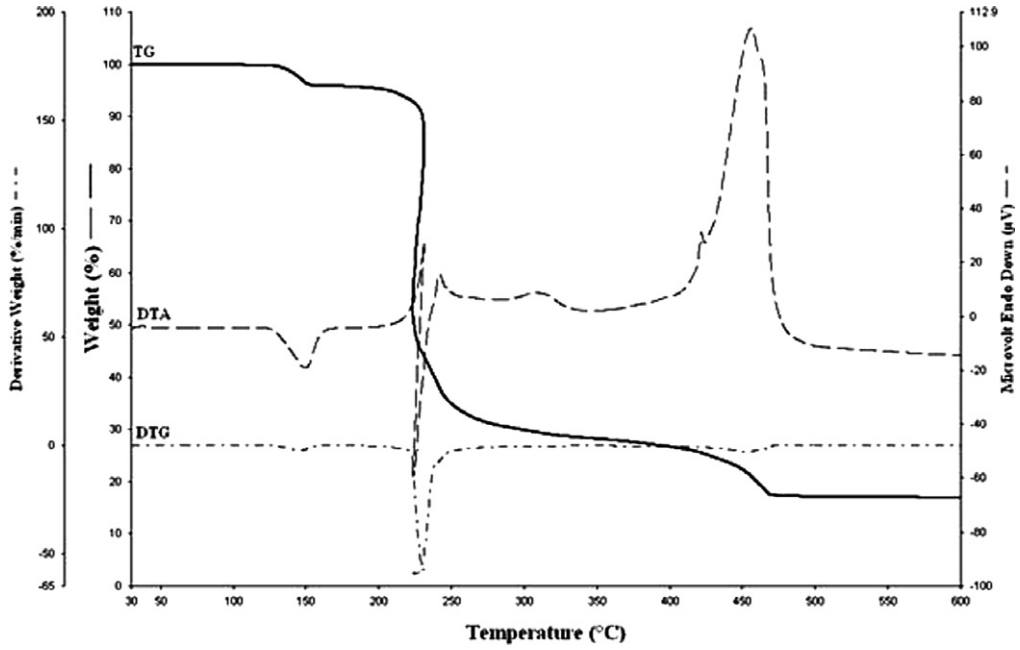

Fig. 3. TG, DTG and DTA curves of **2**.

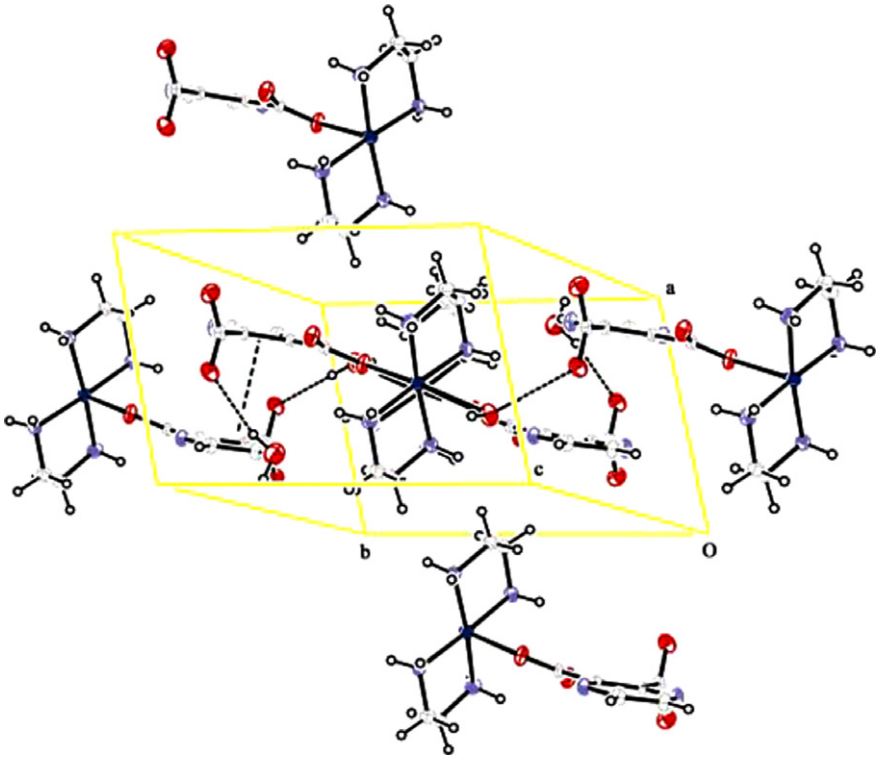

Fig. 5. Packing diagram of **1.**

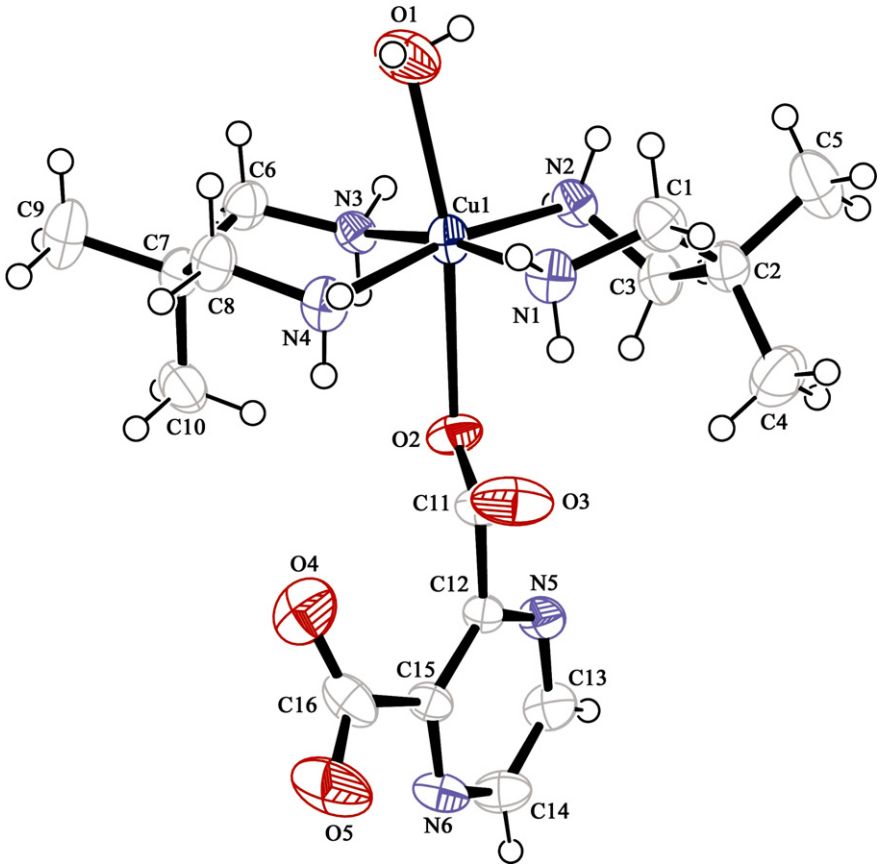

Fig. 6. Ortep III view of **2** with the atom numbering scheme.

The pzdca ligand is almost planar (the r.m.s deviation is 0.0072 Å). The dihedral angles between the pzdca ligand and the carboxyl groups are 16.62° and 81.36° and between the two carboxyl groups, 75.50°.

Details of the hydrogen bonding geometry are given in Table 4. The nitrogen atoms of the pzdca ligands are involved in weak intermolecular hydrogen bonding with the amine group of the en ligand. The oxygen atoms (O1 and O2) of both coordinated water and crystal water molecules are involved in intra- and intermolecular hydrogen bonding with the oxygen atoms of the carboxyl group of the pzdca ligand and the amine group of the en ligands. The intramolecular N1–H6A···O3, N3–H4B···O1 and N4–H3B···O3 bonds have H···O distances of 2.36, 2.63 and 2.54 Å, respectively. The intermolecular O1–H5C···O5^{i}, O1–H5D···O4^{ii}, O6–H6C···O4^{ii} and O6–H6D···O5^{v} bonds have H···O distances of 1.92(2), 2.03(2), 2.16(2) and 2.12(2) Å, respectively ((i): $x+1$, $-y+1$, $-z+2$; (ii): x, $y-1$, z; (v): $x-1$, $y-1$, z). The crystal packing is mainly stabilized by hydrogen bonds. There are also π···π interactions between the Cg3-Cg3^{i} rings (Cg3: N(5)–C(12)–C(15)–N(6)–C(14)–C(13), i: $1-x$, $-y$, $1-z$). Some of these interactions are shown in Fig. 5.

3.4.2. [Cu(pzdca)(H$_2$O)(dmpen)$_2$] (2)

Crystallographic analysis shows that this complex has a mononuclear two-dimensional structure. Moreover, the pyrazine-2,3-dicarboxylate ligand acts as a monodentate ligand through the O atom of the carboxyl group, which has not been reported previously. The asymmetric unit includes [Cu(pzdc)(H$_2$O)(dmpen)$_2$] and the Cu(II) ion is coordinated by one O atom of a carboxyl group from the monodentate pzdca ligand, four N atoms from two dmpen ligands and one O atom from an aqua ligand, forming a distorted octahedral geometry (Fig. 6). The basal coordination plane is formed by the N1, N2, N3 and N4 atoms from the dmpen ligands; [Cu(1)–N(1)$_{dmpen}$ = 2.019(2), Cu(1)–N(2)$_{dmpen}$ = 2.043(2), Cu(1)–N(3)$_{dmpen}$ = 2.012(2) and Cu(1)–N(4)$_{dmpen}$ = 2.046(2) Å] (Table 2). The apical positions are occupied by one oxygen atom of the aqua ligand [Cu(1)–O(1) = 2.379(2) Å] and the one oxygen atom of the pzdca ligand [Cu(1)–O(2) = 2.810(2) Å]. The pzdca ligand is weakly bonded to the copper ion and the Cu(1)–O(2) bond is longer than the equatorial Cu–N bonds due to the Jahn–Teller effect and it is longer than the Cu1–O2 (2.403 (2) Å) bond distance in **1** due to the steric effect of the methyl groups of dmpen ligands.

The Cu(1)–O(2)$_{pzdca}$ bond distances are similar to the corresponding values found in [Cu$_2$(pzdca)$_2$(H$_2$O)$_2$(dmen)$_2$] · 6H$_2$O [2.887(2) Å] [22] and [Cu$_2$(pzdca)$_2$(L)(H$_2$O)$_2$] · 12H$_2$ O [2.552(4) Å] [9], but somewhat longer than that in [Cd(pzdca)(phen)] · H$_2$O [2.310(2) Å] [6], [Ca(Hpzdca)(H$_2$O)$_4$] · NO$_3$ [2.429(2) Å] [24] and {[Eu(pzdca)(NO$_3$)(phen)(H$_2$O)] · H$_2$O}$_n$ [2.344(3) Å] [25].

The pzdca ligand is almost planar (the r.m.s deviation is 0.0111 Å). The dihedral angles between the pzdca ligand and carboxyl groups are 26.76° and 54.92° and between the two carboxyl groups, 52.36°.

The crystal packing of complex is a composite of intermolecular hydrogen bonding, π···π and C–H···π interactions. An intermolecular π···π interaction contact occurs between the two symmetry-related pyrazine rings of the pzdca ligand [Cg3 = N5, N6, C12–C15; Cg3···Cg3^{iv} 3.692(2) Å, (iv): $1-x$, $-y$, $1-z$], while a C–H···π interaction take place between C(9)–H(9A) and the Cg3 ring [C(9)–H(9A)···Cg3^{v} 2.910(2) Å, (v): $1+x$, y, z] (Fig. 7). The crystal is mainly stabilized by strong intermolecular H bonds N(1)–H(1C)···O(4)^{i}, O(1)–H(1E)···O(5)^{iii} and O(1)–H(1F)···O(5)^{i} [(i): $1-x$, $1-y$, $-z$, (iii): x, $1+y$, z]. There are also intramolecular H

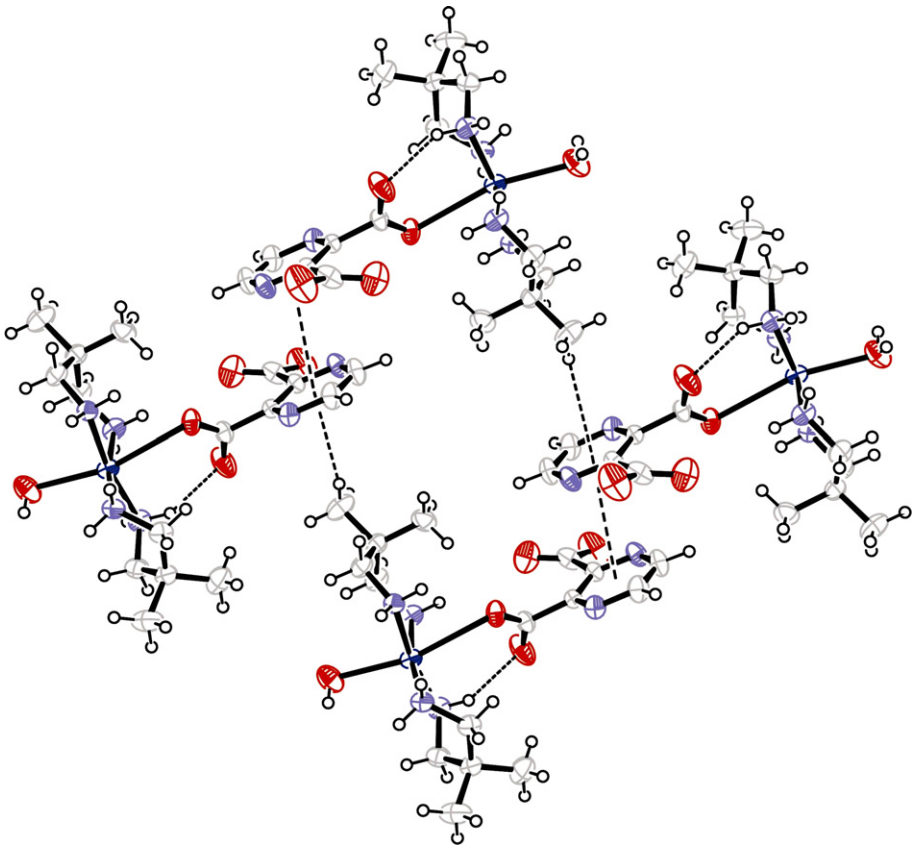

Fig. 7. The π···π and C–H···π interactions of **2**.

bonds between the uncoordinated O3 atom of the carboxyl group and the N1 atom of the dmpen ligand. All of these intermolecular interactions give a two-dimensional network.

4. Conclusion

We have successfully synthesized two novel mononuclear copper(II) complexes with the en ligand, $[Cu(pzdca)(H_2O)(en)_2] \cdot H_2O$ and the dmpen ligand, $[Cu(pzdc)(H_2O)(dmpen)_2]$. In the complexes, the pyrazine-2,3-dicarboxylate ligand exhibits a new coordination mode, though sixteen different other modes have been crystallographically characterized previously. These complexes are the first examples of pzdca ligand exhibiting monodentate coordination mode to the metal ions.

Supplementary data

CCDC 676220 and 675628 contain the supplementary crystallographic data for **1** and **2**. These data can be obtained free of charge via http://www.ccdc.cam.ac.uk/conts/retrieving.html, or from the Cambridge Crystallographic Data Centre, 12 Union Road, Cambridge CB2 1EZ, UK; fax: (+44) 1223-336-033; or e-mail: deposit@ccdc.cam.ac.uk.

Acknowledgments

The authors wish to acknowledge the Faculty of Arts and Sciences, Ondokuz Mayıs University, Turkey, for the use of the Stoe IPDS-II diffractometer (purchased under grant no. F279 of the University Research Fund).

References

[1] C.J. O'Connor, C.L. Klein, R.J. Majeste, L.M. Trefonas, Inorg. Chem. 21 (1982) 64.
[2] H. Xu, H. Ma, M. Xu, W. Zhao, B. GuO, Acta Crystallogr., Sect. E 64 (2008) m104.
[3] R. Burriel, C.J. O'Conner, R.L. Carlin, Inorg. Chem. 24 (1985) 3706.
[4] T. Okubo, M. Kondo, S. Kitagawa, Synth. Met. 85 (1997) 1661.
[5] H.D. Yin, F.H. Li, C.H. Wang, Inorg. Chim. Acta 360 (2007) 2797.
[6] H. Yin, S.X. Liu, Polyhedron 26 (2007) 3103.
[7] X.H. Li, Q. Shi, M.L. Hu, H.P. Xiao, Inorg. Chem. Commun. 7 (2004) 912.
[8] M. Gryz, W. Starosta, J. Leciejewicz, J. Coord. Chem. 58 (2005) 931.
[9] K.Y. Choi, J. Incl. Phen. Macr. Chem. 43 (2002) 195.
[10] S. Konar, S.C. Manna, E. Zangrando, N.R. Chaudhuri, Inorg. Chim. Acta 357 (2004) 1593.
[11] Z. Bi-Song, Chinese J. Struct. Chem. 24 (2005) 478.
[12] Y. Ma, Y.K. He, Z.B. Han, Acta Crystallogr., Sect. E 62 (2006) m2528.
[13] J.Z. Zou, Z. Xu, W. Chen, K.L. Lo, X.Z. You, Polyhedron 18 (1999) 1507.
[14] G. Beobide, O. Castillo, A. Luque, U. Garcia-Coucerio, J.P. Garcia-Teran, P. Roman, Inorg. Chem. 45 (2006) 5367.
[15] M.L. Hu, J.X. Yuan, F. Chen, Q. Shi, Acta Crystallogr., Sect. C 60 (2004) m186.
[16] M. Kondo, T. Okubo, A. Asami, S. Noro, T. Yoshitomi, S. Kitagawa, T. Ishii, H. Matsuzaka, K. Seki, Angew. Chem., Int. Ed. 38 (1999) 1433.
[17] X.J. Zheng, L.P. Jin, S.Z. Lu, Eur. J. Inorg. Chem. (2002) 3356.
[18] C.J. O'Connor, E. Sinn, Inorg. Chem. 20 (1981) 545.
[19] M. Wenkin, M. Devillers, B. Tinant, J.P. Declercq, Inorg. Chim. Acta 258 (1997) 113.
[20] O. Castillo, G. Beobide, A. Luque, P. Román, Acta Crystallogr., Sect. E 59 (2003) m800.
[21] M.S. Wang, L.Z. Cai, G.W. Zhou, G.C. Guo, J.G. Mao, J.S. Huang, Acta Crystallogr., Sect. E 59 (2003) m212.
[22] O.Z. Yeşilel, A. Mutlu, O. Büyükgüngör, J. Coord. Chem., in press.
[23] F. Jaber, F. Charbonnier, R. Faure, J. Chem. Crystallogr. 24 (1994) 681.
[24] J.H. Yang, S.L. Zheng, X.L. Yu, X.M. Chen, Cryst. Growth Des. 4 (2004) 831.
[25] Y.Y. Liu, G.S. Zhu, G.Z. Fan, S.L. Qui, Acta Crystallogr., Sect. C 63 (2007) m159.
[26] G.M. Sheldrick, SHELXS 97 and SHELXL 97. Program for Refinement of Crystal Structures, University of Göttingen, Germany, 1997.
[27] Stoe and Cie (2002). X-AREA (Version 1.18) and X-RED32 (Version 1.04). Stoe and Cie, Darmstadt, Germany, 2001.
[28] L.J. Farrugia, J. Appl. Crystallogr. 30 (1997) 565.
[29] L.J. Farrugia, J. Appl. Crystallogr. 32 (1999) 837.
[30] K. Nakamoto, Infrared and Raman Spectra of Inorganic and Coordination Compounds, 5th ed., Wiley Interscience, New York, 1997. pp. 59–62.

Polyhedron 27 (2008) 2478–2486

Contents lists available at ScienceDirect

Polyhedron

journal homepage: www.elsevier.com/locate/poly

Fine structures of 1-(arylethynylselanyl)naphthalenes: Characteristic features brought by the ethynylselanyl group

Kentaro Yamane [a], Satoko Hayashi [a], Waro Nakanishi [a,*], Takahiro Sasamori [b], Norihiro Tokitoh [b]

[a] Department of Material Science and Chemistry, Faculty of Systems Engineering, Wakayama University, 930 Sakaedani, Wakayama 640-8510, Japan
[b] Institute for Chemical Research, Kyoto University, Gokasho, Uji, Kyoto 611-0011, Japan

ARTICLE INFO

Article history:
Received 19 March 2008
Accepted 15 April 2008
Available online 21 June 2008

Keywords:
1-(Arylethynylselanyl)naphthalenes
Lone pairs
Organic selenium compounds
Structures
Substituent dependence
Through-bond interactions

ABSTRACT

Fine structures of 1-(arylethynylselanyl)naphthalenes [1-(*p*-$YC_6H_4C{\equiv}CSe)C_{10}H_7$: **1**, Y = H (**a**), OMe (**b**), Me (**c**), Cl (**e**), CN (**h**), NO_2 (**i**)] have been determined by X-ray crystallographic analysis. The structures are **A** for **1a–c**, bearing Y that is a non-acceptor, **B** for **1e**, **1h** and **1i**, having Y that is a strong acceptor, where the Se–C_{sp} bond is perpendicular to the naphthyl plane in **A**, but is in the plane in **B**; and **C** is intermediate between **A** and **B** (see Scheme 1). The Y-dependence observed in **1** is just the opposite to the case of 1-(arylselanyl)naphthalenes [1-(*p*-$YC_6H_4Se)C_{10}H_7$]. We call the factor the "*ethynyl effect*", which controls the fine structures of **1**. The structures of **1h** and **1i** are planar or almost planar. The energy lowering effect by the parallel direction between n_p(Se) and n_p(Y) must be responsible for the observations if Y is a strong acceptor. The origin of the ethynyl effect is explained by how effectively n_p(Se) and n_p(Y) interact through the C≡C bond. Crystal packing effects, such as the formation of dimmers, also play an important role in determining the fine structures of **1**. The dimer formation in **1a–c** substantially stabilizes the structures. The π-stacking of naphthyl groups may also contribute to the dimer formation. The structures in solutions are also clarified. Compound **1** exist in the **A** form in solutions, with some equilibration with **B**. The ethynyl effect as the factor that controls the fine structures of **1** is also confirmed in solution. The results are well supported by quantum chemical calculations on the structures, energy profiles and the evaluation of electron affinity. The NMR chemical shifts explain the behavior of **1** in solution.

© 2008 Elsevier Ltd. All rights reserved.

1. Introduction

Weak interactions are of current interest [1–16], since they determine the fine structures of molecules and create the high functionalities of materials. Investigations successfully utilizing weak interactions are increasing, such as in biological and enzymatic activities [17–24], stabilization of folded protein structures [25,26] and supramolecular chemistry [27,28], together with donor–acceptor complexes for electronic materials [29–32]. They are also utilized in the crystal engineering for material development [33–35]. Much attention has also been paid to the ethynyl group in modern physics, chemistry and engineering [36–47]. This group and its derivatives are very important as building blocks when molecules of high functionality are designed [48,49]. It will be of great interest if the ethynyl group is joined to extended hypervalent bonds [10b,10e,10f,10j,10k,10l,10m,10n,16] constructed by group 16 elements.

We intend to construct supramolecular compounds such as **I** [50] and derivatives mainly built by the ethynyl group coordinated to the extended hypervalent 4c–6e bonds of Z_4 (Z = S [10j,16] and Se [10b,10e,16]). It is also of high interest how ethynylchalcogenyl groups operate to control the fine structures. The results will be useful for the design of a system, such as **I**, with high functionality. The effects of ethynylchalcogenyl groups as factors that control fine structures are elucidated by 1-(arylethynylselanyl)naphthalenes [1-(*p*-$YC_6H_4C{\equiv}CSe)C_{10}H_7$ (1-ArC≡CSe-Nap): **1**, Y = H (**a**), OMe (**b**), Me (**c**), F (**d**), Cl (**e**), CN (**h**) and NO_2 (**i**)]. Compounds **1a–e**, **1h** and **1i** have been prepared and the structures determined by X-ray crystallographic analysis.

* Corresponding author. Tel.: +81 73 457 8252; fax: +81 73 457 8253.
E-mail address: nakanisi@sys.wakayama-u.ac.jp (W. Nakanishi).

0277-5387/$ - see front matter © 2008 Elsevier Ltd. All rights reserved.
doi:10.1016/j.poly.2008.04.052

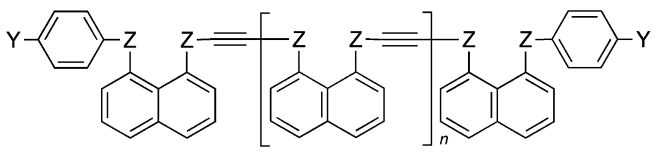

I (Z = S and Se; *n* = 0 and 1)

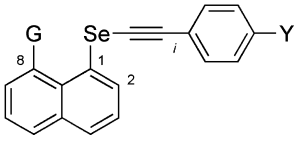

1 (G = H), **2** (G = Cl and Br)

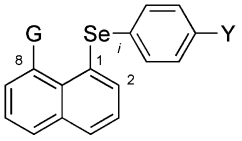

3 (G = H), **4** (G = F, Cl and Br)

	a	b	c	d	e	f	g	h	i
Y =	H	OMe	Me	F	Cl	Br	COOR	CN	NO_2

Naphthalene 1,8-positions supply a good system to investigate weak interactions [10a,10b,10d,10e,10f,10g,10h,10i,10j,16,51–55], since the distance between the non-bonded atoms of the main group elements at those positions are shorter than the sum of van der Waals radii by about 1 Å. The structures of **1** where G is a halogen (**2**) must also be of great interest. Factors to control the fine structures of 1-(arylselanyl)naphthalenes [1-(*p*-YC_6H_4-Se)$C_{10}H_7$: **3**] [11b] and 8-G-1-(*p*-$YC_6H_4Se)C_{10}H_6$ (**4**) [10h] have been clarified based on those determined by X-ray crystallographic analysis. The factors are explained by means of p(Se)–π(Ar/Nap) conjugation for **3** and a non-bonded n_p(G)–σ^*(Se–C) 3c–4e type interaction for **4**.

Structures of the naphthalene system are well explained by the three types, **A**, **B** and **C**, in our definition, where the Se–C_{sp} bond is perpendicular to the naphthyl plane in **A**, is placed on the plane in **B**, and **C** is an intermediate between **A** and **B** [10c,10d,10f,10g,10h,10i,11b]. The **A**, **B** and **C** notations are employed for the structures around the Se–C_{Nap} bonds in **1**. The planar (**pl**), perpendicular (**pd**) and non-planar and non-perpendicular (**np**) notations are also used to specify the structures of **1** around the Se–C≡C–C_{Ar} (abbreviated Se–C_{Ar}) bonds. Scheme 1 illustrates the plausible structures of **1**. Combined notations such as (**A**: **pl**) and (**B**: **pd**) are employed for the structures. The structures of **3** are **B** when Y is a donating group, such as OMe, whereas they are **A** when Y is an acceptor group, such as NO_2 [10h]. We call the results Y-dependence. The magnitude of the p(Se)–π(Ar/Nap) conjugation must be the origin of the Y-dependence in **3**.

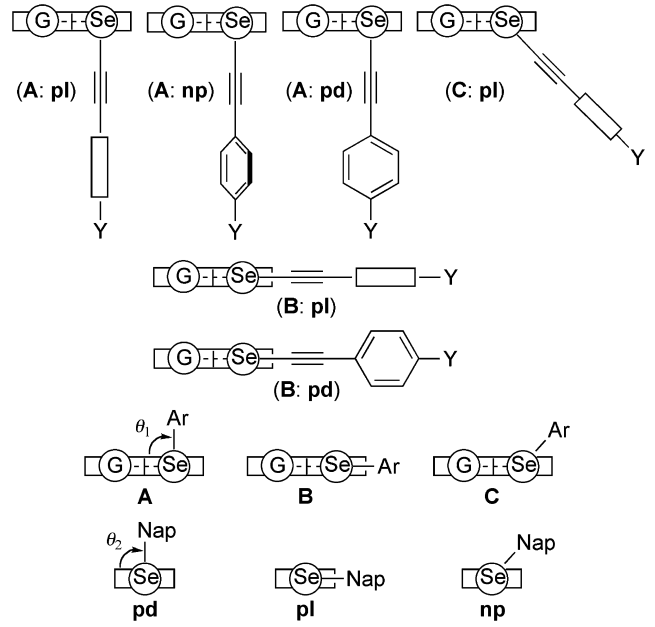

Scheme 1. Plausible structures of **1**, together with the **A**, **B** and **C** and **pd**, **pl** and **np** notations.

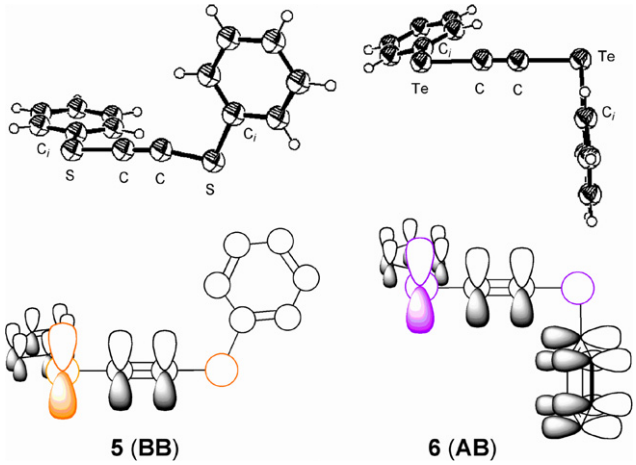

Scheme 2. Structures of **5** (**BB**) and **6**(**AB**), together with the orbital interactions.

The structures of **1** correspond to those of **3**, whereas the structures of **2** correspond to those of **4**. Does Y really control the fine structures of **1**? One may wonder that Y would not have an affect on the conformations of **1**, since the arylethynyl group is essentially unhindered around the C≡C bond. However, **BB** and **AB** structures are reported for the 1,2-di(phenylchalcogenyl)ethynes PhSC≡CSPh (**5**) [56] and PhTeC≡CTePh (**6**) [57], respectively, as shown in Scheme 2 [58]. Each n_p(Z) orbital on both sides of the Z–C≡C–Z framework directs parallel to each of the two π(C≡C) orbitals in **5** and **6**, where the torsion angles of ϕ(C_iZZC_i) are close to 90°. The π(Ph)–n_p(Z)–π(C≡C) conjugations may operate to control the structures of **5** (**BB**) and **6** (**AB**). Similar conjugation must also operate to determine the fine structure of PhSeC≡CSePh (**7**).[1]

Here, we report the fine structures of **1** in crystals, as the first step to clarify the ethynyl effect as a factor that controls fine structures. We call the factor the "*ethynyl effect*" in **1**. The behavior of **1** in solution is also discussed by means of NMR spectroscopy.

2. Experimental

2.1. General experimental considerations

Manipulations were performed under an argon atmosphere with standard vacuum-line techniques. Glassware was dried at 130 °C overnight. Solvents and reagents were purified by standard procedures as necessary. Melting points were measured with a Yanaco MP-S3 apparatus and were uncorrected. NMR spectra were recorded at room temperature on a JEOL AL-300 spectrometer (^{1}H, 300 MHz; ^{13}C, 75 MHz: ^{77}Se, 57 MHz). The ^{1}H, ^{13}C and ^{77}Se chem-

[1] The **AA**, **BB** and **AB** conformers are shown to be stable for **7** and the energies are predicted to be almost equal values of −5342.6801 a.u. with the B3LYP/6-311+G(2d, p) method.

ical shifts are given in parts per million relative to those of Me_4Si, internal $CDCl_3$ of the solvent and external MeSeMe, respectively. Column chromatography was performed on silica gel (Fujishilysia PSQ-100B), acidic and basic alumina (E. Merck).

2.2. Preparation of 1-(arylethynylselanyl)naphthalenes

2.2.1. 1-(Phenylethynylselanyl)naphthalene (**1a**)

Under an argon atmosphere, ethynylbenzene (0.50 g, 4.85 mmol) was dissolved in anhydrous THF (15 mL), and LDA (diisopropylamine (0.52 g, 5.09 mmol) and *n*-BuLi (3.2 mL, 5.09 mmol, 1.62 M)) was added to the solution at 0 °C. After the mixture was stirred for 1 h at 0 °C, 1-naphthylselanyl bromide in anhydrous THF (10 mL) was added to the above solution at 0 °C. The reaction mixture was stirred for 2 h at 0 °C, and allowed to warm up to room temperature. Then, acetone (5 mL) was added, evaporated and dried in vacuo. The crude product was purified by column chromatography (flash column, SiO_2, acidic alumina, hexane). Compound **1a** was isolated in 65% yield as colorless prisms, mp 62.0–63.0 °C. *Anal.* Calc. for $C_{18}H_{12}Se$: C, 70.36; H, 3.94. Found: C, 70.04; H, 3.83%. δ_H (300 MHz; $CDCl_3$; Me_4Si) 7.29–7.36 (m, 3H), 7.41–7.63 (m, 5H), 7.81 (d, *J* 8.2 Hz, 1H), 7.87 (dd, *J* 1.6, 7.6 Hz, 1H), 8.04 (m, 2H); δ_C (75 MHz; $CDCl_3$; Me_4Si) 69.1, 102.9, 123.2, 125.4, 126.3, 126.4, 126.8, 127.3, 128.3, 128.3, 128.6, 128.8, 129.0, 131.8, 132.1, 134.0; δ_{Se} (57 MHz; $CDCl_3$; Me_2Se) 241.4.

2.2.2. 1-(p-Anisylethynylselanyl)naphthalene (**1b**)

A similar method to that described for the preparation of **1a** was used. Compound **1b** was isolated in 61% yield as colorless prisms, mp 99.0–100.0 °C. *Anal.* Calc. for $C_{19}H_{14}OSe$: C, 67.66; H, 4.18. Found: C, 67.91; H, 4.17%. δ_H (300 MHz; $CDCl_3$; Me_4Si) 3.81 (s, 3H), 6.85 (d, *J* 9.0 Hz, 2H), 7.44 (t, *J* 8.0 Hz, 1H), 7.46 (d, *J* 9.0 Hz, 2H), 7.50–7.61 (m, 2H), 7.79 (d, *J* 8.4 Hz, 1H), 7.86 (dd, *J* 1.7, 7.8 Hz, 1H), 7.99–8.06 (m, 2H); δ_C (75 MHz; $CDCl_3$; Me_4Si) 55.3, 67.0, 103.0, 114.0, 115.3, 125.3, 126.3, 126.4, 126.7, 127.7, 128.1, 128.6, 128.7, 132.0, 133.6, 134.0, 160.0; δ_{Se} (57 MHz; $CDCl_3$; Me_2Se) 240.9.

2.2.3. 1-(p-Tolylethynylselanyl)naphthalene (**1c**)

A similar method to that described for the preparation of **1a** was used. Compound **1c** was isolated in 70% yield as light yellow prisms, mp 87.0–88.0 °C. *Anal.* Calc. for $C_{19}H_{14}Se$: C, 71.03; H, 4.39. Found: C, 70.79; H, 4.31%. δ_H (300 MHz; $CDCl_3$; Me_4Si) 2.36 (s, 3H), 7.13 (d, *J* 7.9 Hz, 2H), 7.40 (d, *J* 8.2 Hz, 2H), 7.45 (t, *J* 7.8 Hz, 1H), 7.50–7.62 (m, 2H), 7.80 (d, *J* 8.3, 1H), 7.87 (dd, *J* 1.7, 7.8 Hz, 1H), 8.03 (dd, *J* 1.0, 7.9 Hz, 1H), 8.04 (dd, *J* 1.1, 7.3 Hz, 1H); δ_C (75 MHz; $CDCl_3$; Me_4Si) 21.5, 68.0, 103.1, 120.1, 125.3, 126.3, 126.4, 126.7, 127.5, 128.1, 128.7, 128.8, 129.1, 131.8, 132.1, 134.0, 138.9; δ_{Se} (57 MHz; $CDCl_3$; Me_2Se) 241.4.

2.2.4. 1-(p-Fluorophenylethynylselanyl)naphthalene (**1d**)

A similar method to that described for the preparation of **1a** was used. Compound **1d** was isolated in 67% yield as colorless prisms, mp 87.0–88.0 °C. *Anal.* Calc. for $C_{18}H_{11}FSe$: C, 71.03; H, 4.39. Found: C, 70.79; H, 4.31%. δ_H (300 MHz; $CDCl_3$; Me_4Si) 7.01 (t, *J* 8.8 Hz, 2H), 7.41–7.51 (m, 3H), 7.51–7.63 (m, 2H), 7.81 (d, *J* 8.2 Hz, 1H), 7.87 (dd, *J* 1.6, 7.8 Hz, 1H), 8.02 (dd, *J* 1.1, 7.2 Hz, 1H), 8.05 (dd, *J* 1.1, 8.3 Hz, 1H); δ_C (75 MHz; $CDCl_3$; Me_4Si) 68.9 ($^5J_{C,F}$ 1.7 Hz), 101.6, 115.6 ($^2J_{C,F}$ 22.4 Hz), 119.3 ($^4J_{C,F}$ 3.7 Hz), 125.5, 126.3, 126.5, 126.8, 127.2, 128.4, 128.8, 129.1, 132.2, 133.8 ($^3J_{C,F}$ 7.8 Hz), 134.1, 162.7 ($^1J_{C,F}$ 250.4 Hz); δ_{Se} (57 MHz; $CDCl_3$; Me_2Se) 240.5.

2.2.5. 1-(p-Chlorophenylethynylselanyl)naphthalene (**1e**)

Under an argon atmosphere, 1-chloro-3-ethynylbenzene (0.66 g, 4.83 mmol) was dissolved in anhydrous THF (15 mL), and LDA (diisopropylamine (0.52 g, 5.09 mmol) and *n*-BuLi (3.2 mL, 5.09 mmol, 1.62 M)) was added to the solution at −78 °C. After the mixture was stirred for 1 h at 0 °C, 1-naphthyl-selanylbromide in anhydrous THF (10 mL) was added to the above solution at −78 °C. The reaction mixture was stirred for 2 h at −78 °C, and allowed to warm up to 0 °C. Then, acetone (5 mL) was added, evaporated and dried in vacuo. The crude product was purified by column chromatography (flash column, SiO_2, acidic alumina, hexane). Compound **1e** was isolated in 27% yield as colorless prisms, mp 71.0–72.0 °C. *Anal.* Calc. for $C_{18}H_{11}ClSe$: C, 63.27; H, 3.24. Found: C, 63.26; H, 3.34%. δ_H (300 MHz; $CDCl_3$; Me_4Si) 7.29 (d, *J* 8.8 Hz, 2H), 7.40 (d, *J* 8.9 Hz, 2H), 7.46 (t, *J* 7.8 Hz, 1H), 7.51–7.63 (m, 2H), 7.82 (d, *J* 8.4 Hz, 1H), 7.87 (dd, *J* 1.6, 7.8 Hz, 1H), 8.01 (dd, *J* 1.1 and 7.3 Hz, 1H), 8.06 (dd, *J* 1.0, 8.2 Hz, 1H); δ_C (75 MHz; $CDCl_3$; Me_4Si) 70.6, 101.5, 121.7, 125.5, 126.2, 126.5, 126.9, 127.0, 128.5, 128.7, 128.8, 129.3, 132.2, 132.9, 134.1, 134.6; δ_{Se} (57 MHz; $CDCl_3$; Me_2Se) 241.5.

2.2.6. 1-(p-Cyanophenylethynylselanyl)naphthalene (**1h**) [59]

α-(*p*-Cyanophenylcarbonyl)-α-(naphthylselanyl)phosphorane (**8**) (0.68 g, 1.11 mmol) was heated under vacuum (0.1 mmHg) at 230 °C for 5 min. The crude product was purified by column chromatography (flash column, SiO_2, hexane:benzene = 9:1). Compound **1h** was isolated in 16% yield as yellow prisms, mp 96.0–97.0 °C. *Anal.* Calc. for $C_{19}H_{11}NSe$: C, 68.68; H, 3.34; N, 4.22. Found: C, 68.56; H, 3.49; N, 4.22%. δ_H (300 MHz; $CDCl_3$; Me_4Si) 7.46 (t, *J* 7.8 Hz, 1H), 7.50 (d, *J* 8.7 Hz, 2H), 7.53–7.65 (m, 2H), 7.58 (d, *J* 8.8 Hz, 2H), 7.86 (d, *J* 8.4 Hz, 1H), 7.89 (dd, *J* 1.0, 7.7 Hz, 1H), 8.00 (dd, *J* 1.1, 7.2 Hz, 1H), 8.10 (dd, *J* 1.6, 7.9 Hz, 1H); δ_C (75 MHz; $CDCl_3$; Me_4Si) 75.9, 100.8, 111.4, 118.5, 125.7, 126.2, 126.4, 126.6, 127.1, 127.9, 127.9, 128.8, 129.1, 130.0, 131.8, 132.0, 134.1; δ_{Se} (57 MHz; $CDCl_3$; Me_2Se) 243.9.

2.2.7. α-(p-Cyanophenylcarbonyl)-α-(naphthylselanyl)phosphorane (**8**) [59]

Under an argon atmosphere, (*p*-cyanophenylcarbonylmethylidene)triphenylphosphorane [60] (3.00 g, 7.40 mmol) was dissolved in benzene (30 mL), added to a benzene solution (40 mL) of 1-naphthylselanylbromide at room temperature and stirred for 2 h at room temperature. A white suspension was formed, and the solid was filtered out from the reaction mixture. The filtrate was evaporated and dried in vacuo. The crude product was purified by column chromatography (flash column, SiO_2, CH_2Cl_2). Compound **8** was isolated in 17% yield as yellow prisms, mp 118.0–120.0 °C. *Anal.* Calc. for $C_{19}H_{11}NSe$: C, 72.79; H, 4.29; N, 2.29. Found: C, 73.00; H, 4.63; N, 2.34%. δ_H (300 MHz; $CDCl_3$; Me_4Si) 7.25–7.39 (m, 9H), 7.40–7.51 (m, 5H), 7.54–7.63 (m, 8H), 7.72–7.83 (m, 4H); δ_C (75 MHz; $CDCl_3$; Me_4Si) 52.4 ($^1J_{C,P}$ 92.8 Hz), 53.4, 112.0, 119.0, 125.0, 125.0 ($^3J_{C,P}$ 11.2 Hz), 125.1, 125.6 ($^4J_{C,P}$ 2.5 Hz), 125.9, 126.1 ($^1J_{C,P}$ 90.9 Hz), 128.2, 128.5, 128.5 ($^3J_{C,P}$ 12.3 Hz), 131.2, 131.8, 132.1 ($^4J_{C,P}$ 2.5 Hz), 133.5, 133.7 ($^2J_{C,P}$ 9.3 Hz), 136.8 ($^4J_{C,P}$ 1.9 Hz), 146.5 ($^3J_{C,P}$ 11.2 Hz), 190.9 ($^2J_{C,P}$ 10.6 Hz); δ_{Se} (57 MHz; $CDCl_3$; Me_2Se) 315.4 ($J_{Se,P}$ 8.0 Hz).

2.2.8. 1-(p-Nitrophenylethynylselanyl)naphthalene (**1i**) [59]

α-(*p*-Nitrophenylcarbonyl)-α-(naphthylselanyl)phosphorane (**9**) (0.30 g, 0.79 mmol) was heated under vacuum (0.1 mmHg) at 250 °C for 5 min. The crude product was purified by column chromatography (flash column, SiO_2, hexane:benzene = 4:1). Compound **1i** was isolated in 7% yield as yellow prisms, mp 136.5–137.5 °C. *Anal.* Calc. for $C_{18}H_{11}NO_2Se$: C, 61.38; H, 3.15; N, 3.98. Found: C, 61.23; H, 3.36; N, 3.88%. δ_H (300 MHz; $CDCl_3$; Me_4Si) 7.48 (t, *J* 7.8 Hz, 1H), 7.52–7.62 (m, 2H), 7.55 (d, *J* 9.0 Hz, 2H), 7.87 (d, *J* 7.5 Hz, 1H), 7.90 (d, *J* 7.7 Hz, 1H), 8.02 (dd, *J* 1.1, 7.3 Hz, 1H), 8.12 (dd, *J* 1.3, 8.2 Hz, 1H), 8.17 (d, *J* 9.0 Hz, 2H); δ_C (75 MHz; $CDCl_3$; Me_4Si) 77.4, 100.6, 123.6, 125.8, 126.2,

126.2, 127.1, 128.9, 129.2, 129.9, 130.3, 131.9, 132.4, 134.2, 146.9; δ_{Se} (57 MHz; $CDCl_3$; Me_2Se) 244.9.

2.2.9. α-(p-Nitrophenylcarbonyl)-α-(naphthylselanyl)phosphorane (9) [59]

A similar method to that described for the preparation of **8** was used. Compound **9** was isolated in 33% yield as yellow prisms, mp 135.0–137.0 °C. *Anal.* Calc. for $C_{19}H_{11}NSe \cdot H_2O$: C, 66.67; H, 4.32; N, 2.16. Found: C, 66.43; H, 4.53; N, 2.17%. δ_H (300 MHz; $CDCl_3$; Me_4Si) 7.29 (d, *J* 7.0 Hz, 2H), 7.31–7.41 (m, 7H), 7.45–7.51 (m, 3H), 7.56–7.64 (m, 8H), 7.75 (d, *J* 8.2 Hz, 1H), 7.79–7.83 (m, 3H), 8.06 (d, *J* 8.9 Hz, 2H); δ_C (75 MHz; $CDCl_3$; Me_4Si) 52.9 ($^1J_{C,P}$ 92.0 Hz), 122.7, 124.9, 125.0 ($^3J_{C,P}$ 11.5 Hz), 125.1, 125.9 ($^4J_{C,P}$ 2.9 Hz), 125.9 ($^1J_{C,P}$ 91.1 Hz), 125.6, 126.3, 128.2, 128.5 ($^3J_{C,P}$ 12.5 Hz), 128.7, 131.8, 132.1 ($^4J_{C,P}$ 2.9 Hz), 133.5, 133.7 ($^2J_{C,P}$ 9.6 Hz), 136.6 ($^4J_{C,P}$ 1.9 Hz), 147.7, 148.5 ($^3J_{C,P}$ 11.5 Hz), 190.7 ($^2J_{C,P}$ 10.5 Hz); δ_{Se} (57 MHz; $CDCl_3$; Me_2Se) 314.6 ($J_{Se,P}$ 6.0 Hz).

2.3. X-ray structure determination

Single crystals of **1a–c** and **1e** were obtained by slow evaporation of dichloromethane–hexane at room temperature, and **1h** and **1i** were obtained from an ethyl acetate solution. X-ray diffraction data were collected on a Rigaku/MSC Mercury CCD diffractometer equipped with a graphite-monochromated MoKα radiation source (λ = 0.71070 Å) at 103(2) K. The structures were solved by direct methods (SIR97) and refined by the full-matrix least squares method on F^2 for all reflections (SHELXL-97) [61]. All of the non-hydrogen atoms were refined anisotropically.

2.4. Quantum chemical calculations

Quantum chemical (QC) calculations were performed by employing the 6-311+G(d) basis set of the GAUSSIAN 03 program [62] at the density functional theory (DFT) level of the Becke three-parameter hybrid functionals combined with the Lee–Yang–Parr correlation functional (B3LYP) [63]. QC calculations were also performed by employing the 6-31+G(d) basis set for Se and the 4-31G(d) basis set for other nuclei of the GAUSSIAN 03 program [62] at the Møller–Plesset second order energy correlation (MP2) level [64–66].

3. Results and discussion

3.1. Structures of 1 in crystals

Single crystals were obtained for **1a–c**, **1e**, **1h** and **1i** via slow evaporation of dichloromethane–hexane or ethyl acetate solutions. The X-ray crystallographic analyses were carried out for a suitable crystal of each compound. One type of structure corresponds to **1b**, **1c**, **1e**, **1h** and **1i**, and two-types to **1a** in the crystals. The crystallographic data are collected in Table 1. Figs. 1–4 show the structures of $\mathbf{1a}_A$, **1b**, **1e** and **1i**, respectively. The structures of $\mathbf{1a}_B$, **1c** and **1h** are shown in the Supplementary data. Selected interatomic distances, angles and torsion angles, necessary for the discussion, are collected in Table 2. Scheme 3 summarizes the structures of **1**, together with those of **3**.

As shown in Figs. 1–4 and Table 2, the structure of **1** is **A** (**1** (**A**)) for non-acceptor Y groups, such as H (**a**), OMe (**b**), and Me (**c**), whereas it is **B** for acceptors Y groups (**1** (**B**)), such as Cl (**e**), CN (**h**) and NO_2 (**i**) (Scheme 3). The results are quite a contrast to the case of **3**, where the structure of **3** is **B** when Y is OMe and **A** when Y is Cl and NO_2. The ethynyl group interrupting between *p*-YC_6H_4 and Se changes the structures dramatically: (**B**: **pd**) of **3b** to (**A**: **pd**) of **1b**, (**A**: **pl**) of **3e** to (**B**: **pd**) of **1e**, and (**A**: **pl**) of **3** (Y = CO_2Et) to (**B**: **pl**) of **1i**, where Y = CO_2Et is employed in place of Y = NO_2 for **3**.[2] The direction of Y-dependence in **1** is just the inverse to the case of **3**. We call the factor to determine the fine structure of **1** the "*ethynyl effect*".

The structures of **1a–c** are observed as dimers. Fig. 5 shows the dimer formed from **1a**, which contains $\mathbf{1a}_A$ and $\mathbf{1a}_B$. Dimers of **1b** and **1c** are essentially the same as that of **1a**, and are shown in the Supplementary data. The Se atoms in the **1a** dimer are in short contact with C at the 6′ position of the partner molecule and the Se1—C6′ distance is 3.392 Å. The overlap between the two naphthyl planes must be large in this case.[3] The driving force of the dimer formation must be the energy lowering effect by the π-stacking of the naphthyl groups. The π(C)–σ*(Se–C_{sp}) 3c–4e interaction must also contribute to stabilize the dimers.

How do the electrons in n_p(Se) extend over the orbitals of **1**? The structures of $\mathbf{1a}_A$ (Y = H), **1b** (Y = OMe) and **1c** (Y = Me) are observed as (**A**: **pd**), that of $\mathbf{1a}_B$ (Y = H) as (**A**: **np**), that of **1d** (Y = Cl) as (**B**: **pd**), and those of **1h** (Y = CN) and **1i** (Y = NO_2) as (**B**: **pl**) (see Figs. 1–4 and Scheme 3). Scheme 4 illustrates the orbital interactions in **1** (**A**: **pd**), **1** (**A**: **pl**), **1** (**B**: **pd**) and **1** (**B**: **pl**). How the electrons in n_p(Se) extend over the π-frameworks are explained as: π(C≡C)–n_p(Se) in (**A**: **pd**), n_p(Y)–π(C_6H_4)–π(C≡C)–n_p(Se) in (**A**: **pl**), π(C≡C)–n_p(Se)–π(Nap) in (**B**: **pd**) and n_p(Y)–π(C_6H_4)–π(C≡C)–n_p(Se)–π(Nap) in (**B**: **pl**). **1** (**A**: **pd**) and/or **1** (**B**: **pd**) would be more stable than **1** (**A**: **pl**) and **1** (**B**: **pl**) for Y donating groups, since n_p(Se) is also a good donor. On the contrary, **1** (**A**: **pl**) and/or **1** (**B**: **pl**) must be more stable than **1** (**A**: **pd**) and **1** (**B**: **pd**) for Y acceptor groups. **1** (**A**: **pd**) is detected in crystals when Y = H, OMe and Me, which is in accordance with the observations, although the dimer formation also contributes to stabilize (**A**: **pd**) in **1a–c**. In the case of Y acceptor groups, **1** (**B**: **pd**) is observed in crystals for Y = Cl and **1** (**B**: **pl**) for Y = CN and NO_2. **1** (**B**: **pl**) must be more stable than **1** (**B**: **pd**) for stronger acceptor Y groups due to the wider extension of π-electrons.[4]

3.2. QC calculations

3.2.1. Evaluation of electron affinity (EA) for ArC≡CH and the structures of 1

The structures of **3** are well understood based on the relative magnitudes of the p(Se)–π(Ar) and p(Se)–π(Nap) conjugations [67]. The magnitudes of the conjugations can be estimated by the electron affinity (EA) of PhY and NapH, which are the components of **3**. The structure of **3** is reported to be **A** if π(Ar) stabilizes the electrons in n_p(Se) more effectively than π(Nap) [67]. The efficiency to stabilize the electrons in n_p(Se) can be estimated by the EA of PhY and NapH, the components of **3**. Namely, the structure of **3** is **A**, if EA(PhY) > EA(NapH).

$$EA = -0.900 \times \varepsilon(LUMO) - 1.484 \quad (1)$$

The EA of the molecules can be predicted based on the energy of the LUMO [67]. ε(LUMO) values are calculated with the B3LYP/6-311+G(d,p) method of the GAUSSIAN 03 program [62,63] for *p*-$YC_6H_4C{\equiv}CH$ (**10**), one of the components of **1**, and NapH. The EA of **10** are obtained based on ε(LUMO) by applying Eq. (1) [67]. Table 3

[2] The structure of **3i** is essentially the same as that of **3g**, although that of the former has not been determined by X-ray analysis due to the very thin nature of the crystals.

[3] An Se atom in the **1b** dimer is in short contact with C at the 4′ position of the partner molecule. The overlap between the two naphthyl planes is rather small in this case.

[4] **3** (**B**: **pl**) is not observed as a stable conformer, the steric repulsion between H_2 and H_o must be very large.

Table 1
Crystallographic data for **1a–c**, **1e**, **1h** and **1i**

	1a	1b	1c	1e	1h	1i
Empirical formula	$C_{18}H_{12}Se$	$C_{19}H_{14}OSe$	$C_{19}H_{14}Se$	$C_{18}H_{11}ClSe$	$C_{19}H_{11}NSe$	$C_{18}H_{11}NO_2Se$
Formula weight	307.24	337.28	321.28	341.68	332.25	352.24
Temperature (K)	103(2)	103(2)	103(2)	103(2)	103(2)	103(2)
Crystal system	monoclinic	triclinic	triclinic	triclinic	monoclinic	triclinic
Space group	$P2_1/c$	$P\bar{1}$	$P\bar{1}$	$P\bar{1}$	$P2_1/n$	$P\bar{1}$
Unit cell dimensions						
a (Å)	15.0449(2)	7.4046(2)	7.2417(2)	8.5981(2)	7.0648(2)	6.9474(2)
b (Å)	8.99370(10)	8.2505(2)	8.2484(2)	9.4028(2)	13.8488(4)	7.0900(2)
c (Å)	19.9029(4)	12.6013(4)	12.6209(3)	9.7134(2)	15.0128(3)	14.8742(4)
α (°)	90.00	106.2292(10)	106.7005(10)	72.1791(16)	90.00	93.039(2)
β (°)	97.1408(13)	102.9643(14)	102.6188(11)	79.3822(15)	95.5898(10)	90.9689(15)
γ (°)	90.00	94.905(2)	92.459(3)	68.9784(9)	90.00	100.2889(12)
V (Å^3)	2672.16(7)	711.22(3)	700.12(3)	695.40(3)	1461.85(7)	719.60(3)
Z	8	2	2	2	4	2
D_{calc} (g cm^{-3})	1.527	1.575	1.524	1.632	1.510	1.626
$F(000)$	1232	340	324	340	664	352
Crystal size (mm^3)	0.40 × 0.20 × 0.10	0.30 × 0.12 × 0.02	0.40 × 0.25 × 0.10	0.35 × 0.25 × 0.20	0.15 × 0.10 × 0.02	0.18 × 0.10 × 0.06
μ (cm^{-1})	2.792	2.635	2.667	2.877	2.560	2.615
Reflections collected	22997	5008	4684	4527	12426	6024
Reflections unique	4966	2568	2473	2348	2711	2587
Reflections observed [$I > 2\sigma(I)$]	4157	2446	2466	2282	2427	2533
Parameters	439	191	182	181	234	243
Final R indices R_1	0.0223	0.0238	0.0260	0.0341	0.0249	0.0184
[$I > 2\sigma(I)$] wR_2	0.0562	0.0677	0.0740	0.1024	0.0651	0.0467
R indices (all data) R_1	0.0298	0.0251	0.0273	0.0348	0.0294	0.0188
wR_2	0.0585	0.0682	0.0745	0.1028	0.0682	0.0470
Goodness-of-fit on F^2	1.045	1.186	1.196	1.295	1.064	1.042

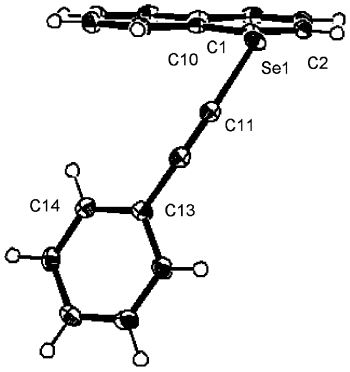

Fig. 1. Structure of **1a**$_A$ (thermal ellipsoids are shown at the 50% probability level).

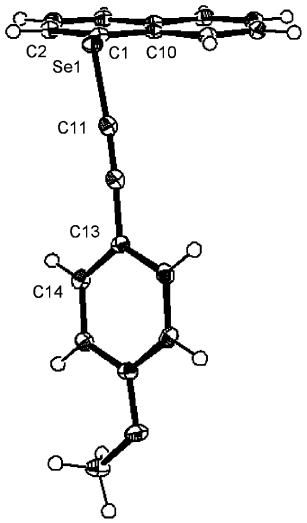

Fig. 2. Structure of **1b** (thermal ellipsoids are shown at the 50% probability level).

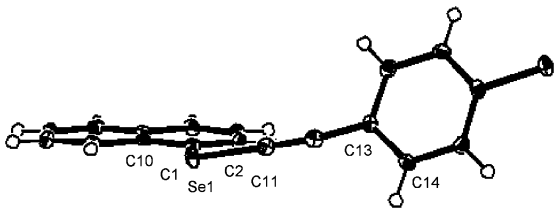

Fig. 3. Structure of **1e** (thermal ellipsoids are shown at the 50% probability level).

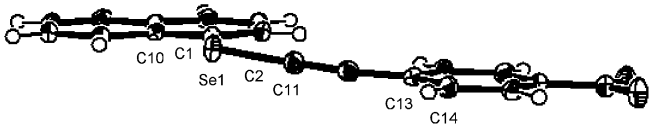

Fig. 4. Structure of **1i** (thermal ellipsoids are shown at the 50% probability level).

shows the evaluated EA values for **10** (Y = OMe, Me, H, Cl, CN and NO_2), together with ε(LUMO). As mentioned above, the structure of **1** is expected to be **A** if EA (**10**) > EA (PhCl) = −0.75 eV. (The structure of **3** (Y = Cl) is **A**.) The EA of **10** are larger than the EA (PhCl) for all Y examined, containing OMe, Me and H. Therefore, it is demonstrated that the structures of **1** can be **A** for all Y examined without the aid of the dimer formation, if the structures of **1** are determined only by the p(Se)–π(Ar) and p(Se)–π(Nap) conjugations.

3.2.2. Dimer formation

QC calculations were also performed on the dimer of **1a** by employing the 6-31+G(d) basis set for Se and the 4-31G(d) basis set for other nuclei of the GAUSSIAN 03 program [62] at the MP2 level [64–66].

Fig. 6 shows the optimized structure for the dimer of **1a**, the Se1–C6′ distance is 3.500 Å. The dimer formed from **1a** is predicted to be more stable than the corresponding monomers by 60.7 kJ mol^{-1} ($\Delta E = 2E$ (monomer) − E (dimer)). The driving force

Table 2
Selected bond distances, angles and torsional angles around the Se atom, observed in **1**

	1a$_A$ (Y = H)	**1a**$_B$ (Y = H)	**1b** (Y = OMe)	**1c** (Y = Me)	**1e** (Y = Cl)	**1h** (Y = CN)	**1i** (Y = NO_2)
r(Se1, C1) (Å)	1.9321(19)	1.9243(18)[a]	1.936(2)	1.933(2)	1.935(2)	1.9335(19)	1.9315(15)
r(Se1, C11) (Å)	1.8406(18)	1.8381(19)[b]	1.847(2)	1.844(2)	1.829(3)	1.825(2)	1.8233(15)
∠C1Se1C11 (°)	98.07(7)	99.68(8)[c]	98.46(9)	99.07(10)	98.92(11)	98.93(9)	98.41(6)
∠C2C1Se1 (°)	117.37(14)	116.77(15)[d]	117.61(16)	117.61(17)	121.26(19)	122.02(15)	122.17(11)
∠C10C1Se1 (°)	121.12(13)	121.74(14)[e]	120.89(15)	120.84(17)	116.86(18)	116.32(14)	116.44(11)
∠C10C1Se1C11 (°)	60.64(15)	62.36(15)[f]	−79.69(17)	−78.92(19)	−169.24(19)	171.59(15)	171.42(11)
∠C1Se1C13C14 (°)	−54.80	−135.72[g]	−58.78	126.88	−123.63	176.47	2.61
Structure	(**A**: **pd**)	(**A**: **np**)	(**A**: **pd**)	(**A**: **pd**)	(**B**: **pd**)	(**B**: **pl**)	(**B**: **pl**)

[a] *r*(Se2, C19).
[b] *r*(Se2, C29).
[c] ∠C19Se2C29.
[d] ∠C20C19Se2.
[e] ∠C28C19Se2.
[f] ∠C28C19Se2C29.
[g] ∠C19Se2C31C32.

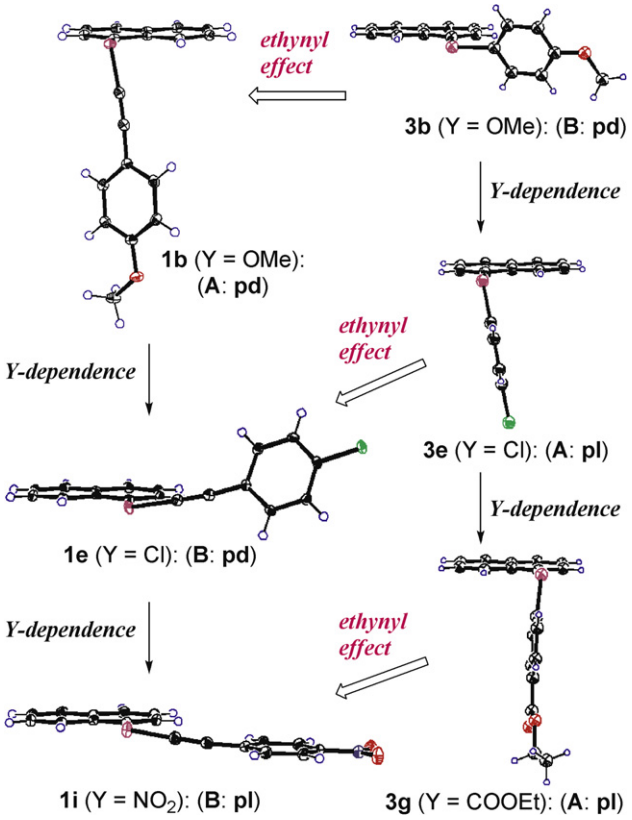

Scheme 3. *ethynyl effect* in **1** and Y-dependence in **1** and **3**.

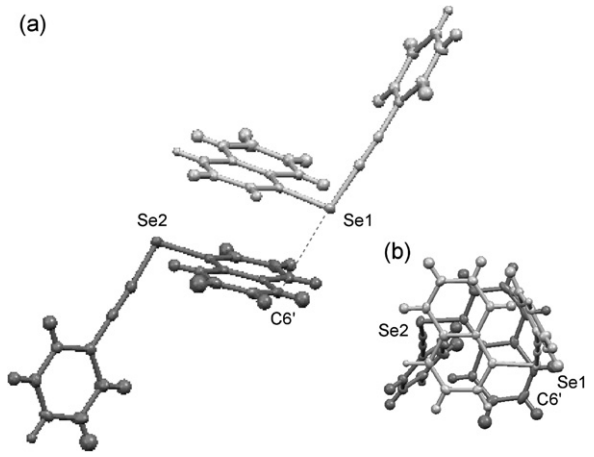

Fig. 5. Dimer formed in **1a**, which contains **1a**$_A$ and **1a**$_B$: (a) a side view (*r*(Se1–C6′): 3.392 Å) and (b) a top view.

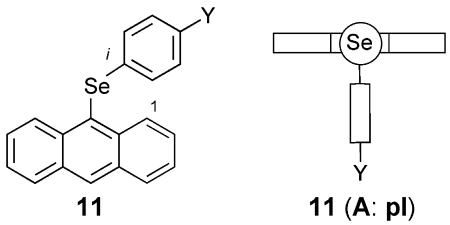

for the dimer formation must be the energy lowering effect of the π-stacking of the naphthyl groups. The 3c–4e interaction of the π(C)–σ*(Se–C_{sp}) type would also contribute to stabilize the dimer structure.

3.3. Behavior of *1* in solution based on NMR spectroscopy

How do **1a**–**e**, **1h** and **1i** behave in solution? ^{1}H, ^{13}C and ^{77}Se NMR chemical shifts were measured in chloroform-*d*. Table 4 collects the $\delta(H_2)$, $\delta(H_8)$ and δ(Se) values. The shift ranges are 0.078, 0.092 and 4.4 ppm, respectively, which are small relative to the usual trends in substituent dependence [68,69]. This must be a reflection of the ethynyl group. It must be the result of the probe site in the NMR spectroscopy being separated far from the *p*-YC_6H_4 group by the ethynyl group.

The structures of **1** in chloroform-*d* solutions are analyzed based on the NMR chemical shifts, which are given in Table 4. The structure of 1-(arylselanly)anthracene [**11**: 1-(*p*-YC_6H_4-Se)$C_{14}H_9$] is established to be the standard of (**A**: **pl**) for all Y in Table 4 [68,69]. Therefore the $\delta(H_1)_{SCS}$ and $\delta(Se)_{SCS}$ values of **11** are employed as the standards for the analysis. Fig. 7 shows the plot of $\delta(H_8$: **1**) versus $\delta(H_1$: **11**). The correlation is shown in Eq. (2) and that for the plot of δ(Se: **1**) versus δ(Se: **11**) is given in Eq. (3).

$$\delta(H_8 : \mathbf{1})_{SCS} = -0.338 \times \delta(H_1 : \mathbf{11})_{SCS} - 0.007 \quad r = 0.991 \qquad (2)$$

$$\delta(Se : \mathbf{1})_{SCS} = 0.096 \times \delta(Se : \mathbf{11})_{SCS} + 0.18 \quad r = 0.960 \qquad (3)$$

The correlation for $\delta(H_8$: **1**) versus $\delta(H_1$: **11**) is good ($r = 0.991$) with a correlation constant (a) of −0.34 ($y = ax + b$: r). The negative value must be the reflection of the inverse direction of the anisotropic effect between the phenyl and the ethynyl groups. Therefore, the structures of **1** are mainly (**A**: **pl**) in solution, which is

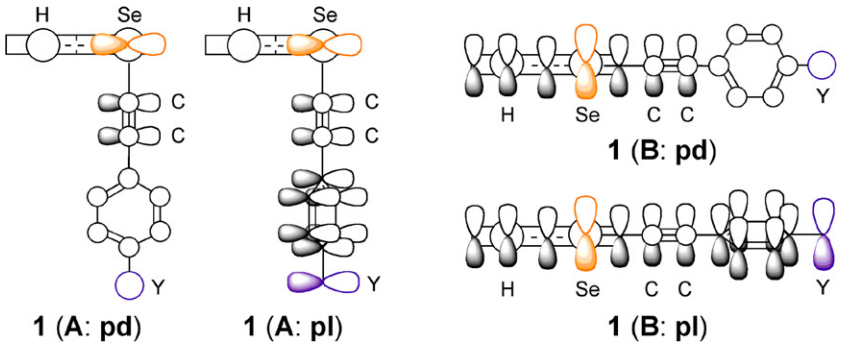

Scheme 4. Orbital interactions in (**A**: **pd**), (**A**: **pl**), (**B**: **pd**) and (**B**: **pl**) in **1**.

Table 3
Evaluated EA based on the calculated energy of the LUMO for PhY and **10**[a]

Y	OMe	Me	H	Cl	CN	NO_2	/NapH[b]	PhCCH[c]
ε(LUMO: PhY)	−0.46[d]	−0.43[d]	−0.48	−0.86	−1.85	−2.92	−1.40[e]	0.51[f]
ε(LUMO: **10**)	−0.95	−1.16	−1.29	−1.55	−2.36	−3.14		−1.02[g]
EA(PhY)	−1.11[e]	−1.09[e]	−1.15[e]	−0.75[e]	0.18	1.01[e]	−0.2	−1.94[f]
EA (**10**)	−0.63	−0.44	−0.32	−0.09	0.65	1.35		−0.57[g]

[a] In eV.
[b] Naphthalene.
[c] Ethynylbenzene.
[d] Based on LUMO+1.
[e] Observed values.
[f] π^*(C≡C).
[g] π^*(PhC≡CH).

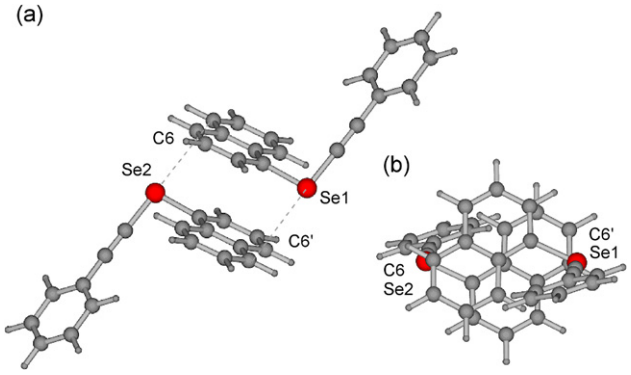

Fig. 6. Optimized structure for the dimer of **1a**: (a) a side view (*r*(Se1–C6′): 3.500 Å) and (b) a top view.

Table 4
^{1}H and ^{77}Se NMR chemical shifts in **1**, together with those in **11**[a,b]

Y	b	c	a	d	e	h	i
1							
$\delta(H_2)_{SCS}$	−0.019	−0.011	0.000[c]	0.005	0.011	0.047	0.059
$\delta(H_8)_{SCS}$	−0.023	−0.014	0.000[d]	0.005	0.012	0.054	0.069
$\delta(Se)_{SCS}$	−0.5	0.0	0.0[e]	−0.9	0.1	2.5	3.5
11							
$\delta(H_1)_{SCS}$	0.045	0.005	0.000[f]	−0.028	−0.075	−0.186	−0.218
$\delta(Se)_{SCS}$	−12.2	−6.6	0.0[g]	−3.6	1.5	26.2	30.3

[a] In $CDCl_3$.
[b] From Me_4Si for δ(H) and from Me_2SeMe for δ(Se).
[c] $\delta(H_2)$ = 7.798.
[d] $\delta(H_8)$ = 8.033.
[e] δ(Se) = 241.4.
[f] $\delta(H_1)$ = 8.884.
[g] δ(Se) = 249.0.

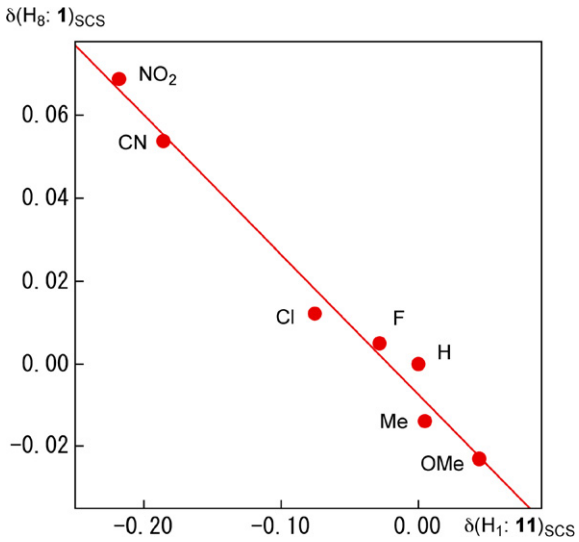

Fig. 7. Plot of $\delta(H_8: \mathbf{1})_{SCS}$ vs. $\delta(H_1{:}\mathbf{1})_{SCS}$.

substantially in accordance with the conclusion obtained from the EA analysis. The inverse effect by the ethynyl group on the structures of **1** is confirmed for non-acceptors Y groups, such as Y = OMe and Me, also in solution. However, the correlation coefficient of 0.991 might be the result of the equilibrium with other conformers such as (**B**: **pd**). The structures of **1** having Y acceptors such as NO_2 and CN seem to equilibrate with (**B**: **pd**), which should also be the reflection of the inverse effect by the ethynyl group.

4. Conclusions

The behavior of ethynylchalcogenyl groups is examined as the factor to control fine structures. Fine structures of

1-(p-$YC_6H_4C{\equiv}CSe$)$C_{10}H_7$ (**1**: Y = H (**a**), OMe (**b**), Me (**c**), Cl (**e**), CN (**h**) and NO_2 (**i**)) are determined by X-ray crystallographic analysis. The structures are (**A**: **pd**) or (**A**: **np**) for **1a–c** bearing non-acceptors Y groups, it is (**B**: **pd**) for **1e** with Y = Cl, and (**B**: **pl**) for **1h** and **1i** with Y being the strong acceptors CN and NO_2. The Y-dependence observed in **1** is just the opposite to the case of 1-(p-YC_6H_4-Se)$C_{10}H_7$ (**3**). The factor to control the fine structures of **1** is called the "*ethynyl effect*". The parallel direction between n_p(Se) and n_p(Y) operates to lower the energy if Y is an acceptor but it destabilize the system for donor Y groups. Therefore, the origin of the ethynyl effect is explained based on the idea how widely the electron in n_p(Se) extends over the π-framework under the conditions for n_p(Se) and n_p(Y). Crystal packing effects giving the formation of dimers also plays an important role in controlling the structures. The structures of **1** in solution are also examined based on NMR chemical shifts, employing the data for (**A**: **pl**) of 1-(arylselanly)anthracene (**11**). The results show that the structures of **1** are mainly (**A**: **pl**) with some equilibria with other conformers such as (**B**: **pd**). The inverse effect of the ethynyl group as the factor to control the structure of **1** in solution is confirmed. The results exhibit that fine structures of arylethynylchalcogenyl compounds can be widely controlled by modulating the electronic conditions around the chalcogen atoms.

Acknowledgments

This work was partially supported by a Grant-in-Aid for Scientific Research (Nos. 16550038 and 19550041) from the Ministry of Education, Culture, Sports, Science, and Technology, Japan.

Appendix A. Supplementary data

CCDC 666789, 666790, 666791, 666792, 666793 and 666794 contain the supplementary crystallographic data for **1a**, **1b**, **1c**, **1e**, **1h** and **1i**. These data can be obtained free of charge via http://www.ccdc.cam.ac.uk/conts/retrieving.html, or from the Cambridge Crystallographic Data Centre, 12 Union Road, Cambridge CB2 1EZ, UK; fax: (+44) 1223-336-033; or e-mail: deposit@ccdc.cam.ac.uk. Supplementary data associated with this article can be found, in the online version, at doi:10.1016/j.poly.2008.04.052.

References

[1] S. Scheiner, Molecular Interactions, From Van der Waals to Strongly Bound Complexes, Wiley, New York, 1997.
[2] K.D. Asmus, Acc. Chem. Res. 12 (1979) 436.
[3] W.K. Musker, Acc. Chem. Res. 13 (1980) 200.
[4] A. Kucsman, I. Kapovits, Non-bonded sulfur–oxygen interaction, in: F. Bernardi, I.G. Csizmadia, A. Mangini (Eds.), Organic Sulfur Chemistry: Theoretical and Experimental Advances, Elsevier, Amsterdam, 1985.
[5] R.S. Glass, S.W. Andruski, J.L. Broeker, Rev. Heteroatom. Chem. 1 (1988) 31.
[6] R.S. Glass, S.W. Andruski, J.L. Broeker, H. Firouzabadi, L.K. Steffen, G.S. Wilson, J. Am. Chem. Soc. 111 (1989) 4036.
[7] R.S. Glass, L. Adamowicz, J.L. Broeker, J. Am. Chem. Soc. 113 (1991) 1065.
[8] N. Furukawa, Bull. Chem. Soc. Jpn. 70 (1997) 2571.
[9] N. Furukawa, K. Kobayashi, S. Sato, J. Organomet. Chem. 611 (2000) 116.
[10] (a) W. Nakanishi, Chem. Lett. (1993) 2121;
(b) W. Nakanishi, S. Hayashi, S. Toyota, Chem. Commun. (1996) 371;
(c) W. Nakanishi, S. Hayashi, H. Yamaguchi, Chem. Lett. (1996) 947;
(d) W. Nakanishi, S. Hayashi, A. Sakaue, G. Ono, Y. Kawada, J. Am. Chem. Soc. 120 (1998) 3635;
(e) W. Nakanishi, S. Hayashi, S. Toyota, J. Org. Chem. 63 (1998) 8790;
(f) S. Hayashi, W. Nakanishi, J. Org. Chem. 64 (1999) 6688;
(g) W. Nakanishi, S. Hayashi, T. Uehara, J. Phys. Chem. A 103 (1999) 9906;
(h) W. Nakanishi, S. Hayashi, J. Org. Chem. 67 (2002) 38;
(i) S. Hayashi, H. Wada, T. Ueno, W. Nakanishi, J. Org. Chem. 71 (2006) 5574;
(j) W. Nakanishi, S. Hayashi, T. Arai, Chem. Commun. (2002) 2416;
(k) W. Nakanishi, S. Hayashi, N. Itoh, Chem. Commun. (2003) 124;
(l) W. Nakanishi, S. Hayashi, N. Itoh, J. Org. Chem. 69 (2004) 1676;
(m) W. Nakanishi, T. Nakamoto, S. Hayashi, T. Sasamori, N. Tokitoh, Chem. Eur. J. 13 (2007) 255;
(n) W. Nakanishi, S. Hayashi, S. Yamaguchi, K. Tamao, Chem. Commun. (2004) 140.
[11] (a) W. Nakanishi, S. Hayashi, H. Kihara, J. Org. Chem. 64 (1999) 2630;
(b) W. Nakanishi, S. Hayashi, T. Uehara, Eur. J. Org. Chem. (2001) 3933.
[12] M. Iwaoka, S. Tomoda, J. Am. Chem. Soc. 116 (1994) 4463.
[13] M. Iwaoka, S. Tomoda, J. Am. Chem. Soc. 118 (1996) 8077.
[14] H. Komatsu, M. Iwaoka, S. Tomoda, Chem. Commun. (1999) 205.
[15] K.-y. Akiba, Chemistry of Hypervalent Compounds, Wiley-VCH, New York, 1999.
[16] W. Nakanishi, Hypervalent chalcogen compounds, in: F.A. Devillanova (Ed.), Handbook of Chalcogen Chemistry: New Perspectives in Sulfur, Selenium and Tellurium, Royal Society of Chemistry, London, 2006. (Chapter 10.3).
[17] F.T. Burling, B.M. Goldstein, J. Am. Chem. Soc. 114 (1992) 2313.
[18] Y. Nagao, T. Hirata, S. Goto, S. Sano, A. Kakehi, K. Iizuka, M. Shiro, J. Am. Chem. Soc. 120 (1998) 3104.
[19] S. Wu, A. Greer, J. Org. Chem. 65 (2000) 4883.
[20] Y. Nagao, H. Iimori, S. Goto, T. Hirata, S. Sano, H. Chuman, M. Shiro, Tetrahedron Lett. 43 (2002) 1709.
[21] E. Meyer, A.C. Joussef, H. Gallardo, A.J. Bortoluzzi, R.L. Longo, Tetrahedron 59 (2003) 10187.
[22] Y. Nagao, T. Honjo, H. Iimori, S. Goto, S. Sano, M. Shiro, K. Yamaguchi, Y. Sei, Tetrahedron Lett. 45 (2004) 8757.
[23] J.C. Taylor, G.D. Markham, J. Biol. Chem. 274 (1999) 32909.
[24] W. Brandt, A. Golbraikh, M. Täger, U. Lendeckel, Eur. J. Biochem. 261 (1999) 89.
[25] M. Iwaoka, S. Takemoto, M. Okada, S. Tomoda, Chem. Lett. (2001) 132.
[26] M. Iwaoka, S. Takemoto, M. Okada, S. Tomoda, Bull. Chem. Soc. Jpn. 73 (2002) 1611.
[27] G.R. Desiraju, Angew. Chem. 107 (1995) 2541.
[28] G.R. Desiraju, Angew. Chem., Int. Ed. Engl. 34 (1995) 2311.
[29] V. Lippolis, F. Isaia, Charge-transfer (C.-T.) adducts and related compounds, in: F.A. Devillanova (Ed.), Handbook of Chalcogen Chemistry: New Perspectives in Sulfur, Selenium and Tellurium, Royal Society of Chemistry, London, 2006. (Chapter 8.2).
[30] C. Rêthorê, M. Fourmiguê, N. Avarvari, Chem. Commun. (2004) 1384.
[31] C. Rêthorê, M. Fourmiguê, N. Avarvari, Tetrahedron 61 (2005) 10935.
[32] C. Rêthorê, N. Avarvari, E. Canadell, P. Auban-Senzier, M. Fourmiguê, J. Am. Chem. Soc. 127 (2005) 5748.
[33] T. Suzuki, H. Fujii, Y. Yamashita, C. Kabuto, S. Tanaka, M. Harasawa, T. Mukai, T. Miyashi, J. Am. Chem. Soc. 114 (1992) 3034.
[34] M. Turbiez, P. Frêre, M. Allain, C. Videlot, J. Ackermann, J. Roncali, Chem. Eur. J. 11 (2005) 3742.
[35] A.F. Cozzolino, I. Vargas-Baca, S. Mansour, A.H. Mahmoudkhani, J. Am. Chem. Soc. 127 (2005) 3184.
[36] P.J. Stang, F. Diederich, Modern Acetylenic Chemistry, VCH, Weinheim, 1995.
[37] F. Diederich, P.J. Stang, R.R. Tykwinski, Acetylene Chemistry: Chemistry, Biology, and Material Science, VCH, Weinheim, 2005.
[38] A.J. Zucchero, J.N. Wilson, U.H.F. Bunz, J. Am. Chem. Soc. 128 (2006) 11872.
[39] E.L. Spitler, L.D. Shirtcliff, M.M. Haley, J. Org. Chem. 72 (2007) 86.
[40] H. Hinrichs, A.J. Boydston, P.G. Jones, K. Hess, R. Herges, M.M. Haley, Chem. Eur. J. 12 (2006) 7103.
[41] J.A. Marsden, M.M. Haley, J. Org. Chem. 70 (2005) 10213.
[42] Y. Jiang, D. Perahia, Y. Wang, U.H.F. Bunz, Macromolecules 39 (2006) 4941.
[43] K. Tahara, S. Furukawa, H. Uji-i, T. Uchino, T. Ichikawa, J. Zhang, W. Mamdouh, M. Sonoda, F.C. De Schryver, S. De Feyter, Y. Tobe, J. Am. Chem. Soc. 128 (2006) 16613.
[44] A. Nomoto, M. Sonoda, Y. Yamaguchi, T. Ichikawa, K. Hirose, Y. Tobe, J. Org. Chem. 71 (2006) 401.
[45] E.E. Nesterov, Z. Zhu, T.M. Swager, J. Am. Chem. Soc. 127 (2005) 10083.
[46] A. Orita, T. Nakano, D.L. An, K. Tanikawa, K. Wakamatsu, J. Otera, J. Am. Chem. Soc. 126 (2004) 10389.
[47] A. Orita, D.L. An, T. Nakano, J. Yaruva, N. Ma, J. Otera, Chem. Eur. J. 8 (2002) 2005.
[48] D.B. Werz, R. Gleiter, J. Org. Chem. 68 (2003) 9400.
[49] See also S. Husebye, E.A. Meyers, R.A. Zingaro, A.L. Braga, J.V. Comasseto, N. Petragnani, Acta Crystallogr., Sect. C 42 (1986) 1789.
[50] Linear alignment of six C_2Se_4 atoms is demonstrated in **I** ($n = 0$) by X-ray crystallographic analysis. K. Yamane, S. Hayashi, W. Nakanishi, unpublished work.
[51] C. Rêthorê, A. Madalan, M. Fourmiguê, E. Canadell, E.B. Lopes, M. Almeida, R. Clerac, N. Avarvari, New. J. Chem. 31 (2007) 1468.
[52] E. Grech, J. Klimkiewicz, J. Nowicka-Scheibe, M. Pietrzak, W. Schilf, A.F. Pozharskii, V.A. Ozeryanskii, S. Bolvig, J. Abildgaard, P.E. Hansen, J. Mol. Struct. 615 (2002) 121.
[53] M. Pietrzak, L. Stefaniak, A.-F. Pozharskii, V.-A. Ozeryanskii, J. Nowicka-Scheibe, E. Grech, G.-A. Webb, J. Phys. Org. Chem. 13 (2000) 35.
[54] C.-L. Perrin, B.K. Ohta, J. Am. Chem. Soc. 123 (2001) 6520.
[55] C.-L. Perrin, B.-K. Ohta, J. Mol. Struct. 644 (2003) 1.
[56] F. Mo, E. Husstad, R.H. Mathiesen, B.C. Hauback, H. Kjøsen, J.A. Haugan, E.H. Mørkved, Z. Kristallogr. 214 (1999) 353.
[57] J. Farran, L. Torres-Castellanos, A. Alvarez-Larena, J.F. Piniella, M.V. Capparelli, J. Organomet. Chem. 654 (2002) 91.
[58] For the structures with Z=O, see, R. Gleiter, D.B. Werz, F. Rominger, E. Zhutov, N.S. Zefirov, M.V. Proskurnina, Eur. J. Org. Chem. (2007) 5834.
[59] A.L. Braga, J.V. Comasseto, N. Petragnani, Synthesis (1984) 240.
[60] The starting α-acylphosphoranes were prepared according to procedures previously described T. Thiemann, K. Umeno, J. Wang, Y. Tabuchi, K. Arima, M.

Watanabe, Y. Tanaka, H. Gorohmaru, S. Mataka, J. Chem. Soc., Perkin Trans. 1 (2002) 2090.
[61] G.M. Sheldrick, SHELXL-97 Program for the Refinement of Crystal Structures, University of Göttingen, Germany, 1997.
[62] M.J. Frisch, G.W. Trucks, H.B. Schlegel, G.E. Scuseria, M.A. Robb, J.R. Cheeseman, J.A. Montgomery Jr., T. Vreven, K.N. Kudin, J.C. Burant, J.M. Millam, S.S. Iyengar, J. Tomasi, V. Barone, B. Mennucci, M. Cossi, G. Scalmani, N. Rega, G.A. Petersson, H. Nakatsuji, M. Hada, M. Ehara, K. Toyota, R. Fukuda, J. Hasegawa, M. Ishida, T. Nakajima, Y. Honda, O. Kitao, H. Nakai, M. Klene, X. Li, J.E. Knox, H.P. Hratchian, J.B. Cross, V. Bakken, C. Adamo, J. Jaramillo, R. Gomperts, R.E. Stratmann, O. Yazyev, A.J. Austin, R. Cammi, C. Pomelli, J.W. Ochterski, P.Y. Ayala, K. Morokuma, G.A. Voth, P. Salvador, J.J. Dannenberg, V.G. Zakrzewski, S. Dapprich, A.D. Daniels, M.C. Strain, O. Farkas, D.K. Malick, A.D. Rabuck, K. Raghavachari, J.B. Foresman, J.V. Ortiz, Q. Cui, A.G. Baboul, S. Clifford, R.L. Cioslowski, B.B. Stefanov, G. Liu, A. Liashenko, P. Piskorz, I. Komaromi, R.L. Martin, D.J. Fox, T. Keith, M.A. Al-Laham, C.Y. Peng, A. Nanayakkara, M. Challacombe, P.M.W. Gill, B. Johnson, W. Chen, M.W. Wong, C. Gonzalez, J.A. Pople, GAUSSIAN 03 (Revision D.02), Gaussian, Inc., Wallingford CT, 2004.
[63] (a) A.D. Becke, Phys. Rev. A 38 (1988) 3098;
(b) A.D. Becke, J. Chem. Phys. 98 (1993) 5648;
(c) C. Lee, W. Yang, R.G. Parr, Phys. Rev. B 37 (1988) 785;
(d) B. Miehlich, A. Savin, H. Stoll, H. Preuss, Chem. Phys. Lett. 157 (1989) 200.
[64] C. Møller, M.S. Plesset, Phys. Rev. 46 (1934) 618.
[65] J. Gauss, J. Chem. Phys. 99 (1993) 3629.
[66] J. Gauss, Ber. Bunsenges, Phys. Chem. 99 (1995) 1001.
[67] W. Nakanishi, S. Hayashi, T. Uehara, Eur. J. Org. Chem. (2001) 3933.
[68] W. Nakanishi, S. Hayashi, D. Shimizu, M. Hada, Chem. Eur. J. 12 (2006) 3829.
[69] S. Hayashi, K. Yamane, W. Nakanishi, J. Org. Chem. 72 (2007) 7587.

Polyhedron 27 (2008) 2487–2493

Contents lists available at ScienceDirect

Polyhedron

journal homepage: www.elsevier.com/locate/poly

Solid state conformational preferences in transition metal complexes double bridged by phosphate and related ligands

José Pérez *, Luis García, Ramón Carrascosa, Eduardo Pérez, José Luis Serrano

Departamento de Ingeniería Minera, Geológica y Cartográfica (Área de Química Inorgánica), Universidad Politécnica de Cartagena, 30202 Cartagena, Murcia, Spain

ARTICLE INFO

Article history:
Received 2 April 2008
Accepted 22 April 2008
Available online 19 June 2008

Keywords:
Conformational analysis
Cambridge Structural Database
Pseudorotation

ABSTRACT

The conformational preferences in the $\{M(\mu\text{-}OPO)\}_2$ core of transition metal complexes double bridged by phosphate and related ligands have been determined using data retrieved from the Cambridge Structural Database by a probabilistic method. The preferred conformations lie on a pseudorotation pathway (*chair* and *twist-chair* conformations). The influence of intra-ring bridges, metal atom, coordination number or ligand in the conformational preferences has been investigated.

© 2008 Elsevier Ltd. All rights reserved.

1. Introduction

Conformational features of organic molecules [1] and metallic complexes [2] have been extensively studied, and the CSD has proved to be a useful tool in both fields [3,4]. It is in particular worth mentioning the contribution of Álvarez and co-workers studying several conformational aspects of transition metal complexes [5,6]. The CSD has been widely applied to life-science research too [7], where it has turned out to be a very useful resource for the rational design of biologically active molecules.

Regarding the system analyzed in this paper, it is significant in the study of metalloenzymes that catalyze the hydrolysis of phosphate ester bonds in biological molecules. A systematic variation of ligands and coordination environments in these biological analogues has provided information about the structure and function of enzymes. Although zinc is the most common metal found in these enzymes, copper(II) complexes have also contributed to the general understanding of these processes [8,9].

Other important research areas involving transition metal complexes double bridged by phosphates and related ligands are the preparation of molecular sieves because of their potential application in ion-exchange, catalysis and separations [10], proton conductivity or non-linear optics.

In spite of the importance of the title compounds, we are not aware of a systematic study about the conformational preferences in the solid state of such complexes. This paper tries to cover this lack.

2. Experimental

The Cambridge Structural Database [1] (CSD) V. 5.28 (November 2006 + an update) was searched for all the structures containing the fragment shown in Fig. 1. The query was filtered so that only the structures without disorder in the ring were retrieved. A total of 881 *refcodes* matched the search, the total number of fragments being 2377. Torsion angles were measured by the CONQUEST 1.9 program [1] and transferred to an ASCII text file for statistical and graphical analysis. Out of these 2377 fragments, 1320 were found to incorporate various types of phosphate moieties (hereafter referred to as phosphates), 916 bis(phosphonate) or bis(phosphonate ester) complexes (hereafter referred to as phosphonates), and 141 bis(phosphinate) complexes (hereafter referred to as phosphinates).

The most probable conformation for each fragment was established by the Classification method using the RingConf software with $\sigma = 10°$ [11]. *Refcodes*, torsion angles and the most probable conformations can be found in the Supplementary data.

A total of 21 possible conformations appear when the core shown in Fig. 1 (that shows topological symmetry D_{2h}) is studied, referring to the 10 canonical conformations of cyclooctane [12]. Fig. 2 shows these 21 conformations with their corresponding point group symmetry; bond distances and angles were not considered in the derivation of these *type* conformations.

The Classification method allows an individual classification of the given structure to be assigned. Based on the values of the torsion angles for a structure, we are able, through the Bayes rule, to

* Corresponding author.
E-mail address: jose.pperez@upct.es (J. Pérez).

0277-5387/$ - see front matter © 2008 Elsevier Ltd. All rights reserved.
doi:10.1016/j.poly.2008.04.053

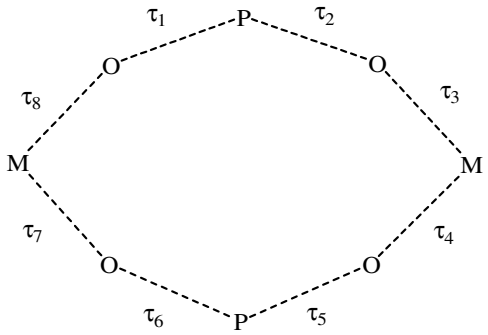

Fig. 1. Substructure used in the conformational study, M = transition metal.

compute the posterior probability that the structure comes from one of the 21 *type* conformations shown in Fig. 2.

3. Results and discussion

The appearance of internal links in the fragment defined in Fig. 1 imposes the most severe conditions to the conformation in the eight-membered ring. Because of this reason we have studied separately three sets of data.

(a) Structures having direct links or one atom bridges in the $\{M(\mu\text{-}OPO)\}_2$ moiety

This set includes the most rigid structures, direct links (or one atom bridges) restrict the conformational freedom. A total of 929 fragments were retrieved from the CSD for this set of data. Most of them correspond to molybdenum complexes. Each of the other metals has less than 10% of the data. Fig. 3 shows the distribution of data by metals.

Only a few conformations from the 21 possible in Fig. 2 are significant for this set of structures. The conformation adopted depends strongly on the kind of bridge. The most abundant types of bridges are:

- M–X–M, X being mostly O and to a minor extent F. 278 fragments contain this bridge, the most frequent conformations in this case are B_1 (36% of fragments), BC_2 (18%) and TCC_1 (17%).
- O–X–O (oxygen atoms in relative positions 1,5), X usually being the metal in the ring (Fig. 1). 235 fragments contain this bridge, conformations are nearly restricted to two kinds: BC_3 (60% of fragments) and TB_1 (38%).

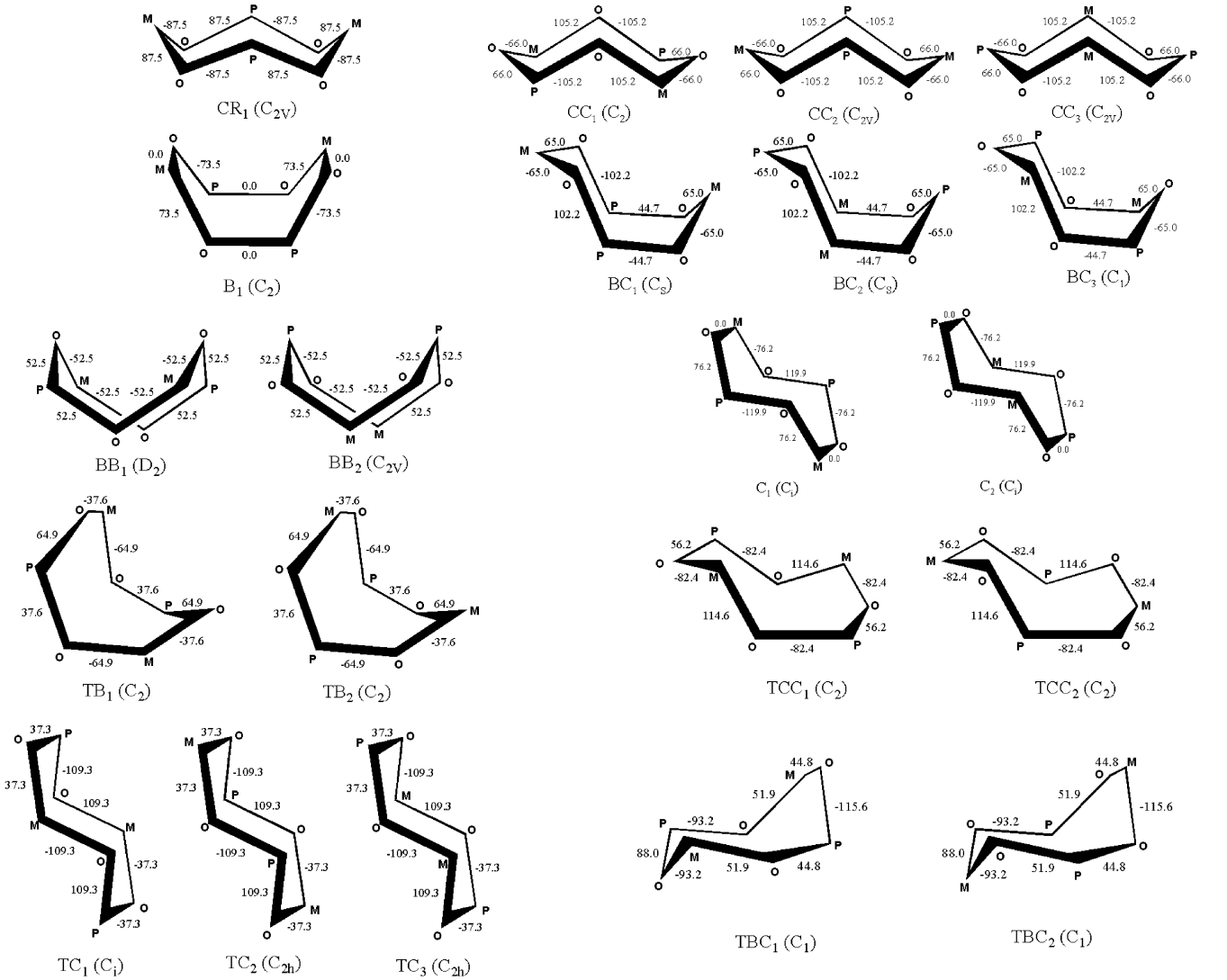

Fig. 2. Conformation type for $\{M(\mu\text{-}OPO)\}_2$. Torsion angles were taken from Ref. [12].

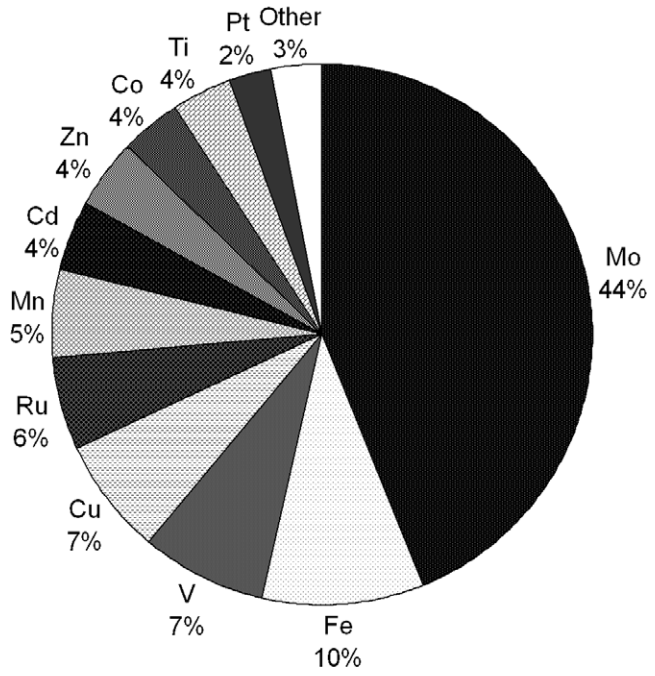

Fig. 3. Relative abundance by metal in set *a*.

- P–X–P, X usually being C. 111 fragments contain this bridge, the most frequent conformations in this case are CC_2 (47%) and BC_1 (30%).
- M···M. 88 fragments contain this bridge, the most frequent conformations in this case are CC_3 (27% of fragments), B_1 (26%) and BC_2 (15%).

There are a significant number of data having at the same time two of the above types of bridge. Forty three data contain both M–X–M and P–X–P bridges and 21 data show P–X–P and M···M links with several metal atoms being represented in these structures. All of them exhibit the BB_2 conformation, which is not the most frequent when there is only one bridge but seems to be the only one compatible with the presence of two bridges simultaneously (Fig. 4).

(b) Structures not included in set *a*

Excluding this way the structures with high constraints in their conformation, the data analysis should allow us to establish the accessible conformations and the influence (if any) of the kind of metal or bridge. Among others, belonging to this set are the polycyclic structures and structures bridged by two or more atoms. In both cases there is still some constraint in the conformation but also some degree of freedom.

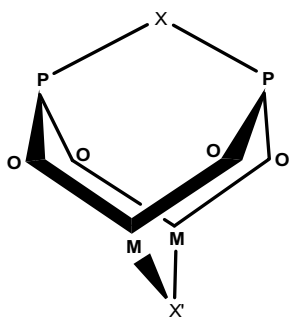

Fig. 4. BB_2 conformation including P–X–P and M–X′–M bridges.

A total of 1448 fragments were retrieved from the CSD for this set. Most of them correspond to zinc complexes (32% of the total); next metals in abundance comprise vanadium (14%), molybdenum (11%) and copper (9%), Fig. 5 shows the distribution of data by metals.

The conformation of these fragments was also assessed using the eight torsion angles in the ring by the Classification method implemented by the authors [11]. A histogram of the conformation assigned to this dataset by this method is shown in Fig. 6. As can be seen the most frequent conformation is C_1 (21% of data), only two more conformations show a frequency higher than 10%: BC_3 and B_1.

Influence of the kind of bridge. In order to determine the influence of the kind of bridge on the conformation, the phosphate, phosphonate and phosphinate bridges were analyzed separately. A total of 888, 457 and 103 fragments of phosphate, phosphonate and phosphinate, respectively, were studied using the Classification method. Histograms showing the frequency for each conformation are shown in Fig. 7.

The histograms for phosphate and phosphonate are very similar. C_1 is the most frequent conformation, it appears in 20% of data approximately, and also in both cases BC_3 and B_1 are the second and third most usual conformations.

Results of the phosphinate structures show similarities and differences with those of the phosphates and phosphonates. Firstly, it is necessary to note that there are far fewer phosphinate bridges than the other kind of bridges. In a similar way C_1 and B_1 are very frequent conformations: 18% and 11% of data, respectively. The principal difference in phosphinate complexes is the high frequency found for TB_1 and BC_2 conformations. This difference can be explained in terms of a statistical distortion of data, as exemplified by the TB_1 conformation. In this case from a total of 19 fragments 15 of them belong to 3 different compounds, furthermore the structure HUWHUC [13] provides 10 fragments. It can be then concluded that there are no significant differences in conformational preferences among phosphates, phosphonates and phosphinates.

Influence of the kind of transition metal atom. In order to investigate the influence of the metal atom in the conformation of the

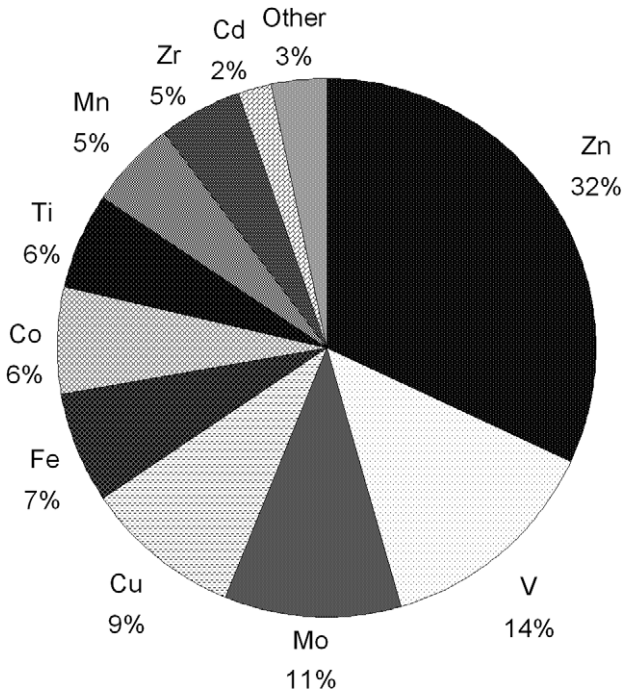

Fig. 5. Relative abundance by metal in set *b*.

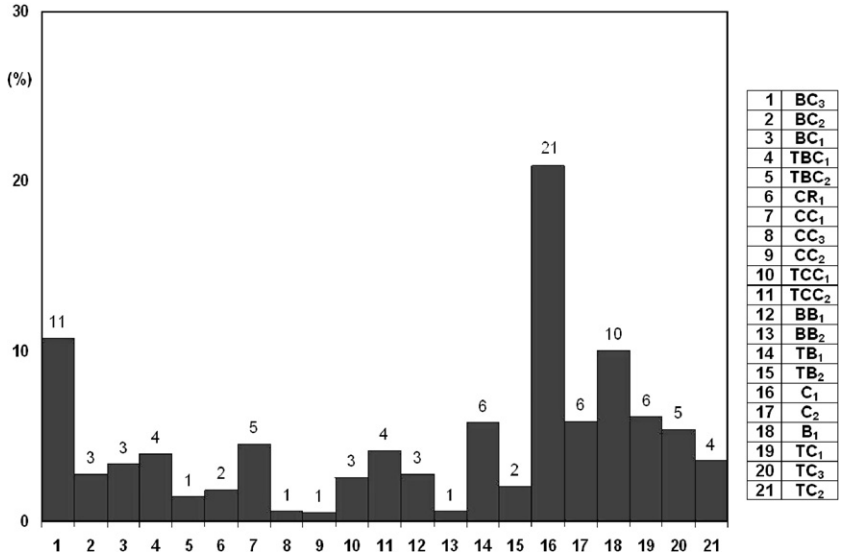

Fig. 6. Frequencies of the most likely conformations for structures included in set *b*.

{M(μ-OPO)}$_2$ core, we performed separated studies by various metals, and the results are summarized in Table 1. As can be seen, conformation C_1 appears in all the metals with a high percentage, indeed even in cobalt (the only case in which C_1 does not appears in Table 1) C_1 appears in 8% of data. Moreover, C_1 is the most frequent conformation in 5 of the 10 metals in Table 1. B_1 and BC_3 conformations also are widely represented through Table 1.

As can be seen in Table 1 there is no correlation between the metal atom or coordination number and the conformation of the {M(μ-OPO)}$_2$ core. Molybdenum and copper complexes show the most defined conformational preferences. In the case of zinc a detailed survey of data reveals the high percentage of the BC_3 conformation is a consequence of a statistical distortion because some *refcodes* supply several fragments. As an example BESJIT [14] and IBOSIB [15] contain 7 and 5 fragments, respectively. This effect is frequent through Table 1 and some significant examples are the following: in the vanadium complexes 21 fragments show a TC_1 conformation, 9 of them belong to the same complex, RARZOZ [16]. In the cobalt complexes 15 fragments show a B_1 conformation, 6 of them belong to the same structure, MEKTUS [17]. In the manganese complexes 16 fragments show a TB_1 conformation, 10 of them belong to the same compound, HUWHUC [13].

In order to elucidate the real influence of the kind of metal and the coordination number, avoiding the statistical distortion induced by *refcodes* with several fragments, we have studied the next set of data.

(c) Structures having only one fragment without internal bridges

Finally, structures having only one fragment without internal bridges were used to establish the conformational preferences when connectivity does not impose any conformational constraint. This set allows the study of conformations avoiding the constraints imposed by internal bridges or polycyclic systems, thus structures in this set have the highest conformational freedom. A total of 285 data fulfilled these conditions, and complexes of Zn (29%), V (18%), Mo (1%), Cu (17%), Fe (8%), Co (6%), Ti (3%), Mn (4%), Zr (3%) and Cd (2%) are included. At the same time all the coordination numbers are significantly represented: 4,4 (35%) 5,5 (25%) and 6,6 (36%).

The most probable conformation was established by the Classification method, and the results are shown in Fig. 8. As can be seen the most frequent conformation is C_1 (21% of data), this result is similar to that obtained in set *b*, but the histogram in Fig. 8 shows significant new features: TC_1 and C_2 are now the second and third most frequent conformations, at the same time B_1 and BC_3 exhibit a much lesser abundance than in set *b* (compare Figs. 8 and 6).

When the data are analyzed separately for each metal the results are more homogeneous than in set *b*. In this case the C_1 conformation is always the most frequent, so it can be concluded that when the influence of having polycyclic systems is removed, the metal atom does not exert a significant influence on the conformation of the ring.

Regarding the coordination number, data were analyzed separately for each possible set (4,4; 5,5 and 6,6) and the results are shown in Table 2. As can be seen, the coordination number cannot be related to the conformation in the {M(μ-OPO)}$_2$ moiety.

The information in Table 2 is completed by other coordination numbers that are also scarcely represented. 4,5 appear in two fragments (CR_1 and B_1); 4,6 appear in one fragment (TC_2); 5,6 appear in six fragments (two BC_3, two BC_2, one BC_1 and one TC_1).

The results shown in Fig. 8 can be rationalized in the next manner: in structures analyzed in set *c* the {M(μ-OPO)}$_2$ core has a high degree of freedom (structures that are not polycyclic and without internal bridges) so the results can be related to the interconversion of conformers.

Conformers of cyclooctane have been grouped in four families: *boat–chair* (conformers BC and TBC), *crown* (TCC, CR, CC), *boat* (BB, TB, B) and *chair* (C, TC). Conformers inside each family can interconvert by a pseudorotational mechanism [18]. In a similar way, the *type* conformations shown in Fig. 2 for the {M(μ-OPO)}$_2$ moiety can be grouped in families whose conformers are able to interconvert by a pseudorotational mechanism. Two more accessible paths for the interconversion of conformations are possible in an analogous mode to that found in cyclooctane [19]. Fig. 9 summarizes the interconversion paths for {M(μ-OPO)}$_2$.

As can be seen in Fig. 9, *chair* and *twist-chair* conformations are situated on a pseudorotation interconversion pathway and it can explain that TC_2, C_1, TC_1, C_2 and TC_3 conformations correspond to 64% of the data in Fig. 8. In a similar way, in the boat family BB_2, TB_2, B_1, TB_1 and BB_1 can interconvert by pseudorotation, and they comprise 18% of the data in Fig. 8. There is also a pseudorotation

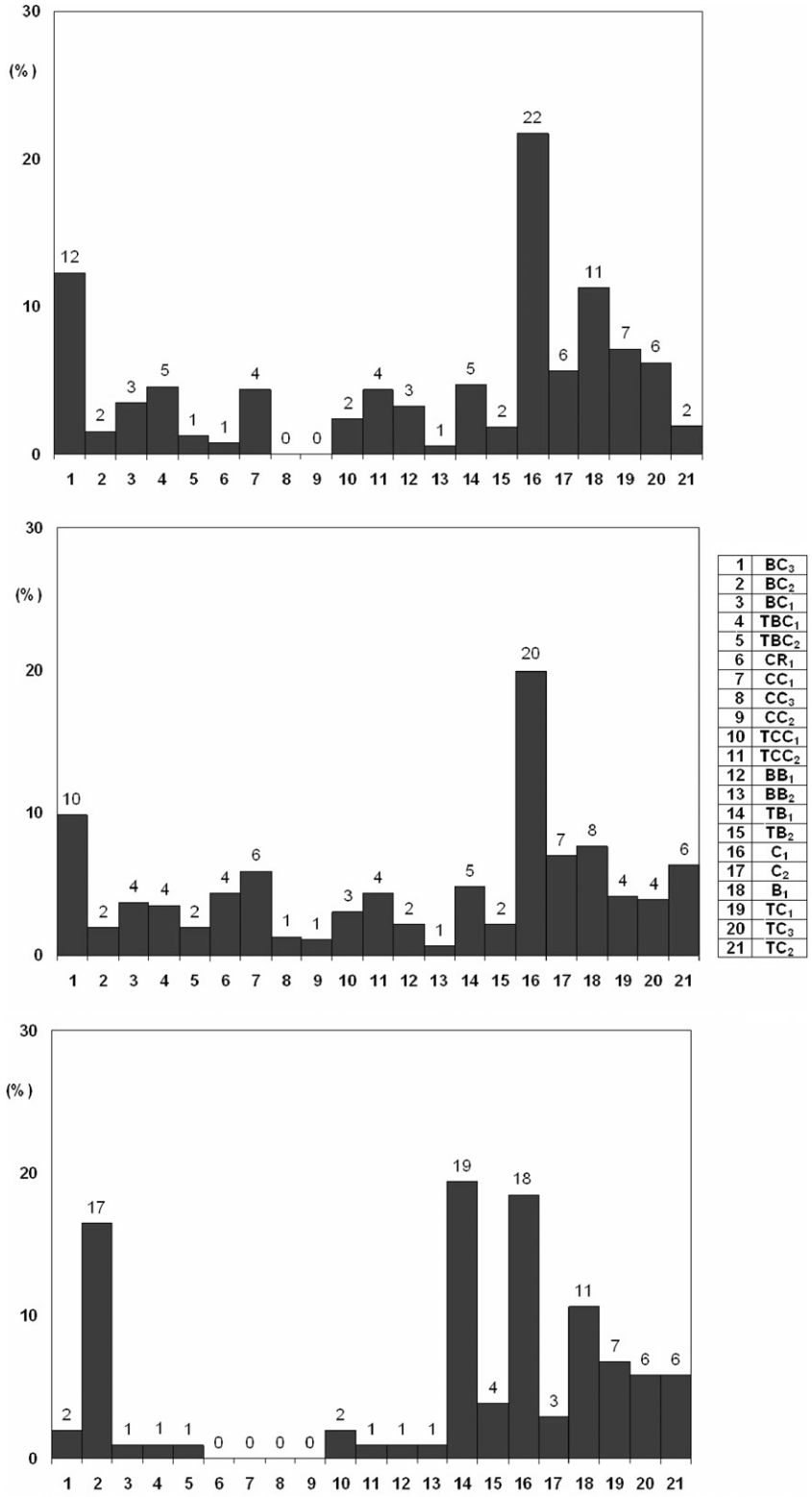

Fig. 7. Frequencies of the most likely conformations in phosphates (top), phosphonates (middle) and phosphinates (bottom) in set *b*.

path for the *boat–chair* family, BC_1, TBC_2, BC_3, TBC_1 and BC_2 group, 12% of the data in Fig. 8.

In order to complete the study of factors that could influence the conformation in the $\{M(\mu\text{-}OPO)\}_2$ core we have tested the role of the terminal ligands coordinated to the metal. Thirteen structures containing the tris(pyrazolyl)borate ligand were found, a high variety of conformations was observed: C_1, C_2, BC_1, BC_2, BC_3, CC_1, TC_1, TC_2, etc. Twelve structures containing the oxalate ligand were retrieved (metal atoms V, Co, Fe and Mn), and again a high variety in the conformation was observed (C_1, C_2, BC_2, BC_3 or TC_1).

Table 1
Conformations for $\{M(\mu\text{-OPO})\}_2$ in transition metal complexes

Metal	Number of fragments	Coordination number[a]	Most frequent conformations
Zn	463	4,4 (86%) 5,5 (10%) 6,6 (3%)	BC_3 (21%) B_1 (11%) C_1 (10%) C_2 (10%)
V	197	4,4 (2%) 5,5 (41%) 6,6 (40%)	TC_3 (13%) TC_1 (11%) BC_3 (10%) C_1 (8%)
Mo	153	6,6 (100%)	C_1 (73%) TBC_1 (14%)
Cu	137	4,4 (12%) 5,5 (72%) 5,6 (6%) 6,6 (6%)	C_1 (47%) B_1 (21%)
Fe	98	4,4 (4%) 5,5 (1%) 5,6 (14%) 6,6 (81%)	C_1 (13%) BC_3 (13%) CC_1 (12%) TCC_2 (12%)
Co	90	4,4 (69%) 5,5 (6%) 6,6 (22%)	B_1 (17%) BC_2 (10%) TCC_1 (9%) TCC_2 (9%)
Ti	84	5,5 (7%) 6,6 (92%)	CC_1 (18%) CR (14%) C_1 (11%) TC_1 (10%)
Mn	77	4,4 (5%) 5,5 (3%) 5,6 (17%) 6,6 (75%)	TB_1 (21%) B_1 (19%) C_1 (16%) CC_1 (12%)
Zr	73	5,5 (1%) 6,6 (97%)	C_1 (18%) TC_3 (12%) BC_3 (11%) B_1 (10%)
Cd	28	5,5 (32%) 6,6 (64%)	BC_3 (18%) C_1 (14%) TBC_1 (11%) B_1 (11%) TC_1 (11%) TC_2 (11%)
Other	48	4,4 (12%) 5,5 (15%) 6,6 (73%)	C_1 (15%) B_1 (15%) TB_1 (13%) TC_1 (13%) TC_3 (13%)

[a] 6,6 include coordination number 6 or higher.

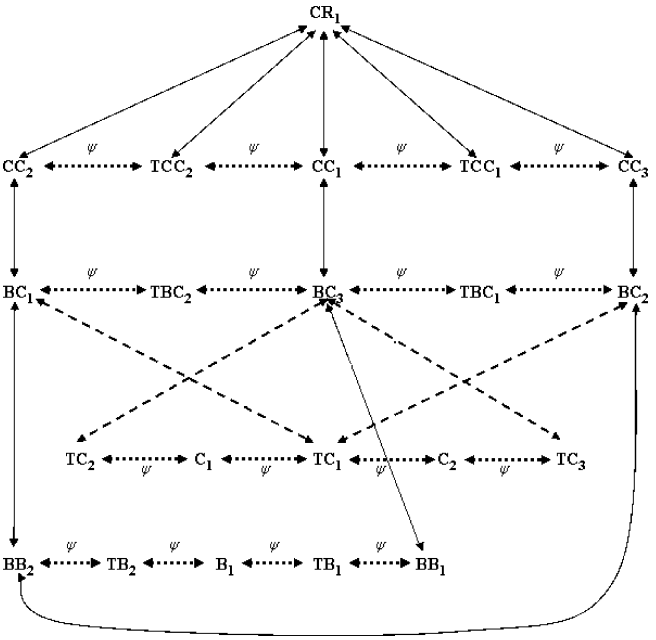

Fig. 9. Interconversions of the $\{M(\mu\text{-OPO})\}_2$ core.

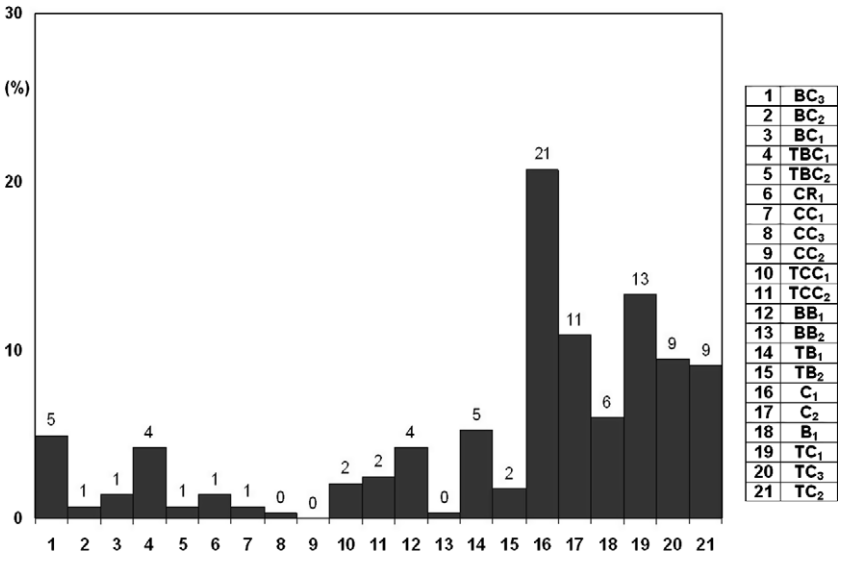

Fig. 8. Frequencies of the most likely conformations in structures included in set *c*.

Table 2
Conformations for $\{M(\mu\text{-OPO})\}_2$ in structures studied in set *c*

Coordination number	Number of data	Most frequent conformations
4,4	100	C_1 (15%) TC_1 (10%) B_1 (10%) BB_1 (10%)
5,5	72	C_1 (32%) TC_1 (14%) C_2 (13%)
6,6	104	C_1 (20%) TC_1 (16%) TC_3 (14%) C_2 (13%)

4. Conclusions

1. The presence of intra-ring bridges in the $\{M(\mu\text{-OPO})\}_2$ moiety is the most determinant factor in the conformation of the eight-membered ring.
   - Structures having two simultaneous links between phosphorus atoms and metal atoms show BB_2 conformations.
   - Structures having O–X–O bridges show BC_3 or TB_1 conformations.
   - Structures having P–X–P bridges show preferably CC_2 or BC_1 conformations.
2. The kind of bridge (phosphate, phosphonate or phosphinate) does not introduce any conformational preference in the $\{M(\mu\text{-OPO})\}_2$ moiety of transition metal complexes.
3. The most frequent conformation in transition metal complexes double bridged by phosphate and related ligands is a *chair* conformation, C_1.
4. When structures without constraints imposed by polycyclic systems or internal bridges are analyzed, the conformations observed can be rationalized in terms of conformation families in pseudorotation pathways:
   - 64% of data show a conformation belonging to the *chair* family (*chair* and *twist-chair* conformations)

- 18% of data show a conformation belonging to the *boat* family (*boat*, *boat–boat* or *twist-boat* conformations)
- 12% of data show a conformation belonging to the *boat–chair* family (*boat–chair* or *twist-boat–chair* conformations)

5. The transition metal or the coordination number in the $\{M(\mu\text{-}OPO)\}_2$ core do not exert a significant influence in the conformation of that ring.

Appendix A. Supplementary data

Supplementary data associated with this article can be found, in the online version, at doi:10.1016/j.poly.2008.04.053.

References

[1] F.H. Allen, Acta Crystallogr., Sect. B 58 (2002) 380.
[2] M. Zimmer, Coord. Chem. Rev. 212 (2001) 133.
[3] F.H. Allen, R. Taylor, Chem. Soc. Rev. 33 (2004) 463.
[4] A.G. Orpen, Chem. Soc. Rev. 22 (1993) 191.
[5] J. Cirera, P. Alemany, S. Álvarez, Chem.-A Eur. J. 10 (1) (2004) 190.
[6] G. Aullón, G. Ujaque, A. Lledos, S. Álvarez, Chem.-A Eur. J. 5 (5) (1999) 1391.
[7] R. Taylor, Acta Crystallogr., Sect. D 58 (2002) 879.
[8] E. Kövári, R. Krämer, J. Am. Chem. Soc. 118 (1996) 12704.
[9] F.H. Fry, P. Jensen, C.M. Kepert, L. Spiccia, Inorg. Chem. 42 (18) (2003) 5637.
[10] A.K. Cheetham, G. Férey, T. Loiseau, Angew. Chem., Int. Ed. 38 (1999) 3268.
[11] M. Kessler, J. Pérez, M.C. Bueso, L. García, E. Pérez, J.L. Serrano, R. Carrascosa, Acta Crystallogr., Sect. B 63 (2007) 869.
[12] F.H. Allen, J.A.K. Howard, N.A. Pitchford, Acta Crystallogr., Sect. B 52 (1996) 882.
[13] A.J. Tasiopoulos, N.C. Harden, K.A. Abboud, G. Christou, Polyhedron 22 (2003) 133.
[14] Y. Xing, G. Li, H. Meng, Z. Shi, Y. Liu, X. Wei, Y. Yang, W. Pang, Inorg. Chem. Commun. 7 (2004) 475.
[15] A.A. Ayi, A. Choudhury, S. Natarajan, S. Neeraj, C.N.R. Rao, J. Mater. Chem. 11 (2001) 1181.
[16] J. Salta, J. Zubieta, J. Clust. Sci. 7 (1996) 531.
[17] R. Sharma, R.P. Sharma, R. Bala, M. Quiros, J.M. Salas, Inorg. Chem. Commun. 9 (2006) 782.
[18] F.A.L. Anet, J. Krane, Tetrahedron Lett. 50 (1973) 5029.
[19] J.B. Hendrickson, J. Am. Chem. Soc. 89 (1967) 7047.

Polyhedron 27 (2008) 2494–2500

Contents lists available at ScienceDirect

Polyhedron

journal homepage: www.elsevier.com/locate/poly

Syntheses, structures and luminescent properties of four d^{10}-metal coordination polymers based on the 2,4,5-tri(4-pyridyl)-imidazole ligand

Xiao-Qiang Liang, Hong-Ping Xiao, Bao-Lin Liu, Yi-Zhi Li, Jing-Lin Zuo *, Xiao-Zeng You *

Coordination Chemistry Institute and the State Key Laboratory of Coordination Chemistry, School of Chemistry and Chemical Engineering, Nanjing University, Hankou Road 9, Nanjing 210093, PR China

ARTICLE INFO

Article history:
Received 27 January 2008
Accepted 25 April 2008
Available online 21 June 2008

Keywords:
d^{10} Metal
2,4,5-Tri(4-pyridyl)-imidazole
Coordination polymers
Supramolecular network
Hydrogen bonding
Photoluminescence

ABSTRACT

Four d^{10}-metal coordination polymers based on the 2,4,5-tri(4-pyridyl)-imidazole ligand (Htpim), $\{[Zn_2(Htpim)_4Cl_4]\cdot 8H_2O\}_n$ (**1**), $\{[Cd(tpim)_2(H_2O)_2]\cdot 4CH_3OH\}_n$ (**2**), $\{[Cu_2(Htpim)(PPh_3)_2I_2]\cdot CH_3CN\}_n$ (**3**) and $\{[Ag(Htpim)](NO_3)\cdot CH_2Cl_2\}_n$ (**4**), have been synthesized and characterized by elemental analyses, IR, thermogravimetric and X-ray structural analyses. Both complexes **1** and **2** show one dimensional ribbon-like structures. Via intermolecular hydrogen bonds, a 2D supramolecular network and 3D framework are formed for **1** and **2**, respectively. Complex **3** shows a 1D zigzag chain with a CuI_2Cu rhomboid dimer. Complex **4** shows a 1D ladder-like polymer with two different metallacycles. The luminescent properties of all the complexes have been studied in the solid state.

© 2008 Elsevier Ltd. All rights reserved.

1. Introduction

In the past few decades, considerable attention has been devoted to the design and syntheses of coordination polymers not only due to their aesthetic architectures and new topologies [1–3], but also because of their potential applications [4–6], such as gas storage [7–9], catalysis [10,11], ion exchange [12,13], photoluminescence [14–19], non-linear optics [20,21] and magnetism [22–26]. Recently, increasing investigations carried out on coordination polymers were focused on the use of the rigid multi-pyridyl ligands, such as 4,4′-bipyridine [27], 2,4,6-tri(4-pyridyl)-1,3,5-triazine [28,29], 5,10,15,20-tetra-4-pyridy-21H,23H-porphine [30] and 2,5-bis(4-pyridyl)-1,3,4-oxadiazole [31,32] as building blocks, because they can afford structural diversities, robustness and stability of metal–organic coordination polymers.

Among the rigid multi-pyridyl ligands, the 2,4,5-tri(4-pyridyl)-imidazole (Htpim) ligand has three pyridine N atoms and two imidazole N atoms (Scheme 1), and is suitable to be a good spacer in the construction of new metal–organic coordination polymers. To our best knowledge, coordination polymers of the Htpim ligand have not been documented so far. Herein, we report the syntheses, crystal structures and luminescent properties of four 1D coordination polymers of d^{10}-metal ions: $\{[Zn_2(Htpim)_4Cl_4]\cdot 8H_2O\}_n$ (**1**), $\{[Cd(tpim)_2(H_2O)_2]\cdot 4CH_3OH\}_n$ (**2**), $\{[Cu_2(Htpim)(PPh_3)_2I_2]\cdot CH_3CN\}_n$ (**3**) and $\{[Ag(Htpim)](NO_3)\cdot CH_2Cl_2\}_n$ (**4**).

2. Experimental

2.1. General procedures

The rigid ligand 2,4,5-tri(4-pyridyl)-imidazole (Htpim) was synthesized according to the literature method [33]. All other reagents and solvents were commercially available and were used without further purification. Elemental analyses for C, H and N were performed on a CHN-O-Rapid analyzer and an Elementar Vario MICRO analyzer. The IR spectra were recorded on a Bruker Vector 22 FT-IR spectrometer using KBr discs in the 4000–400 cm^{-1} range. Thermogravimetric analyses were carried out on a Perkin–Elmer Pyris 1 TGA analyzer from room temperature to 750 °C with a heating rate of 20 °C/min under nitrogen. Photoluminescence analyses for the solid samples were taken on an AMINCO Bowman Series2 luminescence spectrometer.

2.2. Preparation of the complexes

2.2.1. Preparation of $\{[Zn_2(Htpim)_4Cl_4]\cdot 8H_2O\}_n$ (**1**)

A methanolic solution (4 ml) of Htpim (15 mg, 0.05 mmol) was added to an aqueous solution (6 ml) of $ZnCl_2$ (7 mg, 0.05 mmol) with stirring. Orange diamond-like single crystals of **1** were obtained after the mixture was allowed to stand at room temperature for a week. Yield: 44%. *Anal.* Calc. for $C_{72}H_{68}Cl_4N_{20}O_8Zn_2$: C, 53.58; H, 4.25; N, 17.36. Found: C, 53.70; H, 4.65; N, 16.90%. IR (KBr, cm^{-1}): 3445(br), 1614(vs), 1430(s), 1261(m), 1128(s), 1062(m), 1285(m), 1015(w), 839(s), 747(m), 690(s), 614(m), 511(m).

* Corresponding authors. Tel.: +86 25 83593893; fax: +86 25 83314502.
E-mail addresses: zuojl@nju.edu.cn (J.-L. Zuo), youxz@nju.edu.cn (X.-Z. You).

0277-5387/$ - see front matter © 2008 Elsevier Ltd. All rights reserved.
doi:10.1016/j.poly.2008.04.051

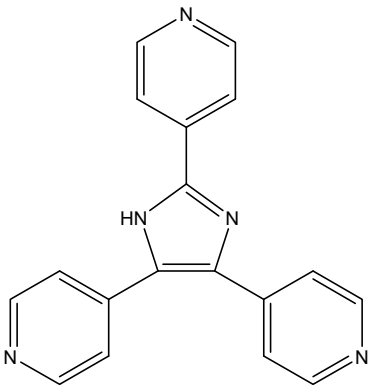

Htpim

Scheme 1. Molecular structure of the ligand.

*2.2.2. Preparation of {[Cd(tpim)$_2$(H$_2$O)$_2$] · 4CH$_3$OH}$_n$ (**2**)*

$Cd(ClO_4)_2 \cdot 6H_2O$ (21 mg, 0.05 mmol) in 10 ml of CH_3OH was layered onto a solution of Htpim (15 mg, 0.05 mmol) in 10 ml of DMF. The resultant solution was allowed to slowly diffuse for several weeks to give yellow plate-like crystals. The crystals were collected, washed with methanol and dried in vacuum. Yield: 32%. *Anal.* Calc. for $C_{40}H_{44}N_{10}O_6Cd$: C, 55.01; H, 5.08; N, 16.04. Found: C, 54.71; H, 5.35; N, 16.74%. IR (KBr, cm^{-1}): 3448(br), 3205(s), 1600(vs), 1504(m), 1429(m), 1341(w), 1245(w), 1213(m), 1149(w), 1061(w), 983(m), 872(w), 839(m), 751(m), 719(m), 689(m), 522(m).

*2.2.3. Preparation of {[Cu$_2$(Htpim)(PPh$_3$)$_2$ I$_2$] · CH$_3$CN}$_n$ (**3**)*

A mixture of CuI (19 mg, 0.10 mmol), Htpim (15 mg, 0.05 mmol), PPh_3 (22.6 mg, 0.10 mmol) in CH_3CN (8 ml) and MeOH (0.2 ml) was sealed in a Teflon-lined stainless steel vessel, heated at 180 °C for 3 days and cooled to room temperature. The reaction mixture was filtered and left to stand at room temperature. Red-dark rod-like crystals suitable for X-ray analysis were obtained by slow evaporation of the solvent over two days. Yield: 20%. *Anal.* Calc. for $C_{56}H_{46}Cu_2I_2N_6P_2$: C, 54.00; H, 3.72; N, 6.74. Found: C, 54.47; H, 3.70; N, 7.10%. IR (KBr, cm^{-1}): 3447(br), 3261(s),

Table 2
Selected bond lengths (Å) and angles (°) for **1**–**4**

Complex **1**			
N(1)–Zn(1)	2.162(3)	Zn(1)–N(5)#2	2.145(3)
Cl(1)–Zn(1)	2.398 (1)		
N(5)#2–Zn(1)–N(5)#3	91.2(2)	N(5)#2–Zn(1)–N(1)	88.3 (1)
N(1)#4–Zn(1)–N(1)	92.4 (1)	N(1)–Zn(1)–Cl(1)	89.11(8)
N(5)#2–Zn(1)–Cl(1)	91.69(7)	N(5)#3–Zn(1)–Cl(1)	86.84(7)
N(1)#4–Zn(1)–Cl(1)	92.34(8)		
Complex **2**			
Cd(1)–O(1)	2.278(3)	Cd(1)–N(1)	2.311(4)
Cd(1)–N(1)	2.311(4)		
O(1)–Cd(1)–N(1)	90.06(1)	O(1)–Cd(1)–N(4)#3	87.5 (1)
O(1)–Cd(1)–N(1)#3	87.7 (1)	N(4)#3–Cd(1)–N(4)	92.9(2)
N(1)–Cd(1)–N(4)#3	87.9(1)	N(1)#3–Cd(1)–N(1)	91.7 (2)
O(1)–Cd(1)–N(4)	94.7(1)		
Complex **3**			
Cu(1)–N(1)	2.086(4)	Cu(1)–P(1)	2.234(2)
Cu(1)–I(1)#1	2.6295(8)	Cu(1)–I(1)	2.6767(8)
Cu(2)–N(2)	2.055(4)	Cu(2)–P(2)	2.234(2)
Cu(2)–I(2)	2.6970(8)	Cu(2)–I(2)#2	2.7059(7)
N(1)–Cu(1)–P(1)	110.8 (2)	N(1)–Cu(1)–I(1)#1	106.3(1)
P(1)–Cu(1)–I(1)#1	112.27(4)	N(1)–Cu(1)–I(1)	106.5 (1)
P(1)–Cu(1)–I(1)	107.46(4)	I(1)#1–Cu(1)–I(1)	113.37(3)
N(1)–Cu(1)–Cu(1)#1	120.9 (2)	P(1)–Cu(1)–Cu(1)#1	128.13(5)
I(1)#1–Cu(1)–Cu(1)#1	57.46(2)	I(1)–Cu(1)–Cu(1)#1	55.91(2)
N(2)–Cu(2)–P(2)	120.1 (1)	N(2)–Cu(2)–I(2)	106.3(1)
P(2)–Cu(2)–I(2)	108.64(4)	N(2)–Cu(2)–I(2)#2	111.6 (1)
P(2)–Cu(2)–I(2)#2	108.04(4)	I(2)–Cu(2)–I(2)#2	100.34(2)
Cu(1)#1–I(1)–Cu(1)	66.63(3)	Cu(2)–I(2)–Cu(2)#2	79.66(2)
Complex **4**			
Ag(1)–N(2)	2.277(5)	Ag(1)–N(1)#1	2.299(4)
Ag(1)–N(4)#2	2.305(5)		
N(2)–Ag(1)–N(1)#1	120.4(2)	N(2)–Ag(1)–N(4)#2	131.0 (2)
N(1)#1–Ag(1)–N(4)#2	101.8(2)		

Symmetry codes: for complex **1**: #3 $-x+1, y-1, -z+1/2$; for complex **2**: #3 $-x, y, -z+3/2$; for complex **3: #1** $-x, -y+2, -z$; **#2** $-x, -y+1, -z+1$; **for complex 4**: #1 $-x+1, -y, -z+1$; #2 $x, y-1, z$.

Table 1
Crystallographic data and details of refinements for complexes **1**–**4**

Complexes	**1**	**2**	**3**	**4**
Empirical formula	$C_{72}H_{68}Cl_4N_{20}O_8Zn_2$	$C_{40}H_{44}CdN_{10}O_6$	$C_{56}H_{46}Cu_2I_2N_6P_2$	$C_{19}H_{15}AgCl_2N_6O_3$
M_r	1614.00	873.25	1245.81	554.14
Crystal system	monoclinic	monoclinic	triclinic	triclinic
Space group	*P*2/*c*	*C*2/*c*	*P*$\bar{1}$	*P*$\bar{1}$
a (Å)	12.087(2)	25.398 (1)	9.0385(7)	8.932(2)
b (Å)	10.032(2)	10.108(4)	13.725(1)	10.603(2)
c (Å)	17.466(3)	19.325(8)	21.870(2)	12.711(3)
α (°)	90	90	78.251(3)	110.191(4)
β (°)	101.142(4)	122.20(2)	84.963 (1)	91.705(5)
γ (°)	90	90	72.862(2)	112.489(4)
V (Å^3)	2077.9(6)	4198(2)	2537.1(4)	1025.6(4)
Z	1	4	2	2
D_{Calc} (g/cm^{-3})	1.290	1.382	1.631	1.794
μ (mm^{-1})	0.768	0.577	2.162	1.279
θ Range (°)	2.03–26.00	1.90–26.00	1.58–26.00	1.74–26.00
Collected reflections	10951	11019	13730	5512
Unique reflections	4086	4114	9695	3924
Parameters	249	258	614	283
F(000)	832	1800	1236	552
T (K)	291(2)	291(2)	291(2)	291(2)
R_1[a], wR_2[b] [$I > 2\sigma(I)$]	0.0592, 0.1224	0.0566, 0.1376	0.0502, 0.0978	0.0490, 0.1103
R_1[a], wR_2[b] (all data)	0.0910, 0.1322	0.0818, 0.1460	0.0864, 0.1046	0.0710, 0.1171
Goodness-of-fit	0.970	1.087	0.970	1.037
Largest peak and hole (e Å^{-3})	0.247, −0.501	0.406, −0.894	0.989, −0.961	0.699, −0.922

[a] $R_1 = \sum ||F_o| - |F_c|| / \sum |F_o|$.
[b] $wR_2 = [\sum w(|F_o^2| - |F_c^2|)^2 / \sum w(|F_o^2|)^2]^{1/2}$.

3048(m), 2253(w), 1952(w), 1637(w), 1602(vs), 1571(m), 1503(s), 1479(m), 1433(s), 1309(w), 1212(m), 1182(m), 1091(m), 1066(w), 831(m), 739(m), 694(s), 519(s), 509(s).

2.2.4. Preparation of $\{[Ag(Htpim)](NO_3)\cdot CH_2Cl_2\}_n$ (**4**)

A buffer layer prepared by mixing MeCN and CH_2Cl_2 (1:1, v/v) was carefully covered on solution of Htpim (15 mg, 0.05 mmol) in CH_2Cl_2/DMF (5 ml, 4:1). Then, a solution containing $AgNO_3$ (8.5 mg, 0.05 mmol) in MeCN (5 ml) was slowly added above the buffer layer. After four weeks, light yellow rod-like crystals formed at the buffer layer. Yield: 35%. *Anal.* Calc. for $C_{19}H_{15}AgCl_2N_6O_3$: C, 41.25; H, 2.55; N, 15.20. Found: C, 41.12; H, 2.83; N, 15.28%. IR (KBr, cm^{-1}): 3446(br), 1606(vs), 1582(s), 1559(w), 1508(w), 1490(w), 1384(s), 1281(m), 1131(w), 1066(w), 1004(w), 833(s), 745(m), 703(w), 688(m), 617(m), 516(w).

Table 3
Hydrogen-bonding geometry parameters (Å, °) for complexes **1**, **2** and **4**

D–H···A	*d*(D–H)	*d*(H···A)	*d*(D···A)	∠(DHA)
Complex **1**				
N3–H3A···O2	0.90	2.08	2.936(5)	158.7
O3–H3Y···N4(#5)	0.85	2.11	2.861(4)	146.3
Complex **2**				
O1–H1Y···O2	0.85	1.80	2.630(4)	164.7
O2–H2A···O1	0.85	1.86	2.630(4)	150.3
O3–H3A···N5(#4)	0.85	1.88	2.722(5)	173.0
Complex **4**				
N3–H3···O2(#4)	0.86(7)	2.07(7)	2.865(7)	154(6)

Symmetry codes: for complex **1**: #5 $x+1, y, z$; for complex **2**: #4 $x-1/2, y+1/2, z-1$; for complex **4**: #4 $-x+2, -y+1, -z+2$.

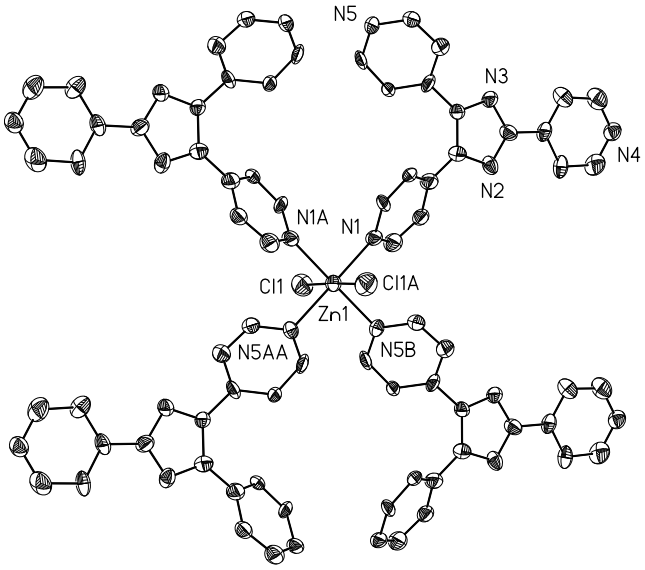

Fig. 1. View of the coordination environment of Zn(II) in complex **1**, thermal ellipsoids are drawn at the 50% probability level. Lattice water molecules and hydrogen atoms have been omitted for clarity.

2.3. X-ray crystallography

Suitable single crystals of **1–4** were selected and mounted on glass fibers in air. X-ray intensity data were collected on a Bruker SMART APEX CCD diffractometer [34] using graphite monochromatized Mo Kα radiation (λ = 0.71073 Å) at 291(2) K. The raw data were reduced and corrected for Lorentz and polarization effects using the SAINT program and for absorption using the SADABS program. The structures were solved by direct methods and refined with the full-matrix least-squares technique using SHELXTL version5.1 [35]. Anisotropic thermal parameters were assigned to all non-hydrogen atoms. The hydrogen atoms were found in a difference Fourier map and the N–H hydrogen atoms were refined with an N–H distance restraint [0.86(7) Å] and $U_{iso}(H) = 1.2U_{eq}(N)$. The remaining hydrogens were added at calculated positions and refined riding on their parent atoms. The crystallographic data are given in Table 1. Selected bond lengths and bond angles are listed in Table 2. The corresponding H-bond data are listed in Table 3.

3. Results and discussion

3.1. Syntheses and IR

The reaction of Htpim with $ZnCl_2$ in MeOH/H_2O afforded compound **1**. Compound **2** was prepared by layering a solution of $Cd(ClO_4)_2\cdot 6H_2O$ in CH_3OH with a Htpim solution in DMF. The hydrothermal reaction of CuI, Htpim and PPh_3 in CH_3CN gave compound **3**. Complex **4** was obtained by the slow diffusion of Htpim in CH_2Cl_2/DMF into $AgNO_3$ in MeCN.

In the IR studies, there is a broad band centered at 3445 cm^{-1} for **1** and it can be assigned to the O–H stretching of the crystalline water molecules. For **2**, the broad band around 3448 cm^{-1} results from the O–H stretching of the crystalline methanol molecules and the coordinated water molecules. For **3** and **4**, the very strong absorptions at 3446 and 3447 cm^{-1} are attributed to the N–H stretching of the ligand. The characteristic absorption band of the crystalline CH_3CN molecules ($\nu_{C\equiv N}$) for **3** appears at 2253 cm^{-1}. For **4**, the characteristic absorption of the NO_3^- anion is at 1384 cm^{-1}. In addition, the absorption bands resulting from the

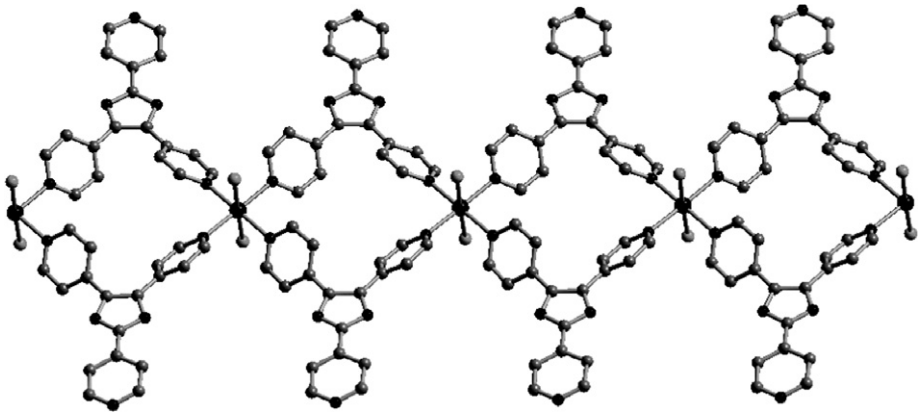

Fig. 2. A ribbon-like chain structure for complex **1**.

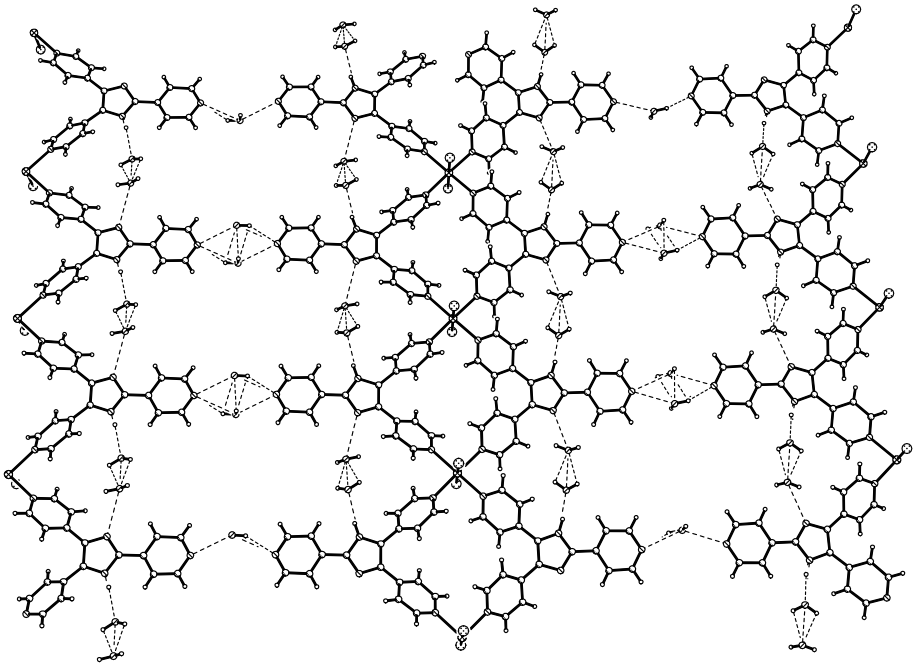

Fig. 3. The 2D layered structure of **1** via intermolecular hydrogen bonds (viewed down the *c* axis).

skeletal vibrations of the aromatic rings of the ligand for all the four complexes appear in the 1400–1600 cm^{-1} region.

3.2. Description of the crystal structures

The X-ray crystallographic analysis reveals that the asymmetric unit of complex **1** contains one ligand molecule, half of one Zn^{2+} ion, one Cl^- ion and two solvated water molecules. As shown in Fig. 1, the Zn(II) center has a slightly distorted octahedral geometry and is six-coordinated with four N atoms of equivalent pyridines from four different ligands in the equatorial plane and two Cl^- ions in the axial sites. The Zn–N distances are 2.162(3) and 2.145(3) Å. The Cl–Zn–Cl bond angle is 177.91(6)°, which is close to a linear geometry. As depicted in Fig. 2, two Zn(II) atoms and two ligands form a 22-membered macrocylic ring and the rings are further connected by the Zn–N coordination bonds to generate a 1D ribbon-like polymer. In the macrometallacycle, the neighboring Zn···Zn diagonal distance is 10.032 Å. Moreover, the hydrogen bond occurring at O3–H3Y···N4(#5) (2.861(4) Å, symmetry code: $x + 1, y, z$) from the uncoordinated N4 atom of the pyridine of the ligand and one solvated water molecule gives rise to a two dimensional network (Fig. 3). In addition, the other solvated water molecule forms an intermolecular hydrogen bond with the N3 atom of imidazole and the N3–H3A···O2 distance is 2.936(5) Å. All the above hydrogen-bonding interactions may stabilize the solid-state structure of **1**.

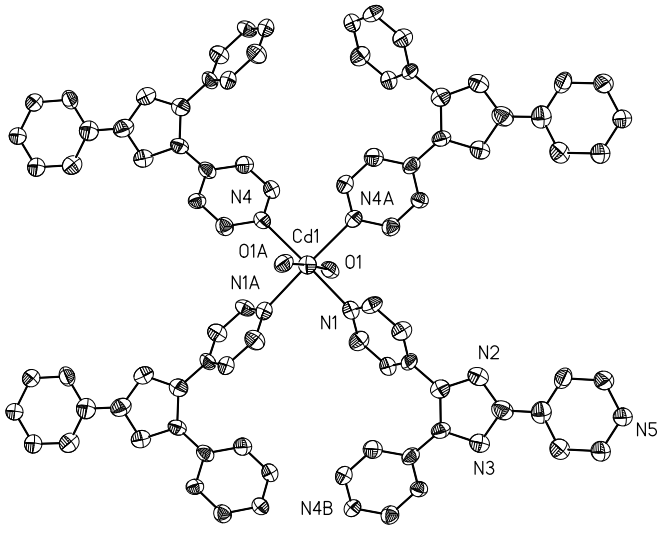

Fig. 4. View of the coordination environment of Cd(II) in complex **2**, thermal ellipsoids are drawn at the 50% probability level. Lattice methanolic, coordinated water molecules and hydrogen atoms have been omitted for clarity.

For **2**, the asymmetric unit consists of one deprotonated ligand, half of one Cd^{2+} ion, one-coordinated aqua molecule and two solvated methanol molecules. As shown in Fig. 4, each Cd(II) center is in an octahedral coordination geometry with four N atoms of equivalent pyridines from four different ligands and two O atoms of two H_2O molecules. It has the same 1D motif as that of complex **1**, as described above. It is noteworthy that the supramolecular architecture of **2** is different from **1**. In complex **2**, the O–H···O and O–H···N hydrogen bonds from coordinated aqua molecules, solvated MeOH molecules and the uncoordinated N atom of the pyridine connect the 1D chain to give a 3D network (Fig. 5). The O1–H1Y···O2 and O2–H2A···O1 distances are 2.630(4) and 2.630(4) Å, and angles are found to be 164.7° and 150.3°, respectively. The O3–H3A···N5(#4) distance is 2.722(5) Å with an angle of 173.0° (symmetry code: $x - 1/2, y + 1/2, z - 1$).

There is one molecule of the Htpim ligand, two molecules of PPh_3, two Cu^+ ions, two I^- ions and one solvated MeCN molecule in the asymmetric unit in the structure of complex **3**. As illustrated in Fig. 6, two Cu(I) centers have the same coordination mode. Each Cu(I) center lies in a distorted tetrahedral coordination sphere which contains of one N atom from pyridine, one P atom from triphenylphosphine and two μ_2-I^- ions. The bond lengths and angles relating to Cu(I) are listed in Table 2. Two μ_2-I^- ions bind to two adjacent Cu(I) centers to give a CuI_2Cu rhomboid dimer, which is further connected to N atoms of the ligands, leading to the formation of a zig-zag chain (Fig. 7). The triphenylphosphine and Htpim

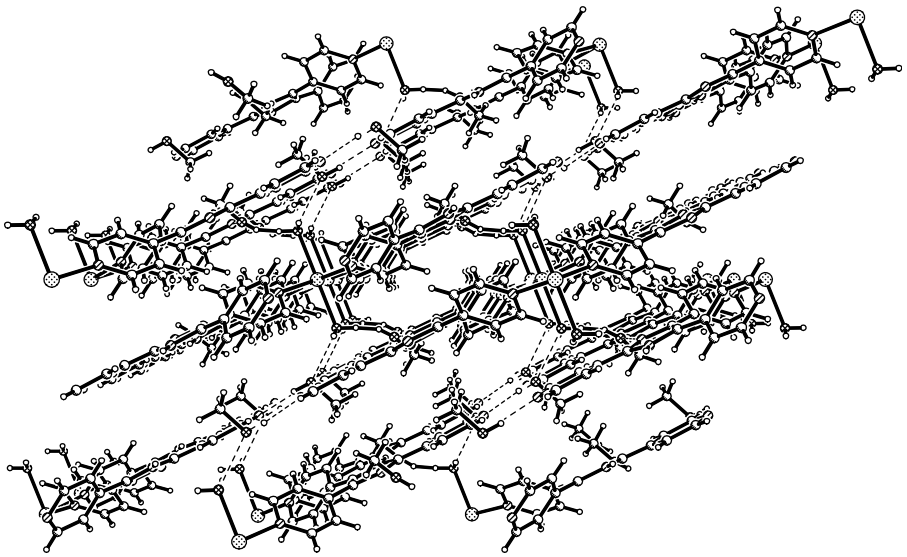

Fig. 5. Crystal packing along the *b*-axis showing the formation of a 3D supramolecular architecture by intermolecular hydrogen bonds.

ligands linking the CuI_2Cu rhomboid dimer are located in *trans* positions.

The asymmetric unit of complex **4** consists of one ligand molecule, one Ag^+ ion, one NO_3^- ion and one solvated CH_2Cl_2 molecule. The Ag(I) center is located in a distorted trigonal arrangement consisting of three N atoms from two equivalent pyridines and one imidazole, as shown in Fig. 8. The Ag–N bond lengths are somewhat different, with relatively longer bond lengths for Ag–N_{py}. As illustrated in Fig. 9, along the symmetry center, the repeating unit is further extended into a 1D ladder-like polymer with two different metallacycles. In the larger one, two Ag (I) atoms and N atoms of equivalent pyridines from two ligands form a 22-membered macrocylic ring with an Ag···Ag diagonal distance of 9.825 Å. In the smaller one, two Ag(I) atoms and N atoms from the pyridine

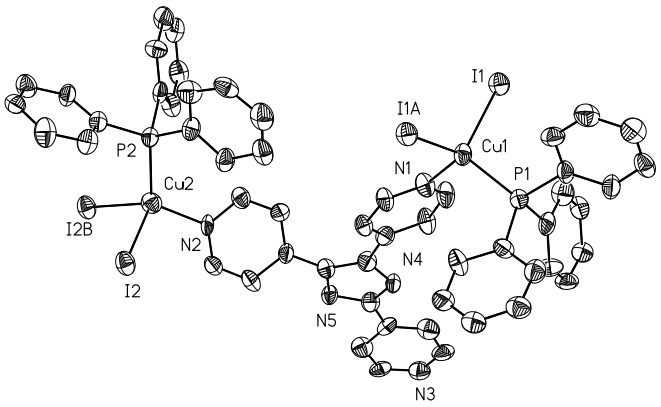

Fig. 6. View of the coordination environment of Cu(I) in complex **3**, thermal ellipsoids are drawn at the 50% probability level. Lattice acetonitrile molecules and hydrogen atoms have been omitted for clarity.

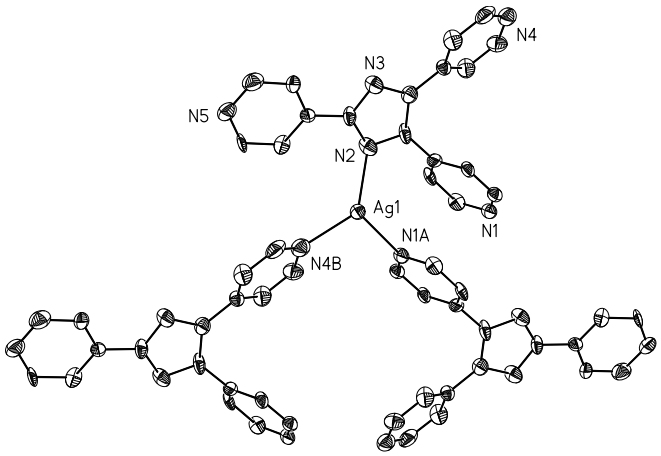

Fig. 8. View of the coordination environment of Ag(I) in complex **4**, thermal ellipsoids are drawn at the 50% probability level. Lattice methylene chloride molecules, nitrate and hydrogen atoms have been omitted for clarity.

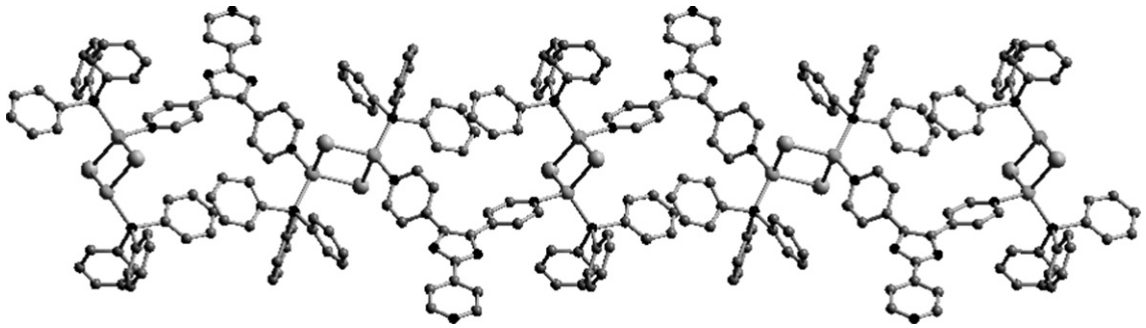

Fig. 7. The zigzag chain structure for complex **3**.

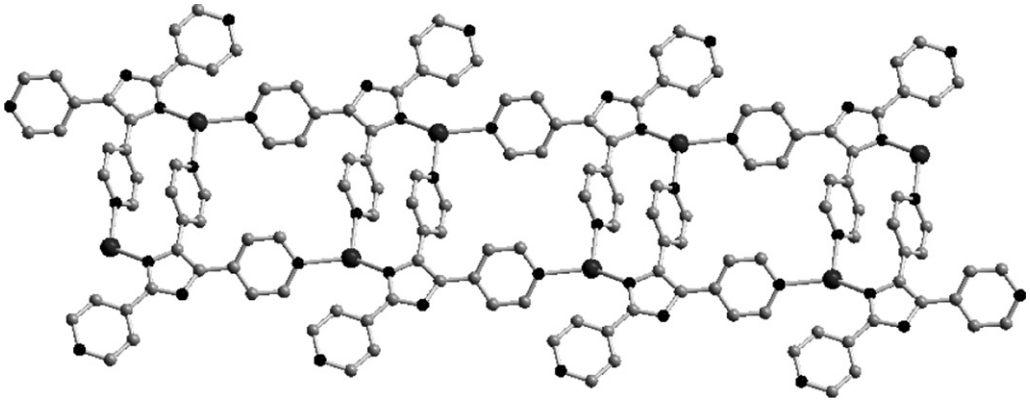

Fig. 9. The ladder-like chain structure for complex **4**.

and imidazole of two ligands form a 14-membered macrocylic ring with an Ag···Ag diagonal distance of 6.948 Å. Additionally, an intermolecular hydrogen bond formed by the N3 atom of imidazole and O2 atom of the NO_3^- ion (N3–H3···O2(#4), symmetry code: $-x+2$, $-y+1$, $-z+2$) makes for the stabilization of the architecture.

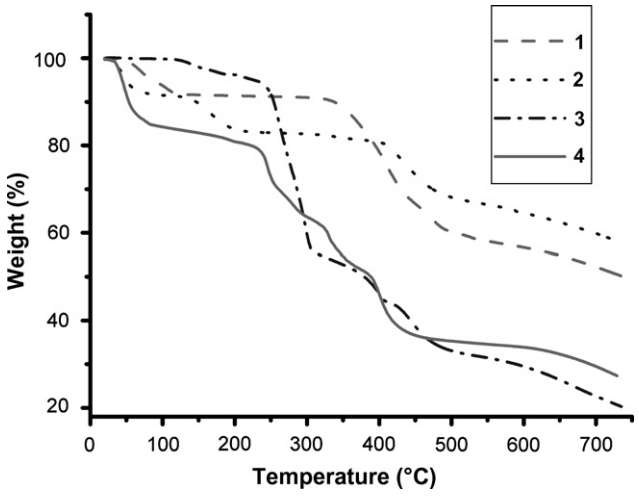

Fig. 10. TGA curves for complexes **1–4**.

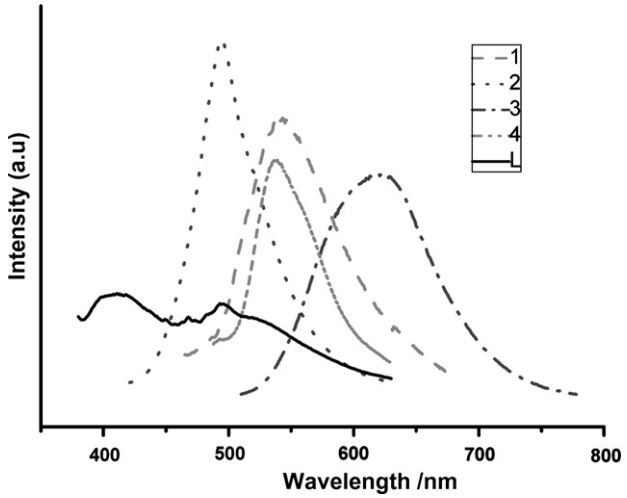

Fig. 11. Emission spectra of **1–4** and the ligand.

3.3. Thermogravimetric analyses

Thermogravimetric analyses (TGA) have been taken on complexes **1–4** by heating to 750 °C under flowing N_2. As shown in Fig. 10, the TGA curve for **1** showed a weight loss between 36 and 157 °C, corresponding to the loss of eight water molecules (8.43% weight loss observed; 8.92% calculated), and the decomposition of the product is observed at ca. 340 °C. Complex **2** displayed two main steps of weight losses: the first step completed the loss of the crystalline methanol molecules at 70 °C (7.43% weight loss observed; 7.34% calculated). The second step occurred between 130 and 230 °C with the loss of two-coordinated water molecules (8.50% weight loss observed; 8.79% calculated). The TGA curve of **3** indicated a weight loss of 3.50% corresponding to the loss of MeCN (calcd. 3.29%) occurring between 120 and 220 °C. Complex **4** lost a guest CH_2Cl_2 molecule in the temperature range of 34–83 °C with a weight loss of 14.76% (calcd. 15.32%).

3.4. Photoluminescent properties

The photoluminescent properties of the free Htpim ligand and compounds **1–4** have been investigated in the solid state at room temperature. As shown in Fig. 11, the free ligand exhibits two emission maxima at 411 and 496 nm upon excitation at 376 nm. The maximum emission peaks of complexes **1** and **4** are located at 540 and 539 nm upon excitation at 362 and 348 nm, respectively. Complex **2** has a very strong emission band centered at 495 nm upon excitation at 375 nm. It is noteworthy that complex **3** displays an emission band in the red region at 623 nm when excited at 346 nm. The emissions could be assigned to a ligand-to-metal charge-transfer (LMCT) transition. Furthermore, the fluorescent intensity of **2** is stronger than compounds **1**, **3** and **4**, which may be attributed to deprotonation of the Htpim ligand in compound **2** [36].

4. Conclusions

In this paper, four new coordination polymers based on a novel rigid multi-pyridyl ligand have been successfully synthesized and characterized. Complexes **1** and **2** have the same one-dimensional motif. Complexes **3** and **4** consist of 1D zigzag and 1D ladder-like chains, respectively. All the complexes reported here, together with the free ligand, display photoluminescence at room temperature.

Acknowledgements

This work was supported by the National Basic Research Program of China (2006CB806104 and 2007CB925103) and the

National Natural Science Foundation of China (20725104 and 20531040).

Appendix A. Supplementary data

CCDC 675098, 675099, 675100 and 675101 contain the supplementary crystallographic data for **1**, **2**, **3** and **4**. These data can be obtained free of charge via http://www.ccdc.cam.ac.uk/conts/retrieving.html, or from the Cambridge Crystallographic Data Centre, 12 Union Road, Cambridge CB2 1EZ, UK; fax: (+44) 1223-336-033, or e-mail: deposit@ccdc.cam.ac.uk. Supplementary data associated with this article can be found, in the online version, at doi:10.1016/j.poly.2008.04.051.

References

[1] K. Biradha, M. Sarkar, L. Rajput, Chem. Commun. (2006) 4169.
[2] A.Y. Robin, K.M. Fromm, Coord. Chem. Rev. 250 (2006) 2127.
[3] V.V. Adrabinska, Coord. Chem. Rev. 251 (2007) 1987.
[4] C. Janiak, J. Chem. Soc., Dalton Trans. (2003) 2781.
[5] D. Maspoch, D.R. Molina, J. Veciana, J. Mater. Chem. 14 (2004) 2713.
[6] Q. Ye, X.S. Wang, H. Zhao, R.G. Xiong, Chem. Soc. Rev. 34 (2005) 208.
[7] T.M. Reineke, M. Eddaoudi, M. Fehr, D. Kelley, O.M. Yaghi, J. Am. Chem. Soc. 121 (1999) 1651.
[8] S. Noro, R. Kitaura, M. Kondo, S. Kitagawa, T. Ishii, H. Matsuzaka, M. Yamashita, J. Am. Chem. Soc. 124 (2002) 2569.
[9] X.S. Wang, S.Q. Ma, D.F. Sun, S. Parkin, H.C. Zhou, J. Am. Chem. Soc. 128 (2006) 16474.
[10] C.D. Wu, A.G. Hu, L. Zhang, W.B. Lin, J. Am. Chem. Soc. 127 (2005) 8940.
[11] İ. Kani, C. Darak, O. Şahin, O. Büyükgüngör, Polyhedron 27 (2008) 1238.
[12] M. Du, Y.M. Guo, S.T. Chen, X.H. Bu, S.R. Batten, J. Ribas, S. Kitagawa, Inorg. Chem. 43 (2004) 1287.
[13] M.H. Shu, C.L. Tu, W.D. Xu, H. B Jin, J. Sun, Cryst. Growth Des. 6 (2006) 1890.
[14] W.T. Chen, M.S. Wang, X. Liu, G.C. Guo, J.S. Huang, Crys. Growth Des. 6 (2006) 2389.
[15] S. Hu, A.J. Zhou, Y.H. Zhang, S. Ding, M.L. Tong, Cryst. Growth Des. 6 (2006) 2543.
[16] M.H. Bi, G.H. Li, J. Hua, Y.L. Liu, X.M. Liu, Y.W. Hu, Z. Shi, S.H. Feng, Cryst. Growth Des. 6 (2007) 2066.
[17] H. Wang, M.X. Li, M. Shao, X. He, Polyhedron 26 (2007) 5171.
[18] F. Jin, H.P. Zhou, X.C. Wang, Z.J. Hu, J.Y. Wu, Y.P. Tian, M.H. Jiang, Polyhedron 26 (2007) 1338.
[19] W.J. Feng, Y. Xu, G.P. Zhou, C.L. Zhang, X.F. Zheng, Inorg. Chem. Commun. 10 (2007) 49.
[20] O.R. Evans, R.G. Xiong, Z.Y. Wang, G.K. Wong, W.B. Lin, Angew. Chem., Int. Ed. 38 (1999) 536.
[21] Q.F. Xu, Q.X. Zhou, J.M. Lu, X.W. Xia, Li. H. Wang, Y. Zhang, Polyhedron 26 (2007) 4849.
[22] Z.G. Gu, Y. Song, J.L. Zuo, X.Z. You, Inorg. Chem. 46 (2007) 9522.
[23] Z.G. Gu, X.H. Zhou, Y.B. Jin, R.G. Xiong, J.L. Zuo, X.Z. You, Inorg. Chem. 46 (2007) 5462.
[24] P. Misra, C.Y. Liao, H.H. Wei, S. Mohanta, Polyhedron 27 (2008) 1185.
[25] F. Setifi, S. Benmansour, S. Triki, C.J. Gómez-García, M. Marchivie, J.Y. Salauün, M. Mustapha, Inorg. Chim. Acta 360 (2007) 3879.
[26] C.D. Ene, F. Tuna, O. Fabelo, C. Ruiz-Pérez, A.M. Madalan, H.W. Roesky, M. Andruh, Polyhedron 27 (2008) 574.
[27] A.J. Fletcher, E.J. Cussen, T.J. Prior, M.J. Rosseinsky, C.J. Kepert, K.M. Thomas, J. Am. Chem. Soc. 123 (2001) 10001.
[28] S.R. Batten, B.F. Hoskins, B. Moubaraki, K.S. Murrayand, R. Robson, Chem. Commun. (2000) 1095.
[29] T. Haneda, M. Kawano, T. Kojima, M. Fujita, Angew. Chem., Int. Ed. 46 (2007) 6643.
[30] T. Ohmura, A. Usuki, K. Fukumori, T. Ohta, M. Ito, K. Tatsumi, Inorg. Chem. 45 (2006) 7988.
[31] M. Du, S.T. Chen, X.H. Bu, Cryst. Growth Des. 2 (2002) 625.
[32] Y.B. Dong, J.P. Ma, R.Q. Huang, Inorg. Chem. 43 (2006) 294.
[33] M.V. Proskurnina, N.A. Lozinskaya, S.E. Tkachenko, N.S. Zefirov, Rus. J. Org. Chem. 38 (2002) 1149.
[34] SMART and SAINT. Area Detector Control and Integration Software, Siemens Analytical X-ray Systems Inc., Madison, WI, 1996.
[35] G.M. Sheldrick, SHELXTL V5.1 Software Reference Manual, Bruker AXS Inc., Madison, WI, 1997.
[36] X.W. Wang, J.Z. Chen, J.H. Liu, Cryst. Growth Des. 7 (2007) 1227.

Polyhedron 27 (2008) 2501–2505

Contents lists available at ScienceDirect

Polyhedron

journal homepage: www.elsevier.com/locate/poly

Synthesis and characterization of organophosphine/phosphite stabilized silver(I) methanesulfonates: Crystal structures of $[Ph_3PAgO_3SCH_3]$ and $[(Ph_3P)_2AgO_3SCH_3]$

Yi-Ying Zhang, Yan Wang, Xian Tao, Ning Wang, Ying-Zhong Shen *

Applied Chemistry Department, School of Material Science and Engineering, Nanjing University of Aeronautics and Astronautics, Nanjing 210016, PR China

ARTICLE INFO

Article history:
Received 24 November 2007
Accepted 27 April 2008
Available online 14 June 2008

Keywords:
Silver(I) methanesulfonates
Organophosphine
Thermogravimetric analysis
Crystal structure

ABSTRACT

Six organophosphine/phosphite stabilized silver(I) methanesulfonates of type $[L_nAgO_3SCH_3]$ (L = Ph_3P, n = 1, **2a**; n = 2, **2b**; n = 3, **2c**; L = $(EtO)_3P$; n = 1, **2d**; n = 2, **2e**; n = 3, **2f**) were synthesized by the reaction of silver methanesulfonates with triphenylphosphine or triethylphosphite in dichloromethane under nitrogen atmosphere. These complexes were obtained in high yields and characterized by elemental analysis, ^{1}H-, ^{13}C{H} NMR, IR spectroscopy and thermogravimetric analysis (TGA), respectively. X-ray single crystal analysis reveals that complex **2a** is a tetramer $[Ph_3PAgO_3SCH_3]_4$ and complex **2b** is a monomer. The thermal stability of **2a** has been studied by applying thermogravimetric analysis. It starts to decompose between 50 and 440 °C in a three-step process. The final residue (Ag) is about 20.50%.

© 2008 Elsevier Ltd. All rights reserved.

1. Introduction

Silver(I) complexes have been widely studied because they have shown a great tendency to form rich structure characteristics [1–6], potential application in catalysis [7] and material science [8,9]. Lewis-base stabilized silver(I) complexes have recently attracted renewed interests, mostly because of their application as precursors in the growth of silver thin films via chemical vapor deposition (CVD) techniques, which could be used as new interconnect material for the future generations of deep submicro integrated circuits because of the lower resistivity and superior electromigration resistance [10–15].

The key to achieve success for CVD, however, is the selection of suitable precursors. As the precursor for CVD, the complexes should have: (i) suitable vapor pressure for transporting it from bubbler to CVD reactor; (ii) suitable thermal decomposition mechanism, (iii) suitable thermal stability which means that it could not decompose during the transportation but decompose easily in the reactor [16,17]. Several organic molecules have been often used as ligands to synthesize the silver complexes, such as β-diketonate and its analogous as the main ligands [18,19], and phosphines as ancillary ligands [20,21]. For example, $[(CH_3)_3CCOCHCOC_3F_7AgPEt_3]$ [22], $[(fod)_3Ag(PPh_3)_5]$ [23] were reported to be successfully used as precursors for the silver film deposition. Lewis-base stabilized silver carboxylates such as $[Ph_3PAgO_2CR]$ [24], $[(Ph_3P)_2AgO_2CC_3F_7]$ [25] are another kind of precursors for silver deposition due to the higher utility of silver (100%) according to the radical decomposition mechanism. But to the best of our knowledge, Lewis-base stabilized silver methanesulfonates have not been reported until now. In order to search for the new kind of silver precursor used in CVD technique, a series of organophosphine stabilized silver(I) sulfonates, $[L_nAgO_3SCH_3]$ (L = Ph_3P, n = 1, **2a**; n = 2, **2b**; n = 3, **2c**; L = $(EtO)_3P$; n = 1, **2d**; n = 2, **2e**; n = 3, **2f**), were synthesized and characterized. The single crystal structures of **2a** and **2b** were determined and discussed. The thermal stability of **2a** has been studied by applying thermogravimetric analysis (TGA) has been studied as well.

2. Experimental

2.1. General procedure

All operations were carried out under an atmosphere of purified nitrogen with standard Schlenk techniques. The solvent dichloromethane (CH_2Cl_2) was purified by distillation from P_2O_5 under N_2. The AgO_3SCH_3 was synthesized by reacting CH_3SO_3H with excessive Ag_2CO_3 in water. ^{1}H NMR were recorded on a Bruker Avance 300 spectrometer operating at 300.130 MHz in the Fourier transform mode; ^{13}C{H} NMR spectra were recorded at 75.467 MHz. Chemical shifts are reported in δ units (parts per million) downfield from tetramethylsilane (δ = 0.0 ppm) with the solvent as the reference signal (^{1}H NMR, $CDCl_3$ δ = 7.26; ^{13}C{H} NMR, $CDCl_3$ δ = 77.55). Infrared spectra were collected on Bruker Vector 22 at room temperature. Elemental analyses were performed on a Perkin–Elmer 240C elemental analyzer. Melting points were observed in sealed capillaries and were uncorrected. Thermogravimetric analysis were performed on a American TA2000/2960

* Corresponding author. Tel.: +86 25 52112904 84765; fax: +86 25 52112626.
E-mail address: yz_shen@nuaa.edu.cn (Y.-Z. Shen).

0277-5387/$ - see front matter © 2008 Elsevier Ltd. All rights reserved.
doi:10.1016/j.poly.2008.04.041

analyzer with a heating rate of 10 °C min^{-1} under nitrogen atmosphere.

2.2. Synthesis

2.2.1. Synthesis of CH_3SO_3Ag (**1**)

Methane sulfonic acid (5 g, 0.052 mol) dissolved in 50 mL of H_2O was added dropwise into a stirred suspended solution of $[Ag_2CO_3]$ (8.7 g, 0.031 mol) in 20 mL of H_2O at 20 °C. The clear solution was obtained by filtration through a pad of celite after stirring the reaction mixture for 1 h at 20 °C. A white solid product was obtained after removing water in Rotary Evaporator and Vacuum Drying Oven at 50 °C. The product was stored under nitrogen and keep in dark place. Yield: 8.8 g (83%, based on Ag_2CO_3).

2.2.2. Synthesis of $Ph_3PAgO_3SCH_3$ (**2a**)

Triphenylphosphine (0.1318 g, 0.5 mmol) dissolved in 20 mL of CH_2Cl_2 was added dropwise into a stirred suspended solution of $[CH_3SO_3Ag]$ (0.1020 g, 0.5 mmol) in 20 mL of CH_2Cl_2 at 0 °C. The clear solution was obtained by filtration through a pad of celite after stirring the reaction mixture for 6 h at 0 °C. A white solid product was obtained after removing all the volatiles in oil-pump vacuo, yield: 0.21 g (91%, based on CH_3SO_3Ag). M.p.: 187 °C dec. *Anal.* Calc. for $C_{19}H_{18}O_3AgPS$: C, 49.05; H, 3.90. Found: C, 48.93; H, 3.85%. ^1H NMR ($CDCl_3$): δ 2.8 (s, 3H, CH_3–H), 7.4–7.6 (m, 15H, Ph–H). $^{13}C\{H\}$ NMR ($CDCl_3$): δ 39.1 (CH_3), 134.3 (J_{PC} = 16.0 Hz, C_6H_5), 132.3 (J_{PC} = 22.4 Hz, C_6H_5), 131.4 (C_6H_5), 129.6 (J_{PC} = 10.36 Hz, C_6H_5). IR (KBr) data (cm^{-1}): 3051 (m), 2962 (m), 1476 (m), 1435 (s), 1388 (m), 1258 (s), 1196 (vs), 1093 (vs), 1023 (vs), 804 (s), 740 (s), 692 (vs), 507 (s).

2.2.3. Synthesis of $(Ph_3P)_2AgO_3SCH_3$ (**2b**)

Complex **2b** as a white solid was obtained following the above procedure, only using $[CH_3SO_3Ag]$ (0.1401 g, 0.69 mmol) and triphenylphosphine (0.3621 g, 1.38 mmol) instead. Yield: 0.477 g (95%, based on AgO_3SCH_3). M.p.: 195 °C dec. *Anal.* Calc. for $C_{37}H_{33}O_3AgP_2S$: C, 61.08; H, 4.57. Found: C, 60.87; H, 4.54. ^1H NMR ($CDCl_3$): δ 2.6 (s, 3H, CH_3), 7.2–7.4 (m, 30H, Ph). $^{13}C\{H\}$ NMR ($CDCl_3$): δ 39.1 (CH_3), 134.4 (J_{PC} = 13.3 Hz, C_6H_5), 132.3 (J_{PC} = 22.3 Hz, C_6H_5), 130.9 (C_6H_5), 129.4 (J_{PC} = 10.36 Hz, C_6H_5). IR (KBr) data (cm^{-1}): 3053 (m), 2959 (m), 1476 (m), 1435 (s), 1392 (m), 1263 (s), 1200 (vs), 1095 (vs), 1039 (vs), 804 (m), 749 (s), 696 (vs), 507 (s).

2.2.4. Synthesis of $(Ph_3P)_3AgO_3SCH_3$ (**2c**)

Complex **2c** was synthesized following the synthesis of **2a** (Section 2.2.1). In this respect, triphenylphosphine (0.4388 g, 1.67 mmol) was reacted with $[AgO_3SCH_3]$ (0.1132, 0.558 mmol). After appropriate work-up (see Section 2.2.1), complex **2c** was obtained as a white solid. Yield: 0.51 g (93%, based on AgO_3SCH_3]). M.p.: 215.2 °C dec. *Anal.* Calc. for $C_{55}H_{48}AgO_3P_3S$: C, 66.74; H, 4.89. Found: C, 66.47; H, 4.62%. ^1H NMR ($CDCl_3$): δ 2.5 (s, 3H, CH_3), 7.2–7.4 (m, 45H, Ph). $^{13}C\{H\}$ NMR ($CDCl_3$): δ 39.4 (CH_3), 134.2 (J_{PC} = 16.06 Hz, C_6H_5), 132.3 (J_{PC} = 23.29 Hz, C_6H_5), 130.7 (C_6H_5), 129.3 (J_{PC} = 9.24 Hz, C_6H_5). IR (KBr) data (cm^{-1}): 3051 (m), 2959 (m), 1480 (m), 1435 (s), 1387 (m), 1260 (s), 1196 (vs), 1087 (s), 1035 (vs), 804 (m), 749 (s), 696 (vs), 507 (s).

2.2.5. Synthesis of $(EtO)_3PAgO_3SCH_3$ (**2d**)

Complex **2d** was synthesized following the synthesis of **2a** (Section 2.2.1). In this respect, $[(EtO)_3P]$ (1.88 g, 11.32 mmol) was reacted with $[AgO_3SCH_3]$ (2.29 g, 11.32 mmol). After appropriate work-up, complex **2d** can be isolated as a colourless liquid. Yield: 3.77 g (90%, based on AgO_3SCH_3). *Anal.* Calc. for $C_7H_{18}O_6AgPS$: C, 22.78; H, 4.92. Found: C, 22.67; H, 4.78%. ^1H NMR ($CDCl_3$): δ 1.2 (t, 9 H, CH_3/CH_3CH_2–, J_{HH} = 7.0), 2.8 (s, 3 H), 4.0 (m, 6H, CH_2/CH_3CH_2–). $^{13}C\{H\}$ NMR ($CDCl_3$): δ 39.2 (CH_3), 16.6 (J_{PC} = 6.5 Hz, CH_3/CH_3CH_2–), 61.4 (J_{PC} = 3.1 Hz, CH_2/CH_3CH_2–). IR (KBr) data (cm^{-1}): 2981 (s), 2929 (m), 2900 (m), 1477 (m), 1444 (m), 1391 (m), 1244 (s), 1207 (s), 1152 (vs), 1095 (m), 1015 (vs), 942, (vs), 764 (vs), 555 (s).

2.2.6. Synthesis of $[(EtO)_3P]_2AgO_3SCH_3$ (**2e**)

Complex **2e** was synthesized following the synthesis of **2a** (Section 2.2.1). In this respect, $[(EtO)_3P]$ (1.4231 g, 8.57 mmol) was reacted with $[AgO_3SCH_3]$ (0.8700 g, 4.285 mmol). After appropriate work-up (see Section 2.2.1), complex **2e** was obtained as a colourless liquid. Yield: 2.09 g (91%, based on AgO_3SCH_3). *Anal.* Calc. for $C_{13}H_{33}O_9AgP_2S$: C, 29.17; H, 6.21. Found: C, 29.03; H, 6.22%. ^1H NMR ($CDCl_3$): δ 1.2 (t, 18H, CH_3/CH_3CH_2–, J_{HH} = 7.0), 2.7 (s, 3H), 4.0 (m, 12H, CH_2/CH_3CH_2–). $^{13}C\{H\}$ NMR ($CDCl_3$): δ 39.2 (CH_3), 16.7 (J_{PC} = 5.6 Hz, CH_3/CH_3CH_2–), 61.3 (J_{PC} = 2.2 Hz, CH_2/CH_3CH_2–). IR (KBr) data (cm^{-1}): 2981 (s), 2934 (m), 2904 (m), 1478 (m), 1444 (s), 1388 (m), 1238 (s), 1208 (s), 1163 (s), 1098 (m), 1020 (vs), 939 (vs), 768 (vs), 531 (s).

2.2.7. Synthesis of $[(EtO)_3P]_3AgO_3SCH_3$ (**2f**)

Complex **2f** was synthesized following the synthesis of **2a** (Section 2.2.1). In this respect, $[(EtO)_3P]$ (1.5644 g, 9.4 mmol) was reacted with $[AgO_3SCH_3]$ (0.6337 g, 3.1 mmol). After appropriate work-up, complex **2f** can be isolated as a colourless liquid. Yield: 2.06 g (93%, based on AgO_3SCH_3). *Anal.* Calc. for $C_{19}H_{48}O_{12}AgP_3S$: C, 32.53; H, 6.90. Found: C, 32.33; H, 6.72%. ^1H NMR ($CDCl_3$): δ 1.2 (t, 27H, CH_3/CH_3CH_2–, J_{HH} = 7.0), 2.6 (s, 3H), 4.0 (m, 18H, CH_2/CH_3CH_2–). $^{13}C\{H\}$ NMR ($CDCl_3$): δ 39.2 (CH_3), 16.6 (J_{PC} = 5.8 Hz, CH_3/CH_3CH_2–), 60.8 (J_{PC} = 3.4 Hz, CH_2/CH_3CH_2–). IR (KBr) data (cm^{-1}): 2982 (vs), 2934 (s), 2902 (m), 1477 (m), 1444 (m), 1391(s), 1241 (s), 1209 (s), 1161 (s), 1098 (m), 1022 (vs), 941 (vs), 764 (vs), 531 (s).

2.3. Single crystal structures of $Ph_3PAgO_3SCH_3$ (**2a**) and $(Ph_3P)_2AgO_3SCH_3$ (**2b**)

Single crystals of **2a** and **2b** could be obtained by cooling a saturated dichloromethane solution to −30 °C. Suitable crystals for X-ray determination were placed in glue under N_2 for they are sensitive to moisture and oxygen. The crystal structure data collection was done on a BRUKER SMART APEX CCD diffractometer using graphite monochromatic Mo Kα radiation (λ = 0.71073 Å) at room temperature. The program SMART [26] was used for determination of the unit cell. Data reduction and integration was carried out with SAINT [26] and absorption corrections were applied using the program SADABS [27]. The structure was solved using direct methods and refined by full-matrix least-squares procedures on F^2 (SHELX-97 [28]). All of the non-hydrogen atoms were refined with anisotropic displacement parameters. Crystallographic data and details on refinement are presented in Table 1. The crystal structures of **2a** and **2b** are drawn using ORTEP [29].

3. Results and discussion

3.1. Synthesis

The phosphine/phosphite stabilized silver(I) methanesulfonates (L = Ph_3P, n = 1, **2a**; n = 2, **2b**; n = 3, **2c**; L = $(EtO)_3P$; n = 1, **2d**; n = 2, **2e**; n = 3, **2f**) were prepared by using $Ph_3P/(EtO)_3P$ reacting with solver(I) methanesulfonate in dichloromethane in stoichiometry at 0 °C under nitrogen atmosphere in high yield (Scheme 1). The complexes were isolated as white solids (**2a**–**2c**) or colourless liquids (**2d**–**2f**). They are very sensitive to temperature, moisture, oxygen as well as light. The complexes are insoluble in cold

Table 1
Crystallographic data and structure refinement details for **2a** and **2b**

Compound	**2a**	**2b**
Formula	$C_{80}H_{80}Ag_4Cl_8O_{12}P_4S_4$	$C_{38}H_{35}AgCl_2O_3P_2S$
Formula weight	2200.64	812.43
Crystal dimensions (mm)	0.4 × 0.5 × 0.6	0.5 × 0.5 × 0.6
Crystal system	tetragonal	monoclinic
Space group	$I4_1/a$	$P2_1/c$
a (Å)	23.993(1)	9.381(1)
b (Å)	23.993(1)	20.165(1)
c (Å)	15.702(1)	19.653(1)
α (°)	90.00	90.00
β (°)	90.00	92.58
γ (°)	90.00	90.00
V [Å^3]	9039.2(8)	3714.1(4)
Z value	4	4
D_{calc} (g/cm^3)	1.617	1.453
Index ranges	$-26 \leqslant h \leqslant 30$, $-30 \leqslant k \leqslant 30$, $-17 \leqslant l \leqslant 19$	$-10 \leqslant h \leqslant 11$, $-13 \leqslant k \leqslant 25$, $-24 \leqslant l \leqslant 24$
$F(000)$	4416	1656
μ(Mo Kα) (mm^{-1})	1.309	0.864
λ (Mo Kα) (Å)	0.71073	0.71073
Temperature (K)	293	293
$2\theta_{max}$ (°)	54	54
Number of reflections measured	4934	7992
Independent reflections observed [$I > 2\sigma(I)$]	4568	6687
Number of refined parameters	254	433
R_1 [$I > 2\sigma(\theta)$][a]	0.0901	0.0624
wR_2 [$I > 2\sigma(\theta)$][b]	0.1592	0.1472
Goodness-of-fit[c]	1.068	1.168
$\Delta\rho_{max}$ (e Å^{-3})	1.01	0.71
$\Delta\rho_{min}$ (e Å^{-3})	−0.61	−0.51

[a] $R_1 = \sum(||F_o| - |F_c||)/\sum|F_o|$; $wR_2 = [\sum(w(F_o^2 - F_c^2)^2)/\sum(wF_o^4)]^{1/2}$.
[b] $w_{2a} = 1/[\sigma^2(F_o^2) + (0.0038P)^2 + 166.3623P]$, $P = (F_o^2 + 2F_c^2)/3$. $w_{2b} = 1/[\sigma^2(F_o^2) + (0.0485P)^2 + 3.1225P]$, $P = (F_o^2 + 2F_c^2)/3$.
[c] $S = [\sum w(F_o^2 - F_c^2)^2]/(n - p)^{1/2}$, n = number of reflections, p = parameters used.

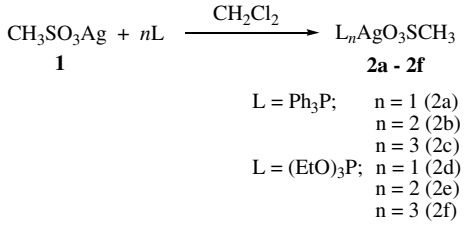

Scheme 1. Synthesis of complexes **2a**–**2f**.

non-polar solvent like petroleum, whereas they are highly soluble in polar or unsaturated hydrocarbons such as methylenechloride, benzene. All the obtained products gave satisfactory elemental analysis results, which were characterized by elemental analysis, IR, ^{1}H NMR, ^{13}C{H} NMR, respectively.

As we know, the typical group vibration of sulfonates shows in the range of 1350–1050 cm^{-1} [30,31]. When the R—SO_3^- anion is "free", that is to say, non-coordinated, it shows local C_{3v}-symmetry with two ν_{so} bands for the symmetrical. Upon coordination to a metal, the C_{3v}-symmetry is broken and for a C_s-symmetrical R–SO_2–O–M moiety and three ν_{SO} bands are observed ($\nu^{as}(SO_2)$; $\nu^{s}(SO_2)$; ν(S–O)). In the case of lithium and sodium salt of the methanesulfonate anion ($CH_3SO_3^-$), the $\nu^{as}(SO_2)$; $\nu^{s}(SO_2)$ are observed at 1233 and 1060 cm^{-1}, respectively (for the NaO_3SCH_3) and $\nu^{as}_{(SO2)}$ (1244 cm^{-1}); $\nu^{s}_{(SO2)}$ (1185 cm^{-1}); $\nu_{(S-O)}$ (1050 cm^{-1}) for LiO_3SCH_3 [32]. In the IR spectra of **2a**–**2f** it shows prominent absorptions in ν_{SO3} region. The absorptions in the range of 1238–1268 cm^{-1} and 1180–1200 cm^{-1} can be interpreted as the asymmetric and symmetric vibration of SO_2, which is the similar as previous reported [33–37]. The absorptions around 1030 cm^{-1} can be assigned as vibration of S–O; which is similar to the reported value [33–37].

The NMR spectra (^{1}H and ^{13}C{H}) were recorded for all six complexes (see Section 2) at room temperature, In ^{1}H NMR, the proton spectra were consistent with the stoichiometries of the complexes. The protons of complexes **2a**–**2c** in the aryl proton region of the ^{1}H NMR spectra were in the range of 7.2–7.6 ppm. The complexes (**2d**–**2f**) are easily distinguished because the resonances of the protons show only two groups. The proton of CH_3 – in CH_3SO_3 – appeared at 2.6–2.8 ppm, which agrees with previous reported [23]. In the ^{13}C{H} NMR spectra of **2a**–**2c** the triphenylphosphine carbon resonances are easily distinguished (in the range of 129.6–134.2 ppm). The carbon resonance of CH_3 – on CH_3SO_3 – shows in the lower field (39.1–39.4 ppm) comparing to that of [$(EtO)_3$P] (ca. 16.7 ppm).

3.2. Single crystal structure of *2a* and *2b*

The X-ray single crystal analysis results indicate that the molecular formula of complex **2a** is $[(Ph_3PAgO_3SCH_3)_4 \cdot 4CH_2Cl_2]$ and complex **2b** is $[(Ph_3P)_2AgO_3SCH_3 \cdot CH_2Cl_2]$. Because of different molar ratio of triphenylphosphine with silver methylsulofonate, complex **2b** is a monomer with each silver atom coordinated by two PPh_3 groups. Complex **2a**, however, is a tetramer with the silver atom coordinated by one PPh_3 group. The molecular structure of **2a** and **2b** are depicted in Fig. 1 and Fig. 2, and selected bond distances (Å) and bond angles (°) are given in Table 2.

Complex **2a** crystallizes in the tetragonal with space group $I4_1/a$, which is composed of a tetramer $[Ph_3PAgO_3SCH_3]_4$ and four molecules of dichloromethane, as shown in Fig. 1. This is different from the reported complex $[Ph_3PAgO_3SCF_3]$ which exists as a trimer [38]. In the tetramer complex, the Ag_4O_4 core of the molecule is regarded as a "cubane-like" framework, with the alternate corners of the cube occupied by the silver atoms and the methanesulfonic oxygen atoms. The phosphorous atoms are approximately apical,

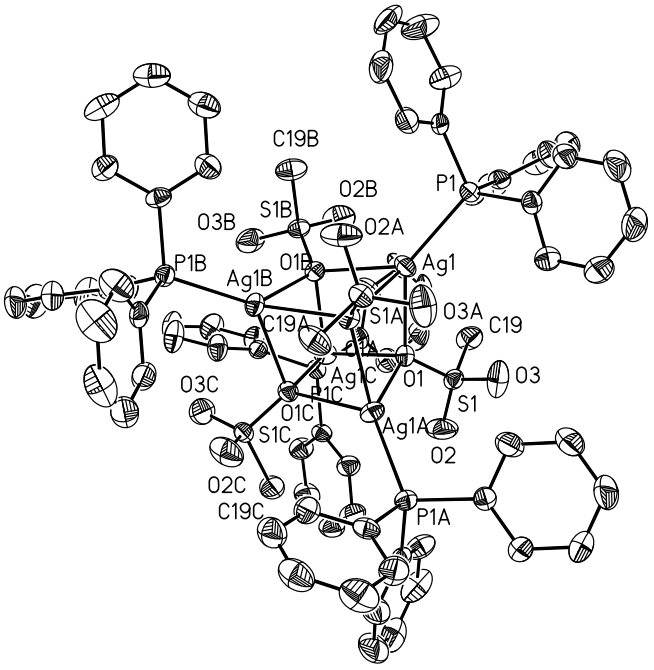

Fig. 1. ORTEP drawing of **2a**, showing 30% probability displacement ellipsoids. The hydrogen atoms and solvent molecules are omitted for clarity.

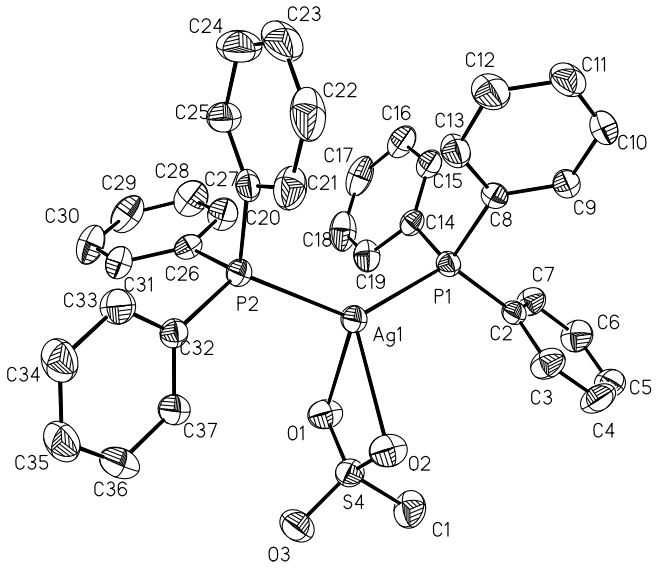

Fig. 2. ORTEP drawing of **2b**, showing 30% probability displacement ellipsoids. The hydrogen atoms and solvent molecules are omitted for clarity.

Table 2
Selected bond distances (Å) and angles (°) for **2a** and **2b**

*Complex **2a***			
Ag(1)–P(1)	2.348(2)	Ag(1)–O(1)	2.389(5)
Ag(1)–O(1)^{b}	2.465(5)	Ag(1)–O(1)^{c}	2.449(5)
P(1)–Ag(1)–O(1)	135.5(1)	P(1)–Ag(1)–O(1)^{b}	133.0(1)
P(1)–Ag(1)–O(1)^{c}	130.8(1)	O(1)–Ag(1)–O(1)^{b}	79.5(2)
O(1)–Ag(1)–O(1)^{c}	78.5(2)	O(1)^{b}–Ag(1)–O(1)^{c}	77.1(2)
Ag(1)–O(1)–Ag(1)^{a}	102.5(2)	Ag(1)^{a}–O(1)–Ag(1)^{b}	100.3(2)
Ag(1)–O(1)–Ag(1)^{b}	98.7(2)		
Complex 2b			
Ag(1)–P(1)	2.434(1)	Ag(1)–P(2)	2.422(1)
Ag(1)–O(1)	2.501(3)	Ag(1)–O(2)	2.552(3)
P(1)–Ag(1)–P(2)	132.4(4)	P(1)–Ag(1)–O(1)	104.0(8)
P(1)–Ag(1)–O(2)	108.9(8)	P(2)–Ag(1)–O(1)	106.6(8)
P(2)–Ag(1)–O(2)	118.3(8)	O(1)–Ag(1)–O(2)	56.5(1)

Symmetry code: a = 5/4 − *y*, 1/4 + *x*, 9/4 − *z*; b = 1 − *x*, 3/2 − *y*, *z*; c = −1/4 + *y*, 5/4 − *x*, 9/4 − *z*.

coordinating to the silver atom, thereby completing a distorted tetrahedral coordination arrangement of the silver atom. The angles of O–Ag–O [79.5(2)°, 77.1(2)°, 78.5(2)°] and Ag–O–Ag [100.7(2)°, 102.5(2)°, 98.7(2)°] are close to 90°, but the former are smaller than the latter, which confirms the deformation of the "cubane" just like other "cubane-like" complexes [39,40]. The P–Ag distance (2.348(2) Å) is close to the sum of covalent radio of P and Ag atoms (2.44 Å) [39] and slightly shorter than other complexes [$(Ph_3P)_2Ag(O_2CC_3F_7)$] 2.406(1) Å [24], [$(Ph_3P)_3Ag(OPhMe_2)$], 2.539(2) Å [41].

Complex **2b** crystallizes in the tetragonal with space group P 2_1/c and exists as a monomer with a molecule of dichloromethane in crystal structure (show in Fig. 2). The silver atom is coordinated by two phosphorus atoms of triphenylphosphine and two methanesulfonic oxygen atoms at the same time. This coordination mode is similar to the reported complex [$(MePh_2P)_2AgO_3SCF_3$] [42] and several silver(I) carboxylates such as [$(Ph_3P)_2Ag(O_2CCH{=}CHCH_2CH_2CH_3)$] [24] and [$(Ph_3P)_2Ag(CO_2CF_3)$], but different from the reported complex [$(Ph_3P)_2AgO_3SCF_3$] [42] which exists as a dimmer. The distances of Ag–P [2.422(1), 2.434(1) Å] are longer than that of [$(R_3P)_2AgO_3SCF_3$] [2.385(8), 2.389(8) Å] and complex **2a** [2.348(2) Å]. The Ag–O distances [2.501(3), 2.552(3) Å] are much shorter than those [2.775(2), 2.854(2) Å] of [$(MePh_2P)_2AgO_3SCF_3$] [42] and much longer than those in complex **2a** [2.389(5), 2.449(5), 2.465(5) Å]. The P–Ag–P angle [132.4(4)°] is much smaller than that [156.2(3)°] of [$(MePh_2P)_2AgO_3SCF_3$] [42], respectively.

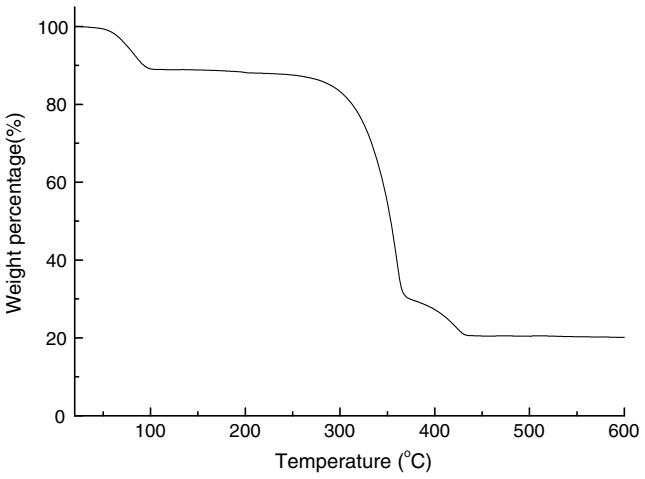

Fig. 3. TG trace of **2a** (heating rate of 10 °C min^{-1}, nitrogen atmosphere).

3.3. Thermogravimetric analysis (TGA)

Thermogravimetric analysis (Fig. 3) was carried-out to determine the relative volatility and evaluate the suitability of complex as possible CVD precursors. These studies are also required to optimize the temperature at which the respective single silver precursor should be maintained during the CVD experiments. Complex **2a**, for example, decomposes between 50 and 440 °C in a three-step process. The first step takes place between 50 and 105 °C with the 10.97% weight loss, the second step is observed in the range of 105–370 °C with the 58.43% weight loss, and the third step is between 370–440 °C with the 10.10% weight loss. The total weight loss is 79.50%. These data show that the percentage of the residue is 20.50% (Ag), which is close to the theoretical value of silver (23.18%) in complex **2a**. The real thermal decomposition mechanism of complex **2a** and other complexes would be studied in the further research.

4. Supplementary data

CCDC 656251 and 666194 contain the supplementary crystallographic data for **2a** and **2b**. These data can be obtained free of charge via http://www.ccdc.cam.ac.uk/conts/retrieving.html, or from the Cambridge Crystallographic Data Centre, 12 Union Road, Cambridge CB2 1EZ, UK; fax: (+44) 1223-336-033; or e-mail: deposit@ccdc.cam.ac.uk.

Acknowledgements

We gratefully acknowledge National 863 Research Project (2006AA03Z219), Natural Science Foundation of Jiangsu province (BK2007199); Foundation for "Liu Da Ren Cai" of Jiangsu Province (06-E-021), the Excellent Project for the Returned Oversea Chinese Scholars, National Defense Industry Committee (R0563-062) and State Education Ministry (N0502-062). The State Postdoctoral Foundation of China (No. 2006040932), the Postdoctoral Foundation of Jiangsu Province (No. 0602008B) and Foundation from NUAA are also acknowledged.

References

[1] M. Dennehy, O.V. Quinzani, M. Jennings, J. Mol. Struct. 841 (2007) 110.
[2] I.G. Dance, Polyhedron 5 (1986) 1037.
[3] B. Krebs, G. Henkel, Angew. Chem., Int. Ed. Engl. 30 (1991) 769.
[4] C. Housecroft, Coord. Chem. Rev. 115 (1992) 141.
[5] R.H. Holm, P. Kennepohl, E.I. Solomon, Chem. Rev. 96 (1996) 2239.
[6] M.C. Hong, W.P. Su, R. Cao, W.J. Zhang, J.X. Lu, Inorg. Chem. 38 (1999) 600.
[7] F. Colombo, R. Annunziata, M. Benaglia, Tetrahedron Lett. 48 (2007) 2687.
[8] K. Ozawa, F. Iso, Y. Nakao, Z.X. Cheng, H. Fujii, M. Hase, H. Yamaguchi, J. Eur. Ceram. Soc. 27 (2007) 2665.
[9] H. Schmidt, Y. Shen, M. Leschke, Th. Haase, K. Hohse-Hoeinghaus, H. Lang, J. Organomet. Chem. 669 (2003) 25.
[10] W. Partenheimer, E.H. Johnson, Inorg. Chem. (11) (1972) 2840.
[11] W. Partenheimer, E.H. Johnson, Inorg. Chem. (12) (1973) 1274.
[12] H.K. Hofstee, J. Boersma, G.J.M. van der Kerk, J. Organomet. Chem. 120 (1976) 313.
[13] W.T. Miller, R.H. Sinder, R.J. Hummel, J. Am. Chem. Soc. 91 (1969) 6532.
[14] Y. Zheng, N.H. Dryden, J.J. Vittal, R.J. Puddephatt, Chem. Mater. 7 (1995) 1696.
[15] M. Wen, M. Munakata, Y.Z. Li, Y. Suenaga, T. Kuroda-Sowa, M. Maekawa, M. Anahata, Polyhedron 26 (2007) 2455.
[16] J. Rickerby, J.H.G. Steinke, Chem. Rev. 102 (2002) 1525.
[17] H.K. Shin, K.M. Chi, J. Farkas, M.J. Hampden-Smith, T.T. Kodas, E.N. Duesler, Inorg. Chem. 31 (1992) 424.
[18] A. Bailey, T.S. Corbitt, M.J. Hampden-Smith, E.N. Duesler, T.T. Kodas, Polyhedron 12 (1993) 1785.
[19] D.A. Edwards, M. Longley, J. Inorg. Nucl. Chem. 40 (1978) 1599.
[20] G. Doyle, K.A. Erickson, D. Van Engen, Organometallics 4 (1985) 830.
[21] D. Gibson, B.F.G. Johnson, J. Lewis, J. Chem. Soc. A. (1970) 367.
[22] S.S. Monim, Z. Yuan, K. Griffiths, P.R. Norton, R.J. Puddephatt, J. Am. Chem. Soc. 117 (1995) 4030.
[23] D.A. Edwards, R.M. Harker, M.F. Mahon, K.C. Molloy, J. Mater. Chem. 9 (1999) 1771.
[24] J.L. Han, Y.Z. Shen, C.X. Li, Y.Z. Li, Y. Pan, Inorg. Chim. Acta 358 (2005) 4417.
[25] D.A. Edwards, R.M. Harker, M.F. Mahon, K.C. Molloy, Inorg. Chim. Acta 328 (2002) 134.
[26] Bruker AXS Inc., SAINT, Area Detector Control and Data Integration and Reduction Software, Madison, WI, USA, 1997.
[27] G.M. Sheldrick, SADABS, Program for Empirical Absorption Correction of Area Detector Data, University of Gottingen, Germany, 1997.
[28] G.M. Sheldrick, SHELX-97, Programs for Crystal Structure Analysis (Release 97-2), University of Gottingen, Germany, 1997.
[29] L. Zsolnai, G. Huttner, ORTEP, University of Heidelberg, Germany, 1994.
[30] L.J. Bellamy, The Infrared Spectra of Complexes Molecules, vol. 1, Chapman and Hall, London, 1975.
[31] M.G. Miles, G. Doyle, R.P. Cooney, R.S. Tobis, Spectrochim. Acta A 25 (1960) 1515.
[32] R.J. Capwell, K.H. Rhee, K.S. Seshadri, Spectrochim. Acta A 24 (1968) 955.
[33] S.M. Chackalackal, F.E. Stafford, J. Am. Chem. Soc. 88 (1966) 4815.
[34] R. Bala, R.P. Sharma, A.D. Bond, J. Mol. Struct. 830 (2007) 198.
[35] C.Y. Panicker, H.T. Varghese, D. Philip, H.I.S. Nogueira, Spectrochim. Acta A 64 (2006) 744.
[36] D. Philip, A. Eapen, G. Aruldhas, J. Solid State Chem. 116 (1995) 217.
[37] D. Jamro, Y. Marechal, J. Phys. Chem. B. 109 (2005) 19664.
[38] R. Terroba, M.B. Hursthouse, M. Lagunab, A. Mendia, Polyhedron 18 (1999) 807.
[39] B.K. Teo, J.C. Calabrese, Inorg. Chem. 15 (1976) 2467.
[40] M.R. Churchill, K.L. Kalra, Inorg. Chem. 13 (1974) 1065.
[41] D.A. Edwards, M.F. Mahon, K.C. Molloy, V. Ogrodnik, Inorg. Chim. Acta 349 (2003) 37.
[42] M. Bardají, O. Crespo, A. Laguna, A.K. Fischer, Inorg. Chim. Acta 304 (2000) 7.

Polyhedron 27 (2008) 2507–2512

Contents lists available at ScienceDirect

Polyhedron

journal homepage: www.elsevier.com/locate/poly

Unexpected differences in the reactivity between MPh_2Cl_2 (M = Pb or Sn) and benzil bis(thiosemicarbazone). X-ray crystal structure of benzil bis(thiosemicarbazonate)lead(II)

Elena López-Torres [a], David G. Calatayud [a], César J. Pastor [b], M[a] Antonia Mendiola [a,*]

[a] Departamento de Química Inorgánica, Avda. Francisco Tomás y Valiente, 7, Universidad Autónoma de Madrid, Cantoblanco, 28049-Madrid, Spain
[b] Servicio Interdepartamental de Investigación Avda. Francisco Tomás y Valiente, 7, Universidad Autónoma de Madrid, Cantoblanco, 28049-Madrid, Spain

ARTICLE INFO

Article history:
Received 27 March 2008
Accepted 30 April 2008
Available online 27 June 2008

Keywords:
Bis(thiosemicarbazone) ligands
Dephenylation process
X-ray diffraction

ABSTRACT

The differences in the reactivity of diphenyllead and diphenyltin dichloride with benzil bis(thiosemicarbazone) LH_6 are explored. The reaction of $PbPh_2Cl_2$ afforded the complex $[Pb(LH_4)]$ **1**, containing the ligand doubly deprotonated and without the phenyl groups bonded to the metal. The reaction with $SnPh_2Cl_2$ in the absence of solvent yielded the complex $[Sn(LH_4)Cl_2]$ **2**. The lead(II) complex, also obtained by the reaction with lead(II) nitrate, was formed by a redistribution of the organolead derivative followed by a reductive elimination reaction, while the tin one was formed by a dephenylation process. Reactions in solution of the organotin derivative are complicated and depending on the working conditions different compounds could be isolated: the organostannoxane $[Sn_2Ph_4ClO(OH)]_2$, which was confirmed by X-ray crystallography, or a complex containing a triazine-3-thione ligand, formed by the loss of one of the thiosemicarbazone arms with subsequent cyclisation. The compounds were characterized by IR, mass spectrometry, ^1H, ^{13}C and ^{119}Sn NMR spectroscopy in solution and in the solid state. The structure of $[Pb(LH_4)]$ has been studied by X-ray diffraction and the ligand acts as a N_2S_2 planar bideprotonated ligand, with the lead(II) ion localized 1.3858 Å over this plane.

© 2008 Elsevier Ltd. All rights reserved.

1. Introduction

Thiosemicarbazones (TSCs) and their metal complexes present a wide range of pharmacological applications, for example as antiviral, antibacterial and anticancer agents [1–6]. These biological activities are often attributed to their chelating ability with metal ions and are normally increased in bis(thiosemicarbazones). Tin complexes are potential anti-tumour and antiviral agents and a number of them have shown to posses activity, the diorganotin(IV) derivatives being the most active [7,8]. On the other hand, the chelating capacity of TSCs can be used to detect and/or remove toxic metals as such lead, copper or mercury [9,10]. The Pb–C bonds are rather weak, and consequently organolead(IV) halides decompose at room temperature, especially when expose to light, although the aryl derivatives are somewhat more stable than the alkyl derivatives [11,12]. The decomposition of dialkyllead dihalides involves a redistribution reaction

$$2PbR_2X_2 \rightarrow PbR_3X + PbRX_3$$

followed by reductive elimination of RX from the unstable monoorganolead derivative

$$PbRX_3 \rightarrow PbX_2 + RX$$

These reactions hinder the synthesis of diorganolead(IV) complexes with anionic ligands and reactions with soft anionic ligands lead very often to Pb(II) and $R_3Pb(IV)$ complexes instead of to the diorganolead(IV) derivative [13,14]. The Sn–C bonds could also be broken in the presence of strong polydentate ligands. In particular, $SnPh_2Cl_2$ and $SnPh_3Cl$ can lose one or more phenyl groups by the reaction with tri or tetradentate ligands [15,16].

Although organolead compounds have been well studied, the main social concern has been focused on lead(II). Recent studies connect lead(II) toxicity with its coordination preferences, because their significant differences from those of important biometals, such as zinc(II), are probably responsible for lead interfering in the normal functions of certain proteins [17]. Due to its environmental relevance, a renaissance of the interest in the coordination chemistry of lead has been observed in recent years [18–22]. The coordination chemistry is mainly determined by two factors: its large size, which permits coordination numbers that range from quasi-one [23] to twelve and its 6s electron pair, which may or may not play a role in the stereochemistry of lead(II) complexes

* Corresponding author.
E-mail address: antonia.mendiola@uam.es (M.A. Mendiola).

0277-5387/$ - see front matter © 2008 Elsevier Ltd. All rights reserved.
doi:10.1016/j.poly.2008.04.055

[24]. When the 6s electrons constitute a stereochemically active lone pair (SALP), they occupy a significant proportion of the coordination sphere of the metal, with the result that bonds with ligand donor atoms tend either to be placed only in the opposite hemisphere or to be shorter in that direction than around the SALP [25].

Following our interest in the coordination chemistry of bis(thiosemicarbazone) ligands with toxic metal ions, in this paper we explore the reactivity of diphenyltin and lead(II) nitrate with the tetradentate ligand LH_6 (Scheme). We also compared it with the reactivity of diphenyllead dichloride, which was previously reported.

2. Experimental

2.1. Physical measurements

Microanalyses were carried out using a Perkin–Elmer 2400 II CHNS/O Elemental Analyser. IR spectra in the 4000–400 cm^{-1} range were recorded in KBr pellets on a Jasco FT/IR-410 spectrophotometer. Fast atom bombardment mass spectra were recorded on a VG Auto Spec instrument using Cs as the fast atom and *m*-nitrobenzylalcohol (*m*NBA) as the matrix. Matrix assisted laser desorption ionisation-time of flight (MALDI-TOF) mass spectra were recorded using a Bruker Reflex III mass spectrometer equipped with a nitrogen laser emitting at 337 nm, using ditranol as the matrix. ^1H spectra were recorded on a Bruker AMX-300 spectrometer using DMSO-d_6 as the solvent; chemical shifts are expressed on the δ scale relative to TMS as an internal reference. ^{119}Sn NMR spectra were recorded in the same spectrometer using $CDCl_3$ as solvent and $SnMe_4$ as a reference. ^{13}C CP/MAS NMR spectra were recorded at 298 K in a Bruker AV400WB spectrometer equipped with a 4 mm MAS NMR probe (magic-angle spinning) and obtained using a cross-polarization pulse sequence. The external magnetic field was 9.4 T and the sample was spun at 10–14 kHz, spectrometer frequencies were set to 100.61 MHz. Chemical shifts are reported relative to TMS, using the CH group of adamantano as a secondary reference (29.5 ppm). ^{119}Sn CP/MAS NMR spectra were recorded at 149.1 MHz, on the same spectrometer using spinning rates of 10 KHz, pulse delays of 30 s, contact times of 8 ms and TPPM high power proton decoupling. Chemical shifts are reported relative to tetramethyltin, using tin(IV) oxide as a secondary reference (−604.3 ppm).

All reagents were obtained from standard commercial sources and were used as received. Methanol, dried Scharlau (max. 0.005% H_2O).

2.2. Synthesis of benzil bis(thiosemicarbazone), LH_6

This was prepared following the procedure previously reported [26]. Selected spectroscopic data: FAB^+ (*m*/*z*): 357 ($[M+1]^+$, 100%), 714 ($[2M+1]^+$, 25%). ^1H NMR (DMSO-d_6, 300 MHz): δ/ppm 9.8 (2H, NH, s), 8.6 (2H, NH_2, s), 8.3 (2H, NH_2, s), 7.7 (4H, Ph, m), 7.4 (6H, Ph, m). ^{13}C CP/MAS NMR (300 MHz): δ/ppm 181.1 (CS); 142.9 (CN); 133.3, 132.4, 130.1 (Ph). IR (KBr, cm^{-1}): 3420, 3386, 3342, 3330, 3210, 3151(s) [ν(NH)], 1608 (w) [ν(CN)], 1581 (s) [$\delta(NH_2)$] and 848 (w) [ν(CS)].

2.3. Synthesis of the complexes

2.3.1. $[Pb(LH_4)]$ (**1**)

A solution of $Pb(NO_3)_2$ (750 mg, 2.30 mmol) in water (5 mL) was mixed with a suspension of LH_6 (540 mg, 1.50 mmol) and $LiOH \cdot H_2O$ (120 mg, 3.00 mmol) in methanol (50 mL). The mixture was stirred for 4 h under reflux. The orange-brown solid that formed was filtered off, washed with hot methanol and dried in vacuo. Yield 59%. M.p.: Decomposes at 199 °C. *Anal.* Calc. for $C_{16}H_{14}N_6S_2Pb$: C, 34.21; H, 2.49; N, 14.97; S, 11.40. Found: C, 34.45; H, 2.69; N, 14.64; S, 11.20%. MS (MALDI-TOF): (*m*/*z*) 563 ($[Pb(LH_4)+1]^+$), 769 ($[Pb_2(LH_4)]^+$), 1330 ($[Pb_3(LH_4)_2]^+$). ^{13}C CP/MAS NMR (300 MHz): δ/ppm 175.9 (CS); 154.7, 150.6 (CN); 138.2, 130.0, 129.5, 127.8, 122.7 (Ph). IR (KBr, cm^{-1}): 3443, 3313 (s) [ν(N–H)], 1565, 1468, 1437 (s) [thioamide II], 768 (w) [ν(CS)]. Crystals suitable for X-ray analysis were obtained from the mother liquor.

This complex was also obtained by reaction of LH_6 and diphenyllead dichloride in methanol in the presence of two moles of $LiOH \cdot H_2O$ [22].

2.3.2. $[Sn(LH_4)Cl_2]$ (**2**)

Diphenyltin dichloride (97 mg, 0.28 mmol) and LH_6 (100 mg, 0.28 mmol) were ground together and transferred to a crucible. The mixture was heated at 110 °C for 12 hours. The orange-brown solid that formed was washed with dichloromethane and dried in vacuo. Yield 83%, M.p.: 260 °C. *Anal.* Calc. for $C_{16}H_{14}N_6S_2Cl_2Sn$: C,

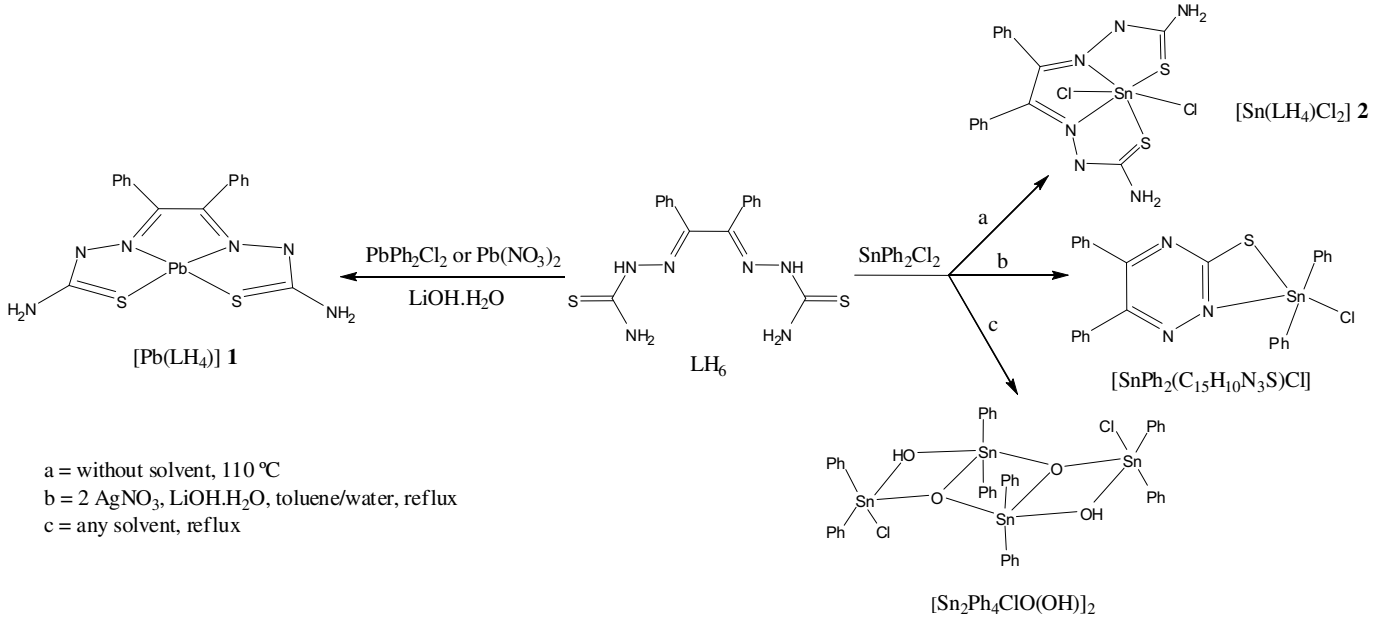

35.32; H, 2.57; N, 15.45; S, 11.73. Found: C, 35.48; H, 2.55; N, 15.64; S, 11.66%. MS (FAB$^+$): (m/z) 509 ([Sn(LH$_4$)Cl]$^+$, 30%). ^{1}H NMR (DMSO-d_6, 300 MHz): δ/ppm 7.9 (4H, NH, s), 7.2–7.0 (10H, Ph, m). ^{13}C CP/MAS NMR (300 MHz): δ/ppm 172.4 (CS); 147.3, 146.3 (CN); 135.2, 133.0, 131.4, 129.5, 127.7 (Ph). ^{119}Sn NMR ($CDCl_3$, 300 MHz,): δ/ppm −550.7. ^{119}Sn CP/MAS NMR (300 MHz): δ/ppm −534. IR (KBr, cm^{-1}) 3450, 3405, 3336, 3297 (s) [ν(N–H)], 1604 (w) [ν(CN)], 1579, 1423 (s) [thioamide II], 823 (w) [ν(CS)].

When the reaction of diphenyltin dichloride was carried out under the same conditions described for the lead(IV) derivative, the starting materials were recovered.

A solution of diphenyltin dichloride (480 mg, 1.40 mmol) in toluene (12 mL) was added over a suspension of LH$_6$ (500 mg, 1.40 mmol) in the same solvent (35 mL). The mixture was heated under reflux for two days. A yellow solid was filtered and identified as LH$_6$. From the orange filtrate, crystals suitable for X-ray study that turned out to be $[Sn_2Ph_4ClO(OH)]_2$ were isolated (Mp 160 °C). The reaction was also carried out under the same conditions but using ethanol, methanol, acetonitrile or DMF, both commercial reagents and dried. In all cases the ligand and the organostannoxane were isolated.

A solution of $AgNO_3$ (290 mg, 1.68 mmol) in distilled water (3 mL) was added to a suspension of $SnPh_2Cl_2$ (290 mg, 0.84 mmol) in the same solvent (3 mL). The mixture was stirred for 30 minutes and filtered off. The filtrate was added slowly, with stirring, to a suspension of LH$_6$ (300 mg, 0.84 mmol) in toluene (40 mL). The mixture was heated under reflux for 24 h. The yellow solid that was separated by filtration was unreacted ligand and $SnPh_2(NO_3)_2$ was isolated from the filtrate. When the same reaction was carried out in the presence of LiOH · H$_2$O, the complex [$SnPh_2(C_{15}H_{10}N_3S)Cl$], containing a triazine-3-thione ligand, was obtained. This complex was previously isolated from the triazine-3-thione ligand and $SnPh_2Cl_2$ in dichloromethane [27].

Table 1
Crystal data and structure refinement for [PbLH$_4$] **1**

Empirical formula	$C_{16}H_{14}N_6PbS_2$
Formula weight	561.64
Temperature (K)	100(2)
Wavelength (Å)	1.54178
Crystal system	orthorhombic
Space group	*Pbca*
Unit cell dimensions	
a (Å)	8.3140(3)
b (Å)	19.3792(11)
c (Å)	21.0592(6)
α (°)	90
β (°)	90
γ (°)	90
Volume (Å^3)	3393.0(2)
Z	8
D_{Calc} (Mg/m^3)	2.199
Absorption coefficient (mm$^{3-1}$)	21.745
F(000)	2128
Crystal size (mm^3)	0.20 × 0.10 × 0.05
Theta range for data collection (°)	4.20–71.29
Index ranges	$-10 \leqslant h \leqslant 10$, $-23 \leqslant k \leqslant 23$, $-25 \leqslant l \leqslant 13$
Reflections collected	18 486
Independent reflections (R_{int})	3190 (0.0838)
Completeness to theta = 71.29° (%)	96.9
Absorption correction	semi-empirical from equivalents
Refinement method	full-matrix least-squares on F^2
Data/restraints/parameters	3190/0/226
Goodness-of-fit on F^2	0.998
Final R indices [I > 2sigma(I)]	R_1 = 0.0358, wR_2 = 0.0799
R indices (all data)	R_1 = 0.0522, wR_2 = 0.0882
Largest difference in peak and hole (e Å^{-3})	1.776 and −1.724

2.4. X-ray crystallography

The crystal data and refinement results are listed in Table 1. Data were collected on a Bruker SMART 6K CCD area-detector three-circle diffractometer with a MAC Science Co., Ltd. Rotating Anode (Cu Kα radiation, λ = 1.54178 Å). The substantial redundancy in data allows empirical absorption corrections (SADABS) [28] to be applied using multiple measurements of symmetry-equivalent reflections. The unit cell parameters were obtained by full-matrix least-squares refinements of 8025 reflections for the complex. The raw intensity data frames were integrated with the SAINT program, which also applied corrections for Lorentz and polarization effects [29].

The software package SHELXTL version 6.10 was used for the space group determination, structure solution and refinement. The structures were solved by direct methods (SHELXS-97) [30], completed with difference Fourier syntheses and refined with full-matrix least-squares using SHELXL-97 minimizing $w(F_o^2 - F_c^2)$. Weighted R factors (R_w) and all goodness-of-fit S are based on F^2; conventional R factors (R) are based on F [31]. All non-hydrogen atoms were refined with anisotropic displacement parameters. Hydrogen atoms were located in a difference Fourier map, although they were positioned geometrically after each cycle of refinement. All scattering factors and anomalous dispersions factors are contained in the SHELXTL 6.10 program library.

3. Results and discussion

3.1. Synthesis

The reaction of LH$_6$ with lead(II) nitrate yielded complex **1**, with a 1:1 lead:ligand ratio and an absence of nitrate groups, in which the ligand has lost two hydrogen atoms. The MALDI-TOF spectrum in the solid state showed a peak at 563 amu, confirming this ratio. There were also weak peaks at 769 and 1330 amu, corresponding to [Pb$_2$(LH$_4$)]$^+$ and [Pb$_3$(LH$_4$)$_2$]$^+$, respectively, due to the strong interactions existing between the molecules. The same complex was obtained by the reaction with diphenyllead dichloride in methanol and in the presence of two moles of lithium hydroxide [22].

The diphenyltin reactions are complicated, giving different compounds depending on the working conditions (solvent, pH, etc.). With $SnPh_2Cl_2$ in the absence of solvent, the complex [Sn(LH$_4$)Cl$_2$] **2** was obtained. Its analytical data suggest the loss of the two phenyl groups and the presence of the two chlorido ligands, which is confirmed by the mass spectrum, with a peak at 509.1 corresponding to [Sn(LH$_4$)Cl]$^+$ (Fig. 1). This complex is obtained by a dephenylation process, as has been described in the literature for other ligands [15,16]. In the presence of solvent, as was indicated in the experimental part, the ligand is recovered and an organostannoxane containing four tin centers bonded by bridging oxygen atoms and hydroxo groups is isolated. Two Sn centers are bonded to two phenyl groups, one chlorido and one hydroxo group and the other two are bonded to two phenyls and the oxygen atoms (Fig. 2). This compound was previously obtained by the partial hydrolysis of diphenyltin dichloride and it was crystallographically characterized [32]. The crystal obtained in this work is triclinic with a space group $P\bar{1}$, which is different to the crystal previously published, which contains two molecules of acetone. In contrast, $SnPh_2(NO_3)_2$ without base does not react and in the presence of lithium hydroxide yields the complex [$SnPh_2(C_{15}H_{10}N_3S)Cl$], containing a triazine ligand formed by the elimination of one TSC arm of LH$_6$ with a subsequent cyclisation, and that has been reported previously [27].

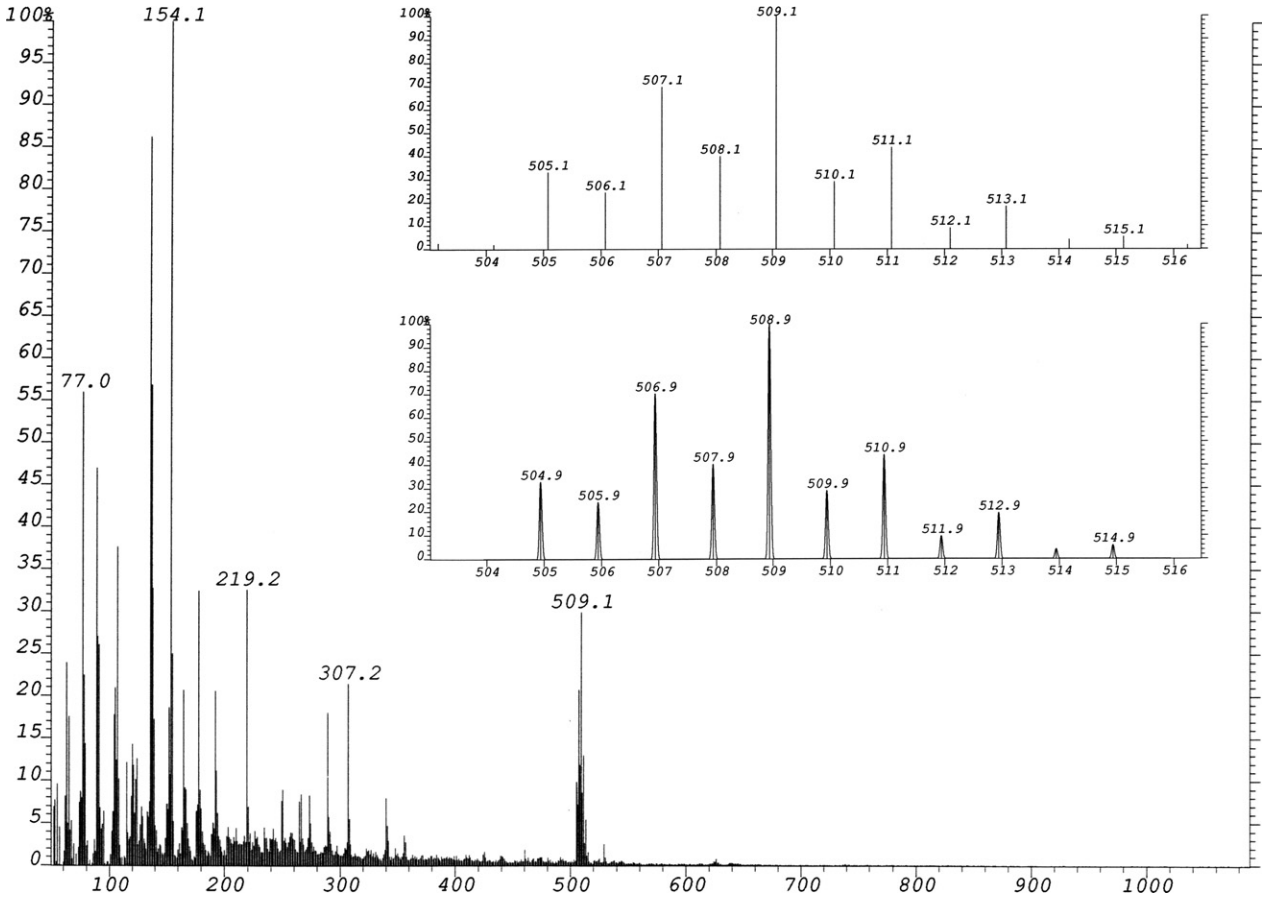

Fig. 1. Mass spectrum of $[Sn(LH_4)Cl_2]$ **2** (theoretical and the experimental isotope distribution in the inset).

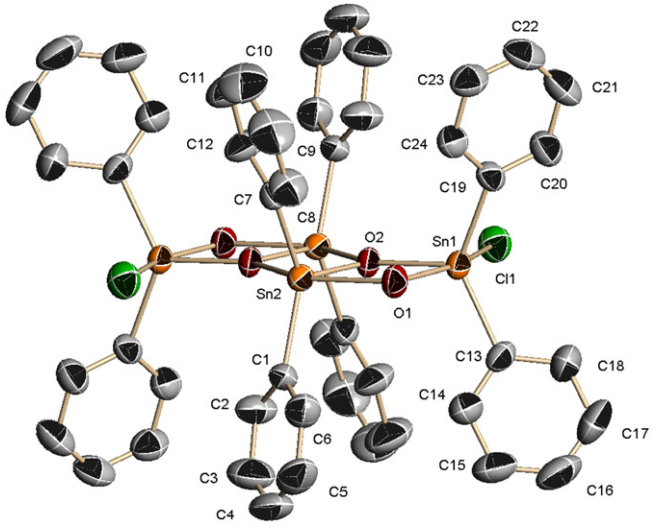

Fig. 2. Crystal structure of $[Sn_2Ph_2ClO(OH)]_2$. Crystal data: $a = 10.3438(2)$ Å, $b = 10.7925(2)$ Å, $c = 11.8431(2)$ Å, $\alpha = 77.6460(10)°$, $\beta = 66.3050(10)°$, $\gamma = 75.5580(19)°$, $R_1 = 0.0253$, $wR_2 = 0.0656$.

These reactions point out the different reactivity of both organoderivatives, since it is not possible to get from $SnPh_2Cl_2$ any complex with the organic groups bonded to the metal, unlike with $PbPh_2Cl_2$ where the complex $[PbPh_2(LH_5)Cl]$ can be synthesised in methanol with one mole of lithium hydroxide [22].

3.2. Spectroscopic studies

In the IR spectra of $[Pb(LH_4)]$ **1** and $[Sn(LH_4)Cl_2]$ **2**, the number of bands corresponding to ν(N–H) decreases, owing to deprotonation, and the remaining bands are displaced with respect to the ligand, probably due to the presence of different networks of hydrogen bonds with respect to the free ligand. The shifts observed in the bands assigned to ν(CN) and ν(CS) are consistent with both groups bonded to the lead or tin atom.

Due to its low solubility or decomposition, a ^{1}H NMR spectrum of complex **1** could not be registered. In the spectrum of $[Sn(LH_4)Cl_2]$ **2** the signal corresponding to the NH protons disappeared, due to the formation of the thiosemicarbazonate anion present in the complex, and the signals of the NH_2 groups were shifted to higher field and merged to form just one signal. The ^{13}C CP/MAS NMR spectra of both complexes were recorded. They show thioamide and imine carbon atoms upfield shifted with respect to the free ligand. The shielding of the thioamide by 4 and 8 ppm for $[Pb(LH_4)]$ and $[Sn(LH_4)Cl_2]$, respectively, is in agreement with the evolution of the thione group to the thiol tautomer when the sulfur atom coordinates to the metal.

It is well known that the ^{119}Sn chemical shift is very sensitive to changes in both the coordination number and the nature of the atoms bonded to tin, so it is a useful tool to determine the environment of this metal in the absence of X-ray data. The ^{119}Sn spectra in solution and in the solid state only showed one signal and the slight difference between the two values indicates that the structure is retained in solution. The chemical shifts are within the range expected for hexa-coordinate complexes [33–36] and agree

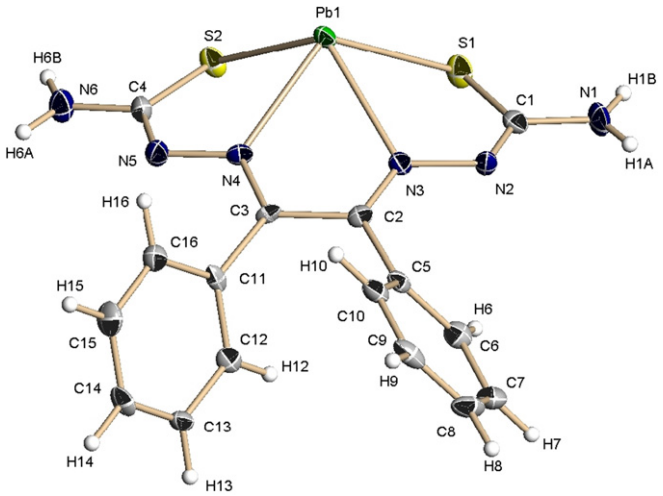

Fig. 3. Molecular structure of [Pb(LH$_4$)] **1**. Ellipsoids are drawn at 50% probability.

Table 2
Selected bond lengths (Å) an angles (°) for [Pb(LH$_4$)] **1**

Pb(1)–N(4)	2.400(5)
Pb(1)–N(3)	2.469(5)
Pb(1)–S(2)	2.7123(16)
Pb(1)–S(1)	2.7866(17)
S(1)–C(1)	1.736(7)
S(2)–C(4)	1.750(7)
C(1)–N(2)	1.332(10)
C(2)–N(3)	1.307(8)
C(2)–C(3)	1.481(8)
C(3)–N(4)	1.334(8)
N(4)–Pb(1)–N(3)	64.41(17)
N(4)–Pb(1)–S(2)	68.89(13)
N(3)–Pb(1)–S(2)	112.79(12)
N(4)–Pb(1)–S(1)	113.49(12)
N(3)–Pb(1)–S(1)	66.59(14)
S(2)–Pb(1)–S(1)	92.84(5)

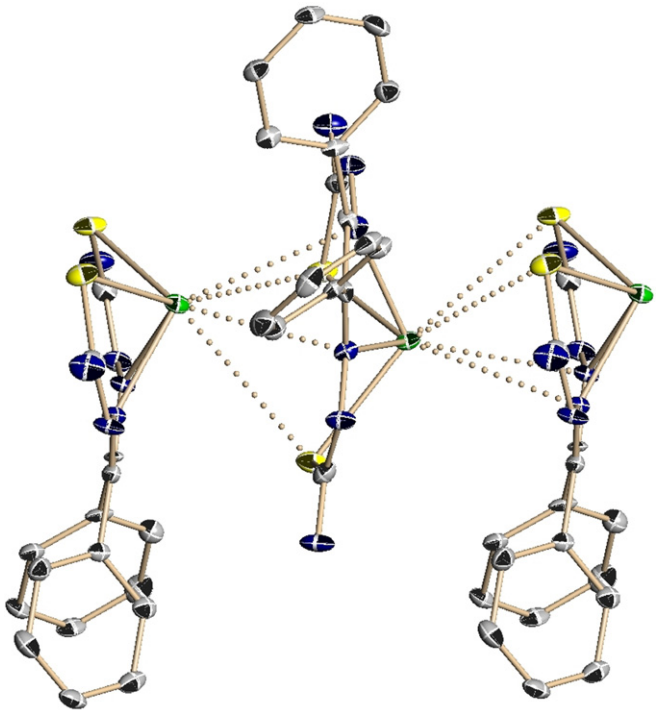

Fig. 4. Secondary interactions Pb-ligand in [Pb(LH$_4$)] along the *a*-axis (symmetry transformations used to generate equivalent atoms: $x + 1/2, y, -z + 1/2 + 1$).

with a $N_2S_2Cl_2$ environment for the tin atom, as the mass data and the ^{13}C NMR spectra have indicated.

3.3. X-ray structure of [Pb(LH$_4$)] *1*

The crystal is made up of discrete [Pb(LH$_4$)] units. This structure rules out the dimeric structure we have previously proposed in view of the mass spectrometry data [22]. The molecular structure is shown together with the numbering scheme in Fig. 3. Selected

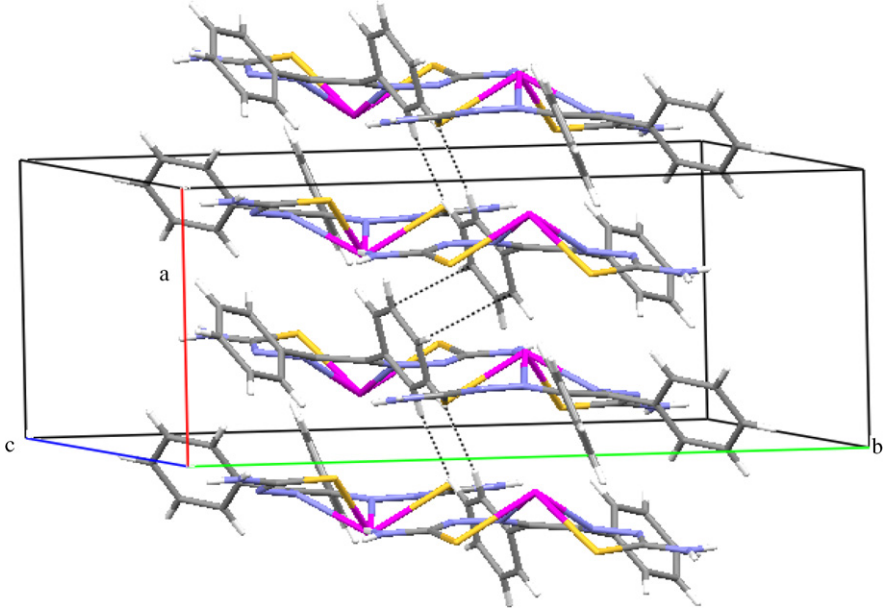

Fig. 5. The unit cell of [Pb(LH$_4$)] showing the stacking within the chains and aromatic interactions linking chains along the *b* and *c*-axes (the hydrogen bonds are omitted for clarity).

bond lengths and angles are summarized in Table 2. The coordination sphere of the lead atom is formed by two sulfurs and two imine nitrogen atoms from the benzil (bisthiosemicarbazonate) ligand. For lead, a coordination number of four is not normally found and only a few cases have been described earlier [21,37,38]. The geometry found in this complex, with all the metal–ligand interactions on the same side of the metal center together with the disposition of the phenyl groups, suggests that the lone pair on the lead center is stereochemically active. This results in a non-spherical charge distribution around the metal and it induces a clear gap in the disposition of the ligand around lead [39]. The four donor atoms of the ligand define the base of a square pyramid, and the Pb(II) cation is 1.3858 Å above this plane. This distortion of the lead atom is greater than that found in other complexes, showing the lone-pair effect that has been previously reported [40,41]. The Pb–N and Pb–S distances in one of the arms are sensitively shorter than in the other, although they are within the normal range. In the lattice (symmetry transformations used to generate equivalent atoms: $x + 1/2$, y, $-z + 1/2 + 1$), the molecules stack along the a-axis, with each Pb center increasing its coordination number to eight by means of two weak Pb···S# bonds [Pb(1)–S(1)# = 3.705 Å, Pb(1)–S(2)# = 3.774 Å] and two weak Pb···N# bonds [Pb(1)–N(3)# = 3.482 Å, Pb(1)–N(4)# 3.497 Å], with distances slightly shorter than the sum of the van der Waals radii (3.55 Å for Pb···N and 3.80 Å for Pb···S). This packing gives rise to polymeric chains with a large Pb···Pb distance of 4.260 Å and in parallel chains, the square-base pyramids are located up and down alternatively (Fig. 4). This induces additional intermolecular interactions based on π–π stacking between the phenyl rings (3.613 Å) linking chains along the b-axis, and CH–CH interactions (3.025 Å) running along the a-axis (Fig. 5). In addition, there is a N(6)–H(6B)–N(2)#1 ($-x + 1/y + 1/z$) hydrogen bond running along the b-axis (d(D–H) 0.88 Å, d(H···A) 2.48 Å, d(D···A) 3.190(8) Å, ∠(DHA) 138.6°). The pseudomacrocyclic coordination mode of the ligand affords three five-member chelate rings, with the C(2)–C(3) bond around 0.35 Å down the N_2S_2 plane. The variation of the distances in the organic backbone with respect to the free benzil bis(thiosemicarbazone) ligand are in the range observed for other complexes in which the ligand is N_2S_2 and is doubly deprotonated [22,42].

Acknowledgements

We thank DGICYT for financial support (Project CT2005-07788/BQU) and the Universidad Autónoma de Madrid for a Grant to David G. Calatayud.

Appendix A. Supplementary data

CCDC 682719 contains the supplementary crystallographic data for [Pb(LH_4)]. These data can be obtained free of charge via http://www.ccdc.cam.ac.uk/conts/retrieving.html, or from the Cambridge Crystallographic Data Centre, 12 Union Road, Cambridge CB2 1EZ, UK; fax: (+44) 1223-336-033; or e-mail: deposit@ccdc.cam.ac.uk. Supplementary data associated with this article can be found, in the online version, at doi:10.1016/j.poly.2008.04.055.

References

[1] D.X. West, A.E. Liberta, S.B. Padhye, R.C. Chikate, P.B. Sonawane, A.S. Kumbhar, R.G. Yeranda, Coord. Chem. Rev. 123 (1993) 49. and references therein.
[2] A.E. Liberta, D.X. West, Biometals 5 (1992) 121.
[3] M. Vázquez, L. Fabbrizzi, A. Taglietti, R.M. Pedrido, A.M. González-Noya, M.R. Bermejo, Angew. Chem., Int. Ed. 43 (2004) 1962.
[4] H. Beraldo, D. Gambino, Mini. Rev. Med. Chem. 4 (2004) 31.
[5] A.G. Quiroga, C. Navarro-Ranninger, Coord. Chem. Rev. 248 (2004) 116.
[6] D.R. Richardson, P.C. Sharpe, D.B. Lovejoy, D. Senaratne, D.S. Kalinowski, M. Islam, P.V. Berhardt, J. Med. Chem. 49 (2006) 6510.
[7] M. Gielen, Coord. Chem. Rev. 151 (1996) 41.
[8] M. Gielen, Appl. Organomet. Chem. 16 (2002) 481.
[9] J. Ruipérez, M.A. Mendiola, M.T. Sevilla, J. Rodríguez-Procopio, L. Hernández, Electroanalysis 14 (2002) 532.
[10] M. Colilla, M.A. Mendiola, J.R. Procopio, M.T. Sevilla, Electroanalysis 17 (2005) 933.
[11] P.G. Harrison, in: G. Wilkinson, F.G.A. Stone, E.W. Abel (Eds.), Comprehensive Organometallic Chemistry, vol. 2, Pergamon Press, Oxford, 1982.
[12] K.A. Jensen, in: P. Grandjean, E.C. Grandjean (Eds.), Biological Effects of Organolead Compounds, CRC Press, Boca Raton, FL, 2000.
[13] J.S. Casas, M.V. Castaño, M.C. Cifuentes, J.C. García-Monteagudo, A. Sánchez, J. Sordo, A. Touceda, J. Organomet. Chem. 692 (2007) 2234.
[14] H.J. Haupt, F. Huber, J. Gmehling, Z. Anorg. Allg. Chem. 390 (1972) 31.
[15] A. Pérez-Rebolledo, G.M. de Lima, N.L. Speziali, O.E. Piro, E.E. Castellano, J.D. Ardisson, H. Baraldo, J. Organomet. Chem. 691 (2006) 3930.
[16] H.D. Yin, S.W. Chen, Inorg. Chim. Acta 359 (2006) 3330.
[17] J.S. Magyar, T.C. Weng, C.M. Stern, D.F. Dye, B.W. Rous, J.C. Payne, B.M. Bridgewater, A. Mijovilovich, G. Parkin, J.M. Zaleski, J.E. Penner-Hahn, H.A. Godwin, J. Am. Chem. Soc. 127 (2005) 9495.
[18] E.S. Claudio, H.A. Godwin, J.S. Magyar, Prog. Inorg. Chem. 51 (2003) 1.
[19] M. Carcelli, G. Corazzari, S. Ianelli, G. Pelizzi, C. Solinas, Inorg. Chim. Acta 353 (2003) 310.
[20] J.S. Casas, E.E. Castellano, J. Ellena, M.S. García-Tastende, A. Sánchez, J. Sordo, M.J. Vidarte, Inorg. Chem. 42 (2003) 2584.
[21] J.S. Casas, E.E. Castellano, J. Ellena, M.S. García-Tastende, A. Sánchez, J. Sordo, A. Touceda, S. Vázquez Rodríguez, Polyhedron 26 (2007) 4228.
[22] D.G. Calatayud, E. López-Tores, M.A. Mendiola, Inorg. Chem. 46 (2007) 10434. and references therein.
[23] J.E. Huheey, E.A. Keiter, R.L. Keiter, in: Inorganic Chemistry, 4th ed., Harper Collins College Publishers, New York, 1993.
[24] R.D. Hancock, in: A.F. Williams, C. Floriani, A.E. Merbach (Eds.), Perspectives in Coordination Chemistry, VCHA:VCH, Basel, 1992.
[25] L. Shimoni-Livny, J.P. Gluske, C.W. Bock, Inorg. Chem. 37 (1998) 1853.
[26] E. López-Torres, M.A. Mendiola, C.J. Pastor, B. Souto Pérez, Inorg. Chem. 43 (2004) 5222.
[27] E. López-Torres, M.A. Mendiola, C.J. Pastor, J.R. Procopio, Eur. J. Inorg. Chem. (2003) 2711.
[28] G.M. Sheldrick, SADABS Version 2.03, Program for Empirical Absorption Corrections, Universiät Göttingen, Göttingen, Germany, 1997–2001.
[29] G.M. Sheldrick, SAINT+NT (Version 6.04) SAX Area-Detector Integration Program, Bruker AXS, Madison, WI, 1997–2001.
[30] G.M. Sheldrick, SHELXTL (Version 6.10) Structure Determination Package, Bruker AXS, Madison, WI, 2000.
[31] G.M. Sheldrick, Acta Crystallogr., Sect. A 46 (1990) 467.
[32] J.F. Vollano, R.Q. Day, R.R. Holmes, Organometallics 3 (1984) 754.
[33] J. Holecek, N. Nädvorník, K. Handlír, A. Lycka, J. Organomet. Chem. 315 (1986) 299.
[34] J.D. Kennedy, W. McFarlane, in: J. Mason (Ed.), Multinuclear NMR, Springer, New York, 1987.
[35] S.J. Langford, M.J. Latter, J. Beckmann, Inorg. Chem. Commun. 8 (2005) 920.
[36] E. López-Torres, A.R. Cowley, J.R. Dilworth, Inorg. Chem. Commun. 10 (2007) 724.
[37] J.S. Casas, M.S. García-Tasende, Coord. Chem. Rev. 209 (2000) 197.
[38] R. Pedrido, M.J. Romero, M.R. Bermejo, A.M. González-Noya, I. García-Lema, G. Zaragoza, Chem. Eur. J. 14 (2008) 500.
[39] N.V. Sidwick, H.M. Powell, Proc. R. Soc. London, Ser. A 176 (1940) 153.
[40] R. Pedrido, M.R. Bermejo, M.J. Romero, M. Vázquez, A.M. González-Noya, M. Maneiro, M.J. Rodrígez, M.I. Fernández, J. Chem. Soc., Dalton Trans. (2005) 572.
[41] R. Pedrido, M.J. Romero, M.R. Bermejo, A.M. González-Noya, M.J. Rodríguez, G. Zaragoza, J. Chem. Soc., Dalton Trans. (2006) 5304.
[42] D.G. Calatayud, E. López-Torres, M.A. Mendiola, C.J. Pastor, J.R. Procopio, Eur. J. Inorg. Chem. (2005) 4401.

Polyhedron 27 (2008) 2513–2518

Contents lists available at ScienceDirect

Polyhedron

journal homepage: www.elsevier.com/locate/poly

Synthesis, spectroscopic characterization, X-ray structure and DFT calculations of five-coordinated chlorocopper(II) complex with bis(3,5-dimethylpyrazol-1-yl)methane

B. Machura [a,*], A. Świtlicka [a], R. Kruszynski [b], J. Kusz [c], R. Penczek [d]

[a] Department of Crystallography, Institute of Chemistry, University of Silesia, 9th Szkolna Street, 40-006 Katowice, Poland
[b] Department of X-ray Crystallography and Crystal Chemistry, Institute of General and Ecological Chemistry, Lodz University of Technology, 116 Żeromski Street, 90-924 Łódź, Poland
[c] Institute of Physics, University of Silesia, 4th Uniwersytecka Street, 40-006 Katowice, Poland
[d] Department of Inorganic and Coordination Chemistry, Institute of Chemistry, University of Silesia, 9th Szkolna Street, 40-006 Katowice, Poland

ARTICLE INFO

Article history:
Received 28 March 2008
Accepted 28 April 2008
Available online 13 June 2008

Keywords:
Copper(II)
Bis(3,5-dimethylpyrazol-1-yl)methane
X-ray structure
DFT calculations

ABSTRACT

The reaction of copper dichloride dihydrate and bis(3,5-dimethylpyrazol-1-yl)methane affords $[Cu\{H_2C(3,5\text{-}Me_2pz)_2\}_2Cl]Cl \cdot 3H_2O$. The compound has been studied by IR, UV–Vis spectroscopy and X-ray crystallography. The electronic structure of the $[Cu\{H_2C(3,5\text{-}Me_2pz)_2\}_2Cl]^+$ cation has been calculated with the density functional theory (DFT) method. The spin-allowed doublet–doublet electronic transitions of $[Cu\{H_2C(3,5\text{-}Me_2pz)_2\}_2Cl]^+$ have been calculated with the time-dependent DFT method, and the UV–Vis spectrum of the title compound has been discussed on this basis.

© 2008 Elsevier Ltd. All rights reserved.

1. Introduction

Bis(pyrazol-1-yl)alkanes and their derivatives constitute a family of stable and flexible bidentate ligands, isoelectronic and isosteric with the well-known bis(pyrazolyl)borates. The coordination properties of bis(pyrazol-1-yl)alkanes may be varied in a rather wide range by introducing substituents into the pyrazole rings. Hence, the donor ability of the ligands is determined by the presence of electron-withdrawing or electron-donating functional groups, and steric factors altered by the introduction of bulky alkyl groups into the rings and the alkane bridge between them [1]. These molecules form a variety of coordination compounds with main group and transition metals [1–3].

Bis(pyrazol-1-yl)methane-copper(II)–complexes have attracted the attention of several research groups during the past three decades. Some bis(3,5-dimethylpyrazol-1-yl)methane-copper(II) complexes of different composition and spectral properties were prepared and characterized so far. In 1979 Jan Reedijk and co-workers reported the preparation of bis(3,5-dimethylpyrazol-1-yl)methane complexes with copper(II) halides and nitrate. These authors isolated compounds of formulas $Cu\{H_2C(3,5\text{-}Me_2pz)_2\}X_2$ ($X = Cl^-$ or Br^-), $Cu\{H_2C(3,5\text{-}Me_2pz)_2\}2X_2$ ($X = Cl^-$, Br^- or NO_3^- and $Cu_3\{H_2C(3,5\text{-}Me_2pz)_2\}_4Cl_6 \cdot EtOH$ trimer [4]. In 1985 the complexes of bis(3,5-dimethylpyrazol-1-yl)methane with copper(II) chloride and nitrate of 1:1 composition were also prepared by Mesubi and Anumba [5]. In 2006 the $Cu\{H_2C(3,5\text{-}Me_2pz)_2\}X_2$ ($X = Cl^-$ or NO_3^- and $Cu\{H_2C(3,5\text{-}Me_2pz)_2\}_2Cl_2 \cdot 2H_2O$ compounds were isolated once again by Potapov and co-workers [6]. For copper(II) nitrate, these authors found formation of only complexes of 1:1 composition independent of the metal to ligand ratio used (1:1 or 1:2). In all the cases, structural conclusions concerning bis(3,5-dimethylpyrazol-1-yl)methane-copper(II) complexes were drawn from spectroscopic and magnetic measurements. X-ray studies for the $Cu\{H_2C(3,5\text{-}Me_2pz)_2\}Cl_2$ were performed in 2007 and revealed distorted tetrahedral geometry about the cooper center [7]. From the structural point of view, the $Cu\{H_2C(3,5\text{-}Me_2pz)_2\}_2$ unit of $Cu\{H_2C(3,5\text{-}Me_2pz)_2\}_2X_2$ compounds may occur either in octahedral geometry leaving two *cis*-positions for X ligands, or in a tetrahedral geometry without space in inner sphere for X ligands, and also in a five-coordinate geometry with one X ligand in inner sphere. The last one geometry has been confirmed very recently by X-ray crystallography in $[Cu\{H_2C(3,5\text{-}Me_2pz)_2\}_2(NO_3)](NO_3)$, $[Cu\{H_2C(3,5\text{-}Me_2pz)_2\}_2(MeOH)](ClO_4)_2 \cdot MeOH$, $[Cu\{H_2C(3,5\text{-}Me_2pz)_2\}_2Cl]_2(CuCl_4) \cdot 2Me_2CO$ and $[Cu\{H_2C(3,5\text{-}Me_2pz)_2\}_2Cl]_2(Cu_2Cl_6) \cdot 3CH_2Cl_2 \cdot H_2O$. The $[Cu\{H_2C(3,5\text{-}Me_2pz)_2\}_2Cl]_2(CuCl_4) \cdot 2Me_2CO$ and $[Cu\{H_2C(3,5\text{-}Me_2pz)_2\}_2Cl]_2(Cu_2Cl_6) \cdot 3CH_2Cl_2 \cdot H_2O$ compounds were prepared by the reaction of bis(3,5-dim-

* Corresponding author.
E-mail addresses: basia@ich.us.edu.pl (B. Machura), rafal.kruszynski@p.lodz.pl (R. Kruszynski).

0277-5387/$ - see front matter © 2008 Elsevier Ltd. All rights reserved.
doi:10.1016/j.poly.2008.04.050

ethylpyrazol-1-yl)methane with copper(II) dichloride dihydrate in molar ratio 4:3 and 1:1, respectively [8].

Here, we present the synthesis, spectroscopic data, crystal, molecular and electronic structure of the $[Cu\{H_2C(3,5\text{-}Me_2pz)_2\}_2Cl]Cl \cdot 3H_2O$ complex. The electronic structure of the $[Cu\{H_2C(3,5\text{-}Me_2pz)_2\}_2Cl]^+$ cation has been determined with the density functional theory (DFT) method, and time-dependent DFT (TD-DFT) calculations have been employed for discussion of the spectroscopic properties in more detail. Currently density functional theory (DFT) is commonly used to examine the electronic structure of transition metal complexes. It meets with the requirements of being accurate, easy to use and fast enough to allow the study of relatively large molecules of transition metal complexes [9].

2. Experimental

2.1. General procedure

Bis(3,5-dimethylpyrazol-1-yl)methane was synthesised according to the literature method [10,11]. The other reagents used to the synthesis were commercially available and were used without further purification. IR spectrum was recorded on a Nicolet Magna 560 spectrophotometer in the spectral range 4000–400 cm^{-1} with the samples in the form of KBr pellets. Electronic spectrum was measured on a spectrophotometer Lab Alliance UV–Vis 8500 in the range 1000–180 nm in dichloromethane solution. Elemental analyses (C H N) were performed on a Perkin–Elmer CHN-2400 analyzer.

2.2. Preparation of $[Cu\{H_2C(3,5\text{-}Me_2pz)_2\}_2Cl]Cl \cdot 3H_2O$

A solution of bis(3,5-dimethylpyrazol-1-yl)methane (1.2 mmol, 025 g) in methanol (15 ml) was added to 0.1 g (0.59 mmol) of $CuCl_2 \cdot 2H_2O$ in 10 ml of water and stirred for 2 h. The resulting solution was kept for evaporation at room temperature, and after a few days green prismatic crystals of $[Cu\{H_2C(3,5\text{-}Me_2pz)_2\}_2Cl]Cl \cdot 3H_2O$ were obtained, filtered off and dried. Yield 75%. The crystals suitable for X-ray investigation were obtained by recrystallization from methanol. IR (KBr; ν/cm^{-1}): 3504 and 3311 (ν_{O-H}, H_2O); 1651(m) and 1630 (m) (δ_{O-H}, H_2O), 1558 and 1468 (ν_{ring}); 1284(β CH) and 1043 (pyrazole ring breathing).

Anal. Calc. for $[Cu\{H_2C(3,5\text{-}Me_2pz)_2\}_2Cl]Cl \cdot 3H_2O$: C, 44.26; H, 6.42; N, 18.77. Found: C, 44.52; H, 6.30; N, 18.29%.

2.3. X-ray diffraction studies

A green crystal of $[Cu\{H_2C(3,5\text{-}Me_2pz)_2\}_2Cl]Cl \cdot 3H_2O$ was mounted on a KM-4-CCD automatic diffractometer equipped with a CCD detector, and used for data collection. X-ray intensity data were collected with graphite monochromated Mo Kα radiation (λ = 0.71073 Å) at 295(1) K. Details concerning crystal data and refinement are given in Table 1. Lorentz, polarization and numerical absorption correction [12] were applied. The structure was solved by the Patterson method and subsequently completed by the difference Fourier recycling. All the non-hydrogen atoms were refined anisotropically using full-matrix, least-squares technique. All the hydrogen atoms were found from difference Fourier synthesis after four cycles of anisotropic refinement, and refined as "riding" on the adjacent carbon atom with individual isotropic temperature factor equal 1.2 times the value of equivalent temperature factor of the aromatic parent atom and equal 1.5 times the value of equivalent temperature factor of the methyl parent carbon atom. SHELXS 97 [13], SHELXL 97 [14] and SHELXTL [15] programs were used for all the calculations. Atomic scattering factors were those incorporated in the computer programs.

Table 1
Crystal data and structure refinement

Empirical formula	$C_{22}H_{38}N_8O_3Cl_2Cu$
Formula weight	597.04
Temperature (K)	200(3)
Wavelength (Å)	0.71073
Crystal system	monoclinic
Space group	$P2_1/c$
Unit cell dimensions	
a (Å)	8.4550(6)
b (Å)	18.679(12)
c (Å)	18.145(12)
β (°)	94.51(7)
V (Å^3)	2856.9(10)
Z	4
D_{calc} (Mg/m^3)	1.388
Absorption coefficient (mm^{-1})	0.989
$F(000)$	1252
Crystal size (mm)	0.05 × 0.07 × 0.42
θ Range for data collection (°)	2.81–25.00
Index ranges	$-10 \leqslant h \leqslant 5$ $-22 \leqslant k \leqslant 21$ $-21 \leqslant l \leqslant 21$
Reflections collected/independent (R_{int})	17320/5002 (0.0614)
Completeness to 2θ = 50.2°	99.6%
Maximum and minimum transmission	0.950 and 0.915
Data/restraints/parameters	5002/0/333
Goodness-of-fit on F^2	1.128
Final R indices [$I > 2\sigma(I)$]	R_1 = 0.0531 wR_2 = 0.1678
R indices (all data)	R_1 = 0.0815 wR_2 = 0.1736
Largest difference peak and hole (e Å^{-3})	0.694 and −0.725

2.4. Computational details

The gas phase geometry of the $[Cu\{H_2C(3,5\text{-}Me_2pz)_2\}_2Cl]^+$ cation was optimized without any symmetry restrictions in the doublet state with the DFT method using the hybrid B3LYP functional of GAUSSIAN 03 [16–18]. The calculations were performed by using the LANL2DZ effective core potential (ECP) set of Hay and Wadt [19] for Cu atom and the standard 6-31+G** basis for chloride and nitrogen, 6 − 31G* for carbon and 6 − 31G for hydrogen atoms.

The electronic spectrum of the $[Cu\{H_2C(3,5\text{-}Me_2pz)_2\}_2Cl]^+$ cation was calculated with the TDDFT method starting from the ground-state geometry optimized in the gas phase. The solvent (methanol) effect was simulated using the polarizable continuum model with the integral equation formalism (IEF-PCM) [20].

3. Results and discussion

The $[Cu\{H_2C(3,5\text{-}Me_2pz)_2\}_2Cl]Cl \cdot 3H_2O$ complex was prepared in good yield by the reaction of bis(3,5-dimethylpyrazol-1-yl)methane with copper(II) dichloride dihydrate in molar ratio 2:1. The elemental analysis of the complex is in good agreement with its formulation. Bands due to bis(3,5-dimethylpyrazol-1-yl)methane ligand vibrations are observed in the range 1580–1000 cm^{-1} in the IR spectrum of $[Cu\{H2C(3,5\text{-}Me_2pz)_2\}_2Cl]Cl \cdot 3H_2O$. The characteristic bands corresponding to the pyrazole ring stretching vibrations appear at 1558 and 1468 cm^{-1}. The peaks at 3504, 3311, 1651 and 1630 cm^{-1} may indicate the existence of molecular lattice water [21].

3.1. Crystal structure

The crystallographic data of $[Cu\{H_2C(3,5\text{-}Me_2pz)_2\}_2Cl]Cl \cdot 3H_2O$ are summarized in Table 1. The asymmetric unit of the title complex consists of the $[Cu\{H_2C(3,5\text{-}Me_2pz)_2\}_2Cl]^+$ cation, chloride ion and three water molecules. A summary of inter- and intramo-

lecular hydrogen bonding contacts detected in the $[Cu\{H_2C(3,5\text{-}Me_2pz)_2\}_2Cl]Cl \cdot 3H_2O$ structure is given in Table 2 [22,23]. The molecules of compound are connected *via* medium strength O–H···O and O–H···Cl intermolecular hydrogen bonds to semiinfinite net extended into two dimensions along crystallography *a0b* plane. The intermolecular C–H···O and C–H···Cl weak hydrogen bonds provide additional stabilization to the hydrogen bonded net. Additionally in the complex molecule can be found weak C–H···N intramolecular hydrogen bond.

The molecular structure of the $[Cu\{H_2C(3,5\text{-}Me_2pz)_2\}_2Cl]^+$ cation is presented in Fig. 1, and the selected bond distances and angles of $[Cu\{H_2C(3,5\text{-}Me_2pz)_2\}_2Cl]^+$ are collected in Table 3. The Cu(II) centre is five-coordinated by four N donors from two $H_2C(3,5\text{-}Me_2pz)_2$ ligands and chloride anion. Upon coordination of two molecules of bis(3,5-dimethylpyrazol-1-yl)methane to the copper, two six-membered cycles (made by the four nitrogen atoms, the copper atom and the carbon atom) are formed, and the formed rings show a *boat* conformation with the copper and the carbon atoms off the plane defined by the four nitrogen atoms (deviations of Cu from N_4 least-squares planes are 0.653(7) and 0.604(8) Å, respectively, for planes N(1)/N(2)/N(3)/N(4) and N(5)/N(6)/N(7)/N(8)). The bite angles of 89.07° and 89.78(17)° show no variation from the values reported for $[Cu_2\{H_2C(3,5\text{-}Me_2pz)\}_4(ta)](ClO_4)_2 \cdot 2H_2O$ [24]. The dihedral angle between the above mentioned N(1)–N(4) and N(5)–N(8) least-squares planes is equal to 63.95(14)°.

The angular structural index parameter τ [25] expressed here as the difference between the bond angles N(7)–Cu(1)–N(1) and N(3)–Cu(1)–Cl(1) divided by 60 has a value of 0.47. Compared with the ideal values of 1 for an equilateral bipyramid and 0 for a square pyramid, the τ descriptor of the examined structure suggests a stereochemistry intermediate between equilateral-bipyramidal and square pyramidal, but on the basis of coordination geometry considerations in terms of scalene bipyramid it can be stated that coordination polyhedron is slightly distorted trigonal bipyramid. The same can be deduced from the bond lengths and angles. Despite the almost linear N(1)–Cu(1)–N(7) angle of 176.17(18)°, the equatorial angles Cl(1)–Cu(1)–N(5), Cl(1)–Cu(1)–N(3) and N(3)–Cu(1)–N(5) are grossly distorted from a regular 120° of an equilateral bipyramid. On the other hand the sum of the N(3)–Cu(1)–Cl(1), N(5)–Cu(1)–Cl(1), N(3)–Cu(1)–N(5) angles is equal to 360.0°, a value typical for scalene bipyramid. Furthermore, the Cu(1)–Cl(1) distance of 2.3099(16) Å is much shorter than found for an apically coordinated Cl atom in a five-coordinate tetragonal-pyramidal copper complexes such as $[Cu(cip)(bipy)Cl_{0.7}(NO_3)_{0.3}](NO_3) \cdot 2H_2O$ (cip = ciprofloxacine) and $[Cu(en)(bipy)Cl](OH) \cdot 3H_2O$ with the Cu–Cl bond distances are 2.549(2) Å and 2.733(2) Å [26,27], but is very similar to that found a five-coordinate trigonal-bipyramidal copper complexes such as $[Cu(phen)_2Cl](OH) \cdot 2MeOH \cdot 6H_2O$ and $[Cu(TBZH)2Cl]Cl \cdot 6H_2O \cdot 6EtOH$ (TBZH = thiabendazole) [28]. Summarizing, in terms of regular polyhedra the coordination geometry is intermediate between trigonal bipyramid and square pyramid, and in terms of irregular polyhedra the coordination geometry is almost ideal scalene bipyramid (Scheme 1).

Table 2
Inter- and intramolecular hydrogen bonding contacts

D–H	A	H···A (Å)	D···A (Å)	D–H···A (°)
O(1)–H(1O)	O(3)#1	2.05	2.888(7)	160.5
O(1)–H(1P)	Cl(1)#2	2.48	3.370(5)	179.8
O(2)–H(2O)	O(1)	1.97	2.845(7)	172.8
O(2)–H(2P)	Cl(2)	2.32	3.185(5)	166.0
O(3)–H(3O)	Cl(2)	2.17	3.137(5)	174.2
O(3)–H(3P)	Cl(1)#3	2.45	3.335(5)	173.5
C(2)–H(2)	O(2)#4	2.52	3.380(7)	153.2
C(5)–H(5C)	N(5)	2.62	3.331(10)	130.9
C(6)–H(6B)	O(2)#1	2.51	3.446(7)	163.2
C(17)–H(17B)	Cl(2)#5	2.63	3.551(6)	158.6
C(19)–H(19)	Cl(2)	2.78	3.654(6)	157.5

Symmetry transformations used to generate equivalent atoms:
#1: $-x+1$, $y-1/2$, $-z+1/2$; #2: $x+1$, y, z; #3: $-x+1$, $y+1/2$, $-z+1/2$; #4: $-x$, $y-1/2$, $-z+1/2$; #5: $x-1$, y, z.

3.2. Geometry optimisation

The geometry of the $[Cu\{H_2C(3,5\text{-}Me_2pz)_2\}_2Cl]^+$ cation was optimized in doublet state using the DFT method with the B3LYP functional. The optimized geometric parameters are gathered in Table 3. In general, the predicted bond lengths are somewhat longer in comparison with the values based upon the X-ray crystal structure data, but the general trends observed in the experimental data are well reproduced in the calculations.

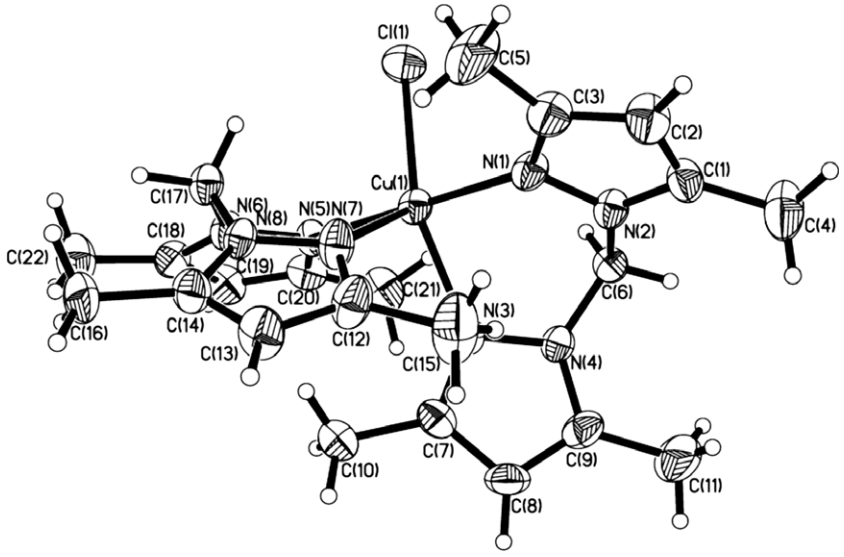

Fig. 1. The molecular structure of the $[Cu\{H_2C(3,5\text{-}Me_2pz)_2\}_2Cl]^+$ cation. Displacement ellipsoids are drawn at 50% probability.

Table 3
The experimental and optimized bond lengths (Å) and angles (°)

	Experimental	Optimized		Experimental	Optimized
Bond lengths			*Bond angles*		
Cu(1)–N(1)	1.996(5)	2.054	N(1)–Cu(1)–N(3)	89.07(18)	87.11
Cu(1)–N(3)	2.105(5)	2.194	N(1)–Cu(1)–N(5)	94.05(18)	97.47
Cu(1)–N(5)	2.193(5)	2.289	N(7)–Cu(1)–N(1)	176.17(18)	174.66
Cu(1)–N(7)	1.991(4)	2.052	N(7)–Cu(1)–Cl(1)	88.87(13)	86.90
Cu(1)–Cl(1)	2.3099(16)	2.345	N(7)–Cu(1)–N(3)	90.51(18)	95.04
			N(7)–Cu(1)–N(5)	89.78(17)	87.00
			N(1)–Cu(1)–Cl(1)	89.45(14)	88.39
			N(3)–Cu(1)–Cl(1)	147.69(13)	141.91
			N(5)–Cu(1)–Cl(1)	118.23(14)	118.41
			N(3)–Cu(1)–N(5)	94.06(18)	99.67

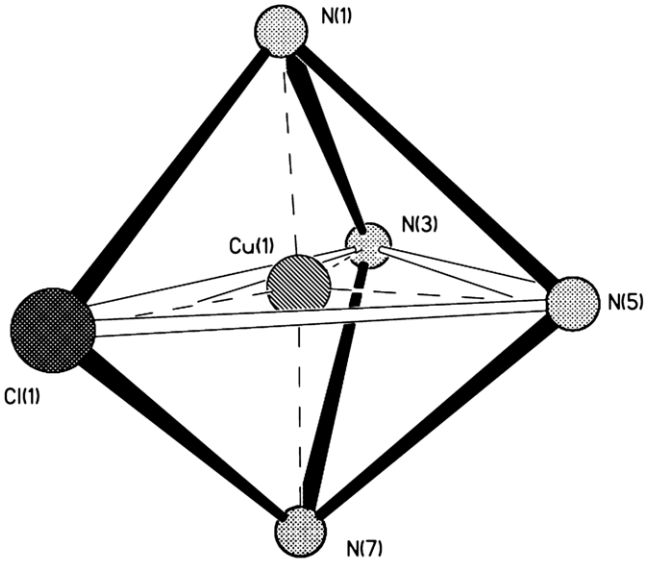

Scheme 1.

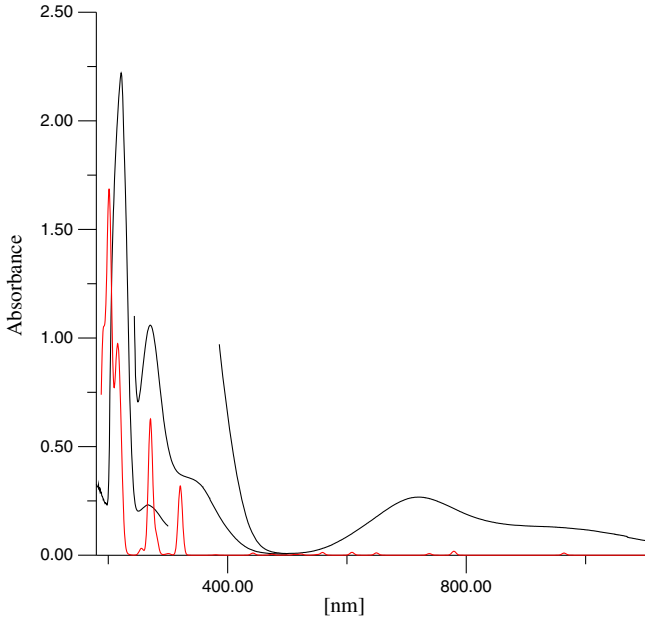

Fig. 2. The experimental (black) and calculated (red) electronic absorption spectra. (For interpretation of the references to colour in this figure legend, the reader is referred to the web version of this article.)

3.3. Electronic spectrum

The nature of the transitions observed in the UV–Vis spectrum of the title complex has been studied by the time-dependent density functional (TDDFT) method. The calculated electronic spectrum of $[Cu\{H_2C(3,5\text{-}Me_2pz)_2\}_2Cl]^+$ in comparison with the experimental one is presented in Fig. 2. Each calculated transition is represented by a gaussian function $y = ce^{-bx^2}$ with the height (c) equal to the oscillator strength and b equal to 0.04 nm^{-2}.

Table 4
The spin-allowed triplet–triplet electronic transitions calculated with the TDDFT method and the assignments of the calculated transitions to the experimental absorption bands

The most important orbital excitations	Character	λ (nm)	E (eV)	f	Experimental Λ (nm) (E (eV)) ε
H-8(β) → L(β)	π(Cl)/d → d	964.0	1.27	0.0003	1011.0 (1.23) 60
H-10(β) → L(β)	π(Cl)/d → d	779.3	1.59	0.0060	738.5 (1.68) 170
H-15(β) → L(β)	d → d				
H(β) → L(β)	π(L)/π(Cl) → d	649.5	1.91	0.0035	
H-3(β) → L(β)	π(L)/π(Cl) → d	608.5	2.04	0.0043	
H-17(β) → L(β)	d → d				
H-2(β) → L(β)	π(L)/π(Cl) → d	559.0	2.22	0.0041	
H-10(β) → L(β)	π(Cl)/d → d	320.6	3.87	0.1064	350.0 (3.54) 1120
H-12(β) → L(β)	n(L) → d	270.7	4.58	0.1967	266.0 (4.66) 3530
H-2(α) → L(α)	π(L)/π(Cl)/d → π*(L)	219.9	5.64	0.0403	221.5 (5.60) 37000
H-6(β) → L + 1(β)	π(L)/π(Cl) → π*(L)	213.1	5.82	0.0495	
H-1(β) → L + 3(β)	π(L)/π(Cl) → π*(L)	201.5	6.15	0.0836	
H(β) → L + 4(β)	π(L)/π(Cl) → π*(L)	201.1	6.17	0.1333	
H-9(β) → L + 1(β)	π(L)/π(Cl)/d → π*(L)	199.5	6.22	0.0582	
H-9(α) → L + 1(α)	π(L)/π(Cl)/d → π*(L)	190.9	6.50	0.0559	
H-10(α) → L + 1(α)	π(L)/π(Cl)/d → π*(L)	190.5	6.51	0.0951	
H-8(β) → L + 3(β)	π(Cl)/d → π*(L)	189.6	6.54	0.0451	

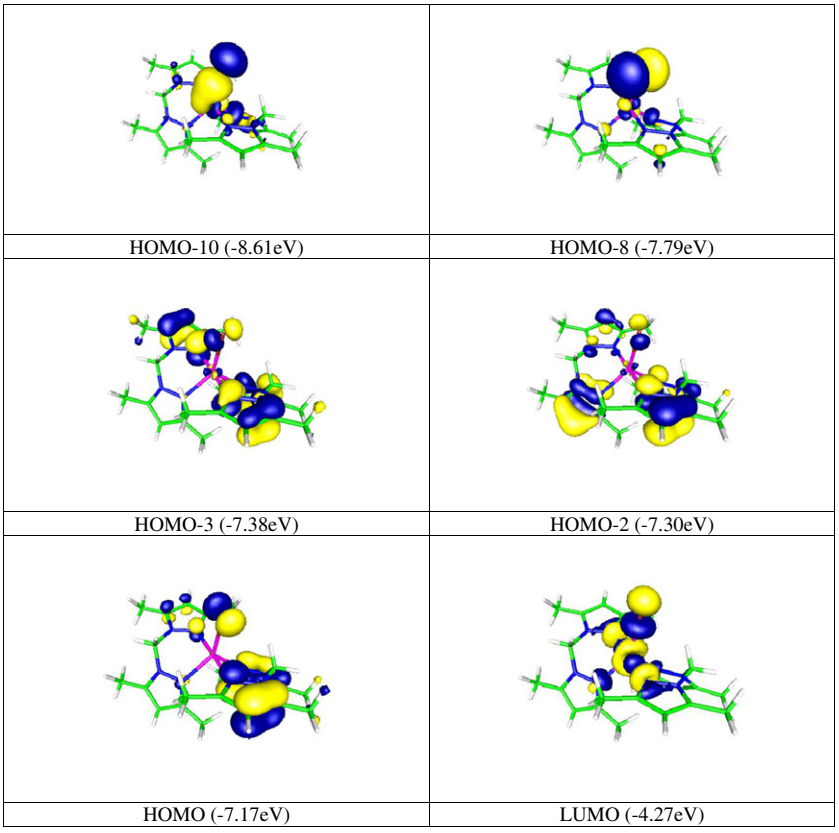

Fig. 3. Contour plots and energy of the selected β-spin HOMO and β-spin LUMO orbitals active in the electronic transitions. The orbitals were plotted with contour values −0.04 (yellow) and 0.04 au (blue). (For interpretation of the references to colour in this figure legend, the reader is referred to the web version of this article.)

Table 4 presents the most important electronic transitions calculated with the TDDFT method for $[Cu\{H_2C(3,5\text{-}Me_2pz)_2\}_2Cl]^+$ and their assignments to the observed absorption bands of the complex. For the high energy part of the spectrum, only transitions with oscillator strengths larger than 0.0400 are listed in Table 4. The assignment of the calculated orbital excitations to the experimental bands was based on an overview of the contour plots and relative energy of occupied and unoccupied molecular orbitals involved in the electronic transitions (Fig. 3).

The TDDFT/PCM calculations show that the two longest wavelength experimental bands at 1011.0 and 738.5 nm originate in the transitions between some lowest β-spin HOMO orbitals and β-spin LUMO orbital. As can be seen from the Fig. 3, the LUMO orbital with β spin is mainly Cu d_z^2 orbital in character, the β-spin HOMO, HOMO-1 and HOMO-2 orbitals are composed of the π-bonding orbitals of bis(3,5-dimethylpyrazol-1-yl)methane and chlorine, the HOMO-3, HOMO-5, HOMO-8 and HOMO-9 are ligand (Cl and bis(3,5-dimethylpyrazol-1-yl)methane) π-bonding orbitals with some contribution of d_{Cu} orbitals, and the HOMO-15 and HOMO-17 are mainly localized on the central ion. Accordingly, the transitions assigned to the two longest wavelength experimental bands can be seen as mixed Cl/bis(3,5-dimethylpyrazol-1-yl)methane → Cu (Ligand–Metal Charge Transfer; LMCT) and d → d (Ligand Field; LF) transitions.

The experimental band at 350.0 nm originates predominately in the transition between β-spin HOMO-10 and β-spin LUMO. As the β-spin HOMO-10 is mainly localized on the chlorine, the absorption band at 350 nm is LMCT transition in nature.

The absorption band at 266.0 nm is also of LMCT character. It can be predominately attributed to the transition from the β-spin HOMO-12 to the β-spin LUMO, and the HOMO-12 is localized on bis(3,5-dimethylpyrazol-1-yl)methane ligand.

The experimental band at 221.5 nm results from the intraligand (IL) and ligand–ligand charge transfer (LLCT) transitions.

4. Conclusion

X-ray studies for the complex of bis(3,5-dimethylpyrazol-1-yl)methane with copper(II) chloride of 2:1 composition revealed five-coordinate geometry about the copper center with one Cl ligand in inner sphere. In terms of regular polyhedra the coordination geometry is intermediate between trigonal bipyramid and square pyramid, and in terms of irregular polyhedra the coordination geometry is almost ideal scalene bipyramid. According to the TDDFT calculations the transitions assigned to the two longest wavelength experimental bands can be seen as mixed Ligand–Metal Charge Transfer and Ligand Field transitions. The reason for this is probably due to the fact that the ligand provide high-lying occupied π bonding orbitals, and as a result the high-lying occupied orbitals are mainly ligand π bonding orbitals in nature.

Supplementary material

CCDC 682987 contains the supplementary crystallographic data for $C_{22}H_{38}N_8O_3Cl_2Cu$. These data can be obtained free of charge via http://www.ccdc.cam.ac.uk/conts/retrieving.html, or from the Cambridge Crystallographic Data Centre, 12 Union Road, Cambridge CB2 1EZ, UK; fax: (+44) 1223-336-033; or e-mail: deposit@ccdc.cam.ac.uk.

Acknowledgements

The GAUSSIAN 03 calculations were carried out in the Wrocław Centre for Networking and Supercomputing, WCSS, Wrocław, Poland under calculational Grant No. 51/96.

References

[1] C. Pettinari, R. Pettinari, Coord. Chem. Rev. 249 (2005) 525.
[2] C. Pettinari, R. Pettinari, Coord. Chem. Rev. 249 (2005) 663.
[3] F.H. Allen, Acta Crystallogr., Sect. B 58 (2002) 380.
[4] 1.J. Reedijk, J. Verbiest, Trans. Met. Chem. 4 (1979) 239.
[5] M. Mesubi, F. Anumba, Trans. Met. Chem. 10 (1985) 5.
[6] A. Potapov, A.I. Khlebnikov, Polyhedron. 25 (2006) 2683.
[7] K. MalinowskaR. Modranka, Acta Crystallogr., Sect. E 63 (2007) m2782.
[8] K. Fujisawa, R. Kanda, Y. Miyashita, K. Okamoto, Polyhedron 27 (2008) 1432.
[9] H. Chermette, Coord. Chem. Rev. 178–180 (1998) 699.
[10] S. Julia, P. Sala, J. Del Mazo, M. Sancho, C. Ochoa, J. Elguero, J.P. Fayet, M.C. Vertut, J. Heterocycl. Chem. 19 (1982) 1141.
[11] E. Díez-Barra, A. de la Hoz, A. Sánchez-Migallón, J. Tejeda, Heterocycles 34 (1992) 1365.
[12] STOE and Cie (1999). X-RED. Version 1.18. STOE and Cie GmbH, Darmstadt, Germany. CRYSALIS RED, Oxford Diffraction Ltd., Version 1.171.29.2.
[13] G.M. Sheldrick, Acta Crystallogr., Sect. A 46 (1990) 467.
[14] G.M. Sheldrick, SHELXL 97. Program for the Refinement of Crystal Structures, University of Göottingen, Germany, 1997.
[15] G.M. Sheldrick, SHELXTL: release 4.1 for Siemens Crystallographic Research Systems (1990).
[16] M.J. Frisch, G.W. Trucks, H.B. Schlegel, G.E. Scuseria, M.A. Robb, J.R. Cheeseman, J.A. Montgomery, Jr., T. Vreven, K.N. Kudin, J.C. Burant, J.M. Millam, S.S. Iyengar, J. Tomasi, V. Barone, B. Mennucci, M. Cossi, G. Scalmani, N. Rega, G.A. Petersson, H. Nakatsuji, M. Hada, M. Ehara, K. Toyota, R. Fukuda, J. Hasegawa, M. Ishida, T. Nakajima, Y. Honda, O. Kitao, H. Nakai, M. Klene, X. Li, J.E. Knox, H.P. Hratchian, J.B. Cross, C. Adamo, J. Jaramillo, R. Gomperts, R.E. Stratmann, O. Yazyev, A.J. Austin, R. Cammi, C. Pomelli, J.W. Ochterski, P.Y. Ayala, K. Morokuma, G.A. Voth, P. Salvador, J.J. Dannenberg, V.G. Zakrzewski, S. Dapprich, A.D. Daniels, M.C. Strain, O. Farkas, D.K. Malick, A.D. Rabuck, K. Raghavachari, J.B. Foresman, J.V. Ortiz, Q. Cui, A.G. Baboul, S. Clifford, J. Cioslowski, B.B. Stefanov, G. Liu, A. Liashenko, P. Piskorz, I. Komaromi, R.L. Martin, D.J. Fox, T. Keith, M.A. Al-Laham, C.Y. Peng, A. Nanayakkara, M. Challacombe, P.M.W. Gill, B. Johnson, W. Chen, M.W. Wong, C. Gonzalez, J.A. Pople, Gaussian 03, Revision B.03, Gaussian, Inc., Pittsburgh, PA, 2003.
[17] A.D. Becke, J. Chem. Phys. 98 (1993) 5648.
[18] C. Lee, W. Yang, R.G. Parr, Phys. Rev. B 37 (1988) 785.
[19] P.J. Hay, W.R. Wadt, J. Chem. Phys. 82 (1985) 299.
[20] M.E. Casida, in: J.M. Seminario (Ed.), Recent Developments and Applications in Modern Density Functional Theory, Theoretical and Computational Chemistry, vol. 4, Elsevier, Amsterdam, 1996.
[21] K. Nakamoto, Infrared and Raman Spectra of Inorganic and Coordination Compounds, 4th ed., Wiley-Interscience, New York, 1986.
[22] G.R. Desiraju, T. Steiner, The Weak Hydrogen Bond in Structural Chemistry and Biology, Oxford University Press, 1999.
[23] G.A. Jeffrey, W. Saenger, Hydrogen Bonding in Biological Structures, Springer-Verlag, 1994.
[24] B. Zhai, W.-Z. Shen, X.-Y. Chen, H-B.H.-B. Song, W. Shi, P. Cheng, Inorg. Chem. Commun. 9 (2006) 1293.
[25] A.W. Addison, T.N. Rao, J. Reedijk, J. Rijn, G.C. Verschoor, J. Chem. Soc., Dalton Trans. (1984) 1349.
[26] H.-Y. Mao, X.-Q. Shen, G. Li, H.-Y. Zhang, Ch. Xu, H.-L. Liu, E.-B. Wang, Q.-A. Wu, H.-W. Hou, Y. Zhu, Polyhedron 23 (2004) 1961.
[27] S.C. Wallis, L.R. Gahan, B.G. Charles, T.W. Hambley, P.A. Duckworth, J. Inorg. Biochem. 62 (1996) 1.
[28] M. Devereux, M. McCann, D. O Shea, R. Kelly, D. Egan, C. Deegan, K. Kavanagh, V. McKee, G. Finn, J. Inorg. Biochem. 98 (2004) 1023.

Polyhedron 27 (2008) 2519–2528

Contents lists available at ScienceDirect

Polyhedron

journal homepage: www.elsevier.com/locate/poly

Synthesis, characterization and magnetostructural correlation studies on three binuclear copper complexes of pyrimidine derived Schiff base ligands

Samik Gupta [a], Sachindranath Pal [b], Anil Kumar Barik [c], Arijit Hazra [a], Somnath Roy [a], Tarak Nath Mandal [a], Shie-Ming Peng [d], Gene-Hsiang Lee [d], M. Salah El Fallah [e,*], Javier Tercero [e], Susanta Kumar Kar [a,*]

[a] Department of Chemistry, University College of Science, University of Calcutta, 92 A.P.C. Road, Kolkata 700 009, West Bengal, India
[b] Department of Chemistry, Sree Chaitanya College, Habra, North 24 Parganas, West Bengal, India
[c] Department of Chemistry, St. Paul's C.M. College, 33/1, Raja Rammohan Roy Sarani, Kolkata 700 009, West Bengal, India
[d] Department of Chemistry, National Taiwan University, Taipei 106, Taiwan, ROC
[e] Departament de Química Inorgànica, Facultat de Química, Universitat de Barcelona, Martí Franquès 1-11, 08028 Barcelona, Spain

ARTICLE INFO

Article history:
Received 5 February 2008
Accepted 6 May 2008
Available online 21 June 2008

Keywords:
Binuclear copper(II) complex
Ferromagnetic
Antiferromagnetic
Pyrimidine derived Schiff base ligands
Magnetostructural correlation

ABSTRACT

Three binuclear Cu(II) complexes of two pyrimidine derived Schiff base ligands, 2-*S*-methyl-6-methyl-4-formyl pyrimidine-*N*(4)-ethyl thiosemicarbazone (HL_1) and salicyl hydrazone of 2-hydrazino-4,6-dimethylpyrimidine (HL_2), have been prepared. HL_1 produces a bis(μ-thiolato) Cu(II) complex co-crystallizing with its mononuclear analog, $[Cu_2(L_1)_2(NO_3)_2][Cu(L_1)(NO_3)]$ (**1**). On the other hand HL_2 shows versatility by producing two different classes of binuclear Cu(II) complexes, a bis(μ-phenoxo) complex $[Cu_2(L_2)_2(NO_3)_2]$ (**2**) and another a (μ-4,4′-bipyridyl) complex, $[Cu_2(L_2)_2(\mu\text{-}4,4'\text{-bipyridyl})(NO_3)_2]$ (**3**) under suitable conditions. All the three complexes show distorted square pyramidal geometry around each Cu atom but to a varied extent. Magnetic behavior of complex **1** shows that it is strongly ferromagnetic in nature whereas compounds **2** and **3** are weakly antiferromagnetic in nature. A magnetostructural correlation study combined with molecular modelling on complexes **1** and **2** has thrown light on the difference on magnetic interaction between the Cu atoms in these two complexes. Various factors that may be responsible for such differences are also explored. A novel and potentially useful pH dependant conversion of **3** to **2** has also been noticed.

© 2008 Elsevier Ltd. All rights reserved.

1. Introduction

The chemistry of dinuclear copper complexes with ligands of biological relevance and with metal centers at close proximity is one of the central themes of current research [1–3] due to their interesting structural, electrochemical and magnetic properties [4] and also because of their relevance to the active sites of several metalloenzymes [5] as synthetic models [6,7]. Apart from the binuclear or polynuclear copper(II) complexes of multidentate donor ligands containing in-built bridging units, synthesis and characterization of di, tri and polynuclear copper complexes using bridging molecules like 4,4′-bipyridyl [8], pyrazine [9] and 1,2 bis(4-pyridyl) ethane [10], etc. are also well documented. These bridging molecules may act singularly or in cooperation with other ligands in the complexes and play a crucial role towards developing diverse innovative structural networks, such as chains, sheets and matrices [11]. Such compounds have found potential applications in catalysis [12], absorption chemistry [13] and molecular magnetism [14].

In the present work we report the synthesis and structural characterization of three dinuclear copper (II) complexes using two pyrimidine based Schiff base ligands, HL_1 and HL_2(Fig. 1). The former one, 2-*S*-methyl-6-methyl-4-formylpyrimidine-*N*(4)-ethyl thiosemicarbazone forms a binuclear bis(μ-thiolato) copper(II) complex (**1**). This complex being pyrimidine derived is a refreshing addition among many other pyridine derived similar complexes [15]. The second chosen ligand HL_2, has restricted electron donating capacity because it produces a five membered and a six membered ring at the metal centers (chelation asymmetry) [16,17]. Hence the metal ion's urge for electrons may be supplemented intrinsically by forming a transaxial bis(μ-phenoxo) dimer or by bridging separate monomeric units through an externally added bridging ligand such as 4,4′-bipyridyl. In this work both the possibilities have been duly exploited in synthesizing complexes **2** and **3** respectively. Further, careful selection of the ligands ensures that the synthesized bis(μ-phenoxo) and the bis(μ-thiolato) complexes **1** and **2** are similar in structure with subtle variations in co-ordination atmosphere for which they are suitable for attempting a magnetostructural correlation study on them. Temperature dependant magnetic

* Corresponding authors. Tel.: +91 033 24322936; fax: +91 033 23519755 (S.K. Kar).
E-mail addresses: salah.elfallah@qi.ub.es (M. Salah El Fallah), skkar_cu@yahoo.co.in (S.K. Kar).

0277-5387/$ - see front matter © 2008 Elsevier Ltd. All rights reserved.
doi:10.1016/j.poly.2008.05.009

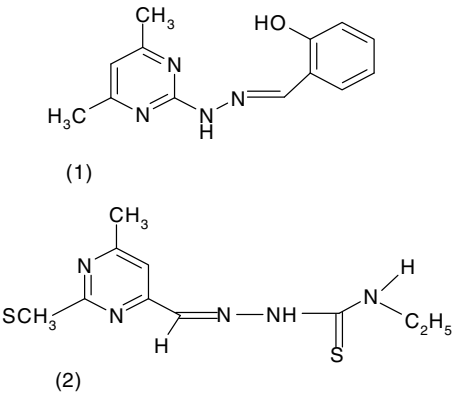

Fig. 1. Representative diagram of ligand HL_2 (**1**) and ligand HL_1 (**2**).

moment studies and molecular modelling have also led to a comparative account of the variation of their magnetic behavior. The 4,4′-bipyridyl bridged complex **3** has been found to have the weakest metal–metal interaction as the metal centers here are far apart.

2. Experimental

2.1. Materials

Ethyl diethoxy acetate and *N*(4)-ethyl-3-thiosemicarbazide, Phosphorus oxychloride, acetyl acetone, urea and hydrazine hydrate were obtained from Aldrich Chemicals, USA and used without further purification. Solvents were also used as received from commercial sources.

2.2. Syntheses

2.2.1. Preparation of ligand HL_1

The ligand HL_1 was synthesized and characterized using the same procedure as reported earlier [18,19].

2.2.2. Preparation of ligand HL_2

The ligand HL_2 was prepared by using 2-hydrazino 4,6-dimethyl pyrimidine and salicylaldehyde in a method similar to that reported by Chiswell and Lions [20]. When a methanolic solution of 1.39 g (10 mmol) of 2-hydrazino 4,6-dimethyl pyrimidine refluxed with a methanolic solution of 1.21 g (10 mmol) of salicylaldehyde for 2 h and the resulting solution kept for slow evaporation, ligand HL_2 separated as crystals from the mother liquor. Filtered and dried in vacuo over fused $CaCl_2$. Yield: 2.20 g (90%). The compound melted with decomposition at 280 °C. IR (ν, cm^{-1}): 3247 (νN–H), 1620 (νC=C), 1566 (νC=NH), 885 (νC_{pym}-H), 1255 (νC–O); ^{1}H NMR (300 MHz, $CDCl_3$, 25 °C, TMS) δ/ppm: (6.68) (s, 1H, C_5–H pyrimidine), (6.8–7.3) (m, 4H, $-C_6H_4$), (8.2) (s,1H, –CH=N–), (12.8) (s, 1H, aromatic-OH), (2.28) (s, 1H, N–H of hydrazone), (2.46–2.53) (m, 6H, CH_3)

2-Hydrazino 4,6-dimethyl pyrimidine was prepared using another literature method [21,22].

2.2.3. Preparation of the complex $[Cu_2(L_1)_2(NO_3)_2][Cu(L_1)(NO_3)]$ (**1**)

The complex **1** was prepared by simply adding an ethanolic solution of hydrated cupric nitrate (1 mmol, 295.5 mg) drop wise to a hot stirred ethanolic solution of ligand HL_1 (0.269 g, 1 mmol). The resulting greenish-yellow solution was refluxed at water bath temperature for 1 h. The solution was filtered and kept for slow evaporation. The dark green compound that separated was filtered off, washed with ice-cold ethanol and dried over fused $CaCl_2$. Yield

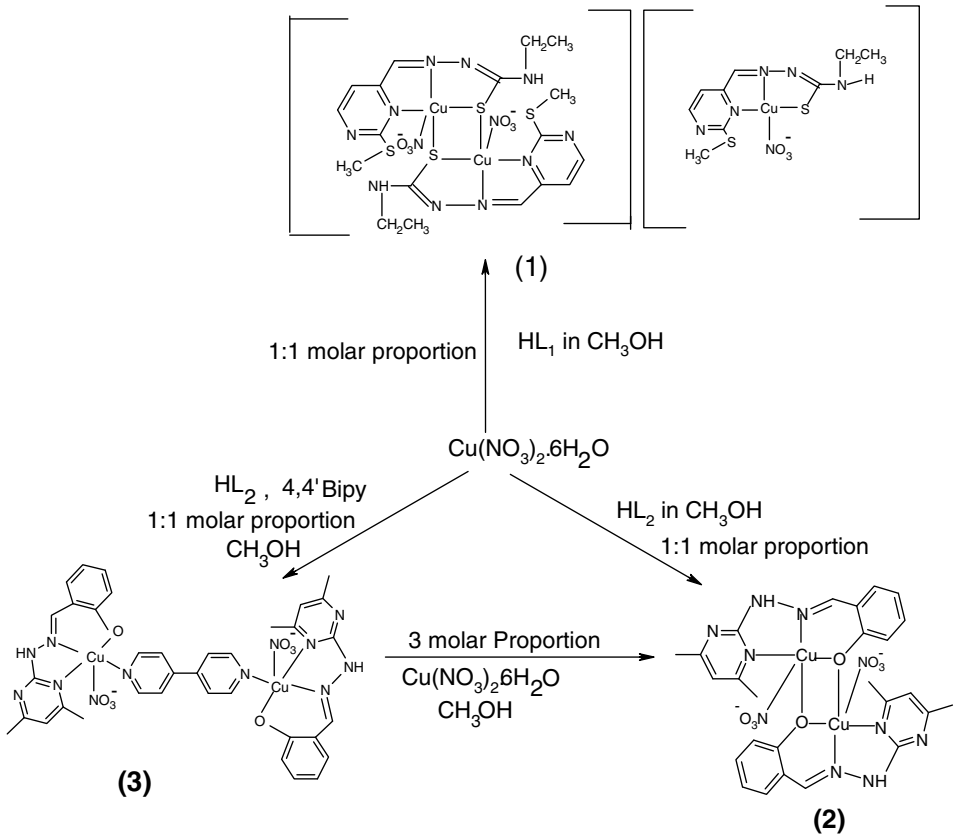

Fig. 2. A scheme showing the method of preparation for the complexes **1**, **2** and **3**.

55%. *Anal.* Calc. for $C_{30}S_6N_{18}O_9H_{42}Cu_3$: C, 30.49; H, 3.18; N, 17.98. Found: C, 30.12; H, 3.56; N, 17.81%. IR (ν, cm^{-1}): 1582 ν(C=N), 1601 ν(C=C), 750 ν(C=S), 800.6 (ν2 of NO_3), 1483, 1292 (ν3 of NO_3). UV–Vis (λ/nm) (ε/L^{-1} mol cm^{-1}): 332.5 (30130)(n → π^* pyrimidine), 434 (10000) (CT, pyrimidine → Cu), 628(440) (d → d). CV E_{pc}/(V): −0.23, −0.92 [$Cu^{II}Cu^{II} \rightarrow Cu^{II}Cu^{I}$, $Cu^{II}Cu^{I} \rightarrow Cu^{I}Cu^{I}$], Epa/(V): +0.40 [$Cu^{II}Cu^{II} \rightarrow Cu^{II}Cu^{III}$].

X-ray quality crystals were grown by slow evaporation of ethanolic solution of the complex at room temperature.

2.2.4. Preparation of the complex $[Cu_2(L_2)_2(4,4'\text{-bipy})(NO_3)_2]$ (**3**)

To a mixture of 4,4′-bipyridyl (1 mmol, 150 mg) and HL_2 (1 mmol, 241 mg) in a methanolic solution (20 ml), of $Cu(NO_3)_2 \cdot 6H_2O$ (1 mmol, 295.5 mg) in the same solvent was added with constant stirring. Immediately, a dirty green precipitate appeared. Stirring was continued for 15 min. The precipitate was filtered off, washed with methanol and dried over fused $CaCl_2$ (Yield 80%). *Anal.* Calc. for $C_{46}N_{14}O_8H_{40}Cu_2$: C, 51.92; H, 3.76; N, 18.43. Found: C, 51.43; H, 3.62; N, 18.59%. IR ν/(cm^{-1}): 1561 ν(C=N) 1611 ν(C=C) 814(ν2 of NO_3) 1304, 1418 (ν3 for NO_3). UV–Vis (λ/nm) (ε/L^{-1} mol cm^{-1}): 332.5 (30130) (n → π^* pyrimidine), 434 (10000) (CT, pyrimidine → Cu), 628 (440) (d → d). CV E_{pc}/(V): −0.42, −0.72 [$Cu^{II}Cu^{II} \rightarrow Cu^{II}$ Cu^{I}, $Cu^{II}Cu^{I} \rightarrow Cu^{I}$ Cu^{I}], Epa/(V): +0.479 [$Cu^{II}Cu^{II} \rightarrow Cu^{II}Cu^{III}$].

The compound was found to be sparingly soluble in common organic solvents; hence X-ray quality crystals were obtained from a mixed solvent of DMF and CH_3OH by slow evaporation.

2.2.5. Preparation of the complex $[Cu_2(L_2)_2(NO_3)_2]$ (**2**)

Method a: The complex **2** was prepared by adding an methanolic solution (10 ml) of $Cu(NO_3)_2 \cdot 6H_2O$ (1 mmol, 295.5 mg) to a methanolic solution (15 ml) of ligand HL_2, (1 mmol, 242 mg) under constant stirring condition. Stirring was continued for half an hour, When dark brown micro crystalline compound separated. It was filtered off, washed with methanol and dried over fused $CaCl_2$. Yield (62%). *Anal.* Calc. for $C_{26}N_{10}O_8H_{24}Cu_2$: C, 41.54 H, 3.19; N, 18.64. Found. C, 41.12; H; 3.52; N,18.69%. IR ν/(cm^{-1}): 1546 ν(C=N), 1607 ν(C=C), 807 (ν2 of NO_3), 1470, 1293 (ν3 of NO_3). UV–Vis (λ/nm) (ε/L^{-1} mol cm^{-1}): 332.5 (32400) (n → π^* pyrimidine), 383 (16000) (Phenoxide → Cu), 429 (19200) (CT, pyrimidine → Cu), 675 (300) (d → d). CV E_{pc}/(V): −0.44, − 0.62 [$Cu^{II}Cu^{II} \rightarrow Cu^{II}Cu^{I}$, $Cu^{II}Cu^{I} \rightarrow Cu^{I}Cu^{I}$], Epa/(V): +0.515 [$Cu^{II}Cu^{II} \rightarrow Cu^{II}Cu^{III}$].

X-ray quality crystals were grown by slow evaporation of a methanolic solution of the complex at room temperature.

Method b: To an ethanolic suspension of complex **3** (223 mg, 0.5 mmol), $Cu(NO3)_2 \cdot 6H_2O$ (1.5 mmol, 443.2 mg) was added and the mixture was refluxed for ca. 2 h at water bath temperature. A brown colored solution resulted during this time along with a blue violet insoluble residue which could not be characterized. It was filtered and kept for slow evaporation. Dark blue crystals of complex **2** was found to deposit from the solution within few days.

2.3. Physical measurements

Elemental analyses (C, H and N), IR spectra (KBr discs, 4000–200 cm^{-1}), ^1H NMR spectra (DMSO-d_6) and UV–Vis spectra (MeCN), were done with a Perkin–Elmer Model 240 C CHN analyzer, a Jasco FTIR model 420 spectrophotometer, and a Hitachi U-3501 spectrophotometer, respectively. Cyclic voltammetry (CV) experiments were carried out using Sycopel Model 77 AEW2 1820F/S instrument. The measurements were performed at 300 K in a DMF solution containing 0.2 M TEAP and 10^{-3}–10^{-4} M Cu(II)–Cu(II) complexes **1**, **2**, **3**, deoxygenated by bubbling with nitrogen. A platinum wire, a platinum coil and a SCE were used as a working, a counter and reference electrodes, respectively. Magnetic susceptibility measurements for compounds **1**, **2** and **3** were carried out on polycrystalline samples, at the Servei de Magnetoquímica of the Universitat de Barcelona, with a Quantum Design SQUID MPMS-XL susceptometer apparatus working in the range 2–300 K under magnetic field of approximately 500 G (2–30 K) and 1000 G (35–300 K). Diamagnetic corrections were estimated from Pascal Tables. The EPR spectra have been recorded on X-band Bruker Spectrometer (ESR 300E), working with an oxford helium liquid cryostat for variable temperature.

2.4. Crystallographic measurements

Relevant crystallographic data are listed in Table 1. Intensity data for **1** and **2** were measured on a Bruker SMART APEX CCD diffractometer and the same for **3** were measured on a NONIUS Kappa-CCD diffractometer, using graphite-monochromated Mo Kα radiation (λ = 0.71073 Å) in the ω–2θ scan mode. These were corrected for Lorentz-polarization effects. The structures were solved by using SHELXS-97 package of program and refined by full matrix least-squares technique based on F^2 (SHELXL-97). Hydrogen atoms were added in the calculated positions. Selected bond angles and bond distances are supplied in Table S1 (Supplementary data). Perspective view of the complexes **1**, **2** and **3** along with the atom numbering schemes are shown in Figs. 3–5.

3. Results and discussion

3.1. Synthesis

The ligand HL_1, used in this work, is prepared using standard literature procedures [18,19]. Ligand HL_1 has been employed to synthesize the bis(μ-thiolato) complex, **1**, while the ligand HL_2 is synthesized for the first time for preparation of the bis(μ-phenoxo) complex, **2**.

With the examples of several other closely related ligand systems to both HL_1 and HL_2 reported earlier as binucleating ligands towards Cu^{2+} ion [23], it seemed worth while to try them out for this purpose and establish a comparative relation between the resulting thiolato and phenoxide bridged complexes with respect to their structures and magnetic behavior. Our pursuit turned fruitful when binuclear copper complexes resulted from both the ligands using $Cu(NO_3)_2$, $6H_2O$ as the precursor. Both ligands act as tridentate mono negative type donors towards Cu^{2+} ion and the complexes obtained were notably similar from the structural point of view barring the bridging donor atoms. Further we extended the purview of this work by attempting the synthesis of 4.4′-bipyridyl and pyrazine bridged dinuclear Cu^{2+} complexes with ligand HL_2. While the 4,4′-bipyridyl bridged complex was easily formed, the attempt with pyrazine was unsuccessful. This is because formation of such a complex would require a close approach of the monomeric bulky units and would exert a severe steric congestion around the bridging pyrazine ring making the species highly unstable. Thus at such a close approach of the monomeric units formation of the phenoxide bridge was favored to a pyrazine bridged binuclear complex.

A most intriguing observation was that the bipyridyl bridged complex, **3**, which is stable in heat (refluxing MeOH temperature), gets transformed to complex **2** when a suspension of **3** in MeOH is refluxed with 3 equiv. of $Cu(NO_3)_2 \cdot 6H_2O$. Within a span of 2 h, complex **3** which was originally insoluble in MeOH became completely soluble to give a brown solution. Slow evaporation of this solution resulted in X-ray quality crystals of **2**. This conversion of **3** to **2** may be attributed to the slight decrease of pH in the resulting solution on addition of excess $Cu(NO_3)_2 \cdot 6H_2O$ to the suspension of **3** in MeOH. Solvolysis of the metal salt causes lowering of pH (4.5–5.0) which is just enough to free the co-ordinated

Table 1
Crystal data and structure refinement for complex **1**, **2**, **3**

Crystal	Complex **1**	Complex **2**	Complex**3**
Empirical formula	$C_{20}H_{28}Cu_2N_{12}O_6S_4$	$C_{26}H_{26}Cu_2N_{10}O_8$	$C_{36}H_{34}Cu_2N_{12}O_8$
Formula weight	787.86	731.65	889.84
Temperature (K)	295(2)	295(2)	150(2)
Crystal system	monoclinic	monoclinic	triclinic
Space group	*P*2(1)/*n*	*P*2(1)/*c*	$P\bar{1}$
Unit cell dimensions			
a (Å)	14.6940(7)	7.5729(3)	7.4141(4)
b (Å)	14.0601(7)	13.1332(6)	9.9865(6)
c (Å)	15.8096(8)	14.8400(7)	12.8196(7)
α (°)	90	90	105.026(1)
β (°)	111.190(1)	96.7425(18)	99.735(1)
γ (°)	90	90	95.096(1)
Volume (Å^3)	3045.4(3)	1465.73(11)	894.70(9)
Z	4	1	2
Absorption coefficient (mm$^{-1)}$	1.729	1.519	1.262
F(000)	1608	748	456
Crystal size (mm)	0.35 × 0.20 × 0.20	0.50 × 0.20 × 0.10	0.30 × 0.13 × 0.05
θ Range for data collection (°)	2.00–27.50	2.76–27.50	2.32–27.50
Reflections collected	24467	11639	11697
Independent reflections (R_{int})	7004 (0.0340)	3347 (0.0585)	4108 (0.0418)
Completeness to θ = 27.50° (%)	100.0	99.8	99.9
Absorption correction	semi-empirical from equivalents	none	semi-empirical from equivalents
Maximum and minimum transmission	0.7236 and 0.5828	0.782 and 0.536	0.9396 and 0.7033
Refinement method	full-matrix least-squares on F^2	full-matrix least-squares on F^2	full-matrix least-squares on F^2
Data/restraints/parameters	7004/0/397	3347/0/210	4108/0/264
Goodness-of-fit on F^2	1.015	1.075	1.008
Final *R* indices [$I > 2\sigma(I)$]	R_1 = 0.0394, wR_2 = 0.0948	R_1 = 0.0459, wR_2 = 0.1314	R_1 = 0.0550, wR_2 = 0.1315
R indices (all data)	R_1 = 0.0552, wR_2 = 0.1026	R_1 = 0.0661, wR_2 = 0.1395	R_1 = 0.0652, wR_2 = 0.1384
Largest difference in peak and hole (e Å^{-3})	0.440 and −0.299	0.804 and −0.404	1.570 and −0.489

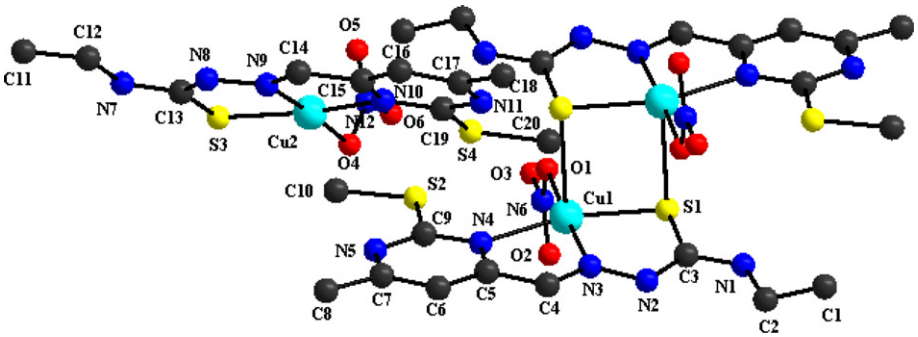

Fig. 3. Structural representation of complex **1**.

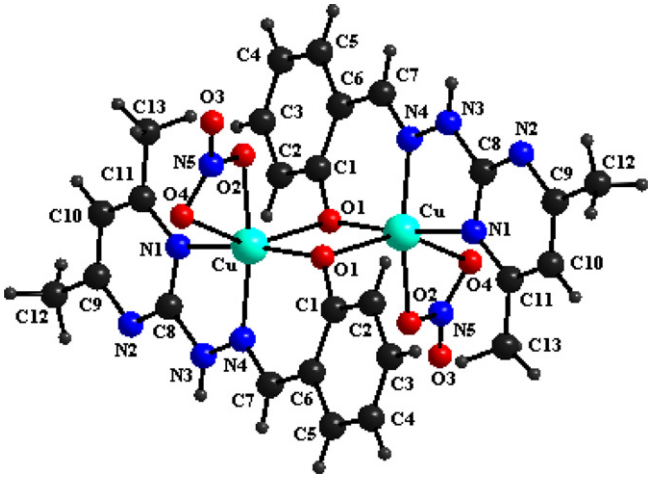

Fig. 4. Structural representation of complex **2**.

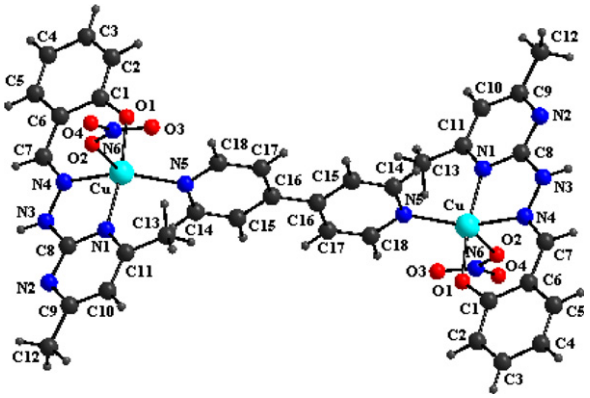

Fig. 5. Structural representation of complex **3**.

4,4′-bipyridyl with a view to protonate it. This slight decrease of pH is however insufficient to protonate other donor atom/ion in the deprotonated prime ligand and thus no change is brought about in the main ligand's binding property. Complex **3** can thus easily get transformed to **2** using the bridging capability of phenoxide ion. The reaction scheme for the preparation of the complexes is shown in Fig. 2.

3.2. Spectroscopic characterization

The ligand HL_1 shows characteristic IR bands for ν(C=N) at 1608 cm^{-1}. This is shifted ca. 26 cm^{-1} towards lower energy in the complex **1** indicating co-ordination via azomethine nitrogen [24]. The ligand HL_1 shows a band at 800 cm^{-1} assigned to ν(C=S), this is also shifted towards the lower frequency to ca. 750 cm^{-1} confirming co-ordination via thiolate sulphur atom in the complex **1**. A band at 272 cm^{-1} may be assigned to $\nu(Cu{-}O_{NO_3})$ consistent with bands at 253–280 cm^{-1} for other nitrato complexes [25]. Moreover two strong bands at 1420 cm^{-1} and 1306 cm^{-1} at a separation of 114 cm^{-1} indicate that the nitrate is bound in monodentate fashion [26].

In the ligand HL_2 the significant bands are observed at 1566 cm^{-1} for ν(C=N), 1620 cm^{-1} for ν(C=C), 2924 cm^{-1} for ν(O–H) and ν(N–H) at 3247 cm^{-1}. Among these the broad band at 2924 cm^{-1} is absent in the complexes **2** and **3** showing that the phenolic –OH is deprotonated in the complexes.

Interestingly, the ν(C=N) band undergoes more deviation towards the lower energy in complex **2** (1546 cm^{-1}) compared to **3** (1561 cm^{-1}). This may be explained as an indirect effect of the difference in co-ordination mode of the phenoxide oxygen of the in **2** and **3**. In **2**, phenoxide ion serves as a bridging ligand. Consequently, the electronic requirement of the copper ions has to be fulfilled more by the other donor atoms (pyrimidine and azomethine nitrogen). Hence the azomethine nitrogen binds more strongly to the copper ions making the C=N bond comparatively weaker. On the other hand in **3** phenoxide ion shares greater responsibility of donation being non-bridging in nature, leaving the azomethine nitrogen rather weakly bound. Similar effects are observed in case of ν(C=C) for complexes **2** and **3**.

In complex **2** the nitrate bands are observed at 807 cm^{-1} (ν2) 1293 cm^{-1} and 1470 cm^{-1}(ν3) indicating that the nitrate bonding mode is bidentate. On the other hand complex **3** the ν3 nitrate vibrations are observed at 1304 cm^{-1} and 1418 cm^{-1} and the ν1 vibration at 841 cm^{-1}. These results signify a monodentate mode of nitrate binding [26].

The ν(C=C) and ν(C=N) peaks for 4,4′-bipy in the complex **3** generally coincide with those of the ligands. An additional peak at 848 cm^{-1} was obtained for 4,4′-bipy [8].

The electronic solution spectra of the complexes were recorded in DMF solution. Complex **1** shows a n–π^* band of the pyrimidine ring at 332.5 nm [27]. A broad band at 434 nm contains the responses for LMCT charge transfer band for pyrimidine → Cu and S → Cu [28]. The n–π^* transition has the highest molar absorption among these bands (ϵ = 30 130 L^{-1} mol cm^{-1}). The d–d transitions occur at much lower energy region and are weak in nature. The broad band at 628 nm is consistent with the broad structured band for square planar (square pyramidal) complexes of copper [29]. Spectra for complex **2** and **3** are almost similar to that of complex **1**. In complex **2**, n–π^* transition is observed at 332 nm, Two very prominent charge transfer bands occur at 383 nm and 429 nm. The former may be assigned to $N_{(pym)}$ → Cu and the latter to $O_{(phenoside)}$ → Cu charge transfer. Much weaker d–d band appears at 675 nm [30]. The CT band in **3** for phenolate → Cu appears at a little higher energy (426 nm) compared to **2** because of the difference of binding mode of the phenolate group in the two compounds. In compound **3** one additional CT band corresponding to $N_{(4,4'bipyridine)}$ → Cu LMCT appears at 344 nm. The d–d transition bands occur at a lower energy in **3** compared to **2** in keeping with the higher distortion of geometry of the copper ion environment. The ϵ value is also considerably higher in the former. In all three complexes intense π–π^* transition bands for ligands are observed at high energy zones.

3.3. Redox behavior

All the complexes show two irreversible cathodic responses at a platinum electrode in DMF solution, with E_{pc} values (versus SCE) at −0.42 V and −0.72 V for complex **3**, 0.44 V and −0.62 V volt for complex **2**, where as the two reductive responses for complex **1** occurs at −0.23 V and −0.92 V. The two reductive responses may be assigned to $Cu^{II}Cu^{II} \rightarrow Cu^{II}Cu^{I}$. and $Cu^{II}Cu^{I} \rightarrow Cu^{I}Cu^{I}$ [4e] reductions. Both reductions are one electron process compared to Fe/Fe^{+} process. The difference of the peak positions for the two reductive responses is indicative of the stability of the electro generated $Cu^{II}Cu^{I}$ mixed valence state [30]. In complex **1** if is found to be maximum. The thiolate bridging donor may have also played a role. However the irreversible nature of the reductions point to the non-supportive nature of the ligand systems towards the structural reorientations required for different preferred co-ordination polyhedra for Cu(II) and Cu(I).

On an anodic scan between 0 and 1.0 V the complexes show one oxidative response for $Cu^{II} \rightarrow Cu^{III}$ between 0.40 and 0.53 V. The peak to peak separation values range between 0.129 and 0.302 V indicating the irreversible nature of the oxidation. Here again the thiolate-bridged complex undergoes oxidation at the least positive potential. Interestingly, despite the presence of a mononuclear asymmetric unit along with thiolate-bridged dimer, complex **1** shows no additional peak in cathodic as well as anodic scan.

3.4. Description of the structure

3.4.1. Structure of $[Cu_2(L_1)_2(NO_3)_2][Cu(L_1)(NO_3)]$ (**1**)

The crystal structure of **1** consists of two crystallographically independent molecules in the asymmetric unit of the complex. One is a binuclear thiolate-bridged pentacoordinated copper(II) complex while the other is its tetracoordinated mononuclear counter part. In the mononuclear unit the ligand acts as a tridentate mono negative NNS donor, using a pyrimidine nitrogen (N10), the azomethine nitrogen (N9) and the thiolato sulphur (S3) atoms. The fourth co-ordination position in the approximately square planar environment of Cu is occupied by the nitrato oxygen atom. The ligand forms two five membered chelate rings at the copper center. The thiol form of the co-ordinated ligand in the complex is evident from the increased C13–S3 bond length (1.736 Å) and decreased C13–N8 bond length (1.334 Å) compared to standard bond lengths observed in thione form of other thiosemicarbazone ligands [31]. The deviation of the copper atom from the mean square plane containing S3N904N10 is negligible. The two chelate rings formed by the ligand are strikingly co-planar with a dihedral angle of less than 1° between the mean planes of Cu2S3C13N8N9 and Cu2N10C15C14N9. This co-planarity of the chelate rings facilitates electron delocalization in the co-ordination sphere rendering enhanced stability to the complex. The thiosemicarbazone bite angles S3Cu2N9 and N10Cu2N9 are observed to be 84.16° and 81.09° respectively while the angular measurements of the trans donor ligands, O4Cu2N9 and S3Cu2N10 are 176.29° and 165.25°, respectively, showing considerable distortion from ideal square planer angles (90° and 180°). However the results are in agreement with those reported for similar mononuclear thiosemicarbazone complexes of copper[32]. The deviation of the copper atom from the basal plane is found to be negligible.

The binuclear unit may simply be regarded as a centrosymmetric dimer of the mononuclear unit, where the two monomeric units are linked by a four membered ring that includes both symmetry related copper atoms and co-ordinated sulphur donors. The local co-ordination environment of each copper comprises of a square pyramidal N_2OS_2 chromophore. The geometry around the copper atoms may be described as distorted square pyramidal. Where the basal plane is occupied by a pyrimidine nitrogen (N4), azomethine nitrogen N(3), a bridging thiolato sulphur (S1) from a mononegative ligand and an oxygen (O1) from a nitrate anion. The apical position is occupied by a bridging thiolate (S1) from another ligand. The bonds formed by the basal ligand atoms with each copper i.e. Cu(1)–S(1), Cu(1)–N(3) and Cu(1)–N(4) are comparable to those observed in the monomeric unit as well as other structurally characterized binuclear thiolato bridged copper complexes [33]. Despite the fact that the co-ordination angles subtended at each copper center is considerably deviated from ideal square planer angles [180° and 90°] (Table S1, Supplementary data), an approximate square pyramidal geometry is established by the calculation of Addison parameter τ, $\tau = (\beta - \alpha)/60°$. In this case α and β are O1Cu1N3 and N4Cu1S1 angles respectively giving a τ value 0.198 [34]. The apical bridging Cu–S bonds are comparatively longer than the basal Cu–S bonds (2.82 Å versus 2.29 Å). The dominant Jahn–Teller distortion characteristics to square pyramidal copper complexes seem to be the reason behind it. The opposite interior angles of the Cu_2S_2 tetragonal core are 86.54° and 93.46°. Thus from the non-equivalence of bond lengths and bond angles it is clear that this is an asymmetric binuclear thiolate double bridged structure. The distance between the two copper atoms is 3.52 Å, comparable to other similar complexes. The Cu_2S_2 core is essentially planer, with all the four atoms sitting in the mean plane. This facilitates the magnetic exchange interaction between the Copper atoms. The mean basal planes at each copper atom through Sl01N3N4 show that there is very little deviation (<0.1 Å) of the atoms from the mean plane. The copper atom is deviated only ca. 0.06 Å towards the apical bridging Sulphur atom. The basal planes of the square pyramid are almost orthogonal with the mean plane of Cu_2S_2 bridge bearing a dihedral angle of 85.9° in each case.

The binding mode of the NO_3^- as the fifth coordinating ligand is worth discussing as nitrate ions are reported to bind metals in monodentate, bidentate and anisobidentate fashion [35]. Based on the available parameters for assigning the nitrate-binding mode [36], it was determined that in both the asymmetric units monodentate fashion of nitrate binding is present. It is found that the nitrate ion is almost planer in the crystal.

A closer look at the crystal lattice shows that the two asymmetric units are networked by profound H-bonding interaction. Each binuclear unit is H-bonded to four mononuclear units. In this case the interaction is between a nitrate oxygen and the Hydrogen of the secondary amine group of the N(4)-substituted thiosemicarbazone.

3.4.2. Structure of the $[Cu_2(L_2)_2(NO_3)_2]$ (**2**)

This dimeric molecule sits on a crystallographically imposed center of inversion forming a bridged dinuclear structure with each copper being five-coordinate. The geometry around each copper may again be described as an approximate square pyramidal arrangement. Three positions in the basal plane being occupied by the tridentate ligand, acting as a monoanionic NNO donor and the fourth position being occupied by a co-ordinated nitrate. A bridging O from the second ligand unit occupies the apical position. The basal mean plane of the square pyramid through the pyrimidine nitrogen (N1), the azomethine nitrogen (N4), the phenoxide (O1) and the nitrate oxygen (O2) does not contain any of these atoms (The deviations range between 0.167 and 0.201 Å). The copper atom is deviated by 0.125 Å towards the apical bridging oxygen. The chelate rings (one five and another six membered) formed by the ligands at each copper center are at a dihedral angle of 9.2°. The angles produced at the axial phenoxide bridge by the basal donors (~374°) shows considerable pyramidal distortion. Overall it may be inferred that complex **2** suffers less distortion ($\tau = 0.157$) from square pyramidal geometry towards TBP geometry than complex **1** in spite of the fact that angular deviations from ideal square planar angles are more pronounced in **2** than **1**. The Cu–O(1) (bridging) bond distance is 2.33 Å whereas the Cu–O(1) (basal) is 1.921 Å are unexceptional [37], as are the other bond lengths in the co-ordination sphere of each copper atom (Table S1, Supplementary data). The distance between the two copper atoms is 3.18 Å which is more to the higher end of the range (2.9–3.34) Å reported for Cu–Cu distances in macrocyclic and non-macrocyclic bis(μ-phenoxo) bridged dicopper complexes [38]. In this complex the Cu_2O_2 core bears dihedral angle of 88.69° with the mean basal plane of each square pyramid. The internal angles produced at the Cu_2O_2 core (96.57° and 83.43°) are comparable to those observed in the Cu_2S_2core of complex **1**.

Unlike complex **1** the nitrate ion is bound to the copper in an anisobidentate fashion. (See Table S2, Supplementary data) however the large nitrate bite angle (118°) supports the view that the second oxygen (04) of the nitrate should be regarded as a sixth co-ordinating ligand approaching vacant the axial end, rather than both oxygens (O2,O4) of nitrate occupying a single co-ordination position in the basal plane. The Cu–O(4) distance of 2.55 Å suggests an weak axial interaction. No appreciable H-bonding interaction is observed of either intra or intermolecular nature. From the Cg–Cg distances it is observed that there is notable π–π interaction between the benzene and pyrimidine ring systems between two separate dimeric molecules. However such interaction if present between aromatic rings belonging to same molecule may be weak in nature.

3.4.3. Structure of $[Cu_2(\mu\text{-}4,4'bipy)(L_2)_2(NO_3)_2]$ (**3**)

The molecular structure of **3** shows two pentacoordinated copper ions bridged by a 4,4′-bipyridyl molecule. The co-ordination environment around each copper may be described as irregular, distorted to an extent of ~50% ($\tau = 0.496$) along the path way from square pyramidal towards trigonal bipyramid. Similar to complex **2**, the ligand (HL_2) acts as tridentate mono negative donor. The only difference is that the phenoxide group (O1) does not operate as a bridging group, i.e. each phenoxide group donates to a single copper ion. The fourth co-ordination position in the basal plane is occupied by the nitrogen (N5) of the bipyridyl bridging ligand. The axial position is occupied by a nitrate donor. In this complex the nitrate acts as a monodentate donor through (O2), the other oxygen (O3) is too far away from the copper ion (3.25 Å) for any appreciable bonding interaction. The Cu–O(2) bonds being the axial one, are found to be the longest (2.247 Å) among all five bond lengths in the co-ordination sphere of each copper (Other bond lengths are in the range 1.89–2.03 Å). The chelate rings formed by the ligand at each copper center are co-planar, bearing a dihedral angle of only 2.09°. This observation is in contrast to complex **2** where a puckering of the chelate rings was observed to accommodate the rigid bis(μ-phenoxo) bridged structure. The two rings of the 4,4′-bipyridyl bridging donor are co-planar to one another in conformation. Hence the compound bears two fold axis of symmetry perpendicular to the plane containing the bipyridyl rings and also a center of symmetry. The distance between the two copper atoms in 11.14 Å which is similar to other bipyridyl bridged binuclear complexes [8–10].

There are two intermolecular H-bonding interactions between the hydrogen of azomethine nitrogen atoms (N3) of a unit with the bonded nitrate oxygen (O2) of another unit. The binuclear complexes thus forms a mixed one dimensional co-ordination polymer

held by both co-ordinate and H-bonds (Fig. S1 in Supplementary data).

3.5. Magnetic studies

3.5.1. Magnetic study on complexes **1** and **2**

The magnetic behavior of the compound **1** is shown in Fig. 7, as a $\chi_M T$ *versus* T plot. At room temperature the $\chi_M T$ value is 0.860 $cm^3\ K\ mol^{-1}$ which is close to the expected value for two uncoupled copper (II) ions with $g = 2.14$. $\chi_M T$ increases slightly with lowering of temperature and reaches a maximum of 0.962 $cm^3\ K\ mol^{-1}$ *ca.* 7.3 K. Below this temperature $\chi_M T$ decreases to a value of 0.833 $cm^3\ K\ mol^{-1}$ at 2 K. The shape of this curve indicates dominant ferromagnetic coupling which result from the interaction of the copper(II) ions through sulphur atoms (thioalkoxo-bridges). The $\chi_M T$ decreasing observed at low-temperature is may be due to the intermolecular antiferromagnetic exchange and/or the presence of the ZFS of the ground state (S = 1).

To determine the exchange parameters *via* sulphur atoms we have used the Bleaney–Bowers expression for an isotropically coupled pair of $S = 1/2$ ions [39], (Eq. (1)) and a Curie–Weiss correction. The best fit parameters for the reproducing satisfactorily the experimental data, as shown in Fig. 6, are $J = +7.6\ cm^{-1}$, $\theta = -0.78$ K and $g = 2.14$ with $R = 1 \times 10^{-5}$ ($R = \sum_i(\chi T_{icalc} - \chi T_{iexp})^2/(\chi T_{iexp})^2$):

$$\chi_M = \frac{Ng^2\mu_B^2}{k_B(T-\theta)}\frac{2\exp(J/k_B)}{1+3\exp(J/k_B)} \quad (1)$$

For compound **2** the global feature of the $\chi_M T$ versus T curve is characteristic of very weak antiferromagnetic interaction in a dinuclear copper(II) complex and/or intermolecular interaction (Fig. 7). The value of $\chi_M T$ at 300 K is 0.951 $cm^3\ mol^{-1}$ K which is as expected for two uncoupled copper(II) ions (0.475 $cm^3\ mol^{-1}$ K per one Cu^{II} with $g = 2.25$). The $\chi_M T$ values are more or less constant at high temperature and then decreases suddenly in the low-temperature region reaching a value of 0.332 $cm^3\ mol^{-1}$ K at 2 K.

The interaction through oxygen atoms was determined by the use of the above equation Eq. (1) The best fit parameters from 300 down to 2 K are found as $J = -1.8\ cm^{-1}$, $\theta = -1.5$ K and $g = 2.25$ with an error $R = 9.8 \times 10^{-6}$ ($R = 1 \times 10^{-5}$) ($R = \sum_i(\chi T_{icalc} - \chi T_{iexp})^2/(\chi T_{iexp})^2$).

The field dependence of magnetization (0–5.0 T) measured at 2 K for compound **1** is shown in Fig. 6b, in the form of M/Nβ (per Cu_2 unit) versus H. The magnetization reaches a value of 2.11 Nβ at 5.0 T which is close to the expected S = 1 value of 2 Nβ for the Cu_2 system, indicating the presence of ferromagnetic interaction between the nearest copper(II) ions. For compound **2** the field dependence of magnetization (0–5.0 T) measured at 2 K is shown in Fig. 7b, reaches a value of 1.7 Nβ near of two electrons but with a particular shape that we cannot fit satisfactory with Brillouin expression for two isolated ion with $S = 1/2$. The curves indicate very slow magnetization which is consistent with a net weak antiferromagnetic interaction.

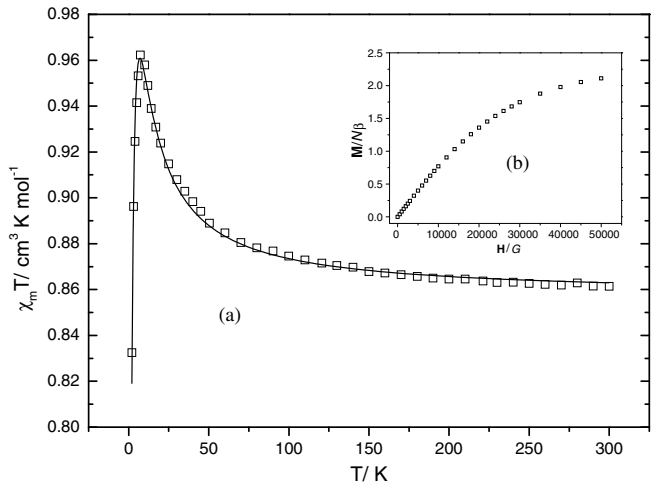

Fig. 6. (a) Plot of the χ_MT vs. T for compound **1**. The squares and solid line are the experimental values and the best fit respectively. (b) The field dependence of magnetization at 2 K for compound **1** (per Cu_2).

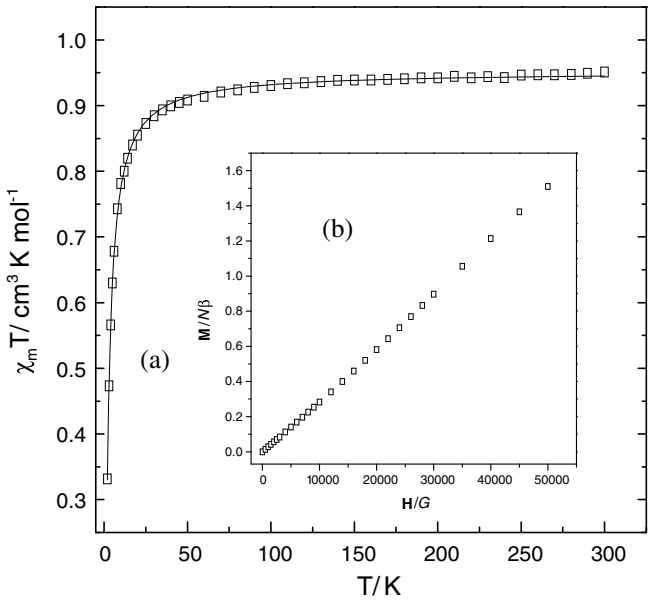

Fig. 7. (a) Plot of the $\chi_M T$ *vs.* T for compound **2**. The squares and solid line are the experimental values and the best fit respectively. (b) The field dependence of magnetization at 2 K for compound **2**.

The EPR spectrum of **1** recorded in X band at 4 K is shown in Fig. S2 (Supplementary data). One band is observed at $g = 2.09$ (3228.66 G for $\nu = 9.460$ GHz), corresponding to the transition $\Delta M_S = \pm 1$. For the compound **2** (Fig. S3, Supplementary data), two bands are located at $g_{\|} = 2.28$ and $g_{\perp} = 2.09$ (2962.77 and 3224.75 G for $\nu = 9.458$ GHz).

In order to evaluate the nature of the interaction with similar topology, via sulphur (thioalkoxo-bridges) and oxygen atoms (alkoxo-bridges) in **1** and **2**, respectively, the experimental atomic co-ordinates were performed to obtain the J values. The calculated $J = +9.9\ cm^{-1}$ for compound **1** are reasonably close to the fit value $+7.6\ cm^{-1}$ but for **2** the calculated J value is $+1.2\ cm^{-1}$ which contradicts the experimental one ($-1.8\ cm^{-1}$).

To clarify this discrepancy, we have modelled the structure of both compounds attempting to understand the influence of the distance, d(Cu–X), in the exchange coupling parameter J between nearest copper(II) (Fig. 8). Therefore, in the model 1 we have varied the Cu–S distance in the range 2.5–2.9 Å in compound **1**. In the model 2, we have varied the Cu–O distance in the range 2.1–2.5 Å in compound **2**. The results of these calculations are reported in Fig. 9 as a J versus d(Cu–X) plots. In the two cases the calculated interactions are ferromagnetic: (i) In the model 1, the calculated J values are varying between +8.0 and $+27.6\ cm^{-1}$ showing a clear parabolic dependence with the Cu–X distance. (ii) A similar trend was observed in the model 2, but with small J values which are varying in the range [+0.3 to $+4.3\ cm^{-1}$].

In previous paper, one of us has analyzed the magnetic properties of alkoxo-bridged dinuclear Cu(II) complexes showing a similar topology of compound **2**. The calculated interactions were also weak and ferromagnetic [40]. In the same way, the calculations of model 2 seem to confirm the weak nature of the interaction. The

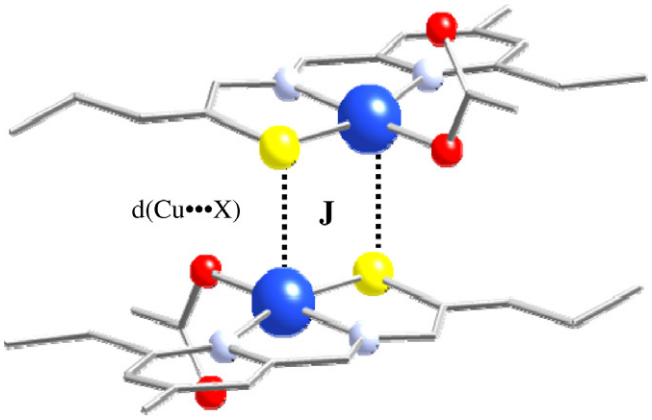

Fig. 8. Molecular structure representation and exchange coupling constant view of compound **1**. The hydrogen atoms are omitted and the non-environment atoms of copper are represented as sticks for clarity. The dotted line represents the apical distance Cu–X that we have varied in mode l for compound **1** and model for compound **2**.

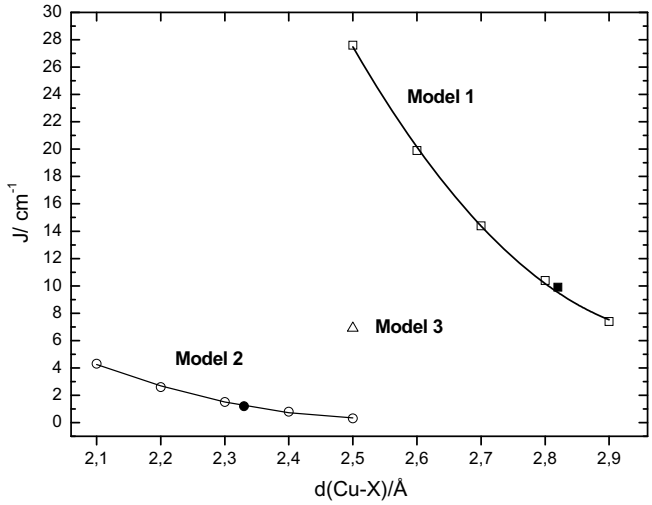

Fig. 9. Variation of the calculated coupling constant as a function of longer distance Cu–X, for **1** (mode1, □) and **2** (model 2, ○). Solids squares and circles represent compound **1** and **2**, respectively. For model 3 (△) see text.

magnetic behavior can easily be rationalized using the Hay–Thibeault–Hoffmann model [41]. If the coupling constant is given by,

$$J = 2K_{ab} - \frac{(\varepsilon_1 - \varepsilon_2)^2}{J_{aa} - J_{ab}}$$

the second term will probably be much smaller, result of the poor overlap between the parallel orbitals on the bridge (Fig. S4, Supplementary data). In such situation, the first term, $2K_{ab}$, is dominating, and leads an overall positive value for the coupling exchange as it shown in compound **1**. In compound **2** this two terms seem to have similar and small values giving a very weak net interaction ferro or antiferromagnetic.

Finally we have substituted in model 1 the sulphur atoms in the bridge by oxygen atoms (with Cu–O distance = 2.5 Å), obtaining a model with a similar bridge of **2** (model 3) but topologically is close to compound **1**. The calculated J value is +6.9 cm^{-1}, which is large than the calculated for compound **2** by the model 2 (Fig. 9). This agrees with the great ferromagnetic J value calculated for compound **1** by model 1, indicating the domain of the $2K_{ab}$ term.

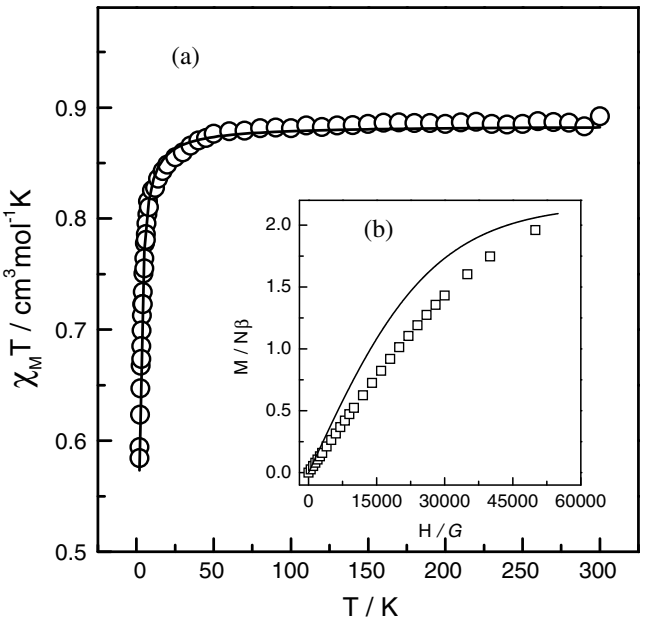

Fig. 10. (a) Plot of the $\chi_M T$ *vs.* T for compound **3**. The squares and solid line are the experimental values and the best fit respectively. (b) The field dependence of magnetization at 2 K for compound **3** (per Cu_2).

*3.5.2. Magnetic study on complex **3***

The magnetic properties of a powder sample of complex **3** are represented as $\chi_M T$ versus T in Fig. 10a. At room temperature, the $\chi_M T$ value of the presented complex is 0.883 $cm^3\ mol^{-1}$ K. This value correspond to two isolated copper(II) ions with one unpaired electron with $g = 2.17$. With decreasing temperature, the $\chi_M T$ value remains almost constant until ca. 25 K and then it decreases sharply, giving the minimum value of 0.594 cm^3 K mol^{-1} at 2 K. The drop in $\chi_M T$ at low-temperatures indicates the presence of a very weak antiferromagnetic coupling between the copper(II) ions.

Analysis of the experimental magnetic data was performed by using the Bleaney–Bowers expression, based on the following isotropic Hamiltonian: $H = -J(S_1 \cdot S_2)$:

$$\chi_M = \frac{Ng^2\mu_B^2}{kT}\frac{2\exp(J/kT)}{1+3\exp(J/kT)} \quad (2)$$

The parameters N, μ_B and k in Eq. (2) have their usual meanings, J = Singlet–triplet splitting. Least-square fitting of experimental data leads to the following parameter $J = -1.6\ cm^{-1}$ and $g = 2.17$.indicating a very weak coupling, as may be expected from the 4,4′-bipyridyl bridge. This weak magnetic exchange can be understood considering the large Cu···Cu distance (11.15 Å).

The very weak antiferromagnetic interaction was confirmed by magnetization measurements at 2 K up to an external field of 5.5 T. At higher field, the magnetization in M/Nβ units indicates a two isolated quasi-saturated $S = 1/2$ system for the compound (Fig. 10b). Comparison of the overall shape of the plot with the Brillouin plot for a fully two isolated ion with $S = 1/2$ system indicates very slower magnetization which consistent with a weak antiferromagnetic interaction.

The EPR of spectra complex **3** at low-temperatures maintain the same shapes and g values as the EPR spectrum at room temperature. The EPR spectrum of the studied compound shows three signals that are quite close and partially overlapped, (see Fig. S5, Supplementary data). The spectrum is a typical rhombic one with three g values at $g_1 = 2.24$, $g_2 = 2.09$ and $g_3 = 2.027$ for the compound. It is necessary to highlight that the foregone signal of $DMs = \pm 2$ for a triplet which should appear in the range 1500–1600 G have not been observed for the complexes **1**, **2** and **3**.

The weak exchange pathways parameter, J; observed in **3** was confirmed by the density functional calculations where the experimental atomic co-ordinates of the compound were performed to obtain the J value, giving -0.3 cm^{-1}. In this compound the spin distribution is mainly localized in d($x^2 - y^2$) orbital as we can observe in the Fig. S6 (Supplementary data) due to the large separation between the Cu(II) paramagnetic centers.

3.6. Computational details

The followed computational strategy to calculate the exchange coupling constants in transition metal complexes was described in previous papers [42–44]. The exchange coupling constants are introduced by a phenomenological Heisenberg Hamiltonian $H = -\sum JS_i \cdot S_j$ (where i and j make reference to the different paramagnetic centers) to describe the interactions between the two paramagnetic transition metals present in the dinuclear complex.

The hybrid B3LYP functional [45] has been used in all calculations as implemented in GAUSSIAN-03 [46] mixing the exact Hartree–Fock-type exchange with Becke's expression for the exchange functional [47] and that proposed by Lee–Yang–Parr for the correlation contribution [48]. Such functional provides calculated J values in excellent agreement with the experimental values [42,49,50]. Basis sets proposed by Schaefer et al. have been employed throughout, triple-ζ quality for the copper atoms [51] and double-ζ for main group elements [52].

4. Conclusion

On a final note, a study on the difference in magnetic behavior of the complexes **1** and **2** has revealed that the major factor in controlling the magnetic interaction between the Cu atoms is the overlap between the parallel orbitals on the bridge. Both the bridging donor atom and the ligand topology are contributory factors for an effective overlap. Further, molecular modelling studies between these two complexes have led to a conclusion that the ligand topology factor dominates the bridging donor atom factor. From a synthetic point of view, ligand HL_2 demonstrates two possible binding modes in complex **2** and **3**. Such versatility in its binding modes has been instrumental in the pH dependant conversion of **3** into **2**. Both the complexes are weakly antiferromagnetic but have slightly different magnetic properties. This phenomenon opens the door towards the potential use of similar ligand systems of multi-utility for the design of metal complexes with magnetic properties tuneable with change of pH of the medium.

Acknowledgements

Acknowledgement is made to the University Grants Commission, New Delhi, India, for awarding a major research project in science [F.30-65/2004(SR)] to S.K. Kar, M. Salah El Fallah and JavierTercero acknowledges the support through grants given by The financial support given by the Spanish (CTQ2006-01759, CTQ2005-08123-C02-02/BQU) and Catalan (2005SGR-00593, 2005SGR-00036) governments. J. Tercero is grateful to the Centre de Computació de Catalunya (CESCA) with a grant provided by Fundació Catalana per a la Recerca (FCR) and the Universitat de Barcelona.

Appendix A. Supplementary data

CCDC 674803, 674804 and 674805 contain the supplementary crystallographic data for the complexes **1**, **2** and **3**. These data can be obtained free of charge via http://www.ccdc.cam.ac.uk/conts/retrieving.html, or from the Cambridge Crystallographic Data Centre, 12 Union Road, Cambridge CB2 1EZ, UK; fax: (+44) 1223-336-033; or e-mail: deposit@ccdc.cam.ac.uk. Other supplementary materials contain epr spectral diagrams at 4 K for complexes **1**, **2**, **3** (Figs. S2, S3, S5), H-bonding mode of complex **3** (Fig. S1), Spin density maps of complexes **1** and **3** (Figs. S4 and S6), table for bond distances of complexes **1**, **2**, **3** (Table S1) and another table containing parameters for assigning the nitrate binding mode of complex **1**, **2**, **3** (Table S2). Supplementary data associated with this article can be found, in the online version, at doi:10.1016/j.poly.2008.05.009.

References

[1] (a) K.D.Karlin, Karlin, Z.Tyeklàr, Tyeklàr, Bioinorganic Chemistry of Copper, Chapman & Hall, New York, 1993;
(b) K.D.Karlin, Karlin, Z.Tyeklàr, Tyeklàr, A.D. Zuberbühler, in: J. Reedijk (Ed.), Bioinorganic Catalysis, Marcel Dekker, New York, 1993, p. 261;
(c) K.D. Karlin, S. Kaderli, A.D. Zuberbühler, Acc. Chem. Res. 30 (1997) 139;
(d) K.D. Karlin, S. Kaderli, A.D. Zuberbühler, W.B. Tolman, Acc. Chem. Res. 30 (1997) 327.
[2] (a) K.D. Karlin, Y. Gultneh, Prog. Inorg. Chem. 35 (1987) 219;
(b) Z. Tyeklàr, K.D. Karlin, Acc. Chem. Res. 22 (1989) 241;
(c) K.D. Karlin, Z. Tyeklàr, Adv. Inorg. Biochem. 9 (1993) 123;
(d) T.N. Sorrell, Tetrahedron 45 (1989) 3;
(e) P.A. Vigato, S. Tamburini, D.E. Fenton, Coord. Chem. Rev. 106 (1990) 25.
[3] (a) (a) N. Kitajima, Adv. Inorg. Chem. 39 (1992) 1;
(b) N. Kitajima, Y. Moro-oka, Chem. Rev. 94 (1994) 737;
(c) L.I. Simàndi, Catalytic Activation of Dioxygen by Metal Complexes, Kluwer, Dordrecht, 1992 (Chapter 5);
(d) E. Spodine, J. Manzur, Coord. Chem. Rev. 119 (1991) 171;
(e) S. Mahapatra, J. Halfen, A.E.C. Wilkinson, G. Pan, C.J. Cramer, L Que.L.Q. Jun, W.B. Tolman, J. Am. Chem. Soc. 117 (1995) 8865.
[4] (a) E.I. Solomon, M.J. Baldwin, M.D. Lowery, Chem. Rev. 92 (1992) 521;
(b) E.I. Solomon, in: T.G. Spiro (Ed.), Copper Proteins, Wiley, New York, 1981. (Chapter 2);
(c) K. Lerch, Life Chem. Rep. 5 (1987) 221;
(d) D.A. Robb, in: R. Lontie (Ed.), Copper Proteins and Copper Enzymes, vol. 2, CRC Press, Boca Raton, FL, 1984;
(e) R. Gupta, S. Mukherjee, R. Mukherjee, J. Chem. Soc., Dalton Trans. (1999) 4025.
[5] C.A. Reed, R.D. Orosz, Spin Coupling Concepts in Bioinorganic Chemistry, in: C.J. O'Connor (Ed.), World Scientific, Singapore, 1993, p. 351.
[6] (a) K.A. Magnus, H. Ton-That, J.E. Carpenter, Chem. Rev. 94 (1994) 727;
(b) E.I. Solomon, U.M. Sundaram, T.E. Machonkin, Chem. Rev. 96 (1996) 2563.
[7] F. Zippel, F. Ahlers, R. Werner, W. Haase, H.-F. Noltine, B. Krebs, Inorg. Chem. 35 (1996) 3409.
[8] A.J. Blake, S.J. Hill, P. Hubberstey, W-S. Li, J. Chem. Soc., Dalton Trans. (1998) 909.
[9] S.K. Ghosh, J. Ribas, P.K. Bharadwaj, Cryst. Eng. Commun. 6 (45) (2004) 250.
[10] R.I. Baldoma, M. Monfort, J. Ribas, X. Solans, M.A. Maestro, Inorg. Chem. 45 (2006) 8144.
[11] (a) R.B. Robson, F. Abrahams, S.R. Batten, R.W. Gable, B.B.F. Hoskins, J. Liu, Supramolecular Architecture, ACS, Washington, DC, 1992. (Chapter 19);
(b) M.Y. Fujita, J. Kwon, S. Washizu, S.K. Ogura, J. Am. Chem. Soc. 116 (1994) 1151;
(c) G.R. Desiraju, Crystal Engineering: The Design of Organic Solids, Elsevier, Amsterdam, 1989;
(d) G.R. Desiraju, Angew. Chem. 107 (1995) 2541;
(e) G.R. Desiraju, Angew. Chem., Int. Ed. Engl. 35 (1995) 2311.
[12] J.S. Seo, D. Whang, H. Lee, S.I. Jun, J. Oh, Y.J. Jeon, K. Kim, Nature 404 (2000) 982. and references cited therein.
[13] M. Kondo, T. Okubo, A. Asami, S. Noro, T. Yoshimoti, S. Kitagawa, T. Ishii, H. Matsukawa, K. Seki, Angew. Chem., Int. Ed. Engl. 38 (1999) 140. and references cited therein.
[14] (a) E. Coronado, P. Delhaes, D. Gatteschi, J.S. Miller (Eds.), Molecular Magnetism: from Molecular Assemblies to DeVices, NATOASI Series E3211996, Kluwer, Dordrecht, The Netherlands;
(b) J.S. Miller, M. Drillon (Eds.), Magnetism: Molecules to Materials, vols. 1–52000–2005, Wiley, New York.
[15] (a) J. Garcia-Tojal, M.K.R. Cortes, L. Lezama, M.I. Arriortua, T.J.T. Rojo, J. Chem. Soc., Dalton Trans. (1994) 2233;
(b) P. Gomez-Saiz, J. Garcia-Tojal, A. Mendina, B. Donadieu, L. Lezama, J.L. Pizarro, M.I. Arriortua, Eur. J. Inorg. Chem. (2003) 518.
[16] N. Gupta, S. Mukerjee, S. Mahapatra, M. Ray, R. Mukherjee, Inorg. Chem. 31 (1992) 39.
[17] D. Ghosh, R. Mukherjee, Inorg. Chem. 37 (1998) 6597.
[18] H. Bredereck, R. Sell, F. Effenberger, Chem. Ber. 97 (1964) 3406.
[19] S. Pal, A.K. Barik, P. Aich, S.M. Peng, G.H. Lee, S.K. Kar, Struct. Chem. 18 (2007) 149.
[20] B. Chiswell, F. Lions, Aust. J. Chem. 22 (1961) 71.
[21] G.M. Kosolapoff, C.H. Roy, J. Org. Chem. 26 (1961) 1895.

[22] M.P.V. Boarland, J.F.W. McOmie, R.N. Timms, J. Chem. Soc. (1952) 4693.
[23] (a) S.C. Ghan, L.L. Koh, P.H. Leung, J.D. Ranford, K.Y. Sim, Inorg. Chim. Acta 23 (1995) 101;
(b) E.W. Ainscough, A.M. Brodie, J.D. Ranford, J.M. Waters, K.S. Murray, Inorg. Chim. Acta 197 (1992) 107.
[24] M. Joseph, V.M. Suni, R.P. Kurup, M. Nethaji, A. Kishore, S.G. Bhat, Polyhedron 23 (2004) 3069.
[25] K. Nakamoto, Infrared and Raman Spectra of Inorganic and Coordination Compounds, 5th ed., Part B, Wiley, New York, p. 88.
[26] N.F. Curtis, Y.E.M. Curtis, Inorg. Chem. 4 (1965) 804.
[27] (a) D.X. West, N.M. Kozub, G.A. Bain, Transition Met. Chem. 21 (1996) 52;
(b) D.X. West, J.S. Ives, J. Krejct, M.M. Salberg, T.L. Zumbahlen, G.A. Bain, A.E. Liberta, J.V. Martinez, S.H. Ortiz, R.A. Toscano, Polyhedron 14 (1995) 2189.
[28] E. Ainscough, A.M. Brodie, N.G. Larsen, Inorg. Chim. Acta 60 (1982) 25.
[29] A.B.P. Lever, Inorganic Electronic Spectroscopy, 2nd ed., Elsevier, Amsterdam, 1984.
[30] S.K. Mandal, L.K. Thompson, K. Nag, J.P. Charland, E.J. Gabe, Inorg. Chem. 26 (1987) 1391.
[31] E. Ainscough, A.M. Bordie, E.N. Bake, R.J. Cresswell, J. Ranford, J.M. Waters, Inorg. Chim. Acta 172 (1990) 185.
[32] V. Philip, V. Suni, M.R.P. Kurup, M. Nethaji, Polyhedron 23 (2004) 1225.
[33] M. Joseph, V. Suni, M.R.P. Kurup, M. Nethaji, A. Kishore, S.G. Bhat, Polyhedron 23 (2004) 3069.
[34] A.W. Addison, T.N. Rao, J. Chem. Soc., Dalton Trans. (1984) 1349.
[35] (a) R. Han, G. Parkin, J. Am. Chem. Soc. 113 (1991) 9707;
(b) C. Kimblin, V.J. Murphy, T. Hascall, B.M. Bridgewater, J.B. Bonanno, G. Parkin, Inorg. Chem. 39 (2000) 967.
[36] G.J. Kleywegt, W.G.R. Wiesmeijer, G.J. Van Driel, W.L. Driessen, J. Reedijk, J.H. Noordik, J. Chem. Soc., Dalton Trans. (1985) 2177.
[37] H. Saimiya, Y. Sunatsuki, M. Kojima, S. Kashino, T. Kambe, M. Hirotsu, H. Akashi, K. Nakajima, T. Tokii, J. Chem. Soc., Dalton Trans. (2002) 3737.
[38] (a) H. Adams, N.A. Bailey, I.K. Campbell, D.E. Fenton, Q.Y. He, J. Chem. Soc., Dalton Trans. (1996) 2233;
(b) D. Black, A.J. Blake, K. Dancey, P. Harrison, A.M. McPartlin, S.P. Parsons, P.A. Tasker, A.G. Whittaker, M. Schröder, J. Chem. Soc., Dalton Trans. (1998) 3953;
(c) Y. Sunatsuki, M. Nakamura, N. Matsumoto, F. Kai, Bull. Chem. Soc. Jpn. 70 (1997) 1851;
(d) M. Vaidyanathan, R. Viswanathan, M. Palaniandavar, T. Balasubramanian, P. Prabhakaran, T.P. Muthiah, Inorg. Chem. 37 (1998) 618.
[39] B. Bleaney, K.D. Bowers, Proc. Roy. Soc. London, Ser. A 214 (1952) 451.
[40] J. Tercero, E. Ruiz, S. Alvarez, A. Rodríguez-Fortea, P. Alemany, J. Mater. Chem. 16 (2006) 2729. and references cited therein.
[41] P.J. Hay, J.C. Thibeault, R. Hoffmann, J. Am. Chem. Soc. 97 (1975) 4884.
[42] E. Ruiz, P. Alemany, S. Alvarez, J. Cano, J. Am. Chem. Soc. 119 (1997) 1297.
[43] E. Ruiz, A. Rodríguez-Fortea, J. Cano, S. Alvarez, P. Alemany, J. Comp. Chem. 24 (2003) 982.
[44] E. Ruiz, J. Cano, S. Alvarez, P. Alemany, J. Comp. Chem. 20 (1999) 1391.
[45] A.D. Becke, J. Chem. Phys. 98 (1993) 5648.
[46] M.J. Frisch, G.W. Trucks, H.B. Schlegel, G.E. Scuseria, M.A. Robb, J.R. Cheeseman, J.A. Montgomery, T. Vreven, K.N. Kudin, J.C. Burant, J.M. Millam, S.S. Iyengar, J. Tomasi, V. Barone, B. Mennucci, M. Cossi, G. Scalmani, N. Rega, G.A. Petersson, H. Nakatsuji, M. Hada, M. Ehara, K. Toyota, R. Fukuda, J. Hasegawa, H. Ishida, T. Nakajima, Y. Honda, O. Kitao, H. Nakai, M. Klene, X. Li, J.E. Knox, H.P. Hratchian, J.B. Cross, C. Adamo, J. Jaramillo, R. Gomperts, R.E. Stratmann, O. Yazyev, A.J. Austin, R. Cammi, C. Pomelli, J. Ochterski, P.Y. Ayala, K. Morokuma, G.A. Voth, P. Salvador, J.J. Dannenberg, V.G. Zakrzewski, S. Dapprich, A.D. Daniels, M.C. Strain, O. Farkas, D.K. Malick, A.D. Rabuck, K. Raghavachari, J.B. Foresman, J.V. Ortiz, Q. Cui, A.G. Baboul, S. Clifford, J. Cioslowski, B.B. Stefanov, G. Liu, A. Liashenko, P. Piskorz, I. Komaromi, R.L. Martin, D.J. Fox, T. Keith, M.A. Al-Laham, C.Y. Peng, A. Nanayakkara, M. Challacombe, P.M.W. Gill, B. Johnson, W. Chen, M.W. Wong, C. Gonzalezm, J. A. Pople, GAUSSIAN 03 (Revision B.4), Pittsburgh, PA, 2003.
[47] A.D. Becke, Phys. Rev. A 38 (1988) 3098.
[48] C. Lee, W. Yang, R.G. Parr, Phys. Rev. B 37 (1988) 785.
[49] E. Ruiz, J. Cano, S. Alvarez, P. Alemany, J. Am. Chem. Soc. 120 (1998) 11122.
[50] E. Ruiz, S. Alvarez, A. Rodríguez-Fortea, P. Alemany, Y. Pouillon, C. Massobrio, in: J.S. Miller, M. Drillon (Eds.), Electronic Structure and Magnetic Behavior in Polynuclear Transition-metal Compounds, Wiley-VCH, Weinheim, 2001.
[51] A. Schaefer, C. Huber, R. Ahlrichs, J. Chem. Phys. 100 (1994) 5829.
[52] A. Schaefer, H. Horn, R. Ahlrichs, J. Chem. Phys. 97 (1992) 2571.

Polyhedron 27 (2008) 2529–2538

Contents lists available at ScienceDirect

Polyhedron

journal homepage: www.elsevier.com/locate/poly

Density functional theory calculations of novel Rh(I) diphosphinite catalysts

Graeme J. Gainsford [a,*], Andrew Falshaw [a], Cornelis Lensink [a], Michael Seth [b]

[a] Industrial Research Limited, P.O. Box 31-310, Lower Hutt, New Zealand
[b] Chemistry Department, University of Calgary, Calgary, Alberta, Canada T2N 1N4

ARTICLE INFO

Article history:
Received 17 March 2008
Accepted 1 May 2008
Available online 13 June 2008

Keywords:
Asymmetric catalysis
DFT calculations
Enantiomeric excess
Rh(I) catalyzed asymmetric hydrogenation
Diphosphinite ligands
Transition state energies

ABSTRACT

Novel Rh(I) diphosphinite catalysts [Rh((*R*,*R*)-3,4-(bis(*O*-diphenylphosphino)-1,2,5,6-tetra-*O*-methyl-*chiro*-inositol)]+ ([Rh-CANDYPHOS]+) and [Rh((*R*,*R*)-3,4-(bis(*O*-diphenylphosphino)-1,2,5,6-tetra-*O*-ethyl-*chiro*-inositol)]+ ([Rh-EtCP]+) have been prepared utilizing naturally-occurring resources. Potential energy surfaces for the catalyzed asymmetric hydrogenation of the prochiral enamides methyl-(*Z*)-α-acetamido cinnamate, methyl-(*Z*)-α-acetamido cinnamic acid and dimethyl itaconate have been surveyed using density function theory (DFT) methods. Key transition states were identified from previous [Rh((*R*,*R*)-DUPHOS)]+ studies for the two diastereoisomeric manifolds [1,2]. Transition state energies were found starting from models based on (1) the X-ray structure of the active complex (CANDYPHOS)(η^4-(*Z*,*Z*)-cyclo-octa-1,5-diene)-rhodium(I) tetrafluoroborate $CHCl_3$ solvate [3] and (2) models in which the complex (without substrate) started with C2 molecular symmetry. The difficulties encountered in calculations of the transition state energies of large cations are outlined and limitations noted. Transition state enthalpy values are compared with the observed experimental free energy differences results and previous studies [1,2]. The predictive aspects of the calculations appear to be limited with the starting models playing an important part in the absolute value of the final energies.

© 2008 Elsevier Ltd. All rights reserved.

1. Introduction

Interest in highly selective asymmetric catalysis continues at a significant level [4] both from synthetic [3] and computational modelling perspectives [2,5–7,20]. In particular we observe that research into asymmetric hydrogenation involving new metal diphosphine/diphosphinite-based compounds [8–13], mono-phosphine/phosphite metal catalysts [9,14–22], including mixtures of chiral and achiral species [23,24], and more recently self-assembled cyclic monophosphanes [25] as well as improved methods for testing their efficiency [26,27] is intense. This is undoubtedly spurred on by the need to produce high value chiral products economically as noted by Knowles [28] and reviewed recently [4]. In passing we note also the considerable interest in "heterogenized"-homogeneous catalysts, where the active catalyst is attached to a heterogeneous framework [4,27,29], reactions involving biphasic [30,31] and continuous hydrogenation membrane systems [32]. An alternative to the quadrant rule [33] used in prediction has also been recently proposed [7] and we note the multiple model calculations of BINOL-based monophosphite Rh catalysts [20]. Finally, for completeness, we record a recent publication which noted that even for the well-studied [Rh(I)-binap]+ catalyzed reactions the mechanism "is still controversial" [34] as to whether it goes via the dihydride pathway (initial formation of dihydride) [35] or the "alkene" or "unsaturated" route [36,37] via an initial Rh-substrate complex (as shown in Scheme 1).

Along with the synthesis of novel homogeneous chiral bis- and mono-phosphinite catalysts, for which both enantiomeric sources were readily available, we were interested to ascertain whether the density functional calculations (DFT) could provide timely and accurate predictions of the enantiomeric excess (ee) for a general reaction with a specific, and with an homologous catalyst. The difficulty of this task was known: DFT energies are usually accurate to a few kcal/mol while ee's require accuracy of 1 kcal/mol. We began with the advantage of previous mechanistic studies providing knowledge of the mechanism of the reaction and of the enantio-determining steps (see full Refs. 2 and 3 in [2]). Although previous papers noted some energy resolution concerns [6], we anticipated that these would be ameliorated through the subtraction of systematic errors in the difference energy calculations for the (two) energy states.

In order to expedite the process, and take advantage of the previous modelling and kinetically-derived mechanisms [2,38], we chose our initial models from those reported for [Rh((*R*,*R*)-DUPHOS)]+ by Feldgus and Landis [1], (hereafter DUPHOS, see Fig. 1) noting that their more comprehensive report [39] suggested different enantiomeric results could result when the substituent at the alpha-carbon site of the enamide was changed.

* Corresponding author. Tel.: +64 4 931 3518; fax: +64 4 931 3142.
E-mail address: g.gainsford@irl.cri.nz (G.J. Gainsford).

0277-5387/$ - see front matter © 2008 Elsevier Ltd. All rights reserved.
doi:10.1016/j.poly.2008.05.011

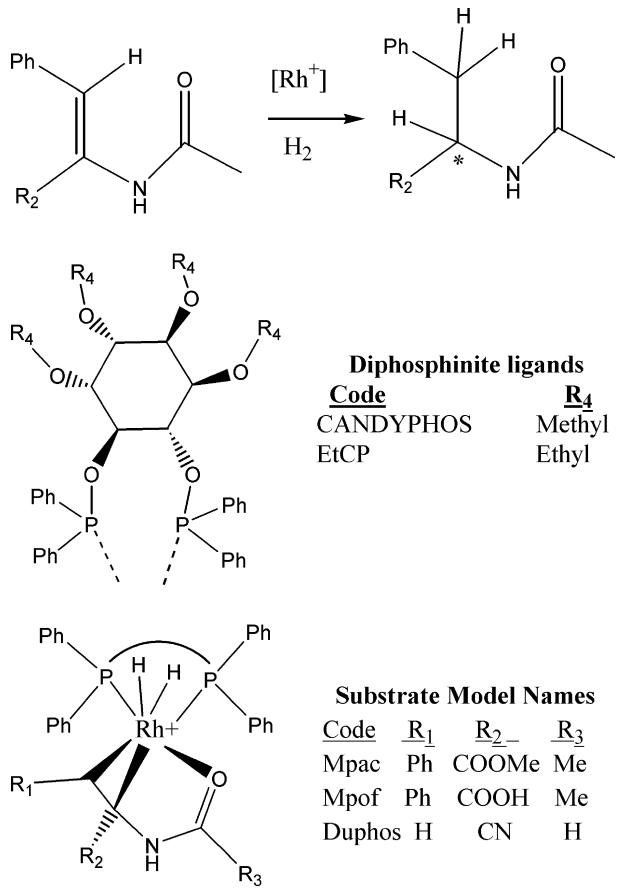

Scheme 1. Overall reaction and model names. *Scheme Key*: Dihydride transition states for the substrate models; for DUPHOS see Ref. [1]. In data tables below, the EtCP-based catalysts are distinguished from the CANDYPHOS ones by the prefix Et (e.g. Mpac and EtMpac).

Our initial calculations with the electron withdrawing cyano group [as in [1]] gave us confidence that we were reproducing both similar energies and geometries (Table 1).

Reference to the compositions shown in Scheme 1 and Fig. 1 show that this work incorporates a new level of detail particularly for the substrate molecule compared with the earlier DUPHOS[1] simplifications. The evaluation involved using a standard Kohn–Sham density functional theory programme suite [40,41] in full DFT mode on two homologous catalysts: [Rh-CANDYPHOS]+ and [Rh-EtCP]+ and three substrates: methyl(*Z*)-α-acetamido cinnamate, methyl(*Z*)-α-acetamido cinnamic acid and dimethyl itaconate (Fig. 1a–c).

2. Results and discussion

We begin this report with an examination of the critical elements of the methodology.

2.1. A. Finding the transition states

The refinement of any model to a transition state (for which the Hessian matrix has a negative eigenvalue) [42] for these molecules is a difficult exercise. A potential energy surface of this dimension will include numerous saddle points and probably several of them in the neighborhood of the saddle point of interest. Ensuring that a transition state search finds the correct saddle point can be a challenge, especially if one or more of the nearby saddle points are lower in energy. In the DUPHOS models [1], there are 4 transition states of significance as recently confirmed in the study by Donoghue et al. [2]. We use the same labels here for the minor and major manifolds (min/MAJ: the major manifolds are labelled in capitals): these are sqpl(SQPL) {the square planar starting complex plus hydrogen molecule}, iid-a‡ (IIDA‡), molh(MOLH), molh‡(MOLH‡) and dihy(DIHY) for the A (approach) series. The highest, and rate determining transition state is the third (MOLH‡) with a typical dihydride H–H distance ~1.28 Å, Rh–H distances ~ 1.6 Å, and H–Rh–H angle ~45° (Table 2; for full description see text and Fig. 6 in Ref. [1]).

For our DUPHOS "proofing" calculations (Table 2), convergence from the provided coordinates was straightforward to the expected values, although the energy differences were rather smaller than previous studies (see Fig. 3 drawn in the Donoghue style [2]). We elected to concentrate on the central transition state (MOLH‡) and the two adjacent states.

2.2. B. Establishing the transition state energies

2.2.1. Reproducibility

In the process of building models from a combination of the X-ray structural parameters for 1L-Rh(CANDYPHOS)+ [3] and the published transition states in DUPHOS, we came to the first decision point: was the reproducibility of electronic energy (and geometry) in the gas-phase calculations for these larger molecules (>100 atoms including Rh) sufficient? Our overall conclusion from a variety of model compounds (the variants of the substrate as we built intermediate models from the CN-bound simplified DUPHOS substrate model to the full methyl(*Z*)-α-acetamido cinnamate (see Fig. 1)) was that the reproducibility was only just adequate (±~0.3 kcal/mol). Our worst agreement of 0.45 kcal/mol occurred when we started from significantly different starting models, using the default integration accuracy parameter of 4.0. In ADF this parameter approximately corresponds to the number of significant figures in the calculated numbers. For all our final calculations therefore we used the more accurate integration accuracy parameter of 5.0.

2.2.2. Convergence parameters

The next decision point concerned the need to establish termination limits for the converging parameters; for any non-linear problem, both the significance level of the calculations and the criteria for three differently determined factors in the ADF package (energy gradient slope, energy differences and distance movement

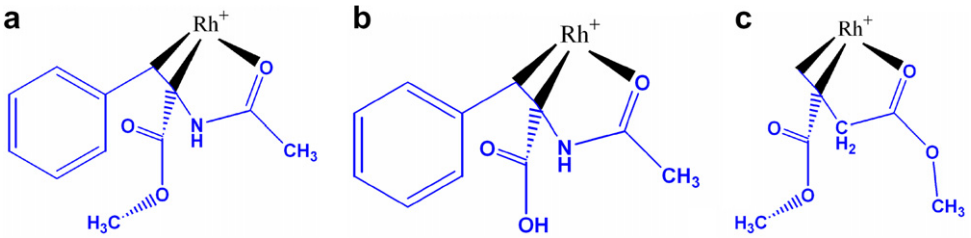

Fig. 1. The target substrates as bound to Rh(I).

Table 1
Initial energies for the key transition state (MOLH‡)

Compound	E-internal	E-electronic	S-Entropy	Total	Δ*E* (total)	Δ*E* (electronic)
MAJ	327.85	−8333.57	0.18409	−8060.61	–	–
MIN	327.92	−8329.67	0.18645	−8057.34	3.27	3.90
Ref. [1]	all *E*'s in kcal/mol				3.61	4.60

Table 2
Selected minor manifold path A transition state data[a]

Transition state	Relative free energy	Relative electronic energy	$H_a \cdots H_b$ (Å)	Rh–H (Å) (average)	H_a–Rh–H_b (*a*) °
molh	12.5	0.1	0.82	1.80	30
molh‡	16.0	4.4	1.23	1.60	45
dihy	13.5	1.2	1.88	1.56	73

[a] *Key*: from [1], see Fig. 2 for definition; all energies kcal/mol.

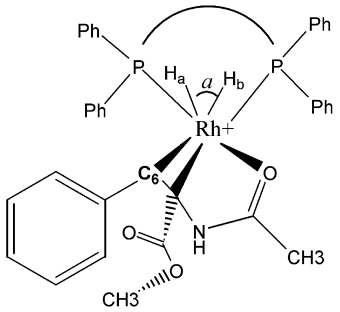

Fig. 2. Mpac1 transition state parameters (Table 2).

for the atoms) must be set to obtain accurate results within a practical refinement time (assuming of course that the refinement does not involve untoward oscillation in energies). The recommended minimum integration limit (of 5 significant figures) in the ADF [40] package was used for final calculations, although a limit of 4 (4.0) was frequently applied for QM/MM runs. A series of trials were run with variations of the limiting ratio for energy, gradient and Cartesian coordinates. Reducing the default parameters to one-tenth of the standard values (i.e. to 0.0001, 0.001 and 0.001) prolonged stable refinements unnecessarily with no significant change in total energy (<0.05 kcal/mol). At the same time, less stable refinements (see saddle point location below) frequently bypassed the requested (using a dihydride H–H distance restraint) or expected saddle points. Using empirical trials we came up with a compromise set of 0.0002 (tolE), 0.01 (tolG) and 0.012 (tolCART) for ADF [40]. It was sometimes necessary to reduce the maximum step size to values as low as 0.005 Å to ensure that the search converged on the saddle point of interest. In a few cases which were consistent with the rather flattened saddle point profiles (see below) these convergence parameters gave final cycles with oscillating enthalpy values, within a range of 0.2 kcal/mol.

2.2.3. Saddle point location: strategy

Our initial success in locating saddle points based on the DUPHOS models was not always repeated for the various models built on the same frameworks in which the DUPHOS ligand was replaced with CANDYPHOS or EtCP and/or the simplified substrates were progressively converted to the actual (experimental) substrates. It is our contention that this reflects different shaped energy surfaces as determined by examining (and plotting) these using the internal reaction coordinate (IRC) feature of the ADF package. An example plot, the XMpof2 MOLH‡ transition state, is given in Fig. 4 to illustrate the commonly observed flat gradients, width and asymmetry.

2.2.4. Starting models

The X-ray structural study result for the CANDYPHOS ligand both bound to Rhodium(I) [3] and free [10] represent ground (and solid) state results. We became concerned that this might not be close enough to the real solution (*in situ)* situation when the CANDYPHOS ligand would (at least initially on release of the

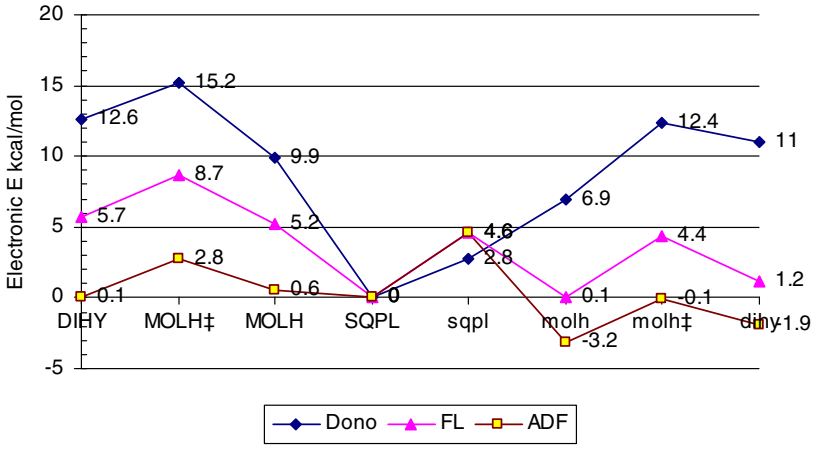

Fig. 3. Calculated enthalpies for DUPHOS models: FL [1], Dono [2], ADF this work.

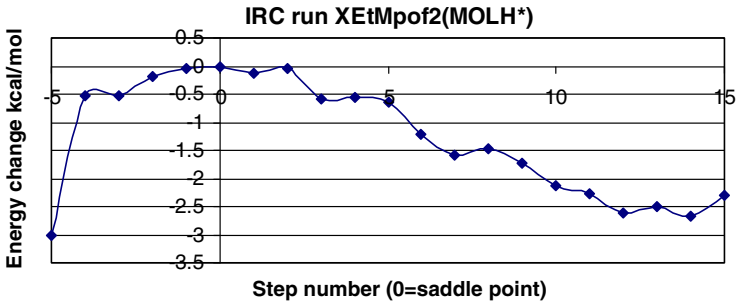

Fig. 4. Enthalpy energy change over the XEtMpof2 saddle point from internal reaction coordinate calculation.

Rh-bound cyclo-octadiene ligand) start from a state with approximate C2-symmetry. Consequently we transformed the X-ray structure-based starting models to a C2-symmetrical state and began a new series of transition state searches. As summarized (Table 3), the transition state attained from this new C2-symmetric start did not convert to the (X) ground-state "non-symmetrical state" found in the crystal structure (Fig. 5) and energies were significantly different: in this case the difference was 6.8 kcal/mol (entries Xmpac2 and C2Mpac2, Table 4). This dramatically emphasizes the requirement that both enantiomers in the two manifolds must be as similar in conformation for a comparative energy to have any meaning. To ensure this point is clear, we have included results for both sets in Tables 3–5 (complex names are prefixed by X or C2 accordingly).

Table 3
Major structural differences (Å,°) in Mpac2 transition state models (Fig. 5A and B)

Atoms	XMpac2	C2Mpac2
Rh–P10	2.264	2.243
Rh–P11	2.388	2.402
Rh–O2	2.164	2.190
Rh–C6	2.172	2.134
P10–Rh–P11	90.4	96.5
P11–Rh–O2	89.3	80.9
O–P11–Rh–P10	−4.8	−33.3
C–O–P11–Rh	−72.9	68.8
P10–Rh–P11–C40	107.9	−140.5
P10–Rh–P11–C39	−132.6	102.4
P11–Rh–P10–C38	−61.9	−74.5
P11–Rh–P10–C37	172.8	161.0

Having recognized that conversion from different conformations of the phenyl rings in the Mpac series was unlikely, we noted that (at least) two different conformations were obvious for the dimethyl itaconate models as shown in Fig. 6. We labelled these Cdmit and CdMeS, respectively (Table 5).

2.2.5. Electronic energies and Gibbs free energies

Our initial trials using DUPHOS suggested that entropy contributions to the transition state energies were small and that zero point energies were not significantly different for the same transition states: room temperature difference of the TS term was 0.7 kcal/mol (Table 1). Although this difference approaches a significant energy, it was anticipated that a cancellation effect would prevail, meaning that electronic energies alone could be used for comparative purposes. The calculation time for the entropy energies is essentially six times the number of atoms longer: so a typical calculation in this 112 atom structure is 672 times one equivalent electronic energy calculation. At present with our 4-cpu cluster, the latter takes around 75 cpu minutes ... the entropy calculation ~36 days! In a recent check calculation using our most studied molecule (Fig. 1a), we found that the difference in vibrational entropy contribution was around 9.4 cal/mol K (cf. 2.4 for DUPHOS) corresponding to a different number of contributing vibrational frequencies leading to an "apparent" entropy difference between the two transition states of 2.5 kcal/mol at room temperature (in this case the total difference between MAJOR and minor energies widened from 4.2 to 6.7 kcal/mol). Moreover, the zero point energies of these two transition states were different by ~0.5 kcal/mol (again increasing the overall difference). We therefore note that the difference in total energy, including the entropy contribution and the

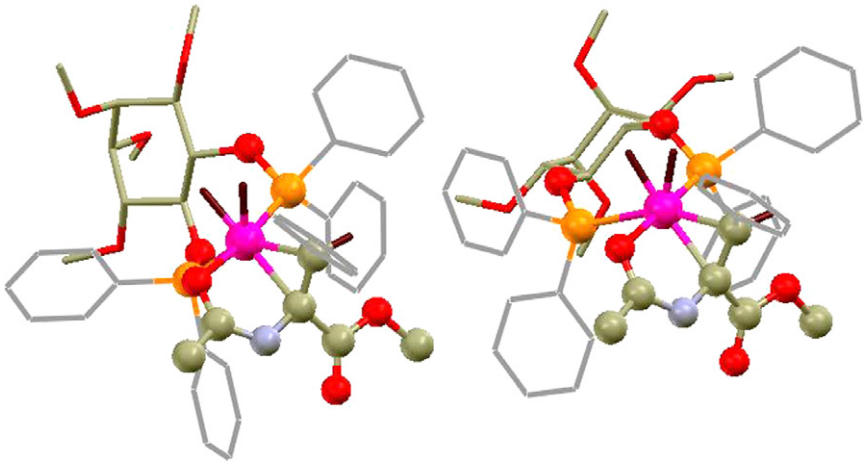

Fig. 5A. XMpac2 (left) and C2Mpac2 (right) final transition state models: only the dihydride and C6 hydrogen atoms are shown. All phenyl groups in stick form; CANDYPHOS with thick bonds. Atom colors: O, red; Rh, pink; P, orange; N, blue; C, gray; H, black. (For interpretation of the references to colour in this figure legend, the reader is referred to the web version of this article.)

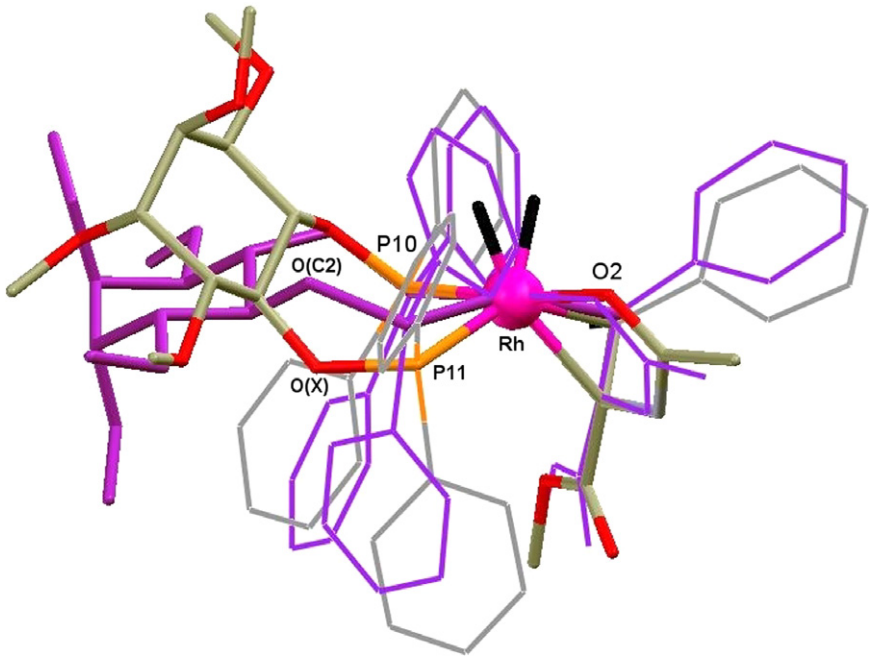

Fig. 5B. Overlap plot of XMpac2 (atoms colored) and C2Mpac2 (in purple) final transition state models (see text). Only the dihydride hydrogens are shown for clarity. All phenyl groups in stick form; CANDYPHOS with thick bonds. Atom colors: as for Fig. 5A. (For interpretation of the references to colour in this figure legend, the reader is referred to the web version of this article.)

Table 4
Calculated transition state electronic energies[a] and MOLH‡ geometry[b] for Cinnamate complexes (see Fig. 1 a and b)

Complex	SQPL (0.0) kcal/mol	MOLH kcal/mol	MOLH‡ kcal/mol	$H_a\cdots H_b$ Å	H_a–Rh–H_b °	$H_a\cdots C_6$ Å	DIHY kcal/mol
DUPHOS MAJ	−8088.8	0.6	2.8	1.24	44.9	2.60	15.8
DUPHOS min	−8084.2	−7.8	−4.7	1.21	43.9	2.52	6.5
XMpac1	−15522.8	0.4	−0.8	1.33	49.1	2.51	3.5
XMpac2	−15528.2	−2.0	0.4	1.28	46.4	2.52	−1.5
C2Mpac1	−15525.7	−1.4	8.6	1.28	47.4	2.61	3.5
C2Mpac2	−15524.4	−2.4	3.4	1.24	45.1	2.47	1.7
XMpof1	−15156.8	1.7	−10	1.37	50.9	2.48	−3.5
XMpof2	−15160.2	−1.4	−0.6[c]	1.22[c]	46.1	2.54	0.1
C2Mpof1	−15159.5	2.3	7.4	1.40	52.1	2.58	8.9
C2Mpof2	−15156.4	−5.8	6.2	1.39	51.6	2.22	2.8
XEtMpac1	−17026.1	0.7	0.1	1.38	51.6	2.41	−5.8
XEtMpac2	−17030.2	−4.7	−2.2	1.29	47.2	2.55	−2.9
XEtMpof1	−16657.6	1.6	−2.3	1.31	48.1	2.53	−5.8
XEtMpof2	−16663.3	0.0	2.4	1.17	42.1	2.52	−1.8

[a] Transition model names Scheme 1[1] & text; Energies are relative to the listed SQPL entries of each row.
[b] For geometry parameters, see Fig. 2 (atom C6 is the alpha carbon atom).
[c] Averaged values.

Table 5
Calculated transition state electronic energies and MOLH‡ geometry for dimethyl itaconate complexes[a]

Complex	SQPL (0.0) kcal/mol	MOLH kcal/mol	MOLH‡ kcal/mol	$H_a\cdots H_b$ Å	H_a–Rh–H_b°	$H_a\cdots C_6$ Å	DIHY kcal/mol
XCdmit1	−14217.9	4.5	3.6	1.61	61.3	2.33	2.6
XCdmit2	−14219.5	−2.0	6.3	1.52	56.8	2.34	0.7
XCdMeS1	−14223.3	−0.8	−0.8[b]	1.35	50.2	2.21	−1.1[c]
XCdMeS2	−14224.1	−2.9	2.0	1.54	58.0	2.32	−1.2
C2CdMeS1	−14226.9	10.9	8.1	1.77	68.2	2.36	7.9
C2CdMeS2	−14223.2	0.7	2.2	1.54	58.0	2.32	2.2
XEtCdMeS1	−15727.2	2.7	−0.2[b]	1.60	61.0	2.42	−5.1
XEtCdMeS2	−15731.8	−0.7	1.9	1.51	56.4	2.34	6.5

[a] See Table 4 for label and layout information.
[b] Obtained using step radius of 0.005 Å.
[c] An alternative adjacent state with energy −5.5 kcal/mol was observed.

zero point correction terms might well be significant at the ~1 kcal/mol level: a reduction in the computation time, and removal of extra vibrating atoms which contribute to the entropy sum, are two features that would be useful in future studies.

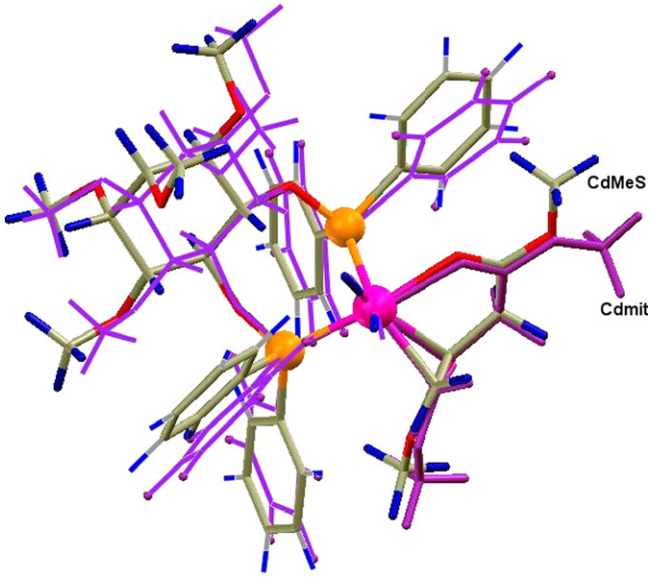

Fig. 6. Superposition of final methyl itaconate transition state models XCdmit1 (in purple) and XCdMes1 (thick bonds with atom colors: O, red; Rh, pink; C, gray; H, blue). Labels indicate the different methyl substrate conformations. (For interpretation of the references to colour in this figure legend, the reader is referred to the web version of this article.)

2.2.6. Comparing like models (the predictive quandary)

We have confirmed that the stereochemistry of the minor and major manifold transition states must be closely aligned also with respect to the dihydride hydrogen geometries. In one case (XMpof2) it was possible to locate transition states with differing H–H distances (1.19 and 1.39 Å) which gave electronic energies differing by 2.5 kcal/mol. On further refinement of both with lower convergence parameters, the energies came closer (within 1 kcal/mol) but with one model not converging in a realistic timeframe: final H–H distances of 1.22 (converged) [quoted in Table 4] and 1.16 Å (oscillating). The models are essentially superimposable (Fig. 7) and serve to warn that care must be taken in comparing similar transition states from the two manifolds. We present a simplified view of this issue in Fig. 8, which maps (using a linear step)

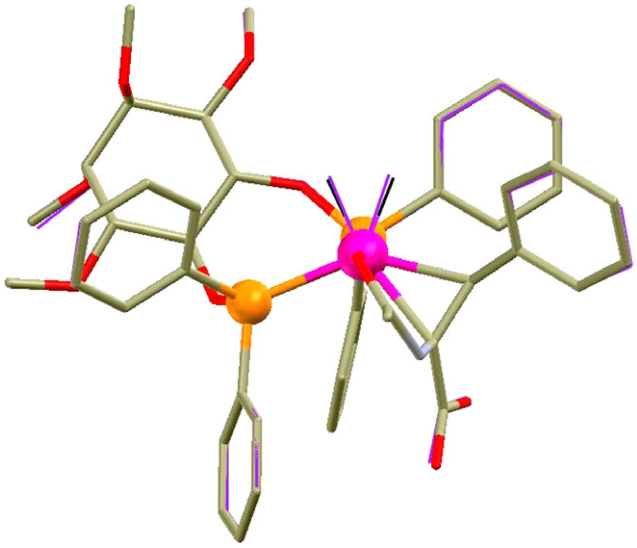

Fig. 7. Overlap of XMof2 transition state models (see text): only the dihydride hydrogen atoms are shown. Converged model with atom colors: O, red; Rh, pink; N, blue; C, gray; H, black. Other model: purple. (For interpretation of the references to colour in this figure legend, the reader is referred to the web version of this article.)

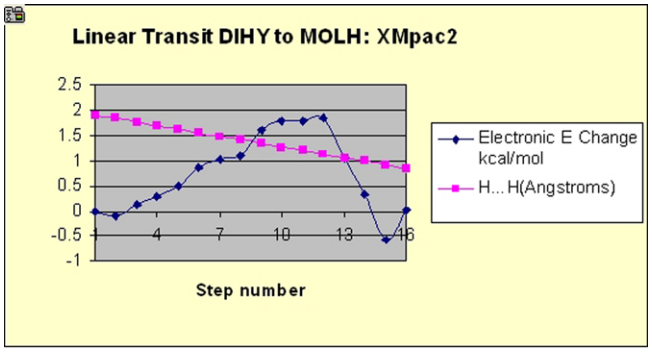

Fig. 8. Energy change vs. H–H dihydride distance (XMpac2 model) (see text).

the energy changes between the DIHY and MOLH models for XMpac2: the energy change compared with the H–H distance is small around the MOLH‡ model region (steps 9–12, Fig. 8).

3. Overall results

We present difference enthalpy results in Tables 4 and 5 and emphasize that the magnitude of the difference between the minor and major manifold transition states is of the order of 0.02% of the total energies by listing the numerical values for the SQPL/sqpl models. Given the notes above about the need to compare similar dihydride geometries, these tables also include the relevant (MOLH‡) dihydride geometric parameters. For comparative purposes, Figs. 9–11 follow the summary format suggested by Donoghue et al. [2] and align with Table 6 which contains the comparative experimental data.

Overall the results indicate that the predicted ee% values are cinnamate > cinnamic acid > itaconate, as observed experimentally. In general, the overall difference magnitudes are much lower than those recently calculated using DFT/ONIOM calculations [2] for the X-ray based starting set, but somewhat similar for the C2-symmetry starting models. Given a choice of model, we would normally take the lowest energy models as being correct but note that the parallel reaction curves suggest the same conclusions. The prediction for the homologous EtCP versus CANDYPHOS based catalysts is mixed with the itaconate and cinnamic acid giving the correct trend, while the cinnamate results are in reverse to the measured value (averaged values 4.1 and 6.4 kcal/mol, respectively). The latter result may well be influenced by other factors, including solvent choice, possibly significant entropy affects and the significance of the DIHY‡ transition state [2].

Another noteworthy aspect of the computations is the relative energy of the square planar starting-complex (the calculations include a non-bound molecule of hydrogen) relative to the transition state energies. This aspect is best shown in the following Figs. 9–11 where the plotted difference values given are relative to the lowest square planar complex in either major or minor manifold (i.e. either sqpl or SQPL models).

3.1. Hydrogenation of methyl-(Z)-α-acetamido-cinnamic acid (Mpof series)

Relative MOLH‡ transition state energies (Fig. 9) are not consistent for the 3 models (see molh‡ & MOLH‡ points), but the relative energies of the square planar starting complexes are quite similar for both manifolds as might be expected. The notable difference is the reversal of chirality predicted from the C2 symmetry-based starting model. Unfortunately no experimental value is available for the EtCP experiment to confirm the lower predicted ee%, though this would be consistent with the Mpac series.

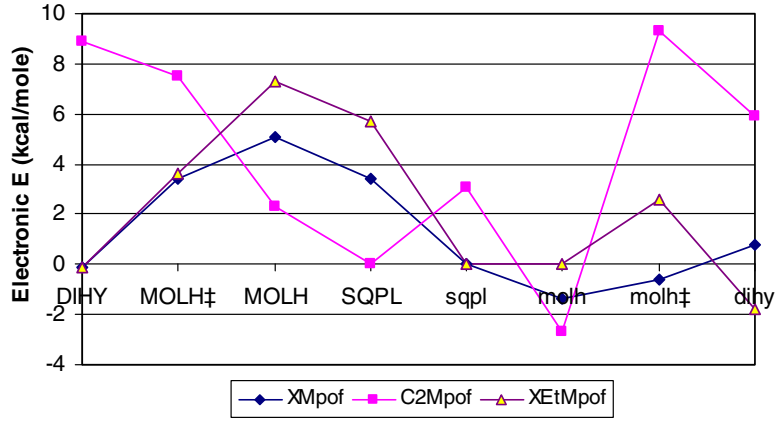

Fig. 9. Calculated enthalpies for substrate methyl(*Z*)-α-acetamido cinnamic acid over pathway A [2] relative to sqpl model.

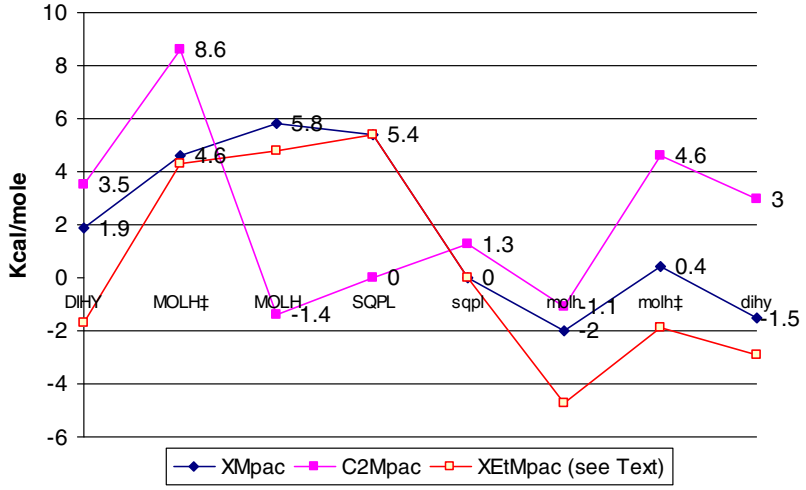

Fig. 10. Calculated enthalpies for substrate methyl(*Z*)-α-acetamido cinnamate over pathway A [2] relative to sqpl model.

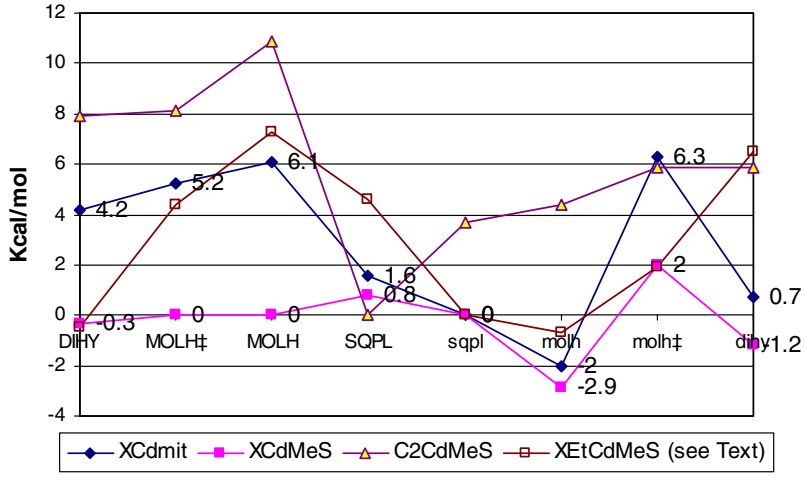

Fig. 11. Calculated enthalpies for substrate dimethyl itaconate over pathway A [2] relative to the sqpl/SQPL model.

3.2. Methyl-(Z)-α-acetamido-cinnamate (Mpac)

For this larger substrate, there is a consistent ee% prediction over the three models (see Fig. 10), with the minor manifold square planar model (sqpl) less stable for both X-ray starting models but not for the C2 model. The relative energies of the molh‡ and molh minor manifold transition states are lower than the starting square-planar complexes, but this comparison is not considered significant given that the starting catalyst is a cyclo-octadiene 6-coordinate complex.

Table 6
Enantiomeric excess: experimental[a] and calculation[b] results

Target	Codename	Experimental (CANDYPHOS)	Calc(X)	Calc (C2)	Exptal (EtCP)	Calc(X)
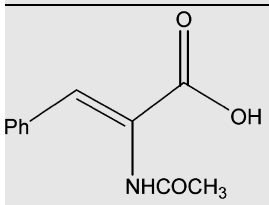	Mpof	76% 1.20 7.6:1	3.0	−1.9	–	1.0
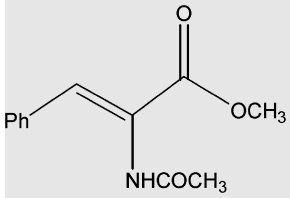	Mpac	95% 2.15 41:1	4.2	4.0	92% 1.90 25:1	6.4
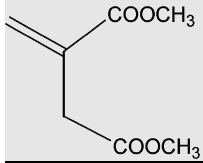	Cdmit/CdMeS	29% 0.35 1.8:1	−1.1, (−2.0)[c]	2.2	51% 0.65 3:1	2.5

[a] Energies are in kcal/mol. Experimental values listed in three ways: ee (%), $\Delta\Delta G^{\circ}$, ~ratio of enantiomers.
[b] Enthalpy energies (ΔH).
[c] For the Cdmit (CdMeS) models (see Table 5).

Table 7
QM/MM calculated Δ(molh‡–MOLH‡) enthalpy electronic difference energies (kcal/mol)

Model	ΔE^{*} (X) (Cp)	ΔE^{*} (C2) (Cp)	ΔG Measured	ΔE^{*} (X)(EtCP)	ΔE^{*} (C2)(EtCP)	ΔG Measured
Mpof	10.1	4.6	1.2	14.0	–	–
Mpac	6.6	5.4	2.15	3.0	9.1	1.90
Cdmit	−7.6	–	0.35	2.0	–	0.65
CdMeS	−7.6	4.4	0.35	−2.5	–	0.65

3.3. Hydrogenation of dimethyl itaconate (Cdmit, CdMes)

The low ee% values observed for this substrate (Table 5) would suggest potential resolution difficulties in the calculation, for the reasons noted above (Fig. 11). The results are surprisingly good in relation to the Mpac and Mpof series. Nevertheless, the transition state geometries were difficult to locate, and show wide variation particularly with respect to the H_a–H_b geometries (Table 5).

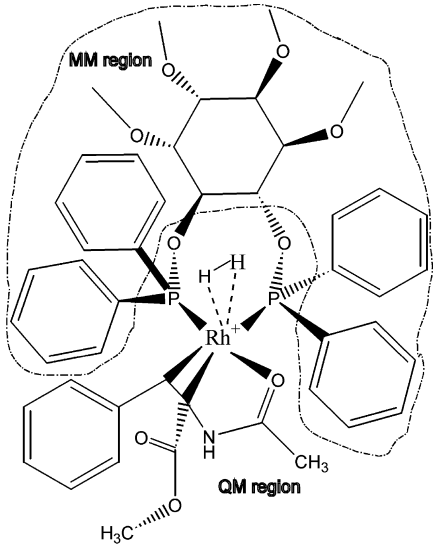

Fig. 12. The division of QM and MM regions in the molecules (Mpac example).

3.4. The QM/MM results

Limitations of QM/MM methods have been identified previously [43]. The QM/MM approach does allow the full system to be treated and "breakout" from starting symmetric geometries to occur, as well as having the bonus of substantial gains in computation time. We present here (Table 7) a summary of our QM/MM trials. Partly as expected from the approximate force constants covering a large part of the molecule (using SYBYL Force Field parameters, 2-layer; see Fig. 12 below), the final energy differences were a poor guide to the ee% values reflecting that the errors involved in this approach are too large.

4. Experimental

4.1. Computational details

DFT calculations were carried out using ADF 2006.01 [40,41] on a cluster of four 3.2 GHz Intel Pentium 4 CPUs with hyperthreading. Each node ran under Redhat 9 Linux configured with OSCAR software from the Open Cluster Group, http://www.openclustergroup.org/. That included the PVM and MPI parallel libraries and PBS (Portable Batch System) used for the queuing and scheduling of batch jobs.

The calculations were carried out within the framework of the generalized gradient approximation (GGA) by using the local den-

sity functional of Voska et al. [44], the exchange correction of Becke [45] and the correlation correction of Perdew [46,47]. Frozen core orbitals were used for all atoms, with the core orbitals for rhodium defined as 1s, 2s, 2p, 3s, 3p and 3d shells. All calculations were spin restricted and relativistic effects were included using the ZORA method [48–50]. Model structures were built from [Rh(CandyPhos)(COD)]+ [3] and the DUPHOS transition state models [1] or locally-programmed C2-symmetric conversions. Substituents were added when required using standard structural data in VEGAZZ[51] and locally written software [52]. The structures were then optimized with respect to their energies using the transition state search algorithm [42] by using double-zeta polarized STO basis sets on all non Rh atoms, and triple-zeta polarized sets for Rh. The division of the atomic coordinates between the QM and MM regions is shown in Fig. 12: the P–C and O–C α link parameters [41] used were 1.28 and 1.44, respectively. A typical sequence involved using a distance restraint on the hydride hydrogens (e.g. H. . .H 1.28 Å) and, in QM/MM runs, the molecular dynamics search using conjugate gradient optimization with a 100 ps for 101 sampled structures heated to a temperature 100–700 K. This final model was then refined under full QM (DFT) calculations with our compromise set of convergent values of 0.0002 (tolE), 0.01 (tolG) and 0.012 (tolCART) with integration limits of 5.0.

4.2. Preparative details

4.2.1. General methods

Manipulations of air sensitive materials were conducted in an argon atmosphere by using either Schlenk techniques or an Innovative Technology dry box. Tetrahydrofuran, ether and toluene were distilled from sodium benzophenone ketal under nitrogen and stored over activated 4 Å molecular sieves. NMR spectra were recorded on an AC300 Bruker spectrometer. Flash column chromatography [53] was carried out on 230–400 silica (Scharlau). Gas chromatographic analysis was performed on a Hewlett–Packard Model 6890. Chiral gas chromatographic separations were accomplished using a Chirasil L-Val (50 m × 0.25 mm, 0.12 μm film thickness) capillary column (Chrompack). Elemental analyses were performed by the Campbell Analytical Laboratory, University of Otago, Dunedin, New Zealand. L-Quebrachitol was obtained from the Rubber Research Institute of Malaysia, Kuala Lumpur, Malaysia. D-Pinitol was obtained from New Zealand Pharmaceuticals Ltd., Palmerston North, New Zealand. Acetamidoacrylate derivatives were synthesized according to literature procedures [54]. (CODRhCl)$_2$ was purchased from Aldrich. All NMR spectra were recorded in $CDCl_3$ unless noted otherwise.

The synthetic pathway that was employed to obtain the diphosphinite ligand was described previously (see ligand D-10 [10]).

4.3. 1,2,5,6-Tetraethyl-chiro-inositol

3,4-Dibenzyl-chiro-inositol [10] (5.0 g, 13.9 mmol) dissolved in dry DMF (150 mL) was treated at 0 °C with NaH (1.5 g, 62.5 mmol) and ethyl bromide (8.76 g, 80.4 mmol). Reaction mixture was allowed to warm to room temperature and stirred overnight. The reaction mixture was quenched with water and extracted with toluene. Removal of the toluene and purification by flash-chromatography (Si-60, hexanes:ethylacetate 4:1) yielded 3,4-dibenzyl-1,2,5,6-tetraethyl-chiro-inositol as a clear oil (4.52 g, yield 69%). This oil was dissolved in ethanol (90 mL), TFA (10 μL) and Pd/C (100 mg) were added, and hydrogenated at 1 atm hydrogen pressure for 4 h. Purification by flash-chromatography (Si-60, hexanes:ethylacetate 3:2) yielded 1,2,5,6-tetraethyl-chiro-inositol (2.97, yield ~100%) as a light orange oil and was committed to the next step without further purification.

^{1}H ($CDCl_3$) 1.22 ppm (m, 12H), 3.2–3.8 (m, 14H).
^{13}C ($CDCl_3$) 15.8 (CH_3), 16.0 (CH_3), 66.1 (CH_3), 67.4 (CH_2), 72.2 (CH), 75.1 (CH), 79.8 (CH).

4.4. 1D-3,4-Bis(O-diphenylphosphino)-1,2,5,6-tetra-O-ethyl-chiro-inositol

The 1,2,5,6-tetra-*O*-ethyl-chiro-inositol (2.28 g, 7.8 mmol), which had been pre-dried azeotropically with dry toluene (2 × 5 mL) and dry pyridine (excess, 4 mL), was added to dry THF (20 mL). The resulting solution was transferred by cannula into a Schlenk tube containing freshly distilled chlorodiphenyl phosphine (3.49, 15.6 mmol) in dry THF (10 mL) under argon. The resulting suspension was stirred at room temperature overnight. The solution was filtered under argon and the solvent removed from the filtrate under vacuum. The remaining solid was washed with dry toluene and filtered. The filtrate was collected and the solvent removed under vacuum to give the diphosphinite as a white solid (5.02 g, 97%). *Anal.* Calc. for $C_{38}H_{46}O_6P$: C, 68.86; H, 6.88. Found: C, 69.08; H, 7.02%.

4.5. 1D-3,4-Bis(O-diphenylphosphino)-1,2,5,6-tetra-O-ethyl-chiro-inositol rhodium cyclooctadiene BF_4

[RhCODCl]$_2$ (123 mg, 0.25 mmol) was dissolved in dichloromethane (4 mL). The ligand (330 mg, 0.5 mmol) dissolved in dichloromethane (5 mL) was added dropwise. The reaction mixture was stirred at room temperature overnight. $AgBF_4$ (97 mg, 0.5 mmol) was added and the reaction mixture stirred for 2 h. The mixture was filtered through Celite® and the solvent removed in vacuo to yield the title compound (480 mg, 100%) as a bright yellow solid. *Anal.* Calc. for $C_{46}H_{59}BF_4O_6P_2Rh$: C, 57.63; H, 6.10. Found: C, 57.40.; H, 6.14%. ^{31}P NMR: 137.6 ppm, J_{Rh-P} −180.7 Hz.

4.6. 1D-3,4-Bis(O-diphenylphosphino)-1,2,5,6-tetra-O-methyl-chiro-inositol rhodium cyclooctadiene BF_4

A solution of 1L-3,4-bis(*O*-diphenylphosphino)-1,2,5,6-tetra-*O*-methyl-chiro-inositol (122 mg, O.20 mmol) in THF (5 mL) was added dropwise to a solution of (RhCODCl)$_2$ (49 mg, 0.10 mmol) in THF (5 mL). The reaction mixture was stirred at room temperature for 17 h. $AgBF_4$ (0.039 g, 0.2 mmol) was added and the reaction mixture stirred for 2 h. Filtration and removal of the solvent yielded an orange solid. Crystallization from $CHCl_3$/ pentane yielded pure title compound as a $CHCl_3$ solvate (0.078 g, 76%). ^{31}P NMR 134.8, J_{Rh-P} = 178 Hz. *Anal.* Calc. for $C_{43}H_{51}BCl_3F_4O_6P_2Rh$: C, 50.54; H, 5.03. Found: C, 50.44; H, 5.00%.

4.7. Hydrogenations

Hydrogenations were carried in 12 mL glass vials equipped with magnetic stirrer bars. The vials were charged with catalyst (0.005 mmol), substrate (1.0 mmol) and solvent (3 mL) inside an inert atmosphere glove box (Innovative Technologies) and placed inside a 300 mL Parr autoclave made from Hastelloy C. In this way several hydrogenation experiments could be carried out at the same time. The autoclave was sealed, taken outside the glovebox and heated to the required temperature using a thermostatic heating mantel. The autoclave was flushed with hydrogen three times before being filled to the required pressure. After the required reaction time the autoclave pressure was reduced to atmospheric pressure and samples of the crude reaction mixture were analyzed by GC.

The GC analysis to obtain conversion and enantiomeric excess were performed on a HP 6890 Series gas chromatography apparatus

using a capillary Supelco GAMMA-DEX 225 (30 m × 0.25 mm × 0.25 μm) column or a SGE CYDEX-B (2 m × 0.32 mm × 0.25 μm) column.

5. Conclusions

Overall, our gas phase calculations (without counterions) supported the observed enantiomeric excess for the catalytic hydrogenation of the prochiral enamides (methyl-(*Z*)-α-acetamido cinnamate, methyl-(*Z*)-α-acetamido cinnamic acid and dimethyl itaconate) using the two homologous Rh(I) bisphosphinite catalysts. The calculations for dimethyl itaconate were not consistent, but the ee% values experimentally observed corresponded to energy differences of <1 kcal/mol. We found that starting models can determine which transition state energies are determined: this raises issues of confidence in predictions as the comparable (other pathway) transition states must represent both the same conformations and comparable "internal" geometries. The observed enthalpy differences are rather smaller than those reported by Feldgus and Landis[1] and Donoghue et al. [2] for the Rh(I)DUPHOS systems.

We have established straightforward chemical routes to two new Rh(I) hydrogenation catalysts based on readily available starting materials.

Our experience in searching for transition state saddle points suggests that a "more intimate" QM/MM relationship would enhance this process, given the difficulty of moving across the energy surface using QM methods alone observed here. Obstacles to the use of DFT calculations for the prediction of enantiomeric excess on larger molecular systems have been identified. Our original intent was to consider other factors, such as solvent effects, but our results suggest that, at the state of current knowledge (mechanism and modeling) such an extension was not justified.

Acknowledgments

This study would not have been possible without the close support of Professor Tom Ziegler (University of Calgary, Calgary, Alberta, Canada). Contributions to the synthetic programme were made by Chris Enright and Joanne Hart. We thank the NZ Foundation for Research Science and Technology for funding (Contract No. CO8X0411).

Appendix A. Supplementary data

The Cartesian coordinates (in XYZ format) for the calculated models in Tables 4 and 5. Supplementary data associated with this article can be found, in the online version, at doi:10.1016/j.poly.2008.05.011.

References

[1] S. Feldgus, C.R. Landis, J. Am. Chem. Soc. 122 (2000) 12714.
[2] P.J. Donoghue, P. Helquist, O. Wiest, J. Org. Chem. 72 (2007) 839.
[3] G.J. Gainsford, A. Falshaw, C. Lensink, Acta Crystallogr., Sect. C 63 (2007) m331.
[4] A.M. Thayer, Chem. Eng. News 83 (2005) 40.
[5] Computational Modeling of Homogeneous Catalysis. Kluwer Academic Publishers, Dordrecht, The Netherlands, 2002.
[6] B.J. Lynch, D.G. Truhlar, J. Phys. Chem. A 105 (2001) 2936.
[7] C. Darcel, D. Moulin, J.C. Henry, M. Lagrelette, P. Richard, P.D. Harvey, S. Juge, Eur. J. Org. Chem. (2007) 2078.
[8] M.T. Reetz, G. Mehler, O.G. Bondarev, Chem. Commun. (2006) 2292.
[9] A.J. Sandee, M. vanderBurg, J.N.H. Reek, Chem. Commun. (2007) 1.
[10] A. Falshaw, G.J. Gainsford, C. Lensink, A.T. Slade, L.J. Wright, Polyhedron 26 (2007) 329.
[11] M. Aghmiz, A. Aghmiz, Y. Diaz, A. Masdeu-Bulto, C. Claver, S. Castillon, J. Org. Chem. 69 (2004) 7502.
[12] T.V. RajanBabu, T.A. Ayers, G.A. Halliday, K.K. You, J.C. Calabrese, J. Org. Chem. 62 (1997) 6012.
[13] C.L. Cai, F.G. Denga, W. Sun, C.G. Xia, Synlett (2007) 3007.
[14] I.D. Gridnev, M. Yasutake, N. Higashi, T. Imamoto,J. Am. Chem. Soc. 123 (2001) 5268.
[15] M.T. Reetz, G. Mehler, Angew. Chem., Int. Ed. 39 (2000) 3889.
[16] D. Ager, A.H.M. Devries, J.G. Devries, Platinum Met. Rev. 50 (2007) 54.
[17] Y. Liu, C.A. Sandoval, Y. Yamaguchi, X. Zhang, Z. Wang, K. Kato, K.L. Ding,J. Am. Chem. Soc. 128 (2006) 14212.
[18] F. Giacomina, A. Meetsma, L. Panella, L. Lefort, A.H.M. de Vries, J.G. de Vries, Angew. Chem., Int. Ed. 46 (2007) 1497.
[19] I.D. Gridnev, C. Fan, P.G. Pringle, Chem. Commun. (2007) 1319.
[20] M.T. Reetz, A. Meiswinkel, G. Mehler, K. Angermund, M. Graf, W. Thiel, R. Mynott, D.G. Blackmond, J. Am. Chem. Soc. 127 (2005) 10305.
[21] S. Enthaler, G. Erre, K. Junge, D. Michalik, A. Spannenberg, F. Marras, S. Gladiali, M. Beller, Tetrahedron: Asymmetr. 18 (2007) 1288.
[22] A.J. Minnaard, B.L. Feringa, L. Lefort, J.G. De Vriest, Acc. Chem. Res. 40 (2007) 1267.
[23] R. Hoen, T.D. Tiemersma-Wegman, B. Procuranti, L. Lefort, J.G. Devries, A.J. Minnaard, B.L. Feringa, Org. Biomol. Chem. 5 (2007) 267.
[24] J.A.F. Boogers, U. Felfer, M. Kotthaus, L. Lefort, G. Steinbauer, A.H.M. de Vries, J.G. de Vries, Org. Proc. Res. Dev. 11 (2007) 585.
[25] M.N. Birkholz, N.V. Dubrovina, H.J. Jiao, D. Michalik, J. Holz, R. Paciello, B. Breit, A. Borner, Chem.-Eur. J. 13 (2007) 5896.
[26] C. Jakel, R. Paciello, Chem. Rev. 106 (2006) 2912.
[27] W.P. Hems, P. Mcmorn, S. Riddel, S. Watson, F.E. Hancock, G.J. Hutchings, Org. Biomol. Chem. 3 (2005) 1547.
[28] W.S. Knowles, J. Chem. Educ. 63 (1986) 222.
[29] J.A. Widegren, R.G. Finke, J. Mol. Catal. A-Chem. 198 (2003) 317.
[30] K. Burgemeister, G. Francio, V.H. Gego, L. Greiner, H. Hugl, W. Leitner, Chem.-Eur. J. 13 (2007) 2798.
[31] J.R. She, L.M. Ye, J. Zhu, Y.Z. Yuan, Catal. Lett. 116 (2007) 70.
[32] L. Greiner, S. Laue, J. Woltinger, A. Liese, Top. Curr. Chem. 276 (2007) 111.
[33] W.S. Knowles, Acc. Chem. Res. 16 (1983) 106.
[34] S. Mori, T. Vreven, K. Morokuma, Chem.-An Asian J. 1 (2006) 391.
[35] I.D. Gridnev, T. Imamoto, Acc. Chem. Res. 37 (2004) 633.
[36] J. Halpern, C.R. Landis, J. Am. Chem. Soc. 109 (1987) 1746.
[37] J.M. Brown, P.A. Chaloner, J. Chem. Soc., Chem. Commun. (1980) 344.
[38] K.V.L. Crepy, T. Imamoto, Adv. Synth. Catal. 345 (2003) 79.
[39] S. Feldgus, C.R. Landis, in: F. Maseras, A. Lledos (Eds.), Computational Modeling of Homogeneous Catalysis, Kluwer Academic Publishers, Dordrecht, 2002. pp. 107–136.
[40] ADF2006.01, SCM, Theoretical Chemistry, Vrije Universiteit, Amsterdam, The Netherlands. http://www.scm.com (2006).
[41] G. te Velde, F.M. Bickelhaupt, S.J.A. van Gisbergen, C. Fonseca Guerra, E.J. Baerends, J.G. Snijders, T. Ziegler, J. Comput. Chem. 22 (2001) 931.
[42] L. Fan, T. Ziegler, J. Am. Chem. Soc. 114 (1992) 10890.
[43] H. Lin, D.G. Truhlar, Theor. Chem. Acc. 117 (2007) 185.
[44] S.H. Vosko, L. Wilk, M. Nusair, Can. J. Phys. 58 (1980) 1200.
[45] A.D. Becke, Phys. Rev. A 38 (1988) 3100.
[46] J.P. Perdew, Phys. Rev. B 33 (1986) 8822.
[47] J.P. Perdew, Phys. Rev. B 34 (1986) 7406.
[48] E. van Lenthe, J.G. Snijders, E.J. Baerends, J. Chem. Phys. (1993) 4597.
[49] E. van Lenthe, J.G. Snijders, E.J. Baerends, J. Chem. Phys. (1994) 9783.
[50] E. van Lenthe, A.E. Ehlers, E.J. Baerends, J. Chem. Phys. (1999) 8943.
[51] A.Pedretti, G.Vistoli, <http://www.vegazz.net/>, 2006.
[52] G.J. Gainsford, C. Lensink, P.N. McGavin, S. White, IRL Report 1885, Industrial Research Limited, Wellington, New Zealand, 2007.
[53] W.C. Still, M. Kahn, A. Mitra, J. Org. Chem. 43 (1978) 2923.
[54] J.P. Genet, C. Pinel, V. Ratovelomananavidal, S. Mallart, X. Pfister, L. Bischoff, M.C.C. Deandrade, S. Darses, C. Galopin, J.A. Laffitte, Tetrahedron: Asymmetr. 5 (1994) 675.

Polyhedron 27 (2008) 2539–2544

Contents lists available at ScienceDirect

Polyhedron

journal homepage: www.elsevier.com/locate/poly

The carbodiphosphorane–CS_2 adduct as a complex ligand: Crystallographic characterization of $[I_2Pt\{S_2CC(PPh_3)_2\}] \cdot CH_2Cl_2$, $[Pt\{S_2CC(PPh_3)_2\}_2][SiF_5]_2 \cdot 2CH_2Cl_2$ and $[(Me)_2PtFI\{S_2CC(PPh_3)_2\}] \cdot 2CH_2Cl_2$

Wolfgang Petz *, Bernhard Neumüller *

Fachbereich Chemie der Philipps-Universität, 35032 Marburg, Germany

ARTICLE INFO

Article history:
Received 17 March 2008
Accepted 6 May 2008
Available online 16 June 2008

Keywords:
Betain-like compounds
Carbodiphosphorane adducts
Chelating ligand
Crystal structures
Platinum compounds

ABSTRACT

The betain-like compound $S_2CC(PPh_3)_2$ (**1**), which is obtained from CS_2 and the double ylide $C(PPh_3)_2$, reacts with $[X_2Pt(COD)]$ (X = Cl, I) in THF to afford the complexes $[X_2Pt\{S_2CC(PPh_3)_2\}]$ (**2**, X = Cl; **3**, X = I) in quantitative yields. Both compounds are insoluble in all usual solvents, and **3** could be characterized by an X-ray analysis. For comparison, the structures of $[Pt(Me)_2FI\{S_2CC(PPh_3)_2\}] \cdot 2CH_2Cl_2$ (**4** · $2CH_2Cl_2$) with Pt^{IV} and $[Pt\{S_2CC(PPh_3)_2\}_2][SiF_5]_2 \cdot 2CH_2Cl_2$ (**5** · $2CH_2Cl_2$) with Pt^{II} are also presented. The compounds are further characterized by ^{31}P NMR and IR spectroscopy.

© 2008 Elsevier Ltd. All rights reserved.

1. Introduction

The Lewis acid CS_2 and the carbodiphosphorane $C(PPh_3)_2$ quantitatively form the yellow addition compound $S_2CC(PPh_3)_2$ (**1**), which has been known for many years [1]. In addition to **1**, further adducts with Lewis acids containing main group [2] or transition metal elements [3] were also described. Recently, we have studied the crystal structure of **1** and its ability as a possible complex ligand.

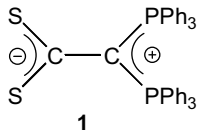

1

Thus, in $[M(CO)_6]$ (M = Cr, Mo, W) two carbonyl groups can be replaced to produce the corresponding $[(CO)_4M\{S_2CC(PPh_3)_2\}]$ complexes, in which **1** acts as a chelating ligand via the two sulfur atoms [4]. The same is true for cationic manganese and cobalt complexes [5]. An alternative coordination mode of **1** was found upon reaction with silver salts containing weakly coordinating anions; Ag_6^{6+} or Ag_4^{4+} clusters are held together by six or four molecules of **1**, respectively, and each S atom contacts up to two Ag atoms [6]. The S_2C–CP_2 bond length in **1** is shorter than a single bond and further shortening occurs upon complex formation, indicating an increase of bond strength. Calculations have shown that in **1** some π interaction exists between the occupied p orbital of the P_2C sp^2 carbon atom and the empty p orbital of the S_2C sp^2 carbon atom [4]. In this publication, we present the results of the reaction of **1** with some platinum complexes.

2. Results and discussion

Reactions of **1** turned out to be highly problematic because **1** is only slightly soluble in THF and insoluble in the usual non-polar solvents, and it decomposes at elevated temperatures or upon prolonged reaction time to give $SPPh_3$ and the heterocummulene S=C=C=PPh_3 [7]. Compound **1** is soluble in CH_2Cl_2 (^{31}P NMR in CH_2Cl_2: 17.11 ppm), but decomposition proceeds more rapidly in this solvent. However, in some cases the reaction products are soluble in THF, which allows sufficient characterization [4].

If a suspension of **1** in THF is treated with the platinum complexes $[X_2Pt(cod)]$ (X = Cl, I) reaction immediately occurs to produce red-brown precipitates of **2** and **3**, respectively, with release of COD. Both products are obtained in about quantitative yields according to the following equation:

$$[X_2Pt(COD)] + S_2CC(PPh_3)_2 \rightarrow [X_2Pt\{S_2CC(PPh_3)_2\}] + COD \qquad (1)$$

* Corresponding authors. Fax: +49 6421 2825653.
E-mail addresses: petz@staff.uni-marburg.de (W. Petz), neumuell@chemie.uni-marburg.de (B. Neumüller).

0277-5387/$ - see front matter © 2008 Elsevier Ltd. All rights reserved.
doi:10.1016/j.poly.2008.05.003

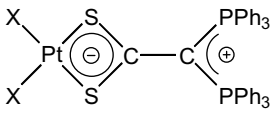

2 (X = Cl), **3** (X = I)

The new platinum complexes **2** and **3** are found to be insoluble in all common solvents including THF and CH_2Cl_2, but are slightly soluble in DMSO. If amorphous **3** from THF is kept in contact with CH_2Cl_2 a kind of mineralization proceeds and the precipitate takes up dichloromethane and is converted into small red crystals. However, the overstanding solution shows no signal in the ^{31}P NMR spectrum confirming the insolubility in this solvent. Unfortunately, no crystals of **2** could be obtained via this way. In the ^{31}P NMR spectra in DMSO singlets at 14.6 ppm (for **2**) and 14.0 ppm (for **3**) were recorded. The solid state IR spectra of **2** and **3** are very similar and contain the same number of bands, which indicate analogous structural properties. Strong absorptions at about 1049 and 1095 cm^{-1} were recorded, which can be assigned to the ν_{as} and ν_s CS_2 vibrations [8]. The related bands in **1** were found at 1067 and 1099 cm^{-1}. A strong band at 1250 cm^{-1} in both compounds can probably be attributed to the vibration of the S_2C–CP_2 bond of the ligand. According to the occupied p orbital at the P_2C carbon atom and the vacant p orbital at the S_2C carbon atom, additional to the σ donor bond a weak and polarized π-interaction is operative [4]. The related band in **1** is found at 1146 cm^{-1} and the shift to higher frequencies upon complex formation can be explained with an increase of the C–C double bond character, which is also expressed in a shorter C–C bond length in **3**.

Additionally, we present the crystal structures of two further compounds with the ligand **1** for comparison. Crystals of the complexes $[(Me)_2PtFI\{S_2CC(PPh_3)_2\}] \cdot 2CH_2Cl_2$ (**4** · $2CH_2Cl_2$) and $[Pt\{S_2CC(PPh_3)_2\}_2][SiF_5]_2 \cdot 2CH_2Cl_2$ (**5** · $2CH_2Cl_2$) were obtained by reacting **1** with a sample of an impure platinum compound which was formed as a result from attempts to fluorinate $[Me_2Pt(cod)]$ (still containing some [Me(I)Pt(cod)]) with XeF_2; the complex $[(CF_3)_2Pt(cod)]$ was expected [9]. The anion $[SiF_5]^-$ may originate from fluorination of some glass or grease by XeF_2.

3. Crystal structures

To get more insight into the nature of the complexes and the bonding situation an X-ray analysis of **3** was performed. Small dark red crystals of **3** · CH_2Cl_2 suitable for an X-ray analysis formed in a suspension of the powder in CH_2Cl_2 at room temperature. To our knowledge, no other platinum(II) compounds with an I_2PtS_2 arrangement are known in which the sulfur atoms come from a CS_2 adduct of the type S_2CR; only two Pt^{IV} complexes with a dithiocarbaminato ligand have been characterized by X-ray analyses [10]. Pt^{II} compounds with this core are described with thiourea derivatives [11], with dimethylsulfoxide [12] or with thioethers [13]. Pt^{II} complexes with other zwitterionic compounds are described with the ligand S_2CPR_3 [14]. For comparison we include the structures of **4** · $2CH_2Cl_2$ and **5** · $2CH_2Cl_2$, which we have obtained as described above. The molecular structures of **3** · CH_2Cl_2, **4** · $2CH_2Cl_2$, and of the cation of **5** · $2CH_2Cl_2$ are depicted in Figs. 1–3. Crystallographic data are listed in Table 1, and distances and angles are summarized in Tables 2–4.

3.1. Crystal structure of **3** · CH_2Cl_2

The environment of the platinum atom is planar as shown by the sum of the bond angles at the Pt atom of 360°; the crystal structure is shown in Fig. 1; the solvent molecule is omitted. On complex formation the ligand **1** undergoes some remarkable changes. The S_2C–CP_2 bond length decreases from 149.4(2) to 141(2) pm indicating an increased double bond character, and together with the S_2C–CP_2 bond lengths of **5** it is the shortest one found in complexes of **1**. The P–C distances to the ylidic carbon atom are slightly longer (mean 178 pm) than those in **1**; only the mean P–C_{Ph} distances are the same as in the free ligand. A slight elongation of the C–S bond length is also observed. These changes in bond lengths upon complex formation can be interpreted in terms of a release of π electron density away from the ylidic carbon atom; the same trends were found in the $(CO)_4M$ adducts [4]. The S–Pt–S angle amounts to 74° and is larger than the corresponding S–M–S angle in the group 6 metal carbonyl derivatives, whereas the S–C–S bite angle is smaller (106°); in going from **1** to **3** a decrease of the bite angle of about 18° occurs, indicating the great

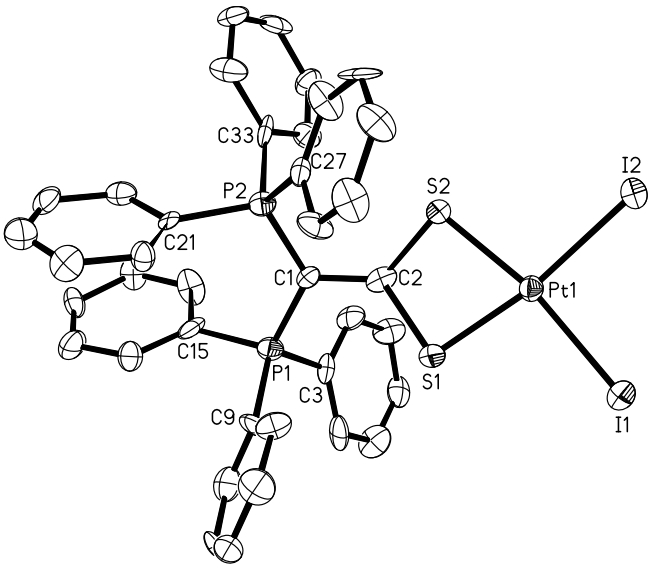

Fig. 1. Molecular structure of **3** · CH_2Cl_2 showing the atom numbering scheme. The ellipsoids are drawn at a 40% probability level; the H atoms at the phenyl rings and the CH_2Cl_2 molecule are omitted for clarity.

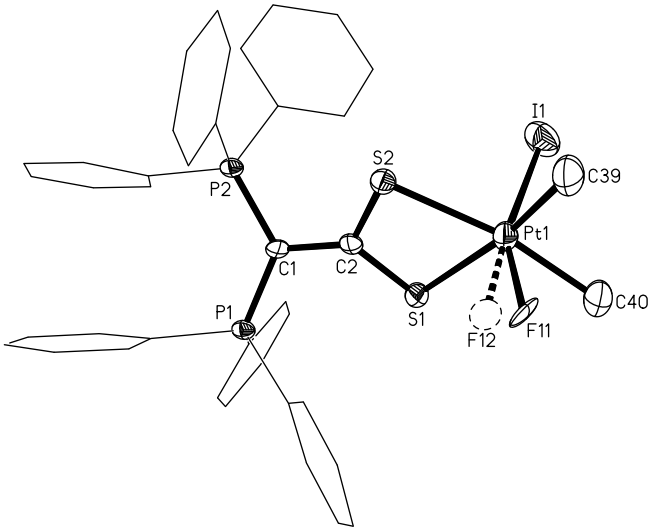

Fig. 2. Molecular structure of **4** · $2CH_2Cl_2$ showing the atom numbering scheme. The ellipsoids are drawn at a 40% probability level; the H atoms at the phenyl rings and the CH_2Cl_2 molecules are omitted for clarity.

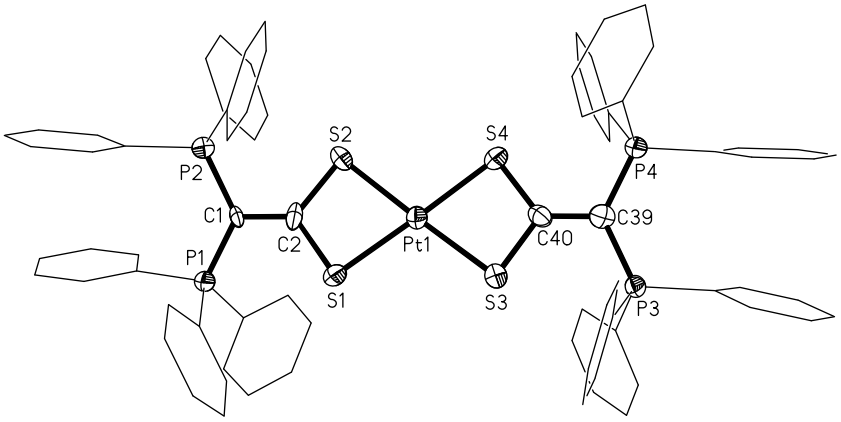

Fig. 3. Molecular structure of the cation of **5** · $2CH_2Cl_2$ omitting the solvent molecules and showing the atom numbering scheme. The ellipsoids are drawn at a 50% probability level; the phenyl groups are represented as thin lines omitting the H atoms for clarity.

Table 1
Crystal data and structure refinement details for the compounds **3** · CH_2Cl_2, **4** · $2CH_2Cl_2$ and **5** · $2CH_2Cl_2$

	3 · CH_2Cl_2	**4** · $2CH_2Cl_2$	**5** · $2CH_2Cl_2$
Formula	$C_{39}H_{32}Cl_2I_2P_2PtS_2$	$C_{42}H_{40}Cl_4FIP_2PtS_2$	$C_{78}H_{64}Cl_4F_{10}P_4PtS_4Si_2$
mw (g/mol)	1146.56	1153.66	1836.57
a (pm)	1104.6(1)	1105.0(1)	1442.1(2)
b (pm)	1832.1(2)	1252.0(2)	1567.7(2)
c (pm)	1965.9(3)	1766.4(2)	1829.8(2)
α (°)	90	71.30(1)	71.10(2)
β (°)	101.88(1)	76.38(1)	82.34(2)
γ (°)	90	74.84(1)	80.40(2)
Crystal size (mm)	0.08 × 0.04 × 0.02	0.29 × 0.2 × 0.05	0.18 × 0.13 × 0.04
Volume ($pm^3 \times 10^6$)	3893.2(8)	2203.2(5)	3845.0(8)
Z	4	2	2
d_{calc} (g/cm^3)	1.956	1.739	1.586
Crystal system	monoclinic	triclinic	triclinic
Space group	$P2_1/c$ (nr. 14)	$P\bar{1}$ (nr. 2)	$P\bar{1}$ (nr. 2)
Diffractometer	IPDS II (Stoe)	IPDS I (Stoe)	IPDS I (Stoe)
Radiation	Mo Kα	Mo Kα	Mo Kα
Temperature (K)	193	193	193
μ (cm^{-1})	55.4	43.3	22.5
$2\theta_{max}$ (°)	52.50	52.24	52.25
Index range	$-13 \leqslant h \leqslant 13$, $-22 \leqslant k \leqslant 22$, $-24 \leqslant l \leqslant 24$	$-12 \leqslant h \leqslant 12$, $-15 \leqslant k \leqslant 15$, $-21 \leqslant l \leqslant 21$	$-17 \leqslant h \leqslant 17$, $-19 \leqslant k \leqslant 19$, $-21 \leqslant l \leqslant 21$
Number of reflections collected	26549	21835	38256
Number of independent reflections (R_{int})	7699 (0.2251)	8068 (0.0674)	14085 (0.235)
Number of observed reflections with $F_0 > 4\sigma(F_0)$	3548	5542	4186
Parameters	434	490	706
Absorption correction	numerical	numerical	numerical
Structure solution	direct methods SIR-92 [19]	direct methods SIR-92 [19]	Patterson method SHELXTL-Plus [20]
Refinement against F^2	SHELXL-97 [21]	SHELXL-97 [21]	SHELXL-97 [21]
H atoms	[a]	[a]	[a]
R_1	0.0762	0.059	0.066
wR_2 (all data)	0.1625	0.1589	0.1441
Maximum electron density left (e/$pm^3 \times 10^{-6}$)	1.18	5.28	1.18

[a] Calculated positions with common displacement parameter.

flexibility of this angle according to the nature of the central metal atom. The dihedral angle between the S_2C and the P_2C planes amounts to 26° and is larger than that in the free ligand **1** (20°). The increased deviation from planarity may be due to interactions of the sulfur atoms with phenyl rings in such that one ring at P(1) is pushing up the sulfur atom S(1) and another one at P(2) is pushing down the S(2) atom, and the shorter S_2C–CP_2 bond in **3** relative to the free ligand brings the phenyl groups closer to the sulfur atoms which causes a further increase of the repulsion. The Pt–I distances (mean 262.5(1) pm) and the Pt–S distances (mean 229.2(4) pm) are typical for compounds of Pt^{II} with a PtS_2I_2 core and a *cis* arrangement of the I atoms; the same is true for the I–Pt–I angle [13a,13b,13c,13d,13e,13f,13g].

3.2. Crystal structure of **4** · $2CH_2Cl_2$

The neutral complex **4** contains Pt^{IV} in a distorted octahedral environment; the crystal structure is depicted in Fig. 2. Other Pt^{IV} compounds with the PtS_2 core are equipped either with dithiocarbaminato ligands [10] or pincer ligands with S donor atoms [15]. In **4** the dihedral angle between the S_2C and the P_2C planes amounts to 35° and is larger than that in **3**. The S_2C–CP_2 bond length is in

Table 2
Selected bond lengths (pm) and angles (°) in **3** · CH_2Cl_2

Bond lengths			
Pt(1)–I(1)	262.2(2)	Pt(1)–I(2)	262.8(1)
Pt(1)–S(1)	228.9(4)	Pt(1)–S(2)	229.5(5)
S(1)–C(2)	176(2)	S(2)–C(2)	170(2)
P(1)–C(1)	180(2)	P(1)–C(3)	186(2)
P(1)–C(9)	181(2)	P(1)–C(15)	181(2)
P(2)–C(1)	175(2)	P(2)–C(21)	180(2)
P(2)–C(27)	182(2)	P(2)–C(33)	183(2)
C(1)–C(2)	141(2)		
Bond angles			
I(1)–Pt(1)–I(2)	92.93(5)	I(1)–Pt(1)–S(1)	95.8(2)
I(1)–Pt(1)–S(2)	169.7(1)	I(2)–Pt(1)–S(1)	171.3(2)
I(2)–Pt(1)–S(2)	97.2(1)	S(1)–Pt(1)–S(2)	74.1(2)
Pt(1)–S(1)–C(2)	89.3(6)	Pt(1)–S(2)–C(2)	90.4(6)
C(1)–P(1)–C(3)	107.6(8)	C(1)–P(1)–C(9)	113.6(9)
C(1)–P(1)–C(15)	113.1(9)	C(3)–P(1)–C(9)	110.9(9)
C(3)–P(1)–C(15)	105.4(8)	C(9)–P(1)–C(15)	105.9(8)
C(1)–P(2)–C(21)	113.3(8)	C(1)–P(2)–C(27)	108.5(9)
C(1)–P(2)–C(33)	115.3(8)	C(21)–P(2)–C(27)	106.8(7)
C(21)–P(2)–C(33)	105.7(8)	C(27)–P(2)–C(33)	106.8(8)
P(1)–C(1)–P(2)	125.1(1)	P(1)–C(1)–C(2)	117.(1)
P(2)–C(1)–C(2)	118.(1)	S(1)–C(2)–S(2)	106.1(9)
S(1)–C(2)–C(1)	125.(1)	S(2)–C(2)–C(1)	129.(1)

Table 3
Selected bond lengths (pm) and angles (°) in **4** · $2CH_2Cl_2$

Bond lengths			
Pt(1)–I(1)	278.2(1)	Pt(1)–S(1)	248.0(2)
Pt(1)–S(2)	243.7(2)	Pt(1)–F(11)	198(1)
Pt(1)–F(12)	210(1)	Pt(1)–C(39)	205(1)
Pt(1)–C(40)	208(1)	S(1)–C(2)	171.4(8)
S(2)–C(2)	170.7(9)	P(1)–C(1)	174.1(8)
P(1)–C(3)	181.7(8)	P(1)–C(9)	180.6(8)
P(1)–C(15)	181.1(8)	P(2)–C(1)	175.8(8)
P(2)–C(21)	181.1(8)	P(2)–C(27)	183.8(8)
P(2)–C(33)	180.5(8)	C(1)–C(2)	145(1)
Bond angles			
I(1)–Pt(1)–S(1)	93.10(6)	I(1)–Pt(1)–S(2)	94.33(6)
I(1)–Pt(1)–F(11)	156.4(4)	I(1)–Pt(1)–F(12)	174.3(4)
I(1)–Pt(1)–C(39)	90.2(4)	I(1)–Pt(1)–C(40)	90.3(4)
S(1)–Pt(1)–S(2)	70.99(8)	S(1)–Pt(1)–F(11)	103.5(5)
S(1)–Pt(1)–F(12)	92.2(4)	S(1)–Pt(1)–C(39)	169.5(4)
S(1)–Pt(1)–C(40)	99.7(4)	S(2)–Pt(1)–F(11)	106.9(4)
S(2)–Pt(1)–F(12)	89.3(4)	S(2)–Pt(1)–C(39)	98.9(4)
S(2)–Pt(1)–C(40)	169.8(4)	F(11)–Pt(1)–C(40)	70.6(6)
F(11)–Pt(1)–C(39)	76.6(6)	F(12)–Pt(1)–C(40)	86.9(6)
F(12)–Pt(1)–C(39)	85.0(6)	Pt(1)–S(1)–C(2)	87.0(3)
C(39)–Pt(1)–C(40)	90.2(6)	C(1)–P(1)–C(3)	109.7(4)
Pt(1)–S(2)–C(2)	88.6(3)	C(1)–P(1)–C(15)	110.3(4)
C(1)–P(1)–C(9)	115.5(4)	C(1)–P(2)–C(21)	113.2(4)
C(1)–P(2)–C(27)	111.9(4)	C(1)–P(2)–C(33)	113.0(4)
P(1)–C(1)–C(2)	119.8(6)	P(1)–C(1)–P(2)	125.4(5)
S(1)–C(2)–S(2)	113.2(5)	P(2)–C(1)–C(2)	114.8(6)
S(2)–C(2)–C(1)	123.5(7)	S(1)–C(2)–C(1)	123.3(7)

between that of **1** and **3** amounting to 145(1) pm. The Pt–S bond lengths are up to 20 pm longer than in the Pt^{II} compounds **3** and **5**, while the C–S distances are only slightly shorter and close to that of the free ligand **1**. The higher charge at the central atom causes the S–C–S bite angle to increase and the S–Pt–S angle to decrease by about 7° and 3°, respectively, relative to the Pt(II) compounds. The F atom is disordered with a 0.5–0.5 distribution, and F(12) occupies more exactly the axial octahedron position while F(11) is slightly bent away from the S atoms. The distance between F(11) and F(12) is about 67 pm. According to our X-ray data there is no possibility to introduce a disorder between the positions of the methyl groups and the fluorine atoms because of the displacement parameters which fit only to the arrangement shown in

Table 4
Selected bond lengths (pm) and angles (°) in the cation of **5** · $2CH_2Cl_2$

Bond lengths			
Pt(1)–S(1)	231.9(4)	Pt(1)–S(2)	228.9(4)
Pt(1)–S(3)	230.8(4)	Pt(1)–S(4)	229.8(5)
S(1)–C(2)	173(2)	S(2)–C(2)	175(2)
S(3)–C(40)	174(2)	S(4)–C(40)	174(2)
P(1)–C(1)	174(2)	P(1)–C(3)	181(2)
P(1)–C(9)	180(2)	P(1)–C(15)	181(2)
P(2)–C(1)	179(2)	P(2)–C(21)	180(2)
P(2)–C(27)	181(2)	P(2)–C(34)	182(2)
P(3)–C(39)	179(2)	P(3)–C(41)	182(2)
P(3)–C(47)	180(2)	P(3)–C(53)	180(2)
P(4)–C(65)	181(2)	P(4)–C(71)	180(2)
C(1)–C(2)	141(2)	C(3)–C(4)	139(2)
Bond angles			
S(1)–Pt(1)–S(2)	74.2(2)	S(1)–Pt(1)–S(3)	107.6(2)
S(1)–Pt(1)–S(4)	178.3(2)	S(2)–Pt(1)–S(3)	178.1(2)
S(2)–Pt(1)–S(4)	104.2(2)	S(3)–Pt(1)–S(4)	74.1(2)
Pt(1)–S(1)–C(2)	89.6(6)	Pt(1)–S(2)–C(2)	89.9(5)
Pt(1)–S(3)–C(40)	89.8(5)	Pt(1)–S(4)–C(40)	90.1(6)
C(1)–P(1)–C(3)	111.4(5)	C(1)–P(1)–C(9)	110.8(5)
C(1)–P(1)–C(15)	110.3(4)	C(3)–P(1)–C(9)	109.0(2)
C(3)–P(1)–C(15)	103.7(2)	C(9)–P(1)–C(15)	111.4(2)
C(1)–P(2)–C(21)	110.0(5)	C(1)–P(2)–C(27)	116.5(5)
C(1)–P(2)–C(34)	106.2(5)	C(21)–P(2)–C(27)	105.9(2)
C(21)–P(2)–C(34)	112.4(2)	C(27)–P(2)–C(34)	105.8(2)
C(39)–P(3)–C(41)	108.1(5)	C(39)–P(3)–C(47)	117.6(5)
C(39)–P(3)–C(53)	110.1(6)	C(41)–P(3)–C(47)	105.5(2)
C(41)–P(3)–C(53)	112.7(2)	C(47)–P(3)–C(53)	102.9(2)
C(39)–P(4)–C(59)	112.8(5)	C(39)–P(4)–C(65)	112.4(6)
C(39)–P(4)–C(71)	118.8(5)	C(59)–P(4)–C(65)	105.4(2)
C(59)–P(4)–C(71)	108.5(2)	C(65)–P(4)–C(71)	108.7(2)
P(1)–C(1)–P(2)	128.2(7)	P(1)–C(1)–C(2)	117.1(1)
P(2)–C(1)–C(2)	115(1)	S(1)–C(2)–S(2)	106.2(8)
S(1)–C(2)–C(1)	127(1)	S(2)–C(2)–C(1)	127(1)
P(3)–C(39)–P(4)	129.2(9)	P(3)–C(39)–C(40)	114(1)
P(4)–C(39)–C(40)	116(1)	S(3)–C(40)–S(4)	106.0(9)
S(3)–C(40)–C(39)	127(1)	S(4)–C(40)–C(39)	127(1)

Fig. 2. The Pt–I distance amounts to 278.2(1) pm and is longer than in other Pt^{IV} compounds with a related ligand arrangement [15]. It is about 16 pm longer than that in **3** to Pt^{II} but 5 pm shorter than the related distance in the tetrameric $[Me_3PtI]$ with a bridging I atom [16]. If we compare terminal and bridging F atoms as in **4** and $[Me_3PtF]_4$, respectively, the terminal one is about 20 pm shorter [17]. The methyl groups are in *trans* position to the sulfur atoms and the Pt–C distances are in the upper range of those in $[Me_3PtX]_4$ complexes [16,17].

3.3. Crystal structure of **5** · $2CH_2Cl_2$

The crystal structure of the dication **5** is shown in Fig. 3. One of the solvent molecules is disordered. The complex contains two molecules of **1** at Pt^{II} as chelating ligands. The dihedral angles between the S_2C and the P_2C planes amount to 19° and 9°, respectively; the environment at the central Pt atom is planar as shown by the sum of the angles of 360.1°, and the deviations of the five atoms from the best plane are very small (Pt(1), S(1), S(2), S(3), S(4) = −1, 0, 1, 0, 1 pm). The S_2C–CP_2 bond lengths are identical with those of **3**; similarly, the S–C–S bite angles and the S–Pt–S angles correspond to those of **3**. The mean Pt–S distance is only slightly longer than that in **3**, but the individual distances differ by about 3 pm, probably due to packing effects. Although compounds with a PtS_4 core are very common in platinum chemistry, cationic compounds with a spiro bicyclic CS_2PtS_2C arrangement have not yet been described. No nearer contacts exist between the cation and the anions. The Si–F distances in the $[SiF_5]^-$ anions range between 153(1) and 160(1) pm at Si(1) and 152(1) and 162(1) pm at Si(2).

4. Conclusion

In contrast to the carbodiphosphorane adducts of CO_2 and COS, which adopt η^1 or η^2 coordination, the CS_2 adduct **1** is found to act only as a chelating ligand towards transition metals as yet. If **1** is connected to Ag^+, aggregates of Ag_4^{4+} or Ag_6^{6+} cluster units are held together by the sulfur atom bonded each to one or two silver atoms [6]. For comparison, the most relevant bond lengths in the compounds **1** and **3**–**5** are summarized in Table 5. Whereas in the starting adduct **1** the S_2C–CP_2 distance is already shorter than a single bond, a further shortening is observed upon complex formation, indicating an increase in double bond character. In the Pt^{II} complexes the related S_2C–CP_2 distances are the shortest ones found as yet with 141(2) pm; they are close to those in aromatic ring systems. This electron release diminishes the P–C (p–σ^*) interaction leading to longer distances. This trend was also observed in the related carbonyl complexes $[(CO)_4MS_2CC(PPh_3)_2]$ where S_2C–CP_2 distances of about 145 pm were found [4]; similar values are also recorded in the silver clusters [6].

Thus, the occupied p orbital of the sp^2 CP_2 carbon atom in **1** and the vacant p orbital at the sp^2 CS_2 carbon atom form a partial double bond which, depending on the nature and charge of the metal, is increased upon coordination of the sulfur atoms at a metal atom. For the first time, we can compare compounds in which **1** is bonded to a metal in different oxidation states. There is a great difference in the coordination of **1** to a Pt^{II} or Pt^{IV} atom with a planar or and octahedral ligand arrangement, respectively. In spite of the higher charge of the central atom in **4** with Pt^{IV} a minor electron release is found, expressed by a longer S_2C–CP_2 bond accompanied by about 16 pm longer (mean) Pt–S distances. The differences in the bonding parameters indicate a weaker bond of the chelating ligand **1** in the complex **4**. Thus, the S_2C–CP_2 double bond character increases in the series **1** < **4** < **3**–**5** corresponding to a decrease of the P–C double bond character in this row. Because **5** is the result of Pt^{II} with weakly coordinating anions, further studies in this field are in progress. Furthermore, the coordination of **1** at Pt^{IV} compounds will also be of interest and the formation of cations with more than one neutral ligand **1**, such as compounds with $[PtS_4X_2]^{2+}$ or $[PtS_6]^{4+}$ cores, will be a challenge for the future.

5. Experimental

All operations were carried out under an argon atmosphere in dried and degassed solvents using Schlenk techniques. The solvents were thoroughly dried and freshly distilled prior to use. The IR spectra were run on a Nicolet 510 spectrometer. For the ^{31}P NMR spectra we used the instrument Bruker AC 200. Elemental analyses were performed by the analytical service of the Fachbereich Chemie der Universität Marburg (Germany). Compound **1** was prepared according to a modified literature procedure [1] by addition of CS_2 to a solution of $C(PPh_3)_2$ in toluene at room temperature. $[Cl_2Pt(cod)]$ and $[I_2Pt(cod)]$ were obtained according to literature procedures [18]. Information concerning the X-ray structure determination is given in Table 1. The residual electron density in **4** · $2CH_2Cl_2$ is near the Pt atom.

Table 5
Comparison of important bond lengths in **1**, **3**, **4** and **5**

	1 [4]	**3**	**4**	**5**
Pt–S (mean)		229.2(4)	245.9(2)	230.4(4)
S–C	169.1(2)	173(2)	171.1(8)	174(2)
S_2C–CP_2	146.9(6)	141(2)	145(1)	141(2)
C–P	175.1(2)	178(2)	175.0(8)	177(2)

5.1. Preparation of $[Cl_2Pt\{S_2CC(PPh_3)_2\}]$ (**2**)

To a suspension of 520 mg (0.85 mmol) of $S_2CC(PPh_3)_2$ (**1**) in about 40 ml THF was added 320 mg (0.85 mmol) $[Cl_2Pt(cod)]$. The yellow suspension immediately turned red-brown. The mixture was stirred magnetically for about 1 h. Then the precipitate was filtered, washed with 1 ml THF and dried in vacuum. Yield 710 mg (95%). ^{31}P NMR (DMSO): 14.56 ppm. IR (Nujol): 1585 vw, 1497 m, 1438 s, 1253 vs, 1197 w, 1163 w, 1098 s, 1069 w, 1043 m, 1027 w, 998 m, 811 m, 749 m, 736 w, 721 m, 714 w, 690 s, 564 w, 556 w, 524 s, 506 s, 492 m (cm^{-1}). *Anal.* Calc. for $[Cl_2Pt\{S_2CC(PPh_3)_2\}]$ (**2**): C, 51.94; H, 3.44. Found: C, 50.38; H 3.65%.

5.2. Preparation of $[I_2Pt\{S_2CC(PPh_3)_2\}]$ (**3**)

In a similar procedure as outlined for the preparation of **2**, the red-brown complex **3** was obtained from 0.66 g (1.08 mmol) $[I_2Pt(cod)]$ and 0.60 g (1.08 mmol) of $S_2CC(PPh_3)_2$ (**1**). The dry red-brown powder was treated with CH_2Cl_2 which produced small dark red crystals of **3** · CH_2Cl_2 during several hours; yield 1.05 g (92%). ^{31}P NMR (DMSO): 13.96 ppm. IR (Nujol): 1586 vw, 1481 m, 1439 s, 1246 vs, 1192 w, 1163 w, 1096 s, 1073 w, 1049 s, 1024 w, 997 m, 806 m, 740 m, 723 m, 711 w, 693 s, 685 s, 570 w, 553 w, 522 s, 509 s, 494 m (cm^{-1}). *Anal.* Calc. for $[I_2Pt\{S_2CC(PPh_3)_2\}]$ (**3**): C, 42.99; H, 2.85. Found: C, 41.64; H, 2.91%.

5.3. Formation of $[Me_2FIPt(S_2CC(PPh_3)_2)]$ (**4**) and $[Pt(S_2CC(PPh_3)_2)_2][SiF_5]_2$ (**5**)

An impure sample obtained from fluorination of $[Me_2Pt(cod)]$/$I_2Pt(cod)]$ with XeF_2 was used [9] for the reaction with **1** in CH_2Cl_2; the anion $[SiF_5]^-$ may originate from fluorination of glass or grease. Few crystals of **4** (small red blocks) and **5** (orange plates) were obtained from CH_2Cl_2 solutions upon layering with *n*-pentane; no further crystalline product was formed. Compound **4**, ^{31}P NMR (CH_2Cl_2): s, 14.8 ppm. Compound **5**, ^{31}P NMR (CH_2Cl_2): s, 13.3 ppm.

Supplementary material

CCDC 667634, 667635 and 667636 contain the supplementary crystallographic data for **3**, **4** and **5**. These data can be obtained free of charge via http://www.ccdc.cam.ac.uk/conts/retrieving.html, or from the Cambridge Crystallographic Data Centre, 12 Union Road, Cambridge CB2 1EZ, UK; fax: (+44) 1223-336-033; or e-mail: deposit@ccdc.cam.ac.uk.

Acknowledgements

We thank the Deutsche Forschungsgemeinschaft for financial support. W.P. is also grateful to the Max-Planck-Society, Munich, Germany, for financial support.

References

[1] C.N. Matthews, J.S. Driscoll, G.H. Birum, J. Chem. Soc. Chem. Commun. (1966) 736.
[2] (a) H. Schmidbaur, C.E. Zybill, D. Neugebauer, Angew. Chem., Int. Ed. Engl. 21 (1982) 310;
(b) H. Schmidbaur, C. Zybill, D. Neugebauer, G. Müller, Z. Naturforsch. 40b (1985) 1293;
(c) W. Petz, C. Kutschera, S. Tschan, F. Weller, B. Neumüller, Z. Anorg. Allg. Chem. 629 (2003) 1235.
[3] (a) W. Petz, F. Weller, J. Uddin, G. Frenking, Organometallics 18 (1999) 619;
(b) J. Sundermeyer, K. Weber, K. Peters, H.G. von Schnering, Organometallics 13 (1994) 2560;
(c) H. Schmidbaur, C.E. Zybill, G. Müller, C. Krüger, Angew. Chem., Int. Ed. Engl. 22 (1983) 729;
(d) J. Vicente, A.R. Singhal, P.G. Jones, Organometallics 21 (2002) 5887.

[4] W. Petz, C. Kutschera, M. Heitbaum, B. Neumüller, G. Frenking, R. Tonner, Inorg. Chem. 44 (2005) 1263.
[5] W. Petz, B. Neumüller, J. Hehl, Z. Anorg. Allg. Chem. 632 (2006) 2232.
[6] W. Petz, B. Neumüller, I. Krossing, Z. Anorg. Allg. Chem. 632 (2006) 859.
[7] C.N. Matthews, J.S. Driscoll, G.H. Birum, Tetrahedron Lett. 46 (1966) 5707.
[8] (a) J. Weidlein, U. Müller, K. Dehnicke, Schwingungsfrequenzen I G, Thieme Verlag Stuttgart, New York, 1981;
(b) H.E. Winberg, D.D. Coffman, J. Am. Chem. Soc. 87 (1965) 2776;
(c) M.L. Ziegler, H. Weber, B. Nuber, O. Serhadle, Z. Naturforsch. 42b (1987) 1411.
[9] J. Lorberth, personal communication.
[10] (a) J. Fornies, A. Martin, R. Navarro, V. Sicilia, P. Villarroya, Organometallics 15 (1996) 1826;
(b) J. Willemse, J.A. Cras, J.G. Wijnhoven, P.T. Beurskens, Rec. Trav. Chim. Pay Bas 92 (1973) 1199.
[11] (a) A.N. Westra, C. Esterhuysen, K.R. Koch, Acta Crystallogr., Sect. C: Cryst. Struct. Commun. 60 (2004) m395;
(b) R. Bardi, A.M. Piazzesi, A. Del Pra, L. Trincia, Acta Crystallogr., Sect. C: Cryst. Struct. Commun. 43 (1987) 1281.
[12] K. Lovqvist, Acta Crystallogr., Sect. C: Cryst. Struct. Commun. 52 (1996) 1921.
[13] (a) G.J. Grant, C.G. Brandow, D.F. Galas, J.P. Davis, W.T. Pennington, E.J. Valente, J.D. Zubkowski, Polyhedron 20 (2001) 3333;
(b) G. Marangoni, B. Pitteri, V. Bertolasi, P. Gilli, Inorg. Chim. Acta 234 (1995) 173;
(c) M. Knorr, H.N. Peindy, F. Guyon, H. Sachdev, C. Strohmann, Z. Anorg. Allg. Chem. 630 (2004) 1955;
(d) H.N. Peindy, F. Guyon, I. Jourdain, M. Knorr, D. Schildbach, C. Strohmann, Organometallics 25 (2006) 1472;
(e) M.H. Johansson, H.P. Engelbrecht, Acta Crystallogr., Sect. E: Struct. Rep. Online (2001) m114;
(f) K. Lovqvist, O.F. Wendt, J.G. Leipoldt, Acta Chem. Scand. 50 (1996) 1069;
(g) A. Oskarsson, B. Noren, C. Svensson, L.I. Elding, Acta Crystallogr. Sect. B: Struct. Sci. 46 (1990) 748.
[14] R. Usón, J. Forniés, M.A. Usón, J.F. Yagüe, P.G. Jones, K. Meyer-Bäse, J. Chem. Soc., Dalton Trans. (1986) 947.
[15] (a) G.S. Hanan, J.E. Kickham, S.J. Loeb, J. Chem. Soc. Chem. Commun. (1991) 893;
(b) G.S. Hanan, J.E. Kickham, S.J. Loeb, Organometallics 11 (1992) 3063.
[16] K.H. Ebert, W. Massa, H. Donath, J. Lorberth, B.-S. Seo, E. Herdtweck, J. Organomet. Chem. 559 (1998) 203.
[17] H. Donath, E.V. Avtomonov, I. Sarraje, K.-H. von Dahlen, M. El-Essawi, J. Lorberth, B.-S. Seo, J. Organomet. Chem. 559 (1998) 191.
[18] C. Clark, L.E. Manzer, J. Organomet. Chem. 59 (1973) 411.
[19] A. Altomare, G. Cascarano, C. Giacovazzo, A. Guagliardi, M.C. Burla, G. Poldori, M. Camalli, SIR-92, Rome, 1992.
[20] G.M. Sheldrick, SHELXTL-Plus, Release 4.2 for Siemens Crystallographic Systems R3, Siemens Analytical X-Ray Instruments Inc., Madison, WI, 1990.
[21] G.M. Sheldrick, SHELXL-97, University of Göttingen, Germany, 1997.

Polyhedron 27 (2008) 2545–2550

Contents lists available at ScienceDirect

Polyhedron

journal homepage: www.elsevier.com/locate/poly

Layered metal succinate/bis(4-pyridylmethyl)piperazine coordination polymers featuring mutual inclined interpenetration

David P. Martin [a], Ronald M. Supkowski [b], Robert L. LaDuca [a,*]

[a] Lyman Briggs College and Department of Chemistry, Michigan State University, E-30 Holmes Hall, East Lansing, MI 48825, USA
[b] Department of Chemistry and Physics, King's College, Wilkes-Barre, PA 18711, USA

ARTICLE INFO

Article history:
Received 10 March 2008
Accepted 8 May 2008
Available online 13 June 2008

Keywords:
Coordination polymer
Succinate
Organodiimine
Mutual inclined interpenetration
Crystal structure

ABSTRACT

Reaction of divalent metal chlorides with succinic acid (H_2suc) and the hydrogen-bonding capable tethering organodiimine bis(4-pyridylmethyl)piperazine (bpmp) in a mixed solvent system has afforded three isostructural coordination polymers: $[M(suc)(bpmp)(H_2O)_2]_n$ (M = Co, **1**; M = Ni, **2**; M = Cu, **3**) Single-crystal X-ray diffraction showed that **1**–**3** possess $[M(suc)(bpmp)(H_2O)_2]_n$ 2D layer motifs. Parallel sets of layer motifs in **1**–**3** aggregate into 2d + 2d → 3D mutually inclined interpenetrated systems, fostered by hydrogen bonding interactions between layers. Spectral and thermal properties of these materials are also discussed.

© 2008 Elsevier Ltd. All rights reserved.

1. Introduction

Over the past decade many researchers have undertaken significant effort towards the synthesis and characterization of metal dicarboxylate and tricarboxylate coordination polymers because of the capability of these materials in diverse applications such as gas storage [1], small molecule shape-selectivity [2], ion-exchange [3], catalysis [4], and optical devices [5]. In these phases, dianionic dicarboxylate ligands not only serve to link metal cations into higher dimensionalities but also provide necessary charge balance, thereby permitting formation of a large number of neutral coordination polymer frameworks that exclude porosity-curtailing smaller anions. A wide range of structural patterns occurs in these systems, based on the disposition of the donor groups within the dicarboxylate moieties, coordination geometry preferences, and an array of available binding carboxylate modes.

While the predominant focus has rested on aromatic dicarboxylates because of their tendency to enforce rigid porous structures, aliphatic -dicarboxylate α,ω-dicarboxylate ligands have also shown their utility in the construction of novel coordination polymers due to their ability to undergo facile conformational interconversions [6–11]. For instance, the succinate dianion (suc, 1,4-butanedioate) has been shown to adopt *anti*, *gauche*, and intermediate conformations when incorporated into coordination polymer systems, thus provoking structurally intriguing frameworks of varying dimensionalities either alone [12–14] or in conjunction with organodiimine co-ligands such as 4,4′-bipyridine (4,4′-bpy) [15,16] or 4,4′-dipyridylamine (dpa) [17].

Recently, we reported the first aromatic dicarboxylate coordination polymers constructed with the aid of bis(4-pyridylmethyl)-piperazine (bpmp, Scheme 1), which exhibited interpenetrated and non-interpenetrated 2D and 3D structural motifs [18]. However, there are currently no reports of aliphatic α,ω-dicarboxylate coordination polymers incorporating this flexible, long, and hydrogen-bonding capable organodiimine tethering ligand to the best of our knowledge. Herein we discuss the synthesis and crystal structures of three isomorphous bpmp-containing succinate coordination polymers exhibiting mutually inclined interpenetration, $[M(suc)(bpmp)(H_2O)_2]_n$ (M = Co, **1**; M = Ni, **2**; M = Cu, **3**). Spectral and thermal properties of these new materials are also reported.

2. Experimental

2.1. General considerations

Metal chlorides and succinic acid (Fisher) were obtained commercially. The organodiimine bis(4-pyridylmethyl)piperazine (bpmp) was prepared via a published procedure [19]. Water was deionized above 3 MΩ in-house. Thermogravimetric analysis was performed on a TA Instruments TGA 2050 Thermogravimetric Analyzer with a heating rate of 10 °C/min up to 900 °C. Elemental analysis was carried out using a Perkin–Elmer 2400 Series II CHNS/O Analyzer. IR spectra were recorded on powdered samples on a Perkin–Elmer Spectrum One instrument.

* Corresponding author. Tel.: +1 5174322268.
E-mail address: laduca@msu.edu (R.L. LaDuca).

0277-5387/$ - see front matter © 2008 Elsevier Ltd. All rights reserved.
doi:10.1016/j.poly.2008.05.008

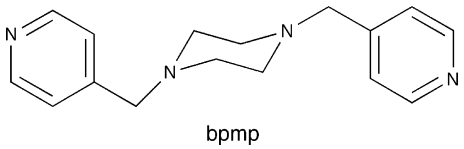

bpmp

Scheme 1.

2.2. Preparation of [Co(suc)(bpmp)(H$_2$O)$_2$]$_n$ (**1**)

$Co(NO_3)_2 \cdot 6H_2O$ (0.054 g, 0.19 mmol), succinic acid (0.022 g, 0.19 mmol) and bpmp (0.100 g, 0.38 mmol) were placed into 10 g (555 mmol) distilled H_2O in a 23 mL Teflon-lined Parr acid digestion bomb (1:1:2:2900 mol ratio). The bomb was sealed and heated at 120 °C for 48 h, whereupon it was cooled slowly in air to 25 °C. Pink blocks of **1** (0.016 mg, 17% yield based on Co) were isolated after washing with distilled water and acetone. Crystals of **1** were stable indefinitely in air. *Anal.* Calc. for $C_{20}H_{28}CoN_4O_6$ (**1**): C, 50.11; H, 5.89; N, 11.69. Found: C, 49.93; H, 5.75; N, 11.83%. IR (cm^{-1}): 3068 w br, 2811 w, 2773 w, 1616 m, 1540 s, 1459 m, 1425 m, 1406 s, 1351 m, 1323 w, 1293 m, 1222 w, 1154 w, 1135 m, 1066 w, 1013 m, 935 w, 878 w, 835 s, 797 s, 724 m, 662 s.

2.3. Preparation of [Ni(suc)(bpmp)(H$_2$O)$_2$]$_n$ (**2**)

$NiCl_2 \cdot 6H_2O$ (0.044 g, 0.19 mmol) and succinic acid (0.022 g, 0.19 mmol) were added to 4 mL of distilled H_2O in a borosilicate glass tube that had been sealed at one end. A solution of bpmp (0.050 g, 0.19 mmol) in 3 mL methanol was then carefully layered on top of the aqueous solution. Blue blocks of **2**(0.016 g, 17% yield based on Ni) were deposited after ~2 weeks on standing. These were filtered, washed with distilled water and acetone, and dried in air. Crystals of **2** were stable indefinitely in air. *Anal.* Calc. for $C_{20}H_{28}NiN_4O_6$ (**2**): C, 50.13; H, 5.89; N, 11.69. Found: C, 49.96; H, 5.63; N, 11.61%. IR (cm^{-1}): 3070 w br, 2905 w, 2810 w, 1618 m, 1538 s, 1441 w, 1425 m, 1406 s, 1389 m, 1351 m, 1324 m, 1293 m, 1221 m, 1154 w, 1135 m, 1013 m, 934 w, 865 w, 837 s, 800 s, 754 m, 726 m, 672 s.

2.4. Preparation of [Cu(suc)(bpmp)(H$_2$O)$_2$]$_n$ (**3**)

The procedure for the synthesis of **2** was followed except for the use of $CuCl_2 \cdot 2H_2O$ (0.044 g, 0.19 mmol) as the metal source. Blue blocks of **3** (0.058 g, 63% yield based on Cu) were obtained. *Anal.* Calc. for $C_{20}H_{28}CuN_4O_6$ (**3**): C, 49.63; H, 5.83; N, 11.58. Found: C, 49.40; H, 5.71; N, 11.46%. IR (cm^{-1}): 3387 w br, 2958 w, 2914 w, 2807 w, 1619 m, 1550 s, 1505 w, 1456 w, 1428 m, 1385 s, 1353 m, 1322 m, 1296 m, 1241 w, 1227 w, 1197 w, 1162 m, 1134 m, 1065 m, 1036 w, 1012 s, 929 w, 883 w, 838 s, 802 s, 673 s, 662 s.

3. X-ray crystallography

Single crystals of all materials were subjected to single crystal X-ray diffraction using a Bruker-AXS APEX II CCD instrument. Reflection data were acquired using graphite-monochromated Mo Kα radiation (λ = 0.71073 Å). The data were integrated via SAINT [20]. Lorentz and polarization effect and empirical absorption corrections were applied with SADABS [21]. The structures were solved using direct methods and refined on F^2 using SHELXTL [22]. All non-hydrogen atoms were refined anisotropically. Hydrogen atoms bound to carbon atoms were placed in calculated positions and refined isotropically with a riding model. The hydrogen atoms bound to all water molecules were found via Fourier difference maps and then refined isotropically with thermal parameters 1.2 times the average U_{ij} values of the atoms to which they are bound. Relevant crystallographic data are listed in Table 1.

Table 1
Crystal and structure refinement parameters for **1–3**

	1	**2**	**3**
Empirical formula	$C_{20}H_{28}CoN_4O_6$	$C_{20}H_{28}N_4NiO_6$	$C_{20}H_{28}CuN_4O_6$
Formula weight	479.39	479.19	484.00
Collection T (K)	173(2)	173(2)	173(2)
Color and habit	pink block	green block	blue block
Crystal size (mm)	0.38 × 0.26 × 0.24	0.18 × 0.16 × 0.15	0.30 × 0.30 × 0.25
λ(Å)	0.71073	0.71073	0.71073
Crystal system	monoclinic	monoclinic	monoclinic
Space group	$P2_1/c$	$P2_1/c$	$P2_1/c$
a (Å)	9.892(8)	9.8842(1)	9.8505(6)
b (Å)	12.351(10)	12.2451(2)	12.6846(7)
c (Å)	8.964(8)	8.9533(1)	8.7731(5)
β (°)	96.197(13)	93.082(1)	95.127(3)
V (Å^3)	1088.9(16)	1082.08(2)	1091.81(11)
Z	2	2	2
D_{calc} (g cm^{-3})	1.462	1.471	1.472
μ (mm^{-1})	0.832	0.941	1.044
Minimum/maximum transmission	0.939/1	0.8496/0.8741	0.7447/0.7803
hkl ranges	$-13 \leqslant h \leqslant 12$, $-16 \leqslant k \leqslant 15$, $-11 \leqslant l \leqslant 11$	$-13 \leqslant h \leqslant 13$, $-16 \leqslant k \leqslant 14$, $-11 \leqslant l \leqslant 11$	$-15 \leqslant h \leqslant 15$, $-20 \leqslant k \leqslant 19$, $-13 \leqslant l \leqslant 14$
Total reflections	12017	16655	17180
Unique reflections	2591	2665	4458
R_{int}	0.0179	0.0441	0.0453
Parameters/restraints	148/3	148/0	150/3
R_1[a] (all data)	0.0258	0.0670	0.0509
R_1[a] ($I > 2\sigma(I)$)	0.0230	0.0401	0.0353
wR_2[b] (all data)	0.0619	0.1013	0.1005
wR_2[b] ($I > 2\sigma(I)$)	0.0599	0.0928	0.0949
Maximum/minimum residual (e$^-$/Å^3)	0.324/−0.285	0.370/−0.542	0.441/−0.742
Goodness-of-fit	1.059		

[a] $R_1 = \sum ||F_o| - |F_c|| / \sum |F_o|$.

[b] $wR_2 = \left\{ \sum [w(F_o^2 - F_c^2)^2] / \sum [wF_o^2]^2 \right\}^{1/2}$.

4. Results and discussion

4.1. Synthesis and spectral characterization

The coordination polymers **1–3** were prepared cleanly either by hydrothermal techniques or via slow diffusion of aqueous solutions of the appropriate metal chloride and succinic acid, with ethanolic solutions of bpmp. The infrared spectra of **1–3** were consistent with their formulations. Sharp bands in the vicinity of ~1600–1200 cm^{-1} mark the stretching modes of the pyridyl rings of the bpmp ligands [23]. Features corresponding to pyridyl ring puckering modes were evident in the region between 820 and 600 cm^{-1}. Asymmetric and symmetric C–O stretching modes of the carboxylate moieties gave rise to very strong, slightly broadened bands at ~1530 and ~1380 cm^{-1}. Broad bands in the region of ~3400–3200 cm^{-1} in all cases represent O–H stretching modes within the ligated water molecules. The broadness of these latter spectral features is caused by the hydrogen bonding mechanisms within **1–3**.

4.2. Structural description of [Co(suc)(bpmp)(H$_2$O)$_2$]$_n$ (**1**)

As revealed by single crystal X-ray diffraction, the asymmetric unit of compound **1** consists of a divalent cobalt ion on a crystallographic inversion center, one bound water molecule, and one-half of a bpmp ligand (Fig. 1). Operation of the inversion center at the cobalt ion produces a $[CoO_4N_2]$ octahedral coordination geometry, with *trans* -disposed pyridyl nitrogen donor atoms from two

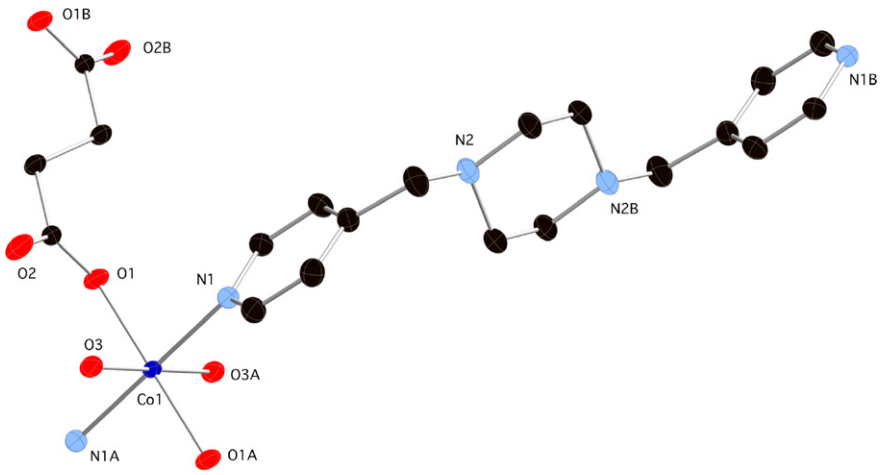

Fig. 1. Coordination environment of **1** with thermal ellipsoids drawn at 50% probability and partial atom numbering scheme. Hydrogen atoms are omitted.

different bpmp ligands situated in axial positions. The equatorial sites are occupied by two *trans* aqua ligands and two oxygen atoms from two different suc ligands. Bond lengths and angles about cobalt are fully consistent with octahedral coordination geometry (Table 2).

Extension of the structure through the *anti*-conformation (four C-atom torsion angle = 180°) bisbridging bismonodentate suc dianions forms one-dimensional (1D) $[Co(suc)(H_2O)_2]_n$ chain motifs parallel to the *c* crystal direction, with a Co···Co distance of 8.964 Å. The covalent connectivity within the chain units is augmented by hydrogen bonding donation from the aquo ligands to the unligated suc carboxylate oxygen atoms. These chains are then connected into a two-dimensional (2D) (4,4) rhomboid grid $[Co(suc)(bpmp)(H_2O)_2]_n$ coordination polymer layer motif, with a through-bpmp Co···Co distance of 15.824 Å (Fig. 2). The incipient void areas within the coordination polymer grid measure 17.652 × 18.706 Å, as determined by through-space Co···Co distances; these grid spaces are nearly rectangular in shape, with Co···Co···Co angles of 86.1° and 93.9°. The $[Co(suc)(bpmp)(H_2O)_2]_n$ 2D dual-ligand layered motifs in **1** contrast with the 1D $[Co(4,4'\text{-bpy})(H_2O)_4]_n$ linear chains observed in the structure of $\{[Co(4,4'\text{-bpy})(H_2O)_4](suc)\}_n$ [15], in which the succinate anions serve asunligated charge-compensating dianions. Within the structure of $[Co(suc)(dpa)_2]_n$, 1D threefold helical $[Co(suc)]_n$ chains are decorated by pendant monodentate dpa ligands [17]. Thus, **1** appears to be a rare example of a cobalt coordination polymer in which both the succinate and organodiimine ligands act as covalent linking agents.

The void spaces within the $[Co(suc)(bpmp)(H_2O)_2]_n$ coordination polymer layers permit mutual inclined 2d + 2d → 3D interpenetration of two parallel sets of layers, coincident with the (−1 1 0) and (−1 −1 0) crystal planes (Fig. 3). Between parallel layers, the nearest Co···Co contact distance is 9.892 Å, corresponding to the *a* lattice parameter. The angle of interpenetration between two members of different parallel layer sets is 77.0°. While there is no direct covalent interaction between interpenetrated layers, structural stability is provided by hydrogen bonding between the aqua ligands in one layer and unligated carboxylate oxygen atoms belonging to suc ligands in another layer. These hydrogen bonding patterns construct supramolecular $[Co(suc)(H_2O)_2]_n$ 1D chain patterns that course along the *b* crystal direction, as seen in Fig. 3. Metrical parameters for the intra- and inter-layer hydrogen bonding interactions in **1** are given in Table 3.

Table 2
Selected bond distance (Å) and angle (°) data for **1–3**

1		**2**	
Co1–O1	2.0624(19)	Ni1–O1	2.0375(15)
Co1–N1	2.1260(18)	Ni1–N1	2.0646(17)
Co1–O3	2.1648(17)	Ni1–O3	2.1202(16)
$O1^{\#1}$–Co1–O1	180.00(5)	$O1^{\#1}$–Ni1–O1	180.00(9)
O1–Co1–$N1^{\#1}$	91.48(4)	$O1^{\#1}$–Ni1–N1	91.12(7)
O1–Co1–N1	88.52(4)	O1–Ni1–N1	88.88(7)
$N1^{\#1}$–Co1–N1	180.00(7)	$N1^{\#1}$–Ni1–N1	180.0
$O1^{\#1}$–Co1–O3	90.82(4)	O1–Ni1–$O3^{\#1}$	91.46(6)
O1–Co1–O3	89.18(4)	O1–Ni1–O3	88.54(6)
$N1^{\#1}$–Co1–O3	87.01(7)	$N1^{\#1}$–Ni1–O3	87.26(6)
N1–Co1–O3	92.99(7)	N1–Ni1–O3	92.74(6)
O3–Co1–$O3^{\#1}$	180.00(5)	$O3^{\#1}$–Ni1–O3	180.0
3			
Cu1–O1	1.9498(9)	$N1^{\#2}$–Cu1–N1	179.999(1)
Cu1–N1	2.0059(11)	N1–Cu1–O3	154.32(4)
Cu–O3	2.5542(10)	O1–Cu1–O3	93.22(4)
		$O3^{\#2}$–Cu1–O3	180.0
$O1^{\#2}$–Cu1–O1	180.0	$O1^{\#2}$–Cu1–O3	86.78(4)
$O1^{\#2}$–Cu1–N1	89.35(4)	O1–Cu1–O3	89.78(4)
O1–Cu1–N1	90.65(4)		

Symmetry transformations to generate equivalent atoms: #1 −*x*, −*y*, −*z*; #2 −*x*, −*y*, −*z* + 1.

4.3. Structural description of $[Ni(suc)(bpmp)(H_2O)_2]_n$ (**2**)

The asymmetric unit of **2** (Fig. 4) is virtually identical to that of **1**, with the exception of the slightly shorter bond lengths (Table 2) imparted by the smaller ionic radius of Ni^{2+}relative to Co^{2+} [24]. As a result, the through-ligand Ni···Ni distances are slightly shorter than the corresponding contact distances in **1**, measuring 8.953 Å and 15.737 Å through the suc and bpmp ligands, respectively. $[Ni(suc)(bpmp)(H_2O)_2]_n$ (4,4) rectangular grid coordination polymer motifs are present in **2**, again with only slight metrical differences with respect to **1**. The through-space Ni···Ni contact distances within the grid measure 17.481 and 18.366 Å, with Ni···Ni···Ni angles of 88.1° and 91.9°. Therefore, the grid apertures more closely approach an idealized rectangular geometry than those in **1**. Parallel sets of layers, coincident with the (−1 1 0) and (−1 −1 0) crystal planes, engage in mutual inclined interpenetration at an angle of 77.7°, very slightly more obtuse than the corresponding angle in **1**. This subtle shift likely arises from the slight contraction of M–O/M–N bond lengths andhydrogen bonding interactions (Table 3) relative to those in **1**.

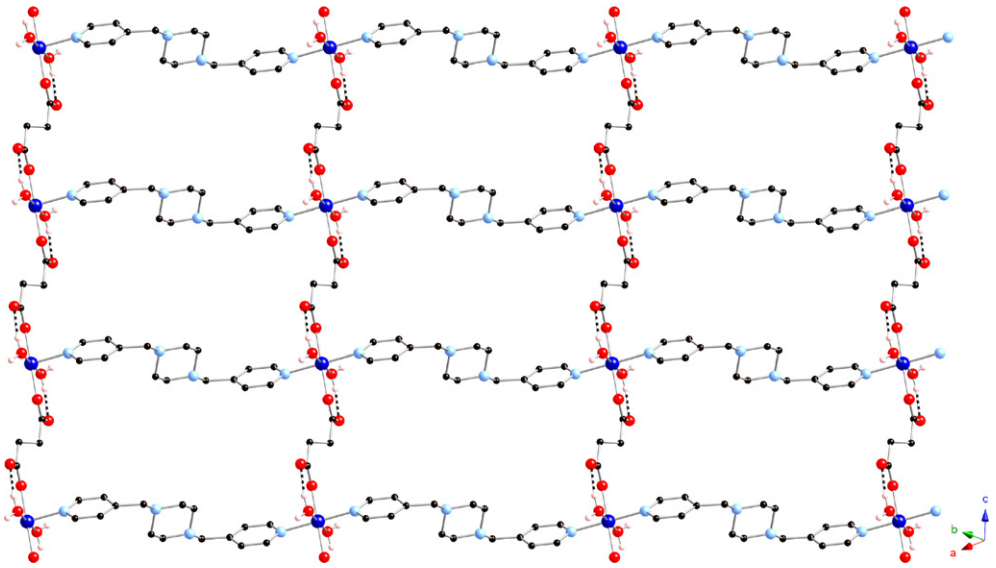

Fig. 2. A single $[Co(suc)(bpmp)(H_2O)_2]_n$ layer in **1**. Hydrogen bonding is indicated as dashed lines.

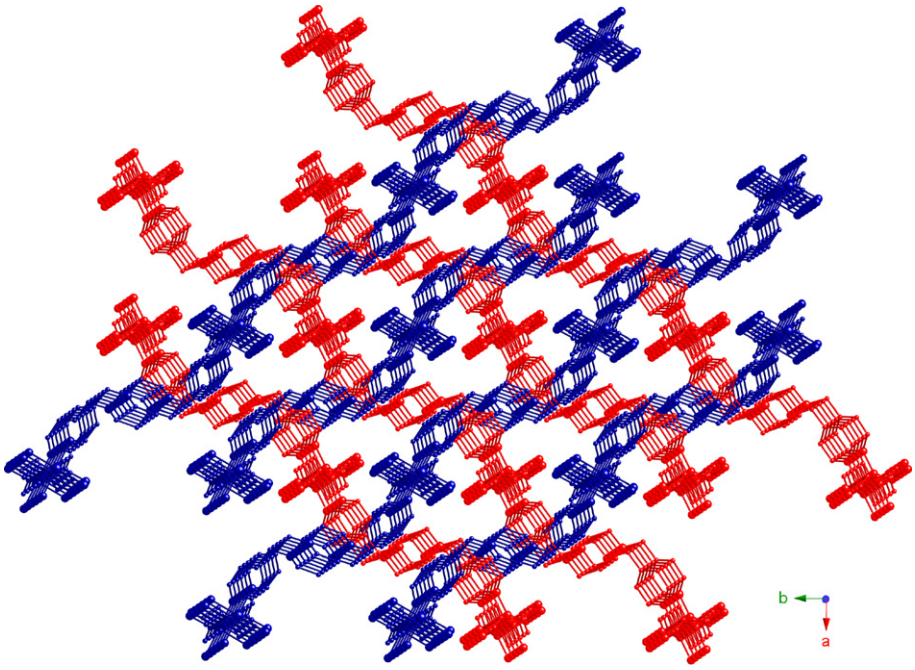

Fig. 3. The system of 2 d + 2d → 3D mutual inclined interpenetration in **1**–**3**.

Table 3
Hydrogen bonding distance (Å) and angle (°) data for **1**–**3**

D–H···A	*d*(H···A)	∠DHA	*d*(D···A)	Symmetry transformation for A
1				
O3–H3A···O2	1.985(13)	175.9(15)	2.822(2)	$-x, y + 1/2, -z + 1/2$
O3–H3B···O2	1.888(13)	160.9(15)	2.706(3)	$-x, -y, -z$
2				
O3–H3A···O2	2.11(3)	173(3)	2.830(2)	$-x, y + 1/2, -z + 1/2$
O3–H3B···O2	1.85(3)	164(2)	2.678(2)	$-x, -y, -z$
3				
O3–H3A···O2	2.053(13)	173.1(16)	2.8651(14)	$x, -y - 1/2, z - 1/2$
O3–H3B···O2	1.912(15)	163(2)	2.7452(14)	

While some frameworks with three-dimensional nickel succinate connectivity have been prepared [13a,14], reports of dual-ligand nickel succinate/organodiimine extended complexes are less common. $\{[Ni(dpa)_2(suc)]Cl\}_n$ displays a unique self-penetrated structure with 6^{10} topology built from the linkage of fourfold interpenetrated $[Ni(dpa)_2]_n$ cationic framework through

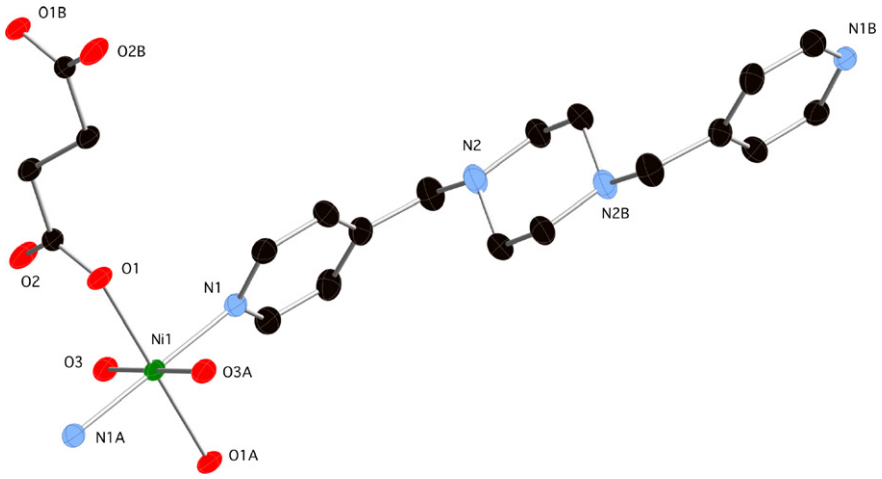

Fig. 4. Coordination environment of **2** with thermal ellipsoids drawn at 50% probability and partial atom numbering scheme. Hydrogen atoms are omitted.

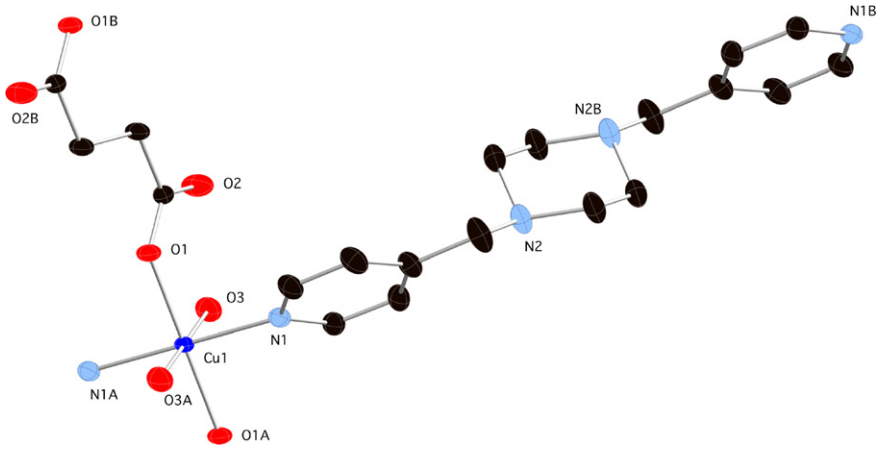

Fig. 5. Coordination environment of **3** with thermal ellipsoids drawn at 50% probability and partial atom numbering scheme. Hydrogen atoms are omitted.

suc ligands [17]. However, the suc ligands in this material only link neighboring nickel atoms between two separate frameworks; no "infinite" nickel succinate building units exist in this structure. Thus, **2** represents an uncommon example of a nickel coordination polymer manifesting extended covalent connectivity through both succinate and organodiimine ligands.

4.4. Structural description of $[Cu(suc)(bpmp)(H_2O)_2]_n$ (**3**)

The asymmetric unit of **3** (Fig. 5) is again very similar to that of **1**, with the exception of the distorted octahedral coordination at copper, imparted by the Jahn–Teller effect of the d^9 Cu^{2+} ion. The oxygen atoms of the two water molecules are positioned 2.554 Å away from each copper atom. Pertinent bond lengths and angles are given in Table 2. $[Cu(suc)(bpmp)(H_2O)_2]_n$ (4,4) rectangular grid coordination polymer motifs are present in **3**, similar to those seen in **1** and **2**. The through-ligand Cu ··· Cu distances are 8.773 Å and 16.060 Å through the suc and bpmp ligands, respectively; these values represent the shortest through-suc and through-bpmp distances within the series **1**–**3**. The through-space Cu ··· Cu contact distances within the grid are 17.873 and 18.717 Å, with Cu ··· Cu ··· Cu angles of 86.9° and 93.1°. The grid apertures in **3** thus deviate more from an idealized rectangular geometry than those in **1** and **2**. Parallel sets of layers, coincident with the (−1 1 0) and (−1 −1 0) crystal planes, engage in mutual inclined interpenetration at an angle of 75.4°. This angle of interpenetration is tighter than the corresponding angles in **1** and **2**, perhaps due to differences in hydrogen bonding provoked by the longer interactions between copper and the ligated water molecules (Table 3).

The structure of **3** can be contrasted with that of its previously reported 4,4′-bipyridine congener $\{[Cu(suc)(4,4'\text{-bpy})(H_2O)_2]2H_2O\}_n$, which possesses a 3D 7^59 (quartz dual) topology formed from 1D $[Cu(suc)(H_2O)_2]_n$ sixfold helices linked through the rigid-rod organodiimine tethers [18]. Fourfold $[Cu(suc)]_n$ helices are observed within the structure of $\{[Cu(suc)(dpa)]0.5H_2O\}_n$, which adopts a doubly interpenetrated 3D 6^58 $CdSO_4$ topology [15,16]. It is thus likely that the specific supramolecular and covalent environment fostered by the longer and more flexible bpmp ligand allows formation of a straight as opposed to a curled $[Cu(suc)(H_2O)_2]_n$ chain motif, resulting in an overall reduction in coordination polymer dimensionality in the case of **3**.

4.5. Thermal analyses

Compound **1** underwent no mass loss until ~125 °C, whereupon ejection of the ligated water molecules occurred obs'd, 7.7% calc'd). (7.5% observed, 7.7% calculated). Between ~150 and ~400 °C a series of mass loss steps totaling 75.3% was observed, consistent with the elimination of the suc and bpmp ligands calc'd). (80.0% calculated). The mass remnant of 17.3% of the original at 500 °C indicated the likely deposition of Co_3O_4 (16.7% predicted). In contrast, the dehydration of compound **3** commenced at ~80 °C, reflective of

the relative weakness of the Cu–O_{water} bonds. A mass loss of 7.5% was completed by 120 °C calc'd (7.4% calculated for two molar equivalents of water). Decomposition of **3** was marked by a mass loss steps totaling 74.0% between ~140 °C and ~500 °C calc'd (79.2% calculated for equivalent 1 equiv. each of suc and bpmp ligands). The 18.5% mass remnant is roughly consistent with the deposition of CuO calc'd). (16.4% calculated). TGA traces for **1** and **3** are shown in Figures S1 and S2, respectively.

5. Conclusions

Three isomorphous divalent metal succinate/bpmp coordination polymers exhibiting mutually inclined interpenetrated layer motifs have been synthesized and structurally characterized, widening the scope of metal-organic extended solids incorporating conformationally flexible ligands. The results hint at an especially rich coordination polymer system in which the aliphatic dicarboxylates components are uniquely suited to adjust to the covalent and supramolecular environments imposed by the presence of organodiimine co-ligands. By extending the aliphatic chain length or including sterically bulky substituents within the dicarboxylate component, or altering nitrogen donor disposition or hydrogen-bonding facility within the flexible organodiimine component, coordination polymers with novel structures and intriguing physicochemical properties are sure to be obtained. Further efforts in this direction are underway in our laboratory and will be reported in due course [25].

Acknowledgements

The authors gratefully acknowledge Michigan State University for financial support of this work. We thank Dr. Rui Huang for elemental analysis and Dr. Richard Staples for assistance with the operation of the Bruker AXS APEX II diffractometer. SDG.

Appendix A. Supplementary data

CCDC 665640, 665641 and 665642 contain the supplementary crystallographic data for **1**, **2** and **3**. These data can be obtained free of charge via http://www.ccdc.cam.ac.uk/conts/retrieving.html, or from the Cambridge Crystallographic Data Centre, 12 Union Road, Cambridge CB2 1EZ, UK; fax: (+44) 1223-336-033; or e-mail: deposit@ccdc.cam.ac.uk. Supplementary data associated with this article can be found, in the online version, at doi:10.1016/j.poly.2008.05.008.

References

[1] (a) J.L.C. Roswell, O.M. Yaghi, Angew. Chem., Int. Ed. Engl. 44 (2005) 4670;
(b) M. Kondo, T. Okubo, A. Asami, S.-I. Noro, T. Yoshitomi, S. Kitagawa, T. Ishii, H. Matsuzaka, Angew. Chem., Int. Ed. 38 (1999) 140;
(c) A.C. Sudik, A.R. Millward, N.W. Ockwig, A.P. Cote, J. Kim, O.M. Yaghi, J. Am. Chem. Soc. 127 (2005) 7110.
[2] (a) J.S. Seo, D. Whang, H. Lee, S.I. Jun, J. Oh, Y.J. Jeon, K. Kim, Nature 404 (2000) 982;
(b) A. Cingolani, S. Galli, N. Masciocchi, L. Pandolfo, C. Pettinari, A. Sironi, J. Am. Chem. Soc. 127 (2005) 6144.
[3] (a) Q.-R. Fang, G.-S. Zhu, M. Xue, J.-Y. Sun, S.-L. Qiu, Dalton Trans. (2006) 2399;
(b) X.-M. Zhang, M.-L. Tong, H.K. Lee, X.-M. Chen, J. Solid State Chem. 160 (2001) 118;
(c) O.M. Yaghi, H. Li, T.L. Groy, Inorg. Chem. 36 (1997) 4292.
[4] (a) S.G. Baca, M.T. Reetz, R. Goddard, I.G. Filippova, Y.A. Simonov, M. Gdaniec, N. Gerbeleu, Polyhedron 25 (2006) 1215;
(b) H. Han, S. Zhang, H. Hou, Y. Fan, Y. Zhu, Eur. J. Inorg. Chem. 8 (2006) 1594;
(c) W. Mori, S. Takamizawa, C.N. Kato, T. Ohmura, T. Sato, Microporous Mesoporous Mater. 73 (2004) 15.
[5] (a) S. Zang, Y. Su, Y. Li, Z. Ni, Q. Meng, Inorg. Chem. 45 (2006) 174;
(b) L. Wang, M. Yang, G. Li, Z. Shi, S. Feng, Inorg. Chem. 45 (2006) 2474;
(c) S. Wang, Y. Hou, E. Wang, Y. Li, L. Xu, J. Peng, S. Liu, C. Hu, New J. Chem. 27 (2003) 1144;
(d) D. Ghoshal, A.K. Ghosh, G. Mostafa, J. Ribas, N.R. Chaudhuri, Inorg. Chim. Acta 360 (2007) 1771;
(e) C. Livage, C. Egger, M. Nogues, G. Férey, Compt. Rend. Acad. Sci. Ser. Chem. 4 (2001) 221.
[6] L.-S. Long, Y.-R. Wu, R.-B. Huang, L.-S. Zheng, Inorg. Chem. 43 (2004) 3798.
[7] R.-F. Hu, Y. Kang, J. Zhang, Z.-J. Li, Y.-Y. Qin, Y.-G. Yao, Z. Anorg. Allgem. Chem. 631 (2005) 3053.
[8] Y.-Q. Zheng, J.-L. Lin, Z.-P. Kong, Inorg. Chem. 43 (2004) 2590.
[9] J.-H. Liao, S.-H. Cheng, H.-L. Tsai, C.-I. Yang, Inorg. Chim. Acta 338 (2002) 1.
[10] N. Hao, E. Shen, Y.-E. Wang, C.-W. Hu, L. Xu, Eur. J. Inorg. Chem. (2004) 4102.
[11] P.S. Mukherjee, S. Konar, E. Zangrando, T. Mallah, J. Ribas, N.R. Chaudhuri, Inorg. Chem. 42 (2003) 2695.
[12] R. Vaidhyanathan, S. Natarajan, C.N.R. Rao, Inorg. Chem. 41 (2002) 5226.
[13] (a) C. Livage, C. Egger, G. Férey, Chem. Mater. 13 (2001) 410;
(b) C. Livage, C. Egger, M. Nogues, G. Férey, Chem. Mater. 11 (1999) 1546;
(c) C. Livage, C. Egger, M. Nogues, G. Férey, J. Mater. Chem. 8 (1998) 2743.
[14] P.M. Forster, A.K. Cheetham, Angew. Chem., Int. Ed. 41 (2002) 457.
[15] S.-M. Ying, J.-G. Mao, Y.-Q. Sun, H.-Y. Zen, Z.-C. Dong, Polyhedron 22 (2003) 3097.
[16] Y.Q. Zheng, Z.P. Kong, Z. Anorg. Allgem. Chem. 629 (2003) 1469.
[17] M.R. Montney, S. Mallika Krishnan, N.M. Patel, R.M. Supkowski, R.L. LaDuca, Crystal Growth Des. 7 (2007) 1145.
[18] D.P. Martin, M.A. Braverman, R.L. LaDuca, Crystal Growth Des. 7 (2007) 2609.
[19] D. Pocic, J.M. Planeix, N. Kyritsakas, A. Jouaiti, H. Abdelaziz, M. Wais, CrystEngComm 7 (2005) 624.
[20] SAINT, Software for Data Extraction and Reduction, Version 6.02, Bruker 2002.
[21] SADABS, Software for Empirical Absorption Correction, Version 2.03, Bruker 2002.
[22] G.M. Sheldrick, SHELXTL, Program forCrystal Structure Refinement, University of Gottingen, Gottingen, Germany, 1997.
[23] M. Kurmoo, C. Estournes, Y. Oka, H. Kumagai, K. Inoue, Inorg. Chem. 44 (2005) 217.
[24] R.D. Shannon, Acta Crystallogr., Sect. A 32 (1976) 751.
[25] D.P. Martin, M.R. Montney, R.M. Supkowski, R.L. LaDuca, unpublished results.

Polyhedron 27 (2008) 2551–2556

Contents lists available at ScienceDirect

Polyhedron

journal homepage: www.elsevier.com/locate/poly

Assembly of new Schiff base ligands derived from vitamin B6 and stabilization through complexation of *N*,*N*′-bis-(pyridoxylideneimine)-*o*-phenylene: Synthesis and X-ray structural features of pyridoxal/*o*-phenylenediamine adducts and of $[UO_2(H_2pyr_2phen)Cl]NO_3$ and $[UO_2(Hpyr_2phen)Cl]$ {pyr_2phen = *N*,*N*′-bis-(pyridoxylideneiminato)$^{2-}$phenylene}

Davi Fernando Back, Gelson Manzoni de Oliveira *, Ernesto Schulz Lang, Jaqueline Pinto Vargas

Departamento de Química, Laboratório de Materiais Inorgânicos, Universidade Federal de Santa Maria, 97105-900 Santa Maria, RS, Brazil

ARTICLE INFO

Article history:
Received 18 February 2008
Accepted 8 May 2008
Available online 13 June 2008

Keywords:
Schiff base ligands
Complex stabilization
Ligands derived from vitamin B6

ABSTRACT

The new Schiff bases ligands **1** and **2** were obtained through reaction of vitamin B6 and *o*-phenylenediamine in methanol, and characterized structurally by X-ray diffractometry. The reaction of **1** with $UO_2(NO_3)_2 \cdot 6H_2O$ leads to the stabilization of *N*,*N*′-bis-(pyridoxylideneimine)-*o*-phenylene, giving $[UO_2(H_2pyr_2phen)Cl]NO_3$ (**3**) and $[UO_2(Hpyr_2phen)Cl]$ (**4**). In the new chelate compounds **3** and **4** the uranium ions are the centers of distorted pentagonal bipyramides, characteristic for the coordination number 7. The positive charge of **3** is counter balanced by NO_3^- ions in the lattice. Deprotonation of an *endo* hydroxyl group of the ligand yields a neutral complex, in the case of **4**. In both complexes a Cl^- ion accomplishes the seventh coordination space around the uranium atom.

© 2008 Elsevier Ltd. All rights reserved.

1. Introduction

It is known that the compounds derived from the vitamin B6 complex (**A**), pyridoxal (PL), pyridoxamine (PM) and pyridoxine (PN) present a reasonable variety of coordination sites with different charges and hard/soft character [1], allowing the statement of a rich coordination chemistry.

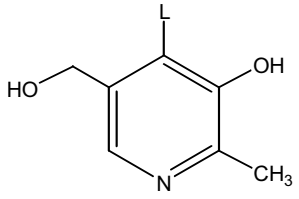

PL: L = CHO; PM: L = CH_2NH_2; PN: L = CH_2OH

The interest for the coordination chemistry of vitamin B6 constituents has increased since Metzler et al. [2] have shown that many different reactions of amino acids are catalyzed by pyridoxal phosphate-containing enzymes [3]. These include, among other important biological reactions, transamination [4], racemization [5], decarboxylation [6] and serine and threonine dehydration [7,8]. Most of these enzymatic reactions have been reproduced by non-enzymatic model reactions in which pyridoxal [9–16] or other appropriate aldehydes [16,17] and a suitable metal salt act as catalysts. For Metzler there is little doubt, therefore, that the catalytic potentialities of pyridoxal phosphate enzymes are basically those of their prosthetic group (the pyridoxal metal complex), and that the non-enzymatic and enzymatic reactions proceed by similar mechanisms.

The Schiff base H_2pyr_2en, *N*,*N*′-bis(pyridoxylideneiminato)ethylene (**B**), derived from the condensation of pyridoxal (PL, **A**) with ethylenediamine (en), is an interesting ligand and a close relative of the vitamin B6 complex.

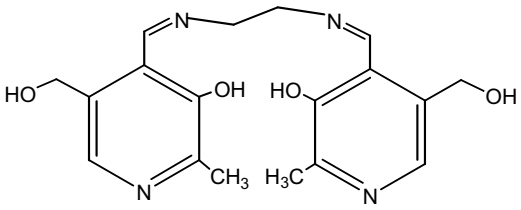

B was developed by Costa Pessoa and co-workers [18] to investigate its possible substitution in compounds of vanadium and the (Schiff base) ligand sal_2en {*N*,*N*′-ethylenediaminebis(salicylideneiminato)}. Given our previous interests in the metallation of

* Corresponding author. Tel.: +55 55 3220 8757; fax: +55 55 3220 8031.
E-mail address: manzoni@quimica.ufsm.br (G. Manzoni de Oliveira).

0277-5387/$ - see front matter © 2008 Elsevier Ltd. All rights reserved.
doi:10.1016/j.poly.2008.05.006

biological ligands [19,20] and the synthesis of chelate salts of uranium with compounds derived from the vitamin B6 complex – like for example $[UO_2(PN)_2(H_2O)]Cl_2$ [21] – we have reported [22] the synthesis and the X-ray structural characterization of the new uranium chelates of 4-pyridoxic acid and *N*,*N*′-bis-(pyridoxylideneiminato)ethylene (**B**), $[UO_2(\beta\text{-pyracinide})_2(H_2O)]$ [23,24] and $[UO_2(H_2pyr_2en^*)DMSO]Cl_2$ ($H_2pyr_2en^*$ = the *diammonium* zwitterionic form of **B**; DMSO = dimethyl sulfoxide). To demonstrate the ability of *N*,*N*′-bis(pyridoxylideneiminato)ethylene to react with further heavy metals, hence stabilizing them as chelate systems, we have synthesized also the chelate complexes $[Th(pyr_2en)_2(H_2O)]$ {pyr_2en = *N*,*N*′-ethylenebis(pyridoxylideneiminato)$^{2-}$}, $[Nd(pyr_2en)(Hpyr_2en)] \cdot 12H_2O$ and [Eu (pyr_2en)($Hpyr_2en$)] [25].

The chemical insertion of larger amino groups (than *en*) between the pyridoxal moieties should lead to Schiff bases with remarkable better chelate ability than **B**, like for example, **C** and **D**

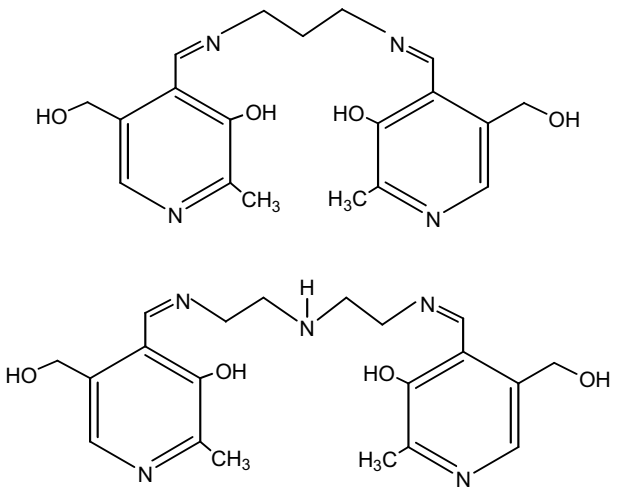

The hydroxyl deprotonation of **C** and **D** gives the dianionic Schiff bases (pyr_2pen)$^{2-}$ *N*,*N*′-bis-(pyridoxylideneiminato)$^{2-}$propylenediamine}, and (pyr_2dien)$^{2-}$ {*N*,*N*′-bis-(pyridoxylideneiminato)$^{2-}$diethylentriamine}, respectively. We have recently reported the synthesis of **C** and **D** and their reactions with $UO_2(NO_3)_2$, as well as the reaction of $Th(NO_3)_4 \cdot 5H_2O$ with **C**, and the synthesis and the X-ray characterization of the new chelate complexes $[Th(pyr_2pen)_2]$, $[UO_2(pyr_2pen)(CH_3OH)]$ and $[UO_2(pyr_2dien)] \cdot 2H_2O$, together with their possible radiological significance [26].

The addition of pyridoxal and *o*-phenylenediamine for the achievement of strategic Schiff base ligands do not proceeds according theoretical predictions (see Section 2). We report now the synthesis and the X-ray characterization of two new addition products of pyridoxal and *o*-phenylenediamine (**1** and **2**), as well the zwitterionic chelate salt $[UO_2(H_2pyr_2phen)Cl]NO_3$ (**3**) and the neutral chelate complex $[UO_2(Hpyr_2phen)Cl]$ (**4**) {pyr_2phen = *N*,*N*′-bis-(pyridoxylideneiminato)$^{2-}$phenylene}. Complexes **3** and **4** are typical examples of stabilization by complexation of unstable assembles – the ligand, in this case –, a very important and worldwide approach adopted in the modern inorganic chemistry to realize many virtually inexistent chemical species.

2. Results and discussion

2.1. Structural features of *1*, *2*, *3* and *4*

The X-ray crystal data and the experimental conditions for the analyses of the addition products of pyridoxal/*o*-phenylenediamine **1** and **2**, and of the complexes $[UO_2(H_2pyr_2phen)Cl]NO_3$ (**3**) and $[UO_2(Hpyr_2phen)Cl]$ (**4**) {pyr_2phen = *N*,*N*′-bis-(pyridoxylideneiminato)$^{2-}$phenylene}, are given in Table 1. Selected bond distances and angles of the title compounds are listed in Tables 2 and 3. Half asymmetric unit of ligand **1** is presented in Fig. 1; the molecular structure (asymmetric unit) of the ligand **2** is shown in Fig. 2. Figs. 3 and 4 display the asymmetric units of complexes **3** and **4**, with atom-labeling scheme. For clarity the H_2O solvate molecules – two in complex **3** and one in complex **4** – are not displayed in Figs. 3 and 4.

In the uranyl complexes **3** and **4** the uranium atoms are the centers of distorted pentagonal bipyramides, characteristic for the coordination number 7. The Schiff base nature of **2** and of the complex ligands are evident in the shorter (double) N–C bond distances: N(2)–C(8) = 1.365(6) Å in **2** (in contrast with the longer N(2)–C(9) bond with 1.402(6) Å), N(3)–C(15) = 1.294(5)/N(2)–C(8) = 1.282(5) Å in **3**, and N(2)–C(8) = 1.294(6)/N(3)–C(15) = 1.280(6) Å in **4** (see Figs. 2–4 and Tables 2 and 3). In **3** and **4** a Cl^- ion accomplishes the seventh coordination space around the uranium(VI) ion; the positive charge of complex **3** – which contains a zwitterionic, neutral ligand – is balanced in the crystal lattice by NO_3^- counter ions. The deprotonation of one *endo* OH group in compound **4** yields a neutral complex. In complexes **3** and **4** becomes evident the (concave) spatial adjustment developed by the ligands to literally grip the uranyl cation, thus stabilizing the compounds (Figs. 3 and 4). The new U complexes described in this work are examples of bimolecular chelate systems not yet reported for this Schiff base ligand. The formation of **3** and **4**, hence the stabilization of the ligand, corroborates the remarkable ability of Schiff bases derived from pyridoxal, to afford the stereochemical and electrical requisites for the achievement of heavy metal chelates with uncommon coordination polyhedra.

2.2. Remarks on stoichiometric and stability

As we have already pointed out, predictions on the chemical behavior of reactions between pyridoxal and *o*-phenylenediamine are not so meaningful.

For example, the reaction of 1 equiv. of pyridoxal with 1 equiv. of *o*-phenylenediamine arises according to the Scheme 1, with mayor reaction of only one NH_2 group of *o*-phenylenediamine, yielding **1** as main component (60%), but also forming compound **2** (40%), in this case, occurring simultaneous reaction of both amino groups and cyclization, under lost of water and hydrogen.

If the reaction is carried out in the relation 1:2 – as shown in Scheme 2 – and in the absence of UO_2^{2+} ions, the obtained product is that one expected alone in the first reaction (**1**), instead of the desired, addition product of single pyridoxal molecules to both amino groups of *o*-phenylenediamine.

The aimed Schiff base not obtained in the preceding reaction is achieved only in the presence of UO_2^{2+} ions, since the desired product is now stabilized as a chelate, according to the Scheme 3. In this chelate salt the Schiff base exhibits a zwitterionic equilibrium, without deprotonation.

The stabilization of the condensed Schiff base ligand can also take place under deprotonation of one *endo* hydroxyl group, giving rise to the neutral chelate **4** (see Figs. 3 and 4). On the contrary of the Schiff base ligands **A**, **B** and **C** (see Section 1), the 1:2 condensation of *o*-phenylenediamine and pyridoxal does not occur in the free state, if this process is attained as demonstrated in the Scheme 2. By direct reaction between pyridoxal and *o*-phenylenediamine the adduct only exists in the chelated form, thus, requiring a template (the uranyl ion) for the assemble (Scheme 3). This should be attributed to the proximity of the two Schiff base centers (separated only by three bonds) in the unachieved adduct of the Scheme

Table 1
Crystal data and structure refinement for **1**, **2**, **3** and **4**

	1	**2**	**3**	**4**
Empirical formula	$C_{28}H_{30}N_6O_4$	$C_{14}H_{13}N_3O_2$	$C_{22}H_{26}ClN_5O_{11}U$	$C_{22}H_{23}ClN_4O_7U$
Formula weight	514.58	255.27	809.96	728.92
T (K)	293(2)	293(2)	293(2)	293(2)
Radiation, λ (Å)	Mo Kα, 0.7107	Mo Kα, 0.7107	Mo Kα, 0.7107	Mo Kα, 0.7107
Crystal system, space group	monoclinic, $P2_1/n$	orthorhombic, *Pbca*	triclinic, $P\bar{1}$	monoclinic, $P2_1/n$
Unit cell dimensions				
a (Å)	12.9277(9)	14.7516(13)	9.2310(15)	10.8761(2)
b (Å)	13.4080(10)	7.3626(5)	11.8550(13)	10.2376(2)
c (Å)	14.7206(11)	23.482(2)	14.026(2)	21.8096(3)
α (°)	90	90	114.80	90
β (°)	99.310(5)	90	94.012(3)	100.2740(10)
γ (°)	90	90	97.95	90
V (Å^3)	2518.0(3)	2550.4(4)	1365.9(3)	2389.46(7)
Z, D_{calc} (g cm^{-3})	4, 1.357	8, 1.330	2, 1.969	4, 2.026
Absorption coefficient (mm^{-1})	0.093	0.092	6.106	6.956
F(000)	1088	1072	780	1392
Crystal size (mm)	0.23 × 0.18 × 0.15	0.77 × 0.24 × 0.12	0.14 × 0.13 × 0.12	0.15 × 0.10 × 0.09
θ Range (°)	2.47–24.75	2.76–24.61	1.90–30.07	2.20–31.03
Index ranges	$-15 \leqslant h \leqslant 15$, $-15 \leqslant k \leqslant 15$, $-17 \leqslant l \leqslant 14$	$-16 \leqslant h \leqslant 16$, $-8 \leqslant k \leqslant 7$, $-24 \leqslant l \leqslant 26$	$-13 \leqslant h \leqslant 12$, $-16 \leqslant k \leqslant 16$, $-19 \leqslant l \leqslant 19$	$-15 \leqslant h \leqslant 15$, $-13 \leqslant k \leqslant 14$, $-31 \leqslant l \leqslant 27$
Reflections collected	23126	9525	33135	31884
Reflections unique (R_{int})	4270 (0.1267)	2100 (0.0829)	7919 (0.0292)	7567 (0.0378)
Completeness to theta maximum (%)	98.9	96.5	98.8	99.1
Absorption correction	GAUSSIAN	semi-empirical from equivalents	semi-empirical from equivalents	semi-empirical from equivalents
Maximum and minimum transmission	1 and 0.825693	1 and 0.867657	1 and 0.876983	1 and 0.874457
Refinement method	full-matrix least-squares on F^2	full-matrix least-squares on F^2	full-matrix least-squares on F^2	full-matrix least-squares on F^2
Data/restraints/parameters	4270/0/343	2100/0/173	7919/3/371	7567/0/323
Goodness-of-fit on F^2	0.926	1.014	1.181	1.044
Final R indices [$I > 2\sigma(I)$]	$R_1 = 0.0698$, $wR_2 = 0.1683$	$R_1 = 0.0798$, $wR_2 = 0.1718$	$R_1 = 0.0239$, $wR_2 = 0.0653$	$R_1 = 0.0362$, $wR_2 = 0.0869$
R indices (all data)	$R_1 = 0.1852$, $wR_2 = 0.2266$	$R_1 = 0.1604$, $wR_2 = 0.2383$	$R_1 = 0.0295$, $wR_2 = 0.0795$	$R_1 = 0.0517$, $wR_2 = 0.0934$
Largest difference in peak and hole (e Å^{-3})	0.286 and −0.210	0.580 and −0.484	2.331 and −1.348	3.063 and −1.419

Table 2
Selected bond lengths (Å) and angles (°) for **1** and **2**

1		**2**	
Bond lengths			
O(2)–C(7)	1.407(5)	O(2)–C(7)	1.419(6)
O(1)–C(2)	1.342(5)	O(1)–C(2)	1.345(5)
N(2)–C(8)	1.282(5)	N(3)–C(8)	1.311(5)
N(2)–C(9)	1.410(6)	N(3)–C(14)	1.374(6)
N(1)–C(1)	1.325(6)	N(1)–C(1)	1.316(6)
N(1)–C(5)	1.331(6)	N(1)–C(5)	1.332(6)
N(3)–C(10)	1.392(6)	N(2)–C(8)	1.365(6)
		N(2)–C(9)	1.402(6)
Bond angles			
C(8)–N(2)–C(9)	121.5(4)	C(8)–N(3)–C(14)	106.7(4)
C(1)–N(1)–C(5)	119.1(4)	C(8)–N(2)–C(9)	105.7(4)
C(14)–C(9)–N(2)	124.4(4)	N(3)–C(8)–N(2)	112.4(4)
C(10)–C(9)–N(2)	116.6(4)	N(3)–C(8)–C(3)	122.8(4)
C(11)–C(10)–N(3)	120.2(5)	N(2)–C(8)–C(3)	124.8(4)
N(3)–C(10)–C(9)	121.0(4)	O(1)–C(2)–C(3)	123.2(4)
N(2)–C(8)–C(3)	120.6(4)	O(1)–C(2)–C(1)	116.6(4)
N(1)–C(1)–C(2)	120.2(4)	N(3)–C(14)–C(9)	109.1(4)
N(1)–C(1)–C(6)	118.6(4)	N(3)–C(14)–C(13)	130.4(5)
N(1)–C(5)–C(4)	125.7(4)	C(10)–C(9)–N(2)	131.5(5)

Table 3
Selected bond lengths (Å) and angles (°) for **3** and **4**

3		**4**	
Bond lengths			
U(1)–O(2)	1.778(3)	U–O(1)	1.771(3)
U(1)–O(1)	1.791(3)	U–O(2)	1.782(3)
U(1)–O(4)	2.246(3)	U–O(3)	2.237(3)
U(1)–O(3)	2.282(3)	U–O(5)	2.274(3)
U(1)–N(2)	2.584(3)	U–N(2)	2.544(3)
U(1)–N(3)	2.594(3)	U–N(3)	2.617(4)
U(1)–Cl	2.7453(11)	U–Cl	2.7596(14)
Bond angles			
O(2)–U(1)–O(1)	175.26(12)	O(1)–U–O(2)	176.53(16)
O(2)–U(1)–O(4)	93.96(12)	O(1)–U–O(3)	88.67(15)
O(1)–U(1)–O(4)	87.95(12)	O(2)–U–O(3)	91.75(16)
O(2)–U(1)–O(3)	90.74(12)	O(1)–U–O(5)	91.38(15)
O(1)–U(1)–O(3)	88.70(12)	O(2)–U–O(5)	89.34(16)
O(4)–U(1)–O(3)	162.52(11)	O(3)–U–O(5)	161.18(12)
O(2)–U(1)–N(2)	90.33(13)	O(1)–U–N(2)	88.78(14)
O(1)–U(1)–N(2)	85.11(12)	O(2)–U–N(2)	88.16(14)
O(4)–U(1)–N(2)	129.00(10)	O(3)–U–N(2)	68.71(11)
O(3)–U(1)–N(2)	67.70(10)	O(5)–U–N(2)	130.11(12)
O(2)–U(1)–N(3)	86.81(13)	O(1)–U–N(3)	89.17(16)
O(1)–U(1)–N(3)	89.89(12)	O(2)–U–N(3)	87.99(14)
O(4)–U(1)–N(3)	67.93(10)	O(3)–U–N(3)	131.73(11)
O(3)–U(1)–N(3)	129.22(10)	O(5)–U–N(3)	67.08(12)
N(2)–U(1)–N(3)	61.61(10)	N(2)–U–N(3)	63.03(11)
O(2)–U(1)–Cl	93.52(11)	O(1)–U–Cl	93.95(13)
O(1)–U(1)–Cl	91.02(10)	O(2)–U–Cl	89.52(11)
O(4)–U(1)–Cl	82.63(7)	O(3)–U–Cl	82.38(9)
O(3)–U(1)–Cl	80.28(8)	O(5)–U–Cl	78.84(9)
N(2)–U(1)–Cl	147.80(8)	N(2)–U–Cl	150.90(9)
N(3)–U(1)–Cl	150.49(8)	N(3)–U–Cl	145.86(9)

2. Worthy of note is the description of a dimeric Cu(II) complex of this ligand, earlier attained by Nepveu et al. [27].

Finally, it has to be enlightened that the syntheses of new Schiff base ligands derived from pyridoxal, as well as their reactions with uranium, thorium and other heavy metals, make part of our researches on modelings for heavy metals damage inhibition in living beings. Nevertheless, only chemical aspects related to the

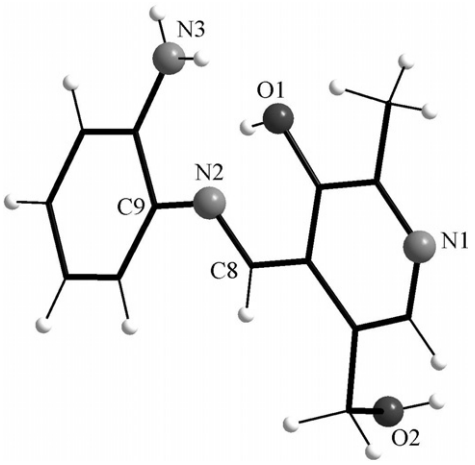

Fig. 1.

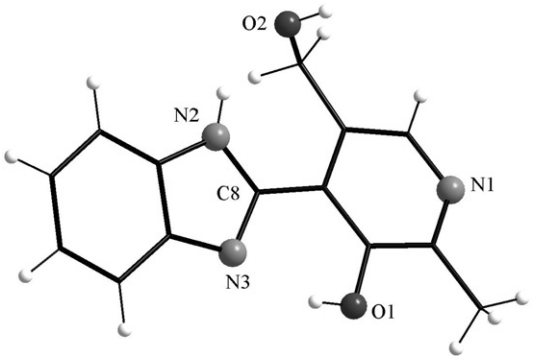

Fig. 2.

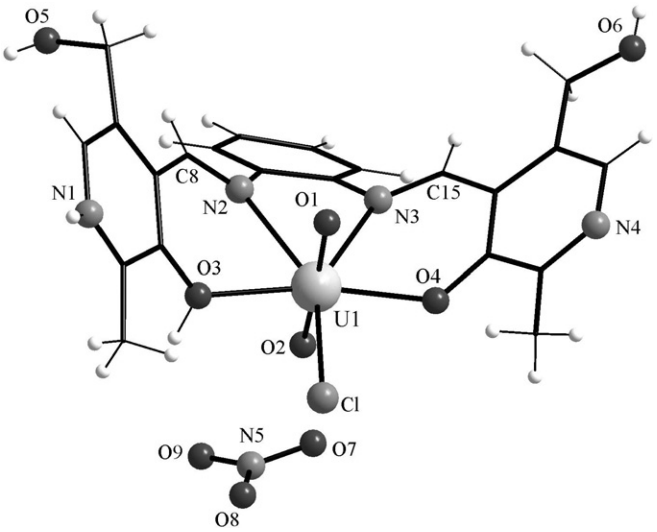

Fig. 3.

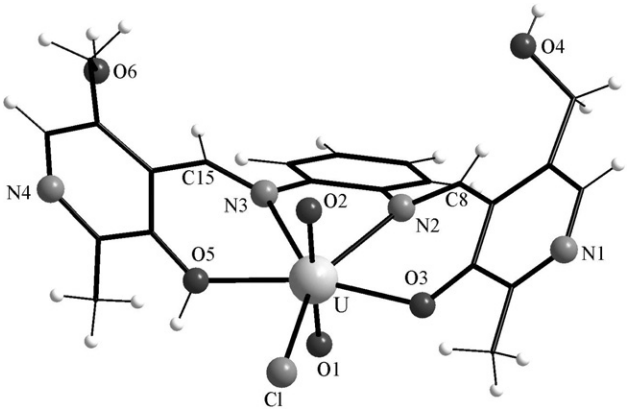

Fig. 4.

synthesis of the title compounds, as well their characterization, will be handled in this communication.

3. Experimental

3.1. Synthesis of the pyridoxal/**o**-phenylenediamine adduct ***1***

Pyridoxal chloridrate (0.208 g, 1 mmol), dissolved in 10 ml of anhydrous methanol, was mixed with 0.040 g (1 mmol) of KOH for the pH adjustment (≈7). The yellow solution was stirred by 15 min. Thereafter, 0.108 g (1 mmol) of 1,2-phenylenediamine was added and the mixture was cooled at 0 °C and stirred under Ar atmosphere by 1 h. The orange precipitate was removed by filtration. The slow evaporation of the remained solution yields yellow crystals, suitable for X-ray analysis. Yield, 84%.

Properties: yellow, wedge-like crystals. $C_{28}H_{30}N_6O_4$ (514.58). Melting point: 182–184 °C. IR (KBr): 3441 [shoulder, ν(O–H)]; 1531 (1412) [strong, (medium), ν(C=C, C=N)$_{py.}$]; 1445 [medium, ν(C–O)$_{ar}$]; 1426 [medium, ν(C–N)$_{aliphatic}$]; 1041 [strong, ν(C–O)$_{alkoh.}$]; 727–627 (broad) [weak, δ(N–H)]. C, H, N – *Anal.* Calc.: C, 65.36; H, 5.83; N, 16.34. Found: C, 65.02; H, 5.39; N, 16.46%.

3.2. Synthesis of the pyridoxal/o-phenylenediamine adduct ***2***

Pyridoxal chloridrate (0.208 g, 1 mmol) and 1,2-phenylenediamine (0.108 g, 1 mmol) were dissolved in 10 ml of anhydrous methanol. The mixture was stirred and kept 15 min in an ultrasound bath at 37 KHz, under precipitation of a red carmine powder. This precipitate was isolated, redissolved in 50 ml of anhydrous ethanol and heated at 70 °C during 2 h. Evaporation of the limpid yellow solution yields after three days yellow crystals, suitable for X-ray analysis. Yield, 87%.

Properties: yellow, tabular crystals. $C_{14}H_{13}N_3O_2$ (255.27). Melting point: 112–115 °C. IR (KBr): 3278–2653 [sh., ν(O–H)]; 1462 (1384) [s, (m), ν(C=C, C=N)$_{py.}$]; 1445 [m, ν(C–O)$_{ar}$]; 1426 [m, ν(C–N)$_{aliphatic}$]; 1025 [s,ν(C–O)$_{alkoh.}$]; 755 [m, δ(N–H)]; 665 [w, δ(N–H)]. C, H, N – *Anal.* Calc.: C, 65.88; H, 5.09; N, 16.47. Found: C, 65.5; H, 5.21; N, 16.02%.

3.3. Synthesis of $[UO_2(H_2pyr_2phen)Cl]NO_3$ (***3***)

Pyridoxal chloridrate (0.101 g, 0.5 mmol) and Na_2CO_3 (0.042 g, 0.5 mmol) were dissolved in 10 ml of methanol. After 15 min stirring the pH of the solution is nearby 7; 0.128 g (0.5 mmol) of the pyridoxal/*o*-phenylenediamine adduct **1** together with $UO_2(NO_3)_2 \cdot 6H_2O$ (0.502 g, 0.5 mmol) were added and the mixture was stirred and refluxed by 1 h. Unstable, but diffractometric measurable crystals were obtained after 24 h. Yield, 30%.

Properties: yellow, air unstable crystals. $C_{22}H_{26}ClN_5O_{11}U$ (809.96). Melting point (decomposition): 205 °C. IR (KBr): 3416 [sh., ν(O–H)]; 1610 [s, ν(C=N)]; 1517, 1430 [m, ν(C=C, C=N)$_{py.}$]; 1438 [m, ν(C–O)$_{ar}$]; 1383 [s, ν(NO$_3$)]; 1039 [s, ν(C–O)$_{alkoh.}$]; 894

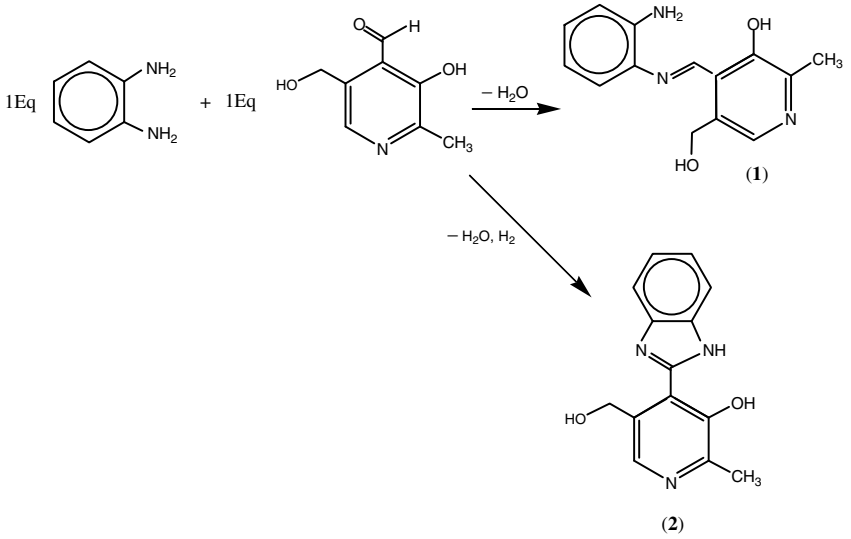

Scheme 1.

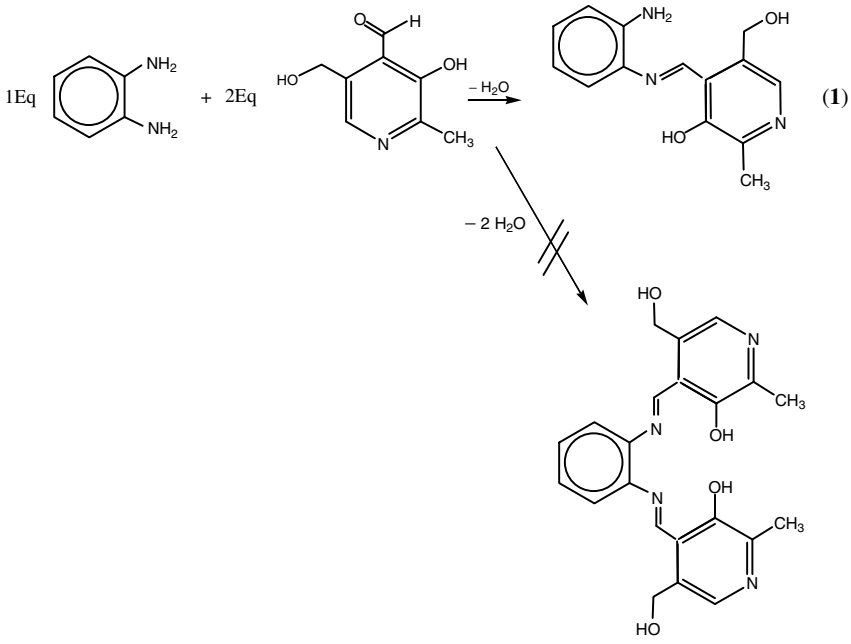

Scheme 2.

[s, δ (O–U–O)]; 768 [w, $\nu(NO_3)$]. C, H, N – *Anal.* Calc.: C, 32.61; H, 3.21; N, 8.64. Found: C, 32.33; H, 3.19; N, 8.36%.

3.4. Synthesis of $[UO_2(Hpyr_2phen)Cl]$ (4)

Pyridoxal chloridrate (0.101 g, 0.5 mmol) and KOH (0.020 g, 0.5 mmol) were dissolved in 10 ml of methanol. After 15 min stirring the pH of the solution is around 7; 0.128 g (0.5 mmol) of the pyridoxal/*o*-phenylenediamine adduct **1** together with $UO_2(NO_3)_2 \cdot 6H_2O$ (0.502 g, 0.5 mmol) were added and the mixture was stirred and refluxed by 1 h. Red crystals suitable for X-ray analysis were obtained after two days. Yield, 45.4%. Unstable yellow crystals, with melting point of 205 °C and 22.4% yield – probably **3** –, can also be isolated from the mother (solution after a few days).

Properties: red, stable crystals. $C_{22}H_{23}ClN_4O_7U$ (728.92). Melting point (decomposition): 262 °C. IR (KBr): 3440 [sh., ν(O–H)]; 1640 [s, ν(C=N)]; 1500, 1420 [m, ν(C=C, C=N)$_{py.}$]; 1438 [m, $\nu(C–O)_{ar}$]; 1040 [s, $\nu(C–O)_{alkoh.}$]; 894 [s, δ (O–U–O)]. C, H, N – *Anal.* Calc.: C, 36.23; H, 3.15; N, 7.68. Found: C, 36.53; H, 3.27; N, 7.76%.

3.5. X-ray structural determination

Data were collected with a Bruker APEX II CCD area-detector diffractometer and graphite-monochromatized Mo Kα radiation. The structures were solved by direct methods using SHELXS [28]. Subsequent Fourier-difference map analyses yielded the positions of the non-hydrogen atoms. Refinements were carried out with the SHELXL package [28]. All refinements were made by full-matrix least-squares on F^2 with anisotropic displacement parameters for all non-hydrogen atoms. Hydrogen atoms were included in the refinement in calculated positions. Crystal data and more details of the data collections and refinements are contained in Table 1.

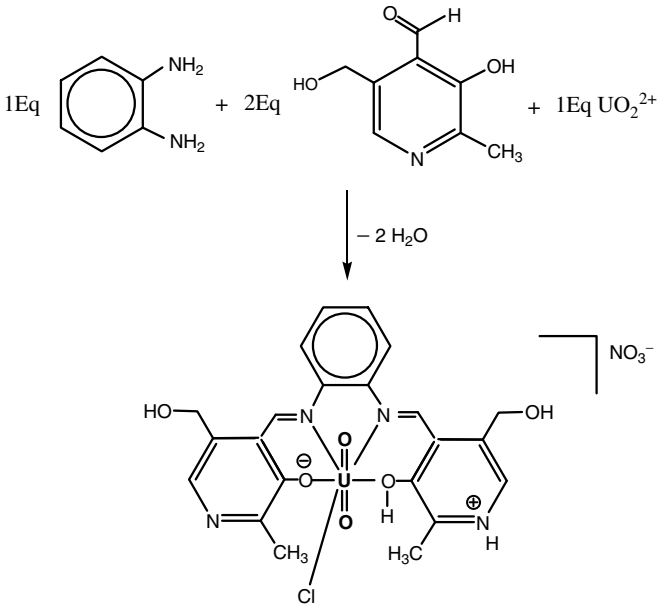

(**3**)

Scheme 3.

Appendix A. Supplementary data

CCDC 678418, 678419, 678420 and 678421 contain the supplementary crystallographic data for **1**, **2**, **3** and **4**. These data can be obtained free of charge via http://www.ccdc.cam.ac.uk/conts/retrieving.html, or from the Cambridge Crystallographic Data Centre, 12 Union Road, Cambridge CB2 1EZ, UK; fax: (+44) 1223-336-033; or e-mail: deposit@ccdc.cam.ac.uk. Supplementary data associated with this article can be found, in the online version, at doi:10.1016/j.poly.2008.05.006.

References

[1] J. Henry, K.A. Acquaye, M.F. Richardson, Inorg. Chim. Acta 201 (1992) 101.
[2] D.E. Metzler, M. Ikawa, E.E. Snell, J. Am. Chem. Soc. 76 (1954) 648.
[3] E.E. Snell, Phys. Rev. 33 (1953) 509.
[4] P.P. Cohen, in: J.B. Sumner, K. Myrbäck (Eds.), The Enzymes, vol. 1, part 2, Academic Press Inc., New York, 1951, p. 1040.
[5] W.A. Wood, I.C. Gunsalus, J. Biol. Chem. 190 (1951) 403.
[6] E.F. Gale, Adv. Enzymol. 6 (1946) 1.
[7] C. Yanofsky, J.L. Reissig, J. Biol. Chem. 202 (1953) 567.
[8] D.E. Metzler, E.E. Snell, J. Biol. Chem. 198 (1952) 363.
[9] D.E. Metzler, J.B. Longenecker, E.E. Snell, J. Am. Chem. Soc. 75 (1953) 2786.
[10] E.E. Snell, J. Am. Chem. Soc. 67 (1945) 194.
[11] D.E. Metzler, E.E. Snell, J. Am. Chem. Soc. 74 (1952) 979.
[12] D.E. Metzler, E.E. Snell, J. Biol. Chem. 198 (1952) 353.
[13] J. Olivard, D.E. Metzler, E.E. Snell, J. Biol. Chem. 199 (1952) 669.
[14] D.E. Metzler, J.B. Longenecker, E.E. Snell, J. Am. Chem. Soc. 76 (1954) 639.
[15] E. Werle, W. Koch, Biochem. Z. 319 (1949) 305. (in German).
[16] D.E. Metzler, J. Olivard, E.E. Snell, J. Am. Chem. Soc. 76 (1954) 644.
[17] M. Ikawa, E.E. Snell, J. Am. Chem. Soc. 76 (1954) 653.
[18] I. Correia, J. Costa Pessoa, M.T. Duarte, R.T. Henriques, M.F.M. Piedade, L.F. Veiros, T. Jakusch, T. Kiss, Á. Dörnyei, M.M.C.A. Castro, C.F.G.C. Geraldes, F. Avecilla, Chem. Eur. J. 10 (2004) 2301.
[19] L.L. Marques, G. Manzoni de Oliveira, E. Schulz Lang, R.A. Burrow, Z. Naturforsch. 60b (2005) 318.
[20] E. Schulz Lang, L.L. Marques, G. Manzoni de Oliveira, Z. Naturforsch. 60b (2005) 1264.
[21] E. Bonfada, G. Manzoni de Oliveira, D.F. Back, E. Schulz Lang, Z. Anorg. Allg. Chem. 631 (2005) 878.
[22] D.F. Back, G. Manzoni de Oliveira, E. Schulz Lang, J. Inorg. Biochem. 100 (2006) 1698.
[23] D. Heyl, J. Am. Chem. Soc. 70 (1948) 3434.
[24] L.J. Daniel, M.L. Scott, L.C. Norris, G.F. Heuser, J. Biol. Chem. 160 (1945) 265.
[25] D.F. Back, É. Bonfada, G. Manzoni de Oliveira, E. Schulz Lang, J. Inorg. Biochem. 101 (2007) 709.
[26] D.F. Back, G. Manzoni de Oliveira, J.P. Vargas, E. Schulz Lang, G. Tabarelli, J. Inorg. Biochem. 102 (2008) 666.
[27] F. Nepveu, F. Dahan, R. Haran, P. Cassoux, J.J. Bonnet, J. Cryst. Spectroc. Res. 14 (1984) 129.
[28] G.M. Sheldrick, Acta Crystallogr., Sect. A 64 (2008) 112.

Polyhedron 27 (2008) 2557–2562

Contents lists available at ScienceDirect

Polyhedron

journal homepage: www.elsevier.com/locate/poly

Coordination and separation studies of the uranyl ion with *iso*-butyramide based ligands: Synthesis and structures of $[UO_2(NO_3)_2(^iC_3H_7CON\{^iC_4H_9\}_2)_2]$ and $[UO_2(C_6H_5COCHCOC_6H_5)_2(^iC_3H_7CON\{^iC_3H_7\}_2)]$

S. Kannan [a,*], Sadhan B. Deb [b], J.S. Gamare [a], M.G.B. Drew [c]

[a] Fuel Chemistry Division, Bhabha Atomic Research Center, Trombay, Mumbai, Maharastra 400 085, India
[b] Radioanalytical Chemistry Division, Bhabha Atomic Research Centre, Mumbai 400 085, India
[c] School of Chemistry, The University of Reading, P.O. Box 224, Whiteknights, Reading RG6 6AD, UK

ARTICLE INFO

Article history:
Received 25 March 2008
Accepted 9 May 2008
Available online 13 June 2008

Keywords:
iso-Butyramide
Coordination chemistry
Precipitation
Separation
Uranium(VI)
Lanthanum(III)
Thorium(IV)
Crystal structure

ABSTRACT

The coordination chemistry of *iso*-butyramide based ligands such as: $^iC_3H_7CON(^iC_3H_7)_2$, $^iC_3H_7CON(C_4H_9)_2$ and $^iC_3H_7CON(^iC_4H_9)_2$ with $[UO_2(NO_3)_2 \cdot 6H_2O]$, $[UO_2(OO)_2 \cdot 2H_2O]$ {where OO = $C_4H_3SCOCHCOCF_3$ (TTA), $C_6H_5COCHCOCF_3$ (BTA) and $C_6H_5COCHCOC_6H_5$ (DBM)}, $[Th(NO_3)_4 \cdot 6H_2O]$ and $[La(NO_3)_3 \cdot 6H_2O]$ has been evaluated. Structures for the compounds $[UO_2(NO_3)_2(^iC_3H_7CON\{^iC_4H_9\}_2)_2]$ and $[UO_2(C_6H_5COCHCOC_6H_5)_2(^iC_3H_7CON\{^iC_3H_7\}_2)]$ have been determined by single crystal X-ray diffraction methods. Preliminary separation studies from nitric acid medium using the amide $^iC_3H_7CON(^iC_4H_9)_2$ with U(VI), Th(IV) and La(III) ions showed the selective precipitation of uranyl ion from the mixture. Thermal study of the compound $[UO_2(NO_3)_2(^iC_3H_7CON(^iC_4H_9)_2)_2]$ in air revealed that the ligands can be destroyed completely on incineration.

© 2008 Elsevier Ltd. All rights reserved.

1. Introduction

Actinide coordination chemistry is very important for the development of new technology concerning the safe processing and storage of irradiated nuclear fuel materials [1–3]. The selective separation of uranium-233 from the mixture of thorium and other fission products is an important step [4a] in the advanced heavy water reactor (AHWR) technology [4b] of the Indian atomic energy program, where upon the thorium oxide is used as a fuel material. In recent years, incinerable organic amide based extractants have proved to be of particular interest in the process chemistry of lanthanides and actinides from the nitric acid medium [5]. It is reported that the *N*,*N*′-2,ethylhexyl *iso*-butyramide shows selective extraction property for the uranium(VI) ion from a mixture containing thorium(IV) or plutonium(IV) ion [6]. The solvent extraction method needs many steps such as: extraction, stripping, precipitation and purification during the reprocessing of fuel materials. The neutral *N*-cyclohexyl,2-pyrrolidone ligand shows selective precipitation of uranium(VI) ion (up to 68%) from the mixture containing various other ions [7] and with this ligand only two steps are required namely precipitation and purification. The selectivity of *N*-cyclohexyl,2-pyrrolidone ligand was explained on the basis of a strong complexing nature of this ligand towards the uranyl nitrate compared to those of other metal nitrate ions. We have reported recently that *iso*-butyramide based amide ligands show an excellent coordination property towards the uranyl group and form air and moisture stable halide and thiolato complexes [8,9]. The stability of these complexes was explained on the basis of very strong bonding between the amide and uranyl group. The observed bond distances in these complexes are much shorter in length compared to those of any of the uranyl-amide [10–12], uranyl-phosphine oxide [13–17] and uranyl-pyrrolidone [18,19] complexes reported. The strong complexing ability of the *iso*-butyramide based ligand promoted us to study their complexing behavior towards uranyl nitrate, thorium nitrate, lanthanum nitrate and uranyl bis(β-diketonate) to investigate whether it was feasible to use these ligands for separation purposes and the results of these studies are reported herein.

2. Experimental

2.1. General considerations

All the starting materials and other chemicals were reagent grade and were used as received. All the amides [8] and uranyl

* Corresponding author. Tel.: +91 22 25594574; fax: +91 22 25505151.
E-mail address: skannan@magnum.barc.ernet.in (S. Kannan).

0277-5387/$ - see front matter © 2008 Elsevier Ltd. All rights reserved.
doi:10.1016/j.poly.2008.05.010

bis(β-diketonates) [20] were prepared according to the reported methods. FTIR spectra were obtained on a JASCO-610 FTIR spectrometer and the samples were mounted as a Nujol mull. The ^{1}H NMR spectra in $CDCl_3$, on a Brucker 500 MHz spectrometer and the peak positions are calibrated with respect to the internal residual solvent peaks. Elemental analyses were performed by the Analytical Chemistry Division of Bhabha Atomic Research Centre, Mumbai. The TG/DTA for the compound $[UO_2(NO_3)_2(^iC_3H_7CON^iBu_2)_2]$ was recorded on a Mettler TGA-851E instrument under the flow of an air. Elemental compositions in the precipitated $[UO_2(NO_3)_2(^iC_3H_7CON^iBu_2)_2]$ and the supernatant solution were analyzed via an ITAL-TXRF instrument.

2.2. Synthesis of $[UO_2(NO_3)_2\{^iC_3H_7CON(^iC_3H_7)_2\}_2]$ (**1**)

To a solution of $^iC_3H_7CON(^iC_3H_7)_2$ (450 mg, 2.6 mmol) in $CHCl_3$, solid $[UO_2(NO_3)_2 \cdot 6H_2O]$ (502 mg, 1.0 mmol) was added and stirred for few minutes until all $[UO_2(NO_3)_2 \cdot 6H_2O]$ dissolves to give a clear solution. This solution was filtered and layered with *iso*-octane. The solution on slow evaporation deposited a yellow crystalline solid, which was filtered, washed with hexane and dried. Yield: 700 mg (95%). Elemental *Anal.* Calc. for $[UO_2(NO_3)_2(^iC_3H_7CON\{^iC_3H_7\}_2)_2]$, $C_{20}H_{42}N_4O_{10}U$: C, 32.6; H, 5.7; N, 7.6. Found: C, 32.3; H, 5.5; N, 7.5%. IR (KBr, Nujol): ν/cm^{-1} 1570 (CO), 930 (O=U=O). ^{1}H NMR (25 °C, $CDCl_3$): δ 1.40 (d, 7 Hz, 12H, CH_3, $N^iC_3H_7$), 1.57 (d, 7 Hz, 6H, CH_3, $^iC_3H_7$), 3.29 (br, 1H, CH, $^iC_3H_7$), 4.26 (br, 2H, CH, $N^iC_3H_7$).

2.3. Synthesis of $[UO_2(NO_3)_2\{^iC_3H_7CON(C_4H_9)_2\}_2]$ (**2**)

Compound **2** was prepared similarly to **1** by taking $^iC_3H_7CON(C_4H_9)_2$ (460 mg, 2.31 mmol) and $[UO_2(NO_3)_2 \cdot 6H_2O]$ (450 mg, 0.89 mmol). Yield: 730 mg (92%). Elemental *Anal.* Calc. for $[UO_2(NO_3)_2\{^iC_3H_7CON(C_4H_9)_2\}_2]$, $C_{24}H_{50}N_4O_{10}U$: C, 36.4; H, 6.3; N, 7.1. Found: C, 36.1; H, 6.1; N, 7.0%. IR (KBr, Nujol mull): ν/cm^{-1} 1571 (CO), 932 (O=U=O). ^{1}H NMR (25 °C, $CDCl_3$): δ 0.67 (t, 7 Hz, 3H, CH_3, NC_4H_9), 0.97 (m, 2H, CH_2, NC_4H_9), 1.07 (t, 7 Hz, 3H, CH_3, NC_4H_9), 1.43 (d, 6H, CH_3, $^iC_3H_7$), 1.53 (m, 2H, CH_2, NC_4H_9), 1.67 (m, 2H, CH_2, NC_4H_9), 1.86 (m, 2H, CH_2, NC_4H_9), 3.25 (br, 1H, CH, $^iC_3H_7$), 3.63 (m, 4H, NCH_2, NC_4H_9).

2.4. Synthesis of $[UO_2(NO_3)_2\{^iC_3H_7CON(^iC_4H_9)_2\}_2]$ (**3**)

Compound **3** prepared similarly to **1** by taking $^iC_3H_7CON(^iC_4H_9)_2$ (454 mg, 2.28 mmol) and $[UO_2(NO_3)_2 \cdot 6H_2O]$ (502 mg, 1.0 mmol). Yield: 725 mg (91.5%). Elemental *Anal.* Calc. for $[UO_2(NO_3)_2\{^iC_3H_7CON(^iC_4H_9)_2\}_2]$, $C_{24}H_{50}N_4O_{10}$ U: C, 36.4; H, 6.3; N, 7.1. Found: C, 36.3; H, 6.2; N, 7.0%. IR (KBr, Nujol mull): ν/cm^{-1} 1571 (CO), 931 (O=U=O). ^{1}H NMR (25 °C, $CDCl_3$): δ 0.73 (d, 7 Hz, 6H, CH_3, $N^iC_4H_9$), 1.29 (d, 7 Hz, 6H, CH_3, $N^iC_4H_9$), 1.43 (d, 7 Hz, 6H, CH_3, $^iC_3H_7$), 2.23 (m, 2H, CH, $N^iC_4H_9$), 3.34 (br, 1H, CH, $^iC_3H_7$), 3.5 (m, 4H, CH_2, $N^iC_4H_9$).

2.5. Synthesis of $[UO_2(C_4H_3SCOCHCOCF_3)_2\{^iC_3H_7CON(^iC_3H_7)_2\}]$ (**4**)

To a chloroform solution of $[UO_2(C_4H_3SCOCHCOCF_3)_2 \cdot 2H_2O]$ (500 mg, 0.66 mmol), $^iC_3H_7CON(^iC_3H_7)_2$ (120 mg, 0.70 mmol) was added and refluxed for 30 min. The resultant solution was filtered and layered with *iso*-octane. The solution on slow evaporation yielded an orange colored product. This was filtered, washed with hexane and dried. Yield: 550 mg (93%). Elemental *Anal.* Calc. for $[UO_2(C_4H_3SCOCHCOCF_3)_2\{^iC_3H_7CON(^iC_3H_7)_2\}]$, $C_{26}H_{29}NO_7S_2F_6U$: C, 35.3; H, 3.3; N, 1.6. Found: C, 35.0; H, 3.5; N, 1.2%. IR (KBr, Nujol): ν/cm^{-1} 1565 (CO, $^iC_3H_7CON(^iC_3H_7)_2$), 1600–1630 (CO, $C_4H_3SCOCHCOCF_3$), 919 (O=U=O). ^{1}H NMR (25 °C, $CDCl_3$): δ 1.43 (br, CH_3, $N^iC_3H_7$), 1.56 (br, CH_3, $^iC_3H_7$), 3.32 (br, CH, $^iC_3H_7$), 4.36 (br, NCH, $N^iC_3H_7$), 6.77, 6.81 (s, CH, $C_4H_3SCOCHCOCF_3$), 7.17–7.33, 7.77–7.85, 8.25–8.30 (m, C_4H_3S, $C_4H_3SCOCHCOCF_3$).

2.6. Synthesis of $[UO_2(C_4H_3SCOCHCOCF_3)_2\{^iC_3H_7CON(^iC_4H_9)_2\}]$ (**5**)

Compound **5** was prepared similarly to **4** by taking $[UO_2(C_4H_3SCOCHCOCF_3)_2 \cdot 2H_2O]$ (500 mg, 0.66 mmol) and $^iC_3H_7CON(^iC_4H_9)_2$ (140 mg, 0.70 mmol). Yield: 580 mg (95%). Elemental *Anal.* Calc. for $[UO_2(C_4H_3SCOCHCOCF_3)_2\{^iC_3H_7CON(^iC_4H_9)_2\}]$, $C_{28}H_{33}NO_7S_2F_6U$: C, 36.9; H, 3.6; N, 1.5. Found: C, 36.7; H, 3.4; N, 1.1%. IR (KBr, Nujol): ν/cm^{-1} 1571 (CO, $^iC_3H_7CON(^iC_4H_9)_2$), 1600–1630 (CO, $C_4H_3SCOCHCOCF_3$), 916 (O=U=O). ^{1}H NMR (25 °C, $CDCl_3$): δ 0. 72 (d, CH_3, $N^iC_4H_9$), 1.17 (d, CH_3, $N^iC_4H_9$), 1.47 (d, CH_3, $^iC_3H_7$), 2.24 (m, CH, $N^iC_4H_9$), 3.34 (br, CH, $^iC_3H_7$), 3.5–3.6 (m, NCH_2, $N^iC_4H_9$), 6.77, 6.82 (s, CH, $C_4H_3SCOCHCOCF_3$), 7.33, 7.50–7.85, 8.25–8.29 (m, C_4H_3S, $C_4H_3SCOCHCOCF_3$).

2.7. Synthesis of $[UO_2(C_6H_5COCHCOCF_3)_2\{^iC_3H_7CON(^iC_3H_7)_2\}]$ (**6**)

Compound **6** was prepared similarly to **4** by taking $[UO_2(C_6H_5COCHCOCF_3)_2 \cdot 2H_2O]$ (450 mg, 0.611 mmol) and $^iC_3H_7CON(^iC_3H_7)_2$ (110 mg, 0.64 mmol).Yield: 490 mg (92%). Elemental Anal. Calc. for $[UO_2(C_6H_5COCHCOCF_3)_2\{^iC_3H_7CON(^iC_3H_7)_2\}]$, $C_{30}H_{33}$- NO_7F_6U: C, 41.3; H, 3.8; N, 1.6. Found: C, 41.0; H, 3.5; N, 1.2%. IR (KBr, Nujol): ν/cm^{-1} 1565 (CO, $^iC_3H_7CON(^iC_3H_7)_2$), 1604–1630 (CO, $C_6H_5COCHCOCF_3$), 918 (O=U=O). ^{1}H NMR (25 °C, $CDCl_3$): δ 1.34 (br, CH_3, $N^iC_3H_7$), 1.64 (br, CH_3, $^iC_3H_7$), 3.32 (br, CH, $^iC_3H_7$), 4.36 (br, NCH, $N^iC_3H_7$), 6.98, 7.01 (s, CH, $C_6H_5COCHCOCF_3$), 7.60–7.72, 8.57–8.37 (m, C_6H_5, $C_6H_5COCHCOCF_3$).

2.8. Synthesis of $[UO_2(C_6H_5COCHCOCF_3)_2\{^iC_3H_7CON(^iC_4H_9)_2\}]$ (**7**)

Compound **7** was prepared similarly to **4** by taking $[UO_2(C_6H_5COCHCOCF_3)_2 \cdot 2H_2O]$ (450 mg, 0.61 mmol) and $^iC_3H_7CON(^iC_4H_9)_2$ (125 mg, 0.63 mmol). Yield: 505 mg (92%). Elemental *Anal.* Calc. for $[UO_2(C_6H_5COCHCOCF_3)_2\{^iC_3H_7CON(^iC_4H_9)_2\}]$, $C_{32}H_{37}NO_7F_6U$: C, 42.7; H, 4.1; N, 1.6. Found: C, 42.5; H, 4.4; N, 1.4%. IR (KBr, Nujol): ν/cm^{-1} 1570 (CO, $^iC_3H_7CON(^iC_4H_9)_2$), 1603–1630 (CO, $C_6H_5COCHCOCF_3$), 915 (O=U=O). ^{1}H NMR (25 °C, $CDCl_3$): δ 0.74 (d, CH_3, $N^iC_4H_9$), 1.18 (d, CH_3, $N^iC_4H_9$), 1.50 (d, CH_3, $^iC_3H_7$), 2.25 (m, CH, $N^iC_4H_9$), 3.38 (br, CH, $^iC_3H_7$), 3.5–3.7 (m, NCH_2, $N^iC_4H_9$), 6.99 (s, CH, $C_6H_5COCHCOCF_3$), 7.59–7.77, 8.57–8.60 (m, C_6H_5, $C_6H_5COCHCOCF_3$).

2.9. Synthesis of $[UO_2(C_6H_5COCHCOC_6H_5)_2\{^iC_3H_7CON(^iC_3H_7)_2\}]$ (**8**)

Compound **8** was prepared similarly to **4** by taking $[UO_2(C_6H_5COCHCOC_6H_5)_2 \cdot 2H_2O]$ (400 mg, 0.532 mmol) and $^iC_3H_7CON(^iC_3H_7)_2$ (95 mg, 0.55 mmol). Yield: 440 mg (93%). Elemental *Anal.* Calc. for $[UO_2(C_6H_5COCHCOC_6H_5)_2\{^iC_3H_7CON(^iC_3H_7)_2\}]$, $C_{40}H_{43}NO_7U$: C, 54.1; H, 4.8; N, 1.6. Found: C, 54.0; H, 4.6; N, 1.4%. IR (KBr, Nujol): ν/cm^{-1} 1591 (CO, $C_6H_5COCHCOC_6H_5$), 1572 (CO, $^iC_3H_7CON(^iC_3H_7)_2$), 921 (O=U=O). ^{1}H NMR (25 °C, $CDCl_3$): δ 1.38 (br, CH_3, $N^iC_3H_7$), 1.56 (br, CH_3, $^iC_3H_7$), 3.27 (br, CH, $^iC_3H_7$), 4.35 (br, NCH, $N^iC_3H_7$), 7.40 (s, CH, $C_6H_5COCHCOC_6H_5$), 7.50–7.7, 8.42–8.60 (m, C_6H_5, $C_6H_5COCHCOC_6H_5$).

2.10. Synthesis of $[UO_2(C_6H_5COCHCOC_6H_5)_2\{^iC_3H_7CON(^iC_4H_9)_2\}]$ (**9**)

Compound **9** was prepared similarly to **4** by taking $[UO_2(C_6H_5COCHCOC_6H_5)_2 \cdot 2H_2O]$ (400 mg, 0.532 mmol) and $^iC_3H_7CON(^iC_3H_7)_2$ (110 mg, 0.55 mmol). Yield: 420 mg (86%). Elemental *Anal.* Calc. for $[UO_2(C_6H_5COCHCOC_6F_5)_2\{^iC_3H_7CON(^iC_3H_7)_2\}]$, $C_{40}H_{43}NO_7U$: C, 54.1; H, 4.8; N, 1.6. Found: C, 54.0; H, 4.6; N, 1.4%. IR (KBr, Nujol): ν/cm^{-1} 1580 (CO, $^iC_3H_7CON(^iC_3H_7)_2$), 1591 (CO, $C_6H_5COCHCOC_6H_5$), 922 (O=U=O). ^{1}H NMR (25 °C, $CDCl_3$): δ

0. 72 (d, CH_3, $N^iC_4H_9$), 1.32 (d, CH_3, $N^iC_4H_9$), 1.45 (d, CH_3, $^iC_3H_7$), 2.22 (m, CH, $N^iC_4H_9$), 3.32 (br, CH, $^iC_3H_7$), 3.4–3.6 (m, NCH_2, $N^iC_4H_9$), 7.41 (s, CH, $C_6H_5COCHCOC_6H_5$), 7.52–7.7, 8.40–8.60 (m, C_6H_5, $C_6H_5COCHCOC_6H_5$).

2.11. Reaction of $^iC_3H_7CON(^iC_4H_9)_2$ with $Th(NO_3)_4 \cdot 6H_2O$

To a solution of $^iC_3H_7CON(^iC_4H_9)_2$ (500 mg, 2.5 mmol) in $CHCl_3$, solid [$Th(NO_3)_4 \cdot 6H_2O$] (600 mg, 1.02 mmol) was added and stirred for 12 h. No reaction between the amide and $Th(NO_3)_4 \cdot 6H_2O$ was observed due to the presence of an insoluble starting material. Ten millilitres of methanol was added to the solution and stirred for another 6 h. The clear solution was evaporated to dryness and the hygroscopic material was subjected to IR spectral analysis. IR (KBr, Nujol): ν/cm^{-1} 1640 (CO), 3600–3200 (br, H_2O).

2.12. Reaction of $^iC_3H_7CON(^iC_4H_9)_2$ with $La(NO_3)_3 \cdot 6H_2O$

This reaction was performed similarly to that of $Th(NO_3)_4 \cdot 6H_2O$ by taking the amide (650 mg, 3.27 mmol) and $La(NO_3)_3 \cdot 6H_2O$ (450 mg, 1.03 mmol). The resultant hygroscopic material was subjected to the IR spectral studies. IR (KBr, Nujol): ν/cm^{-1} 1639 (CO), 3600–3200 (br, H_2O).

2.13. Solvent extraction studies

Distribution studies were performed by using a solution of $^iC_3H_7CON(^iC_4H_9)_2$ in toluene (0.2 F) with the required aqueous phase spiked with ^{233}U or ^{239}Pu tracers in a thermostated water bath for 1 h at 25 ± 0.1 °C. Assay of organic and aqueous phases were done in duplicate by alpha counting using a dioxane based liquid scintillator for ^{233}U and ^{239}Pu. The distribution ratio (D) is defined as the ratio of the concentration of uranium in the organic phase to that of the aqueous phase.

2.14. Separation studies

Stock solutions containing 5 g of $Th(NO_3)_4 \cdot 6H_2O$, 300 mg of $La(NO_3)_3 \cdot 6H_2O$ and 500 mg of $UO_2(NO_3)_2 \cdot 6H_2O$ were prepared in 10 ml of 1, 2, 3 and 6 M HNO_3. This solution was layered with 1 g of $^iC_3H_7CON(^iC_4H_9)_2$ amide and allowed to stand for over night. This process deposited yellow crystalline solid material, which was filtered, washed with water, hexane and dried. The supernatants and the solutions of yellow solid in ethanol were used for the elemental analysis using the total reflection X-ray fluorescence (TXRF) method.

2.15. X-ray diffraction studies of **3** and **8**

Data for **3** and **8** were measured with the Mo Kα radiation (λ = 0.71073 Å) at 150 K using the Oxford Instruments X-Calibur CCD System. The crystals were positioned at 50 mm from the Image Plate. Three hundred and twenty-one frames were measured with a counting time of 10 s. Data analysis was carried out with the CRYSALIS program [21a]. The structures were solved using direct methods with the SHELXS97 program [21b]. All non-hydrogen atoms in these structures were refined with anisotropic thermal parameters. The hydrogen atoms bonded to carbon atoms were included in the geometric positions and given thermal parameters equivalent to 1.2 times those of the atoms to which they attached. Empirical absorption corrections were carried out using the ABSPACK program [21c]. The structures were refined to convergence on F^2 using SHELXL97 [21d]. Selected crystallographic data for **3** and **8** are summarized in Table 1.

Table 1
Crystal and structural refinement details for **3** and **8**

	3	**8**
Empirical formula	$C_{24}H_{50}N_4O_{10}U$	$C_{40}H_{43}NO_7U.\ 0.5C_7H_8$
Formula weight	792.71	933.85
Crystal system	triclinic	orthorhombic
Space group	$P\bar{1}$	*Pbca*
a (Å)	9.4263(13)	16.2338(7)
b (Å)	9.5422(13)	20.988(4)
c (Å)	10.1230(11)	23.5467(16)
α (°)	75.567(10)	90
β (°)	81.956(10)	90
γ (°)	69.296(13)	90
Volume (Å^3)	823.51(18)	8022.8(17)
Z (formula unit)	1	8
Calculated density (g/cm^3)	1.598	1.546
Reflections collected/unique	5695/4591	41 448/11 663
Data/restraints/parameters	4591/0/184	11 663/12/464
Goodness of fit on F^2	0.953	0.738
Final R_1 indices [$I > 2\sigma(I)$]	0.0750	0.0509
wR_2 indices (all data)	0.1883	0.1544

$w = 1/[\sigma^2(F_o^2) + (0.1579P)^2 + 0.000P]$ for **3**, $w = 1/[\sigma^2(F_o^2) + (0.0706P)^2 + 0.000P]$ for **8**, where $P = (F_o^2 + 2F_c^2)/3$ for **3** and **8**.

3. Results and discussion

3.1. Complexation study of ***iso*-butyramide ligands with the uranyl nitrate**

The complexing ability of $^iC_3H_7CON(^iC_3H_7)_2$, $^iC_3H_7CON(C_4H_9)_2$ and $^iC_3H_7CON(^iC_4H_9)_2$ with uranyl nitrate was studied by using elemental analysis, IR and NMR spectroscopic techniques. The reaction of [$UO_2(NO_3)_2 \cdot 6H_2O$] with the *iso*-butyramide ligands yielded the compounds **1**–**3**. The C, H and N analysis revealed that the ratio of ligand to uranyl nitrate is 1:2 in all these compounds. The IR spectra of **1**–**3** show that the water molecules from the starting compound [$UO_2(NO_3)_2 \cdot 6H_2O$] are completely replaced by the ligand and that the ligand is bonded through the carbamoyl oxygen atom to the uranyl group.

The observed frequency differences for a carbamoyl ($\Delta\nu_{CO}$ = 68–70 cm^{-1}, where $\Delta\nu_{CO} = \nu_{CO(\text{free ligand})} - \nu_{CO(\text{coordinated})}$) group are consistent with the supposition that the carbamoyl group is bonded to the uranyl group directly in the reported compounds. These differences are comparable in magnitude with those of the $[UO_2Cl_2(^iC_3H_7CON\{^iC_3H_7\}_2)_2]$, $[UO_2Br_2(^iC_3H_7CON\{^{sec}C_4H_9\}_2)_2]$ [8], $[UO_2(C_6H_3Cl_2S)_2(^iC_3H_7CON\{^iC_4H_9\}_2)_2]$ [9], $[UO_2(NO_3)_2(N\text{-cyclohexyl,2-pyrrolidone})_2]$ [18] and $[UO_2(NO_3)_2(1,3\text{-dimethyl,2-imidazolidone})_2]$ [19] complexes and much higher in magnitude compared to those observed in other amides or malonamides uranyl complexes [5,22]. The ^1H NMR spectra of **1**–**3** show that the CH proton of the *iso*-propyl group is deshielded by ca. 0.5–0.6 ppm with respect to the free ligand, indicating that the ligand is coordinated to the uranyl group in solution also. It is apparent from the elemental analysis and IR spectral results that ligands are acting as monodentate ligand in compounds **1**–**3** in the solid state to give similar structures to those observed in the compounds of pyrrolidone [18,19] or other monodentate amides [10–12] with the uranyl nitrate. Interestingly, all these complexes are air and moisture stable crystalline solids, having good solubility in $CHCl_3$ and CH_2Cl_2, and can be used as a starting compound for further reactions. The structure of **3** has been determined by single crystal X-ray diffraction methods, which confirms the IR and elemental analysis results.

3.2. Molecular structure of **3**

The molecular structure of **3** is shown in Fig. 1 and the selected interatomic bond distances and angles for are given in Table 2. The

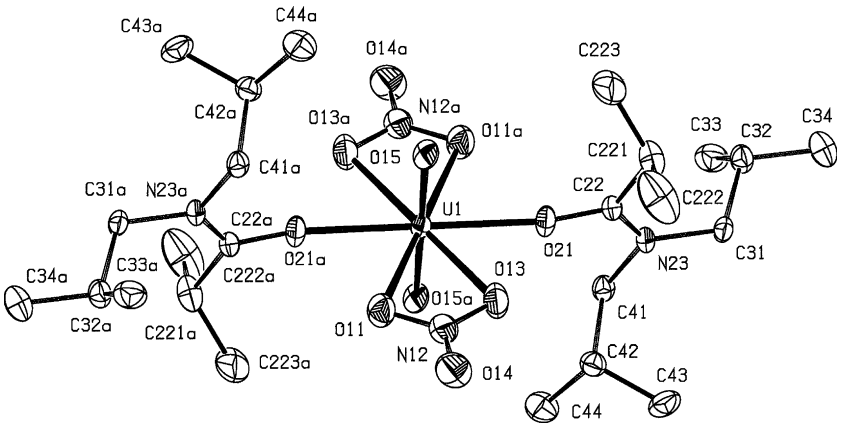

Fig. 1. Molecular structure of **3** (hydrogen atoms omitted for the clarity).

structure contains a crystallographic center of symmetry with the uranium atom surrounded by eight oxygen atoms in a hexagonal bi-pyramidal geometry. Two uranyl oxygen atoms occupy the axial positions. There are two bidentate nitrate ligands in the hexagonal equatorial plane together with two carbamoyl oxygen atoms from the two monodentate *iso*-butyramide ligands. These six oxygen atoms are approximately coplanar to within an r.m.s. of 0.042 Å.

This type of co-ordination is similar to that observed in the compounds of the mono-functional ligands, phosphine oxide, phosphates and amides or pyrrolidones with uranyl nitrate such as: $[UO_2(NO_3)_2(OPPh_3)_2]$ [13], $[UO_2(NO_3)_2(OP\{OEt\}_3)_2]$ [14], $[UO_2(NO_3)_2(OPBu_3)_2]$ [15], $[UO_2(NO_3)_2(TPPPO)_2]$ [16], $[UO_2(NO_3)_2(OP\{OCH_3\}_3)_2]$ [17], $[UO_2(NO_3)_2(DMF)_2]$ [10], $[UO_2(NO_3)_2(N$-cyclohexyl,2-pyrrolidone$)_2]$ [18] and $[UO_2(NO_3)_2(1,3$,dimethyl, 2-imidazolidone$)_2]$ [19]. The U–O(amide) distance (2.349(1) Å) in **3** is much shorter in length compared to those of earlier reported uranyl nitrate–amide compounds such as: $[UO_2(NO_3)(DMF)_2]$ (2.397(6) Å) [10], $[UO_2(NO_3)_2($tetrabutylglutaramide$)_2]$ (2.378(6) Å) [11], $[UO_2(NO_3)_2($dibutyldecanamide$)_2]$ (2.37(2) Å) [12] and $[UO_2(NO_3)_2(^iC_3H_7)_2NCOCH_2CON(^iC_3H_7)_2]$ (2.41(2) Å) [22] and comparable in magnitude with those of $[UO_2(NO_3)_2(N$-cyclohexyl,2-pyrrolidone$)_2]$ (2.347(4) Å) [18] and $[UO_2(NO_3)_2(OPBu_3)_2]$ (2.347(6) Å) [15]. The observed average U–O(NO_3) bond distance 2.531(1) Å is normal [10–19]. The angles subtended at the metal atom show that the uranium atom has a slightly distorted hexagonal bi-pyramidal geometry.

Table 2
Important bond distances (Å) and angles (°) for **3** and **8**

Compound **3**			
U1–O11	2.527(7)	U1–O13	2.535(8)
U1–O15	1.756(6)	U1–O21	2.349(6)
N12–O11	1.264(11)	N12–O13	1.276(11)
N12–O14	1.229(12)	C22–O21	1.264(9)
O11–U1–O13	50.4(2)	O11–U1–O15	90.1(3)
O11–U1–O21	114.9(2)	O13–U1–O15	88.3(3)
O13–U1–O21	64.6(2)	O15–U1–O21	91.4(3)
U1–O21–C22	171.2(6)		
Compound **8**			
U1–O1	1.770(5)	U1–O2	1.776(5)
U1–O11	2.361(5)	U1–O15	2.352(5)
U1–O21	2.359(5)	U1–O25	2.333(5)
U1–O31	2.379(5)	O31–C32	1.273(8)
O1–U1–O2	179.0(2)	O1–U1–O11	88.6(2)
O1–U1–O15	92.8(2)	O1–U1–O21	90.4(2)
O1–U1–O25	86.7(2)	O1–U1–O31	89.3(2)
U1–O31–C32	159.8(5)		

The shorter bond lengths observed in this compound can be explained on the basis of a strong π bonding interaction between the filled p orbitals of oxygen atom with those of the vacant d/f orbitals of the uranyl group, which lead to the opening of the U–O–C bond angle from 130° to 140° (normally observed in number of metal–amide compounds [23]) to 171.2(6)°. The observed bond lengths and the U–O–C bond angles are compatible with the earlier reported correlation diagram for the uranyl nitrate–amide compounds [19]. In particular, the characteristic of shorter bond distances and wider bond angles are reported for the *iso*-butyramide based ligands in the compounds of $[Th(NCS)_4(^iC_3H_7CON\{^iC_3H_7\}_2)_3]$ [24], $[UO_2Cl_2(^iC_3H_7CON\{^iC_3H_7\}_2)_2]$, $[UO_2Br_2(^iC_3H_7CON\{^{sec}C_4H_9\}_2)_2]$ [8] and $[UO_2(C_6H_3Cl_2S)_2(^iC_3H_7CON\{^iC_4H_9\}_2)_2]$ [9].

3.3. Complexation study of iso-butyramide with the uranyl bis(β-diketonates)

The reaction of $^iC_3H_7CON(^iC_3H_7)_2$ and $^iC_3H_7CON(^iC_4H_9)_2$ with $[UO_2(OO)_2 \cdot 2H_2O]$ (OO = TTA, BTA or DBM) yielded the compounds **4–9**. The C, H, N analyses revealed that the ratio of ligand to metal is 1:1 in all these compounds. The IR spectra of all these compounds show that the water molecules from the starting compounds $[UO_2(OO)_2 \cdot 2H_2O]$ are replaced completely by the ligands. The spectra show further that the ligands are bonded through the carbamoyl oxygen atoms to the metal ion. ($\Delta\nu_{CO}$ = 70–75 cm^{-1}, where $\Delta\nu_{CO} = \nu_{CO(free\ ligand)} - \nu_{CO(coordinated)}$). The ^1H NMR of the compounds show that CH protons of the *iso*-propyl group is deshielded (ca. 0.5–0.6 ppm) with respect to the free ligand, indicating that the ligand is bonded to the uranyl bis(β-diketonte) in solution also. The structure of compound **8** has been determined by single crystal X-ray diffraction methods, which confirms the spectral and analyses results.

3.4. Molecular structure of *8*

The molecular structure of **8** is shown in Fig. 2 together with the numbering scheme and selected interatomic bond distances and angles are given in Table 2. There is a disordered toluene molecule refined with 50% occupancy in the asymmetric unit which is not shown. The structure shows that the uranyl group is bonded to two $C_6H_5COCHCOC_6H_5$ groups and an amide group to give a coordination number of seven. The amide ligand acts as a monodentate ligand and is bonded through the carbamoyl oxygen atoms to the uranyl bis(β-diketonates). Four oxygen atoms from two $C_6H_5COCHCOC_6H_5$ groups, one oxygen atom from the amide ligand and two oxygen atoms of uranyl group form a pentagonal bi-pyramidal geometry around the uranium(VI) ion. The five contributing

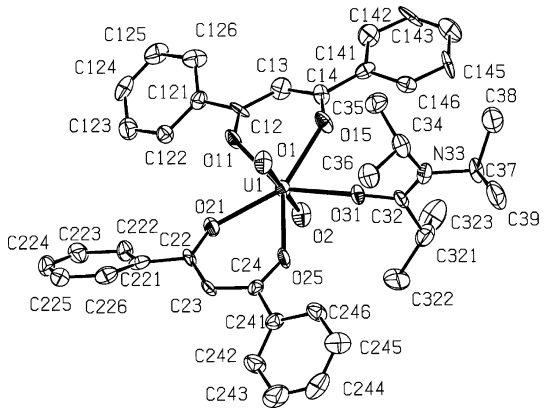

Fig. 2. The structure of **8** (hydrogen atoms omitted for the clarity).

oxygen atoms in the equatorial plane show an r.m.s. deviation of 0.062 Å. Similar structures are also observed in the compounds of phosphine oxide, sulfoxide, N-oxide, ketones and amides with the uranyl bis(β-diketonates) viz; $[UO_2(DBM)_2(OPPh_3)]$ [25a], $[UO_2(DBM)_2(C_6H_5SOCH_3)]$ [25b], $[UO_2(TTA)_2(C_5H_5NO)]$ [25c], $[UO_2(DBM)_2$ (camphor) [25d] and $[UO_2(DBM)_2\{C_4H_9CON(C_5H_{11})(C_4H_9)\}]$ [25e]. The observed metal to amide oxygen distance in **8** (2.379(5) Å) is shorter in length compared to those value reported in $[UO_2(DBM)_2\{C_4H_9CON(C_5H_{11})(C_4H_9)\}]$ (2.42 Å) [25e]. The shortest bond distance observed in compound **8** compared to those observed in $[UO_2(DBM)_2\{C_4H_9CON(C_5H_{11})(C_4H_9)\}]$ can be explained once again on the basis of strong interaction between the amide oxygen and uranyl group, which results in opening of U–O–C bond angle to 159.8(5)°. The longer bond distances in **8** compared to those in **3** can be explained on the basis of a bulkier phenyl group of the β-diketonate units, which may not allow the donor group to come closer to uranyl group compared to those of the less bulkier nitrate groups.

3.5. Complexation study of $^iC_3H_7CON(^iC_4H_9)_2$ with $Th(NO_3)_4 \cdot 6H_2O$ and $La(NO_3)_3 \cdot 6H_2O$

The IR spectra of the product obtained from the reaction between $^iC_3H_7CON(^iC_4H_9)_2$ and $Th(NO_3)_4 \cdot 6H_2O$ or $La(NO_3)_3 \cdot 6H_2O$ show the presence of an uncoordinated carbonyl group (1639 cm^{-1}) and water molecules (3600–3200 cm^{-1}). This shows clearly that there is no reaction between the amide ligand and metal nitrates. However, the uranyl nitrate forms a strong complex with the same amide under identical conditions.

3.6. Thermal studies of the compound **3**

Thermogravimetric (TG) and differential thermal analyses (DTA) of **3** (see the supporting information) were carried out to see whether the bonded ligands can be destroyed completely on heating. These compounds decompose in two steps to give U_3O_8 as a final product without any other impurities as revealed by the powder X-ray diffraction methods.

3.7. Extraction studies of U(VI) and Pu(IV) with $^iC_3H_7CON(^iC_4H_9)_2$ from nitric acid medium

The extraction studies were carried out by using the ligand $^iC_3H_7CON(^iC_4H_9)_2$ in toluene with the U(VI) and Pu(IV) ions in tracer level (using the ^{233}U and ^{239}Pu) from nitric acid medium to assess the feasibility of using this ligand (0.2 F for both the U(VI) and Pu(IV)) for the extraction purpose. Distribution ratios (D) for U(VI) and Pu(IV) as a function of nitric acid concentrations (Fig. 3) shows

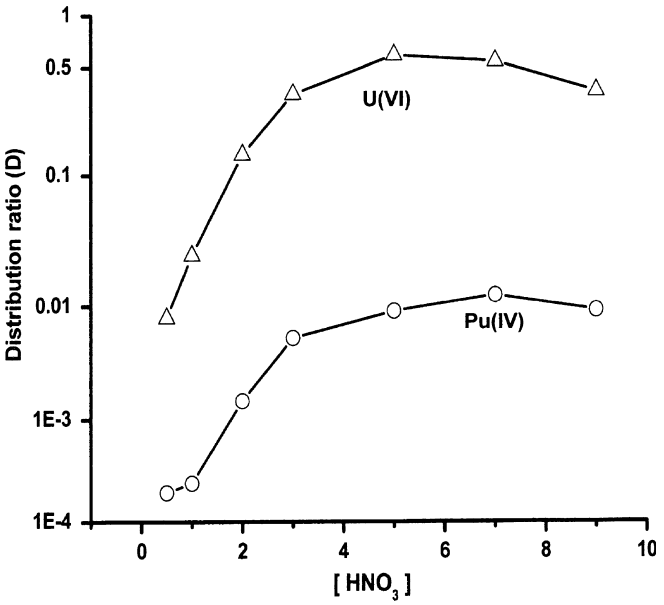

Fig. 3. Variation of distribution ratio for U(VI) and Pu(IV) with HNO_3.

clearly that observed distribution values are very low for both the U(VI) and Pu(IV) under the acid concentrations of 1–10 M. However, under any acid concentration, the D for Pu(IV) is much smaller than those of U(VI). This observation is completely contradictory to the data reported for any of the extractants (either mono-functional or bi-functional) with that of Pu(IV) ($D_{Pu(IV)} \gg D_{U(IV)}$ always) [5a,5b,5c,5d] and agrees well with the result reported for the *iso*-butyramide based extractant [6]. This shows clearly that the uranium can be selectively separated from plutonium or vice versa.

3.8. Selective separation of uranium from thorium by using $^iC_3H_7CON(^iC_4H_9)_2$ ligand

The total reflection X-ray fluorescence (TXRF) spectrum of the supernatant (see the supporting information) clearly shows that more than 98% of the uranium is precipitated from a mixture of thorium, lanthanum and uranium. The TXRF spectrum of the ethanolic solution of the precipitated product shows (see the supporting information) clearly that the precipitate contains more than 98% of uranium and less than 0.2% of thorium and 0% La. It confirms that the uranium is selectively precipitated as its nitrate complex from the solution leaving the thorium and lanthanum ions. This study clearly demonstrates that the uranium can be selectively separated from the mixture of thorium and lanthanum in an equivalent manner to that of the *N*-cyclohexyl,2-pyrrolidone type of ligands. Further work is in progress to investigate the separation of uranium in presences of other lanthanide ions and fission products.

4. Conclusions

Studies on the coordination ability of the *iso*-butyramide based ligands with the uranyl(VI) nitrate show that the ligands act as monodentate ligand and form 1:2 complexes. The studies further show that the ligands are un-reactive towards the thorium(IV) and lanthanum(III) nitrates. Preliminary precipitation studies show that the U(VI) can be selectively separated as an uranyl nitrate amide complex from the solution containing the mixture of U(VI), Th(IV) and La(III) ions. TG/DTA experiments show that the

uranyl nitrate–amide compound can be completely converted in to U_3O_8 without any other impurities.

Supplementary material

X-ray crystallographic files in CIF format for **3** and **8**, IR, ^{1}H NMR spectra and TG/DTA of **3** and TXRF spectra of the Th, U and La mixture, uranyl nitrate precipitate and the supernatant are deposited to the editor as supporting information. Crystallographic data may be obtained from the Cambridge Crystallographic Data Center, by quoting the reference number CCDC: 680831 and 680832. Copies of this information may be obtained free of charge from The Director, CCDC, 12, Union Road, Cambridge, CB21EZ, UK (fax: +44-1223-336-033; email: deposit@ccdc.cam.ac.uk or www: http://www.ccdc.cam.ac.uk).

Acknowledgements

We wish to thank, the Head, Analytical Chemistry Division, BARC, for carbon, hydrogen and nitrogen analysis, the Head, National NMR facilities, TIFR, Mumbai for NMR spectra, Kum. S. Dhara for TXRF, Dr. N.K. Kulkarni for TG/DTA, Dr. S.K. Aggarwal, Head, Fuel Chemistry Division and Dr. K.L. Ramakumar, Head, Radioanalytical Chemistry Division for their support. We also wish to thank the EPSRC (UK) and the University of Reading for funds for the Oxford Diffraction CCD system.

References

[1] L.R. Morss, N.M. Edelstein, J. Fuger, J.J. Katz, The Chemistry of the Actinide and Transactinide Elements, Springer, The Netherlands, 2006.
[2] C.J. Burns, M.P. Neu, H. Boukhalfa, K.E. Gutowshi, N.J. Bridges, R.D. Rogers, in: J.A. McCleverty, T.J. Meyer, G.F.R. Parkin (Eds.), Comprehensive Coordination Chemistry II, vol. 3, Elsevier, Oxford, 2004, p. 189.
[3] M. Ephritikhine, Dalton Trans. (2006) 2501.
[4] (a) S. Kant, Int. J. Nucl. Ener. Sci. Tech. 1 (2005) 204;
(b) R.K. Sinha, A. Kakodkar, Nucl. Eng. Des. 236 (2006) 683.
[5] (a) C. Musikas, Inorg. Chim. Acta 140 (1987) 197;
(b) C. Madic, M.J. Hudson, High Level Liquid Waste Partitioning by Means of Completely Incinerable Extractants, European Commission, Nuclear Science and Technology, EU18038EN, Luxembourg, 1998.;
(c) L. Nigond, C. Musikas, C .C. Cullerdier, Solv. Extr. Ion Exch. 12 (1994) 261;
(d) L. Nigond, N. Condamines, P.Y. Cordier, J. Livert, C. Madic, C .C. Cullerdier, C. Musikas, Sep. Sci. Technol. 30 (1995) 2075;
(e) Y. Sasaki, Y. Sugo, S. Suzuki, S. Tachimori, Solv. Extr. Ion Exch. 19 (2001) 91;
(f) S. Tachimori, Y. Sasaki, S. Suzuki, Solv. Extr. Ion Exch. 20 (2002) 687;
(g) Z. Zhu, Y. Sasaki, H. Suzuki, S. Suzuki, T. Kimura, Anal. Chim. Acta 527 (2004) 163.
[6] (a) P.N. Pathak, R. Veeraraghavan, D.R. Prabhu, G.R. Mahajan, V.K. Manchanda, Sep. Sci. Technol. 34 (1999) 2601;
(b) P.N. Pathak, L.B. Kumbhare, V.K. Manchanda, Solv. Extr. Ion Exch. 19 (2001) 105;
(c) V.K. Manchanda, P.N. Pathak, Sep. Purif. Technol. 35 (2004) 85.
[7] T.R. Varga, M. Sato, Zs. Fazekas, M. Harada, Y. Ikeda, H. Tomiyasu, Inorg. Chem. Commun. 3 (2000) 637.
[8] S. Kannan, C.L. Barnes, P.B. Duval, Chem. Commun. (2005) 5997.
[9] S. Kannan, C.L. Barnes, P.B. Duval, Inorg. Chem. 44 (2005) 9137.
[10] J.M. Gil, F.J.M. Gil, A. Perales, J. Fayos, M.M. Ripoll, Acta Crystallogr., Sect. C 39 (1983) 44.
[11] P. Charpin, M. Lance, M. Nierlich, D. Vigner, Acta Crystallogr., Sect. C 43 (1987) 442.
[12] P. Charpin, M. Lance, M. Nierlich, D. Vigner, Acta Crystallogr., Sect. C 42 (1986) 560.
[13] N.W. Alcock, M.M. Roberts, D. Brown, Dalton Trans. (1985) 25.
[14] B. Kanellakopulos, E. Dornberger, R. Maier, B. Nuber, H.G. Stammler, M.L. Ziegler, Z. Anorg. Allg. Chem. 619 (1993) 593.
[15] J.H. Burns, Inorg. Chem. 20 (1981) 3868.
[16] A.R. de Aquino, G. Bombieri, P.C. Isolani, G. Vicentini, J. Zukerman Schpector, Inorg. Chim. Acta 306 (2000) 101.
[17] G. Agostini, G. Giacometti, D.A. Clemente, M. Vicentini, Inorg. Chim. Acta 62 (1982) 237.
[18] T.R. Varga, A.C. Benyei, Z. Fazekas, H. Tomiyasu, Y. Ikeda, Inorg. Chim. Acta 342 (2003) 291.
[19] N. Koshino, M. Harada, M. Nogami, Y. Morita, T. Kikuchi, Y. Ikeda, Inorg. Chim. Acta 358 (2005) 1857.
[20] K.M. Abubacker, N.S.K. Prasad, J. Inorg. Nucl. Chem. 16 (1961) 296.
[21] (a) CRYSALIS program, Oxford Diffraction Ltd., 2005.;
(b) G.M. Sheldrick, SHELXS, Program for Crystal Structure Solution, University of Gottingen, Gottingen, Germany, 1997.;
(c) ABSPACK Program, Oxford Diffraction Ltd., 2005.;
(d) G.M. Sheldrick, SHELXL, Program for Crystal Structure Refinement, University of Gottingen, Gottingen, Germany, 1997.
[22] G.J. Lumetta, B.K. McNamara, B.M. Rapko, R.L. Sell, R.D. Rogers, G. Broker, J.E. Hutchison, Inorg. Chim. Acta 309 (2000) 103.
[23] O. Clements, B.M. Rapko, B.P. Hay, Coord. Chem. Rev. 170 (1998) 203.
[24] K.W. Bagnall, F. Benetollo, E. Forsellini, G. Bombieri, Polyhedron 11 (1992) 1765.
[25] (a) S. Alagar, M. Subha Nandhini, R.V. Krishnakumar, S. Kannan, S. Natarajan, Acta Crystallogr., Sect. E 59 (2003) m524;
(b) S. Kannan, V. Venugopal, M.R.A. Pillai, P.A. Droege, C.L. Barnes, Polyhedron 15 (1996) 97;
(c) S. Kannan, A. Usman, H.K. Fun, Polyhedron 21 (2002) 2403;
(d) S. Kannan, M.R.A. Pillai, V. Venugopal, P.A. Droege, C.L. Barnes, Inorg. Chim. Acta 254 (1997) 113;
(e) S. Rajagopal, S. Kannan, V. Venugopal, R.V. Krishnakumar, M. Subha Nandhini, S. Natarajan, J. Chem. Res. (2003) 468.

Polyhedron 27 (2008) 2563–2568

Contents lists available at ScienceDirect

Polyhedron

journal homepage: www.elsevier.com/locate/poly

Ruthenium monoterpyridine complexes with 2,6-bis(benzoxazol-2-yl)pyridine as an ancillary ligand: Synthesis, structure and spectral studies

Amardeep Singh, Gopal Das, Biplab Mondal *

Department of Chemistry, Indian Institute of Technology Guwahati, North Guwahati, Assam 781039, India

ARTICLE INFO

Article history:
Received 6 February 2008
Accepted 2 May 2008
Available online 28 June 2008

Keywords:
Ruthenium
Terpyridine
2,6-Bis(benzoxazol-2-yl)pyridine
Structure
Spectra

ABSTRACT

Ruthenium monoterpyridine complexes, $[\mathbf{1}]^+$ and $[\mathbf{2}]^{2+}$, with 2,6-bis(benzoxazol-2-yl)pyridine as an ancillary ligand, L, have been synthesized and characterized by UV–Vis, FT-IR and ^{1}H NMR spectroscopic techniques. The formulations of the complexes were confirmed by the single crystal structure of their perchlorate salts. In both complexes, the Ru^{II} center is hexa-coordinated in a distorted geometry. In complex $[\mathbf{1}]^+$, the ancillary ligand L behaves as a bidentate ligand; in $[\mathbf{2}]^{2+}$, however, it binds the metal center as a tridentate ligand. The central pyridine nitrogen of terpyridine ($N_{p,trpy}$) is in a *cis* position with respect to the central pyridine nitrogen of the ancillary ligand ($N_{p,benz}$) in complex $[\mathbf{1}]^+$ and in a *trans*-position in complex $[\mathbf{2}]^{2+}$. The *cis* orientation of $N_{p,trpy}$ and $N_{p,benz}$ in complex $[\mathbf{1}]^+$ forces L to behave as bidentate. The quasi-reversible Ru^{II}/Ru^{III} couple appears at 0.90 and 1.44 V versus SCE in the case of complex $[\mathbf{1}]^+$ and $[\mathbf{2}]^{2+}$, respectively. $[\mathbf{1}]^+$, in the presence of aqueous $AgNO_3$, affords $[\mathbf{2}]^{2+}$ through an intramolecular dissociative interchange pathway.

© 2008 Elsevier Ltd. All rights reserved.

1. Introduction

Strong metal to ligand charge-transfer transitions, facile electron-transfer properties and long lived ^{3}MLCT excited states of ruthenium–polypyridine complexes make them effective for designing photochemical and electrochemical devices [1–7]. In this direction, a variety of ruthenium–terpyridine complexes incorporating different kinds of bidentate and tridentate ancillary ligands have been synthesized in recent years [8–17]. However, ruthenium–monoterpyridine chemistry with the tridentate 2,6-bis(benoxazol-2-yl)pyridine ligand, structurally analogous to the triimine 2,2′:6′,2″-terpyridine, has not yet been explored, though its chemistry with some transition metals like copper, iron and zinc has been studied well [18,19]. Due to extensive π-delocalization, the rigid planar tridentate ligand will afford a well defined structure for its complexes [18,19] and by virtue, like terpyridine, can bind a metal center in a meridional fashion with a bite angle of about 79°.

In the present study, we have synthesized a ruthenium monoterpyridine complex $[\mathbf{1}]^+$ with the tridentate ancillary ligand, 2,6-bis(benzoxazol-2-yl)pyridine (L). The complex $[\mathbf{1}]^+$, in presence of aqueous silver nitrate solution, undergoes an intramolecular dissociative interchange type reaction to afford complex $[\mathbf{2}]^{2+}$.

2. Experimental

2.1. Materials

The starting complex Ru(trpy)Cl_3 [trpy: 2,2′:6′,2″-terpyridine] was prepared according to the reported procedure [20]. 2,2′:6′,2″-terpyridine and 2,6-pyridinedicarboxylic acid were obtained from Aldrich, USA. 2-Aminophenol was purchased from Loba Chemie, India. Other chemicals and solvents were reagent grade and were used as received. For spectroscopic and electrochemical studies HPLC grade solvents were used. Commercial tetraethyl ammonium bromide was converted into pure tetraethyl ammonium perchlorate by following the available procedure [21].

2.2. Physical measurements

UV–Vis spectra were recorded with a Perkin Elmer Lambda-25 spectrophotometer. FT-IR spectra were taken on a Perkin Elmer spectrophotometer with samples prepared as KBr pellets. Solution electrical conductivity was checked using a Systronic 305 conductivity bridge. ^{1}H NMR spectra were obtained with a 400 MHz Varian FT spectrometer. Cyclic voltammetric, differential pulse voltammetric and coulometric measurements were carried out using a PAR model 273A electrochemistry system. A glassy carbon working electrode, platinum auxiliary electrode and an aqueous saturated calomel reference electrode (SCE) were used in a three electrode configuration. The supporting electrolyte was $[NBu_4]ClO_4$ and the solute concentration was $\sim 10^{-3}$ M. The half-wave poten-

* Corresponding author. Tel.: +91 3612582317; fax: +91 3612582349.
E-mail address: biplab@iitg.ernet.in (B. Mondal).

0277-5387/$ - see front matter © 2008 Elsevier Ltd. All rights reserved.
doi:10.1016/j.poly.2008.05.022

tial E^0_{298} was set equal to $0.5(E_{pa} + E_{pc})$, where E_{pa} and E_{pc} are the anodic and cathodic cyclic voltammetric peak potentials, respectively. All experiments were carried out under a dinitrogen atmosphere and were uncorrected for junction potentials. The elemental analyses were carried out with a Perkin Elmer elemental analyser.

2.3. Crystallography

X-ray diffraction data for the complexes were collected on Bruker 3-circle SMART Apex diffractometer with CCD area detectors, using graphite monochromated Mo Kα ($\lambda = 0.71073$ Å) radiation, with increasing ω (width of 0.3° per frame) at a scan speed of 3 s/frame. The structures were solved by direct methods and refined by full-matrix least squares against F^2 for all data, using SHELXTL software [22]. Multi-scan empirical absorption corrections were applied to the data using the program SADABS [23]. All the non-hydrogen atoms were refined anisotropically. The hydrogen atoms were located from the difference Fourier maps and refined. Structural illustrations have been drawn with ORTEP-3 for Windows [24].

2.4. Synthesis of the ligand L

A mixture of pyridine 2,6-dicarboxylic acid (835 mg, 5 mmol) and 2-aminophenol (1.09 g, 10 mmol) in 10 ml *ortho*-phosphoric acid was refluxed for 8 h. It was then cooled down to room temperature and poured into 200 ml pre-cooled water with constant stirring, which resulted in a dark brown precipitate. The precipitate, on washing with 20% sodium carbonate solution, afforded the dark colored ligand, L. It was then recrystallized from hot methanolic solution (yield = 40%).

Elemental *Anal.* Calc.: C, 72.84; H, 3.54; N, 13.41. Found: C, 72.87; H, 3.53; N, 13.39%. ^{1}H NMR data (400 MHz, in $CDCl_3$) δ_{ppm}: 8.52 (d, 2H), 8.10 (t, 1H), 7.85 (d, 2H), 7.73 (d, 2H), 7.46–7.39 (m, 4H).

2.4.1. Synthesis of the complex [*1*](ClO$_4$)

$Ru^{III}(trpy)Cl_3$(200 mg; 0.44 mmol) and the ligand, L (144 mg; 0.46 mmol) were dissolved in 20 ml ethanol, and NEt_3 (0.7 mmol) was added dropwise to the mixture. It was then heated to reflux with constant stirring for 4 h. Then the volume of the mixture was reduced to 5 ml under reduced pressure and a pre-cooled saturated aqueous $NaClO_4$ solution was added. The mixture was kept in a refrigerator overnight. The dark precipitate that formed was filtered off and washed with ice cold distilled water. The product was dried in vacuo over P_4O_{10}. It was then passed through a silica gel column with a CH_2Cl_2/CH_3CN solvent mixture. The reddish brown color complex, [**1**](ClO$_4$) was separated with 4:1 CH_2Cl_2:CH_3CN. Yield: ~45%, 165 mg. Elemental *Anal.* Calc. for complex [**1**]ClO$_4$: C, 52.19; H, 2.81; N, 10.74. Found: C, 52.18; H, 2.83; N, 10.76%. ^{1}H NMR data (400 MHz, in DMSO-d_6) δ_{ppm}: 8.80 (d, 1H), 8.73 (d, 1H), 8.54 (d, 2H) 8.3 (d, 1H), 8.14 (d, 2H), 8.03 (t, 2H), 7.96 (d, 1H), 7.84 (t, 2H), 7.64–7.60 (m, 3H), 7.54 (d, 1H), 7.45 (t, 2H), 7.36 (t, 2H), 7.10 (t, 2H).

2.4.2. Synthesis of the complex [*2*](ClO$_4$)$_2$

The complex [**1**]ClO$_4$ (100 mg, 0.12 mmol) was dissolved in a minimum volume of acetonitrile. To this, an aqueous $AgNO_3$ solution (0.15 M, 10 ml) was added and then heated to reflux for 1 h with constant stirring. The reaction mixture was then cool down to room temperature and filtered through a sintered glass crucible to get rid off the precipitated AgCl. After reducing the volume of the clear filtrate to ~2 ml, a pre-cooled saturated $NaClO_4$ solution (~2 ml) was added, and the resulting solution was kept in a refrigerator overnight. The precipitated complex [**2**](ClO$_4$)$_2$ was filtered off as a brown microcrystalline material. It was then dried under vacuum over P_4O_{10}. Yield: ~68%, 70 mg. Elemental *Anal.* Calc. for complex [**2**](ClO$_4$)$_2 \cdot H_2O$: C, 46.89; H, 3.45; N, 9.66. Found: C, 46.21; H, 3.33; N, 9.72%. ^{1}H NMR data (400 MHz, in DMSO-d_6) δ_{ppm}: 9.15 (d, 2H), 8.92 (d, 2H), 8.70 (d, 2H) 8.60 (t, 2H), 7.93 (d, 2H), 7.60 (t, 4H), 7.41 (d, 2H), 7.25 (t, 4H), 6.20 (d, 2H).

2.5. Crystallographic data

2.5.1. Complex [*1*](ClO$_4$)

CCDC No. 652460, $C_{34}H_{22}Cl_2N_6O_6Ru$, $M = 782.55$, orthorhombic, $a = 19.7242(3)$, $b = 15.7100(2)$, $c = 19.9264(3)$ Å, $V = 6174.54(15)$ Å^3, space group *Pbca*, $Z = 8$, $T = 298(2)$ K, μ(Mo Kα) = 0.740 mm^{-1}, $F(000) = 3152$, Goodness-of-fit = 1.033; final R indices: $R_1 = 0.0344$ [$I > 2\sigma(I)$], $wR_2 = 0.0801$; R indices (all data): $R_1 = 0.0536$, $wR_2 = 0.0898$.

2.5.2. Complex [*2*](ClO$_4$)$_2$H$_2$O

CCDC No. 652461, $C_{34}H_{22}C_{l2}N_6O_{11}Ru$, $M = 862.55$, monoclinic, $a = 8.6420(2)$, $b = 21.3292(6)$, $c = 19.0073(5)$ Å, $\beta = 91.274(2)$, $V = 3502.69(16)$ Å^3, space group $P2(1)/c$, $Z = 4$, $T = 298(2)$ K, μ (Mo Kα) = 0.671 mm^{-1}, $F(000) = 1736$, Goodness-of-fit = 0.971; final R indices: $R_1 = 0.0547$ [$I > 2\sigma(I)$], $wR_2 = 0.1362$; R indices (all data): $R_1 = 0.0823$, $wR_2 = 0.1570$.

3. Results and discussion

The tridentate ligand L has been synthesized by a modified reported route [25]. The reaction of L with the ruthenium–terpyridine precursor $Ru(trpy)Cl_3$ in ethanol initially afforded a dark solution, from which a dark colored solid mass has been isolated on addition of excess saturated aqueous $NaClO_4$ solution (Scheme 1). Chromatographic purification of the crude product on a silica gel column using a CH_3CN–CH_2Cl_2 mixture (1:4) as the eluent results in a reddish complex [**1**]$^+$ as its perchlorate salt (yield, 45%), followed by other products.

Complex [**1**]$^+$ exhibits satisfactory elemental analyses. The formulation of the complex has been further supported by FT-IR and ^{1}H NMR spectroscopy (Supplementary data, Figs. S1 and S2). The formation of [**1**]ClO$_4$ has also been authenticated by its single crystal X-ray structure.

Complex [**1**]$^+$, when heated for 1 h with constant stirring in the presence of aqueous $AgNO_3$ solution, affords complex [**2**]$^{2+}$ (Scheme 1). The formation of [**2**]$^{2+}$ was authenticated by elemental analysis, FT-IR and ^{1}H NMR spectroscopy, and by its single crystal X-ray structure.

3.1. Crystal structure analyses

X-ray quality single crystals were grown by slow diffusion of an acetonitrile solution of the complexes into benzene followed by the slow evaporation technique. The ORTEP plot of [RuL(terpy)Cl](ClO$_4$), [**1**]ClO$_4$, is shown in Fig. 1. In the monomeric complex, The Ru center is in a distorted octahedral arrangement with a RuN_5Cl coordination environment (Table 1). The largest distortion of the octahedral geometry is due to the geometrical constraints of the terpy ligand, which is shown by small N–Ru–N angles (Table 1) [26–29]. The ligand L is bonded to the metal center in a bidentate fashion. Both the central pyridine nitrogen atoms are in a *cis* orientation and the pyridine nitrogen atom of L is *trans* to the Cl^- ion. The nitrogen from one benzoxazole ring is in a *trans* position with respect to the central pyridine nitrogen of terpyridine. As a result, the second benzoxazole ring becomes distant from the ruthenium center and hence is not coordinated to the metal. The Ru–N distances are in the range 1.962(2)–2.122(19) Å. The average bite angles involving terpyridine/L in [**1**]ClO$_4$ are 79.50(4) and 78.59(13)°.

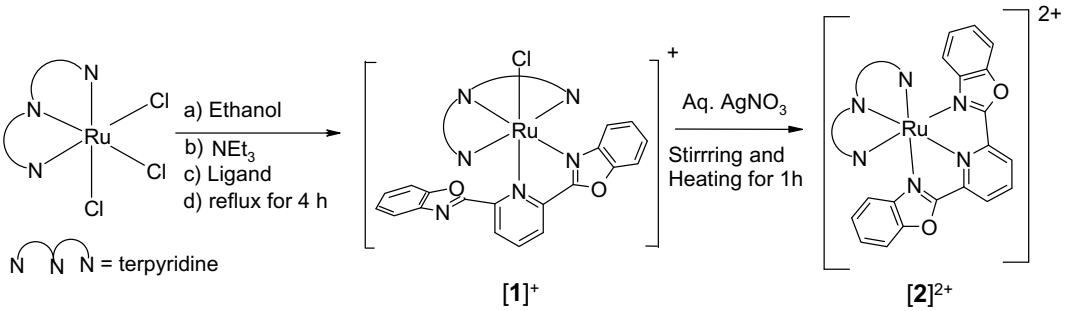

Scheme 1.

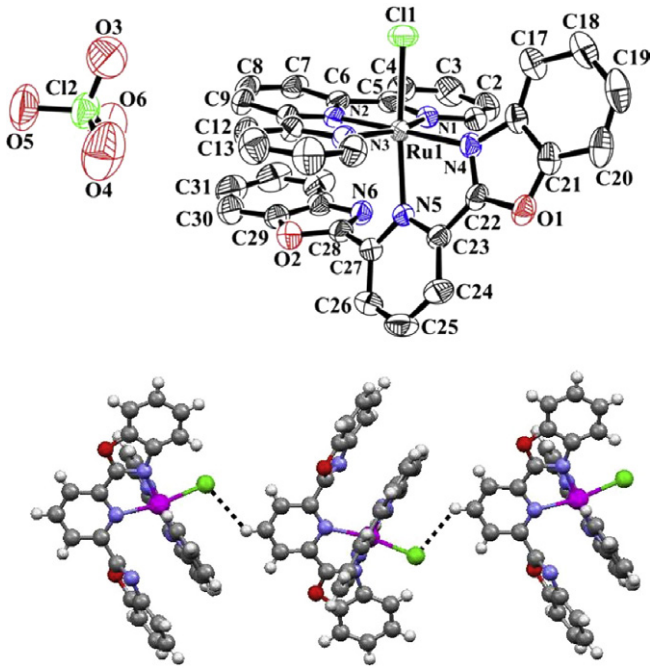

Fig. 1. ORTEP plot with 50% thermal ellipsoids (top) and an infinite chain formed by C–H···Cl interactions in complex [**1**]ClO_4.

Table 1
Selected bond lengths (Å) and bond angles (°)

	[**1**] ClO_4	[**2**]$(ClO_4)_2$. H_2O
Ru(1)–N(1)	2.064(2)	2.077(4)
Ru(1)–N(2)	1.962(2)	1.986(4)
Ru(1)–N(3)	2.069(2)	2.083(4)
Ru(1)-N(4)	2.087(2)	2.098(4)
Ru(1)–N(5)	2.122(19)	2.006(4)
Ru(1)–Cl(1)	2.381(7)	
Ru(1)–N(6)		2.075(4)
N(1)–Ru(1)–N(2)	79.58(9)	78.83(18)
N(1)–Ru(1)–N(3)	159.37(8)	157.48(17)
N(1)–Ru(1)–N(4)	103.25(8)	90.69(18)
N(1)–Ru(1)–N(5)	99.34(8)	99.94(18)
N(1)–Ru(1)–N(6)		93.88(16)
N(2)–Ru(1)–N(3)	79.83(8)	78.66(17)
N(2)–Ru(1)–N(4)	177.11(8)	104.65(16)
N(2)–Ru(1)–N(5)	102.62(8)	177.41(16)
N(2)–Ru(1)–N(6)		99.94(16)
N(3)–Ru(1)–N(4)	97.33(8)	95.66(16)
N(3)–Ru(1)–N(5)	86.33(8)	102.53(17)
N(4)–Ru(1)–N(5)	77.66(8)	77.58(17)
N(5)–Ru(1)–Cl(1)	170.20(6)	
N(5)–Ru(1)–N(6)		77.83(16)

The bond distances and angles match well with the reported analogous ruthenium–terpy complexes [26–29]. The Ru^{II}–Cl distance, 2.3815(7) Å, in [**1**]ClO_4 is comparable to that observed in [Ru(trpy)(biq)Cl]PF_6 (biq = 2,2′-bisquinoline), 2.378(2) Å [30], but is smaller than that in other Ru^{II} complexes with a N_5Cl coordination core [31–33]. The metal bonded Cl atom forms a weak intermolecular C–H···Cl type hydrogen bond with the adjacent ligand in the solid-state, which leads to the formation of an infinite chain along the crystallographic *a* axis (Fig. 1b). One of the benzoxazole rings of L is in the plane with its central pyridine ring, while the other is in an almost perpendicular orientation. In the crystal structure both the aromatic rings form π-stacking interactions, which remain in the same plane in the solid-state. It is interesting to note that the ruthenium center is separated from the outside environment and is in buried inside the hydrophobic environment. The counter anions are lined up in a zig-zag fashion along the crystallographic *a* axis. The structure contains alternate hydrophobic and hydrophilic layers (Supplementary data, Fig. S3).

The ORTEP plot of [RuL(terpy)]$(ClO_4)_2 \cdot H_2O$, [**2**]$(ClO_4)_2 \cdot H_2O$, is shown in Fig. 2. In this complex, the RuN_6 chromophore binds the ruthenium center in a distorted octahedral geometry (Table 1). The hydrogen atoms for the solvent water molecule were not located in the electron density map. The Cl^- ion in the complex [**1**]ClO_4 has been replaced by the nitrogen atom (N6) of one of the benzoxazole moieties, which was on the opposite side of the axial Cl atom in [**1**]ClO_4. Unlike in [**1**]ClO_4, here the pyridine nitrogen of the ligand is in a *trans* orientation with respect to the central pyridine nitrogen of terpyridine. Moreover, the ligand is bonded to Ru in a tridentate fashion with both benzoxazole nitrogens in axial positions. The Ru–N distances in the complex [**2**]$(ClO_4)_2 \cdot H_2O$ are in the range 1.986(4)–2.098(4) Å. The average bite angles involving terpyridine/L are 79.80(18) and 78.32(18)°. In the solid-state there are no π-stacking interactions in this complex. Similar to the complex [**1**]ClO_4, several weak C–H···O type hydrogen bonding interactions are present in the solid-state. The metal ion is also buried inside the hydrophobic core of the molecule. Perchlorate anions and water molecules form a hydrogen bonded network in complex [**2**]$(ClO_4)_2 \cdot H_2O$. The oxygen atoms of the benzoxazole unit are in the periphery of the hydrophobic sphere. In [**2**]$(ClO_4)_2 \cdot H_2O$, counter anions along with water of crystallization formed the hydrophilic hemisphere, which is in a face-to-face arrangement in alternate layers. Complex [**2**]$(ClO_4)_2 \cdot H_2O$ formed alternate rows of square boxes in the solid-state along the crystallographic *a* axis (see Supplementary data, Fig. S4).

3.2. UV–Vis spectroscopic studies

Both the complexes, $[\mathbf{1}]^+$ and $[\mathbf{2}]^{2+}$, exhibit strong MLCT transitions in the visible region in acetonitrile solvent (Fig. 3). For complex $[\mathbf{1}]^+$, a band appears at 521 nm ($\varepsilon = 5960\ M^{-1}\ cm^{-1}$) and in the case of complex $[\mathbf{2}]^{2+}$, at 452 nm ($\varepsilon = 4880\ M^{-1}\ cm^{-1}$). The

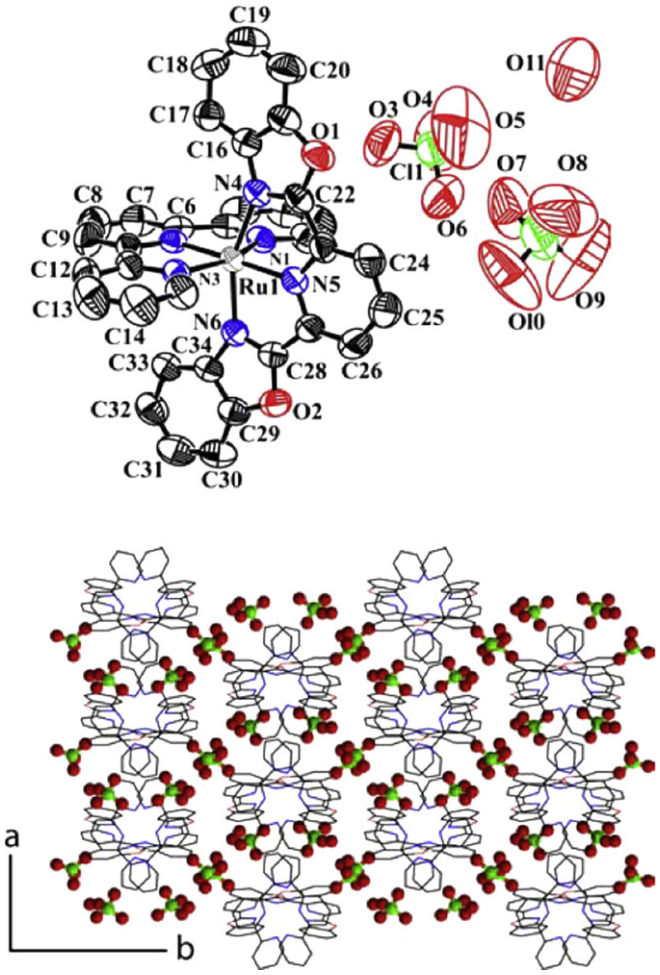

Fig. 2. ORTEP Plot with 50% thermal ellipsoids (top) and packing diagram (below) of complex $[\mathbf{2}](ClO_4)_2 \cdot H_2O$.

intra-ligand $\pi \rightarrow \pi^*$ transitions appear at 318, 272 nm ($\varepsilon = 26600$ and 17050 $M^{-1}\,cm^{-1}$) and 304, 270 nm ($\varepsilon = 23650$ and 15060 $M^{-1}\,cm^{-1}$) for complexes $[\mathbf{1}]^+$ and $[\mathbf{2}]^{2+}$, respectively. It is interesting to note that the MLCT band in $[Ru^{II}(trpy)(bbp)]^{2+}$ appears at 475 nm [trpy = 2,2′:6′,2″-terpyridine; bbp = 2,6-bis(benzimidazoly-2yl)pyridine] [34]. This may be attributed to the weaker π-acceptor properties of the ligand L compared to trpy or bbp [34].

The broad band at 1080–1100 cm^{-1} followed by a band at ~625 cm^{-1} in the FT-IR spectra of the complexes confirms the presence of the perchlorate anion (Supplementary data, Fig. S1). The molar conductivities (Λ_M) of complexes $[\mathbf{1}]^+$ and $[\mathbf{2}]^{2+}$, in acetonitrile solvent are 124 and 216 $\Omega^{-1}\,cm^2\,mol^{-1}$, respectively; which are consistent with the 1:1 and 1:2 electrolytic natures of $[\mathbf{1}]^+$ and $[\mathbf{2}]^{2+}$, respectively. The diamagnetic nature of the complexes is indicative of the presence of Ru(II) with a low-spin d^6 configuration.

3.3. ^1H NMR spectra

The ^1H NMR spectra of complexes $[\mathbf{1}]^+$ and $[\mathbf{2}]^{2+}$ were recorded in DMSO-d_6 solvent [Supplementary data, Figs. S2 and S3]. Both the complexes exhibit the calculated number of aromatic signals, overlapping between 6 and 10 ppm. In both the complexes, the symmetrical terpyridine moiety shows only six signals as expected. In $[\mathbf{1}]^+$, the ancillary ligand, L, due to its bidentate coordination mode, exhibits all eleven signals; whereas, in $[\mathbf{2}]^{2+}$, as L binds the ruthenium center in a symmetrical tridentate fashion, it shows only six signals. Attempts were not made to assign the individual signals because of the overlapping nature of the spectra.

3.4. Electrochemistry

The electron-transfer properties of the complexes $[\mathbf{1}]^+$ and $[\mathbf{2}]^{2+}$ have been studied in acetonitrile solvent versus SCE. The one electron reversible Ru^{II}/Ru^{III} couple appears at 0.90 and 1.44 V in the case of complex $[\mathbf{1}]^+$ and $[\mathbf{2}]^{2+}$, respectively. A representative voltammogram of complex $[\mathbf{1}]^+$ is shown in Fig. 4. The replacement of the strong donor chloride in $[\mathbf{1}]^+$ by the 'N'-donor from the benzoxazole derivative in $[\mathbf{2}]^{2+}$ results in the positive shift of the oxidation potential by ~0.54 V.

The same Ru^{II}/Ru^{III} couple appears at 1.30 and 1.11 V in the case of the complexes $[Ru^{II}(trpy)_2]^{2+}$ and $[Ru^{II}(trpy)(bbp)]^{2+}$, respectively [34,35]. The stronger ligand field strength of trpy compared to bbp or L results in the greater stabilization of the Ru(II) d_π orbitals. On the other hand, poly-imidazole or -oxazole derivatives are known as better σ-donors and weaker π-acceptors than polypyridine derivatives. The effect of these factors is reflected in the shift of the oxidation potential of the Ru^{II}/Ru^{III} couple.

The formation of $[\mathbf{2}](ClO_4)_2$ from $[\mathbf{1}]ClO_4$ can take place either *via* a five coordinated intermediate species [intermediate I] (dissociative mechanism) or through a dissociative interchange type reaction pathway [intermediate II] (Scheme 2).

However, when the same reaction was carried out in the presence of azide, pyridine or thiocyanate, no incorporation of the

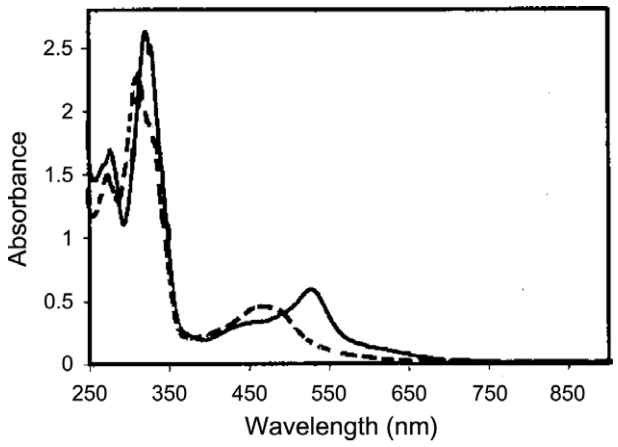

Fig. 3. UV–Vis spectra of $[\mathbf{1}]^+$ (solid line) and $[\mathbf{2}]^{2+}$ (dashed line) in acetonitrile solvent.

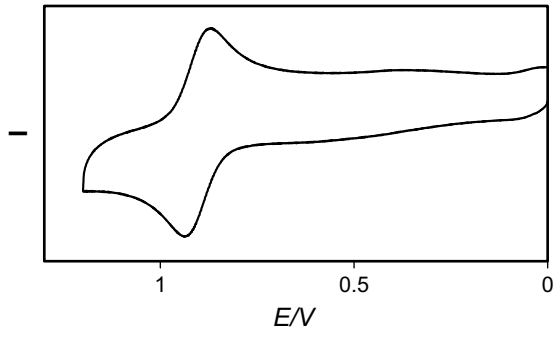

Fig. 4. Cyclic voltammogram of complex $[\mathbf{1}]^+$ in acetonitrile, SCE, TBAP supporting electrolyte, glassy carbon working electrode.

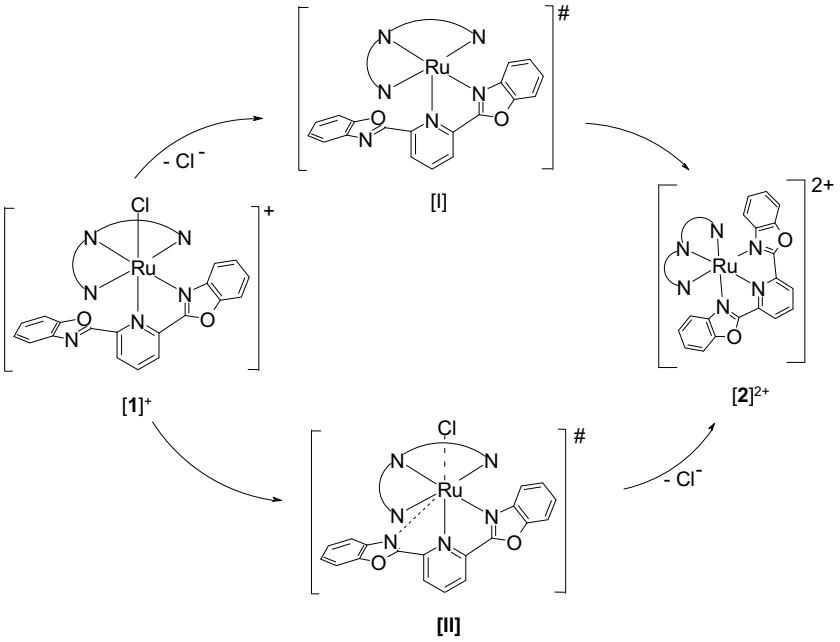

Scheme 2.

azide, pyridine or thiocyanate was found; which, in turn, indicates that the formation of $[\mathbf{2}](ClO_4)_2$ takes place through the dissociative interchange type reaction pathway rather than a dissociative mechanism which involves a pentacoordinated intermediate.

4. Conclusions

In conclusion, the present study demonstrates the synthesis, characterization, electron-transfer properties and structural aspects of a set of ruthenium monoterpyridine complexes with 2,6-bis(benzoxazol-2-yl)pyridine as an ancillary ligand. Complex $[\mathbf{1}]^+$ undergoes an intramolecular dissociative interchange type substitution in the presence of aqueous $AgNO_3$ solution to afford complex $[\mathbf{2}]^{2+}$. Complex $[\mathbf{2}]^{2+}$ represents an unique example where the ruthenium center is encapsulated by a hydrophobic and a hydrophilic hemisphere, which are in planes perpendicular to each other.

Acknowledgements

The author would like to acknowledge their sincere gratitude to the Department of Chemistry, Central Instrumentation Facility, Indian Institute of Technology Guwahati, India. We are also thankful to the Department of Science and Technology, India for the FIST funded X-ray diffractometer.

Appendix A. Supplementary data

CCDC 652460 and 652461 contain the supplementary crystallographic data for $[\mathbf{1}]ClO_4$ and $[\mathbf{2}](ClO_4)_2H_2O$. These data can be obtained free of charge via http://www.ccdc.cam.ac.uk/conts/retrieving.html, or from the Cambridge Crystallographic Data Centre, 12 Union Road, Cambridge CB2 1EZ, UK; fax: (+44) 1223-336-033; or e-mail: deposit@ccdc.cam.ac.uk. FT-IR spectra in KBr pellets, ^1H NMR spectra, H–H correlation spectra of the complexes $[\mathbf{1}]^+$ and $[\mathbf{2}]^{2+}$, the cyclic voltammogram of complex $[\mathbf{2}]^{2+}$ and the packing diagrams for both complexes. Supplementary data associated with this article can be found, in the online version, at doi:10.1016/j.poly.2008.05.022.

References

[1] F. Scandola, C.A. Bignozzi, M.T. Indelli, in: K. Kalyanasundaram, M. Gratzel (Eds.), Photosensitization and Photocatalysis Using Inorganic and Organometallic Compounds, Kluwer, Dordrecht, 1993, p. 161.
[2] K. Kalyanasundaram, Coord. Chem. Rev. 28 (1989) 2920.
[3] J.P. Sauvage, J.P. Collin, J.C. Chambron, S. Guillerez, C. Coudret, V. Balzani, F. Barigelletti, L. De Cola, L. Flamigni, Chem. Rev. 94 (1994) 993.
[4] C.M. Hartshorn, K.A. Maxwell, P.S. White, J.M. DeSimon, T.J. Meyer, Inorg. Chem. 40 (2001) 601.
[5] B. Gholamkhass, K. Koike, N. Negishi, H. Hori, K. Takeuchi, Inorg. Chem. 40 (2001) 756.
[6] A. Doveletoglou, S.A. Adeyemi, T.J. Meyer, Inorg. Chem. 35 (1996) 4127.
[7] M. Ebadi, A.B.P. Lever, Inorg. Chem. 38 (1999) 467.
[8] H. Chao, G. Yang, G.-Q. Xue, H. Li, H. Zang, I.D. Williams, L.-N. Ji, X.-M. Chen, X. -Y. Li, J. Chem. Soc., Dalton Trans. (2001) 1326.
[9] H. Sugimito, K. Tsuge, K. Tanaka, J. Chem. Soc., Dalton Trans. (2001) 57.
[10] Y.-Q. Fang, N.J. Taylor, G.S. Hanan, F. Loiseau, R. Passalacqua, S. Campagna, H. Nierengarten, D.A. Van, J. Am. Chem. Soc. 124 (2002) 7912.
[11] T.-a. Koizumi, T. Tomon, K. Tanaka, Organometallics 22 (2003) 970.
[12] M. Shiotsuki, T. Suzuki, K. Iida, Y. Ura, K. Wada, T. Kondo, T. Mitsudo, Organometallics 22 (2003) 1332.
[13] S. Bonnet, J.-P. Collin, J.-P. Sauvage, E. Schofield, Inorg. Chem. 43 (2004) 8346.
[14] J. wang, G.S. Hanan, F. Loiseau, S. Campagna, Chem. Commun. (2004) 2068.
[15] J.H. Alstrum-Acevedo, M.K. Brennaman, T.J. Meyer, Inorg. Chem. 44 (2005) 6802.
[16] S. Patra, B. Sarkar, S. Ghumaan, M.P. Patil, S.M. Mobin, R.B. Sunoj, W. Kaim, G.K. Lahiri, J. Chem. Soc., Dalton Trans. (2005) 1188.
[17] K.J. Arm, G.J.A. Williams, J. Chem. Soc., Dalton Trans. (2006) 2172.
[18] S. Ruttimann, C.M. Moreau, A.F. Williams, G. Bernardinelli, A.W. Addison, Polyhedron 11 (1992) 635.
[19] C. Piguet, B. Bocquet, E. Mueller, A.F. Williams, Helv. Chim. Acta 72 (1989) 323.
[20] K. Hutchison, J.C. Morris, T.A. Nile, J.L. Walsh, D.W. Thompson, J.D. Petersen, J.R. Schoonover, Inorg. Chem. 38 (1999) 2516.
[21] D.T. Sawyer, A. Sobkowiak, J.L. Roberts Jr., Electrochemistry for Chemists, 2nd ed., Wiley, New York, 1995.
[22] G.M. Sheldrick, SHELXS-97, University of Gottingen, Germany, 1997.
[23] G.M. Sheldrick, SADABS: Software for Empirical Absorption Correction, University of Gottingen, Institut fur Anorganische Chemieder Universitat, Tammanstrasse 4, D-3400 Gottingen, Germany, 1999–2003.
[24] L.J. Farrugia, J. Appl. Crystallogr. 30 (1997) 565.
[25] A.W. Addison, P.J. Burke, J. Heterocycl. Chem. 12 (1981) 4455.
[26] S. Sarkar, B. Sarkar, N. Chanda, S. Kar, S.M. Mobin, J. Fiedler, W. Kaim, G.K. Lahiri, Inorg. Chem. 44 (2005) 6092.

[27] N. Chanda, D. Paul, S. Kar, S.M. Mobin, A. Datta, V.G. Puranik, K.K. Rao, G.K. Lahiri, Inorg. Chem. 44 (2005) 3499.
[28] N. Chanda, S.M. Mobin, V.G. Puranik, A. Datta, M. Niemeyer, G.K. Lahiri, Inorg. Chem. 43 (2004) 1056.
[29] B. Mondal, V.G. Puranik, G.K. Lahiri, Inorg. Chem. 41 (2002) 5813.
[30] A.M.E. Boelrijk, J. Reedijk, J. Mol. Catal. 89 (1994) 63.
[31] B. Mondal, M.G. walawalkar, G.K. Lahiri, J. Chem. Soc., Dalton Trans. (2000) 4209.
[32] C.J. Cathey, E.C. Constable, M.J. Hannon, D.A. Tocher, M.D. Ward, J. Chem. Soc., Chem. Commun. (1990) 621.
[33] R.J. Forster, A. Boyle, J.G. Vos, R. Hage, A.H.J. Dijkhuis, R.A.G. DeGraff, J.G. Haasnoot, R. Prins, J. Reedijk, J. Chem. Soc., Dalton Trans. (1990) 121.
[34] D. Mishra, A. Barbieri, C. Sabatini, M.G.B. Drew, H.M. Figgie, W.S. Sheldrick, S.K. Chattopadhyay, Inorg. Chim. Acta 360 (2007) 2231.
[35] R.P. Thummel, S. Chirayil, Inorg. Chim. Acta 154 (1988) 77.

Polyhedron 27 (2008) 2569–2576

Contents lists available at ScienceDirect

Polyhedron

journal homepage: www.elsevier.com/locate/poly

Mononuclear and dinuclear iron thiocyanate and selenocyanate complexes of tris-pyrazolylmethane ligands

A. Abibat Salaudeen, Colin A. Kilner, Malcolm A. Halcrow *

School of Chemistry, University of Leeds, Woodhouse Lane, Leeds LS2 9JT, UK

ARTICLE INFO

Article history:
Received 5 February 2008
Accepted 13 May 2008
Available online 17 June 2008

Keywords:
Iron
Dinuclear complexes
Crystal structure
Magnetic properties

ABSTRACT

Treatment of $Fe(NCE)_2$ (E = S or Se) with 1 equiv. of tris-(3,5-dimethylpyrazol-1-yl)methane (tpm′) yields dimeric $[\{Fe(NCE)(\mu\text{-}NCE)(tpm')\}_2]$. These dimers are cleaved in MeCN solution, yielding isolable $[Fe(NCE)_2(tpm')(NCMe)]$, whose solvent ligands can be substituted by moderately basic heterocycle donors to give $[Fe(NCE)_2(tpm')(py)]$, $[Fe(NCS)_2(tpm')(im)]$ or $[\{Fe(NCE)_2(tpm')\}_2(\mu\text{-}4,4'\text{-bipy})]$. The monodentate heterocycles in the latter compounds are readily lost in most solvents, regenerating the dimeric starting materials. $[Fe(NCS)_2(tpm')(py)]$ was also prepared by reacting $[Fe(NCS)_2(py)_4]$ with tpm′. The mononuclear compounds are all high-spin between 5 and 300 K, despite mostly having regular coordination geometries and tpm′ ligand conformations that should in principal favour spin-crossover. Analogous products containing unsubstituted tris-(pyrazol-1-yl)methane (tpm) could not be isolated, but the crystal structure of the double salt $[Fe(tpm)_2][Fe(NCS)_5(py)]$, containing a new iron(III) anion, is described.

© 2008 Elsevier Ltd. All rights reserved.

1. Introduction

There is strong continued interest in the synthesis and structural and physical chemistry of spin-crossover materials, whose magnetic moment, dielectric constant and colour can all be switched reversibly upon application of temperature, light or other physical stimuli [1]. By far the majority of spin-crossover research is performed using six-coordinate iron(II) complexes of N-donor ligands, since that is the metal–ligand combination that most reliably exhibits the phenomenon, and is most likely to show novel physical behaviour when it does. Most known spin-crossover compounds of this type can be grouped into two classes, of formula $[FeL_6]^{2+}$ (where L is an amine or imine ligand, or an N-donor group in a larger polydentate ligand framework) or $[Fe(NCE)_2L_4]$ (where $NCE^- = NCS^-$, $NCSe^-$ or another N-donor pseudohalide) [2]. With this in mind, as part of our own continuing research in this area [3] we decided to pursue complexes of formula $[Fe(NCE)_2(tpm)L]$. We were particularly interested in polynuclear compounds containing multiple $[Fe(NCE)_2(tpm)]$ centres linked by bridging heterocyclic ligands, whose iron centres could undergo spin-crossover independently of each other. The interplay between covalently linked spin centres in spin-crossover compounds can lead to unusual cooperative switching behaviour that is not found in mononuclear complexes [4].

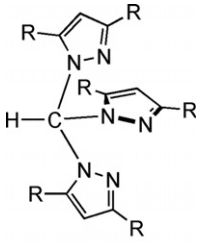

Several iron complexes of tris-pyrazolylmethane ligands are known. Salts of $[Fe(tpm)_2]^{2+}$ are low-spin at room temperature but can undergo thermal spin-transitions on heating [5–9]. Several homoleptic complexes of analogous ligands substituted at the pyrazole rings also undergo spin-crossover, at reduced temperatures that are more tractable for detailed study [9–11]. Heteroleptic half-sandwich complexes of tris-pyrazolylmethane coligands are less common, although mononuclear $[Fe(tpm)(solv)_3]^{2+}$ (solv = H_2O or CH_3CN) [12], $[Fe(tpm)(NCS)_2]$ [5,6] and a small number of dinuclear and polynuclear complexes containing $[Fe(tpm)]^{2+}$ centres [13,14] have been reported. All of the latter are high-spin at room temperature and below, where that has been measured.

* Corresponding author. Fax: +44 113 343 6565.
E-mail address: M.A.Halcrow@leeds.ac.uk (M.A. Halcrow).

0277-5387/$ - see front matter © 2008 Elsevier Ltd. All rights reserved.
doi:10.1016/j.poly.2008.05.013

2. Experimental

All manipulations were carried out in air, using undried reagent-grade solvents. Tris(3,5-dimethylpyrazol-1-yl)methane (tpm′) [15], $[Fe(NCS)_2(py)_4]$ [16] and $[Fe(NCS)_2(pyz)_2]$ [17] were prepared by the reported methods, while all other organic and inorganic reagents were purchased commercially and used as supplied.

2.1. Synthesis of [{Fe(NCS)(μ-NCS)(tpm′)}$_2$] (**1**)

A methanolic solution (40 cm^3) of $Fe[ClO_4]_2 \cdot 6H_2O$ (1.45 g, 4.0 mmol) and a pinch of ascorbic acid was added gradually to a solution of NaNCS (0.64 g, 8.0 mmol) in MeOH (80 cm^3). Tpm′ (1.19 g, 4.0 mmol) in MeOH (40 cm^3) was added to the solution, yielding a white precipitate. This was collected by filtration, washed with MeOH and dried under reduced pressure. Yield 1.10 g, 58%. Calc. for $C_{36}H_{44}Fe_2N_{16}S_4$: C, 46.0; H, 4.71; N, 23.8; S, 13.6. Found: C, 45.6; H, 4.65; N, 23.5; S, 13.4%. ESMS: *m*/*z* 882 $[^{56}Fe_2(tpm')_2(NCS)_3]^+$, 412 $[^{56}Fe(tpm')(NCS)]^+$. IR (Nujol): 2115, 2076 (ν{N=CS}) cm^{-1}.

2.2. Synthesis of [{Fe(NCSe)(μ-NCSe)(tpm′)}$_2$] (**2**)

Method as for (**1**), using KNCSe (1.15 g, 8.0 mmol). The product precipitated from MeOH as an off-white powder. Yield 1.48 g, 65%. Calc. for $C_{36}H_{44}Fe_2N_{16}Se_4$: C, 38.3; H, 3.93; N, 19.9. Found: C, 38.1; H, 3.90; N, 19.6%. ESMS: *m*/*z* 1024 $[^{56}Fe_2(tpm')_2(NCSe)_3]^+$. IR (Nujol): 2115, 2081 (ν{N=CSe}) cm^{-1}.

2.3. Synthesis of [Fe(NCS)$_2$(tpm′)(CH$_3$CN)] · H$_2$O (**3** · H$_2$O)

A solution of **1** (0.24 g, 0.25 mmol) in acetonitrile (30 cm^3) was refluxed for 90 min. The solution was cooled to room temperature and concentrated to *ca.* 5 cm^3 volume. Slow diffusion of diethyl ether vapour through the filtered solution gave pale brown crystals of the product, contaminated by unreacted **1** as a white powder that was removed by decantation. Yield 0.11 g, 49%. Calc. for $C_{20}H_{25}FeN_9S_2 \cdot H_2O$: C, 45.4, H, 5.14; N, 23.8; S, 12.1. Found: C, 45.7; H, 5.15; N, 24.2; S, 12.3%. ESMS: *m*/*z* 882 $[^{56}Fe_2(tpm')_2(NCS)_3]^+$, 412 $[^{56}Fe(tpm')(NCS)]^+$. IR (Nujol): 2304, 2271 (ν{N≡CCH$_3$}), 2083 (ν{N=CS}) cm^{-1}.

2.4. Synthesis of [Fe(NCSe)$_2$(tpm′)(CH$_3$CN)] (**4**)

Method as for **3**, starting from **2** (0.28 g, 0.25 mmol). The product formed pale yellow crystals from MeCN/Et$_2$O. Yield 0.11 g, 45%. Calc. for $C_{20}H_{25}FeN_9Se_2$: C, 39.7; H, 4.16; N, 20.8. Found: C, 39.9; H, 4.30; N, 21.0%. ESMS: *m*/*z* 458 $[^{56}Fe(tpm')(NCSe)]^+$. IR (Nujol): 2302, 2270 (ν{N≡CCH$_3$}), 2083 (ν{N=CSe}) cm^{-1}.

2.5. Synthesis of [Fe(NCS)$_2$(tpm′)(py)] (**5**)

2.5.1. Method A

Solutions of tpm′ (0.30 g, 1.0 mmol) and $[Fe(NCS)_2(py)_4]$ (0.49 g, 1.0 mmol) in dichloromethane (both 25 cm^3) were slowly mixed at room temperature, and the resultant solution heated to reflux for 40 min. The cooled, violet solution was concentrated to *ca.* 10 cm^3, and filtered. Slow diffusion of excess diethyl ether vapour into the solution gave dark red crystals of the product. Yield 0.42 g, 85%. Calc. for $C_{23}H_{27}FeN_9S_2$: C, 50.3; H, 4.95; N, 22.9; S, 11.7%. Found: C, 50.0; H, 4.90; N, 23.0; S, 11.5%. ESMS: *m*/*z* 412 $[^{56}Fe(tpm')(NCS)]^+$. IR (Nujol): 2071 (ν{N=CS}) cm^{-1}.

2.5.2. Method B

Solutions of pyridine (0.12 g, 1.5 mmol) in acetonitrile (10 cm^3), and of **1** (0.24 g, 0.25 mmol) in acetonitrile (20 cm^3), were slowly mixed, and the resultant solution was refluxed for 30 min. The cooled solution was concentrated to *ca.* 5 cm^3 volume and filtered. Slow diffusion of diethyl ether vapour into the solution afforded yellow microcrystals. Yield 0.14 g, 51%. Calc. for $C_{23}H_{27}FeN_9S_2$: C, 50.3; H, 4.95; N, 22.9; S, 11.7. Found: C, 50.3; H, 4.95; N, 23.1; S, 11.6%. ESMS: *m*/*z* 412 $[^{56}Fe(tpm')(NCS)]^+$. IR (Nujol): 2070, 2093 (ν{N=CS}) cm^{-1}.

Table 1
Experimental details for the single crystal structure determinations in this work

	3 · 2CH$_3$CN	**4** · 2CH$_3$CN	**5**	**7**	**9** · 4CH$_3$CN	**10** · 2CH$_3$CN
Molecular formula	$C_{24}H_{31}FeN_{11}S_2$	$C_{24}H_{31}FeN_{11}Se_2$	$C_{23}H_{27}FeN_9S_2$	$C_{21}H_{26}FeN_{10}S_2$	$C_{54}H_{64}Fe_2N_{22}Se_4$	$C3_4H_{31}Fe_2N_{20}S_5$
M_r	593.57	687.37	549.51	538.49	1448.81	991.79
Crystal size (mm)	0.27 × 0.19 × 0.06	0.27 × 0.19 × 0.06	0.37 × 0.26 × 0.13	0.35 × 0.18 × 0.18	0.25 × 0.16 × 0.13	0.28 × 0.16 × 0.03
Crystal system	monoclinic	monoclinic	orthorhombic	monoclinic	monoclinic	triclinic
Space group	$P2_1/c$	$P2_1/c$	$Pbcn$	Pc	$P2_1/c$	$P\bar{1}$
a (Å)	20.1302(3)	20.329(4)	13.9471(8)	11.8189(9)	10.5104(1)	10.7022(11)
b (Å)	8.2149(2)	8.3348(17)	18.0365(11)	13.8628(10)	18.6983(3)	13.2986(13)
c (Å)	20.2154(3)	20.501(4)	44.403(3)	17.8777(14)	16.4693(3)	16.2971(16)
α (°)						80.012(4)
β (°)	119.1000(10)	119.29(3)		110.193(5)	101.8905(6)	79.139(5)
γ (°)						77.033(4)
V (Å^3)	2920.99(9)	3029.4(11)	11169.9(12)	2749.1(4)	3167.20(8)	2198.9(4)
Z	4	4	16	4	2	2
T (K)	150(2)	150(2)	150(2)	150(2)	150(2)	150(2)
ρ_{calc} (g cm^{-3})	1.350	1.507	1.307	1.301	1.519	1.498
μ (mm^{-1})	0.694	2.934	0.718	0.729	2.811	0.950
Measured reflections	40078	70731	233433	54849	50024	68210
Independent reflections	6688	7732	16684	11769	7270	16435
R_{int}	0.064	0.036	0.034	0.054	0.105	0.029
Observed reflections [$I > 2\sigma(I)$]	5257	6136	12600	9430	5539	12502
Data, restraints, parameters	6688, 0, 352	7732, 0, 352	16684, 0, 643	11769, 2, 625	7270, 6, 406	16435, 0, 555
$R(F)$[a], $wR(F^2)$[b]	0.038, 0.109	0.030, 0.075	0.049, 0.127	0.039, 0.089	0.038, 0.096	0.038, 0.093
Goodness-of-fit	1.028	1.029	1.116	1.013	1.021	1.019
$\Delta\rho_{min}$, $\Delta\rho_{max}$ (e Å^{-3})	−0.50, 0.48	−1.03, 1.04	−0.74, 0.80	−0.29, 0.47	−0.76, 0.81	−1.10, 1.35
Flack parameter				−0.020(10)		

[a] $R = \sum[|F_o| - F_c|]/\sum|F_o|$.
[b] $wR = [\sum w(F_o^2 - F_c^2)/\sum wF_o^4]^{1/2}$.

2.6. Synthesis of [Fe(NCSe)$_2$(tpm′)(py)] (**6**)

Method B for **5** was followed, using **2** (0.28 g, 0.25 mmol). Slow diffusion of diethyl ether vapour into the filtered reaction mixture gave yellow crystals of the product. Yield 0.16 g, 58%. Calc. for $C_{23}H_{27}FeN_9Se_2$: C, 42.9; H, 4.23; N, 19.6. Found: C, 43.1; H, 4.20; N, 19.7%. ESMS: *m*/*z* 458 [^{56}Fe(tpm′)(NCSe)]$^+$. IR (Nujol): 2076 (ν{N=CSe}) cm^{-1}.

2.7. Synthesis of [Fe(NCS)$_2$(tpm′)(im)] (**7**)

A solution of imidazole (0.10 g, 1.5 mmol) in acetonitrile (10 cm^3) was gradually added to a solution of **1** (0.24 g, 0.25 mmol) in acetonitrile (20 cm^3). The resultant solution was refluxed for 30 min, then cooled and concentrated to *ca.* 5 cm^3 volume. Slow diffusion of diethyl ether vapour into the filtered solution afforded red crystals. Yield 0.09 g, 37%. Calc. for $C_{21}H_{26}FeN_{10}S_2$: C, 46.8; H, 4.87; N, 26.0; S, 11.9. Found: C, 47.0; H, 4.90; N, 26.1; S, 11.8%. ESMS: *m*/*z* 412 [^{56}Fe(tpm′)(NCS)]$^+$. IR (Nujol): 2070 (ν{N=CS}) cm^{-1}.

2.8. Synthesis of [{Fe(NCS)$_2$(tpm′)}$_2$(μ-4,4′-bipy)] · H$_2$O (**8** · H$_2$O)

Method as for **7**, using, 4′-bipy (0.16 g, 1.0 mmol). Slow diffusion of diethyl ether vapour into the filtered reaction mixture gave dark red crystals. Yield 0.11 g, 45%. Calc. for $C_{46}H_{52}Fe_2N_{18}S_4 \cdot H_2O$: C, 49.6; H, 4.88; N, 22.6; S, 11.5. Found: C, 49.6; H, 4.75; N, 22.2; S, 11.5%. ESMS: *m*/*z* 882 [^{56}Fe$_2$(L)$_2$(NCS)$_3$]$^+$. IR (Nujol): 2079, 2058 (ν{N=CS}) cm^{-1}.

2.8.1. Synthesis of [{Fe(NCSe)$_2$(tpm′)}$_2$(μ-4,4′-bipy)] (**9**)

Method as for **7**, using **2** (0.28 g, 0.25 mmol) and 4,4′-bipy (0.16 g, 1.0 mmol). The product formed orange crystals from acetonitrile/diethyl ether. Yield 0.19 g, 60%. Calc. for $C_{46}H_{52}Fe_2N_{18}Se_4$: C, 43.0; H, 4.08; N 19.6. Found: C, 43.0; H, 4.35; N, 19.9%. ESMS: *m*/*z* 1024 [^{56}Fe$_2$(tpm′)$_2$(NCSe)$_3$]$^+$. IR (Nujol): 2061 (ν{N=CSe}) cm^{-1}.

2.9. Single crystal X-ray structure determinations

Single crystals of [Fe(tpm)$_2$][Fe(NCS)$_5$(py)] · 2CH$_3$CN (**10** · 2CH$_3$CN) were obtained from a reaction of [Fe(NCS)$_2$(py)$_4$] and 1 equiv. tpm in acetonitrile, following method A described above for **5**. Slow diffusion of diethyl ether vapour into the concentrated reaction mixture yielded a small number of dark red crystals, contaminated by a sticky white impurity. All other single crystals in this work were grown by slow diffusion of diethyl ether vapour into acetonitrile solutions of the preformed products. Experimental details for the structure determinations are given in Table 1. Diffraction data for **3** · 2CH$_3$CN and **9** · 4CH$_3$CN were

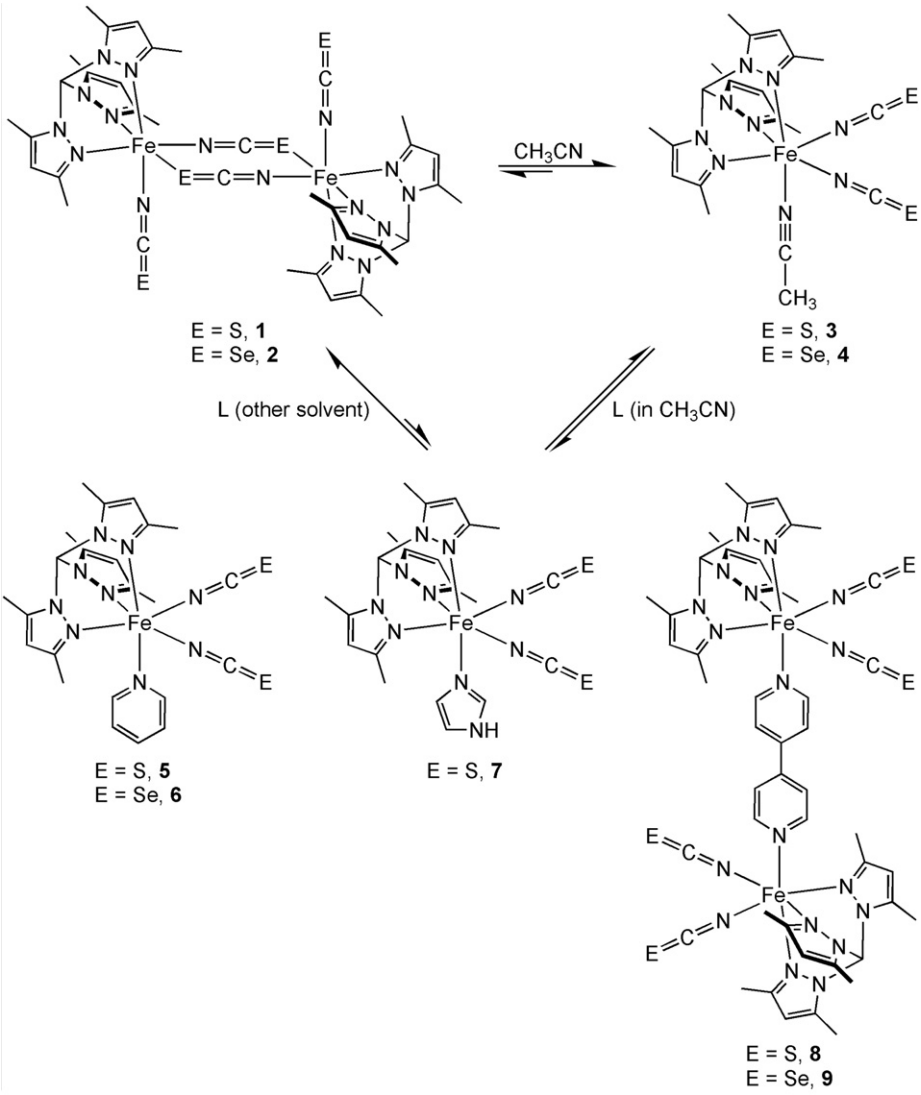

Scheme 1. Solution stabilities of the [Fe(NCE)$_2$(tpm′)L] complexes in this work.

measured on a Nonius KappaCCD area detector diffractometer, using graphite-monochromated Mo Kα radiation (λ = 0.71073 Å) from a sealed tube source. The other four datasets were obtained using a Bruker X8 Apex diffractometer using graphite-monochromated Mo Kα radiation generated by a rotating anode. The structures were all solved by direct methods [18], then developed by least squares refinement on F^2 [19].

The asymmetric units of **5** and **7** contain two unique molecules, labelled 'A' and 'B', while that of **9** · $4CH_3CN$ contains half a formula unit with the 4,4′-bipy ligand spanning the crystallographic inversion centre at 1/2, 1/2, 1/2. There are two half-cations in the asymmetric unit of **10** · $2CH_3CN$, also labeled 'A' and 'B', whose iron atoms lie on the inversion centres 0, 1/2, 0 and 1/2, 1/2, 1/2, and a complete anion lying on a general position. One of the two unique solvent molecules in **9** · $4CH_3CN$ is disordered over two equally occupied sites, which were refined using the fixed restraints C–C = 1.45(2), C≡N = 1.14(2) and 1,3-C···N = 2.59(2) Å. No disorder was detected in any of the other structures. All non-H atoms in all six structures were refined anisotropically, and all H atoms were placed in calculated positions and refined using a riding model, with methyl group torsions allowed to refine freely.

3. Other measurements

Electrospray mass spectra were obtained using a Waters Micromass LCT TOF spectrometer, from MeCN solution. C, H, N and S microanalyses were performed by the University of Leeds Department of Chemistry microanalytical service. NMR spectra were obtained using a Bruker DPX300 spectrometer, operating at 300.1 MHz (^{1}H) or 75.5 MHz (^{13}C). Infra-red spectra were obtained as KBr disks, between 400 and 4000 cm^{-1} using a Nicolet Avatar 360 spectrophotometer. Variable temperature magnetic susceptibility measurements were obtained in the solid state using a Quantum Design SQUID magnetometer in an applied field of 1000 G. Diamagnetic corrections for the sample (from Pascal's constants [20]) and the sample holder were applied to the data.

4. Results and discussion

Our first approach towards this work was to react tpm or tpm′ with preformed iron(II) thiocyanato precursors. Treatment of $[Fe(NCS)_2(py)_4]$ (py = pyridine) [16] with 1 equiv. of tpm′ in refluxing CH_2Cl_2 yielded dark red crystalline $[Fe(NCS)_2(tpm')(py)]$ (compound **5**, see below) in 85% yield. A similar reaction using tpm did not afford a clean product, however. Some insight into this result was provided when recrystallisation of the crude product from MeCN/Et_2O gave a small number of crystals, of formula $[Fe^{II}(tpm)_2][Fe^{III}(NCS)_5(py)] \cdot 2CH_3CN$ (see below). Although we were unable to isolate a bulk sample of that compound in pure form, it is clearly the product of a ligand disproportionation reaction, with concomitant aerobic oxidation of a fraction of the iron content of the sample. Since the desired product in this initial study (**5**) was obtained using tpm′ but not tpm, the subsequent work described below employed exclusively tpm′ as tridentate ligand. No reaction was observed between $[Fe(NCS)_2(pyz)_2]$ (pyz = pyrazine) [17] and either tpm or tpm′, in CH_2Cl_2 or MeCN. This presumably reflects the insolubility of that 3D coordination polymer iron(II) starting material [21].

In order to find a more general route to $[Fe(NCE)_2(tpm')L]$ (E = S, Se) compounds, the base-free starting materials "$[Fe(NCE)_2(tpm')]$" were synthesised by reacting tpm′ in MeOH with 1 equiv. of $Fe(NCE)_2$ (formed *in situ* from $[Fe[ClO_4]_2 \cdot 6H_2O$ and 2 equiv. NaNCS or KNCSe, in the presence of ascorbic acid to inhibit aerial oxidation of the iron). The white solid products precipitated from the reaction mixtures in *ca.* 60% yield. We assign dinuclear structures to these products, $[\{Fe(NCE)(\mu\text{-}NCE)(tpm')\}_2]$ (E = S, **1**; E = Se, **2**) for two reasons. First, is the observation of a very strong molecular ion corresponding to $[Fe_2(NCE)_3(tpm')_2]^+$ by electrospray mass spectrometry, at m/z = 992 for **1** (E = S) and 1024 for **2** (E = Se). Second, is the presence of two strong peaks in the triple bond region of their IR spectra, one at 2076–2081 cm^{-1} and the other at 2115 cm^{-1}. These can be assigned to the ν{CN} stretches from terminal and bridging thiocyanato or selenocyanato groups, respectively [22]. In that regard, the IR spectra resemble that of the only comparable dinuclear iron(II) compound to have been crystallographically characterised, $[\{Fe(NCS)(\mu\text{-}NCS)(Me_3tacn)\}_2]$ (Me_3tacn = 1,4,7-trimethyl-1,4,7-triazacyclononane), which exhibits ν{CN} = 2020 and 2070 cm^{-1} [23]. While crystalline $[\{Fe(NCNCN)(\mu\text{-}NCNCN)(tpm)\}_2]$ has a similar dinuclear structure to that proposed for **1** and **2** [13], syntheses of apparently distinct forms of $[Fe(NCS)_2(tpm)]$ with mononuclear (ν{CN} = 2058 cm^{-1}) [6] and "polymeric" (2060, 2095 and 2105 cm^{-1}) structures [5] have been

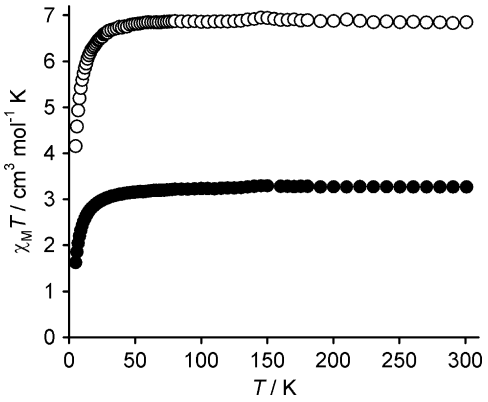

Fig. 1. Variable temperature magnetic data for **5** (red form, ●) and **8** · H_2O (○). Data from **6** and **7** are essentially identical to those of **5**, while the behaviour of **9** closely resembles that of **8** · H_2O.

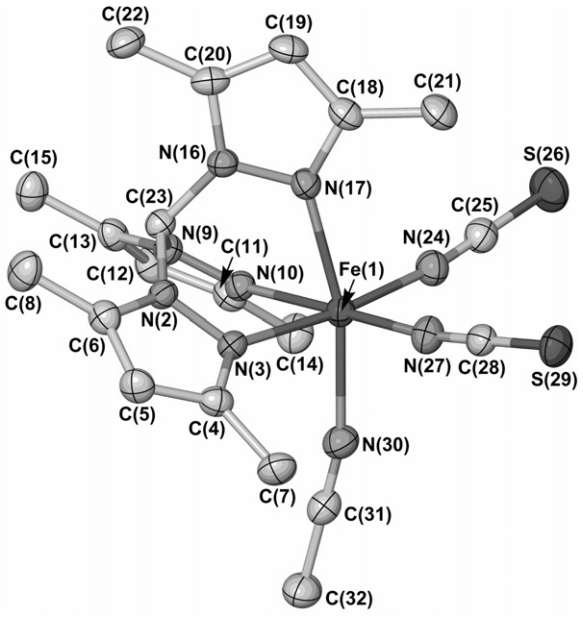

Fig. 2. View of the $[Fe(NCS)_2(tpm')(NCCH_3)]$ molecule in the crystal structure of **3** · $2CH_3CN$. All H atoms have been removed, and thermal ellipsoids are at the 50% probability level. The $[Fe(NCSe)_2(tpm')(NCCH_3)]$ molecule in **4** · $2CH_3CN$ is visually indistinguishable from the one shown, and uses the same atom numbering scheme with 'S' replaced by 'Se'.

reported before. Notably, the IR spectra of both the latter materials are quite distinct from those of **1** and **2**.

Recrystallisation of **1** or **2** from MeCN/Et_2O affords isostructural, solvated crystals of [Fe(NCE)$_2$(tpm′)(NCCH$_3$)] (E = S, **3**; E = Se, **4**), showing that the $[Fe_2(\mu\text{-NCE})_2]^{2+}$ bridges in **1** and **2** can be cleaved by Lewis bases. Compound **4** is obtained in pure form by this method but **3** is always contaminated by unreacted **1**, that can be removed from the freshly prepared crystals by decantation. Treatment of **1** or **2** with a 3-fold excess of pyridine, imidazole or 4,4′-bipyridine in refluxing MeCN affords polycrystalline [Fe(NCE)$_2$(tpm′)(py)] (E = S, **5**; E = Se, **6**), [Fe(NCS)$_2$(tpm′)(im)] (**7**; im = imidazole) and [{Fe(NCE)$_2$(tpm′)}$_2$(μ-bipy)] (E = S, **8**; E = Se, **9**) after the usual work-up. Reaction of **2** with imidazole gave an impure product, for reasons that are unclear, while reactions using pyrazine (pyz) as base afforded **3** and **4** instead of the desired [Fe(NCE)$_2$(tpm′)(pyz)] or [{Fe(NCE)$_2$(tpm′)}$_2$(μ-pyz)]. The choice of solvent is important in these reaction, since analogous procedures carried out in CH_2Cl_2, $CHCl_3$ or $MeNO_2$ led to unchanged **1** and **2** as the only isolable products. Recrystallisation of preformed **3**-**9** from a chlorinated solvent also caused their decomposition to **1** or **2**.

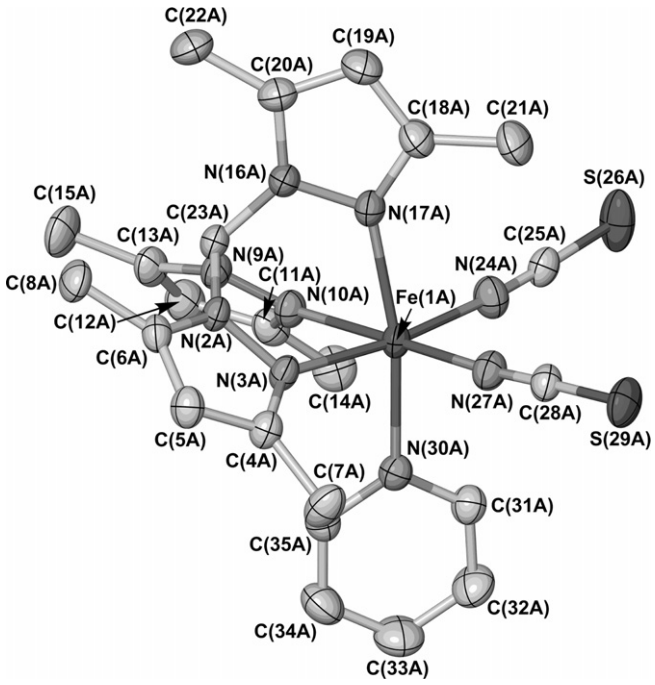

Fig. 3. View of the [Fe(NCS)$_2$(tpm′)(py)] molecule A in the crystal structure of **5**. All H atoms have been removed, and thermal ellipsoids are at the 50% probability level. Molecule B shows only small visual differences from molecule A, and uses the same atom numbering scheme.

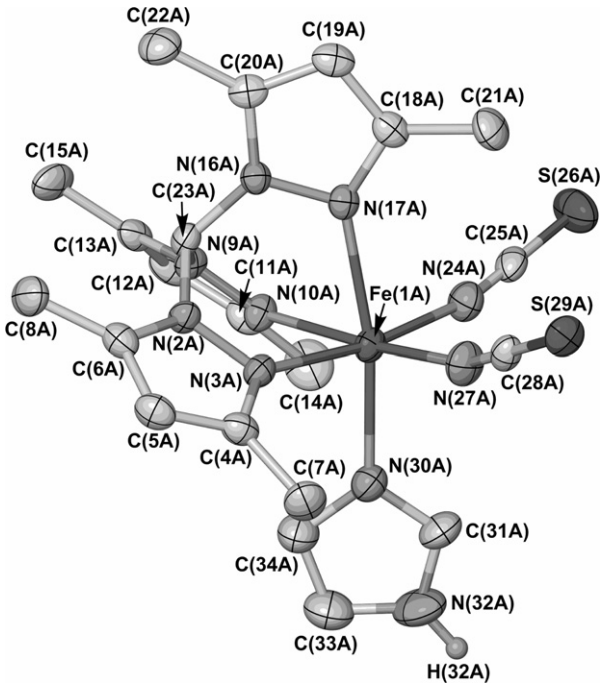

Fig. 4. View of the [Fe(NCS)$_2$(tpm′)(im)] molecule A in the crystal structure of **7**. All C-bound H atoms have been removed, and thermal ellipsoids are at the 50% probability level. Molecule B shows only small visual differences from molecule A, and uses the same atom numbering scheme.

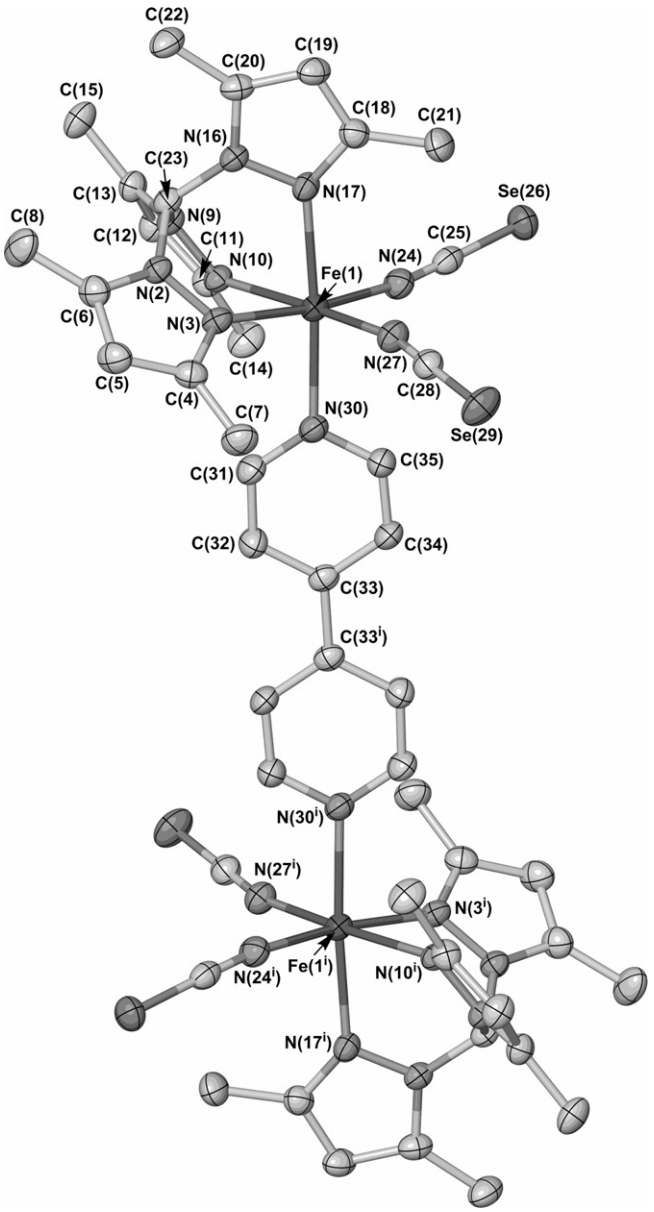

Fig. 5. View of the [{Fe(NCSe)$_2$(tpm′)}$_2$(μ-4,4′-bipy)] molecule in the crystal structure of **9** · 4CH$_3$CN. All H atoms have been removed, and thermal ellipsoids are at the 50% probability level. Symmetry code: (i) $1-x$, $1-y$, $1-z$.

These results imply that the monodentate 'L' ligand in [Fe(NCE)$_2$(tpm′)L] is only weakly coordinated and is readily lost in solution, leading to precipitation of sparingly soluble **1** and **2** from most solvents (Scheme 1). In acetonitrile solution the weakly binding solvent is present in large excess, and the more soluble **3** and **4** are the dominant species in that solvent. The CH_3CN ligand in **3** and **4** is itself substituted by stronger bases, so that **5**–**9** can be crystallised from acetonitrile but not from other solvents (Scheme 1). Presumably, pyrazine is not basic enough to displace CH_3CN from **3** and **4** under these conditions.

Interestingly, **5** was isolated in two crystal forms from different solvents, with red and yellow colouration (the crystal structure described below is of the red crystals). Both forms are solvent-free by microanalysis, but show slightly different IR spectra (see below). In the absence of a crystal structure of the yellow polymorph, the cause of their different colouration is unclear.

The dried solids **3**–**9** all analyse cleanly as the solvent-free compounds, except for **3** and **8** whose microanalyses are more consistent with monohydrate formulations, **3** · H_2O and **8** · H_2O. The water content in **3** · H_2O presumably arises from partial replacement of the lattice solvent in freshly prepared crystals (see below) by atmospheric moisture upon exposure to air. Their Nujol mull IR spectra all contain one strong ν{CN} vibration at between 2058 and 2093 cm^{-1}, except for the yellow form of **5** and **8** · H_2O where two peaks were seen in this range. These values are typical for high-spin iron(II) isothiocyanato and isoselenocyanato complexes [21,24]. The weak doublet in the triple bond region expected from a coordinated acetonitrile molecule was also present in the IR spectra of **3** · H_2O and **4**, around 2270 and 2303 cm^{-1} [25]. Electrospray mass spectra of **3** · H_2O–**9** all show the molecular ions $[Fe_2(NCE)_3(tpm')_2]^+$ and/or $[Fe(NCE)(tpm')]^+$ only, with no peaks attributable to the parent octahedral adducts being observed. Their paramagnetic ^{1}H NMR spectra in $CDCl_3$ are also unusually broadened for high-spin iron(II) species, and could not be unambiguously analysed. Both these latter observations are consistent with our conclusion, that the monodentate ligands in these compounds are very labile in solution.

Variable temperature magnetic measurements were performed on powder samples of **5**–**9**. All the compounds show an effectively constant $\chi_M T$ between 50 and 300 K, at 3.3–3.4 cm^3 mol^{-1} K for **5**–**7** and 6.7–6.8 cm^3 mol^{-1} K for **8** · **H_2O** and **9** (Fig. 1). These are typical values for high-spin mononuclear and dinuclear iron(II) centres, and their invariability over this temperature range shows the compounds all remain high-spin on cooling [20]. In all cases, $\chi_M T$ decreases increasingly rapidly on further cooling below 50 K, which is not caused by a spin-transition but reflects zero-field splitting of the $S = 2$ iron spin manifold [20]. Notably there is no unambiguous evidence for superexchange between the iron centres in **8** · H_2O and **9**, which must therefore be very weak. That is reasonable, given that the only intramolecular pathway for superexchange between the metal atoms is nine covalent bonds long.

Single crystal *X*-ray structures were obtained from crystals of **3** · 2CH_3CN, **4** · 2CH_3CN, the red crystal form of **5**, **7** and **9** · 4CH_3CN (Figs. 2–5). Single crystals of **8** grown from acetonitrile/diethyl ether are apparently isostructural with **9** · 4CH_3CN but suffered from twinning [unit cell data: monoclinic, 2/*m*, $a = 10.6434(14)$, $b = 18.755(2)$, $c = 16.245(2)$ Å, $\beta = 99.523(8)°$, $V = 3198.1(7)$ Å^3 at 150 K]. All the compounds for which a full refinement was obtained contain the expected six-coordinate iron(II) centres, with Fe–N bond lengths in the usual range for high-spin compounds (Table 2) [26]. The crystals of **5** and **7** both contain two unique molecules in their asymmetric units, whose metric parameters show only small differences. The dinuclear molecule of **9** spans a crystallographic inversion centre, giving a single unique iron centre; the intramolecular Fe...Fe distance in that compound is

Table 3
Selected structural indices for the [Fe(NCS)$_2$(tpm′)L] complexes in this work (Å, °)

	av. Fe–N	$\sum$	Φ	τ
3 · 2CH_3CN	2.1789(7)	56.5(2)	56	3.3(1)
4 · 2CH_3CN	2.1850(7)	52.8(2)	61	3.2(1)
5, molecule A	2.1852(8)	49.1(3)	50	8.9(1)
5, molecule B	2.1908(8)	49.6(2)	48	8.5(1)
7, molecule A	2.197(1)	45.2(4)	32	7.0(2)
7, molecule B	2.197(1)	49.5(3)	50	10.4(2)
9 · 4CH_3CN	2.1807(8)	46.0(3)	65	15.5(2)

See text for definitions of $\sum$, Φ and τ.

Table 2
Selected bond lengths (Å) and angles (°) in the single crystal X-ray structures of the [Fe(NCS)$_2$(tpm′)L] complexes in this work

	3 · 2CH_3CN	**4** · 2CH_3CN	**5**		**7**		**9** · 4CH_3CN
			Molecule A	Molecule B	Molecule A	Molecule B	
Fe(1)–N(3)	2.2262(16)	2.2221(16)	2.2377(18)	2.2433(17)	2.247(3)	2.248(2)	2.203(2)
Fe(1)–N(10)	2.2156(16)	2.2103(17)	2.2257(18)	2.2250(19)	2.215(2)	2.247(3)	2.243(2)
Fe(1)–N(17)	2.2322(16)	2.2375(16)	2.2060(19)	2.2489(18)	2.294(2)	2.233(2)	2.200(2)
Fe(1)–N(24)	2.0848(18)	2.1021(18)	2.115(2)	2.100(2)	2.121(3)	2.130(3)	2.120(2)
Fe(1)–N(27)	2.1017(18)	2.1179(19)	2.1013(19)	2.107(2)	2.119(3)	2.147(3)	2.100(2)
Fe(1)–N(30)	2.2131(19)	2.2200(18)	2.2254(19)	2.2203(19)	2.183(3)	2.177(3)	2.218(2)
N(3)–Fe(1)–N(10)	82.21(6)	83.18(6)	83.12(7)	83.74(7)	84.01(9)	83.96(9)	80.75(8)
N(3)–Fe(1)–N(17)	81.03(6)	81.46(6)	82.13(7)	81.39(6)	80.79(9)	80.42(9)	82.70(8)
N(3)–Fe(1)–N(24)	172.92(6)	173.62(6)	172.60(7)	174.14(7)	171.46(10)	173.14(10)	172.03(9)
N(3)–Fe(1)–N(27)	92.81(6)	93.04(7)	92.89(7)	90.29(7)	89.96(11)	91.32(10)	91.06(9)
N(3)–Fe(1)–N(30)	87.72(6)	87.72(6)	92.45(7)	87.54(7)	91.41(10)	90.99(9)	95.31(8)
N(10)–Fe(1)–N(17)	82.09(6)	82.40(6)	83.18(7)	81.68(6)	81.61(9)	82.93(9)	84.30(8)
N(10)–Fe(1)–N(24)	92.21(6)	92.26(7)	90.88(7)	92.07(8)	91.29(10)	91.51(10)	92.40(8)
N(10)–Fe(1)–N(27)	174.75(6)	175.80(6)	175.84(7)	173.01(7)	171.29(10)	174.16(10)	171.80(8)
N(10)–Fe(1)–N(30)	87.75(6)	88.12(6)	86.28(7)	89.90(7)	91.02(10)	87.12(10)	91.15(8)
N(17)–Fe(1)–N(24)	93.93(6)	93.55(7)	92.89(8)	93.98(7)	91.49(10)	93.95(10)	92.62(8)
N(17)–Fe(1)–N(27)	95.55(6)	95.26(7)	95.12(7)	93.88(7)	91.24(10)	92.91(10)	94.20(9)
N(17)–Fe(1)–N(30)	165.74(7)	166.36(6)	168.65(7)	166.73(7)	169.75(10)	167.46(10)	175.27(8)
N(24)–Fe(1)–N(27)	92.63(7)	91.36(7)	93.00(8)	93.62(8)	93.88(11)	92.87(11)	95.72(9)
N(24)–Fe(1)–N(30)	96.44(7)	96.62(7)	91.48(8)	96.57(8)	95.81(11)	93.93(10)	88.85(9)
N(27)–Fe(1)–N(30)	93.72(7)	93.57(7)	95.11(7)	93.46(8)	95.42(11)	96.42(10)	90.11(9)
Fe(1)–N(24)–C(25)	172.63(17)	173.97(17)	173.5(2)	172.9(2)	168.7(3)	169.4(3)	168.6(2)
Fe(1)–N(27)–C(28)	171.84(17)	171.72(18)	174.59(19)	171.3(2)	161.4(3)	175.8(2)	167.2(2)

11.5617(7) Å. Intermolecular N–H···S hydrogen bonding between imidazole and NCS^- ligands occurs in **7**, leading to a 2D hydrogen bond array with a strongly puckered 6^3 honeycomb topology. There are no noteworthy intermolecular interactions in the other crystals.

Several structural indices have been used to quantify different types of angular structural distortion in six-coordinate metal complexes [27]. This can have a bearing on whether a high-spin complex undergoes spin-crossover on cooling, because a compound may be trapped in its high-spin state if its metal coordination sphere or ligand conformation exhibits a large angular structural distortion compared to the expected low-spin structure [11,28–30]. The angular motion of the ligands that would accompany spin-crossover would then be inhibited by intermolecular contacts. The most general ways of quantifying any angular distortion of a six-coordinate complex from an ideal octahedral geometry are *via* two indices. First is $\sum$, which measures local angular distortions of the octahedral donor set (Eq. (1)):

$$\sum = \sum_{i=1}^{12} |90 - \alpha_i| \quad (1)$$

where α_i are the twelve *cis*-N–Fe–N angles in the coordination sphere [27]. Second is Θ, which defines the degree of trigonal distortion of the N donor atoms from an octahedral geometry towards a trigonal prism (Eq. (2)):

$$\Theta = \sum_{j=1}^{24} |60 - \theta_j| \quad (2)$$

where θ_j are the 24 unique N–Fe–N angles measured on the projection of two triangular faces of the octahedron along their common pseudo-threefold axis [31]. An ideal octahedron would give $\sum$ and $\Theta = 0$. Compounds **3**–**9** exhibit a narrow range of values for $\sum$ and Θ that are unusually low for high-spin iron(II) complexes (Table 3) [27,31], showing they have near-regular octahedral coordination geometries.

Also listed in Table 3 is τ, the average of the three Fe(1)–N–N–C(23) torsions to the tpm′ pyrazolyl groups. This has a strong bearing on the ability of homoleptic complexes of tris-pyrazolylborate or tris-pyrazolylmethane derivatives to undergo spin-crossover, which is inhibited when τ is large [11,29,30]. The τ values exhibited by **3**–**9** span the previously observed range, encompassing values that should be both consistent (**3**–**5**) and inconsistent (**9**) with a thermal spin-transition [29]. Hence, there are no consistent angular distortions in these molecules that could explain why none of them undergoes spin-crossover.

The asymmetric unit of $[Fe(tpm)_2][Fe(NCS)_5(py)] \cdot 2CH_3CN$ (**10** · $2CH_3CN$) contains two unique, centrosymmetric $[Fe(tpm)_2]^{2+}$ half-cations, and a whole $[Fe(NCS)_5(py)]^{2-}$ anion lying on a general position (Fig. 6, Table 4). The cations are clearly low-spin at the temperature of measurement (150 K), consistent with other salts

Table 4
Selected bond lengths (Å) and angles (°) in the single crystal X-ray structure of $[Fe(tpm)_2][Fe(NCS)_5(py)] \cdot 2CH_3CN$ (**10** · $2CH_3CN$)

Fe(1A)–N(3A)	1.9735(12)	Fe(18)–N(19)	2.2125(13)
Fe(1A)–N(8A)	1.9714(11)	Fe(18)–N(25)	2.0676(14)
Fe(1A)–N(13A)	1.9829(12)	Fe(18)–N(28)	2.0296(14)
Fe(1A)–N(3A)	1.9721(12)	Fe(18)–N(31)	2.0198(14)
Fe(1A)–N(8A)	1.9649(11)	Fe(18)–N(34)	2.0826(14)
Fe(1A)–N(13B)	1.9737(11)	Fe(18)–N(37)	2.0571(16)
N(3A)–Fe(1A)–N(3A^{ii})	180	N(19)–Fe(18)–N(25)	86.89(5)
N(3A)–Fe(1A)–N(8A)	87.78(5)	N(19)–Fe(18)–N(28)	88.23(5)
N(3A)–Fe(1A)–N(8A^{ii})	92.22(5)	N(19)–Fe(18)–N(31)	88.48(6)
N(3A)–Fe(1A)–N(13A)	86.93(5)	N(19)–Fe(18)–N(34)	86.74(5)
N(3A)–Fe(1A)–N(13A^{ii})	93.07(5)	N(19)–Fe(18)–N(37)	176.65(5)
N(8A)–Fe(1A)–N(8A^{ii})	180	N(25)–Fe(18)–N(28)	88.74(6)
N(8A)–Fe(1A)–N(13A)	87.49(5)	N(25)–Fe(18)–N(31)	174.85(6)
N(8A)–Fe(1A)–N(13A^{ii})	92.51(5)	N(25)–Fe(18)–N(34)	90.74(6)
N(13A)–Fe(1A)–N(13A^{ii})	180	N(25)–Fe(18)–N(37)	91.60(6)
N(3B)–Fe(1B)–N(3B^{i})	180	N(28)–Fe(18)–N(31)	88.86(6)
N(3B)–Fe(1B)–N(8B)	87.53(5)	N(28)–Fe(18)–N(34)	174.97(6)
N(3B)–Fe(1B)–N(8B^{i})	92.47(5)	N(28)–Fe(18)–N(37)	94.72(6)
N(3B)–Fe(1B)–N(13B)	87.74(5)	N(31)–Fe(18)–N(34)	91.26(6)
N(3B)–Fe(1B)–N(13B^{i})	92.26(5)	N(31)–Fe(18)–N(37)	93.14(6)
N(8B)–Fe(1B)–N(8B^{i})	180	N(34)–Fe(18)–N(37)	90.29(6)
N(8B)–Fe(1B)–N(13B)	87.25(5)		
N(8B)–Fe(1B)–N(13B^{i})	92.75(5)		
N(13B)–Fe(1B)–N(13B^{i})	180		

Symmetry codes: (i) $1-x, 1-y, 1-z$; (ii) $-x, 1-y, -z$.

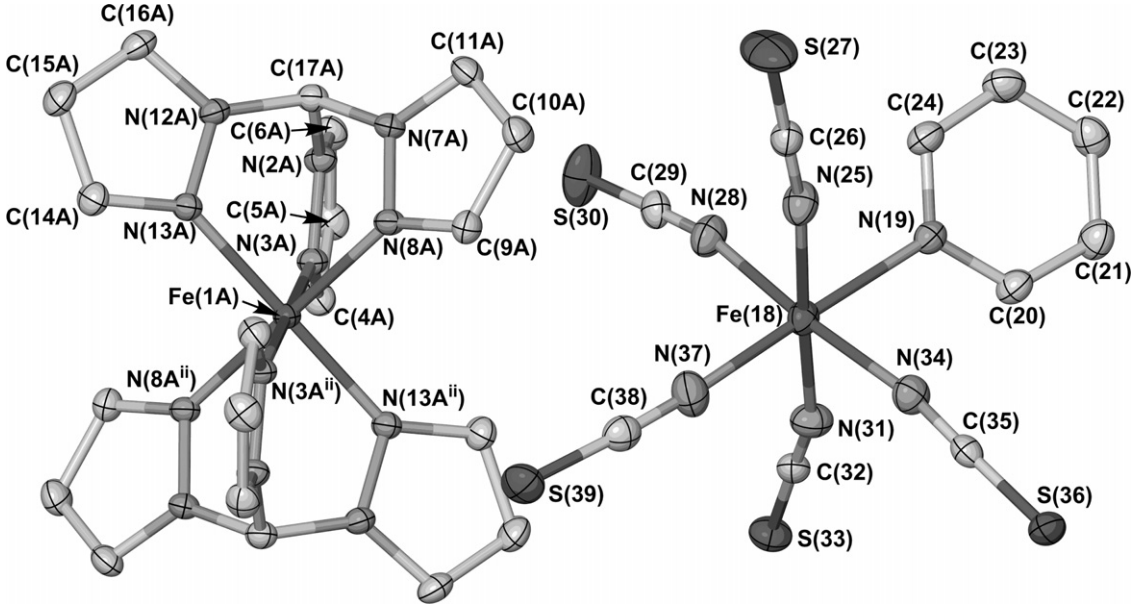

Fig. 6. View of the $[Fe(tpm)_2]^{2+}$ cation A, and the $[Fe(NCS)_5(py)]^{2-}$ anion, in the crystal structure of **10** · $2CH_3CN$. All H atoms have been removed, and thermal ellipsoids are at the 50% probability level. Cation B is visually indistinguishable from cation A, and uses the same atom numbering scheme. Symmetry code: (ii) $-x, 1-y, -z$.

of $[Fe(tpm)_2]^{2+}$ which are all low-spin at room temperature [5–9]. The $[Fe(NCS)_5(py)]^{2-}$ anion is new, and shows Fe–N distances that are consistent with a high-spin iron(III) centre [26]. The Fe–N(pyridine) bond is substantially longer than the five Fe–NCS bonds, reflecting its lower π-donor character. While the Fe–NCS distances vary between 2.0198(14) and 2.0826(14) Å, there is no obvious correlation between these parameters and the position of the NCS^- ligands relative to the pyridine donor. Unfortunately, no magnetochemical or spectroscopic characterisation of **10** was possible, owing to the very small amounts of pure material available.

5. Conclusion

The $[Fe_2(\mu\text{-}NCE)_2]^{2+}$ (E = S or Se) bridge in **1** and **2** is cleaved in acetonitrile solution, yielding the mononuclear adducts $[Fe(NCE)_2(tpm')(NCMe)]$ (**3** and **4**) whose solvent ligands can be substituted by moderately basic heterocycle donors to give $[Fe(NCE)_2(tpm')L]$ (L = pyridine, imidazole or 1/2[4,4′-bipy]; **5**-**9**). The monodentate 'L' ligands in **5**–**9** are only weakly coordinated, being readily lost in solvents other than acetonitrile to reform **1** and **2**. Analogous complexes of the unsubstituted tpm ligand could not be isolated, apparently owing to competing ligand disproportionation reactions. Crystals of $[Fe(tpm)_2][Fe(NCS)_5(py)] \cdot 2CH_3CN$ (**10** · $2CH_3CN$), containing the new $[Fe^{III}(NCS)_5(py)]^{2-}$ anion, were isolated from one such reaction. Compounds **5**-**9** are all high-spin between 5 and 300 K, despite mostly having regular coordination geometries and tpm′ ligand conformations that should favour spin-crossover. Presumably, the ligand field exerted by the $[Fe(NCE)_2(tpm')L]$ donor set is too weak to make the low-spin forms of the compounds accessible.

Acknowledgements

The authors thank Dr. H. J. Blythe (University of Sheffield) for the susceptibility measurements, and the EPSRC for funding.

Appendix A. Supplementary data

CCDC 672295, 672296, 672297, 672298, 672299 and 672300 contain supplementary crystallographic data for **10** · $2CH_3CN$, **5**, **7**, **3** · $2CH_3CN$, **9** · $4CH_3CN$ and **4** · $2CH_3CN$. These data can be obtained free of charge via http://www.ccdc.cam.ac.uk/conts/retrieving.html, or from the Cambridge Crystallographic Data Centre, 12 Union Road, Cambridge CB2 1EZ, UK; fax: (+44) 1223-336-033; or e-mail: deposit@ccdc.cam.ac.uk. Supplementary data associated with this article can be found, in the online version, at doi:10.1016/j.poly.2008.05.013.

References

[1] P. Gütlich, H.A. Goodwin (Eds.), Spin Crossover in Transition Metal Compounds I–III, Top. Curr. Chem. 233–235 (2004).
[2] M.A. Halcrow, Polyhedron 26 (2007) 3523. and references cited therein.
[3] (a) M.A. Halcrow, Coord. Chem. Rev. 249 (2005) 2880. and references cited therein;
(b) C. Carbonera, J.S. Costa, V.A. Money, J. Elhaïk, J.A.K. Howard, M.A. Halcrow, J.-F. Létard, Dalton Trans. (2006) 3058;
(c) R. Pritchard, C.A. Kilner, M.A. Halcrow, Chem. Commun. (2007) 577;
(d) V.A. Money, C. Carbonera, J. Elhaïk, M.A. Halcrow, J.A.K. Howard, J.-F. Létard, Chem. Eur. J. 13 (2007) 5503;
(e) H.Z. Lazar, T. Forestier, S.A. Barrett, C.A. Kilner, J.-F. Létard, M.A. Halcrow, Dalton Trans. (2007) 4276.
[4] (a) A.B. Gaspar, M.C. Muñoz, J.A. Real, J. Mater. Chem. 16 (2006) 2522;
(b) A. Bousseksou, G. Molnár, J.A. Real, K. Tanaka, Coord. Chem. Rev. 251 (2007) 1822.
[5] F. Mani, Inorg. Nucl. Chem. Lett. 15 (1979) 297.
[6] L.D. Field, B.A. Messerle, L.P. Soler, T.W. Hambley, P. Turner, J. Organomet. Chem. 655 (2002) 146.
[7] J.J. McGarvey, H. Toftlund, A.H.R. Al-Obaidi, K.P. Taylor, S.E.J. Bell, Inorg. Chem. 32 (1993) 2469.
[8] P.A. Anderson, T. Astley, M.A. Hitchman, R.F. Keene, B. Moubaraki, K.S. Murray, B.W. Skelton, E.R.T. Tiekink, H. Toftlund, A.H. White, Dalton Trans. (2000) 3505.
[9] D.L. Reger, C.A. Little, A.L. Rheingold, M. Lam, L.M. Liable-Sands, B. Rhagitan, T. Concolino, A. Mohan, G.J. Long, V. Briois, F. Grandjean, Inorg. Chem. 40 (2001) 1508.
[10] (a) D.L. Reger, C.A. Little, A.L. Rheingold, M. Lam, T. Concolino, A. Mohan, G.J. Long, Inorg. Chem. 39 (2000) 4674;
(b) D.L. Reger, C.A. Little, V.G. Young Jr., M. Pink, Inorg. Chem. 40 (2001) 2870;
(c) D.L. Reger, D.J. Elgin, M.D. Smith, F. Grandjean, L. Rebbouh, G.J. Long, Eur. J. Inorg. Chem. (2004) 3345;
(d) H. Paulsen, L. Duelund, A. Zimmermann, F. Averseng, M. Gerdan, H. Winkler, H. Toftlund, A.X. Trautwein, Monatsh. Chem. 134 (2003) 295;
(e) B. Moubaraki, B.A. Leita, G.J. Halder, S.R. Batten, P. Jensen, J.P. Smith, J.D. Cashion, C.J. Kepert, J.-F. Létard, K.S. Murray, Dalton Trans. (2007) 4413.
[11] D.L. Reger, C.A. Little, M.D. Smith, A.L. Rheingold, K.-C. Lam, T.L. Concolino, G.J. Long, R.P. Hermann, F. Grandjean, Eur. J. Inorg. Chem. (2002) 1190.
[12] (a) D.L. Reger, C.A. Little, A.L. Rheingold, R. Sommer, G.J. Long, Inorg. Chim. Acta 316 (2001) 65;
(b) P.G. Edwards, A. Harrison, P.D. Newman, W. Zhang, Inorg. Chim. Acta 359 (2006) 3549.
[13] S.R. Batten, J. Bjernemose, P. Jensen, B.A. Leita, K.S. Murray, B. Moubaraki, J.P. Smith, H. Toftlund, Dalton Trans. (2004) 3370.
[14] (a) Z.-G. Gu, J.-L. Zuo, Y. Song, C.-H. Li, Y.-Z. Li, X.-Z. You, Inorg. Chim. Acta 358 (2005) 4057;
(b) Z.-G. Gu, Q.-F. Yang, W. Liu, Y. Song, Y.-Z. Li, J.-L. Zuo, X.-Z. You, Inorg. Chem. 45 (2006) 8895.
[15] D.L. Reger, T.C. Grattan, K.J. Brown, C.A. Little, J.J.S. Lamba, A.L. Rheingold, R.D. Sommer, J. Organomet. Chem. 607 (2000) 120.
[16] N.E. Erickson, N. Sutin, Inorg. Chem. 5 (1966) 1834.
[17] J.S. Haynes, A. Kostikas, J.R. Sams, A. Simopoulos, R.C. Thompson, Inorg. Chem. 26 (1987) 2630.
[18] G.M. Sheldrick, Acta Crystallogr., Sect. A 46 (1990) 467.
[19] G.M. Sheldrick, SHELXL-97, Program for the Refinement of Crystal Structures, University of Göttingen, 1997.
[20] C.J. O'Connor, Prog. Inorg. Chem. 29 (1982) 203.
[21] J.A. Real, G. De Munno, M.C. Muñoz, M. Julve, Inorg. Chem. 30 (1991) 2701.
[22] K. Nakamoto, Infrared and Raman Spectra of Inorganic and Coordination Compounds Part B, 5th ed., Wiley Interscience, New York, 1997. p 116.
[23] K. Pohl, K. Wieghardt, B. Nuber, J. Weiss, J. Chem. Soc., Dalton Trans. (1987) 187.
[24] (a) See e.g., P. Coronel, A. Barraud, R. Claude, O. Kahn, A. Ruaudel-Teixier, J. Zarembowitch, J. Chem. Soc., Chem. Commun. (1989) 193;
(b) D.C. Figg, R.H. Herber, J.A. Potenza, Inorg. Chem. 31 (1992) 2111;
(c) C.L. Zilverentant, G.A. van Albada, A. Bousseksou, J.G. Haasnoot, J. Reedijk, Inorg. Chim. Acta 303 (2000) 287;
(d) D. Zhu, Y. Xu, Z. Yu, Z. Guo, J. Sang, T. Liu, X. You, Chem. Mater. 14 (2002) 838;
(e) G. Brehm, M. Reiher, B. Le Guennic, M. Leibold, S. Schindler, J. Raman Spectrosc. 37 (2006) 108.
[25] H. Endres, in: G. Wilkinson, R.D. Gillard, J.A. McCleverty (Eds.), Comprehensive Coordination Chemistry, vol. 2, Pergamon, Oxford, 1987, p. 264 (Chapter 13.7).
[26] E. König, Prog. Inorg. Chem. 35 (1987) 527.
[27] P. Guionneau, M. Marchivie, G. Bravic, J.-F. Létard, D. Chasseau, Top. Curr. Chem. 234 (2004) 97.
[28] (a) J.M. Holland, J.A. McAllister, C.A. Kilner, M. Thornton-Pett, A.J. Bridgeman, M.A. Halcrow, J. Chem. Soc., Dalton Trans. (2002) 548;
(b) J. Elhak, D.J. Evans, C.A. Kilner, M.A. Halcrow, Dalton Trans. (2005) 1693;
(c) J. Elhak, C.A. Kilner, M.A. Halcrow, Dalton Trans. (2006) 823;
(d) C.A. Kilner, M.A. Halcrow, Polyhedron 25 (2006) 235.
[29] D.L. Reger, J.R. Gardinier, J.D. Elgin, M.D. Smith, D. Hautot, G.J. Long, F. Grandjean, Inorg. Chem. 45 (2006) 8862.
[30] D.L. Reger, J.D. Elgin, M.D. Smith, G.F. Grandjean, L. Rebbouh, G.J. Long, Polyhedron 25 (2006) 2616.
[31] M. Marchivie, P. Guionneau, J.-F. Létard, D. Chasseau, Acta Crystallogr., Sect. B 61 (2005) 25.

Polyhedron 27 (2008) 2577–2584

Contents lists available at ScienceDirect

Polyhedron

journal homepage: www.elsevier.com/locate/poly

Syntheses, crystal structures and magnetic properties of tricyanomethanide-containing bis(2-pyrimidylcarbonyl)amidate copper(II) complexes

Consuelo Yuste [a], Danielle Cangussu de Castro Gomes [a,b], Harry Adams [c], Jim A. Thomas [c,*], Francesc Lloret [a], Miguel Julve [a,*]

[a] Departament de Química Inorgànica/Instituto de Ciencia Molecular, Universitat de València, Polígono La Coma s/n, 46980 Paterna (València), Spain
[b] Departamento de Química, Centro Federal de Educaçâo Tecnológica de Minas Gerais, Av. Amazonas 5253, Belo Horizonte-MG, 30480-000, Brazil
[c] Department of Chemistry, Daiton Building, University of Sheffield, Brook Hill, Sheffield S3 7HF, United Kingdom

ARTICLE INFO

Article history:
Received 9 April 2008
Accepted 12 May 2008
Available online 26 June 2008

Keywords:
Copper(II)
Coordination chemistry
Crystallography
Magnetism
Tricyanomethanide ligand

ABSTRACT

Three new copper(II) complexes of formulae [Cu(bpcam)(tcm)(H_2O)] · 2H_2O (**1**), [Cu(bpcam)(tcm)(H_2O)] (**2**) and [Cu(bpcam)(tcm)]$_n$ (**3**) [bpcam = bis(2-pyrimidylcarbonyl)amidate and tcm = tricyanomethanide] have been prepared and their structures determined by single crystal X-ray diffraction. Complexes **1** and **2** are mononuclear species where each copper atom is five-coordinated in a somewhat distorted square pyramidal environment with a tridentate bpcam ligand and a terminally bound tcm group building the basal plane and a water molecule in the apical position. Compound **3** is a uniform copper(II) chain where the [Cu(bpcam)]$^+$ units are connected through single μ-1,5-tcm bridges which link one equatorial position at one copper atom with the apical position of the adjacent copper. The intrachain meal–metal separation in **3** is 7.678(2) Å. Magnetic susceptibility measurements of **3** in the temperature range 1.9–295 K show the occurrence of a weak intrachain antiferromagnetic interaction [$J = -0.39$ cm^{-1} with the Hamiltonian being defined as $\hat{H} = -J\sum_i \hat{S}_i \cdot \hat{S}_{i+1}$]. This value of the magnetic coupling is analyzed through simple orbital symmetry considerations and compared with those observed through this bridge in other magneto-structurally characterized copper(II) complexes.

© 2008 Elsevier Ltd. All rights reserved.

1. Introduction

Coordination polymers containing dicyanamide [$N(CN)_2^-$, dca] and tricyanomethanide [$N(CN)_3^-$, tcm] as bridging ligands have been the subject of a recent review which focused on their structures and magnetic properties [1]. These two ligands have several points in common such as their Lewis base character, negative charge, planar stereochemistry (C_{2v} and D_{3h} points groups for dca and tcm, respectively) and potentially coordinating nitrile-nitrogen atoms which provide a five-atom superexchange pathway (a three-atom pathway being also accessible only for dca). The discovery of long range magnetic ordering in the binary d-block series of complexes α-M(dca)$_2$ [2–5] and the wide range of *nD* (*n* = 0–3) structural motifs for [M(dca)$_x$L$_y$] ternary species (*L* is a terminal or bridging coligand, *x* = 1 or 2 and *y* = 1 or 2) [1,6–10], largely account for the great interest in the coordination chemistry of dca in the last decade.

The large number of magneto-structural studies on dca-containing metal complexes contrasts with the small number of reports with the related tcm ligand [1,11]. These reports have shown that tcm can adopt four coordination modes in its metal complexes, one being terminal (μ_1) and the other three bridging ($\mu_{1,5}$, $\mu_{1,5,7}$ and $\mu_{1,1,5,7}$) (see Scheme 1). One appealing feature of tcm is the possibility to design triangular magnetically frustrated systems in the μ-1,5,7 bridging mode [12]. To date, only weak magnetic interactions between the paramagnetic metal ions across bridging tcm have been observed [1,11a–e,11g–i,12]. However, this lack of information on its behaviour as a ligand and also the possibility of generating new structural *nD* metal–organic frameworks motivated us to pursue a further investigation into the coordination chemistry of tcm.

In the framework of our previous magneto-structural studies on polynuclear copper(II) complexes and heterometallic species obtained by reacting the stable [Cu(bpca)]$^+$ and [Cu(bpcam)]$^+$ [bpca = bis-(2-pyridylcarbonyl)amidate and bpcam = 2-bis(2-pyrimidylcarbonyl)amidate] building blocks with potentially bridging ligands or preformed complexes which can act as ligands [6b,13,14], we obtained three tcm-containing complexes of formula [Cu(bpcam)(tcm)(H_2O)] · 2H_2O (**1**), [Cu(bpcam)(tcm)(H_2O)]

* Corresponding authors.
E-mail addresses: james.thomas@sheffield.ac.uk (J.A. Thomas), miguel.julve@uv.es (M. Julve).

0277-5387/$ - see front matter © 2008 Elsevier Ltd. All rights reserved.
doi:10.1016/j.poly.2008.05.015

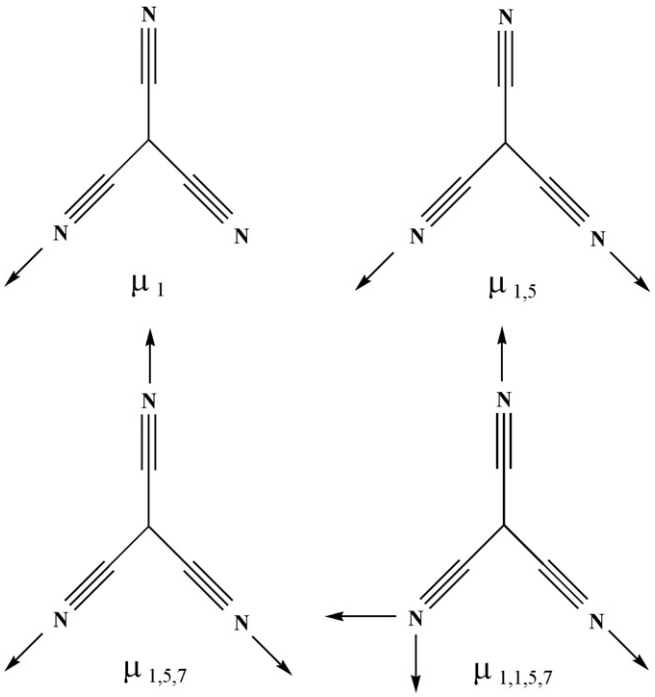

Scheme 1. Coordination modes of the tricyanomethanide.

(**2**) and [Cu(bpcam)(tcm)]$_n$ (**3**). Complexes **1** and **2** are discrete mononuclear species whereas **3** is a chain compound. The preparation and structural characterization of **1**–**3** are presented here together with the variable-temperature magnetic study of **3**.

2. Experimental

2.1. Materials

[Cu(bpcam)(H_2O)$_3$]$NO_3 \cdot 2H_2O$ was prepared by the copper(II)-assisted hydrolysis of the tpymt ligand, as previously reported [15]. Potassium tricyanomethanide was purchased from commercial sources and used and received. Elemental analysis (C, H, N) were conducted by the Microanalytical Service of the Universitat de València.

2.2. Synthesis

2.2.1. [Cu(bpcam)(tcm)(H_2O)] · 2H_2O (**1**)

Compound **1** was obtained as dark green octagonal plates from an aqueous solution (50 cm^3) containing [Cu(bpcam)(H_2O)$_3$]-(NO_3)(H_2O)$_2$ (0.05 mmol) and Ktcm (0.05 mmol) by slow evaporation at room temperature. They were collected by filtration on filter paper, washed with a small amount of cold water and kept in a desiccator over calcium(II) chloride. The yield is practically quantitative. *Anal.* Calc. for $C_{14}H_{12}CuN_8O_5$ (**1**): C, 38.59; H, 2.75; N, 25.71. Found: C, 38.31; H, 2.68; N, 25.54%.

2.2.2. [Cu(bpcam)(tcm)(H_2O)] (**2**) and [Cu(bpcam)(tcm)]$_n$ (**3**)

X-ray quality crystals of **2** and **3** were grown by slow diffusion in an H-shaped tube of aqueous solutions [Cu(bpcam)(H_2O)$_3$]-$NO_3 \cdot 2H_2O$ (0.1 mmol) in one arm and Ktcm (0.1 mmol) in the other one. Both arms were filled with water and cover with parafilm to avoid evaporation. The diffusion was complete after one month at room temperature. Two types of crystals were obtained: dark green parallelepipeds (**2**) and pale green plates (**3**), the former being the main product. They were separated manually, washed with a small amount of cold water and dried on filter paper. The yield is practically quantitative. *Anal.* Calc. for $C_{14}H_8CuN_8O_3$ (**2**): C, 42.07; H, 2.00; N, 28.02. Found: C, 41.92; H, 1.94; N, 27.90%. *Anal.* Calc. for $C_{14}H_6CuN_8O_2$ (**3**): C, 44.05; H, 1.57; N, 29.34. Found: C, 43.90; H, 1.51; N, 29.21%.

2.3. Physical techniques

Infrared spectra of **1**–**3** were recorded with a Bruker IF S55 spectrophotometer as KBr pellets in the 4000–400 cm^{-1} region. The magnetic susceptibility measurements on a polycrystalline sample of **3** were performed in the temperature range 1.9–295 K with a Quantum Design SQUID susceptometer, using an applied magnetic field of 1000 G. Diamagnetic corrections of the constituent atoms of **3** were estimated from Pascal's constants [16] as -163×10^{-6} cm^3 mol^{-1}. A value of 60×10^{-6} cm^3 mol^{-1} was used for the temperature-independent paramagnetism (tip) of the copper(II) ion.

2.4. X-ray data collection and structure refinement

Diffraction data for complexes **1**–**3** were collected at 150(2) K with a Bruker Smart CCD area detector diffractometer equipped with Oxford Cryosystems low temperature system. Crystal parameters and refinement results are listed in Table 1. The reflections of **1**–**3** were measured from a hemisphere of data collected of frames each covering 0.3° in ω. They were corrected for Lorentz and polarization effects and for absorption by semipirical methods based on symmetry-equivalent and repeated reflections through SADABS [17a]. The values of the minimum and maximum transmission coefficients are 0.7679 and 0.8359 (**1**), 0.6141 and 0.6533 (**2**) and 0.6344 and 0.9401 (**3**). The three structures were solved by direct methods and refined by full-matrix least-squares methods on F^2. All non-hydrogen atoms were refined anisotropically. Hydrogen atoms for **1**–**3** were placed geometrically and refined with a riding model and with U_{iso} constrained to be 1.2 times U_{eq} of the carrier atom. The refinements for all reflections converged at final R/wR values which are listed in Table 1. The values of the minimum

Table 1
Summary of crystal data and structure refinement for [Cu(bpcam)(tcm)(H_2O)] · 2H_2O (**1**), [Cu(bpcam)(tcm)(H_2O)] (**2**) and [Cu(bpcam)(tcm)]$_n$ (**3**)[a]

Compound	**1**	**2**	**3**
Formula	$C_{14}H_{12}CuN_8O_5$	$C_{14}H_8CuN_8O_3$	$C_{14}H_6CuN_8O_2$
Formula weight	435.86	399.82	381.81
Crystal system	monoclinic	triclinic	monoclinic
Space group	$P2_1/n$	$P\bar{1}$	$P2_1/n$
a (Å)	10.951(7)	7.129(1)	10.390(2)
b (Å)	12.074(8)	10.271(1)	18.438(4)
c (Å)	14.009(9)	10.350(2)	7.6784(15)
α (°)	90	97.515(2)	90
β (°)	112.795(7)	94.894(2)	105.57(3)
γ (°)	90	93.854(2)	90
U (Å)^3	1707(19)	746.9(2)	1416.9(5)
Z	4	2	4
D_{Calc} (Mg m^{-3})	1.695	1.779	1.790
μ (MoKα) (mm^{-1})	1.328	1.501	1.571
Maximum θ (°)	2.02–29.06	1.99–28.58	3.69–25.77
Reflection collected	13891	8575	12902
Independent reflection	4247	3426	2713
R_{int}	0.0478	0.0308	0.0541
Reflection [$I > 2s(I)$]	3363	2821	1982
Data/restrain/parameters	4247/0/253	3426/0/259	2713/0/226
Goodness-of-fit (GOF) on F^2	1.062	1.242	1.055
R [$I > 2\sigma(I)$]	0.0363	0.0370	0.0422
wR [$I > 2\sigma(I)$]	0.0817	0.0990	0.0958
R (all data)	0.0513	0.0484	0.0730
wR (all data)	0.0877	0.1030	0.1082

[a] Details in common: T = 150(2) K and λ = 0.71073 Å.

Table 2
Selected interatomic distances (Å) and angles (°) for [Cu(bpcam)(tcm)(H_2O)] · 2H_2O (**1**) and [Cu(bpcam)(tcm)(H_2O)] (**2**) with esds in parentheses

	1	**2**
Copper environment		
Cu(1)–N(3)	1.937(2)	1.935(2)
Cu(1)–N(6)	1.958(2)	1.953(2)
Cu(1)–N(5)	2.019(2)	2.035(2)
Cu(1)–N(1)	2.027(2)	2.036(2)
Cu(1)–O(1W)	2.275(2)	2.280(2)
N(3)–Cu(1)–N(6)	173.12(8)	171.45(10)
N(3)–Cu(1)–N(5)	81.60(7)	81.20(9)
N(6)–Cu(1)–N(5)	96.76(7)	101.49(10)
N(3)–Cu(1)–N(1)	81.47(8)	81.60(9)
N(6)–Cu(1)–N(1)	99.31(8)	95.24(9)
N(5)–Cu(1)–N(1)	161.94(7)	162.60(9)
N(3)–Cu(1)–O(1W)	94.37(8)	96.05(8)
N(6)–Cu(1)–O(1W)	92.48(8)	92.33(8)
N(5)–Cu(1)–O(1W)	99.01(7)	88.17(8)
N(1)–Cu(1)–O(1W)	88.50(7)	95.96(8)
Tricyanomethanide ligand		
C(11)–C(12)	1.400(3)	1.396(4)
C(11)–C(13)	1.420(3)	1.419(4)
C(11)–C(14)	1.417(3)	1.421(4)
N(6)–C(12)	1.148(3)	1.156(4)
N(7)–C(13)	1.155(3)	1.150(4)
N(8)–C(14)	1.150(3)	1.155(4)
C(12)–N(6)–Cu(1)	166.8(2)	173.0(2)
N(6)–C(12)–C(11)	177.8(3)	179.0(3)
C(12)–C(11)–C(13)	119.1(2)	121.1(3)
C(12)–C(11)–C(14)	121.4(2)	119.8(2)
C(13)–C(11)–C(14)	119.5(2)	119.4(2)
N(7)–C(13)–C(11)	178.6(3)	178.4(3)
N(8)–C(14)–C(11)	177.5(3)	179.2(3)
D–H···A	D···A (Å)	H···A (Å)	D–H···A (°)
Compound ***1***			
Hydrogen bonds[a,b]			
O(1W)–H(1WB)···O(1a)	2.817(2)	2.02	156.2
O(1W)–H(4WA)···O(3W)	2.666(2)	1.82	172.5
O(2W)–H(2WB)···N(4b)	2.959(3)	2.13	164.4
O(2W)–H(2WA)···O(1W)	2.849(2)	2.03	162.0
O(3W)–H(3WB)···O(2Wc)	2.749(3)	1.90	171.9
O(3W)–H(3WA)···O(1b)	2.966(3)	2.17	155.7
Compound ***2***			
Hydrogen bonds[a,c]			
O(1W)–H(1W)···O(2a)	2.758(3)	2.003(33)	170(4)
O(1W)–H(2W)···O(1b)	2.753(3)	2.171(31)	146(4)

[a] D = donor and A = acceptor.
[b] Symmetry operations used to generate equivalent atoms: (a) = $-x+2$, $-y+1$, $-z+2$; (b) = $x-1/2$, $-y+1/2$, $z-1/2$; (c) = $-x+3/2$, $y-1/2$, $-z+3/2$.
[c] Symmetry operations used to generate equivalent atoms: (a) = $x+1$, y, z; (b) = $-x$, $-y+2$, $-z+1$.

Table 3
Selected interatomic distances (Å) and angles (°) for [Cu(bpcam)(tcm)]$_n$ (**3**) with esds in parentheses

Copper environment			
Cu(1)–N(1)	2.008(3)	Cu(1)–N(6)	1.971(3)
Cu(1)–N(3)	1.948(3)	Cu(1)–N(7b)	2.163(3)
Cu(1)–N(5)	1.998(3)		
N(1)–Cu(1)–N(3)	82.16(13)	N(3)–Cu(1)–N(6)	153.82(13)
N(1)–Cu(1)–N(5)	163.82(13)	N(3)–Cu(1)–N(7b)	105.24(12)
N(1)–Cu(1)–N(6)	96.57(14)	N(5)–Cu(1)–N(6)	96.25(14)
N(1)–Cu(1)–N(7b)	95.88(14)	N(5)–Cu(1)–N(7b)	91.35(14)
N(3)–Cu(1)–N(5)	81.98(13)	N(6)–Cu(1)–N(7b)	100.91(13)
Tricyanomethanide ligand			
N(6)–C(12)	1.149(5)	C(11)–C(12)	1.390(5)
N(7)–C(13)	1.142(5)	C(11)–C(13)	1.401(5)
N(8)–C(14)	1.145(5)	C(11)–C(14)	1.410(6)
C(13)–N(7)–Cu(1a)	162.5(3)	C(12)–N(6)–Cu(1)	164.5(3)
N(7)–C(13)–C(11)	176.0(4)	C(13)–C(11)–C(14)	119.1(3)
N(8)–C(14)–C(11)	179.0(4)	C(13)–C(11)–C(12)	121.2(3)
N(6)–C(12)–C(11)	177.8(3)	C(12)–C(11)–C(14)	119.7(3)

[a] Symmetry transformations used to generate equivalent atoms: (a) $x, y, z-1$; (b) $x, y, z+1$.

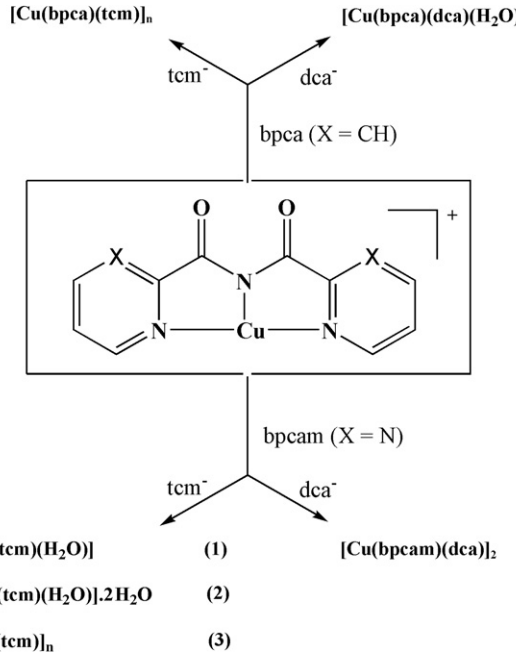

Scheme 2. Complex formation between the bis(2-aryl/pyrimidylcarbony)amidate-copper(II) and the dca and tcm ligands.

and maximum final electron density peaks are −0.640 and 0.418 (**1**), −0.410 and 0.545 (**2**), and −0.410 and 1.029 e Å^{-3} (**3**). A weighting scheme $w = 1/[\sigma(F_o)^2 + (mP)^2 + nP]$ where $P = (F_o + 2F_c^2)/3$ with $m = 0.0330$ (**1**), 0.0484 (**2**) and 0.0573 (**3**) and $n = 0.7152$ (**1**), 0.0000 (**2**), and 1.8442 (**3**) was used in the latter stages of refinement. Complex scattering factors were taken from the program package SHELXTL [17b] as implemented on the Viglen Pentium computer. The graphical manipulations were performed with the XP utility of the SHELXTL system [17c] and the DIAMOND program [17d]. Selected bond lengths and angles are given in Tables 2 (**1** and **2**) and 3 (**3**).

3. Results and discussion

3.1. Synthesis and infrared spectra of *1*–*3*

The coordination of the bpca and bpcam to the coper(II) ion as tridentate ligands through the imido and two pyridyl (bpca) or two pyrimidyl (bpcam) nitrogen atoms affords the very robust [Cu(bpca)]$^+$ and [Cu(bpcam)]$^+$ entities which are shown in Scheme 2. The complex formation of these units with the polynitrile ligands tcm and dca afford the dinuclear complexes [Cu(bpca)(dca)(H_2O)]$_2$ [6b] and [Cu(bpcam)(dca)(H_2O)]$_2$ [13i] and the chain compounds [Cu(bpca)(tcm)]$_n$ [13i] and [Cu(bpcam)(tcm)]$_n$ (**3**) where double $\mu_{1,3}$-dca (dinuclear) and single $\mu_{1,5}$-tcm bridges (chain) link the adjacent copper atoms. However, analogues of the mononuclear species [Cu(bpcam)(tcm)(H_2O)] · 2H_2O (**1**) and [Cu(bpcam)(tcm)-(H_2O)] (**2**) were not observed for the parent bpca-containing system.

The infrared spectra of **1**–**3** show a sharp and strong peak in the range 1730–1720 cm^{-1} [ν_{as}(CO) vibration of the imide group] which is indicative of the presence of coordinated bpcam ligand [13g–i,14b,15]. The high-frequency region of the ir spectra of **1** and **2** is dominated by a strong and broad absorption in the range

3500–3350 cm^{-1} [ν(OH) stretching vibration] which is due to the presence of coordinated (**1** and **2**) and crystallization (**1**) water molecules that are involved in hydrogen bonds [18]. The peaks corresponding to the ν(C≡N) stretches of the tcm ligand in **1**–**3** occur in the range 2260–2170 cm^{-1}: two sharp and strong absorptions at 2237 and 2175 cm^{-1} for **1** and **2** and three peaks at 2260w, 2203s and 2187vs for **3** (comparable to the single absorption at 2178s cm^{-1} in the IR spectrum of Ktcm). A comparison of these absorption patterns with those previously reported for structurally characterized tcm-containing copper(II) complexes [11a,i,j,13i] suggests the presence of monodentate (**1** and **2**) and $\mu_{1,5}$-bridging modes [**3**] for the tcm ligand, which is confirmed by the structures of **1**–**3** (see below).

3.2. Description of the structures

3.2.1. [Cu(bpcam)(tcm)(H_2O)] · 2H_2O (**1**) and [Cu(bpcam)(tcm)(H_2O)] (**2**)

The crystal structures of **1** and **2** contain the same neutral unit of formula [Cu(bpcam)(tcm)(H_2O)], the difference between the structures being the presence of molecules of water of crystallization in the former compound [Figs. 1 (**1**) and 2 (**2**)]. The neutral mononuclear units are interlinked through hydrogen bonds involving the coordinated (**1** and **2**) and non-coordinated water molecules (**1**) as well as the carbonyl-oxygen (**1** and **2**) and one of the free pyrimidyl-nitrogen (**1**) atoms of the bpcam ligand (see end of Table 2) affording the sheet (**1**) and ladder (**2**) supramolecular motifs shown in Figs. 3 (**1**) and 4 (**2**).

The copper atom [Cu(1)] in **1** and **2** is five-coordinated in a somewhat distorted square pyramidal CuN_4O geometry, the values of the trigonality parameter τ being 0.19 (**1**) and 0.16 (**2**) [τ = 0 and 1 for ideal square pyramid and trigonal bipyramid, respectively] [19]. The basal plane is formed by three nitrogen atoms of the tridentate bpcam ligand [Cu–N bonds varying in the range 1.937(2)–2.027(2) (**1**) and 1.935(2)–2.036(2) Å (**2**)] and a nitrile-nitrogen from a terminally bound tcm ligand [Cu(1)–N(6) = 1.958(2) (**1**) and 1.953(2) Å (**2**)], whereas the apical position is occupied by a water molecule [Cu(1)–O(1W) = 2.275(2) (**1**) and 2.280(2) Å (**2**)]. The values of the Cu–N(bpcam) bond lengths agree with those observed in other bpcam-containing copper(II) complexes [13g–i,14b,15]. The angles in the basal plane are distorted from that of an ideal square planar geometry [values varying in the range 81.20(9)–81.60(7)°] mainly due to the steric constraints geometry of the tridentate bpcam ligand subtending two five-membered chelate rings at the copper atom. The atoms defining the basal plane are practically coplanar with maximum deviations of 0.007(1) (**1**) and 0.041(1) Å (**2**) at N(3). The copper atom is displaced by 0.121(1) (**1**) and 0.100(1) Å (**2**) from the basal plane towards O(1w).

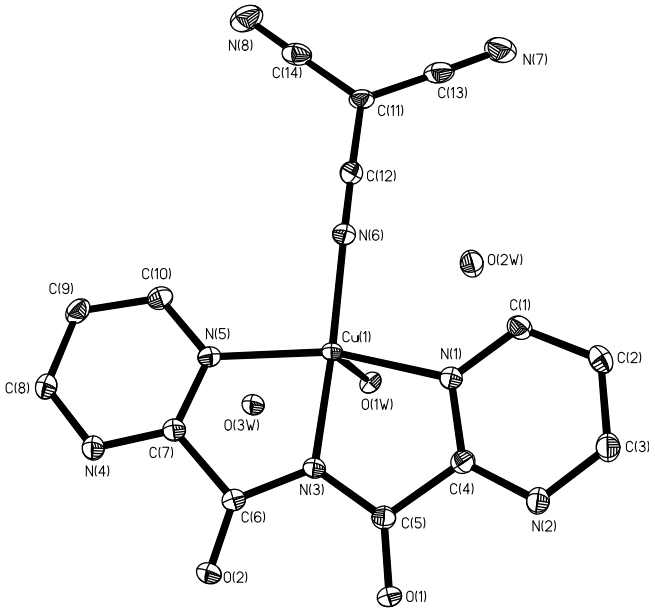

Fig. 1. A perspective view of the molecular structure of **1** showing atom numbering adopted. Hydrogen atoms are omitted for clarity.

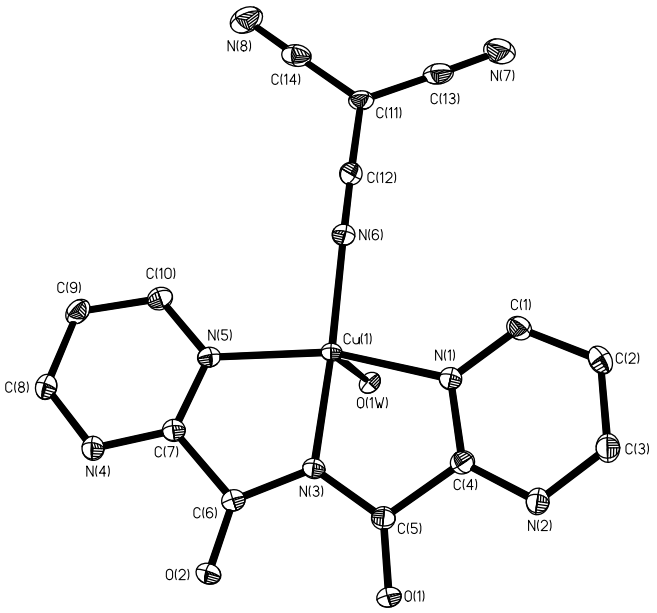

Fig. 2. A perspective view of the molecular structure of **2** showing atom numbering adopted. Hydrogen atoms are omitted for clarity.

The pyrimidyl rings of the bpcam ligand are planar and the values of the dihedral angle between them are 13.24(2) (**1**) and 5.52(1)° (**2**). Bond lengths and angles within the bpcam ligand are in agreement with those reported previously [13g–i,14b,15]. The tcm ligand is planar and the value of the dihedral angle between this group and the equatorial plane at the copper atom is 13.9(1)° for **1** and 14.6(1)° for **2**. The structural parameters of the tcm group indicate localized single C–C and triple C≡N bonds with values for the angles at the central carbon atom [C(11)] and C–C–N fragments varying in the ranges 119.1(2)–121.4(2) (**1**)/119.4(4)–121.1(3)° (**2**) and 177.5(3)–178.6(3) (**1**)/178.4(3)–179.2(3)° (**2**), as expected for sp^2 and sp hybridizations of the appropriate carbon atoms.

The values of the shorter intermolecular copper–copper distance are 6.348(3) [Cu(1)···Cu(1a); (a) = $-x$, $-y$, $1-z$] and 6.607(4) Å [Cu(1)···Cu(1b); (b) = $1-x$, $2-y$, $1-z$] for (**1**) and (**2**), respectively.

3.2.2. [Cu(bpcam)(tcm)]$_n$ (**3**)

This compound has a uniform chain structure with the tcm group adopting a $\mu_{1,5}$-bridging mode between the [Cu(bpcam)] units (Fig. 5). The neutral chains extend along the c axis in a zigzag fashion and they are stacked in a zipper arrangement in the *bc* plane (Fig. 6).

The copper atom is five-coordinated in a distorted square pyramidal surrounding, with τ = 0.17. The equatorial positions are occupied by three bpcam-nitrogen atoms [N(1), N(3) and N(5)] and a nitrile-nitrogen [N(6)] from a tcm group whereas the apical position is occupied by a nitrile-nitrogen [N(7b)] from another tcm ligand. The larger deviation from the mean equatorial plane is

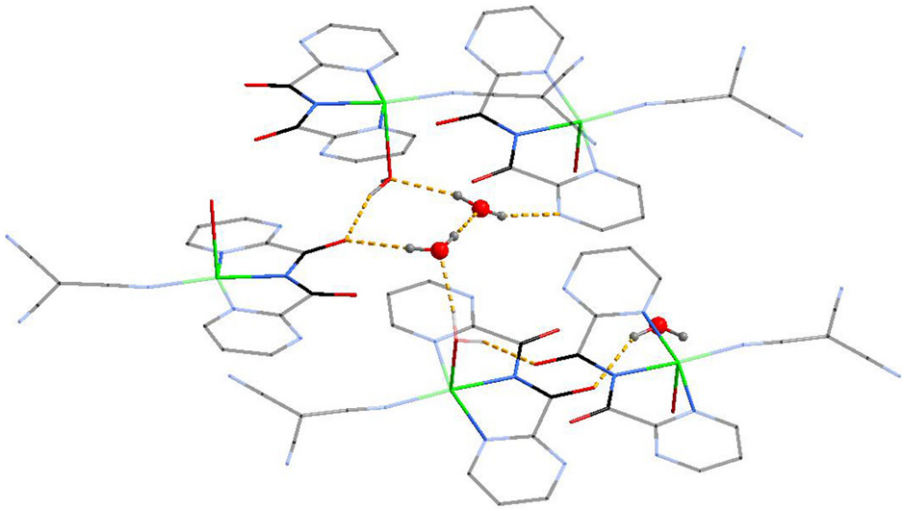

Fig. 3. View of a fragment of the layered structure of **1** in the *ab* plane through hydrogen bonds (yellow broken lines). (For interpretation of the references to colour in this figure legend, the reader is referred to the web version of this article.)

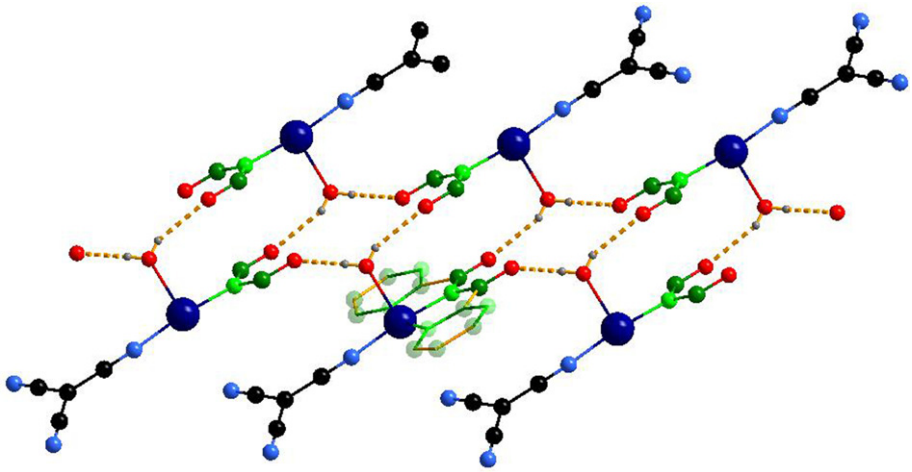

Fig. 4. View of the hydrogen bonding pattern in **2** (yellow broken lines) which leads to a ladder-like motif running parallel to the *a* axis. (For interpretation of the references to colour in this figure legend, the reader is referred to the web version of this article.)

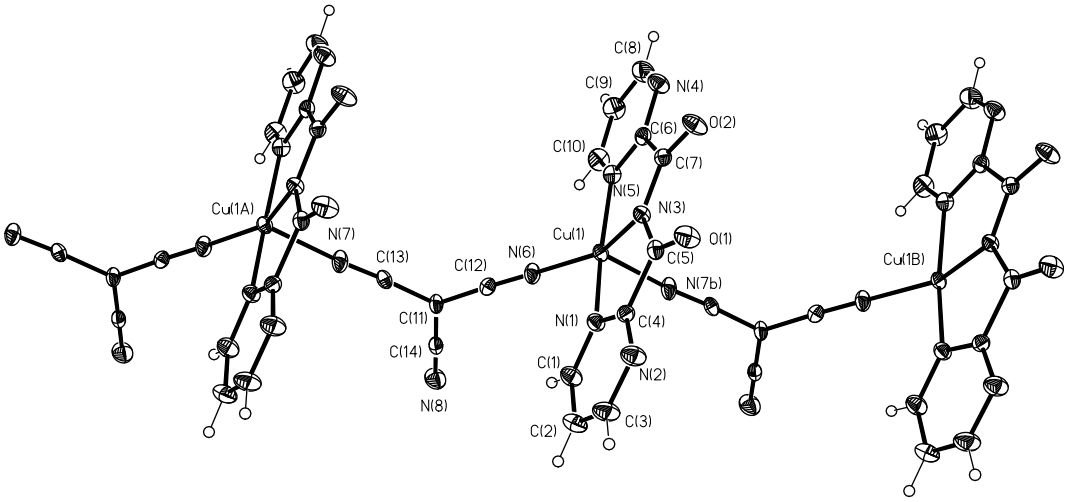

Fig. 5. View of a fragment of the chain structure of **3** with atom numbering.

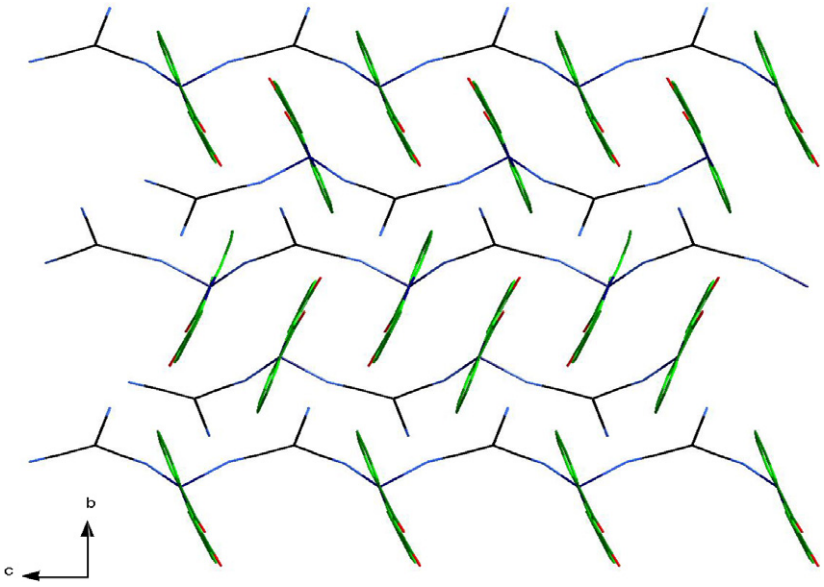

Fig. 6. A view of the stacking of the chains of **3** in the *bc* plane.

0.176(3) Å for N(3) and the copper atom is displaced by 0.284(4) Å from this mean plane toward the apical nitrile-nitrogen. The values of the dihedral angle between the mean basal plane and those of the bpcam and tcm ligands are 10.28(6) and 82.25(8)°, respectively.

As in **1** and **2**, the bpcam ligand adopts a tridentate coordination mode with the inner copper to amido-nitrogen bond being shorter than the outer copper to pyrimidine-nitrogen bonds. The pyrimidyl rings of the bpcam ligand are planar and the dihedral angle between them is 4.94(2)°. The values of the C–C and C–N bond lengths and the C–C–C bond angles of the tcm ligand in **3** remain in rather narrow ranges 1.390(5)–1.410(6) Å, 1.142(5)–1.149(5) Å and 119.1(3)–121.2(3)°, respectively. This is in agreement with almost ideal sp^2 hybridization for the central carbon atom. This single and asymmetric μ-1,5-bridging mode for the tcm ligand has been previously observed in related uniform copper(II) chains $\{[Cu(terpy)(tcm)]\cdot tcm\}_n$ (terpy = 2,2′:6′,2″-terpyridine) [11j] and $[Cu(bpca)(tcm)]_n$ [13i] with values of the intrachain metal–metal separation of 7.469(19) and 7.688(3) Å, respectively [to be compared to 7.678(2) Å for Cu(1)···Cu(1a) in **3**]. The shortest interchain copper–copper distance in **3** is 4.409(9) Å [Cu(1)···Cu(1c); (c) = 2 − *x*, −*y*, 2 − *z*], a value which is much shorter than the analogous intrachain separation.

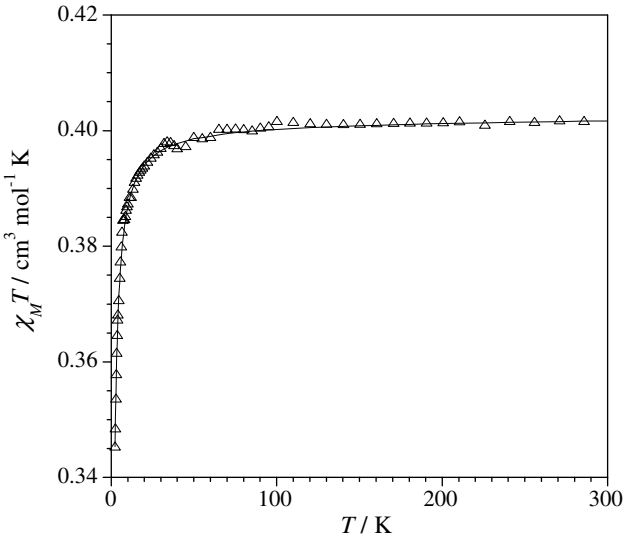

Fig. 7. Thermal dependence of the $\chi_M T$ product for **3**: (Δ) experimental data; (−) best-fit curve through Eq. (1) (see text).

*3.2.3. Magnetic properties of **3***

The magnetic properties of **3** in the form of $\chi_M T$ versus T plot [χ_M is the magnetic susceptibility per copper(II) ion] are shown in Fig. 7. Curie law behaviour for a magnetically isolated copper(II) ion is observed in the temperature range 290–100 K ($\chi_M T$ being practically constant and equal to ca. 0.40 cm^3 mol^{-1} K). The smooth decrease of $\chi_M T$ at $T < 100$ K to reach a minimum value of 0.345 cm^{-1} at 1.9 K is indicative of weak antiferromagnetic coupling in this compound.

Given the one-dimensional structure of **3**, the magnetic data were analyzed through the numerical expression [20] for a uniform chain of local spin doublets [Eq. (1)] which is derived from the isotropic Hamiltonian in Eq. (2)

$$\chi_M = (N\beta^2 g^2/kT)[(0.25 + 0.074975x + 0.075235x^2) / [1.0 + 0.9931x + 0.172135x^2 + 0.757825x^3] \quad (1)$$

$$\hat{H} = -J\sum_i \hat{S}_i \cdot \hat{S}_{i+1} \quad (2)$$

where $x = |J|/kT$ and J is the exchange coupling constant describing the magnetic interaction between the two nearest-neighbour spin doublets. Best-fit parameters through Eq. (1) leads to the following parameters: $J = -0.30$ cm^{-1}, $g = 2.07$ and $R = 1.6 \times 10^{-5}$ (R is the agreement factor defined as $\sum_i[(\chi_M T)_{obs(i)} - (\chi_M T)_{calc(i)}]^2 / \sum_i[(\chi_M T)_{obs(i)}]^2$).

The magnetic coupling in **3** is very weak and antiferromagnetic. Its value is within those observed in other copper(II) complexes through asymmetric single- and double $\mu_{1,5}$-tcm bridges, as shown in Table 4. The out-of-plane exchange pathway involved in **3** and in the other complexes of this table is the origin of the small overlap between the magnetic orbitals of the adjacent copper(II) ions, the unpaired electron of each copper(II) ion being essentially located in the equatorial plane with a weak spin density on the axial position. Under these conditions, a weak magnetic interaction between the copper(II) ions is predicted. Thus, the tcm bridge appears to be a poor mediator of magnetic interactions when adopting the $\mu_{1,5}$-bridging mode in the equatorial axial exchange pathway.

Table 4
Selected magneto-structural data for single and double μ-1,5-tcm bridged copper(II) complexes[a]

Compound[b]	Nuclearity	No. tcm bridges	Cu–N_{ax}[c] (Å)	$d_{Cu\cdots Cu}$[d] (Å)	J[e] (cm^{-1})	Ref.
$\{[Cu(terpy)(tcm)]\cdot tcm\}_n$	Chain	1	2.124(2)	7.469(1)	−0.086	[11j]
$[Cu(pyim)(tcm)_2]_n$	Chain	1	2.193(2)	7.4889(4)	−0.09	[11j]
$[Cu(2,3\text{-dbq})(tcm)_2]_n$	Chain	1	2.158(1)	7.446(1)	−0.18	[11i]
$[Cu(bpcam)(tcm)]_n$	Chain	1	2.163(3)	7.678(2)	−0.39	This work
$[Cu(bpca)(tcm)]_n$	Chain	1	2.210(2)	7.688(3)	−0.64	[13i]
$[Cu(tn)(tcm)_2]_n$	Chain	1	2.341(2)	7.5157(4)	−0.70	[11a]
		2	2.729(3)	7.7455(4)		
$[Cu_4(bpz)_4(tcm)_8]$	Tetranuclear	1	2.883(4)	7.969(2)	−0.04	[11j]
		2	2.174(3)/2.247(3)	7.469(1)	−1.21	
$[Cu(bipy)(tcm)_2]_n$	Chain	2	2.467(2)/2.659(2)	7.520(1)/7.758(1)	+0.11	[11j]
$[Cu_2(Hpz)(tcm)_4]$	Dinuclear	2	2.472(4)	[g]	+3.2[f]	[21]

[a] The equatorial-axial exchange pathway in involved in the whole series.
[b] Abbreviations used: pyim = 2-(2-pyridyl)imidazole; terpy = 2,2′:6′,2″-terpyridine; 2,3-dpq = 2,3-bis(2-pyridyl)quinoxaline; tn = 1,3-diaminopropane; bpz = 2,2′-bipyrazine; bipy = 2,2′-bipyridine.
[c] Value of the axial copper to tcm-nitrogen bond.
[d] Copper–copper separation through bridging tcm.
[e] Value of the magnetic coupling.
[f] This value is the Curie–Weiss term θ.
[g] Value not given by the authors.

4. Conclusions

Complex formation between the $[Cu(bpcam)]^+$ unit and the polynitrile ligand tcm affords two mononuclear complexes (**1** and **2**) and a uniform copper(II) chain where the tcm ligand adopts the monodentate and $\mu_{1,5}$-bridging coordination modes. A weak intrachain antiferromagnetic coupling occurs in **3** illustrating once more the poor ability of this bridge to transmit magnetic interactions between the magnetic centres separated by more than 7.0 Å. Finally, this work and previous reports show that the high stability of the preformed complex $[Cu(bpcam)]^+$ in aqueous solution facilitates the preparation of mono- and homo- and heterometallic polynuclear complexes using bridging linkers as coligands. The extension of bpcam-based coordination chemistry to other spin carriers will allow a wide variety magnetic compounds with an increased number of exchange pathways to be prepared.

Acknowledgements

Thanks are due to the Spanish Ministry of Science and Education (Project CTQ-2007-61690) and the Royal Society for financial support. Two of us, C.Y. and D.C.C.G., acknowledge the Ministerio Español de Educación y Ciencia and the Ministério da Educaçâo do Brasil (CAPES/COFECUB) for pre- and post-doctoral grants, respectively.

Appendix A. Supplementary data

CCDC 684300, 684301 and 684302 contain the supplementary crystallographic data for **1**, **2** and **3**, respectively. These data can be obtained free of charge via http://www.ccdc.cam.ac.uk/conts/retrieving.html, or from the Cambridge Crystallographic Data Centre, 12 Union Road, Cambridge CB2 1EZ, UK; fax: (+44) 1223-336033; or e-mail: deposit@ccdc.cam.ac.uk.

References

[1] S.R. Batten, K.S. Murray, Coord. Chem. Rev. 246 (2003) 103.
[2] S.R. Batten, P. Jensen, B. Moubaraki, K.S. Murray, R. Robson, Chem. Commun. (1998) 439.
[3] M. Kurmoo, C.J. Kepert, New J. Chem. 22 (1998) 1515.
[4] J.L. Manson, C.R. Kmety, Q.Z. Huang, J.W. Lynn, G.M. Bendele, S. Pagola, P.W. Stephens, L.M. Liable-Sands, A.L. Rheingold, A.J. Epstein, J.S. Miller, Chem. Mater. 10 (1998) 2552.
[5] C.R. Kmety, Q. Huang, J.W. Flynn, R.W. Erwin, J.L. Manson, S. McCall, J.E. Crow, K.L. Stevenson, J.S. Miller, A.J. Epstein, Phys. Rev. B 62 (2000) 5576.
[6] (a) J. Luo, M. Hong, J. Weng, Y. Zhao, R. Cao, Inorg. Chim. Acta 329 (2002) 59; (b) B. Vangdal, J. Carranza, F. Lloret, M. Julve, J. Sletten, J. Chem. Soc., Dalton Trans. (2002) 566; (c) J. Carranza, C. Brennan, J. Sletten, F. Lloret, M. Julve, J. Chem. Soc., Dalton Trans. (2002) 3164; (d) H.Z. Kou, Y. He, Chem. Lett. 32 (2003) 902; (e) J. Carranza, C. Brennan, J. Sletten, J.M. Clemente-Juan, F. Lloret, M. Julve, Inorg. Chem. 42 (2003) 8176; (f) C.X. Zhang, Z.Q. Liu, D.Z. Liao, Z.H. Jiang, S.P. Yan, Inorg. Chim. Acta 357 (2004) 376; (g) J. Carranza, J. Sletten, F. Lloret, M. Julve, Inorg. Chim. Acta 357 (2004) 3304; (h) S. Konar, S. Dalai, J. Ribas, M.G.B. Drew, E. Zangrando, N.R. Chaudhuri, Inorg. Chim. Acta 357 (2004) 4208; (i) J.L. Manson, J.A. Schlueter, H.J. Koo, M.H. Whangbo, Inorg. Chem. 43 (2004) 4007.
[7] (a) E.Q. Gao, S.Q. Bai, Z.M. Wang, C.H. Yan, Dalton Trans. (2003) 1759; (b) C. Paraschiv, J.P. Sutter, M. Schmidtmann, A. Müller, M. Andruh, Polyhedron 22 (2003) 1611; (c) W. Dong, Q.L. Wang, Z.Q. Liu, D.Z. Liao, Z.H. Jiang, S.P. Yan, P. Cheng, Polyhedron 22 (2003) 3315; (d) H.L. Sunn, S. Gao, B.Q. Ma, S.R. Batten, CrystEngComm 6 (2004) 579; (e) D. Armentano, G. De Munno, F. Guerra, M. Julve, F. Lloret, Inorg. Chem. 45 (2006) 4626.
[8] (a) D. Ghoshal, G. Mostafa, T.K. Maji, E. Zangrando, T.H. Lu, J. Ribas, N.R. Chaudhuri, New J. Chem. 28 (2004) 1204; (b) G.S. Papaefstathiou, A. Escuer, F.A. Mautner, C. Raptopoulou, A. Terzis, S.P. Perlepes, R. Vicente, Eur. J. Inorg. Chem. (2005) 879.
[9] (a) S. Martín, M.G. Barandika, J.M. Ezpeleta, R. Cortés, J.I. Ruiz de Larramendi, L. Lezama, T. Rojo, J. Chem. Soc., Dalton Trans. (2002) 4275; (b) D. Ghoshal, H. Bialas, A. Escuer, M. Font-Bardía, T.K. Maji, J. Ribas, X. Solans, R. Vicente, E. Zangrando, N.R. Chaudhuri, Eur. J. Inorg. Chem. (2003) 3929; (c) R. Boca, M. Boca, M. Gembicky, L. Jäger, C. Wagner, H. Fuess, Polyhedron 23 (2004) 2337; (d) J. Luo, X.G. Zhou, S. Gao, L.H. Weng, Z.H. Shao, C.M. Zhang, Y.R. Li, J. Zhang, R.F. Cai, Inorg. Chem. Commun. 7 (2004) 669; (e) S. Komar, S. Dalai, P.S. Mukherjee, M.G.B. Drew, J. Ribas, N.R. Chaudhuri, Inorg. Chim. Acta 358 (2005) 957; (f) E. Colacio, I.B. Maimoun, F. Lloret, J. Suárez-Varela, Inorg. Chem. 44 (2005) 3771.
[10] A.Q. Wu, F.K. Zheng, W.T. Chen, L.Z. Cai, G.C. Guo, J.S. Huang, Z.C. Dong, Y. Takano, Inorg. Chem. 43 (2004) 4839.
[11] (a) F. Thétiot, S. Triki, J. Sala Pala, S. Golhen, Inorg. Chim. Acta 350 (2003) 314; (b) R. Boca, M. Gembicky, R. Herchel, W. Haase, L. Jäger, C. Wagner, H. Ehrenberg, H. Fuess, Inorg. Chem. 42 (2003) 6965; (c) S.R. Batten, J. Bjernemose, P. Jensen, B.A. Leita, K.S. Murray, B. Moubaraki, J.P. Smith, H. Toflund, Dalton Trans. (2004) 3370; (d) J.L. Manson, J.A. Schlueter, Inorg. Chim. Acta 357 (2004) 3975; (e) H.L. Sun, B.Q. Ma, S. Gao, S.R. Batten, Cryst. Growth Des. 5 (2005) 1331; (f) Z.H. Shao, J. Luo, R.F. Cai, X.G. Zhou, L.H. Weng, Z.X. Chen, Acta Crystallogr. C60 (2004) m250; (g) J. Luo, Z.H. Shao, E.Q. Gao, C.F. Wang, R.F. Cai, X.G. Zhou, Inorg. Chem. Commun. 9 (2006) 196; (h) L.F. Jones, L. O'Dea, D.A. Offermann, P. Jensen, B. Moubaraki, K.S. Murray, Polyhedron 25 (2006) 360; (i) C. Yuste, A. Bentama, S.E. Stiriba, D. Armentano, G. De Munno, F. Lloret, M. Julve, Dalton Trans. (2007) 5190; (j) C. Yuste, D. Armentano, N. Marino, L. Cañadillas-Delgado, F.S. Delgado, C. Ruiz-Pérez, D.P. Rillema, F. Lloret, M. Julve, Dalton Trans. (2008) 1583.

[12] (a) R. Feyerherm, A. Loose, H. Nojiri, J. Magn. Magn. Mater. 272–276 (2004) 1054;
(b) R. Feyerherm, A. Loose, S. Landsgesell, J.L. Manson, Inorg. Chem. 43 (2004) 6633.
[13] (a) I. Castro, J. Faus, M. Julve, M. Mollar, A. Monge, E. Gutiérrez-Puebla, Inorg. Chim. Acta 161 (1989) 97;
(b) I. Castro, J. Faus, M. Julve, Y. Journaux, J. Sletten, J. Chem. Soc., Dalton Trans. (1991) 2533;
(c) I. Castro, J. Sletten, J. Faus, M. Julve, Y. Journaux, F. Lloret, S. Alvarez, Inorg. Chem. 31 (1992) 1889;
(d) J. Sletten, M. Julve, F. Lloret, I. Castro, G. Seitz, K. Mann, Inorg. Chim. Acta 250 (1996) 219;
(e) I. Castro, M.L. Calatayud, J. Sletten, F. Lloret, J. Cano, M. Julve, K. Seitz, K. Mann, Inorg. Chem. 38 (1999) 4680;
(f) M.L. Calatayud, I. Castro, J. Sletten, F. Lloret, M. Julve, Inorg. Chim. Acta 300–302 (2000) 846;
(g) D. Cangussu, H.O. Stumpf, F. Lloret, M. Julve, V. González, H. Adams, J.A. Thomas, Inorg. Chim. Acta 358 (2005) 1113;
(h) D. Cangussu, H.O. Stumpf, H. Adams, J.A. Thomas, F. Lloret, M. Julve, Inorg. Chim. Acta 358 (2005) 2292;
(i) D. Cangussu, L.M. Toma, H.O. Stumpf, H. Adams, J.A. Thomas, F. Lloret, M. Julve, Polyhedron 27 (2008) 559.
[14] (a) R. Lescouëzec, G. Marinescu, J. Vaissermann, F. Lloret, J. Faus, M. Andruh, M. Julve, Inorg. Chim. Acta 350 (2003) 131;
(b) L.M. Toma, R. Lescouëzec, D. Cangussu, R. Llusar, J. Mata, S. Spey, J.A. Thomas, F. Lloret, M. Julve, Inorg. Chem. Commun. 8 (2005) 382.
[15] (a) E.I. Lerner, S.J. Lippard, J. Am. Chem. Soc. 98 (1976) 5397;
(b) E.I. Lerner, S.J. Lippard, Inorg. Chem. 16 (1977) 1546.
[16] A. Earnshaw, Introduction to Magnetochemistry, Academic Press, London, 1968.
[17] (a) G.M. Sheldrick, SADABS, Siemens Energy and Automation Inc., Madison, WI, USA, 1996;
(b) G.M. Sheldrick, SHELXTL/PC, An Integrated System for Solving and Refining Crystal Structures from Diffraction Data, Revision 5.1, Bruker AXSINC., Madison, WI, USA, 1998;
(c) SHELXTL, Version 6.14, Bruker AXS Inc., Madison, WI, USA, 2001;
(d) DIAMOND, Version 2.1d, Crystal Impact GbR, CRYSTAL IMPACT K, Brandeburg & H. Putz GBR, Bonn, Germany, 2000.
[18] K. Nakamoto, Infrared and Raman Spectra of Inorganic and Coordination Compounds, 4th ed., Wiley, New York, 1986. p. 228.
[19] A.W. Addison, T.N. Rao, J. Reedijk, J. Van Rijn, G.C. Verschoor, J. Chem. Soc., Dalton Trans. (1984) 1349.
[20] W.E. Estes, D.P. Gavel, W.E. Hatfield, D. Hodgson, Inorg. Chem. 17 (1978) 1415.
[21] J. Kozisek, M. Hvastijova, J. Kohout, J. Mrozinski, H. Köhler, J. Chem. Soc., Dalton Trans. (1991) 1773.

Polyhedron 27 (2008) 2585–2594

Contents lists available at ScienceDirect

Polyhedron

journal homepage: www.elsevier.com/locate/poly

Influence of some reaction conditions on the obtaining of tetra- and dinuclear zinc complexes of some Schiff bases derived from 2,6-diformyl-4-alkyl-phenols

Matilde Fondo [a], Ana M. García-Deibe [a,*], Noelia Ocampo [a], Jesús Sanmartín [b,*], Manuel R. Bermejo [b]

[a] Dpto. de Química Inorgánica, Fac. de Ciencias, Campus de Lugo, Univ. de Santiago de Compostela, 27002 Lugo, Spain
[b] Dpto. de Química Inorgánica, Fac. de Química, Campus Sur, Univ. de Santiago de Compostela, 15782 Santiago de Compostela, Spain

ARTICLE INFO

Article history:
Received 9 April 2008
Accepted 13 May 2008
Available online 24 June 2008

Keywords:
Macrocycle
Schiff base
Acetate bridge
Dinuclear complex
Tetranuclear complex
Zinc

ABSTRACT

A template 2:2:4 condensation of 2,6-diformyl-4-methyl-phenol, triethylenetetramine and zinc acetate gave rise to the crystallisation of $[\{Zn_4(H_4L^1)(OAc)_4\}\{Zn(OAc)_3(H_2O)\}(OAc)] \cdot 7H_2O$ (**1** · $7H_2O$), being H_6L^1 a macrocyclic diphenolate Schiff base ligand. Changing some operation conditions, other template reactions yielded dinuclear complexes of the type $Zn_2(L^n)(OAc) \cdot xH_2O$, where H_3L^n (n = 2, 3) are podant triphenolate Schiff base ligands derived from a 3:1 condensation of the corresponding 2,6-diformyl-4-alkyl-phenol (alkyl = Me or Bu^t, respectively) and triethylenetetramine. After recrystallisation, these two latter complexes could be X-ray characterised as $Zn_2(L^2)(OAc) \cdot 1.25H_2O \cdot 0.5MeCN$ (**2** · $1.25H_2O$ · 0.5MeCN), and $Zn_2(L^3)(OAc)$ (**3**). Furthermore, after addition of a 3:1 molar ratio of 2-amino-4-methyl-phenol to **3**, this underwent imidazolidine hydrolysis and a double imine condensation, yielding $Zn_2(L^4)(OAc)(HOAc) \cdot 2H_2O$ (**4** · $2H_2O$), where H_3L^4 is an acyclic pentadentate Schiff base derived from the 1:2 condensation of 2,6-diformyl-4-*tert*-butyl-phenol and 2-amino-4-methyl-phenol.

© 2008 Elsevier Ltd. All rights reserved.

1. Introduction

The cyclic Schiff base H_6L^1 (Scheme 1), derived from the 2:2 condensation of 2,6-diformyl-4-methyl-phenol and triethylenetetramine, was first obtained by Kahwa et al. in dinuclear lanthanide complexes [1]. The partial hydrolysis of these macrocyclic dinuclear complexes in mildly acid alcohol solutions resulted in mononuclear complexes of a podant Schiff base (H_3L^2, Scheme 1) [2]. Since then, several tetra- or dinuclear complexes of the mentioned macrocycle [3,4], and its *N*-alkylated derivatives [5,6] have been prepared by template reactions using a 1:1:2 (phenol:amine:metal salt) molar ratio.

During last years we have been working on the coordination chemistry of three-armed triphenolate Schiff bases derived from substituted salicylaldehydes and triethylenetetramine [7–10]. Now, we are presenting our studies on the influence of some reaction conditions when we attempted to obtain polynuclear complexes of some ligands derived from 2,6-diformyl-4-alkyl-phenols (alkyl = methyl or *tert*-butyl, Scheme 1). We have focused our attention on the susceptibility to hydrolysis of their N–C–N and C=N groups. Template reactions have been assayed employing 3:1:2, 1.5:1:2 and 1:1:2 phenol:amine:zinc acetate molar ratios. The use of a diamagnetic ion as zinc(II) has facilitated the identification of the reaction products through NMR techniques.

2. Results and discussion

It was reported that the success in the obtaining of macrocyclic complexes of *N*-alkylated derivatives of H_6L^1 (Scheme 1) arrives when the metal salt and the corresponding phenol are firstly mixed under aerobic conditions, and then, the tetraamine is added to this mixture. In contrast, no macrocyclic complexes were obtained when amine and metal salt were mixed in methanol, and the corresponding phenol subsequently added to the resulting solution, both in aerobic or anaerobic conditions [5].

The essence of the synthetic mechanism reported for these macrocyclic complexes [5] is the formation of two intermediates in methanol solution under aerobic conditions: $[M_2(phenol)(OAc)_2]^+$, which is air-stable, and $[M_2(1{:}1\ SB)(OAc)_2]^+$ (Scheme 2). Dimerisation by a double imine condensation of this second type of intermediate would afford the tetranuclear complexes desired.

In our case study (Scheme 2), the coordination of two zinc(II) ions to 2,6-diformyl-4-methyl-phenol to form $[Zn_2(phenol)(OAc)_2]^+$ seems to be a key factor in the activation of the C=O sites, favouring their reactivity, as it increases their electrophile character, and allowing the formation of the diphenolate macrocyclic Schiff base ligand H_6L^1. This could be confirmed by solving the crystal structure of $[\{Zn_4(H_4L^1)(OAc)_4\}\{Zn(OAc)_3(H_2O)\}(AcO)] \cdot 7H_2O$, **1** · $7H_2O$, which crystallised from the corresponding reaction mixture.

Although high temperatures and a moisture-laden atmosphere are not crucial factors, their concurrence does not favour the obtaining of this type of macrocyclic complexes, since hydrolysis could occur. In fact, the heating and vacuum concentration of the

* Corresponding authors.
E-mail addresses: qianadei@usc.es (A.M. García-Deibe), qisuso@usc.es (J. Sanmartín).

0277-5387/$ - see front matter © 2008 Elsevier Ltd. All rights reserved.
doi:10.1016/j.poly.2008.05.016

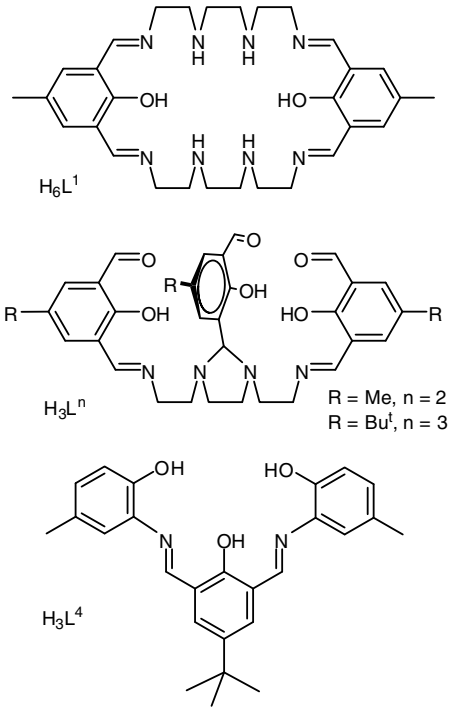

Scheme 1. Ligands used in this work.

yellowish mother liquor obtained after crystallisation of **1** · $7H_2O$, gave rise to the more stable dinuclear neutral complex $[Zn_2(L^2)(OAc)]$, **2** (Scheme 2), which contains a three-armed triphenolate Schiff base ligand $(L^2)^{3-}$, and whose presence was undoubtedly confirmed by NMR. This complex seems to result from an acid hydrolysis of two of the C=N groups of H_6L^1 to yield C=O ones, what joint to the losing of two of the metal ions and three of the acetate ligands, appears to lead to an imidazolidine condensation between adjacent secondary amine sites of the tetraamine, and one of the formyl groups of the 2,6-diformyl-4-methylphenol originated by the hydrolysis of the macrocycle. The characterisation of **1** · $7H_2O$ provides evidence of the presence in the reaction medium of limited amounts of water, being its presence essential for the hydrolysis process that these macrocyclic complexes can undergo [2].

Neutral dinuclear acyclic complexes of the type $[Zn_2(L^n)(OAc)] \cdot xH_2O$ (n = 2–3) have been also obtained by template methods employing 3:1:2, and even 1.5:1:2, (phenol:amine:zinc acetate) molar ratios. Thus, reaction stoichiometry does not seem to be a crucial factor in the success of these template syntheses. However, the order in which the reagents are added to the reaction medium could influence the final product by means of a change in the mechanism of the reaction (Scheme 3, top).

The isolation of H_3L^3, by stirring a methanol solution containing 2,6-diformyl-4-*tert*-butyl-phenol and triethylenetetramine in 3:1 molar ratio, supports the formation of the free ligand prior to the obtaining of $[Zn_2(L^n)(OAc)] \cdot H_2O$ (n = 2–3) complexes, when phenol and amine are firstly mixed, and the metal salt subsequently added to the resulting solution. The stability of the acyclic triphenolate Schiff base ligand sharply contrasts with the marked instability of the macrocyclic diphenolate Schiff base ligand [2].

Finally, the obtaining of $Zn_2(L^4)(OAc)(HOAc) \cdot 2H_2O$, **4** · $2H_2O$ (Scheme 3, bottom) evidences that **3** · $2H_2O$ undergoes an imidazolidine hydrolysis process in the presence of 2-amino-4-methylphenol at room temperature, showing the vulnerability of N–C–N bonds. Thus, it seems reasonable to suppose that **3** · $2H_2O$ undergoes hydrolysis to afford the air-stable $[Zn_2(phenol)(OAc)_2]^+$

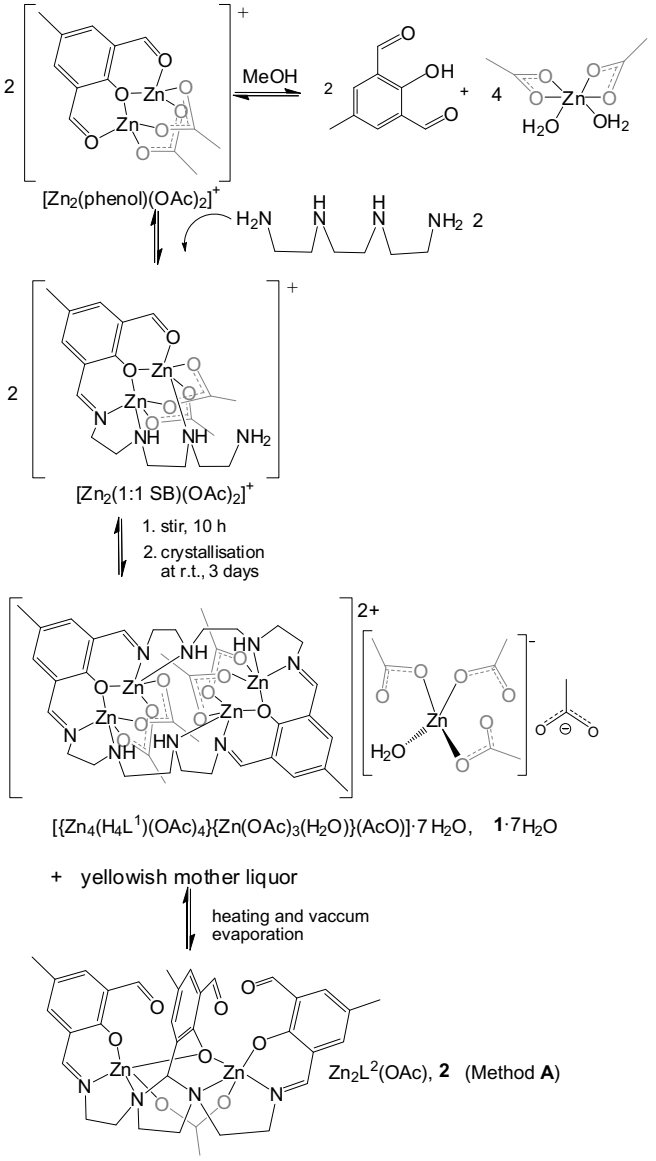

Scheme 2. Synthetic route used to obtain **1** · $7H_2O$ and **2** (Method **A**). The formation of $[Zn_2(phenol)(OAc)_2]^+$ and $[Zn_2(1:1\ SB)(OAc)_2]^+$ species as intermediates had been proposed by Sakiyama et al. [5].

(Schemes 2 and 3). Finally, the 1:2 condensation of this latter compound with 2-amino-4-methyl-phenol would yield **4** · $2H_2O$.

2.1. Crystal structure of 1 · $7H_2O$

X-ray diffraction analyses have revealed that single crystals directly obtained from the reaction mixture described in Scheme 2 contain in its unit cell co-crystallised $[Zn_4(H_4L^1)(OAc)_4]^{2+}$, $[Zn(OAc)_3(H_2O)]^-$, and acetate anions in a 2:2:2 ratio, with disordered water molecules captured in the crystal lattice. Its asymmetric unit only contains half molecule of each one of the two cations, one mononuclear anion, as well as an acetate anion. The macrocyclic ligand involved in $[Zn_4(H_4L^1)(OAc)_4]^{2+}$ is the result of the 2:2 condensation of 2,6-diformyl-4-methyl-phenol with triethylenetetramine. Selected bond distances and angles for all these species are listed in Table 1. An ORTEP view of one of the two $[Zn_4(H_4L^1)(OAc)_4]^{2+}$ cations is shown in Fig. 1, while $[Zn(OAc)_3(H_2O)]^-$ is shown in Fig. 2, together with the atom-numbering schemes for both complexes.

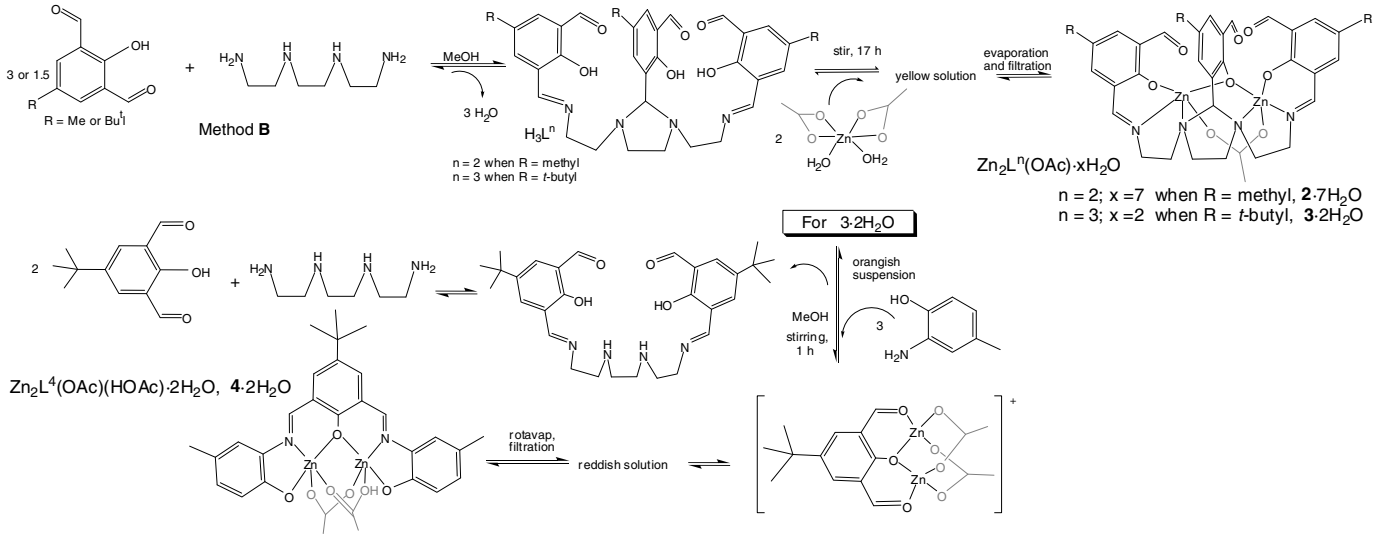

Scheme 3. Synthetic route used to obtain dinuclear acyclic complexes **2** · 7H_2O and **3** · 2H_2O (Method **B**, top); and proposed mechanism for the imidazolidine hydrolysis of **3** · 2H_2O (bottom) leading to obtain **4** · 2H_2O.

Table 1
Selected geometric parameters for **1** · 7H_2O

$[Zn_4(H_2L^1)(OAc)_4]^+$				$[Zn(OAc)_3(H_2O)]^-$	
Zn11–O13	1.970(5)	Zn21–O23	1.961(5)	Zn3–O5	1.964(5)
Zn11–O11	1.974(5)	Zn21–O21	1.946(5)	Zn3–O3	1.984(5)
Zn11–N102	2.008(5)	Zn21–N202	2.006(6)	Zn3–O1	1.984(5)
Zn11–O101	2.075(5)	Zn21–O201	2.119(5)	Zn3–O3W	2.021(5)
Zn11–N101	2.151(6)	Zn21–N201	2.164(6)	O1–C1	1.247(9)
Zn12–O10	1.981(5)	Zn22–O20	1.983(5)	O2–C1	1.245(10)
Zn12–O12	1.996(5)	Zn22–O22	1.970(5)	O3–C3	1.240(8)
Zn12–N103	2.012(6)	Zn22–N203	2.024(6)	O4–C3	1.248(9)
Zn12–O101	2.097(4)	Zn22–O201	2.092(5)	O5–C5	1.272(9)
Zn12–N104	2.149(5)	Zn22–N204	2.133(6)	O6–C5	1.234(9)
O10–C10	1.242(8)	O20–C20	1.264(8)		
O11–C10	1.244(8)	O21–C20	1.254(8)		
O12–C12	1.253(9)	O22–C22	1.248(9)		
O13–C12	1.237(8)	O23–C22	1.251(9)		
O13–Zn11–O11	125.69(19)	O21–Zn21–O23	126.1(2)	O5–Zn3–O3	131.3(2)
O13–Zn11–N102	121.4(2)	O21–Zn21–N202	116.7(2)	O5–Zn3–O1	111.9(2)
O11–Zn11–N102	112.5(2)	O23–Zn21–N202	117.0(2)	O3–Zn3–O1	102.6(2)
O13–Zn11–O101	94.3(2)	O21–Zn21–O201	93.75(19)	O5–Zn3–O3W	101.0(2)
O11–Zn11–O101	93.18(19)	O23–Zn21–O201	91.62(19)	O3–Zn3–O3W	110.2(2)
N102–Zn11–O101	88.7(2)	N202–Zn21–O201	88.0(2)	O1–Zn3–O3W	93.7(2)
O13–Zn11–N101	88.9(2)	O21–Zn21–N201	94.7(2)		
O11–Zn11–N101	91.7(2)	O23–Zn21–N201	88.9(2)		
N102–Zn11–N101	82.6(2)	N202–Zn21–N201	82.2(2)		
O101–Zn11–N101	171.06(19)	O201–Zn21–N201	169.19(19)		
O10–Zn12–O12	124.3(2)	O22–Zn22–O20	122.8(2)		
O10–Zn12–N103	117.8(2)	O22–Zn22–N203	116.8(2)	*OAc*	
O12–Zn12–N103	117.7(2)	O20–Zn22–N203	120.2(2)	O7–C7	1.280(10)
O10–Zn12–O101	93.19(19)	O22–Zn22–O201	95.71(19)	O8–C7	1.260(9)
O12–Zn12–O101	93.0(2)	O20–Zn22–O201	90.68(19)		
N103–Zn12–O101	87.2(2)	N203–Zn22–O201	87.5(2)	O7–C7–O8	124.3(8)
O10–Zn12–N104	93.0(2)	O22–Zn22–N204	93.3(2)		
O12–Zn12–N104	90.7(2)	O20–Zn22–N204	90.9(2)		
N103–Zn12–N104	82.3(2)	N203–Zn22–N204	81.6(2)		
O101–Zn12–N104	169.3(2)	O201–Zn22–N204	168.2(2)		
Zn11–O101-Zn12	100.12(18)	Zn22–O201–Zn21	99.95(19)		

Hydrogen atoms potentially bonded to their N or O atoms were studied with particular care, in order to determine the neutral or ionic nature of each one of the species. Thus, in the case of $[Zn_4(H_4L^1)(OAc)_4]^{2+}$ (Fig. 1), ΔF maps showed electron densities at chemically reasonable positions near to the amine N atoms of the macrocyclic ligand, and which could be assumed with full occupancies. This does not occur for any acetate group, neither coordinated nor free, what joint to their geometric parameters have leaded to be considered as anions in all the cases. Hence, the mononuclear complex $[Zn(OAc)_3(H_2O)]^-$ is acting as one of the two monoanionic counterions that each $[Zn_4(H_4L^1)(OAc)_4]^{2+}$ complex needs to achieve electric neutrality.

Each one of the zinc ions corresponding to the macrocyclic complex is bonded to one imine and one amine N atoms, one

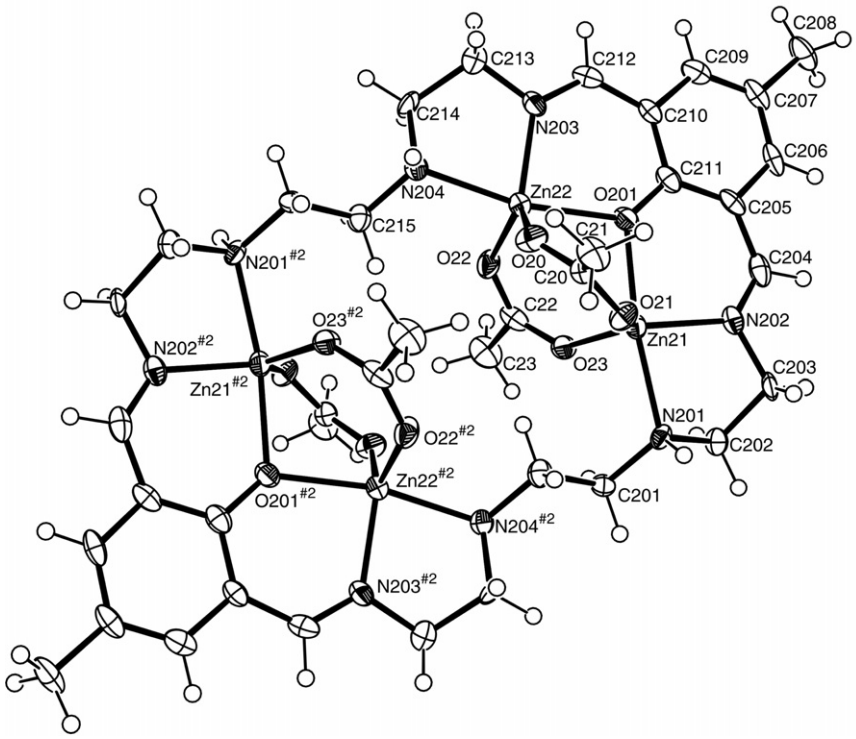

Fig. 1. An ORTEP view of the molecular structure of one of the $[Zn_4(H_4L^1)(OAc)_4]^{2+}$, complexes. The other molecule of this cationic complex present in the unit cell is totally equivalent, being its numbering scheme comparable, but with 1 as first figure. Ellipsoids are drawn at 50% probability.

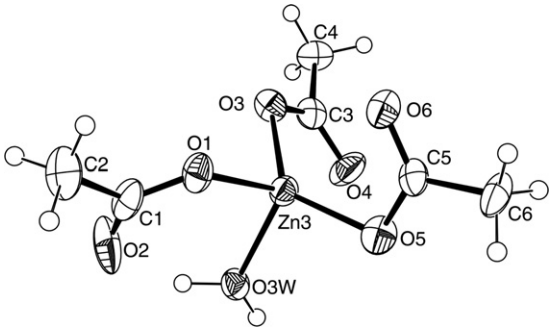

Fig. 2. An ORTEP view of the molecular structure of $[Zn(OAc)_3(H_2O)]^-$. Ellipsoids are drawn at 50% probability.

μ_2-bridging phenolate O atom, and two O atoms corresponding to two μ_2-η^1:η^1 bridging acetate groups, what affords ZnO_3N_2 coordination polyhedra. Their geometries are markedly distorted from regular trigonal-bipyramids, with the phenolate O atom and the amine N atom at their apexes. The $Zn–O_{(phen)}$ and $Zn–O_{(OAc)}$ distances of the macrocyclic complex fall in the range commonly found for zinc(II) complexes with these donor atoms [7,8,11]. The $Zn–N_{(imine)}$ and $Zn–N_{(amine)}$ distances are similar to those found for complexes containing related three-armed ligands [7,8].

The geometry around the metal ion in $[Zn(OAc)_3(H_2O)]^-$ can be depicted as an irregular tetrahedron formed by four O atoms, one of the coordinated water molecule, and the other from monodentate acetate anions (Fig. 2). It must be noted that O4 and O6, can be considered as secondarily bonded to the zinc ion. These interactions are responsible for the distortion of the coordination polyhedron. Selected bond distances and angles are also given in Table 1. The $Zn–O_{(AcO)}$ lengths found in $[Zn(OAc)_3(H_2O)]^-$ can be considered in the range expected in four-coordinated carboxylate zinc complexes [12], being $Zn–O_{(water)}$ also consistent with similar bond lengths [13].

Finally, an intricate H bonding scheme involving the water molecules solvated and the different acetate groups significantly contributes to the crystal packing.

2.2. Crystal structures of $2 \cdot 1.25H_2O \cdot 0.5MeCN$ and 3

Single crystals of $\mathbf{2} \cdot 1.25H_2O \cdot 0.5MeCN$ (Fig. 3) and **3** (Fig. 4) were obtained from recrystallisation of $\mathbf{2} \cdot 7H_2O$ and $\mathbf{3} \cdot 2H_2O$ (Scheme 3), respectively, and as indicated in Section 4. Their X-ray diffraction analyses showed that both compounds consisted of neutral dinuclear complexes with three-armed Schiff base ligands, and some water and solvent molecules as solvates.

The spatial array of the podant triphenolate Schiff base ligands $(L^2)^{3-}$ and $(L^3)^{3-}$ are similar in their respective complexes. These ligands use each one of their N_2O compartments to allocate a zinc atom. Both zinc centres are doubly bridged by a phenolate O atom of the central arm, and by an acetate group acting as a μ_2-η^1:η^1 bridge, what gives rise to ZnN_2O_3 coordination chromophores. These adopt distorted square pyramidal dispositions around the metal centres, with the acetate oxygen atoms at the apexes of their respective distorted pyramids.

Main distances and angles for $\mathbf{2} \cdot 1.25H_2O \cdot 0.5MeCN$ and **3** are listed in Tables 2 and 3, respectively. All the distances and angles are in the range of those expected for this type of complexes [7,8,11], and reflect the symmetry of their phenolate bridges. However, it should be noted that the apical $Zn–O_{(AcO)}$ distances are the shortest ones, as occurred in the macrocyclic complexes, what leads to some distortion of the coordination polyhedra.

A curious feature of $\mathbf{2} \cdot 1.25H_2O \cdot 0.5MeCN$ arises from the conformation adopted by one of O atoms (O18a) of its carbonyl groups, which is disordered on two different occupation sites (0.52 and 0.48, for O18a and O18b, respectively). This leads to the chirality of part of the molecules of this complex (52%) in the solid state,

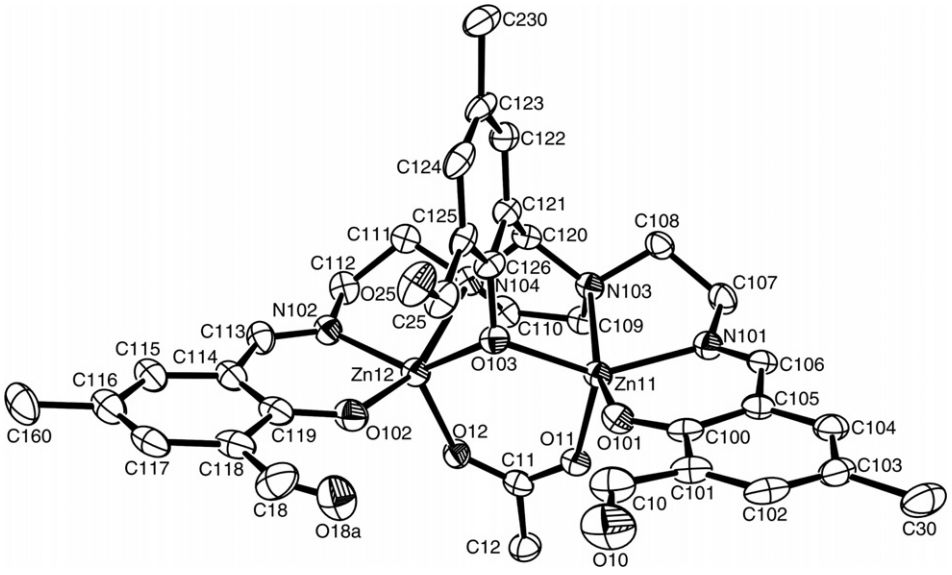

Fig. 3. An ORTEP view of the molecular structure of **2**. Only one of the disordered sites (O18a, 52% occupation) is shown in the figure, and being this the only one involved in the H bonding scheme. Ellipsoids are drawn at 40% probability.

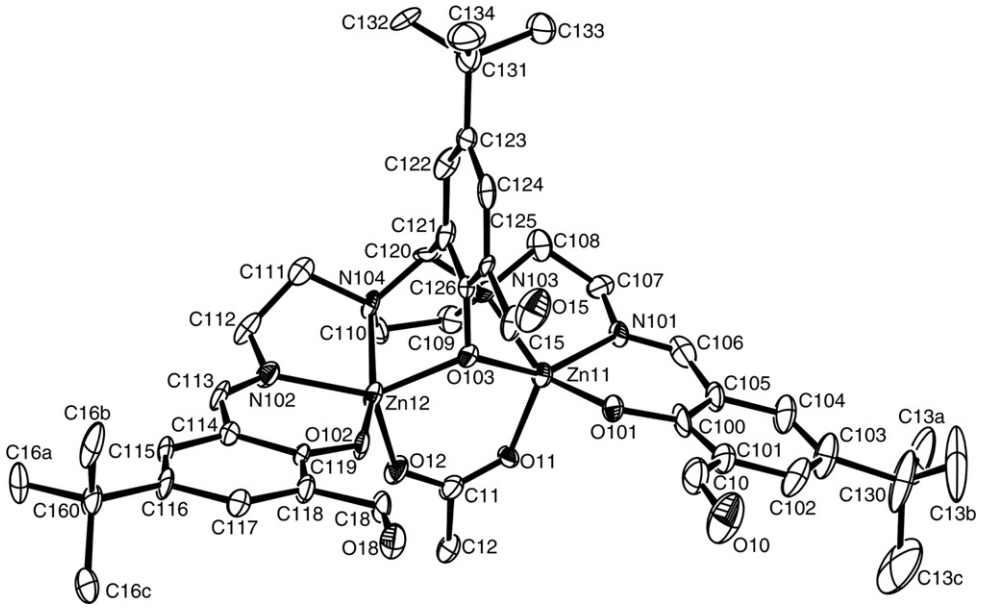

Fig. 4. An ORTEP view of the molecular structure of one of the complex molecules included in the asymmetric unit of **3**. Ellipsoids are drawn at 40% probability.

as this disparity avoids the C_s symmetry that the other 48% of the achiral molecules present, and being only the most occupied site involved in the H bond scheme. In fact, this crystal corresponds to a non-centrosymmetric polar group as *R*3*c*. The correction of the absolute structure was confirmed by the low value observed for the Flack's parameter [14].

2.3. Physicochemical characterisation of the dinuclear complexes

The formation of the complexes **1**, **2, 3** and **4** was evidenced in solid state by microanalytical data and IR spectroscopy, whereas ^{1}H NMR spectroscopy and ESI-MS data show the preservation of the acetate complexes in solution, at least during the time employed in these experiments.

From the current NMR results (Fig. 5), and considering the ligand symmetry of $(L^2)^{3-}$ and $(L^2)^{3-}$, the observation of two separate signals for each methylene group (*e.g.* 3.83 and 2.61 ppm for H_2C–N=C) in the spectra of **2** · 7H_2O and **3** · 2H_2O must be consequence of a diastereotopic nature of these geminal protons, on the NMR timescale at room temperature. This is indicative of a non-planar arrangement for the triethylenetetramine residue in **2** · 7H_2O and **3** · 2H_2O, and reveals a certain kinetic stability of these complexes in DMSO solution. Moreover, the chemical non-equivalence between the free formyl, as well as alkyl, substituents in $(L^n)^{3-}$ is clearly observed through their corresponding chemical shifts.

All the complexes present a signal near to 2 ppm in their ^{1}H NMR spectra that is in agreement with the coordination of the acetate ligand to the metal centres, while a peak near to 4 ppm indicates the permanence of the imidazolidine ring in solution of complexes **2** and **3**. This signal corresponding to the HCN_2 proton disappears in the case of **1** · 7H_2O and **4** · 2H_2O, what is indicative

Table 2
Selected bond distances and angles for **2** · 1.25H_2O · 0.5MeCN

Zn11–O11	1.976(2)	Zn12–O12	1.943(2)
Zn11–O101	2.004(2)	Zn12–O103	1.981(2)
Zn11–O103	2.012(2)	Zn12–O102	1.987(3)
Zn11–N101	2.043(3)	Zn12–N102	2.018(3)
Zn11–N103	2.285(3)	Zn12–N104	2.438(3)
O11–Zn11–O101	102.48(10)	O12–Zn12–O103	105.84(10)
O11–Zn11–O103	103.13(10)	O12–Zn12–O102	105.99(11)
O101–Zn11–O103	90.57(10)	O103–Zn12–O102	92.61(11)
O11–Zn11–N101	111.54(11)	O12–Zn12–N102	113.05(11)
O101–Zn11–N101	89.90(11)	O103–Zn12–N102	138.05(11)
O103–Zn11–N101	144.35(11)	O102–Zn12–N102	91.39(12)
O11–Zn11–N103	101.51(10)	O12–Zn12–N104	96.17(10)
O101–Zn11–N103	155.96(10)	O103–Zn12–N104	83.19(9)
O103–Zn11–N103	85.50(10)	O102–Zn12–N104	157.74(10)
N101–Zn11–N103	79.86(11)	N102–Zn12–N104	77.74(11)
		Zn11–O103–Zn12	113.84(11)

Table 3
Selected bond distances and angles for **3**

Zn11–O11	1.972(5)	Zn21–O21	1.953(6)
Zn11–O101	1.993(5)	Zn21–O201	1.982(6)
Zn11–O103	1.999(5)	Zn21–O203	1.988(4)
Zn11–N101	2.022(6)	Zn21–N201	2.013(4)
Zn11–N103	2.349(6)	Zn21–N203	2.388(7)
Zn12–O12	1.982(5)	Zn22–O22	1.974(5)
Zn12–O102	1.991(5)	Zn22–O202	1.985(5)
Zn12–O103	2.010(5)	Zn22–O203	1.997(5)
Zn12–N102	2.028(6)	Zn22–N202	2.018(6)
Zn12–N104	2.322(6)	Zn22–N204	2.294(6)
O11–Zn11–O101	106.4(2)	O21–Zn21–O201	105.0(3)
O11–Zn11–O103	104.5(2)	O21–Zn21–O203	106.6(2)
O101–Zn11–O103	92.5(2)	O201–Zn21–O203	92.8(3)
O11–Zn11–N101	108.3(2)	O21–Zn21–N201	108.0(2)
O101–Zn11–N101	90.0(2)	O201–Zn21–N201	91.0(3)
O103–Zn11–N101	144.9(2)	O203–Zn21–N201	142.9(2)
O11–Zn11–N103	99.4(2)	O21–Zn21–N203	99.4(2)
O101–Zn11–N103	153.9(2)	O201–Zn21–N203	155.2(2)
O103–Zn11–N103	84.9(2)	O203–Zn21–N203	83.8(2)
N101–Zn11–N103	77.9(2)	N201–Zn21–N203	77.8(3)
O12–Zn12–O103	105.2(2)	O22–Zn22–O203	107.0(2)
O12–Zn12–O102	104.5(2)	O22–Zn22–O202	104.5(2)
O103–Zn12–O102	90.22(19)	O203–Zn22–O202	88.9(2)
O12–Zn12–N102	110.5(2)	O22–Zn22–N202	110.0(3)
O103–Zn12–N102	143.0(2)	O203–Zn22–N202	142.0(2)
O102–Zn12–N102	90.0(2)	O202–Zn22–N202	90.2(2)
O12–Zn12–N104	98.9(2)	O22–Zn22–N204	97.7(2)
O103–Zn12–N104	85.9(2)	O203–Zn22–N204	87.7(2)
O102–Zn12–N104	156.5(2)	O202–Zn22–N204	157.6(2)
N102–Zn12–N104	79.5(2)	N202–Zn22–N204	79.0(2)
Zn11–O103–Zn12	112.5(2)	Zn22–O203–Zn21	111.0(2)

of the hydrolysis of this ring. The observation of imine, aromatic, methylene and methyl signals in the spectrum of **1** · 7H_2O supports the preservation of the diphenolate Schiff $(H_4L^1)^{2-}$.

The limited number of signals observable in the NMR spectrum of **4** · 2H_2O (Fig. 6) allows an unequivocal full assignment of the signals corresponding to $(L^4)^{3-}$. Thus, the presence of the imine and *tert*-butyl signals, which had been already observed in the spectrum of **3** · 2H_2O, are two clear evidences to support the formation of the triphenolate Schiff. An additional peak at 2.20 ppm reveals the presence of the methyl groups from the 2-amino-4-methyl-phenol residues of $(L^4)^{3-}$. Moreover, the integration value observed for the signal assigned to the methyl group of the acetate ligand in the spectrum of **4** · 2H_2O is coherent with a 6:2 ratio for methyl:imine protons and supports the $Zn_2(L^4)(OAc)(HOAc) \cdot 2H_2O$ formula deduced from elemental analysis and mass spectroscopy. The remaining four signals, two singlets and two "doublets" (in appearance) show the expected chemical shifts.

The observation of a very strong IR band at about 1675 cm^{-1}, which is assignable to $\nu(C{=}O)_{(formyl)}$, is coherent with the presence of free formyl groups in **2** · 7H_2O and **3** · 2H_2O. On the contrary, no bands at the mentioned value can be observed in the **4** · 2H_2O spectrum (Fig. 7), supporting the formation of a new Schiff base ligand derived from a 1:2 condensation of 2,6-diformyl-4-*tert*-butyl-phenol and 2-amino-4-methyl-phenol, this is $(L^4)^{3-}$.

The IR spectra of all these complexes exhibit two intense bands assignable to ν_a(COO) and ν_s(COO) modes that support the presence of coordinated acetate groups. Fig. 7 shows these and other significant bands for **4** · 2H_2O. The Δ value [$\Delta = \nu_a(COO) - \nu_s(COO)$] of about 135 cm^{-1}, which is close to those reported for other acetate bridged complexes [15,16], points to a bidentate bridging behaviour.

3. Conclusions

The reaction stoichiometry does not seem to be a key factor in the obtaining of dinuclear complexes of three-armed triphenolate Schiff base ligands, derived from a 3:1 condensation of 2,6-diformyl-4-alkyl-phenol and triethylenetetramine, whereas the order in which the reagents are added to the reaction medium seems to be more important, although not deciding in the final product (macrocyclic tetranuclear or acyclic dinuclear complexes), if water and acid species are present in enough amounts to hydrolyse the tetranuclear cyclic complexes.

The instability in methanol solution of the tetra- and dinuclear complexes of H_6L^1 and H_3L^3, respectively, lies in the vulnerability of their respective C=N and N–C–N groups to hydrolysis. This occurs in mildly acid methanol solutions with limited amounts of water.

4. Experimental

4.1. Materials and methods

Chemicals of the highest commercial grade available (Aldrich) were used as received, without further purification. Elemental analyses were performed on a Carlo Erba EA 1108 analyser. Positive electrospray ionisation mass spectra were recorded on a LC/MSD Hewlett Packard 1100 spectrometer, using methanol as solvent. NMR spectra were recorded on Bruker spectrometers, using DMSO-d_6 or $CDCl_3$ as solvents. FTIR spectra were recorded as KBr pellets on a Bio-Rad FTS 135 spectrophotometer in the range 4000–600 cm^{-1}. These characterisation analyses were performed at the in-house services (CACTUS).

4.2. Single crystal X-ray diffraction analyses

Crystallographic data at 100 K were collected on a Smart CCD-1000 diffractometer for **1** · 7H_2O, while those corresponding to **2** · 1.25H_2O · 0.5MeCN and **3** were collected on an APEX-II CCD Bruker diffractometer. Graphite monochromated Mo Kα radiation (λ = 0.71073 Å) from a fine focus sealed tube source has been used in the three cases. The computing data reduction, with correction for Lorentz and polarisation factors, was done using XPREP software [17]. Crystal and refinement data for these compounds are summarised in Table 4.

Despite attempts made to select a single crystal, finally a twinned one was selected for data collection corresponding to **1** · 7H_2O. Its structure was identified as a non-merohedral twin using RLATT. The collected reflections were processed with the program CELLNOW, which found two twin components. The absorption

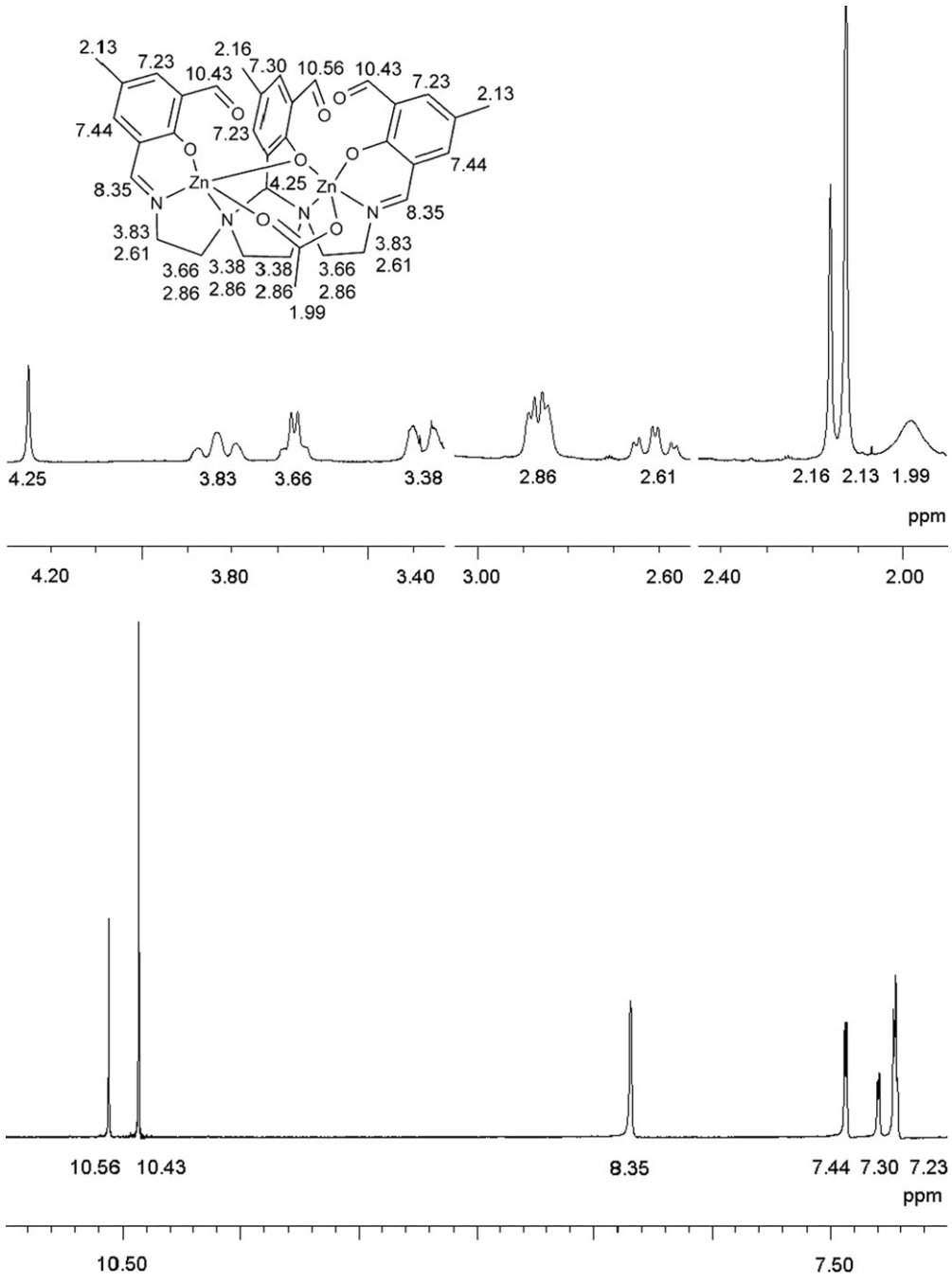

Fig. 5. ^{1}H NMR spectrum of **2** · 7H_2O in DMSO-d_6. Chemical shifts are below their corresponding signals.

correction was applied using TWINABS [18]. The final refinements were performed with all unique reflections using the HKLF 5 format in SHELXL-97 [19]. The ratio of the two twin components were approximately 0.73:027.

Multi-scan absorption corrections were performed with the help of the SADABS routine [20] for **2** · 1.25H_2O · 0.5MeCN and **3**. Although some twinned crystals had been previously selected for **3**, this feature was not detected for the data set whose results are shown herein. However, the quality of these data was not completely satisfactory. In fact, the contribution of the electron density of disordered solvated molecules (methanol, acetonitrile and/or water) had to be subtracted from the measured structure factors using SQUEEZE [21]. After this, subsequent refinement then converged with *R* factors and parameter errors significantly better than those obtained for all attempts made to model the solvent disorder, and being the largest residual peaks adjacent to zinc ions. Up to eleven voids (2594.5 Å^3, 25.3% of the volume) were found in the unit cell of **3**, but only two of them, around two special positions, were actually significant. These two voids, of about 1207 Å^3, meant 90 e each one, so it was difficult to determine the actual nature of the solvated molecules, especially for this type of complexes, which usually favour intricate H bonding schemes and considerable solvatation [7–10]. Despite these inconveniences, the quality of the refinement appear to be reasonable, since these data allowed determining the molecular structure of this complex, which is clearly defined and totally similar for both complex molecules found in the asymmetric unit (Table 3).

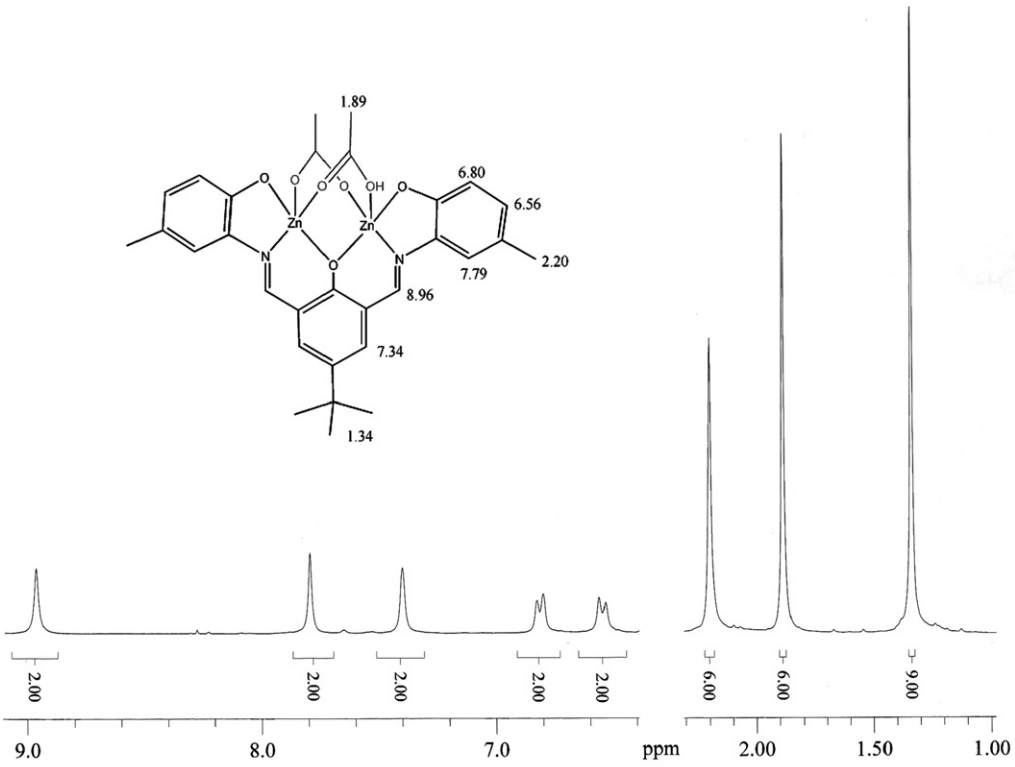

Fig. 6. ^{1}H NMR spectrum of **4** · 2H_2O in DMSO-d_6. Integration values are indicated below their corresponding signals.

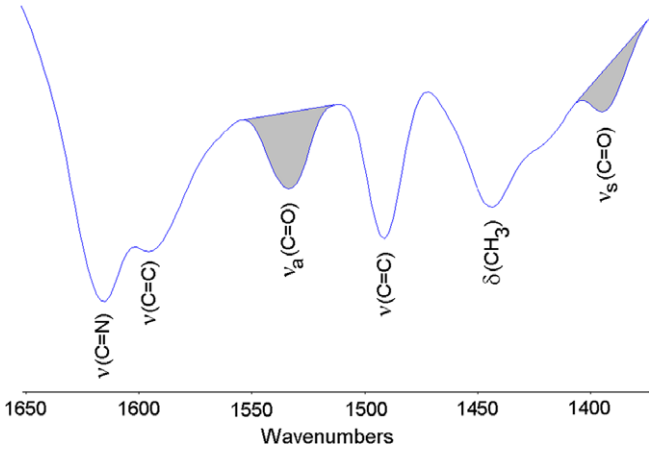

Fig. 7. Partial view of the IR spectrum of **4** · 2H_2O. Bands attributed to ν_a(COO) and ν_s(COO) have been shaded.

The structures were solved by a combination of the direct methods, using SHELXS-97 [19] or DIRDIF99 [22], and difference Fourier syntheses, and refined against F^2 by the full-matrix least-squares technique, using the SHELXL-97 program [19], via WINGX [23]. Non-hydrogen atoms were anisotropically refined for all complex molecules, but some atoms corresponding to disordered sites or solvated molecules with partial occupancies were isotropically treated.

In all cases, H atoms attached to C atoms were included in the model at geometrically calculated positions, and refined in a riding mode using SHELXL [19] default parameters, whereas those bonded to O or N atoms were objectively found on Fourier difference maps. These positions were studied with particular care for **1** · 7H_2O, in order to determine the neutral or ionic nature of each one of the species, as indicated above. The coordinates of hydrogen atoms bonded to N or O atoms were freely refined, but their isotropic thermal parameters were set at 1.2 times the isotropic equivalent of the attached atom. This was not always possible for disordered and/or low-occupancy atoms corresponding to solvated water molecules, so several H atoms could not be found.

*R*3*c* symmetry deduced from a statistical analysis of data collected for **2** · 1.25H_2O · 0.5MeCN was confirmed by successful refinement in this non-centrosymmetric space group. The absolute structure was determined from the Flack parameter [14], $x = -0.008(9)$.

4.3. Ligand synthesis

H_3L^3 could be obtained by stirring a methanol solution containing 2,6-diformyl-4-*tert*-butyl-phenol and triethylenetetramine in 3:1 molar ratio (Scheme 2) for 6 h. Vacuum concentration of the resulting solution, and then, addition of diethyl ether yielded a yellow solid that was filtered, washed with diethyl ether, and dried in vacuum. ^{1}H NMR spectrum showed that the solid was H_3L^3 with their starting compounds as insignificant impurities.

H_3L^3. Yellow powder. ^{1}H NMR (300 MHz, $CDCl_3$, ppm) 14.00 (s, 2H, *H*O), 11.10 (s, 1H, *H*O), 10.24 (s, 2H, *H*CO), 10.11(s, 1H, *H*CO), 8.28 (s, 2H, *H*CN), 7.88 (s, 2H, H_{arom}), 7.66 (s, 1H, H_{arom}), 7.51 (s, 1H, H_{arom}), 7.43 (s, 2H, H_{arom}), 4.10 (s, 1H, *H*CN_2), 3.62–2.76 (12H, H_{aliph}), 1.29 (s, 18H, H_3C).

4.4. Complexes syntheses

4.4.1. 1 · 7H_2O

This compound was obtained when 2,6-diformyl-4-methyl-phenol (0.110 g, 0.67 mmol) and zinc(II) acetate dihydrate (0.295 g, 1.34 mmol) were firstly mixed in methanol (60 mL), and then the tetraamine (0.098 g, 0.67 mmol) added to this mixture (Scheme 2). The resulting solution was stirred for 10 h, and then

Table 4
Crystal data and structure refinement for **1** · 7H_2O,**2** · 1.25H_2O · 0.5MeCN and **3**

Compound	**1** · 7H20 [{$Zn_4(H_4L^1)(OAc)_4$} {$Zn(OAc)_3(H_2O)$}(OAc)] · 7H_2O	**2** · 1.25H_2O · 0.5MeCN $Zn_2(L^2)(OAc)$ · 0.5MeCN · 1.25H_2O	**3** $Zn_2(L^3)(OAc)$
Empirical formula	$C_{46}H_{76}N_8O_{26}Zn_5$	$C_{36}H_{39.83}N_{4.50}O_{9.25}Zn_2$	$C_{44}H_{54}N_4O_8Zn_2$
Formula weight	1484.00	814.30	897.65
Crystal system	triclinic	trigonal	monoclinic
Space group	$P\bar{1}$ (No. 2)	$R3c$ (No. 161)	$P2_1/n$ (No. 14)
Unit cell dimensions			
a (Å)	15.363(2)	27.3374(8)	25.816(2)
b (Å)	15.466(2)	27.3374(8)	13.0040(11)
c (Å)	16.084(2)	26.3641(17)	31.171(3)
α (°)	73.622(2)	90	90
β (°)	65.784(2)	90	102.008(4)
γ (°)	63.607(2)	120	90
Volume (Å^3)	3098.7(7)	17063.1(13)	10235.6(15)
Z	2	18	8
D_{calc} (Mg/m^3)	1.590	1.426	1.165
Absorption coefficient (mm^{-1})	1.993	1.324	0.985
F(000)	1532	7584	3760
Crystal size (mm)	0.34 × 0.12 × 0.07	0.26 × 0.10 × 0.08	0.67 × 0.15 × 0.04
θ Range for data collection (°)	2.16–24.89	2.40–26.40	1.34–23.30
Index ranges	$-16 \leqslant h \leqslant 18$, $-17 \leqslant k \leqslant 18$, $0 \leqslant l \leqslant 19$	$-29 \leqslant h \leqslant 0$, $0 \leqslant k \leqslant 34$, $-32 \leqslant l \leqslant 32$	$-28 \leqslant h \leqslant 28$, $0 \leqslant k \leqslant 14$, $0 \leqslant l \leqslant 34$
Reflection collected/independent reflections (R_{int})	63209, 10741 (0.0626)	228502/7728 (0.0630)	73831/14778 (0.0950)
Data/restraints/parameters	10741/0/790	7728/1/498	14778/0/1080
Goodness-of-fit on F^2	1.055	0.963	0.924
Final R indices [$I > 2\sigma(I)$]	R_1 = 0.0601, wR_2 = 0.1572	R_1 = 0.0344, wR_2 = 0.0829	R_1 = 0.0756, wR_2 = 0.1777
R indices (all data)	R_1 = 0.1139, wR_2 = 0.1777	R_1 = 0.0440, wR_2 = 0.0861	R_1 = 0.1425, wR_2 = 0.1989
Largest difference in peak and hole (e Å^{-3})	0.983 and −0.884	0. 411 and −0.225	0.904 and −1.079

was allowed to stand at ambient temperature in an open flask. Yellow single crystals suitable for X-ray diffraction studies were deposited within 3 days. After this time, concentration of the mother liquor on a rotavap yielded a yellow powdery solid, latter NMR characterised as **2**, which was filtered, washed with diethyl ether, and dried in vacuum.

1 · 7H_2O: Yellow powder (0.14 g); *Anal.* Calc. for $C_{46}H_{82}N_8O_{26}Zn_5$ (M, 1489 g mol^{-1}): C, 37.07; H, 5.51; N, 7.52. Found: C, 38.28; H, 5.22; N, 6.91%. FTIR (KBr, cm^{-1}): ν(O–H) 3419(b,m), ν(C=N) 1647(vs), $\nu_a(COO_{ionic})$ 1598(vs,br), $\nu_a(COO_{bridge})$ 1547(vs), $\nu_s(COO_{ionic})$ 1437(vs,br), $\nu_s(COO_{bridge})$ 1399(vs), ν(C–N) 1333(m); ^{1}H NMR (300 MHz, DMSO-d_6, ppm) 8.49 (s, *H*CN), 7.36 (s, H_{arom}), 3.69 (m, H_2C–N=C), 2.88 (m, H_2C–H_2C–N=C), 2.22 (s, H_3C), 1.76 (s, $H_3C_{(OAc)}$).

4.4.2. Compounds 2 and 3

As commented above, **2** can be obtained by concentration of the mentioned mother liquor of **1** (Method **A**). Likewise, **2** · 7H_2O and **3** · 2H_2O were obtained by stirring a methanol solution containing the corresponding 2,6-diformyl-4-alkyl-phenol (alkyl = Me or Bu^t), triethylenetetramine and zinc(II) acetate dihydrate in 3:1:2 molar ratio for 17 h (Scheme 2) (Method **B**). Thus, when 2,6-diformyl-4-alkyl-phenols (1.20 mmol), and triethylenetetramine (0.058 g, 0.40 mmol) were firstly mixed in methanol (20 mL), and about 15 min later, $Zn(OAc)_2(H_2O)_2$ (0.176 g, 0.80 mmol) was added to the resulting suspensions, yellow solutions were obtained. Vacuum concentration of these solutions and the subsequent addition of diethyl ether yielded yellow solids that were filtered, washed with diethyl ether, and dried in vacuum. Recrystallisation at room temperature of these solids in a acetonitrile:ethanol 1:1 mixture gave rise to crystal suitable for X-ray diffraction studies of **2** · 1.25H_2O · 0.5MeCN and **3**.

Similar template reactions, employing the same reaction conditions mentioned above, but with 1.5:1:2 (phenol:amine:metal salt) molar ratios led to the formation of **2** · 6H_2O and **3** · 6H_2O (Method **C**), although these yields were not so good as those obtained for **2** · 7H_2O and **3** · 2H_2O (Method **B**).

2 · *7H$_2$O* (*Method **B***): Yellow powder (0.20 g, 56%); *Anal.* Calc. for $C_{35}H_{36}N_4O_8Zn_2$ · 7H_2O (M, 896.80 g mol^{-1}): C, 46.83; H, 5.57; N, 6.24. Found: C, 46.72; H, 4.85; N, 6.19%. m/z (ESI$^+$-MS, methanol, 150 V): 793.4 (100%) [Zn_2L^2(OAc)+Na]$^+$; FTIR (KBr, cm^{-1}): ν(O–H) 3450(b,m), ν(C=O)$_{(formyl)}$ 1673(vs), ν(C=N) 1635(vs), ν_a(COO) 1535(vs), ν_s(COO) 1399(s), ν(C–N) 1339(m); ^{1}H NMR (300 MHz, DMSO-d_6, ppm) 10.56(s, 1H, *H*CO), 10.43 (s, 2H, *H*CO), 8.35 (s, 2H, *H*CN), 7.44 (s, 2H, H_{arom}), 7.30 (s, 1H, H_{arom}), 7.23 (s, 3H, H_{arom}), 4.25 (s, 1H, *H*CN_2), 3.83 (m, 2H, J = 12.4 Hz, H_2C), 3.66 (m, 2H, J = 4.1 Hz, H_2C), 3.38 (m, 2H, J = 9.4 Hz, H_2C), 2.86 (m, 4H, J = 9.4, 4.1 Hz, H_2C), 2.61 (m, 2H, J = 12.4, 3.6 Hz, H_2C), 2.16 (s, 3H, H_3C), 2.13 (s, 6H, H_3C), 1.99 (s, 3H, $H_3C_{(OAc)}$).

2 · *6H$_2$O (Method **C***): Yellow powder (0.13 g, 18%); *Anal.* Calc. for $C_{35}H_{36}N_4O_8Zn_2$ · 6H_2O (M, 878.80 g mol^{-1}): C, 47.79; H, 5.46; N, 6.37. Found: C, 47.22; H, 5.02; N, 6.41%. The remaining characterisation data are totally similar to those corresponding to **2** · 7H_2O.

3 · *2H$_2$O* (*Method **B***): Yellow powder (0.24 g, 64%); *Anal.* Calc. for $C_{44}H_{54}N_4O_8Zn_2$ · 2H_2O (M, 932.76 g mol^{-1}): C, 56.61; H, 6.22; N, 6.00. Found: C, 56.01; H, 6.20; N, 5.65%. m/z (ESI$^+$-MS, methanol, 150 V): 921.2 (100%) [Zn_2L^3(OAc)+Na]$^+$, FTIR (KBr, cm^{-1}): ν(O–H) 3440(b,m), ν(C=O) 1676(vs), ν(C=N) 1635(vs), ν_a(COO) 1530(vs), ν_s(COO) 1399(s), ν(C–N) 1339(m); ^{1}H NMR (300 MHz, DMSO-d_6, ppm) 10.62(s, 1H, *H*CO), 10.46 (s, 2H, *H*CO), 8.46 (s, 2H, *H*CN), 7.65 (s, 2H, H_{arom}), 7.55 (s, 1H, H_{arom}), 7.50 (s, 2H, H_{arom}), 7.42 (s, 1H, H_{arom}), 4.35 (s, 1H, *H*CN_2), 3.85 (m, 2H, J = 12.4 Hz, H_2C), 3.69 (m, 2H, J = 4.4 Hz, H_2C), 3.42 (m, 2H, J = 12.7 Hz, H_2C), 2.88 (m, 4H, J = 8.9, 4.3 Hz, H_2C), 2.56 (m, 2H, J = 12.6, 3.2 Hz, H_2C), 2.04 (s, 3H, $H_3C_{(OAc)}$), 1.20 (s, 18H, H_3C), 1.19 (s, 9H, H_3C).

3 · *6H$_2$O* (*Method **C***): Yellow powder (0.13 g, 30%); *Anal.* Calc. for $C_{44}H_{54}N_4O_8Zn_2$ · 6H_2O (M, 1004.82 g mol^{-1}): C, 52.55; H, 6.57; N, 5.57. Found: C, 52.43; H, 5.77; N, 5.57%. The remaining characterisation data are absolutely analogous to those corresponding to **3** · 2H_2O.

4.4.3. ***4*** · *2H$_2$O*

4 · 2H_2O was obtained by stirring an orangish methanolic suspension (20 mL) containing **3** · 2H_2O (0.58 g, 0.622 mmol) and 2-

amino-4-methyl-phenol (0.23 g, 1.865 mmol) in 1:3 molar ratio for 1 h (Scheme 3). Vacuum concentration of the resulting reddish solution, and afterwards, addition of diethyl ether yielded a red solid that was filtered, washed with diethyl ether, and dried in vacuum.

4 · $2H_2O$: Red powder (0.31 g, 71%); *Anal.* Calc. for $C_{30}H_{32}N_2O_7Zn_2 \cdot 2H_2O$ (M, 698.8 g mol^{-1}): C, 51.52; H, 5.15; N, 4.01. Found: C, 51.85; H, 5.64; N, 4.08%. m/z (ESI$^+$-MS, methanol, 100 V): 663.0 (100%) $[Zn_2L^4(OAc)(HOAc)]^+$, FTIR (KBr, cm^{-1}): ν(O–H) 3430(b,m), ν(C=N) 1615(vs), ν_a(C=C) 1595(vs), ν_a(COO) 1533(s), ν_s(C=C) 1491(vs), δ (CH_3) 1443(s), ν_s(COO) 1395(s), ν(C–N) 1323(m); ^{1}H NMR (300 MHz, DMSO-d_6, ppm) 8.94 (s, 2H, *H*CN), 7.77 (s, 2H, H_{arom}), 7.38 (s, 2H, H_{arom}), 6.80 (d, 2H, H_{arom}), 6.52 (d, 2H, H_{arom}), 2.20 (s, 6H, H_3C), 1.88 (s, 6H, $H_3C_{(OAc)}$), 1.33 (s, 9H, H_3C).

Acknowledgement

The authors are grateful to Xunta de Galicia (PGIDIT06PXIB209043PR) for financial support.

Appendix A. Supplementary data

CCDC 676569, 676570 and 676571 contain the supplementary crystallographic data for this paper. These data can be obtained free of charge via http://www.ccdc.cam.ac.uk/conts/retrieving.html, or from the Cambridge Crystallographic Data Centre, 12 Union Road, Cambridge CB2 1EZ, UK; fax: (+44) 1223-336-033; or e-mail: deposit@ccdc.cam.ac.uk. Supplementary data associated with this article can be found, in the online version, at doi:10.1016/j.poly.2008.05.016.

References

[1] I.A. Kahwa, J. Selbin, Y.C.-Y. Hsieh, R.A. Laine, Inorg. Chim. Acta 118 (1986) 179.
[2] I.A. Kahwa, F.R. Fronczek, J. Selbin, Inorg. Chim. Acta 148 (1988) 273.
[3] H. Sakiyama, K. Motoda, H. Okawa, S. Kida, Chem. Lett. (1991) 1133.
[4] K. Motoda, H. Sakiyama, N. Matsumoto, H. Okawa, D.E. Fenton, J. Chem. Soc., Dalton Trans. (1995) 3419.
[5] H. Sakiyama, K. Tokuyama, Y. Matsumura, H. Okawa, J. Chem. Soc., Dalton Trans. (1993) 2329.
[6] H. Sakiyama, K. Tokuyama, J. Nishio, N. Matsumoto, H. Okawa, S. Kida, Chem. Lett. (1992) 1021.
[7] M. Fondo, A.M. García-Deibe, M.R. Bermejo, J. Sanmartín, A.L. Llamas-Saiz, J. Chem. Soc., Dalton Trans. (2002) 4746.
[8] M. Fondo, A.M. García-Deibe, N. Ocampo, J. Sanmartín, M.R. Bermejo, Dalton Trans. (2004) 2135.
[9] M. Fondo, N. Ocampo, A.M. García-Deibe, M. Corbella, M.S. El Fallah, J. Cano, J. Sanmartín, M.R. Bermejo, Dalton Trans. (2006) 4905.
[10] M. Fondo, A.M. García-Deibe, N. Ocampo, J. Sanmartín, M.R. Bermejo, Dalton Trans. (2007) 414.
[11] H. Montgomery, E.C. Lingafelter, Acta Crystallogr., Sect. C 16 (1963) 748.
[12] W. Clegg, I.R. Little, B.P. Straughan, Acta Crystallogr., Sect. C 42 (1986) 1701.
[13] T. Ishioka, A. Murata, Y. Kitagawa, K.T. Nakamura, Acta Crystallogr., Sect. C 53 (1997) 1029.
[14] H.D. Flack, Acta Crystallogr., Sect. A 39 (1983) 876.
[15] S. Pal, J.W. Gohdes, W.C.A. Wilish, W.H. Armstrong, Inorg. Chem. 31 (1992) 713.
[16] K. Wieghardt, U. Bossek, L. Zsolnai, G. Huttner, G. Blondin, J.J. Girerd, F. Babonneau, J. Chem. Soc., Chem. Commun. (1987) 651.
[17] XPREP, Reciprocal Space Exploration, Bruker AXS Inc., Madison, WI, USA, 2007.
[18] G.M. Sheldrick, TWINABS, University of Göttingen, Germany, 2002.
[19] G.M. Sheldrick, shelx-97 (shelxs 97 and shelxl 97), Programs for Crystal Structure Analyses, University of Göttingen, Germany, 1998.
[20] G.M. Sheldrick, SADABS, Program for Scaling and Correction of Area Detector Data, University of Göttingen, Germany, 1996.
[21] (a) A.L. Spek, Acta Crystallgr., Sect. A 46 (1990) C34;
(b) A.L. Spek, PLATON, A Multipurpose Crystallographic Tool, Utrecht University Utrecht, The Netherlands, 1998.
[22] P.T. Beurskens, G. Beurskens, R. de Gelder, S. Garcia-Granda, R.O. Gould, R. Israel, J.M.M. Smits, Crystallography Laboratory, University of Nijmegen, The Netherlands, 1999.
[23] L.J. Farrugia, J. Appl. Crystallogr. 32 (1999) 837.

Polyhedron 27 (2008) 2595–2602

Contents lists available at ScienceDirect

Polyhedron

journal homepage: www.elsevier.com/locate/poly

Infinite chains constructed from flexible bis(benzimidazole)-based ligands

Hui Jiang, Ying-Ying Liu, Jian-Fang Ma *, Wen-Li Zhang, Jin Yang

Key Lab of Polyoxometalate Science, Department of Chemistry, Northeast Normal University, Changchun 130024, People's Republic of China

ARTICLE INFO

Article history:
Received 8 April 2008
Accepted 20 May 2008
Available online 1 July 2008

Keywords:
Coordination polymers
Bis(benzimidazole)
Carboxylate
Sulfonate

ABSTRACT

Two neutral ligands, $L^1 \cdot 2H_2O$ and $L^2 \cdot H_2O$, and seven complexes, $[Cu(pmb)_2(L^1)]$ (**1**), $[Cu(pmb)_2(L^2)]$ (**2**), $[Cu(Ac)_2(L^2)] \cdot 4H_2O$ (**3**), $[Cu(4\text{-aba})_2(L^2)]$ (**4**), $[Ag(4\text{-ts})(L^1)(H_2O)]$ (**5**), $[Ag_2(epes)_2(L^1)] \cdot 2H_2O$ (**6**), $[Ag(1,5\text{-nds})_{0.5}(L^2)] \cdot 0.5C_2H_5OH \cdot H_2O$ (**7**) [where L^1 = 1,1′-(1,4-butanediyl)bis(2-methylbenzimidazole); L^2 = 1,1′-(1,4-butanediyl)bis(2-ethylbenzimidazole), pmb = *p*-methoxybenzoate anion; Ac = acetate anion; 4-aba = 4-aminobenzoate anion; 4-ts = *p*-toluenesulfonate anion; epes = *N*-(2-hydroxyethyl)piperazine-*N*′-(2-ethanesulfonate) anion; 1,5-nds = 1,5-naphthalenedisulfonate anion], have been synthesized and characterized by elemental analysis, IR, and single-crystal X-ray diffraction. The L^1 and L^2 ligands in compounds **1**–**7** act as bridging ligands, linking metal ions into chain structures. The chains in compounds **3**, **4** and **6** interlace with each other by hydrogen bonds to generate 3D supramolecular structures. In compound **5**, π–π interactions between adjacent L^1 ligands hold the chains to a supramolecular layer. In compound **7**, the sulfonate anions act as counterions in the framework. The thermal stabilities of **3**, **6** and **7**, and the luminescent properties for **5**–**7** in the solid states are also discussed.

© 2008 Elsevier Ltd. All rights reserved.

1. Introduction

The crystal engineering of supramolecular architecture based on metal and organic building blocks has been rapidly expanding in recent years owing to their novel and diverse topologies and potential applications in host-guest chemistry, catalysis, electrical conductivity, and magnetism [1–12]. Generally, extended high-dimensional networks can be obtained by the assembly of lower dimensional coordination polymers via noncovalent intermolecular forces such as hydrogen-bonding and π–π stacking interactions [13–17]. According to previous reports, bis(imidazole) ligands are excellent candidates for the construction of extended architectures and supramolecular architectures [18–24]. Carboxylate and sulfonate anions have also been proven to be good candidates for the formation of supramolecular structures because they can be regarded not only as hydrogen-bonding acceptor but also as hydrogen-bonding donors. In this study, copper and silver ions, bis(benzimidazole) ligands (Scheme 1), and carboxylate and sulfonate anions (Scheme 2) are selected as the reactants. We describe the successful syntheses of seven novel compounds: $[Cu(pmb)_2(L^1)]$ (**1**), $[Cu(pmb)_2(L^2)]$ **(2)**, $[Cu(Ac)_2(L^2)] \cdot 4H_2O$ (**3**), $[Cu(4\text{-aba})_2(L^2)]$ (**4**), $[Ag(4\text{-ts})(L^1)(H_2O)]$ (**5**), $[Ag_2(epes)_2(L^1)] \cdot 2H_2O$ (**6**), and $[Ag(1,5\text{-nds})_{0.5}(L^2)] \cdot 0.5C_2H_5OH \cdot H_2O$ (**7**). All crystal structures have been determined by single-crystal X-ray diffraction, and the compounds are also characterized by IR and elemental analyses.

2. Experimental

2.1. Materials and methods

All reagents and solvents for syntheses were purchased from commercial sources and used without further purification. The C, H, and N elemental analysis was conducted on a Perkin–Elmer 240C elemental analyzer. ^1H NMR spectra were recorded at 500 MHz with TMS as internal standard. The FT-IR spectra were recorded from KBr pellets in the range 4000–400 cm^{-1} on a Mattson Alpha-Centauri spectrometer. TGA was performed on a Perkin–Elmer TG-7 analyzer heated from room temperature to 600 °C under nitrogen. The luminescent properties of compounds **5**–**7** were measured on a Perkin–Elmer LS55 spectrometer.

2.2. Syntheses of the ligands and metal complexes

2.2.1. Synthesis of $L^1 \cdot 2H_2O$

A mixture of NaOH (1.18 g, 30 mmol) and 2-methylbenzimidazole (3.96 g, 30 mmol) in acetone (50 mL) was stirred at room temperature to give a clear solution, then 1,4-dibromobutane (3.24 g, 15 mmol) and NaI (0.1 g) were added. The mixture was stirred at 50 °C for 10 h. After removing the acetone, 50 mL water was poured and a brown solid formed. The solid was recrystallized from a mixture of water and ethanol (v:v = 4:1) to give L^1 as a light brown crystalline solid. Yield: 85% based on 2-methylbenzimidazole. *Anal.* Calc. for $C_{20}H_{22}N_4 \cdot 2H_2O$: C, 67.77; H, 7.39; N, 15.81. Found: C, 67.56; H, 7.58; N, 15.80%. IR (KBr) ν/cm^{-1}: 1665 (vw), 1615 (w), 1515 (s), 1474 (m), 1461 (s), 1439 (m), 1406 (vs), 1359

* Corresponding author. Tel./fax: +86 431 85098620.
E-mail address: jianfangma@yahoo.com.cn (J.-F. Ma).

0277-5387/$ - see front matter © 2008 Elsevier Ltd. All rights reserved.
doi:10.1016/j.poly.2008.05.019

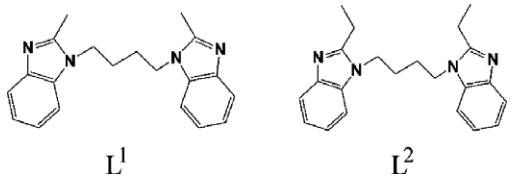

Scheme 1. Structures of the bis(benzimidazole) ligands in this work.

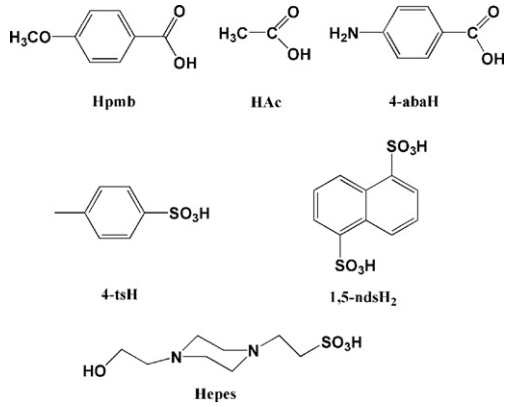

Scheme 2. Structures of the acids in this work.

(m), 1331 (w), 1287 (m), 1232 (m), 1126 (vw), 1009 (w), 929 (vw), 750 (s), 731 (vs), 668 (w), 432 (vw). ^{1}H NMR (500 MHz, $CDCl_3$) δ/ppm: 1.85 (4H, multiplet, C–CH_2–C), 2.54 (6H, s, CH_3), 4.07 (4H, multiplet, N–CH_2) 7.21-7.24 (6H, multiplet, aromatic protons), 7.68–7.70 (2H, multiplet, aromatic protons).

2.2.2. Synthesis of $L^2 \cdot H_2O$

The same synthetic method as for L^1 was used except that 2-methylbenzimidazole was replaced by 2-ethylbenzimidazole (4.38 g, 30 mmol). Yield: 80% based on 2-ethylbenzimidazole. *Anal.* Calc. for $C_{22}H_{26}N_4 \cdot H_2O$: C, 72.50; H, 7.74; N, 15.37. Found: C, 72.26; H, 7.68; N, 15.57%. IR (KBr) ν/cm^{-1}: 2966 (m), 2933 (m), 1661 (vw), 1614 (m), 1514 (m), 1462 (vs), 1415 (s), 1375 (s), 1334 (w), 1318 (m), 1280 (s), 1236 (m), 1179 (vw), 1153 (m), 1070 (m), 1016 (w), 922 (vw), 801 (w), 741 (vs), 610 (m), 430 (w). ^{1}H NMR (500 MHz, $CDCl_3$) δ/ppm: 1.44(6H, triplet, CH_3), 1.87(4H, multiplet, C–CH_2–C), 2.81(4H, quartet, N–CH_2–Me), 4.08 (4H, multiplet, N–CH_2), 7.22-7.26 (6H, multiplet, aromatic protons), 7.73-7.75 (2H, multiplet, aromatic protons).

*2.2.3. Synthesis of [Cu(pmb)$_2$(L^1)] (**1**)*

A mixture of $CuCl_2 \cdot 2H_2O$ (0.171 g, 1 mmol), NaOH (0.08 g, 2 mmol) and Hpmb (0.304 g, 2 mmol) in ethanol was stirring for 10 min at room temperature. Then L^1 (0.318 g, 1 mmol) was added to the solution with stirring for 30 min and a purple precipitate was obtained. The precipitate was dissolved by dropwise addition of ammonia (5 M). Suitable purple single crystals were obtained by slow evaporation of the solution at room temperature. The crystals were collected, washed with water, and dried in air. Yield: 75% based on $CuCl_2 \cdot 2H_2O$. *Anal.* Calc. for $C_{36}H_{36}CuN_4O_6$ (M_r = 684.23): C, 63.19; H, 5.30; N, 8.19. Found: C, 63.21; H, 5.19; N, 8.06%. IR (cm^{-1}): 2952 (w), 2829 (w), 1604 (s), 1566 (w), 1513 (m), 1455 (m), 1414 (m), 1365 (s), 1250 (s), 1161 (m), 1099 (w), 1032 (m), 849 (w), 782 (m), 741 (m).

*2.2.4. Synthesis of [Cu(pmb)$_2$(L^2)] (**2**)*

The same synthetic method as for **1** was used except that L^1 was replaced by L^2 (0.348 g, 1 mmol). Yield: 73% based on $CuCl_2 \cdot 2H_2O$. *Anal.* Calc. for $C_{38}H_{40}CuN_4O_6$ (M_r = 712.28): C, 64.08; H, 5.66; N, 7.87. Found: C, 63.96; H, 5.53; N, 7.92%. IR (cm^{-1}): 3596 (w), 2960 (w), 2831 (w), 1601 (s), 1458 (m), 1413 (m), 1371 (s), 1245 (s), 1161 (m), 1026 (m), 851 (m), 780 (m), 739 (s), 693 (w).

*2.2.5. Synthesis of [Cu(Ac)$_2$(L^2)] $\cdot$ 4H$_2$O (**3**)*

A mixture of $CuCl_2 \cdot 2H_2O$ (0.171 g, 1 mmol), NaOH (0.080 g, 2 mmol) and HAc (0.120 g, 2 mmol) in ethanol was stirring for 10 min at room temperature. Then L^2 (0.348 g, 1 mmol) was added to the solution with stirring for 30 min and a purple precipitate was obtained. The precipitate was dissolved by dropwise addition of ammonia (5 M). Suitable purple single crystals were obtained by slow evaporation of the solution at room temperature. The crystals were collected, washed with water, and dried in air. Yield: 75% based on $CuCl_2 \cdot 2H_2O$. *Anal.* Calc. for $C_{36}H_{36}CuN_4O_6$ (684.23): C, 63.19; H, 5.30; N, 8.19. Found: C, 63.21; H, 5.19; N, 8.06%. IR (cm^{-1}): 3899 (w), 3859 (m), 3801 (w), 3742 (s), 3673 (m), 3624 (m), 1679 (w), 1646 (s), 1630 (s), 1541 (m), 1515 (s), 1456 (m), 1425 (s), 675 (s).

*2.2.6. Synthesis of [Cu(4-aba)$_2$(L^2)] (**4**)*

The same synthetic method as for **2** was used except that HAc was replaced by 4-abaH (0.274 g, 2 mmol). Yield: 73% based on $CuCl_2 \cdot 2H_2O$. *Anal.* Calc. for $C_{36}H_{38}CuN_6O_4$ (682.26): C, 63.38; H, 5.61; N, 12.32. Found: C, 63.76; H, 5.53; N, 12.56%. IR (cm^{-1}): 3311 (m), 3209 (w), 2937 (w), 1632 (s), 1599 (s), 1558 (m), 1466 (m), 1413 (m), 1354 (s), 1306 (s), 1218 (w), 1166 (m), 1068 (w), 850 (m), 785 (s).

*2.2.7. Synthesis of [Ag(4-ts)(L^1)(H$_2$O)] (**5**)*

A mixture of Ag_2CO_3 (0.028 g, 0.1 mmol), 4-tsH (0.034 g, 0.2 mmol) and L^1 (0.0318 g, 0.1 mmol) in ethanol (10 mL) was stirring for 30 min at room temperature. The mixture was dissolved by dropwise addition of ammonia (5 M). Suitable colorless single crystals were obtained by slow evaporation of the solution at room temperature. Yield: 66% based on Ag_2CO_3. *Anal.* Calc. for $C_{27}H_{31}AgN_4O_4S$ (615.49): C, 52.69; H, 5.08; N, 9.10. Found: C, 52.72; H, 5.04; N, 9.09%. IR (cm^{-1}): 3726 (m), 3047 (w), 2939 (w), 1605 (w), 1512 (m), 1454 (m), 1409 (s), 1359 (m), 1227 (s), 1187 (s), 1008 (s), 817 (m), 746 (s), 675 (s), 561 (w).

*2.2.8. Synthesis of [Ag$_2$(epes)$_2$(L^1)] $\cdot$ 2H$_2$O (**6**)*

The same synthetic method as for **5** was used except that 4-tsH was replaced by Hepes (0.048 g, 0.2 mmol). Yield: 68% based on Ag_2CO_3. *Anal.* Calc. for $C_{36}H_{60}Ag_2N_8O_{10}S_2$ (1044.78): C, 41.39; H, 5.79; N, 10.73. Found: C, 41.58; H, 5.64; N, 10.78%. IR (cm^{-1}): 3794 (w), 3726 (m), 3664 (w), 3282 (m), 2942 (m), 2850 (m), 1453 (s), 1414 (s), 1377 (s), 1174 (s), 1032 (s), 935 (m), 767 (s), 674 (w), 589 (w).

*2.2.9. Synthesis of [Ag(1,5-nds)$_{0.5}$(L^2)] $\cdot$ 0.5C$_2$H$_5$OH $\cdot$ H$_2$O (**7**)*

The same synthetic method as for **5** was used except that 4-tsH was replaced by 1,5-ndsH$_2$ (0.029 g, 0.1 mmol) and L^1 was replaced by L^2 (0.348 g, 1 mmol). Yield: 68% based on Ag_2CO_3. *Anal. Calc. for $C_{27}H_{35}AgN_4O_{5.5}S$ (638.53): C, 50.79; H, 5.52; N, 8.77. Found: C, 51.58; H, 5.64; N, 8.78%. IR (cm^{-1}): 3729 (m), 3661 (m), 3046 (m), 2938 (m), 1598 (m), 1507 (w), 1455 (s), 1414 (s), 1300 (w), 1227 (s), 1185 (s), 1117 (s), 1009 (s), 745 (s), 675 (s), 553 (w), 404 (w).*

2.3. X-ray crystallography

Single-crystal X-ray diffraction data for compounds **1** and **7** were recorded on a Bruker Apex CCD diffractometer with graphite-monochromated Mo Kα radiation (λ = 0.71073 Å) at 293 K. Crystallographic data for compounds **$L^1 \cdot 2H_2O$**, **$L^2 \cdot H_2O$**, and **2–6** were collected on a Rigaku RAXIS-RAPID single-crystal

diffractometer with Mo Kα radiation (λ = 0.71073 Å) at 293 K. Absorption corrections were applied using multi-scan technique. All the structures were solved by Direct Method of SHELXS-97 [25] and refined by full-matrix least-squares techniques using the SHELXL-97 program [26]. Non-hydrogen atoms were refined with anisotropic temperature parameters. The disordered ligands in compounds **6** was refined using isotropic C atoms split over two sites, with a total occupancy of 1. The hydrogen atoms of the organic ligands were refined as rigid groups. Some water and ethanol H atoms in compound $\mathbf{L^2 \cdot H_2O}$ and **7** could not be positioned reliably. Other H atoms of water molecules were located from difference Fourier maps.

3. Results and discussion

3.1. Syntheses of the compounds

As well known, the reactions of transition metals with carboxylates or sulfonates and neutral ligands in aqueous solution often result in the formation of insoluble materials, presumably because of the fast coordination of them to form polymeric structures. In this paper, the crystals of compounds **1**–**7** were obtained by using crystallization process through evaporating an ammoniacal solution of them. These compounds were synthesized by allowing a solution of transition metals with carboxylates or sulfonates and

Table 1
Crystal data and structure refinements for compounds $\mathbf{L^1 \cdot 2H_2O}$, $\mathbf{L^2 \cdot H_2O}$ and **1**–**7**

	$\mathbf{L^1 \cdot 2H_2O}$	$\mathbf{L^2 \cdot H_2O}$	**1**
Formula	$C_{20}H_{26}N_4O_2$	$C_{22}H_{28}N_4O$	$C_{38}H_{38}ZnN_4O_5$
Formula weight	354.45	364.48	696.09
Crystal system	monoclinic	monoclinic	monoclinic
Space group	*P*21/*n*	*C*2/*c*	*P*2/*c*
a (Å)	17.527(10)	16.604(10)	10.796(3)
b (Å)	4.815(3)	8.722(7)	8.987(3)
c (Å)	22.375(12)	15.858(9)	19.052(7)
α (°)	90	90	90
β (°)	91.49(2)	114.37(2)	94.20(2)
γ (°)	90	90	90
V (Å^3)	1887.6(18)	2092(2)	1843.5(11)
Z	4	4	2
D_{calc} (g cm^{-3})	1.247	1.157	1.254
F(000)	760	784	728
R_{int}	0.0726	0.0325	0.0345
Goodness-of-fit on F^2	1.045	1.115	1.037
R_1[a] [$I > 2\sigma$ (*I*)]	0.0768	0.0726	0.0523
wR_2[b]	0.1811	0.1997	0.1540
	2	**3**	**4**
Formula	$C_{40}H_{40}ZnN_4O_4$	$C_{26}H_{40}CuN_4O_8$	$C_{36}H_{38}CuN_6O^4$
Formula weight	706.13	600.16	682.26
Crystal system	monoclinic	monoclinic	monoclinic
Space group	*P*2/*c*	*P*21/*c*	*C*2/*c*
a (Å)	10.861(4)	9.442(3)	14.468(5)
b (Å)	8.856(3)	10.672(6)	11.561(6)
c (Å)	19.466(6)	13.975(8)	20.676(7)
α (°)	90	90	90
β (°)	95.51(2)	96.76(2)	106.74(1)
γ (°)	90	90	90
V (Å^3)	1863.7(11)	1398(12)	3312(2)
Z	2	2	4
D_{calc} (g cm^{-3})	1.258	1.425	1.368
F(000)	740	634	1428
R_{int}	0.0691	0.0217	0.0399
Goodness-of-fit on F^2	1.042	1.054	1.041
R_1[a] [$I > 2\sigma(I)$]	0.0651	0.0281	0.0635
wR_2[b]	0.1659	0.0752	0.1703
	5	**6**	**7**
Formula	$C_{27}H_{31}AgN_4O_4S$	$C_{36}H_{60}Ag_2N_8O_{10}S_2$	$C_{28}H_{34}AgN_4O_{4.50}S$
Formula weight	615.49	1044.78	638.52
Crystal system	orthorhombic	triclinic	triclinic
Space group	*Pnma*	$P\bar{1}$	$P\bar{1}$
a (Å)	10.585(1)	9. 835(3)	8.376(5)
b (Å)	16.189(2)	14.530(6)	11.688(5)
c (Å)	15.527(2)	16.349(8)	14.103(7)
α (°)	90	71.16(2)	87.79(2)
β (°)	90	73.392(2)	85.33(2)
γ (°)	90	77.83(1)	85.19(2)
V (Å^3)	2660.6(5)	2100.7(15)	1370.5(12)
Z	4	2	2
D_{calc} (g cm^{-3})	1.537	1.652	1.547
F(000)	1264	1076	658
R_{int}	0.0221	0.0340	0.0215
Goodness-of-fit on F^2	1.079	1.036	1.106
R_1[a] [$I > 2\sigma(I)$]	0.0390	0.0516	0.0375
wR_2[b]	0.1059	0.1320	0.1129

[a] $R_1 = \Sigma||F_o| - F_c||/\Sigma|F_o|$.
[b] $wR_2 = \{\Sigma[w(|F_o|^2 - |F_c|^2)^2]/\Sigma[w(|F_o|^2)^2]\}^{1/2}$.

L (L = L^1 or L^2) ligands in a mixed solution of ethanol and ammonia (5 M) to evaporate slowly. All the compounds are insoluble in water and common organic solvents, but they can be dissolved in a concentrated solution of ammonia by segregating the L^1 or L^2 ligands from metal cations. With a 1:2:1 molar ratio of M^{II}: HX: L, **1**–**4** were isolated. The reaction mixtures produce crystals with Ag_2CO_3:HX:L^1 = 1:2:1 for **5** and **6**, and Ag_2CO_3:H_2X:L = 1:1:1 for **7**. Crystallographic data are summarized in Table 1. Selected bond distances and angles for $L^1 \cdot 2H_2O$, $L^2 \cdot H_2O$ and compounds **1**–**7** are listed in Table S1 (Supplementary data).

3.2. Descriptions of crystal structures

3.2.1. Structure of $L^1 \cdot 2H_2O$ and $L^2 \cdot H_2O$

The structure of $L^1 \cdot 2H_2O$ contains discrete L^1 molecules and lattice waters (see Fig. S1 in the Supplementary data). For the L^1 molecule, the dihedral angle between two benzimidazole rings is 47.4°. The guest water molecules are hydrogen-bonded to the N atoms of the L^1 ligands, and the L^1 ligands act as anchors for holding the water clusters. In the case of $L^1 \cdot 2H_2O$, the water clusters which are associated by strong O–H···O hydrogen bonds arrange themselves to form a chain structure (Fig. S2). This supramolecular water chain is associated with the host by O–H···N hydrogen bonds. In $L^1 \cdot 2H_2O$, O1W shows a 4-coordinate mode, and the O2W shows a 2-coordinate mode (Table S2). The discrete L^1 molecules are bridged through the hydrogen-bonding interactions between the water molecules and the N atoms to form an overall two-dimensional supramolecular structure (Fig. S3). The presence of water molecules in the structure can play an important role in stabilizing the supramolecular structure because of the formation of hydrogen bonds. It is similar to $L^1 \cdot 2H_2O$, the structure of $L^2 \cdot H_2O$ contains discrete L^2 molecules and lattice water (Fig. S4).

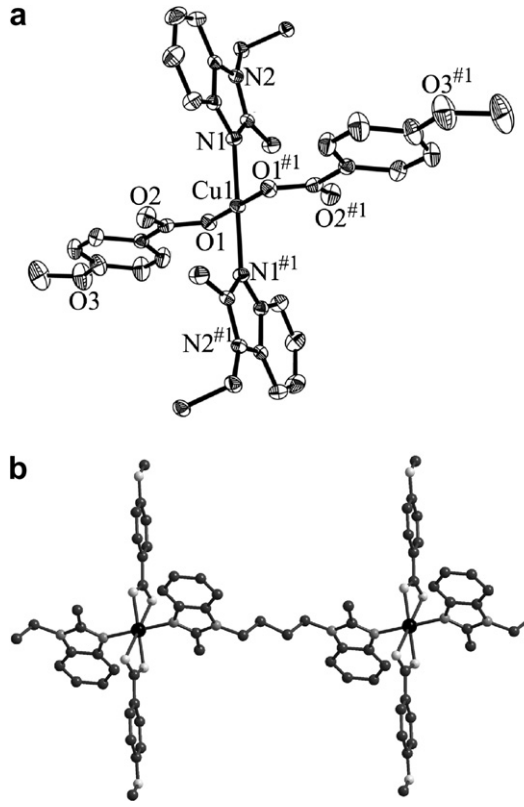

Fig. 1. (a) ORTEP diagram showing the coordination environment for Cu atom in **1**. (b) The infinite zigzag chain of **1**.

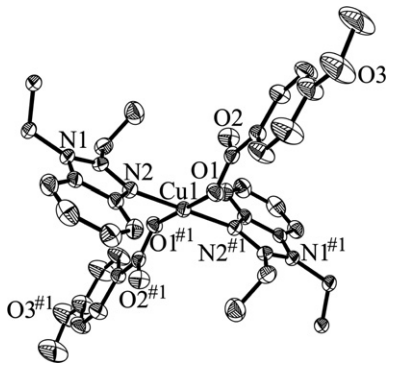

Fig. 2. ORTEP diagram showing the coordination environment for Cu atom in **2**.

3.2.2. Structure of $[Cu(pmb)_2(L^1)]$ (**1**)

Compound **1** shows chains formed by L^1 ligands connecting Cu^{II} atoms. As shown in Fig. 1a, Cu^{II} lies on a crystallographic inversion centre and each Cu^{II} is four-coordinated, forming square planar coordination geometry. The Cu^{II} is coordinated by two nitrogen atoms from two L^1 and two oxygen atoms from two pmb anions. The Cu(1)–N distance of 1.991(3) Å and the Cu(1)-O distance of 1.956(2) Å fall in the range of normal Cu–O [27–29] and Cu–N [29,30] distances. The pmb ligands exhibit monodentate coordination mode to link Cu^{II} centers. The Cu atoms are bridged by L^1 ligands to form an infinite chain (Fig. 1b), with two benzimidazolyl rings of L^1 ligand being parallel to each other.

3.2.3. Structure Description of $[Cu(pmb)_2(L^2)]$ (**2**)

The structure of **2** is similar to compound **1** except L^1 was replaced by L^2 ligands. The structure of **2** is shown in Fig. 2. Cu^{II} cations are bridged by L^2 ligands to form a chain just as that observed in compound **1**. (Fig. S5)

3.2.4. Structure of $[Cu(Ac)_2(L^2)] \cdot 4H_2O$ (**3**)

Part of the structure of compound **3** is shown in Fig. 3a. Cu^{II} cation lies at an inversion center and is six-coordinated by four oxygen atoms from two Ac anions and two nitrogen atoms from two L^2 ligands. The Cu–N distances are 2.029(1) Å, which are similar to the reported distances [31,32], while the Cu–O distances of 2.543 Å in axial positions are much longer than the average values, owing to the Jahn–Teller effect. Each Ac anion in **3** exhibits bidentate chelating coordination mode. Cu^{II} centers are connected by L^2 ligands to form an infinite wavelike chain (Fig. 3b). Compound **3** contains a unique supramolecular organization of these polymeric chains. These polymeric chains are arranged on parallel levels in different propagating directions, rotated by 81.5° on passing from one level to the successive one, thus resulting in an ABAB sequence (Fig. 3c) [33–35].

There exists a $(H_2O)_4$ cluster linked by O1W and O2W atoms (Fig. 3d). Hydrogen-bonding data indicate that the coordinated water molecule (O1W) acts as a donor and is hydrogen-bonded to the carboxylate oxygen atoms O1 and water molecule O2W; and O2W donates to $O2^{\#3}$ and $O1W^{\#4}$ [36,37]. As well-known, water molecule has two hydrogen atoms and two lone-electron pairs which enable it to participate in four hydrogen bonds in a tetrahedral configuration, but it also frequently shows a 3-coordinate configuration [38]. In compound **3**, both of the O1W and O2W show 3-coordinate modes. As shown in Fig. 4d, if we neglect L^2 ligands, the $(H_2O)_4$ clusters link Cu^{II} ions and Ac anions to form a supramolecular layer. The polymeric infinite chains in **3** are bridged through the hydrogen-bonding interactions to form a 3D supramolecular structure (Fig. 3e).

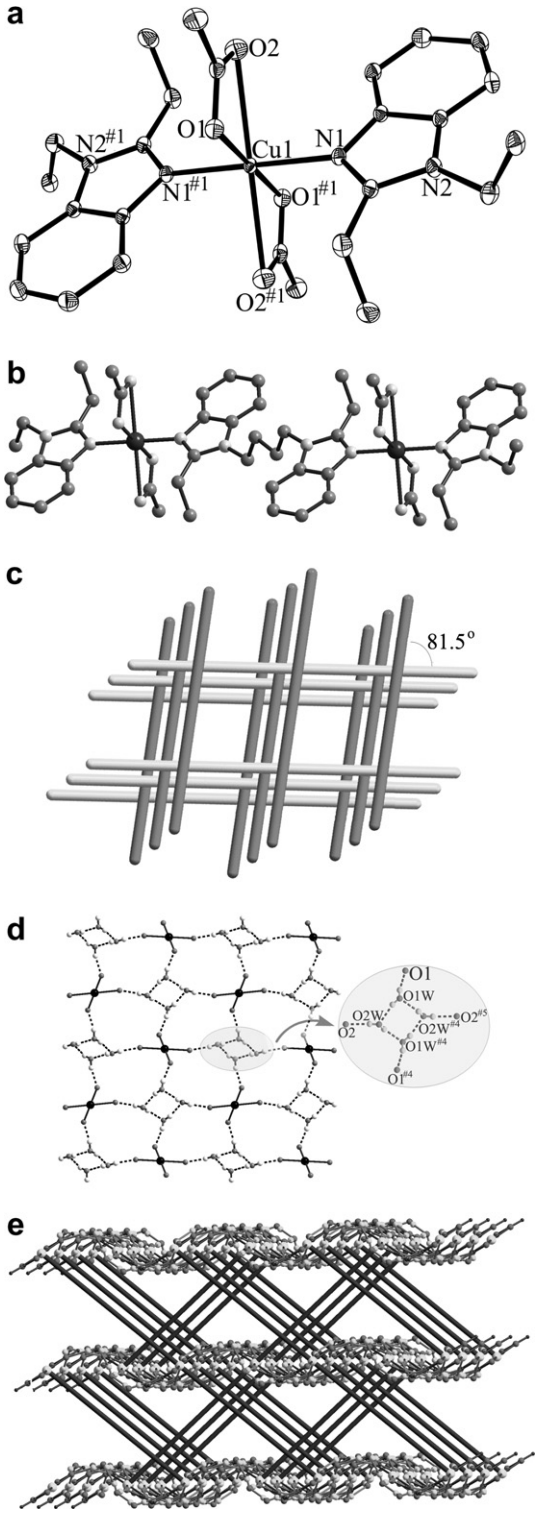

Fig. 3. (a) ORTEP diagram showing the coordination environment for Cu atom in **3**. Hydrogen atoms have been omitted for clarity. (b) The infinite zigzag chain. (c) Rod-packing picture of the chains spanning two different directions (light gray and medium gray) in **3**. (d) The supramolecular layer formed by hydrogen bonds without L^2 (H-bonds: dashed lines). (e) The 3D supramolecular structure linked by hydrogen bonds (black lines: L^2 ligands).

3.2.5. Structure of $[Cu(4\text{-}aba)_2(L^2)]$ (**4**)

As shown in Fig. 4a, Cu^{II} ion lies on a crystallographic inversion center and each Cu^{II} ion is four-coordinated, forming a square planar coordination geometry. The Cu^{II} is coordinated by two nitrogen atoms from two L^2 and two oxygen atoms from two 4-aba anions.

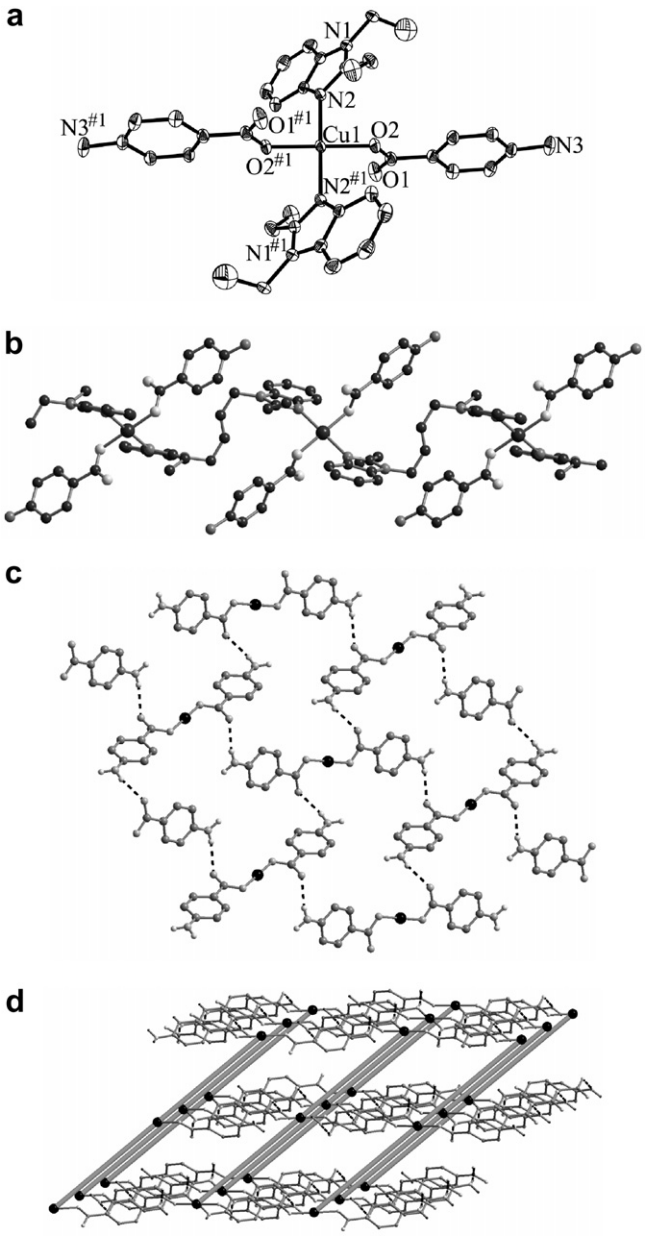

Fig. 4. (a) ORTEP diagram showing the coordination environment for Cu atom in **4**. Hydrogen atoms have been omitted for clarity. (b) The infinite zigzag chain. (c) The supramolecular layer formed by hydrogen bonds without L^2. (H-bonds: dashed lines) (d) The 3D supramolecular structure linked by hydrogen bonds. (Gray lines: L^2 ligands).

The 4-aba anions exhibit monodentate coordination mode to link Cu^{II} centers. The Cu atoms are bridged by L^2 ligands to form an infinite chain (Fig. 4b).

In the compound **4**, hydrogen bonds are present between the hydrogen atoms of the amino group and the carboxylate group of adjacent 4-aba anions. The N···O distances are 2.976(6) Å, which are similar to the reported distances [39–41]. As shown in Fig. 4c, if we neglect L^2 ligands, the hydrogen bonds link Cu^{II} ions and 4-aba anions to form a supramolecular layer. The polymeric infinite chains in **4** are bridged through the hydrogen-bonding interactions to form a 3D supramolecular structure (Fig. 4d).

3.2.6. Structure of $[Ag(4\text{-}ts)(L^1)(H_2O)]$ (**5**)

As shown in Fig. 5a, the silver ion shows a distorted tetrahedral coordination geometry, and is coordinated by two nitrogen atoms from two L^1 ligands (Ag–N = 2.270(2) Å), one sulfonate oxygen

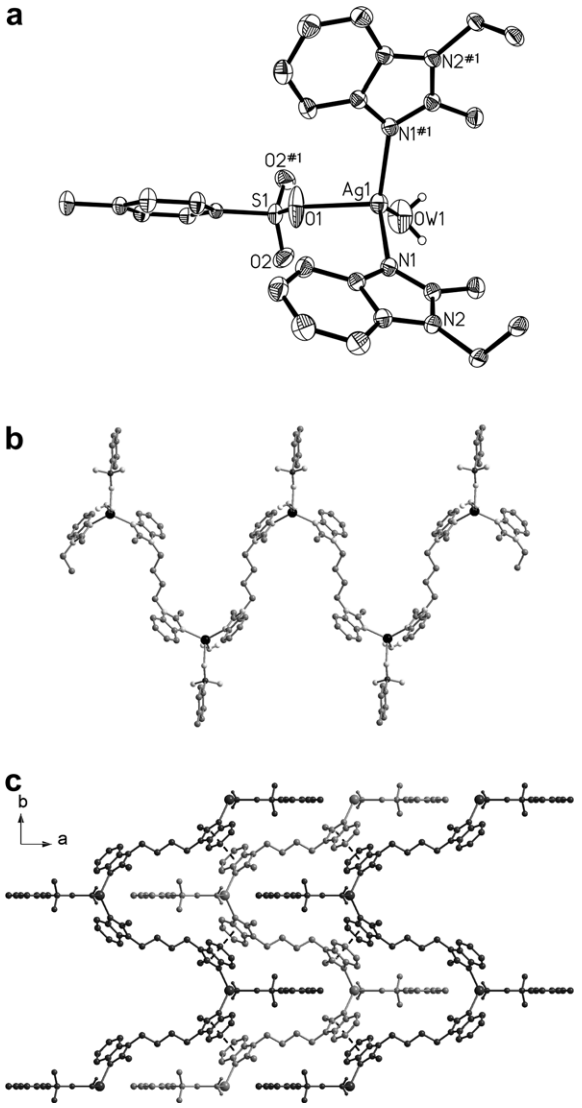

Fig. 5. (a) ORTEP diagram showing the coordination environment for Ag atom in **5**. Hydrogen atoms have been omitted for clarity. (b) The infinite wavelike chain of **5**. (c) View of the π–π interactions.

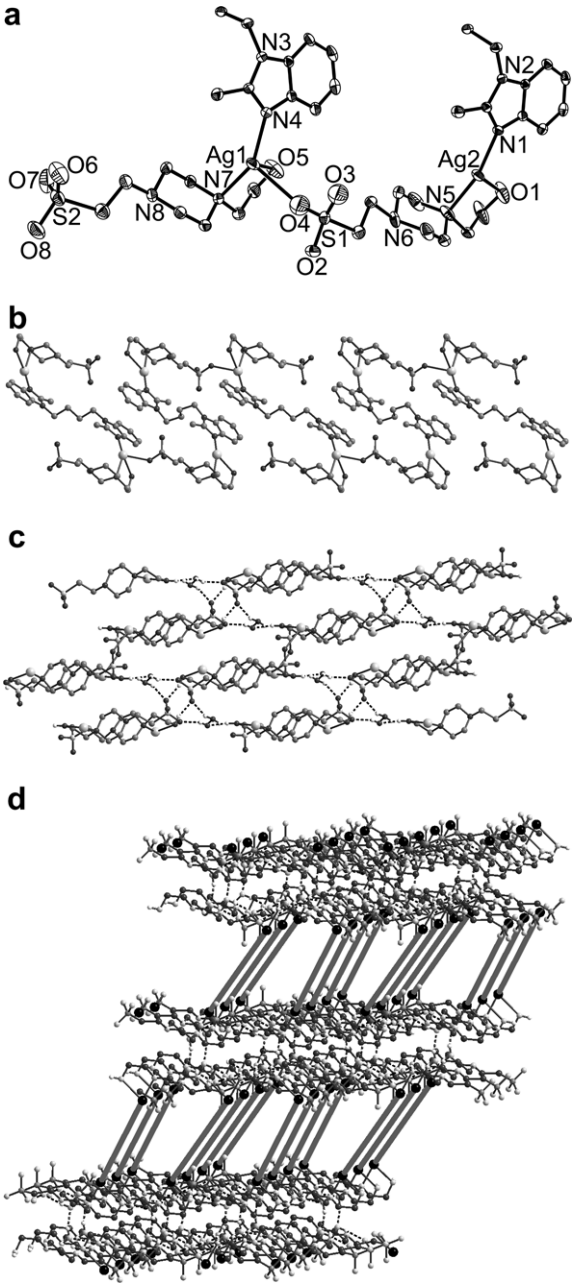

Fig. 6. (a) ORTEP diagram showing the coordination environment for Ag atom in **6**. Hydrogen atoms have been omitted for clarity. (b) The infinite zigzag chain of **6**. (c) The supramolecular layer formed by hydrogen bonds without L^1 of **6** (H-bonds: dashed lines). (d) The 3D supramolecular structure linked by hydrogen bonds. (H-bonds: dashed lines; gray lines: L^2 ligands).

atom (Ag–O = 2.434(3) Å), and one aqua ligand (Ag–O1W = 2.277(4) Å). The Ag–O bond lengths are similar to the normal distances in the related compound (AgOTs) [42]. The Ag cations are bridged by L^1 ligands to form a wavelike chain (Fig. 5b).

Aromatic–aromatic or π–π interactions engendered by aromatic–aromatic stacking are important non-covalent intermolecular forces similar to hydrogen bonding. They can contribute to self-assembly or molecular recognition when extended structures are formed from building blocks with aromatic moieties [43–46]. In compound **5**, there exist π–π stacking interactions between benzimidazole rings of the L^1 ligands, which link the wavelike chains to a supramolecular layer. The centroid-to-centroid distance is 3.61 Å (Fig. 5c).

3.2.7. Structure of $[Ag_2(epes)_2(L^1)] \cdot 2H_2O$ (**6**)

As shown in Fig. 6a, there are two crystallographically unique silver ions in the structure of **6**. Ag1 ion has a distorted tetrahedral geometry consisting of four bonds from one sulfonate oxygen atom, one oxygen atom from hydroxyl group, two nitrogen atoms from one epes anion and one L^1 ligand. Ag2 ion is three-coordinate with a distorted T-shape geometry composed of one hydroxyl oxygen atom from epes anion and two nitrogen atoms from one epes anion and one L^1 ligand. There are two kinds of crystallographically unique epes anions in the structure. One epes anion exhibits bidentate coordination mode to link Ag^I center with its hydroxyl group and nitrogen atom, and the other tridentate epes anion coordinates to two different silver ions with sulfonate oxygen atom, hydroxyl group and nitrogen atom. In the crystal structure of **6**, silver ions are bridged by L^1 ligands to form a polymeric 'S' chain (Fig. 6b).

If we neglect L^2 ligands, sulfonate anions, hydroxyl groups and water molecules are connected by hydrogen bonds to form a double layer (Fig. 6c and Fig. S6). The polymeric infinite chains in **6** are bridged through the hydrogen-bonding interactions to form a 3D supramolecular structure (Fig. 6d).

*3.2.8. Structure of [Ag(1,5-nds)$_{0.5}$(L^2)] · 0.5C_2H_5OH · H_2O (**7**)*

In compounds **5** and **6**, the anions are monosulfonate, in compound **7**, the 1,5-nds was selected as a disulfonate anion. Single X-ray analysis reveals compound **7** possesses chain structure. As shown in Fig. 7a, the Ag^I cation is coordinated by two N atoms from two L^2 ligands. Metal ions are bridged by L^2 molecules to form an infinite zigzag chain. In compound **7**, 1,5-nds anions act as counterions in the framework. This phenomenon may be due to the weak coordination ability of the sulfonate anions. The polymeric chains are arranged in a parallel mode (Fig. 7b).

3.3. Discussion

3.3.1. The effect of the neutral ligands on the structure of the complexes

L^1 and L^2 ligands display similar bidentate bridging coordination mode with two aromatic N atoms coordinating to two metal ions in compounds **1**–**7**. The similar frameworks may be expected when the L^1–L^2 are used. Indeed, compounds **1** and **2** have the similar structures.

In fact, the fine tunability is realized by changing the conformation of the neutral ligands (Scheme 3). In $L^1 \cdot 2H_2O$, the L^1 ligands adopt the zigzag conformation, the two benzimidazole rings of the L^1 ligands has a dihedral angle of 47.3° (Scheme 3a). In compounds **1** and **5**, L^1 ligands also adopt zigzag conformations, but with the benzimidazole rings of L^1 ligands being parallel to each other (Scheme 3b). In compound **6**, L^1 ligands adopt zigzag and 'S' conformations (Scheme 3b and 3c). Similar conformation changes occur for L^2 ligands. In $L^2 \cdot H_2O$, the L^2 ligands adopt zigzag conformations (Scheme 3a′). In compounds **2**, **3**, and **7**, L^2 ligands also adopt zigzag conformations (Scheme 3b′). In compound **4**, L^2 ligands adopt 'S' conformations (Scheme 3c′).

3.3.2. The effect of the anions on the structure of the complexes

From the structures of **1**–**7**, it can be seen that the anions play a very important role in the construction of the frameworks. Each of pmb, Ac and 4-aba anions contain one carboxylate group, and coordinates to only one metal ion, acting as a terminal ligand. And the related complexes (**2**–**4**) contain only one kind of connector (L^1 or L^2), and show chain structures. The 4-ts anion contains one sulfonate group, and coordinates to only one metal ion, acting as a terminal ligand. And the related complex (**5**) contains only one kind of connector (L^1), and shows a chain structure. In compound **6**, epes anion adopts two kinds of coordination modes. One kind of epes anion exhibits bidentate chelating coordination mode to link Ag^I centers with their hydroxyl groups and N atom, and the other kind of epes anion acts as an interesting tridentate ligand, coordinating to two different silver ions by their sulfonate oxygen atom, hydroxyl group and nitrogen atom. The 4-aba and epes anions containing –OH and $–NH_2$ groups have a potential for hydrogen-bonding interactions to construct supramolecular architectures. Compounds **4** and **6** show 3D supramolecular structures containing hydrogen-bonding interactions.

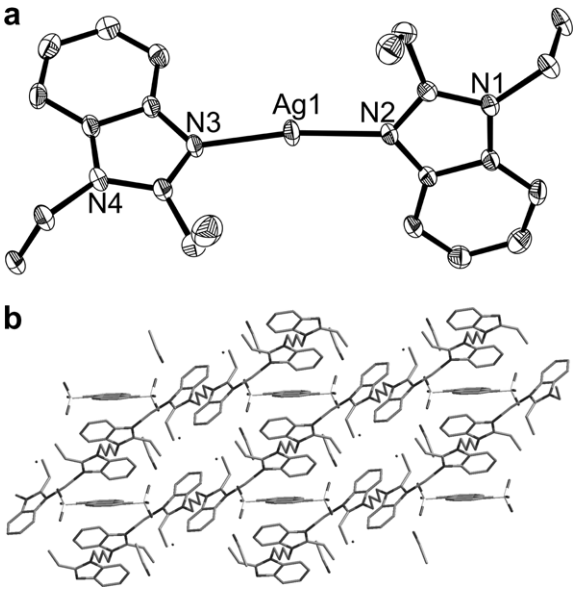

Fig. 7. (a) ORTEP diagram showing the coordination environment for Ag atom in **7**. Hydrogen atoms have been omitted for clarity. (b) Packing diagram of compound **7**.

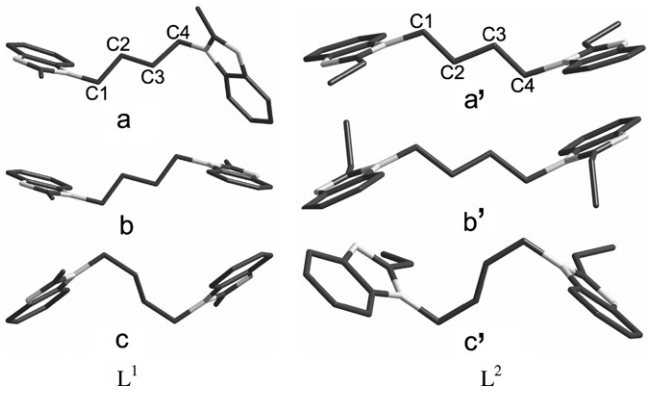

Scheme 3. Conformation of the L^1 and L^2.

3.4. Thermal analysis

In order to characterize the compounds more fully in terms of thermal stability, their thermal behaviors were studied by TGA. The experiments were performed on samples consisting of numerous single crystals of **3**, **6** and **7** under N_2 atmosphere with a heating rate of 10 °C/min (Figs. S7–S9 in the Supplementary data).

For compound **3**, the weight loss in the range of room temperature to 45 °C corresponds to the departure of water molecules (a weight loss of 1.67% is smaller than the calculated value, 10.5%, probably resulting from a very slow liberation of the water molecules from **3** at room temperature) [47]. For compound **6**, the weight loss in the range from room temperature to 156 °C corresponds to the departure of water molecules (obsd 3.9%, calcd 3.6%). The anhydrous compound begins to decompose at 230 °C. For compound **7**, the weight loss in the range from room temperature to 280 °C corresponds to the departure of water and ethanol. The decomposition of the anhydrous compound occurs at 325 °C.

3.5. Luminescent properties

Luminescent compounds are of great current interest because of their various applications in chemical sensors, photochemistry and electroluminescent (EL) display [48–50]. The photoluminescent properties of compounds **5–7** were studied at room temperature. The solid-state photoluminescent spectra of **5–7**, and the neutral

Table 2
The wavelengths of the emission maximums and excitation (nm)

Compound	5	6	7
λ_{em}	435	388, 483	358
λ_{ex}	309	315	310

ligands L^1 and L^2 are depicted in Fig. S10. The wavelengths of the emission maximums and excitation are listed in Table 2.

The free ligands display luminescence with emission maximums at 371 and 515 nm for L^1 and 365 nm for L^2, respectively (λ_{ex} = 295 nm), which are attributed to the $\pi \rightarrow \pi^*$ transitions. Compound **5** exhibits a peak at 435 nm which is probably due to ligand-to-metal charge transfer (LMCT) transition. Similar LMCT has been reported in many metal–organic coordination polymers [51–53]. Compound **6** exhibits two main peaks at 388 and 483 nm upon excitation at 315 nm. The peak at 388 nm would be assigned to $\pi \rightarrow \pi^*$ transition of neutral ligand, while the peaks at 483 nm would be attributed to the emission of LMCT. The main peak of compound **7** exhibits at 358 nm (λ_{ex} = 310 nm), which is probably due to the $\pi \rightarrow \pi^*$ transition of neutral ligand because similar peak also appears for the free bis(benzimidazole) ligand [54–56].

4. Conclusion

In summary, seven metal coordination polymers based on L^1–L^2 ligands and six kinds of different anions have been synthesized and characterized. The results of this study not only illustrate that the neutral ligands play an important role in the construction of coordination polymers, but also illustrate that the coordination modes of anions and the coordination behavior of metal ions can also have an influence on the final frameworks. It is anticipated that more metal complexes containing neutral ligands and carboxylate or sulfonate anions with interesting structures as well as physical properties will be synthesized.

Acknowledgements

We thank the Program for New Century Excellent Talents in Chinese University (NCET-05-0320), Program for Changjiang Scholars and Innovative Research Teams in Chinese University, and the Analysis and Testing Foundation of Northeast Normal University for support.

Appendix A. Supplementary data

CCDC 683110, 683111, 683112, 683113, 683114, 683115, 683116, 683117, and 683118 contain the supplementary crystallographic data for **1**, **2**, **3**, **4**, **5**, **6**, **7**, and **8**. These data can be obtained free of charge via http://www.ccdc.cam.ac.uk/conts/retrieving.html, or from the Cambridge Crystallographic Data Centre, 12 Union Road, Cambridge CB2 1EZ, UK; fax: (+44) 1223-336-033; or e-mail: deposit@ccdc.cam.ac.uk. Supplementary data associated with this article can be found, in the online version, at doi:10.1016/j.poly.2008.05.019.

References

[1] R. Robson, B.F. Abrahams, S.R. Batten, R.W. Gable, B.F. Hoskins, J. Liu, Supramolecular Architecture, American Chemical Society, Washington, DC, 1992. p. 256.
[2] J.M. Lehn, Supramolecular Chemistry: Concepts and Perspectives, VCH, Weinheim, Germany, 1995. (Chapter 9).
[3] S.R. Batten, R. Robson, Angew. Chem., Int. Ed. 37 (1998) 1460.
[4] P.J. Hagrman, D. Hagrman, J. Zubieta, Angew. Chem., Int. Ed. 38 (1999) 2638.
[5] M.D. Hollingsworth, Science 29 (2002) 2410.
[6] O.R. Evans, W.-B. Lin, Acc. Chem. Res. 35 (2002) 511.
[7] J.W. Steed, J.L. Atwood, Supramolecular Chemistry, Wiley, Chichester, UK, 2000.
[8] S. Subramanian, M. Zaworotko, Coord. Chem. ReV. 127 (1994) 357.
[9] J.R. Fredericks, A.D. Hamilton, in: J.P. Stang, M.W. Hosseini (Eds.), Comprehensive Supramolecular Chemistry, vol. 9, Pergamon, Oxford, UK, 1996. (Chapter 16).
[10] B.J. Holliday, C.A. Mirkin, Angew. Chem., Int. Ed. 40 (2001) 2022.
[11] T.M. Reineke, M. Eddaoudi, D. Moler, M. O'Keeffe, O.M. Yaghi, J. Am. Chem. Soc. 122 (2000) 4843.
[12] S. Leininger, B. Olenyuk, P.J. Stang, Chem. Rev. 100 (2000) 853.
[13] Z.N. Chen, H.X. Zhang, K.B. Yu, K.C. Zheng, H. Cai, B.S. Kang, J. Chem. Soc., Dalton Trans. 7 (1998) 1133.
[14] M.L. Tong, Y.M. Wu, S.L. Zheng, X.M. Chen, T. Yuen, C.L. Lin, X.Y. Huang, J. Li, New J. Chem. 12 (2001) 1482.
[15] D. Vujovic, H.G. Raubenheimer, L.R. Nassimbeni, J. Chem. Soc., Dalton Trans. 4 (2003) 631.
[16] D. Ghoshal, T.K. Maji, G. Mostafa, T.H. Lu, N.R. Chaudhuri, Cryst. Growth Des. 3 (2003) 9.
[17] P. Yin, S. Gao, L.M. Zheng, X.Q. Xin, Chem. Mater. 15 (2003) 3233.
[18] G.-H. Cui, J.-R. Li, J.-L. Tian, X.-H. Bu, S.R. Batten, Cryst. Growth Des. 5 (2005) 1775.
[19] J.-F. Ma, J.-F. Liu, Y. Xing, H.-Q. Jia, Y.-H. Lin, J. Chem. Soc., Dalton Trans. (2000) 2403.
[20] J.-F. Ma, J. Yang, G.-L. Zheng, L. Li, J.-F. Liu, Inorg. Chem. 42 (2003) 7531.
[21] J. Yang, J.-F. Ma, Y.-Y. Liu, S.-L. Li, G.-L. Zheng, Eur. J. Inorg. Chem. (2005) 2174.
[22] F.-F. Li, J.-F. Ma, S.-Y. Song, J. Yang, Cryst. Growth Des. 6 (2006) 209.
[23] J. Yang, J.-F. Ma, Y.-Y. Liu, J.-C. Ma, H.-Q. Jia, N.-H. Hu, Eur. J. Inorg. Chem. (2006) 1208.
[24] Y.-Y. Liu, J.-F. Ma, J. Yang, Z.-M. Su, Inorg. Chem. 46 (2007) 3027.
[25] G.M. Sheldrick, SHELXS-97, Programs for X-ray Crystal Structure Solution, University of Göttingen, Göttingen, 1997.
[26] G.M. Sheldrick, SHELXL-97, Programs for X-ray Crystal Structure Refinement, University of Göttingen, Göttingen, Germany, 1997.
[27] Q. Zhang, B.-H. Ye, C.-X. Ren, X.-M.Z. Chen, Anorg. Allg. Chem. 629 (2003) 2053.
[28] R. Cao, Q. Shi, D.-F. Sun, M.-C. Hong, W.-H. Bi, Y.-J. Zhao, Inorg. Chem. 41 (2002) 6161.
[29] Y.-F. Zeng, F.-C. Liu, J.-P. Zhao, S. Cai, X.-H. Bu, J. Ribas, Chem. Commun. (2006) 2227.
[30] J.M. Holland, X.-M. Liu, J.-P. Zhao, F.E. Mabbs, C.A. Kilner, M. Thornton-Pett, M.A.J. Halcrow, Chem. Soc., Dalton Trans. (2000) 3316.
[31] Y.-F. Zeng, F.-C. Liu, J.-P. Zhao, S. Cai, X.-H. Bu, J. Ribas, Chem. Commun. (2006) 2227.
[32] J.M. Holland, X.-M. Liu, J.-P. Zhao, F.E. Mabbs, C.A. Kilner, M. Thornton-Pett, M.A. Halcrow, J. Chem. Soc., Dalton Trans. (2000) 3316.
[33] X.-L. Wang, C. Qin, E.-B. Wang, Cryst. Growth Des. 6 (2006) 439.
[34] X.-L. Wang, C. Qin, E.-B. Wang, L. Xu, Cryst. Growth Des. 6 (2006) 2061.
[35] X.-L. Wang, C. Qin, E.-B. Wang, Z.-M. Su, Chem. Eur. J. 12 (2006) 2680.
[36] S. Supriya, S.K. Das, New J. Chem. 27 (2003) 1568.
[37] J. Tao, Z.-J. Ma, R.-B. Huang, L.-S. Zheng, Inorg. Chem. 43 (2004) 6133.
[38] G.A. Jeffrey, H. Maluszynska, Acta Crystallogr., Sect. B 46 (1990) 546.
[39] F.P. Pruchnik, M. Bańbuła, Z. Ciunik, H. Chojnacki, M. Latocha, B. Skop, T. Wilczok, A. Opolski, J. Wietrzyk, A. Nasulewicz, Eur. J. Inorg. Chem. (2002) 3214.
[40] R.H. Wang, F.L. Jiang, Y.f. Zhou, L. Han, M.C. Hong, Inorg. Chim. Acta 358 (2005) 545.
[41] T.A. George, H.H. Hammud, S. Isber, Polyhedron 25 (2006) 2721.
[42] G.K.H. Shimizu, G.D. Enright, C.I. Ratcliffe, G.S. Rego, J.L. Reid, J.A. Ripmeester, Chem. Mater. 10 (1998) 3282.
[43] D.B. Amabilino, J.F. Stoddart, Chem. Rev. 95 (1995) 2725.
[44] C.G. Claessens, J.F. Stoddart, J. Phys. Org. Chem. 10 (1997) 254.
[45] K.A. Hirsch, S.R. Wilson, J.S. Moore, Chem. Eur. J. 3 (1997) 765.
[46] C.J. Janiak, Chem. Soc., Dalton Trans. (2000) 3885.
[47] Z. Huang, H.-B. Song, M. Du, S.-T. Chen, X.-H. Bu, Ribas, J. Inorg. Chem. 43 (2004) 931.
[48] Q.G. Wu, M. Esteghamatian, N.-X. Hu, Z. Popovic, G. Enright, Y. Tao, D'Iorio, S. Wang, Chem. Mater. 12 (2000) 79.
[49] J.E. McGarrah, Y.J. Kim, M. Hissler, R. Eisenberg, Inorg. Chem. 40 (2001) 4510.
[50] G.D. Santis, L. Fabbrizzi, M. Licchelli, A. Poggi, A. Taglietti, Angew. Chem., Int. Ed. Engl. 35 (1996) 202.
[51] X.-Z. Sun, Z.-L. Huang, H.-Z. Wang, B.-H. Ye, X.-M. Chen, Z. Anorg. Allg. Chem. 631 (2005) 919.
[52] N. Kaltsoyannis, J. Chem. Soc., Dalton Trans. (1997) 1.
[53] S.-L. Zheng, J.-H. Ying, X.-L. Yu, X.-M. Chen, W.-T. Wang, Inorg. Chem. 43 (2004) 830.
[54] X. Shi, G. Zhu, Q. Fang, G. Wu, G. Tian, R. Wang, D. Zhang, M. Xue, S. Qiu, Eur. J. Inorg. Chem. (2004) 185.
[55] X.-M. Zhang, M.-L. Tong, M.-L. Gong, X.-M. Chen, Eur. J. Inorg. Chem. (2003) 138.
[56] G. Tian, G.-S. Zhu, Q.-R. Fang, X.-D. Guo, M. Xue, J.-Y. Sun, S.-L. Qiu, J. Mol. Struct. 787 (2006) 45.

Polyhedron 27 (2008) 2603–2611

Contents lists available at ScienceDirect

Polyhedron

journal homepage: www.elsevier.com/locate/poly

Novel platinum(II) compounds with *N*-benzylidenebenzylamines: Synthesis, crystal structures and the effect of *cis* or *trans* geometry on cycloplatination

Margarita Crespo [a,*], Raquel Martín [a], Teresa Calvet [b], Mercè Font-Bardía [b], Xavier Solans [b,✠]

[a] Departament de Química Inorgànica, Universitat de Barcelona, Diagonal 647, 08028 Barcelona, Spain
[b] Departament de Cristal·lografia, Mineralogia i Dipòsits Minerals, Universitat de Barcelona, Martí i Franquès s/n, 08028 Barcelona, Spain

ARTICLE INFO

Article history:
Received 31 March 2008
Accepted 5 May 2008
Available online 10 June 2008

Dedicated to the memory of Xavier Solans; he will always be with us

Keywords:
Platinum
N-donor ligands
Cyclometallation
cis–trans Isomers
Crystal structure

ABSTRACT

Coordination compounds with a *trans*-stereochemistry were prepared for ligands (4-ClC_6H_4)CH=NCH_2(4′-ClC_6H_4) (**L_a**), (2,4,6-$Me_3C_6H_2$)CH=NCH_2(4′-ClC_6H_4) (**L_b**) and (2,6-$Cl_2C_6H_3$)CH=NCH_2(4′-ClC_6H_4) (**L_c**) and were shown to be precursors of the corresponding cyclometallated compounds. The reactions between *cis*-[$PtCl_2$(dmso)$_2$] and ligands ArCH=NCH_2(4′-ClC_6H_4) (Ar = 2-BrC_6H_4 (**L_d**); 2-ClC_6H_4 (**L_e**); C_6F_5 (**L_f**); 2,6-$F_2C_6H_3$ (**L_g**)) under previously described conditions for cycloplatination of *N*-benzylidenebenzylamines gave a cyclometallated compound only for imine **L_f**; the other imines produced coordination compounds with a *cis* arrangement from which cyclometallation could not be achieved. Formation of either *cis* or *trans* coordination compounds [$PtCl_2$(**L**)dmso] (**L** = *N*-benzylidenebenzylamine) can be related to steric effects and to the *E*/*Z* configuration of the C=N bond. All compounds were fully characterized including structure determinations for *trans*-[$PtCl_2${(4-ClC_6H_4)CH=NCH_2(4′-ClC_6H_4)}$SOMe_2$] (**2a**), *trans*-[$PtCl_2${(2,6-$Cl_2C_6H_3$)CH=NCH_2(4′-ClC_6H_4)}$SOMe_2$] (**2c**) and the amine derivative *trans*-[$PtCl_2$(4-$ClC_6H_4CH_2NH_2$)$SOMe_2$] (**2**) obtained as a by-product.

© 2008 Elsevier Ltd. All rights reserved.

1. Introduction

Cyclometallation of N-donor ligands by platinum and palladium has remained as one of the major topics in organometallic chemistry [1]. Recently *cis*-[$PtCl_2$(dmso)$_2$] has become an useful substrate for direct cycloplatination, and numerous examples have been reported including tridentate [C,N,X] (X = N [2], S [3] and O[4]) as well as bidentate [C,N] systems derived from imines [5], oximes [6], pyridines[7] or even tertiary amines leading to either mono [8] or dinuclear [9] compounds.

Coordination compounds [$PtCl_2$(**L**)dmso] (**L** = nitrogen donor ligand) with a *trans* geometry have been postulated as precursors to the cyclometallated derivatives [5c,10] and crystal structures of these compounds confirm the proposed *trans* arrangement [5c,8c,10,11]. However, these results do not address specifically whether only *trans* isomer of the precursor or also *cis* isomer may lead to successful cyclometallation.

In view of these facts, the synthesis of novel coordination compounds [$PtCl_2$(**L**)dmso] (**L** = nitrogen donor ligand) was envisaged in this work in order to ascertain whether their *cis* or *trans* arrangement is decisive for a successful cyclometallation process. We have recently reported the reactions of *cis*-[$PtCl_2$(dmso)$_2$] with bifunctional *N*-benzylidenebenzylamines of general formula ArCH-NCH_2(4′-ClC_6H_4) leading to either *endo* (containing the imine functionality) or *exo* cyclometallated platinum compounds [12]. These ligands along with similar ones with *ortho* substituents of different bulk were selected for this study.

2. Results and discussion

2.1. Coordination compounds as precursors to cycloplatinated derivatives

Initial work was carried out for imines (4-ClC_6H_4)CH=NCH_2(4′-ClC_6H_4) (**L_a**), (2,4,6-$Me_3C_6H_2$)CH=NCH_2(4′-ClC_6H_4) (**L_b**) and (2,6-$Cl_2C_6H_3$)CH=NCH_2(4′-ClC_6H_4) (**L_c**) for which cyclometallated derivatives **3a**, **3b** and **3c** (see Chart 1) have been previously prepared in a "one-pot" synthesis using *cis*-[$PtCl_2$(dmso)$_2$] as metallating agent [12]. The aim of isolating the corresponding coordination compounds is (i) to determine the *cis* or *trans* arrangement and (ii) to confirm that these compounds are intermediates in the cycloplatination process.

The reaction of the imine 4-ClC_6H_4CH=NCH_2(4′-ClC_6H_4) with *cis*-[$PtCl_2$(dmso)$_2$] in refluxing methanol for 4 h produced the corresponding aldehyde and the amine derivative *trans*-[$PtCl_2$(4-$ClC_6H_4CH_2NH_2$)$SOMe_2$] (**2**) which was characterized crystallographically. This result suggests hydrolysis of the imine with adventitious water in the solvent, a process that has been reported for palladium or platinum compounds under metallation

* Corresponding author. Tel.: +34 934039132; fax: +34 934907725.
E-mail address: margarita.crespo@qi.ub.es (M. Crespo).
✠ Deceased.

0277-5387/$ - see front matter © 2008 Elsevier Ltd. All rights reserved.
doi:10.1016/j.poly.2008.05.001

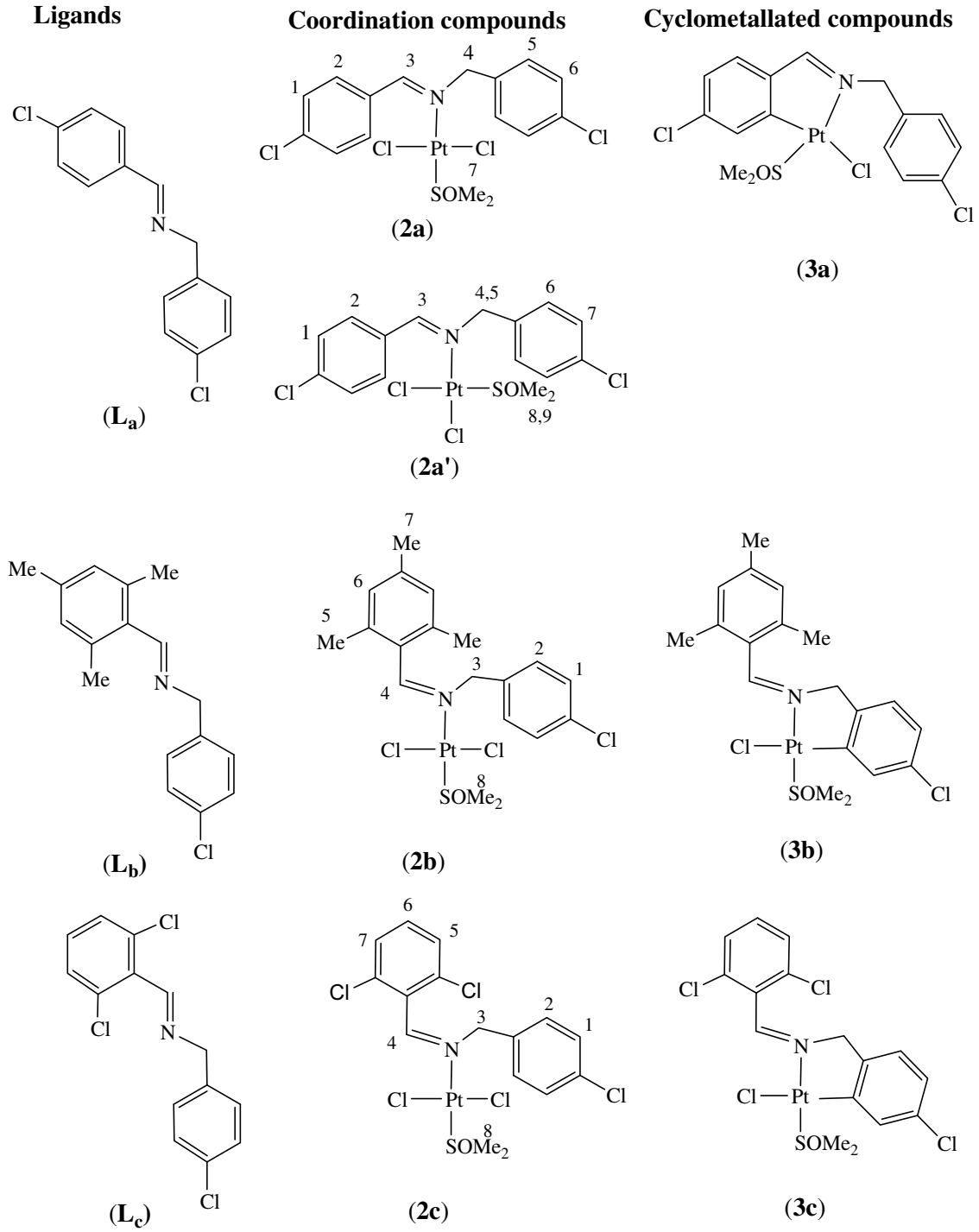

Chart 1.

conditions [2a]. When the reaction was carried out in refluxing dry toluene, hydrolysis was avoided and a mixture of *trans* and *cis*-$[PtCl_2\{(4\text{-}ClC_6H_4)CH{=}NCH_2(4'\text{-}ClC_6H_4)\}SOMe_2]$ (**2a** and **2a**′ shown in Chart 1) was produced. Suitable crystals for structure resolution of the *trans* isomer were obtained. The ^{1}H NMR spectra of the *cis* and *trans* isomers display distinct features. For the *cis* isomer, both the methylene hydrogen atoms and the methyl groups of the dimethylsulfoxide ligand appear as non-equivalent which suggest a low symmetry, and the imine hydrogen displays a large *J*(H–Pt) value (117.4 Hz) which is consistent with the presence of a chloro ligand in a *trans* position and with an *E* conformation[1] of the imine as confirmed by a 2D-NOESY experiment. Conversely, for the *trans* isomer both the methylene hydrogen atoms and the methyl groups of the dimethylsulfoxide ligand appear as equivalent and the *J*(H–Pt) for the imine hydrogen is reduced (84.5 Hz) compared to the *cis* isomer which is consistent with the presence of a dimethylsulfoxide li-

[1] *Z*/*E* conformation has been assigned as for the free imine (not taking into account the platinum coordination to the nitrogen).

gand in a *trans* position to the nitrogen atom. The presence of a cross-peak signal between the imine and the methylene protons in a 2D-NOESY NMR spectrum supports an *E* conformation across the C=N bond.

The reactions of imines $\mathbf{L}_b$ and $\mathbf{L}_c$ with *cis*-[$PtCl_2(dmso)_2$] were also studied in refluxing toluene and produced the corresponding compounds *trans*-[$PtCl_2\{(2,4,6\text{-}Me_3C_6H_2)CHNCH_2(4'\text{-}ClC_6H_4)\}SOMe_2$] (**2b**) and *trans*-[$PtCl_2\{(2,6\text{-}Cl_2C_6H_3)CHNCH_2(4'\text{-}ClC_6H_4)\}SOMe_2$] (**2c**). For these compounds, both the methylene hydrogen atoms and the methyl groups of the dimethylsulfoxide ligand appear as equivalent as expected for a *trans* stereochemistry. The *J*(H–Pt) values for the imine hydrogen of **2b** and **2c** are consistent with a *Z* conformation across the C=N bond [13] since it is reduced (37.2 and 42.6 Hz, respectively) compared to that of **2a** (84.5 Hz).

In order to confirm that *trans*-[$PtCl_2(4\text{-}ClC_6H_4CH{=}NCH_2(4'\text{-}ClC_6H_4))SOMe_2$] (**2a**) is a precursor to the cyclometallated compound **3a**, the coordination compound was dissolved in toluene and treated with an equimolar amount of sodium acetate dissolved in methanol. Refluxing the mixture for 48 h produced quantitative formation of the cyclometallated compound **3a**, thus confirming that the coordination compound is an intermediate in the cyclometallation process which requires the presence of added base. Analogous reactions carried out for *trans*-[$PtCl_2\{(2,4,6\text{-}Me_3C_6H_2)CHNCH_2(4'\text{-}ClC_6H_4)\}SOMe_2$] (**2b**) in refluxing toluene and for *trans*-[$PtCl_2\{(2,6\text{-}Cl_2C_6H_3)CHNCH_2(4'\text{-}ClC_6H_4)\}SOMe_2$] (**2c**) in refluxing methanol lead to the corresponding *exo*-metallacycles **3b** and **3c**.

However, an analogous experiment carried out with a mixture of *trans* and *cis*-[$PtCl_2(4\text{-}ClC_6H_4CH{=}NCH_2(4'\text{-}ClC_6H_4))SOMe_2$] (**2a**/**2a**′) gave a mixture of the cyclometallated compound **3a** and the *cis* coordination compound **2a**′ which was recovered unchanged. This result suggests that only the *trans* isomer may lead to cyclometallation.

2.2. Crystal structures of *trans*-[$PtCl_2(4\text{-}ClC_6H_4CH_2NH_2)SOMe_2$] (**2**), *trans*-[$PtCl_2\{(4\text{-}ClC_6H_4)CH{=}NCH_2(4'\text{-}ClC_6H_4)\}SOMe_2$] (**2a**) and *trans*-[$PtCl_2\{(2,6\text{-}Cl_2\ C_6H_3)CHNCH_2(4'\text{-}ClC_6H_4)\}SOMe_2$] (**2c**)

Crystals of compounds **2**, **2a** and **2c** were grown from dichloromethane–methanol. The crystal structures are composed of discrete molecules separated by van der Waals interactions. The structures of **2** and **2c** consist of the packing in the asymmetric unit of four and two independent molecules, respectively, in both cases with bond parameters equal within experimental error [3σ]. The structures are shown in Figs. 1–3 and selected molecular dimensions are listed in Table 1. The molecular structures confirm the geometries predicted from spectroscopic data. The coordination sphere of platinum is square-planar with two mutually *trans* chloro ligands, a S-bound dimethylsulfoxide and the N-donor ligand completing the coordination sphere. The angles between adjacent atoms in the coordination sphere of platinum lie in the range 85.9–95.36° (**2**), 88.40–93.77° (**2a**) and 87.67–94.16° (**2c**). Pt–Cl, Pt–N and Pt–S bond lengths are well within the range of values obtained for similar complexes of platinum [8c,10,11].

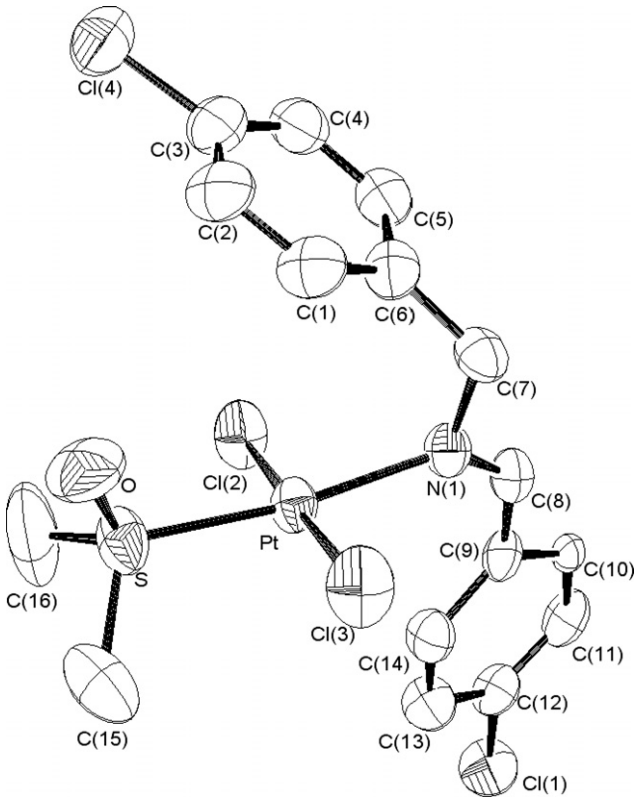

Fig. 2. Molecular structure of **2a**.

For **2a**, the configuration at the C=N moiety is *E* which is the adequate arrangement for formation of an *endo*-metallacycle through activation of a C–H bond at the benzal ring. The Pt···H(14)–C(14) distance is only 2.651 Å, a smaller value than the one observed for the *ortho* hydrogen atoms of the benzylamine (3.161 Å) which suggest that formation of an *endo*-cycle from **2a** is more favoured than that of an *exo* derivative, as experimentally observed [12]. For **2c**, the configuration at the C=N moiety is *Z*, a form that allows formation of an *exo*-cycle [12] and the shortest distance between platinum and the *ortho* hydrogen atoms is 3.289 Å for Pt···H(110)–C(110). For **2a** and **2c**, the distances between platinum

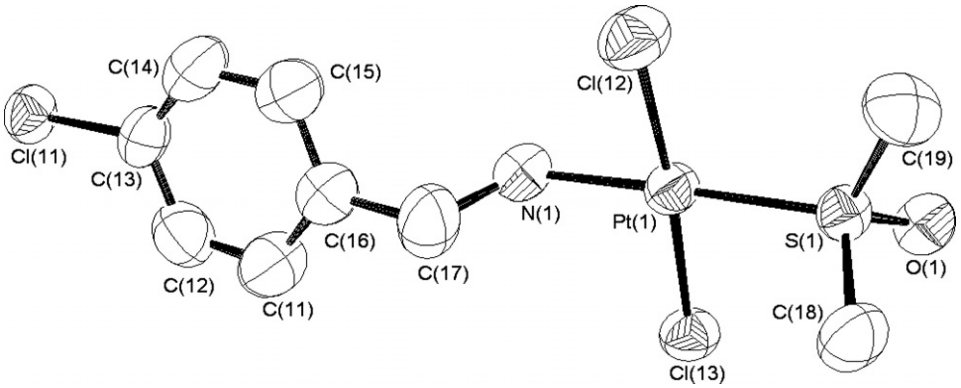

Fig. 1. Molecular structure of **2** (molecule 1).

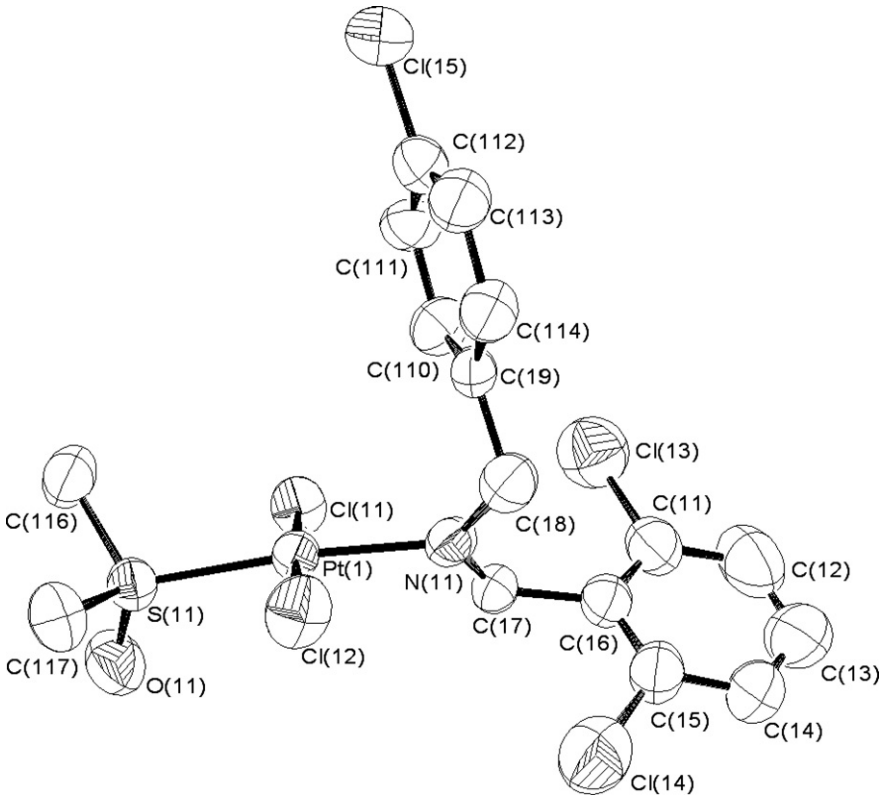

Fig. 3. Molecular structure of **2c** (molecule 1).

Table 1
Selected bond lengths (Å) and angles (°) with estimated standard deviations

Compound **2** (molecule 1)		Compound **2a**		Compound **2c** (molecule 1)	
Pt(1)–N(1)	2.079(10)	Pt–N(1)	2.050(8)	Pt(1)–N(11)	2.070(6)
Pt(1)–S(1)	2.214(2)	Pt–S	2.222(3)	Pt(1)–S(11)	2.2202(19)
Pt(1)–Cl(13)	2.280(2)	Pt–Cl(3)	2.301(4)	Pt(1)–Cl(11)	2.288(3)
Pt(1)–Cl(12)	2.287(3)	Pt–Cl(2)	2.303(3)	Pt(1)–Cl(12)	2.305(3)
N(1)–C(17)	1.443(16)	N(1)–C(8)	1.304(12)	N(11)–C(17)	1.276(8)
C(16)–C(17)	1.523(17)	N(1)–C(7)	1.514(13)	N(11)–C(18)	1.482(10)
N(1)–Pt(1)–Cl(13)	85.9(3)	N(1)–Pt–Cl(3)	88.6(3)	N(11)–Pt(1)–Cl(11)	89.4(2)
S(1)–Pt(1)–Cl(13)	89.01(9)	S–Pt–Cl(3)	88.40(14)	S(11)–Pt(1)–Cl(11)	87.67(8)
N(1)–Pt(1)–Cl(12)	90.0(3)	N(1)–Pt–Cl(2)	89.5(3)	N(11)–Pt(1)–Cl(12)	88.7(2)
S(1)–Pt(1)–Cl(12)	95.36(10)	S–Pt–Cl(2)	93.77(14)	S(11)–Pt(1)–Cl(12)	94.16(9)
C(17)–N(1)–Pt(1)	118.2(8)	C(6)–C(7)–N(1)	111.1(9)	N(11)–C(18)–C(19)	109.5(7)
N(1)–C(17)–C(16)	113.7(10)	C(7)–N(1)–C(8)	117.0(8)	C(17)–N(11)–C(18)	122.0(6)
		N(1)–C(8)–C(9)	129.4(9)	N(11)–C(17)–C(16)	124.9(7)

and *ortho* C–H bonds are in the range reported for an analogous compound with a coordinated aryl oxime (3.153 Å), described as an intermediate in the cyclometallation process [10]. The distances between platinum and *ortho* hydrogen atoms observed for the 4-chlorobenzylamine derivative **2** are considerably greater (4.668 Å is the shortest distance for molecule 1) and, consistently, the cyclometallation of 4-chlorobenzylamine did not occurred so readily as for the benzylidenebenzylamine $\mathbf{L}_a$ [12].

2.3. Reactions of *cis*-[$PtCl_2(dmso)_2$] with ligands $ArCH{=}NCH_2(4'\text{-}ClC_6H_4)$ ($Ar = 2\text{-}BrC_6H_4$ ($\mathbf{L}_d$); $2\text{-}ClC_6H_4$ ($\mathbf{L}_e$); C_6F_5 ($\mathbf{L}_f$); $2,6\text{-}F_2C_6H_3$ ($\mathbf{L}_g$))

In order to complete this study, the reactions of *cis*-[$PtCl_2$-$(dmso)_2$] with ligands $\mathbf{L}_d$–$\mathbf{L}_g$ which had not been tested so far towards cycloplatination, were also studied. The *N*-benzylidenebenzylamine ligands $\mathbf{L}_d$–$\mathbf{L}_g$ were prepared by a condensation reaction of 4-chlorobenzylamine with the corresponding aldehyde. They were formed as single isomers and the expected *E* configuration of the C=N bond was confirmed by a cross-peak between the imine and the methylene protons in the 2D-NOESY NMR spectra taken for $\mathbf{L}_d$ and $\mathbf{L}_f$ (see Chart 2).

Ligands $\mathbf{L}_d$ and $\mathbf{L}_e$ might in principle lead to either *endo* (containing the imine functionality) or *exo* five-membered metallacycles. Ligands $\mathbf{L}_f$ and $\mathbf{L}_g$ contain fluoro substituents in the *ortho* positions of the benzal ring and, although intramolecular C–F bond activation for analogous ligands has been reported at electron rich platinum(II) substrates [14], this process is not expected in principle for an electrophilic substrate such as *cis*-[$PtCl_2(dmso)_2$]; therefore, formation of an *exo*-metallacycle through C–H activation in the benzylamine ring is more likely. As shown in Chart 3, both *endo*- and *exo*-cycles can be formed from the *E* form, while only *exo*-cycles are possible for the *Z* form.

Initially, the reactions of imines $\mathbf{L}_d$-$\mathbf{L}_g$ were carried out using *cis*-[$PtCl_2(dmso)_2$], the imine and CH_3CO_2Na in a 1:1:2 ratio and heat-

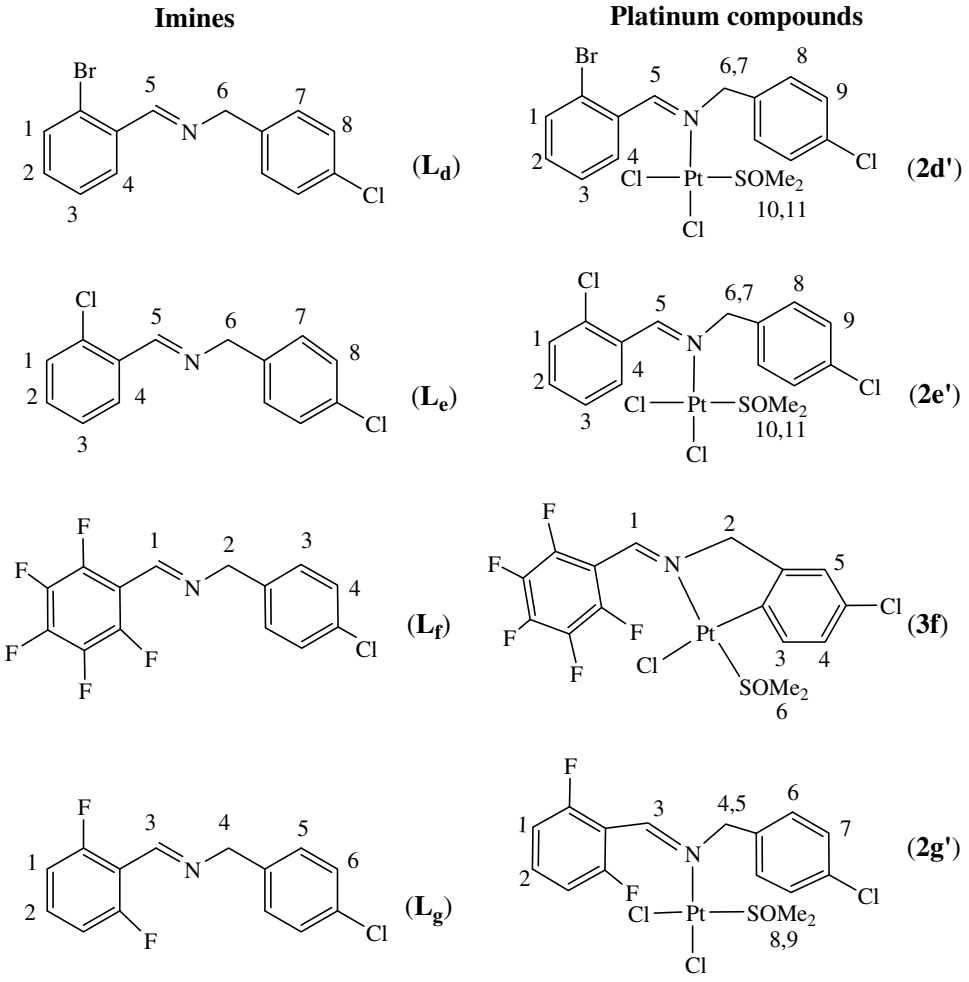

Chart 2.

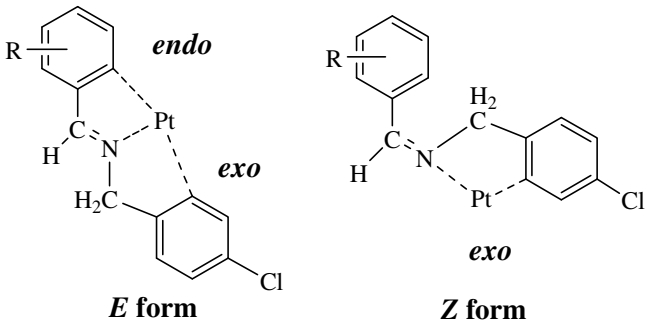

Chart 3.

ing the obtained mixture in refluxing methanol during 48 h. According to the NMR spectra of the crude products, only one platinum compound was detected in each reaction, along with formation of metallic platinum and the corresponding aldehyde. Due to decomposition processes of the platinum compounds as well as to hydrolysis of the imines, low yields were obtained. After work-up of the reaction mixtures, a cyclometallated compound was obtained in extremely low yield for imine $C_6F_5CHNCH_2(4\text{-}C_6H_4Cl)$ ($\mathbf{L}_f$) while the other imines produced coordination compounds with a *cis* arrangement. The proposed structures are shown in Chart 2. For imine $\mathbf{L}_e$, the reaction time was increased up to six days, however the *cis* coordination compound was again the only product and no evidence of formation of the corresponding cyclometallated compound was observed.

With the aim of achieving the syntheses of cyclometallated derivatives, the reactions of imines $\mathbf{L}_d$ and $\mathbf{L}_e$ were tested under more drastic conditions. A molar ratio [Pt]:[**L**]:[acetate] = 1:1:1 was used; sodium acetate was dissolved in a small amount of methanol and added to a solution of imine and *cis*-$[PtCl_2(dmso)_2]$ in toluene and the mixture was refluxed for 48 h under nitrogen. Since a higher concentration of the base could favour the cyclometallation process, a molar ratio [Pt]:[**L**]:[acetate] = 1:1:2 was also tested for both reactions. In all cases, the coordination compounds described above were obtained with similar yields to those obtained when methanol was used as a solvent.

Attempts to obtain the corresponding cyclometallated compound were also carried out using the coordination compound **2e**′ as starting material. In one experiment, compound **2e**′ was dissolved in toluene, sodium acetate dissolved in methanol was added and the mixture was heated under reflux for 48 h; in another experiment, coordination compound **2e**′ in the solid state was heated at 145 °C in an oven for three days following a literature procedure for cycloplatination of a benzophenone imine [11]. In both cases, the coordination compound was recovered and longer reaction times lead only to partial decomposition with no evidence of cyclometallation.

The obtained compounds were characterized by ^1H, ^{13}C (**2e**′), ^{19}F (**3f** and **2g**′), COSY ^1H–^1H (**2d**′), NOESY ^1H–^1H (**2e**′, **3f** and **2g**′) and gHSQC ^1H–^{13}C (**2e**′, **3f** and **2g**′) NMR spectra, mass spectrometry

and elemental analyses (except for **3f** due to its low stability). For compound **3f**, the presence of only three crossing peaks in the aromatic region of the {^{1}H–^{13}C}-heterocorrelation spectra can be taken as evidence of cyclometallation leading to an *exo*-metallacycle and the presence of a cross-peak signal between the imine and the methylene protons in a 2D-NOESY NMR spectrum supports an *E* conformation across the C=N bond [1]. Coordination compounds **2d′**, **2e′** and **2g′** display analogous NMR spectral features to those described in the previous section for compound **2a′**. In addition, the presence of 6 (**2e′**) or 4 (**2g′**) crossing peaks in the aromatic region of the {^{1}H–^{13}C}-heterocorrelation spectra confirms that intramolecular C–H activation did not occur in these reactions. A *cis* arrangement of these coordination compounds is consistent with all the spectral data. In addition, the NOESY NMR spectrum of **2e′** indicates that each methyl of the dimethylsulfoxide ligand is close to one of the aromatic rings of the imine.

The very low yield obtained for cyclometallated compound **3f** was not totally unexpected taking into account the low stability of *exo*-metallacycles as previously observed for ligand 2,4,6-$Me_3C_6H_2CHNCH_2(4'\text{-}ClC_6H_4)$ [12]. More striking is the failure to obtain cyclometallated derivatives for ligands $\mathbf{L}_d$, $\mathbf{L}_e$ and $\mathbf{L}_g$ which are analogous to the *N*-benzylidenebenzylamines previously studied ($\mathbf{L}_a$–$\mathbf{L}_c$) for which cyclometallation was successful. This result could be related to the *cis* arrangement of the coordination compounds derived from $\mathbf{L}_d$, $\mathbf{L}_e$ and $\mathbf{L}_g$ versus the *trans* geometry of $\mathbf{L}_a$, $\mathbf{L}_b$ and $\mathbf{L}_c$ derivatives.

In an attempt to obtain the corresponding *trans* isomer, the reaction of imine $\mathbf{L}_e$ with *cis*-[$PtCl_2(dmso)_2$] was studied under the conditions used for imines $\mathbf{L}_a$, $\mathbf{L}_b$ and $\mathbf{L}_c$, which consist in refluxing the mixture in toluene for 4 h. In contrast to the results obtained for the latter imines, the reaction of $\mathbf{L}_e$ produced exclusively the *cis* isomer of the coordination compound **2e′** without traces of the *trans* isomer. In an analogous procedure for imine $\mathbf{L}_f$, no reaction was observed and the starting materials were recovered; this suggests that the low basicity of the imine bearing an electron-withdrawing group such as C_6F_5 inhibits the coordination to platinum.

3. Conclusions

In agreement with previously suggested mechanism for the cyclometallation process [5c,8c,10], the results here obtained show that cycloplatination is successful for those ligands leading to a *trans* isomer of the coordination compound ($\mathbf{L}_a$, $\mathbf{L}_b$ and $\mathbf{L}_c$), while the cyclometallation process is inhibited for those ligands leading to a *cis* isomer of the coordination compound ($\mathbf{L}_d$, $\mathbf{L}_e$ and $\mathbf{L}_g$). Crystal structures for *trans* complexes **2a** and **2c** indicate a suitable arrangement of these compounds as precursors of *endo* (**3a**) and *exo* (**3c**) metallacycles, respectively. Unfortunately, suitable crystals for structure determination of the *cis* coordination compounds could not be obtained. It is expected, however, that steric effects are important due to the mutual proximity of dimethylsulfoxide and imine ligands in an *E* conformation. In order to minimize the steric effects, it is likely that both aryl rings of the imine ligand would be tilted away from the coordination plane in an arrangement which is not suitable for cyclometallation. In addition, for the *cis* isomer there is only one Pt–Cl *cis* to the N-donor ligand and available for cyclometallation.

It has been reported in the literature that the reaction between *cis*-[$PtCl_2(dmso)_2$] and nitrogen donor ligands lead to formation of *trans*-[$PtCl_2$(**L**)dmso] [15] in a substitution process that takes place with stereo-chemical change as shown in Eq. (1).

$$cis\text{-}[PtCl_2(dmso)_2] + L \rightarrow trans\text{-}[PtCl_2(\mathbf{L})dmso] + dmso \quad (1)$$

In addition, slow *trans* to *cis* isomerization might be observed since complexes having the *cis* configuration are usually more stable than the *trans* compounds [16]. Further studies indicated that if there is a high steric hindrance due to *ortho* substituents in the ligand, direct formation of the *cis* isomer takes place [15]. These results are related to the position of the entering ligand in the five-coordinate intermediate or transition state: axial for non-bulky ligands and equatorial for bulky ligands.

The results here reported can be rationalized on steric grounds taking into account that upon coordination to metal centres, *N*-benzylidenebenzylamines of considerable size might reduce the steric hindrance through *E* to *Z* isomerization around the imine bond [13,17]. Therefore, three distinct types of coordination compounds [$PtCl_2$(**L**)dmso] have been obtained: (i) The less bulky ligand $\mathbf{L}_a$ produced a *trans* isomer with an *E* conformation of the imine which in the absence of added base isomerizes partially to the *cis* isomer **2a′**, but in the presence of CH_3CO_2Na gives the corresponding cyclometallated compound **3a**; (ii) Ligands $\mathbf{L}_d$, $\mathbf{L}_e$ and $\mathbf{L}_g$ containing, respectively, one bromo, one chloro or two fluoro substituents in the *ortho* positions of the benzal ring are sterically more demanding than ligand $\mathbf{L}_a$ and direct formation of the *cis* isomers **2d′**, **2e′** and **2g′** takes place; therefore, cyclometallation is inhibited; (iii) The bulkier ligands $\mathbf{L}_b$ and $\mathbf{L}_c$ adopt a *Z* conformation of the imine to reduce the steric hindrance upon coordination and this allows formation of *trans* isomers **2b** and **2c** which are precursors of cyclometallated compounds **3b** and **3c**. In conclusion, the combined effect of steric hindrance due to *ortho* substituents and of the *E* or *Z* configuration of the C=N bond seems decisive on the formation of either *cis* or *trans* coordination compounds of *N*-benzylidenebenzylamines and, consequently, on the success of the cyclometallation process.

4. Experimental

4.1. General

Toluene (ACS) and methanol (ACS; max. 0.005 H_2O) were used as received from commercial sources.

Microanalyses were performed at Serveis Cientifico-tècnics (Universitat de Barcelona) and at Servei de Recursos Científics i Tècnics (Universitat Rovira i Virgili, Tarragona).

Mass spectra were performed at Servei d'Espectrometria de Masses (Universitat de Barcelona). Electrospray mass spectra were carried out in a LC/MSD-TOF spectrometer using H_2O–CH_3CN 1:1 to introduce the sample. CI mass spectra were carried out in a HP-5988A spectrometer using NH_3. NMR spectra were performed at Unitat de RMN d'Alt Camp (Universitat de Barcelona). ^{1}H, ^{13}C and ^{19}F spectra were recorded by using Varian Unity 300 (^{1}H, 300 MHz; ^{19}F, 282.2 MHz), Mercury-400 (^{1}H, 400 MHz; ^{13}C, 100.6 MHz; ^{19}F, 376.5 MHz) and Varian Inova DMX-500 (^{1}H, 500 MHz; ^{1}H–^{1}H-COSY; ^{1}H–^{1}H-NOESY, ^{1}H–^{13}C-gHSQC) spectrometers, and referenced to $SiMe_4$ (^{1}H, ^{13}C), and $CFCl_3$ (^{19}F). δ values are given in ppm and *J* values in Hz. Abbreviations used: s = singlet; d = doublet; t = triplet; m = multiplet; br = broad; NMR labelling as shown in Charts 1 and 3.

4.2. Preparation of the compounds

4-Chlorobenzylamine was used as received from commercial sources. *cis*-[$PtCl_2(dmso)_2$] [18] and ligands $\mathbf{L}_a$, $\mathbf{L}_b$ and $\mathbf{L}_c$ [12] were prepared using reported procedures.

4.2.1. Preparation of the ligands

Compounds $\mathbf{L}_d$–$\mathbf{L}_g$ were prepared from the reaction of 0.507 g (2.7 mmol) of 2-bromobenzaldehyde ($\mathbf{L}_d$), 0.509 g (3.6 mmol) of 2-chlorobenzaldehyde ($\mathbf{L}_e$), 0.503 g (2.6 mmol) of pentafluorobenzaldehyde ($\mathbf{L}_f$) or 0.506 g (3.6 mmol) of 2,6-difluorobenzaldehyde

($\mathbf{L_g}$) with an equimolar amount (0.396 g ($\mathbf{L_d}$), 0.511 g ($\mathbf{L_e}$), 0.371 g ($\mathbf{L_f}$), 0.511 g ($\mathbf{L_g}$)) of 4-chlorobenzylamine in dichloromethane (20 mL) with an excess of Na_2SO_4. The mixture was stirred under reflux for 2 h and filtered. The solvent was removed in a rotary evaporator to yield white ($\mathbf{L_d}$, $\mathbf{L_e}$) or yellow ($\mathbf{L_f}$, $\mathbf{L_g}$) solids. (2-BrC_6H_4)$CHNCH_2$(4′-ClC_6H_4) ($\mathbf{L_d}$): Yield 708 mg (85%). ^{1}H NMR (400 MHz, $CDCl_3$): δ = 8.77 [s, 1H, H^5], 8.06 [dd, ^3J(H–H) = 7.8, ^4J(H–H) = 1.8, 1H, H^4], 7.58 [dd, ^3J(H–H) = 8.0, ^4J(H–H) = 1.2, 1H, H^1], 7.36–7.24 [m, 6H, $H^{2,3,7,8}$], 4.82 [s, 2H, H^6]. CI-MS (NH_3) *m*/*z*: 308.2 $[M]^+$. (2-ClC_6H_4)$CHNCH_2$(4′-ClC_6H_4) ($\mathbf{L_e}$): Yield 818 mg (86%). ^{1}H NMR (400 MHz, $CDCl_3$): δ = 8.84 [s, 1H, H^5], 8.08 [dd, ^3J(H–H) = 7.8, ^4J(H–H)=1.8, 1H, H^4], 7.38–7.26 [m, 6H, $H^{1,2,3,7,8}$], 4.82 [s, 2H, H^6]. (C_6F_5)$CHNCH_2$(4-ClC_6H_4) ($\mathbf{L_f}$): Yield 648 mg (78%). ^{1}H NMR (400 MHz, $CDCl_3$): δ = 8.50 [s, 1H, H^1], 7.36–7.25 [m, 4H, $H^{3,4}$], 4.86 [s, 2H, H^2]. ^{19}F NMR (376.5 MHz, $CDCl_3$): δ = −138.67 [dd, 2F, *J*(F–F) = 24.4; 8.0, F^{ortho}], −146.68 [t, 1F, *J*(F–F) = 21.8, F^{para}], −157.83 [td, 2F, *J*(F–F) = 21.8; 8.0, F^{meta}]. CI-MS (NH_3) *m*/*z*: 320.3 $[M+H]^+$. (2,6-$F_2C_6H_3$)$CHNCH_2$(4′-ClC_6H_4) ($\mathbf{L_g}$): Yield 746 mg (78%). ^{1}H NMR (400 MHz, $CDCl_3$): δ = 8.60 [s, 1H, H^3], 7.39–7.23 [m, 5H], 7.00–6.92 [m, 2H], 4.85 [s, 2H, H^4]. ^{19}F NMR (282.2 MHz, $CDCl_3$): δ = -113.67 [t, ^3J(F–H) = 7.0, 2F]. CI-MS (NH_3) *m*/*z*: 266.7 $[M+H]^+$.

4.2.2. Preparation of platinum compounds

$[PtCl_2\{(4\text{-}ClC_6H_4)CHNCH_2(4'\text{-}ClC_6H_4)\}SOMe_2]$ (**2a**/**2a′**) was obtained from 0.322 g (0.76 mmol) of *cis*-$[PtCl_2(dmso)_2]$ and 0.200 g (0.76 mmol) of the imine $\mathbf{L_a}$ which were allowed to react in dry toluene (50 mL) at 100 °C for 4 h. Unreacted *cis*-$[PtCl_2(dmso)_2]$ was removed by filtration of the reaction mixture, the solvent was removed in a rotary evaporator and the residue was re-crystallized in dichloromethane–methanol, yielding a first crop of orange-yellow crystals of **2a** (yield 66 mg; 14.3%) followed by pale-yellow solid which was a mixture of **2a** and **2a′** (yield 115 mg; 24.7%) and a final crop of **2a′** (yield 45 mg; 9.8%). Total yield 226 mg (48.8%). **2a**: ^{1}H NMR (500 MHz, $CDCl_3$): δ = 8.62 [d, $^3J(H^1–H^2)$ = 8.6, 2H, H^1], 8.28 [t, $^3J(^{195}Pt–H^3)$ = 84.5, $^4J(H^4–H^3)$ = 1.5, 1H, H^3], 7.51 [d, $^3J(H^1–H^2)$ = 8.6, 2H, H^2], 7.45–7.40 [m, 4H, $H^{5,6}$], 5.21 [d, $^4J(H^4–H^3)$ = 1.5, 2H, H^4], 3.34 [s, 6H, H^7]. gHSQC (500 MHz): δ = 168.2 [C^3], 132.1 [C^1], 132.0 [C^5], 129.1 [C^6], 128.9 [C^2], 66.6 [C^4], 43.4 [C^7]. Compound **2a′**: ^{1}H NMR (300 MHz, $CDCl_3$): 8.65 [s, ^3J(Pt–H^3) = 117.4, 1H, H^3], 8.65 [d, $^3J(H^1–H^2)$ = 8.4, 2H, H^1], 7.68 [d, $^3J(H^6–H^7)$ = 8.5, 2H, H^6], 7.58 [d, $^3J(H^1–H^2)$ = 8.4, 2H, H^2], 7.46 [d, $^3J(H^6–H^7)$ = 8.5, 2H, H^7], 5.52 [dd, $^2J(H^4–H^5)$ = 13.5, $^4J(H^3–H^4)$ = 1.9, 1H, H^4], 4.94 [d, $^2J(H^4–H^5)$ = 13.6, ^3J(Pt–H^5) = 54.4, 1H, H^5], 2.67 [s, br, 3H, H^8], 2.65 [s, br, 3H, H^9]. *Anal.* Calc. for $C_{16}H_{17}Cl_4NOPtS$: C, 31.59; H, 2.82; N, 2.30; S, 5.27. Found: C, 31.9; H, 3.0; N, 2.4; S, 5.2%.

$[PtCl_2(4\text{-}ClC_6H_4CH_2NH_2)SOMe_2]$ (**2**) was obtained as a by-product in the reaction of equimolar amounts of *cis*-$[PtCl_2(dmso)_2]$ and imine $\mathbf{L_a}$ (see above) carried out in refluxing methanol. The solvent was removed in a rotary evaporator and the residue was re-crystallized in dichloromethane–methanol at low temperature. Orange-yellow crystals of **4** were obtained. ^{1}H NMR (300 MHz, $CDCl_3$): δ = 7.34 [d, $^3J(H^1–H^2)$ = 8.6, 2H, H^2], 7.28 [d, $^3J(H^1–H^2)$ = 8.7, 2H, H^1], 4.61 [s, 2H, H^4], 4.02 [m, 2H, H^3], 3.41 [s, $^3J(^{195}Pt–H^5)$ = 23.7, 6H, H^5]. ESI-MS, *m*/*z*: 502.99 $[M+NH_4]^+$; 485.96 $[M]^+$; 449.98 $[M-Cl]^+$; 414.01$[M-2Cl]^+$. *Anal.* Calc. for $C_9H_{14}Cl_3NOPtS$: C, 22.25; H, 2.90; N, 2.89; S, 6.60. Found: C, 22.5; H, 3.0; N, 2.9; S, 6.6%.

$[PtCl_2\{(2,4,6\text{-}Me_3C_6H_2)CHNCH_2(4'\text{-}ClC_6H_4)\}SOMe_2]$ (**2b**) was obtained from 0.079 g (0.187 mmol) of *cis*-$[PtCl_2(dmso)_2]$ and 0.051 g (0.184 mmol) of the imine $\mathbf{L_b}$ which were allowed to react in toluene under reflux for 4 h. The solvent was removed in a rotary evaporator and the residue was dried in vacuo. Upon addition of diethylether a yellow solid was obtained, filtered and dried in vacuo (yield 73.5 mg; 64.9%). ^{1}H NMR (400 MHz, $CDCl_3$): 9.05 [s, ^3J(Pt–H^4) = 37.2, 1H, H^4], {7.33 [d, $^3J(H^1\text{-}H^2)$ = 8.8, 2H], 7.29 [d, $^3J(H^1–H^2)$ = 8.8, 2H], $H^{1,2}$}, 6.94 [s, 2H, H^6], 4.78 [d, $^3J(H^3–H^4)$ = 1.6, 2H, H^3], 3.30 [s, 6H, H^8], 2.32 [s, 3H, H^7]; 2.27 [s, 6H, H^5]. gHSQC (400 MHz): δ = 169.7 [C^4], 131.9 [C^2], 129.3 [C^6], 129.0 [C^1], 57.9 [C^3], 43.8 [C^8], 21.1 [C^7], 19.2 [C^5]. ESI-MS, *m*/*z*: 580.06 $[M-Cl]^+$; 616.04 $[M+H]^+$; 633.06 $[M+NH_4]^+$. *Anal.* Calc. for $C_{19}H_{24}Cl_3NOPtS \cdot H_2O$: C, 36.0; H, 4.1; N, 2.2; S: 5.1. Found: C, 36.04; H, 3.98; N, 2.25; S, 5.55%.

$[PtCl_2\{(2,6\text{-}Cl_2C_6H_3)CHNCH_2(4'\text{-}ClC_6H_4)\}SOMe_2]$ (**2c**) was obtained from 142 mg (0.34 mmol) of *cis*-$[PtCl_2(dmso)_2]$ and 100 mg (0.34 mmol) of the imine $\mathbf{L_c}$ which were allowed to react in refluxing toluene (50 mL) at 100 °C for 4 h. The solvent was removed in a rotary evaporator and the residue was re-crystallized in dichloromethane–methanol, yielding **2c** (yield 140 mg; 64%). ^{1}H NMR (400 MHz, $CDCl_3$): 8.92 [t, $^3J(H^3–H^4)$ = 1.5, ^3J(Pt–H^4) = 42.6, 1H, H^4], 7.43 [s, 3H, $H^{5,6,7}$], {7.36 [d, $^3J(H^1–H^2)$ = 8.0, 2H], 7.33 [d, $^3J(H^1–H^2)$ = 8.0, 2H], $H^{1,2}$}, 4.92 [d, $^3J(H^3–H^4)$ = 1.5, ^3J(Pt–H^3) = 27.6, 2H, H^3], 3.30 [s, ^3J(Pt–H^8) = 16.8, 6H, H^8]. ESI-MS, *m*/*z*: 640.91 $[M+H]^+$, 604.93 [M−Cl], 568.96 [M−2Cl]. *Anal.* Calc. for $C_{16}H_{16}Cl_3NOPtS$: C, 29.90; H, 2.51; N, 2.18; S, 4.99. Found: C, 29.8; H, 2.6; N, 2.3; S, 4.9%.

$[PtCl_2\{(2\text{-}BrC_6H_4)CHNCH_2(4'\text{-}ClC_6H_4)\}SOMe_2]$ (**2d′**) was obtained from 0.207 g (0.49 mmol) of *cis*-$[PtCl_2(dmso)_2]$, 0.151 g (0.489 mmol) of imine $\mathbf{L_d}$ and 80 mg (0.975 mmol) which were allowed to react in refluxing methanol (30 mL) for 48 h. The reaction mixture was filtered, the solvent was removed in a rotary evaporator and the residue was re-crystallized in dichloromethane–methanol, yielding a light yellow solid which was filtered in vacuo. Yield 81.2 mg (25.4%). ^{1}H NMR (400 MHz, $CDCl_3$): δ = 9.35 [dd, $^3J(H^3–H^4)$ = 7.7, $^4J(H^2–H^4)$ = 1.6, 1H, H^4], 8.87 [s, ^3J(Pt–H^5) = 115.0, $^4J(H^5–H^6)$ = 1.9, 1H, H^5], 7.69–7.63 [m, 2H, $H^{1,3}$], 7.67 [d, $^3J(H^8–H^9)$ = 8.3, 2H, H^8], 7.51 [td, $^3J(H^2–H^{1,3})$ = 7.7, $^4J(H^2–H^4)$ = 1.7, 1H, H^2], 7.47 [d, $^3J(H^8–H^9)$ = 8.4, 2H, H^9], 5.6 [dd, $^2J(H^6–H^7)$ = 13.4, $^4J(H^5–H^6)$ = 1.9, 1H, H^6], 4.94 [d, $^2J(H^6–H^7)$ = 13.4, 1H, H^7], 2.63 [s, br, 3H, H^{10}], 2.48 [s, br, 3H, H^{11}]. *Anal.* Calc. for $C_{16}H_{17}BrCl_3NOPtS$: C, 29.44; H, 2.63; N, 2.15; S, 4.91. Found: C, 30.0; H, 2.8; N, 2.3; S, 4.6%.

$[PtCl_2\{(2\text{-}ClC_6H_4)CHNCH_2(4'\text{-}ClC_6H_4)\}SOMe_2]$ (**2e′**) was obtained from 0.242 g (0.573 mmol) of *cis*-$[PtCl_2(dmso)_2]$, 0.151 g (0.572 mmol) of imine $\mathbf{L_e}$ and 93 mg (1.134 mmol) of sodium acetate, using the procedure reported for **2d′**. Yield 166.2 mg (47.7%). ^{1}H NMR (500 MHz, $CDCl_3$): δ = 9.36 [dd, $^3J(H^3–H^4)$ = 5.7, $^4J(H^2–H^4)$ = 3.6, 1H, H^4], 8.95 [s, ^3J(Pt–H^5) = 120.2, 1H, H^5], 7.67 [d, $^3J(H^8–H^9)$ = 8.4, 2H, H^8], 7.60 [d, $^3J(H^3–H^4)$ = 5.9, $^4J(H^2–H^4)$ = 3.4, 2H, $H^{2,3}$], 7.51–7.50 [m, 1H, H^1], 7.47 [d, $^3J(H^8–H^9)$ = 8.4, 2H, H^9], 5.58 [dd, $^2J(H^6–H^7)$ = 13.3, $^4J(H^5–H^6)$ = 1.9, 1H, H^6], 4.95 [d, $^2J(H^6–H^7)$ = 13.3, ^3J(Pt–H^7) = 56.3, 1H, H^7], 2.62 [s, ^3J(Pt–H^{10}) = 22.8, 3H, H^{10}], 2.48 [s, ^3J(Pt–H^{11}) = 22.8, 3H, H^{11}]. ^{13}C NMR (100.6 MHz, $CDCl_3$): δ = 161.05 [1C, C^7], 136.00 [1C, C^6], 135.24 [1C, C^9], 133.66 [1C, C^3], 132.97 [1C, C^1], 132.84 [2C, C^{10}], 132.69 [1C, C^{12}], 130.20 [1C, C^5], 129.89 [1C, C^2], 129.17 [2C, C^{11}], 126.77 [1C, C^4], 69.78 [1C, C^8], 43.66 [1C, C^{13}], 43.44 [1C, C^{14}]. ESI-MS, *m*/*z*: 626.98 $[M+NH_4]^+$. *Anal.* Calc. for $C_{16}H_{17}Cl_4NOPtS$: C, 31.59; H, 2.82; N, 2.30; S, 5.27. Found: C, 31.6; H, 3.2; N, 2.3; S, 6.2%.

$[PtCl\{C_6F_5CHNCH_2(4\text{-}ClC_6H_3)\}SOMe_2]$ (**3f**) was obtained from 0.203 g (0.480 mmol) of *cis*-$[PtCl_2(dmso)_2]$, 0.154 g (0.481 mmol) of imine $\mathbf{L_f}$ and 79 mg (0.963 mmol) of sodium acetate, using the procedure reported for **2d′**. Yield 20 mg (6.6%). ^{1}H NMR (500 MHz, $CDCl_3$): δ = 8.69 [d, ^3J(Pt–H^1) = 82.9, $^4J(H^1–H^2)$ = 1.4, 1H, H^1], 8.01 [d, ^3J(Pt–H^5) = 50.9, $^4J(H^5–H^{3,4})$ = 1.7, 1H, H^5], 7.08 [t, J(Pt–$H^{3,4}$) = 20.2, $J(H^5–H^{3,4})$ = 2.0, 2H, $H^{3,4}$], 5.05 [s, ^3J(Pt–H^2) = 25.2, 2H, H^2], 3.47 [s, 6H, H^6]. ^{19}F NMR (376.5 MHz, $CDCl_3$): δ = −150.93 [t, *J*(F–F) = 20.8, 1F, F^{para}], −163.83 [dd, *J*(F–F) = 20.5; 5.7, 2F, F^{ortho}], −169.48 [td, *J*(F–F) = 18.4; 2.1, 2F, F^{meta}]. gHSQC (500 MHz) δ = 154.0 [C^1], 133.6 [C^5], {120.5, 124.5 [C^3, C^4]}, 68.5 [C^2], 44.5 [C^6]. ESI-MS, *m*/*z*: 663.46 $[M+2H_20]^+$.

$[PtCl_2\{(2,6\text{-}F_2C_6H_3)CHNCH_2(4'\text{-}ClC_6H_4)\}SOMe_2]$ (**2g′**) was obtained from 0.242 g (0.573 mmol) of *cis*-$[PtCl_2(dmso)_2]$, 0.151 g (0.572 mmol) of imine $\mathbf{L}_g$ and 93 mg (1.134 mmol) of sodium acetate, using the procedure reported for **2d′**. Yield 36.5 mg (10.0%). ^{1}H NMR (500 MHz, $CDCl_3$): δ = 8.80 [s, ^3J(Pt–H^3) = 120.2, 1H, H^3], 7.64 [d, ^3J(H^6–H^7) = 8.4, 2H, H^6], 7.61–7.58 [m, 1H, H^2], 7.47 [d, ^3J(H^6–H^7) = 8.4, 2H, H^7], 7.11 [t, ^3J(H^1–H^2) = 8.2, ^3J(H^1–F) = 8.2, 2H, H^1], 5.71 [dd, ^2J(H^4–H^5) = 13.5, ^4J(H^3–H^4) = 1.8, 1H, H^4], 5.05 [d, ^2J(H^4–H^5) = 13.5,1H, H^5], 2.75 [s, br, 3H, H^8], 2.64 [s, br, 3H, H^9]. ^{19}F NMR (376.5 MHz, $CDCl_3$): δ = −104.00 [t, ^3J(F–H^1) = 7.0]. gHSQC (500 MHz) δ = 162.9 [C^3]; 134.0 [C^2]; 132.6 [C^6]; 128.9 [C^7], 112.0 [C^1]; 69.8 [C^4]; 42.0 [C^8]. ESI-MS, *m*/*z*: 1237.95 $[2M+H_2O]^+$; 1182.95 $[2M-Cl]^+$; 626.99 $[M+H_2O]^+$; 573.99 $[M-Cl]^+$; 538.02 $[M-2Cl]^+$. *Anal.* Calc. for $C_{16}H_{16}Cl_3F_2NOPtS$: C, 31.51; H, 2.64; N, 2.30; S, 5.26. Found: C, 31.9; H, 2.9; N, 2.4; S, 5.3%.

4.3. X-ray structure analysis for 2, 2a and 2c

Prismatic crystals were selected and mounted on a MAR 345 diffractometer. Unit cell parameters were determined from 6776 (**2**), 309 (**2a**) and 7029 (**2c**) reflections ($3° < \theta < 31°$) and refined by least-squares methods. Intensities were collected with graphite mono-chromatized Mo Kα radiation. 28622 (**2**), 9983 (**2a**) and 9836 (**2c**) reflections were measured in the range $2.60° < \theta < 30.00°$ (**2**), $3.06° < \theta < 30.00°$ (**2a**) or $2.73° < \theta < 32.34°$ (**2c**). 12272 (**2**), 5345 (**2a**) and 7929 (**2c**) reflections were assumed as observed applying the condition $I > 2\sigma(I)$. Lorentz polarization and absorption corrections were made for **2** and **2c**.

The structures were solved by direct methods using SHELXS program [19], and refined by full-matrix least-squares method with SHELXL97 computer program using 28622 (**2**), 9983 (**2a**) and 9836 (**2c**) reflections. The function minimized was $\sum w||F_o|^2 - |F_c|^2|^2$, where $w = [\sigma^2(I) + (0.0501P)^2 + 11.8165P]^{-1}$ (**2**), $[\sigma^2(I) + (0.0986P)^2 + 3.6436P]^{-1}$ (**2a**) or $[\sigma^2(I) + (0.0734P)^2 + 4.1280P]^{-1}$ (**2c**) and $P = (|F_o|^2 + 2|F_c|^2)/3$. *f*, *f′* and *f″* were taken from International Tables of X-ray Crystallography [20]. All hydrogen atoms were computed and refined using a riding model with an isotropic temperature factor equal to 1.2 times the equivalent temperature factor of the atom to which they are linked. Further details are given in Table 2.

Table 2
Crystallographic and refinement data

	Compound **2**	Compound **2a**	Compound **2c**
Empirical formula	$C_9H_{14}Cl_3NOPtS$	$C_{16}H_{17}Cl_4NOPtS$	$C_{16}H_{16}Cl_5NOPtS$
Molecular weight	485.71	608.26	642.70
Temperature (K)	293(2)	293(2)	293(2)
Wavelength (Å)	0.71073	0.71073	0.71073
Crystal system, space group	triclinic, $P\bar{1}$	monoclinic, $P2_1$	monoclinic, $P2_1/c$
Unit cell dimensions			
a (Å)	13.603(7)	11.126(6)	9.890(6)
b (Å)	14.699(5)	7.842(3)	32.240(15)
c (Å)	16.323(6)	12.127(4)	13.289(5)
α (°)	67.60(2)	90	90
β (°)	89.04(3)	109.93(2)	97.76(3)
γ (°)	77.35(2)	90	90
Volume (Å^3)	2936(2)	994.7(7)	4198(4)
Z; D_{calc} (Mg m^{-3})	8; 2.198	2; 2.031	8; 2.034
Absorption coefficient (mm^{-1})	10.225	7.699	7.425
F(000)	1824	580	2448
Crystal size (mm)	0.1 × 0.1 × 0.2	0.09 × 0.05 × 0.05	0.2 × 0.1 × 0.1
θ Range for data collection (°)	2.60–30	3.06–30	2.73–32.34
Reflections collected/ unique (R_{int})	28622/14588 (0.0947)	9983/5596 (0.0714)	9836/9836 (0.0370)
Completeness to θ	85.1 (θ = 30.00)	98.2 (θ = 30.00)	78.1 (θ = 25.00)
Refinement method	full-matrix least-squares on F^2	full-matrix least-squares on F^2	full-matrix least-squares on F^2
Data/restraints/ parameters	14588/5/578	5596/1/218	9836/8/457
Goodness-of-fit on F^2	1.087	1.118	1.146
Final *R* indices [$I > 2\sigma(I)$]	R_1 = 0.0547, wR_2 = 0.1449	R_1 = 0.0593, wR_2 = 0.1568	R_1 = 0.0452, wR_2 = 0.1392
R indices (all data)	R_1 = 0.0612, wR_2 = 0.1511	R_1 = 0.0624, wR_2 = 0.1630	R_1 = 0.0547, wR_2 = 0.1450
Largest difference in peak and hole (e Å^{-3})	0.916 and −0.763	0.970 and −0.922	0.883 and −0.916

5. Supplementary data

CCDC 68025, 68026 and 68027 contain the supplementary crystallographic data for **2**, **2a** and **2c**. These data can be obtained free of charge via http://www.ccdc.cam.ac.uk/conts/retrieving.html, or from the Cambridge Crystallographic Data Centre, 12 Union Road, Cambridge CB2 1EZ, UK; fax: (+44) 1223-336-033; or e-mail: deposit@ccdc.cam.ac.uk.

Acknowledgement

This work was supported by the Ministerio de Ciencia y Tecnología (Project: CTQ2006-02007/BQU).

References

[1] (a) A.D. Ryabov, Synthesis (1985) 233;
(b) V.V. Dunina, O.A. Zalevskaya, V.M. Potapov, Russ. Chem. Rev. 57 (1988) 434;
(c) A.D. Ryabov, Chem. Rev. 90 (1990) 403;
(d) P. Espinet, M.A. Esteruelas, L.A. Oro, J.L. Serrano, E. Sola, Coord. Chem. Rev. 117 (1992) 215;
(e) C. Navarro-Ranninger, I. López-Solera, J.M. Pérez, J.R. Masaguer, C. Alonso, Appl. Organomet. Chem. 7 (1993) 57;
(f) M. Albrecht, M. Lutz, A.L. Spek, G. van Koten, Nature (2000) 406;
(g) M. Albrecht, G. van Koten, Angew. Chem., Int. Ed. 40 (2001) 3750;
(h) J. Dupont, M. Pfeffer, J. Spencer, Eur. J. Inorg. Chem. (2001) 1917;
(i) I. Omae, Coord. Chem. Rev. 248 (2004) 995;
(j) J. Dupont, C.S. Consorti, J. Spencer, Chem. Rev. 105 (2005) 252.
[2] (a) J. Bravo, C. Cativiela, R. Navarro, E.P. Urriolabeitia, J. Organomet. Chem. 650 (2002) 157;
(b) S. Pérez, C. López, A. Caubet, X. Solans, M. Font-Bardía, New J. Chem. 27 (2003) 975;
(c) M. Crespo, M. Font-Bardía, J. Granell, M. Martínez, X. Solans, Dalton Trans. (2003) 3763;
(d) A. Capapé, M. Crespo, J. Granell, M. Font-Bardía, X. Solans, J. Organomet. Chem. 690 (2005) 4309.
[3] (a) X. Riera, A. Caubet, C. López, V. Moreno, X. Solans, M. Font-Bardía, Organometallics 19 (2000) 1384;
(b) X. Riera, C. López, A. Caubet, V. Moreno, X. Solans, M. Font-Bardía, Eur. J. Inorg. Chem. (2001) 2135.
[4] C. López, A. Caubet, S. Pérez, X. Solans, M. Font-Bardía, E. Molins, Eur. J. Inorg. Chem. (2006) 3974.
[5] (a) L. Ding, D.P. Zou, Y.J. Wu, Polyhedron 17 (15) (1998) 2511;
(b) C. López, A. Caubet, S. Pérez, X. Solans, M. Font-Bardía, Chem. Commun. (2004) 540;
(c) Y.J. Wu, L. Ding, H.X. Wang, Y.H. Liu, H.Z. Yuan, X.A. Mao, J. Organomet. Chem. 535 (1997) 49.
[6] (a) L. Alexandrova, O.G. D'yachenko, G.M. Kazankov, V.A. Polyakov, P.V. Samuleev, E. Sansores, A.D. Ryabov, J. Am. Chem. Soc. 122 (2000) 5189;
(b) A.D. Ryabov, G.M. Kazankov, I.M. Panyashkina, O.V. Grozovsky, O.G. Dyachenko, V.A. Polyakov, L.M. Kuz'mina, J. Chem. Soc., Dalton Trans. (1997) 4385;
(c) A.D. Ryabov, S. Otto, P.V. Samuleev, V.A. Polyakov, L. Alexandrova, G.M. Kazankov, S. Shova, M. Revenco, J. Lipkowski, M.H. Johansson, Inorg. Chem. 41 (16) (2002) 4286.
[7] (a) A.D. Ryabov, I.M. Panyashkina, V.A. Polyakov, A. Fischer, Organometallics 21 (2002) 1633;
(b) S. Tollari, S. Cenini, A. Penoni, G. Granata, G. Palmisano, F.J. Demartin, J. Organomet. Chem. 608 (2000) 34.
[8] (a) R. Annunziata, S. Cenini, F. Demartin, G. Palmisano, S. Tollari, J. Organomet. Chem. 496 (1995) C1;
(b) M.D. Meijer, E. de Wolf, M. Lutz, A.L. Spek, G.P.M. van Klink, G. van Koten, Organometallics 20 (2001) 4198;
(c) P.R.R. Ranatunge-Bandarage, B.H. Robinson, J. Simpson, Organometallics 13 (1994) 500;

(d) A.D. Ryabov, I.M. Panyashkina, A.V. Polyakov, J.A.K. Howard, L.G. Kuz'mina, M.S. Datt, C. Sacht, Organometallics 17 (1998) 3615.
[9] (a) C.E.L. Headford, R. Mason, P.R. Ranatunge-Bandarage, B.H. Robinson, J. Simpson, J. Chem. Soc., Chem. Commun. (1990) 601;
(b) M.D. Meijer, A.W. Kleij, M. Lutz, A.L. Spek, G. van Koten, J. Organomet. Chem. 640 (2001) 166;
(c) M.D. Meijer, A.W. Kleij, B.S. Williams, D. Ellis, M. Lutz, A.L. Spek, G.P.M. van Klink, G. van Koten, Organometallics 21 (2002) 264;
(d) P.R.R. Ranatunge-Bandarage, N.W. Duffy, S.M. Johnston, B.H. Robinson, J. Simpson, Organometallics 13 (1994) 511.
[10] S. Otto, A. Chanda, P.V. Samuleev, A.D. Ryabov, Eur. J. Inorg. Chem. (2006) 2561.
[11] Y.Y. Scaffidi-Domianello, A.A. Nazarov, M. Haukka, M. Galanski, B. Keppler, J. Schneider, P. Du, R. Eisenberg, V.Y. Kukuskin, Inorg. Chem. 46 (11) (2007) 4469.
[12] (a) A. Capapé, M. Crespo, J. Granell, A. Vizcarro, J. Zafrilla, M. Font-Bardía, X. Solans, Chem. Commun. (2006) 4128;
(b) A. Capapé, M. Crespo, J. Granell, M. Font-Bardía, X. Solans, Dalton Trans. (2007) 2030.
[13] M. Crespo, M. Font-Bardía, X. Solans, J. Organomet. Chem. 691 (2006) 1897.
[14] (a) C.M. Anderson, M. Crespo, G. Ferguson, A.J. Lough, R.J. Puddephatt, Organometallics 11 (1992) 1177;
(b) O. López, M. Crespo, M. Font-Bardía, X. Solans, Organometallics 16 (1997) 1233.
[15] G. Annibale, M. Bonivento, L. Cattalini, M.L. Tobe, J. Chem. Soc., Dalton Trans. (1992) 3433.
[16] (a) F.D. Rochon, J.R.L. Priqueler, Can. J. Chem. 82 (2004) 649;
(b) N. Nédélec, F.D. Rochon, Inorg. Chim. Acta 319 (2001) 95.
[17] R. Bosque, M. Crespo, E. Evangelio, M. Font-Bardía, X. Solans, J. Organomet. Chem. 690 (2005) 2062.
[18] (a) J.H. Price, A.N. Williamson, R.F. Schramm, B.B. Wayland, Inorg. Chem. 11 (6) (1972) 1280;
(b) V.Y. Kukushkin, A.J. L Pombeiro, C.M.P. Ferreira, L.I. Elding, Inorg. Synth. 33 (2002) 189.
[19] G.M. Sheldrick, SHELXS97, A Computer Program for Crystal Structure Determination, University of Göttingen, Germany, 1997.
[20] International Tables of X-ray Crystallography, vol. IV, Kynoch Press, Birmingham, UK, 1974. p. 99, 149.

Polyhedron 27 (2008) 2612–2624

Contents lists available at ScienceDirect

Polyhedron

journal homepage: www.elsevier.com/locate/poly

12-Tungstophosphoric acid supported on inorganic oxides as heterogeneous and reusable catalysts for the selective preparation of alkoxymethyl ethers and their deprotections under different reaction conditions

Iraj Mohammadpoor-Baltork *, Majid Moghadam *, Shahram Tangestaninejad, Valiollah Mirkhani, Arsalan Mirjafari

Department of Chemistry, Catalysis Division, University of Isfahan, Isfahan 81746-73441, Iran

ARTICLE INFO

Article history:
Received 23 February 2008
Accepted 2 May 2008
Available online 3 June 2008

Keywords:
Alkoxymethylation
12-Tungstophosphoric acid
Silica gel
Zirconia
Microwave irradiation

ABSTRACT

A wide variety of primary and secondary alcohols were efficiently converted to their corresponding methoxymethyl (MOM) and ethoxymethyl (EOM) ethers in the presence of catalytic amounts of supported $H_3PW_{12}O_{40}$ on silica gel and zirconia at room temperature and under microwave irradiation at solvent-free conditions, whereas, phenols and tertiary alcohols remained intact under the same reaction conditions. Deprotection of these ethers to their parent alcohols was also achieved using these heterogeneous catalysts in ethanol, as a green solvent, under reflux conditions and microwave irradiation. Selective deprotection of primary and secondary MOM- and EOM-ethers in the presence of phenolic and tertiary ones, methyl and benzyl ethers, esters and trimethylsilyl ethers was achieved by these reagent systems. The present methodology offers several advantages such as short reaction times, high yields, simple procedure, heterogeneous reaction conditions, selectivity, non-toxicity and reusability of the catalysts.

© 2008 Published by Elsevier Ltd.

1. Introduction

The use of Keggin-type heteropoly acids (HPAs) as homogeneous or heterogeneous catalysts for organic synthetic processes has been developed for important industries related to fine chemicals, pharmaceutical and food industries [1]. HPAs have several advantages such environmentally benign, reusability, non-corrosive and fewer disposal problems as catalysts which make them economically and environmentally attractive. Heteropoly acids, especially $H_3PW_{12}O_{40}$, have received great attention among the acid catalysts, because of their high acid strength and selectivity properties [2]. A major disadvantage of bulk HPAs, when used as catalysts, lies in their low specific surface area, less than 10 $m^2\ g^{-1}$, which can be improved by immobilization on the solid supports [3]. Procedures for supporting HPAs on different carriers and also their characterization are covered in the literature [3,4]. Several organic transformations using supported HPAs such as Diels–Alder reaction [5], oxidative dehydrogenation of alcohols and amines [6], olefin hydration [7], synthesis of dihydropyrimidinones [8], esterification reactions [9], preparation of oximes [10] and synthesis of oxazolines, imidazolines and thiazolines [11] has been reported in the literature.

The selective protection and deprotection of hydroxyl groups have occupied a unique position in organic synthesis because of the fundamental importance of hydroxyl groups in multi-step synthesis of complex natural products [12]. Alkoxymethyl groups have been induced as suitable protecting groups for alcohols in organic synthesis. These protecting groups provide a number of significant advantages such as ease of introduction and stability toward a wide variety of conditions including many organometallic reagents, reducing and oxidizing agents [13]. Alkoxymethyl ethers are frequently prepared by the reactions of alcohols with formaldehyde dimethyl acetal (FDMA) or formaldehyde diethyl acetal (FDEA) [14]. Deprotection of these ethers to their corresponding alcohols under mild conditions is of practical importance and several methods and catalysts have been reported for these transformations [14h,15]. However, some of the reported methods suffer from one or more disadvantages such as harsh reaction conditions, high reaction temperature, long reaction times, high cost or toxicity of the reagents and tedious work-up. Consequently, introduction of efficient and selective methods for the preparation of alkoxymethyl ethers and their deprotection using inexpensive, relatively non-toxic, easy handling and environmentally friendly catalysts is of practical importance and is still in demand.

The utility of microwave irradiation to carry out organic reactions has now become a regular feature. The main benefits of performing the reaction under microwave conditions are the significant rate enhancements and the higher product yields that

* Corresponding authors. Tel.: +98 311 7932705; fax: +98 311 6689732.
E-mail addresses: imbaltork@sci.ui.ac.ir (I. Mohammadpoor-Baltork), majidmoghadamz@yahoo.com, moghadamm@chem.ui.ac.ir (M. Moghadam).

0277-5387/$ - see front matter © 2008 Published by Elsevier Ltd.
doi:10.1016/j.poly.2008.05.002

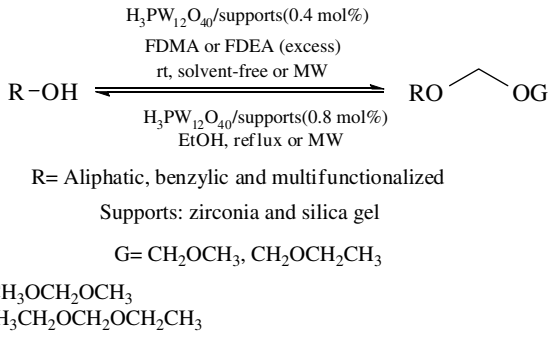

Scheme 1.

can be observed. A key advantage of modern scientific microwave apparatus is the ability to control reaction conditions very specifically, monitoring temperature, pressure and reaction times [16].

In continuation of our research on protection and deprotection reactions [17], we now report the use of $H_3PW_{12}O_{40}$ (TPA) supported on inorganic oxides such as silica gel and zirconia as heterogeneous, relatively non-toxic and reusable catalysts for conversion of primary and secondary benzylic and aliphatic alcohols with FDMA and FDEA to their corresponding methoxymethyl (MOM) and ethoxymethyl (EOM) ethers at room temperature under solvent-free conditions and also deprotection of these ethers in a green solvent, ethanol, under reflux conditions. These reactions were also performed under microwave irradiation (Scheme 1).

2. Experimental

All materials were purchased from Merck chemical company. All products were identified by comparison of their physical and spectral data with those of authentic samples. ^{1}H NMR spectra were recorded in a $CDCl_3$ solution on a Bruker-AC 500 MHz spectrometer. IR spectra were recorded on a Shimadzu IR-435 spectrophotometer. Melting points were determined using Stuart Scientific SMP2 apparatus. The microwave system used for these experiments includes the following items: Micro-SYNTH labstation, complete with glass door, dual magnetron system with pyramid-shaped diffuser, 1000 Watt delivered power, exhaust system, magnetic stirrer, "quality pressure" sensor for flammable organic solvents, ATCFO fiber optic system for automatic temperature control.

2.1. General procedure for the preparation of EOM- and MOM-ethers at room temperature

To a solution of alcohol (3 mmol) and FDEA (15 mmol) or FDMA (21 mmol), supported TPA (0.03 g, 0.4 mol%) was added and the mixture was stirred at room temperature for the appropriate time according to Tables 2 and 3. The progress of the reaction was monitored by TLC (eluent: cyclohexane/ethyl acetate, 4:1). After completion of the reaction, the catalyst was separated by filtration and washed with cold EtOH (10 mL). The filtrate was evaporated and the crude product was purified by column chromatography on silica gel (eluent: cyclohexane/ethyl acetate, 4:1) to afford the pure product.

2.2. General procedure for the preparation of EOM- and MOM-ethers under microwave irradiation

All reactions were carried out at 53–56 °C, with 150 W applied power in a 100 mL round-bottom flask provided with two openings equipped with a glass condenser.

To a mixture of alcohol (3 mmol) and FDEA (15 mmol) or FDMA (21 mmol), supported TPA (0.03 g, 0.4 mol%) was added and the mixture was irradiated with MW for appropriate time as mentioned in Tables 2 and 3. After completion of the reaction (monitored by TLC, eluent: cyclohexane/ethyl acetate, 4:1), the catalyst was filtered and washed with cold EtOH (10 mL). Evaporation of the solvent under reduced pressure and purification by a silica gel column gave the pure product.

2.3. General procedure for the cleavage of EOM- and MOM-ethers under reflux conditions

A mixture of alkoxymethyl ether (1 mmol) and supported TPA (0.06 g, 0.8 mol%) in EtOH (8–10 mL) was stirred under reflux conditions for the appropriate time according to Tables 5 and 6. After completion of the reaction (TLC analysis), the mixture was cooled to room temperature and the catalyst was separated by filtration and washed with cold EtOH (10 mL). Evaporation of the filtrate and purification of the crude product by a silica gel column (eluent: cyclohexane/ethyl acetate, 4:1) afforded the pure product.

2.4. General procedure for the cleavage of EOM- and MOM-ethers under microwave irradiation

All reactions were carried out at 72–75 °C, with 250 W applied power in a 100 mL round-bottom flask provided with two openings equipped with a glass condenser.

A mixture of alkoxymethyl ether (1 mmol) and supported TPA (0.06 g, 0.8 mol%) in EtOH (8–10 mL) was irradiated with MW for the appropriate time according to Tables 5 and 6. After completion of the reaction (TLC analysis), the mixture was cooled to room temperature and the catalyst was separated by filtration and washed with cold EtOH (10 mL). The filtrate was evaporated and the crude product was purified by a silica gel column (eluent: cyclohexane/ethyl acetate, 4:1) to afford the pure alcohol.

Table 1
Optimization of conditions for the protection of benzyl alcohol with FDMA

Entry	Catalyst	Catalyst amount (mol%)							
		0.2		0.3		0.4		0.5	
		Time (h)	Yield[b] (%)	Time (h)	Yield[b] (%)	Time (h)	Yield[b] (%)	Time (h)	Yield[b] (%)
1	TPA/SiO_2	6	47	4	59	1	93	1	93
2	TPA/ZrO_2	7	44	7	54	2	90	2	90
3	ZrO_2[a]	24	0						
4	SiO_2[a]	24	0						
5	TPA	7	23	6	29	2	45	1	25

[a] Reaction was performed in the presence of 50 mg of silica gel or zirconia.
[b] Isolated yields.

Table 2
Protection of alcohols with TPA supported on silica gel at room temperature and under MW irradiation

Entry	Alcohol	Formation of EOM-ether (a)		Formation of MOM-ether (b)	
		Yield[a] (%) (Time, min)		Yield[a] (%) (Time, min)	
		RT	MW	RT	MW
1	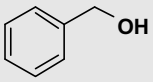	93 (60)	93 (2)	94 (60)	91 (1.5)
2	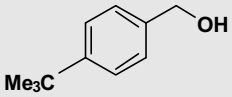	94 (60)	94 (1)	97 (45)	94 (1)
3	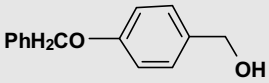	97 (120)	90 (1.5)	94 (60)	90 (1.5)
4	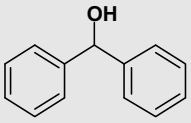	94 (120)	93 (3.5)	93 (120)	87 (2.5)
5[b]	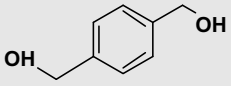	91 (150)	91 (2.5)	93 (150)	90 (2.5)
6	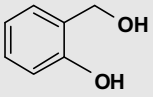	89 (60)	88 (3)	84 (120)	90 (1.5)
7	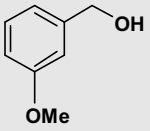	80 (90)	93 (2)	93 (60)	92 (1.5)
8	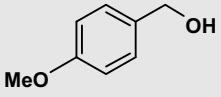	85 (120)	96 (2)	88 (90)	92 (1.5)
9	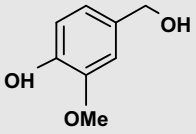	92 (90)	89 (3)	89 (60)	87 (3)
10	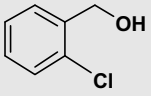	91 (60)	91 (1.75)	94 (45)	90 (0.5)
11	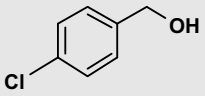	93 (45)	98 (0.5)	97 (45)	97 (0.5)
12	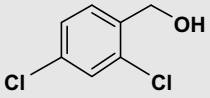	97 (45)	91 (1)	91 (45)	95 (1)
13	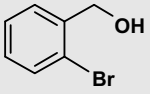	91 (60)	97 (0.5)	93 (45)	96 (0.5)
14	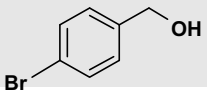	97 (45)	97 (0.5)	96 (45)	97 (0.5)

Table 2 (*continued*)

Entry	Alcohol	Formation of EOM-ether (a)		Formation of MOM-ether (b)	
		Yield[a] (%) (Time, min)		Yield[a] (%) (Time, min)	
		RT	MW	RT	MW
15	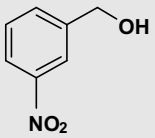	89 (180)	89 (3)	91 (180)	91 (2.5)
16	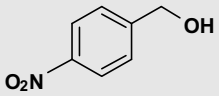	79 (210)	92 (5)	74 (210)	90 (5.5)
17	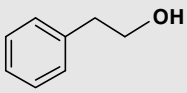	94 (60)	93 (2)	97 (60)	94 (1.5)
18	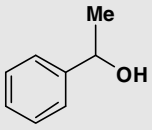	80 (210)	90 (2.5)	84 (180)	93 (2)
19	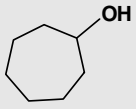	94 (105)	94 (2.5)	94 (105)	92 (2.5)
20	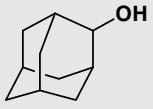	94 (90)	88 (2)	94 (90)	91 (2)
21	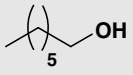	95 (60)	94 (1)	93 (60)	90 (1)
22	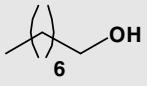	94 (60)	94 (1)	94 (60)	92 (1)

[a] Isolated yields.
[b] 0.8 mol% of the catalyst was used.

3. Results and discussion

3.1. Preparation of the supported 12-tungstophosphoric acid

The supported TPAs (TPA–SiO_2 and TPA–ZrO_2) catalysts were prepared by the method of incipient wetness. In a typical procedure, a 400 mg portion of TPA was dissolved in deionized water (50 mL) and impregnated drop-wise onto 1600 mg high surface area SiO_2 (Cabosil 20) and ZrO_2 (purchased from Merck) supports under constant agitation. The resulting pastes were dried at 110 °C for 4 h and then calcined at 250 °C for 4 h [18].

FT-IR spectra can be used as a powerful technique for the investigation of surface interaction between TPA and inorganic supports. Pure TPA compounds display infrared bands at 1080 cm^{-1} (P–O), 985 (W=O), 887 (W–O_c–W) and 807 cm^{-1} (W–O_b–W) [2,19]. The FT-IR spectrum of TPA–SiO_2 shows bands at 982 (W=O), 899 and 819 cm^{-1} (W–O–W) and the band assigned to P–O vibrations is masked by SiO_2 broad vibrations. The FT-IR spectrum of TPA–ZrO_2 shows bands at 1072 (P–O), 966 (W=O), 870 and 817 cm^{-1} (W–O–W) [20].

The TPA loading on the supports, which were calculated from W content in supported-TPA catalysts, was determined by neutron activation analysis. The amounts of W loading on the supported catalysts were 29.75 ± 0.9 (0.13 mmol/g) and 24.10 ± 0.8 (0.11 mmol/g) for TPA–SiO_2 and TPA–ZrO_2, respectively.

3.2. Protection reactions

First, we studied the reaction of benzyl alcohol with FDMA in the presence of supported TPAs in order to find the best reaction conditions. The reaction was performed in the presence of different molar ratios of FDMA and catalysts. The optimum condition used for the protection of benzyl alcohol with these heterogenized catalysts, was alcohol, FDMA and catalyst, in a molar ratio of 1:7:0.004, at room temperature under solvent-free conditions (Table 1, entries 1 and 2).

In order to show the role of the catalysts, the protection of benzyl alcohol was carried out with silica gel and zirconia alone in the absence of TPA. The experimental results showed that the alcohol remained intact under this condition (Table 1, entries 3 and 4). Comparison of TPA in supported and pure forms in the protection of benzyl alcohol showed that the activity of supported catalysts is higher than the bulk form (Table 1, entry 5).

The protection of benzyl alcohol with FDMA was also investigated in the presence of these catalysts under microwave irradiation. The highest yield of the product was obtained at the power

Table 3
Protection of alcohols with TPA supported on zirconia at room temperature and under MW irradiation

Entry	Alcohol	Formation of EOM-ether (a)		Formation of MOM-ether (b)	
		Yield[a] (%) (Time, min)		Yield[a] (%) (Time, min)	
		RT	MW	RT	MW
1	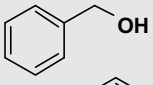	90 (120)	91 (2.5)	84 (150)	88 (1.5)
2	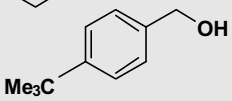	87 (120)	91 (1.5)	96 (150)	91 (1.5)
3	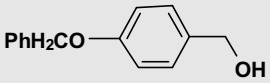	89 (90)	91 (1.5)	83 (120)	87 (1.5)
4	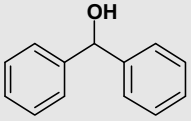	89 (120)	87 (4.5)	90 (150)	87 (3.5)
5[b]	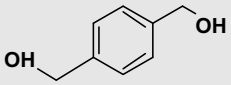	88 (150)	90 (3)	80 (150)	90 (3)
6	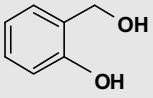	92 (150)	88 (3)	94 (150)	87 (2.5)
7	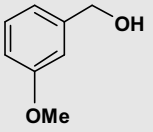	82 (180)	93 (2.5)	94 (120)	91 (2.5)
8	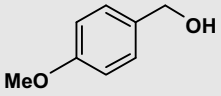	87 (150)	91 (2)	88 (180)	90 (2)
9	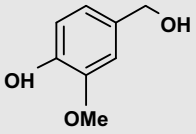	82 (120)	83 (3)	89 (180)	86 (3)
10	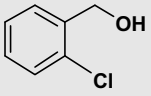	95 (90)	90 (2)	95 (90)	92 (1)
11	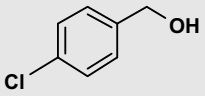	95 (90)	93 (0.5)	94 (120)	94 (0.5)
12	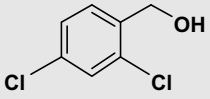	93 (60)	91 (2)	90 (150)	91 (1.5)
13	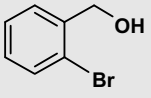	92 (120)	96 (1)	94 (120)	96 (1)
14	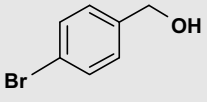	91 (120)	93 (0.5)	95 (90)	92 (0.5)
15	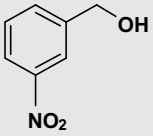	71 (210)	86 (3)	73 (210)	88 (2.5)

Table 3 (*continued*)

Entry	Alcohol	Formation of EOM-ether (a)		Formation of MOM-ether (b)	
		Yield[a] (%) (Time, min)		Yield[a] (%) (Time, min)	
		RT	MW	RT	MW
16	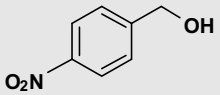	79 (360)	87 (5)	74 (360)	86 (5.5)
17	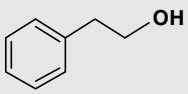	80 (210)	90 (2.5)	91 (150)	91 (1.5)
18	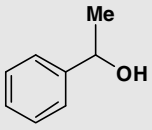	83 (240)	90 (2.5)	91 (150)	91 (3)
19	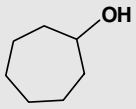	94 (105)	94 (2.5)	94 (105)	92 (2.5)
20	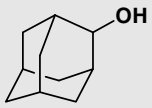	87 (150)	85 (3)	83 (120)	84 (3)
21	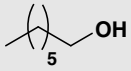	95 (60)	94 (1)	93 (60)	90 (1)
22	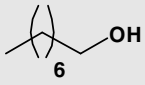	91 (120)	93 (1.5)	87 (120)	91 (1.5)

[a] Isolated yields.
[b] 0.8 mol% of the catalyst was used.

Table 4
Competitive protection of alcohols and phenol in the presence of TPA/silica gel (I) and TPA/ZrO_2 (II)[a]

Entry	Substrates	Product[b]	R	Yield[c] (%)	
				I	II
1	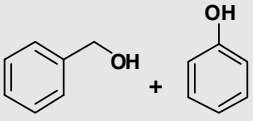	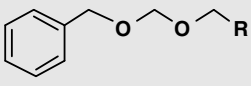	H Me	94 93	84 90
2	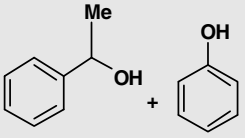	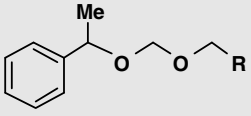	H Me	80 84	91 83
3	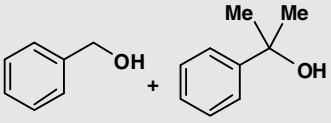	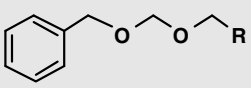	H Me	94 93	84 90
4	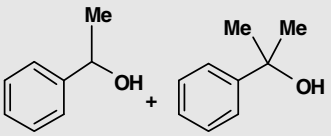	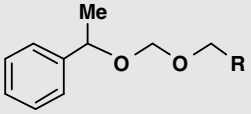	H Me	80 84	91 83

[a] Reaction conditions: alcohol or phenol (1 mmol), FDEA (5 mmol) or FDMA (7 mmol), supported TPA (0.03 g, 0.4 mol%).
[b] Phenol and tertiary alcohol remained intact in the reactions mixture.
[c] Isolated yields.

Table 5
Deprotection of MOM- and EOM-ethers with TPA supported on silica gel under reflux condition and MW irradiation

Entry	Ether	Cleavage of EOM-ether (a)		Cleavage of MOM-ether (b)	
		Yield[a] (%) (Time, min)		Yield[a] (%) (Time, min)	
		Thermal	MW	Thermal	MW
1	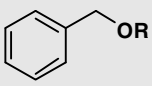	81 (240)	88 (19)	79 (240)	85 (19)
2	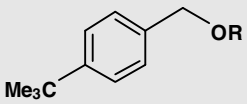	79 (150)	79 (22)	89 (180)	83 (18)
3	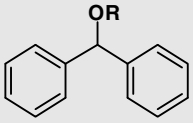	73 (330)	90 (15)	81 (270)	92 (14)
4[b]	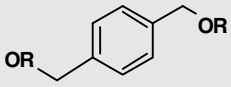	73 (300)	83 (23)	83 (270)	87 (21)
5	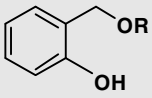	80 (150)	80 (23)	90 (180)	79 (21)
6	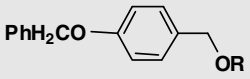	79 (240)	86 (19)	83 (180)	88 (19)
7	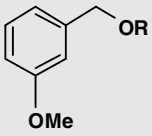	82 (120)	77 (24)	88 (180)	76 (26)
8	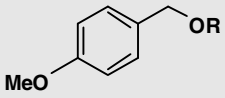	89 (150)	81 (25)	78 (180)	78 (24)
9	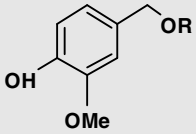	80 (180)	82 (22)	85 (150)	80 (22)
10	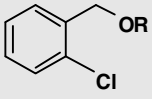	78 (150)	86 (21)	87 (120)	88 (20)
11	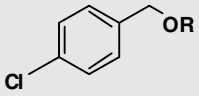	81 (150)	87 (20)	90 (120)	86 (20)
12	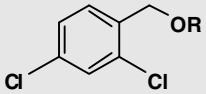	83 (150)	81 (25)	80 (210)	83 (22)
13	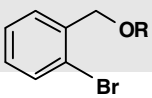	80 (180)	86 (21)	85 (120)	87 (20)

Table 5 (*continued*)

Entry	Ether	Cleavage of EOM-ether (a)		Cleavage of MOM-ether (b)	
		Yield[a] (%) (Time, min)		Yield[a] (%) (Time, min)	
		Thermal	MW	Thermal	MW
14	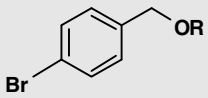	81 (120)	86 (19)	90 (120)	89 (18)
15	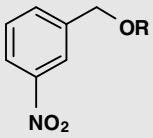	81 (210)	80 (27)	83 (210)	81 (25)
16	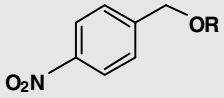	89 (210)	75 (29)	84 (210)	78 (26)
17	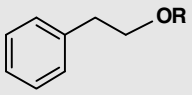	80 (300)	81 (25)	77 (150)	85 (22)
18	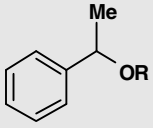	87 (240)	84 (21)	85 (120)	81 (19)
19	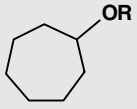	84 (180)	86 (24)	82 (180)	86 (22)
20	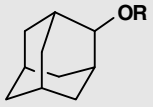	83 (180)	85 (25)	84 (180)	84 (23)
21	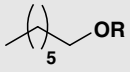	81 (240)	80 (22)	82 (240)	84 (22)
22	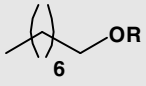	77 (240)	79 (24)	80 (240)	80 (22)

[a] Isolated yields.
[b] 1.6 mol% of the catalyst was used.

of 150 W. At this power, the temperature of the reaction vessel was measure to be 53–56 °C.

Under the optimized reaction conditions, various primary and secondary benzylic and saturated alcohols reacted with FDMA and FDEA in the presence of these catalysts at room temperature and under microwave irradiation to afford the corresponding MOM- and EOM-ethers in high yields (Tables 2 and 3). While phenols and tertiary alcohols remained intact in the reaction mixture under the same conditions. The results show that the reaction times are considerably shorter under microwave irradiation. The acceleration of reactions by microwave mainly results from two effects: thermal effect and specific microwave effect [16c,16d]. Thermal effect (dielectric heating) resulting from material-microwave interaction which allows fast and uniform distribution and conversion of microwave energy into heat. Specific microwave effect can be expected for the polar mechanism, when the polarity is increased during the reaction from the ground state (GS) toward the transition state (TS). For the protection reactions under investigation, it seems that stabilization of the transition state is more effective than that of the ground state, and therefore, the reactivity is enhanced as a result of decreased activation energy.

It is noteworthy that in multifunctional compounds containing both benzylic and phenolic hydroxyl groups, only benzylic hydroxyl groups were transformed to their corresponding ethers with excellent chemoselectivity (Tables 2 and 3, entries 6 and 9). Also competitive protection of primary and secondary alcohols in the presence of phenols and tertiary alcohols were investigated. In this manner, a mixture of primary alcohol (1 mmol) and phenol (1 mmol) was reacted with FDMA (7 mmol) or FDEA (5 mmol) in the presence of supported TPA (0.03 g, 0.4 mol%) and it was found

Table 6
Deprotection of MOM- and EOM-ethers with TPA supported on zirconia under reflux condition and MW irradiation

Entry	Ether	Cleavage of EOM-ether (a)		Cleavage of MOM-ether (b)	
		Yield[a] (%) (Time, min)		Yield[a] (%) (Time, min)	
		Thermal	MW	Thermal	MW
1	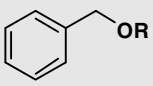	71 (210)	84 (22)	73 (240)	80 (21)
2	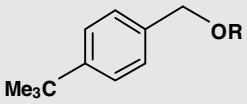	81 (210)	75 (24)	80 (210)	79 (22)
3	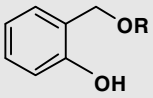	79 (180)	80 (28)	81 (120)	78 (29)
4[b]	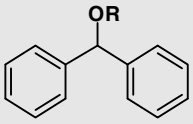	81 (210)	78 (17)	89 (210)	84 (20)
5	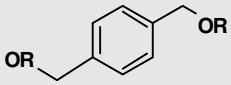	79 (150)	81 (23)	83 (150)	83 (22)
6	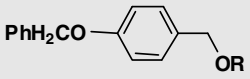	88 (120)	80 (22)	81 (120)	80 (23)
7	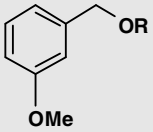	85 (120)	76 (27)	88 (150)	79 (29)
8	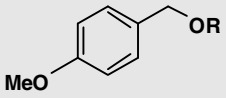	89 (150)	76 (26)	89 (120)	78 (23)
9	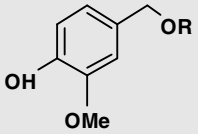	83 (120)	76 (29)	81 (210)	78 (26)
10	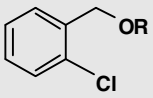	81 (150)	76 (25)	83 (120)	77 (25)
11	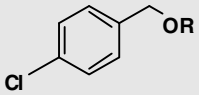	83 (180)	85 (27)	80 (180)	87 (28)
12	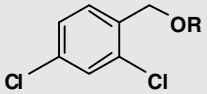	80 (240)	80 (27)	80 (210)	81 (25)
13	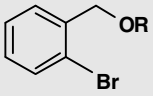	72 (240)	73 (28)	74 (180)	75 (26)

Table 6 (*continued*)

Entry	Ether	Cleavage of EOM-ether (a)		Cleavage of MOM-ether (b)	
		Yield[a] (%) (Time, min)		Yield[a] (%) (Time, min)	
		Thermal	MW	Thermal	MW
14	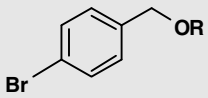	82 (210)	77 (24)	87 (180)	83 (24)
15	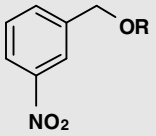	81 (150)	71 (33)	85 (150)	70 (30)
16	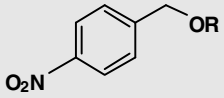	75 (240)	70 (37)	79 (240)	73 (35)
17	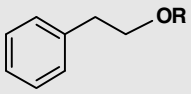	82 (210)	80 (27)	90 (150)	81 (25)
18	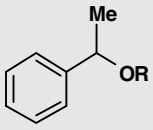	73 (180)	74 (22)	71 (180)	80 (21)
19	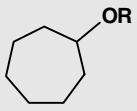	84 (180)	86 (24)	82 (180)	86 (22)
20	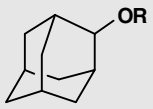	84 (180)	785 (25)	87 (180)	75 (25)
21	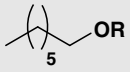	81 (240)	80 (22)	82 (240)	84 (22)
22	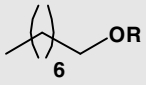	90 (120)	74 (26)	81 (180)	76 (24)

[a] Isolated yields.
[b] 1.6 mol% of the catalyst was used.

that only primary alcohol was converted to the corresponding ether and the phenol remained intact in the reaction mixture (Table 4, entry 1). Under the same reaction conditions, secondary alcohol was selectively converted to the corresponding ether in the presence of phenol (Table 4, entry 2). Treatment of a mixture of primary alcohol (1 mmol) and tertiary alcohol (1 mmol) with FDMA (7 mmol) or FDEA (5 mmol) in the presence of supported TPA (0.03 g, 0.4 mol%), resulted exclusively in the protection of primary alcohol (Table 4, entry 3). Under these conditions in a mixture of secondary and tertiary alcohols, only secondary alcohol was selectively transformed to the corresponding ether (Table 4, entry 4). Therefore, the results indicate that the present method is potentially applicable for the chemoselective protection of primary and secondary alcohols in the presence of phenols and tertiary alcohols (Table 4).

3.3. Deprotection reactions

Deprotection of these ethers was also investigated under thermal and microwave irradiation. At first, deprotection reaction of EOM-ether of benzyl alcohol was conducted with different amounts of supported catalysts in order to find the optimized reaction conditions. The maximum yields were obtained with 0.8 mol% of supported catalysts in refluxing EtOH. Under microwave irradiation, the best results were obtained at the power of 250 W. At this power, the temperature of the reaction vessel was measure to be 72–75 °C.

Under the above-mentioned conditions, a wide variety of primary and secondary EOM- and MOM-ethers were deprotected in the presence of supported catalysts in EtOH under reflux conditions and microwave irradiation to afford the corresponding alco-

Table 7
Competitive deprotection of MOM- and EOM-ethers of alcohols and phenol in the presence of TPA/SiO_2 (I) and TPA/ZrO_2 (II)[a]

Entry	Substrates	Products	Yield[b] (%) I	Yield[b] (%) II	Time (h)
1	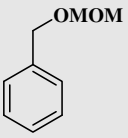 + 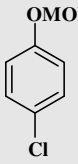	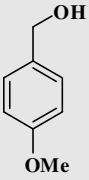 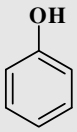	79 11	73 7	4
2	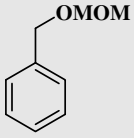 + 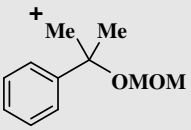	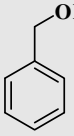 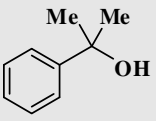	79 16	73 10	4
3	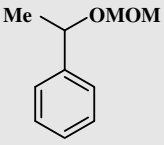 + 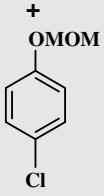	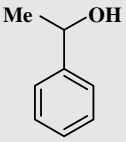 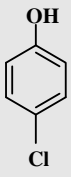	85 11	71 7	4
4	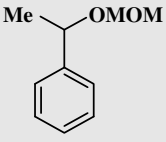 + 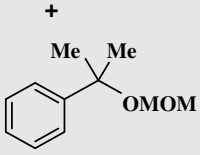	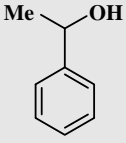 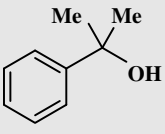	85 16	71 10	4
5	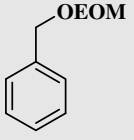 + 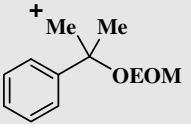	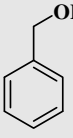 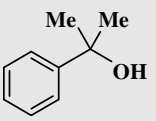	81 13	71 12	4
6	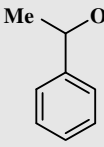 + 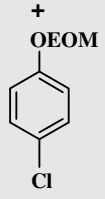	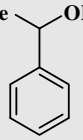 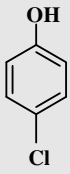	87 9	73 8	4

[a] Reaction conditions: MOM- and EOM- ether of alcohol and phenol (1 mmol), supported TPA (0.06 g, 0.8 mol%).
[b] Isolated yields.

hols in high yields (Tables 5 and 6). The results showed that the reaction times were considerably shorter under microwave irradiation. As mentioned in the protection reactions, in the deprotection reactions under microwave irradiation, the thermal and specific microwave effects increases the reaction rates.

In order to explore the general applicability of this method, several competitive deprotection reactions were also investigated using these catalysts. As can be seen, interesting selectivities were observed. When an equimolar mixture of primary or secondary MOM- and EOM-ethers and phenolic MOM- and EOM-ethers was reacted with supported TPA (0.06 g, 0.8 mol%), primary and secondary ethers were deprotected to their parent alcohols with high selectivity (Table 7, entries 1, 3 and 6). Selective deprotection of primary and secondary MOM- and EOM-ethers was also achieved in the presence of tertiary MOM- and EOM-ethers (Table 7, entries 2, 4 and 5). Also, this method can be selectively applied for the chemoselective deprotection of these ethers in the presence of other hydroxyl protecting groups such as benzyl, methyl ethers (Tables 5 and 6, entries 6–9), acetates and trimethylsilyl ethers (Table 8) using these catalytic systems. These selectivities can be considered as useful practical achievements in deprotection reactions.

3.4. Recyclability and reusability of the catalyst

The reusability and recycling of the supported catalysts were tested in the reaction of benzyl alcohol with FDEA. After completion of the reaction, supported catalysts were separated by filtration and washed with cold EtOH. The recovered catalysts were reused six consecutive runs. The filtrates were used for determination of catalyst leaching. Addition of fresh benzyl alcohol and FDEA to the filtrates and only 2–3% of product was detected by GC. The amount of tungsten loading after each consecutive runs was determined by NAA. These results showed that only trace amounts of catalyst are leached from supports (Table 9).

4. Conclusion

In conclusion, we have successfully developed a convenient and efficient protocol for the protection of alcohols as MOM- and EOM-ethers at room temperature and under microwave irradiation at solvent-free conditions and deprotection of these ethers to their parent alcohols in ethanol, as a green solvent, under reflux conditions and microwave irradiation using 12-tungstophosphoric acid supported on silica gel and zirconia as heterogeneous catalysts.

Table 8
Competitive deprotection of EOM- and MOM- ethers of alcohols, acetates and trimethylsilyl ethers in the presence of TPA/SiO_2 (I) and TPA/ZrO_2 (II)

Entry	Substrates	Products	Yield (%)[a]		Time (h)
			I	II	
1	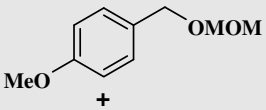	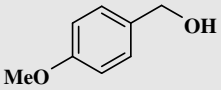	78	89	
	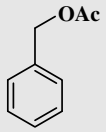	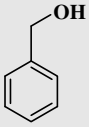	20	10	3
2	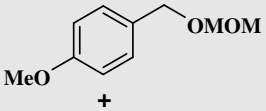	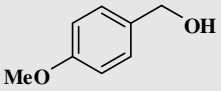	78	89	
	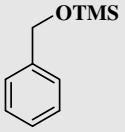	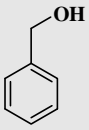	12	9	3
3	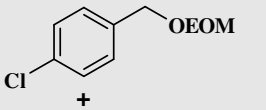	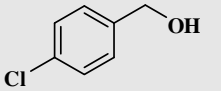	81	81	
	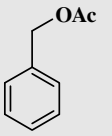	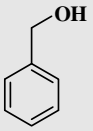	18	17	3
4	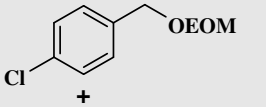	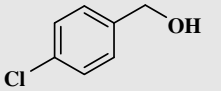	81	81	
	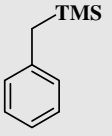	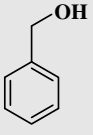	9	7	3

[a] Isolated yields.

High yields, short reaction times, operational simplicity, excellent chemoselectivity and low cost, easy availability, non-toxicity and reusability of the catalysts are other noteworthy advantages of the present method which makes this procedure a useful and attractive addition to the currently available methods.

Table 9
The recycling of the catalysts in the protection of benzyl alcohol with FDEA in the presence of TPA/SiO_2 and TPA/ZrO_2 at room temperature

Run	TPA/SiO_2			TPA/ZrO_2		
	Yield[a] (%)	Time (h)	W[b] (%)	Yield[a] (%)	Time (h)	W[b] (%)
1	93	1	29.60 ± 0.9	90	2	23.90 ± 0.8
2	91	1	29.10 ± 0.8	88	2	23.60 ± 0.8
3	91	1	28.90 ± 0.9	86	2	23.30 ± 0.8
4	90	1	28.70 ± 0.8	85	2	23.10 ± 0.8
5	88	1	28.40 ± 0.9	85	2	23.00 ± 0.8
6	86	1	28.10 ± 0.9	84	2	22.80 ± 0.8

[a] Isolated yields.
[b] Determined by NAA.

Acknowledgement

We thankful to the Centre of Excellence of Chemistry of University of Isfahan (CECUI) for financial support of this work.

References

[1] (a) H. Firouzabadi, A.A. Jafari, J. Iran Chem. Soc. 2 (2005) 85;
(b) M.T. Pope, Heteropoly and Isopoly Oxometalates, Springer-Verlag, Berlin, 1993.
[2] (a) Y. Izumi, K. Urabe, M. Onaka, Zeolite, Clay and Heteropoly Acid in Organic Reactions, Kodansha/VCH, Tokyo, 1992;
(b) I.V. Kozhevnikov, Chem. Rev. 98 (1999) 171.

[3] I.V. Kozehevnikov, K.R. Kloetstra, A. Sinnema, H.W. Zandbergen, H. van Bekkum, J. Mol. Catal. A: Chem. 114 (1996) 287.
[4] (a) F. Marme, G. Coudurier, J.C. Vidrine, Micropor. Mesopor. Mater. 22 (1998) 151;
(b) N. Nowinska, R. Fiedorov, J. Adamiec, J. Chem. Soc., Faraday Trans. 87 (1991) 749;
(c) M.E. Chimienti, L.R. Pizzio, C.V. Càceres, M.N. Blanco, Appl. Catal. A: Gen. 208 (2001) 7.
[5] G.J. Meuzelaar, L. Maat, R.A. Sheldon, I.V. Kozhevnikov, Catal. Lett. 45 (1997) 249.
[6] R. Neumann, M. Levin, J. Org. Chem. 56 (1991) 5707.
[7] M. Misono, N. Nojiri, Appl. Catal. 64 (1990) 1.
[8] R. Fazaeli, S. Tangestaninejad, H. Aliyan, M. Moghadam, Appl. Catal. A: Gen. 309 (2006) 44.
[9] M.A. Schweglar, H. van Bekkum, N.A. de Munck, Appl. Catal. 74 (1991) 191.
[10] R. Fazaeli, S. Tangestaninejad, H. Aliyan, Catal. Commun. 8 (2007) 205.
[11] I. Mohammadpoor-Baltork, M. Moghadam, S. Tangestaninejad, V. Mirkhani, S.F. Hojati, Polyhedron 27 (2008) 750.
[12] M. Schelhaas, H. Waldmann, Angew. Chem., Int. Ed. Engl. 35 (1996) 2056.
[13] (a) T.W. Greene, P.G.M. Wuts, Protective Groups in Organic Synthesis, Wiley, New York, 1991;
(b) P.J. Kocienski, Protecting Groups, Georg Thieme, Stuttgart, 1994.
[14] (a) G.A. Olah, A. Husain, B.G.B. Gupta, S.C. Narang, Synthesis 896 (1983);
(b) M.L. Kantam, P.L. Santhi, Synlett 429 (1993);
(c) B. Karimi, L. Mamani, Tetrahedron Lett. 44 (2003) 6051;
(d) K. Niknam, M.A. Zolfigol, A. Khorramabadi-Zad, R. Zare, M. Shayegh, Catal. Commun. 7 (2006) 494;
(e) M.A. Zolfigol, M. Shiri, Mendeleev Commun. 165 (2005);
(f) K. Niknam, M.A. Zolfigol, M. Shayegh, R. Zare, J. Chin. Chem. Soc. 54 (2007) 1067;
(g) R.L. Danheiser, K.R. Romines, H. Koyama, S.K. Gee, C.R. Johnson, J.R. Medich, Org. Synth. 71 (1992) 133;
(h) G.V.M. Sharma, K.L. Reddy, P.S. Lakshmi, P.R. Krishna, Tetrahedron Lett. 45 (2004) 9229.
[15] (a) E.J. Corey, D.H. Hua, S.P. Seitz, Tetrahedron Lett. 25 (1984) 3;
(b) D.A. Goff, R.N. Harris, J.C. Bottaro, C.D. Bedford, J. Org. Chem. 51 (1986) 4711;
(c) B.F. Marcune, S. Karady, U.H. Dolling, T. Novak, J. Org. Chem. 64 (1999) 2446;
(d) T.R. Boehlow, J.J. Harburn, C.D. Spilling, J. Org. Chem. 66 (2001) 3111;
(e) A.S.-Y. Lee, Y.-J. Hu, S.-F. Chu, Tetrahedron 57 (2001) 2121;
(f) J.P. Deville, V. Behar, J. Org. Chem. 66 (2001) 4097;
(g) C. Ramesh, N. Ravindranath, B. Das, J. Org. Chem. 68 (2003) 7101;
(h) J.M. Keith, Tetrahedron Lett. 45 (2004) 2739.
[16] (a) C.O. Kappe, Angew. Chem., Int. Ed. 43 (2004) 6250;
(b) R.S. Varma, Green Chem. 1 (1999) 43;
(c) L. Perreux, A. Loupy, Tetrahedron 57 (2001) 9199;
(d) P. Lidstrom, J. Tierney, B. Wathey, J. Westman, Tetrahedron 57 (2001) 9225.
[17] (a) I. Mohammadpoor-Baltork, H. Aliyan, J. Chem. Res. (S) (1999) 272;
(b) I. Mohammadpoor-Baltork, H. Aliyan, Synth. Commun. 29 (1999) 2741;
(c) I. Mohammadpoor-Baltork, H. Aliyan, Indian J. Chem. B 38 (1999) 1223;
(d) I. Mohammadpoor-Baltork, M.K. Amini, S. Farshidipoor, Bull. Chem. Soc. Jpn. 73 (2000) 2775;
(e) H. Firouzabadi, I. Mohammadpoor-Baltork, S. Kolagar, Synth. Commun. 31 (2001) 905;
(f) I. Mohammadpoor-Baltork, B. Kharamesh, S. Kolagar, Synth. Commun. 32 (2002) 1633;
(g) A. Bamoniri, M.A. Zolfigol, I. Mohammadpoor-Baltork, B.F. Mirjalili, J. Iran. Chem. Soc. 3 (2006) 85;
(h) I. Mohammadpoor-Baltork, M.M. Khodaei, H. Ahankar, Lett. Org. Chem. 3 (2006) 768.
[18] (a) M. Misono, N. Misono, K. Katamura, A. Kasai, Y. Konishi, K. Sakata, T. Okuhara, Y. Yoneda, Bull. Chem. Soc. Jpn. 55 (1982) 400;
(b) T.H. Chang, J. Chem. Soc., Faraday Trans. 91 (1995) 375;
(c) M. Fournier, R. Thouvenot, C. Rocchiccioli-Deltcheff, J. Chem. Soc., Faraday Trans. 87 (1991) 349;
(d) G.D. Yadav, N. Kirthivasan, J. Chem. Soc., Faraday Trans. 91 (1995).
[19] (a) K.W. Lee, N. Mizuno, T. Okuhara, M. Misono, Bull. Chem. Soc. Jpn. 62 (1998) 1731;
(b) B.W.L. Southward, J.S. Vaughan, C.T.O. Connor, J. Catal. 153 (1995) 293.
[20] (a) T. Okuhura, N. Mizuno, M. Misono, Adv. Catal. 41 (1996) 113;
(b) L.A.M. Cardoso, W. Alves Jr., A.R.E. Gonzaga, L.M.G. Aguiar, H.M.C. Andrade, J. Mol. Catal. A: Chem. 209 (2004) 189;
(c) E. Lopez-Salinas, J.G. Hernandez-Cortez, I. Schifter, E. Torres-Garcia, J. Navarrete, A. Gutierrez-Carrillo, T. Lopez, P.P. Lottici, D. Bersani, Appl. Catal. A: Gen. 193 (2000) 215;
(d) J.A. Dias, M.C. Rangel, S.C.L. Dias, E. Caliman, F.A.C. Garcia, Appl. Catal. A: Gen. 329 (2007) 189.

Polyhedron 27 (2008) 2625–2633

Contents lists available at ScienceDirect

Polyhedron

journal homepage: www.elsevier.com/locate/poly

Cu^{II} acetate complexes involving N,N,O donor Schiff base ligands: Mono-atomic oxygen bridged dimers and alternating chains of the dimers and $Cu_2(OAc)_4$

Biswarup Sarkar [a,b], Michael G.B. Drew [c], Marta Estrader [d], Carmen Diaz [d], Ashutosh Ghosh [a,*]

[a] Department of Chemistry, University College of Science, University of Calcutta, 92, A.P.C. Road, Kolkata 700 009, India
[b] Bolpur College, Bolpur 731 204, West Bengal, India
[c] School of Chemistry, The University of Reading, P.O. Box 224, Whiteknights, Reading RG66AD, UK
[d] Departament de Química Inorgànica, Universitat de Barcelona, Marti i Franques 1-11, 08028 Barcelona, Spain

ARTICLE INFO

Article history:
Received 4 April 2008
Accepted 5 May 2008
Available online 16 June 2008

Keywords:
Copper
Acetate bridge
Schiff base
X-ray structures
Magnetic properties

ABSTRACT

Two tridentate N,N,O donor Schiff bases, HL^1 (4-(2-ethylamino-ethylimino)-pentan-2-one) and HL^2 (3-(2-amino-propylimino)-1-phenyl-butan-1-one) on reaction with Cu^{II} acetate in presence of triethyl amine yielded two basal-apical, mono-atomic acetate oxygen-bridging dimeric copper(II) complexes, $[Cu_2L^1_2(OAc)_2]$ (**1**), $[Cu_2L^2_2(OAc)_2]$ (**2**). Whereas two other similar tridentate ligands HL^3 (4-(2-amino-propylimino)-pentane-2-one) and HL^4 (3-(2-amino-ethylimino)-1-phenyl-butan-1-one) under the same conditions produced a mixture of the corresponding dimers and a one-dimensional alternating chain of the dimer and copper acetate moiety, $[Cu_4L^3_2(OAc)_6]_n$ (**3**) and $[Cu_4L^4_2(OAc)_6]_n$ (**4**), formed by a very rare μ_3 bridging mode of the acetate ion. All four complexes (**1**–**4**) have been characterized by X-ray crystallography. The isotropic Hamiltonian, $H = -JS_1S_2$ has been used to interpret the magnetic data. Magnetic measurements of **1** and **2** in the temperature range 2–300 K reveal a very weak antiferromagnetic coupling for both complexes ($J = -0.56$ and -1.19 cm^{-1} for **1** and **2**, respectively).

© 2008 Elsevier Ltd. All rights reserved.

1. Introduction

The Schiff bases derived from the mono-condensation of diamines e.g. 1,2-diaminothane, 1,3-diaminopropane, etc. and β-diketone e.g. acetyl- or 1-benzoylacetone are a group of mono-negative N,N,O donor ligands that react readily with Cu^{II} to form mono-, di-, or trinuclear complexes depending upon the coligand present. For examples, a neutral monodentate coligand like pyridine or imidazole results in the formation of mono-nuclear square planar complexes [1] whereas an azide or chloride ion yields dinuclear species [2]. Dinuclear complexes can also be obtained by bridging the mono-nuclear units by 4,4′-bipyridine [3]. On the other hand, a μ_3-OH bridged trinuclear copper(II) complex is formed in a slightly alkaline solution with such ligands [4]. With acetate coligands, two complexes have so far been structurally characterized [5] and both of them are mono-atomic acetate oxygen bridged dimers. Variable temperature magnetic measurements of one of the compounds have also been carried out and showed very weak antiferromagnetic coupling [5a].

The carboxylate group is one of the most widely used bridging ligands for designing polynuclear metal complexes with interesting magnetic properties. Normally, each of the two oxygen atoms of a carboxylate group are bonded to a different metal atom to form M–O–C–O–M bridging in one of the *syn–syn*, *syn–anti*, and *anti–anti* modes [6]. The occurrence of M–O–M bridges via one oxygen atom of the carboxylate ligand is relatively scarce. There are some examples of unsymmetrical mono-atomic acetate oxygen bridged copper(II) complexes in the literature [5,7,8]. Variable temperature magnetic measurements of those complexes reveal that they can be either ferromagnetic [8b] or antiferromagnetic [5a,8a,8c,8d]. Till now, there is no clear magneto-structural correlation for such magnetic pathways. Therefore, we have tried to synthesize similar complexes using four different N,N,O donor Schiff base ligands, 4-(2-ethylamino-ethylimino)-pentan-2-one (HL^1), 3-(2-amino-propylimino)-1-phenyl-butan-1-one (HL^2), 4-(2-amino-propylimino)-pentan-2-one (HL^3) and 3-(2-amino-ethylimino)-1-phenyl-butan-1-one (HL^4) (Scheme 1) and the results are presented in this paper. With ligands L^1 and L^2, we have obtained pure mono-atomic acetate oxygen bridged dinuclear complexes and have characterized them both structurally and magnetically. But for the other two ligands (L^3 and L^4), the products were not pure dinuclear species and we failed to grow any single crystals suitable for X-ray analysis. Instead, we have succeeded in obtaining single crystals of the minor products, which are present in the product and characterized them by single crystal X-ray analysis. The crystal structures reveal that in both cases the structures of these minor products are one-dimensional novel chains of alternating dimer and copper acetate moieties.

* Corresponding author. Fax: +91 33 23519755.
E-mail address: ghosh_59@yahoo.com (A. Ghosh).

0277-5387/$ - see front matter © 2008 Elsevier Ltd. All rights reserved.
doi:10.1016/j.poly.2008.05.004

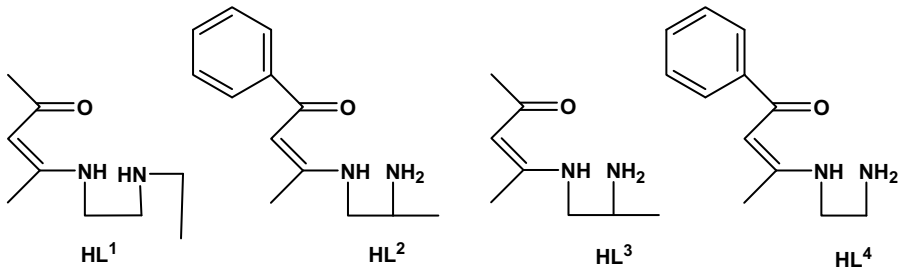

Scheme 1.

2. Experimental

The diamines, 1-benzoylacetone and acetylacetone were purchased from Lancaster Chemical Co. They were of reagent grade and used without further purification.

2.1. Synthesis of the ligands, HL^1 (4-(2-ethylamino-ethylimino)-pentan-2-one), HL^2 (3-(2-amino-propylimino)-1-phenyl-butan-1-one), HL^3 (4-(2-amino-propylimino)-pentane-2-one) and HL^4 (3-(2-amino-ethylimino)-1-phenyl-butan-1-one)

The four mono-condensed tridentate Schiff base ligands HL^1–HL^4 were prepared by half-condensation of the respective diamine with the corresponding β-diketone (acetylacetone or 1-benzoylacetone) under the condition of high dilution in chloroform as reported earlier [4,9].

*2.2. Synthesis of complexes $[Cu_2L^1_2(OAc)_2]$ (**1**), $[Cu_2L^2_2(OAc)_2]$ (**2**), $[Cu_4L^3_2(OAc)_6]_n$ (**3**) and $[Cu_4L^4_2(OAc)_6]_n$ (**4**)*

The clear methanol solution (20 cm^3) of the Schiff bases (2 mmol), were added to the suspension of copper(II) acetate monohydrate (2 mmol, 0.199 g) in methanol (10 cm^3) and the mixed solutions were stirred well. Triethylamine (1.5 mmol, 0.2 cm^3) was added dropwise with constant stirring. For all four complexes, a small amount of green hydrolyzed product which separated immediately during the addition of triethylamine was filtered off. The filtrates were kept several days in a refrigerator to yield bluish green crystalline products. Dark green hexagonal single crystal of **1** was obtained on dissolving the bluish green precipitate in methanol and keeping the resulting solution several days at room temperature. Greenish mass of **2** was obtained next day. Single crystals of **2**, **3** and **4**, suitable for X-ray diffraction analysis were obtained by slow diffusion of *n*-hexane into a dichloromethane solution of the respective compounds.

Complex **1**: Yield: 0.11 g (49%). Calc. for $C_{22}H_{44}Cu_2N_4O_8$ (619.70): C, 42.64; H, 7.16; N, 9.04. Found: C, 42.73; H, 7.19; N, 9.01%. λ_{max}/nm (ε_{max}/$dm^3\,mol^{-1}\,cm^{-1}$) (acetonitrile), 613 (89.3) and 320 (18 700). IR: $\tilde{\nu} = 3178$ [ν(N–H)]; 1589 [$\nu(COO^-)$] cm^{-1}.

Complex **2**: Yield: 0.13 g (56%). Calc. for $C_{31}H_{42}Cl_2Cu_2N_4O_6$ (764.67): C, 48.69; H, 5.54; N, 7.33. Found: C, 48.57; H, 5.59; N, 7.31%. λ_{max}/nm (ε_{max}/$dm^3\,mol^{-1}\,cm^{-1}$) (acetonitrile), 609 (95.2) and 323 (18 400). IR: $\tilde{\nu} = 3152$, 3257 [ν(N–H)]; 1591 [$\nu(COO^-)$] cm^{-1}.

The analytical data of the crystalline solids of **3** and **4** which were obtained from the mother liquor correspond neither to the dimeric species nor to the one-dimensional chain compounds as characterized by X-ray analysis. Instead, the data suggest that they are probably a mixture of these two types of complexes. Moreover, the proportions of the two species in the mixture differ when the syntheses are repeated. Therefore, the analytical data are not presented here.

2.3. Physical measurements

Elemental analyses (C, H, N) were performed using a Perkin–Elmer 240C elemental analyzer. IR spectra in KBr (4500–500 cm^{-1}) were recorded using a Perkin–Elmer RXI FT-IR spectrophotometer.

Table 1
Crystal data

Complexes	**1**	**2**	**3**	**4**
Formula	$[Cu_2L^1_2(OAc)_2]$, H_2O	$[Cu_2L^2_2(OAc)_2]$, CH_2Cl_2	$[Cu_4L^1_2(OAc)_6]_n$	$[Cu_4L^2_2(OAc)_6]_n$
Empirical formula	$C_{22}H_{44}Cu_2N_4O_8$	$C_{31}H_{42}Cl_2Cu_2N_4O_6$	$C_{28}H_{48}Cu_4N_4O_{14}$	$C_{36}H_{48}Cu_4N_4O_{14}$
Formula weight	619.70	764.67	918.86	1014.94
Data measurement, temperature	Mar Image Plate, 298 K	Oxford Instruments CCD, 150 K	Oxford Instruments CCD, 150 K	Mar Image Plate 298 K
Crystal system	triclinic	monoclinic	triclinic	monoclinic
Space group	$P\bar{1}$	$P2_1/n$	$P\bar{1}$	$C2/c$
a (Å)	8.807(10)	12.9930(15)	8.1420(6)	24.20(3)
b (Å)	9.026(10)	18.6964(19)	9.6925(7)	9.879(12)
c (Å)	10.058(12)	15.0956(18)	13.0849(10)	18.54(2)
α (°)	86.66(1)	(90)	69.52(1)	(90)
β (°)	77.40(1)	110.04(1)	88.05(1)	97.13(1)
γ (°)	71.60(1)	(90)	89.61(1)	(90)
V ($Å^3$)	740.4(15)	3445.1(7)	966.8(1)	4398(8)
Z	1	4	1	4
ρ_{calc} (mg m^{-3})	1.390	1.474	1.578	1.533
Collected reflections (R_{int})	4462 (0.0307)	21 365 (0.0604)	6780 (0.0268)	7834 (0.0430)
Unique data/restraints/ parameters	2536/0/167	9671/0/401	5382/0/227	3509/0/266
Final R indices [$I > 2\sigma(I)$] R_1	0.0405	0.0747	0.0436	0.0765
wR_2	0.1081	0.1913	0.1147	0.1598
R indices (all data) R_1	0.0440	0.1602	0.0638	0.1184
wR_2	0.1103	0.2100	0.1206	0.1728
Maximum, minimum peak (e/A^3)	0.386, −0.805	1.304, −0.931	1.193, −1.031	0.528, −0.327

Electronic spectra in methanol (1200–350 nm) were recorded in a Hitachi U-3501spectrophotometer.

2.4. Crystallographic studies

The independent reflections for complexes **1** and **4** were measured with Mo Kα radiation using the MARresearch Image Plate System. The crystals were positioned at 70 mm from the Image Plate. One Hundred frames were measured at 2° intervals at 298 K with a counting time of 2 min. Data analysis was carried out with the XDS program [10]. Data for **2** and **3** were measured on an Oxford Diffraction X-Calibur with a CCD at 150 K. 321 frames were measured for 10 s. Mo Kα radiation was used. Data analysis was carried out with the CRYSALIS program [11]. All four structures

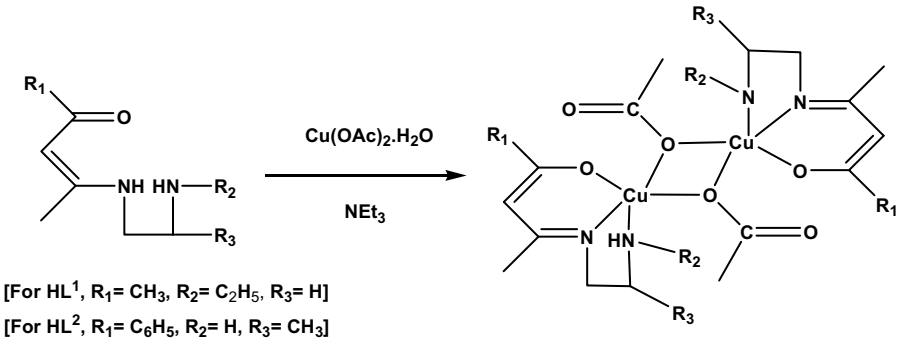

Scheme 2a.

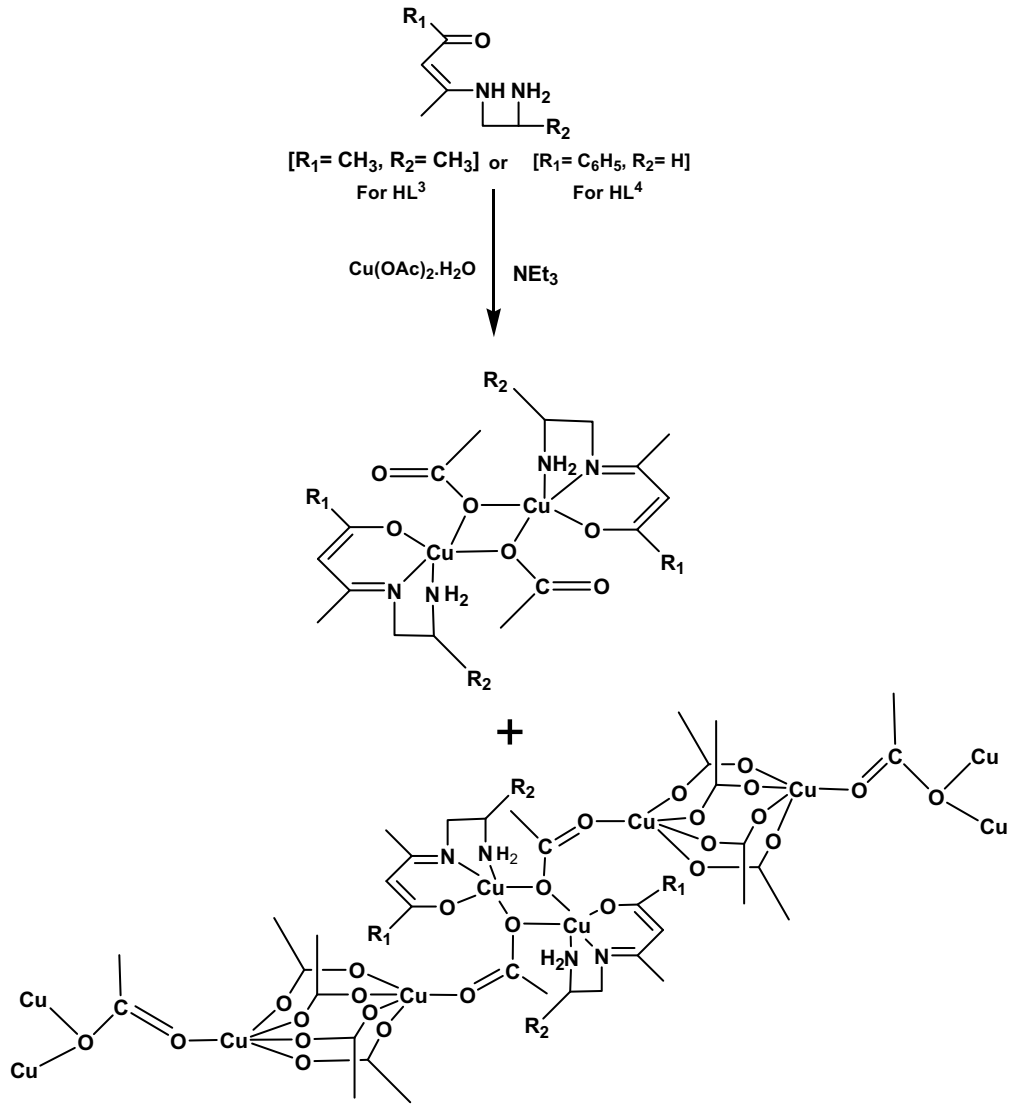

Scheme 2b.

were solved using direct methods with the SHELXS97 program [12]. The hydrogen atoms bonded to carbon were included in geometric positions and given anisotropic displacement parameters proportional to those of the atom to which they were attached and refined on F^2. Non-hydrogen atoms were refined with anisotropic displacement parameters. Empirical absorption corrections were carried out using DIFABS [13] for **1** and **4** and ABSPACK [14] for **2** and **3**. Structures were refined using the SHELXL97 program [12]. Significant crystallographic data are summarized in Table 1.

2.5. Magnetic studies

The magnetic measurements were carried out in the "Servei de Magnetoquimica (Universitat de Barcelona)" on polycrystalline samples (20 mg) with a Quantum Design SQUID MPMSXL magnetometer in the temperature range of 2–300 K and the magnetic field was 0.1 T. The diamagnetic corrections were evaluated from Pascal's constants. EPR spectra were recorded on powder samples at X-band frequency with a Bruker 300E automatic spectrometer, varying the temperature between 4 and 300 K.

3. Results and discussion

The two tridentate ligands HL^1 and HL^2 (Scheme 1) on treatment with the methanol solution of copper acetate monohydrate and triethylamine yield the dinuclear complexes **1** and **2**, respectively, in pure form (Scheme 2a). However, under the same conditions, the other two ligands, HL^3 and HL^4 (Scheme 1), yield a mixture of products as is evident from analytical, spectral and variable temperature magnetic susceptibility data. The products consist of mostly the dimers (similar to **1** and **2**) along with some other minor products. The proportions of the dimers and the minor products change with the variations in metal: ligand ratios and even for different batches of preparation keeping the same metal:ligand ratio. Unfortunately, in spite of several attempts, we failed either to isolate pure dimers with these two ligands (HL^3 and HL^4) or to get diffraction quality single crystals of them. However, during our attempt of crystallization we obtained a few single crystals of the minor products. X-ray analysis reveals that an unreacted copper acetate moiety joins the dimers to form a one-dimensional alternating chain of the dimers and copper acetate (Scheme 2b).

3.1. IR and electronic spectra

Compound **1** contains a non-coordinating water molecule, which is clear from the well-defined band at 3423 cm^{-1} in its IR spectra. It displays a single sharp band at 3178 cm^{-1} due to the N–H stretching vibration, whereas complex **2** displays two bands at 3152 and 3257 cm^{-1} characteristic of the asymmetric and symmetric stretching vibrations of NH_2 group. The attributions of the IR spectra in the 1300–1600 cm^{-1} region are difficult due to the appearance of several absorption bands from both Schiff base ligands and acetate. The strong bands at 1589 cm^{-1} with a shoulder at 1610 cm^{-1} for complex **1** and 1591 cm^{-1} with a shoulder at 1615 cm^{-1} for complex **2** are likely to be due to the overlapping of bands from Schiff bases with the antisymmetric stretching mode of the carboxylate group. The shoulders at 1610 and 1615 cm^{-1} for complexes **1** and **2**, respectively, may be attributed to the ν_{as}(CO) of the CH_3COO^- group [5a]. The symmetric stretching modes for the carboxylate are observed at 1390 and 1401 cm^{-1}. The separations between the two peaks (Δ) are 220 and 214 cm^{-1} for complexes **1** and **2**, respectively. For monodentate carboxylate, the Δ value is usually higher and for bidentate symmetrical chelate the Δ is much lower. For classical carboxylate bridges (Cu–O–C–O–Cu), the value of Δ is usually of ca. 180 cm^{-1} [15]. The Δ values of complexes **1** and **2** are higher than the classical bridges but lower than the monodentate one substantiating the non-symmetric bridging mode of the carboxylate in the complexes. The strong absorption bands at 1518 and 1517 cm^{-1} for complexes **1** and **2**, respectively, are attributed to ν(CN) of the corresponding ligands.

The electronic spectra of these complexes were recorded in acetonitrile solution. Both the complexes show single absorption band (613 and 609 for complexes **1** and **2**, respectively). The positions of these bands are consistent with the observed square-based geometry around the copper centre [16]. The charge-transfer bands are observed at 320 and 323 nm for complexes **1** and **2**, respectively.

3.2. Description of structures of complexes *1*, *2*, *3* and *4*

3.2.1. Complexes *1* and *2*

The structures of **1** and **2** consist of dinuclear units, $[Cu_2L_2(OAc)_2]$ and a solvent molecule which is water in **1** and dichloromethane in **2**. Bond distances and angles are listed in Table 2 and S1. The dimeric unit of **1** contains a crystallographic centre of symmetry. Although there is no crystallographically imposed symmetry in **2**, the structure has an approximate centre of symmetry and in essential details is equivalent to that of **1**. The molecular structures of **1** and **2**, together with the atom-numbering scheme are shown in Figs. 1 and 2, respectively. In these structures, the coordination geometry around the copper atom can be considered to consist of a five-coordinate (4 + 1) distorted square-base pyramid. The basal plane consists of one oxygen and two nitrogen atoms from the respective deprotonated Schiff base ligands and a carboxylate oxygen while the apical site is occupied by one oxygen atom of another acetate anion that is basal to the second copper atom in the dimer of the complexes.

In **1** the four donor atoms, O(11), N(15), N(18) and O(31) that constitute the equatorial plane are approximately coplanar with distances −0.078(1), 0.080(1), −0.076(1) and 0.074(1) Å from the least squares plane through them. The copper atom is 0.040(1) Å from this plane towards the bridging oxygen. The Cu–N bond length is as expected shorter at 1.954(3) Å to the trigonal N(15) than to the tetrahedral N(18) at 2.059(3) Å while the Cu–O bond lengths to the ligand oxygen Cu(1)–O(11) 1.948(3) Å is similar to that of the acetate oxygen, Cu(1)–O(31) 1.978(3) Å. The Cu–O(31′) (1 − *x*, 1 − *y*, −*z*) axial bond (2.508(3) Å) is much longer than the equatorial distances as is expected for Jahn–Teller distorted system. The Addison parameter (τ) [17] which is an index of distortion from the square-pyramidal to the trigonal-bipyramidal geometry is calculated to be 0.09.

Table 2
Bond distances (Å) for the complexes

Compounds	1	2	3	4
Cu(1)–O(11)	1.948(3)	1.920(4)	1.915(2)	1.942(8)
Cu(1)–O(31)	1.978(3)	1.972(3)	1.979(2)	1.998(8)
Cu(1)–N(15)	1.954(3)	1.939(4)	1.933(3)	1.936(9)
Cu(1)–N(18)	2.059(3)	2.017(4)	2.001(2)	2.028(9)
Cu(1)–O(31′)	2.508(3)		2.433(2)	2.500(8)
Cu(1)–O(41)		2.501(3)		
Cu(2)–O(21)		1.942(3)		
Cu(2)–N(25)		1.951(4)		
Cu(2)–N(28)		2.011(4)		
Cu(2)–O(31)		2.429(3)		
Cu(2)–O(41)		1.962(3)	1.969(2)	1.971(9)
Cu(2)–O(33)			2.124(2)	2.134(6)
Cu(2)–O(51)			1.983(3)	1.966(8)
Cu(2)–O(43″)			1.962(2)	1.961(8)
Cu(2)–O(53″)			1.964(2)	1.923(8)

Symmetry code: ′ = 1 − *x*, 1 − *y*, −*z* (complex **1**), ′ = 1 − *x*, 1 − *y*, 1 − *z*, ″ = 1 − *x*, 1 − *y*, −*z* (complex **3**) and ′ = −*x*, 2 − *y*, −*z*; ″ = −*x* + 1/2, −*y* + 3/2, −*z* (complex **4**).

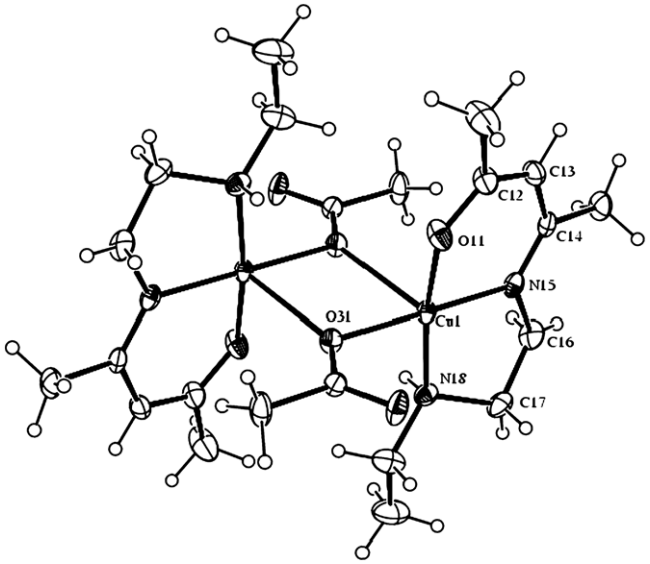

Fig. 1. ORTEP view of complex **1** with ellipsoids at 25% probability.

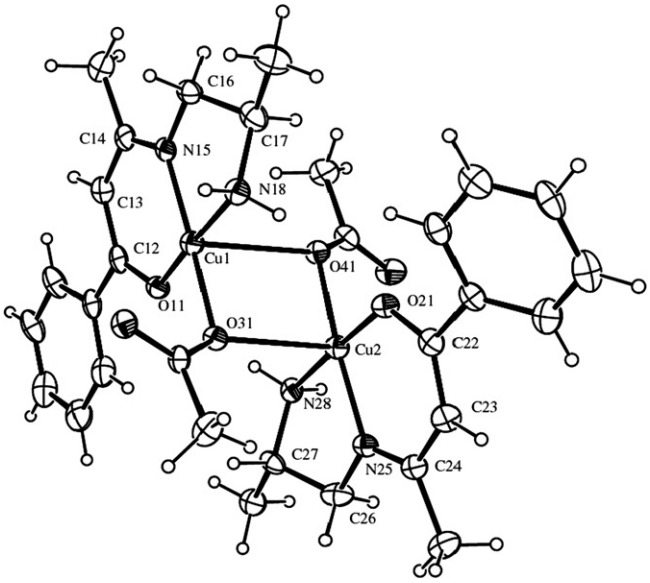

Fig. 2. ORTEP view of complex **2** with ellipsoids at 25% probability.

In **2**, the four coordinating atoms [O(11), N(15), N(18) and O(31)] in the equatorial plane around Cu(1) deviate from the mean plane through them by −0.072(2), 0.074(2), −0.074(2) and 0.072(2) Å, respectively. The Cu^{II} ion is almost coplanar; the deviation is only 0.004(2) Å from the plane towards the apical atom O(41). Whereas, the four atoms [O(21), N(25), N(28) and O(41)] in the equatorial plane of Cu(2) deviate from the mean plane through them by 0.058(2), −0.060(2), 0.059(2) and −0.057(2) Å, respectively. The Cu^{II} ion is displaced by 0.065(2) Å from the plane towards the apical atom O(31). The bond lengths to terminal NH_2 (Cu(1)–N(18) 2.017(4), Cu(2)–N(28) 2.011(4) Å), unsaturated N (Cu(1)–N(15) 1.939(4), Cu(2)–N(25) 1.951(4) Å) and terminal oxygen (Cu(1)–O(11) 1.920(4), Cu(2)–O(21) 1.942(3) Å) are similar to those of **1**. The two axial bonds (Cu(1)–O(41) 2.501(3), Cu(2)–O(31) 2.429(3) Å) by which the two monomeric units are joined to form the dimer are as expected much longer. The Addison parameters (τ) which is 0 for an ideal square planar geometry and 1 for ideal trigonal bipyramid [17], are 0.10 and 0.03 for Cu(1) and Cu(2), respectively, indicating a slight distortion from square planar geometry. The dihedral angle between the bridging Cu(1)–O(31)-Cu(1) plane and mean basal plane of the copper "square bipyramid" in complex **1** is 88.6°; the corresponding average value for complex **2** is 85.4°.

The six membered chelate ring formed by the acetylacetone or benzoylacetone moiety (for complexes **1** and **2**, respectively) is essentially planar and the interatomic distances and angles of the ring are similar. The five-membered chelate ring incorporating the dimethylene fragments from the starting diamines show different conformations in complexes **1** and **2**. In complex **1** this ring is an envelope on C(17) [q = 0.447(3) Å and ϕ = 296.3(3)°] whereas in **2** the ring is an envelope on C27 and half-chair conformation twisted on C(17)–C(18) [q = 0.412(6) Å and ϕ = 117.8(6)°] [18].

In complex **1**, the crystallized water molecule forms strong H-bonds with the amine hydrogen, uncoordinated oxygen atom of the acetate group and the oxygen atom of the ligand to form a one-dimensional supramolecular structure. The oxygen atom (O1) acts as an acceptor for an H-bond involving the H18 from the amine group and it forms two donor hydrogen bonds to O11 and O33′ (−x, 1 − y, −z) (Fig. 3, Table 3). In complex **2** (Fig. S1, Table 3) all the amine hydrogen are involved in hydrogen bonding. H18b and H28a form intra-dimer H-bonds with the oxygen atom of the chelated Schiff base ligand whereas H18a and H28b links the neighboring dimers through H-bonds with O43′ (1/2 + x, 1/2 − y, 1/2 + z) and O33″ (−1/2 + x, 1/2 − y, −1/2 + z), respectively, to form a one-dimensional network.

In both complexes there is no considerable π-stacking interaction between the aromatic rings. However, the C16–H16a bond of each molecule of **2** interacts with the phenyl group of the neighboring molecules (1 − x, 1 − y, 1 − z) by means of weak C_{sp^3}–H···π (phenyl) supramolecular contact to generate a two-dimensional network (the distance H16a···centroid A is 2.65(3) Å), angle between C16–H16a···C_g (ring A) is 169(4)° and the distance C16···C_g (ring A) is 3.612(6) Å (Fig. S2). The C_{sp^3}–H···π contact distance is typical for this type of interaction [19].

3.2.2. Complexes *3* and *4*

The structures of **3** and **4** (Figs. 4 and 5, respectively) are composed of one-dimensional polymeric chains that contain alternating $[Cu_2L_2(OAc)_2]$ and $Cu_2(OAc)_4$ units, each lying on a crystallographic centre of symmetry and are connected by acetate groups in the very rare μ_3-*syn–anti–anti* bridging mode. The structures of the dinuclear units, $[Cu_2L^3_2(OAc)_2]$ and $[Cu_2L^4_2(OAc)_2]$ of complexes **3** and **4**, respectively, are very similar to those of the $[Cu_2L^1_2(OAc)_2]$ and $[Cu_2L^2_2(OAc)_2]$ units of complex **1** and **2**, respectively. Like complexes **1** and **2**, the coordination geometry around copper atom of these dinuclear units can also be considered to consist of a five-coordinate (4+1) distorted square-base pyramid. The basal plane consists of one oxygen and two nitrogen atoms from the respective Schiff base ligand and a carboxylate oxygen while the apical site is occupied by one oxygen atom of another acetate anion that is basal to the second copper atom in the dimer of the complexes. All the bond distances and bond angles of these dinuclear units (Table 2 and Table S1) are comparable to those of complexes **1** and **2** and also to similar other reported complexes [5,8a].

In the dinuclear, $[Cu_2L^3_2(OAc)_2]$ unit of complex **3**, the four donor atoms [O(11), N(15), N(18) and O(31)] in the equatorial plane deviate from the mean plane through them by 0.117(1), −0.120(1), 0.120(1) and −0.116(1) Å, respectively. Cu^{II} ion is displaced 0.014(1) Å from the plane towards the apical atom O31′ (1 − x, 1 − y, 1 − z). In the $[Cu_2L^4_2(OAc)_2]$ unit of complex **4**, the deviations of O11, N15, N18 and O31 from the mean plane through them are −0.104(4), −0.107(4), 0.105(4) and −0.102(4) Å, respectively. The Cu^{II} ion is also displaced 0.016(1) Å from this plane towards the apical atom O31′ (−x, 2 − y, −z). The τ values [17] for these

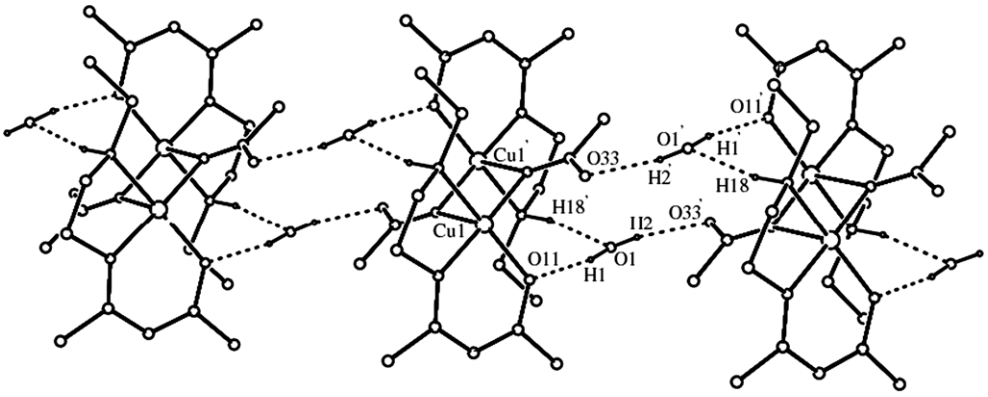

Fig. 3. H-bonding network in complex **1**.

Table 3
Hydrogen bonding distances (Å) and angles (°) for the complexes

Compound	D–H···A	D–H	D···A	A···H	∠D–H···A
1	O1–H1···O11	0.78(3)	2.864(5)	2.08(3)	168(4)
	O1–H2···O33′	0.83(4)	2.796(5)	1.97(4)	169(4)
	N18–H18···O1′	0.91	2.971(5)	2.07	169
2	N18–H18a···O43′	0.90	3.185(6)	2.39	146
	N18–H18b···O21	0.90	3.390(5)	2.56	154
	N28–H28a···O11	0.90	3.285(5)	2.46	153
	N28–H28b···O33″	0.90	3.081(6)	2.21	163
3	N18–H18a···O11′	0.90	3.161(4)	2.33	154
	N18–H18b···O51	0.90	3.307(4)	2.41	173
4	N18–H18b···O41	0.90	3.097(11)	2.20	175
	N18–H18a···O11′	0.90	3.187(12)	2.35	154

Symmetry codes: ′ = $-x$, $1-y$, $-z$ (complex **1**), ′ = $1/2+x$, $1/2-y$, $1/2+z$; ″ = $-1/2+x$, $1/2-y$, $-1/2+z$ (complex **2**), ′ = $1-x$, $1-y$, $1-z$ (complex **3**), ′ = $-x$, $2-y$, $-z$ (complex **4**).

dinuclear units are 0.044 and 0.039 Å for complexes **3** and **4**, respectively. The five-membered chelate ring containing the diamine fragment assumes an envelope conformation on C17 for both the complexes [18].

Unlike complexes **1** and **2**, the other oxygen atom (O33) of the bridging acetate of the dinuclear, $[Cu_2L_2(OAc)_2]$ unit of complexes **3** and **4** is coordinated however not to Cu(1) but rather to the copper(II) atom Cu(2) of the $[Cu_2(OAc)_4]$ unit to form the one-dimensional chains. The $[Cu_2(OAc)_4]$ units contain four bridging acetate ligands in the familiar $\eta^1:\eta^1:\mu$ coordination mode [20]. The overall geometry of the $[Cu_2(OAc)_4]$ units of **3** and **4** is as expected with a Cu···Cu distances of 2.615(1) and 2.635(1) Å for **3** and **4**, respectively. The distances are slightly larger than the 2.614(2) Å in $[Cu_2(OAc)_4(H_2O)_2]$ [21]. The axial bridging O(33)–Cu(2) distances at 2.124(2) and 2.135(6) Å for complexes **3** and **4**, respectively, are slightly shorter than the Cu–O (water) distance at 2.161(2) in $[Cu_2(OAc)_4(H_2O)_2]$ [21]. Other bond distances and angles for these units are fairly similar to those found for $[Cu_2(OAc)_4(H_2O)_2]$ [21].

There are several structurally characterized compounds in which the axial water of the copper acetate dimer is replaced by a coordinating atom from another complex moiety to form high-nuclearity complexes [20,22]. However, the one-dimensional structures of complexes **3** and **4** are rather unusual as they exhibit a very rare μ_3-*syn–anti–anti* bridging mode of the acetate group. In most of the complexes of this type, a carboxylate ion usually bridges the copper acetate dimer with the other complex moiety by the familiar μ_2-mode [20,22]. In the only previously reported example with a μ_3 acetate bridge, the acetate ion bridges two copper(II) acetate dimer and a copper(I) ion from a bis(triethylphosphite)-copper(I) moiety in *syn–syn–anti* mode [23]. Therefore, to our knowledge, complexes **3** and **4** are the first examples of structures which show a μ_3-*syn–anti–anti* bridging mode of the acetate to join copper(II) acetate dimer with another Cu(II) complex moiety.

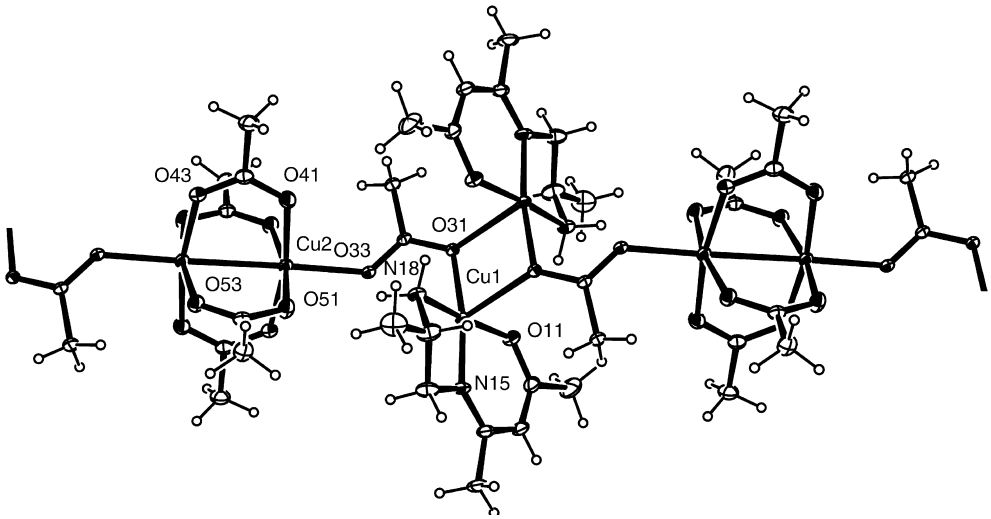

Fig. 4. ORTEP view of complex **3** with ellipsoids at 25% probability.

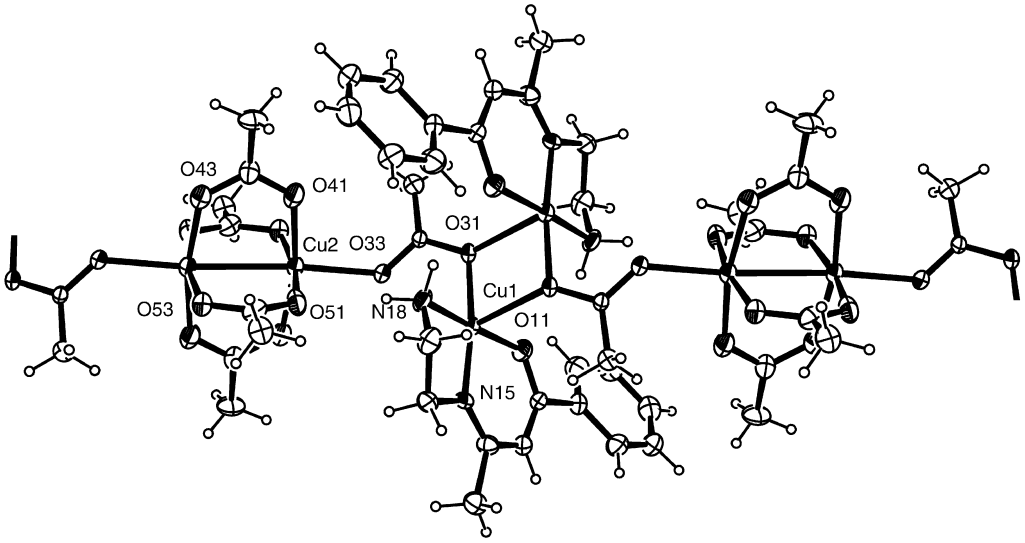

Fig. 5. ORTEP view of complex **4** with ellipsoids at 25% probability.

One of the amine hydrogen atoms, H18a of both **3** and **4** forms strong hydrogen bond with the corresponding Schiff base oxygen atom O11′ within the dimeric unit, whereas the other amine hydrogen, H18b forms a hydrogen bond with O51 for complex **3** and with O41 for complex **4** of an acetate group of the attached $[Cu_2(OAc)_4]$ core (Figs. S3 and S4).

3.3. Magnetic properties of the complexes *1* and *2*

The temperature dependence of the magnetic susceptibility data in the form of $\chi_M T$ versus T and χ_M versus T plots, for complexes **1** and **2**, are shown in Figs. 6a and 7a, respectively (χ_M being the magnetic susceptibility per $[Cu]_2$ unit). The $\chi_M T$ values at 300 K for **1** and **2** are 0.81 and 0.88 $cm^3\ mol^{-1}$ K, respectively which is as expected for two magnetically quasi-isolated spin doublets ($g > 2.00$). When the systems are cooled down, the $\chi_M T$ value remains constant to approximately 20 K for **1** and 50 K for **2** and below these temperatures decreases reaching the values of 0.72 and 0.66 $cm^3\ mol^{-1}$ K, respectively. The profile of the curves indicates the presence of weak antiferromagnetic exchange interactions between the Cu^{II} ions. The isotropic Heisenberg Dirac van Vleck (HDvV) Hamiltonian (Eq. (1)) is the main term used to interpret the magnetic data.

$$H = -JS_1S_2 \tag{1}$$

The Bleaney–Bowers equation (Eq. (2)) was used to fit the experimental data for the two complexes [24].

$$\chi_M = \frac{Ng^2\beta^2}{kT}\cdot\frac{2\exp(J/k_T)}{1+3\exp(J/kT)} \tag{2}$$

The best fit parameters are: $J = -0.56\ cm^{-1}$, $g = 2.09$ and $R = 5 \times 10^{-5}$ for **1** and $J = -1.19\ cm^{-1}$, $g = 2.17$ and $R = 3 \times 10^{-5}$ for **2** ($R = \sum_i(\chi_M T_{icalc} - \chi_M T_{iexp})^2/\sum_i(\chi_M T_{iexp})^2$). Complexes **1** and **2** show a slightly distorted square-pyramidal geometry, so the unpaired electron of the Cu^{II} ion lies in a mainly $d_{x^2-y^2}$ orbital, and there is very small unpaired electron density on the apical, out-of plane ligand. Since in all the present compounds the super exchange pathways involve out-of plane unpaired electron density, a weak exchange interaction may be anticipated. The small values of J parameters, for complexes **1** and **2**, have also been manifested by the curves of the reduced magnetization ($M/N\beta$) versus H compared with the hypothetical Brillouin law for two isolated copper(II) ions. As shown in Figs. 6b and 7b the experimental curves lie slightly bellow the theoretical Brillouin curve, indicating very small antiferromagnetic coupling.

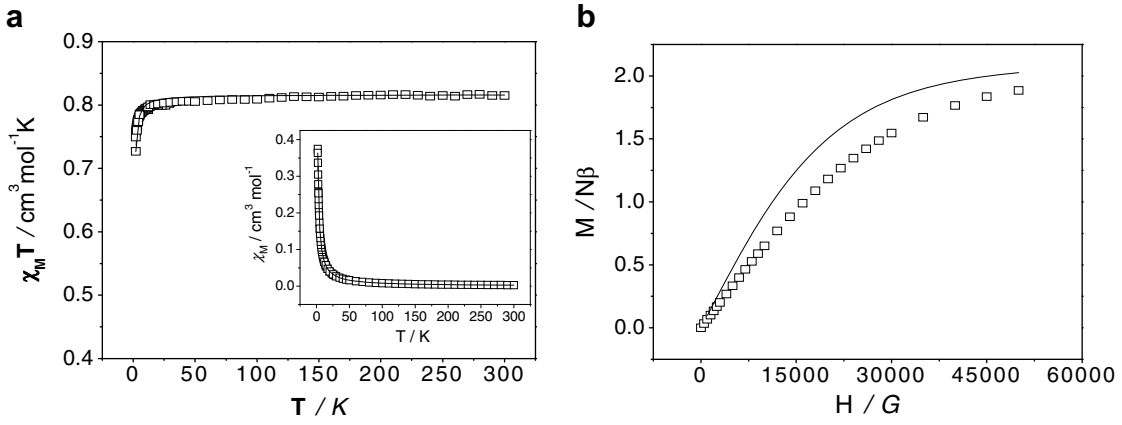

Fig. 6. (a) Plot of the $\chi_M T$ vs. T in the range 2–300 K for **1**. Inset: plot of χ_M vs. T. Solid lines show the best fit obtained. (b) Plot of the reduced magnetization ($M/N\beta$) vs. H for **1** (solid lines represent the Brillouin law for two isolated copper(II) ions).

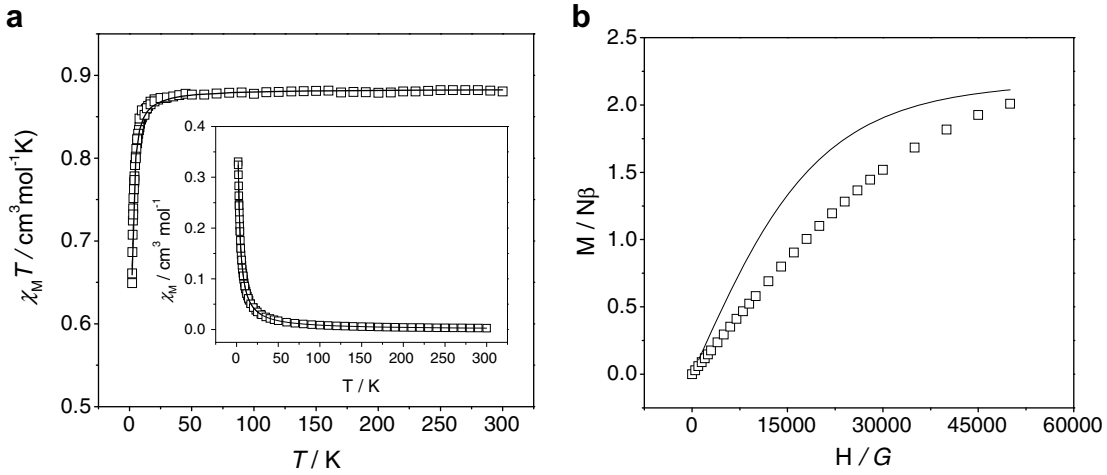

Fig. 7. (a) Plot of the $\chi_M T$ vs. T in the range 2–300 K for **2**. Inset: plot of χ_M vs. T. Solid lines show the best fit obtained. (b) Plot of the reduced magnetization ($M/N\beta$) vs. H for **2** (solid lines represent the Brillouin law for two isolated copper(II) ions).

3.3.1. EPR spectra

The X-band EPR spectra of powdered samples of complexes **1** and **2** were recorded on powder samples varying the temperature between 4 and 298 K. There is no appreciable change in the spectrum in changing the temperature of the sample from room temperature to 4 K. The pattern (Fig. 8) is typical for a square-pyramidal Cu^{II} [25]. The simulated parameters are the following: $g_{\|} = 2.25$ and $g_{\perp} = 2.05$ for **1**, and $g_{\|} = 2.23$ and $g_{\perp} = 2.05$ for **2**.

3.3.2. Discussion

From the structural point of view, in each dimer of complex **1** the ligand environment of the copper atoms is identical owing to crystallographic inversion symmetry and exhibits a 1D structure built of well separated chains in which the dimer units are connected by weakly hydrogen bonded water molecules. In complex **2** the dimer is not centrosymmetric, and therefore the two Cu–O–Cu bridges are dissimilar. The dimer units are linked by van der Waals interactions to form a 2D structure (Fig. S2). Taking into account the structural features the calculated J value for complex **2** is approximately the average of the two J intra values along the two Cu–O–Cu sides.

The magnetic pathway in the complexes is the Cu_2O_2 core. The magnetic properties of this core have been exhaustively studied from an experimental and theoretical point of view but only when the two O atoms occupy equatorial–equatorial positions with respect to copper(II) ions [26]. In contrast, the number of similar complexes containing this Cu_2O_2 core with the two O atoms in equatorial–axial positions is less abundant [5a,8,27] and no general trends have been reported relating the sign of the coupling constant and Cu–O–Cu angles. For such a bridging mode, the relative orientation of the magnetic orbitals centred on the metal ions is highly unfavorable for a strong magnetic coupling. The magnetic orbital for copper(II) ions in a square pyramidal environment is of the $d_{x^2-y^2}$-type; the x and y axes are roughly defined by the equatorial bonds. Some admixture of the d_{z^2} orbital is present as a result of trigonal distortion. The magnetic coupling is very weak because it is the result of the interaction of a $d_{x^2-y^2}$-type orbital with a d_{z^2}-type orbital having a very small spin density. The small J values can be positive (F) or negative (AF) depending upon subtle structural changes which is yet to be defined clearly. The literature shows that the absolute J value mainly depends on the axial Cu–O distances: if this length is ca. 2.3–2.5 Å (the most frequent cases), J lies between 8 and 0.5 cm^{-1} (ferromagnetically coupled systems) [8b,27] and -0.5 to -1 cm^{-1} (antiferromagnetically coupled systems) [5a,8a,8c,8d]. In complexes **1** and **2**, the central Cu_2O_2 core is equatorial–axial coordinated with the axial Cu–O lengths (2.508(4) Å in **1**, 2.501(3) and 2.433(2) Å in complex **2**). Thus, the antiferromagnetic coupling in both complexes is comparable to the values reported in the literature for similar systems. Furthermore, the Addison parameters for both the complexes indicate that the spin density on the apical position should be small, corroborating the small magnitude of the J values.

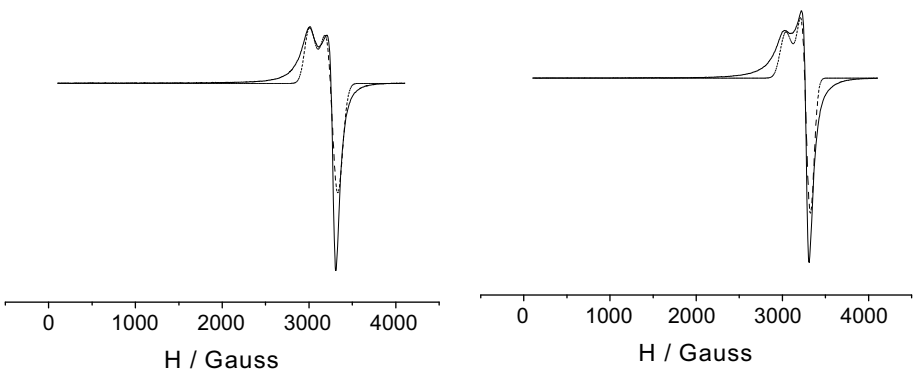

Fig. 8. The X-band EPR spectra of powdered samples and simulated EPR spectra (dotted lines) of complexes **1** and **2** at 4 K.

4. Conclusions

The N,N,O donor Schiff bases obtained by the reaction of acetyl-/benzoylacetone with diamines react with Cu^{II} acetate to yield dinuclear complexes containing mono-atomic acetate oxygen bridge – a relatively rare bridging mode of the carboxylate group. Synthesis of such complexes may also be accompanied by the formation of a one-dimensional alternating chain of the dimer and unreacted copper acetate in which a very rare μ_3-*syn–anti–anti* bridging mode of the acetate ion is observed. The variable temperature magnetic study of the two dimers shows very weak antiferromagnetic coupling caused by the basal-apical, mono-atomic acetate oxygen-bridge. The results corroborate the fact that for such bridging mode, the magnetic coupling is always very small but it can be either ferromagnetic or antiferromagnetic depending upon the subtle structural features that are yet to be understood.

Acknowledgements

We thank EPSRC and the University of Reading for funds for the Image Plate and X-Calibur diffractometers and the Spanish Government (Grant BQU2003-00539).

Appendix A. Supplementary data

Diagrams for H-bonding interactions of **2**, **3** and **4**, C–H–π interactions of **2**, and Table for bond angles of complexes **1**–**4**. CCDC 676657, 676658, 676659 and 676660 contain the supplementary crystallographic data for **1**, **2** and **3**. These data can be obtained free of charge via http://www.ccdc.cam.ac.uk/conts/retrieving.html, or from the Cambridge Crystallographic Data Centre, 12 Union Road, Cambridge CB2 1EZ, UK; fax: (+44) 1223-336-033; or e-mail: deposit@ccdc.cam.ac.uk. Supplementary data associated with this article can be found, in the online version, at doi:10.1016/j.poly.2008.05.004.

References

[1] (a) M.S. Ray, A. Ghosh, G. Mukhopadhyay, M.G.B. Drew, J. Coord. Chem. 56 (2003) 1141;
(b) J.P. Costes, J.P. Laurent, Inorg. Chim. Acta 134 (1987) 245.
[2] (a) B. Sarkar, M.S. Ray, M.G.B. Drew, C.Z. Lu, A. Ghosh, J. Coord. Chem. 60 (2007) 2165;
(b) M.S. Ray, A. Ghosh, R. Bhattacharya, G. Mukhopadhyay, M.G.B. Drew, J. Ribas, Dalton Trans. (2004) 252;
(c) M.S. Ray, A. Ghosh, S. Chaudhuri, M.G.B. Drew, J. Ribas, Eur. J. Inorg. Chem. (2004) 3110;
(d) M. Kwiatkowski, E. Kwiatkowski, A. Olechnowicz, Inorg. Chim. Acta 37 (1989) 158;
(e) M. Kwiatkowski, E. Kwiatkowski, A. Olechnowicz, Inorg. Chim. Acta 117 (1991) 82;
(f) J.P. Costes, F. Dahan, J. Ruiz, P. Laurent, Inorg. Chim. Acta 239 (1995) 53.
[3] C. Biswas, S. Chattopadhyay, M.G.B. Drew, A. Ghosh, Polyhedron 26 (2007) 4411.
[4] (a) B. Sarkar, M.S. Ray, M.G.B. Drew, A. Figuerola, C. Diaz, A. Ghosh, Polyhedron 25 (2006) 3084;
(b) B. Sarkar, M.S. Ray, Y.Z. Li, Y. Song, A. Figuerola, E. Ruiz, J. Cirera, J. Cano, A. Ghosh, Chem. Eur. J. 13 (2007) 9297. and references cited therein;
(c) J.P. Costes, F. Dahan, J.P. Laurent, Inorg. Chem. 25 (1986) 413;
(d) M.S. Ray, S. Chattopadhyay, M.G.B. Drew, A. Figuerola, J. Ribas, C. Diaz, A. Ghosh, Eur. J. Inorg. Chem. (2005) 4562;
(e) P. Mukherjee, M.G.B. Drew, M. Estrader, C. Diaz, A. Ghosh, Inorg. Chim. Acta 361 (2008) 161.
[5] (a) J.P. Costes, F. Dahan, J.P. Laurent, Inorg. Chem. 24 (1985) 1018. and references cited therein;
(b) M. Becht, T. Gerfin, K.H. Dahmen, Helv. Chim. Acta 77 (1994) 1288.
[6] (a) A.K. Ghosh, D. Ghoshal, E. Zangrando, J. Ribas, N.R. Chaudhuri, Inorg. Chem. 46 (2007) 3057;
(b) C. Biswas, P. Mukherjee, M.G.B. Drew, C.J.G. Garcia, J.M.C. Juan, A. Ghosh, Inorg. Chem. 46 (2007) 10771. and references cited therein;
(c) J. Pasan, J. Sanchiz, C. Ruiz-Perez, F. Lloret, M. Julve, Eur. J. Inorg. Chem. (2004) 4081. and references cited therein;
(d) J. Pasan, J. Sanchiz, C. Ruiz-Perez, F. Lloret, M. Julve, Inorg. Chem. 44 (2005) 7794.
[7] (a) S.R. Breeze, S. Wang, L. Chen, J. Chem. Soc., Dalton Trans. (1996) 1341;
(b) S. Wang, K.D.L. Smith, Z. Pang, M.J. Wagner, Chem. Commun. (1992) 1594;
(c) G. Mezei, M.R. Carrillo, R.G. Raptis, Inorg. Chim. Acta 357 (2004) 372;
(d) R. Hamalainen, M. Ahlgren, U. Turpeinen, Acta Crystallogr., Sect. B 38 (1982) 1577;
(e) N.A. Bailey, D.E. Fenton, J.R. Tate, P.M. Thomas, J. Chem. Soc., Dalton Trans. (1985) 1471.
[8] (a) B. Chiari, J.H. Helms, O. Piovesana, T. Tarantelli, P.F. Zanazzi, Inorg. Chem. 25 (1986) 870;
(b) A.M. Greenaway, C.J. O'Connor, J.W. Overman, E. Sinn, Inorg. Chem. 20 (1981) 1508;
(c) B. Chiari, J.H. Helms, O. Piovesana, T. Tarantelli, P.F. Zanazzi, Inorg. Chem. 25 (1986) 2408;
(d) B. Conerney, P. Jensen, P.E. Kruger, B. Moubaraki, K.S. Murray, Cryst. Eng. Commun. 5 (2003) 454.
[9] (a) E. Kwiatkowski, M. Kwiatkowski, A. Olechnowiez, Inorg. Chim. Acta 90 (1984) 45;
(b) H. Adams, N. A Bailey, I.S. Bard, D.E. Fenton, J.P. Costes, G. Cros, J.P. Laurent, Inorg. Chim. Acta 101 (1985) 7;
(c) M. Kwiatkowski, G. Bandoli, J. Chem. Soc., Dalton Trans. (1992) 379;
(d) J.P. Costes, F. Dahan, A. Dupuis, J.P. Laurent, J. Chem. Soc., Dalton Trans. (1998) 1307;
(e) M.S. Ray, A. Ghosh, S. Chaudhuri, M.G.B. Drew, J. Ribas, Eur. J. Inorg. Chem. (2004) 3110;
(f) J.P. Costes, F. Dahan, J.M.D. Vera, J.P. Laurent, J. Ruiz, J. Sotiropoulos, Inorg. Chem. 33 (1994) 3908.
[10] W. Kabsch, J. Appl. Crystallogr. 21 (1988) 916.
[11] CRYSALIS, Oxford Diffraction, Oxford Diffraction Ltd., Abingdon, England, 2006.
[12] G.M. Sheldrick, Acta Crystallogr., Sect. A 64 (2008) 112.
[13] N. Walker, D. Stuart, Acta Crystallogr., Sect. A 39 (1983) 158.
[14] ABSPACK Program, Oxford Instruments, 2005.
[15] K. Nakamoto, J. Fujita, S. Tanaka, M. Kobayashi, J. Am. Chem. Soc. 79 (1957) 4904.
[16] B.J. Hathaway, A.A.G. Tomlinson, Coord. Chem. Rev. 5 (1970) 1.
[17] A.W. Addison, T.N. Rao, J. Reedijk, J. van Rijn, G.C. Verschoor, J. Chem. Soc., Dalton Trans. (1984) 1349.
[18] (a) D. Cremer, J.A. Pople, J. Am. Chem. Soc. 97 (1975) 1354;
(b) J.C.A. Boyens, J. Cryst. Mol. Struct. 8 (1978) 31.
[19] (a) Z. Lu, P. Gamez, I. Mutikainen, U. Turpeinen, J. Reedijk, Cryst. Growth Des. 7 (2007) 1669;
(b) M. Nishio, Cryst. Eng. Commun. 6 (2004) 130. and references cited therein.
[20] (a) C.A. Crawford, E.F. Day, W.E. Streib, J.C. Huffman, G. Christou, Polyhedron 13 (1994) 2933. and references cited therein;
(b) A. Neels, H.S. Evans, A. Escuer, R. Vicente, Inorg. Chem. 34 (1995) 1946;
(c) B. Chiari, O. Piovesana, T. Tarantelli, P.F. Zanazzi, Inorg. Chem. 27 (1988) 3246.
[21] (a) A. Elmali, Turk. J. Phys. 24 (2000) 667;
(b) G.M. Brown, R. Chidambaram, Acta Crystallogr., Sect. B 29 (1973) 2393.
[22] (a) S.P. Perlepes, E. Libby, W.E. Streib, K. Folting, G. Christou, Polyhedron 11 (1992) 923;
(b) Y.Y. Wang, Q. Shi, Q.Z. Shi, Y.C. Gao, X. Hou, Polyhedron 19 (2000) 891;
(c) M. Koman, D. Valigura, E. Durcanska, G. Ondrejovic, Chem. Commun. (1984) 381;
(d) B. Chiari, O. Piovesana, T. Tarantelli, P.F. Zanazzi, Inorg. Chem. 32 (1993) 4834.
[23] R.L. Beddoes, J.A. Conner, D. Dubowski, A.C. Jones, O.S. Mills, R. Price, J. Chem. Soc., Dalton Trans. (1981) 2119.
[24] B. Bleaney, K. Bowers, Proc. Roy. Soc. London, A 214 (1952) 451.
[25] (a) D.E. Billing, B.J. Hathaway, Coord. Chem. Rev. 5 (1970) 143;
(b) R. Barbuchi, A. Bencini, D. Gatteschi, Inorg. Chem. 16 (1977) 2117.
[26] (a) E. Ruiz, P. Alemany, S. Alvarez, J. Cano, J. Am. Chem. Soc. 119 (1997) 1297;
(b) E. Ruiz, P. Alemany, S. Alvarez, J. Cano, Inorg. Chem. 36 (1997) 3683.
[27] (a) G.A. Van Albada, I. Mutinaiken, O. Roubeau, U. Turpeinen, J. Reejijk, Inorg. Chim. Acta 331 (2002) 208;
(b) S. Sain, T.K. Maji, G. Mostafa, T.H. Lu, J. Ribas, J. Tercero, N.R. Chaudhuri, Polyhedron 22 (2003) 625. and references cited therein;
(c) R. Baldoma, M. Monfort, J. Ribas, X. Solans, M.A. Maestro, Inorg. Chem. 45 (2006) 8144.

Polyhedron 27 (2008) 2634–2642

Contents lists available at ScienceDirect

Polyhedron

journal homepage: www.elsevier.com/locate/poly

Assembly molecular architectures based on structural variation of metalloligand [Cu(PySal)$_2$] (PySal = 3-pyridylmethylsalicylideneimino)

Xiu-Jian Wang [a,b,*], Hong-Xia Jian [a], Zi-Ping Liu [a], Qing-Ling Ni [a], Liu-Cheng Gui [a], Lin-Hua Tang [a]

[a] School of Chemistry and Chemical Engineering, Guangxi Normal University, Guilin 541004, PR China
[b] State Key Laboratory of Coordination Chemistry, Nanjing University, Nanjing 210093, PR China

ARTICLE INFO

Article history:
Received 7 April 2008
Accepted 6 May 2008
Available online 4 June 2008

Keywords:
Metalloligand
3-Pyridylmethylsalicylideneimine
The building unit
Structural variation

ABSTRACT

A versatile neutral metalloligand [Cu(PySal)$_2$] (**1**) (PySal = 3-pyridylmethylsalicylidene-imino) was exploited as a building unit to construct five complexes {Cu[Cu(PySal)$_2$]$_2$}(ClO$_4$)$_2$ (**2**), {Cd[Cu(PySal)$_2$]$_2$(H$_2$O)$_2$]} (NO$_3$)$_2$ · 2H$_2$O · 4CH$_3$OH (**3**), {Zn[μ_2-Cu(PySal)$_2$]Cl$_2$}$_n$ · nCH$_3$OH (**4**), {Hg[μ_2-Cu(PySal)$_2$]I$_2$}$_n$ (**5**) and {Cd[μ_2-Cu(PySal)$_2$]Cl$_2$}$_n$ · nCH$_2$Cl$_2$ (**6**). [Cu(PySal)$_2$] acts as a chelating ligand in discrete complexes **2** and **3** with unbound anions, but as a bis-monodentate bridging ligand in polymers **4**, **5** and **6** when halogen anions coordinated cooperatively to metal cations. The coordination geometry of Cu^{2+} is well-defined square planar in bridging [Cu(PySal)$_2$], analogous to that in free metalloligand (**1**), but it is distorted square planar in chelating [Cu(PySal)$_2$].

© 2008 Elsevier Ltd. All rights reserved.

1. Introduction

The design and construction of metal-organic architectures has been received considerable attention not only because of their intrinsic aesthetic appeal in structures but also because of their potential application in catalysis, molecular adsorption, magnetism, non-linear optics and molecular sensing [1–8]. A variety of molecular architectures, such as multiple helicates, cages, grids, two-dimensional sheets, diamondoid networks and porous framework [9–12], have been prepared by the self-assembly of metal ions and organic ligands. The diversity of the structures and new topology are attributed to the selection of metal centers as well as the organic building blocks. The rigid ligands, allowing for a certain control of steric consequence in the assembly process, are usually used to develop metal-organic framework. The use of non-rigid (semi-rigid or flexible) ligands to construct well-shaped molecular architectures is far less common, partly due to the less predictable assembly process [13]. However, the lability and adaptability of flexible ligand can increase the structural diversity and functionality of metal-organic framework [14,15]. In addition, compounds that are capable of rotational motion in response to outside driving forces such as light, heat, or electric fields are intriguing for the development of molecular devices [16].

Metalloligand, the aggregate of metal ion and pure organic ligand, has been taken much interest recently due to its extra oriented donor atoms and well-defined geometry. Exploitation of metalloligand with *exo*-oriented donor atoms for bonding can give more easy access to target structure accommodated by the preconstructed geometry of metalloligand. Many examples have been shown that the use of metalloligands as building blocks is effective not only in the construction of the desired structures but also to design the spatial arrangement of metal ions and to tune the metal–metal interactions [17–28].

In this paper, we report a metalloligand [Cu(PySal)$_2$] **1**, which is prepared by reaction of organic ligand 3-pyridylmethylsalicylideneimine (HPySal) with Cu(Ac)$_2$. This copper-containing ligand not only contains two "free" pyridyl N donors which can coordinate to the external metal ions, but also possesses the nature of flexibility owing to the presence of a –CH$_2$– spacer between pyridyl ring and salicylideneimine moiety. The flexible rotation of pyridyl moiety can meet the requirement of coordination environment of external metal ion to exhibit different spatial conformation. In addition, the flexible coordination geometry of copper(II) ion between square planar and tetrahedral endows [Cu(PySal)$_2$] with adaptability. Based on the building block [Cu(PySal)$_2$], five compounds {Cu[Cu(PySal)$_2$]$_2$}(ClO$_4$)$_2$ (**2**), {Cd[Cu(PySal)$_2$]$_2$(H$_2$O)$_2$]} (NO$_3$)$_2$ · 2H$_2$O · 4CH$_3$OH (**3**), {Zn[μ_2-Cu(PySal)$_2$]Cl$_2$}$_n$ · nCH$_3$OH (**4**), {Hg[μ_2-Cu(PySal)$_2$]I$_2$}$_n$ (**5**) and {Cd[μ_2-Cu(PySal)$_2$]Cl$_2$}$_n$ · nCH$_2$Cl$_2$ (**6**) (Scheme 1) are isolated. The building unit of [Cu(PySal)$_2$], as a bis(pyridyl) ligand, can adopt chelating coordination mode or bis-monodentate bridging mode to construct architectures (Chart 1).

2. Experimental

2.1. Synthesis

All chemicals were of reagent grade and were used as received without further purification. The IR spectrum was recorded as KBr

* Corresponding author. Address: School of Chemistry and Chemical Engineering, Guangxi Normal University, Guilin 541004, PR China.
E-mail address: wang1_xj@yahoo.com.cn (X.-J. Wang).

0277-5387/$ - see front matter © 2008 Elsevier Ltd. All rights reserved.
doi:10.1016/j.poly.2008.05.005

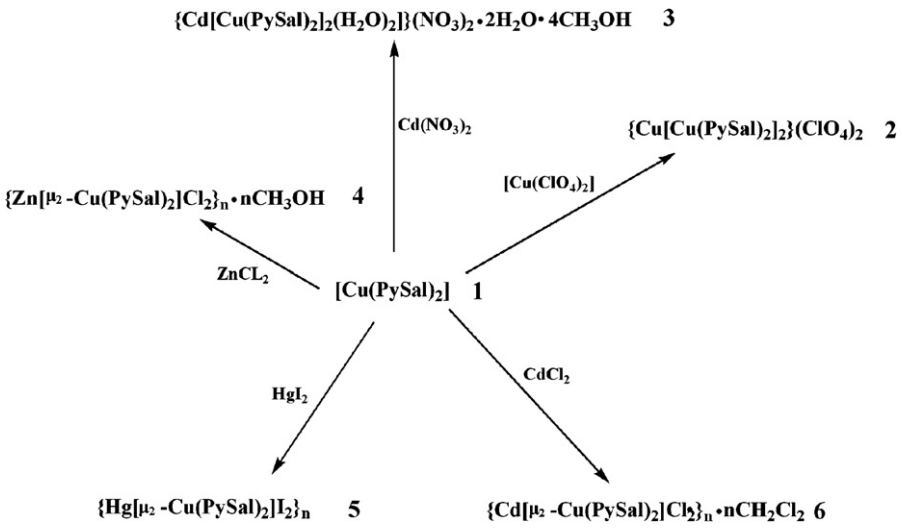

Scheme 1.

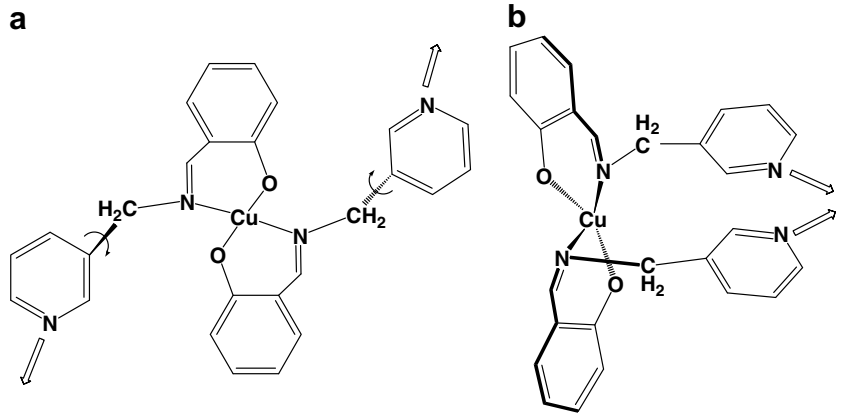

Chart 1. The coordination mode of $[Cu(PySal)_2]$. (a) The bridging mode; (b) The chelating mode.

pellets on a Perkin Elmer FT-IR spectrometer in the 4000–450 cm^{-1}. Elemental analyses for C, H, and N were performed on a Carlo ERBA 1106 analyzer. 3-Pyridylmethylsalicylideneimine (HPySal) was synthesized according to Ref. [29].

*2.1.1. Preparation of $[Cu(PySal)_2]$ (**1**)*

$Cu(Ac)_2 \cdot 2H_2O$ (0.0410 g, 0.20 mmol) was added to a stirring solution of HPySal (0.0852 g, 0.40 mmol) in CH_2Cl_2/CH_3OH (20 mL with 1:1 ratio), and the resulting deep green solution was allowed to stir for another 4 h. By diffusion of diethyl ether into the filtrate, the block deep green crystals were formed for X-ray diffraction analysis. Yield: 0.0830 g, 85%. *Anal.* Calc. for $C_{26}H_{22}N_4O_2Cu$: C, 64.20; H, 4.53; N, 11.52. Found: C, 64.17; H, 4.59; N, 11.48%. IR(cm^{-1}): 1615(s), 1601(m), 1543(m), 1470(m), 1437(s), 1330(m), 1201(m), 1044(m), 754(m), 705(m), 679(m).

*2.1.2. Preparation of $\{Cu[Cu(PySal)_2]_2\}(ClO_4)_2$ (**2**)*

A solution of **1** (0.0972 g, 0.2 mmol) in CH_2Cl_2 (10 mL) was added into a stirring solution of $Cu(ClO_4)_2$ (0.0262 g, 0.1 mmol) in CH_3OH (10 mL), and immediate precipitation of a deep green solid was observed. The mixture was allowed to stir for an additional 1 h to complete precipitate, then the precipitation collected by filtration was washed using CH_3OH and CH_2Cl_2 for two times, respectively, and dried under a vacuum. Yield: 0.1190 g, 85%. *Anal.* Calc. for $C_{52}H_{44}N_8O_{12}Cl_2Cu_3$: C, 50.55; H, 3.56; N, 9.07. Found: C, 50.02; H, 3.23; N, 9.44%. IR(cm^{-1}): 1624(s), 1609(m), 1535(m), 1466(m), 1450(m), 1430(m), 1321(m), 1121(s), 1094(s), 765(m), 706(m), 625(m). Suitable block deep green crystals were grown from the diffusion of diethyl ether into a THF solution of complex **2**.

*2.1.3. Preparation of $\{Cd[Cu(PySal)_2]_2(H_2O)_2]\}(NO_3)_2 \cdot 2H_2O \cdot 4CH_3OH$ (**3**)*

A solution of **1** (0.0972 g, 0.2 mmol) in CH_2Cl_2 (10 mL) was added into a stirring solution of $Cd(NO_3)_2 \cdot 2H_2O$ (0.0272 g, 0.1 mmol) in CH_3OH (10 mL). After allowed to stir for an additional 4 h, diethyl ether was diffused into the mixture solution. Two weeks later, the block red crystals were grown up suitable for X-ray diffraction. Yield: 0.0563 g, 40%. *Anal.* Calc. for $C_{56}H_{68}N_{10}O_{18}Cu_2Cd$: C, 47.73; H, 4.84; N, 9.94. Found: C, 47.45; H, 4.97; N, 9.53%. IR(cm^{-1}): 1620, 1601, 1537, 1469, 1452, 1437, 1428, 1384, 1324, 1150, 1128, 761, 707, 614.

*2.1.4. Preparation of $\{Zn[\mu_2\text{-}Cu(PySal)_2]Cl_2\}_n \cdot nCH_3OH$ (**4**)*

A solution of $ZnCl_2$ (0.0136 g, 0.1 mmol) in CH_3OH (10 mL) was layered onto a solution of **1** (0.0486 g, 0.1 mmol) in CH_2Cl_2 (10 mL). Two weeks later, block green crystals were collected for X-ray diffraction measure. Yield: 0.0348 g, 56%. *Anal.* Calc. for $C_{27}H_{26}N_4O_3CuZnCl_2$: C, 49.54; H, 3.98; N, 8.56. Found: C, 49.95; H, 3.62; N, 8.32%. IR(cm^{-1}): 1616(s), 1586(m), 1540(s), 1471(m), 1452(s), 1433(m), 1399(m), 1328(s), 765(s), 705(m).

*2.1.5. Preparation of {Hg[μ_2-Cu(PySal)$_2$]I$_2$}$_n$ (**5**)*

To a solution of **1** (0.0486 g, 0.1 mmol) in CH_2Cl_2 (10 mL) was dropped a solution of HgI_2 (0.0454 g, 0.10 mmol) in methanol (10 mL), and immediate precipitation of red solid was observed. After stirring for an additional 1 h, 5 ml DMF was added into the mixture to dissolve the precipitation. The resulting solution was layered by diethyl ether for 1 week to give block deep green crystals. Yield: 0.0378 g, 40%. *Anal.* Calc. for $C_{26}H_{22}N_4O_2CuHgI_2$: C, 33.17; H, 2.34; N, 5.95. Found: C, 33.475 H, 2.48; N, 6.30%. IR(cm^{-1}): 1619(s), 1599(m), 1539(m), 1470(m), 1452(m), 1429(m), 1331(m), 787(m), 753(m), 702(m).

*2.1.6. Preparation of {Cd[μ_2-Cu(PySal)$_2$]Cl$_2$}$_n \cdot n$CH$_2$Cl$_2$ (**6**)*

A solution of $CdCl_2 \cdot 2.5H_2O$ (0.0219 g, 0.1 mmol) in CH_3OH (10 mL) was layered onto a solution of **1** (0.0486 g, 0.1 mmol) in CH_2Cl_2 (10 mL). Three weeks later, block green crystals were collected for X-ray diffraction measure. Yield: 0.0250 g, 35%. *Anal.* Calc. for $C_{26.5}H_{23}N_4O_2Cl_3CuCd$: C, 44.68; H, 32.31; N, 7.87. Found: C, 44.35; H, 3.23; N, 7.87%. IR(cm^{-1}): 1614(s), 1538(s), 1472(m), 1448(s), 1431(m), 1338(s), 752(s), 708(s), 577(m).

2.2. Crystal structure determination

Crystals were mounted on glass fibers. Data were collected on a Bruker SMART CCD diffractometer using graphic-monochromated Mo Kα radiation (λ = 0.71073) at 293 K and the ω scan mode. The structures were solved with direct method on F^2 with full matrix least-squares methods using SHELXS-97 [30] and SHELXL-97 [31] programs, respectively. Except as mentioned, all non-hydrogen atoms were refined anisotropically. The hydrogen atoms were constrained to idealized geometries and assigned isotropic displacement parameters equal to 1.2- or 1.5-times the U_{iso} values of their respective parent atoms. Thermal ellipsoid diagrams were shown at 30% probability. In **2**, two perchloride anions were disordered over special position with two chlorine atoms at 25% occupancy. Both O6 and O7 were set to 50% occupancy. The anions were left isotropic and the largest residual electron density peaks (2.78–1.10 e/Å^3) were associated with them. In **3**, the solvent molecules of water and methanol were just suggested by elemental microanalysis of crystals from the same batch, and crystallographically modeled due to severely disordered. Geometric restraints were applied to the nitrate anions, and the largest residual electron density peaks (1.29 e/Å^3) were still associated with them. All solvent molecules and nitrate anions were left with isotropic thermal parameters. No hydrogen atoms were assigned on coordination water, crystalline water and methanol molecules. In **5**, the largest residual electron density peaks (2.78–1.10 e/Å^3) were associated with I^- and Hg^{2+} ions. In **6**, solvent CH_2Cl_2molecule, which laid on a symmetry element, was modeled at 50% occupancy with isotropic thermal parameters. Because of symmetry, only one-half molecule was located on the different Fourier map. Crystallographic data for these complexes are showed in Table 1, while the selected bond distances and angles are showed in Table 2.

3. Result and discussion

*3.1. Crystal structure description of **1***

When 3-pyridylmethylsalicylideneimine (HPySal) reacted with $Cu(Ac)_2 \cdot 2H_2O$ in dichloro- methane at room temperature (1:2 metal-to-ligand ratio), neutral complex **1** was obtained in quantitative yield with a formula of Cu(PySal)$_2$. This compound is air-stable and only soluble in organic solvents such as CH_2Cl_2, $CHCl_3$, THF, 1,2-dichloroethane, 1,1,2,2,-tetrachloromethane, not soluble in more polar solvents such as H_2O, DMF, CH_3CN, CH_3OH, CH_3COCH_3, and non-polar solvents. X-ray diffraction analysis shows that complex **1** is centro-symmetric with Cu^{2+} at the inversion center (Fig. 1). The asymmetric unit contains half a metal atom and one PySal entity. The copper center is well-suited for square planar coordination consisted of two phenolate-O and two imine-N atoms from two PySal ligands in a trans arrangement. The pyridyl nitrogen atoms in PySal do not take part in coordination. The bond distances and angles around Cu are similar as expected in other copper complexes of salicylideneimine ligands [32,33]. The chelating rings are in the same plane as the benzene rings forming a large common plane. Two pyridyl rings locate on the opposite sides of the coordination plane pointing in opposite directions, presumably to minimize the steric hindrance. The torsion angle of C7–N1–C8–C9 is −103.5° and the dihedral angle between pyridyl ring and the coordination plane is 86.1°. The separation of two pyridyl nitrogen atoms is 10.828(4) Å, significantly longer than that in 4,4′-bipyridine (7.12(3) Å), but comparable to those of 1,2-bis(4-pyridy)ethane (9.385(5) Å) and 1,2-bis(4-pyridyl)-ethyne (9.685(4) Å) [24].

The important structure feature of **1** is the presence of two uncoordinated nitrogen atoms of pyridyl rings which can endow complex **1** with a potential metalloligand to assemble the external transition metals to produce new coordination complexes, as well as the flexibility from the versatile co-ordination geometry of cop-

Table 1
Crystallographic data for complexes **1**, **2**, **3**, **4**, **5** and **6**

Complex	1	2	3	4	5	6
Formula	$C_{26}H_{22}$ N_4O_2Cu	$C_{52}H_{44}$ $N_8O_{12}Cl_2Cu_3$	$C_{56}H_{60}$ $N_{10}O_{18}CdCu_2$	$C_{27}H_{26}N_4O_3C_{12}CuZn$	$C_{26}H_{22}N_4O_2I_2CuHg$	$C_{26.50}H_{23}N_4O_2Cl_3CdCu$
F_w	486.02	1234.47	1400.62	654.33	940.41	711.78
Crystal system	monoclinic	tetragonal	tetragonal	orthorhombic	monoclinic	monoclinic
Space group	$P2_1/n$	$P4/ncc$	$P\bar{4}2_1c$	$Pnma$	$P2_1/m$	$C2/c$
a (Å)	10.1147(15)	18.3858(10)	18.4188(11)	13.677(3)	6.6031(12)	27.620(2)
b (Å)	9.0238(14)	18.3858(10)	18.4188(11)	22.383(5)	25.306(5)	14.4643(13)
c (Å)	12.3071(19)	15.1821(17)	17.537(2)	8.6211(19)	8.5574(16)	7.2112(6)
α (°)	90	90	90	90	90	90
β (°)	107.377(3)	90	90	90	91.415(3)	98.941(2)
γ (°)	90	90	90	90	90	90
V (Å^3)	1072.0(3)	5132.1(7)	5949.6(9)	2639.1(10)	1429.5(5)	2845.9(4)
Z	2	4	4	4,	2	4
ρ_{calc} (Mg/m^3)	1.506	1.598	1.546	1.647	2.185	1.760
μ (mm^{-1})	1.051	1.408	1.142	1.955	8.296	1.903
Total number of data	5329	36759	26316	16999	8279	14676
Number of unique data	2105	3180	5242	2828	3210	2791
Number of parameters	151	169	334	184	169	171
R_1 [$I > 2\sigma(I)$]	0.0356	0.0914	0.0679	0.0391	0.0542	0.0493
wR_2 [$I > 2\sigma(I)$]	0.0913	0.2450	0.1869	0.0906	0.1455	0.1287

Table 2
Selected bonded distances (Å) and angles (°) for complexes

1					
Cu1–O1	1.887(2)	Cu(1)–N1	2.004(2)	N1–C8	1.478(3)
O1–C1	1.307(3)	N1–C7	1.286(3)		
O1–Cu1–N1	91.7(1)	C7–N1–C8	115.3(2)	O1–Cu1–N1A	88.3(1)
Symmetry code: A: $-x$, $-y$, $-z$					
2					
Cu1–O1	1.874(5)	Cu1–N1	1.988(6)	Cu2–N2	2.023(5)
O1–Cu1–O1A	151.6(4)	O1–Cu1–N1	93.8(2)	O1–Cu1–N1A	94.5(2)
N1–Cu1–N1A	145.3(3)	N2–Cu2–N2A	91.9(3)	N2–Cu2–N2B	172.7(3)
N2–Cu2–N2C	88.6(3)				
Symmetry codes: A: $y + 3/2$, $x - 3/2$, $-z - 3/2$; B: $-x + 1/2$, $-y - 5/2$, z; C: $-y - 1$, $-x - 1$, $-z - 3/2$					
3					
Cu1–O1	1.872(7)	Cu1–O2	1.877(6)	Cu1–N1	1.963(9)
Cu1–N3	1.969(8)	Cd1–N4	2.250(8)	Cd1–N2	2.307(7)
Cd1–O3	2.342(1)	Cd1–O4	2.413(1)		
O1–Cu1–O2	158.3(3)	O1–Cu1–N1	92.6(3)	O1–Cu1–N3	91.3(3)
O2–Cu1–N1	89.3(3)	O2–Cu1–N3	93.4(3)	N1–Cu1–N3	162.5(3)
N2–Cd1–O3	94.1(2)	N2–Cd1–O4	85.9(2)	N2–Cd1–N4	90.5(3)
N2–Cd1–N2A	171.8(5)	N2–Cd1–N4A	89.4(3)	N4–Cd1–O3	90
N4–Cd1–O4	90	O3–Cd1–O4	180		
Symmetry code: A: $-x$, $-y + 1$, z					
4					
Zn1–N2	2.053(3)	Zn1–Cl1	2.202(2)	Zn1–Cl2	2.227(1)
Cu1–O1	1.882(2)	Cu1–N1	2.000(3)		
O1–Cu1–N1	91.9(1)	O1–Cu1–N1A	88.1(1)	N2–Zn1–N2B	105.8(2)
N2–Zn1–Cl1	110.5(1)	N2–Zn1–Cl2	105.7(1)	Cl1–Zn1–Cl2	118.0(1)
Symmetry codes: A: $-x - 1$, $-y + 1$, $-z$; B: x, $-y + 1/2$, z					
5					
Hg1–N2	2.437(7)	Hg1–I1	2.633(2)	Hg1–I2	2.645(1)
Cu1–O1	1.881(6)	Cu1–N1	2.013(7)		
O1–Cu1–N1	91.5(3)	O1–Cu1–N1B	88.5(3)	N2–Hg1–N2A	92.3(4)
N2–Hg1–I1	103.7(2)	N2–Hg1–I2	102.4(2)	I1–Hg1–I2	141.93(7)
Symmetry codes: A: x, $-y + 1/2$, z; B: $-x + 1$, $-y + 1$, $-z + 1$					
6					
Cu1–O1	1.888(4)	Cu1–N1	2.003(4)	Cd1–N2	2.374(4)
Cd1–Cl1	2.589(1)	Cd1–Cl1B	2.685(1)		
O1–Cu1–N1	91.3(2)	O1–Cu1–N1D	88.7(2)	N2–Cd1–N2A	83.0(2)
N2–Cd1–Cl1	163.7(1)	N2–Cd1–Cl1A	90.6(1)	N2–Cd1–Cl1B	84.6(1)
N2–Cd1–Cl1C	97.1(1)	Cl1–Cd1–Cl1A	97.1(1)	Cl1–Cd1–Cl1B	81.4(4)
Cl1–Cd1–Cl1C	97.2(1)	Cl1A–Cd1–Cl1C	81.4(4)	Cd1–Cl1–Cd1B	98.6(4)
Symmetry codes: A: $-x + 1$, y, $-z - 1/2$; B: $-x + 1$, $-y + 1$, $-z$; C: x, $-y + 1$, $z - 1/2$; D: $x + 3/2$, $-y + 3/2$, $-z - 1$					

per(II) ion and the freely rotating pyridyl moieties which make [Cu(PySal)$_2$] labile to meet the coordination requirement of the external metal ions. By the rotation of pyridyl moieties, [Cu(PySal)$_2$] can take on a variety of conformations.

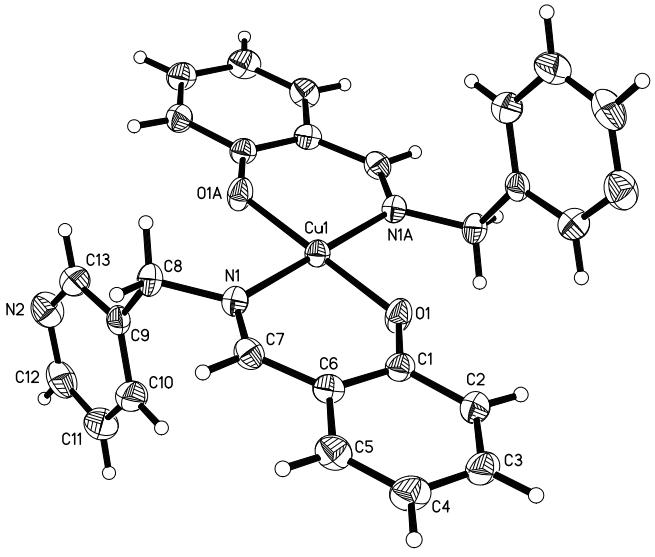

Fig. 1. ORTEP of complex **1** showing the numbering scheme.

3.2. Crystal structure description of *2* and *3*

When **1** was associated with Cu(ClO$_4$)$_2$ and Cd(NO$_3$)$_2$, respectively, trinuclear complexes **2** and **3** were isolated. X-ray diffraction analysis reveals that the building block of [Cu(PySal)$_2$], whose spatial configuration is totally different from that of free metalloligand **1**, takes chelating coordination mode to connect external metal ion through pyridyl nitrogen atoms. The geometry of Cu^{2+} ion in the building block is distorted square planar, significantly deviated from ideal square planar in the process of [Cu(PySal)$_2$] chelating to the external metal ions. Both of pyridyl moieties locate at the same side of distorted square plane. The long arms of methylenepyridine, like pincers, are agile to clamp metals. Complex **2** is composed of two building units of [Cu(PySal)$_2$] and one [Cu(ClO$_4$)$_2$] molecule (Fig. 2). The asymmetric unit contains half a building block. A crystallographically imposed twofold axis that passes through Cu1 bisects the building unit. The O1–Cu1–O1A and N1–Cu1–N1A angles exhibit that the geometry of Cu1 is largely deviated from ideal square plane. However, the bond distances of Cu1–O and Cu1–N are comparable to the corresponding values in **1**. Cu2 has a square planar geometry composed of four crystallographically identical pyridyl nitrogen atoms from two [Cu(PySal)$_2$] units, with the mean deviation of the CuN$_4$ plane of 0.094 Å. The

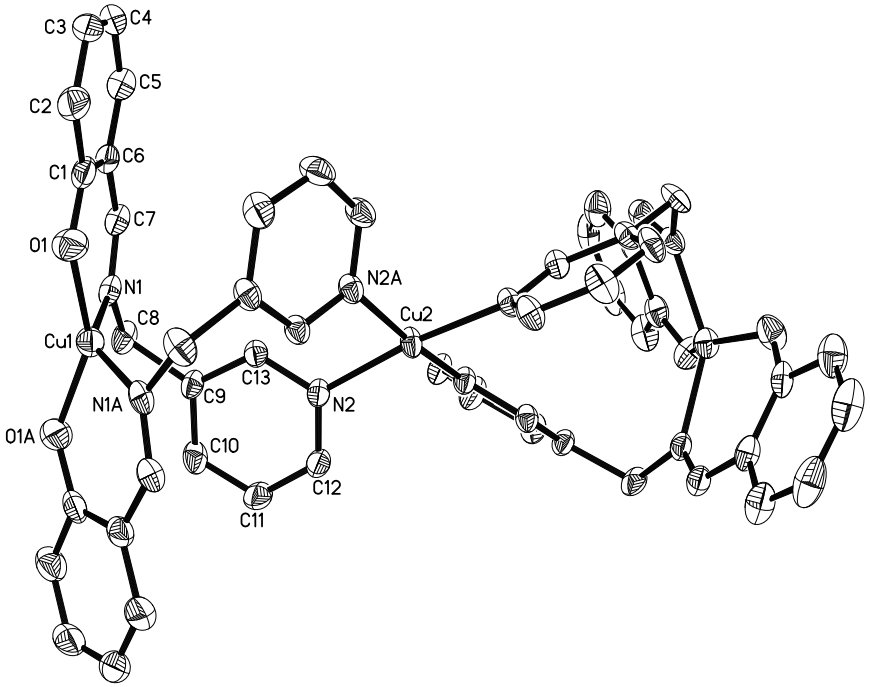

Fig. 2. The cation ORTEP of **2** showing the numbering scheme.

Cu2–N2 distance of 2.023(5) Å is within the normal range observed in bipyridyl Cu^{2+} complexes [34–36]. Counterions anions ClO_4^- are unbound and located between cations. Due to an active electron delocalization, the Cu–N-heterocyclic chelate rings exhibit some degree of "metalloaromaticity" [37]. So intermolecular $\pi\cdots\pi$ interactions between chelate and phenyl rings are observed (the ring-centroid distance of 4.37 Å and dihedral angle of 4°) in the packing structure of **2**[38]. It is surprising that complex **2** was also prepared by reaction of **1** with $[Cu(en)_2](ClO_4)_2$ or $[Cu(phen)_2](ClO_4)_2$ (en = 1,2-ethylenediamine, phen = 1,10-phenanthroline). The chelating ligand of en or phen being replaced by $[Cu(PySal)_2]$ demonstrates that the building block of $[Cu(PySal)_2]$ with long flexible arms is of very strong chelating ability. Complex **3** is composed of two $[Cu(PySal)_2]$, one $Cd(NO_3)_2$, two coordinated water molecules, four CH_3OH and two crystalline water molecules. The crystalline solvents of CH_3OH and H_2O are disordered. The asymmetric unit contains one building block. Two building blocks, whose geometric configuration similar to that in **2**, chelate to Cd^{2+} ion (Fig. 3), but the angles of O–Cu–O and N–Cu–N show that the deviation from ideal square plane in **3** is slightly smaller than that in **2**. The geometry of Cd^{2+} can be described as slightly distorted octahedron with the basal plane occupied by four pyridyl nitrogen atoms from two equivalent $[Cu(PySal)_2]$, and two apical sites associated with two aqua donors. The Cd–O distances are comparable to those in other known Cd complexes containing coordinated water molecules, but the Cd–N distances are shorter than those found in dipyridyl Cd complexes [39,40]. No intermolecular $\pi\cdots\pi$ interactions are observed. The solvents and unbound counterions anions are located between cations. Due to disorder, the weak interactions between solvents, anions and cations are not discussed.

Both **2** and **3** are discrete trinuclear complexes in which the anions are unbound, only as counterions. The geometric flexibility of Cu ion and the free rotating methylpyridine make $[Cu(PySal)_2]$ can adopt chelating coordination mode. It can be predicted that multi-dimensional complexes would be constructed if the building block

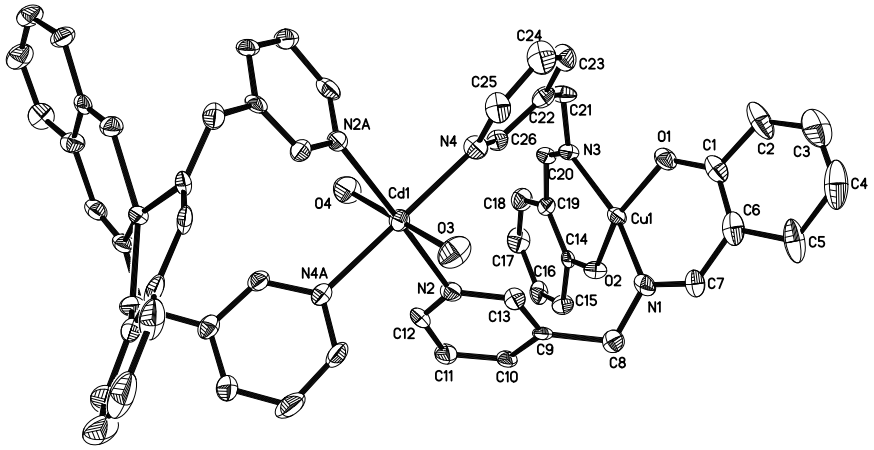

Fig. 3. The cation ORTEP of **3** showing the numbering scheme.

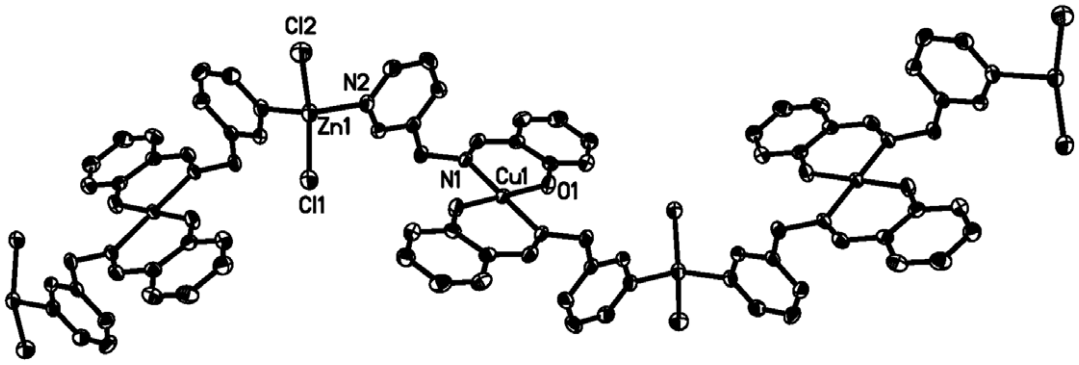

Fig. 4. 1D $[Cu(PySal)_2]/[ZnCl_2]$ polymer of **4**.

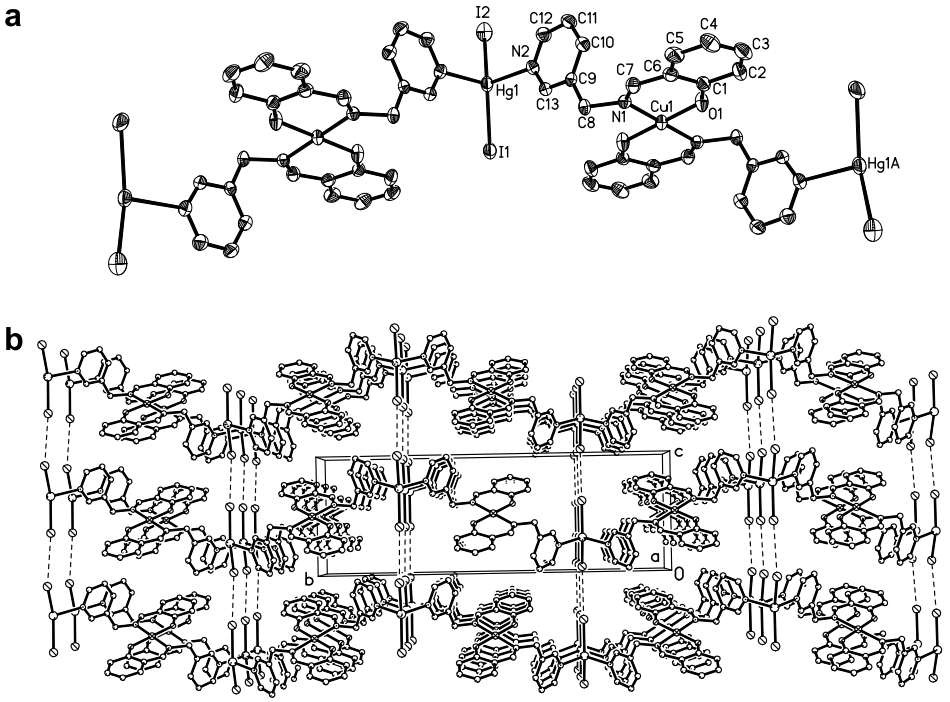

Fig. 5. (a) 1D $[Cu(PySal)_2]/[HgI_2]$ chain of **5**. (b) 3D structure in the solid state constructed by π···π and I···I weak interactions between chains.

of $[Cu(PySal)_2]$ adopts bridging coordination mode in the assembly process. Thus neutral bulky PPh_3 was internationally introduced into molecular architecture to increase steric hindrance and expected to induce the building block taking bridging mode, but it was found that $[Cu(PySal)_2]$ was still inclined to perform as chelating mode in complex $\{Cu(PPh_3)(CH_3CN)[Cu(PySal)_2]\}(BF_4)$.[1]

3.3. Crystal structure description of *4*, *5* and *6*

In order to avoid the presence of unbound anions and to investigate further the coordination behavior of metalloligand $[Cu(PySal)_2]$, the neutral metal halides MX_2(M = Zn, Cd, Hg; X = Cl or I) were associated with experiments. The mixed-metal coordination polymers $\{Zn[\mu_2\text{-}Cu(PySal)_2]Cl_2\}_n \cdot nCH_3OH$ (**4**), $\{Hg[\mu_2\text{-}Cu(PySal)_2]I_2\}_n$ (**5**) and $\{Cd[\mu_2\text{-}Cu(PySal)_2]Cl_2\}_n \cdot nCH_2Cl_2$ (**6**) were obtained. They are air-stable and exhibit low solubility in all common solvents. The single-crystal structural determination reveals that the structures of these three compounds are distinctly different from discrete complexes **2** and **3**. The building unit $[Cu(PySal)_2]$ acts as bridging coordination mode in these three polymers.

Polymer **4** is composed of the building block, $ZnCl_2$ and CH_3OH molecules. Each $[Cu(PySal)_2]$ links two incorporated Zn^{2+} ions and each Zn^{2+} ion is coordinated by two $[Cu(PySal)_2]$ units to generate one-dimensional zigzag $[Cu(PySal)_2]/[ZnCl_2]$ chain along the *b*-axis (Fig. 4). The Zn^{2+} cation adopts a distorted geometry (N–Zn–N and Cl–Zn–Cl angles of *ca.* 105.76° and 118.03°, respectively) and its coordination geometry is composed of two Cl^- anions and two pyridyl nitrogen atoms from two neighboring units of $[Cu(PySal)_2]$. The bond distances of Zn–N and Zn–Cl are comparable to those in similar compounds [41,42]. The shortest separations of Zn···Zn, Cu···Cu and Zn···Cu within the chain are 14.515 Å, 11.171 Å and 7.257 Å, respectively. CH_3OH molecules are located between chains. No special interactions such as π–π interactions are observed between adjacent chains. The conformation of free metalloligand is virtually retained in complex **4**: the building block is

[1] Structural analysis of $[Cu(PPh_3)(CH_3CN)[Cu(PySal)_2](BF_4)$ by X-ray diffraction shows that the building unit of $[Cu(PySal)_2]$ chelates to $[Cu(PPh_3)(CH_3CN)]$ moiety. Triclinic, space group, $P\bar{1}$, a = 12.352(2), b = 14.003(3), c = 14.595(3) Å, α = 87.606(3), β = 82.639(3), γ = 65.819(3)°, V = 2283.8(7) Å^3.

centro-symmetric with Cu^{2+} at the inversion centre; the coordination geometry of Cu^{2+} is square planar and the pyridyl rings locate on the opposite sides of the coordination plane pointing in opposite directions. The torsion angle of C7–N1–C8–C9 (−106.6°), the dihedral angle between pyridyl ring and the coordination plane (87.5°) and the bond distances around Cu^{2+} are also comparable to the corresponding values in **1**. But the separation between pyridyl nitrogen atoms in the building unit $[Cu(PySal)_2]$ is 11.142 Å, a little longer than that in **1** (10.828(4) Å).

For complex **5** obtained when the building unit of $[Cu(PySal)_2]$ was associated with HgI_2, a rather similar structure as **4** was observed. Each $[Cu(PySal)_2]$ bridges two Hg^{2+} ions and each Hg^{2+} ion is coordinated by two $[Cu(PySal)_2]$ units to generate one-dimensional zigzag $[Cu(PySal)_2]/[HgI_2]$ chains along the *b*-axis (Fig. 5). The geometry of Hg^{2+} can be described as significantly distorted tetrahedral and its coordination geometry is composed of two I^- anions and two pyridyl nitrogen atoms from two neighboring units of $[Cu(PySal)_2]$. The shortest separations of Hg···Hg, Cu···Cu and Hg···Cu within the chain are 15.147 Å, 12.653 Å and 7.573 Å, respectively. Interchain π···π weak interactions are observed between the chelating rings around Cu^{2+} cations and phenyl rings (ring-centroid distance of 3.60 Å), which lead to the stack of chains along the crystallographic *a*-axis. These π-stacking interactions between metallo-aromaticity-chelate and aryl rings are usually observed in crystal structures [37,38]. Taking into account of the ionic radius of I^- to be 2.06 Å [43], the I···I distance of 3.977(2) Å between adjacent polymers indicates the formation of I···I weak interactions which lead to the chains array along the crystallographic *c*-axis. Both of interchain π···π interactions and I···I weak interactions lead to chains packing into three-dimen-

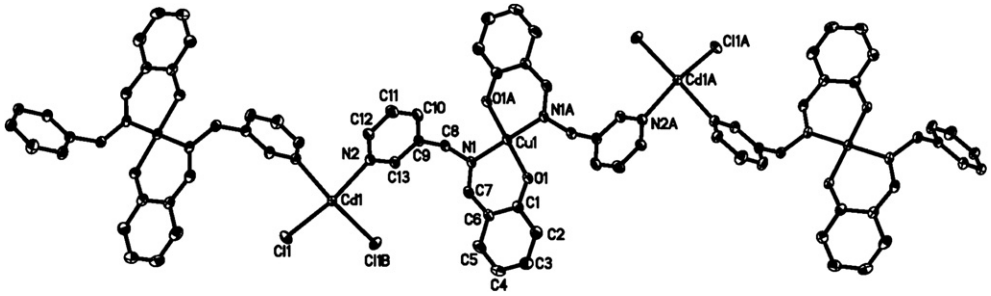

Fig. 6. 1D $[Cu(PySal)_2]/[CdCl_2]$ chain in **6**.

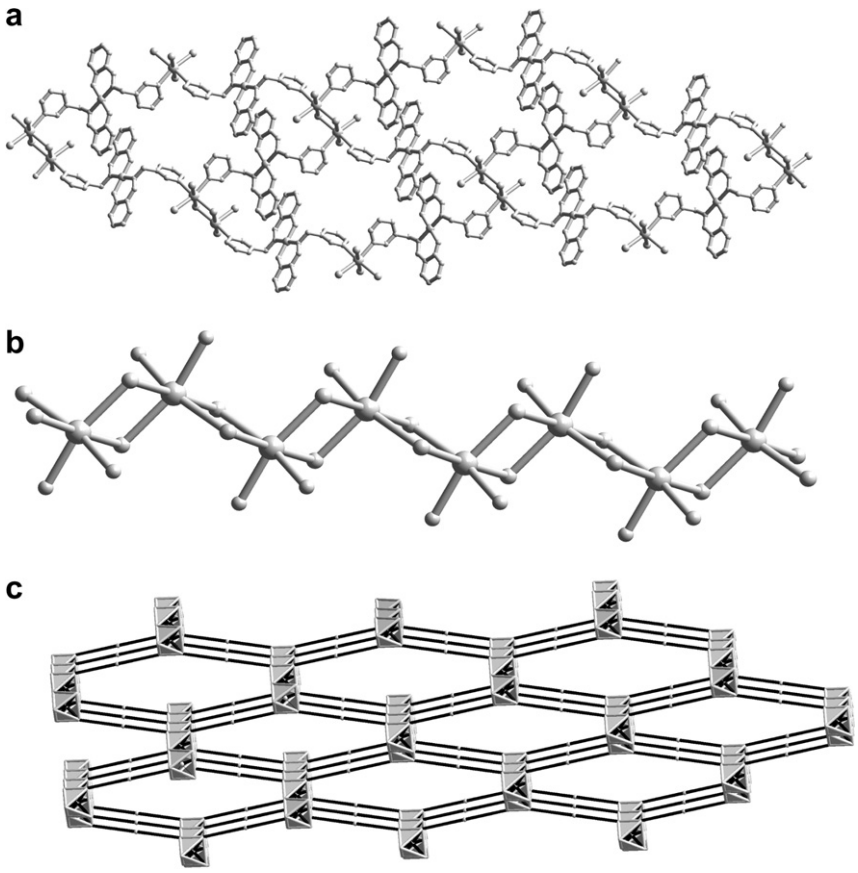

Fig. 7. (a) 2D sheet formed by double μ_2-Cl bridges linking adjacent chains in **6**; (b) 1D inorganic $[Cd(\mu_2\text{-}Cl)_2N_2]_n$ chain in **6**; (c) Schematic representation of 3D structure of **6** constructed by $[Cu(PySal)_2]$ units connecting inorganic chains $[Cd(\mu_2\text{-}Cl)_2]_n$ (polyhedral chains, inorganic chains $[Cd(\mu_2\text{-}Cl)_2]_n$; sticks, $[Cu(PySal)_2]$ units).

sional supramolecular structure (Fig. 5). The building unit [Cu(PySal)$_2$] in **5**, also retains the basic conformation of **1**. The bond parameters around Cu^{2+} and the torsion angle of C7–N1–C8–C9 (−102.3°) are close to the corresponding values in **1**, but the dihedral angle between pyridyl ring and the coordination plane is 95.1°, larger than that in **1**.

The establishment of complex **6** is based on [Cu(PySal)$_2$] and $CdCl_2$ building blocks. X-ray diffraction analysis shows **6** is composed of [Cu(PySal)$_2$], $CdCl_2$ and CH_2Cl_2. The synthetic precursor of [Cu(PySal)$_2$] adopts bridging mode *cis*-coordinating to cadmium cation (Fig. 6). Each [Cu(PySal)$_2$] links two neighboring $CdCl_2$ and each $CdCl_2$ links two [Cu(PySal)$_2$] units to generate a 1D zigzag metal-organic [Cu(PySal)$_2$]/[$CdCl_2$] chain along the crystallographic *a*-axis, as observed in above-mentioned complexes **4** and **5**. The significant difference is that these chains in **6** are further interconnected by double μ_2-Cl bridges between Cd centers into 3D noninterpenetrating network which contains one-dimensional zigzag inorganic chains of [Cd(μ_2-Cl)$_2$]$_n$ along the crystallographic *c*-axis (Fig. 7). In other words, if the inorganic [Cd(μ_2-Cl)$_2$]$_n$ chains can be treated as secondary building units (SUBs), the construction of 3D network in **6** can be also described as adjacent 1D SUBs of [Cd(μ_2-Cl)$_2$]$_n$ connected by [Cu(PySal)$_2$] units (Fig. 7c). The four adjacent SUBs are connected by [Cu(PySal)$_2$] units to form a 1D open channel. Each SUB is shared by four adjacent channels. The channels are filled by CH_2Cl_2 molecules and the phenyl rings of [Cu(PySal)$_2$] units, resulting in the total potential solvent-accessible volume is only 17.6% (501.4 $Å^{-3}$ per 2845.9 $Å^{-3}$) [44].

Within the 1D metal-organic [Cu(PySal)$_2$]/[$CdCl_2$] chain, the neighboring Cd···Cd, Cu···Cu and Cd···Cu separations are 15.795 Å, 14.803 Å and 7.897 Å, respectively. The separation between the two pyridyl nitrogen atoms in the [Cu(PySal)$_2$] unit is 11.820 Å, 1.0 Å longer than that in **1**. π···π weak interactions are observed between phenyl rings (the centroid distance of 3.788 Å) from adjacent 1D [Cu(PySal)$_2$]/[$CdCl_2$] chains, which could make, to some extent, contribution to the formation of 3D network [45].

The cadmium centers are crystallographically identical and lie in distorted octahedral *cis*-{Cd(μ_2-Cl)$_4$N$_2$} coordination spheres. The nitrogen donors are provided by pyridyl rings of [Cu(PySal)$_2$] units. Cadmium-centered octahedrons in inorganic chains are edge-shared. The bond length of Cd-μ_2-Cl (2.589 Å, 2.685 Å) and the angle of Cd-μ_2-Cl–Cd (98.6°) are similar to those observed in other analogous [Cd(μ_2-Cl)$_2$]$_n$ inorganic chains [46,47]. The bond length of Cd–N (2.376 Å) is longer than that in complex **3**. In [Cu(PySal)$_2$], the torsion angle of C7–N1–C8–C9 (85.5°) and the dihedral angle between pyridyl ring and the coordination plane (72.1°) are distinctly different from those in complex **1**, exhibiting the large-angle rotation of pyridyl groups. However, the basic conformation in free metalloligand of **1** is retained in complex **6**.

In the three compounds containing [Cu(PySal)$_2$]/[MX_2] chains, the building units of [Cu(PySal)$_2$] acts as a bridging ligand, and their spatial conformation and geometric parameters are analogous, even close to those in free metalloligand of **1**. The conformational changes of [Cu(PySal)$_2$] in these polymers are completed through the rotation of labile pyridine groups to meet the need of overall structures.

4. Conclusion

Metalloligand **1**, of which the functionality originates from mobile components, can adopt not only bidentate chelating mode, but also bridging mode in the process of metal-organic construction. The flexibility in [Cu(PySal)$_2$] (the geometric variation of Cu ion and the free rotation of methylpyridine moiety) is intrinsic for the metalloligand to meet the coordination requirement of different molecular architectures such as discrete and multi-dimensional structures. [Cu(PySal)$_2$] is inclined to perform as chelating mode with unbond anions. Nevertheless, the bridging coordination mode is preferred for [Cu(PySal)$_2$] in the presence of halogen anion ligand.

Acknowledgements

This work is financially sponsored by the National Natural Foundation of China (No. 20463001), the National Natural Foundation of Guangxi Province (No. 0832100) and State Key Laboratory of Coordination Chemistry, Nanjing University, China. We are also appreciated for Prof. Bei-Sheng Kang in Sun Yat-Sen University to provide help for crystal data collection.

Appendix A. Supplementary data

CCDC 639213, 639214, 639215, 639216, 639217 and 639218 contains the supplementary crystallographic data for complexes **1**, **2**, **3**, **4**, **5** and **6**. These data can be obtained free of charge via http://www.ccdc.cam.ac.uk/conts/retrieving.html, or from the Cambridge Crystallographic Data Centre, 12 Union Road, Cambridge CB2 1EZ, UK; fax: +44 1223 336 033; or e-mail:deposit@ccdc.cam.ac.uk. Supplementary data associated with this article can be found, in the online version, at doi:10.1016/j.poly.2008.05.005.

References

[1] N.L. Rosi, J. Kim, M. Eddaoudi, B. Chen, M. O'Keeffe, O.M. Yaghi, J. Am. Chem. Soc. 127 (2005) 1504.
[2] J.T. Hupp, K.R. Poeppelmeier, Science 309 (2005) 2008.
[3] S. Kitagawa, R. Kitaura, S. Noro, Angew. Chem., Int. Ed. 43 (2004) 2334.
[4] R.J. Hill, D.L. Long, N.R. Champness, P. Hubberstey, M. Schröder, Acc. Chem. Res. 38 (2005) 335.
[5] E. Coronado, J.R. Galan-Mascaros, C.J. Gomez-Garcia, V. Laukhin, Nature 408 (2000) 447.
[6] H. Kisida, H. Matsuzaki, H. Okamoto, T. Manabe, M. Yamashita, Y. Taguchi, Y. Tokura, Nature 405 (2000) 929.
[7] C. Janiak, Dalton Trans. (2003) 2781.
[8] R. Robson, J. Chem. Soc., Dalton Trans. (2000) 3735.
[9] S.P. Argent, H. Adams, T. Riis-Johannessen, J.C. Jeffery, L.P. Harding, W. Clegg, R.W. Harrington, M.D. Ward, Dalton Trans. (2006) 4996.
[10] B.J. O'Keefe, P.J. Steel, CrystEngComm 9 (2007) 222.
[11] F. Zhang, M.C. Jennings, R.J. Puddephatt, Chem. Commun. (2007) 1496.
[12] X.-D. Chen, M. Du, T.C.W. Mak, Chem. Commun. (2005) 4417.
[13] C.-L. Chen, J.-Y. Zhang, C.-Y. Su, Eur. J. Inorg. Chem. (2007) 2997.
[14] W. Zhuang, X. Zheng, L. Li, D. Liao, H. Ma, L. Jin, CrystEngComm 9 (2007) 653.
[15] S.-N. Wang, J. Bai, Y.-Z. Li, M. Scheer, X.-Z. You, CrystEngComm 9 (2007) 228.
[16] S. Horike, R. Matsuda, D. Tanaka, S. Matsubara, M. Mizuno, K. Endo, S. Kitagawa, Angew. Chem., Int. Ed. 45 (2006) 1.
[17] B. Chen, F.R. Fronczek, A.W. Maverick, Inorg. Chem. 43 (2004) 8209.
[18] J.K. Clegg, K. Gloe, M.J. Hayter, O. Kataeva, L.F. Lindoy, B. Moubaraki, J.C. McMurtrie, K.S. Murray, D. Schilter, Dalton Trans. (2006) 3977.
[19] S. Kitagawa, S. Noro, T. Nakamura, Chem. Commun. (2006) 701.
[20] K.-T. Youm, M.G. Kim, J. Ko, M.-J. Jun, Angew. Chem., Int. Ed. 24 (2006) 4003.
[21] V.D. Vreshch, A.B. Lysenko, A.N. Chernega, J.A.K. Howard, H. Krautscheid, J. Sieler, K.V. Domasevitch, Dalton Trans. (2004) 2899.
[22] L. Öhrström, K. Larsson, Dalton Trans. (2004) 347.
[23] S.R. Halper, L. Do, J.R. Stork, S.M. Cohen, J. Am. Chem. Soc. 128 (2006) 15255.
[24] V.D. Vreshch, A.N. Chernega, J.A.K. Howard, J. Sieler, K.V. Domasevitch, Dalton Trans. (2003) 1707.
[25] L. Carlucci, G. Ciani, F. Porta, D.M. Proserpio, L. Santagostini, Angew. Chem., Int. Engl. 41 (2002) 1907.
[26] B.F. Abrahams, B.F. Hoskins, D.M. Michail, R. Robson, Nature 369 (1994) 727.
[27] S.S. Kaye, J.R. Long, J. Am. Chem. Soc. 127 (2005) 6506.
[28] L.M. Toma, F.S. Delgado, C. Ruiz-Pérez, R. Carrasco, J. Cano, F. Lloret, M. Julve, Dalton Trans. (2004) 2836.
[29] Z. Cimerman, R. Kiralj, N. Galić, J. Mol. Struct. 323 (1994) 7.
[30] G.M. Sheldrick, SHELXS-97, University of Göttingen, Germany, 1997.
[31] G.M. Sheldrick, SHELXL-97, Program for Crystal Structure Refinement, University of Göttingen, Germany, 1997.
[32] M.K. Saha, D.K. Dey, B. Samanta, A.J. Edwards, W. Clegg, S. Mitra, Dalton Trans. (2003) 488.
[33] T. Akitsu, Y. Einaga, Polyhedron 24 (2005) 2933.
[34] M.A. Withersby, A.J. Blake, N.R. Champness, P.A. Cooke, P. Hubberstey, A.L. Realf, S.J. Teat, M. Schröder, J. Chem. Soc., Dalton Trans. (2000) 3261.

[35] S. Noro, R. Kitaura, M. Kondo, S. Kitagawa, T. Ishii, H. Matsuzaka, M. Yamashita, J. Am. Chem. Soc. 124 (2002) 2568.
[36] B. Murphy, M. Aljabri, A.M. Ahmed, G. Murphy, B.J. Hathaway, M.E. Light, T. Geilbrich, M.B. Hursthouse, Dalton Trans. (2006) 357.
[37] H.H. Monfared, Z. Kalantari, M.-A. Kamyabi, C. Janiak, Z. Anorg. Allg. Chem. 633 (2007) 1945.
[38] D. Sredojevi, G.A. Bogdanovi, Z.D. Tomi, S.D. Zari, CrystEngComm 9 (2007) 793.
[39] Y.-B. Dong, M.D. Smith, R.C. Layland, H.-C. Zur Loye, J. Chem. Soc., Dalton Trans. (2000) 775.
[40] M.-L. Tong, S.-L. Zheng, X.-M. Chen, Polyhedron 19 (2000) 1809.
[41] U. Siemeling, I. Scheppelmann, B. Neumann, A. Stammler, H.-G. Stammler, J. Frelek, Chem. Commun. (2003) 2236.
[42] Y. Gao, B. Twamley, J.M. Shreeve, Organometallics 25 (2006) 3364.
[43] M. Winter, WebElements periodic table, http://www.webelements.com.
[44] A.L.J. Spek, Appl. Crystallogr. 36 (2003) 7.
[45] C. Janiak, J. Chem. Soc., Dalton Trans. (2000) 3885.
[46] C.-D. Wu, A. Hu, L. Zhang, W. Lin, J. Am. Chem. Soc. 127 (2005) 8940.
[47] D.M. Ciurtin, M.D. Smith, H.-C. Zur Loye, Dalton Trans. (2003) 1245.

Polyhedron 27 (2008) 2643–2649

Contents lists available at ScienceDirect

Polyhedron

journal homepage: www.elsevier.com/locate/poly

Cyanooxo molybdenum(IV) complexes with 2-pyrazinecarbonitrile and 2-pyrazinecarboxylate: Crystallographic and spectroscopic studies reveal metal-assisted nitrile hydrolysis

Dariusz Matoga, Janusz Szklarzewicz *, Krzysztof Lewiński

Faculty of Chemistry, Jagiellonian University, Ingardena 3, 30-060 Kraków, Poland

ARTICLE INFO

Article history:
Received 18 January 2008
Accepted 30 April 2008
Available online 13 June 2008

Keywords:
Molybdenum
Cyano
Complexes
Hydrolysis
Nitrile
Carboxylate

ABSTRACT

The pH-control of a reaction between tetracyanooxomolybdate(IV) and 2-pyrazinecarbonitrile (pcn), in aqueous-ethanolic solution under ambient conditions, affords the Mo(IV) mixed-ligand complex anions $[Mo(CN)_4O(pcn)]^{2-}$ (**1**) or $[Mo(CN)_4O(Hpca)]^{2-}$ (**2**) with a monodentately bound 2-pyrazinecarboxylic acid (Hpca), resulting from metal-assisted organonitrile hydrolysis. The acid undergoes slow rearrangement to a bidentate mode in $[Mo(CN)_3O(pca)]^{2-}$ (**3**), which is confirmed by means of UV–Vis spectroscopy. The nitrile hydrolysis, favored by the basic conditions, has been ascertained by elemental analyses as well as IR, ^1H and ^{13}C NMR spectroscopy. The use of Hpca instead of pcn in the synthetic procedure results in the direct formation of $[Mo(CN)_3O(pca)]^{2-}$ (**3**) with the bidentate 2-pyrazinecarboxylate. The coordination versatility of 2-pyrazinecarboxylate toward cyanooxomolybdenum(IV) complexes is demonstrated by the IR and UV–Vis spectroscopy of solids with $[Mo(CN)_4O(Hpca)]^{2-}$ and $[Mo(CN)_3O(pca)]^{2-}$ ions, and the definitive evidence for the structure of $[Mo(CN)_3O(pca)]^{2-}$ is provided by single-crystal X-ray crystallography. The chemical formulations of all the complexes, isolable as $[PPh_4]^+$ salts, have been verified with microanalyses, spectroscopic measurements and X-ray crystal structures of **1** and **3**.

© 2008 Elsevier Ltd. All rights reserved.

1. Introduction

Mixed-ligand cyanooxocomplexes of molybdenum(IV) and tungsten(IV) are of considerable interest in coordination chemistry in part because of their biological relevance as well as interesting properties and reactivity. Such complexes are also of structural interest, given the versatility of the incorporated hetero-donor ligands in terms of coordination numbers, ligand denticity and structural isomerism.

Tetracyanooxometallates in aqueous solution are labile for substitution which makes them attractive starting materials and allows for the introduction of various other monodentate or polydentate ligands such as, for instance, biologically relevant Schiff bases [1–6]. Recently, it has been shown that some products of these reactions, $[M^{IV}(CN)_4O(L)]^{n-}$ ions (M = Mo, W; L = monodentate ligand), are reactive toward small molecules such as O_2 and NO [7–12]. The binding of molecular oxygen by transition metal complexes is of tremendous importance in that the products act as reagents, catalysts or key intermediates in selective oxidation reactions. Moreover, complexes that bind atmospheric oxygen at the metal centre can be treated as models for oxygen transport systems in living organisms [13,14]. The interest in nitrosyl metal complexes, on the other hand, results to a large degree from the revealed role for nitric oxide as a key physiological regulator [15,16].

In this work, we report on the synthesis and physicochemical properties of $[Mo(CN)_4O(Hpca)]^{2-}$ (Hpca = 2-pyrazinecarboxylic acid), $[Mo(CN)_4O(pcn)]^{2-}$ (pcn = 2-pyrazinecarbonitrile) and $[Mo(CN)_3O(pca)]^{2-}$complexes, as well as the crystal structures of the latter two ions. The complexes were obtained in the pursuit of relevant molybdenum precursors for small molecule activation and the 2-pyrazinecarbonitrile ligand seemed interesting for us also in terms of the versatile reactivity of the coordinated nitriles [17–20]. In the case of the tetracyanocomplexes, the synthetic route involves the reaction of 2-pyrazinecarbonitrile with the $[Mo(CN)_4O(H_2O)]^{2-}$ and $[Mo(CN)_4O(OH)]^{3-}$ ions that remain in a pH-dependent equilibrium. Interestingly, two different products are isolated as $[PPh_4]^+$ salts, depending on the synthetic conditions. The differences between these products are elucidated spectroscopically and crystallographically. The complexes are compared in particular with a tricyanooxo complex, $[Mo(CN)_3O(pca)]^{2-}$, obtained directly from Hpca and the tetracyanooxomolybdate(IV) starting material. Such a coordination versatility of 2-pyrazinecarboxylate has not been observed for any organic ligands in the mixed-ligand cyanooxo complexes of molybdenum(IV) reported to date.

* Corresponding author. Tel.: +48 12 6632231; fax: +48 12 6340515.
E-mail address: szklarze@chemia.uj.edu.pl (J. Szklarzewicz).

0277-5387/$ - see front matter © 2008 Elsevier Ltd. All rights reserved.
doi:10.1016/j.poly.2008.04.048

2. Experimental

2.1. Materials and methods

Potassium sodium tetracyanooxomolybdate(IV) hexahydrate, $K_3Na[Mo(CN)_4O_2]\cdot 6H_2O$, was synthesized according to a literature method [21]. All other chemicals were of analytical grade (Aldrich) and were used as supplied. Carbon, hydrogen and nitrogen were determined using an Euro EA 3000 elemental analyzer. Solid samples for IR spectroscopy were compressed as KBr pellets and the IR spectra were recorded on a Bruker EQUINOX 55 FT-IR spectrophotometer. Electronic absorption spectra were measured with a Shimadzu UV-2101PC scanning spectrophotometer. Diffuse reflectance spectra were measured in $BaSO_4$ pellets with $BaSO_4$ as a reference using a Shimadzu 2101 PC equipped with an ISR-260 attachment. The magnetic susceptibility measurements were carried out by the Gouy method on an analytical balance, Radwag WPA120, at room temperature with $VOSO_4\cdot 5H_2O$ as a standard. ^1H and ^{13}C NMR spectra were recorded on a Bruker AVANCE II 300 MHz instrument; the spectra were measured in CD_3OD or CD_3CN at 293 K.

2.2. Synthesis of $[PPh_4]_2[Mo(CN)_4O(pcn)]\cdot 2H_2O$ (**1**)

$K_3Na[Mo(CN)_4O_2]\cdot 6H_2O$ (0.20 g, 0.42 mmol) was dissolved in water (10 ml). To the stirring solution (pH ≈ 11) hydrochloric acid (3.0 M) was added dropwise until a pH value of 8.5 was reached, followed by addition of 2-pyrazinecarbonitrile (0.100 ml, 1.12 mmol) in ethanol (3 ml). The resultant purple solution was treated with an aqueous solution (3 ml) of $[PPh_4]Cl$ (0.32 g, 0.85 mmol). Green crystals of **1** (yield: 0.24 g, 55%), which deposited within a few hours, were filtered off, washed with water and dried in air at room temperature. *Anal.* Calc. for $C_{57}H_{47}MoN_7O_3P_2$: C, 66.09; H, 4.57; N, 9.46. Found: C, 66.07; H, 4.27; N, 9.29%. IR (KBr, cm^{-1}): ν_{MoO} 979s, ν_{CN} 2091s. ^1H NMR (300 MHz, CD_3OD, 293 K): δ (ppm) 8.89 (d, 1H of pcn, J = 3 Hz), 8.47 (d, 1H of pcn, J = 2 Hz), 8.41 (m, 1H of pcn), 7.74–8.01 (40H of $[PPh_4]^+$). ^{13}C NMR (300 MHz, CD_3OD, 293 K): δ (ppm) 117.45, 118.64, 130.19, 130.37, 134.44, 134.58, 135.29, 135.32 (C of $[PPh_4]^+$), 138.72, 142.20, 142.67, 152.02, 158.10 (C of pcn, CN^-). UV–Vis (solid state) λ, nm: 645, 488, 376, 318, 274, 232, 210. Visible [EtOH solution: λ, nm (ε, $dm^3\ mol^{-1}\ cm^{-1}$)]: 625 (120), 487 (270), 404 (200).

2.3. Synthesis of $[PPh_4]_2[Mo(CN)_4O(Hpca)]\cdot 2H_2O$ (**2**)

$K_3Na[Mo(CN)_4O_2]\cdot 6H_2O$ (0.30 g, 0.62 mmol) was dissolved in water (12 ml). To the stirring solution 2-pyrazinecarbonitrile (0.100 ml, 1.12 mmol) was added followed by ethanol (2 ml). The resultant solution at pH ≈ 11 was stirred for *ca.* 15 min and then treated with $[PPh_4]Cl$ (0.48 g, 1.3 mmol) and hydrochloric acid (3.0 M) which was added dropwise until a pH value of 8.5 was reached. Purple crystals of **2** (yield: 0.40 g, 69%), which deposited within a few hours, were filtered off, washed with water and dried in air at room temperature. *Anal.* Calc. for $C_{57}H_{48}MoN_6O_5P_2$: C, 64.90; H, 4.59; N, 7.97. Found: C, 65.22; H, 4.75; N, 8.39%. IR (KBr, cm^{-1}): ν_{MoO} 973m, ν_{CN} 2091s, ν_{CO} 1670s, 1692s. ^1H NMR (300 MHz, CD_3OD, 293 K): δ (ppm) 9.26 (d, 1H of Hpca, J = 2 Hz), 8.81 (d, 1H of Hpca, J = 3 Hz), 8.72 (m, 1H of Hpca), 7.74–8.01 (40H of $[PPh_4]^+$). ^{13}C NMR (300 MHz, CD_3OD, 293 K): δ (ppm) 117.46, 118.65, 130.18, 130.34, 134.44, 134.58, 135.28, 135.32 (C of $[PPh_4]^+$), 143.45, 143.51, 147.18 (C of Hpca, CN^-). UV–Vis (solid state) λ, nm: 590sh, 540, 386, 325, 274, 232, 211. Hydrogen atoms labelling scheme for **2** is the same as that for **1**.

2.4. Synthesis of $[PPh_4]_2[Mo(CN)_3O(pca)]\cdot 3H_2O$ (**3**)

$K_3Na[Mo(CN)_4O_2]\cdot 6H_2O$ (1.86 g, 3.87 mmol) was dissolved in water (30 ml). To the stirring solution 2-pyrazinecarboxylic acid (0.48 g, 3.87 mmol) was added followed by ethanol (8 ml). The resultant solution was treated with $[PPh_4]Cl$ (2.90 g, 7.74 mmol) and hydrochloric acid (3.0 M) was added dropwise until a pH value of 8.5 was reached. Purple crystals of **3** (yield: 1.50 g, 38%), which deposited within one day, were filtered off, washed with water and dried in air at room temperature. The product is also obtainable from $[Mo(CN)_4O(Hpca)]^{2-}$ as a result of slow rearrangement of the Hpca ligand to a bidentate mode, what have been observed by means of UV–Vis spectroscopy. *Anal.* Calc. for $C_{56}H_{49}MoN_5O_6P_2$: C, 64.31; H, 4.72; N, 6.70. Found: C, 64.56; H, 4.52; N, 6.48%. IR (KBr, cm^{-1}): ν_{MoO} 953s, ν_{CN} 2104s, ν_{CO} 1641s. ^1H NMR (300 MHz, CD_3CN, 293 K): δ (ppm) 9.10 (d, 1H of pca^-, J = 3 Hz), 8.62 (s, 1H of pca^-), 8.22 (d, 1H of pca^-, J = 3 Hz), 7.60–7.91 (40H of $[PPh_4]^+$). ^{13}C NMR (300 MHz, CD_3CN, 293 K): δ (ppm) 117.93, 117.98, 130.91, 131.07, 135.27, 135.41, 136.02, 136.07 (C of $[PPh_4]^+$), 140.63, 144.34, 144.68 (C of pca, CN^-). UV–Vis (solid state) λ, nm: 590sh, 541, 410sh, 318, 274, 231, 212. Visible [EtOH solution: λ, nm (ε, $dm^3\ mol^{-1}\ cm^{-1}$)]: 585sh, 516 (9300).

2.5. Crystallographic data collection and structure refinement

The crystals of **1** and **3** suitable for X-ray analysis were selected from the materials prepared as described in Section 2. Intensity data were collected on a Nonius Kappa CCD diffractometer using graphite monochromated Mo Kα radiation, λ = 0.7107 Å. The crystal data and details of data collection and structure refinement parameters are summarized in Table 1. The positions of most atoms were determined by direct methods, other non-hydrogen atoms were located in difference Fourier maps. The hydrogen atoms of water molecules O2 and O3 in **1** and O21 in **3** were located in difference Fourier maps and were refined with restraints on bond lengths and angles. The water molecules O22 and O24 and disordered water O23A and O23B in **3** were refined with an occupancy factor equal to 0.5. No hydrogen atoms of these water molecules could be reliably located and refined. The hydrogen atoms of aromatic rings (phenyl rings and 2-pyrazinecarbonitrile) were refined in idealized positions using a riding model with isotropic displacement parameters. The structures were solved using SIR92 [22] and refined by the SHELXL program [23].

Table 1
Crystal data and structure refinement parameters for **1** and **3**

	1	**3**
Empirical formula	$C_{57}H_{47}MoN_7O_3P_2$	$C_{56}H_{49}MoN_5O_6P_2$
Formula weight	1035.90	1045.88
Crystal size (mm)	0.30 × 0.25 × 0.10	0.17 × 0.12 × 0.10
Crystal system	triclinic	triclinic
Space group	$P\bar{1}$	$P\bar{1}$
a (Å)	13.5070(3)	13.4550(1)
b (Å)	13.6720(3)	13.5150(2)
c (Å)	16.9100(6)	16.6940(2)
α (°)	69.503(1)	87.740(1)
β (°)	88.891(1)	69.466(1)
γ (°)	62.529(1)	62.121(1)
V (Å^3)	2557.0(1)	2484.3(1)
Z	2	2
T (K)	293(2)	100(2)
D_{calc} (Mg/m^3)	1.345	1.398
μ (mm^{-1})	0.371	0.385
Reflections measured	15314	20311
Reflections unique	8928	11336
Reflections observed [$I > 2\sigma(I)$]	7455	8878
R indices [$I > 2\sigma(I)$]	R = 0.0433	R = 0.0474
	wR_2 = 0.1060	wR_2 = 0.1122
S	1.069	1.028

3. Results and discussion

3.1. General remarks for the syntheses

It was found earlier that there are two complexes susceptible to ligand substitution in aqueous solutions of $K_3Na[Mo(CN)_4O_2] \cdot 6H_2O$. One of them is the $[Mo(CN)_4O(OH)]^{3-}$ ion, prevailing in alkaline media (pH > 9.7), whose OH^- ligand can be slowly replaced by cyanide or a monodentate organic ligand L forming $[Mo(CN)_4OL]^{n-}$ complexes [24]. Under less alkaline conditions (pH < 9.7) the $[Mo(CN)_4O(H_2O)]^{2-}$ ion predominates and substitution reactions become considerably faster. Similarly as for the hydroxo complex, the reaction of the aqua complex with monodentate ligands L leads to $[Mo(CN)_4OL]^{n-}$ complexes, whereas the introduction of bidentate ligands, not observed for the hydroxo complex, results in the formation of $[Mo(CN)_3O(LL)]^{n-}$ ions.

Since our first synthetic goal in this work was to introduce 2-pyrazinecarbonitrile (pcn) to the coordination sphere of cyanooxomolybdates(IV), we decided to decrease the initial pH of the solution with the tetracyanooxomolybdate(IV) substrate from *ca.* 11 to 8.5, taking into account both faster substitution reactions for labile $[Mo(CN)_4O(H_2O)]^{2-}$ ions as well as the fact that free nitriles are known to undergo hydrolysis to carboxylates in alkaline and acidic media. The addition of pcn followed by $[PPh_4]^+$ cations under these conditions has resulted in the isolation of compound **1** with a preserved pendant nitrile group in the pcn ligand. On the other hand, when the 2-pyrazinecarbonitrile ligand was introduced to a tetracyanooxomolybdate(IV) solution already at pH = 11, with the resulting mixture being left for some time at this pH, salt **2** containing a monodentate carboxylate ligand was isolated from the solution after $[PPh_4]^+$ addition combined with a pH decrease. This observation confirms that the nitrile has undergone hydrolysis. The main question arises whether it is a free nitrile that hydrolyses at pH = 11 and then is coordinated to a metal centre, or it is a process involving a nitrile already bound to a Mo centre. In order to answer that question we carried out additional experiments with 2-pyrazinecarboxylic acid (Hpca). We have observed that the reaction of the $[Mo(CN)_4O(H_2O)]^{2-}$ ion with 2-pyrazinecarboxylic acid (pH = 8.5) results in the exclusive formation of the $[Mo(CN)_3O(pca)]^{2-}$ ion, isolated as compound **3**. In more alkaline solutions (pH = 11) this reaction did not proceed. One could therefore expect that the hydrolysis of the free nitrile should result in a free carboxylate and as a consequence should lead to compound **3**. Thus, the formation of product **2** could not have been accounted for, as observed in alkaline tetracyanooxomolybdate(IV) solutions. This suggests that the process of 2-pyrazinecarbonitrile hydrolysis follows binding of the nitrile to a molybdenum centre and is metal-assisted. This explanation is additionally supported by the fact that hydrolysis of free nitriles is generally slow [13,19] whereas the formation of **2** in high yield is relatively fast.

The obtained product **2** with coordinated 2-pyrazinecarboxylic acid indicates that the hydrolysis reaction is a two-stage process, which involves two consecutive attacks of hydroxide/water nucleophiles. The initial one produces 2-pyrazinehydroxyimine that may tautomerize to 2-pyrazinecarboxamide, which in turn generates 2-pyrazinecarboxylic acid upon further hydrolysis. Interestingly, the resulting acid undergoes slow rearrangement to a bidentate mode, which has been observed by means of UV–Vis spectroscopy. The reactions involved in the syntheses of **1**, **2** and **3** are summarized in Scheme 1.

3.2. Crystal structures

The crystal structure of **1** contains the $[Mo(CN)_4O(pcn)]^{2-}$ anion, two $[PPh_4]^+$ cations and two water molecules in the asymmetric part of the unit cell (Fig. 1). The packing of molecules in **1** is similar to that found in the crystal structure of $[PPh_4]_2[M(CN)_4O(pz)] \cdot 3H_2O$ [11]. The tetraphenylphosphonium

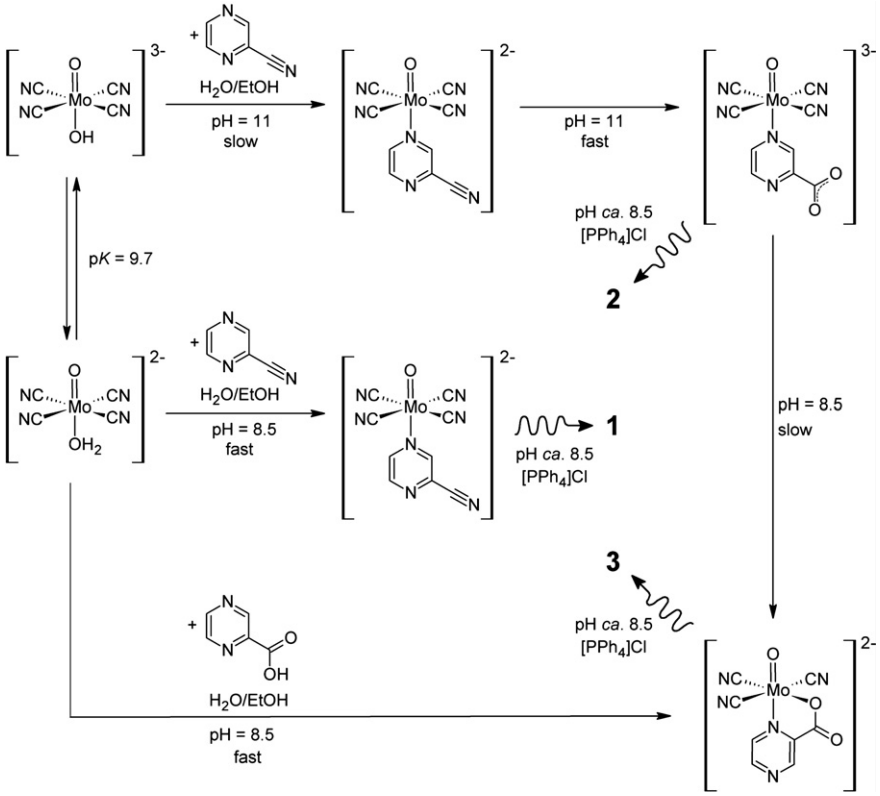

Scheme 1. Synthetic routes to Mo(IV) complexes with 2-pyrazinecarbonitrile and 2-pyrazinecarboxylate.

cations form infinite chains in the [100] direction, stabilized by alternating face-to-face and face-to-edge π stacking. Chains of $[PPh_4]^+$ cations, related by a translation along the *c* axis, separate layers of anions parallel to the *ac* plane. Water molecules O2 and O3 are located between the tetraphenylphosphonium chains and form a four-membered ring around the centre of symmetry. These water molecules make a network of hydrogen bonds that through bonds to cyano ligands connect pairs of tetracyanides from two separate layers. The observed hydrogen bond distances for **1** are: N1–O2 2.973 Å, N2–O3 2.904 Å, O2–O3 2.866 Å, O2–O3′ 2.808 Å. The cyano ligands are also involved in weak interactions to aromatic C–H groups. The $[Mo(CN)_4O(pcn)]^{2-}$ anions in **1**, related by a centre of symmetry, make pairs connected by weak hydrogen bonds, C6–H6···N3. The anion is also an acceptor in a weak hydrogen bond, C76–H76···N4, to the phenyl ring of a tetraphenylphosphonium cation.

The asymmetric unit cell in the crystal structure of **3** contains the $[Mo(CN)_3O(pca)]^{2-}$ anion, two $[PPh_4]^+$ cations and water molecules (Fig. 1). Only is water O21 well ordered with full occupancy, the other water molecules have occupancy factors equal to 0.5 and occupy four alternative positions. Similarly, as in the structure of **1**, the tetraphenylphosphonium cations form infinite chains in the [010] direction stabilized by alternating face-to-face and face-to-edge π stacking. Chains of $[PPh_4]^+$ cations related by a translation along the *c* axis separate layers of $[Mo(CN)_4O(pca)]^{2-}$ anions parallel to the *bc* plane. Water molecules O21, O22, O23 and O24 are located between tetraphenylphosphonium chains and make strong hydrogen bonds with one of the cyano ligands (C3–N3) and non-coordinated carboxylate oxygen O12. The observed hydrogen bond distances for **3** are: N3–O21 2.841 Å, O11–O24 2.772 Å, O12–O22 2.745 Å.

The structures of complex anions in **1** and **3** are presented in Figs. 2 and 3, and selected bond lengths and angles are listed in Table 2. The complex ions $[Mo(CN)_4O(pcn)]^{2-}$ and $[Mo(CN)_4O(Hpca)]^{2-}$ exhibit distorted octahedral geometries with four equatorial cyano ligands as well as oxo and cyanopyrazine ligands that occupy axial positions. The cyano ligands are displaced from the equatorial plane toward the nitrile ligand and the average O1–Mo–C angle is 100.68° for **1**. The average Mo–C and C–N bond distances in **1** were found to be 2.154 and 1.150 Å. In the case of salt **3**, the 2-pyrazinecarboxylate ligand coordinates in a bidentate mode to the molybdenum(IV) centre to afford a distorted octahedral geometry with a *trans*(*O*,*O*)-$[MoO_2C_3N]$ core (Fig. 3). The cyano ligands in **3** are more displaced from the equatorial plane away from the oxo ligand than in **1** and the average O1–Mo–C angle is 101.85°, whereas the N atom, occupying the fourth equatorial site, lies on the plane (the O1–Mo–N4 angle is 89.91°). The O11 atom is located *trans* to the Mo-oxo group. This indicates that O11 is coordinated first during the complex formation (replacing a labile aqua ligand) and this step is followed by the replacement of the cyano ligand by the N4 nitrogen atom. The average Mo–C and C–N bond distances were found to be the same as in tetracyano complexes and their averages are 2.159 and 1.156 Å, respectively. All observed distances within the anion are very similar to those found in other complexes of this type, $[Mo(CN)_3O(pic)]^{2-}$ [24] and $[Mo(CN)_3O(ensal)]^{2-}$ [3] (where Hpic = picolinic acid and Hensal = *N*-salicylideneethylenediamine).

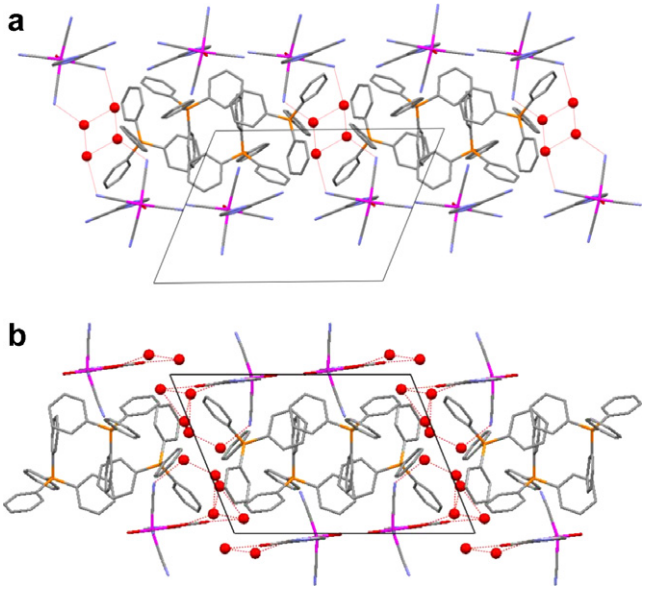

Fig. 1. Partial view of the structure of (a) $[PPh_4]_2[Mo(CN)_4O(pcn)] \cdot 2H_2O$ (**1**) along the *a* direction and (b) $[PPh_4]_2[Mo(CN)_3O(pca)] \cdot 3H_2O$ (**3**) along the *b* direction. H atoms are omitted for clarity. Hydrogen bonds with oxygen atoms as proton acceptors are represented by dotted lines.

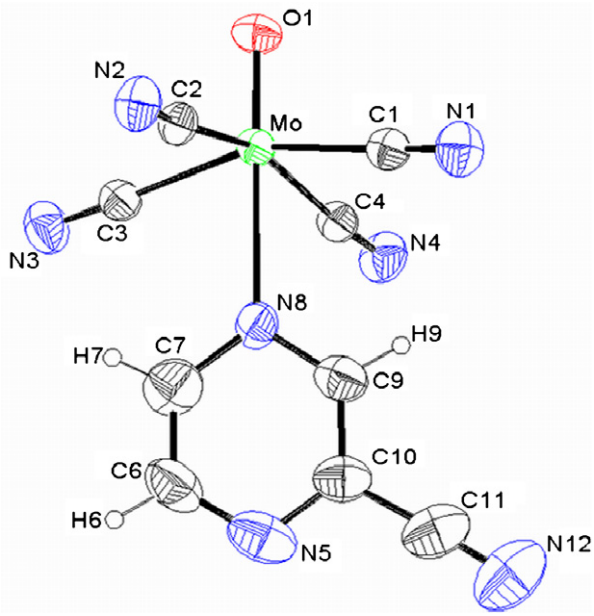

Fig. 2. Structure of $[Mo(CN)_4O(pcn)]^{2-}$ in **1** with the atom labelling scheme and 30% displacement ellipsoids.

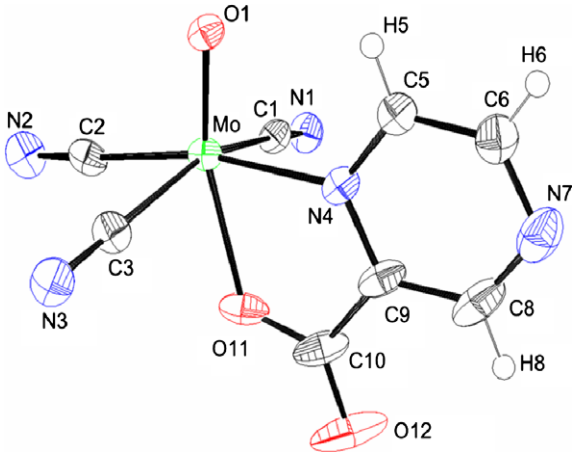

Fig. 3. Structure of $[Mo(CN)_3O(pca)]^{2-}$ in **3** with the atom labelling scheme and 50% displacement ellipsoids.

Table 2
Selected bond lengths (Å) and angles (deg) for $[PPh_4]_2[Mo(CN)_4O(pcn)] \cdot 2H_2O$ (**1**) and $[PPh_4]_2[Mo(CN)_3O(pca)] \cdot 3H_2O$ (**3**) with estimated standard deviations in parentheses

1		**3**	
Bond lengths			
Mo–O1	1.653(2)	Mo–O1	1.681(2)
Mo–C1	2.144(4)	Mo–C1	2.168(3)
Mo–C2	2.159(3)	Mo–C2	2.140(3)
Mo–C3	2.148(4)	Mo–C3	2.169(3)
Mo–C4	2.163(3)	Mo–N4	2.171(3)
Mo–N8	2.538(3)	Mo–O11	2.195(2)
C1–N1	1.161(5)	C1–N1	1.153(4)
C2–N2	1.144(4)	C2–N2	1.153(4)
C3–N3	1.146(4)	C3–N3	1.162(4)
C4–N4	1.145(4)	N4–C5	1.356(4)
N8–C9	1.358(5)	N4–C9	1.353(4)
N8–C7	1.413(6)	C5–C6	1.385(5)
C9–C10	1.372(6)	C6–N7	1.335(5)
N5–C10	1.349(6)	C8–N7	1.325(5)
N5–C6	1.400(7)	C8–C9	1.412(5)
C6–C7	1.345(7)	C9–C10	1.484(5)
C10–C11	1.463(8)	C10–O11	1.286(5)
C11–N12	1.171(7)	C10–O12	1.233(4)
Bond angles			
O1–Mo–C1	102.37(13)	O1–Mo–C1	101.37(10)
O1–Mo–C2	100.89(12)	O1–Mo–C2	103.55(11)
O1–Mo–C3	100.09(13)	O1–Mo–C3	100.64(11)
O1–Mo–C4	99.38(12)	O1–Mo–N4	89.91(10)
O1–Mo–N8	175.66(11)	O1–Mo–O11	161.80(10)
N1–C1–Mo	179.3(3)	N1–C1–Mo	175.6(3)
N2–C2–Mo	175.0(3)	N2–C2–Mo	175.2(3)
N3–C3–Mo	178.4(3)	N3–C3–Mo	174.1(3)
N4–C4–Mo	176.5(3)	O11–Mo–C1	80.03(10)
N8–Mo–C1	79.33(12)	O11–Mo–C2	94.65(11)
N8–Mo–C2	83.16(12)	O11–Mo–C3	80.74(10)
N8–Mo–C3	78.37(12)	O11–Mo–N4	71.92(10)
N8–Mo–C4	76.62(11)	O11–C10–C9	113.4(3)
N12–C11–C10	177.9(7)	O12–C10–C9	120.2(4)
		O11–C10–O12	126.4(4)

3.3. Spectroscopic properties

The IR spectra of compounds **1**, **2** and **3** exhibit the same absorption bands characteristic for $[PPh_4]^+$ cations as well as those assignable to the vibrations within the complex ions. These spectra within the 800–2200 cm^{-1} range are presented in Fig. 4. The absorption of ν(Mo–O) in **1** (979 cm^{-1}) is slightly higher in energy than that observed in **2** (973 cm^{-1}) and it is the highest of all ν(Mo–O) values reported to date for analogous $[Mo(CN)_4O(L)]^{n-}$ complexes with monodentate ligands L having a nitrogen atom in the *trans* position to the Mo–O bond (Table 3).

These high ν(Mo–O) absorptions in **1** and **2** suggest weak bonding of 2-pyrazinecarbonitrile and 2-pyrazinecarboxylic acid and are consistent with short Mo–O1 and long Mo–N8 bond distances, as determined in the X-ray crystal structures of **1** (Table 2). The position of ν(Mo–O) in **3** is 953 cm^{-1} which is in agreement with values reported for analogous tricyanooxo complexes with κ^2-*N*,*O* ligands [24,30,31]. In the C–N stretching region one strong band is observed for each salt, at 2091 cm^{-1} (**1**, **2**) and at 2104 cm^{-1} (**3**) (Fig. 4). In compound **1** this band is broader and it can be assigned to the stretching vibrations of four cyano ligands and the nitrile substituent in the aromatic ring. It is consistent with their similar C–N bond lengths (1.170 Å for the nitrile and 1.15 Å on average for the four cyano ligands). The observed energy of the stretching vibration of the nitrile substituent in **1** is lower than that of free 2-cyanopyrazine (2241 cm^{-1}), which indicates a weakening of the nitrile bond upon coordination [32]. The carbonyl groups in **2** and **3** are conspicuous by their characteristic absorptions at 1670, 1692 (**2**) and 1641 cm^{-1} (**3**) (Fig. 4).

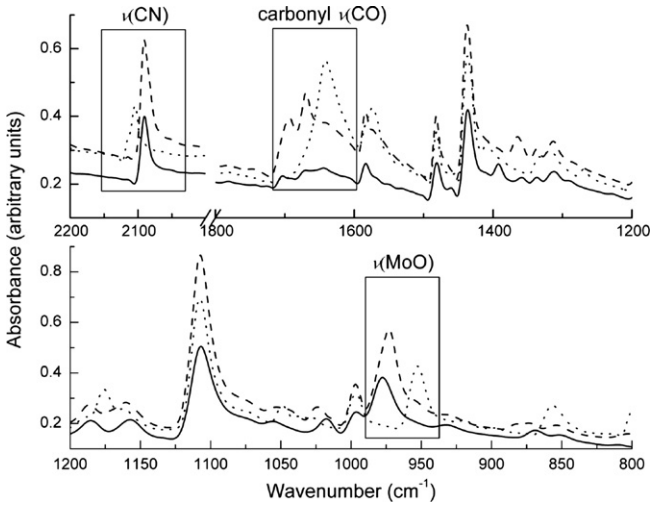

Fig. 4. The IR spectra of **1**(solid line), **2** (dashed line) and **3** (dotted line) in the 800–2200 cm^{-1} region.

Table 3
The IR absorptions, ν(Mo–O) (cm^{-1}), of tetracyanooxomolybdates(IV) with N-donor monodentate ligands *trans* to the Mo–O bond

Salt	ν(Mo–O)
$Cs_2Na[Mo(CN)_4O(N_3)]$	953[i]
$[N(PPh_3)_2]_2[Mo(CN)_4O(MeCN)]$	940[ii]
$[PPh_4]_2[Mo(CN)_4O(MeCN)]$	940[ii]
$[N(PPh_3)_2]_2[Mo(CN)_4O(en)]$[a]	958[iii]
$[N(PPh_3)_2]_2[Mo(CN)_4O(pn)]$[b]	958[iii]
$[PPh_4]_2[Mo(CN)_4O(tmen)]$[c]	937[iii]
$[PPh_4]_2[Mo(CN)_4O(tnmat)]$[d]	964[iii]
$[PPh_4]_2[Mo(CN)_4O(teat)]$[e]	960[iii]
$[PPh_4]_2[Mo(CN)_4O(hmta)]$[f]	925[iii]
$[PPh_4]_2[Mo(CN)_4O(CNEt)]$	964[iii]
$[PPh_4]_2[Mo(CN)_4O(CNCH_2Ph)]$	976[iii]
$[PPh_4]_2[Mo(CN)_4O(CNCH_2C_6H_4CH_2Br)]$	927[iii]
$[PPh_4]_2[Mo(CN)_4O(hmpa)]$[g]	954[iii]
$[PPh_4]_2[Mo(CN)_4O(NCH)] \cdot 5H_2O$	940[iv]
$[PPh_4]_2[Mo(CN)_4O(pz)] \cdot 3H_2O$[h]	974[v]
$[PPh_4]_2[Mo(CN)_4O(py)] \cdot 2H_2O$[j]	963[vi]
$[PPh_4]_2[Mo(CN)_4O(NH_3)] \cdot 2H_2O$	961[vii]
$[PPh_4]_2[Mo(CN)_4O(pcn)] \cdot 2H_2O$	979[viii]
$[PPh_4]_2[Mo(CN)_4O(Hpca)] \cdot 2H_2O$	973[viii]

[a] en = ethylenediamine.
[b] pn = 1,3-propylenediamine.
[c] tmen = tetramethylethylenediamine.
[d] tnmat = 2,4,6-trinitrilemethyleneamine-1,3,5-triazine.
[e] teat = 2,4,6-triethyleneamine-1,3,5-triazine.
[f] hmta = hexamethylenetetramine.
[g] hmpa = hexamethylphosphoramide.
[h] pz = pyrazine.
[j] py = pyridine.
[i] Refs. [25,26].
[ii] Ref. [8].
[iii] Ref. [27].
[iv] Ref. [28].
[v] Ref. [9].
[vi] Ref. [11].
[vii] Ref. [29].
[viii] This work.

Magnetic susceptibility measurements carried out by Gouy method at room temperature for salts **1**, **2** and **3** confirm that all the solids are diamagnetic.

The ^1H NMR spectra for solutions of **1** and **2** exhibit signals for the protons of the organic ligands and aromatic rings of the $[PPh_4]^+$ cations. The position of the phenyl resonances in the 7.74–8.01 ppm range is the same for both complexes. The considerable

difference between the complexes is observed for the signals of the substitued pyrazine ligands. The resonances of 2-pyrazinecarbonitrile protons in **1** are observed at 8.41, 8.47 and 8.89 ppm which are in agreement with various pyrazine nitrile derivatives [32,33]. The presence of the COOH substituent in the pyrazine ligand of **2** is manifested by the downfield shifts of positions of the heteroaromatic protons (8.72, 8.81 and 9.26 ppm) compared to **1**. These protons are less shielded in **2** as the electron density is more shifted towards the electron-withdrawing carboxylic group.

The reflectance and solution UV–Vis spectra of **1** and **2** contain bands for the tetraphenylphosphonium cations and the organic ligand (2-pyrazinecarbonitrile or 2-pyrazinecarboxylic acid) within the UV region (<350 nm) as well as bands of lower energy ascribed to d–d transitions. The visible part of these spectra closely resembles those of other $[Mo(CN)_4O(L)]^{n-}$ ions [9,11,30]. The intensities of all these bands are relatively low ($\varepsilon < 300\ dm^3\ mol^{-1}\ cm^{-1}$). However, in the case of **2** it is difficult to determine the molar absorptivities of the d–d bands in solution since the weakly bonded monodentate Hpca is slowly released and rebound in a bidentate mode as pca^-, forming complex **3**. Thus, minute impurities of **3** with very intense bands always affect the spectrum of **2**.

As is usually the case with molybdenum(IV) tricyanoxo complexes with organic ligands, the electronic spectrum of **3** is dominated by a high-intensity absorption attributable to a metal-to-ligand charge transfer (MLCT) transition between the molybdenum and carboxylate ligand [5,24,30]. Additionally, a band corresponding to a d–d transition, obscured by the intense MLCT transition, is observed as a shoulder (Fig. 5). The MLCT band is strongly solvatochromic whereas the position of the lower-energy d–d absorption only slightly depends on the solvent used for measurement, as a result of borrowing intensity from the adjacent MLCT band. The band positions with their corresponding intensities of **3** in various solvents are presented in Table 4. The shifts in the MLCT band energies (E_{abs}) correlate well with the Gutmann "acceptor number" (AN) of the solvent (Fig. 6) [34]. The explanation of the acceptor number dependence can be based on interactions between the coordinated organic ligand and solvent molecules. The greater the hydrophobic nature of solvent used, the stronger its interaction with the carboxylate, which results in the ligand's stabilization and lowering of its energy levels. Among all the solvents used the stabilization of the ligand is the highest for acetone and the lowest for water, which is in agreement with the observed E_{abs}(MLCT) values in these solvents.

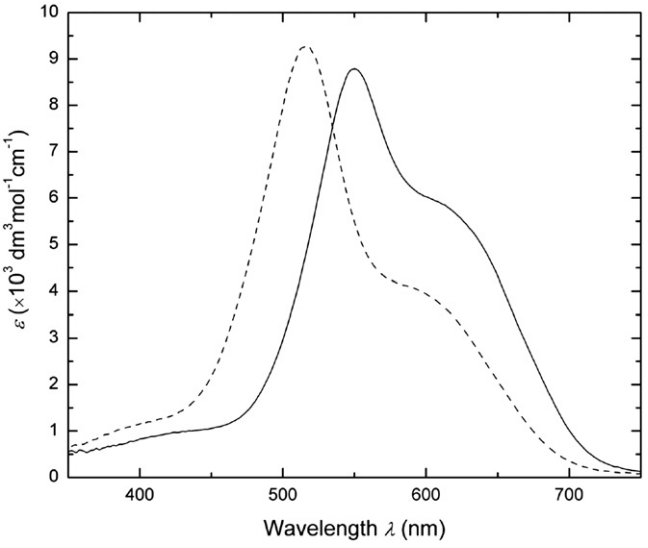

Fig. 5. Electronic spectrum of **3** in acetone (solid line) and EtOH (dashed line).

Table 4
Band positions and intensities of **3** in various solvents

Solvent	Acceptor number (AN)	λ, nm (ε, $\times 10^3\ dm^3\ mol^{-1}\ cm^{-1}$)
H_2O	54.8	483 570sh
MeOH	41.3	509 (8.1) 582sh
EtOH	37.1	516 (9.3) 585sh
2-PrOH	33.5	527 593sh
$CHCl_3$	23.1	532 (9.5) 596sh
CH_2Cl_2	20.4	532 (10.1) 595sh
MeCN	19.3	530 (9.8) 597sh
DMSO	19.3	539 (9.8) 598sh
DMF	16.0	546 (10.1) 604sh
Acetone	12.5	550 (8.8) 603sh

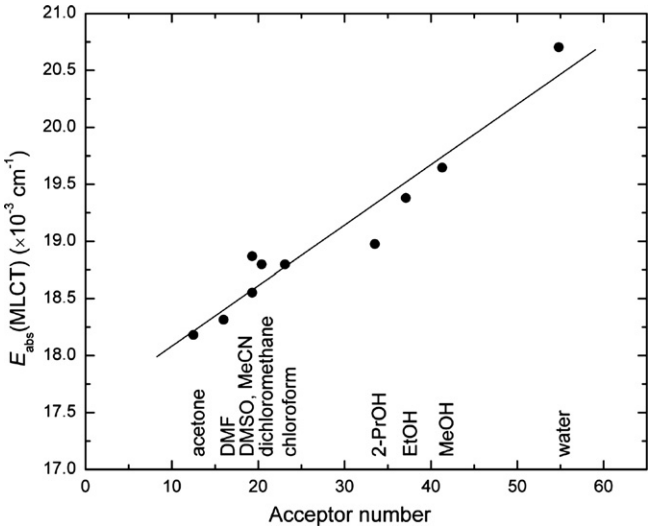

Fig. 6. Shifts in E_{abs}(MLCT) of **3** with acceptor number (AN). The correlation is $E_{abs}(\text{MLCT}, \times 10^{-3}\ cm^{-1}) = (0.053 \pm 0.0051)\text{AN} + (17.55 \pm 0.16) \times 10^{-3}$ with $R^2 = 0.97$.

4. Conclusion

This report has focused attention on the pH-dependent behavior of the molybdate(IV) system $[Mo(CN)_4O(OH)]^{3-}/[Mo(CN)_4O(H_2O)]^{2-}$ in the presence of 2-pyrazinecarbonitrile. Crystallographic and spectroscopic data have revealed that two complexes, $[Mo(CN)_4O(pcn)]^{2-}$ and $[Mo(CN)_4O(Hpca)]^{2-}$, are obtainable in this system; the former via a pure substitutional synthetic route and the latter as a result of metal-assisted nitrile hydrolysis. Interestingly, the resulting acid (Hpca) undergoes slow rearrangement to a bidentate mode yielding $[Mo(CN)_3O(pca)]^{2-}$. The coordination versatility of the 2-pyrazinecarboxylate ion has been demonstrated in the isolated $[Mo(CN)_3O(pca\text{-}\kappa^2\text{-}N,O)]^{2-}$ and $[Mo(CN)_4O(Hpca)]^{2-}$ products.

Appendix A. Supplementary data

CCDC 675046 and 675047 contain the supplementary crystallographic data for **1** and **3**. These data can be obtained free of charge

via http://www.ccdc.cam.ac.uk/conts/retrieving.html, or from the Cambridge Crystallographic Data Centre, 12 Union Road, Cambridge CB2 1EZ, UK; fax: (+44) 1223-336-033; or e-mail: deposit@ccdc.cam.ac.uk. Supplementary data associated with this article can be found, in the online version, at doi:10.1016/j.poly.2008.04.048.

References

[1] B. Burda, J. Burgess, S.A. Parsons, A. Samotus, J. Szklarzewicz, Transit. Met. Chem. 20 (1995) 291.
[2] J. Szklarzewicz, A. Samotus, J. Burgess, J. Fawcett, D.R. Russell, J. Chem. Soc., Dalton Trans. (1995) 3057.
[3] B. Nowicka, A. Samotus, J. Szklarzewicz, F. Heinemann, H. Kisch, J. Chem. Soc., Dalton Trans. (1998) 4009.
[4] J. Szklarzewicz, Transit. Met. Chem. 26 (2001) 189.
[5] J. Szklarzewicz, A. Samotus, Transit. Met. Chem. 27 (2002) 769.
[6] A. Midura, J. Szklarzewicz, W. Łasocha, Transit. Met. Chem. 28 (2003) 918.
[7] H. Arzoumanian, J.F. Petrignani, M. Pierrot, F. Ridouane, J. Sanchez, Inorg. Chem. 27 (1988) 3377.
[8] H. Arzoumanian, M. Pierrot, F. Ridouane, J. Sanchez, Transit. Met. Chem. 16 (1991) 422.
[9] D. Matoga, J. Szklarzewicz, A. Samotus, J. Burgess, J. Fawcett, D.R. Russell, Polyhedron 19 (2000) 1503.
[10] J. Szklarzewicz, D. Matoga, A. Samotus, J. Burgess, J. Fawcett, D.R. Russell, Croat. Chem. Acta 74 (2001) 529.
[11] D. Matoga, J. Szklarzewicz, A. Samotus, K. Lewiński, J. Chem. Soc., Dalton Trans. (2002) 3587.
[12] D. Matoga, J. Szklarzewicz, J. Fawcett, Polyhedron 24 (2005) 1533.
[13] M.L. Tobe, J. Burgess, in: Inorganic Reaction Mechanisms, Addison Wesley Longman Limited, Essex, 1999 (Chapter 10).
[14] I.M. Klotz, D.M. Kurtz Jr., Chem. Rev. 94 (1994) 567.
[15] G.B. Richter-Addo, P. Legzdins, J. Burstyn, Chem. Rev. 102 (2002) 857.
[16] J.A. Olabe, L.D. Slep, in: J.A. McCleverty, T.J. Meyer (Eds.), Comprehensive Coordination Chemistry II, vol. 2, Elsevier, Oxford, UK, 2004 (Chapter 1.31).
[17] A.J.L. Pombeiro, V.Y. Kukushkin, in: J.A. McCleverty, T.J. Meyer (Eds.), Comprehensive Coordination Chemistry II, vol. 1, Elsevier, Oxford, UK, 2004, p. 639 (Chapter 1.34).
[18] E.C. Constable, in: Metals and Ligand Reactivity, Springer, Weinheim, Germany, 1995, p. 65 (Chapter 4.2).
[19] V.Y. Kukushkin, A.J.L. Pombeiro, Inorg. Chim. Acta 358 (2005) 1.
[20] V.Y. Kukushkin, A.J.L. Pombeiro, Chem. Rev. 102 (2002) 1771.
[21] A. Samotus, M. Dudek, A. Kanas, J. Inorg. Nucl. Chem. 37 (1975) 943.
[22] A. Altomare, G. Cascarano, G. Giacovazzo, A. Guagliardi, M.C. Burla, G. Polidori, M. Camalli, J. Appl. Crystallogr. 27 (1994) 435.
[23] G.M. Sheldrick, SHELXL 97, University of Göttingen, Germany, 1997.
[24] J. Szklarzewicz, A. Makula, D. Matoga, J. Fawcett, Inorg. Chim. Acta 358 (2005) 1749.
[25] S.S. Basson, J.G. Leipoldt, I.M. Potgieter, A. Roodt, Inorg. Chim. Acta 103 (1985) 121.
[26] A. Roodt, J.G. Leipoldt, S.S. Basson, I.M. Potgieter, Transit. Met. Chem. 15 (1990) 439.
[27] H. Arzoumanian, A. Bouraoui, V. Lazzeri, M. Rajzmann, H. Teruel, New J. Chem. 16 (1992) 965.
[28] J.P. Smit, W. Purcell, A. Roodt, J.G. Leipoldt, J. Chem. Soc., Chem. Commun. (1993) 1388.
[29] J. Szklarzewicz, D. Matoga, K. Lewiński, Inorg. Chim. Acta 360 (2007) 2002.
[30] A. Samotus, J. Szklarzewicz, D. Matoga, Bull. Pol. Acad. Sci. Chem. 50 (2002) 145.
[31] J. Szklarzewicz, Transit. Met. Chem. 26 (2001) 1.
[32] SDBSWeb: <http://riodb01.ibase.aist.go.jp/sdbs/> (National Institute of Advanced Industrial Science and Technology, 2007-11-05).
[33] V. Opletalova, A. Patel, M. Boulton, A. Dundrova, E. Lacinova, M. Prevorova, M. Appeltauerova, M. Coufalova, Collect. Czech. Chem. Commun. 61 (1996) 1093.
[34] V. Gutmann, in: The Donor–Acceptor Approach to Molecular Interactions, Plenum Press, New York, 1980, p. 27 (Chapter 2.3).

Polyhedron 27 (2008) 2650–2654

Contents lists available at ScienceDirect

Polyhedron

journal homepage: www.elsevier.com/locate/poly

Mono- and polynuclear Cu(II) coordination compounds that contain diazine ligands

Jamie L. Manson [a,*], Jeffrey Donovan [a], Brendan Twamley [b]

[a] Department of Chemistry and Biochemistry, Eastern Washington University, 226 Science, 526 5th Street, Cheney, WA 99004, USA
[b] University Research Office, University of Idaho, Moscow, ID 83844, USA

ARTICLE INFO

Article history:
Received 19 February 2008
Accepted 8 May 2008
Available online 18 June 2008

Keywords:
Low-dimensional
Copper
Diazine, coordination polymer
Molecular magnet

ABSTRACT

$Cu(OTf)_2(2\text{-mepyz})_2(H_2O)_2$ (2-mepyz = 2-methylpyrazine; $OTf^- = CF_3SO_3^-$ = triflate), **1**, and $Cu(OTf)_2(H_2O)_2(pyz)$ (pyz = pyrazine), **2**, consist of monomeric and polymeric structures, respectively. Both compounds contain octahedral Cu(II) metal centers surrounded by *trans*-coordinated OTf^-, H_2O, and diazines, either 2-mepyz in the case of **1** or pyz in **2**. In **1**, O–H···O(triflate) hydrogen bonds link CuO_4N_2 monomers into quasi-1D chains which are joined via O–H···N interactions to afford a three-dimensional (3D) network. Pyz ligands in **2** link CuO_4N_2 octahedra into linear chains similar to $Cu(NO_3)_2(pyz)$. Magnetically, neither **1** or **2** show indications for long-range magnetic ordering (LRO) above 2 K. Least-squares fits of the magnetic susceptibility data, $\chi(T)$, to a Bonner–Fisher uniform chain model gave $2J/k_B = -0.005(1)$ and $-6.0(1)$ K for compounds **1** and **2**, respectively, indicative of negligible and moderate antiferromagnetic coupling between spin-1/2 Cu(II) ions. Inter-chain magnetic interactions seem to be negligible for both systems.

© 2008 Elsevier Ltd. All rights reserved.

1. Introduction

Low-dimensional molecule-based magnets comprised of spin-1/2 ions represent an area of intense research interest [1–8]. Spin-1/2 ions such as Cu(II) have been used extensively owing to the lack of single-ion anisotropy leading to more easily interpretable magnetic behaviors. The single spin involved is also more amenable to theoretical investigations.

From a crystal engineering perspective, there are many ways in which the paramagnetic spin-bearing units can be arranged in the solid state which ultimately depends on the choice of organic synthons. The coordinative properties of the synthons dictate the number of ligands to be used, geometrical constraints, and the number of synthons that will attach to the metal ion. Owing to its good Lewis basicity, pyrazine (pyz) is arguably one of the most successfully utilized synthons in crystal design. As hydrogen atoms in the parent pyz molecule are replaced by alkyl groups (Scheme 1), the basicity decreases due to increased steric hindrance, however, there are numerous compounds known to possess mono- or bidentate diazine derivatives that are coordinated to Cu(II) ions. Examples that possess either bridging or mono-coordinate dimethyl-substituted pyrazine ligands include $Cu(NCO)_2(2\text{-mepyz})_2$ [9], $Cu(NO_3)_2(2\text{-mepyz})$ [10], $CuBr_2(2,3\text{-me}_2\text{pyz})$ [11], $Cu_2(HCO_2)_4(2,3\text{-me}_2\text{pyz})$ [12], $CuCl_2(2,5\text{-me}_2\text{pyz})$ [13], $CuCl_2(2,5\text{-me}_2\text{pyz})(CH_3CN)$ [14], $CuCl_2(2,6\text{-me}_2\text{pyz})$ [13], and $[Cu(2,6\text{-me}_2\text{pyz})_4]SiF_6$ [15].

Structural modification can also be achieved by varying the size, molecular shape and charge of the counter-anion. Excluding halides, numerous anions (including coordinating and weakly-coordinating types) such as ClO_4^- [2,16], BF_4^- [4], NO_3^- [10], PF_6^- [16], SO_4^{2-} [17], $CH_3CO_2^-$ [18], and many others are frequently employed in the design of functional molecule-based solids. In our quest to self-assemble novel magnetic materials comprised of molecular building blocks we have combined triflate anions with pyrazine and 2-mepyz. These efforts lead to new molecular and polymeric structures, namely $Cu(OTf)_2(2\text{-mepyz})_2(H_2O)_2$ (**1**) and $Cu(OTf)_2(H_2O)_2(pyz)$ (**2**), respectively, where mono-coordinate 2-mepyz or bridging pyz ligands are involved. Our continued use of pyz and its various substituted variants is driven by our desire to understand and ultimately control the magnetic behavior of complex magnetic solids.

2. Experimental

2.1. Synthesis

Compound **1** was prepared by slow dropwise addition of 2-methylpyrazine (1.52 mmol, 0.1435 g) to a 5-mL CH_3CN solution of $Cu(OTf)_2$ (0.762 mmol, 0.2758 g) to afford a deep blue solution. Crystalline plates suitable for X-ray structure determination were obtained by slow evaporation of the solvent over a 5-week period. The material was collected by vacuum filtration and gently dried (0.3215 g, 72% yield). Compound **2** was synthesized by dissolving each reactant, $Cu(OTf)_2$ (0.781 mmol, 0.2846 g) and pyrazine (1.56 mmol, 0.1260 g), in 5 mL of a 50:50 v:v mixture containing

* Corresponding author. Tel.: +1 509 359 2878; fax: +1 509 359 6973.
E-mail address: jmanson@mail.ewu.edu (J.L. Manson).

0277-5387/$ - see front matter © 2008 Elsevier Ltd. All rights reserved.
doi:10.1016/j.poly.2008.05.007

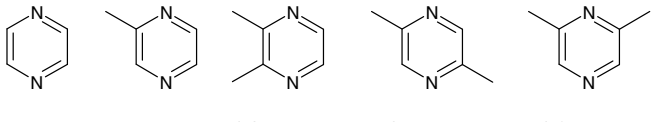

Scheme 1. Parent pyrazine molecule and its dimethyl-substituted variants.

H_2O/CH_3CN. The two solutions were gently mixed to give a dark blue solution from which large pale blue crystals of **2** were obtained upon slow evaporation of the solvent over a period of 2 months. The crystals were collected by vacuum filtration and carefully dried to produce 0.3222 g of solid in 86% yield.

2.2. X-ray crystallography

Crystals of compound **1** and **2** were removed from the flask, a suitable crystal was selected of each, attached to a glass fiber and data were collected at 297(2) K using a Bruker/Siemens SMART APEX X-ray diffractometer (Mo Kα radiation, $\lambda = 0.71073$ Å). Data were measured using omega scans of 0.3° per frame for 5 s, and a partial and full sphere of data was collected. A total of 1324 and 2400 frames were collected with a final resolution of 0.83 and 0.77 Å for **1** and **2**, respectively. Cell parameters were retrieved using SMART [19] software and refined using SAINTPLUS [20] on all observed reflections. Data reduction and correction for Lp and decay were performed using the SAINTPLUS software. Absorption corrections were applied using SADABS [21]. Structures were solved by direct methods and refined by least-squares method on F^2 using the SHELXTL [22] program package. Analysis of systematic absences led to the solution and refinement of the structures of **1** and **2** in the space groups $P2_1/n$ (#14) and $C2/c$ (#15), respectively. The triflate anion in **1** was found to be disordered in two positions (70:30%) and only the non-carbon and oxygen atoms were refined anisotropically. All non-hydrogen atoms were refined anisotropically in **2**. No decomposition was observed during data collection. Details of the data collection and refinement are given in Table 1 and selected bond lengths and angles can be found in Table 2. Further details are provided in the Supplementary data.

Table 1
Crystallographic data and structure refinement parameters

	1	2
Formula	$C_{12}H_{16}CuF_6N_4O_8S_2$	$C_6H_8CuF_6N_2O_8S_2$
Molecular weight	585.95	477.80
Crystal system, space group	monoclinic, $P2(1)/n$	monoclinic, $C2/c$
a (Å)	11.5197(10)	13.002(2)
b (Å)	7.5615(6)	6.8016(12)
c (Å)	12.6908(11)	18.261(3)
β (°)	100.288(2)°	105.299(3)
V (Å^3)	1087.67(16)	1557.7(4)
Z	2	4
T (K)	297(2)	298(2)
λ (Å)	0.71073	0.71073
ρ_{calc} (Mg/m^3)	1.789	2.037
μ (mm^{-1})	1.294	1.779
$F(000)$	590	948
Crystal size (mm^3)	0.64 × 0.54 × 0.05	0.43 × 0.32 × 0.09
θ Range (°)	2.20 to 25.25	2.31 to 27.46
Index ranges	$-13 \leqslant h \leqslant 13$, $-9 \leqslant k \leqslant 6$, $-15 \leqslant l \leqslant 13$	$-16 \leqslant h \leqslant 16$, $-8 \leqslant k \leqslant 8$, $-23 \leqslant l \leqslant 23$
Number of reflections collected	9024	10551
Number of independent reflections (R_{int})	1965 (0.0245)	1792 (0.0266)
Data/restraints/parameters	1965/20/178	1792/0/115
Goodness-of-fit	1.080	1.042
R_1[a] [$I > 2\sigma(I)$]	0.0652	0.0323
wR_2[a] [$I > 2\sigma(I)$]	0.1834	0.0851
Largest difference in peak, hole (e Å^{-3})	0.824, −0.941	0.532, −0.243

[a] $R_1 = \sum||F_o| - |F_c||/\sum|F_o|$; $wR_2 = \{\sum[w(F^2_o - F^2_c)^2]/\sum[w(F^2_o)^2]\}^{1/2}$.

Table 2
Selected bond lengths (Å) and bond angles (°) for $Cu(OTf)_2(2\text{-mepyz})_2(H_2O)_2$ (**1**) and $Cu(OTf)_2(H_2O)_2(pyz)$ (**2**)

1		2	
Cu(1)–N(1)	2.011(4)	Cu(1)–N(1)	2.024(2)
Cu(1)–O(3)	1.968(3)	Cu(1)–N(4A)	2.024(2)
Cu(1)–O(4A)	2.420(4)	Cu(1)–O(1)	1.966(2)
Cu(1)–O(4B)	2.423(6)	Cu(1)–O(2)	2.402(2)
S(1A)–O(1A)	1.428(8)	S(1)–O(2)	1.434(2)
S(1A)–O(2A)	1.423(8)	S(1)–O(3)	1.425(2)
S(1A)–O(4A)	1.443(6)	S(1)–O(4)	1.422(2)
S(1A)–C(6A)	1.816(9)	S(1)–C(5)	1.821(3)
C(6A)–F(1A)	1.39(1)	C(5)–F(1)	1.323(3)
C(6A)–F(2A)	1.31(1)	C(5)–F(2)	1.306(4)
C(6A)–F(3A)	1.27(1)	C(5)–F(3)	1.315(4)
N(1)–C(2)	1.332(6)	N(1)–C(2)	1.329(2)
C(1)–C(2)	1.382(7)	C(2)–C(3)	1.386(3)
N(1)–Cu(1)–N(1A)	180	N(1)–Cu(1)–N(4A)	180
N(1)–Cu(1)–O(3)	89.5(2)	N(1)–Cu(1)–O(1)	90.68(4)
N(1)–Cu(1)–O(4A)	85.7(2)	O(2)–Cu(1)–O(2A)	178.45(8)
O(3)–Cu(1)–O(3A)	180	N(4A)–Cu(1)–O(1)	89.32(4)
O(4A)–Cu(1)–O(4AA)	180	N(4A)–Cu(1)–O(2)	89.22(4)
O(3)–Cu(1)–O(4A)	84.7(2)	O(1)–Cu(1)–O(1A)	178.63(8)
C(2)–N(1)–Cu(1)	121.1(3)	C(2)–N(1)–Cu(1)	120.9(1)
S(1A)–O(4A)–Cu(1)	151.8(5)	S(1)–O(2)–Cu(1)	134.2(1)
O(2A)–S(1A)–O(4A)	116.4(5)	O(2)–S(1)–O(3)	114.5(1)
F(1A)–C(6A)–F(2A)	101.3(10)	F(1)–C(5)–F(2)	109.0(3)
C(2)–N(1)–C(3)	117.8(4)	C(2)–N(1)–C(2A)	118.2(2)

2.3. Magnetic properties

A Quantum Design MPMS-5XL ac/dc SQUID magnetometer equipped with an RSO transport was used to measure the temperature-dependence of the magnetization. Appropriate amounts of polycrystalline samples of **1** and **2** were loaded into pharmaceutical gelatin capsules, placed inside a plastic drinking straw and affixed to the end of a carbon fiber rod. Samples were mounted in the magnetometer at 295 K and zero-field cooled to 2 K. The magnetic field was charged to 1-kOe and data collected upon warming to room temperature. All magnetic data were corrected for core diamagnetism using Pascal's constants.

3. Results and discussion

The crystal structures of **1** and **2** were determined by conventional X-ray crystallographic techniques and both Cu(II) coordination spheres are shown in Fig. 1. Both compounds feature identical coordination environments with donor atoms of the same type positioned *trans* to one another. The Cu(II) ions in both compounds exhibit the usual Jahn-Teller (4+2) distortion with the Cu–O(triflate) bond distances the longest at 2.420(4) and 2.423(6) Å for **1** and 2.402(2) Å for **2**. The Cu(II) ion in **1** lies on an inversion center while the metal and ligand atoms N(1) and N(4) occupy the two-fold rotation axis in **2**. The CuO_4N_2 octahedron is significantly more distorted in **1** than in **2** with the bond angles O(3)–Cu(1)–O(4A) = 84.7(2)° and O(1)–Cu(1)–O(2) = 88.21(7)°, respectively, exhibiting the greatest deviation from the ideal 90° angle. All observed geometric parameters found for the 2-mepyz and parent pyz ligands in **1** and **2** are in agreement with previously reported structures [2,4,9–15].

The methyl substituents in **1** are distal to the Cu–N coordinate bond which prevents ligation of the second nitrogen atom, thus limiting the lattice dimensionality to molecular. Each molecule is linked to nearest-neighbors through O(1A)···H(3A)–O(3) hydrogen

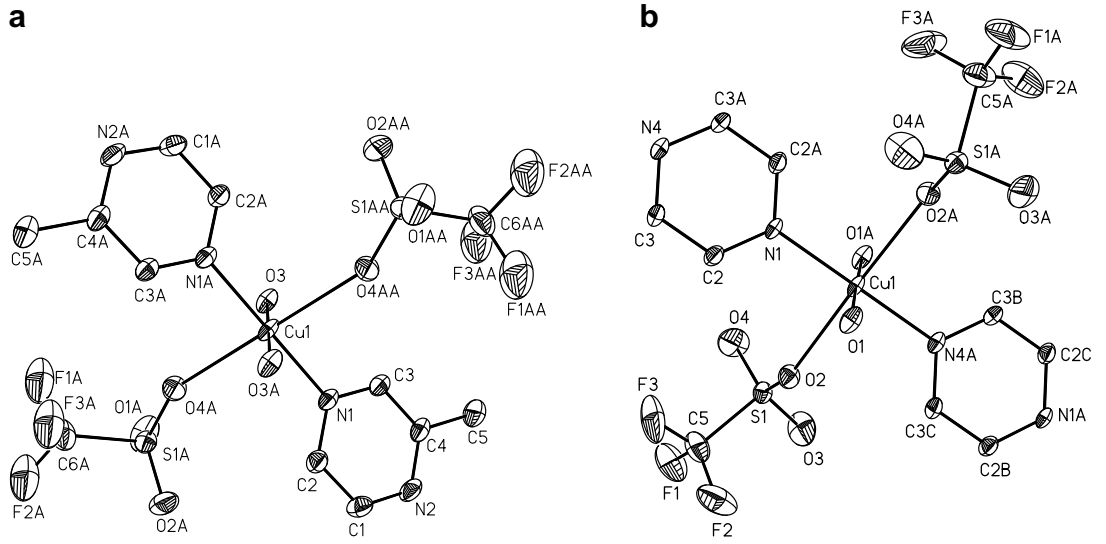

Fig. 1. Thermal displacement diagrams (30%) and atom labeling schemes for (a) $Cu(OTf)_2(2\text{-mepyz})_2(H_2O)_2$ (**1**) and $Cu(OTf)_2(H_2O)_2(pyz)$ (**2**). Only the highest occupied triflate molecule (70%) is shown in (a). Hydrogen atoms have been omitted for clarity.

bonds as shown in Fig. 2a to form a chain that runs along the *b*-axis. These pseudo-chains are linked further by additional N(2)···H(3B)–O(3) hydrogen bonds to form sheets (Fig. 2b) that lie in the *bc*-plane. This particular packing motif is interesting as it produces a distorted triangular lattice where two edges are comprised of N(2)···H(3B)–O(3) hydrogen bonds with a Cu···Cu distance of ca. 8.6 Å. The remaining edge is the O(1A)···(3A)–O(3) bond and is ~1 Å shorter with a Cu···Cu distance of ca. 7.6 Å. The vertices of each triangle are occupied by Cu(II) ions.

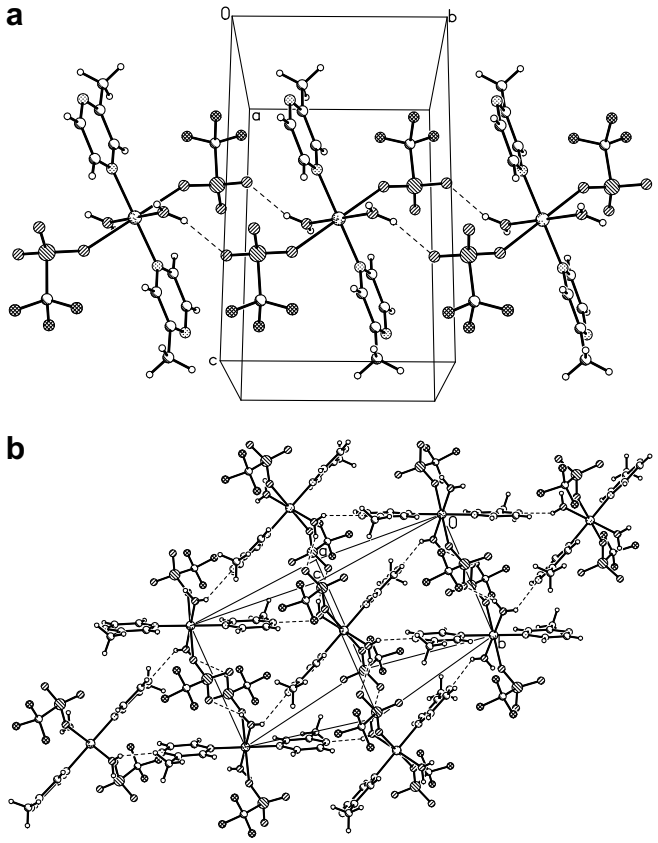

Fig. 2. (a) Portion of a hydrogen bonded chain found in **1**. Only the OTf^- anion with the highest occupancy is shown for clarity. (b) Molecular packing arrangement of **1** viewed approximately perpendicular to the (101) plane. Dashed lines indicate intermolecular hydrogen bonds.

For compound **2**, pyrazine ligands join CuO_4N_2 octahedra into a linear chain as shown in Fig. 3a, giving intrachain Cu···Cu separations of 6.8016(2) Å (*i.e.*, the length of the *b*-axis). The chains are linked via O(3)···H(1B)–O(1) and O(4)···H(1A)–O(1) hydrogen bonds to afford sheets in the *ab*-plane (Fig. 3b) which stack along the *c*-direction. All pyrazine rings are co-planar and align exactly parallel with the *c*-axis, corresponding to a O(1)–Cu(1)–N(1)–C(2) torsion angle of 62.4(1)°. From Fig. 3b it can be seen that hexagonal channels exist in **2** owing to H-bond formation between both protons of the H_2O molecule and triflate oxygen atoms with pyz ligands passing through the center.

In addition to **1** and **2**, several other Cu(II) coordination complexes also exist that contain either coordinated or non-coordinated triflate anions. For example, a search of the Cambridge Crystal Database [23] yielded one molecular complex, namely $[Cu(2,2'\text{-bipy})(H_2O)_2(OTf)_2]$ (bipy = bipyridine) [24], that has a similar CuO_4N_2 core. This complex is composed of coordinated 2,2′-bipy, two triflate anions and two H_2O ligands where the latter aqua ligands are *cis* to one another and occupy the same plane as the chelated 2,2'-bipy ligand. Other related complexes that contain Cu(II) ions and 2-mepyz ligands include $[Cu(2\text{-mepyz})_4(H_2O)X]X$ ($X = NO_3^-$ or ClO_4^-) [25,26], $[Cu(2\text{-mepyz})_4(ClO_4)_2]$[27] and $[Cu(2\text{-mepyz})_2(H_2O)_2(ClO_4)_2]$ [28].

The bulk magnetic properties of **1** and **2** were determined by conventional SQUID magnetometry and the data plotted as χ versus T are shown in Fig. 4. While data was obtained between 2 and 300 K only the region below 80 K are shown to highlight the differing magnetic behavior. Compound **1** is essentially paramagnetic and does not show a maximum in χ versus T down to 2 K suggesting the presence of very weak magnetic interactions. In order to determine the extent of interaction between Cu(II) sites the data were fitted to a Curie–Weiss law, $\chi = g^2S(S+1)/8(T-\theta)$, where g is the Landé value and θ is the Weiss constant. The resulting least-squares fit between 2 and 300 K yielded $g = 2.127(1)$ and $\theta = +0.27(7)$ K with the slightly positive θ-value indicating a very weak ferromagnetic coupling. In order to verify whether the interaction along either the N(2)···H(3B)–O(3) or O(1A)···H(3A)–O(3) pathway is plausible, we fitted the same χ versus T data to a Bon-

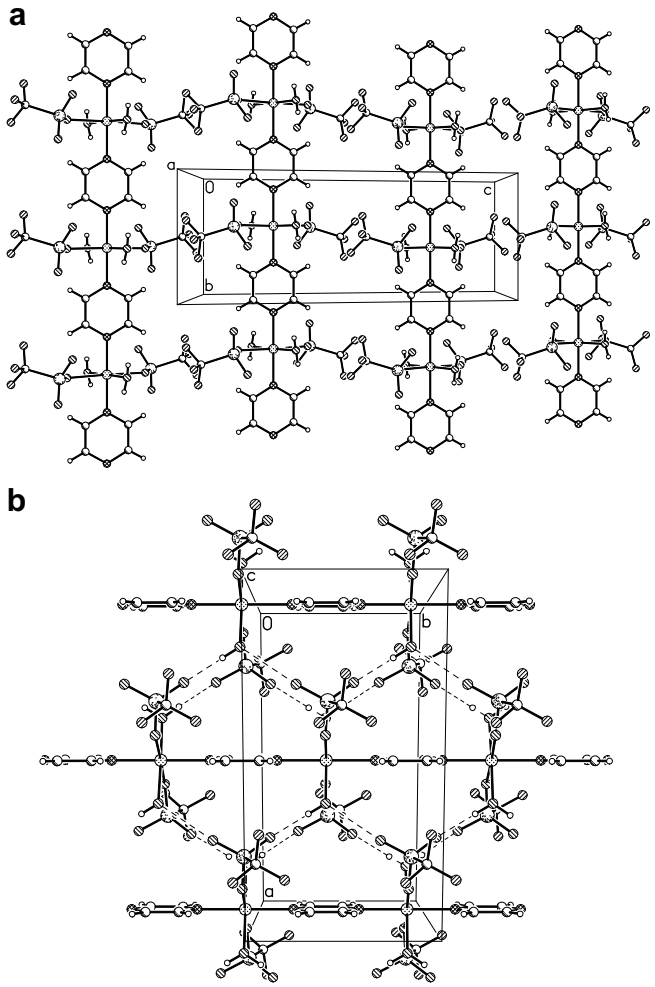

Fig. 3. (a) Crystal packing of linear chains in compound **2** viewed down the *a*-axis. (b) Packing of chains in **2** viewed parallel to the *c*-axis.

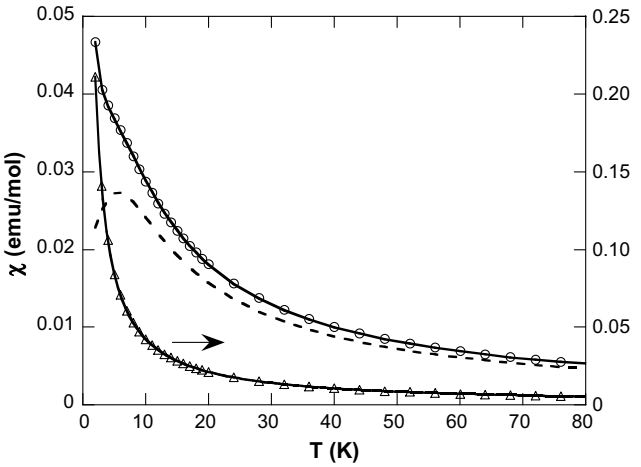

Fig. 4. Temperature-dependence of the magnetic susceptibility for **1** (△) and **2** (○) measured in a 1-kOe external field. The solid lines represent least-squares fits of the data as described in the text. The dashed line is the calculated Bonner–Fisher magnetic susceptibility for compound **2** using the same parameters as previously described however for $\rho = 0$.

ner–Fisher [24] chain model which gave good agreement for $g = 2.128(1)$ and $2J/k_B = -0.005(1)$ K. The Curie–Weiss and Bonner–Fisher results reflect ambiguity in the sign of the very weak, and possibly negligible, interaction. A plot of χT versus T is essentially invariant as the temperature changes, consistent with the apparently negligible exchange interaction.

In contrast to **1**, the temperature-dependence of χ for **2** does show indication for more significant magnetic coupling. As the data are plotted on a per mole basis, the susceptibility of **2** is reduced by a factor of ~5 owing to the presence of stronger antiferromagnetic interactions. While a maximum in χ versus T is not detectable there is clearly anomalous behavior below 10 K. From Fig. 4 it can also be seen that χ versus T rises much more slowly for **2** than it does for **1**, again suggestive of a stronger magnetic interaction. A similar fit of these data to a Curie–Weiss law ($T \geqslant 20$ K) afforded $g = 2.152(1)$ and $\theta = -2.5(1)$ K which suggests antiferromagnetic coupling between Cu(II) spins. Because the structure of **2** consists of polymeric Cu-pyz-Cu chains, we also fitted χ versus T over the entire temperature range to a Bonner–Fisher [28] chain model compensating for any possible spin-1/2 paramagnetic impurity, ρ, in the sample. This fit yielded excellent agreement for $g = 2.133(1)$, $2J/k_B = -6.0(1)$ K, temperature-independent paramagnetism (TIP) = 60×10^{-6} emu/mol and $\rho = 0.0296(1)$. Omission of ρ from the fit would lead to a broad maximum at ~5.6 K (dashed line in Fig. 4) using the same g, $2J$ and TIP values. Close inspection of χ versus T between 2 and 5 K reveals a discontinuous feature that, had an impurity not been present, would have likely displayed a broad maximum associated with short-range spin correlations. We believe the chain model to be the most appropriate because the $d_{x^2-y^2}$ magnetic orbital occupies the CuN_2O_2 (oxygen from H_2O ligands) plane; the lobe directed along the N–Cu–N axis subsequently overlaps with the $2p_z$ orbital of the pyz bridge. An additional inter-chain interaction as mediated by $H_2O\cdots OTf^-$ hydrogen bonds [Cu···Cu = 7.337 Å] does not appear plausible due to overlap between the other lobe of the $d_{x^2-y^2}$ magnetic orbital and the non-magnetic d_{z^2} orbital of next-nearest-neighbor Cu(II) sites. This claim is substantiated by the fact that inclusion of a mean-field correction term, zJ' [29], does not improve the quality of the fit.

To conclude, we have synthesized and structurally and magnetically characterized two new Cu(II) coordination compounds. Both systems contain triflate ions that participate extensively in hydrogen bond interactions. While triflate is generally considered to be a weakly-coordinating anion, it does occupy two sites of the Cu(II) coordination sphere which reduces the lattice (and spin) dimensionality in both cases. Likewise, H_2O ligands take up two additional sites. Future synthetic efforts will be to employ non-aqueous media in an effort to eliminate the possibility of H_2O coordination and subsequently increase the lattice and spin dimensionality.

Acknowledgements

This work was supported by an award from Research Corporation (J.L.M.). The Bruker (Siemens) SMART APEX diffraction facility was established at the University of Idaho with the assistance of the NSF-EPSCoR program and the M. J. Murdock Charitable Trust, Vancouver, WA, USA.

Appendix A. Supplementary data

CCDC 685979 and 685980 contain the supplementary crystallographic data for **1** and **2**. These data can be obtained free of charge via http://www.ccdc.cam.ac.uk/conts/retrieving.html, or from the Cambridge Crystallographic Data Centre, 12 Union Road, Cambridge CB2 1EZ, UK; fax: (+44) 1223-336-033; or e-mail: deposit@ccdc.cam.ac.uk. Supplementary data associated with this article can be found, in the online version, at doi:10.1016/j.poly.2008.05.007.

References

[1] J.L. Manson, T. Lancaster, J.A. Schlueter, S.J. Blundell, M.L. Brooks, F.L. Pratt, C.L. Nygren, H.-J. Koo, D. Dai, M.-H. Whangbo, Inorg. Chem. 46 (2007) 213.
[2] T. Lancaster, S.J. Blundell, M.L. Brooks, P.J. Baker, F.L. Pratt, J.L. Manson, M.M. Conner, F. Xiao, C.P. Landee, F.A. Chaves, S. Soriano, M.A. Novak, T. Papageorgiou, A.D. Bianchi, T. Herrmannsdorfer, J. Wosnitza, Phys. Rev. B 75 (2007) 094421.
[3] T. Lancaster, S.J. Blundell, M.L. Brooks, P.J. Baker, F.L. Pratt, J.L. Manson, C.P. Landee, C. Baines, Phys. Rev. B 73 (2006) 020410(R).
[4] J.L. Manson, M.M. Conner, J.A. Schlueter, T. Lancaster, S.J. Blundell, M.L. Brooks, F.L. Pratt, T. Papageorgiou, A.D. Bianchi, J. Wosnitza, M.-H. Whangbo, Chem. Commun. (2006) 4894.
[5] F.M. Woodward, A.S. Albrecht, C.M. Wynn, C.P. Landee, M.M. Turnbull, Phys. Rev. B 65 (2002) 144412.
[6] F.M. Woodward, C.P. Landee, J. Giantsidis, M.M. Turnbull, C. Richardson, Inorg. Chim. Acta 324 (2001) 324.
[7] R.D. Willett, C. Galeriu, C.P. Landee, M.M. Turnbull, B. Twamley, Inorg. Chem. 43 (2004) 3804.
[8] R.D. Willett, B. Twamley, W. Montfrooij, G.E. Granroth, S.E. Nagler, D.W. Hall, J.-H. Park, B.C. Watson, M.W. Meisel, D.R. Talham, Inorg. Chem. 45 (2006) 7689.
[9] T. Otieno, S.J. Rettig, R.C. Thompson, J. Trotter, Inorg. Chem. 32 (1993) 4384.
[10] S. Amaral, W.E. Jensen, C.P. Landee, M.M. Turnbull, F.M. Woodward, Polyhedron 20 (2001) 1317.
[11] B.M. Wells, C.P. Landee, M.M. Turnbull, F.F. Awwadi, B. Twamley, J. Mol. Catal. A: Chem. 228 (2005) 117.
[12] M. Barquin, M.J. Gonzalez Garmendia, L. Larrinaga, E. Pinilla, M.R. Torres, Z. Anorg. Allg. Chem. 631 (2005) 2210.
[13] F.F. Awwadi, C.P. Landee, M.M. Turnbull, B. Twamley, B.M. Wells, Polyhedron 24 (2005) 2153.
[14] C. Nather, J. Greve, Acta. Crystallogr., Sect. C 57 (2001) 1388.
[15] M.M. Conner, A.C. McConnell, J.A. Schlueter, J.L. Manson, J. Low Temp. Phys. 142 (2006) 273.
[16] F.M. Woodward, P.J. Gibson, G.P. Jameson, C.P. Landee, M.M. Turnbull, R.D. Willett, Inorg. Chem. 46 (2007) 4256.
[17] Y.Q. Zheng, J.-L. Lin, Z. Anorg. Allg. Chem. 629 (2003) 1622.
[18] T. Ohmura, A. Usuki, K. Fukumori, T. Ohta, M. Ito, K. Tatsumi, Inorg. Chem. 45 (2006) 7988.
[19] SMART: v. 5.632, Bruker AXS, Madison, WI, 2005.
[20] SAINTPLUS: v. 7.23a, Data Reduction and Correction Program, Bruker AXS, Madison, WI, 2004.
[21] SADABS: v. 2004/1, An Empirical Absorption Program, Bruker AXS Inc., Madison, WI, 2004.
[22] G.M. Sheldrick, SHELXTL: v. 6.14, Structure Determination Software Suite, Bruker AXS Inc., Madison, WI, 2004.
[23] F.H. Allen, Acta Crystallogr., Sect. B 58 (2002) 380.
[24] L. Carlucci, G. Ciani, A. Gramaccioli, D.M. Proserpio, S. Rizzato, Cryst. Eng. Commun. 2 (2000) 154. (CCDC refcode WOPPAS).
[25] T. Otieno, A.T. Pinkston, N.C. Johnson, S. Parkin, Acta. Crystallogr., Sect. E 58 (2002) m328. (CCDC refcode LOXYAY).
[26] C. Navas, M.M. Turnbull, C. Giogas, C.P. Landee, W. Zhang, G. Pon, R. Willett, Polyhedron 12 (1993) 1019. (CCDC refcodes WEGZUD and WEGZOX).
[27] M. Maekawa, S. Kitagawa, T. Tanimura, M. Munakata, T. Yonezawa, Anal. Sci. 8 (1992) 899. (CCDC refcode PEJJIX).
[28] J.C. Bonner, M.E. Fisher, Phys. Rev. 135 (1964) A640.
[29] A.P. Ginsberg, M.E. Lines, Inorg. Chem. 11 (1972) 2289.

Polyhedron 27 (2008) 2655–2661

Contents lists available at ScienceDirect

Polyhedron

journal homepage: www.elsevier.com/locate/poly

Synthesis and chromatographic study of methyl-2,3-*O*-isopropylidene-5-dimethylarsinoyl-β-D-ribofuranoside and methyl-2,3-*O*-isopropylidene-5-deoxy-5-dimethylthioarsinoyl-β-D-ribofuranoside

Attila Gyepes [a], Richárd Schäffer [a], Gábor Bajor [b], Ágnes Woller [a,*], Péter Fodor [a]

[a] Department of Applied Chemistry, Corvinus University of Budapest, Villányi út 29-31, H-1114 Budapest, Hungary
[b] Department of Inorganic Chemistry, Budapest University of Technology and Economics, Műegyetem rkp. 3-9, H-1111 Budapest, Hungary

ARTICLE INFO

Article history:
Received 3 April 2008
Accepted 30 April 2008
Available online 16 June 2008

Keywords:
Arsenosugars
Methyl-2,3-*O*-isopropylidene-5-dimethylarsinoyl-β-D-ribofuranoside
Methyl-2,3-*O*-isopropylidene-5-deoxy-5-dimethyl-thioarsinoyl-β-D-ribofuranoside
Gas chromatography
Thin-layer chromatography
Trimethylsilylation

ABSTRACT

The synthesis of two riboside-containing arsenic compounds, methyl-2,3-*O*-isopropylidene-5-dimethylarsinoyl-β-D-ribofuranoside and methyl-2,3-*O*-isopropylidene-5-deoxy-5-dimethyl-thioarsinoyl-β-D- ribofuranoside is presented in this paper. Intermediates and final products of the synthesis were examined by gas chromatography and thin layer chromatography. The purity of the products was assessed by NMR spectroscopy. Trimethylsilylation was used to volatilise sugar compounds and thus use of the costly HPLC–MS technique was avoided. The results affirmed the presence of tautomers in case of arsenosugars.
© 2008 Elsevier Ltd. All rights reserved.

1. Introduction

There are an increasing number of papers dealing with arsenic containing ribosides (called arsenosugars) present in sea and freshwater organisms. In marine algae arsenic occurs predominantly as arsenosugar [1], further sources of dietary arsenosugar exposure include herbivorous marine molluscs such as oysters, mussels and clams [2]. Several arsenosugar compounds have already been identified in marine organisms [3,4] and only few studies have been published on the potential health hazard of these compounds [5]. The lack of arsenic toxicity reported in humans after consumption of large amounts of seafood and seaweed suggests that these arsenic compounds are not acutely toxic [6]. However, chronic toxicity of these arsenic compounds should be considered.

Several papers have been published on the synthetic preparation of such arsenosugar compounds [7–9]. The most convenient way to determine the identity and the purity of intermediates and final products is the use of HPLC–MS techniques. Since sugars are easily volatilised by the use of adequate derivatives, the less expensive TLC and GC techniques may replace the costly HPLC–MS technique as far as purity assessment is concerned, while NMR spectroscopy can give information on the structure of molecules.

This article describes the synthetic preparation of two arsenosugars and their characterisation by TLC, GC and NMR spectroscopy. Known methods [7,8] were used for the synthesis of arsenosugars, with some modifications compared to the referred procedures.

The preparation of different arsenosugar compounds is useful for the assessment of potential health risks of a certain kind of food and for improving our understanding of arsenic biochemistry.

2. Experimental

2.1. Chemicals and reagents

D-Ribose (98%) was purchased from Sigma–Aldrich Co. (St. Louis, MO, USA), the sephadex G-25 (50–150 μm) was supplied by Pharmacia Fine Chemicals AB (Uppsala, Sweden). Sulfuric acid (96%), potassium hydrogen carbonate, propanone (Ph. Eur.), hydrochloric acid (37%), chloroform, anhydrous sodium sulfate, ethyl acetate (EtOAc), ethanol (EtOH, 99 %), *N*,*N*-dimethylmethanamide (DMF, puriss), sodium bromide (puriss), hexane, sulfur and hydrogen peroxide (30%) were purchased from Reanal Finomvegyszergyár ZRt. (Budapest, Hungary). *N*,*O*-bis(trimethylsilyl) trifluoroacetic amide (BSTFA, >99%) was obtained from Fluka. Methanol (MeOH, HPLC

* Corresponding author. Tel.: +36 1 482 6164; fax: +36 1 466 4272.
E-mail address: agnes.woller@uni-corvinus.hu (Á. Woller).

0277-5387/$ - see front matter © 2008 Elsevier Ltd. All rights reserved.
doi:10.1016/j.poly.2008.04.049

Table 1
Chrompack CP-9000 gas chromatographic parameters used in the experiments

Column	RH-5 ms$^+$ capillary column (30 m × 0.25 mm I.D. × 0.25 μm), Chromatix Separation Sciences Inc. (Jackson, CA, USA)
Injection temperature	250 °C
Detector	flame ionisation detector (FID)
Detector temperature	250 °C
Carrier gas	N_2 (99.9995%)
N_2 inlet pressure	35 kPa
Temperature program 1	at 85 °C for 2 min, then heat until 325 °C at a ramp rate of 12 °C/min, where held for 15 min
Temperature program 2	at 125 °C for 2 min., then heat until 325 °C at a ramp rate of 10 °C/min, where held for 10 min
Sample injected	1 μl
Derivatisation	2 mg sample/ 200 μl Py/50 μl BSTFA

grade) was purchased from Carlo-Elba, kiesel gel 40(70–230 mesh), pyridine (Py, dried, pro anal.) and methanesulfonyl chloride (MsCl for synthesis) from Merck (Whitehouse Station, NJ, USA). Tetrahydrofuran (THF) and diethyl ether (Et_2O) were HPLC grade solvents from Romil (Cambridge, UK). Sodium dimethyl arsine (Me_2AsNa) was prepared at the Department of Inorganic Chemistry, Budapest University of Technology and Economics (Budapest, Hungary) following the procedures published by Burrows and Turner [10] and Feltham et al. [11]. Reagents were all of analytical reagent grade except those specified. The purity of argon gas used for the reactions was 99.95%. Distilled water was used except for the water extraction processes where ultra-pure water (Millipore, Guyancourt, France) was used.

2.2. Apparatus

Investigation of the synthesised compounds was carried out on a Chrompack CP-9000 gas chromatograph and kieselgel 60 F254 (aluminium sheet) TLC plates (Merck). The gas chromatographic parameters used are shown in Table 1. Mass spectrometric detection and NMR spectroscopy was used for identification and confirmation of the synthesised products. An API 3200 LC–MS–MS (Applied Biosystems, Foster City, CA, USA) system was used in the electrospray ionisation (ESI) mode applying 30 eV collision energy. A Bruker Avance 500 MHz NMR spectrometer was used for the NMR studies. Spectra were taken at ^{1}H: 500 MHz and ^{13}C: 125 MHz in deuterochloroform.

2.3. Trimethylsilylation

For the GC analyses of the sugar-derivatives a silylation method was used, as the compounds to be analysed have low volatility and are quite heat sensitive. BSTFA was applied as a silylating agent. This method results in highly volatile trimethylsilyl derivatives where active hydrogen atoms of the substrate are substituted for trimethylsilyl groups. The resulting sugar-derivatives have lower

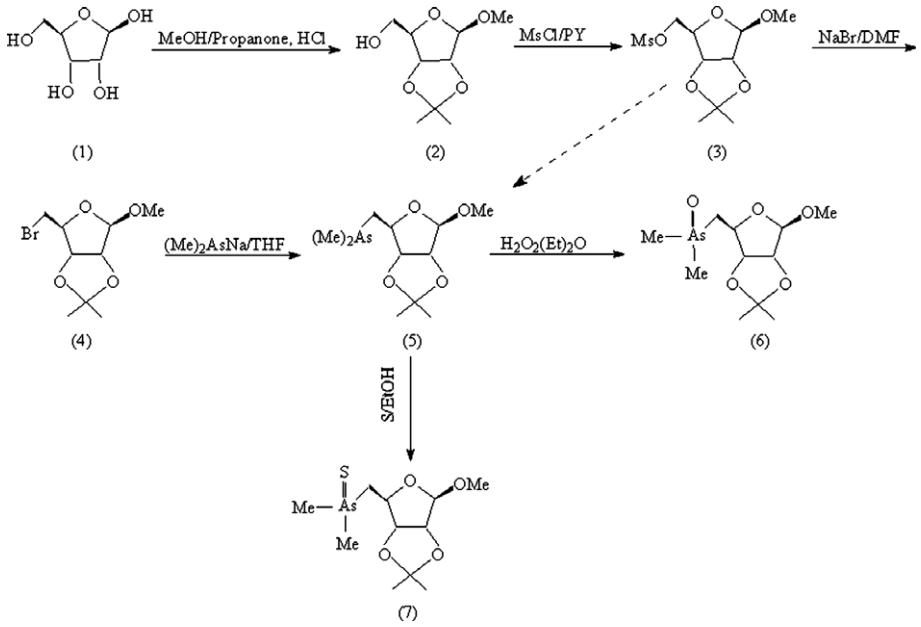

Fig. 1. Structure of ribose, intermediates and the final products formed by means of the synthesis process. (**1**) D-Ribose, (**2**) methyl-2,3-*O*-isopropylidene-β-D-ribofuranoside, (**3**) methyl 2,3-*O*-isopropylidene-5-*O*-mesyl-β-D-ribofuranoside, (**4**) methyl 2,3-*O*-isopropylidene-5-deoxy-5-bromo-β-D-ribofuranoside, (**5**) dimethyl (methyl-2,3-*O*-isopropylidene-5-deoxy-β-D-ribofuranose-5-yl) arsine, (**6**) methyl-2,3-*O*-isopropylidene-5-dimethyl-arsinoyl-β-D-ribofuranoside, (**7**) methyl-2,3-*O*-isopropylidene-5-deoxy-5-dimethyl-thioarsinoyl-β-D-ribofuranoside.

Table 2
Characterisation results of the intermediates and final products

Synthesised intermediates and products	Product weight (g)	Purity (%)	Yield (%)	$R_{f(TLC)}$	Purity according to NMR analysis
2	11	98.5 (GC)	62.2	0.64 [*EtOAc:nC$_6$1:1*]	Pure
3	2.75	99.5 (GC)	95	0.73 [*EtOAc:nC$_6$1:1*]	Pure
4	4	>95 (TLC)	90	*0.95* [*EtOAc:nC$_6$1:1*]	Pure
5	5.65	≈50 (GC)	57.4		Acceptable purity
6	1.15	>86.5 (GC)	57.5	0.34 [*EtOAc:MeOH 1:1*]	Pure
7	0.422	>*98*(GC)	80	0.85 [*EtOAc:MeOH 1:1*]	Pure

polarity and are less heat sensitive, thus this quantitative silylation method makes these derivatives suitable for GC and GC–MS studies.

3. Syntheses

3.1. Methyl 2,3-*O*-isopropylidene-β-D-ribofuranoside (*2*)

Compound **2** was obtained from D-ribose (**1**) by following Lerner's procedure [12]. D-Ribose (13 g), propanone (50 ml), MeOH (50 ml) and cc. HCl (1.4 ml) were heated under reflux for 2 h. The solution was cooled to room temperature and neutralised with saturated $KHCO_3$ (50 ml). After concentration under vacuum, water and $CHCl_3$ were added to the concentrate. The organic phase was washed with water, dried over Na_2SO_4 and evaporated. The product **2** was obtained in a yield of 11 g as a yellowish oil.

3.2. Methyl 2,3-O-isopropylidene-5-O-mesyl-β-D-ribofuranoside (*3*)

A mixture of 2 g of **2**, dry Py (70 ml) and MsCl (4.5 ml) was stirred for 2 h. The solution was poured into a mixture of icy water and H_2SO_4 then extracted with $CHCl_3$ (5 × 10 ml). The Py free extract

Table 3
^{1}H NMR (δ; 500 MHz), ^{13}C NMR (δ; 125 MHz) data and *J*-coupling values (Hz) of the synthesised compound

	2	3	5	6	7
H-1	4.97	4.98	4.92	4.97	4.97
H-2	4.48	4.60	4.62	4.66	4.64
H-3	4.83	4.73	4.76	4.69	4.70
H-4	4.42	4.23	4.46	4.55	4.62
H-5a	3.69	4.19	2.51	2.50	2.50
H-5b	3.61	4.12	2.27	2.50	2.27
Other	3.43(OMe); 1.48 and 1.32(CMe_2)	3.27(OMe); 3.22(OMs); 1.39 and 1.27(CMe_2)	2.29(OMe); 1.64 and 1.63($AsMe_2$); 1.38 and 1.25(CMe_2)	3.40(OMe); 1.84($AsOMe_2$); 1.48 and 1.32(CMe_2)	3.89(OMe); 1.86 and 1.87($AsSMe_2$); 1.49 and 1.32(CMe_2)
C-1	110.0	108.9	109.5	110.7	110.6
C-2	85.8	84.3	84.3	85.0	85.1
C-3	81.5	80.8	80.8	81.8	82.6
C-4	88.3	83.3	83.3	84.9	83.3
C-5	64.0	69.7	36.4	37.8	40.0
Other	55.5(OMe); 26.3 and 24.7(CMe_2); 111.8(CMe_2)	54.6(OMe); 36.8(OMs); 26.3 and 24.7(CMe_2); 111.9(CMe_2)	54.8(OMe); 15.4 and 15.0($AsMe_2$); 26.3 and 24.7(CMe_2); 111.6(CMe_2)	55.9 (OMe); 16.3 ($AsOMe_2$); 26.5 and 25.0(CMe_2); 113.1(CMe_2)	55.6(OMe); 19.7 and 18.7($AsSMe_2$); 26.5 and 25.0(CMe_2); 113.0(CMe_2)
$J_{1,2}$					
$J_{2,3}$	5.9	5.9	6.1	6.0	6.0
$J_{3,4}$					
$J_{4,5a}$	2.3	7.0	6.2	7.3	9.9
$J_{4,5b}$	3.2		8.5	7.3	4.7
$J_{5a,5b}$	13.0	10.2	13.7		15.5

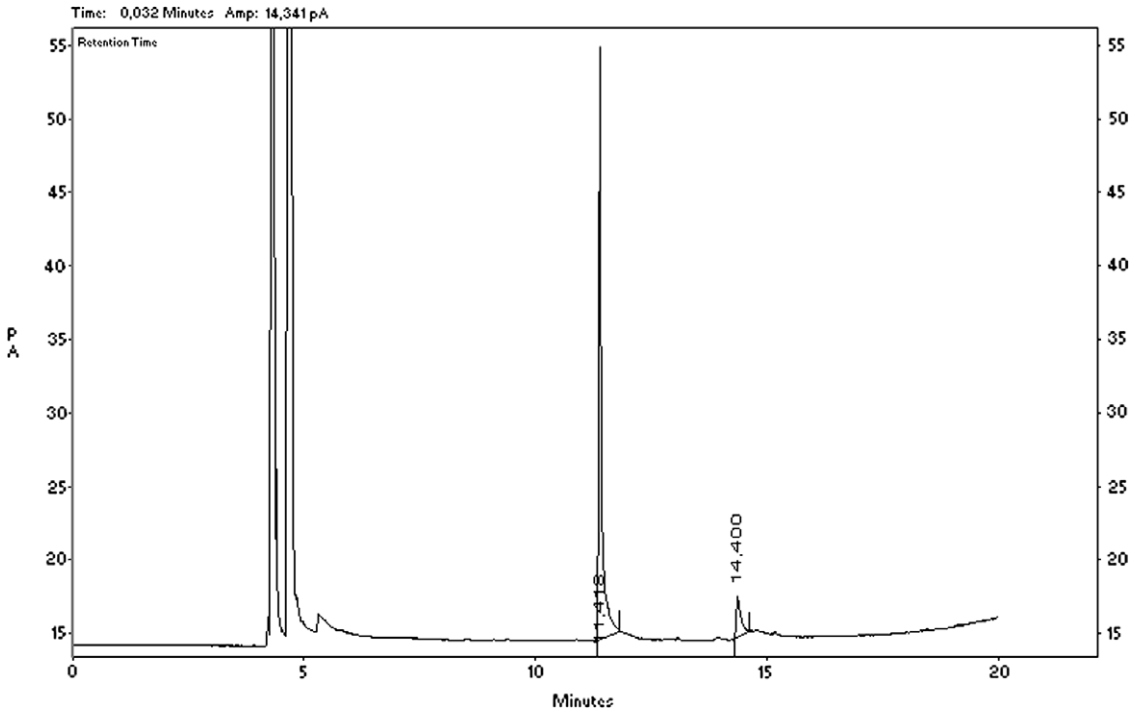

Fig. 2. GC chromatogram of methyl-2,3-*O*-isopropylidene-5-dimethyl-arsinoyl-β-D-ribofuranoside (**6**) in pyridine. Retention time: 11.4 min.

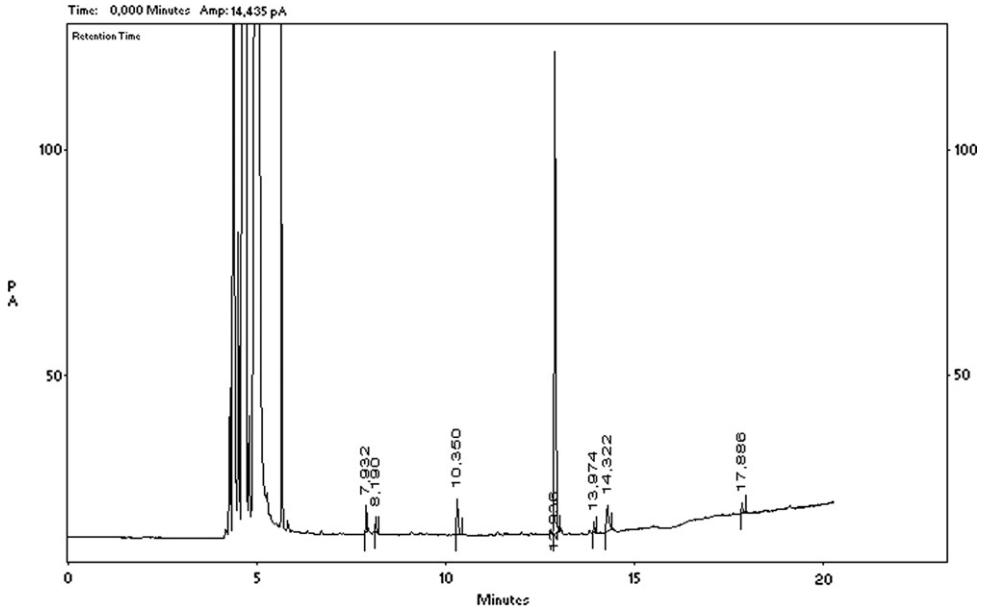

Fig. 3. GC chromatogram of the trimethylsilyl derivative of methyl-2,3-*O*-isopropylidene-5-dimethyl-arsinoyl-β-D-ribofuranoside (**6**). Retention time: 12.9 min.

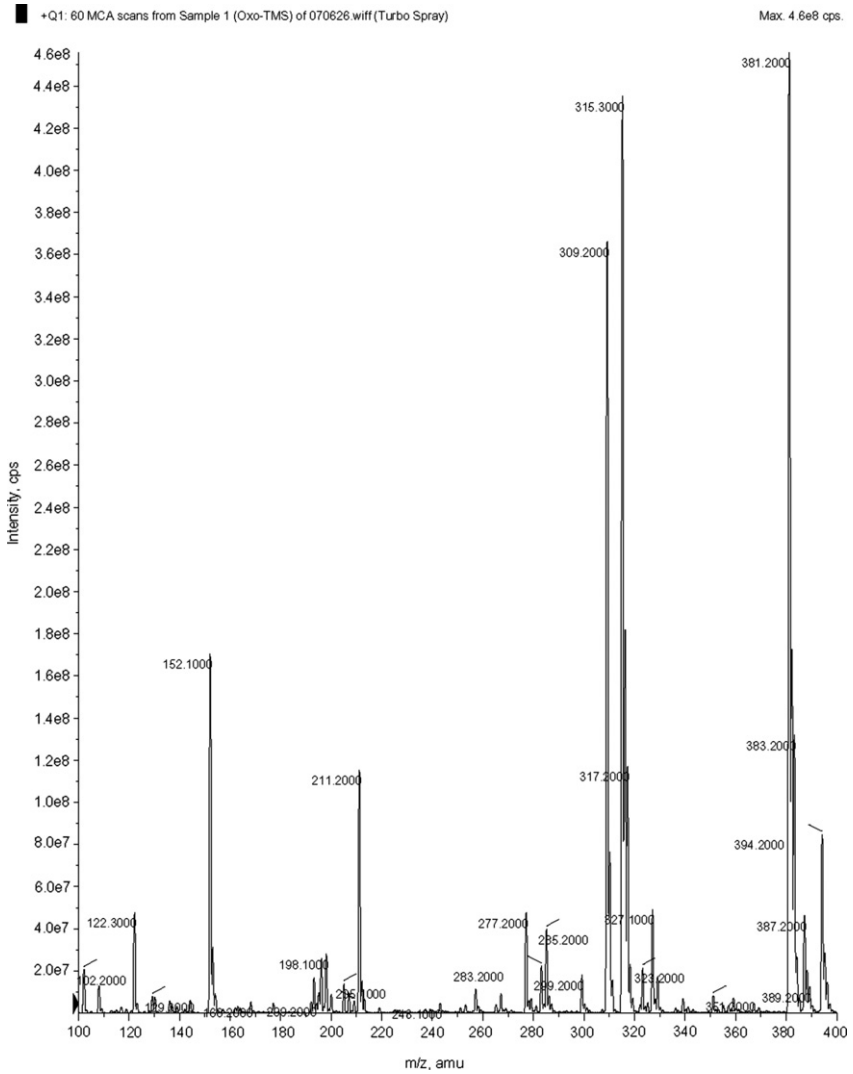

Fig. 4. ESI–MS–MS spectrum of the trimethylsilyl derivative of methyl-2,3-*O*-isopropylidene-5-dimethyl-arsinoyl-β-D-ribofuranoside (**6**) taken in the +Q1mode.

was washed with $KHCO_3$ solution and water. Drying of the extract and evaporation afforded 2.75 g of **3** as yellowish crystals.

3.3. Methyl 2,3-O-isopropylidene-5-deoxy-5-bromo-β-D-ribofuranoside (*4*)

A mixture containing 4.57 g of **3**, DMF (70 ml) and NaBr (1.8 g) was heated under reflux for 1.5 h. TLC was used to check the reaction endpoint. The reaction mixture was poured into icy water (300 ml). After extraction with $CHCl_3$ (4×10 ml), the organic phase was washed with water, dried over Na_2SO_4 and evaporated. Four grams of **4** was obtained as an orange oil.

3.4. Dimethyl (methyl-2,3-O-isopropylidene-5-deoxy-β-D-ribofuranose-5-yl) arsine (*5*)

A round-bottomed flask was charged with a solution of THF (120 ml) and Me_2AsNa (~5 g) under an argon atmosphere. While continuously flushing and stirring, a solution of **4** in THF (8.6 g) was added to the flask in drops (over 30 min). The reaction mixture was chilled and extracted with $CHCl_3$ (5×30 ml). The organic phase was dried over Na_2SO_4 and evaporated. The oily residue was dissolved in Et_2O (50 ml), filtered on a silica gel column and distilled. The product **5** was obtained in a yield of 5.65 g as a yellow oil.

3.5. Methyl-2,3-O-isopropylidene-5-dimethyl-arsinoyl-β-D-ribofuranoside (*6*)

1.9 g of **5** were dissolved in Et_2O (40 ml) and H_2O_2 (2.5 ml) was added to the solution dropwise under constant stirring (over 10 min, 20 °C). After 1.5 h the reaction mixture was extracted several times with ultra-pure water (50 ml and 5×10 ml). The water extracts were combined and washed with Et_2O (2×10 ml), then distilled to obtain 1.15 g of a white syrup **6**.

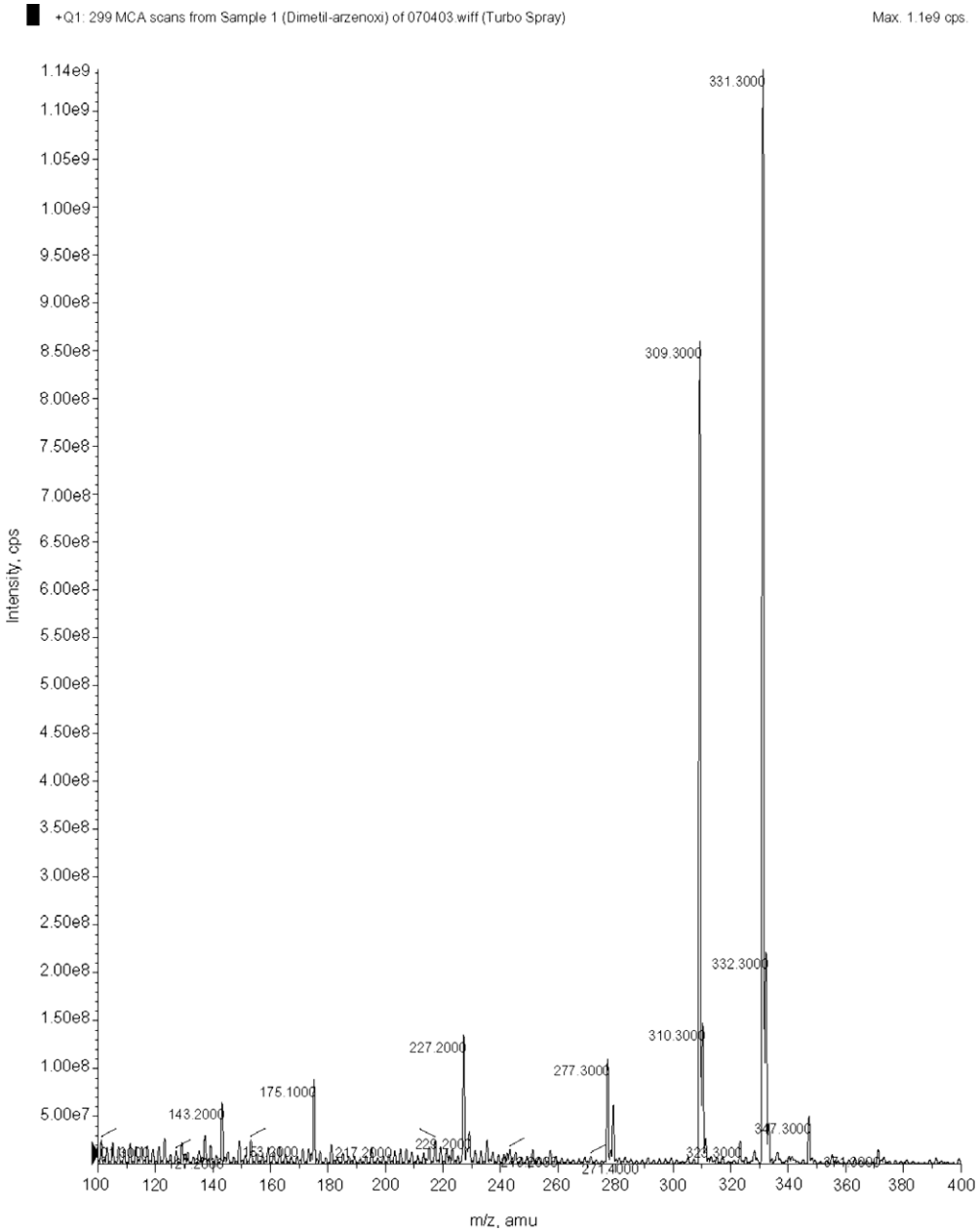

Fig. 5. ESI–MS–MS spectrum of methyl-2,3-O-isopropylidene-5-dimethyl-arsinoyl-β-D-ribofuranoside (**6**) in MeOH (+Q1mode.)

3.6. Methyl-2,3-O-isopropylidene-5-deoxy-5-dimethyl-thioarsinoyl-β-D-ribofuranoside (7)

To a solution of 1.1 g of **5** and EtOH (25 ml), finely powdered sulfur (1.4 g) was added. The mixture was refluxed and heated for 5 h under an argon atmosphere. The solution was cooled down, filtered and evaporated. The residue was dissolved in MeOH (10 ml) and filtered on a Sephadex G-25 column (4 × 10 cm). Finally, the concentrate was dissolved in hot MeOH (5 ml) and was put in a refrigerator to crystallize. The yellowish crystals that formed were separated and washed with cold MeOH and Et_2O. Drying resulted in 0.422 g of **7**.

4. Results and discussion

The known naturally occurring arsenosugars are exclusively organic arsinoyl and thioarsinoyl compounds built on the ribofuranose ring. Our primary goal was the synthesis and characterisation of such compounds using D-ribose as a starting material. First, several ribose derivatives were prepared, offering a good possibility to be followed up as intermediates of subsequent synthesis steps. Such derivates were 2,3-*O*-isopropylidene-riboside and methyl-ribofuranoside. These compounds, with a knowledge of chromatographic theory, could predict the retention behaviour of the synthesised intermediates without the use of standard solutions.

The first product was the methyl 2,3-*O*-isopropylidene-β-D-ribofuranoside (**2**), resulting from the reaction of D-ribose with MeOH and propanone (1:1) in the presence of HCl (Fig. 1). The hydroxyl group located at C5 position of **2** can easily be converted to the corresponding mesylate or tosylate. The use of methanesulfonyl chloride might be more advantageous than that of tosyl chloride, as the former yields a shorter reaction time. The resulting product is easily cleaned after pyridine and acid residues have been eliminated. The methyl 2,3-*O*-isopropylidene-5-*O*-mesil-β-D-ribofuranoside (**3**) was obtained as yellowish crystals. The synthesis

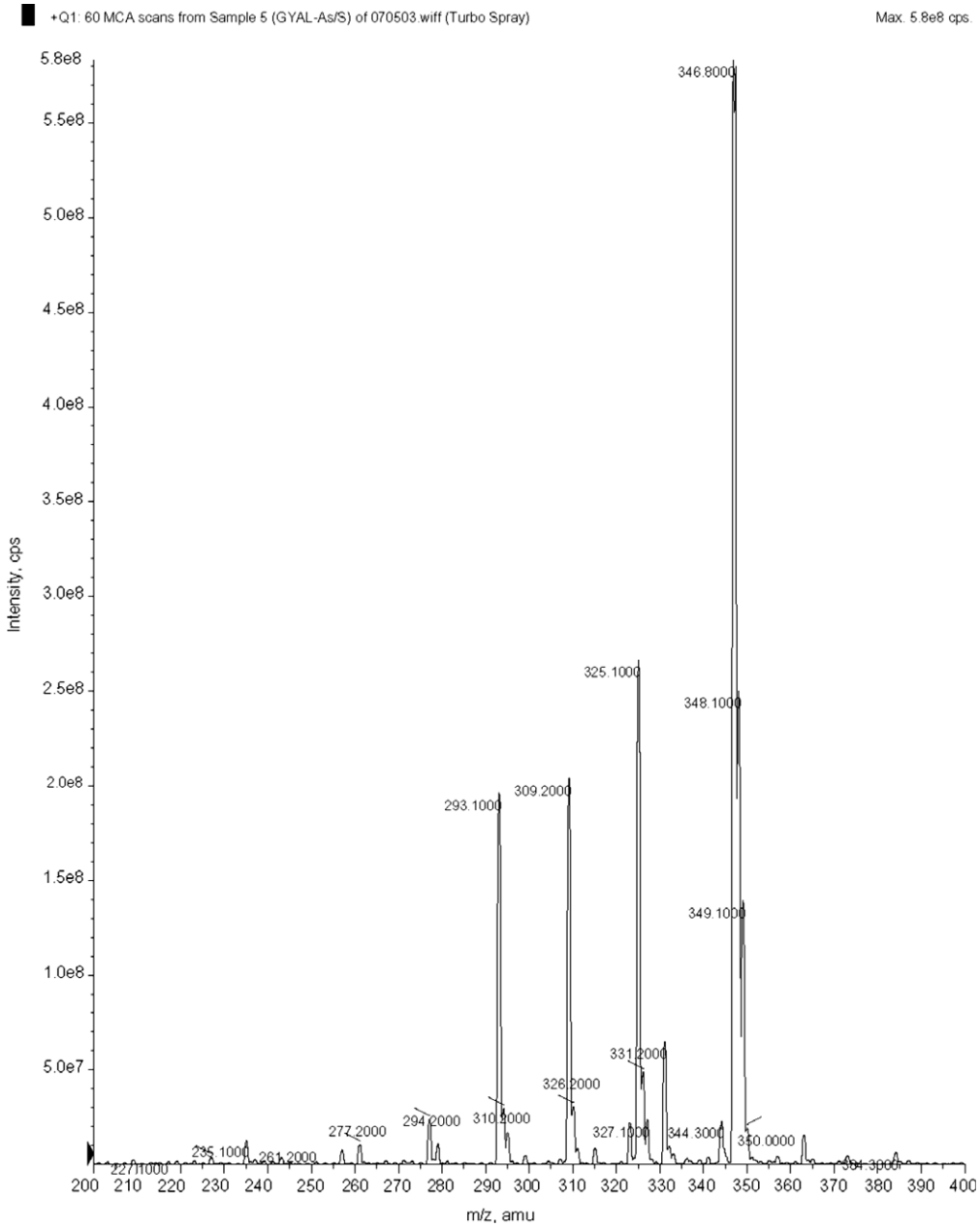

Fig. 6. ESI–MS–MS spectrum of methyl-2,3-*O*-isopropylidene-5-deoxy-5dimethyl-thioarsinoyl-β-D-ribofuranoside (**7**) in MeOH (+Q1mode).

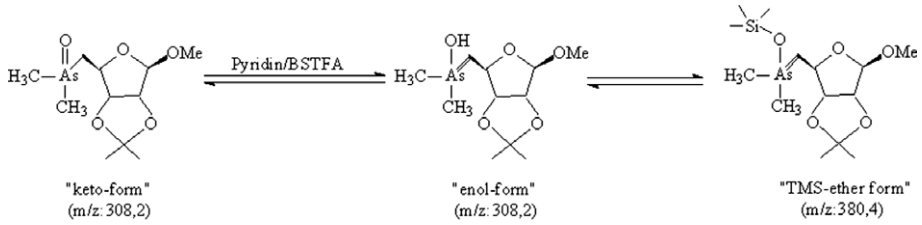

Fig. 7. Equilibrium processes among the keto-, enol- and trimethylsilycated forms (TMS) of methyl-2,3-*O*-isopropylidene-5-dimethyl-arsinoyl-β-D-ribofuranoside.

of methyl 2,3-*O*-isopropylidene-5-deoxy-5-bromo-β-D-ribofuranoside (**4**) was carried out in the presence of DMF solvent and NaBr at a reflux temperature for 1.5 h. A sodium dimethyl arsine reagent was used for the dimethyl arsine side chain construction in dry THF solution, along with continuous stirring and argon flushing. We should emphasize that this substitution reaction works directly from the mesylate intermediate **3** as well, as our NMR spectroscopy studies have proven. The resulting dimethyl (methyl-2,3-*O*-isopropylidene-5-deoxy-β-D-ribofuranose-5-yl) arsine (**5**) was isolated as a yellow oil. The oxidation reaction of the arsinoyl compound takes place easily in the presence of H_2O_2 and Et_2O. The reaction completed in 1.5 h and the resulting final product **6** was isolated as a colourless syrup. The thioarsinoyl analogue **7** was prepared in EtOH from **5** by adding sulfur to the solution. The mixture was held under an argon atmosphere, heated to the reflux temperature of EtOH and refluxed, thus avoiding the presence of oxidized side products. After cleaning steps were carried out, the final product **7** was crystallised from MeOH. Results of TLC, GC and NMR spectroscopy measurements for the characterisation and identification of the synthesis intermediates and products are seen in Tables 2 and 3.

In the case of the arsinoyl final product **6**, it was noticed that the oxygen atom (oxo-group), bonded to the arsenic by a $\sigma + \pi$ bond, was silylised in the presence of a strong trimethylsilycating agent (BSTFA), presumably after tautomerisation. Comparing the chromatograms of Figs. 2 and 3 it can be seen that the peak of the *O*-trimethylsilyl-ether of **6** is sharper and more symmetrical than the tailing peak of the "silyl-free" arsenosugar **6**, due to a more effective volatilisation in the GC. LC–MS–MS studies have supported that the silylation was successful. Fig. 4 shows the MS spectrum of the trimethylsilyl derivative of **6** where the trimethylsilyl-ether parent ion *m*/*z*: 381.2 dominates. Fig. 5 shows the mass spectrum of the arsinoyl compound **6**, here two parent ions, the protonated arsenosugar (*m*/*z*: 309.3) and its sodium-adduct (*m*/*z*: 331.3) are the most intense peaks. As in the case of the thio-analogue, compound **7** silylation was unsuccessful. Its mass spectrum (Fig. 6) is dominated by its sodium-adduct (*m*/*z*: 346.8).

In the case of **6** the mass of the trimethylsilyl-ether parent ion (*m*/*z*: 381.2) proves the deprotonation of the terminal methylene-group. This finding seems to support the assumption of Pergantis et al. [13] on the proposed fragmentation routes of an oxo-arsenosugar.

Keto–Enol tautomerism is characteristic for adequately substituted compounds containing an oxo-group, and the conversion of the enol to the keto form in a base catalysed environment proceeds easily. For these reactions one of the most convenient solvents is pyridine as a base, using it along with BSTFA as a trimethylsilycating agent. The LC–MS–MS results obtained seem to support the assumption of Pergantis and his co-workers [13] that tautomerism also takes place in the case of arsenosugars. Fig. 7 shows the interconversion among the keto-, enol- and trimethylsilycated forms of the arsinoyl compound **6**.

Acknowledgements

We thank János Kuszmann his kind help in the synthesis of the sugars. Special thanks to Ferenc Szederkényi for his advice on the interpretation of chromatographic results.

References

[1] M. Morita, Y. Shibata, Appl. Organomet. Chem. 4 (1990) 181.
[2] X.C. Le, M. Ma, V.W.M. Lai, in: W.R. Chappell, C.O. Abernathy, R.L. Calderon (Eds.), Arsenic Exposure and Health Effects, Elsevier Science, Amsterdam, 1999, p. 69.
[3] J.S. Edmonds, K.A. Francesconi, Mar. Pollut. Bull. 26 (1993) 665.
[4] K.A. Francesconi, W. Goessler, S. Panutrakul, K.J. Irgolic, Sci. Total Environ. 221 (1998) 139.
[5] P. Andrewes, D.M. Demarini, K. Funasaka, K. Wallace, V.W.M. Lai, H.S. Sun, W.R. Cullen, K.T. Kitchin, Environ. Sci. Technol. 38 (2004) 4140.
[6] J. Borak, H.D. Hosgood, Regul. Toxicol. Pharmacol. 47 (2007) 204.
[7] J. Liu, D.H. O'Brien, K.J. Igorlic, Appl. Organomet. Chem. 10 (1996) 13.
[8] J. Liu, D.H. O'Brien, K.J. Igorlic, Appl. Organomet. Chem. 10 (1996) 1.
[9] D.P. McAdam, A.M.A. Perera, R.V. Stick, Aust. J. Chem. 40 (1987) 1901.
[10] G.J. Burrows, E.E. Turner, J. Chem. Soc. 117 (1920) 1373.
[11] R.D. Feltham, A. Kasenally, R.S. Nyholm, J. Organometal. Chem. 7 (1967) 285.
[12] L.M. Lerner, Carbohydr. Res. 53 (1977) 177.
[13] S.A. Pergantis, S. Wangkarn, K.A. Francesconi, J.E. Thomas-Oates, Anal. Chem. 72 (2000) 357.

Polyhedron 27 (2008) 2662–2666

Contents lists available at ScienceDirect

Polyhedron

journal homepage: www.elsevier.com/locate/poly

Co(II/III) coordinated pyridine alcoholate ligand generated through metal assisted nucleophilic addition to a C=O function: Temperature dependent synthesis of a mononuclear complex and a neutral cubane cluster

Sumanta Kumar Padhi *, Rojalin Sahu

Department of Chemistry, Indian Institute of Technology Guwahati, Guwahati 781 039, Assam, India

ARTICLE INFO

Article history:
Received 16 April 2008
Accepted 5 May 2008
Available online 27 June 2008

Keywords:
Pyridine alcoholate ligand
Optical properties
Magnetism
Neutral cubane

ABSTRACT

The synthesis and characterization of pyridine alcoholate ligand coordinated Co(II/III) metal complexes are reported. The characterization includes elemental analysis, spectral, magnetism, and X-ray crystallographic studies. Water readily shows nucleophilic addition to the C=O group upon coordination of the 2-pyridyl ring of the ligands, forming a *gem*-diol form of $(2\text{-py})_2CO$. By coordinating through the two pyridine nitrogen atoms and one oxygen atom from the newly formed *gem*-diol, the ligand becomes tridentate rather than bidentate, as might be expected. Two spin allowed ($^1A_{1g} \rightarrow {}^1T_{1g}$ and $^1A_{1g} \rightarrow {}^1T_{2g}$) d ← d transitions are observed in the electronic spectra of the strong field octahedral Co(III) complex and the $^1A_{1g} \rightarrow {}^1T_{2g}$ transition is obscured by intense MLCT bands. In $[Co\{OC(OH)(2\text{-pyridyl})_2\}_2][OAc] \cdot 4H_2O$ (**1**) the cationic part shows a N_4O_2 coordinated octahedral geometry for the Co(III) species with two di-(pyridyl)-ketone hydrate (DPKH) moieties coordinated in a tridentate fashion. The tetranuclear cluster molecule of $[Co_4\{OC(OH)(2\text{-pyridyl})_2\}_4[OAc]_4] \cdot 7H_2O$ (**2**) has a cubane core with alternate vertices occupied by Co(II) and oxygen atoms, consisting of two interpenetrating tetrahedra. In complex **2** the $1/\chi'_M$ *versus* T plot fitted with the simple Curie–Weiss law $1/\chi'_M = C/(T-\theta)$, and shows an antiferromagnetic behavior with $C = 8.14$ and $\theta = -69.26 \pm 0.06$ K.

© 2008 Elsevier Ltd. All rights reserved.

1. Introduction

One domain of coordination chemistry which has flourished in recent years is the synthesis of complex polynuclear architectures via self-assembly processes involving suitably designed ligands and transition metal ions. The development of routes and strategies for the synthesis of polynuclear complexes (clusters) of 3d metals in moderate oxidation states is of great importance because these species provide substantial impetus for development in several fields, including bioinorganic chemistry, magnetochemistry, materials chemistry and solid-state physics [1]. The ligand di-2-pyridyl ketone has recently been proved to be a central player in 3d-metal cluster chemistry. There continues to be great interest in the synthesis and study of polynuclear metal complexes (clusters) containing paramagnetic 3d metals in intermediate oxidation states [2]. There are various reasons for this, not least of which is the aesthetically pleasing nature of some of these species [3]. From an applications point of view, however, efforts in this area are part of the continuing search for new examples of molecular species which can function as nanoscale magnetic particles or the so-called single-molecule magnets (SMMs) [4]. Research on single-molecule magnets (SMMs) has been one of the most active fields in the past decade, and is still rapidly expanding. SMMs not only show dramatic architectures, but also provide almost ideal systems for investigating the coexistence of classic and quantum effects, and are hopeful for applications in information storage and quantum computing in the future [5]. The cubane-like structure of tetranuclear metal complexes is a characteristic motif in coordination chemistry of different metal ions and this structural motif, with a close spatial alignment of metal centres, is important also in the chemistry of transition metals where it may have an essential impact on considering possible magnetic and catalytical properties of the compounds [6]. Oxo-bridged cluster complexes of transition metals have recently been the subjects of study because these complexes could provide a fundamental basis for the study of redox and ligand substitution reactions vital to metal catalyzed autoxidation processes [7]. "*Binary* ligand blend" reactions involving (i) the monoanion $(2\text{-py})_2C(OH)O^-$ or the dianion $(2\text{-py})_2CO_2^{2-}$ of the *gem*-diol form of di-2-pyridyl ketone $(2\text{-py})_2CO$ and carboxylates and (ii) the monoanion $(2\text{-py})_2C(OR)O^-$ of the hemiacetal form of $(2\text{-py})_2CO$ and carboxylates have been explored with the belief that they might foster formation of discrete polynuclear metal systems [8]. The reactions of $(2\text{-py})_2CO$ with metal ions have been well studied over the years [9,10]. Water readily shows nucleophilic addition to the C=O group upon coordination of the

* Corresponding author. Tel.: +91 361 258 3620; fax: +91 361 258 2349.
E-mail address: sumanta@iitg.ernet.in (S.K. Padhi).

0277-5387/$ - see front matter © 2008 Elsevier Ltd. All rights reserved.
doi:10.1016/j.poly.2008.05.024

2-pyridyl ring of the ligands, forming the *gem*-diol form of (2-py)$_2$CO. The hydration reaction is unusual since ketones are not normally hydrated to any appreciable extent in aqueous media, unless flanked by very strong electron withdrawing groups such as Cl or F. By coordinating through the two pyridine nitrogen atoms and one oxygen atom from the newly formed *gem*-diol, the ligand becomes tridentate rather than bidentate, as might be expected.

2. Experimental

2.1. Materials

Chemicals like dipyridyl ketone were purchased from Aldrich, USA. $Co(OAc)_2 \cdot 4H_2O$ was purchased from Merck India Limited. All chemicals and solvents were of reagent grade and used as received without further purification.

2.2. Instrumentation and methods

FT-IR spectra in the range 4000–400 cm^{-1} were recorded using a Perkin–Elmer Spectrum One in KBr disc.

2.3. X-ray crystallography

Single crystal X-ray crystallographic data were collected using a Bruker SMART APEX-CCD diffractometer with Mo Kα radiation (λ = 0.71073 Å). The intensity data were corrected for Lorentz and polarization effects and empirical absorption corrections were applied using the SAINT program [11]. The structure was solved by direct methods using SHELXS-97 and non-hydrogen atoms located from the difference Fourier maps were refined anisotropically by full-matrix least-squares on F^2 using SHELXL-97 [11]. The hydrogen atoms were included in calculated positions and refined isotropically using a riding model.

2.4. Magnetic properties

The AC susceptibility was measured as a function of temperature at an AC field amplitude of 22 A/m by employing the mutual inductance bridge method and using a Perkin–Elmer (model 7265) dual phase lock-in-amplifier. The solid-state AC magnetic susceptibility of the tetranuclear cluster molecule **2** was recorded at an oscillator frequency of 333 Hz at 6 Oe; the magnetic field was generated using a Walker electromagnet. The temperature variation was achieved using a commercial closed cycle helium refrigerator cryostat equipped with a LakeShore Temperature Controller (model-331). The temperature was measured using a LakeShore calibrated GaAlAs sensor with an accuracy of better than ±50 mK.

2.5. Syntheses

2.5.1. $[Co\{OC(OH)(2\text{-pyridyl})_2\}_2][OAc] \cdot 4H_2O$ (**1**)

To 25 mL of a methanolic solution of 500 mg (2.71 mmol) of dipyridyl ketone (DPK), 1.35 g (5.42 mmol) 2 × 10 mL of a methanolic solution of $Co(OAc)_2 \cdot 4H_2O$ were added. The reaction mixture was stirred for 1.5 h, after which a pink colored solution was obtained. The reaction mixture was left for crystallization. After a week block-like crystals were obtained and washed with ice-cold methanol. Yield: 1.75 g (55%). IR (KBr), cm^{-1}: 1613 (C=N$_{py}$), 1476. *Anal.* Calc. for $C_{24}H_{29}N_4O_{10}Co$: C, 48.69; H, 4.90; N, 9.47. Found: C, 48.72; H, 4.95; N, 9.55%.

2.5.2. $[Co_4\{OC(OH)(2\text{-pyridyl})_2\}_4[OAc]_4] \cdot 7H_2O$ (**2**)

Synthetically the procedure for **2** was similar to that of **1**, but a dark pink colored solution was obtained after refluxing for 2.5 h. The reaction mixture was left for crystallization. After a week block-like crystals were obtained and washed with ice-cold methanol. Yield: 40%. IR (KBr), cm^{-1}: 1614 (C=N$_{py}$), 1474. *Anal.* Calc. for $C_{52}H_{64}N_8O_{24}Co_4$: C, 43.91; H, 4.50; N, 7.88. Found: C, 44.08; H, 4.61; N, 7.72%.

3. Results and discussion

3.1. Optical properties

The excitation spectra for the complexes (Fig. 1) were recorded in the region 200–1100 nm. In all of these complexes, four dominant bands were observed. Of these, the first two bands are at higher energies with high ε values and were attributed to intraligand $\pi^* \leftarrow \pi$ or $\pi^* \leftarrow$ n excitations. The remaining two bands (Bands III and IV) present MLCT character and d $\leftarrow$ d transitions of Co(III), respectively. Table 1 presents the excitation and ε values for the Gaussian fitted UV–Vis spectra of complexes **1** and **2**. The shape of the electronic spectra and the low extinction coefficients are suggestive of an octahedral configuration around the Co(III) ion. In general two spin allowed ($^1A_{1g} \rightarrow {}^1T_{1g}$ and $^1A_{1g} \rightarrow {}^1T_{2g}$) d $\leftarrow$ d transitions are observed in the electronic spectra of strong field octahedral Co(III) complexes. In many nitrogen donor Co(III) complexes the $^1A_{1g} \rightarrow {}^1T_{2g}$ transition is obscured by the intense MLCT bands. The intensities of the $^1A_1 \rightarrow {}^1T_1$ transitions are high due to "intensity stealing". In case of tetranuclear Co(II) cluster **2** two d–d transitions appear at 517 and 455 nm, and two MLCT bands are observed at 295 and 256 nm [12].

3.2. Molecular structure

The molecular structures of $[Co\{OC(OH)(2\text{-pyridyl})_2\}_2][OAc] \cdot 4H_2O$ (**1**) and $[Co_4\{OC(OH)(2\text{-pyridyl})_2\}_4[OAc]_4] \cdot 7H_2O$ (**2**) were determined by X-ray crystallography. The crystallographic data and refinement parameters are summarized in Table 2.

3.2.1. $[Co\{OC(OH)(2\text{-pyridyl})_2\}_2][OAc] \cdot 4H_2O$ (**1**)

The cationic part shows a N_4O_2 coordinated octahedral geometry for the Co(III) species with the two di-(pyridyl)-ketone hydrate (dpkH) moieties coordinated in a tridentate fashion. A perspective view of **1** is shown in Fig. 2. In this case, the hydrated dpkH stabilizes the high oxidation state of the metal centre, owing to the presence of a σ-donor oxygen atom where Co(III) gets neutralized by two deprotonated hydroxyl groups and a counter anionic acetate. The coordinated pendant generates two puckered five membered rings. The dihedral angle ∠Co1–N2–C7–C6 of 4.52(0.73)° is higher than that of ∠Co1–N1–C5–C6, −0.03(0.75)°, and similarly in the another moiety ∠Co1–N4–C18–C17, 6.84(0.80)°, is less than that of ∠Co1–N3–C16–C17, −2.99(0.76)°. The *trans* coordinated pyridyl rings are almost linear, ∠N1–Co1–N4 and ∠N2–Co1–N3 being 178.8(4)° and 179.0(3)°, respectively, but ∠O1–Co1–O2 deviates from linearity by 2.3°. The equatorially coordinated Co–N (N1, N2) bonds are longer than the axially coordinated Co–O1, whereas in the next moiety the equatorially coordinated Co–N (N3, N4) bonds are shorter than the axially coordinated Co–O2 bond. The molecular packing of **1** generates 3D-bilayers through hydrogen bonding (Fig. 3), where a layer of hydrogen bonded acetate and water molecules links to another cationic complex layer through hydrogen bonding.

3.2.2. $[Co_4\{OC(OH)(2\text{-pyridyl})_2\}_4[OAc]_4] \cdot 7H_2O$ (**2**)

The tetranuclear cluster molecule of **2** has a cubane core with the alternate vertices occupied by Co(II) and oxygen atoms. It consists of two interpenetrating tetrahedra, one of four Co(II) atoms and another of four μ_3-oxygen atoms originating from (2-

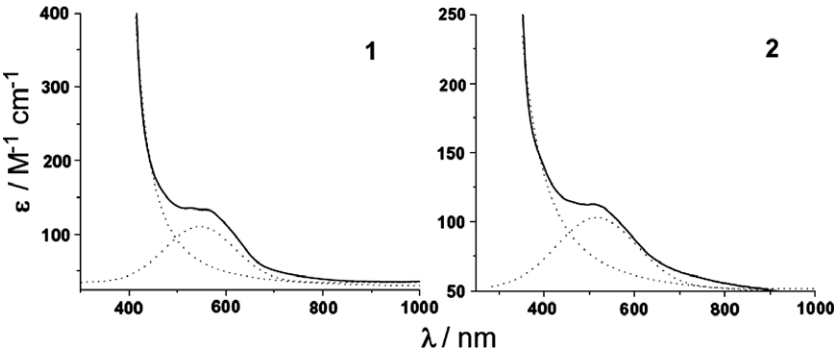

Fig. 1. UV–Vis spectra of **1** and **2**, dotted lines are the Gaussian fitted lines.

Table 1
Electronic excitation data for complexes **1** and **2**

Compound	Band I, sh		Band II		Band III, sh		Band IV	
	λ (nm)	log ε	λ (nm)	log ε	λ (nm)	log ε	λ (nm)	log ε
1	213	3.71	255	3.57	495	1.75	550	1.87
2	256	3.61	295	2.94	455	1.62	517	1.73

Table 2
Crystallographic data and refinement parameters

Metal complex	**1**	**2**
Empirical formula	$C_{24}H_{29}N_4O_{10}Co$	$C_{52}H_{64}N_8O_{24}Co_4$
CCDC number	627293	645238
Formula weight	591.47	1420.85
T (K)	296(2)	296(2)
Wavelength (Å)	0.71073	0.71073
Crystal system	triclinic	monoclinic
Space group	*P*1	$P2_1/c$
a (Å)	8.5042(10)	18.8549(11)
b (Å)	8.7269(10)	15.3133(9)
c (Å)	9.3648(11)	22.5864(12)
α (°)	86.306(6)	
β (°)	78.259(6)	92.377(3)
γ (°)	75.349(6)	
V (Å^3)	658.28(13)	6515.8(6)
Z	1	4
D_{Calc} (g cm^{-3})	1.502	1.467
μ (mm^{-1})	0.719	1.083
Goodness-of-fit on F^2[a]	1.055	1.000
$R[I > 2\sigma(I)]$	$R_1 = 0.0513$[b], $wR_2 = 0.1352$[c]	$R1 = 0.0382$[b], $wR_2 = 0.1096$[c]
R indices (all data)	$R_1 = 0.0628$[b], $wR_2 = 0.1454$[c]	$R_1 = 0.0413$[b], $wR_2 = 0.1118$[c]

[a] GOF $= [\sum[w(F_o^2 - F_c^2)^2]/M - N]^{1/2}$ (M = number of reflections, N = number of parameters refined).
[b] $R_1 = \sum||F_o| - |F_c||/\sum|F_o|$.
[c] $wR_2 = [\sum[w(F_o^2 - F_c^2)^2]/\sum[w(F_o^2)^2]]$.

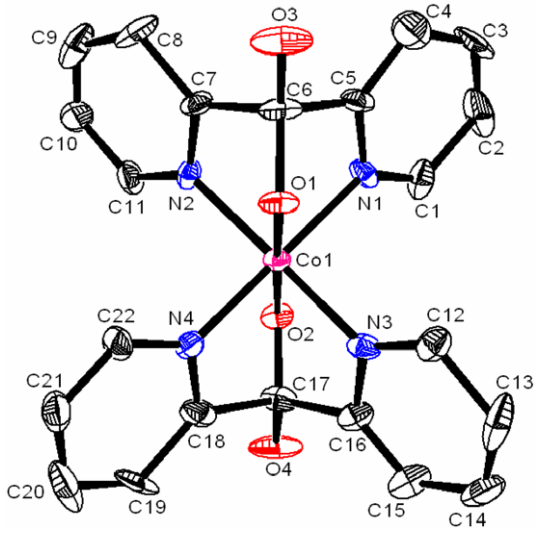

Fig. 2. ORTEP (30% probability) of the cationic species in **1** (hydrogens are omitted for clarity).

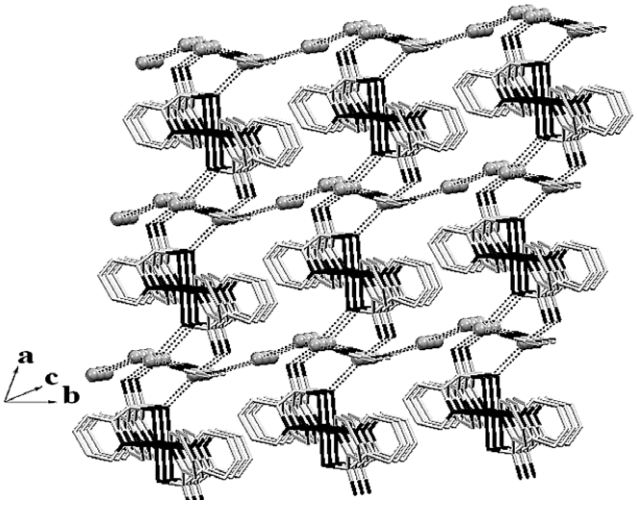

Fig. 3. Molecular packing of **1**, 3D-bilayers generated through hydrogen bonding.

py)$_2$C(OH)O$^-$ ligands. In addition to three μ_3-oxygen atoms, each Co(II) atom is coordinated to two N atoms belonging to two different (2-py)$_2$C(OH)O$^-$ ligands and to a monodentate acetate anion, satisfying an octahedral environment. A perspective view of **2** is shown in Fig. 4. Here each Co(II) atom is coordinated by one N_2O_4 chromophore system with a distorted octahedral geometry. One oxygen atom of each (2-py)$_2$C(OH)O$^-$ ligands remains protonated, without binding to any metal centre. The resultant mono anion functions as a $\eta^1{:}\eta^3{:}\eta^1{:}\mu_3$ ligand forming two five membered CoNCCO chelating rings with two Co(II) metal centres which share a common C–O bridge. There are two types of Co–O(μ_3) bond for each metal ion, where one bond is elongated compared to the adjacent one. The average ∠Co(1)–O–Co(2) angle of 97.16° is lower as compared to the average ∠Co(3)–O–Co(4) angle, 98.07°. A large number of intracubane hydrogen bonds are present in **2**, which reinforce the framework of the cubes. Each hydroxyl group of (2-py)$_2$C(OH)O$^-$ is intramolecularly hydrogen bonded strongly to an O atom from a monodentate acetate anion. One notable feature is that the non-coordinating oxygen atoms in the hydroxyl group

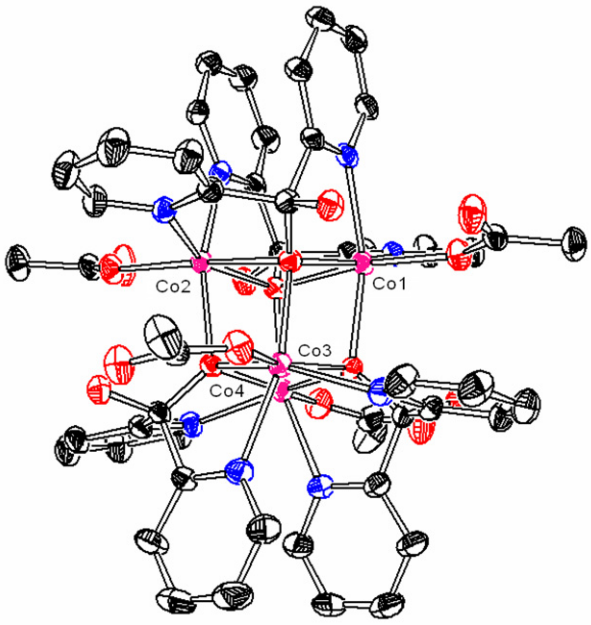

Fig. 4. ORTEP (30% probability) of **2** (hydrogens are omitted for clarity).

in $(2\text{-py})_2C(OH)O^-$ and the terminal acetate participate in intracubane hydrogen bonding. One chair type hydrogen bonding is noticed between the solvated water molecules and the non-coordinating oxygen atoms in the hydroxyl group in $(2\text{-py})_2C(OH)O^-$ and the terminal acetate. The chair consists of two five membered and a central rectangular hydrogen bonding. The water molecules are in a chain in the chair hydrogen bonding where each side is occupied by three water molecules. Besides those interactions, there are π–π stacked interactions, C1···C2 along $-x+1, -y, -z+1$ and C1···C1 along $-x+1, -y, -z+1$, of 3.159(4) and 3.355(3) Å, respectively.

3.3. Magnetic studies

The tetranuclear cluster molecule **2** exhibits a $\chi'_M T$ value of 6.53 $cm^3\ mol^{-1}\ K$ at 293 K, where a spin-only value of 7.3 $cm^3\ mol^{-1}\ K$ is expected for four uncoupled Co(II) centres with a ground state $^4T_1(S = 3/2)$ with $g = 2$, where χ'_M is the molar AC susceptibility for the real component. The important reason for this difference is that the orbital contribution to the magnetic moment is significant as the orbital degeneracy of this state is not quenched. The $\chi'_M T$ value continuously decreases upon cooling from a value of 6.53 $cm^3\ mol^{-1}\ K$ at 293 K to a value of 3.02 $cm^3\ mol^{-1}\ K$ at 25 K. The $\chi'_M T$ value deceases steadily from 293 to 100 K, but below 100 K it decreases suddenly. The χ'_M value increases continuously from a value of 0.0232 $cm^3\ mol^{-1}$ at 293 K to 0.0751 $cm^3\ mol^{-1}$ at 25 K. The overall behavior is a clear indication of an antiferromagnetic nature present in **2** below 100 K. Analysis of the coupling constants of the cobalt(II) tetramer is difficult by means of an effective Hamiltonian based on four $S = 3/2$ spins due to the large anisotropy of this ion [13]. The experimental data were fitted with the help of ORIGIN 6.0 software, using the expression derived from the isotropic Heisenberg Hamiltonian $H = -J_1(S_1S_4 + S_2S_3) - J_2(S_1S_2 + S_3S_4) - J_3(S_1S_3 + S_2S_4)$. The best fit parameters were $J_1 = -21.86\ cm^{-1}$, $J_2 = -14.81\ cm^{-1}$, $J_3 = -10.55\ cm^{-1}$ and $g = 2.03$. The $1/\chi'_M$ *versus* T plot shown in Fig. 5 was fitted with the simple Curie–Weiss law $\chi'_M = C/(T-\theta)$, which shows an antiferromagnetic behavior with $C = 8.14$ and $\theta = -69.26 \pm 0.06$ K. The effective magnetic moment (μ_{eff}) was calculated from the least square fitting and is 3.63 BM per cobalt atom.

4. Conclusion and perspectives

Water readily shows nucleophilic addition to the C=O group upon coordination of the 2-pyridyl ring of the ligands, forming the *gem*-diol form of $(2\text{-py})_2CO$. By coordinating through the two pyridine nitrogen atoms and one oxygen atom from the newly formed *gem*-diol, the ligand becomes tridentate rather than bidentate, as might be expected. The tetranuclear cluster molecule of $[Co_4\{OC(OH)(2\text{-pyridyl})_2\}_4[OAc]_4] \cdot 7H_2O$ (**2**) has a cubane core with alternate vertices occupied by Co(II) and oxygen atoms, consisting of two interpenetrating tetrahedra. The $1/\chi'_M$ *versus* T plot fitted with the simple Curie–Weiss law $\chi'_M = C/(T-\theta)$, and shows an antiferromagnetic behavior with $C = 8.14$ and $\theta = -69.25 \pm 0.06$ K.

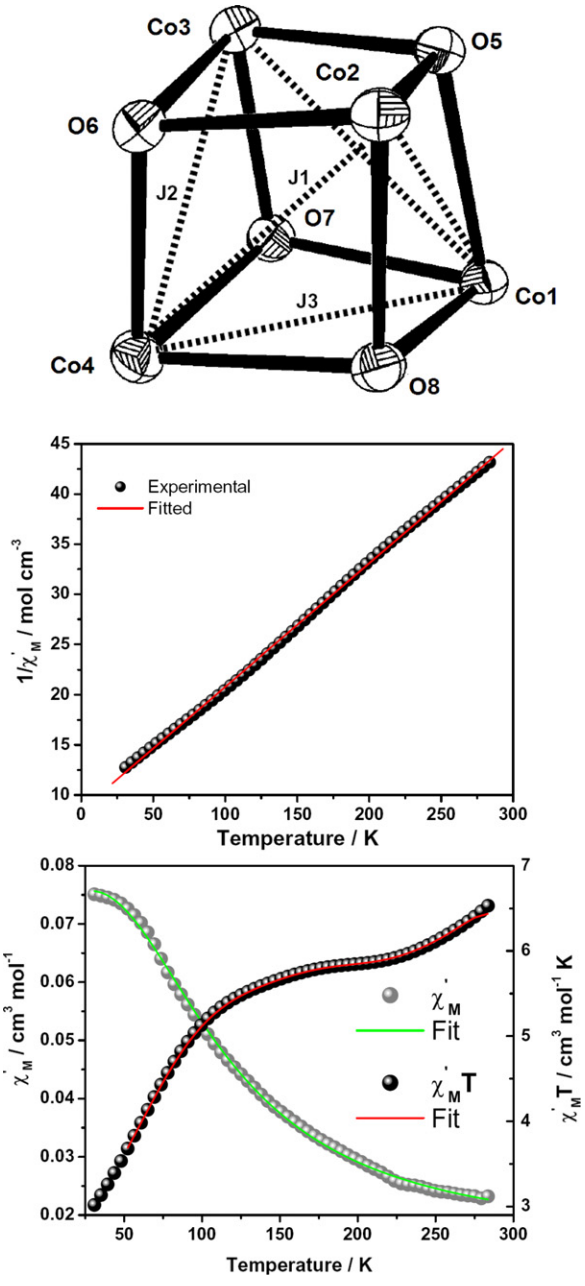

Fig. 5. Assignments of J values and AC susceptibility plot in **2**.

Supplementary data

CCDC 627293 and 645238 contain the supplementary crystallographic data for this paper. These data can be obtained free of charge via http://www.ccdc.cam.ac.uk/conts/retrieving.html, or from the Cambridge Crystallographic Data Centre, 12 Union Road, Cambridge CB2 1EZ, UK; fax: (+44) 1223-336-033, or e-mail: deposit@ccdc.cam.ac.uk.

Acknowledgements

Dr. V. Manivannan is acknowledged in affording the proper accomplishment and giving us the opportunity to communicate this paper. We are grateful to the Department of Science and Technology (DST) New Delhi for establishing the single crystal X-ray diffractometer facility under FIST scheme. The authors are thankful to Babulal Das for X-ray data and CIF IIT Guwahati for VSM facilities, and Dr. S. Ravi for AC susceptibility measurements.

References

[1] (a) R.M. Cinco, A. Rompel, H. Visser, G. Aromi, G. Christou, K. Sauer, M.P. Klein, V.K. Yachandra, Inorg. Chem. (38) (1999) 5988;
(b) G. Christou, D. Gatteschi, D.N. Hendrickson, R. Sessoli, MRS Bull. 25 (2000) 1;
(c) D. Gatteschi, R. Sessoli, A. Cornia, Chem. Commun. (2000) 725;
(d) R.E.P. Winpenny, J. Chem. Soc., Dalton Trans. (2002) 1.

[2] (a) R.E.P. Winpenny, Adv. Inorg. Chem. 52 (2001) 1;
(b) R.E.P. Winpenny, J. Chem. Soc., Dalton Trans. (2002) 1.

[3] (a) A.J. Tasiopoulos, A. Vinslava, W. Wernsdorfer, K.A. Abboud, G. Christou, Angew. Chem., Int. Ed. 43 (2004) 2117;
(b) M. Murugesu, K.A. Abboud, G. Christou, J. Chem. Soc., Dalton Trans. (2003) 4552;
(c) S. Langley, M. Helliwell, J. Raftery, E.I. Tolis, R.E.P. Winpenny, Chem. Commun. (2004) 142;
(d) L.F. Jones, E.K. Brechin, D. Collison, A. Harrison, S.J. Teat, W. Wernsdorfer, Chem. Commun. (2002) 2974;
(e) T.K. Paine, E. Rentschler, T. Weyhermüller, P. Chaudhuri, Eur. J. Inorg. Chem. (2003) 3167;
(f) J. Overgaard, B.B. Iversen, S.P. Palii, G.A. Timco, N.V. Gerbeleu, F.K. Larsen, Chem. Eur. J. 8 (2002) 2775;
(g) X. Liu, J.A. McAllister, M.P. de Miranda, E.J.L. McInnes, C.A. Kilner, M.A. Halcrow, Chem. Eur. J. 10 (2004) 1827;
(h) T.S.M. Abedin, L.K. Thompson, D.O. Miller, E. Krupicka, Chem. Commun. (2003) 708;
(i) M. Murugesu, C.E. Anson, A.K. Powell, Chem. Commun. (2002) 1054;
(j) G.L. Abati, A. Cornia, A.C. Fabretti, A. Caneschi, D. Gatteschi, Inorg. Chem. 37 (1998) 1430.

[4] (a) D. Gatteschi, R. Sessoli, Angew. Chem., Int. Ed. 42 (2003) 268;
(b) G. Christou, D. Gatteschi, D.N. Hendrickson, MRS Bull. 25 (2000) 66.

[5] (a) R. Sessoli, D. Gatteschi, Angew. Chem., Int. Ed. 42 (2003) 268;
(b) M. Murugesu, W. Wernsdorfer, K.A. Abboud, G. Christou, Angew. Chem., Int. Ed. 44 (2005) 892;
(c) E.K. Berchin, Chem. Commun. (2005) 5141;
(d) D. Gatteschi, R. Sessoli, A. Cornia, Chem. Commun. (2000) 725;
(e) M.P. Shores, J.J. Sokol, J.R. Long, J. Am. Chem. Soc. 124 (2002) 2279;
(f) E.J. Schelter, A.V. Prosvirin, K.R. Dunbar, J. Am. Chem. Soc. 126 (2004) 15004;
(g) Y. Song, P. Zhang, X.M. Ren, X.F. Shen, Y.Z. Li, X.Z. You, J. Am. Chem. Soc. 127 (2005) 3708.

[6] (a) M.A. Banares, L. Dauphin, V. Calvo-Perez, T.P. Fehlner, E.E. Wolf, J. Catal. 152 (1995) 396;
(b) B.C. Gates, Catalytic Chemistry, Wiley-Interscience, New York, 1992.

[7] R.E.P. Winpenny, in: J.A. McCleverty, T.J. Meyer (Eds.), Comprehensive Coordination Chemistry, vol. 7, Pergamon Press, Oxford, 2004, p. 125 (Chapter 7.3).

[8] (a) C.J. Milios, E. Kefalloniti, C.P. Raptopoulou, A. Terzis, R. Vicente, N. Lalioti, A. Escuer, S.P. Perlepes, Chem. Commun. (2003) 819;
(b) N. Lalioti, C.P. Raptopoulou, A. Terzis, A.E. Aliev, I.P. Gerothanassis, E. Manessi-Zoupa, S.P. Perlepes, Angew. Chem., Int. Ed. 40 (2001) 3211;
(c) A. Tsohos, S. Dionyssopoulou, C.P. Raptopoulou, A. Terzis, E.G. Bakalbassis, S.P. Perlepes, Angew. Chem., Int. Ed. 38 (1999) 983;
(d) V. Tangoulis, C.P. Raptopoulou, S. Paschalidou, E.G. Bakalbassis, S.P. Perlepes, A. Terzis, Angew. Chem., Int. Ed. Engl. 36 (1997) 1083;
(e) V. Tangoulis, C.P. Raptopoulou, A. Terzis, S. Paschalidou, S.P. Perlepes, E.G. Bakalbassis, Inorg. Chem. 36 (1997) 3996.

[9] (a) M.-L. Long, S.-L. Zheng, J.-X. Shi, Y.-X. Tong, H.K. Lee, X.-M. Chen, J. Chem. Soc., Dalton Trans. (2002) 1727;
(b) S.B. Jedner, H. Schwöppe, H. Nimir, A. Rompel, D.A. Brown, B. Krebs, Inorg. Chim. Acta 340 (2002) 181;
(c) S.R. Breeze, S. Wang, J.E. Greedan, N.P. Raju, Inorg. Chem. 35 (1996) 6944.

[10] (a) K.N. Crowder, S.J. Garcia, R.L. Burr, J.M. North, M.H. Wilson, B.L. Conley, P.E. Fanwick, P.S. White, K.D. Sienerth, R.M. Granger II, Inorg. Chem. 43 (2004) 72;
(b) G. Crundwell, B.L. Westcott, R. Coffey, M. Zeller, A.D. Hunter, Inorg. Chim. Acta 355 (2003) 432;
(c) J. Woltz, B.L. Westcott, G. Crundwell, M. Zeller, A.D. Hunter, S.O. Sommerer, Acta Crystallogr., Sect. E 58 (2002) 609;
(d) A.K. Boudalis, F. Dahan, A. Bousseksou, J.-P. Tuchagues, S.P. Perlepes, J. Chem. Soc., Dalton Trans. (2003) 3411;
(e) E. Katsoulakou, N. Lalioti, C.P. Raptopoulou, A. Terzis, E. Manessi-Zoupa, S.P. Perlepes, Inorg. Chem. Commun. 5 (2002) 719;
(f) S. Zhou, W.W. Brennessel, R.G. Harrison, L. Que Jr., Inorg. Chim. Acta 337 (2002) 32;
(g) M.G. Barandika, Z. Serna, R. Cortes, L. Lezama, M.K. Urtiaga, M.I. Arriortua, T. Rojo, Chem. Commun. (2001) 45;
(h) Z.E. Serna, R. Cortes, M.K. Urtiaga, M.G. Barandika, L. Lezama, M.I. Arriortua, T. Rojo, Eur. J. Inorg. Chem. (2001) 865;
(i) M.-L. Tong, H.K. Lee, Y.-X. Tong, X.-M. Chen, T.C.W. Mak, Inorg. Chem. 39 (2000) 4666;
(j) V. Tangoulis, C.P. Raptopoulou, S. Paschalidou, A. Tsohos, E.G. Bakalbassis, A. Terzis, S.P. Perlepes, Inorg. Chem. 36 (1997) 5270;
(k) A.C. Deveson, S.L. Heath, C.J. Harding, A.K. Powell, J. Chem. Soc., Dalton Trans. (1996) 3173;
(l) A.N. Papadopoulos, V. Tangoulis, C.P. Raptopoulou, A. Terzis, D.P. Kessissoglou, Inorg. Chem. 35 (1996) 559.

[11] (a) G.M. Sheldrick, SADABS, University of Göttingen, Göttingen, Germany, 1996.;
(b) SMART and SAINT, Siemens Analytical X-ray Instruments Inc., Madison, WI, 1996.;
(c) G.M. Sheldrick, SHELXS-97 and SHELXL-97, University of Göttingen, Göttingen, Germany, 1997.

[12] (a) A.B.P. Lever, Inorganic Electronic Spectroscopy, Elsevier, Amsterdam, 1986;
(b) J.D. Ortego, M. Seymour, Polyhedron 1 (1982) 29;
(c) A. Grirrane, A. Pastor, E. A'lvarez, C. Mealli, A. Ienco, D. Masi, A. Galindo, Inorg. Chem. Commun. 8 (2005) 463.

[13] (a) C.J. O'Connor, Prog. Inorg. Chem. 29 (1982) 203;
(b) O. Kahn, Molecular Magnetism, Wiley–VCH, 1993;
(c) D.K. Arcon, K. Prassides, p-Electron magnetism, in: J. Veciana (Ed.), Structure and Bonding, vol. 100, Springer, Berlin, 2001, p. 129;
(d) A. Tsohos, S. Dionyssopoulou, C.P. Raptopoulou, A. Terzis, E.G. Bakalbassis, S.P. Perlepes, Angew. Chem., Int. Ed. 38 (1999) 983;
(e) G.S. Papaefstathiou, A. Escuer, F.A. Mautner, C. Raptopoulou, A. Terzis, S.P. Perlepes, R. Vicente, Eur. J. Inorg. Chem. (2005) 879;
(f) Z.E. Serna, M.K. Urtiaga, M.G. Barandika, R. Cortes, S. Martin, L. Lezama, M.I. Arriortua, T. Rojo, Inorg. Chem. 40 (2001) 4550;
(g) G.S. Papaefstathiou, A. Escuer, C.P. Raptopoulou, A. Terzis, S.P. Perlepes, R. Vicente, Eur. J. Inorg. Chem. (2001) 1567;
(h) K.S. Murray, Adv. Inorg. Chem. 43 (1995) 261.

Polyhedron 27 (2008) 2667–2671

Contents lists available at ScienceDirect

Polyhedron

journal homepage: www.elsevier.com/locate/poly

Synthesis, characterization and X-ray crystal structure of the trigonal-planar copper(I) complex $[Cu(MIBI)_3]^+$ (MIBI = 2-methoxyisobutylisocyanide)

Micol Pasquali, Valeria Ferretti, Adriano Duatti *

Laboratory of Nuclear Medicine, Department of Radiological Sciences, and Centre for Structural Diffractometry, Department of Chemistry, University of Ferrara, 44100 Ferrara, Italy

ARTICLE INFO

Article history:
Received 18 February 2008
Accepted 13 May 2008
Available online 27 June 2008

Keywords:
Trigonal-planar copper complexes
Copper isocyanide complexes
Cu-MIBI
^{99m}Tc-MIBI

ABSTRACT

The synthesis, spectroscopic and chromatographic characterization, and X-ray crystal structure of the complex tris(2-methoxyisobutylisocyano) copper(I) tetrafluoroborate, $[Cu(MIBI)_3][BF_4]$, is reported. The Cu atom lies on threefold axis and is bonded to three 2-methoxyisobutylisocyano ligands in a perfect trigonal-planar coordination. The calculated and experimental powder-diffraction spectra of this complex are also reported.

© 2008 Elsevier Ltd. All rights reserved.

1. Introduction

Mononuclear copper(I) complexes with isocyanide derived ligands is a well-established class of organometallic compounds [1]. Usually, these complexes display a tetrahedral geometry with four isocyanide ligands bound to the same Cu^+ ion through the carbon atom of the carbon–nitrogen triple bond. However, an interesting feature of this category of complexes comes from the fact that they may also exist in a trigonal-planar arrangement, in which only three isocyanide ligands are coordinated to the same metal center. Commonly, this behavior is interpreted by considering the strength of the π-acceptor interaction between the electron-rich Cu(I) atom and the isocyanide ligand [2].

The ligand 2-methoxyisobutylisocyanide (MIBI) occupies a relevant position in nuclear cardiology since it is employed for the preparation of the heart perfusion imaging agent ^{99m}Tc-MIBI (commercial name, Cardiolite®) [3]. This monocationic organometallic radiopharmaceutical is formed by a Tc(I) atom coordinated to six MIBI ligands in an octahedral geometry. Interestingly, the routine preparation of this imaging agent in hospital radiopharmacies is carried out through a ligand exchange reaction between the four-coordinated Cu(I) complex $[Cu(MIBI)_4]^+$ and the *in situ* formed Tc^+ ion.

The synthesis of $[Cu(MIBI)_4]^+$ was reported previously along with X-ray crystal structure determination of the corresponding tetrafluoroborate salt [4]. As expected, X-ray diffraction data showed that this complex has a tetrahedral coordination geometry with four MIBI ligands bound to the same Cu(I) center. In another publication, the synthesis of the three-coordinated complex $[Cu(MIBI)_3]^+$ was also described [5]. However, no structural characterization of this complex has been reported so far.

This study reports the synthesis, characterization and X-ray crystal structure of the tetrafluoroborate salt of the complex $[Cu(MIBI)_3]^+$. Based on structural data, the powder-diffraction spectrum of this complex was calculated and compared with the same spectrum as experimentally determined. Comparison between the powder-diffraction spectra of the four-coordinated and three-coordinated Cu(I) complexes with MIBI ligand is also reported.

2. Experimental

2.1. Materials

The ligand 2-methoxyisobutylisocyanide (IUPAC name: 2-methoxy-2-methylpropan isocyanide) was obtained from ABX, Radeberg, Germany. The compounds $[Cu(CH_3CN)_4][BF_4]$ [6] and $[Cu(MIBI)_4][BF_4]$ [4] were prepared as reported elsewhere. All laboratory chemicals and solvents (Fluka) were reagent grade and used without further purification.

2.2. Instrumentation

Elemental analyses (C, H, N) were performed on a Carlo Erba 1106 elemental analyzer. FT-IR spectra were recorded on a Nicolet 510P Fourier-transform spectrometer in the range 4000–200 cm^{-1} in KBr mixtures using a Spectra-Tech diffuse-reflectance collector

* Corresponding author. Tel.: +39 0532 455354; fax: +39 0532 236589.
E-mail address: dta@unife.it (A. Duatti).

0277-5387/$ - see front matter © 2008 Elsevier Ltd. All rights reserved.
doi:10.1016/j.poly.2008.05.018

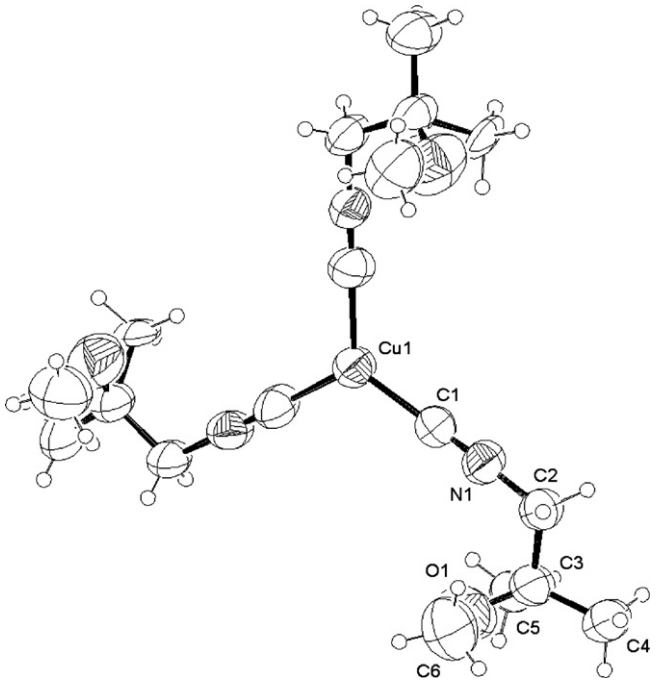

Fig. 1. ORTEPIII [11] view and atom numbering scheme for the tris(2-methoxyisobutylisocyano) copper(I) cation. Ellipsoids are drawn at 40% probability.

accessory. Proton NMR spectra were collected on a Bruker AC-300 instrument using $SiMe_4$ as internal reference. Positive ion fast atom bombardment mass spectra (FAB^+ MS) of selected complexes in an NBA matrix were recorded on a VG 30-250 spectrometer (VG Instrument) at the probe temperature. Xe was used as the primary beam gas, and the ion gun was operated at 8 keV (ca. 1.28×10–15 J) and 100 μA.

2.3. Synthesis

The complex $[Cu(MIBI)_3][BF_4]$ was prepared as reported previously [5] with only minor modification as briefly described below.

$[Cu(CH_3CN)_4][BF_4]$ (1.07 g, 3.38 mmol) and chloroform (40 mL) were placed in a round-bottom flask equipped with a magnetic bar. The mixture was stirred for 5 min, at room temperature and under a nitrogen atmosphere. $[Cu(MIBI)_4][BF_4]$ (6.13 g, 10.2 mmol) was then added and the reaction mixture was further stirred to form a clear solution. Stirring was continued for additional 30 min and, then, the solvent was evaporated under reduced pressure to obtain a semi-solid residue, which was dried with a high-vacuum pump to give a white solid. This solid was dissolved in a chloroform (50 mL)/ethyl acetate (50 mL) mixture followed by addition of diethyl ether (≈150 mL) to form a cloudy suspension. This suspension was kept at low temperature (4 °C) overnight to yield a microcrystalline solid, which was filtered and dried under vacuum. Yield, 5.2 g (78%).

Crystals suitable for X-ray diffraction were obtained by dissolving part of the solid product (1.2 g) in a mixture of acetone (60 mL) and *n*-propanol (20 mL), and by allowing the resulting solution to slowly evaporate, at room temperature, under air atmosphere. Crystals were collected when some residual solvent was still present (≈10 mL) and, then, washed with *n*-propanol and diethyl ether.

Elemental *Anal.* Calc. for $C_{15}H_{33}N_3O_3CuBF_4$: C, 44.14; H, 6.79; N, 8.58. Found: C, 44.17; H, 6.82; N, 8.51%.

FT-IR (KBr, cm^{-1}): 2982–2839 ν(C–H), 2215 ν(N≡C), 1080 ν(B–F) and ν(C–O–C).

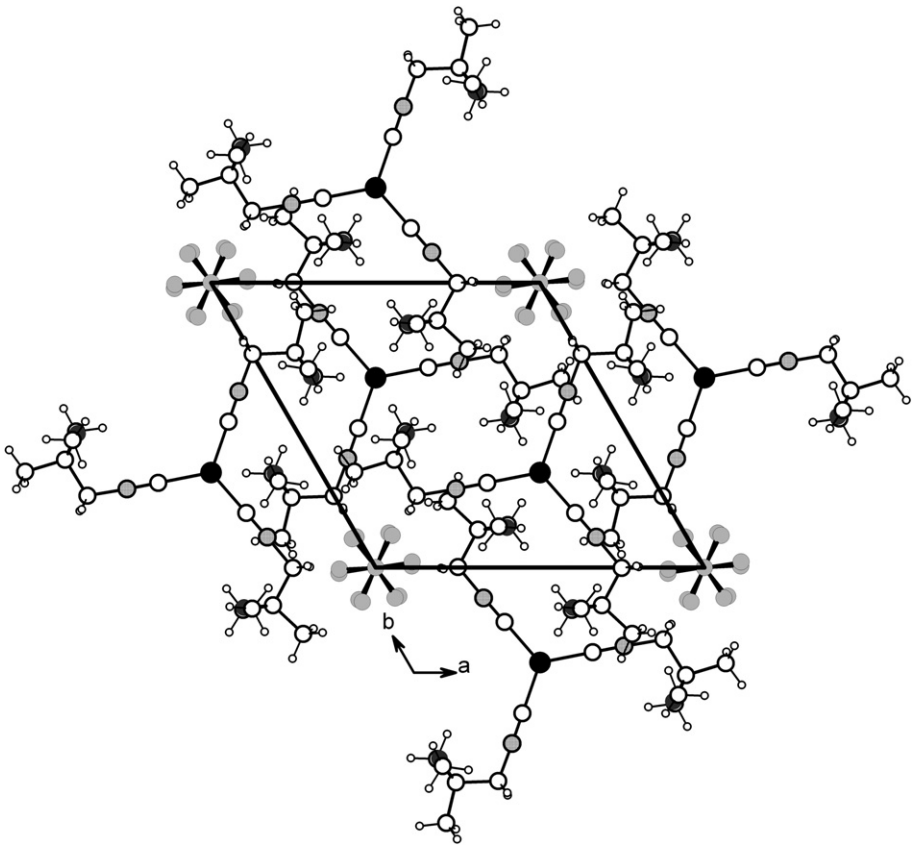

Fig. 2. Packing diagram (view along *c*).

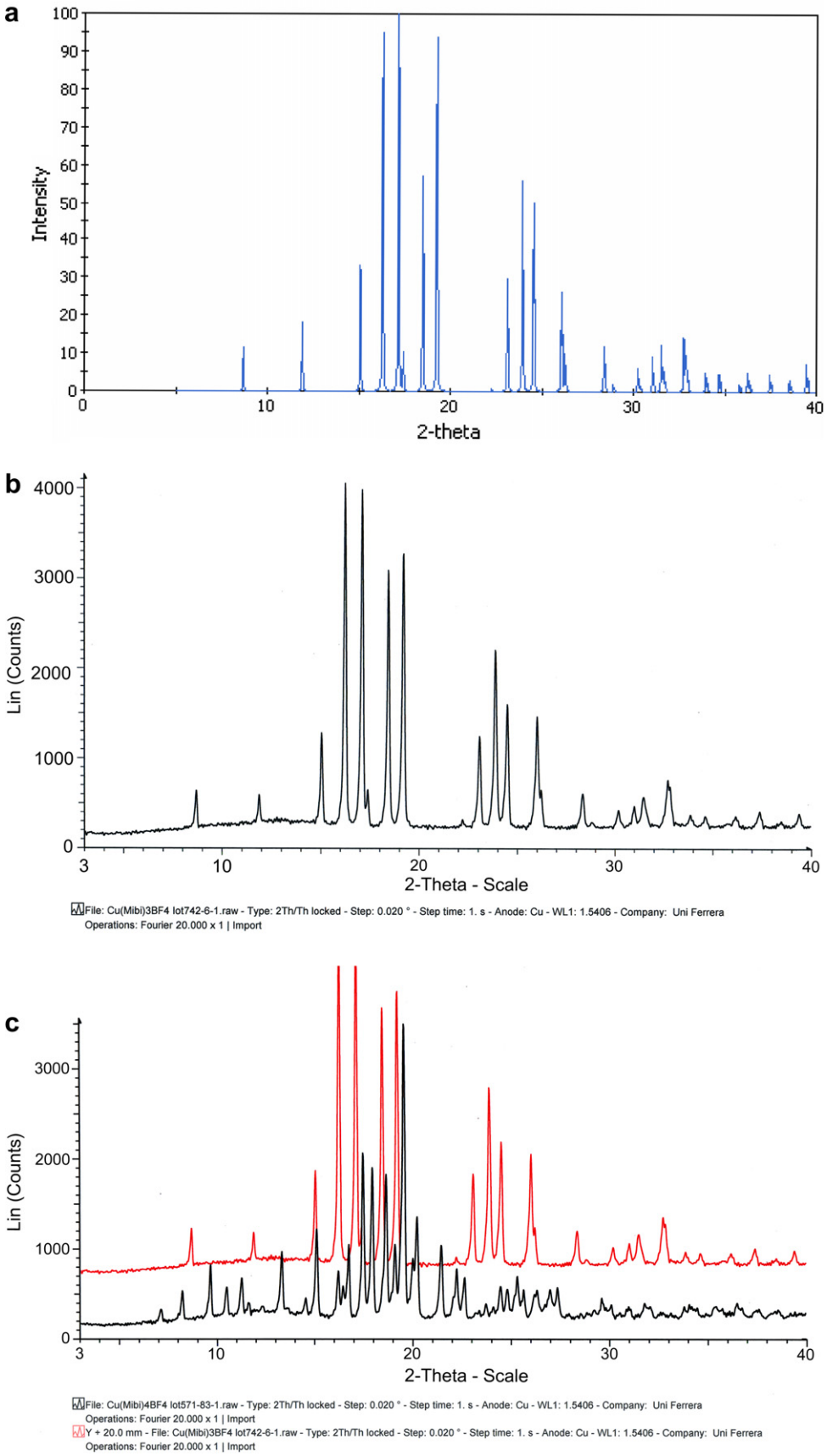

Fig. 3. Calculated [MaterialStudio system of programs, Accelrys Inc., 2003] (a) and experimental (b) powder-diffraction spectrum of the title compound. (c) Superimposed experimental spectra of $[Cu(MIBI)_3][BF_4]$ (upper) and $[Cu(MIBI)_4][BF_4]$ (space group: $P2_12_12_1$, cell parameters: $a = 15.198(2)$, $b = 21.478(4)$, $c = 10.095(3)$).

^{1}H NMR ($CDCl_3$, ppm): 1.25 (s, CH_3), 3.23 (s, OCH_3), 3.67 (s, CH_2).

^{13}C NMR ($CDCl_3$, ppm): 22.58 (s, CH_3), 50.13 (s, OCH_3), 52.03 (s, CH_2), 73.40 (s, CH_2C), 137.60 (broad, N≡C).

FAB$^+$ MS (*m/z*): 404, 402 [M^+], 291, 289 [M^+−MIBI].

2.4. Chromatography

High performance liquid chromatography (HPLC) was performed on a System Gold Instrument equipped with a programmable solvent Module 126, a scanning detector Module 166, and a radioisotope detector Module 170 (Beckman Instruments, Fullerton, CA, USA). Chromatographic analyses were carried out on a Restek Allure Basic column (150 × 4.6 mm, ∅ = 5 μm) using the following conditions. Mobile phase: A = ammonium acetate, B = CH_3CN; gradient: 0–10 min, B = 50%, 10–15 min, B = 100%.

2.5. X-ray crystallography and powder diffraction

Data collection was performed on a Nonius Kappa CCD area detector diffractometer using graphite-monochromatized Mo Kα radiation (λ = 0.71073 Å). All intensities were corrected for Lorentz polarization and absorption effects [7]. The structure was solved by direct methods with the SIR97 program [8] and refined on F^2 by full-matrix least-squares methods with anisotropic non-H atoms using SHELXL-97 [9]. Hydrogen atoms were included on calculated positions, riding on their carried atoms. All other calculations were performed using the program PARST [10]. Molecular drawing was obtained using ORTEPIII [11].

Crystal data for tris(2-methoxyisobutylisocyano) copper(I) tetrafluoroborate: crystal dimensions, 0.41 × 0.23 × 0.20 mm, F_w = 489.83 g/mol, hexagonal, space group, $P6_3$, a = 11.7517(3) Å, c = 10.8845(3) Å, V = 1301.79(6) Å^3, Z = 2, D_{Calc} = 1.250 g cm^{-3}, $F(000)$=512, μ(Mo Kα) = 0.887 mm^{-1}, T = 295 K. Measured, independent and observed reflections: 17895, 2091, 1630 [$I > 2\sigma(I)$], R(int) 0.0361, 127 parameters; R [on $F^2 > 2\sigma(F^2)$], wR (on F^2), S: 0.051, 0.157, 1.04.

Powder-diffraction spectra were recorded, at room temperature, on a Bruker D-8 Advance diffractometer with graphite-monochromatized Cu Kα radiation (λ = 1.5406 Å). The data were recorded at 2θ steps of 0.02° with 1 s/step.

3. Results and discussion

The complex $[Cu(MIBI)_3]^+$ was prepared by ligand exchange between the four-coordinated complexes $[Cu(MIBI)_4]^+$ and $[Cu(CH_3CN)_4]^+$. Formally the reaction can be thought to proceed through the transfer of one-coordinated MIBI ligand from each of three $[Cu(MIBI)_4]^+$ complexes to a single $[Cu(CH_3CN)_4]^+$, with the concomitant release of four CH_3CN ligands. This hypothetical exchange yields four molecules of the three-substituted $[Cu(MIBI)_3]^+$ complex as illustrated in the reaction diagram below:

$$3[Cu(MIBI)_4]^+ + [Cu(CH_3CN)_4]^+ \rightarrow 4[Cu(MIBI)_3]^+ + 4\ CH_3CN.$$

Characterization of this compound was carried out by elemental analysis, and by spectroscopic and chromatographic methods. Solid-state and structural determinations were conducted by X-ray powder and single-crystal diffraction studies.

HPLC chromatography showed only a single peak at 8.1 min, thus suggesting the presence of a definite compound.

In the FAB mass spectrum of $[Cu(MIBI)_3]^+$, collected in the positive ion mode, a peak doublet was found at 404, 402 corresponding to the parent ion with the expected isotopic ratio (isotopic abundance, ^{63}Cu = 69.1% and ^{65}Cu = 30.9%). An additional peak was observed at 291, 289 and was associated with the fragment $[Cu(MIBI)_2]^+$ generated through the loss of one MIBI ligand.

The FT-IR spectrum of $[Cu(MIBI)_3]^+$ was consistent with the presence of MIBI ligands coordinated to the metal center. Similarly, ^{1}H and ^{13}C NMR spectra showed characteristic resonance peaks corresponding to functional groups of coordinated MIBI ligands. Interestingly, both FT-IR and NMR spectra of $[Cu(MIBI)_3]^+$ do not substantially differ from those recorded for the four-coordinated complex $[Cu(MIBI)_4]^+$. This result can be easily interpreted by considering that key factors in determining the positions of both vibrational bands and resonance peaks are much dependent on the nature of functional groups of the coordinated ligands and on their reciprocal position within the structure of the metal complex. When the symmetry of the complex leads all the coordinated ligands to become geometrically equivalent, and there is no change in the electronic density on the metal, no significant spectroscopic differences are expected between two closely related complexes differing only in the number of identical ligands bound to the same metal ion.

This observation clearly indicates that the complex $[Cu(MIBI)_3]^+$ should possess a geometry in which the three-coordinated MIBI ligands are all equivalent, and that differences between the four- and three-coordinated complexes should arise mainly at the solid-state. This prediction was nicely confirmed by results of X-ray studies carried out on these two complexes. In particular, the structure of single crystals of $[Cu(MIBI)_3][BF_4]$, obtained from acetone/*n*-propanol, provided unambiguous assignment of the identity of the three-coordinated complex.

Fig. 1 reports the X-ray crystal structure of the compound $[Cu(MIBI)_3][BF_4]$. The Cu atom lies on special position (threefold axis) and is bonded to three 2-methoxyisobutylisocyano ligands in a perfect trigonal-planar coordination with the two terminal methyl groups disordered over two almost equivalent positions (occupancies: 0.4 and 0.6). The cations are isolated and there are no interactions between adjacent copper atoms (Cu···Cu distance: 8.698 Å). The Cu–C1 bond length of 1.917(3) Å is in good agreement with those found in other similar Cu trigonal complexes, which are in the range 1.88–1.95 Å (16 compounds retrieved from the Cambridge Structural Database [12]). The other relevant bond distances involving the bound CN group, C1–N1 = 1.142(4) Å and N1–C2 = 1.435(4) Å, do not show any significant discrepancy from structural parameters of similar groups. The tetrafluoroborate anion is positioned as well on a threefold axis with the fluorine atoms disordered over two non-equivalent positions. In the crystal the different units interact with each other through weak C–H···O and C–H···F intermolecular interactions, mean H···F and H···O interaction distances being 2.42 and 2.45 Å, respectively, for C–H···X angles >140°. The packing diagram is shown in Fig. 2. Comparable weak interactions are found in the crystal structure of $[Cu(MIBI)_4][BF_4]$ [4], showing mean H···F and H···O distances of 2.40 and 2.70 Å, respectively.

Structural data allowed to calculate the theoretical X-ray powder spectrum of $[Cu(MIBI)_3][BF_4]$ as illustrated in Fig. 3a. This appears almost superimposable with the same spectrum determined experimentally (Fig. 3b). Comparison between powder spectra of $[Cu(MIBI)_3][BF_4]$ and $[Cu(MIBI)_4][BF_4]$ is reported in Fig. 3c. These spectra clearly show that physico-chemical differences between the two Cu(I) complexes mainly occur at the solid-state as a result of the different chemical composition and structural geometry.

4. Conclusion

The three-coordinated trigonal-planar Cu(I) complex $[Cu(MIBI)_3]^+$ has been structurally characterized and its spectroscopic properties compared with those of the four-coordinated analogue $[Cu(MIBI)_4]^+$. Experimental findings showed that there exist no significant differences in stretching frequencies and magnetic reso-

nance signals between four- and three-coordinated MIBI ligands, thus indicating that the electronic density and metal–ligand bond strengths are almost the same in the two complexes. Moreover, both tetrahedral and trigonal-planar geometries determine a perfect equivalence of coordinated MIBI ligands that contributes to further averaging of the properties of the two copper complexes.

Acknowledgements

The authors thank Mr. Gabriele Bertocchi for providing X-ray powder spectral data.

Appendix A. Supplementary data

CCDC 676490 contains the supplementary crystallographic data for $[Cu(MIBI)_3][BF_4]$. These data can be obtained free of charge via http://www.ccdc.cam.ac.uk/conts/retrieving.html, or from the Cambridge Crystallographic Data Centre, 12 Union Road, Cambridge CB2 1EZ, UK; fax: (+44) 1223-336-033, or e-mail: deposit@ccdc.cam.ac.uk.

References

[1] F.A. Cotton, G. Wilkinson, C.A. Murillo, M. Bochmann, Advanced Inorganic Chemistry, 6th ed., John Wiley & Sons, New York, 1999.
[2] J.L. Wardell (Ed.), Comprehensive Organometallic Chemistry II, vol. 3, Elsevier Science Ltd., 1995.
[3] J.P. Norenberg, M.P. Vaidya, W.B. Hladik III, D.R. Pathak, J.L. Born, T.L. Anderson, T.R. Carroll, J. Nucl. Med. Technol. 33 (2005) 34.
[4] B. Deicas, D. Gambino, C. Kremer, E. Kremer, A. Mombrù, L. Suescum, R. Mariezcurrena, O. González, A. Rey, L. Mallo, A. Leon, Polyhedron 16 (1997) 2397.
[5] T. Iqbal, J.H. Cain, Jr., J.J. Spek, Cryst. Struct. Commun. 11 (1982) 413.
[7] R.H. Blessing, Acta Crystallogr., Sect. A 51 (1995) 33.
[8] A. Altomare, M.C. Burla, M. Camalli, G.L. Cascarano, C. Giacovazzo, A. Guagliardi, A.G.G. Moliterni, G. Polidori, R. Spagna, J. Appl. Crystallogr. 32 (1999) 115.
[9] G.M. Sheldrick, SHELX97, "Program for crystal structure refinement", University of Göttingen, Germany, 1997.
[10] M. Nardelli, J. Appl. Crystallogr. 28 (1995) 659.
[11] M.N. Burnett, C.K. Johnson, Report ORNL-6895, Oak Ridge National Laboratory, Oak Ridge, TN, USA, 1996.
[12] F.H. Allen, S. Bellard, M.D. Brice, B.A. Cartwright, A. Doubleday, H. Higgs, T. Hummelink, B.G. Hummelink-Peters, O. Kennard, W.D.S. Motherwell, J. Rodgers, D.G. Watson, Acta Crystallogr., Sect. B 35 (1979) 2331.

Polyhedron 27 (2008) 2672–2680

Contents lists available at ScienceDirect

Polyhedron

journal homepage: www.elsevier.com/locate/poly

pH-dependent self-assembly of copper(II) complexes with a new imidazole-containing polyamine ligand: Synthesis, structure and magnetic property

Zhao-Peng Qi [a], Zheng-Shuai Bai [a], Qing Yuan [a], Taka-aki Okamura [b], Kai Cai [a], Zhi Su [a], Wei-Yin Sun [a,*], Norikazu Ueyama [b]

[a] Coordination Chemistry Institute, State Key Laboratory of Coordination Chemistry, School of Chemistry and Chemical Engineering, Nanjing University, Nanjing 210093, China
[b] Department of Macromolecular Science, Graduate School of Science, Osaka University, Toyonaka, Osaka 560-0043, Japan

ARTICLE INFO

Article history:
Received 21 April 2008
Accepted 16 May 2008
Available online 18 June 2008

Keywords:
Imidazole-containing ligand
Copper(II)
pH-dependent
Magnetic property

ABSTRACT

Four copper(II) complexes were synthesized by reactions of new imidazole-containing polyamine ligand N^1-(2-aminoethyl)-N^1-(1*H*-imidazol-4-ylmethyl)-ethane-1,2-diamine (HL) with $Cu(ClO_4)_2 \cdot 6H_2O$ under different pH and their structures were characterized by X-ray crystallography. Interestingly, the complexes have diverse structures from protonated ligand $[H_3(HL)][CuCl_4] \cdot Cl$ (**1**), dinuclear $[Cu_2(HL)_2Cl](ClO_4)_3 \cdot H_2O$ (**2**), one-dimensional chain polynuclear $\{[Cu(L)](ClO_4)\}_n$ (**3**) to cyclic-tetranuclear $[Cu_4(L)_4](ClO_4)_4 \cdot 3CH_3CN$ (**4**) coordination compounds by varying reaction pH from acidic to basic. The results indicate that the reaction pH has great impact on the formation and structure of the complexes. The magnetic measurements show that there are antiferromagnetic interactions between the Cu(II) centers with $g = 2.09$, $J = -39.0\ cm^{-1}$ and $g = 2.17$, $J = -36.8\ cm^{-1}$ for **3** and **4**, respectively.

© 2008 Elsevier Ltd. All rights reserved.

1. Introduction

In the past few years, imidazole-containing ligands have been extensively investigated due to their versatile use as building blocks in supramolecular and biomimic chemistry [1,2], as well as in new functional materials [3]. Among the reported studies, the switching function of metal complexes controlled by pH is particularly interested since the imidazole group can be deprotonated at high pH to give oligomeric or polymeric frameworks with imidazolate bridging. For instance, the Cu(II) complexes can be converted from monomer to certain oligomer or polymer, which are determined by the nature of the ligand such as linkage position of imidazole (1-, 2- or 4-imidazole), steric effect, etc. [3d,3e,3f,3g,3h,3i]. However, in the most reported cases, the ligands are Schiff-base or reduced Schiff-base, and the interconversions occurred between monomer and certain oligomer or polymer [3c,3d,3e,3f,3g,3h,3i], and only very recently, tripodal imidazole-containing ligands were reported to form tetranuclear and hexanuclear complexes [4].

We focus our attention on construction and property of metal complexes with imidazole-containing organic ligands [5]. For example, we have reported copper(II) and zinc(II) complexes that can fix atmosphere carbon dioxide (CO_2), which are the first examples of polymeric carbonate complexes with supramolecular use of polyamine ligand with imidazole pendant, namely N^1-(2-aminoethyl)-N^1-(2-imidazolethyl)-ethane-1,2-diamine (L1, Scheme 1) [5e]. As an extension of our previous work, we designed and synthesized a new imidazole-containing polyamine ligand N^1-(2-aminoethyl)-N^1-(1*H*-imidazol-4-ylmethyl)-ethane-1,2-diamine (HL, Scheme 1), by varying the spacer from $-CH_2CH_2-$ in L1 to $-CH_2-$ in HL between the polyamine and imidazole groups, and the linkage position of 1-imidazole in L1 to 4-imidazole in HL. Reactions of HL with $Cu(ClO_4)_2 \cdot 6H_2O$ were carried out under different pH and complexes with diverse structures from protonated ligand $[H_3(HL)][CuCl_4] \cdot Cl$ (**1**), dinuclear $[Cu_2(HL)_2Cl](ClO_4)_3 \cdot H_2O$ (**2**), one-dimensional chain polynuclear $\{[Cu(L)](ClO_4)\}_n$ (**3**) to cyclic-tetranuclear $[Cu_4(L)_4](ClO_4)_4 \cdot 3CH_3CN$ (**4**) coordination compounds were isolated (Scheme 2). Herein, the synthesis, structure of the four compounds, and the magnetic property of **3** and **4** are reported.

2. Experimental

2.1. Synthesis of the ligand HL · 4HCl

The NH_2 groups of diethylenetriamine were protected by phthalic anhydride as described previously [5e]. The protected product (1.8 g, 5.0 mmol) was allowed to react with imidazole-4-aldehyde (0.48 g, 5.0 mmol) in mixture of methanol (50 ml) and chloroform

* Corresponding author. Fax: +86 25 83314502.
E-mail address: sunwy@nju.edu.cn (W.-Y. Sun).

0277-5387/$ - see front matter © 2008 Elsevier Ltd. All rights reserved.
doi:10.1016/j.poly.2008.05.012

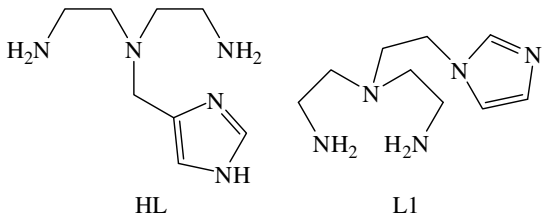

Scheme 1. The imidazole-containing polyamine ligands HL and L1.

(50 ml) for 2 h, then sodium cyanoborohydride (0.32 g, 5.0 mmol) was added in small portions in 3 h. After the resulting solution was stirred for one day at room temperature, the solution was evaporated under reduced pressure. The residual was extracted by CH_2Cl_2 from aqueous phase, and the organic phase was dried over Na_2SO_4 and evaporated to give pale oil. Then concentrated hydrochloric acid (30 ml) was added, and the mixture was boiled for 8 h, and filtered. The filtrate was evaporated to dryness, after recrystallization from ethanol, HL · 4HCl was obtained as white powder (0.95 g, 63%). ^{1}H NMR: (D_2O, 500 MHz): δ = 8.63 (s, 1H), 7.41 (s, 1H), 3.82 (s, 2H), 3.08 (t, 4H), 2.76 (t, 4H) ppm.

2.2. Synthesis of the complexes

2.2.1. Synthesis of $[H_3(HL)][CuCl_4] \cdot Cl$ (**1**)

A methanol solution (3 ml) of HL · 4HCl (16.5 mg, 0.0500 mmol) was added to a methanol solution (3 ml) of $Cu(ClO_4)_2 \cdot 6H_2O$ (18.6 mg, 0.0500 mmol), and the solution was stirred for 10 min, then filtered. The filtrate was diffused by diethyl ether for two days, during which time yellow crystals appeared. The crystal is very deliquescent in air. Yield: (72%). IR: (KBr, cm^{-1}): 3444 (br), 3182 (s), 3129 (s), 2964 (m), 2902 (m), 1625 (m), 1601 (m), 1574 (m), 1504 (m), 1445 (m), 1369 (m), 1319 (w), 1171 (w), 1078 (w), 1029 (w), 987 (w), 948 (w), 833 (w), 769 (w), 685 (m), 624 (m).

2.2.2. Synthesis of $[Cu_2(HL)_2Cl](ClO_4)_3 \cdot H_2O$ (**2**)

An aqueous solution (3 ml) of HL · 4HCl (16.5 mg, 0.0500 mmol) was added to an aqueous solution (3 ml) of $Cu(ClO_4)_2 \cdot 6H_2O$ (18.6 mg, 0.0500 mmol), and the solution was stirred, then 0.5 M NaOH was added dropwise to pH ca. 5.5. Blue crystals were obtained by slow evaporation of the solution in air for several days. Yield: (65%). *Anal.* Calc. for $C_{16}H_{36}Cl_4Cu_2N_{10}O_{13}$: C, 22.70; H, 4.26; N, 16.56. Found: C, 22.57; H, 4.35; N, 16.44%. IR: (KBr, cm^{-1}): 3337 (s), 3285 (s), 2973 (w), 2921 (w), 1625 (m), 1595 (m), 1469 (m), 1451 (m), 1378 (w), 1319 (w), 1276 (w), 1103 (vs), 1082 (vs), 994 (m), 940 (m), 895 (m), 848 (m), 658 (m), 624 (m).

2.2.3. Synthesis of $\{[Cu(L)](ClO_4)\}_n$ (**3**)

An aqueous solution (3 ml) of HL · 4HCl (16.5 mg, 0.0500 mmol) was added to an aqueous solution (3 ml) of $Cu(ClO_4)_2 \cdot 6H_2O$ (18.6 mg, 0.0500 mmol), and the resulted solution was adjusted to pH ca. 7 with 0.5 M NaOH while stirring. About 10 min later, it was filtered, and the filtrate was allowed to stand for several days, green block crystals were obtained. Yield: (55%). *Anal.* Calc. for $C_{16}H_{32}Cl_2Cu_2N_{10}O_8$: C, 27.81; H, 4.63; N, 20.28. Found: C, 27.77; H, 4.71; N, 20.39%. IR: (KBr, cm^{-1}): 3366 (s), 3336 (s), 3284 (s), 2921 (w), 2880 (w), 1601 (m), 1470 (m), 1358 (w), 1312 (w), 1244 (w), 1220 (w), 1114 (vs), 980 (m), 951 (w), 885 (w), 825 (w), 655 (w), 624 (m).

2.2.4. Synthesis of $[Cu_4(L)_4](ClO_4)_4 \cdot 3CH_3CN$ (**4**)

An aqueous solution (3 ml) of HL · 4HCl (16.5 mg, 0.0500 mmol) was added to an aqueous solution (3 ml) of $Cu(ClO_4)_2 \cdot 6H_2O$ (18.6 mg, 0.0500 mmol), and the resulted solution was adjusted to pH ca. 9 with 0.5 M NaOH while stirring, the solution becomes cloudy immediately. Then 2 ml of CH_3CN was added to give a clear

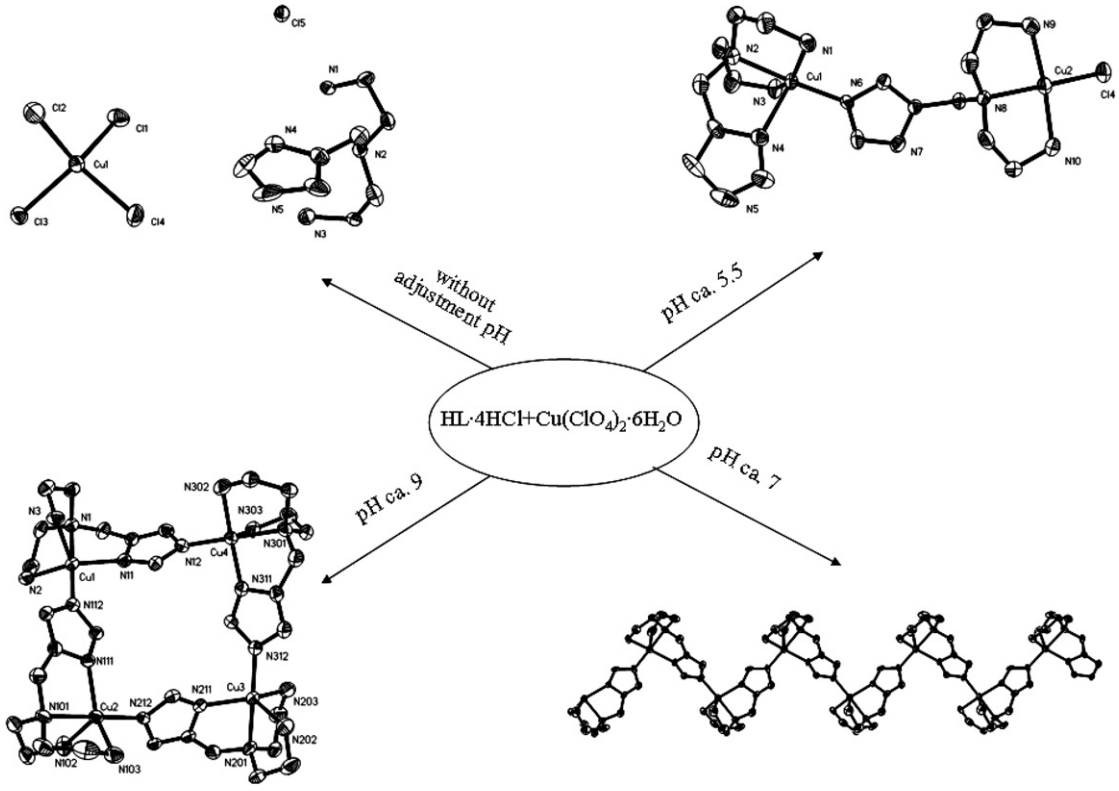

Scheme 2. Schematic drawing for formation of **1**–**4** under different solution pH.

solution, after stirred for another 10 min, it was filtered, and the filtrate was allowed to stand for several days, and blue crystals were isolated. Yield: (85%). *Anal.* Calc. for $C_{32}H_{64}Cl_4Cu_4N_{20}O_{16}$ (noncoordinated CH_3CN molecules were lost upon drying): C, 27.53; H, 4.58; N, 20.07. Found: C, 27.98; H, 4.55; N, 20.36%. IR: (KBr, cm^{-1}): 3340 (s), 3242 (s), 2925 (w), 2877 (w), 1602 (m), 1469 (s), 1356 (w), 1312 (w), 1236 (w), 1209 (m), 1113(vs), 981 (m), 954 (m), 884 (w), 823 (w), 779 (w), 654 (w), 625 (m).

Caution! Perchlorate salts of metal complexes with organic ligands are potentially explosive. Only small amounts of materials should be prepared, and the samples should be handled with caution.

2.3. Physical measurements

All commercially available chemicals are of reagent grade and used as received without further purification. Elemental analyses for C, H and N were made on a Perkin–Elmer 240C elemental analyzer. Infrared (IR) spectra were recorded on a Bruker Vector22 FT-IR spectrophotometer by using KBr pellets. Magnetic measurements were performed in a MPMS-SQUID magnetometer at a field of 2000 G on powder samples in a Teflon capsule in the range of 1.8–300 K.

2.4. X-ray crystallography

The unit cell parameters were determined and the data collected at 293 K with a Bruker SMART CCD system equipped with monochromated Mo Kα radiation (λ = 0.71073 Å) for **1–3**. Empirical absorption corrections were applied to the data using the SADABS program [6]. Structures of **1**–**3** were solved by the direct methods and refined by full-matrix least-squares on F^2 using the SHELXL-97 programs [7]. Crystallographic data of **4** was collected at 200 K on a Rigaku RAXIS-RAPID Imaging Plate diffractometer with graphite monochromated Mo Kα radiation (λ = 0.71075 Å). The structure of **4** was solved by direct methods using SIR92, expanded using Fourier techniques DIRDIF94 and refined using SHELXL-97 programs [7,8]. All the non-hydrogen atoms were refined anisotropically on F^2 by full-matrix least-squares techniques. The hydrogen atoms were generated geometrically. All calculations were performed using the TEXSAN crystallographic software package of Molecular Structure Corporation [9]. Crystallographic data for **1–4** are listed in Table 1. Selected bond lengths and angles for complexes **1–4** are listed in Table 2. C4 atom of **1** is disordered in two positions with an occupation of 0.5, for clarity, only one of these sites is shown.

3. Results and discussion

3.1. Description of the crystal structures of complexes *1–4*

3.1.1. $[H_3(HL)][CuCl_4] \cdot Cl$ (*1*)

When the hydrochloride salt of the ligand HL · 4HCl was used to react with $Cu(ClO_4)_2 \cdot 6H_2O$ directly without adjustment of reaction pH, yellow crystals were obtained. The crystallographic analysis revealed that the structure of **1** consists of protonated $[H_3(HL)]^{3+}$ cation, $[CuCl_4]^{2-}$ anion, and one chloride ion as shown in Fig. 1a. It is reasonable that the ligand did not coordinate with Cu(II) atoms under the experiment conditions since the amino and imidazole groups in the ligand are protonated and thus loss coordination ability with the metal atom. On the other hand, the Cu(II) atom is coordinated by four chloride ions to form a $[CuCl_4]^{2-}$ unit with distorted tetrahedral geometry. The Cu–Cl bond distances are from 2.231(2) Å to 2.252(2) Å, and the Cl–Cu–Cl angles fall in the range of 97.77(8)° and 134.38 (8)° (Table 2), which are similar to the reported ones [1a,10].

The protonated $[H_3(HL)]^{3+}$ cations are joined together through N–H···Cl5 hydrogen bonds to form an infinite one-dimensional (1D) chain structure (Fig. 1b). The adjacent 1D chains are further connected together by C–H···Cl and N–H···Cl ($[CuCl_4]^{2-}$ anion) hydrogen bonds to form a three-dimensional (3D) structure (Fig. 1c). The hydrogen-bonding data are summarized in Table S1.

3.1.2. $[Cu_2(HL)_2Cl](ClO_4)_3 \cdot H_2O$ (*2*)

When the reaction solution of HL · 4HCl and $Cu(ClO_4)_2 \cdot 6H_2O$ was adjusted to pH ca. 5.5, a new complex **2** was isolated as blue crystals. There are one dinuclear $[Cu_2(HL)_2Cl]^{3+}$ cation, three perchlorate anions and one lattice water molecule in the asymmetric unit of **2**. As shown in Fig. 2a, the dinuclear $[Cu_2(HL)_2Cl]^{3+}$ unit contains two independent Cu(II) centers with different coordination

Table 1
Crystallographic data for complexes **1–4**

Complex	1	2	3	4
Empirical formula	$C_8H_{20}Cl_5CuN_5$	$C_{16}H_{36}Cl_4Cu_2N_{10}O_{13}$	$C_{16}H_{32}Cl_2Cu_2N_{10}O_8$	$C_{38}H_{73}Cl_4Cu_4N_{23}O_{16}$
Formula weight	427.08	845.45	690.5	1504.15
Crystal system	orthorhombic	orthorhombic	orthorhombic	monoclinic
Space group	$P2_12_12_1$	$P2_12_12_1$	$Pna2_1$	$P2_1/c$
Crystal size (mm)	0.25 × 0.2 × 0.18	0.2 × 0.15 × 0.12	0.15 × 0.12 × 0.1	0.3 × 0.2 × 0.05
a (Å)	9.167(3)	8.0100(19)	23.440(4)	13.4743(19)
b (Å)	11.438(4)	15.801(4)	11.6384(19)	33.605(3)
c (Å)	16.558(6)	24.727(6)	9.6917(15)	14.545(2)
β (°)	90.00	90.00	90.00	104.449(7)
V (Å^3)	1736.2(11)	3129.6(13)	2644.0(7)	6377.9(14)
Z	4	4	4	4
D_{calc} (g cm^{-3})	1.634	1.794	1.735	1.566
μ (mm^{-1})	2.021	1.776	1.872	1.561
F(000)	868	1728	1416	3096
2θ max (°)	50.0	50.0	50.0	50.0
Independent reflections	3061	5508	3828	11201
Observed reflections ($I > 2\sigma(I)$)	2683	3575	2823	7421
Parameters refined	181	406	343	769
R_{int}	0.0575	0.0828	0.1143	0.0919
R_1 ($I > 2\sigma(I)$)[a]	0.0564	0.0513	0.0929	0.0853
wR_2 (all data)[b]	0.1108	0.0950	0.1796	0.2460
Goodness-of-fit on F^2	1.076	1.021	1.134	1.015

[a] $R_1 = \sum||F_o| - |F_c||/\sum|F_o|$.
[b] $wR_2 = |\sum w(|F_o|^2 - |F_c|^2)|/\sum|w(F_o)^2|^{1/2}$.

Table 2
Selected bond lengths (Å) and angles (°) for complex **1–4**

$[H_3(HL)][CuCl_4] \cdot Cl$ (**1**)			
Cu1–Cl1	2.231(2)	Cu1–Cl2	2.233(2)
Cu1–Cl3	2.233(2)	Cu1–Cl4	2.252(2)
Cl1–Cu1–Cl2	103.74(8)	Cl1–Cu1–Cl3	134.38(8)
Cl1–Cu1–Cl4	97.77(8)	Cl2–Cu1–Cl3	98.63(7)
Cl2–Cu1–Cl4	128.02(9)	Cl3–Cu1–Cl4	98.88(8)
$[Cu_2(HL)_2Cl](ClO_4)_3 \cdot H_2O$ (**2**)			
Cu1–N1	1.999(5)	Cu1–N2	2.057(6)
Cu1–N3	1.997(5)	Cu1–N4	2.218(6)
Cu1–N6	1.965(6)	Cu2–N8	2.038(5)
Cu2–N9	1.996(5)	Cu2–N10	1.992(6)
Cu2–Cl4	2.247(2)		
N1–Cu1–N2	85.1(2)	N1–Cu1–N3	150.4(2)
N1–Cu1–N4	105.9(2)	N1–Cu1–N6	94.2(2)
N2–Cu1–N3	83.8(2)	N2–Cu1–N4	82.7(2)
N2–Cu1–N6	176.4(2)	N3–Cu1–N4	99.8(2)
N3–Cu1–N6	95.2(2)	N4–Cu1–N6	100.9(2)
N8–Cu2–N9	85.3(2)	N8–Cu2–N10	84.6(2)
N9–Cu2–N10	161.5(3)	N8–Cu2–Cl4	167.17(2)
N9–Cu2–Cl4	96.52(2)	N10–Cu2–Cl4	96.84(2)
$\{[Cu(L)](ClO_4)\}_n$ (**3**)			
Cu1–N2	2.01(1)	Cu1–N3	2.19(1)
Cu1–N4	2.04(1)	Cu1–N5	2.04(1)
Cu1–N6	1.95(1)	Cu2–$N1^{\#1}$	1.96(1)
Cu2–N7	2.01(1)	Cu2–N8	2.06(1)
Cu2–N9	2.15(1)	Cu2–N10	2.068(9)
N2–Cu1–N3	103.5(5)	N2–Cu1–N4	81.7(4)
N2–Cu1–N5	143.6(5)	N2–Cu1–N6	99.7(5)
N3–Cu1–N4	82.6(5)	N3–Cu1–N5	106.2(5)
N3–Cu1–N6	103.2(5)	N4–Cu1–N5	81.8(4)
N4–Cu1–N6	173.5(5)	N5–Cu1–N6	93.6(5)
N1–Cu2–$N7^{\#1}$	99.3(5)	N1–Cu2–$N8^{\#1}$	175.6(5)
N1–Cu2–$N9^{\#1}$	94.1(5)	N1–Cu2–$N10^{\#1}$	99.4(5)
N7–Cu2–N8	82.7(4)	N7–Cu2–N9	111.8(5)
N7–Cu2–N10	133.1(5)	N8–Cu2–N9	81.6(5)
N8–Cu2–N10	81.8(4)	N9–Cu2–N10	109.2(5)
$[Cu_4(L)_4](ClO_4)_4 \cdot 3CH_3CN$ (**4**)			
Cu1–N1	2.085(7)	Cu1–N2	2.041(7)
Cu1–N3	2.183(7)	Cu1–N11	1.990(6)
Cu1–N112	1.955(7)	Cu2–N101	2.072(6)
Cu2–N102	2.154(8)	Cu2–N103	2.043(7)
Cu2–N111	1.998(6)	Cu2–N212	1.953(6)
Cu3–N201	2.062(7)	Cu3–N202	2.129(8)
Cu3–N203	2.060(7)	Cu3–N211	1.988(6)
Cu3–N312	1.947(7)	Cu4–N301	2.070(8)
Cu4–N302	2.039(8)	Cu4–N303	2.153(9)
Cu4–N311	1.974(7)	Cu4–N12	1.941(7)
N1–Cu1–N2	82.2(3)	N1–Cu1–N3	83.1(3)
N1–Cu1–N11	82.4(3)	N1–Cu1–N112	177.1(3)
N2–Cu1–N3	104.5(3)	N2–Cu1–N11	143.1(3)
N2–Cu1–N112	96.6(3)	N3–Cu1–N11	106.6(3)
N3–Cu1–N112	99.7(3)	N11–Cu1–N112	97.1(3)
N212–Cu2–N111	98.6(2)	N212–Cu2–N103	94.3(3)
N111–Cu2–N103	133.0(3)	N212–Cu2–N101	178.3(3)
N111–Cu2–N101	82.7(3)	N103–Cu2–N101	83.9(3)
N212–Cu2–N102	97.7(3)	N111–Cu2–N102	113.0(3)
N103–Cu2–N102	109.7(4)	N101–Cu2–N102	82.9(3)
N312–Cu3–N211	97.7(3)	N312–Cu3–N203	94.5(3)
N211–Cu3–N203	139.3(3)	N312–Cu3–N201	176.4(3)
N211–Cu3–N201	82.4(3)	N203–Cu3–N201	83.2(3)
N312–Cu3–N202	100.2(3)	N211–Cu3–N202	110.9(3)
N203–Cu3–N202	104.9(4)	N201–Cu3–N202	83.1(3)
N12–Cu4–N311	97.7(3)	N12–Cu4–N302	95.8(3)
N311–Cu4–N302	137.4(4)	N12–Cu4–N301	177.9(3)
N311–Cu4–N301	81.6(3)	N302–Cu4–N301	83.4(3)
N12–Cu4–N303	98.2(3)	N311–Cu4–N303	109.7(3)
N302–Cu4–N303	108.0(4)	N301–Cu4–N303	83.9(3)

Symmetry transformation used to generate equivalent atoms: #1 *x*, *y*, −1 + *z*.

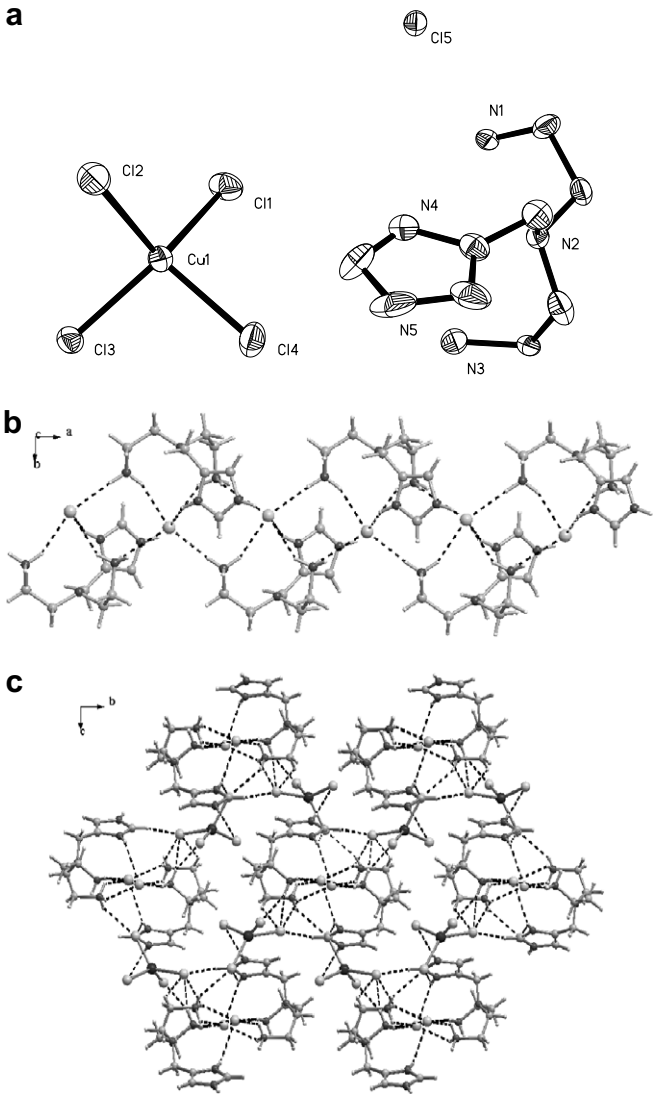

Fig. 1. (a) ORTEP drawing of **1** with thermal ellipsoids set to 30% probability level, the hydrogen atoms were omitted for clarity. (b) View of 1D chain structure of **1** with hydrogen bonds indicated by dashed lines. (c) The 3D structure of **1** with hydrogen bonds indicated by dashed lines.

geometry, namely the Cu1 atom is five-coordinated by three amino nitrogen atoms from one HL and two imidazole nitrogen atoms from two different HL ligands with an average Cu–N bond distance of 2.047(6) Å. The bond angles around Cu1 are in the range of 82.7(2)–176.4(2)° (Table 2). The coordination geometry around Cu1 atom is a distorted square pyramid as indicated by an index τ value of 0.43 as defined by Addison et al.: $\tau = 0$ for an ideal square pyramid and $\tau = 1$ for a perfect trigonal-bipyramid [11]. On the other hand, the Cu2 atom is four-coordinated by three amino nitrogen atoms from one HL ligand and one chloride atom with distorted square planar geometry. The average Cu–N distance around Cu2 is 2.008(6) Å, and the Cu–Cl distance is 2.247(2) Å, the bond angles around Cu2 are ranging from 84.6(2) to 167.17(2)° (Table 2). It should be noticed that the deprotonation of the two imidazole groups at N5 and N7 positions did not occur, and thus they did not participate in the coordination under pH at ca. 5.5.

The dinuclear $[Cu_2(HL)_2Cl]^{3+}$ cations are linked into an infinite 1D zigzag chain by perchlorate anions through C–H···O1 and

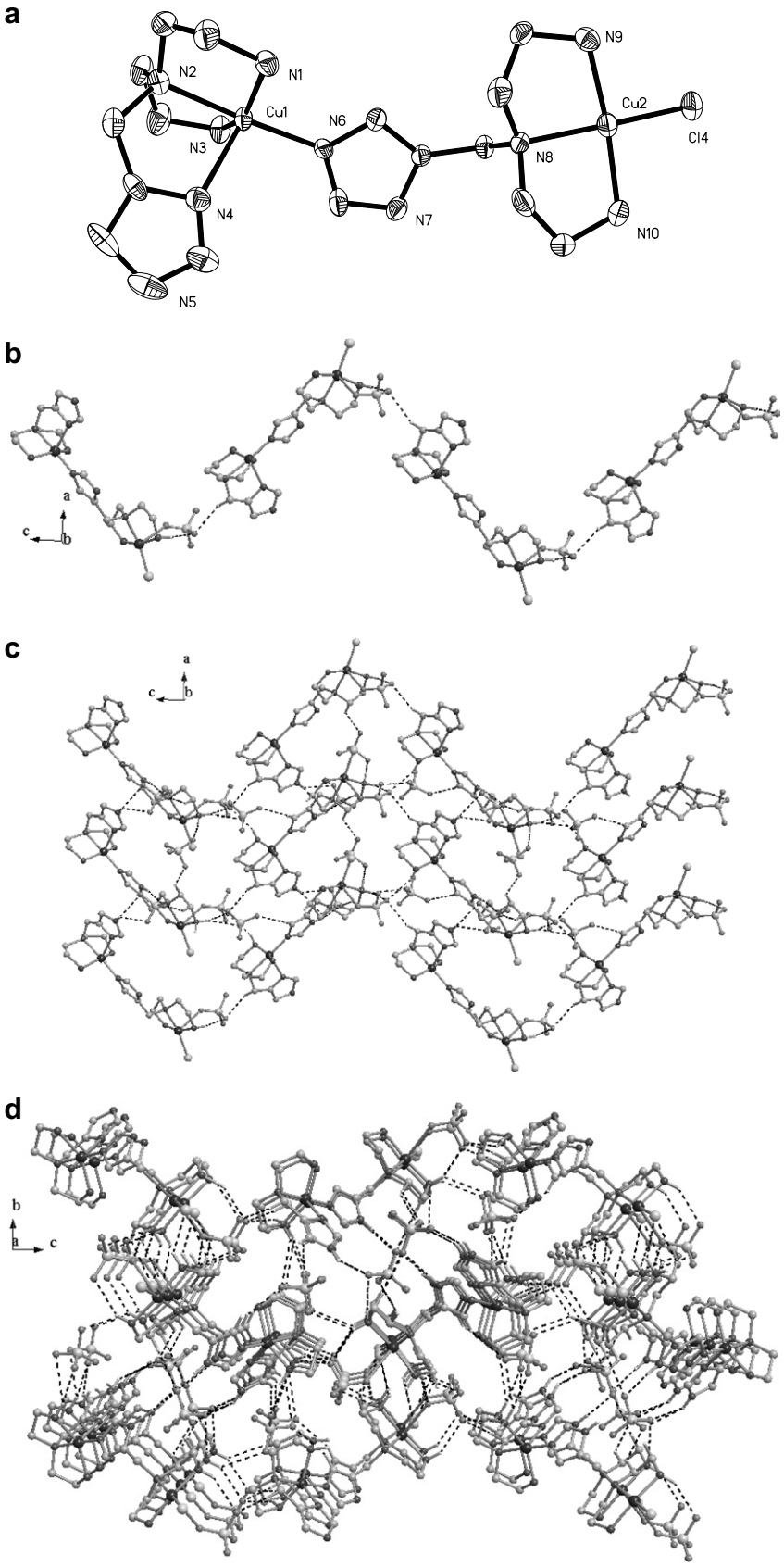

Fig. 2. (a) View of the dinuclear complex of **2** with thermal ellipsoids set to 30% probability level, the hydrogen atoms, perchlorate anions, and uncoordinated water molecules were omitted for clarity. (b) View of 1D zigzag chain structure of **2** with hydrogen bonds indicated by dashed lines. (c) The 2D network of **2** with hydrogen bonds indicated by dashed lines. (d) The 3D framework of **2** with hydrogen bonds indicated by dashed lines.

N–H···O1 hydrogen bonds (Fig. 2b). The 1D chains are further joined together to form two-dimensional (2D) network by C–H···O and N–H···O (perchlorate anion) hydrogen bonds (Fig. 2c), which produce a 3D framework through C–H···O, N–H···O (perchlorate anion), and C–H···Cl4, N–H···Cl4 hydrogen bonds as listed in Table S1 (Fig. 2d).

3.1.3. $\{[Cu(L)](ClO_4)\}_n$ (**3**)

When the pH of the reaction solution was further raised to ca. 7, complex **3** was obtained as green crystals and the result of crystallographic analysis confirmed that the imidazole group of the HL ligand deprotonated to give L^- and as a result each imidazole group acts as imidazolate bridging to coordinate with two metal atoms. As illustrated in Fig. 3a, there are two different Cu(II) centers and two independent L^- ligands in the repeat unit of **3**. The Cu1 atom is five-coordinated by four nitrogen atoms from one L^- ligand and one imidazolate nitrogen atom from another L^- ligand, with an average Cu1–N separation of 2.04(1) Å. There is no structural preference for the coordination geometry of Cu1, since the τ value is calculated to be 0.49 [11]. The Cu2 atom is also five-coordinated which is similar to that in Cu1, but the coordination geometry around Cu2 is a distorted trigonal-bipyramid since the τ value is 0.71 [11]. The average Cu2–N distance is 2.05(1) Å. On the other hand, each L^- ligand, using its two imidazolate nitrogen atoms, acts as a bridge to link two Cu(II) atoms to generate a zigzag chain structure (Fig. 3b). Then, the 1D chains are further connected through C–H···O and N–H···O (perchlorate anion) hydrogen bonds to form 3D structure (Fig. 3c).

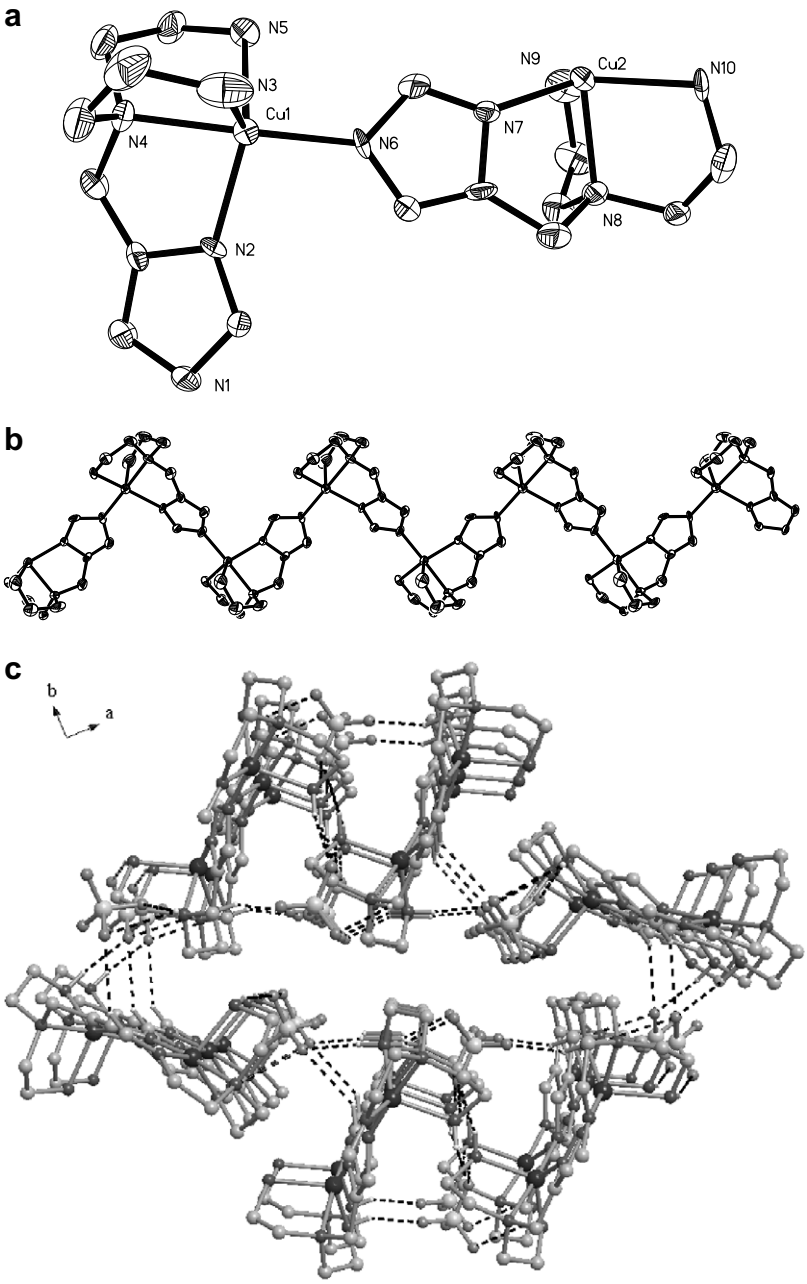

Fig. 3. (a) ORTEP drawing of **3** showing the coordination environment with thermal ellipsoids set to 30% probability level, the hydrogen atoms, and perchlorate anions were omitted for clarity. (b) View of the infinite 1D zigzag chain structure of **3**, the hydrogen atoms and perchlorate anions were omitted for clarity. (c) The 3D structure of **3** with hydrogen bonds indicated by dashed lines.

*3.1.4. $[Cu_4(L)_4](ClO_4)_4 \cdot 3CH_3CN$ (**4**)*

In order to further investigate the influence of pH on the formation and structure of the complex, the pH of the reaction solution was adjusted to ca. 9 and complex **4** was generated. It is interesting to find that the imidazole group of the HL ligand in **4** also deprotonated as observed in **3**, however, the structures of **3** and **4** are totally different. As shown in Fig. 4a, the structure of **4** consists of one cyclic-tetranuclear $[Cu_4(L)_4]^{4+}$ cation, four perchlorate anions, and three non-coordinated acetonitrile molecules. All the Cu(II) atoms have the same coordination environment with

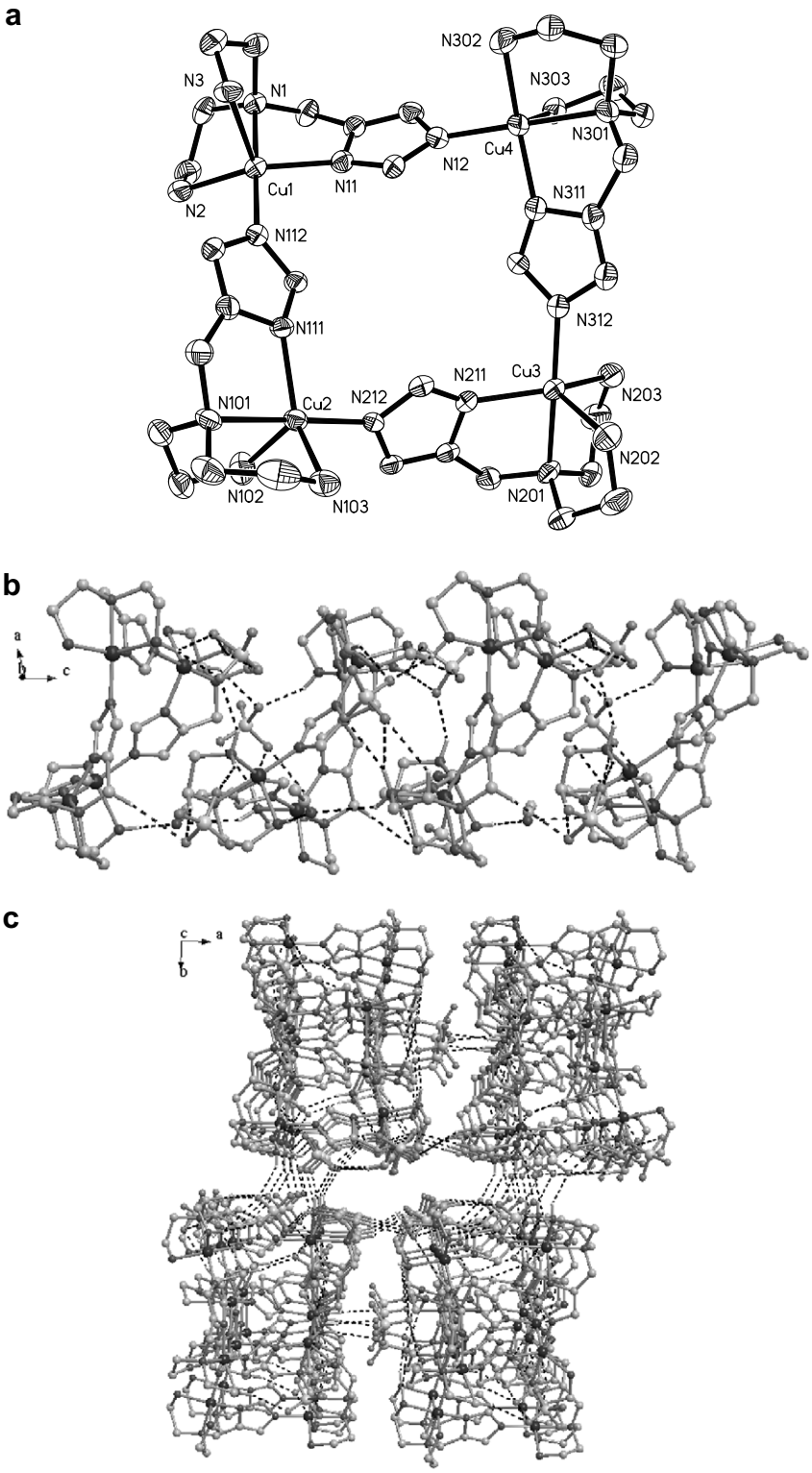

Fig. 4. (a) View of the cyclic-tetranuclear complex of **4** with thermal ellipsoids set to 30% probability level. The perchlorate anions, acetonitrile molecules and hydrogen atoms were omitted for clarity. (b) The 1D chain structure of **4** with hydrogen bonds indicated by dashed lines. (c) The 3D framework of **4** with hydrogen bonds indicated by dashed lines. The acetonitrile molecules are omitted for clarity.

trigonal-bipyramid coordination geometry, but different bond lengths and angles as listed in Table 2. Each Cu(II) atom is five-coordinated by four nitrogen atoms from one ligand, and one imidazolate nitrogen atom from another ligand with the Cu–N bond distances in the range of 1.941(7)–2.183(7) Å.

The $[Cu_4(L)_4]^{4+}$ cations are linked through C–H···O and N–H···O (perchlorate anion) hydrogen bonds to form 1D chain structure (Fig. 4b), and the 1D chains are further connected to form 3D framework by C–H···O and N–H···O (perchlorate anion) hydrogen bonds, with acetonitrile molecules filled in the vacancy (Fig. 4c).

3.2. Magnetic property of **3** and **4**

As observed in the crystal structure, the adjacent copper(II) atoms in complexes **3** and **4** are bridged by imidazolate groups and thus their magnetic property is interested. Variable-temperature magnetic susceptibility measurements were performed on crystalline sample of **3** and **4** in the temperature range of 1.8–300 K, and the results in plots of $\chi_M T$ versus T and χ_M versus T are shown in Fig. 5. For **3**, the value of $\chi_M T$ at 300 K is estimated at 0.35 emu K mol^{-1}, which is smaller than that of spin-only value 0.375 emu K mol^{-1} for S = 1/2. When the temperature is lowered, the $\chi_M T$ decreases gradually to 0.0028 emu K mol^{-1} at 1.8 K. The χ_M versus T curve shows a maximum at about 70 K. The facts clearly indicate the antiferromagnetic interactions between the Cu(II) atoms in **3**. The magnetic susceptibility data were interpreted by the Bonner and Fisher model for a 1D infinite-chain structure for $J < 0$, where the Hamiltonian is $\widehat{H} = -2J\sum S_i\, S_{i+1} J$ is the intra-chain exchange coupling constant [3c,3f,3i]. The least-squares fitting was carried above 10 K including paramagnetic impurity ρ, and the best-fit parameters are $g = 2.09$, $J = -39.0$ cm^{-1}, $\rho = 0.002$ and the linear agreement factor is $R = 0.9992$. The $J = -39.0$ cm^{-1} is compatible with those of the imidazolate-bridged 1D chain complexes reported previously [3c,3f,3i]. The magnetic behavior of **4** is shown in Fig. 5b, the value of $\chi_M T$ at 300 K is estimated at 1.20 emu K mol^{-1}, which is smaller than the spin-only value of 1.50 emu K mol^{-1} for the Cu_4 unit. The $\chi_M T$ decreases gradually from room temperature to 1.8 K and the χ_M versus T curve shows a maximum at about 80 K, which means the operation of antiferromagnetic interactions between the copper(II) atoms. The magnetic susceptibility data were analyzed by a cyclic-tetranuclear structure model [3c,3e,3i,4], where the Hamiltonian is $\widehat{H} = -2J(S_1S_2 + S_2S_3 + S_3S_4 + S_4S_1)$. The least-squares fitting was carried above 10 K including paramagnetic impurity ρ, and the best-fit parameters are $g = 2.17$, $J = -36.8$ cm^{-1}, $\rho = 0.007$ and the linear agreement factor is $R = 0.9999$. Similar results have been reported previously for the cyclic-tetranuclear complexes [3c,3e,3i,4].

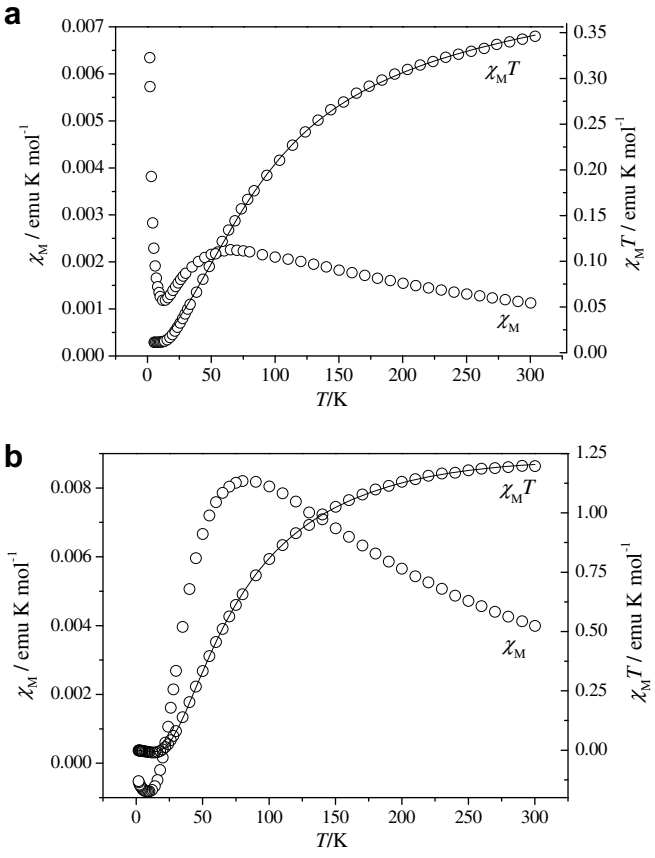

Fig. 5. Temperature dependences of magnetic susceptibility χ_M and χ_MT for **3** and **4**. The solid lines represent the fitted curve: (a) **3**; (b) **4**.

4. Conclusions

In summary, we have designed and synthesized a new tripodal polyamine ligand HL, and investigated its reactions with $Cu(ClO_4)_2 \cdot 6H_2O$ under different pH. Interestingly, it can realize the self-assembly from protonated ligand $[H_3(HL)][CuCl_4] \cdot Cl$ (**1**), dinuclear $[Cu_2(HL)_2Cl](ClO_4)_3 \cdot H_2O$ (**2**), one-dimensional chain polynuclear $\{[Cu(L)](ClO_4)\}_n$ (**3**) to cyclic-tetranuclear $[Cu_4(L)_4](ClO_4)_4 \cdot 3CH_3CN$ (**4**) coordination compounds from acidic to basic conditions. The results indicate that the reaction solution pH has great impact on the assembly process of the complexes and their structures. The magnetic investigation revealed that the imidazolate bridging between the adjacent Cu(II) atoms mediates the antiferromagnetic interactions.

Acknowledgements

This work was financially supported by the National Science Fund for Distinguished Young Scholars (Grant No. 20425101), the National Natural Science Foundation of China (Grant Nos. 20731004 and 20721002) and the National Basic Research Program of China (Grant No. 2007CB925103).

Appendix A. Supplementary data

CCDC 683649, 683650, 683651 and 683652 contain the supplementary crystallographic data for **1**, **2**, **3** and **4**. These data can be obtained free of charge via http://www.ccdc.cam.ac.uk/conts/retrieving.html, or from the Cambridge Crystallographic Data Centre, 12 Union Road, Cambridge CB2 1EZ, UK; fax: (+44) 1223-336-033; or e-mail: deposit@ccdc.cam.ac.uk. Supplementary data associated with this article can be found, in the online version, at doi:10.1016/j.poly.2008.05.012.

References

[1] (a) R.L. Sang, L. Xu, Inorg. Chem. 44 (2005) 373;
(b) B.-B. Ding, Y.-Q. Weng, Z.-W. Mao, C.K. Lam, X.-M. Chen, B.-H. Ye, Inorg. Chem. 44 (2005) 8836;
(c) X.-C. Huang, J.-P. Zhang, X.-M. Chen, J. Am. Chem. Soc. 126 (2004) 13218;
(d) X.-C. Huang, J.-P. Zhang, Y.-Y. Lin, X.-L. Yu, X.-M. Chen, Chem. Commun. (2005) 2232;
(e) R. Atencio, M. Chacon, T. Gonzalez, A. Briceno, G. Agrifoglio, A. Sierraalta, Dalton Trans. (2004) 505;
(f) M. Tadokoro, K. Isober, H. Uekusa, Y. Ohashi, J. Toyoda, K. Tashiro, K. Nakasuji, Angew. Chem., Int. Ed. 38 (1999) 95;
(g) M. Tadomoro, K. Nakasuji, Coord. Chem. Rev. 198 (2000) 205;
(h) E. Colacio, M. Ghazi, R. Kivekas, M. Klinga, F. Lloret, J.M. Moreno, Inorg. Chem. 39 (2000) 2770;
(i) Y. Sunatsuki, H. Ohta, M. Kojima, Y. Ikuta, Y. Goto, N. Matsumoto, S. Iijima,

H. Akashi, S. Kaizaki, F. Dahan, J. Tuchagues, Inorg. Chem. 43 (2004) 4154;
(j) I. Katsuki, Y. Motoda, Y. Sunatsuki, N. Matsumoto, T. Nakashima, M. Kojima, J. Am. Chem. Soc. 124 (2002) 629.

[2] (a) B. Verdejo, S. Blasco, E. García-España, F. Lloret, P. Gaviña, C. Soriano, S. Tatay, H.R. Jiménez, A. Doménech, J. Latorre, Dalton Trans. (2007) 4726;
(b) R.A.N. Silva, V. Drago, A.S. Mangrich, W.A. Ortiz, W.A.C. Passos, M.C.B. Oliveira, H. Terenzi, Inorg. Chem. 42 (2003) 8353;
(c) S.-A. Li, D.-F. Li, D.-X. Yang, Y.-Z. Li, J. Huang, K.-B. Yu, W.-X. Tang, Chem. Commun. (2003) 880;
(d) S.-A. Li, J. Xia, D.-X. Yang, Y. Xu, D.-F. Li, M.-F. Wu, W.-X. Tang, Inorg. Chem. 41 (2002) 1807;
(e) H. Ohtsu, Y. Shimazaki, A. Odani, O. Yamauchi, W. Mori, S. Itoh, S. Fukuzumi, J. Am. Chem. Soc. 122 (2000) 5733;
(f) T. Gajda, R. Krämer, A. Jancsó, Eur. J. Inorg. Chem. (2000) 1635;
(g) E. Kimura, Y. Kurogi, M. Shionoya, M. Shiro, Inorg. Chem. 30 (1991) 4524.

[3] (a) M.A. Alam, R.R. Koner, A. Das, M. Nethaji, M. Ray, Cryst. Growth Des. 7 (2007) 1818;
(b) M.A. Alam, M. Nethaji, M. Ray, Angew. Chem., Int. Ed. 42 (2003) 1940;
(c) W.A. Alves, G. Cerchiaro, A. Paduan-Filho, D.M. Tomazela, M.N. Eberlin, A.M.D.C. Ferreira, Inorg. Chim. Acta 358 (2005) 3581;
(d) Y. Sunatsuki, Y. Motoda, N. Matsumoto, Coord. Chem. Rev. 226 (2002) 1999;
(e) Y. Shii, Y. Motoda, T. Matsuo, F. Kai, T. Nakashima, J.P. Tuchagues, N. Matsumoto, Inorg. Chem. 38 (1999) 3513;
(f) M. Mimura, T. Matsuo, T. Nakashima, N. Matsumoto, Inorg. Chem. 37 (1998) 3553;
(g) N. Matsumoto, Y. Mizuguchi, G. Mago, S. Eguchi, H. Miyasaka, T. Nakashima, J.P. Tuchagues, Angew. Chem., Int. Ed. 36 (1997) 1860;
(h) T. Nozaki, H. Ushio, G. Mago, N. Matsumoto, H. Okawa, Y. Yamakawa, T. Anno, T. Nakashima, J. Chem. Soc., Dalton Trans. (1994) 2339;
(i) N. Matsumoto, T. Nozaki, H. Ushio, K. Motoda, M. Ohba, G. Mago, H. Okawa, J. Chem. Soc., Dalton Trans. (1993) 2157.

[4] T. Higa, M. Moriya, Y. Shimazaki, T. Yajima, F. Tani, S. Karasawa, M. Nakano, Y. Naruta, O. Yamauchi, Inorg. Chim. Acta 360 (2007) 3304.

[5] (a) X.-F. Wang, Y. Lv, T. Okamura, H. Kawaguchi, G. Wu, W.-Y. Sun, N. Ueyama, Cryst. Growth Des. 7 (2007) 1125;
(b) W.-L. Meng, G.-X. Liu, T. Okamura, H. Kawaguchi, Z.-H. Zhang, W.-Y. Sun, N. Ueyama, Cryst. Growth Des. 6 (2006) 2092;
(c) Z.-H. Zhang, Y. Song, T. Okamura, Y. Hasegawa, W.-Y. Sun, N. Ueyama, Inorg. Chem. 45 (2006) 2896;
(d) L.-Y. Kong, H.-F. Zhu, Y.-Q. Huang, T. Okamura, X.-H. Lu, Y. Song, G.X. Liu, W.-Y. Sun, N. Ueyama, Inorg. Chem. 45 (2006) 8098;
(e) L.-Y. Kong, Z.-H. Zhang, H.-F. Zhu, H. Kawaguchi, T. Okamura, M. Doi, Q. Chu, W.-Y. Sun, N. Ueyama, Angew. Chem., Int. Ed. 44 (2005) 4352;
(f) W. Zhao, Y. Song, T. Okamura, J. Fan, W.-Y. Sun, N. Ueyama, Inorg. Chem. 44 (2005) 3330;
(g) H.-F. Zhu, J. Fan, T. Okamura, W.-Y. Sun, N. Ueyama, Cryst. Growth Des. 5 (2005) 289;
(h) J. Fan, L. Gan, H. Kawaguchi, W.-Y. Sun, K.-B. Yu, W.-X. Tang, Chem. Eur. J. 9 (2003) 3965;
(i) J. Fan, H.-F. Zhu, T. Okamura, W.-Y. Sun, W.-X. Tang, N. Ueyama, Chem. Eur. J. 9 (2003) 4724;
(j) J. Fan, H.-F. Zhu, T. Okamura, W.-Y. Sun, W.-X. Tang, N. Ueyama, Inorg. Chem. 42 (2003) 158;
(k) J. Fan, W.-Y. Sun, T. Okamura, W.-X. Tang, N. Ueyama, Inorg. Chem. 42 (2003) 3168;
(l) S.-Y. Wan, J. Fan, T. Okamura, H.-F. Zhu, X.-M. Ouyang, W.-Y. Sun, N. Ueyama, Chem. Commun. (2002) 2520.

[6] G.M. Sheldrick, SADABS, Program for Bruker Area Detector Absorption Correction, University of Göttingen, Germany, 1997.

[7] (a) DIRDIF-94: P.T. Beurskens, G. Admiraal, G. Beurskens, W.P. Bosman, R. de Gelder, R. Israel J.M.M. Smits, The DIRDIF-94 Program System, Technical Report of the Crystallography Laboratory, University of Nijmegen, The Netherlands, 1994.;
(b) G.M. Sheldrick, SHELXS-97, Program for Solution of Crystal Structures, University of Göttingen, Germany, 1997.

[8] SIR92: A. Altomare, M.C. Burla, M. Camalli, M. Cascarano, C. Giacovazzo, A. Guagliardi, G. Polidori, J. Appl. Crystallogr. 27 (1994) 435.

[9] TEXSAN: Crystal Structure Analysis Package, Molecular Structure Corporation, The Woodlands, TX, 1999.

[10] (a) F.F. Awwadi, R.D. Willett, B. Twamley, Cryst. Growth Des. 7 (2007) 624;
(b) R.D. Willett, F.F. Awwadi, R. Butcher, S. Haddad, B. Twamley, Cryst. Growth Des. 3 (2003) 301;
(c) A. Panja, S. Goswami, N. Shaikh, P. Roy, M. Manassero, R.J. Butcher, P. Banerjee, Polyhedron 24 (2005) 2921.

[11] A.W. Addison, T.N. Rao, J. Reedijk, J. Van Rijn, G.C. Verschoor, J. Chem. Soc., Dalton Trans. (1984) 1349.

Polyhedron 27 (2008) 2681–2687

Contents lists available at ScienceDirect

Polyhedron

journal homepage: www.elsevier.com/locate/poly

Anion dependent formation of Ag(I) complexes of multidentate azine ligands: Synthesis and structural study

Chih-Yu Wu, Chen-Shiang Lee, Sachindranath Pal, Wen-Shu Hwang *

Department of Chemistry, National Dong Hwa University, 1, Sec. 2, Da-Hsueh Road, Shoufeng, Hualien 974, Taiwan, ROC

ARTICLE INFO

Article history:
Received 1 November 2007
Accepted 12 May 2008
Available online 28 June 2008

Keywords:
Azine
Ag(I) complexes
Anion influence
Supramolecular chemistry

ABSTRACT

The extended structures of Ag-complexes of the azine based ligands phenyl-2-pyridyl ketone azine ($\mathbf{L_1}$) and di-2-pyridyl ketone azine ($\mathbf{L_2}$) are reported, and focus is made on the investigation of the influence of the anion and supramolecular interactions on the self-assembly. Using $AgNO_3$, $AgClO_4$ and CF_3COOAg salts as starting materials for both ligands in acetonitrile, we observed the formation of the dinuclear complexes $[Ag_2(\mathbf{L_1})_2](NO_3)_2$ (**1a**), $[Ag_2(\mathbf{L_1})_2](ClO_4)_2$ (**1b**), from $\mathbf{L_1}$, the tetranuclear complexes $[Ag_4(\mathbf{L_2})_2(NO_3)(CH_3CN)_2](NO_3)_3$ (**2a**), $[Ag_4(\mathbf{L_2})_2(CF_3COO)_3CH_3CN](CF_3COO)$ (**2b**) and the linear chain polynuclear complex $\{[Ag_3(\mathbf{L_2})_2](ClO_4)_3\}_n$ (**3**) from $\mathbf{L_2}$. The X-ray structures show that the molecular geometry depends on the choice of anion. The silver centers have distorted tetrahedral coordination geometry in all the complexes. Weak hydrogen bonding and other interactions result in 2-D and 3-D networks in these complexes.

© 2008 Elsevier Ltd. All rights reserved.

1. Introduction

Azine and its derivatives are well known and are a useful class of organic compounds [1]. These compounds display important biological properties, are of importance for drug development [2], and are also used to develop supramolecular chemistry [1,3]. Supramolecular materials are found in a variety of applications including separation and host–guest interactions [4], catalytic properties [5], gas storage [6], non-linear optics [7] and magnetism [8]. So the design of metal–organic coordination polymers of supramolecular architecture, using non-covalent interactions such as electrostatic, hydrogen bonding and π-stacking, is an important area for supramolecular chemists and crystal engineers [9]. The formation of supramolecules is largely affected by the organic ligands, the nature of the metal ions, counter anions and other factors [10]. The role of anions in supramolecular chemistry is of enormous interest because of its application in ion pair recognition and anion exchange [11]. Recently, metallosupramolecular systems have been described for various types of ligands in which the anion and solvent play an important role in the design of the molecular architecture [9,11a,12]. As a soft acid the Ag(I) ion plays a central role in the formulation of such supramolecular assemblies, it favors stable coordination to soft bases like unsaturated nitrogen and sulfur [13]. There has only been a limited structural study of azine ligand based Ag-complexes [1b,3a,14]. Here we report the anion dependent formation of new Ag(I) complexes with pyridyl ketone azines.

2. Experimental

2.1. General

The solvents and reagents were purchased from general sources and were used without further purification. $\mathbf{L_1}$ and $\mathbf{L_2}$ were prepared according to the literature [1b,14a]. NMR spectra were recorded on a Bruker DX-300 NMR spectrometer (^{1}H, 300 MHz). Chemical shifts were referenced to TMS and deuterated acetonitrile (Acros) was used as the solvent. IR spectra were recorded using a Jasco FTIR 410 instrument. Mass spectra were measured on a Micromass Platform II spectrometer. Elemental analyses were carried out using a Perkin–Elmer 2400, 2400II elemental analyzer.

2.2. Synthesis of the complexes$[(\mathbf{L_1})_2Ag_2](NO_3)_2$ (**1a**) and $[(\mathbf{L_1})_2Ag_2](ClO_4)_2$ (**1b**)

$\mathbf{L_1}$ (0.362 g, 1 mmol) was dissolved in 10 ml acetonitrile. To this solution $AgNO_3$/$AgClO_4$ salt (1 mmol) was added with stirring. After 6 h a light yellow precipitate was collected by filtration. After washing with ether and drying under vacuum **1a** (81% yield)/**1b** (88% yield) was obtained.

Complex **1a**: ^{1}H NMR (CD_3CN) δ (ppm): 7.11 (d, 2H, J = 7.2 Hz), 7.25 (t, 2H, J = 8.1 Hz), 7.33 (d, 1H, J = 8.1 Hz), 7.52 (tt, 1H, J = 7.5 Hz), 7.67 (ddd, 1H, J = 7.8 Hz), 7.97 (td, 1H, J = 7.8 Hz), 8.38 (dt, 1H, J = 4.8 Hz); IR (KBr film, cm^{-1}) $\nu_{C=N}$: 1578, 1559,

* Corresponding author. Tel.: +886 3 8632001; fax: +886 3 8632000.
E-mail address: hws@mail.ndhu.edu.tw (W.-S. Hwang).

0277-5387/$ - see front matter © 2008 Elsevier Ltd. All rights reserved.
doi:10.1016/j.poly.2008.05.025

Table 1
Crystal data and structure refinement parameters for complexes **1a**, **1b**, **2b** and **3**

Compound	**1a**	**1b**	**2b**	**3**
Formula	$C_{48}H_{36}Ag_2N_{10}O_6$	$C_{48}H_{36}Ag_2Cl_2N_8O_8$	$C_{54}H_{41}Ag_4F_{12}N_{13}O_{11}$	$C_{44}H_{32}Ag_3Cl_3N_{12}O_{12}$
Formula weight	1064.61	1139.49	1707.48	1350.78
Crystal size (mm)	0.07 × 0.07 × 0.06	0.08 × 0.08 × 0.07	0.1 × 0.1 × 0.08	0.09 × 0.09 × 0.08
T (K)	273 (2)	273 (2)	293 (2)	273 (2)
Crystal system	monoclinic	monoclinic	triclinic	monoclinic
Space group	$P2(1)/c$	$P2(1)/c$	$P\bar{1}$	Pc
a (Å)	12.6475(3)	17.3461(6)	14.4930(2)	20.7930(13)
b (Å)	33.8450(9)	15.1473(6)	15.2040(2)	9.4019(6)
c (Å)	12.2745(3)	19.4393(7)	15.3180(3)	25.0609(16)
α (°)			67.5800(10)	
β (°)	109.0160(10)	112.1050(10)	79.7690(10)	143.208(2)
γ (°)			84.7340(10)	
V (Å3)	4967.4(2)	4732.2(3)	3069.53(8)	2934.2(3)
Z	4	4	2	2
D_{Calc} (g cm^{-3})	1.445	1.599	1.847	1.529
μ (mm^{-1})	0.85	1.00	1.36	1.19
θ Range (°)	2.3–19.4	2.4–23.5	2.0–25.0	2.2–19.8
Number of data unique/collected	9258/52 346	12 286/55 168	10 732/25 969	22 298/13 237
R_1/wR_2 [$I > 2\sigma(I)$]	0.129/0.373	0.046/0.147	0.049/0.173	0.055/0.127
Goodness-of-fit	1.19	1.01	1.048	1.036

$\nu_{NO_3^-}$: 1384; MS (FAB): m/z 1065, 1061 [M]$^+$. *Anal.* Calc. for $C_{48}H_{36}Ag_2N_{10}O_6$: C, 54.14; H, 3.38; N, 13.16. Found: C, 53.98; H, 3.42; N, 13.08%.

Complex **1b**: ^{1}H NMR (CD_3CN) δ (ppm): 7.10 (d, 2H, J = 7.2 Hz), 7.27 (t, 2H, J = 7.5 Hz), 7.35 (d, 1H, J = 7.8 Hz), 7.52 (tt, 1H, J = 7.5 Hz), 7.68 (ddd, 1H, J = 6.6 Hz), 7.97 (td, 1H, J = 7.8 Hz), 8.33 (dt, 1H, J = 5.1 Hz); IR (KBr film, cm^{-1}) $\nu_{C=N}$: 1578, 1559, $\nu_{ClO_4^-}$: 1084; MS (FAB): m/z 1041, 1035 [M−ClO_4]$^+$. *Anal.* Calc. for $C_{48}H_{36}Ag_2Cl_2N_8O_8$: C, 50.59; H, 3.18; N, 9.83. Found: C, 50.73; H, 3.24; N, 9.90%.

2.3. Synthesis of complexes $[(\mathbf{L_2})_2Ag_4(NO_3)(CH_3CN)_2](NO_3)_3$ (**2a**) and $\{[(\mathbf{L_2})_2Ag_3](ClO_4)_3\}_n$ (**3**)

Ligand $\mathbf{L_2}$ (0.364 g, 1 mmol) was dissolved in 10 ml of acetonitrile. To this solution $AgNO_3$/$AgClO_4$ salt (2 mmol) was added with stirring. After 4 h the reaction mixture was concentrated and a yellow precipitate appeared immediately. The precipitate was collected by filtration, washed with ether and dried under vacuum to give complex **2a** (yield 78%)/**3** (yield 72%).

Complex **2a**: ^{1}H NMR (CD_3CN) δ (ppm): 7.29 (d, 1H, J = 8.1 Hz), 7.45 (ddd, 1H, J = 7.8 Hz), 7.60 (m, 2H), 7.88 (m, 2H), 8.34 (d, 1H, J = 4.5 Hz), 8.41 (d, 1H, J = 5.1 Hz); IR (KBr film, cm^{-1}): $\nu_{C=N}$: 1583, 1564, $\nu_{NO_3^-}$: 1384. MS (FAB): m/z 1350, 1342 [M−2(CH_3CN)−NO_3]$^+$, 1288, 1280 [M−2(CH_3CN)−2(NO_3)]$^+$, 1224, 1216 [M−2(CH_3CN)−3(NO_3)]$^+$. *Anal.* Calc. for $C_{48}H_{38}Ag_4N_{18}O_{12}$: C, 38.66; H, 2.55; N, 16.91. Found: C, 38.59; H, 2.63; N, 16.80%.

Complex **3**: ^{1}H NMR (CD_3CN) δ (ppm): 7.27 (d, 1H, J = 8.1 Hz), 7.52 (ddd, 1H, J = 7.8 Hz), 7.59 (m, 2H), 7.88 (m, 2H), 8.34 (d, 1H, J = 4.5 Hz), 8.40 (d, 1H, J = 5.1 Hz); IR (KBr film, cm^{-1}): $\nu_{C=N}$: 1591, 1564, $\nu_{ClO_4^-}$: 1090; MS (FAB): m/z 1467, 1453 [M +Ag]$^+$; 1358, 1349, 1346 [M]$^+$. *Anal.* Calc. for $C_{44}H_{34}Ag_3Cl_3N_{12}O_{13}$ (**3** · H_2O): C, 38.57; H, 2.48; N, 12.27. Found: C, 38.46; H, 2.54; N, 12.18%.

2.4. Synthesis of complex $[(\mathbf{L_2})_2Ag_4(CF_3COO)_3](CF_3COO)$ (**2b**)

Ligand $\mathbf{L_2}$ (0.364 g, 1 mmol) was dissolved in 10 ml of acetonitrile. To this solution $AgOOCCF_3$ salt (2 mmol) was added with

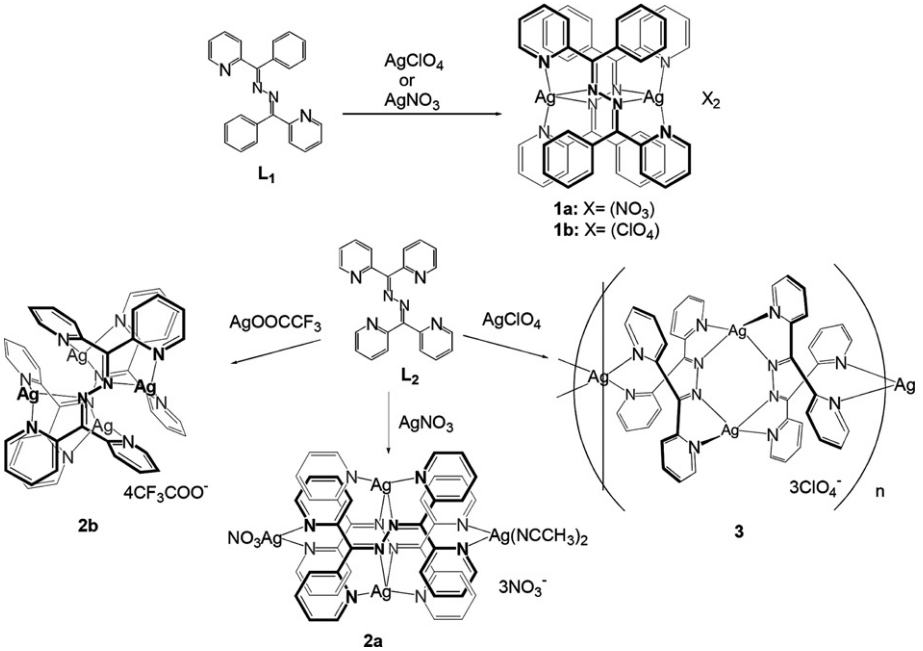

Scheme 1.

stirring. After 4 h the yellow solution was concentrated and stirred with a large volume of ether. The precipitate that formed was collected by filtration and dried under vacuum to give complex **2b** (76% yield). ^{1}H NMR (CD_3CN) δ (ppm): 7.25 (dt, 1H, J = 7.8 Hz), 7.61 (m, 2H), 7.71 (d, 1H, J = 7.8 Hz), 7.93 (ddd, 2H, J = 9.3 Hz), 8.38 (dt, 1H, J = 7.8 Hz), 8.43 (d, 1H, J = 5.1 Hz); IR (KBr film, cm^{-1}) $\nu_{C=N}$: 1581, 1562; $\nu_{CF_3COO^-}$: 1684. MS (FAB): m/z 1502, 1494 $[M-(CF_3COO)]^+$. *Anal.* Calc. for $C_{52}H_{38}Ag_4F_{12}N_{12}O_{11}$ (**2b** · $3H_2O$): C, 37.45; H, 2.28; N, 10.08. Found: C, 37.44; H, 2.24; N, 9.98%.

2.5. X-ray diffraction studies

X-ray quality crystals of all the complexes were grown by the slow diffusion of ether into an acetonitrile solution of the complexes. Single crystals were mounted on a glass fiber and the X-ray diffraction intensity data were measured on a Bruker Smart APEXII CCD XRD. The intensity data were collected at 273 K. All data were collected with the ω scan technique using graphite monochromatic Mo Kα radiation (λ = 0.71073 Å). All non-hydrogen atoms were refined with anisotropic displacement parameters and hydrogen atoms were included at calculated positions. The structures were solved by direct methods using the SHELXS-97 computer program and refined by full-matrix least-squares methods on F^2 using SHELXL-97 [15]. The crystal data and structure refinement parameters for complexes **1a**, **1b**, **2b**, and **3** are tabulated in Table 1. Although the main complex cation of the structure of **1a** is correct, there exists an unknown high electron density which could not be resolved with proper chemical meaning. In the structure of complex **2b**, there are some unreasonable displacement parameters for some C atoms and short C–C distances on the F_3CCOO^- anion groups due to the unsolved disorder problem.

3. Result and discussion

To investigate Ag(I) chemistry in the presence of different anions, complexes **1a**, **1b**, **2a**, **2b** and **3** were prepared. The formation of complexes is given in Scheme 1. X-ray quality crystals of **1a**, **1b**, **2a**, **2b**, and **3** were grown by diffusing ether into an acetonitrile solution of the complexes. In all the complexes, $\mathbf{L_1}$ acts as a tetradentate ligand and $\mathbf{L_2}$ acts as a hexadentate one, using their all possible N-donor sites. A similar structure of nitrate complex **2a** had been reported [14a] where it crystallized in the space group $P2_1/c$.

Except for the coordination of anions or solvents, the coordination environments of the Ag(I) centers of the complexes of ligand $\mathbf{L_1}$ are almost same, in the presence of different anions, but the packing of the crystals are different for different anions. For the complexes of $\mathbf{L_2}$, both the coordination environment and the packing of the crystals are different with different anions. Nitrate and trifluoroacetate complexes are tetranuclear with different coordination environments of the Ag(I) centers whereas the perchlorate complex has a polynuclear chain structure. It is important to note that the main chromophore contains $Ag_2(N_{az})_4(N_{py})_4$ units for the perchlorate and nitrate complexes of both ligands. The structural motif of the main chromophore is given in Fig. 1. In this chromophore two Ag centers and two azine (N–N) bridges form a six member distorted ring.

3.1. Crystal structures of complexes

3.1.1. Molecular structures of *1a* and *1b*

X-ray crystal structure determination of **1a** and **1b** lead to the formulation $[Ag_2(\mathbf{L_1})_2](NO_3)_2$ and $[Ag_2(\mathbf{L_1})_2](ClO_4)_2$, respectively. The structures indicated that both complexes are dimeric (Figs. 2 and 3a), with each Ag(I) center coordinated by two pyridine N-atoms from each of the two ligands. Two Ag(I) ions are also doubly bridged by azine (N–N) groups. In this way each Ag(I) center is tetra-coordinated, but their geometry is far from tetrahedral (π-type geometry) due to twisting of the ligands. The Ag–Naz distances are much longer than the Ag–Npy distances in both complexes (Table 2). The Ag–Npy distances are comparable with those reported for similar complexes [14,16] whereas the Ag–Naz distances are longer than similar bonds reported in other Ag–azine bridge complexes [14b]. This is due to the steric crowding of the substituted phenyl rings. The two ligands lie above and below the line made between the two Ag(I) centers. The ligands undergo a twist due to the coordination to the metal centers and form a double helical structure [17]. The twist conformation of the ligands as well as the rings also prevents the formation of an intramolecular π–π interaction. The Ag–Ag separation in both complexes (average 4.829 Å) indicates that there is no argentophilic interaction.

In the perchlorate complex **1b**, C–H···π interactions also generate a two-dimensional network (Fig. 3b, H···π distance range 2.74–2.83 Å, H···centroid distance 3.50 Å). Moreover, the perchlorate

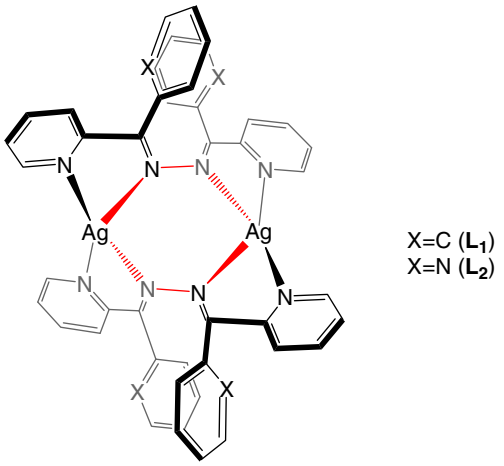

Fig. 1. The structural motif of the main chromophore in complexes **1a**, **1b**, **2a** and **3**.

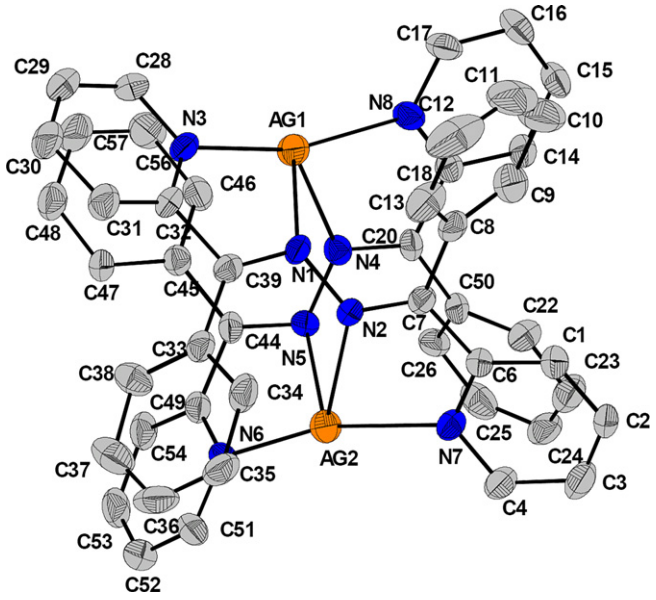

Fig. 2. ORTEP view of **1a** showing 30% probability ellipsoids. Anions and hydrogen atoms are omitted for clarity.

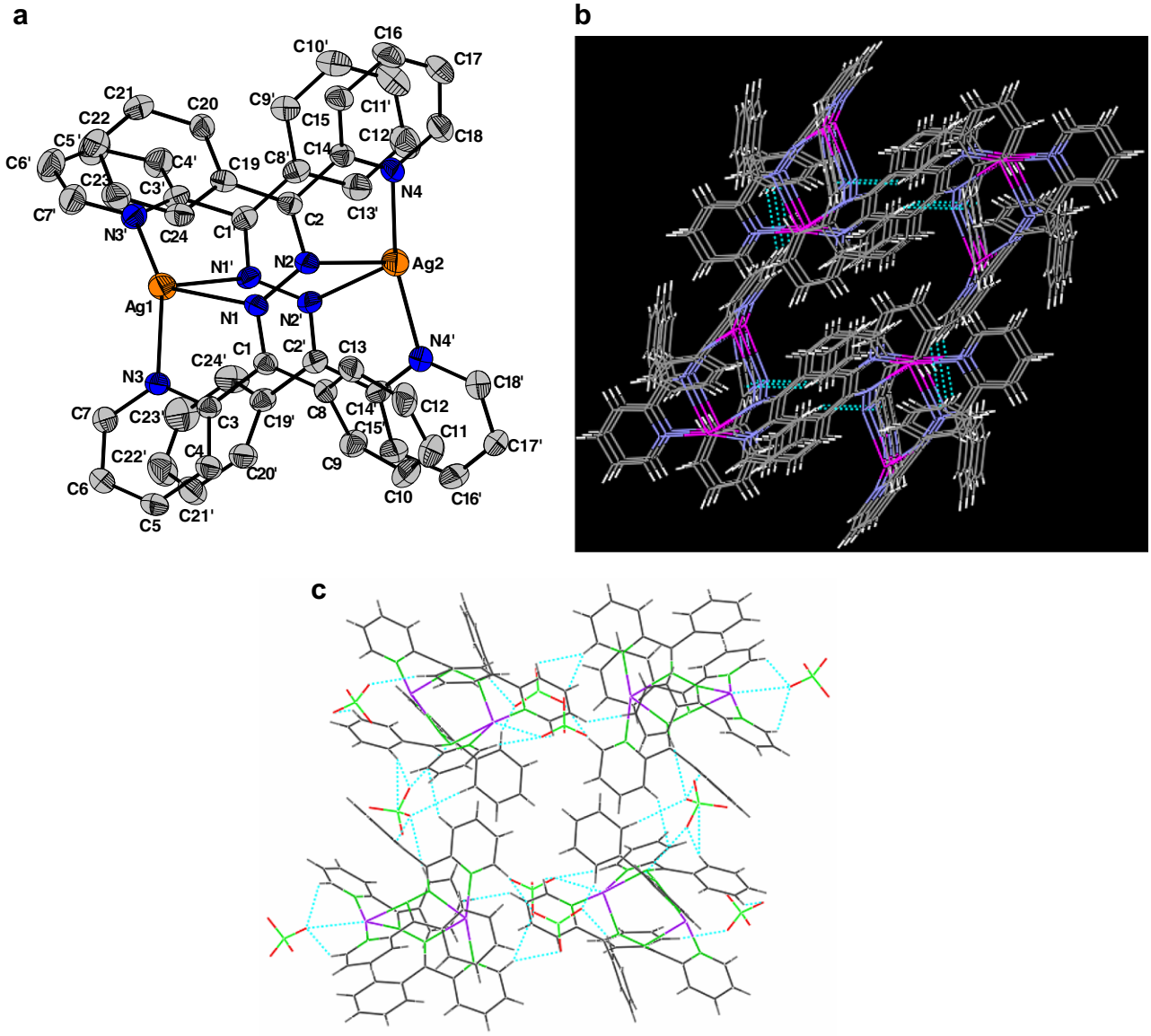

Fig. 3. (a) ORTEP view of **1b** showing 30% probability ellipsoids. Anions and hydrogen atoms are omitted for clarity. (b) C–H···π interactions between molecules to form the 2-D network in complex **1b**. (c) View of the 3-D network of C–H···O and C–H···π interactions in complex **1b**.

groups also make a number of short O···H–C interactions [9a] in the range 2.38–2.66 Å (Fig. 3c). The perchlorate ions contact the pyridine ring protons and benzene ring protons, which may be involved in the stabilization of the solid state structure. Weak C–H···π interactions also help to make a three-dimensional (3-D) network structure.

*3.1.2. Molecular structure of **2b***

The X-ray analysis of **2b** reveals that the asymmetric unit of the complex contains a discrete polynuclear $Ag_4(\mathbf{L_2})_2$ moiety formed by the assembly of four Ag atoms and two ligand molecules. The unit cell contains two of the above complete units with six coordinated trifluoroacetate (F_3CCOO^-), two coordinated acetonitrile (CH_3CN), two free F_3CCOO^- ions and six water molecules. Unlike the nitrate complex, the complex crystallizes in the triclinic system with space group $P\bar{1}$. An ORTEP plot of the discrete unit is shown in Fig. 4.

The coordination environment of each Ag(I) center is completely different from the nitrate complex **2a** [14a]. Among the four Ag(I) centers in the nitrate complex, two Ag(I) ions are coordinated by two azine N-atoms from two ligands and two pyridine N-atoms also from two ligands. Each of the other two Ag(I) ions is coordinated by two pyridine N-atoms from two ligands and a nitrate ion or acetonitrile solvent molecule. Whereas, in the trifluoroacetate complex each of the three Ag(I) centers Ag1, Ag2 and Ag4 completes its three coordination position with the same donor atoms – one azine N-atom and two pyridine N-atoms, and the fourth coordination position is satisfied by either F_3CCOO^- or CH_3CN. One azine N-donor and one pyridine N-donor of a ligand form a five member chelate ring with each Ag center. The remaining Ag3 center is coordinated by two pyridine nitrogen atoms and a F_3CCOO^- ion. The Ag–N_{py} distances around all the Ag centers are in the range 2.250–2.323 Å (Table 2), similar to those found in other pyridine N-donor Ag(I) complexes [12a,14b,16,18] and longer than other reported complexes [3,13b]. The Ag–N_{az} distances are quite a lot longer than the Ag–Npy distances, but are similar to those found in the reported azine bridged Ag complex **2a** [14a] and also longer than another reported Ag complex [14b]. The N–Ag–N angles around the Ag centers are quite dissimilar from one Ag center to

Table 2
Selected bond lengths and angles

Atom		Bond distances (Å)		Bond angles (°)
		$Ag–N_{py}$	$Ag–N_{az}$	
1a	Ag1	2.192(10) (N3)	2.409(9) (N4)	N3–Ag1–N8 = 161.1(4), N3–Ag1–N4 = 128.1(3)
		2.222(10) (N8)	2.525(9) (N1)	N8–Ag1–N4 = 70.7(3), N3–Ag1–N1 = 70.1(3)
				N8–Ag1–N1 = 115.8(3), N4–Ag1–N1 = 88.8(3)
	Ag2	2.253(9) (N7)	2.460(10) (N2)	N6–Ag2–N7 = 158.9(3), N6–Ag2–N2 = 130.5(3)
		2.219(9) (N6)	2.662(6) (N5)	N6–Ag2–N5 = 68.67(2), N7–Ag2–N2 = 69.0(3)
1b	Ag1	2.198(3) (N3′)	2.435(3) (N1)	N3′–Ag1–N3 = 152.35(11), N3′–Ag1–N1 = 136.18(11)
		2.245(3) (N3)	2.659 (N1′)	N3–Ag1–N1 = 69.39(10), N1′–Ag1–N1 = 83.54(9)
				N1′–Ag1–N3 = 113.65(11), N3′–Ag1–N1′ = 68.19(11)
	Ag2	2.206(3) (N4)	2.446(3) (N2′)	N4–Ag2–N4′ = 164.85(12), N4–Ag2–N2′ = 124.74(10)
		2.228(3) (N4′)	2.583(3) (N2)	N4′–Ag2–N2′ = 70.24(11), N4–Ag2–N2 = 69.29(10)
				N4′–Ag2–N2 = 113.60(11), N2′–Ag2–N2 = 84.13(10)
2b	Ag1	2.250(5) (N8)	2.539(5) (N2)	N8–Ag1–N1 = 131.27(18), N8–Ag1–N13 = 99.6(2)
		2.267(5) (N1)	2.353(7) (N13)	N1–Ag1–N13 = 99.6(2), N8–Ag1–N2 = 119.34(16)
			(CH_3CN)	N1–Ag1–N2 = 69.15(15), N13–Ag1–N2 = 136.9(2)
	Ag2	2.276(5) (N5)	2.604(4) (N6)	N5–Ag2–N4 = 135.72(18), N5–Ag2–O1 = 112.2(2)
		2.323(5) (N4)	2.414(5) (O1)	N4–Ag2–O1 = 86.34(19), N5–Ag2–N6 = 66.78(15)
			(F_3CCOO^-)	N4–Ag2–N6 = 112.85(15), O1–Ag2–N6 = 154.04(17)
	Ag3	2.231(5) (N10)	2.447(5) (O3)	N10–Ag3–N12 = 142.57(16), N10–Ag3–O3 = 115.93(18)
		2.270(5) (N12)	(F_3CCOO^-)	N12–Ag3–O3 = 89.30(18)
	Ag4	2.259(5) (N9)	2.586(4) (N7)	N9–Ag4–N11 = 130.92(16), N9–Ag4–O5 = 125.80(18)
		2.313(5) (N11)	2.333(5) (O5)	N11–Ag4–O5 = 89.25(17), N9–Ag4–N7 = 117.53(15)
			(F3CCOO$^-$)	N11–Ag4–N7 = 67.54(14), O5–Ag4–N7 = 110.50(16)
3	Ag1	2.229(7) (N6)	2.516(6) (N2)	N6–Ag1–N6 = 171.4(2), N6–Ag1–N2 69.5(2)
		2.240(6) (N6′)	2.537(5) (N2′)	N6′–Ag1–N2 = 118.9(2), N6–Ag1–N2′ = 117.2(2)
				N6′–Ag1–N2′ = 68.2(2), N2–Ag1–N2′ = 78.17(18)
	Ag2	2.226(6) (N5)	2.475(5) (N1)	N5–Ag2–N5′ = 169.4(2), N5–Ag2–N1 = 69.4(2)
		2.265(6) (N5′)	2.561(6) (N1′)	N5′–Ag2–N1 = 121.1(2), N5′–Ag2–N1′ = 69.1(2)
	Ag3	2.307(6) (N3)		N5′–Ag2–N1 = 121.1(2), N5–Ag2–N1′ = 114.5(2)
		2.339(6) (N4′i)		N3–Ag3–N4′i = 101.2(2), N3–Ag3–N4 = 121.3(2)
		2.344(6) (N4)		N4′i–Ag3–N4 = 106.8(2), N3–Ag3–N3′i = 117.0(2)
		2.330(6) (N3′i)		N4′i–Ag3–N3′i = 118.2(2), N4–Ag3–N3′i = 93.1(2)

Symmetry codes for **3** (i) $x, y-1, z$.

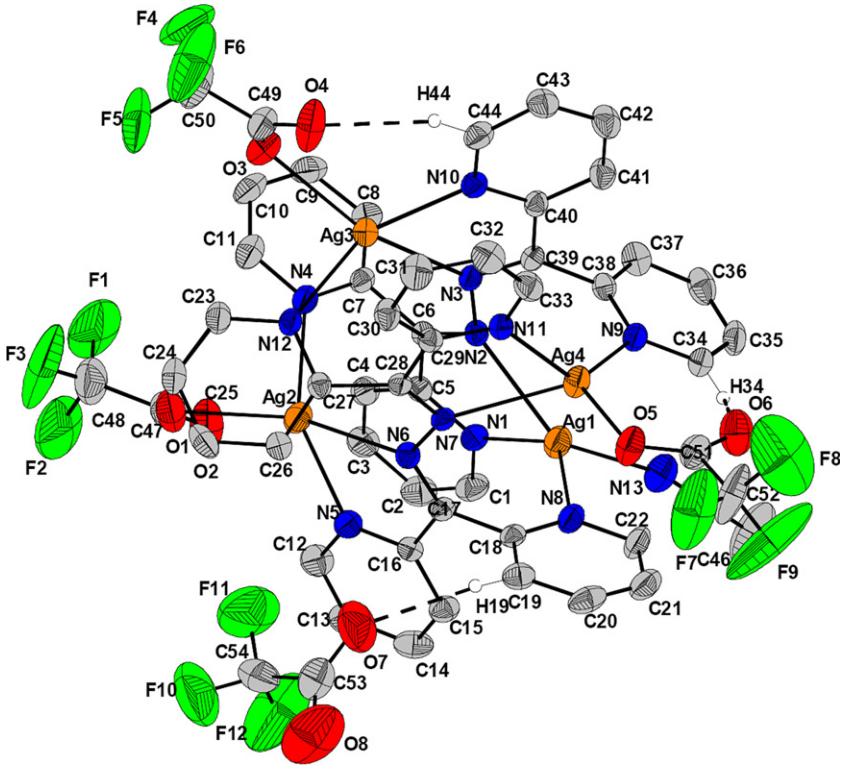

Fig. 4. ORTEP view of **2b** showing 30% probability ellipsoids. Anions and hydrogen atoms are omitted for clarity.

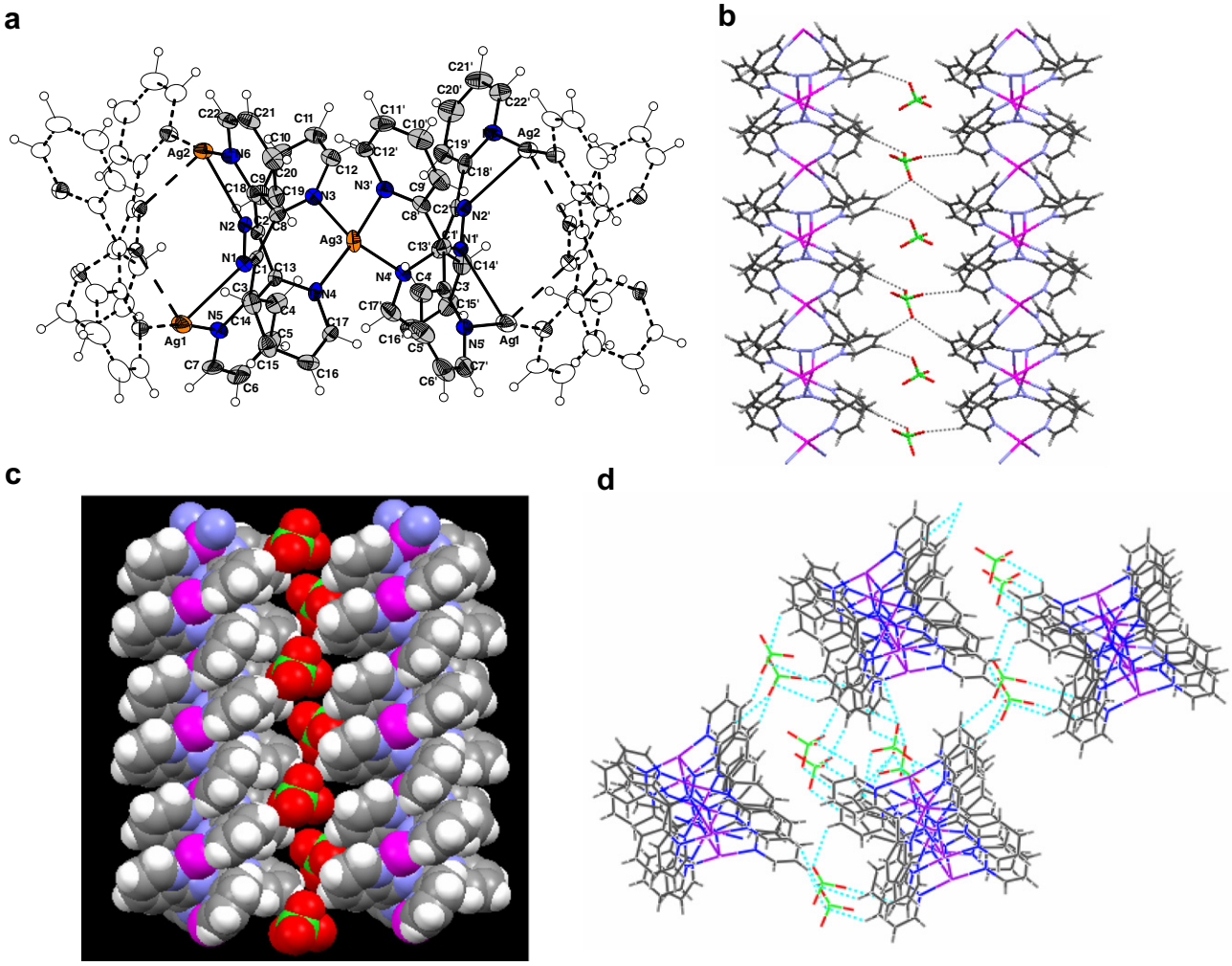

Fig. 5. (a) ORTEP view of **3** showing 30% probability ellipsoids. Anions and hydrogen atoms are omitted for clarity. (b) View of hydrogen bonding by perchlorate between two linear chains in complex **3**. (c) Space-filling 2-D structure showing hydrogen bonding in complex **3**. (d) 3-D packing diagram of complex **3**.

the next (Table 2). The Ag2 and Ag4 centers are bridged by two azine N-atoms of one ligand, but the Ag1 and Ag3 centers are not bridged by the two azine N-atoms of another ligand. Only the Ag1 center is coordinated to one azine nitrogen whereas the large Ag3–N_{az}3 distance (2.778 Å) indicates that there is no bonding due to the strained conformation of the ligand. The large Ag–Ag distances also indicate that there is no argentophilic interaction.

3.1.3. Molecular structure of ***3***

The structure of the cation of **3** is a polymer of stoichiometry $[Ag_3(\mathbf{L_2})_2]^{3+}$, in which each tetrapyridyl azine ligand coordinates three Ag(I) centers (Fig. 5a). All the Ag centers are tetra-coordinated but they are also far from a tetrahedral geometry. Each ligand is bidentate to each Ag center. Each of the Ag1 and Ag2 centers in $[Ag_3(\mathbf{L_2})_2]^{3+}$ has a four coordinate pseudo-tetrahedral or π-type geometry with a coordination sphere consisting of two pyridine N-donors from two ligands and two azine N-donors from two ligands. The Ag3 center in $[Ag_3(\mathbf{L_2})_2]^{3+}$ also has a four coordinate distorted tetrahedral geometry with a coordination sphere consisting of two pyridine N-donors from the same ligand and two other pyridine N-donors from another ligand of another $[Ag_3(\mathbf{L_2})_2]^{3+}$ unit.

The two pyridine rings of the same or different ligands are not co-planar. The dihedral angle (79.63°) of the two pyridine rings which coordinate to Ag1 and Ag2 means that they are almost perpendicular to each other. The dihedral angle of the other two pyridine rings which coordinate to Ag3 is 54.87°. The repetition of the $[Ag_3(\mathbf{L_2})_2]^{3+}$ unit form the linear polynuclear chain. In a closer look, the Ag3 centers helped to form the extended linear chain in the molecule and the linear chains are linked into a two-dimensional (2-D) (Fig. 5b and c) and three-dimensional (3-D) (Fig. 5d) network through C–H···O hydrogen bonding interactions involving pyridine ring protons with perchlorate ions (H···O distance range 2.5–2.68 Å).

4. Conclusions

Four coordination complexes constructed by self assembly of azine based ligands and Ag ions have been structurally characterized. This structural analysis revealed a great difference in the crystal packing due to the influence of the anion symmetry. Such variation in the environment of a complex molecule is termed as 'Chemical Frustration' [9a]. In these complexes, various weak interactions and hydrogen bonding generate 2-D or 3-D networks.

Appendix A. Supplementary data

CCDC 663164, 663165, 663166 and 663167 contain the supplementary crystallographic data for **3**, **1b**, **2b** and **1a**. These data can

be obtained free of charge via http://www.ccdc.cam.ac.uk/conts/retrieving.html, or from the Cambridge Crystallographic Data Centre, 12, Union Road, Cambridge CB2 1EZ, UK; Fax: (+44) 1223-336-033; or e-mail: deposit@ccdc.cam.ac.uk.

Acknowledgements

Financial support from the National Science Council (Taiwan, ROC) and National Dong Hwa University are gratefully acknowledged.

References

[1] (a) R. Cohen, B. Rybtchinski, M.K. Gandelman, L.J.W. Shimon, J.M.L. Martin, D. Milstein, Angew. Chem., Int. Ed. Engl. 42 (2003) 1949;
(b) E. Amadei, M. Carcelli, S. Ianelli, P. Cozzini, P. Pelagatti, C. Pelizzi, J. Chem. Soc., Dalton Trans. (1998) 1025.
[2] A.I. Khodair, P. Bertrand, Tetrahedron 54 (1998) 4859.
[3] (a) A.R. Kennedy, K.G. Brown, D. Graham, J.B. Kirkhouse, M. Kittner, C. Major, C.J. McHugh, P. Murdoch, W.E. Smith, New J. Chem. 29 (2005) 826;
(b) D. Dragancea, V.B. Arion, S. Shova, E. Rentschler, N.V. Gerbeleu, Angew.Chem., Int. Ed. Engl. 44 (2005) 7938.
[4] (a) M. Aoyagi, K. Biradha, M. Fujita, J. Am. Chem. Soc. 121 (1999) 7457;
(b) A. Tanatani, M.J. Moi, J.S. Moore, J. Am. Chem. Soc. 123 (2001) 1792;
(c) K. Biradha, C. Seward, M.J. Zaworotko, Angew. Chem. 111 (1999) 584;
(d) K. Biradha, C. Seward, M.J. Zaworotko, Angew. Chem., Int. Ed. Engl. 38 (1999) 492.
[5] (a) Y. Aoyama, Top. Curr. Chem. 165 (1998) 131;
(b) D.M. Bassani, V. Darcos, S. Mahony, J.P. Desvergne, J. Am. Chem. Soc. 122 (2000) 8795.
[6] (a) J.L.C. Rowsell, A.R. Millward, K.S. Park, O.M. Yaghi, J. Am. Chem. Soc. 126 (2004) 5666;
(b) H.K. Chae, D.Y. Siberio-Perez, J. Kim, Y.B. Go, M. Eddaoudi, A.J. Matzger, M. O'Keeffe, O.M. Yaghi, Nature 427 (2004) 523.
[7] (a) M. Muthuraman, R. Masse, J.F. Nicold, G.R. Desiraju, Chem. Mater. 13 (2001) 1473;
(b) O. König, H.B. Bürgi, T. Armbruster, J. Hulliger, T. Weber, J. Am. Chem. Soc. 119 (1997) 10632.
[8] (a) O. Kahn, Acc. Chem. Res. 33 (2000) 1;
(b) J.S. Miller, Inorg. Chem. 39 (2000) 4392.
[9] (a) M.J. Hannon, C.L. Painting, E.A. Plummer, L.J. Childs, N.W. Alcock, Chem. Eur. J. 8 (2002) 2225;
(b) M.D. Stephenson, M.J. Hardie, Cryst. Growth Des. 6 (2006) 423.
[10] X. Xu, Y. Lu, E. Wang, Y. Ma, X. Bai, Cryst. Growth Des. 6 (2006) 2029.
[11] (a) M.O. Awaleh, A. Badia, F. Brisse, Cryst. Growth Des. 6 (2006) 2674;
(b) Q.G. Zhai, X.Y. Wu, S.M. Chen, Z.G. Zhao, C.Z. Lu, Inorg. Chem. 46 (2007) 5046.
[12] (a) B. Hasenknopf, J.M. Lehn, N. Boumediene, A. Dupont-Gervais, A. Van Dorsselaer, B.O. Kneisel, D. Fenske, J. Am. Chem. Soc. 119 (1997) 10956;
(b) R.D. Schnebeck, E. Freisinger, B. Lippert, Angew. Chem., Int. Ed. Engl. 38 (1999) 168;
(c) J.S. Fleming, K.L.V. Mann, C.A. Carraz, E. Psillakis, J.C. Jeffery, J.A. McCleverty, M.D. Ward, Angew. Chem. 110 (1998) 1315;
(d) P.L. Jones, K.J. Byrom, J.C. Jeffery, J.A. McCleverty, M.D. Ward, Chem. Commun. (1997) 1361;
(e) S.L. James, D.M.P. Mingos, A.J.P. White, D.J. Williams, Chem. Commun. (1998) 2323;
(f) D.A. McMorran, P.J. Steel, Angew. Chem., Int. Ed. Engl. 37 (1998) 3295;
(g) R.D. Schnebeck, E. Freisinger, B. Lippert, Angew. Chem. 111 (1999) 235;
(h) D.A. McMorran, P.J. Steel, Angew. Chem. 110 (1998) 3495;
(i) N. Gimeno, R. Vilar, Coord. Chem. Rev. 250 (2006) 3161;
(j) R. Vilar, D.M.P. Mingos, A.J.P. White, D.J. Williams, Angew. Chem., Int. Ed. Engl. 37 (1998) 1258;
(k) G. Bianchi, E. Garcia-Espaňa, K. Bowman-James, Supramolecular Chemistry of Anions, Wiley-VCH, Weinheim, Germany, 1997;
(l) R.M. Silva, M.D. Smith, J.R. Gardinier, Inorg. Chem. 45 (2006) 2132.
[13] (a) G.K. Patra, I. Goldberg, Cryst. Growth Des. 3 (2003) 321;
(b) N.L.S. Yue, M.C. Jennings, R.J. Puddephatt, Inorg. Chem. 44 (2005) 1125.
[14] (a) C.J. Sumby, P.J. Steel, New J. Chem. 29 (2005) 1077;
(b) G. Dong, H. Cheng, C. Y Duan, C.Q. Quin, Q.J. Meng, New J. Chem. 26 (2002) 796.
[15] G.M. Sheldrick, SHELX-97: Program for Solution of Crystal Structures, University of Göttingen, Germany, 1997.
[16] V. Patroniak, A.R. Stefankiewicz, J.M. Lehn, M. Kubicki, Eur. J. Inorg. Chem. (2005) 4168.
[17] (a) C.J. Fang, C.Y. Duan, H. Mo, C. He, Q.J. Meng, Y.J. Liu, Y.H. Mei, Z.M. Wang, Organometallics 20 (2001) 2525;
(b) C. He, C.Y. Duan, C.J. Fang, Q.J. Meng, J. Chem. Soc., Dalton Trans. (2000) 2419;
(c) C.J. Fang, C.Y. Duan, C. He, Q.J. Meng, Chem Commun. (2000) 1187;
(d) M.J. Hannon, S. Bunce, A.J. Clarke, N.W. Alcock, Angew. Chem., Int. Ed. Engl. 38 (1999) 1277;
(e) M.J. Hannon, C.L. Painting, N.W. Alcock, Chem. Commun. (1999) 2023.
[18] Y.B. Dong, X. Zhao, R.Q. Huang, M.D. Smith, H.C. zur Loye, Inorg. Chem. 43 (2004) 5603.

Polyhedron 27 (2008) 2688–2692

Contents lists available at ScienceDirect

Polyhedron

journal homepage: www.elsevier.com/locate/poly

A europium(II) complex with bis-pyridino-18-crown-6

Jens Christoffers [a], Przemysław Starynowicz [b,*]

[a] Institut für Reine und Angewandte Chemie, Carl von Ossietzky-Universität Oldenburg, D-26111 Oldenburg, Germany
[b] Wydział Chemii, Uniwersytet Wrocławski, ul. F. Joliot-Curie 14, 50-383 Wrocław, Poland

ARTICLE INFO

Article history:
Received 18 March 2008
Accepted 7 May 2008
Available online 1 July 2008

Keywords:
Divalent europium
Bis-pyridine-18-crown-6
Structure
Spectroscopy
Density functional calculations

ABSTRACT

A new Eu(II) complex, bis(perchlorato)(bis-pyridino-18-crown)europium(II), has been obtained in the crystalline form by electrolytic reduction. The metal ion is 10-coordinated and its surrounding consists of four macrocycle O atoms, two N ones and four O atoms from perchlorate anions. The compound shows a very broad absorption band, starting gently from 600 nm towards the UV region, and two weak luminescence bands with maxima at 430 and 500 nm. The performed density functional theory (DFT) calculations have shown that the absorption results from mixed f–d, f–s and charge transfer transitions. The possible mechanism of luminescence is also discussed.

© 2008 Elsevier Ltd. All rights reserved.

1. Introduction

Macrocycles are an important class of ligands in the chemistry of divalent lanthanides because they stabilize to some extent this oxidation state. The Ln(II) complexes that have been investigated extensively feature complexes of crown ethers (with O donors) and cryptands [1,2]. These compounds generally show efficient blue luminescence in solutions and in the solid state. The derivatives of crown ethers with both O and N donors have been devoted less attention and to the best of the authors' knowledge no complexes of Ln(II) with crown ethers containing pyridine rings have been reported. Such a compound could be helpful in gaining insight into some questions relating to the blue emission of divalent europium, namely: (a) the presence of pyridine fragments coordinated to the Eu^{2+} cation would allow the assessment of the impact of the antenna effect on the luminescent properties of the metal centre (such an effect plays an important role in enhancing the luminescent efficiency of trivalent lanthanide complexes [3]), (b) it would be interesting to know the impact of the aromatic π electrons located directly near the Eu^{2+} cation on the spectroscopic properties of the latter. Apart from that, the donor pyridine N atoms are less basic than in azacrown ethers which may result in easier complexation of the ligand under mild (non-anhydrous) conditions (the competition from the hydrogen cations being less severe). Therefore for the present study a ligand of this type, bis-pyridino-18-crown-6 or 3,6,10,13-tetraoxa-1(2,6),8(2,6)-dipyridinacyclotetradecaphan, has been chosen. Generally, only a few examples of metal complexes with this macrocycle or its substituted derivatives have been reported so far; these include a cadmium compound [4], an yttrium and a few lanthanide(III) complexes [5]. According to what has been said above, the purpose of the present work is to investigate the coordination ability of bis-pyridino-18-crown-6 towards Eu(II) and to determine the structure and spectroscopic properties of the obtained compound.

2. Experimental

2.1. Synthesis

2.1.1. 3,6,10,13-Tetraoxa-1(2,6),8(2,6)-dipyridinacyclotetradecaphan

The ligand was obtained according to the method previously described [6]. NaH (0.671 g, 16.8 mmol, 60% in mineral oil) was added at room temperature to a solution of ethylene glycol (0.440 g, 7.11 mmol) in abs. THF (100 ml). The reaction mixture was stirred for 30 min at 23 °C then a solution of 2,6-bis(bromomethyl)pyridine (1.88 g, 7.11 mmol) in abs. THF (100 ml) was added dropwise. After 6 days stirring at 23 °C, H_2O (30 ml) was added to the mixture, the layers were separated and the aqueous layer was extracted with DCM (3 × 30 ml). The combined organic layers were dried over anhydrous $MgSO_4$ and the solvent was removed under reduced pressure. After column chromatography with Al_2O_3 (DCM with a gradient to MeOH) and sublimation (0.14 mbar, 135°C), bis-pyridino-18-crown-6 (126 mg, 0.381 mmol, 11%) was obtained as a colourless crystalline solid. M.p.: 133 °C, Lit.: 147–148 °C; R_f (SiO_2, DCM:MeOH = 1:1) = 0.15–0.44; ^1H NMR (300 MHz, $CDCl_3$): δ = 3.76 (s, 8H), 4.56 (s, 8H), 7.23 (d, J = 7.7 Hz, 4H), 7.61 (t, J = 7.7 Hz, 2H) ppm; $^{13}C\{^1H\}$ NMR

* Corresponding author.
E-mail address: psta@wchuwr.pl (P. Starynowicz).

0277-5387/$ - see front matter © 2008 Elsevier Ltd. All rights reserved.
doi:10.1016/j.poly.2008.05.028

(75 MHz, $CDCl_3$): δ = 69.84 ($4CH_2$), 73.53 ($4CH_2$), 120.40 (4CH), 136.68 (2CH), 157.91 (4C) ppm; IR (ATR): λ^{-1} = 3064 (w), 2956 (m), 2921 (m), 2889 (m), 2852 (m), 2005 (w), 1592 (s), 1579 (m), 1458 (m), 1442 (s), 1369 (m), 1355 (m), 1301 (m), 1258 (m), 1242 (m), 1134 (vs), 1156 (s), 1089 (s), 1027 (s), 986 (m), 881 (m), 838 (m), 802 (s) cm^{-1}.

2.1.2. Bis(perchlorato)(bis-pyridino-18-crown)europium(II)

One hundred milligrams (0.28 mmol) of Eu_2O_3 was dissolved in a small excess of 60% $HClO_4$, evaporated until white fumes appeared, cooled down, and the resulting slurry was dissolved in a few ml of methanol (*caution*!). The resulting solution was placed in the cathode compartment of an electrolyzer provided with a pool Hg cathode and the anode compartment separated from the cathode space with a frit. Then 100 mg (0.30 mmol) of the bis-pyridino-18-crown-6 ligand was added to the solution (in this way the initial solution contained an excess of Eu, which served merely to increase the conductivity). A few drops of perchloric acid diluted with a few ml of methanol was the anolyte. Yellow crystals of the complex formed after approximately 6 h of electrolytic reduction performed at a controlled potential (−1.3 V with respect to the saturated calomel electrode). It was observed that further electrolysis led to redissolution of the complex, probably due to reduction of the pyridine rings.

2.2. X-ray analysis

The appropriate crystal was cut from a larger one, mounted on a Kuma KM4 diffractometer equipped with a CCD counter and measured at 160 K. The structure was solved using Patterson and subsequent difference Fourier maps. The hydrogen atoms were placed in positions calculated from the geometry. The final refinement was anisotropic for all non-H atoms. The computations were performed with SHELXS97 and SHELXL97 programs [7], and the molecular graphic was prepared with DIAMOND [8]. Pertinent details are given in Table 1.

Table 1
Crystal data and structure refinement details

Empirical formula	$C_{18}H_{22}Cl_2EuN_2O_{12}$
Formula weight	681.24
Temperature (K)	160(2)
Wavelength (Å)	0.71073
Crystal system, space group	monoclinic, $P2_1/n$
Unit cell dimensions	
a (Å)	11.579(6)
b (Å)	12.978(7)
c (Å)	15.331(7)
β (°)	90.78(4)
Volume (Å^3)	2304(2)
Z, Calculated density (Mg/m^3)	4, 1.964
Absorption coefficient (mm^{-1})	3.022
F(000)	1348
Crystal size (mm)	0.29 × 0.18 × 0.11
θ Range for data collection (°)	2.72–28.80
Index ranges	$-14 \leqslant h \leqslant 15$, $-17 \leqslant k \leqslant 16$, $-20 \leqslant l \leqslant 19$
Reflections collected/unique [R_{int}]	16 299/5625 [0.0312]
Completeness to 2θ = 28.80° (%)	93.4
Absorption correction	analytical
Maximum and minimum transmission	0.782 and 0.598
Refinement method	full-matrix least-squares on F^2
Data/restraints/parameters	5625/0/316
Goodness-of-fit on F^2	0.953
Final R indices [$I > 2\sigma(I)$]	$R(F)$ = 0.0312, $R_w(F^2)$ = 0.0654
R indices (all data)	$R(F)$ = 0.0505, $R_w(F^2)$ = 0.0765
Largest difference in peak and hole (e Å^{-3})	1.411 and −0.461

2.3. Spectroscopy

The absorption spectrum of the complex was taken on a Cary 500 Scan spectrophotometer at room temperature. The sample was prepared by grinding a small amount of the compound with paraffin oil between two quartz glass plates. The emission spectra of both the complex and the free ligand were recorded at 77 K using a Spectra Pro 750 monochromator, equipped with a Hamamatsu R928 photomultiplier and 1200 l/mm grating blazed at 500 nm. The samples were excited with 320 nm light. The ligand, under these conditions, did not show any emission.

2.4. Theoretical calculations

The electronic structure of the complex molecule was calculated using the density functional approach with the ADF suite of programs [9]. In the first step the geometrical structure was optimized to get acceptable positions of the H atoms, keeping the coordinates of the non-H atoms frozen. The electron density functional used was Perdew–Wang exchange and the correlation functional (PW91 [10]) and the basis was TZ2P+ with the core frozen up to 4d for Eu [denoted hereinafter as TZ2P + (4d), etc.] and TZ2P for the remaining atoms with the core frozen up to 2p for Cl and 1s functions frozen for C, N and O. The scalar relativity was included using the ZORA [11] method, and basis functions scaled to ZORA, supplied with the ADF packet, were used. The second step included freezing of all the coordinates, computing the electronic structure of the molecule with various electron density functionals and simulating the spectra with the supplied time-dependent DFT [12]. The functionals tested were: PW91 [10] and SAOP [13]. The tested combinations of functionals and bases were the following: (**I**) – PW91, TZ2P + (4d) for Eu, TZ2P(2p) for Cl, TZ2P(1s) for C, N, O and TZ2P for H; (**II**) – PW91, TZ2P+ for Eu and TZ2P for the rest; (**III**) – SAOP and the bases like in the preceding variant; (**IV**) – PW91 and QZ4P for all atoms. The relativity treatment was as previously described.

3. Results and discussion

3.1. Structure

The coordination of the Eu^{2+} cation in the present compound follows that found in the bis(perchlorato-*O*,*O*′) (18-crown-6)europium(II) complex [2c], namely two bidentate perchlorate anions occupy the axial positions, and the six equatorial coordination sites are occupied by the donor atoms (4 O and 2 N) of the macrocycle ligand, see Fig. 1. In this way the metal ion is deca-coordinate. The Eu–O_{crown} distances (presented inTable 2) are similar to those

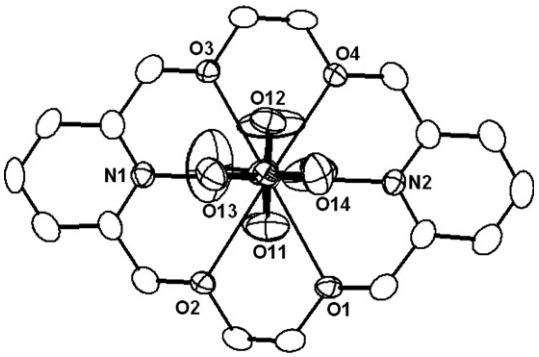

Fig. 1. A view of the complex molecule together with the atom labelling. The Eu and Cl2 atoms are eclipsed by Cl1, and likewise: O21 by O11, O22 by O12, O23 by O14 and O24 by O13.

Table 2
Eu–O and Eu–N bond lengths (Å)

Eu–O1	2.712(3)
Eu–O2	2.686(3)
Eu–O3	2.665(3)
Eu–O4	2.653(3)
Average Eu–O_{crown}	2.679(26)
Eu–N1	2.719(3)
Eu–N2	2.719(3)
Average Eu–N	2.719
Eu–O11	2.692(3)
Eu–O12	2.783(3)
Eu–O21	2.771(4)
Eu–O22	2.744(4)
Average Eu–$O_{perchlorate}$	2.748(41)

in other complexes of Eu(II) with crown ethers (15-crown-5, benzo-15-crown-5, 18-crown-6, benzo-18-crown-6, 12-crown-4) [2], the latter distances being in the range 2.640(3)–2.760(11) Å. The Eu–$O_{perchlorate}$ bond lengths are generally slightly longer than those observed in the 18-crown-6 complex, which were between 2.628(7) and 2.727(8) Å, average 2.680(50) Å. As Eu–N distances, to the best of the authors' knowledge, have not been reported for Eu(II)–crown ether complexes, it is necessary to invoke other Eu(II) compounds where such bonds are present. Inspection of some carboxylate complexes (ethylenediaminetetraacetates [14], nitrilotriacetates [15] and diethylenetriaminepentaacetate [16]) and bis(triethanolamine)europium diperchlorate [17] reveals that these distances are rather short in the present compound in comparison to those in the former ones, which were in the range 2.725(5)–2.888(6) Å, and this is the most probably brought about by steric reasons. The mutual twisting of the pyridine planes is 36.5° and is similar to that observed in the related light lanthanide(III) complexes [5], 36.9° for Ce and 38.3° for Pr. This suggests that the metal ion utilizes almost the maximum capacity of the macrocycle cavity; for metals with a smaller ionic radius this angle grows to 50.2° in the case of Gd, and 52.4° for Y. The structure is composed only of neutral complex molecules, which means that the crystal network is held together by weak intermolecular forces.

3.2. Spectroscopy

The absorption spectrum is essentially featureless (Fig. 2). The absorption starts to rise gently at approximately 600 nm; as a consequence the spectrum is somewhat different from those recorded for other yellow Eu(II) compounds, diaqua(μ_3-acetato)(acetato-*O*)(acetic acid-*O*)europium(II) [18] and bis(guanidinium) (ethylenediaminetetraacetato)europate(II) [14b], where the growth of the absorption started at 450 and 490 nm, respectively, and was sharper. The peak at 270 nm is due to $\pi \rightarrow \pi^*$ transitions within the pyridine rings.

Introduction of pyridine fragments changes profoundly the luminescent properties of the present complex in comparison with its analogue, bis(perchlorato-*O*,*O*′)(18-crown-6)europium(II) [2c]. First, the emission intensity is practically quenched at room temperature and is weak at 77 K. Second, the spectrum is composed of two rather weak bands (Fig. 3), with maxima at approximately 430 (23 300 cm^{-1}) and 500 nm (20 000 cm^{-1}). The first band lies in the range typical for Eu(II)–crown ether complexes [1,2], whereas the latter is unexpected and distinguishes the present compound from the other Eu(II)–crown ether complexes, where usually one luminescence band (or two closely overlapping bands) is (are) observed.

3.3. Electronic structure

In order to find a plausible explanation of such spectroscopic behaviour, density functional calculations have been undertaken. The following discussion will be based mostly on model **II** (see Section 2.4), unless otherwise stated, and for spin α electrons. The approach with SAOP (model **III**) gave all the virtual orbitals shifted significantly towards higher energies, and in the case of **IV** the interpretation is obscured by large correlations among the basis functions. The outcome from model **I** was practically identical with that of **II**.

The seven 4f orbitals of Eu^{2+} constitute the highest occupied ones and they lie well above the other occupied levels – the difference between the energy of the lowest 4f orbital and the next lower occupied one, which represents non-bonding electrons of oxygen atoms from the perchlorate anions, is 26 100 cm^{-1}. The difference between the lowest and the highest energy of the 4f electrons is 2000 cm^{-1}. The LUMO (located 630 cm^{-1} above the HOMO) and three following states are the empty π^* orbitals of

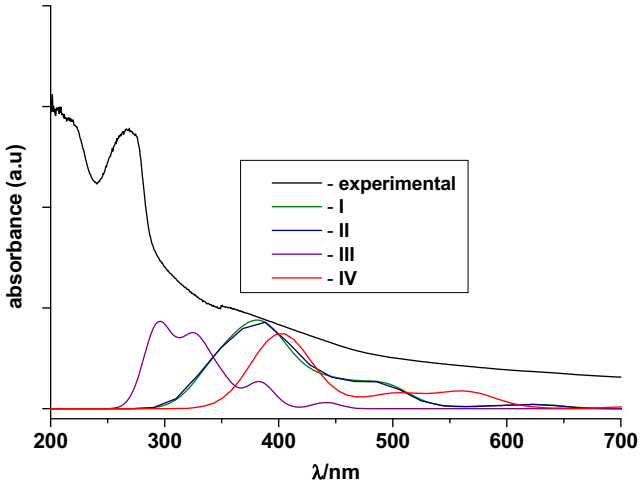

Fig. 2. The experimental and simulated absorption spectra of (bis-pyridino-18-crown)-bis(perchlorato)europium(II). The Roman numerals of the simulated curves refer to the models described in Section 2 (theoretical calculations). (For interpretation of the references to colours in this figure legend, the reader is referred to the web version of this article.)

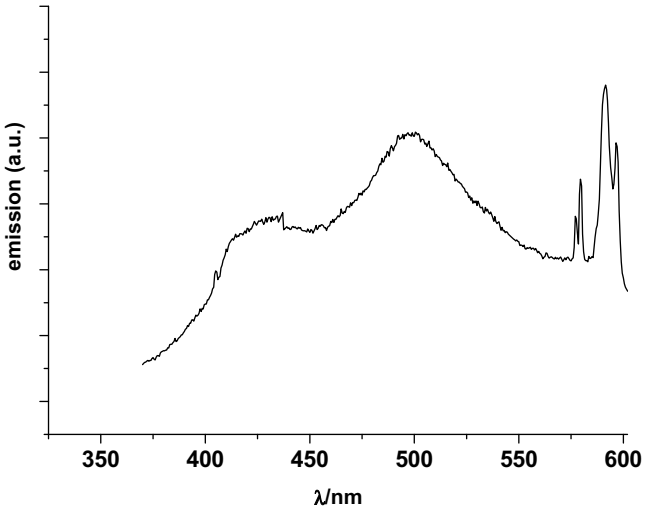

Fig. 3. The luminescence spectrum of (bis-pyridino-18-crown)-bis(perchlorato)europium(II); the peaks at the right side come from a Eu(III) impurity.

the pyridine fragments. The next virtual orbital, hereinafter labelled as **A**, 15600 cm^{-1} above the HOMO (22500 cm^{-1} in model **III** and 13100 cm^{-1} in model **IV**), is composed mostly of 1s and 2s functions of hydrogen atoms from the CH_2–O–CH_2CH_2–O–CH_2 fragments. In all the models this orbital had a non-negligible contribution from the 6s and 7s functions of europium. It is perhaps worth noting that analogous functions also appeared in a calculated orbital, 13600 cm^{-1} above the HOMO, in an ytterbium(II) complex with dimethyl oxydiacetate, $[Yb(CH_3OOCCH_2OCH_2COOCH_3)_3]^{2+}$ [19]. The four next levels, labelled as **B**, up to ca. 20500 cm^{-1}, are of a similar type, i.e. they are built up basically from the 1s and 2s functions of H atoms (mostly of the CH_2–O–CH_2CH_2–O–CH_2 fragments). The two upper of these orbitals also have small admixtures of 5,6d functions of Eu and 3s of Cl. The subsequent orbital, at approximately 22100 cm^{-1}, has a remarkable contribution from the 6s function of Eu and from the 3s functions of Cl. In the range of interest (up to 35000 cm^{-1}) there are no pure 5d europium levels; the largest share of this function in a virtual orbital was 57% (24700 cm^{-1} above the HOMO). The energy diagram, where orbitals with significant participation of the metal functions have been singled out, is shown in Fig. 4.

The simulated spectra (computed for the first 150 excitations), shown in Fig. 2, render rather well the gentle rise of absorption. They are basically composed of three groups of excitations, all starting from the 4f orbitals of Eu^{2+}. The first one, ranging from 650 to 550 nm (15400–18200 cm^{-1}), is composed of very weak transitions to the orbital **A**. The second set, from 550 to 450 nm (18200–22200 cm^{-1}), is formed by transitions to the **B** levels. The third group, the most intense, in the range 450–350 nm (22200–28600 cm^{-1}), includes transitions to the ten virtual orbitals above the **B** ones. These transitions are of various natures, including charge transfer excitations to both the ether and the pyridine fragments of the macrocyle, perchlorate anions and those with partial f–d and/or f–s character. Near the shorter wavelength limit of this area excitations from the occupied orbitals in the perchlorate groups to the empty π^* orbitals of the pyridine fragments also begin to appear.

The diagram presented in Fig. 4 allows a possible rationalization of the emission spectrum. It may be noticed that the difference between the energies of the luminescence band maxima, 3200 cm^{-1}, matches rather well the gap between the two higher and the two lower π^* orbitals of the pyridine fragments (3070 cm^{-1} for **I** and **II**, 3720 cm^{-1} for **III** and 3280 for **IV**). Adding 23300 cm^{-1} (the 430 nm emission band) to the energies of the lower π^* orbitals, or 20000 cm^{-1} (the 500 nm emission) to the energies of the higher π^* orbitals, a value of approximately 24000 cm^{-1} will be obtained which is close to the energies of the two orbitals with significant participation of 5d and/or 6,7s functions of europium. It may therefore be presumed that the observed 500 nm emission consists of transitions from one or both of these levels to the two upper π^* orbitals of the pyridine. To illustrate this point the quasi-5d orbital at 24700 cm^{-1} and the highest pyridine π^* one are shown together in Fig. 5. Analogously, two lower π^* levels would be the final states for the emission at 430 nm. It should be noticed, however, that because of the small difference between the LUMO and HOMO and after taking into account possible involvement of the vibrational components of the final state(s) and the limitations of the calculation accuracy, it is also possible that the 430 nm band is the result of the transitions to the 4f levels of Eu. The present data do not unequivocally show whether the former or the latter pathway (or both) are active in this case.

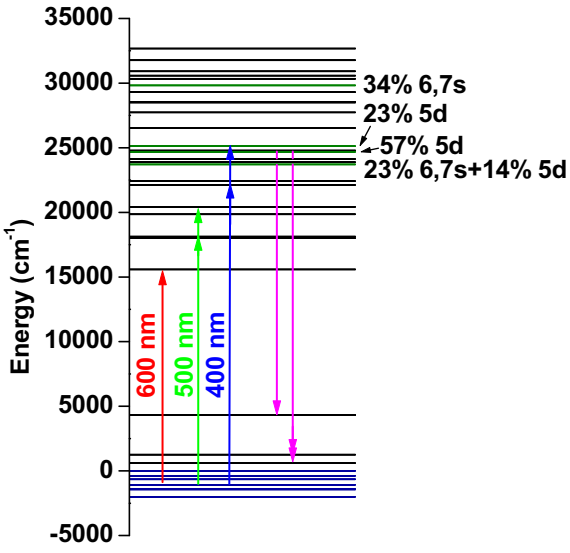

Fig. 4. A scheme of calculated energy levels. The occupied 4f orbitals of Eu are marked in blue and the virtual orbitals with considerable participation of Eu functions – in green. The possible ways of light absorption and emission are shown by red, green, blue and magenta arrows. The energies are given with respect to the HOMO. (For interpretation of the references to colour in this figure legend, the reader is referred to the web version of this article.)

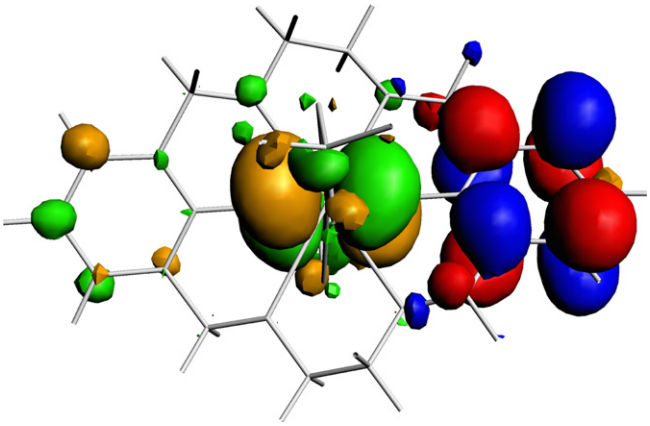

Fig. 5. The highest pyridine-part π^* orbital (blue–red) together with the *quasi*-5d orbital of Eu (green–yellow). (For interpretation of the references to colour in this figure legend, the reader is referred to the web version of this article.)

The luminescence mechanisms described above may shed some light on the reasons of the low observed emission intensity. Discharge of the excited state to the π^* levels of the pyridine fragments reduces the intensity of the 5d–4f transition, and radiationless energy transfer deteriorates the efficiency of the 5d → π^* radiative path, which results in an overall decrease of the luminescence intensity.

The Mulliken charges were 1.75 for Eu, 1.78–1.79 for Cl, −0.90 to −0.91 for the ether oxygen atoms, −0.61 to −0.71 for the oxygen atoms in the perchlorate anions, −0.70 in the case of N atoms, 0.76–0.81 for the aliphatic carbon atoms, 0.08–0.28 for the carbon atoms in the pyridine rings, −0.13 to −0.19 for the H atoms in the aliphatic part of the macrocycle and −0.09 to −0.10 for the H atoms that are part of the pyridine fragments.

4. Conclusions

During the electrolytic reduction of a methanolic solution of europium tris(perchlorate) and bis-pyridino-18-crown-6, a decacoordinate complex of Eu(II) with perchlorate anions directly bonded to the metal cation was formed. The absorption spectrum is apparently structureless; this is a consequence of a plethora of various transitions of diverse characters: metal-to ligand charge transfers, f–d and f–s transitions, and also perchlorate–pyridine

excitations, accumulating from 600 nm towards shorter wavelengths. The weak luminescence of the complex is presumably due to the transitions from the *quasi*-5d levels of europium to π^* orbitals in the pyridine rings, as well as to europium 4f orbitals. The presence of the pyridine conjugated π electron system in the vicinity of Eu^{2+} exerts a deleterious impact on the luminescence efficiency of the complex.

Acknowledgements

The authors would like to thank Michael Rössle for the synthesis of the macrocycle, Ing. Halina Trelińska-Nowak for recording the absorption spectra, and Dr. Paula Gawryszewska and Dr. Jerzy Sokolnicki for the luminescence spectra. The ADF calculations have been carried out at the Wrocław Centre for Networking and Supercomputing (http://www.wcss.wroc.pl), grant No. 58.

Appendix A. Supplementary data

CCDC 676612 contains the supplementary crystallographic data for bis(perchlorato)(bis-pyridino-18-crown)europium(II). These data can be obtained free of charge via http://www.ccdc.cam.ac.uk/conts/retrieving.html, or from the Cambridge Crystallographic Data Centre, 12 Union Road, Cambridge CB2 1EZ, UK; fax: (+44) 1223-336-033; or e-mail: deposit@ccdc.cam.ac.uk.

References

[1] J. Jiang, N. Higashiyama, K. Machida, G. Adachi, Coord. Chem. Rev. 17 (1998) 1.
[2] (a) P. Starynowicz, K. Bukietyńska, Eur. J. Inorg. Chem. (2002) 1835;
(b) P. Starynowicz, K. Bukietyńska, S. Gołąb, W. Ryba-Romanowski, J. Sokolnicki, Eur. J. Inorg. Chem. (2002) 2344;
(c) P. Starynowicz, Polyhedron 22 (2003) 337.
[3] e.g. N. Sabbatini, M. Guardigli, J.-M. Lehn, Coord. Chem. Rev. 123 (1993) 201.
[4] Ch.-J. Li, H. Wang, J.-M. Dou, D.-Ch. Li, D.-Q. Wang, Acta Crystallogr., Sect. E: Struct. Rep. Online 62 (2006) m2136.
[5] T. Hamada, K. Manabe, S. Ishikawa, S. Nagayama, M. Shiro, S. Kobayashi, J. Am. Chem. Soc. 125 (2003) 2989.
[6] M. Newcomb, G.W. Gokel, D.J. Cram, J. Am. Chem. Soc. 96 (1974) 6810.
[7] (a) G.M. Sheldrick, SHELXS-97, Program for Structure Solution, University of Göttingen, 1997;
(b) G.M. Sheldrick, SHELXL-97, Program for Structure Refinement, University of Göttingen, 1997.
[8] DIAMOND – Visual Crystal Structure Information System, CRYSTAL IMPACT, Postfach 1251, D-53002 Bonn, Germany.
[9] (a) G. te Velde, F.M. Bickelhaupt, S.J.A. van Gisbergen, C. Fonseca Guerra, E.J. Baerends, J.G. Snijders, T. Ziegler, J. Comput. Chem. 22 (2001) 931;
(b) C. Fonseca Guerra, J.G. Snijders, G. te Velde, E.J. Baerends, Theor. Chem. Acc. 99 (1998) 391;
(c) E.J. Baerends, J. Autschbach, A. Bérces, C. Bo, P.M. Boerrigter, L. Cavallo, D.P. Chong, L. Deng, R.M. Dickson, D.E. Ellis, M. van Faassen, L. Fan, T.H. Fischer, C. Fonseca Guerra, S.J.A. van Gisbergen, J.A. Groeneveld, O.V. Gritsenko, M. Grüning, F.E. Harris, P. van den Hoek, H. Jacobsen, L. Jensen, G. van Kessel, F. Kootstra, E. van Lenthe, D.A. McCormack, A. Michalak, V.P. Osinga, S. Patchkovskii, P.H.T. Philipsen, D. Post, C.C. Pye, W. Ravenek, P. Ros, P.R.T. Schipper, G. Schreckenbach, J.G. Snijders, M. Solà, M. Swart, D. Swerhone, G. te Velde, P. Vernooijs, L. Versluis, O. Visser, F. Wang, E. van Wezenbeek, G. Wiesenekker, S.K. Wolff, T.K. Woo, A.L. Yakovlev, T. Ziegler, ADF2005.01, SCM, Theoretical Chemistry, Vrije Universiteit, Amsterdam, The Netherlands. <http://www.scm.com>.
[10] J.P. Perdew, J.A. Chevary, S.H. Vosko, K.A. Jackson, M.R. Pederson, D.J. Singh, C. Fiolhais, Phys. Rev. B 46 (1992) 6671.
[11] (a) E. van Lenthe, E.J. Baerends, J.G. Snijders, J. Chem. Phys. 99 (1993) 4597;
(b) E. van Lenthe, E.J. Baerends, J.G. Snijders, J. Chem. Phys. 101 (1994) 9783;
(c) E. van Lenthe, A.E. Ehlers, E.J. Baerends, J. Chem. Phys. 110 (1999) 8943.
[12] (a) S.J.A. van Gisbergen, J.G. Snijders, E.J. Baerends, Comput. Phys. Commun. 118 (1999) 119;
(b) A. Rosa, E.J. Baerends, S.J.A. van Gisbergen, E. van Lenthe, J.A. Groeneveld, J.G. Snijders, J. Am. Chem. Soc. 121 (1999) 10356.
[13] P.R.T. Schipper, O.V. Gritsenko, S.J.A. van Gisbergen, E.J. Baerends, J. Chem. Phys. 112 (2000) 1344.
[14] (a) P. Starynowicz, J. Alloys Compd. 269 (1998) 67;
(b) R. Janicki, A. Mondry, P. Starynowicz, Z. Anorg. Allg. Chem. 631 (2005) 2475.
[15] P. Starynowicz, Polyhedron 22 (2003) 2761.
[16] L. Burai, É. Tóth, S. Seibig, R. Scopelliti, A.E. Merbach, Chem. Eur. J. 6 (2000) 3761.
[17] P. Starynowicz, J. Alloys Compd. 323–324 (2001) 159.
[18] P. Starynowicz, Polyhedron 14 (1995) 3573.
[19] P. Starynowicz, J. Chem. Soc., Dalton Trans. (2007) 2779.

Polyhedron 27 (2008) 2693–2697

Contents lists available at ScienceDirect

Polyhedron

journal homepage: www.elsevier.com/locate/poly

Synthesis, crystal engineering, and magnetic properties of an anionic 4-terpyridone based copper(II) azide supramolecule containing dinuclear–mononuclear cocrystal

Chun-Yuan Liao [a], Malabika Nayak [b], Ho-Hsiang Wei [a,*], Sasankasekhar Mohanta [b,*]

[a] Department of Chemistry, Tamkang University, Tamsui 25137, Taiwan
[b] Department of Chemistry, University of Calcutta, 92 A. P. C. Ray Road, Kolkata 700 009, India

ARTICLE INFO

Article history:
Received 11 December 2007
Accepted 19 May 2008
Available online 2 July 2008

Keywords:
Magnetic properties
4-Terpyridone
Cocrystal
Hydrogen-bond
Tetracopper(II)
Azide-bridged

ABSTRACT

Synthesis, crystal engineering, and magnetic properties of an anionic 4-terpyridone (L) based three-dimensional supramolecule, $[Cu^{II}_2(L)_2(\mu_{1,1}\text{-}N_3)_2]\cdot 2[Cu^{II}(L)(N_3)(H_2O)]\cdot 6H_2O$ (**1**), have been described in the present investigation. The title compound crystallizes in the monoclinic space group *C2/c* with the following unit cell parameters: $a = 27.803(7)$ Å, $b = 14.361(4)$ Å, $c = 16.071(4)$ Å, $\beta = 99.09(2)°$, and $Z = 4$. In this compound, one dinuclear $[Cu^{II}_2(L)_2(\mu_{1,1}\text{-}N_3)_2]$ unit is cocrystallized with two mononuclear $[Cu^{II}(L)(N_3)(H_2O)]$ units. In both the dinuclear and mononuclear species, 4-terpyridone chelates to the metal centers in its anionic form. The coordination environment of the metal ions is distorted square pyramidal. Eight O–H···O type strong hydrogen bonds involving the oxygen of anionic 4-terpyridone ligand and water molecules link the components of **1** into a three-dimensional framework. Excluding the atoms except the water molecules and ligand oxygens, the topology is a two-dimensional network. The mononuclear $[Cu^{II}(L)(N_3)(H_2O)]$ moiety is appended from this sheet, while the neighboring sheets are interlinked by the dinuclear $[Cu^{II}_2(L)_2(\mu_{1,1}\text{-}N_3)_2]$ unit to add the third dimension of the overall three-dimensional structure of the title compound.

© 2008 Elsevier Ltd. All rights reserved.

1. Introduction

The successful development of crystal engineering strategies relies first on developing, understanding, and rationalizating intermolecular interactions in the context of crystal packing, followed by the subsequent utilization and exploitation of this understanding in the design of new solids with predictable structural properties [1]. Several types of intermolecular interactions and topologies resulted therein have been explored in recent years.

4-Terpyridone is known to coordinate to the metal ions in its enolic form (LH) [2]. With an expectation that H–O–pyridine–M–pyridine–O–H fragment in $[M(LH)_2]^{n+}$ species may act as hydrogen bond donor/acceptor and thus may be a potential supramolecular synthon, an enolic 4-terpyridone based nickel(II) dicyanamide supramolecule, $[Ni^{II}(LH)_2](dicyanamide)_2\cdot 2H_2O$ has been previously reported [2b] and therefore it is expected that new compounds derived from 4-terpyridone will generate interesting hydrogen-bonded topologies. If the metal-4-terpyridone fragments are bridged by azide ligands, the derived compound will also be interesting for its magnetic properties. It may be mentioned that azide bridged coordination compounds of paramagnetic metal ions have been one of the most widely studied systems in molecular magnetism [3–8]. Several magnetostructural correlations, both experimental [3–6] and theoretical [6,7], in azide-bridged systems have been developed and the derived ideas have been successfully utilized for the construction of multidimensional systems to exhibit long-range magnetic ordering [3a,8].

To explore further the possibility of 4-terpyridone containing metal complexes to develop extended architecture and to enlighten the magnetic properties of azide-bridged system, we describe here the synthesis, crystal engineering, and magnetic properties of an anionic 4-terpyridone (L) based three-dimensional supramolecule $[Cu^{II}_2(L)_2(\mu_{1,1}\text{-}N_3)_2]\cdot 2[Cu^{II}(L)(N_3)(H_2O)]\cdot 6H_2O$ (**1**) which contains cocrystallized dinuclear and mononuclear complex units.

2. Experimental

2.1. Materials and methods

All the reagents and solvents were purchased from commercial sources and used as received. Elemental (C, H, and N) analyses were performed on a Perkin–Elmer 2400 II analyzer. IR spectra were recorded in the region 400–4000 cm^{-1} on a Perkin–Elmer

* Corresponding authors. Fax: +91 33 23519755 (S. Mohanta); fax: +886 2 26209924 (H.-H. Wei).
E-mail addresses: tkwei@mail.tku.edu.tw (H.-H. Wei), sm_cu_chem@yahoo.co.in (S. Mohanta).

0277-5387/$ - see front matter © 2008 Elsevier Ltd. All rights reserved.
doi:10.1016/j.poly.2008.05.027

RXIFT spectrophotometer with samples as KBr disks. Variable-temperature (2–300 K) magnetic susceptibility measurements were carried out with a Quantum Design MPMS SQUID magnetometer. Diamagnetic corrections were estimated from the Pascal constants.

2.2. Synthesis

An aqueous solution (10 mL) containing copper(II) nitrate trihydrate (0.24 g, 1 mmol) and sodium azide (0.26 g, 4 mmol) was dropwise added with stirring to an ethanol solution (30 mL) containing 4-terpyridone (0.25 g, 1 mmol). After a few minutes a green precipitate started to deposit. The stirring was continued for an additional period of 2 h. Then the green compound was collected by filtration and washed with ethanol. Recrystallization on diffusing ethanol to dimethylformamide solution of the green compound yielded green crystalline compound containing diffractable single crystals. Yield: 0.137 g (35%). *Anal.* Calc. for $C_{60}H_{56}N_{24}O_{12}Cu_4$: C, 46.21; H, 3.62; N, 21.56. Found: C, 46.30; H, 3.53; N, 21.45%. IR (KBr/cm^{-1}): water 3380 br; azide 2102 sh, 2071 sh, 2051 s.

2.3. Determination of crystal structure

The crystal data are summarized in Table 1. Diffraction data were collected on a Siemens P4 diffractometer in the ω–2ϑ scan mode using graphite-monochromated Mo Kα radiation having $\lambda = 0.71073$ Å. Three standard reflections were periodically monitored and showed no significant variation over data collection. The accurate unit cells were obtained by means of least-squares fittings of 25 centered reflections. The intensity data were corrected for Lorentz and polarization effects, and multi-scan absorption correction was made. A total of 5719 reflections were collected in the range $2\theta = 3.96$–$50.04°$ with $0 \leqslant h \leqslant 33$, $0 \leqslant k \leqslant 17$, and $-19 \leqslant l \leqslant 18$, of which 5597 independent reflections ($R_{int} = 0.0329$) were used for structure determinations. The structures were solved by direct and Fourier methods and refined by full-matrix least-squares methods based on F^2 with the programs SHELXS-97 and SHELXL-97 [9]. The final least-squares refinements (R_1) based on $I > 2\sigma(I)$ converged to 0.0470.

3. Results and discussion

3.1. Description of structure

The asymmetric unit of the structure of $[Cu^{II}_2(L)_2(\mu_{1,1}\text{-}N_3)_2] \cdot 2[Cu^{II}(L)(N_3)(H_2O)] \cdot 6H_2O$ (**1**) contains one and a half of a dinuclear $[Cu^{II}_2(L)_2(\mu_{1,1}\text{-}N_3)_2]$ unit, one mononuclear $[Cu^{II}(L)(N_3)(\text{-}H_2O)]$ moiety and three water molecules ($H_2O(4)$, $H_2O(5)$, and $H_2O(6)$) as solvent of crystallization. As one and a half of the whole molecule are symmetry related to the other half, the composition of the title compound is $[Cu^{II}_2(L)_2(\mu_{1,1}\text{-}N_3)_2] \cdot 2[Cu^{II}(L)(N_3)(H_2O)] \cdot 6H_2O$ (**1**) consisting of a dinuclear $[Cu^{II}_2(L)_2(\mu_{1,1}\text{-}N_3)_2]$ unit in which two metal centers are bridged by two end-on azide ligand, two mononuclear $[Cu^{II}(L)(N_3)(H_2O)]$ moieties in which azide is a monodentate terminal ligand, and six water molecules as solvent of crystallization. The dinuclear and mononuclear units are shown in Fig. 1, while selected bond lengths and angles of the coordination environment of the metal centers are listed in Table 2. The copper(II) center in the bis(azide)-bridged unit is pentacoordinated; the remaining three coordination positions are occupied by three nitrogens of 4-terpyridone. The metal center in the mononuclear $[Cu^{II}(L)(N_3)(H_2O)]$ unit is also pentacoordinated with a terminal azide ligand, three nitrogens of 4-terpyridone and a water molecule. The composition of both the dinuclear and mononuclear moieties indicate that 4-terpyridone is present in the title compound as monoanionic form resulted due to the deprotonation of the secondary amine group in the reaction mixture.

The stereochemistry of the metal ions in both the dinuclear and mononuclear units are distorted square pyramidal. The τ ($(\beta - \alpha)/60$, where β and α are the largest and second largest bond angles, respectively) values in the pentacoordinated environment of Cu(1) and Cu(2) are 0.27 and 0.09, respectively, indicating that the geometry around both the metal centers are distorted square pyramidal and the extent of distortion is much greater for Cu(1) [10]. In the case of the copper(II) ion (Cu(1)) in the dinuclear unit, three nitrogens (N(1), N(2), N(3)) of anionic 4-terpyridone and one nitrogen (N(4)) of a bridging azide ligand define the basal plane, while the apical position is occupied by a nitrogen (N(4A)) of the second bridging azide. For the metal center (Cu(2)) in the mononuclear unit, the basal plane is defined by three nitrogens (N(7), N(8), and N(9)) of anionic 4-terpyridone and a nitrogen (N(10)) of the terminal azide group, while the water oxygen O(3) occupies the apical position. The Cu–N distances involving anionic 4-terpyridone fall into two distinct ranges; those (Cu(1)–N(2) = 1.910(3) Å and Cu(2)–N(8) = 1.919(3) Å) involving the central rings are shorter than the bond lengths (Cu(1)–N(1) = 2.027(4) Å, Cu(1)–N(3) = 2.016(4) Å, Cu(2)–N(7) = 2.048(4) Å, and Cu(2)–N(9) = 2.057(4) Å) involving the terminal rings. The fourth bond length (Cu(1)–N(4) = 1.935(3) Å and Cu(2)–N(10) = 1.955(4) Å) in the basal plane with the bridging azide (for Cu(1)) or terminal azide (for Cu(2)) lies in the range of the short and long bond distances involving anionic 4-terpyridone. In contrast, as expected due to Jahn–Teller distortion, the bond distance (Cu(1)–N(4A) = 2.552(4) Å and Cu(2)–O(3) = 2.242(4) Å) involving the apical ligand is much longer. In addition to the differences in the metal–ligand bond distances, the distortion of the coordination environment can also be evidenced from the *transoid* angles (158.92(13)° and 174.97(16)° for Cu(1); 157.91(14)° and 163.28(18)° for Cu(2)) in the basal plane as well as from the wide range of the *cisoid* angles (79.68(14)–103.64(15)° for Cu(1); 79.38(15)–103.36(19)° for Cu(2)). The metal centers in the dinuclear unit are separated by 3.2679(13) Å with Cu–N–Cu bridge angles of 92.44(15)°.

Eight O–H···O type hydrogen bonds involving oxygens (O(1) and O(2)) of anionic 4-terpyridone ligand and water molecules ($H_2O(3)$, $H_2O(4)$, $H_2O(5)$, and $H_2O(6)$) link the components of **1** into a three-dimensional framework (*vide infra*). As summarized in Table 3, the donor···acceptor contacts of the hydrogen bonds lie in the range 2.68–2.86 Å indicating that the hydrogen bonds can be considered as strong. The understanding of the hydrogen bonding interactions and analyses of the topology resulted therein can be better understood as fragments. As shown down the crystallographic *a* axis in Fig. 2, the topology excluding the atoms except

Table 1
Crystallographic data of **1**

Empirical formula	$C_{60}H_{56}N_{24}O_{12}Cu_4$
Formula weight	1559.49
Crystal system	monoclinic
Space group	*C*2/*c*
a (Å)	27.803(7)
b (Å)	14.361(4)
c (Å)	16.071(4)
β (°)	99.09(2)
V (Å^3)	6337(3)
Z	4
T (K)	293(2)
λ(Mo Kα) (Å)	0.71073
D_{calcd} (g cm^{-3})	1.635
μ (mm^{-1})	1.408
Number of reflections collected	5719
Number of independent reflections	5597
R_1[a]/wR_2[b] ($I > 2\sigma(I)$ data)	0.0470/0.0897
R_1[a]/wR_2[b] (all data)[a]	0.0907/0.1045

[a] $R_1 = [\sum||F_o| - |F_c||/\sum|F_o|]$.
[b] $wR_2 = [\sum w(F_o^2 - F_c^2)^2/\sum w(F_o^2)^2]^{1/2}$.

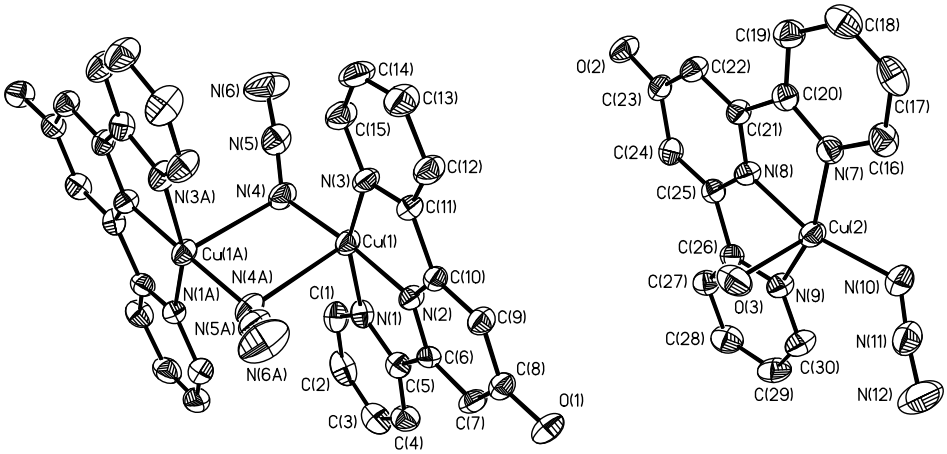

Fig. 1. ORTEP representation of the dinuclear $[Cu^{II}_2(L)_2(\mu_{1,1}\text{-}N_3)_2]$ and mononuclear $[Cu^{II}(L)(N_3)(H_2O)]$ units in $[Cu^{II}_2(L)_2(\mu_{1,1}\text{-}N_3)_2] \cdot 2[Cu^{II}(L)(N_3)(H_2O)] \cdot 6H_2O$ (**1**) with atom-labeling schemes. Hydrogen atoms of the organic ligand as well as water molecules of crystallization are omitted for clarity. Symmetry code: (A) $1 - x, y, 0.5 - z$.

Table 2
Selected bond lengths (Å) and angles (°) of **1**

Cu(1)–N(1)	2.027(4)
Cu(1)–N(2)	1.910(3)
Cu(1)–N(3)	2.016(4)
Cu(1)–N(4)	1.935(3)
Cu(1)–N(4A)	2.552(4)
Cu(2)–N(7)	2.048(4)
Cu(2)–N(8)	1.919(3)
Cu(2)–N(9)	2.057(4)
Cu(2)–N(10)	1.955(4)
Cu(2)–O(3)	2.242(4)
Cu(1)···Cu(1A)	3.2679(13)
N(1)–Cu(1)–N(3)	158.92(13)
N(2)–Cu(1)–N(4)	174.97(16)
N(4A)–Cu(1)–N(1)	91.38(13)
N(4A)–Cu(1)–N(2)	89.61(13)
N(4A)–Cu(1)–N(3)	95.96(14)
N(4A)–Cu(1)–N(4)	87.32(15)
N(1)–Cu(1)–N(2)	79.68(14)
N(1)–Cu(1)–N(4)	96.40(15)
N(2)–Cu(1)–N(3)	80.64(14)
N(3)–Cu(1)–N(4)	103.64(15)
Cu(1)–N(4)–Cu(1A)	92.44(15)
N(7)–Cu(2)–N(9)	157.91(14)
N(8)–Cu(2)–N(10)	163.28(18)
O(3)–Cu(2)–N(7)	92.75(16)
O(3)–Cu(2)–N(8)	92.70(16)
O(3)–Cu(2)–N(9)	95.60(16)
O(3)–Cu(2)–N(10)	103.36(19)
N(7)–Cu(2)–N(8)	79.38(15)
N(7)–Cu(2)–N(10)	95.02(17)
N(8)–Cu(2)–N(9)	79.83(15)
N(9)–Cu(2)–N(10)	102.84(18)

Symmetry code: A, $1 - x, y, 0.5 - z$.

Table 3
Geometries (distances in Å and angles in °) of the hydrogen bonds in **1**

D–H···A	H···A	D···A	D–H···A
O(3)–H(3AO)···O(4D)	1.94	2.77	165.2
O(3)–H(3BO)···O(5)	1.94	2.68	177.1
O(4)–H(4AO)···O(2)	1.92	2.85	168.4
O(4)–H(4BO)···O(6E)	2.12	2.79	164.6
O(5)–H(5AO)···O(2E)	2.03	2.70	167.3
O(5)–H(5BO)···O(1)	1.95	2.85	172.5
O(6)–H(6AO)···O(1F)	2.00	2.83	168.7
O(6)–H(6BO)···O(1)	2.12	2.86	165.6

Symmetry codes: see Fig. 2.

the water molecules and ligand oxygens is a two-dimensional network. It is clear from this figure that the coordinated water molecule ($H_2O(3)$) acts as a double donor, while three solvated water molecules ($H_2O(4)$, $H_2O(5)$, and $H_2O(6)$) behaves as double donor and single acceptor. Regarding the ligand oxygens O(1) and O(2), while the former behaves as a triple acceptor, the later acts as a double acceptor. The two-dimensional sheet can be considered (Fig. 2) as the repetition of fused one 4-member and two 5-member rings of hydrogen-bonded oxygen centers.

Six oxygen centers are the members of the above-mentioned two-dimensional sheet. Two of them, O(3) and O(2), are parts of the mononuclear complex unit $[Cu^{II}(L)(N_3)(H_2O)]$. Clearly, the mononuclear $[Cu^{II}(L)(N_3)(H_2O)]$ unit is appended from the sheet

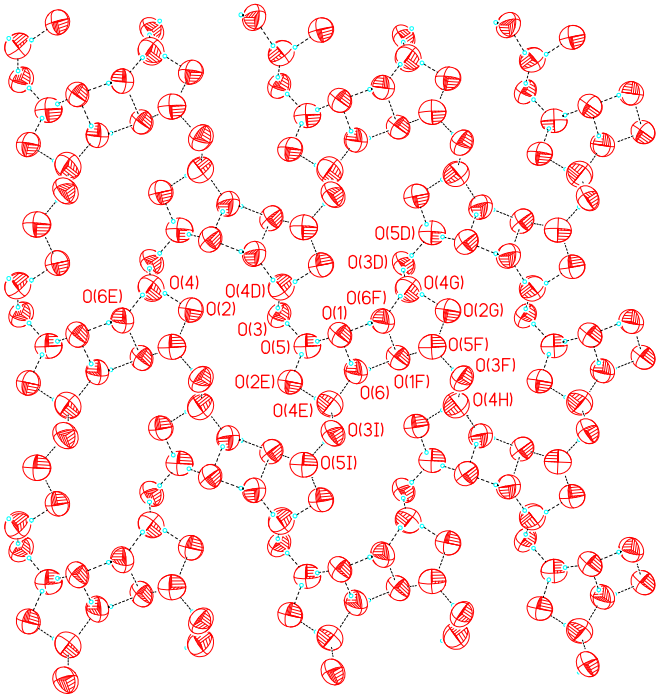

Fig. 2. Perspective view down the crystallographic *a* axis to demonstrate the two-dimensional sheet formed due to the hydrogen bonds involving ligand oxygens (O(1) and O(2)) and water molecules ($H_2O(3)$, $H_2O(4)$, $H_2O(5)$, and $H_2O(6)$). All other atoms are omitted for clarity. Symmetry codes: (D) $x, 1 - y, 0.5 + z$; (E) $0.5 - x, 1.5 - y, -z$; (F) $0.5 - x, 1.5 - y, 1 - z$; (G) $x, y, 1 + z$; (H) $0.5 - x, 1.5 - y, 0.5 - z$; (I) $0.5 - x, 0.5 + y, 0.5 - z$.

(Fig. 3). Another member, O(1), is part of the bis(azide)-bridged dinuclear $[Cu^{II}_2(L)_2(\mu_{1,1}\text{-}N_3)_2]$ unit. While ligand oxygen O(1) is one end of the dinuclear unit, the symmetry related ligand oxygen O(1A) is the other end of the dinuclear unit (Fig. 1). Therefore, two sheets in which O(1) and O(1A) are members, respectively, may be considered as interlinked by the dinuclear $[Cu^{II}_2(L)_2(\mu_{1,1}\text{-}N_3)_2]$ unit to result in the third dimension of the structure (Fig. 3). An extended view down the crystallographic *c* axis of the three-dimensional framework containing two-dimensional sheets interlinked by the dinuclear $[Cu^{II}_2(L)_2(\mu_{1,1}\text{-}N_3)_2]$ unit is shown in Fig. 3.

3.2. Magnetic properties

Variable-temperature (2–300 K) magnetic behavior of the title compound is shown in Fig. 4 in the form of $\chi_M T$ versus T plots. The $\chi_M T$ value at 300 K is 1.65 $cm^3\ mol^{-1}$ K, which is slightly greater than the spin-only $\chi_M T$ value of four Cu^{II} ions with $g = 2$. On lowering of temperatures, $\chi_M T$ increases to 1.85 $cm^3\ mol^{-1}$ K at 15 K. On further lowering of temperatures, $\chi_M T$ diminishes very rapidly to 1.65 $cm^3\ mol^{-1}$ K at 2 K. The profile indicates that there exists ferromagnetic interaction in this molecule. The interaction between dinuclear and mononuclear units in this molecule should be small because the metal centers in two types of units are separated as Cu(dinuclear)–terpyridone···water–Cu(mononuclear) (O(1)···O(5)···O(3) part in Fig. 2) or Cu(dinuclear)–terpyridone···terpyridone–Cu(mononuclear) (O(1)···O(5)···O(2E) part in Fig. 2). Therefore, the two mononuclear copper(II) moieties should only influence the $\chi_M T$ values as a known amount of paramagnetic impurity. Considering molecular field approximation (zJ') for the possible weak dinuclear···mononuclear interaction and the same value for the magnetic moment (μ_{Cu}) of the copper(II) centers in the mononuclear fragments, the theoretical expression for the molar magnetic susceptibility (χ_M) of a system having one exchange-coupled dicopper(II) and two mononuclear copper(II) moieties can be derived as [11].

$$\chi_M = \frac{\chi^1_M}{1 - 2zJ'\chi^1_M/N\beta^2g^2} \tag{1}$$

where

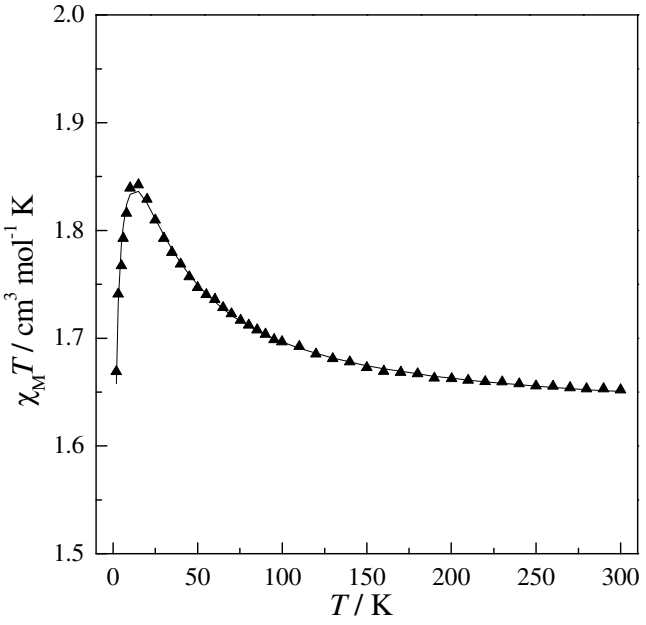

Fig. 4. $\chi_M T$ versus T plots for **1**. The solid lines represent the simulated curves.

$$\chi^1_M = \frac{7.997\chi_D T + 2\mu^2_{Cu}}{7.997T}$$

with

$$\chi_D = \frac{N\beta^2g^2}{kT}\frac{2e^{2J/kT}}{1 + 3e^{2J/kT}}$$

Least-squares fitting of the experimental data with Eq. (1) leads to $J = 15.0\ cm^{-1}$, $zJ' = -0.082\ cm^{-1}$, $g = 2.06$, and $\mu_{Cu} = 1.82$ BM; the agreement factor (R) defined as $[\sum\{(\chi_M T')_{obs} - (\chi_M T')_{calc}\}^2 / \sum(\chi_M T')^2_{obs}]$ is 2.85×10^{-3}. It may be mentioned that on fixing $\mu_{Cu} = 1.73$ BM simulation converges with $J = 15.0\ cm^{-1}$, $zJ' = -0.10\ cm^{-1}$, $g = 2.15$, and $R = 2.85 \times 10^{-3}$. However, in this case little deviation occurs in the temperature range 300–150 K (Fig. S1).

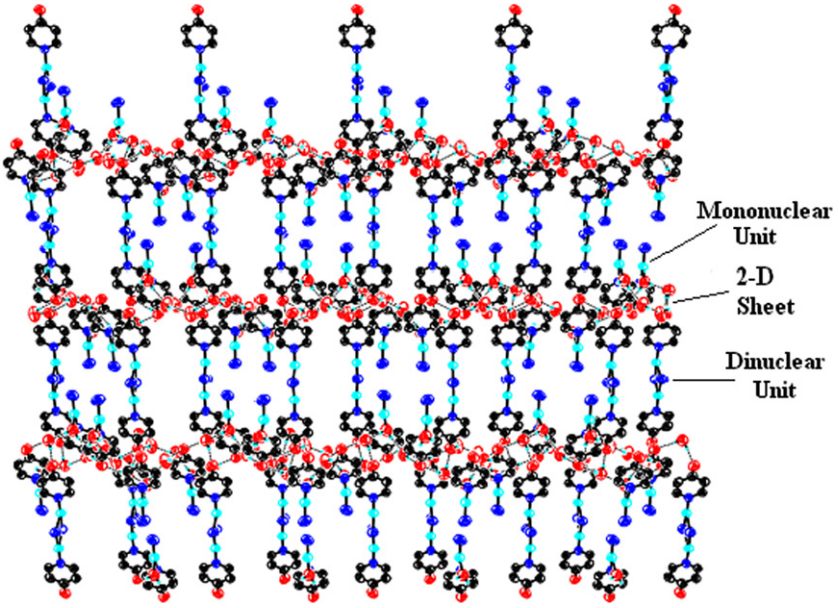

Fig. 3. Perspective view down the crystallographic *c* axis to demonstrate the interlinking of the two-dimensional oxygen sheets in Fig. 2 by the dinuclear $[Cu^{II}_2(L)_2(\mu_{1,1}\text{-}N_3)_2]$ unit to result in the creation of overall three-dimensional architecture in **1**. Terminal rings of anionic 4-terpyridone, N(5), N(6), N(11), and N(12) are omitted for clarity.

Magnetic properties of azide-bridged dicopper(II) systems have been extensively studied, both experimentally and theoretically [3a–5,7a,7c]. It has been realized that end-to-end (EE)-bridged and end-on (EO)-bridged compounds exhibit antiferromagnetic and ferromagnetic interaction, respectively, [3a–5]. According to established magneto-structural correlations for the EO-bridged dicopper(II) systems having both the bridging azide nitrogens in equatorial positions, the extent of ferromagnetic interaction depends on Cu–N–Cu bridge angle and Cu–N distance [7a,7c]. As the angle decreases below ca. 105°, the interaction becomes more and more ferromagnetic. To be mentioned that as the magnetic orbitals for copper(II) is $d_{x^2-y^2}$, there arises significant extent of spin density in the equatorial sites when the two coordinated azide nitrogens occupy equatorial positions resulting strong ferromagnetic interaction; $J = 85\ cm^{-1}$ and $52\ cm^{-1}$ have been reported for two such dicopper(II) compounds [4a,4b]. In contrast, as the two bridging azide ligands occupy axial and equatorial positions in the title compound, the magnetic orbitals are directed along only one azide moiety. Again, the axial bond length (2.552(4) Å) becomes much longer than the equatorial bond distance (1.935(3) Å). These result in high spin density in the equatorial position and low spin density in the axial position. Therefore, although the title compound displays low value of Cu–N–Cu bridge angle (92.44(15)°), it exhibits weak ferromagnetic interaction ($J = 15\ cm^{-1}$). It may be mentioned that similar weak ferromagnetic interaction have been observed previously in related compounds [5].

4. Conclusions

The synthesis, crystal engineering, and magnetic properties of an anionic 4-terpyridone (L) based three-dimensional supramolecule, $[Cu^{II}_2(L)_2(\mu_{1,1}\text{-}N_3)_2]\cdot 2[Cu^{II}(L)(N_3)(H_2O)]\cdot 6H_2O$ (**1**), have been described in the present investigation. An important aspect of the title compound is that it contains cocrystallized and self-assembled dinuclear and mononuclear metal complexes. It is an important addition in the family containing a few examples of cocrystals of metal complexes [11,12]. In contrast to the previously reported supramolecule $[Ni^{II}(LH)_2](dicyanamide)_2\cdot 2H_2O$ [2b] which contains neutral and enolic 4-terpyridone, the presence of anionic 4-terpyrodone is another interesting aspect of the present investigation. Again, O–pyridine–M–$(\mu\text{-}N_3)_2$–pyridine–O and O–pyridine–M moieties in the title compound have been found as potential supramolecular synthon. Regarding the ability to create a multidimensional assembly, the O–pyridine–M–$(\mu\text{-}N_3)_2$–pyridine–O moiety (as in **1**) can be considered as similar to H–O–pyridine–M–pyridine–O–H moiety (as in $[M(LH)_2]^{2+}$) and 4,4′-bipyridine or 4,4′-bipyridine-*N*,*N*′-dioxide [1e,2b,13]; Finally, two-dimensional hydrogen bonded sheet created due to the interactions involving oxygen centers of anionic 4-terpyridone and water molecules in the title compound may be considered as an important example in the area of supramolecular chemistry and crystal engineering. Moreover, the title compound is an addition in the family of end-on azide-bridged compounds which exhibit weak ferromagnetic interaction due to the axial–equatorial occupation.

Acknowledgements

Financial support from National Science Council, Taiwan (NSC95-2113-M032-005) and Department of Science and Technology, the Government of India (SR/S1/IC–27/2002), and is gratefully acknowledged. M.N. thanks CSIR, Government of India, for providing a fellowship.

Appendix A. Supplementary data

CCDC 665405 contains the supplementary crystallographic data for this paper. These data can be obtained free of charge via http://www.ccdc.cam.ac.uk/conts/retrieving.html, or from the Cambridge Crystallographic Data Centre, 12 Union Road, Cambridge CB2 1EZ, UK; fax: (+44) 1223-336-033; or e-mail: deposit@ccdc.cam.ac.uk. Supplementary data associated with this article can be found, in the online version, at doi:10.1016/j.poly.2008.05.027.

References

[1] (a) J.-P. Sauvage (Ed.), Transition Metals in Supramolecular Chemistry, Perspectives in Supramolecular Chemistry, vol. 5, Wiley, England, 1999;
(c) G.R. Desiraju (Ed.), The Crystal as a Supramolecular Entity, Perspectives in Supramolecular Chemistry, vol. 2, Wiley, England, 1996;
(c) D. Braga, F. Grepioni, A.G. Orpen, Crystal Engineering: from Molecules and Crystals to Materials, Kluwer Academic Publishers, Dordrecht, 1999;
(d) B. Moulton, M.J. Zaworotko, Chem. Rev. 101 (2001) 1629;
(e) A.J. Blake, N.R. Champness, P. Hubberstey, M.A. Withersby, M. Schröder, Coordin. Chem. Rev. 183 (1999) 117.
[2] (a) A.B. Gaspar, M.C. Munoz, V. Niel, J.A. Real, Inorg. Chem. 40 (2001) 9;
(b) M. Nayak, R. Koner, S. Evans, S. Mohanta, Cryst. Growth Des. 5 (2005) 1907.
[3] (a) O. Kahn, Molecular Magnetism, VCH Publications, New York, 1993. see also references cited therein;
(b) J. Ribas, A. Escuer, M. Monfort, R. Vicente, R. Cortés, L. Lezama, T. Rojo, Coordin. Chem. Rev. 193–195 (1999) 1027;
(c) A. Escuer, C.J. Harding, Y. Dussarl, J. Nelson, V. McKee, R. Vicente, Dalton Trans. (1999) 223;
(d) C.S. Hong, J.-E. Koo, S.-K. Son, Y.S. Lee, Y.-S. Kim, Y. Do, Chem. Eur. J. 7 (2000) 4243;
(e) S. Mohanta, K.K. Nanda, R. Werner, W. Haase, A.K. Mukherjee, S.K. Dutta, K. Nag, Inorg. Chem. 36 (1997) 4656.
[4] (a) S. Sirakov, I. Bkouche-Waksman, O. Kahn, Inorg. Chem. 23 (1984) 490;
(b) S.S. Tandon, L.K. Thompson, M.E. Manuel, J.N. Bridson, Inorg. Chem. 33 (1994) 5555;
(c) G.A. van Albada, M.T. Lakin, N. Veldman, A.L. Spek, J. Reedijk, Inorg. Chem. 34 (1995) 4910;
(d) J. Comarmond, P. Plumere', J.-M. Lehn, Y. Agnus, R. Louis, R. Weiss, O. Kahn, I. Morgenstern-Badarau, J. Am. Chem. Soc. 104 (1982) 6330.
[5] (a) J.P. Costes, F. Daham, J. Ruiz, J.P. Laurent, Inorg. Chim. Acta 239 (1995) 53;
(b) L. Li, D. Liao, Z. Jiang, S. Yan, Polyhedron 20 (2001) 681.
[6] (a) M. Monfort, I. Resino, J. Ribas, X. Solans, M. Font-Bardia, P. Rabu, M. Drillon, Inorg. Chem. 39 (2000) 2572;
(b) R. Vicente, A. Escuer, Polyhedron 14 (1995) 2133.
[7] (a) M.-F. Charlot, O. Kahn, M. Chaillet, C. Larrieu, J. Am. Chem. Soc. 108 (1986) 2574;
(b) C. Adamo, V. Barone, A. Bencini, F. Totti, I. Ciafini, Inorg. Chem. 38 (1999) 1996;
(c) E. Ruiz, J. Cano, S. Alvarez, P. Alemany, J. Am. Chem. Soc. 120 (1998) 11122.
[8] (a) B.-Q. Ma, H.-L. Sun, S. Gao, G. Su, Chem. Mater. 13 (2001) 1946;
(b) M. Monfort, I. Resino, J. Ribas, H. Stoeckli-Evans, Angew. Chem., Int. Ed. Engl. 39 (2000) 191;
(c) A. Escuer, R. Vicente, M.A.S. Goher, F.A. Mautner, Inorg. Chem. 36 (1997) 3440;
(d) A. Escuer, R. Vicente, F.A. Mautner, M.A.S. Goher, M.A.M. Abu-Youssef, Chem. Commun. (2002) 64.
[9] (a) G.M. Sheldrick, SHELXS-97: A Program for Crystal Structure Solution, University of Göttingen, Göttingen, Germany, 1997;
(b) G.M. Sheldrick, SHELXL-97: A Program for Crystal Structure Refinement, University of Göttingen, Göttingen, Germany, 1993.
[10] A.W. Addison, T.N. Rao, J. Reedijk, J. van Rijn, G.C. Verschoor, Dalton Trans. (1984) 1349.
[11] (a) M. Nayak, R. Koner, H.-H. Lin, U. Flörke, H.-H. Wei, S. Mohanta, Inorg. Chem. 45 (2006) 10764;
(b) M. Nayak, S. Hazra, P. Lemoine, R. Koner, C.R. Lucas, S. Mohanta, Polyhedron 27 (2008) 1201.
[12] (a) C.-C. Chou, C.-C. Su, H.-L. Tsai, K.-H. Lii, Inorg. Chem. 44 (2005) 628;
(b) M. Palaniandavar, R.J. Butcher, A.W. Addison, Inorg. Chem. 35 (1996) 467;
(c) R.C. Holz, L.C. Thompson, Inorg. Chem. 32 (1993) 5251;
(d) P. Jones, R.S. Vagg, P.A. Williams, Inorg. Chem. 23 (1984) 4110;
(e) W.J. Evans, T.J. Boyle, J.W. Ziller, Inorg. Chem. 31 (1992) 1120.
[13] D.-L. Long, A.J. Blake, N.R. Champness, C. Wilson, M. Schröder, J. Am. Chem. Soc. 123 (2001) 3401.

Polyhedron 27 (2008) 2698–2704

Contents lists available at ScienceDirect

Polyhedron

journal homepage: www.elsevier.com/locate/poly

Synthesis and characterization of ruthenium(II) azoimine-diphosphine mixed-ligand complexes

Mousa Al-Noaimi [a,*], Musa I. El-Barghouthi [a], Mohammad El-khateeb [b], Obada S. Abdel-Rahman [a], Helmar Görls [c], Robert J. Crutchley [d]

[a] Chemistry Department, Faculty of Science, The Hashemite University, Zarqa, Jordan
[b] Chemistry Department, Jordan University of Science and Technology, Irbid 22110, Jordan
[c] Institut für Anorganische und Analytische Chemie, Friedrich-Schiller-Universtät Jena, August-Bebel Strasse 2, Jena 07743, Germany
[d] Chemistry Department, Carleton University, Ottawa, Ontario, Canada K1S 5B6

ARTICLE INFO

Article history:
Received 13 March 2008
Accepted 13 May 2008
Available online 9 July 2008

Keywords:
Ruthenium
Complexes
Azomethine
X-ray structures
Electrochemistry
Spectroelectrochemistry

ABSTRACT

A novel family of the general type *cis*-[Ru^{II}(dppe)LCl_2] {L = $C_6H_5N{=}NC(COCH_3){=}NAr$, Ar = 2,4,6-trimethylphenyl (L_1), 2,5-dimethylphenyl (L_2), 4-tolyl (L_3), phenyl (L_4), 4-methoxyphenyl (L_5), 4-chlorophenyl (L_6), 4-nitrophenyl (L_7), 2,5-dichlorophenyl (L_8); dppe = $Ph_2P(CH_2)_2PPh_2$} has been synthesized. These complexes have been characterized through analytical, spectroscopic (IR, UV–Vis, and NMR) and electrochemical (cyclic voltammetry) techniques. In addition, complex **4** (where L = L_4) has been further characterized by X-ray diffraction analysis. Crystallographic, electrochemical and electronic spectral data are all consistent with the azomethine ligands possessing strong π-acceptor properties. These π-acceptor properties can be "tuned" by a judicious choice of substituent on the azomethine ligand.

© 2008 Elsevier Ltd. All rights reserved.

1. Introduction

Ruthenium(II) complexes with heterocyclic N-donor bidentate ligands such as 2,2′-bipyridine (bpy) and its dervatives are of interest because of their fascinating electron-transfer, photochemical and catalytic properties [1,2]. The metal-to-ligand charge-transfer properties of these complexes have been extensively studied by UV–Vis absorption and electrochemical investigations [3]. Correlations have been found between charge transfer (CT) energies and the difference between ligand and ruthenium couples [4]. An arylazoheterocyclic ligand which contains an imine group in a heterocyclic backbone with a pendant azo group such as 2-(arylazo)pyridine (aap) coordinates to a metal ion as an azoimine (–N=N–C=N–) bidentate ligand [5,6]. This type of ligand is a strong π-acceptor, stronger than 2,2′-bipyridine and other N-donor heterocyclic ligands, and stabilizes the lower oxidation states of ruthenium [7,8]. Because of this interesting property, we have developed several arylamidrazone ligands (L) [9,10].

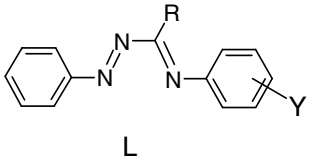

L

Ru(II) complexes containing tertiary phosphines have been extensively studied from a synthetic viewpoint, and their performance as catalysts are well-known [11]. More recently, there has been an increased interest in mixed-ligand ruthenium(II) complexes containing both soft P donor atoms and hard N-containing ligands. This interest is a result of the unique electronic properties that this combination of ligands is able to transmit to the metal center [12–14].

With the aim of contributing to the understanding of how geometric and electronic factors, imposed by a combination of mixed ligands (N and P types), influence the electronic properties of the metal center, we have prepared a family of *cis*-[Ru(L)(dppe)Cl_2] complexes bearing the azoimine ligands L and the P-bidentate bis(1,2-diphenylphosphino)ethane (dppe) ligand. Changing the substituents (Y) on the ligand L is expected to vary the π-acceptor properties on these bidentate ligands. Consequently, this will also "tune" the electronic properties of the ruthenium and

* Corresponding author. Tel.: +962 777296245.
E-mail address: manoaimi@hu.edu.jo (M. Al-Noaimi).

0277-5387/$ - see front matter © 2008 Elsevier Ltd. All rights reserved.
doi:10.1016/j.poly.2008.05.026

consequently the energy of the MLCT bands. The spectral studies, redox properties and single crystal X-ray structure (for complex **4**) of the newly synthesized family will be described in this work.

2. Experimental

2.1. Materials

The reagents: aniline derivatives, ruthenium trichloride hydrate, bis(diphenylphosphino)ethane, lithium chloride and solvents (reagent grade) were purchased from Aldrich and were used as received. Tetrabutylammonium hexafluorophosphate (TBAH), purchased from Aldrich, was recrystallized twice from 1:1 ethanol/water solution and then vacuum dried at 110 °C. Hydrazonyl chlorides were prepared according to the reported procedures [14]. The synthesis and the physical characterization of the ligands L_3, L_4, L_5,L_6 and L_7 have been described previously [9].

2.2. Arylamidrazones (L): general procedure

The arylamidrazones (L) were synthesized by refluxing 20 mmol of arylamine, triethylamine (2.4 g, 24 mmol) and (3.9 g, 20 mmol) of hydrazonyl chloride in 5.0 mL ethanol for 2 h. Condensing the solution followed by cooling produced a yellow solid which was recrystallized from ethanol.

2.2.1. 1-(2,4,6-Trimethylphenylimino)-1-(phenylhydrazono)-propan-2-one (L_1)

Yield (3.2 g, 54%). *Anal. Calc. for* $C_{18}H_{19}N_3O$: C, 73.70; H, 6.53; N, 14.32. Found: C,73.42; H, 6.50; N, 14.11%. *UV–Vis in acetonitrile:* λ_{max} (ε_{max}/M^{-1} cm^{-1}): 368 (8.09×10^4), 276 (4.69×10^4), 254 (6.24×10^4). IR (cm^{-1}): ν(N=N) 1479, ν(C=N) 1599, ν(C=O) 1674. ^{1}H NMR ($CDCl_3$, δ ppm): 6.62 (s, 1H, H3), 6.67 (d, 2H, H11, H7), 6.8 (t, 1H, H9), 7.05 (s, 1H, H5), 7.15 (t, 2H, H10, H8), 2.57 (3H, s, $COCH_3$), 2.30 (s, 3H, CH_3 position 4), 2.15 (s, 6H, CH_3 positions 2 and 6). M.p.: 144–146 °C.

2.2.2. 1-(2,5-Dimethylphenylimino)-1-(phenylhydrazono)-propan-2-one (L_2)

Yield (3.2 g, 58%). *Anal. Calc. for* $C_{17}H_{17}N_3O$: C, 73.10; H, 6.13; N, 15.04. Found. C, 73.41; H, 6.03; N, 15.19%. *UV–Vis in acetonitrile:* λ_{max} (ε_{max}/M^{-1} cm^{-1}): 380 (8.83×10^4), 284 (5.24×10^4), 214 (6.90×10^4). IR (cm^{-1}): ν(N=N) 1507, ν(C=N) 1578, ν(C=O) 1665. ^{1}H NMR ($CDCl_3$, δ ppm): 7.26 (d, 2H, H11, H7), 7.06 (t, 2H, H10, H8), 6.96 (t, 1H, H9), 6.95 (d, 1H, H4), 6.76 (d, 1H, H3), 6.50 (s, 1H, H6), 2.62 (s, 3H, $COCH_3$), 2.28 (s, 3H, CH_3 position 5), 2.19 (s, 3H, CH_3 position 2). M.p.: 114–116 °C.

2.2.3. 1-(2,5-Dichlorophenylimino)-1-(phenylhydrazono)-propan-2-one (L_8)

Yield (3.9 g, 61%). *Anal.* Calc. for $C_{15}H_{11}N_3OCl_2$: C, 56.27; H, 3.46; N, 13.12. Found: C, 56.40; H, 3.48; N, 13.24%. UV–Vis in acetonitrile: λ_{max} (ε_{max}/M^{-1} cm^{-1}): 380 (9.01×10^4), 297 (5.38×10^4), 245 (7.02×10^4). IR (cm^{-1}): ν(N=N) 1493, ν(C=N) 1590, ν(C=O) 1652. ^{1}H NMR (in $CDCl_3$, δ ppm): 7.26 (d, 2H, H11, H7), 7.06 (t, 2H, H10, H8), 6.95 (d, 1H, H4), 6.90 (t, 1H, H9), 6.76 (d, 1H, H3), 6.50 (s, 1H, H6), 2.62 (s, 3H, $COCH_3$). M.p.: 153–155 °C.

2.3. General procedure for the syntheses of the cis-[Ru(dppe)(L)Cl_2] complexes

Ruthenium trichloride. trihydrate (0.26 g, 1.0 mmol) and (1.0 mmol) of (L) were dissolved in 100 mL of absolute ethanol under argon. After refluxing for 1 h, 1.0 mmol of bis(diphenylphosphino)ethane (dppe) was added to the solution. The reaction was heated for an additional 2 h, followed by the addition of excess LiCl (0.50 g, 11.8 mmol). After allowing the reaction mixture to reflux for an additional 1 h, the solvent was then removed by rotary evaporator. The crude product was dissolved in dichloromethane, filtered and washed with water to remove the unreacted ruthenium trichloride and lithium chloride. The filtrate was reduced to 20 mL and purified by chromatography (50×3 cm) on alumina grade (III). The first pale yellow band, thought to be the azomethine ligand (L) was eluted with hexane. Acetone was used to elute the second dark-red band of the product. The complex was recrystallized easily as dark red platelets from a slowly evaporating solution of dichloromethane.

2.3.1. cis-[Ru(dppe)(L_1)Cl_2] CH_2Cl_2 (**1**)

Yield (0.40 g, 47%). *Anal. Calc. for* $C_{25}H_{22}N_6O_3Cl_2Ru \cdot CH_2Cl_2$: C, 58.98; H, 4.89; N, 4.64%. Found: C, 58.78; H, 4.78; N, 4.75%. *UV–Vis in acetonitrile:* λ_{max} (ε_{max}/M^{-1} cm^{-1}): 378 (4.562×10^3), 516 (5.642×10^3), 802 (1.83×10^3). IR (cm^{-1}): ν(N=N) 1434, ν(C=N) 1536, ν(C=O) 1711.^{1}H NMR ($CDCl_3$, δ ppm): 2.2 (s, 6H, CH_3 position 2 and 6), 2.47 (s, 3H, CH_3 position 4), 2.53 (m, 2H, PCH_2), 2.76 (s, 3H, $COCH_3$), 3.02 (m, 2H, PCH_2), 6.11 (s, 2H, H3), 6.21 (s, 2H, H5), 7.68 (t, 2H, H8, H10), 6.81 (t, 1H, H9), 6.88 (m, 6H, PPh_2), 7.15 (m, 8H, PPh_2), 7.33 (m, 6H, PPh_2), 7.56 (d, 2H, H11, H7). ^{31}P NMR ($CDCl_3$, δ ppm): 41.36 (d), 35.60 (d).

2.3.2. cis-[Ru(dppe)(L_2)Cl_2] · H_2O (**2**)

Yield (0.34 g, 40%). *Anal. Calc. for* $C_{43}H_{41}Cl_2N_3OP_2Ru \cdot H_2O$: C, 59.52; H, 4.99; N, 4.84. Found: C, 59.77; H, 4.77; N, 4.47%. *UV–Vis in acetonitrile:* λ_{max} (ε_{max}/M^{-1} cm^{-1}): 362 (6.688×10^3), 512 (5.146×10^3), 800 (2.50×10^2). IR (cm^{-1}): ν(N=N) 1429, ν(C=N) 1536, ν(C=O) 1711. ^{1}H NMR ($CDCl_3$, δ ppm): 2.20 (s, 3H, CH_3 position 2), 2.47 (s, 3H, CH_3 position 5), 2.53 (m, 2H, PCH_2), 2.76 (s, 3H, $COCH_3$). 3.02 (m, 2H, PCH_2), 6.11 (s, 1H, H6), 6.44 (d, 2H, H3), 6.50 (s, 1H, H4), 6.82 (t, 1H, H9), 6.88 (m, 6H, PPh_2), 7.15 (m, 8H, PPh_2), 7.33 (m, 6H, PPh_2), 7.56 (d, 2H, H10, H8), 7.68 (t, 2H, H11, H7). ^{31}P NMR ($CDCl_3$, δ ppm): 42.03 (d), 36.08 (d).

2.3.3. cis-[Ru(dppe)(L_3)Cl_2] · H_2O (**3**)

Yield (0.35 g, 42%). *Anal. Calc. for* $C_{42}H_{39}Cl_2N_3OP_2Ru \cdot H_2O$: C, 59.09; H, 4.84; N, 4.92. Found: C, 59.41; H, 5.18; N, 4.51%. *UV–Vis in acetonitrile:* λ_{max} (ε_{max}/ M^{-1} cm^{-1}): 374 (7.449×10^3), 506 (6.55×10^3), 804 (3.12×10^2). IR (cm^{-1}): ν(N=N) 1434, ν(C=N) 1552., ν(C=O) 1715. ^{1}H NMR (in $CDCl_3$, δ ppm): 2.26 (s, 3H,CH_3, $COCH_3$), 2.53 (m, 2H, PCH_2), 2.95 (m, 2H, PCH_2), 6.42 (d, 2H, H3, H5), 6.49 (d, 2H, H2, H6), 6.70 (t, 1H, H9), 6.73 (m, 2H, PPh_2), 6.93 (m, 6H, PPh_2), 7.17 (m, 6H, PPh_2), 7.34 (m, 6H, PPh_2), 7.58 (t, 2H, H11, H7), 7.67 (t, 2H, H10, H8), ^{31}P NMR ($CDCl_3$, δ ppm): 41.33 (d), 35.61 (d).

2.3.4. cis-[Ru(dppe)(L_4)Cl_2] (**4**)

Yield (0.44 g, 53%). *Anal. Calc. for* $C_{41}H_{37}Cl_2N_3OP_2Ru$: C, 59.93; H, 4.54; N, 5.11. Found: C, 59.29; H, 4.59; N, 4.86%. *UV–Vis in acetonitrile:* λ_{max} (ε_{max}/M^{-1} cm^{-1}): 378 (6.40×10^3), 504 (5.684×10^3), 800 (2.71×10^2). IR (cm^{-1}): ν(N=N) 1435, ν(C=N) 1485, ν(C=O) 1711. ^{1}H NMR ($CDCl_3$, δ ppm): 2.62 (m, 2H, PCH_2), 2.66 (s, 3H, $COCH_3$), 3.18 (m, 2H, PCH_2), 6.46 (d, 2H, H2, H6), 6.49 (d, 2H, H11, H7), 6.7 (t, 2H, H9), 6.80 (t, 1H, H4), 7.0 (m, 7H, PPh_2), 7.18 (m, 7H, PPh_2), 7.35 (m, 6H, PPh_2), 7.58 (t, 2H, H3, H5), 7.67 (t, 2H, H8, H10). ^{31}P NMR ($CDCl_3$, δ ppm): 40.56 (d), 35.72 (d).

2.3.5. cis-[Ru(dppe)(L_5)Cl_2] (**5**)

Yield (0.35 g, 41%). *Anal. Calc. for Ru* $C_{42}H_{39}Cl_2N_3O_2P_2$: C, 59.23; H, 4.62; N, 4.93. Found: C, 59.51; H, 4.87; N, 4.88%. *UV–Vis in acetonitrile:* λ_{max} (ε_{max}/M^{-1} cm^{-1}): 378 (6.015×10^3), 509 (7.04×10^3), 806 (2.73×10^2). IR (cm^{-1}): ν(N=N) 1435, ν(C=N) 1506, ν(C=O) 1711. ^{1}H NMR ($CDCl_3$, δ ppm): 2.31 (s, 3H, $COCH_3$), 2.57 (m, 2H,

PCH_2), 2.97 (m, 2H, PCH_2), 3.77 (s, 3H, OCH_3), 6.57 (t, 1H, H9), 6.59 (d, 2H, H2, H6), 6.79 (t, 3H, PPh_2), 6.97 (m, 6H, PPh_2), 7.21 (m, 6H, PPh_2), 7.36 (m, 5H, PPh_2), 7.47 (d, 2H, H3, H5), 7.61 (d, 2H, H11, H7), 7.70 (t, 2H, H10, H8). ^{31}P NMR ($CDCl_3$, δ ppm): 42.33 (d), 36.03 (d).

2.3.6. cis-[Ru(dppe)(L_6)Cl_2] (**6**)

Yield (0.33 g, 38%). *Anal. Calc. for $C_{41}H_{36}Cl_3N_3OP_2Ru$: C, 57.52; H, 4.24; N, 5.91. Found: C, 57.34; H, 4.63; N, 5.70%. UV–Vis in acetonitrile:* λ_{max} (ε_{max}/M^{-1} cm^{-1}): 378 (7.343×10^3), 502 (6.464×10^3), 806 (2.22×10^2). IR (cm^{-1}): ν(N=N) 1486, ν(C=N) 1540, ν(C=O) 1712. ^{1}H NMR ($CDCl_3$, δ ppm): 2.41 (s, 3H, $COCH_3$), 2.54 (m, 2H, PCH_2), 3.02 (m, 2H, PCH_2), 6.45 (d, 2H, H3, H5), 6.55 (d, 2H, H2, H6), 7.59 (d, 2H, H11, H7), 7.66 (t, 2H, H10, H8), 6.70 (t, 2H, PPh_2), 6.73 (t, 1H, H9), 7.03 (m, 6H, PPh_2), 7.22 (m, 6H, PPh_2). 7.34 (m, 6H, PPh_2), 7.76 (d, 2H, H11). ^{31}P NMR ($CDCl_3$, δ ppm): 42.01 (d), 36.10 (d).

2.3.7. cis-[Ru(dppe)(L_7)Cl_2] · CH_2Cl_2 (**7**)

Yield (0.39 g, 45%). *Anal. Calc. for $C_{41}H_{36}Cl_2N_4O_3P_2Ru \cdot CH_2Cl_2$: C, 53.01; H, 4.02; N, 5.89. Found: C, 52.82; H, 3.91; N, 5.92%. UV–Vis in acetonitrile:* λ_{max} (ε_{max}/M^{-1} cm^{-1}): 496 (5.277×10^3). IR (cm^{-1}): ν(N=N) 1491, ν(C=N) 1599, ν(C=O) 1675. ^{1}H NMR ($CDCl_3$, δ ppm): 2.60 (m, 2H, PCH_2), 2.64 (s, 3H, $COCH_3$), 3.18 (m, 2H, PCH_2), 6.47 (t, 2H, H10, H8), 6.52 (t, 2H, H3, H5), 6.73 (t, 2H, PPh_2), 6.83 (t, 1H, H9), 6.91 (m, 4H, PPh_2), 7.41 (m, 7H, PPh_2), 7.58 (d, 2H, H2, H6), 7.63 (m, 7H, PPh_2), 7.67 (d, 2H, H11, H7).^{31}P NMR ($CDCl_3$, δ ppm): 40.38 (d), 35.14 (d).

2.3.8. cis-[Ru(dppe)(L_8)Cl_2] (**8**)

Yield (0.36 g, 40%). *Anal.* Calc. for $C_{41}H_{37}Cl_2N_3OP_2Ru$: C, 55.30; H, 3.96; N, 4.72. Found: C, 54.91; H, 4.10; N,4.87%. UV–Vis in acetonitrile: λ_{max} (ε_{max}/M^{-1} cm^{-1}): 382 (8.343×10^3). 501 (3.195×10^3), 866 (1.81×10^3). IR (cm^{-1}): ν(N=N) 1491, ν(C=N) 1592, ν(C=O) 1707.^{1}H NMR ($CDCl_3$, δ ppm): 2.55 (s, 3H, $COCH_3$), 2.57 (m, 2H, PCH_2), 3.14 (m, 2H, PCH_2), 6.47 (t, 2H, H10, H8), 6.58 (d, 2H, H11, H7), 6.71 (t, 2H, PPh_2), 6.83 (t, 1H, H9), 6.91 (m, 6H, PPh_2), 7.18 (m, 6H, PPh_2), 7.36 (m, 6H, PPh_2), 7.08 (s, 1H, H6), 7.59 (d, 1H, H4), 7.61 (d, 1H, H3).^{31}P NMR ($CDCl_3$, δ ppm): 41.27 (d), 35.68 (d).

2.4. Instrumentation

Cyclic voltammetry studies were performed in 99.8% anhydrous acetonitrile (Aldrich, HPLC grade) using a BAS CV-27W voltammetric analyzer and plotted on a BAS XY recorder. Three electrodes were utilized in this system, two platinum-disk working and counter (auxiliary) electrodes (BAS, 1.6-mm diameter), and a silver wire pseudo-reference electrode with ferrocene (0.665 V versus NHE) as an internal reference [15]. To control the temperature, a Haake D8-G refrigerated bath and circulator was used to maintain the cell temperature at 25.0 ± 0.1 °C. Tetrabutylammonium hexafluorophosphate (0.1 M) was twice recrystallized and vacuum dried at 120 °C, and used as the supporting electrolyte. Spectroscopic data were obtained using Cary 5 spectrophotometer. Spectroelectrochemistry for complex **4** was performed using an OTTLE (Optically Transparent Thin Layer Electrochemistry) cell [16]. The cell had interior dimensions of roughly 1 × 2 cm with a path length of 0.2 cm and was fitted with an Ag/AgCl reference electrode. ITO (indium–tin oxide) coated glass served as working and counters electrodes and was purchased from Delta-Technologies. Spectra were obtained on Cary 5 spectrophotometer versus appropriate background of solvent and electrolyte at a scan rate of 1800 nm/min. The potential was controlled by the same BAS CV-27 which was used for cyclic voltammetry. At any given potential, the system was allowed to come to equilibrium ($i \approx 0$ μA) before the spectrum was taken. IR spectra were measured using a FT-IR JASCO model 420. Nuclear magnetic resonances (^{1}H and ^{31}P NMR) spectra were measured on a Bruker-Avance 400 MHz spectrometer at 400 MHz and 161.3 MHz, respectively. All chemical shifts are reported in ppm downfield of TMS (^{1}H) or 85% phosphoric acid (^{31}P) and referenced using the chemical shifts of residual solvent resonances. Elemental analyses were carried out on a Eurovector E.A.3000 instrument using copper sample tubes.

2.5. Crystallography

Dark red crystals of *cis*-[Ru(dppe)(L_4)Cl_2] (**4**) suitable for structural determination were obtained by recrystallization from a dichloromethane solution. X-ray data were collected by a Nonius Kappa CCD diffractometer with a graphite monochromator λ(Mo Kα) = 0.71073 Å. Selected crystal data of **4** are presented in Table 1. The structure was solved by direct methods using SHELXS-97 [17] and refined by full-matrix least-square procedures on $|F|^2$, using SHELX-97 [18]. All non-hydrogen atoms were refined anisotropically and the hydrogen atom positions were refined using the atom corresponded riding model [19]. The structure was determined by the refinement of the Flack x parameter.

3. Results and discussion

3.1. Synthesis

The azomethine ligands (L_1–L_8) used in this study were prepared by the reaction of hydrazonyl chloride **1** with the appropriate aniline derivative **2** according to Scheme 1. The structure of these ligands was confirmed by ^{1}H NMR Spectroscopy and elemental analyses. The synthesis of *cis*-[Ru(dppe)LCl_2] was achieved by the stepwise addition of the azoimine ligands, dppe and then an excess of lithium chloride.

Table 1
Crystal data and structure refinement for complex **4**

Empirical formula	C_{43} $H_{41}C_{16}N_3OP_2Ru$
Formula weight	991.50
Temperature (K)	183(2)
Wavelength (Å)	0.71073
Crystal system	monoclinic
Space group	*P*2(1)/*n*
Unit cell dimensions	
a (Å)	11.2878(3)
b (Å)	17.5181(3)
c (Å)	22.6299(6)
α (°)	90
β (°)	100.465(1)
γ (°)	90
V (Å^3)	4400.42(18)
Z	4
D_{calc} (Mg/m^3)	1.497
Absorption coefficient (mm^{-1})	0.831
F(000)	2016
Crystal size (mm^3)	0.05 × 0.05 × 0.04
θ Range for data collection (°)	2.17–27.48
Index ranges	$-14 \leqslant h \leqslant 13$ $-22 \leqslant k \leqslant 22$ $-27 \leqslant l \leqslant 29$
Reflections collected	29621
Independent reflections (R_{int})	10061 (0.0522)
Completeness to theta = 27.48°	99.7%
Absorption correction	none
Refinement method	full-matrix least-squares on F^2
Data/restraints/parameters	10061/0/499
Goodness-of-fit on F^2	1.007
Final *R* indices [$I > 2\sigma(I)$]	R_1 = 0.0517, wR_2 = 0.1249
R indices (all data)	R_1 = 0.0798, wR_2 = 0.1397
Largest difference peak, hole (e Å^{-3})	1.140, −1.223

$R_1 = \sum||F_o| - |F_c||/\sum|F_o|$; $wR_2 = \{\sum[w(F_o^2 - F_c^2)^2]/\sum[w(F_o^2)^2]\}^{1/2}$.

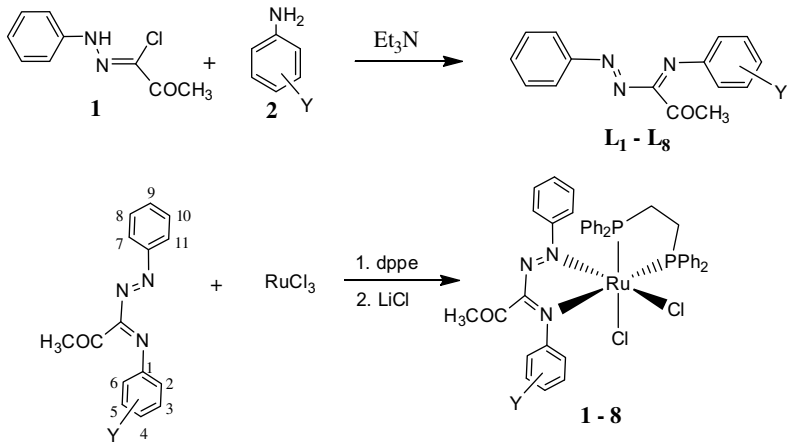

Scheme 1.

Substituent (Y)	2,4,6-Trimethyl	2,5-Dimethyl	4-CH_3	H	4-OCH_3	4-Cl	4-NO_2	2,5-Dichloro
Ligand (L)	L_1	L_2	L_3	L_4	L_5	L_6	L_7	L_8
Complex	**1**	**2**	**3**	**4**	**5**	**6**	**7**	**8**

The neutral complexes **1–8** are air stable and diamagnetic, and their structures were confirmed by ^{1}H and ^{31}P NMR spectra and X-ray diffraction for complex **4**. The aromatic region in the ^{1}H NMR spectra of complexes **1–8** consists of several coupled multiplets due to the aromatic protons of the phenyl rings of the dppe ligand and the phenyl rings of the azoimine ligands. The ^{31}P{^{1}H} NMR spectra of complexes **1–8** showed two doublets in the range 35–42 ppm. It is proposed that the more shielded phosphorus atom is the one trans to the nitrogen while the deshielded P is trans to Cl [20]. In their IR-spectra, all the complexes show bands in the range 1660–1712 cm^{-1} assignable to the C=O stretching frequency of the acetyl group. The intense bands in the ranges 1560–1590 and 1430–1500 cm^{-1} were assigned to the C=N and N=N stretching bands of the azoimine ligands, respectively.

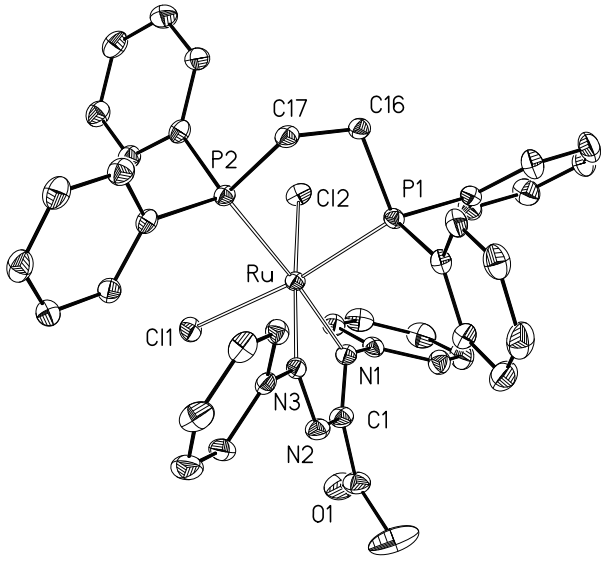

Fig. 1. Thermal ellipsoid plot (30%) of complex **4**. Hydrogen atoms are omitted for clarity.

3.2. Crystal structure

The crystal structure of complex **4** has been solved by X-ray diffraction analysis and its ORTEP plot is depicted in Fig. 1. The main crystallographic data are reported in Table 1. Selected bond distances and angles are found in Table 2. Compound **4** crystallizes in the centrosymmetrical space group *P*2(1)/*n*. The geometry around Ru is distorted octahedral with Ru–N, Ru–P and Ru–Cl bond lengths of 2.027, 2.348 and 2.416 Å, respectively. These data are within the range of bond lengths found for Ru(II) complexes containing these atoms [21]. In this structure, there are two salient features that are worth mentioning: one is the trans influence exerted by the phosphine ligand, which resulted in an elongation of the Ru–Cl distances of **4** (average 2.416 Å) compared to the reported values for *trans*-[Ru(bpy)LCl_2] [22]. The Ru–Cl2 bond length (2.4021(10) Å) trans to the azoimine N atom is shorter than the Ru–Cl1 bond distance of 2.4308(10) Å trans to the P atom of the dppe ligand. This may due to a stronger trans influence of the P versus N donor atom. This trans influence can also be observed in the Ru–N azoimine bonds [Ru–N3], trans to Cl: 1.969(3) Å, Ru–N1, trans to P: 2.084(3) Å. The Ru–P bond lengths of **4** (2.3645(10), 2.332(9) Å) are comparable to Ru–P bond lengths in other reported systems [23].

The second interesting character is that the Ru–N3 [N (azo)] bond distance (1.969(3) Å) is shorter than the Ru–N1 [N (methine)] bond distance (2.084(3) Å), and is also shorter than Ru–N (azo) bond distances for other reported azo-pyridines complexes [24]. This shortening is due to greater π-back donation from the Ru–d orbital to the empty π* orbital of the azoimine ligand and may indicate that the M–L π interaction is localized in the M–azo fragment [24].

3.3. Electrochemistry

The electron-transfer behavior of the complexes in acetonitrile solution was examined by cyclic voltammetry and the corresponding results are summarized in Table 3. As a representative example, the cyclic voltammogram for complex **4** is shown in Fig. 2. Two one-electron reduction steps are observed in the range −0.29 to −0.71 V versus NHE and are localized at the azo group, analogous to the azopyridine systems [23]. Our concern here is the quasi-reversible single oxidation wave which lies between 1.40 and 1.55 V. This wave is assigned to Ru(III/II) and occurs at more positive potentials compared to

Table 2
Bond lengths [Å] and angles [°] for complex **4**

Bond lengths [Å]		Bond angles [°]			
Ru–N(3)	1.969(3)	N(3)–Ru–N(1)	77.12(12)	P(2)–Ru–Cl(1)	90.81(3)
Ru–N(1)	2.084(3)	N(3)–Ru–P(1)	99.19(9)	Cl(2)–Ru–Cl(1)	90.49(4)
Ru–P(1)	2.3320(9)	N(1)–Ru–P(1)	100.50(9)	C(18)–P(1)–Ru	114.33(13)
Ru–P(2)	2.3645(10)	N(3)–Ru–P(2)	103.02(9)	C(16)–P(1)–Ru	106.16(13)
Ru–Cl(2)	2.4021(10)	N(1)–Ru–P(2)	175.44(9)	C(24)–P(1)–Ru	123.79(13)
Ru–Cl(1)	2.4308(9)	P(1)–Ru–P(2)	84.01(3)	C(36)–P(2)–Ru	122.68(13)
N(2)–N(3)	1.321(4)	N(3)–Ru–Cl(2)	171.38(9)	C(17)–P(2)–Ru	108.28(13)
N(2)–C(1)	1.366(5)	N(1)–Ru–Cl(2)	94.51(9)	C(30)–P(2)–Ru	114.40(12)
N(1)–C(1)	1.295(5)	P(1)–Ru–Cl(2)	84.22(4)	C(1)–N(1)–C(4)	118.7(3)
P(1)–C(18)	1.827(4)	P(2)–Ru–Cl(2)	85.17(3)	C(1)–N(1)–Ru	110.4(3)
P(1)–C(16)	1.830(4)	N(3)–Ru–Cl(1)	86.72(9)	C(4)–N(1)–Ru	130.3(2)
P(2)–C(36)	1.827(4)	N(1)–Ru–Cl(1)	84.64(9)	P(2)–Ru–Cl(1)	90.81(3)
P(2)–C(17)	1.829(4)	P(1)–Ru–Cl(1)	172.87(4)	Cl(2)–Ru–Cl(1)	90.49(4)

Table 3
Cyclic voltammetry and electronic spectroscopy data of the *cis*-[Ru(dppe)(L)Cl_2] complexes

Complex number	Cyclic voltammetric data $E_{1/2}$ [V][a]					Electronic spectroscopic data[b]
	$(E^0_{1/2})_{ox}$	$(E^0_{1/2})_{red}$	$(E^{0M}_{1/2})$[c]	Azo(0/−)[d]	(ΔE^0)[e]	λ_{max} (nm) (E_{MLCT})[f]
1	1.50	1.41	1.46	−0.27	1.73	(516) 55.41
2	1.52	1.42	1.47	−0.28	1.75	(512) 55.84
3	1.53	1.45	1.49	−0.28	1.77	(506) 56.50
4	1.52	1.48	1.50	−0.28	1.78	(504) 56.73
5	1.52	1.44	1.48	−0.28	1.76	(509) 56.17
6	1.57	1.49	1.53	−0.28	1.81	(502) 56.95
7	1.59	1.51	1.55	−0.29	1.84	(496) 57.64
8	1.60	1.50	1.55	−0.27	1.82	(501) 57.07

[a] Solvent MeCN, supporting electrolyte Bu_4NPF_6 (0.1 M), scan rate (0.1 V s), Pt-disk working electrode, Pt-wire auxiliary electrode, reference electrode Ag at 25 °C.
[b] Solvent MeCN.
[c] $E^{0M}_{1/2} = (E^0_{pa} + E^0_{pc})/2$
[d] The cathodic peak maximum.
[e] $\Delta E^{0M} = E^0_{1/2} - \text{Azo}(0/-)$.
[f] MLCT=[28591/λ_{max} (nm)] kCal mol^{-1}.

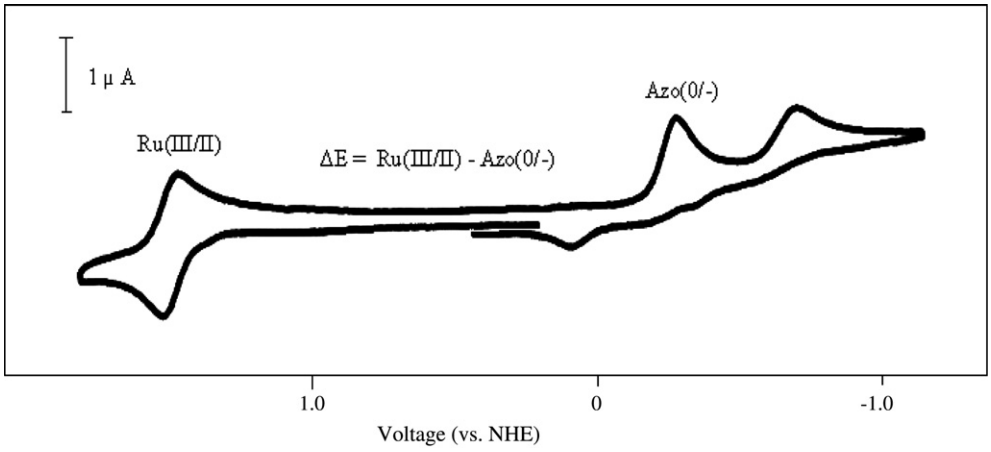

Fig. 2. Cyclic voltammogram for complex **4** in acetonitrile 0.1 M TBAH at 25 °C, data reported in *V* versus NHE with scan rate of 0.1 V/s.

the analogous dihalo ruthenium(II) complexes [24]. The Ru(III/II) couples of these complexes are among the highest in ruthenium(II) chemistry. The large positive shift (300 mV) for this family (compared to Ru(L)(bpy)Cl_2 complexes [9,10]) results from the strong π-acceptor properties of the dppe ligand (t2(Ru) → d(P)-backbonding [25]) compared to bpy. This couple is slightly affected by changing the substituent on the azo-imine auxiliary ligand and is shifted to more positive potentials upon replacing the donating methyl group with the more withdrawing nitro group.

3.4. Spectroelectrochemistry

The electronic spectral data for the *cis*-[Ru(dppe)LCl_2] complexes were collected in acetonitrile. The transitions below 400 nm are of the intra-ligand charge transfer ($\pi \rightarrow \pi^*$) type and are not considered further. The complexes exhibit multiple transitions in the visible region. A high intensity ($\varepsilon \sim 10^4$) transition at 500–550 nm is assigned to the MLCT transition [26]. Spectroelectrochemistry of **4** in DMF solution (Fig. 3) was performed in order to obtain the visible electronic absorption spectra of the

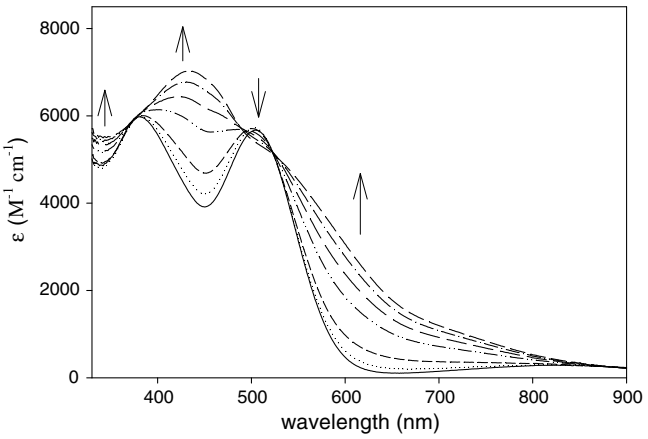

Fig. 3. Spectroelectrochemical oxidation of complex **4** in DMF, 0.1 M TBAH, 25 °C.

Ru(III) oxidation state. As seen in Fig. 3, oxidation of this complex results in a decrease in the band centered at 504 nm that we have assigned to a MLCT transition. The concomitant growth of a broad absorbance at $\lambda > 550$ nm is assigned to Cl-to-Ru(III) ($p\pi \rightarrow d\pi^*$) ligand-to-metal charge transfer transitions and the band centered at 435 nm is assigned to an azoimine-to-Ru(III) LMCT.

The MLCT band of the Ru(II) mononuclear complex and its electrochemistry provide information about the relative energies of the complex's metal and ligand-based orbitals. The change in $d\pi$-orbital energy can be measured experimentally using cyclic voltammetry to obtain the potential of the Ru(III/II) couple, which shifts to more positive potentials as the metal orbitals are stabilized. This has been demonstrated, for example, by the replacement of σ-donating amine ligands with pyridine-type ligands by Crutchley et al. [27]. For Ru(L)(dppe)Cl_2 complexes, electron withdrawing groups shift the Ru(III/II) couple approximately 100 mV positive relative to their donating analogues. This stabilization, however, does not result in a large shift in the MLCT band energy of the Ru(II) complexes, due to the equivalent stabilization of the orbitals involved in the MLCT events (the HOMO and the LUMO azoimine ligand).

The difference in the two successive redox responses at positive and negative values relative to NHE [$\Delta E^0 = E^{0M}_{1/2} - E^0_L(0/-)$] may be correlated with the MLCT transitions. The electronic excitation may be considered as an intramolecular redox process [27,28] and the spin-allowed MLCT transition is expected to correlate linearly with ΔE^0. The least squares plot of E_{MLCT}(kcal mol^{-1}) against

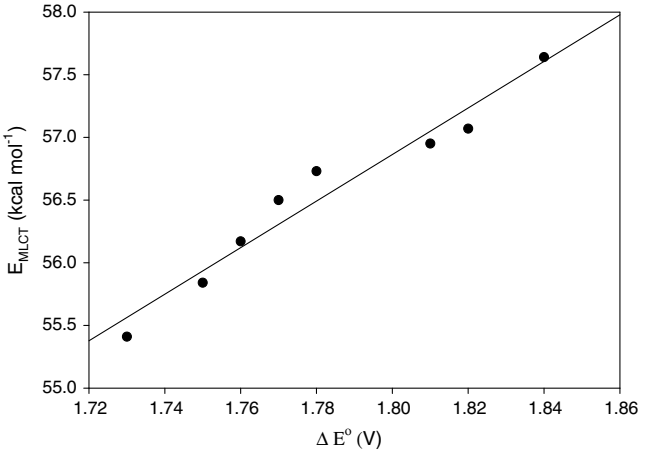

Fig. 4. Linear correlation between MLCT band energies and ΔE^0 (V).

ΔE^0 ($\Delta E^0 = E^{0M}_{1/2} - \mathrm{Azo}(0/-)$) among the entire group of complexes (Fig. 4) corresponds to Eq. (1), with a correlation coefficient of 0.956. A similar correlation has been observed for bpy, arylazopyridine and arylazoimidazole complexes [6–8b].

$$E_{MLCT} = 18.6\Delta E^0 + 23.4 \quad (1)$$

Comparative electrochemistry of [Ru(L)(bpy)Cl_2] [9,10] and [Ru(L)(dppe)Cl_2] complexes showed a positive shift of ~0.3 V in the Ru(III,II) and ~0.2 V in the L(0/−1) couples of the latter complexes. A more convincing explanation is that the much weaker σ-donor strength of bis(diphenylphosphino)ethane causes the metal ion to have a significantly higher effective nuclear charge relative to that of the bipyridyl analogues, and may cause the stabilization of the metal d orbitals. For the ruthenium complexes, the difference between metal oxidation and ligand reduction ($\Delta E^0 = E^{0M}_{1/2} - \mathrm{Azo}(0/-)$) is the same for both families. Thus, the essential identity in the charge-transfer transitions is consistent.

The spectroscopic and electrochemical results may be compared with the literature reported data of 2-(arylazo)pyridine (aap) and its phosphine derivatives $[Ru(aap)_2(dppe)]^{+2}$ [29]. The data reveal that t_2(Ru) is better stabilized in the present series of complexes than in the aap complexes. This may be due to the better π-acidity of the arylamidrazone ligand system (L) than that of 2-(arylazo)pyridine (aap) derivatives.

4. Conclusions

Eight ruthenium (II) complexes, *cis*-[Ru(dppe)LCl_2], where dppe is bis(diphenylphosphino)ethane and L is an azomethine ligand, were synthesized and characterized by crystallography, spectroscopic and electrochemical methods. Cyclic voltammetry studies of the *cis*-[Ru(dppe)LCl_2] complexes showed reversible ruthenium-based oxidation–reduction processes and irreversible ligand-based reductions. The electronic effect of the substituents on the azomethine ligand was shown in the ruthenium couple. This couple is shifted to more positive potentials when stronger electron-withdrawing substituents were introduced. The electronic absorption spectra of these complexes showed a strong band in the visible region which was assigned to a (Ru(II)-to-azomethine) MLCT transition.

5. Supplementary data

CCDC 680294 contains the supplementary crystallographic data for **4**. These data can be obtained free of charge via http://www.ccdc.cam.ac.uk/conts/retrieving.html, or from the Cambridge Crystallographic Data Centre, 12 Union Road, Cambridge CB2 1EZ, UK; fax: (+44) 1223-336-033; or e-mail: deposit@ccdc.cam.ac.uk.

Acknowledgements

Authors would like to thank the Hashemite University (Jordan) for their research support. R.J.C. would like to thank the Natural Sciences and Engineering Council of Canada for its support.

References

[1] J. Reedijk, G. Wilkinson, R.D. Gillard, J.A. McCleverty (Eds.), Comprehensive Coordination Chemistry, vol. 2, Pergamon Press, Oxford, 1987, p. 73.
[2] W.T. Wong, Coord. Chem. Rev. 131 (1994) 45.
[3] (a) H.P. Ross, M. Boldaji, D.P. Rillema, C.B. Blanton, R.P. White, Inorg. Chem. 28 (1989) 1013;
(b) K. Haarmann, Master Thesis, University Fribourg, 1986.;
(c) D.P. Rillema, G. Allen, T. J Meyer, D. Conrad, Inorg. Chem. 22 (1983) 1617;
(d) J.C. Curtis, B.P. Sullivan, T.J. Meyer, Inorg. Chem. 22 (1983) 224.
[4] (a) R. Languri, J.J. Morris, W.C. Stanley, E.T. Bell-Loncella, M. Turner, W.J. Boyko, C.A. Bessel, Inorg. Chim. Acta 315 (2001) 53;

(b) X.-J. Yang, C. Janiak, J. Heinze, F. Drepper, P. Mayer, H. Piotrowski, P. Klüfers, Inorg. Chim. Acta 318 (2001) 103.
[5] W. Kaim, Coord. Chem. Rev. 219–221 (2001) 463.
[6] T.K. Misra, D. Das, C. Sinha, P. Ghosh, C.K. Pal, Inorg. Chem. 37 (1998) 1672.
[7] (a) B.K. Santra, G.A. Thakur, P. Pramanic, G.K. Lahiri, Inorg. Chem. 35 (1996) 3050;
(b) J. Chakravarty, S. Bhattacharya, Trans. Met. Chem. 20 (1995) 138;
(c) M. Kakoti, S. Chaudhury, A.K. Deb, S. Goswami, Polyhedron 12 (1993) 783.
[8] (a) N. Bag, G.K. Lahiri, A. Chakravorty, Inorg. Chem. 31 (1992) 40;
(b) B.K. Ghosh, A. Chakravorty, Coord. Chem. Rev. 95 (1989) 239.
[9] M. Al-Noaimi, H. Saadeh, S. Haddad, M. El-Barghouthi, M. El-khateeb, R. Crutchley, Polyhedron 26 (2007) 3675.
[10] M. Al-Noaimi, R.J. Abdel-Jalil, S. Haddad, R. Al-Far, R.J. Crutchley, Inorg. Chim. Acta 359 (2006) 2395.
[11] (a) M. Berthod, G. Mignani, G. Woodward, M. Lemaire, Chem. Rev. 105 (2005) 1801;
(b) Q. Xia, H. Ge, Z. Liu, K. Su, Chem. Rev. 105 (2005) 1603.
[12] (a) M. Rahman, P. Prince, J. Steed, K. Hii, Organometallics 21 (2002) 4927;
(b) P. Braunstein, F. Naud, A. Pfaltz, S. Rettig, Organometallics 19 (2000) 2676;
(c) W. Baratta, E. Herdtweck, K. Siega, M. Toniutti, P. Rigo, Organometallics 24 (2005) 1660;
(d) T. Ohkuma, C. Sandoval, R. Srinivasan, Q. Lin, Y. Wei, K. Muniz, R. Noyori, J. Am. Chem. Soc. 127 (2005) 8288.
[13] A. Yu, E.A.S. Litke, A.S. Litke, T.V. Mezentseva, Y.M. Grigor'ev, G.N. Lyalin, Russ. J. Gen. Chem. 72 (2002) 1164.
[14] N.F. Eweiss, A. Osman, J. Heterocycl. Chem. 17 (1980) 1713.
[15] T. Gennett, D.F. Milner, M.J. Weaver, J. Phys. Chem. 89 (1985) 2787.
[16] (a) M. Kejeik, M. Danek, F. Hartl, J. Electroanal. Chem. 317 (1991) 179;
(b) C. Evans, Ph.D. Thesis Carleton University, 1997.
[17] Bruker, Programs SAINT-NT, version 6.0; SAINT, version 7.12A; SADABS, version 2.10; XPREP, version 5.1. Bruker AXS Inc., Madison,WI, USA, 2003.
[18] G.M. Sheldrick, Acta Crystallogr., Sect. A: Fund, Crystallogr. 46 (1990) 467.
[19] G.M. Sheldrick, SHELXS-97 (Release 97-2), University of Göttingen, Germany, 1997.
[20] (a) S.L. Queiroz, A.A. Batista, G. Oliva, M.P.T. Gambardella, R.H.A. Santos, K.S. MacFarlane, S.J. Rettig, B.R. James, Inorg. Chim. Acta 267 (1998) 209;
(b) A.A. Batista, L.A. Cordeiro, G. Oliva, O.R. Nascimento, Inorg. Chim. Acta 258 (1997) 131.
[21] (a) I. Romero, M. Rodrı'guez, A. Llobet, M. Collomb-Dunand-Sauthier, A. Deronzier, T. Parella, H. Stoeckli-Evans, J. Chem. Soc., Dalton Trans. (2000) 1689;
(b) J. Polam, L. Porter, J. Coord. Chem. 29 (1993) 109;
(c) M. Akita, Y. Takahashi, S. Hikichi, Y. Moro-oka, Inorg. Chem. 40 (2001) 169.
[22] I. Wyman, K. Robertson, T. Cameron, J. Swarts, M. Aquino, Inorg. Chim. Acta 359 (2006) 3092.
[23] (a) T.K. Misra, D. Das, C. Sinha, P. Ghosh, C.K. Pal, Inorg. Chem. 37 (1998) 1672;
(b) P.K. Santra, T.K. Misra, D. Das, C. Sinha, A.M.Z. Slawin, J.D. Woollins, Polyhedron 18 (1999) 2869.
[24] S. Goswami, L.F. Falvello, A. Chakravorty, Inorg. Chem. 26 (1987) 3365.
[25] (a) S. Goswami, A.R. Chakravarty, A. Chakravorty, Inorg. Chem. 21 (1982) 2173;
(b) B.K. Ghosh, A. Chakravorty, Coord Chem. Rev. 95 (1989) 239;
(c) B.P. Sullivan, D. Salmon, T.J. Meyer, Inorg. Chem. 17 (1978) 3334.
[26] (a) T.K. Misra, D. Das, C. Sinha, P. Ghosh, C.K. Pal, Inorg. Chem. 37 (1998) 1672;
(b) S. Goswami, A.R. Chakravarty, A. Chakravorty, Inorg Chem. 21 (1982) 2173;
(c) B.K. Ghosh, A. Chakravorty, Coord. Chem. Rev. 95 (1989) 239.
[27] P. Mosher, G. Yap, R. Crutchley, Inorg. Chem. 40 (2001) 550.
[28] (a) R. Crutchley, B. Lever, Inorg. Chem. 2 (1982) 2276;
(b) R.J. Crutchley, K. McCaw, F.L. Lee, E.J. Gabe, Inorg. Chem. 29 (1990) 2576.
[29] S. Goswami, A.R. Chakravarty, A. Chakravorty, Inorg. Chem. 21 (1982) 2737.

Polyhedron 27 (2008) 2705–2709

Contents lists available at ScienceDirect

Polyhedron

journal homepage: www.elsevier.com/locate/poly

Studies on an enantiomeric pair of dimeric copper(II) metallomacrocyclic complexes

Wei Huang *, Zhaolian Chu, Juechao Jiang

State Key Laboratory of Coordination Chemistry, Coordination Chemistry Institute, School of Chemistry and Chemical Engineering, Nanjing University, Nanjing 210093, PR China

ARTICLE INFO

Article history:
Received 15 April 2008
Accepted 14 May 2008
Available online 26 June 2008

Keywords:
Chiral ligand
Enantiomeric pair
Dimeric copper(II) complex
Metallomacrocyclic complex
Circular dichroism

ABSTRACT

An enantiomeric pair of [1+2] dimeric copper(II) metallomacrocyclic complexes, (*S*,*S*)-**1** and (*R*,*R*)-**2**, prepared from the cleavage of Schiff base C=N double bonds and ring-degradation of their respective chiral [3+3] macrocyclic ligands, are studied in this paper. X-ray single-crystal diffraction determination for (*S*,*S*)-**1** and (*R*,*R*)-**2** reveals that novel dimeric structures are formed where two complementary weak Cu–O coordinative bonds between the formaldehydo O atoms and the copper(II) centers are present and the separations between the dimeric copper(II) centers are 5.546(4) Å in (*S*,*S*)-**1** and 5.555(3) Å in (*R*,*R*)-**2**. The intrinsic chiral differences of these two copper(II) complexes are demonstrated by their circular dichroism (CD) spectra.

© 2008 Elsevier Ltd. All rights reserved.

1. Introduction

Macrocyclic Schiff bases and related polyamine derivatives have been extensively studied since the first syntheses of homodinuclear macrocyclic complexes via template condensation in the beginning of the 1970s [1]. Depending on the shape of the formyl and amino precursors and/or the metal ion template used, different ring sizes can be attained during the cyclization reaction. The cleavage of Schiff base C=N double bonds and the ring-degradation of macrocycles often take place due to the size matching effect of the macrocycles, the restriction of the coordination geometry of the central metals and the counterions used. A newly published review paper on recent developments of compartmental macrocyclic Schiff bases [2] related polyamine derivatives and some other previous reviews can be found in the literature [3–10].

In our systematic work, a variety of chiral and achiral metallomacrocyclic complexes have been synthesized by sodium(I) template condensation [11–18]. We have newly acquired [2+2], [2+1] and [1+2] kinds of ring-contraction metal complexes from chiral or racemic [3+3] macrocyclic ligands [19], including [2+2] dinuclear macrocyclic copper(II) and [2+1] compartmental dinuclear copper(II) complexes produced by using $Cu(NO_3)_2 \cdot 3H_2O$ as the metal source. In this paper, we report a novel enantiomeric pair of dimeric [1+2] copper(II) metallomacrocyclic complexes (*S*,*S*)-**1** and (*R*,*R*)-**2**, obtained using $Cu(OAc)_2 \cdot 3H_2O$ as the metal source.

2. Experimental

2.1. Materials and measurements

The enantiopure (1*R*,2*R*) and (1*S*,2*S*) cyclohexane-1,2-diamines were purchased directly from Aldrich. 4-Chloro-2,6-diformylphenol was prepared by an improved oxidation method using active manganese(IV) dioxide [20]. The [3+3] macrocyclic compounds were synthesized *via* the sodium(I) template Schiff base condensation of 4-chloro-2,6-diformylphenol and the corresponding chiral cyclohexane-1,2-diamines, as reported previously [19]. The other reagents were of analytical grade from commercial sources and were used without any further purification.

Elemental analyses were measured with a Perkin–Elmer 1400C analyzer. Infrared spectra (4000–400 cm^{-1}) were collected on a Nicolet FT-IR 170X spectrophotometer at 25 °C using KBr plates. Electrospray ionization mass spectra (ESI-MS) were recorded on a Finnigan MAT SSQ 710 mass spectrometer in the scan range 100–1200 amu. UV–Vis spectra were recorded on a Shimadzu UV-3100 double-beam spectrometer using a Pyrex cell with a path length of 10 mm at room temperature. The circular dichroism (CD) spectra were measured with a JASCO J-810 spectropolarimeter using the same solutions as those for the UV–Vis determination. TGA–DTA data were recorded by a CA Instruments DTA–TGA 2960 type simultaneous analyzer heating from 20.00 °C to 700.00 °C at 10 °C/min. The optical rotation values were determined via a WZZ-115 digital auto-polarimeter.

2.2. Preparation for complexes (*S*,*S*)-**1** and (*R*,*R*)-**2**

As illustrated in Scheme 1, the (*S*,*S*) and (*R*,*R*) [3+3] macrocyclic ligands (0.0788 g, 0.1 mmol) were dissolved in 20 mL ethanol,

* Corresponding author. Tel.: +86 25 83686526; fax: +86 25 83314502.
E-mail address: whuang@nju.edu.cn (W. Huang).

0277-5387/$ - see front matter © 2008 Elsevier Ltd. All rights reserved.
doi:10.1016/j.poly.2008.05.020

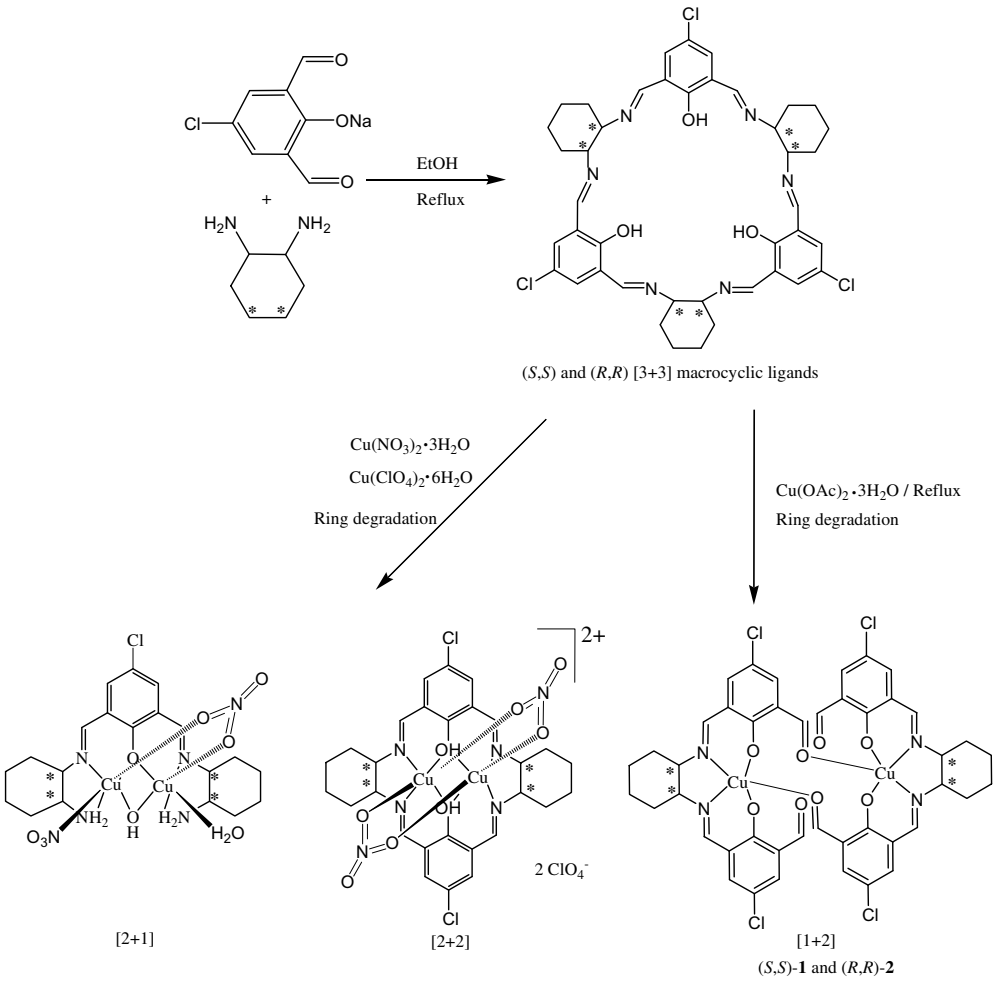

Scheme 1. Schematic illustration of the preparation of (*S*,*S*)-**1** and (*R*,*R*)-**2** in the present study.

respectively, and then an ethanol solution (10 mL) of $Cu(OAc)_2 \cdot 3H_2O$ (0.0707 g, 0.3 mmol) was added dropwise. After 2 h of reflux, the mixture was cooled to room temperature and condensed to nearly 5 mL with a rotatory evaporator. The resultant solids, (*S*,*S*)-**1** and (*R*,*R*)-**2**, were collected in yields of 73% and 75%. (*S*,*S*)-**1**: *Anal.* Calc. for $Cu_2C_{44}H_{36}N_4O_8Cl_4$: C, 51.93; H, 3.57; N, 5.51. Found: C, 51.88; H, 3.49; N, 5.56%. Main FT-IR absorptions (KBr pellets, cm^{-1}): 3452 (m), 2925 (m), 1636 (s), 1542 (s), 1434 (s), 1390 (m), 1316 (m), 1206 (m), 1179 (m), 1035 (m), 968 (w). ESI-MS in methanol: *m*/*z*: $[(S,S)\text{-}\mathbf{1} \cdot CH_3OH]^+$, 1048.8 (100%); $[(S,S)\text{-}\mathbf{1} \cdot 3H_2O]^{2+}/2$, 536.2 (40%). UV–Vis (in ethanol, nm): λ_{max} = 242, 364. $[\alpha]^{20}_D$ = +319 (*c* = 0.1 g/100 mL in ethanol). (*R*,*R*)-**2**: *Anal.* Calc. for $Cu_2C_{44}H_{36}N_4O_8Cl_4$: C, 51.93; H, 3.57; N, 5.51. Found: C, 51.87; H, 3.54; N, 5.49%. Main FT-IR absorptions (KBr pellets, cm^{-1}): 3452 (m), 2924 (m), 1636 (s), 1543 (s), 1434 (s), 1390 (m), 1316 (m), 1206 (m), 1179 (m), 1035 (m), 968 (w). ESI-MS in methanol: *m*/*z*: $[(R,R)\text{-}\mathbf{2} \cdot CH_3OH]^+$ 1048.8, (100%); $[(R,R)\text{-}\mathbf{2} \cdot 3H_2O]^{2+}/2$, 536.2 (37%). UV–Vis (in ethanol, nm): λ_{max} = 242, 364. $[\alpha]^{20}_D$ = −313 (*c* = 0.1 g/100 mL in ethanol). Single-crystal samples of (*S*,*S*)-**1** and (*R*,*R*)-**2** suitable for X-ray diffraction measurement were grown from an acetonitrile/ethanol (v/v = 2:1) mixture by slow evaporation in air at room temperature.

2.3. X-ray crystallographic analysis

Single crystals of (*S*,*S*)-**1** and (*R*,*R*)-**2** were glue-covered and mounted on glass fibers and used for data collection on a Rigaku Mercury CCD area-detector at 291 K using graphite mono-chromated Mo Kα radiation (λ = 0.71073 Å). The collected data were reduced by using the program CRYSTALCLEAR [21] and empirical absorption corrections were done. The original data files generated by CRYSTALCLEAR were transformed to SHELXTL97 format by the TEXSAN program [22]. The crystal systems were determined by laue symmetry and the space groups were assigned on the basis of systematic absences using XPREP. The structures were solved by direct methods and refined by the least-squares method on F^2_{obs} using the SHELXTL-PC software package [23]. All non-hydrogen atoms were refined on F^2 by the full-matrix least-squares procedure using anisotropic displacement parameters and all hydrogen atoms were geometrically located with a riding model and isotropic thermal parameters fixed to 1.2 times the equivalent isotropic *U* of their respective parent atoms (1.5 times for the oxygen atoms). All calculations were carried out with the SHELXTL-PC program package. A summary of crystal data, experimental details and refinement results for (*S*,*S*)-**1** and (*R*,*R*)-**2** is listed in Table 1. Selected bond distances and bond angles involving the copper(II) ions are given in Table 2, while versatile hydrogen bonding interactions are tabulated in Table 3.

3. Results and discussion

3.1. Syntheses and spectral characterization

In the process of metal ion complexation, the size matching effect of macrocycles, the restriction of the central metal coordination geometry and the nature of different counterions are believed to play significant roles in the macrocyclic Schiff base

Table 1
Crystallographic data and structural refinements for complexes (*S*,*S*)-**1** and (*R*,*R*)-**2**

Compound	(*S*,*S*)-**1**	(*R*,*R*)-**2**
Empirical formula	$C_{44}H_{36}Cl_4Cu_2N_4O_8$	$C_{44}H_{36}Cl_4Cu_2N_4O_8$
Formula weight	1017.67	1017.67
Crystal size (mm^3)	0.10 × 0.10 × 0.20	0.10 × 0.10 × 0.20
Crystal system	monoclinic	monoclinic
Space group	$P2_1$	$P2_1$
a (Å)	9.143(2)	9.147(2)
b (Å)	19.875(4)	19.866(4)
c (Å)	11.914(2)	11.880(2)
α (°)	90	90
β (°)	101.97(3)	101.68(3)
γ (°)	90	90
V ($Å^3$)	2118.0(7)	2114.0(7)
Z, D_{Calc} (Mg/m^3)	2, 1.596	2, 1.599
$F(000)$	1036	1036
μ (mm^{-1})	1.316	1.319
h_{min}/h_{max}	−11/10	−11/9
k_{min}/k_{max}	−21/25	−23/25
l_{min}/l_{max}	−15/15	−15/15
Reflections collected/unique (R_{int})	8292/7309 (0.0491)	8195/7651 (0.0571)
Parameters	559	559
Flack parameter	0.022(17)	0.018(13)
Maximum/minimum transmissions	0.8796/0.7787	0.8794/0.7784
Final R indices [$I > 2\sigma(I)$]	R_1 = 0.0587, wR_2 = 0.1141	R_1 = 0.0459, wR_2 = 0.1059
R indices (all data)	R_1 = 0.0702, wR_2 = 0.1190	R_1 = 0.0506, wR_2 = 0.1081
Goodness-of-fit on F^2	1.029	1.070
Maximum/minimum, $\Delta\rho$ ($e\,Å^{-3}$)	0.506/−0.451	0.534/−0.411

Table 2
Selected bond lengths (Å) and angles (°) for complexes (*S*,*S*)-**1** and (*R*,*R*)-**2**

	(*S*,*S*)-**1**	(*R*,*R*)-**2**
Cu(1)–O(1)	1.950(4)	1.942(3)
Cu(1)–O(2)	1.913(4)	1.912(3)
Cu(1)–N(1)	1.953(5)	1.958(4)
Cu(1)–N(2)	1.963(4)	1.960(3)
Cu(1)–O(7)	2.401(4)	2.400(3)
Cu(2)–O(3)	1.926(4)	1.933(3)
Cu(2)–O(4)	1.913(4)	1.917(3)
Cu(2)–N(3)	1.948(5)	1.950(4)
Cu(2)–N(4)	1.971(4)	1.968(3)
Cu(2)–O(5)	2.406(4)	2.405(3)
O(2)–Cu(1)–O(1)	90.16(18)	90.02(14)
O(2)–Cu(1)–N(1)	165.39(18)	165.21(14)
O(1)–Cu(1)–N(1)	93.07(18)	92.70(14)
O(2)–Cu(1)–N(2)	93.05(18)	92.99(14)
O(1)–Cu(1)–N(2)	175.88(19)	176.24(14)
N(1)–Cu(1)–N(2)	83.18(19)	83.83(15)
O(2)–Cu(1)–O(7)	98.02(18)	98.17(13)
O(1)–Cu(1)–O(7)	84.86(16)	84.89(12)
N(1)–Cu(1)–O(7)	96.46(18)	96.55(13)
N(2)–Cu(1)–O(7)	97.23(17)	96.91(13)
O(4)–Cu(2)–O(3)	89.48(18)	89.62(14)
O(4)–Cu(2)–N(3)	176.82(18)	176.71(13)
O(3)–Cu(2)–N(3)	93.0(2)	92.96(14)
O(4)–Cu(2)–N(4)	92.54(18)	92.74(14)
O(3)–Cu(2)–N(4)	165.66(18)	165.10(13)
N(3)–Cu(2)–N(4)	84.57(19)	84.24(14)
O(4)–Cu(2)–O(5)	94.38(17)	94.49(13)
O(3)–Cu(2)–O(5)	87.91(15)	87.81(12)
N(3)–Cu(2)–O(5)	87.71(18)	87.65(13)
N(4)–Cu(2)–O(5)	106.07(17)	106.64(13)

ring-contraction and formation of the final products. In this work, when $Cu(OAc)_2 \cdot 3H_2O$ was used as the metal source to react with the chiral [3+3] macrocyclic ligands, a new type of dimeric [1+2] copper(II) metallomacrocyclic complex was isolated in relatively high yields. Here the presence of different counterions (OAc^- or NO_3^-) is supposed to be responsible for the formation of the resultant products. The formaldehydo O atoms derived from the cleavage of Schiff base C=N double bonds, which have relatively weak coordination ability, can further coordinate with the copper(II) centers, thus forming novel dimeric macrocyclic structures. In contrast, the nitrate anions occupy some of the coordination sites of central copper(II) ions in the case of the previously reported [2+2] chiral dinuclear macrocyclic copper(II) and [2+1] compartmental dinuclear copper(II) complexes (Scheme 1) [19].

Table 3
Weak C–H···O hydrogen bonding interactions (Å, °) in complexes (*S*,*S*)-**1** and (*R*,*R*)-**2**

D–H···A	D–H	H···A	D···A	∠DHA	
(*S*,*S*)-**1**					
C(7)–H(7)···O(6)	0.93	2.52	3.415(8)	162.0	2 − *x*, 1/2 + *y*, −*z*
C(29)–H(29)···O(8)	0.93	2.54	3.430(9)	159.0	1 − *x*, −1/2 + *y*, −*z*
C(31)–H(31)···O(1)	0.98	2.46	3.303(6)	144.0	−1 + *x*, *y*, *z*
(*R*,*R*)-**2**					
C(7)–H(7)···O(6)	0.93	2.52	3.414(6)	162.0	−*x*, −1/2 + *y*, −*z*
C(29)–H(29)···O(8)	0.93	2.53	3.418(6)	159.0	1 − *x*, 1/2 + *y*, −*z*
C(31)–H(31)···O(1)	0.98	2.44	3.276(5)	143.0	1 + *x*, *y*, *z*

Spectral characterization of (*S*,*S*)-**1** and (*R*,*R*)-**2** reveals that they exhibit very similar behavior except for their CD spectra and optical rotation values. Positive ESI-MS spectra in methanol solutions of (*S*,*S*)-**1** and (*R*,*R*)-**2** show predominant peaks centered at m/z = 1048.8 (see Supplementary data), which are in agreement with the presence of $[(S,S)\text{-}\mathbf{1} \cdot CH_3OH]^+$ or $[(R,R)\text{-}\mathbf{2} \cdot CH_3OH]^+$ species. In addition, doubly charged peaks of medium intensity corresponding to $[(S,S)\text{-}\mathbf{1} \cdot 3H_2O]^{2+}/2$ or $[(R,R)\text{-}\mathbf{2} \cdot 3H_2O]^{2+}/2$ species, at m/z = 536.2, are also observed. All the ESI-MS peaks have been calculated and verified by using the numbers and natural isotopic abundances of the atoms [24].

In their UV–Vis spectra (inset in Fig. 1), the intense adsorption peak at 242 nm is assigned to the π–π* transition of the phenolic rings and the band at 364 nm is assigned to the π–π* transition of the azomethine chromophore. The sign patterns of the CD spectra suggest an intrinsic chiral difference of the enantiomeric pair. It is found that (*S*,*S*)-**1** gives cotton effects that are the mirror image of (*R*,*R*)-**2** (Fig. 1). The first cotton effect of (*S*,*S*)-**1** is positive, but for (*R*,*R*)-**2**, it is negative. In contrast to the corresponding electronic absorption band at 364 nm, their CD bands split into 356 (+) nm and 423 (−) nm with opposite cotton effects, which can be attributed to the split π–π* azomethine transition. On the other hand, one CD peak appears at 273 nm, corresponding to the UV–Vis absorption at 242 nm. In addition, there is a weak d–d transition

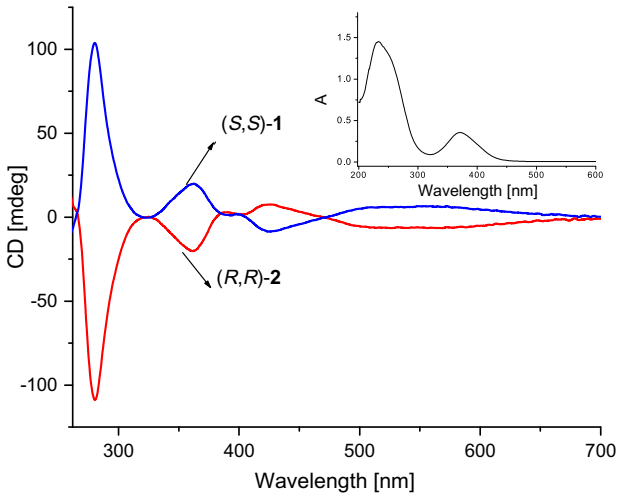

Fig. 1. CD and UV–Vis (inset) spectra of (*S*,*S*)-**1** and (*R*,*R*)-**2** in ethanol.

absorption observed in the long wavelength range at 500–700 nm. The sign patterns of the CD spectra suggest that conformers of negative chirality predominate in the solutions of the [3+3] (*R*,*R*)-macrocycle, whereas conformers of positive chirality predominate in those of the [3+3] (*S*,*S*)-macrocycle.

Both complexes show similar thermal stability because of the same molecular formulae. They are stable in the temperature range 293–571 K, and then a continuous weight loss is found, indicative of the decomposition of the copper(II) complexes.

3.2. Crystal structures of (*S*,*S*)-**1** and (*R*,*R*)-**2**

The molecular structures of (*S*,*S*)-**1** and (*R*,*R*)-**2**, with the atom-numbering scheme, are shown in Fig. 2. The X-ray crystal structural studies indicate that they have the same chiral space group $P2_1$ and their unit cell parameters are identical within experimental error. However, the carbon atoms of the cyclohexane-1,2-diamine moieties in (*S*,*S*)-**1** and (*R*,*R*)-**2** present different configurations, in which all four chiral carbon atoms are in the *S* configuration in (*S*,*S*)-**1** and in the *R* configuration for (*R*,*R*)-**2**, which are in agreement with those of the starting materials. Reasonable Flack parameters

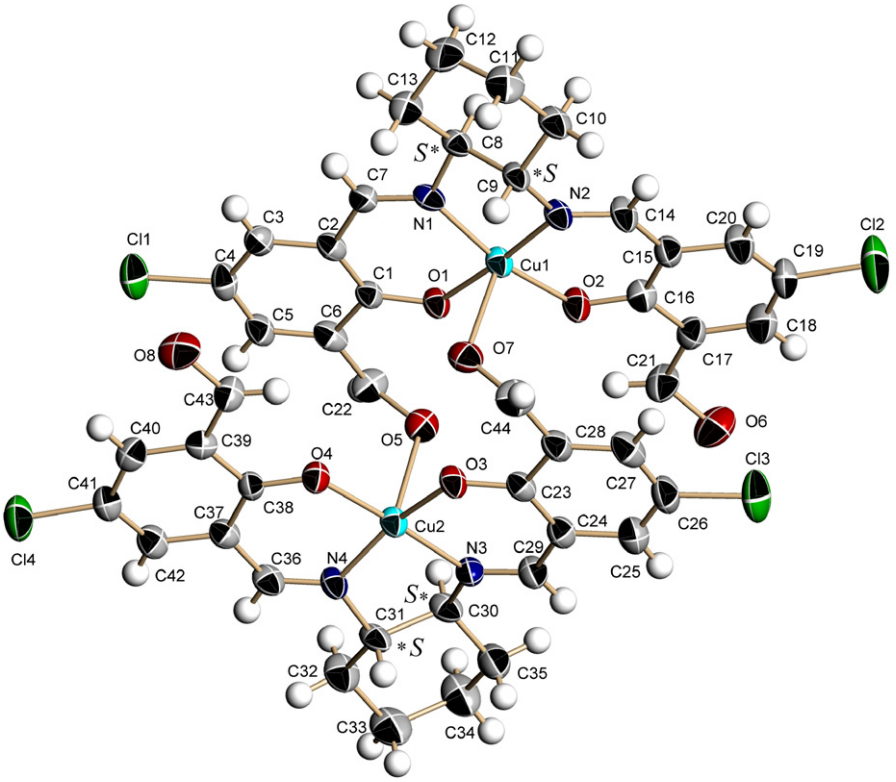

Fig. 2. ORTEP diagram (50% thermal probability) of the molecular structure of (*S*,*S*)-**1** with the atom-numbering scheme, where the chiral carbon atoms are marked.

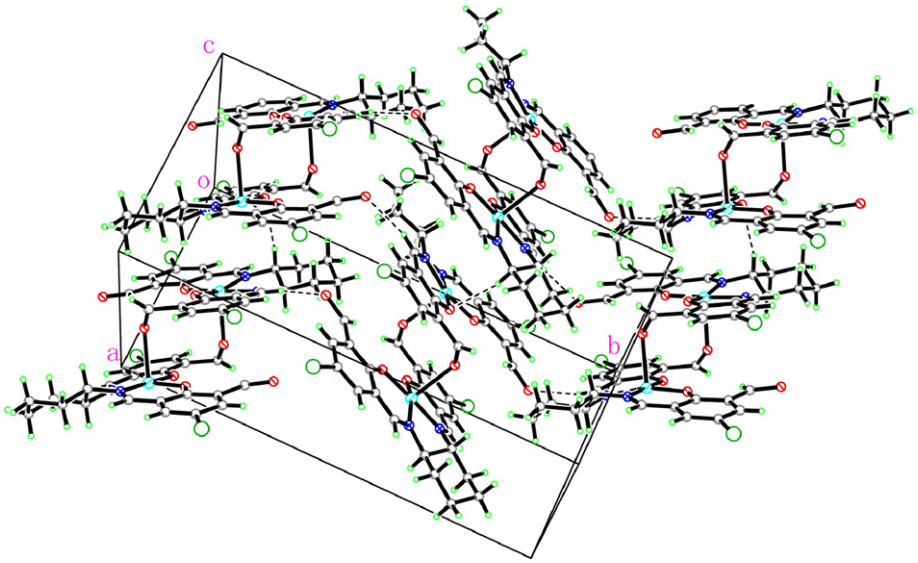

Fig. 3. A crystal packing view of (*S*,*S*)-**1**, together with the unit cell.

0.022(17) in (*S*,*S*)-**1** and 0.018(13) in (*R*,*R*)-**2** demonstrate the right specification of chirality [25].

Each molecular structure consists of a dimer of mononuclear copper(II) units, including the [1+2] compartmental Schiff base. The monomers are linked by two complementary weak Cu–O coordinative bonds where the formaldehydo O atoms act as donors. Each copper(II) center in (*S*,*S*)-**1** and (*R*,*R*)-**2** shows a five-coordinate pyramidal coordination geometry, where two imino N atoms and two phenolato O atoms constitute the basal plane, with Cu–N bond lengths in the range 1.953(5)–1.963(4) Å and Cu–O bond lengths in the range 1.912(3)–1.950(4) Å. The geometry of the coordination basal planes of the (*S*,*S*)-**1** and (*R*,*R*)-**2** monomers is comparable with a previously reported six-coordinate mononuclear Mn(II) complex [26]. However, each apical position of coordination of (*S*,*S*)-**1** and (*R*,*R*)-**2** is occupied by one formaldehydo O atom from another moiety, with a relatively weak coordination ability: longer Cu–O apical bond lengths of 2.401(4) and 2.400(3) Å are observed for (*S*,*S*)-**1** and (*R*,*R*)-**2**, respectively. Each macrocycle in (*S*,*S*)-**1** and (*R*,*R*)-**2** is essentially coplanar and the separations between the dimeric copper(II) centers are 5.546(4) Å in (*S*,*S*)-**1** and 5.555(3) Å in (*R*,*R*)-**2**. The dihedral angles between the intramolecular phenolic planes are 8.3° and 5.8° in (*S*,*S*)-**1** and 8.1° and 5.4° in (*R*,*R*)-**2**. The dihedral angles between the phenolic planes from each compartmental half-macrocycle are 2.4–6.4° in (*S*,*S*)-**1** and 2.6–6.2° in (*R*,*R*)-**2**.

Additionally, the hydrogen-bonding patterns in (*S*,*S*)-**1** and (*R*,*R*)-**2** are identical, in which C–H···O hydrogen bonds play an important role in the crystal packing of the complexes (Fig. 3). Atoms O(6) and O(8) form intermolecular C–H···O hydrogen bonds with the imino hydrogen atoms. In addition, the phenolato oxygen atom O(1) forms a C–H···O hydrogen bond with the hydrogen atom bonded to atom C(31) of the chiral cyclohexane-1,2-diamine.

4. Conclusion

By using $Cu(OAc)_2 \cdot 3H_2O$ as the metal source, an enantiomeric pair of [1+2] dimeric copper(II) metallomacrocyclic complexes, (*S*,*S*)-**1** and (*R*,*R*)-**2**, were obtained by means of the cleavage of Schiff base C=N double bonds and the degradation of their respective chiral [3+3] macrocyclic ligands, where novel dimeric structures are formed by two complementary weak Cu–O coordinative bonds between the formaldehydo O atoms and the copper(II) centers. These two copper(II) products are different from our previously reported [2+2] dinuclear macrocyclic copper(II) and [2+1] compartmental dinuclear copper(II) complexes yielded by using $Cu(NO_3)_2 \cdot 3H_2O$ as the metal source, although similar experimental conditions were used. The size matching effect of the macrocycles, the restriction of the coordination geometry of the copper(II) ion and the nature of counterions used (CH_3COO^- versus NO_3^-) in this comparative study are believed to determine the configuration of the resulting complexes.

Acknowledgements

W.H. would like to acknowledge the Major State Basic Research Development Programs (Nos. 2006CB806104 and 2007CB925101), the National Natural Science Foundation of China (No. 20301009) and the Scientific Research Foundation for the Returned Overseas Chinese Scholars, State Education Ministry for financial aid.

Appendix A. Supplementary data

CCDC 684881 and 684882 contain the supplementary crystallographic data for (*S*,*S*)-**1** and (*R*,*R*)-**2**. These data can be obtained free of charge via http://www.ccdc.cam.ac.uk/conts/retrieving.html, or from the Cambridge Crystallographic Data Centre, 12 Union Road, Cambridge CB2 1EZ, UK; fax: (+44) 1223-336-033; or e-mail: deposit@ccdc.cam.ac.uk. The ESI-MS spectrum of (*S*,*S*)-**1** is also attached for reference. Supplementary data associated with this article can be found, in the online version, at doi:10.1016/j.poly.2008.05.020.

References

[1] N.H. Pilkington, R. Robson, Aust. J. Chem. 23 (1970) 2226.
[2] P.A. Vigato, S. Tamburini, L. Bertolo, Coord. Chem. Rev. 251 (2007) 1311.
[3] P. Zanello, S. Tamburini, P.A. Vigato, G.A. Mazzochin, Coord. Chem. Rev. 77 (1987) 165.
[4] D.E. Fenton, P.A. Vigato, Coord. Chem. Rev. 17 (1988) 89.
[5] P.A. Vigato, S. Tamburini, D.E. Fenton, Coord. Chem. Rev. 106 (1990) 25.
[6] P. Guerriero, P.A. Vigato, D.E. Fenton, P.C. Hallier, Acta Chem. Scand. 46 (1992) 1025A.
[7] P. Guerriero, S. Tamburini, P.A. Vigato, Coord. Chem. Rev. 134 (1995) 17.
[8] A.E. Martell, J. Perutka, D. Kong, Coord. Chem. Rev. 216–217 (2001) 55.
[9] A. Erxleben, Coord. Chem. Rev. 246 (2003) 203.
[10] S. Tamburini, P.A. Vigato, Coord. Chem. Rev. 248 (2004) 1718.
[11] W. Huang, Z.L. Chu, S.H. Gou, T. Ogawa, Polyhedron 26 (2007) 1483.
[12] W. Huang, H.B. Zhu, S.H. Gou, Coord. Chem. Rev. 250 (2006) 414.
[13] W. Huang, D.H. Hu, S.H. Gou, S. Chantrapromma, H.K. Fun, Y. Xu, Q.J. Meng, Inorg. Chim. Acta 342 (2003) 9.
[14] W. Huang, S.H. Gou, H.F. Qian, D.H. Hu, S. Chantrapromma, H.K. Fun, Q.J. Meng, Eur. J. Inorg. Chem. (2003) 947.
[15] W. Huang, S.H. Gou, D.H. Hu, S. Chantrapromma, H.K. Fun, Q.J. Meng, Inorg. Chem. 41 (2002) 864.
[16] W. Huang, S.H. Gou, D.H. Hu, S. Chantrapromma, H.K. Fun, Q.J. Meng, Inorg. Chem. 40 (2001) 1712.
[17] S.H. Gou, M. Qian, Z. Yu, C.Y. Duan, X.F. Sun, W. Huang, J. Chem. Soc., Dalton Trans. 21 (2001) 3232.
[18] S.H. Gou, W. Huang, M. Qian, Q.D. Zeng, Trends Inorg. Chem. 7 (2001) 15.
[19] Z.L. Chu, W. Huang, L. Wang, S.H. Gou, Polyhedron 27 (2008) 1079.
[20] W. Huang, S.H. Gou, D.H. Hu, Q.J. Meng, Synth. Commun. 30 (2000) 1555.
[21] Molecular Structure Corporation & Rigaku Corporation, CRYSTALCLEAR, Version 1.3. MSC, 9009 New Trails Drive, The Woodlands, TX 77381-5209, USA, and Rigaku, Toyko, Japan, 2001.
[22] Molecular Structure Corporation & Rigaku Corporation, TEXSAN, Version 1.11. MSC, 9009 New Trails Drive, The Woodlands, TX 77381-5209, USA, and Rigaku, Toyko, Japan, 2000.
[23] G.M. Sheldrick, SHELXTL (Version 6.10), Software Reference Manual, Bruker AXS, Inc., Madison, Wisconsin (USA), 2000.
[24] J.D. Lee, Talanta 20 (1973) 1029.
[25] H.D. Flack, Acta Crystallogr., Sect. A 39 (1983) 876.
[26] S.R. Korupoju, N. Mangayarkarasi, S. Ameerunisha, E.J. Valente, P.S. Zacharias, J. Chem. Soc., Dalton Trans. (2000) 2845.

Polyhedron 27 (2008) 2710–2720

Contents lists available at ScienceDirect

Polyhedron

journal homepage: www.elsevier.com/locate/poly

Preparation and *cis*-to-*trans* transformation study of square-planar $[Pt(L_n)_2Cl_2]$ complexes bearing cytokinins derived from 6-benzylaminopurine (L_n) by view of NMR spectroscopy and X-ray crystallography

Lucie Szüčová [a], Zdeněk Trávníček [a,*], Igor Popa [a,b], Jaromír Marek [a,c]

[a] Department of Inorganic Chemistry, Faculty of Science, Palacký University, CZ-771 47 Olomouc, Czech Republic
[b] Laboratory of Growth Regulators, Palacký University and Institute of Experimental Botany AS CR, CZ-783 71 Olomouc, Czech Republic
[c] Institute of Experimental Biology, Faculty of Science, Masaryk University, CZ-625 00 Brno, Czech Republic

ARTICLE INFO

Article history:
Received 8 April 2008
Accepted 20 May 2008
Available online 24 June 2008

Keywords:
Pt(II) complexes
Cytokinins
NMR spectroscopy
X-ray structures
In vitro cytotoxicity

ABSTRACT

Mononuclear, square-planar platinum(II) complexes involving derivatives of aromatic cytokinins as the ligands, and having the general formula *cis*-$[Pt(L_n)_2Cl_2]$ (**1–3**) and *trans*-$[Pt(L_n)_2Cl_2]$ (**4–6**), where $n = 1–3$, L_1 = 2-chloro-6-(benzylamino)-9-isopropylpurine, L_2 = 2-chloro-6-[(4-methoxybenzyl)amino]-9-isopropylpurine and L_3 = 2-chloro-6-[(2-methoxybenzyl)-amino]-9-isopropylpurine, have been synthesized and characterized by elemental analysis, MALDI-TOF mass, FT IR, ^1H, ^{13}C, ^{15}N and ^{195}Pt NMR spectral measurements. Dynamic *cis*-to-*trans* isomerization process of complex **1** in *N*,*N*′-dimethylformamide (DMF) has been investigated by means of multinuclear NMR spectroscopy. The solid-state structures of **1, 4** · $(DMF)_2$, and **5** have been determined by single crystal X-ray analysis. X-ray structures revealed that the heterocyclic ligands are coordinated to platinum *via* nitrogen atom N(7) in all the complexes studied. *In vitro* cytotoxicity of the prepared complexes against MCF7, G361, K562, and HOS has been evaluated. Owing to low solubility of the complexes in water, the cytotoxicity has been only tested up to 5 μM concentration. Unfortunately, all complexes have been found to be non-cytotoxic in the accessible concentration range.

© 2008 Elsevier Ltd. All rights reserved.

1. Introduction

Nowadays, there is indisputable fact that a platinum drug called *Cisplatin*, i.e. *cis*-diamminedichloridoplatinum(II), of which the cytotoxic effects were discovered by Rosenberg et al. in the 1960s [1], and some its derivatives, represent a unique class of antineoplastic drugs used in current chemotherapy [2,3]. A high number of recently prepared *cis* and/or *trans*-$[Pt(L)_2Cl_2]$ (L = amine) complexes showed the possibility to inhibit cell division and growth of cancer cells [4]. This attribute initiated a great interest in the potential application of these inorganic substances in the treatment of tumors [4]. At present, novel potential platinum-based anticancer agents are still intensively studied with the intention to improve their therapeutic profiles to overcome their side effects and acquired resistance to the drugs [5,6]. Thus, an identification of *cis*/*trans* isomers was found to play a crucial role in the characterization of the above mentioned types of Pt(II) complexes because *cis* and *trans* isomers were found to possess substantially different cytotoxic effects when tested against various cancer cell lines [7]. This fact gave rise the reason to study the stereochemistry and geometric isomerism of square-planar complexes of the type $[Pt(L)_2X_2]$ (where L = a monodentate *N*-donor ligand, X = halide) in solid state as well as in solution. Above all, *cis*-to-*trans* isomerization of square–planar Pt(II) complexes in solution is still a subject of great interest. The formation of the *trans* isomer in a process which was supposed to give the *cis* isomer gave impulse to focus on this phenomenon, especially if this effect was already observed and determined, e.g. for $[Pt(L)_2Cl_2]$ complexes with L = aniline, 2,5-dimethyl-aniline or *p*-toluidine [8], cyclobutylamine [9], cyclohexylamine [10], and cycloheptylamine [11], Moreover, *cis*-to-*trans* isomerization reactions of $[Pt(L)_2X_2]$ complexes, where X = Cl, Br or NO_3^-, and L = pyridine or pyrimidine [12,13], ketoxime [14], and pyridine [15], were also previously reported. Generally, it may be concluded that the situation regarding the isomerization process may be a bit complicated in a solution mainly because of the fact that *trans*-isomers may be formed unexpectedly during the synthetic pathway or re-crystallization of *cis*-isomers from some solvents [9,10]. For that reason, the monitoring of *cis*-isomer behavior in solution was showed to be very contributing. For instance, *cis* and *trans*-$[Pt(amine)_2I_2]$ complexes were studied using ^{195}Pt NMR spectrometry in DMF and their *cis*-to-*trans* isomerization was observed [16]. Similarly, the geometric isomers distribution in case of platinum(II) complexes of the type $[M(L)_2X_2]$, where M = Pt or Pd, L = *N*-benzoyl-*N*′-propylthiourea, X = Cl, Br or I, in chloroform was studied by ^{195}Pt and ^1H NMR

* Corresponding author. Tel.: +420 585634944; fax: +420 585634954.
E-mail address: zdenek.travnicek@upol.cz (Z. Trávníček).

0277-5387/$ - see front matter © 2008 Elsevier Ltd. All rights reserved.
doi:10.1016/j.poly.2008.05.021

spectrometry and their *cis*-to-*trans* isomerization process was also investigated [17].

Besides the above-mentioned publications regarding the *Cisplatin*-like complexes, there exists a great number of scientific papers concerning with the preparation, characterization and biological activity testing of *cis* and *trans* Pt-complexes as well as the papers describing the conditions and rules for their DNA binding. Among them, the following may be highlighted as examples, e.g. [18–21].

Based on these facts, we focused our attention on the preparation and characterization of isomerically pure Pt(II) complexes bearing derivatives of plant growth hormones called cytokinins as N-donor ligands and on their *cis*-to-*trans* isomerization processes in solutions. One group of cytokinins, i.e. a class of natural or artificial plant growth regulators discovered in the 1950s [22–24], is represented by compounds bearing a 6-benzylaminopurine moiety. Cytokinins play a very important role in plant growth and development, including the promotion of cell division, senescence and apical dominance regulation, and nutritional signals transmission [25–27]. Since the 1990s, some cytokinin derivatives based on 2,6,9-trisubstituted purine moiety have been extensively studied due to their activity in the regulation of the eukaryotic cell cycle, more specifically, due to their significant inhibition of cyclin-dependent kinases (CDKs) [28,29]. The CDKs are protein kinase enzymes playing a considerable role in regulation of the cell cycle [30]. Some of these CDK inhibitors, e.g. 2-[2-(hydroxyl-ethyl)amino]-6-benzylamino-9-methylpurine (*Olomoucine*), 2-[3-(hydroxypropyl)amino]-6-benzylamino-9-isopropylpurine (*Bohemine*), and 2-{[1-(hydroxylmethyl)-propyl]-amino}-6-benzylamino-9-isopropylpurine (*Roscovitine*, also named as seliciclib or CYC202) were also found effective against the proliferation of some human cancer cell lines both *in vitro* and *in vivo* [31,32]. The reason why we use derivatives of aromatic cytokinins and/or cyclin-dependent kinase inhibitors derived from 6-benzylaminopurine as the ligands for the preparation of transition metal complexes is that the cytotoxicity may be improved after the coordination of these organic molecules to a suitable transition metal ion, *e.g.* to Pt(II) and Pd(II) [33,34], Cu(II) [35], Zn(II) [36] or Co(II) [37], as we have found in the case of complexes prepared previously in our laboratory. Up to now, the dynamic *cis*-to-*trans* isomerization process of Pt(II) complexes involving the above-discussed organic molecules has not been investigated using NMR spectrometry yet. However, the *cis*-to-*trans* isomerization process was previously investigated in the case of Pd(II) complexes of the type $[Pd(L)_2Cl_2]$, where L = cytokinins derived from 6-benzyalminopurine [34].

In this paper, we describe the preparation of a series of isomerically pure *cis* and *trans*-Pt(II) complexes of the general formula *cis*-$[Pt(L_n)_2Cl_2]$ and *trans*-$[Pt(L_n)_2Cl_2]$, where $n = 1–3$, L_1 = 2-chloro-6-(benzylamino)-9-isopropylpurine (**1, 4**), L_2 = 2-chloro-6-[(4-methoxybenzyl)-amino]-9-isopropylpurine (**2, 5**), L_3 = 2-chloro-6-[(2-methoxybenzyl)amino]-9-isopropylpurine (**3, 6**). The complexes have been fully characterized by means of elemental analysis, MALDI-TOF, FT IR and multinuclear NMR spectra, and complexes **1**, **4** and **5** also by single crystal X-ray analysis. The complexes were also investigated for their cytotoxic effects *in vitro* against four human cancer cell lines: MCF7, K 562, G 361 and HOS. The *cis*-to-*trans* isomerization process of the complexes in DMFA solutions was studied by means of ^{1}H, ^{13}C, ^{15}N and ^{195}Pt NMR spectroscopy.

2. Experimental

2.1. Materials

$PtCl_2$ was used as received from Sigma–Aldrich Co. The organic ligands 2-chloro-6-benzylamino-9-isopropylpurine (L_1), 2-chloro-6-[(4-methoxybenzyl)amino]-9-isopropylpurine (L_2) and 2-chloro-6-[(2-methoxybenzyl)amino]-9-isopropylpurine (L_3) were prepared by methods described in the literature [34]. Schematic representations of all the ligands used in this study including atom numbering are depicted in Fig. 1. Organic solvents used for the syntheses were purchased from Lachema Co., while *N*,*N*′-dimethylformamide-d_7 (99.5%) used for NMR spectroscopy was purchased from Sigma–Aldrich Co.

2.2. Synthesis of the complexes

2.2.1. General procedure for the preparation of cis-$[Pt(L_n)_2Cl_2]$ (**1–3**), $L_n = L_1–L_3$

An appropriate ligand (1 mmol) was dissolved in chloroform (15 mL) and added to a mixture of $PtCl_2$ (0.09 g, 0.5 mmol) in the same solvent (10 mL). The reaction mixture was stirred at −18 °C for 15 days. Obtained yellow or light orange solutions were filtered and the filtrate let to stand at room temperature. Yellowish or dark

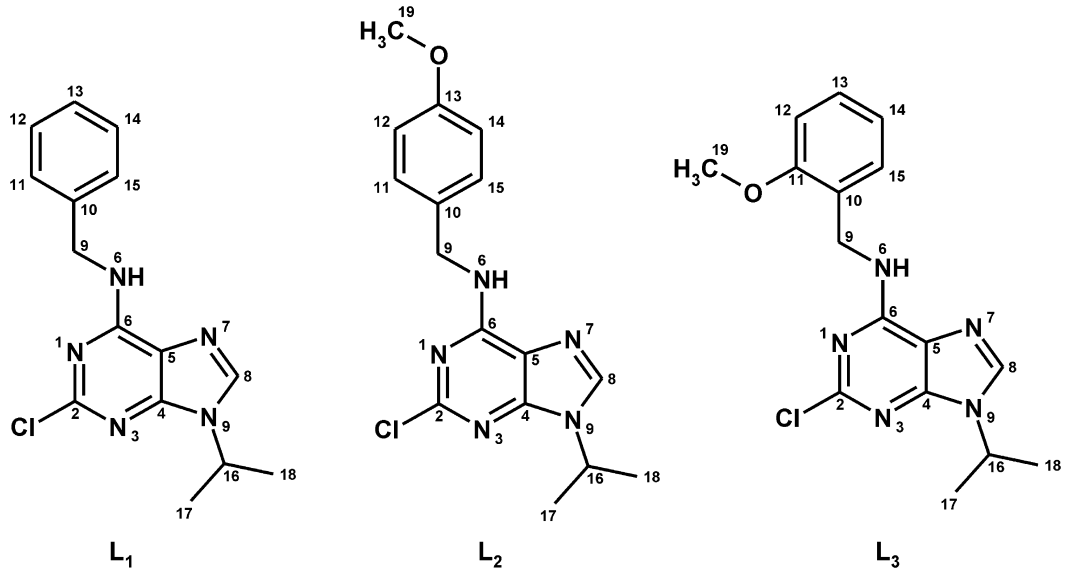

Fig. 1. A representation of organic molecules, including atom numbering scheme, used as ligands L_1–L_3.

yellow precipitates appeared after several days, which were filtered off, and dried in a vacuum desiccator over KOH.

*2.2.1.1. cis-[Pt(L$_1$)$_2$Cl$_2$] (**1**).* The complex was re-crystallized from chloroform and yellowish crystals suitable for X-ray crystallography were obtained by free evaporation of the solvent used. Yield: 76%. λ_M = 0.5 Ω cm^2 mol^{-1} in acetone, 0.8 Ω cm^2 mol^{-1} in DMF. FT-IR (KBr, cm^{-1}): 3342 (s, ν_{N-H}); 3092 (w, $\nu_{(C-H)ar}$); 1617 (vs, $\nu_{(C=N)ar}$), 1168 (m, $\nu_{(C-Cl)ar}$). FT-IR (Nujol, cm^{-1}): 348 (s, ν_{Pt-Cl}), 362 (vs, ν_{Pt-Cl}), 532 (vs, ν_{Pt-N}), 547 (s, ν_{Pt-N}). ^{1}H NMR (300 MHz, DMF-d_7, 300 K): δ 9.37 (1H, t, J = 6.0 Hz, N6H), δ 9.25 (1H, bs, C8H), δ 7.46 (2H, d, J = 7.3 Hz, C11,15H), δ 7.33 (2H, tt, J_a = 7.3 Hz, J_b = 1.5 Hz, C12,14H), δ 7.27 (1H, tt, J_a = 7.3 Hz, J_b = 1.5 Hz, C13H), δ 4.82 (1H, sep, J = 6.8 Hz, C16H), δ 4.90 (2H, s, C9H), δ 1.58 (6H, d, J = 6.8 Hz, C17,18H). ^{13}C NMR (75 MHz, DMF-d_7, 300 K): 155.10 (C6), 154.23 (C2), 149.88 (C4), 142.17 (C8), 139.32 (C10), 128.94 (C12,14), 127.84 (C11,15), 127.57 (C13), 116.37 (C5), 49.64 (C16), 45.02 (C9), 22.14 (C17,18). ^{15}N NMR (30 MHz, DMF-d_7, 340 K): 231.92 (N1), 184.54 (N9), 141.62 (N7), 99.05 (N6). ^{195}Pt (65 MHz, DMF-d_7, 300 K): −2017.88. MALDI-TOF-MS m/z: (positive mode) 906 (calc. for [M+K]$^+$), 906; 890.1 (calc. for [M+Na]$^+$) 890; 868.1 (calc. for [M+H]$^+$) 868; 833 (calc. for [{M−Cl}+H]$^+$) 833; 798 (calc. for [{M−2Cl}+H]$^+$) 798; 302 (calc. for [L+H]$^+$) 302. *Anal.* Calc. for $C_{30}H_{32}N_{10}Cl_4Pt$ (**1**): C, 41.4; H, 3.7; N, 16.1. Found: C, 41.5; H, 3.7; N, 15.9%.

*2.2.1.2. cis-[Pt(L$_2$)$_2$Cl$_2$] (**2**).* The complex was re-crystallized from chloroform. Yield: 70%. λ_M = 0.9 Ω cm^2 mol^{-1} in acetone, 2.0 Ω cm^2 mol^{-1} in DMF. FT-IR (KBr, cm^{-1}): 3316 (s, ν_{N-H}), 3103 (m, $\nu_{(C-H)ar}$); 1614 (vs, $\nu_{(C=N)ar}$), 1226 (s, ν_{Car-O}), 1033 (m, $\nu_{(C-O)alif}$), 1176 (m, $\nu_{(C-Cl)ar}$). FT-IR (Nujol, cm^{-1}): 340 (s, ν_{Pt-Cl}), 349 (m, ν_{Pt-Cl}), 521 (s, ν_{Pt-N}), 532 (s, ν_{Pt-N}). ^{1}H NMR (300 MHz, DMF-d_7, 300 K): δ 9.29 (1H, t, J = 6.1 Hz, N6H), δ 9.20 (1H, bs, C8H), δ 7.41 (2H, d, J = 8.6 Hz, C11,15H), δ 6.89 (2H, dd, J_a = 8.6 Hz, J_b = 2.2 Hz, C12,14H), δ 4.81 (1H, sep, J = 6.8 Hz, C16H), δ 4.82 (2H, s, C9H), 3.80 (3H, s, C19H), δ 1.57 (6H, d, J = 6.8 Hz, C17,18H). ^{13}C NMR (75 MHz, DMF-d_7, 300 K): 159.55 (C13), 155.10 (C6), 154.16 (C2), 149.84 (C4), 142.17 (C8), 131.00 (C10), 129.32 (C11,15), 116.38 (C5), 114.37 (C12,14), 55.51 (C19), 49.65 (C16), 44.55 (C9), 22.06 (C17,18). ^{15}N NMR (30 MHz, DMF-d_7, 340 K): 231.10 (N1), 184.47 (N9), 141.94 (N7), 100.70 (N6). ^{195}Pt (65 MHz, DMF-d_7, 300 K): −2017.36. MALDI-TOF-MS m/z: (positive mode) 966 (calc. for [M+K]$^+$), 966; 950.0 (calc. for [M+Na]$^+$) 950; 928 (calc. for [M+H]$^+$) 928; 893 (calc. for [{M−Cl}+H]$^+$) 893; 858 (calc. for [{M−2Cl}+H]$^+$) 858; 332 (calc. for [L+H]$^+$) 332. *Anal.* Calc. for $C_{32}H_{36}N_{10}O_2Cl_4Pt$ (**2**): C, 41.3; H, 3.9; N, 15.1. Found: C, 41.3; H, 3.9; N, 15.0%.

*2.2.1.3. cis-[Pt(L$_3$)$_2$Cl$_2$] (**3**).* The complex was re-crystallized from chloroform. Yield: 80%. λ_M = 1.5 Ω cm^2 mol^{-1} in acetone, 1.8 Ω cm^2 mol^{-1} in DMF. FT-IR (KBr, cm^{-1}): 3317 (s, ν_{N-H}), 3101 (w, $\nu_{(C-H)ar}$); 1620 (vs, $\nu_{(C=N)ar}$), 1243 (m, ν_{Car-O}), 1029 (m, $\nu_{(C-O)alif}$), 1163 (m, $\nu_{(C-Cl)ar}$). FT-IR (Nujol, cm^{-1}): 336 (s, ν_{Pt-Cl}), 345 (s, ν_{Pt-Cl}), 527 (s, ν_{Pt-N}), 549 (s, ν_{Pt-N}). ^{1}H NMR (300 MHz, DMF-d_7, 300 K): δ 9.32t (1H, t, J = 6.2 Hz, N6H), δ 9.15 (1H, bs, C8H), δ 7.38 (1H, bs, C15H), δ 7.29 (1H, t, J = 7.9 Hz, C13H), δ 7.06 (1H, d, J = 8.2 Hz, C12H), δ 6.86 (1H, t, J = 7.9 Hz, C14H), δ 4.79 (1H, sep, J = 6.8 Hz, C16H), δ 4.91 (2H, d, J = 6.0 Hz, C9H), δ 3.97 (3H, s, C19H), δ 1.55 (6H, d, J = 6.4 Hz, C17,18H). ^{13}C NMR (75 MHz, DMF-d_7, 300 K): 158.15 (C11), 155.12 (C6), 154.27 (C2), 149.79 (C4), 142.24 (C8), 129.17 (C13), 128.49 (C15), 126.42 (C10), 120.64 (C14), 116.37 (C5), 111.02 (C12), 56.05 (C19), 49.66 (C16), 40.90 (C9), 22.04 (C17,18). ^{15}N NMR (30 MHz, DMF-d_7, 340 K): 231.68 (N1), 184.50 (N9), 142.53 (N7), 98.32 (N6). ^{195}Pt (65 MHz, DMF-d_7, 300 K): −2023.06. MALDI-TOF-MS m/z: (positive mode) 966 (calc. for [M+K]$^+$), 966; 950.0 (calc. for [M+Na]$^+$) 950; 928 (calc. for [M+H]$^+$) 928; 332 (calc. for [L+H]$^+$) 332. *Anal.* Calc. for $C_{32}H_{36}N_{10}O_2Cl_4Pt$: C, 41.3; H, 3.9; N, 15.1. Found: C, 41.0; H, 3.9; N, 15.2%.

*2.2.2. General procedure for the preparation of trans-[Pt(L$_n$)$_2$Cl$_2$] (**4–6**), L$_n$ = L$_1$–L$_3$*

0.5 mmol of each of the *cis*-Pt isomers (**1**–**3**) was dissolved in DMF (10 mL). The solution was heated up to 50 °C and stirred for 15 min. Then, the solution was filtered and let to crystallize at the room temperature. The crystals of the complexes, in the case of **4** suitable for X-ray analysis, were obtained after 21 days.

*2.2.2.1. trans-[Pt(L$_1$)$_2$Cl$_2$] (**4**).* Dark yellow crystals suitable for X-ray crystallography were obtained by slow evaporation of the solvent. Yield: 50%. λ_M = 0.9 Ω cm^2 mol^{-1} in acetone, 2.4 Ω cm^2 mol^{-1} in DMF. FT-IR (KBr, cm^{-1}): 3331 (s, ν_{N-H}), 3110 (m, $\nu_{(C-H)ar}$); 1623 (vs, $\nu_{(C=N)ar}$), 1163 (m, $\nu_{(C-Cl)ar}$). FT-IR (Nujol, cm^{-1}): 348 (vs, ν_{Pt-Cl}), 542 (vs, ν_{Pt-N}). ^{1}H NMR (300 MHz, DMF-d_7, 300 K): δ 9.05 (1H, t, J = 6.0 Hz, N6H), δ 8.97 (1H, s, C8H), δ 7.56 (2H, dd, J_a = 7.3 Hz, J_b = 1.5 Hz, C11,15H), δ 7.35 (2H, tt, J_a = 7.3 Hz, J_b = 1.5 Hz, C12,14H), δ 7.28 (1H, tt, J_a = 7.3 Hz, J_b = 1.5 Hz, C13H), δ 4.95 (1H, sep, J = 6.8 Hz, C16H), δ 4.92 (2H, d, J = 6.2 Hz, C9H), δ 1.63 (6H, d, J = 6.8 Hz, C17,18H). ^{13}C NMR (75 MHz, DMF-d_7, 300 K): 155.15 (C6), 153.91 (C2), 149.60 (C4), 143.34 (C8), 138.77 (C10), 128.97 (C12,14), 128.05 (C11,15), 127.48 (C13), 115.99 (C5), 49.87 (C16), 45.24 (C9), 22.29 (C17,18). ^{15}N NMR (30 MHz, DMF-d_7, 340 K): 231.87 (N1), 224.80 (N3), 183.83 (N9), 133.20 (N7), 100.10 (N6). ^{195}Pt (65 MHz, DMF-d_7, 300 K): −2061.63. MALDI-TOF-MS m/z: (positive mode) 890.1 (calc. for [M+Na]$^+$) 890; 868 (calc. for [M+H]$^+$) 868; 833 (calc. for [{M−Cl}+H]$^+$) 833; 798 (calc. for [{M−2Cl}+H]$^+$) 798; 302 (calc. for [L+H]$^+$) 302. *Anal.* Calc. for $C_{30}H_{32}N_{10}Cl_4Pt$ (**4**): C, 41.4; H, 3.7; N, 16.1. Found: C, 41.5; H, 3.7; N, 16.0%.

*2.2.2.2. trans-[Pt(L$_2$)$_2$Cl$_2$] (**5**).* Orange crystals suitable for X-ray crystallography were obtained after slow evaporation of the solvent used. Yield: 65%. λ_M = 0.8 Ω cm^2 mol^{-1}. λ_M = 2.5 Ω cm^2 mol^{-1} in acetone, 3.2 Ω cm^2 mol^{-1} in DMF. FT-IR (KBr, cm^{-1}): 3300 (s, ν_{N-H}), 3120 (m, $\nu_{(C-H)ar}$); 1622 (vs, $\nu_{(C=N)ar}$), 1218 (s, ν_{Car-O}), 1028 (m, $\nu_{(C-O)alif}$), 1177 (m, $\nu_{(C-Cl)ar}$). FT-IR (Nujol, cm^{-1}): 347 (s, ν_{Pt-Cl}), 525 (s, ν_{Pt-N}). ^{1}H NMR (300 MHz, DMF-d_7, 300 K): δ 8.94 (1H, t, J = 6.0 Hz, N6H), δ 8.91 (1H, s, C8H), δ 7.49 (2H, dd, J_a = 8.6 Hz, J_b = 2.2 Hz, C11,15H), δ 6.90 (2H, dd, J_a = 8.6 Hz, J_b = 2.2 Hz, C12,14H), δ 4.94 (1H, sep, J = 6.8 Hz, C16H), δ 4.81 (2H, d, J = 6.06 Hz, C9H), 3.79 (3H, s, C19H), δ 1.64 (6H, d, J = 6.8 Hz, C17,18H). ^{13}C NMR (75 MHz, DMF-d_7, 300 K): 159.68 (C13), 155.28 (C6), 153.85 (C2), 149.60 (C4), 143.28 (C8), 130.45 (C10), 129.68 (C11,15), 116.06 (C5), 114.41 (C12,14), 55.51 (C19), 49.94 (C16), 44.95 (C9), 22.06 (C17,18). ^{15}N NMR (30 MHz, DMF-d_7, 340 K): 232.18 (N1), 224.68 (N3), 184.19 (N9), 133.66 (N7), 102.52 (N6). ^{195}Pt (65 MHz, DMF-d_7, 300 K): −2064.02. MALDI-TOF-MS m/z: (positive mode) 928 (calc. for [M+H]$^+$) 928; 893 (calc. for [{M−Cl}+H]$^+$) 893; 858 (calc. for [{M−2Cl}+H]$^+$) 858; 332 (calc. for [L+H]$^+$) 332. *Anal.* Calc. for $C_{32}H_{36}N_{10}O_2Cl_4Pt$ (**5**): C, 41.3; H, 3.9; N, 15.1. Found: C, 41.4; H, 3.8; N, 15.4%.

*2.2.2.3. trans-[Pt(L$_3$)$_2$Cl$_2$] (**6**).* Yield: 50%. λ_M = 0.9 Ω cm^2 mol^{-1} in acetone, 2.1 Ω cm^2 mol^{-1} in DMF. FT-IR (KBr, cm^{-1}): 3344 (s, ν_{N-H}), 3095 (w, $\nu_{(C-H)ar}$); 1619 (vs, $\nu_{(C=N)ar}$), 1244 (s, ν_{Car-O}), 1027 (m, $\nu_{(C-O)alif}$), 1166 (m, $\nu_{(C-Cl)ar}$). FT-IR (Nujol, cm^{-1}): 340 (s, ν_{Pt-Cl}), 530 (s, ν_{Pt-N}). ^{1}H NMR (300 MHz, DMF-d_7, 300 K): δ 9.00 (1H, t, J = 6.2 Hz, N6H), δ 9.02 (1H, s, C8H), δ 7.49 (1H, d, J = 7.9 Hz, C11,15H), δ 7.38 (1H, t, J = 7.9 Hz, C13H), δ 7.04 (1H, d, J = 8.2 Hz, C12H), δ 6.87 (1H, t, J = 7.9 Hz, C14H), δ 4.95 (1H, sep, J = 6.8 Hz, C16H), δ 4.88 (2H, d, J = 6.0 Hz, C9H), δ 3.82 (3H, s, C19H), δ 1.64 (6H, d, J = 6.8 Hz, C17,18H). ^{13}C NMR (75 MHz, DMF-d_7, 300 K):

158.03 (C11), 155.28 (C6), 154.13 (C2), 149.69 (C4), 143.37 (C8), 129.28 (C13), 128.62 (C15), 126.26 (C10), 120.73 (C14), 116.11 (C5), 111.02 (C12), 55.78 (C19), 49.88 (C16), 40.90 (C9), 22.04 (C17,18). ^{15}N NMR (30 MHz, DMF-d_7, 340 K): 231.76 (N1), 184.20 (N9), 133.98 (N7), 99.34 (N6). ^{195}Pt (65 MHz, DMF-d_7, 300 K): −2066.07. MALDI-TOF-MS *m*/*z*: (positive mode) 928 (calc. for $[M+H]^+$) 928; 893 (calc. for $[\{M-Cl\}+H]^+$) 893; 858 (calc. for $[\{M-2Cl\}+H]^+$) 858; 332 (calc. for $[L+H]^+$) 332. *Anal.* Calc. for $C_{32}H_{36}N_{10}O_2Cl_4Pt$ (**6**): C, 41.3; H, 3.9; N, 15.1. Found: C, 41.2; H, 4.0; N, 15.0%.

2.3. Physical measurements

Elemental analysis (C,H,N) was performed on the EA1112 Flash analyzer (ThermoFinnigan). Thin layer chromatography (TLC) of the prepared organic molecules was performed using a $CHCl_3$/CH_3OH/NH_4OH (8:2:0.1) mobile phase and carried out using Silica Gel 60 WF_{254} plates (Merck Co.). Positive ion MALDI-TOF mass spectra were measured in the reflection mode on a Microflex MALDI-TOF LRF20 mass spectrometer equipped with a nitrogen laser operating at 337 nm (Bruker Daltonik). MALDI-TOF-MS data of the studied complexes were measured acetone solutions (0.5 mM final concentration). Saturated solution of α-cyano-4-hydroxycinnamic acid in a 50%/0.2% acetonitrile/trifluoroacetic acid solution was used as a MALDI matrix. An aliquot of the sample solution in acetone (5 μL) and 5 μL of the matrix solution were premixed in a test tube. Then, 0.5 μL of the mixture was pipetted onto the target plate and allowed to dry at ambient temperature. Spectra were accumulated from 20 to 50 laser shots at a laser repetition rate of 10 Hz. The instrument was calibrated externally using a mixture of peptide standards. Acquired spectra were processed by FLEXANALYSIS 2.4 software (Bruker Daltonik). Post-source decay (PSD) spectra were recorded in 15 segments with each succeeding segment representing a 10% reduction in reflectron voltage. About 100 shots were averaged per segment. Segment spectra were pasted, calibrated and smoothed using the program FLEXANALYSIS 2.4. Conductivity measurements were performed on a Cond340i/SET conductometer (WTW, Germany) in DMF solution (10^{-3} M) at 25 °C. Far FT-IR spectra were measured using the Nujol technique in the range of 150–600 cm^{-1}, whilst mid FT-IR spectra were obtained by the KBr pellets technique between 400 and 4000 cm^{-1}, both using a NEXUS 670 FT-IR spectrometer (Thermo Nicolet). ^{1}H and ^{13}C NMR spectra were recorded on a Bruker Avance 300 spectrometer at 300 K. The samples were prepared by dissolving the ligands $\mathbf{L}_1$–$\mathbf{L}_3$ and complexes **1–6** in deuterated *N*,*N*′-dimethylformamide (DMF-d_7). The internal reference standard used for ^{1}H and ^{13}C NMR measurements was tetramethylsilane (TMS). ^{15}N NMR chemical shifts were measured relatively to the DMF-d_7 solvent (adjusted to 104.7 ppm). The individual ^{1}H and ^{13}C signals were assigned and refined by means of 2D correlation experiments of ^{1}H–^{1}H *gs*-COSY, ^{1}H–^{13}C *gs*-HMQC and ^{1}H–^{13}C *gs*-HMBC experiments. ^{15}N chemical shifts for the ligands $\mathbf{L}_1$–$\mathbf{L}_3$ and complexes **1–6** were obtained at natural abundance by ^{1}H–^{15}N *gs*-HMQC and ^{1}H–^{15}N *gs*-HMBC experiments and the spectra were recorded at 340 K.

2.4. X-ray crystallography

Diffraction data for single crystals of *cis*-Pt(II) complex of **1** and *trans*-Pt(II) complexes of **4** · $(DMF)_2$ and **5** were collected on an Xcalibur diffractometer (Oxford Diffraction) with Mo Kα (monochromator Enhance, Oxford Diffraction) radiation and ω-scan rotation techniques. The data were collected to maximum θ value of 25° and processed using the CRYSALIS software package (Oxford Diffraction, Ltd.) [38]. A multi-scan absorption correction integrated in the CRYSALIS software was applied on the data of all three complexes. All three structures were determined by direct methods using SHELXS-97 and refined anisotropically on F^2 using full-matrix least-squares procedure by SHELXL-97 [39]. H-atoms were positioned geometrically, with C–H distances of 0.95–1.00 Å and N–H distances of 0.88 Å, and with U_{iso}(H) values of 1.2U_{eq}(C,N). Most of atoms of the L_1 ligand in **1**, methyl groups of the isopropyl moiety in **4** · $(DMF)_2$, and all atoms of the isopropyl moiety as well as chlorine atom of the L_2 ligand in **5** were refined as disordered over two positions. Moreover, because of the disordered nature of the part of the structure in the case of **1**, isotropic restraints were placed on the anisotropic thermal parameters of some atoms of the L_1 ligand. All structural figures were made with DIAMOND [40].

2.5. Cytotoxicity testing

Cytotoxicity values of IC_{50} for complexes **1–6** and for the ligands L_1–L_3 were determined by a calcein AM assay. Human cancer cell lines *in vitro* were used as follows: malignant melanoma (G361), chronic myelogenous leukaemia (K562), osteogenic sarcoma (HOS), and breast adenocarcinoma (MCF7). The technique of the biological activity testing has been previously described in greater detail [33]. All the experiments were repeated in triplicate. The presented IC_{50} values are represented by arithmetic mean values, with a maximal deviation of 15%. All the ligands and complexes were first dissolved in DMF and then immediately diluted in water to a final DMF concentration of 0.6%.

3. Results and discussion

3.1. Synthetic aspects and conductivity measurement results

Scheme 1 illustrates the synthetic pathway that led to the preparation both L_n organic molecules, used as ligands, and *cis*-$[Pt(L_n)_2Cl_2]$ (**1–3**) and *trans*-$[Pt(L_n)_2Cl_2]$ (**4–6**) complexes. As the first step of the complex syntheses, *cis* isomers were prepared. Yellow to light orange solutions appeared after mixing the reactants at the temperature of −18 °C. Then, the reaction mixtures were filtered off in order to remove visible residues originating from initial $PtCl_2$ and let to stand at the temperature of −18 °C for next few days. Yellow precipitates, which appeared after this time period, were collected by filtration and re-crystallized from chloroform (**1–3**). *Trans* isomers were obtained after dissolving of the powdery samples of the appropriate *cis* isomers in DMF. The whole procedure was supported by heating up to 50 °C. Based on our next experiences, *trans* isomers could be also obtained by elongation of the reaction time by several weeks supported by heating (60–70 °C). Generally, it is known that a *cis-to-trans* isomerization process of square-planar Pt(II) complexes can be caused both by recrystallization of *cis* isomers from various solvents (e.g. acetone [9–11], DMF [41], $CHCl_3$ [17]) or solid state thermal heating [14].

All the complexes behave as non-electrolytes both in acetone and DMF solutions with the conductivity values found within the interval of 0.5–2.5 and 1.2–3.2 Ω cm^2 mol^{-1} in acetone, and DMF, respectively. The obtained conductivity values are consistent with the literature data obtained for other complex non-electrolytes [42].

3.2. Mass and FT IR spectral studies

The positive ion MALDI-TOF mass spectra were carried out for all complexes **1–6**. They showed molecular ion $[M+H]^+$ peaks in the spectra of complexes **1–3**, and moreover, the $[M+K]^+$ molecular adduct ions also appeared. Fig. 2 depicts the isotopic distribution of the molecular peak obtained for complex **1** compared to the calculated one obtained using the MASSLYNXTM software taking into

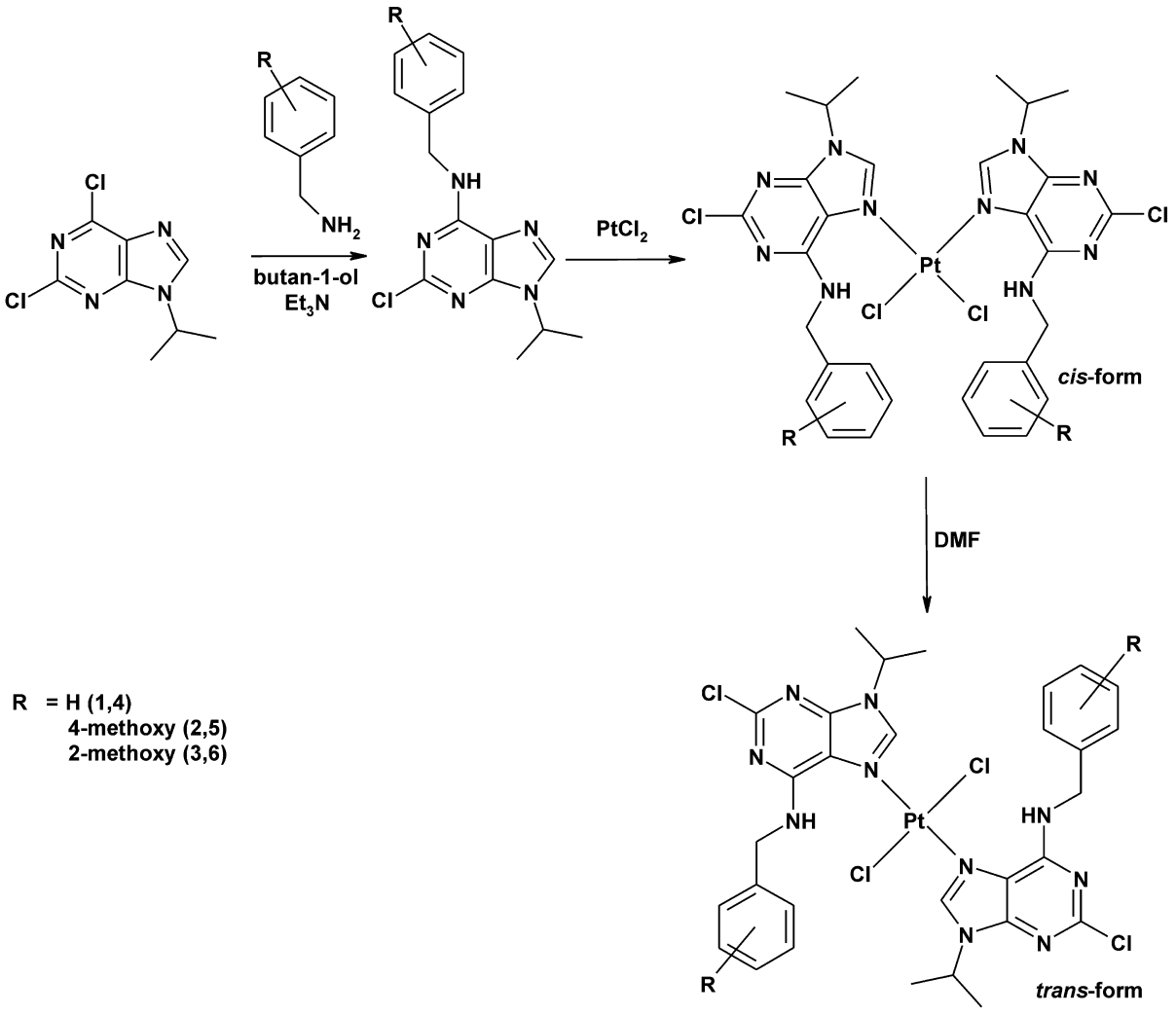

Scheme 1. Schematic representation of the synthesis of ligands and *cis* (**1**–**3**) and *trans* (**4**–**6**) Pt(II) complexes.

account the isotopic representation of all the atoms within the molecule [43]. For complexes **1–4**, there were also found $[M+Na]^+$ molecular adduct ions. Generally, the formation of adducts with Na^+ and K^+ is typical for this type of complexes [44]. All the complexes, except for **3**, showed at least two fragments, *i.e.* $[\{M-Cl\}+H]^+$ and $[\{M-2Cl\}+H]^+$. Moreover, the molecular peak of the appropriate ligand, $[L+H]^+$, appeared in all spectra of the complexes.

FT-IR spectra of both the ligands L_1–L_3 and complexes **1–6** were measured in the region of 150–4000 cm^{-1}. Characteristic bands confirming the presence of organic ligands in complexes **1–6** were observed in the region of 600–4000 cm^{-1} [45]. The bands were found and assigned as follows: strong bands between 3300 and 3342 cm^{-1} are assignable to $\nu_{(N-H)}$, weak to medium bands between 3092 and 3120 cm^{-1} are assignable to $\nu_{(C-H)ar}$, very strong bands between 1614 and 1623 cm^{-1} may be attributed to $\nu_{(C=N)ar}$ and medium bands between 1163 and 1177 cm^{-1} are assignable to $\nu_{(C-Cl)ar}$. The majority of the bands found between 660 and 900 cm^{-1} can be assigned to skeletal vibrations of a purine moiety of the organic ligands which is present in the complexes studied. Medium to strong bands between 1218 and 1244 cm^{-1} and 1027 and 1033 cm^{-1} attributable to $\nu_{(Car-O)}$, and $\nu_{(C-O)aliph}$, respectively, were found in FT IR spectra of complexes **2**, **3**, **5** and **6**, containing ligands L_2 and L_3. Some new bands appeared in the spectra of the complexes in comparison with free organic ligands in the region between 150 and 600 cm^{-1}. Strong or very strong bands between 340 and 362 cm^{-1} assignable to ν(Pt–Cl) and between 521 and 549 cm^{-1} attributable to $\nu_{(Pt-N)}$ were found [46]. For *cis*-complexes, these bands were splitted into two peaks as compared to *trans*-isomers which clearly supports the *cis*-to-*trans* transformation process in case of the Pt(II) complexes studied.

3.3. Multinuclear NMR studies

Multinuclear NMR study of complexes **1–6** and the ligands L_1–L_3 was performed by means of ^1H, ^{13}C, ^{15}N and ^{195}Pt NMR spectroscopy. Chemical shifts of the selected atoms of the free ligands L_1–L_3 and complexes **1–6**, as found in ^1H and ^{13}C NMR spectra, are given in Table 1, while the ^{15}N NMR and ^{195}Pt NMR spectral data are given in Table 2. Observed signals were assigned and refined by means of ^1H–^1H COSY, ^1H–^{13}C HMQC and ^1H–^{13}C HMBC experiments. The signals found in ^1H and ^{13}C NMR spectra confirmed the presence of organic ligands L_1–L_3 in complexes **1–6** and also proved the coordination of these organic molecules to the central Pt(II) ion. The manner of the ligand L_1–L_3 coordinations to Pt(II) can be deduced from the coordination shifts $\Delta\delta$ ($\Delta\delta = \delta_{complex} - \delta_{ligand}$) as found in both ^1H and ^{13}C NMR spectra of the free ligands and complexes. It is evident from ^1H and ^{13}C spectral data given in Table 1 that the greatest coordination shifts in ^1H NMR spectra were found for the N6H ($\Delta\delta$ = 0.35–0.94 ppm, downfield) and

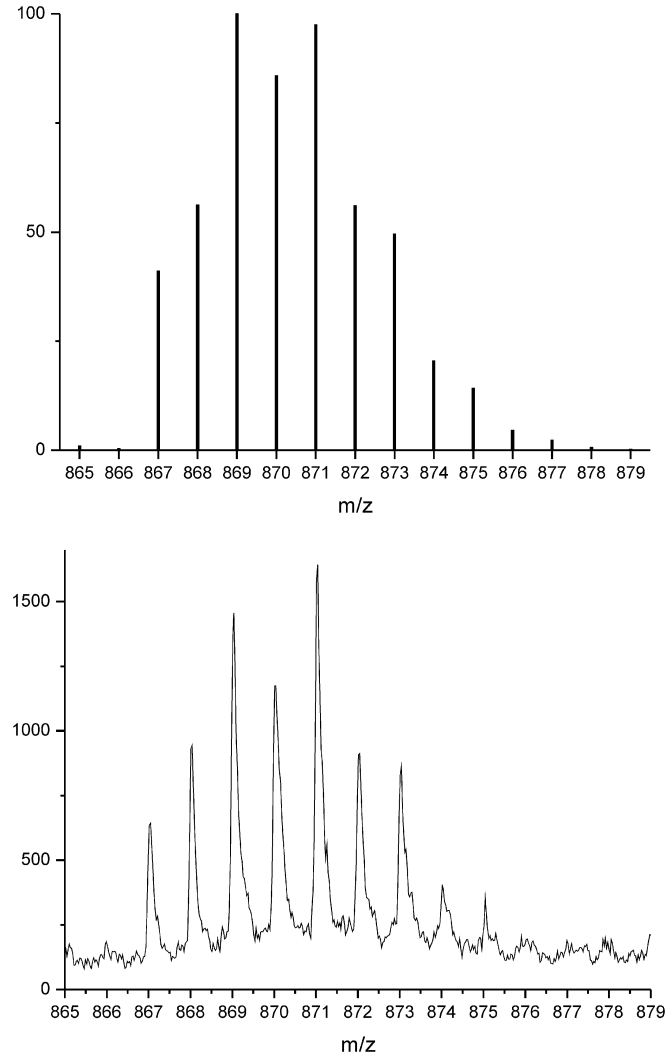

Fig. 2. A representation of the isotopic distribution of the molecular ion of **1** compared to the calculated one obtained using the MASSLYNX software taking into account isotope representation of all the atoms within the molecule.

C8H ($\Delta\delta$ = 0.65–0.97 ppm, downfield) atoms which are situated close to the N7 atom, i.e. to a position where the coordination to platinum(II) [33,34] or palladium(II) [34] can be expected on the basis of our previous findings. These results could be also supported by ^{13}C NMR spectral data, where the greatest chemical shifts were observed for the C5 ($\Delta\delta$ = 3.28–3.69 ppm, upfield) and C8 ($\Delta\delta$ = 2.13–3.33 ppm, downfield) atoms which are adjacent to a coordination site represented by the N7 atom. The signals found in ^{15}N NMR spectra were obtained at natural abundance by long-lasting two dimensional heteronuclear correlation ^{1}H–^{15}N *gs*-HMQC and ^{1}H–^{15}N *gs*-HMBC experiments. Presumable coordination *via* the N7 atom can be also supported by ^{15}N NMR spectral data given in Table 2, from which it is obvious that the greatest coordination shift as compared to the free ligands occurred at the N7 atom ($\Delta\delta$ = 97.67–106.55 ppm, upfield). The chemical shifts of N1, N3, N6 and N9 remained without significant changes, i.e. $\Delta\delta$ were found to be within the interval of 0.80–10.07 ppm that means they are non-significantly influenced by the organic ligand coordinations to platinum. The N7 atom chemical shifts observable in the spectra of the ligands and complexes demonstrably revealed that the coordination of the 6-benzylaminopurine derived ligands to the central platinum(II) ion proceeds *via* the N7 position of the purine moiety.

Generally, it is known, that very important conclusions about the oxidation state of the central Pt ion, stereochemistry, chromophore and isomer types can be obtained from ^{195}Pt NMR experiments, where the significant differences between $\delta(^{195}\text{Pt})$ chemical shifts assignable to *cis* and *trans* complexes are supposed to be observed. It can be evident from the $\delta(^{195}\text{Pt})$ chemical shifts listed in Table 2 that those ones assignable to *cis* isomers **1–3** appeared within the interval of −2017.36 and −2023.06 ppm, while the signals observed for *trans* isomers **4–6** were found between −2061.63 and −2066.07 ppm. The values obtained for complexes **1–3** are in a good agreement with those found for similar complexes of the type *cis*-[Pt(L)$_2$Cl$_2$] (L = methyl derivatives of pyridine), where the $\delta(^{195}\text{Pt})$ values were observed within the interval between −1998 and −2021 ppm [16]. With regard to the fact that we have already studied square-planar platinum(II) complexes bearing 6-benzylaminopurine moiety recently, we can state that the $\delta(^{195}\text{Pt})$ chemical shift values found for *cis*-complexes **1–3** are in good agreement with those determined for Pt(II) complexes of similar structural type and composition published previously [33]. As for *trans*-complexes **4–6**, it is interesting that the observed $\delta(^{195}\text{Pt})$ values between −2061.63 and −2066.07 ppm are shifted to higher fields in comparison with literature data given for similar type of complexes like *trans*-[Pt(L)$_2$Cl$_2$] (L = methyl derivatives of pyridine) being −1948 and −1973 ppm [15]. On the other hand, the achieved values are very close to those published elsewhere, e.g. −2101 ppm for *trans*-[Pt(NH$_3$)$_2$Cl$_2$] [47].

3.3.1. Cis-to-trans isomerization NMR study

It has been known for a long time that square-planar Pt(II) complexes with *cis* arrangement of the type *cis*-[Pt(L)$_2$X$_2$] (where L = NH$_3$ or its derivatives, X = halide) can be transformed into *trans* isomers by re-crystallization from various solvents or by their heating [8–11]. That is why, we decided to prove this ability in the case of the Pt(II) complexes **1–3** involving 6-benzylaminopurine derivatives. A series of 1D (^{1}H, ^{13}C, ^{195}Pt) and 2D (^{15}N *gs*-HMQC and ^{1}H–^{15}N *gs*-HMBC) NMR experiments were per-

Table 1
Selected ^{1}H and ^{13}C NMR spectral data (δ, ppm) for L$_1$–L$_3$ and **1–6**

Compound	^{1}H NMR (ppm)				^{13}C NMR (ppm)		
	N6H	C8H	C2	C4	C5	C6	C8
L$_1$	8.67	8.28	153.96	150.57	119.68	156.11	140.04
L$_2$	8.59	8.26	153.96	150.52	119.66	156.01	139.96
L$_3$	8.38	8.29	154.02	150.54	119.75	156.35	140.04
1 *cis*-[Pt(L$_1$)$_2$Cl$_2$]	9.37 (0.70)	9.25 (0.97)	154.23 (0.27)	149.88 (−0.89)	116.37 (−3.31)	155.10 (−1.01)	142.17 (2.13)
2 *cis*-[Pt(L$_2$)$_2$Cl$_2$]	9.29 (0.70)	9.20 (0.94)	154.16 (0.20)	149.84 (−0.68)	116.38 (−3.28)	155.10 (−0.91)	142.17 (2.21)
3 *cis*-[Pt(L$_3$)$_2$Cl$_2$]	9.32 (0.94)	9.15 (0.86)	154.27 (0.25)	149.79 (−0.75)	116.37 (−3.38)	155.12 (−1.23)	142.24 (2.20)
4 *trans*-[Pt(L$_1$)$_2$Cl$_2$]	9.05 (0.38)	8.97 (0.69)	153.91 (−0.05)	149.60 (−0.97)	115.99 (−3.69)	155.15 (−0.96)	143.34 (3.30)
5 *trans*-[Pt(L$_2$)$_2$Cl$_2$]	8.94 (0.35)	8.91 (0.65)	153.85 (−0.11)	149.60 (−0.92)	116.06 (−3.60)	155.28 (−0.73)	143.28 (3.32)
6 *trans*-[Pt(L$_3$)$_2$Cl$_2$]	9.00 (0.62)	9.02 (0.73)	154.13 (0.11)	149.69 (−0.85)	116.11 (−3.64)	155.28 (−1.07)	143.37 (3.33)

Coordination chemical shifts ($\Delta\delta = \delta_{complex} - \delta_{ligand}$) are given in parentheses.

Table 2
Selected ^{15}N NMR spectral data (δ, ppm) for $\mathbf{L_1}$–$\mathbf{L_3}$ and **1**–**6** and ^{195}Pt NMR chemical shifts obtained for **1**–**6**

Compound	N1	N3	N6	N7	N9	^{195}Pt
$\mathbf{L_1}$	227.30	224.00	93.57	239.75	178.70	
$\mathbf{L_2}$	227.32	223.69	95.32	240.15	178.57	
$\mathbf{L_3}$	227.47	223.97	89.27	240.20	178.73	
1 *cis*-$[Pt(L_1)_2Cl_2]$	231.92 (4.62)		99.05 (5.48)	141.62 (−98.13)	184.54 (5.84)	−2017.88
2 *cis*-$[Pt(L_2)_2Cl_2]$	231.10 (3.78)		100.70 (5.38)	141.94 (−98.21)	184.47 (5.90)	−2017.36
3 *cis*-$[Pt(L_3)_2Cl_2]$	231.68 (4.21)		98.32 (9.05)	142.53 (−97.67)	184.50 (5.77)	−2023.06
4 *trans*-$[Pt(L_1)_2Cl_2]$	231.87 (4.57)	224.80 (0.80)	100.10 (6.53)	133.20 (−106.55)	183.83 (5.13)	−2061.63
5 *trans*-$[Pt(L_2)_2Cl_2]$	232.18 (4.86)	224.68 (0.99)	102.52 (7.20)	133.66 (−106.49)	184.19 (5.62)	−2064.02
6 *trans*-$[Pt(L_3)_2Cl_2]$	231.76 (4.29)		99.34 (10.07)	133.98 (−106.22)	184.20 (5.47)	−2066.07

Coordination chemical shifts ($\Delta\delta = \delta_{complex} - \delta_{ligand}$) are given in parentheses.

formed during six months to obtain necessary data for the study of the *cis*-to-*trans* isomerization process in DMF. Although these measurements were performed for all complexes **1–3**, we decided to describe and interpret NMR data regarding the process for complex **1** only because the obtained results were fully comparable for all the studied complexes. Regarding the proper experiment, the sample was measured 20 min after dissolving complex **1** in DMF, and subsequently after one, three and six months. An example of the ^{1}H–^{15}N *gs*-HMBC experiment performed for complex **1** taken one month after the sample dissolution together with its comparison to the spectra of the corresponding free ligand L_1 is presented in Fig. 1A (see Supplementary data). The presence of both *cis* and *trans* isomers (i.e. complexes **1** and **3**) can be clearly seen from the last-mentioned figure. The same conclusion may be drawn from the ^{1}H NMR experiments of complex **1**. The ^{1}H NMR spectra of complex **1**, showing the integral intensities of hydrogen atoms belonging to N6 and C8 atoms measured after 20 min, and 1, 3, and 6 months, as well as proving the presence of both isomers are depicted in Fig. 3. While a trace signal (3%) belonging to the *trans*-isomer can be seen in the spectrum of complex **1** taken 20 min after dissolving of the sample in DMF, after one month, the *cis*-to-*trans* ratio changed approximately to 6:3. Subsequently, the content of *trans* isomer increased gradually and pure *trans* isomer occurred six months after the beginning of the experiment. On the basis of the above described experiments we can state that the *trans* arrangement of the studied complexes is much more stable than the *cis* one in the DMF solutions. Moreover, the performed experiments gave us clear conclusions regarding the time-dependent stability of *cis* complexes **1–3** in DMF and showed us another possibility how to prepare *trans* isomers in a pure form.

In the quest to better describe the solution behavior of *cis*-complexes **1–3**, we were also trying to determine what is occurring with the complexes in a DMF/water mixture. For that reason, complex **1** was dissolved in DMF-d_7:D_2O mixture in 9:1 (v/v) ratio, and we tried to obtain the signals of some hydroxo or aqua species {i.e *cis*-$[Pt(L_n)_2(OH)_2]$ or *cis*-$[Pt(L_n)_2(H_2O)_2]^{2+}$} that were expected to be formed after dissolving the sample in the mentioned solvent mixture. We could not use higher content of water in the mixture due to low solubility of the prepared complexes in water. The sample was measured in time intervals after 20 min, one week, and 1, 3, and 6 months. We used nearly the same experiment formerly in the case of analogous Pd(II) complexes bearing similar types of ligands, where the signals proving the presence of $[Pd(L)_2(OH)_2]$ species were detected [34]. Unfortunately, we were not successful to observe any obvious NMR signals of $(OH)^-$ group in the case of Pt(II)-complexes **1–3**. This might be caused by the fact that the studied Pt(II) complexes are even less soluble than analogous Pd(II) ones in the same solvent mixture used and the complex concentrations were under the detectable limit of the device used. However, the formation of *cis*-$[Pt(L_n)_2(OH)_2]$ or *cis*-$[Pt(L_n)_2(H_2O)_2]^{2+}$ species in the mixture used may be supported by a simple, but very sensitive, analytical experiment. $AgNO_3$ was added to the solution of complex **1** in the DMF/water (9:1) mixture after one week of standing in room temperature. After this time period, a white precipitate originating from AgCl formed and it showed that chlorine anions had to leave the complex in the solvent. To support assumption that organic ligands remain coordinated to platinum, we simultaneously performed additional NMR experiments. It has been found that complex **1** is sufficiently kinetically inert to hold the organic ligands within the inner coordination sphere of platinum, because signals belonging to the uncoordinated ligands were not detected by means of ^{1}H and ^{13}C NMR measurements. It clearly supports conclusion that *cis*-$[Pt(L_n)_2(OH)_2]$ or *cis*-$[Pt(L_n)_2(H_2O)_2]^{2+}$ species are forming in the mixture of solvents used.

3.4. X-ray molecular structures

Crystallographic data and refinement details for complexes **1**, **4** · $(DMF)_2$ and **5** are summarized in Table 3, while the selected bond lengths and angles are given in Table 4. All important hydrogen-bonding interactions were generated by PARST95 [48].

3.4.1. Molecular and crystal structures of cis-$[Pt(L_1)_2Cl_2]$ (**1**)

The molecular structure of **1** is shown in Fig. 4 (DIAMOND) [40]. The central Pt(II) ion is coordinated by two chlorido and two L_1 ligands through the N7 atoms of the adenine units forming a *cis*-square-planar coordination around the central atom. The Pt–N and Pt–Cl bond distances are comparable with the average bond lengths of 2.027(4) and 2.291(1) Å, respectively, found in related $PtCl_2N_2$ complexes deposited in the Cambridge Structural Database [49]. Most of atoms of one of two L_1 ligands are disordered over two positions. A degree of the disorder can be seen from different positions of adenine moieties and phenyl rings (see Fig. 4). The adenine moieties are turned in the plane of adenine to each other around the center of rotation lying in the N7A atom about 10.3–13.7°. If Cg1 and Cg2 are defined as the centroids of the first and second disordered phenyl rings, then the Cg1···Cg2 distance is 1.9948(2) Å and the dihedral angle between the rings is 41.8(3)°. Two adenine moieties originating from two L_1 ligands (or three, if we consider the disorder in the case of one L_1 ligand) are almost perpendicular to each other [dihedral angles are 93.6(1)° and 93.4(2)°], and the angle between the platinum coordination plane (i.e. a $PtCl_2N_2$ chromophore) and the purine moiety is 65.13(7)°, 72.80(13)° and 71.99(14)°, respectively. The platinum atom deviates significantly from the planarity of the imidazole ring of the first L_1 ligand [the out-of-plane deviation is 0.2807(3) Å] probably as the result of an intramolecular hydrogen-bonding interactions (N6–H···Cl1: N6···Cl1 = 3.275(5) Å; ∠DHA = 141°; where D = a donor atom, H = the corresponding hydrogen atom, A = an acceptor atom), while the deviations of platinum from the other two disordered imidazole rings are notably lower [0.0636(3) and 0.0745(3) Å].

In the crystal packing, the individual molecules of **1** are connected through strong intermolecular C–H···Cl hydrogen-bonding interactions (C8–H···Cl1: H···Cl1 = 2.65 Å, ∠DHA 171°; 2.54 Å,

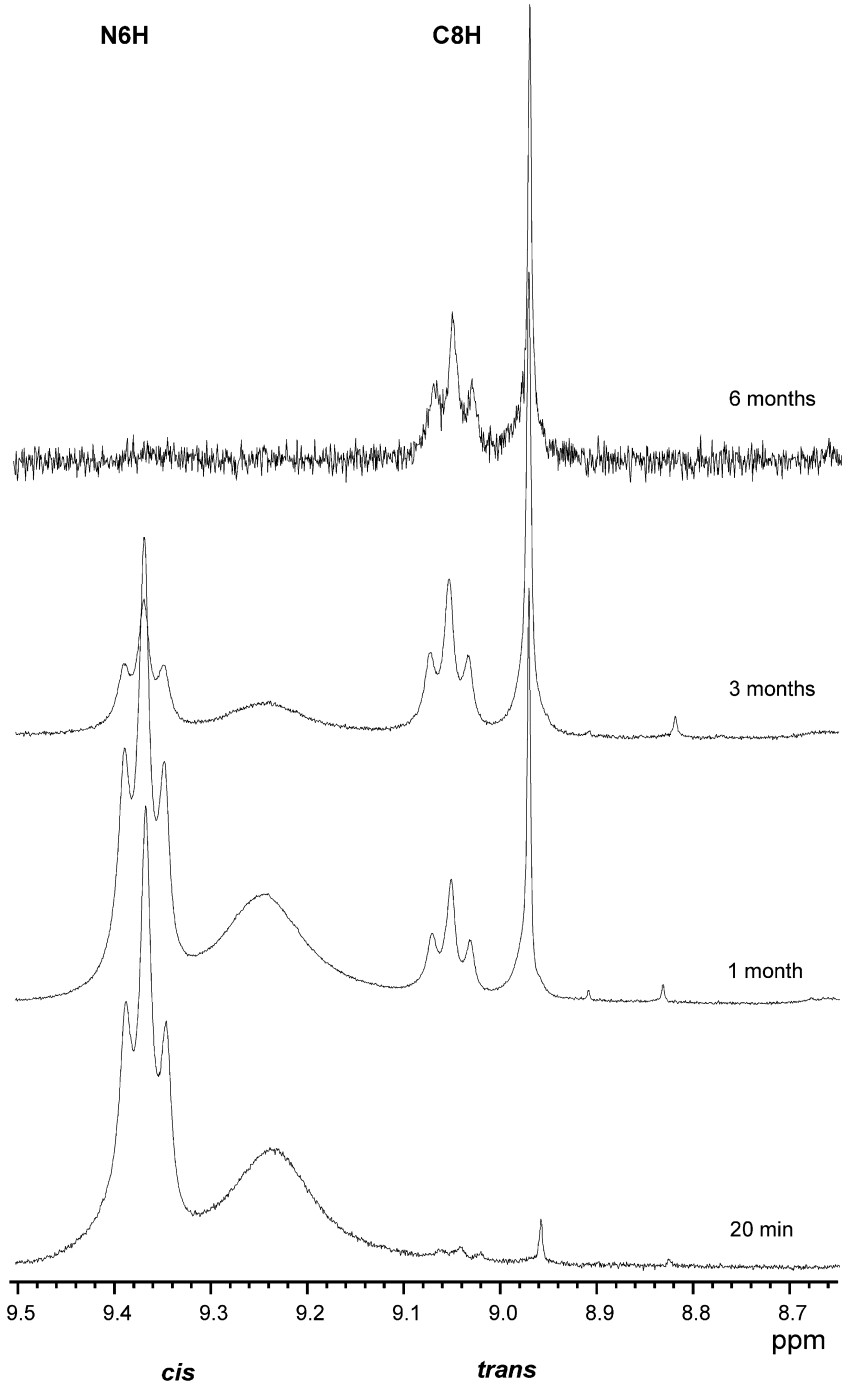

Fig. 3. Selected part of ^{1}H NMR spectra of **1** showing the transformation of *cis* into *trans* isomer of the complex based on the changes of the N6H and C8H signals in dependence on time.

178°; and 2.77 Å; 146°; respectively). The non-bonding intermolecular interactions may be considered to be the main reason of the ligand disorder. Whilst the first position of the disordered L_1 is stabilized by a π interaction [Cl3A···C5: 3.247(8) Å], the second position is stabilized by a π–π stacking interaction [the distance between adjacent parallel imidazole planes is 3.3858 Å].

3.4.2. Molecular and crystal structures of trans-[Pt(L$_1$)$_2$Cl$_2$] (4 · (DMF)$_2$)

The molecular structure of **4** · $(DMF)_2$ (see Fig. 5) revealed a centrosymmetric *trans*-square-planar complex in which the Pt(II) ion is coordinated by two chlorido and two L_1 ligands through the N7 atoms of the adenine moieties [Pt–N: 2.009(2) Å; Pt–Cl: 2.2846(7) Å; N–Pt–Cl: 91.87(7)°]. The Pt(II) ion lies slightly out of the plane of the imidazole ring [the out-of-plane deviation is 0.1332(4) Å]. Similarly to complex **1**, the L_1 ligand is also partially disordered in methyl groups of the isopropyl moiety in the crystal structure of **4** · $(DMF)_2$, i.e. each of the two terminal methyl groups is disordered over two positions. The corresponding methyl groups are turned towards each other about 28° around the axis of rotation lying on the N9–C16 bond. The purine moiety is slightly bent [the dihedral angle between the imidazole and pyrimidine rings is 3.06(13)°] and almost perpendicular to the plane of phenyl group [the dihedral angle is 88.4(1)°].

Table 3
Crystallographic data and refinement for **1**, **4** · $(DMF)_2$ and **5**

	1	**4** · $(DMF)_2$	**5**
Formula	$C_{30}H_{32}Cl_4N_{10}Pt$	$C_{36}H_{46}Cl_4N_{12}O_2Pt$	$C_{32}H_{36}Cl_4N_{10}O_2Pt$
M (g mol^{-1})	869.55	1015.74	929.60
T (K)	110(2)	110(2)	105(2)
λ (Å)	0.71073	0.71073	0.71073
Crystal system	triclinic	monoclinic	monoclinic
Space group	$P\bar{1}$	$P2_1/n$	$P2_1/c$
a (Å)	11.2275(5)	9.2726(8)	8.1507(4)
b (Å)	12.4605(5)	19.8713(16)	15.6503(7)
c (Å)	14.1821(6)	11.0317(11)	14.1585(6)
α (°)	85.638(3)	90	90
β (°)	66.747(4)	96.886(7)	101.086(4)
γ (°)	69.128(4)	90	90
V (Å^3)	1698.46(14)	2018.0(3)	1772.37(14)
Z	2	2	2
D_{calc} (g cm^{-3})	1.700	1.672	1.742
μ (Mo Kα) (mm^{-1})	4.483	3.791	4.306
Crystal size (mm)	0.35 × 0.30 × 0.30	0.35 × 0.10 × 0.10	0.30 × 0.30 × 0.25
Crystal shape and color	yellow prism	orange prism	orange prism
T_{min}/T_{max}	0.82926/1.00000	0.61972/1.00000	0.84874/1.00000
Number data measured	14312	16816	12907
Unique data (R_{int})	5992 (0.0172)	3555 (0.0155)	3126 (0.0164)
Observed data [$I > 2\sigma(I)$]	5313	3175	2576
Final R_1[a], wR_2[b] (observed data)	0.0310, 0.0772[c]	0.0206, 0.0475[d]	0.0251, 0.0626[e]
Final R_1[a], wR_2[b] (all data)	0.0375, 0.0800[c]	0.0245, 0.0493[d]	0.0358, 0.0689[e]
ρ_{max}, ρ_{min} (e Å^{-3})	2.282, −1.813	0.710, −0.295	0.694, −0.586

Where [a] $R = \sum(|F_o| - |F_c|)/\sum|F_o|$, [b] $wR_2 = [\sum w(|F_o| - |F_c|)^2/\sum(F_o)^2]^{1/2}$, [c] $w = 1/[\sigma^2(F_o) + (0.0375P)^2 + 10P]$, [d] $w = 1/[\sigma^2(F_o) + (0.015P)^2 + 10P]$, [e] $w = 1/[\sigma^2(F_o) + (0.025P)^2 + 10P]$ and $P = (F_o^2 + 2F_c^2)/3$.

Table 4
Selected bond lengths (Å) and angles (°) for **1**, **4** · $(DMF)_2$ and **5**

	1	**4** · $(DMF)_2$	**5**
Bond lengths			
Pt(1)–N(7)	2.032(4)	2.009(2)	2.008(4)
Pt(1)–N(7A)	2.022(4)	2.009(2)	2.008(4)
Pt(1)–Cl(1)	2.2873(14)	2.2846(7)	
Pt(1)–Cl(1A)		2.2846(7)	
Pt(1)–Cl(2)	2.2834(13)		2.2954(11)
Bond angles			
N(7)–Pt(1)–Cl(2)	178.63(12)		91.02(11)
N(7)–Pt(1)–Cl(1A)		88.13(7)	
N(7A)–Pt(1)–N(7)	89.74(16)	180.0	180.0
N(7A)–Pt(1)–Cl(1A)		91.87(7)	
N(7A)–Pt(1)–Cl(2)	88.98(12)		88.98(11)
N(7A)–Pt(1)–Cl(1)	179.17(13)	88.13(7)	
N(7)–Pt(1)–Cl(1)	90.04(12)	91.87(7)	
Cl(2)–Pt(1)–Cl(1)	91.25(5)		
Cl(1A)–Pt(1)–Cl(1)		180.0	
Cl(2)–Pt(1)–Cl(2A)			180.0

Symmetry transformations used to generate equivalent atoms labelled A for **4** · $(DMF)_2$: $-x+1, -y+1, -z+1$; for **5**: $-x+1, -y+1, -z+1$.

The crystal packing of **4** · $(DMF)_2$ is stabilized by hydrogen-bonding interactions involving chlorine and some atoms of DMF (e.g. C8–H···O1: H···O1 = 2.16 Å; ∠DHA = 176°; C20–H20C···Cl1: H···Cl1 = 2.78 Å; ∠DHA = 155°; C20–H20A···Cl1: H···Cl1 = 2.81 Å; ∠DHA 148°) forming infinite linear complex–$(DMF)_2$–complex chains.

3.4.3. Molecular and crystal structures of trans-$[Pt(L_2)_2Cl_2]$ (**5**)

The central part of the molecular structure of **5** (see Fig. 6) is very similar to that of **4** · $(DMF)_2$. The complex is centrosymmetric

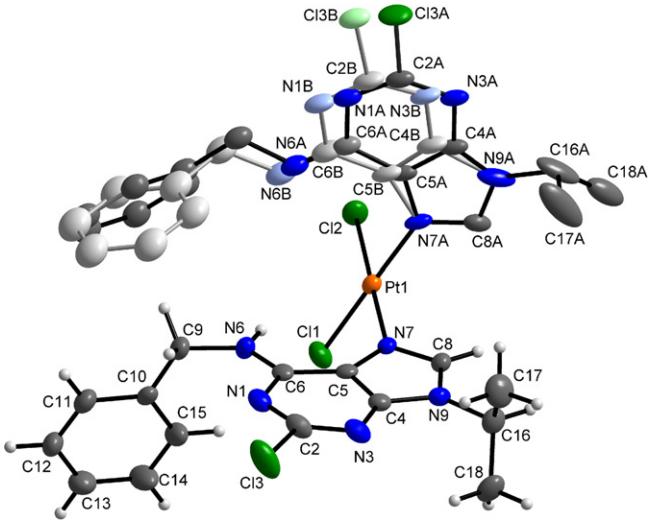

Fig. 4. Molecular structure of complex **1**, showing the atom numbering scheme. Thermal ellipsoids are drawn at the 40% probability level. Some of atoms are disordered over two positions. Some of H-atoms were omitted for clarity.

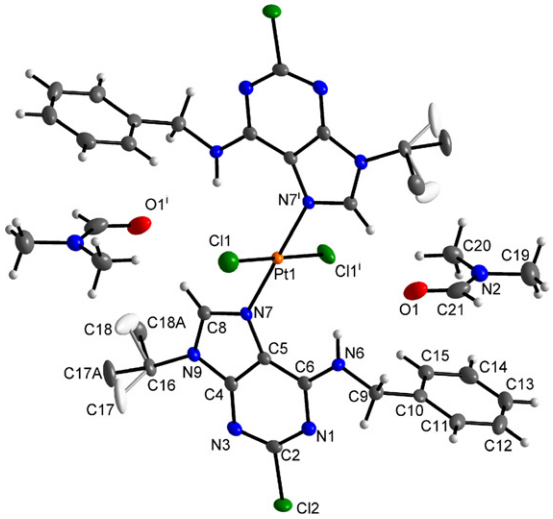

Fig. 5. Molecular structure of the centrosymmetric complex **4** · $(DMF)_2$, showing the atom numbering scheme [symmetry code: (i) $1-x, 1-y, 1-z$]. Some of atoms are disordered over two positions. H-atoms belonging to the disordered part of the molecule were omitted for clarity.

with a *trans*-square-planar coordination around the central Pt(II) ion which is coordinated by two chlorido and two L_2 ligands via the N7 atoms [Pt–N: 2.008(4) Å; Pt–Cl: 2.2954(11) Å; N–Pt–Cl: 91.02(11)°]. The platinum(II) ion lies significantly out of the plane of the imidazole ring [the deviation is 0.1956(1) Å]. The isopropyl group and chlorine atom of the L_2 ligand is disordered over two positions. Atoms of the isopropyl group are turned towards each other around the N9–C16 rotation axis about 31.891(2)°. The purine moiety is also slightly bent [the dihedral angle between the imidazole and pyrimidine rings is 5.23(2)°]. The main structural differences between **4** · $(DMF)_2$ and **5** are in intra- and intermolecular interactions. While the interactions in the crystal structure of **4** · $(DMF)_2$ are affected by the presence of DMF molecules, their absence in **5** result in a more compact molecular packing. The phenyl group of one L_2 ligand in **5** is stabilized by π-interactions with the purine of the other L_2 ligand [if Cg1 is the centroid of the phenyl ring of the first L_2, H8···Cg1 distance is 3.07 Å, H8 distance from

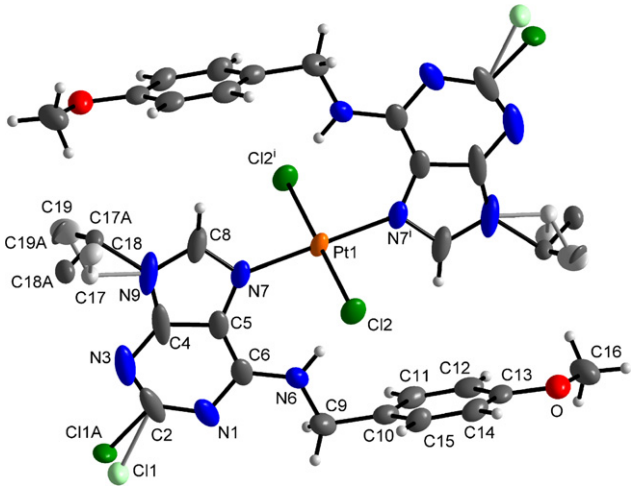

Fig. 6. Molecular structure of the centrosymmetric complex **5**, showing the atom numbering scheme [symmetry code: (i) $1-x, 1-y, 1-z$]. Thermal ellipsoids are drawn at the 50% probability level. Some of atoms are disordered over two positions. H-atoms belonging to the disordered part of the molecule were omitted for clarity.

the plane of the phenyl ring is 3.04 Å, and the dihedral angle between the purine and phenyl moieties is 77.35(13)°]. The crystal packing is further stabilized by intramolecular hydrogen bonds N6–H···Cl2 [N6···Cl2 = 3.281(5) Å; ∠DHA = 139°] and intermolecular Cl···N π–π interactions [Cl2···N1: 3.289(6) Å] arranging molecules of **5** into infinite linear chains.

3.4.4. Crystal structure summary

Generally, the Pt–N and Pt–Cl bond distances in complexes **1**, **4** · $(DMF)_2$ and **5** are in the range of 2.008–2.032 Å, and 2.2834–2.2954 Å, respectively. They are quite comparable to those found for the *trans*-$[PtCl_2(L)_2]$ complex involving two coordinated 2-chloro-6-[(3-hydroxybenzyl)amino]-9-isopropylpurine ligands (L) [50] and also to the average bond lengths found for the Pt–N and Pt–Cl bond lengths (2.02, and 2.29 Å, respectively) in related $PtCl_2N_2$ complexes as reported in the Cambridge Structural Database [49]. In all the discussed complexes, the central platinum atom deviates significantly from the planarity of purine moieties. The degree of deformation of organic ligands within the complexes is markedly influenced by non-bonding intramolecular and intermolecular interactions.

3.5. Biological activity

Complexes **1–6** were screened for their cytotoxic effects *in vitro* against four human cancer cell lines: MCF7, G361, K562 and HOS. Based on the fact that the prepared complexes **1–6** were only slightly soluble in water, and the testing procedure necessarily uses water as a medium, we were limited by the solubility of the complexes in water. That is why we could only prepare water solutions with the complex concentrations being maximally 5 μM. At higher concentrations, the complexes precipitated from the water medium. Unfortunately, the complexes showed to be non-cytotoxic within this low concentration range.

4. Conclusions

We have prepared and fully characterized six new *cis* and *trans* square-planar Pt(II) complexes involving derivatives of plant growth hormones, called cytokinins, derived from 6-benzylaminopurine moiety, and having a general formula of $[Pt(L_n)_2Cl_2]$. X-ray molecular structures of the complexes *cis*-$[Pt(L_1)_2Cl_2]$ (**1**), *trans*-$[Pt(L_1)_2Cl_2]$ (**4** · $(DMF)_2$), and *trans*-$[Pt(L_2)_2Cl_2]$ (**5**) have been determined and supported the composition and stereochemistry following from other physical techniques used for the characterization of the complexes. Moreover, the dynamic *cis*-to-*trans* isomerization process in DMF solutions, as well as the behavior of the complexes in a DMF/water solution has been investigated by the means of multinuclear NMR spectroscopy. The obtained results elucidated and extended our knowledge about time-dependent solution behavior of these complexes. All the complexes were tested *in vitro* against four human cancer cell lines (MCF7, G361, K562 and HOS). The tested compounds could only be tested at low concentrations (up to 5 μM) because of their low solubility in water which is a necessary medium in the testing procedure used. Unfortunately, at this concentration, the complexes, as well as the initial free ligands, showed no cytotoxicity.

Acknowledgements

This work was funded by The Ministry of Education, Youth and Sports of the Czech Republic (a Grant No. MSM6198959218). The authors thank to Assoc. Prof. Marek Šebela, PhD for performing of MALDI-TOF experiments and Ms. Olga Hustáková for her help with biological testing.

Appendix A. Supplementary data

CCDC 683645, 683646 and 683647 contain the supplementary crystallographic data for **1**, **4** · $(DMF)_2$, and **5**. These data can be obtained free of charge via http://www.ccdc.cam.ac.uk/conts/retrieving.html, or from the Cambridge Crystallographic Data Centre, 12 Union Road, Cambridge CB2 1EZ, UK; fax: (+44) 1223-336-033; or e-mail: deposit@ccdc.cam.ac.uk. Supplementary data associated with this article can be found, in the online version, at doi:10.1016/j.poly.2008.05.021.

References

[1] B. Rosenberg, L. Van Camp, T. Krigas, Nature 205 (1965) 698.
[2] E. Wong, Ch.M. Giandomenico, Chem. Rev. 99 (1999) 2451.
[3] R.R. Barefoot, J. Chromatogr. B 751 (2001) 205.
[4] Ch.X. Zhang, S.J. Lippard, Curr. Opin. Chem. Biol. 7 (2003) 481.
[5] L.R. Kelland, S.Y. Sharp, C.F. O'Neill, F.I. Raynaud, P.J. Beale, I.R. Judson, J. Inorg. Biochem. 77 (1999) 111.
[6] Y. Najarjeh, J.M. Perez, C. Navarro-Ranninger, D. Gibson, J. Med. Chem. 45 (2002) 5189.
[7] Y.N. Kukushkin, Platinum Met. Rev. 35 (1991) 28.
[8] P.C. Kong, F.D. Rochon, Inorg. Chim. Acta 61 (1982) 269.
[9] C.J.L. Lock, M. Zvagulis, Inorg. Chem. 20 (1981) 1817.
[10] C.J.L. Lock, M. Zvagulis, Acta Crystallogr., Sect. B 36 (1980) 2140.
[11] J.P. Bradford, R. Faggiani, C.J.L. Lock, Acta Crystallogr., Sect. B 37 (1981) 243.
[12] P.C. Kong, F.D. Rochon, Can. J. Chem. 57 (1979) 526.
[13] P.C. Kong, F.D. Rochon, Can. J. Chem. 59 (1981) 3293.
[14] V.Y. Kukushkin, D. Tudela, Y.A. Izotova, V.K. Belsky, A.I. Stash, Polyhedron 17 (1998) 2455.
[15] Ch. Tessier, F.D. Rochon, Inorg. Chim. Acta 322 (2001) 37.
[16] F.D. Rochon, V. Buculei, Inorg. Chim. Acta 357 (2004) 2218.
[17] K.R. Koch, Y. Wang, A. Coetzee, J. Chem. Soc., Dalton Trans. (1999) 1013.
[18] J. Reedijk, PNAS 100 (2003) 3611.
[19] O. Nováková, J. Kašpárková, J. Malina, G. Natile, V. Brabec, Nucleic Acids Res. 31 (2003) 6450.
[20] G. McGowan, S. Pearsons, P.J. Sadler, Inorg. Chem. 44 (2005) 7459.
[21] J. Vinje, E. Sletten, AntiCancer Agents Med. Chem. 7 (2007) 35.
[22] D.S. Letham, New Zeal. J. Bot. 1 (1964) 336.
[23] C.O. Miller, F. Skoog, M.H. Von Saltza, F.M. Strong, J. Am. Chem. Soc. 77 (5) (1955) 1392.
[24] F. Skoog, H.Q. Hamzi, A.M. Szweykowska, N.J. Leonard, K.L. Carraway, T. Fujii, J.P. Helgeson, R.N. Leoppky, Phytochemistry 6 (9) (1967) 1169.
[25] P.J. Davies, Plant Hormones. Biosynthesis, Signal Transduction, Action, Kluwer Academic Publishers, Dordrecht, The Netherlands, 2004.
[26] S. Gan, R.M. Amasino, Science 270 (1995) 1986.

[27] G. Haberer, J.J. Kieber, Plant Physiol. 128 (2002) 354.
[28] M. Legraverend, P. Tunnah, M. Noble, P. Ducrot, O. Ludwig, D.S. Grierson, M. Leost, L. Meijer, J. Endicott, J. Med. Chem. 43 (2000) 1282.
[29] M.J. Moon, S.K. Lee, J.W. Lee, W.K. Song, S. W Kim, J.I. Kim, C. Cho, S.J. Choi, Y.C. Kim, Bioorg. Med. Chem. 14 (2006) 237.
[30] R.M. Goldsteyn, Cancer Lett. 217 (2005) 129.
[31] W.F. DeAzevedo, S. Leclerc, L. Meijer, L. Havlíček, M. Strnad, S.H. Kim, Eur. J. Biochem. 243 (1997) 518.
[32] F.I. Raynaud, S.R. Whittaker, P.M. Fisher, S. McClue, M.I. Walton, S.E. Barrie, M.D. Garrett, P. Rogers, S.J. Clarke, L.R. Kelland, M. Valenti, L. Brunton, S. Eccles, D.P. Lane, P. Workman, Clin. Cancer Res. 11 (13) (2005) 4875.
[33] L. Szüčová, Z. Trávníček, M. Zatloukal, I. Popa, Bioorg. Med. Chem. 14 (2006) 479.
[34] Z. Trávníček, L. Szüčová, I. Popa, J. Inorg. Biochem. 101 (2007) 477.
[35] M. Maloň, Z. Trávníček, M. Maryško, J. Marek, K. Doležal, J. Rolčík, M. Strnad, Transition Met. Chem. 27 (2002) 580.
[36] Z. Trávníček, V. Kryštof, M. Šipl, J. Inorg. Biochem. 100 (2006) 214.
[37] A. Klanicová, Z. Trávníček, I. Popa, M. Čajan, K. Doležal, Polyhedron 25 (2006) 1421.
[38] CRYSALIS RED and CRYSALIS CCD, Version 1.171.23, Oxford Diffraction Ltd., Abingdon, England, 2006.
[39] G.M. Sheldrick, Acta Crystallogr., Sect. A 46 (1990) 467.
[40] K. Brandenburg, DIAMOND (Release 3.1e), Grystal Impact GbR, Bonn, Germany, 2006.
[41] P.C. Kong, F.D. Rochon, Inorg. Chim. Acta 83 (1984) 65.
[42] W.J. Geary, Coord. Chem. Rev. 7 (1971) 81.
[43] MASSLYNXTM, version 4.0, Waters, Milford, MA, USA, 2005.
[44] W. Henderson, J.S. McIndoe, Mass Spectrometry of Inorganic and Organometallic Compounds, John Wiley & Sons, Ltd., Chichester, England, 2005.
[45] C.J. Pouchert, The Aldrich Library of Infrared Spectra, Aldrich Chemical Company Press, Milwaukee, USA, 1981.
[46] K. Nakamoto, Infrared and Raman Spectra of Inorganic and Coordination Compounds. Part B: Applications in Coordination, Organometallic and Bioinorganic Chemistry, John Wiley & Sons Ltd., New York, England, 1991.
[47] F.H. Appleton, F.J. Pesch, M. Wienken, S. Menzer, B. Lippert, Inorg. Chem. 31 (1992) 4410.
[48] M. Nardelli, J. Appl. Crystallogr. 28 (1995) 659.
[49] F.H. Allen, Acta Crystallogr., Sect. B 58 (2002) 380.
[50] Z. Trávníček, J. Marek, L. Szüčová, Acta Crystallogr., Sect. E 62 (2006) m1 482.

Polyhedron 27 (2008) 2721–2729

Contents lists available at ScienceDirect

Polyhedron

journal homepage: www.elsevier.com/locate/poly

The use of electrospray ionization tandem mass spectrometry on the structural characterization of novel asymmetric metallo-organic supermolecules, based on pentafluorophenylporphyrins and ruthenium complexes

Emmanuel Zimmermman Moreira [a], Luiz Alberto Beraldo de Moraes [a], Marcos Nogueira Eberlin [b], Yassuko Iamamoto [a], Sofia Nikolaou [c,*]

[a] Departamento de Química da Faculdade de Filosofia Ciências e Letras de Ribeirão Preto, Universidade de São Paulo, Brazil
[b] Laboratorio ThoMSon de Espectrometria de Massas, Instituto de Química da Universidade Estadual de Campinas, UNICAMP, Brazil
[c] Departamento de Física e Química da Faculdade de Ciências Farmacêuticas de Ribeirão Preto, Universidade de São Paulo, Av. do Café s/n, 14040-903 Ribeirão Preto, SP, Brazil

ARTICLE INFO

Article history:
Received 8 February 2008
Accepted 20 May 2008
Available online 23 June 2008

Keywords:
μ-Oxo ruthenium trinuclear complexes
Porphyrins
Ruthenium–bipyridine complexes
Mass spectrometry
HF neutral loss
NMR
Photophysical properties

ABSTRACT

The novel asymmetric metallo-organic triads *cis*- and *trans*-[B(4-py)BPFPH$_2${Ru$_3$O(Ac)$_6$(py)$_2$}{Ru(bpy)$_2$Cl}](PF$_6$)$_2$ (**5a,b**) for which *cis*- and *trans*-B(4-py)BPFPH$_2$ = 5,10-bis(pentafluorophenyl)-15,20-bis(4-pyridyl)porphyrin and 5,15-bis(pentafluorophenyl)-10,20-bis(4-pyridyl)porphyrin, respectively; Ac = acetate; py = pyridine and bpy = 2,2′-bipyridine, as well as their corresponding monosubstituted dyads *cis*- and *trans*-[B(4-py)BPFPH$_2${Ru$_3$O(Ac)$_6$(py)$_2$}]PF$_6$ (**4a,b**) have been structurally characterized via electrospray ionization mass spectrometry (ESI-MS and ESI-MS/MS). The ESI-MS of dyads **4a,b** display two characteristic Ru-multicomponent clusters of isotopologue ions corresponding to singly charged ions **4a,b**$^+$ of *m/z* 1629 and doubly charged ions [**4a,b**+H]$^{2+}$ of *m/z* 815 and the triads **5a,b** are detected by ESI-MS as the intact doubly charged cluster of isotopologue ions of *m/z* 1039 [**5a,b**]$^{2+}$. The ESI-MS/MS of **4a,b**$^+$, [**4a,b**+H]$^{2+}$ and [**5a,b**]$^{2+}$ reveal characteristic dissociation pathways, which confirm the structural assignments providing additional information on the intrinsic binding strengths of the gaseous ions. Although the gas-phase behavior of each pair of isomers was rather similar, the less symmetric dyads **4a,b** are distinguished via the ^{1}H NMR spectral profile of the pyrrolic signals. Exploratory photophysical assays have shown that both modifying motifs alter the porphyrinic core emission profile, opening the possibility to use these asymmetric systems as photophysical devices.

© 2008 Elsevier Ltd. All rights reserved.

1. Introduction

Electrospray ionization mass spectrometry (ESI-MS) as well as its tandem version (ESI-MS/MS) have been increasingly used for the structural characterization of organometallic [1], metallo-organic [2], inorganic molecules [3] and supermolecules and their ionic forms [4]. ESI is particularly suited for such species due to its ability to transfer, via an unique and gentle ion evaporation process, pre-formed ions directly from solutions to the gas phase environment of mass spectrometers [5]. ESI-MS is also advantageous for the structural characterization of organometallic and inorganic complexes owing to detailed structural information on both metal cores and ligands, isotope profiles, and high sensitivity, therefore requiring reduced amounts of sample as those required for other conventional techniques, such as NMR and cyclic voltammetry, which are more commonly applied to characterize organometallic and inorganic complexes [6].

Regarding the compounds of interest to this work, porphyrins and metalloporphyrins are molecules of great interest particularly in chemistry, biology and physics, also featuring important industrial applications. They display useful properties such as the ability to mimic biologically-active structures like cytochrome P450 monooxygenases, to act as catalysts and as photosensitizers in photodynamic therapy [7]. Recently, ESI-MS(/MS) has been applied with success to characterize these molecules [8], as well as supramolecular extended structures based on the porphyrinic core [9].

On the other hand, μ-oxo triruthenium acetates complexes constitute a versatile class of molecules that display rich electrochemical behavior, including electrochromism, and interesting spectroscopic and catalytic properties [10]. Relevant work has been done using these triruthenium carboxylates as modifying motifs to porphyrins [11], as building blocks in extended structures which feature electron transfer reactions [12], as well as acceptors for photoinduced transfer reactions in supramolecular assemblies [13]. Their well known chemistry has recently allowed researchers to

* Corresponding author. Tel.: +55 16 36024712; fax: +55 16 36331092.
E-mail address: sofian@fcfrp.usp.br (S. Nikolaou).

0277-5387/$ - see front matter © 2008 Elsevier Ltd. All rights reserved.
doi:10.1016/j.poly.2008.05.014

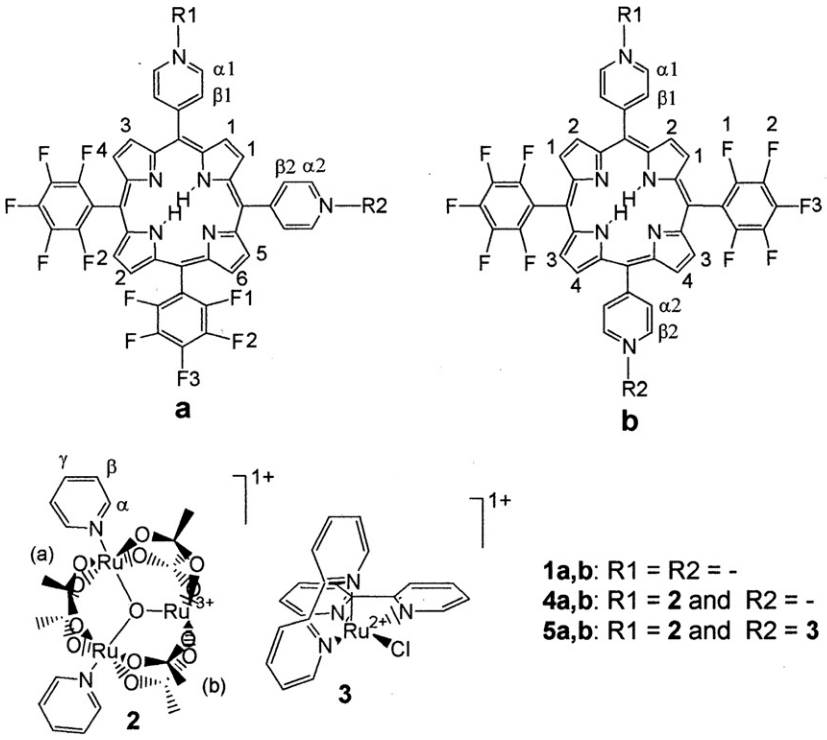

Fig. 1. Structures of the compounds studied herein and labels for NMR assignments.

plan novel clusters with important properties, such as controlled and reversible NO or CO delivery [14]. With respect to the [Ru(bpy)$_3$] moiety, this and related ruthenium polypyridine complexes have been extensively explored and their chemical, electrochemical and spectroscopic (photophysical) behaviors well-described in the literature [15].

This work focuses the structural characterization, via ESI-MS(/MS) and ^{1}H and ^{19}F NMR analysis, of a series of substituted pentafluoropyridylporphyrins synthesised by a suitable approach designed in order to obtain the asymmetric metallo-organic dyads **4a,b** and triads **5a,b** (Fig. 1). It is also presented a brief spectroscopic characterization, as well as preliminary photophysical data. Usually, triads such as **5** are composed by a porphyrin central chromophore and peripheral organic electron donor and acceptor units, which are designed to mimic the active centers of the natural photosynthetic systems. Those triads are able to generate excited states of charge separation and thus convert light into chemical energy [16]. For the novel asymmetric metallo-organic systems **5a,b** that we have prepared, the ruthenium trinuclear complex **2** may act as an electron acceptor owing to its ability to participate in photoinduced electron and energy transfers [13], and the [Ru(bpy)$_2$] moiety **3** would act as a tunable unit able to display either the acceptor or the donating ability, depending on the experiment conditions [17].

2. Experimental

All the reactants were commercially available and used without further purification. The compounds [Ru(bpy)$_2$Cl$_2$] · 2H$_2$O, [Ru$_3$O(Ac)$_6$(py)$_2$(CH$_3$OH)]PF$_6$ and *cis*- and *trans*-B(4-py)BPFPH$_2$(5,10-bis(pentafluorophenyl)-15,20-bis(4-pyridyl)porphyrin and 5,15-bis(pentafluorophenyl)-10,20-bis(4-pyridyl)porphyrin, respectively) were synthesized according to reported procedures [18]. The description of the purification and isolation of the *cis*- and *trans*-pentafluoropyridylporphyrins isomers is detailed elsewhere [19].

2.1. Synthesis of cis- and trans-[B(4-py)BPFPH$_2${Ru$_3$O(Ac)$_6$(py)$_2$}]PF$_6$ (dyads **4a,b**)

About 51.3 mg of [Ru$_3$O(Ac)$_6$(py)$_2$(CH$_3$OH)]PF$_6$ (5.1×10^{-5} mol) was dissolved in 70 mL of dichloromethane and the resulting solution were slowly dropped into a solution of 45 mg (5.6×10^{-5} mol) of *cis*- or *trans*-[B(4-py)BPFPH$_2$], dissolved in 5 mL of dichloromethane. The reaction mixture was magnetically-stirred for 24 h, at room temperature under aerobic conditions. The resulting solution was evaporated to dryness and the purple solid obtained was purified by chromatography in a neutral alumina column of approximately 20 cm high and 2.5 cm of diameter. The solvent used for elution was dichloromethane and the fractions eluted from the column were identified by their UV–Vis absorption spectra. For both dyads **4a,b**, the first fraction eluted was identified as unreacted porphyrin; the following fraction apparently contained mixtures with variable amounts of porphyrin and ruthenium complex. The third fraction contained dyads **4** and the last fraction contained the symmetric, bi-substituted triads *cis*- and *trans*-[B(4-py)BPFPH$_2${Ru$_3$O(Ac)$_6$(py)$_2$}$_2$](PF$_6$)$_2$ (*m/z* 1229 for the cations *cis*- or *trans*-[B(4-py)BPFPH$_2${Ru$_3$O(Ac)$_6$(py)$_2$}$_2$]$^{2+}$; *cis*-[B(4-py)BPFPH$_2$ {Ru$_3$O(Ac)$_6$(py)$_2$}$_2$](PF$_6$)$_2$ $\eta = 6\%$; *trans*-[B(4-py)BPFPH$_2${Ru$_3$O(Ac)$_6$ (py)$_2$}$_2$](PF$_6$)$_2$ $\eta = 9\%$). **4a** ($\eta = 31$); λ_{max}(dichloromethane)/nm ($\log \varepsilon$/dm^3 cm^{-1} mol^{-1} and assignment [18]) 414 (5.5, Soret), 510 (4.4, $Q_{y(1,0)}$), 545 (3.9, $Q_{y(0,0)}$), 587 (4.1, $Q_{x(1,0)}$), 655 (4.0, $Q_{x(0,0)}$) and 691 (4.0, intra-cluster). **4b** ($\eta = 45$); λ_{max}(dichloromethane)/nm ($\log \varepsilon$/dm^3 cm^{-1} mol^{-1} and assignment) 414 (5.4, Soret), 510 (4.4, $Q_{y(1,0)}$), 545 (3.8, $Q_{y(0,0)}$), 587 (4.0, $Q_{x(1,0)}$), 655 (3.9, $Q_{x(0,0)}$) and 691 (3.9, intra-cluster).

2.2. Synthesis of cis- and trans-[B(4-py)BPFPH$_2${Ru$_3$O(Ac)$_6$(py)$_2$}{Ru(bpy)$_2$Cl}](PF$_6$)$_2$ (triads **5a,b**)

About 37.9 mg of dyad **4a,b** (2.1×10^{-5} mol) and 12.2 mg of [Ru(bpy)$_2$Cl$_2$] (2.5×10^{-5} mol) were dissolved in 10 mL of dichlo-

romethane and allowed to react during 48 h, under gentle heat, magnetic stirring and aerobic conditions. The reaction media was then dropped into an alcoholic saturated solution of NH_4PF_6 and, after 2 h, was evaporated to dryness, yielding a black solid. The crude material were purified by chromatography in a neutral alumina column of approximately 20 cm high and 2.5 cm of diameter; the solvent used for elution was a 1% mixture (v/v) of ethanol: dichloromethane and the fractions eluted from the column were identified by their UV–Vis absorption spectra. The products of interest were collected as the third fraction eluted from the column. **5a** (η = 30%); λ_{max}(dichloromethane)/nm ($\log \varepsilon$/dm^3 cm^{-1} mol^{-1} and assignment) 296 (4.4, π–π^*), 417 (5.0, Soret), 511 (4.0, *Qy*(1,0)), 545 (3.7, $Q_{y(0,0)}$), 587 (3.7, $Q_{x(1,0)}$), 650 (3.4, $Q_{x(0,0)}$) and 691 (3.5, intra-cluster). **5b** (η = 6%); λ_{max}(dichloromethane)/nm ($\log \varepsilon$/dm^3 cm^{-1} mol^{-1}and assignment) 295 (4.3, π–π^*), 416 (4.8, Soret), 512 (3.9, *Qy*(1,0)), 548 (3.5, $Q_{y(0,0)}$), 588 (3.6, $Q_{x(1,0)}$), 650 (3.4, $Q_{x(0,0)}$) and 690 (3.4, intra-cluster).

2.3. Physical measurements

The mass spectrometric experiments were performed using a high-resolution hybrid quadrupole (q) and orthogonal time-of-flight (TOF) mass spectrometer (QTOF from Waters Micromass, UK) operating in the positive ion mode at ca. 5000 resolving power. The temperature of the nebulizer was 150 °C and the cone voltage was 30 V. The ESI-MS/MS experiments were performed via Q1 selection of the ion or cluster of ions of interest followed by collision-induced dissociation (CID) with argon in the collision hexapole at energies ranging from 10 to 20 eV and TOF-MS analysis of the ionic fragments. Samples were dissolved in a 1:1 methanol/water solution acidified by the addition of 0.1% formic acid. The ^{1}H, COSY (^{1}H–^{1}H, not shown) and ^{19}F NMR data were collected on a Bruker Advanced DRX 400MHz spectrometer (Bruker Biospin, Bremen, Germany), from 1×10^{-2} mol dm^{-3} $CDCl_3$ solutions. The electronic spectra were recorded on a HP 8453 spectrophotometer, from 1×10^{-5} mol dm^{-3} dichloromethane solutions. Steady-state emission and excitation spectra were recorded on a Spex Fluorolog 2 spectrophotometer (excitation slit = 10 and emission slit = 20), at room temperature in a four faced 1 cm × 1 cm quartz cuvette, from approximately 5×10^{-6} mol dm^{-3} degassed dichloromethane solutions. The quantum yields were calculated from degassed CH_2Cl_2 solutions, using the known value of ϕ_s for $TPPH_2$ (tetraphenyl porphyrin) at room temperature (ϕ_s = 0.099) and the integrated areas under the emission curve corrected by the relative absorbance at the excitation wavelength [17a,20].

3. Results and discussion

3.1. Synthesis

Obtaining the monosubstituted dyads **4a,b** is not a trivial task, since both coordination sites of the precursor isomers **1a,b** (the pyridyl group) are equivalent. Nevertheless, the synthetic approach proposed here is based on the use of sub-stoichiometric amounts of the modifying motif (in this case the trinuclear ruthenium complex **2**), and the addition of a diluted solution of the complex to a more concentrated solution of the porphyrinic core, in order to warranty local excess of porphyrin. Besides that, the reaction was submitted to soft conditions (room temperature and magnetic stirring), and care was taken not to extend the reaction too long, minimizing it to further yield high quantities of the bisubstituted product. This synthetic strategy, along with the adsorption chromatography purification, allowed one to obtain the monosubstituted dyads (η = 31% and η = 45% for **4a** and **4b**, respectively) in higher yield, although the coordination of two trinuclear complexes molecules to the central core has occured to some extent, yielding smaller amounts of the bisubstituted symmetric byproduct, which was collected as the last fraction from the chromatographic column.

In the particular case of compounds **5a,b**, once one of the coordination sites of the porphyrinic center was already compromised with the bond to complex **2**, there was no need to have a rigid control on the synthetic conditions, and the asymmetric triads were obtained by the use of a slight excess of the $[Ru(bpy)_2]$ substituent and a more concentrated reaction medium.

3.2. ESI-MS(/MS)

The porphyrins **1a,b** as well as the dyads **4a,b** and triads **5a,b** show nearly identical gas-phase behaviour, therefore we will comment only on the ESI-MS results for the *cis*-isomers (a). ESI-MS detects the model *cis*-porphyrin **1a** as a cluster of singly-charged mono-protonated molecule [**1a**+H]$^+$ of *m/z* 797 (only the *m/z* of the most intense ion within the isotope cluster will be mentioned). Note that mono-protonation may occur either on a central N atom of the porphyrin ring or on an N hetero-atom of the pyridyl groups. The cluster from the doubly protonated molecule [**1a**+2H]$^{2+}$ of *m/z* 398.5 was not observed at all, indicating that the addition of a second proton to the porphyrin molecule is unfavourable, at least for the gaseous molecule. The gaseous [**1a**+H]$^+$ of *m/z* 797 was then selected and dissociated via 20 eV collisions with argon (spectrum not shown). Interestingly, dissociation occurs to great extent by several successive losses of HF molecules (20 Da). These sequential losses must therefore require substantial molecular rearrangements that are accessed likely due to the lack of alternative less energy-demanding direct bond cleavages.

The ESI-MS of the model compound $[Ru_3O(Ac)_6(py)_2(CH_3OH)]PF_6$, that is **2** · PF_6, display a multicomponent cluster of isotopologue ions of *m/z* 863 mostly characteristic of the Ru_3 composition (ruthenium is a multiple isotope element: ^{104}Ru (18.7%), ^{102}Ru (31.6%), ^{101}Ru (17.0%), ^{100}Ru (12.6%), ^{99}Ru (12.7%), ^{98}Ru (1.88%) and ^{96}Ru (5.52%)). This ion is ascribed to the methanol adduct of **2**$^+$ (Fig. 2) that is, $[Ru_3O(Ac)_6(py)_2(CH_3OH)]^+$. This whole isotopologue cluster of singly charged ions was therefore selected and subjected to 20 eV collision induced dissociation (CID). Extensive CID occurs (Fig. 2) yielding first $[Ru_3O(Ac)_6(py)_2]^+$ of *m/z* 831, that is **2**$^+$. This preferential loss of methanol over pyridine is consistent with the binding strength of both ligands, that is, also in gas phase methanol is more loosely bonded to Ru than py, mimicking the solution behaviour [3]. After methanol loss, successive losses of the two more strongly bonded pyridine ligands (py) occurs thus yielding the fragment ions of *m/z* 751 and *m/z* 672, which are assigned, respectively to $[Ru_3O(Ac)_6py]^+$ and $[Ru_3O(Ac)_6]^+$. The fragment ion of *m/z* 751 dissociates further by an unexpected and interesting process that involves the loss of four acetate (Ac) ligands. We rationalize this dissociation by the release of two neutral dimeric molecules of Ac_2 composition, thus yielding the $[Ru_3O(Ac)_2(py)]^+$ fragment of *m/z* 516. This fragment ion fragments further by pyridine loss to form $[Ru_3O(Ac)_2]^+$ of *m/z* 437.

The ESI-MS of the acidified water:methanol solution of dyad **4a** (spectrum not shown) displays predominantly two prominent clusters of isotopologue ions of similar abundances. In one cluster of *m/z* 1629, the ions are separated by one *m/z* unit indicating that they are singly charged species, ascribed therefore to **4a**$^+$. The other of *m/z* 815 displays ions separated by 1/2 *m/z* unit, and is ascribed to the mono-protonated and therefore doubly charged ion [**4a**+H]$^{2+}$. Fig. 3 shows the ESI-MS/MS of both **4a**$^+$ and [**4a**+H]$^{2+}$.

The gaseous **4a**$^+$ of *m/z* 1629 (Fig. 3a) dissociates promptly upon 20 eV collisions with argon by sequential losses of the peripheral pyridine ligands, yielding the cluster of isotopologues singly-charged ions [**4a**-py]$^+$ and [**4a**-2py]$^+$ of *m/z* 1550 and *m/z* 1471,

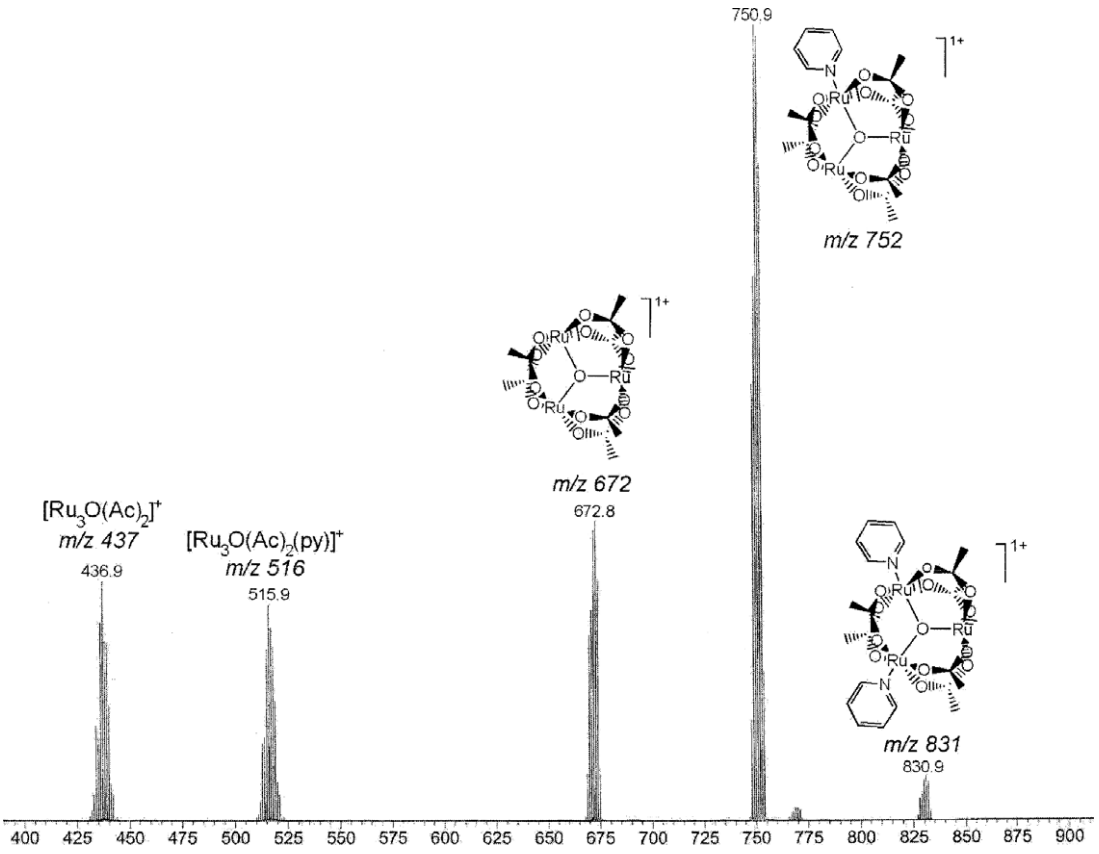

Fig. 2. ESI-MS/MS for 20 eV CID of $[Ru_3O(Ac)_6(py)_2]^+$ of *m/z* 831. Proposed structures and dissociation pathways for the fragment ions are shown as inserts. The parent species $[Ru_3O(Ac)_6(py)_2(CH_3OH)]^+$ of *m/z* 863 dissociates completely and is not detected.

respectively. It dissociates also to form the isotopologue cluster of **2**$^+$ ions of *m/z* 831 due to the loss of the entire porphyrin ligand hence due to the dissassembly of the supramolecular dyad. It was previously reported [9c] that for a similar supramolecular system in which a tetra-pyridyl porphyrin is modified exclusively with the $[Ru(bpy)_2Cl]$ fragment, CID fails to form supramolecular species via the loss of peripheral 2,2′-bipyridine ligand (a fragment that would be analogous to [**4a**-py]$^+$). Instead, only the successive cleavage of the Ru–pyridyl bond was observed thus yielding the two fragments composing the supermolecular assembly. For that assembly, the chelate effect stabilizes the Ru–bpy bond making it stronger than the Ru–pyridyl bond. For **4a**$^+$ however, we observe a different behaviour: the three fragments and their relative abundances, [**4a**-py]$^+$ > [**4a**-2py]$^+$ = [**2**]$^+$ and the absence of any additional effect such as the chelate one lead us to conclude that at least for the unprotonated **4a**$^+$ species, the bond of the $[Ru_3O]$ core to the porphyrin through the pyridyl group (the one that sustain the supramolecular assembly), is as strong as the bond of the $[Ru_3O]$ to the peripheral pyridine ligands.

In Fig. 3a we also observe that **4a**$^+$ of *m/z* 1629 dissociates to form a cluster of singly charged (separated by one *m/z* unit) isotopologue ions of *m/z* 752, which corresponds to [**2**-py]$^+$. Being the most abundant fragment ion, we assume that probably [**2**-py]$^+$ is originated not solely from **2**$^+$ of *m/z* 831, but also from [**4a**-py]$^+$ of *m/z* 1550. Further fragmentation of **4a**$^+$ also occurs to originate less abundant ions such as $[Ru_3O(Ac)_2py]^+$ and $[Ru_3O(Ac)_2]^+$ of *m/z* 516 and *m/z* 437, respectively.

The ESI-MS/MS of the isotopologue cluster of [**4a**+H]$^{2+}$ ions of *m/z* 815 is quite unique and illustrative (Fig. 3b). It shows that the ion loses the peripheral pyridine ligand of 89 Da to form the doubly charged cluster of supramolecular species [**4a**+H-py]$^{2+}$ of *m/z* 775, separated by 1/2 *m/z* units. This loss reinforces the indication that the Ru–porphyrin bond is quite strong. Due to pyridyl–Ru bond cleavage, [**4a**+H]$^{2+}$ of *m/z* 815 also dissociate by "charge partitioning" to form two singly charged species: the singly charged cluster of isotopologue ions [**1a**+H]$^+$ of *m/z* 797 (with a much less diverse isotope pattern) and **2**$^+$ of *m/z* 831 (a diverse Ru_3-isotope pattern) both containing ions separated by one *m/z* unit. Note that **2**$^+$ undergoes further dissociation by the loss of one peripheral pyridine, yielding the cluster of singly charged isotopologue ions [**2**-py]$^+$ of *m/z* 752.

The ESI-MS of the triad **5a** solution shows that ESI is able to gently transfer to the gas phase the doubly charged ion **5a**$^{2+}$ of *m/z* 1039 with spatially separated charge sites, detecting it unambiguously as a characteristic cluster of isotopologue ions separated by 1/2 *m/z* unit. The ESI-MS data shows therefore that the synthetic approach reported herein to obtain the assymmetrical **5a,b** isomeric supermolecules was successful. To obtain structural confirmation for **5a**, and for clarity and illustration, the ESI-MS/MS of the ions of *m/z* 1039 (in fact a mixture of isobaric Ru-isotopologue ions) selected from the multicomponent cluster of isotopologue ions of **5a**$^{2+}$ (see inset) was acquired (Fig. 4). Scheme 1 depicts the "charge partitioning" dissociation pattern proposed for **5a**$^{2+}$.

The doubly charged **5a**$^{+2}$ ions of *m/z* 1039 dissociates mainly by "charge partitioning" to yield two pairs of singly charged cations, that is, (i) **4a**$^+$ of *m/z* 1630 and $[B(4\text{-py})BPFPH_2\{Ru(bpy)_2Cl\}]^+$ of *m/z* 1247 and (ii) **2**$^+$ of *m/z* 833 and **3**$^+$ of *m/z* 449. The fragment **4a**$^+$ undergoes further dissociation by the loss of its peripheral pyridine ligand to yield [**4a**-py]$^+$ of *m/z* 1551.

3.3. NMR spectroscopy

Table 1 summarize the tentative assignment of the observed NMR signals for **1a,b** (^{1}H and ^{19}F) and **4a,b** (^{1}H). ^{19}F-RMN spectra

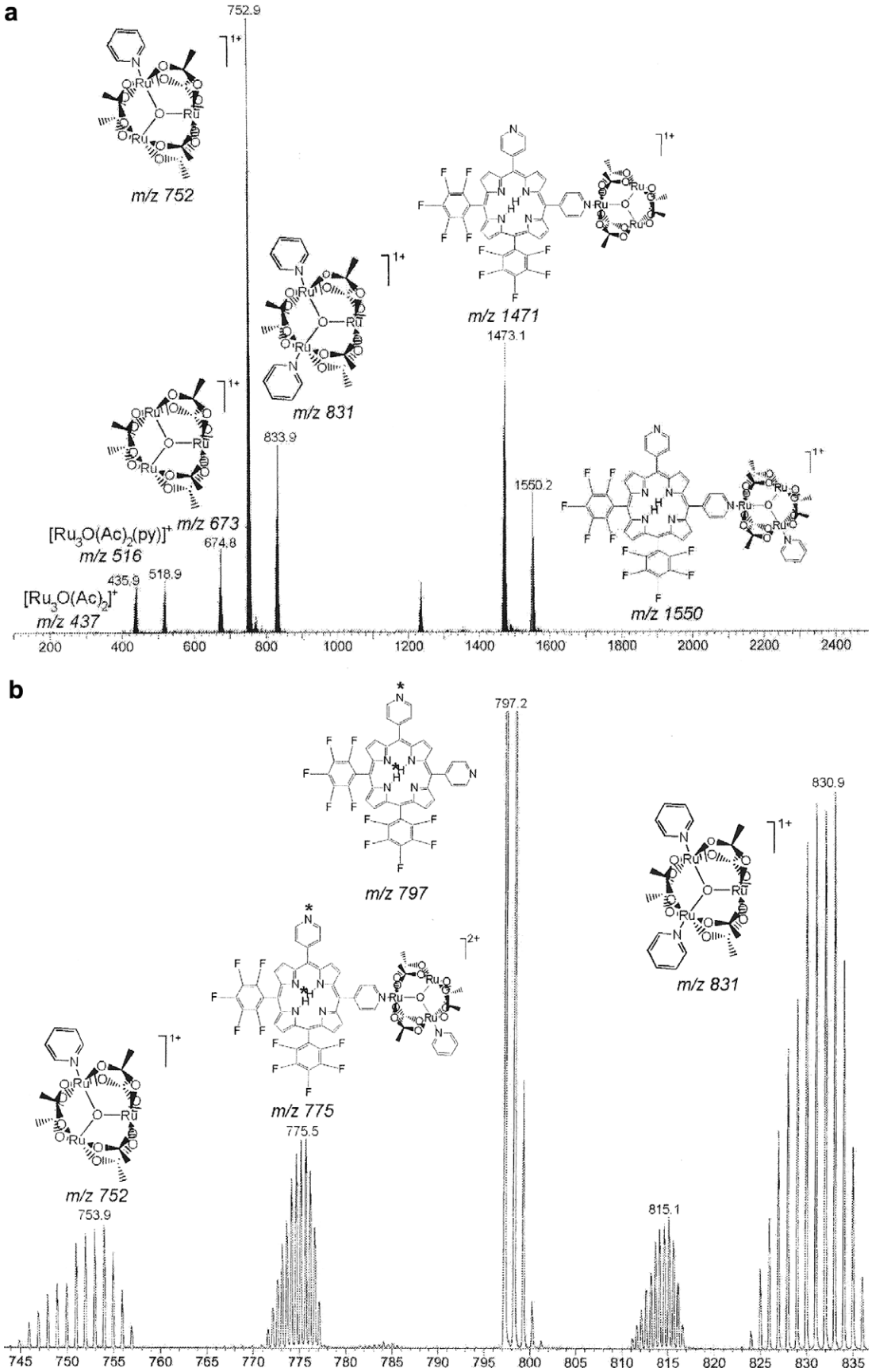

Fig. 3. ESI-MS/MS for 20 eV CID of: (a) $\mathbf{4a}^{+}$ of *m/z* 1629 and (b) $[\mathbf{4a}+H]^{2+}$ of *m/z* 815.

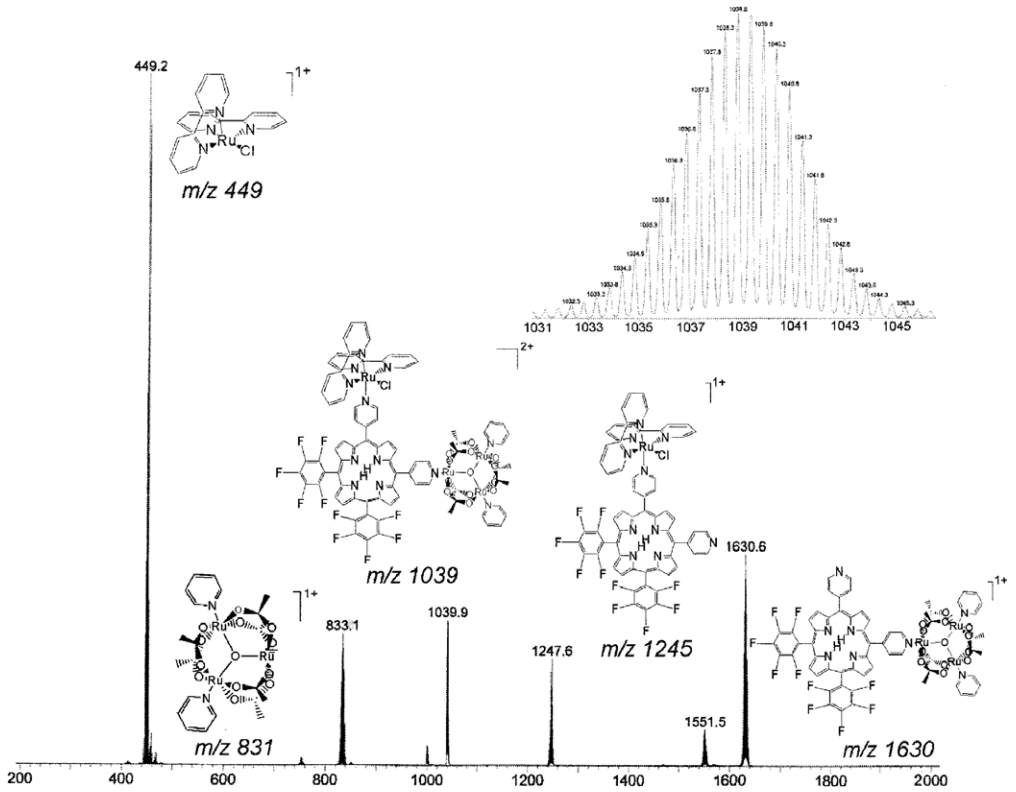

Fig. 4. ESI-MS/MS for 15 eV CID of $\mathbf{5a}^{2+}$ of *m/z* 1039. The inset shows the full cluster of isotopologue ions of $\mathbf{5a}^{2+}$ detected by ESI-MS.

are quite useful to characterize fluorinated porphyrins [21]. As expected for isomers **1a** and **1b**, the ^{19}F-RMN spectra display three sets of signals corresponding to the *ortho*, meta and *para* fluorines. Each signal appears as a doublet and two triplets, respectively, and show no significant variations on the chemical shifts values between the *cis* to the*trans* isomer. The pyrrolic ^{1}H signals of the *cis*-porphyrin isomer 1, however, which were expected to appear as a set of two doublets and two singlets [22], are superimposed into two distorted doublets, each of them integrating to four protons. This spectral profile almost converges to the one observed for the *trans* isomer 1b (two doublets), making it hard to identify the precursors isomers by the ^{1}H NMR spectra. Nevertheless, the coordination of **2** to one pyridyl position of the *cis* and *trans*-dyads **4a,b** lowers the molecular symmetry, leading to different patterns of resonances in the aromatic region of the ^{1}H spectra, making therefore the isomers distinguishable.

Concerning the $[Ru_3O(Ac)_6(py)_2]$ moiety, the δ values follow the pattern dictated by the paramagnetic anisotropy of the $[Ru_3O]$ core, which contains one unpaired electron [6c,10]. For the ^{1}H spectra, this effect promotes large shifts to higher field on the pyridinic protons α, β, γ, α1 and β1, which tend to vanish with distance, suggesting that the pseudo-contact is the main paramagnetic interaction mechanism operating in these molecules.

3.4. Absorption spectra and exploratory photophysical essays

In terms of the absorption spectra of dyads **4a,b** and triads **5a,b**, the coordination of the ruthenium complexes to the precursors **1a,b** causes very little perturbation on the spectra profiles, resulting in spectra which are a summation of the bands observed in the electronic spectra of each building block that composes the supermolecules (see Section 2 for λ_{max} and assignments).

Exciting isomers **1a,b** in one of their Q band leads to the typical porphyrin emission, centered around 645 and 705 nm, assigned to a fluorescence band with vibrational structure ($Q_{0,0}$ and $Q_{0,1}$ respectively, Table 2) [23]. In spite of the absorption spectra suggest poor electronic coupling among the units composing the supermolecules, going to dyads **4a,b**, one can observe that the coordination of the triruthenium compound **2** to porphyrins **1a,b** leads to a significant decrease in the fluorescence quantum yield (ϕ) and the rise of another emission band, with very low intensity, centered at 770 nm. The coordination of the second substituent (compound **3**), yielding triads **5a,b** leads to a further decrease of ϕ, but do not introduce any modification on the spectra profile.

Although it was not possible to do a selective excitation, due to band overlap in the UV–Vis spectra, triads **5a,b** were excited at 490 nm (approximately the λ_{max} of the $[Ru(bpy)_2]$ MLCT transition) and neither emission from the ruthenium chromophore nor an increase in the ϕ values of the porphyrin emission were observed. In fact, the excitation spectra (not shown) were recorded monitoring all the three observed emission bands and, in all cases the spectra reproduces exclusively the spectral profile of the porphyrin (Soret and four Q bands). This result, and the low emission quantum yield observed for the supermolecules show that there is no contribution from electronic levels of the peripheral units to the porphyrin emission and that these units are quenching that emission. In the particular case of the 770 nm band, it has been assigned to a porphyrin phosphorescence [23], which might appear when there is direct sensitization of the porphyrin triplet state by energy transfer, or when the rate of intersystem crossing (ISC) is high [24]. The absence of any bands of the **2** and **3** units in the excitation spectra of triads **5a,b** excludes the first argument exposed above. Therefore, it seems that the coordination of two ruthenium compounds to the porphyrinic core has simply favored ISC by the heavy atom effect. This explanation also holds for dyads **4a,b**.

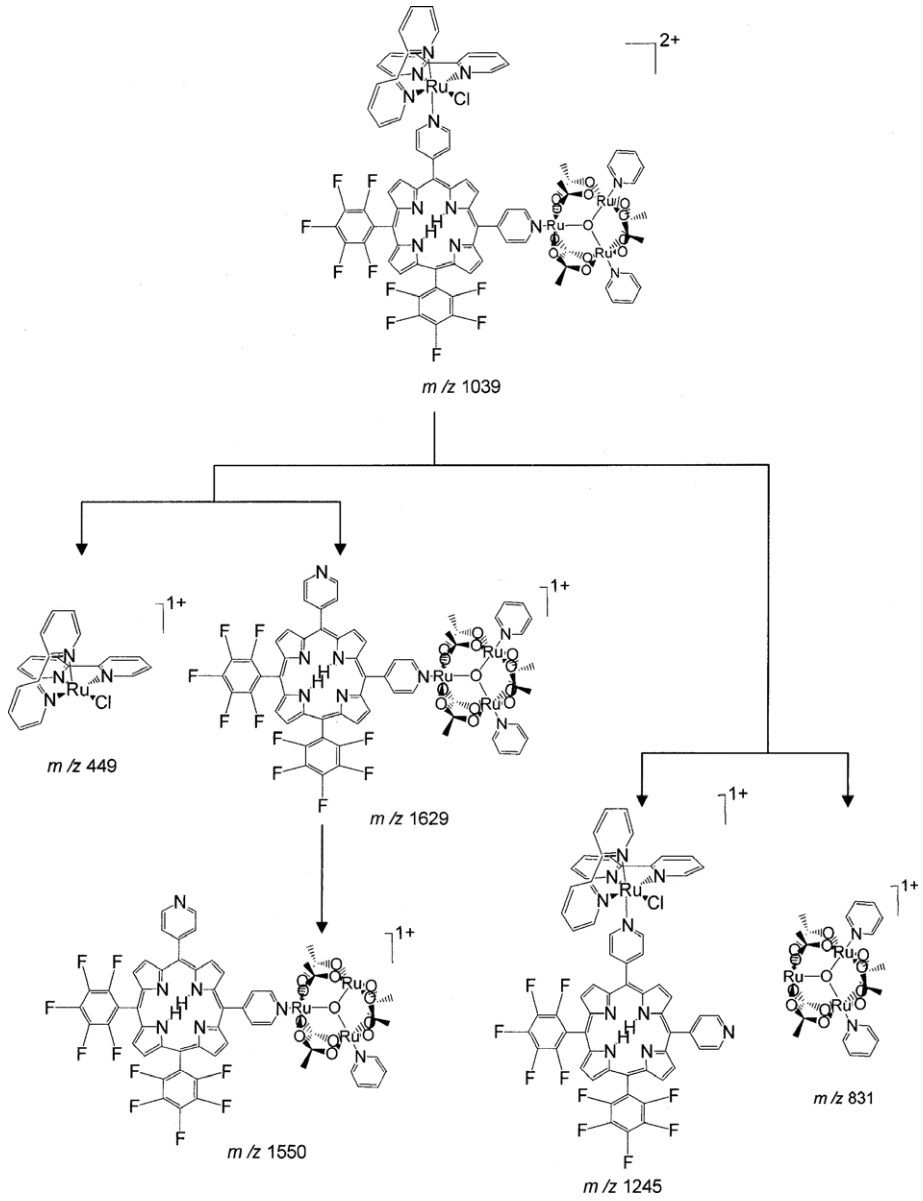

Scheme 1. Dissociation pattern of triad **5a**.

On a qualitative basis, the preliminary data presented here allows one to point out some interesting aspects: concerning the triruthenium compound **2**, it could quench the porphyrin fluorescence by a reabsorption interference, since it has an absorption band centered around 690 nm, which matches the emission bands at 650 nm/710 nm. However, there are a few literature examples in which the triruthenium compound is able to quench a $[Ru(bpy)_2]$ chromophore by both photoinduced energy and electron transfers [13a] and quench Zn porphyrins and Zn phtalocyanines by photoinduced electron transfer mechanism [13c,25]. Therefore, in the present case it is possible to propose that the porphyrinic core emission is partially quenched by an electron transfer to the triruthenium moiety.

For triads **5a,b** there is the additional effect of the $[Ru(bpy)_2Cl]$ modifying complex. The porphyrin singlet state might be transfering excitation energy to the $MLCT^3$ (metal to ligand charge transfer) of the metal complex, since the energy of this state [15b] is close to that of the emitting state of the porphyrinic core. If this is so, one would expect to detect the emission of the $[Ru(bpy)_2Cl]$ chromophore. However, in the particular case of ruthenium–bipyridine complexes whose coordination sphere is completed with a chloro ligand, the $MLCT^3$ is normally quenched by a low lying d–d state, which decays by non-radiative (vibrational) pathways [15b,26]. In all cases, the existence of a phosphorescence band, which arises from an ISC process, also contributes to the decrease of the porphyrin ϕ_{fl}.

Finally, although it was demonstrated here that the electronic coupling of the units which composes compound **4a,b** and **5a,b** is rather low, it is worth mentioning that, as far as we consider the present data, it seems that the difference in the position of the coordinating pyridyl groups on the porphyrinic core does not disturb the electronic properties of the molecules under investigation. Consequently, it was not detected significant differences in the spectroscopic behaviour of the isomers studied. Yet, the positional isomerism is manifested in the NMR measurements results for compounds **1a,b** and **4a,b**, since the symmetry of molecules might be directly addressed by this technique.

Table 1
Tentative assignment of the observed ^{1}H and ^{19}F chemical shifts (δ/ppm) for compound **1a,b** and **4a,b** from 1×10^{-2} mol dm^{-3} $CDCl_3$

	1a	1b	4a	4b
1H				
H1	8.92, 4H, m[a]	8.92, 4H, d	8.81, 2H, br	8.65, 2H, d
H2	≡H1	≡H1	8.76, 2H, br	8.83, 2H, d
H3	≡H1	8.86, 4H, d	≡ H2	8.16, 2H, d
H4	8.86, 4H, m	≡H3	8.19, 1H, br	8.77, 2H, d
H5	≡H4		8.65, 2H,br	
H6	≡H4		8.13, 1H, br	
H7	≡H4		≡ H5	
Inner H	−2.88, 2H, s	−2.92, 2H, s	−3.15, s	−3.20, 2H, s
Hα1	9.08, 4H, d	9.08, 4H, d	1.28, br	1.24, 2H, br
Hβ1	8.16, 4H, d	8.18, 4H, d	6.59, br	6.56, 2H, br
$H\alpha_2$	≡α1	≡α1	9.03, d	9.02, 2H, d
$H\beta_2$	≡β1	≡β1	8.04, d	8.08, 2H, d
Hα			0.19, br	0.12, 4H, br
Hβ			5.69, br	5.67, 4H, br
Hγ			6.34, t	6.35, 2H, t
CH_3 (a)			5.16, s	5.19, 6H, s
CH_3 (b)			5.04, s	5.06, 12H, s
19F[b]				
F1	−140.32, d	−141.49, d		
F2	−165.15, m	−165.18, m		
F3	−155.23, t	−155.22, t		

[a] m = multiplet, s = singlet, d = doublet, t = triplet and br = broad signal.
[b] $CF_3C_6H_5$ was used as internal standard in $CDCl_3$ solution; to facilitate comparison with the literature data [21], the reported values were converted to a scale based on the residual signal of $CFCl_3$ by summing −63, 72 ppm.

Table 2
Photophysical data for compounds **1a,b**; **4a,b** and **5a,b**[a]

	λ_{emi} (nm)	λ_{exc} (nm)	ϕ[b]
1a	647, 707	510	0.035
1b	643, 707	510	0.046
4a	647, 705, 770	510	0.0014
4b	646, 708, 770	510	0.0010
5a	649, 712, 770	510	0.00061
5b	648, 709, 770	510	0.00062

[a] Data collected from CH_2Cl_2 degassed solutions at room temperature.
[b] Fluorescence quantum yield.

4. Conclusions

Using ESI-MS and ESI-MS/MS, we have been able to gently transfer to the gas phase the corresponding cationic species **4a,b**$^{+}$ and **5a,b**$^{2+}$ present in solutions of dyads **4a,b** and triads **5a,b**, respectively. Using ESI-MS/MS and by performing CID of isolated gaseous ions, and by following changes in characteristic isotope patters and charge states, we have been able to characterize these gaseous ions via their structurally diagnostic dissociation chemistries. The ESI-MS(/MS) data, besides demonstrating the success of the synthetic approach used to prepare dyads **4a,b** and assymmetric triads **5a,b**, shows that these species constitute another series of gaseous ions with stable, long-lived supramolecular assemblies. The molecular *cis* or *trans* conformation of these species has been found to have no particular effect on their intrinsic dissociation chemistry. Via ESI-MS/MS, it was also possible to access information on the relative bond strengths of these supermolecular ions. For the singly charged dyads **4a,b**$^{+}$, no significant differences were observed for the cleavage of the Ru–pyridine bond or the Ru–pyridyl bond, showing that the supramolecular arrangement is supported by a strong coordinative bond. However, as expected for the doubly charged triad ions **5a,b**$^{2+}$, no preferential cleavage of the Ru–pyridyl bond was observed as opposed to the Ru–bipyridine bond, which is stabilized by the chelate effect, being thus stronger than the interaction that keeps the integrity of the triads.

Regarding the photophysical behaviour of triads **5a,b**, any further comments based on the data presented here would be too speculative. Nevertheless, this work has shown that the coordination of the triruthenium compounds do quench the porphyrin luminescence, thus acting as a final acceptor of excitation energy. Under the conditions investigated here, the $[Ru(bpy)_2Cl]$ unit is also playing the function of excitation energy acceptor. Measurements at low temperature and different solvents are underway in our laboratories in order to evaluate if variations in experimental conditions would lead to a system where the $[Ru(bpy)_2]$ unit would act as a donor of excitation energy and also to get a better understanding on the mechanisms of the porphyrin luminescence quenching by the substituents **2** and **3**.

Acknowledgements

This work was supported by the São Paulo State Research Foundation (FAPESP), the Brazilian National Research Council (CNPq – RENAMI) and Instituto do Milênio de Materiais Complexos (CNPq – MCT). We would like to thank Prof. O.A. Serra and Dr. Cláudio Neri (both from FFCLRP – USP) for the use of the Spex Fluorolog 2 spectrophotometer and the kind help on the photophysical experiments.

References

[1] (a) C. Chevrin, J. Le Bras, A. Roglans, D. Harakat, J. Muzart, New J. Chem. 31 (1) (2007) 121;
(b) P. Wang, G.R. Newcome, C. Wesdemiotis, Int. J. Mass Spectrom. 255 (2006) 86.
[2] O. Bortolini, V. Conte, Mass Spectrom. Rev. 25 (5) (2006) 724.
[3] M.N. Eberlin, D.M. Tomazela, K. Araki, A.D.P. Alexiou, A.L.B. Formiga, H.E. Toma, S. Nikolaou, Organometallics 25 (13) (2006) 3245.
[4] (a) H.E. Toma, S. Nikolaou, M.N. Eberlin, D.M. Tomazela, Polyhedron 24 (2005) 731;
(b) F.C. Gozzo, L.S. Santos, R. Augusti, C.S. Consorti, J. Dupont, M.N. Eberlin, Chem. Eur. J. 10 (2004) 6187;
(c) M. Vazquez, M.R. Bermejo, M. Licchelli, A.M. Gonzalez-Nova, R.M. Pedrido, C. Sangregorio, L. Sorace, A.M. Garcia-Deibe, J. Satunartin, Eur. J. Inorg. Chem. (2005) 3479.
[5] (a) A.E.M. Crotti, R.L. Vessecchi, J.L.C. Lopes, N.P. Lopes, Quím Nova 29 (2) (2006) 287;
(b) R.B. Cole, in: Electrospray Mass Spectrometry, John Wiley, New York, 1997;
(c) R. Colton, A. D'Agostinho, J.C. Traeger, Mass Spectrom. Rev. 14 (1995) 79.
[6] (a) M. Zamora, S. Herrero, J. Losada, I. Cuadrado, C.M. Casado, B. Alonso, Organometallics 26 (10) (2007) 2688;
(b) J.L. Vera, F.R. Roman, E. Melendez, Bioinorg. Med. Chem. 14 (24) (2006) 8683;
(c) S. Nikolaou, M. Uemi, H.E. Toma, Spec. Lett. 3 (3) (2001) 267.
[7] (a) F.S. Vinhado, P.R. Martins, A.P. Masson, D.G. Abreu, E.A. Vidoto, Y. Iamamoto, O.R. Nascimento, J. Mol. Catal. A: Chem. 188 (2002) 141;
(b) M.A. Schiavon, L.S. Iwamoto, A.G. Ferreira, Y. Iamamoto, M.V.B. Zanoni, M.D. Assis, J. Braz. Chem. Soc. 11 (2000) 458;
(c) C.M.C.P. Manso, E.A. Vidoto, H.C. Sacco, J.R. Lindsay-Smith, P.R. Martins, A.G. Ferreira, Y. Iamamoto O.R. Nascimento, J. Mol. Catal. A: Chem. 150 (1999) 141;
(d) K. Lang, J. Mosinger, D.M. Wagnerová, Coord. Chem. Rev. 248 (3–4) (2004) 321.
[8] (a) R.A. Izquierdo, C.M. Barros, M.G. Santana-Marques, A.J. Ferrer-Correia, E.M.P. Silva, F. Giuntini, M.A.F. Faustino, J.P.C. Tome, A.C. Tome, A.M.S. Silva, C.P.M.S. Neves, J.A.S. Cavaleiro, A.F. Peixoto, M.M. Pereira, A.A.C.C. Pais, J. Am. Soc. Mass Spectrom. 18 (2) (2007) 218;
(b) E.M.P. Silva, V.V. Serra, A.O. Ribeiro, J.P.C. Tome, P. Domingues, M.A.F. Faustino, M.G.P.M.S. Neves, A.C. Tome, J.A.S. Cavaleiro, A.J. Ferrer-Correia, Y. Iamamoto, M.R.M. Domingues, Rapid Commun. Mass Spectrom. 20 (23) (2006) 3605;
(c) K.S.F. Lau, M. Sadilek, G.E. Khalil, M. Gouterman, C. Bruckner, J. Am. Chem. Soc. Mass Spectrom. 16 (12) (2005) 1915.
[9] (a) K. Kano, H. Kitagishi, C. Dagallier, M. Kodera, T. Matsuo, T. Hyashi, Y. Hisaeda, S. Hirota, Inorg. Chem. 45 (11) (2006) 4448;
(b) T. Haino, T. Fujii T, Y. Fukazawa, J. Org. Chem. 71 (7) (2006) 2572;
(c) D.M. Tomazela, F.C. Gozzo, I. Mayer, R.M. Engelmann, K. Araki, H.E. Toma, M.N. Eberlin, J. Mass Spectrom. 39 (10) (2004) 1161;

(d) S. Arai, S. Ishihara, S. Takeoka, H. Ohkawa, T. Shibue, H. Nishide, Rapid Commun. Mass Spectrom. 18 (18) (2004) 2065.
[10] H.E. Toma, K. Araki, A.D.P. Alexiou, S. Nikolaou, S. Dovidauskas, Coord. Chem. Rev. 219–221 (2001) 187.
[11] (a) H. Winnischofer, V.Y. Otake, S. Dovidauskas, M. Nakamura, H.E. Toma, K. Araki, Electrochim. Acta 49 (22–23) (2004) 3711;
(b) S. Dovidauskas, H.E. Toma, K. Araki, H.C. Sacco, Y. Iamamoto, Inorg. Chim. Acta 305 (2) (2000) 206.
[12] (a) B.J. Lear, S.D. Glover, J.C. Salsman, C.H. Londergan, C.P. Kubiak, J. Am. Chem. Soc. 129 (2007) 12772;
(b) H.E. Toma, S. Nikolaou, J. Chem. Res. (S). (2000) 326;
(c) H. Kido, H. Nagino, T. Ito, Chem. Lett. (1996) 745.
[13] (a) S. Nikolaou, H.E. Toma, J. Chem. Soc., Dalton Trans. (2002) 352;
(b) H. Kunkely, A. Vogler, Inorg. Chem. Commun. 4 (2001) 689;
(c) M. Otake, M. Itou, Y. Araki, O. Ito, H. Kido, Inorg. Chem. 44 (23) (2005) 8581.
[14] (a) S. Ye, W. Zhou, M. Abe, T. Nishida, L. Cui, K. Uosaki, M. Osawa, Y. Sasaki, J. Am. Chem. Soc. 126 (24) (2004) 7434;
(b) M. Itou, Y. Araki, H. Kido, Inorg. Chem. 45 (16) (2006) 6114.
[15] (a) V. Balzani, G. Bergamini, F. Marchioni, P. Ceroni, Coord. Chem. Rev. 250 (11–12) (2006) 1254. and references cited therein;
(b) A. Juris, V. Balzani, F. Barigelletti, S. Campagna, P. Belser, A. Vonzelewsky, Coord. Chem. Rev. 84 (1988) 85.
[16] (a) G. Kodis, Y. Terazono, P.A. Liddell, J. Andreasson, V. Garg, M. Hambourger, T.A. Moore, A.L. Moore, D. Gust, J. Am. Chem. Soc. 128 (6) (2006) 1818;
(b) R.E. Palacios, S.L. Gould, C. Herrero, M. Hambourger, A. Brune, G. Kodis, P.A. Lidell, J. Kennis, A.N. Macpherson, D. Gust, T.A. Moore, A.L. Moore, Pure Appl. Chem. 77 (6) (2005) 1001.
[17] (a) K. Araki, H. Winnischofer, F.M. Engelmann, H.E. Toma, P. Losco, J. Porphyr. Phthaloc. 6 (1) (2002) 33;
(b) P.A. Anderson, F.R. Keene, T.J. Meyer, J.A. Moss, G.F. Strouse, J.A. Treadway, J. Chem. Soc., Dalton Trans. 20 (2002) 3820.
[18] (a) B.P. Sullivan, D.J. Salmon, T.J. Meyer, Inorg. Chem. 17 (12) (1978) 3334;
(b) J.A. Baumann, D.J. Salmon, S.T. Wilson, T.J. Meyer, W.E. Hatifield, Inorg. Chem. 17 (12) (1978) 3342;
(c) A.D. Adler, F.R. Longo, W. Shjergalis, J. Am. Chem. Soc. 86 (15) (1964) 3145.
[19] E.Z. Moreira, in: Synthesis and characterization of pentafluorophenyl-porphyrins substituted with ruthenium complexes, MS Thesis, São Paulo University, 2007.
[20] S.F. McClanahan, R.F. Dallinger, F.J. Holler, J.R. Kincard, J. Am. Chem. Soc. 107 (1985) 4853.
[21] E.R. Birnbaum, J.A. Hodge, M.W. Grinstaff, W.P. Schaefer, L. Henling, J.A. Labinger, J.E. Bercaw, H.B. Gray, Inorg. Chem. 34 (14) (1995) 3625.
[22] G.Z.G. Meng, B.R. James, K.A. Skov, Can. J. Chem. 72 (1994) 1894.
[23] T.P. Wijesekera, D. Dolphin, Metalloporphyrins in Catalytic Oxidations, Marcel Deker Inc., New York, 1994.
[24] V. Balzani, F. Scandola, in: Supramolecular Photochemistry, Ellis Horwood, Chichester, UK, 1991.
[25] M. Itou, M. Otake, Y. Araki, O. Ito, H. Kido, Inorg. Chem. 44 (5) (2005) 1580.
[26] J.C. Curtis, J.S. Berstein, T.J. Meyer, Inorg. Chem. 24 (1985) 385.

Polyhedron 27 (2008) 2731–2738

Contents lists available at ScienceDirect

Polyhedron

journal homepage: www.elsevier.com/locate/poly

Synthesis, characterization, crystal structures, *in vitro* and *in vivo* antitumor activity of palladium(II) and zinc(II) complexes with 2-formyl and 2-acetyl pyridine N(4)-1-(2-pyridyl)-piperazinyl thiosemicarbazone

Dimitra Kovala-Demertzi [a,*], Alexandros Alexandratos [a], Athanassios Papageorgiou [b], Paras Nath Yadav [a], Panagiotis Dalezis [b], Mavroudis A. Demertzis [a]

[a] Department of Chemistry, University of Ioannina, 45110 Ioannina, Greece
[b] Symeonidio Research Center, Theagenio Cancer Hospital, Thessaloniki, Greece

ARTICLE INFO

Article history:
Received 9 January 2008
Accepted 9 April 2008
Available online 23 July 2008

Keywords:
Palladium(II, zinc(II)) complexes
Thiosemicarbazonato complexes
Crystal structure
Spectroscopic studies
Anti-tumor activity

ABSTRACT

The present paper includes synthesis and spectral characterization of the novel prepared palladium(II) and zinc(II) complexes with 2-formyl pyridine N(4)-1-(2-pyridyl)-piperazinyl thiosemicarbazone, HFo4Npypipe, **1** and the 2-acetyl pyridine N(4)-1-(2-pyridyl)-piperazinyl thiosemicarbazone, HAc4Npypipe, **2**. The Pd(II) complexes [PdCl(Fo4Npypipe)], **3**, [PdCl(Ac4Npypipe)], **4** and the Zn(II) complexes [$ZnCl_2$(Fo4Npypipe)], **5** and [$ZnCl_2$(Ac4Npypipe)], **6** have been characterized by elemental analyses and spectroscopic studies. The crystal structure of the complexes [PdCl(Fo4Npippy)], **3** and [PdCl(Ac4Npippy)], **4**, have been solved by single-crystal X-ray diffraction. The electronic, IR, UV/Vis, and NMR spectroscopic data of the complexes are reported. The results of the cytotoxic activity of **1**–**6** have been evaluated *in vitro* against the cells of three human cancer cell lines: MCF-7, T24, A-549 and a mouse L-929 (a fibroblast-like cell line cloned from strain L). For selected compounds **2** and **6** the acute toxicity and antitumor activity were evaluated on leukemia P388-bearing mice. The Zn(II) compounds **5** and **6** are considered as agents with potential antitumor activity, and can therefore be candidates for further stages of screening *in vitro* and/or *in vivo*.

© 2008 Elsevier Ltd. All rights reserved.

1. Introduction

Tsc's are among the most potent inhibitors of ribonucleotide reductase, RR, activity. RR catalyzes the synthesis of deoxyribonucleotides from their ribonucleotide precursors and as such is responsible for maintaining a balanced supply of the deoxyribonucleotides required for DNA synthesis and repair. Strong positive correlation has been established between RR activity and the rate of replication of cancer cells. The mechanism of action of Tscs is due to their ability to inhibit the biosynthesis of DNA, possibly by blocking the enzyme ribonucleotide diphosphate reductase, binding to the nitrogen bases of DNA, hindering or blocking base replication and creation of lesions in DNA strands by oxidative rupture [1].

The chemistry of transition metal complexes of thiosemicarbazone, Tsc's, has been receiving considerable attention largely because their broad profile of pharmacological activity affords a diverse variety of compounds with different activities [2]. The biological properties of Tsc's are often related to metal ion coordination. Firstly, lipophilicity, which controls the rate of entry into the cell, is modified by coordination and some side effects may decrease upon complexation. In addition, the complex can exhibit bioactivities which are not shown by the free ligand [3–9]. The combination of Tsc's with agents like platinum(II) and palladium(II) that damage DNA produces synergistic inhibition of tumor growth and may lead to improvements in the effectiveness of cancer chemotherapy regimens [3–9]. Zinc is the second most prominent trace metal in the human body after iron. Zinc deficiency may cause growth effects, although unlike copper and iron few noxious effects of excess zinc have been observed. Zinc is essential for growth and developments and plays an important role in various biological systems and is a vital component an essential cofactor, critical for numerous cellular processes and may be a major regulatory ion in the metabolism of cells. Zinc is cytoprotective and suppresses apoptotic pathways. Also, zinc plays a role in brain, where it has a specific function as a neuromodulator in addition to its other typical cellular functions [10].

The present work is an extension of previously studied platinum(II), palladium(II) and zinc(II) complexes of 2-acetylpyridine-thiosemicarbazones and 2-carbaldehyde thiosemicarbazone with potentially interesting biological activities [5–9]. The present paper includes synthesis and spectral characterization of the newly prepared palladium(II) and zinc(II) complexes with 2-formylpyridine

* Corresponding author. Tel.: +30 2651098425; fax: +30 2651098786.
E-mail address: dkovala@cc.uoi.gr (D. Kovala-Demertzi).

0277-5387/$ - see front matter © 2008 Elsevier Ltd. All rights reserved.
doi:10.1016/j.poly.2008.04.009

N(4)-1-(2-pyridyl)-piperazinyl thiosemicarbazone, HFo4Npypipe, **1** and the 2-acetyl pyridine N(4)-1-(2-pyridyl)-piperazinyl thiosemicarbazone, HAc4Npypipe, **2** and the crystal structure of the complexes [PdCl(Fo4Npippy)], **3** and [PdCl(Ac4Npippy)], **4**. The cytotoxic activities of **1**–**6** have been evaluated *in vitro* against the cells of three human cancer cell lines: MCF-7 (human breast cancer cell line), T24 (bladder cancer cell line), A-549 (non-small cell lung carcinoma) and a mouse L-929 (a fibroblast-like cell line cloned from strain L). For selected compounds **2** and **6** the acute toxicity and antitumor activity were evaluated on leukemia P388-bearing mice.

2. Experimental

2.1. General and instrumental

Solvents were purified and dried according to standard procedures. Infrared and far-infrared spectra were recorded on a Perkin Elmer Spectrum GX Fourier transform spectrophotometer using KBr pellets (4000–400 cm^{-1}) and Nujol mulls dispersed between polyethylene disks (400–40 cm^{-1}). UV–Vis spectra were acquired with a JASCO V-570 UV/Vis/NIR spectrophotometer. The ^1H (250.13 MHz) spectra were obtained on a Bruker AMX-400 spectrometer at room temperature with the signal of the free DMSO or $CHCl_3$ (at 2.49 and 7.24 ppm, respectively) as a reference. Cross-peaking of heteronuclear multiple quantum correlation (HMQC) and heteronuclear multiple bond correlation (HMBC) gradient-assisted spectra **1** and **2** were performed. Elemental analyses, C, H, N and S were performed on a Carlo Erba EA (model 1108).

2.1.1. Preparation of the ligands

*2-Formyl pyridine N(4)-1-(2-pyridyl)-piperazinyl thiosemicarbazone (HFoPy4PyPiz), **1** and 2-acetyl pyridine N(4)-1-(2-pyridyl)-piperazinyl thiosemicarbazone (HAcPy4PyPiz), **2***: 4-methyl-4-phenyl-3-thiosemicarbazide was prepared according to the method described by Scovil [11]. The crude product, 4-methyl-4-phenyl-3-thiosemicarbazide, was recrystallized from a mixture of EtOH and distilled water (3:1). To a solution of 4-methyl-4-phenyl-3-thiosemicarbazide (0.905 g, 5 mmol) in CH_3CN (5 ml), 1-(2-pyridyl) piperazine (8 ml, 5 mmol) and 2-formyl pyridine (0.47 ml, 5 mmol) or 2-acetyl pyridine (0.56 ml, 5 mmol) were added. The mixture was refluxed for 25 min and then left standing in a refrigerator for 12 h. The resulting yellow precipitates were filtered off, washed with cold CH_3CN, recrystallized from CH_3CN and dried in vacuo over silica gel, and then at 40 °C in vacuo over P_4O_{10} for 3 h. **1**: Yield: 62%. Mp 159 °C. IR (cm^{-1}): 3141m, ν(NH); 2970, 2835s, $\nu(CH_2)$; 1599s, ν(C=N); 1561s, δ(NH); 1102ms, ν(NN); 922s, ν(C=S); 643ms, δ(py). UV–Vis: ($CHCl_3$)λ/cm^{-1} ($\log\varepsilon$) 31,545 (3.30); (DMF) λ/cm^{-1} ($\log\varepsilon$) 32,400 (4.18). *Anal.* Calc. for $C_{16}H_{18}N_6S$ (M_W: 326.42): C, 58.9; H, 5.6; N, 25.7; S, 9.8. Found: C, 59.0; H, 5.8; N, 25.9; S, 9.7%. Compound **2**: Yield: 43%. Mp 142 °C. IR (cm^{-1}): 3231w, ν(NH); 2995w, 2848 m, $\nu(CH_2)$; 1595s, ν(C=N); 1560m, δ(NH); 1087m, ν(NN); 941ms, ν(C=S); 649m, δ(py). UV–Vis: ($CHCl_3$)λ/cm^{-1} ($\log\varepsilon$) 32 790 (3.17), 25 060 (3.02); (DMF) λ/cm^{-1} ($\log\varepsilon$) 33 420 (3.78). *Anal.* Calc. for $C_{17}H_{20}N_6S$ (M_W: 340.45): C, 59.9; H, 5.9; N, 24.7; S, 9.4. Found: C, 59.7; H, 6.6; N, 25.1; S, 10.2.

2.1.2. Preparation of the complexes

*Chloro(2-formyl pyridine N(4)-1-(2-pyridyl)-piperazinyl-thiosemicarbazonato) palladium(II) [PdCl(FoPy4PyPiz)], **3** and chloro(2-acetyl pyridine N(4)-1-(2-pyridyl)-piperazinyl thiosemicarbazonato) palladium(II) ([PdCl(AcPy4PyPiz)], **4***: To lithium tetrachloropalladate, prepared *in situ* from $PdCl_2$ (0.1241 g, 0.7 mmol) and LiCl (0.847 g, 2 mmol), in MeOH (5 ml), was added a soln. of ligand **1** (0.1827 g, 0.56 mmol) or **2** (0.1908 g, 0.56 mmol) in MeOH (5 ml). The mixture was stirred for 24 h at RT and then left in a refrigerator for 24 h. The resulting orange precipitate was filtered off, washed with cold MeOH and Et_2O, recrystallized from MeOH and dried *in vacuo* over silica gel, and then at 70° *in vacuo* over P_4O_{10} for 2 h. Compound **3**: Yield: 83%. Orange powder. Mp 245 °C (dec.) IR (cm^{-1}): 3051m, 2933s, $\nu(CH_2)$; 1639s, 1609s, ν(C=N); 1389w, ν(NCS); 1231s, ν(NN); 885w, ν(C=S); 463m, ν(PdN); 386m, ν(PdS); 346m, ν(Pd–Cl); 315m, $\nu(PdN_{Py})$. UV–Vis: ($CHCl_3$) λ/cm^{-1} ($\log\varepsilon$) 32 360 (3.07), 25 445 (3.07), 20 060 (2.56)sh; (DMF) λ/cm^{-1} ($\log\varepsilon$) 32 790 (3.17), 26 040 (3.15), 21 010 (2.67)sh. *Anal.* Calc. for $C_{16}H_{17}N_6SPdCl$ (M_W: 467.3): C, 41.2; H, 3.9; N, 18.0; S, 6.8. Found: C, 41.1; H, 3.7; N, 18.0; S, 6.9%. Compound **4**: Yield: 73%. Orange powder. Mp 275 °C (dec.). IR (cm^{-1}): 2917m, $\nu(CH_2)$; 1643s, 1615s, ν(C=N); 1106w, ν(NN); 880w, ν(C=S); 655m, δ(py); 467m, ν(PdN); 384s, ν(PdS); 342s ν(Pd–Cl); 283s, $\nu(PdN_{Py})$. UV–Vis: ($CHCl_3$)λ/cm^{-1} ($\log\varepsilon$) 31 845 (3.22), 25 770 (3.17), 20 920 (2.74)sh; (DMF) λ/cm^{-1} ($\log\varepsilon$) 32 360 (3.20), 26 455 (3.13), 21 230 (2.66)sh. *Anal.* Calc. for $C_{17}H_{19}N_6SPdCl$ (M_W: 481.3): C, 42.4; H, 4.0; N, 17.6; S, 6.7. Found: C, 42.8; H, 4.11; N, 17.1; S, 5.9.

*Dichloro(2-formylpyridine N (4)-1-(2-pyridyl)-piperazinyl thiosemicarbazonato)zinc(II), [$ZnCl_2$(HFoPy4PyPiz)], **5** and dichloro(2-acetyl pyridine N(4)-1-(2-pyridyl)-piperazinyl thiosemicarbazonato)zinc(II), [$ZnCl_2$ (HAcPy4PyPiz)]*, **6**: To a soln. of $ZnCl_2$ (0.1362 g, 1 mmol) in EtOH (25 ml) ligand **1** (0.3264 g, 1 mmol) or **2** (0.3404 g, 1 mmol) were added. The mixture was refluxed for 2 h. The yellow precipitate was filtered off, washed with cold EtOH, recrystallized from EtOH, dried *in vacuo* over silica gel, and re-dried at 50 °C *in vacuo* over P_4O_{10} for 12 h. Compound **5**: Yield: 83%. Yellow powder. Mp 264 °C. IR (cm^{-1}): 3089w, ν(NH); 2865 m, $\nu(CH_2)$; 1643s, ν(C=N); 1604s, δ(NH); 1129s, ν(NN) 894m, ν(C=S); 665m, δ(py); 457m, ν(Zn–N); 365m, ν(ZnS); 325s, 304ms ν(Zn–Cl); 268s, $\nu(Zn–N_{Py})$. UV–Vis: (DMF) λ/cm^{-1} ($\log\varepsilon$) 32 405 (4.05), 24 415 (4.26). *Anal.* Calc. for $Zn(C_{16}H_{18}N_6S)Cl_2$ (M_W: 462.73): C, 41.5; H, 3.9; N, 18.2; S, 6.9. Found: C, 41.5; H, 4.4; N, 18.3; S, 7.0%. Compound **6**: Yield: 76%. Yellow powder. Mp 265 °C. IR (cm^{-1}): 3477w, 3414w, 3254s, ν(NH); 3000m, 2866m, $\nu(CH_2)$; 1639s, ν(C=N); 1616s, δ(NH); 1110ms, ν(NN); 813s, ν(C=S); 670w, δ(py); 464m, ν(Zn–N); 411s, ν(Zn–S); 325m, 305ms, ν(Zn–Cl); 269ms, $\nu(Zn–N_{Py})$. UV–Vis: (DMF) λ/cm^{-1} ($\log\varepsilon$) 32 575 (4.18), 24 840 (4.17), 23 855 (4.07). *Anal.* Calc. for $Zn(C_{17}H_{20}N_6S)Cl_2$ (M_W: 476,71): C, 42.8; H, 4.2; N, 17.6; S, 6.7. Found: C, 42.9; H, 4.3; N, 17.6; S, 6.7%.

2.2. X-ray crystallography

A summary of the crystal data, experimental details and refinement results are listed in Table 1. All measurements of crystals were performed on a Bruker-P4 diffractometer. Data were collected at 293 K using Mo Kα radiation (λ = 0.71073 Å) and the ω-scan technique, and corrected for Lorentz and polarization effects. A semi-empirical absorption correction (Ψ-scans) was made. Cell constants and an orientation matrix for data collection were obtained by least-squares refinement of the diffraction data from 25 reflections in the range $2.33 < \theta < 24.99$ for **3** and $2.48 < \theta < 26.81$ for **4**. The structure was solved by direct methods (program SHELXS SHELXS-97) and refined by the full-matrix least-squares method on all F^2 data using the WINGX version of SHELXL SHELXL-97 programs [12]. Non-hydrogen atoms were refined with anisotropic displacement parameters; all hydrogen atoms were located in their calculated positions (C–H 0.93–0.97 Å) and refined using a riding model for **3** and **4**. Atomic scattering factors are from "International Tables for X-ray Crystallography" and molecular graphics were performed from PLATON2001 [12].

2.3. In vitro growth inhibition assay

Compounds: Test solutions of the compounds tested (1 mg/ml) were prepared by dissolving the substance in 100 μl of DMSO com-

Table 1
Crystal data and structure refinement for **3** and **4**

	3	**4**
Empirical formula	$C_{16}H_{17}Cl\ N_6PdS$	$C_{17}H_{19}ClN_6PdS$
Formula weight	467.27	481.27
Temperature (K)	293(2)	293(2)
Wavelength (Å)	0.71073	0.71073
Crystal system	monoclinic	monoclinic
Space group	*P*21/*c* (No. 14)	*P*21/*c* (No. 14)
Unit cell dimensions		
a (Å)	13.984(2)	7.624(1)
b (Å)	11.558(1)	28.030(4)
c (Å)	11.819(2)	8.602(1)
α (°)	90	90
β(°)	107.58(1)	94.79(1)
γ °	90	90
Volume (Å^3)	1821.1(4)	1831.8(4)
Z, D_{calc} (Mg/m^3)	4, 1.704	4, 1.745
Absorption coefficient (mm^{-1})	1.292	1.287
F(000)	936	968
Crystal size (mm)	0.16 × 0.16 × 0.20	0.15 × 0.15 × 020
Reflections collected/unique	3125/3125 [*R*(int) = 0.0225]	4154/3860 [*R*(int) = 0.0325]
Data [$I > 2\sigma(I)$]	2594	1319
Absorption correction	empirical (DIFABS)	empirical (DIFABS)
Data/restraints/parameter	3125/0/226	3860/0/236
Goodness-of-fit on F^2	0.986	0.946
Final *R* indices [$I > 2\sigma(I)$]	R_1 = 0.0290, wR_2 = 0.0723	R_1 = 0.0406 wR_2 = 0.0681
Largest difference in peak and hole (e/Å^3)	0.322 and −0.246	0.348 and −0.362

pleted with 900 μl of tissue culture medium. Afterwards, the tested compounds were diluted in culture medium to reach the final concentrations of 100, 10, 1, and 0.1 ng/μl. The solvent (DMSO) in the highest concentration used in test did not reveal any cytotoxic activity. *Cells*: The cell lines are maintained in the Cell Culture Collection of the University of Ioannina. Twenty-four hours before addition of the tested agents, the cells were plated in 96-well plates at a density of 10^4 cells per well. The MCF-7 cells were cultured in the D-MEM (Modified Eagle's Medium) medium supplemented with 1% antibiotic and 10% fetal calf serum. L-929 cells were grown in Hepes-buffered RPMI 1640 medium supplemented with 10% fetal calf serum, penicillin (50 U/ml) and streptomycin (50 mg/ml). A-549 cells were grown in F-12K Ham's medium supplemented with 1% glutamine, 1% antibiotic/antimycotic, 2% $NaHCO_3$ and 10% fetal calf serum. The cell cultures were maintained at 37 °C in a humid atmosphere saturated with 5% CO_2. Cell number was counted by the Trypan blue dye exclusion method. MCF-7, L-929 and A-549 cells were determined by the sulforhodamine B assay [13], while T24 cells by the MTT assay [14]. The *in vitro* tests were performed as described previously [9a,9c].

2.4. In vivo antitumor experiments [15]

Mice: Male and female DBA/2 and BDF/1 (C57BL x DBA/2) that were 8–10 weeks old and weighed 20–25 g were used for toxicity studies and antitumor evaluation. The mice were obtained from the Experimental Laboratory of Theagenion Anticancer Institute, and kept in sterile cages under conditions of constant temperature and humidity, with water and food. Lymphocytic P388 Leukemia was maintained in ascetic form in DBA/2 mice by injection of 10^6 cells into the peritoneal cavity at 6-day intervals.

Compounds: For intraperitoneal treatment, stock solutions of the compounds used in this study were made immediately before use. They were suspended in corn oil in the desired concentration following initial dissolution in a small amount of 10% dimethylsulfoxide. This concentration by itself produced no observable toxic effect. A drop of Tween 80 was added. The estimation of acute toxicity and the antitumor evaluation were performed as described previously [5b,5c,6b].

3. Results and discussion

3.1. Synthetic aspects

HFo4Npypipe and HAc4Npypipe were synthesized by the condensation of 3-methyl-3-phenyl-thiosemicarbazide synthesized according to Scovil [11], formyl pyridine or 2-acetyl pyridine and 1-(2-pyridyl)-piperazine. The Pd(II) complexes [PdCl(FoPy4PyPiz)], **3** *and* [PdCl(AcPy4PyPiz)], **4** were prepared by reacting lithium tetrachloropalladate (Li_2PdCl_4) – prepared *in situ* from $PdCl_2$ and LiCl – with the **1** or **2** in MeOH solution in a molar ratio of 1:1. It has been found that palladium(II) promotes deprotonation of thiosemicarbazones in the presence of methanolic solutions [6–8]. The Zn(II) complexes [$ZnCl_2$(HFoPy4PyPiz)], **5** and [$ZnCl_2$(HAcPy4-PyPiz)], **6** were prepared by refluxing $ZnCl_2$ with the **1** or **2** in EtOH solution in a molar ratio of 1:1. The formula of these Pd(II) and Zn(II) complexes were confirmed by elemental analysis, spectroscopic studies and for **3** and **4** by X-ray analysis. The stoichiometries of the complexes indicate that Pd(II) is coordinated by the singly charged anion Fo4Npypipe$^-$ and Ac4Npypipe$^-$ in **3** and **4**, while Zn(II) is coordinated by the neutral molecule HFo4Npypipe and HAc4Npypipe in **5** and **6**. For details, (see Section 2).

3.2. Structural characterization

Complexes **3** and **4** were recrystallized from MeCN and dimethylformamide, respectively, to furnish orange prisms suitable for single-crystal X-ray analysis. Selected interatomic distances and bond angles are collected in Table 2. Anionic **1** and **2** act as tridentate ligands coordinating to the Pd^{II} center through the pyridyl N-atom, N(1), the azomethine N-atom, N(2), and the thiolato S-atom, Figs. 1 and 2. The ligand shows a (*Z*, *E*, *Z*)-configuration for these three donor centers, respectively. The S–C bond distance is consistent with an increased single-bond character, and both thioamide C=N distances indicate increased double-bond character. The ligands are planar, as indicated by the dihedral angle between the mean planes of the pyridyl ring and the chelate ring Pd–S–C–N–N, as well as between the mean planes of the pyridyl ring and the Pd–N–C–C–N, with values of only 2.6(2)°, 0.8(2)° and 1.5(3)° and 1.0(3)° for **3** and **4**, respectively. The dihedral angle between the mean planes of the N(4)-1-(2-pyridyl) and the piperazinyl ring is 9.3(2)° and 71.2(4)° for **3** and **4**, respectively. The monomers of **3** form hydrogen-bonded dimers linked by two hydrogen bonds C(2)–H(2)···Cl involving the C(2)H(2) hydrogen atom and the chloro atom and vice versa of centrosymetrically related pairs of

Table 2
Selected bond distances (Å) and angles for **3** and **4**

3		**4**	
Pd–N(2)	1.948(2)	Pd(1)–N(2)	1.953(6)
Pd–N(1)	2.067(3)	Pd(1)–N(1)	2.049(6)
Pd–S	2.242(1)	Pd(1)–S(1)	2.271(3)
Pd–Cl	2.299(1)	Pd(1)–Cl(1)	2.297(2)
S–C(7)	1.764(3)	S(1)–C(8)	1.783(8)
N(1)–C(1)	1.335(5)	N(1)–C(5)	1.347(10)
N(1)–C(5)	1.354(4)	N(1)–C(1)	1.348(10)
N(2)–Pd–N(1)	81.07(10)	N(2)–Pd(1)–N(1)	80.0(3)
N(2)–Pd–S	84.53(8)	N(2)–Pd(1)–S(1)	85.2(2)
N(1)–Pd–S	165.36(7)	N(1)–Pd(1)–S(1)	165.3(2)
N(2)–Pd–Cl	177.25(7)	N(2)–Pd(1)–Cl(1)	177.2(2)
N(1)–Pd–Cl	97.79(7)	N(1)–Pd(1)–Cl(1)	97.1 (2)
S–Pd–Cl	96.71(3)	S(1)–Pd(1)–Cl(1)	97.6(1)

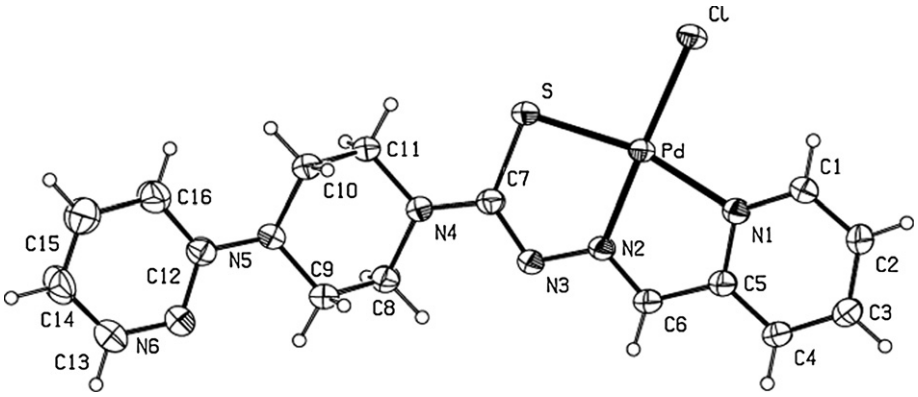

Fig. 1. Molecular structure of [PdCl(FoPy4PyPiz)], **3**.

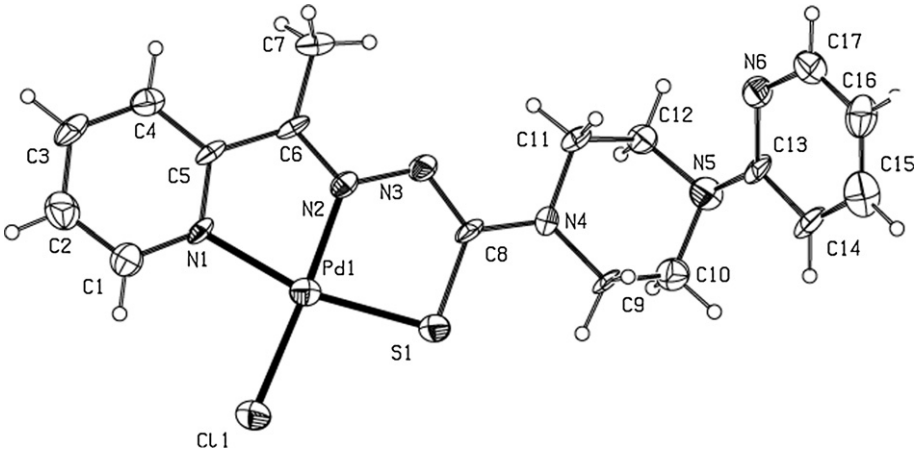

Fig. 2. Molecular structure of [PdCl(AcPy4PyPiz)], **4**.

molecules. The observed hydrogen-bonding pattern is of the double DA = AD type. The same chloro atoms of the dimers participates in intermolecular hydrogen bonds of C–H–Cl type. The dimmers are connected by two intermolecular bonds C(4)–H(4)···Cl and C(6)–H(6)···Cl, Fig. 3, Table 3. Also, C–H-π and double weak π → π interactions are observed in **3**. The most significant π → π interactions being that between the pair of rings N(1)–C(1)–C(2))–C(3)–C(4))–C(5) and N(6)–C(13)–C(14))–C(15)–C(16))–C(12) at a center to center separation of 4.165(3) Å. Intermolecular H-bonding, π → π, and CH → π interactions help to stabilize the structure, Fig. 4. The monomers of **4** are connected by strong π–π interactions in dimmers and are arranged in a head to tail fashion.

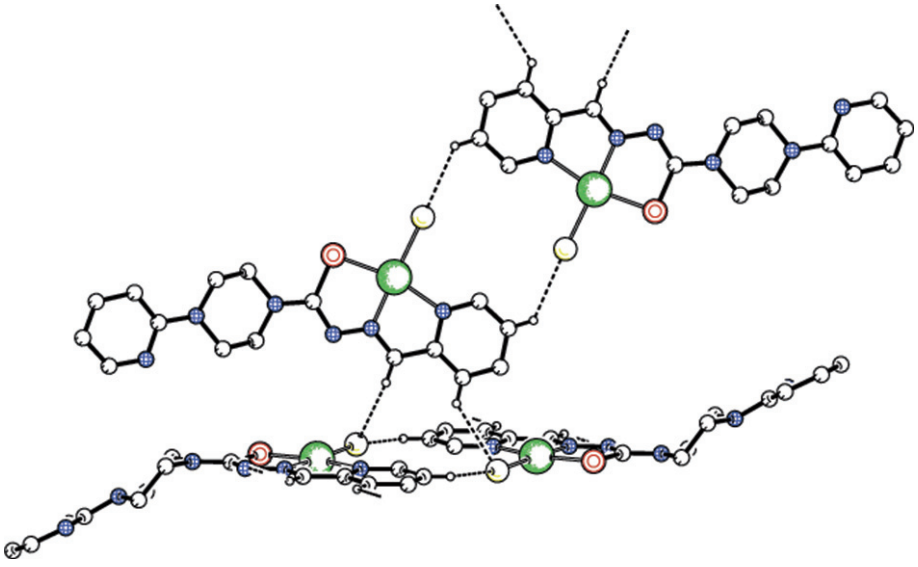

Fig. 3. Arrangement of the intermolecular hydrogen bonds in [PdCl(FoPy4PyPiz)], **3**.

Table 3
Inter- and intra-molecular hydrogen bonds for **3** and π–π interactions and intramolecular hydrogen bonds for **4**

D	H	A[b]	D···A	H···A	D–H···A
Inter- and intra-molecular hydrogen bonds for **3**					
C(2)[i]	H(2)	Cl	3.482(5)	2.78	133
C(4)[ii]	H(4)	Cl	3.424(5)	2.70	135
C(6)[iii]	H(6)	Cl	3.610(4)	2.73	157
C(8)	H(8A)	N(3)	2.736(5)	2.30	107
C(9)	H(9A)	N(6)	2.705(6)	2.33	102
C(11)	C(11A)	S	3.025(4)	2.48	115
		Cg–Cg[b]	β[c]	CgI-Perp[d]	CgJ-Perp[e]
π–π, *and intra-molecular hydrogen bonds for* **4**					
Cg(1) → Cg(2)[iv]		3.782(4)	17.91	3.610	3.599
Cg(1) → Cg(3)[v]		3.644(4)	15.54	3.493	3.510
Cg(2) → Cg(3)[v]		3.706(5)	18.92	3.501	3.506
D	H	A[b]	D···A	H···A	D–H···A
C(7)	H(7C)	N(3)	2.782(12)	2.36	106
C(11)	H(11B)	N(3)	2.674(10)	2.55	103
C(9)	H(9A)	S	3.039(9)	2.55	111

Cg(3) and Cg(5) refer to the centroids N(1)–C(1)–C(2))–C(3)–C(4))–C(5) and N(6)–C(13)–C(14))–C(15)–C(16) –C(12) resp., Cg(1) and Cg(2) refer to the centroids Pd(1)–S–C(7)–N(3)–N(2) and Pd(1)–N(2)–C(5)–C(4)–N(1). D and A refers to donor and acceptor, respectively.

[a] Symmetry transformations (i), $-x, -y, 2-z$; (ii) $-x, 1/2+y, 3/2-z$; (iii) $x, 1/2-y, -1/2+z$; (iv) $2-x, -y, 1-z$; $1-x, -y, 1-z$.

[b] Cg–Cg is the distance between ring centroids.

[c] Where β is the angle Cg(I) → Cg(J).

[d] CgI-Perp is the perpendicular distance of Cg(I) on ring J.

[e] CgJ-Perp is the perpendicular distance of Cg(J) on ring I.

Double strong π–π interactions connect the pair of rings PdN(2)N(3)C(8)S and N(1)C(1)C(2)C(4)C(5) at a center separation of 3.644(4), Fig. 5, Table 3.

3.3. Spectroscopy

Infrared spectroscopy: The significant IR bands of Pd(II) and zinc(II) complexes are close in energy to those found in other compounds with tridentate coordination [4–9]. The coordination of the azomethine N-atom to the M(II) center was suggested in the IR spectra of complexes **3**–**6**, relative to those of the free ligands, by a shift of the ν(C=N) band to lower frequencies, along with the occurrence of a ν(N–N) band to higher frequency. Furthermore, the presence of a band at *ca.* 450–460 cm^{-1} was assigned to ν(M–N). The thioamide band, which contains considerable ν(CS) character, was less intense in the complexes and found at a lower frequency, suggesting coordination of the metal through sulfur after deprotonation for **3** and **4**. Coordination of the thiolato S-atom was further indicated by a decrease in the energy of the thioamide band, as well as by the presence of a band at *ca.* 360–380 cm^{-1} assignable to ν(M–S). The band at 346 and 348 cm^{-1} is assigned to ν(Pd–Cl) for **3** and **4**, respectively. Bands at 325, 304 cm^{-1} and at 325, 305 cm^{-1} are assigned to ν(Zn–Cl) for **5** and **6**, respectively.

UV/Vis absorption spectra: The electronic absorption spectra of **1** and **2** in (DMF solution) exhibit bands at *ca.* 32400 and 33420 cm^{-1}, respectively, and are due to $n \rightarrow \pi^*$ transitions. This band is associated with the azomethine functions of the thiosemicarbazone moieties [9]. The bands of the Zn(II) complexes **5** and **6**, in the same solvent, are exhibited bands at 23855–24840 and at

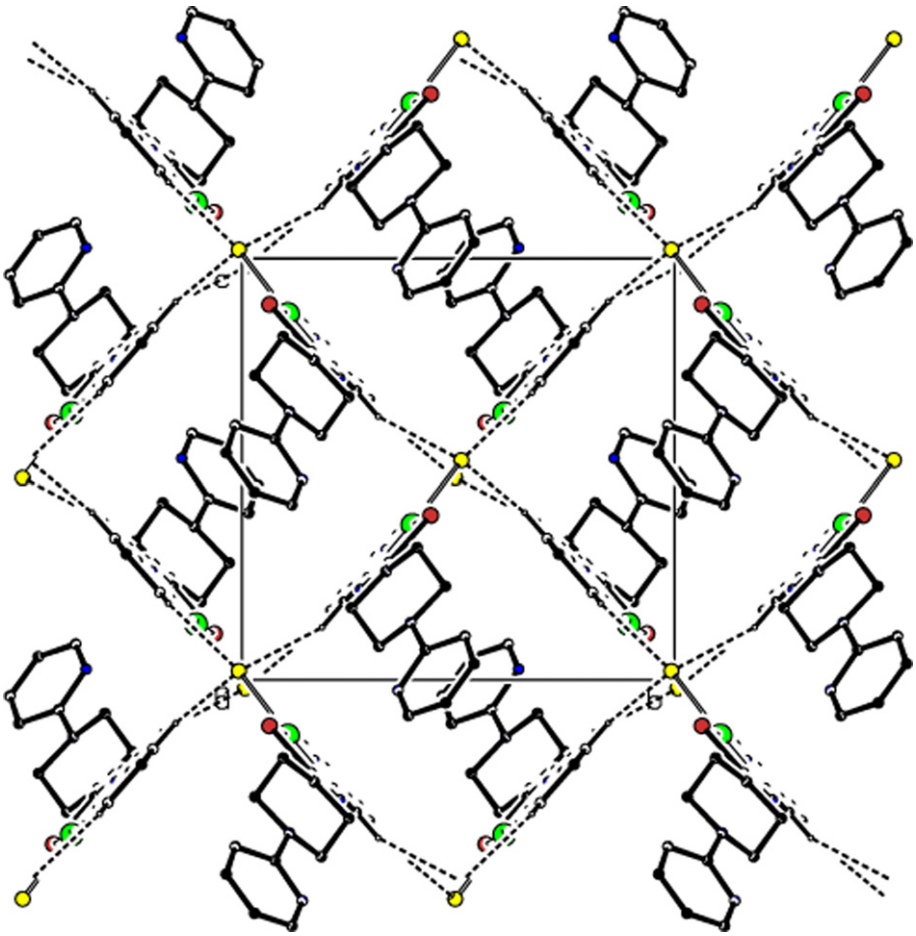

Fig. 4. A view of the extended network of [PdCl(FoPy4PyPiz)], **3**, along the *a* axis.

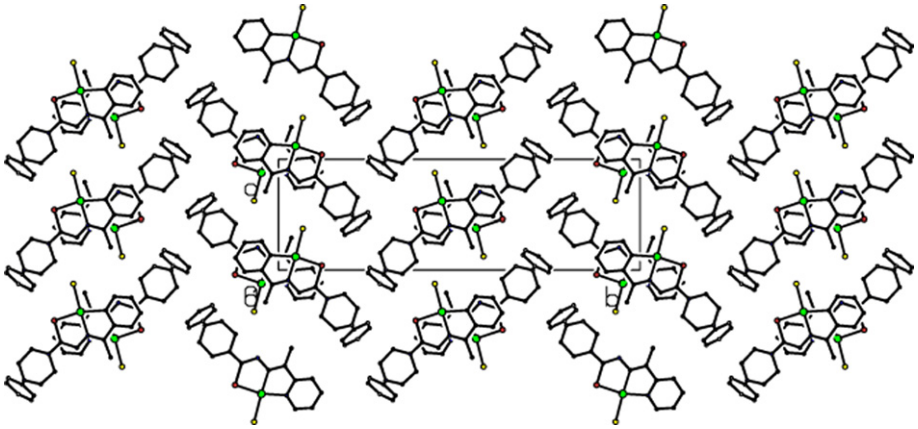

Fig. 5. A view of the extended network of [PdCl(AcPy4PyPiz)], **4**, along the *a* axis.

32 400–32 575 cm^{-1}. The absorptions in the ultraviolet region are assignable to transitions within the ligand orbitals and that in the visible region is probably due to charge transfer transition involving ligand and metal orbitals, transitions from S → Zn and N → Zn [9]. The electronic spectra of complexes **3** and **4** were indicative of square-planar geometries. In the visible region, three spin-allowed S → S (d → d) transitions can be expected. However, strong charge-transfer (CT) transitions interfered preventing the observation of all these predicted bands. The very intense band at about 21 000 cm^{-1} is assignable to a combination of sulfur → Pd(II), nitrogen (pyridyl) → Pt(II) charge transfer (L(p) → MCT) and Pd(II) d–d bands. The strong band at about 26 000 cm^{-1} is assignable to a combination of metal–ligand charge transfer (M → LCT) and d–d bands [5–9].

NMR Spectra: Peak assignments were based on ^{2}D NMR data (^{1}H, ^{1}H-COSY, ^{1}H,^{13}C-HMQC, ^{1}H,^{13}C-HMBC). In the ^{1}H NMR spectra of the ligand **1** and **2** H–N(3) resonated at *ca.* (H) 11.50 and 9.12, respectively, indicating that this H-atom is involved in H-bonding [6]. This resonance was absent in the spectra of the corresponding Pd(II) complexes, which indicated deprotonation of H–**N**(**3**) and, thus, anionic thiosemicarbazone moieties. The absence of peaks corresponding to the imino protons in **3** and **4** indicates that the ligands are present in the deprotonated form. These changes suggest that deprotonation and metallation exists and the structure of the complexes **3** and **4** in the solid state persists in $(CD_3)_2SO$ solution. In the ^{1}H and ^{13}C NMR spectra of the Pd(II) and Zn(II) complexes **3**–**6** the hydrogen and carbon atoms of the pyridyl ring H–C(1) were shifted upon coordination, which indicated variations in the electron density of the pyridyl ring These signals were shifted downfield, in accord with an decreased electron density at these sites in the complexes. The C=S resonance of the thiosemicarbazone moiety in **2** resonated at 180.95 ppm. In the complexes **3** and **5**, downfield shifts were observed, indicating decreased electron density from the thiolato C-atoms [6]. The C=S resonance of the thiosemicarbazone moiety in **2** resonated at 182.71 ppm and in the complexes **4** and **6**, upfield shifts were observed, indicating in-

Table 4
Proton and ^{13}C NMR data[a]

Compound	C(1)**H**	C(2)**H**	C(3)**H**	C(4)**H**	C(6)**H**	C(7)**H** C(8)**CH$_3$**	N(3)**H**	N(4)-Piperazinyl	N(4)-Pyridyl			
								CH$_2$	C(14)**H**	C(15)**H**	C(16)**H**	C(17)**H**
HFoPy4PyPiz	8.58d	7.36t	7.82–7.89m	7.73–7.82m	8.20s		11.45s	4.04t 3.65t	6.84d	7.58t	6.66t	8.13d
HAcPy4PyPiz	8.10d	7.49–7.58m	7.94b	7.49–7.58m		2.62s	8.65s 9.12s	3.51t 4.06s	6.84d	7.58m	6.67m	8.11d
PdCl(FoPy4PyPiz)	8.52d	7.64	8.18t	7.81d	8.03s			3.98t 3.86	7.29d	7.99t	6.97t	8.12d
PdCl(AcPy4PyPiz)	8.58d	7.68t	8.21t	7.88		2.41s		3.69s 3.92s	7.19d	7.90d	6.91t	8.11d
$ZnCl_2$(HFoPy4PyPiz)	8.52b	7.53b	8.57b	7.84t	8.48b		11.53	3.76d 4.15t	7.12d	7.83m	6.86t	8.03d
$ZnCl_2$(HAcPy4PyPiz)	8.08d	7.60m	7.78t	7.89d		2.55s	8.71s	3.76t 4.15t	7.19d	6.88m	6.81m	8.11d

	C(2)	**C(3)**	**C(4)**	**C(5)**	**C(6)**	**C=N**	**C=S**	**CH$_2$**	**C(14)**	**C(15)**	**C(16)**	**C(17)**	**C(18)**	**C(8)**
HFoPy4PyPiz	153.51	124.17 126.12	136.95	116.69	149.6	144.17	180.95	43.77 49.74	158.66	106.92 107.17	137.74	113.32	147.71	
HAcPy4PyPiz	149.44	124.52	137.73	124.52	147.70	137.73	182.71	43.87 48.15	158.78	107.23	137.73	113.30	147.70	12.89
PdCl(FoPy4PyPiz)	158.87	126.54	142.05	126.45	149.29	147.35	181.86	45.62	158.79	113.32	141.15	113.32	148.41	
PdCl(AcPy4PyPiz)	156.98	127.19	141.96	124.05	148.39	148.89	180.13	45.58 47.81	159.30	106.06	133.03	114.4	146.84	14.14
$ZnCl_2$(HFoPy4PyPiz)	155.4	122.7	140.97	121.76	155.78	143.14	181.60	44.98 47.3	156.0	109.8	138.13	113.53	149.21	
$ZnCl_2$(HAcPy4PyPiz)	156.79	126.8	141.30	122.9	152.87	148.16	180.51	43.27 45.82	159.34	108.75	139.14	115.03	149.53	14.26

[a] in $(CD_3)_2SO$.

creased electron density at this site on complexation and due probably to back π-bonding for thiolato sulfur [6] (see Table 4).

3.4. Pharmacology. In vitro growth inhibition assay

Pt(II) complexes of *N*4-ethyl 2-formyl and 2-acetylpyridine thiosemicarbazones showed cytotoxicity and were found to be able to overcome the cisplatin resistance of A2780/Cp8 cells [9]. Pt(II) or Pd(II) complexes with 2-acetyl pyridine N(4)-ethyl-thiosemicarbazone, HAc4Et were tested in a panel of human tumor cell lines of different origins (breast, colon, and ovary cancers), and cisplatin-refractory/resistant cell lines and were found to exhibit very remarkable growth inhibitory activities with mean IC_{50} values of 0.9–0.5 nM and support the hypothesis that both $[Pt(Ac4Et)_2]$ and $[Pd(Ac4Et)_2]$ complexes can be characterized by cellular pharmacological properties distinctly different from those of cisplatin [9b].

The compounds **1**–**6** were tested *in vitro* against the cells of three human cancer cell lines: MCF-7 (human breast cancer cell line), T24 (bladder cancer cell line), A-549 (non-small cell lung carcinoma) and a mouse fibroblast L-929 cell line. The results of cytotoxic activity *in vitro* are expressed as IC_{50} – the concentration of compound (in M) that inhibits a proliferation rate of the tumor cells by 50% as compared to control untreated cells.

The $ZnCl_2$ and K_2PdCl_4 exhibit very poor cytotoxic activity in all these four lines. In the case of L-929 and A-549 cell lines the ligands and the complexes are in the same μM range less cytotoxic compared to *cis-platin*. In this case the observed cytotoxicity is probably due to the cytotoxicity of the ligands **1** and **2** and the metal complexes may be a vehicle for activation of the ligand as the cytotoxic agent. The IC_{50} value for HAc4Npypipe against the A-549 cell line is 16.6 μM and for the Zn(II) complex is 8.08 μM. The two thiosemicarbazones and the metal complexes exhibited cytotoxic activity against the MCF-7 and T-24 cell lines in a μM range better than to *cis-platin.*

Table 5 shows that complex $[ZnCl_2(Ac4Npypipe)]$, **6**, is 43 and four times more active than *cis-platin* in the T24 and MCF-6 cell lines, respectively. Also, complex $[ZnCl_2(Fo4Npypipe)]$, **5**, is four and 33 times more active than *cis-platin* in the T24 and MCF-6 cell lines, respectively. The cytotoxic activity shown by these Zn(II) compounds **5** and **6** against MCF-7 and T24 cell lines indicate that coupling of **1** and **2** to Zn(II) metal center result in metallic complexes with important biological properties and remarkable cytotoxic activity, since they are display IC_{50} values in a μM range better to that of the antitumor drug *cis-platin*. Thus, the Zn(II) compounds **5** and **6** are considered as agents with potential antitumor activity, and can therefore be candidates for further stages of screening *in vitro* and/or *in vivo*.

3.5. In vivo antitumor experiments

Also the acute toxicity and antitumor activity were evaluated on leukemia P388-bearing mice for selected compounds **2** and **6**. The acute toxicity and the antitumor activities of these compounds were correlated with the related complexes of 2-formylpyridine and 2-acetylpyridine thiosemicarbazone, HFoTsc and HAcTsc, respectively, [5,6].

The ligand HAc4Npypipe causes a high acute toxicity and does not display antitumor activity, while the complex $[ZnCl_2(Ac4Npypipe)]$ shows reduction of the toxicity, and very high increase of survival time of the drug treated leukemia bearing mice, Table 6. The ligand is achieving a *T*/*C*% value of 113 and the zinc(II) complex of 285. Also, one of the mice was cured and was considered as long-term survivor. The long-term survivors are defined as mice alive 90 days after tumor inoculation.

Probably the zinc(II) complex, $[ZnCl_2(Ac4Npypipe)]$, may interact better with DNA and/or proteins than the other compounds. In conclusion, these experiments showed that the activity of the metal complex) $[ZnCl_2(Ac4Npypipe)]$ is different compared with the activity of the ligand alone and probably represent independent cytotoxic entities. It was surprising and not predictable that among these compounds the zinc compound, $[ZnCl_2(Ac4Npypipe)]$ was more effective than other related palladium compounds. The re-

Table 6
Acute toxicity and antitumor activity of the ligand, **2**, its Zn(II) complex **6** and related Tsc's and Pd(II) complexes on leukemia P388-bearing BDF1

Compound	LD_{50}[a]	LD_{10}[a]	MST ± SD[b] (days)	*T*/*C*%[b]	Cures
Controls	–	saline	10.00 ± 0.41	100	0/6
2	34	12	11.3 ± 0.61	113	0/6
HAcTsc[c]	25	10	10 9.0 + 0.19	106	0/6
HFoTsc[d]		20	11.25 ± 0.21	129	0/6
[Pd(AcTsc)Cl][c]	80	50	9.4 ± 0.22	111	0/6
[Pd(AcTsc)$_2$][c]	65	40	10.8 ± 0.25	127	0/6
[Pd(FoTsc)Cl][d]		38	11.50 ± 0.19	132	0/6
[Pd(FoTsc)$_2$][d]		150	13.00 ± 0.25	149	0/6
6	46	18	**21.5 ± 0.58**	**285**	**1/6**
cis-Platin[e]			22.6 ± 6.5	138	

[a] LD_{50} and LD_{10} (dosage μg/g body wt) values were estimated graphically: percent deaths due to the toxicity of each dose are shown on the ordinate, while the administered doses are indicated on the abscissa on semi-logarithmic paper. LD_{50} and LD_{10} = lethal doses for 50% and 10%, respectively, of the mice used (10 animals per dose).

[b] LD_{10} was given as a single dose on the first day after tumor transplantation for antitumor evaluation. MST, mean survival time; *T*/*C*%, median survival time of the drug-treated animals versus corn oil-treated controls (C).

[c,d] Where HFoTsc and HAcTsc is the related pyridine-2-carbaldehyde and 2-acetylpyridine Tsc, respectively [Ref. [5a,b,6a]].

[e] Ref. [16]; dose 3 mg/kg.

Table 5
The *in vitro* activity of **1**, **2** and its Pd(II), Zn(II) complexes and related Zn(II) complexes [9a] (expressed as IC_{50} (M)) against MCF-7, T-24, A-549 and L-929 cancer cell lines

Compounds	MCF-7	T-24	L-929	A-549
1	2.24×10^{-6}	3.77×10^{-6}	7.96×10^{-6}	1.75×10^{-6}
2	2.70×10^{-6}	2.64×10^{-6}	7.84×10^{-6}	16.6×10^{-6}
HFoTsc[a]	$<0.55 \times 10^{-6}$	2.55×10^{-6}	inactive	
HAcTsc[a]	0.55×10^{-6}	2.06×10^{-6}	2.16×10^{-6}	
[$ZnCl_2$(HFoTsc)] · H_2O[a]	3.29×10^{-6}	1.73×10^{-6}	inactive	
[$ZnCl_2$(HAcTsc)][a]	1.36×10^{-6}	1.06×10^{-6}	1.57×10^{-6}	
3	83.9×10^{-6}	4.89×10^{-6}	214.01×10^{-6}	12.8×10^{-6}
4	3.75×10^{-6}	5.2×10^{-6}	160.05×10^{-6}	113.0×10^{-6}
5	$\mathbf{<0.21 \times 10^{-6}}$	9.79×10^{-6}	1.60×10^{-6}	10.6×10^{-6}
6	2.20×10^{-6}	$\mathbf{0.96 \times 10^{-6}}$	19.90×10^{-6}	8.08×10^{-6}
$ZnCl_2 \cdot 1.5H_2O$	605.30×10^{-6}	$>605.30 \times 10^{-6}$	734.05×10^{-6}	281.55×10^{-6}
K_2PdCl_4	306.05×10^{-6}	$>306.05 \times 10^{-6}$	$>306.05 \times 10^{-6}$	$>306.05 \times 10^{-6}$
***cis*-Platin**	8.00×10^{-6}	41.7×10^{-6}	0.70×10^{-6}	1.53×10^{-6}

[a] Ref. [9a]; where HFoTsc and HAcTsc is the related pyridine-2-carbaldehyde and 2-acetylpyridine Tsc, respectively.

sults of the anti-tumor activity encourage this kind of investigations in order to select and synthesize more effective chemotherapeutics.

Acknowledgements

Thanks are due to the Hellenic State Scholarship Foundation (IKY) for financial support to P.N.Y. We thank the Centrum of X-ray Crystallography of the University of Ioannina and Assoc. Professor Dr. S. Skoulika for the X-ray data collection. We also thank the NMR center of the University of Ioannina for measurements.

Appendix A. Supplementary material

CCDC 671219 and 671218 contain the supplementary crystallographic data for **3** and **4**. These data can be obtained free of charge via http://www.ccdc.cam.ac.uk/conts/retrieving.html, or from the Cambridge Crystallographic Data Centre, 12 Union Road, Cambridge CB2 1EZ, UK; fax: (+44) 1223-336-033; or e-mail: deposit@ccdc.cam.ac.uk. Supplementary data associated with this article can be found, in the online version, at doi:10.1016/j.poly.2008.04.009.

References

[1] (a) R.A. Finch, M.-C. Liu, S.P. Grill, W.C. Rose, R. Loomis, K.M. Vasquez, Y.-C. Cheng, A.C. Sartorelli, Biochem. Pharmacol. 59 (2000) 983. and refs. cit. therein;
(b) D.R. Richardson, Crit. Rev. Oncol./Hemat. 42 (2002) 267. and refs. cit. therein.
[2] (a) S. Padhye, R.C. Chikate, P.B. Sonawane, A. Kumbhar, R. Yerande, D.X. West, A. Liberta, Coordin. Chem. Rev. 123 (1993) 49;
(b) A.E. Liberta, D.X. West, Biometals 5 (1992) 121;
(c) J.G. Cory, A.H. Cory, G. Rappa, A. Lorico, M.C. Liu, T.-S. Lin, A.C. Sartorelli, Biochem. Pharmacol. 48 (1994) 335.
[3] (a) H. Beraldo, D. Gambino, Mini Rev. Med. Chem. 4 (2004) 159;
(b) Z. Afrasiabi, E. Sinn, J. Chen, Y. Ma, S. Padhye, Toxicol. Appl. Pharmacol. 197 (2004) 40.
[4] (a) A. Gomez Quiroga, C. Navarro Ranninger, Coordin. Chem. Rev. 248 (2004) 119;
(b) A.G. Quiroga, J.M. Pérez, I. López-Solera, J.R. Masaquer, A. Luque, P. Román, A. Edwards, C. Alonso, C. Navarro-Ranninger, J. Med. Chem. 41 (1998) 1399.
[5] (a) D. Kovala-Demertzi, M.A. Demertzis, E. Filiou, A.A. Pantazaki, P.N. Yadav, J.R. Miller, Y. Zheng, D.A. Kyriakidis, Biometals 16 (2003) 411;
(b) Z. Iakovidou, E. Mioglou, D. Mourelatos, A. Kotsis, M.A. Demertzis, A. Papagoorgiou, P.N. Yadav, D. Kovala-Demertzi, Anticancer Drugs 12 (2001) 65;
(c) D. Kovala-Demertzi, M.A. Demertzis, V. Varagi, A. Papageorgiou, D. Mourelatos, E. Mioglou, Z. Iakovidou, A. Kotsis, Chemotherapy 44 (1998) 421.
[6] (a) D. Kovala-Demertzi, P. Nath Yadav, M.A. Demertzis, M. Coluccia, J. Inorg. Biochem. 78/4 (2000) 347;
(b) A. Papageorgiou, Z. Iakovidou, D. Mourelatos, E. Mioglou, L. Boutis, A. Kotsis, D. Kovala-Demertzi, A. Domopoulou, D.X. West, M.A. Demertzis, Anticancer Res. 17 (1997) 247;
(c) D. Kovala-Demertzi, A. Domopoulou, M.A. Demertzis, G. Valle, A. Papageorgiou, J. Inorg. Biochem. 68 (1997) 147.
[7] (a) D. Kovala-Demertzi, M.A. Demertzis, J.R. Miller, C. Papadopoulou, C. Dodorou, G. Filousis, J. Inorg. Biochem. 86 (2001) 555;
(b) D. Kovala-Demertzi, J.R. Miller, N. Kourkoumelis, S.K. Hadjikakou, M.A. Demertzis, Polyhedron 18 (1999) 1005;
(c) D. Kovala-Demertzi, A. Domopoulou, M.A. Demertzis, A. Papageorgiou, D.X. West, Polyhedron 16 (20) (1997) 3625.
[8] (a) P. Nath Yadav, M.A. Demertzis, D. Kovala-Demertzi, S. Skoulika, D.X. West, Inorg. Chim. Acta 349 (2003) 30;
(b) M.A. Demertzis, P. Nath Yadav, D. Kovala-Demertzi, Helv. Chim. Acta 89 (9) (2006) 1959;
(c) D. Kovala-Demertzi, N. Kourkoumelis, M.A. Demertzis, J.R. Miller, C.S. Frampton, J.K. Swearingen, D.X. West, Eur. J. Inorg. Chem. (2000) 727.
[9] (a) D. Kovala-Demertzi, P.N. Yadav, J. Wiecek, S. Skoulika, T. Varadinova, M.A. Demertzis, J. Inorg. Biochem. 100 (2006) 1558;
(b) D. Kovala-Demertzi, A. Boccarelli, M.A. Demertzis, M. Coluccia, Chemotherapy 53 (2007) 148;
(c) D. Kovala-Demertzi, A. Galani, N. Kourkoumelis, J.R. Miller, M.A. Demertzis, Polyhedron 26 (2007) 2871.
[10] (a) W. Maret, BioMetals 14 (2001) 187;
(b) G.K. Walkup, S.C. Burdette, S.J. Lippard, R.Y. Tsien, J. Am. Chem. Soc. 122 (23) (2000) 5644;
(c) H.L. Hellmich, C.J. Frederickson, D.S. DeWitt, R. Saban, M.O. Parsley, R. Stephenson, M. Velasco, T. Uchida, M. Shimamura, D.S. Prough, Neurosci. Lett. 355 (3) (2004) 221.
[11] J.P. Scovill, Phosphorus Sulfur Silicon 60 (1991) 15.
[12] (a) G.M. Sheldrick, SHELXS86, Acta Crystallogr., Sect. A 46b(990) 467.;
(b) G.M. Sheldrick, SHELXL-97, Program for Crystal Structure Refinement, University of Göttingen, 1997;
(c) L.J. Farrugia, J. Appl. Crystallogr. 32 (1999) 837;
(d) A.L. Spek, PLATON, A Multipurpose Crystallographic Tool, A Program for the Automated Generation of a Variety of Geometrical Entities, Utrecht University, Utrecht, The Netherlands, 2001.
[13] P. Skehan, R. Storeng, D. Scudiero, A. Monks, J. Mcmahon, D. Vistica, J.T. Warren, H. Bokesch, S. Kenney, M.R. Boyol, J. Natl. Cancer. Inst. 82 (1990) 1107.
[14] (a) M. Ohno, T. Abe, J. Immunol. Meth. 145 (1991) 199;
(b) T.J. Sabo, V.M. Dinovic, G.N. Kaluderovic, T.P. Stanojkovic, G.A. Bogdanovic, Z.D. Juranic, Inorg. Chim. Acta 358 (2005) 2239;
(c) T. Mosman, J. Immunol. Methods 65 (1983) 55.
[15] A.Goldin, Z. Sofina, A. Syrkin, National Cancer Inst Monograph (USA) No. 55, 1980.
[16] J.H. Burchenal, T. O'Toole, K. Kalaher, J. Chisholm, Cancer Res. 37 (1977) 4098.

Polyhedron 27 (2008) 2739–2742

Contents lists available at ScienceDirect

Polyhedron

journal homepage: www.elsevier.com/locate/poly

Synthesis and characterization of intermediate sitting-atop (i-SAT) complexes of free base *meso*-tetraarylporphyrins and tin(IV) chloride

Hossein Dehghani *, Mehrnoosh Babaahmadi

Department of Chemistry, Faculty of Science, University of Kashan, Kashan 87317-51167, Iran

ARTICLE INFO

Article history:
Received 14 April 2008
Accepted 19 May 2008
Available online 17 July 2008

Keywords:
Porphyrin
i-SAT complex
Tin(IV) chloride
Donor
Acceptor

ABSTRACT

The reaction of *meso*-tetraarylporphyrins ($H_2T(X)PP$) with $SnCl_4$ affords green intermediate sitting-atop (i-SAT) complexes, [$(H_2T(X)PP)SnCl_4$]. UV–Vis, ^1H NMR and ^{13}C NMR spectral data show that the porphyrin core of the complexes is distorted, thus two nitrogen atoms of the pyrrolenine groups on one side of the porphyrin plane act as electron donors to the tin center of $SnCl_4$. The intermediate sitting-atop (i-SAT) complex is formed each time during the incorporation of the metal center, where in the intermediate state the pyrrolic protons still remain on the porphyrin.

© 2008 Elsevier Ltd. All rights reserved.

1. Introduction

Understanding the metallation of porphyrins has long been important in biochemistry because of their central role in photosynthesis, biological redox processes, and oxygen transport [1–10]. Depending on their size, charge and spin multiplicity, metal ions can fit into the central hole of the porphyrin ring, forming regular metalloporphyrins, or several of them are located out of the ligand plane, resulting in sitting-atop (SAT) complexes. Most of the natural metalloporphyrins are of the regular type, i.e. their metal centers are located within the plane of the macrocyclic ligand as a consequence of their fitting size. Their ionic radii are in the range 55–80 pm, corresponding to the sphere in the porphyrin core surrounded by the four pyrrolic nitrogens. While the symmetry group of the free base porphyrins is D_{2h} due to the two hydrogen atoms on the diagonally located pyrrolic nitrogens, the coplanar (regular) metalloporphyrins (without these protons) are of higher symmetry (D_{4h}) [11]. Deviating from regular porphyrins, in the sitting-atop complexes, the metal centers are located out of the ligand plane, distorting it and causing lower symmetry (C_{4v} "dome" or S_4 "saddle"). These sitting-atop complexes are called stable sitting-atop (s-SAT) complexes. Another type of sitting-atop complex is the intermediate sitting-atop (i-SAT) complex and it is known as an intermediate in the metallation of porphyrins. In the i-SAT complexes, similar to the molecular complexes of porphyrins, the metal connects to the pyrrolenine nitrogens and the two pyrrolic protons remain on the porphyrin. It is reported that porphyrins are only capable of forming 1:2 molecular complexes with tin(IV) compounds such as $Sn(CH_3)Br_3$, $SnPhCl_3$, $Sn(CH_3)_2Cl_2$, $Sn(Ph)_2Cl_2$ and $Sn(Ph)_2Br_2$ [12–17]. This article presents the synthesis and spectroscopic characterization of the 1:1 molecular complexes or intermediate sitting-atop (i-SAT) complexes of *meso*-tetraarylporphyrins (Fig. 1) with $SnCl_4$. The suitable selection of $SnCl_4$ meant that we could be prepare i-SAT complexes of tin(IV) with *meso*-tetraarylporphyrins.

2. Experimental

2.1. Materials and measurements

Tin(IV) chloride, benzaldehyde and various substituted benzaldehydes (3-CH_3, 4-CH_3, 3-OCH_3, 4-OCH_3, 4-isopropyl) were obtained from Merck and were used without further purification. Pyrrole was purchased from Merck and was distilled before use. Chloroform and acetone (Merck) were dried over anhydrous calcium chloride for 3 days and distilled before use. Other solvents that were employed for the synthesis of the porphyrins and i-SAT complexes were obtained from Merck and Fluka, and were used as received. The substituted *meso*-tetraarylporphyrins were prepared by the literature methods [18].

The NMR spectra (^1H and ^{13}C) were recorded on a Bruker 400 Ultrashield spectrometer in $CDCl_3$. The residual $CHCl_3$ in the conventional 99.8% atom D $CDCl_3$ gives a signal at $\delta = 7.26$ ppm, which was used for calibration of the chemical shift scale. FT-IR spectra were recorded on a Magna 550 Nicolet spectrometer using KBr pellets. The UV–Vis measurements were obtained with a GBC cintra 6

* Corresponding author. Tel.: +98 361 555 5333; fax: +98 361 555 2935.
E-mail address: dehghani@kashanu.ac.ir (H. Dehghani).

0277-5387/$ - see front matter © 2008 Elsevier Ltd. All rights reserved.
doi:10.1016/j.poly.2008.05.017

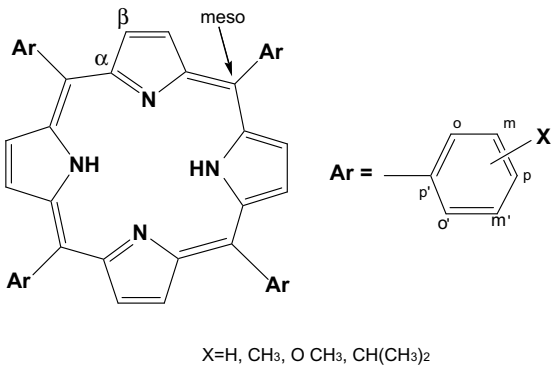

Fig. 1. *meso*-Tetraarylporphyrins, $H_2T(X)PP$.

UV–Vis spectrophotometer. The molar conductance was measured on a METROHM 644 conductometer.

2.2. Preparation of the i-SAT complexes

0.05 mmol $SnCl_4$ was dissolved in 5 ml acetone and added to 0.05 mmol of the *meso*-tetraarylporphyrins in 15 ml chloroform and the mixture was stirred for 15 min. Evaporation of the solvent at room temperature produced the green i-SAT complexes, $[(H_2T(X)PP)SnCl_4]$, without an excess amount of the porphyrins or $SnCl_4$. The progress of the reaction was monitored by UV–Vis spectra. The porphyrins completely changed to the i-SAT complexes and the mixture did not show an absorption band (Soret band) related to the free base *meso*-tetraarylporphyrins. The results of elemental analyses for the i-SAT complexes formed from the porphyrins and $SnCl_4$, which were dried in a vacuum oven for 12 h at 55–60 °C were consistent with $[(H_2T(X)PP)SnCl_4]$.

$[(H_2TPP)SnCl_4]$: *Anal.* Calc. for $C_{44}H_{30}N_4SnCl_4$: C, 60.38; H, 3.45; N, 6.40. Found: C, 59.55; H, 3.18; N, 6.23%. ^1H NMR ($CDCl_3$), δ (ppm): 0.30 (s, 2H, NH), 8.61-8.63 (d, 8H, o), 7.92–8.02 (d, 12H, m,p), 8.59 (s, 8H, β).

$[(H_2T(4\text{-}CH_3)PP)SnCl_4]$: *Anal.* Calc. for $C_{48}H_{38}N_4SnCl_4$: C, 61.89; H, 4.11; N, 6.04. Found: C, 61.63; H, 3.90; N, 5.85%. ^1H NMR ($CDCl_3$): δ 0.35 (s, 2H, NH), δ 2.79 (s, 12H, CH_3), δ 8.49-8.51 (d, 8H, o), δ 7.80–7.82 (d, 8H, m), δ 8.55 (s, 8H, β).

$[(H_2T(3\text{-}CH_3)PP)SnCl_4]$: *Anal.* Calc. for $C_{48}H_{38}N_4SnCl_4$: C, 61.89; H, 4.11; N, 6.04. Found: C, 61.57; H, 4.01; N, 5.91%. ^1H NMR ($CDCl_3$), δ (ppm): 0.24 (s, 2H, NH), 2.84 (s, 12H, CH_3), 8.53 (br., 8H, o, o′), 7.88–7.92 (t, 4H, m), 7.77–7.79 (d, 4H, p), 8.59 (s, 8H, β).

$[(H_2T(4\text{-}OCH_3)PP)SnCl_4]$: *Anal.* Calc. for $C_{48}H_{38}N_4O_4SnCl_4$: C, 57.91; H, 3.85; N, 5.63. Found: C, 57.65; H, 3.70; N, 5.51%. ^1H NMR ($CDCl_3$), δ (ppm): 0.56 (s, 2H, NH), 4.18 (s, 12H, OCH_3), 8.53–8.55 (d, 8H, o), 7.54–7.56 (d, 8H, m), 8.47 (s, 8H, β).

$[(H_2T(3\text{-}OCH_3)PP)SnCl_4]$: *Anal.* Calc. for $C_{48}H_{38}N_4O_4SnCl_4$: C, 57.91; H, 3.85; N, 5.63. Found: C, 57.63; H, 3.69; N, 5.56%. ^1H NMR ($CDCl_3$), δ (ppm): 0.23 (s, 2H, NH), 4.16 (s, 12H, OCH_3), 8.17 (br., 8H, o, o′), 7.88–7.92 (t, 4H, m), 7.51–7.53 (d, 4H, p), 8.63 (s, 8H, β).

$[(H_2T(4\text{-}CH(CH_3)_2)PP)SnCl_4]$: *Anal.* Calc. for $C_{56}H_{54}N_4SnCl_4$: C, 64.45; H, 5.22; N, 5.37. Found: C, 64.23; H, 5.01; N, 5.07%. ^1H NMR ($CDCl_3$), δ (ppm): 0.30 (br., 2H, NH), 1.60–1.62 (s, 24H, CH_3), 3.34–3.37 (s, 4H, CH), 8.52–8.54 (d, 8H, o), 7.87–7.89 (d, 8H, m), 8.57 (s, 8H, β).

3. Results and discussion

The UV–Vis spectrum of H_2TPP shows five absorption bands at 416.7 (Soret), 516.8, 551.5, 592.0 and 648.0 nm [19–27], but the $[(H_2TPP)SnCl_4]$ complex shows two new absorption bands at 444.3 (Soret) and 659.1 nm, Fig. 2. Upon the addition of $SnCl_4$ to H_2TPP, the UV–Vis spectrum of the porphyrin is 11–28 nm red shifted. This is an evidence for an increase of the π-resonance interaction in the aryl rings with the porphyrin nucleus in going from H_2TPP to the $[(H_2TPP)SnCl_4]$ complex, which would be produced by the deformation of the porphine core [19–27]. The results of the UV–Vis spectra for the i-SAT complexes are listed in Table 1. The UV–VIS spectra for the titration of tin(IV) chloride into $H_2T(4\text{-}CH_3)PP$ (0.25:1, 0.5:1, 0.75:1, 1:1, 1:1.5 and 1:2) showed the molar ratio of the metal to ligand in the i-SAT complex was 1:1. An excess amount of tin(IV) chloride more than the 1:1 molar ratio had no measurable effect on the UV–Vis spectra of the studied complexes.

^1H NMR spectral data for the mixing of different equivalents of $SnCl_4$ (0.25, 0.5, 0.75, 1.0, 1.5 and 2.0) with H_2TPP showed that the complexation between H_2TPP and $SnCl_4$ had a 1:1 molar ratio. Further, these results indicate that using an amount of $SnCl_4$ less than that of free base H_2TPP leads to a superimposition of the porphyrin and the related i-SAT complex, and an excess of $SnCl_4$ more than the 1:1 molar ratio causes no changes in the spectrum of the i-SAT complex. The reaction of $SnCl_4$ with H_2TPP, similar to the molecular complexation of the porphyrin [19–26] or its diprotonation [28], leads to an upfield shift of the β-protons (0.26 ppm) and

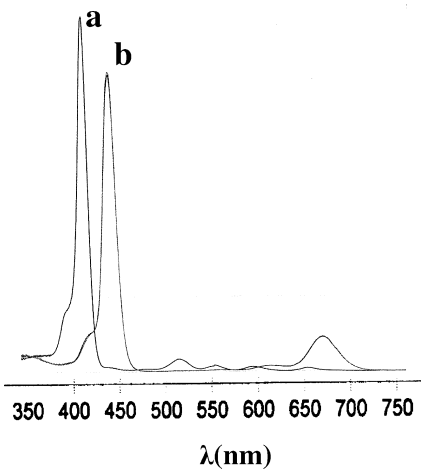

Fig. 2. UV–Vis spectra of (a) H_2TPP and (b) $[(H_2TPP)SnCl_4]$ complex.

Table 1
UV–Vis spectral data of the *meso*-tetraarylporphyrins and $[(H_2T(X)PP)SnCl_4]$ complexes in $CHCl_3$

Compounds	λ_{max} (nm)
H_2TPP	416.7(S), 516.8, 551.5, 592.0, 648.0
$[(H_2TPP)SnCl_4]$	444.3, 659.1
$\Delta\lambda$[a]	27.6, 11.1
$H_2T(4\text{-}CH_3)PP$	418.3(S), 518.4, 554.0, 593.0, 649.0
$[(H_2T(4\text{-}CH_3)PP)SnCl_4]$	448.4(S), 670.1
$\Delta\lambda$[a]	30.1, 21.1
$H_2T(3\text{-}CH_3)PP$	418.2(S), 517.5, 550.6, 590.0, 647.2
$[(H_2T(3\text{-}CH_3)PP)SnCl_4]$	446.2(S), 662.8
$\Delta\lambda$[a]	28.0, 15.6
$H_2T(4\text{-}OCH_3)PP$	419.5(S), 520.5, 557.1, 596.0, 653.0
$[(H_2T(4\text{-}OCH_3)PP)SnCl_4]$	453.6(S), 688.7
$\Delta\lambda$[a]	34.1, 35.7
$H_2T(3\text{-}OCH_3)PP$	418.9(S), 517.0, 550.3, 590.3, 646.6
$[(H_2T(3\text{-}OCH_3)PP)SnCl_4]$	449.9(S), 660.9
$\Delta\lambda$[a]	31.0, 14.3
$H_2T(4\text{-}CH(CH_3)_2)PP$	419.7(S), 519.2, 555.1, 594.4, 650.4
$[(H_2T(4\text{-}CH(CH_3)_2)PP)SnCl_4]$	448.4(S), 670.1
$\Delta\lambda$[a]	28.7, 19.7

(S): Soret band.
[a] $\Delta\lambda$: Red shifts for the bands of the porphyrins upon SAT complexation.

downfield shifts of the N–H signal (3.06 ppm) and aryl ring protons. The chemical shifts of the NH and β-proton for the *meso*-tetraarylporphyrins and the related i-SAT complexes are listed in Table 2. The chemical shift direction of the NH and β-protons signals of the i-SAT complex, $[(H_2TPP)SnCl_4]$, was similar to the related molecular complexes of the porphyrins. The observed ^1H NMR and UV–Vis spectral shifts upon the SAT complexation of $H_2T(4\text{-}OCH_3)PP$ with $SnCl_4$ was more than the other studied porphyrins (Tables 1 and 2). This result was obtained because of the π-resonance effect and low steric hindrance of the *para*-methoxy group. The spectral shifts of the *para*-substituents were more than the related *meta*-substituents. This is explained by the low steric hindrance of the *para*-groups compared to the *meta*-groups. Further, these results show that the π-resonance effect is more important than σ-induction effect [19,20].

The ^{13}C NMR spectrum of $H_2T(4\text{-}CH_3)PP$ showed seven sharp signals (one signal for the CH_3 group (19.9 ppm) and six signals for the porphine core) and aryl rings ((120.5 (C_{meso}), 127.8 ($C_{m,m'}$), 137.7 (C_p), 131.4 (C_β), 134.9 ($C_{o,o'}$), 139.7 ($C_{p'}$) ppm)) [24,25]. The complexation of $H_2T(4\text{-}CH_3)PP$ with $SnCl_4$ leads to changes in the ^{13}C NMR spectrum of the porphyrin. The new peaks were revealed at 21.7 (CH_3), 122.4 (C_{meso}), 127.8 (C_β), 129.2 ($C_{m,m}$), 137.5(C_p), 139.0 ($C_{o,o'}$), 140.3 ($C_{p'}$) and 146.1 ($C\alpha$) ppm. The observed changes upon the SAT complexation were the same as the diprotonation [28] and molecular complexation of the *meso*-tetraarylporphyrins with π- or σ-acceptors [19,20,24,25].

The UV–Vis, ^1H NMR and ^{13}C NMR spectral correspondences between the molecular complexes produced from various acceptors with *meso*-tetraarylporphyrins [19,20] or H_4TPP^{2+} [28] and $[(H_2TPP)SnCl_4]$ proposed a similar porphyrin core in all of the species, with non-coplanar pyrrole rings tilted alternatively up and down. In the proposed structure, the lone pairs of two pyrrolenine nitrogens act as electron donors to one molecule of $SnCl_4$, and so two hydrogen atoms of pyrroles (N–H) still remain on the macrocycle, Fig. 3. In the FT-IR spectrum of the free base *meso*-tetraarylporphyrin is observed a N–H stretching band at 3320 cm^{-1} [29] that did not show a considerable change upon SAT complexation with $SnCl_4$. Furthermore, as mentioned above, the ^1H NMR spectra of the SAT complexes showed that the two protons on the pyrrole nitrogens still remained on the porphyrins. These data are in complete correspondence with the proposed structure in Fig. 3, but the observation of a singlet for the β-protons in the ^1H NMR spectrum of the $[(H_2TPP)SnCl_4]$ complex is in contrast with the unsymmetrical pyrrole rings in the proposed structure. This

Table 2
^1H NMR spectral data of the *meso*-tetraarylporphyrins and $[(H_2T(X)PP)SnCl_4]$ complexes

Compounds	N–H	H_β
H_2TPP	−2.76	8.85
$[(H_2TPP)SnCl_4]$	0.30	8.59
$\Delta\delta$	3.06	−0.26
$H_2T(4\text{-}CH_3)PP$	−2.77	8.85
$[(H_2T(4\text{-}CH_3)PP)SnCl_4]$	0.35	8.55
$\Delta\delta_1$	3.12	−0.30
$H_2T(3\text{-}CH_3)PP$	−2.75	8.88
$[(H_2T(3\text{-}CH_3)PP)SnCl_4]$	0.24	8.59
$\Delta\delta$	2.99	−0.29
$H_2T(4\text{-}OCH_3)PP$	−2.75	8.86
$[(H_2T(4\text{-}OCH_3)PP)SnCl_4]$	0.56	8.51
$\Delta\delta$	3.31	−0.35
$H_2T(3\text{-}OCH_3)PP$	−2.75	8.90
$[(H_2T(3\text{-}OCH_3)PP)SnCl_4]$	0.23	8.63
$\Delta\delta$	2.98	−0.27
$H_2T(4\text{-}CH(CH_3)_2)PP$	−2.74	8.86
$[(H_2T(4\text{-}CH(CH_3)_2)PP)SnCl_4]$	0.30	8.57
$\Delta\delta$	3.04	−0.29

$\Delta\delta$: Chemical shifts of the proton signals for the porphyrins upon SAT complexation.

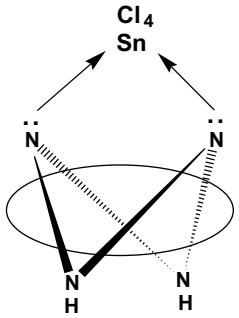

Fig. 3. Two pyrrolenine nitrogen atoms of the porphyrin act as electron donors to a tin center of $SnCl_4$.

can be explained by ring inversion of the saddled core conformation of the porphyrin, which is fast on the NMR timescale [19,20,27].

A comparison of the molar conductivity of the SAT complexes and the related diprotonated species indicates that the synthesized complexes are completely different from the diprotonated porphyrin species, although the spectral data of two species are similar. The measurement of molar conductivity in acetone solution showed the SAT complexes were not electrolytes. This was completely in accordance to the proposed formula of the SAT complexes, Fig. 3. In contrast, the molar conductivities of $[H_4T(X)PP]Cl_2$ in methanol were in accordance with 1:2 electrolytes [30].

The compounds SnR_2Cl_2 and $SnRCl_3$ (R = Me, Ph) reacted with *meso*-tetraarylporphyrins with the formation of 2:1 (acceptor:donor) molecular complexes, whereas $SnCl_4$ has produced 1:1 complexes with the free base porphyrins. The quantity of chlorine atoms in the $SnCl_4$ molecule are more than for SnR_2Cl_2 and $SnRCl_3$ molecules. The chlorine atom has higher electronegativity and lower steric hindrance than methyl and phenyl groups. Consequently, $SnCl_4$ is a better acceptor than SnR_2Cl_2 and $SnRCl_3$ and can accept two lone pairs from the porphyrin molecule for the formation of the complexes with a 1:1 (donor:acceptor) mole ratio.

4. Conclusion

Tin(IV) chloride and *meso*-tetraarylporphyrins ($H_2T(X)PP$) reacted with the formation of i-SAT complexes, $[(H_2T(X)PP)SnCl_4]$. The UV–Vis, ^1H NMR and ^{13}C NMR spectral data showed the porphyrin core of the SAT complexes, similar to the molecular complexes of *meso*-tetraarylporphyrins with various acceptors [19–25] and porphyrin diacids [28], is deformed and two nitrogen atoms of pyrrolenine are situated to one side of the porphyrin plane and act as electron donors to a tin atom of $SnCl_4$.

Acknowledgement

This work was partly supported by the Kashan University Research Council.

References

[1] C.K. Mathews, K.E. Van Holde, K.G. Ahern, Biochemistry, Addison Wesley Longman, San Francisco, 2000.
[2] R.H. Garrett, C.M. Grisham, Biochemistry, Saunders College Publishing, Fort Worth, 1999.
[3] G. Knör, A. Strasser, Inorg. Chem. Commun. 8 (2005) 471.
[4] G. Knör, ChemBiochem 2 (2001) 593.
[5] G. Knör, Coord. Chem. Rev. 171 (1998) 61.
[6] D.R. McMillin, K.M. McNet, Chem. Rev. 98 (1998) 1201.
[7] M.D. Lim, I.M. Lorkovic, P.C. Ford, J. Inorg. Biochem. 99 (2005) 151.
[8] B.O. Fernandez, I.M. Lorkovic, P.C. Ford, Inorg. Chem. 43 (2004) 593.
[9] G.G. Martirosyan, A.S. Azizyan, T.S. Kurtikyan, P.C. Ford, Chem. Commun. (2004) 1488.

[10] P.D. Beer, D.P. Cormode, J.J. Davis, Chem. Commun. (2004) 414.
[11] S.Y. Ma, Chem. Phys. Lett. 332 (2000) 603.
[12] M. Asadi, A. Zabardasti, J. Ghasemi, Polyhedron 21 (2002) 683.
[13] M. Asadi, A. Zabardasti, V. Karimvand, J. Ghasemi, Polyhedron 21 (2002) 1255.
[14] M. Asadi, A. Zabardasti, J. Ghasemi, Bull. Chem. Soc. Jpn. 75 (2002) 1137.
[15] A. Zabardasti, M. Mirzaeian, Chem. Lett. 35 (2006) 1348.
[16] D. Mohajer, E. Sakhtemanian, S. Rayati, S. Zakavi, Spectrochim. Acta Part A 69 (2008) 998.
[17] A. Zabardasti, M. Asadi, A. Kakanejadifard, J. Heterocycl. Chem. 43 (2006) 1157.
[18] (a) A.M.d A.R. Gonsalves, J.M.T.B. Varejao, M.M. Pereira, J. Heterocycl. Chem. 28 (1991) 635;
(b) A.D. Adler, F.R. Longo, J.H. Finarelli, J. Goldmacher, J. Assour, L. Korsakoff, J. Org. Chem. 32 (1967) 476.
[19] H. Dehghani, A.R. Ansari Sardrood, Polyhedron 26 (2007) 4263.
[20] H. Dehghani, A.R. Ansari Sardrood, Bull. Chem. Soc. Jpn. 80 (2007) 518.
[21] H. Dehghani, F. Fathi, Dyes Pigments 77 (2008) 323.
[22] H. Dehghani, M.R. Mansournia, Polyhedron 27 (2008) 849.
[23] H. Dehghani, F. Fathi, J. Porph. Phthal. 11 (2007) 742.
[24] D. Mohajer, H. Dehghani, J. Chem. Soc. Perkin Trans. 2 (2000) 199.
[25] D. Mohajer, H. Dehghani, Bull. Chem. Soc. Jpn. 73 (2000) 1477.
[26] D. Mohajer, S. Rayati, New J. Chem. 27 (2003) 242.
[27] D. Mohajer, S. Zakavi, S. Rayati, M. Zahedi, N. Safari, H.R. Khavasi, S. Shahbazian, New J. Chem. 28 (2004) 1600.
[28] (a) E.C.A. Ojadi, R.I. Walter, H. Linschitz, J. Phys. Chem. 97 (1993) 13308;
(b) M. Meot-Ner, A.D. Adler, J. Am. Chem. Soc. 97 (1975) 5107;
(c) A. Stone, E.B. Fleischer, J. Am. Chem. Soc. 90 (1968) 2735.
[29] H.H. Limbach, J. Henning, J. Stulz, J. Chem. Phys. 78 (1983) 5432.
[30] W.J. Geary, Coord. Chem. Rev. 7 (1971) 81.

characterization, electrochemistry, DNA-binding potential and antibacterial activity of the resulting complexes. The general structure of the ligands used in this study is given in Chart 1.

2. Experimental

2.1. Reagents and materials

Analytical or chemically pure grade chemicals were used for the preparation of ligands. $RuCl_3 \cdot 3H_2O$ purchased from Himedia was used as supplied. Protein free herring sperm ds DNA obtained from SRL chemicals was stored at 0–4 °C. All the spectroscopic DNA titrations were carried out in Tris–HCl buffer [0.197 g (5 mmol) of Tris–HCl and 0.73 g (50 mmol) NaCl] are dissolved in double distilled water and the pH was adjusted to 7.1 using 1 mM NaOH solution before making up to 250 ml) at room temperature. A solution of herring sperm DNA (0.1 g) in Tris–HCl buffer (10 ml) gave a ratio of UV absorbance at 260 and 280 nm of ca. 1.8–1.9:1 indicating that the DNA was sufficiently free of protein [25]. The DNA concentration per nucleotide was determined by absorption spectroscopy using the molar absorption coefficient (6600 M^{-1} cm^{-1}) at 260 nm [26]. Distilled dmso was used for the preparation of the starting complex and for the preparation of solutions of complexes for DNA-binding studies. Purified dry methanol was used to record the electronic spectra of the complexes. Commercially available TBAP was properly dried and used as supporting electrolyte for recording cyclic voltammograms of the complexes. The starting complex *cis*-$[RuCl_2(dmso)_4]$ was prepared according to the method reported by Evans et al. [27] and the ligands were prepared by refluxing an ethanolic solution of the aldehyde or ketone with thiosemicarbazide as described in the literature [28].

2.2. Physical measurements

A Nicolet Avatar Model FT-IR spectrophotometer was used to record the IR spectra (4000–400 cm^{-1}) of the free ligands and the complexes. Electronic spectral measurements (800–250 nm) and absorption titrations (DNA binding) were carried out with a Systronics 119 UV–Vis spectrophotometer. ^1H NMR spectra were recorded on Varian-Australia AMX-400 instrument. Micro analyses (C, H, N and S) were performed on a Vario EL III Elementar analyzer. The electrochemical analyzer (CHI 1120A) equipped with a three electrode compartment consisting of Platinum disc working electrode, Platinum wire counter electrode and Ag/AgCl reference electrode was used to record the cyclic voltammograms of the complexes.

2.3. Syntheses

2.3.1. Synthesis of cis-$[RuCl_2(dmso)_4]$

$RuCl_3 \cdot 3H_2O$ (1 g) was refluxed in dmso (5 ml) for 5 min. The solution rapidly turned orange brown and the volume was reduced to half using rotary evaporator. When acetone (20 ml) was added to the solution a yellow precipitate separated out. The precipitate was washed with acetone and ether and dried in vacuum.

2.3.2. Synthesis of ligands

An ethanolic solution of the corresponding aldehyde or ketone (0.01 mol) with thiosemicarbazide (0.01 mol) was heated under reflux for 4–5 h. Then the reaction mixture was cooled to get the respective thiosemicarbazone as precipitate. The precipitate was washed with ethanol and dried.

2.3.3. $[RuCl_2(dmso)_2(petsc)]$ (**1**)

cis-$[RuCl_2(dmso)_4]$ (0.1 g; 0.21 mmol) and the ligand petsc (0.040 g; 0.21 mmol) were heated under reflux in ethanol (30 ml) for 4 h during which a brownish solid separated. The solvent was evaporated on a rotary evaporator and the product was dried under vacuum. Finally, the product was washed with ether several times to get shiny brown crystalline complex. Yield, 73 mg; 67%. Elemental *Anal.* Calc. for $C_{13}H_{23}N_3S_3O_2Cl_2Ru$ (521.53): C, 29.93; H, 4.44; N, 8.06; S, 18.44. Found: C, 29.68; H, 4.12; N, 8.31; S, 18.17%. IR (KBr, cm^{-1}): $\nu(NH_2$ (asy)), 3381(w); $\nu(NH_2$ (sym)), 3303(w); ν(NH), 3128(w); ν(C=N), 1625 (s); ν(C=S), 736(w) (asy, asymmetric; sym, symmetric; s, strong; w, weak). UV/Vis (dmso) λ, nm (ε, mol^{-1} cm^{-1} l): 270 (9780), 294 (6620). ^1H NMR ([D_6]-dmso, δ ppm): 2.38 (s, H_3C–C=N, 3H), 3.2–3.5 (group of peaks, dmso, 12H), 3.64 (s, NH_2, 2H), 6.98–7.27 (multiplet, aromatic protons, 5H), 11.23 (s, –NH, 1H).

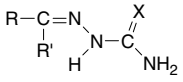

Ligand	R	R'	X	Name	Abbreviation
L1	C_6H_5	CH_3	S	1-Phenyl-ethanone thiosemicarbazone	petsc
L2	*p*-$C_6H_4CH_3$	CH_3	S	1-*p*-Tolyl-ethanone thiosemicarbazone	tetsc
L3	C_4H_3S	H	S	Thiophene-2-carbaldehyde thiosemicarbazone	tctsc
L4	C_4H_3O	H	S	Furan-2-carbaldehyde thiosemicarbazone	fctsc
L5	*p*- $C_6H_4OCH_3$	H	S	4-Methoxybenzaldehyde thiosemicarbazone	mbtsc
L6	*p*- $C_6H_4OCH_3$	CH_3	S	1-(4-Methoxy-phenyl)-ethanone thiosemicarbazone	mptsc
L7	*p*- C_6H_4Cl	CH_3	S	2-Chlorobenzaldehyde thiosemicarbazone	cbtsc
L8	C_6H_5	H	O	Benzaldehyde semicarbazone	bzsc

Chart 1. General structure of the ligands.

*2.3.4. [$RuCl_2(dmso)_2(tetsc)$] (**2**)*

The complex was prepared as described in Section 2.3.3. by the reaction of *cis*-[$RuCl_2(dmso)_4$] (0.1 g; 0.21 mmol) with the ligand tetsc (0.043 g; 0.21 mmol). Yield: 72 mg; 64%. Elemental *Anal.* Calc. for $C_{14}H_{25}N_3S_3O_2Cl_2Ru$ (535.56): C, 31.39; H, 4.70; N, 7.84; S, 17.96. Found: C, 31.48; H, 4.47; N, 7.59; S, 17.77%. IR (KBr, cm^{-1}): $\nu(NH_2$ (asy + sym)), 3434(b,w); ν(NH), 3147(w); ν(C=N), 1625(s); ν(C=S), 740(w) (asy, asymmetric; sym, symmetric; s, strong; w, weak). UV/Vis (dmso) λ, nm (ε, mol^{-1} cm^{-1} L): 272 (9840), 291(7700). ^{1}H NMR ([D_6]-dmso, δ ppm): 1.64 (s, –CH_3, 3H), 2.45 (s, H_3C–C=N, 3H), 3.1–3.4 (group of peaks, dmso, 12H), 3.62 (s, –NH_2, 2H), 6.7–7.3 (multiplet, aromatic protons, 4H), 10.87 (s, –NH, 1H).

*2.3.5. [$RuCl_2(dmso)_2(tctsc)$] (**3**)*

The complex was prepared as described in Section 2.3.3. by the reaction of *cis*-[$RuCl_2(dmso)_4$] (0.1 g; 0.21 mmol) with the ligand tctsc (0.039 g; 0.21 mmol). Yield: 67 mg; 62%. Elemental *Anal.* Calc. for $C_{10}H_{19}N_3S_4O_2Cl_2Ru$ (513.53): C, 23.38; H, 3.72; N, 8.18; S, 24.97. Found: C, 23.29; H, 3.95; N, 8.39; S, 24.76%. IR (KBr, cm^{-1}): $\nu(NH_2$ (asy + sym)), 3380(b,w); ν(NH), 3142(w); ν(C=N), 1629(s); ν(C=S), 720(w) (asy, asymmetric; sym, symmetric; s, strong; w, weak). UV/Vis (dmso) λ, nm (ε, mol^{-1} cm^{-1} L): 295 (15230), 314 (11530). ^{1}H NMR ([D_6]-dmso, δ ppm): 3.2–3.4 (group of peaks, dmso, 12H), 4.22 (s, –NH_2, 2H), 7.05–7.35 (multiplet, aromatic protons, 3H), 8.17 (s, H–C=N, 1H), 11.24 (s, –NH, 1H).

*2.3.6. [$RuCl_2(dmso)_2(fctsc)$] (**4**)*

The complex was prepared as described in Section 2.3.3. by the reaction of *cis*-[$RuCl_2(dmso)_4$] (0.1 g; 0.21 mmol) with the ligand fctsc (0.035 g; 0.21 mmol). Yield: 70 mg; 64%. Elemental *Anal.* Calc. for $C_{10}H_{19}N_3S_3O_3Cl_2Ru$ (497.46): C, 24.14; H, 3.84; N, 8.44; S, 19.33. Found: C, 24.33; H, 3.72; N, 8.69; S, 19.45%. IR (KBr, cm^{-1}): $\nu(NH_2$ (asy + sym)), 3410(b,w); ν(NH), 3138(w); ν(C=N), 1618(s); ν(C=S), 759(w) (asy, asymmetric; sym, symmetric; s, strong; w, weak). UV/Vis (dmso) λ, nm (ε, mol^{-1} cm^{-1} L): 287 (16930), 302 (16510). ^{1}H NMR ([D_6]-dmso, δ ppm): 3.2–3.4 (group of peaks, dmso, 12H), 3.75 (s, –NH_2, 2H), 6.6–7.8 (multiplet, aromatic protons, 3H), 8.09 (s, H–C=N, 1H), 11.00 (s, –NH, 1H).

*2.3.7. [$RuCl_2(dmso)_2(mbtsc)$] (**5**)*

The complex was prepared as described in Section 2.3.3. by the reaction of *cis*-[$RuCl_2(dmso)_4$] (0.1 g; 0.21 mmol) with the ligand mbtsc (0.044 g; 0.21 mmol). Yield: 74 mg; 66%. Elemental *Anal.* Calc. for $C_{13}H_{23}N_3S_3O_3Cl_2Ru$ (537.53): C, 29.04; H, 4.31; N, 7.81; S, 17.89. Found: C, 28.81; H, 4.16; N, 7.59; S, 18.02%. IR (KBr, cm^{-1}): $\nu(NH_2$ (asy)), 3411(w); $\nu(NH_2$ (sym)), 3292(w); ν(NH), 3148(w); ν(C=N), 1602(s); ν(C=S), 680(w) (asy, asymmetric; sym, symmetric; s, strong; w, weak). UV/Vis (dmso) λ, nm (ε, mol^{-1} cm^{-1} L): 287 (18680). ^{1}H NMR ([D_6]-dmso, δ ppm): 3.0–3.4 (group of peaks, dmso, 12H), 3.54 (s, –NH_2, 2H), 3.71 (s, –OCH_3, 3H), 7.1–7.9 (multiplet, aromatic protons, 4H), 8.27 (s, H–C=N, 1H), 11.29 (s, –NH, 1H).

*2.3.8. [$RuCl_2(dmso)_2(mptsc)$] (**6**)*

The complex was prepared as described in Section 2.3.3. by the reaction of *cis*-[$RuCl_2(dmso)_4$] (0.1 g; 0.21 mmol) with the ligand mptsc (0.047 g; 0.21 mmol). Yield: 82 mg; 71%. Elemental *Anal.* Calc. for $C_{14}H_{25}N_3S_3O_3Cl_2Ru$ (551.56): C, 30.48; H, 4.56; N, 7.61; S, 17.44. Found: C, 30.25; H, 4.41; N, 7.39; S, 11.11%. IR (KBr, cm^{-1}): $\nu(NH_2$ (asy)), 3405(w); $\nu(NH_2$ (sym)) 3353(w); ν(NH), 3156(w); ν(C=N), 1598(s); ν(C=S), 696(w) (asy, asymmetric; sym, symmetric; s, strong; w, weak). UV/Vis (dmso) λ, nm (ε, mol^{-1} cm^{-1} L): 277 (7980). ^{1}H NMR ([D_6]-dmso, δ ppm): 2.45 (s, H_3C–C=N, 3H), 3.1–3.6 (group of peaks, dmso, 12H), 3.81 (s, –NH_2, 2H), 3.87 (s, –OCH_3, 3H), 7.0–7.3 (multiplet, aromatic protons, 4H), 11.14 (s, –NH, 1H).

*2.3.9. [$RuCl_2(dmso)_2(cbtsc)$] (**7**)*

The complex was prepared as described in Section 2.3.3. by the reaction of *cis*-[$RuCl_2(dmso)_4$] (0.1 g; 0.21 mmol) with the ligand cbtsc (0.045 g; 0.21 mmol). Yield: 86 mg; 74%. Elemental *Anal.* Calc. for $C_{13}H_{22}N_3S_3O_2Cl_3Ru$ (555.98): C, 28.08; H, 3.98; N, 7.55; S, 17.30. Found: C, 28.24; H, 3.77; N, 7.38; S, 17.54%. IR (KBr, cm^{-1}): $\nu(NH_2$ (asy)), 3360(w); $\nu(NH_2$ (sym)), 3326(w); ν(NH), 3124(w); ν(C=N), 1625(s); ν(C=S), 680(w) (asy, asymmetric; sym, symmetric; s, strong; w, weak). UV/Vis (dmso) λ, nm (ε, mol^{-1} cm^{-1} L): 281 (13780), 312 (8620). ^{1}H NMR ([D_6]-dmso, δ ppm):, 2.48 (s, H_3C–C=N, 3H), 3.1–3.4 (group of peaks, dmso, 12H), 3.74 (s, –NH_2, 2H), 7.4–7.8 (multiplet, aromatic protons, 4H), 10.96 (s, –NH, 1H).

*2.3.10. [$RuCl_2(dmso)_2(bzsc)$] (**8**)*

cis-[$RuCl_2(dmso)_4$] (0.1 g; 0.21 mmol) and the ligand bzsc (0.034 g; 0.21 mmol) were heated under reflux in ethanol (30 ml) for 6 h. Slow evaporation of the solvent after reduction to 50% gave orange crystals suitable for single crystal XRD studies. Yield: 74 mg; 72%. Elemental *Anal.* Calc. for $C_{12}H_{21}N_3S_2O_3Cl_2Ru$ (491.440): C, 29.32; H, 4.29; N, 8.55; S, 13.04. Found: C, 29.54; H, 4.08; N, 8.71; S, 12.88%. IR (KBr, cm^{-1}): $\nu(NH_2$ (asy)), 3325(w); $\nu(NH_2$ (sym)), 3252(w); ν(NH), 3148(w); ν(C=N), 1625(s); ν(C=O), 1665(s) (asy, asymmetric; sym, symmetric; s, strong; w, weak). UV/Vis (dmso) λ, nm (ε, mol^{-1} cm^{-1} L): 276 (10780), 308 (7620). ^{1}H NMR ([D_6]-dmso, δ ppm): 3.1–3.4 (group of peaks, dmso, 12H), 3.82 (s, –NH_2, 2H), 7.5–7.9 (multiplet, aromatic protons, 5H), 8.35 (s, –CH=N, 1H), 11.15 (s, –NH, 1H).

2.4. Crystallographic structure determination

X-ray diffraction measurements were performed on a Nonius Kappa CCD (with Oxford Cryostream) diffractometer with graphite monochromatized Mo Kα radiation. The structure was solved by direct methods and refinements were carried out by full-matrix least-square techniques. The hydrogen atoms were treated by a mixture of independent and constrained refinement. The following computer programs were used: structure solution SIR-97 [29], refinement SHELXL-97 [30], molecular diagrams, ORTEP-3 [31] for windows.

2.5. Antimicrobial screening

The bacterial stains, *Escherichia coli* NCIM 2831, *Staphylococcus aureus* NCIM 2492, *Staphylococcus epidermidis* NCIM 2493, *Klebsiella pneumoniae* NCIM 5082 and *Shigella sonnei* MTCC 2957 were used in the study. Agar-well diffusion method [32] was employed for the determination of antimicrobial activities. Minimum inhibitory concentrations (MICs) of the compounds against test organisms were determined by broth micro dilution method. All the tests were performed in duplicate and repeated twice. Modal values were selected.

2.5.1. Agar-well diffusion method

Compounds were weighed and dissolved in dimethyl sulphoxide (dmso). Compounds were filter sterilized using a 0.45 μm membrane filter. Each microorganism was suspended in sterile saline and diluted at ca.106 colony forming units (cfu/mL). They were flood inoculated onto the surface of Mueller Hinton Agar (MHA). The wells (8 mm in diameter) were cut from the agar and 0.1 mL of solution was delivered into them. After incubation for 24 h at 37 °C, all plates were examined for any zones of growth inhibition, and the diameter of these zones were measured in millimeters.

2.5.2. Determination of minimum inhibitory concentration (MIC)

A microdilution broth susceptibility assay was used as recommended [33] by NCCLS for determination of MIC. All the tests were

performed in Mueller–Hinton Broth (MHB) supplemented with Tween 80 detergent (final concentration of 0.5% (v/v)). Bacterial stains were cultured overnight at 37 °C in MHA. Test strains were suspended in MHB to give a final density of 5 × 105 cfu/ml and these were confirmed by viable counts. Geometric dilutions of the compounds were prepared in a 96-well microtiter plate, including one growth control (MHB + Tween 80) and one sterility control (MHB + Tween 80 + Compound). Plates were incubated under normal atmospheric conditions at 37 °C for 24 h. The MIC of kanamycin and oxytetracycline was individually determined in parallel experiments in order to control the sensitivity of the test organisms. The bacterial growth was indicated by the presence of a white "pellet" on the well bottom.

3. Results and discussion

As the onset of this investigation, the synthesis of thiosemicarbazones was carried out as described in Section 2. On analyzing the ligands for characterization through IR spectroscopy, a sharp peak at 1649 cm^{-1} which is characteristic of ν(C=O) was observed for the ligand (L8) synthesized by condensing benzaldehyde and thiosemicarbazide Based on this observation, the ligand was supposed to be benzaldehyde semicarbazone rather than the expected benzaldehyde thiosemicarbazone. The reactions of the ligands (L1–L7) with the starting complex in 1:1 mole ratio in ethanol yielded complexes of the type $[RuCl_2(dmso)_2(L)]$ (L = thiosemicarbazones) and that of L8 resulted in a complex of the formula $[RuCl_2(dmso)_2(bzsc)]$ (bzsc = benzaldehyde semicarbazone) which is evident from its single crystal XRD data (presented in Section 3.3.). Thus, it becomes manifest that the reaction of benzaldehyde with thiosemicarbazide in ethanol has lead to the formation of benzaldehyde semicarbazone through the conversion of >C=S (of the expected benzaldehyde thiosemicarbazones) to >C=O. Therefore, it is presumed that adventitious water in ethanol should have effected the transformation *in situ* after the formation of thiosemicarbazone as proposed in the tentative mechanism (Scheme 1).

3.1. IR and UV–Vis spectra

The prominent IR regions of interest pertaining to the complexes are furnished in Section 2. The spectra of the free thiosemicarbazone ligands (L1–L7) show peaks of concern around 3400–3250 (two peaks), 3160–3120 and 1615–1585 cm^{-1} attributed to the symmetric and asymmetric stretching of NH_2, ν(NH) and ν(C=N), respectively. The weak to medium intensity band around 782–716 cm^{-1} in the ligands are assigned to ν(C=S). The question of thione-thiol tautometism in the ligands is ruled out because no bands were observed in the region near 2570 cm^{-1}, which is characteristic of ν(C–SH) [34]. This corroborates that the ligands are in thione form in the solid state. In the IR spectra of the ligand L8, besides other characteristic bands, a strong absorption at 1649 cm^{-1} was found and tentatively assigned as due to ν(C=O). In the IR spectra of the complexes, a considerable decrease (5–10 cm^{-1}) for **5** and **6** and increase (5–45 cm^{-1}) for all other complexes in the ν(C=N) frequency shows the coordination of the azomethine nitrogen. The bands due to $\nu(NH_2)$ and ν(NH) almost remain practically unaltered supporting the non-coordination of NH_2 nitrogen and the presence of thione form of the ligand after complex formation. A small negative shift of 10–40 cm^{-1} in ν(C=S) in complexes **1**–**7** shows the neutral coordination of thioamide sulfur. Similarly, the positive shift of ν(C=O) to 1666 cm^{-1} in complex **8**, suggests the neutral coordination of amide oxygen to ruthenium. The peak at 915 cm^{-1}, characteristic of ν(SO)(O-bonded) exhibited by the precursor *cis*-$[RuCl_2(dmso)_4)]$ is absent in the new complexes and thus it is perceived that the ligands act as neutral bidentate donors replacing one O-bonded dmso and one S-bonded dmso from the precursor, which is in accord with a previous study [27].

The electronic spectra of all the complexes were identical showing weak absorptions in the ultraviolet region. The absorption maximum and molar extinction coefficients are given in Section 2. The bands are assignable to transitions within the ligand orbitals (intraligand $\pi \rightarrow \pi^*$ or $n \rightarrow \pi^*$) [35,36].

3.2. ^{1}H NMR spectra

The ^{1}H NMR spectra of the complexes recorded in $[D_6]$-dmso exhibited narrow signals. Comparison of the spectra of the precursor, *cis*-$[RuCl_2(dmso)_4]$ with that of the new complexes seemed inevitable in order to predict the nature of bonding mode of dmso in the new complexes. Out of the six singlets appeared in the ^{1}H NMR spectra of *cis*-$[RuCl_2(dmso)_4]$ at δ 3.50, 3.48, 3.43, 3.32, 2.72 and 2.66 ppm due to six sets of chemically different protons, the peak at δ 2.66 ppm has been assigned to free dmso which resulted from the 10% dissociation of O-bonded dmso. Similarly the peak at δ 2.72 ppm has been attributed to the O-bonded dmso since the methyl resonance is close to that of free dmso (δ 2.50). The other peaks appearing in a group have been assigned to S-bonded dmso and the integration of these peaks had not been possible owing to their proximity and their sharing the same broad base line [27]. Thus it becomes obvious that the group of peaks appearing in the new complexes around $\sim\delta$ 3.0–3.6 ppm should be attributed to S-bonded dmso resonances. The lack of any peak at δ 2.7 ppm for any of the new complexes implied the absence of O-bonded dmso in the complexes and supported the same point inferred from the IR spectra and evidenced by the crystal structure of **8**. The resonance around δ 2.5 ppm in all the complexes is due to the solvent. The Ar-methyl protons in **2** resonated at δ 1.64 ppm. The NH_2 protons in all the complexes gave single resonance peak in the range δ 3.54–4.22. The protons of CH_3–C=N in **1**, **2**, **6** and **7** appeared as a singlet in the range at δ 2.38–2.48. The singlets observed at δ 3.71 (complex **5**) and δ 3.87 (complex **6**) are due to methoxy protons. The protons of the methyl group in **3** and **4** gave resonance at δ 2.2 ppm. The aromatic/heterocyclic ring protons were observed in the range 6.6–7.9 ppm as multiplets. The azomethine (HC=N) proton in **3**, **4**, **5** and **8** resonated in the range δ 8.09–8.35 ppm. The appearance of a singlet in all the complexes around δ 10.87–11.23 ppm is due to NH proton which is matching with the IR observation that the chelating ligand coordinates in its keto form to the metal. From the foregoing discussions, it can be established that the semicarbazone/thiosemicarbazone ligands behave as neutral bidentate donors replacing one O-bonded dmso and one S-bonded dmso from the precursor.

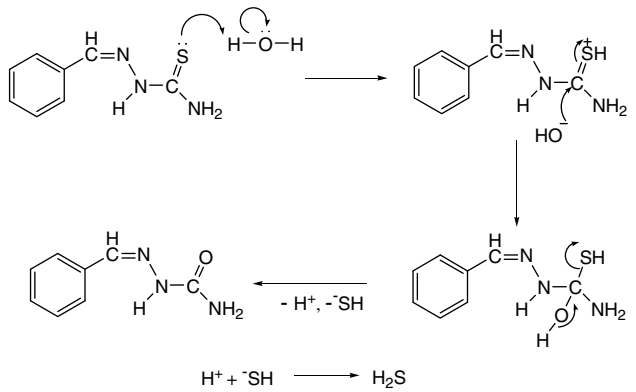

Scheme 1. Tentative mechanism for the conversion of >C=S to >C=O.

Table 1
Crystallographic data for **8**

Chemical formula	$C_{12}H_{21}Cl_2N_3O_3RuS_2$
Formula weight	491.41
Crystal color, habit	orange-yellow, fragment
Crystal dimensions (mm^3)	$0.23 \times 0.15 \times 0.12$
Crystal system	orthorhombic
Space group	$P2_12_12_1$
a (Å)	9.1078(12)
b (Å)	12.729(2)
c (Å)	16.318(3)
V (Å^3)	1891.8(5)
Z	4
D_{Calc} (Mg m^{-3})	1.725
μ (mm^{-1}) (Mo Kα)	1.346
T (K)	115
Reflections collected	35798
Unique reflections	4316
Reflections [$I \geqslant 2\sigma(I)$]	4035
$F(000)$	992
θ_{max} (°)	27.5
R_{int}	0.054
R [$F^2 \geqslant 2\sigma(F^2)$]	0.037
wR [F^2]	0.087
Goodness of fit on F^2	1.056
Largest peak and hole (e Å^{-3})	1.52 and −1.03

3.3. X-ray crystallography of $[RuCl_2(dmso)_2(bzsc)]$ (**8**)

The structural study of this complex gains importance because the synthesis of this complex attempted previously by Vieites et al. by reacting *trans*-$[RuCl_2(dmso)_4]$ with benzaldehyde semicarbazone in methanol has not afforded any isolable complex and the characterization was limited only to the ^{1}H NMR spectra of the reaction mixture [37]. Unlike their synthesis, in our case, X-ray quality single crystals of the complex could be obtained by following the simple procedure given in Section 2.3.8. The complex crystallizes in the orthorhombic space group $P2_12_12_1$. The compound forms enantiopure crystals, as evidenced by the space group and the value of Flack parameter, −0.01(4) [38] and Hooft parameter, 0.008(11) [39]. However the complex itself does not contain chiral species, and is meso, with potential mirror symmetry. We thus assume that the compound crystallizes as a conglomerate, with individual crystals of each hand in the macroscopic sample.

The details on data collection, refinement and unit cell parameters are collected in Table 1. Fig. 1 shows the ORTEP drawing of **8** and Table 2 presents the selected geometrical parameters that are essential for the discussion. The molecular structure of **8** shows that the coordination sphere around Ru(II) is S_2Cl_2NO. The coordination polyhedron of the ruthenium ion can be described as distorted octahedron. The distortion in the complex from ideal octahedral geometry is due to the small bite angle of the ON chelate of semicarbazone ligand and the bending of chloride ligands towards the chelate which is evident from the angles O1–Ru1–N1 = 77.23(13), Cl1–Ru1–Cl2 = 171.62(4)°.

The average Ru–Cl bond lengths Ru1–Cl1 = 2.4154(12); Ru1–Cl2 = 2.3960(12) Å are slightly longer than found in $[RuCl_2(dmso)_2$(5-nitro-2-furaldehyde semicarbazone)] [Ru1–Cl12 = 2.386(4); Ru1–Cl11 = 2.394(4) Å] [8]. This length is shorter than that found in *cis*-$[RuCl_2(dmso)_4]$ (average Ru–Cl = 2.42 Å) and comparable with that found in the *trans* isomer [Ru–Cl = 2.402(2) Å] which is in agreement with the greater *trans* influence of dmso that weakens the Ru–Cl bond in *cis*-$[RuCl_2(dmso)_4]$ [40]. Similarly, the two Ru–S bond lengths [Ru1–S1 = 2.2054(12); Ru1–S2 = 2.2436(11) Å] are significantly shorter than the four equal Ru–S bonds [2.352(2) Å] in *trans*-$[RuCl_2(dmso)_4]$ and mean Ru–S bond length of 2.25(1) Å in $[Ru(dmso)_6]^{2+}$ [41] which shows the diminished competition between two dmso ligands for π-back donation in **8**. This stronger Ru^{2+}–S bonds in comparison with the Ru^{3+}–S bonds in similar Ru(III) complexes{Ru1–S1 = 1.461(3) Å in $[(dmso)_2H$-[*trans*-$Ru(dmso)_2Cl_4]$; Ru–S2 = 2.330(2), Ru–S3 = 2.351(1) Å in *mer*-$[Ru(dmso)_3Cl_3]$ and Ru1–S1 = 2.295(2) Å in [pyH]*trans*-$[RuCl_4$-(dmso)(py)]} [9,11] is in accordance with the better donation of d-electron density of less positive Ru(II) to sulfur atoms of dmso than by Ru(III) centre.

The complex is stabilized by intermolecular and intramolecular hydrogen bonds. The hydrogen bonding geometries for the complex is given in Table 3. The C–H···O (azomethine carbon, C2 is hydrogen bonded to the oxygen atom of the dmso) type intramolecular hydrogen bonds exhibited by the complex is noteworthy.

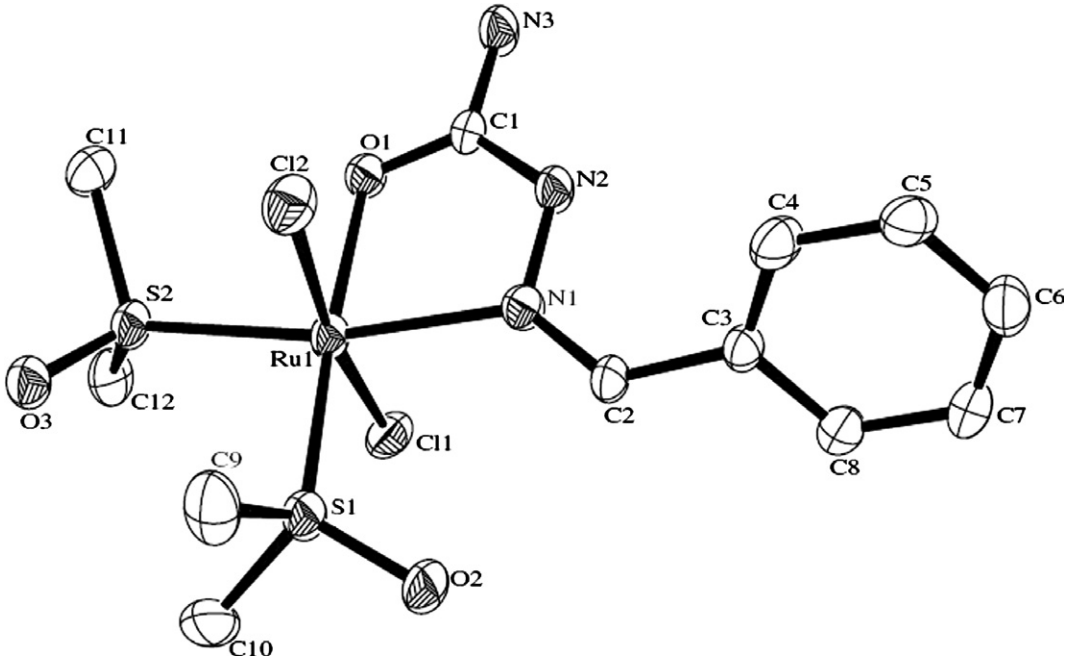

Fig. 1. ORTEP style drawing of **8** with 50% probability of thermal ellipsoids. Hydrogen atoms are omitted for clarity.

Table 2
Selected geometrical parameters for **8**

Bond distances (Å)			
Ru1–N1	2.123(4)	Ru1–S2	2.2436(11)
Ru1–O1	2.100(3)	Ru1–Cl1	2.4154(12)
Ru1–S1	2.2054(12)	Ru1–Cl2	2.3960(12)
S1–O2	1.484(3)	S2–O3	1.490(4)
Bond angles (°)			
O1–Ru1–N1	77.23(13)	S1–Ru1–Cl2	94.10(5)
O1–Ru1–S1	175.83(9)	S2–Ru1–Cl2	89.94(5)
N1–Ru1–S1	98.60(10)	O1–Ru1–Cl1	87.79(9)
O1–Ru1–S2	91.14(9)	N1–Ru1–Cl1	87.41(11)
N1–Ru1–S2	167.93(10)	S1–Ru1–Cl1	92.07(5)
S1–Ru1–S2	93.03(4)	S2–Ru1–Cl1	95.41(4)
O1–Ru1–Cl2	85.65(9)	Cl2–Ru–Cl1	171.62(4)
N1–Ru1–Cl2	86.05(11)	C9–S1–O2	106.6(3)
C11–S2–C12	99.7(3)	C10–S1–O2	104.3(2)
C9–S1–C10	99.9(3)	C11–S2–O3	107.4(2)
		C12–S2–O3	106.6(3)

Table 3
Hydrogen-bonding distances (Å) and angles(°) for **8**

D–H···A	D–H	H···A	D···A	D–H···A
N2–H2N···Cl1^{i}	0.89(6)	2.49(6)	3.281(4)	149(5)
N3–H31N···O3^{ii}	0.95(6)	2.03(6)	2.937(5)	160(5)
N3–H32N···Cl1^{i}	0.80(6)	2.55(6)	3.256(4)	147(5)
C2–H2···O2	0.95	2.14	2.962(6)	143.5

Symmetry codes (i) $1-x$, $1/2+y$, $1/2-z$ and (ii) $1/2+x$, $3/2-y$, $-z$.

Table 4
Cyclic voltammetric data of the complexes in dmso

Complex	Ru(II)/Ru(I)[a] $E_{1/2}/V$ (ΔEp/mV)	(Cl)/(Cl$^-$)[b] $E_{1/2}/V$ (ΔEp/mV)	dmso based reduction[d]
(**1**)	−1.02 (350)	0.90[c]	−0.75
(**2**)	−0.70 (200)	1.06 (300)	−0.20
(**3**)	−0.66 (360)	1.07 (340)	−0.20
(**4**)	−0.72 (240)	0.90[c]	−0.28
(**5**)	−0.73 (300)	1.08 (400)	−0.20
(**6**)	−0.72 (240)	1.08 (360)	−0.24
(**7**)	−0.75 (140)	1.05 (300)	−0.40
(**8**)	−0.76 (160)	1.09 (340)	−0.24

[a] Reduction couple.
[b] Oxidation couple.
[c] Irreversible, Ep_a value.
[d] Irreversible, Ep_c value.

By analogy of the structure of **8**, a similar structure is proposed for other thiosemicarbzone complexes **1**–**7**, whose spectral characterization supports the neutral bidentate coordination of the SN chelate to ruthenium.

3.4. Cyclic voltammetric studies

The electron transfer properties of the new Ru(II) complexes were examined by cyclic voltammetry with dmso solutions ($\sim 1 \times 10^{-3}$ M) using 0.1 M TBAP as supporting electrolyte. The redox potentials measured relative to Ag/AgCl electrode at a scan rate of 0.1 V/s are reported in Table 4. All the complexes were electroactive in the sweep range ±1.5 V and displayed well-defined one-electron quasi-reversible coupled redox wave on either side of the reference electrode besides an irreversible peak at less negative potentials with respect to the coupled redox wave at the negative side of Ag/AgCl electrode. A prototype showing all the voltammetric features is shown Fig. 2. The oxidative couple exhibited by the complexes with formal potentials in the range 1.05–1.09 V (in complexes **1** and **4**, the cathodic counterpart of this couple is ill-defined) is ascribed to the oxidation of a slowly dissociated chloride ion [9,42]. This dissociation in turn accompanies Ru(II)/Ru(I) reduction occurring in the range −0.66 to −1.02 V and this range is concurrent with literature values [43,44]. Further dissociation of chloride has not been evidenced previously [9] for *trans*-$[Ru(dmso)_2Cl_4]^{2-}$ ion and thus the same is expected for the new complexes and also substantiated by the lack of any other reduction wave at more negative potentials than that for Ru(II)/Ru(I) reduction process. Also the dissociation of two chloride ions is unlikely since it will lead to the formation of Ru(0) species which is highly unstable. The other irreversible reduction wave in the range −0.18 to −0.40 V for **2**–**8** and at −0.75 V for **1** could not be thought of semicarbazone/thiosemicarbazones-based reduction for two reasons. Firstly, these ligand-based reductions occur at more negative potentials, almost at the negative-end of the chosen potential window here. The other reason is the observance of a similar peak at −0.15 V in the cyclic voltammogram of the precursor, *cis*-$[RuCl_2(dmso)_4]$ obtained under identical experimental conditions. Thus, this irreversible reduction may be attributed to coordinated dmso. This reduction potential is affected in the complexes due to coordinated semicarbazone/thiosemicarbazones. Nevertheless no correlation could be made out for this with the electronic nature of the ligands.

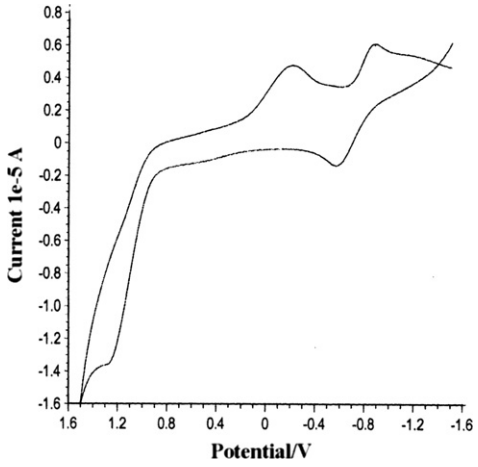

Fig. 2. Cyclic voltammogram of **6**.

3.5. UV–Vis spectra of the complexes in the presence of buffered herring sperm DNA solution

In general, metal complexes can bind to DNA via both covalent and non-covalent interactions [45–47]. These different modes of binding can be monitored by following the changes in the wavelength and intensity of absorption of a particular peak exhibited by the unbound complex. A decrease in absorbance (hypochromism) or an increase in absorbance (hyperchromicity) upon addition of DNA to a compound in solution is indicative of an interaction between these molecules [48].

In a typical experiment, the absorption titration was carried out with a complex of final concentration $\sim 1 \times 10^{-4}$ M and varying the concentration of herring sperm DNA. The concentration of the DNA stock solution was calculated to be 3.7878×10^{-3} M. The addition of DNA to the complex was achieved by adding buffered DNA (in different mixing ratios (r = [DNA]/[Ru-complex]) to the complex (0.3 mL) while maintaining the total volume a constant (3 mL). All the complexes showed single peak in the Tris–HCl buffer in the range 264–329 nm due to intraligand transitions. The change in wavelength and absorbance of this peak in the unbound complex was monitored as increasing amounts of DNA were added

Table 5
Change in UV–Vis spectra of (**1**)–(**8**) upon the gradual addition of herring sperm DNA[a]

Complex	$r = 0$		$r = 1$		$r = 2$		$r = 3$	
	λ_{max} (nm)	$\varepsilon_{max} \times 10^3$	λ_{max} (nm)	$\varepsilon_{max} \times 10^3$	λ_{max} (nm)	$\varepsilon_{max} \times 10^3$	λ_{max} (nm)	$\varepsilon_{max} \times 10^3$
1	264	18.341	264	23.348	264	25.040	264	25.994
2	264	16.076	267	22.432	269	24.970	270	25.816
3	273	6.138	270	9.560	265	17.265	264	19.400
4	302	11.089	304	11.935	305	13.204	306	13.838
5	283	10.610	283	9.682	283	9.682	283	9.682
6	276	8.557	273	11.082	270	12.340	268	14.440
7	307	16.559	309	17.828	312	18.251	313	18.674
8	257	4.483	305	7.867	311	10.033	324	10.033

[a] Concentration of the complexes $\sim 10^{-4}$ M in dmso; concentration of DNA = 3.7878×10^{-3} in Tris–HCl buffer (pH 7.1); r = [DNA]/[complex].

Table 6
Antibacterial activity data of the complexes

Compound	*Escherichia coli*		*Shigella sonnei*		*Klebsiella pneumoniae*		*Staphylococcus epidermidis*		*Staphylococcus aureus*	
	WD[a]	MIC[b]	WD	MIC	WD	MIC	WD	MIC	WD	MIC
2	18	56	12	78	NA	NT	NA	NT	NA	NT
3	NA	NT	NA	NT	NA	NT	10	61	10	82
4	14	64	13	69	14	55	NA	NT	NA	NT
6	18	58	17	58	NA	NT	NA	NT	NA	NT
7	NA	NT	NA	NT	NA	NT	12	63	12	77
8	15	62	12	74	12	58	14	58	13	63
Oxytetracycline	30	15	37	8	30	8	44	8	32	7
Kanamycin	32	18	48	9	35	10	60	11	40	10

NA – not active; NT – not tested.
[a] WD, disc diffusion method as recommended by NCCLS. Diameter of zone of inhibition (mm) including well diameter 8 mm. One hundred micrograms of both compound and antibiotics were used.
[b] MIC, minimum inhibitory concentration. Values given as μg/ml for both compounds and antibiotics.

and the results are recorded in Table 5. Except **1** and **5**, all the other complexes show small red shift or blue shift with a considerable hypochromism. These changes are indicative of interaction of the complexes with DNA [49].

3.6. Antibacterial activity

The antibacterial activity of the complexes as a measure of inhibition zone as well as minimum inhibitory concentration (MIC) against three Gram negative (*E. coli*, K. pneumoniae, S. sonnei) and two Gram positive (*S. aureus*, S. epidermidis) bacteria have been evaluated and the results are listed in Table 6. Since **1** and **5** showed an inhibition zone of 12 mm only against *S. sonnei* and were inactive against all other species, they were not tested further. The results show that none of the new ruthenium complexes were anywhere near as active as either oxytetracycline or kanamycin.

4. Conclusions

An interesting series of Ru(II)-dmso thiosemicarbazone complexes along with a semicarbazone complex has been synthesized and characterized. The XRD structure of previously ill-characterized [$RuCl_2$(dmso)$_2$(benzaldehyde semicarbazone)] has been reported which also supports the conversion of benzaldehyde thiosemicarbazone to benzaldehyde semicarbazone during ligand preparation. The electrochemistry and preliminary DNA-binding studies of the complexes with herring sperm ds-DNA has also been carried out. The complexes have been screened for their antibacterial activity against five pathogenic bacteria.

Appendix A. Supplementary data

CCDC 608057 contains the supplementary crystallographic data for 8. These data can be obtained free of charge via http://www.ccdc.cam.ac.uk/conts/retrieving.html, or from the Cambridge Crystallographic Data Centre, 12 Union Road, Cambridge CB2 1EZ, UK; fax: (+44) 1223-336-033, or e-mail: deposit@ccdc.cam.ac.uk.

References

[1] D.-L. Ma, C.-M. Che, F.-M. Siu, M. Yang, K.-Y. Wong, Inorg. Chem. 46 (2007) 740.
[2] V.B. Arion, E. Reisner, M. Fremuth, M.A. Jakupec, B.K. Keppler, V.Y. Kukushkin, A.J.L. Pombeiro, Inorg. Chem. 42 (2003) 6024.
[3] M. Ravera, S. Baracco, C. Cassino, P. Zanello, D. Osella, Dalton Trans. (2004) 2347.
[4] G. Sava, E. Alessio, A. Bergamo, G. Mestroni, Topics in Biological Inorganic Chemistry, in: M.J. Clarke, P.J. Sadler (Eds.), Metallo-pharmaceuticals, vol. 1, Springer, Berlin, 1999, p. 143.
[5] E. Alessio, G. Mestroni, A. Bergamo, G. Sava, Metal ions in biological systems, in: A. Sigel, H. Sigel, M. Dekker (Ed.), Metal Ions and Their Complexes in Medication and in Cancer Diagnosis and Therapy, vol. 42, New York, 2004, p. 323.
[6] E. Alessio, G. Mestroni, A. Bergamo, G. Sava, Curr. Topics Med. Chem. 4 (2004) 1525.
[7] B. Bratsos, E. Serli, N. Zangrando, E. Katsaros, Alessio, Inorg. Chem. 46 (2007) 975.
[8] L. Otero, P. Nobilia, D. Gambino, H. Cerecetto, M. González, J.A. Ellena, O.E. Piro, Inorg. Chim. Acta 344 (2003) 85.
[9] E. Alessio, G. Balducci, M. Calligaris, G. Costa, W.M. Attia, G. Mestroni, Inorg. Chem. 30 (1991) 609.
[10] E. Alessio, G. Balducci, A. Lutman, G. Mestroni, M. Calligaris, W.M. Attia, Inorg. Chim. Acta 203 (1993) 205.
[11] Q.A. de Paula, A.A. Batista, O.R. Nascimento, A.J. da Costa-Filho, M.S. Schultz, M.R. Bonfadini, G. Oliva, J. Braz. Chem. Soc. 11 (5) (2000) 530.
[12] G. Sava, S. Pacor, G. Mestroni, E. Alessio, Anticancer Drugs 3 (1992) 25.
[13] G. Sava, S. Pacor, G. Mestroni, E. Alessio, Clin. Exp. Metastasis 10 (1992) 273.
[14] C. Monti-Bragadin, M. Giacca, L. Dolzani, M. Tamaro, Inorg. Chim. Acta 137 (1987) 31.
[15] G. Sava, S. Zorzet, T. Giraldi, G. Mestroni, G. Zassinovich, Eur. J. Cancer Clin. Oncol. 20 (1984) 841.
[16] S. Cauci, E. Alessio, G. Mestroni, F. Quadrifoglio, Inorg. Chim. Acta 137 (1987) 19.
[17] D.X. West, S.B. Padhye, P.B. Sonawane, Struct. Bond. 76 (1991) 1. and Refs therein.
[18] S.N. Pandeya, J.R. Dimmock, Pharmazie 48 (1993) 659. and Refs. therein.
[19] S. Padhye, G.B. Kauffman, Coord. Chem. Rev. 63 (1985) 127.
[20] J.G. Cory, A.H. Cory, G. Rappa, A. Lorico, M.-C. Liu, T.-S. Lin, A.C. Sartorelli, Biochem. Pharmacol. 48 (1994) 335.

[21] D. Kovala-Demertzi, P.N. Yadav, M.A. Demertzis, M. Coluccia, J. Inorg. Biochem. 78 (2000) 347.
[22] J.P. Scovill, D.L. Klayman, C.F. Franchino, J. Med. Chem. 25 (1982) 1261.
[23] M.J.M. Campbell, Coord. Chem. Rev. 15 (1975) 279.
[24] Z. Lakovidou, A. Papageorgiou, M.A. Demertzis, E. Mioglou, D. Mourelatos, A. Kotsis, P.N. Yadav, D. Kovala-Demertzi, Anti-Cancer Drugs 12 (2001) 65.
[25] J. Marmur, J. Mol. Biol. 3 (1961) 208.
[26] M.F. Reichmann, S.A. Rice, C.A. Thomas, P. Doty, J. Am. Chem. Soc. 76 (1954) 3047.
[27] I.P. Evans, A. Spencer, G. Wilkinson, J. Chem. Soc., Dalton Trans. (1973) 204.
[28] R.L. de Lima, L.R.deS. Teixeira, T.M.G. Carneiro, H. Beraldo, J. Braz. Chem. Soc. 10 (3) (1999) 184.
[29] M.C. Altomare, M. Burla, G. Camalli, C. Cascarano, A. Giacovazzo, A.G.G. Guagliardi, G. Moliterni, R. Polidori, J. Appl. Crystallogr. 32 (1999) 115.
[30] G.M. Sheldrick, SHELXL-97 A Program for Structure Refinement, University of Göttingen, Göttingen, Germany, 1997.
[31] L.J. Farrugia, J. Appl. Crystallogr. 30 (1997) 565.
[32] NCCLS (National Committee for Clinical Laboratory Standards), Performance standards for antimicrobial disk susceptibility test, 6th ed. Approved standard, Wayne, PA, M2-A6, 1997.
[33] NCCLS (National Committee for Clinical Laboratory Standards), Performance standards for antimicrobial susceptibility testing; 9th International supplement, Wayne, PA, M100-S9, 1999.
[34] K.H. Reddy, P.S. Reddy, P.R. Babu, Trans. Met. Chem. 25 (2000) 154.
[35] S. Grguric-Sipka, C.R. Kowol, S.-M. Valiahdi, R. Eichinger, M.A. Jakupec, A. Roller, S. Shova, V.B. Arion, B.K. Keppler, Eur. J. Inorg. Chem. (2007) 2870.
[36] M. Ashok, V. Ravinder, A.V.V.S. Prasad, Trans. Met. Chem. 32 (2007) 23.
[37] M. Vieites, P. Buccino, L. Otero, M. Gonzalez, O.E. Piro, R.S. Delgado, C.M.R.S. Anna, E.J. Barreiro, H. Cerecetto, D. Gambino, Inorg. Chim. Acta 358 (2005) 3065.
[38] H.D. Flack, Acta Crystallogr., Sect. A 39 (1983) 876.
[39] R.W.W. Hooft, L.H. Straver, A.L. Spek, J. Appl. Crystallogr. 41 (2008) 96.
[40] E. Alessio, G. Mestroni, G. Nardin, W.M. Attia, M. Calligaris, G. Sava, S. Zorzet, Inorg. Chem. 27 (1998) 4099.
[41] A.R. Davies, F.W.B. Einstein, N.P. Farrell, B.R. James, R.S. McMillan, Inorg. Chem 17 (1978) 1965.
[42] B. Serli, E. Zangrando, E. Iengo, G. Mestroni, L. Yellowless, E. Alessio, Inorg. Chem. 41 (2002) 4033.
[43] K.N. Kumar, R. Ramesh, Polyhedron 24 (2005) 1885.
[44] Y.-P. Tian, M.-L. Zhang, Z.-J. Hu, H.-M. Hu, J.-Y. Wu, X.-J. Zhang, X.-T. Tao, M.-H. Jiang, H.-P. Chen, S. Chantrapromma, H.-K. Fun, Trans. Met. Chem. 30 (2005) 778.
[45] H.H. Thorp, J. Inorg. Organomet. Polymers 3 (1993) 111.
[46] A.M. Pyle, J.K. Barton, Prog. Inorg. Chem. 38 (1990) 413.
[47] S.J. Lippard, Acc. Chem. Res. 11 (1978) 211.
[48] D.R. Richardson, P.C. Sharpe, D.B. Lovejoy, D. Senaratne, D.S. Kalinowski, M. Islam, P.V. Bernhardt, J. Med. Chem. 49 (2006) 6510.
[49] M. Baldini, M. Belicchi-Ferrari, F. Bisceglie, G. Pelosi, S. Pinelli, P. Tarasconi, Inorg. Chem. 42 (2003) 2049.

on a Varian E-112 (X band, 9.1 GHz) spectrometer at a microwave power of 1 mW and a modulation amplitude of 0.5 gauss, and the spectra were collected using a quartz dewar. Diphenylpicrylhydrazyl (dpph, $g = 2.0037$) was used to calibrate the spectra. Magnetic measurements were carried out on polycrystalline samples with a Quantum Design MPMS XL SQUID susceptometer operating at a magnetic field of 0.1 T between 2 and 300 K. The diamagnetic corrections were evaluated from Pascal's constants. Elemental analyses (C, H, N) were performed on a Perkin–Elmer 2400 Series II Elemental Analyzer.

2.2. Synthesis of the complexes

$[Fe^{III}(HL)][BPh_4]$ (**1**). H_3L (129 mg, 0.25 mmol) was added to a solution of $FeCl_3 \cdot 6H_2O$ (68 mg, 0.25 mmol) in methanol (10 ml) and the resulting violet solution was stirred at room temperature for 1 h. Addition of Et_3N (0.104 ml, 0.75 mmol) resulted in a deep brown colored solution which yielded a deep brown crystalline product after addition of $NaBPh_4$ (85 mg, 0.25 mmol) on slow evaporation. The product was collected by filtration and washed with cold water. Deep brown crystals were obtained by layering the product with DCM/hexane. Yield: 0.179 g, 80%. *Anal.* Calc. for $C_{55}H_{62}BFeN_4O_3$: C, 73.39; H, 6.92; N, 6.32. Found: C, 73.85; H, 6.99; N, 6.26%. UV–Vis (λ_{max}/nm (ε/$M^{-1}\,cm^{-1}$) CH_3CN solution): 500 (5549), 275 (18373). IR (KBr)/cm^{-1}: ν(C–O) 1270; ν(Fe–O) 690. E_{pa} (Fe^{III}/Fe^{II}): −0.191 V (irr.).

$[Fe_2^{III}L(OAC)_2]BPh_4$ (2). A solution containing H_3L (129 mg, 0.25 mmol) and $FeCl_3 \cdot 6H_2O$ (135 mg, 0.5 mmol) in 15 ml methanol was stirred at room temperature. After 15 min sodium acetate (123 mg, 1.5 mmol) was added, followed by $NaBPh_4$ (171 mg, 0.5 mmol) after an additional 30 min. Stirring was continued for 1 h and a deep blue solid started separating; it was evaporated to dryness and the resulting solid was washed thoroughly with water. The deep blue solid was dried in vacuum and recrystallized from methanol. Yield: 0.213 g, 76%. *Anal.* Calc. for $C_{60}H_{73}BFe_2N_4O_9$: C, 64.51; H, 6.52; N, 5.05. Found: C, 64.45; H, 6.59; N, 5.01%. UV–Vis (λ_{max}/nm (ε/$M^{-1}\,cm^{-1}$) CH_3CN solution): 545 (59964), 321 (18295), 275 (36565). IR (KBr)/cm^{-1}: ν(C–O) 1270; ν(Fe–O) 694; ν(O_2CMe) 1564 and 1452. E_{pa} (Fe^{III}/Fe^{II}): −0.131 V.

2.3. Crystallographic studies

Single crystals suitable for X-ray crystallographic analysis of the complex $[Fe^{III}(HL)][BPh_4]$ were obtained by diffusing a dichloromethane solution of the complex into hexane and that of $[Fe_2^{III}L(OAc)_2][BPh_4] \cdot H_2O \cdot CH_3OH$ was obtained from a methanolic solution by slow evaporation. The X-ray intensity data were collected on a Bruker AXS SMART APEX CCD diffractometer (Mo Kα, $\lambda = 0.71073$ Å) at 293 K. The detector was placed at a distance of 6.03 cm from the crystal. A total of 606 frames were collected with a scan width of 0.3° in different settings of φ. The data were reduced in SAINTPLUS [8] and an empirical absorption correction was applied using the SADABS package [8]. The metal atoms were located by the Patterson Method and the rest of the non-hydrogen atoms emerged from successive Fourier synthesis. The structures were refined by a full-matrix least-square procedure on F^2. All non-hydrogen atoms were refined anisotropically. All hydrogen atoms were directly located in different Fourier maps. All calculations were performed using the SHELXTL V 6.14 program package [9]. Molecular structure plots were drawn using ORTEP [10]. Relevant crystal data are given in Table 1.

2.4. Computational details

All the calculations were carried out with the Density Functional Theory (DFT) [11] method and the calculations have been performed using the B3LYP exchange correlation function, [12] as implemented in the GAUSSIAN03 (G03) program package [13]. The geometry of complexes **1** and **2** were fully optimized in the gas phase using the 6-31G basis set [14] for the H, C, N, O atoms and the 6-31+g(d) basis set for iron without any symmetry constrain.

Table 1
Crystal data and structure refinement parameters for complexes **1** and **2**

	Complex **1**	Complex **2**
Formula	$C_{55}H_{62}BFeN_4O_3$	$C_{60}H_{73}BFe_2N_4O_9$
Formula weight	893.75	1116.73
Crystal system	monoclinic	triclinic
Space group	$C12/C1$	$P\bar{1}$
a (Å)	36.273(7)	10.947(2)
b (Å)	10.608(2)	14.656(3)
c (Å)	28.959(6)	18.701(4)
α (°)	90.00	71.439(4)
β (°)	119.08(3)	86.525(4)
γ (°)	90.00	74.833(4)
V (Å^3)	9738(3)	2744.5(10)
Z	8	2
D_{calc} (Mg m^{-3})	1.219	1.351
μ (mm^{-1})	0.357	0.590
θ (°)	1.61 - 25.00	1.52 - 24.00
T (K)	293(2)	293(2)
R_1,[a] wR_2[b] [$I > 2\sigma(I)$]	0.0755, 0.1213	0.1197, 0.2676
Goodness-of-fit (GOF) on F^2	1.102	1.216

[a] $R_1 = \sum |F_o| - |F_c| / \sum |F_o|$.
[b] $wR_2 = [\sum w(F_o^2 - F_c^2)^2 / \sum w(F_o^2)^2]^{1/2}$.

3. Results and discussion

The trianionic N_4O_3 coordinating ligand [7] has been used for the present study. The ligand possesses two sets of mono-acidic ONN chelating donor sites along with a central phenolate group. The reaction of $FeCl_3 \cdot 6H_2O$ with H_3L in a ratio 2:1 in the presence of sodium acetate offered a μ-phenoxo μ-acetato bridged diiron(III) complex of the formula $[Fe_2^{III}L(OAc)_2]^+$, (**2**$^+$) in good yields. Interestingly, when the same reaction was carried out with a 1:1 metal-to-ligand ratio in the presence of excess triethylamine instead of sodium acetate it yielded mononuclear $[Fe^{III}(HL)]^+$, **1**$^+$. The Fe(III) complexes are isolated as salts of the BPh_4^- anion.

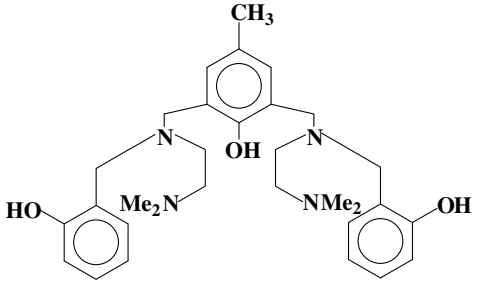

H_3L

The $\nu_{(C-Ophenolate)}$ vibrations in both cases are observed around 1270 cm^{-1}. Complex **2** displays carboxylate stretches near 1564 and 1452 cm^{-1}. The splitting between the two peaks is 112 cm^{-1}, which indicates that the carboxylate group bridges the two iron ions in a *syn–syn* fashion [15a].

The UV–vis spectra of the complexes were recorded in acetonitrile (CH_3CN) solution and display two well resolved peaks along with a shoulder. The absorption near 500–545 nm is probably due to a phenolate(axial) → Fe(III) or phenolate(equatorial) → Fe(III) LMCT transition [15b,c]. The band near 300 nm is associated with ligand π–π^* transition.

All the complexes are electroactive at a platinum electrode versus SCE in acetonitrile solution. Complexes **1** and **2** exhibit an anodic response at −0.191 and −0.131 V, respectively. The voltammogram response is probably due to Fe(III) → Fe(II) and Fe(III)–Fe(III) → Fe(III)–Fe(II) reduction couples [16], respectively.

4. Crystal structures

The molecular structures of **1** and **2** · H_2O · CH_3OH have been determined by the X-ray diffraction method. The molecular views of the cationic part of the complexes are shown in Figs. 1 and 2, respectively. Selected bond parameters are listed respectively in Tables 2 and 3.

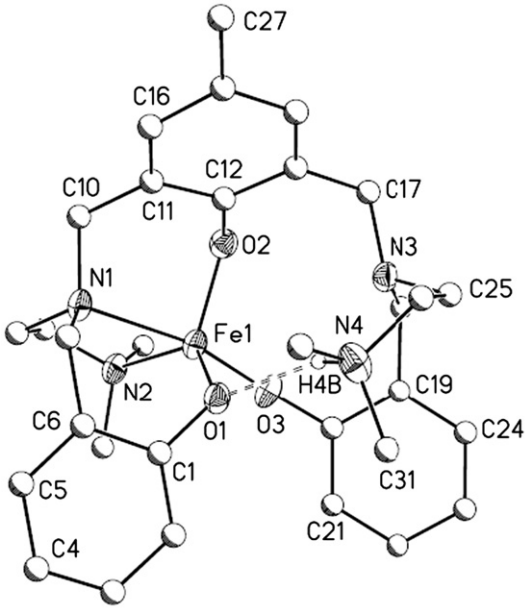

Fig. 1. Perspective view and atom-labelling scheme for [$Fe^{III}LH^+$]. All non-hydrogen atoms are represented by their 30% thermal probability ellipsoids.

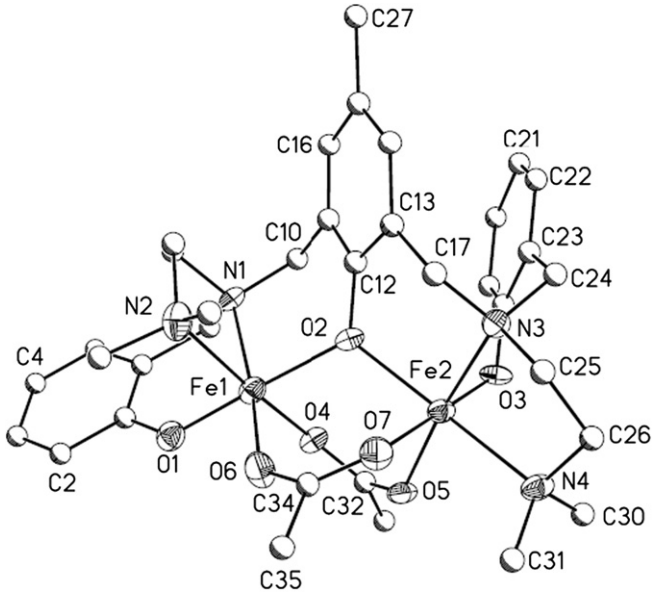

Fig. 2. Perspective view and atom-labelling scheme for [$Fe^{III}_2L(OAC)_2]^+$. All non-hydrogen atoms are represented by their 30% thermal probability ellipsoids.

[Fe^{III}(HL)][BPh_4] (**1**). The coordination environment around the iron atom in [$Fe^{III}LH^+$] is a distorted trigonal bipyramid (τ = 0.84) [17]. The ONN donor atoms along with the central phenolato group occupy four coordinating sites in which the terminal phenolate and tripodal nitrogen occupy equatorial positions whereas the central phenolate and terminal phenolate groups are *trans* to each other in the axial sites. The fifth coordination position is occupied by the terminal phenolato group of another ONN site of H_3L and the other two nitrogen atoms remain uncoordinated. It is interesting to note that the pentadentate nitrogen becomes protonated in the complex. In the lattice, the protonated N–*H* atom is hydrogen bonded with the coordinated O(1), the O(1)···N(4) distance being 2.833(6) Å. The involvement in hydrogen bonding of the O(1) atom explains the large Fe(1)–O(1) bond distance. The Fe–O(phenoxide) bond distances reveal that all three phenol groups are coordinated to iron(III) as phenoxides. The observed Fe–O bond distances (Fe(1)–O(1), 1.900(3), Fe(2)–O(2), 1.849(3) and Fe(1)–O(3), 1.872(3) Å) are shorter than the average octahedral Fe–O(phenoxide) bond distance of 1.92 Å. Fe–N bond distances are usual and span the range 2.15–2.31 Å [4b].

[FeIII2L(OAc)2][BPh4] · H_2O · CH_3OH, 2 · H_2O · CH_3OH. For the cationic part of the complex, two iron centers are bridged by the

Table 2
Selected bond distances (Å) and angles (°) for **1**, calculated parameters are given in parentheses

Distances	
Fe(1)–O(1)	1.900(3) [1.945]
Fe(1)–O(2)	1.849(3) [1.890]
Fe(1)–O(3)	1.872(3) [1.875]
Fe(1)–N(1)	2.316(3) [2.398]
Fe(1)–N(2)	2.157(3) [2.173]
Angles	
O(1)–Fe(1)–O(2)	116.48(12) [119.9]
O(1)–Fe(1)–O(3)	95.66(11)
O(2)–Fe(1)–O(3)	102.89(12)
O(1)–Fe(1)–N(1)	84.88(11)
O(2)–Fe(1)–N(1)	88.46(11)
O(3)–Fe(1)–N(1)	166.88(13) [164.07]
O(1)–Fe(1)–N(2)	129.32(13)
O(2)–Fe(1)–N(2)	110.77(13)
O(3)–Fe(1)–N(2)	90.72(12)
N(1)–Fe(1)–N(2)	78.97(12)

Table 3
Selected bond distances (Å) and angles (°) for **2**, calculated parameters are given in parentheses

Distances			
Fe(1)–O(1)	1.874(8) [1.860]	Fe(2)–O(2)	2.061(6) [2.052]
Fe(1)–O(2)	2.063(7) [2.098]	Fe(2)–O(3)	1.864(7) [1.864]
Fe(1)–O(4)	2.041(7) [2.082]	Fe(2)–O(5)	1.975(7) [1.990]
Fe(1)–O(6)	1.981(8) [1.997]	Fe(2)–O(7)	2.047(8) [2.118]
Fe(1)–N(1)	2.177(8) [2.208]	Fe(2)–N(3)	2.175(8) [2.218]
Fe(1)–N(2)	2.258(10) [2.272]	Fe(2)–N(4)	2.215(8) [2.233]
Angles			
O(1)–Fe(1)–O(2)	174.1(3)	O(2)–Fe(2)–O(3)	97.0(3)
O(1)–Fe(1)–O(4)	88.8(3)	O(2)–Fe(2)–O(5)	96.8(3)
O(1)–Fe(1)–O(6)	92.1(3)	O(2)–Fe(2)–O(7)	83.1(3)
O(2)–Fe(1)–O(4)	85.9(3)	O(3)–Fe(2)–O(5)	91.5(3)
O(4)–Fe(1)–O(6)	98.1(3)	O(3)–Fe(2)–O(7)	179.1(3)
O(2)–Fe(1)–O(6)	91.2(3)	O(5)–Fe(2)–O(7)	89.3(3)
O(1)–Fe(1)–N(1)	88.5(3)	O(2)–Fe(2)–N(3)	88.9(3)
O(2)–Fe(1)–N(1)	89.2(3)	O(3)–Fe(2)–N(3)	90.0(3)
O(4)–Fe(1)–N(1)	93.3(3)	O(5)–Fe(2)–N(3)	173.8(3)
O(6)–Fe(1)–N(1)	168.6(3)	O(7)–Fe(2)–N(3)	89.2(3)
O(1)–Fe(1)–N(2)	91.7(3)	O(2)–Fe(2)–N(4)	164.6(3)
O(2)–Fe(1)–N(2)	93.5(3)	O(3)–Fe(2)–N(4)	95.5(3)
O(4)–Fe(1)–N(2)	174.9(3)	O(5)–Fe(2)–N(4)	91.9(3)
O(6)–Fe(1)–N(2)	87.0(4)	O(7)–Fe(2)–N(4)	84.3(3)
N(1)–Fe(1)–N(2)	81.7(3)	N(3)–Fe(2)–N(4)	82.0(3)
Fe(1)– O(2)– Fe(2)	115.81(16)		

central phenolate (O(2)) of the heptadentate ligand and two bidentate *syn–syn* acetato groups, leading to a triply bridged dinuclear species with Fe(1)–Fe(2) = 3.496(9) Å. The remaining coordinating sites of each iron are occupied by the ONN donor atoms of the ligand. The positions of the donor atoms in both iron centers are not identical. The bridging phenolato (O(2)) group in the coordination sphere of Fe(1) is *trans* to a terminal phenoxo group while that in Fe(2) is *trans* to the pentadentate nitrogen atom (N(4)). The Fe(1)–O(2)–Fe(2) bridging angle is 115.81(16)°. The Fe–O(terminal phenolato) span the range 1.864–1.874 Å. The Fe–O(bridging), Fe–N and Fe–O(acetate) distances are normal [5].

5. Optimized geometry

The geometry optimization for the cationic part of complexes **1** and **2** is performed in the gas phase with the complexes in their highest spin state. The geometries are optimized using the crystal coordinates as the initial coordinates. The gas phase optimized structures in both cases are shown in Figs. 3a and b, respectively. The crystal structural parameters of $\mathbf{1}^{+}$ and $\mathbf{2}^{+}$ (Tables 1 and 2) are in excellent agreement with the optimized parameters.

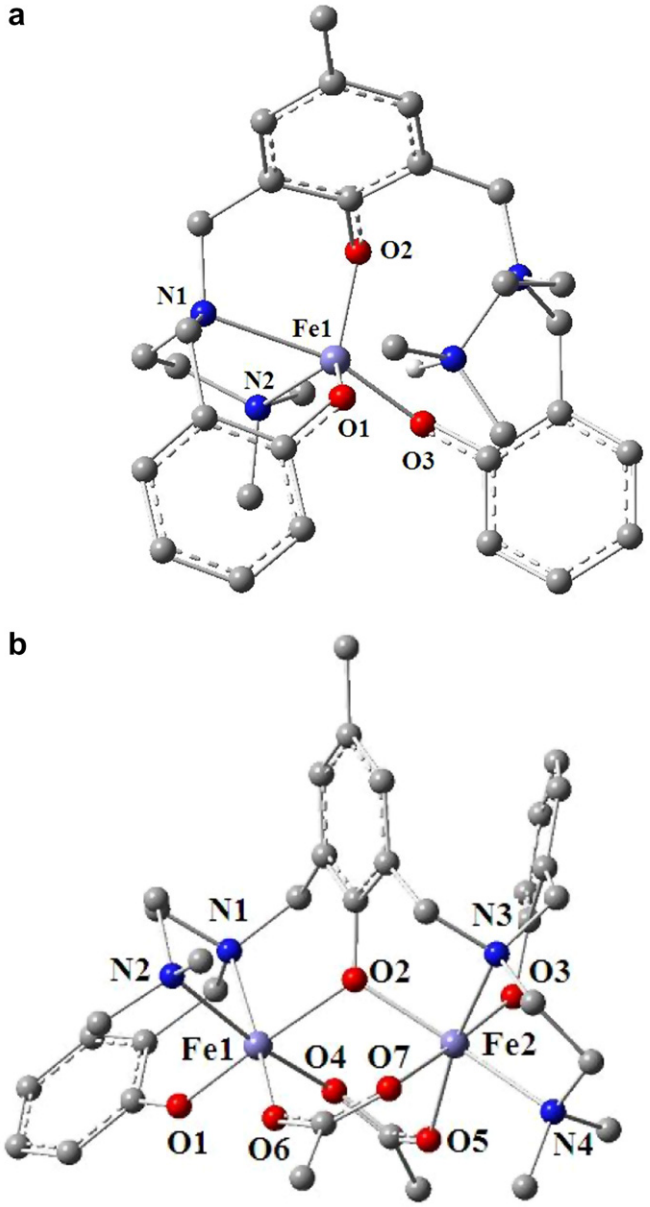

Fig. 3. Optimized molecular structure of (a) $[Fe^{III}LH^{+}]$ and (b) $[Fe^{III}_2L(OAC)_2]^{+}$ (Fe: Cyan, N: Blue, O: Red, C: Grey). Hydrogen atoms are excluded for clarity. (For interpretation of the references to colour in this figure legend, the reader is referred to the web version of this article.)

6. EPR spectra

Complex **2** is EPR silent, both in the solid state and in solution. However, in frozen solution complex **1** exhibits an EPR signal near $g = 4.2$ (Fig. 4a). The spectral feature is associated with a rhombically distorted high-spin iron(III) complex [15c,18].

7. Magnetic studies

Variable temperature magnetic susceptibility measurements were performed in the range 2–300 K. The plot of $\chi_M T$ versus T and an inset plot of χ_M versus T are shown in Fig. 4b. The effective magnetic moment at 300 K is 7.49 emu cm^{-1} K and this decreases rapidly to 0.62 emu cm^{-1} K at 2 K, which is a characteristic feature of weak antiferromagnetic interactions. The spin Hamiltonian used to simulate the $\chi_M T$ versus T curve is

$$H = -JS_1S_2$$

where $S_1 = S_2 = 5/2$. The best fit of the $\chi_M T$ versus T curve yielded $J = -14.4(4)$ cm^{-1}, $g = 2.04(2)$ and $\rho = 0.06(1)$.

The weak antiferromagnetic interaction is a characteristic feature of diiron(III) complexes interacting *via* (μ-O) bis(μ-acetato)/(μ-OH) bis(μ-acetato). It has been documented in the literature that the exchange coupling between two iron(III) centers in such a class of complexes take place through Fe(III)–(μ-O)–Fe(III)/Fe(III)–(μ-OH)–Fe(III) bonds and the strength of the exchange primarily depends on the Fe–O(bridge) bond distance; whereas the Fe(III)–O(bridge)–Fe(III) angle has a secondary role [6b]. In the present case, the weak antiferromagnetic coupling is a direct consequence of the large Fe–O(bridging) distance, 2.061 Å, and the exchange coupling is comparable with other reported (μ-$O_{phenoxo}$)bis(μ-acetato) complexes [5].

CASSCF and CASPT2 [19] calculations have been performed for a theoretical investigation of the exchange coupling of complex **2** using 6-31G and ANO-DZP [20] basis sets. The calculated J values are listed in Table 4. For the CASPT2 calculation the model structure **3** has been used, keeping the coordination environment

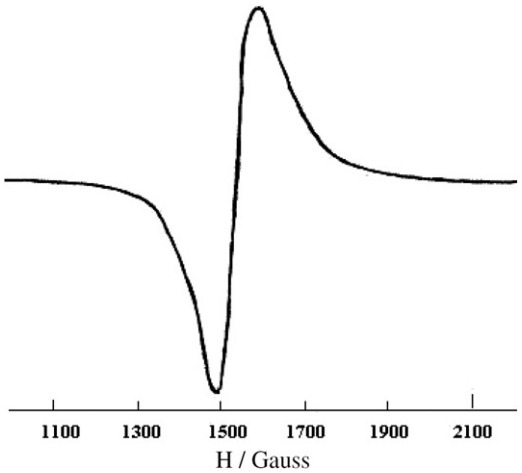

Fig. 4a. X-band EPR spectra for **2** in frozen solution (CH_2Cl_2/Toluene) at 77 K. Instrument settings: microwave frequency, 9.1 GHz; microwave power, 1 mW; modulation frequency,100 kHz; modulation amplitude, 0.5 G; sweep center, 2100 G.

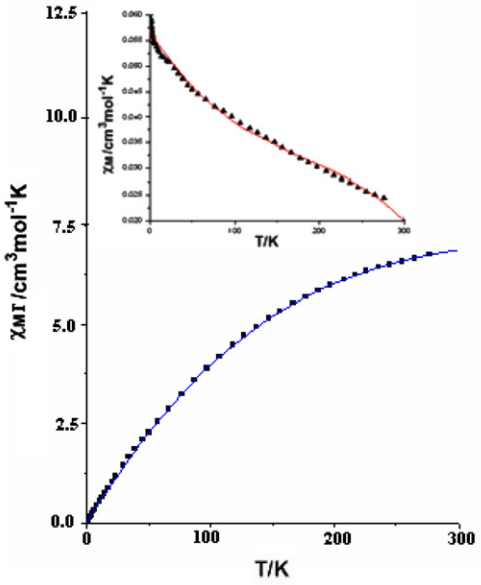

Fig. 4b. $\chi_M T$ vs. T for **2**. Solid line shows the best fit obtained. Inset plot of χ_M vs. T.

Table 4
Calculated J values (in cm^{-1}) for complex **2** and model **3**

Basis	Molecule	CASSCF	CASPT2
6-31G	**2**	−3.3	
	3	−3.0	−21.7
ANO-DZP	**3**	−2.8	−20.9

around the iron centers unchanged. It has been documented that this has little or no influence on the magnetic coupling as long as the geometry of the core of the molecule and the nature of the atoms directly coordinated to the metal ions remain the same [21]. In the present case the CASSCF results for the real and the model complex confirm the small effect of the modelling and the results are almost identical (Table 4). The calculated J value is in agreement with the experimental result.

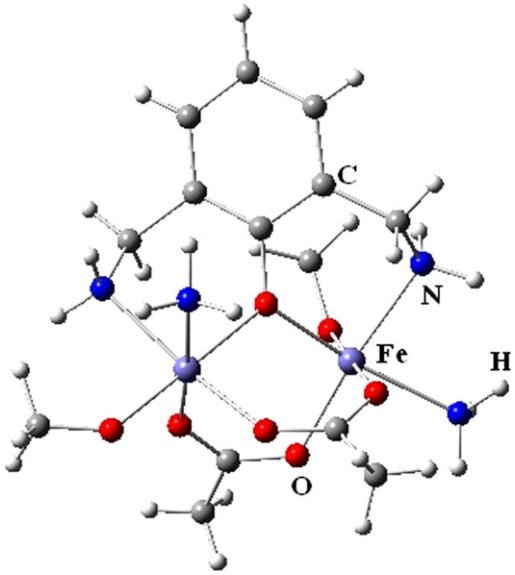

8. Conclusion

In summary, we have synthesized and characterized mononuclear and dinuclear iron(III) complexes incorporating a N_4O_3 coordinating heptadentate ligand. Interestingly in the mononuclear complex the ligand binds in the N_2O_3 form. Variable temperature magnetic moment measurements have been performed in the case of the dinuclear species. The optimized geometries, in both cases, are in good agreement with the X-ray structures. The study of different Fe(III) species using various O,N-coordinating ligands, along with theoretical investigations, are in progress.

Acknowledgements

Financial support from the Council of Scientific and Industrial Research, New Delhi, India, the Department of Science and Technology, New Delhi, India and the University Grant Commission, New Delhi is greatly acknowledged. We are also thankful to DST for the data collection on the CCD facility setup at the Indian Institute of Science, Bangalore, India under the IRHPA-DST program and the department of Chemistry, IIT Guwahati. The author also acknowledges SAIF, IIT Bombay, India for EPR measurements and lastly the financial support from the Spanish Government (Grant No. BQU2000/0791).

Appendix A. Supplementary material

CCDC 682156 and 682155 contain the supplementary crystallographic data for **1** and **2**. These data can be obtained free of charge via http://www.ccdc.ac.uk/conts/retrieving.html, or from the Cambridge Crystallographic Data Centre, 12 Union Road, Cambridge CB2 1EZ, UK; email: deposit@ccdc.cam.ac.uk.

References

[1] (a) Y. Tshuva, S.J. Lippard, Chem. Rev. 104 (2004) 987;
(b) H.A.O. Hill, P.J. Sadler, A.J. Thomson (Eds.), Metal Sites in Proteins and Models Iron Centers, Springer-Verlag, Berlin, Heidelberg, 1999.
[2] (a) P.F. Hennart, D.J. Brasseur, J.B. Delogne-Desnoeck, M.M. Dramaix, C.E. Robyn, Am. J. Clin. Nutr. 53 (1991) 32;
(b) L. Que Jr., R.Y.N. Ho, Chem. Rev. 90 (1990) 2607;
(c) D.C. Harris, P. Aisen, in: T.M. Loehr (Ed.), Iron Carriers and Iron Proteins, VCH, New York, 1989, p. 239;
(d) P. Aisen, in: T.M. Loehr (Ed.), Iron Carriers and Iron Proteins, VCH, New York, 1989, p. 353;
(e) L. Que Jr., in: T.M. Loehr (Ed.), Iron Carriers and Iron Proteins, VCH, New York, 1989, p. 467;
(f) R.E. Feeney, S.S. Komatsu, Struct. Bond. (Berl.) 1 (1966) 149.
[3] (a) E.Y. Tshuva, S.J. Lippard, Chem. Rev. 104 (2004) 987;
(b) E.I. Solomon, T.C. Brunold, M.I. Davis, J.N. Kemsley, S.K. Lee, N. Lehnert, F. Neese, A.J. Skulan, Y.S. Yang, J. Zhou, Chem. Rev. 100 (2000) 235;
(c) J. Du Bois, T.J. Mizoguchi, S.J. Lippard, Coord. Chem. Rev. 200 (2000) 443;
(d) B.J. Wallar, J.D. Lipscomb, Chem. Rev. 96 (1996) 2625;
(e) D.M. Kurtz, Chem. Rev. 90 (1990) 585.
[4] (a) Q. Pan, W. Jiang, Z. Liao, T. Zhang, C. Liu, Inorg. Chem. 45 (2006) 490;
(b) M. Velusamy, R. Mayilmurugan, M. Palaniandavar, Inorg. Chem. 43 (2004) 6284;
(c) M. Velusamy, M. Palaniandavar, Inorg. Chem. 42 (2003) 8283;
(d) I.A. Setyawati, S.J. Rettig, C. Orvig, Can. J. Chem. 77 (1999) 2033;
(e) D.D. Cox, S.J. Benkovic, L.M. Bloom, F.C. Bradley, M.J. Nelson, L. Que Jr., D.E. Wallick, J. Am. Chem. Soc. 110 (1988) 2026;
(f) L. Que Jr., R.C. Kolanczyk, L.S. White, J. Am. Chem. Soc. 109 (1987) 5373;
(g) Y. Nishida, H. Shimo, S. Kida, J. Chem. Soc., Chem. Commun. (1984) 1611.
[5] (a) T. Glaser, T. Lügger, R. Hoffmann, Eur. J. Inorg. Chem. (2004) 2356;
(b) Y. Hayashi, T. Kayatani, H. Sugimoto, M. Suzuki, K. Inomata, A. Uehara, Y. Mizutani, T. Kitagawa, Y. Maeda, J. Am. Chem. Soc. 117 (1995) 11220;
(c) H. Nie, S.M.J. Aubin, M.S. Mashuta, C. Wu, J.F. Richardson, D.N. Hendrickson, R.M. Buchanan, Inorg. Chem. 34 (1995) 2382;
(d) V.D. Campbell, E.J. Parsons, W.T. Pennington, Inorg. Chem. 32 (1993) 1773;
(e) B.P. Murch, F.C. Bradley, P.D. Boyle, V. Papaefthymiou, L. Que Jr., J. Am. Chem. Soc. 109 (1987) 7993.
[6] (a) J. Jullien, G. Juhasz, P. Mialane, E. Dumas, C.R . Mayer, J. Marrot, E. Riviere, E.L. Bominaar, E. Munck, F. Secheresse, Inorg. Chem. 45 (2006) 6922;
(b) J.H. Rodriguez, J.K. McCusker, J. Chem. Phys. 116 (2002) 6253;
(c) Z. Chen, Z. Xu, L. Zhang, F. Yan, Z. Lin, J. Phys. Chem. A 105 (2001) 9710.

[7] A. Mondal, S. Sarkar, D. Chopra, T.N. Guru Row, K. Pramanik, K.K. Rajak, Inorg. Chem. 44 (2005) 703.
[8] Bruker (1998), SMART, SAINT, SADABS, XPREP, SHELXTL, Bruker AXS Inc. Madison. Wisconsin, USA.
[9] G.M. Sheldrick, SHELXTL, version 5.03, Siemens Analytical Instruments Inc: Madison, WI, 1994.
[10] C.K. Johnson, ORTEP. Report ORNL-5138, Oak Ridge National Laboratory. Oak Ridge, TN, 1976.
[11] R.G. Parr, W. Yang, Density-Functional Theory of Atoms and Molecules, Oxford University Press, Oxford, UK, 1989.
[12] A.D. Becke, J. Chem. Phys. 98 (1993) 5648.
[13] M.J. Frisch, G.W. Trucks, H.B. Schlegel, G.E. Scuseria, M.A. Robb, J.R. Cheeseman, J.A. Montgomery, Jr., T. Vreven, K.N. Kudin, J.C. Burant, J.M. Millam, S.S. Iyengar, J. Tomasi, V. Barone, B. Mennucci, M. Cossi, G. Scalmani, N. Rega, G.A. Petersson, H. Nakatsuji, M. Hada, M. Ehara, K. Toyota, R. Fukuda, J. Hasegawa, M. Ishida, T. Nakajima, Y. Honda, O. Kitao, H. Nakai, M. Klene, X. Li, J.E. Knox, H.P. Hratchian, J.B. Cross, V. Bakken, C. Adamo, J. Jaramillo, R. Gomperts, R.E. Stratmann, O. Yazyev, A.J. Austin, R. Cammi, C. Pomelli, J.W. Ochterski, P.Y. Ayala, K. Morokuma, G.A. Voth, P. Salvador, J.J. Dannenberg, V.G. Zakrzewski, S. Dapprich, A.D. Daniels, M.C. Strain, O. Farkas, D.K. Malick, A.D. Rabuck, K. Raghavachari, J.B. Foresman, J.V. Ortiz, Q. Cui, A.G. Baboul, S. Clifford, J. Cioslowski, B.B. Stefanov, G. Liu, A. Liashenko, P. Piskorz, I. Komaromi, R.L. Martin, D.J. Fox, T. Keith, M.A. Al-Laham, C.Y. Peng, A. Nanayakkara, M. Challacombe, P.M.W. Gill, B. Johnson, W. Chen, M.W. Wong, C. Gonzalez, J.A. Pople, Gaussian Inc., Wallingford CT, 2004.
[14] J.S. Binkley, J.A. Pople, W.J. Hehre, J. Am. Chem. Soc. 102 (1980) 939.
[15] (a) G. Deacon, R.J. Phillips, Coord. Chem. Rev. 33 (1980) 227;
(b) C.A. Brown, G.J. Rennar, R.L. Musselman, E.I. Solomon, Inorg. Chem. 34 (1995) 688;
(c) L. Casella, M. Gullotti, A. Pintar, L. Messori, A. Rockenbauer, M. Gyorl, Inorg. Chem. 26 (1987) 1031.
[16] (a) J. Mukherjee, V. Balamurugan, R. Gupta, R. Mukherjee, J. Chem. Soc., Dalton Trans. (2003) 3686;
(b) S. Singh, V. Mishra, J. Mukherjee, N. Seethalekshmi, R. Mukherjee, J. Chem. Soc., Dalton Trans. (2003) 3392.
[17] C. O'Sullivan, G. Murphy, B. Murphy, B. Hathaway, J. Chem. Soc., Dalton Trans. (1999) 835.
[18] (a) M.I. Scullane, L.K. White, N.0. Chasteen, J. Magn. Reson. 47 (1982) 383;
(b) W.T. Oosterhuis, Struct. Bond. (Berl.) 20 (1974) 59;
(c) G. Lang, R. Aasa, K. Garbett, R.J.P. Williams, J. Chem. Phys. 55 (1971) 4539;
(d) R. Aasa, J. Chem. Phys. 52 (1970) 3919.
[19] G. Karlstrom, R. Lindh, P.-A. Malmqvist, B.O. Roos, U. Ryde, V. Veryazov, P.-O. Widmark, M. Cossi, B. Schimmelpfennig, P. Neogrady, L. Seijo, Comput. Mater. Sci. 28 (2003) 222.
[20] E. Bordas, R. Caballol, C. de Graaf, J. Mol. Struct. (Theo. Chem.) 173 (2005) 727.
[21] D. Munoz, C. de Graaf, F. Illas, J. Comp. Chem. 25 (2004) 1234.

Recently, Steiner et al. reported that the reaction of hexaprotic phosphazene $\{2\text{-}(MeO)(C_6H_4NH)\}_6P_3N_3$ with excess (12 equiv.) *n*BuLi in THF produced a monomeric dodecanuclear complex incorporating six enolate ligands [10]. We report here the synthesis of novel lanthanide complexes incorporating amido and enolate ligands having the general formula $(CH_2{=}CHO)Ln[2,6\text{-}(i\text{Pr})_2C_6H_3NSiMe_3]_2(\mu\text{-}Cl)Li(THF)_3$, by the one-pot reaction of *N*-trimethylsilyl-2,6-diisopropylaniline 2,6-$(i\text{Pr})_2C_6H_3NHSiMe_3$ with excess *n*BuLi in THF, followed by treatment with 1 equiv. of $LnCl_3$. The reactivity of this kind of complexes with aromatic aldehydes is also reported.

2. Results and discussion

The structurally characterized rare earth metal complexes incorporating amido and enolate mixed ligands $(CH_2{=}CHO)Ln[2,6\text{-}(i\text{Pr})_2C_6H_3NSiMe_3]_2(\mu\text{-}Cl)Li(THF)_3$ (Ln = Y(**1**), Yb(**2**)) were synthesized for the first time by the one-pot reaction of *N*-trimethylsilyl-2,6-diisopropylaniline 2,6-$(i\text{Pr})_2C_6H_3NHSiMe_3$ with 1.5 equiv. of *n*BuLi in THF, followed by treatment with $LnCl_3$ in good yields (Scheme 1). The complexes are soluble in toluene, benzene, THF and CH_2Cl_2, but only slightly soluble in *n*-hexane. These complexes were well characterized by spectroscopic methods and elemental analyses. Their structures were additionally determined by X-ray diffraction study (Figs. 1 and 2).

The ^{1}H NMR spectrum of complex **1** exhibited resonances at 6.90, 4.24 and 4.20 ppm, which can be attributed to the corresponding proton resonances of the enolate ligand OCH=CH$_2$ in the complex. The resonances of the enolate ligand exhibited coupling. The proton resonances of the enolate ligand of the complex

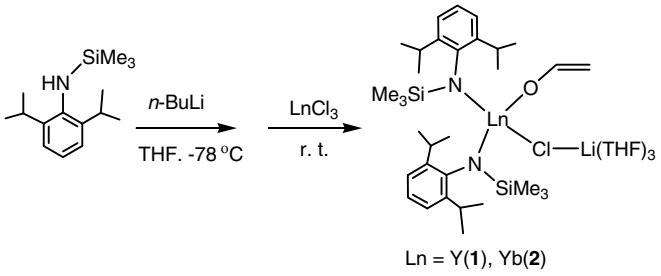

Scheme 1.

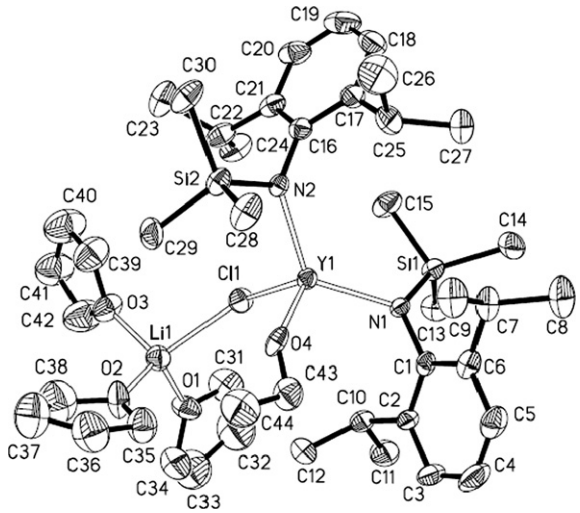

Fig. 1. Molecular structure of complex **1**, hydrogen atoms are omitted for clarity.

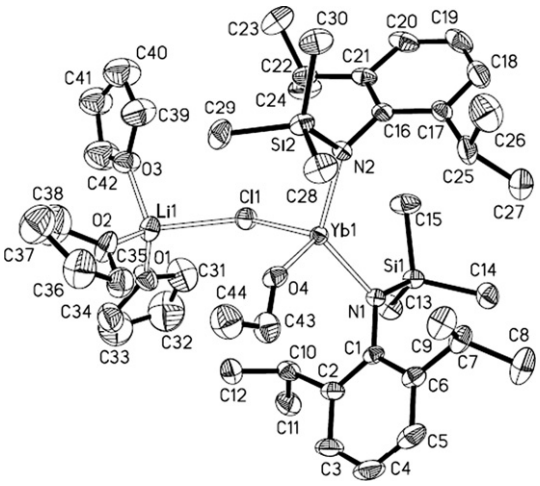

Fig. 2. Molecular structure of complex **2**, hydrogen atoms are omitted for clarity.

can be compared with those of the enolate ligand in $(Cp'Y)_4(OCH{=}CH_2)(\mu\text{-}O)(\mu\text{-}H)_5(THF)$ [6], $[(C_5H_5)_2Y(\mu\text{-}OCH{=}CH_2)]_2$ or $[(CH_3C_5H_4)_2Y(\mu\text{-}OCH{=}CH_2)]_2$ [7], and LiOCH = CH$_2$ [11]. Each IR spectrum of complex **1** or **2** contains a very broad strong band around 1650 cm^{-1}, which can be attributable to the C=C bond of the enolate and the phenyl ring stretch.

In order to search for the origination of the enolate ligand of the above complexes, 2,6-$(Et)_2C_6H_3NHSiMe_3$ was treated with *n*BuLi in *n*-hexane at first, followed by treatment with 1/2 or 1/3 equiv. of YCl_3 in THF respectively, and complexes with the formula $[2,6\text{-}(Et)_2C_6H_3NSiMe_3]_2Y(THF)(\mu\text{-}Cl)_2Li(THF)_2$ (**3**) and $\{[2,6\text{-}(Et)_2C_6H_3NSiMe_3]_3YCl\}[Li(THF)_4]$ (**4**) were isolated (Scheme 2). The complexes were well characterized by spectroscopic methods and elemental analyses. The elemental analyses data are in agreement with the loss of THF molecules, which is common in lanthanide chemistry. The structures of complexes **3** and **4** were determined by single crystal X-ray analyses. These results suggested that (1) the produced lithium amide Li(2,6-$(i\text{Pr})_2C_6H_3NSiMe_3$) is not responsible for the resulting enolate ligand in complexes **1** and **2**; (2) YCl_3 cannot react with THF leading to the formation of the enolate ligand. Evidence that *n*BuLi can react with THF leading to the cleavage of the THF ring to produce a lithium enolate and ethylene is reported, and this process has been monitored by NMR spectroscopy [11]. Thus, the enolate ligand in complexes **1** and **2** is believed to have come from the cleavage of the THF molecule by *n*BuLi. To further prove the above conclusion, the

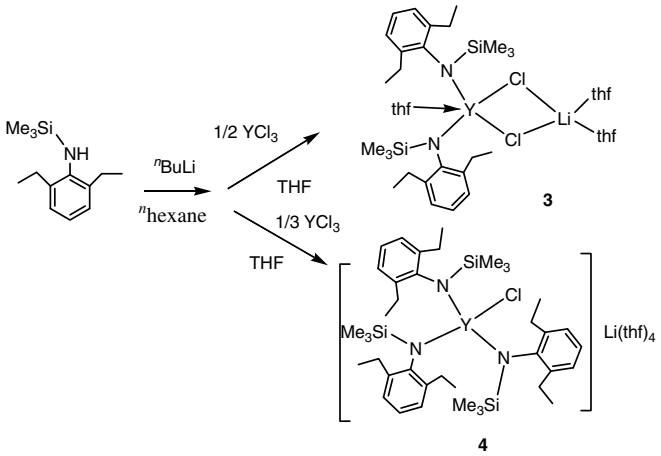

Scheme 2.

product of the reaction of *N*-trimethylsilyl-2,6-diethylaniline with 1.5 equiv. of *n*BuLi was analyzed by ^{1}H NMR spectroscopy. The spectra clearly indicated the formation of Li[2,6-$(Et)_2C_6H_3NSiMe_3$)] and LiOCH = CH_2, and the existence of three coordinated THF molecules.

X-ray analyses confirmed that complexes **1** and **2** consisted of two amido ligands, an enolate ligand and a bridged chlorine atom connected with a lithium atom coordinated by three THF molecules. The central rare earth metal of each complex is coordinated by two nitrogen atoms of the amido ligand, an oxygen atom of the enolate ligand and a chlorine atom. The central yttrium atom in complex **3** is coordinated by two nitrogen atoms of the amido ligand, one oxygen atom of a THF molecule and two chlorine atoms (Fig. 3). The central yttrium atom in complex **4** is coordinated by three nitrogen atoms of the amido ligand and one chlorine atom

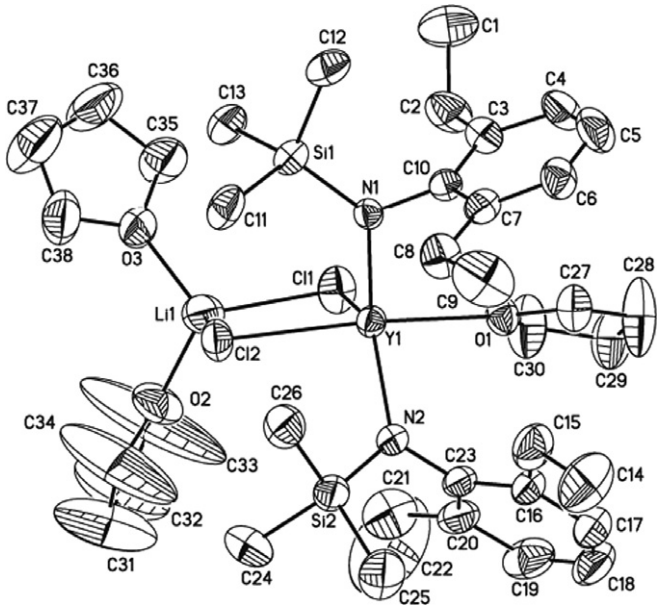

Fig. 3. Molecular structure of complex **3**, hydrogen atoms are omitted for clarity.

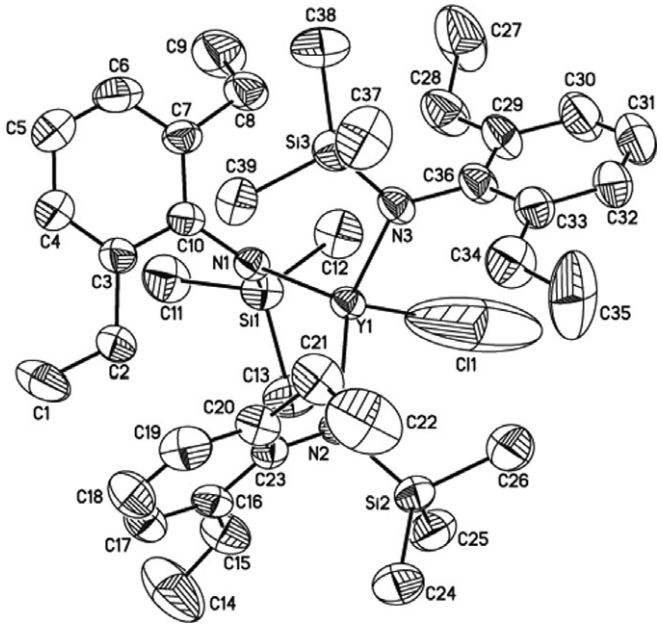

Fig. 4. The structure of the anion in **4**, hydrogen atoms are omitted for clarity.

Table 1
Selected bond distances (Å) and angles (°) for **1**, **2**, **3** and **4**

1		**2**	
Y(1)–O(4)	2.103(7)	Yb(1)–O(4)	2.070(6)
Y(1)–O(4′)	2.104(2)	Yb(1)–O(4′)	2.067(9)
Y(1)–N(1)	2.229(5)	Yb(1)–N(1)	2.188(5)
Y(1)–N(2)	2.254(6)	Yb(1)–N(2)	2.201(5)
Y(1)–Cl(1)	2.603(2)	Yb(1)–Cl(1)	2.552(2)
Cl(1)–Li(1)	2.394(2)	Cl(1)–Li(1)	2.401(2)
Li(1)–O(1)	1.93(2)	Li(1)–O(1)	1.92(2)
Li(1)–O(2)	1.90(2)	Li(1)–O(2)	1.86(2)
Li(1)–O(3)	1.89(2)	Li(1)–O(3)	1.90(2)
C(43)–C(44)	1.351(10)	C(43)–C(44)	1.344(9)
O(4)–Y(1)–N(1)	107.1(3)	O(4)–Yb(1)–N(1)	106.1(3)
O(4)–Y(1)–N(2)	102.7(3)	O(4)–Yb(1)–N(2)	102.3(3)
N(1)–Y(1)–N(2)	126.9(2)	N(1)–Yb(1)–N(2)	127.61(2)
O(4)–Y(1)–Cl(1)	105.4(3)	O(4)–Yb(1)–Cl(1)	105.2(3)
N(1)–Y(1)–Cl(1)	105.98(2)	N(2)–Yb(1)-Cl(1)	106.01(2)
N(2)–Y(1)–Cl(1)	107.08(15)	N(1)–Yb(1)–Cl(1)	107.70(2)
Li(1)–Cl(1)–Y(1)	136.3(4)	Li(1)–Cl(1)–Yb(1)	136.1(3)
3		**4**	
Y(1)–N(1)	2.228(3)	Y(1)–N(1)	2.302(5)
Y(1)–N(2)	2.252(4)	Y(1)–N(2)	2.292(5)
Y(1)–O(1)	2.404(3)	Y(1)–N(3)	2.289(5)
Y(1)–Cl(1)	2.657(2)	Y(1)–Cl(1)	2.621(2)
Y(1)–Cl(2)	2.638(2)	Li(1)–O(1)	1.97(2)
Cl(2)–Li(1)	2.370(2)	Li(1)–O(2)	1.95(2)
Cl(1)–Li(1)	2.331(2)	Li(1)–O(3)	1.89(2)
O(2)–Li(1)	1.90(2)	Li(1)–O(4)	1.89(2)
O(3)–Li(1)	1.92(2)	N(2)–Y(1)–N(1)	118.04(18)
N(1)–Y(1)–N(2)	120.22(14)	N(3)–Y(1)–N(1)	115.39(18)
N(1)–Y(1)–O(1)	101.27(12)	N(3)–Y(1)–N(2)	116.58(19)
N(2)–Y(1)–O(1)	92.57(13)	N(3)–Y(1)–Cl(1)	98.5(2)
N(1)–Y(1)–Cl(2)	93.10(9)	N(2)–Y(1)–Cl(1)	99.04(18)
N(2)–Y(1)–Cl(2)	91.91(10)	N(1)–Y(1)–Cl(1)	104.35(19)
O(1)–Y(1)–Cl(2)	160.16(10)		
O(1)–Y(1)–Cl(1)	80.87(10)		
N(1)–Y(1)–Cl(1)	111.46(10)		
N(2)–Y(1)–Cl(1)	128.16(11)		
Cl(2)–Y(1)–Cl(1)	81.17(5)		
Cl(1)–Li(1)–Cl(2)	94.3(4)		
O(2)–Li(1)–O(3)	105.5(5)		

(Fig. 4). The bond angles of N–Ln–N, Cl–Ln–O, N–Ln–Cl, O–Ln–N (Ln = Y, Yb), in the range 102.7(3)–126.9(2)° (Table 1) for complex **1**, 102.3(3)–127.61(19)° (Table 1) for complex **2**, and 98.5(2)–118.04(18)° for complex **4**, are deviated from the ideal tetrahedral angle. Thus the coordination geometry around the central metal of complexes **1**, **2** and **4** can be described as a distorted tetrahedral. The bond angles of O(1)–Y(1)–Cl(2), N(1)–Y(1)–N(2), N(1)–Y(1)–Cl(1) and N(2)–Y(1)–Cl(1) are 160.16(10), 120.22(14), 111.46(10) and 128.16(11)° (Table 1), respectively in complex **3**, largely deviated from the ideal trigonal bipyramidal bond angles, so the coordination geometry of the central yttrium in complex **3** can be described as pseudo-trigonal bipyramidal with O(1) and Cl(2) at the axial positions.

The Y–N distances are 2.229(5) and 2.254(6) Å, with an average of 2.242(6) Å, in **1**, which is comparable to the average distance of 2.194(5) Å found in **2**, and that of 2.240(4) Å in **3** and 2.294(5) Å in **4**, if the ionic radii difference between the central metal is taken into account. The average Y–N distance of 2.242(6) Å in **1** is similar to that of 2.243(4) Å found in [η^5-$(CH_2)_2(C_9H_6)_2$]YN($SiMe_3$)$_2$ [12]. But the average Yb–N bond distance of 2.194(5) Å found in **2** is slightly longer than that of 2.162(5) Å found in [η^5-$(CH_2)_2(C_9H_6)_2$]YbN($SiMe_3$)$_2$ [13], this difference can be attributable to ionic and steric effects [14]. The Yb–Cl distance of 2.552(2) Å found in **2** is equal to that of 2.552(2) Å found in [$(Me_3Si)_2$-N]$_3$Yb(μ-Cl)Li(THF)$_3$ [13a]. The Y–Cl distance of 2.603(2) Å found in **1** is longer than the Yb–Cl distance of 2.552(2) Å found in **2** due to the ionic radii difference. The Y–Cl distance of 2.603(2) Å found in **1** is shorter than those of 2.648(2) Å in **3** and 2.621(2) Å

in **4**, probably due to steric effects. The Ln–Cl bond distances found in the above complexes are comparable to those found in $Ln\{N[Si(Me)_2CH_2CH_2Si(Me)_2]\}(\mu\text{-}Cl)Li(L)_3$ (L = THF or Et_2O) [15]. The yttrium–oxygen distance of 2.104(10) Å is shorter than those of 2.275(3) and 2.290(3) Å found in $[(CH_3C_5H_4)_2Y(\mu\text{-}OCH{=}CH_2)]_2$ [7] The Li(1)–Cl(1)–Y(1) angle of 136.3(4)° in **1** is comparable to that of 136.1(3)° found in **2**, but these angles are significantly smaller than the corresponding Li–Cl–Ln angles of 175 ± 1° found in $[(Me_3Si)_2N]_3Ln(\mu\text{-}Cl)Li(THF)_3$ (Ln = Yb, Sm, Eu) [16], and those of 170 ± 2° found in $Ln\{N[Si(Me)_2CH_2CH_2Si(Me)_2]\}(\mu\text{-}Cl)Li(L)_3$ (L = THF or Et_2O) [15].

The C=C double bond distances of the enolate, 1.351(10) Å in **1** and 1.344(4) Å in **2**, are slightly longer than the standard 1.34 Å expected for the C=C bond in ethylene, they are also longer than that of 1.287(8) Å for the C=C double bond of the enolate found in $[(CH_3C_5H_4)_2Y(\mu\text{-}OCH{=}CH_2)]_2$ [7].

It has been well documented that the Aldol reaction proceeds through an enolate intermediate when the reaction is carried out in an inorganic base medium [8]. We have found that lanthanide amides $[(Me_3Si)_2N]_3Ln(\mu\text{-}Cl)Li(THF)_3$ can initiate the disproportionation reaction of aromatic aldehydes to give the corresponding amides and alcohols [9]. In order to search for the influence of the rare earth metals on the reactivity or selectivity of the amido and enolate ligands with aromatic aldehydes (Scheme 3), the reactivity of the lanthanide complexes **1** and **2** with aromatic aldehydes was explored.

First, a model reaction of 4-bromobenzyl aldehyde with a stoichiometric amount of the yttrium complex **1** was tested (Scheme 4, Table 2). It was found that the reaction can proceed in different solvents such as toluene, CH_2Cl_2 and THF (Table 2, entries 1–3), but the outputs of the reaction products are higher in CH_2Cl_2 than for reactions carried out in other solvents such as THF and toluene. It was found that only the disproportionation products of the corresponding amide and alcohol instead of the Aldol reaction product could be isolated, suggesting that the amido ligand could selectively react with aromatic aldehydes. The outputs of the reaction products were influenced by the reaction temperatures. Low yields of the products could be obtained when the reaction was carried out at moderately higher temperatures. It should be noted that a small amount of imines could be detected when the reaction was carried out at moderately higher temperatures, but the imines is decomposed to aldehydes during workup. Thus, the conditions for doing the following experiments were fixed as room temperature reaction, employing CH_2Cl_2 as the solvent.

Table 2
Conditions and results of the reaction of 4-bromobenzyl aldehyde with a stoichiometric amount of yttrium complex **1**[a]

Entry	Temperature (°C)	Solvent	Time (d)	Yield of amide[b]
1	r. t.	Toluene	2	49
2	r. t.	CH_2Cl_2	2	68
3	r. t.	THF	2	35
4	50	CH_2Cl_2	2	41
5	80	THF	2	23

[a] Aldehyde:yttrium complex = 4:1 (mol ratio).
[b] Isolated yield based on the yttrium complex.

A series of aromatic aldehydes can selectively react with the amido group of the lanthanide complexes **1** and **2** to produce the corresponding disproportionation products of amides and alcohols (Scheme 5, Table 3), and no Aldol reaction products were found to any detectable degree, indicating that the electron-deficient lanthanide metal has a great influence on the reactivity of the enolate group. The substituents on the aromatic aldehydes could be either electron-donating groups such as CH_3^-, CH_3O^- and Me_2N^- or electron-withdrawing ones such as Cl^-, Br^-, O_2N^- and F_3C^-. However, the electronic effects of the substituent groups have an influence on the output of the reactions. When the substituents are electron-donating groups such as CH_3^-, CH_3O^- and Me_2N^- or electron-withdrawing ones such as Cl^- and Br^-, the main products of amides and alcohols (>50% yield based on the lanthanide complexes) could be isolated, and only a trace or a very small amount of the corresponding imines could be detected from the reaction mixture. When the substituents are O_2N^- and F_3C^-, the output of the imines increased as the output of the amides and alcohols decreased. The corresponding imines could be isolated under the workup conditions, and they were well characterized (Fig. 5), however, in all other cases the imine products could not be isolated under the workup conditions. These results are different to our previous work on the reaction of lanthanide amides $[(Me_3Si)_2N]_3Ln(\mu\text{-}Cl)Li(THF)_3$ with aromatic aldehydes, producing the corresponding amides and alcohols as the only products [9a], with no imine products being found to any detectable degree.

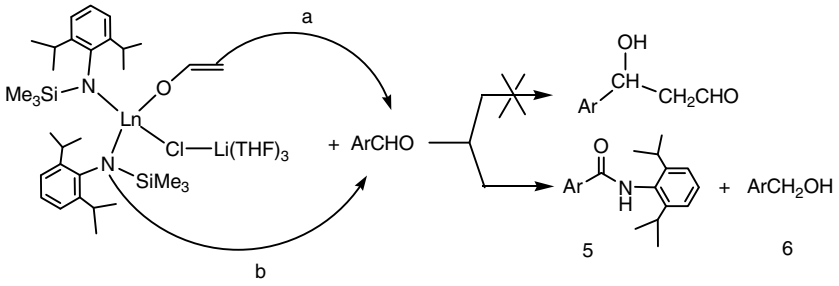

Scheme 3.

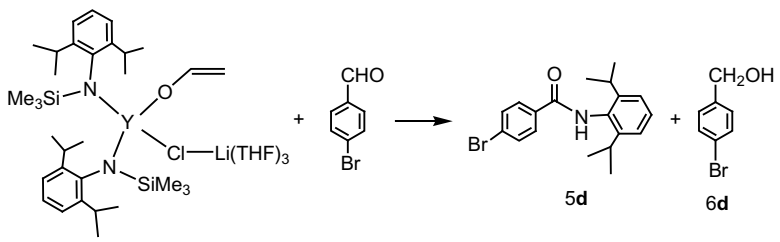

Scheme 4.

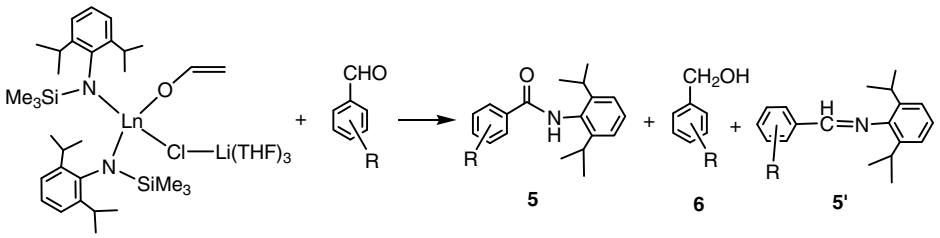

Scheme 5.

Table 3
Results of the reaction of aromatic aldehydes with a stoichiometric amount of lanthanide complex **1** and **2a**

Entry	Ar-	Time	Product of **5**	Yield of **5** (%)[b]	Product of **6**	Yield of **6** (%)[b]	Yield of product **5′**
1	4-$CH_3C_6H_4$–	2	**5a**	88[c] (87)[d]	**6a**	85 (83)	Trace
2	4-$CH_3OC_6H_4$–	2	**5b**	73 (75)	**6b**	67 (69)	Trace
3	4-ClC_6H_4–	2	**5c**	74 (67)	**6c**	69 (65)	Trace
4	4-BrC_6H_4–	2	**5d**	68 (49)	**6d**	65 (47)	Trace
5	4-$Me_2NC_6H_4$–	2	**5e**	54 (59)	**6e**	51 (57)	Trace
6	4-$O_2NC_6H_4$–	2	**5f**	51 (55)	**6f**	49 (52)	32 (39)
7	4-$F_3CC_6H_4$–	2	**5g**	53 (49)	**6g**	47 (44)	38 (37)
8	C_6H_5–	3	**5h**	49 (47)	**6h**	47 (45)	Trace

Conditions: [a]CH_2Cl_2 as a solvent, room temperature. [b]isolated yield based on lanthanide complex. [c]Data are obtained from the reaction of the aldehydes with yttrium complex **1**. [d]Data in the parenthesis are obtained from the reaction of the aldehydes with ytterbium complex **2**.

We have found that the reaction of lithium amide $(Me_3Si)_2NLi$ with aromatic aldehydes in the presence of $LnCl_3$, or the stoichiometric reaction of $[(Me_3Si)_2N]_3Ln(\mu\text{-}Cl)Li(THF)_3$ with aromatic aldehydes, yielded the corresponding disproportionation products of amides and alcohols. No imine product has been detected in the reaction [9a]. For comparison, the reaction of the lithium amide $\{[2,6\text{-}(i\text{Pr})_2C_6H_3](Me_3Si)N\}Li$ with some selected aromatic aldehydes catalyzed by YCl_3 was investigated (Scheme 6). The reaction goes smoothly producing the disproportionation products of amides and alcohols in the presence of 5 mol% YCl_3 (Table 4) in satisfactory yields. The substituents on the aromatic aldehydes can be either electron-donating groups such as CH_3^- and CH_3O^- or electron-withdrawing ones such as Cl^-, Br^- and O_2N^-. The major differences between the stoichiometric reactions of the lanthanide complexes **1** or **2** with aldehydes and the catalytic reaction of lithium amide with the aldehydes are: (1) no imine products have been detected in all cases (Table 4); and (2) the output of the corresponding amides and alcohols are improved significantly when the substituents on the aromatic aldehydes are electron-withdrawing ones such as O_2N^- and F_3C^- (Table 4, entries 5 and 6) under almost the same reaction conditions. These results are somewhat different to our previous work, which may be due to the coordinated enolate ligand's effect on the reactions. We have proposed that the reaction of lithium amide $(Me_3Si)_2NLi$ with aromatic aldehydes in the presence of $LnCl_3$ goes through lanthanide amides $[(Me_3Si)_2N]_3Ln(\mu\text{-}Cl)Li(THF)_3$ as intermediates. It is reported that the reaction of lithium amides $\{[2,6\text{-}(i\text{Pr})_2C_6H_3](Me_3Si)N\}Li$ with lanthanide chlorides $LnCl_3$ produced the lanthanide amides $\{[2,6\text{-}(i\text{Pr})_2C_6H_3](Me_3Si)N\}_3Ln$ [17]. On the basis of these results, we can conclude that the reaction of lithium amide $\{[2,6\text{-}(i\text{Pr})_2C_6H_3](Me_3Si)N\}Li$ with aldehydes in the presence of YCl_3 may go through a similar mechanism as in our previous work, which has been demonstrated as a Cannizzaro type disproportionation [9a]. The reaction involves the addition of the amido group from the lanthanide metal center to one molecule of aldehyde to give the intermediate $\{ArCH(O)N(SiMe_3)[C_6H_3\text{-}2,6\text{-}(i\text{Pr})_2]\}^-$ (**A**), which leads to the oxidation of the aldehyde by transferring the hydride from the intermediate (**A**) to another molecule of aldehyde to produce the amide precursor, leading to the reduction of the aldehyde, $ArCH_2O^-$. The final products of amide and alcohols could be isolated after workup. The formation of imine products in the stoichiometric reactions of lanthanide complex **1** or **2** with aromatic aldehydes may be due to the influence of the coordinated enolate ligand in the complexes. However, further work on this detail should be carried out.

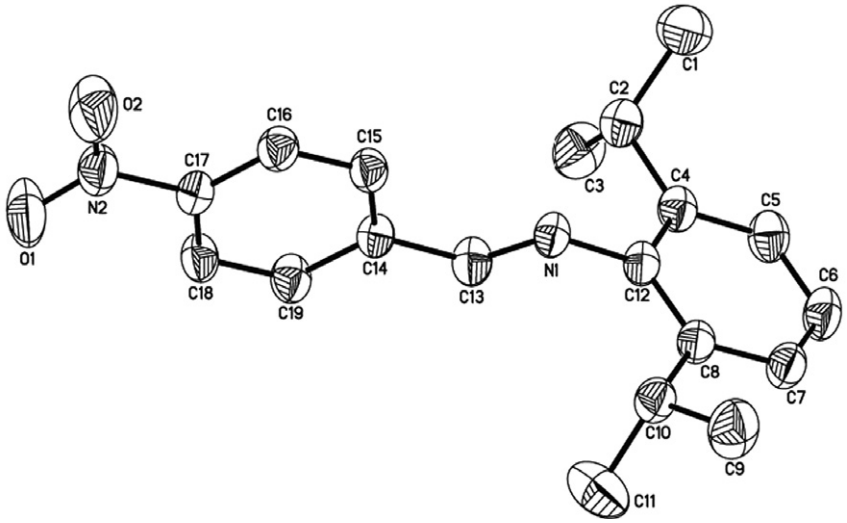

Fig. 5. Molecular structure of **5f′**, hydrogen atoms are omitted for clarity.

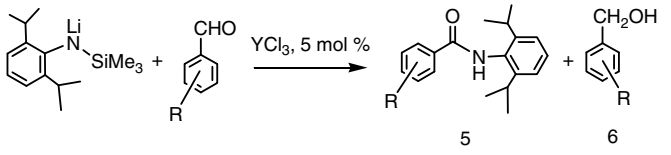

Scheme 6.

Table 4
Reaction of lithium amide {[2,6-(iPr)$_2$C$_6$H$_3$](Me$_3$Si)N}Li with aromatic aldehydes catalyzed by YCl$_3$[a]

Entry	Ar–	Solvent	Time	Product of **5**	Yield of **5** (%)[b]	Product of **6**	Yield of **6** (%)[b]
1	4-CH$_3$C$_6$H$_4$–	Toluene	3	**5a**	76	**6a**	73
2	4-CH$_3$OC$_6$H$_4$–	Toluene	3	**5b**	70	**6b**	65
3	4-ClC$_6$H$_4$–	Toluene	2	**5c**	75	**6c**	74
4	4-BrC$_6$H$_4$–	Toluene	2	**5d**	72	**6d**	70
5[c]	4-O$_2$NC$_6$H$_4$–	CH_2Cl_2	2	**5f**	81	**6f**	75
6[c]	4-F$_3$CC$_6$H$_4$–	CH_2Cl_2	2	**5g**	83	**6g**	79
7	C$_6$H$_5$–	Toluene	3	**5h**	86	**6h**	79

Conditions: [a]5 mol% YCl$_3$, 80 °C; [b]isolated yield based on the lithium amide; [c]room temperature reaction.

3. Conclusion

We have for the first time rationally synthesized novel rare earth metal complexes incorporating amido and enolate mixed ligands by a one-pot reaction. The experimental results suggest that this method may be applied to the synthesis of complexes incorporating amido and enolate mixed ligands. Investigation on the reactivity of this kind of lanthanide complex indicates that the amido ligand of the complex can selectively react with aromatic aldehydes to afford the disproportionation products of amides and alcohols, suggesting that the Lewis acid property of the rare earth metals have a great influence on the reactivity of the enolate ligand. When the enolate is coordinated with the rare earth metals; it showed no reactivity with aromatic aldehydes. This kind of complex has compatibility for substituents on the aromatic aldehyde ring such as Cl^-, Br^-, F_3C^-, O_2N^- and other electron-donating groups. The outputs of the reaction were influenced by the substituents on the aromatic aldehydes ring, the solvents and the ligands of the lanthanide complexes. The results of the reaction of the lithium amide {[2,6-(iPr)$_2$C$_6$H$_3$](Me$_3$Si)N}Li with aromatic aldehydes in the presence of a catalytic amount of YCl$_3$ suggested that the method for the preparation of the amides from aldehydes by a one step reaction may be extended to reaction of other lithium amides with aldehydes. Further investigation on the reactivity of other lithium amides with aldehydes in the presence of lanthanide compounds is now in progress in our laboratory.

4. Experimental

4.1. Materials and methods

All syntheses and manipulations of air and moisture-sensitive materials were carried out in flamed dried Schlenk-type glassware on a Schlenk line. All solvents were refluxed and distilled over either finely divided LiAlH$_4$ or sodium benzophenone ketyl under argon prior to use unless otherwise noted. 2,6-(iPr)$_2$C$_6$H$_3$NHSiMe$_3$ 2,6-(Et)$_2$C$_6$H$_3$NHSiMe$_3$ [17] and LnCl$_3$ [18] (Ln = Yb, Y) were prepared according to the literature procedures. CDCl$_3$ was dried over activated 4 Å molecular sieves. Elemental analysis data were obtained on a Perkin–Elmer 2400 Series II elemental analyzer. IR spectra were recorded on a BIO-RAD FTS-40 spectrometer (CsI crystal plate, Nujol and Fluoroble mulls). Melting points were determined in sealed capillaries and are reported without correction. ^{1}H NMR and ^{13}C NMR spectra for analyses of compounds were recorded on a Bruker Avance-300 NMR spectrometer in benzene-d_6 for the lanthanide complexes, and in CDCl$_3$ for organic compounds, and chemical shifts for ^{1}H and ^{13}C NMR spectra were referenced to the internal solvent resonances.

4.2. Preparation of (CH$_2$=CHO)Y[2,6-(iPr)$_2$C$_6$H$_3$NSiMe$_3$]$_2$(μ-Cl)Li(THF)$_3$ (**1**)

To a THF solution of 2,6-(^{i}Pr)$_2$C$_6$H$_3$NHSiMe$_3$ (5.90 g, 23.6 mmol) at −78 °C was slowly added an n-hexane solution of nBuLi (20.6 mL, 35.8 mmol). The temperature of the reaction mixture was then gradually raised to room temperature after the addition. The mixture was stirred at room temperature for another 12 h. The reaction mixture was then transferred to a suspension of YCl$_3$ (2.31 g, 11.8 mmol) in THF. The reaction mixture was stirred at room temperature for 6 h, and then at 60 °C overnight. The solvent was pumped off. The residue was washed with 15 mL of n-hexane. The solid was extracted with a mixture of toluene and n-hexane (2:3, v/v) at 50 °C. Colorless crystals were obtained upon cooling the extracts at −10 °C for several days (6.27 g, 60%). M.p.: 82–84 °C (dec.). ^{1}H NMR (300 MHz, C$_6$D$_6$, δ in ppm): 7.32–7.16 (m, 6H, C$_6H_3$), 6.90 (dd, 1H, J = 12.9 Hz, J = 5.4 Hz, CH=CH$_2$), 4.24 (dd, 1H, J = 12.9 Hz, J = 1.2 Hz, CH=CH_2), 4.20 (dd, 1H, J = 5.4 Hz, J = 1.2 Hz, CH=CH_2), 3.12 (m, 4H, CH(CH$_3$)$_2$), 3.50 (m, 12H, OC$_4H_8$), 1.46 (m, 12H, OC$_4H_8$), 1.25–1.23 (m, 24H, CH(CH_3)$_2$), 0.50 (s, 18H, Si(CH_3)$_3$). IR (Nujol and Fluoroble mulls, cm^{-1}): ν 2961 (w), 2870 (s), 1651 (vs), 1441 (m), 1383 (m), 1327 (w), 1252 (vs), 1196 (w), 1044 (w), 907 (s), 843(s). *Anal.* Calc. for C$_{44}$H$_{79}$ClLiN$_2$O$_4$Si$_2$Y: C, 59.54; H, 8.97; N, 3.16. Found: C, 59.26; H, 9.13; N, 3.00%.

4.3. Preparation of (CH$_2$=CHO)Yb[2,6-(iPr)$_2$C$_6$H$_3$NSiMe$_3$]$_2$(μ-Cl)Li(THF)$_3$ (**2**)

This complex was prepared as yellow crystals in 61% yield from the reaction of 2,6-(iPr)$_2$C$_6$H$_3$NHSiMe$_3$ (4.45 g, 17.8 mmol) with nBuLi (15.5 mL, 26.9 mmol) in THF, followed by treatment with YbCl$_3$ (2.49 g, 8.9 mmol) by applying the procedures similar to those used for the preparation of **1**. M.p.: 86–88 °C (dec.). IR (Nujol and Fluoroble mulls, cm^{-1}): 2960 (s), 2870 (w), 1632 (vs), 1462 (m), 1363 (m), 1263 (w), 1092 (w), 1057 (w), 745 (w). *Anal.* Calc. for C$_{44}$H$_{79}$ClLiN$_2$O$_4$Si$_2$Yb (971.70): C, 54.39; H, 8.19; N, 2.88. Found: C, 54.12; H, 8.03; N, 2.98%.

4.4. Preparation of [2,6-(Et)$_2$C$_6$H$_3$NSiMe$_3$]$_2$Y(THF)(μ-Cl)$_2$Li(THF)$_2$ (**3**)

To a Schlenk flask containing an n-hexane solution of 2,6-(Et)$_2$C$_6$H$_3$NHSiMe$_3$ (2.78 g, 12.6 mmol) was added nBuLi (10.6 mL, 13.0 mmol) at −78 °C. The reaction mixture temperature was slowly raised to room temperature, and it was stirred for another 12 h at room temperature. The excess nBuLi was filtered off and washed with n-hexane, then 30 mL of THF was added. To the THF solution of the resulting lithium amide Li[2,6-(Et)$_2$C$_6$H$_3$NSiMe$_3$], was added YCl$_3$ (1.23 g, 6.3 mmol). The reaction mixture was stirred at room temperature overnight, and then at 60 °C for another 24 h. The solvent was evaporated under reduced pressure. The residue was extracted with toluene and n-hexane mixed solvents (1:1, v/v, 2 × 10 mL), the extraction was combined and concentrated. Colorless crystals were obtained upon standing the concentrated solution at −20 °C for several days (3.54 g, 83%). M.p.: 86–88 °C. ^{1}H NMR (300 MHz, C$_6$D$_6$, δ in ppm): 7.20–6.94 (m, 6H), 3.37–3.26 (m, 4H), 2.97–2.88 (m, 8H), 1.46–1.33 (m, 4H), 1.24–1.19 (m, 12H), 0.46–0.34 (m, 18H). IR (KBr, cm^{-1}): 3406 (w), 2966 (s), 2874 (w), 1624 (s), 1454 (s), 1253 (vs), 1107

(m), 1060 (w), 902 (m), 840 (w), 748 (w). *Anal.* Calc. for $C_{30}H_{52}Cl_2LiN_2OSi_2Y$ (**3**-2THF) (679.67): C, 53.01; H, 7.71; N, 4.12. Found C, 52.81; H, 7.36; N, 3.75%.

4.5. Preparation of {[2,6-(Et)$_2$C$_6$H$_3$NSiMe$_3$]$_3$YCl}[Li(THF)$_4$] (**4**)

This complex was prepared as colorless crystals in 75% yield from the reaction of 2,6-$(Et)_2C_6H_3NHSiMe_3$ (4.59 g, 20.8 mmol) with *n*BuLi (17.4 mL, 21.4 mmol) in *n*-hexane, followed by treatment with YCl_3 (1.35 g, 6.9 mmol) in THF, by employing procedures similar to those used for the preparation of complex **3**. ^{1}H NMR (300 MHz, C_6D_6, δ in ppm): 7.19–6.92 (m, 6H), 3.35–3.25 (m, 4H), 2.95–2.88 (m, 8H), 1.45–1.30 (m, 4H), 1.24–1.19 (m, 12H), 0.46–0.34 (m, 18H). IR (KBr, cm^{-1}): 2962 (s), 2874 (m), 2330 (w), 1631 (s), 1454 (s), 1373 (w), 1253 (vs), 1111 (s), 1057 (m), 906 (s), 840 (m), 748 (w). *Anal.* Calc. for $C_{43}H_{74}ClLiN_3OSi_3Y$ (**4**-3THF) (864.62): C, 59.73; H, 8.63; N, 4.86. Found: C, 59.49; H, 8.63; N 4.97%.

4.6. Reaction of N-trimethylsilyl-2, 6-diethylaniline with nBuLi

To a Schlenk flask containing a tetrahydrofuran (THF) solution of 2,6-$(Et)_2C_6H_3NHSiMe_3$ (0.278 g, 1.26 mmol) was added *n*BuLi (1.60 mL, 2.0 mmol) at −78 °C. The reaction mixture temperature was slowly raised to room temperature after the addition, and it was stirred for another 12 h at room temperature. The excess *n*BuLi was filtered off and washed with *n*-hexane. The solvents were pumped off, and the solid product was dried under vacuum. ^{1}H NMR (300 MHz, C_6D_6, δ in ppm): 7.08–7.06 (m, 6 H), 6.69 (dd, 1H, J = 12.5 Hz, J = 6.9 Hz, C*H*=CH$_2$), 3.99 (dd, 1H, J = 12.5 Hz, J = 1.2 Hz, CH=C*H*$_2$), 3.72 (dd, 1H, J = 6.9 Hz, J = 1.2 Hz, CH=C*H*$_2$), 3.43 (m, 12H, OC$_4$*H*$_8$), 2.94 (t, 8H, J = 7.2 Hz, C*H*$_2$CH$_3$), 1.45 (m, 12H, OC$_4$*H*$_8$), 1.32 (t, J = 7.2 Hz, 12H, CH$_2$C*H*$_3$), 0.24 (s, 18H, Si(C*H*$_3$)$_3$). This clearly shows the formation of Li[2, 6-$(Et)_2C_6H_3NSiMe_3$], LiOCH = CH_2 and the existence of three coordinated THF molecules.

4.7. Reaction of complexes **1** or **2** with aromatic aldehydes

A 30 mL Schlenk tube was charged with the complex (1 mmol) under dried argon. To the flask were added CH_2Cl_2 (3 mL) and the aromatic aldehydes (4 mmol). The reaction mixture was stirred at room temperature for 2–3 days; the mixture was then quenched with diluted HCl (0.1 M, 1. 0 mL). The mixture was extracted with acetyl acetate, and the extracts were dried over $MgSO_4$ and filtered. The solvent was removed by rotary evaporation. The residue was purified with a flash chromatography column (10:1 *n*-hexane:acetyl acetate, v/v) to give the corresponding products. In the case of the reactions of aromatic aldehydes having strong electron-withdrawing groups, such as O_2N^- and F_3C^-, with stoichiometric amounts of complexes **1** or **2**, the imine products could be isolated and characterized under the experimental conditions.

4.8. Reaction of lithium amide {[2,6-(iPr)$_2$C$_6$H$_3$](Me$_3$Si)N}Li with aromatic aldehydes catalyzed by YCl$_3$

A 30 mL Schlenk tube was charged with YCl_3 (5 mol%). To the tube were added solvent (toluene, or CH_2Cl_2, 3 mL), lithium amide [2,6-(iPr)$_2$C$_6$H$_3$NSiMe$_3$]Li (1 mmol) and the aromatic aldehyde (2 mmol). The reaction mixture was stirred at a certain temperature for a fixed interval; the mixture was then quenched with diluted HCl (0.1 M, 1. 0 mL). The mixture was extracted with acetyl acetate, and the extracts were dried over $MgSO_4$ and filtered. The solvent was removed by rotary evaporation. The residue was purified with flash chromatography column (10:1 *n*-hexane:acetyl acetate, v/v) to give the corresponding products.

4.9. X-ray crystallography

A suitable crystal of each of the complexes **1**, **2**, **3**, **4** and **5f′** was mounted in a sealed capillary. Diffraction was performed on a Siemens SMART CCD-area detector diffractometer using graphite-monochromated Mo Kα radiation (λ = 0.71073 Å); temperature

Table 5
Crystallographic data and structure refinement details for **1**, **2**, **3**, **4** and and **5′**

	1	**2**	**3**	**4**	**5f′**
Empirical formula	$C_{44}H_{79}ClLiN_2O_4Si_2Y$	$C_{44}H_{79}ClLiN_2O_4Si_2Yb$	$C_{38}H_{68}Cl_2LiN_2O_3Si_2Y$	$C_{55}H_{98}ClLiN_3O_4Si_3Y$	$C_{19}H_{22}N_2O_2$
Formula weight	887.57	971.70	823.87	1080.93	310.39
Crystal system	triclinic	triclinic	orthorhombic	monoclinic	monoclinic
Space group	$P\bar{1}$	$P\bar{1}$	$Pna2_1$	$P2_1/n$	$P2_1/c$
a (Å)	13.123(2)	13.041(2)	37.272(2)	18.494(2)	8.4963(2)
b (Å)	13.266(2)	13.246(2)	12.2901(8)	17.872(2)	28.2166(7)
c (Å)	16.606(3)	16.579(3)	10.0790(7)	19.879(3)	8.1526(2)
α (°)	85.256(3)	85.127(2)	90	90	90
β (°)	84.929(3)	84.736(3)	90	97.657(2)	117.122(2)
γ (°)	66.722(3)	66.766(2)	90	90	90
V (Å^3)	2641.7(7)	2616.7(7)	4617.0(5)	6511.9(14)	1739.56(7)
T (K)	294(2)	294(2)	293(2)	293(2)	293(2)
$\rho_{calc.}$ (g/cm^3)	1.116	1.233	1.175	1.103	1.185
Z	2	2	4	4	4
F(000)	952	1014	1724	2328	664
Reflections collected	13552	13397	38934	55588	9238
Unique reflections	9282	9185	9993	15001	3051
R_{int}	0.056	0.036	0.050	0.111	0.031
Parameters refined	538	538	453	629	213
λ (Å); Mo Kα	0.71073	0.71073	0.71073	0.71073	0.71073
μ (mm^{-1})	1.236	1.920	1.463	1.032	0.077
θ Range (°)	1.67–25.02	1.68–25.02	1.74–27.52	1.41–27.60	1.44–25.00
Goodness-of-fit (GOF) on F^2	0.984	1.027	1.016	0.960	1.031
R [$I > 2\sigma(I)$]	0.070	0.053	0.053	0.088	0.045
wR_2 (all data)	0.229	0.138	0.143	0.318	0.121
Largest difference in peak and hole (e Å^{-3})	0.459 and −0.377	1.875 and −1.763	0.401 and −0.335	2.433 and −1.502	0.142 and −0.135

294(2) K; ψ and ω scan technique; SADABS effects and empirical absorption were applied in the data corrections. All the structures were solved by direct methods (SHELXS-97) [19], completed by subsequent difference Fourier syntheses and refined by full-matrix least-square calculations based on F^2 (SHELXS-97) [19]. See Table 5 for crystallographic data.

Acknowledgments

This work was co-supported by the National Natural Science Foundation of China (Grant Nos. 20672002 and 20702001), the program for the NCET (Grant No. NCET-04-0590). The Grant from Anhui Province and Anhui Education Department (Grant Nos. 2007Z016, TD200707). We are also grateful for the assistance of Prof. Bao-hui Du and Ji-ping Hu in running IR and NMR spectra.

Appendix A. Supplementary data

CCDC 684085, 684086, 684087, 684088 and 684089 contain the supplementary crystallographic data for **1**, **2**, **3**, **4** and **5f'**. These data can be obtained free of charge via www.ccdc.ac.uk/conts/retrieving.html or from the Cambridge Crystallographic Data Centre, 12 Union Road, Cambridge CB2 1EZ, UK; fax: (+44) 1223-336-033; or e-mail: deposit@ccdc.cam.ac.uk. Supplementary data associated with this article can be found, in the online version, at doi:10.1016/j.poly.2008.05.030.

References

[1] (a) M. Zimmermann, K.W. Törnroos, R. Anwander, Angew. Chem., Int. Ed. 46 (2007) 3126;
(b) M.T. Gamer, P.W. Roesky, S.N. Konchenko, P. Nava, R. Ahlrichs, Angew. Chem., Int. Ed. 45 (2006) 4447;
(c) C.N. Carlson, J.M. Veauthier, K.D. John, D.E. Morris, Chem. Eur. J. 14 (2008) 422;
(d) M. Rastätter, A. Zulys, P.W. Roesky, Chem. Commun. (2006) 874;
(e) S. Hong, T.J. Marks, Acc. Chem. Res. 37 (2004) 673;
(f) Y. Horino, T. Livinghouse, Organometallics 23 (2004) 12;
(g) A.A. Trifonov, G.G. Skvortsov, D.M. Lyubov, N.A. Skorodumova, G.K. Fukin, E.V. Baranov, V.N. Glushakova, Chem. Eur. J. 12 (2006) 5320;
(h) Y. Yao, Z. Zhang, H. Peng, Y. Zhang, Q. Shen, J. Lin, Inorg. Chem. 45 (2006) 2175;
(i) R. Gauvin, A. Mortreux, Chem. Commun. (2005) 1146;
(j) F. Bonnet, A. Hillier, A. Collins, S. Dubberley, P. Mountford, J. Chem. Soc., Dalton Trans. (2005) 421;
(k) M.T. Gamer, M. Rastätter, P.W. Roesky, A. Steffens, M. Glanz, Chem. Eur. J. 11 (2005) 3165;
(l) Y. Nakayama, H. Yasuda, J. Organomet. Chem. 689 (2004) 4489;
(m) H. Ma, T.P. Spaniol, J. Okuda, Angew. Chem., Int. Ed. 45 (2006) 7818;
(n) S. Arndt, K. Beckerle, P.M. Zeimentz, T.P. Spaniol, J. Okuda, Angew. Chem., Int. Ed. 44 (2005) 7473.
[2] (a) J. Zhao, T.J. Marks, Organometallics 25 (2006) 4763;
(b) P.W. Roesky, T.E. Müller, Angew. Chem., Int. Ed. 42 (2003) 2708;
(c) A.M. Kawaoka, M.R. Douglass, T.J. Marks, Organometallics 22 (2003) 4630;
(d) G. Zi, L. Xiang, H. Song, Organometallics 27 (2008) 1242;
(e) X. Xu, X.Y. Xu, Y. Chen, J. Sun, Organometallics 27 (2008) 758;
(f) S. Datta, M.T. Gamer, P.W. Roesky, Organometallics 27 (2008) 1207;
(g) S.B. Amin, T.J. Marks, Angew. Chem., Int. Ed. 47 (2008) 2006;
(h) H.F. Yuen, T.J. Marks, Organometallics 27 (2008) 155.
[3] W.J. Evans, D. Drummond, J. Am. Chem. Soc. 110 (1988) 2772.
[4] W.J. Evans, J.W. Grate, L.A. Hughes, H. Zhang, J.L. Atwood, J. Am. Chem. Soc. 107 (1985) 3728.
[5] (a) W.J. Evans, D. Drummond, J. Am. Chem. Soc. 108 (1986) 7440;
(b) W.J. Evans, L.A. Hughes, D. Drummond, H. Zhang, J.L. Atwood, J. Am. Chem. Soc. 108 (1986) 1722.
[6] T. Shima, Z. Hou, J. Am. Chem. Soc. 128 (2006) 8124.
[7] (a) W.J. Evans, R. Dominguez, T.P. Hanusa, Organometallics 5 (1986) 1291;
(b) Z. Wu, Z. Xu, X. You, X. Zhou, Y. Xing, Z. Jin, J. Chem. Soc., Chem. Commun. (1993) 1494;
(c) Z. Wu, Z. Xu, X. You, X. Zhou, X. Huang, J. Organomet. Chem. 483 (1994) 107.
[8] G.T.W. Solomons, C.B. Fryhle, Organic Chemistry, 8th ed., John Wiley & Sons Inc., New York, 2004.
[9] (a) L. Zhang, S. Wang, S. Zhou, G. Yang, E. Sheng, J. Org. Chem. 71 (2006) 3149;
(b) S. Seo, T.J. Marks, Org. Lett. 10 (2008) 317;
(c) H. Berberich, P.W. Roesky, Angew. Chem. 110 (1998) 1618;
(d) H. Berberich, P.W. Roesky, Angew.Chem., Int. Ed. 37 (1998) 1569.
[10] F. Rivals, A. Steiner, Chem. Commun. (2001) 1426.
[11] T.R. Hoye, B.M. Eklov, T.D. Ryba, M. Voloshin, L.J. Yao, Org. Lett. 6 (2004) 953.
[12] S. Zhou, S. Wang, G. Yang, Q. Li, L. Zhang, Z. Yao, Z. Zhou, H. Song, Organometallics 26 (2007) 3755.
[13] (a) E. Sheng, S. Wang, G. Yang, S. Zhou, L. Cheng, K. Zhang, Z. Huang, Organometallics 22 (2003) 684;
(b) A.T. Gilbert, B.L. Davis, T.J. Emge, R.D. Broene, Organometallics 18 (1999) 2125.
[14] R.D. Shannon, Acta Crystallogr. A32 (1976) 751.
[15] O. Just, W.S. Rees Jr., Inorg. Chem. 40 (2001) 1751.
[16] S. Zhou, S. Wang, G. Yang, X. Liu, E. Sheng, K. Zhang, L. Cheng, Z. Huang, Polyhedron 22 (2003) 1019.
[17] H. Schumann, J. Winterfeld, C. Esther, E. Rosenthal, H. Hemling, L. Esser, Z. Anorg. Allg. Chem. 621 (1995) 122.
[18] M.D. Taylor, C.P. Carter, J. Inorg. Nucl. Chem. 24 (1962) 387.
[19] G.M. Sheldrick, SHELXTL, version 5.10, Bruker Analytical X-ray Systems Inc., Madison, WI, 1997.

studied platinum(IV) complexes with different axial ligands where the cytotoxicity increase was observed in the following order: OH < $OOCCH_3$ < Cl < $OOCCF_3$ [9,15,18]. The above compounds suggest a weak correlation between the chemical structure of the platinum(IV) complex and their cytotoxicity. That is why platinum(IV) complexes with other equatorial N-donors, such as 1,2,4-triazolo [1,5-*a*]pyrimidines (tp) have been studied [22]. These heterocycles have a structure similar to purine and adenine (Fig. 1); their fused ring system differing by having the pyrimidine nitrogen atom in a bridge-head position with the disappearance of the proton of the five-membered ring. Due to the similarity of both systems, coordination compounds of 1,2,4-triazolo[1,5-*a*]pyrimidines can be considered as a model system for various naturally occurring metal coordination compounds.

Previously papers demonstrated that dichloride platinum(II) complexes with 1,2,4-triazolo[1,5-*a*]pyrimidine revealed a high antitumor activity [23,24], e.g., *cis*-platinum(II) compounds with HmtpO (5-methyl-1,2,4-triazolo[1,5-*a*]pyrimidin-7(*4H*)-one) [23], dbtp (5,7-ditertbutyl-1,2,4-triazolo[1,5-*a*]pyrimidine) [24] and dptp (5,7-diphenyl-1,2,4-triazolo[1,5-*a*]pyrimidine) [24] had good *in vitro* cytotoxic activity against the cells of rectal, breast and bladder cancer.

In our continuing efforts to develop new platinum antitumors prodrugs, we have reported the synthesis, molecular characterization and antiproliferative activity *in vitro* of the new Pt(IV) compounds: $PtCl_4(tp)_2$ (**1**), $PtCl_4(dmtp)_2$ (**2**), $PtCl_4(dbtp)_2$ (**3**), $PtCl_4(HmtpO)_2$ (**4**). In addition the crystal structure of $(H_2mtpO)_2PtCl_6$ (**5**) has been determined.

2. Experimental

2.1. Materials

Pt of 99.9% purity was purchased from the Polish State Mint, whereas 3-amino-1,2,4-triazole (98%), 2,4-pentanedione (99%), 5-methyl-*s*-triazolo[1,5-*a*]pyrimidine-7-ol (98%), 5,7-dimethyl-*s*-triazolo[1,5-*a*]pyrimidine (98%) and 2,2,6,6-tetramethyl-3,5-heptanedione (98%) were from Aldrich. A water solution of H_2PtCl_6 was prepared using a standard procedure. 5,7-Ditertbutyl-1,2,4-triazolo[1,5-*a*]pyrimidine was prepared according to the Bülow and Haas method [25] by the reaction of 3-amino-1,2,4-triazole with 2,2,6,6-tetramethyl-3,5-heptanedione [26].

2.2. Instrumentation

The content of C, H and N was determined by elemental semimicroanalysis. Thermogravimetric analyses were performed with a SDT-2960 TA Instruments (samples – 5 mg, heating range 25–1000 °C, heating rate 3.5 deg/min, N_2 atmosphere). IR spectra were measured with a Perkin–Elmer Spectrum-2000 FT–IR spectrometer, using KBr (400–4000 cm^{-1}) and polyethylene discs (100–400 cm^{-1}). The $^1H\{^{13}C\}$ HSQC, $^1H\{^{13}C\}$ HMBC and $^1H\{^{15}N\}$ HMQC spectra were performed with a Varian INOVA-500 NMR spectrometer equipped with an inverse Nalorac Z-gradient shielded probe. The solvent was DMF-d_7 or DMSO-d_6; the concentrations of the saturated solutions being ca. 0.01–0.05 M, the temperature being 298 K. The reference standard was TMS for ^1H and ^{13}C; CH_3NO_2 (external) for ^{15}N and K_2PtCl_6 (external) for ^{195}Pt.

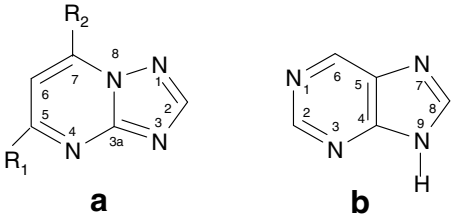

Fig. 1. IUPAC numbering of: (a) 1,2,4-triazolo[1,5-*a*]pyrimidine R_1, R_2 = H (tp); R_1, R_2 = CH_3 (dmtp); R_1, R_2 = $C(CH_3)_3$ (dbtp); R_1 = CH_3, R_2 = O (HmtpO); (b) purine molecule.

2.3. Preparation of the platinum(IV) complexes

*$PtCl_4(tp)_2$ (**1**)* and *$PtCl_4(dmtp)_2$ (**2**)* were obtained by the reaction of H_2PtCl_6 with tp or dmtp in M:L molar ratio of 1:2 [27].

*$PtCl_4(dbtp)_2$ (**3**).* To a solution of 330 μl of H_2PtCl_6 (0.10 mmol) in 10 cm^3 of water, a solution of dbtp (0.0465 g, 0.20 mmol) in 25 cm^3 of ethanol was added. The reaction mixture was stirred at room temperature for 24 h. The solution was slowly evaporated and after a few days a yellow precipitate was obtained. The solid was filtered off and washed with acetone and diethyl ether, and dried in vacuum. Yield: 0.0738 g (92%). *Anal.* Calc. for $C_{26}H_{40}Cl_4N_8Pt$: C, 38.9; N, 14.0; H, 5.0. Found: C, 39.2; N, 14.0; H, 5.3%.

*$PtCl_4(HmtpO)_2 \cdot 3H_2O$ (**4**).* 330 μl of H_2PtCl_6 (0.1 mmol) was added to 10 ml water. Next a solution of HmtpO (0.0366 g, 0.24 mmol) in 5 cm^3 of 1 M HCl was added dropwise. The solution was stirred at room temperature for 24 h. The solution was slowly evaporated and after a few days a yellow precipitate was obtained. The solid was filtered off and washed with water and diethyl ether, and dried in vacuum. Yield: 0.0714 g (92%). *Anal.* Calc. for $C_{12}H_{18}Cl_4N_8O_5Pt$: C, 20.8; N, 16.2; H, 2.6. Found: C, 21.0; N, 16.5; H, 2.3%. The content of water in (**4**) was confirmed by thermogravimetric analyses. The first endothermic step in range 240–270 °C corresponds to a mass loss on the TG curve which can be correlated with detachment of three water molecules and Cl_2 (calcd 18.1%, exp. 18.3%). The next endothermic processes (275–860 °C) can be related to decomposition of (**4**) leaving platinum as the final product.

*$[H_2mtpO]_2[PtCl_6]$ (**5**).* This compound was isolated by slow evaporation of $PtCl_4(HmtpO)_2$ (**4**) from a mixture of water and n-hexane (5:1 v/v) (pH 1) giving crystals suitable for X-ray analysis (*vide infra*).

2.4. X-ray structure determination

$[H_2mtpO]_2[PtCl_6]$ (**5**) crystallized in the monoclinic space group $P2_1/n$. The X-ray data was collected at 293(2) K with an Oxford Sapphire CCD diffractometer, using MoKα radiation (λ = 0.71073 Å) and the ω–2θ method. A shape-based numerical absorption correction was applied with minimum and maximum transmissions of 0.3811 and 0.1971. The structure was solved by Patterson methods and refined with the full-matrix least-squares method on F^2 with the use of the SHELX-97 program package [28]. The data collection and refinement processes are summarized in Table 1.

2.5. Cells

The following established *in vitro* human cancer cell lines were studied: SW707 (rectal adenocarcinoma), HCV29T (bladder cancer) and HL-60 (human acute promyelocytic leukemia).

Cells were patted in 96-well sterile plates (Sarstedt, Costar) at a density of 10^4 cells per well (in 100 μl of culture medium) and incubated for 24 h. The tested complexes **1**–**4** were added to the final concentrations from 0.1 to 100 μg/cm^3 and the incubation was continued for an additional 72 h. The results of the cytotoxic activity *in vitro* were expressed as an IC_{50} – the dose of compound (in μM) that inhibits the proliferation rate of the tumors cells by 50% as compared to the control untreated cells. The details of this technique were described by Skehan [29]. The antiproliferative activity *in vitro* against SW707 and HCV29T cell lines were performed by

Table 1
Crystal data and structure refinement for (**5**)

Identification code	$[H_2mtpO]_2[PtCl_6]$ (**5**)
Empirical formula	$C_{12}H_{14}Cl_6N_8O_2Pt$
Formula weight	710.10
Temperature (K)	293(2)
Wavelength (Å)	0.71073
Crystal system, space group	monoclinic, $P2_1/n$
Unit cell dimensions	
a (Å)	7.602(2)
b (Å)	20.441(4)
c (Å)	7.608(2)
α (°)	90
β (°)	117.30(3)
γ(°)	90
Volume (Å^3)	1050.5(4)
Z, Calculated density (Mg/m^3)	2, 2.245
Absorption coefficient (mm^{-1})	7.470
F(000)	676
Crystal size (mm)	0.32 × 0.20 × 0.16
Theta range for data collection (°)	3.17–30.98
Index ranges	$-9 \leqslant h \leqslant 10$ $-29 \leqslant k \leqslant 20$ $-9 \leqslant l \leqslant 11$
Reflections collected/unique [R_{int}]	7027/3083 [0.0447]
Data/restraints/parameters	3083/12/134
Goodness-of-fit on F^2	1.193
Final R indices [$I > 2\sigma(I)$]	R_1 = 0.0754, wR_2 = 0.1964
R indices (all data)	R_1 = 0.0816 wR_2 = 0.1993
Largest difference in peak and hole (e Å^{-3})	2.703 and −2.918

using the SRB test [24], whereas against HL-60 tumors cell the MTT test was used [30].

3. Results and discussion

3.1. NMR spectroscopy

The multinuclear NMR spectral data of (**1**) and (**2**) have been reported [27], hence here we present only the ^{1}H, ^{13}C, ^{15}N and ^{195}Pt NMR data for $PtCl_4(dbtp)_2$ in DMF-d_7 and $PtCl_4(HmtpO)_2$ in DMSO-d_6. The chemical shifts of the heterocyclic ligands protons in the platinum(IV) complexes are listed in Table 2. The ^{1}H NMR spectrum of $PtCl_4(dbtp)_2$ exhibits two characteristic signals at 9.34 ppm (t) H(2) and 7.43 ppm (s) H(6). However the ^{1}H NMR spectrum changed with time and after 1 h three different sets of signals (**3**, **3a**, **3b**) appeared (Table 2). In the latter solvent the ^{1}H NMR chemical shift of H(2) and H(6) were 9.45, 7.57 ppm for **3a** and 9.27, 7.58 ppm for **3b**. Probably all the complexes (**3**, **3a**, **3b**) are rotamers (HH (head-to-head) and HT (head-to-tail), formed by the restrained rotation of the dbtp ligand around the Pt–N(3) bond (Fig. 2). This phenomenon is probably affected by the steric hindrance of the bulky *tert*-butyl group.

In the case of the spectrum of (**4**), three hydrogen signals (10.52 ppm (s) N(4)–H, 8.52 ppm (t) H(2) and 6.17 ppm (s) H(6)) are present. In comparison to the free ligand spectrum, the signals

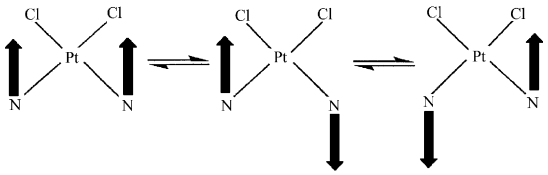

Fig. 2. The possible HH and HT conformers of $PtCl_4(dbtp)_2$. The equatorial ligands are presented only for clarity.

were shifted upon coordination, Δ_{coord} coordination shift ($\Delta_{coord} = \delta_{complex} - \delta_{ligand}$), towards the low field region. The most significant coordination shift was observed for H(2) (0.35–0.81 ppm) (Table 2). However these changes do not confirm unambiguously which of the heterocyclic nitrogen atoms (N(1) or N(3)) is engaged in the formation of a platinum–nitrogen bond. This problem was solved by means of ^{15}N–^{1}H HETCOR spectral analysis (Table 2). In the ^{15}N NMR spectra resonance lines at: −108.9, −247.3, −121.0 and −161.7 ppm for (**3**) and −111.4, −252.4, −255.7 and −157.7 ppm for (**4**) were *detected* (Table 2). In comparison to the free ligand spectra, all the signals in the spectra of the complexes are shielded upon platination. However the highest coordination shift (Δ_{coord} = 87–115 ppm) was observed for the N(3) signals (Table 2), which indicates the monodentate coordination to Pt(IV) in solution. Moreover the ^{15}N resonances of N(3), in (**3**) were observed at much higher fields, than for the platinum(II) analog [24]. Shift towards higher frequencies comes from the higher shielding of the N ligating sites upon coordination. The latter cannot be related only to a σ donation effect from the N atom in the heterocycle to Pt(IV). The second effect which causes an increase of electron density on coordinating nitrogen atom can be correlated with inter- and intramolecular interactions, which influence on the chemical shift of the nitrogen atoms.

The proposed coordination mode of the triazolopyrimidine ligands to the platinum(IV) ion can also be elucidated by ^{13}C NMR spectra, which are more commonly observed and registered. In the ^{13}C NMR spectra of the complexes, the signals of the carbon atoms adjacent to the N(3) coordination site, i.e. C(2) and C(3a) are shielded (Δ_{coord} in the range 2.6–4.1 ppm), whereas the signals of C(5), C(6) and C(7) were deshielded (Δ_{coord} between 2.3–3.8 ppm), except for the signals of (**4**), where the opposite shift was observed. The shielding of carbon atoms adjacent to the coordination site N(3), as well as the deshielding of the other carbons and protons inside the heterocyclic ring, has already been described by us for some Pt(II) chloride complexes with triazolopyrimidine derivatives.

The ^{195}Pt NMR chemical shifts of the studied complexes are listed in Table 3. The ^{195}Pt resonance in the spectra of the platinum(IV) compounds were observed between −113 and 69 ppm, which is characteristic for octahedral platinum(IV) complexes where two adjacent corners are occupied by nitrogen atoms and the other four positions by chlorides [20,31–33]. However, the ^{195}Pt NMR signals for the complexes with triazolopyrimidine (**3**) and (**4**) are observed at a lower field than those reported for Pt(IV) complexes with other N-donor ligands: −145 ppm for $PtCl_4(NH_3)_2$ in H_2O [33]; −150 ppm

Table 2
^{1}H and ^{15}N NMR chemical shifts (δ) of the platinum(IV) complexes

Compound	H(2)	H(6)	N(1)	N(3)	N(4)	N(8)
(**3**) $PtCl_4(dbtp)_2$ in DMF-d_7	9.34 (+0.70)	7.43 (+0.16)	−108.9 (−1.3)	−247.3 (−94.2)	−121.0 (−5.2)	−161.7 (−3.0)
(**3a**) $PtCl_4(dbtp)_2$ in DMF-d_7	9.45 (+0.81)	7.57 (+0.30)	−107.4 (+0.2)	−268.0 (−114.9)	−122.2 (−6.4)	−161.4 (−2.7)
(**3b**) $PtCl_4(dbtp)_2$ in DMF-d_7	9.27 (+0.63)	7.58 (+0.31)	−109.1 (−1.5)	−252.2 (−99.1)	−121.5 (−5.7)	−162.4 (−3.7)
(**4**) $PtCl_4(HmtpO)_2$ in DMSO-d_6	8.52 (+0.35)	6.17 (+0.35)	−111.4 (−0.6)	−252.4 (−86.7)	−255.7 (−3.0)	−157.7 (−2.4)
(**5**) $[H_2mtpO]_2[PtCl_6]$ in DMSO-d_6	8.28 (+0.11)	6.05 (+0.23)	[a]	[a]	[a]	[a]

[a] Was not recorded.

Table 3
^{13}C and ^{195}Pt NMR chemical shifts (δ) of the platinum(IV) complexes

Compound	^{13}C					^{195}Pt
	C(2)	C(3a)	C(5)	C(6)	C(7)	δPt
(**3**) $PtCl_4(dbtp)_2$ in DMF-d_7	152.2 (−3.1)	151.6 (−4.9)	179.7 (+3.8)	108.2 (+3.6)	160.2 (+2.3)	−30
(**3a**) $PtCl_4(dbtp)_2$ in DMF-d_7	152.3 (−3.0)	151.0 (−5.5)	180.4 (+4.5)	109.0 (+4.4)	160.6 (+2.7)	−113
(**3b**) $PtCl_4(dbtp)_2$ in DMF-d_7	153.2 (−2.1)	151.5 (−5.0)	180.8 (+4.1)	108.6 (+4.0)	160.4 (+2.5)	−113
(**4**) $PtCl_4(HmtpO)_2$ in DMSO-d_6	147.6 (−4.1)	147.9 (−2.6)	150.2 (−1.3)	101.2 (+3.2)	153.6 (−2.2)	69
(**5**) $[H_2mtpO]_2[PtCl_6]$ in DMSO-d_6	150.2 (−1.5)	149.1 (−1.4)	150.4 (−1.1)	98.9 (+0.9)	156.4 (+0.6)	[a]

[a] Was not recorded.

for $PtCl_4(HMI)_2$, where HMI = hexamethyleneimine, in acetone [32]; −252 ppm for $PtCl_4$(1,4-dach) in acetone [20]; −358 ppm for $PtCl_4$(Hyp), where Hyp = hypoxantine, in DMSO-d_6 [31].

3.2. IR spectra

The frequencies of the two most characteristic bands of the pyrimidine and imidazole ring skeleton vibrations after coordination appeared at higher frequencies by 18–24 and 15–19 cm^{-1}, respectively. The observed shifts are bigger than for Pt(II) chloride complexes with other 1,2,4-triazolo[1,5-*a*]pyrimidines [27]. This may be caused by the fact that due to the coordination by N(3), the tp ring double bonds (C=N, C=C) reveal a more pronounced double bond character [34].

For the ionic pair (**5**) the discussed bands are significantly shifted towards higher frequencies (21–28 cm^{-1}), which can be the result of either N(3) protonation or formation of hydrogen bonds. In the IR spectrum of (**5**) we also observed an intensive band of rich structure in the 2500–2700 cm^{-1} range, characteristic for the $(N–H)^+$ stretching vibration for salts of tertiary amines [35]. Its presence is in agreement with the X-ray structure where the protonated H_2mtpO^+ species was observed.

The far-IR spectra of the complexes show ligand vibrations as well as new bands originating from Pt–Cl and Pt–N stretchings. The spectra of (**3**) and (**4**) exhibit one new strong broad absorption band in region 328–339 cm^{-1}. The frequencies of these bands are similar to those found in the spectra of Pt(IV) chloride complexes with 1,4-dach in the equatorial position (325–350 cm^{-1}) [36,37] this band and was assigned to a Pt–Cl stretching vibration. The vibrations in the range 227–287 cm^{-1} can be assigned to Pt–N stretching modes.

3.3. Cytotoxic activity

The antitumors activity *in vitro* of the platinum(IV) compounds (**1–4**) have been tested against HL-60, SW707 and HCV29T tumors cells. The results, expressed as the concentration of the compound required to kill the tumor cell by 50% (IC_{50}), are listed in Table 4. Cisplatin was used as a reference substance. We noticed that treatment of tumor cells with the platinum(IV) complexes (**1–4**) display an antiproliferative effect. However, the new platinum complexes (**1**) and (**2**) exhibit negligible cytotoxicity (IC_{50} 170–43.3 μM). Their IC_{50} parameters indicate that $PtCl_4(tp)_2$ and $PtCl_4(dmtp)_2$ have revealed generally lower immunostimulating activity than cisplatinum (Table 4) against the studied tumor cell lines. In contrast, (**3**) and (**4**) were more cytotoxic than **1** and **2** (Table 4). $PtCl_4(HmtpO)_2$ and $PtCl_4(dbtp)_2$ display relatively low IC_{50} values (1.1–57 μM) against the tumor cell lines and they seem to have significant cytotoxic activity. In addition, it should be noted that $PtCl_4(dbtp)_2$ is also expected to be more reactive than (**4**). For example, against HCV29T, $PtCl_4(dbtp)_2$ presents relatively high antitumor activity, (with an IC_{50} value of 1.1 μM) which is a 50 times lower concentration than for the platinum(IV) analog $PtCl_4(HmtpO)_2$ (Table 4).

Table 4
Cytotoxicity of platinum(IV) complexes against HL-60, HCV29T and SW707 tumors cells

Compound	Cell line/IC_{50} (μM) ± SD		
	HL-60	SW707	HCV29T
(**1**) $PtCl_4(tp)_2$	43.3 ± 1.2	>170.0	121.3 ± 1.4
(**2**) $PtCl_4(dmtp)_2$	48.3 ± 3.0	113.0 ± 26.0	94.7 ± 15.0
(**3**) $PtCl_4(dbtp)_2$	1.1 ± 0.7	1.5 ± 1.1	1.1 ± 1.0
(**4**) $PtCl_4(HmtpO)_2$	35.0 ± 3.5	[a]	56.6 ± 5.3
cis-$PtCl_2(NH_3)_2$	11.0 ± 4.6	16.3 ± 1.5	2.3 ± 1.5

[a] Was not recorded.

Against HL-60 and SW707, compounds (**3**) revealed IC_{50} values in the range 1.1–4.7 μM, which indicates moderate antiproliferative activity. In addition, the high cytotoxic values for compound (**3**) were even 10 times higher than the clinically used cisplatin against the human tumors models.

Thus, from the anticancer screening data complex (**3**) demonstrated strong cytotoxic activity *in vitro* and may be recommended for further preclinical studies. The research on lethal toxicity in experimental animals and on antitumors activity *in vivo* in transplantable mouse tumors models will be described in future work.

With regard to structure–activity relationships, it is apparent that the antitumor activity of the platinum(IV) compounds containing 1,2,4-triazolo[1,5-*a*]pyrimidines correlates with the size of the alkyl group in the heterocyclic ligands. The highest antitumor activity was achieved with sterically bulky group, introduced by the two *tert* butyl groups of the heterocycle, which are responsible for the hydrogen-bond properties and this may be reflected in an increase in the lipophilicity and its interaction with cellular components.

A similar relationship between cytotoxicity and the type of heterocycle were noted for platinum(II) complexes with the same triazolopyrimidine ligands [24,38]. Here, the best activity against tumors cell lines has been detected for *cis*-$PtCl_2(dbtp)_2$ and *cis*-$PtCl_2(dptp)_2$, which contain bulky groups (*tert*butyl or phenyl) in the heterocyclic ring [24]. The cytotoxicity data indicate that the antitumor activity of the studied platinum(II) compounds containing 1,2,4-triazolo[1,5-*a*]pyrimidines depends directly on the geometry of platinum(II) and the kinds of ligands and heterocyclic ligands involved.

Careful interpretation of the cytotoxic data for the Pt(II) and Pt(IV) complexes confirm the influence of the geometry and type of heterocyclic ligand on the antitumors activity (Table 4) [38]. Consistently, the octahedral complexes (**1–4**) are also more cytotoxic than their square-planar platinum(II) analogues. For example, against SW707, the value of IC_{50} for $PtCl_4(dbtp)_2$ is five times lower than for *cis*-$PtCl_2(dbtp)_2$ (Fig. 3). Perhaps this observation could serve as a reasonable basis for designing new strategies in finding antitumor drugs based on platinum(IV) complexes.

3.4. Crystal structure of $[H_2mtpO]_2[PtCl_6]$

Fig. 4 shows a perspective view of the crystal along with its atomic labelling. Selected bond lengths and bond angles are given in Table 5.

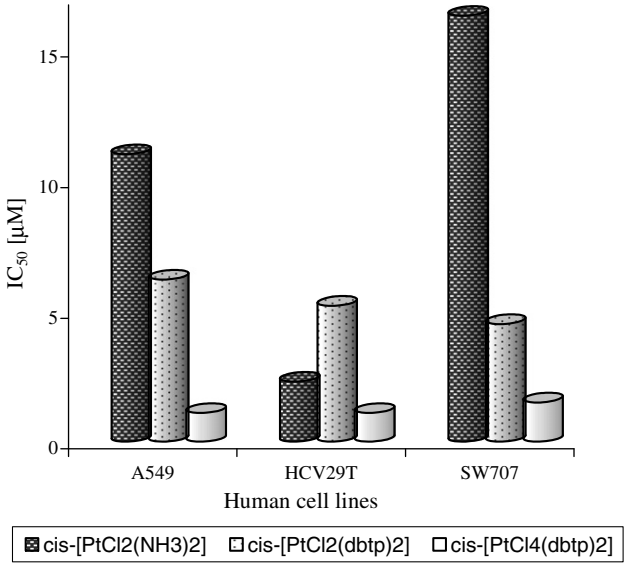

Fig. 3. Comparative chart of the antiproliferative activity in vitro for platinum complexes with 5,7-ditertbutyl-1,2,4-triazolo[1,5-*a*]pyrimidine (dbtp) against tumor cells.

The slight discrepancy between the final R_1 value of 0.0754 and R_{int} = 0.0447 are observed, despite the numerical absorption correction applied. This difference can be explained by the thermal displacement of the H_2mtpO$^+$ cations, as is seen on Fig. 4. The small librations of that moiety, in particular for O(71) and the C(6)–C(7)–N(8)–N(1) fragment of the ring system, cannot be described in a most satisfactory way with the anisotropic displacement parameters during the refinement. Also no discrete positions of the atoms for the cation could be defined to improve the model.

Complex (**5**) is an ionic pair consisting of two N(3)-monoprotonated H_2mtpO$^+$ cations and one octahedral $[PtCl_6]^{2-}$ anion. The Pt(IV) of the hexachloroplatinate ion is located on the center of symmetry. Therefore the asymmetric part of the reported structure contains a half of the $[PtCl_6]^{2-}$ anion. The asymmetric part of the structure is completed by one H_2mtpO$^+$ cation. A small distortion of the octahedral geometry was found for the complex anion, with Cl–Pt–Cl angles in the asymmetric part varying from 88.9(2)° to 90.8(2)°. Due to the centrosymmetric structure of that anion, the chlorides related by the center of symmetry occupy the trans positions with the valence angles being 180°. Such a phenomenon is not unusual and has been described for $[N(CH_3)_4]_2[PtCl_6]$ [39], $[N(C_2H_5)_4]_2[PtCl_6]$ [40], $[NH_2(CH_3)_2]_2[PtCl_6]$ [41], (9-MeGuH)$_2$[PtCl$_6$] [42] (9-MeGuH = 9-methylguaninium cation) and (dmtpH$^+$)$_2$[PtCl$_6$] [27]. The lengths of the Pt–Cl bonds vary from 2.308(4) to 2.313(3) Å.

Table 5
Selected bond lengths (Å) and angles (°) for $[H_2mtpO]_2[PtCl_6]$ (**5**)

Bond		Angle	
Pt(1)–Cl(1)#1	2.308(4)	Cl(1)#1–Pt(1)–Cl(1)	180.0
Pt(1)–Cl(1)	2.308(4)	Cl(1)#1–Pt(1)–Cl(3)#1	89.2(2)
Pt(1)–Cl(3)#1	2.310(3)	Cl(1)–Pt(1)–Cl(3)#1	90.8(2)
Pt(1)–Cl(3)	2.310(3)	Cl(1)#1–Pt(1)–Cl(3)	90.8(2)
Pt(1)–Cl(2)#1	2.313(3)	Cl(1)–Pt(1)–Cl(3)	89.2(2)
Pt(1)–Cl(2)	2.314(3)	Cl(3)#1–Pt(1)–Cl(3)	180.0
C(2)–N(3)	1.36(2)	Cl(1)#1–Pt(1)–Cl(2)#1	91.1(2)
N(1)–C(2)	1.23(2)	Cl(1)–Pt(1)–Cl(2)#1	88.9(2)
N(1)–N(8)	1.36(2)	Cl(3)#1–Pt(1)–Cl(2)#1	90.0(1)
C(2)–N(3)	1.36(2)	Cl(3)–Pt(1)–Cl(2)#1	90.03(1)
N(3)–C(3A)	1.309(18)	Cl(1)#1–Pt(1)–Cl(2)	88.9(2)
C(3A)–N(4)	1.286(17)	Cl(1)–Pt(1)–Cl(2)	91.1(2)
C(3A)–N(8)	1.35(2)	Cl(3)#1–Pt(1)–Cl(2)	90.0(1)
N(4)–C(5)	1.40(3)	Cl(3)–Pt(1)–Cl(2)	90.0(1)
C(5)–C(6)	1.26(3)	Cl(2)#1–Pt(1)–Cl(2)	180.0(2)
C(5)–C(51)	1.55(2)	C(2)–N(3)–C(3A)	105.2(13)
C(6)–C(7)	1.53(3)	N(4)–C(3A)–N(3)	136.2(14)
C(7)–O(71)	1.16(2)	O(71)–C(7)–N(8)	127(2)
C(7)–N(8)	1.42(2)	O(71)–C(7)–C(6)	126(2)

Operators for generating equivalent atoms: # $[-x, 1-y, -z]$.

The valence geometry of the H_2mtpO$^+$ cation is similar to that reported for the HmtpO structures. However, few statistically significant differences have been found between the structure of the H_2mtpO$^+$ cation reported here and the HmtpO ligand coordinated to Pt via the N(3) atom in *cis*-$PtCl_2(NH_3)$(HmtpO) and *cis*-$PtCl_2$(HmtpO)$_2$·4H_2O [43]. In the structure reported here the distances N(1)–C(2) and C(3A)–N(4) [1.23(2) and 1.286(17) Å, respectively] are significantly shorter than the corresponding distances reported for the platinum complexes [1.301(7)–1.317(15) and 1.352(6)–1.362(12), respectively]. Also the valence angle N(1)–C(2)–N(3) of 116.1(17)° is larger than the equivalent angle in the HmtpO ligand (average 112.8°), while the N(3)–C(3A)–N(8) angle of 104.8(13)° is smaller than those reported for the complexes (average 108.2°). That seems to reflect the different electron density distribution within the pyrimidine ring moiety between the protonated and coordinated species.

There is a small bend of the H_2mtpO$^+$ ring system, with the dihedral angle between the best planes of the five-membered N(1)–C(2)–N(3)–C(3A)–N(8) and six-membered C(3A)–N(4)–C(5)–C(6)–C(7)–N(8) rings being 1.8(9)°.

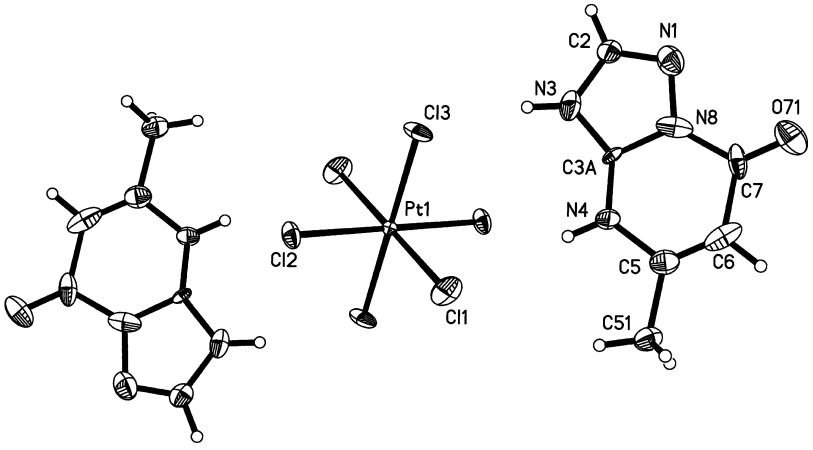

Fig. 4. ORTEP drawing with the atomic labelling scheme for $[H_2mtpO]_2[PtCl_6]$.

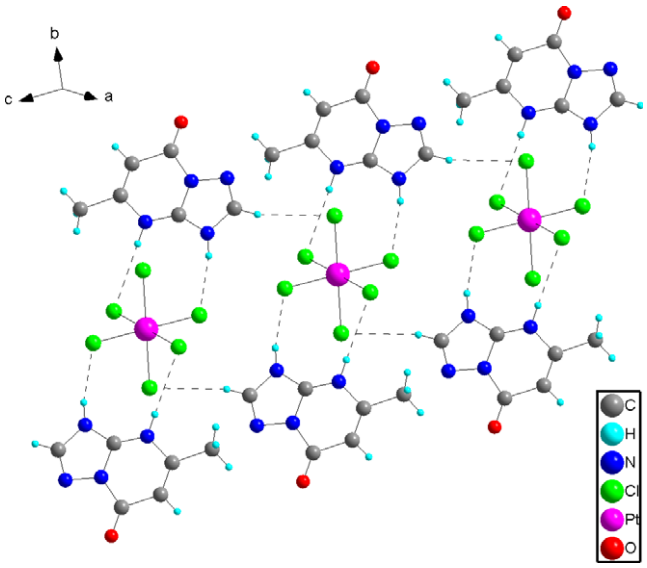

Fig. 5. Intermolecular hydrogen bonding in $[H_2mtpO]_2[PtCl_6]$.

The structure reveals the presence of two H-bonds involving both N–H groups of the ring moiety and chloride ions. The N(3)Cl(3) $[x+1,y,z+1]$ distance is 3.095(15) Å and the N(3)–H(3A)···Cl(3) $[x+1,y,z+1]$ angle is 167.5°. The corresponding values for the N(4)–H(4A)···Cl(1) $[x+1,y,z+1]$ interaction are 3.506(15) Å and 177.5°, respectively. These interactions link the complex anion with the pair of neighboring organic cations (Fig. 5). The C(2)–H group forms an interaction to Cl(2) $[-1+x,y,z]$, with a C(2)···Cl distance of 3.720(17) Å (Fig. 5).

Analysis of the interactions within the ion pair constituting the asymmetric unit of the reported structure reveals the relatively short distances between Cl(1) and the center of gravity of the five-membered ring and between Cl(2) and the center of gravity of the five-membered ring, being 3.520 and 3.769 Å respectively. Also the O(71) atom is positioned near the H_2mtpO^+ $[1/2+x,1/2-y,1/2+z]$ ring system, the distances to the centers of gravity of the five-membered and six-membered rings being 2.915 and 2.844 Å, respectively.

4. Conclusion

The observed monodentate coordination via N(3) may be regarded as representative for triazolopyrimidines and analogous to N(9) complexation in purine. The highest antitumor activities have been observed for platinum(IV) complexes contain a bulky *tert*-butyl group in the heterocycle ring. These results indicate that tetrachloride platinum(IV) complexes with bulky ligands might be a promising source of new metal-based antitumor activity. Perhaps this observation could serve as a reasonable basis for designing new antitumor platinum(IV) prodrugs.

Acknowledgement

This work was supported in part by Grant 551/Ch-CM from Nicolaus Copernicus University.

Appendix A. Supplementary data

CCDC 679071 contains the supplementary crystallographic data for (**5**). These data can be obtained free of charge via http://www.ccdc.cam.ac.uk/conts/retrieving.html, or from the Cambridge Crystallographic Data Centre, 12 Union Road, Cambridge CB2 1EZ, UK; fax: (+44) 1223-336-033; or e-mail: deposit@ccdc.cam.ac.uk. Supplementary data associated with this article can be found, in the online version, at doi:10.1016/j.poly.2008.05.032.

References

[1] P.J. O'Dwyer, J.P. Stevenson, S.W. Johnson, in: B. Lippert (Ed.), Cisplatin in Chemistry and Biochemistry of a Leading Anticancer Drug, Wiley-VCH, Weinheim, 1999, p. 31.
[2] K.M. Comess, S.J. Lippard, in: S. Neidle, M. Waring (Eds.), Molecular Aspects of Anticancer Drug-DNA Interaction, MacMillan, London, 1993, p. 134.
[3] E. Wong, C.M. Giandomenico, Chem. Rev. 99 (1999) 2451.
[4] J. Reedijk, PNAS 100 (2003) 3611.
[5] L. Ronconi, P.J. Sadler, Coord. Chem. Rev. 251 (2007) 1633.
[6] M.D. Hall, T.W. Hambley, Coord. Chem. Rev. 232 (2002) 49.
[7] H.-B. Kraatz, N. Metzel-Nolte, Concepts and Models in Bioinorganic Chemistry, Wiley-VCH Verlag GmbH & Co. KGaA, Weinheim, 2006.
[8] E.L. Weaver, R.N. Bose, J. Inorg. Biochem. 95 (2003) 231.
[9] S. Choi, C. Filotto, M. Bisanzo, S. Delaney, D. Lagasee, J.L. Whiworth, A. Jusko, Ch. Li, N.A. Wood, J. Willingham, A. Schwenker, K. Spaulding, Inorg. Chem. 37 (1998) 2500.
[10] T.W. Hambley, A.R. Battle, G.B. Deacon, E.T. Lawrenz, G.D. Fallon, B.M. Gatehouse, L.K. Webster, S. Rainone, J. Inorg. Biochem. 77 (1999) 3.
[11] L.T. Ellis, H.M. Er, T.W. Hambley, Aust. J. Chem. 48 (1995) 793.
[12] R. Song, K. Mook, Y.S. Sohn, Bull. Korean Chem. Soc. 21 (2000) 1000.
[13] M. Galanski, B.K. Keppler, Inorg. Chim. Acta 265 (1997) 271.
[14] T.J. Sabo, V.M. Dinović, G.N. Kaluderović, T.P. Stanojković, G.A. Bogdanović, Z.D. Juranić, Inorg. Chim Acta 358 (2005) 2239.
[15] H.J. Kim, K.M. Kim, R. Song, Y.S. Sohn, Inorg. Chim. Acta 358 (2005) 415.
[16] S.R.A. Khan, S. Huang, S. Shamsuddin, S. Inutsuka, K.H. Whitmire, Z.H. Siddik, A.R. Khokhar, Bioorg. Med. Chem. 8 (2000) 515.
[17] R. Song, S.Y. Park, Y.-S. Kim, Y. Kim, S.-J. Kim, B.T. Ahn, Y.S. Sohn, J. Inorg. Chem. 96 (2003) 339.
[18] A.R. Khokhar, S. Al-Baker, S. Shamsuddin, Z.H. Siddik, J. Med. Chem. 40 (1997) 112.
[19] S. Shimsuddin, C.C. Santillan, J.L. Stark, K.H. Whitmire, Z.H. Siddik, A.R. Khokhar, J. Inorg. Biochem. 71 (1998) 29.
[20] S. Shimsuddin, I. Takahashi, Z.H. Siddik, A.R. Khokhar, J. Inorg. Biochem. 61 (1996) 291.
[21] M.D. Hall, S. Amjadi, M. Zhang, P.J. Beale, T.W. Hambley, J. Inorg. Biochem. 98 (2004) 1614.
[22] J. Salas, M.A. Romero, M.P. Sanchez, M. Quiros, Coord. Chem. Rev. 193–195 (1999) 1119.
[23] J.A.R. Navarro, J.M. Salas, M.A. Romero, R. Vilaplana, F. Gonzáles-Vilchez, R. Faure, J. Med. Chem. 41 (1998) 332.
[24] I. Łakomska, E. Szłyk, J. Sitkowski, L. Kozerski, J. Wietrzyk, M. Pełczyńska, A. Nasulewicz, A. Opolski, J. Inorg. Biochem. 98 (2004) 167.
[25] C. Bülow, K. Haas, Berichte 42 (1909) 4638.
[26] A. Grodzicki, E. Szłyk, L. Pazderski, A. Goliński, Magn. Res. Chem. 34 (1996) 725.
[27] E. Szłyk, L. Pazderski, I. Łakomska, A. Surdykowski, T. Głowiak, J. Sitkowski, L. Kozerski, Polyhedron 21 (2002) 343.
[28] G.M. Sheldrick, T.M. Schneider, Methods Enzymol. 277B (1997) 319.
[29] P. Skehan, R. Storeng, D. Scudiero, A. Monks, J. McMahon, D. Vistica, J.T. Warren, H. Bokesch, S. Kenney, M.R. Boyol, J. Natl. Cancer. Inst. 82 (1990) 1107.
[30] I. Łakomska, L. Pazderski, J. Sitkowski, L. Kozerski, M. Pełczyńska, A. Nasulewicz, A. Opolski, E. Szłyk, J. Mol. Struct. 707 (2004) 241.
[31] A.S. Gaballa, J. Mol. Struct. 782 (2006) 204.
[32] M.S. Ali, J.H. Thurston, K.H. Whitmire, A.R. Khokhar, Polyhedron 21 (2002) 2659.
[33] B.M. Still, P.G.A. Kuman, J.R. Aldrich-Wright, W.S. Price, Chem. Soc. Rev. 36 (2007) 665.
[34] M. Quiros, J.M. Salas, M.P. Sanches, A.L. Beauchamp, X. Solans, Inorg. Chim. Acta 204 (1993) 213.
[35] R.M. Silverstein, F.X. Webster, Spectrometric Identification of Organic Compounds, John Wiley, New York, 1998, p. 103.
[36] K. Nakamoto, Infrared and Raman Spectra, pp. 147–148, 156.
[37] S. Shamsuddin, I. Takahashi, Z.H. Siddik, A.R. Khokhar, J. Inorg. Biochem. 61 (1996) 91.
[38] I. Łakomska, Inog. Chim. Acta (2008) accepted for publication.
[39] R.W. Berg, I. Sotofle, Acta Chem. Scand. A 32 (1978) 241.
[40] M.S.D. Elyouloi, M.H. Ben Ghozlen, Y. Milk, A. Daoud, Phys. Status Solidi A 98 (1986) 435.
[41] D.D. Makitova, O.N. Krasochka, L.V. Atormyan, I.P. Lavrentev, Yu.M. Shulga, L.V. Revenko, M.L. Khidekel, Koord. Khim. 13 (1987) 383.
[42] A. Terzis, D. Mentzafos, Inorg. Chem. 22 (1983) 1140.
[43] I. Łakomska, A. Wojtczak, J. Sitkowski, L. Kozerski, E. Szłyk, Polyhedron 26 (2007) 803.

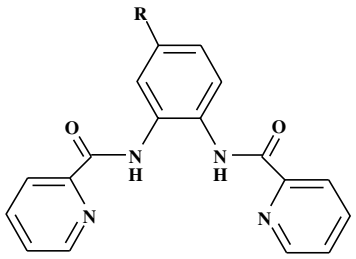

R	Ligand
CH_3	H_2Mebpb
Cl	H_2cbpb

Scheme 1.

of a representative complex, *trans*-[Co(Mebpb)(prldn)$_2$]ClO_4, has been determined. The IR, UV–Vis, and ^{1}H NMR spectra of the complexes are also reported and discussed. The electrochemical behavior of the complexes has also been investigated with the goal of evaluating the effects of axial ligation and equatorial substitution on their redox properties.

2. Experimental

2.1. Materials and general methods

All solvents and chemicals were of commercial reagent grade and used as received from Aldrich and Merck. Elemental analyses were performed by using a Perkin–Elmer 2400II CHNS-O elemental analyzer. UV–Vis spectra were recorded on a Jasco V-570 spectrophotometer. Infrared spectra (KBr pellets) were obtained on a Jasco 680-plus FT-IR spectrophotometer. The ^{1}H NMR spectra of the complexes were obtained on a Bruker AVANCE DR X500 (500 MHz) spectrometer. Proton chemical shifts are reported in parts per million (ppm) relative to an internal standard of Me_4Si. Cyclic voltammograms were recorded by using a Sama Research Analyzer M-500. Three electrodes were utilized in this system, a glassy carbon working electrode, a platinum disk auxiliary electrode, and Ag wire as reference electrode. The glassy carbon working electrode (Metrohm 6.1204.110) with 2.0 ± 0.1 mm diameter was manually cleaned with 1 μm alumina polish prior to each scan. Tetrabutylammonium hexafluorophosphate (TBAH) was used as supporting electrolyte. Acetonitrile was dried over CaH_2. The solutions were deoxygenated by purging with Ar for 5 min. All electrochemical potentials were calibrated versus internal $Fc^{+/0}$ (E^0 = 0.40 V versus SCE) couple under the same conditions [32].

Caution: Perchlorate salts with organic compounds are potentially explosive and should be handled with care.

2.2. Synthesis

2.2.1. H_2Mebpb

4-Methyl-1,2-phenylenediamine was recrystallized from hot ligroin before use. The ligand was prepared according to the method described in the literature with some modification [18]. To a solution of 2-pyridinecarboxylic acid (7.38 g, 60 mmol) in pyridine (25 mL) in a two-necked round-bottom flask equipped with mechanical stirrer was added a solution of 4-methyl-1,2-phenylenediamine (3.66 g, 30 mmol) in 5 mL pyridine, and the mixture stirred at 40 °C for 40 min. Triphenylphosphite (15.6 mL, 60 mmol) was then added dropwise and the reaction mixture was stirred at 90–100 °C for 4 h. Upon cooling to room temperature the product precipitated as a microcrystalline solid. The resulting precipitate was filtered off, washed with ethanol (20 mL), and recrystallized from a mixture of methanol and water (2:1 v/v). Yield (70%). m.p. 168–169 °C. FT-IR (KBr, cm^{-1}) ν_{max}: 3302 (s, N–H), 1689, 1659 (s, C=O), 1589 (m, C=C), 1520 (m, C–N). UV–Vis: λ_{max} (nm) (ε, L M^{-1} cm^{-1}) (CH_3CN): 300 (9427), 267 (15662), 219 (26563).

2.2.2. H_2cbpb

H_2cbpb was synthesized by a procedure similar to that for H_2Mebpb, but 4-chloro-1,2-phenylenediamine was used instead of 4-methyl-1,2-phenylenediamine. The product was recrystallized from ethanol. Yield (70%). m.p. 196–198 °C. *Anal.* Calc. for $C_{18}H_{13}N_4O_2Cl$: C, 61.28; H, 3.71; N, 15.88. Found: C, 61.28; H, 3.61; N, 15.81%. FT-IR (KBr, cm^{-1}) ν_{max}: 3297 (s, N–H), 1697, 1661 (s, C=O), 1588 (m, C=C), 1506 (s, C–N). UV–Vis: λ_{max} (nm) (ε, L M^{-1} cm^{-1}) (CH_3CN): 300 (10735), 267 (18627), 211 (35942). ^{1}H NMR ($CDCl_3$, 300 MHz): δ = 10.32, 10.19 (2H, NH_{amidic}, s), 8.56 (2H_a, dd, J = 9.8, 4.4), 8.31 (2H_d, d, J = 7.8), 8.03 (1H_g, d, J = 7.8), 7.92 (2H_c, dd, J = 7.7, 7.7), 7.81 (1H_e, d, J = 8.6), 7.48 (2H_b, m), 7.26 (1H_f, d, J = 8.0).

2.2.3. Synthesis of trans-[Co(Mebpb)(prldn)$_2$] ClO_4 (**1a**)

To a solution of $Co(CH_3COO)_2 \cdot 4H_2O$ (62.3 mg, 0.25 mmol) in methanol (20 mL) was added a boiling solution of H_2Mebpb (83.1 mg, 0.25 mmol) in methanol (30 mL). To this solution was added dropwise 9.07 mmol (0.75 mL) of pyrrolidine and air was bubbled through the reaction mixture for 3 h. The final reaction mixture was filtered, a solution of 0.25 mmol (30.6 mg) of $NaClO_4 \cdot H_2O$ in methanol was slowly added to the filtrate, and the resulting solution was stirred for 5 min. Dark blue crystals were obtained by slow evaporation of methanol. The crystals were isolated by filtration, washed with methanol, and dried in vacuum. Yield: 75%. *Anal.* Calc. for $C_{27}H_{32}N_6O_6ClCo$: C, 51.4; H, 5.11; N, 13.32. Found: C, 50.73; H, 5.29; N, 13.11%. FT-IR (KBr, cm^{-1}) ν_{max}: 3168 (s, N–H), 1626 (s, C=O), 1599 (s, C=C), 1571 (s, C–N), 1109, 1087 (s, Cl–O). UV–Vis: λ_{max} (nm) (ε, L M^{-1} cm^{-1}) (CH_3CN): 625 (180), 418 (6686). ^{1}H NMR (CD_3CN, 500 MHz): δ = 1.29 (8H_i, m), 1.55, 2.12 (8H_h, m), 2.39 (3H, CH_3, s), 3.30 (2H, amine NH, br s), 6.94 (1H_f, d, J = 8.2), 8.00–8.39 (6H $_{b,c,d}$, m), 8.71 (1H_g, s), 8.75 (1H_e, d, J = 8.2), 9.46 (2H_a, dd, 5.2, 5.2).

2.2.4. Synthesis of trans-[Co(cbpb)(prldn)$_2$] PF_6 (**1b**)

To a solution of $Co(CH_3COO)_2 \cdot 4H_2O$ (62.3 mg, 0.25 mmol) in methanol–ethanol (2:1 v/v) (20 mL) was added a boiling solution of H_2cbpb (88.2 mg, 0.25 mmol) in methanol–ethanol (2:1 v/v) (30 mL). To this solution was added dropwise 9.07 mmol (0.75 mL) of pyrrolidine and air was bubbled through the reaction mixture for 3 h. The volume of the reaction mixture was increased to 75 mL by adding methanol and the final solution was filtered. A solution of 0.25 mmol (40.6 mg) of ammonium hexafluorophosphate in methanol–ethanol (2:1v/v) (25 mL) was slowly added to the filtrate and the resulting solution stirred for 5 min. Green-blue crystals were obtained by slow evaporation of solvent. The crystals were isolated by filtration, washed with cold methanol, and dried in vacuum. Yield: 75%. *Anal.* Calc. for $C_{29}H_{29}N_6O_2ClPF_6Co$: C, 44.81; H, 4.19; N, 12.05. Found: C, 44.54; H, 4.09; N, 11.91%. FT-IR (KBr, cm^{-1}) ν_{max}: 3171 (s, N–H), 1629 (s, C=O), 1600 (s, C=C), 1563 (s, C–N), 842 (s, PF_6). UV–Vis: λ_{max} (nm) (ε, L M^{-1} cm^{-1}) (CH_3CN): 611 (188), 410 (7354). ^{1}H NMR (CD_3CN, 500 MHz): δ = 1.30 (8H_i, m), 1.52, 2.12 (8H_h, m), 3.28 (2H, NH_{amine}, br s), 7.11 (1H_f, bd, J = 8.6), 7.99–8.41 (6$H_{b,c,d}$, m), 8.82–8.83 (2H, H_e, H_g), 9.42 (2H_a, bd, J = 4.8).

2.2.5. Synthesis of trans-[Co(Mebpb)(pprdn)$_2$]ClO_4 (**2a**)

To a solution of $Co(CH_3COO)_2 \cdot 4H_2O$ (62.3 mg, 0.25 mmol) in 20 mL ethanol–methanol (1:2 v/v) was added a boiling solution of H_2Mebpb (83.1 mg, 0.25 mmol) 30 mL ethanol–methanol (1:2

v/v). To this solution was added dropwise 7.58 mmol (0.75 mL) of piperidine and air was bubbled through the reaction mixture for 3 h. The final reaction mixture was filtered and a solution of 0.25 mmol (30.6 mg) of $NaClO_4 \cdot H_2O$ in methanol was added slowly to the filtrate. Dark green-blue crystals were obtained by slow evaporation of solvent. The crystals were isolated by filtration, washed with a mixture of ethanol and methanol (1:2 v/v), and dried in vacuum. Yield: 80%. *Anal.* Calc. for $C_{29}H_{36}N_6O_6ClCo$: C, 52.85; H, 5.51; N, 12.75. Found: C, 52.32; H, 6.1; N, 12.2%. FT-IR (KBr, cm^{-1}) ν_{max}: 3162 (s, N–H), 1626 (s, C=O), 1599 (s, C=C), 1565 (s, C–N), 1111, 1087 (s, Cl–O). UV–Vis: λ_{max} (nm) (ε, $L\,M^{-1}\,cm^{-1}$) (CH_3CN): 682 (193), 417 (6532). ^1H NMR (CD_3CN, 500 MHz): δ = 0.91–1.28 ($12H_{i,j}$, m), 1.40–2.22 ($8H_h$, m), 2.39 (3H, CH_3, s), 2.45 (2H, NH_{amine}, br s), 6.93 ($1H_f$, d, J = 7.9), 8.00–8.41 ($6H_{b,c,d}$, m), 8.71 (H_g, s), 8.75 (H_e, d, 8.2) 9.39 ($2H_a$, br d, J = 5.0).

2.2.6. Synthesis of trans-[Co(cbpb)(pprdn)$_2$]PF_6 (**2b**)

This complex was prepared by the same method as for **1b** except that piperidine was used instead of pyrrolidine. Dark green-blue crystals were obtained after 5 days; they were filtered off, washed with a small amount of cold methanol, and dried in vacuum. Yield: 65%. *Anal.* Calc. for $C_{28}H_{33}N_6O_2ClPF_6Co$: C, 46.39; H, 4.58; N, 11.59. Found: C, 45.52; H, 4.52; N, 11.25%. FT-IR (KBr, cm^{-1}) ν_{max}: 3173 (s, N–H), 1627 (s, C=O), 1600 (s, C=C), 1562 (s, C–N), 841 (s, PF_6). UV–Vis: λ_{max} (nm) (ε, $L\,M^{-1}\,cm^{-1}$) (CH_3CN): 656 (205), 409 (7434). ^1H NMR (CD_3CN, 500 MHz): δ = 0.9–1.29 ($12H_{i,j}$, m), 1.35–2.22 ($8H_h$, m), 2.47 (2H, NH_{amine}, br s), 7.12 ($1H_f$, d, J = 8.6), 7.95–8.45 ($6H_{b,c,d}$, m), 8.83–8.87 (2H, H_e, H_g), 9.36 ($2H_a$, br d, J = 4.8).

2.2.7. Synthesis of trans-[Co(Mebpb)(mrpln)$_2$] ClO_4 (**3a**)

To a solution of $Co(CH_3COO)_2 \cdot 4H_2O$ (62.3 mg, 0.25 mmol) in methanol (5 mL) was added a solution of H_2Mebpb (83.1 mg, 0.25 mmol) in acetone (50 mL). To this solution was added dropwise morpholine (8.61 mmol, 0.75 mL) and air was bubbled through the reaction mixture for 3 h. The final reaction mixture was filtered and a solution of 0.25 mmol (30.6 mg) of $NaClO_4 \cdot H_2O$ in acetone was added slowly to the filtrate. Dark green-blue crystals were isolated by filtration, washed with a mixture of acetone and methanol (1:9 v/v), and dried in vacuum. Yield: 70%. *Anal.* Calc. for $C_{27}H_{32}N_6O_8ClCo$: C, 48.92; H, 4.86; N, 12.68. Found: C, 48.01; H, 5.18; N, 12.64%. FT-IR (KBr, cm^{-1}) ν_{max}: 3141 (m, N–H), 1626 (s, C=O), 1599 (s, C=C), 1566 (m, C–N), 1111, 1091 (s, Cl–O). UV–Vis: λ_{max} (nm) (ε, $L\,M^{-1}\,cm^{-1}$) (CH_3CN): 689 (198), 412 (8134). ^1H NMR (CD_3CN, 500 MHz): δ = 1.65–1.95 ($8H_h$, overlaps with solvent signals), 2.39 (3H, CH_3, s), 2.97 (2H, NH_{amine}, br s), 3.20 ($8H_i$, m), 6.95 ($1H_f$, d, J = 7.9), 8.02–8.44 ($6H_{b,c,d}$, m), 8.73 ($1H_g$, s), 8.75 ($1H_e$, d, J = 8.2), 9.42 ($2H_a$, br d, J = 4.9).

2.2.8. Synthesis of trans-[Co(cbpb)(mrpln)$_2$] ClO_4 (**3b**)

To a solution of $Co(CH_3COO)_2 \cdot 4H_2O$ (24.9 mg, 0.1 mmol) in methanol–ethanol (2:1 v/v) (20 mL) was added a solution of H_2cbpb (35.3 mg, 0.1 mmol) in methanol–ethanol (2:1 v/v) (30 mL). To this solution was added dropwise morpholine (8.61 mmol, 0.75 mL) and air was bubbled through the reaction mixture for 3 h. The volume of the reaction mixture was increased to 75 mL by adding methanol and the final solution was filtered. A solution of 0.1 mmol (12.2 mg) of $NaClO_4 \cdot H_2O$ in methanol–ethanol (2:1 v/v) (25 mL) was slowly added to the filtrate and the resulting solution stirred for 5 min. Green-blue crystals were obtained by slow evaporation of solvent. The crystals were isolated by filtration, washed with mixture of diethyl ether and methanol (1:9 v/v) and dried in vacuum. Yield: 65%. *Anal.* Calc. for $C_{26}H_{29}N_6O_8Cl_2Co$: C, 45.69; H, 4.28; N, 12.29. Found: C, 45.35; H, 4.29; N, 12.00%. FT-IR (KBr, cm^{-1}) ν_{max}: 3169 (m, N–H), 1626 (s, C=O), 1600 (s, C=C), 1562 (s, C–N), 1119, 1089 (s, ClO_4). UV–Vis: λ_{max} (nm) (ε, $L\,M^{-1}\,cm^{-1}$) (CH_3CN): 663 (232), 405 (7061). ^1H NMR (CD_3CN, 500 MHz): δ = 1.61, 2.98 ($8H_h$, m), 3.55 (2H, NH_{amine}, br s), 3.21 ($8H_i$, m), 7.09 ($1H_f$, m), 7.81–8.48 ($6H_{b,c,d}$, m), 8.82–8.91 ($2H_{e,g}$, m), 9.39 ($2H_a$, br d, J = 4.8).

2.2.9. Synthesis of trans-[Co(Mebpb)(bzlan)$_2$] ClO_4 (**4a**)

To a solution of $Co(CH_3COO)_2 \cdot 4H_2O$ (24.9 mg, 0.1 mmol) in methanol (20 mL) was added a boiling solution of H_2 Mebpb (33.2 mg, 0.1 mmol) in methanol (30 mL). To this solution was added dropwise 6.86 mmol (0.75 mL) benzylamine and air was bubbled through the reaction mixture for 3 h. The final reaction mixture was filtered and a solution of 0.1 mmol (12.2 mg) of $NaClO_4 \cdot H_2O$ in methanol was added slowly to the filtrate. Dark green-blue crystals were isolated by filtration, washed with a mixture of ethanol and diethyl ether (9:1 v/v), and dried in vacuum. Yield: 65%. *Anal.* Calc. for $C_{33}H_{32}N_6O_6ClCo$: C, 56.38; H, 4.59; N, 11.95. Found: C, 56.10; H, 4.52; N, 11.84%. FT-IR (KBr, cm^{-1}) ν_{max}: 3251, 3214, 3135 (m, m, s, N–H), 1628 (s, C=O), 1601 (s, C=C), 1566 (s, C–N), 1094, 1081 (s, Cl–O). UV–Vis: λ_{max} (nm) (ε, $L\,M^{-1}\,cm^{-1}$) (CH_3CN): 610 (235), 414 (7013). ^1H NMR (CD_3CN, 500 MHz): δ = 2.42 (3H, CH_3, s), 2.74 ($4H_h$, m), 2.91 (4H, NH_{2amine}, br s), 6.74 ($4H_i$, bd), 7.09–7.15 ($6H_{j,k}$, m), 6.96($1H_f$,d, J = 8.2), 7.94–8.35 ($6H_{b,c,d}$, m), 8.75 ($1H_g$, s), 8.78 ($1H_e$, d, J = 8.2), 9.41 ($2H_a$, dd, J = 4.6, 4.6, 4.6).

2.2.10. Synthesis of trans-[Co(cbpb)(bzlan)$_2$] PF_6 (**4b**)

This complex was prepared by the same method as for **1b** except that benzylamine was used instead of pyrrolidine. Dark green-blue crystals were obtained after one week; they were filtered off, washed with a mixture of ethanol and diethyl ether (9:1 v/v), and dried in vacuum. Yield: 65%. *Anal.* Calc. for $C_{32}H_{29}N_6O_2ClPF_6Co$: C, 49.98; H, 3.80; N, 10.93. Found: C, 49.11; H, 3.80; N, 10.66%. FT-IR (KBr, cm^{-1}) ν_{max}: 3213, 3133 (m, N–H), 1629 (s, C=O), 1601 (s, C=C), 1562 (s, C–N), 843 (s, PF_6). UV–Vis: λ_{max} (nm) (ε, $L\,M^{-1}\,cm^{-1}$) (CH_3CN): 607 (224), 408 (7210). ^1H NMR (CD_3CN, 500 MHz): δ = 2.74 ($4H_h$, m), 3.05 (4H, NH_{2amine}, br s), 6.75 ($4H_i$, bd, 7.6), 7.05–7.16 ($7H_{j,k,f}$, m), 7.96–8.33 ($6H_{b,c,d}$, m), 8.73–8.76 ($2H_{e,g}$, m), 9.41 ($2H_a$, br d).

2.3. X-ray crystallography

Dark blue crystals of **1a** suitable for X-ray crystallography were obtained from methanol. Data were collected at 150 K, on a Nonius KappaCCD diffractometer (Mo Kα radiation, λ = 0.71069 Å) using

Table 1
Crystal data and structure refinement for (**1a**)

Chemical formula	$[C_{27}H_{32}CoN_6O_2]^+ClO_4^-$
Formula weight	631.0
Crystal system	triclinic
Space group	$P\bar{1}$
a (Å)	9.382(5)
b (Å)	11.788(5)
c (Å)	13.361(5)
α (°)	84.155(5)
β (°)	81.886(5)
γ (°)	82.339(5)
V (Å^3)	1444.6(11)
Z, D_{Calc} (g cm^{-3})	2, 1.451
Crystal size (mm)	0.40 × 0.40 × 0.35
μ (mm^{-1})	0.738
Reflections collected	29046
Independent reflections (R_{int})	5671 (0.0293)
Transmission factors	0.757–0.782
Refined parameters	381
Goodness-of-fit on F^2	1.108
R ($F^2 > 2\sigma$)	0.0680
R_w (F^2, all data)	0.2070
Maximum and minimum electron density (e Å^{-3})	1.89 and −1.22

the COLLECT [33] program. Cell refinement and data reduction were performed with EVALCCD [34]. Crystal data, together with other relevant information on structure determination, are listed in Table 1. An empirical absorption correction, based on repeated and equivalent reflections, was carried out using SADABS [35]. The structure was solved by SIR97 [36] and refined, against F^2, by SHELXTL [37]. Anisotropic displacement parameters were assigned to all the non-hydrogen atoms. Hydrogen atoms were placed in idealized positions and allowed to ride on their respective parent atoms. The major residual electron density features are close to the anion, which is probably subject to unresolved disorder.

3. Results and discussion

3.1. Synthesis

All complexes were prepared by the following general method. To a solution of $Co(CH_3COO)_2 \cdot 4H_2O$ in an appropriate solvent was added an equimolar amount of ligand in an appropriate solvent. A vigorous stream of air was passed through this solution, to which was gradually added excess amine. The air oxidation was continued for a period of 3 h, during which the color changed from red-brown to green-blue. Dark green-blue crystals of these complexes were obtained in good yield (65–80%).

3.2. Description of structure of trans-[Co(Mebpb)(prldn)$_2$]ClO$_4$ (**1a**)

To the best our knowledge, this is only the second reported structure of a $[Co^{III}(bpb)(amine)_2]^+$ complex containing neutral *N*-donor axial ligands. Fig. 1 shows the molecular structure of **1a** with the atomic numbering scheme. The structure exhibits a distorted octahedral environment around cobalt. Selected bond angles and distances are listed in Table 2. As expected, the ligand ($Mebpb^{2-}$) in **1a** binds to the trivalent metal ion (Co^{III}) via two pyridine N atoms and two amido N atoms in the equatorial plane of the octahedron. There are two pyrrolidine molecules attached to the metal to fill its axial sites. All Co–N bond distances are within the range

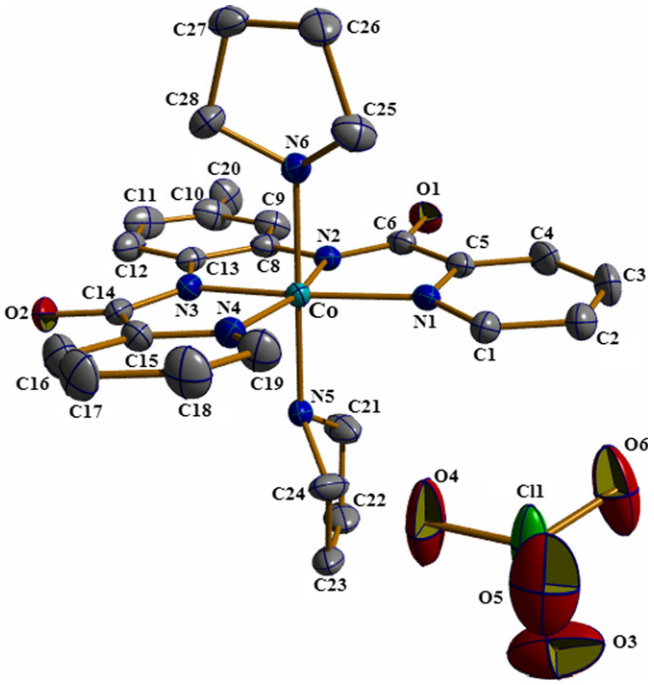

Fig. 1. The asymmetric unit of complex **1a** with the atom labeling scheme. Displacement ellipsoids are drawn at the 50% probability level; H atoms are omitted for clarity.

Table 2
Selected bond lengths (Å) and angles (°) for (**1a**)

Bond lengths	
Co–N1	1.997(3)
Co–N2	1.892(3)
Co–N3	1.892(3)
Co–N4	1.994(3)
Co–N5	1.992(3)
Co–N6	2.012(3)
Bond angles	
N1–Co–N2	82.88(13)
N1–Co–N3	166.85(14)
N1–Co–N4	110.63(13)
N1–Co–N5	90.16(13)
N1–Co–N6	89.36(13)
N2–Co–N3	84.10(14)
N2–Co–N4	166.28(13)
N2–Co–N5	92.86(13)
N2–Co–N6	88.43(13)
N3–Co–N4	82.46(14)
N3–Co–N5	88.69(13)
N3–Co–N6	92.08(13)
N4–Co–N5	89.59(13)
N4–Co–N6	89.32(13)
N5–Co–N6	178.57(13)

1.892(3)–2.012(3) Å, and are indicative of a low-spin $(t_{2g})^6$ configuration of the central Co^{III} ion [22].

Of the four Co–N bonds in the equatorial plane, the Co–N_{amide} bond distances [Co–N2 = 1.892(3) Å and Co–N3 = 1.892(3) Å], which are comparable to the Co–N_{amide} values [1.885(2) Å and 1.891(1) Å] in *trans*-[Co^{III}(bpb)(prldn)$_2$]NCS, are indicative of strong bonding between the deprotonated amide nitrogens and the cobalt center. This is in agreement with the fact that the deprotonated amide nitrogen is a very strong σ-donor. The deprotonated mode of coordination of the amide nitrogen atoms is also evident from the absence of the amide proton signals in the ^{1}H NMR spectrum of complex **1a** (*vide infra*). The bond distances to the pyridine nitrogen atoms [Co–N1 = 1.997(3) Å and Co–N4 = 1.994(3) Å] are longer than those to N2 and N3, which is in accord with the lower donor ability of the pyridine nitrogen atoms. The N–Co–N bond angles in the equatorial plane consist of one which is larger than 90° [N1–Co–N4 = 110.63(13)°] and three smaller bite angles [N1–Co–N2 = 82.88(13)°, N2–Co–N3 = 84.10(14)°, and N3–Co–N4 = 82.46(14)°]. This indicates that there might be some strain in the coordination due to the rigid geometry of the ligand. The dihedral angle between the two pyridyl rings of the ligand is 15.0°. The dihedral angles between the central benzene plane and the two pyridyl rings are 10.7° and 5.5°. This observation can be attributed to the close intramolecular contact that occurs between the two H atoms in the 6-positions of the pyridyl rings; the H1···H18 distance of 2.05 Å is significantly less than the sum of the van der Waals radii (2.40 Å). The effect would be expected to be more pronounced if the ligand were perfectly planar [38]. The C–O, $C_{pyridyne}$–N, and $C_{carboxy}$–N bond distances agree well with those reported for related complexes [16,20,39–41].

All *cis* N_{eq}–Co–N_{ax} bond angles are within 3° of the ideal right-angle. The *trans*-axial N5–Co–N6 unit with a bond angle of 178.57(13)° is essentially linear. The distances between the cobalt atom and the two axial nitrogen donor atoms differ only slightly [Co–N5 = 1.992(3) Å and Co–N6 = 2.012(3) Å] and compare well with the Co–N distances found in *trans*-[Co^{III}(bpb)(prldn)$_2$]NCS [25].

A further interesting feature of the structure of **1a** is the intermolecular hydrogen bonding (Table 3). The structure consists of chains of cations linked by rather strong N–H···O=C hydrogen bonds zig-zagging along the *c* axis (Fig. 2); the anions are not involved in hydrogen bonding.

Table 3
Hydrogen bond lengths (Å) and angles (°) for (**1a**)

D–H···A	D–H (Å)	H···A (Å)	D···A (Å)	D–H···A (°)
N5–H5···O2A	0.83(5)	2.06(5)	2.847(4)	159(4)
N6–H6···O1B	0.87(5)	2.07(5)	2.896(4)	158(4)

Symmetry operations for equivalent atoms: (A) $1-x$, $1-y$, $1-z$ and (B) $1-x$, $1-y$, $-z$.

3.3. Spectroscopic studies

The octahedral geometry of complex **1a** is evident from the X-ray structure analysis (Fig. 1). An octahedral *trans* structure for other complexes (**2a**–**4a**, **1b**–**4b**) can be inferred based on the similarity of the spectroscopic data of these complexes with those of complex **1a**. The FT-IR data of the complexes are listed in Section 2. Meaningful information regarding the bonding sites of the ligand molecules can be obtained by comparing the IR spectra of the cobalt complexes with those of the uncomplexed ligands. In the IR spectra of H_2Mebpb and H_2cbpb a band characteristic of the NH group is observed in the 3295–3305 cm^{-1} region. The disappearance of this band in the IR spectra of the complexes confirms that the ligands coordinate in their deprotonated form [17]. The bands corresponding to the amine N–H stretching vibrations are shifted to lower frequencies by about 98–265 cm^{-1} relative to the uncoordinated amines, which is in accord with expectation. Two sharp C=O stretching vibration bands at 1689 and 1659 cm^{-1} for H_2Mebpb and 1661 and 1697 cm^{-1} for H_2cbpb are shifted to lower frequencies upon coordination of the deprotonated amide, which is in agreement with the data reported for related complexes [31]. The C–N stretching vibration of medium intensity appearing at 1520 cm^{-1} for H_2Mebpb and at 1506 cm^{-1} for H_2cbpb undergoes a significant shift to higher frequencies in the corresponding complexes. This displacement is to be expected because of the resonance enhancement in the deprotonated amide which in turn leads to strengthening of the C–N bond [17]. The stretching vibrations due to the perchlorate and hexafluorophosphate anions appear in the 1080–1120 cm^{-1} and 840–846 cm^{-1} regions, respectively [42].

The UV–Vis data are presented in the Experimental section. The electronic spectra of the *trans*-[Co^{III}(Mebpb)(amine)$_2$]ClO_4 complexes (**1a**–**4a**) consist of ligand field transitions with low intensity ($180 < \varepsilon < 235$) which, depending on the axial amine ligand field strength, appear in the 610–689 nm region, and intense LMCT

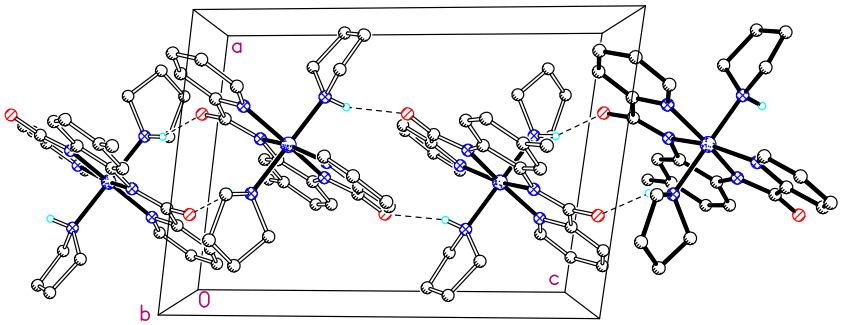

Fig. 2. A view, along the *b* axis, of the packing of **1a**. Hydrogen bonding is shown as dashed lines. Anions have been omitted, together with H atoms not involved in the hydrogen bonding.

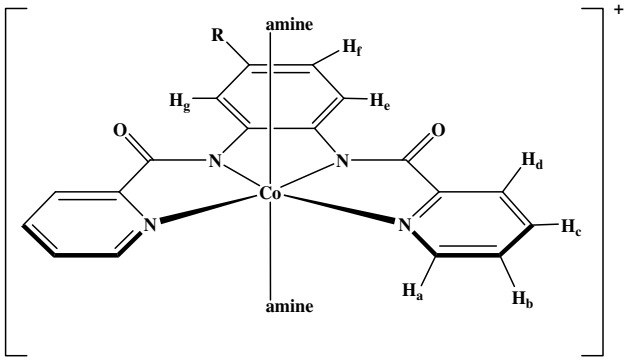

Amine	Compound	
	R	
	CH_3	Cl
Pyrrolidine	*1a*	*1b*
Piperidine	*2a*	*2b*
Morpholine	*3a*	*3b*
Benzylamine	*4a*	*4b*

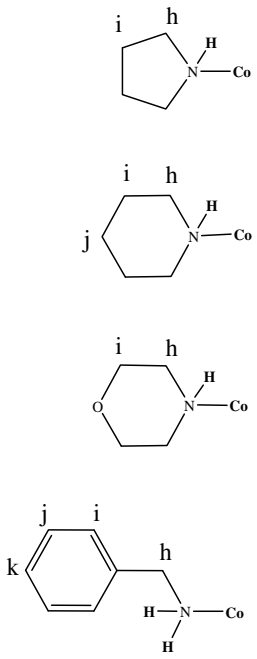

Scheme 2.

transitions appearing in the 412–418 nm region. Similar transitions have been observed in the electronic absorption spectra of *trans*-[Co^{III}(cbpb)(amine)$_2$]X complexes (**1b–4b**) with a blue shift of about 3–25 nm in the position of all the absorption bands relative to those of *trans*-[Co^{III}(Mebpb)(amine)$_2$]ClO_4 complexes (d–d transitions, 607–656 nm and CT transitions, 405–410 nm).

The ^{1}H NMR spectroscopic measurements were performed on samples in CD_3CN and $CDCl_3$ solutions. Scheme 2 displays the labeling system. The assignments are based on comparisons with corresponding rhodium(III), iridium(III), organocobalt(III) and ruthenium(II) complexes and by integrated area ratios [17,18,43–45].

The absence of the amido N–H resonance in the spectra of the complexes indicates that the ligand is coordinated to cobalt in its deprotonated form. The proton signals of the equatorial amide ligand in the complexes are generally shifted downfield relative to the free ligand. As expected, the most significant downfield shifts correspond to the protons *ortho* to the pyridyl nitrogen, H_a, and *ortho* to the nitrogen substituent on the diamido benzene group, $H_{e,g}$ [44]. The broad doublet of doublet at *ca.* δ = 9.39–9.46 is assigned to H_a.

Although the chemical shifts of H_f were found to be virtually unaffected by the axial ligand, chemical shifts of $H_{e,g}$ and H_a of the cobalt complexes varied significantly. In general, δ ($H_{e,g}$) changes in the same direction as δ (H_a) but to a larger extent. The changes in the chemical shift of H_c and H_d are in line with the donor ability of the axial ligands and the UV–Vis spectral data. The trend observed in δ (H_c, H_d) for complexes **1a–4a**, bzlan > prldn > pprdn > mrpln, conforms to the σ-donating strength of the axial ligands, which in turn is evident from the electrochemistry of these complexes.

The appearance of the signals due to the amine protons indicates the coordination of two amine ligands in the axial positions. Aside from the aromatic protons of benzylamine which appear at about 6.74–7.12 ppm, other proton resonances of the axial amines appear between about 0.91 and 3.55 ppm.

The ^{1}H NMR spectra of *trans*-[Co^{III}(cbpb)(amine)$_2$]$^+$ complexes (**1b–4b**) show features similar to those observed for *trans*-[Co^{III}-(Mebpb)(amine)$_2$]$^+$ complexes. As expected, the protons on the benzene ring exhibit slight downfield shifts in the peak positions in the [Co^{III}(cbpb)(amine)$_2$]$^+$ complexes, demonstrating the electron-withdrawing effect of chloro substitution in the equatorial $cbpb^{2-}$ ligand.

3.4. Electrochemistry

Cyclic voltammograms of the ligands and complexes in acetonitrile solutions with 0.1 M [N(*n*-Bu)$_4$]PF_6 as the supporting electrolyte were recorded at a glassy carbon working electrode. The approximate concentrations of the compounds were 1×10^{-3}–10^{-6} M.

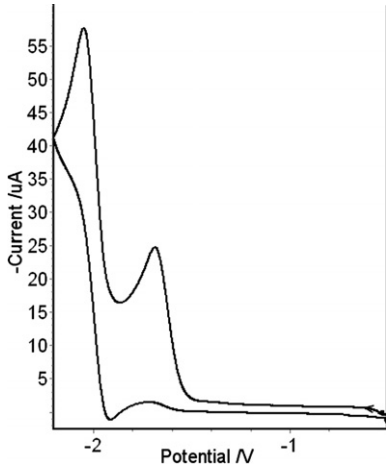

Fig. 3. Cyclic voltammogram of H_2Mebpb ligand in acetonitrile solution at 298 K. Scan rate: 100 mV s^{-1}, $c = 2.8 \times 10^{-3}$ M.

3.4.1. Electrochemistry of the ligands

The cyclic voltammograms of the ligands and their complexes were conducted at 25 °C under an argon atmosphere. It is evident from the cyclic voltammogram of H_2Mebpb, displayed in Fig. 3, that the ligand is electroactive over a range from −0.5 to −2.2 V. Two ligand-centered reductions are observed at −1.89 V and −2.2 V (Fig. 3). These reductions are attributed to the pyridyl rings and are shifted to more positive values in the corresponding complexes (Table 4). The tendency of the ligand towards reduction is apparently increased due to the transfer of electron density to the metal center [46].

The cyclic voltammogram of H_2cbpb shows features similar to those observed for H_2bpb, with an anodic shift in the peak positions resulting from the electron-withdrawing nature of the chloro substitution in the H_2cbpb ligand.

3.4.2. Electrochemistry of the complexes in the absence of amines

The reduction potentials for the cobalt complexes are summarized in Table 4. The cyclic voltammogram of the representative complex, *trans*-[Co^{III}(Mebpb)(pprdn)$_2$]ClO_4 (**2a**), is shown in Fig. 4a. An interesting observation in the cyclic voltammetric measurements of these cobalt(III) complexes is the presence of a nearly reversible oxidative response in the range of $E_{1/2}$ = 0.98–1.01 V (Fig. 4, Table 4) (the first oxidation process, which can be assigned as mainly ligand-centered, occurs at virtually identical potentials).

The next reduction peak observed over the range of −0.31 to −0.53 V in (**1a–4a)** complexes, and −0.22 to −0.49 V in (**1b–4b)** complexes, is metal-centered. This is supported by the relative sensitivity of Co^{III}/Co^{II} reduction potentials to the nature of the axial amine ligand. From the E_{pc1} values (Table 4), it is evident that

Table 4
Redox potentials of (**1a–4a**) and (**1b–4b**) cobalt complexes in acetonitrile[a]

No.	Compound	$E_{1/2}$[b]	Epc1	Epa1	Epc2	Epa2	Epc3	Epa3	Epc4	Epa4
1a	[Co(Mebpb)(Prldn)$_2$]ClO_4	1.01	−0.53	−0.14		−1.28	−1.42		−2.08	−2.0
2a	[Co(Mebpb)(Pprdn)$_2$]ClO_4	1.03	−0.42	−0.01		−1.24	−1.39		−2.06	−1.99
3a	[Co(Mebpb)(Mrpln)$_2$]ClO_4	1.04	−0.31	0.03		−1.23	−1.40		−2.09	−2.01
4a	[Co(Mebpb)(Bzlan)$_2$]ClO_4	0.98	−.049	−0.05		−1.26	−1.38		−2.05	−1.97
1b	[Co(cbpb)(Prldn)$_2$]PF_6	1.16	−0.48	−0.13	−1.28	−1.19	−1.41	−1.32	−2.00	−1.92
2b	[Co(cbpb)(Pprdn)$_2$]PF_6	1.16	−0.35	−0.06	−1.23	−1.17	−1.38	−1.32	−2.00	−1.92
3b	[Co(cbpb)(Mrpln)$_2$]ClO_4	1.19	−0.22	0.33	−1.24	−1.15	−1.35	−1.31	−2.00	−1.93
4b	[Co(cbpb)(Bzlan)$_2$]PF_6	1.12	−0.49	−0.002	−1.25	−1.13	−1.43	−1.32	−2.01	−1.92

[a] Potentials are vs. $Fc^{+/0}$ in 0.1 M TBAH, T = 293 K. Scan rate 100 mV/s. Approximate concentrations: 1×10^{-3}–10^{-6} M.
[b] $E_{1/2} = 0.5(E_c + E_a)$.

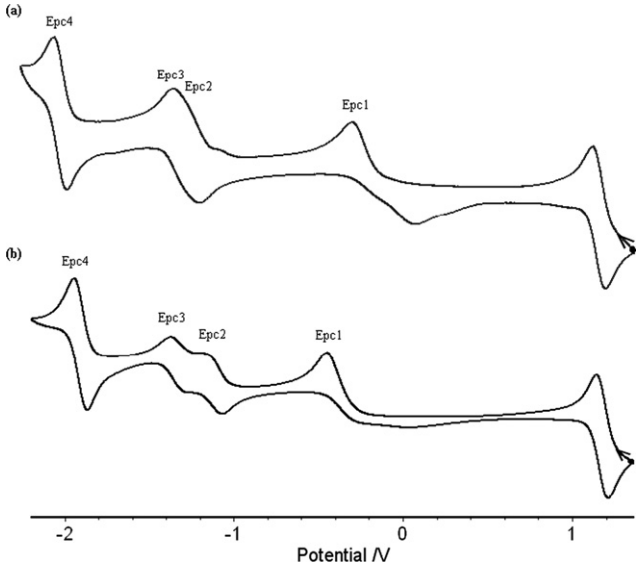

Fig. 4. Cyclic voltammograms of $[Co^{III}(Mebpb)(pprdn)_2]ClO_4$, $c = 1.8 \times 10^{-3}$ M (a), and $[Co^{III}(cbpb)(bzlan)_2]PF_6$, $c = 1.2 \times 10^{-3}$ M (b), in acetonitrile at 298 K. Scan rate, 100 mV s^{-1}.

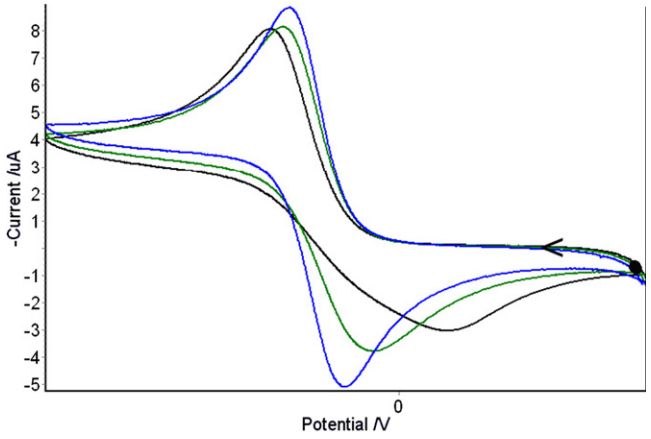

Fig. 5. Cyclic voltammograms of $[Co^{III}(Mebpb)(pprdn)_2]ClO_4$, **2a**, at different piperidine concentrations ratios (0, — black), (50, — green), (100, — blue) in acetonitrile containing 0.1 M TBAH as supporting electrolyte at 298 K. Scan rate 100 mV s^{-1}, $c = 1.5 \times 10^{-3}$ M. (For interpretation of the references to colour in this figure legend, the reader is referred to the web version of this article.)

stronger axial ligands shift the reduction potentials to more negative values. In general the Co^{III}/Co^{II} reductions for all these complexes are electrochemically irreversible in nature [19]. Accordingly, we assume that the lack of reversibility observed (Fig. 4) is most likely due to the loss of axial ligands from the cobalt(II) complex, because the electron is added to the antibonding d_{z^2} orbital [47].

$$[Co^{III}(Mebpb)(amine)_2]^+ + e^- \overset{MeCN}{\rightarrow} [Co^{II}(Mebpb)] + 2\ amine \qquad (1)$$

Owing to the very facile substitution of the axial ligands in the reduced form of these cobalt(III) complexes, electrochemical reversibility for the Co^{III}/Co^{II} couple is not observed. The oxidation of $[Co^{II}(Mebpb)(MeCN)]$ adduct occurs at much higher potentials.

The Co^{III}/Co^{II} cathodic wave in all $[Co^{III}(Mebpb)(amine)_2]^+$ complexes is followed by two overlapping redox waves, resulting from the combination of the Co^{II}/Co^{I} couple [48] and the redox couple corresponding to one of the pyridyl rings (Fig. 4a). In the $[Co^{III}(cbpb)(amine)_2]^+$ complexes, however, these couples are resolved (Fig. 4b). The final electrochemically reversible reduction couple observed in the voltammograms is related to the second pyridyl ring, that appears between $E_{1/2} = -2.01$ and -2.05 V for $[Co^{III}(Mebpb)(amine)_2]^+$ and at $E_{1/2} = -1.96$ V for $[Co^{III}(cbpb)(amine)_2]^+$ complexes. Additional evidence produced in substantiation of this fact are the results obtained from the cyclic voltammetric studies of the Ni(Mebpb) complex, that shows only two reduction waves in the range -1.57 to -2.04 V, attributed to the consecutive reduction of the two pyridyl rings [49]. Similar results have been reported for Ni(bpb) and Ni(bpen) complexes by Fenton et al. [46].

The σ-donor strength of the axial ligands also has a significant influence on the Co^{III}/Co^{II} reduction process, and the tendency of Co^{III} towards reduction increases as the axial ligand becomes a weaker donor. These observations are compatible with the ^{H} NMR and UV–Vis spectroscopic data.

A similar behavior has been found for $[Co^{III}(cbpb)(amine)_2]^+$ complexes. Fig. 4b shows the cyclic voltammogram of $[Co^{III}(cbpb)(bzlan)_2]PF_6$ (**4b**) as an example. In general the redox couples of $[Co^{III}(cbpb)(amine)_2]^+$ complexes are shifted to more positive values relative to those of the corresponding $[Co^{III}(Mebpb)(amine)_2]^+$ complexes, demonstrating the electron-withdrawing effect of chloro substitution on the electron density of the system. Similar results have been reported by Che et al. [16,43] and Ray and Mukherjee [19].

3.4.3. Electrochemistry of the complexes in the presence of amines. It is well established that in many *trans*-$[Co^{III}(N_2O_2)(L)_2]^+$ Schiff base complexes, the first irreversible reduction process (Co^{III}/Co^{II}) can become quasi-reversible under controlled concentration conditions [47,50]. In an attempt to examine the possibility of reversible electrochemical behavior in analogous amido complexes, the electrochemistry of $[Co^{III}(Mebpb)(pprdn)_2]ClO_4$ was carried out in the presence of excess amine. In the absence of additional amine the first reduction processes of (Co^{III}/Co^{II}) is electrochemically irreversible ($\Delta E = 410$ mV). Upon addition of excess amine, the oxidation wave of Co(II) is shifted towards more negative potentials (Fig. 5) ($\Delta E = 107$ mV), indicating the increased formation of six-coordinated adducts; i.e. the electrode process is preceded by a reversible chemical reaction

$$[Co^{II}(Mebpb)] + \text{excess amine} [Co^{III}(Mebpb)(amine)_2]^+ + e^- \qquad (2)$$

The redox potential of the Co(II/I) couple is not significantly changed by the addition of excess amine and can be regarded as approximately independent.

4. Conclusion

The combination of spectroscopic, crystallographic, and electrochemical measurements we have described has illustrated the main features of the coordination and redox chemistry of the *trans*-$[Co^{III}(Mebpb)(amine)_2]ClO_4$ and *trans*-$[Co^{III}(cbpb)(amine)_2]PF_6$ complexes. The coordination geometry around the Co^{III} center in these complexes is distorted octahedral. Electrochemical studies reveal that the first reduction process Co^{III}/Co^{II} is irreversible and strongly influenced by the nature of the axial amines. When the axial ligands are changed from morpholine to pyrrolidine a change in the Co^{III}/Co^{II} cathodic peak of 220 mV for Mebpb complexes and 260 mV for cbpb complexes is observed. This process becomes quasi-reversible upon the addition of excess amine. The two redox waves, resulting from the combination of the Co^{II}/Co^{I} couple and the redox couple corresponding to one of the pyridyl rings, overlap in $[Co(Mebpb)(amine)_2]^+$, but are resolved in $[Co(cbpb)(amine)_2]^+$ complexes. In general, the redox couples of $[Co(cbpb)(amine)_2]^+$ complexes are shifted to more positive values relative to those of the corresponding $[Co(Mebpb)(amine)_2]^+$ com-

plexes due to the electron-withdrawing effect of chloro substitution.

Acknowledgement

Partial support of this work by the Isfahan University of Technology Research Council is gratefully acknowledged.

Appendix A. Supplementary data

CCDC 681508 contains the supplementary crystallographic data for **1a**. These data can be obtained free of charge via http://www.ccdc.cam.ac.uk/conts/retrieving.html, or from the Cambridge Crystallographic Data Centre, 12 Union Road, Cambridge CB2 1EZ, UK; fax: (+44) 1223-336-033, or e-mail: deposit@ccdc.cam.ac.uk. Supplementary data associated with this article can be found, in the online version, at doi:10.1016/j.poly.2008.05.031.

References

[1] C. Jubert, A. Mohamadou, C. Gerard, S. Brandes, A. Tabard, J.P. Barbier, Inorg. Chem. Commun. 6 (2003) 900.
[2] J. Lin, J.Y. Zhang, Y. Xu, X.K. Ke, Z. Guo, Acta Crystallogr., Sect. C 57 (2001) 192.
[3] D.A. Conlon, N. Yasuda, Adv. Synth. Catal. 343 (2001) 137.
[4] H. Kurosaki, R.K. Sharma, S. Aoki, T. Inoue, Y. Okamoto, Y. Sugiura, M. Doi, T. Ishida, M. Otsuka, M. Goto, J. Chem. Soc., Dalton Trans. (2001) 441.
[5] J. Zhang, Q. Liu, C. Duan, Y. Shao, J. Ding, Z. Miao, X.-Z. You, Z. Guo, J. Chem. Soc., Dalton Trans. (2002) 591.
[6] W.-H. Leung, J.-X. Ma, V.W.-W. Yam, C.-M. Che, C.-K. Poon, J. Chem. Soc., Dalton Trans. (1991) 1071.
[7] B.M. Trost, I. Hachiya, J. Am. Chem. Soc. 120 (1998) 1104.
[8] S.R. Collinson, T. Gelbrich, M.B. Hursthouse, J.H.R. Tucker, Chem. Commun. (2001) 555.
[9] I. Huc, M.J. Krische, D.P. Funeriu, J.-M. Lehn, Eur. J. Inorg.Chem. (1999) 1415.
[10] J.D. Epperson, L.-J. Ming, G.R. Baker, G.R. Newkome, J. Am. Chem. Soc. 123 (2001) 8583.
[11] U. Beckmann, E. Bill, T. Weyhermuller, K. Wieghardt, Inorg. Chem. 42 (2003) 1045.
[12] M. Ray, D. Ghosh, Z. Shirin, R. Mukherjee, Inorg. Chem. 36 (1997) 3568.
[13] C.-M. Che, W.-H. Leung, C.-K. Li, H.-Y. Cheng, S.M. Peng, Inorg. Chim. Acta 196 (1992) 43.
[14] M. Ray, S. Mukerjee, R.J. Mukherjee, Chem. Soc. Dalton Trans. (1990) 3635.
[15] A.K. Patra, R. Mukherjee, Inorg. Chem. 38 (1999) 1388.
[16] S.-T. Mak, W.-T. Wong, V.W.-W. Yam, T.-F. Lai, C.-M. Che, J. Chem. Soc., Dalton Trans. (1991) 1915.
[17] R.L. Chapman, R.S. Vagg, Inorg. Chim. Acta 33 (1979) 227.
[18] D.J. Barnes, R.L. Chapman, R.S. Vagg, E.C. Walton, J. Chem. Eng. Data 23 (1978) 349.
[19] M. Ray, R.N. Mukherjee, Polyhedron 11 (1992) 2929.
[20] M. Ray, R. Mukherjee, J.F. Richardson, R.M. Buchanan, J. Chem. Soc., Dalton Trans. (1993) 2451.
[21] A. Hori, T. Ozawa, H. Yoshida, Y. Imod, Y. Kufibayashi, E. Nakano, N. Azuma, Inorg. Chim. Acta 281 (1998) 207.
[22] S.K. Dutta, U. Beckmann, E. Bill, T. Weyhermuller, K. Wieghardt, Inorg. Chem. 39 (2000) 3355.
[23] A.K. Patra, M. Ray, R. Mukherjee, Inorg. Chem. 39 (2000) 652.
[24] J.M. Rowland, M.L. Thornton, M.M. Olmstead, P.K. Mascharak, Inorg. Chem. 40 (2001) 1069.
[25] M. Amirnasr, K.J. Schenk, S. Meghdadi, Inorg. Chim. Acta 338 (2002) 19.
[26] S.L. Jain, P. Bhattacharyya, H.L. Milton, A.M.Z. Slawin, J.A. Crayston, J.D. Woollins, J. Chem. Soc., Dalton Trans. (2004) 862.
[27] O. Belda, C. Moberg, Coord. Chem. Rev. 249 (2005) 727.
[28] J. Singh, G. Hundal, R. Gupta, Eur. J. Inorg. Chem. (2008) 2052.
[29] Z.N. Zahran, D.R. Powell, G.B. Richter-Addo, Inorg. Chim. Acta 359 (2006) 3084.
[30] S. Meghdadi, H.R. Khavasi, S. Nalchigar, Acta Crystallogr., Sect. E 62 (2006) o5492.
[31] S. Meghdadi, M. Amirnasr, V. Langer, A. Zamanpoor, Can. J. Chem. 84 (2006) 971.
[32] N.G. Connelly, W.E. Geiger, Chem. Rev. 96 (1996) 877.
[33] Nonius, COLLECT, Nonius BV, Delft, The Netherlands, 1998.
[34] A.J.M. Duisenberg, L.M.J. Kroon-Batenburg, A.M.M. Schreurs, J. Appl. Crystallogr. 36 (2003) 220.
[35] G.M. Sheldrick, SADABS, Göttingen University, Germany, 2006.
[36] A. Altomare, M.C. Burla, M. Camalli, G.L. Cascarano, C. Giacovazzo, A. Guagliardi, A.G.G. Moliterni, G. Polidori, R. Spagna, J. Appl. Crystallogr. 32 (1999) 115.
[37] G.M. Sheldrick, SHELXTL Version 6, Bruker AXS Inc., Madison, WI, USA, 2001.
[38] W.-T. Wong, C.-M. CHE, Acta Crystallogr., Sect. C 50 (1994) 1407.
[39] N. Azuma, T. Ozawa, S. Tsuboyama, J.Chem. Soc., Dalton Trans. (1994) 2609.
[40] A.K. Patra, R. Mukherjee, Polyhedron 18 (1999) 1317.
[41] Y. Yang, F. Diederich, J.S. Valentine, J. Am. Chem. Soc. 113 (1991) 7195.
[42] K. Nakamoto, Infrared and Raman Spectra of Inorganic and Coordination Compounds Part II: Application in Coordination, Organometallic and Bioinorganic Chemistry, 5th ed., Wiley Interscience, New York, 1997.
[43] S.-T. Mak, V.W.-W. Yam, C.-M. Che, J. Chem. Soc., Dalton Trans. (1990) 2555.
[44] C.F. Fortney, R.E. Shepherd, Inorg. Chem. Commun. 7 (2004) 1065.
[45] C.F. Fortney, S.J. Geib, F.-T. Lin, R.E. Shepherd, Inorg. Chim. Acta 358 (2005) 2921.
[46] C.L. Weeks, P. Turner, R.R. Fenton, P.A. Lay, J. Chem. Soc., Dalton Trans. (2002) 931.
[47] A. Bottcher, T. Takeuchi, K.I. Hardcastle, T.J. Meade, H.B. Gray, D. Cwikel, M. Kapon, Z. Dori, Inorg. Chem. 36 (1997) 2498.
[48] A.K. Patra, M. Ray, R. Mukherjee, J. Chem. Soc., Dalton Trans. (1999) 2461.
[49] A. Amiri, M. Amirnasr, S. Meghdadi, K. Mereiter, V. Ghodsi, A. Gholami, submitted for publication.
[50] M. Amirnasr, R. Vafazadeh, A. Mahmoudkhani, Can. J. Chem. 80 (2002) 1196.

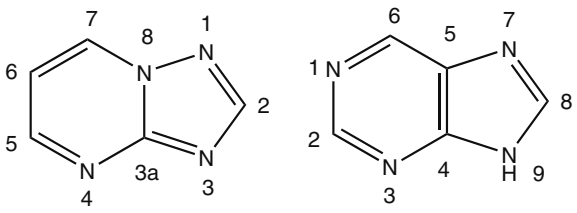

Fig. 1. The basic skeleton of 1,2,4-triazolo[1,5-*a*]pyrimidines and purines.

2. Experimental

2.1. Synthesis of the compounds

1,2,4-Triazolo-[1,5-*a*]pyrimidine (tp), 5,7-dimethyl-1,2,4-triazolo-[1,5-*a*]pyrimidine (dmtp), 1,10-phenanthroline (phen), ethylenediamine (en), $Cu(ClO_4)_2 \cdot 6H_2O$ and $Cu(NO_3)_2 \cdot 3H_2O$ were purchased from Aldrich and used without further purification.

2.1.1. $[Cu(H_2O)(phen)(tp)_2](ClO_4)_2 \cdot H_2O$ (**1**) and $[Cu(H_2O)(phen)(dmtp)_2](ClO_4)_2$ (**2**)

Firstly a green solution was obtained by mixing an aqueous solution of $Cu(ClO_4)_2 \cdot 6H_2O$ (1 mmol, 10 mL) and another one of the appropriate ligand tp (**1**) or dmtp (**2**) (1 mmol, 10 mL). After adding 1,10-phenanthroline dissolved in ethanol (1 mmol, 5 mL) a green precipitate of $Cu(phen)_2(ClO_4)_2 \cdot H_2O$ immediately appeared, which was filtered, washed with water and ethanol. The filtered solution was allowed to evaporate at room temperature and, after several days, blue crystals suitable for X-ray studies were isolated. Elemental analysis data: Compound **1**: *Anal.* Calc. for $C_{22}H_{20}Cl_2CuN_{10}O_{10}$: C, 36.8; H, 2.8; N, 19.5. Found: C, 37.4; H, 2.6; N, 19.8%. Compound **2**: *Anal.* Calc. for $C_{26}H_{26}Cl_2CuN_{10}O_9$: C, 41.3; H, 3.5; N, 18.5. Found: C, 41.3; H, 3.5; N, 18.4%.

2.1.2. $[Cu(NO_3)(H_2O)(phen)(tp)](NO_3)$ (**3**)

The complex was obtained by mixing three solutions, 10 mL each, one containing 1 mmol of $Cu(NO_3)_2 \cdot 3H_2O$, other 1 mmol of tp and the third 1 mmol of 1,10-phenanthroline. The two first solutions are aqueous and the last is ethanolic. After few days blue crystals suitable for X-ray study were obtained. Elemental analysis data: *Anal.* Calc. for $C_{17}H_{14}CuN_8O_7$: C, 40.4; H, 2.8; N, 22.2. Found: C, 40.8; H, 2.7; N, 22.6%.

2.1.3. $[Cu(H_2O)_2(en)(tp)_2](ClO_4)_2$ (**4**) and $[Cu(H_2O)_2(en)(dmtp)_2](ClO_4)_2$ (**5**)

Firstly two aqueous solutions of $Cu(ClO_4)_2 \cdot 6H_2O$ (1 mmol, 10 mL) and the appropriate ligand (tp (**4**) or dmtp (**5**)) (1 mmol, 10 mL) were mixed. After adding 0.5 mmol (34 μL) of ethylenediamine, it was left to stand at room temperature, blue crystals suitable for X-ray studies were isolated. Elemental analysis data: Compound **4**: *Anal.* Calc. for $C_{12}H_{20}Cl_2CuN_{10}O_{10}$: C, 24.1; H, 3.4; N, 23.4. Found: C, 24.3; H, 4.0; N, 23.8%. Compound **5**: *Anal.* Calc. for $C_{16}H_{28}Cl_2CuN_{10}O_{10}$: C, 29.3; H, 4.3; N, 21.4. Found: C, 29.6; H, 4.6; N, 22.0%.

2.1.4. $[Cu_2(OH)(H_2O)_{2.5}(tp)_5](ClO_4)_3(H_2O)_{1.5}$ (**6**)

Two solutions of $Cu(ClO_4)_2 \cdot 6H_2O$ (1 mmol, 10 mL) and tp (1 mmol, 10 mL) in 0.01 M NaOH were mixed. The mixture was allowed to evaporate at room temperature and, after one week, light blue crystals suitable for X-ray studies were obtained. Elemental analysis data: *Anal.* Calc. for $C_{25}H_{29}Cl_3Cu_2N_{20}O_{17}$: C, 26.9; H, 2.6; N, 25.1. Found: C, 27.1; H, 2.9; N, 25.7%.

2.2. Instrumentation

Microanalysis of C, H and N were performed in a Fisons Instruments EA-1008 analyser. Thermal behaviour was studied under an air flow in Shimadzu TGA-50 and Shimadzu DSC-50 equipments, at heating rates of 20 °C min^{-1} and 10 °C min^{-1}, respectively. Reflectance diffuse spectra were made on a VARIAN model CARY-5E spectrophotometer. EPR spectra of powdered samples were recorded at room temperature on a Bruker ESP-300E spectrometer, operating at X-band (9–10 GHz) while the magnetic susceptibility measurements, in the temperature range of 2–300 K, were carried out on powdered samples using a Quantum Design MPMS-XL SQUID (all this equipment is sited at the Centre of Scientific Instrumentation of the University of Granada). IR spectra were recorded on a ThermoNicolet IR 200 spectrometer using KBr pellets.

2.3. Crystallography

Data were collected, at room temperature for **3** and **4** and at 100 K for the rest of the samples, in a Bruker SMART APEX CCD system with Mo Kα radiation (λ = 0.7107 Å). Data were corrected for absorption (multi-scan, transmission ranges, 0.8305–0.7330, 0.7944–0.7122, 0.673–0.545, 0.822–0.614, 0.7013–0.6392 and 0.8659–0.7245 for **1**–**6**, respectively). The structures were solved by the heavy atom method and anisotropically refined in F^2 using SHELXL-97 [17]. There are two non-coordinated nitrate anions in **3** placed in binary axes, one of them disordered between two equally populated positions. Two water molecules in **6** have been refined with half occupancy. Hydrogen atoms of the heterocycles and auxiliary ligands were placed in ideal positions whereas those of water molecules (except the half occupancy ones in **6**) were refined with fixed O–H distance. Isotropic thermal parameters of all H atoms fixed to 1.2 times the equivalent isotropic thermal parameter of their parent atoms. Table 1 summarizes the crystallographic data for the six compounds.

3. Results and discussion

3.1. X-ray structure of the ternary copper complexes

All ternary copper(II) complexes (**1**–**5**) are mononuclear with the triazolopyrimidine ligands monodentately coordinated to the metal via the nitrogen atom at position 3 and the auxiliary ligand (ethylenediamine, en or 1,10-phenanthroline, phen) bidentately attached closing a five-member chelate ring. The geometry around the metal atom is square-pyramidal when the auxiliary ligand is phen (**1**, **2**, **3**) and tetragonally distorted octahedral when the auxiliary ligand is en (**4**, **5**). Figs. 2–4 display the structures of all these complexes. Distances and angles in the coordination sphere are listed in Table 2. These distances agree well with bibliographic data for Cu complexes of both triazolopyrimidine ligands and amine ligands [11]. The trigonality indexes [18] calculated for the five-coordinate compounds are 0.142, 0.187 and 0.022, respectively for **1**, **2** and **3** indicating that the geometries are in fact much closer to tetragonal pyramidal than to trigonal bipyramidal.

Both the triazolopyrimidine moiety and the auxiliary ligands occupy basal or equatorial coordination positions. For compound **3**, in which only one tp molecule is present, the fourth position in the basal plane is occupied by one oxygen atom of the coordinated nitrate anion. The axial positions are filled by one (**1**, **2**, **3**) or two (**4**, **5**) water molecules at a longer distance in typical Cu(II) Jahn–Teller distorted environments. In the two later compounds, distances Cu–water are long enough to let us consider the compounds as quasi-square planar (4+2). A weak interaction of the metal with a second oxygen atom of the coordinated nitrate anion

Table 1
Crystal data and structure refinement for the structures

	(**1**)	(**2**)	(**3**)	(**4**)	(**5**)	(**6**)
Empirical formula	$C_{22}H_{20}Cl_2CuN_{10}O_{10}$	$C_{26}H_{26}Cl_2CuN_{10}O_9$	$C_{17}H_{14}CuN_8O_7$	$C_{12}H_{20}Cl_2CuN_{10}O_{10}$	$C_{16}H_{28}Cl_2CuN_{10}O_{10}$	$C_{25}H_{29}Cl_3Cu_2N_{20}O_{17}$
Formula weight	718.92	757.01	505.90	598.82	654.92	1115.11
Crystal system	triclinic	monoclinic	monoclinic	monoclinic	monoclinic	monoclinic
Space group	$P\bar{1}$	$P2_1/c$	$P2/n$	$P2_1/c$	$P2_1/c$	$P2_1/c$
a (Å)	9.5677(5)	12.1033(5)	14.8687(9)	13.3507(8)	14.2694(6)	13.2076(7)
b (Å)	12.4114(6)	18.1364(7)	7.3470(5)	14.2757(9)	8.7680(4)	22.2625(10)
c (Å)	13.3517(6)	14.2061(5)	18.2668(11)	13.0530(8)	23.9159(10)	14.1257(7)
α (°)	75.465(1)	90	90	90	90	90
β (°)	71.674(1)	102.712(1)	95.563(1)	114.735(1)	117.222(1)	102.797(1)
γ (°)	78.059(1)	90	90	90	90	90
V (Å^3)	1442.71(12)	3041.9(2)	1986.1(2)	2259.5(2)	2660.8(2)	4050.3(3)
Z	2	4	4	4	4	4
r (g cm^{-3})	1.655	1.653	1.692	1.760	1.635	1.829
μ (mm^{-1})	1.015	0.965	1.162	1.276	1.091	1.347
Crystal size (mm^3)	0.35 × 0.33 × 0.19	0.41 × 0.32 × 0.25	0.41 × 0.37 × 0.37	0.65 × 0.25 × 0.16	0.46 × 0.36 × 0.35	0.36 × 0.27 × 0.11
Unique reflections	6543	7160	4523	5104	6253	9546
R ($I > 2s(I)$)	0.0306	0.0284	0.0451	0.0526	0.0484	0.0604
wR_2 (all data)	0.0826	0.0781	0.1388	0.1518	0.1403	0.1626

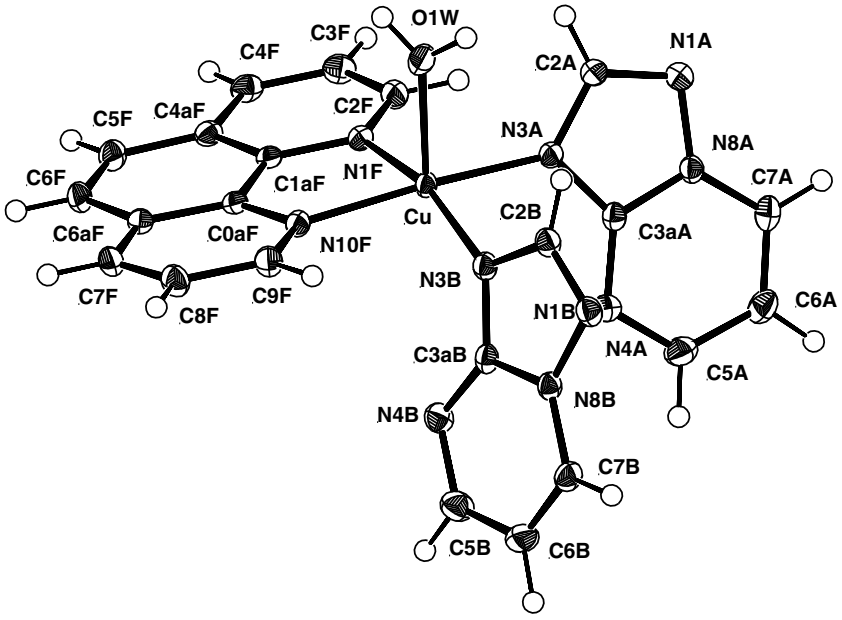

Fig. 2. View of the cationic complex $[Cu(H_2O)(phen)(tp)_2]^{2+}$ in compound **1**. The cation $[Cu(H_2O)(phen)(dmtp)_2]^{2+}$ in compound **2** is analogous to this.

(distance, 2.634(2) Å) is observed in compound **3**. The rotation around the Cu–N3 bonds seems to be quite easy since the dihedral angle between the equatorial coordination plane and the average triazolopyrimidine plane is rather variable (37–83°) and apparently conditioned by the repulsion between the ligands and the interactions with neighbouring species. In compound **3**, the tp ligand has its hexagonal ring pointing to the same side of the coordinated water molecule, this orientation being supported by a intramolecular H-bond (distance O1W···N4, 2.871(3) Å) whereas in compounds **1** and **2**, the orientation of tp or dmtp is just the opposite with relative head–head disposition.

The complex cations in **1** and **2** are associated in couples with the two cations related by an inversion centre and linked by a well-defined stacking interaction between the auxiliary ligands. Stacking interaction between the phen moieties is also observed in compound **3** but, in this case, it leads to the formation of rows of cations along the *b* axis. The formation of these couples of cations in **1** and **2** may explain why the coordination number in these complexes is five, the sixth coordination position being hindered by the other component of the couple. Water molecules form H-bonds towards oxygen atoms of the anions and non-coordinated N atoms of tp and dmtp (N1,N4) of neighbouring complexes.

The charge of the cationic complexes is balanced by two interstitial perchlorate anions placed in general positions in compounds **1**, **2**, **4**, **5** whereas for compound **3** there are two crystallographically independent non-coordinated nitrate moieties both placed in binary axes. An additional interstitial water molecule is present in the asymmetric unit of **1**.

It is clear that the nature of both the auxiliary ligand and the counteranion influences the geometry around the metal atom. The entrance of one nitrate anion (with higher coordination ability than perchlorate) in the coordination sphere of **3** leaves only one free equatorial coordination position available for the triazolopyrimidine ligands, which may explain why the relation Cu:tp is 1:2 for **1**, **2**, **4** and **5** and 1:1 for **3**, despite the fact that all reaction mixtures were initially 1:1. The stacking of phen ligands may explain why the coordination number is clearly five (it may be regarded as 5+1 for **3**) when the auxiliary ligand is phen and 4+2 when

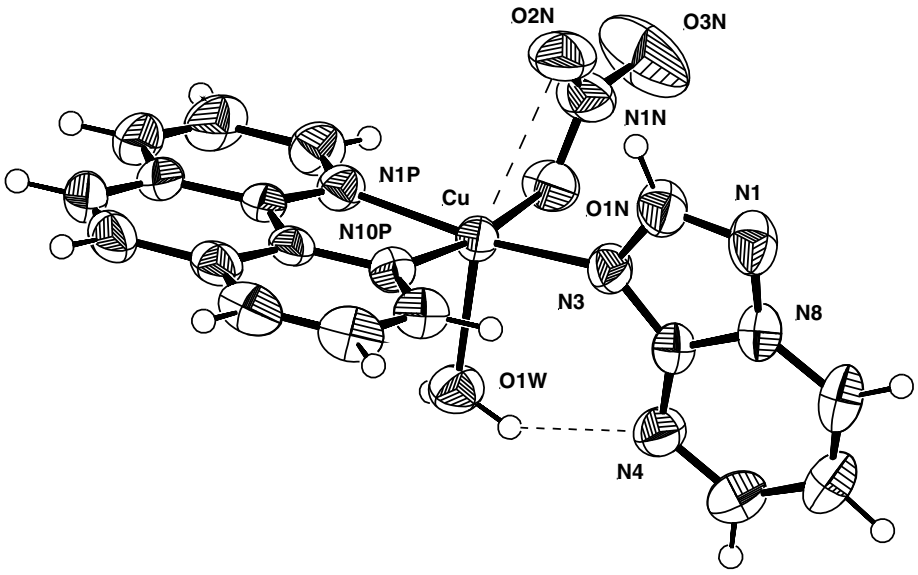

Fig. 3. View of the cationic complex $[Cu(NO_3)(H_2O)(phen)(tp)]^+$ in compound **3**.

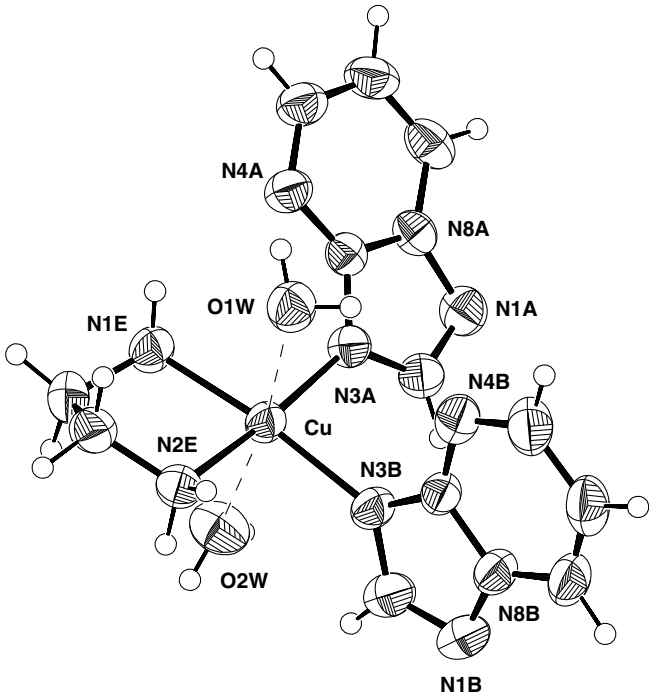

Fig. 4. View of the cationic complex $[Cu(H_2O)_2(en)(tp)_2]^{2+}$ in compound **4**. The cation $[Cu(H_2O)_2(en)(dmtp)_2]^{2+}$ in compound **5** is analogous to this.

Table 2
Distances (Å) in the coordination sphere and angles (°) in the basal plane of complexes **1**–**5**

	(**1**)	(**2**)	(**3**)	(**4**)	(**5**)
Cu–N3	1.9980(14) 2.0175(15)	1.9800(13) 2.0037(13)	1.993(2)	2.024(3) 2.028(3)	2.002(2) 2.015(2)
Cu–Na	2.0039(14) 2.0276(15)	2.0202(12) 2.0260(12)	2.008(2) 2.016(2)	2.011(3) 2.017(3)	2.008(2) 2.012(2)
Cu–On			1.9944(19)		
Cu–Ow	2.1891(14)	2.2397(11)	2.2155(19)	2.482(3) 2.494(3)	2.502(2) 2.518(2)
N3–Cu–N3	89.43(6)	90.70(5)		90.86(11)	90.79(9)
Na–Cu–Na	81.71(6)	81.90(5)	81.91(8)	84.77(12)	84.70(10)
N3–Cu–Na	93.29(6) 93.65(6) 172.05(6) 163.53(6)	95.23(5) 91.96(5) 177.07(5) 165.88(5)	93.44(9) 169.56(9)	92.42(11) 92.37(12) 174.78(12) 173.51(12)	91.52(9) 92.95(9) 176.22(9) 171.82(9)
N3–Cu–On			91.23(9)		
Na–Cu–On			92.17(9) 170.85(8)		

Na = nitrogen atom of phen of en, On = oxygen atom of nitrate, Ow = oxygen atom of water.

the auxiliary ligand is en, for which stacking interactions are absent. The presence of the methyl groups at positions 5 and 7 does not seem to influence appreciably the geometry of the cations.

3.2. X-ray structure of the dinuclear compound

Dinuclear complexes of 1,2,4-triazolo-[1,5-*a*]-pyrimidine derivatives with the heterocycle bridging two metal atoms through their nitrogen atoms in positions 3 and 4 have been described for several metals including Cu(I) [19], Ag(I) [20,21], Pd(II) [22] and Pt(II) [23,24]. This coordination mode mimics the behaviour of purine bases like adenine or hypoxanthine bridging metal atoms through N3 and N9 [25–27]. For Cu(II), such compounds have only been described for triazolopyrimidines bearing an ionizable H-atom which is removed raising the pH thus increasing the coordination capability of the ligand [15]. If such strategy is attempted with ligands like tp or dmtp without ionizable protons, the result is usually just the precipitation of $Cu(OH)_2$. Nevertheless, we have succeeded in obtaining a dinuclear compound with the ligand tp by raising only slightly the pH using 0.01 M NaOH as reaction medium. The compound, isolated as X-ray suitable crystals, exhibits the formula $[Cu_2(OH)(H_2O)_{2.5}(tp)_5](ClO_4)_3 \cdot 1.5H_2O$ (**6**). A view of the dinuclear cation of this compound is displayed in Fig. 5.

The asymmetric unit of this compound contains two non-equivalent copper atoms. Two equatorial positions of each of them are occupied by N3-monodentate tp moieties, whereas the other two are occupied by two different species bridging the metal atoms, one hydroxydo group and one tp molecule linked through N3 to one of the metal atoms (Cu1) and through N4 to the other (Cu2). Cu–N3 distances for the terminal tp ligands range from 2.007(3) to 2.028(3) Å, this range being similar to that found in the above

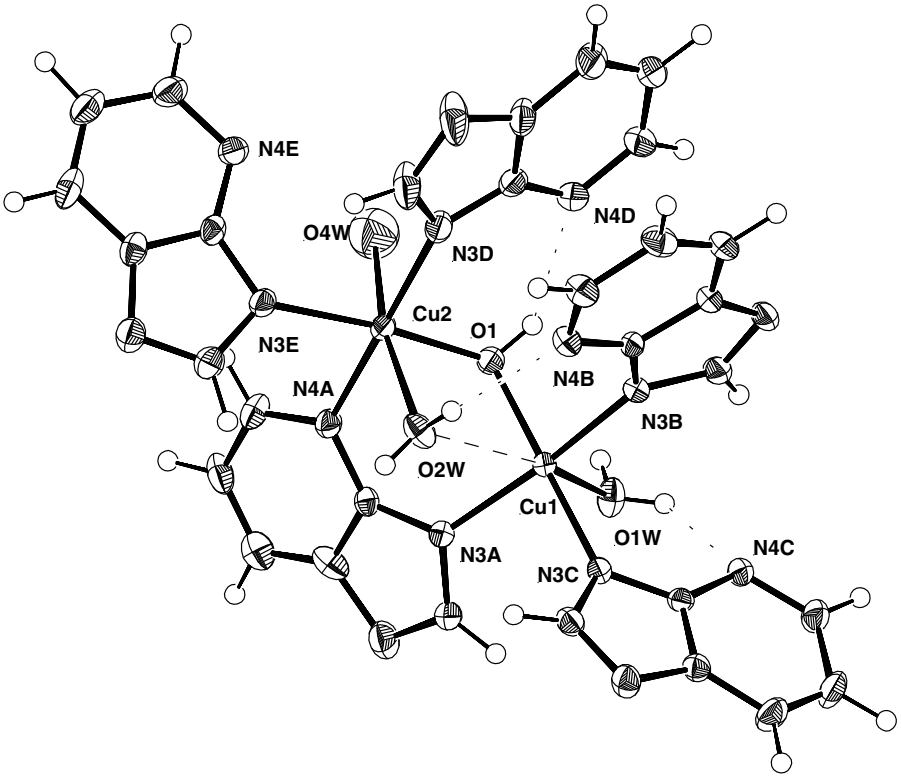

Fig. 5. View of the dinuclear complex $[Cu_2(OH)(H_2O)_{2.5}(tp)_5]^{3+}$ in compound **6**. The water molecule O4W has half occupancy and therefore should be present only in half of the complexes in the crystal.

described mononuclear complexes. Distances for the bridging tp moiety are, as expected, slightly longer (Cu1–N3 = 2.045(3) and Cu2–N4 = 2.063(3) Å) whereas the hydroxydo group is strongly attached to both copper atoms as usual for this species (Cu1–OH = 1.928(3) and Cu2–OH = 1.913(3) Å) but with a rather wide Cu–O–Cu angle (114.61(13)°) probably forced by the simultaneous presence of the bridging tp ligand. Both equatorial planes are not coplanar (dihedral angle 63.79(9)°) and the bridging tp ligand forms a dihedral angle of 28.54(9)° with the equatorial plane of Cu1 and an angle of 43.92(8)° with the equatorial plane of Cu2.

The axial positions of both metal atoms are occupied by water molecules with different structural roles. One of them (O1W) is attached to Cu1 with a distance of 2.300(3) Å whereas a second one (O2W) is linked to Cu2 at 2.412(3) Å, the latter also weakly interacting with Cu1 (distance, 2.697(4) Å) so it might be considered as a third asymmetric bridging ligand between the metal atoms. According to this, the coordination mode of Cu1 may be regarded as "4+1+1". Another water molecule (O4W) does not refine acceptably if considered with full occupancy and, after some trial and error, has finally been introduced in the refinement process with half occupancy, its distance to Cu2 being 2.441(9) Å. Therefore the coordination polyhedra of Cu2 is a square pyramid (4+1) for half of the Cu2 atoms present in the sample and a distorted octahedron (4+2) for the other half.

The hydroxydo group and the coordinated water molecules form intramolecular hydrogen bonds towards the N4 atom of terminal tp ligands thus contributing to stabilize the complex, the corresponding distances are OH···N4D = 2.866(4), O1W···N4C = 2.856(4) and O2W···N4B = 2.858(4) Å.

The charge of the cationic dinuclear complex is balanced by three perchlorate anions. A full-occupancy and another half-occupancy non-coordinated water molecules complete the asymmetric unit.

As told above, the N3,N4 bridging coordination mode for triazolopyrimidine ligands has been reported in previous papers. Nevertheless, this dinuclear complex is novel because it is the first time that this coordination mode is displayed in Cu(II) complexes with triazolopyrimidine derivatives without exocyclic oxygen atoms and also because of the presence of two different bridging ligands (tp and OH). The simultaneous presence of N3-monodentate and N3,N4-bridging modes in the same complex had been only previously observed for a Pt compound containing the anionic form of 4,7-dihydro-5-methyl-7-oxo-1,2,4-triazolo[1,5-*a*]pyrimidine ($mtpO^-$) in $[(mtpO)(NH_3)_2Pt(\mu\text{-}mtpO)Pt(bpy)(OH)](NO_3)\cdot 6H_2O$ [24] (where bpy = 2,2′-bipyridine).

3.3. Spectral and thermal studies

The 1500–1700 cm^{-1} region of the infrared spectra of the free heterocycles displays three bands for tp (1621, 1534 and 1515 cm^{-1}) and two for dmtp (1638 and 1548 cm^{-1}). Szłyk et al. [28] have assigned these bands by comparison with the previously assigned spectra of purine and adenine [29] suggesting that the higher wavenumber band is due to a vibration mode of the whole triazolopyrimidine moiety (ν_{tp}) whereas the other are due to pyrimidine ring modes (ν_{py} for dmtp, split into ν_{py1} and ν_{py2} for tp). These bands are only slightly affected by the coordination, with a displacement of the three bands of tp and the ν_{py} band of dmtp to higher wavenumber and a displacement of ν_{tp} band of dmtp to lower wavenumbers.

The presence of the anions is indicated by the typical stretching vibrations of perchlorate (1146, 1112 and 1087 cm^{-1} (**1**), 1144, 1119 and 1085 cm^{-1} (**2**), 1093 cm^{-1} (**4**), 1147, 1114 and 1087 cm^{-1} (**5**) and 1093 cm^{-1} (**6**)) or nitrate (1385 cm^{-1} (**3**)). The spectra also show broad bands around 3500–3400 cm^{-1}, easily assignable to ν(O–H) of water.

The first step of the thermal decomposition of the isolated complexes is the dehydration process. Complexes **1**, **2**, **3** and **5** display well-defined weight losses in the range 47–152 °C which agree well with the number of water molecules indicated by their elemental analysis. For **4** and **6** the experimental values for weight losses are lower than theoretical values and dehydration enthalpies cannot be reliably obtained from the integration of the peaks in the DSC diagrams since the dehydration partially occurs at room temperature. Dehydration takes place in a single step (endothermic peaks in the range 57–133 °C) except for **5** and **6** for which two well-defined stages are observed (peaks at 87 and 134 °C (**5**) and 58 and 141 °C (**6**)). After this, the decomposition of anions takes place followed of the pyrolysis of organic moiety that normally occurs in several steps (200–900 °C).

The diffuse reflectance spectra for all compounds present a only broad and asymmetric band with a maximum in the range 15 600–16 800 cm^{-1} that can be assigned for a d–d transition in a d^9 configuration with distorted octahedral or square-pyramidal geometries [30].

3.4. Magnetic and EPR studies

The X-band EPR spectra have been recorded for the polycrystalline powdered samples at room temperature. Compounds **1**, **2**, **3** and **5** present a spectrum made up by single very broad asymmetric band attributable to an unresolved anisotropic spectrum with an average g value of 2.06–2.07. The spectrum of compound **4** presents better resolution, with a slightly orthorhombic signal (g_1 = 2.16, g_2 = 2.09, g_3 = 2.06). The dinuclear complex **6** is EPR silent at room temperature, probably due to the broadening of the signal caused by the magnetic interaction between the copper atoms inside the complex.

The magnetic susceptibility of the six complexes has been measured in the 2–300 K range, at the magnetic field 10^4 Oe for all samples except **5** where a 5×10^3 Oe magnetic field was used. Experimental data were corrected for diamagnetism using the Pascal constants [31]. The magnetic data of the ternary copper complexes, **1**–**5**, are typical of magnetically diluted compounds and their magnetic behaviour can be described by the Curie law. The calculated μ_{eff} values (1.82–1.91 BM) are in the expected range for mononuclear Cu(II) complexes with similar geometry [11].

On the other hand, compound **6** displays a smooth decrease of $\chi_M T$ (where χ_M is the magnetic susceptibility per pair of copper(II) ions) as the temperature decreases from a value of 0.79 cm^3 K mol^{-1} at room temperature to a value of 0.19 cm^3 K mol^{-1} at 2 K, which is indicative of antiferromagnetic interactions between the metal centres. Nevertheless, no susceptibility maximum is observed and the data cannot be acceptably fit to the Bleany–Bowers equation for copper dimers [32], which do not let us to calculate an accurate $2J$ value. This may be due to the presence of the partial occupancy water molecule attached to one of the metal atoms (see above) which means that we have, in fact, two different dinuclear species present at the compound with possible different magnetic parameters. Alternatively, the data have been fitted to the Curie–Weiss law [33], the antiferromagnetic interaction being thus quantified by the negative value of θ (−9.424 K). From the Curie constant, a value of 1.81 BM for the effective magnetic moment when $T \to \infty$ has been calculated. The observed antiferromagnetic interaction is much weaker than that for $[Cu_2(biim)_2(5tpO)_2(H_2O)](ClO_4)_2 \cdot 5.5H_2O$ [15], compound with two triazolopyrimidine bridges and also much weaker than that expected for a dinuclear compound with two hydroxydo bridges and a Cu–O–Cu angle like that present in compound **6** [34].

Acknowledgements

This work was supported by a project of the Ministry of Education and Science of Spain (Project: CTQ-2005-00329/BQU) and the Junta de Andalucía (FQM195). C.R. Maldonado is grateful for a FPU grant from the Ministry of Education and Science of Spain.

Appendix A. Supplementary material

CCDC 674879 and 674884 contains the supplementary crystallographic data for this paper. These data can be obtained free of charge via http://www.ccdc.cam.ac.uk/conts/retrieving.html, or from the Cambridge Crystallographic Data Centre, 12 Union Road, Cambridge CB2 1EZ, UK; fax: (+44) 1223-336-033; or e-mail: deposit@ccdc.cam.ac.uk. Supplementary data associated with this article can be found, in the online version, at doi:10.1016/j.poly.2008.06.001.

References

[1] G. Fischer, Adv. Heterocycl. Chem. 57 (1993) 81.
[2] J.P. Cornelissen, R.A.G. De Graaff, J.G. Haasnoot, R. Prins, J. Reedijk, M. Biagini-Cingi, A.M. Manotti-Lanfredi, A. Tiripicchio, Polyhedron 8 (1989) 2313.
[3] G.A. Van Albada, R.A.G. De Graaff, J.G. Haasnoot, J. Schild, J. Reedijk, Acta Crystallogr., Sect. C 47 (1991) 946.
[4] M.A. Romero, J.M. Salas, M. Quirós, M.P. Sánchez, J. Romero, D. Martín, Inorg. Chem. 33 (1994) 5477.
[5] M. Biagini-Cingi, A.M. Manotti-Lanfredi, A. Tiripicchio, J.G. Haasnoot, J. Reedijk, Inorg. Chim. Acta 72 (1983) 81.
[6] J.G. Haasnoot, W.L. Driessen, J. Reedijk, Inorg. Chem. 23 (1984) 2803.
[7] T.L.F. Favre, J.G. Haasnoot, J. Reedijk, Polyhedron 5 (1986) 1405.
[8] E.J. Dirks, J.G. Haasnoot, A.J. Kinneging, J. Reedijk, Inorg. Chem. 26 (1987) 1902.
[9] J.M. Salas, M.A. Romero, C. Enrique, R. Sirera, Acta Crystallogr., Sect. C 49 (1993) 1902.
[10] J.A.R. Navarro, M.A. Romero, J.M. Salas, M. Quirós, E.R.T. Tiekink, Inorg. Chem. 36 (1997) 4988.
[11] J.A.R. Navarro, M.A. Romero, J.M. Salas, J. Molina, E.R.T. Tiekink, Inorg. Chim. Acta 274 (1998) 53.
[12] A. Grodzicki, E. Szłyk, A. Wojtczak, G. Wrzeswz, L. Pazderski, T. Muziol, Polyhedron 18 (1999) 519.
[13] M. Abul-Haj, M. Quirós, J.M. Salas, Acta Crystallogr., Sect. E 59 (2003) m903.
[14] M. Biagini-Cingi, A.M. Manotti-Lanfredi, A. Tiripicchio, J.P. Cornelissen, J.G. Haasnoot, J. Reedijk, Inorg. Chim. Acta 129 (1987) 217.
[15] M. Abul-Haj, M. Quirós, J.M. Salas, J.A. Dobado, J.M. Molina, M.G. Basallote, M.A. Máñez, Eur. J. Inorg. Chem. (2002) 811.
[16] J.M. Salas, M.A. Romero, M.P. Sánchez, M. Quirós, Coord. Chem. Rev. 193 (1999) 1119.
[17] G.M. Sheldrick, SHELXL-97, University of Göttingen, Germany, 1997.
[18] A.W. Addison, T.N. Rao, J Chem. Soc., Dalton Trans. (1984) 1349.
[19] J.G. Haasnoot, T.L.F. Favre, W. Hinrichs, J. Reedijk, Angew. Chem., Int. Ed. 27 (1988) 856.
[20] M.A. Romero, J.M. Salas, M. Quirós, M.P. Sánchez, J. Molina, J. El Bahraoui, R. Faure, J. Mol. Struct. 354 (1995) 189.
[21] J.A.R. Navarro, J.M. Salas, M.A. Romero, R. Faure, J. Chem. Soc., Dalton Trans. (1998) 901.
[22] J.A.R. Navarro, M.A. Romero, J.M. Salas, J. Chem. Soc., Dalton Trans. (1997) 1001.
[23] J.A.R. Navarro, M.A. Romero, J.M. Salas, M. Quirós, J. El Bahraoui, J. Molina, Inorg. Chem. 35 (1996) 7829.
[24] J.A.R. Navarro, M.A. Romero, J.M. Salas, M. Quirós, Inorg. Chem. 36 (1997) 3277.
[25] P. De Meester, A.C. Skapski, J. Chem. Soc. Part A (1971) 2167.
[26] A. Terzis, A.L. Beauchamp, R. Rivest, Inorg. Chem. 12 (1973) 1166.
[27] E. Sletten, Acta Crystallogr., Sect. B 26 (1970) 1609.
[28] E. Szłyk, A. Grodzicki, L. Pazderski, E. Bednarek, B. Kamiénski, Polyhedron 19 (2000) 965.
[29] M.J. Nowak, H. Rostkowska, L. Lapinski, J.S. Kwiatkowski, J. Leszczynski, Spectrochim. Acta Part A 50 (1994) 1081.
[30] A.B.P. Lever, Inorganic Electronic Spectroscopy, Elsiever, Amsterdam, 1986.
[31] S.J. Lippard, Progress in Inorganic Chemistry, vol. 29, John Wiley & Sons, United States, 1982.
[32] B. Bleany, K.D. Bowers, Proc. R. Soc. Lond. Ser. A 214 (1952) 451.
[33] F.E. Mabbs, D.J. Machin, Magnetism and Transition Metal Complexes, Champman and Hall Ltd., United Kingdom, 1973.
[34] V.H. Crawford, H.W. Richardson, J.R. Wasson, D.J. Hodgson, W.E. Hatfield, Inorg. Chem. 15 (1976) 2107.

Table 1
Chemical structures and abbreviations of salicyl derivatives examined

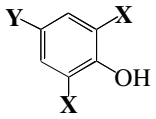

Ligand	X	Y
Salicylic acid (**Ac**)	–COOH –H	–H
Salicyl alcohol (**Ol**)	$-CH_2OH$ –H	–H
2,6-Bis(hydroxymethyl)-*p*-cresol (**LMe**)	$-CH_2OH$ $-CH_2OH$	$-CH_3$
3,5-Bis(hydroxymethyl)-4-hydroxybenzoic acid (**LAc**)	$-CH_2OH$ $-CH_2OH$	–COOH

2.2. Preparation of 3,5-bis(hydroxymethyl)-4-hydroxybenzoic acid (*LAc*) and *LAc* loaded resin

The 3,5-bis(hydroxymethyl)-4-hydroxybenzoic acid ethyl ester was prepared according to the literature methods [21–23]. A mixture of 4-hydroxybenzoic acid ethyl ester (50.0 g, 0.301 mol), formaldehyde (63 cm^3 of 37% solution in water, 0.72 mol) and NaOH (13.8 g, 0.331 mol) was heated at 40 °C for 11 days in water (190 cm^3), and then, it was acidified with 7% aqueous HCl. Filtration and recrystallization from a mixed solvent of benzene and ethanol afforded the 3,5-bis(hydroxymethyl)-4-hydroxybenzoic acid ethyl ester as a yellow powder. The powder (30 g, 0.14 mol) and KOH (32 g, 0.48 mol) were dissolved in 150 cm^3 of water and heated at 80 °C for half a day. The reaction mixture was allowed to cool, acidified with 35% aqueous HCl, and filtered off. The product was washed with water and dried in air, yielding 18 g (0.088 mol, 63% yield) of **LAc** as a pale-yellow powder.

LAc (10.0 g, 50.5 mmol) and NaOH (2.36 g, 57.6 mmol) were dissolved in 200 cm^3 of water, and then, the solution was added to 12.0 g of a strong-base type anion-exchange resin, Dowex 1-X8 (100–200 mesh) of the Cl^- form. The mixture was shaken for one day at 25 °C in a thermostatic shaking apparatus. The resulting resin was filtered off, washed thoroughly with water, and dried in air to give 14.7 g of the **LAc** loaded resin. The amounts of the unfixed ligand were estimated from the absorbances of the reaction solution and the washings at 249 nm.

2.3. NMR measurements

The ^1H NMR spectra were recorded by a JEOL JNM-GX270 spectrometer to identify the synthesized ligand **LAc**. TMS was used as the internal reference. The ^{11}B NMR spectra were recorded by a JEOL JNM-GSX500 spectrometer with a 10 mm multinuclear probe at 25 °C located at the Center of Advanced Instrumental Analysis, Kyushu University. The standard NMR parameters were as follows: an observed frequency of 160.0 MHz, a flip angle of *ca.* 90° (36 μs), a pulse repetition time of 1 s and a spectral width of 31 kHz. Sample tubes made of PTFE (poly(tetrafluoroethylene)) were employed for the measurements. Overlapping NMR signals were resolved into individual peaks by a Lorentzian curve-fitting method. A sample solution (I = 0.10 mol dm^{-3}, KCl) containing known amounts of boric acid/borate and ligand was prepared. The pH of the solution was adjusted with 0.04 mol dm^{-3} acetate buffer, phosphate buffer, HEPES (2-[4-(2-hydroxyethyl)-1-piperazinyl]ethanesulfonic acid) buffer or ammonia buffer, and measured by a Horiba pH meter, Model F-22. After being allowed to stand for about 1 day, the solution was used for the ^{11}B NMR measurements. The chemical shifts were reported with respect to BF_3–OEt_2 as the external standard.

2.4. Molecular modeling calculations

Molecular modeling calculations were carried out for the complexes of boric acid with salicyl alcohol (**Ol**) and 2,6-bis(hydroxymethyl)-*p*-cresol (**LMe**). First, the molecular-mechanics (MM) method was applied for all models using MM+ method in HyperChem ver. 6.03 (Hypercube, Inc.) [24]. Semi-empirical molecular-orbital calculations were then done in a vacuum mode for the obtained structures of the complexes using the MOPAC2002 [25] of CAChe 6.1.1 version (Fujitsu Ltd., Japan) [26]. The AM1 method was employed for these calculations and the heat of formation (HOF) was evaluated. Single-point energy and optimization calculations of the complex models were then conducted by Becke's three-parameter hybrid method with LYP correlation (B3LYP) method in the GAUSSIAN98 program package [27]. The 6-31G(d) basis set was employed for all atoms.

2.5. Boric acid adsorption

The adsorption behavior of boric acid onto the **LAc** loaded resin was investigated by the batch technique. The effect of pH on the adsorption was examined as follows: An appropriate amount of the dry adsorbent was added to 20 cm^3 of an aqueous solution containing a known amount of boric acid/borate. The solution pH was adjusted with 0.02 mol dm^{-3} acetate buffer, HEPES buffer, or ammonia buffer, and with the addition of a small amount of KOH or HCl solution, which caused the ionic strength of the solution to range from 0.02 to 0.04 mol dm^{-3}. The mixture was mechanically shaken for 3–5 days at 25 °C in a thermostated water bath. The equilibrated solution was then filtered through a 0.45 μm membrane filter and the pH of the solution measured. The boron concentration in the equilibrated solution was measured by absorption spectrophotometry (SHIMADZU UV-2200) using an Azomethine H [20,28–30] or ICP-MS (Agilent 7500 c).

The column test was performed using a 1.00 cm (i.d.) × 2.86 cm column packed with the **LAc** loaded resin (1.00 g on a dry-weight basis) at 25 °C in a thermostated room. The volume of the swelled resin was 2.21 cm^3. A 10.0 mmol dm^{-3} boric acid/borate solution was continuously fed to the column at the flow rate of 0.52 cm^3 min^{-1}. Every 10 cm^3 of effluent from the column was collected and the concentration of boric acid/borate was spectrophotometrically determined. The quantity of the boron adsorbed onto the resin was calculated by subtracting the boric acid/borate concentration in the equilibrated solution from the initial concentration. The leakage of the ligand from the resin was estimated from the absorbance at 249 nm.

3. Results and discussion

3.1. Boric acid–salicylic acid system

The ^{11}B NMR chemical shifts provide direct information about the boron species formed in solution, and the relative signal intensities of the boron species are proportional to the concentration of the respective species [8–10,12,13,15]. Fig. 1 shows the ^{11}B NMR spectra for boric acid/borate solutions (pH 4) containing salicylic acid (**Ac**). Two signals due to the borate complexes with six-membered ring structures were observed at 2.9 and 3.3 ppm besides the free boric acid signal. The relative signal intensities of the complexes depend on the concentration ratio of the ligand to boric acid/borate. At pHs higher than 5, the peak at 3.3 ppm was not observed even at a high salicylic acid concentration, and the relative intensity of the peak at 2.9 ppm was independent of the solution pH in the pH range from 4 to 8 at a constant ligand to boric acid/borate concentration ratio.

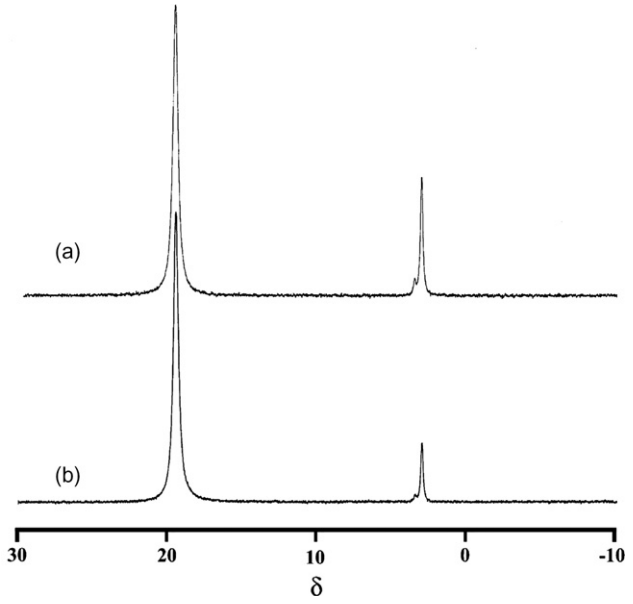

Fig. 1. ^{11}B NMR spectra for solutions containing 10.0 mmol dm^{-3} boric acid/borate and (a): 19.7 mmol dm^{-3} or (b): 9.80 mmol dm^{-3} salicylic acid at pH 4.

Salicylic acid has two functional groups relating to the acid dissociation reactions expressed as follows:

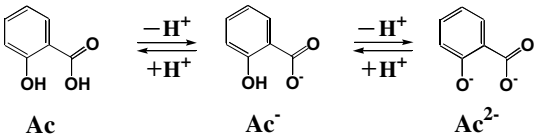

(1)

$$K_{a1(\mathbf{Ac})} = [H^+][\mathbf{Ac}^-]/[\mathbf{Ac}] \quad (2)$$

$$K_{a1(\mathbf{Ac})} = [H^+][\mathbf{Ac}^{2-}]/[\mathbf{Ac}^-] \quad (3)$$

The acid dissociation constants of the salicylic acid, $K_{a1(\mathbf{Ac})}$ and $K_{a2(\mathbf{Ac})}$, are $10^{-2.98}$ and $10^{-13.61}$ (I = 0.1 mol dm^{-3}, 25 °C), respectively [31]. The acid dissociation constant of boric acid, $K_{a(B)}$, is reported as $10^{-9.05}$ (I = 0.1 mol dm^{-3}, 25 °C) [3]. Considering the acid dissociation reactions of the respective species, almost all of the salicylic acid is present as $\mathbf{Ac}^-$ in Eq. (1) and the free boron as $B(OH)_3$ under the conditions that only one complex peak was observed at 2.9 ppm in the ^{11}B NMR spectra. On the other hand, another peak at 3.3 ppm appeared at a lower pH where salicylic acid exists as both $\mathbf{Ac}^-$ and **Ac** species. These results can be explained by two complexation reactions. One is the reaction of boric acid with the deprotonated salicylic acid, $\mathbf{Ac}^-$, to form the 1:1 monochelate complex which gives the signal at 2.9 ppm. The other is the condensation reaction between the 1:1 monochelate complex and the fully protonated salicylic acid, **Ac**, to yield the 1:2 bischelate complex which gives the signal at 3.3 ppm.

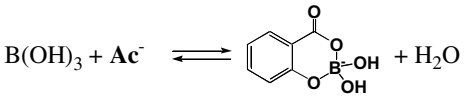

(4)

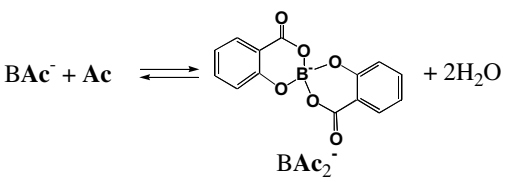

(5)

The formation constants are then defined by Eqs. (6) and (7), respectively.

$$K_{f(\mathbf{BAc})} = [\mathbf{BAc}^-]/([B(OH)_3][\mathbf{Ac}^-]) \quad (6)$$

$$K_{f(\mathbf{BAc2})} = [\mathbf{BAc}_2^-]/([\mathbf{BAc}^-][\mathbf{Ac}]) \quad (7)$$

The deprotonated salicylic acid has a carboxy group with a strong nucleophilicity and the trigonal planar boric acid has an empty orbital to accept an electron pair from the ligand. Therefore, boric acid accepts an electron pair through the nucleophilic attack of the deprotonated carboxy group, followed by the condensation reaction with the phenolic hydroxy group of the ligand to form the 1:1 monochelate complex. The monochelate complex then only reacts with the fully protonated salicylic acid through the condensation reaction to give the 1:2 bischelate complex and two water molecules. The formation constants were estimated from the ^{11}B NMR signal intensity data. The calculated values of $K_{f(\mathbf{BAc})}$ and $K_{f(\mathbf{BAc2})}$ were constant at $10^{1.05 \pm 0.01}$ and $10^{2.15 \pm 0.03}$, respectively (Table 2).

When boric acid/borate reacts with polyhydroxy compounds to form borate complexes with six-membered ring structures, the 1:1 monochelate complex gives a signal around 1.1 ppm, and the 1:2 bischelate one gives a new peak around 0.5 ppm [12,13,15]. The chemical shifts in both the monochelate and bischelate complexes with salicylic acid are lower field values compared to the corresponding complexes in the polyol systems. Furthermore, the bischelate complex gave the lower field signal relative to the monochelate one in contrast to the polyol systems. The aromatic ring of the salicylic acid should slightly decrease the electron density of the boron atom in the complex *via* the oxygen atom, which brings about the deshielding effect. Such phenomena were also observed for the complexation of boric acid with salicyl alcohol derivatives as will be shown later.

3.2. Boric acid–salicyl alcohol derivative system

Salicyl alcohol derivatives have two different kinds of hydroxy groups; *i.e.*, alcoholic and phenolic hydroxy groups. The alcoholic hydroxy group is always available for the condensation reaction with the hydroxy group of the boron species. The phenolic hydroxy group is available not only for the condensation reaction, but also for the nucleophilic attack on the empty orbital of boric acid. The acid dissociation constants of the salicyl alcohol derivatives were potentiometrically determined to be $10^{-9.54}$ for the salicyl alcohol (**Ol**), $10^{-9.44}$ for 2,6-bis(hydroxymethyl)-*p*-cresol (**LMe**) and $10^{-8.57}$ for 3,5-bis(hydroxymethyl)-4-hydroxybenzoic acid (**LAc**) as shown in Table 2.

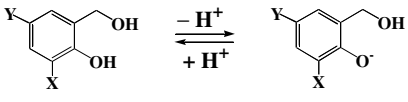

(8)

Table 2
^{11}B NMR chemical shifts and formation constants of boric acid complexes with salicyl derivatives (I = 0.10 mol dm^{-3}, KCl, 25 °C)

Ligand	pK_{a1}	pK_{a2}	Complex	δ	log K_f
Salicylic acid (**Ac**)	2.98*	13.61*	$\mathbf{BAc}^-$	2.9	1.05 ± 0.01
			$\mathbf{BAc}_2^-$	3.3	2.15 ± 0.03
Salicyl alcohol (**Ol**)	9.54		$\mathbf{BOl}^-$	1.6	3.60 ± 0.01
			$\mathbf{BOl}_2^-$	1.8	1.50 ± 0.06
2,6-Bis(hydroxymethyl)-*p*-cresol (**LMe**)	9.44		$\mathbf{BLMe}^-$	1.7	4.23 ± 0.03
			$\mathbf{B(LMe)}_2^-$	1.9	2.45 ± 0.10
3,5-Bis(hydroxymethyl)-4-hydroxybenzoic acid (**LAc**)	4.20	8.57	$\mathbf{BLAc}^{2-}$	1.8	3.74 ± 0.04
			$\mathbf{B(LAc)}_2^{3-}$	2.0	2.42 ± 0.09

* Data from Ref [29].

In addition to the phenolic hydroxy group, **LAc** has a carboxy group for **Y**, and the acid dissociation constant was determined to be $10^{-4.20}$ (Table 2). Considering the acid dissociation reactions of the respective species, it is expected that boric acid forms 1:1 monochelate and 1:2 bischelate complexes with these salicyl alcohol derivatives as follows:

$$B(OH)_3 + \mathbf{L}^- \rightleftharpoons \mathbf{BL}^- + H_2O \quad (9)$$

$$\mathbf{BL}^- + \mathbf{L} \rightleftharpoons \mathbf{BL}_2^- + 2H_2O \quad (10)$$

Boric acid would accept the electron pair through the nucleophilic attack of the deprotonated phenolic hydroxy groups, followed by the condensation reaction with the alcoholic hydroxy group of the ligand to form the 1:1 monochelate complex as expressed by Eq. (9). The monochelate complex should then react with the protonated salicyl alcohol moieties through the condensation reaction to give the 1:2 bischelate complex and two water molecules as expressed by Eq. (10).

The ^{11}B NMR measurements were performed for the boric acid solutions containing **Ol**, **LMe** or **LAc**. As an example, the NMR spectra for the salicyl alcohol are shown in Fig. 2. Two signals due to complexes were observed at 1.8–1.6 ppm and 2.0–1.8 ppm for all the examined salicyl alcohol derivatives. In the same way as that for the salicylic acid system, the higher and lower field signals were assigned to the 1:1 monochelate and 1:2 bischelate complexes, respectively. The formation constants of the 1:1 monochelate and 1:2 bischelate complexes were calculated using the equilibrium concentrations estimated from the ^{11}B NMR signal intensities. The evaluated formation constants are summarized in Table 2 together with the chemical shift values of the chelate complexes. Both bis(hydroxymethyl)phenol derivatives (**LMe** and **LAc**) form highly stable complexes in the salicyl derivatives examined. The overall formation constants of the 1:2 bischelate complexes for **LMe** and **LAc** are comparable to those of the most stable bischelate complexes reported so far (approximately 10^6) [20,32].

Even if the fact that the bis(hydroxymethyl)phenol derivatives have two hydroxymethyl groups available for the chelate complex formation at the ortho position is considered, the stabilities of the complexes are too high compared to the salicyl alcohol; the statistical contribution to the $\log K_f$ value is only 0.30, however, the difference between the values estimated by the NMR method is 1.58, as shown in Table 2. In order to obtain structural and thermodynamic information, we carried out molecular modeling calculations for the 1:2 complexes of boric acid with the salicyl alcohol derivatives, **Ol** and **LMe**. The optimized structures of the 1:2 complexes are shown in Fig. 3. The bond lengths of B–O in the optimized complexes were 1.52–1.42 Å, which agreed well with the values in the Cambridge Structural Database (CSD) [33]. No appreciable difference in the bond length among the salicyl alcohol derivatives was observed. The standard enthalpy change (ΔH°) for the overall complexation (Eq. (11)) was evaluated from the estimated heat of formation as follows: $\Delta H^\circ = -178.694$ kJ/mol for $B\mathbf{Ol}_2^-$ and -194.408 kJ/mol for $B(\mathbf{LMe})_2^-$.

$$B(OH)_3 + \mathbf{L}^- + \mathbf{L} \rightleftharpoons B\mathbf{L}_2^- + 3H_2O \quad (11)$$

Molecular modeling calculations have clarified that the complexation with the bis(hydroxymethyl)phenol derivatives is highly favorable in enthalpy.

Fig. 4 shows the pH dependence of the equilibrium concentrations of the boron species in a large excess of the ligand **LAc**. In the pH range of 6–9, the −3 charged 1:2 bischelate complex prevails in the solution. This calculation provides useful information to optimize the conditions for the boron-selective adsorption utilizing the complexation between the boric acid and the ligand **LAc**.

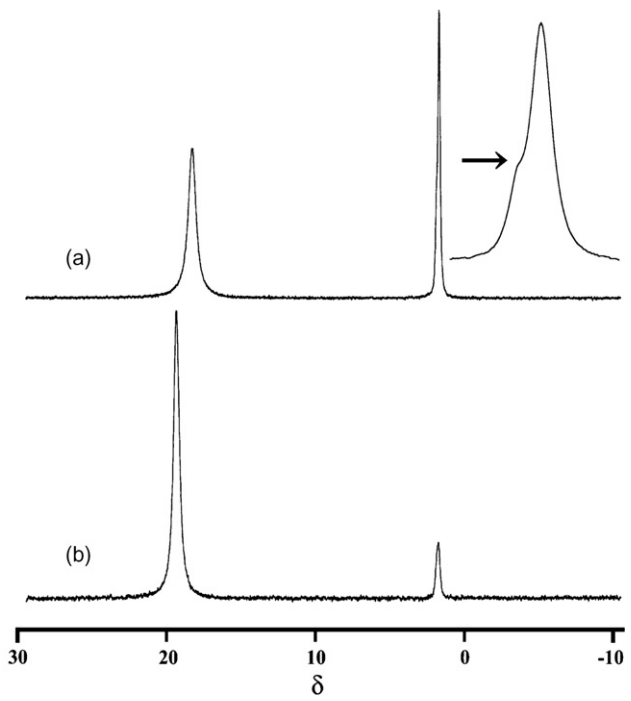

Fig. 2. ^{11}B NMR spectra for solutions containing 9.99 mmol dm^{-3} boric acid/borate and 10.0 mmol dm^{-3} salicyl alcohol at different pH ((a): pH 8.1, (b): pH 7.1).

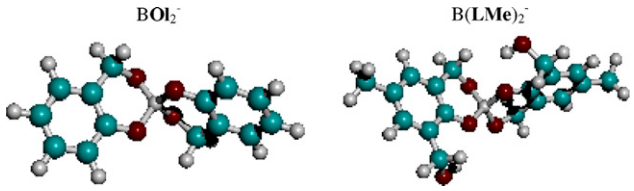

Fig. 3. Optimized structures of the 1:2 complexes of boric acid with $\mathbf{Ol}^-$ and $\mathbf{LMe}^-$.

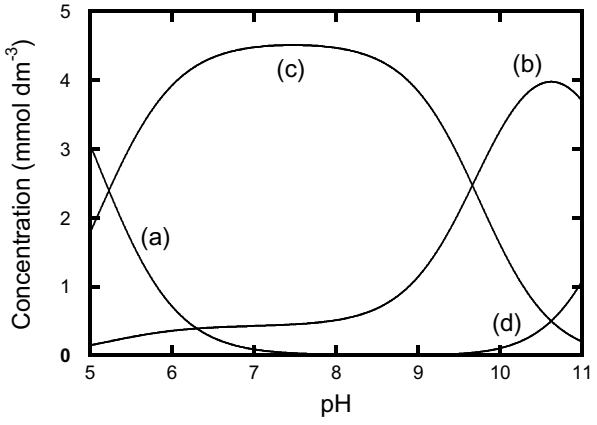

Fig. 4. pH dependent equilibrium concentrations of boron species for a solution containing 5 mmol dm^{-3} boric acid/borate and 50 mmol dm^{-3} **LAc**. (a): $B(OH)_3$; (b): $B(\mathbf{LAc})^{2-}$; (c): $B(\mathbf{LAc}_2)^{3-}$; (d): $B(OH)_4^-$.

3.3. Boron adsorption onto the **LAc** loaded anion-exchange resin

The adsorption of boric acid onto an anion-exchange resin using the ligand **LAc**–boric acid complexation was examined. The **LAc**–boric acid complexes have the negative charges of −2 for the 1:1 monochelate and −3 for the 1:2 bischelate complexes. Therefore, boric acid will be selectively adsorbed onto the strong-base type anion-exchange resin loaded with **LAc**. The boron-selective adsorbent was prepared by mixing the resin beads with the ligand solution. The amount of the ligand fixed into the resin was estimated to be 1.40 mmol g^{-1} by subtracting the amount of the ligand remaining in the solution from the initial amount.

Fig. 5 shows the pH dependence of the boron adsorption onto the **LAc** loaded resin. Boron was adsorbed all over the pH range under the experimental conditions. In particular, almost all of the boron was removed from the neutral solutions. Boron exists as the borate anion in an alkaline solution, however, the selectivity of the borate anion toward the Dowex 1-X8 resin was too low to contribute to the adsorption. The boron uptake is definitely a consequence of the formation of the chelate complexes. Fig. 6 shows the pH dependent adsorption capacities of boron and the ligand **LAc** toward an anion-exchange resin (Dowex 1-X8). The concentration ratios of boron to the ligand in the resin were almost constant, and slightly greater than 50% in the pH range of 4–10. This indicates that the boron species adsorbed onto the resin is predominantly present as the −3 charged 1:2 bischelate complex, and that the formation of the 1:1 monochelate complex makes a relatively low contribution to the overall boron adsorption. The decrease in the amounts of adsorbed boron in the weakly acidic or basic solution is due to the decrease in the conditional formation constants. In order to estimate the formation constants of the chelate complexes of boric acid with the ligand **LAc** in the adsorbent, we have carried out a Langmuir analysis for the adsorption of boron onto the **LAc** loaded resin at the optimum pH of 7. Leakage of the ligand from the resin was less than 1.6% under the experimental conditions. The quotient, $\overline{C}_B/([\overline{B(OH)_3}]\overline{C}_L)$, is given by the following equation:

$$\frac{\overline{C}_B}{[\overline{B(OH)_3}]\overline{C}_L} = \frac{[\overline{B(OH)_3}] + [\overline{B(OH)_4^-}] + [\overline{B\mathbf{LAc}^{2-}}] + [\overline{B(\mathbf{LAc})_2^{3-}}]}{[\overline{B(OH)_3}]([\overline{\mathbf{LAc}^-}] + [\overline{\mathbf{LAc}^{2-}}] + [\overline{B\mathbf{LAc}^{2-}}] + 2[\overline{B(\mathbf{LAc})_2^{3-}}])} \quad (12)$$

where the upper bar refers to the resin phase, and $\overline{C}_L$ (mmol g^{-1}) and $\overline{C}_B$ (mmol g^{-1}) are the total amounts of **LAc** and boron adsorbed onto the resin on a dry-weight basis, respectively. Judging from the strong adsorbability, $[\overline{B(\mathbf{LAc})_2^{3-}}]$ is much higher than $[\overline{B(OH)_3}] + [\overline{B(OH)_4^-}] + [\overline{B\mathbf{LAc}^{2-}}]$, and therefore we can get the following equation for a low boron loading condition:

$$\frac{[\overline{B(OH)_3}]}{\overline{C}_B} = \frac{1}{\overline{\beta}_{f(\mathbf{BLAc2})}} \frac{(\overline{K}_{a2(\mathbf{LAc})} + [\overline{H^+}])^2}{\overline{K}_{a2(\mathbf{LAc})}\overline{C}_L^2[\overline{H^+}]} + 2\frac{[\overline{B(OH)_3}]}{\overline{C}_L} \quad (13)$$

where $\overline{\beta}_{f(\mathbf{BLAc2})}$ (mol^{-2} dm^6) is the overall formation constant of the 1:2 bischelate complex (the main boron species adsorbed) in the resin phase.

$$\overline{\beta}_{f(\mathbf{BLAc2})} = [\overline{B(\mathbf{LAc})_2^{3-}}]/([\overline{B(OH)_3}][\overline{\mathbf{LAc}^{2-}}][\overline{\mathbf{LAc}^-}]) \quad (14)$$

Since $B(OH)_3$ has no charge, $[\overline{B(OH)_3}]$ can be replaced with the concentration of boric acid in the equilibrated solution. According to Eq. (13), the value on the left was plotted versus $[\overline{B(OH)_3}]$. A good linear relationship was obtained as shown in Fig. 7. From the slope, we estimated the total amount of **LAc** adsorbed to be $\overline{C}_L = 1.5$ mmol g^{-1}, which agrees well with the estimated amount of 1.40 mmol g^{-1} from the absorbance change at 249 nm.

In our previous studies [34,35], the hydrogen ion concentration in an anion-exchange resin had been estimated from the ^{31}P NMR chemical shift of phosphorus oxoanions adsorbed onto the resin. A linear relationship was obtained between the pH values in the resin phase and in the equilibrated solution:

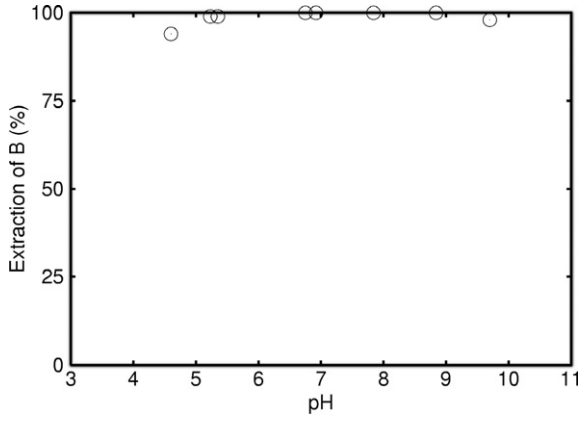

Fig. 5. Extraction percentage of boron by the anion-exchange resin presorbed with **LAc**. Solution (3.0 mmol dm^{-3} boric acid/borate): 20 cm^3; Resin: 0.20 g; Shaking time 3 d at 25 °C.

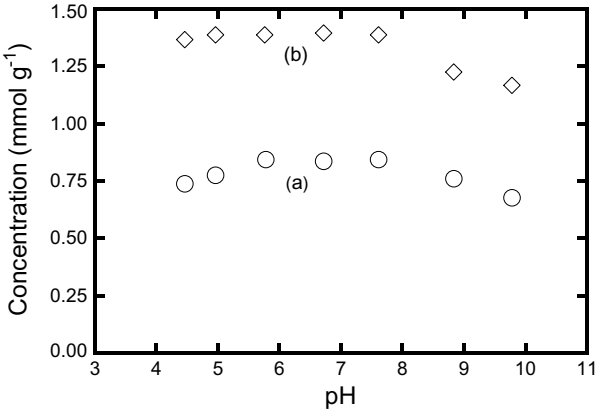

Fig. 6. Adsorption capacity of boron and the ligand **LAc** toward the anion-exchange resin as a function of pH (amounts of (a) boron and (b) ligand adsorbed onto 1 g of dried resin). Solution (30 mmol dm^{-3} boric acid/borate): 20 cm^3; Resin: 0.20 g; shaking time 3 d at 25 °C.

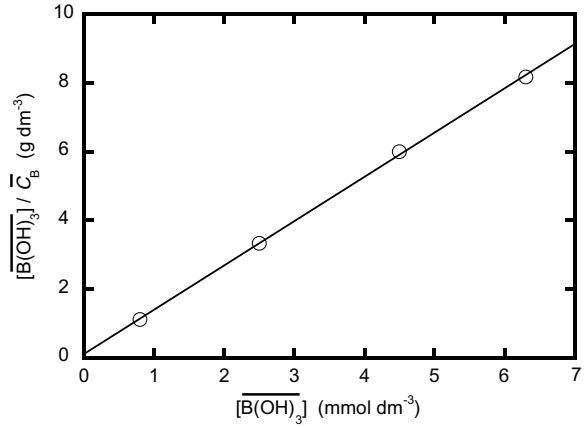

Fig. 7. Langmuir plot for the adsorption of boron onto the anion-exchange resin presorbed with **LAc** at pH 7. Solution (0.02 mol dm^{-3} HEPES): 20 cm^3; Resin: 0.20 g; Shaking time 3 d at 25 °C.

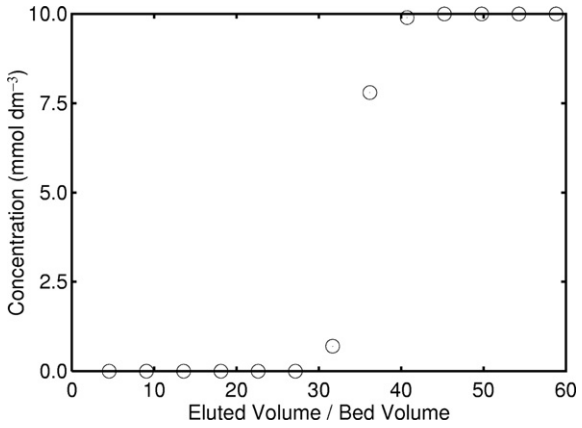

Fig. 8. Column breakthrough profile of boron for the anion-exchange resin presorbed with **LAc** at 25 °C. Flow rate: 0.5 $cm^3\ min^{-1}$; solution: 10 mmol dm^{-3} boric acid/borate; resin: 1.00 g (bed volume: 2.21 cm^3).

$$-\log[\overline{H^+}] = -a\log[H^+] + b \quad (15)$$

where $a \approx 1$ and $b = 0.52$–0.61 for the strong-base type anion-exchange resin of the Cl^- form at $I = 0.1$ mol dm^{-3} (NaCl). This relationship was interpreted as proof of the Donnan relation. We then made a rough estimate of the hydrogen ion concentration in the **LAc** loaded resin by Eq. (15) with $a = 1$ and $b = 0.5$. By assuming $\overline{K}_{a2(\mathbf{LAc})} = K_{a2(\mathbf{LAc})}$, we evaluated the overall formation constant of the 1:2 bischelate complex in the resin phase, $\overline{\beta}_{f(\mathbf{BLAc2})}$, to be $10^{5.0}$ at 25 °C from the intercept of the plot in Fig. 7. The constant in the resin phase roughly agrees with those of the salicyl alcohol derivatives in aqueous solutions (Table 2).

Fig. 8 shows a column breakthrough profile for the **LAc** loaded resin. A flow rate of 0.52 $cm^3\ min^{-1}$ is equal to a space velocity of 14 beds h^{-1}. About 0.72 mmol of boric acid, which is almost half the amount of **LAc** loaded, was removed. Therefore, the prepared resin efficiently removes boric acid/borate from aqueous solutions up to the total boron adsorption capacity at a relatively high flow rate.

4. Conclusion

The interaction of boric acid with salicylic acid, salicyl alcohol and bis(hydroxymethyl)phenol derivatives has been examined in order to develop boron-selective adsorbents having these derivatives as anchor groups. Boric acid accepts the electron pair through the nucleophilic attack of the ligand, followed by the condensation reaction, to form the 1:1 monochelate complex. The monochelate complex then reacts with the ligand through the condensation reaction to give the 1:2 bischelate complex. Bis(hydroxymethyl)phenol derivatives form highly stable chelate complexes among the examined salicyl derivatives. The anion-exchange resin presorbed with 3,5-bis(hydroxymethyl)-4-hydroxybenzoate had a strong adsorbability of boron over a wide pH range. The adsorbent quantitatively removes boron up to approximately half the amount of the ligand loaded onto the resin. The boron species adsorbed onto the resin is predominantly present as the −3 charged 1:2 bischelate complex. The formation constant of the 1:2 bischelate complex with 3,5-bis(hydroxymethyl)-4-hydroxybenzoate in the resin phase was estimated to be $\overline{\beta}_{f(\mathbf{BLAc2})} = 5.0$, which almost agreed with those of the salicyl alcohol derivatives in aqueous solutions. Polyalcohol compounds interact with borate, therefore, functional groups, such as *N*-methyl-glucamine, contribute to the boron uptake from a slightly alkaline solution with the highest degree of efficiency [1–4]. On the contrary, in the bis(hydroxymethyl)phenol derivative system, the optimum pH for the boron adsorption was in the neutral range, so that the presorbed resin will be suitable for the adsorption and/or removal of boron from natural water without any troublesome pretreatment.

Acknowledgements

We thank Dr. Hirofumi Sakashita and Dr. Yoshinori Miura of the Center of Advanced Instrumental Analysis, Kyushu University, for their help in obtaining the ^{11}B NMR data. This work was partially supported by the Salt Science Research Foundation (No. 0621-2006).

References

[1] R. Kunin, A.F. Preuss, Ind. Eng. Chem., Prod. Res. Dev. 3 (1964) 304.
[2] U. Schide, E. Uhlemann, React. Polym. 18 (1992) 155.
[3] K. Yoshimura, Y. Miyazaki, F. Ota, S. Matsuoka, H. Sakashita, J. Chem. Soc., Faraday Trans. 94 (1998) 683.
[4] Y. Inukai, Y. Tanaka, T. Matsuda, N. Mihara, K. Yamada, N. Nambu, O. Itoh, T. Doi, Y. Kaida, S. Yasuda, Anal. Chim. Acta 511 (2004) 261.
[5] K. Yoshimura, R. Kariya, T. Tarutani, Anal. Chim. Acta 109 (1979) 115.
[6] M. Matsumoto, T. Matsui, K. Kondo, J. Chem. Eng. Jpn. 32 (1999) 190.
[7] Y. Inukai, Y. Kaida, S. Yasuda, Anal. Chim. Acta 343 (1997) 275.
[8] K. Yoshimura, Y. Miyazaki, S. Sawada, H. Waki, J. Chem. Soc., Faraday Trans. 92 (1996) 651.
[9] C. Shao, Y. Miyazaki, S. Matsuoka, K. Yoshimura, H. Sakashita, Macromolecules 33 (2000) 19.
[10] Y. Miyazaki, C. Shao, S. Matsuoka, K. Yoshimura, J. Ion Exchange 14 (Supplement) (2003) 33.
[11] H. Maeda, H. Egawa, A. Jyo, Sep. Sci. Technol. 30 (1995) 3545.
[12] J.G. Dawber, S.I.E. Green, J. Chem. Soc., Faraday Trans. 1 82 (1986) 3407.
[13] J.G. Dawber, S.I.E. Green, J.C. Dawber, S. Gabrail, J. Chem. Soc., Faraday Trans. 1 84 (1988) 41.
[14] R. Pizer, P.J. Ricatto, Inorg. Chem. 33 (1994) 2402.
[15] Y. Miyazaki, K. Yoshimura, S. Matsuoka, Y. Miura, H. Sakashita, K. Ishimaru, Polyhedron 22 (2003) 909.
[16] T.M. Suzuki, D.A.P. Tanaka, T. Yokoyama, Y. Miyazaki, K. Yoshimura, J. Chem. Soc., Dalton Trans. (1999) 1639.
[17] C. Shao, S. Matsuoka, Y. Miyazaki, K. Yoshimura, Analyst 127 (2002) 1614.
[18] C. Shao, S. Matsuoka, Y. Miyazaki, K. Yoshimura, T.M. Suzuki, D.A.P. Tanaka, J. Chem. Soc., Dalton Trans. (2000) 3136.
[19] C. Shao, S. Matsuoka, Y. Miyazaki, K. Yoshimura, Anal. Sci. 17 (Supplement) (2001) i1475.
[20] H. Matsuo, Y. Miyazaki, H. Takemura, S. Matsuoka, H. Sakashita, K. Yoshimura, Polyhedron 23 (2004) 955.
[21] J. de Mendoza, P.M. Nietro, P. Prados, C. Sánchez, Tetrahedron Lett. 46 (1990) 671.
[22] H. Takemura, K. Yoshimura, I.U. Khan, T. Shinmyozu, T. Inazu, Tetrahedron Lett. 33 (1992) 5775.
[23] I.U. Khan, H. Takemura, M. Suenaga, T. Shinmyozu, T. Inazu, J. Org. Chem. 58 (1993) 3158.
[24] HyperChem Release 6.03, Serial No.12-600-1500800089, Hypercube Inc.
[25] J.J.P. Stewart, MOPAC Manual, 6th ed., United States Air Force Academy, Colorad Springs, 1990.
[26] CAChe Release 6.1.1, Serial No. 1502700302, Fujitsu Ltd., Japan.
[27] M.J. Frisch, G.W. Truck, H.B. Schlegel, G.E. Scuseria, M.A. Robb, J.R. Cheeseman, V.G. Zakrzewski, J.A. Montgomery Jr., R.E. Stratmann, J.C. Burant, S. Dapprich, J.M. Millam, A.D. Daniels, K.N. Kudin, M.C. Strain, O. Farkas, J. Tomasi, V. Barone, M. Cossi, R. Cammi, B. Mennucci, C. Pomelli, C. Adamo, S. Clifford, J. Ochterski, G.A. Petersson, P.Y. Ayala, Q. Cui, K. Morokuma, D.K. Malick, A.D. Rabuck, K. Raghavachari, J.B. Foresman, J. Cioslowski, J.V. Ortiz, A.G. Boboul, B.B. Stefnov, G. Liu, A. Liaschenko, P. Piskorz, L. Komaromi, R. Gomperts, R.L. Martin, D.J. Fox, T. Keith, M.A. Al-Laham, C.Y. Peng, A. Nanayakkara, C. Gonzalez, M. Challacombe, P.M.W. Gill, B. Johnson, W. Chen, M.W. Wong, J.L. Andres, M. Head-Gordon, E.S. Replogle, J.A. Pople, Gaussian 98, Revision X, Gaussian Inc., Pittsburgh, PA, 1998.
[28] W.D. Basson, R.G. Böhmer, D.A. Stanton, Analyst 94 (1969) 1135.
[29] R.A. Edwards, Analyst 105 (1980) 139.
[30] K. Nose, M. Zenki, Y. Shimoishi, Bunseki Kagaku 42 (1993) 351.
[31] D.D. Perrin, Nature 182 (1958) 741.
[32] R.G. Charles, J. Org. Chem. 22 (1957) 677.
[33] K. Benner, P. Klufers, Carbohydr. Res. 327 (2000) 287.
[34] A. Marton, Y. Miyazaki, Prog. Colloid Polym. Sci. 117 (2001) 153.
[35] A. Marton, H. Sakashita, Y. Miura, E. Hiramatsu, Y. Miyazaki, Talanta 59 (2003) 217.

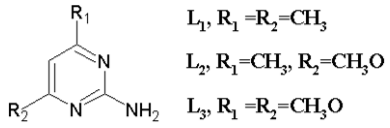

Chart 1. Structural drawings of ligands L_1–L_3.

and $[Ag(L_3)(ClO_4)]_n$ [L_1 = 2-amino-4,6-dimethylpyrimidine; L_2 = 2-amino-4-methoxy-6-methylprimidine; L_3 = 2-amino-4,6-dimethoxyprimidine]. The research results indicate that the nature of counter anions and the ligands have great influence on the formation and structure of metal–organic frameworks.

2. Experimental

2.1. Caution!

Perchlorate salts in the presence of organic ligands are potentially explosive and heating has to be avoided. Only small amounts of the materials should be prepared, and handled with care.

2.2. Materials and instruments

All starting materials were of reagent quality and were obtained from commercial sources without further purification. Infrared spectra were recorded on a Nicolet AVATAT FT-IR360 spectrometer as KBr pellets in the frequency range 4000–400 cm^{-1}. The elemental analyses (C, H, N contents) were determined on a CE instruments EA 1110 analyzer. Photoluminescence measurements were performed on a Hitachi F-4500 fluorescence spectrophotometer with solid powder on a 1 cm quartz round plate at room temperature.

2.3. Synthesis of complexes

2.3.1. Synthesis of complex $[Ag(L_1)(CF_3SO_3)(H_2O)]_n$ (**1**)

A methanol solution (5 ml) of L_1 (47 mg, 0.5 mmol) was slowly diffused into an aqueous solution (5 ml) of silver trifluoromethylsulfonate $AgCF_3SO_3$ (130 mg, 0.5 mmol) in a test tube. Colorless rod-like crystals of **1** were formed at the interface of the solvent in three weeks and were obtained in 55% yield. *Anal.* Calc. for $AgC_7H_{11}N_3O_4F_3S$: C, 21.12; H, 2.78; N, 10.55. Found: C, 21.19; H, 2.70; N, 10.62%. IR (cm^{-1}): 3421 (s), 3331 (m), 3171 (br), 1656 (m), 1589 (m), 1467 (m), 1384 (m), 1285 (s), 1254 (s), 1164 (m), 1040 (s), 950 (m), 825 (m), 794 (m), 638 (m), 554 (m), 520 (m).

2.3.2. Synthesis of complex $[Ag_4(L_1)_4(CF_3CO_2)_4]_n$ (**2**)

The synthesis of **2** was similar to that of **1**, but with silver trifluoroacetate $AgCF_3CO_2$ (0.5 mmol) instead of $AgCF_3SO_3$. Colorless crystals of **2** were obtained in 67% yield. *Anal.* Calc. for $Ag_4C_{32}H_{32}N_{12}O_8F_{12}$: C, 33.04; H, 2.77; N, 14.45. Found: C, 33.07; H, 2.71; N, 14.50%. IR (cm^{-1}): 3396 (s), 3301 (m), 1685 (s), 1654 (m), 1595 (m), 1569 (m), 1467 (m), 1431 (m), 1391 (m), 1366 (w), 1207 (s), 1134 (m), 1039 (m), 985 (w), 927 (w), 838 (m), 804 (m), 723 (m), 567 (m), 547 (m), 467 (w).

2.3.3. Synthesis of complex $[Ag_2(L_1)_4(ClO_4)_2]$ (**3**)

To a solution of silver perchlorate $AgClO_4$ (208 mg, 1 mmol) in water (3 ml) was added a solution of L_1 (123 mg, 1 mmol) in a water–methanol (5:5 v/v, 10 mL) at 60 °C. A small amount of white precipitate was removed from the resulting solution. X-ray-quality crystals of **3** as colorless block-like were obtained by slow evaporation at room temperature after one week. They were washed with a small volume of cold methanol and diethyl ether. Yield: ca. 65% yield. *Anal.* Calc. for $Ag_2C_{24}H_{36}N_{12}O_8Cl_2$: C, 31.77; H, 4.00; N, 18.53. Found: C, 31.84; H, 3.94; N, 18.63%. IR (cm^{-1}): 3396 (s), 3313 (m), 3138 (br), 1654 (s), 1594 (m), 1568 (m), 1475 (m), 1453 (m), 1384 (s), 1233 (m), 1026 (m), 961(m), 834 (m), 825 (m), 788 (m), 729 (m), 567 (m), 547 (m), 474 (m).

2.3.4. Synthesis of complex $[Ag(L_2)(ClO_4)]_n$ (**4**)

The synthesis of **4** was similar to that of **3**, but with ligand L_2 (1 mmol) instead of ligand L_1. Colorless crystals were obtained in 50% yield. *Anal.* Calc. for $AgC_6H_9N_3O_5Cl$: C, 20.80; H, 2.62; N, 12.13. Found: C, 20.85; H, 2.55; N, 12.08%. IR (cm^{-1}): 3367 (s), 3314 (w), 3183 (m), 3023 (m), 1637 (s), 1585 (s), 1458 (m), 1384 (s), 1346 (m), 1204 (m), 1152 (m), 1023 (m), 938 (m), 839 (w), 798 (m), 782 (m), 646 (m), 585 (w), 546 (w).

2.3.5. Synthesis of complex $[Ag(L_3)(ClO_4)]_n$ (**5**)

The synthesis of **5** was similar to that of **3**, but with ligand L_3 (1 mmol) instead of ligand L_1. Colorless crystals were obtained in 60% yield. *Anal.* Calc. for $AgC_6H_9N_3O_6Cl$: C, 22.04; H, 2.77; N, 12.85. Found: C, 21.85; H, 2.90; N, 12.92%. IR (cm^{-1}): 3413 (m), 3312 (m), 3192 (m), 3025 (m), 1637 (s), 1581 (s), 1452 (m), 1384 (s), 1215 (m), 1151 (m), 1102 (m), 1047 (m), 928 (m), 794 (m), 786 (m), 671 (m), 564 (w), 512 (w).

2.4. X-ray crystallography

Single crystals of these complexes with appropriate dimensions were mounted on a glass fiber and used for data collection. Data was collected on a Bruker-AXS CCD diffractometer equipped with a graphite-monochromated Mo Kα radiation source (λ = 0.71073 Å) at 298 K for **1** and **2** and at 173 K for **3**–**5**. All absorption corrections were performed with the SADABS program [24a]. All the structures were solved by direct methods using SHELXS-97 [24b] and refined by full-matrix least-squares techniques using SHELXL-97 [24c]. All the non-hydrogen atoms were treated anisotropically. The positions of hydrogen atoms were generated geometrically. The crystallographic details of **1**–**5** are summarized in Table 1. Selected bond lengths and bond angles of **1**–**5** are displayed in Table 2.

3. Results and discussion

3.1. Construction

The syntheses of complexes **1**–**5** are summarized in Scheme 1 in the Supplementary data. The formation of the products is not significantly affected by changes of the reaction mole ratio of ligands to metal ions, and the resultant crystals are insoluble in water and common organic solvents. The reactions of L_1 with $AgCF_3SO_3$ and $AgCF_3CO_2$ yield 1D zigzag chain structure (**1**), 1D ladder network (**2**), respectively. The different structure of complexes **1**–**2** is caused by the difference in coordination ability and geometry of the counter anions. In contrast to the bridge coordination of $CF_3CO_2^-$ anions in **2**, weak mono-coordination of $CF_3SO_3^-$ anions occurred in **1**. The trifluoromethylsulfonate anions locate to the one side of the 1D chain and link the adjacent 1D chains to form a 1D ladder structure *via* O(w)–H···O($CF_3SO_3^-$) hydrogen bonds. On the other hand, the structures of complexes **3–5** are directed by the different ligands adopted in the reaction system: the reaction of $AgClO_4$ with L_1 yields a dimer (**3**). The reaction of $AgClO_4$ with L_2 leads to a 2D grid network (**4**). When L_3 is used, a 1D zigzag chain (**5**) (if the Ag···Ag interactions are excluded) different from that of **1** is obtained, which further connected into 3D framework through N–H···O intermolecular hydrogen bonds and Ag···O weak interaction. In complexes **3**–**5**,

Table 1
Crystallographic data for complexes **1**–**5**

Complexes	**1**	**2**	**3**	**4**	**5**
Formula	$AgC_7H_{11}N_3O_4F_3S$	$Ag_4C_{32}H_{32}N_{12}O_8F_{12}$	$Ag_2C_{24}H_{36}N_{12}O_8Cl_2$	$AgC_6H_9N_3O_5Cl$	$AgC_6H_9N_3O_6Cl$
M_r	398.12	1372.18	907.29	346.48	362.48
Crystal system	orthorhombic	triclinic	triclinic	monoclinic	orthorhombic
Space group	*Pbca*	$P\bar{1}$	$P\bar{1}$	$P2_1/n$	*Pccn*
a (Å)	14.256(8)	10.862(3)	7.3094(3)	8.1291(1)	14.2842(3)
b (Å)	12.635(7)	11.119(3)	8.5764(4)	10.8255(2)	11.7549(2)
c (Å)	15.689(9)	11.559(3)	13.4415(5)	12.0301(2)	12.6474(2)
α (°)	90	116.979(5)	96.464(3)	90	90
β (°)	90	106.079(5)	93.870(3)	102.786(2)	90
γ (°)	90	100.616(5)	100.107(3)	90	90
Z	8	1	1	4	8
V (Å^3)	2826(3)	1114.4(6)	820.99(6)	1032.42(3)	2123.62(7)
D_{calc} (g cm^{-3})	1.871	2.045	1.835	2.229	2.268
μ (mm^{-1})	1.620	1.843	1.421	2.222	2.172
F(000)	1568	668	456	680	1424
Number of unique reflections	3000	3842	3163	2005	2313
Number of observed reflections [$I > 2\sigma(I)$]	2136	3339	2794	1880	1960
Parameters	175	307	217	145	154
Goodness-of-fit	0.974	1.104	1.032	1.060	1.015
Final *R* indices [$I > 2\sigma(I)$]	$R_1 = 0.0488$, $wR_2 = 0.1091$	$R_1 = 0.0537$, $wR_2 = 0.1366$	$R_1 = 0.0291$, $wR_2 = 0.0795$	$R_1 = 0.0187$, $wR_2 = 0.0447$	$R_1 = 0.0192$, $wR_2 = 0.0494$
R indices (all data)	$R_1 = 0.0704$, $wR_2 = 0.1196$	$R_1 = 0.0616$, $wR_2 = 0.1424$	$R_1 = 0.0341$, $wR_2 = 0.0813$	$R_1 = 0.0206$, $wR_2 = 0.0453$	$R_1 = 0.0250$, $wR_2 = 0.0512$
Largest difference peak and hole (e Å^{-3})	0.939 and −1.131	1.216 and −0.523	0.770 and −0.540	0.522 and −0.481	0.453 and −0.487

Table 2
Selected bond distances (Å) and angles (°) for **1**–**5**

Complex **1**					
Ag(1)–N(1)	2.226(3)	Ag(1)–N(1)	2.235(3)	Ag(1)–O(1w)	2.521(3)
Ag(1)–O(1)	2.691(3)				
N(1)–Ag(1)–N(2)	150.1(1)	N(1)–Ag(1)–O(1w)	108.4(1)		
N(2)–Ag(1)–O(1w)	99.4(1)	O(1)–Ag(1)–O(1w)	80.3(1)		
Complex **2**					
Ag(1)–N(3)	2.254(5)	Ag(1)–O(3)	2.332(5)	Ag(1)–O(1)	2.382(5)
Ag(1)–N(2)	2.423(4)	Ag(2)–N(6)	2.166(4)	Ag(2)–N(4)	2.172(4)
Ag(2)–O(2)	2.485(5)	Ag(2)–O(3)	2.674(5)		
N(3)–Ag(1)–O(3)	140.8(2)	N(3)–Ag(1)–O(1)	114.8(2)		
O(3)–Ag(1)–O(1)	91.4(2)	N(3)–Ag(1)–N(2)	110.2(2)		
O(3)–Ag(1)–N(2)	94.6(2)	O(1)–Ag(1)–N(2)	95.7(2)		
N(6)–Ag(2)–N(4)	158.3(2)	N(6)–Ag(2)–O(2)	97.5(2)		
N(4)–Ag(2)–O(2)	102.4(2)	N(6)–Ag(2)–O(3)	101.6(2)		
N(4)–Ag(2)–O(3)	83.6(2)	O(2)–Ag(2)–O(3)	100.2(2)		
Complex **3**					
Ag(1)–N(1)	2.286(3)	Ag(1)–N(4)	2.235(2)	Ag(1)–N(2)^{i}	2.448(2)
Ag(1)^{i}–N(2)	2.252(9)				
N(4)–Ag(1)–N(1)	147.36(9)	N(4)–Ag(1)–N(2)^{i}	118.60(9)		
N(1)–Ag(1)–N(2)^{i}	92.27(8)				
Complex **4**					
Ag(1)–N(2)	2.213(2)	Ag(1)–N(1)	2.257(2)	Ag(1)–O(1)	2.627(3)
Ag(1)–O(3)	2.639(4)				
N(2)–Ag(1)–N(1)	141.61(7)	O(1)–Ag(1)–O(3)	78.98(7)		
Complex **5**					
Ag(1)–N(1)	2.172(2)	Ag(1)–N(3)^{i}	2.183(2)	Ag(1)–Ag(1)^{ii}	3.3764(4)
N(1)–Ag(1)–N(3)^{i}	167.11(6)	N(1)–Ag(1)–Ag(1)^{ii}	95.36(5)		
N(3)–Ag(1)–Ag(1)^{ii}	79.21(4)				

Symmetry transformations used to generate equivalent atoms: (i), $-x+2$, $-y+1$, $-z+1$, for **3**. (i), x, $-y+1/2$, $z+1/2$; (ii), $-x+1/2$, $-y+1/2$, z, for **5**.

2-aminopyrimidyl derivatives adopt similar coordination modes, a bidentate N,N′-donor ligands binding with silver atoms, while the different substitutions of 2-aminopyrimidyl ligands in the same substitutional positions in the three complexes result in distinct structural motifs. Thus, we have reason to believe that subtle structural changes of ligands might create a tuning effect on the formation of crystal structures. Additionally, as far as certain ligand such as L_1 concerned, the structure of complexes (**1**–**3**) can be controlled by different counter anions. Furthermore, the overall architecture in complexes **1**–**5** may partly be ascribed to the N–H···O interactions between the amino groups of pyrimidyl ligands and the counter anions.

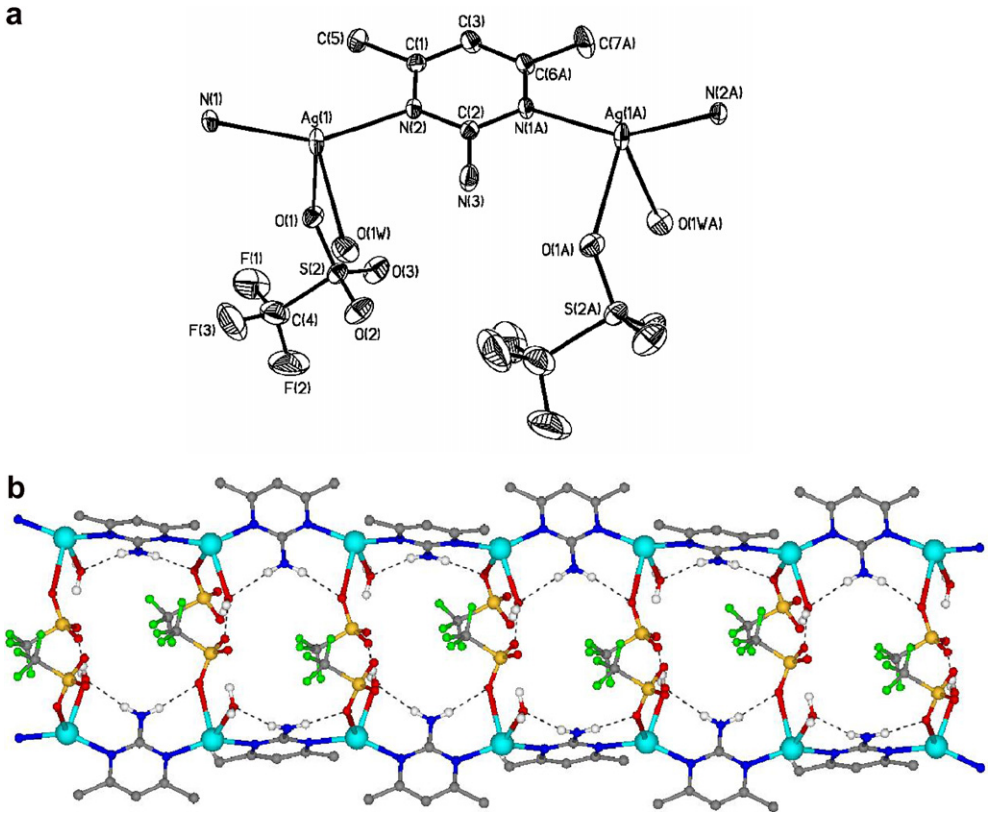

Fig. 1. (a) Crystal structure of **1** with the coordination environment around the silver(I) center (ellipsoids at 40% probability). (b) A view along the *a* axis of the 1D motif in **1**. Hydrogen atoms in methyl and phenyl groups are omitted for clarity. Ag stressed in bigger ball ( ).

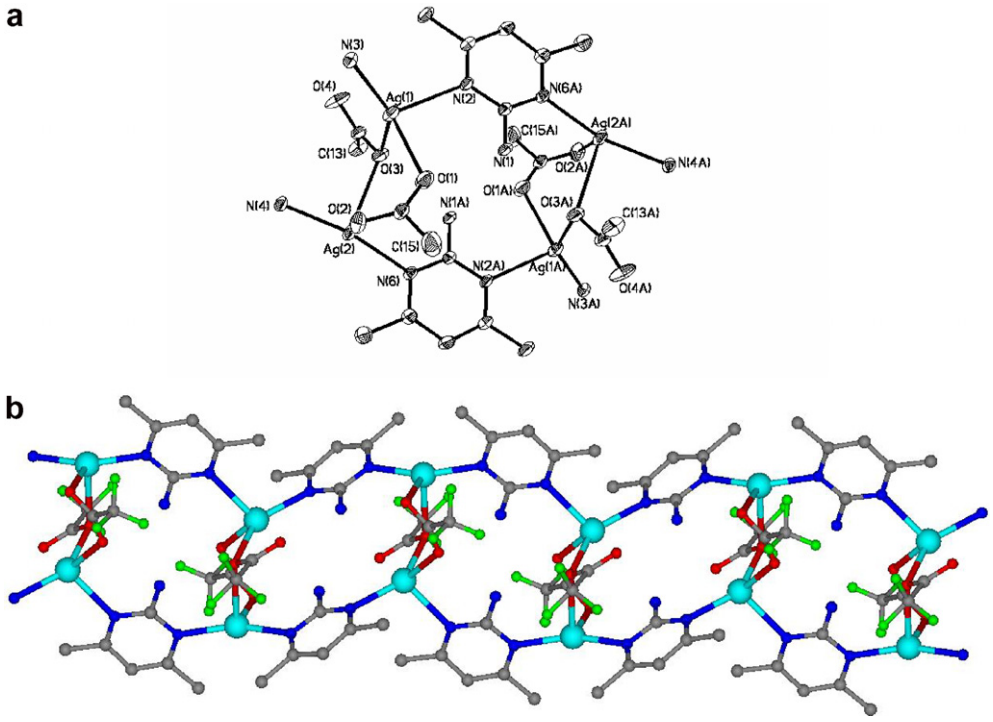

Fig. 2. (a) Perspective view shows the molecular and crystal structure of **2,** the fluorine atoms on C13, C15, C13A and C15A are omitted for clarity. (b) A packing diagram showing the 1D ladder structure in **2**. All hydrogen atoms are omitted for clarity. Ag stressed in bigger ball ( ).

3.2. Description of crystal structures

3.2.1. Crystal structures of $[Ag(L_1)(CF_3SO_3)(H_2O)]_n$ (**1**), $[Ag_4(L_1)_4(CF_3CO_2)_4]_n$ (**2**) and $[Ag_2(L_1)_4(ClO_4)_2]$ (**3**)

To investigate the effect of counter anions on the structure of silver(I) complexes, the reactions of L_1 with $AgCF_3SO_3$, $AgCF_3CO_2$ and $AgClO_4$ were carried out, respectively, and complexes **1**–**3** were isolated. The X-ray crystallographic analysis shows that **1** crystallizes in the orthorhombic space group *Pbca* and has an infinite 1D zigzag chain structure. As depicted in Fig. 1a, the basic repeat is a distorted tetragonal four-coordinate AgO_2N_2 unit, which comprises a unidentate association to one O-atom donor from one anion $CF_3SO_3^-$, one O-atom donor from one coordinated water, and two independent pyrimidine hetero-nitrogens [Ag(1)–N(1) = 2.226(3) Å; Ag(1)–N(2) = 2.235(3) Å] in a distinctly nonlinear geometry [N(1)–Ag(1)–N(2) = 150.1(1)°] forming zigzag chains. The deviation from linear geometry is due to the weak interaction between Ag atom and O atom on the water molecule [Ag(1)–O(1w) = 2.521(3) Å]. The average Ag–N distance in **1** is agreement with those reported in literature, such as $[\{Ag(pts)\}_2(L_1)_3]_n$ [22b] and $[Ag(L_1)(NO_3)]_n$ [22h] (pts = *p*-toluenesulfonate). The anions $CF_3SO_3^-$ are weakly bonded to Ag(I) ions with Ag–O distances of 2.691(3) Å. All anions are oriented to the one side of the 1D chain. In the 1D chain, intramolecular hydrogen bonds are observed involving the amino group of the L_1 with the oxygen atoms on the coordinated $CF_3SO_3^-$ anion, and on the coordinated water molecule, respectively [2.914(4) and 2.950(4) Å for N(3)···O(1w) and N(3)···O(1A), respectively, symmetry for A: $-x + 1/2, y + 1/2, z$]. The chains in **1** are interlinked by means of intermolecular hydrogen bonds in which two coordinated water molecules of adjacent chains and one trifluoromethylsulfonate anion are involved [O(1w)···O(2) = 2.823(5), O(1w)···O(3B) = 2.764(4); symmetry code: B = $x - 1/2, y, -z + 1/2$] to generate 1D ladder structure (Fig. 1b).

Complex **2** crystallizes in the space group $P\bar{1}$ and has a 1D ladder structure. The structure of **2** with the atom labeling is displayed in Fig. 2a. Each four-coordinate Ag which adopts a slightly distorted tetrahedral geometry is coordinated by a μ_1-O of one $CF_3CO_2^-$ [2.382(5) and 2.485(5) Å for Ag(1)–O(1) and Ag(2)–O(2)], a μ_2-O of the other $CF_3CO_2^-$ [2.332(5) and 2.674(5) Å for Ag(1)–O(3) and Ag(2)–O(3)], and two bridging L_1 pyrimidine nitrogen donors, and the angle of O–Ag–O [91.4(2)° for O(3)–Ag(1)–O(1)] is responsible for the slightly distorted tetrahedral geometry of Ag^+ ions. Due to the coordination ability of the $CF_3CO_2^-$ is stronger than the $CF_3SO_3^-$, the Ag–O bond lengths in **2** are shorter than the corresponding ones in **1**, indicative of strong interactions between oxygen and silver. The most remarked feature is that the $[Ag_4(L_1)_4(CF_3CO_2)_4]$ cores in **2** are interlinked together *via* the bridging L_1 groups to generate a 1D ladder motif (Fig. 2b). In the motif, every ring of the ligands is nearly parallel to the adjacent corresponding ring and the intrachain and interchain Ag···Ag separation is 3.843 and 6.463 Å, respectively. In addition, hydrogen bonds

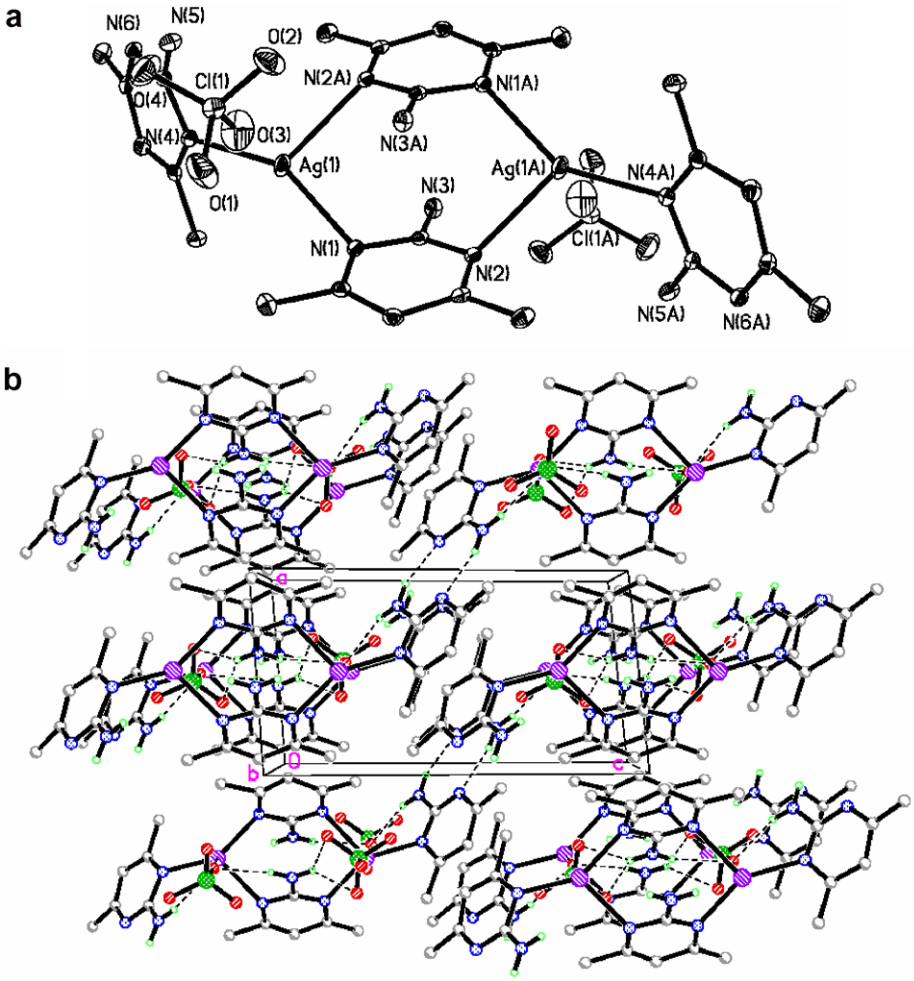

Fig. 3. (a) ORTEP drawing of **3** with 40% probability displacement ellipsoids. (b) A view of the 3D packing diagram in **3**. Hydrogen atoms in methyl and phenyl groups are omitted for clarity.

between the free amino groups on the L_1 ligands and $CF_3CO_2^-$ anions [H···N, 1.97–2.10 Å, N···O, 2.824–2.947 Å, N–H···O, 152.3–177.6°] contribute to the stabilization of the structure of **2** (Fig. S1).

Complex **3** also crystallizes in triclinic space group $P\bar{1}$. Unlike polymer **1** and **2**, **3** is a binuclear Ag^I complex. The asymmetric unit of **3** consists of one Ag^I, two L_1 ligands. Each silver(I) atom in **3** is coordinated by one nitrogen atom from η^1-L_1 and two nitrogen atoms from two different μ_2-L_1 ligands with distorted triangular coordination geometry as shown in Fig. 3a. The bond distances and bond angles around Ag1 range from 2.235(2) to 2.448(2) Å and 92.27(8)° to 147.36(9)°. These bonds distances are slightly longer than the corresponding values for **1**. It is noteworthy that two μ_2-L_1 ligands connect two Ag atoms to form an eight-membered M_2L_2 binuclear ring, rather than to form a 1D chain as observed in **1**. The Ag_2N_4 eight-member ring reveals a chair-like conformation. Each dimeric $[Ag_2(L_1)_4]$ unit is hydrogen bonded to two other units to form a 1D chain resulting from N–H···N hydrogen bonds (Fig. S2). The 1D chains further interact in the form of π–π attractions between pyrimidyl whose rings are arranged in offset face-to face mode to produce an infinite 2D layer framework structure (Fig. S3). The centroid–centroid distance of pyrimidyl in **3** is about 3.37 Å, which indicates a strong π–π stacking. An extended 3D supramolecular structure arises from further hydrogen bonds between oxygen atoms of perchlorate anions and the uncoordinated amino groups on the L_1 ligands (Fig. 3b).

3.2.2. Crystal structure of $[Ag(L_2)(ClO_4)]_n$ (**4**)

To investigate the influence of ligands on the structure of self-assembly product further, we carried out the reaction of $AgClO_4$ with ligand L_2 instead of L_1 under the same reaction conditions as **3**. A new coordination polymer **4** with a different structure was obtained. The crystallographic studies reveal that complex **4** which conforms to the space group $P2_1/n$, exists in the solid state as a 2D grid network structure and the L_2 ligand adopts the coordination mode as we predicted. Fig. 4a depicts a view with atom numbering the molecule. Each central Ag(I) cation has distorted tetragonal geometry, which is confined by two nitrogen atoms [2.257(2) and 2.213(2) Å for Ag(1)–N(1) and Ag(1)–N(2)] from two pyrimidine rings, and weakly coordinated by two oxygen atoms [Ag(1)–O(1), 2.627(3) Å; Ag(1)–O(3A), 2.639(4) Å] from two different perchlorate groups. The average Ag–N distances in **4** are comparable to those found in **1**. As shown in Fig. 4b, each

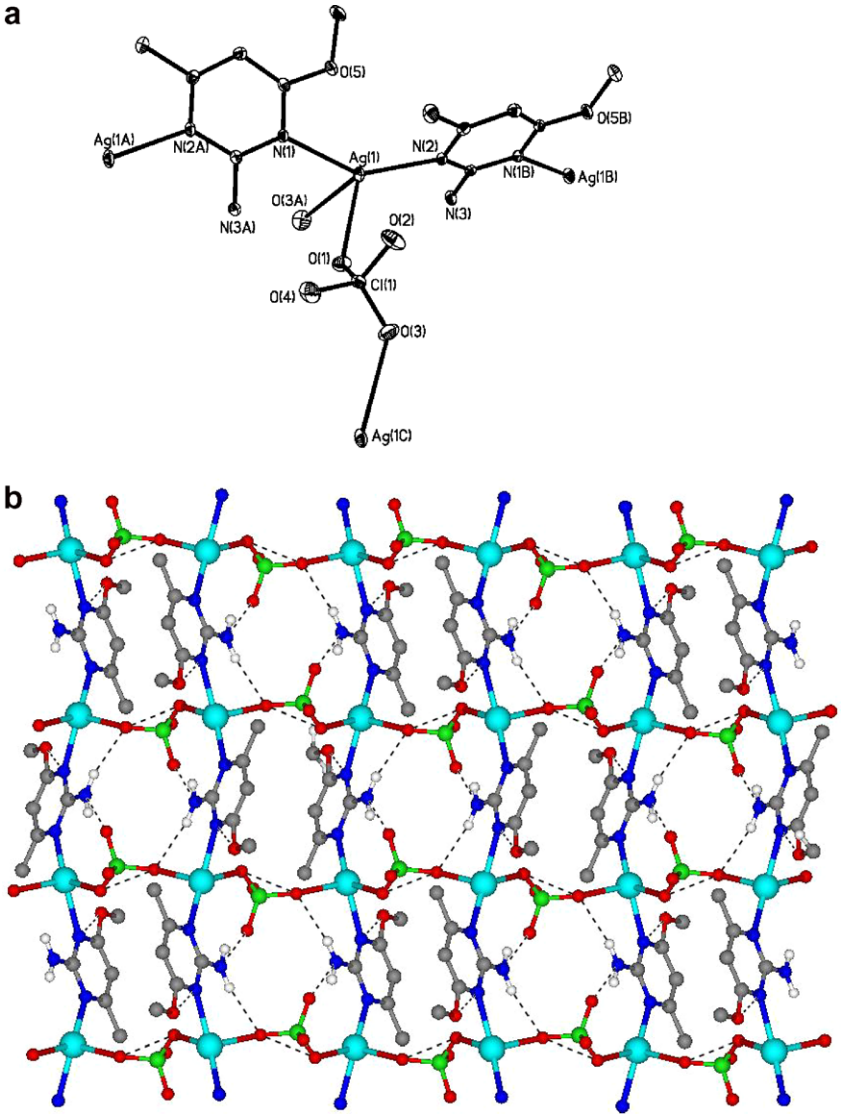

Fig. 4. (a) Crystal structure of **4** with the coordination environment around the silver(I) center (ellipsoids at 40% probability). (b) A view along the *a* axis of the 2D grid network in **4**. Hydrogen atoms in methyl, methoxy and phenyl groups are omitted for clarity. Ag stressed in bigger ball ( ).

L_2 ligand links two Ag atoms to form a zigzag chain which is different from that is described for **1** or **2** (Fig. S4). The adjacent chains are further connected by ClO_4^- groups to generate microporous metal–organic framework which exhibits intriguing tetragonal channels (Fig. 4b). The framework is further stabilized by intermolecular N–H···O hydrogen bonds where oxygen atoms of perchlorate anions serve as acceptors while hydrogen atoms of the free amino group of the L_2 ligand act as donors [2.955(3) and 3.046(3) Å for N(3)···O(4) and N(3)···O(1), respectively] (Fig. 4b). Obvious changes were observed from the structures of **3** and **4**, and the dimension of the complexes increase from 0D(**3**) to 2D(**4**). It is noteworthy that striking structural difference between **3** and **4** simply caused by a subtle difference in the ligand structure, *i.e.*, the replacement of 4-position of methyl group by methoxy group. On the basis of the above results, it may be concluded that structural major transformation between **3** and **4** may partially be attributed to steric effect of substituted groups of ligands.

3.2.3. Crystal structure of $[Ag(L_3)(ClO_4)]_n$ (**5**)

Since L_1 and L_2 ligands give distinct structures (**1**–**4**), it is of interest to examine the effect of other 2-aminopyrimidyl ligands that could possibly coordinate with silver ions. Thus when the L_3 ligand is chosen to react with $AgClO_4$ under the otherwise same conditions as **3** or **4**, a new complex **5** is obtained. The crystal of **5** conforms to the space group *Pccn* and its structure with the atom labeling is displayed in Fig. 5a. The connectivity of the ligands with metals of **5** is similar to that seen in the previous structures **1–4**. The central Ag(I) ion, which is coordinated by two N atoms [2.172(2) and 2.183(2) Å for Ag(1)–N(1) and Ag(1)–N(3B)] from two pyrimidine rings, has a distinctly nonlinear geometry [N(1)–Ag(1)–N(3B) = 167.11(6)°]. The average Ag–N distance in **5** is slightly shorter than the corresponding values for **1**. Each L_3 ligand links two Ag atoms to form a zigzag chain which is similar to that described for **4** and the adjacent chains are further connected by Ag···Ag weak metal–metal interactions to generate one-dimensional ladder structure along *a* axis (Fig. S6). The Ag···Ag separation in the proximal zigzag chains is 3.376 Å, which is slightly shorter than the summed van der Waals radius of two silver atoms (3.44 Å) [25], indicating there are weak interactions between two Ag(I) ions in different zigzag chains. The neighbored 1D ladder structures further interlinked into 3D framework through N–H···O intermolecular hydrogen bonds in the form of chair-like conformations (Fig. S7) where oxygen atoms of perchlorate anions serve as acceptors while hydrogen atoms of NH_2 groups of the pyrimidine rings act as donors: N(2)···O(4A) = 2.978(3) and N(2)···O(3B) = 2.973(3) Å [symmetry codes: (A) = *x*, $-y + 1/2$, $z-1/2$; (B) = $-x + 1$, $y + 1/2$, $-z + 3/2$] and Ag···O weak interactions (Ag···O = 2.731 Å for anion) [26] (Fig. 5b).

3.3. Photoluminescence properties

The mixed inorganic–organic hybrid coordination polymers have been investigated for fluorescence properties and for potential applications. However, owing to the intense spin–orbital cou-

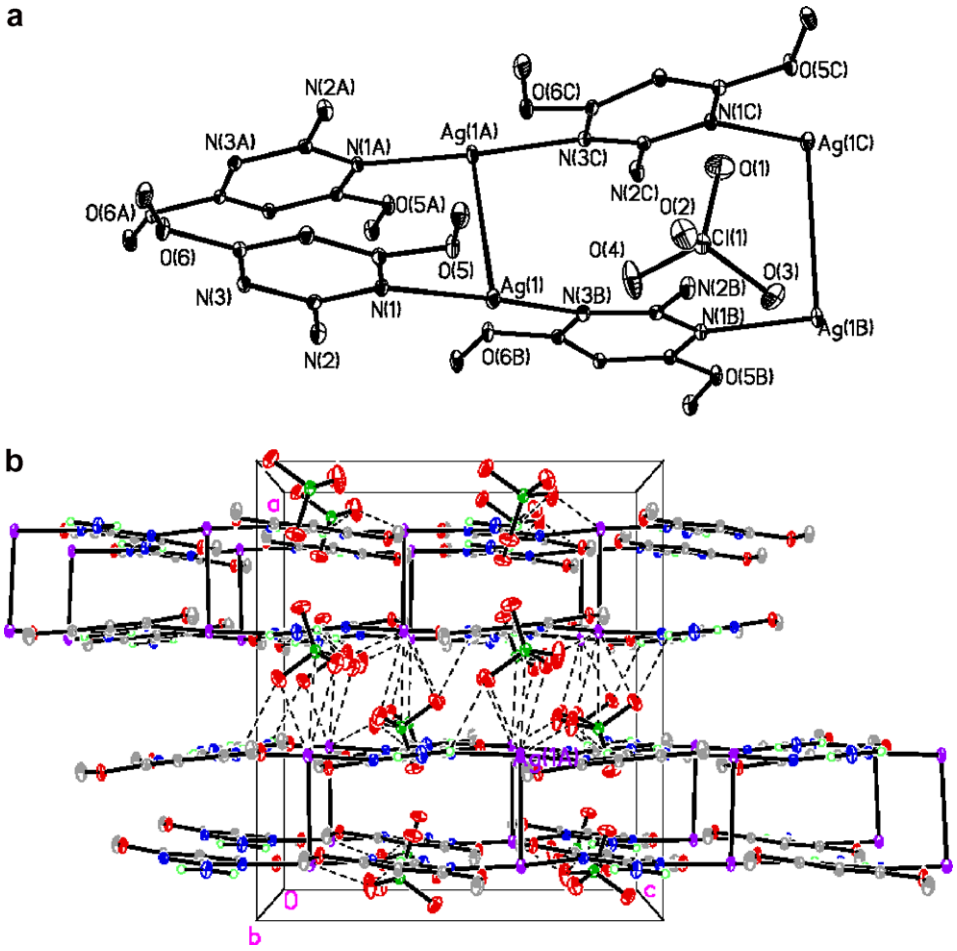

Fig. 5. (a) Local coordination around the silver atoms in **5** with the ellipsoids drawn at the 40% probability level. (b) A view of the 3D framework in **5** constructed by N–H···O hydrogen bonds, Ag···O weak interactions. Hydrogen atoms in methoxy and phenyl groups are omitted for clarity.

pling of Ag(I), most of luminescent Ag(I) complexes exhibit luminescence at low temperature [27] and Ag(I) complexes which exhibit luminescence at room temperature are few [28]. The complexes **1**–**5** reported herein represent room-temperature luminescent Ag-containing polymeric complexes [29].

The solid-state fluorescence data for both free ligands and the complexes **1–5** at room temperature are shown in Table S2. When excited at room temperature at 280 nm, complexes **1**–**5** exhibit some low-energy emission bands, which have shapes and positions similar to the free ligands L_1–L_3. The emissions are neither metal-to-ligand charge (MLCT) nor ligand-to-metal charge transfer (LMCT) in nature and probably can be assigned to the intraligand π_L—π_L^* transitions fluorescent emission (LLCT) because very similar emissions are also observed for the free ligands.

4. Conclusions

In this study, five new complexes with interesting structural motifs have been successfully synthesized from the various rigid ligands L_1, L_2, and L_3 and varied silver salts. The analysis of the crystallographic data of **1–5** clearly shows that the overall architecture of the crystals is not only controlled by the nature of the rigid ligands present in the moiety, but by different counter anions. To the best of our knowledge, the ligands L_2 and L_3 are for the first time employed in coordination chemistry of metal silver. Table S3 shows the cation–anion interaction, metal geometry and structure in complexes **1–5**. Moreover, the photoluminescent properties of free ligands L_1–L_3, and complexes **1**–**5** have been examined.

Acknowledgments

This work was financially supported by the National Natural Science Foundation of China (Nos. 20571062 and 20721001) and the National Basic Research Program of China (2007CB815301).

Appendix A. Supplementary data

CCDC 668535, 652464, 668536, 668537 and 668538 contain the supplementary crystallographic data for **1**–**5**. These data can be obtained free of charge via http://www.ccdc.cam.ac.uk/conts/retrieving.html, or from the Cambridge Crystallographic Data Centre, 12 Union Road, Cambridge CB2 1EZ, UK; fax: (+44) 1223-336-033; or e-mail: deposit@ccdc.cam.ac.uk. Supplementary data associated with this article can be found, in the online version, at doi:10.1016/j.poly.2008.06.003.

References

[1] M. Fujita, M. Tominaga, K. Suzuki, M. Kawano, T. Kusukawa, Angew. Chem., Int. Ed. 43 (2004) 5621.
[2] (a) X.Y. Wang, L. Wang, Z.M. Wang, S. Gao, J. Am. Chem. Soc. 128 (2006) 674; (b) X.L. Wang, C. Qin, N.B. Wang, Angew. Chem., Int. Ed. 44 (2005) 5824.
[3] O.R. Evans, W. Lin, Acc. Chem. Res. 35 (2002) 511.
[4] S. Kitagawa, R. Kitaura, S.I. Noro, Angew. Chem., Int. Ed. 43 (2004) 2334.
[5] S.L. James, Chem. Soc. Rev. 32 (2003) 276.
[6] C.N.R. Rao, S. Natarajan, R. Vaidhyanathan, Angew. Chem., Int. Ed. 43 (2004) 1466.
[7] S. Kitagawa, R. Kitaura, S. Noro, Angew. Chem., Int. Ed. 43 (2004) 2334.
[8] M.J. Rosseinsky, Micropor. Mesopor. Mater. 73 (2004) 15.
[9] J.L.C. Rowsell, O.M. Yaghi, Micropor. Mesopor. Mater. 73 (2004) 3.
[10] A.K. Cheetham, C.N.R. Rao, R.K. Feller, Chem. Commun. (2006) 4780.
[11] O.M. Yaghi, M. O'Keeffe, N.W. Ockwig, H.K. Chae, M. Eddaoudi, J. Kim, Nature 423 (2003) 705.
[12] (a) C.K.V. Sharma, R.D. Rogers, Chem. Commun. (2003) 1808; (b) E.Q. Gao, A.L. Cheng, Y.X. Xu, C.H. Yan, M.H. He, Cryst. Growth Des. 5 (2005) 1005; (c) N.S. Oxtoby, N.R. Champness, CrystEngComm. 7 (2005) 284.
[13] (a) M.L. Tong, B.H. Ye, J.W. Cai, X.M. Chen, S.W. Ng, Inorg. Chem. 37 (1998) 2645; (b) M. Oh, C.L. Stern, C.A. Mirkin, Inorg. Chem. 44 (2005) 2647; (c) M.B. Zaman, K. Udachin, J.A. Ripmeester, Inorg. Chem. 44 (2005) 5047; (d) A.N. Khlobystov, N.R. Champness, M. Schroder, J. Am. Chem. Soc. 125 (2003) 6753.
[14] (a) R.P. Feazell, C.E. Carson, K.K. Klausmeyer, Eur. J. Inorg. Chem. (2005) 3287; (b) R.P. Feazell, C.E. Carson, K.K. Klausmeyer, Inorg. Chem. 45 (2006) 2627; (c) R.P. Feazell, C.E. Carson, K.K. Klausmeyer, Inorg. Chem. 45 (2006) 2635; (e) R.P. Feazell, C.E. Carson, K.K. Klausmeyer, Inorg. Chem. 45 (2006) 935.
[15] A.J. Blake, N.R. Champness, P. Hubberstey, W.S. Li, M.A. Withersby, M. Schroder, Coord. Chem. Rev. 183 (1999) 117.
[16] D.B. Leznoff, B.Y. Xue, R.J. Batchelor, F.W.B. Einstein, B. Patrick, Inorg. Chem. 40 (2001) 6026.
[17] M. Munakata, L.P. Wu, T. Kuroda-Sowa, Adv. Inorg. Chem. 46 (1999) 173.
[18] (a) L. Carlucci, G. Ciani, D.M. Proserpio, A. Sironi, Angew. Chem., Int. Ed. Engl. 34 (1995) 1895; (b) G.K.H. Shimizu, G.D. Enright, C.I. Ratcliffe, J.A. Ripmeester, D.D.M. Wayner, Angew. Chem., Int. Ed. Engl. 37 (1998) 1407; (c) G.K.H. Shimizu, G.D. Enright, C.I. Ratcliffe, K.F. Preston, J.L. Reid, J.A. Ripmeester, Chem. Commun. (1999) 1485.
[19] (a) R. Lescouezec, F. Lloret, M. Julve, M. Verdaguer, Inorg. Chem. 41 (2002) 818; (b) A.Q. Wu, F.K. Zheng, G.C. Guo, Inorg. Chem. 43 (2004) 4839.
[20] (a) E. Tynan, P. Jensen, P.E. Kruger, CrystEngComm. 7 (2005) 90; (b) E. Tynan, P. Jensen, P.E. Kruger, Chem. Commun. (2004) 776; (c) Y.Q. Huang, Z.L. Shen, T. Okamura, Y. Wang, X.F. Wang, W.Y. Sun, J.Q. Yu, N. Ueyama, Dalton Trans. (2008) 204.
[21] C. Seward, W.L. Jia, R.Y. Wang, G.D. Enright, S. Wang, Angew. Chem., Int. Ed. Engl. 43 (2004) 2933.
[22] (a) K. Aoki, M. Inaba, S. Teratani, H. Yamazaki, Y. Miyashita, Inorg. Chem. 33 (1994) 3018; (b) G. Smith, B.A. Cloutt, D.E. Lynch, K.A. Byriel, C.H.L. Kennard, Inorg. Chem. 37 (1998) 3236; (c) C.V.K. Sharma, S.T. Griffin, R.D. Rogers, Chem. Commun. (1998) 215; (d) C.V.K. Sharma, R.D. Rogers, Cryst. Eng. 1 (1998) 18; (e) H. Cai, H.M. Hu, W.Z. Chen, H.G. Zhu, X.Z. You, Chem. Lett. (1999) 221; (f) D.R. Armstrong, F. Benevelli, A.D. Bond, et al., Inorg. Chem. 41 (2002) 1492; (g) C.K. Terajima, H. Miyasaka, T. Ishii, K. Sugiura, M. Yamashita, Inorg. Chim. Acta 332 (2002) 210; (h) Y.H. Wang, K.L. Chu, H.C. Chen, et al., Cryst. Eng. 8 (2006) 84.
[23] Y.N. Chi, K.L. Huang, F.Y. Cui, Y.Q. Xu, C.W. Hu, Inorg. Chem. 45 (2006) 10605.
[24] (a) R.H. Blessing, Acta. Crystallogr., Sect. A 51 (1995) 33; (b) G.M. Sheldrick, SHELXS 97: Program for Crystal Structure Solution, University of Göttingen: Göttingen, Germany, 1997.; (c) G.M. Sheldrick, SHELXL 97: Program for Crystal Structure Refinement, University of Göttingen: Göttingen, Germany, 1997.
[25] A. Bondi, J. Phys. Chem. 68 (1964) 44.
[26] (a) O.M. Yaghi, H. Li, J. Am. Chem. Soc. 118 (1996) 295; (b) M.A. Withersby, A.J. Blake, N.R. Champness, P. Hubberstey, W.S. Li, M. Schroder, Angew. Chem., Int. Ed. Engl. 36 (1997) 2327; (c) P. Lin, R.A. Henderson, R.W. Harrington, W. Clegg, C.D. Wu, X.T. Wu, Inorg. Chem. 43 (2004) 181.
[27] (a) V.W.W. Yam, K.K.W. Lo, W.K.M. Fung, C.R. Wang, Coord. Chem. Rev. 171 (1998) 17; (b) P.D. Harvey, D. Fortin, Coord. Chem. Rev. 171 (1998) 351.
[28] (a) M.L. Tong, X.M. Chen, B.H. Ye, L.N. Ji, Angew. Chem., Int. Ed. 38 (1999) 2237; (b) S.L. Zheng, M.L. Tong, S.D. Tan, Y. Wang, J.X. Shi, Y.X. Tong, H.K. Lee, X.M. Chen, Organometallics 20 (2001) 5319; (c) V.W.W. Yam, K.K.W. Lo, C.R. Wang, K.K. Cheng, Inorg. Chem. 35 (1996) 5116; (d) X.C. Huang, S.L. Zheng, J.P. Zhang, X.M. Chen, Eur. J. Inorg. Chem. (2004) 1024; (e) V.J. Catalano, H.M. Kar, J. Garnas, Angew. Chem., Int. Ed. 38 (1999) 1979; (f) D. Fortin, M. Drouin, M. Turcotte, P.D. Harvey, J. Am. Chem. Soc. 119 (1997) 531; (g) Y.Q. Wei, K.C. Wu, B.T. Zhuang, Z.F. Zhou, J. Mol. Struct. 751 (2005) 143; (h) Y.Q. Wei, K.C. Wu, B.T. Zhuang, Z.F. Zhou, M.X. Zhang, C.P. Liu, Z. Anorg. Allg. Chem. 631 (2005) 1532.
[29] (a) Y.B. Dong, G.X. Jin, M.D. Smith, R.Q. Huang, B. Tang, H.C. zur Loye, Inorg. Chem. 41 (2002) 4909; (b) Q.X. Liu, F.B. Xu, Q.S. Li, X.S. Zeng, X.B. Leng, Y.L. Chou, Z.Z. Zhang, Organometallics 22 (2003) 309.

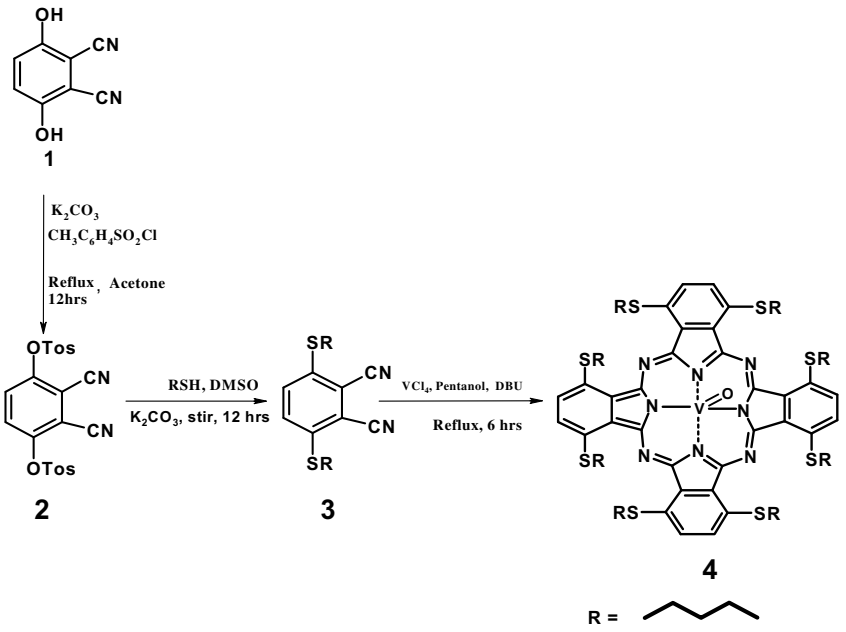

Scheme 1. Synthesis of OVPc derivative **4**.

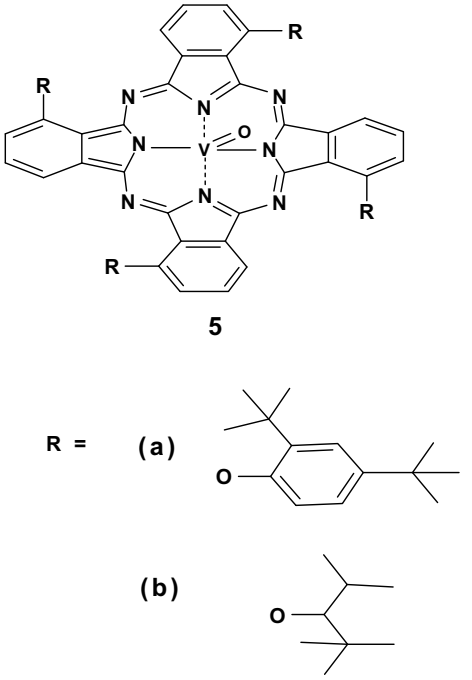

Fig. 1. Molecular structure of reported OVPc [21].

2. Experimental

2.1. Materials

Vanadium tetrachloride, dimethylsulfoxide (DMSO), 1-pentanethiol, 1,8-diazabicyclo{5.4.0}-undec-7-ene(DBU), tetrabutylammonium tetrafluoroborate ($TBABF_4$) and 1-pentanol were purchased from Sigma Aldrich. Potassium carbonate, deuterated chloroform ($CDCl_3$), 2,3-dicyanohydroquinone, *p*-toluenesulfonyl chloride, chloroform ($CHCl_3$) and dichloromethane (DCM), tetrahydrofuran (THF), toluene were procured from Merck. Solvents were dried and/or distilled before use. Column chromatography was performed on Silica Gel 60 (0.04–0.063 mm). Thin layer chromatography was performed on Silica Gel 60P F_{254}.

2.2. Electrochemical methods

Cyclic (CV) and square wave (SWV) voltammetry data were obtained with Autolab potentiostat PGSTAT 30 (Eco Chemie, Utretch, The Netherlands) driven by the General Purpose Electrochemical Systems data processing software (GPES, software version 4.9, Eco Chemie), using a three-electrode set-up with glassy carbon electrode (GCE, 3 mm diameter) as a working electrode, platinum wire as counter electrode and Ag|AgCl wire as pseudo-reference electrode. The potential response of Ag|AgCl pseudo-reference in aqueous conditions was less than the Ag|AgCl (3 M KCl) by 0.015 ± 0.003. Electrochemical experiments were performed in dry DCM containing tetrabutylammonium tetrafluoroborate ($TBABF_4$) as a supporting electrolyte. Prior to scans, the working electrode was polished with alumina paste on a Buehler felt pad, followed by washing with deionised water and rinsing with DCM. Square wave parameters were: step potential 5 mV; amplitude 20 mV at a frequency of 25 Hz. Spectroelectrochemical data were obtained using a home made optically transparent thin-layer electrochemical (OTTLE) cell which was connected to a Bioanalytic Systems (BAS) CV 27 voltammograph.

2.3. Equipment

UV/Vis spectra were recorded on a Cary 50 UV/Vis/NIR spectrophotometer. IR (KBr) was recorded on a Perkin–Elmer spectrum 2000 FTIR spectrometer. Elemental analyses were also performed at University of Cape Town. Low resolution mass spectra electron impact (EIMS) were recorded on a Finnigan MAT GCQ mass spectrometer at 70 eV for complexes **2** and **3**. For complex **4** low resolution atmospheric pressure chemical ionisation (APCI) mass spectra were recorded on a Finnigan MAT LCQ ion trap mass spectrometer equipped with XCALIBUR software.

2.4. Synthesis

For the synthesis of phthalonitriles (**2** and **3**), a procedure similar to that reported in literature [25,26] was employed with slight modification as follows:

2.4.1. 3,6-Bis(4′-methylphenylsulfonyloxy) phthalonitrile (**2**)

p-Toluenesulfonyl chloride (5.16 g, 27 mmol) was added to a mixture of 2,3-dicyanohydroquinone (**1**, 2 g, 12.5 mmol) and potassium carbonate (6.9 g, 50 mmol) in acetone (15 ml). The mixture was heated to reflux for 2 h. Thin layer chromatography (TLC) was performed to determine the consumption of compound **1**. The mixture was cooled to room temperature and poured into water (40 ml). The mixture was stirred for 1 h in water. The light brown product was filtered and oven dried. Yield: 4.51 (79%) IR [(KBr) ν_{max}/cm^{-1}]: 3432, 3239, 3085, 2243, 2226 (CN), 1504, 1449, 1315, 1279, 1204, 1174, 1142, 1021, 1004, 979, 934, 847, 749, 694, 638, 614. LREI-MS *m*/*z*: Calc. 469; found [M^+] 468.

2.4.2. 3,6-Di(pentathio)-4,5-dicyanobenzene (**3**)

1-Pentathiol (2.39 g, 22.9 mmol) was dissolved in DMSO under a nitrogen atmosphere and 3,6-bis(4′-methylphenylsulfoloxy phthalonitrile) (**2**, 4.30 g, 9.18 mmol) was added. The mixture was stirred for 15 min and finely ground anhydrous potassium carbonate (5.07 g, 36.7 mmol) was added portion-wise for 2 h while stirring. The mixture was stirred under a nitrogen atmosphere for 12 h. Water was added and the aqueous phase extracted using chloroform (3 × 50 ml). The extracts were further treated with 5% sodium carbonate solution (2 × 250 ml). The solution was further treated with water (2 × 250 ml) and the solvent was evaporated off using a rotavapor. The product was recrystallised from ethanol. Yield: 2.19 g (71.7%). IR [(KBr)ν_{max}/cm^{-1}]: 3084, 2951, 2930, 2864, 2378 (S–C), 2225 (C≡N), 1444, 1283, 1202, 1181, 1173, 1145, 877, 847, 827, 725, 547, 447. ^{1}H NMR ($CDCl_3$): δ, ppm 7.49 (2-H, s, Ar-H), 3.02–2.99 (4-H, t, $-CH_2$), 1.71–1.63 (4-H, m, $-CH_2$) 1.46–1.37 (4-H, m, $-CH_2$), 1.36–1.28 (4-H, m, $-CH_2$), 0.91–0.88 (6-H, t, $-CH_3$). LREI-MS *m*/*z*: Calc. 333; found [M^+] 332.

2.4.3. 1,4,8,11,15,18,22,25-Octapentylthiophthalocyaninato vanadium(IV) oxide (**4**)

A solution of 3,6-di(pentathio)-4,5-dicyanobenzene (**3,** 0.4 g, 1.20 mmol) in 1-pentanol (3.5 ml) was refluxed under a nitrogen atmosphere and vanadium(IV) tetrachloride (0.069 g, 0.40 mmol) was added. After the addition of DBU (0.13 ml, 0.857 mmol) heating under reflux was continued for 6 h. The mixture was cooled and column chromatography over silica was done (eluent: chloroform).

Yield: 0.24 g (42%). UV–Vis (DCM): λ_{max} (nm) (log ε) 344 (3.96) 754 (3.46) 850 (4.24). IR [(KBr) ν_{max}/cm^{-1}]: 2955, 2916, 2853, 2363 (S–C), 1555, 1456, 1357, 1306, 1281, 1221, 1208, 1186, 1147, 1112, 1075, 992, 925 (V=O), 810, 794, 775, 759, 741, 584, 533. ^{1}H NMR (600 MHz, $CDCl_3$): δ, ppm 7.42 (8H, s, Ar-H), 2.93 (16H, t, $-CH_2$), 1.75 (16H, m, $-CH_2$), 1.47 (16H, m, $-CH_2$), 1.35 (16H, m, $-CH_2$), 0.90 (24H, t, $-CH_3$). *Anal.* Calc. for $C_{72}H_{96}N_8S_8OV$: C, 61.90; H, 6.92; N, 8.02; S, 18.36. Found: C, 61.53; H, 7.04; N, 7.56; S, 18.25%. LRAPCI-MS *m*/*z*: Calc. for $C_{72}H_{96}N_8S_8OV$: 1396.9; found [M^+] 1396.

3. Results and discussion

3.1. Spectroscopic characterisation

The synthesised complex **4** is soluble in solvents such as DCM, $CHCl_3$, THF and toluene. A good yield (42%) for the synthesised **4** was obtained. The new compound was characterised using IR, NMR, UV/Vis and mass spectra and by elemental analysis. The disappearance of the sharp C≡N vibration at ~2225 cm^{-1} confirmed the cyclotetramerisation of the phthalonitrile **3** and typical V=O stretch appearing as a medium band at 925 cm^{-1}. ^{1}H NMR spectrum of complex **4** is simple since the complex is octa substituted hence has isomeric purity. The ^{1}H NMR spectrum showed a singlet integrating for 8 observed at 7.42 ppm, for the Pc ring, and the methylene and methyl proton shifts belonging to the thio-alkyl side chain were clearly observed in the ^{1}H NMR spectrum and integrated correctly. The mass spectra of complex **4** showed a molecular ion peak at *m*/*z* 1396.

The UV/Vis spectrum of the complex **4** is shown in Fig. 2. It is known that red-shifting of absorption spectra is a function of the solvent's refractive index [27], and Table 1 also shows a shift to the red with increase in the solvents' refractive indexes. The Q band is observed at 850 nm in dichloromethane. A broad band between 500 and 600 is probably due to charge transfer. Bands in this region for neutral MPc complexes have been shown to be of charge transfer in nature [28]. The colour of the synthesised complex is purple. The observed colour is due to the fact that the Q band is moved out of the red region of the visible spectrum, which is the region that normally determines the colour of MPcs. The large red shift of the Q band is due to the large electron-donating ability of the sulfur groups. The Q band of complex **4** is red shifted by 160 nm and 209 nm (Table 1) compared to unsubstituted OVPc and $OVPcF_{16}$, respectively, making it the most highly red-shifted OVPc derivative, absorbing in the near infrared region. The reported complexes **5a** and **5b** contained oxygen rather than sulfur bridges to the alkyl substituent, and as stated above oxo complexes are less red shifted (larger HOMO–LUMO gap) than thiol complexes which are more red shifted (smaller HOMO–LUMO gap).

The red-shifting to near infrared region in MPc complexes is highly dependent on the central metal. Alkyl thio MPc containing

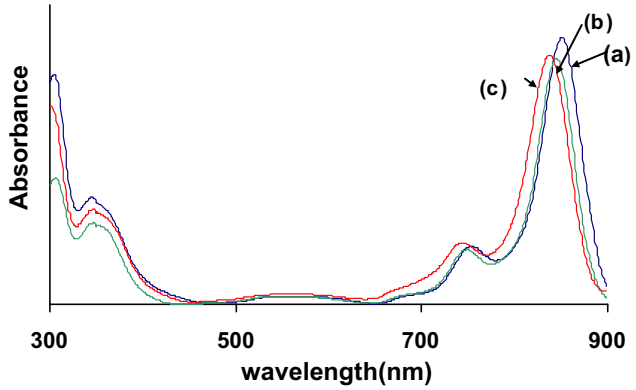

Fig. 2. UV–Vis spectrum of **4** in (a) DCM (b) $CHCl_3$ and (c) THF. Concentration = ~1.1×10^{-5} mol dm^{-3}.

Table 1
UV–Visible spectra of OVPc derivatives in DCM, unless otherwise stated

Complex[a]	Q band maxima (nm)	Ref.
4 (OV[Pc(SC_5H_{11})$_8$])	850 (DCM) 841 ($CHCl_3$) 834 ((THF) 830 (toluene)	This work
OV[Pc(OC_6H_3(*t*-Bu)$_2$)$_4$][b]	736	[21]
OV[Pc(C_8H_{17})$_4$][b]	742	[21]
OVPc	690	[29]
OV(PcF_{16})	641	[23]

[a] *t*-Bu = *tert*-butyl.
[b] Solvent = DMF.

transition metals such as Fe and Co, do not show the NIR absorption and they remain blue or green in colour [29–31]. However alkylthio substituted Mn(III)Pc (α or β substituted) and Ti(IV)Pc complexes show red shifting [32–34]. Mn(III)Pc and Ti(IV)Pc complexes octasubstituted with pentylthio groups gave Q band maxima at 893 and 808 nm, respectively in dichloromethane. Mn(III)Pc complex shows a red shifted Q band (with a brown solution) even in the absence of substituents [34], while Mn(II)Pc does not show red-shifting and is blue or green in colour depending on substituents. On electrochemical reduction of Mn(III)Pc or Ti(IV)Pc derivatives, a blue shift of the Q band is observed [32–34], with a change of colour to green or blue. The observation of NIR absorption for complex **4**, containing V(IV) central metal, suggests that NIR absorption is favoured for MPc complexes containing central metals in a high oxidation state. The red shift is a result of the lowering of the HOMO–LUMO gap, by either destabilising the HOMO or stabilising the LUMO by the central metal.

Complex (**4**) did not show aggregation and Beer's law was obeyed for concentrations lower than 3×10^{-5} M.

3.2. Voltammetric and spectroelectrochemical characterisation

The cyclic (CV) and square wave (SWV) voltammetries of **4** were performed in de-aerated DCM containing $TBABF_4$ as electrolyte, Fig. 3. Two oxidations and three reduction couples are observed. This is one of the few OVPc complexes which show two oxidation peaks [21]. The half-wave potentials ($E_{1/2}$) for complex **4** are summarised in Table 2 together with reported data for some OVPc derivatives. The redox processes for complex **4** are labelled **I** ($E_{1/2}$ = 0.59 V), **II** ($E_{1/2}$ = 0.97 V), **III** ($E_{1/2}$ = −0.58 V), and **IV** ($E_{1/2}$ = −0.93 V), **V** ($E_{1/2}$ = −1.18 V), versus Ag|AgCl in Fig. 2. All the redox

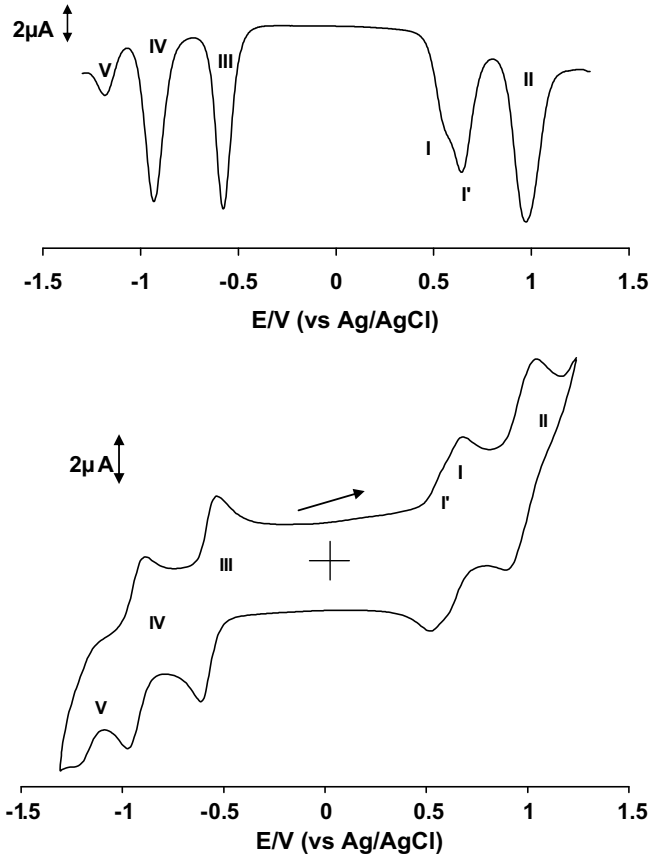

Fig. 3. Cyclic and square wave voltammograms of **4** in DCM containing $TBABF_4$. Scan rate = 100 mV s^{-1}.

processes showed both the cathodic and anodic components. The cathodic to anodic peak separation (ΔE) ranged from 90 to 120 mV, suggesting slow electron transfer. A ΔE value of 90 mV was obtained for ferrocene. The cathodic to anodic peak current ratio (I_{pc}/I_{pa}) were near unity. For all redox couples, plots of peak current (I_p) versus the square root of scan rate ($v^{1/2}$) were linear, thus suggesting diffusion control at the electrode surface. Table 2 also shows that complex **4** containing sulfur groups (due to the electron donating nature of the sulfur group) is more easily oxidised than the complexes containing oxo groups though different substituents are attached. It would therefore be expected that complex **4** would be more difficult to reduce; this is the case in Table 2 when comparing with fluorinated $OVPcF_{16}$. Also comparing complex **4** with other complexes in Table 2, which exhibited only ring based oxidation and reduction processes, we would expect the former also to show only ring based processes since the peak potentials are comparable except for slight differences due to the different substituents. Also the redox processes are in the range for ring-based processes in MPc complexes [22].

The first oxidation process showed an overlap of two peaks labelled **I′** and **I**. The overlap is probably due to aggregation at concentrations used for cyclic voltammetry. Such closely spaced cyclic voltammograms are associated with aggregation [22]. On dilution of the solution, there was disappearance process **I′**, only one process remained as **I**. The nature of the couples as well as the number of electrons transferred was confirmed by spectroelectrochemistry below.

Spectroelectrochemical studies using optically transparent thin layer electrode (OTTLE) cell gave more insight into the origin of the redox couples observed during voltammetric studies of the complexes. Fig. 4a shows the spectral changes observed during the reduction of **4** at potentials of process **III**. At the high concentrations used for the OTTLE cell, the original spectrum before reduction is broad due to aggregation. Aggregation in MPc complexes is usually depicted as a coplanar association of rings progressing from monomer to dimer and higher order complexes. It is dependent on the concentration, nature of the solvent, nature of substituents, complexed metal ions and temperature [35]. In the aggregated state the electronic structure of the complexed phthalocyanine rings are perturbed resulting in alternation of the ground and excited state electronic structures [36], thus broadening of the spectra.

Upon reduction, there is a blue shift in the Q band from 853 to 680 nm and at the same time the colour of the complex changed from purple to green, Fig. 4a. These spectral changes occurred with a clear isosbestic point at 731 nm. The number of electrons transferred (n) was calculated to be approximately 1.

Metal-based redox processes can be identified using UV–Vis spectra since a definite shift in the Q band (without much change in intensity) is generally observed [34]. Spectral changes in Fig. 4a are not similar to those observed for ring reduction in OVPc derivatives ($OV[Pc(OC_6H_3(t\text{-}Bu)_2)_4]$ and $OV[Pc(C_8H_{17})_4]$) [21], in that new weak bands were observed at 571, 618 and 646 nm upon reduction of the latter complexes. For complex **4**, the peak 680 is quite intense, but since only ring based processes have been reported [21,34,37] for VPc complexes, the spectral changes observed in Fig. 4a may be associated with ring based reduction (to Pc(-3) species), with differences in absorption band intensity and positions being due to differences in substituents.

The green colour of ring reduced VPc derivative (**4**) observed in this work, is uncommon in phthalocyanine chemistry, where reduction leads to purplish colour. The green colour is due to the fact that the shift of the main absorption band is to 680 nm, while in general for Pcs, the main (weak) absorption bands occur between 500 and 600 nm [28,38]. The peak at 680 nm is intense relative to the original species with a reduction in $\log \varepsilon$ of only 20%

Table 2
Electrochemical data for OVPc derivatives

Complex[a]	$V^{III}Pc^{-3}/V^{III}Pc^{-4}$ (**V**)	$V^{III}Pc^{-2}/V^{III}Pc^{-3}$ (**IV**)	$V^{IV}Pc^{-2}/V^{III}Pc^{-2}$ (**III**)	$V^{IV}Pc^{-2}/V^{IV}Pc^{-1}$ (**I**)	$V^{IV}Pc^{-1}/V^{IV}Pc^{0}$ (**II**)	Ref.
4 (OV[Pc(SC_5H_{11})$_8$])	(−1.18) −1.14	(−0.93) −0.89	(−0.58) −0.54	(0.59) 0.68	(0.97) 1.02	This work
Reported OVPc complexes						
5a OV[Pc(OC_6H_3(*t*-Bu)$_2$)$_4$][b]	−2.07	−1.12	−0.62	0.76	1.21	[21]
5b OV[Pc(C_8H_{17})$_4$][b]	−1.94	−0.97	−0.51	0.94	1.34	[21]
OV[Pc(Bu)$_4$]	–	−1.08	−0.58	0.94	–	[22]
OV(PcF_{16})	−1.41	−0.62	−0.29	0.85(irr)[c]	–	[23]

Unless otherwise stated, the data collected in DCM containing $TBABF_4$. Potentials vs. SCE unless otherwise stated. Values in Brackets vs. Ag|AgCl. A conversion factor of $E_{½}$ (SCE) = $E_{½}$ (Ag|AgCl) + 0.045 V has been applied.
[a] *t*-Bu = *tert*-butyl.
[b] In DMF containing TBAP.
[c] irr = irreversible.

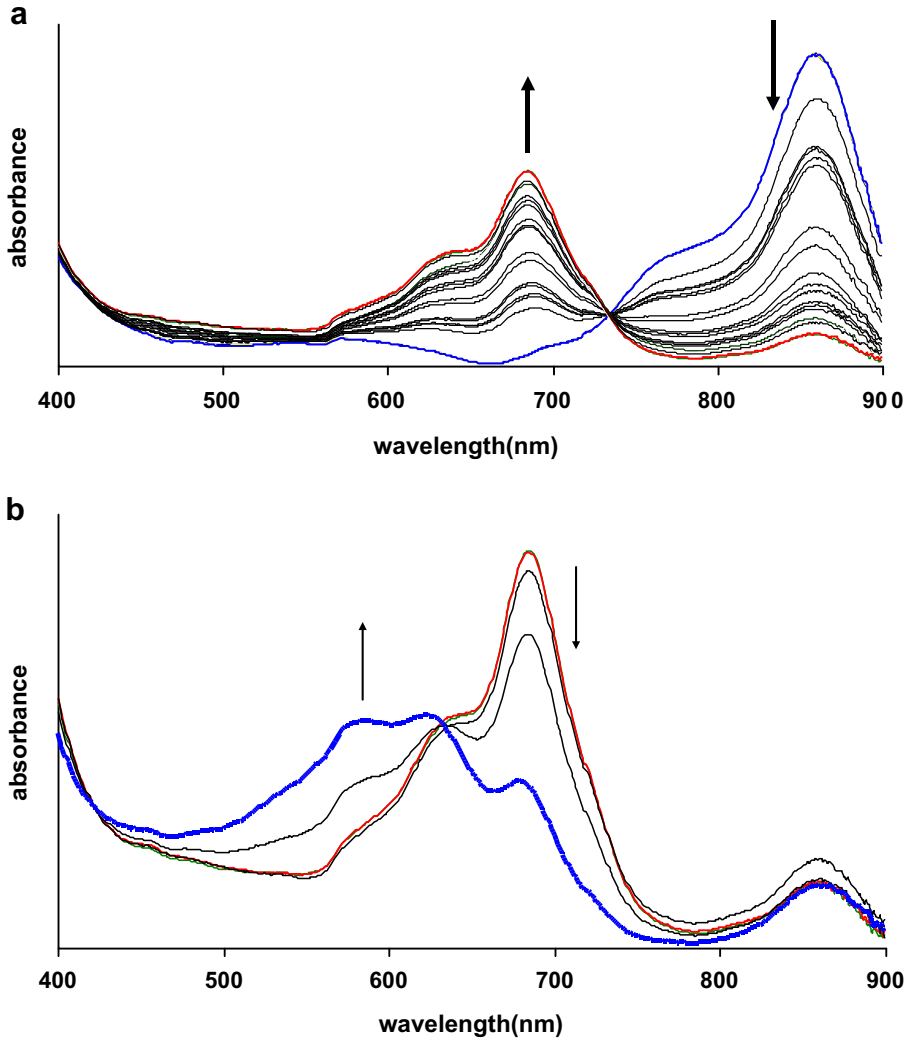

Fig. 4. UV–Vis spectral changes for **4** observed using controlled potential electrolysis at (a) −0.7 V, (b) −1.2. First spectrum in (b) is the same as the last spectrum in (a). Electrolyte = DCM containing 0.1 M $TBABF_4$. Electrolysis time was 30 min for each redox process.

(assuming complete transformation) compared to the more common ring reduction in Pcs with large reduction in intensity upon reduction.

Fig. 4b shows spectral changes observed on further reduction at potentials of couple **IV**. There was emergence of new peaks at 578 and 620 nm. The spectral changes shown in Fig. 4b are similar to those observed for other OVPc derivatives, (OV[Pc(OC_6H_3(*t*-Bu)$_2$)$_4$] and OV[Pc(C_8H_{17})$_4$]) which were assigned to ring based processes [21]. Thus spectral changes shown in Fig. 4b are assigned to the formation of Pc^{4-} species, hence the couple $V^{IV}Pc^{3-}/V^{IV}Pc^{4-}$. Process V may be assigned to further ring reduction and the formation of $V^{IV}Pc^{5-}$.

Spectroelectrochemical characterisation was done to determine the origin of the oxidation couples. Fig. 5 shows the spectroelectro-

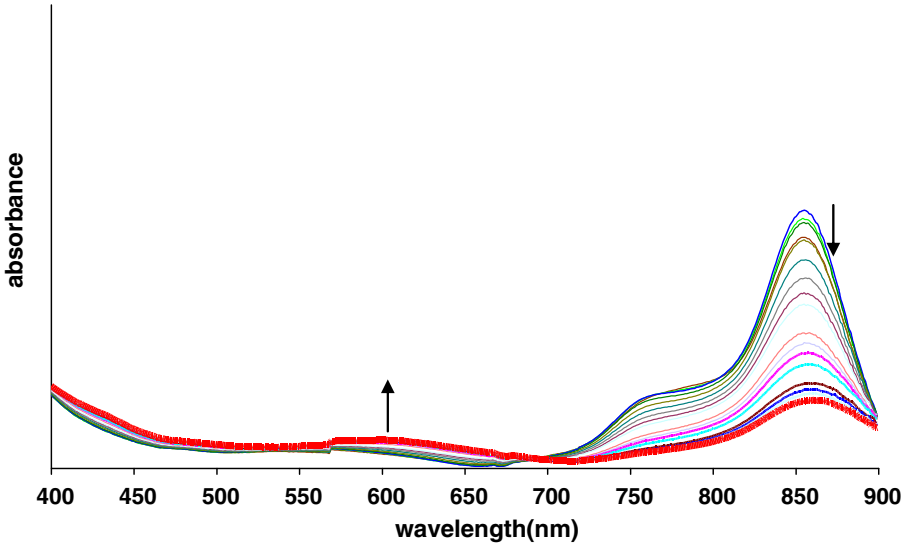

Fig. 5. UV–Vis spectral changes for **4** observed using controlled potential electrolysis at 0.8 V electrolyte = DCM containing 0.1 M $TBABF_4$. Electrolysis time was 30 min.

chemical changes observed upon oxidation at the potential of process **I**. Oxidation at the potential of peak **I** showed the decrease in intensity of the Q band and formation of a weak new peak around the 500–700 nm region, this is indicative of a ring based process and assigned to the oxidation of $V^{IV}Pc^{2-}$ to $V^{IV}Pc^{1-}$, Fig. 5.

Based on the electrochemical data above, we assign processes **I**–**V** as follows:

$$V^{IV}Pc^{2-} \rightarrow V^{IV}Pc^{1-} + e^{-} (\text{process } \mathbf{I}) \quad (1)$$

$$V^{IV}Pc^{1-} \rightarrow V^{IV}Pc^{0} + e^{-} (\text{process } \mathbf{II}) \quad (2)$$

$$V^{IV}Pc^{2-} + e^{-} \rightarrow V^{IV}Pc^{3-} (\text{process } \mathbf{III}) \quad (3)$$

$$V^{IV}Pc^{3-} + e^{-} \rightarrow V^{IV}Pc^{4-} (\text{process } \mathbf{IV}) \quad (4)$$

$$V^{IV}Pc^{4-} + e^{-} \rightarrow V^{IV}Pc^{5-} (\text{process } \mathbf{V}) \quad (5)$$

4. Conclusion

A vanadium phthalocyanine which absorbs in the red region, 850 nm in DCM, has been synthesised. This complex has potential in applications as near-IR absorbers are used in optical recording materials and in IR radiation filters. The electrochemical data reveals five redox processes. The spectroelectrochemical data revealed ring based processes, with spectra of the reduced species being different from the other VPc derivatives in that ring reduction does not result in considerable loss in intensity.

Acknowledgements

This work has been supported by the National Research Foundation of South Africa (NRF GUN = 2053657) as well as Rhodes University. G.M. thanks NRF Scarce skills for graduate scholarships.

References

[1] C.C. Leznoff, A.B.P. Lever (Eds.), in: Phthalocyanines: Properties and Applications, vol. 1–4, VCH Publishers, New York, 1989–1996.
[2] G. Guillaud, J. Simon, J.P. Germain, Coordin. Chem. Rev. 180 (1998) 1433.
[3] C.G. Claessens, W.J. Blau, M. Cook, M. Hanack, R.J.M. Nolte, T. Torres, D. Wöhrle, Monatsh. Chem. 132 (2001) 3.
[4] D. Williams, S.G. Latham, C.M.J. Powles, M.A. Powell, R.C. Chittick, A.P. Sparks, N. Collings, J. Phys. D 21 (1988) 154.
[5] N.B. McKeown, Chem. Ind. (1992) 92.
[6] A.J. Duro, G. de la Torre, J. Barber, J.L. Serrano, T. Torres, Chem. Mater. 8 (1996) 1061.
[7] G.J. Clarkson, N.B. McKeown, K.E. Treacher, J. Chem. Soc., Perkin Trans. I (1995) 1817.
[8] G. de la Torre, P. Vasquez, F. Agulló-López, Adv. Mater. 9 (1997) 265.
[9] G. de la Torre, P. Vaquez, F. Agulló-López, T. Torres, J. Mater. Chem. 8 (1998) 1671.
[10] H. Ali, J.E. van Lier, Chem. Rev. 99 (1999) 2379.
[11] K. Katrin, A. Nihal, C. Tracy, B. David, M. Hasan, Cancer Res. 60 (2000) 5984.
[12] D. Phillips, Pure Appl. Chem. 67 (1995) 117.
[13] R. Bonnett, Chem. Soc. Rev. 24 (1995) 19.
[14] S.B. Brown, T.G. Truscott, Chem. Brit. 29 (1993) 955.
[15] C.M. Allen, W.M. Sharman, J.E. van Lier, J. Porphyr. Phthalocya. 5 (2001) 1.
[16] P. Kivits, R. Debouts, J. Van Der Veen, J. Appl. Phys. A26 (1981) 101.
[17] D. Gu, Q. Chen, J. Shu, X. Tang, F. Gan, S. Shen, K. Liu, H. Xu, Thin Solid Films 257 (1995) 88.
[18] G. Long, B. Snedecker, K. Bartosh, M.L. Werner, A. Sen, Can. J. Chem. 79 (2001) 1026.
[19] A.W. Snow, in: K.M. Kadish, K.M. Smith, R. Guilard (Eds.), Porphyrin Handbook, Phthalocyanines: Properties and Materials, vol. 17, Academic Press, New York, 2003.
[20] R.M. Christie, Dyes Pigments 27 (1995) 35.
[21] Z. Jiang, Z. Ou, N. Chen, J. Wang, J. Huang, J. Shao, K.M. Kadish, J. Porphyr. Phthalocya. 9 (2005) 352.
[22] A.B.P. Lever, E.R. Milaeva, G. Speier, in: C.C. Leznoff, A.B.P. Lever (Eds.), Phthalocyanines: Properties and Applications, vol. 3, VCH Publishers, New York, 1993.
[23] M. Handa, A. Suzuki, S. Shoji, K. Kasuga, K. Sogobe, Inorg. Chem. Acta 230 (1995) 41.
[24] P. Tau, T. Nyokong, Polyhedron 25 (2006) 1802.
[25] J. Morita, H. Nakatsiju, T. Misaki, Y. Tanabe, Green Chem. 7 (2005) 714.
[26] A. Gürek, Ö. Bekaroğlu, J. Chem. Soc., Dalton Trans. (1994) 1422.
[27] A.O. Ogunsipe, M.D. Maree, T. Nyokong, J. Mol. Struct. 650 (2003) 131.
[28] J. Mark, M.J. Stillman, in: K.M. Kadish, K.M. Smith, R. Guilard (Eds.), Porphyrin Handbook, Phthalocyanines: Spectroscopic and Electrochemical Characterization, vol. 16, Academic Press, New York, 2003.
[29] B.O. Agboola, K.I. Ozoemena, T. Nyokong, Electrochim. Acta 51 (2006) 6470.
[30] B. Agboola, K. Ozoemena, T. Nyokong, Electrochim. Acta 51 (2006) 4379.
[31] F. Matemadombo, M.D. Maree, K.I. Ozoemena, P. Westbroek, T. Nyokong, J. Porphyr. Phthalocya. 9 (2005) 484.
[32] B. Agboola, K.I. Ozoemena, P. Westbroek, T. Nyokong, Electrochim. Acta 52 (2007) 2520.
[33] G. Mbambisa, P. Tau, E. Antunes, T. Nyokong, Polyhedron 26 (2007) 5355.
[34] M.J. Stillman, T. Nyokong, in: C.C. Leznoff, A.B.P. Lever (Eds.), Phthalocyanines: Properties and Applications, vol. 1, VCH, New York, 1989. Chapter 3.
[35] H. Enkelkamp, R.J.M. Nolte, J. Porphyr. Phthalocya. 4 (2000) 454.
[36] D.D. Dominguez, A.W. Snow, J.S. Shirk, R.G.S. Pong, J. Porphyr. Phthalocya. 5 (2001) 582.
[37] M. L'Her, A. Pondaven, in: K.M. Kadish, K.M. Smith, R. Guilard (Eds.), Porphyrin Handbook, Phthalocyanines: Spectroscopic and Electrochemical Characterization, vol. 16, Academic Press, New York, 2003.
[38] M.J. Stillman, in: C.C. Leznoff, A.B.P. Lever (Eds.), Phthalocyanines: Properties and Applications, vol. 3, VCH Publishers, New York, 1993 (Chapter 5).

Unicom UV-2 Spectrometer. ^{1}H NMR and ^{13}C NMR spectra were recorded on a Bruker 300 spectrometer instrument. The cyclic voltammetry (CV) and differential pulse voltammetry (DPV) measurements were carried out with a Gamry Reference 600 potentiostat/galvanostat controlled by an external computer and utilizing a three-electrode configuration at 25 °C. The working electrode was a Pt disc with a surface area of 0.071 cm^2. The surface of the working electrode was polished with a diamond suspension before each run. A Pt wire served as the counter electrode. A saturated calomel electrode (SCE) was employed as the reference electrode and separated from the bulk of the solution by a double bridge. Ferrocene was used as an internal reference. Electrochemical grade TBAP in extra pure THF was employed as the supporting electrolyte at a concentration of 0.10 mol dm^{-3}. High purity N_2 was used to remove dissolved O_2 for at least 15 min prior to each run and to maintain a nitrogen blanket during the measurements. IR compensation was also applied to the CV scans to further minimize the potential control error. Mass spectra were acquired on a Voyager-DE™ PRO MALDI-TOF mass spectrometer (Applied Biosystems, USA) equipped with a nitrogen UV-Laser operating at 337 nm. Spectra were recorded both in linear and reflectron modes with an average of 50 and 100 shots for the linear and reflectron modes, respectively. A-cyano-4-hydroxycinnamic acid (CHCA) and 3-indole acrylic acid MALDI matrix were used and prepared in chloroform at a concentration of 20 mg/mL for **2**. MALDI samples were prepared by mixing sample solutions (4 mg/mL) with the matrix solution (1:10 v/v) in a 0.5 mL eppendorf® micro tube. Finally 1 μL of this mixture was deposited on the sample plate, dried at room temperature and then analyzed. 3-Indole acrylic acid (IAA) (20 mg/mL in acetonitrile) matrix for **3** and **4** and α-cyano-4-hydroxycinnamic acid (ACCA) (15 mg/mL 1:1 water–acetonitrile) MALDI matrix for **5** were prepared. MALDI samples were prepared by mixing the complex (2 mg/mL in acetonitrile) with the matrix solution (1:10 v/v) in a 0.5 mL eppendorf® micro tube. Finally 1 μL of this mixture was deposited on the sample plate, dried at room temperature and then analyzed as described elsewhere [24].

2.1. Synthesis

2.1.1. 4-(3,5-Bis(trifluoromethyl)phenoxy)-phthalonitrile (*1*)

3,5-Bis(trifluoromethyl) phenol (1.62 g, 1.36 mmol) was dissolved in 10.0 cm^3 dry DMF under N_2. Finely ground anhydrous K_2CO_3 (~1.25 g, 1.73 mmol) was added to this solution. After efficient stirring for 0.5 h, 4-nitrophthalonitrile (1.00 g, 5.07 mmol) in DMF (~10 cm^3) was added dropwise at 35 °C over a period of 0.5 h. After the reaction mixture was kept at this temperature under a N_2 atmosphere for 3 days, the solution was cooled to room temperature. Then, the crude compound was poured into ice-water (~200 cm^3). The creamy precipitate that formed was filtered and washed several times with water until the washings became neutral. It was chromatographed over a silica gel column using a mixture of $CHCl_3$:MeOH (100:5 (v:v)) as eluent, giving a powder, 4-(3,5-bis-(trifluoromethyl)phenoxy)-phthalonitrile (**1**). Finally, the pure powder was dried in a vacuum.

Yield: 1.81 g (87.3%); m.p.: 95 °C. *Anal.* Calc. for $C_{16}H_6F_6N_2O$: C, 53.95; H, 1.70; N, 7.86. Found: C, 53.54; H, 1.75; N, 7.73%. IR (Thin film, disc) ν/cm^{-1}: 3107 (w), 3077 (w), 3047 (w, *Ar-H*), 2236 (st, *–C≡N*), 1591 (*C=C*), 1570 (*C=N*), 1488, 1463, 1366 (*–C–F*), 1275 (Ar-O-Ar), 1254, 1212, 1171, 1121, 1002, 970, 918, 880, 846, 699, 680. ^{1}H NMR (300) (DMSO-d_6) δ (ppm): 8.22 (d, 2H, *ortho* to Ar-CN group), 7.88 (d, 1H, meta to Ar-CN), 7.84 (s, 1H, *ortho* to CN), 7.70 (d, 1H, ortho to CF_3), 7.55 (d, 1H, *ortho* to CF_3), 7.14 (s, 1H, ortho to CF_3 and Ar-O–). ^{13}C NMR (DMSO-d_6) δ (ppm): 160.38 (Ar-*C*–O), 156.05 (Ar-*C*–O and *ortho* to CF_3), 137.06 (Ar-*C*–CF_3), 133.75 (Ar-*C*–C≡N), 133.86 (Ar-*C*–CCF_3), 132.41 (*para* to Ar-C–CF_3), 125.21 (Ar-*C*–C–O), 124.32 (Ar-*C*–CF_3), 121.59 (C–*C*F_3), 119.75 (Ar-C–*C*F_3), 117.54 (Ar-C–C≡N), 116.49 (Ar-C–*C*≡N), 116.02 (Ar-C–*C*≡N), 110.30 (Ar-*C*–C≡N). EI/MS: *m*/*z* (%): 356.02 $[M]^+$.

2.1.2. 2(3),9(10),16(17),23(24)-Tetrakis-4′-(3,5-bis(trifluoromethyl)phenoxy)-phthalocyaninatozinc(II) Zn(Pc) (*2*)

A mixture of **1** (0.10 g, 0.28 mmol), anhydrous $Zn(acac)_2$ (0.017 g, 0.10 mmol) and quinoline (~1 cm^3) in a sealed tube was heated with efficient stirring at 170–180 °C for about 8 h under a N_2 atmosphere. After cooling to room temperature, the resulting waxy solid was washed several times successively with hexane and methanol to remove any inorganic and organic impurities until the filtrate was clear. The blue product was isolated by silica gel column chromatography first with $CHCl_3$ and then with THF:$CHCl_3$ (1:1 (v:v)) as the eluent. Pure **2** was obtained as a blue powder following column chromatography over silica gel (eluent: $CHCl_3$:MeOH; 10:1, and then THF) and then dried in vacuum. This product is readily soluble in CH_2Cl_2, $CHCl_3$, THF, pyridine, DMF and DMSO.

Yield: 0.032 g (28.65%). *Anal.* Calc. for $C_{64}H_{246}N_8O4_8Zn$ (1488 g/mol): C, 51.58; H, 1.22; N, 7.52. Found: C, 51.46; H, 1.17; N, 7.28%. FTIR (KBr thin film) ν/cm^{-1}: 3077 (w, broad, *Ar-H*), 1754 (w), 1606 (*C=C*), 1487, 1460, 1365 (st, *C–F*), 1336, 1274, 1230, 1170, 1083, 1044, 1002, 959, 945, 921, 878, 776, 745, 734, 700, 680. ^{1}H NMR (300) (DMSO-d_6) δ (ppm): 8.23–8.18 (d, 2H, *ortho* to Ar-CN group), 7.85–7.82 (d, 1H, *meta* to Ar-CN), 7.72 (s, 1H, *ortho* to CN), 7.58–7.32 (m, br, 3H, *ortho* to CF_3 and *ortho* to CF_3 and Ar-O–). UV–Vis (THF, λ_{max}/nm: 677, 648, 611, 353. MS (MALDI-TOF, 3-indole acrylic acid, 10 mg/mL in acetonitrile as the matrix): *m*/*z* (100%): 1488 $[M+H]^+$.

2.1.3. 2(3),9(10),16(17),23(24)-Tetrakis-4′-(3,5-bis(trifluoromethyl)phenoxy)-phthalocyaninatocopper Cu(Pc) (II) (*3*)

A similar preparation method to that of complex **2** was used to obtain the blue powder of **3** by using compound **1** (0.150 g, 0.405 mmol), quinoline (0.5 cm^3) and anhydrous $CuCl_2$ (left one night in an oven at 110 °C) (0.013 g, 0.107 mmol). The desired compound is slightly soluble in $CHCl_3$ and CH_2Cl_2, has excellent solubility in acetone and THF, and is less soluble in DMF and DMSO.

Yield: 0.013 g (12.31%). *Anal.* Calc. for $C_{64}H_{246}N_8O4_8Cu$ (1487 g/mol): C, 51.64; H, 1.63; N, 7.53. Found: C, 51.60; H, 1.62; N, 7.47%. FTIR (KBr thin film) ν/cm^{-1}: 3068 cm^{-1} (w, Ar-H, broad), 1739 (w), 1668 (w) 1607 (*C=C*), 1508, 1459, 1407, 1365 (st, *–C–F*), 1274 (*Ar-O-Ar*), 1233, 1169, 1122 (st), 1084, 1050, 1002, 959, 947, 878, 847, 827, 782, 747, 700, 680. UV–Vis (THF), λ_{max}/nm: 674, 642, 608, 340; MS (MALDI-TOF, 3-indole acrylic acid (IAA) as the matrix): *m*/*z* (%):1487 $[M+H]^+$.

2.1.4. 2(3),9(10),16(17),23(24)-Tetrakis-4′-(3,5-bis(trifluoromethyl)-phenoxy)-phthalocyaninatocobalt (II) Co(Pc) (*4*)

A similar preparation method to that of complex **2** was used to obtain the blue powder of **4** by using a mixture of compound **1** (0.150 g, 0.405 mmol), anhydrous $CoCl_2$ (left one night in an oven at 110 °C) (ca. 0.013 g, 0.107 mmol) and quinoline (0.5 cm^3). Complex **4** is soluble in CH_2Cl_2, $CHCl_3$, acetone and THF, and is less soluble in DMF and DMSO.

Yield: 0.016 g (15.23%). *Anal.* Calc. for $C_{64}H_{24}N_8O_4Co$ (1483 g/mol): C, 51.80; H, 1.63; N, 7.55. Found: C, 51.72; H, 1.65; N, 7.40%. FTIR (KBr thin film) ν/cm^{-1}: 3069 cm^{-1} (w, Ar-H, broad), 1728 (w), 1606 (*C=C*), 1525 (w), 1459, 1412, 1364 (st, *–C–F*), 1274 (*Ar-O-Ar*), 1234, 1170, 1124 (st), 1085, 1057, 1002 (w), 961, 948, 878, 847, 825, 786, 752, 727, 700, 680. UV–Vis (THF), λ_{max}/nm: 665, 635, 601, 327; MS (MALDI-TOF, 3-indole acrylic acid (IAA) as the matrix): *m*/*z* (%): 1483 $[M+H]^+$.

*2.1.5. 2(3),9(10),16(17),23(24)-Tetrakis-4′-(3,5-bis(trifluoromethyl)phenoxy)-phthalocyaninatonickel (II) Ni(Pc) (**5**)*

A similar preparation method to that of complex **2** gave the blue powder of **5** by using compound **1** (0.150 g, 0.405 mmol), quinoline (0.5 cm^3) and anhydrous $NiCl_2$ (left one night in an oven at 110 °C) (0.013 g, 0.107 mmol). Complex **5** is soluble in CH_2Cl_2, $CHCl_3$, acetone anad THF and is less soluble in DMF and DMSO.

Yield: 0.015 g (14.30%). *Anal.* Calc. for $C_{64}H_{24}N_8O_4Ni$ (1482 g/mol): C, 51.81; H, 1.63; N, 7.55. Found: C, 51.77; H, 1.64; N, 7.42%. FTIR (KBr thin film) ν/cm^{-1}: 3072 cm^{-1} (w, Ar-H, broad), 1723 (w), 1608 (*C*═*C*), 1535 (w), 1459, 1416, 1367 (st, –*C*–*F*), 1275 (*Ar*-*O*-*Ar*), 1236, 1170, 1124 (st), 1086, 1051, 1001, 962, 948, 878, 848, 827, 786, 748, 727, 700, 680. UV–Vis (THF), λ_{max}/nm: 666, 635, 601, 332. MS (MALDI-TOF, 3-indole acrylic acid, 10 mg/mL in acetonitrile as the matrix): *m*/*z* (100%): 1483 $[M+H]^+$.

3. Results and discussion

3.1. Synthesis and characterization

Novel phthalocyanines (**2**–**5**) were prepared by the templated cyclization of 4′-(3,5-bis(trifluoromethyl)phenoxy)-phthalonitrile and anhydrous $Zn(OAc)_2$, $CuCl_2$, $CoCl_2$ and $NiCl_2$ in the presence of high boiling quinoline at 170–185 °C under a N_2 atmosphere in the presence of 1,8-diazabicyclo [5.4.0] undec-7-ene (DBU) as a strong base (Scheme 1). The blue cyclotetramerization products, MPc's (M = Zn, Cu, Co and Ni), were purified by column chromatography and were obtained in a moderate yield (28.65% for **2**, 12.31% for **3**, 15.23% for **4** and 14.30% for **5**). Elemental analysis results and the spectral data (^{1}H NMR, FTIR and MALDI-TOF-MS) of the new products are consistent with the assigned formulations. The blue-green phthalocyanine products were isolated as a mixture of isomers, as expected. The presence of isomers could be verified by the slight broadening encountered in the UV–Vis absorption bands and broadening in the ^{1}H NMR spectra as compared with the spectra of octa-substituted phthalocyanines composed of a single isomer [13,14,21,24]. The six peripheral fluoro atoms confer increased solubility of the complexes in both halogenated solvents ($CHCl_2$ and $CHCl_3$) and more polar solvents such as acetone and thf. The solubility of complex **3** and **5** are also affected by the central metal ion; these complexes show slightly lower solubility than **2** and **4** in halogenated solvents.

A strong –*C*–*F* stretching band, with a small shift, and the disappearance of the –*CN* band at 2236 cm^{-1} after phthalocyanine formation were identified in the FTIR spectra. Aliphatic and aromatic –*C*–*H* and ═*C*–*H* peaks at above and below 3000 cm^{-1}, and the remaining spectra are closely similar to that of compound **1** and provide easy diagnosis.

The ^{1}H NMR spectrum of complex **2** was almost identical to that of the starting compound **1**, except for small chemical shifts. The aromatic protons in the lower field region of the ^{1}H NMR spectrum and twelve different aromatic carbon atoms between 110 and 160 ppm in the ^{13}C NMR spectrum are the instinctive indicator signals for **1**. It is likely that the rather broad bands in the case of **2** are probably due to chemical exchange associated with an aggregation–disaggregation equilibria that occurs at the high concentrations used in the NMR measurements. The production of a mixture of four positional isomers are expected to cause broadening of the bands and the chemical shifts [11,14,21].

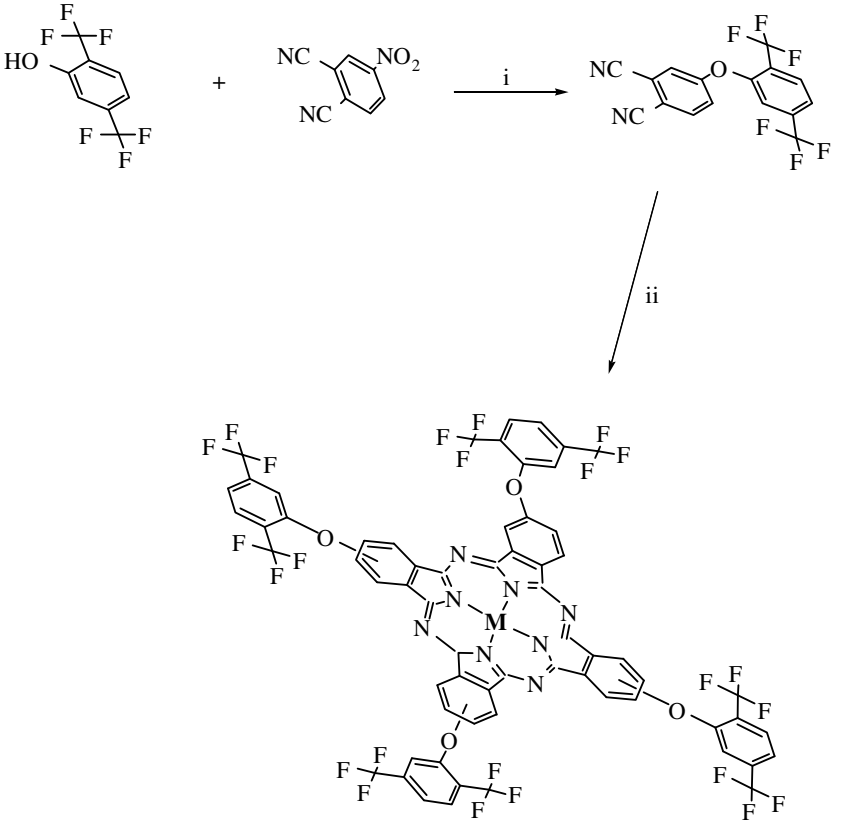

Scheme 1. Synthetic route of 4-(3,5-bis-(trifluoromethyl)-phenoxy)-phthalonitrile and its metallophthalocyanines (M = Zn(II), Cu(II), Co(II) and Ni(II)): (i) 3,5-bis-(trifluoromethyl)-phenol, 4-nitrophthalonitrile and K_2CO_3 in dmf at 40 °C for 72 h; (ii) anhydrous $Zn(acac)_2$, $CuCl_2$, $CoCl_2$ and $NiCl_2$, DBU, quinoline.

The UV–Vis spectra of the phthalocyanine complexes exhibit characteristic Q and B bands. Two principle π–π^* transitions are seen for phthalocyanines: a Q-band (~550–700 nm, a π–π^* transition from the highest occupied molecular orbital (HOMO) to the lowest unoccupied molecular orbital (LUMO) of the complexes) and a B-band (~300–350 nm, a deeper π–π^* transition from the HOMO's (a_{1u} and a_{2u}) to the LUMO (e_g)) [14,25]. The Q-band absorptions in the UV–Vis absorption spectra of the phthalocyanines (**2**, **3**, **4** and **5**) were observed as a single high intensity band due to a π–π^* transition at 677, 674, 665 and 666 nm, respectively, with shoulders on the slightly higher energy side of the Q-bands, as shown in Fig. 1. The positions of the absorption bands of the complexes are different from each other due to the effect of the ionic radius of the metal center [14,24]. The effect of *O*-substitution on the periphery for all phthalocyanines when compared with those of the *S*-substituted derivatives causes a shift in the Q-bands to shorter wavelengths [13,15,17,18,26–28].

The positive ion MALDI-MS spectrum of **2** is given in Fig. 2. Many different MALDI matrices were tried to find an intense molecular ion peak and low fragmentation under the MALDI-MS conditions for this complex. 3-Indole acrylic acid MALDI matrix yielded the best MALDI-MS spectrum, as seen in Fig. 2. The peak group representing the protonated molecular ion of the **2** was observed starting with a 1488 Da mass and finishing with 1494 Da, following each other by 1 Da mass differences. This type of mass distribution results from the isotopic mass distribution of carbon (mainly ^{13}C) and the isotopes of **2**. In the MALDI-MS spectrum of the complex, only the protonated molecular ion peak was observed, with no fragment ions. It is clear that no leaving group was available for this complex because of the high stability of the complex under the MALDI matrix conditions and also under the laser energy. The protonated molecular ion peak was observed at 1487 Da for **3**, with the other isotopic peaks mainly resulting from the isotopic distribution of the components of **3**, and this distribution exactly overlapped with the mass of the **3** calculated theoretically from its elemental composition (Fig. 3). Beside the protonated molecular ion peak of the complex, no peak was observed between the 500 and 2500 Da mass range, eliminating the presence of any other impurity or fragment ions under the laser shots. Beyond the protonated molecular ion peak of **4**, its MALDI spectrum showed a very clear spectrum and no fragmentations. The protonated molecular ion peak of **4** was observed at 1484 with the other three peaks following each other by a 1 Da mass difference. This peak group is because of the isotopic distribution of cobalt and carbon in the complex structure [14,24]. The best MALDI-MS spectrum of this complex was obtained using α-cyano-4-hydroxycinnamic acid with (ACCA), and it showed only one fragment peak at low intensity around 1380 Da mass. When 3-indole acrylic acid and other conventional matrices (except ACCA) were used, more fragmentations and broad peaks were obtained in each case. The protonated molecular ion peak of **5** was obtained at 1483 Da with a few other low intensity fragment peaks in the positive ion and reflectron mode MALDI-MS spectrum. The molecular ion peak showed an isotopic peak distribution because of the isotopic distribution of both nickel and carbon. In the case of **5**, some fragmentations were observed. This showed that the stability of **5** is lower than complexes **3** and **4**. [14].

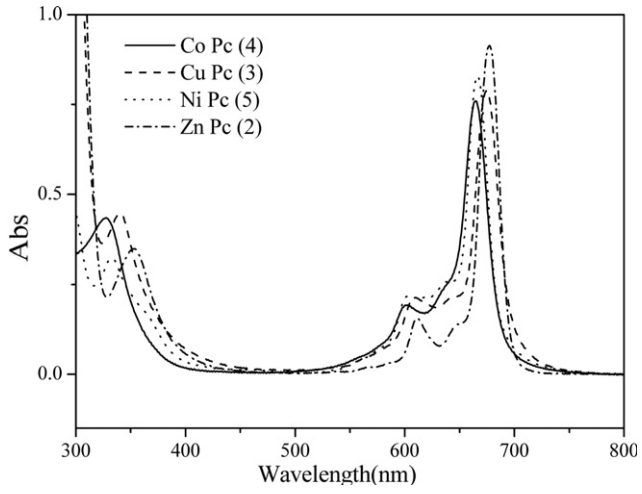

Fig. 1. UV–Vis spectra of the metallophthalocyanines (**2–5**) in THF.

3.2. Electrochemical measurements

The electrochemical behaviors of the phthalocyanines (**2**–**5**) were investigated by cyclic voltammetry (CV) and differential pulse voltammetry (DPV) on a platinum working electrode in THF. The half-wave potential values ($E_{1/2}$) vs SCE are summarized in Table 1.

As shown in the CVs in Fig. 4, complex **4** undergoes a one-electron oxidation and three one-electron reduction reactions within the electrochemical window of TBAP/THF. The DPV of the complex confirms the recorded redox processes clearly (Fig. 4C) [29,30]. The CV and DPV show the aggregation of the complex in solution. As shown in Fig. 4A, the first reduction couple (III) is very broad and irreversible. When the solution is diluted, this couple is split into two waves (Fig. 4B). This behavior shows the existence of an aggregation–disaggregation equilibrium of the species. Thus, first

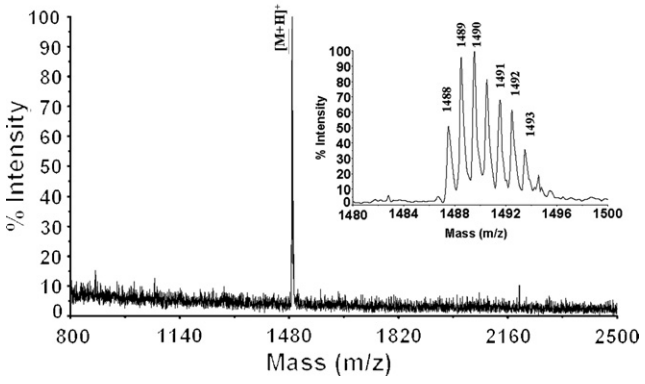

Fig. 2. Positive ion and reflectron mode MALDI-MS spectrum of **2** obtained in 3-indoleacrylic acid MALDI matrix. Inset spectrum shows the expanded molecular mass region of **2**.

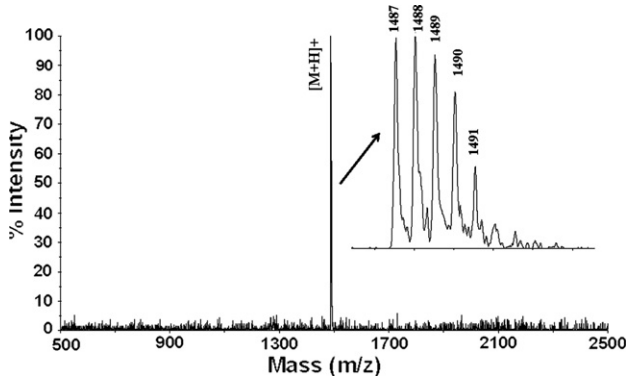

Fig. 3. Positive ion and reflectron mode MALDI-MS spectrum of **3** obtained in 3-indoleacrylic acid MALDI matrix. Inset spectrum shows the expanded molecular mass region of **3**.

Table 1
Voltammetric data for the complexes

Complexes	([a]$E_{1/2}$ (V)); ([b]ΔE_p (mV))					Ref.
	Oxd. 2	Oxd. 1	Red. 1	Red. 2	Red. 3	
ZnPc (**2**)		1.22 (65)	−0.67 (76)	−1.10 (85)		Tw
CuPc (**3**)		1.15 (80)	−0.77 (65)	−1.13 (62)		Tw
CoPc (**4**)	1.13 (110)	0.75 (130)	−0.21 (130)			
(−0.56)[c]	−1.29 (110)		Tw			
NiPc (**5**)		1.11 (145)	−0.65 (160)	−1.02 (145)	−1.93[d]	Tw
ZnPc (in DMSO)[e]		0.73	−0.74	−1.10	−1.43	[14]
CuPc (in DMSO)[e]		0.18[h]	−0.73	−1.03	−1.42	[14]
CoPc (in DMSO)[e]		0.46	−0.36	−1.27		[14]
NiPc (in DMSO)[f]			−0.62	−1.21	−1.67	[19]
ZnPc (in DMSO)[g]		0.67	−0.73	−1.13	−1.43	33]
CoPc (in DMSO)[g]	0.99	0.49	−0.36	−1.27	−1.83	[33]

Tw: This work.
[a] $E_{1/2} = (E_{pa} + E_{pc})/2$ at 0.100 V s^{-1}.
[b] $\Delta E_p = E_{pa} + E_{pc}$ at 0.100 V s^{-1}.
[c] Resulting from the aggregated species.
[d] Recorded with DPV.
[e] Substituted with tetrakis(6-hydroxyhexylsulfanyl) moieties.
[f] Substituted with tetra-aminophenyl sulfanyl moieties.
[g] Substituted with tetrakis-6-(-thiophene-2-carboxylate)-hexylthio moieties.
[h] Resulted from the adsorption of the complex on the working electrode.

one of the split peaks results from the monomeric form and the second one from the aggregated form of the complex. To indicate the effect of the switching potential to the peak character, the CVs were recorded with different switching potentials. However there was no significant effect to the reversibility and peak current of the redox waves. The first oxidation and first reduction processes occur on the metal center only for the Mn, Fe and Co phthalocyanine derivatives in polar solvents. For the Ni, Cu and Zn phthalocyanines, the redox processes take place on the Pc ring [31]. According to these studies, the first reduction process of **4** could be assigned easily to the Co^{II}/Co^{I} transformation, and the remaining processes to the phthalocyanine ring. All the predicted redox processes are given in Eq. (1). As shown in Table 1, all the redox processes are shifted toward positive potentials as a result of the increased electron-withdrawing ability of the trifluorophenyl substituents with respect to tetra-(propanediolsulfanyl) tetrachloro CoPc [32], tetrakis(6-hydroxyhexylsulfanyl) CoPc [14], tetrakis 2-aminophenylsulfanyl CoPc [19] and tetrakis-6-(-thiophene-2-carboxylate)-hexylthio CoPc [33], characterized in our previous studies.

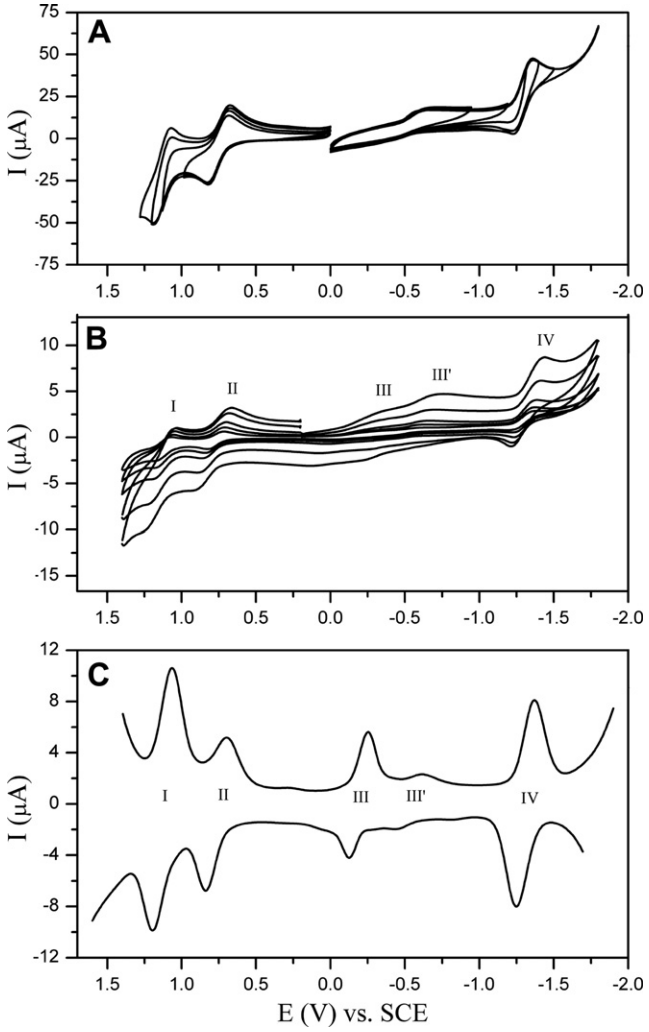

Fig. 4. (A) CVs of **4** (5.0×10^{-4} mol dm^{-3}) recorded with different switching potentials at 0.100 V s^{-1} scan rate. (B) CVs of **4** (1.0×10^{-4} mol dm^{-3}) recorded at various scan rates. (C) DPV of **4** at 0.100 V s^{-1} scan rate on Pt in THF/TBAP.

tials (Fig. 5C), however there is no significant difference for the redox reaction reversibility and peak currents due to the different

$$[Co^{III}Pc^{-1}]^{2+} \underset{1.13\ V}{\overset{-e^-}{\Leftrightarrow}} [Co^{II}Pc^{-1}]^{1+} \underset{0.75\ V}{\overset{-e^-}{\Leftrightarrow}} [Co^{II}Pc^{-2}] \underset{-0.21\ V}{\overset{+e^-}{\Leftrightarrow}} [Co^{I}Pc^{-2}]^{1-} \left\{ \begin{array}{l} \text{agg.} \Updownarrow \text{disagg.} \\ [Co^{II}Pc^{-2}]_{agg.} \underset{-0.56\ V}{\overset{+e^-}{\Leftrightarrow}} [Co^{I}Pc^{-2}]^{1-} \end{array} \right\} \underset{-1.29\ V}{\overset{+e^-}{\Leftrightarrow}} [Co^{I}Pc^{-3}]^{2-} \quad (1)$$

As shown in Fig. 5, **2**, **3** and **5** represent very similar well-resolved CVs. They undergo a one-electron oxidation and two one-electron reductions within the electrochemical window of TBAP/THF. The main difference is the aggregation tendency of **2**. As shown in Fig. 5A, the first reduction wave is split into two peaks. Diluting the solution decreases the peak current of the wave assigned to the aggregated species more than those of the monomeric species reduction wave. These observations support the aggregation behavior of the complex. The CV of **5** was recorded with different switching potentials. Because of the electro-inactive metal center of the complexes, all of these processes are attributed to the successive removal of electrons from, or addition of electrons to, the macrocycle orbitals. The HOMO–LUMO gaps of the complexes are comparable with those of common metallophthalocyanines (~1.300–1.700 V). A positive potential shift of the redox processes due to the electron-withdrawing nature of the triflorophenyl substituents with respect to the metallophthalocyanines characterized in our previous study [14,19,32,33] was also observed.

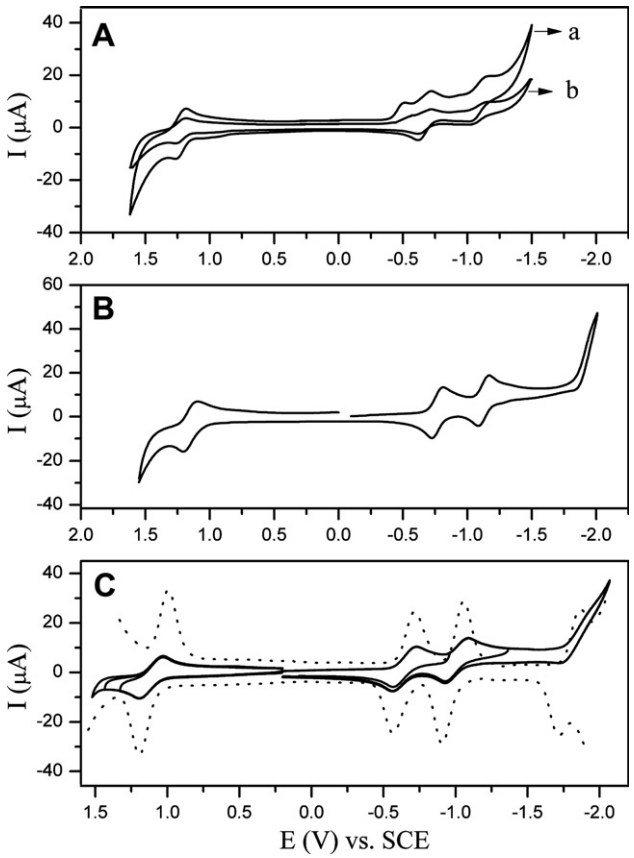

Fig. 5. (A) CVs of **2** ($a = 5.0 \times 10^{-4}$ mol dm^{-3} and $b = 2.5 \times 10^{-4}$ mol dm^{-3}). (B) CVs of **3** (5.0×10^{-4} mol dm^{-3}). (C) Solid lines: CVs of 5 recorded with different switching potentials. Dot lines: DPVs of **5** (5.0×10^{-4} mol dm^{-3}) at 0.100 V s^{-1} scan rate on Pt in THF/TBAP.

Acknowledgements

We thank the Research Funds of Sakarya University, DPT-2004 (Project No. 2003K120970) and TUBİTAK (Project No. TBAG: 108T094; MAG-106M286).

References

[1] C.C. Leznoff, A.B.P. Lever (Eds.), Phthalocyanines: Properties and Applications, vols. 1–4, VCH Publishers, New York, 1989–1996.
[2] N.B. Mc Keown, Phthalocyanine Materials: Synthesis, Structure and Function, Cambridge University Press, Cambridge, 1998.
[3] J.J. Simon, H.J. Andre, Molecular Semiconductors, Springer, Berlin, 1985.
[4] M.J. Cook, Adv. Mater 7 (1995) 877.
[5] Y. Sadaoka, T.A. Jones, W. Göpel Sens, Actuators 1 (1990) 148.
[6] J. Jiang, K. Kasuga, D.P. Arnold, in: H.S. Nalwa (Ed.), Supramolecular Photosensitive and Electroactive Materials, Academic Press, San Diego, CA, 2001, p. 188.
[7] A. Koca, M.K. Şener, M.B. Koçak, A. Gül, Int. J. Hydrogen Energy 31 (2006) 2211.
[8] H. Aga, A. Aramata, Y. Hisaeda, J. Electroanal. Chem. 437 (1997) 111.
[9] J.H. Zagal, Coord. Chem. Rev. 119 (1992) 89.
[10] E. Hamuryudan, Dyes Pigments 68 (2–3) (2006) 151.
[11] M. Kandaz, S.L.J. Michel, B.M. Hoffman, J. Porphyr. Phthalocyan. 7 (2003) 700.
[12] Y. Lu, R.G. Reddy, Electrochim. Acta 52 (2007) 256.
[13] M. Kandaz, I. Yılmaz, Ö. Bekaroğlu, Polyhedron 19 (2000) 115.
[14] M.N. Yarasir, M. Kandaz, A. Koca, B. Salih, Polyhedron 26 (2007) 1139.
[15] M. Kandaz, Ö. Bekaroğlu, Chem. Ber. 135 (1997) 1833.
[16] Ş. Abdurrahmanoğlu, A.R. Özkaya, M. Bulut, Ö. Bekaroğlu, J. Chem. Soc., Dalton Trans. (2004) 4022.
[17] M. Selçukoğlu, E. Hamuryudan, Dyes Pigments 74 (2007) 17.
[18] R.J. Li, X.X. Zhang, P.H. Zhu, D.K.P. Ng, N. Kobayashi, J.Z. Jiang, Inorg. Chem. 45 (5) (2006) 2327.
[19] M. Kandaz, M.N. Yaraşır, A. Koca, Ö. Bekaroğlu, Polyhedron 21 (2002) 255.
[20] B.A. Bench, W.W. Brennessel, H.-J. Lee, S.M. Gorun, Angew. Chem., Int. Ed. 41 (2002) 750.
[21] S. Wei, D. Huang, L. Li, Q. Meng, Dyes Pigments 56 (2003) 1.
[22] J.H. Wang, A.K. Khanamiryan, C.C. Leznoff, J. Porphyr. Phthalocyan. 8 (11) (2004) 1293.
[23] J.G. Young, W. Onyebuagu, J. Org. Chem. 55 (1990) 2155.
[24] M.N. Yarasir, M. Kandaz, A. Koca, B. Salih, J. Porphyr. Phthalocyan. 10 (2006) 1022.
[25] M. Gouterman, D. Dolphin, The Porphyrins, vol. 1, Springer, London, 1990. p. 123.
[26] M. Kandaz, Ö. Bekaroğlu, J. Porphyr. Phthalocyan. 3 (1999) 339.
[27] M. Durmus, T. Nyokong, Inorg. Chem. Commun. 10 (2007) 332.
[28] A. Kalkan, S. Guner, Z.A. Bayir, Dyes Pigments 74 (2007) 636.
[29] P.T. Kissinger, W.R. Heineman, Laboratory Techniques in Electroanalytical Chemistry, 2nd ed., Marcel Dekker, New York, 1996.
[30] A.J. Bard, L.R. Faulkner, Electrochemical Methods: Fundamentals and Applications, 2nd ed., Wiley, New York, 2001.
[31] A.B.P. Lever, E.R. Milaeva, G. Speier, in: C.C. Leznff, A.B.P. Lever (Eds.), The Redox Chemistry of Metallophthalocyanines in Solution in Phthalocyanines: Properties and Applications, vol. 3, VCH, New York, 1993.
[32] M. Kandaz, H.S. Çetin, A. Koca, A.R. Özkaya, Dyes Pigments 74 (2007) 298.
[33] M.N. Yarasir, M. Kandaz, B.F. Senkal, A. Koca, B. Salih, Dyes Pigments 77 (2008) 7.

temperature range 100–200 °C at low pressure, and exhibit rather good stability during storage and use [8,10], which is rather rare for barium and strontium volatile compounds. Nevertheless, [Ba(hfa)$_2$(tetraglyme)] demonstrates a relatively high melting point of 150 °C, so it must be sublimed into the reactor feed stream. Meanwhile, MOCVD techniques with precursor liquid delivery are well-known and applied for deposition of AEE-containing thin films [10]. Therefore, the development of low-melting AEE precursors, which should be liquid and provide constant surface areas for evaporation and transport during deposition experiments is of interest, especially for barium.

Marks and co-workers [11] have proposed to reduce the melting points of [Ba(hfa)$_2$($CH_3O(CH_2CH_2O)_nCH_3$)] by increasing the number of ether fragments ($n > 4$) and by the introduction of bulky R^1 and R^2 substituents in the polyglyme ligands. In this way, the complexes [Ba(hfa)$_2$($R^1O(CH_2CH_2O)_nR^2$)] with melting points down to 50 °C were obtained, but decomposition and low volatility of some such complexes were observed under heating. This is caused by impossibility of coordination of all the polyglyme oxygen atoms to the barium ion, which leads to additional intermolecular interactions and complicates evaporation.

In contrast to Marks and co-workers [11], Fragala and co-workers [12] suggested the use of glyme ligands with short chains ($n = 1$ or 2, corresponding to monoglyme or diglyme) for the synthesis of low-melting precursors, and such volatile, low-melting mixed ligand complexes with diglyme were obtained for hexafluoroacetylacetonates of lanthanides [12], lead(II) [13] and cobalt(II) [14].

However, the complexes of AEE hexafluoroacetylacetonates with diglyme have not been described yet. Here we report the synthesis, X-ray structures, thermal behavior and mass spectrometric study of [Ca(hfa)$_2$(diglyme)(H_2O)] (**I**), [Sr(hfa)$_2$(diglyme)(H_2O)] (**II**) and [Ba(hfa)$_2$(diglyme)$_2$] (**III**).

2. Experimental

Analytically pure hexane, metallic Ba, $CaCO_3$, $SrCO_3$ and $BaCO_3$ from Reakhim (Russia) were used without further purification. Hhfa (P&M Invest, Russia, 98%) and diglyme (Fluka, 99%) were preliminary distilled under reduced pressure.

The C, H and N contents were determined by conventional elemental analysis. The calcium and strontium contents were determined titrimetrically. IR spectra were recorded on a Perkin–Elmer 1600 FTIR spectrometer as Nujol and hexachlorobutadiene mulls between KBr plates in the region 4000–400 cm^{-1}. ^{1}H and ^{13}C NMR spectra were obtained using a Bruker Avance-400 (400 MHz, $CDCl_3$/TMS). TG curves at low pressure (0.01 torr) were recorded on a ULVAC SINKU-RIKO TA-7000 analyzer with a 10 °C min^{-1} heating rate.

2.1. Synthesis of [Ca(hfa)$_2$(diglyme)(H_2O)] (**I**), [Sr(hfa)$_2$(diglyme)(H_2O)] (**II**), [Ba(hfa)$_2$(diglyme)$_2$] (**III**)

MCO_3 (4 mmol, M = Ca, Sr, Ba) was added to a Hhfa and diglyme mixture (molar ratio 1:2:1 or 1:2:2) in hexane (40 ml) followed by continuous stirring for 2 h at 50 °C, until full dissolution of MCO_3. White crystalline precipitates were obtained after slow solvent evaporation in air. Yield: ~90–95%.

Anal. Calc. for $C_{16}H_{18}F_{12}O_8Ca$: C, 31.69; H, 2.99; Ca, 6.61. Found: C, 32.63; H, 3.07; Ca, 6.45. IR, cm^{-1}: 3640–3340 ν(O–H); 2960–2840 ν(C–H); 1661 ν(C=O); 1527, 1510 ν(C=C); 1248, 1187, 1132 ν(C–F); 1472 $\delta(CH_2)$; 1455 $\delta(CH_3)$; 1067 ν(C–O–C). ^{1}H NMR ($CDCl_3$), ppm: δ 6.01 (s, 2H, CH), 3.81 (tr, 4H, CH_2), 3.73 (tr, 4H, CH_2), 3.41 (s, broad, 6H, OCH_3 + 2H, H_2O); ^{13}C ($CDCl_3$), ppm: δ 177.1 (quartet, CO), 122.1, 119.3, 115.9 (s, CF_3), 86.8 (s, CH), 71.1, 69.4 (s, CH_2CH_2), 59.7 (s, OCH_3). M.p. 109 °C.

Anal. Calc. for $C_{16}H_{18}F_{12}O_8Sr$: C, 29.39; H, 2.77; Sr, 13.40. Found: C, 29.53; H, 2.78; Sr, 13.07. IR, cm^{-1}: 3640–3390 ν(O–H); 2960–2850 ν(C–H); 1676 ν(C=O); 1532, 1514 ν(C=C); 1256, 1194, 1142, ν(C–F); 1470 $\delta(CH_2)$; 1458 $\delta(CH_3)$; 1072 ν(C–O–C). ^{1}H NMR ($CDCl_3$), ppm: δ 5.94 (s, 2H, CH), 3.72 (tr, 4H, CH_2), 3.67 (tr, 4H, CH_2), 3.41 (s, broad, 6H, OCH_3 + 2H, H_2O); ^{13}C ($CDCl_3$), ppm: δ 175.8 (tr, CO), 122.3, 119.4, 116.6 (s, CF_3), 87.9 (s, CH), 71.4, 69.8 (s, CH_2CH_2), 59.1 (s, OCH_3). M.p. 122 °C.

Anal. Calc. for $C_{22}H_{30}F_{12}O_{10}Ba$: C, 32.23; H, 3.69. Found: C, 32.21; H, 3.72; IR, cm^{-1}: 2942–2844 ν(C–H); 1674 ν(C=O); 1532

Table 1
Crystal and refinement data

	[Ca(hfa)$_2$(diglyme)(H_2O)] (**I**)	[Sr(hfa)$_2$(diglyme)(H_2O)] (**II**)	[Ba(hfa)$_2$(diglyme)$_2$] (**III**)	[Ba(hfa)$_2$(diglyme)$_2$] (**III***)
Formula	$C_{16}H_{18}CaF_{12}O_8$	$C_{16}H_{18}F_{12}O_8Sr$	$C_{22}H_{30}F_{12}O_{10}Ba$	$C_{22}H_{30}F_{12}O_{10}Ba$
Formula weight	606.38	653.92	819.80	819.80
Diffractometer	Bruker APEX II	Bruker APEX II	Bruker Smart 1000	Enraf-Nonius CAD-4
Data collection method	φ and ω scans	φ and ω scans	φ and ω scans	ω/1.33θ scans
T (K)	100(2)	100(2)	143(2)	293(2)
Crystal system	monoclinic	monoclinic	triclinic	monoclinic
Space group	$P2_1/n$	$P2_1/n$	$P\bar{1}$	$C2/c$
a (Å)	17.0254(7)	17.6449(11)	9.4484(16)	11.5431(9)
b (Å)	18.3627(7)	18.1523(11)	9.6588(17)	15.4702(11)
c (Å)	17.8369(7)	17.7294(11)	18.681(3)	18.969(2)
α (°)	90	90	97.954(9)	90
β (°)	117.063(1)	117.7646(11)	95.743(7)	101.217(8)
γ (°)	90	90	106.915(5)	90
V (Å^3)	4965.8(3)	5024.9(5)	1597.6(5)	3322.7(5)
Z	8	8	2	4
Color, habit	colorless, prism	colorless, prism	colorless, prism	colorless, prism
Crystal dimensions (mm)	0.63 × 0.40 × 0.35	0.34 × 0.25 × 0.23	0.50 × 0.24 × 0.20	0.52 × 0.25 × 0.28
D_{calc} (g cm^3)	1.622	1.729	1.704	1.639
μ (mm^{-1})	3.81	2.272	1.360	1.308
Unique reflections (R_{int})	13058 (0.0319)	12526 (0.076)	8332 (0.022)	4839 (0.051)
Observed reflections [$I > 2\sigma(I)$]	10010	7377	7400	3307
Parameters	769	671	411	235
$R[F^2 > 2\sigma(F^2)]$, $wR(F^2)$	0.0436, 0.0914	0.046, 0.109	0.038, 0.094	0.046, 0.127
Goodness-of-fit on F^2	1.001	0.969	1.03	1.15
Absorption correction	multi-scan APEX II [16]	multi-scan APEX II [16]	multi-scan SADABS [17]	GAUSSIAN [18]
T_{max}, T_{min}	0.629, 0.612	0.623, 0.512	0.773, 0.550	0.751, 0.700
ρ_{min}, ρ_{max} (e Å^3)	−1.11, 1.19	−0.66, 0.89	−1.20, 1.73	−0.67, 0.68

ν(C=C); 1252, 1190, 1142, ν(C–F); 1470 $\delta(CH_2)$; 1458 $\delta(CH_3)$; 1074 ν(C–O–C). ^{1}H NMR ($CDCl_3$), ppm: δ 5.82 (s, 2H, CH), 3.69 (quartet, 8H, CH_2), 3.60 (quartet, 8H, CH_2), 3.41 (s, 12H, OCH_3); ^{13}C ($CDCl_3$), ppm: δ 174.6 (quartet, CO), 122.5, 119.7, 116.8 (CF_3), 86.5 (s, CH), 71.6, 69.6 (s, CH_2CH_2), 58.6 (s, OCH_3). M.p. 83 °C.

The same complex **III** was synthesized by the interaction of metallic Ba (4.23 mmol) with a mixture of Hhfa and diglyme (molar ratio 1:2:2) in hexane (40 ml) under continuous stirring for 8 h at 50 °C, followed by the separation of unreacted Ba pieces and slow solvent evaporation in air. Yield ~70%.

2.2. X-ray crystal structure determination

X-ray quality single-crystals were grown by recrystallization from hexane solution. The single-crystal X-ray diffraction data were collected on Bruker APEX II, Bruker SMART 1000 (with CCD area detectors) and Enraf-Nonius CAD-4 diffractometers (Mo Kα, λ = 0.71073 Å, graphite monochromator). The structures were solved by direct methods and refined with the full-matrix F^2 least-squares technique (SHELXTL PLUS) [15]. The hydrogen atoms of the water molecules were found on difference Fourier synthesis. Other H atoms were placed in idealized positions and refined using a riding model with fixed isotropic thermal parameters. Pertinent details are given in Table 1.

2.3. Mass spectrometry

The mass spectra of **I**–**III** were recorded on a MS 1301 spectrometer having a 50–1500 amu mass range using 65 eV ionizing electrons. The complexes were vaporized from a Knudsen effusion cell. The ratio of evaporation surface to surface of the effusion hole was about 600. The cell temperature was measured with a Pt/Pt(Rh) thermocouple (±2°). The main ion peaks in the mass spectra of **I**–**III** are presented in Tables 5 and 6.

3. Results and discussion

3.1. Synthesis

Two main methods for the synthesis of mixed ligand AEE β-diketonates $[M(dik)_2Q_n]$ are known and used in MOCVD precursor preparation: (i) the interaction between oligomeric homoleptic $[M(dik)_2]_x$ or heteroleptic $[M(dik)_2(Solv)]_x$ (Solv = H_2O, Et_2O or EtOH, $x \leqslant 3$) complexes with neutral donor ligands Q; (ii) the *in situ* reaction of the ethoxides with Hdik and Q [1,19]. A rich variety of monomeric mixed ligand AEE β-diketonates have been prepared, including the complexes of AEE hexafluoroacetylacetonates with polyglymes $CH_3O(CH_2CH_2O)_nCH_3$ ($n \geqslant 3$) [1]. However, for such precursors to be useful MOCVD sources, these methods are too expensive and have several inherent limitations: in method (i), the necessity of the synthesis and purification of the starting homoleptic β-diketonates; in method (ii), the use of air/moisture-sensitive metal ethoxides. An effective simple strategy of synthesis based on the high acidity of Hhfa ($pK_a \sim 4.5$ [20]) was developed for $[M(hfa)_2(CH_3O(CH_2CH_2O)_nCH_3)]$ ($n \geqslant 3$) – the *in situ* interaction of AEE oxide, hydroxide or carbonate with Hhfa and $CH_3O(CH_2CH_2O)_nCH_3$ ($n \geqslant 3$) in EtOH or hydrocarbons in a stoichiometric ratio (method (iii)). In this method, the interaction of MCO_3 ($M(OH)_2$ or MO) with Hhfa results in the formation of hydrated $[M(hfa)_2(H_2O)_x]$, followed by replacement of the water molecules and saturation of the AEE ion coordination sphere by donor oxygen atoms of polyglyme ligands, forming 5-membered chelate rings with the central AEE ions. In the case of polyglymes with $n \geqslant 3$, the number of oxygen atoms is large enough ($\geqslant 4$) for saturation of the AEE coordination sphere, together with four oxygen atoms from two hfa^- ligands, and formation of mixed ligand complexes containing no water molecules. In complexes $[M(hfa)_2(CH_3O(CH_2CH_2O)_nCH_3)]$ ($n \geqslant 3$) the typical coordination number (CN) for Ca and Sr is equal to 8, and for the larger Ba, CN $\geqslant$ 9 (up to 10 in the complexes with polyglymes) [11].

In this work for the synthesis of mixed ligand complexes with diglyme we used method (iii) with starting MCO_3. Diglyme contains only three oxygen atoms, which can form two chelate rings with central metal ions. In the syntheses with a molar ratio $[MCO_3]$:[diglyme] = 1:1, one would expect the formation of hydrated complexes $[M(hfa)_2(diglyme)(H_2O)_m]$, where $m = 1$ for Ca and $\geqslant 1$ for the larger Sr and Ba. In fact the complexes $[M(hfa)_2(diglyme)(H_2O)]$ (M = Ca, Sr) were obtained, but the barium complex contained two diglyme molecules – $[Ba(hfa)_2(diglyme)_2]$ in spite of the starting molar ratio of 1:1. The composition of the complexes formed did not change when the starting molar ratio $[MCO_3]$:[diglyme] was equal to 1:2. The data of elemental analysis, IR spectroscopy and NMR confirm the formation of **I–III**. Notice that **III** was prepared from metallic Ba as a starting reagent too, but the yield of product was about 20% lower than in the synthesis from $BaCO_3$ because the surface of metallic Ba is less than that of crystalline barium carbonate. Additionally metallic Ba does not react totally, as with time its surface is covered by thin layer of product and the reaction stops.

The difference in the composition of the calcium, strontium and barium complexes is attributable to the ionic radii of these elements. The ionic radii of Ca and even Sr are not so large for the coordination of a second diglyme molecule in the chelate mode, and coordination in the bridging mode does not occur owing to the presence of water molecules in the reaction mixture. However when the same method (iii) was used for the synthesis of lead(II) complexes, the anhydrous dimers $[Pb(hfa)_2(\mu\text{-}\eta^3{:}\eta^1\text{-diglyme})]_2$ formed in spite of water presence in the reaction mixture in toluene [13]. It means that the composition and structure of hexafluoroacetylacetonate complexes with diglyme depend not only on the synthesis method and ionic radii, but also on the electronic configuration of the central ion: for CN = 8 the ionic radii of Sr^{2+} (1.40 Å) and Pb^{2+} (1.46 Å) are close to each other. The bridging mode of the diglyme coordination was described in the complex $[Ba(thd)_2(diglyme)]_2$ (Hthd = 2,2,6,6,-tetramethylheptane-3,5-dione), prepared via the reaction of $[Ba_4(thd)_8]$ and diglyme in absolute *n*-hexane and under a dry atmosphere [21].

Only in the case of the largest barium ion is the coordination of a second diglyme molecule possible in the chelating mode. The formation of four diglyme chelate rings stabilizes the mixed ligand complex so strongly that $[Ba(hfa)_2(diglyme)_2]$ forms even in the presence of water and at a $[MCO_3]$:[diglyme] molar ratio of 1:1. A similar situation was described in the synthesis of mixed ligand complexes of lanthanide hexafluoroacetylacetonates with the bidentate ligands Dipy and Phen [22,23].

Finally, a significant reduction in the melting point of AEE diglyme complexes, compared to the tetraglyme complexes, has been observed only for the barium compound (from 125 °C [8] to 83 °C). This is caused by its structural features disordering of the CF_3 groups and the presence of only weak van der Waals intermolecular interactions.

3.2. Structures of the complexes

3.2.1. The structure of $[Ca(hfa)_2(diglyme)(H_2O)]$ (*I*) and $[Sr(hfa)_2(diglyme)(H_2O)]$ (*II*)

Complexes **I** and **II** are isostructural and their crystal structures are built by the packing of two crystallographically non-equivalent molecules $[M(hfa)_2(diglyme)(H_2O)]$ (I^* and I′, II^* and II′) which differ only slightly in the mutual orientation of the hfa^- anions and diglyme ligands in the coordination polyhedron of the central ions.

The independent molecules are combined into dimers by means of four hydrogen bonds between the oxygen atoms of the hfa^- anions and the hydrogen atoms of H_2O molecules (Figs. 1 and 2, Table 2).

In both independent $[M(hfa)_2(diglyme)(H_2O)]$ molecules, the M^{2+} cations have a distorted anti-prismatical coordination (CN = 8) formed by four O atoms (O1–O4 or O1′–O4′) of two chelating hfa^- anions, three O atoms (O5–O7 or O5′–O7′) of the diglyme ligand and one O atom (O1w or O2w) from a water molecule. The oxygen atoms of the diglyme and water ligands lie in an equatorial plane with the hfa^- ligands situating respectively above and below the plane in an approximately orthogonal relationship (dihedral angles 84.3°/89.7° for I*/I′ and 88.8°/84.8° for II*/II′, respectively). The Ca^{2+} ion is displaced from the mean planes of the hfa^- anions by 0.14–0.33 Å for I* and 0.55–0.64 Å for I′. In the structure of **II**, a similar displacement of Sr^{2+} occurs only in II* (0.57–0.68 Å).

In the structures of both **I** and **II**, the $M–O_{hfa}$ bond distances are slightly shorter than the $M–O_{diglyme}$ distances (Table 2). The average $M–O_{hfa}$ and $M–O_{diglyme}$ bond distances increase by 0.11 and 0.07 Å, respectively, from **I** to **II**, which agrees with the difference in ionic radii of Ca^{2+} and Sr^{2+} with CN = 8 (0.14 Å). The M–O bonds inside the same chelate rings forming by hfa^-, as well as by the diglyme ligands, vary in lengths (Table 2), which is rather typical for alkaline and rare earth element β-diketonates and their mixed ligand complexes with predominantly ionic bond nature [24,25]. The $M–O_{water}$ bond distances are the shortest among M–O bonds in coordination polyhedrons of both Ca^{2+} and Sr^{2+} (2.37 and 2.52 Å, respectively).

The literature data about the structures of calcium and strontium β-diketonate complexes with polyglymes are few in number [1]. As for hexafluoroacetylacetonate complexes, only two structures of calcium compounds have been published – $[Ca(hfa)_2$-(tetraglyme)] (**IV**) [19] and $[Ca_2(hfa)_4$(heptaglyme)] (**V**) [20], and to our knowledge, no structures of strontium hexafluroacetylacetonates with glyme ligands have been published as yet. In spite of the difference in the numbers of donor oxygen atoms in diglyme (three), tetraglyme (five) and heptagyme (eight), the gross molecular structures of **I**, **IV** and **V** are similar: a distorted anti-prismatic coordination of the calcium ions with CN = 8, equatorial positions of glyme oxygen atoms and nearly orthogonal arrangements of chelating hfa^- ligands. These general structural features lead one to compare the average Ca–O bond distances in structures of **I**, **IV** and **V** (Table 3). In all these structures a regular correlation in $Ca–O_{hfa}$ and $Ca–O_{glyme}$ bond distances occurs, however, in **I** these distances are the longest. For the $Ca–O_{glyme}$ bonds, this can be explained from the viewpoint of structure stabilization due to the macrochelate effect: in **IV** and **V** the glyme ligands form three chelate rings, in **I** there are only two.

In the case of non-fluorinated AEE β-diketonates, the dimeric complex $[Sr_2(thd)_4(diglyme)_2(\mu\text{-}H_2O)]$ with CN = 8 and a bridging water molecule has been described [26]. In this complex the average $Sr–O_{dik}$ distance is about 0.06 Å shorter and the $Sr–O_{diglyme}$ is about 0.06 Å longer than the corresponding values in **II**, which is caused by the difference between the Lewis acidity of $Sr(thd)_2$ and $Sr(hfa)_2$. The $Sr–OH_2$ distance is 0.45 Å longer than that in **II** due to the bridging function of the water molecule.

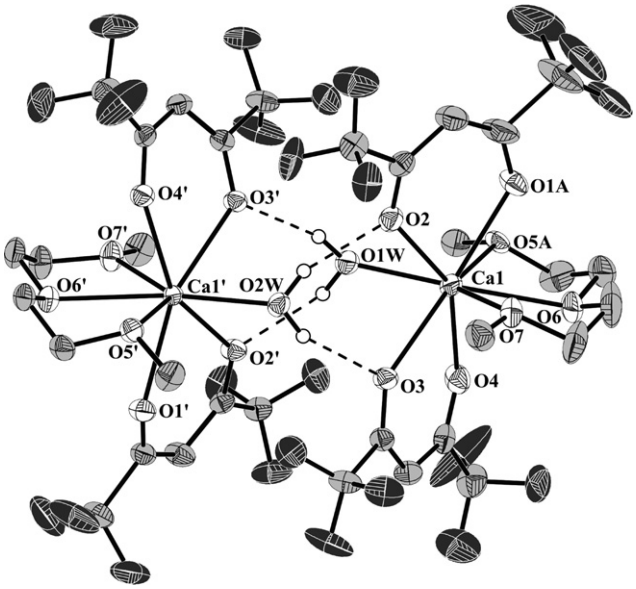

Fig. 1. Molecular structure of $[Ca(hfa)_2(diglyme)(H_2O)]$. H-atoms are partially omitted for clarity. Dash lines show intermolecular hydrogen bonds. For disordered atoms only one position is shown.

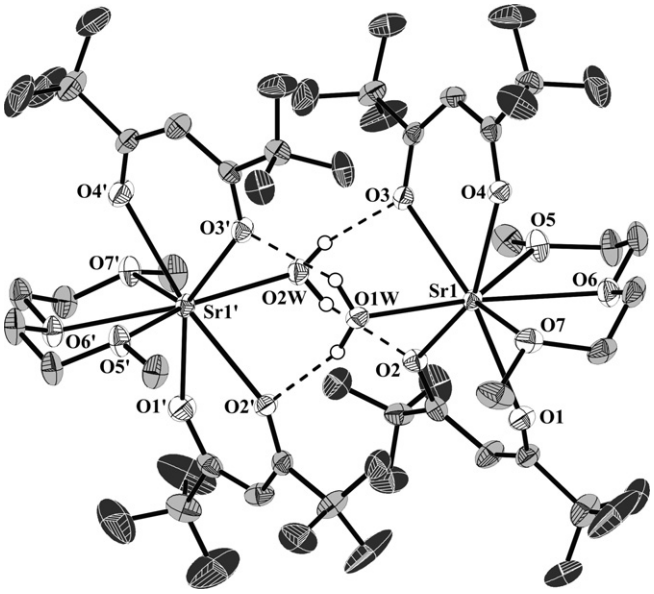

Fig. 2. Molecular structure of $[Sr(hfa)_2(diglyme)(H_2O)]$. H-atoms are partially omitted for clarity. Dash lines show intermolecular hydrogen bonds.

Table 2
Selected geometric parameters for $[Ca(hfa)_2(diglyme)(H_2O)]$ (**I**) and $[Sr(hfa)_2$(diglyme)$(H_2O)]$ (**II**)

	I* (M = Ca1)	**I′** (M = Ca1′)	**II*** (M = Sr1)	**II′** (M = Sr1′)
Bond distances (Å)				
M–O$_{hfa}$				
M–O1A[a]	2.454(9)	2.3936(13)	2.516(2)	2.521(3)
M–O1B[a]	2.305(10)			
M–O2	2.4474(13)	2.4802(12)	2.606(2)	2.612(2)
M–O3	2.4720(13)	2.4462(12)	2.543(2)	2.567(2)
M–O4	2.4001(15)	2.4021(13)	2.538(2)	2.532(3)
M–O$_{glyme}$				
M–O5A[a]	2.532(4)	2.5414(12)	2.597(2)	2.584(2)
M–O5B[a]	2.577(8)			
M–O6	2.4896(14)	2.5109(13)	2.635(3)	2.618(2)
M–O7	2.4788(16)	2.4762(14)	2.632(2)	2.632(2)
M–O1w	2.3614(14)	2.3705(13)	2.517(2)	2.521(2)
Hydrogen-bond geometry (Å, °)				
	D···A	D–H···A	D···A	D–H···A
O1w–H···O2′	2.8914(19)	143	2.834(3)	159
O1w–H···O3′	2.8011(16)	162	2.843(4)	146
O2w–H···O2	2.8681(18)	155	2.852(4)	154
O2w–H···O3	2.8551(17)	156	2.823(3)	164

[a] Atoms are disordered.

Table 3
The average Ca–O bond distances (Å) in the structures of **I**, **IV** and **V**

	$Ca–O_{hfa}$	$Ca–O_{glyme}$
I	2.43	2.55
IV [19]	2.40	2.47
V [20]	2.39	2.50

3.2.2. Structure of $[Ba(hfa)_2(diglyme)_2]$ (*III*)

The crystal structure of **III** consists of monomeric molecules with CN = 10 (Fig. 3). The coordination polyhedron of the Ba^{2+} central ion is formed by four oxygen atoms (O1–O4) of two chelating hfa^- anions and six O atoms (O5–O10) of two diglyme ligands (Table 4), and it is rather difficult to describe its geometry exactly.

The diglyme ligands are coordinated on one side of the Ba^{2+} cation (the dihedral angle between the O5–O6–O7 and O8–O9–O10 planes is 79°) while the hfa^- anions are on the other side. In **III**, the Ba^{2+} cation is displaced from the planes of the hfa^- anions by 0.22 Å (O1–C1–C2–C3–O2) and 0.07 Å (O3–C6–C7–C8–O4).

Such a "*cis*"-arrangement of ancillary ligands is typical for mixed ligand complexes with the general formula $[M(hfa)_2(Q)_2]$ and with the CN of the alkaline earth cations equal to 8, for example $[Ba(hfa)_2(Phen)_2]$ [27] and $[Sr(hfa)_2(Dipy)_2]$ [28]. This is in contrast to the non-fluorinated or asymmetrical incompletely fluorinated β-diketones analogues, in which the ancillary ligands are in the "*trans*"-position: $[M(thd)_2(Phen)_2]$ (M = Ca, Sr, Ba) [29], $[Ba(pta)_2(Phen)_2]$ (Hpta = 1,1,1-trifluoro-5,5-dimethyl-hexahe-2,4-dione) [30]. In our opinion, this difference in the mutual arrangement of ligands in the $[M(hfa)_2(Q)_2]$ molecules is caused by the increasing role of the crystal structure packing effects in complexes with fluorinated β-diketones [27].

Among the barium β-diketonate mixed ligand complexes there is only one with diglyme as the ancillary ligand – $[Ba(thd)_2(diglyme)]_2$ [21], which has a dimeric structure with a 7 + 1 coordination number of Ba^{2+} and in which the association into dimers is caused by weak bridging functions of O atoms from diglyme. The high coordination number, equal to 10, occurs in the complex $[Ba(hfa)_2(pentaglyme')]$ (**VI**) [pentaglyme′ = $CH_3O(CH_2CH_2O)_5C_2H_5$], where all six oxygen atoms of pentaglyme are coordinated by barium and are situated in nearly a meridional plane [11].

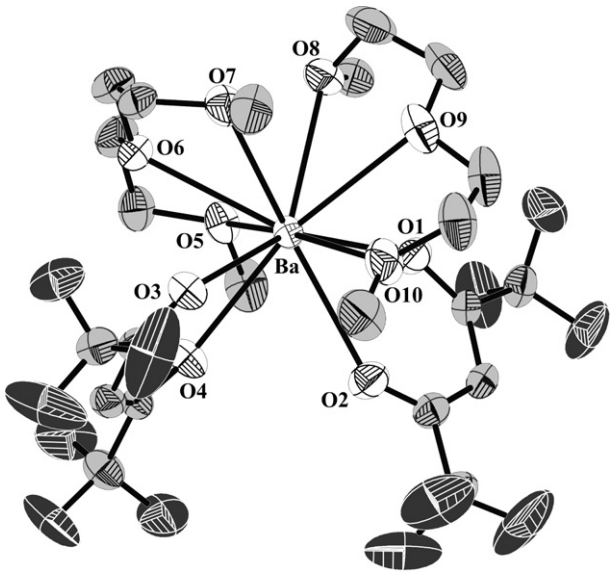

Fig. 3. Molecular structure of $[Ba(hfa)_2(diglyme)_2]$. H-atoms are omitted for clarity.

Table 4
Bond distances (Å) for $[Ba(hfa)_2(diglyme)_2]$ (**III**) and $[Ba(hfa)_2(pentaglyme')]$ (**VI**) [11]

Bond length (Å)	III	III*	VI
$Ba–O_{hfa}$			
Ba–O1	2.720(2)	2.725(3)	2.806(3)
Ba–O2	2.778(2)	2.757(3)	2.775(3)
Ba–O3	2.715(2)	2.725(3)	2.763(3)
Ba–O4	2.753(2)	2.757(3)	2.819(3)
$Ba–O_{glyme}$			
Ba–O5	2.881(2)	2.933(4)	2.842(3)
Ba–O6	2.892(2)	2.941(5)	2.887(3)
Ba–O7	2.910(2)	2.908(4)	2.813(3)
Ba–O8	2.940(3)	2.908(4)	2.827(3)
Ba–O9	2.914(3)	2.941(5)	2.865(3)
Ba–O10	2.909(3)	2.933(4)	2.845(3)

In structure **III** the average $Ba–O_{hfa}$ distance (2.74 Å) is shorter then the same one in **VI** (2.79 Å), but the average $Ba–O_{glyme}$ distances of both diglyme ligands (2.89 and 2.92 Å) are longer than the average $Ba–O_{glyme}$ distance (2.84 Å) in **VI**, which originates from the macrochelate effect in pentaglyme.

The temperature of 143 K for data collection of **III** was chosen due to the fact that further cooling leads to a significant increase of mosaicity and the appearance of additional satellite reflections. It must be mentioned that consequent heating of a single crystal makes it possible to obtain an initial diffraction pattern. Such behavior of a single crystal can be caused by a phase transition or by the anisotropic contraction of the crystal. Surprisingly, in addition to the above possible phase transition below 143 K, we have found that in the temperature range 193–213 K the crystal system changes from triclinic (space group $P\bar{1}$) to monoclinic. The corresponding phase transition was detected in the DSC-curve in this temperature region.

The crystal structure of $[Ba(hfa)_2(diglyme)_2]$ was also determined at 293 K (**III*** in Tables 1 and 4). With the temperature increase, the flexibility of the $[Ba(hfa)_2(diglyme)_2]$ molecule grows, its framework does not vary significantly but the adequacy of the structure determination diminishes (Table 4). The analysis of XRD data array gives no way to determine the space group definitely. The description of the crystal structure in both groups *Cc* and *C*2/*c* gives practically the same results (R_1 values are 3.9% and 4.6%, respectively). In this paper, the results obtained in the more symmetrical *C*2/*c* group are given. In **III*** the average $Ba–O_{hfa}$ distance is still retained (2.74 Å) while the average $Ba–O_{diglyme}$ distances of both diglyme ligands (2.93 Å) are longer than the same ones in **III** (2.89 and 2.92 Å, Table 4).

3.3. Thermal analysis

The thermal behavior of **I–III** has been studied by thermal gravimetric anaysis (TG) at low pressure (Fig. 4). For **I** the TG curve shows two main stages of weight loss (Fig. 4). The weight loss (3%) occurring in the temperature range 50–70 °C corresponds to removal of one water molecule (calc. 3%). The main weight loss (95%) takes place in the temperature range 125–160 °C and the evaporation of the mixed ligand complex $Ca(hfa)_2(diglyme)$ is mainly responsible for the weight loss at this stage. For **I**, the total weight loss is equal to 100% at 200 °C.

Complex **II** undergoes three major stages of weight loss upon heating (Fig. 4). The weight loss for first stage (80–150 °C) is equal to 16% and corresponds to dehydration (calc. 2.7%) and partial elimination of diglyme (total elimination of diglyme – 19%). However, these two processes could not be completely separated from each other. The main weight loss (70%, 150–250 °C) could be caused by three simultaneous processes: elimination of the diglyme residuary part, evaporation of $Sr(hfa)_2(diglyme)$ and evapora-

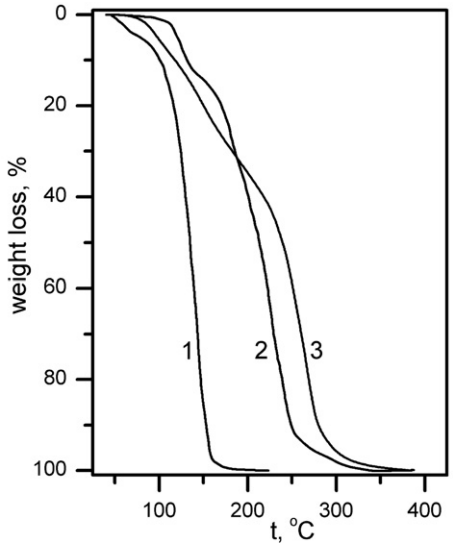

Fig. 4. TG curves for $[Ca(hfa)_2(diglyme)(H_2O)]$ (**1**), $[Sr(hfa)_2(diglyme)(H_2O)]$ (**2**) and $[Ba(hfa)_2(diglyme)_2]$ (**3**).

tion of $Sr(hfa)_2$. In the third stage (250–400 °C) the weight loss could be attributed to $Sr(hfa)_2$ evaporation. In this temperature range the TG-curves of **II** and $Sr(hfa)_2$ are very similar.

In the case of **III**, the TG-curve has two main stages. The first one, in the temperature range 120–250 °C, corresponds to elimination of two diglyme molecules (calc. 31.4%, found 32%). In the second stage (250–400 °C) the evaporation of $Ba(hfa)_2$ takes place. The total weight loss is equal to 100%.

A mass spectrometry study was performed to confirm the processes taking place on the heating of **I**–**III** complexes.

3.4. Mass spectrometry

Under the mass spectrometry experiments (10^{-5} torr), complexes **I** and **II** lose water molecules forming $[Ca(hfa)_2(diglyme)]$ and $[Sr(hfa)_2(diglyme)]$, respectively, under sample degasifying treatment at room temperature (298 K). This is consistent with the data of the TG analysis for **I** and **II**.

3.4.1. [Ca(hfa)$_2$(diglyme)]

The mass spectra of $[Ca(hfa)_2(diglyme)]$ were recorded in the temperature range 298–340 K (Table 5). The analysis of the curves of ionization efficiency, obtained for the main species, shows that the vapor phase over $[Ca(hfa)_2(diglyme)]$ consists of the mixed ligand complex molecules. From the results of full isothermal evaporation experiments it was found that the intensities of the all ion currents were constant during evaporation and the mixed ligand complex $[Ca(hfa)_2(diglyme)]$ sublimed quantitatively (without formation of a non-volatile residue in the Knudsen cell). On the basis of these data, there are grounds for believing that the mixed ligand complex $[Ca(hfa)_2(diglyme)]$ sublimes in the selected temperature range:

$$[Ca(hfa)_2(diglyme)]\ (s) = [Ca(hfa)_2(diglyme)]\ (g) \quad (1)$$

The saturated vapor pressure values of $[Ca(hfa)_2(diglyme)]$ were calculated according to the Hertz–Knudsen equation. At 325 K the vapor pressure of $[Ca(hfa)_2(diglyme)]$ is equal to 2.45×10^{-1} Pa. Based on the temperature dependence of the ion current intensities for the three ions $[Ca(hfa)_2(diglyme)]^+$, $[Ca(hfa)(diglyme)]^+$ and $[Ca(hfa)]^+$, the standard enthalpy of $[Ca(hfa)_2(diglyme)]$ sublimation was calculated:

$$\Delta_s H^0([Ca(hfa)_2(diglyme)],\ s.,\ T) = 99.8 \pm 8.3\ \text{kJ/mol}$$

Table 5
Intensities of the main ion currents (relative units) in the mass spectra of **I** (T = 325 K) and **III** (T = 450 K)

$[Ca(hfa)_2(diglyme)]$		$Ba(hfa)_2(diglyme)_2$	
Ion	I (%)	Ion	I (%)
$[Ca(hfa)-F]^+$	1	$[Ba(hfa)-CH]^+$	80
$[Ca(hfa)]^+$	17	$Ba(hfa)^+$	100
$[Ca(hfa)(diglyme)^-OC(CF_3)CH]^+$	3	$[Ba_2(hfa)+CO]^+$	20
$[Ca(hfa)+OCH_3(CH_2)_2O]^+$	1	$[Ba_2(hfa)+OCC]^+$	80
$[Ca(hfa)(diglyme)]^+$	100	$[Ba_2(hfa)+OCCF_3]^+$	17
$[Ca(hfa)_2(diglyme)-2CF_3]^+$	1	$[Ba_2(hfa)_2+CO]^+$	15
$[Ca(hfa)_2(diglyme)]^+$	6	$[Ba_2(hfa)_2+OCC]^+$	79
$[CH_3O(CH_2)_2]^+$	6	$Ba_2(hfa)_3^+$	60
		$[Ba_3(hfa)_4-OCCF_3CH]^+$	4
		$Ba_3(hfa)_4^+$	10
		$Ba_3(hfa)_5^+$	6

and the temperature dependence of the saturated vapor pressure can be approximated by the equation:

$$\ln P_{[Ca(hfa)_2(diglyme))]}\ (\text{Pa}) = -(12\,004 \pm 1000)/T + (34.6 \pm 2.0)298\text{–}340\ K.$$

3.4.2. [Sr(hfa)$_2$(diglyme)]

For $[Sr(hfa)_2(diglyme)]$ the sublimation is a more complicated process and its dependence on temperature has been found and studied. The mass spectra $[Sr(hfa)_2(diglyme)]$ were recorded in the temperature range 310–457 K (Table 6). At a temperature below 340 K the ions formed from the mixed ligand complex $[Sr(hfa)_2(diglyme)]$ were present in the spectra. Below 320–325 K the ions $[CH_3O(CH_2)_2]^+$ and $[CH_3OCH_2]^+$, corresponding to the ionization of diglyme molecules, were not detected. In the temperature range 330–400 K these ions were detected but their ion current intensities decreased down to the point of disappearance at 410 K.

Really, the mass spectra at 410 K (Table 6) and at higher temperatures were practically identical to the spectra of $[Sr(hfa)_2]$, and the vapor phase contained mainly the dimeric molecules $[Sr(hfa)_2]_2$.

The full isothermal evaporation experiments performed at all the temperatures studied confirm that the thermal behavior of $[Sr(hfa)_2(diglyme)]$ can be described by three partially overlapping processes:

$$[Sr(hfa)_2(diglyme)]\ (s) = [Sr(hfa)_2(diglyme)]\ (g) \quad 310\text{–}340\ K \quad (5)$$

$$[Sr(hfa)_2(diglyme)]\ (s) = Sr(hfa)_2\ (s) + n\ \text{diglyme}\ (g)\ (n < 1) \quad 330\text{–}410\ K \quad (6)$$

$$2\,Sr(hfa)_2\ (s) = [Sr(hfa)_2]_2\ (g) \quad 380\text{–}457\ K \quad (7)$$

The complex $[Sr(hfa)_2(diglyme)]$ sublimes (5) only in the narrow temperature range of 310-340 K. Based on the temperature dependence of the ion current intensities for $[Sr(hfa)_2(diglyme)]^+$, the standard enthalpy of $[Sr(hfa)_2(diglyme)]$ sublimation was estimated:

Table 6
Intensities of the main ion currents (relative units) in the mass spectra of **II** at 330 K and 410 K

T = 330 K		T = 410 K			
Ion	I (%)	Ion	I (%)	Ion	I (%)
$Sr(hfa)^+$	26	$[Sr_2(hfa)-CH(CF_3)_2]^+$	110	$[Sr_2(hfa)_3-OC(CF_3)_2]^+$	82
$[Sr(hfa)(diglyme)]^+$	100	$Sr(hfa)^+$	35	$[Sr_2(hfa)_3-OCCF_3]^+$	2
$[Sr(diglyme)OH]^+$	48	$[Sr_2(hfa)+OCC]^+$	100	$[Sr_2(hfa)_3-2F]^+$	12
$[Sr(hfa)_2(diglyme)]^+$	3	$[Sr(hfa)_2-2CF_3]^+$	40	$Sr_3(hfa)_3^+$	18
$[CH_3O(CH_2)_2]^+$	150	$[Sr(hfa)_2-CF_3]^+$	30	$[Sr_2(hfa)_3+OCCF_2]^+$	1
$[CH_3OCH_2]^+$	50			$[Sr_2(hfa)_4-OCCF_3]^+$	8

$\Delta_s H^0([Sr(hfa)_2(diglyme)],\ s.,\ T) \geqslant 82$ kJ/mol 310—340 K.

On increasing the temperature, the removal of diglyme (6) and evaporation of $[Sr(hfa)_2]$ (7) occurrs. The estimation of the standard enthalpy of $[Sr(hfa)_2]_2$ evaporation was made according to the second thermodynamic law, based on the data of six independent experiments in the temperature range 380–410 K:

$\Delta_s H^0([Sr(hfa)_2]_2,\ T) \leqslant 177 \pm 10$ kJ/mol 380—410 K

3.4.3. [Ba(hfa)$_2$(diglyme)$_2$]

For $[Ba(hfa)_2(diglyme)_2]$ the mass spectra were measured in the temperature range 330–485 K. The results of the full isothermal experiments show that in the temperature range 330–380 K the vapor phase contains only diglyme molecules and the spectra are very similar to that for pure diglyme in the same temperature range. With increasing temperature the current intensities of the $[CH_3O(CH_2)_2]^+$ and $[CH_3OCH_2]^+$ ions decreased and disappeared from the spectra at $T > 430$ K. The peaks of barium-containing ions appeared in the spectra above 380 K, however the mixed ligand ions were not found. Above 430 K the spectra had invariable character (Table 5), which is very similar to that for pure $[Ba(hfa)_2]$, consisting in the trimeric form in the vapor phase [31]. Thus, the sublimation of $[Ba(hfa)_2(diglyme)_2]$ proceeds with the removal of both diglyme molecules and can be described by two consecutive processes:

$$[Ba(hfa)_2(diglyme)_2]\ (s) = Ba(hfa)_2\ (s) + 2\,diglyme\ (g), \quad (8)$$

$$3\,Ba(hfa)_2\ (s) = [Ba(hfa)_2]_3\ (g). \quad (9)$$

The standard enthalpy value of $[Ba(hfa)_2]_3$ sublimation, which was made according the second thermodynamic law, based on the data of six independent experiments:

$\Delta_s H^0([Ba(hfa)_2]_3,\ T) = 183.2 \pm 4.5$ kJ/mol 430—480 K,

is in good agreement with that obtained in [31]:

$\Delta_s H^0([Ba(hfa)_2]_3) = 181.3 \pm 1.5$ kJ/mol 420—470 K.

Thus, the data of thermal analysis at low pressure and mass spectrometry showed that the stability of the mixed ligand complexes $[M(hfa)_2(diglyme)_n]$ to the removal of diglyme molecules under heating decreases in the row **I** > **II** ≈ **II**. Only **I** evaporates as the mixed ligand complex after water removal and it is in line with the decrease of Lewis acidity in the row $Ca(hfa)_2$–$Sr(hfa)_2$–$Ba(hfa)_2$. However, such low thermal stability of the diglyme mixed ligand complexes with both $Sr(hfa)_2$ and $Ba(hfa)_2$ is slightly unexpected. In the literature the thermal behaviors of the similar mixed ligand complexes $[Sr(hfa)_2(Dipy)_2]$ [28] and $[Ba(hfa)_2(Phen)_2]$ [27] have been described and it has been found that $[Sr(hfa)_2(Dipy)_2]$ sublimes intact but the sublimation of $[Ba(hfa)_2(Phen)_2]$ is carried out in two stages: the removal of one Phen ligand and then the sublimation of $[Ba(hfa)_2(Phen)]$. Even for non-fluorinated complexes $[M(thd)_2(Phen)_2]$ (M = Ca, Sr), where $M(thd)_2$ is a weaker Lewis acid than $M(hfa)_2$, the same two-stage scheme with the removal of only one ancillary ligand and the sublimation of $[M(thd)_2(Phen)]$ was found [29]. Diglyme as the ancillary ligand, containing three donor oxygen atoms and forming two chelate rings with the central ion, should be stronger bound together with barium or strontium hexafluoroacetylacetonates than the Dipy or Phen ancillary ligands. In our opinion, the thermal behavior feature of **II** and **III** can be explained with the respect to the rather high volatility of diglyme in comparison with Dipy and Phen. The intensive diglyme evaporation at rather low temperature results in the undesirable thermal dissociation: $[M(hfa)_2Q_n]\ (s) \rightarrow M(hfa)_2\ (s) + nQ\ (g)$ in contrast to the mixed ligand complexes with the low volatile Dipy and Phen. The results obtained give evidence on the important role of $M(dik)_2$ and Q volatility correlation in the thermal stability features of AEE mixed ligand β-diketonates $[M(dik)_2Q_n]$ used as MOCVD precursors.

4. Conclusions

By way of an example of mixed ligand complexes of AEE hexafluoroacetylacetonates with diglyme, this work demonstrated once again a wide variety of compositions, structures and properties typical for the coordination chemistry of AEE β-diketonates. Although the same synthetic procedure was applied for Ca, Sr and Ba compounds, their compositions differed. The complex $[Ba(hfa)_2(diglyme)_2]$ demonstrated an unexpected high stability in solution that originated probably from a macrochelate effect, because the large Ba ions allow the arrangement of two diglyme ligands instead of water in their coordination sphere (CN = 10). Smaller in size, Ca and Sr ions coordinate only one diglyme ligand together with a water molecule, reaching CN = 8. According to the X-ray structural analysis, all the mixed ligand complexes obtained are molecular crystals. In the crystal structures of $[M(hfa)_2(diglyme)(H_2O)]$ (M = Ca, Sr) water molecules take part in intermolecular hydrogen bonds. In spite of this, the water molecules are weakly kept in the crystal lattice and are removed in vacuum (room temperature at 10^{-5} torr or 50–70 °C at 10^{-2} torr) producing unhydrous $[M(hfa)_2(diglyme)]$. The stability of the mixed ligand complexes $[M(hfa)_2(diglyme)_n]$ to removal of diglyme molecules under heating decreases by changing M in the order Ca > Sr ≈ Ba. According to the mass spectrometry data, both diglyme ligands are fully removed by heating $[Ba(hfa)_2(diglyme)_2]$ up to 330 K and the vapor phase consists of trimeric $[Ba(hfa)_2]_3$ molecules at $T > 430$ K. $[Ca(hfa)_2(diglyme)]$ sublimes in the 298–330 K temperature range. The thermal behavior of $[Sr(hfa)_2(diglyme)]$ combines the features of both neighbouring complexes: it sublimes in the very narrow temperature range of 310–330 K, then removes diglyme at higher temperatures (340–410 K) and finally evaporates as dimeric molecules of $[Sr(hfa)_2]_2$ at $T > 410$ K.

The mentioned variety of compositions, structures, properties of the complexes synthesized and studied is caused by the specific features of AEE coordination chemistry, namely by the interplay of three factors – the increase of ionic radii in the row Ca–Sr–Ba, the predominantly ionic bond nature that allows significant variability in the geometry of the coordination sphere, as well as the ability of AEE ions to saturate their coordination sphere by any donor molecules available in the reaction mixture during synthesis.

Acknowledgement

The Material Engineering Faculty of Israel Institute of Technology (Technion) is cordially acknowledged for initiation of this work.

Appendix A. Supplementary data

CCDC 682256, 682257, 682254 and 682255 contains the supplementary crystallographic data for this paper. These data can be obtained free of charge via http://www.ccdc.cam.ac.uk/conts/retrieving.html, or from the Cambridge Crystallographic Data Centre, 12 Union Road, Cambridge CB2 1EZ, UK; fax: (+44) 1223-336-033; or e-mail: deposit@ccdc.cam.ac.uk. Supplementary data associated with this article can be found, in the online version, at doi:10.1016/j.poly.2008.06.021.

References

[1] D.J. Otway, W.S. Rees Jr., Coord. Chem. Rev. 210 (2000) 279.
[2] N.P. Kuzmina, L.I. Martynenko, Russ. J. Inorg. Chem. 47 (2002) 555.
[3] M. Tiitta, L. Niinisto, Chem. Vap. Dep. 3 (1) (1997) 167.

[4] F. Maury, J. Phys. IV France 5 (5) (1995) 449.
[5] K.M. Fromm, E.D. Gueneau, Polyhedron 23 (2004) 1479.
[6] R.C. Mehrotra, R. Bohra, D.P. Gaur, Metal β-Diketonates and Allied Derivatives, Academic Press, London, 1978. 427 p.
[7] J.A.T. Norman, G.P. Pez, J. Chem. Soc., Chem. Commun. (1991) 971.
[8] R. Gardinier, D.W. Brown, P.S. Kirlin, Chem. Mater. 3 (6) (1991) 1053.
[9] T. Marks, Pure Appl. Chem. 67 (2) (1995) 313.
[10] G.G. Condorelli, G. Malandrino, I.L. Fragalà, Coord. Chem. Rev. 251 (2007) 1931.
[11] J.A. Belot, D.A. Neumayer, C.J. Reedy, D.B. Studebaker, B.J. Hinds, C.L. Stern, T.J. Marks, Chem. Mater. 9 (1997) 1638.
[12] G. Malandrino, I.L. Fragalà, Coord. Chem. Rev. 250 (2006) 1605.
[13] W.J. Evans, D.B. Rego, J.W. Ziller, Polyhedron 25 (2006) 2691.
[14] A. Gulino, I. Fragalà, Inorg. Chim. Acta 358 (2005) 4466.
[15] G.M. Sheldrick, SHELXTL v. 5.10, Structure Determination Software Suite, Bruker AXS, Madison, WI, USA, 1998.
[16] Bruker APEX2 Software Package, Bruker AXS Inc., 5465, East Cheryl Parkway, Madison, WI 5317, 2005.
[17] G.M. Sheldrick, SADABS v.2.01, Bruker/Siemens Area Detector Absorption Correction Program, Bruker AXS, Madison, WI, USA, 1998.
[18] V. Petricek, M. Dusek, L. Palatinus, JANA2000. Structure Determination Software Programs, Institute of Physics, Praha, Czech Republic, 2000.
[19] S.R. Drake, S.A.S. Miller, D.J. Williams, Inorg. Chem. 32 (1993) 3227.
[20] V.-C. Arunasalam, I. Baxter, S.R. Drake, M.B. Hursthouse, K.M.A. Malik, S.A.S. Miller, D.M.P. Mingos, D.J. Otway, J. Chem. Soc., Dalton Trans. (1997) 1331.
[21] S.R. Drake, M.B. Hursthouse, K.M.A. Malik, S.A.S. Miller, Inorg. Chem. 32 (1993) 4653.
[22] D.R. van Staveren, G.A. van Albada, J.G. Haasnoot, H. Kooijman, A.M.M. Lanfredi, P.J. Nieuwenhuizen, A.L. Spek, F. Ugozzoli, T. Weyhermuller, J. Reedijk, Inorg. Chim. Acta 315 (2001) 163.
[23] A.Yu. Rogachev, L.H. Minacheva, V.S. Sergienko, I.P. Malkerova, A.S. Alikhanyan, V.V. Stryapan, N.P. Kuzmina, Polyhedron 24 (2005) 723.
[24] L.I. Martynenko, N.P. Kuzmina, A.N. Grigorev, Russ. J. Inorg. Chem. 43 (1998) 1038.
[25] L.I. Martynenko, N.P. Kuzmina, A.N. Grigorev, Koord. Khim. (Russ. Coord. Chem.) 21 (1995) 515.
[26] S.R. Drake, M.B. Hursthouse, K.M.A. Malik, S.A.S. Miller, J. Chem. Soc., Chem. Commun. (1993) 478.
[27] N. Kuzmina, M. Ryazanov, S. Troyanov, Polyhedron 18 (1999) 2177.
[28] Y. Shen, Y. Pan, G. Dong, X. Sun, X. Huang, Polyhedron 17 (1998) 69–73.
[29] I.E. Soboleva, S.I. Troyanov, N.P. Kuz'mina, V.K. Ivanov, L.I. Martynenko, Yu.T. Struchkov, Koord. Khim. (Russ. Coord. Chem.) 21 (1995) 688.
[30] N. Kuzmina, M. Ryazanov, S. Troyanov, V. Kezko, Russ. J. Inorg. Chem. 45 (2000) 38.
[31] M.V. Ryazanov, S.I. Troyanov, I.P. Malkerova, A.S. Alikhanyan, N.P. Kuzmina, Russ J. Inorg. Chem. 46 (2001) 256.

section into the bridge, which breaks the conjugation, as *e.g.* in Q = 1,2-bi(4-pyridyl)ethane (105 mV, $K_c = 60$) [6], considerably decreases ΔE_f, but does not exclude electronic and magnetic through-bridge interactions. However, few examples of complexes containing completely saturated bridges have been described in the literature, *e.g.* cyclic piperazine-1,4-diyl, Q = NC_4H_8N (560 mV, $K_c = 3 \times 10^9$) [10].

We have shown [11,12] that bimetallic complexes with $\{Mo(NO)(Tp^{Me2})X\}^+$ (X denotes Cl or Br) core incorporating saturated *n*-alkanediolate bridges exhibit two chemically reversible one-electron reduction processes. The separations between these processes, being the largest for the complex with a C_2 bridge (310 mV, $K_c = 1.7 \times 10^5$; Mo···Mo distance >6 Å) decrease by *ca.* 100 mV per CH_2 group for C_2 to C_4 bridges. Starting with C_5 bridge the electrochemical interactions could not be detected. The reappearance of a measurable separation between the redox potentials in fluorinated C_5 analogue $[\{Mo(NO)(Tp^{Me2})Cl\}_2\{OCH_2(CF_2)_3CH_2O\}]$ ($\Delta E_f = 70$ mV), in spite of both bridges imposing the same Mo···Mo distance, is significant and can be explained partly by through-bond interactions enabled by inductive effect of fluorine atoms transmitted through the σ-bond framework. This effect also manifested itself in an anodic shift of *ca.* 300 mV of the first reduction potential, which reflects LUMO stabilization in comparison with a non-fluorinated bimetallic complex. A different solvent reorganization effects cannot be excluded in these two cases.

These findings posed a challenge to prospective theoretical research on the nature of electrochemical interactions in bimetallic complexes with saturated bridging ligands. On the other hand, quick development of quantum chemistry methods (especially DFT) in the last few years prompted us to undertake DFT studies on weakly coupled metallic centers in complexes constructed from $\{M(NO)(Tp^{Me2})\}^{2+}$ core, one or two saturated bridges and/or Cl^- ligands. Such modeling has already been used more and more widely to examine mixed-valence compounds [13,14], recently also for nitrosyl complexes containing tris(3,5-dimethylpyrazol-1-yl)hydroborate ligand [15], what encouraged us to undertake the research presented in this paper.

In this work we focus on the stabilization of reduced mixed-valence species incorporating single and double ethane-1,2-diolate bridges: $[\{Mo(NO)(Tp^{Me2})Cl\}_2\{O(CH_2)_2O\}]$ (**A**) and $[Mo(NO)(Tp^{Me2})\{O(CH_2)_2O\}]_2$ (**B**). Monometallic analogue (**M**) $[Mo(NO)(Tp^{Me2})Cl\{O(CH_2)_2OH\}]$ serves for comparative analysis. Calculated geometries, electron affinities and NO stretching frequencies are correlated with experimental X-ray, CV and IR spectral data, where available, in order to as well validate DFT results as draw conclusions regarding localization of additional electron after electrochemical reduction. Electrochemical data for monometallic and singly bridged complex have already been published [11]. Stretching frequencies of NO for monometallic and singly bridged species in solution are given in this work. Unfortunately, doubly bridged bimetallic complex was not soluble in any solvent allowing for electrochemical studies.

2. Methodology

2.1. Experimental

The complexes $[\{Mo(NO)(Tp^{Me2})Cl\}_n\{O(CH_2)_2OH_{2-n}\}]$ ($n = 1$ or 2) were prepared according to the literature [11]. The reduced forms of these species were prepared by addition of cobaltocene to solutions of the neutral complexes in dichloromethane freshly distilled from CaH_2 under argon. Infrared spectra for singly bridged complex with its monometallic analogue reported in this work were recorded using a Bio-Rad FTS 175C spectrophotometer in CH_2Cl_2 solutions.

2.2. Models

All calculations in this paper were conducted on mimetic models in which outer methyl groups of tris(3,5-dimethylpyrazol-1-yl)hydroborate ligand were cut off to avoid additional energy inaccuracy due to nearly free rotation of these groups. Secondly it helped to decrease computational problem size. Methyl groups next to nitrosyl ligand were retained since they appeared to be important for keeping proper geometry of NO group and bridging unit. Therefore all compounds presented here contain hydrotris(3-methylpyrazol-1-yl)borato ligand.

Starting geometry of bimetallic doubly bridged complex (**B**) was obtained from crystallographic structure of $[Mo(NO)(Tp^{Me2})\{O(CH_2)_2O\}]_2$ [11]. This structure is highly symmetric having C_{2h} point group symmetry. Both monometallic complex (**M**) and bimetallic singly bridged complex (**A**) starting structures were prepared from computed equilibrium geometry of **B**. Complex **A** has C_i symmetry, which was used to prepare the starting structure of this species. Geometries of neutral complexes, monoanions and dianions were optimized independently. Symmetry constraints were used during geometry optimization of non-reduced **A** and **B** compounds. On the contrary, computations for singly and doubly reduced complexes of **A** and **B** were carried both with and without imposing symmetry.

2.3. DFT calculations

Calculations were performed using GAUSSIAN03 [16] within both unrestricted and restricted DFT with hybrid B3LYP functional, widely used in mixed-valence theoretical studies [13,14], and LanL2DZ [17–19] basis set (denoted as BS1), with effective core potential on heavy atoms (molybdenum and chlorine atoms). Additional polarization and diffuse functions were added for chlorine atoms [20]. For BS1 geometries, additional single-point calculations were performed with the extended basis set labeled as BS2 being of triple zeta quality with polarization functions for all atoms. This basis set was constructed using def2TZVPP [21,22] for molybdenum and def2TZVP [21,23] for other atoms. Additionally, for selected properties the performance of non-hybrid OLYP [24] potential was tested in smaller basis BS1.

Vacuum equilibrium geometries were used to estimate solvent effects by means of the self-consistent reactions field (SCRF) method called polarizable continuum model (PCM) [25]. Dielectric constant of actual dichloromethane solvent ($\varepsilon = 8.93$) and UFF scheme for cavity generation were used for single-point computations. IR spectra were calculated for gas phase models using standard harmonic approximation for equilibrium geometries. Contour plots of spin densities were prepared using GABEDIT [26].

3. Results and discussion

3.1. Experimental results

The electrochemical results reported for $[\{Mo(NO)(Tp^{Me2})Cl\}_2\{O(CH_2)_2O\}]$ (**A**) (first reduction process at $E_f = -1.11$ V *vs.* Fc/Fc^+; separation $\Delta E_f = 310$ mV) [11] indicate that the mixed-valence $\{16e{:}17e\}^-$ form of **A** is accessible by the reduction of the neutral precursor $\{16e{:}16e\}$ using cobaltocene ($E_f = -1.34$ V *vs.* Fc/Fc^+). We chose the chloride complex, since voltammetric studies of the iodo complexes revealed that the reduction is followed by the dissociation of I^-, which may disturb the reduction process. The IR spectrum of $\mathbf{A}^-$ in dichloromethane exhibits two NO stretching vibrations, at 1605 and 1542 cm^{-1} ($\Delta\nu_{NO} = 63$ cm^{-1}) instead of one (1680 cm^{-1}) in the neutral precursor or monometallic analogue (Table 10). This shows that this species is valence-trapped

on the IR timescale (*ca.* 10^{-13} s) and can be classified as Class I in the Robin-Day scheme (double minimum on the potential-energy curve).

3.2. Equilibrium geometries

Optimized geometries of **A** and **B** are shown in Fig. 1 and Tables 1 and 2, respectively. Computed geometrical parameters show good agreement with available X-ray crystal structure (Table 2). Even the distance between two molybdenum atoms, which is crucial for electronic interactions investigation but could be very sensitive to any inaccuracies in computed geometry, is reasonably reproduced. In singly bridged complex **A** this distance is greater by nearly 1.3 Å (25%) than in **B**. As a result of close packing, the crystal unit cell of **B** contains two nonequivalent molecules having slightly different geometries; therefore two experimental structure data are shown in Table 2.

Addition of an extra electron triggers symmetry breaking in examined compounds. In both complexes **A** and **B** molybdenum centers become nonequivalent after first reduction. Values of selected bonds and angles in molybdenum's neighborhood are given in Tables 3 and 4. The most dramatic difference relates to distances between molybdenum and bridging oxygen ($\Delta R \sim 6\%$) or chlorine ($\Delta R \sim 5\%$), also the distances molybdenum–nitrosyl ($\Delta R \sim 0.4\%$) and nitrogen–oxygen ($\Delta R \sim 1.5\%$) differ between nonequivalent centers; molybdenum–molybdenum separation changes after reduction by nearly 2%.

Second reduction leads to triplet dianions with selected geometrical parameters shown in Tables 5 and 6 for **A** and **B**, respectively. The inspection of the tables indicates that differences between both molybdenum centers become insignificant in doubly reduced complexes.

As mentioned above, computations for singly and doubly reduced complexes were performed both with and without symmetry constraints. The comparison between energies of equilibrium structures of symmetric and asymmetric singly reduced compounds indicates the stabilization of the asymmetric ones (Table 7), with larger effect for singly bridged compound **A**. Additional single-point BS2 calculations confirm these results. The stabilization of asymmetric structures for singly and doubly bridged species equals to 0.162 eV and 0.037 eV for BS1 and was increased to 0.201 eV and 0.048 eV for BS2, respectively. The energetic stabilization of asymmetric structures and differences in geometries of molybdenum neighborhood confirm nonequivalence of molybdenum atoms in mixed-valence single reduced complexes and, what follows, substantial localization of additional electron. Stabilization of asymmetric structure with extra electron trapped on one molyb-

Table 1
Selected bond distances (Å) and angles (°) for complex **A**

Distance (Å)		Angle (°)	
Mo(1)–N(2)	2.26	N(1)–Mo(1)–N(2)	177.5
Mo(1)–N(1)	1.78	N(1)–Mo(1)–O(2)	99.2
Mo(1)–O(2)	1.91	N(2)–Mo(1)–O(2)	83.3
N(1)–O(1)	1.23	Mo(1)–N(1)–O(1)	179.3
O(2)–C(1)	1.44	O(2)–Mo(1)–Cl	97.5
C(1)–C(2)	1.54	N(1)–Mo(1)–Cl	92.2
Mo(1)–Cl	2.44	Mo(1)–O(2)–C(1)	144.7
Mo(1)–Mo(2)	6.66		

Table 2
Selected bond distances (Å) and angles (°) for complex **B** (experimental values in parentheses)

Distance (Å)		Angle (°)	
Mo(1)–N(2)	2.28 (2.26, 2.26)	N(1)–Mo(1)–N(2)	175.0 (177.6, 177.4)
Mo(1)–N(1)	1.78 (1.77, 1.73)	N(1)–Mo(1)–O(2)	98.9 (99.7, 99.0)
Mo(1)–O(2)	1.93 (1.86, 1.91)	N(2)–Mo(1)–O(2)	84.2 (81.8, 82.6)
N(1)–O(1)	1.24 (1.25, 1.24)	Mo(1)–N(1)–O(1)	176.0 (175.0, 175.0)
O(2)–C(1)	1.44 (1.46, 1.39)	O(2)–Mo(1)–O′(2)	101.0 (101.7, 102.2)
C(1)–C(2)	1.54 (1.49, 1.52)	Mo(1)–O(2)–C(1)	137.4 (137.0, 136.3)
Mo(1)–Mo(2)	5.37 (5.28, 5.28)		

Table 3
Selected bond distances (Å) and angles (°) for singly reduced complex **A**

Distance (Å)			Angle (°)		
Mo center	$Mo^{(1)}$	$Mo^{(2)}$	Mo center	$Mo^{(1)}$	$Mo^{(2)}$
Mo–N(1)	1.78	1.78	N(1)–Mo–O(2)	100.4	99.5
Mo–O(2)	1.88	2.04	O(2)–Mo–Cl	99.4	91.8
Mo–Cl	2.46	2.56	N(1)–Mo–Cl	92.7	94.9
N(1)–O(1)	1.23	1.26	Mo–N(1)–O(1)	178.1	177.6

Table 4
Selected bond distances (Å) and angles (°) for singly reduced complex **B**

Distance (Å)			Angle (°)		
Mo center	$Mo^{(1)}$	$Mo^{(2)}$	Mo center	$Mo^{(1)}$	$Mo^{(2)}$
Mo–N(1)	1.78	1.78	N(1)–Mo–O(2)	99.6	101.0
Mo–O(2)	1.92	2.04	N(1)–Mo–O′(2)	99.6	100.8
Mo–O′(2)	1.92	2.04	O(2)–Mo–O′(2)	103.3	92.1
N(1)–O(1)	1.25	1.27	Mo–N(1)–O(1)	174.9	175.0

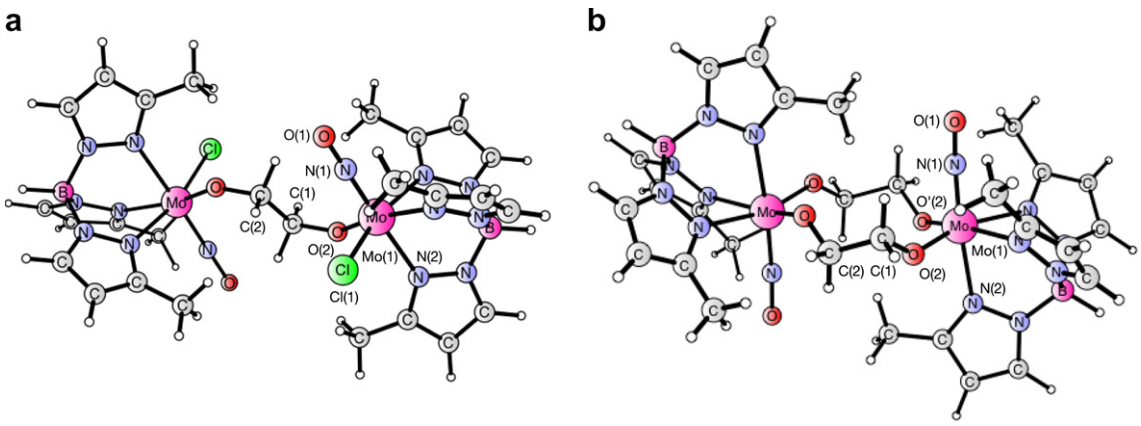

Fig. 1. Computed equilibrium geometries of complexes **A** (a) and **B** (b).

Table 5
Selected bond distances (Å) and angles (°) for doubly reduced complex **A**

Distance (Å)			Angle (°)		
Mo center	$Mo^{(1)}$	$Mo^{(2)}$	Mo center	$Mo^{(1)}$	$Mo^{(2)}$
Mo–N(1)	1.78	1.78	N(1)–Mo–O(2)	101.2	101.2
Mo–O(2)	2.01	2.01	O(2)–Mo–Cl	93.3	93.3
Mo–Cl	2.56	2.56	N(1)–Mo–Cl	96.1	96.1
N(1)–O(1)	1.26	1.26	Mo–N(1)–O(1)	174.1	174.1

Table 6
Selected bond distances (Å) and angles (°) for doubly reduced complex **B**

Distance (Å)			Angle (°)		
Mo center	$Mo^{(1)}$	$Mo^{(2)}$	Mo center	$Mo^{(1)}$	$Mo^{(2)}$
Mo–N(1)	1.78	1.78	N(1)–Mo–O(2)	99.5	99.5
Mo–O(2)	2.05	2.05	N(1)–Mo–O′(2)	100.1	100.1
Mo–O′(2)	2.05	2.05	O(2)–Mo–O′(2)	95.4	95.4
N(1)–O(1)	1.28	1.28	Mo–N(1)–O(1)	173.1	173.0

Table 7
Stabilization energy of asymmetric structures for singly reduced complexes **A** and **B** with respect to symmetric ones (B3LYP calculations)

Complex	Stabilization (eV)	
	BS1	BS2[a]
A	0.162	0.201
B	0.037	0.048

[a] Single-point for BS1 geometry.

denum site may be rather underestimated here due to known tendency of B3LYP to favor delocalized solutions [27].

3.3. Analysis of electron affinities

The investigations of mixed-valence compounds carried out most commonly by electrochemical experiments provide information about the strength of the electronic metal–metal interactions, measured as the splitting between the redox potentials of metal centers (ΔE_f). The splitting may be well approximated by the difference between the first and second electron affinity, denoted as $EA^{(1)}$ and $EA^{(2)}$ (in the case of reduction) or ionization potentials (in the case of oxidation) of a mixed-valence complex.

Electron affinities of **A** and **B** shown in Table 8 were calculated as the differences between total energies of neutral and singly reduced ($EA^{(1)}$) or singly reduced and doubly reduced ($EA^{(2)}$) complexes. Table 8 lists also the differences between computed first and second electron affinities that may be directly compared with experimental ΔE_f listed in the last row of Table 8. Comparison of electron affinities calculated in gas phase and with PCM solvent model indicates that solvent effects play crucial role in stabilization of negatively charged complexes. Calculations with significantly bigger BS2 basis set, in which description of negatively charged species should be of better quality, do not change trends in electron affinities neither in vacuum nor in PCM solvent model. Moreover, even rough solvent model such as PCM provides reasonable agreement with experimental data already at the simplest level. The description of electron affinity differences is improved in extended basis set, the introduction of non-hybrid OLYP functional for solvent model also complies with the experiment. However, one has to be aware that PCM methodology depends on the choice of cavity parameters, which brings additional uncertainty to computed energies thus by no means do we claim quantitative reproduction of the experiment.

Table 8
Electron affinities for neutral and negatively charged complexes **A** and **B**

	Electron affinity (eV)			
	A		**B**	
	In vacuum	In solvent	In vacuum	In solvent
$EA^{(1)}$				
B3LYP/BS1	−2.40	−3.78	−1.39	−2.77
B3LYP/BS2[a]	−2.10	−3.52	−1.24	−2.68
OLYP/BS1[a]	−1.91	−3.29	−1.14	−2.43
$EA^{(2)}$				
B3LYP/BS1	−0.19	−3.66	0.92	−2.64
B3LYP/BS2[a]	0.05	−3.32	1.13	−2.34
OLYP/BS1[a]	0.20	−3.16	1.56	−1.94
$EA^{(2)} - EA^{(1)}$				
B3LYP/BS1	2.20	0.12	2.30	0.14
B3LYP/BS2[a]	2.14	0.19	2.37	0.34
OLYP/BS1[a]	2.11	0.13	2.73	0.49
ΔE_f^{exp}		0.31[b]		

[a] Single-point calculations for geometries optimized with B3LYP/BS1.
[b] From Ref. [11].

3.4. Analysis of spin densities

Spin density plots for singly reduced complex **A** and **B** are shown on Fig. 2a and 2b, respectively. Localization of an extra electron on one molybdenum center is clearly visible, however, some delocalization (about 10% – see Table 9) occurs in the case of compound **B** with double bridge, where the distance between molybdenum atoms is nearly 25% smaller than in complex **A**. The plots indicate also that the additional electron is partly delocalized towards NO ligand, with antiferromagnetic coupling. This phenomenon has already been reported in the literature both for mononuclear and binuclear metal-nitrosyl complexes [28–30], however, here it may be overestimated due to the tendency of UDFT to favor delocalized solutions [23] and to suffer from spin contamination [24,25]. Data collected in Table 9 bring additional evidence that the injected electron is trapped on $Mo^{(1)}$.

After second reduction the two molybdenum centers become again equivalent. Spin density on NO ligand may be taken as qualitative fingerprint of metal to ligand π-backdonation enhanced by spurious electron density on Mo center after reduction. Both the increase of the basis set and in particular the use of non-hybrid functional increase delocalization of the extra electron towards the second molybdenum center. Nevertheless, this does not change qualitative picture of an electron predominantly trapped on one molybdenum. In the OLYP case the increase of electron delocalization goes in line with known tendency of non-hybrid potentials, favoring delocalized solutions in comparison to hybrid ones [31]. Smaller values of Mo and NO spin densities in **B** than in **A** may be additionally rationalized by to the lack of chlorine ligand in the former case.

3.5. Analysis of IR spectra

In experimental IR spectra after first reduction, both nitrosyl stretching frequencies are shifted towards red, but the splitting of 63 cm^{-1} is registered. Theoretical computations go in line with the experiment, however, the shift of nitrosyl stretching frequency for non-reduced center in $\mathbf{A}^-$ and $\mathbf{B}^-$ is underestimated. Therefore computed splitting of nitrosyl stretching frequencies in singly reduced compound **A** is bigger by 30 cm^{-1} than the experimental value. Nevertheless, both experiment and theory nicely corroborate the issue of electron trapping on IR time scale. Similar situation occurs in singly reduced complex **B** – calculated nitrosyl vibrational bands are split, but due to partial delocalization of the extra electron the splitting is smaller than in **A**. Unfortunately, experimental IR spectra for **B** are not available thus only

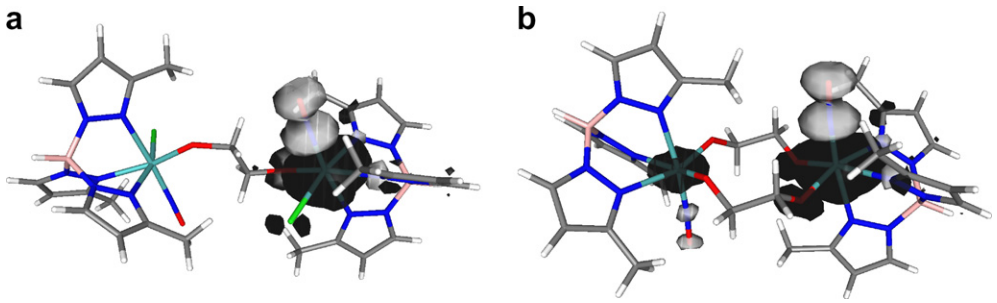

Fig. 2. Spin density plots for singly reduced complexes **A** (a) and **B** (b) (contour value 0.002).

Table 9
Spin densities on Mo atoms and NO ligands in singly reduced complexes **A** and **B**

Complex	Functional/basis	$Mo^{(1)}$	$Mo^{(2)}$	$NO^{(1)}$	$NO^{(2)}$
A					
	B3LYP/BS1	1.26	0.00	0.37	0.00
	B3LYP/BS2[a]	1.10	0.07	0.21	0.04
	OLYP/BS1[a]	1.00	0.14	0.20	0.04
B					
	B3LYP/BS1	1.14	0.10	0.35	0.04
	B3LYP/BS2[a]	0.96	0.04	0.15	0.00
	OLYP/BS1[a]	0.74	0.29	0.15	0.06

[a] Single-point calculations for geometries optimized with B3LYP/BS1.

Table 10
Experimental and calculated IR frequencies for neutral and one-electron reduction products for monometallic (**M**) or singly (**A**) and doubly (**B**) bridged bimetallic complexes

Complex		ν_{NO} (cm^{-1})		$\Delta\nu_{NO}$[a] (cm^{-1})
		Neutral	Singly reduced	
M	Exp	1680	1600	–
	Calc	1652	1549	
A	Exp	1680	1605, 1542	63
	Calc	1645	1640, 1547	93
B	Exp	1642[b]	–[c]	–[c]
	Calc	1603	1575, 1489	86

[a] $\Delta\nu_{NO}$ denotes the difference between reduced and non-reduced molybdenum center in bimetallic complexes.
[b] Data from Ref. [11], obtained in KBr disc.
[c] Complex **B** was insoluble in solvents other than $CHCl_3$, which is unsuitable for

theoretical analysis is possible here. On the contrary, the two nitrosyl stretching vibrations calculated for doubly reduced complexes have the same frequency (1545 cm^{-1} in the case of **A** and 1476 cm^{-1} for **B**), slightly lower than the frequency of nitrosyl bound to reduced Mo in singly reduced species, due to additional electrostatic interaction with the second reduced metal center.

Calculated shifts of NO stretching frequencies are consistent with the increase of NO bond distances (Tables 1–6) and metal to ligand π-backdonation ability estimated from spin density transfer towards NO. Nearly linear geometry of NO ligand in neutral complexes would comply with classification of diamagnetic ($S = 0$) and nearly linear MoNO moieties into nitrosonium category [32]. Neither NO bond length nor low IR frequency, however, do correspond to the assumption of NO^+ ligand. Reduction of Mo centers yields more radical character on NO; linearity of Mo–NO fragment is retained what may be attributed to geometrical constraints imposed by surrounding CH_3 groups from hydrotris(3-methylpyrazol-1-yl)borate ligand. In summary, no quantitative agreement of calculated and measured IR spectra could be expected here since theoretical NO frequencies could be calculated only in vacuum whereas experiment was done in solution. Nevertheless, both experiment and theory properly describe qualitative features of IR spectra for neutral and reduced bimetallic complexes; the dependence of NO stretching frequencies on the degree of electron density localization is properly described and helps to understand the nature of mixed-valence compounds.

4. Conclusions

Electronic structure of mixed-valence states of two bimetallic hydrotris(3-methylpyrazol-1-yl)borato molybdenum nitrosyl complexes and their reduced forms has been theoretically investigated. Computed IR spectra, geometrical and energetic parameters show good agreement with experimental results, which allows for the validation of our computational scheme for such large molecules. DFT modeling showed to be capable of describing symmetry-broken structures with the electron trapped on one reduced Mo center in mixed-valence complexes; however, some electron delocalization through the saturated bridge may be also directly evidenced here.

DFT calculations have shown that the nonequivalence of molybdenum centers in mixed-valence compound is energetically favorable and in both investigated bimetallic complexes an extra electron is localized on one of the molybdenum centers. Therefore both compounds should be considered as Class I complexes according to Robin-Day classification. However, in the doubly bridged complex (**B**) partial electron delocalization occurs, which may suggest that saturated bridging ligands could play a role in the strengthening of electronic interactions and, what follows, shifting the complex into Class II category.

In addition, calculating and experimental infrared spectra confirm the assumption of electron localization yielding Class I labeling, stemming from geometry, energetic and spin density discussions. As could be expected, stretching vibrations of NO bound to two molybdenum centers in singly reduced complexes are diversified. After addition of the second electron this difference vanishes. This reasoning corroborates electron localization in mixed-valence compounds prepared from **A** and **B**. Again, in the case of doubly bridged complex (**B**) partial delocalization occurs, while in singly bridged compound (**A**) it is much less significant.

Present work may be regarded as a first part (concentrating on short bridging ligands) of a bigger project that concerns the study of possible mechanisms of electron transfer trough saturated bridges in $\{Mo(NO)Tp\}^{2+/1+}$ complexes, undertaken in our group.

Acknowledgments

The computations were performed at the Academic Computer Centre CYFRONET AGH (Grant Nos. MNiSW/SGI2800/UJ/133/2006 and MNiSW/SGI3700/UJ/133/2006).

All figures of the molecular models were created using xyz-viewer software by Sven de Marothy (from Stockholm University).

References

[1] J.A. McCleverty, M.D. Ward, Acc. Chem. Res. 31 (1998) 842.
[2] M.D. Ward, Chem. Soc. Rev. 24 (1995) 121.
[3] P.J.F. de Rege, S.A. Williams, M.J. Therien, Science 269 (1995) 1409.
[4] A. Wlodarczyk, G.A. Doyle, J.P. Maher, J.A. McCleverty, M.D. Ward, J. Chem. Soc., Chem. Commun. (1997) 769.
[5] A. Wlodarczyk, J.P. Maher, J.A. McCleverty, M.D. Ward, J. Chem. Soc., Chem. Commun. (1995) 2397.
[6] S.L.W. McWhinnie, C.J. Jones, J.A. McCleverty, D. Collison, F.E. Mabbs, J. Chem. Soc., Chem. Commun. (1990) 940.
[7] C. Creutz, H. Taube, J. Am. Chem. Soc. 95 (1973) 1086.
[8] A. Wlodarczyk, J.P. Maher, J.A. McCleverty, M.D. Ward, J. Chem. Soc., Dalton Trans. (1997) 3287.
[9] S.L.W. McWhinnie, J.A. Thomas, T.A. Hamor, C.J. Jones, J.A. McCleverty, David Collison, F.E. Mabbs, C.J. Harding, L.J. Yellowlees, M.G. Hutchings, Inorg. Chem. 35 (1996) 760.
[10] N. Al Obaidi, T.A. Hamor, C.J. Jones, J.A. McCleverty, K. Paxton, J. Chem. Soc., Dalton Trans. (1987) 2653.
[11] P.P. Romańczyk, M.N. Guzik, A.J. Włodarczyk, Polyhedron 26 (2007) 1182.
[12] A.J. Włodarczyk, P.P. Romańczyk, S.S. Kurek, W. Nitek, J.A. McCleverty, Polyhedron 27 (2008) 783.
[13] S.B. Braun-Sand, O. Wiest, J. Phys. Chem. A 107 (2003) 285.
[14] D. Yokogawa, H. Sato, Y. Nakao, S. Sakaki, Inorg. Chem. 46 (2007) 1966.
[15] V.K. Landry, K. Pang, S.M. Quan, G. Parkin, J. Chem. Soc., Dalton Trans. (2007) 820.
[16] M.J. Frisch, G.W. Trucks, H.B. Schlegel, G.E. Scuseria, M.A. Robb, J.R. Cheeseman, J.A. Montgomery, Jr., T. Vreven, K.N. Kudin, J.C. Burant, J.M. Millam, S.S. Iyengar, J. Tomasi, V. Barone, B. Mennucci, M. Cossi, G. Scalmani, N. Rega, G.A. Petersson, H. Nakatsuji, M. Hada, M. Ehara, K. Toyota, R. Fukuda, J. Hasegawa, M. Ishida, T. Nakajima, Y. Honda, O. Kitao, H. Nakai, M. Klene, X. Li, J.E. Knox, H.P. Hratchian, J.B. Cross, V. Bakken, C. Adamo, J. Jaramillo, R. Gomperts, R.E. Stratmann, O. Yazyev, A.J. Austin, R. Cammi, C. Pomelli, J.W. Ochterski, P.Y. Ayala, K. Morokuma, G.A. Voth, P. Salvador, J.J. Dannenberg, V.G. Zakrzewski, S. Dapprich, A.D. Daniels, M.C. Strain, O. Farkas, D.K. Malick, A.D. Rabuck, K. Raghavachari, J.B. Foresman, J.V. Ortiz, Q. Cui, A.G. Baboul, S. Clifford, J. Cioslowski, B.B. Stefanov, G. Liu, A. Liashenko, P. Piskorz, I. Komaromi, R.L. Martin, D.J. Fox, T. Keith, M.A. Al-Laham, C.Y. Peng, A. Nanayakkara, M. Challacombe, P.M.W. Gill, B. Johnson, W. Chen, M.W. Wong, C. Gonzalez, J.A. Pople, GAUSSIAN 03, Revision D.01, Gaussian, Inc., Wallingford, CT, 2004.
[17] P.J. Hay, W.R. Wadt, J. Chem. Phys. 82 (1985) 270.
[18] P.J. Hay, W.R. Wadt, J. Chem. Phys. 82 (1985) 284.
[19] P.J. Hay, W.R. Wadt, J. Chem. Phys. 82 (1985) 299.
[20] C.E. Check, T.O. Faust, J.M. Bailey, B.J. Wright, T.M. Gilbert, L.S. Sunderlin, J. Phys. Chem. A 105 (2001) 8111.
[21] F. Weigend, M. Haser, H. Patzelt, R. Ahlrichs, Chem. Phys. Lett. 294 (1998) 143.
[22] D. Andrae, U. Haeussermann, M. Dolg, H. Stoll, H. Preuss, Theor. Chim. Acta 77 (1990) 123.
[23] F. Weigend, R. Ahlrichs, Phys. Chem. Chem. Phys. 7 (2005) 3297.
[24] N.C. Handy, A.J. Cohen, Mol. Phys. 99 (2001) 403.
[25] M. Cossi, N. Rega, G. Scalmani, V. Barone, J. Chem. Phys. 114 (2001) 5691.
[26] A.R. Allouche, GABEDIT is a free Graphical User Interface for Computational Chemistry Packages. Available from: <http://gabedit.sourceforge.net/>.
[27] M. Lundberg, Per E.M. Siegbahn, J. Chem. Phys. 122 (2005) 224103.
[28] M. Jaworska, Z. Stasicka, New J. Chem. 29 (2005) 604.
[29] M. Jaworska, Z. Stasicka, J. Organomet. Chem. 689 (2004) 1703.
[30] M. Jaworska, Polyhedron 26 (2007) 3247.
[31] J.N. Harvey, Annu. Rep. C, Phys. Chem. 102 (2006) 203.
[32] F. Roncaroli, M. Videla, L.D. Slep, J.A. Olabe, Coord. Chem. Rev. 251 (2007) 1903.

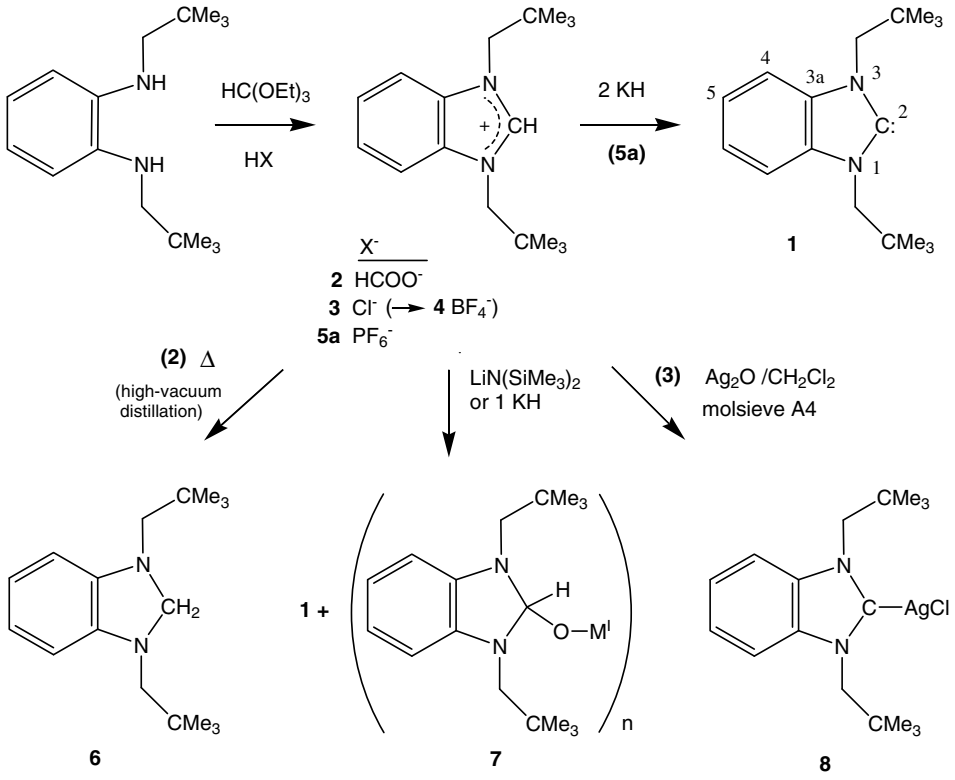

Scheme 1. Formation and deprotonation of anellated *N*,*N*′-dineopentyl-imidazolium salts.

N,*N*′-dimethyl- and dibutylbenzimidazolium formate [14]. The ^{1}H and ^{13}C NMR data are in accordance with those recently reported [6].

Deprotonation of **2** by $LiN(SiMe_3)_2$ in THF furnished mainly the corresponding carbene, but accompanied by a small amount of a lithium salt $\mathbf{7_{Li}}$ that displays similar solution NMR data to a known NHC–KOH adduct, In the solid state the latter is a tetramer anellated imidazolium compound bound at a $(KO^{-})_4$-cluster with distorted cubane structure as the anion, but in solution it disproportionates into the corresponding dihydroimidazole and imidazol-2-one coordinating the potassium oxide [12a]. $\mathbf{7_{Li}}$ is thought to be the corresponding lithium compound, a formal addition product of **1** and LiOH, formed by traces of moisture originating from the aqueous formic acid, that in solution disproportionates into **6** and dineopentyl-benzimidazol-2-one coordinated at Li_2O, and thus displays two sets of signals with equal intensity.

To avoid contamination by water, the benzimidazolium chloride **3** was prepared by cyclocondensation of *N*,*N*′-dineopentyl-1,2-diaminobenzene with triethyl orthoformate in the presence of anhydrous ethereal HCl. Carbon analyses of **3** were not satisfactory, but conversion to the well-defined tetrafluoroborate **4** by treatment with $AgBF_4$ confirmed its composition. As starting material for the synthesis of **1** the hexafluorophosphate **5a**, formed directly by orthoformate condensation in the presence of stoichiometric amounts of NH_4PF_6, proved to be superior. As expected, the protons in position 2 of the anellated imidazolium salts **2–5** are quite acidic and appear in the ^{1}H NMR spectra at low field. The proton chemical shifts depend somewhat on the solvent and the anion. In CD_3CN they are more strongly shifted for the polarizing anion chloride than the weakly coordinating PF_6^{-} anion (**3** $\delta = 9.77$, **5a** $\delta = 8.87$), while in the highly polar O-donor solvent DMSO-d_6 the stronger downfield shift is observed also in the case of weakly coordinating anions (**4** $\delta = 9.70$, **5a** $\delta = 9.71$). The CH-acidity leads to more or less strong H–D exchange, visible by low-intensity H-2 proton and superimposed $\{^{1}H\}^{13}CH$-2 singlet and ^{13}CD-2 triplet signals, but rates or amounts of this exchange were not systematically studied. Attempts to deprotonate the benzimidazolium salts **3** or **5a** on the NMR scale with an equimolar amount of $LiN(SiMe_3)_2$ in toluene or THF did not display the signals of **1** but again the two sets assigned to the disproportion products of $\mathbf{7_{Li}}$. The use of two equivalents of the base provided the carbene in high yield, but accompanied by the second equivalent of $LiN(SiMe_3)_2$ and $HN(SiMe_3)_2$. A convenient synthesis of free **1** in high yield and on a preparative scale proved to be the deprotonation of **5a** by potassium hydride in THF in 1:1, or better in 1:2 molar ratio. The excess KH did not cause reduction but improved the yield. The deprotonation of **3** by KH (1:1) in THF was found to be less suitable and gave only 50 mol% of **1** along with some $\mathbf{7_K}$ and unidentified contamination. The formation of dimers, which might be favored by the presence of the imidazolium salts (proton catalysis) [15], was not observed, probably because of steric hindrance by the neopentyl substituents.

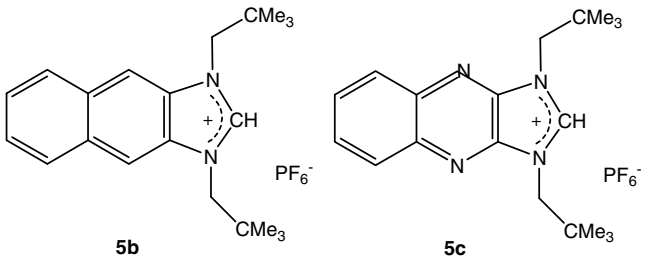

Compounds 5b and 5c

The two closely related hexafluorophosphates **5b** and **5c** were obtained by reaction of the respective aromatic diamines with triethyl orthoformate in the presence of stoichiometric amounts of NH_4PF_6

Table 1
Selected ^{1}H and ^{13}C NMR data (δ in ppm)

Compound (solvent)	**3** (CD_3CN)	**2** (D_2O)	**5a** (DMSO-d_6)	**5b** [12a] (DMSO-d_6)	**5c**[12b] (DMSO-d_6)	**8** (CD_2Cl_2)
δ_H (ppm)						
C^{II}–H	9.77	9.29	9.71 (8.87)[a]	9.92	10.50	
CH_2	4.35	4.23	4.40 (4.29)	4.48	4.49	4.27
H_{But}	1.05	0.90	1.01 (1.04)	1.07	1.11	1.10
H_{aryl1}	7.66; 7.91	7.64; 7.81	7.69, 8.16 (7.68; 7.91)	8.75		7.38;7.54
H_{aryl2}				7.66; 8.19	8.09; 8.38	
δ_C (ppm)						
C^{II}	144.1	144.6	143.6	147.6	153.2	193.2
CH_2	58.4	60.0	56.8	57.0	56.4	62.0
C_{bridge}	133.4	134.48	132.0	130.8; 131.2	138.2; 140.4	136.4
C_{aryl1}	115.0; 127.6	116.3; 129.1	114.2; 126.4	111.9		114.41 125.3
C_{aryl2}				126.6; 128.2	128.9; 131.2	
C_{But}	34.14	35.16	33.12	33.2	33.0	35.8
C_{But}	27.57	29.04	27.00	27.1	27.1	30.5

[a] ^{1}H NMR data in parentheses measured in CD_3CN.

in moderate yields. The NMR spectra of **5a**, **5b** and **5c** in DMSO-d_6 show the expected trends of $\delta = 9.71$ (**5a**), 9.92 (**5b**) and 10.50 ppm (**5c**) in the proton NMR spectrum and $\delta = 143.57$ (**5a**), 147.57 (**5b**) and 153.16 ppm (**5c**) in the ^{13}C {^{1}H} NMR spectrum (Table 1). The downfield shift of either the H-2-proton or the C-2-carbon atom is seemingly dependent upon the electron-withdrawing effect of the anellated aromatic ring system in the order quinoxaline > naphthalene > benzene, as predicted by the anellation effect [16].

Reaction of **3** with Ag_2O in methylene chloride affords the AgCl adduct of **1** in nearly quantitative yield (98% isolated). The silver complex is soluble in CH_2Cl_2 and in THF and somewhat light-sensitive.

3. Crystal and molecular structures

Structures of *N*,*N*′-disubstituted imidazolium salts with very short C–H···O hydrogen bonds to oxoanions such as NO_3^-, SO_4^{2-}, $S_2O_7^{2-}$ $CF_3SO_3^-$ or ClO_4^- [2f], HCO_3^- [17] or phenolates [4] have already been reported, but structure reports of anellated species of this type [18] or with carboxylate anions [19] are rare.

A single-crystal X-ray study of **2** · 2HCOOH, taken from the original mother liquor, indicated hydrogen bonding between the formic acid molecules and also between the oxygen atoms of the formate anion and the acidic hydrogen atom at C-2 (Fig. 1). However, disorder of one of the formic acid molecules prevented acceptable refinement, and we therefore present no details of this structure beyond the structural motif.

The formate anion and the formic acid molecules form an unbranched linear chain held together by hydrogen bonding. It is reasonable to assume that the benzimidazolium cation uses its acidic H-2 proton to hydrogen bond to an oxygen atom of the formate anion. This seems to be the case, but we cannot unambiguously distinguish between the formate and the formic acid entities.

Compound **3**·CH_2Cl_2 (Fig. 2) crystallises in the monoclinic space group $P2_1/c$ with four formula units in the unit cell. The bond lengths and angles lie in the expected ranges (Table 2).

The packing (Fig. 3) involves six C–H···Cl interactions, five of them involving the chloride anion (three within the asymmetric unit), the H-1 atom (in ring position 2) prominently amongst them (C1–H1 95(2), H1···Cl1 262(2) pm). Five of these combine to produce layers parallel to the *ab* plane; H13B···Cl1 and the short contact Cl3···Cl1 354.0(2) pm connect the layers.

Compound **5a** (Fig. 4) crystallises in the monoclinic, non-centrosymmetric space group *Pc* with two molecules in the unit cell. The bond lengths and angles lie in the expected ranges with the N1–C2–N3 angle at 111.06(12)° (Table 2). The similarity of the shortest H···F distance from the hydrogen atom at the carbene carbon (H1···F(6) 244(2) pm; C···F 301.83(16) pm) to other F···H contacts in **5a** (242–264 pm; C···F 339.24(17)–352.42(18) pm) and the small variation of the P–F bond lengths (159.36(9)–

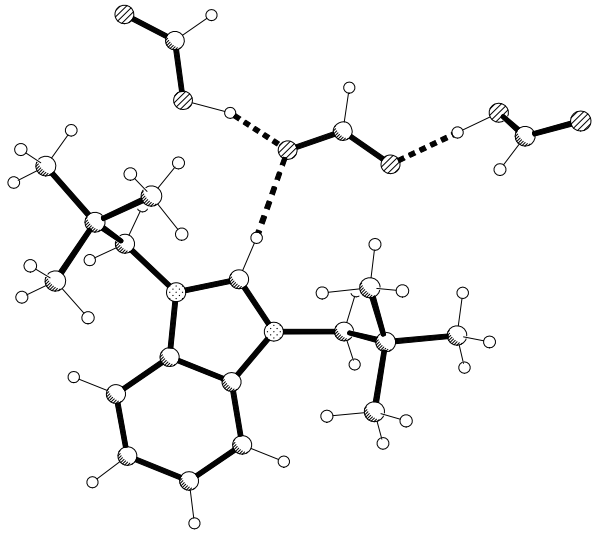

Fig. 1. Simplified qualitative structure of **2** · 2HCOOH; one HCOOH is, however, appreciably disordered.

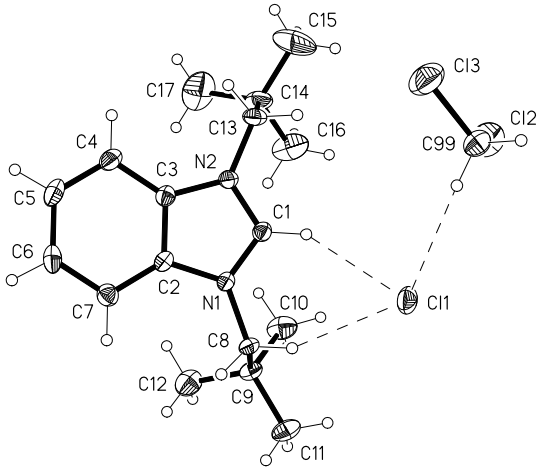

Fig. 2. Structure of **3** · CH_2Cl_2 in the crystal (ellipsoids with 50% probability).

Table 2
Selected bond lengths (pm) and angles (°)

Compound	**3**	**5a**	**5b**	**5c**	**8**
Bond lengths (pm)					
$C^{II}(1)$–H(1)	95(2)	94.7(16)	90(4)	90	
N–C^{II}	132.4(3); 133.5(2)	132.95(17); 133.01(17)	132.4(5); 133.1(5)	133.3(4); 133.4(4)	135.72(18); 135.86(17)
N–C_{ring}	139.4(2); 139.4(3)	140.05(17); 140.05(17)	140.5(5); 139.7(5)	139.3(4); 139.4(4)	139.21(18); 139.56(18)
N–C_{alk}	147.1(2); 147.4(3)	147.53(16); 147.23(15)	147.5(5); 147.9(5)	147.2(4); 147.2(4)	146.84(18); 146.71(17)
C=C	139.5(3)	139.50(19)	140.4(5)	141.4(4)	140.1(2)
C–Ag					208.45(14)
Ag–Cl					233.56(14)
Bond angle (°)					
N–C^{II}–N	110.94(17)	111.06(12)	111.3(4)	112.0(3)	106.21(12)
C–N–C^{II}	107.73(16); 108.13(16)	107.86(11); 107.97(11)	107.9(3); 108.1(3)	107.2(2); 107.5(2)	110.96(12); 110.68(11)
C–N–C_{alk}	124.17(16); 127.69(17); 124.19(17); 128.08(16)	125.16(11); 126.97(11); 124.93(11); 126.96(11)	123.8(3); 128.2(3); 124.6(3); 127.3(3)	126.7(2); 125.9(2); 125.1(2); 127.4(2)	123.23(11); 126.02(11); 123.34(12); 125.67(12)
C^{II}–Ag–Cl					175.88(4)
N–C^{II}–Ag					127.56(10); 126.19(10)

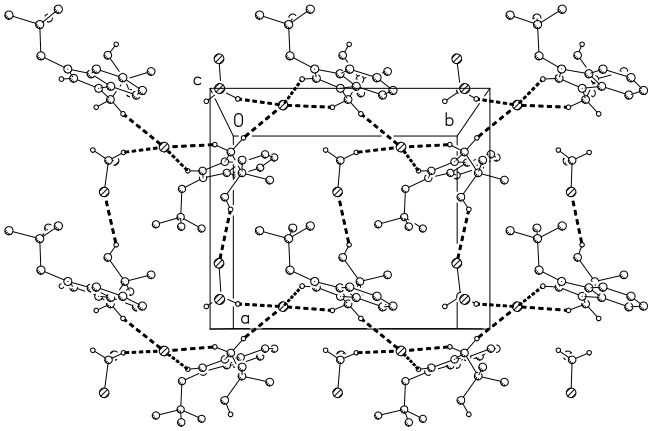

Fig. 3. Packing of **3** · CH_2Cl_2. Layer parallel to the *ab* plane at $z \approx 1/4$.

160.97(9) pm), indicates the absence of unusually short (strong) hydrogen bonds. As was found in non-anellated imidazolium tetrafluoroborates [20], the C1–H···F contact may be regarded as a

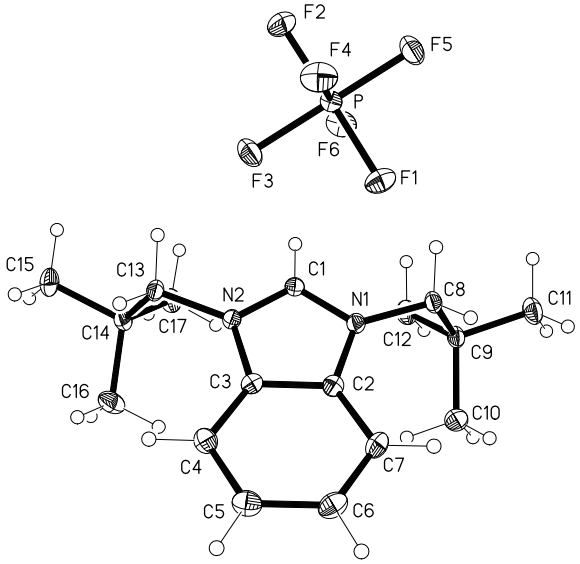

Fig. 4. Structure of **5a** in the crystal (ellipsoids with 30% probability).

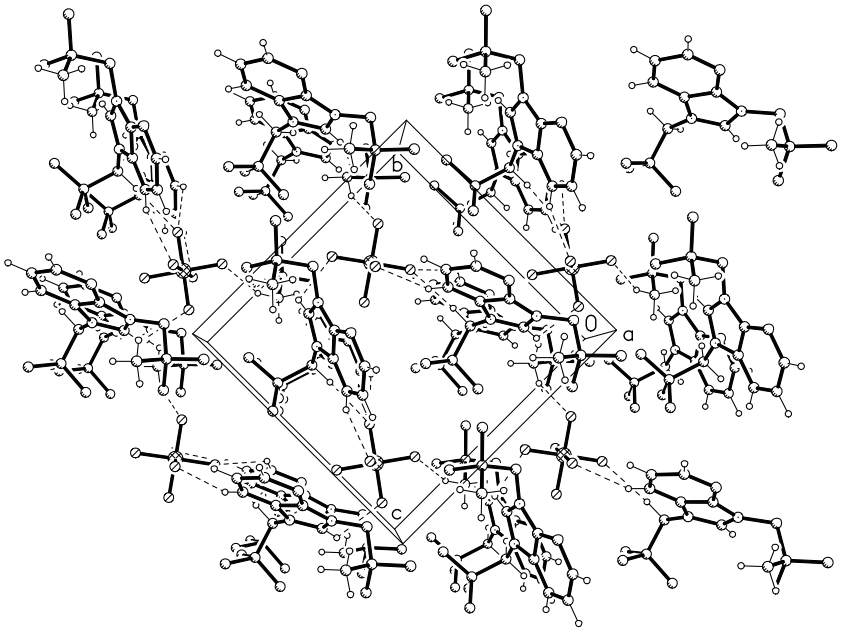

Fig. 5. Packing of **5a**; shortest contacts are shown as dotted lines.

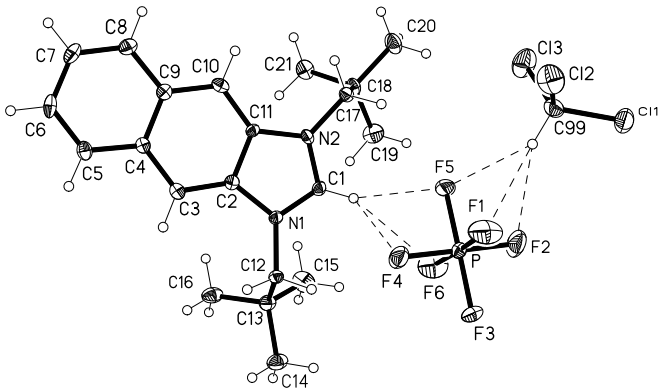

Fig. 6. Structure of **5b** in the crystal (ellipsoids with 30% probability).

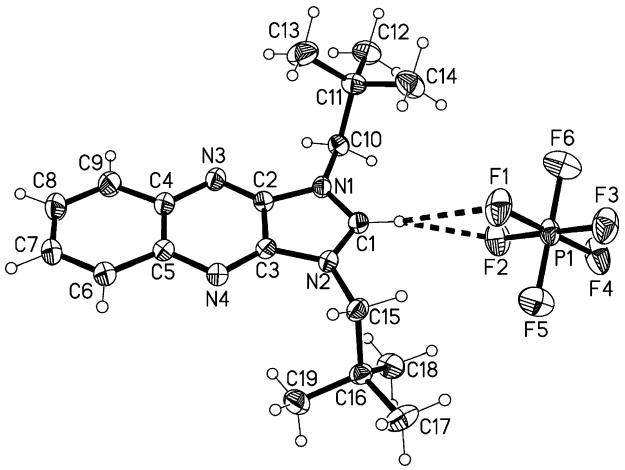

Fig. 7. Molecular structure of **5c** (ellipsoids with 50% probability).

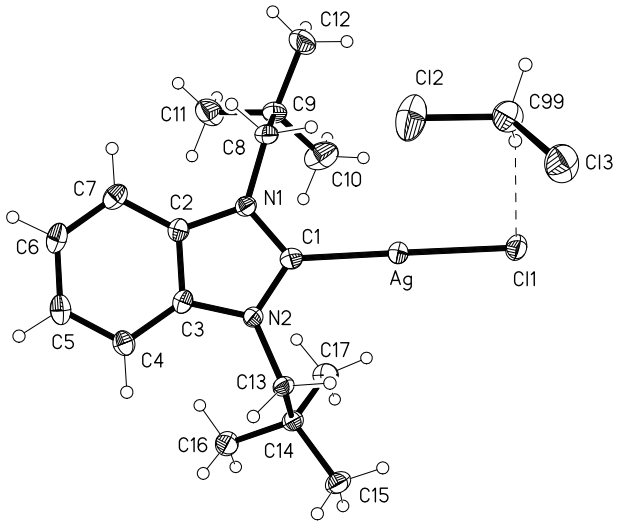

Fig. 8. Molecular structure of **8** · CD_2Cl_2 (ellipsoids with 50% probability).

weaker packing effect rather than a directed interaction. The packing of **5a**, with columns of cations and anions parallel to the *a* axis, is depicted in Fig. 5.

For comparison, the structures of related, but differently anellated naphtho- and quinoxalino[2,3-d]imidazolium hexafluorophosphates **5b** and **5c** were also studied. Compound **5b** (Fig. 6) crystallises in the monoclinic space group $P2_1/c$ with four molecules in the unit cell, compound **5c** (Fig. 7) in the triclinic space group $P\bar{1}$ with two molecules in the unit cell. The bond lengths and angles of both compounds lie in the expected ranges and are very similar to those of **5a** and **3** (Table 2).

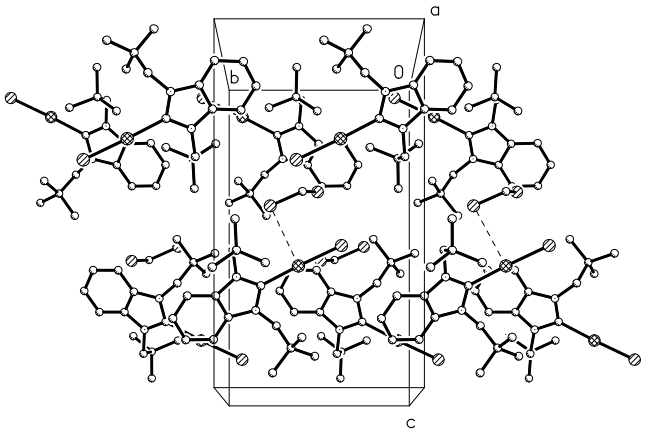

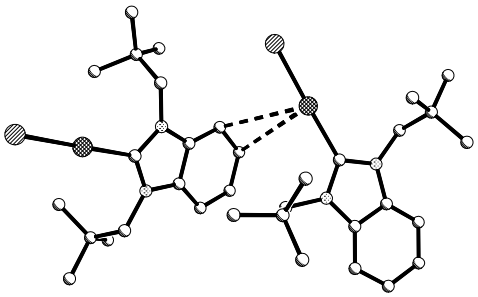

Fig. 9. General packing showing Ag···Cl contacts (a) and intermolecular silver–carbon contacts (b) in the crystal of **8** · CD_2Cl_2.

The packing in both the naphtho- and quinoxalino-anellated imidazolium hexafluoro-phosphates involves some short C–H···F contacts (several involving H1 at the carbenic carbon, Figs. 6,7). However, the overall packing patterns display no clearly recognisable motifs such as ribbons or layers.

Compound **8** is isolobal with the carbene-H···X adducts by virtue of its $4d^{10}5s^1$ electron configuration and preference for twofold coordination, and represents the carbene complex structure with similar molecular architecture (Fig. 8). However, the metal is much larger than hydrogen and possesses d-electrons for back bonding, which limits this comparison. Compound **8** crystallises in the monoclinic space group $P2_1/n$ with four molecules in the unit cell.

The silver atom shows the well-known linear coordination sphere for Ag(I,) with a chloro and a carbene ligand. The C–Ag–Cl angle is 175.88° and thus deviates slightly from linearity. This deviation may be caused by a close contact of the silver atom to the C4–C5 bond of a second carbene moiety in the packing (Ag···C4 340 pm, Ag···C5 367 pm; operator $0.5 - x$, $0.5 + y$, $0.5 - z$) (Fig. 9). Such silver aryl interactions are known, but have been observed in only one silver NHC complex, the naphtho-anellated analogue of **8** [12a], which forms dimers (Ag···C5 343 pm, Ag···C6 311 pm, Ag···C7 358 pm). There is also a contact of 358.39(6) pm from the silver atom to Cl(2) of the solvent, and one of 269 pm from a solvent deuterium to the chloro ligand, both within the asymmetric unit. There are no Ag···Ag interactions in the crystal. The C^{II}–Ag and C^{II}–N bond lengths in **8** are similar to those reported for other NHC–Ag complexes [9a,21–24] and do not indicate any systematic effect of anellation on the bond lengths. As compared to the ligand **1** [6] the NCN angle is markedly larger (by ca. 3°), but the C^{II}–N bonds are not significantly shorter in **8** (difference ca. 1 pm and thus within 3σ). Other bond lengths of **8** (Table 2) are similar to those in related compounds. The resemblance of the structural

motif in **8** to that frequently encountered [9a] in [Ag(NHC)][$AgBr_2$] complexes is noticeable, whereby the aryl formally takes the place of the $AgBr_2$ unit.

4. Conclusions

1,3-Dineopentyl-benzimidazol-2-ylidene (**1**) is available easily and in high yield by ring closure of 1,2-di(neopentylamino)benzene with orthoformate in the presence of NH_4PF_6 and deprotonation with excess KH in THF. Stoichiometric amounts of KH and other bases such as $LiN(SiMe_3)_2$ or KH/KO*t*Bu proved less suitable. Crystal structure analyses of various anellated imidazolium salts, for comparison each *N*,*N*′-dineopentyl substituted, displayed neither significant changes nor systematic trends of bond lengths and angles within the five-membered ring. The ^1H and ^{13}C NMR chemical shifts of the CH(2) nuclei, which are particularly sensitive to the π-electron density, indicate however the electronic influence of the anellated ring and are downfield shifted as a result of electron-withdrawing anellation.

5. Experimental

General remarks: All reactions were carried out in carefully dried, freshly distilled solvents. Reactions with air- or moisture-sensitive compounds were conducted under an argon atmosphere using Schlenk techniques. The synthesis of hexafluorophosphate **5b** was reported earlier [12a], other chemicals were purchased. NMR spectra were recorded on a multinuclear FT NMR spectrometer ARX300 (Bruker) at 300.1 (^1H), 75.5 (^{13}C), and 121.5 (^{31}P) MHz. Shift references are tetramethylsilane for ^1H and ^{13}C and H_3PO_4 (85%) for ^{31}P. Assignment numbers are given in Scheme 1. Coupling constants refer to J_{HH} unless stated otherwise. Assignments are based on CH–COSY NMR experiments, proton-decoupled and DEPT ^{13}C NMR spectra for selected compounds. Melting points (uncorrected) were determined with a Sanyo Gallenkamp melting point apparatus, elemental analysis with a CHNS-932 analyzer from LECO using standard conditions.

5.1. 1,3-Dineopentyl-benzimidazolium formate · formic acid solvates (2 · HCOOH and 2 · 2HCOOH) (2)

Formic acid (0.4 mL, 85% in water, 8.86 mmol) was added to a solution of *N*,*N*′-dineopentyl 1,2-diaminobenzene (1.42 g, 5.71 mmol) in triethyl orthoformate (15 mL), and the resulting solution was heated at 70 °C for 15 h. Hexane (10 mL) was layered slowly over the solution at room temperature, and the product was allowed to crystallize. After some days the off-white crystals were separated, washed with hexane and dried in vacuum to give 1.71 g (85%) of **2** · HCOOH, mp 124 °C. (Before drying, the crystals contain two molecules of formic acid, as discussed above.) ^1H NMR (CH–COSY, D_2O): δ = 0.90 (s, 18H, CMe_3), 4.23 (s, 4H, NCH_2), 7.64 (m, 2H, 5-H), 7.81 (m, 2H, 4-H), 8.33 (s, 2H, $HCOO^-$), 9.29(s, 1H, 2-H); $^{13}C\{^1H\}$ NMR (CH–COSY, D_2O): δ = 29.0 (*C*Me_3), 35.2 (*C*Me_3), 60.0 (NCH_2), 116.3 (C-4), 129.1 (C-5), 134.5 (C-3a), 144.6 (C-2), 170.7 ($HCOO^-$); MS (EI, 70 eV, 345 °C): *m*/*z* (%) = 261 (13), 260 (76), 259 (100) [M^+−2HCOOH], 258 (33), 257 (10), 203 (52), 202 (72) [$M-C_4H_8^+$], 133 (51), 132 (35), 131 (43); Elemental Anal. Calc. (%) for $C_{19}H_{30}N_2O_4$ (350.46): C, 65.12; H, 8.63; N, 7.99. Found: C, 64.84; H, 8.47; N, 8.37%.

5.2. High vacuum thermolysis of 2 · HCOOH to 1,3-dineopentyl-benzimidazoline (6)

Thermolytic distillation of **2** · HCOOH (300 mg, 0.86 mmol) at 170 °C (bath)/10^{-5} bar afforded 215 mg (96%) of *N*,*N*′-dineopentyl-benzimidazoline **6**. The ^1H and ^{13}C NMR data are in accordance with those recently reported [6].

5.3. 1,3-Dineopentyl-benzimidazolium chloride (3)

Ethereal HCl (3.62 mL, 0.5 M, 1.81 mmol) was added to a solution of *N*,*N*′-dineopentyl 1,2-diaminobenzene (450 mg, 1.81 mmol) in triethyl orthoformate (15 mL), and the resulting mixture was stirred for 16 h at ambient temperature. The precipitate was filtered off, repeatedly washed with hexane and recrystallized from CH_3CN to give 523 mg (98%) colorless crystals of **3**, mp >300 °C. Alternatively, NH_4Cl (509 mg, 9.51 mmol), *N*,*N*′-dineopentyl 1,2-diaminobenzene (2.36 g, 9.51 mmol) and triethyl orthoformate (15 mL) were heated at 100 °C overnight in a rectification apparatus and the mixture worked up as above affording 2.53 g (90%) of **3**. Single crystals of **3** · CH_2Cl_2 were grown from CH_2Cl_2 solution by overlayering with *n*-hexane; selected bond lengths and angle bond see Table 2, crystal data see Table 3. ^1H NMR (CD_3CN): δ = 1.05 (s, 18H, CMe_3), 4.35 (s, 4H, NCH_2), 7.66 (m, 2H, 5-H), 7.91 (m, 2H, 4-H), 9.77 (s, 1H, 2-H); $^{13}C\{^1H\}$ NMR (CD_3CN): δ = 27.6 (*C*Me_3), 34.1 (*C*Me_3), 58.4 (NCH_2), 115.0 (C-4), 127.6 (C-5), 133.4 (C-3a), 144.1 (C-2); MS (EI, 70 eV, 345 °C): *m*/*z* (%) = 259 (2) [M^+−Cl], 258 (3), 257 (3), 202 (11) [$M-C_4H_8^+$], 132 (6), 131 (7); Elemental Anal. Calc. (%) for $C_{17}H_{27}N_2Cl$ (294.87): H, 9.23; N, 9.50. Found: H, 9.19; N, 9.43%.

5.4. 1,3-Dineopentyl-benzimidazolium tetrafluoroborate (4)

$AgBF_4$ (764 mg, 3.92 mmol) was added to a solution of **3** (1.15 g, 3.90 mmol) in 15 mL CH_3CN. The suspension was stirred for 1 day at room temperature (light protected) and filtered. The solvent was removed in vacuum to give 1.25 g (92%) crystals of **5**, mp 247–249 °C. ^1H NMR (DMSO-d_6): δ = 1.00 (s, 18H, CMe_3), 4.41 (s, 4H, NCH_2), 7.69 (m, 2H, 5-H), 8.16 (m, 2H, 4-H), 9.70 (s, 1H, 2-H); ^{13}C NMR (DMSO-d_6): δ = 27.0 (*C*Me_3), 33.1 (*C*Me_3), 56.8 (NCH_2), 114.2 (C-4), 126.4 (C-5), 132.0 (C-3a), 143.7 (C-2); Elemental Anal. Calc. (%) for $C_{17}H_{27}N_2BF_4$ (346.22): H, 7.86; N, 8.09. Found: H, 7.83; N, 7.94%.

5.5. 1,3-Dineopentyl-benzimidazolium hexafluorophosphate (5a)

N,*N*′-Dineopentyl 1,2-diaminobenzene (1.01 g, 4.06 mmol), NH_4PF_6 (663 mg, 4.06 mmol), and triethyl orthoformate (15 mL) were heated to 130 °C for 6 h in a rectification apparatus to separate ethanol from the reaction mixture. The solution was then allowed to cool to room temperature, the product was precipitated and washed with hexane (3× each 10 mL). The solid was dissolved in CH_3CN and the solution filtered, and the volatiles were removed in vacuum to give 1.55 g (94%) of **5a**, mp 221 °C. Single crystals grew from saturated solution in acetonitrile (selected bond lengths and angles Table 2, crystal data in Table 3). ^1H NMR (CD_3CN): δ = 1.04 (s, 18H, CMe_3), 4.29 (s, 4H, NCH_2), 7.68 (m, 2H, 5-H), 7.91 (m, 2H, 4-H), 8.87 (s, 0.4H, 2-H); ^1H NMR (DMSO-d_6): δ = 1.01 (s, 18H, CMe_3), 4.40 (s, 4H, NCH_2), 7.69 (m, 2H, 5-H), 8.16 (m, 2H, 4-H), 9.71 (s, 1H, 2-H); ^{13}C NMR (DMSO-d_6): δ = 27.0 (*C*Me_3), 33.1 (*C*Me_3), 56.8 (NCH_2), 114.2 (C-4), 126.4 (C-5), 132.0 (C-3a), 143.6 (C-2); ^{31}P NMR (DMSO-d_6): δ = −143.1 (sept, $^1J_{PF}$ = 711.3 Hz); Elemental Anal. Calc. (%) for $C_{21}H_{29}N_2PF_6$ (404.37): C, 50.49; H, 6.73; N, 6.93. Found: C, 50.62; H, 6.89; N, 7.00%.

5.6. Deprotonation experiments

Deprotonation by LiN(SiMe$_3$)$_2$. A solution of $LiN(SiMe_3)_2$ prepared from *n*BuLi in *n*-hexane and $(Me_3Si)_2NH$ (HMDS) in the given solvent was added at the given temperature to a suspension of the anellated imidazolium salt in the given solvent.

Table 3
Crystal data and structure refinement of the anellated NHC complexes **3** · CH_2Cl_2, **5a–c** and **8** · CH_2Cl_2

Identification code	**3** · CH_2Cl_2	**5a**	**5b**	**5c**	**8** · CH_2Cl_2
Empirical formula	$C_{18}H_{29}Cl_3N_2$	$C_{17}H_{27}F_6N_2P$	$C_{22}H_{29}DCl_3F_6N_2P$	$C_{19}H_{27}F_6N_4P$	$C_{18}H_{26}D_2AgCl_3N_2$
Formula weight	379.78	404.38	574.81	456.42	488.65
Temperature (K)	133(2)	133(2)	133(2)	173(2)	133(2)
Wavelength (pm)	71.073	71.073	71.073	71.073	71.073
Crystal system	monoclinic	monoclinic	monoclinic	triclinic	monoclinic
Space group	$P2_1/c$	Pc	$P2_1/c$	$P\bar{1}$	$P2_1/n$
Unit cell dimensions					
a (pm)	1041.18(9)	809.22(8)	1007.11(17)	847.46(4)	1191.27(8)
b (pm)	1208.88(10)	1091.90(12)	1463.8(2)	1100.41(6)	1016.46(8)
c (pm)	1654.30(14)	1110.93(12)	1839.2(3)	1216.25(6)	1783.80(12)
α (°)	90	90	90	80.561(2)	90
β (°)	93.729(2)	93.922(4)	90.406(4)	83.767(3)	101.314(4)
γ (°)	90	90	90	87.336(3)	90
Volume (10^6 pm^3)	2077.8(3)	979.30(18)	2711.4(8)	1111.8(1)	2118.0(3)
Z	4	2	4	2	4
D_{calc} (Mg/m^3)	1.214	1.371	1.408	1.363	1.532
Absorption coefficient (mm^{-1})	0.442	0.198	0.452	0.186	1.333
F(000)	808	424	1184	476	992
Crystal size (mm^3)	0.26 × 0.15 × 0.13	0.40 × 0.20 × 0.17	0.30 × 0.25 × 0.20	0.48 × 0.09 × 0.08	0.32 × 0.30 × 0.17
Theta range for data collection (°)	1.96–28.28	2.52–30.02	1.11–26.22	2.33–29.00°	1.90–30.03
Index ranges	$-13 \leqslant h \leqslant 13$, $-16 \leqslant k \leqslant 16$, $-22 \leqslant l \leqslant 22$	$-11 \leqslant h \leqslant 11$, $-15 \leqslant k \leqslant 15$, $-15 \leqslant l \leqslant 15$	$-12 \leqslant h \leqslant 12$, $-18 \leqslant k \leqslant 18$, $-22 \leqslant l \leqslant 22$	$-11 \leqslant h \leqslant 11$, $-14 \leqslant k \leqslant 14$, $-16 \leqslant l \leqslant 16$	$-16 \leqslant h \leqslant 16$, $-14 \leqslant k \leqslant 14$, $-25 \leqslant l \leqslant 25$
Reflections collected	37648	10968	33939	49101	40553
Independent reflections (R_{int})	5143 (0.0565)	5571 (0.0244)	5417 (0.1104)	5805 (0.0556)	6188 (0.0284)
Completeness to theta	(=28.00°) 100.0%	(=30.00°) 99.6%	(=26.00°) 100.0%	98.2%	(=30.00°) 99.9%
Absorption correction	semi-empirical from equivalents	none	none	semi-empirical from equivalents	semi-empirical from equivalents
Refinement method	full-matrix least-squares on F^2	full-matrix least-squares on F^2	full-matrix least-squares on F^2	full-matrix least-squares on F^2	full-matrix least-squares on F^2
Data/restraints/parameters	5143/0/218	5571/2/245	5417/0/312	5805/0/276	6188/0/223
Goodness-of-fit on F2	1.045	0.969	1.046	1.073	1.035
Final R indices [$I > 2$sigma(I)]	$R_1 = 0.0505$, $wR_2 = 0.1080$	$R_1 = 0.0302$, $wR_2 = 0.0682$	$R_1 = 0.0549$, $wR_2 = 0.1142$	$R_1 = 0.0581$, $wR_2 = 0.1381$	$R_1 = 0.0225$, $wR_2 = 0.0567$
R indices (all data)	$R_1 = 0.0823$, $wR_2 = 0.1222$	$R_1 = 0.0341$, $wR_2 = 0.0697$	$R_1 = 0.1193$, $wR_2 = 0.1335$	$R_1 = 0.0915$, $wR_2 = 0.1475$	$R_1 = 0.0293$, $wR_2 = 0.0590$
Largest difference in peak and hole (e 10−6 pm−3)	0.427 and −0.309	0.287 and −0.272	0.475 and −0.337	0.380 and −0.357	0.863 and −0.532

Table 4
Generation of **1** or **7**[a] by deprotonation with $LiN(SiMe_3)_2$ or KH

Exp.	NHC−H+X$^-$ (mg, mmol)	Base[b] (mL/mg, mmol)	Solvent (mL) Temperature (°C)	Products **1**, (**6** + **7**′) (mol%)
1	**2** (500, 1.43)	*n*BuLi (1.91, 2.87), HMDS (0.61, 2.87)	THF (5+10) −78 to 20	92, 8
2	**3** (500, 1.70)	*n*BuLi (1.06, 1.70), HMDS (0.36, 1.70)	Toluene (5+10) −78 to 20	–, >95 (234 mg solid)
3	**3** (300, 1.01)	*n*BuLi (0.67, 1.01), HMDS (0.21, 1.01)	THF (5+10) −78 to 20	–, >95 (176 mg solid)
4	**3** (207, 0.70)	*n*BuLi (0.87, 1.39), HMDS (0.29, 1.40)	Toluene (5+10) −78 to 20	>95, – and $(Me_3Si)N$-species
5	**3** (445, 1.51)	KH (30%) (202, 1.51)	THF (20) 20	50, 25 (and unknown; 160 mg solid)
6	**5a** (1730, 4.28)	KH (30%) (570, 4.27)	THF (20) 20	90, 10[c]
7	**5a** (274, 0.68)	KH (30%) (181, 1.35)	THF (10) −78 to 20	>95, –

[a] Product analysis is based on solution NMR spectra. The solid compound **7** disproportionates in solution and displays two equal intense NMR signal sets of **6** and 1,3-dineopentyl-benzimidazol-2-one, coordinated at M^I (**7**′).
[b] *n*BuLi and HMDS (mL, mmol), KH, KO*t*Bu (mg).
[c] After distillation 860 mg (78%) **1**, bp 10^{-5} Torr/110 °C (bath), contamination by **6** + **7**′ ⩽ 3%.

Deprotonation by KH or KH in the presence of catalytic amounts (5 mol%) of KOtBu. A suspension of the anellated imidazolium salt in THF was added at the given temperature to a suspension of 30% KH in mineral oil, washed beforehand with THF.

Work up and characterization. The mixture was allowed to warm to room temperature (if prepared at low temperature) and stirred overnight. After filtration the solvent was removed in vacuum. If THF was used, the residue was extracted with diethyl ether and the ether evaporated (separation from salts soluble in THF). The oily or solid residue was dissolved in C_6D_6, and ^{1}H and ^{13}C NMR spectra were measured. The ratios of **1** and **7**, which in solution disproportionates into **6** + **7**′, are given in Table 4 and refer to the integration of the characteristic NCH_2 proton signals and/or to the intensity ratio of the ^{13}C-signals of CH-4 and CH-5. The NMR data for **1** and **6** correspond to known values [6,7]. **7**′: ^{1}H NMR (C_6D_6): δ = 0.93 (s, 18H, CH_3), 3.47 (s, 4H, NCH_2), 6.73 (m, 2H, 4-H), 6.94 (m, 2H, 5-H); ^{13}C NMR (C_6D_6): δ = 29.1 (CMe_3), 35.3 (CMe_3), 53.3 (NCH_2), 109.2 (CH-4), 121.3 (CH-5), 132.2 (C_q-3a), 156.8 (C=O).

5.7. 1,3-Dineopentyl-quinoxalino[2,3-d]imidazolium hexafluorophosphate (**5c**)

2,3-Dineopentylamino-quinoxaline (1.50 g, 5.00 mmol), NH_4PF_6 (815 mg, 5.00 mmol) and triethyl orthoformate (15 mL) were heated to 120 °C for 5h in a rectification apparatus to separate ethanol from the reaction mixture. After cooling to room temperature a solid precipitated and was washed with hexane (3 × 10 mL). Then the product was extracted with CH_3CN to give 1.19 g (52%) colourless crystals of **5c**, mp >300 °C. Single crystals grew from saturated solution in acetonitrile (selected bond lengths and angles

Table 2, crystal data in Table 3). ^{1}H (CH–COSY) NMR (DMSO-d_6): δ = 1.11 (s, 18H, CH_3); 4.49 (s, 4H, NCH_2), 8.09 (m, 2H, 6-H), 8.38 (m, 2H, 5-H), 10.50 [in CD_2Cl_2 9.66] (s, 1H, 2-H). ^{13}C (FIDRES 0.332; CH–COSY) NMR (DMSO-d_6): δ = 27.1 (quart, ^1J = 126 Hz, CMe_3), 33.0 (s, $CqMe_3$), 56.4 (t br, ^1J = 144 Hz, NCH_2), 128.9 ($^1J \approx 167$ Hz, CH-5), 131.2 ($^1J \approx 170$ Hz, CH-6), 138.2 (dd, $^3J_{C-H2}$ = 6.6, $^3J_{C-H(neop)}$ = 3.7 Hz, C_q-3a), 140.4 (m, C_q-4a), 153.2 (dpent, ^1J = 221, ^3J = 5 Hz, {^{1}H}: s and t, $^1J_{CD}$ = 84.7 Hz, C_q-2; t). Elemental Anal. Calc. for $C_{19}H_{27}F_6N_4P$ (456.41): C, 50.00; H, 5.96; N, 12.28. Found: C, 49.86; H, 6.00; N, 12.15%.

5.8. (1,3-Dineopentyl-benzimidazol-2-ylidene)silver chloride (**8**)

Ag_2O (117 mg, 0.51 mmol) was added to a solution of **3** (300 mg, 1.02 mmol) in 10 mL of CH_2Cl_2. The suspension was stirred for 24 h at ambient temperature, filtered and washed with CH_2Cl_2. The solvent of the filtrate was partly removed in vacuum (residual solution ca. 2 mL), hexane (4 mL) was added, and the resulting white precipitate was separated and recrystallized. Drying in vacuum led to 202 mg (98%) colorless **8**, mp 220 °C. ^{1}H NMR (CD_2Cl_2): δ = 1.10 (s, 18H, CMe_3), 4.27 (s, 4H, NCH_2), 7.38 (m, 2H, 5-H), 7.54 (m, 2H, 4-H); ^{13}C{^{1}H} NMR (CD_2Cl_2): δ = 30.5 (CMe_3), 35.8 (CMe_3), 62.0 (NCH_2), 114.4 (C-4), 125.3 (C-5), 136.4 (d, $^3J(^{13}C–^{107/109}Ag) \approx 7.6$ Hz, C-3a), 193.2 (2d, $^1J(^{13}C–^{107/109}Ag)$ = 234.9, 271.0 Hz, C-2); MS (EI, 70 eV, 345 °C): *m*/*z* (%) = 367 (11), 365 (13), 366 (18), 364 (17) [M^+–Cl], 258 (38) [M^+–AgCl], 257 (74), 202 (100), 145 (25), 132 (32), 131 (34); Elemental Anal. Calc. (%) for $C_{17}H_{26}N_2AgCl$ (401.73): C, 50.83; H, 6.52. Found: C, 51.02; H, 6.76%; single crystals of **8** · CD_2Cl_2 formed in the NMR tube; selected bond lengths and angles see Table 2, crystal data see Table 3.

5.9. Crystal structure analyses

X-ray diffraction data for **3**, **5a**, **5b** and **8** were recorded at 133 K; on a Bruker SMART 1000-CCD diffractometer, and for **5c** at 173 K on a Bruker/Nonius Apex X8-CCD diffractometer. All measurements were performed using monochromated Mo Kα-radiation. The data of **3**, **5c** and **8** were corrected for absorption effects using the SADABS procedure [25]. The structures were solved by Direct Methods (SHELXS-97) [26] and refined by full-matrix least-squares methods on F^2 for all unique reflections (SHELXL-97) [26]. All non-hydrogen atoms were refined anisotropically. H-atoms were calculated assuming idealized geometries and refined using riding models or rigid methyl groups. Exceptions are the acidic H-atoms of **3**, **5a** and **5b** attached to C1, which were refined freely. *Special features*: For compound **5a** the Flack parameter refined to –0.02(5). Compound **5b** was a pseudo-merohedral twin by 180° rotation about **a**, and the twinning ratio was 68:32%.

Crystallographic data are given in Table 3 and selected bond lengths and angles in Table 2.

6. Supplementary data

CCDC 686030, 271543, 686031, 685607 and 271545 contain the supplementary crystallographic data for **3**, **5a–c** and **8**. These data can be obtained free of charge via http://www.ccdc.cam.ac.uk/conts/retrieving.html, or from the Cambridge Crystallographic Data Centre, 12 Union Road, Cambridge CB2 1EZ, UK; fax: (+44) 1223-336-033; or e-mail: deposit@ccdc.cam.ac.uk.

Acknowledgements

Funding for this project was provided by the Department of Biochemistry at Ernst-Moritz-Arndt-University Greifswald. A DAAD scholarship (F.U.) is acknowledged. We thank B. Witt for numerous NMR measurements.

References

[1] (a) P. Wasserscheid, W. Keim, Angew. Chem. 112 (2000) 3926;
(b) P. Wasserscheid, W. Keim, Angew. Chem., Int. Ed. 39 (2000) 3773;
(c) J. Dupont, R.F. De Soluza, P.A.Z. Suarez, Chem. Rev. 102 (2002) 3667.
[2] (a) W.A. Herrmann, C. Köcher, Angew. Chem. 109 (1997) 2256;
(b) W.A. Herrmann, C. Köcher, Angew. Chem., Int. Ed. 36 (1997) 2163;
(c) A.J. Arduengo III, Acc. Chem. Res. 32 (1999) 913;
(d) D. Bourissou, O. Guerret, F.P. Gabbaï, G. Bertrand, Chem. Rev. 100 (2000) 39;
(e) T. Weskamp, V.P.W. Böhm, W.A. Herrmann, J. Organomet. Chem. 600 (2000) 12;
(f) N. Kuhn, A. Al-Sheikh, Coord. Chem. Rev. 249 (2005) 829;
(g) F.E. Hahn, Angew. Chem. 118 (2006) 1374;
(h) F.E. Hahn, Angew. Chem., Int. Ed. 45 (2006) 1348;
(i) F.E. Hahn, M. Jahnke, Angew. Chem. 120 (2008) 3166;
(j) F.E. Hahn, M. Jahnke, Angew. Chem., Int. Ed. 47 (2008) 3122. And lit. cited therein.
[3] (a) H.-W. Wanzlick, H.-J. Schönherr, Angew. Chem. 80 (1968) 154;
(b) H.-W. Wanzlick, H.-J. Schönherr, Angew. Chem., Int. Ed. Engl. 7 (1968) 141;
(c) K. Öfele, J. Organomet. Chem. 12 (1968) P42.
[4] (a) A.J. Arduengo III, S.F. Gamper, M. Tamm, J.C. Calabrese, F. Davidson, H.A. Craig, J. Am. Chem. Soc. 117 (1995) 572;
(b) J.A. Cowan, J.A.C. Clyburne, M.G. Davidson, R. L.W. Harris, J.A.K. Howard, P. Küpper, M.A. Leech, S.P. Richards, Angew. Chem. 114 (2002) 1490;
(c) J.A. Cowan, J.A.C. Clyburne, M.G. Davidson, R.L.W. Harris, J.A.K. Howard, P. Küpper, M.A. Leech, S.P. Richards, Angew. Chem., Int. Ed. 41 (2002) 1432.
[5] N. Kuhn, T. Kratz, Synth. (1993) 561.
[6] F.E. Hahn, L. Wittenbecher, R. Boese, D. Bläser, Chem. Eur. J. 5 (1999) 1931.
[7] (a) W.M. Boesveld, B. Gehrhus, P.B. Hitchcock, M.F. Lappert, P.v.R. Schleyer, Chem. Commun. (1999) 755;
(b) B. Gehrhus, P.B. Hitchcock, M.F. Lappert, J. Chem. Soc., Dalton Trans. (2000) 3094.
[8] O. Kühl, Chem. Soc. Rev. 36 (2007) 592.
[9] (a) J.C. Garrison, W.J. Youngs, Chem. Rev. 105 (2005) 3978;
(b) H.M.J. Wang, I.J.B. Lin, Organometallics 17 (1998) 972.
[10] E. Diez-Barra, J. Guerra, V. Hornillos, S. Merino, J. Tejeda, J. Organomet. Chem. 690 (2005) 5654.
[11] L.N. Appelhans, D. Zuccaccia, A. Kovacevic, A.R. Chianese, J.R. Miecznikowski, A. Macchioni, E. Clot, O. Eisenstein, R.H. Crabtree, J. Am. Chem. Soc. 127 (2005) 16299.
[12] (a) S. Saravanakumar, A.I. Oprea, M.K. Kindermann, P.G. Jones, J. Heinicke, Chem. Eur. J. 12 (2006) 3143;
(b) S. Saravanakumar, M.K. Kindermann, J. Heinicke, M. Köckerling, Chem. Comm. (2006) 640.
[13] T.L. Amyes, S.T. Diver, J.P. Richard, F.M. Rivas, K. Toth, J. Am. Chem. Soc. 126 (2004) 4366.
[14] M.I. Korotkikh, G.F. Rayenko, O.P. Shvaika, Dopovidi Natsional'noi Akademii Nauk Ukraini (2001) 130.
[15] R.W. Alder, M.E. Blake, L. Chaker, J.N. Harvey, F. Paolini, J. Schütz, Angew. Chem. 116 (2004) 6020.
[16] (a) O. Kühl, P. Lönnecke, J. Heinicke, Polyhedron 20 (2001) 2215;
(b) O. Kühl, P. Lönnecke, J. Heinicke, New. J. Chem. 26 (2002) 1304;
(c) O. Kühl, Coord. Chem. Rev. 248 (2004) 411;
(d) J. Heinicke, O. Kühl, in Organosilicon Chemistry, in: N. Auner, J. Weis (Eds.), From Molecules to Materials V, VCH, Weinheim, 2005;
(e) L. Pause, M. Robert, J. Heinicke, O. Kühl, J. Chem. Soc., Perkin Trans. 2 (2001) 1383;
(f) O. Kühl, P. Lönnecke, J. Heinicke, Inorg. Chem. 42 (2003) 2836;
(g) O. Kühl, K. Lifson, W. Langel, Eur. J. Org. Chem. (2006) 2336.
[17] A. Abu-Rayyan, Q. Abu-Salem, N. Kuhn, C. Maichle-Mößmer, M. Steimann, G. Henkel, Z. Anorg. Allg. Chem. 634 (2008) 823.
[18] G. Steiner, A. Krajete, H. Kopacka, K.-H. Ongania, K. Wurst, P. Preishuber-Pflügl, B. Bildstein, Eur. J. Inorg. Chem. (2004) 2827.
[19] T. Ishida, M. Doi, H. Ueda, M. Inoue, G.M. Sheldrick, J. Am. Chem. Soc. 110 (1988) 2286.
[20] N. Kuhn, M. Walker, M. Steinmann, Z. Naturforsch. 57b (2002) 248.
[21] (a) D. Nemcsok, K. Wichmann, G. Frenking, Organometallics 23 (2004) 3640;
(b) X. Hu, I. Castro-Rodriguez, K. Olsen, K. Meyer, Organometallics 23 (2004) 755;
(c) X. Hu, Y. Tang, P. Gantzel, K. Meyer, Organometallics 22 (2003) 612.
[22] T. Ramnial, C.D. Abernethy, M.D. Spicer, I.D. McKenzie, I.D. Gay, J.A.C. Clyburne, Inorg. Chem. 42 (2003) 1391.
[23] (a) K.M. Lee, H.M.J. Wang, I.J.B. Lin, J. Chem. Soc., Dalton Trans. (2002) 2852;
(b) S.K. Schneider, W.A. Herrmann, E. Herdtweck, Z. Anorg. Allg. Chem. 629 (2003) 2363.
[24] A.J. Arduengo III, H.V.R. Dias, J.C. Calabrese, F. Davidson, Organometallics 12 (1993) 3405.
[25] SADABS, Bruker AXS Inc., Madison, WI, USA, 2003.
[26] G. M. Sheldrick, SHELXS-97 and SHELXL-97, Programs for the Solution and Refinement of Crystal Structures, University of Göttingen, 1997.

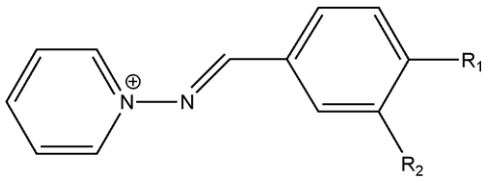

R_1	R_2	Abbreviation
NO_2	H	p-NO_2Bz-1-APy
CH_3	H	p-CH_3Bz-1-APy
Br	H	p-BrBz-1-APy
Cl	H	p-ClBz-1-APy
H	NO_2	m-NO_2Bz-1-APy

Scheme 1. Structures of cations in salts **1**–**5**.

absorption in the 750–1000 nm region, while **1** exhibits intense absorption from the UV/Visible to near-IR regions (200–1100 nm).

2. Experimental

2.1. Chemicals and reagents

All reagents and chemicals were purchased from commercial sources and used without further purification.

2.2. Physical measurements

Elemental analyses were performed with an Elementar Vario EL III analytic instrument. IR spectra were recorded on a Bruker Vector 22 Fourier Transform Infrared Spectrometer (170SX) (KBr disc). ^{1}H NMR spectra were carried out with an AVANCE AV-300 NMR spectrometer and the chemical shifts were measured relative to the TMS signal. UV–Vis absorption spectra in the solid state and solution were taken using a Cary 5000 UV–Vis–NIR and a Lambda 35 UV/Vis spectrophotometer, respectively.

2.3. Preparations for ***1–5***

2.3.1. Materials

Disodium maleonitriledithiolate (Na_2mnt)[14] and 1-aminopyridinium iodide ([1-APy]I) [15] were synthesized following the respective published procedures. The Schiff base derivatives, [RBz-1-Apy]I, were prepared employing a similar procedure described in the literature [16].

2.3.2. [p-NO_2Bz-1-Apy]$_2$[Ni(mnt)$_2$] (***1***)

Na_2mnt (456 mg, 2.5 mmol) and $NiCl_2 \cdot 6H_2O$ (297 mg, 1.25 mmol) were mixed under stirring in MeOH (30 mL) at room temperature. Subsequently, a solution of [*p*-NO_2Bz-1-Apy]I (887 mg, 2.5 mmol) in MeOH (15 mL) was added to the mixture, and the brown precipitate that was immediately formed was filtered off, and washed with MeOH. The crude product was recrystallized in acetone (20 mL) to give dark-brown crystals. Yield: 76%. *Anal.* Calc. for $C_{32}H_{20}N_{10}O_4S_4Ni$: C, 48.31; H, 2.54; N, 17.61. Found: C, 48.76; H, 2.66; N, 17.93%. IR spectrum (KBr, cm^{-1}): 2192.6 (s) for $\nu_{C\equiv N}$ and 1480.7 (s) for $\nu_{C=C}$ of mnt^{2-}, 1628. 7 (m) for $\nu_{C=N}$ of Schiff base, and 1343.3 (s) for ν_{-NO_2}. 1H NMR (300 MHz and acetone-d_6): δ 9.77 (s, 1H, –N=CH–), 9.56–9.53 (d, 2H, pyridyl), 8.86–8.80 (t, 1H, pyridyl), 8.54–8.40 (m, 6H, phenyl and pyridyl).

The similar procedures were used to prepare the complexes **2–5**.

2.3.3. [p-BrBz-1-Apy]$_2$[Ni(mnt)$_2$] (***2***)

Dark-brown color and yield: 73%. *Anal.* Calc. for $C_{32}H_{20}N_8Br_2S_4Ni$: C, 44.52; H, 2.34; N, 12.98. Found: C, 44.58; H, 2.21; N, 13.26%. IR spectrum (KBr, cm^{-1}): 2194.5 (s), 2213.7 (sh) for $\nu_{C\equiv N}$ and 1472.9 (s) for $\nu_{C=C}$ of mnt^{2-}, 1624.4 (s) for $\nu_{C=N}$ of Schiff base. ^{1}H NMR (300 MHz and acetone-d_6): δ 9.50 (s, 1H, –N=CH–), 9.48–9.45 (d, 2H, pyridyl), 8.86–8.80 (t, 1H, pyridyl), 8.47–8.42 (t, 2H, pyridyl), 8.09–8.06 (d, 2H, phenyl), 7.89–7.85 (d, 2H, phenyl).

2.3.4. [p-ClBz-1-Apy]$_2$[Ni(mnt)$_2$] (***3***)

Dark-brown color and yield: 75%. *Anal.* Calc. for $C_{32}H_{20}Cl_2N_8S_4Ni$: C, 49.63; H, 2.60; N, 14.47. Found: C, 49.96; H, 2.54; N, 14.76%. IR spectrum (KBr, cm^{-1}): 2195.2 (s) and 2213.2 (sh) for $\nu_{C\equiv N}$ and 1475.9 (s) for $\nu_{C=C}$ of mnt^{2-}, 1626.4 (m) for $\nu_{C=N}$ of Schiff base. ^{1}H NMR (300 MHz and acetone-d_6): δ 9.52 (s, 1H, –N=CH–), 9.50–9.45 (d, 2H, pyridyl), 8.85–8.78 (t, 1H, pyridyl), 8.46–8.40 (t, 2H, pyridyl), 8.18–8.10 (d, 2H, phenyl), 7.72–7.67 (d, 2H, phenyl).

2.3.5. [p-MeBz-1-Apy]$_2$[Ni(mnt)$_2$] (***4***)

Dark-brown color and yield: 79%. *Anal.* Calc. for $C_{34}H_{26}N_8S_4Ni$: C, 55.66; H, 3.58; N, 15.28. Found: C, 55.83; H, 3.51; N, 15.49%. IR spectrum (KBr, cm^{-1}): 2195.1 (s), 2212.2 (sh) for $\nu_{C\equiv N}$ and 1475.5 (s), 1486.4 (m) for $\nu_{C=C}$ of mnt^{2-}, 1620.2 (m) for $\nu_{C=N}$ of Schiff base. ^{1}H NMR (300 MHz and acetone-d_6): δ 9.39 (s, 1H, –N=CH–), 9.43–9.41 (d, 2H, pyridyl), 8.83–8.77 (t, 1H, pyridyl), 8.45–8.40 (t, 2H, pyridyl), 8.02–7.969 (d, 2H, phenyl), 7.49–7.46 (d, 2H, phenyl), 2.48 (s, 3H, –CH_3).

2.3.6. [m-NO_2Bz-1-Apy]$_2$[Ni(mnt)$_2$] (5)

Dark-brown color and yield: 69%. *Anal.* Calc. for $C_{32}H_{20}N_{10}O_4S_4Ni$: C, 48.31; H, 2.54; N, 17.61. Found: C, 48.23; H, 2.30; N, 18.00%. IR spectrum (KBr, cm^{-1}): 2191.9 (s), 2210.8 (sh) for $\nu_{C\equiv N}$ and 1475.2 (s) for $\nu_{C=C}$ of mnt^{2-}, 1625.8 (m) for $\nu_{C=N}$ of Schiff base and 1355.3 (s) for ν_{-NO_2}. 1H NMR (300 MHz and acetone-d_6): δ 9.76 (s, 1H, –N=CH–), 9.56–9.54 (d, 2H, pyridyl), 8.92 (s, 1H, phenyl), 8.88–8.82 (t, 1H, pyridyl), 8.62–8.58 (t, 2H, pyridyl), 8.50–8.45 (m, 2H, phenyl), 8.01–7.96 (t, 1H, phenyl).

The single crystals of **1**–**5** suitable for X-ray analysis were obtained by diffusing diethyl ether into the solution of the corresponding [RBz-1-Apy]$_2$[Ni(mnt)$_2$] compound in acetone for 7–10 days.

2.4. X-ray crystallography

The diffraction data for **1**–**5** were collected at 296K with graphite-monochromated Mo Kα (λ = 0.71073 Å) on a CCD area detector (Bruker-SMART). Data reductions and absorption corrections were performed with the SAINT and SADABS software packages, respectively [17]. Structures were solved by the direct method and refined by the full-matrix least-squares procedure on F^2 using SHELXL-97 program [18]. All non-hydrogen atoms were refined anisotropically, and the hydrogen atoms were introduced at calculated positions. The crystallographic details about data collection and structure refinement are summarized in Table 1.

2.5. DFT calculation details

All calculations were carried out with the GAUSSIAN98 program [19] by density functional theory (DFT) and time-dependent DFT (TDDFT). Becke's three-parameter functional [20] combined with Lee-Yang-Parr's correlation functional [21,22] (B3LYP) and 6-31+G(d,p) [23] basis set were employed for the molecular geometric optimizations for the five [RBz-1-Apy]$^+$ cations as well as

Table 1
Crystal and structural refinement data of **1**–**5**

Compound	**1**	**2**	**3**	**4**	**5**
Chemical formula	$C_{32}H_{20}N_{10}O_4S_4Ni$	$C_{32}H_{20}N_8Br_2S_4Ni$	$C_{32}H_{20}N_8Cl_2S_4Ni$	$C_{34}H_{26}N_8S_4Ni$	$C_{32}H_{20}N_{10}O_4S_4Ni$
CCDC No.	675156	675159	675158	675157	675160
Formula weight	795.53	863.33	774.41	733.58	795.53
Temperature (K)	296(2)	296(2)	296(2)	296(2)	296(2)
Wavelength (Å)	0.7107	0.7107	0.7107	0.7107	0.7107
Crystal system	monoclinic	monoclinic	triclinic	monoclinic	monoclinic
Space group	$P2_1/n$	$P2_1/n$	$P\bar{1}$	$P2_1/n$	$P2_1/n$
a (Å)	14.0617(12)	9.6824(18)	7.5422(9)	9.4530(8)	13.6126(17)
b (Å)	13.2431(11)	16.111(3)	10.5043(12)	6.8680(6)	6.9530(9)
c (Å)	18.9457(15)	21.799(4)	11.3160(13)	26.201(2)	18.914(2)
α (°)	90	90	70.9870(10)	90	90
β (°)	103.6620(10)	95.653(3)	83.741(2)	91.0530(10)	104.839(2)
γ (°)	90	90	82.064(2)	90	90
V(Å^3) (Z)	3428.3(5)/4	3384.0(11)/4	837.52(17)/1	1700.7(3)/2	1730.5(4)/2
Density (g cm^{-3})	1.541	1.695	1.535	1.432	1.527
Abs coeff. (mm^{-1})	0.864	3.219	1.026	0.854	0.856
$F(000)$	1624	17200	394	756	812
Data collect θ range	1.63–25.09	1.57–25.50	1.91–25.08	1.55–25.50	1.66–25.50
Index range	$-16 \leqslant h \leqslant 15$ $-15 \leqslant k \leqslant 15$ $-17 \leqslant l \leqslant 22$	$-11 \leqslant h \leqslant 11$ $-19 \leqslant k \leqslant 17$ $-26 \leqslant l \leqslant 24$	$-7 \leqslant h \leqslant 8$ $-12 \leqslant k \leqslant 12$ $-13 \leqslant l \leqslant 13$	$-11 \leqslant h \leqslant 11$ $-8 \leqslant k \leqslant 8$ $-31 \leqslant l \leqslant 22$	$-16 \leqslant h \leqslant 16$ $-8 \leqslant k \leqslant 6$ $-18 \leqslant l \leqslant 22$
Reflns collected	16754	17394	4237	8380	8661
Independent reflns	6079	6275	2932	3139	3222
R_{int}	0.0222	0.1029	0.0159	0.0206	0.093
Refinement method on F^2	Full-matrix least-squares				
Data/restraints/parameters	6079/0/461	6275/0/424	2932/0/214	3139/0/215	3222/0/232
Goodness-of-fit on F^2	1.05	0.869	1.053	1.032	0.867
Final R indices [$I > 2\delta(I)$]	$R_1 = 0.0307$, $wR_2 = 0.0855$	$R_1 = 0.0459$, $wR_2 = 0.0789$	$R_1 = 0.0331$, $wR_2 = 0.0941$	$R_1 = 0.0344$, $wR_2 = 0.0924$	$R_1 = 0.0412$, $wR_2 = 0.0931$
R indices (all data)	$R_1 = 0.0378$, $wR_2 = 0.0896$	$R_1 = 1.1066$, $wR_2 = 0.0873$	$R_1 = 0.0396$, $wR_2 = 0.0986$	$R_1 = 0.0444$, $wR_2 = 0.0972$	$R_1 = 0.0675$, $wR_2 = 0.1026$
Residual (e Å^{-3})	0.341 and −0.262	0.548 and −0.405	0.313 and −0.251	0.456 and −0.183	0.459 and −0.273

$R_1 = \sum(||F_o| - |F_c||)/\sum|F_o|$, $wR_2 = \sum w(|F_o|^2 - |F_c|^2)^2/\sum w\,(|F_o|^2)^2]^{1/2}$.

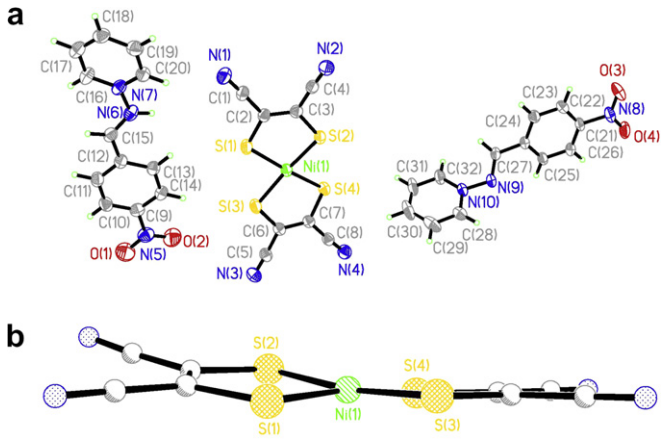

Fig. 1. (a) ORTEP view of **1** with thermal ellipsoids at the 30% probability level; (b) the molecular configuration shows a distorted anionic geometry.

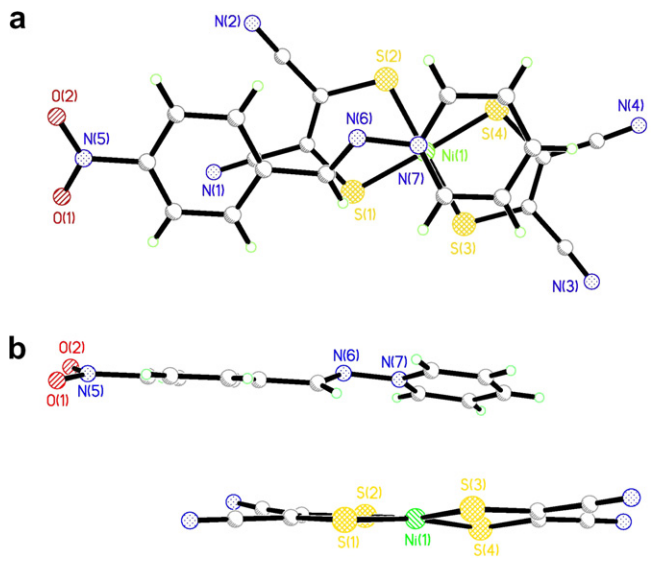

Fig. 2. The arrangement between adjacent anion and cation (a) top view and (b) side view in the crystal of **1**.

TDDFT calculations for the [*p*-NO_2Bz-1-Apy]$^+$ cation; the geometric optimization for the $[Ni(mnt)_2]^{2-}$ anion was performed at B3LYP level, and 6-31+G(d,p) basis set were employed for C, N and S atoms, while LANL2DZ [24] basis set for Ni atom. The TDDFT calculations for the $[Ni(mnt)_2]^{2-}$ anion were carried out at BPW91/LANL2DZ level. The lowest 20 singlet-singlet transitions were computed by TDDFT calculations for both the $[Ni(mnt)_2]^{2-}$ anion and the [*p*-NO_2Bz-1-Apy]$^+$ cation.

3. Results and discussion

3.1. Description of crystal structures

[*p*-NO_2Bz-1-Apy]$_2$[Ni(mnt)$_2$] (1): Complex **1** crystallizes in monoclinic system with $P2_1/n$ space group, as shown in Fig. 1a, an asymmetric unit consists of one $[Ni(mnt)_2]^{2-}$ anion and two [*p*-NO_2Bz-1-Apy]$^+$ cations. The bond lengths and angles in two crystallographically nonequivalent cations are comparable to each other, whereas the interplanar angles are very different between the pyridine and benzene rings (14.99(10)° and 72.24(6)°, respectively). For the $[Ni(mnt)_2]^{2-}$ anion, the Ni-S lengths range from 2.1666(6) to 2.1758(6) Å, and two S–Ni–S bite angles have the same magnitude of 92.52(2)°, these bonding parameters are comparable to the reported values [25]; of particular note is the large deviation from the square-planar environment around the Ni atom, as demonstrated in Fig. 1b, with the dihedral angle between the S1–Ni–S2 and S3–Ni–S4 mean planes being 10.99(6)°. In most

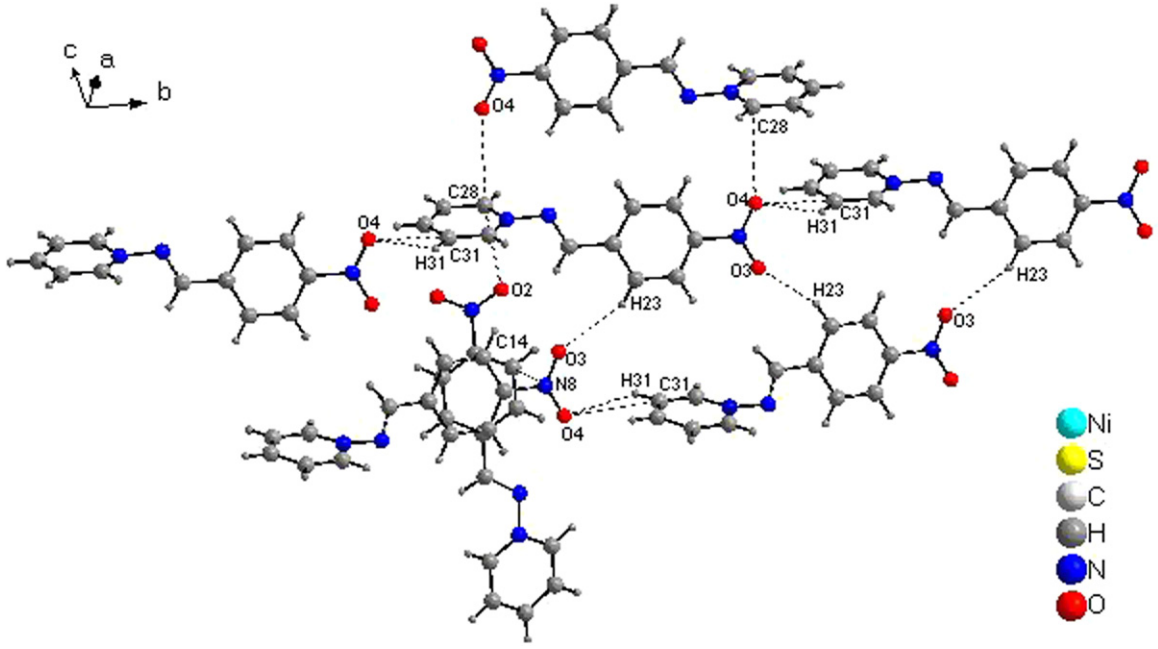

Fig. 3. Schematic represents the shorter interatomic contacts between the adjacent cations in crystal of **1**.

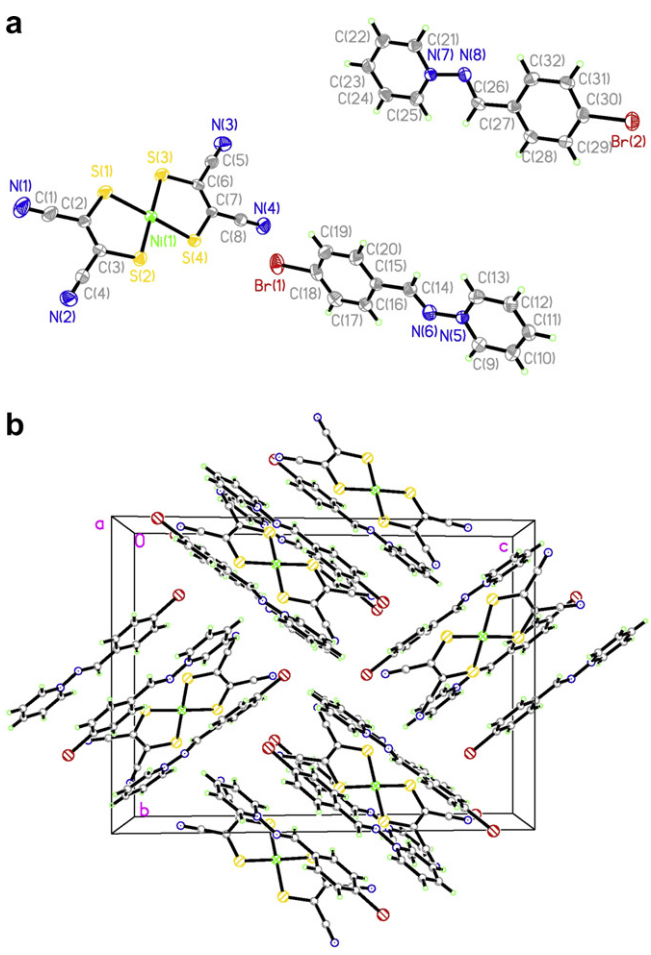

Fig. 4. (a) ORTEP drawing (with thermal ellipsoids at the 30% probability level) and (b) the packing diagram show no close packing interaction in the crystal for **2**.

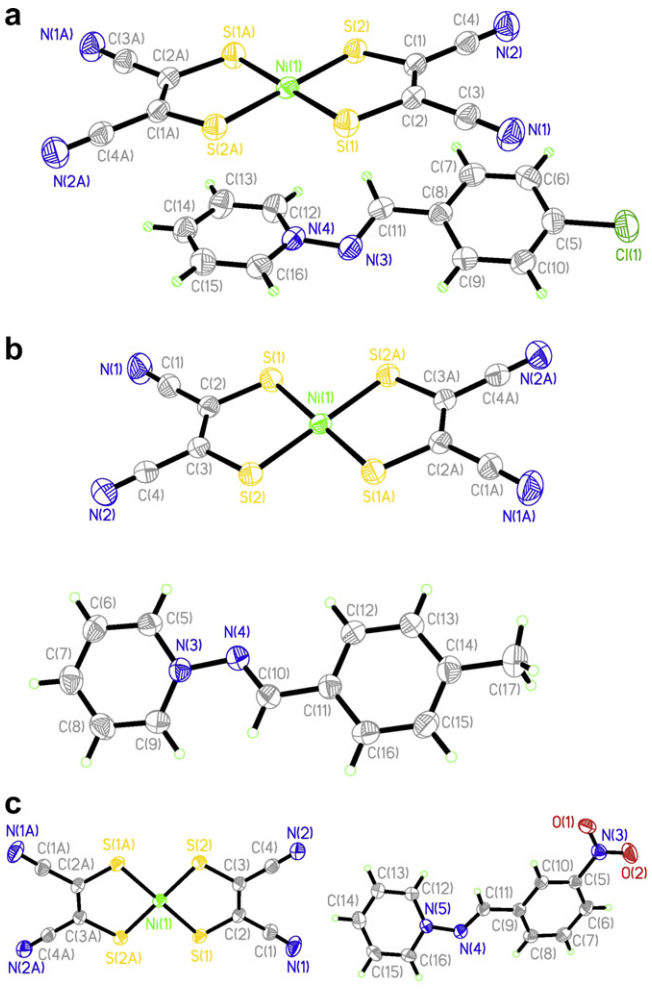

Fig. 5. Molecular structures for complexes (a) **3** (b) **4** and (c) **5**, respectively.

Table 2
Selected bonding lengths (Å) and angles (°) in the anions as well as the dihedral angles (ϕ(Py–Ph)/°) between the pyridine and benzene rings in the cations for **1**–**5**

Compound ***1***					
Ni1–S1	2.1760(6)	S3–Ni1–S4	92.51(2)	S4–Ni1–S1	172.67(2)
Ni1–S2	2.1710(6)	S3–Ni1–S2	172.16(2)	S2–Ni1–S1	92.52(2)
Ni1–S3	2.1670(6)	S4–Ni1–S2	87.56(2)	[a]ϕ(Py–Ph)1	14.99(10)
Ni1–S4	2.1689(6)	S3–Ni1–S1	88.41(2)	[a]ϕ(Py–Ph)2	72.24(6)
Compound ***2***					
Ni1–S3	2.1645(14)	S3–Ni1–S1	87.32(5)	S1–Ni1–S4	177.46(6)
Ni1–S1	2.1657(13)	S3–Ni1–S2	177.38(6)	S2–Ni1–S4	88.24(5)
Ni1–S2	2.1696(14)	S1–Ni1–S2	92.09(5)	[a]ϕ (Py–Ph)1	2.91(24)
Ni1–S4	2.1703(13)	S3–Ni1–S4	92.46(5)	[a]ϕ (Py–Ph)2	4.65(22)
Compound ***3***					
Ni1–S1	2.1632(7)	S1–Ni1–S2	92.07(2)	ϕ (Py–Ph)	21.29(13)
Ni1–S2	2.1744(7)	S1–Ni1–S2 (2 − *x*, 1 − *y*, 1 − *z*)	87.93(2)		
Compound ***4***					
Ni1–S1	2.1614(3)	S1–Ni1–S2	92.356(10)	ϕ (Py–Ph)	12.45(3)
Ni1–S2	2.1719(3)	S1–Ni1–S2 (2 − *x*, 2 − *y*, −*z*)	87.644(10)		
Compound ***5***					
Ni1–S1	2.1650(7)	S1–Ni1–S2	92.17(3)	ϕ (Py–Ph)	34.35(7)
Ni1–S2	2.1766(8)	S1–Ni1–S2 (2 − *x*, 1 − *y*, −*z*)	87.83(3)		

[a] The dihedral angles between the benzene and pyridine ring in two crystallographically independent cations for complexes **1** and **2**.

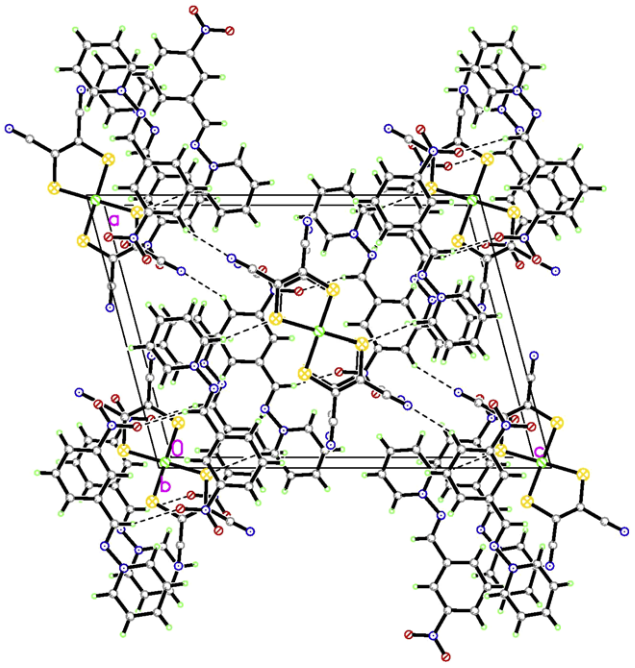

Fig. 6. Packing diagram for **5** which shows approximately separated stacks of the cations and anions along the direction of crystallographic *b*-axis.

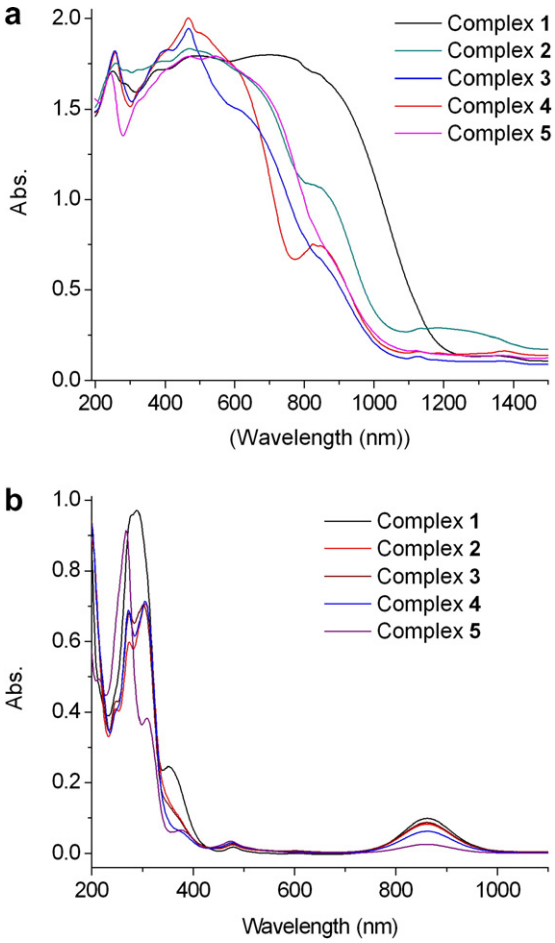

Fig. 7. (a) Diffuse reflectance spectra in solid states and (b) absorbance spectra in acetonitrile solutions for complexes **1**–**5** (with $c = 5.0 \times 10^{-6}$ mol L^{-1} for each complex).

cases, the transition metal ion in a bis(1,2-dithiolato)metal complex favors a planar coordination environment. However, the distorted square planar coordination geometry around a metal centre has also been observed [26,27]. For example, in the cases of the metal centre being Mn^{2+}, Fe^{3+} or Co^{2+} ions in the complexes $[RBzPy]_2[Fe_2(mnt)_4]$ [28], $[Bu_4N]_2[Fe_2(mnt)_4]$ [29], $[Bu_4N]_2[Fe_2(edt)_4]$ [30], $[Et_4N]_2[Mn_2(edt)_4]$ [31], $Co_2[S_2C_2(CF_3)_2]$ [32] and $[Bu_4N]_2[Co_2(S_2C_6Cl_4)_4]$ [33], the deviation from planarity is mainly caused by dimerization via M···S interactions. For bis(1,2-dithiolato)cuprate(II) complexes, notably, there are a few cases of a significantly non-planar environment around a tetra-coordinate Cu^{2+} centre resulting from the weakly intermolecular interactions between the cation and anion [13a,34]. Theoretical investigation for the $[Cu(mnt)_2]^{2-}$ complex further disclosed that the energy gap between distorted and perfect square-planar coordination geometry is not much higher than the values of the crystal packing forces. As a result, the configuration preference for the $[Cu(mnt)_2]^{2-}$ complexes will be controlled by the combination of a variety of intermolecular interactions [35]. For the bis(1,2-dithiolato)nickelate(II) species, reports of significant non-planar environment

Table 3
Optical properties of complexes **1**–**5** ($c = 5.0 \times 10^{-6}$ mol L^{-1}) in acetonitrile

λ_{max} (nm) (ε (M^{-1} cm^{-1}))					
Compound ***1***					
246 (90800)	278 (191260)	289 (194194)	353 (51080)	479 (3678)	862 (19698)
Compound ***2***					
248 (81916)	274 (119674)	305 (141358)	367 (22442)	478 (4982)	862 (16692)
Compound ***3***					
248 (86172)	275 (136238)	301 (140698)	366 (21670)	478 (5282)	863 (17418)
Compound ***4***					
248 (80822)	273 (137686)	305 (142830)	382 (11360)	477 (6084)	863 (12690)
Compound ***5***					
214 (98854)	268 (182790)	308 (76428)	374 (13336)	474 (6920)	862 (5218)

around a tetra-coordinate Ni^{2+} ion are very rare, only eight complexes having dihedral angle more than 10° between the mean planes of two S–Ni–S chelate rings have been reported to the best of our knowledge [36] (the corresponding analyses of crystal structures retrieved from the Cambridge Structural Database (CCDC, conquest version 1.3, August, 2007)) [37]. To better understand why there are distortions in the Ni^{2+} coordination environment, we performed the geometry optimization for the $[Ni(mnt)_2]^{2-}$ ion in DFT theoretical framework, and the results revealed that square-planar geometry is the more stable configuration (optimization geometry see Fig. S1). Meanwhile, we inspected the molecular packing and found two notable points: (1) as demonstrated in Fig. 2, there exist close packing interactions between the anion and the cation containing O1 atom, the pyridine ring is almost parallel to the mean plane of the anionic moiety Ni1/S3/S4/C5/C6/C7/C8/N3/N4 with a dihedral angle of 0.54(7)°, the benzene ring makes a dihedral angle of 7.92(8)° with the anionic moiety of Ni1/S1/S2/C1/C2/C3/C4/N1/N2, and the shortest interatomic distance is only 3.394(3) Å for C2···C15; (2) there exist some shorter interatomic separations between the adjacent cations (see Fig. 3), such as N8···C14($1 + x$, $1 + y$, z) = 3.187(3) Å, O2···C28 ($0.5 - x$, $-0.5 + y$, $1.5 - z$) = 3.159(3) Å, O3···H23 ($1.5 - x$, $0.5 + y$, $1.5 - z$) = 2.6354 Å, O4···C31 ($2 - x$, $2 - y$, $2 - z$) = 3.193(3) Å and O4···H31 ($2 - x$, $2 - y$, $2 - z$) = 2.4841 Å, respectively. Therefore, we might conclude that the deviation from planarity for the $[Ni(mnt)_2]^{2-}$ anion in **1** is mainly arisen from intermolecular packing interactions.

Crystal of **2** belongs to monoclinic system with space group $P2_1/n$, and an asymmetric unit contains an anion and two crystallographically independent cations (Fig. 4a), which is similar to **1**. The Ni–S bond lengths and S–Ni–S bite angles are comparable to those in **1**. The crystal structure distinctions from **1** concern three aspects: (1) the $[Ni(mnt)_2]^{2-}$ anion exhibits perfect square-planar geometry; (2) two crystallographically independent [*p*-BrBz-1-Apy]$^+$ cations show almost planar molecular conformations with very similar dihedral angles between the pyridine and benzene rings (2.91(24)° and 4.65(22)°, respectively); (3) as shown in Fig. 4b, the anions and the cations show the slippage arrangement, therefore there is no close packing interactions between the anions and the cations.

Crystal of **3** belongs to triclinic system with space group $P\bar{1}$, and both complexes **4** and **5** crystallize in monoclinic system with space group $P2_1/n$. The molecular structures for **3–5** are displayed in Fig. 5, respectively, and the common structural feature for these three complexes is that an asymmetric unit is composed of one cation and one half of anion, and the Ni^{2+} ion locates at an inversion center. This leads to the Ni^{2+} ion possessing the perfect square-planar coordination environment; additionally, the cation shows a non-planar conformation in each complex. The bond lengths and angles in the $[Ni(mnt)_2]^{2-}$ anions are normal, and the selected bonding parameters for **3–5** are summarized in Table 2. The anions and cations arrange in a slippage fashion, as a consequence, no significant π···π stacking interactions between the anions and cations are observed in the crystals of **3–5** (see Fig. 6 as well as Figs. S3 and S4), which are analogous to **2** but distinct from **1**. It is noteworthy that the structural difference of the cation between **1** and **5** just concerns the position of NO_2 group in the benzene ring, whereas the fashions of the cations and anions are big difference, the slippage arrangement between anion and cation in **5** leads to the overlap of NO_2 group of benzene ring with mnt^{2-} moiety of $[Ni(mnt)_2]^{2-}$ anion, which gives rise to the shorter intermolecular contacts, 3.387(3) Å of C3···O1 ($1 + x$, y, z), 3.453(3) Å of C2···N3 ($1 + x$, y, z) and 3.444(3) Å of N1···C6 ($0.5 - x$, $0.5 + y$, $0.5 - z$).

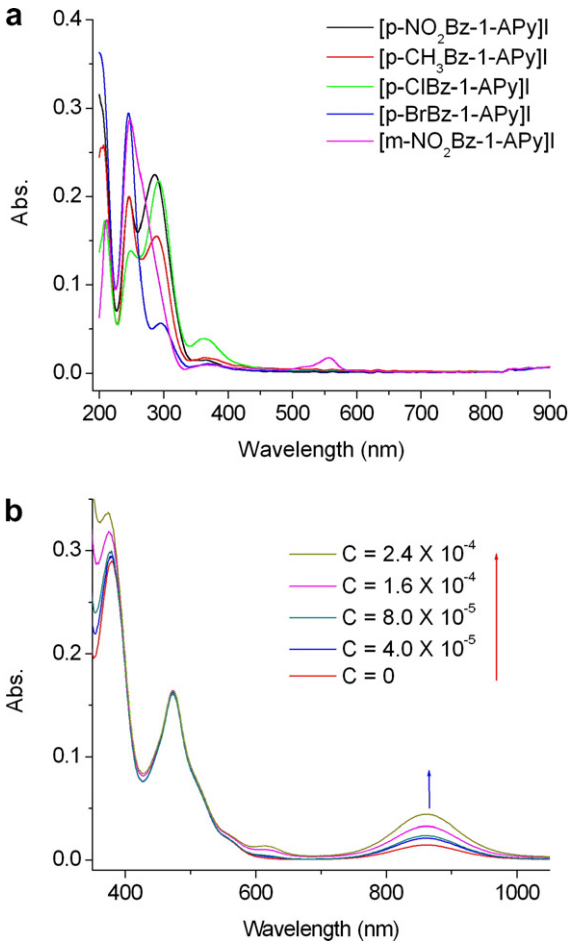

Fig. 8. Electronic absorption spectra in acetonitrile for (a) the compounds [RBz-1-Apy]I (b) $[Bu_4N]_2[Ni(mnt)_2]$ ($c = 5.0 \times 10^{-5}$ mol L^{-1}) with different concentration of [*p*-NO_2Bz-1-Apy]I (c = 0, 4.0×10^{-5}, 8.0×10^{-5}, 1.6×10^{-4} and 2.4×10^{-4} mol L^{-1}).

3.2. UV–Vis–NIR spectra

The UV–Vis–NIR spectra of **1–5** complexes for solids are shown in Fig. 7a. In the solid state, complexes **2–5** show the intense absorption in the UV/visible region (200–700 nm) with a moderately intense absorption band (centered at around 870 nm and the low energy absorption tail extend up to ca. 1000 nm) in the near-IR region. The spectral shape of **1** is strikingly different from the other four, in which a very strong absorption is observed from the UV/Visible to near-IR region and its low energy absorption tail extends up to ca. 1200 nm. Such different spectroscopic features between **1** and the other four complexes will be further discussed in the theoretic analysis section. The UV–Vis–NIR spectra of **1–5** in acetonitrile ($c = 5.0 \times 10^{-6}$ mol L^{-1}) are shown in Fig. 7b, and the absorption spectral properties are listed in Table 3. From these we can summarize: (1) the investigated complexes exhibit different spectral shape in the range of 200–400 nm, and a series of bands have high molar absorptions ($\varepsilon > 10^4$); (2) both the maxima position and the intensity are independent of the cation for the band centered at 473 nm; (3) the maxima position is almost independent of cation, whereas the intensity depends on the cation for the band centered at around 862 nm. A series of bands with high molar extinction coefficients in 200–400 nm region originate from the $\pi \rightarrow \pi^*$ transitions within the cation and anion. For a better understanding of the nature of two bands in the visible and near IR regions (473 and ~862 nm), the UV–Vis–NIR spectra for the corresponding iodide compounds ([RBz-1-Apy]I) of the cations in acetonitrile are presented in Fig. 8a, and the spectroscopic data are listed in Table 4. From Fig. 8a, it can be found that no absorption band appears in more than the 420 nm spectral region for [*p*-NO_2Bz-1-Apy]I, [*p*-BrBz-1-Apy]I, [*p*-ClBz-1-Apy]I and [*p*-CH_3Bz-1-Apy]I; while the compound, [*m*-NO_2Bz-1-Apy]I, possesses a weak

Table 4
Optical properties of compounds [RBz-1-Apy]I ($c = 1.0 \times 10^{-5}$ mol L^{-1}) in acetonitrile

λ_{max} (nm (ε (M^{-1} cm^{-1}))					
[*p*-NO_2Bz-1-Apy]I					
201 (32650)	205 (31680)	209 (28350)	246 (20760)	286 (22720)	366 (1499)
[*p*-BrBz-1-Apy]I					
	205 (39060)	210 (34470)	245 (33950)	296 (5870)	369 (1069)
[*p*-ClBz-1-Apy]I					
203 (15580)	207 (17710)	210 (29350)	248 (14160)	292 (22150)	364 (3908)
[*p*-CH_3Bz-1-Apy]I					
203 (26390)	206 (29330)	212 (22370)	246 (21190)	287 (15820)	363 (1791)
[*m*-NO_2Bz-1-Apy]I					
	205 (12990)	211 (20450)	247 (29760)	291 (10800)	370 (931)

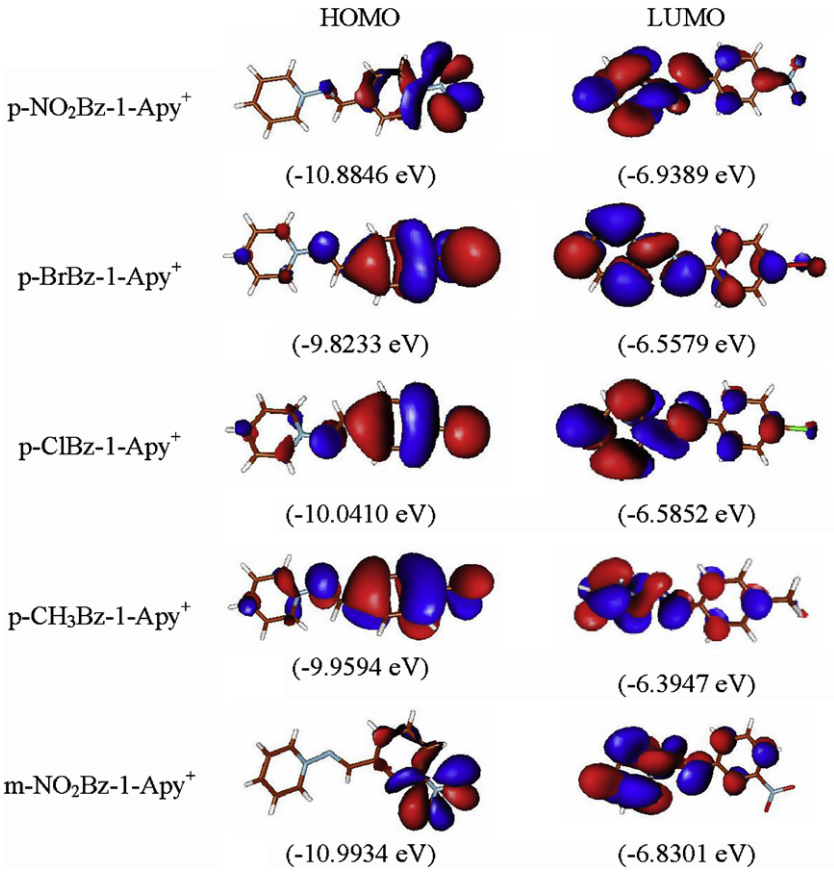

Fig. 9. The frontier orbitals and the corresponding energy levels of RBz-1-Apy^+ cations.

Table 5
Main calculated transitions for the $[Ni(mnt)_2]^{2-}$ anion and the five cations

Transition	Coeff	*E*/eV (nm)	Oscillator	Assignment
p-NO_2Bz-1-Apy$^+$ cation				
HOMO − 1 → LUMO	0.67518	3.5010 (354)	0.0252	$\pi \rightarrow \pi^*$
HOMO − 5 → LUMO	0.35860	4.4958 (276)	0.3379	$\pi \rightarrow \pi^*$
HOMO − 2 → LUMO + 1	0.54836			
HOMO − 7 → LUMO	0.12932	4.8249 (257)	0.0195	$\pi \rightarrow \pi^*$
HOMO − 6 → LUMO	0.14244			
HOMO − 5 → LUMO	0.40996			
HOMO − 5 → LUMO + 1	0.14952			
HOMO − 2 → LUMO + 1	−0.25066			
HOMO − 2 → LUMO + 2	−0.30124			
HOMO − 1 → LUMO + 2	−0.10610			
HOMO → LUMO + 2	−0.16392			
HOMO − 6 → LUMO	0.50367	5.1875(239)	0.0264	$\pi \rightarrow \pi^*$
HOMO − 5 → LUMO	0.11033			
HOMO − 5 → LUMO + 2	−0.23402			
HOMO − 3 → LUMO + 1	−0.10216			
HOMO − 3 → LUMO + 2	0.25423			
HOMO − 3 → LUMO + 3	−0.14382			
HOMO − 2 → LUMO + 2	0.19742			
HOMO − 4 → LUMO + 2	−0.26100	5.3468 (232)	0.0131	$\pi \rightarrow \pi^*$
HOMO − 4 → LUMO + 3	−0.14906			
HOMO − 1 → LUMO + 3	0.61903			
p-BrBz-1-Apy$^+$ cation				
HOMO → LUMO	0.66994	2.9512 (420)	0.3401	$\pi \rightarrow \pi^*$
HOMO − 4 → LUMO	0.14432	4.0360 (307)	0.4033	$\pi \rightarrow \pi^*$
HOMO → LUMO + 1	0.52755			
HOMO → LUMO + 2	−0.36934			
HOMO − 5 → LUMO	0.67140	4.4849 (276)	0.1526	$\pi \rightarrow \pi^*$
HOMO − 6 → LUMO	0.52312	5.1244 (242)	0.0183	$\pi \rightarrow \pi^*$
HOMO − 4 → LUMO + 1	0.15483			
HOMO − 4 → LUMO + 2	0.19186			
HOMO − 3 → LUMO + 1	−0.22022			
HOMO − 3 → LUMO + 2	−0.28258			
HOMO − 3 → LUMO + 1	−0.12451	5.3212 (233)	0.0577	$\pi \rightarrow \pi^*$
HOMO − 1 → LUMO + 1	−0.15866			
HOMO − 1 → LUMO + 5	−0.16066			
HOMO → LUMO + 3	0.60899			
HOMO − 6 → LUMO	0.11982	5.5813 (222)	0.0163	$\pi \rightarrow \pi^*$
HOMO − 4 → LUMO	0.11671			
HOMO − 4 → LUMO + 1	−0.19485			
HOMO − 4 → LUMO + 2	0.15854			
HOMO − 3 → LUMO + 1	0.47111			
HOMO − 3 → LUMO + 2	−0.31167			
HOMO → LUMO + 3	0.10947			
HOMO − 8 → LUMO	0.10442	5.6932 (217)	0.1047	$\pi \rightarrow \pi^*$
HOMO − 4 → LUMO + 1	0.54255			
HOMO − 4 → LUMO + 2	−0.22721			
HOMO − 3 → LUMO + 1	0.20406			
HOMO − 3 → LUMO + 2	−0.19224			
p-ClBz-1-Apy$^+$ cation				
HOMO → LUMO	0.66783	3.1217 (397)	0.3391	$\pi \rightarrow \pi^*$
HOMO → LUMO + 1	−0.10043			
HOMO − 4 → LUMO	0.13604	4.2161 (294)	0.4602	$\pi \rightarrow \pi^*$
HOMO − 3 → LUMO	−0.14752			
HOMO → LUMO + 1	0.48485			
HOMO → LUMO + 2	−0.39045			
HOMO − 1 → LUMO + 1	0.61237	4.4987 (276)	0.0236	$\pi \rightarrow \pi^*$
HOMO − 1 → LUMO + 2	−0.23846			
HOMO → LUMO + 3	0.22008			
HOMO − 4 → LUMO	−0.21398	4.7331 (262)	0.0366	$\pi \rightarrow \pi^*$
HOMO − 3 → LUMO	0.56442			
HOMO − 3 → LUMO + 1	0.11744			
HOMO → LUMO + 1	0.11486			
HOMO − 5 → LUMO	0.12689	5.0318 (246)	0.0337	$\pi \rightarrow \pi^*$
HOMO − 4 → LUMO	0.58647			
HOMO − 3 → LUMO	0.30239			
HOMO − 5 → LUMO	0.53893	5.1718 (240)	0.0261	$\pi \rightarrow \pi^*$
HOMO − 4 → LUMO	−0.11465			
HOMO − 4 → LUMO + 2	0.10004			
HOMO − 3 → LUMO + 1	−0.24172			
HOMO − 3 → LUMO + 2	−0.26576			
HOMO − 3 → LUMO + 1	−0.16226	5.5274 (224)	0.0972	$\pi \rightarrow \pi^*$
HOMO − 1 → LUMO + 1	−0.13516			
HOMO − 1 → LUMO + 5	−0.21049			
HOMO → LUMO + 3	0.58320			

Table 5 (*continued*)

Transition	Coeff	*E*/eV (nm)	Oscillator	Assignment
HOMO − 5 → LUMO	0.24957	5.8668 (211)	0.0366	$\pi \rightarrow \pi^*$
HOMO − 5 → LUMO + 1	0.27536			
HOMO − 5 → LUMO + 2	−0.23177			
HOMO − 4 → LUMO	−0.12440			
HOMO − 4 → LUMO + 1	−0.24205			
HOMO − 3 → LUMO + 1	0.14971			
HOMO − 3 → LUMO + 2	0.42649			
p-CH_3Bz-1-Apy$^+$ cation				
HOMO → LUMO	0.66394	3.1695 (391)	0.3071	$\pi \rightarrow \pi^*$
HOMO − 1 → LUMO	0.68726	3.3833 (366)	0.0366	$\pi \rightarrow \pi^*$
HOMO − 2 → LUMO	−0.19469	4.3069 (288)	0.2485	$\pi \rightarrow \pi^*$
HOMO − 1 → LUMO + 1	−0.19667			
HOMO − 1 → LUMO + 2	−0.31554			
HOMO → LUMO+1	0.12404			
HOMO → LUMO + 2	0.49973			
HOMO − 2 → LUMO	−0.22205	4.4053 (281)	0.2691	$\pi \rightarrow \pi^*$
HOMO − 1 → LUMO + 1	0.32387			
HOMO − 1 → LUMO + 2	0.44659			
HOMO → LUMO + 2	0.28124			
HOMO → LUMO + 3	0.16393			
HOMO − 3 → LUMO	0.54529	5.1895 (239)	0.0240	$\pi \rightarrow \pi^*$
HOMO − 2 → LUMO + 1	−0.40455			
HOMO − 5 → LUMO	0.14870	5.4103 (229)	0.0417	$\pi \rightarrow \pi^*$
HOMO − 4 → LUMO	0.63904			
HOMO − 2 → LUMO	0.14463			
HOMO − 5 → LUMO + 2	−0.14107	5.6275 (220)	0.0623	$\pi \rightarrow \pi^*$
HOMO − 4 → LUMO + 2	−0.10703			
HOMO − 2 → LUMO	−0.12564			
HOMO − 2 → LUMO + 1	0.19376			
HOMO − 2 → LUMO + 2	0.57618			
HOMO − 1 → LUMO + 2	−0.12118	5.7941 (214)	0.0773	$\pi \rightarrow \pi^*$
HOMO − 1 → LUMO + 5	−0.26253			
HOMO − 1 → LUMO + 6	−0.11401			
HOMO → LUMO + 3	0.57610			
HOMO − 7 → LUMO	−0.22280	6.3716 (195)	0.1034	$\pi \rightarrow \pi^*$
HOMO − 5 → LUMO + 2	−0.10257			
HOMO − 4 → LUMO	−0.11528			
HOMO − 4 → LUMO + 1	0.14794			
HOMO − 4 → LUMO + 2	0.42816			
HOMO − 1 → LUMO + 3	−0.28868			
HOMO → LUMO + 5	−0.23778			
m-NO_2Bz-1-Apy$^+$ cation				
HOMO − 2 → LUMO	0.66779	3.7177 (333)	0.0083	$\pi \rightarrow \pi^*$
HOMO − 1 → LUMO	0.13371			
HOMO − 2 → LUMO	−0.13002	3.7267 (333)	0.3551	$\pi \rightarrow \pi^*$
HOMO − 1 → LUMO	0.65505			
HOMO − 1 → LUMO + 1	−0.10942			
HOMO − 4 → LUMO	0.69406	4.1745 (297)	0.0119	$\pi \rightarrow \pi^*$
HOMO − 2 → LUMO	−0.12395	4.4645 (278)	0.0467	$\pi \rightarrow \pi^*$
HOMO − 2 → LUMO + 1	0.49101			
HOMO − 2 → LUMO + 3	−0.12352			
HOMO − 1 → LUMO + 1	0.34917			
HOMO − 1 → LUMO + 3	0.26483			
HOMO − 6 → LUMO	−0.10706	4.6176 (269)	0.1820	$\pi \rightarrow \pi^*$
HOMO − 5 → LUMO	0.37939			
HOMO − 2 → LUMO + 1	0.30567			
HOMO − 1 → LUMO + 1	−0.39862			
HOMO − 1 → LUMO + 3	0.13284			
HOMO → LUMO + 1	0.11296			
HOMO − 7 → LUMO	−0.11678	4.8517 (256)	0.0678	$\pi \rightarrow \pi^*$
HOMO − 6 → LUMO	−0.10695			
HOMO − 5 → LUMO	0.39285			
HOMO − 5 → LUMO + 1	0.11267			
HOMO − 4 → LUMO + 1	−0.13360			
HOMO − 2 → LUMO + 1	−0.24449			
HOMO − 2 → LUMO + 3	−0.18613			
HOMO − 1 → LUMO + 1	0.26640			
HOMO − 1 → LUMO+2	−0.19164			
HOMO − 1 → LUMO + 3	0.14146			
HOMO − 4 → LUMO + 1	0.40887	5.0043 (248)	0.0217	$\pi \rightarrow \pi^*$
HOMO − 2 → LUMO + 1	−0.17088			
HOMO − 2 → LUMO + 2	0.27945			
HOMO − 2 → LUMO + 3	0.24592			
HOMO − 1 → LUMO + 3	0.35378			

(*continued on next page*)

Table 5 (*continued*)

Transition	Coeff	*E*/eV (nm)	Oscillator	Assignment
HOMO − 4 → LUMO + 1	−0.43415	5.0809 (244)	0.0288	π → π*
HOMO − 4 → LUMO + 3	0.14462			
HOMO − 2 → LUMO + 3	0.47305			
HOMO − 1 → LUMO + 3	0.14603			
HOMO − 5 → LUMO	−0.19567	5.1608 (240)	0.3855	π → π*
HOMO − 5 → LUMO + 1	−0.13020			
HOMO − 4 → LUMO + 1	−0.21656			
HOMO − 4 → LUMO + 3	0.10578			
HOMO − 2 → LUMO + 1	−0.11655			
HOMO − 2 → LUMO + 3	−0.29738			
HOMO − 1 → LUMO + 1	−0.17559			
HOMO − 1 → LUMO + 3	0.37426			
HOMO − 1 → LUMO + 4	−0.11584			
HOMO − 6 → LUMO	0.54197	5.2308 (237)	0.0529	π → π*
HOMO − 5 → LUMO + 1	−0.12275			
HOMO − 5 → LUMO + 2	−0.28212			
HOMO − 1 → LUMO + 2	−0.19438			
$[Ni(mnt)_2]^{2-}$ anion				
HOMO − 3 → LUMO + 1	0.15392	1.4979 (828)	0.0082	d-d + MLCT + π → π*
HOMO → LUMO + 2	0.65490			
HOMO − 4 → LUMO + 1	−0.16856	2.6828 (462)	0.0046	MLCT + π → π*
HOMO − 4 → LUMO + 2	−0.44567			
HOMO − 3 → LUMO + 2	0.50577			
HOMO − 8 → LUMO	0.41204	3.1539 (393)	0.0318	d-d + MLCT + π → π*
HOMO − 4 → LUMO + 2	0.42320			
HOMO − 3 → LUMO + 1	0.30580			

absorption band centered at 555 nm in the region of 420–900 nm, such a weak absorbance can be assigned to the IPCT transition from I^- to m-NO_2Bz-1-Apy$^+$ ions [12a–d]. Therefore, the two bands centered at 473 nm and ~862 nm in Fig. 7b might originate from the transition in $[Ni(mnt)_2]^{2-}$ or IPCT transition between the cation and the anion. Thus, we further investigated the influence of the concentration of the [*p*-NO_2Bz-1-Apy]$^+$ cation on the spectroscopic feature of the $[Ni(mnt)_2]^{2-}$ anion in acetonitrile (where the concentration of $(Bu_4N)_2[Ni(mnt)_2]$ is 5.0×10^{-5} mol L^{-1}), and the results are shown in Fig. 8b. As the concentration of [*p*-NO_2Bz-1-Apy]$^+$ cation increases, the intensity of the band at 473 nm does not change while the band at 862 nm obviously increases and the band becomes broadened. Accordingly, the band with maximum at 473 nm can be attributed to the intramolecular electronic transition in the $[Ni(mnt)_2]^{2-}$ anion, which is in agreement with the analysis in the literature [38]. In the UV–Vis–NIR spectrum of $(Bu_4N)_2[Ni(mnt)_2]$ in acetonitrile, the band at 862 nm was also observed with $\varepsilon = 289$, which was interpreted as a parity forbidden d–d type transition [38]. In our case, the observation that absorption intensity increases with higher concentration of cation demonstrates that the IPCT transition should also contribute to the broad and moderate band at 862 nm.

3.3. DFT and TDDFT analyses

The IPCT band position depends on the energy gap between the donor HOMO and the acceptor LUMO, as for complexes **1**–**5**, the donor ($[Ni(mnt)_2]^{2-}$ anion) are the same for each complex, therefore, only the energy level of the cationic LUMO affects the relative position of the IPCT band. Fig. 9 shows the Kohn-Sham frontier orbitals and their levels for each cation in complexes **1**–**5**. From this two conclusions can be drawn: (1) the cationic HOMO contributes mainly from the orbitals of the benzene molecule as well as the substituent group; (2) the cationic LUMO is essentially composed of the orbitals of the pyridine molecule, and the substituent group has a negligible contribution to the cationic LUMO. This finding implies the cationic features (electronic property, steric hindrance and so on) have minor influence on the LUMO orbitals of the investigated cations (the maximum energy difference is 0.5442 eV between *p*-NO_2Bz-1-Apy$^+$ and *p*-CH_3Bz-1-Apy$^+$ species). As a result, it can be understandable that IPCT band position (the broad near IR absorbance band) is almost independent of the substituent group feature in the benzene ring of cation in acetonitrile solution. TDDFT calculations were further performed for the five cations together with the $[Ni(mnt)_2]^{2-}$ anion, and the transition states, excitation energies, CI coefficients, and oscillator strengths are given in Table 5. For five cations, except for *p*-BrBz-1-Apy$^+$, the calculations disclosed that no absorption exists over 400 nm region, and these results are in agreement with the experimental spectra. The discrepancy between calculation and experiment spectra for *p*-BrBz-1-Apy$^+$ could be attributed to the poor asymptotic behavior of the exchange-correlation potential of the TD-DFT method [39]. And for the $[Ni(mnt)_2]^{2-}$ anion, the transitions HOMO → LUMO + 2 and HOMO − 3 → LUMO + 1 give rise to a modest absorption band at 827 nm. As illustrated in Fig. 10, the HOMO − 3 is mainly contributed from the d_{z^2} orbital of Ni^{2+} ion, and the HOMO and LUMO + 1 have largely the character of the π orbitals of mnt^{2-} ligands with small contributions from the $d_{x^2-y^2}$ orbital of Ni^{2+} ion. Contrastively, the LUMO + 2 is virtually a pure ligand orbital, so the lower frequency absorbance band (~862 nm in experimental absorbance spectra) can be assigned to combined transitions of partial forbidden d–d, allowed d–π* (MLCT in the

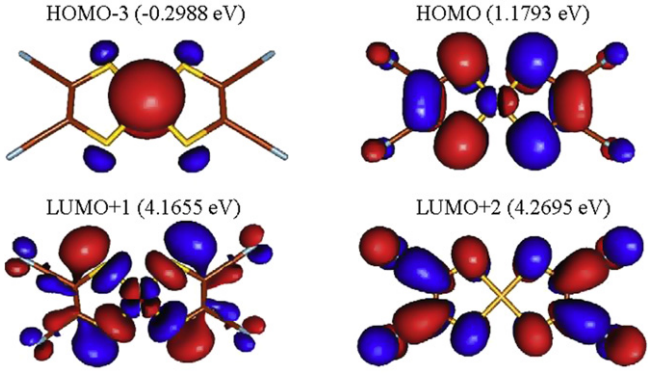

Fig. 10. The orbitals of the $[Ni(mnt)_2]^{2-}$ anion which are involved in the near-IR absorbance bands.

$[Ni(mnt)_2]^{2-}$ anion) and π–π^* (in the mnt^{2-} ligand) as well as the IPCT transition. And now, the observation could be well understood that the solid UV–Vis–NIR spectroscopic feature of **1** is different from those of the other four complexes in the low energy region, on the one hand, the very close packing interactions between the anions and the cations in **1** could broaden the low energy absorption band [40]; on the other hand, the geometric optimization indicates that the perfect planar molecular geometry is the most stable configuration for the $[Ni(mnt)_2]^{2-}$ anion. Thus, the heavy distortion of the anionic molecular geometry in **1** could raise the energy level of its HOMO, which gives rise to the IPCT band red-shift [11], and two factors mentioned above probably cause **1** having a more broaden band in the low energy region than those of other four complexes in the solid state.

4. Conclusions

We presented the UV–Vis–NIR spectra in both solid state and acetonitrile solution for five ion-pair complexes based on $[Ni(mnt)_2]^{2-}$ and the benzylidene-1-aminopyridinium derivatives. In the solid state, complexes **2**–**5** show similar spectral features, namely, the intense absorption in the UV/visible region with the moderate absorbance in the near IR region of 750–1000 nm, while complex **1** exhibits the intense absorbance from UV/visible to near IR region (200–1100 nm). Such a spectral feature makes this compound an excellent candidate as a near-IR dye for DSSC and Q-switching laser. The unique spectral property of **1** can be attributed to its distinctive crystal structure features, the strong intermolecular $\pi\cdots\pi$ stacking interactions between the anions and the cations as well as the heavy deviation from the planarity of the anionic geometry. DFT and TDDFT calculations disclosed that the near-IR absorbance bands in **1**–**5** are assigned to the combined transitions of d–d, MLCT and π–π^* in the $[Ni(mnt)_2]^{2-}$ anion as well as the IPCT transition from the HOMO of the $[Ni(mnt)_2]^{2-}$ anion to the LUMO of the RBz-1-Apy$^+$ cation. For **1**–**5**, the IPCT band position is almost independent of the substituent group features in the benzene ring of the cation due to the substituent group in the benzene ring has only a very minor contribution to the cationic LUMO, and that modifying the molecular structure of the pyridine moiety could adjust the IPCT band property for the ion-pair complexes of pyridinium derivatives with $[Ni(mnt)_2]^{2-}$.

Acknowledgements

The authors thank the Science and Technology Department of Jiangsu Province, PR China, and the Nature Science Foundation of China for financial support (Grant Nos.: BK2007184 and 10774076). J.X. thanks Brett M. Paterson and Ryan Gilbert-Wilson for reading the manuscript and also acknowledges the financial support of the Australian Research Council.

Appendix A. Supplementary data

CCDC 675156, 675157, 675158, 675159 and 675160 contain the supplementary crystallographic data for complexes **1**–**5**. These data can be obtained free of charge via http://www.ccdc.cam.ac.uk/conts/retrieving.html, or from the Cambridge Crystallographic Data Centre, 12 Union Road, Cambridge CB2 1EZ, UK; fax: (+44) 1223-336-033; or e-mail: deposit@ccdc.cam.ac.uk. Supplementary data associated with this article can be found, in the online version, at doi:10.1016/j.poly.2008.06.008.

References

[1] T. Horiuchi, H. Miura, K. Sumioka, S. Uchida, J. Am. Chem. Soc. 126 (2004) 12218.
[2] (a) U. Bach, D. Lupo, P. Comte, J.E. Moser, F. Weissörtel, J. Salbeck, H. Spreitzer, M. Grätzel, Nature 395 (1998) 583;
(b) B. Oregan, M. Grätzel, Nature 414 (2001) 338.
[3] (a) A. Islam, H. Sugihara, K. Hara, L.P. Singh, R. Katoh, M. Yanagida, Y. Takahashi, S. Murata, H. Arakawa, Inorg. Chem. 40 (2001) 5371;
(b) S. Nakade, Y. Saito, W. Kubo, T. Kitamura, Y. Wada, S. Yanagida, J. Phys. Chem. B 107 (2003) 8607.
[4] K.D. Benkstein, N. Kopidakis, J. van de Lagemaat, A.J. Frank, J. Phys. Chem. B 107 (2003) 7759.
[5] E. Stathatosa, P. Lianos, V. Jovanovskib, B. Orel, J. Photochem. Photobiol. A: Chem. 169 (2005) 57.
[6] C. Klein, Md.K. Nazeeruddin, P. Liska, Davide Di Censo, N. Hirata, E. Palomares, J.R. Durrant, M. Grätzel, Inorg. Chem. 44 (2005) 178.
[7] H.J. Snaith, A.J. Moule, C. Klein, K. Meerholz, R.H. Friend, M. Grätzel, Nano Lett. 11 (2007) 3372.
[8] W.M. Campbell, K.W. Jolley, P. Wagner, K. Wagner, P.J. Walsh, K.C. Gordon, L. Schmidt-Mende, M.K. Nazeeruddin, Q. Wang, M. Grätzel, D.L. Officer, J. Phys. Chem. C 111 (2007) 11760.
[9] J. He, G. Benkö, F. Korodi, T. Polívka, R. Lomoth, B. Åkermark, L. Sun, A. Hagfeldt, V. Sundströ, J. Am. Chem. Soc. 124 (2002) 4922.
[10] (a) J.-J. Cid, J.-H. Yum, S.-R. Jang, M.K. Nazeeruddin, E. Martínez-Ferrero, E. Palomares, J. Ko, M. Grätzel, T. Torres, Angew. Chem., Int. Ed. 46 (2007) 8358;
(b) M. Velusamy, K.R.J. Thomas, J.T. Lin, Y.-C. Hsu, K.-C. Ho, Org. Lett. 7 (2005) 1899.
[11] (a) Z.S. Herman, R.F. Kirchner, G.H. Loew, U.T. Mueller-Westerhoff, A. Nazal, M.C. Zerner, Inorg. Chem. 21 (1982) 46;
(b) A. Endo, S. Matsumoto, J. Mizuguchi, J. Phys. Chem. A 103 (1999) 8193.
[12] (a) W.E. Geiger Jr., A.H. Maki, J. Phys. Chem. 76 (1971) 2387;
(b) E.M. Kosower, P.E. Klinedinst Jr., J. Am. Chem. Soc. 78 (1956) 3493;
(c) E.M. Kosower, J. Am. Chem. Soc. 78 (1956) 5700;
(d) E.M. Kosower, J. Am. Chem. Soc. 80 (1958) 3253;
(e) H. Güsten, L. Klasinc, J. Phys. Chem. 76 (1972) 2452.
[13] (a) V. Madhu, S.K. Das, Polyhedron 23 (2004) 1235;
(b) F. Bigoli, P. Deplano, M.L. Mercuri, M.A. Pellinghelli, L. Pilia, G. Pintus, A. Serpe, E.F. Trogu, Inorg. Chem. 41 (2002) 5241;
(c) H.-J. Lee, D.-Y. Noh, Polyhedron 19 (2000) 425;
(d) C. Handrosch, R. Dinnebier, G. Bondarenko, E. Bothe, F. HeinemannH. Kisch, Eur. J. Inorg. Chem. (1999) 1259;
(e) J.-F. Bai, J.-L. Zuo, W.-L. Tan, W. Ji, Z. Shen, H.-K. Fun, K. Chinnakali, I.A. Razak, X.-Z. You, C.-M. Che, J. Mater. Chem. 9 (1999) 2419;
(f) F. Bigoli, P. Deplano, F.A. Devillanova, V. Lippolis, P.J. Lukes, M.L. Mercuri, M.A. Pellinghelli, E.F. Trogu, J. Chem. Soc., Chem. Commun. (1995) 371;
(g) G. Schmauch, F. Knoch, H. Kisch, Chem. Ber. 127 (1994) 287;
(h) I. Nunn, B. Eisen, R. Benedix, H. Kisch, Inorg. Chem. 33 (1994) 5079;
(i) H. Kisch, Coordin. Chem. Rev. 125 (1993) 155;
(j) W. Dmler, H. Kisch, New J. Chem. 15 (1991) 649.
[14] A. Davison, H.R. Holm, Inorg. Synth. 10 (1967) 8.
[15] G. Richard, M. Alwin, Chem. Ber. 92 (1959) 2521.
[16] (a) E.N. Kurkutova, O.I. Levina, A.K. Sheynkman, E.A. Gladkikh, Zh. Strukt. Khin. 17 (1976) 881;
(b) Z.F. Tian, X.M. Ren, Y.Z. Li, Y. Song, Q.J. Meng, Inog. Chem. 46 (2007) 8102.
[17] Software packages SMART and SAINT, Siemens Analytical X-ray Instrument Inc., Madison, WI, 1996.
[18] G.M. Sheldrick, SHELXL-97, Program for the Refinement of Crystal Structure, University of Göttingen, Germany, 1997.
[19] M.J. Frisch, G.W. Trucks, H.B. Schlegel, G.E. Scuseria, M.A. Robb, J.R. Cheeseman, V.G. Zakrzewski, J.A. Montgomery Jr., R.E. Stratmann, J.C. Burant, S. Dapprich, J.M. Millam, A.D. Daniels, K.N. Kudin, M.C. Strain, O. Farkas, J. Tomasi, V. Barone, M. Cossi, R. Cammi, B. Mennucci, C. Pomelli, C. Adamo, S. Clifford, J. Ochterski, G.A. Petersson, P.Y. Ayala, Q. Cui, K. Morokuma, P. Salvador, J.J. Dannenberg, D.K. Malick, A.D. Rabuck, K. Raghavachari, J.B. Foresman, J. Cioslowski, J.V. Ortiz, A.G. Baboul, B.B. Stefanov, G. Liu, A. Liashenko, P. Piskorz, I. Komaromi, R. Gomperts, R.L. Martin, D.J. Fox, T. Keith, M.A. Al-Laham, C.Y. Peng, A. Nanayakkara, M. Challacombe, P.M.W. Gill, B. Johnson, W. Chen, M.W. Wong, J.L. Andres, C. Gonzalez, M. Head-Gordon, E.S. Replogle, J.A. Pople, Gaussian 98, Revision A.11, Gaussian, Inc., Pittsburgh, PA, 2001.
[20] A.D. Becke, J. Chem. Phys. 98 (1993) 5648.
[21] C. Lee, W. Yang, R.G. Parr, Phys. Rev. B 37 (1988) 785.
[22] B. Miehlich, A. Savin, H. Stoll, H. Preuss, Chem. Phys. Lett. 157 (1989) 200.
[23] (a) R. Ditchfield, W.J. Hehre, J.A. Pople, J. Chem. Phys. 54 (1971) 724;
(b) M.S. Gordon, Chem. Phys. Lett. 76 (1980) 163.
[24] (a) W.R. Wadt, P.J. Hay, J. Chem. Phys. 82 (1985) 284;
(b) P.J. Hay, W.R. Wadt, J. Chem. Phys. 82 (1985) 299.
[25] X.M. Ren, C.Y. Duan, H.Z. Zhu, Q.J. Meng, C.J. Hu, C.S. Lu, Y.J. Liu, Trans. Met. Chem. 26 (2001) 295.
[26] M. Melnik, M. Kabesova, J. Coordin. Chem. 50 (2000) 323.
[27] C.L. Beswick, J.M. Schulman, E.I. Stiefel, Progr. Inorg. Chem. 52 (2004) 55.
[28] X.M. Ren, P.H. Wu, W.W. Zhang, Q.J. Meng, X.Y. Chen, Trans. Met. Chem. 27 (2002) 394.
[29] W.C. Hamilton, I. Bernal, Inorg. Chem. 6 (1967) 2003.
[30] M.R. Snow, J.A. Ibers, Inorg. Chem. 12 (1973) 249.
[31] (a) T. Costa, J.R. Dorfman, K.S. Hagen, R.H. Holm, Inorg. Chem. 22 (1983) 4091;
(b) G. Christou, J.C. Huffman, J. Chem. Soc., Chem. Commun. (1983) 558.
[32] J.H. Enemark, W.N. Lipscomb, Inorg. Chem. 4 (1965) 1729.

[33] M.J. Baker-Hawkes, Z. Dori, R. Eisenberg, H.B. Gray, J. Am. Chem. Soc. 90 (1968) 4253.
[34] (a) B.R. Serr, C.E.L. Headford, O.P. Anderson, C.M. El1iot, C.K. Schauer, K. Akabori, K. Spartalian, W.E. Hatfield, B.R. Rohrs, Inorg. Chem. 29 (1990) 2663;
(b) D. Snaathorst, H.M. Doesburg, J.A.A.J. Perenboom, C.P. Keijzers, Inorg. Chem. 20 (1981) 2526.
[35] X.M. Ren, Z.P. Ni, S. Noro, T. Akutagawa, S. Nishihara, T. Nakamura, Y.X. Sui, Y. Song, Cryst. Growth Des. 6 (2006) 2530.
[36] (a) O. Jeannin, J. Delaunay, F. Barriere, M. Fourmigue, Inorg. Chem. 44 (2005) 9763;
(b) S.A. Baudron, N. Avarvari, P. Batail, Inorg. Chem. 44 (2005) 3380;
(c) B.S. Lim, D.V. Fomitchev, R.H. Holm, Inorg. Chem. 40 (2001) 4257;
(d) M.R. Bryce, A.J. Moore, A.S. Batsanov, J.A.K. Howard, L.M. Goldenberg, C. Pearson, M.C. Petty, B.K. Tanner, Synth. Met. 86 (1997) 1839;
(e) S.Q. Sun, B. Zhang, P.J. Wu, D.B. Zhu, J. Chem. Soc., Dalton Trans. (1997) 277;
(f) M. Lemke, F. Knoch, H. Kisch, J. Salbeck, Chem. Ber. 128 (1995) 131;
(g) K.T. Youm, Y. Kim, Y. Do, M.J. Jun, Inorg. Chim. Acta 310 (2000) 203;
(h) C. Zhang, H.K. Reddy, R.K. Chadha, G.N. Schrauzer, J. Coordin. Chem. 26 (1992) 117.
[37] The CSD 3D Graphics Search System: F.H. Allen, Acta Crystallogr., Sect. B 58 (2002) 380.
[38] S.I. Shupacke, E. Billig, R.J.H. Clark, R. Williams, H. Gray, J. Am. Chem. Soc. 86 (1964) 4564.
[39] X. Zhou, Q.-J. Pan, B.-H. Xia, M.-X. Li, H.-X. Zhang, A.-C. Tung, J. Phys. Chem. A 111 (2007) 5465.
[40] A. Ajayaghosh, Acc. Chem. Res. 38 (2005) 449.

Carbide Co. and treated by means of general procedure before use [25]. Other reagents and solvents were purchased commercially and used without further purification unless specially noted. Doubly distilled water was used to prepare buffer solutions.

2.2. Preparation of ligands and complexes

5,5′-Dimethyl-2,2′-dipyridyl was purchased from Aldrich Chemical Co. 5,5′-Dibromomethyl-2,2′-dipyridyl, $L^1Br_2 \cdot 4H_2O$ and L^2Br_2 were synthesized and characterized according to our previous method [23]. *cis*-$[Ru(phen)_2Cl_2] \cdot 2H_2O$ was prepared and characterized according to the literature procedures [26].

2.2.1. $[Ru(phen)_2(L^1)](PF_6)_4 \cdot 3CH_3CN$ (**1**)

A mixture of *cis*-$[Ru(phen)_2Cl_2] \cdot 2H_2O$ (0.28 g, 0.5 mmol), $L^1Br_2 \cdot 4H_2O$ (0.31 g, 0.5 mmol) and ethylene glycol (30.0 cm^3) was heated at 130 °C under the protection of argon for 6 h, during which the solution turned red. The solution was cooled to room temperature. After filtration dropwise addition of saturated NH_4PF_6 resulted in a red-orange precipitate which was filtered and recrystallized with CH_3CN/CH_3OH (1:1, v/v), and red single crystals were obtained. Yield: 0.60 g (70.6%). *Anal. Calc. for $C_{54}H_{65}F_{24}N_{11}P_4Ru$ (1549.09): C, 41.87; H, 4.23; N, 9.95. Found: C, 41.58; H, 4.20; N, 9.88%.*

2.2.2. $[Ru(phen)_2(L^2)](PF_6)_4 \cdot 1.5CH_3OH \cdot 0.5H_2O$ (2)

This complex was obtained by a similar procedure described for complex **1**. L^2Br_2 (0.36 g, 0.5 mmol) was used instead of $L^1Br_2 \cdot 4H_2O$. The crude product was recrystallized with CH_3CN/CH_3OH (1:1, v/v), red single crystals were obtained. Yield: 0.53 g (64.7%). *Anal. Calc. for $C_{61.5}H_{80}F_{24}N_8O_2P_4Ru$ (1644.24): C, 44.92; H, 4.90; N, 6.81. Found: C, 44.95; H, 4.92; N, 6.84%.*

2.3. General methods

Elemental analyses (C, H and N) were carried out with a Perkin–Elmer 240 C elemental analyzer. UV–Vis and emission spectra were measured on Perkin–Elmer Lambda-850 spectrophotometer and Ls55 spectrofluorophotometer, and circular dichroism (CD) spectra were measured on a Jasco J-810 spectropolarimeter.

Buffer (5 mM tris(hydroxymethyl)aminomethane (Tris) hydrochloride, 50 mM NaCl, pH 7.2) was used for absorption titration, emission titration, equilibrium dialysis, and viscosity experiments. Solutions of CT-DNA in buffer gave a ratio of UV absorbance at 260 and 280 nm of 1.8–1.9:1, indicating that the DNA was sufficiently free of protein [27]. The concentration of CT-DNA was determined spectrophotometrically assuming a molar absorption is 6600 M^{-1} cm^{-1} (260 nm) [28].

The absorption and emission titration of the Ru(II) complexes were performed by using a fixed complex concentration to which increments of the DNA stock solution were added. The concentration of the $[Ru(phen)_2(L)]^{4+}$ solution was 10 μM. Complex-DNA solutions were allowed to incubate for 5 min before the absorption spectra were recorded. Titrations for each sample were repeated at least three times. The intrinsic binding constant K_b of a complex to CT-DNA was determined from Eq. (1) [29–32], where [DNA] is the concentration of DNA in base pair, ε_a is the extinction coefficient (A_{abs}/[M]) observed for the absorption band at a given DNA concentration, ε_f and ε_b are the extinction coefficient for the free Ru(II) complex and the extinction coefficient for the Ru(II) complex in the fully bound form, respectively; K_b is the equilibrium binding constant in M^{-1}, C_t is the total Ru(II) complex concentration, and s is the binding site size. Eq. (1) has been applied to absorption titration data for noncooperative metallointercalator binding to CT-DNA.

$$(\varepsilon_a - \varepsilon_f)/(\varepsilon_b - \varepsilon_f) = (b - (b^2 - 2K_b^2 C_t[DNA]/s)^{1/2}/2K_b C_t \quad (1a)$$

$$b = 1 + K_b C_t + K_b[DNA]/2s \quad (1b)$$

Equilibrium dialysis was carried out in the dark and held at room temperature for 12 h with 5 mL of CT-DNA (1.0 mM) sealed in a dialysis bag and 10 mL of the Ru(II)-polypyridyl complex (50 μM) outside the bag. The bandwidth was 1 nm and the response time was 1 s. For each CD spectrum, repeated at least three times, spectral data were collected at 0.1 nm intervals with a scan speed of 300 nm min^{-1}. DNA was dialyzed thoroughly prior to the experiments. For the equilibrium dialysis and CD studies, blank experiment of the complex was also been carried out, and did not show obvious CD signal.

Viscosity measurements were carried out using an Ubbelohde viscometer maintained at a constant temperature of 30.0 ± 0.1 °C in a thermostatic bath. DNA samples with an approximate average length of 200 base pairs were prepared by sonication in order to minimize complexities arising from DNA flexibility [33]. Flow time was measured with a digital stopwatch. Each sample was measured three times and an average flow time was calculated. Data are presented as $(\eta/\eta^0)^{1/3}$ versus binding ratio ([Ru]/[DNA]) [34], where η is the viscosity of DNA in the presence of complex and η^0 is the viscosity of DNA alone.

2.4. X-ray crystallography

Single crystal X-ray diffraction experiments were carried out with a Bruker Smart Apex CCD area detector at 173(2) and 293(2) K for complexes **1** and **2**, respectively. The dimensions of crystals of complexes **1** and **2** used for X-ray diffraction analysis were 0.48 × 0.40 × 0.38 mm (**1**) and 0.52 × 0.41 × 0.20 mm (**2**), respectively. Data collection was performed with Mo Kα radiation (k = 0.71073 Å) for **1** and Cu Kα radiation (k = 1.54178 Å) for **2**. Absorption corrections were applied by using the SADABS program [35]. The structures were solved by direct methods, and all non-hydrogen atoms were refined anisotropically by least-squares on F^2 using the SHELXTL program [36]. These were first refined isotropically and then anisotropically. The hydrogen atoms of the ligands were placed in calculated positions with fixed isotropic thermal parameters and the structures factor calculations were included in the final stage of full-matrix least-squares refinement. A summary of the crystal data was given in Table 1.

3. Results and discussion

3.1. Description of the molecular structures

Figs. 1 and 2 depict the structures of complexes **1** and **2**, respectively. Selected bond distances and bond angles of complexes **1** and **2** are given in Table 2. Both complexes contain a six-coordinated ruthenium atom chelated by two phen ligands and one dicationic L ligand. The coordination geometry about the ruthenium atom is a distorted octahedron, with a bite angle of 79.5° in **1** and 79.2° in **2** averaged over three bidentate ligands. This distortion from an ideal octahedral geometry is due to the customary narrow bite angles of the bipyridine moieties, as observed in some other ruthenium complexes [37]. The mean Ru–N bond length for **1** (2.065 Å) and **2** (2.068 Å) are typical value for this type of Ru(II) complex (2.059–2.069 Å) [38,39]. The torsion angles between pyridine pairs of two bpy ligands of the complexes are nonequivalent, **1** being 15.6° and **2** being 2.8°.

3.2. Absorption spectra

The absorption spectra of both Ru(II) complexes are characterized by two intense ligand-centered transitions (LC) in the UV re-

Table 1
Crystallographic data for complexes **1** · $3CH_3CN$ and **2** · $1.5CH_3OH$ · $0.5H_2O$

Complex	**1** · $3CH_3CN$	**2** · $1.5CH_3OH$ · $0.5H_2O$
Empirical formula	$C_{54}H_{65}F_{24}N_{11}P_4Ru$	$C_{61.5}H_{80}F_{24}N_8O_2P_4Ru$
Formula weight	1549.12	1644.28
Temperature (K)	173(2)	293(2)
Wavelength (Å)	0.71073	1.54178
Crystal system, space group	triclinic, $P\bar{1}$	monoclinic, $P2(1)/c$
a (Å)	12.4079(13)	13.1497(2)
b (Å)	14.8052(16)	25.6450(5)
c (Å)	19.639(2)	21.4886(4)
α (°)	68.906(2)	90.00
β (°)	83.196(2)	119.085(2)
γ (°)	80.752(2)	90.00
Volume (Å^3)	3314.9(6)	7234.8(2)
Z	2	4
D_{calc} (g cm^{-3})	1.552	1.510
$F(000)$	1572	3364
Crystal size (mm)	0.48 × 0.40 × 0.38	0.52 × 0.41 × 0.20
θ Range for data collection (°)	1.49–26.00	2.69–62.19
Limiting indices	$-15 \leqslant h \leqslant 15$, $-18 \leqslant k \leqslant 18$,$-24 \leqslant l \leqslant 24$	$-14 \leqslant h \leqslant 14$, $-28 \leqslant k \leqslant 29$,$-27 \leqslant l \leqslant 27$
Reflections collected	12806	33260
Independent reflections	10536 (R_{int} = 0.0234)	10863 (R_{int} = 0.0298)
Goodness-of-fit on F^2	1.061	0.909
R_1/wR_2 [$I > 2\sigma(I)$][a]	0.0581/0.1655	0.0460/0.1346
R_1/wR_2 (all data)	0.0708/0.1803	0.0631/0.1469
Largest differences in peak (e A^{-3})	1.284/−0.964	1.277/−0.553

[a] $R_1 = \sum||F_o| - |F_c||/\sum|F_o|$, $wR_2 = [\sum w(F_o^2 - F_c^2)2/\sum w(F_o^2)^2]^{1/2}$.

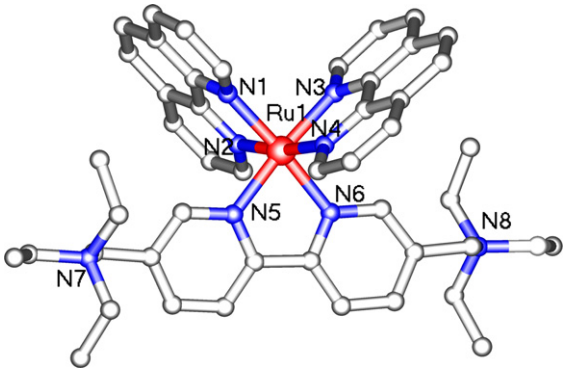

Fig. 1. X-ray crystal structure of **1**. All the hydrogen atoms are omitted for clarity.

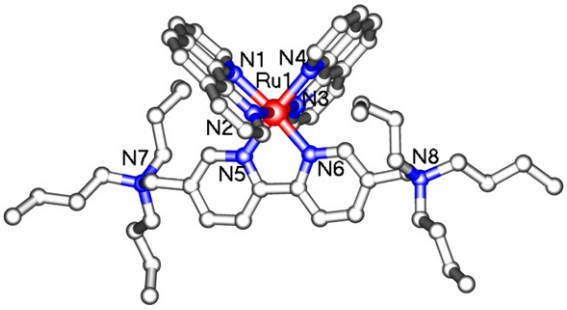

Fig. 2. X-ray crystal structure of **2**. All the hydrogen atoms are omitted for clarity.

gion, at 263, 293 nm for **1** and 262, 294 nm for **2**, and a metal-to-ligand charge transfer (MLCT) in the visible region, at 430 and 437 nm for **1** and **2**, respectively. The visible bands around 430 nm arise from the metal ($d\pi$) to the ligand (π^*) charge transfer (MLCT) transitions, and the ultraviolet bands around 260 nm and 295 nm belong to $\pi \rightarrow \pi^*$ transitions of the ligands. When DNA is added into the solution, different hypochromism (H%), as defined by $H\% = 100\%\ (A_{free} - A_{bound})/A_{free}$, is observed for both LC and MLCT transition absorptions. Hypochromism and red shifting changes indicate weak interactions between the DNA bases and the complexes and such results are consistent with the geometry of the main ligands. Although the two complexes have only subtle differences, the difference in behavior of the complexes with different main ligands in terms of spectral properties is distinct. The electronic spectral traces of the complexes titrated with DNA are shown in Fig. 3. The other related data were shown in Table 3.

To compare quantitatively the affinity of these complexes towards DNA, the intrinsic binding constants K_b of these complexes to DNA are determined by monitoring the changes of absorbance in the MLCT band with increasing concentration of DNA. The intrinsic binding constants K_b of complexes **1** and **2** obtained were 7.73×10^4 M^{-1} and 2.50×10^4 M^{-1}, respectively, from the decay of

Table 2
Selected bond lengths (Å) and angles (°) for metal environments of complexes **1** and **2**

	1	**2**
Ru(1)–N(1)	2.059(3)	2.072(3)
Ru(1)–N(2)	2.064(3)	2.067(3)
Ru(1)–N(3)	2.061(3)	2.067(3)
Ru(1)–N(4)	2.067(3)	2.081(4)
Ru(1)–N(5)	2.066(3)	2.054(3)
Ru(1)–N(6)	2.074(3)	2.064(3)
N(1)–Ru(1)–N(2)	79.8(1)	79.4(1)
N(1)–Ru(1)–N(3)	89.2(1)	96.6(1)
N(1)–Ru(1)–N(4)	93.9(1)	88.2(1)
N(1)–Ru(1)–N(5)	96.5(1)	96.4(1)
N(1)–Ru(1)–N(6)	175.5(1)	173.4(1)
N(2)–Ru(1)–N(3)	93.8(1)	172.6(1)
N(2)–Ru(1)–N(4)	171.2(1)	93.9(1)
N(2)–Ru(1)–N(5)	87.0(1)	91.8(1)
N(2)–Ru(1)–N(6)	99.6(1)	96.3(1)
N(3)–Ru(1)–N(4)	79.8(1)	79.7(1)
N(3)–Ru(1)–N(5)	174.3(1)	94.8(1)
N(3)–Ru(1)–N(6)	95.2(1)	88.1(1)
N(4)–Ru(1)–N(5)	100.0(1)	173.2(1)
N(4)–Ru(1)–N(6)	87.1(1)	97.2(1)
N(5)–Ru(1)–N(6)	79.0(1)	78.6(1)

Table 3
Absorption spectra (λ_{max}/nm) and DNA-binding constants K_b ($\times 10^4\ M^{-1}$) of **1** and **2**

Complex	λ_{max} (free)	λ_{max} (bound)	$\Delta\lambda$ (nm)	H (%)	K_b ($10^4\ M^{-1}$)	s
1	430	437	7	8.22	7.73 ± 0.1	0.62 ± 0.07
	293	294	1	8.63		
	263	263	0	18.66		
2	437	439	2	6.60	2.50 ± 1.3	0.43 ± 0.1
	294	295	1	7.93		
	262	263	1	10.37		

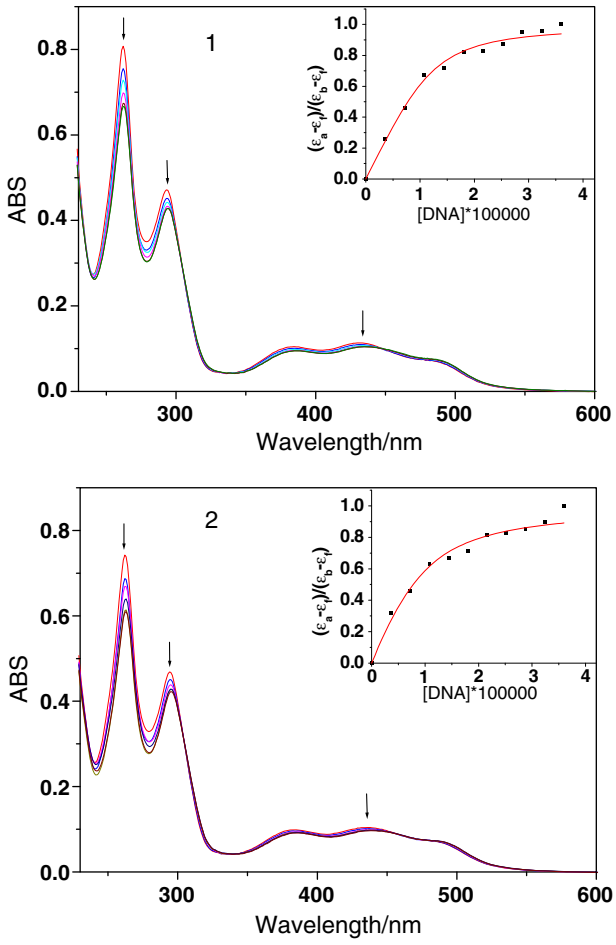

Fig. 3. Absorption spectra of **1** and **2** in Tris buffer (pH 7.2) in the presence of increasing amounts of CT-DNA. [Ru] = 10 μM, [DNA] = 0–120 μM from top to bottom. Arrows indicate the change in absorbance upon increasing the DNA concentration. Inset: plot of $(\varepsilon_a - \varepsilon_f)/(\varepsilon_b - \varepsilon_f)$ vs. [DNA] and the nonlinear fit for the titration of DNA to Ru(II) complexes.

the absorbance. The binding constant K_b of 1 is greater than that of **2**, showing the DNA-binding affinity of **1** stronger than that of **2**. The K_b values of the two complexes we studied in this paper are much smaller than those observed for many DNA intercalative complexes of type $[Ru(phen)_2L]^{2+}$: $K_b = 5.1 \times 10^6\ M^{-1}$ for $[Ru(phen)_2dppz]^{2+}$ (dppz = dipyrido[3,2-*a*:2′,3′-*c*]phenazine]) [31], $1.2 \times 10^5\ M^{-1}$ for $[Ru(phen)_2(actatp)]^{2+}$ (actatp = acenaphthereno[1,2-*b*]-1,4,8,9-tetraazariphenylence) [32] and $1.1 \times 10^5\ M^{-1}$ for $[Ru(phen)_2(PPIP)]^{2+}$ (2-(4′-phenoxy-phenyl)imidazo[4,5-*f*][1,10]-phenanthroline) [40]. It is interesting to find the intrinsic binding activity of complexes **1** and **2** are much higher than $[Ru(phen)_3]^{2+}$ ($0.55 \times 10^4\ M^{-1}$) and their analogue $[Ru(phen)_2(bpy)](PF_6)_2$ ($0.36 \times 10^4\ M^{-1}$) [41]. Although the mechanism is not clear, it is also important since the increasing of the charge of the ligands can enhance the affinity of complexes and DNA.

3.3. Emission spectra

Upon excitation using a wavelength of 430 and 436 nm for complexes **1** and **2** respectively, both of the complexes can emit fluorescence with a maximum wavelength of about 630 nm. The results of the emission titration for these complexes with DNA are shown in Fig. 4. The fluorescence intensity of these complexes increased with the increase of DNA concentration, reaching a maximum at the ratio of [DNA]/[Ru] ≈ 20:1, at which there is a 3.71- and 2.96-fold increase in the fluorescence intensity of the complexes compared with that in the absence of DNA for **1** and **2,** respectively. The results suggest that both of the complexes can be protected from solvent water molecules by the hydrophobic environment inside the DNA helix, since that the butyl has a bigger sterical hindrance than ethyl, complex **1** can be protected more efficiently than complex **2**.

3.4. Enantioselective binding studies

Circular dichroic spectra can provide information about the chirality of spectroscopically active species in solution. The *rac*-metal complexes give a zero CD but show induced circular dichroic (ICD)

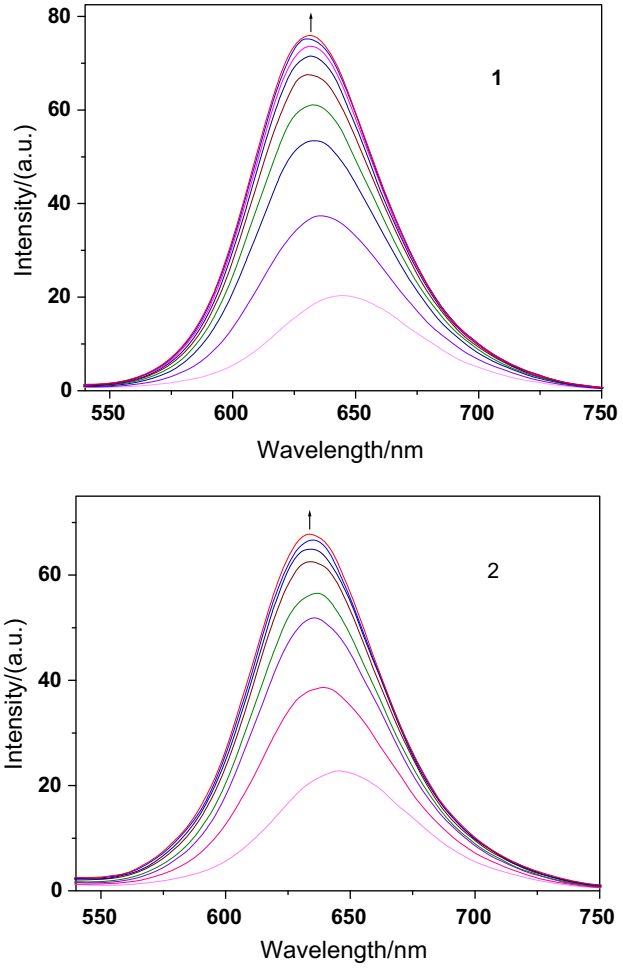

Fig. 4. Emission spectra of **1** and **2** in Tris buffer (pH 7.2) in the presence of increasing amounts of CT-DNA, [Ru] = 10 μM, [DNA] = 0–200 μM. Arrow shows the emission intensity changes upon increasing DNA concentrations.

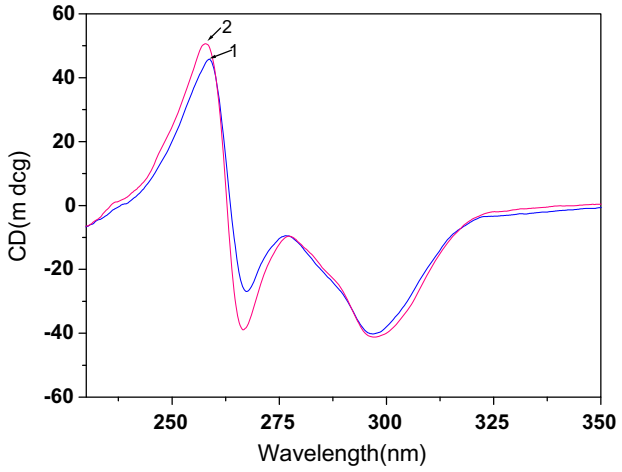

Fig. 5. CD spectra of **1** and **2** in 5 mM Tris–HCl and 50 mM NaCl (pH 7.2) in the presence of CT-DNA, [Ru] = 50 μM, [DNA] = 1.0 mM.

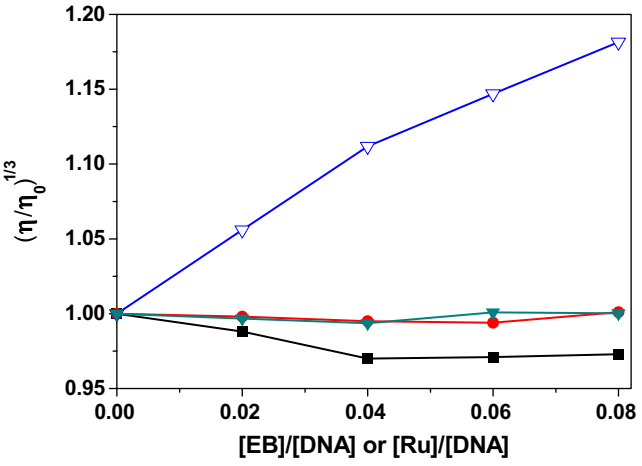

Fig. 6. Effects of increasing amounts of **1** (■), **2** (●), EB(▽) and $Ru(bpy)_3^{2+}$ (▼) on the relative viscosities of CT-DNA at 30 ± 0.1 °C, [DNA] = 0.5 mM, r = [Ru]/[DNA] ($\times 10^{-2}$).

signals on enantiopreferential binding to DNA providing further and definitive confirmation for their DNA binding [42,13]. Thus, the CD spectral technique has been used to study the enantiopreferential DNA binding of *rac*-metal complexes. According to the proposed binding model [43,44], the Δ-enantiomer of the complex, a right-handed propeller-like structure, will display a greater affinity than the Λ-enantiomer with the right-handed calf-thymus DNA helix, due to the appropriate steric matching. Therefore, the enantiospecific binding of complex to DNA can be observed clearly from circular dichroism spectra.

The CD spectra in the UV region of 230–350 nm for complexes **1** and **2** after their racemic solution has been dialyzed against DNA are shown in Fig. 5. Both of the dialysates of the Ru(II) complexes show strong CD signals consist of a positive (258 nm) and two negative bands (267 and 297 nm). This is typical of exciton coupled ICD arising due to enantiopreferential binding of the Δ-enantiomer of the *rac*-complex and/or ligand–ligand interactions among DNA bound/unbound complexes [45]. The CD spectra results indicate that both complexes show good enantioselectivity when binding with DNA, and the Δ-enantiomers reveal the potential to bind preferentially to right-handed CT-DNA.

3.5. Viscosity studies

Optical photophysical probes provide necessary, but not sufficient clues to support a binding model. Hydrodynamic measurements (i.e., viscosity and sedimentation) that are sensitive to length change are regarded as the least ambiguous and the most critical tests of a binding model in solution in the absence of crystallographic structural data [12,46,47]. A classical intercalation model results in lengthening the DNA helix as base pairs are separated to accommodate the bound ligand, leading to the increase of DNA viscosity. In contrast, a semi-intercalation of ligand could bend (or kink) the DNA helix, reduce its effective length, and concomitantly, its viscosity. In addition, some complexes such as $[Ru(bpy)_3]^{2+}$, which interacts with DNA by an electrostatic binding mode, have no influence on DNA viscosity [48].

The changes in relative viscosity of rod-like CT-DNA in the presence of $[Ru(phen)_2(L)]^{4+}$ (L^1 or L^2), EB (ethidium bromide = 3,8-diamino-5-ethyl-6-phenylphenanthridinium bromide) and $[Ru(bpy)_3]^{2+}$ are shown in Fig. 6. EB, a well-known DNA intercalator, increases the relative viscosity strongly by lengthening the DNA double helix through intercalation. On the contrary, $[Ru(bpy)_3]^{2+}$, which binds to DNA in the electrostatic mode, exerts essentially no effect on DNA viscosity. As can be seen from Fig. 6, the viscosity of DNA decreases with increasing concentration of **1**, which is consistent with bending or kinking of the helix upon binding *rac*-Ru(II) complex to DNA [45]. In contrast, the viscosity of DNA remains almost unchanged upon addition of **2**. The results suggest that the binding modes of complexes **1** and **2** are different and **1** may partially intercalate between DNA base-pairs while **2** most likely interact with DNA in an electrostatic binding mode.

4. Conclusion

Two new Ru(II) complexes $[Ru(phen)_2(L)]^{4+}$ where the ligand L contains dicationic pendants have been synthesized. The experimental and theoretical studies show that the main ligand with dicationic pendants can cause some interesting differences in the properties of the resulting complexes. The results indicate that **1** has a greater DNA affinity than **2**. It is a very interesting finding that the two complexes reveal good enantioselectivity when binding with DNA. In addition, the experimental results suggest that complexes **1** and **2** bind to DNA in different modes, i.e., **1** by semi-intercalation and **2** by electrostatic binding mode.

Acknowledgments

We are grateful to the National Natural Science Foundation of China, the Doctoral Program of Higher Education, the Natural Science Foundation of Guangdong Province, the Planned Item of Science and Technology of Guangdong Province, the Item of Tackle Key Problem of Science and Technology of Guangzhou City, and National Basic Research Program of China (973 Program No. 2007CB815306).

Appendix A. Supplementary data

CCDC 675928 and 675929 contain the supplementary crystallographic data for complexes **1** and **2**. These data can be obtained free of charge via http://www.ccdc.cam.ac.uk/conts/retrieving.html, or from the Cambridge Crystallographic Data Centre, 12 Union Road, Cambridge CB2 1EZ, UK; fax: (+44) 1223-336-033; or e-mail: deposit@ccdc.cam.ac.uk. Supplementary data associated with this article can be found, in the online version, at doi:10.1016/j.poly.2008.06.009.

References

[1] L.N. Ji, X.H. Zou, J.G. Liu, Coordin. Chem. Rev. 216–217 (2001) 513.
[2] K.E. Erkkila, D.T. Odom, J.K. Barton, Chem. Rev. 99 (1999) 2777.
[3] J.K. Barton, Science 233 (1986) 727.
[4] D.S. Sigman, A. Mazumder, D.M. Perrin, Chem. Rev. 93 (1993) 2295.
[5] R. Caspar, L. Musatkina, A. Tatosyan, H. Amouri, M. Gruselle, C. Guyard-Duhayon, R. Duval, C. Cordier, Inorg. Chem. 43 (2004) 7986.
[6] J.G. Vos, J.M. Kelly, J. Chem. Dalton Trans. (2006) 4869.
[7] M.J. Hannon, Chem. Soc. Rev. 36 (2007) 280.
[8] S.O. Kelley, J.K. Barton, Science 283 (1999) 375.
[9] B.A. Jackson, V.Y. Alekseyev, J.K. Barton, Biochemistry 38 (1999) 4655.
[10] C. Metcalfe, J.A. Thomas, Chem. Soc. Rev. 32 (2003) 215.
[11] J.K. Barton, J.M. Goldberg, C.V. Kumar, N.J. Turro, J. Am. Chem. Soc. 108 (1986) 2081.
[12] S. Satyanarayana, J.C. Dabrowiak, J.B. Chaires, Biochemistry 32 (1993) 2573.
[13] C. Hiort, B. Nordén, A. Rodger, J. Am. Chem. Soc. 112 (1990) 1971.
[14] M. Eriksson, M. Leijon, C. Hiort, B. Nordén, A. Gräslund, Biochemistry 33 (1994) 5031.
[15] L.M. Wilhelmsson, F. Westerlund, P. Lincoln, B. Nordén, J. Am. Chem. Soc. 124 (2002) 102092.
[16] S. Shi, J. Liu, J. Li, K.C. Zheng, C.P. Tan, L.M. Chen, L.N. Ji, J. Chem. Soc. Dalton Trans. (2005) 2038.
[17] M. Mariappan, B.G. Maiya, Eur. J. Inorg. Chem. (2005) 2164.
[18] M.J. Han, L.H. Gao, Y.Y. Lu, K.Z. Wang, J. Phys. Chem. B 110 (2006) 2364.
[19] C.B. Spillane, J.L. Morgan, N.C. Fletcher, J.G. Collins, F.R. Keene, Dalton Trans. (2006) 3122.
[20] F. Gao, H. Chao, J.Q. Wang, Y.X. Yuan, B. Sun, Y.F. Wei, B. Peng, L.N. Ji, J. Biol. Inorg. Chem. 12 (2007) 1015.
[21] G.J. Ryan, S. Quinn, T. Gunnlaugsson, Inorg. Chem. 47 (2008) 401.
[22] E. Kövári, R. Krämer, J. Am. Chem. Soc. 118 (1996) 12704.
[23] Y. An, Y.Y. Lin, H. Wang, H.Z. Sun, M.L. Tong, L.N. Ji, Z.W. Mao, J. Chem. Soc., Dalton Trans. (2006) 2066.
[24] Y. An, M.L. Tong, L.N. Ji, Z.W. Mao, J. Chem. Soc., Dalton Trans. (2007) 1250.
[25] J.K. Barton, A.T. Danishefsky, G.M. Goldberg, J. Am. Chem. Soc. 106 (1984) 2172.
[26] B.P. Sullivan, D.J. Salmon, T.J. Meyer, Inorg. Chem. 17 (1978) 3334.
[27] J. Marmur, J. Mol. Biol. 3 (1961) 208.
[28] M.E. Reichmann, S.A. Rice, C.A. Thomas, P. Doty, J. Am. Chem. Soc. 76 (1954) 3047.
[29] M.T. Carter, M. Rodriguez, A. J Bard, J. Am. Chem. Soc. 111 (1989) 8901.
[30] S.R. Smith, G.A. Neyhart, W.A. Karlsbeck, H.H. Thorp, New J. Chem. 18 (1994) 397.
[31] R.B. Nair, E.S. Teng, S.L. Kirkland, C. Murphy, Inorg. Chem. 37 (1998) 139.
[32] H. Deng, H. Xu, Y. Yang, H. Li, H. Zou, L.H. Qu, L.N. Ji, J. Inorg. Biochem. 97 (2003) 207.
[33] J.B. Chaires, N. Dattagupta, D.M. Crothers, Biochemistry 21 (1982) 3933.
[34] G. Cohen, H. Eisenberg, Biopolymers 8 (1969) 45.
[35] G.M. Sheldrick, SADABS 2.05, University of Göttingen, 2002.
[36] SHELXTL 6.10, Bruker Analytical Instrumentation, Madison, WI, USA, 2000.
[37] B.K. Santra, M. Menon, C.K. Pal, G.K. Lahiri, J. Chem. Soc., Dalton Trans. (1997) 1387.
[38] D.P. Rillema, D.S. Jones, C. Woods, H.A. Levy, Inorg. Chem. 31 (1992) 2935.
[39] B.H. Ye, X.M. Chen, T.X. Zeng, L.N. Ji, Inorg. Chim. Acta 240 (1995) 5.
[40] L.F. Tan, H. Chao, H. Li, Y.J. Liu, B. Sun, W. Wei, L.N. Ji, J. Inorg. Biochem. 99 (2005) 513.
[41] P.U. Maheswari, V. Rajendiran, M. Palaniandavar, R. Thomas, G.U. Kulkarni, Inorg. Chim. Acta 359 (2006) 4601.
[42] S. Delaney, M. Pascaly, P. Bhattarcharya, K. Han, J.K. Barton, Inorg. Chem. 41 (2002) 1966.
[43] J.K. Barton, A.L. Raphael, J. Am. Chem. Soc. 106 (1984) 2466.
[44] C.V. Kumar, J.K. Barton, N.J. Turro, J. Am. Chem. Soc. 107 (1985) 5518.
[45] P.U. Maheswari, V. Rajendiran, M. Palaniandavar, R. Parthasarathi, V. Subramanian, J. Inorg. Biochem. 100 (2006) 3.
[46] S. Satyanarayana, J.C. Dabrowiak, J.B. Chaires, Biochemistry 31 (1992) 9319.
[47] X.H. Zou, B.H. Ye, H. Li, Q.L. Zhang, H. Chao, J.G. Liu, L.N. Ji, X.Y. Li, J. Biol. Inorg. Chem. 6 (2001) 143.
[48] J.G. Liu, B.H. Ye, H. Li, Q.X. Zhen, L.N. Ji, Y.H. Fu, J. Inorg. Biochem. 76 (1999) 265.

N^6-R-adenine **N^6,N^6-diR-adenine**

R = propyl, pentyl, hexyl, benzyl R = butyl

Scheme 1.

$[Ru^{III}Cl_4(DMSO)[H\text{-}(BAP)]] \cdot 0.5H_2O$ (**5**) have been spectroscopically characterized (BAP = N^6-benzylaminopurine). Moreover, in an attempt to obtain similar complexes from $RuCl_3 \cdot 3H_2O$ in DMSO/HCl [16] or from *cis*-$[RuCl_2(DMSO)_4]$ in EtOH/HCl we have obtained a microcrystalline solid of an outer-sphere complex of Ru(II), $[H\text{-}(BAP)][Ru^{II}Cl_3(DMSO)_3]$ (**6**). A similar crystalline Ru(II) complex has been isolated with the creatinine bioligand, $[H\text{-}(creat)][Ru^{II}Cl_3(DMSO)_3]$ (**7**) which has been structurally solved by X-ray diffraction for comparison purposes.

2. Experimental

2.1. Materials, analysis and physical measurements

All organic, including 6-benzylaminopurine (BAP) and creatinine, and inorganic ($RuCl_3 \cdot xH_2O$) reagents were used without further purification (Sigma and Aldrich). The starting complexes $[(DMSO)_2H][trans\text{-}Ru^{III}Cl_4(DMSO)_2]$ and $(NH_4)[trans\text{-}Ru^{III}Cl_4(DMSO)_2]$ were synthesized according to the procedure of Alessio et al. [16] and *cis*-$[RuCl_2(DMSO)_4]$ to the method reported by Evans et al. [17].

Tris–HCl, [tris(hydroxymethyl)aminomethane] hydrochloride, and HEPES, [4-(hydroxyethyl)-1-piperazineethanesulfonic acid] were obtained from ICN (Spain). pBR322 plasmid DNA and DTT (1,4-dithio-DL-threitol) were from Boehringer Mannheim (Germany). EDTA and ethydium bromide were from Sigma and ultrapure agarose was obtained from Pronadisa (Spain).

Elemental analyses were carried out using Carlo-Erba models 1106 and 1108 and Thermo Finningan Flash 1112 microanalysers. Infrared spectra (KBr pellets) were recorded on a Bruker IFS 66 and on a Nicole Impact 400. UV–Vis spectra were recorded on a Varian Cary 300 Bio UV–Vis spectrophotometer. ^1H and ^{13}C NMR spectra were obtained with a Bruker AMX 300 spectrometer. Proton and carbon chemical shifts in dimethylsulfoxide (DMSO-d_6), chloroform ($CDCl_3$) and deuterated water (D_2O) solutions were referenced itself to DMSO-d_6 [^1H NMR δ(DMSO) = 2.47 ppm ^{13}C NMR δ(DMSO) = 40.0 ppm], to $CDCl_3$ [^1H NMR $\delta(CDCl_3)$ = 7.26 ppm ^{13}C NMR $\delta(CDCl_3)$ = 77.0 ppm] and to D_2O [^1H NMR δ(D_2O) = 4.79 ppm], respectively. Conductivity measurements were carried out on a Crison 525 conductimeter at 25 °C.

2.2. Syntheses

2.2.1. Synthesis of N^6-substituted adenines

These ligands were obtained according to previously described methods [18,19]: a suspension of 0.5 g (3.2 mmol) of 6-chloropurine in 10 ml of *n*-butanol and 1.5 ml of triethylamine was refluxed with the required amount (3.2 mmol) of the corresponding amine during several hours. The resulting solution was evaporated in vacuum, yielding a syrup which was treated with concentrated ammonium hydroxide and evaporated again. The resulting solids were filtered off and washed with cold water and cold acetone to remove the triethylammonium hydrochloride impurities. Dissolution of these compounds in HCl 2 M or in EtOH/HCl yields the corresponding salt. Yields, elemental analyses, and ^1H NMR data are included in Table 1, and IR data of protonated ligands is discussed in Table 4. A more complete spectroscopic characterization of these ligands synthesized and their respective hydrochloride salts is included as Supplementary data.

2.2.2. Synthesis of $[Ru^{III}Cl_4(DMSO)[H\text{-}(N^6\text{-pentyladenine})]]$ (**1**), $[Ru^{III}Cl_4(DMSO)[H\text{-}(N^6\text{-hexyladenine})]]$ (**2**), $[Ru^{III}Cl_4(DMSO)\text{-}[H\text{-}(N^6\text{-dibutyladenine})]]$ (**3**), $[Ru^{III}Cl_4(DMSO)[H\text{-}(N^6\text{-propyladenine})]] \cdot 0.5EtOH$ (**4**) and $[Ru^{III}Cl_4(DMSO)[H\text{-}(BAP)]] \cdot 0.5H_2O$ (**5**)

A 0.05 mmol sample of $[NH_4][trans\text{-}RuCl_4(DMSO)_2]$ was dissolved in 5 ml of EtOH/HCl (0.1 M). The resulting solution was stirred for 5 min at room temperature and 0.1 mmol of the ligand dissolved in 2 ml of EtOH/HCl (0.1 M) were added. The orange solution was stirred for 15 min until a deep orange solution was obtained. Orange crystals appeared in the solution after 24 h. The crystals were filtered off and dried in vacuum. Yield 40%.

*2.2.2.1. $[Ru^{III}Cl_4(DMSO)[H\text{-}(N^6\text{-pentyladenine})]]$ (**1**).* Anal. Calc. for $C_{12}H_{22}N_5OSCl_4Ru$: C, 27.33; H, 4.21; N, 13.28. Found: C, 27.86; H, 4.27; N, 13.03%. IR (cm^{-1}): 3485w,br, 1665vs, 1620m, 1579m, 1444m, 1404m, 1378w, 1340w, 1067s, 1019s, 428w. UV–Vis (methanol): λ 280 (ε 1.1×0^4), 400 (1.94×10^3 M^{-1} cm^{-1}). Λ_M/Ω^{-1} cm^2 mol^{-1} (10^{-3} mol dm^{-3} in DMSO, 25 °C) = 8.

*2.2.2.2. $[Ru^{III}Cl_4(DMSO)[H\text{-}(N^6\text{-hexyladenine})]]$ (**2**).* Anal. Calc. for $C_{13}H_{24}N_5OSCl_4Ru$: C, 28.84; H, 4.47; N, 12.94. Found: C, 29.00; H, 4.40; N, 12.85%. IR (cm^{-1}): 3500w,br, 1663vs, 1620m, 1579m, 1441m, 1403m, 1377m, 1340w, 1066s, 1019s, 427w. UV–Vis (methanol): λ 277 (ε 1.57×10^4), 400 (1.58×10^3 M^{-1} cm^{-1}). Λ_M/Ω^{-1} cm^2 mol^{-1} (10^{-3} mol dm^{-3} in DMSO, 25 °C) = 7.

*2.2.2.3. $[Ru^{III}Cl_4(DMSO)[H\text{-}(N^6,N^6\text{-dibutyladenine})]]$ (**3**).* Anal. Calc. for $C_{15}H_{27}N_5OSCl_4Ru$: C, 31.70; H, 4.79; N, 12.32. Found: C, 31.59; H, 4.76; N, 12.09%. IR (cm^{-1}): 3470w,br, 1635vs, 1607vs, 1562m, 1461s, 1402s, 1370m, 1340m, 1080s, 1023s, 691w, 427w. UV–Vis (methanol): λ 288 (ε 2.08×10^4), 399 (3.39×10^3 M^{-1} cm^{-1}). Λ_M/Ω^{-1} cm^2 mol^{-1} (10^{-3} mol dm^{-3} in DMSO, 25 °C) = 14.

*2.2.2.4. $[Ru^{III}Cl_4(DMSO)[H\text{-}(N^6\text{-propyladenine})]] \cdot 0.5EtOH$ (**4**).* Anal. Calc. for $C_{12}H_{24}N_5O_{1.5}SCl_4Ru$: C, 25.30; H, 4.05; N, 13.41. Found: C, 25.22; H, 3.87; N, 13.54%. IR (cm^{-1}): 3480w,br, 1658vs, 1614m, 1570m, 1445s, 1403m, 1335w, 1271w, 1114m, 1067s, 1018m, 430m. UV–Vis (methanol): λ 275 (ε 1.08×10^4), 400 (1.82×10^3 M^{-1} cm^{-1}). Λ_M/Ω^{-1} cm^2 mol^{-1} (10^{-3} mol dm^{-3} in DMSO, 25 °C) = 8.

*2.2.2.5. $[Ru^{III}Cl_4(DMSO)[H\text{-}(BAP)]] \cdot 0.5H_2O$ (**5**).* Anal. Calc. for $C_{14}H_{19}N_5O_{1.5}SCl_4Ru$: C, 30.23; H, 3.44; N, 12.59. Found: C, 30.35; H, 3.46; N, 12.29%. IR (cm^{-1}): 3445m,br, 1656s, 1573m, 1449m, 1409m, 1375m, 1342m, 1065s, 1023m, 432w, UV–Vis (DMSO): λ 282 (ε 6.3×10^3), 405 (1.35×10^3 M^{-1} cm^{-1}). Λ_M/Ω^{-1} cm^2 mol^{-1} (10^{-3} mol dm^{-3} in DMSO, 25 °C) = 9.

2.2.3. Synthesis of $[H\text{-}(BAP)][Ru^{II}Cl_3(DMSO)_3]$ (**6**)

Attempts to prepare a similar product from the *cis*-$[RuCl_2(DMSO)_4]$ in EtOH/HCl (0.1 M) yield the outer-sphere Ru(II) complex, $[H\text{-}(BAP)][Ru^{II}Cl_3(DMSO)_3]$ (**6**). *Anal.* Calc. for $C_{18}H_{32}N_5O_3S_3Cl_3Ru$: C, 32.26; H, 4.81; N, 10.45. Found: C, 32.54; H, 4.64; N, 10.11%. IR (cm^{-1}): 3456w,br, 1652s, 1607m, 1571m, 1509m, 1487m, 1475m, 1453m, 1393m, 1347m, 1095s, 1019s, 424m, ^1H NMR, δ (D_2O): 8.45br s [1H, C(2)–H], 8.35s [1H, C(8)–H], 7.40m [5H, C_6H_5], 4.92br s [2H, C(10)–H], 3.50s [6H, $(CH_3)_3SO$], 3.49s [6H, $(CH_3)_3SO$], 3.39s [6H, $(CH_3)_3SO$]. ^1H NMR, δ (DMSO-d_6): 10.09br s [1H, N(6)–H], 8.62s [1H, C(2)–H], 8.56s [1H, C(8)–H], 7.30m [5H, C_6H_5], 4.85br s [2H, C(10)–H], 2.29s [18H, $(CH_3)_3SO$]. UV–Vis

Table 1
Yield, elemental analyses, and ^{1}H NMR data of prepared ligands

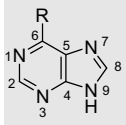	Ligand	Yield (%)	Elemental Analyses Found/Calc.			^{1}H NMR data (DMSO-d_6)
			%C	%H	%N	
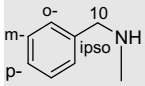	BAP · HCl	70	54.7 55.1	4.5 4.6	26.7 26.8	10.36br t [1H, N(6)-H], 8.65s [1H, C(2)–H], 8.61s [1H, C(8)–H], 7.38br d [2H, *o*-C_6H_5, J_{est} = 6.6 Hz], 7.32br t [2H, *m*-C_6H_5, J_{est} = 6.6 Hz], 7.28br t [1H, *p*-C_6H_5, J_{est} = 6.6 Hz], 4.85br d [2H, C(10)–H, J_{est} = 5.7 Hz]
	$AdeC_3$	70	54.3 54.2	6.3 6.3	39.8 39.6	12.84s [1H, N(9)–H], 8.13s [1H, C(2)–H], 8.04s [1H, C(8)–H], 7.60br s [1H, N(6)–H], 3.40br s [2H, C(10)–H], 1.57br hex [2H, C(11)–H, J_{est} = 7.2 Hz], 0.86t [3H, C(12)–H, J_{est} = 7.2 Hz]
	$AdeC_3HCl$	50	41.5 41.4	6.1 6.1	30.2 30.1	9.95br t [1H, N(6)–H], 8.58s [1H, C(2)–H], 8.54s [1H, C(8)–H], 3.54br m [2H, C(10)–H], 1.57 hex [2H, C(11)–H, J_{est} = 7.2 Hz], 0.93t [3H, C(12)–H, J_{est} = 7.2 Hz]
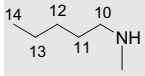	$AdeC_5$	60	57.7 57.3	7.4 7.5	33.4 33.4	12.74br s [1H, N(9)–H], 8.12s [1H, C(2)–H], 8.03s [1H, C(8)–H], 7.58br s [1H, N(6)–H], 3.42br s [2H, C(10)–H], 1.56br m [2H, C(11)–H], 1.27br m [4H, C(12)–H/C(13)–H], 0.83br t [3H, C(14)–H, J_{est} = 7.2 Hz]
	$AdeC_5HCl$	70	49.9 49.7	6.7 6.7	28.8 29.0	9.619br s [1H, N(6)–H], 8.54s [1H, C(2)–H], 8.48s [1H, C(8)–H], 1.61br quint [2H, C(11)–H, J_{est} = 6.9 Hz], 1.26br m [4H, C(12)–H/C(13)–H], 0.84br t [3H, C(14)–H, J_{est} = 6.9 Hz]
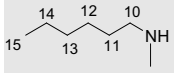	$AdeC_6$	25	60.3 60.3	7.8 7.8	32.2 31.9	12.84br s [1H, N(9)–H], 8.12s [1H, C(2)–H], 8.02s [1H, C(8)–H], 7.58br s [1H, N(6)–H], 3.43br s [2H, C(10)–H], 1.53br t [2H, C(11)–H], 1.25br s [6H, C(12)–H/C(13)–H/C(14)–H], 0.82br s [3H, C(15)–H]
	$AdeC_6HCl$	30	51.8 51.6	7.1 7.1	27.2 27.4	9.57br s [1H, N(6)–H], 8.53s [1H, C(2)–H], 8.47s [1H, C(8)–H], 1.61br quint [2H, C(11)–H], 1.31br m [2H, C(12)–H], 1.26br m [4H, C(13)–H/C(14)–H], 0.83br t [3H, C(15)–H, J_{est} = 6.9 Hz]
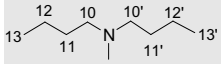	$AdediC_4$	30	62.8 63.2	8.6 8.6	28.2 28.3	12.87br s [1H, N(9)–H], 8.12s [1H, C(2)–H], 8.04s [1H, C(8)–H], 3.91br s [4H, C(10)–H/C(10′)–H], 1.57br quint [4H, C(11)–H/C(11′)–H, J_{est} = 7.2 Hz], 1.29br hex [4H, C(12)–H/C(12′)–H, J_{est} = 7.2 Hz], 0.88 t [6H, C(13)–H/C(13′)–H, J_{est} = 7.2 Hz]
	$AdediC_4HCl$	45	54.5 55.0	7.7 7.8	24.5 24.7	8.40s [1H, C(2)–H], 8.35s [1H, C(8)–H], 3.84br s [4H, C(10)–H/C(10′)–H], 1.62br quint [4H, C(11)–H/C(11′)–H], 1.33br hex [4H, C(12)–H/C(12′)–H, J_{est} = 7.5 Hz], 0.89t [6H, C(13)–H/C(13′)–H, J_{est} = 7.5 Hz]

s = singlet; d = doblet; t = triplet; quint = quintuplet; hex = hexaplet; br = broad; J_{est} = estimated coupling constant.

(methanol): λ 358 (ε 319 × M^{-1} cm^{-1}). Λ_M/Ω^{-1} cm^2 mol^{-1} (10^{-3} mol dm^{-3} in DMSO, 25°C) = 50.

Although complex (**6**) and the structurally solved [H-(creat)][$Ru^{II}Cl_3(DMSO)_3$] (**7**) present the same anion complex unit (see Section 3), comparison of their powder X-ray diffraction patterns revealed that both compounds do not have the same packing. Details of the synthesis and description of the structure of the creatinine complex (**7**) are included in the Supplementary data (Appendix B).

2.3. X-ray crystallography

Suitable crystals of (**1**), (**2**), (**3**) and (**7**) were selected for X-ray single crystal diffraction experiments and mounted at the tip of glass fibres on an Enraf-Nonius CAD4 diffractometer producing graphite monochromated Mo Kα radiation (λ = 0.71073 Å). In each case, after the random search of 25 reflections, the indexation procedure gave rise to the cell parameters (see Table 2 for a summary of the crystal data). Intensity data were collected in the ω–2θ scan mode and corrected for Lorenz and polarization effects. The absorption correction was performed following the empirical Ψ-scan [20] (**7**) and DIFABS [21] (**1**, **2** and **3**) methods. The structural resolution procedure was made using the WInGX package [22]. Solving for structure factor phases was performed by SIR2002 [23] (**7**) and SIR2004 [24] (**1**, **2** and **3**), and the full matrix refinement by SHELXL97 [25] for all of them. Non-H atoms were refined anisotropically and H-atoms were introduced in calculated positions and refined riding on their parents atoms except for protonation sites (**1**, **2** and **3**). H-atoms of protonation [H(3)] were located in Fourier maps and refined isotropically. A summary of refinement parameters can also be seen in Table 2. In **1**, **2** and **3**, the coordinated DMSO present rotational disorder which has been modelled assuming two fragments with complementary occupancies. Also, the aliphatic chain of the adenines has been split in two (**1**) or four (**2**) different positions to account for the observed disorder.

2.4. Preparation of adducts DNA–metal complexes

Fifteen nanograms of pBR322 DNA were incubated in an appropriate volume with the required complex concentration corresponding to the molar ratio ri = 0.5. Ruthenium complexes were dissolved in HEPES buffer (4 mM HEPES, 10 mM KCl and 2 mM $MgCl_2$, pH 7.4). The different solutions were passed through 0.2 nm FPO30/3 filters (Scheicher & Schuell, Germany). The incubation was run at 37 °C for 4 h.

2.5. Atomic force microscopy (sample preparation and imaging)

Samples were prepared by placing a drop (3 μl) of DNA solution or DNA–metal solution onto freshly cleaved green mica (Ted Pella, Inc., CA, US). After adsorption for 5 min at room temperature, the sample was gently rinsed with MilliQ water and dried under a stream of compressed argon gas. Imaging was performed using a multimode atomic force microscope with a Nanoscope IIIa controller (Veeco/Digital Instruments, Santa Barbara, CA, USA) operating in air and at room temperature (t = 23 ± 2 °C) and a relative humidity (RH) always lower than 45%. Commercially available cantilevers (NCH Pointprobe, Nanosensors, Norderfriedrichskoog, Germany) were used for tapping mode scanning with a root mean square amplitude of 0.7 V (~9 nm) and a drive frequency of ~300 kHz. Images were captured in height mode at a scan rate of ~1 Hz in a 512 × 512 pixel format.

Table 2
Selected crystallographic data for the compounds **7**, **1**, **2** and **3**

Identification code	**7**	**1**	**2**	**3**
Empirical formula	$C_{10}H_{26}Cl_3N_3O_4RuS_3$	$C_{12}H_{22}Cl_4N_5ORuS$	$C_{13}H_{24}Cl_4N_5ORuS$	$C_{15}H_{28}Cl_4N_5ORuS$
Formula weight	555.94	527.28	541.30	569.36
T (K)	293(2)	294(2)	294(2)	294(2)
Wavelength (Å)	0.71073	0.71073	0.71073	0.71073
Crystal system	orthorhombic	orthorhombic	orthorhombic	monoclinic
Space group	*Pnaa*	$P2_12_12_1$	$P2_12_12_1$	$P2_1/c$
a (Å)	14.107(3)	7.6917(15)	7.826(3)	13.105(3)
b (Å)	16.589(3)	13.101(3)	13.311(4)	12.979(3)
c (Å)	17.594(2)	20.008(5)	20.350(7)	14.771(3)
β (°)				113.97(3)
V (Å^3)	4117.4	2016.2(8)	2119.9(13)	2295.7(10)
Z	8	4	4	4
D_{calc} (Mg/m^3)	1.794	1.737	1.696	1.647
Absorption coefficient (mm^{-1})	1.475	1.422	1.355	1.255
F(000)	2256	1060	1092	1156
Crystal size (mm^3)	0.78 × 0.16 × 0.12	0.37 × 0.28 × 0.12	0.45 × 0.06 × 0.03	0.27 × 0.15 × 0.15
θ Range for data collection (°)	2.22–30.41	1.86–24.99	1.83–24.98	1.7–26.96
Index ranges	$-20 \leqslant h \leqslant 0$	$-9 \leqslant h \leqslant 9$	$-9 \leqslant h \leqslant 9$	$-16 \leqslant h \leqslant 15$
	$-23 \leqslant k \leqslant 0$	$0 \leqslant k \leqslant 15$	$0 \leqslant k \leqslant 15$	$0 \leqslant k \leqslant 16$
	$0 \leqslant l \leqslant 25$	$0 \leqslant l \leqslant 23$	$0 \leqslant l \leqslant 24$	$0 \leqslant l \leqslant 18$
Reflections collected	6223	3522	3704	5008
Independent reflections	6223	3522	3704	5008
Completeness to final theta (%)	99.8	99.8	100	100
Absorption correction	Ψ-scan	empirical (DIFABS)		
Maximum and minimum transmission	0.8429 and 0.7352	0.8479 and 0.6213	0.9605 and 0.5808	0.8341 and 0.728
Refinement method	Full-matrix least-squares on F^2			
Data/restraints/parameters	6223/0/224	3522/393/290	3704/553/400	5008/81/281
Goodness-of-fit on F^2	1.018	0.828	0.896	1.003
Final R indices [$I > 2\sigma(I)$]	$R_1 = 0.0340$	$R_1 = 0.0729$	$R_1 = 0.0764$	$R_1 = 0.0589$
	$wR_2 = 0.0945$	$wR_2 = 0.1124$	$wR_2 = 0.1108$	$wR_2 = 0.1387$
R indices (all data)	$R_1 = 0.0597$	$R_1 = 0.215$	$R_1 = 0.223$	$R_1 = 0.1054$
	$wR_2 = 0.0993$	$wR_2 = 0.1415$	$wR_2 = 0.1398$	$wR_2 = 0.1553$
Absolute structure parameter		0.00 (TWIN refinement)	−0.05(13)	
Largest difference peak and hole (e Å^{-3})	1.369 and −0.577	0.54 and −0.868	0.471 and −0.673	0.772 and −0.576

2.6. Gel electrophoresis of drug-pBR322 complexes

pBR322 DNA aliquots (0.25 μg/mL) were incubated in TE buffer (10 mM Tris–HCl, 1 mM EDTA, pH 7.5) at molar ratio ri = 0.50 for electrophoresis study. Incubation was carried out in the dark at 37 °C for 24 h. 4 μL of charge marker were added to aliquots parts of 20 μL of the compound–DNA complex. The mixture was electrophoresed in agarose gel (1% in TBE buffer, Tris–Borate–EDTA) for 5 h at 1.5 V/cm. Afterwards, the DNA was dyed with ethydium bromide solution (0.75 μg/mL in TBE) for 6 h. A sample of free DNA was used as control. The experiment was carried out in an ECOGEN horizontal tank connected to a PHARMACIA GPS 200/400 variable potential power supply and the gel was photographed with an image Master VDS, Pharmacia Biotech.

3. Results and discussion

3.1. Description of X-ray structures [$Ru^{III}Cl_4$(DMSO)[H-(N^6-pentyladenine)]] (**1**), [$Ru^{III}Cl_4$(DMSO)[H-(N^6-hexyladenine)]] (**2**) and [$Ru^{III}Cl_4$(DMSO)[H-(N^6,N^6-dibutyladenine)]] (**3**)

The zwitterionic inner-sphere complexes (**1**), (**2**) and (**3**) (Figs. 1–3) present slightly distorted octahedral coordination around Ru(III) ion with four chlorido ligands in the basal plane and the two axial positions occupied by a S atom of a DMSO molecule and the N(9) atom present in the corresponding purine ring. These complexes show a similar disposition to that found in NAMI-A [4].

Previous crystallographic studies have demonstrated that the most probable site of coordination on unsubstituted purines is the imidazole N(9) nitrogen atom. When N(9) is blocked, N(7) is the site of coordination and there are only few exceptions that violate these general guidelines [26].

All Ru(III) complexes show metal–nitrogen [2.139(12) for (**1**), 2.113(12) for (**2**) and 2.141(4) Å for (**3**)] and metal–sulfur bond lengths [2.272(5) for (**1**), 2.264(5) for (**2**) and 2.2629(16) for (**3**)], comparable to those of related complexes [13,15,27]. The Ru–Cl bond distances [ranging from 2.325(4) to 2.359(4) Å for (**1**), 2.329(4) to 2.350(4) Å for (**2**) and 2.3439(18) to 2.3607(17) Å for (**3**)] are in agreement with published values found in the related structures above mentioned. The same can be mentioned with the *cis* angles around the metal which vary between 86.7(3)° and 94.14(17)° for (**1**), 87.6(3)° and 94.49(18)° for (**2**) and 87.73(14)° and 93.39(7)° for (**3**), while the *trans* angles are between 176.44(19)° and 178.5(4)° for (**1**), 177.80(18)° and 177.25(17)° for (**2**) and 176.34 (15)° and 177.56(6)° for (**3**). On the other hand, a comparison between the protonated adenines [(**1**), (**2**) and (**3**)] and neutral adenine shows a more significant increment of the C(2)–N(3)–C(4) angle which is in agreement with N(3) protonation [26]. Selected bond distances and angles are shown in Table 3.

As observed previously [15], in the three complexes the protonated adenine ligand is involved in an intramolecular hydrogen bond with *cis* chlorido ligand: N(3)–H···Cl = 2.68 for (**1**), 2.60 for (**2**) and 2.54 for (**3**).

By comparison of powder X-ray diffraction patterns of complex (**6**) and the structurally solved [H-(creat)][$Ru^{II}Cl_3$(DMSO)$_3$] (**7**) it is possible to deduce that both compounds do not have the same packing. Detailed description of the structure of the outer-sphere creatinine complex [H-(creat)][$Ru^{II}Cl_3$(DMSO)$_3$] (**7**) is included in the Supplementary data. The anion has a facial octahedral structure with three chlorido ligands and three DMSO (coordinated

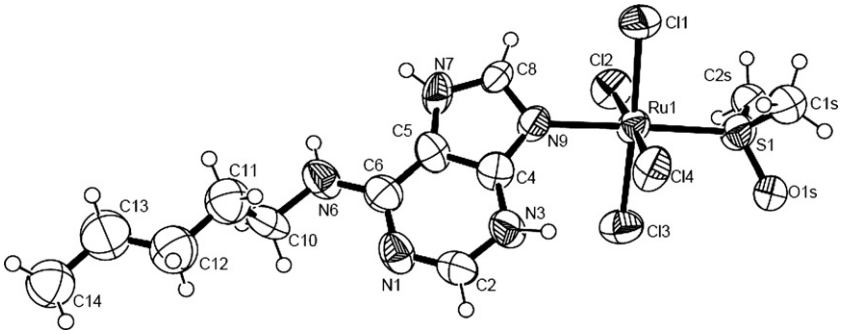

Fig. 1. ORTEP of [$Ru^{III}Cl_4$(DMSO)[H-(N^6-pentyladenine)]] (**1**). Displacement ellipsoids are drawn at 50% probability level and H atoms are drawn as circles of arbitrary radii.

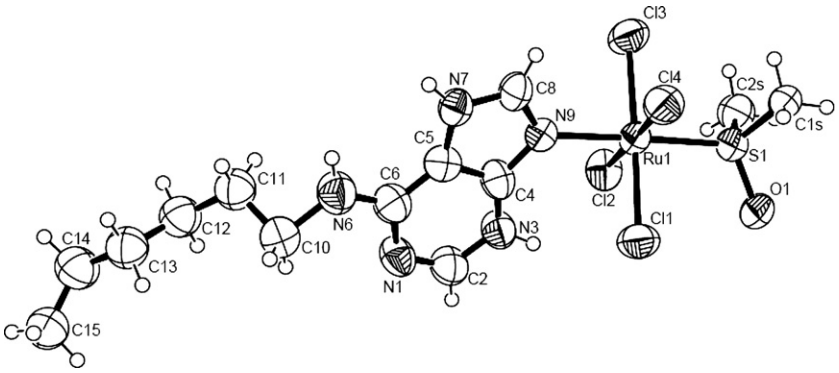

Fig. 2. ORTEP of [$Ru^{III}Cl_4$(DMSO)[H-(N^6-hexyladenine)]] (**2**). Displacement ellipsoids are drawn at 50% probability level and H atoms are drawn as circles of arbitrary radii.

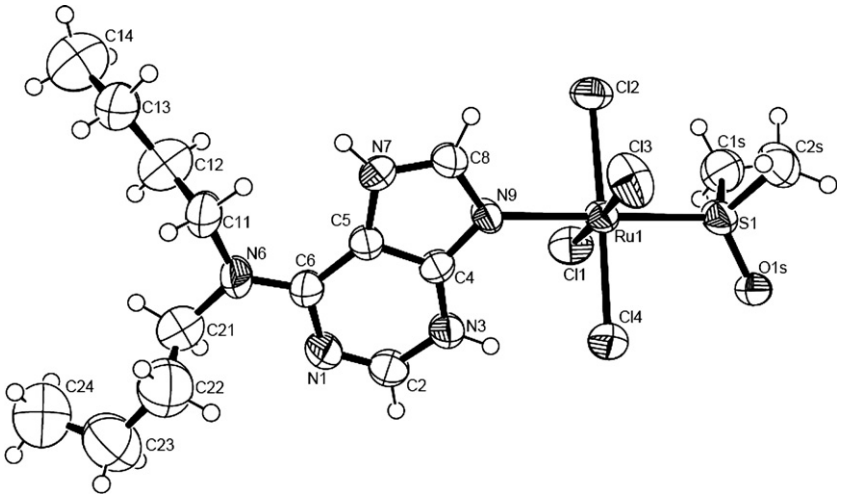

Fig. 3. ORTEP of [$Ru^{III}Cl_4$(DMSO)[H-(N^6-dibutyladenine)]] (**3**). Displacement ellipsoids are drawn at 50% probability level and H atoms are drawn as circles of arbitrary radii.

via *S*) molecules (Fig. 4). Selected bond distances and angles are shown in Table 2 of Supplementary data.

3.2. Infrared spectra

The IR spectra of inner-sphere complexes, [$Ru^{III}Cl_4$(DMSO)[H-(N^6-pentyladenine)]] (**1**), [$Ru^{III}Cl_4$(DMSO)[H-(N^6-hexyladenine)]] (**2**), [$Ru^{III}Cl_4$(DMSO)[H-(N^6,N^6-dibutyladenine)]] (**3**), [$Ru^{III}Cl_4$(DMSO)[H-(N^6-propyladenine)]] · 0.5EtOH (**4**) and [$Ru^{III}Cl_4$(DMSO)[H-(BAP)]] · 0.5H_2O (**5**) were compared with those of protonated ligands. Tentative band assignments (cm^{-1}) for N^6-substituted adenines according to literature [28–30] and some characteristic changes in the complex bands are shown in Table 4. The most relevant features are related to the binding between the Ru(III) and a nitrogen atom of the purine ring [bond through the N(9) atom of adenine and protonation of the N(3) atom]. These changes are: (i) very small shifts on the bands related to [δ(NHR)] and [δ(C=N–H)] of protonated N^6-substituted adenine which indicate the zwitterionic form of the complexes. The bands appearing at 1662–1668 cm^{-1} and 1611–1615 cm^{-1} show small shifts probably as a consequence of a change in H-bonding (in complex **3**, only one band is observed at 1637 cm^{-1}); (ii) The 1513–1520 cm^{-1} band assignable to ν[C(4)–N(9)] + δ[C(8)–H] + δ[CH_2] disappears in all spectra of the complexes; iii) The band at *ca.* 1460 cm^{-1} related

Table 3
Selected bond lengths (Å) and bond angles (°) for complexes **1–3**

[Ru^{III}Cl$_4$(DMSO)][H-(N^6-pentyladenine)]] **1**			
Ru(1)–S(1)	2.272(5)	Ru(1)–Cl(1)	2.325(4)
Ru(1)–N(9)	2.139(12)	Ru(1)–Cl(2)	2.342(4)
S(1)–O(1S)	1.48(2)	Ru(1)–Cl(3)	2.328(5)
		Ru(1)–Cl(4)	2.359(4)
N(9)–Ru(1)–S(1)	178.5(4)	N(9)–Ru(1)–Cl(1)	88.5(4)
S(1)–Ru(1)–Cl(1)	92.77(17)	N(9)–Ru(1)–Cl(2)	86.7(3)
S(1)–Ru(1)–Cl(2)	94.14(17)	N(9)–Ru(1)–Cl(3)	88.6(4)
S(1)–Ru(1)–Cl(3)	90.09(17)	N(9)–Ru(1)–Cl(4)	90.6(3)
S(1)–Ru(1)–Cl(4)	88.55(16)	Cl(1)–Ru(1)–Cl(3)	176.44(19)
Cl(1)–Ru(1)–Cl(2)	88.47(18)	Cl(3)–Ru(1)–Cl(2)	89.21(17)
Cl(1)–Ru(1)–Cl(4)	92.03(17)	Cl(3)–Ru(1)–Cl(4)	90.16(16)
Cl(2)–Ru(1)–Cl(4)	177.24(17)	C(2)–N(3)–C(4)	118.4(17)
C(6)–N(1)–C(2)	119.2(17)		
[Ru^{III}Cl$_4$(DMSO)][H-(N^6-hexyladenine)]] **2**			
Ru(1)–S(1)	2.264(5)	Ru(1)–Cl(1)	2.329(4)
Ru(1)–N(9)	2.113(12)	Ru(1)–Cl(2)	2.350(4)
S(1)–O(1S)	1.561(19)	Ru(1)–Cl(3)	2.337(4)
		Ru(1)–Cl(4)	2.346(4)
N(9)–Ru(1)–S(1)	177.6(4)	N(9)–Ru(1)–Cl(1)	88.4(3)
S(1)–Ru(1)–Cl(1)	90.43(16)	N(9)–Ru(1)–Cl(2)	89.8(3)
S(1)–Ru(1)–Cl(2)	88.10(16)	N(9)–Ru(1)–Cl(3)	89.6(3)
S(1)–Ru(1)–Cl(3)	91.62(16)	N(9)–Ru(1)–Cl(4)	87.6(3)
S(1)–Ru(1)–Cl(4)	94.49(18)	Cl(1)–Ru(1)–Cl(3)	177.80(18)
Cl(1)–Ru(1)–Cl(2)	89.43(16)	Cl(3)–Ru(1)–Cl(2)	91.42(16)
Cl(1)–Ru(1)–Cl(4)	89.63(16)	Cl(3)–Ru(1)–Cl(4)	89.43(16)
Cl(2)–Ru(1)–Cl(4)	177.25(17)	C(2)–N(3)–C(4)	118.9(8)
C(6)–N(1)–C(2)	117.8(8)		
[Ru^{III}Cl$_4$(DMSO)][H-(N^6-dibutyladenine)]] **3**			
Ru(1)–S(1)	2.2629(16)	Ru(1)–Cl(1)	2.3439(18)
Ru(1)–N(9)	2.141(4)	Ru(1)–Cl(2)	2.3607(17)
S(1)–O(1S)	1.515(10)	Ru(1)–Cl(3)	2.3465(18)
		Ru(1)–Cl(4)	2.3511(17)
N(9)–Ru(1)–S(1)	176.34(15)	N(9)–Ru(1)–Cl(1)	87.42(14)
S(1)–Ru(1)–Cl(1)	89.02(7)	N(9)–Ru(1)–Cl(2)	87.73(14)
S(1)–Ru(1)–Cl(2)	91.40(6)	N(9)–Ru(1)–Cl(3)	90.14(14)
S(1)–Ru(1)–Cl(3)	93.39(7)	N(9)–Ru(1)–Cl(4)	90.10(14)
S(1)–Ru(1)–Cl(4)	90.84(6)	Cl(1)–Ru(1)–Cl(3)	177.10(7)
Cl(1)–Ru(1)–Cl(2)	89.99(7)	Cl(3)–Ru(1)–Cl(2)	88.34(7)
Cl(1)–Ru(1)–Cl(4)	91.00(7)	Cl(3)–Ru(1)–Cl(4)	90.57(8)
Cl(2)–Ru(1)–Cl(4)	177.56(6)	C(2)–N(3)–C(4)	117.4(6)
C(6)–N(1)–C(2)	121.0(5)		

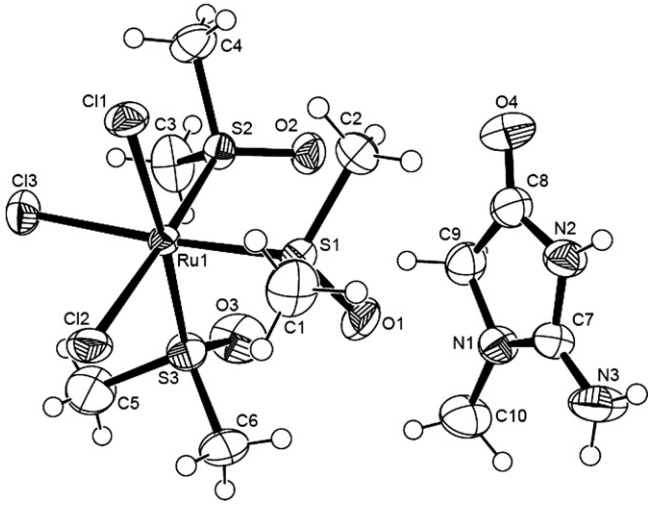

Fig. 4. ORTEP of [H-creat][Ru^{II}Cl$_3$(DMSO)$_3$] (**7**). Displacement ellipsoids are drawn at 50% probability level and H atoms are drawn as circles of arbitrary radii.

to ν[C(8)–N(9)] splits into a shoulder at *ca.* 1480 cm^{-1} and a medium intensity band between 1440 and 1460 cm^{-1}. These features agree with the coordination of Ru to the N(9) atom of the adenine ligand. Finally, strong bands at *ca.* 1070 cm^{-1} assignable to ν(S=O) of the S-bonded DMSO molecules and *ca.* 1020 cm^{-1} [ρ_r(CH$_3$)] as well as a weak intensity peak at *ca.* 430 cm^{-1} related to ν(Ru–S) modes, are observed in all the complexes.

The IR spectrum of the outer-sphere complex [H-(BAP)][Ru^{II}Cl$_3$(DMSO)$_3$] (**6**) was compared with that of [H-(creat)][Ru^{II}Cl$_3$(DMSO)$_3$] (**7**) (See Supplementary data). Both spectra are typical of *fac*-[Ru^{II}Cl$_3$(DMSO)$_3$]$^-$ units in which two strong bands are observed. The first one at 1095 cm^{-1} with small shoulder at *ca.* 1080 cm^{-1} due to ν(S=O) of the S-bonded DMSO molecules and the second at 1019 cm^{-1} corresponding to ρ_r(CH$_3$). The bands due to ν(ring) exhibit essentially the same pattern of that observed for the protonated ligand with important differences with respect to the spectra of the inner-sphere complexes. The medium intensity peak at 428 cm^{-1} is related to ν(Ru–S).

3.3. ^{1}H NMR spectra of Ru(II) compounds

The ^{1}H NMR spectrum of [H-(BAP)][Ru^{II}Cl$_3$(DMSO)$_3$] (**6**) in D$_2$O shows three singlets between 3.37 and 3.27 ppm attributed to the methyl protons of dimethylsulphoxide [31]. The presence of more than one signal in D$_2$O results from the formation of different aquospecies as has been previously reported in the literature [16]. In a few days, the solution turns to greenish gray and the signals of the spectrum show a progressive broadening and shifting which are indicative of decomposition of the complex and presence of paramagnetic Ru(III) species. On the other hand, the corresponding spectrum in DMSO-d_6 shows only one signal for the six equivalent methyl groups of dimethylsulphoxide at 3.29 ppm, as it was expected. Similar results are obtained in the corresponding creatinine complex [H-(creat)][Ru^{II}Cl$_3$(DMSO)$_3$] (**7**).

3.4. Electronic spectra

The electronic spectra of the **1–4** complexes were obtained in methanol solution and are suggestive of octahedral geometry around Ru(III). As observed in similar Ru(III) compounds a band centred at 400 nm with charge-transfer character is observed [($\varepsilon = 1.94 \times 10^3$) for **1**; ($1.58 \times 10^3$) for **2**; ($3.39 \times 10^3$) for **3** and ($1.82 \times 10^3$) for **4**]. The electronic spectrum of complex **5** was performed in DMSO solution due to its low solubility in MeOH, [405 nm ($\varepsilon = 1.35 \times 10^3$)]. Moreover, an important band corresponding to the $\pi \rightarrow \pi^*$ transition of the protonated adenine ring, is present [280 (1.1×10^4) for **1**; 277 (1.57×10^4) for **2**; 288 (2.08×10^4) for **3**, 275 (1.08×10^4) for **4** and 282 (6.3×10^3) for **5**]. A freshly solution was used in all our measurements in order to avoid the known hydrolysis processes of these Ru(III) complexes in methanol [16].

The electronic spectrum of the complex [H-(BAP)][Ru^{II}Cl$_3$(DMSO)$_3$] (**6**) was obtained in a freshly prepared methanol solution and is suggestive of octahedral geometry around Ru(II). The observed band at 358 ($\varepsilon = 319$) nm is assigned to the transition $^1A_{1g} \rightarrow {}^1T_{1g}$.

3.5. Ruthenium complexes–plasmidic DNA interactions

Atomic force microscopy and electrophoretic mobility (Figs. 5 and 6, respectively) were used to verify the interactions of isolated ruthenium complexes and DNA pBR322. Plasmidic DNA was incubated for 4 h at 37 °C with the series of complexes **1–5** at identical concentrations.

In Fig. 5a plasmid pBR322 DNA without previous treatment, in mixed covalently closed circular (ccc) and open (oc) forms, was AFM imaged. AFM images of the same DNA treated with the complexes **1–5** are presented in Fig. 5b–f. There are not noticeable differences in the images corresponding to the different complexes.

Table 4
Selected IR bands (cm^{-1}) for the complexes and tentative assignments

	$AdeC_5 \cdot HCl$	(**1**)	$AdeC_6 \cdot HCl$	(**2**)	$AdediC_4 \cdot HCl$	(**3**)	$AdeC_3 \cdot HCl$	(**4**)	$BAP \cdot HC1$	(**5**)	(**6**)
δ(NHR)	1668s	1665s	1665s	1663s		1635s	1668s	1659s	1662s	1656vs	1652vs
δ[C=N–H] ν(ring)	1615m	1620m	1614m	1620w	1637s	1607s	1615m	1618m	1611m	1618sh	1607m
	1578w	1579w	1578m	1579w	1580s	1562m	1582m	1576m	1574m	1573m	1571m
	1519m		1518m		1520m		1519w		1513m		1509w
		ov.(sh)*		ov.(sh)	1483m	ov.(sh)		1487s		ov.(sh)	
ν(ring)**	1463s				1467sh	1460m	1470w	1457m	1450m	1449m	1453m
		1444m	1456m	1441m	1456m		1437m	1426m			
	1396m	1404m	1395m	1403m	1410m	1402m	1395m	1399m	1394m	1409m	1393m
	1373w	1378w	1374m	1377m	1376m	1370m	1385m	1377m		1375m	
	1346w	1340w	1345m	1340w	1350m	1350m	1345m	1340m*	1344m	1342m	1347m
ν(S=0)		1112m		1111m		1108sh		ov.(sh)		1117m	
(DMSO)		1067s		1066s		1080s		1066s		1065s	1095s
$\rho_r(CH_3)$		1019s		1019s		1023m		1017s		1023m	1019m
ν(Ru–S)		428w		427w		427w		427m		432w	424m

* [ν = stretching, δ = bending, s = strong, m = medium, w = weak, br = broad, sh = shoulder, ov. = overlapping].
** ν (ring bands) Refs. [28–30]: 1513–1520 cm^{-1}: ν[C(4)–N(9)] + δ[C(8)–H] + δ[CH_2]; 1450–1467 cm^{-1}: δ[C(2)–H] + ν[C(8)–N(9)] + δ[C(8)–H].

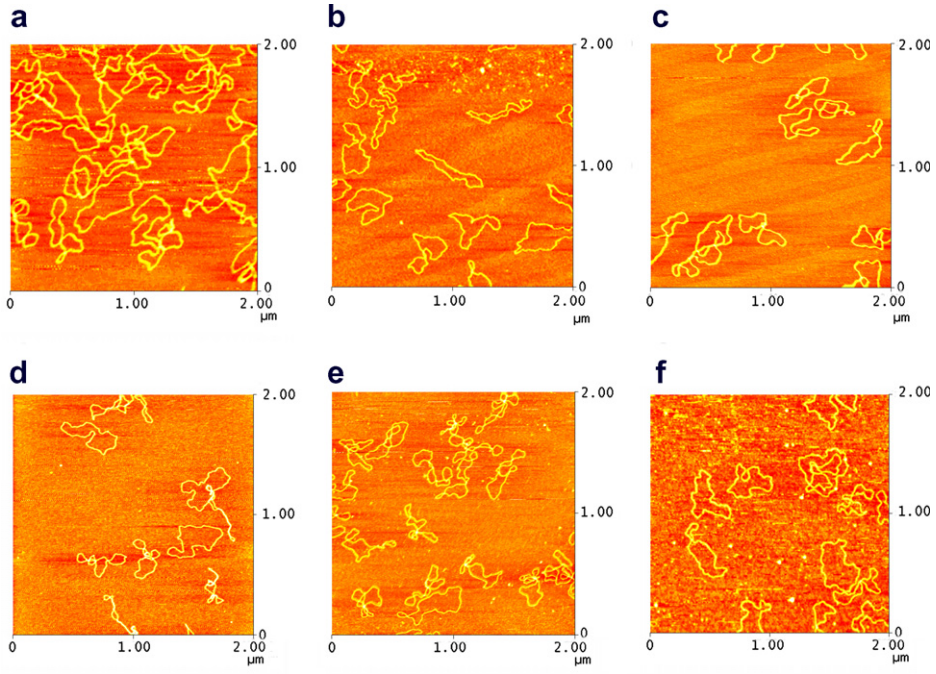

Fig. 5. Plasmidic DNA pBR322 (a), incubated in presence of: [$Ru^{III}Cl_4$(DMSO)[H-(N^6-pentyladenine)]] (**1**), (b); [$Ru^{III}Cl_4$(DMSO)[H-(N^6-hexyladenine)]] (**2**) (c); [$Ru^{III}Cl_4$(DMSO)[H-(N^6-dibutyladenine)]] (**3**) (d); [$Ru^{III}Cl_4$(DMSO)[H-(N^6-propyladenine)]]·0.5EtOH (**4**) (e). [$Ru^{III}Cl_4$(DMSO)[H-(BAP)]] · 0.5H_2O (**5**) (f). In all cases, Ru:DNA base pairs relationship is 1:20 (each circular plasmid has 4361 base pairs).

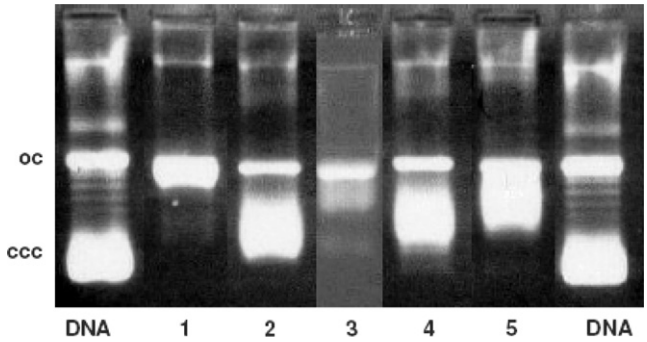

Fig. 6. Electrophoresis experiments: Plasmidic DNA pBR322 (DNA control), incubated in presence of: [$Ru^{III}Cl_4$(DMSO)[H-(N^6-pentyladenine)]] (**1**), [$Ru^{III}Cl_4$-(DMSO)[H-(N^6-hexyladenine)]] (**2**), [$Ru^{III}Cl_4$(DMSO)[H-(N^6-dibutyladenine)]] (**3**), [Ru^{III}-Cl_4(DMSO)[H-(N^6-propyladenine)]] · 0.5EtOH (**4**), [$Ru^{III}Cl_4$(DMSO)[H-(BAP)]] · 0.5H_2O (**5**).

Probably the type of interaction is identical for all the series and the variation of the nature and length of the chain do not affect it. However, in all of them, kinks can be observed confirming interaction with DNA in agreement with electrophoretic mobility results. Nuclease activity is not observed in the different complexes and the modifications indicated confirm that these complexes do not cleave the pBR322 plasmid DNA. They yield more coiled and/or more associated plasmids which are in agreement with different types of interactions between these ruthenium complexes and the corresponding DNA: ruthenium covalent binding to the heterocyclic nitrogens, intercalation of the adenine ring and electrostatic interaction of the protonated nitrogens and the phosphate groups of other plasmidic units.

The influence of the compounds on the tertiary structure of DNA was determined by its ability to modify the electrophoretic mobility of the covalently closed circular (ccc) and open (oc) forms of pBR322 plasmid DNA. Fig. 6 shows, from left to right,

the mobility of the native pBR322 plasmid DNA and the plasmid DNA incubated with the compounds **1–5**. The behavior of the gel electrophoretic mobility of these two forms, ccc and oc, of pBR322 plasmid and DNA ruthenium compounds adducts (Fig. 6) presents differences in comparison to the DNA pattern. Incubation with complexes (**1**) and (**3**) show that only the form oc of DNA is present, while in case of the other compounds (**2**), (**4**) and (**5**) the DNA pattern is modified showing a wide band with lower mobility than ccc form of free plasmid control as it was observed previously [15]. Probably, the insertion of the purine ligand in the double helix origins opening of the DNA forms. We are aware that under physiological conditions ruthenium compounds are prone to various hydrolytic processes [2,17,22,57] but the exact study of such reactions was out of the scope of this work.

Acknowledgements

We are grateful to Dirección General de Investigación Projects CTQ2006-09339/BQU and CTQ2005-01834 for financial support. FMA and MB-O acknowledge grants of Conselleria d'Economia, Hisenda i Innovació (Govern de les Illes Balears).

Appendix A. Supplementary data

CCDC 676147, 676148, 676149 and 676150 contains the supplementary crystallographic data for **7**, **1**, **2** and **3**. These data can be obtained free of charge via http://www.ccdc.cam.ac.uk/conts/retrieving.html, or from the Cambridge Crystallographic Data Centre, 12 Union Road, Cambridge CB2 1EZ, UK; fax: (+44) 1223-336-033; or e-mail: deposit@ccdc.cam.ac.uk. Supplementary data associated with 373 this article can be found, in the online version. Supplementary data associated with this article can be found, in the online version, at doi:10.1016/j.poly.2008.06.013.

References

[1] M.J. Clarke, F. Zhu, D.R. Frasca, Chem. Rev. 99 (1999) 2511.
[2] M.J. Clarke, Coord. Chem. Rev. 236 (2003) 209.
[3] E. Reisner, V.B. Arion, M.F.C. Guedes da Silva, R. Lichtenecker, A. Eichinger, B.K. Keppler, V.Y. Kukushkin, A.J. Pombeiro, Inorg. Chem. 43 (2004) 7083.
[4] G. Sava, E. Alessio, A. Bergamo, G. Mestroni, in: M.J. Clarke, P.J. Sadler (Eds.), Topics in Biological Inorganic Chemistry, vol. 1, Springer, Berlin, 1999, pp. 143–170.
[5] E. Alessio, G. Mestroni, A. Bergamo, G. Sava, in: A. Sigel, H. Sigel (Eds.), Metal Ions in Biological Systems, vol. 42, M. Dekker, New York, 2004, pp. 323–351.
[6] J.M. Redemaker-Lakhai, D. van der Bongard, D. Pluim, J.H. Beijnen, J.H.M. Schellens, Clin. Cancer Res. 10 (2004) 3717.
[7] I. Bratsos, B. Serli, E. Zangrando, N. Katsaros, E. Alessio, Inorg. Chem. 46 (2007) 975.
[8] J. Malina, O. Novakova, B.K. Keppler, E. Alessio, V. Brabec, J. Biol. Inorg. Chem. 6 (2001) 435.
[9] D.W. Mok, M.C. Mok, Annu. Rev. Plant Physiol. Plant Mol. 89 (2001) 89.
[10] M. Malon, Z. Trávnícek, M. Marysko, R. Zboril, M. Maslán, J. Marek, K. Dolezal, J. Rolcík, V. Krystof, M. Strnad, Inorg. Chim. Acta 323 (2001) 119.
[11] Z. Travnicek, I. Popa, M. Cajan, R. Herchel, J. Marek, Polyhedron 26 (2007) 5271. and references therein.
[12] I. Turel, M. Pecanac, A. Golobic, E. Alessio, B. Serli, Eur. J. Inorg. Chem. (2002) 1928.
[13] I. Turel, M. Pecanac, A. Golobic, E. Alessio, B. Serli, A. Bergamo, G. Sava, J. Inorg. Biochem. 98 (2004) 393.
[14] C. Price, M.R.J. Elsegood, W. Clegg, N.H. Rees, A. Houlton, Angew. Chem., Int. Ed. Engl. 36 (1997) 1762.
[15] A. García-Raso, J.J. Fiol, A. Tasada, M.J. Prieto, V. Moreno, I. Mata, E. Molins, T. Bunic, A. Golobic, I. Turel, Inorg. Chem. Commun. 8 (2005) 800.
[16] E. Alessio, G. Balducci, G.M. Calligaris, G. Costa, W.M. Attia, G. Mestroni, Inorg. Chem. 30 (1991) 609.
[17] I.P. Evans, A. Spencer, G. Wilkinson, J. Chem. Soc., Dalton Trans. (1973) 204.
[18] J.H. Lister, J. Chem. Soc. (1960) 3394.
[19] A. García-Raso, J.J. Fiol, F. Bádenas, A. Tasada, X. Solans, M. Font-Bardia, M.G. Basallote, M.A. Máñez, M.J. Fernández-Trujillo, D. Sánchez, J. Inorg. Biochem. 93 (2003) 141.
[20] A.C.T. North, D.C. Phillips, F.S. Mathews, Acta Crystallogr., Sect. A 24 (1968) 351.
[21] N. Walker, D. Stuart, Acta Crystallogr., Sect. A 39 (1983) 158.
[22] L.J. Farrugia, J. Appl. Crystallogr. 32 (1999) 837.
[23] M.C. Burla, M. Camalli, B. Carrozzini, G.L. Cascarano, C. Giacovazzo, G. Polidori, R. Spagna, J. Appl. Crystallogr. 36 (2003) 1103.
[24] M.C. Burla, R. Caliandro, M. Camalli, B. Carrozzini, G.L. Cascarano, L. De Caro, C. Giacovazzo, G. Polidori, R. Spagna, J. Appl. Crystallogr. 38 (2005) 381.
[25] G.M. Sheldrick, SHELXL97, Program for Crystal Structure Analysis (Release 97-2), University of Göttingen, Göttingen, Germany, 1997.
[26] D.J. Hodgson, in: S.J. Lippard (Ed.), Prog. Inorg. Chem, vol. 23, John Wiley and Sons, New York, 1977, pp. 211–254. and references therein.
[27] A.H. Velders, A. Bergamo, E. Alessio, E. Zangrando, J.G. Haasnoot, C. Casarsa, M. Cocchietto, S. Zorzet, G. Sava, J. Med. Chem. 47 (2004) 1110.
[28] M. Tsuboi, S. Takahashi, I. Harada, in: J. Duchesne (Ed.), Physiochemical Properties of Nucleic Acids, vol. 2, Academic Press, London, 1973, pp. 91–145.
[29] M. Tsuboi, in: P.O.P. Ts'O (Ed.), Basic Principles in Nucleic Acid Chemistry, vol. 1, Academic Press, New York, 1974, pp. 406–416.
[30] G. Cervantes, J.J. Fiol, A. Terrón, V. Moreno, J.A. Alabart, M. Aguiló, M. Gómez, X. Solans, Inorg. Chem. 29 (1990) 5168.
[31] R.S. McMillan, A. Mercer, B.R. James, J. Trotter, J. Chem. Soc., Dalton Trans. (1975) 1006.

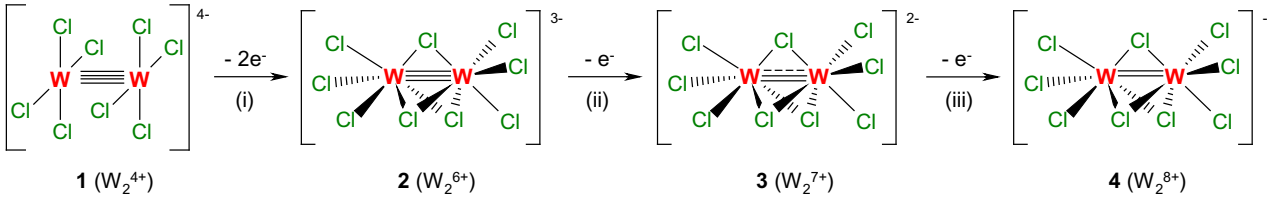

Scheme 1.

However, despite the rich and facile redox chemistry of the ditungsten center W_2^{n+} ($n = 4, 6, 7$) the application of these complexes in catalysis has been largely unexploited. This can be attributed to several reasons. In aqueous or aqueous acidic media (HCl 3–12 M) the chemistry of the alkali salts of these compounds is in general complex in nature and only **2** is stable [15–17]. In organic media **1**$Na_4(THF)_x$ is stable in THF up to 0 °C and the salts of **2**–**4** with organic cations are soluble and stable in inert organic solvents (CH_2Cl_2, THF), but the synthetic utility of the W_2^{n+} redox couples is impeded by: (a) the great ease of oxidation of **1** to **2** and the difficulty of reducing **2** to **1**; (b) the failure to perform the **2** → **3** oxidation in a convenient and controlled manner; and (c) the inability to obtain **4** directly from the oxidation of **1**–**3**. Additional complications arise from disproportionation and/or comproportionation reactions between **2**, **3** and **4** influenced by the solvent(s), the nature of the counter organic ion(s) and the presence of the halide ligand [10]. Finally, a major obstacle is the complexities entailed by the different synthetic methods for their preparation, especially of the salts with organic cations, which are elaborate or serendipitous.

Attempts to prepare salts of **1** with organic cations from the WCl_4 reduction with Na/Hg amalgam in toluene or THF produced respectively the two- or three-electron oxidized complexes **2**$(HTMPP)_3$ and **3**$(PPN)_2$ (yield 50%), despite the neutral or even reducing conditions. Efforts to obtain **2a** or **2**$(Et_4N)_3$ by mimicking the synthesis of the $[Mo_2(\mu\text{-}Cl)_3Cl_6]^{3-}$ analog [18] e.g. the comproportionation reaction of the halocarbonylmolybdates $[Mo(CO)_5Cl]^-$ with anhydrous molybdenum halides is not applicable with tungsten. Indeed, reaction of $[W(CO)_5Cl]^-$ with WCl_6 in CH_2Cl_2 in the presence of TBACl gives a mixture of $[WCl_6]^-$, $[WCl_6]^{2-}$ and **3a** in low yield (~20%) [19].

The cation exchange pathway from the alkaline salts of **2** [20–24] (addition of TBACl into solutions of **2**K_3 in concentrated hydrochloric acid) has been previously reported [25–29], but the yield is notoriously low, variable, and no experimental details are given. In addition, this methodology requires the demanding synthesis of the alkaline salts obtained from the reduction of the WO_4^{2-} ion in aqueous HCl solutions chemically, electrochemically (**2**K_3) [30,31] or from the oxidation of **1**$Na_4(THF)_x$ (**2**Na_3) [32], and $[W_2(mhp)_4]$ (**2**Cs_3) [33] by $HCl_{(g)}$ in THF or CH_3OH, respectively. Oxidation of **2a** obtained from the latter route with molecular chlorine in CH_2Cl_2 provides **3a** along with decomposition products [13]. Another example of formation of a relevant W_2^{7+} derivative has been the isolation of $TPP[W_2(\mu\text{-}Cl)_3Cl_5(THF)]$ (**5**) formed from the one-electron photochemical oxidation (induced by visible light) of $TPP[W_2(\mu\text{-}Cl)_3Cl_4(THF)_2]$ (**6**) by CCl_4 [34].

Herein, as a part of our studies in exploiting the reactivity of multiply bonded clusters [35] we report novel insights in the redox chemistry of the aforementioned complexes in organic media, by chemical and electrochemical means. This resulted not only in developing new effective preparative methods for the synthesis of **2a**,**b** and **3a**,**b**, but also in conditions where the bimetallic W_2^{n+} ($n = 6, 7$) redox couple becomes functional and a potential candidate for mediating stoichiometric or catalytic oxidations of organic compounds [36].

2. Experimental

2.1. Starting materials

Starting materials and solvents were purchased from Sigma–Aldrich and are of the highest available purities. Chlorobenzene was purchased from Fluka. **1**$Na_4(THF)_x$ [6], **2**K_3 [30], **4**(TEBA) [10], $PhICl_2$ [37], and PhIO [38] were prepared according to literature procedures. TBACl was purified by recrystallization from acetone. Toluene was distilled over Na, THF and diethyl ether over Na/Ph_2CO, MeCN, CH_2Cl_2, and chlorobenzene over P_2O_5 in an inert atmosphere. Acetone was distilled over Drierite. Carbon tetrachloride was fractionally distilled. $HCl_{(g)}$ was passed through a trap containing concentrated H_2SO_4 and subsequently through a tube containing silicon oxide and activated charcoal. DMSO was used without further purification. All solvents were degassed by three freeze-pump-thaw cycles, with the exception of water and methanol, which were degassed by bubbling nitrogen or argon for 0.5 h. All operations were performed under a dinitrogen (99.999%) or argon (99.999%) atmosphere, using Schlenk techniques on an inert gas/vacuum manifold or in a drybox (O_2, H_2O < 1 ppm).

2.2. Physical techniques

UV–Vis spectra were measured on a Hitachi U-2000 or a Varian Cary 50 Bio spectrophotometer. GC–MS experiments were performed on a Varian 3400 CX GC coupled to a Varian Saturn 2000 MS (Column 30 m × 0.25 mm ID, 0.25 μm, DB5-MS; injection 1 μL, 50:1 split; flow 1 mL/min-He, constant flow; oven 50 °C/hold 3.00 min, 7 °C/min to 150 °C, 50 °C/min to 280 °C, 280 °C/hold 2.12 min, 5 °C/min to 300 °C, 300 °C/hold 4.00 min; injector 280 °C; transfer line 280 °C; MSD scan range 10–600 amu). Dihydrogen was detected by gas chromatography (GC; Varian 90-P). Mass spectrometric analyses were done using electrospray ionization on a Thermo-Finnigan TSQ7000 triple-quadrupole. The heated inlet capillary was kept at 250 °C and the electrospray needle voltage was 4.5 kV. All other voltages were optimized to maximize ion transmission and minimize unwanted fragmentation and were determined during the regular tuning and calibration of the instrument. Nitrogen sheath gas was supplied to the electrospray source at 80 psi. Samples were infused into the source at a rate of 10 μL/min using a 500 μL Gastight syringe (Hamilton, Reno, NV) in a Pump 11 syringe pump (Harvard Apparatus, Holliston, MA). The same analyses were also done using a Fisons VG Quattro with a VG Biotech ionization source and CH_2Cl_2 or acetonitrile solutions were infused directly. The capillary voltage was 3.0 or 3.5 V, and the orifice to skimmer potential (cone voltage) was varied between 15 and 45 V depending on sensitivity. The source temperature was 353 K. Mass spectra were recorded with a scan range of m/z 200–2000 for positive and negative ions. EPR measurements were obtained with an upgraded Bruker ER-200D spectrometer interfaced with a personal computer and equipped with an Oxford ESR 900 cryostat, an Anritsu MF76A frequency counter, and a Bruker 035 M NMR gaussmeter. The Signal-Channel unit was replaced with an SR830 digital lock-in amplifier from Stanford Research. The perpendicular

4I02ST cavity was used, and the microwave frequency was 9.41 GHz. Atomic Absorption analyses were done with a GF AAS (Varian SpectrAA-640Z) instrument with Zeeman background correction. Electrochemical measurements were performed with an AUTOLAB PGSTAT100 electrochemical work station (EcoChemie B.V.) in the dry box. Cyclic voltammetry was performed using a Au disk electrode (1.6 mm in diameter) as the working electrode, a thin Pt foil as the counter electrode (8 cm^2) and a Ag/Ag^+ (0.01 M $AgNO_3$ and 0.1 M $TBAPF_6$ in MeCN) non-aqueous reference electrode with a prolonged bridge (0.1 M $TBAPF_6$ in MeCN). The working electrode was polished using successively 6, 3, 1 μm diamond paste on a DP-Nap polishing cloth, all obtained from Struers (Westlake, OH), washed with water, acetone and air-dried. The Pt foil and Pt gauge electrodes were cleaned in a $1 \div 4$ (v/v) $H_2O_2 \div$ concentrated H_2SO_4 solution and oven-dried. The concentration of the samples was 3 mM and the concentration of $TBAPF_6$ (supporting electrolyte) was 0.1 M. The potential sweep rate varied in the limits of 10–1000 mV/s. All of the voltammograms were compensated for the solution resistance. Bulk electrolysis was conducted in the dry-box with a three-compartment H-cell with compartments separated by 1 cm diameter fritted glass discs (Ace Glass 10–20 μm pore diameter). The working electrode and the counter electrode compartments were made of 25 mL screw-cap vials. Holes were drilled through the cup of the working electrode compartment allowing placement of a BAS Au-disk working electrode for monitoring, if necessary, the progress of the electrolysis, a thin Pt foil to be used as the working electrode during electrolysis, and a bridge to the reference electrode. A Pt-gauge electrode was placed in the counter electrode compartment. Electrolysis was carried out until the faradaic current decayed below 2% of its initial value.

2.3. Preparation of **2a** and **2b** by cation exchange

To a degassed mixture of **2**K_3 (0.804 g, 1.0 mmol) and TBACl (0.834 g, 3.0 mmol) was added methylene chloride (30 mL) and the mixture was stirred for 24 h. After filtration, the solution was concentrated (~10 mL). The addition of excess diethyl ether (20 mL) under stirring for 30 min yielded a green precipitate, which was separated by filtration and dried. The solid was recrystallized from methylene chloride/diethyl ether. Yield: 1.16 g (82%) of **2a**. UV–Vis (CH_2Cl_2): λ_{max} (ε_M) 462 (3600), 602 (33), 760 (23) nm ($M^{-1}\,cm^{-1}$). ESI-MS, *m*/*z*: 1413.86 ([**2a**+H]$^+$), 343.28 ($[W_2Cl_9]^{2-}$), 360.72 ($[WCl_5]^-$), 616.73 ($[W_2Cl_7]^-$), 651.69 ($[W_2Cl_8]^-$), 929.07 ($[TBAW_2Cl_9]^-$).

The same procedure was followed with TPPCl (1.124 g, 3.0 mmol) instead of TBACl yielding 1.26 g (74%) of **2b**. UV–Vis (CH_2Cl_2): λ_{max} (ε_M) 462 (4300), 608 (38), 760 (26) nm ($M^{-1}\,cm^{-1}$).

2.4. Preparation of **2a** and **2b** by cation exchange from the biphasic system H_2O/CH_2Cl_2

To a degassed mixture of **2**K_3 (0.804 g, 1.0 mmol) and TBACl (0.834 g, 3.0 mmol) or TPPCl (1.124 g, 3.0 mmol) was added methylene chloride (20 mL) and the mixture was stirred for 4 h. Then water (10 mL) was added and stirring continued for another 20 min. The aqueous layer was separated, water (10 mL) was added again and the mixture was kept under stirring for 1 h. This procedure was repeated once more and, after removing the water, the solution was concentrated under vacuum and diethyl ether (20 mL) was added. The precipitate formed was recrystallized from acetone/diethyl ether and was dried under vacuum. Yield: 1.26 g (86%) of **2a**, 1.33 g (78%) of **2b**.

2.5. Preparation of **2a** and **2b** from WCl_4

To a degassed mixture of WCl_4 (3.26 g, 10.0 mmol) and TBACl (4.17 g, 15.0 mmol) or TPPCl (5.63 g, 15.0 mmol) was added toluene (20 mL). The mixture was transferred to another flask, which contained Na/Hg 0.44% w/w (104.5 g, 20.0 mmol Na) and was stirred for 24 h, filtered through Celite, and stripped under vacuum. The residue was dissolved in acetonitrile (10 mL), filtered, concentrated, and cooled at −20 °C to yield a green precipitate. This was filtered, recrystallized from acetonitrile and dried under vacuum. Yield: 6.36 g (90%) of **2a**, 7.34 g (86%) of **2b**. *Anal.* Calc. for $C_{48}H_{108}N_3W_2Cl_9$ **2a**: C, 40.77; H, 7.70; N, 2.97. Found: C, 40.69; H, 7.64; N, 2.87%. *Anal.* Calc. for $C_{72}H_{60}P_3W_2Cl_9$ **2b**: C, 50.72; H, 3.55. Found: C, 50.55; H, 3.49%.

2.6. Preparation of **2a** from $W(CO)_6$ and Me_3SiCl

To a degassed mixture of $W(CO)_6$ (1.05 g, 3.0 mmol) and TBACl (0.840 g, 3.0 mmol) was added chlorobenzene (20 mL) and the mixture was heated to reflux with constant stirring for 15 min. Then, Me_3SiCl (15 mL) was added and the reaction mixture was refluxed for another 7 h. The solution was then cooled down to room temperature and the solvent was removed under vacuum. The gelatinous residue was dissolved in methylene chloride (10 mL). The addition of excess diethyl ether (20 mL) yielded a green precipitate, which was separated by filtration. This procedure was repeated 4 times and the product was finally dried under vacuum. Yield: 1.58 g (74%).

2.7. Preparation of **3a** and **3b** from the biphasic system HCl (6 M)/CH_2Cl_2

To a degassed mixture of **2**K_3 (0.804 g, 1.0 mmol),) and TBACl (0.834 g, 3.0 mmol) was added methylene chloride (10 mL) and aqueous HCl 6 M (10 mL) and the mixture was stirred for 20 min. The aqueous layer was removed, aqueous HCl 6 M (10 mL) was added again and the mixture was kept under stirring for 30 min. The organic phase was collected and the solution was concentrated (~5 mL). Addition of excess diethyl ether (20 mL) under stirring for 30 min yielded a blue-violet precipitate, which was separated by filtration and dried. The solid was recrystallized by dissolving in acetone/diethyl ether and was dried under vacuum. Yield: 1.02 g (87%) of **3a**. UV–Vis (CH_2Cl_2): λ_{max} (ε_M) 576 (2400), 734 (1500) nm ($M^{-1}\,cm^{-1}$). ESI-MS, *m*/*z*: 326 ($[WCl_4]^-$), 360.5 ($[WCl_5]^-$), 651.5 ($[W_2Cl_8]^-$), 929 ($[TBAW_2Cl_9]^-$).

The same procedure was followed with TPPCl (1.124 g, 3.0 mmol) instead of TBACl yielding 1.36 g (>99%) of **3b**. UV–Vis (CH_2Cl_2): λ_{max} (ε_M) 582 (2500), 732 (1550) nm ($M^{-1}\,cm^{-1}$). ESI–MS, *m*/*z*: 1704.07 ([**3b** + TPP]$^+$), 341.78 ($[W_2Cl_9]^{2-}$), 360.72 ($[WCl_5]^-$).

2.8. Preparation of **3a** by oxidation of **2a**

2.8.1. Oxidation by $HCl_{(g)}$

Compound **2a** (0.141 g, 0.15 mmol) was dissolved in methylene chloride (5 mL) and $HCl_{(g)}$ was bubbled through the solution until the color changed from green to blue-violet. The solution was concentrated to half volume and upon addition of diethyl ether (5 mL) under stirring, a blue-violet precipitate was yielded, which was separated by filtration and dried under vacuum. Yield: 0.109 g (93%) of **3a**.

The same reaction in acetonitrile or THF afforded similar yields.

2.8.2. Oxidation by metal halides

To a degassed mixture of **2a** (0.141 g, 0.1 mmol) and anhydrous $CuCl_2$ (0.013 g, 0.1 mmol) was added methylene chloride (5 mL) and the mixture was stirred for 20 min, followed by filtration. The addition of excess diethyl ether (20 mL) under stirring for 30 min yielded a blue-violet precipitate, which was separated by filtration and dried under vacuum. Yield: 0.107 g (91%) of **3a**.

The same procedure was followed with the other metal chlorides employed in this study: $FeCl_3$ (0.016 g, 0.1 mmol), $HgCl_2$ (0.027 g, 0.1 mmol), $SnCl_2$ (0.019 g, 0.1 mmol), $AlCl_3$ (0.013 g, 0.1 mmol) all of which afforded similar yields (90–92%).

Examination of the products by Atomic Absorption shows negligible amounts of Cu, Fe, Hg, Sn, Al.

2.8.3. Oxidation by CCl_4

Compound **2a** (0.070 g, 0.050 mmol) was dissolved in methylene chloride (20 mL) and excess of carbon tetrachloride (2 mL) was added. The solution was stirred for 3 h in the dark or in the presence of visible light. The addition of excess diethyl ether (40 mL) under stirring yielded a blue-violet precipitate, which was separated by filtration and dried under vacuum. Yield: 0.035 g (60%) of **3a**.

Similarly, the reaction of **2a** in CCl_4, where it is insoluble, and stirring overnight produced **3a** in nearly quantitative yield.

2.8.4. Oxidation by $PhICl_2$

Compound **2a** (0.021 g, 0.15 mmol) and $PhICl_2$ (0.021 g, 0.075 mmol) were dissolved in methylene chloride (7.5 mL) and the solution was stirred for 10 min followed by filtration. The addition of excess diethyl ether (20 mL) under stirring yielded a blue-violet precipitate, which was separated by filtration and dried. Yield: 0.153 g (87%) of **3a**.

2.9. Preparation of *3a* and *3b* from $W(CO)_6$ (with Cl-donors)

2.9.1. 1,2-$C_2H_4Cl_2$

To a degassed mixture of $W(CO)_6$ (2.46 g, 7.0 mmol) and TBACl (1.95 g, 7.0 mmol) or TPPCl (2.63 g, 7.0 mmol) was added chlorobenzene (30 mL) and the mixture was heated to reflux with constant stirring for 15 min. 1,2-Dichloroethane (15 mL) was added and the mixture was refluxed further for 7 h. The solution was cooled at room temperature. Addition of diethyl ether (20 mL) yielded a blue-violet precipitate, which was separated by filtration and dried. The solid was recrystallized from acetonitrile. Yield: 5.25 g (85%) of **3a**, 4.89 g (89%) of **3b**. *Anal.* Calc. for $C_{32}H_{72}N_2W_2Cl_9$ **3a**: C, 32.80; H, 6.19; N, 2.39. Found: C, 32.66; H, 6.02; N, 2.29%. *Anal.* Calc. for $C_{48}H_{40}P_2W_2Cl_9$ **3b**: C, 42.22; H, 2.95. Found: C, 41.5; H, 2.79%.

2.9.2. $PhICl_2$

To a degassed mixture of $W(CO)_6$ (1.05 g, 3.0 mmol) and TBACl (0.840 g, 3.0 mmol) or TPPCl (1.12 g, 3.0 mmol) was added chlorobenzene (20 mL) and the mixture was heated to reflux with constant stirring for 15 min. Then, $PhICl_2$ (1.44 g, 5.25 mmol) was added in portions under continuous stirring. After the addition was complete, the reaction mixture was refluxed for another 5 h. The solution was then cooled at room temperature. The addition of excess diethyl ether (20 mL) yielded a blue-violet precipitate, which was separated by filtration and dried under vacuum. Yield: 1.39 g (79%) of **3a**, 1.49 g (73%) of **3b**.

2.10. Formation of *3b* by bulk electrolysis

A 3.0 mM solution of **2b** in CH_2Cl_2, containing also 0.1 M of supporting electrolytic salt ($TBAPF_6$) was placed in the working electrode compartment of the electrolytic cell. The middle compartment and the counter electrode compartments were filled with a supporting electrolyte solution in CH_2Cl_2 of the same concentration. Electrodes were placed in the working and the counter electrode compartments as described above. Based on the cyclic voltammogram of **2**, a potential in the mass transfer-controlled region for the oxidation of **2b** to **3b** 0.750 V was applied on the Pt foil working electrode and current was allowed to pass under constant stirring until its value fell below 2% of its original one. During the course of the electrolysis the color of the solution changed quickly from green to violet. The quantitative conversion of **2b** into **3b** was monitored spectrophotometrically by taking aliquots. Although **3b** was not isolated, based on the extinction coefficient of **3**, the oxidation of **2b** to **3b** was quantitative (>99%).

2.11. Reaction of *3a* with $PhCH_2OH$

Compound **3a** (19.5 mg, 25.0 μmol) was dissolved under anaerobic conditions in methylene chloride (5 mL) followed by addition of $PhCH_2OH$ (2.6 μl, 2.7 mg, 25.0 μmol) and TBACl (7.0 mg, 25.0 μmol). The mixture was stirred for 24 h under Ar at $T = 298$ K. At the end of the reaction the solvent was removed under vacuum and the products (PhCHO: 18%, $PhCH_2Cl$: 27%) were characterized by GC–MS, ^1H and ^{13}C NMR.

3. Results and discussion

3.1. Synthetic aspects

Scheme 2 summarizes the major synthetic routes explored in this work.

We have encountered difficulties while preparing **2a** via the cation exchange route. The yield was low, variable and occasionally gray residues insoluble to common organic solvents were formed. In the case of **2b** only the latter were obtained. These are, most likely, mixed salts of the type $\mathbf{2}(TPP)_{3-x}K_x$, ($x = 1, 2$) deriving from incomplete cation exchange and are insoluble in aqueous media and sparingly soluble in organic solvents [39,40].

This method can be improved by adding $\mathbf{2}K_3$ into solutions of CH_2Cl_2 containing the organic cation and provides after 24 h of stirring **2a**,**b** in ~80% yield. Since $\mathbf{2}K_3$ is stable both in H_2O and in aqueous HCl 6–12 M, the procedure can be further improved in terms of purification, by carrying the exchange in biphasic media ($\mathbf{2}K_3/H_2O/CH_2Cl_2$/organic salt, yield 78%). Interestingly, when aqueous HCl 6–12 M was used ($\mathbf{2}K_3$/HCl 6–12 M/CH_2Cl_2/organic salts), the green color of the organic layer containing **2a**,**b** changes to blue-violet, due to the formation of **3a**,**b**, as evidenced by UV–Vis, indicating a facile one-electron oxidation of **2a**,**b** by HCl. This was independently verified from the reaction of **2a**,**b** in CH_2Cl_2 with carefully purified $HCl_{(g)}$. Fast conversion to **3a**,**b** occurs at room temperature in a nearly quantitative manner, with the products being stable in excess of $HCl_{(g)}$. The reaction is slower in polar solvents (THF, MeCN), and does not proceed in protic ones (MeOH, H_2O, aqueous HCl 6–12 M) or in equimolar mixtures of CH_2Cl_2/MeOH. The oxidation can be also carried out heterogeneously, simply by addition of acidic silica to solutions of **2a**,**b** in CH_2Cl_2 under vigorous stirring.

Similarly, under the same conditions and with comparable efficiency, Lewis acids ($AlCl_3$, $SnCl_2$ in CH_2Cl_2) or metal halide oxidants, such as $FeCl_3$, $CuCl_2$, and $HgCl_2$ (in CH_2Cl_2, THF, MeCN) induce the same oxidation.

Also, addition of CCl_4 to a green solution of **2a**,**b** in CH_2Cl_2 results in formation of **3a**,**b** within 3 h. The reaction proceeds also in the dark in contrast to the conversion of **5** to **6**, where visible light is required [34]. The solid state interaction of green **2a**,**b** with CCl_4 yields blue-violet crystals of **3a**,**b** after stirring overnight. Detection in the reaction products of C_2Cl_6 (by GC–MS) indicates that the reaction proceeds through Cl-atom abstraction via homolytic cleavage of a C–Cl bond in CCl_4.

The high tendency of the W^{4}–W bonds to be oxidized by hydrohalic acids is a recurrent and general property which has been responsible for the slow development of the chemistry of W_2^{4+}

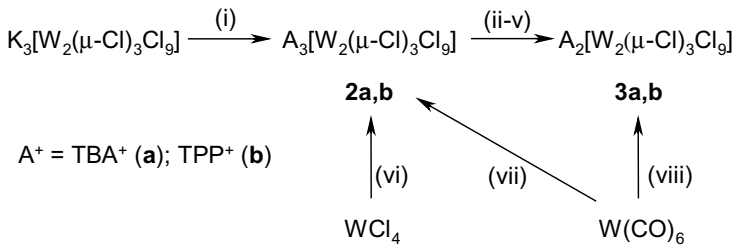

Scheme 2. Synthetic pathways for the preparation of the **2a**,**b** and **3a**,**b** complexes: (i) CH_2Cl_2, TBACl or TPPCl, r.t., t = 24 h, or CH_2Cl_2/H_2O, TBACl or TPPCl, r.t., t = 4 h. (ii) CH_2Cl_2, $HCl_{(g)}$, r.t., t = 20 min, or CH_2Cl_2/aqueous HCl 6 M, TBACl or TPPCl, r.t., t = 20 min. (iii) CH_2Cl_2, $FeCl_3$ or $CuCl_2$ or $HgCl_2$ or $SnCl_2$ or $AlCl_3$, r.t., t = 20 min. (iv) Bulk electrolysis in CH_2Cl_2, E = 0.750 V. (v) CH_2Cl_2, CCl_4, r.t., t = 3 h. (vi) Toluene, Na/Hg, TBACl or TPPCl, r.t., t = 24 h. (vii) $W(CO)_6$, Me_3SiCl, TBACl, chlorobenzene, reflux, t = 7 h. (viii) Chlorobenzene, 1,2-dichloroethane, TBACl or TPPCl, reflux, t = 7 h.

complexes [1]. Mechanistically, the first step of the overall two-electron oxidation process (Eq. (1)) proceeds presumably via the formation of the $[W_2(\mu\text{-}H)(\mu\text{-}Cl)_2Cl_6]^{3-}$ hydride.

$$Na_4[W_2Cl_8](THF)_x \overset{THF,HCl_{(g)}}{\underset{-78\,^\circ C}{\rightarrow}} [HW_2Cl_9]^{4-} \text{ or } [HW_2Cl_8]^{3-} \overset{HCl_{(g)}}{\rightarrow} Na_3[W_2Cl_9] + H_2 + Cl^- \quad (1)$$

IR evidence obtained from the low temperature (−10 °C) reaction of $[W_2(TFA)_4]$ (TFA = trifluoroacetate anion) with concentrated hydrochloric acid supports this reaction sequence [41]. Further support is provided by the isolation and structural characterization of $[W_2(\mu\text{-}H)(\mu\text{-}Cl)Cl_2(O_2CPh)_2(^nBu_3P)_2]$ [42], $[W_2(\mu\text{-}H)(\mu\text{-}Cl)Cl_4(dppm)_2]$ [43], $[W_2(\mu\text{-}H)(\mu\text{-}Cl)Cl_5(Etpy)_4]$ [44], $[Mo_2(\mu\text{-}H)(\mu\text{-}Cl)_2Cl_6]^{3-}$ [45], $[MoW(\mu\text{-}H)(\mu\text{-}Cl)_2Cl_6]^{3-}$ [46] deriving from analogous genuine HCl additions to the $W\equiv W$, $Mo\equiv W$, and $Mo\equiv Mo$ bonds contained in the $[W_2Cl_4(^nBu_3P)_4]$, $[W_2Cl_4(dppm)_2]$ (dppm = $Ph_2CH_2CH_2Ph_2$), $[W_2(mph)_4]$, $[Mo_2(\mu\text{-}CH_3COO)_4]$, $K_4[Mo_2Cl_8]$ and $[MoW(\mu\text{-}^tBuCOO)_4]$ precursors. There is no evidence in the literature concerning the intimate details of the subsequent steps leading to the formation of **2**.

The ability of $W\equiv W$ bonds to undergo further an overall one-electron oxidation by protic acids in aprotic media (**2a**,**b**, CH_2Cl_2, $HCl_{(g)}$), in contrast to their stability in protic solvents (**2**K_3, aqueous HCl 6–12 M) can be attributed, at least in part, to solvation effects of the proton [47], and also to the exact nature of **2a**,**b** due to solvent dependent ligand mobility and/or *fsbo-esbo* equilibria [1,48]. Although we have detected formation of H_2 (by GC) we have not managed yet to isolate any intermediate or obtain spectroscopic evidence (UV–Vis) from the reaction of **2a** with $HCl_{(g)}$ or with stoichiometric amounts of non-complexing protonic acids (HBF_4, CF_3SO_3H) in CH_2Cl_2 or MeCN.

These findings constitute simple and facile routes for the preparation of **3a**,**b**, and also, they point out that the PPN^+ may be responsible for the three-electron oxidation of **1**$Na_4(THF)_x$ [9]. However, when we repeated the reaction replacing PPNCl with TBACl or TPPCl, instead of **3a**,**b**, pale green-gray insoluble residues were obtained. In contrast, the same reaction in toluene instead of THF provides **2a**,**b** in high yield (∼90%). Attempts to reduce **2a**,**b** to **1a**,**b** with amalgams of Na, Zn, Al in THF at low temperature (−10 to 0 °C) were not successful.

Furthermore, the direct high yield preparation of **3a**,**b** has been possible by paralleling McCarley's method for the synthesis of the $(^nPr_4N)_2[W_2(\mu\text{-}Br)_3Br_6]$ analog [12]. Thus, reaction of $W(CO)_6$ in boiling PhCl in the presence of the organic salts employing $PhICl_2$ or 1,2-$C_2H_4Cl_2$ as oxidants and halide sources, instead of WCl_6 or WCl_4, gives the desired products. In the first case, slow stepwise addition of the $PhICl_2$ to the reaction mixture is required in order to minimize overoxidation, whereas in the second case the reaction proceeds cleanly in a nearly quantitative manner (yield ∼95%). In contrast, when Me_3SiCl was used under the same conditions **2a** is isolated in 74% yield, but formation of a gelatinous residue makes the purification difficult.

Oxidation of **2a**,**b** with $PhICl_2$ or PhIO in CH_2Cl_2 is more convenient than with Cl_2 and gives **3a**,**b** in ∼80% yield. Attempts to obtain **4a**,**b** from the stoichiometric oxidation of **3a**,**b** as above were not successful, producing colorless solutions.

3.2. Electrochemical studies

The oxidation of **2b** was investigated by cyclic voltammetry in CH_2Cl_2, CH_3CN and DMSO. Pertinent data are summarized in Table 1. As shown spectroelectrochemically (*vide infra*), **2b** undergoes two well-separated oxidations to **3b** and **4b**:

$$\mathbf{2b}(W_2^{6+}) \underset{+e^-}{\overset{-e^-}{\rightleftharpoons}} \mathbf{3b}(W_2^{7+}) \underset{+e^-}{\overset{-e^-}{\rightleftharpoons}} \mathbf{4b}(W_2^{8+})$$

From the $i_{p,a}/i_{p,c}$ and the voltammetric peak-to-peak separation ($\Delta E_{p\text{-}p}$) values it is concluded that within the time scale of cyclic voltammetry at 0.02–1.0 V s^{-1} the first oxidation wave is both chemically and kinetically reversible in all three solvents. The second oxidation is chemically irreversible in DMSO and CH_3CN, in accord with the observed instability of **4** upon dissolution in these solvents. The case of CH_2Cl_2, however, is worth commenting on (see Fig. 1). Although at first glance the second oxidation wave may seem to lack chemical reversibility ($i_{p,a}/i_{p,c}$ = 1.39), voltammograms normalized by dividing the faradaic current by the square root of the potential sweep rate are fully superimposable over a wide range of sweep rates, indicating that both waves are fully chemically *as well as* kinetically reversible. That is, if in analogy to what is observed in DMSO and CH_3CN, the second wave in CH_2Cl_2 was chemically irreversible, then the return part of the first wave would be also compromised, because after a potential excursion through **4b** there would be less **3b** available to be re-reduced to **2b** in the reverse sweep. Therefore, we are forced to attribute the high $i_{p,a}/i_{p,c}$ value (=1.39) for the second wave in CH_2Cl_2 to large differences in the diffusion coefficients of **2b**/**3b** on one hand and of **4b** on the other. Indeed, considering the homogeneous comproportionation reaction of **4b** with **2b** [49,50], and based on the fact that the $i_{p,a}$ values for both waves are about equal ($i_{p,a}(1)/i_{p,a}(2) \sim 0.92$), we conclude that the diffusion coefficients of **2b** and **3b** are about equal as well. Thus we can attribute the high $i_{p,a}/i_{p,c}$ value for the second wave entirely to differences in diffusion coefficients, D_i, and we can set $i_{p,a}/i_{p,c} = (D_{\mathbf{3b}}/D_{\mathbf{4b}})^{1/2}$, meaning that $D_{\mathbf{3b}}/D_{\mathbf{4b}}$ = 1.9. The lower diffusion coefficient of **4b** implies extensive ion pairing, namely that in CH_2Cl_2 the $\{W_2^{8+}\}$ species exists in close association with its counter ions.

Bulk electrolysis of **2b** in CH_2Cl_2 at 0.750 V for 14 min using an H-cell afforded **3b** quantitatively. The reaction was monitored by UV–Vis (Fig. 2). The two isosbestic points (402 and 508 nm; Fig. 2, right) indicate clean conversion of **2b** to **3b**. Fig. 2, left shows absorption spectra of **3b** and **4b** for comparison. The absorption

Table 1
Electrochemical data for the oxidation of **2b** in three different solvents[a]

Solvent	First wave			Second wave			
	$E_{1/2}$ (V)	$\Delta E_{p\text{-}p}$ (mV)	$i_{p,a}/i_{p,c}$	$E_{p,a}(2)$ (V)	$E_{1/2}$ (V)	$\Delta E_{p\text{-}p}$ (mV)	$i_{p,a}/i_{p,c}$
CH_2Cl_2	−0.741	68	0.98	0.014	−0.021	69	1.39
DMSO	−0.711	63	1.08	0.004		168	3
CH_3CN	−0.664	74	1.06	0.130		[b]	[b]

[a] All potentials reported vs. the Fc^+/Fc couple; data derived from voltamograms at 0.1 V s^{-1}.
[b] No discernible re-reduction wave.

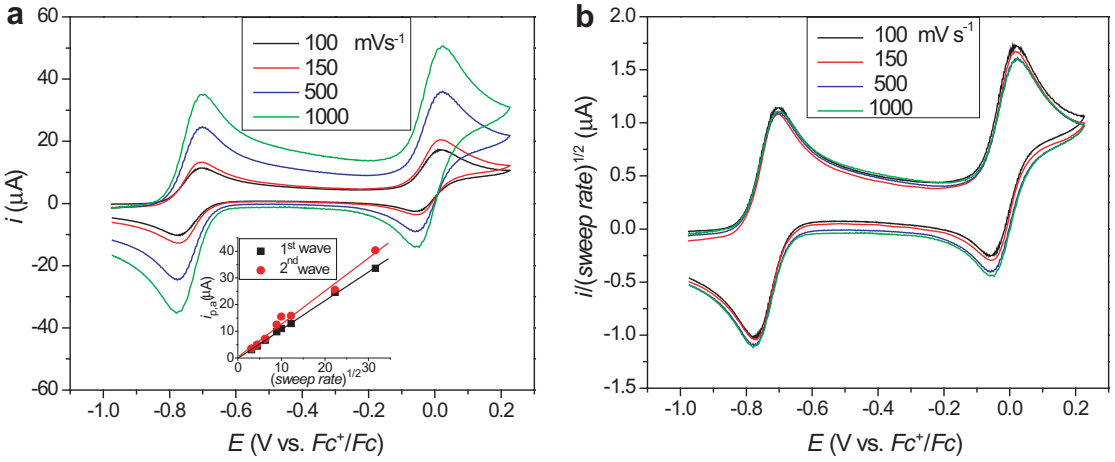

Fig. 1. (a) Cyclic voltammetry of **2b** (3.0 mM) in CH_2Cl_2/0.1 M $TBAPF_6$ with a Au-disk electrode (1.6 mm in diameter) at various sweep rates, as indicated. Inset: Randles–Sevcic plots for the anodic parts of both waves. (b) Same curves as in part (a), divided by the square root of the sweep rate. Experiments were carried out in a dry-box.

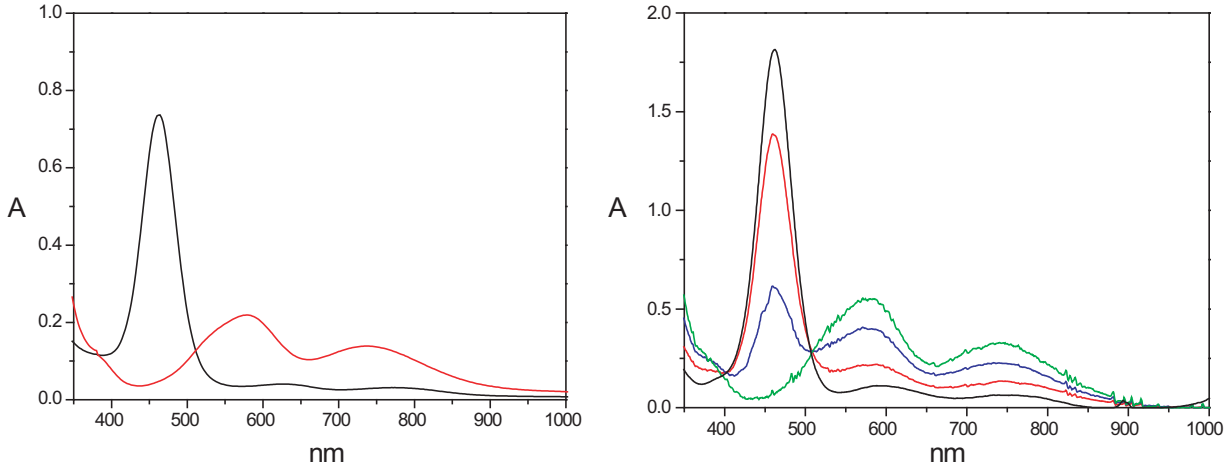

Fig. 2. Left: electronic absorption spectra of **2b** (2×10^{-4} M, black) and **3b** (9×10^{-5} M, red) in CH_2Cl_2. The two spectra were taken independently, in different solutions. Right: successive spectra during the bulk electrolysis of **2b** in CH_2Cl_2 (5×10^{-4} M) at 0.750 V; $t = 0$ s (black), $t = 30$ s (red), $t = 7$ min (blue), $t = 14$ min (green). (For interpretation of the references to colour in this figure legend, the reader is referred to the web version of this article.)

maxima are similar to those reported in the literature [9,25,51] Electrolysis at 1.100 V for another 1 min gave a mixture of **3b** and **4b**, as shown by the UV–Vis spectrum of the reaction mixture (for **4b** λ_{max} (ε_M) 650 (825), 530 (370), 360 (sh), and 305 (22 600) nm (M^{-1} cm^{-1}) [10]). The degree of conversion of **3b** to **4b** could not be calculated accurately, because the bands of the two species are overlapping. The formation of **4b** was confirmed from the second derivative spectra ($d^2A/d\lambda^2$). Electrolysis at higher potentials and/or for longer time periods resulted in decomposition products, which were not pursued further. These results are consistent with previous reports on electrolysis of $\mathbf{2}K_3$ in a basic aluminum chloride/methyl-3-ethyl-imidazolium chloride molten salt [52].

3.3. ESI-MS spectra

Electrospray ionization mass spectrometry was additionally used for the characterization of **2a**,**b** and **3a**,**b**. The experimental isotope clusters obtained are in agreement with the theoretical masses and isotope patterns. The ESI(+) spectra showed signals centered at $m/z = 1415.86$ and 1704.70, which are attributed to

Table 2
Peaks observed in the ESI-MS spectra of **2a**, **3a**,**b**

Compound	*m/z* experimental	*m/z* calculated	Fragment
2a	1413.82	1414	$[\mathbf{2a}+H]^+$
	343.28	343.5	$[W_2Cl_9]^{2-}$
	360.72	361	$[WCl_5]^-$
	616.73	617	$[W_2Cl_7]^-$
	651.69	652	$[W_2Cl_8]^-$
	929.07	929	$[TBAW_2Cl_9]^-$
3a	326	326	$[WCl_4]^-$
	360.5	361	$[WCl_5]^-$
	651.5	652	$[W_2Cl_8]^-$
	929	929	$[TBAW_2Cl_9]^-$
3b	1704.07	1704	$[\mathbf{3b}+TPP]^+$
	341.78	343.5	$[W_2Cl_9]^{2-}$
	360.72	361	$[WCl_5]^-$

($[\mathbf{2a}+H]^+$) and ($[\mathbf{3b}+TPP]^+$) respectively. In the ESI(−) spectra the most characteristic peaks were at *m/z* = 929.07 ($[TBAW_2Cl_9]^-$), and 341.78 ($[W_2Cl_9]^{2-}$). Other signals were also present, attributable to di- or mononuclear fragments, as shown in Table 2. **4**(TEBA) was too sensitive to obtain reliable spectra.

3.4. Electron paramagnetic resonance

The EPR spectra of **2a**, **3a** and **4**(TEBA) in CH_2Cl_2 solutions were taken at room and at 25 K temperatures and are shown in Fig. 3. All spectra exhibit a simple derivative shape signal at $g = 1.75$, except for **3a**, which shows an additional weak peak at $g = 2.8$ at 25 K. The **2a** signal is weak and the *g* value is compatible with previously reported powder spectra of $\mathbf{2}K_3$ and $\mathbf{2}Cs_3$ at 77 K [53]. The **4**(TEBA) signal is asymmetric.

3.5. Reactions of *3a,b* with $PhCH_2OH$

Compounds **2a**,**b** are inactive towards $PhCH_2OH$ at ambient temperature. In contrast, **3a**,**b** are anaerobically reduced to **2a**,**b** (**3a**,**b**/$PhCH_2OH$/TBACl or TPPCl = 1/1/1, $t = 24$ h), as was confirmed by the electronic absorption spectrum (CH_2Cl_2, $T = 298$ K) of the reaction solution, producing PhCHO (18%) and $PhCH_2Cl$ (27%). No PhCOOH was detected. The ability of **3** to oxidize $PhCH_2OH$ resembles partly to that of the hexanuclear clusters $[M_6X_{14}]^-$ (M = Mo, X = Cl; M = W, X = Br) reported previously [36]. The system is under investigation, and details of the mechanism of this reaction, as well as chemical and electrochemical catalytic studies with $PhCH_2OH$ and other organic substrates will be reported in due course.

4. Conclusions

The principal results of this work can be summarized as following:

(i) New simple and facile high-yield chemical and electrochemical synthetic routes for **2a**,**b** and especially for **3a**,**b**, have been developed, which are expected to facilitate studies of their functionality in organic media;

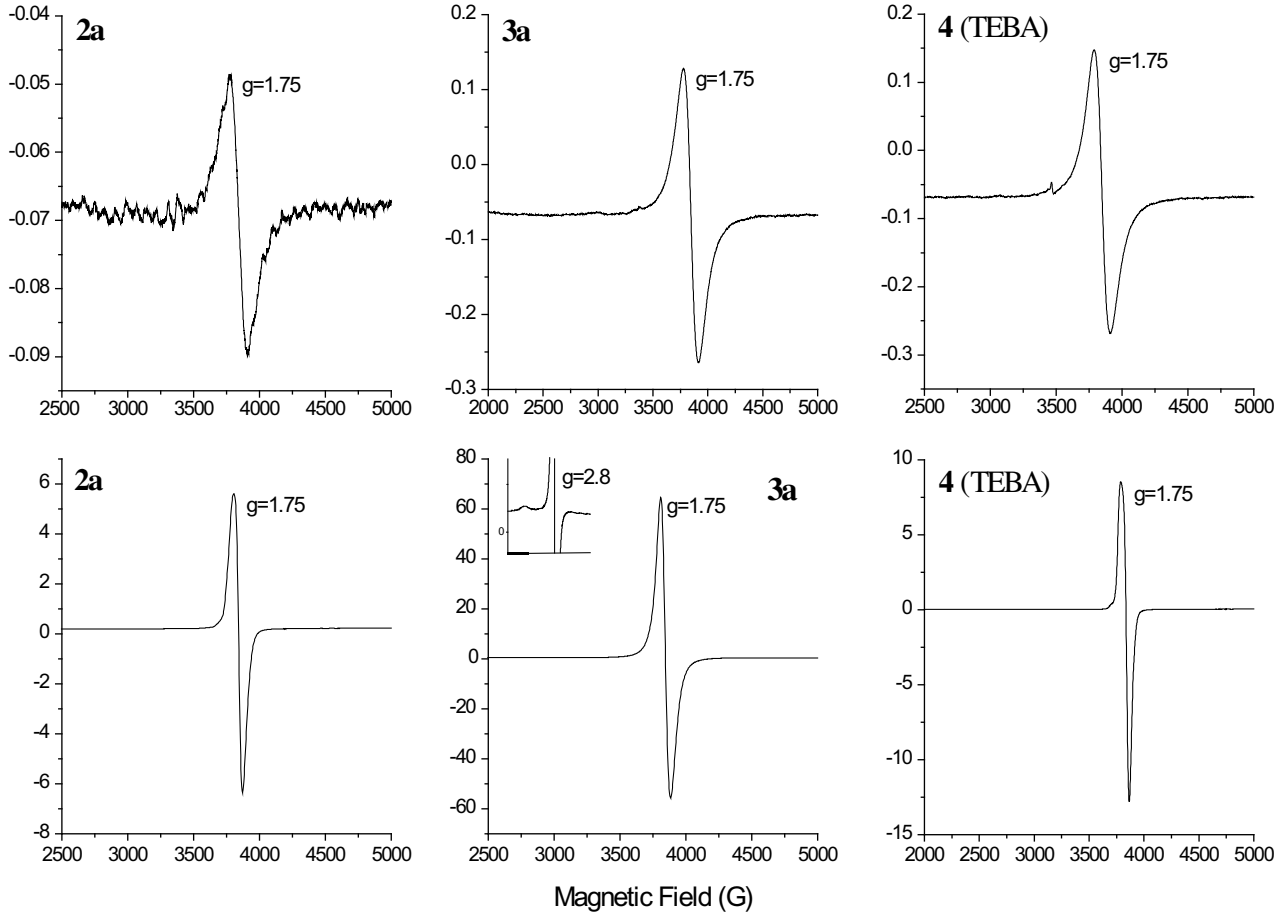

Fig. 3. X-band EPR spectra of **2a**, **3a**, and **4**(TEBA) in CH_2Cl_2 solution at room (top) and at 25 K (bottom) temperatures. Conditions: 9.4 GHz, modulation 10 Gpp, mW power of 50 mW. The EPR of **4**(TEBA) at 25 K was recorded with a modulation of 1Gpp, which translates in a multiplication factor of 10 if it is to be compared with the others.

(ii) The $W^{\equiv}W$ bonds contained in **2a**,**b** are capable of undergoing facile one-electron oxidation in aprotic organic solvents by protons or Lewis acids, in sharp contrast to their stability in acidic protic media (CH_3OH, $HCl_{(aq)}$ 6–12 M);

(iii) Complex **3** acts as a convenient anaerobic one-electron oxidant of $PhCH_2OH$ to PhCHO. Future studies are directed towards elucidating the mechanism of this reaction, tuning the reactivity of **3a**,**b**, and making the **2**/**3** redox-couple of potential utility in catalytic oxidations of alcohols and other organic substrates.

Acknowledgements

We thank the Special Account for Research Grants of the University of Athens (70/4/3342), and the EPEAEK II "PYTHAGORAS" (70/3/7327) (co-funded by the European Social Fund and National Resources) for financial assistance. We also thank Mr. George Karapanagos at the Institute of Materials Science, NCSR "Demokritos", Greece, for obtaining the EPR spectra and Dr. Nathan Leigh at the University of Missouri-Columbia for obtaining the ESI-MS spectra.

References

[1] F.A. Cotton, R.A. Walton (Eds.), Multiple Bonds Between Metal Atoms, third ed., Springer, 2005.
[2] R.H. Holm, P. Kennepohl, E.I. Solomon, Chem. Rev. 96 (1996) 2239.
[3] R.D. Adams, F.A. Cotton (Eds.), Catalysis by Di- and Polynuclear Metal Cluster Complexes, Wiley VCH, New York, 1999.
[4] O.S. Alexeev, B.C. Gates, Ind. Eng. Chem. Res. 42 (2003) 1571.
[5] Chemical and Engineering News (C&EN) September 14, 76 (1998) 33.
[6] F.A. Cotton, G.N. Mott, R.R. Schrock, L.G. Sturgeoff, J. Am. Chem. Soc. 104 (1982) 6781.
[7] W.H. Watson Jr., J. Waser, Acta Crystallogr. 11 (1958) 689.
[8] K.R. Dunbar, L.E. Pence, Acta Crystallogr., Sect. C. c47 (1991) 23.
[9] F.A. Cotton, L.R. Falvello, G.N. Mott, R.R. Schrock, L.G. Sturgeoff, Inorg. Chem. 22 (1983) 2621.
[10] V. Kolesnichenko, D.C. Swenso, L. Messerle, Chem. Commun. (1998) 2137.
[11] R.A. Walton, D. DeMarco, T. Nimry, Inorg. Chem. 19 (1980) 575.
[12] J.L. Templeton, R.A. Jacobson, R.E. McCarley, Inorg. Chem. 16 (1977) 3320.
[13] W.H. Delphin, R.A.D. Wentworth, J. Am. Chem. Soc. 95 (1973) 7920.
[14] L.B. Anderson, F.A. Cotton, D. DeMarco, A. Fang, W.H. Ilsley, B.W.S. Kolthammer, R.A. Walton, J. Am. Chem. Soc. 103 (1981) 5078.
[15] R.C. Young, J. Am. Chem. Soc. 54 (1932) 4515.
[16] J.J. Lingane, L.A. Small, J. Am. Chem. Soc. 71 (1949) 973.
[17] E. König, Inorg. Chem. 2 (1963) 1238.
[18] W.H. Delphin, R.A.D. Wentworth, Inorg. Chem. 13 (1974) 2037.
[19] W.H. Delphin, R.A.D. Wentworth, Inorg. Chem. 12 (1973) 1914.
[20] O. Olsson, Z. Anorg. Allg. Chem. 88 (1914) 49.
[21] R.B. Saillant, J.L. Hayden, R.A.D. Wentworth, Inorg. Chem. 6 (1967) 1497.
[22] R. Usel, R. Pribil, Coll. Czech. Chem. Commun. (1938) 330.
[23] E.L. Goodenow, C.S. Garner, J. Am. Chem. Soc. 77 (1955) 5268.
[24] H.B. Jonassen, A.R. Tarsey, S. Cantor, G.F. Helfrich, Inorg. Synth. 51 (1957) 139.
[25] R. Saillant, R.A.D. Wentworth, J. Am. Chem. Soc. 91 (1969) 2174.
[26] P.W. Clark, R.A.D. Wentworth, Inorg. Chem. 8 (1969) 1223.
[27] J.R. Ebner, D.L. McFadden, D.R. Tyler, R.A. Walton, Inorg. Chem. 15 (1976) 3014.
[28] G.L. Hawkins, C.S. Garner, J. Am. Chem. Soc. 80 (1958) 2946.
[29] A. Nagasawa, Y. Sasaki, B. Wang, S. Ikari, T. Ito, Chem. Lett. (1987) 1271.
[30] O. Collenberg, A. Guthe, Z. Anorg, Allg. Chem. 134 (1924) 317.
[31] R.A. Laudise, R.C. Young, Inorg. Synth. 6 (1960) 149.
[32] R.R. Schrock, L.G. Sturgeoff, P.R. Sharp, Inorg. Chem. 22 (1983) 2801.
[33] F.A. Cotton, P.E. Fanwick, R.H. Niswander, J.C. Secutowski, J. Am. Chem. Soc. 100 (1978) 4725.
[34] D.J. Bergs, M.H. Chisholm, K. Folting, J.C. Huffman, K.A. Stahl, Inorg. Chem. 27 (1988) 2950.
[35] D. Neuman, P. Paraskevopoulou, N. Psaroudakis, K. Mertis, R.J. Staples, P. Stavropoulos, Inorg. Chem. 39 (2000) 5530.
[36] J.A. Jackson, R.D. Mussell, D.G. Nocera, Inorg. Chem. 32 (1993) 4643.
[37] H.J. Lucas, E.R. Kennedy, Org. Synth. 22 (1942) 69.
[38] H. Saltzman, J.G. Sharefkin, Org. Synth. 5 (1973) 658.
[39] P.W. Smith, A.G. Wedd, J. Chem. Soc. A (1970) 2447.
[40] I.E. Grey, P.W. Smith, Aust. J. Chem. 24 (1971) 73.
[41] A.P. Sattelberger, K.W. McLaughlin, J.C. Huffman, J. Am. Chem. Soc. 103 (1981) 2880.
[42] F.A. Cotton, G.N. Mott, J. Am. Chem. Soc. 104 (1982) 5978.
[43] P.E. Fanwick, W.S. Harwood, R.A. Walton, Inorg. Chem. 26 (1987) 242.
[44] R.T. Carlin, R.E. McCarley, Inorg. Chem. 28 (1989) 2604.
[45] A. Bino, F.A. Cotton, Angew. Chem., Int. Ed. Engl. 18 (1979) 332.
[46] V. Katović, R.E. McCarley, Inorg. Chem. 17 (1978) 1268.
[47] U. Koelle, New. J. Chem. 16 (1992) 157.
[48] W.E. Streib, R.B. Jackson, Inorg. Chem. 10 (1971) 1760.
[49] A. Dass, N. Leventis, Electrochim. Acta 50 (2005) 4134.
[50] N. Leventis, W.S. Oh, X. Gao, A.M.M. Rawashdeh, Anal. Chem. 75 (2003) 4996.
[51] W. Trogler, Inorg. Chem. 19 (1980) 697.
[52] T.B. Scheffler, C.L. Hussey, Inorg. Chem. 23 (1984) 1926.
[53] P.D.W. Boyd, P.W. Smith, A.G. Wedd, Aust. J. Chem. 22 (1969) 653.

semicarbazone complexes, Quiroga and Navarro have observed the sensible increase in the number of studies of their antibacterial, antiviral, antifungal and antitumour activity [12]. For instance, a report of Cu^{II}, Zn^{II}, Cd^{II} or Hg^{II} complexes with thiosemicarbazone derived from vanillin shows their activity against pathogen fungus belonging to the groups *Alternaria* (sp.), *Paecilomyces* (sp.) and *Pestalotia* (sp.) [13].

In the present work we have chosen thiosemicarbazones with the group 2-ethoxy-3-methoxy-benzaldehyde, which can be considered a ester derivative similar of vanillin, and the fragment *fac*-$[Re(CO)_3]^+$. Besides the interesting bioinorganic properties mentioned above, the exploration of the coordinative behaviour of these ligands against tricarbonylrhenium(I) and the structures resulting of their molecular association and their spectroscopic behaviour, is also worth to be studied.

2. Results and discussion

2.1. Synthesis and spectroscopic characterization

The ligands derived from 2-ethoxy-3-methoxy-benzaldehyde thiosemicarbazone were obtained by refluxing a mixture methanol/water solution for 2 h (Scheme 1).

Reaction of the three ligands with *fac*-$[ReX(CO)_3(CH_3CN)_2]$ afforded six adducts (Scheme 2) with general formula *fac*-$[ReX(CO)_3(HL)]$ (**1**).

Elemental analysis and mass spectrometry confirmed the stoichiometry $[ReX(CO)_3(HL)]$. The mass spectra of the metallic species contains a signal corresponding to the molecular ion, although the peak due to the species $[M-X]^+$ is more intense.

Furthermore, facial geometry around the rhenium atom is suggested by the three strong bands $\nu(C{\equiv}O)$ in IR (sometimes collapsed) in the range 1889–2027 cm^{-1}. The ligand bands corresponding to the N–H groups appear between 3181 and 3508 cm^{-1} and are hardly modified by coordination. Regarding the typical bands from the thiosemicarbazide fragment, the frequencies of the band C=N, in the free ligands in the range 1543–1556 cm^{-1}, shift to the region 1555–1630 cm^{-1} in the spectra of all the complexes. Nevertheless, the band corresponding to the C=S mode shifts from 783 to 788 cm^{-1} in free ligands to 740–771 cm^{-1} in the rhenium complexes, in agreement with the coordination of the ligand by the sulfur atom. This behaviour has been observed in other TSC complexes and it is consistent with the S,N coordination of the ligand [8,11,14,15].

In general, all proton signals in the ^1H NRM spectra in acetone-d_6 of the complexes are shifted at low field (around 0.5 ppm) respect the free ligands. Differently, the signal of the N(2)–H proton moves around 2 ppm. Similar behaviour has been observed in rhenium(I) complexes of hydrazones [16] and thiosemicarbazones [11,14], where the N(2)–H group is a member of the chelate ring resulting after the S,N-coordination. However, when the thiosemicarbazone is coordinated as a S-monodentate ligand, the N(2)–H proton signal behaves as the rest of the ligand signals [10].

To explore the influence of temperature and nature of the rhenium precursor in the reaction product, the reaction of HL^1 with $[ReX(CO)_5]$ were tested in toluene. In the bromine derivative, the

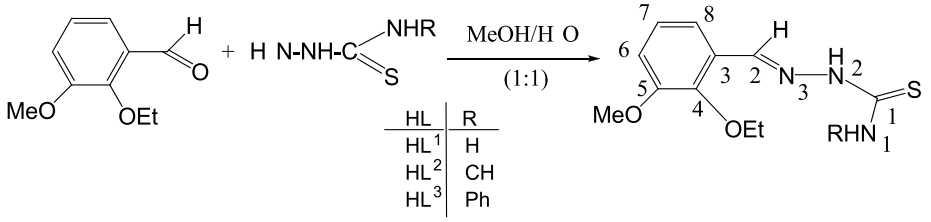

HL	R
HL^1	H
HL^2	CH
HL^3	Ph

Scheme 1.

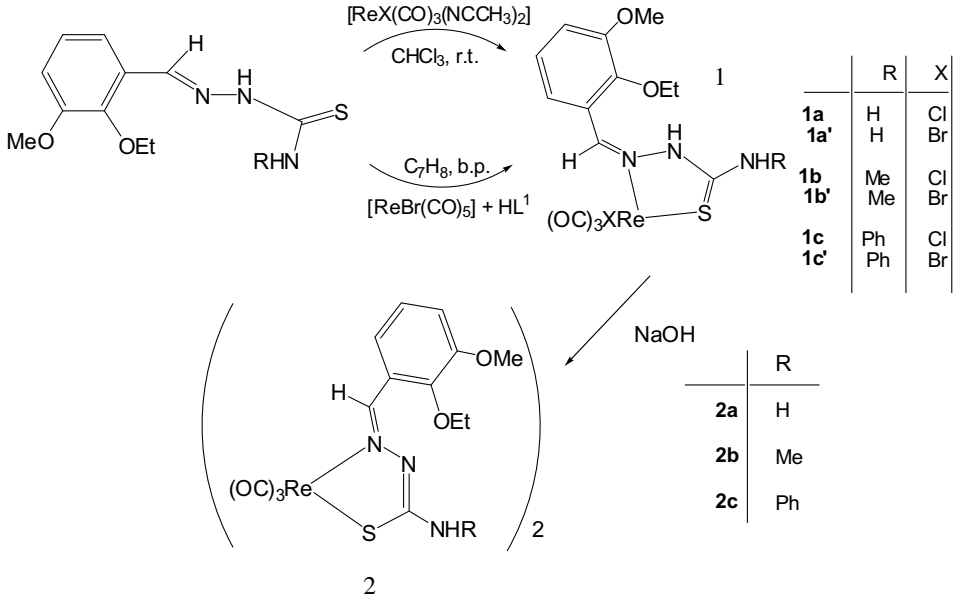

	R	X
1a	H	Cl
1a'	H	Br
1b	Me	Cl
1b'	Me	Br
1c	Ph	Cl
1c'	Ph	Br

	R
2a	H
2b	Me
2c	Ph

Scheme 2.

characterization of the product showed the formation of the same adduct, $[ReBr(CO)_3(HL^1)]$ (**1a′**), exclusively. However when the chloride derivative was used, the spectroscopic data suggested the coexistence of the compound **1a** and also some product derivate of the deprotonation.

On the other hand, the X-ray study of the crystals obtained from methanol solutions **1b** and **1c** showed the formation of binuclear thiosemicarbazonate complexes (Scheme 2). In a process similar to observed in the rhenium(I) complex of ferrocenylaldehyde thiosemicarbazone [11], the deprotonation of the TSC ligand induces the labilization of the halogen in a position occupied by sulfur atom from other TSC coordinated.

These complexes **2a**, **2b** and **2c** were obtained by reaction of bromine derivatives, **1a′**, **1b′** and **1c′**, with NaOH in methanol. In all of them, the three carbonyl IR bands are consistent with the facial geometry around rhenium atom, and the ν(C=S) bands at 714–740 cm^{-1}, suggest some weakening of the bond. The vibration frequencies of C=N bonds shift to a larger wavenumbers than in free ligands (1610–1710 cm^{-1}).

The ^1H NMR spectra of these compounds in acetone-d_6 show all the proton signals shifted at low field respect to the free ligands and as expected the signals for N(2)–H are absent.

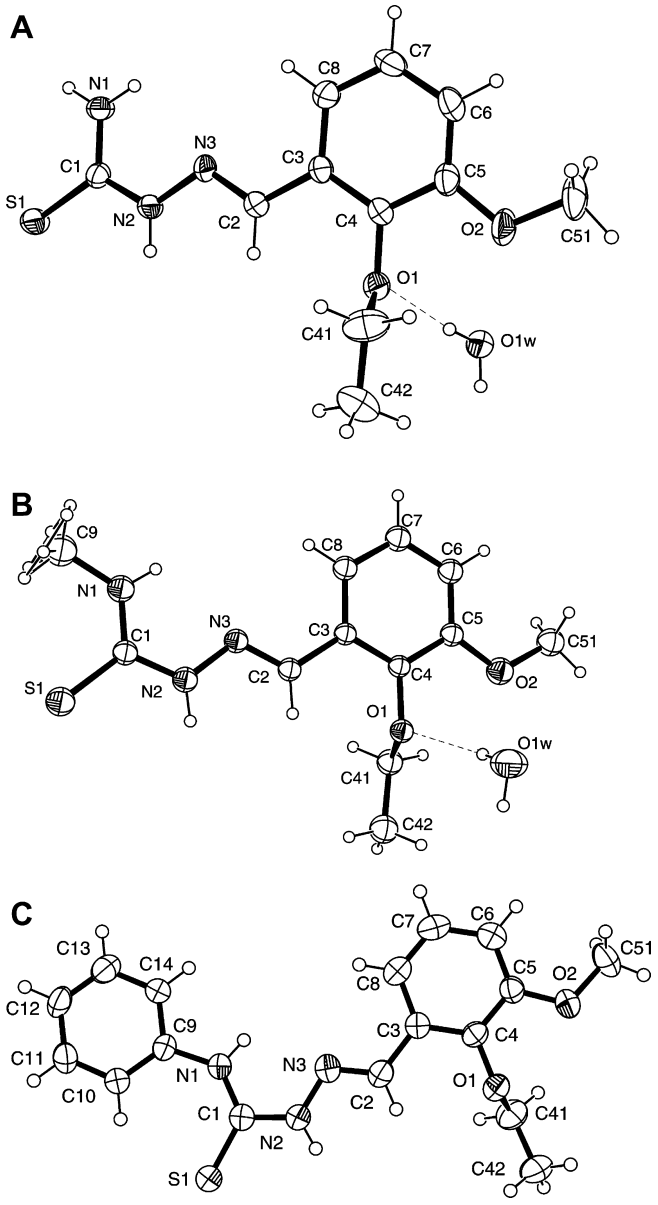

Fig. 1. Molecular structures of $HL^1 \cdot H_2O$ (A), $HL^2 \cdot 1/2H_2O$ (B) and HL^3 (C).

2.2. Crystal and molecular structure of the ligands

The molecular structures of the free ligands are shown in Fig. 1 along with the atomic numbering scheme used. Crystal data and selected bond lengths and angles are listed in Tables 1 and 2, respectively.

Ligands HL^1 and HL^2 crystallized as mono- and hemi-hydrates, respectively, and the water molecule is linked by hydrogen bond to the oxygen atom of the ethoxy group (O(1)W). The role of this molecule in both structures is discussed in detail below. In HL^2, two TCS ligand molecules per asymmetric unit were identified showing differences between distances and angles statistically insignificant and, consequently, the average values are including in Table 2.

In all the cases, the distances C(1)–S(1), C(2)–N(3), N(2)–N(3) and N(2)–C(1) suggest that, in spite of the usual delocalization of π electrons along the thiosemicarbazide chain [17], the canonical form of the free ligand depicted in Scheme 1 is likely the main form in solid state.

The molecular structure of these ligands shows *E* configuration around C(1)–N(2), N(2)–N(3), N(3)–C(2) and C(2)–C(3) bonds. However, *Z* configuration in the C(1)–N(1) bond has been linked with the existence of intramolecular hydrogen-bonding interactions N(1)–H···N(3). The distance N(1)–N(2) decrease from $HL^1 \approx HL^2 > HL^3$ (Table 3). Before conclude that the shortening is due to the increasing of the interaction strength, note that the angle N(1)–C(1)–S(1) widen following the same path. Thus, these findings are also compatible with the increase of steric hindrance of the R group linked to N(1) and the sulfur atom.

In the three cases, the molecule of the ligand can be considered planar: the angles between the ideal plane of the thiosemicarbazide chain N(1)/S(1)/C(1)/N(2)/N(3)/C(2) and the carbon atoms that define the phenyl ring are 7.34(3)°, 6.67(8)° and 2.4(2)° for HL^1, HL^2 and HL^3, respectively.

Table 1
Crystal data, data collection and refinement of the structures of $HL^1 \cdot H_2O$, $HL^2 \cdot 1/2H_2O$ and HL^3

Compound	$HL^1 \cdot H_2O$	$HL^2 \cdot 1/2H_2O$	HL^3
Empirical formula	$C_{11}H_{17}N_3O_3S$	$C_{12}H_{18}N_3O_{2.5}S$	$C_{17}H_{19}N_3O_2S$
Molecular weight	271.34	276.35	329.41
Space group	*C2/c*	$P2_1/n$	*C2/c*
Unit cell dimensions			
a (Å)	20.260(5)	14.893(3)	30.219(6)
b (Å)	7.0868(19)	10.0714(17)	5.6664(11)
c (Å)	20.581(5)	19.671(3)	20.127(4)
β (°)	113.081(5)	101.779(3)	101.714(4)
V (Å^3)	2718.4(12)	2888.4(8)	3374.6(12)
Z	8	8	8
D_{calc} (Mg/m^3)	1.326	1.271	1.297
μ (mm^{-1})	0.243	0.227	0.205
θ Range (°)	2.19–28.04	1.92–28.05	2.07–28.03
Reflections collected	7029	14981	7626
Independent reflections (R_{int})	3010 (0.0863)	6149 (0.0297)	3408 (0.0518)
Maximum/minimum transmission	0.969/0.672	0.930/0.894	0.966/0.865
Goodness-of-fit on F^2	0.775	1.065	0.906
Final R_1/wR_2 indices [$I > 2\sigma(I)$]	0.0548/ 0.0909	0.0444/ 0.1127	0.0648/ 0.1603
R_1/wR_2 indices (all data)	0.1902/ 0.1160	0.0765/ 0.1243	0.1445/ 0.1957

Table 2
Selected bond lengths (Å) and bond angles (°) for $HL^1 \cdot H_2O$, $HL^2 \cdot 1/2H_2O$ and HL^3

	$HL^1 \cdot H_2O$	$HL^2 \cdot 1/2H_2O$[a]	HL^3
S(1)–C(1)	1.691(3)	1.686(11)	1.681(4)
N(1)–C(1)	1.320(3)	1.323(3)	1.329(4)
N(1)–C(9)		1.442(3)	1.414(4)
N(2)–C(1)	1.340(3)	1.352(2)	1.349(4)
N(2)–N(3)	1.376(3)	1.374(2)	1.373(4)
N(3)–C(2)	1.276(3)	1.276(2)	1.275(4)
C(2)–C(3)	1.462(4)	1.464(3)	1.456(5)
N(1)–C(1)–N(2)	117.7(2)	116.8(18)	114.2(3)
N(1)–C(1)–S(1)	122.6(2)	124.2(15)	127.9(3)
N(2)–C(1)–S(1)	119.8(2)	119.0(16)	117.9(3)
C(1)–N(2)–N(3)	119.8(2)	120.1(17)	120.8(3)
C(2)–N(3)–N(2)	114.7(2)	115.8(17)	115.3(3)
N(3)–C(2)–C(3)	120.7(3)	120.9(19)	121.5(3)
C(1)–N(1)–C(9)		124.7(18)	132.9(3)

[a] Average values and standard deviation estimated by the expressions $x = (\sum x_j/\sigma_j^2)/\sum 1/\sigma_j^2$ and $\sigma^2(x) = 1/\sum 1/\sigma_j^2$.

Table 3
Parameters (Å, °) of H-bonding interactions in $HL^1 \cdot H_2O$, $HL^2 \cdot 1/2H_2O$ and HL^3

D–H···A[a]	d(D–H)	d(H···A)	d(D···A)	∠(DHA)
HL1 · H2O				
N(1)–H(1A)···N(3)	0.86	2.29	2.637(3)	104.5
N(1)–H(1A)···O(1W)	0.86	2.22	2.965(3)	145.2
N(2)–H(2)···S(1)#1	0.86	2.54	3.394(3)	171.1
N(1)–H(1B)···O(1W)#2	0.86	2.39	3.136(4)	145.2
O(1W)–H(1W)···S(1)#2	0.83(3)	2.58(4)	3.330(3)	150(3)
O(1W)–H(2W)···O(1)#3	0.91(4)	2.02(4)	2.923(4)	175(4)
HL2 · ½H2O				
N(1A)–H(1A)···N(3A)	0.86	2.23	2.624(2)	107.8
N(1B)–H(1B)···N(3B)	0.86	2.27	2.652(2)	107.3
N(1A)–H(1A)···O(1W)	0.86	2.28	2.988(3)	139.5
N(2A)–H(2AN)···S(1B)	0.86	2.59	3.4365(18)	167.5
N(2B)–H(2BN)···S(1A)	0.86	2.55	3.3900(18)	165.4
O(1W)–H(1W)···O(1A)#4	0.88(3)	2.15(3)	3.009(3)	164(3)
HL3				
N(1)–H(1)···N(3)	0.86	2.13	2.601(3)	113.9
N(2)–H(2)···S(1)#5	0.86	2.64	3.441(3)	154.5

[a] Symmetry transformations used to generate equivalent atoms: #1 = $-x$, y, $-z+½$; #2 = $-x$, $-y+2$, $-z+1$; #3 = $-x-½$, $y+½$, $-z+½$; #4 = $-x$, $-y$, $-z$; #5 = $-x$, $-y-1$, $-z+1$.

The molecular association in $HL^1 \cdot H_2O$ is strongly dominated by the presence of the water molecule. Two HL^1 molecules are associated with two water molecules by N(1)–H···O(1W) interactions (Table 3) showing in both cases the water molecule an acceptor hydrogen behaviour (Fig. 2A). The interaction between a sulfur atom from TSC and the water, which is now a H-bond donor, probably assists to the formation of these "virtual molecular-tetramer". These units are associated by N(2)–H···S(1) interactions along the *c* axis. In turn, these chains are associated by hydrogen bonds between water and the oxygen atoms, O(1), from a neighbouring ethoxy group in the brick-wall-like arrangement showed in Fig. 2B.

As mentioned before, two molecules of HL^2 can be observed per asymmetric unit. Though important differences are not observed in molecular distances and angles, the differences become more marked when the crystal packing is considered. One of the HL^2 molecules is associated with other, crystallographically equivalent (labelled A in Fig. 2C) by two water molecules as in HL^1, involving two hydrogen bonds pairs N(1A)–H···O(1W) and O(1W)–H···O(1A) (Table 3). These molecules are also associated with molecules non-crystallographically equivalent (labelled B) by N(2A)–H···S(1B) and N(2B)–H···S(1A) interactions (Fig. 2C). These units formed by four ligand molecules and two water molecules are packed by weak contacts O(1W)–H···π, in a herringbone pattern as usually observed in aromatic derivatives.

The HL^3 molecules are also coupled N(2)–H···S(1)#5 by hydrogen bond (Fig. 2E) and the dimers are associated in a herringbone pattern by weak interactions involving methoxy and aromatic C–H groups as H-donors and oxygen atom (ethoxy) or π-clouds as acceptors, respectively (Fig. 2F).

2.3. Crystal and molecular structure of $[ReBr(HL^1)(CO)_3] \cdot ½C_7H_8$ (**1a′** · **½C₇H₈**)

Single crystals of the complex **1a′**, obtained from the mother liquor (toluene) contains one solvent molecule per each two molecules of the complex. The toluene molecule is in the cell origin and, consequently, disordered. In the final model we have considered the methyl group on two alternate positions with occupation factors 50% and the aromatic ring centre at the origin. Moreover, two independent molecules that correspond to the two enantiomer of the *fac* configuration (OC-6-33) appear in the asymmetric, although there are also differences concerning the relative orientation of the aromatic ring and the bromo ligand.

The molecular structure of (**1a′** · **½C₇H₈**) together the numbering scheme used is depicted in Fig. 3A. Crystal data and relevant interatomic distances and angles relative to the coordination sphere are included in Tables 4 and 5, respectively.

The ligand HL^1 is coordinated to Re(I) through the sulfur and azomethine nitrogen N(3) atoms. This coordination mode changes the configuration of the bond C(1)–N(2) from *E*, observed in the structure of free ligand HL^1 (*vide supra*), to *Z* to forms a five-membered chelate ring. This ring is approximately planar and the angles respect to the aromatic ring are 39.4(3)° (Re(1) molecule) and 50.3(4)° (Re(2) molecule). The rhenium atom is octahedrally coordinated to three carbonyl carbon atoms in *fac* arrangement, a bromine atom, the azomethine nitrogen and the sulfur atom of the thiosemicarbazone, main distortion being in the angle S–Re–N (<80°) due to the formation of the chelate ring. The bond distances in Re–N(3), Re–S and Re–Br are statistically equivalent in both molecules and they are very similar to observed previously in others *fac*-$Re(CO)_3$ adducts with TSC chelate ligands [8,9,11,14].

Aside the change of the configuration in the bond C(1)–N(2), the coordination of HL^1 to rhenium modifies also the configuration about the C(2)–N(3) bond to *Z*. Both changes and the non-planar structure of the ligand are likely due to steric hindrances between the aromatic ring, and its ether group, with the fragment $\{Re(CO)_3\}$.

Finally, respect to the molecular structure, the non-planar structure of TSC and the metallic fragment asymmetry, allows the coexistence of two possible distributions of 2-ethoxy-3-methoxy-benzaldehyde fragment: one with the group positioned to the direction occupied by the bromine atom and the other in the opposite direction. Both are in the crystal and probably coexist also in solution but, in contrast to ferrocenyl derivatives, they no produce different signals in the ^1H NMR spectrum [11].

The description of the molecular packing in the crystal is complex since the two enantiomers are associated in different fashion. Beside the weak C–H···acceptor interactions, the Re(1) molecule is associated with other symmetrically equivalent molecules (Fig. 3B) by hydrogen bonds between N–H azomethine and thioamide groups and the bromine atom (N(1A)–H(1A1)···Br(1)#1 = 0.86, 2.557, 3.372(8) Å, 158.54; N(2A)–H(2A2)···Br(1) = 0.86, 2.939, 3.465(8) Å, 147.78°; #1 = $-x+2$, $-y+2$, $-z+1$). These associations, and the metric values from these interactions, have been observed in other rhenium(I) thiosemicarbazones derived from ferrocenylcarbaldehyde [11] and β-keto esters [14]. In the present case, the two interactions are reinforced by an additional interaction which involve the thioamide nitrogen and the ethoxy group from the partner molecule.

In addition, the interactions between molecules containing Re(2) atom, involve the bromine atom in a very similar way to

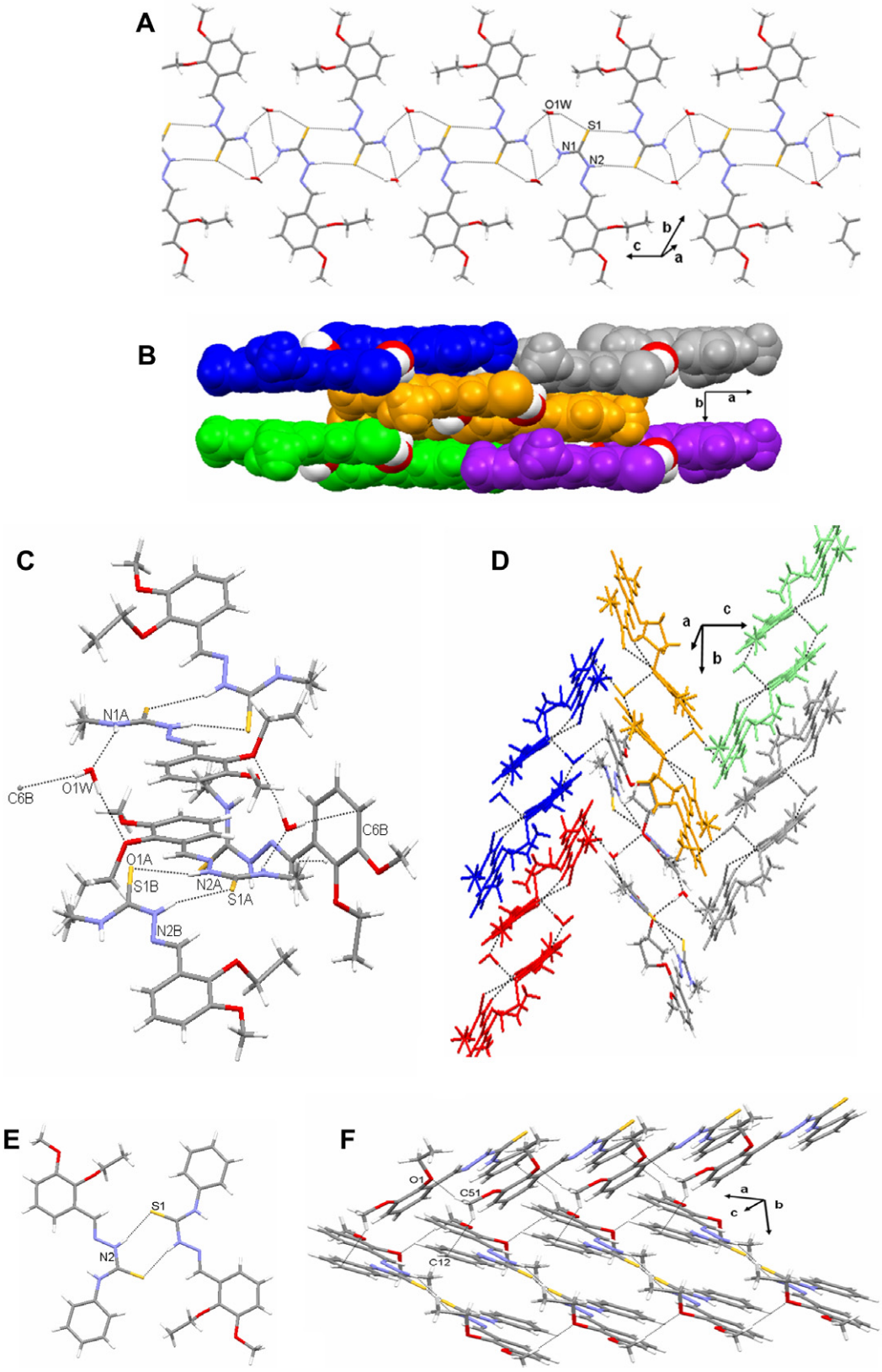

Fig. 2. Supramolecular association in $HL^1 \cdot H_2O$ (A and B), $HL^2 \cdot \frac{1}{2}H_2O$ (C and D) and HL^3 (E and F).

Re(1) molecules, but now, the N(1B)–H group establishes H-bonds (N(1B)–H(1B2)···O(1B)$^{\#2}$ = 0.86, 2.50, 2.934(11) Å, 111.9°; N(1B)–H(1B2)···O(2B)$^{\#2}$ = 0.86, 2.19, 3.042(10) Å, 171.5°; #2 = $-x$, $1-y$, $-z$) with the ether groups of a neighbouring molecule. Consequently, dimers are associated in chains running parallel to *a* axis (Fig. 3C).

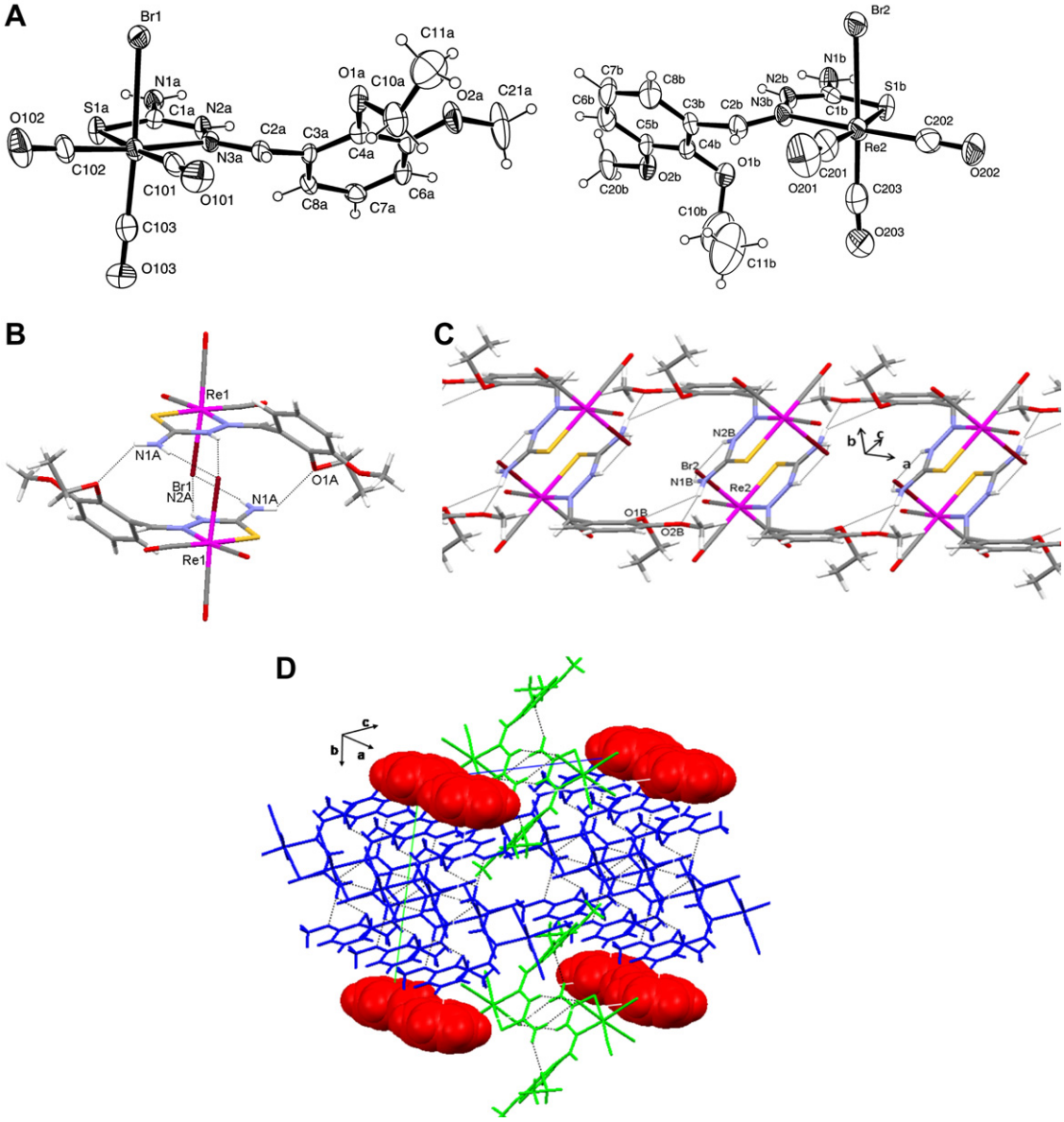

Fig. 3. The molecular structure (A) and crystal packing (B–D) in **1a**′ · **½C$_7$H$_8$**.

Finally, the molecular packing is completed with weak interactions between donor C–H groups and carbonyl as acceptors and can be described considering the packing of the chains of Re(2) molecules, in *b* direction, hosts the Re(1) dimers and toluene molecules (Fig. 3D).

*2.4. Crystal and molecular structure of [Re$_2$(L^2)$_2$(CO)$_6$] (**2b**) and [Re$_2$(L^3)$_2$(CO)$_6$] · 2CH$_3$OH (**2c** · 2CH$_3$OH)*

Single crystals of **2b** and **2c** were obtained by slow concentration from methanol solutions of the previously isolated adducts. The observed disorder of the methyl or the ethoxy group was modulated by refinement of two alternate positions for these groups with occupancies of 80% and 25%. Crystal and structure refinement data for both compounds are showed in Table 4. Relevant length bonds and angles are included in Table 5 meanwhile the molecular structures, showing the numbering scheme used are depicted in Fig. 4.

The ligand deprotonation and the interaction of the rhenium with the sulfur atom of a neighbouring molecule at the position occupied by the halogen atom creates dimers. A difference between both, is that in **2c** this interaction produces centrosymmetric dimers, similar to observed in the ferrocenylcarbaldehyde thiosemicarbazonates [11] but in **2b** both thiosemicarbazonate groups are in the same side of the Re$_2$S$_2$ fragment. This different group orientation and the formation of the Re$_2$S$_2$ diamond, does not impose important differences in bond lengths and angles (Table 6).

The rhenium atoms retains its octahedral coordination, but now interacts with two sulfur atoms, and the sulfur belonging to the partner in the dimer, is farther away than its own sulfur. In fact, the Re–S–Re bridge is relatively asymmetric, as in others dimer structures based on this type of interaction [18,19]. In the diamond Re$_2$S$_2$, the bond angles close to 90° and the distance Re–Re is too long (>3.75 Å) for means any significant bonding interaction.

As observed in ferrocenyl derivatives [11], the Re–N(3) and Re–S(1A) distances are statistically equivalents to the observed in **1a**′. However, the C(1)–S(1) distance is longer than in the free ligands or the adduct **1b**, in agree with a higher thiol character. In addition, the angle between the plane of benzaldehyde ring and the TSC

Table 4
Crystal data and structure refinement of rhenium(I) complexes

Compound	**1a′ · ½C$_7$H$_8$**	**2b**	**2c · 2(CH$_3$OH)**
Empirical formula	$C_{15.5}H_{15}N_3O_5SReBr$	$C_{30}H_{32}N_6O_{10}S_2Re_2$	$C_{40}H_{36}N_6O_{10}S_2Re_2$
Formula weight	623.49	1073.14	1325.44
Space group	$P\bar{1}$	$P2_1/c$	$P\bar{1}$
Unit cell dimensions			
a (Å)	8.0343(9)	10.6586(9)	7.9039(6)
b (Å)	15.5310(17)	16.9065(15)	12.6770(9)
c (Å)	16.9500(18)	21.3813(19)	13.6465(10)
α (°)	93.907(2)		64.4370(10)
β (°)	98.804(2)	91.009(2)	82.0500(10)
γ (°)	96.164(2)		89.9540(10)
V (Å^3)	2070.3(4)	3852.3(6)	1218.99(16)
Z	4	4	1
D_{calc} (Mg/m^3)	2.000	1.850	1.806
μ (mm^{-1})	7.930	6.588	5.177
θ Range (°)	1.88–28.03	1.91–28.03	1.78–28.01
Reflections collected	13435	24785	8019
Independent reflections (R_{int})	9455 (0.0462)	9143 (0.0857)	5596 (0.0223)
Maximum/minimum transmission	0.530/0.357	0.433/0.279	0.541/0.233
Goodness-of-fit on F^2	0.966	0.997	1.097
Final R_1/wR_2 indices [$I > 2\sigma(I)$]	0.0527/0.0945	0.0521/0.1150	0.0264/0.0652
R_1/wR_2 indices (all data)	0.1382/0.1209	0.1371/0.1481	0.0311/0.0781

Table 5
Relevant interatomic distances (Å) and angles (°) for the complex [ReBr(CO)$_3$(HL^1)] · **½C$_7$H$_8$** (**1a′** · **½C$_7$H$_8$**)

Re(1)–C(101)	1.919(12)	Re(2)–C(201)	1.933(16)
Re(1)–C(102)	1.869(12)	Re(2)–C(202)	1.893(13)
Re(1)–C(103)	1.875(13)	Re(2)–C(203)	1.794(18)
Re(1)–N(3A)	2.196(8)	Re(2)–N(3B)	2.204(8)
Re(1)–S(1A)	2.462(3)	Re(2)–S(1B)	2.455(3)
Re(1)–Br(1)	2.6380(12)	Re(2)–Br(2)	2.6452(14)
S(1A)–C(1A)	1.682(10)	S(1B)–C(1B)	1.680(11)
N(1A)–C(1A)	1.318(11)	N(1B)–C(1B)	1.312(12)
C(1A)–N(2A)	1.346(11)	C(1B)–N(2B)	1.350(11)
N(2A)–N(3A)	1.374(10)	N(2B)–N(3B)	1.359(10)
C(102)–Re(1)–C(101)	86.6(5)	C(202)–Re(2)–C(201)	90.0(5)
C(102)–Re(1)–C(103)	89.4(5)	C(203)–Re(2)–C(202)	86.9(6)
C(103)–Re(1)–C(101)	88.9(4)	C(203)–Re(2)–C(201)	89.6(7)
C(102)–Re(1)–N(3A)	174.5(4)	C(202)–Re(2)–N(3B)	174.5(5)
C(103)–Re(1)–N(3A)	95.7(4)	C(203)–Re(2)–N(3B)	93.3(5)
C(101)–Re(1)–N(3A)	95.4(4)	C(201)–Re(2)–N(3B)	95.5(4)
C(102)–Re(1)–S(1A)	98.6(3)	C(202)–Re(2)–S(1B)	95.4(4)
C(103)–Re(1)–S(1A)	92.4(3)	C(203)–Re(2)–S(1B)	92.2(6)
C(101)–Re(1)–S(1A)	174.7(3)	C(201)–Re(2)–S(1B)	174.4(3)
N(3A)–Re(1)–S(1A)	79.3(2)	N(3B)–Re(2)–S(1B)	79.1(2)
C(102)–Re(1)–Br(1)	88.8(3)	C(202)–Re(2)–Br(2)	94.8(4)
C(103)–Re(1)–Br(1)	176.2(3)	C(203)–Re(2)–Br(2)	178.2(4)
C(101)–Re(1)–Br(1)	94.4(3)	C(201)–Re(2)–Br(2)	89.9(5)
N(3A)–Re(1)–Br(1)	85.97(19)	N(3B)–Re(2)–Br(2)	85.0(2)
S(1A)–Re(1)–Br(1)	84.54(8)	S(1B)–Re(2)–Br(2)	88.17(9)
N(2A)–C(1A)–S(1A)	122.7(8)	N(2B)–C(1B)–S(1B)	122.2(8)
C(1A)–N(2A)–N(3A)	121.0(8)	C(1B)–N(2B)–N(3B)	121.7(8)
C(2A)–N(3A)–N(2A)	118.0(8)	C(2B)–N(3B)–N(2B)	117.3(8)

plane (12° and 15° in **2b** and 9.5° in **2c**) shows a more planar ligand in complexes **2b** and **2c** than in **1a′**.

In the supramolecular structure of **2b**, dimers are associated by hydrogen bonds between the N–H thioamide nitrogen group and the oxygen atom of the ethoxy group of a neighbour dimer (N(1A)–H(1A2)···O(1A)$^{\#1}$ = 0.86, 2.268, 2.934(7) Å, 134.32°; #1 = 1 − x, ½ + y, ½ − z). This interaction links the units [Re$_2$(L^2)$_2$(CO)$_6$] in chains running parallel along b axis (Fig. 4C).

In **2c**, the presence of methanol affects the association of the centrosymmetric dimers. The two molecules of methanol are symmetrically independents and they are associated by O(2M)–H···O(1M) bonds and at the same time, one of them establishes a hydrogen chelate bond with two oxygen atoms of the methoxy and ethoxy group (O(1M)–H(1M)···O(2) = 0.82, 2.083, 2.844(8) Å, 154.08°; O(1M)–H(1M)···O(1) = 0.82, 2.592, 3.221(7) Å, 134.56°). The other methanol molecule behaves as hydrogen bond acceptor with the N–H group of a neighbour dimer (N(1)–H(1)···O(2M)$^{\#1}$ = 0.86, 1.976, 2.830(8) Å, 171.65°; #1 = −x, −y, 2 − z). These interactions make ribbons running transverse to the crystallographic directions a and b.

3. Experimental

3.1. Materials and methods

All solvents used for synthesis were dried over appropriate drying agents, degassed using a vacuum line and distilled under an Ar atmosphere [20]. Adducts [ReX(CO)$_3$(CH$_3$CN)$_2$] were synthesized by Farona and Kraus' published methods [21] from the corresponding [ReX(CO)$_5$] [22].

Elemental analyses were carried out on a Fisons EA-1108. Melting points (mp) were determined on a Gallenkamp MFB-595 and are uncorrected. Mass spectra were recorded on a VG Autospec Micromass spectrometer operating under FAB conditions (nitrobenzyl alcohol matrix). Infrared spectra were recorded from KBr pellets on a Bruker Vector 22FT. The ^{1}H NMR spectra were obtained on a Bruker ARX-400 spectrometer from acetone-d_6 solutions.

3.2. General synthesis of the ligands HL^1, HL^2 and HL^3

To a mixture of a water solution (15 mL) of thiosemicarbazide and a methanol solution (15 mL) of 2-ethoxy-3-methoxy-benzaldehyde was added one $H_2SO_{4(c)}$ drop. To avoid the precipitation of 2-ethoxy-3-methoxy-benzaldehyde some methanol (about 15 mL) was added. The reaction mixture was heated under reflux for 2 h. The resulting solid was filtered off and vacuum dried over KOH/CaCl$_2$. Single crystals were obtained after slow evaporation of the mother liquor.

3.2.1. Data for HL^1

Thiosemicarbazide (500 mg, 5.49 mmol)/2-ethoxy-3-methoxybenzaldehyde (0.5 mL, 3.08 mmol). White crystalline solid. Yield: 1783 mg (89.2%). M.p.: 185 °C. *Anal.* Calc. for $C_{11}H_{15}N_3O_2S$: C, 52.1; H, 6.0; N, 16.6; S, 12.6. Found: C, 52.2; H, 6.1; N, 16.4; S, 12.6%. Mass spectrum [m/z (%)]: 254.11(100) [M]$^+$. IR data (KBr, cm^{-1}): 3482m, 3442m, 3282m ν(NH); 1543s ν(C=N); 783w ν(C=S). ^{1}H NMR data (ppm): 10.55s (1) δ(N(2)–H); 8.55s (1) δ(C(2)–H); 7.83s (1) δ(N(1)–H); 7.62m (1) δ(C(7)–H); 7.43s (1) δ(N(1)–H); 7.05s (1) δ(C(6,8)–H); 7.04s (1) δ(C(6,8)–H); 4.06m (2) δ(O(4)–R^2); 3.85s (3) δ(O(5)–R^3); 1.34m (3) δ(O(4)–R^2).

3.2.2. Data for HL^2

4-Methyl-3-thiosemicarbazide (500 mg, 4.75 mmol)/2-ethoxy-3-methoxybenzaldehyde (0.5 mL, 3.08 mmol). Yellow crystalline solid. Yield: 810 mg (81.0%). M.p.: 154 °C. *Anal.* Calc. for $C_{12}H_{17}N_3O_2S$: C, 51.9; H, 6.4; N, 15.7; S, 11.9. Found: C, 51.6; H, 6.8; N, 15.5; S, 11.7%. Mass spectrum [m/z (%)]: 268.09(100) [M]$^+$. IR data (KBr, cm^{-1}): 3508m, 3334m, 3311m ν(NH); 1556s ν(C=N); 788w ν(C=S). ^{1}H NMR data (ppm): 10.49s (1) δ(N(2)–H); 8.52s (1) δ(C(2)–H); 8.26s (1) δ(N(1)–H); 7.57m (1) δ(C(7)–H); 7.05s (1) δ(C(6,8)–H); 7.04s (1) δ(C(6,8)–H); 4.05m (2) δ(O(4)–R^2); 3.84s (3) δ(O(5)–R^3); 3.14d (3) δ(N(1)–R^1); 1.34t (3) δ(O(4)–R^2).

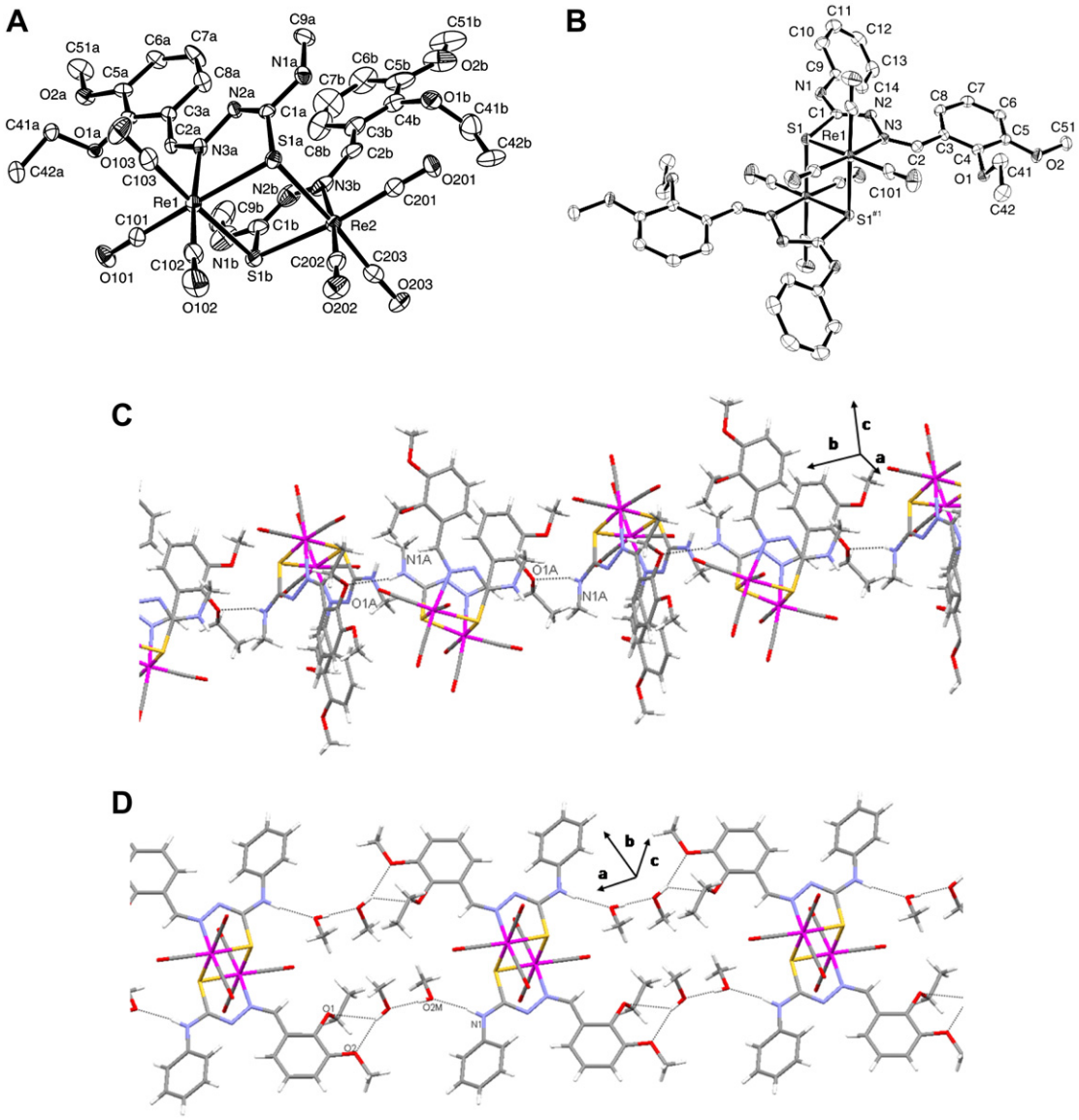

Fig. 4. Molecular structures (hydrogen atoms are omitted for clarity) and the crystal packing in **2b** (A and C) and **2c** · 2(CH_3OH) (B and D).

3.2.3. Data for HL^3

4-Phenyl-3-thiosemicarbazide (500 mg, 2.99 mmol)/2-ethoxy-3-methoxybenzaldehyde (0.5 mL, 3.08 mmol). White crystalline solid. Yield: 771 mg (77.1%). M.p.: 204 °C. *Anal.* Calc. for $C_{17}H_{19}N_3O_2S$: C, 61.9; H, 5.9; N, 12.7; S, 9.7. Found: C, 61.7; H, 6.0; N, 12.7; S, 9.6%. Mass spectrum [*m*/*z* (%)]: 330.09(100) $[M]^+$. IR data (KBr, cm^{-1}): 3508m, 3333m, 3298m ν(NH); 1556s ν(C=N); 788w ν(C=S). ^1H NMR data (ppm): 10.77s (1) δ(N(2)–H); 9.88s (1) δ(N(1)–H); 8.64s (1) δ(C(2)–H); 7.75d (1) δ(C(7)–H); 7.73d (2) δ(N(1)–R^1); 7.36t (2) δ(N(1)–R^1); 7.19t (1) δ(N(1)–R^1); 7.06s (1) δ(C(6,8)–H); 7.05s (1) δ(C(6,8)–H); 4.10m (2) δ(O(4)–R^2); 3.88s (3) δ(O(5)–R^3); 1.36m (3) δ(O(4)–R^2).

*3.3. General synthesis of the complexes [ReX(CO)$_3$(HL)] (**1**)*

To a solution of the corresponding HL ligand in freshly distilled chloroform (15 mL) was added the corresponding equimolecular quantity of *fac*-[ReX(CO)$_3$(CH_3CN)$_2$] (X = Cl, Br). The yellow mixture was stirred at room temperature for 1 h. The resulting yellow solution was concentrated *in vacuo* to *ca.* 3 mL and stored at room temperature after dropwise addition of diethyl ether until saturation. Yellow solid formed was filtered off and vacuum dried.

*3.3.1. Data for **1a** (HL^1, X = Cl)*

Yield: 227 mg (89.7%). M.p.: 177 °C. *Anal.* Calc. for $C_{14}H_{15}ClN_3O_5SRe$: C, 30.1; H, 2.7; N, 7.5; S, 5.7. Found: C, 29.9; H, 2.6; N, 7.3; S, 5.4%. Mass spectrum [*m*/*z* (%)]: 559 (16.3) $[M]^+$, 524 (100) $[M-Br]^+$, 467 (26.3) $[M-2CO]^+$, 438 (9.7) $[M-3CO]^+$. IR data (KBr, cm^{-1}): 3442m ν(NH); 2027vs, 1922vs, 1903vs $\nu(CO_{fac})$; 1630vs ν(C=N); 757w ν (C=S). ^1H NMR data (ppm): 12.49s (1) δ(N(2)–H); 8.78s (1) δ(C(2)–H); 8.20s (2) δ(N(1)–H); 7.47d (1) δ(C(6)–H); 7.23m (2) δ(C(7,8)–H); 4.18m (2) δ(O(4)–R^2); 3.89s (3) δ(O(5)–R^3); 1.27t (3) δ(O(4)–R^2).

*3.3.2. Data for **1a′** (HL^1, X = Br)*

Yield: 240 mg (88.6%). M.p.: 195–202 °C. *Anal.* Calc. for $C_{14}H_{15}BrN_3O_5SRe$: C, 27.8; H, 2.5; N, 6.7; S, 5.3. Found: C, 27.5; H, 2.3; N, 6.1; S, 5.1%. Mass spectrum [*m*/*z* (%)]: 603 (19.7) $[M]^+$, 524 (100) $[M-Br]^+$, 467 (24.3) $[M-2CO]^+$, 438 (10.3) $[M-3CO]^+$. IR data (KBr, cm^{-1}): 3441m, 3420m ν(NH); 2027vs, 1923vs,

Table 6
Relevant interatomic distances (Å) and angles (°) of $[Re_2(L^2)_2(CO)_6]$ (**2b**) and $[Re_2(L^3)_2(CO)_6] \cdot 2CH_3OH$ (**2c** $\cdot 2CH_3OH$)

	2b	**2c** $\cdot 2(CH_3OH)$
Re(1)–N(3A)/N(3)	2.191(9)	2.202(3)
Re(1)–S(1A)/S(1)	2.458(3)	2.4588(8)
Re(1)–S(1B)/S(1)[a]	2.549(3)	2.5467(9)[a]
Re(1)–C(103)	1.903(14)	1.914(4)
Re(1)–C(101)	1.918(12)	1.917(4)
Re(1)–C(102)	1.936(13)	1.915(4)
Re(2)–N(3B)	2.213(12)	
Re(2)–S(1B)	2.470(3)	
Re(2)–S(1A)	2.557(3)	
Re(2)–C(203)	1.894(14)	
Re(2)–C(202)	1.901(14)	
Re(2)–C(201)	1.921(13)	
S(1A)/S(1)–C(1A)/C(1)	1.780(11)	1.790(3)
C(1A)/C(1)–N(2A)/N(2)	1.276(12)	1.303(5)
N(2A)/N(2)–N(3A)/N(3)	1.384(10)	1.403(3)
C(2A)/C(2)–N(3A)/N(3)	1.285(11)	1.299(5)
S(1B)–C(1B)	1.754(15)	
C(1B)–N(2B)	1.311(16)	
N(2B)–N(3B)	1.281(14)	
C(2B)–N(3B)	1.413(16)	
N(3A)/N(3)–Re(1)–S(1A)/S(1)	79.0(2)	77.19(7)
N(3A)/N(3)–Re(1)–S(1B)/S(1)[a]	90.3(2)	83.56(7)[a]
S(1A)/S(1)–Re(1)–S(1B)/S(1)[a]	82.84(9)	82.02(3) [a]
N(3B)–Re(2)–S(1B)	77.5(4)	
N(3B)–Re(2)–S(1A)	90.9(3)	
S(1B)–Re(2)–S(1A)	82.43(9)	
Re(1)–S(1A)–Re(2)/Re(1)[a]	96.95(9)	97.98(3) [a]
Re(2)–S(1B)–Re(1)	96.88(10)	
C(1A)/C(1)–N(2A)/N(2)–N(3A)/N(3)	117.8(9)	114.0(3)
C(2A)/C(2)–N(3A)/N(3)–N(2A)/N(2)	116.4(9)	116.5(3)
C(1B)–N(2B)–N(3B)	115.2(15)	
C(2B)–N(3B)–N(2B)	110.2(13)	

[a] Equivalents atoms generated by symmetry transformations: $x+1$, $-y+1$, $-z+1$.

1905vs $\nu(CO_{fac})$; 1624s ν(C=N); 757w ν(C=S). ^{1}H NMR data (ppm): 12.53s (1) δ(N(2)–H); 8.72d (1) δ(C(2)–H); 8.19s (2) δ(N(1)–H); 7.37s (1) δ(C(6)–H); 7.21m (2) δ(C(7,8)–H); 4.17m (2) δ(O(4)–R^2); 3.86d (3) δ(O(5)–R^3); 1.23m (3) δ(O(4)–R^2).

This compound was also obtained as **1a**′ $\cdot$ ½C_7H_8 crystals by heating a solution of HL^1 and $[ReBr(CO)_5]$ in toluene for 20 h. Yield: 143 mg (50%).

3.3.3. Data for ***1b*** *(HL^2, X = Cl)*

Yield: 162 mg (72.3%). M.p.: 190–202 °C. *Anal.* Calc. for $C_{15}H_{17}ClN_3O_5SRe$: C, 31.4; H, 3.0; N, 7.3; S, 5.6. Found: C, 31.9; H, 3.2; N, 7.5; S, 5.5%. Mass spectrum [*m*/*z* (%)]: 573 (13.0) $[M]^+$, 538 (100) $[M-Br]^+$, 481 (21.4) $[M-2CO]^+$, 453 (8.8) $[M-3CO]^+$. IR data (KBr, cm^{-1}): 3398m ν(NH); 2023vs, 1899vs $\nu(CO_{fac})$; 1576s ν(C=N); 757w ν(C=S). ^{1}H NMR data (ppm): 12.41s (1) δ(N(2)–H); 8.77s (1) δ(C(2)–H); 8.17s (1) δ(N(1)–H); 7.45d (1) δ(C(6)–H); 7.27d (2) δ(C(7,8)–H); 7.21m (1) δ(C(7,8)–H); 4.18m (2) δ(O(4)–R^2); 3.90d (3) δ(O(5)–R^3); 3.18d (3) δ(N(1)–R^1); 1.27t (3) δ(O(4)–R^2).

3.3.4. Data for ***1b***′ *(HL^2, X = Br)*

Yield: 219 mg (83.6%). M.p.: 219 °C. *Anal.* Calc. for $C_{15}H_{17}BrN_3O_5SRe$: C, 29.2; H, 2.8; N, 6.8; S, 5.2. Found: C, 29.4; H, 2.9; N, 6.7; S, 5.1%. Mass spectrum [*m*/*z* (%)]: 617 (10.0) $[M]^+$, 538 (100) $[M-Br]^+$, 509 (8.6) $[M-CO]^+$, 481 (21.1) $[M-2CO]^+$, 453 (12.6) $[M-3CO]^+$. IR data (KBr, cm^{-1}): 3445m, 3283m ν(NH); 2023vs, 1930vs, 1906vs $\nu(CO_{fac})$; 1596s ν(C=N); 771w ν(C=S). ^{1}H NMR data (ppm): 12.37s (1) δ(N(2)–H); 8.67s (1) δ(C(2)–H); 8.14s (1) δ(N(1)–H); 7.35s (1) δ(C(6)–H); 7.20m (2) δ(C(7,8)–H); 4.16m (2) δ(O(4)–R^2); 3.86d (3) δ(O(5)–R^3); 3.14t (3) δ(N(1)–R^1); 1.23m (3) δ(O(4)–R^2).

3.3.5. Data for ***1c*** *(HL^3, X = Cl)*

Yield: 69 mg (34.8%). M.p.: 214 °C. *Anal.* Calc. for $C_{20}H_{19}ClN_3O_5SRe$: C, 37.7; H, 3.0; N, 6.6; S, 5.0. Found: C, 37.6; H, 3.0; N, 6.6; S, 5.0%. Mass spectrum [*m*/*z* (%)]: 635 (7.4) $[M]^+$, 600 (29.0) $[M-Br]^+$, 543 (7.7) $[M-2CO]^+$. IR data (KBr, cm^{-1}): 3441m ν(NH); 2026vs, 1916vs, 1889vs $\nu(CO_{fac})$; 1555s ν(C=N); 743w ν(C=S). ^{1}H NMR data (acetone-d_6, ppm): 12.56s (1) δ(N(2)–H); 10.24s (1) δ(N(1)–H); 8.91d (1) δ(C(2)–H); 7.48m (5) δ(N(1)–R^1); 7.38m (1) δ(C(6)–H); 7.26m (2) δ(C(7,8)–H); 4.18m (2) δ(O(4)–R^2); 3.90d (3) δ(O(5)–R^3); 1.25t (3) δ(O(4)–R^2).

3.3.6. Data for ***1c***′ *(HL^3, X = Br)*

Yield: 177 mg (76.6%). M.p.: 193 °C. *Anal.* Calc. for $C_{20}H_{19}BrN_3O_5SRe$: C, 35.4; H, 2.8; N, 6.2; S, 4.7. Found: C, 35.6; H, 2.8; N, 6.1; S, 4.9%. Mass spectrum [*m*/*z* (%)]: 679 (11.8) $[M]^+$, 600 (100) $[M-Br]^+$, 571 (10.4) $[M-CO]^+$, 543 (16.3) $[M-2CO]^+$, 514 (14.2) $[M-3CO]^+$. IR data (KBr, cm^{-1}): 3441m ν(NH); 2024vs, 1924vs, 1898vs $\nu(CO_{fac})$; 1565s ν(C=N); 740w ν(C=S). ^{1}H NMR data (ppm): 12.54s (1) δ(N(2)–H); 10.20s (1) δ(N(1)–H); 8.85d (1) δ(C(2)–H); 7.45m (5) δ(N(1)–R^1); 7.35m (1) δ(C(6)–H); 7.24m (2) δ(C(7,8)–H); 4.15m (2) δ(O(4)–R^2); 3.86d (3) δ(O(5)–R^3); 1.21m (3) δ(O(4)–R^2).

3.4. General synthesis of complexes $[Re_2(L)_2(CO)_6]$ (**2**)

To a solution of the corresponding adduct *fac*-$[ReBr(CO)_3(HL)]$ **1,** in 15 mL of dry methanol was added the corresponding equimolar amount of NaOH. The yellow mixture was refluxing for 1 h. The pale yellow solid formed was filtered out and vacuum dried.

3.4.1. Data for ***2a*** *(L^1)*

Yield: 36 mg (21.1%). M.p.: 215–250 °C. *Anal.* Calc. for $C_{28}H_{28}N_6O_{10}S_2Re_2$: C, 30.1; H, 2.7; N, 7.5; S, 5.7. Found: C, 29.9; H, 2.6; N, 7.3; S, 5.4%. Mass spectrum [*m*/*z* (%)]: 1046 (39.5) $[M]^+$. IR data (KBr, cm^{-1}): 3448m, ν(NH); 2021vs, 1908vs $\nu(CO_{fac})$; 1737m ν(C=N); 717w ν(C=S). ^{1}H NMR data (ppm): 9.22s (1) δ(N(1)–H), 8.85s (1) (C(2)–H); 7.78s (1) δ(N(1)–H); 7.65s (1) δ(C(6,8)–H); 7.24s (1) δ(C(6,8)–H); 7.07s δ(C(7)–H); 4.16m (2) δ(O(4)–R^2); 3.88s (3) δ(O(5)–R^3); 1.33t (3) δ(O(4)–R^2).

3.4.2. Data for ***2b*** *(L^2)*

Yield: 64 mg (59.8%). M.p.: 248–253 °C. *Anal.* Calc. for $C_{30}H_{32}N_6O_{10}S_2Re_2$: C, 33.5; H, 3.0; N, 7.8; S, 5.9. Found: C, 33.3; H, 2.8; N, 7.7; S, 5.6%. Mass spectrum [*m*/*z* (%)]: 1074 (9.8) $[M]^+$. IR data (KBr, cm^{-1}): 3443m, 3376m ν(NH); 2028vs, 2015vs, 1917vs, 1895vs $\nu(CO_{fac})$; 1714s ν(C=N); 740w ν(C=S). ^{1}H NMR data (ppm): 8.49s (2) δ(N(1)–H, C(2)–H); 7.63d (1) δ(C(6,8)–H); 7.14d (1) δ(C(6,8)–H); 7.05t δ(C(7)–H); 4.15m (2) δ(O(4)–R^2); 3.87s (3) δ(O(5)–R^3); 2.86s (3) δ(N(1)–R^1); 1.35t (3) δ(O(4)–R^2). Single yellow crystals of **2b** suitable for X-ray diffraction were obtained by slow evaporation of a methanol solution of **1b**.

3.4.3. Data for ***2c*** *(L^3)*

Yield: 21 mg (19.5%). M.p.: >250 °C. *Anal.* Calc. for $C_{40}H_{36}N_6O_{10}S_2Re_2$: C, 40.0; H, 3.0; N, 7.0; S, 5.3. Found: C, 39.9; H, 2.9; N, 6.9; S, 5.1%. Mass spectrum [*m*/*z* (%)]: 1198 (71.4) $[M]^+$. IR data (KBr, cm^{-1}): 3430m ν(NH); 2021vs, 1923vs $\nu(CO_{fac})$; 1707m ν(C=N); 715w ν(C=S). ^{1}H NMR data (ppm): 9.56s (1) δ(N(1)–H); 8.87s (1) δ(C(2)–H); 7.77d (2) δ(C(6,8)–H); 7.46d (1), 7.36t (2), 7.30d (2) δ(N(1)–R^1); 7.09t (1) δ(C(7)–H); 4.24m (1), 4.16m (1) δ(O(4)–R^2); 3.92s (3) δ(O(5)–R^3); 1.32t (3) δ(O(4)–R^2). Yellow single crystals of **2c** $\cdot$ 2(CH_3OH) suitable for X-ray diffraction were obtained by slow evaporation of a methanol solution of **1c**.

3.5. X-ray data collection, structure determination and refinement

Crystallographic data were collected on a Bruker SMART CCD-1000 diffractometer at 293 K using graphite monochromated Mo Kα radiation (λ = 0.71073 Å), and were corrected for Lorentz, polarization and absorption effects [23]. The structures were solved by direct methods using the program SHELX 97 [24]. All non-hydrogen atoms were refined with anisotropic thermal parameters. Hydrogen atoms were inserted at calculated positions and refined as riders [24]. Graphics were produced with PLATON [25] and MERCURY [26].

Acknowledgements

This research was supported by the European Rural Development Found and The Directorates General for Research of Galician Government and Spanish Ministry of Education and Science through projects PGIDIT06PXIB314373PR and CTQ2006-05642/BQU.

Appendix A. Supplementary data

CCDC 683875, 683876, 683877, 683678, 683679 and 683680 contain the supplementary crystallographic data for $HL^1 \cdot H_2O$, $HL^2 \cdot ½H_2O$, $HL^3 \cdot$ **½C$_7$H$_8$**, **2b**, **2c** $\cdot$ 2(CH_3OH). These data can be obtained free of charge via http://www.ccdc.cam.ac.uk/conts/retrieving.html, or from the Cambridge Crystallographic Data Centre, 12 Union Road, Cambridge CB2 1EZ, UK; fax: (+44) 1223-336-033; or e-mail: deposit@ccdc.cam.ac.uk.

References

[1] F. Zobi, B. Spingler, T. Fox, R. Alberto, Inorg. Chem. 42 (2003) 2818.
[2] F. Zobi, O. Blacque, H. Schmalle, B. Spingler, R. Alberto, Inorg. Chem. 43 (2004) 2087.
[3] F. Zobi, B. Spingler, R. Alberto, ChemBioChem 6 (2005) 1397.
[4] K.P. Maresca, J.F. Kronauge, J. Zubieta, J.W. Babich, Inorg. Chem. Commun. 10 (2007) 1409.
[5] M.J.M. Campbell, Coord. Chem. Rev. 15 (1975) 279.
[6] J.S. Casas, M.S. García-Tasende, J. Sordo, Coord. Chem. Rev. 209 (2000) 197.
[7] D.X. West, S.B. Padhye, P.B. Sonawane, Struct. Bond. (Berlin) 76 (1991) 1.
[8] I.G. Santos, U. Abram, R. Alberto, E. Vázquez-López, A. Sánchez, Inorg. Chem. 43 (2004) 1834.
[9] G. Pereiras-Gabián, E.M. Vázquez-López, U. Abram, Z. Anorg. Allg. Chem. 630 (2004) 1665.
[10] R. Carballo, J.S. Casas, E. García-Martínez, G. Pereiras-Gabián, A. Sánchez, U. Abram, E.M. Vázquez-López, CrystEngComm 7 (2005) 113.
[11] R. Carballo, J.S. Casas, E. García-Martínez, G. Pereiras-Gabián, A. Sánchez, J. Sordo, E.M. Vázquez-López, J.C. García-Monteagudo, U. Abram, J. Organomet. Chem. 656 (2002) 1.
[12] A.G. Quiroga, C. Navarro Ranninger, Coord. Chem. Rev. 248 (2004) 119.
[13] K.N. Thimmaiah, G.T. Chandrappa, W.D. Lloyd, C. Párkány, Trans. Met. Chem. (1985) 299.
[14] R. Carballo, J.S. Casas, E. García-Martínez, G. Pereiras-Gabián, A. Sánchez, J. Sordo, E.M. Vázquez-López, Inorg. Chem. 42 (2003) 6395.
[15] G. Pereiras-Gabián, E.M. Vázquez-López, H. Braband, U. Abram, Inorg. Chem. 44 (2005) 834.
[16] P. Barbazán, R. Carballo, U. Abram, G. Pereiras-Gabián, E.M. Vázquez-López, Polyhedron 25 (2006) 3343.
[17] G.J. Palenik, D.F. Rendle, W.S. Carter, Acta Crystallogr., Sect. B 30 (1974) 2390.
[18] G. Thiele, G. Liehr, E. Lindner, Chem. Ber. 107 (1974) 442.
[19] G. Thiele, G. Liehr, E. Lindner, J. Organomet. Chem. 70 (1974) 427.
[20] D.D. Perrin, W.L.F. Armarego, Purification of Laboratory Chemicals, 3rd ed., Oxford, 1988.
[21] M.F. Farona, K.F. Kraus, Inorg. Chem. 9 (1970) 1700.
[22] S.P. Schmidt, W.C. Trogler, F. Basolo, Inorg. Synth. 28 (1990) 160.
[23] G.M. Sheldrick, SADABS, University of Göttingen, Germany, 1996.
[24] G.M. Sheldrick, SHELX-97, Program for the Solution and Refinement of Crystal Structures, v.2, University of Göttingen, Germany, 1997.
[25] A.L. Spek, PLATON, 2002, v. 21.08.03, University of Utrecht, The Netherlands, 2002.
[26] I.J. Bruno, J.C. Cole, P.R. Edgington, M.K. Kessler, C.F. Macrae, P. McCabe, J. Pearson, R. Taylor, Acta Crystallogr., Sect. B 58 (2002) 389.

Aldrich Chemical Company, Inc. USA and were used as received. The precursor complexes $[\{(\eta^6\text{-arene})RuCl(\mu\text{-}Cl)\}_2]$, $[(\eta^6\text{-arene})RuCl_2(PyCN)]$ (arene = benzene and *p*-cymene), $[(\eta^5\text{-}C_5H_5)RuCl(PPh_3)_2]$ and $[(\eta^5\text{-}C_5Me_5)MCl(\mu\text{-}Cl)\}_2]$ (M = Rh and Ir) and the ligand (1,2-diphenylimino)acenaphthene (Ph-BIAN) were prepared and purified according to the published procedures [11,5f]. Microanalysis and FAB mass spectra were acquired from the Sophisticated Analytical Instrument Facility, Central Drug Research Institute, Lucknow. Electronic and luminescence spectra were recorded on a Shimadzu UV-1601 and Perkin–Elmer LS-45 spectrofluorophotometers, respectively. NMR spectra were acquired on a JEOL AL 300 MHz spectrometer, where chemical shifts were referenced to internal tetramethylsilane for ^{1}H NMR and phosphorous trichloride for ^{31}P NMR at room temperature.

2.2. Synthesis and characterization of $[(\eta^6\text{-}C_6H_6)RuCl(Ph\text{-}BIAN)]BF_4$ (**1**)

(a) To a suspension of the chloro-bridged dimeric ruthenium complex $[\{(\eta^6\text{-}C_6H_6)RuCl(\mu\text{-}Cl)\}_2]$ (0.502 g, 1.0 mmol) in methanol (25 mL), Ph-BIAN (0.664 g, 2.0 mmol) was added and the suspension was stirred at room temperature for ~10.0 h. Slowly it dissolved and gave a clear brown-black solution. It was filtered through Celite to remove any solid impurities. The filtrate was treated with NH_4BF_4 dissolved in methanol and left for slow crystallization. The dark brown product thus obtained was separated by filtration, washed with diethyl ether and dried under *vacuum*. It was further recrystallized from dichloromethane/diethyl ether. Yield: 0.471 g (68 %). *Anal.* Calc. (%) for $C_{30}ClF_4H_{22}N_2BRu$: C, 52.02; H, 3.18; N, 4.05. Found: C, 51.94; H, 2.83; N, 4.24%. FAB-MS: m/z = 547 (547) [M^+]; 512 (512) [$M-Cl^+$]. ^{1}H NMR (δ ppm, 300 MHz, $CDCl_3$, 298 K): 8.05 (d, 2H, J = 7.5 Hz), 7.99 (d, 2H, J = 7.2 Hz), 7.85 (d, 2H, J = 6.9 Hz), 7.73 (t, 2H, J = 6.6 Hz), 7.61 (m, 4H, J = 8.1 Hz), 7.44 (t, 2H, J = 7.5 Hz), 6.92 (d, 2H, J = 7.2 Hz), 5.58 (s, 6H). UV–Vis: λ_{max} (ε, dm^3 mol^{-1} cm^{-1}) = 706 (5.8×10^3), 446 (1.9×10^4), 300 (3.9×10^4), 256 (4.1×10^4) nm. Emission: λ_{em} (λ_{ex}, $\Phi/10^{-6}$) = 577 (446, 1.9) nm.

(b) Alternately, complex **1** can be synthesized by the reaction of $[(\eta^6\text{-}C_6H_6)RuCl_2(PyCN)]$ with Ph-BIAN in methanol under stirring conditions at room temperature.

2.3. Synthesis and characterization of $[(\eta^6\text{-}C_{10}H_{14})RuCl(Ph\text{-}BIAN)]BF_4$ (**2**)

This was prepared following the above synthetic procedure for **1** using $[\{(\eta^6\text{-}C_{10}H_{14})RuCl(\mu\text{-}Cl)\}_2]$ (0.612 g, 1.0 mmol) in place of $[\{(\eta^6\text{-}C_6H_6)RuCl(\mu\text{-}Cl)\}_2]$. Red brown, Yield: 0.531 g (71 %). *Anal.* Calc. (%) for $BC_{34}ClF_4H_{30}N_2Ru$: C, 54.55; H, 4.01; N, 3.74. Found: C, 53.88; H, 3.82; N, 3.57%. FAB-MS: m/z = 603 (603) [M^+]; 568 (568) [$M-Cl^+$]. ^{1}H NMR (δ ppm, 300 MHz, $CDCl_3$, 298 K): 7.99 (d, 2H, J = 8.1 Hz), 7.93 (d, 2H, J = 6.6 Hz), 7.82 (d, 2H, J = 6.3 Hz), 7.74 (t, 2H, J = 6.9 Hz), 7.62 (m, 4H), 7.43 (t, 2H, J = 8.1 Hz), 6.89 (d, 2H, J = 6.9 Hz), 5.33 (s, 4H), 2.51 (sep., 1H, J = 6.9 Hz), 1.99 (s, 3H), 1.09 (d, 6H, J = 6.9Hz). UV–Vis: λ_{max} (ε, dm^3 mol^{-1} cm^{-1}) = 462 (2.3×10^4), 310 (3.9×10^4), 255 (4.1×10^4) nm. Emission: λ_{em} (λ_{ex}, $\Phi/10^{-6}$) = 547 (462, 1.8) nm.

2.4. Synthesis and characterization of $[(\eta^5\text{-}C_5H_5)Ru(PPh_3)(Ph\text{-}BIAN)]BF_4$ (**3**)

A suspension of the ruthenium complex $[(\eta^5\text{-}C_5H_5)RuCl(PPh_3)_2]$ (0.728 g, 1.0 mmol) in methanol (25 mL) was treated with Ph-BIAN (0.332 g, 1.0 mmol) and the solution was refluxed for ~10.0 h. The resulting dark purple-black solution was filtered through Celite, and a saturated methanolic solution of NH_4BF_4 was added to the filtrate and left for slow crystallization. The dark purple-black product thus obtained was filtered and washed with diethyl ether and dried under vacuum. The product was further recrystallized from dichloromethane/diethyl ether. Yield: 0.584 g (69 %). *Anal.* Calc. (%) for $BC_{47}F_4H_{36}N_2PRu$: C, 66.58; H, 4.25; N, 3.30. Found: C, 65.98; H, 4.11; N, 3.87%. FAB-MS: m/z = 763 (760) [M^+]; 500 (498) [$M-PPh_3^+$]. ^{1}H NMR (δ ppm, 300 MHz, $CDCl_3$, 298 K): 8.13 (d, J = 8.1 Hz), 8.01 (d, J = 7.0 Hz), 7.91 (t, J = 7.1 Hz), 7.71 (t, J = 6.9 Hz), 7.60 (m), 4.65 (s). ^{31}P NMR (δ ppm, 120 MHz, $CDCl_3$): 43.29 (s). UV–Vis: λ_{max} (ε, dm^3 mol^{-1} cm^{-1}) = 561 (1.9×10^4), 323 (2.6×10^4), 244 (4.1×10^4) nm. Emission: λ_{em} (λ_{ex}, $\Phi/10^{-6}$) = 617 (561, 0.9) nm.

2.5. Synthesis and characterization of $[(\eta^5\text{-}C_5(CH_3)_5)RhCl(Ph\text{-}BIAN)]BF_4$ (**4**)

This was prepared following the above synthetic procedure for **1** using $[\{(\eta^5\text{-}C_5(CH_3)_5)RhCl(\mu\text{-}Cl)\}_2]$ (0.618 g, 1.0 mmol) in place of $[\{(\eta^6\text{-}C_6H_6)RuCl(\mu\text{-}Cl)\}_2]$. Red brown, Yield: 0.499 g (72 %). *Anal.* Calc. (%) for $BC_{34}ClF_4H_{31}N_2Rh$: C, 58.87; H, 4.47; N, 4.04. Found: C, 58.68; H, 4.82; N, 4.37%. ^{1}H NMR (δ ppm, 300 MHz, $CDCl_3$, 298 K): 7.98 (d, 2H, J = 8.1 Hz), 7.95 (d, 2H, J = 7.8 Hz), 7.83 (d, 2H, J = 7.5 Hz), 7.71–7.52 (m, 6H), 7.41 (t, 1H, J = 8.1Hz), 6.91 (d, 2H, J = 6.9 Hz), 1.33 (s, 15H). UV–Vis: λ_{max} (ε, dm^3 mol^{-1} cm^{-1}) = 375 (3.5×10^4), 314 (3.9×10^3), 257 (4.1×10^4) nm.

2.6. Synthesis and characterization of $[(\eta^5\text{-}C_5(CH_3)_5)IrCl(Ph\text{-}BIAN)]BF_4$ (**5**)

This was prepared following the above synthetic procedure for **1** using $[\{(\eta^5\text{-}C_5(CH_3)_5)IrCl(\mu\text{-}Cl)\}_2]$ (0.796 g, 1.0 mmol) in place of $[\{(\eta^6\text{-}C_6H_6)RuCl(\mu\text{-}Cl)\}_2]$. Red brown, Yield: 0.547 g (70 %). *Anal.* Calc. (%) for $BC_{34}ClF_4H_{31}N_2Ir$: C, 52.17; H, 3.96; N, 3.58. Found: C, 52.31; H, 3.82; N, 3.77%. ^{1}H NMR (δ ppm, 300 MHz, $CDCl_3$, 298K): 8.02 (d, 2H, J = 8.1 Hz), 7.99 (d, 2H, J = 6.9 Hz), 7.78 (d, 2H, J = 7.8 Hz), 7.71–7.52 (m, 6H), 7.43 (t, 2H, J = 7.8 Hz), 6.99 (d, 2H, J = 7.5 Hz), 1.31 (s, 15H). UV–Vis: λ_{max} (ε, dm^3 mol^{-1} cm^{-1}) = 435 (2.2×10^4), 319 (3.9×10^4), 244 (4.0×10^4) nm.

3. Results and discussion

3.1. Synthesis and characterization of the complexes **1**–**5**

The cationic mononuclear complexes $[(\eta^6\text{-arene})Ru(Ph\text{-}BIAN)Cl]^+$ (η^6-arene = benzene, **1** and *p*-cymene, **2**) (Scheme 1) have been synthesized by the reactions of the arene ruthenium precursor complexes $[\{(\eta^6\text{-arene})RuCl(\mu\text{-}Cl)\}_2]$ with Ph-BIAN in methanol at room temperature. Complexes **1** and **2** were also prepared by the reaction of the complexes $[(\eta^6\text{-arene})RuCl_2(PyCN)]$ (η^6-arene = benzene **1,** *p*-cymene, **2**; PyCN = 4-cyanopyridine) with Ph-BIAN in methanol. It was observed that in the reactions of the arene ruthenium complexes containing 4-cyanopyridine $[(\eta^6\text{-arene})RuCl_2(PyCN)]$ with Ph-BIAN, the coordinated 4-cyanopyridine gets substituted by Ph-BIAN to afford the complexes **1** and **2**. This observation is consistent with our earlier findings on the analogous arene ruthenium $[(\eta^6\text{-arene})RuCl_2(PyCN)]$ and 3:3-bis allyl ruthenium complexes $[(\eta^3\text{:}\eta^3\text{-}C_{10}H_{16})RuCl_2(PyCN)]$ incorporating 4-cyanopyridine, where the respective bases (EPh_3, E = P, As, Sb; bipy, phen) displaced the metal bound 4-cyanopyridine [12]. Treatment of $[(\eta^5\text{-}C_5H_5)RuCl(PPh_3)_2]$ with Ph-BIAN in refluxing methanol led to the formation of the cationic ruthenium complex $[(\eta^5\text{-}C_5H_5)Ru(Ph\text{-}BIAN)(PPh_3)]^+$ (Scheme 1), which was isolated as the BF_4^- salt.

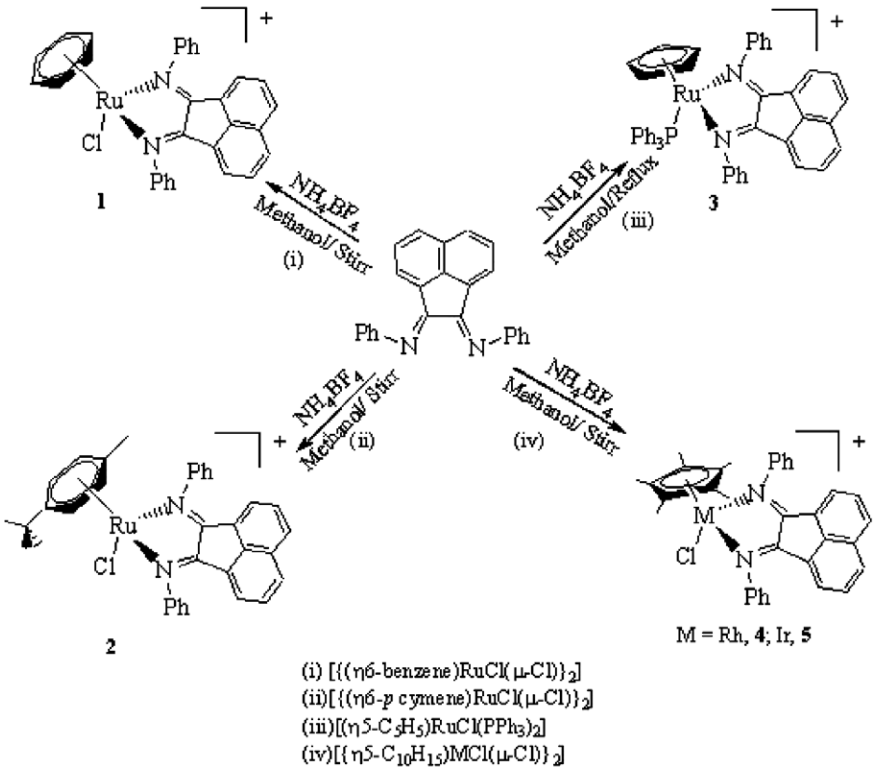

Scheme 1.

The pentamethylcyclopentadienyl complexes $[(\eta^5\text{-}C_5Me_5)M(Ph\text{-}BIAN)Cl]^+$ [M = Rh (**4**), Ir (**5**)] were obtained by the reactions of the chloro-bridged dimeric complexes $[\{(\eta^5\text{-}C_5Me_5)MCl(\mu\text{-}Cl)\}_2]$ [M = Rh and Ir] with two equivalents of Ph-BIAN in methanol and these were isolated as BF_4^- salts.

Spectral and analytical data of complexes **1**–**5** corroborate well to the proposed formulations. FAB-MS spectra of the complexes displayed prominent peaks corresponding to the molecular ion fragment. Representative spectra of **1**–**3** are shown in Fig. 1. Complexes **1** and **2** displayed the loss of chloride in the first step, whereas **3** displayed the loss of the coordinated triphenylphosphine. In these complexes the metal to Ph-BIAN bond is stronger and remains intact. The FAB-MS spectral results corroborate well to the proposed formulation of the complexes.

^{1}H NMR spectral data of the complexes, along with their assignments, are recorded in the experimental section. In the ^{1}H NMR spectra of complexes **1** and **2**, the protons associated with the arene moiety and Ph-BIAN displayed downfield shifts as compared to that in the precursor complexes and uncoordinated ligand, respectively. The ^{1}H NMR spectrum of complex **1** exhibited resonances at δ 8.05 (d, 2H), 7.99 (d, 2H), 7.85 (d, 2H), 7.73 (t, 2H), 7.62 (t, 4H), 7.44 (t, 2H) and 6.92 (d, 2H) ppm corresponding to Ph-BIAN protons and at δ 5.58 (s) ppm corresponding to the coordinated η^6-C_6H_6 ring protons. Similarly, in the ^{1}H NMR spectrum of complex **2** Ph-BIAN protons resonated at δ 7.99 (d, 2H, 8.1 Hz), 7.93 (d, 2H, 6.6 Hz), 7.82 (d, 2H, 6.3 Hz), 7.74 (t, 2H, 6.9 Hz), 7.62 (m, 4H), 7.43 (t, 2H, 8.1 Hz) and 6.89 (d, 2H, 6.9 Hz) ppm, while the protons associated with the *p*-cymene ring resonated at δ 5.33 (s, 4H), 2.51 (sep, 1H, 6.9 Hz), 1.99 (s, 3H) and 1.09 (d, 6H, 6.9 Hz) ppm. It was observed that the protons corresponding to Ph-BIAN resonated at almost same position in all the complexes. Further, the protons associated with the η^5-C_5H_5 ring in complex **3** resonated at 4.65 ppm and the methyl protons corresponding to the pentamethylcyclopentadienyl rings in complexes **4** and **5** appeared as a singlet at ~1.30 ppm. The position and integrated intensity of the various signals corresponded well to the formulation of respective complexes. In the ^{31}P NMR spectrum of complex **3**, the ^{31}P nuclei of the coordinated triphenylphosphine resonated as a singlet in the normal range at 43.29 ppm.

Electronic and emission spectral data for all the complexes are recorded in the experimental section. Comparative electronic spectra for the mononuclear complexes **1**–**5** are shown in Fig. 2. The electronic spectra of the ruthenium complexes **1** and **2** displayed bands at ~446, 310 and 255 nm. On the basis of its intensity and position, the lower energy absorption band at 446 nm has been assigned to a [Ru(II) → π^* Ph-BIAN] metal-to-ligand charge transfer (MLCT), where the high-lying filled orbital is localized on the metal centre and the low-lying empty orbital is localized on Ph-BIAN. Bands at around 300 nm could be attributed to intra-ligand π–π^* transitions. Similar trends of absorptions have been observed in the electronic spectra of complexes **3**–**5**.

The luminescence properties of complexes **1**–**3** were examined at room temperature in dichloromethane, Fig. 3. Upon excitation at their respective excitation bands (in parentheses), the complexes exhibited moderate emissions [577 nm (446 nm) for **1**, 547 nm (462 nm) for **2** and 617 nm (561 nm) for **3**]. The emission spectra were found to be parallel to their respective absorption bands, therefore these bands may be assigned to the ^{3}MLCT energy state of $Ru_{d\pi}$-$BIAN_{\pi^*}$. The observed results could be attributed to the fact that the excited state energy can be fine tuned with different substituents on the ligands that can be either electron donating or electron withdrawing [1c,1d,1e,13]. Emission from arene ruthenium complexes is often quenched following a non-radiative deactivation pathway [14]. Further, the non-radiative decay could be hindered by a judicious choice of ligands that controls the energy gap between the lowest excited energy state and the ground state (Table 1).

3.2. Solid-state characterization of complex *5*

Suitable crystals with distinct morphology were grown from a dichloromethane solution and diethylether by slow diffusion. The

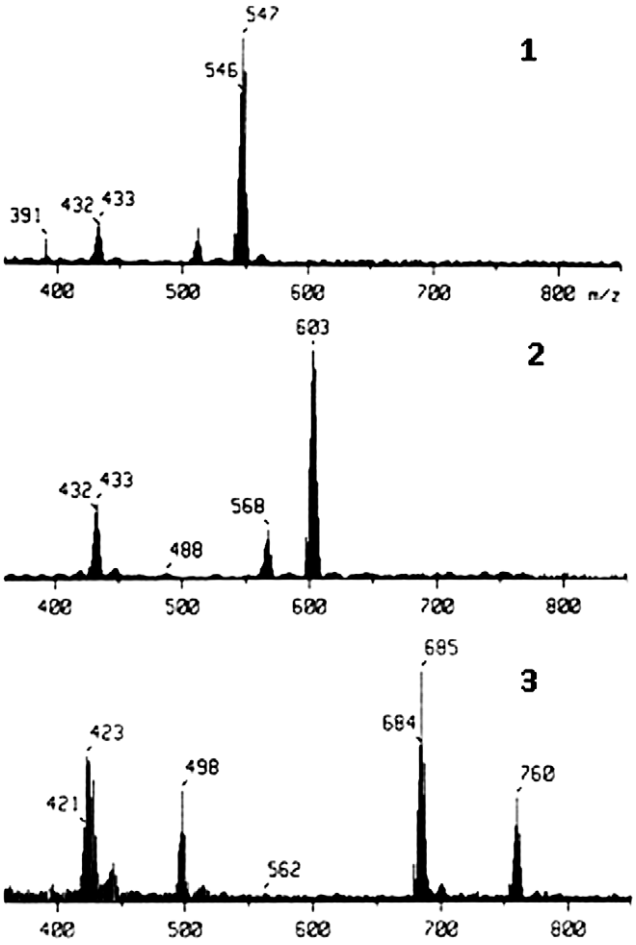

Fig. 1. FAB mass spectra of **1**–**3**.

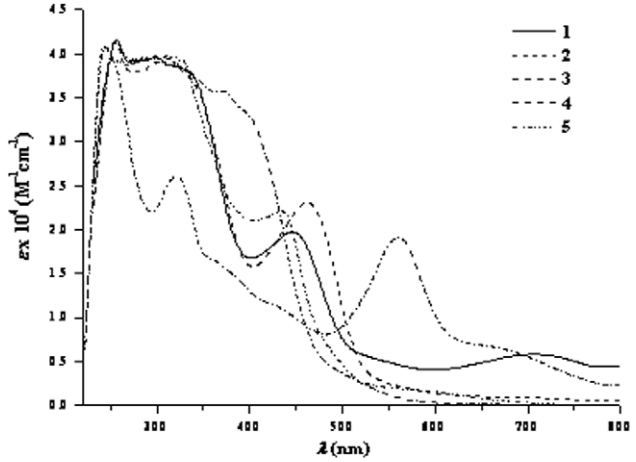

Fig. 2. Electronic spectra of **1**–**5** in dichloromethane.

ORTEP [15] depiction, including the atom-numbering scheme for the complex cation of **5**, is shown in Fig. 4, and the selected crystallographic data and bond parameters are listed in Tables 2 and 3, respectively. Complex **5** crystallizes in the orthorhombic crystal system with the *Pnma* space group. The coordination geometry about the metal centre Ir(1) is completed by nitrogen N(1) of PhBIAN, chloride ligand Cl(1) and $C_5Me_5(Cp^*)$ in η^5-coordination mode. Considering C_5Me_5 as a single coordination site, the overall

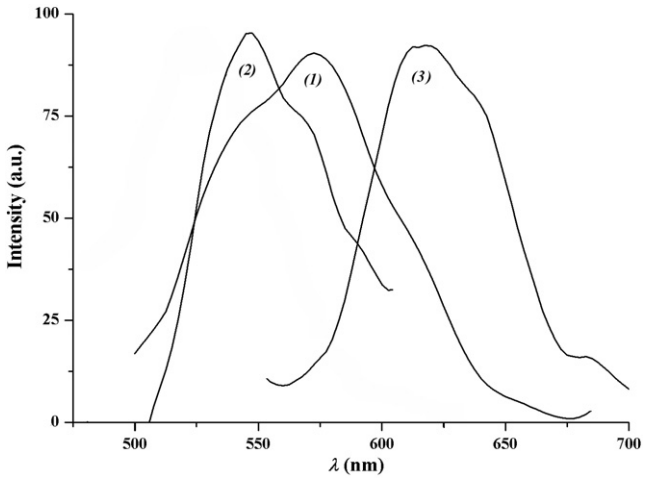

Fig. 3. Emission spectra of **1**–**3** in dichloromethane solution.

Table 1
Crystallographic data for **5**

Empirical formula	$C_{6.18}H_{5.64}B_{0.18}Cl_{0.18}F_{0.73}Ir_{0.18}N_{0.36}$
Formula weight	142.19
Wavelength (Å)	0.71073
Crystal system	orthorhombic
Space group	*Pnma*
Unit cell dimensions	
a (Å)	12.073(2)
b (Å)	16.432(3)
c (Å)	15.775(3)
α (°)	90
β (°)	90
γ (°)	90
Volume (Å^3)	3129.4(11)
Z	22
D_{calc} (Mg/m^3)	1.660
Reflections collected/unique (R_{int})	28 948/3706 (0.0730)
Data/restraints/parameters	3706/0/211
Goodness-of-fit on F^2	0.998
Final *R* indices [$I > 2\sigma(I)$]	$R_1 = 0.0431$, $wR_2 = 0.1164$
R indices (all data)	$R_1 = 0.0488$, $wR_2 = 0.1210$

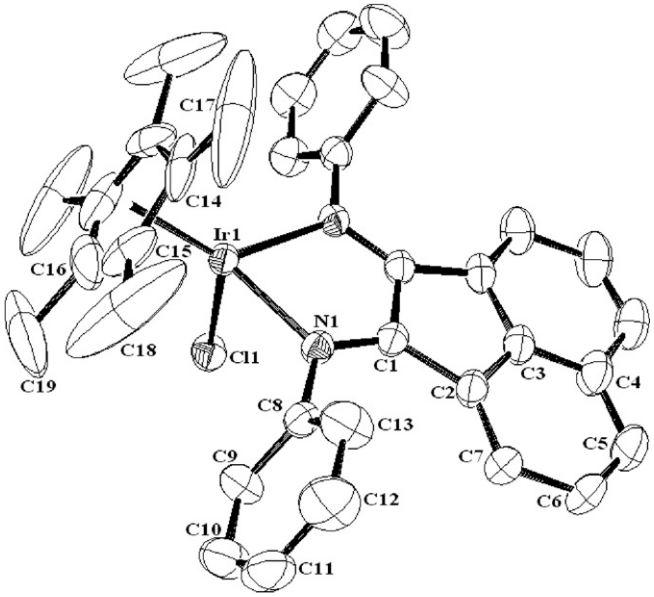

Fig. 4. ORTEP view of **5** with 30% ellipsoid probability.

Table 2
Important bond parameters (Å, °) for **5**

Ir(1)–N(1)	2.101(4)
Ir(1)–C(14)	2.133(8)
Ir(1)–C(16)	2.145(7)
Ir(1)–C(15)	2.166(6)
Ir–Ccp*	2.151
Ir–Cct	2.151
Ir(1)–Cl(1)	2.4047(18)
C–C(C5Me5)	1.368
C(C5Me5)–C(C5*Me*5)	1.473
C(1)–N(1)	1.299(7)
C(1)–C(2)	1.467(7)
C(1)–C(1)#1	1.473(10)
N(1)–Ir(1)–N(1)	76.9

Table 3
Hydrogenation of terephthalaldehyde with M-BIAN in H_2O at a S/C ratio of 100

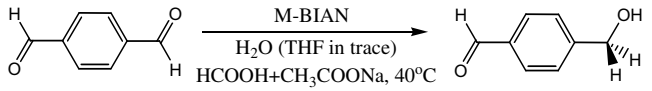

Catalyst	% Con	*t* (h)	TOF[a] (h^{-1})
RuB-BIAN (**1**)	>99	7	14
RuPC-BIAN (**2**)	>99	3	33
RuCP-BIAN (**3**)	>99	10	10
Rh-BIAN (**4**)	>99	0.75	133
Ir-BIAN (**5**)	>99	2	50

[a] Based on >99 % conversion.

coordination geometry about the metal centre is a typical *piano-stool* geometry. The average Ir—C_{cp^*} distance is 2.151 Å (range 2.133–2.166 Å; Ir–C_{ct} 1.810 Å) [16,17a]. The Ir–Cl and Ir–N distances are normal and have values of 2.4047 and 2.101 Å, respectively [16a–18]. The chelating N–Ir–N bite for the coordination of the imino nitrogen of Ph-BIAN is 76.9°. The arrangement of phenyl rings with respect to the acenaphthene ring is almost orthogonal, with a dihedral angle of 71.97°. The acenaphthene ring is planar with a deviation of 0.76°. The C–C(C_5Me_5) bond lengths in C_5Me_5 are in the range 1.25–1.472 Å, with an average value of 1.368 Å, and the exterior C(C_5Me_5)–C(C_5Me_5) average bond length is 1.473 Å. The C–C bond lengths within the Cp^* ring and the C–CH_3 bond lengths are normal [19].

3.3. Catalytic application of complexes *1*–*5*

To evaluate the selectivity and efficiency of complexes **1**–**5** as catalysts towards the reduction of the mono/di-formyl group, terephthalaldehyde was used as a model substrate. Hydrogenation was initiated by introducing formic acid–sodium acetate and terephthalaldehyde (1.0 mmol) in water (a few drops of freshly distilled THF was used to dissolve the catalyst) and air at 40 °C with 1% catalyst. All the complexes were found to catalyze the hydrogenation of terephthalaldehyde to produce 4-hydroxymethybenzaldehyde in aqueous solution (Table 3). It was observed that in all cases only one formyl group of terephthalaldehyde was selectively reduced. Further, we found that the rhodium complex Rh-BIAN (**4**) led to almost complete conversion of terephthalaldehyde into 4-hydroxymethybenzaldehyde in 45 min. The analogous iridium complex Ir-BIAN (**5**) was less active as compared to the rhodium complex Rh-BIAN (**4**) and complete conversion of the substrate took place in 2 h. RuPC-BIAN (**2**) required 3 h for the same reduction and RuCP-BIAN (**3**) is least effective in this regard. Among the ruthenium *p*-cymeme and benzene complexes, the ruthenium *p*-cymene complex (**2**) is more effective than its benzene (**1**) analogue. This may be due to the inductive effect of the isopropyl and methyl substituents on the capped arene ligand. Further, Rh-BIAN was also found to catalyze the hydrogenation of 2-acetyl-naphthalene, however only 20% conversion was achieved even after 10 h.

4. Conclusion

In conclusion, in this work a new series of mononuclear *piano-stool* complexes [(η^6-arene)Ru(Ph-BIAN)Cl]BF_4 [η^6-arene = C_6H_6 (**1**), $C_{10}H_{14}$ (**2**)], [(η^5-C_5H_5)Ru(Ph-BIAN)PPh_3]BF_4 (**3**) and [(η^5-C_5Me_5)M(Ph-BIAN)Cl]BF_4 [M = Rh (**4**), Ir (**5**)] have been synthesized using a highly conjugated diimine ligand with a rigid acenaphthene skeleton. Apart from the non-radiative nature of arene ruthenium complexes, the reported complexes were found to be luminescent at room temperature in dichloromethane. Furthermore, it has been shown that complexes **1**–**5** effectively catalyze the reduction of terephthalaldehyde, and among these the rhodium complex [(η^5-C_5Me_5)Rh(Ph-BIAN)Cl]BF_4 (**4**) is an effective hydrogenating catalyst for use in water and air, and delivers faster rates without requiring inert gas protection or substrate solubility in water.

Crystallographic data: Crystals suitable for single crystal X-ray diffraction analyses for **5** were grown from dichloromethane and diethyl ether at room temperature using the diffusion technique. Preliminary data on the space group and unit cell dimensions as well as intensity data were collected on a R-AXIS RAPID II diffractometer using graphite monochromatized Mo Kα radiation. The structure was solved by direct methods and refined using SHELX 97 [20]. The non-hydrogen atoms were refined with anisotropic thermal parameters. The H-atoms attached to carbon atoms were included as a fixed contribution and were geometrically calculated and refined using the SHELX riding model.

5. Supplementary data

CCDC 670670 contains the supplementary crystallographic data for complex **5**. These data can be obtained free of charge via http://www.ccdc.cam.ac.uk/conts/retrieving.html, or from the Cambridge Crystallographic Data Centre, 12 Union Road, Cambridge CB2 1EZ, UK; fax: (+44) 1223-336-033; or e-mail: deposit@ccdc.cam.ac.uk.

Acknowledgements

Thanks are due to the Council for Scientific and Industrial Research, New Delhi for providing financial assistance through the scheme HRDG, 01(1784)/02/EMR-II and for a Senior Research Fellowship to S.K.S. Thanks are also due to the Head, Department of Chemistry, Banaras Hindu University, Varanasi (UP) and the National Institute of Advanced Industrial Science and Technology (AIST), Ikeda, Osaka, Japan for extending facilities. We also thank Mr. Atish Chandra (Department of Chemistry, Banaras Hindu University, Varanasi 221 005) for his help in monitoring the catalytic reactions.

References

[1] (a) K.K.-W. Lo, C.-K. Li, K.-W. Lau, N. Zhu, J. Chem. Soc., Dalton Trans. (2003) 4642;
(b) W.R. Browne, C.M. O'Connor, H.P. Hughes, R. Hage, O. Walter, M. Doering, J.F. Gallagher, J.G. Vos, J. Chem. Soc., Dalton Trans. (2002) 4048;
(c) Y. Zhang, K.D. Ley, K.S. Schanze, Inorg. Chem. 35 (1996) 7102;
(d) C.E. Whittle, J.A. Weinstein, M.W. George, K.S. Schanze, Inorg. Chem. 40 (2001) 4053;

(e) W. Lu, M.C.W. Chen, N. Zhu, C.-M. Che, Z. He, K.-Y. Wong, Chem. Eur. J. 9 (2003) 6155.
[2] (a) S.D. Ittel, L.K. Johnson, Chem. Rev. 100 (2000) 1169;
(b) F. Ragaini, S. Cenini, E. Borsani, M. Dompe, E. Gallo, Organometallics 20 (2001) 3390;
(c) S. Niibayashi, K. Matsubara, M. Haga, H. Nagashima, Organometallics 33 (2004) 635;
(d) I.L. Fedushkin, N.M. Khvoinova, A.Y. Baurin, G.K. Fukin, V.K. Cherkasov, M.P. Bubnov, Inorg. Chem. 43 (2004) 7807;
(d) A.M. Kluwer, T.S. Koblenz, T. Jonischkeit, K. Woelk, C.J. Elsevier, J. Am. Chem. Soc. 127 (2005) 15470;
(e) M. Gasperini, F. Ragaini, Organometallics 23 (2004) 995;
(f) J.H. Groen, C.J. Elsevier, K. Vrieze, W.J.J. Smeets, A.L. Speck, Organometallics 15 (1996) 3445;
(g) J.H. Groen, J.G.P. Delis, P.W.N.M. van Leeuwen, K. Vrieze, Organometallics 16 (1997) 68;
(h) J.G.P. Delis, J.H. Groen, K. Vrieze, P.W.N.M. van Leeuwen, N. Veldman, A.L. Speck, Organometallics 16 (1997) 551.
[3] (a) R. van Asselt, C.J. Elsevier, Organometallics 11 (1992) 1999;
(b) G. Reeske, C.R. Hoberg, N.J. Hill, A.H. Cowley, J. Am. Chem. Soc. 128 (2006) 2800.
[4] (a) M.W. van Laren, C.J. Elsevier, Angew. Chem., Int. Ed. 38 (1999) 3715;
(b) R. van Belzen, H. Hoffmann, C.J. Elsevier, Angew. Chem., Int. Ed. Engl. 36 (1997) 1743;
(c) E. Shirakawa, T. Hiyama, J. Organomet. Chem. 653 (2002) 114.
[5] (a) R.A. Klein, P. Witte, R. van Belzen, J. Fraanje, K. Goubitz, M. Numan, H. Schenk, J.M. Ernsting, C.J. Elsevier, Eur. J. Inorg. Chem. (1998) 319;
(b) R. van Asselt, C.J. Elsevier, W.J.J. Smeets, A.L. Speck, Inorg. Chem. 33 (1994) 1521;
(c) C.J. Adams, N. Fey, J.A. Weinstein, Inorg. Chem. 45 (2006) 6105;
(d) L.K. Johnson, C.M. Killian, M. Brookhant, J. Am. Chem. Soc. 117 (1995) 6414;
(e) F. Ragaini, M. Gasperini, E. Gallo, P. Macchi, Chem. Commun. (2005) 1031;
(f) F. Ragaini, S. Cenini, S. Tollari, G. Tummolillo, R. Beltrami, Organometallics 18 (1999) 928;
(g) S. Cenini, F. Ragaini, S. Tollari, D. Paone, J. Am. Chem. Soc. 118 (1996) 11964.
[6] (a) S. Arseniyadis, K.S. Kyler, D.S. Watt, Org. React. 31 (1984) 1;
(b) W.A. Herrmann, C.W. Kohlpaintner, Angew. Chem., Int. Ed. 32 (1993) 1524.
[7] (a) X. Wu, D. Vinci, T. Ikariya, J. Xiao, Chem. Commun. (2005) 4447;
(b) P. Govindaswamy, J. Canivet, B. Therrien, G. Süss-Fink, P. Štěpnička, J. Ludvík, J. Organomet. Chem. 692 (2007) 3664.
[8] (a) D. Morales-Morales, C. Grause, K. Kasaoka, R. Redon, R.E. Cramer, C.M. Jensen, Inorg. Chim. Acta 300–302 (2000) 958;
(b) R.J. Cross, A.R. Kennedy, K.W. Muir, J. Organomet. Chem. 487 (1995) 227.
[9] J.P. Collman, L.S. Hegedus, J.R. Norton, R.G. Finke, in: Principles and Applications of Organotransition Metal Chemistry, University Science, Mill Valley, CA, 1987, p. 241.
[10] D.D. Perrin, W.L.F. Armango, D.R. Perrin, Purification of Laboratory Chemicals, Pergamon, Oxford, UK, 1986.
[11] (a) M.A. Bennett, T.N. Huang, T.W. Matheson, A.K. Smith, Inorg. Synth. 21 (1982) 74;
(b) R.A. Zelonka, M.C. Baird, Can. J. Chem. (1972) 3063;
(c) G.S. Ashby, M.I. Bruce, I.B. Tomkins, R.C. Wallis, Aust. J. Chem. 32 (1979) 1003;
(d) M.I. Bruce, B.C. Hall, N.N. Zaitseva, B.W. Skelton, A.H. White, J. Chem. Soc., Dalton Trans. (1998) 1793;
(e) B.L. Booth, R.N. Haszeldine, M. Hill, J. Chem. Soc. A (1969) 1299;
(f) C. White, A. Yates, P.M. Maitilis, Inorg. Synth. 29 (1992) 228;
(g) C.W. Glynn, M.M. Turnbull, Transition Met. Chem. 27 (2002) 822.
[12] (a) D.K. Gupta, A.N. Sahay, D.S. Pandey, N.K. Jha, P. Sharma, G. Espinosa, A. Cabrera, M.C. Puerta, P. Valerga, J. Organomet. Chem. 568 (1998) 13;
(b) A.N. Sahay, D.S. Pandey, M.G. Walwalkar, J. Organomet. Chem. 605 (2000) 74.
[13] P.A. Anderson, F.R. Keene, T.J. Meyer, J.A. Moss, G.F. Strouse, J.A. Treadway, J. Chem. Soc., Dalton Trans. (2002) 3820.
[14] (a) G.D. Marco, A. Bartolotta, V. Ricevuto, S. Campagna, G. Denti, L. Sabatino, G.D. Rosa, Inorg. Chem. 30 (1991) 270;
(b) S. Campagna, C.D. Pietre, F. Loiseau, B. Maubert, N. McClenaghan, R. Passalacqua, F. Puntoriero, V. Ricevuto, S. Serroni, Coord. Chem. Rev. 229 (2002) 67.
[15] L.J. Farrugia, J. Appl. Crystallogr. 30 (1997) 565.
[16] (a) D.L. Davies, O. Al-Duaij, J. Fawcett, M. Giardiello, S.T. Hilton, D.R. Russell, J. Chem. Soc., Dalton Trans. (2003) 4132;
(b) H. Amouri, C. Guyard-Duhayon, J. Vaissermann, Inorg. Chem. 41 (2002) 397.
[17] (a) T. Scheiring, J. Fiedler, W. Kaim, Organometallics 20 (2001) 1437;
(b) H. Aneetha, P.S. Zacharias, B. Srinivas, G.H. Lee, Y. Wong, Polyhedron 18 (1999) 299.
[18] (a) A. Buryak, K. Severin, J. Am. Chem. Soc. 127 (2005) 3700;
(b) C. Pettinari, R. Pettinari, M. Fianchini, F. Marchetti, B.W. Skeleton, A.H. White, Inorg. Chem. 44 (2005) 7933.
[19] P. Paul, B. Tyagi, A.K. Bilakhia, D. Parthsarthi, M.M. Bhadbhade, E. Suresh, G. Ramchandraiah, Inorg. Chem. 37 (1998) 5733.
[20] G.M. Sheldrick, SHELX-97: Programme for Refinement of Crystal Structures, University of Göttingen, Göttingen, Germany, 1997.

2. Experimental

2.1. General and physical measurements

Solvents were purchased from Aldrich and dried by usual procedures. *Trans*-[Pt(N_4CR)$_2$(PPh_3)$_2$] **1** [R = Me **1a**, Et **1b**, Ph **1c**], *trans*-[Pt(CN)(N_4CEt)(PPh_3)$_2$] **4** and *cis*-[Pt(N_3)$_2$(PPh_3)$_2$] **5** were prepared according to published procedures [12,20]. C, H and N elemental analyses were carried out by the Microanalytical Service of the Instituto Superior Técnico. ^{1}H, ^{13}C and ^{31}P{^{1}H} NMR spectra (in $CDCl_3$) were measured on a Varian Unity 300 spectrometer at ambient temperature. The chemical shifts (δ) are expressed in ppm relative to Si(Me)$_4$ (^{1}H and ^{13}C) or 85% H_3PO_4 (^{31}P). *J* values are in Hertz. Infrared spectra (4000–400 cm^{-1}) were recorded on a Bio-Rad FTS 3000MX and a Jasco FT/IR-430 instruments in KBr pellets and the wavenumbers are in cm^{-1}.

Electrospray mass spectra of 5-substituted-1*H*-tetrazoles were carried out with an ion-trap instrument (Varian 500-MS LC Ion Trap Mass Spectrometer) equipped with an electrospray (ESI) ion source. The solutions (in CH_2Cl_2) were continuously introduced into the mass spectrometer source with a syringe pump at a flow rate of 10 μL/min. The drying gas temperature was maintained at 350 °C and dinitrogen was used as nebulizer gas at a pressure of 35 psi. Scanning was performed from *m/z* = 50–1500. The compounds were observed in the negative mode (capillary voltage = −4000 V). The microwave irradiation experiments were undertaken in a focused microwave CEM Discover reactor (10 mL, 13 mm diameter, 300 W) which is fitted with a rotational system and an IR detector of temperature.

2.2. Compounds preparation

2.2.1. *trans*-[Pt(5-phenethyltetrazolato)$_2$(PPh_3)$_2$] (**1d**)

(i) By refluxing: A solution of *cis*-[Pt(N_3)$_2$(PPh_3)$_2$] **5** (0.080 g, 0.10 mmol) in $NCCH_2CH_2Ph$ (8 mL) was refluxed for 12 h whereupon the solvent was removed *in vacuo*. The oily residue was treated with diethyl ether to obtain, upon stirring, a white semicrystalline solid. This was washed repeatedly with 5 mL portions of water, and then with ethanol and lastly with diethyl ether. Recrystallization from a chloroform/diethyl ether mixture gave off-white crystals of *trans*-[Pt(5-phenethyltetrazolato)$_2$(PPh_3)$_2$] **1d**.

(ii) By focused microwave irradiation: In this method, identical amounts of the reagents described above were added to a cylindrical Pyrex tube which was then placed in the focused microwave reactor. The system was left under irradiation for 1 h at 100 °C. The solvent was then removed *in vacuo* and the resulting oily residue was treated in a manner similar to that described above to obtain a white crystalline solid of **1d**. Yield: 52% (method i) and 50% (method ii). IR (cm^{-1}): 1629 (C=N). ^{1}H NMR ($CDCl_3$), δ 2.51 (m, 8H, CH_2), 7.11–7.51 (m, 40H, aromatic). ^{13}C{^{1}H} NMR ($CDCl_3$), δ 27.19 (CH_2), 34.47 (CH_2), 125.84–141.79 ($C_{aromatic}$), 164.46 (C=N). ^{31}P{^{1}H} NMR ($CDCl_3$), δ 16.51 (J_{Pt-P} = 2726 Hz). *Anal.* Calc. for $PtC_{54}H_{48}N_8P_2$: C, 60.79; H, 4.50; N, 10.50. Found: C, 60.49; H, 4.30; N, 10.39%.

2.2.2. *trans*-[Pt(C≡CPh)$_2$(PPh_3)$_2$] (**7a**)

A solution of *cis*-[Pt(N_3)$_2$(PPh_3)$_2$] **5** (0.080 g, 0.10 mmol) in ethynylbenzene (3 mL) was taken in a cylindrical Pyrex tube which was then placed in the focused microwave reactor. The system was irradiated for 1 h at 100 °C. Then the mixture was cooled and excess of diethyl ether was added to precipitate a yellow compound which was isolated by filtration and washed with diethyl ether and dried at room temperature. The resultant compound **7a** was recrystallized from a dichloromethane and diethyl ether solvent mixture. Yield: 65%. IR (cm^{-1}): 2109 (C≡C). ^{1}H NMR ($CDCl_3$), δ 6.27–6.92 (m, 10H, C_6H_5), 7.33–7.86 (m, 30H, P(C_6H_5)). ^{31}P{^{1}H} NMR ($CDCl_3$), δ 18.60 (J_{Pt-P} = 2650 Hz). *Anal.* Calc. for $PtC_{52}H_{40}P_2$: C, 67.75; H, 4.37. Found: C, 67.32; H, 4.46%. Due to poor solubility no reliable results were obtained for ^{13}C NMR spectroscopy.

2.2.3. *trans*-[Pt(*p*-MeC_6H_4C≡C)$_2$(PPh_3)$_2$] (**7b**)

This compound was prepared by a similar method to that used for **7a**, but by using 1-ethynyl-4-methylbenzene as the solvent. Yield: 62%. IR (cm^{-1}): 2105 (C≡C). ^{1}H NMR ($CDCl_3$), δ 2.16 (s, 6H, CH_3), 6.16–6.73 (m, 8H, C_6H_4), 7.34–7.82 (m, 30H, P(C_6H_5)). ^{31}P{^{1}H} NMR ($CDCl_3$), δ 18.55 (J_{Pt-P} = 2655 Hz). *Anal.* Calc. for $PtC_{54}H_{44}P_2$: C, 68.27; H, 4.67. Found: C, 67.98; H, 4.82%. Due to poor solubility no reliable results were obtained for ^{13}C NMR spectroscopy.

2.2.4. *trans*-dicyano bis(triphenylphosphine)platinum(II) complex 2 and 5-substituted-1H-tetrazoles

This compound was prepared in identical ways starting from **1a**, **1c**, **1d**, **7a** or **7b** by refluxing any of these complexes in propionitrile for 24 h. The following synthesis is described as a representative case.

A solution of *trans*-[Pt(N_4CCH_3)$_2$ (PPh_3)$_2$] **1a** (0.088 g, 0.10 mmol) in NCEt (8 mL) was refluxed for 24 h whereupon the solvent was removed to half of its volume *in vacuo*. The reaction mixture was left to cool to room temperature and was treated with diethyl ether (5 mL). The white solid **2** was isolated by filtration and washed with diethyl ether for several times and chromatographic purification of the complex on SiO_2 was carried out using dichloromethane/diethyl ether (10:1). The mother liquor was evaporated to dryness and the resulting compound was identified as 5-methyl-1*H*-tetrazole.

A slight modification was followed when starting from *trans*-[Pt(5-ethyltetrazolato)$_2$(PPh_3)$_2$] **1b**. When refluxing its solution in propionitrile, the intermediate complex *trans*-[Pt(CN)(5-ethyltetrazolato)(PPh_3)$_2$] **4** started to precipitate after 6 h, whereupon 5 mL of DMF (dimethylformamide) was added to solubilize the complex, thus allowing the reaction to proceed further.

2.2.5. *trans*-[Pt(CN)$_2$(PPh_3)$_2$] (**2**)

Yield: 60%. IR (cm^{-1}): 2129 (C≡N). ^{1}H NMR ($CDCl_3$), δ 7.43–7.72 (m, 30H, aromatic). ^{13}C{^{1}H} NMR ($CDCl_3$), δ 125.70 (C≡N), 128.49–141.08 ($C_{aromatic}$). ^{31}P{^{1}H} NMR ($CDCl_3$), δ 14.42 (J_{Pt-P} = 2377 Hz). *Anal.* Calc. for $PtC_{38}H_{30}N_2P_2$: C, 59.14; H, 3.92; N, 3.63. Found: C, 59.13; H, 3.90; N, 3.25%.

2.2.6. 5-Methyl-1H-tetrazole (**3a**)

Yield: 70%. IR (cm^{-1}): 1629 (C=N). ^{1}H NMR ($CDCl_3$), δ 2.60 (s, 3H, CH_3). ^{13}C{^{1}H} NMR ($CDCl_3$), δ 9.18 (CH_3), 153.21 (C=N). ESI-MS, *m/z* 83 [M−H]$^-$.

2.2.7. 5-Ethyl-1H-tetrazole (**3b**)

Yield: 75%. All the spectroscopic and ESI-MS data are in agreement with those reported earlier [18].

2.2.8. 5-Phenyl-1H-tetrazole (**3c**)

Yield: 80%. IR (cm^{-1}): 1636 (C=N). ^{1}H NMR ($CDCl_3$), δ 7.43–8.16 (m, 5H, aromatic). ^{13}C{^{1}H} NMR ($CDCl_3$), δ 126.34–133.93 ($C_{aromatic}$), 158.49 (C=N). ESI-MS, *m/z* 145 [M−H]$^-$.

2.2.9. 5-Phenethyl-1H-tetrazole (**3d**)

Yield: 77%. IR (cm^{-1}): 1634 (C=N). ^{1}H NMR ($CDCl_3$), δ 3.09 (t, J_{HH} = 9 Hz, 2H, CH_2), 3.24 (t, J_{HH} = 9 Hz, 2H, CH_2), 7.12–7.54 (m, 5H, aromatic). ^{13}C{^{1}H} NMR ($CDCl_3$), δ 25.40 (CH_2), 33.64 (CH_2), 126.58–139.61 ($C_{aromatic}$), 155.94 (C=N). ESI-MS, *m/z* 173 [M−H]$^-$.

Table 1
Summary of crystal data, data collection and structure refinement for the X-ray diffraction study of complexes **2** and **7a**

	2	**7a**
Empirical formula	$C_{38}H_{30}N_2P_2Pt$	$C_{52}H_{40}P_2Pt$
Formula weight	771.66	921.86
Crystal system	triclinic	orthorhombic
Space group	$P\bar{1}$	Pbca
a (Å)	9.1519(20)	18.051(2)
b (Å)	9.6660(26)	9.5650(11)
c (Å)	10.3888(22)	22.929(2)
α (°)	109.959(13)	90
β (°)	90.901(14)	90
γ (°)	108.283(16)	90
V (Å^3)	812.4(4)	3958.9(8)
Z	1	4
ρ (g cm^{-3})	1.577	1.547
μ(Mo Kα)	4.445	3.662
Number of reflections measured	7409	28382
Number of reflections unique	2805	8069
Number of reflections observed	2802	4091
R_{int}	0.0339	0.0410
R_1, wR_2 (all data)	0.0243, 0.0572	0.0797, 0.0611
R_1, wR_2 (obs. refl.)	0.0242, 0.0572	0.0262, 0.0476
Goodness-of-fit	1.034	0.913

2.3. Single-crystal X-ray crystallography

Single crystals of **2** were obtained by diffusing diethyl ether in dichloromethane solutions of the complex. X-ray diffraction suitable crystals of **7a** were obtained by slow evaporation of the reaction mixture.

X-ray intensity data were measured at 150 K on a Bruker AXS-KAPPA APEX II CCD-based diffractometer (Mo Kα radiation, λ = 0.71073 Å) using omega scans of 0.5° per frame, and a full sphere of data was obtained. Raw data frame integration and corrections were performed with Bruker SAINT. An empirical absorption correction was applied with SADABS. Direct methods structure solution were performed with SHELXS-97 package [21] and refined with SHELXL-97 [22] with the WinGX graphical user interface [23]. All hydrogens were inserted in calculated positions. Least square refinement with anisotropic thermal motion parameters for all the non–hydrogen atoms and isotropic for the remaining atoms were employed. Crystallographic parameters and residuals are given in Table 1.

3. Results and discussion

The phenethyltetrazolato complex *trans*-[Pt(N$_4$CR)$_2$(PPh$_3$)$_2$] **1d** (R = CH$_2$CH$_2$Ph) was prepared by using either the traditional refluxing method or by microwave irradiation (M.W.) as reported in a previous paper for the synthesis of the analogous complexes **1a** (R = Me), **1b** (R = Et) and **1c** (R = Ph) [12]. Treatment of any of these complexes with an excess of propionitrile in refluxing conditions leads ultimately to the dicyano-Pt^{II} compound *trans*-[Pt(CN)$_2$(PPh$_3$)$_2$] **2**, isolated as a white crystalline solid in moderate yield (*ca.* 60%), with concomitant formation of the corresponding 5-substituted-1*H*-tetrazoles **3** in good yields (*ca.* 80%) (Scheme 1).

The dicyano-complex **2** was synthesized and reported for the first time by Bailar et al. [24], using [PtCl$_2$(PPh$_3$)$_2$] and KCN as the source of the cyano-ligand. When starting from *trans*-[Pt(N$_4$CEt)$_2$(PPh$_3$)$_2$] **1b**, the addition of a small amount of DMF is required to prevent the precipitation of the intermediate mono-cyano complex *trans*-[Pt(CN)(N$_4$CEt)(PPh$_3$)$_2$] **4**. This intermediate has been isolated by a method described elsewhere [12] and converts to *trans*-[Pt(CN)$_2$(PPh$_3$)$_2$] **2** by dissolving in DMF and then refluxing a propionitrile solution for 24 h (Scheme 2).

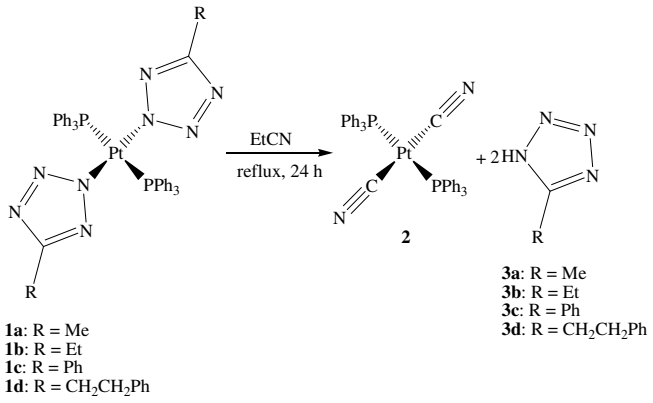

Scheme 1.

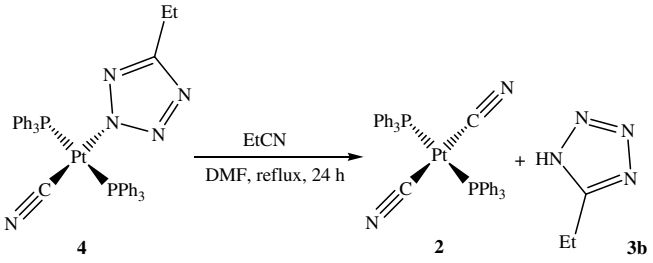

Scheme 2.

In all the above cases the dicyano-complex **2** precipitates on addition of diethyl ether and is further purified chromatographically using dichloromethane/diethyl ether as eluent. Evaporation of the mother liquor provides the respective 5-substitued-1*H*-tetrazole **3** (Scheme 1) as an off-white solid.

The dialkynyl complexes *trans*-[Pt(C≡CR′)$_2$(PPh$_3$)$_2$] **7** (R′ = Ph **7a**, *p*-MeC$_6$H$_4$ **7b**), analogous to the dicyano compound **2**, were obtained by reaction of *cis*-[Pt(N$_3$)$_2$(PPh$_3$)$_2$] **5** with ethynylbenzene **6a** or 1-ethynyl-4-methylbenzene **6b**, respectively (reaction a, Scheme 3), under focused microwave irradiation (1 h, 100 °C, 300 W). This unexpected overall replacement of the azide ligands by alkynyl groups occurs instead of the anticipated formation of triazolato complexes upon metal-promoted [2+3] cycloaddition

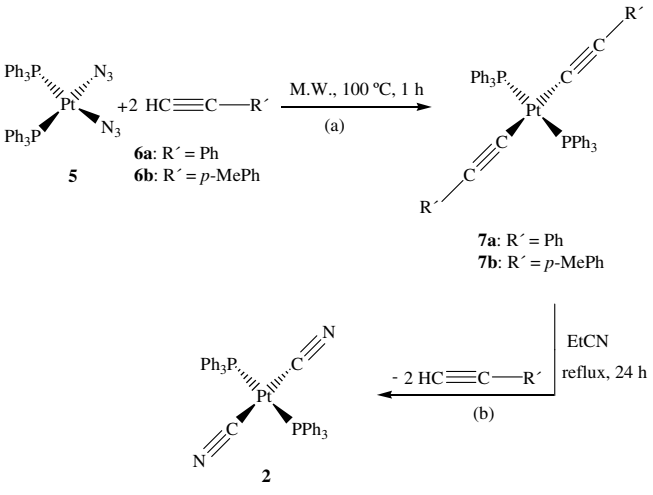

Scheme 3.

between the ligated azides and the alkynes. Complex **7a** was previously synthesized [25] starting from *cis*-$[PtCl_2(PPh_3)_2]$. Both **7a** and **7b** have been characterized by means of IR, ^1H, and $^{31}P\{^1H\}$ NMR spectroscopies, elemental analyses and X-ray crystallographically (for complex **7a**). The observed spectroscopic data are in accordance with those of related alkynyl complexes reported elsewhere [26]. The dialkynyl complexes **7a** and **7b** also furnish the dicyano-platinum complex **2** upon refluxing in propionitrile for 24 h (reaction b, Scheme 3).

The formation of the dicyano-platinum(II) complex **2** is believed to proceed, in all the cases, *via* activation of the C–CN bond in propionitrile. In fact, all the attempts to transform the bis(tetrazolato) complexes **1** or the dialkynyl complexes **7** into **2** in the absence of propionitrile have failed (the starting materials were then recovered quantitatively), namely when a CH_2Cl_2 solution of **1** or **7** was refluxed for 36 h or heated under focused M.W. irradiation (2 h, 100 °C), also in solid phase (SiO_2) without solvent. These results indicate that propionitrile is the precursor of the cyanide ligand in complex **2**.

A possible pathway for the conversion of the bis(tetrazolato) complexes **1** or the dialkynyl compounds **7** into **2** is proposed in Scheme 4. It involves an oxidative addition of propionitrile (which thus undergoes NC–C bond cleavage) to Pt^{II} to give a cyano-ethyl-Pt^{IV} intermediate (reaction a, Scheme 4), followed by β-elimination from the ethyl ligand to form ethylene, and reductive elimination of the corresponding 5-substituted-1*H*-tetrazole **3** or alkyne **6** to yield the mixed cyano-tetrazolato or cyano-alkynyl platinum(II) complex, respectively (reaction b, Scheme 4). In most of the cases the high solubility of these mono-cyano complexes in propionitrile allows the reaction to proceed further towards a second oxidative addition of EtCN and reductive elimination step (reaction c, Scheme 4), ultimately giving the dicyano-complex **2**. The evolution of ethylene gas assists in driving these reactions. Efforts to isolate the intermediate mixed cyano-tetrazolato or cyano-alkynyl complexes failed except in the case of *trans*-$[Pt(N_4CEt)_2(PPh_3)_2]$ **1b** where *trans*-$[Pt(CN)(N_4CEt)(PPh_3)_2]$ **4** precipitates from the reaction mixture due to its poor solubility in propionitrile. Quantitative recovery of complex **1a** or **1c** upon prolonged refluxing in benzonitrile or in acetonitrile, respectively, *i.e.* N≡CR solvents with R groups which can not undergo β-elimination, reinforces the proposed mechanistic pathway.

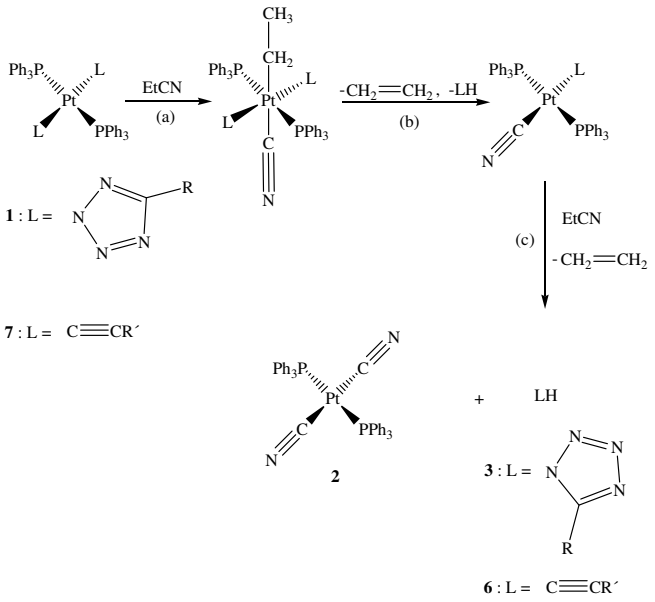

Scheme 4.

Table 2
Selected bond distances (Å) and angles (°) for complexes **2** and **7a**

	2	7a
Bond lengths		
Pt1–P1	2.3210(12)	2.3118(7)
Pt1–C1	1.987(5)	2.004(3)
N1–C1	1.154(7)	
C1–C2		1.204(4)
Bond angles		
P1–Pt1–C1	88.25(13)	86.68(8)
P1–Pt1–C1[a]	91.75(13)	93.34(8)
Pt1–C1–C2		173.0(2)
Pt1–C1–N1	176.8(4)	

[a] Symmetry operation to generate equivalent atom: $-x, -y, -z$.

The 5-substituted-1*H*-tetrazoles **3** were isolated in good yields (*ca.* 80%) and characterized by IR, ^1H and ^{13}C NMR spectral data and electrospray mass spectrometry (ESI-MS). The ^{13}C NMR resonances of the tetrazole ring carbon atoms *C*=N (153.2–159.9 ppm) are observed at a higher field than those of the corresponding complex precursors **1** (*ca.* 164 ppm).

The obtained complex **2** was characterized by elemental analysis, IR and ^1H, $^{13}C\{^1H\}$ and $^{31}P\{^1H\}$ spectroscopies. The IR band at 2129 cm^{-1} and the ^{13}C resonance at 125.7 ppm confirm the presence of the cyano ligand in the complex [27]. In the $^{31}P\{^1H\}$ NMR spectrum, the $J(^{31}P\text{-}^{195}Pt)$ value of 2726 Hz is typical for the *trans* configuration in solution [28].

The single-crystal X-ray diffraction structural analyses of **2** and **7a** confirm the formulations of the respective complexes. Selected bond lengths and angles and crystallographic data are given in Tables 1 and 2. The crystal structure of *trans*-$[Pt(CN)_2(PPh_3)_2]$ with one methanol molecule as solvent of crystallization was reported previously [29].

In both compounds **2** and **7a**, the metal center is essentially square-planar, the Pt atoms lie on inversion centers and the bulky PPh_3 ligands are mutually *trans* (Figs. 1 and 2). The bond lengths

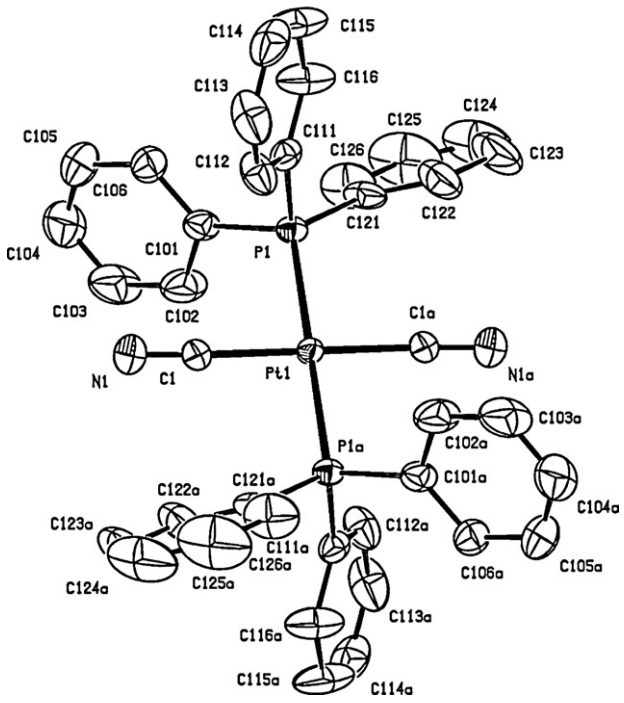

Fig. 1. Molecular structure of *trans*-$[Pt(CN)_2(PPh_3)_2]$ **2** with atomic numbering scheme (ellipsoids are drawn at 50% probability).

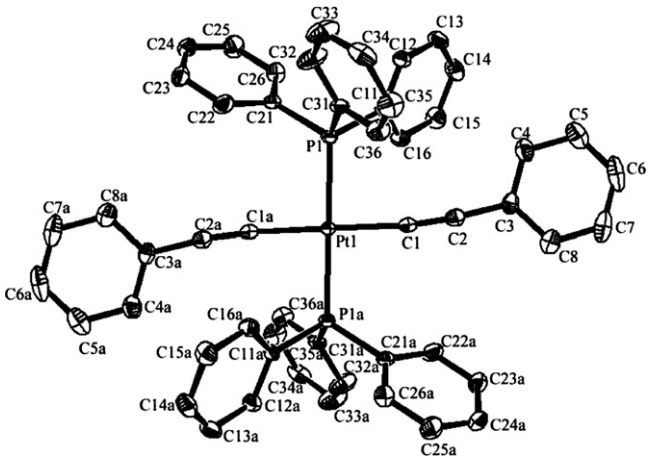

Fig. 2. Molecular structure of *trans*-[Pt(C≡CPh)$_2$(PPh$_3$)$_2$] **7a** with atomic numbering scheme (ellipsoids are drawn at 50% probability).

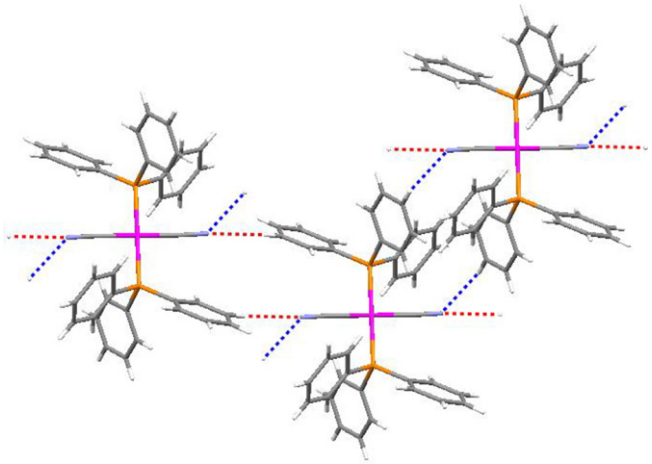

Fig. 3. A three-dimensional sheet of **2**. The C–H···N weak hydrogen bonding interactions that sustain the sheets are shown as dots (blue dots refer to the H114···N1 interaction and the red dots to the H123···N1 interaction). (For interpretation of the references to colour in this figure legend, the reader is referred to the web version of this article.)

between the platinum ion and the donating atoms are within the ranges reported for related Pt(II) complexes [30].

The centrosymmetric molecules of **2** are connected by a set of C–H···N weak hydrogen bonding interactions, which arrange the molecules into three-dimensional sheets (Fig. 3) since the nitrogen N1 lone pair of one molecule is oriented towards the phenyl hydrogen atoms H114 and H123, of two other molecules. The H114···N1 and H123···N1 distances for these interactions are 2.55 Å and 2.74 Å, respectively.

4. Conclusion

In this work, we have shown that both the bis(tetrazolato) and the dialkynyl complexes *trans*-[Pt(N$_4$CR)$_2$(PPh$_3$)$_2$] and *trans*-[Pt(C≡CR′)$_2$(PPh$_3$)$_2$], respectively, react with propionitrile to furnish dicyano-complex *trans*-[Pt(CN)$_2$(PPh$_3$)$_2$] *via* an unusual oxidative addition (involving NC–C bond cleavage of two propionitrile molecules) followed by a reductive elimination process. It also provides an alternative metal-assisted route to prepare 5-substituted-1*H*-tetrazole compounds in an easy and convenient way. The extension of these methods to the preparation of (i) other cyano-complexes, namely of the types [Pt(CN)$_2$L$_2$] and [Pt(CN)$_2$X$_2$L$_2$] (X = single-electron donating ligand, L = two-electron donor ligand), without the need to use toxic chemicals (such as an alkali metal cyanide) and (ii) other 5-substituted tetrazoles (simply by changing the R group of the organonitrile NCR precursors), are worth to be pursued.

Acknowledgements

This work has been partially supported by the Fundação para a Ciência e a Tecnologia (FCT) and its POCI 2010 program (FEDER funded) (Portugal). S.M. and J.L. express gratitude to the FCT for their post-doc. fellowships (grants SFRH/BPD/14690/2003 and SFRH/BPD/20927/2004).

Appendix A. Supplementary data

CCDC 680289 and 680290 contain the supplementary crystallographic data for **7a** and **2**. These data can be obtained free of charge via http://www.ccdc.cam.ac.uk/conts/retrieving.html, or from the Cambridge Crystallographic Data Centre, 12 Union Road, Cambridge CB2 1EZ, UK; fax: (+44) 1223-336-033; or e-mail: deposit@ccdc.cam.ac.uk. Supplementary data associated with this article can be found, in the online version, at doi:10.1016/j.poly.2008.06.031.

References

[1] (1) R.R. Wexler, W.J. Greenlee, J.D. Irvin, M.R. Goldberg, K. Prendergast, R.D. Smith, P.B.M.W.M. Timmermans, J. Med. Chem. 39 (1996) 625;
(b) B. Schmidt, B. Schieffer, J. Med. Chem. 46 (2003) 2261;
(c) T. Tanaka, T. Ohida, Y. Yamamoto, Chem. Pharm. Bull. 52 (2004) 830.
[2] V.A. Ostrovskii, M.S. Pevzner, T.P. Kofmna, M.B. Shcherbinin, I.V. Tselinskii, Targets Heterocycl. Syst. 3 (1999) 467.
[3] R.N. Butler, in: A.R. Katritzky, C.W. Rees, E.F.V. Scriven (Eds.), Comprehensive Heterocyclic Chemistry, vol. 4, Pergamon, Oxford, UK, 1996.
[4] W.G. Finnegan, R.A. Henry, R. Lofquist, J. Am. Chem. Soc. 80 (1958) 3908.
[5] (a) D.P. Curran, S. Hadida, S.-Y. Kim, Tetrahedron 55 (1999) 8997;
(b) S.J. Wittenberger, B.G. Donner, J. Org. Chem. 58 (1993) 4139.
[6] (a) A. Kumar, R. Narayanan, H. Shechter, J. Org. Chem. 61 (1996) 4462;
(b) B.E. Huff, M.A. Staszak, Tetrahedron Lett. 34 (1993) 8011.
[7] K. Koguro, T. Oga, S. Mitsui, R. Orita, Synthesis (1998) 910.
[8] Z.P. Demko, K.B. Sharpless, J. Org. Chem. 66 (2001) 7945.
[9] D. Amantini, R. Beleggia, F. Fringuelli, F. Pizzo, L. Vaccoro, J. Org. Chem. 69 (2004) 2896.
[10] M.L. Kantam, K.B. Shiva Kumar, C. Sridhar, Adv. Synth. Catal. 347 (2005) 1212.
[11] L.V. Myznikov, J. Roh, T.V. Artamonova, A. Hrabalek, G.I. Koldobskii, Russ. J. Org. Chem. 43 (2007) 765.
[12] S. Mukhopadhyay, J. Lasri, M.A. Januário Charmier, M.F.C. Guedes da Silva, A.J.L. Pombeiro, Dalton Trans. (2007) 5297.
[13] W.P. Fehlhammer, M. Fritz, Chem. Rev. 93 (1993) 1243.
[14] (a) J.A. Connor, D. Gibson, R. Price, J. Chem. Soc., Dalton Trans. (1986) 2741;
(b) J.A. Connor, D. Gibson, R. Price, J. Chem. Soc., Perkin Trans. 1 (1987) 619.
[15] S.M. Peng, D.S. Liaw, Inorg. Chim. Acta 113 (1986) L11.
[16] S.M. Peng, Y. Wang, S.L. Wang, M.C. Chuang, Y. Le Page, E.J. Gabe, J. Chem. Soc., Chem Commun. (1981) 329.
[17] (a) A.J.L. Pombeiro, Inorg. Chem. Commun. 4 (2001) 585;
(b) A.J.L. Pombeiro, M.F.C. Guedes da Silva, R.A. Michelin, Coord. Chem. Rev. 218 (2001) 43;
(c) A.J.L. Pombeiro, M.F.C. Guedes da Silva, J. Organomet. Chem. 617–618 (2001) 65;
(d) M.F.C. Guedes da Silva, M.A.N.D.A. Lemos, J.J.R. Fraústo da Silva, A.J.L. Pombeiro, M.A. Pellinghelli, A. Tiripicchio, J. Chem. Soc., Dalton Trans. (2000) 373;
(e) M.F.C. Guedes da Silva, J.J.R. Fraústo da Silva, A.J.L. Pombeiro, M.A. Pellinghelli, A. Tiripicchio, J. Chem. Soc., Dalton Trans. (1996) 2763.
[18] S.S.P.R. Almeida, M.F.C. Guedes da Silva, J.J.R. Fraústo da Silva, A.J.L. Pombeiro, J. Chem. Soc., Dalton Trans. (1999) 467.
[19] (a) T. Schaub, C. Döring, U. Radius, Dalton Trans. (2007) 1993;
(b) J.J. Garcia, N.M. Brunkan, W.D. Jones, J. Am. Chem. Soc. 124 (2002) 9547;
(c) G.W. Parshall, J. Am. Chem. Soc. 96 (1974) 2360.
[20] J. Erbe, W. Beck, Chem. Ber. 116 (1983) 3867.
[21] G.M. Sheldrick, Acta Crystallogr., Sect. A 46 (1990) 467.
[22] G.M. Sheldrick, SHELXL-97, University of Gottingen, Germany, 1997.
[23] L.J. Farrugia, J. Appl. Crystallogr. 32 (1999) 837.
[24] J.C. Bailar Jr., H. Itatani, J. Am. Chem. Soc. 89 (1967) 1592.

[25] H. Masai, K. Sonogachira, N. Hagihara, J. Organomet. Chem. 26 (1971) 271.
[26] R. D'Amato, A. Furlani, M. Colapietro, G. Portalone, M. Casalboni, M. Falconieri, M.V. Russo, J. Organomet. Chem. 627 (2001) 13.
[27] (a) J.S. Field, R.J. Haines, L.P. Ledwaba, R. McGuire Jr., O.Q. Munro, M.R. Low, D.R. McMillin, Dalton Trans. (2007) 192;
(b) G.N. Richardson, U. Brand, H. Vahrenkamp, Inorg. Chem. 38 (1999) 3070;
(c) J.A. Rahn, D.J. O'Donnell, A.R. Palmer, J.H. Nelson, Inorg. Chem. 28 (1989) 2631.
[28] M.F.C. Guedes da Silva, E.M.P.R.P. Branco, Y. Wang, J.J.R. Fraústo da Silva, A.J.L. Pombeiro, R. Bertani, R.A. Michelin, M. Mozzon, F. Benetollo, G. Bombieri, J. Organomet. Chem. 490 (1995) 89.
[29] R.J. Staples, Md. N.I. Khan, S. Wang, J.P. Fackler Jr., Acta Crystallogr., Sect. C 48 (1992) 2213.
[30] (a) A.J. Deeming, G. Hogarth, M.-Y. Lee, M. Saha, S.P. Redmond, H. Phetmung, A.G. Orpen, Inorg. Chim. Acta 309 (2000) 109;
(b) M. Ravera, R. D'Amato, A. Guerri, J. Organomet. Chem. 690 (2005) 2376.

complexes [4,13,16] of two related *N*-substituted mono-dpa derivatives have been investigated as part of biologically orientated studies.

As an extension of the above we now report the results of an investigation of the interaction of the '*N*-methylene substituted' dpa derivatives **2**–**8** with copper(II) and **1**, **4**–**6** with palladium(II).

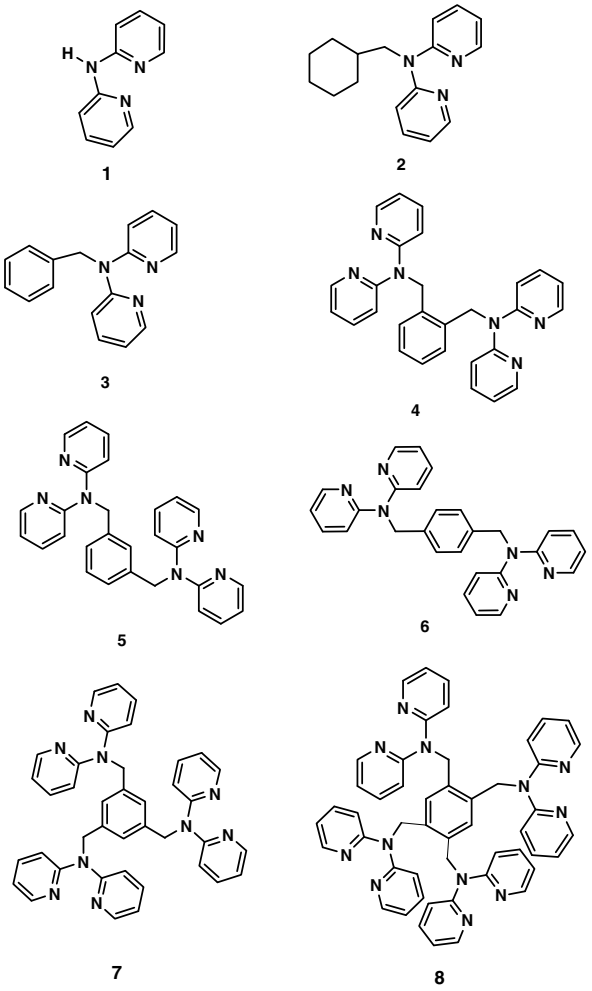

2. Experimental

2.1. Physical methods

Electrospray (ES) mass spectra were recorded using a Micromass LCT-TOF mass spectrometer; EI and FAB spectra were recorded using a Kratos MS80RFA mass spectrometer. HRMS were determined on samples loaded in dichloromethane and run in an acetonitrile matrix. Melting points are uncorrected. NMR spectra were determined on a DRX-500 Bruker spectrometer or on Varian 300 and 500 MHz spectrometers.

2.2. Ligand synthesis

The syntheses of the di-2-pyridylamine derivatives di-2-pyridylaminomethylbenzene (**3**) [14,17,18], 1,2-bis(di-2-pyridylaminomethyl)benzene (**4**) [14], 1,3-bis(di-2-pyridylaminomethyl)benzene (**5**) [14], and 1,4-bis(di-2-pyridylaminomethyl)benzene (**6**) [14] and 1,3,5-tris(di-2-pyridylaminomethyl)benzene (**7**) [14] have been reported previously. Di-2-pyridylamine was obtained commercially.

2.2.1. *N*-Cyclohexylmethyl-2,2′-dipyridylamine (**2**)

To 2,2′-dipyridylamine (0.952 g, 5.56 mmol) in DMF (5 mL) was added finely ground KOH (0.81 g; 14.4 mmol). Bromomethylcyclohexane (0.984 g, 5.56 mmol) in DMF (3 mL) was added dropwise and the reaction mixture was stirred for 24 h at room temperature; a colour change to bright yellow occurred. The solvent was removed under reduced pressure and the pale yellow solid that remained was dissolved in water and extracted with chloroform (4×100 mL). The combined chloroform extracts were dried over $MgSO_4$. The solution was filtered and the solvent was removed from the filtrate under reduced pressure to yield the crude product which was purified on a chromatographic column (Silica Gel KG 60) employing CH_2Cl_2–MeOH (95:5) as eluent; 0.8 g of the crude product yielded 0.08 g of pure product as a yellow oil (the first fraction eluted from the column). ESI-MS $m/z = 268$ $[M+H]^+$; ^1H NMR ($CDCl_3$) δ 8.30 (dd, 2H, H1), 7.47 (t, 2H, H3), 7.05 (d, 2H, $3J = 8.4$ Hz, H4), 6.80 (t, 2H, H2), 4.04 (s, 2H, H6), 1.81 (m, 1H, H7), 1.58–1.71 (m, 5H, H8, H9, H11, H12), 1.12 (m, 3H, H10, H11, H14, H15), 0.96 (m, 2H, H16, H17). ^{13}C NMR ($CDCl_3$): δ 157.0 (C5), 148.0 (C1), 137.1 (C3), 116.8 (C2), 114.9 (C4), 54.0 (C6), 37.2 (C7), 30.9 (C8, C9, C14, C15), 26.5 (C12, C13), 25.9 (C10, C11, C16, C17).

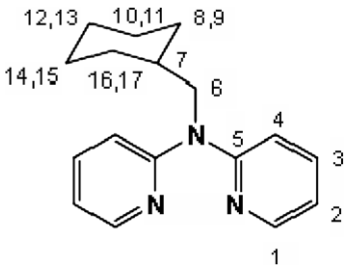

2.2.2. 1,2,4,5-Tetrakis(di-2-pyridylaminomethyl)benzene (**8**)

Di-2-pyridylamine (1.00 g, 5.84 mmol) and potassium hydroxide (1.31 g, 23.4 mmol) were stirred in DMSO for 1 h, 1,2,4,5-tetrakis(bromomethyl)benzene (0.642 g, 1.89 mmol) was added and the solution stirred for a further 48 h. Addition of water gave a yellow precipitate which was washed with water and then recrystallised from a chloroform–petroleum ether mixture. Yield: 0.396 g (34%); m.p. 238–241 °C. Calc. for $C_{50}H_{42}N_{12} \cdot 2H_2O$: C, 70.90; H, 5.47; N, 19.84. Found: C, 71.03; H, 5.36; N, 20.01%. ES-MS $m/z = 811$ $[M+H]^+$. HRMS: calc. for $[C_{50}H_{43}N_{12}]^+$ 811.3729; found 811.3734. ^1H NMR ($CDCl_3$): δ 8.16 (d, 8H, H1), 7.33 (br, 8H, H3), 7.14 (s, 2H, H8), 6.84 (d, 8H, H4), 6.78 (dd, 8H, H2), 5.42 (s, 8H, H6). ^{13}C NMR ($CDCl_3$): δ 156.8 (C5), 148.0 (C1), 137.0 (C3), 133.6 (C7), 123.6 (C8), 116.9 (C2), 114.5 (C4), 52.1(C6).

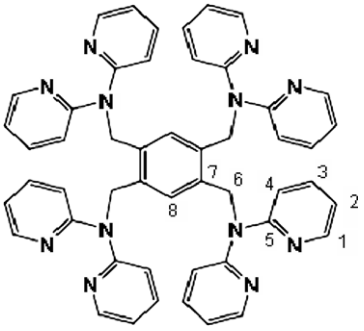

2.3. Complex synthesis

2.3.1. [Cu(2)(μ-Cl)Cl]$_2$

$CuCl_2 \cdot 2H_2O$ (34 mg, 0.20 mmol) in warm ethanol (5 mL) was added with stirring to **2** (54 mg, 0.20 mmol) in warm ethanol (5 mL). Diffusion of diethylether vapour overnight into this solution yielded green crystals. These were separated, washed with ether, and dried in air. Yield: 58 mg (72%); m.p. >218 °C (decomp.). Calc. for $C_{34}H_{42}Cl_4Cu_2N_6$: C, 50.81; H, 5.27; N, 10.46. Found: C, 50.43; H, 5.10; N, 10.31%. ESI-MS m/z = 635 $[2L+Cu+Cl]^+$, 268 $[L+H]^+$.

2.3.2. [Cu(3)(μ-Cl)Cl]$_2 \cdot H_2O$

$CuCl_2 \cdot 2H_2O$ (20 mg; 0.12 mmol) in warm ethanol (5 mL) was added with stirring to a warm solution of **3** (30 mg, 0.12 mmol) in ethanol (5 mL). Diffusion of diethylether vapour over several days into this solution yielded green crystals. These were separated, washed with ether, and dried in air. Yield: 39 mg (82%); m.p. > 202 °C (decomp.). Calc. for $C_{34}H_{30}Cl_4Cu_2N_6{\cdot}H_2O$: C, 50.44; H, 3.98; N, 10.38. Found: C, 50.83; H, 3.61; N, 10.44%. A crystal was subsequently removed from the ethanol reaction solution and used directly (without air drying) for the X-ray structure determination; the structure analysis showed it to be the di-ethanol solvate, $[Cu(3)(\mu\text{-}Cl)(Cl)]_2 \cdot 2C_2H_5OH$.

2.3.3. [Cu$_2$(4)(NO$_3$)$_4$]

$Cu(NO_3)_2 \cdot 2.5H_2O$ (23.0 mg, 0.095 mmol) in methanol (5 mL) was added to a dichloromethane solution (5 mL) of **4** (20.0 mg, 0.045 mmol). On standing a blue solid precipitated that was collected and dried under vacuum. Yield: 25 mg (67%); m.p. 261–263 °C (decomp.). Calc. for $C_{28}H_{24}N_{10}O_{12}Cu_2$: C, 41.03; H, 2.95; N, 17.09. Found: C, 40.99; H, 3.08; N, 17.06%.

2.3.4. [Cu$_2$(5)(NO$_3$)$_4$] · 2CH$_3$OH

$Cu(NO_3)_2 \cdot 2.5H_2O$ (22.8 mg, 0.094 mmol) in methanol (5 mL) was added to **5** (20.0 mg, 0.045 mmol) in dichloromethane (5 mL). On standing a blue crystalline product precipitated. This was collected, dissolved in methanol, and recrystallised via vapour diffusion of ether into the methanol solution. The product was collected by filtration and dried under vacuum. Yield: 22 mg (54%); m.p. > 175 °C (decomp.). Calc. for $C_{28}H_{24}N_{10}O_{12}Cu_2 \cdot 2CH_3OH$: C, 40.77; H, 3.65; N, 15.85. Found: C, 40.57; H, 3.26; N, 15.96%.

2.3.5. [Cu$_2$(6)(CH$_3$OH)$_2$(NO$_3$)$_4$]

$Cu(NO_3)_2 \cdot 2.5H_2O$ (23.6 mg, 0.098 mmol) in methanol (5 mL) was added to a dichloromethane solution (5 mL) of **6** (19.9 mg, 0.045 mmol). On standing blue crystals formed which were found suitable for X-ray crystallography. They were collected by filtration and dried under vacuum. Yield: 23 mg (59%); m.p. 275–277 °C (decomp.). Calc. for $C_{30}H_{32}N_{10}O_{14}Cu_2$: C, 40.77; H, 3.65; N, 15.85. Found: C, 40.81; H, 3.46; N, 16.03%.

2.3.6. [Cu$_4$(8)](NO$_3$)$_4$] · 4H$_2$O

$Cu(NO_3)_2 \cdot 2.5H_2O$ (26.3 mg, 0.109 mmol) in methanol (5 mL) was added to **8** (20.5 mg, 0.025 mmol) in dichloromethane (5 mL). The solution was concentrated by slow evaporation to give a blue crystalline solid that was collected by filtration and dried under vacuum. Yield: 23.5 mg (58%); m.p. 224–227 °C (dec.). Calc. for $C_{50}H_{42}N_{20}O_{24}Cu_4.4H_2O$: C, 36.77, H, 3.09, N, 17.15. Found: C, 37.20; H, 2.78; N, 16.75%.

2.3.7. [Pd(1)$_2$](PF$_6$)$_2$ · 2CH$_3$OH

$Pd(OAc)_2$ (2.2 mg, 0.01 mmol) in methanol (10 mL) was added to a stirred solution of **1** (1.8 mg, 0.01 mmol) in methanol (5 mL) followed by NH_4PF_6 (5 mg, 0.03 mmol) in methanol (3 mL) and the solution was stirred for 3 h at room temperature. It was then filtered and the filtrate allowed to stand at 4 °C over several weeks to yield a small number of orange-yellow crystals, one of which was used directly for the X-ray structure determination. ^{1}H NMR (DMSO-d_6): δ 11.6 (s, 1H), 8.10 (t, 2H), 7.60 (t, 6H), 7.26 (t, 6H), 7.10 (d, 6H), 4.05 (br, 1H, HO–CH$_3$), 3.08 (s, 3H, H3C–OH).

2.3.8. [Pd$_2$(4)Cl$_4$]

$PdCl_2$ (16.6 mg, 0.094 mmol) in 2 M hydrochloric acid (2 mL) was added to a dichloromethane–methanol solution (1:1; 8 mL) of **4** (20.2 mg, 0.045 mmol). A pale yellow solid precipitated. This was collected, washed with methanol, and dried under vacuum. Yield: 29 mg (81%); m.p. > 330 °C. Calc. for $C_{28}H_{24}N_6Cl_4Pd_2$: C, 42.08; H, 3.03; N, 10.52. Found: C, 41.85; H, 2.81; N, 10.24%.

2.3.9. [Pd$_2$(4)(OAc)$_4$]

$Pd(OAc)_2$ (29 mg, 0.13 mmol) in a 1:1-mixture of THF/toluene (8 mL) was added dropwise to **4** (29 mg, 0.060 mmol) in dichloromethane (3 mL). Yellow-orange crystals formed over several days. These were isolated, washed with ether, and dried under vacuum. Yield 42 mg (79%); m.p. > 240 °C (decomp.) Calc. for $C_{34}H_{36}N_6O_8Pd_2$: C, 48.43; H, 4.07; N, 9.41. Found: C, 48.15; H, 4.13; N, 9.12%. ^{1}H NMR (DMSO-d_6): δ 8.10 (d, 4H), 7.91 (d, 4H), 7.79 (t, 4H), 7.10–7.22 (m, 8H), 6.24 (br, s, 4H).

2.3.10. [Pd$_2$(5)Cl$_4$]

$PdCl_2$ (17.5 mg, 0.099 mmol) in 2 M hydrochloric acid (2 mL) was added to a dichloromethane–methanol solution (1:1; 8 mL) of **5** (20.9 mg, 0.047 mmol). Immediately a pale yellow precipitate formed that was collected, washed with methanol, and dried under vacuum. Yield: 27 mg (81%); m.p. 300–301 °C (decomp.). Calc. for $C_{28}H_{24}N_6Cl_4Pd_2$: C, 42.08; H, 3.03; N, 10.52. Found: C, 42.03; H, 2.93; N, 10.32%.

2.3.11. [Pd$_2$(6)Cl$_4$]

$PdCl_2$ (16.6 mg, 0.094 mmol) in 2 M hydrochloric acid (2 mL) was added to a dichloromethane–methanol solution (1:1; 8 mL) of **6** (19.9 mg, 0.045 mmol). A pale yellow precipitate formed that was collected, washed with methanol and dried under vacuum. Yield: 29 mg (80%); m.p. > 330 °C. Calc. for $C_{28}H_{24}N_6Cl_4Pd_2$: C, 42.08; H, 3.03; N, 10.52. Found: C, 41.97; H, 3.01; N, 10.24%.

2.3.12. [Pd$_2$(6)(OAc)$_4$] · CH$_2$Cl$_2$

$Pd(OAc)_2$ (23 mg, 0.103 mmol) in a 1:1-mixture of THF/toluene (8 mL) was added dropwise to **6** (23 mg, 0.051 mmol) in dichloromethane (3 mL). The solution was let stand and after two days bright yellow crystals had formed. These were isolated, washed with ether, and dried under vacuum. Yield: 32 mg (65%); m.p. > 240 °C (decomp.). Calc. for $C_{34}H_{36}N_6O_8Pd_2 \cdot CH_2Cl_2$: C, 45.49; H, 3.92; N, 8.60. Found: C, 45.92; H, 3.87; N, 8.97%. ^{1}H–NMR (DMSO-d_6): δ 8.24 (d, 4H), 7.95 (t, 4H), 7.86 (s, 4H), 7.45 (d, 4H), 7.23 (t, 4H), 5.41 (s, 4H).

2.4. Solvent extraction experiments

Liquid–liquid extraction experiments were performed at 23 ± 1 °C in microcentrifuge tubes (2 cm^3) with a phase ratio $V_{(org)}$:$V_{(aq)}$ of 1:1 (500 μL each). The aqueous phase contained $[Cu(ClO_4)_2]$ (1×10^{-4} M), sodium perchlorate (5×10^{-3} M) as supporting anion and the zwitterionic buffer system, HEPES/NaOH, at pH 7.2; as a precaution, the pH of the aqueous phase was monitored before and after each experiment with the aid of a InLab423 pH electrode. The organic phase contained a known concentration of ligand in chloroform (1×10^{-3} M). All experiments involved the mechanical shaking of the two-phase system for 30 min by which time equilibrium was reached (as established by preliminary

experiments). At the end of this time, the phases were separated, centrifuged and the depletion of the metal ion concentrations in the aqueous phase was measured using an ICP-MS (ELAN 9000/ Perkin Elmer) spectrometer.

2.5. Crystallography

Structures $[Cu(\mathbf{2})(\mu\text{-}Cl)Cl]_2$, $[Cu(\mathbf{3})(\mu\text{-}Cl)Cl]_2 \cdot 2C_2H_5OH$, $[Pd(\mathbf{1})_2](PF_6)_2 \cdot 2CH_3OH$, $[Pd_2(\mathbf{4})(OAc)_4] \cdot 4H_2O$ and $[Pd_2(\mathbf{6})(OAc)_4] \cdot 2CH_2Cl_2$ were collected on a Nonius Kappa CCD with ω and φ scans to approximately 53° 2θ at either 293(2) or 198(2) K. Data collections were undertaken with COLLECT [19], cell refinement with Dirax/lsq [20], and data reduction with EvalCCD [21]. Structure $[Cu_2(\mathbf{6})(CH_3OH)_2(NO_3)_4]$ was collected at 168(2) K with a Siemens CCD area detector with ω and φ scans to approximately 52° 2θ. Data integration and reduction were undertaken with SAINT and XPREP [22]. Each structure was solved by direct methods using SHELXS-97 [23]. Both diffractometers employed graphite-monochromated Mo Kα radiation generated from a sealed tube (0.71073 Å). Multi-scan empirical absorption corrections were applied to all data sets using the program SADABS [24]. All structures were refined and extended with SHELXL-97 [25]. In general, ordered non-hydrogen atoms with occupancies greater than 0.5 were refined anisotropically. Partial occupancy carbon, nitrogen and oxygen atoms were refined isotropically. Carbon-bound hydrogen atoms were included in idealised positions and refined using a riding model. Oxygen and nitrogen-bound hydrogen atoms that were structurally evident in the difference Fourier map were included and refined with bond length and angle constraints. Specific refinement details follow below. Tables of bonds, angles and H-bond geometries are presented in the ESI.

2.5.1. $[Cu(2)(\mu\text{-}Cl)Cl]_2$

Formula $C_{34}H_{42}Cl_4Cu_2N_6$, *M* 803.62, monoclinic, space group $P2_1/n$(#14), *a* 10.614(1), *b* 12.951(1), *c* 13.312(1) Å, *β* *99.74(1)*°, *V* 1803.5(3) Å^3, D_{calc} 1.480 g cm^{-3}, *Z* 2, crystal size 0.40 by 0.30 by 0.05 mm, colour green, habit plate, temperature 293(2) Kelvin, λ(Mo Kα) 0.71073 Å, μ(Mo Kα) 1.509 mm^{-1}, $T(\text{SADABS})_{min,max}$ 0.5836, 0.9284, $2\theta_{max}$ 52.00, *hkl* range −13 12, −15 15, −16 16, *N* 23057, N_{ind} 3531(R_{merge} 0.0585), *N*obs 2513 ($I > 2\sigma(I)$), *N*var 188, residuals* $R_1(F)$ 0.0538, $wR_2(F^2)$ 0.1419, GoF(all) 1.144, $\Delta\rho_{min,max}$ −0.688, 1.127 e Å^{-3}, *A* 0.0580, *B* 2.2400.

2.5.1.1. Specific details. The cyclohexyl rings are disordered and were modelled over two positions with equal occupancies. A number of restraints and constraints were necessary to facilitate realistic modelling in this region. Each of the carbon atoms in the rings were refined with identical thermal parameters.

2.5.2. $[Cu(3)(\mu\text{-}Cl)Cl]_2 \cdot 2C_2H_5OH$

Formula $C_{38}H_{42}Cl_4Cu_2N_6O_2$, *M* 883.66, triclinic, space group $P\bar{1}$(#2), *a* 7.467(1), *b* 8.460(1), *c* 16.422(1) Å, *α* *96.43(1)*°, *β* *97.23(1)*°, *γ* 104.80(1)°, *V* 983.70(19) Å^3, *D*calc 1.492 g cm^{-3}, *Z* 1, crystal size 0.98 by 0.21 by 0.07 mm, colour blue, habit plate, temperature 293(2) K, λ(Mo Kα) 0.71073 Å, μ(Mo Kα) 1.394 mm^{-1}, $T(\text{SADABS})_{min,max}$ 0.3143, 0.9087, $2\theta_{max}$ 54.00, *hkl* range −9 9, −9 9, −20 20, *N* 16407, *N*ind 3888(R_{merge} 0.0244), N_{obs} 3268 ($I > 2\sigma(I)$), N_{var} 236, residuals* $R_1(F)$ 0.0318, $wR_2(F^2)$ 0.0846, GoF(all) 1.079, $\Delta\rho_{min,max}$ −0.468, 0.662 e Å^{-3}, *A* 0.0401, *B* 0.6659.

2.5.3. $[Pd(\mathbf{1})_2](PF_6)_2 \cdot 2CH_3OH$

Formula $C_{22}H_{26}F_{12}N_6O_2P_2Pd$, *M* 802.83, triclinic, space group $P\bar{1}$(#2), *a* 8.170(1), *b* 8.560(1), *c* 10.968(1) Å, *α* *84.42(1)*°, *β* *81.61(1)*°, *γ* *74.76(1)*°, *V* 730.76(14) Å^3, D_{calc} 1.824 g cm^{-3}, *Z* 1, crystal size 0.31 by 0.16 by 0.09 mm, colour colourless, habit block, temperature 198(2) K, λ(Mo Kα) 0.71073 Å, μ(Mo Kα) 0.855 mm^{-1}, $T(\text{SADABS})_{min,max}$ 0.7774, 0.9270, $2\theta_{max}$ 52.00, *hkl* range −10 10, −10 10, −13 13, *N* 15943, N_{ind} 2866 (R_{merge} 0.0454), N_{obs} 2674 ($I > 2\sigma(I)$), N_{var} 212, residuals* $R_1(F)$ 0.0279, $wR_2(F^2)$ 0.0687, GoF(all) 1.101, $\Delta\rho_{min,max}$ −0.714, 0.607 e Å^{-3}, *A* 0.0358, *B* 0.3469.

2.5.4. $[Pd_2(\mathbf{6})(OAc)_4] \cdot 2CH_2Cl_2$

Formula $C_{38}H_{40}Cl_4N_6O_8Pd_2$, *M* 1063.36, monoclinic, space group $P2_1/c$(#14), *a* 9.073(1), *b* 13.903(1), *c* 17.021(1) Å, *β* *99.46(1)*°, *V* 2117.9(3) Å^3, D_{calc} 1.667 g cm^{-3}, *Z* 2, crystal size 0.33 by 0.27 by 0.18 mm, colour yellow, habit block, temperature 293(2) K, λ(Mo Kα) 0.71073 Å, μ(Mo Kα) 1.159 mm^{-1}, $T(\text{SADABS})_{min,max}$ 0.7010, 0.8185, $2\theta_{max}$ 56.00, *hkl* range −11 11, −18 18, −22 22, *N* 44135, N_{ind} 5079(R_{merge} 0.0326), N_{obs} 4107 ($I > 2\sigma(I)$), N_{var} 264, residuals* $R_1(F)$ 0.0380, $wR_2(F^2)$ 0.1120, GoF(all) 1.069, $\Delta\rho_{min,max}$ −0.793, 1.268 e Å^{-3}, *A* 0.0571, *B* 2.5642.

2.5.5. $[Pd_2(\mathbf{4})(OAc)_4] \cdot 4H_2O$

Formula $C_{36}H_{44}N_6O_{12}Pd_2$, *M* 965.57, orthorhombic, space group *Pccn*(#56), *a* 13.263(1), *b* 14.559(1), *c* 23.120(1) Å, *V* 4464.4(5) Å^3, D_{calc} 1.437 g cm^{-3}, *Z* 4, crystal size 0.40 by 0.21 by 0.21 mm, colour yellow, habit block, temperature 293(2) K, λ(Mo Kα) 0.71073 Å, μ(Mo Kα) 0.866 mm^{-1}, $T(\text{SADABS})_{min,max}$ 0.7232, 0.8390, $2\theta_{max}$ 50.80, *hkl* range −10 15, −17 16, −27 26, *N* 20125, N_{ind} 4047 (R_{merge} 0.0567), N_{obs} 3148 ($I > 2\sigma(I)$), N_{var} 273, residuals* $R_1(F)$ 0.0734, $wR_2(F^2)$ 0.2027, GoF(all) 1.219, $\Delta\rho_{min,max}$ −0.623, 1.067 e Å^{-3}, *A* 0.0788, *B* 17.6798.

2.5.5.1. Specific details. There is a region of disordered solvent present within the lattice. Attempts were made to refine this as a variety of different solvents including toluene, thf and dichloromethane. The results, however, were not satisfactory. As such, the electron density associated with this region was modelled as isotropic water molecules. The hydrogen atoms of these water molecules could not be located in the Fourier difference map and so were not modelled. In total there are six positions modelled with a total occupancy of 3.1 per complex molecule. In addition there is one ordered anisotropic water molecule (occupancy 0.45) modelled.

2.5.6. $[Cu_2(\mathbf{6})(CH_3OH)_2(NO_3)_4]$

Formula $C_{30}H_{32}Cu_2N_{10}O_{14}$, *M* 883.74, monoclinic, space group $P2_1/n$(#14), *a* 8.336(3), *b* 13.148(5), *c* 16.660(6) Å, *β* *91.955(5)*°, *V* 1824.9(11) Å^3, D_{calc} 1.608 g cm^{-3}, *Z* 2, crystal size 0.37 by 0.20 by 0.12 mm, colour blue, habit block, temperature 168(2) K, λ(Mo Kα) 0.71073 Å, μ(Mo Kα) 1.247 mm^{-1}, $T(\text{SADABS})_{min,max}$ 0.778, 0.861, $2\theta_{max}$ 52.88, *hkl* range −4 10, −16 16, −20 20, *N* 14750, N_{ind} 3651(R_{merge} 0.0394), N_{obs} 2538 ($I > 2\sigma(I)$), N_{var} 257, residuals* $R_1(F)$ 0.0355, $wR_2(F^2)$ 0.0827, GoF(all) 0.985, $\Delta\rho_{min,max}$ −0.350, 0.296 e Å^{-3}, *A* 0.0454, *B* 0.0000.

* $R_1 = \sum||F_o| - |F_c||/\sum|F_o|$ for $F_o > 2\sigma(F_o)$; $wR_2 = (\sum w(F^2_o - F^2_c)^2/\sum(wF^2_c)^2)^{1/2}$ all reflections $w = 1/[\sigma^2(F^2_o) + (AP)^2 + BP]$ where $P = (F^2_o + 2F^2_c)/3$.

3. Results and discussion

3.1. Copper(II) complexes

New copper(II) complexes incorporating the dpa derivatives **2**–**8** were synthesised during the present study. Reaction of the cyclohexylmethylene substituted 2,2′-dipyridylamine derivative **2** with copper(II) chloride in ethanol followed by ether vapour diffusion into the reaction solution yielded a green crystalline species of type $[Cu(\mathbf{2})(\mu\text{-}Cl)Cl]_2$. The X-ray structure (Fig. 1) of this product revealed a μ-dichloro bridged dimer, disposed around an inversion centre, containing five-coordinate copper(II) ions, with the latter separated by 3.73 Å. The N_2Cl_3 coordination sphere is best

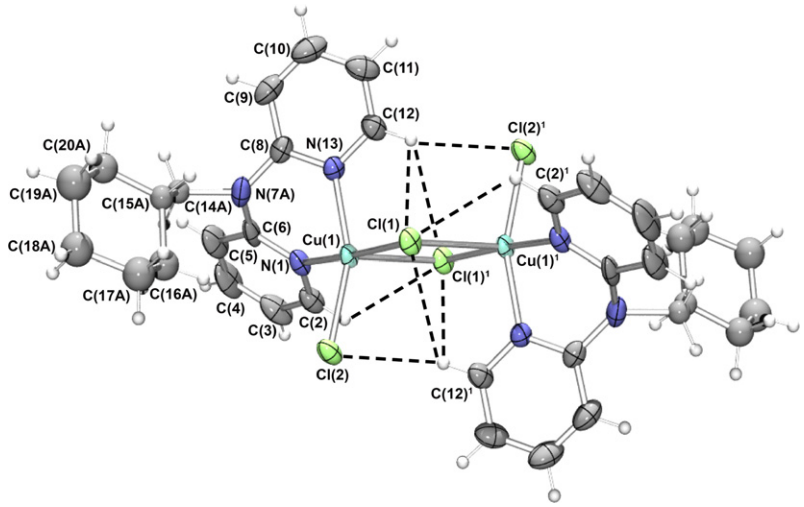

Fig. 1. ORTEP [27] representation of $[Cu(\mathbf{2})(\mu\text{-}Cl)Cl]_2$ shown with 30% probability ellipsoids. The second disordered position of the cyclohexane rings is omitted for clarity. Symmetry code used for generating equivalent atoms: $-x$, $1-y$, $1-z$. Dashed lines indicate H···Cl interactions.

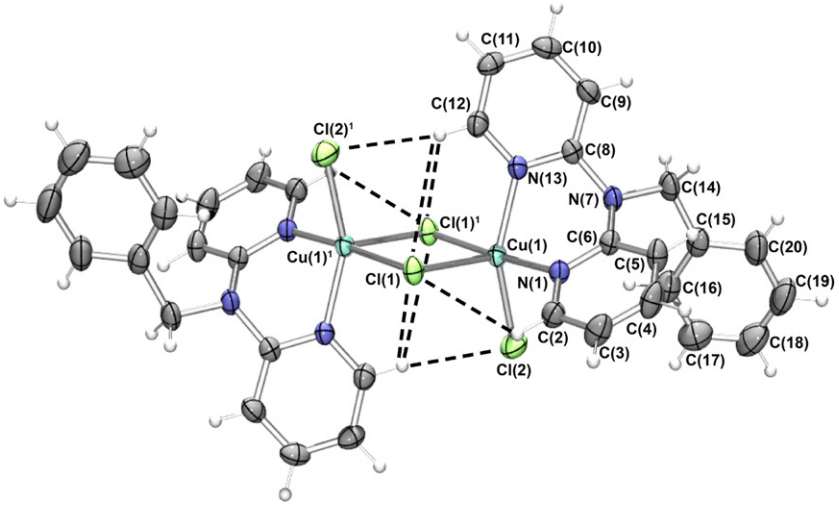

Fig. 2. ORTEP [27] representation of the dimer complex unit $[Cu(\mathbf{3})(\mu\text{-}Cl)Cl]_2 \cdot 2C_2H_5OH$ (thermal ellipsoids at 50% level) with solvent molecules omitted for clarity. Symmetry code used for generating equivalent atoms: $2-x$, $1-y$, $1-z$. Dashed lines indicate H···Cl interactions.

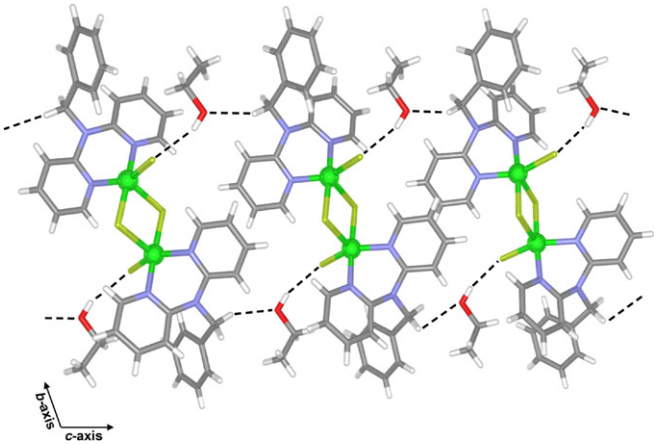

Fig. 3. A schematic representation of part of the $[Cu(\mathbf{3})(\mu\text{-}Cl)Cl]_2 \cdot 2C_2H_5OH$ crystal lattice viewed down the *a*-axis.

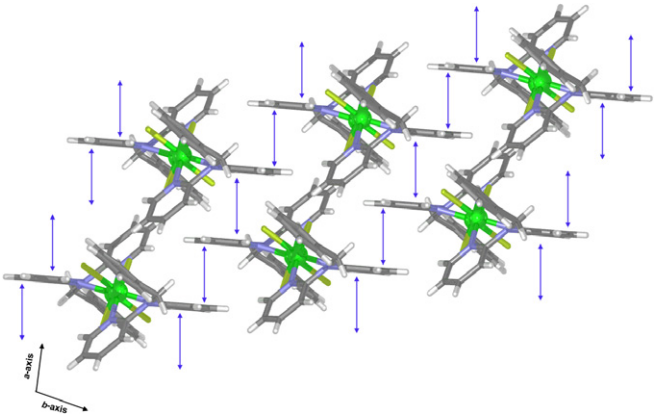

Fig. 4. A schematic representation of the 2-D sheet-like motif formed through offset face-to-face π–π interactions in $[Cu(\mathbf{3})(\mu\text{-}Cl)Cl]_2 \cdot 2C_2H_5OH$; π–π interactions indicated by arrows.

described as a distorted square pyramid ($\tau = 0.33$) [26]. The dimeric arrangement is stabilised by a number of intramolecular C–H···Cl-interactions between the metal-bound Cl^- ligand and pyridyl hydrogen atoms. (C(12)–H(12)···Cl(2)^1 = 2.75 Å; C(2)–H(2)···Cl(1)^1 = 2.96 Å; C(12)–H(12)···Cl(1) = 2.85 Å, C(12)–H(12)···Cl(1)^1 = 3.27 Å). These interactions are shown as dashed lines in Fig. 1.

[Cu(**3**)(μ-Cl)Cl]$_2 \cdot 2C_2H_5OH$ was synthesised in an analogous fashion to the above dinuclear complex, [Cu(**2**)(μ-Cl)Cl]$_2$, and both X-ray structures (Fig. 2) are very similar (the former is again disposed around an inversion centre), with the coordination sphere of each copper centre being slightly closer to a trigonal bipyramidal in the structure incorporating **3** (τ, Cu(1) = 0.46) [26]. Again, the overall arrangement is stabilised by a number of weak pyridine H-chloride interactions, the strongest of which occurs between H(12) and Cl(2)^1 (=2.45 Å); these interactions are indicated by dashed lines in Fig. 2.

In contrast to the cyclohexylmethylene-containing structure just discussed, ethanol solvent molecules are present in the lattice of the corresponding benzyl-containing derivative, [Cu(**3**)(μ-Cl)Cl]$_2 \cdot 2C_2H_5OH$. Each ethanol oxygen atom is hydrogen bonded to one of the coordinated chloride ions: (O(21)–H(21)···Cl(2), 2.45 Å); in addition, each ethanol oxygen acts as an acceptor for a weak contact from one of the methylene hydrogen atoms (C(14)–H(14A)···O(21) 2.60 Å). The latter results in the formation of a one-dimensional ribbon-like arrangement which propagates

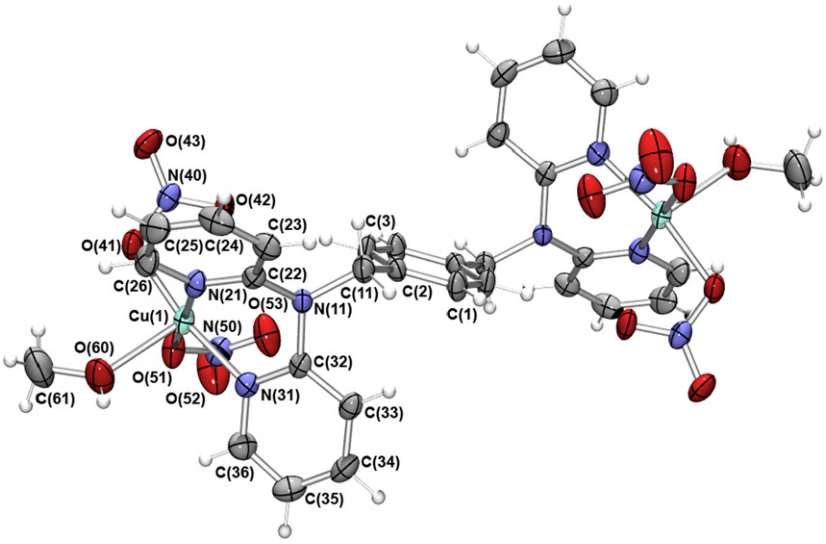

Fig. 5. ORTEP [27] depiction of the X-ray structure of [Cu_2(**6**)$(CH_3OH)_2(NO_3)_4$] shown with 50% probability ellipsoids. Symmetry code for generating equivalent atoms: $-x$, $-y$, $2 - z$.

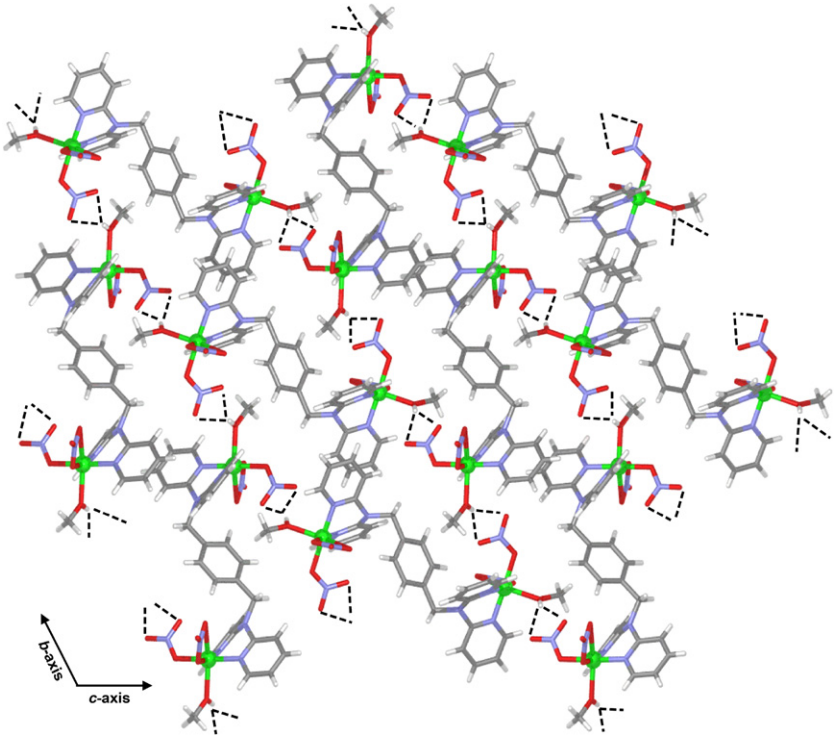

Fig. 6. The two-dimensional sheet-like arrangement formed via H-bonding interactions between [Cu_2(**6**)$(CH_3OH)_2(NO_3)_4$] units.

down the crystallographic *c*-axis. A schematic representation of a section of this packing is presented in Fig. 3.

The substitution of a phenyl ring for the cyclohexane ring clearly increases the possibility of π–π interactions occurring within the lattice of $[Cu(\mathbf{3})(\mu\text{-}Cl)Cl]_2 \cdot 2C_2H_5OH$ when compared to $[Cu(\mathbf{2})(\mu\text{-}Cl)Cl]_2$. Indeed, no significant π–π interactions were observed in the crystal packing of the latter, while there are two distinct offset face-to-face π–π interactions present in the lattice of $[Cu(\mathbf{3})(\mu\text{-}Cl)Cl]_2 \cdot 2C_2H_5OH$. The stacking occurs exclusively between alternate N(13)-containing rings throughout the lattice (centroid–centroid 3.73 Å, $\beta = 17.5°$ [28]; there is a second weak interaction, centroid–centroid 4.44 Å, β 40.5°, with the closest C–C distance C(10)–C(11) being 3.44 Å). These interactions result in the formation of a two-dimensional sheet-like motif extending in the *ab*-plane (Fig. 4). Each of these sheets is linked by the hydrogen bonds described above to form an overall three-dimensional polymeric arrangement.

As observed previously for the silver complexes of **4**–**6** [14], complexes of **4** could be expected to bind in a bis-bidentate fashion towards a single metal ion, while **5** and **6** might complex with two metal ions, one to each of the dpa sites. The latter arrangement is confirmed by the X-ray structure of $[Cu_2(\mathbf{6})(CH_3OH)_2(NO_3)_4]$ (Fig. 5); this product crystallised in the monoclinic space group $P2_1/n$, with the complex disposed around an inversion centre. In contrast to the two structures discussed above, each copper ion in this complex has a square-pyramidal geometry ($\tau = 0.02$) [26], with two pyridyl nitrogen donors and two monodentate nitrate anions occupying the basal plane and a coordinated methanol molecule bound in the apical position. The copper–copper separation is 11.206(1) Å.

The packing for the $[Cu_2(\mathbf{6})(CH_3OH)_2(NO_3)_4]$ complex shows that each dinuclear complex unit is linked through O–H···O hydrogen bonds involving coordinated methanol on one complex and the oxygen atom of a nitrate anion on an adjacent complex. The presence of these interactions results in the two-dimensional pattern illustrated in Fig. 6; a number of weak pyridyl hydrogen–oxygen interactions interconnect these layers.

3.1.1. Liquid–liquid extraction studies

Comparative two-phase solvent extraction experiments (water/chloroform) were carried out for copper(II) perchlorate in the aqueous phase at pH 7.2 (HEPES/NaOH buffer) and ligands **1**–**3**, **5**, **7** or **8** in the chloroform phase. Under the conditions employed, the extraction of copper into the chloroform phase was negligible for the single dpa derivatives (<4% which is within experimental error of zero) whereas the bis-dpa derivative, **6**, and the tri-dpa derivative, **7**, showed marginal extraction at 6% and 7%, respectively. In contrast, the tetrakis-derivative, **8**, gave 36% extraction of the copper(II) perchlorate under identical conditions. As expected, increasing the number of DPA subunits (with presumably a corresponding increase in the lipophilicity) thus results in increased extraction efficiency for the above ligand series.

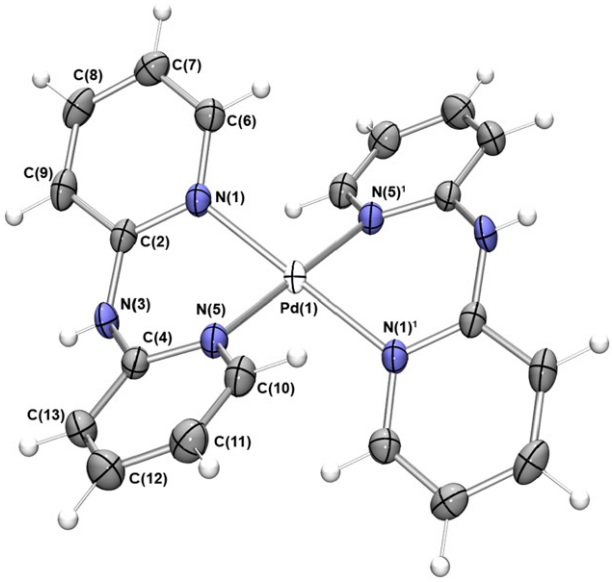

Fig. 7. ORTEP [27] plot of $[Pd(\mathbf{1})_2]^{2+}$ showing atom labels (thermal ellipsoids at the 50% probability level). Counter ion and solvent molecules are omitted for clarity. Symmetry code used for generating equivalent atoms: $1-x, -y, -z$.

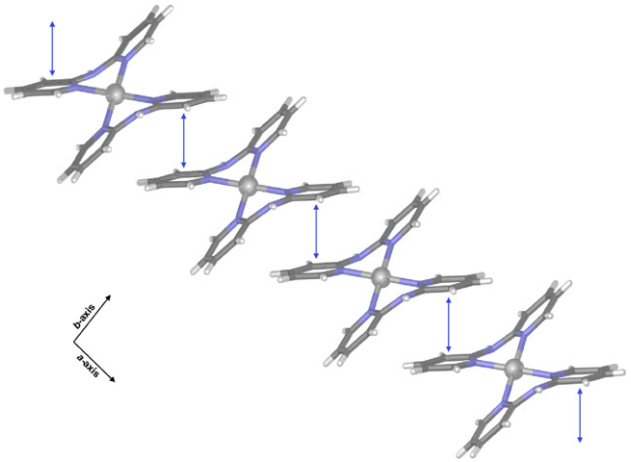

Fig. 9. A schematic representation of the chain formed by π–π interactions present in $[Pd(\mathbf{1})_2](PF_6)_2 \cdot 2CH_3OH$.

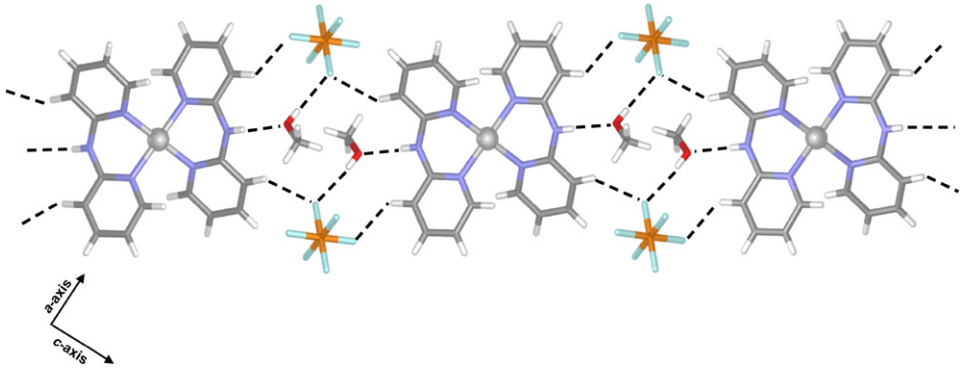

Fig. 8. Schematic representation of the one-dimensional polymeric chain formed through hydrogen bonding interactions between $[Pd(\mathbf{1})_2](PF_6)_2 \cdot 2CH_3OH$ units.

3.2. Palladium(II) complexes

As expected, the X-ray structure of $[Pd(\mathbf{1})_2](PF_6)_2 \cdot 2CH_3OH$ confirms that two 2,2′-dipyridylamine ligands bind in a bidentate fashion via their pyridyl nitrogen atoms to the palladium(II) centre in a square planar manner. An ORTEP [27] plot of the $[Pd(\mathbf{1})_2]^{2+}$ cation is shown in Fig. 7. The palladium to nitrogen bond lengths of 2.02 Å and N–Pd–N bond angles (for example, N(1)–Pd(1)–N(5) = 86°) are both within the expected range for square planar palladium(II) complexes of this type. The palladium(II) ion is located on an inversion centre. The combination of the flexible central nitrogen atom, N(3), which displays some sp^2 character (C(2)–N(3)–C(4) = 127°) and steric effects between the pyridyl rings, results in each of the dpa moieties bowing somewhat from the plane formed by the metal ion and donor atoms. This is reflected in the C(6)–N(1)–N(5)^1–C(10)^1 torsion angle of 60°.

The crystal packing for $[Pd(\mathbf{1})_2](PF_6)_2 \cdot 2CH_3OH$ (Fig. 8) is characterised by significant hydrogen bond interactions between the complex cation, the PF_6 counter ion and the methanol solvate molecules. The N–H···O interactions between the secondary amine nitrogens and methanol oxygens show a nearly ideal geometry (N–H···O, 2.11 Å; 176°). As well as the hydrogen bonding interactions, there are a number of pyridine hydrogen–fluorine interactions. These latter interactions result in the formation of a one-dimensional chain arrangement (Fig. 8). A number of other weaker phenylene hydrogen–fluorine interactions are also present in the lattice with H–F distances between 2.44 and 2.53 Å.

In addition to the above, offset face-to-face π–π-stacking occurs between pyridine rings to link the adjacent hydrogen bonded chains of the type described above, (centroid–centroid 3.65 Å, β = 12.3° [28]), resulting in a two-dimensional motif. The π–π-stacking and 'bowing' present in the cations is illustrated in Fig. 9.

The structures of the $[Pd_2(\mathbf{4})(OAc)_4] \cdot 4H_2O$ and $[Pd_2(\mathbf{6})(OAc)_4] \cdot 2CH_2Cl_2$ incorporating the isomeric ligands **4** and **6** exhibit some similar features. Both complexes are dinuclear, with each palladium centre showing square planar coordination in which two cis pyridyl nitrogen and two cis acetate oxygen atoms surround each metal centre (see Figs. 10 and 11). Each palladium ion lies only 0.01 Å and 0.03 Å out of the N_2O_2-donor planes for the complexes incorporating **4** and **6**, respectively. Selected bond lengths and angles for both complexes are given in the ESI.

An intramolecular, face-to-face, π–π interaction is present in the structure of $[Pd_2(\mathbf{4})(OAc)_4] \cdot 4H_2O$ (Fig. 10). In addition, the non-coordinated oxygen atom of each acetate ligand acts as an acceptor for hydrogen bonding from the hydrogen of a solvate water molecule. Individual complex units are connected by intermolecular O–H···O hydrogen bonds (O(1w)–H(2w)···O(2), 2.3 Å, 127°; O(1w)–H(1w)···O(4), 2.69 Å, 91°), resulting in a two-dimensional motif which propagates in the *ab*-plane as shown schematically in Fig. 12. There are also a number of weak pyridyl hydrogen–oxygen interactions present within the lattice.

In a similar manner to that occurring in the structure of $[Cu_2(\mathbf{6})(NO_3)_4] \cdot 2MeOH$ discussed previously, $[Pd_2(\mathbf{6})(OAc)_4] \cdot 2CH_2Cl_2$ (Fig. 11) is disposed around an inversion centre such that half the complex is present in the asymmetric unit. However, in contrast to the copper(II)-containing structure there are few significant formal interactions present within the lattice. Analysis of the crystal packing of this complex reveals a number of weak intermolecular C–H···O interactions involving methylene (H11) and aryl (H14B) hydrogen atoms. The geometries of these C–H···O (acetate) interactions are similar to those reported previously for a related palladium acetate complex (C···O = 3.47–3.65 Å) [29]. Other weak intramolecular C–H···N interactions are also present (see ESI).

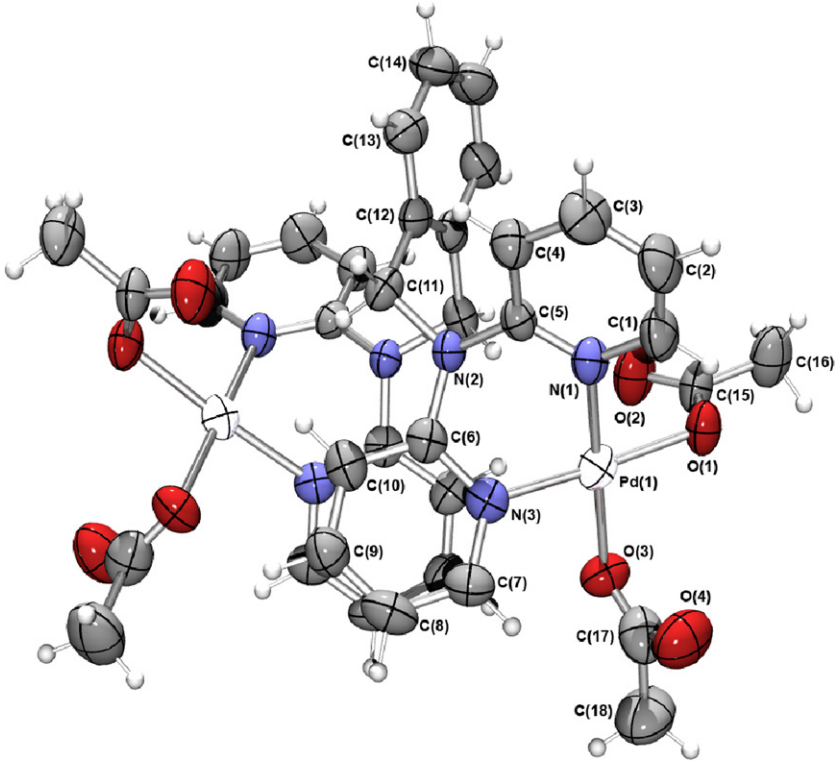

Fig. 10. ORTEP [27] representation of $[Pd_2(\mathbf{4})(OAc)_4] \cdot 4H_2O$ shown with 50% probability ellipsoids. Solvent molecules removed for clarity. Symmetry code used for generating equivalent atoms: ½ − *x*, ½ − *y*, *z*.

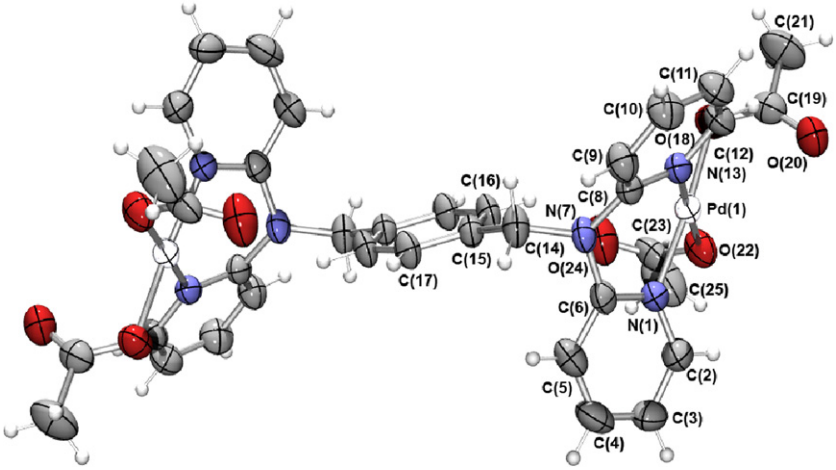

Fig. 11. ORTEP [27] representation of $[Pd_2(\mathbf{6})(OAc)_4] \cdot 2CH_2Cl_2$ shown with 50% probability ellipsoids. Solvent molecules omitted for clarity. Symmetry code used for generating equivalent atoms: $-x, 1-y, 1-z$.

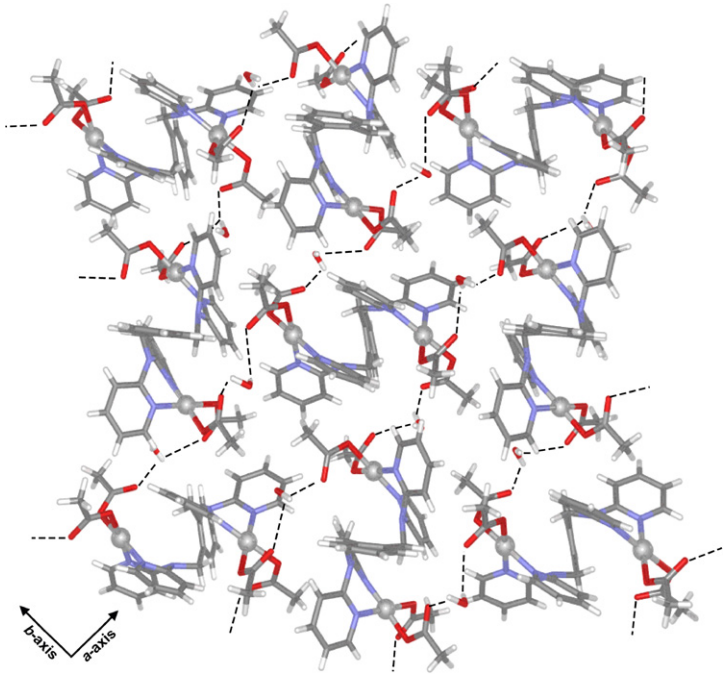

Fig. 12. Schematic representation of the two-dimensional hydrogen bonded network in $[Pd_2(\mathbf{4})(OAc)_4] \cdot 4H_2O$. Dashed lines represent hydrogen bonding interactions.

4. Concluding remarks

The interaction of copper(II) and palladium(II) with an extended series of linked dipyridylamine derivatives has been explored and shown to result in a diverse range of interesting coordination geometries and lattice architectures, with the latter ranging from essentially discrete to three-dimensional polymeric. Liquid–liquid ($H_2O/CHCl_3$) extraction experiments involving copper(II) in the aqueous phase and **1–3, 5,7** and **8** in the organic phase show that the efficiency of extraction depends markedly on the number of dpa-subunits in the ligand employed, with the tetrakis-dpa derivative **8** acting as the most efficient extractant for copper of the six ligands investigated.

Acknowledgements

We thank the Australian Research Council, the Royal Society of New Zealand Marsden Fund and the Deutsche Forschungsgemeinschaft for support. B.A. gratefully acknowledges the Max-Buchner-Stiftung for a research grant. O.K. acknowledges the DFG for assistance under Grant 36RUS 17/20/06 and Prof. P. Metz for access to X-ray facilities at TU Dresden.

Appendix A. Supplementary data

CCDC 682093, 682094, 682095, 682096, 682097 and 682098 contain the supplementary crystallography data for this paper. These data can be obtained free of charge via http://www.ccdc.cam.ac.uk/conts/retrieving.html, or from the Cambridge Crystallographic Data Centre, 12 Union Road, Cambridge CB2 1EZ, UK; fax: (+44) 1223-336-033; or e-mail: deposit@ccdc.cam.ac.uk. Supplementary data associated with this article can be found, in the online version, at doi:10.1016/j.poly.2008.06.036.

References

[1] (a) S. Youngme, N. Chaichit, C. Pakawatchai, S. Booncoon, Polyhedron 21 (2002) 1279;
(b) S. Youngme, N. Chaichit, N. Koonsaeng, Inorg. Chim. Acta 335 (2002) 36;
(c) M.J. Plater, M.R.S.J. Foreman, J.M.S. Skakle, R.A. Howie, Inorg. Chim. Acta 332 (2002) 135;
(d) S. Youngme, N. Chaichit, Polyhedron 21 (2002) 247;
(e) H. Zhu, M. Strobele, Z. Yu, Z. Wang, H.J. Meyer, X. You, Inorg. Chem. Commun. 4 (2001) 577.

[2] (a) See for example: D.A. Benson, I. Karsch-Mizrachi, D.J. Lipman, J. Ostell, B.A. Rapp, D.L. Wheeler, Genbank Nucl. Acids Res. 28 (2000) 15;
(b) S. Youngme, J. Phatchimkun, N. Chaichit, Acta Crystallogr., Sect. C 62 (2006) m602;
(c) S. Youngme, J. Phatchimkun, N. Chaichit, C. Pakawatchai, I. Mutikainen, U. Turpeinen, J. Coord. Chem. 59 (2006) 1813;
(d) H. Chowdhury, S.H. Rahaman, R. Ghosh, S.K. Sarkar, M. Corbella, B.K. Ghosh, Inorg. Chem. Commun. 9 (2006) 276;
(e) S. Youngme, J. Phatchimkun, U. Suksangpanya, C. Pakawatchai, G.A. van Albada, M. Quesada, J. Reedijk, Inorg. Chem. Commun. 9 (2006) 242;
(f) R. Carballo, B. Covelo, N. Fernández-Hermida, A.B. Lago, E.M. Vázquez-López, Z. Anorg. Allg. Chem. 633 (2007) 1791;
(g) R. Carballo, A. Castiñeiras, B. Covelo, A.B. Lago, E.M. Vázquez López, Z. Anorg. Allg. Chem. 633 (2007) 687;
(h) S. Youngme, T. Chotkhun, N. Chaichit, Acta Crystallogr., Sect. C 63 (2007) m59;
(i) S. Youngme, P. Phuengphai, N. Chaichit, I. Mutikainen, U. Turpeinen, B.M. Murphy, J. Coord. Chem. 60 (2007) 131;
(j) S. Youngme, J. Phatchimkun, C. Pakawatchai, S. Prabpaic, P. Kongsaereec, Acta Crystallogr., Sect. C 63 (2007) m45;
(k) S. Youngme, J. Phatchimkun, U. Suksangpanya, C. Pakawatchai, N. Chaichit, P. Kongsaeree, J. Krzystek, B. Murphy, Polyhedron 26 (2007) 871.

[3] J. Chen, X. Wang, Y. Shao, J. Zhu, Y. Zhu, Y. Li, Q. Xu, Z. Guo, Inorg. Chem. 40 (2007) 3306.

[4] A.K. Paul, H. Mansuri-Torshizi, T.S. Srivastava, S.J. Chavan, M.P. Chitnis, J. Inorg. Biochem. 50 (1993) 9.

[5] W.-R. Yao, Z.-H. Liu, Q.-F. Zhang, Acta Crystallogr., Sect. C 59 (2003) m139.

[6] (a) C. Seward, S. Wang, Comments Inorg. Chem. 26 (2005) 103;
(b) C.R.K. Glasson, L.F. Lindoy, G.V. Meehan, Coord. Chem. Rev. 252 (2008) 940.

[7] (a) P. Gamez, P. de Hoog, O. Roubeau, M. Lutz, W.L. Driessen, A.L. Spek, J. Reedijk, Chem. Commun. (2002) 1488;
(b) P. Gamez, P. de Hoog, M. Lutz, A.L. Spek, J. Reedijk, Inorg. Chim. Acta 351 (2003) 319;
(c) de Hoog, P. Gamez, M. Leuken, O. Roubeau, B. Krebs, J. Reedijk, Inorg. Chim. Acta 357 (2004) 213;
(d) S. Demeshko, G. Leibeling, S. Dechert, F. Meyer, Dalton Trans. (2004) 3782;
(e) C. Seward, W.-l. Jia, R.-Y. Wang, S. Wang, Inorg. Chem. 43 (2004) 978;
(f) J.-S. Yang, Y.-D. Lin, Y.-H. Lin, F.-L. Liao, J. Org. Chem. 69 (2004) 3517;
(g) W.-L. Jia, D.-R. Bai, T. McCormick, Q.-D. Liu, M. Motala, R.-Y. Wang, C. Seward, Y. Tao, S. Wang, Chem. Eur. J. 10 (2004) 994.

[8] (a) J. Pang, Y. Tao, S. Freiberg, X.-P. Yang, M. D'Iorio, S. Wang, J. Mater. Chem. 12 (2002) 206;
(b) Q.-D. Liu, W.-L. Jia, G. Wu, S. Wang, Organometallics 22 (2003) 3781;
(c) L. Aubouy, P. Gerbier, N. Huby, G. Wantz, L. Vignau, L. Hirsch, J.-M. Janot, New J. Chem. 28 (2004) 1086;
(d) J.-S. Yang, Y.-D. Lin, Y.-H. Chang, S.-S. Wang, J. Org. Chem. 70 (2004) 6066;
(e) Y. Kang, C. Seward, D. Song, S. Wang, Inorg. Chem. 42 (2003) 2789;
(f) C. Seward, W.-L. Jia, R.-Y. Wang, G.D. Enright, S. Wang, Angew. Chem., Int. Ed. 43 (2004) 2933.

[9] M. Kapnisti, A.G. Hatzidimitriou, Struct. Chem. 18 (2007) 331.

[10] (a) C.J. Sumby, P.J. Steel, Organometallics 22 (2003) 2358;
(b) C.J. Sumby, P.J. Steel, Inorg. Chim. Acta 360 (2007) 2100.

[11] Y. Wang, Y. Mizubayashi, M. Odoko, N. Okabe, Acta Crystallogr., Sect. C 61 (2005) m67.

[12] (a) I. Puscasu, C. Mock, M. Rauterkus, A. Rondigs, G. Tallen, S. Gangopadhyay, J.E.A. Wolff, B. Krebs, Z. Anorg. Allg. Chem. 627 (2001) 1292;
(b) M.J. Rauterkus, S. Fakih, C. Mock, I. Puscasu, B. Krebs, Inorg. Chim. Acta 350 (2003) 355.

[13] S. Fakih, W.C. Tung, D. Eierhoff, C. Mock, B. Krebs, Z. Anorg. Allg. Chem. 631 (2005) 1397.

[14] B. Antonioli, D.J. Bray, J.K. Clegg, K. Gloe, K. Gloe, O. Kataeva, L.F. Lindoy, J.C. McMurtrie, P.J. Steel, C.J. Sumby, M. Wenzel, Dalton Trans. (2006) 4783.

[15] T. Chao, Y. Shao, N. Gan, Q. Xu, Z. Guo, Inorg. Chem. 43 (2004) 4761.

[16] (a) I. Puscasu, C. Mock, M. Rauterkus, A. Rondigs, G. Tallen, S. Gangopadhyay, J.E.A. Wolff, B. Krebs, Z. Anorg. Allg. Chem. 627 (2001) 1292;
(b) M.J. Rauterkus, S. Fakih, C. Mock, I. Puscasu, B. Krebs, Inorg. Chim. Acta 350 (2003) 355;
(c) C. Tu, J. Lin, Y. Shao, Z. Guo, Inorg. Chem. 42 (2003) 5795.

[17] L. Song, W.C. Trogler, J. Organomet. Chem. 452 (1993) 271.

[18] Y. Oh, J. Korean Chem. Soc. 44 (2000) 507.

[19] Nonius BV, Delft, The Netherlands, 1998.

[20] A.J.M. Duisenberg, J. Appl. Crystallogr. 25 (1992) 92.

[21] A.J.M. Duisenberg, L.M.J. Kroon-Batenburg, A.M.M. Schreurs, J. Appl. Crystallogr. 36 (2003) 220.

[22] Bruker, SMART, SAINT and XPREP, Bruker Analytical X-ray Instruments Inc., Madison, Wisconsin, USA, 1995.

[23] G.M. Sheldrick, Acta Crystallogr., Sect. A 46 (1990) 467.

[24] G.M. Sheldrick, SADABS: Empirical Absorption and Correction Software, University of Göttingen, Institut für Anorganische Chemie der Universität, Tammanstrasse 4, D-3400 Göttingen, Germany, 1999–2003.

[25] G.M. Sheldrick, SHELX-97: Programs for Crystal Structure Analysis, University of Göttingen, Institut für Anorganische Chemie der Universität, Tammanstrasse 4, D-3400 Göttingen, Germany, 1997.

[26] A.W. Addison, T.N. Rao, J. Reedijk, J. van Rijn, G.C. Verschoor, Dalton Trans. (1984) 1349.

[27] L.J. Farrugia, J. Appl. Crystallogr. 30 (1999) 565.

[28] (a) M. Nishio, M. Hirota, Y. Umezawa, The CH/π Interaction (Evidence, Nature and Consequences), Wiley VCH, New York, 1998;
(b) C. Janiak, J. Chem. Soc., Dalton Trans. (2000) 3885.

[29] C. Seward, J. Pang, S. Wang, Eur. J. Inorg. Chem. (2002) 1390.

a tridentate ligand L generated *in situ*, and two chlorides directly bonded to Cu(II). The formation of the tridentate ligand is unexpected as the starting materials in the stated molar proportions are used as a synthetic protocols for the preparation of biguanides [7]. Here we report role of the *in situ* generated tridentate ligand on the self-assembly of the superstructure of the molecular complex **1**.

2. Experimental

2.1. Materials and measurements

All reactions were carried out in aerobic condition and in water solvent. Cyanamide (Lancaster), dicyandiamide (Aldrich) and ethylenediamine dihydrochloride (Fluka) were used as received. All other chemicals were of reagent grade and used without further purification. The elemental analyses were done using a Perkin–Elmer 2400 Series-II elemental analyzer. The IR spectra were recorded from KBr pellets at a range of 500–4000 cm^{-1} on a Perkin–Elmer RXI FT-IR spectrophotometer with a spectral resolution of 4 cm^{-1}. UV–Vis spectral data were obtained from Shimadzu UVPC 1601 spectrophotometer. EPR spectral data were recorded using Varian E-109C spectrometer fitted with a liquid nitrogen quartz dewar, 9.1 GHz microwave frequency, 100 kHz modulation, 30 dB power, 3200 G sweep center, 4000 G sweep width, 240 s sweep time. Diphenylpicrylhydrazyl (dpph, $g = 2.0037$) was used to calibrate the spectra. Electrochemical measurements were done in nitrogen atmosphere with a three-electrode setup, consisting of a glassy carbon working, a saturated calomel reference and a Pt wire auxiliary electrodes using a EG&G PARC electrochemical analysis system, model 250/5/0. An ECDA-Pt02 platinum disk electrode obtained from Con-Serv Enterprises, India, and a planar EG&G PARC G0229 glassy carbon milli electrode were used as the working electrodes in cyclic voltammetry. The measurements (1.0 mM Cu(II) complex) were done in aqueous solution in presence of 0.1 M KCl as supporting electrolyte at 25 °C and the data are uncorrected for junction potentials. Room temperature Magnetic moment was measured by using a PAR-155 vibrating sample magnetometer. Solution conductivity was measured by a Systronics (India) direct reading conductivity meter (model 304).

2.2. Synthesis of the complex $[CuLCl_2] \cdot H_2O$ (**1**) [L = 1-(2-aminoethyl)biguanide] (**1**)

To an aqueous solution of 0.10 mol cyanamide (NH_2CN) added 0.05 mol ethylenediamine dihydrochloride (in 25 mL water). 0.025 mol $CuCl_2 \cdot 2H_2O$ (in 25 mL water) was added into this solution. The solution mixture was then either kept for ~2 months at room temperature (25–30 °C) when deep blue crystals suitable for X-ray analysis were separated or refluxed at ~80 °C for 10 h when the same blue crystals were formed on cooling to room temperature. The crystals were separated by filtration, washed with ethanol and dried in air. Alternatively, using dicyandiamide (0.05 mol, half of the cyanamide) instead of cyanamide and following the same procedures as described above resulted in the formation of **1** as confirmed by X-ray crystallography. The compound **1** can be prepared in high yield (80%, based on Cu) in either way. *Anal.* Calc. for $C_4H_{12}Cl_2N_6Cu \cdot H_2O$: C, 16.18; H, 4.72; N, 28.32. Found: C, 16.24; H, 4.79; N, 28.18%. Selected IR peaks (KBr/cm^{-1}): ν(C–N) 1308 (w) and 1267 (m), ν(N–H) 3300 (s) and 3231 (s), ν(C–H) 2940 (m) and ν(O–H) 3435 (sh).

2.3. X-ray crystallographic study

Suitable single crystals of complex **1** were mounted on a Siemens Smart CCD diffractometer equipped with a graphite-monochromated Mo Kα radiation ($\lambda = 0.71073$ Å) at 298(2) K. Absorption corrections were performed using the SADABS program after the diffracting frames were reduced [8]. The structure was solved by the direct methods and refined by full-matrix least-squares fitting on F^2 by SHELXTL-97 [9]. All non-hydrogen atoms were refined with anisotropic thermal parameters. H atoms of C and N atoms were located at geometrically calculated positions and treated by a mixture of independent and constrained refinement. H atoms of the water molecule were located from difference Fourier maps.

3. Results and discussion

3.1. Synthetic observations

The tridentate ligand, L, $H_2N–(CH_2)_2–N{=}C(NH_2)–NH–C(NH_2){=}NH$, is formed *in situ* in the reaction media in presence of Cu^{2+} resulting in complex **1**. In an attempt to remove Cu^{2+} from **1** to isolate the ligand by passing H_2S gas through the aqueous solution of **1** resulted in decomposition of the ligand though Cu(II) can be quantitatively removed as CuS. We have also verified that the tridentate ligand L cannot be synthesized separately in absence of Cu^{2+}. We thus conclude that the Cu^{2+} acts as a template in the synthesis of **1**. Though we are unable to uncover the exact role of Cu^{2+} for the formation of this tridentate ligand but we have verified that similar synthetic procedure failed when Ni^{2+}, Co^{2+}, Zn^{2+}, Fe^{2+} or Fe^{3+} salts were used instead of Cu^{2+}. A possible route for the formation of the ligand L might be proposed as the one-ended attack of one amine group of ethylenediamine to the cyanamide and in turn another cyanamide, Scheme 1 (or one dicyandiamide instead of two molecules of cyanamide, Scheme 2) and simultaneous rearrangements of protons is presented in Schemes 1 and 2. It might also be possible (but could not be resolved at present) that two cyanamide molecules at first dimerises to form dicyandiamide which then reacts with ethylenediamine (Scheme 2).

3.2. Physico-chemical observations

The complex **1** shows magnetic moment ($\mu_{eff} = 1.65$ BM at 25.0 °C) corresponding to a single unpaired electron. Complex **1** is highly soluble in water and conductivity measurements (438 Ω^{-1} cm^2 M^{-1}) established its 1:2 electrolytic nature in aqueous media [10] indicating that the two chlorides become free from Cu(II) in aqueous media. An aqueous solution of **1** shows spectral peaks at 650 nm ($\varepsilon = 48$ M^{-1} cm^{-1}) and a shoulder at 960 nm ($\varepsilon = 11$ M^{-1} cm^{-1}).

3.3. X-ray crystallographic study

3.3.1. Description of the crystal structure of $[CuLCl_2] \cdot H_2O$ ($L = H_2N–(CH_2)_2–N{=}C(NH_2)–NH–C(NH_2){=}NH$, a tridentate ligand formed in situ in the reaction media)

Fig. 1 presents the structure of **1**, $[CuLCl_2] \cdot H_2O$ [L = 1-(2-aminoethyl) biguanide], showing N_3Cl_2 coordination that results in square pyramid geometry where three N and Cl1 occupy the base of the square pyramidal coordination environment while Cl2 occupies the apical position. The Cu–N bonds in **1** range from 1.917(4) to 1.975(4) Å, similar to those in complexes of $[CuL(NCS)] \cdot SCN$ and $[CuL(cyanoguanidine)] \cdot SO_4 \cdot H_2O$ [11,12], in which four N atoms coordinated to Cu(II) cation in a square plane. The Cu–Cl bonds have two models, their bond distances being 2.327(2) and 2.906(2) Å, respectively. Compared to other coordinated forms of CuN2Cl2 and CuN3Cl [13,14], the Cu–Cl bond lengths are much longer in **1**. The Cu–Cl2 long bond is expected for a d^9 system due to Jahn–Teller effect. The Cu1–Cl2 apical bond (2.906(2) Å)

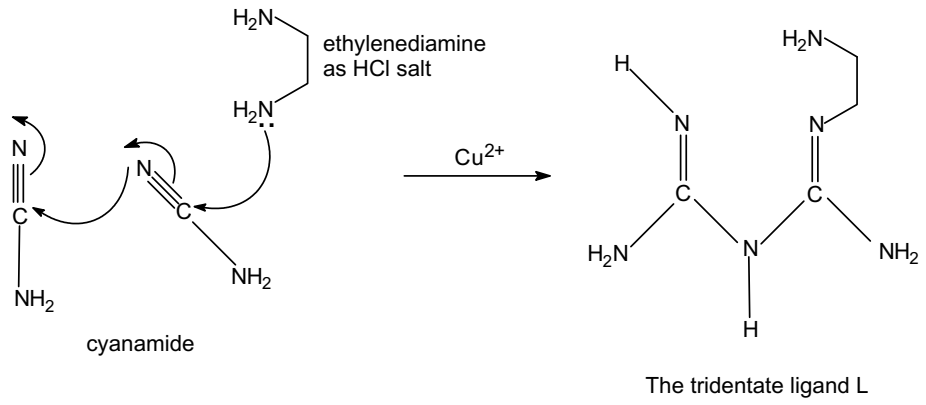

Scheme 1.

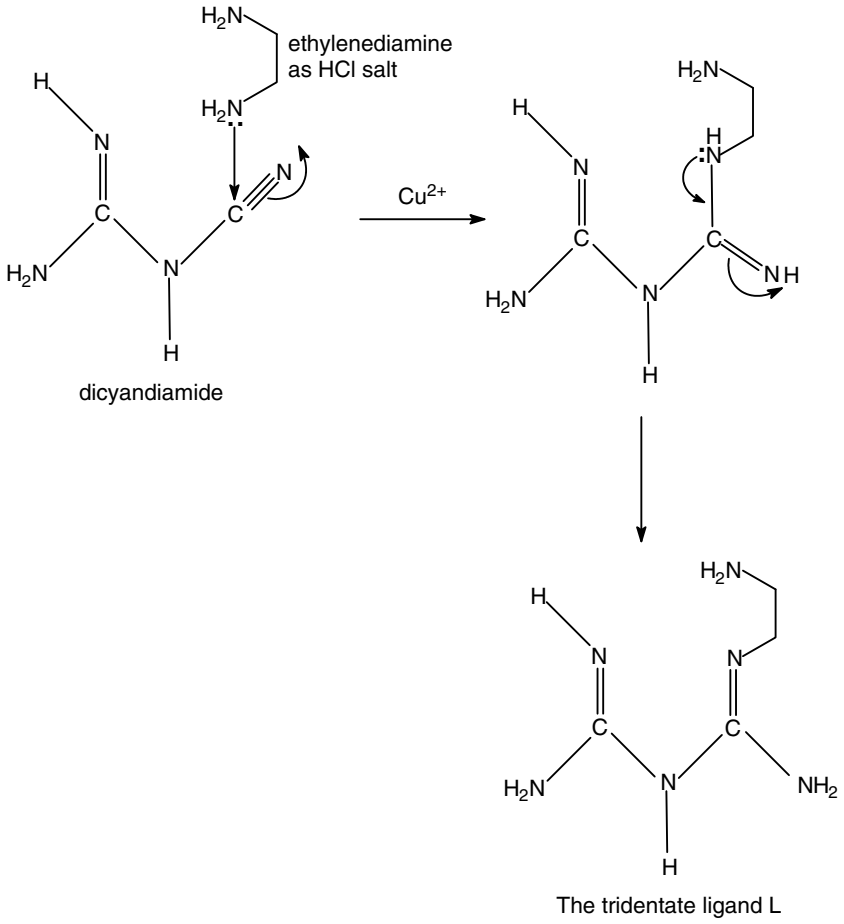

Scheme 2.

length is quiet high indicating predominantly ionic nature of this bond compared to Cu1–Cl1 equatorial bond. The tridentate ligand, L, formed *in situ*, binds to the Cu(II) in a meridional fashion with the Cu–N bond distances ranging from 1.918(4)–1.978(4) Å. The five-membered chelate ring is puckered while the adjacent six-membered ring is planar, the planarity being attributed to the π-cloud delocalisation. This is evident from the N–C bond lengths, which are considerably shorter in the six-membered ring. Even in the six-membered ring, N(1)–C(4) [1.296(6) Å] and N(2)–C(3) [1.299(6) Å] are shorter than the other N–C bonds [1.350(6)–1.389(6) Å] that suggests the π-electron density is somewhat more localized over the two terminal N–C bonds in the six-membered ring.

The overall 3D supramolecular built-up of the complex is the result of the self-assembly of a primary supramolecular dimeric unit (Fig. 2) through multi directional self-recognition. This multiway self-recognition has been facilitated by the active participation of a solvent water molecule. Monomeric units give rise to centrosymmetric supramolecular dimers through strong hydrogen bonds N4–H4···Cl2^{iv} and N5–H5B···Cl2^{iv} (iv = $1-x,-y,2-z$). These dimeric units self-recognize each other through N6–H6A···Cl1^{v} (v = $x,-1+y,z$) hydrogen bond and assemble along the *b* axis. This self-assem-

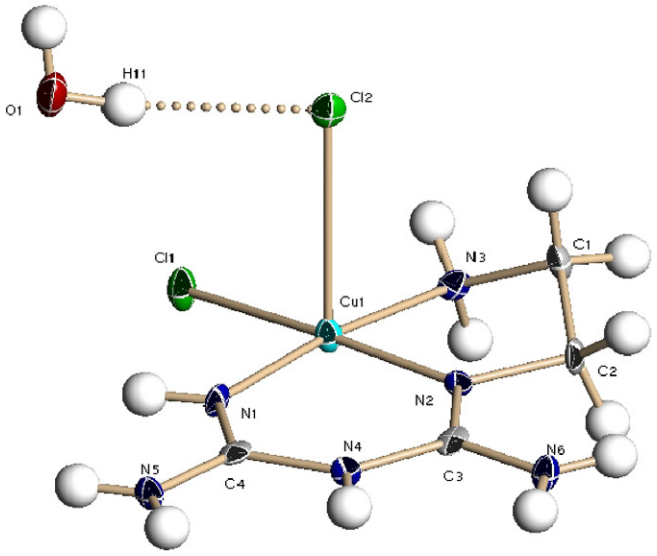

Fig. 1. ORTEP and atom-numbering scheme for $[CuLCl_2] \cdot H_2O$ (**1**), dotted line is for hydrogen bond.

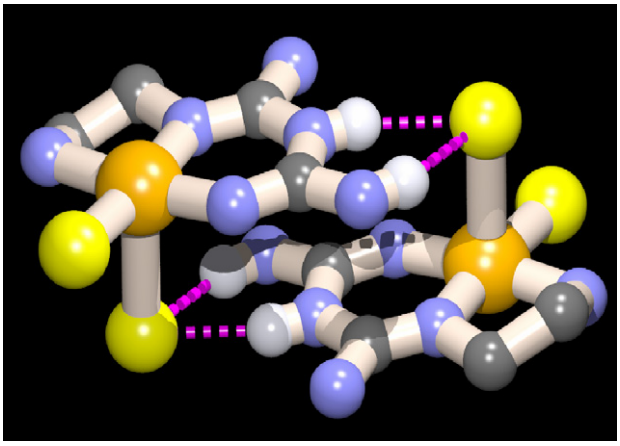

Fig. 2. N–H···Cl hydrogen bond assisted supramolecular dimer. Color code: N, dark turquoise; Cl, bright gold; C, gray; H, silver; Cu, bronze. (For interpretation of the references to colour in figure legends, the reader is referred to the web version of this article.)

bly is reinforced with the participation of a water molecule (O1) that act as acceptor for N6–H6B···O1^{iv}, N1–H1···O1^{i}, N5–H5A···O1^{i} (i = 1 − *x*,1 − *y*,2 − *z*; iv = 1 − *x*,−*y*,2 − *z*) hydrogen bonds and donor for O1–H11···Cl2 hydrogen bonds (Fig. 3). The water molecules also cross-link adjacent dimeric units along *a* axis through O1–H12···Cl1^{vi} (vi = 1 + *x*,*y*,*z*) hydrogen bond and lead the 2D-layered assembly of the dimeric units (Fig. 4). Water in this supramolecular assembly has acted as a T type connector establishing contact among three adjacent dimeric units. It is to be noted that a single water molecule in this 2D assembly has taken part in five hydrogen bonding contacts and thus stabilized the supramolecular assembly in a crucial way.

Self-recognition of dimeric units along the crystallographic *c* axis through complementary N3–H3A···Cl2^{iii} and N3–H3A···Cl1^{ii} (ii = −*x*,1 − *y*,1 − *z*; iii = −1 + *x*,*y*,*z*) hydrogen bonds help the 3D supramolecular assembly of the 2D layers (Fig. 5). Crystallographic data and structural refinements are summarized in Table 1 while the selected bond parameters are shown in Table 2. Hydrogen bond distances and angles are presented in Table 3.

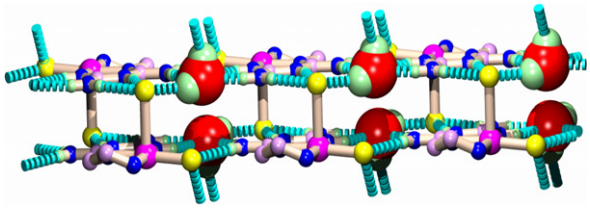

Fig. 3. Assembly of dimers along *b*-axis through self-recognition via N6–H6A···Cl1^{v} (v = *x*,−1 + *y*,*z*) hydrogen bond that is reinforced by water molecules. Color code: O, red; Cu, pink; N, blue; H, aquamarine; Cl, bright gold.

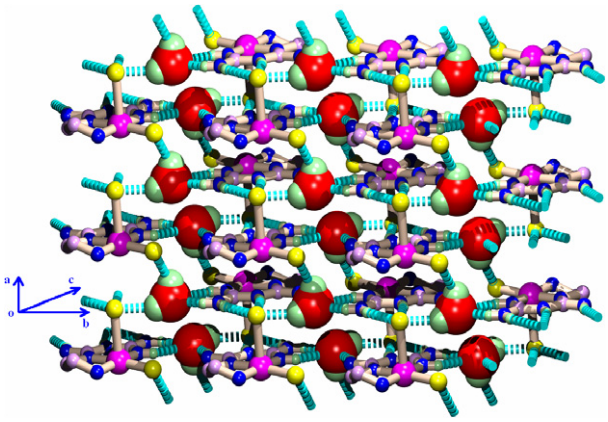

Fig. 4. The water assisted 2D supramolecular assembly of the dimeric units in the *ab* plane. Color code: O, red; Cu, pink; N, blue; H, aquamarine; Cl, bright gold.

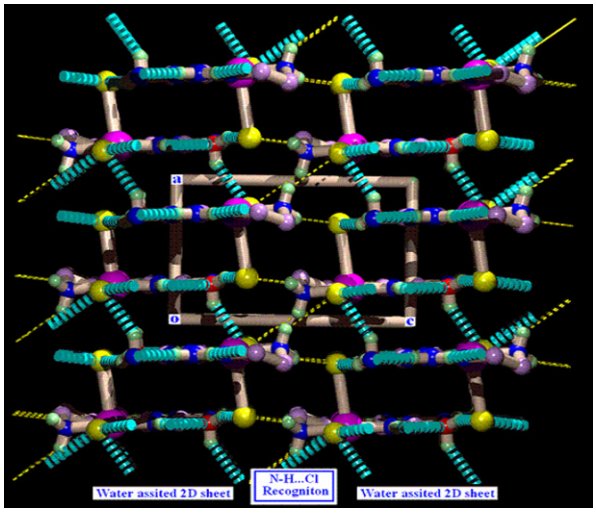

Fig. 5. Packing of 2D layers through self-recognition. Color code: O, red; Cu, pink; N, blue; H, aquamarine; Cl, bright gold.

3.4. Electrochemical studies

Cyclic voltammetric study of **1** in aqueous medium displayed an irreversible reductive response at −0.65 V versus SCE (Fig. 6) which is assignable to Cu^{II}/Cu^{I} redox couple. The anodic counterparts are at −0.13 V and 0.05 V. The peak at −0.13 V in the reverse scan is associated with a narrow width of anodic response with a large peak current and is possibly due to surface adsorbed Cu metal [15]. However, the peak at 0.05 V is not observable on scanning between 700 and −500 mV that possibly indicates the peak at 0.05 V

Table 1
Crystallographic data for **1**

Formula	$C_4H_{12}Cl_2CuN_6 \cdot H_2O$
M	296.65
Crystal system	triclinic
Space group	$P\bar{1}$
a (Å)	6.281(1)
b (Å)	8.603(1)
c (Å)	10.633(1)
α (°)	68.386(2)
β (°)	88.607(2)
γ (°)	87.018(2)
V (Å^3)	533.44(9)
Z	2
D_{calc} (g/cm^3)	1.847
μ (mm^{-1})	2.53
T (K)	298(2)
$F(000)$	302
Crystal size	0.46 × 0.34 × 0.08
Data/restraint/parameters	1864/0/127
Reflections collected	2871
Unique reflections	1864
Goodness-of-fit	0.902
$R_1[I > 2\sigma(I)]$	0.034
$wR_2[I > 2\sigma(I)]$	0.076
R_1 (all data)	0.055
wR_2 (all data)	0.076
$(\Delta/\sigma)_{max}$	0.001
Residuals (e Å^{-3})	0.54, −0.50

Table 2
Selected bond lengths (Å) and angles (°) for **1**

Cu1–N1	1.917(4)	Cu1–Cl1	2.327(2)
Cu1–N2	1.964(4)	Cu1–Cl2	2.906(2)
Cu1–N3	1.975(4)		
N1–Cu1–N2	90.9(2)	N3–Cu1–Cl1	93.0(1)
N1–Cu1–N3	173.1(2)	N1–Cu1–Cl2	96.6(1)
N2–Cu1–N3	84.1(2)	N2–Cu1–Cl2	91.8(1)
N1–Cu1–Cl1	91.7(1)	N3–Cu1–Cl2	88.4(1)
N2–Cu1–Cl1	174.6(1)	Cl1–Cu1–Cl2	92.6(1)

Table 3
Hydrogen-bond parameters (Å, °) for **1**

Cg(I)[a] → Cg(J)	D–H	H···A	D···A	D–H···A
N1–H1···O1[i]	0.86	2.60	3.325(6)	143.3
N3–H3A···Cl1[ii]	0.90	2.74	3.481(4)	140.9
N3–H3A···Cl2[iii]	0.90	2.84	3.491(5)	130.4
N4–H4···Cl2[iv]	0.86	2.33	3.159(4)	162.7
N5–H5A···O1[i]	0.86	2.11	2.928(6)	158.4
N5–H5B···Cl2[iv]	0.86	2.44	3.230(4)	153.8
N6–H6A···Cl1[v]	0.86	2.44	3.273(4)	163.3
N6–H6B···O1[iv]	0.86	2.30	3.119(5)	159.8
O1–H11···Cl2	0.88	2.37	3.167(4)	150.9
O1–H12···Cl1[vi]	0.87	2.47	3.233(4)	147.2

[i] $1-x, 1-y, 2-z$; [ii] $x, 1-y, 1-z$; [iii] $1+x, y, z$; [iv] $1-x, -y, 2-z$; [v] $x, -1+y, z$; [vi] $1+x, y, z$.

is not associated with any oxidation of Cu(II) leading to Cu(III), rather may be assigned to reoxidation of deposited Cu on electrode.

3.5. EPR studies

The EPR spectroscopy is particularly informative for understanding the electronic structure of Cu(II) complexes [16,17]. The nearly axial features of the well-resolved X-band spectrum (Fig. 7) of the mononuclear **1** in the frozen state (water:ethylene glycol = 1:1 v/v, 77 K) with $g_{||}$ (2.276) > $g_{\perp}$ (2.035) > 2.00 and $A_{||}$ (170×10^{-4} cm^{-1}) > $A_{\perp}$ (60×10^{-4} cm^{-1}), are consistent with a typical monomeric tetragonal Cu(II) environment and a $^1B_1$ $d_{x^2-y^2}$ ground state [18]. The g tensor and A tensor values are quite similar for Cu(II) in an analogous pseudoplanar N_2O_2 equatorial environment [19]. Conductivity measurements of **1** in solution indicated loss of two chloride ions and thus in mixed water–ethylene glycol solvent an overall N_2O_2 coordination seems feasible. The apparent similarity in the hyperfine coupling and g-values is clearly indicative of the orbital containing unpaired electron (SOMO) involves a predominant metal contribution. Consequently, an alternative hypothetical ground electronic state with an unpaired electron localized mainly on the ligand ($Cu^{III}L^{2-}$) is clearly ruled out. This fact, that is the localization of larger spin density on the Cu nucleus as is expected for lower electronegativity of the ligand (lower pi-acidity) is further supported by the considerably high $A_{||}$ value [20].

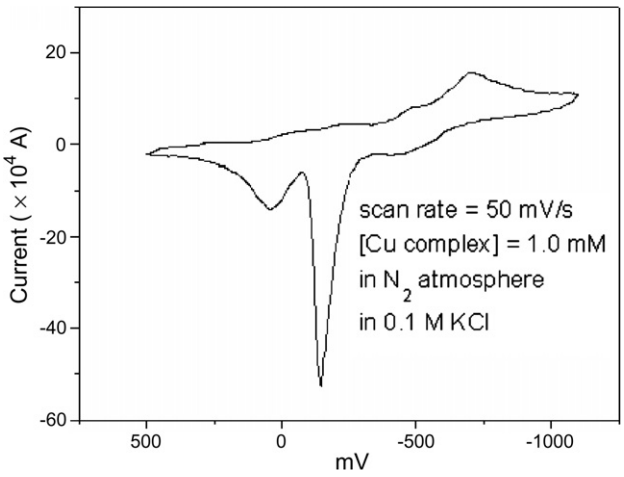

Fig. 6. Cyclic volammogram of **1**. Experimental conditions are shown within the figure.

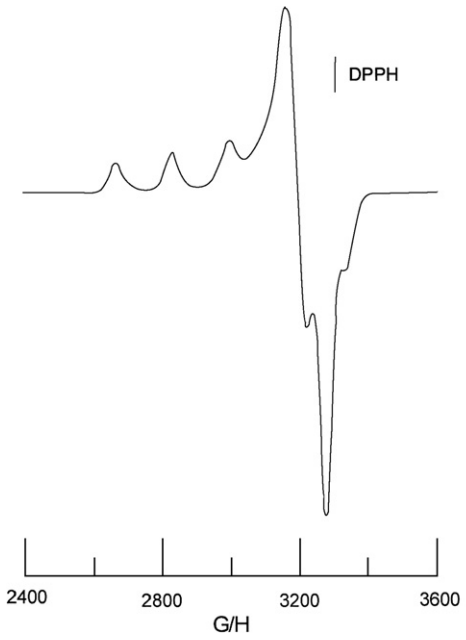

Fig. 7. EPR spectrum of **1** at 77 K.

Acknowledgements

Financial assistance received by S.M. from the Department of Chemistry, Jadavpur University under the UGC-CAS programme is

thankfully acknowledged. S.M. is also thankful to his departmental colleague Dr. Kausikisankar Pramanik for many helpful discussions. M.L.Z. acknowledges National Natural Science Foundation of China (Grant No.: 20471033) and Province Natural Foundation of Shanxi province of China (Grant No.: 20051013) as well as the Overseas Returned Scholar Foundation of Shanxi province of China in 2006 for financial support. A.D. thankfully acknowledges University Grants Commission (New Delhi) for a minor research project (Project No. F. PSW-028/05-06 (ERO)).

Appendix A. Supplementary data

CCDC 298150 contains the supplementary crystallographic data for **1**. These data can be obtained free of charge via http://www.ccdc.cam.ac.uk/conts/retrieving.html, or from the Cambridge Crystallographic Data Centre, 12 Union Road, Cambridge CB2 1EZ, UK; fax: (+44) 1223-336-033; or e-mail: deposit@ccdc.cam.ac.uk.

References

[1] [a] C. Janiak, Dalton Trans. (2003) 2781;
[b] B. Moulton, M.J. Zaworotko, Chem. Rev. 101 (2001) 1629;
[c] J.-M. Lehn, Proc. Natl. Acad. Sci. USA 99 (2002) 4763.
[2] [a] R.-G. Xiong, J. Zhang, Z.-F. Chen, X.-Z. You, C.-M. Che, H.-K. Fun, Dalton Trans. (2001) 780;
[b] A. Rodriguez-Diéguez, J. Cano, R. Kiveka1s, A. Debdoubi, E. Colacio, Inorg. Chem. 46 (2007) 2503;
[c] X.-M. Chen, M.-L. Tong, Acc. Chem. Res. 40 (2007) 162.
[3] [a] B.E. Turner, A.G. Kislyakov, H.S. Liszt, N. Kaifu, Astrophys. J. 201 (1975) L149;
[b] A.P.C. Mann, D.A. Williams, Nature 283 (1980) 721.
[4] G. Steinman, R.M. Lemmon, M. Calvin, Proc. Natl. Acad. Sci. USA 2 (1964) 27.
[5] A. Schimpl, R.M. Lemmon, M. Calvin, Science 147 (1965) 149.
[6] [a] B. Bann, S.A. Miller, Chem. Rev. 58 (1958) 131;
[b] A.J.L. Pombeiro, Inorg. Chim. Acta 198–200 (1992) 179.
[7] P. Ray, Chem. Rev. 61 (1961) 313. Structurally, cyanamide is half of dicyandiamide that is used for the preparation of biguanides.
[8] G.M. Sheldrick, SADABS, University of Göttingen, Germany, 2000.
[9] G.M. Sheldrick, SHELXS97 and SHELXL97, University of Göttingen, Germany, 1997.
[10] J. Lewis, T.D. O'Donoghue, P.R. Raithby, J. Chem. Soc., Dalton Trans. (1979) 1383.
[11] G.D. Andreetti, L. Coghi, M. Nardelli, P.S. Sgarabotto, J. Cryst. Mol. Struct. 1 (1971) 147.
[12] L. Coghi, A. Mangia, M. Nardelli, G. Pelizzi, L. Sozzi, Chem. Commun. (1968) 1475.
[13] D.A. Harvey, C.J.L. Lock, Acta Crystallogr., Sect. C 42 (1986) 799.
[14] S. Das, P. Banerjee, S.-M. Peng, G.-H. Lee, J. Kim, S. Goswami, Inorg. Chem. 45 (2006) 562.
[15] B.K. Santra, P.A.N. Reddy, M. Nethaji, A.R. Chakravarty, Inorg. Chem. 41 (2002) 1328.
[16] B.J. Hathaway, D.E. Billing, Coord. Chem. Rev. 5 (1970) 143.
[17] B.J. Hathaway, Struct. Bond. (Berlin) 57 (1984) 55.
[18] [a] E.I. Solomon, M.J. Baldwin, M.D. Lowery, Chem. Rev. 92 (1992) 521;
[b] B.J. Hathaway, in: G. Wilkinson, R.D. Gillard, J.A. McCleverty (Eds.), Comprehensive Coordination Chemistry, vol. 5, Pergamon Press, Oxford, UK, 1987, p. 663.
[19] [a] R. Miyamoto, Y. Ohba, M. Iwaizumi, Inorg. Chem. 31 (1992) 3138;
[b] M.L. Colon, S.Y. Qian, D. Vanderveer, X.R. Bu, Inorg. Chim. Acta 357 (2004) 83.
[20] M.F. Ottaviani, F. Mantali, N.J. Turro, D.A. Tomalia, J. Phys. Chem. B 101 (1997) 158.

2. Experimental

Potassium tetraorganodichalcogenoimidodiphosphinates were prepared according to literature methods: K[(SPMe$_2$)(SPPh$_2$)N] [14], K[(SPPh$_2$){OP(OEt)$_2$}N], K[(OPPh$_2$){OP(OEt)$_2$}N] [15]. Solvents were purified by standard procedures and were freshly distilled prior to use. IR spectra were recorded in the range 4000–400 cm^{-1} in KBr pellets on a Jasco FTIR-615 machine. Mass spectra were recorded on a FINNIGAN MAT 8200 instrument (CI). EPR spectra were recorded at 77 K and at room temperature on a Bruker ESP 300 spectrometer operating in X-band, equipped with an ER 035 M Bruker NMR gaussmeter and a HP 3530B Hewlett–Packard microwave frequency counter, and only at room temperature on a X-band Radiopan SE/X 2543 Spectrometer, respectively. All g factors were determined with ±0.05 accuracy. Magnetic measurements in the temperature range of 1.8–300 K were carried out on powdered samples of complex **3**, at a magnetic field of 0.5 T and at 2 K in the range of 0–5 T, using a Quantum Design SQUID based MPMSXL-5 type magnetometer. Corrections are based on subtracting the sample-holder signal and the contribution $\chi_D = 1181 \times 10^{-6}$ cm^3 mol^{-1} was estimated from the Pascal constants [16]. Elemental analyses were performed on a VarioEL analyzer.

2.1. Preparation of bis[P,P-dimethyl-P′,P′-diphenyl-dithioimidodiphosphinato]manganese(II), Mn[(SPMe$_2$)(SPPh$_2$)N]$_2$ (**1**)

A reaction mixture of K[(SPMe$_2$)(SPPh$_2$)N] (0.515 g, 1.420 mmol) and MnCl$_2 \cdot$ 4H$_2$O (0.140 g, 0.707 mmol) in methanol (50 ml) was stirred at room temperature for 24 h. The solvent was completely removed in vacuum and the remaining solid was extracted with toluene. The clear solution was concentrated in vacuum, yielding the title compound as a colourless crystalline product. Yield: 0.261 g (52%), m.p. 119–120 °C. *Anal.* Calc. for C$_{28}$H$_{32}$MnN$_2$P$_4$S$_4$: C, 47.79; H, 4.58; N, 3.98. Found: C, 47.68; H, 4.52; N, 3.97%. IR (cm^{-1}): 1197s, br [ν_{as}(P$_2$N)], 589s [ν(*Ph*PS)], 571s [ν(*Me*PS)]. CI$_{pos}$ MS (*m*/*z*, %): 703 (42) [M$^+$], 324 (100) [{(SPMe$_2$)(SPPh$_2$)N}$^+$]. CI$_{neg}$ MS (*m*/*z*, %): 703 (18) [M$^-$], 324 (57) [{(SPMe$_2$)(SPPh$_2$)N}$^-$], 110 (100) [(SPMe$_2$ + NH$_3$)$^-$].

Compounds **2** and **3** were similarly prepared:

*Bis[P,P-diethoxy-P′,P′-diphenyl-P′-thioimidodiphosphinato] manganese(II)], Mn[(SPPh$_2$){OP(OEt)$_2$}N]$_2$ (**2**)* from K[(SPPh$_2$){OP(OEt)$_2$}N] (0.720 g, 1.769 mmol) and MnCl$_2 \cdot$ 4H$_2$O (0.175 g, 0.883 mmol). Yield: 0.315 g (45%), m.p. 95 °C. *Anal.* Calc. for C$_{32}$H$_{40}$MnN$_2$O$_6$S$_2$P$_4$: C, 48.55; H, 5.09; N, 3.54. Found: C, 48.61; H, 5.05; N, 3.55%. IR (cm^{-1}): 1265vs [ν_{as}(P$_2$N)], 1104s [ν(PO)], 1033vs, br [ν(POC)], 599s [ν(PS)]. CI$_{pos}$ MS (*m*/*z*, %): 792 (100) [(M+H)$^+$], 370 (92) [{(SPPh$_2$){OP(OEt)$_2$}NH}$^+$]. CI$_{neg}$ MS (*m*/*z*, %): 792 (12) [(M+H)$^-$], 368 (100) [{(SPPh$_2$){OP(OEt)$_2$}N}$^-$], 336 (26) [{(PPh$_2$){OP(OEt)$_2$}N}$^-$].

*Bis[P,P-diethoxy-P′,P′-diphenyl-imidodiphosphinato]manganese(II) water solvate, Mn[(OPPh$_2$){OP(OEt)$_2$}N]$_2$(H$_2$O) (**3**)* from K[(OPPh$_2$){OP(OEt)$_2$}N] (0.151 g, 1.317 mmol) and MnCl$_2 \cdot$ 4H$_2$O (0.130 g, 0.658 mmol). Yield: 0.36 g (70%), m.p. 100–102 °C. *Anal.* Calc. for C$_{32}$H$_{42}$MnN$_2$O$_9$P$_4$: C, 49.43; H, 5.44; N, 3.60. Found: C, 49.75; H, 5.18; N, 3.65%. IR (cm^{-1}): 1244vs [ν_{as}(P$_2$N)], 1157vs, 1143vs [ν(PO)], 1067vs, 1041vs [ν(POC)]. CI$_{pos}$ MS (*m*/*z*, %): 759 (52) [{Mn{(OPPh$_2$){OP(OEt)$_2$}N}$_2$}$^+$], 353 (100) [{(OPPh$_2$){OP(OEt)$_2$}NH}$^+$]. CI$_{neg}$ MS (*m*/*z*, %): 760 (12) [{Mn{(OPPh$_2$){OP(OEt)$_2$}N}$_2$+H}$^-$], 352 (100) [{(OPPh$_2$){OP(OEt)$_2$}N}$^-$], 336 (26) [{(PPh$_2$){OP(OEt)$_2$}N}$^-$].

3. Crystal structure determination

Colourless block crystals of Mn[(SPMe$_2$)(SPPh$_2$)N]$_2$ (**1**) and Mn[(OPPh$_2$){OP(OEt)$_2$}N]$_2$(H$_2$O) (**3**) were attached with epoxy glue on cryoloops. The data were collected on a Bruker SMART APEX CCD diffractometer using graphite-monochromated Mo Kα radiation (λ = 0.71073 Å). Data reduction was performed using the SAINT-PLUS software and the data were corrected for absorption effects using the SADABS program [17]. The details of the crystal structure determination and refinement are given in Table 1.

Table 1
Crystal data and structure refinement for Mn[(SPMe$_2$)(SPPh$_2$)N]$_2$ (**1**) and Mn[(OPPh$_2$){OP(OEt)$_2$}N]$_2$(H$_2$O) (**3**)

	1	**3**
Empirical formula	C$_{28}$H$_{32}$MnN$_2$P$_4$S$_4$	C$_{64}$H$_{84}$Mn$_2$N$_4$O$_{18}$P$_8$
Formula weight	703.62	1554.99
Temperature (K)	297(2)	297(2)
Wavelength (Å)	0.71073	0.71073
Crystal system	monoclinic	triclinic
Space group	*P*2(1)/*c*	*P*2(1)/*n*
a (Å)	15.0259(11)	11.9760(9)
b (Å)	11.9642(9)	13.5226(10)
c (Å)	19.1422(14)	13.6310(11)
α (°)	90	108.6870(10)
β (°)	106.0830(10)	106.4710(10)
γ (°)	90	97.7490(10)
Volume (Å^3)	3306.6(4)	1942.4(3)
Z	4	1
D_{calc} (g/cm^3)	1.413	1.329
Absorption coefficient (mm^{-1})	0.867	0.555
F(000)	1452	810
Crystal size (mm)	0.29 × 0.23 × 0.21	0.30 × 0.29 × 0.22
θ Range for data collections (°)	2.03 to 25.00	1.68 to 26.37
Reflections collected	23505	20991
Independent reflections (*R*(int))	5835 (0.0497)	7887 (0.0413)
Maximum and minimum transmissions	0.8388 and 0.7871	0.8877 and 0.8513
Refinement method	Full-matrix least-squares on F^2	
Data/restraints/parameters	5835/0/356	7887/0/456
Goodness-of-fit on F^2	1.154	1.146
Final *R* indicies [I > 2sigma(I)]	R_1 = 0.0560, wR_2 = 0.1206	R_1 = 0.0667, wR_2 = 0.1424
R indicies (all data)	R_1 = 0.0692, wR_2 = 0.1261	R_1 = 0.0881, wR_2 = 0.1525
Largest difference in peak and hole (e Å^{-3})	0.458 and −0.238	0.573 and −0.271

Cell refinement gave cell constants corresponding to monoclinic (**1**) and triclinic (**3**) cells. The structures were solved by direct methods [18] and refined using the SHELXTL [19] version of SHELX-97 [20]. Compound **3** is centrosymmetric with an inversion centre in the middle of the Mn$_2$O$_2$ ring and thus half of the molecule is generated by symmetry. The hydrogen atoms were refined with a riding model and a mutual isotropic thermal parameter, excepting the hydrogen atoms from the water molecule in **3**, which were located on the difference map and refined at a O–H distance of 0.82(5) and 0.80(5) Å, respectively. C16 in **3** is disordered and was refined over two positions with 49% and 51% occupancy. The drawings were created with the DIAMOND program [21].

4. Results and discussion

Manganese(II) complexes were obtained in moderate yields by salt metathesis reactions between MnCl$_2 \cdot$ 4H$_2$O and the potassium salt of the appropriate tetraorganodichalcogenoimidodiphosphinic acid, in a 1:2 molar ratio.

$$MnCl_2 \cdot 4H_2O + 2K[(XPR_2)(YPR'_2)N] \rightarrow Mn[(XPR_2)(YPR'_2)N]_2(nH_2O) + 2KCl + (4-n)H_2O$$

X = Y = S; R = Ph, R′ = Me; $n = 0$ (**1**)

X = S, Y = O; R = Ph, R′ = OEt; $n = 0$ (**2**)

X = Y = O; R = Ph, R′ = OEt; $n = 1$ (**3**)

The complexes were isolated as colourless (**1** and **3**) or slight pink (**2**) solids and were characterized by mass spectrometry, IR and EPR spectroscopy. For compounds **1** and **3** the crystal and molecular structure was determined by single-crystal X-ray diffraction.

In the CI mass spectra of the title compounds either the molecular or the pseudo-molecular ions appear with high or medium intensity, *i.e.* $[Mn\{(SPPh_2)(SPMe_2)N\}_2]^+$ (*m/z* 703, 42%), $[Mn\{(SPPh_2)\{OP(OEt)_2\}N\}_2 + H]^+$ (*m/z* 792, 100%) and $[Mn\{(OPPh_2)\{OP(OEt)_2\}N\}_2]^+$ (*m/z* 759, 52%) for **1**, **2** and **3**, respectively. For derivative **3** the dimeric species or fragments with a higher mass than that corresponding to the monomeric species were not observed by chemical ionization.

The IR spectra are consistent with the coordination of the ligand units in the deprotonated form, through both chalcogen atoms. The strong absorption bands observed for the Mn(II) complexes in the ranges 1250–1200, 1150–1110 and 600–550 cm^{-1} were assigned to $\nu_{as}(P_2N)$, ν(PO) and ν(PS) stretching vibrations, respectively, in comparison with the potassium salts used as starting materials [14,15].

The EPR spectra of the manganese(II) complexes are expected to display a fine structure of five lines. However, only for compounds **2** and **3** the fine structure was observed, while for the derivative **1** only a broad band was found at room temperature ($g = 1.94$), due probably to the paramagnetic ion clusters present in this sample. The line width (390 Gs for **1**, 502 Gs and 400 Gs for the central line of **2** and **3**, respectively) is consistent with a strong crystal field around the paramagnetic ions. This behaviour might be explained by the strong interaction with the crystal field created by the ligands and the covalent interactions between the Mn(II) ion and the ligands. The *g* values determined at room temperature for the compounds **2** and **3** (2.01 and 2.03, respectively) are also consistent with strong covalent interactions. Theoretical calculations allowed us to determine the crystal field constant D (431 Gs) for the species **3**, which exhibits a fine structure. In the case of this polycrystalline material we average the θ angle between the direction of the magnetic induction and the symmetry axes of the magnetic centre from 0 to $\pi/2$ in the Spin Hamiltonian [22].

The EPR spectrum of the complex **3** at 4.2 K exhibits a single broad line with $g = 1.98$, $\Delta H_{pp} = 565$ Gs (ΔH_{pp} = peak to peak linewidth) and shows a partial resolved hyperfine structure due to the interaction between the transition inside Krammer's doublet (±1/2) and the ^{55}Mn(II) nuclear spin $I = 5/2$, of a value about 95 Gs (Fig. 1).

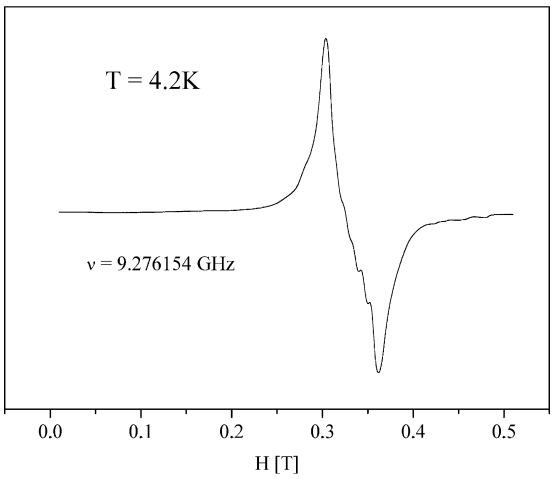

Fig. 1. EPR spectrum of **3** at 4.2 K.

4.1. Crystal and molecular structure of $Mn[(SPMe_2)(SPPh_2)N]_2$ (**1**)

The molecular structure of **1** was determined by single-crystal X-ray diffraction. Important bond distances and angles are listed in Table 2.

The crystal of **1** consists of distinct monomeric units separated by normal van der Waals distances. An ORTEP-like diagram with the atom numbering scheme is given in Fig. 2.

The dithioato ligand units behave monometallic biconnective, resulting in a *spiro*-bicyclic system with a slightly distorted tetrahedral MnS_4 core (S–Mn–S bond angles in the range 106.3–113.9°). One of the endocyclic angles is larger [S(3)–Mn(1)–S(4) 111.02(4)°], while the other one [S(1)–Mn(1)–S(2) 109.32(4)°] is close to the tetrahedral value of 109.5°. The dihedral angle between the S(1)/Mn(1)/S(2) and S(3)/Mn(1)/S(4) planes is 87.46(4)°, larger than those observed for $Mn[(SPPh_2)_2N]_2$ (86.8°) [7] and $Mn[(SPPr^i_2)(SPPh_2)N]_2$ [78.99(3)°] [8], and slightly smaller than that one found for $Mn[(SPPr^i_2)_2N]_2$ [88.12(1)°] [8]. The Mn–S bond distances [av. 2.423(1) Å] are similar to those found in $Mn[(SPPh_2)_2N]_2$ [av. 2.443(12) Å] [7].

Table 2
Selected interatomic distances (Å) and angles (°) in $Mn[(SPPh_2)(SPMe_2)N]_2$ (**1**)

Mn(1)–S(1)	2.4354(12)	Mn(1)–S(3)	2.4438(12)
Mn(1)–S(2)	2.4136(12)	Mn(1)–S(4)	2.4001(12)
S(1)–P(1)	2.0159(14)	S(3)–P(3)	2.0177(14)
S(2)–P(2)	2.0213(14)	S(4)–P(4)	2.0155(15)
N(1)–P(1)	1.595(3)	N(2)–P(3)	1.582(3)
N(1)–P(2)	1.591(3)	N(2)–P(4)	1.591(3)
S(1)–Mn(1)–S(2)	109.31(4)	S(3)–Mn(1)–S(4)	111.02(4)
S(1)–Mn(1)–S(3)	113.90(4)	S(2)–Mn(1)–S(4)	108.11(4)
S(1)–Mn(1)–S(4)	106.33(4)	S(2)–Mn(1)–S(3)	108.02(4)
Mn(1)–S(1)–P(1)	105.10(5)	Mn(1)–S(3)–P(3)	104.70(5)
Mn(1)–S(2)–P(2)	99.59(5)	Mn(1)–S(4)–P(4)	99.63(5)
N(1)–P(1)–S(1)	118.68(12)	N(2)–P(3)–S(3)	118.53(12)
N(1)–P(2)–S(2)	115.90(12)	N(2)–P(4)–S(4)	118.27(13)
P(1)–N(1)–P(2)	129.5(2)	P(3)–N(2)–P(4)	134.7(2)

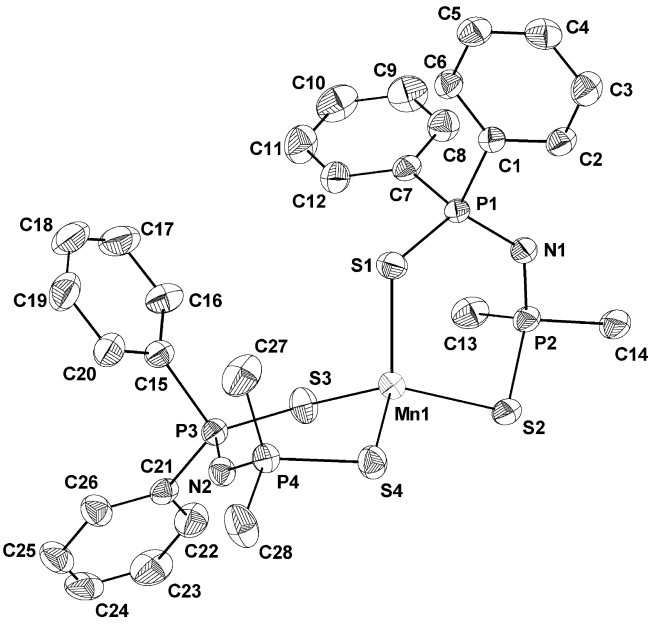

Fig. 2. ORTEP plot at 40% probability and atom numbering scheme for **1**. For clarity, the hydrogen atoms are omitted.

The two six-membered MnS_2P_2N chelate rings are not planar and display twisted chair conformations with the Mn(1)/N(1) and Mn(1)/N(2) atoms, respectively, in apices. In contrast, twisted boat conformations were observed for other reported dithioato derivatives, *i.e.* $Mn[(SPPh_2)_2N]_2$ [7] and $Mn[(SPPr^i_2)_2N]_2$ [8] (with phosphorus and sulfur atoms in the apices) or $Mn[(SPPr^i_2)(SPPh_2)N]_2$ [8] (with manganese and nitrogen atoms in apices), respectively.

The phosphorus–sulfur [range of 2.0155(15)–2.0213(14) Å] and phosphorus–nitrogen [range of 1.582(3)–1.595(3) Å] distances, respectively, are intermediate between the single and the double bonds [cf. $Ph_2P(=S)–N=P(–SMe)Ph_2$ [23]: P=S 1.954(1) Å, P–S 2.071(1) Å, P=N 1.562(2) Å, P—N 1.610(2) Å. The P–N–P angles are different in the two ligand moieties [P(1)–N(1)–P(2) 129.5(2) and P(3)–N(2)–P(4) 134.7(2)°], both being considerably larger in comparison with the free acid [P–N–P 126.1(4)°] [24], and thus suitable to accommodate around the metal centre.

Table 3
Selected interatomic distances (Å) and angles (°) in $Mn[(OPPh_2)\{OP(OEt)_2\}N]_2(H_2O)$ (**3**)[a]

Mn(1)–O(1)	2.088(2)	Mn(1)–O(3)	2.102(2)
Mn(1)–O(2)	2.168(2)	Mn(1)–O(4)	2.237(2)
		Mn(1)–O(4a)	2.247(2)
Mn(1)–O(9)	2.271(3)		
O(1)–P(1)	1.508(2)	O(3)–P(3)	1.500(3)
O(2)–P(2)	1.496(2)	O(4)–P(4)	1.503(2)
O(5)–P(2)	1.572(3)	O(7)–P(5)	1.556(3)
O(6)–P(2)	1.573(3)	O(8)–P(5)	1.577(3)
N(1)–P(1)	1.595(3)	N(2)–P(3)	1.587(3)
N(1)–P(2)	1.553(3)	N(2)–P(4)	1.567(3)
O(1)–Mn(1)–O(4)	174.98(9)	O(3)–Mn(1)–O(4a)	169.96(9)
O(2)–Mn(1)–O(9)	163.68(10)		
O(1)–Mn(1)–O(2)	93.52(9)	O(4)–Mn(1)–O(2)	91.15(9)
O(1)–Mn(1)–O(3)	92.32(9)	O(4)–Mn(1)–O(3)	88.92(9)
O(1)–Mn(1)–O(9)	93.73(11)	O(4)–Mn(1)–O(9)	81.29(11)
O(1)–Mn(1)–O(4a)	97.51(9)	O(4)–Mn(1)–O(4a)	81.11(9)
O(2)–Mn(1)–O(3)	97.16(10)	O(9)–Mn(1)–O(4a)	80.26(10)
O(3)–Mn(1)–O(9)	97.13(11)	O(4a)–Mn(1)–O(2)	84.31(9)
Mn(1)–O(4)–Mn(1a)	98.89(9)		
Mn(1a)–O(4)–P(4)	125.07(13)	Mn(1)–O(3)–P(3)	131.25(15)
Mn(1)–O(2)–P(2)	127.83(13)	Mn(1)–O(4)–P(4)	126.95(14)
		Mn(1a)–O(4)–P(4)	130.33(13)
O(1)–P(1)–N(1)	119.60(15)	O(3)–P(3)–N(2)	118.24(15)
O(2)–P(2)–N(1)	117.87(15)	O(4)–P(4)–N(2)	117.29(15)
P(1)–N(1)–P(2)	130.2(2)	P(3)–N(2)–P(4)	128.2(2)

[a] Symmetry equivalent positions (−*x*, −*y*, −*z*) are given by "a".

4.2. Crystal and molecular structure of $Mn[(OPPh_2)\{OP(OEt)_2\}N]_2(H_2O)$ (**3**)

Selected bond distances and angles for **3** are listed in Table 3 and the ORTEP-like diagram with the atom numbering scheme is given in Fig. 3.

The crystal contains discrete dimer associations in which the metal centres are bridged by the oxygen atoms of the $OP(OEt)_2$ groups from two ligand units acting as bimetallic triconnective moieties, thus resulting in a fused tricyclic $Mn_2O_4P_4N_2$ system. The other two ligands chelate each a metal atom, resulting in an overall structure which resembles that found in the dimeric $[Mn\{(OPPh_2)_2N\}_2]_2$ [9]. However some significant differences have to be noted. The central four-membered Mn_2O_2 ring in the dimer of the title compound **3** is planar, while it is slightly folded in the related $[Mn\{(OPPh_2)_2N\}_2]_2$. This behaviour is consistent with a larger nonbonding Mn···Mn distance in **3** than in $[Mn\{(OPPh_2)_2N\}_2]_2$ [3.4073(6) Å versus 3.378(3) Å].

The overall conformation of the $[Mn\{(OPPh_2)_2N\}_2]_2$ dimer might be described as *cis*, *i.e.* with the six-membered MnO_2P_2N rings formed by ligands of the same type placed on the same side of the four-membered Mn_2O_2 ring (Fig. 4 a) [9]. By contrast, the fused tricyclic $Mn_2O_4P_4N_2$ system in the dimer of **3** is considerably flattened, with equivalent atoms of the six-membered MnO_2P_2N rings deviated on opposite sides of the central planar Mn_2O_2 core [deviations from Mn_2O_2 plane: O(3) 0.042, P(3) 0.226, N(2) −0.160 Å, and P(4) 0.419 Å, respectively]. The chelate MnO_2P_2N rings are placed on opposite sides of this flattened tricyclic system and the overall conformation in the dimer of **3** might be described as *trans* (Fig. 4 b).

The oxygen atom from a water molecule completes a distorted octahedral coordination geometry around the manganese atoms in the dimer of **3**, in contrast with the trigonal bipyramidal geometry observed for the related $[Mn\{(OPPh_2)_2N\}_2]_2$ analogue [9]. Moreover, the water molecules are involved in hydrogen bonding with

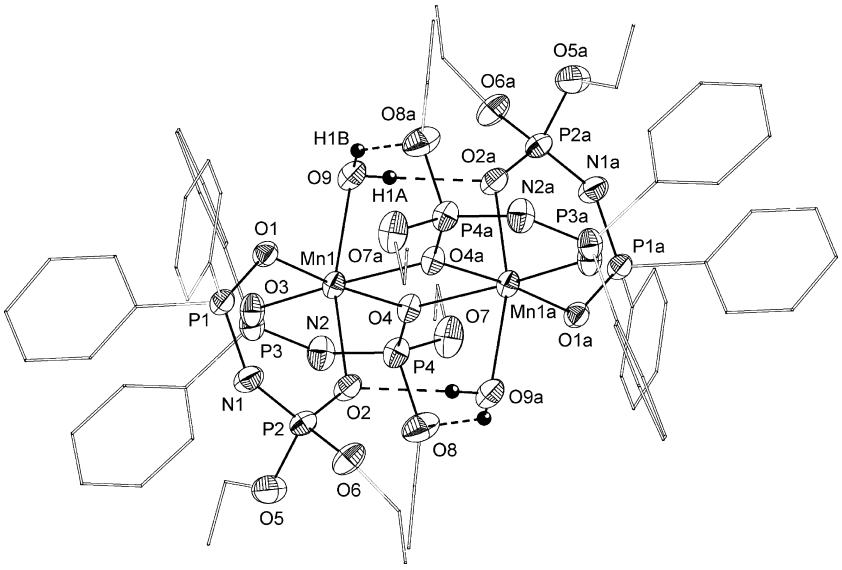

Fig. 3. ORTEP plot of the dimer unit in the crystal of **3**. The atoms are drawn with 30% probability ellipsoids [symmetry equivalent atoms (−*x*, −*y*, −*z*) are given by "a"]. For clarity, the hydrogen atoms, other than water hydrogens, are omitted.

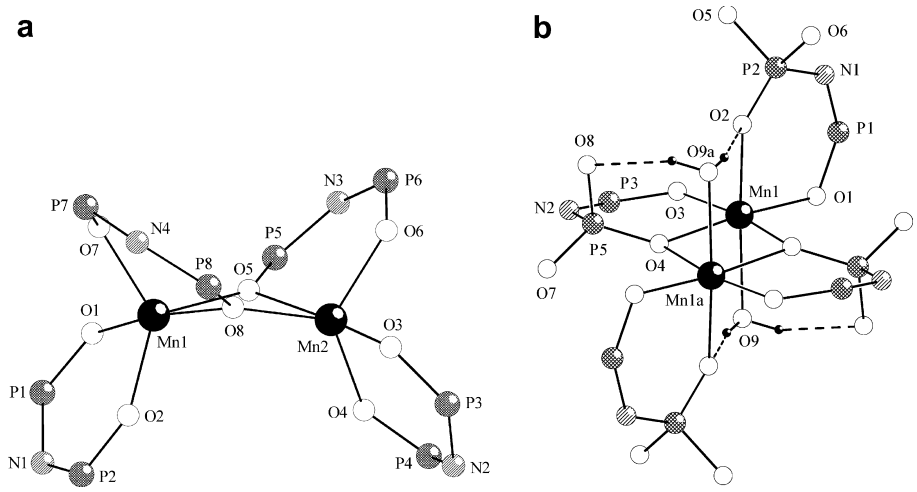

Fig. 4. Dimer cores in (a) $[Mn\{(OPPh_2)_2N\}_2]_2$ [9], and (b) title compound **3**. For clarity, the hydrogen atoms, other than water hydrogens, and the carbon atoms are omitted.

the oxygen atom connected to the metal centre from the chelating ligand [H(1A)···O(2a) 2.05 Å] and one oxygen atom of an ethoxy group from the bridging ligand [H(1B)···O(8a) 2.30 Å], respectively (Fig. 3).

The monometallic biconnective MnO_2P_2N rings show distorted chair conformations with nitrogen and manganese atoms in apices, while for the bridging ligands the corresponding MnO_2P_2N rings exhibit distorted boat conformations, with bridging O(4) and P(3) atoms in apices.

The Mn–O distances in the Mn–O–Mn bridge are equivalent [Mn(1)–O(4) 2.237(2), Mn(1)–O(4a) 2.247(2) Å] and considerably longer than the Mn(1)–O(3) bond distance [2.102(2) Å] in the same ligand unit. Even longer is the Mn–O_{water} bond distance [Mn(1)–O(9) 2.271(3) Å]. For the monometallic biconnective ligand moiety the Mn–O bonds are also not equivalent [Mn(1)–O(1) 2.088(2), Mn(1)–O(2) 2.168(2) Å], a behaviour which contrasts with that observed for the ligand moieties exhibiting a similar, but symmetric, coordination pattern in the related $[Mn\{(OPPh_2)_2N\}_2]_2$ dimer [9].

The phosphorus–nitrogen [range 1.553(3)–1.595(3) Å] and phosphorus–oxygen distances [range 1.496(2)–1.508(2) Å], respectively, are of a magnitude intermediate between a single and a double bond, thus suggesting some delocalization of the π electrons on the OPNPO system in all four ligand units (cf. $[(Me_3Si)_2N–P(=N^tBu)S]_2$ [25]: P=N 1.529(2) Å, P–N 1.662(2) Å; $Ph_2P(O)OH$ [26]: P=O 1.486(6) Å, P–O 1.526(6) Å).

4.3. Magnetic properties

The magnetic behaviour of complex **3** in the form of $\chi_{Mn}T$ versus T curve is shown in Fig. 5 (χ_{Mn} is the molar magnetic susceptibility per Mn(II) ion). The value of $\chi_{Mn}T$ product at room temperature is 4.87 $cm^3\ mol^{-1}\ K$ ($\mu_{eff.}$ = 6.24 B.M.), which is slightly larger than that calculated for $S = 5/2$ with $g = 2$ (4.375 $cm^3\ mol^{-1}\ K$, $\mu_{eff.}$ = 5.92 B.M.). Upon lowering the temperature, $\chi_{Mn}T$ decreases gradually and reaches a value of 0.61 $cm^3\ mol^{-1}\ K$ at 1.8 K.

The temperature variation of χ_{Mn}^{-1}, from room temperature down to 10 K, follows a Curie–Weiss law ($\chi_M = C/(T - \Theta)$), with C = 5.36 $cm^3\ mol^{-1}\ K$ and $\Theta = -28.9$ K. Below 10 K, the slope of χ_{Mn}^{-1} changes (inset to Fig. 5). The magnetic susceptibility can be analyzed using the isotropic spin Hamiltonian: $H = -2JS_1S_2$. The temperature dependence of the magnetic susceptibility is given by the equation [27]:

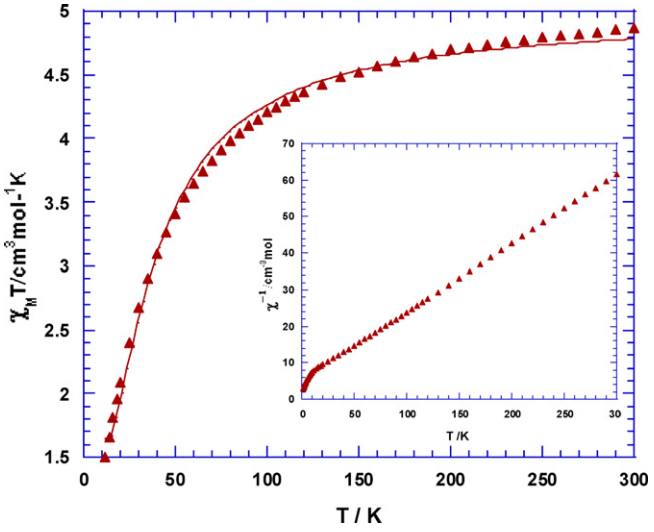

Fig. 5. Plot of $\chi_{Mn}T$ vs. T in the temperature range 10–300 K for **3**. The solid line represents the best fit to the experimental data with the parameters reported in the text (inset: temperature dependence of χ_{Mn}^{-1}).

$$\chi_{Mn} = \frac{Ng^2\beta^2}{kT}\frac{55 + 30e^{5x} + 14e^{9x} + 5e^{12x} + e^{14x}}{11 + 9e^{5x} + 7e^{9x} + 5e^{12x} + 3e^{14x} + e^{15x}}, \qquad x = \frac{-2J}{kT}$$

Additional interdimer interactions have been introduced in the frame of the mean-field approximation [28]:

$$\chi_{Mn}^{corr} = \frac{\chi_{Mn}}{1 - \frac{2J'}{N\beta^2g^2}\chi_{Mn}}$$

zJ' is the intermolecular exchange parameter and z is the number of the nearest neighbours. Least-square fit to the experimental data gives $J = -3.5\ cm^{-1}$, $zJ' = -1.0\ cm^{-1}$, g = 1.99.

5. Supplementary data

CCDC 656244 and 656245 contain the supplementary crystallographic data for **1** and **3**. These data can be obtained free of charge via http://www.ccdc.cam.ac.uk/conts/retrieving.html, or from the Cambridge Crystallographic Data Centre, 12 Union Road, Cambridge CB2 1EZ, UK; fax: (+44) 1223-336-033; or e-mail: deposit@ccdc.cam.ac.uk.

Acknowledgements

This work was supported by the Romanian Ministry of Education and Research (Grant CERES 4-62/2004) and the Polish Ministry of Science and Higher Education (Grant No. 1T09A 12430).

References

[1] J.D. Woollins, J. Chem. Soc., Dalton. Trans. (1996) 2893.
[2] C. Silvestru, J.E. Drake, Coord. Chem. Rev. 223 (2001) 117.
[3] O. Siiman, Inorg. Chem. 20 (1981) 2285 and references cited therein.
[4] J.J.R.F. da Silva, R.J.P. Williams, The Biological Chemistry of the Elements, second ed., Oxford University Press, 2001 (Chapter 14).
[5] U. Bossek, H. Hummel, T. Weyhermueller, K. Wieghardt, S. Russell, L. van der Wolf, U. Kolb, Angew. Chem., Int. Ed. Engl. 35 (1996) 1552. and references cited therein.
[6] J.D. Martin, R.F. Hess, Chem. Commun. (1996) 2419.
[7] O. Siiman, H.B. Gray, Inorg. Chem. 13 (1974) 1185.
[8] D. Maganas, S.S. Staniland, A. Grigoropoulos, F. White, S. Parsons, N. Robertson, P. Kyritsis, G. Pneumatikakis, Dalton Trans. (2006) 2301.
[9] I. Szekely, C. Silvestru, J.E. Drake, G. Balazs, S.I. Farcas, I. Haiduc, Inorg. Chim. Acta 299 (2000) 247.
[10] I. Szekely, J.E. Drake, C. Silvestru, Phosphorus, Sulfur and Silicon 124 and 125 (1997) 557.
[11] N. Zuniga-Villarreal, C. Silvestru, M. Reyes-Lezama, S. Hernandez-Ortega, C. Alvarez Toledano, J. Organomet. Chem. 496 (1995) 169.
[12] N. Zuniga-Villarreal, M. Reyes-Lezama, G. Espinosa, J. Organomet. Chem. 626 (2001) 113.
[13] N. Zuniga-Villarreal, M. Reyes-Lezama, S. Hernandez-Ortega, C. Silvestru, Polyhedron 17 (1998) 2679.
[14] R. Roesler, C. Silvestru, G. Espinosa-Perez, I. Haiduc, R. Cea-Olivares, Inorg. Chim. Acta 241 (1996) 47.
[15] G. Balazs, J.E. Drake, C. Silvestru, I. Haiduc, Inorg. Chim. Acta 287 (1999) 61.
[16] E. König, Magnetic Properties of Coordination and Organometallic Transition Metal Compounds, Springer, Berlin, 1966.
[17] SAINT-PLUS 2001, Bruker AXS Inc., Madison, WI, 2001.
[18] G.M. Sheldrick, Acta Crystallogr. Sect. A 46 (1990) 467.
[19] SHELXTL, Bruker AXS Inc., Madison, WI, 2000.
[20] G.M. Sheldrik, SHELX-97, Universität Göttingen, Germany, 1997.
[21] DIAMOND—Visual Crystal Structure Information System, Release 3.1d, CRYSTAL IMPACT GbR, Bonn, Germany, 2006.
[22] A. Nicula, I. Ursu, S. Nistor, Rev. Roum. Phys. 10 (1965) 229.
[23] I. Ghesner, A. Soran, C. Silvestru, J.E. Drake, Polyhedron 22 (2003) 3395.
[24] C. Silvestru, R. Roesler, J.E. Drake, J. Yang, G. Espinoza-Perez, I. Haiduc, Dalton Trans. (1998) 73.
[25] S. Pohl, Chem. Ber. 109 (1976) 3122.
[26] D. Fenske, R. Mattes, J. Loens, K.-F. Tebbe, Chem. Ber. 106 (1973) 1139.
[27] A. Earnshaw, J. Lewis, J. Chem. Soc. (1961) 396.
[28] J.S. Smart, Effective Field Theories of Magnetism, W.B. Saunders Comp., Philadelphia and London, 1966.

the form of coordination compounds, modulates the effect of the ligand itself [21]. The structure of quinic acid is that of a polyfunctional natural ligand containing an α-hydroxycarboxylic acid moiety on one side of the molecule and three alcoholic moieties on the other side. Hence, its chemical structure provides efficient anchors to metal ionic targets, exemplified through variable binding modes in a diverse spectrum of metal ionic geometries.

In view of the known accumulation [22–24] and toxicity of Al(III) in plants, animals and humans, its toxic manifestations entail a deep knowledge of its chemistry at the molecular level. Therefore, the aqueous speciation of this metallotoxin in binary and ternary systems, containing readily available cellular targets, is a valuable source of information. Through the aqueous speciation of such Al(III) binary and ternary systems, soluble and potentially bioavailable forms of the metal ion arise with suitable substrate ligands. It is likely that such Al(III) forms participate in molecular processes linked to that metal ion's toxicity. Poised to delineate the molecular chemistry involved in the establishment of Al(III) toxicity in cellular fluids, we launched efforts targeting the interactions of Al(III) with the natural binder D-(−)-quinic acid. To this end, we herein report on (a) the aqueous speciation of the binary Al(III)–quinic acid system, (b) pH-specific synthetic efforts to characterize species projected through the aqueous speciation of the binary Al(III)–quinic acid system, and (c) the association of the physicochemical profile of specific soluble and potentially bioavailable forms of Al(III)–quinate species, with the biological activity of that metal ion.

2. Experimental

2.1. Materials and methods

All experiments were carried out under aerobic conditions. Nanopure quality water was used for all the reactions. $Al(NO_3)_3 \cdot 9H_2O$, $AlCl_3 \cdot 6H_2O$ and quinic acid were purchased from Aldrich. Potassium hydroxide was supplied by Fluka. The Al(III) stock solution used for potentiometric measurements was prepared from recrystallized $AlCl_3 \cdot 6H_2O$ and its metal ion concentration was determined gravimetrically through its oxinate. The stock solution contained 0.1 M HCl to prevent hydrolysis of the metal ion. The exact concentrations of the ligand solution were determined by potentiometric titration, using the Gran method [25].

2.2. Physical measurements

FT-Infrared spectra were recorded on a Perkin Elmer 1760X FT-infrared spectrometer. A ThermoFinnigan Flash EA 1112 CHNS elemental analyser was used for the simultaneous determination of carbon, and hydrogen (%). The analyser is based on the dynamic flash combustion of the sample (at 1800 °C) followed by reduction, trapping, complete GC separation and detection of the products. The instrument is (a) fully automated and controlled by a PC via the Eager 300 dedicated software, and (b) capable of handling solid, liquid or gaseous substances.

A TA Instruments, model Q 600, system was used to run the simultaneous TGA–DSC experiments. The instrument mass precision is 0.1 μg. About 20 mg of sample was placed in an open alumina sample pan for each experiment. High purity helium and air (80/20 in N_2/O_2) were used at a constant flow rate of 100 mL/min, depending on the conditions required for running the experiment(s). During the experiments, the sample weight loss and rate of weight loss were recorded continuously under dynamic conditions, as a function of time or temperature, in the range 30–1000 °C. Prior to activating the heating routine program, the entire system was purged with the appropriate gas for 10 min, at a rate of 400 mL/min, to ensure that the desired environment was established.

2.3. Solid-state NMR

High resolution solid-state ^{13}C magic angle spinning (MAS) NMR spectra were measured at 100.63 MHz on a Bruker MSL400 NMR spectrometer, capable of high power ^1H-decoupling. The spinning rate used for the ^1H–^{13}C cross polarization and magic angle spinning experiments was 5 kHz at ambient temperature (25 °C). Each solid-state spectrum was the result of the accumulation of 200 scans. The recycle delay used was 4 s, the 90° pulse was 5 μs and the contact time was 1 ms. All the solid-state spectra were referenced to adamantane, which showed two peaks at 26.5 and 37.6 ppm, respectively, and to the external reference of TMS.

2.4. Solution NMR

The samples for solution NMR studies were prepared by dissolving the crystalline complex in D_2O, at concentrations in the range 0.02–0.10 M. The NMR spectra were recorded on a Bruker AM360 (^{13}C) spectrometer. Chemical shifts (δ) are reported in ppm relative to the internal reference, TMS.

2.5. pH-potentiometric measurements

The stability constants of the proton and Al(III) complexes of the title ligand were determined by pH-potentiometric titrations of 25 mL samples in the pH range 2–9 or until precipitation occurred, under a purified argon atmosphere. Care was taken to ensure that titrimetric data were recorded and collected under conditions taking into consideration the kinetically sluggish Al(III). Duplicate titrations were performed. The reproducibility of the titrations was within 0.005 pH units. Titration points obtained when 5 min was not enough to attain pH equilibrium were omitted from the evaluation. The ionic strength was adjusted to 0.2 M with KCl. The temperature was maintained during the measurements at 25 ± 0.1 °C. The titrations were performed with a carbonate-free KOH solution of known concentration (ca. 0.2 M). The ligand concentration was 0.002, 0.004 or 0.008 M and the metal:ligand ratios were 0:1, 1:1, 1:2 or 1:4. All other experimental conditions were the same as in earlier studies [26,27].

The pH was measured with a computer-controlled Molspin titration system elaborated for titrations at low concentrations and a Metrohm 6.0234.100 combined glass electrode, calibrated for hydrogen ion concentration according to Irving et al. [28]. The concentration stability constants $\beta_{pqr} = [M_pA_qH_r]/[M]^p[A]^q[H]^r$ were calculated with the PSEQUAD computer program [29,30]. The uncertainties (3SD values) of the stability constants are given in the parentheses in Table 3. The stability constants used for the hydroxo species of Al(III) were taken from Ref. 30 and are corrected to $I = 0.2$ M using the Davies equation: −5.49 for $[AlH_{-1}]^{2+}$, −13.54 for $[Al_3H_{-4}]^{5+}$, −108.62 for $[Al_{13}H_{-32}]^{7+}$ and −23.40 for $[AlH_{-4}]^{-}$.

2.6. Preparation of the complex $K[Al(C_7H_{11}O_6)_3] \cdot (OH) \cdot 4H_2O$

A quantity of $Al(NO_3)_3 \cdot 9H_2O$ (0.25 g, 0.68 mmol) was placed in a flask and dissolved in 5.5 mL of H_2O. Subsequently, quinic acid (0.39 g, 2.0 mmol) was added slowly with continuous stirring. The solution was heated to 50 °C for 1 h until all of the reagents dissolved, and then it was cooled. Aqueous KOH was then added slowly to adjust the pH to a final value of 4.0. The resulting solution was stirred overnight. The following morning, addition of cold ethanol at 4 °C resulted, after a couple of weeks, in the deposition of a colorless crystalline material. The crystals were isolated by filtration and dried in vacuo. The yield was 0.34 g (~70%). *Anal.* Calc. for **1**, $K[Al(C_7H_{11}O_6)_3] \cdot (OH) \cdot 4H_2O$, $AlC_{21}H_{42}KO_{23}$, M.W. 728.63: C, 34.58; H, 5.76. Found: C, 34.41; H, 5.87%.

3. X-ray crystallography

3.1. Crystal structure determination

X-ray quality crystals of compound **1** were grown from mixtures of water–ethanol solutions. A single crystal, with dimensions 0.26 × 0.22 × 0.20 mm, was mounted on the tip of a glass fiber with epoxy glue. Single crystal analysis was carried out on a Bruker SMART 1K CCD diffractometer. The frame data were acquired with the SMART software [31] using Mo Kα radiation (λ = 0.71073 Å). Final values of the cell parameters were obtained from the least-squares refinement of the positions of 807 reflections. A total of 1271 thirty-second frames were collected in three sets with 0.3° ω-scans. The frames were then processed using the SAINT software [32] to provide the *hkl* file corrected for Lorentz and polarization effects. No absorption correction was applied. Further experimental crystallographic details: for **1**, θ range for data collection = 1.92–23.2°; number of reflections collected/unique/used, 14960/1641[$R_{(int)}$ = 0.0245]/1580; 154 parameters refined; $F(000)$ = 1536; $(\Delta\rho)_{max}/(\Delta\rho)_{min}$ = 0.842/−0.285 e/Å^3; goodness-of-fit = 1.111; R/R_w (for all data), 0.0481/0.1427. Table 1 summarizes the crystallographic structural and refinement parameters.

The structure was solved by direct methods using the SHELX-90 program [33] and refined by least-squares methods on F^2, SHELXL-97 [34], incorporated in SHELXTL, Version 5.1 [35]. The initial E-maps yielded all non-hydrogen atom positions. Hydrogen atoms on carbon atoms were geometrically positioned and left riding on their parent atoms during the structure refinement. Hydrogen atom positions, which belong to water or hydroxyl groups, were first determined from E-maps, brought to reasonable distances from their parent oxygen atoms, and then fixed. The final assignment satisfies electroneutrality for the entire compound, on the premise that the aluminum ions are formally in the oxidation state +3. All non-hydrogen atoms were refined anisotropically.

4. Results and discussion

4.1. Synthesis

The synthesis of compound **1** was pursued through the facile reaction of Al(III) with quinic acid in aqueous media. The pH, at which the reaction was run, was 4.0. The adjustment of the pH was achieved with aqueous KOH. The stoichiometric reaction leading to the isolation of **1** is shown below (Reaction (1)):

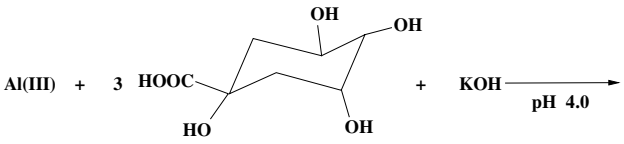

$K[Al(C_7H_{11}O_6)_3]\cdot(OH)$ + 3 H$^+$ Reaction 1

The compound was isolated in the pure crystalline form upon addition of ethanol to the reaction mixture at 4 °C. Elemental analysis of the isolated colorless crystalline material suggested the molecular formulation $K[Al(C_7H_{11}O_6)_3]\cdot(OH)\cdot 4H_2O$. Further spectroscopic inspection by FT-IR revealed the presence of quinates bound to Al(III), thus confirming the aforementioned formulation (**1**).

Compound **1** is soluble in water, but insoluble in organic solvents, like methanol, acetonitrile, chlorinated solvents ($CHCl_3$, CH_2Cl_2), toluene and DMF. The material is stable in air at room temperature for extended periods of time.

4.2. X-ray crystallographic structure of $K[Al(C_7H_{11}O_6)_3]\cdot(OH)\cdot 4H_2O$ (**1**)

The X-ray crystal structure of **1** reveals the presence of a lattice comprised of $[Al(C_7H_{11}O_6)_3]$ units and K^+ ions counteracted by discrete OH^- ions. The compound crystallizes in the cubic space group $P2_13$. The ORTEP diagram along with a perspective view of **1** is shown in Figs. 1 and 2. Selected interatomic distances and bond angles for **1** are listed in Table 2. The structure consists of a mononuclear core unit assembled by a central Al(III) ion surrounded by three quinate ligands. The latter moieties bind to the metal ion through the carboxylate and protonated alcoholic oxygens O(1′) and O(3), respectively. Formation of the Al(III) assembly proceeds through the formation of a five-membered ring, rendering the

Table 1
Summary of Crystal, Intensity Collection and Refinement Data for $K[Al(C_7H_{11}O_6)_3]\cdot(OH)\cdot 4H_2O$ (**1**)

	1
Formula	$C_{21}H_{42}AlKO_{23}$
Formula weight	728.63
T (K)	293(2)
Wavelength	Mo Kα 0.71073
Space group	$P2_13$ (No.198)
a (Å)	15.0093(9)
b (Å)	15.0093(9)
c (Å)	15.0093(9)
α (°)	90
β (°)	90
γ (°)	90
V (Å^3)	3381.3(4)
Z	4
D_{calc}/D_{measd} (Mg m^{-3})	1.431/1.45
Absorption coeffient (μ), mm^{-1}	0.271
Range of h,k,l	−13→19, −16→16, −16→16
Goodness-of-fit on F^2	1.111
R indices[a]	R = 0.0470, R_w = 0.1414[b]

[a] R values are based on F values, R_w values are based on F^2. $R = \frac{\sum||F_o|-|F_c||}{\sum(|F_o|)}$, $R_w\sqrt{\sum[w(F_o^2-F_c^2)^2]/\sum[w(F_o^2)^2]}$.

[b] [1580 refs $I > 2\sigma(I)$].

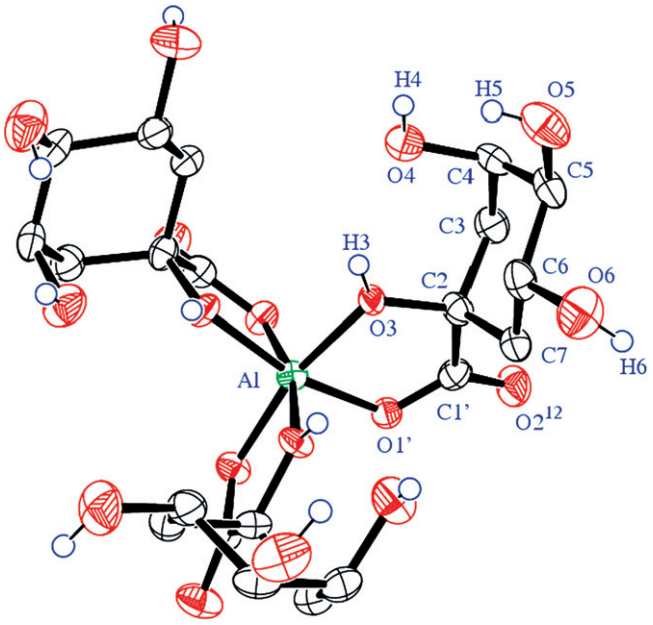

Fig. 1. Labelled ORTEP plot of the $[Al(C_7H_{11}O_6)_3]$ assembly with thermal ellipsoids drawn at the 30% probability level. Hydrogen atoms have been included for alcoholic moieties.

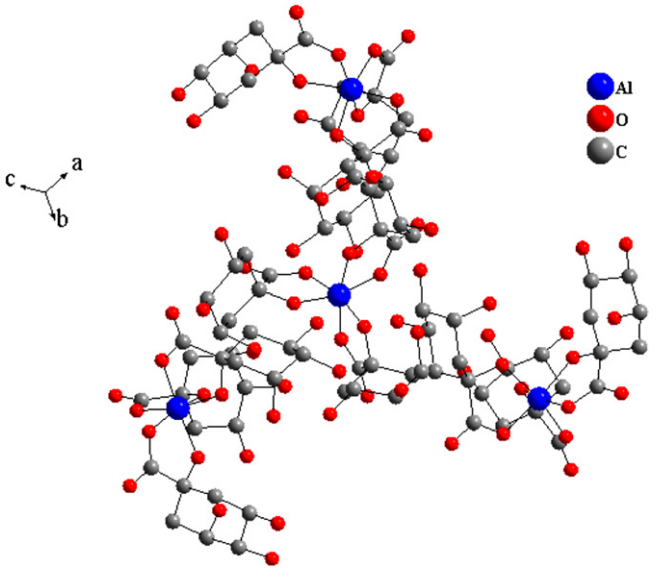

Fig. 2. Perspective view of the arrangement of Al–quinate units along the diagonal of the unit cell.

Table 2
Bond lengths (Å) and angles (°) in $K[Al(C_7H_{11}O_6)_3] \cdot (OH) \cdot 4H_2O$ (**1**)

Distances (Å)	
Al(1)–O(1)	1.876(2)
Al(1)–O(3)	1.891(2)
Angles (°)	
O(1)–Al(1)–O(1)′	90.57(11)
O(1)–Al(1)–O(3)	166.03(9)
O(1)–Al(1)–O(3)′	101.03(10)
O(1)–Al(1)–O(3)″	81.65(9)
O(3)′–Al(1)–O(3)	88.45(11)

Symmetry operation (′): $-y + 3/2, -z + 1, x - 1/2$; (″) $z + 1/2, -x + 3/2, -y + 1$.

arising species quite stable. Therefore, the six coordination sites around Al(III) are taken up by the three quinate ligands bound in the same bidentate fashion. The rest of the alcoholic groups of the quinate ligands do not bind Al(III), dangling away from its coordination sphere. The overall coordination geometry in **1** is distorted octahedral. Charge balance consideration and inspection of the bond lengths of the alcoholic and carboxylate groups indicate that the ligand is singly deprotonated, with the site of deprotonation being the terminal carboxylate group, while the α-alcoholic moiety remains protonated.

The Al–O bond distances in **1** are in line with those in other Al(III) oxygen-containing complexes, like $(NH_4)_5[Al(C_6H_4O_7)_2] \cdot 2H_2O$ (**2**) (1.844(3)–1.961(3) Å) [36], $(NH_4)_4[Al(C_6H_4O_7)(C_6H_5O_7)] \cdot 3H_2O$ (**3**) (1.836(1)–1.959(1) Å) [37], the dinuclear $(NH_4)_4[Al_2(C_6H_4O_7)(C_6H_5O_7)_2] \cdot 4H_2O$ (**4**) (1.835(3)–1.932(3) Å) [38], the trinuclear $(NH_4)_5[Al_3(C_6H_4O_7)_3(OH)(H_2O)] \cdot (NO_3) \cdot 6H_2O$ (**5**) [39] (1.832(5)–1.935(5) Å), and the M(III)–O distances in the congener complexes $(NH_4)_3[Ga(C_2O_4)_3] \cdot 3H_2O$ (1.961–1.976 Å) [40], $(NH_4)_4[Ga(C_6H_4O_7)(C_6H_5O_7)] \cdot 3H_2O$ (1.893(1)–2.058(1) · Å) and $(NH_4)_5[Ga(C_6H_4O_7)_2] \cdot 2H_2O$ (1.902(2)–2.056(2) Å). The Al–O distances are also similar to M(III)–O distances observed in other mononuclear M(III)–hydroxycarboxylate complexes such as $(NH_4)_5[Fe(C_6H_4O_7)_2] \cdot 2H_2O$ (1.953(2)–2.068(2) · Å) [41,42], $(NH_4)_3[Ga(C_6H_5O_7)_2] \cdot 4H_2O$ (1.890(2)–2.054(2) · Å) [43], and $(NH_4)_4[Cr(C_6H_4O_7)(C_6H_5O_7)] \cdot 3H_2O$ (1.933(2)–1.993(2) · Å) [44].

The protonated alcoholic moiety participates in hydrogen bonding interactions. Therefore, the presence of potassium ions along with the discrete OH^- groups in the lattice and the solvent water molecules further stabilizes the above-mentioned network, contributing to the stability of the crystal lattice in **1**.

4.3. FT-IR spectroscopy

The FT-infrared spectrum of **1** in KBr revealed the presence of vibrationally active carboxylate groups. Thus, antisymmetric as well as symmetric vibrations for the carboxylate groups in the coordinated quinate ligand were present in the spectrum. Specifically, antisymmetric stretching vibrations $\nu_{as}(COO^-)$ for the carboxylate carbonyls appeared between 1676 cm^{-1} and 1653 cm^{-1} for **1**. Symmetric vibrations $\nu_s(COO^-)$ for the same groups emerged in the range between 1384 cm^{-1} and 1365 cm^{-1} for **1**. The frequencies of the observed carbonyl vibrations were shifted to lower values in comparison to the corresponding vibrations in free quinic acid, thereby indicating changes in the vibrational status of the quinate ligand upon binding to the Al(III) ion [45]. The difference between the symmetric and antisymmetric stretches, $\Delta(\nu_{as}(COO^-) - \nu_s(COO^-))$, was greater than 200 cm^{-1}, indicating that the carboxylate groups of the quinate ligand were either free or coordinated to Al(III) in a monodentate fashion [46]. The latter contention was subsequently confirmed by the X-ray crystallography. All of the above assignments were in agreement with past observations in mononuclear $Al(III)O_6$ complexes [47], and in line with previous reports on carboxylate-containing ligands bound to metal ions [36,48–55].

4.4. Solid-state NMR spectroscopy

The MAS ^{13}C-NMR spectrum of **1** is consistent with the coordination mode of quinate around the Al(III) ion. The spectrum showed several discrete peak features. Two of those lie in the high field region, whereas the rest lie at lower fields. The two peaks in the high field region (34.4 and 40.7 ppm), were attributed to the C(6) and C(2) carbons, respectively, of the CH_2 groups in the quinate ligands bound to the central Al(III) ion. The resonances at 67.0, 71.3, 74.5 and 79.0 ppm were assigned to the C(5), C(3), C(4) and C(1) carbons, respectively, of the bound quinate. The signal at 180.0 ppm in the lower field region was assigned to the carboxylate carbon C(7) coordinated to the Al(III) central ion. This signal was shifted to lower fields in comparison to the corresponding signal in the free quinic acid. A similar pattern of ^{13}C resonances was observed in the case of mononuclear complexes containing other α-hydroxycarboxylate ligands (i.e. citrate), such as $(NH_4)_5[Al(C_6H_4O_7)_2] \cdot 2H_2O$ [36].

4.5. Solution NMR spectroscopy

The solution ^{13}C NMR spectrum of complex **1** was measured in D_2O (Fig. 3). The spectrum revealed the presence of several resonances. The two resonances in the high field region (38.9 and 43.2 ppm), were attributed to the C(6) and C(2) carbons, respectively, of the CH_2 groups in the quinate ligands bound to the central Al(III) ion. The resonances at 69.7, 74.0, 77.8 and 81.7 ppm were assigned to the C(5), C(3), C(4) and C(1) carbons, respectively, of the bound quinate. The signal at 183.6 ppm in the lower field region was assigned to the carboxylate carbon C(7) coordinated to the Al(III) central ion. This signal was shifted to lower fields in comparison to the corresponding signal in the free quinic acid. The shift was ~1.2 ppm downfield and was comparable to that observed in the MAS ^{13}C solid-state spectrum of **1**. It is worth noting that the pattern of resonances observed was similar to that observed in the solid state ^{13}C-MAS NMR spectrum of **1**. Further inquiry, however, into the solution ^1H NMR spectroscopy of compound **1** in D_2O revealed the presence of free quinate in equilibrium with

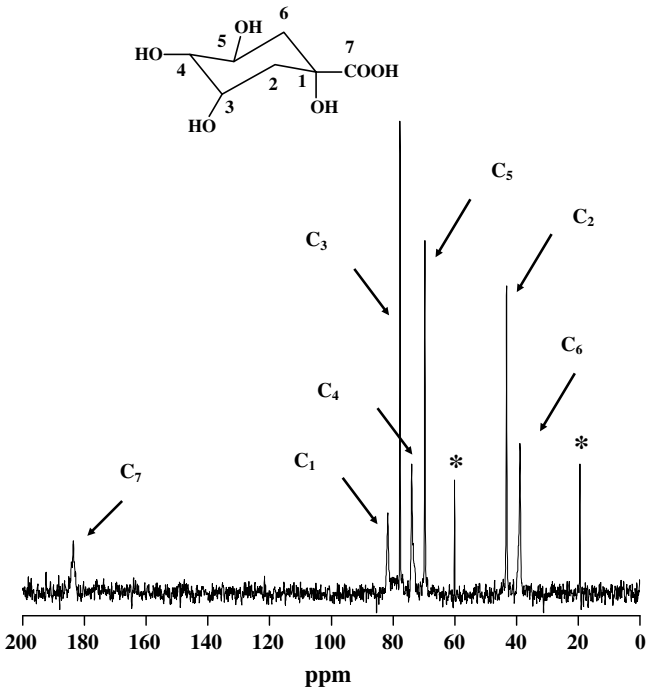

Fig. 3. ^{13}C NMR of **1** in solution (D_2O), at the autogenous pH. The signals marked with a star (*) belong to ethanol from the reaction mixture.

the species under investigation (See Supplementary data). Collectively, the data in solution support the presence of a mononuclear complex like **1,** but not identical in composition with that in the solid state.

4.6. Speciation studies

Potentiometric titrations were carried out on the ligand quinic acid alone and the binary system Al(III)–quinic acid in various metal ion to ligand molar ratios. Quinic acid contains only one dissociable proton in the measurable pH range (pK(HA) = 3.34(2)). The alcoholic hydroxyl groups are very weakly acidic dissociating up to pH ~ 13. For the titratable quinate carboxylate group, the pK_a value of 3.34 was obtained and was found to be very close to the values reported by Clifford (3.40) [56] and Luethy-Krause et al. (3.36) [57]. The obtained metal ion-ligand titration curves were evaluated with different potential speciation models. As quinic acid contains an α-hydroxycarboxylate moiety, the speciation model found for lactic acid [58,59] was tested first. An acceptable fit between the experimental and calculated titration curves for the binary Al(III)–quinic acid system was achieved by considering the species $[Al(H_2O)_6]^{3+}$ (Al), $[AlL]^{2+}$ (LH = $C_7H_{12}O_6$, L = $C_7H_{11}O_6^-$), $[AlLH_{-1}]^+$, $[AlLH_{-3}]^-$, $[AlL_2H_{-1}]^0$, the dinuclear form $[Al_2L_2H_{-4}]^0$, the polynuclear form $[Al_{13}L_4H_{-32}]^{3+}$, and the mononuclear $[AlH_{-4}]^-$ species toward the end of the investigated pH range. The fit was reasonably good in the overall employed pH and concentration range, indicating that the adopted speciation model was satisfactorily defined. Other binary Al(III):quinate complexes, including variably protonated and deprotonated species, were rejected by the computer program (PSEQUAD) during the computational process. The omission of any of the metal–ligand species decreased the fit by at least 30%. Accordingly, it can be stated that the suggested speciation model, with stability constants listed in Table 3, is the best model describing the solution state of the Al(III)–quinate system in the pH and concentration range studied. The uncertainties (3SD values) of the stability constants are given in parentheses. The pH range of their optimal formation is also reported. The species emerging from the speciation distribution of the binary system are basically in line with the overall structural characteristics encountered in species **1**, which was synthesized and isolated in the solid state. The collective data, however, indicate that the 3 × (COO^-, OH) type six-coordinate octahedral geometry, observed in the solid state species **1**, does not persist in solution in the whole pH range up to neutral pH.

Table 3
Proton (log$K$) and Al(III)–quinate complex formation constants (logβ) at I = 0.15 M (NaCl) and 25 °C[a]

Species	Quinic acid	logβ	pH range of participating species
	HL ($C_7H_{12}O_6$)	3.34(2)	
Al			2–5.5
AlL		1.84(3)	2–5
$AlLH_{-1}$		−1.05(2)	2–6.5
$AlLH_{-3}$		−11.48(5)	4–9
AlL_2H_{-1}		1.50(8)	2–6.5
$Al_2L_2H_{-4}$		−8.96(9)	4–7
$Al_{13}L_4H_{-32}$		−95.99(14)	5–6.5
AlH_{-4}		−23.4	7–9
Number of points		236	
Fitting parameter[b]		0.0106	

[a] Charges from the various species are omitted for reasons of clarity.
[b] Goodness of fit between the experimental and the calculated titration curves, expressed in mL of titrant.

On the basis of the analytical and crystallographic data, the alcoholic group of the quinate retains its proton upon binding to Al(III). Thus, there is no expected pH-dependence of the deprotonation of that group and the specific mode of binding to Al(III) over the investigated pH range. However, it has been proven by pH-potentiometric, NMR and CD spectroscopic methods that Al(III) may induce deprotonation of the weakly acidic alcoholic-OH group in various α-hydroxycarboxylic acids (such as lactic acid, malic acid, citric acid) [60,61]. The titration curves in the absence and presence of Al(III) suggest clearly formation of the mononuclear 1:1 complexes $[Al(H_2O)_6]^{3+}$, $[AlL]^{2+}$ and $[AlLH_{-1}]^+$, and the 1:2 complex $[AlL_2H_{-1}]^0$ in the acidic region up to pH 5. In the early part of that range, the predominant species is $[Al(H_2O)_6]^{3+}$. The latter three species $[AlL]^{2+}$, $[AlLH_{-1}]^+$ and $[AlL_2H_{-1}]^0$ contain a singly deprotonated quinate ligand bound to Al(III). As the pH of the aqueous solution increases from 2 to 5, the fraction of the mononuclear species such as $[AlL]^{2+}$, $[AlLH_{-1}]^+$ and $[AlL_2H_{-1}]^0$ increases progressively. Around pH 4.5, the predominant species is $[AlLH_{-1}]^+$. Towards the end of the specific pH range, new species such as the mononuclear $[AlLH_{-3}]^-$, and the dinuclear form $[Al_2L_2H_{-4}]^0$ arise.

In the pH range 5–7, three species emerge, namely $[AlLH_{-3}]^-$, $[Al_2L_2H_{-4}]^0$ and the polynuclear cluster form $[Al_{13}L_4H_{-32}]^{3+}$. In the pH range 5–5.5, the predominant species is the dinuclear species $[Al_2L_2H_{-4}]^0$, gradually growing in from the latter part of the previously described pH range and reaching a maximum around 5.2. Slowly emerging in the same pH range is the mononuclear $[AlLH_{-3}]^-$ species, which eventually predominates over the entire range of values beyond 5.5. Slightly above that pH value, a polynuclear assembly of Al(III) ions bound to quinates, namely $[Al_{13}L_4H_{-32}]^{3+}$, emerges as a participant, albeit at a minor fraction compared to the other two species. In a fashion similar to the Al(III)–lactic acid system, what was suggested as $[Al_2L_2H_{-4}]^0$ and $[Al_{13}L_4H_{-32}]^{3+}$ are oligo(poly)nuclear hydroxo species [58,59].

Albeit not definitively proven, it is worth noting that the dinuclear species $[Al_2L_2H_{-4}]^0$ may originate from the previously emerging $[AlLH_{-1}]^0$ species, for which a clear picture of the coordination mode of quinate was proposed. On these grounds, dinuclear com-

plex formation through the mononuclear species as a synthon could be perceived to proceed through (a) employment of the coordinated quinate carboxylate group binding to an adjacent $[AlLH_{-1}]^+$ species unit (and vice versa) through the second oxygen anchor, (b) utilization of the alcoholic moiety as a bridge between abutting $[AlLH_{-1}]^+$ units, and (c) deprotonation of coordinated water molecule(s) leading to OH^- moieties potentially acting as template bridges to the adjacently located $[AlLH_{-1}]^+$ units. Thus, hydroxo bridged dinuclear assembly formation could be promoted. This thesis is consistent with the fact that hydroxo and dihydroxo bridges are a characteristic feature in Al(III) complexation chemistry, leading to dinuclear species in the solid state. Representative examples of such species are complexes of trivalent metal ions such as $[(Al_3(C_6H_4O_7)_2(OH)_2(H_2O)_4]_2 \cdot (NO_3) \cdot 6H_2O$ [62], $Na_6[Al_6(C_6H_6O_8)_4(OH)_8] \cdot 21H_2O$ [63], $[Al_{13}(\mu_3\text{-}OH)_6(\mu_2\text{-}OH)(C_6H_8NO_5)_6(H_2O)_6] \cdot (NO_3)_3$ [64], and $[Al_2(OH)_2(C_4H_5NO_4)_2(H_2O)_2]$ [65], and Cr(III) i.e. $([(H_2O)_4Cr(OH)_2Cr(H_2O)_4]^{4+}$ [66,67], $[Cr(tpa)(OH)]_2(ClO_4)_4\ 4H_2O$ [68], $[Cr(gly)_2(OH)]_2$ [69,70] and $[Cr(pic)_2(OH)]_2^{4+}$ [71]), already reported in the literature. Analogous chemistry has been observed in the case of Cu(II) and VO(II). On similar grounds, all of these metal ions were shown to be able to induce deprotonation of the weakly acidic alcoholic-OH function in various hydroxyl group derivatives when the OH group lies adjacent to another strongly coordinating donor group [58,59,72–74].

What emerges as a noteworthy observation from the aqueous speciation scheme is the 1:1 and 1:2 Al(III):quinate stoichiometry for the majority of the species present in it. In both cases of Al(III):quinate ratios, the binding mode of the quinate ligand(s) could be either through the carboxylate group or through the carboxylate and α-alcoholate groups, while the remaining polyol functionalities do not enter the coordination sphere of Al(III). It appears that the bidentate coordination of α-hydroxycarboxylate containing ligands through carboxylate groups may also be preferred in other divalent or trivalent metal ions, such as Cu(II) [72], Co(II) [75], Al(III)[73] and VO(II) [74]. Accordingly, it is very probable that the deprotonated species between Al(III) and quinic acid form isomeric structures and the coordination sphere of the metal ion is filled by monodentate or bidentate bound quinate, hydroxo and water ligands. The additional H_{-1} in species, such as $[AlLH_{-1}]^+$, $[AlL_2H_{-1}]^0$, could emerge upon dissociation of the α-OH group and coordination of the incipient α-O^- group or dissociation of a coordinated water molecule from $[AlL]^{2+}$ and $[AlL_2]^+$. Considering the data in this pH range, it appears that $\log K(AlL_2H_{-1})$ (characteristic for the equilibrium $AlLH_{-1} + L \rightleftarrows AiL_2H_{-1}$) is 2.55 and is similar to the $\log K(AlL)$ value of 1.84, indicating that only one ligand molecule is coordinated via a deprotonated alcoholate. The second ligand is bound to Al(III) in a (COO^-, OH) fashion. This value also indicates favorable formation for $[AlL_2H_{-1}]^0$ over that of $[AlLH_{-1}]^+$, due to charge neutralization. As a matter of fact, the two species coexist in the same pH range, with the former species comprising 30% of the total Al(III) fraction compared to ~50% for the latter species at pH ~ 4.5 (Fig. 4).

In the high pH zone, from 7 to 9, the two species present are $[AlLH_{-3}]^-$ and $[AlH_{-4}]^-$, both mononuclear in nature. In the first case, the mixed hydroxo $[AlLH_{-3}]^-$ species might exhibit isomeric binding modes. To this end, one formulation could include a singly deprotonated quinate, three hydroxides originating from the deprotonation of an equivalent number of bound water molecules, with the coordinated quinate preventing precipitation of $Al(OH)_3$ [76]. In the other binding mode, quinate coordinates in a bidentate (COO^-, O^-) fashion and only two OH^- ions are ionized in the coordination sphere of the metal ion. The $[AlLH_{-3}]^-$ species is the only species present around pH 7 and is the predominant species of the physiological pH range and even beyond that. The second species, $[AlH_{-4}]^- = [Al(OH)_4]^-$ ($\log \beta_{1-4} = -23.4$), emerges as a minor tetrahedral Al(III) species after pH 7 and reaches a maximum of 35% of the total fraction of Al(III) toward the high end of the investigated pH range. In a fashion similar to the Al(III)–lactate system, polynuclear species such as $Al_2L_2H_{-4}$ and $Al_{13}L_4H_{-32}$ also form in the pH range 4–7, in a significant but lower concentration than in the former system, probably due to the larger spatial requirement of the quinate ligand.

4.7. Thermal studies

The thermal decomposition of the title complex was studied by TGA–DSC under an atmosphere of oxygen (Fig. 5). The complex $K[Al(Quinic)_3] \cdot (OH) \cdot 4H_2O$ (**1**) is thermally stable up to 30 °C. From that point on, a fairly broad heat process points to the dehydration of **1**, with the release of lattice water molecules between 30 and 180 °C, signifying an endothermic process. The observed weight loss amounts to 9.63%, a value close to the calculated value of 9.88% based on the molecular formula of the title complex. Beyond the specific temperature, it appears that the quinate ligand loses its integrity. In a second step, the release of carbon dioxide is observed from the compound between 180 °C and 225 °C. The observed weight loss amounts to 6.13%, a value very close to the calculated value of 6.04% based on the molecular formula of the title complex. Subsequently, consecutive steps ensue between 225 and 500 °C that are associated with further decomposition of the organic part of the molecule. No clear plateaus are reached in these stages, suggesting that the derived products are unstable and

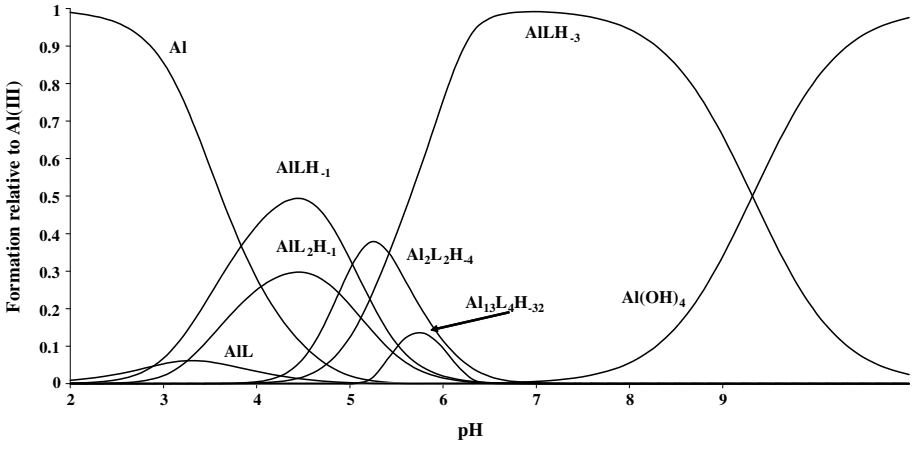

Fig. 4. Speciation curves for complexes forming in the Al(III)–quinic acid system; c_{Al} = 0.001 mol dm^{-3}, c_{ligand} = 0.003 mol dm^{-3}. Charges are omitted for clarity.

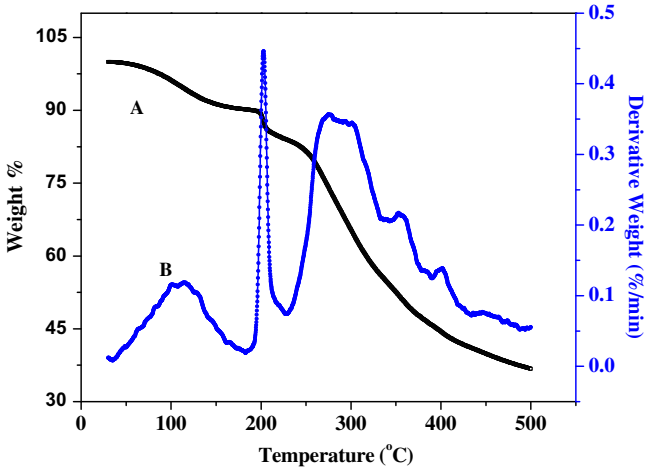

Fig. 5. TGA (A) and DSC (B) analysis of **1**.

decompose further. The total weight loss of 86.8% due to the decomposition of the title complex is reached at 518 °C, with no further loss up to 800 °C. This value is in good agreement with the calculated weight loss derived upon the thesis that the product at that temperature (500 °C) is Al_2O_3. The DSC profile of the complex exhibits clear features that correspond to the aforementioned TGA processes. Collectively, the specified number of observed processes very likely reflects discrete mechanistic steps for the decomposition pathways of **1**.

5. Discussion

5.1. A closer look at the aqueous Al(III)–quinic acid chemistry

As a metallotoxin, Al(III) has been linked to a number of pathological conditions in plants (soil acidity complex) [77] and humans (Alzheimer's disease) [11,12,16]. In both cases, its cellular toxicity entails a diverse aqueous chemistry at the molecular level, that, in turn, is linked to the existence of soluble and bioavailable forms of that metal ion influencing its chemical reactivity. To this end, understanding Al(III) toxicity is closely tied to well-characterized soluble forms of Al(III) that can promote its reactivity with physiological targets through ensuing ternary interactions. Drawn by the paucity of such well-defined forms of Al(III) in aqueous media that promote interactions leading to aberrant cellular (neuro)physiologies, a structural speciation approach was adopted encompassing pH-dependent synthetic reactions between Al(III) and the physiological substrate D-(−)-quinic acid. At the optimally established pH 4, the new binary species $K[Al(C_7H_{11}O_6)_3]\cdot(OH)\cdot 4H_2O$ (**1**) arose and was isolated in a pure crystalline form. The physicochemical characterization of **1** projected structural and chemical properties relating to the following:

(a) The arisen aqueous chemistry in this binary system under the employed conditions is linked to the formation of discrete complexes of Al(III) bearing quinate ligands. The specificity of the reaction pH was crucial in deriving the new material in a pure and crystalline form. pH-specific synthesis had previously been successfully applied in the case of soluble metal-hydroxycarboxylate species involving trivalent (Al(III), Ga(III), Fe(III)) [36,37,41] and divalent metal ions (Co(II), Mn(II)) [49,50].

The physicochemical properties of **1** contribute significantly to understanding its nature both in the solid state and in solution (*vide infra*). In this regard, delineation of the composition of the coordination sphere of Al(III) in solution reflects distinct structural features on species arising from the interaction of the metal ion with natural O-containing low molecular mass substrates in biologically relevant media. The fact that in solution species such as $[AlL_2]^+$ or $[AlL_2H_{-1}]^0$ may arise consolidates further the emergence of Al(III)–O_6 moieties (very likely octahedral, albeit not unequivocally delineated as such by NMR beyond pH 4–5 due to parallel formation of $Al(OH)_3$) in aqueous media through binary and ternary interactions of Al(III) with O-containing targets. The so arisen interactions could reflect a general multifactorial contribution to $[AlL_2]^+$ or $[AlL_2H_{-1}]^0$ emergence as a speciation participant, primarily influenced by factors such as pH, ligand deprotonation state, H-bond formation and others. Along with the thermal behavior, the overall data formulate a well-defined physicochemical profile for **1**, supporting its solid-state nature and its solution signature.

(b) The structural characterization of **1** reveals distinct traits of the interaction between Al(III) and quinic acid. Firstly, the mode of coordination of the ligand with the metal ion is specific and derives from the propensity of the α-hydroxycarboxylate moiety to promote metal ion binding. A key factor driving this particular reactivity of Al(III) is the formation of stable five-membered rings for the quinate ligands bound to Al(III). Secondly, the employment of the alcoholic moiety of the α-hydroxycarboxylate group to bind Al(III) is marked by a retention of the proton on the specific oxygen (as evidenced by the solid-state structure of the isolated species **1**). The aqueous speciation work, however, provides further insight into the chemical behavior of the quinate ligand anchored to Al(III). Specifically, both singly ionized quinate as well as doubly ionized quinate moieties appear to anchor to Al(III), giving rise to binding isomers for specific species such as $[AlLH_{-1}]^+$ and $[AlL_2H_{-1}]^0$. This behavior may imply similarities to the aqueous Al(III) chemistry at pH values lower or higher than the one employed here, or to the chemistry of other divalent/trivalent metal ions with the same ligand. In no cases so far, however, have doubly deprotonated quinate-containing mononuclear octahedral metal complexes been synthesized and isolated, thus projecting the interconnection of the inherent chemical properties of the various metal ions with the complexity and diversity of species present in aqueous media. To this end, the possibility that the Al(III)–quinate binary system would give rise to new, thus far elusive, species in a pH-dependent fashion cannot be discounted.

(c) The three alcoholic groups almost diametrically located with respect to the α-hydroxycarboxylate moiety play totally different roles. They do not participate in the formation of five-member metallacyclic rings, like the α-hydroxycarboxylate moiety does, which further stabilizes the entire mononuclear complex. In the case of divalent metal ions, such as Mn(II) [78], participating in binary systems with quinic acid, the terminal alcoholic moieties were variably involved in the formulation of the coordination sphere of the metal ion, differentiating the structural environment of abutting Mn(II) ions in the arising solid-state lattice, without losing their protons. Specifically, one of the polyolic group members acts as a bridge between adjacently located metal ion centers, leading to the formation of dinuclear species $[Mn_2(C_7H_{11}O_6)_4]_n\cdot nH_2O$ infinitely extended in a polymeric and molecular lattice. Even though that behavior was observed in the crystalline state only, it projects the potential affinity of polyol functionalities for metal ion coordination, such as Al(III), as ligand terminals on diverse physiological substrates interacting with it in biologically relevant fluids.

5.2. Correlation of structural diversity in the aqueous binary Al(III)–quinate speciation with the synthetic chemistry

The aqueous speciation in the binary Al(III)–quinic acid system (Fig. 4) can be described satisfactorily by considering the presence of (a) 1:1 Al(III)–quinate complexes in the form $[AlL_n(H_{-1})_p]^{q+}$ ($n = 0$, $p = 0$, q = 3; $n = 1$, $p = 1$, q = 1; $n = 1$, $p = 0$, $q = 2$), the neutral $[AlL_2H_{-1}]^0$ and dinuclear $[Al_2L_2H_{-4}]^0$ forms, the anionic

$[AlL_n(H_{-1})_p]^{q-}$ ($n = 0$, $p = 4$, $q = 1$; $n = 1$, $p = 3$, $q = 1$) and polynuclear $[Al_{13}L_4H_{-32}]^{3+}$ forms, and (b) 1:2 mononuclear Al(III)–quinate species $[AlL_2H_{-1}]^0$.

On the basis of the aforementioned observations, it is logical to juxtapose the results of the aqueous speciation with the solid-state structure of compound **1** and its physicochemical properties in the solid state and in solution. To that end, the solid-state structure of **1** suggests the existence of an octahedral Al(III) central metal ion surrounded by three singly deprotonated quinate ligands, thus filling all of the six available coordination sites. In solution, the NMR data obtained for **1** upon dissolution and at the equilibrium state suggest that (a) the species does not retain its solid-state structure in solution, thereby releasing quinate away from the coordination sphere of Al(III), and (b) even the binding mode of the quinate may change from (COO^-, OH) to (COO^-, O^-) coordination. Consistent with this general behavior is the suggestion offered by the aqueous speciation that, in the pH range investigated synthetically, there are two species prevailing. These are $[AlLH_{-1}]^+$ and $[AlL_2H_{-1}]^0$. Consequently: (a) the fact that **1** has been isolated in the solid state with the specific molecular lattice composition and physicochemical properties reflects the lattice dynamics of Al(III)–quinate complexation in the solid state, and (b) $[AlL_2H_{-1}]^0$ might be the species that **1** dissociates to upon dissolution in water at the autogenous pH (consistent with the pH range at which the synthesis of **1** was pursued).

The aforementioned remarks lend further credence to the notion that $[AlL_2H_{-1}]^0$, a zero-valent complex (like **1**), is likely the arising species in solution consistent with the potential reactions shown below:

$$[AlL_3]^0 \rightleftarrows [AlL_2]^+ + L^-$$

$$[AlL_2]^+ \rightleftarrows [AlL_2H_{-1}]^0 + H^+$$

To a first approximation, dissociation of $[AlL_3]^0$ to $[AlL_2]^+$ is followed by further deprotonation of one of the Al(III)–bound water molecules, or one of the α-OH groups of the quinate molecules, leading to the formation of $[AlL_2H_{-1}]^0$. Thus, (a) the mononuclear octahedral complex, isolated in the solid state, affords upon dissolution another mononuclear, presumably octahedral complex, containing fewer quinates (two), (b) the charge of $[AlL_3]^0$ (**1**) in the solid state (zero) is maintained upon dissolution of the complex and the formation of the emerging complex $[AlL_2H_{-1}]^0$. The chemical and potential biological repercussions of that property could be relevant to molecular mechanisms of Al(III) toxicity.

From a structural point of view, the quinate ligand is configured so as to promote formation of variable size species extending from low molecular mass complexes to high molecular mass aqueous assemblies. In analogy to other α-hydroxycarboxylate metal ion binders, such as lactic acid, citric acid, malic acid, etc., a chemistry of such breadth would be expected to afford dinuclear and potentially multinuclear Al(III)–quinate clusters. Consistent with this notion is the suggestion offered by the aqueous speciation distribution of this binary system that the dinuclear complex $[Al_2L_2H_{-4}]^0$ exists in the pH range 4–7 and a higher nuclearity cluster $[Al_{13}L_4H_{-32}]^{3+}$ is present in the pH range 5–6.5. With regard to the binding mode of the di- and polynuclear species, the most likely assumption concerning the $Al_2L_2H_{-4}$ complex would be the tentative formula $[Al_2(OH)_2(H_{-1}L)_2]^0$, i.e. a dihydroxo-bridged species in which both quinate ions are doubly deprotonated and bound in a bidentate fashion around the $Al_2(OH)_2$ core. A similar core structure has been reported in $[Al_2(\mu\text{-}OH)_2(\text{nitrilotriacetate})_2]^-$ [79]. Concerning the high-nuclearity species $Al_{13}L_4H_{-32}$, we have no clear suggestion as to the binding mode of quinate in this species. It should be mentioned, however, that for a similar polynuclear species bearing the hydrolytic $[Al_{13}O_4(OH)_{24}]^{7+}$ core and thought to arise upon interaction of Al(III) with lactate, ^{27}Al NMR studies by Marklund and Öhman [58] concluded that in fact the species was not a complex to which lactate ions were coordinated. These assumptions are consistent with the existence of structural features not unlike those encountered in (1) dinuclear oxo- or hydroxo-bridges seen in species such as $K_2[Cr_2(C_6H_6NO_6)_2(OH)_2]\cdot 6H_2O$ [80], $Ba[\{Fe(nta)(H_2O)\}_2O]\cdot 4H_2O$ [81], $[Ga(heidi)(H_2O)]_2$ [82], $[Al(heidi)(H_2O)]_2$ [64] and $[Fe(heidi)(H_2O)]_2$ [83,84], which have been synthesized and isolated, and (2) polynuclear species that could emerge from the herein investigated binary system. As to the latter category of species, the importance of the M:ligand ratio in achieving high nuclearity species has been noted as a key factor in the chemistry of a number of trivalent metal ions like Fe(III), Al(III), Ga(III) and others. Thus, species such as $[Fe_{19}(\mu_3\text{-}O)_6(\mu_3\text{-}OH)_6(\mu_2\text{-}OH)_8(heidi)_{10}(H_2O)_{12}]^+$, $[Fe_{17}(\mu_3\text{-}O)_4(\mu_3\text{-}OH)_6(\mu_2\text{-}OH)_{10}(heidi)_8(H_2O)_{12}]^{3+}$ [83], $[Al_{13}(\mu_3\text{-}OH)(\mu_2\text{-}OH)_{12}(heidi)_6(H_2O)_6]^{3+}$ [64], $[Ga_8(\mu_3\text{-}OH)(\mu_2\text{-}OH)_8(heidi)_4(H_2O)_4(py)_2]^{2+}$ [82] and $[Ga_{13}(\mu_3\text{-}OH)(\mu_2\text{-}OH)_{12}(heidi)_6(H_2O)_6]^{3+}$ [82] have been synthesized. On the basis of the above remarks, pertinent synthetic and physicochemical studies are currently in progress in our lab to complement the already conducted aqueous speciation studies.

5.3. From the aqueous chemistry of the binary Al(III)–quinate system to toxicity

Aside from humans, most plants are fairly sensitive to Al(III) toxicity, a major factor affecting significantly crop productivity in agriculture [77,85] around the world. Therefore, essential in understanding the toxicity of Al(III) at the cellular level, is an in-depth knowledge of the (bio)chemistry of that metal ion with intracellular and/or extracellular targets of variable mass and distinct biological activity. A key contributor to that knowledge is (a) the aqueous speciation of binary/ternary systems of a kinetically sluggish Al(III) with its elicited targets as a function of pH and molecular stoichiometry, and (b) the structure and properties of soluble and bioavailable species of Al(III)–L (substrate) species partaking of the requisite speciation [86]. To this end, the herein described complex **1** is a good example of a species, which (a) in the solid state contains the key physicochemical characteristics of an efficient metal ion binder (ligand to metal ratio, structural features, etc.) anchored onto Al(III), as previously proposed for plant tea organic acids interacting with that metal ion [87,88], (b) in solution, turns into mononuclear Al(III) species bearing a variable metal:ligand ratio while concurrently retaining the overall solid-state characteristics of the binary species, and (c) gives rise to $[AlL_2H_{-1}]^0$, bearing a net neutral charge, presenting a soluble Al(III) entity poised to traverse cellular structures (e.g. membranes) and participate in further chemical reactivity by eliciting interactions from variable mass and structure cellular targets involved in cytosolic and nuclear processes (i.e. cellular-neuronal integrity, degeneration, etc.). Further synthetic chemistry targeting such well-defined yet elusive aqueous Al(III)–quinate pH-structural variants, components of the speciation of that binary system, are under way.

6. Conclusions

The work presented here, projects the nature of the aqueous interactions between Al(III) and a natural O-containing substrate, ultimately leading to well-defined complexes in the solid state and in solution. Both the aqueous speciation study and the invoked synthetic approaches offer invaluable data adumbrating the profile of soluble species in the binary Al(III)–quinate system through the correlation of their structural properties in those two phases. Given the importance of binary and ternary interactions of Al(III) with variable mass cellular targets, understanding the nature and physicochemical properties of **1** in the solid state and in solution is the first step in the delineation of the complex distribution of Al(III)–

quinate species and any related Al(III)–(O-substrate) interactions under conditions dictated by cellular environmental factors and biological settings [89]. Undoubtedly, the contribution of the pH-dependent synthetic chemistry to the investigation of (a) the molecular processes involving this otherwise kinetically sluggish Al(III), and (b) the relationships to molecular neuro(toxic) effects in higher organisms and humans, is significant. To the degree that soluble and bioavailable Al(III)-bound (α-hydroxy)carboxylate-containing biological targets, such as $[AlL_2H_{-1}]^0$, are likely involved in chemical processes underlying (neuro)toxic effects in biological media, further synthetic and solution studies on this specific, as well as other hydroxycarboxylate-bearing binary systems, are expected to shed light on their nature. Work along these lines is currently in progress in our labs.

Acknowledgments

This work was supported by a "Pythagoras" grant from the National Ministry of Education and Religious Affairs, and by a "PENED" grant co-financed by the E.U. European Social Fund (75%) and the Greek Ministry of Development-GSRT (25%), and by the Hungarian Research Fund (OTKA No. NI61786).

Appendix A. Supplementary data

CCDC 678110 contains the supplementary crystallographic data for $K[Al(C_7H_{11}O_6)_3] \cdot (OH) \cdot 4H_2O$ (**1**). These data can be obtained free of charge via http://www.ccdc.cam.ac.uk/conts/retrieving.html, or from the Cambridge Crystallographic Data Centre, 12 Union Road, Cambridge CB2 1EZ, UK; fax: (+44) 1223-336-033; or e-mail: deposit@ccdc.cam.ac.uk. Supplementary data associated with this article can be found, in the online version, at doi:10.1016/j.poly.2008.06.029.

References

[1] P. Nayak, Environ. Res. 89 (2002) 101.
[2] A. Campbell, E.Y. Yang, M. Tsai-Turton, S.C. Bondy, Brain Res. 933 (2002) 60.
[3] V. Rondeau, Rev. Environ. Health 17 (2002) 107.
[4] H. Meiri, E. Banin, M. Roll, A. Rouesseau, Prog. Neurobiol. 40 (1993) 89.
[5] G.B. Van der Voet, M.F. Van Ginkel, F.A. de Wolff, Toxicol. Appl. Pharm. 99 (1989) 90.
[6] D.N.S. Kerr, M.K. Ward, in: H. Sigel, A. Sigel (Eds.), Metal Ions in Biological Systems, vol. 24, Marcel Dekker, Inc., New York, NY, 1988, p. 217 (Chapter 6).
[7] H.H. Malluche, Nephrol. Dial. Transplant. 17 (Suppl. 2) (2002) 21.
[8] J.B. Cannata-Andia, J.L. Fernandez-Martin, Nephrol. Dial. Transplant. 17 (Suppl. 2) (2002) 9.
[9] D. Pratico, K. Uryu, S. Sung, S. Tang, J.Q. Trojanowski, V.M. Lee, FASEB J. 16 (2002) 1138.
[10] M.J. Hull, J.L. Abraham, Hum. Pathol. 33 (2002) 819.
[11] C. Exley, J. Alzheimer's Dis. 3 (2001) 551.
[12] V. Rondeau, D. Commenges, in: C. Exley (Ed.), Aluminium and Alzheimer's Disease: The Science that Describes the Link, Elsevier Science, New York, 2001.
[13] V. Rondeau, D. Commenges, H. Jacqmin-Gadda, J.-F. Dartigues, Am. J. Epidemiol. 152 (2000) 59.
[14] G.D. Fasman, C.D. Moore, Proc. Natl. Acad. Sci. USA 91 (1994) 11232.
[15] M. Clauberg, J.G. Joshi, Proc. Natl. Acad. Sci. USA 90 (1993) 1009.
[16] C. Exley, J.D. Birchall, J. Theor. Biol. 159 (1992) 83.
[17] D. Stead, Lett. Appl. Microbiol. 18 (1994) 112.
[18] E. Haslam, Shikimic Acid: Metabolism and Metabolites, Wiley & Sons, NY, 1993.
[19] A.J. Pittard (Ed.), *Escherichia coli* and Salmonella: Cellular and Molecular Biology, ASM Press, Washington, DC, 1996.
[20] R. Bentley, Crit. Rev. Biochem. Mol. Biol. 25 (1990) 307.
[21] S.E. Castillo-Blum, N. Barbra-Behrens, Coord. Chem. Rev. 196 (2000) 3.
[22] G.E. Hutchinson, Quart. Rev. Biol. 18 (1943) 1.
[23] T. Watanabe, M. Osaki, T. Yoshihara, T. Tadano, Plant Soil 201 (1998) 165.
[24] T.P. Flaten, Coord. Chem. Rev. 228 (2002) 385.
[25] G. Gran, Acta Chem. Scand. 4 (1950) 559.
[26] D. Sanna, G. Micera, P. Buglyo, T. Kiss, J. Chem. Soc., Dalton Trans. (1996) 87.
[27] M. Dyba, M. Jezowska-Bojczuk, E. Kiss, T. Kiss, H. Kozlowski, Y. Leroux, D. El Manouni, J. Chem. Soc., Dalton Trans. (1996) 1119.
[28] H.M. Irving, M.G. Miles, L.D. Petit, Anal. Chim. Acta 38 (1967) 475.
[29] L. Zekány, I. Nagypál, in: D. Leget (Ed.), Computational Methods for the Determination of Stability Constants, Plenum, New York, 1985.
[30] L.O. Öhman, S. Sjöberg, Acta Chem. Scand. 36 (1982) 47.
[31] SMART-NT Software Reference Manual, Version 5.059, Bruker AXS, Inc., Madison, WI, 1998.
[32] SAINT+Software Reference Manual, Version 6.02, Bruker AXS, Inc., Madison, WI, 1999.
[33] G.M. Sheldrick, SHELXS-90, Program for the Solution of Crystal Structure, University of Göttingen, Germany, 1986.
[34] G.M. Sheldrick, SHELXL-97, Program for the Refinement of Crystal Structure, University of Göttingen, Germany, 1997.
[35] SHELXTL-NT Software Reference Manual, Version 5.1, Bruker AXS, Inc., Madison, WI, 1998.
[36] M. Matzapetakis, C.P. Raptopoulou, A. Terzis, A. Lakatos, T. Kiss, A. Salifoglou, Inorg. Chem. 38 (1999) 618.
[37] M. Matzapetakis, M. Kourgiantakis, M. Danakali, C.P. Raptopoulou, A. Terzis, A. Lakatos, T. Kiss, I. Banyai, L. Iordanidis, T. Mavromoustakos, A. Salifoglou, Inorg. Chem. 40 (2001) 1734.
[38] M. Dakanali, C.P. Raptopoulou, A. Terzis, A. Lakatos, I. Banyai, T. Kiss, A. Salifoglou, Inorg. Chem. 42 (2003) 252.
[39] T.L. Feng, P.L. Gurian, M.D. Healy, A.R. Barron, Inorg. Chem. 29 (1990) 408.
[40] N. Bulc, L. Golic, J. Siftar, Acta Crystallogr., Sect. C 40 (1984) 1829.
[41] M. Matzapetakis, C.P. Raptopoulou, A. Tsohos, B. Papefthymiou, N. Moon, A. Salifoglou, J. Am. Chem. Soc. 120 (1998) 13266.
[42] I. Shweky, A. Bino, D.P. Goldberg, S.J. Lippard, Inorg. Chem. 33 (1994) 5161.
[43] P. O'Brien, H. Salacinski, M. Motevalli, J. Am. Chem. Soc. 119 (1997) 12695.
[44] C. Gabriel, C.P. Raptopoulou, A. Terzis, V. Tangoulis, C. Mateescu, A. Salifoglou, Inorg. Chem. 46 (2007) 2998.
[45] G.B. Deacon, R. Philips, J. Coord. Chem. Rev. 33 (1980) 227.
[46] C. Djordjevic, M. Lee, E. Sinn, Inorg. Chem. 28 (1989) 719.
[47] K. Nakamoto, Infrared and Raman Spectra of Inorganic and Coordination Compounds, 5th ed., John Wiley and Sons, Inc., New York, 1997 (Part B).
[48] P. Panagiotidis, E.T. Kefalas, C.P. Raptopoulou, A. Terzis, T. Mavromoustakos, A. Salifoglou, Inorg. Chim. Acta 361 (2008) 2210.
[49] M. Matzapetakis, M. Dakanali, C.P. Raptopoulou, V. Tangoulis, A. Terzis, N. Moon, J. Giapintzakis, A. Salifoglou, J. Biol. Inorg. Chem. 5 (2000) 469.
[50] M. Matzapetakis, N. Karligiano, A. Bino, M. Dakanali, C.P. Raptopoulou, V. Tangoulis, A. Terzis, J. Giapintzakis, A. Salifoglou, Inorg. Chem. 120 (2000) 4044.
[51] W.P. Griffith, T.D. Wickins, J. Chem. Soc. A (1968) 397.
[52] N. Vuletic, C. Djordjevic, J. Chem. Soc., Dalton Trans. (1973) 1137.
[53] M. Kaliva, T. Giannadaki, C.P. Raptopoulou, V. Tangoulis, A. Terzis, A. Salifoglou, Inorg. Chem. 40 (2001) 3711.
[54] M. Tsaramyrsi, D. Kavousanaki, C.P. Raptopoulou, A. Terzis, A. Salifoglou, Inorg. Chim. Acta 320 (2001) 47.
[55] M. Matzapetakis, M. Kourgiantakis, M. Dakanali, C.P. Raptopoulou, A. Terzis, A. Lakatos, T. Kiss, I. Banyai, L. Iordanidis, T. Mavromoustakos, A. Salifoglou, Inorg. Chem. 40 (2001) 1734.
[56] M. Clifford, Tea Coffee Trade J. 159 (1987) 35.
[57] B. Luethy-Krause, I. Pfenninger, W. Landolt, Trees – Struct. Func. 4 (1990) 198.
[58] E. Marklund, L.O. Öhman, Acta Chem. Scand. 44 (1990) 228.
[59] T. Kiss, I. Sóvágó, R.B. Martin, J. Pursiainen, J. Inorg. Biochem. 55 (1994) 53.
[60] R.B. Martin, in: Aluminium in Biology and Medicine, Ciba Foundation Symposium 169, Wiley, Chichester, 1992, p. 5. and references cited therein.
[61] T. Kiss, E. Farkas, Perspect. Bioinorg. Chem. 3 (1996) 199. and references cited therein.
[62] S.A. Malone, P. Cooper, S.L. Heath, Dalton Trans. (2003) 4572.
[63] P. Klufers, G. Kramer, H. Piotrowski, J. Senker, Z. Naturforsch., B: Chem. Sci. 57 (2002) 1446.
[64] S.L. Heath, P.A. Jordan, I.D. Johnson, G.R. Moore, A.K. Powell, M. Helliwell, J. Inorg. Biochem. 59 (1995) 785.
[65] S.P. Petrosyants, M.A. Malyarik, A.B. Ilyukhin, Russ. J. Inorg. Chem. 40 (1995) 765.
[66] L. Spiccia, H. Stoeckli-Evans, W. Marty, R. Giovanoli, Inorg. Chem. 26 (1987) 474.
[67] J.A. Laswick, R.A. Plane, J. Am. Chem. Soc. 81 (1959) 3564.
[68] D.J. Hodgson, M.H. Zietlow, H.E. Pedersen, M.H. Toftlund, Inorg. Chim. Acta 149 (1988) 111.
[69] J.T. Veal, W.E. Hatfield, D.Y. Jeter, J.C. Hempel, D.J. Hodgson, Inorg. Chem. 12 (1973) 342.
[70] J.T. Veal, D.Y. Jeter, J.C. Hempel, R.P. Eckberg, W.E. Hatfield, D.J. Modgson, Inorg. Chem. 12 (1973) 2928.
[71] K. Michelsen, Acta Chem. Stand. Ser. A 30 (1976) 521.
[72] E. Kiss, T. Kiss, M. Jezowska-Bojczuk, J. Coord. Chem. 40 (1996) 157.
[73] A. Lakatos, I. Bányai, R. Bertani, P. Decock, T. Kiss, Eur. J. Inorg. Chem. (2001) 461.
[74] T. Kiss, P. Buglyo, D. Sanna, G. Micera, P. Decock, D. Dewaele, Inorg. Chim. Acta 239 (1995) 45.
[75] M. Matzapetakis, M. Dakanali, C.P. Raptopoulou, V. Tangoulis, A. Terzis, J. Giapintzakis, A. Salifoglou, J. Biol. Inorg. Chem. 5 (2000) 469.
[76] M. Kilyén, I. Labádi, E. Tombácz, T. Kiss, Bioinorg. Chem. Appl. 1 (2003) 321.
[77] L.V. Kochian, D.L. Jones, in: R.A. Yokel, M.S. Golub (Eds.), Research Issues in Aluminum Toxicity, Taylor & Francis, Washington, DC, 1997, p. 69.
[78] M. Menelaou, C.P. Raptopoulou, A. Terzis, V. Tangoulis, A. Salifoglou, Eur. J. Inorg. Chem. (2006) 1957.
[79] G.C. Valle, G.G. Bombi, B. Corain, M. Favarato, P. Zatta, J. Chem. Soc., Dalton Trans. (1989) 1513.
[80] T. Moseley, J.O.W. Norris, E. Williams, in: Techniques and Mechanisms in Gas Sensing, Adam Hilger Series on Sensors, I.O.P. Publishing, Bristol, 1991.

[81] S.L. Heath, A.K. Powell, H.L. Utting, M. Helliwell, J. Chem. Soc., Dalton Trans. (1992) 305.
[82] J.C. Goodwin, S.J. Teat, S.L. Heath, Angew. Chem., Int. Ed. 43 (2004) 4037.
[83] S.L. Heath, A.K. Powell, Angew. Chem., Int. Ed. Engl. 31 (1992) 191.
[84] A.K. Powell, S.L. Heath, D. Gatteschi, L. Pardi, R. Sessoli, G. Spina, F. Del Giallo, F. Pieralli, J. Am. Chem. Soc. 117 (1995) 2491.
[85] H.R. von Uexküll, E. Mutert, Plant Soil 171 (1995) 1.
[86] A. Salifoglou, Coord. Chem. Rev. 228 (2002) 297.
[87] K. Takeda, T. Yamashita, A. Takahashi, C.F. Timberlake, Phytochemistry 29 (1990) 1089.
[88] C.F. Timberlake, J. Gem. Sot. 561 (1959) 2795.
[89] A. Salifoglou, in: M. Gielen, E.R.T. Tiekink (Eds.), Metallotherapeutic Drugs & Metal-based Diagnostic Agents: The Use of Metals in Medicine, John Wiley & Sons Ltd., England, 2005, p. 65.

2.2. Physical measurements

Elemental analyses were carried out on a Carlo Erba Model 1108 and Perkin–Elmer 240B microanalyser. IR spectra were recorded on a Bruker IFS-66V spectrophotometer as KBr disks (4000–400 cm^{-1}) or polyethylene-sandwiched Nujol mulls (500–100 cm^{-1}). Electronic spectra were obtained on a Shimadzu UV-3101PC spectrophotometer equipped with a reflectance accessory. X-band EPR spectra of the complexes were obtained in 3 mm pyrex tubes with a Bruker EMX spectrometer using a conventional Dewar insert at liquid nitrogen temperature and Cr^{II} as the reference. Room temperature magnetic moments were determined on a DSM-8 magnetic susceptibility balance, and the instrument was calibrated using nickel metal.

2.3. X-ray crystallography

Suitable single crystals were mounted on a glass fiber and these samples were used for data collection. Data were collected at room temperature and with Mo Kα radiation ($\lambda = 0.71073$ Å) on a Bruker SMART CCD 1000 diffractometer. The data were processed with SAINT [14] and corrected for absorption using SADABS [15]. The structures were solved by direct methods [16], which revealed the position of all non-hydrogen atoms. These atoms were refined on F^2 by a full-matrix least-squares procedure using anisotropic displacement parameters [17]. Hydrogen atoms were located in difference maps (**1** and **3**) or placed geometrically, but the OH^- and H_2O hydrogen atoms were located unambiguously from difference Fourier maps (**2** and partly in **4**). All hydrogen atoms were included as fixed contributions riding on attached atoms with isotropic atomic displacement parameters constrained to be 1.2 times those of their carrier atoms. Criteria for a satisfactory complete analysis were the ratios of *rms* shift to standard deviation less than 0.001 and no significant features in final difference maps. Atom scattering factors were taken from the International Tables for Crystallography [18]. Crystal and refinement data are listed in Table 1.

2.4. Preparation of the complexes

2.4.1. Synthesis of $[Cu(bpy)(\mu_2\text{-MANO})]_2 \cdot 8H_2O$ (**1**), $[Cu(bpy)(MANO)] \cdot 4H_2O$ (**2**), and $[Cu_4(_3\text{-}OH)_2(_2\text{-}MANO)_2(bpy)_4](phglyo)_2 \cdot 8H_2O$ (**3**)

To a stirred suspension of $Cu_2CO_3(OH)_2$ (0.100 g, 0.452 mmol) in distilled water (15 mL) were added a solution of mandelic acid (0.138 g, 0.907 mmol) in water (10 mL) and then *bpy* (0.142 g, 0.909 mmol). The mixture was heated under reflux for 3 h and was then stirred at room temperature for a further 7 d. The resulting blue solution was filtered and slow evaporation of the solvent in air at room temperature afforded micro-crystals of **1**, which were separated by filtration. The resulting solution was left in open air, and slow evaporation of the solvent at room temperature gave a few blue crystals of **2** suitable for a single-crystal X-ray analysis. Finally, after about ten weeks, an unidentified brown solid and crystals of **3** were obtained from the final solution and these were easily separated. A similar result for **3** has been obtained by passing a strong flow of air through the dissolution for 12 days.

*2.4.1.1. $[Cu(bpy)(\mu_2\text{-MANO})]_2 \cdot 8H_2O$ (**1**).* Yield: 61% (122 mg), based on $C_{36}H_{44}Cu_2N_4O_{14}$ ($M_r = 883.83$). *Anal.* calc. C, 48.9; H, 5.0; N, 6.3. Found: C, 49.4; H, 5.1; N, 6.2%. IR (KBr pellets, cm^{-1}): 3388 m,br ν(OH), 1654 m,br δ(OH), 1600 $\nu_{as}(CO_2)$, 1499 m, 1446 m ν(bpy, C=N + C=C), 1391 m $\nu_s(CO_2)$, 640 w, 422 w (bpy, ring), 338 w ν(CuO), 264 w ν(CuN). UV–Vis (λ_{max}, cm^{-1}) in solid state: 23690, 16110, 15600, 14347. EPR (room temperature): $g_{||} = 2.26$, $g_{\perp} = 2.10$.

*2.4.1.2. $[Cu(bpy)(MANO)] \cdot 4H_2O$ (**2**).* Yield: 28% (90 mg), based on $C_{18}H_{22}CuN_2O_7$ ($M_r = 441.92$). *Anal.* calc. C, 48.9; H, 5.0; N, 6.3. Found: C, 49.2; H, 4.8; N, 6.3%. IR (KBr pellets, cm^{-1}): 3422 m,br ν(OH), 1622 s, br δ(OH), 1592 s $\nu_{as}(CO_2)$, 1492 m, 1446 m ν(bpy, C=N + C=C), 1358 m,br $\nu_s(CO_2)$, 636 w, 426 w (bpy, ring), 394 w ν(CuO), 280 w ν(CuN). UV–Vis (λ_{max}, cm^{-1}) in solid state: 23697, 17270, 15925. μ_{eff} (BM): 1.82. EPR (room temperature): $g_{||} = 2.24$, $g_{\perp} = 2.06$.

Table 1
Crystal data and structure refinement for $[Cu(bpy)(\mu_2\text{-MANO})]_2 \cdot 8H_2O$ (**1**), $[Cu(bpy)(MANO)] \cdot 4H_2O$ (**2**), $[Cu_4(\mu_3\text{-}OH)_2(\mu_2\text{-}MANO)_2(bpy)_4](phglyo)_2 \cdot 8H_2O$ (**3**) and $[Cu_4(\mu_3\text{-}OH)_2(\mu_2\text{-}OH)_2(OH_2)_2(phen)_4](Bza)_2(OH)_2 \cdot 5H_2O$ (**4**)

Compound	**1**	**2**	**3**	**4**
Empirical formula	$C_{36}H_{44}Cu_2N_4O_{14}$	$C_{18}H_{22}CuN_2O_7$	$C_{72}H_{72}Cu_4N_8O_{22}$	$C_{62}H_{62}Cu_4N_8O_{17}$
Formula weight	883.83	441.92	1655.54	1445.36
Crystal system	triclinic	monoclinic	triclinic	triclinic
Space group	$P\bar{1}$ (No. 2)	$P2_1/c$ (No. 14)	$P\bar{1}$ (No. 2)	$P\bar{1}$ (No. 2)
Unit cell dimensions				
a (Å)	10.299(2)	12.146(2)	10.384(2)	10.136(3)
b (Å)	10.575(2)	17.869(2)	12.469(2)	13.322(3)
c (Å)	19.504(4)	9.149(1)	13.663(3)	13.690(3)
α (°)	94.174(4)	90	89.183(3)	78.081(4)
β (°)	92.242(4)	104.584(2)	78.866(3)	68.782(4)
γ (°)	113.965(3)	90	83.853(3)	75.433(4)
Volume ($Å^{-3}$)	1930.4(7)	1921.7(4)	1775.5(6)	1654.2(7)
Z	2	4	1	1
D_{calc} (Mg/m^3)	1.521	1.527	1.548	1.451
Absorption coefficient (mm^{-1})	1.174	1.180	1.265	1.341
$F(000)$	916	916	852	742
Crystal size	0.21 × 0.18 × 0.09	0.53 × 0.27 × 0.23	0.41 × 0.10 × 0.05	0.29 × 0.11 × 0.09
θ Range (°)	1.05–26.40	1.73–26.42	1.52–26.42	1.59–26.37
Limiting indices (h,k,l)	−12/12, −13/13, 0/24	−15/14, 0/22, 0/11	−12/13, −15/15, 0/17	−11/12, −16/16, 0/17
Reflections collected/unique (R_{int})	20224/7840 (0.0431)	16435/3928 (0.0251)	16723/7237 (0.0509)	11631/6611 (0.0506)
Completeness to θ (%)	99.1	99.5	98.8	97.6
Maximum/minimum transmission	0.9017/0.7906	0.7731/0.5736	0.9394/0.6250	0.8888/0.6971
Data/parameters	7840/505	3928/253	7237/478	6611/412
Goodness-of-fit on F^2	1.035	1.079	0.943	0.917
Final R indices	$R_1 = 0.0610$, $wR_2 = 0.1545$	$R_1 = 0.0300$, $wR_2 = 0.0751$	$R_1 = 0.0506$, $wR_2 = 0.1058$	$R_1 = 0.0822$, $wR_2 = 0.2257$
R indices (all data)	$R_1 = 0.1358$, $wR_2 = 0.1966$	$R_1 = 0.0425$, $wR_2 = 0.0822$	$R_1 = 0.1232$, $wR_2 = 0.1241$	$R_1 = 0.1630$, $wR_2 = 0.2601$
Largest difference in peak/hole (e $Å^{-3}$)	0.765/−0.843	0.296/−0.287	0.516/−0.674	1.794/−0.924

2.4.1.3. [$Cu_4(\mu_3\text{-}OH)_2(\mu_2\text{-}MANO)_2(bpy)_4](phglyo)_2 \cdot 8H_2O$ (3). Yield: <5% (10 mg), based on $C_{72}H_{72}Cu_4N_8O_{22}$ (M_r = 1653.54). *Anal.* calc. C, 52.2; H, 4.4; N, 6.8. Found: C, 50.6; H, 4.7; N, 6.7%. IR (KBr pellets, cm^{-1}): 3430 m,br ν(OH), 1610sh δ(OH), 1605 s $\nu_{as}(CO_2)$, 1518 m, 1429sh *ν*(bpy, C═N + C═C), 1384 m,br $\nu_s(CO_2)$, 642 w, 431 w (bpy, ring), 398 w *ν*(CuO), 293 w *ν*(CuN). Owing to the extremely low yield, magnetic characterization was not carried out.

*2.4.2. Synthesis of [$Cu_4(_3\text{-}OH)_2(_2\text{-}OH)_2(OH_2)_2(phen)_4](Bza)_2(OH)_2 \cdot 5H_2O$ (**4**)*

To a stirred suspension of $Cu_2CO_3(OH)_2$ (0.100 g, 0.452 mmol) in distilled water (15 mL) were added a solution of mandelic acid (0.138 g, 0.907 mmol) in water (10 mL) and then phen (0.180 g, 0.908 mmol). The mixture was heated under reflux for 3 h and then magnetic stirring was maintained at room temperature for a week. The resulting greenish-blue solid was filtered off, washed with water and dried over calcium chloride. This solid was not identified. After about six weeks, the resulting solution was left in open air, and slow evaporation of the solvent at room temperature gave a few greenish single crystals of **4** suitable for X-ray diffraction studies and these were separated by hand. Yield: <10% (13 mg), based on $C_{62}H_{62}Cu_4N_8O_{17}$ (M_r = 1445.36). *Anal.* calc.: C, 51.5; H, 4.3; N, 7.8. Found: C, 51.7; H, 4.8; N, 7.4%. IR (KBr pellets, cm^{-1}): 3363 s,br *ν*(OH), 1612 s,br *δ*(OH), 1586 s $\nu_{as}(CO_2)$, 1519 w, 1427 m *ν*(phen, C═N + C═C), 1387 m,br $\nu_s(CO_2)$, 628 w, 430 w (bpy, ring), 384 w *ν*(CuO), 255 w *ν*(CuN). Owing to the extremely low yield, magnetic characterization was not carried out. A similar result has been obtained by passing a strong flow of air through the dissolution for eight days.

3. Results and discussion

Aqueous solutions resulting from reactions between $Cu_2(OH)_2CO_3$, mandelic acid (H_2MANO) and 2,2′-bipyridine (bpy) or 1,10-phenanthroline (phen), after prolonged exposure to air, yield crystals of $[Cu(bpy)(\mu_2\text{-}MANO)]_2 \cdot 8H_2O$ (**1**), $[Cu(bpy)(MANO)] \cdot 4H_2O$ (**2**), $[Cu_4(\mu_3\text{-}OH)_2(\mu_2\text{-}MANO)_2(bpy)_4](phglyo)_2 \cdot 8H_2O$ (**3**) or $[Cu_4(\mu_3\text{-}OH)_2(\mu_2\text{-}OH)_2(OH_2)_2(phen)_4](Bza)_2(OH)_2 \cdot 5H_2O$ (**4**), where phglyo is the phenylglyoxylate anion and Bza is the benzoate anion, respectively. These reactions do not occur under anaerobic conditions.

In the 3000–3500 cm^{-1} region, the IR spectra of complexes show two bands, generally of medium intensity, corresponding to OH stretching vibrations. The strong band around 1605–1585 cm^{-1} is attributable to ν_{asym}(OCO), and the band between 1355 and 1390 cm^{-1} to ν_{sym}(OCO). The values of $\Delta\nu = \nu_{asym}(O\text{-}CO) - \nu_{sym}(OCO)$, 199–234 cm^{-1}, are typical of monodentate carboxylato groups [19] and very similar to those found in copper(II)/α-hydroxycarboxylato/1,10-phen or bpy systems [20]. The bands around 1490 and 1450 cm^{-1} are due to the C═C and C═N stretching modes of the coordinated diimine molecules. On the other hand weak bands at 640 and 420 cm^{-1} correspond to the pyridine ring deformations. A weak band around 400 cm^{-1} is assignable to *ν*(CuO), and the band between 250 and 300 cm^{-1} is tentatively identified as due to *ν*(CuN) [21].

The electronic (diffuse reflectance) spectra of complexes **1** and **2** show three broad bands in the visible region. A band is observed at 23700 cm^{-1} and must be due to metal-ligand charge-transfer processes (MLCT) probably $\pi \rightarrow d_{x^2-y^2}$ and d_{z^2} (Cu^{II}). In contrast to other copper(II) complexes, in this case there does not seems to be a clear correlation between the position of the maximum of this band and the coordination geometry or the nature of the ligand coordinated to the metal. The band that is observed in the lower energy region of the spectrum, between 17270 and 15600 cm^{-1}, correspond to a d–d transition [22].

3.1. Description of crystal structures

*3.1.1. Structure of $[Cu(bpy)(_2\text{-}MANO)]_2 \cdot 8H_2O$ (**1**)*

The asymmetric unit is formed by two half molecules (**I** and **II**). The structure of the molecule **I** of $[Cu(bpy)(\mu_2\text{-}MANO)]_2$, is shown in Fig. 1. These compounds consist of a centrosymmetric dimer in which the non-carboxy mandelato oxygens bridge between copper atoms that are each chelated by a *bpy* molecule and are also coordinated by a carboxy mandelato oxygen. The resulting coordination polyhedra are square pyramids (Addison's τ = 0.14 in **I** and 0.11 in **II** [23]) with the copper atom at the center of a base plane defined by the *bpy* nitrogen atoms, the carboxy oxygen and one of the bridging alkoxide oxygen atoms. As one would expect in square pyramidal copper complexes, the Cu-apex distance Cu1–O13[a], 2.269(4)/2.292(4) Å, is longer than the bond lengths in the base [Cu1–O13 = 1.938(4)/1.935(4) Å] due to the $\sigma^*(d_{z^2})^2\sigma^*(d_{x^2-y^2})^1$ configuration of the copper(II) ion (Table 2). The oxygen bridge is thus very asymmetric, in spite of the overall symmetry of the dimer. The basal Cu–O distance and the Cu–N distances [1.987(1)–2.017(1) Å] are within the usual range for complexes of copper(II) with chelating *bpy*, bridging alkoxido and non-bridging carboxylato ligands [24]. The axial Cu–O distance is similar to those found in other dimers with asymmetric alkoxido bridges [25]. However, the narrow Cu–O–Cu bridging angles [92.54(17)/87.71(15)° in **I** and 90.28(6)° in **II**] mean that the Cu···Cu distance in the dimer is only 3.0491(15)/3.0582(14) Å, and according to magneto-structural correlations for bis-alkoxide bridged cooper dimers [26–28] the acute Cu–O–Cu. angle would lead to a ferromagnetic coupling in compound **1**.

The half-dimer that forms the asymmetric unit is not completely flat. In **I** the deviations from the least-squares planes of the 2,2′-bipyridine and mandelato ligands are 0.043(6) and 0.108(4) Å, respectively, for C22 and C11. These two least-squares planes (represented by N11—N12 and O11—O13) make a dihedral angle of 38.1(2)° and the copper atom lies 0.231(2) Å nearer to O13[a] than the base plane of the coordination polyhedron. The corresponding distances and angles in **II** are 0.021(6) Å (C49), 0.080(3) Å (C31), 38.9(2)° (N31—N32 and O21—O23) and 0.240(2) Å (O23[a]), respectively.

The packing in the lattice is dominated by different hydrogen bonding networks (Table 3). There are hydrogen bonds between

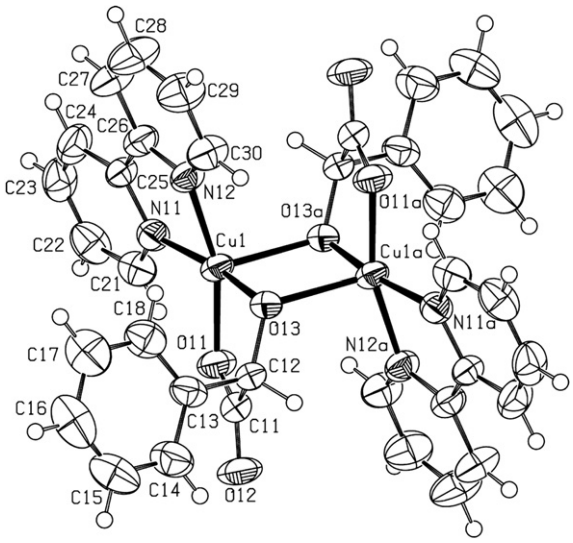

Fig. 1. Perspective view of **1** (molecule **I**), showing 50% probability ellipsoids for the non-hydrogen atoms and the numbering scheme for the atoms in the molecule. For the sake of clarity crystallization water molecules have been omitted.

Table 2
Selected interatomic bond distances (Å) and angles (°) for [Cu(bpy)(μ2-MANO)]2 · 8H2O (**1**) and [Cu(bpy)(MANO)] · 4H2O (**2**)

Compound	**1**		**2**
	Molecule **I**	Molecule **II**[a]	
Cu1–O11	1.952(4)	1.928(4)	1.8984(15)
Cu1–O13	1.938(4)	1.935(3)	1.8899(15)
Cu1–N11	1.988(5)	1.996(4)	1.9885(18)
Cu1–N12	2.015(5)	1.998(5)	1.9825(17)
Cu1–O13[a]	2.269(4)	2.292(4)	
O13–Cu1–O11	85.11(17)	85.39(15)	86.68(6)
O11–Cu1–N11	93.38(19)	93.44(17)	92.70(7)
O13–Cu1–N11	170.67(18)	169.28(19)	174.53(8)
O11–Cu1–N12	162.04(19)	162.26(19)	173.66(7)
O13–Cu1–N12	97.45(18)	96.66(17)	99.21(7)
N11–Cu1–N12	81.2(2)	81.26(18)	81.67(7)
O11–Cu1–O13[a]	97.02(16)	97.63(16)	
O13–Cu1–O13[a]	87.46(17)	87.71(15)	
N11–Cu1–O13[a]	101.87(17)	103.00(17)	
N12–Cu1–O13[a]	100.85(17)	100.06(17)	

Symmetry transformations: $-x+1, -y, -z$; $-x+1, -y+1, -z+1$.
[a] Atoms labelled as Cu2, O21, O23, N21 and N22.

the water molecules and between one of these and the uncoordinated mandelato oxygen (O12, O22). In the crystals, however, these sets of hydrogen bonds result in the water molecules binding together the stepped chains of dimers that are created in the [1 0 0] and [0 1 0] directions for molecules **I** and **II**, respectively, through π–π interactions between the pyridine rings of one half-dimer and those of the opposite half-dimer of a neighboring molecule [centroid–centroid distances 3.754(4)/3.934(4) Å]. The interconnections of dimers and water molecules result in 1D chains with base vectors [1 1 0] (Fig. 2).

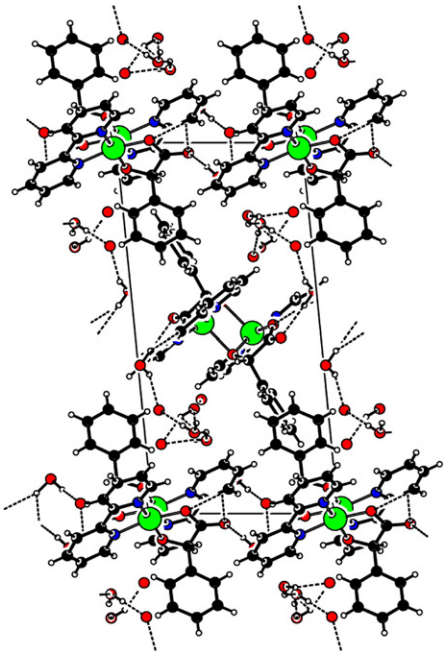

Fig. 2. View of the crystal cell and hydrogen bonds of **1** in the plane *bc*.

3.1.2. Structure of [Cu(bpy)(MANO)] · 4H2O (*2*)

Relevant bond distances and angles are given in Table 2. A molecular representation of the neutral complex is shown in Fig. 3. The copper atom is coordinated to the nitrogen atoms of the single *bpy* ligand and two oxygen atoms belonging to a dideprotonated bidentate mandelato ligand (which like *bpy* forms a five-membered chelate ring), giving rise to a square-planar environment (mean deviation = 0.0682 Å) in which the copper atom lies in the least-squares plane defined by the four nitrogen and oxygen atoms [0.0235(9) Å]. The Cu–N distances are longer than the Cu–O distances and similar to the Cu–N distances in **1**. However, the square-planar coordination geometry leads to the Cu–O distance being shorter than the Cu–O distance in **1** (Table 2). In the complex there are stacking interactions between the *bpy* rings of neighboring molecules, with an inter-ring distance of 3.824(2) Å and these are chelate-ring type [centroid–centroid distance 3.523(1) Å]. Finally, the presence of water of crystallization gives rise to an infinite 3D framework of hydrogen bonds (Table 3).

Table 3
Main hydrogen bonds (in Å and °) for [Cu(bpy)(μ2-MANO)]2 · 8H2O (**1**) and [Cu(bpy)(MANO)] · 4H2O (**2**)

D–H···A	*d*(D–H)	*d*(H···A)	*d*(D···A)	∠(DHA)
Compound ***1***				
O1–H1A···O6	1.05	1.86	2.840(10)	154.8
O1–H1B···O7	1.09	1.78	2.715(13)	141.1
O2–H2A···O22[b]	0.94	2.24	3.063(7)	145.7
O2–H2A···O21[b]	0.94	2.29	3.149(8)	150.4
O2–H2B···O8[c]	0.98	1.95	2.732(15)	134.7
O3–H3A···O12[d]	0.90	2.02	2.844(9)	152.3
O3–H3B···O12[a]	1.05	2.18	2.871(9)	121.5
O3–H3B···O11[a]	1.05	2.28	3.261(9)	155.2
O4–H4A···O8[c]	0.85	1.74	2.591(19)	177.6
O4–H4B···O6	0.85	2.05	2.901(12)	179.6
O5–H5A···O4[e]	1.03	1.99	2.929(16)	149.7
O5–H5B···O7	1.09	1.87	2.750(15)	134.6
O5–H5B···O1	1.09	2.18	2.993(14)	129.1
Symmetry transformations: a = $-x+1, -y, -z$; b = $-x+1, -y+1, -z+1$; c = $x-1, y, z$; d = $x+1, y+1, z$; e = $x+1, y, z$.				
Compound ***2***				
O1–H1A···O12[a]	0.77	2.08	2.823(2)	162.3
O1–H1B···O12[b]	0.93	1.94	2.845(3)	161.3
O2–H2A···O13	0.93	1.92	2.836(2)	166.8
O2–H2B···O2[b]	0.72	2.02	2.734(4)	168.2
O3–H3A···O1	0.91	1.84	2.750(3)	174.9
O3–H3B···O2	0.82	1.98	2.738(3)	153.0
O4–H4A···O13[c]	0.91	1.94	2.819(2)	161.9
O4–H4B···O3	0.92	2.00	2.761(3)	138.9
Symmetry transformations: a = $x-1, y, z$; b = $-x+1, -y, -z$; c = $-x+1, -y, -z+1$.				

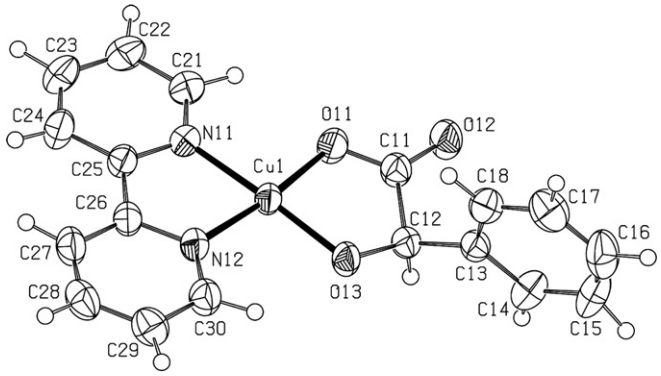

Fig. 3. Perspective view of **2**, showing 50% probability ellipsoids for the non-hydrogen atoms and the numbering scheme of the atoms in the molecule.

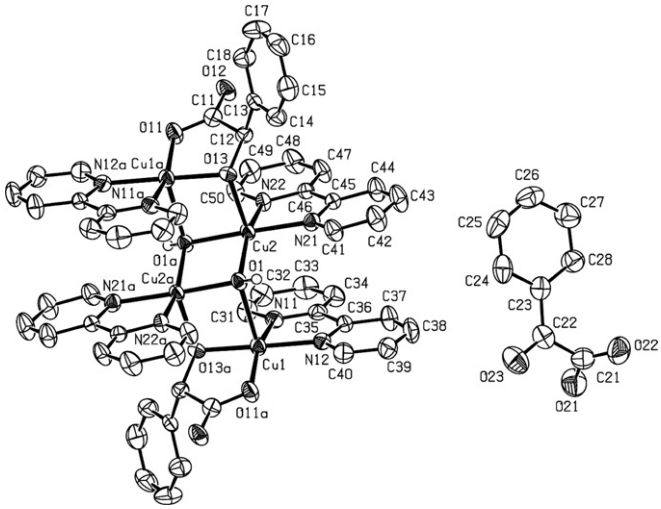

Fig. 4. Perspective view of **3**, showing 50% probability ellipsoids for the non-hydrogen atoms and the numbering scheme of the atoms in the molecule. For the sake of clarity crystallization water molecules and hydrogen atoms have been omitted.

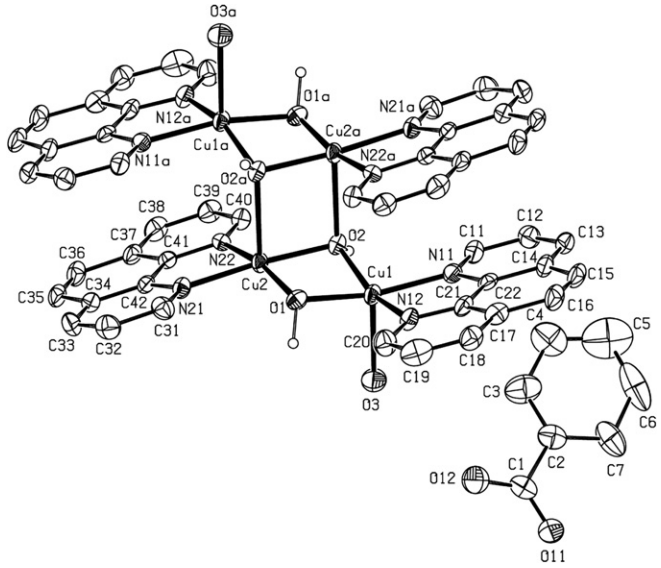

Fig. 5. Perspective view of **4**, showing 30% probability ellipsoids for the non-hydrogen atoms and the numbering scheme of the atoms in the molecule. For the sake of clarity crystallization water molecules and hydrogen atoms have been omitted.

Table 4
Selected interatomic bond distances (Å) and angles (°) for $[Cu_4(\mu_3\text{-}OH)_2(\mu_2\text{-}MANO)_2(bpy)_4](phglyo)_2 \cdot 8H_2O$ (**3**) and $[Cu_4(\mu_3\text{-}OH)_2(\mu_2\text{-}OH)_2(OH_2)_2(phen)_4](Bza)_2(OH)_2 \cdot 5H_2O$ (**4**)

Compound	3	4
Cu1–O1	2.385(3)	1.928(6)
Cu1–O2		1.942(5)
Cu1–O3		2.240(6)
Cu1–O13[a]	1.909(3)	
Cu1–O11[a]	1.922(3)	
Cu1–N11	1.992(4)	2.022(7)
Cu1–N12	1.979(4)	2.017(6)
Cu2–O1	1.959(3)	1.917(5)
Cu2–O2		1.953(5)
Cu2–O2[a]		2.342(5)
Cu2–O13	2.208(3)	
Cu2–N21	2.002(4)	2.010(7)
Cu2–N22	2.026(4)	
		2.031(6)
O1–Cu1–O2		81.9(2)
O1–Cu1–N12	95.88(12)	95.2(2)
O2–Cu1–N12		157.6(3)
O1–Cu1–N11	98.72(12)	167.0(2)
O2–Cu1–N11		96.3(2)
N12–Cu1–N11	81.26(15)	81.6(3)
O1–Cu1–O3		95.7(2)
O2–Cu1–O3		107.4(2)
N12–Cu1–O3		95.7(2)
N11–Cu1–O3		97.1(3)
O13[a]–Cu1–O11[i]	86.36(13)	
O13[a]–Cu1–N12	178.75(14)	
O11[a]–Cu1–N12	94.89(14)	
O13[a]–Cu1–N11	97.54(14)	
O11[a]–Cu1–N11	158.19(15)	
O13[a]–Cu1–O1	83.93(11)	
O11[a]–Cu1–O1	103.04(12)	
O1–Cu2–O2		81.9(2)
O1–Cu2–N21	98.65(13)	96.3(3)
O2–Cu2–N21		175.3(2)
O1–Cu2–N22	156.85(13)	165.8(2)
O2–Cu2–N22		99.0(2)
N21–Cu2–N22	80.62(14)	81.7(3)
O1–Cu2–O2[a]		99.4(2)
O2–Cu2–O2[a]		85.0(2)
N21–Cu2–O2[a]		99.5(2)
N22–Cu2–O2[a]		94.8(2)
O1–Cu2–O1[a]	79.99(12)	
O1[a]–Cu2–N21	178.28(14)	
O1[a]–Cu2–N22	100.21(13)	
O1–Cu2–O13	103.27(11)	
O1[a]–Cu2–O13	87.71(11)	
N21–Cu2–O13	93.64(13)	
N22–Cu2–O13	99.87(13)	

Symmetry transformations: a = $-x$, $-y$, $-z$; a = $1-x$, $1-y$, $-z$.

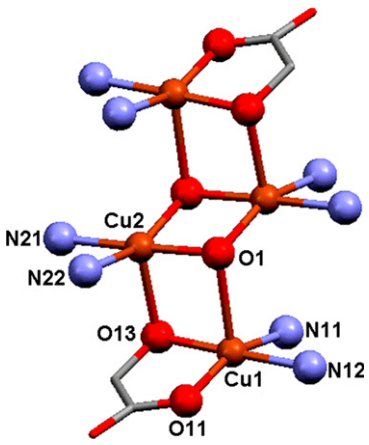

Fig. 6. $Cu_4(OH)_2O_2$ core of **3**.

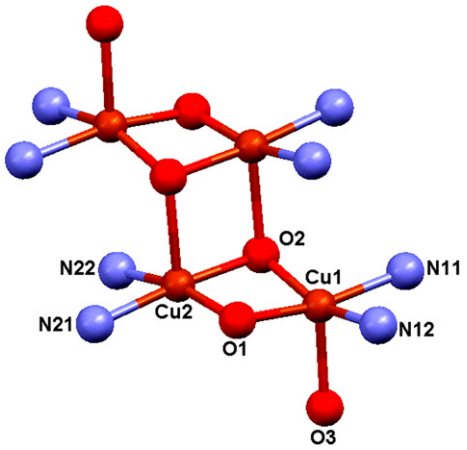

Fig. 7. $Cu_4(OH)_4$ core of **4**.

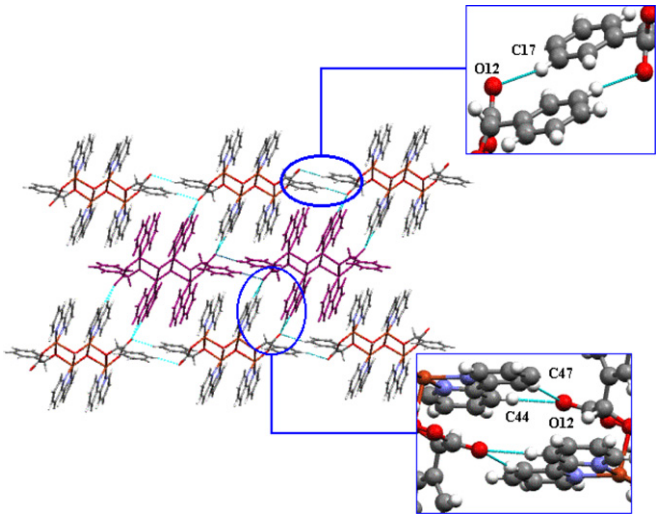

Fig. 8. 2D layer formed by the tetranuclear complex cations in **3** (view down the *c*-axis).

*3.1.3. Structures of $[Cu_4(_3\text{-}OH)_2(_2\text{-}MANO)_2(bpy)_4](phglyo)_2 \cdot 8H_2O$ (**3**) and $[Cu_4(_3\text{-}OH)_2(_2\text{-}OH)_2(OH_2)_2(phen)_4](Bza)_2(OH)_2 \cdot 5H_2O$ (**4**)*

Compounds **3** and **4** are tetranuclear copper(II) complexes with chair-like stepped cubane structures. The molecular structures and atom-labelling schemes are shown for **3** and **4** in Figs. 4 and 5, respectively. Selected bond distances and angles are presented in Table 4.

The structure of **3** consists of divalent $[Cu_4(\mu_3\text{-}OH)_2(\mu_2\text{-}MANO)_2(bpy)_4]^{2+}$ cations (MANO = dianionic mandelato), phenylglyoxylate anions and water molecules. The crystal structure of **4** consists of tetravalent $[Cu_4(OH)_4(phen)_4(H_2O)_2]^{4+}$ complex cations, benzoate and hydroxide anions and H_2O molecules. In this compound the colour of the crystals and the coordination geometry suggest an oxidation state +2 for the copper ions, consequently in order to preserve charge neutrality 6 OH^- groups are required. As we describe later the oxygen atoms labelled as O3 and O6 are involved in a typical hydrogen pattern with two benzoate anions, but the hydrogen atoms of these oxygen atoms could not be successful located in the structure calculation, therefore there is uncertainty about the correspondence of O3 or O6 with a OH^- group.

The two compounds have different Cu_4O_4 cores. In **3** the core is $Cu_4(OH)_2O_2$ (Fig. 6), with a triple-bridging OH and the alkoxide oxygen of the mandelato ligand acting as a bridge between two copper atoms. However, in **4** the $Cu_4(OH)_4$ core (Fig. 7) is formed by triple-bridging and double-bridging OH ligands.

In both compounds the two crystallographically independent copper atoms are pentacoordinated with similar coordination arrangements but different environments. In both cases the coordination polyhedra are essentially square pyramids (geometry 4 + 1), but with a different degree of distortion towards trigonal bipyramid for each compound. The trigonality index τ [23] for the metal centers in **3** the values are 0.34 (Cu1) and 0.36 (Cu2) and in **4** is 0.16 for the two copper atoms, showing the greater distortion of the polyhedra in the first compound.

In **4** the material coordination environment for each Cu is distinct: two nitrogen atoms provided by a phen ligand and two OH bridging ligands ($O1_{\mu_2}$ and $O1_{\mu_3}$) form the equatorial planes around Cu1 and Cu2, but the axial sites are occupied by a ligand (O3) for Cu1 and by an OH μ_3-bridging ligand ($O2^i$) for Cu2. The basal distances are in the range 1.917–2.022 Å and the longer Cu1–O3 (2.240 Å) and Cu2–$O2^i$ (2.342 Å) distances result from the Jahn–Teller distortion around the metal atoms. This axial-equatorial bridge formed by the hydroxide ion at Cu2 is unusual even for hy-

Table 5
Main hydrogen bonds (in Å and °) for $[Cu_4(\mu_3\text{-}OH)_2(\mu_2\text{-}MANO)_2(bpy)_4](phglyo)_2 \cdot 8H_2O$ (**3**) and $[Cu_4(\mu_3\text{-}OH)_2(\mu_2\text{-}OH)_2(OH_2)_2(phen)_4](Bza)_2(OH)_2 \cdot 5H_2O$ (**4**)

D–H···A	*d*(D–H)	*d*(H···A)	*d*(D···A)	∠(DHA)
Compound ***3***				
O1–H1···$O2^b$	0.94	2.00	2.919(4)	166.2
O2–H2A···$O4^c$	1.05	1.71	2.745(5)	168.8
O2–H2B···$O5^d$	1.05	1.90	2.886(6)	154.1
O3–H3A···$O12^e$	0.96	1.99	2.925(5)	166.0
O4–H4A···O21	0.96	2.04	2.773(6)	131.2
O5–H5A···$O21^f$	0.92	1.97	2.843(6)	157.8
O5–H5B···O3	0.83	2.05	2.871(6)	170.0
C17–H17···$O12^g$	0.93	2.53	3.443(6)	166.0
C44–H44···$O12^e$	0.93	2.27	3.199(6)	178.0
C47–H47···$O12^e$	0.93	2.35	3.273(6)	171.0
Symmetry transformations: b = $-x$, $-y$, $1-z$; c = $1-x$, $-y$, $1-z$; d = $-x$, $1-y$, $1-z$; e = $-x$, $1-y$, $-z$; f = $1-x$, $1-y$, $1-z$; g = $1-x$, $1-y$, $-z$				
Compound ***4***				
O1–H1A···$O11^b$	1.05	1.79	2.786(9)	158.3
O2–H2A···O5	0.74	2.59	3.322(9)	175.0
O3···O6			2.723(11)	
O6···O12			2.772(12)	
O6···O5			3.249(11)	
O7···$O12^c$			3.161(21)	
Symmetry transformations: b = $-x$, $1-y$, $1-z$; c = $-x$, $-y$, $1-z$.				

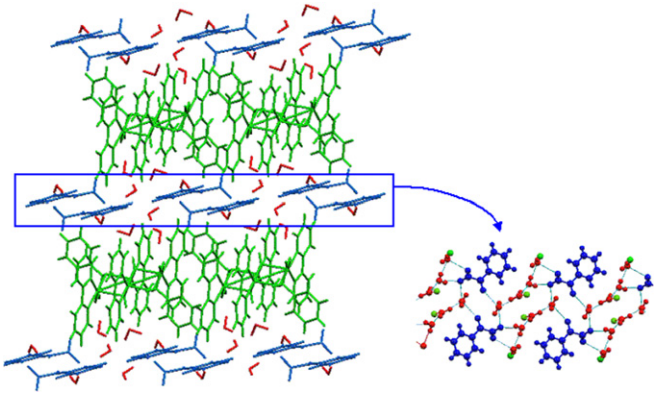

Fig. 9. 3D network in **3** (view down *b*-axis).

droxo-bridged copper(II) dimers [29] but has also been found in some tetranuclear copper hydroxo-complexes [30]. The Cu—OH_{μ_2} distances [1.928(6) and 1.917(5) Å], as expected, are shorter than the Cu—OH_{μ_3} distances [1.942(5) and 1.953(5) Å].

In **3**, the coordination environments around the Cu atoms are also different. The basal plane around Cu1, with bond distances in the range 1.909–1.992 Å, is formed by two nitrogen atoms of one bpy molecule and by the two oxygen atoms of one dianionic bidentate chelating mandelato molecule. The apical position is occupied by the triple-bridging OH ligand at 2.385(3) Å. The equatorial plane of Cu2, with bond distances in the range 1.959–2.026 Å, consists of two nitrogen atoms (bpy) as well as two oxygen atoms from two OH ligands. The axial site is occupied by the bridging alkoxide oxygen of the mandelato ligand at a distance of 2.208(3) Å. The shortest Cu–Cu distances are 3.0015(12) Å in **3** and 2.9011(13) Å in **4**, which rules out the existence of direct Cu to Cu interactions such as those observed, e.g. in copper acetate (2.64 Å) [31].

In both compounds the four Cu atoms form flat rhomboids with sides of length 2.9011(13) Å (Cu1–Cu2) and 3.5225(15) Å (Cu1–Cu2^a, a = 1 − *x*, 1 − *y*, −*z*) in **4** and 3.4964(9) Å (Cu1–Cu2) and 3.1023(9) Å (Cu–Cu2^a, a = −*x*, −*y*, −*z*) in **3**. The short diagonals of the rhomboids (Cu2–Cu2^a) are 3.177(7) Å in **4** and 3.0015(12) Å in **3** and the long diagonals (Cu1–Cu1^a) are 5.617(2) Å in **4** and 5.890 Å in **3**.

The "step structures" are defined by three four-membered rings. These rings in **4** are the strictly planar Cu2–O2–Cu2^a–O2^a ring, because there is an inversion center in the middle of this core, and the other two four member ring, Cu2–O1–Cu1–O2 and Cu^a–O1^a–Cu2^a–O2^a, also related by symmetry, which have a dihedral angle between them of 75.0°. In **3** the planar ring is Cu2–O1–Cu2^a–O1^a and the non-planar ring is Cu1–O13–Cu2–O1, with a dihedral angle of 85.8°.

In both tetranuclear compounds the supramolecular organization results from the combination of several weak intermolecular interactions and these are briefly described below.

In **3** the cationic species are assembled through CH···O-type hydrogen bonding to give 2D layers parallel to (001) (Fig. 8). The C···O distances are in the range 3.199–3.443 Å (Table 5). In all of these interactions the acceptor is the uncoordinated oxygen atom (O12) of the MANO ligand and the donors are CH-bpy and CH-MANO groups, as represented in Fig. 8. In this way each cation interacts with four neighboring ones. The 2D layer is also stabilized by π–π stacking interactions between the bpy rings, where the shortest distance between the center of the rings is 3.719 Å and these have a dihedral angle of 3.15°.

These sheets are linked by strong hydrogen bonding between the lattice water, the phglyo anions and the hydroxo and mandelato ligands of cations [Ow···Ophglyo; Ow···Ow; Ow···OMANO and OH(cation)···Ow]. As a result, a chain of hydrogen-bonded phglyo

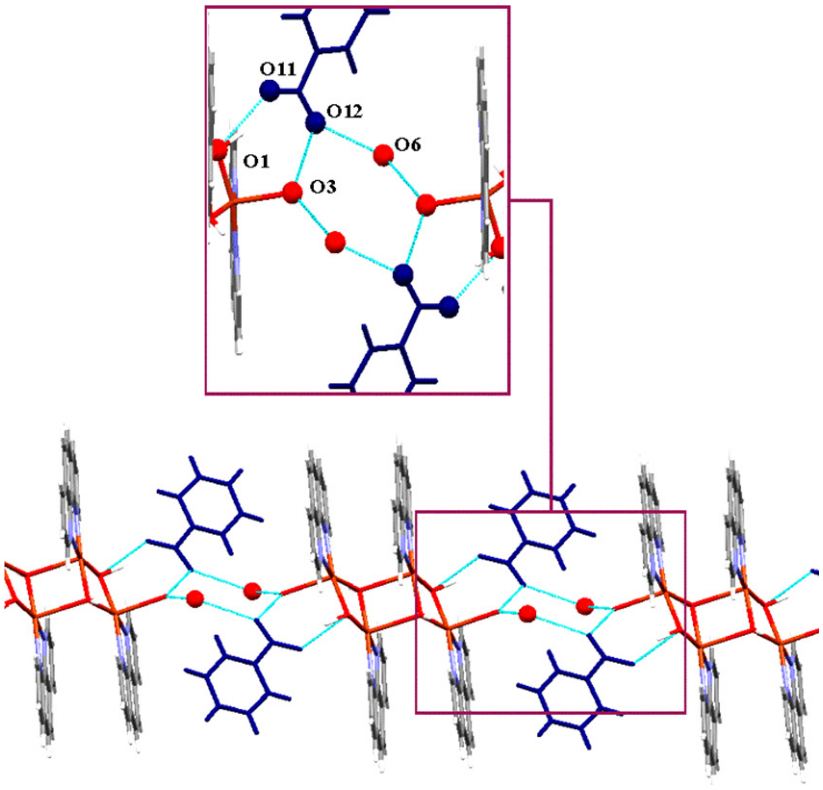

Fig. 10. 1D linkage by hydrogen bonds in **4** (view down the *b*-axis).

anions and water lattice molecules join the sheets of cations, as represented in Fig. 9. The O···O distances (Table 5) range between 2.745 and 2.925 Å.

In **4** a 1D chain, which is represented in Fig. 10, is formed by strong hydrogen bonding, with O···O distances in the range 2.723–2.786 Å (Table 5), showing a characteristic hexagonal pattern involving two benzoate anions, two O6 atoms and the coordinated O3 and the μ_2-OH (O1) of two tetranuclear cationic species.

On the other hand, owing to the interdigitation of phen rings, the neighboring 1D chains are self-assembled into 2D sheets through π–π interactions that are characterized by distances of 3.632(5) and 3.736(5) Å and interplanar dihedral angles α of 2.97° and 1.43°, indicating the parallelism of the phen rings (Fig. 11). The interactions C(15)H(phen)···O3 between chains, with a C···O distance of 3.48(1) Å, also contributes to the formation of this 2D sheet.

The intercalation of benzoate anions on both sides of the sheets expands the structure into a 3D network (Fig. 12). As a result of this intercalation, the aromatic ring planes of benzoate anions overlap in an offset or displaced geometry with significant ring slippage [32], to the extent that there are only limited atom-atom interactions, with the shortest distance being 3.47(3) Å for C4···C5 (1 − *x*, −*y*, 1 − z). In the resulting 3D structure the water molecules of crystallization other than O6 (labelled as O5, O7 and O8) are weakly linked by hydrogen bonding with D···A distances greater than 3.2 Å (Table 5), as shown in Fig. 13.

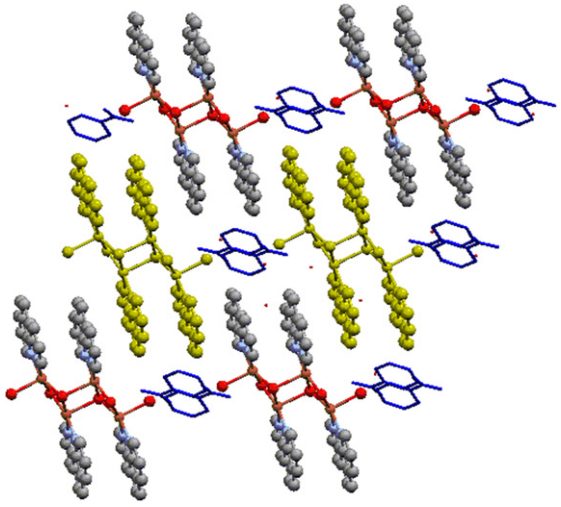

Fig. 11. π–π Stacking interactions between the chains of **4** (view down the *b*-axis).

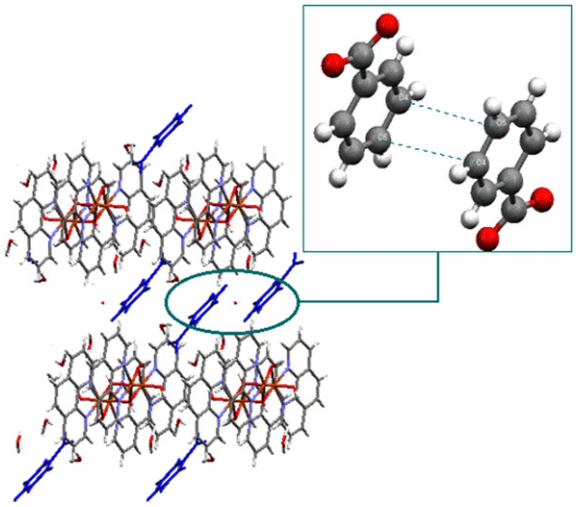

Fig. 12. Interaction between the 2D sheets through the benzoate anions in **4** (down the *c*-axis).

3.2. Oxidative cleavage mechanism

Numerous kinetic studies have been carried out on hydroxy-acid oxidation reactions, particularly using H_2MANO and different oxidizing agents such as (2,2′-bipyridine)copper(II) permanganate [33], potassium permanganate in acid solution [34], lead tetraacetate [35], benzo-dipteridine with Zn^{2+}, Co^{2+} or Ni^{2+} ions and the presence of a basic amine (such as Et_3N) in MeCN or *t*-BuOH [13,36], polyanilines and salts of transition metals such as copper(II) or iron(III) chlorides [37], O_2 and copper(II) [38] or cobalt(II) chlorides [39]. In all cases, it was concluded that the possible pathway for oxidative H_2MANO cleavage follows two different routes depending on the catalytic pathway, giving rise to the formation of benzoic acid (HBza) and/or benzaldehyde (Bz). According to these findings, as well as the results of our own studies, we propose the two routes summarized in Scheme 1.

Route 'a' involves an initial step for the dehydrogenation of H_2MANO and formation of phenylglyoxylic acid (Hphglyo) (1) and a second step for its oxidative decarboxylation to HBza (2) or its decarboxylation to Bz (3). Alternatively, route 'b', which also consists of two steps, begins with oxidative decarboxylation to give Bz (3) followed by the easy and expected oxidation of this aldehyde to HBz.

This dual mechanism has been confirmed by studies in which $CoCl_2$ was used as a catalyst. The results showed that route 'a' for the oxidation of phglyo to Bza is a very slow process, whereas route 'b' for the oxidation of Bz to Bza is a very fast reaction [39].

Our experimental results proved that the phenylglyoxylate anion is included in the formula of compound **3** as a result of the reaction between H_2MANO and Cu^{II} in the presence of bpy. On the other hand, the benzoate anion is also present in compound **4** as a result of a similar reaction, but with phen instead of bpy.

On the basis of the similarities between our studies and those carried out with $CoCl_2$ as a catalyst [39], it seems clear that the specific structure of the aromatic diimine used plays a very important role in determining the route that is followed in the catalytic reaction. Thus, when the reaction in question occurs in the presence of bpy, H_2MANO will be converted in Hphglyo by route 'a' and, be-

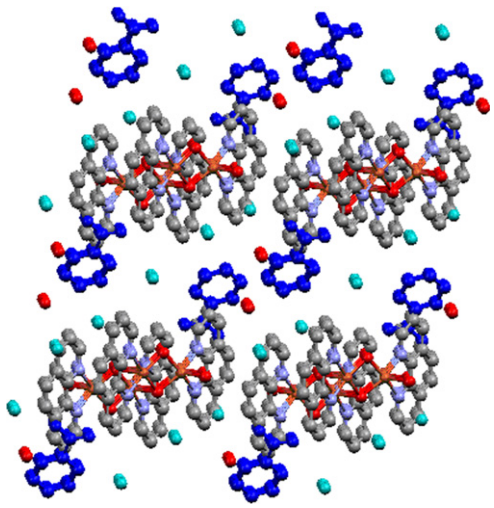

Fig. 13. 3D network in **4**, showing the water molecules of crystallization.

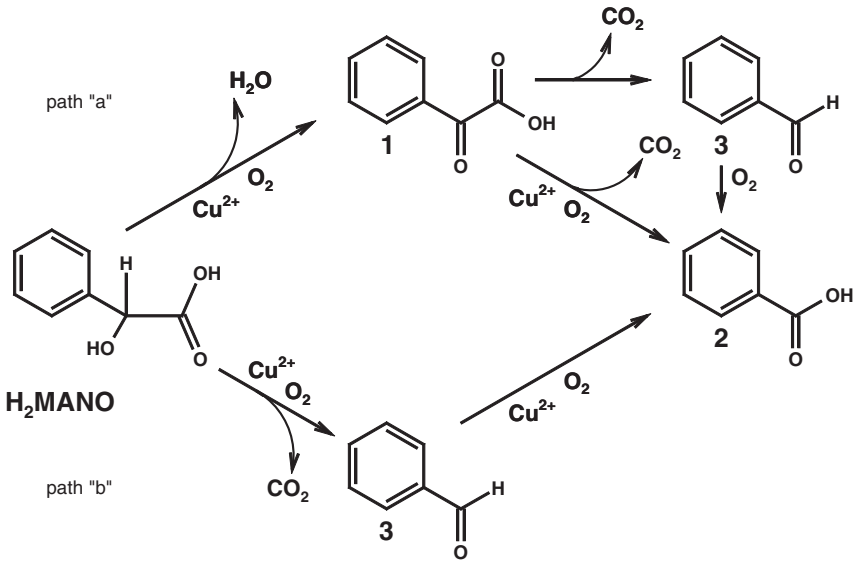

Scheme 1.

cause oxidative decarboxylation of phglyo to Bza is very slow, compound **3** crystallizes with phglyo as a counter-anion. In contrast, when the reaction occurs in the presence of phen, H_2MANO will be converted to Bz by route 'b'. In this case, the rapid oxidation of Bz to Hbza means that compound **4** crystallizes with Bza as a counter-anion.

4. Conclusions

The Cu^{II}/O_2 system in aqueous basic media constitutes a path for the oxidative decarboxylation of mandelic acid. Phenylglyoxylic acid or benzoic acid are obtained, depending on nature of the diimine ancillary ligands. The reaction exhibits an autocatalytic nature and follows two stages, as one of the products [a ternary copper(II) complex] enhances the rate of the reaction. The reaction also represents a confirmation of oxidative decarboxylation of mandelic acid proposed by other authors [39] and, more importantly, the results provide crystallographic evidence to support the oxidation of mandelic acid in the presence of a transition metal ion.

5. Supplementary data

CCDC 665140, 665139, 638839 and 638840 contain the supplementary crystallographic data for **1**, **2**, 3 and **4**. These data can be obtained free of charge via http://www.ccdc.cam.ac.uk/conts/retrieving.html, or from the Cambridge Crystallographic Data Centre, 12 Union Road, Cambridge CB2 1EZ, UK; fax: (+44) 1223-336-033; or e-mail: deposit@ccdc.cam.ac.uk.

Acknowledgements

We thank the Spanish Ministry of Education and Science for financial support (Ref. CTQ2006-15329-C02/BQU and CTQ2006-05642/BQU).

References

[1] (a) J.M. Anderson, J.K. Kochi, J. Am. Chem. Soc. 92 (1970) 2450;
(b) Y.T. Jeon, C.P. Lee, P.M. Mariano, J. Am. Chem. Soc. 113 (1991) 8847;
(c) D. Wang, H.P. Schuchmann, C. von Sonntag, Z. Naturforsch. 48b (1993) 761;
(d) M. Xu, P. Wan, Chem. Commun. 21 (2000) 2147.
[2] (a) J. Rivhard, D. Job, Eur. J. Biochem. 44 (1974) 359;
(b) L.P. Candeias, L.K. Folkes, M. Porssa, J. Parrick, P. Wardman, Biochemistry 35 (1996) 102;
(c) M. Bonifacic, I. Stefanic, G.L. Hug, D.A. Armstrong, K.-D. Asmus, J. Am. Chem. Soc. 120 (1998) 9930;
(d) C. Cervellati, F. Dallocchio, C.M. Bergamini, P.F. Cook, Biochemistry 44 (2005) 2432;
(e) P.K. Grzyska, M.J. Ryle, G.R. Monterosso, J. Lui, D.P. Ballou, R.P. Hausinger, Biochemistry 44 (2005) 3845;
(f) P.Z. Gatzeva-Topalova, A.P. May, M.C. Sousa, Biochemistry 44 (2005) 5328.
[3] (a) L. Eberson, in: S. Patai (Ed.), The Chemistry of Carboxylic Acids, Wiley-Interscience, New York, 1962;
(b) H.J. Schäfer, Angew. Chem., Int. Ed. Engl. 20 (1981) 911.
[4] J.A. Howard, Chem. Peroxides (1983) 235.
[5] J. Paczkowski, D.C. Neckers, in: V. Balzani (Ed.), Electron Transfer in Chemistry, vol. 5, Wiley-VCH, New York, 2001.
[6] I.R. Gould, J.R. Lenhard, A.A. Muenter, S.A. Godleski, S. Farid, J. Am. Chem. Soc. 122 (2000) 11934.
[7] V.M. Paradkar, T.B. Latham, D.H. Demko, Synlett (1995) 1059, and references cited therein.
[8] K.K. Banerji, J. Chem. Res. (S) 193 (M) (1978) 2561.
[9] R. Stewart, Oxidation Mechanisms, Application to Organic Chemistry, W.A. Benjamin Inc., New York, 1964.
[10] M. Sugumaran, Biochemistry 25 (1986) 4489.
[11] R.G. Johnson, R.K. Ingham, Chem. Rev. 56 (1956) 219.
[12] B.C.L. Weedon, Quart. Rev. 6 (1952) 380.
[13] H. Ohshiro, K. Mitsui, N. Ando, Y. Ohsawa, W. Koinuma, H. Takahashi, S. Kondo, T. Nabeshima, Y. Yano, J. Am. Chem. Soc. 123 (2001) 2478.
[14] Bruker, SMART and SAINT, Area Detector Control and Integration Software, Bruker Analytical X-ray Instruments Inc., Madison, WI, USA, 1997.
[15] G.M. Sheldrick, SADABS, Program for Empirical Absorption Correction of Area Detector Data, University of Göttingen, Germany, 1997.
[16] G.M. Sheldrick, Acta Crystallogr., Sect. A 46 (1990) 467.
[17] G.M. Sheldrick, SHELXL-97, Program for the Refinement of Crystal Structures, University of Göttingen, Germany, 1997.
[18] A.J.C. Wilson, International Tables for Crystallography, vol. C, Kluwer Academic Publications, Dordrecht, The Netherlands, 1995.
[19] G.B. Deacon, R.J. Phillips, Coord. Chem. Rev. 33 (1980) 227.
[20] R. Carballo, B. Covelo, S. Balboa, A. Castiñeiras, J. Niclós, Z. Anorg. Allg. Chem. 627 (2001) 948.
[21] K. Nakamoto, Infrared and Raman Spectra of Inorganic and Coordination Compounds, 3rd ed., Wiley, New York, 1978.
[22] A.B.P. Lever, Inorganic Electronic Spectroscopy, 2nd ed., Elsevier, Amsterdam, 1986.
[23] A.W. Addison, T.N. Rao, J. van Rijn, G.C. Verschoor, J. Chem. Soc., Dalton Trans. (1984) 1349.
[24] H.-B. Bürgi, J.D. Dunitz (Eds.), Structure Correlations, vol. 2, VCH, Weinheim, 1994.
[25] K.D. Karlin, Q.-F. Gan, A. Farooq, S. Liu, J. Zubieta, Inorg. Chem. 29 (1990) 2549.
[26] D.J. Hodgson, Prog. Inorg. Chem. 19 (1975) 173.
[27] P.J. Hay, J.C. Thibeaulf, R. Hofman, J. Am. Chem. Soc. 97 (1975) 4884.
[28] (a) M. Handa, N. Koga, S. Kida, Bull. Chem. Soc. Jpn. 61 (1988) 3853;
(b) E. Ruiz, S. Alvarez, P. Alemany, J. Chem. Soc., Chem. Commun. (1998) 2767.
[29] K.D. Karlin, Y. Gultneh, J.C. Hayes, J. Zubieta, Inorg. Chem. 23 (1984) 519.
[30] (a) I.I. Mathews, H. Manohar, J. Chem. Soc., Dalton Trans. (1991) 2139;
(b) Y.Q. Zheng, J-L. Lin, Z. Anorg. Allg. Chem. 628 (2002) 203;
(c) R. Carballo, B. Covelo, E.M. Vázquez-López, E. García-Martínez, A. Castiñeiras, Z. Anorg. Allg. Chem. 628 (2002) 907;

(d) J-H. Yu, H-Y. Bie, J-Q. Xu, J. Lu, X. Zhang, Inorg. Chem. Commun. 7 (2004) 1205.
[31] F. Hanic, D. Stempelová, K. Hanicová, Acta Crystallogr. 17 (1964) 633.
[32] C. Janiak, J. Chem. Soc., Dalton Trans. (2000) 3885.
[33] B.K. Satsangi, S. Kothari, J. Ind. Chem. Soc. 74 (1971) 16.
[34] S.A. Farokhi, S.T. Nadibewoor, Can. J. Chem. 82 (2004) 1372.
[35] Y. Pocker, B.C. Davis, J. Org. Chem. 40 (1975) 1625.
[36] (a) K. Mitsui, Y. Ohsawa, T. Kobayashi, T. Nabeshima, J. Chem. Soc., Chem. Commun. (1993) 1719;
(b) N. Ando, Y. Osawa, T. Nabeshima, Y. Yano, Chem. Lett. (1996) 381.
[37] M. Higuchi, I. Ikeda, T. Hirao, J. Org. Chem. 62 (1997) 1072.
[38] H.R. Bj?rsvik, L. Lignovi, F. Minisci, Org. Proc. Res. Dev. 4 (2000) 534.
[39] I. Favier, E. Duñach, D. Hebrault J.-R. Desmurs, New J. Chem. 28 (2004) 62.

binuclear copper(II) complexes containing hexa (amine compartment) and tetra (imine compartment) coordination sites. The amine compartment consists of two secondary nitrogens, two tertiary nitrogens and two phenolic oxygens (N4O2), whilst the imine compartment comprises of two imine nitrogens and two phenolic oxygens (N2O2). In these systems, one metal is in a 6-coordinate site and the other is in a 4-coordinate site, if a ligand like ClO_4^- is coordinated, this site can be made into a 5-coordinate site [14,15]. The antimicrobial studies of the complexes are also discussed.

2. Experimental

2.1. Analytical and physical measurements

Elemental analysis of the complexes were obtained using a Haereus CHN rapid analyzer. ^{1}H NMR spectra were recorded using a JEOL GSX 400 MHZ NMR spectrometer. Electronic spectral studies were carried out on a Hitachi 320 spectrophotometer in the range 200–1100 nm. IR spectra were recorded on a Shimadzu FTIR 8300 series spectrophotometer on KBr disks in the range 4000–400 cm^{-1}. Molar conductivity was measured using an Elico digital conductivity bridge model CM-88 using a freshly prepared solution of the complex in dimethylformamide. The atomic absorption spectral data were recorded using a Varian spectra AA-200 model atomic absorption spectrophotometer. Mass spectra were obtained on a JEOL SX-102 (FAB) mass spectrometer. Cyclic voltammograms were obtained on a CHI-600A electrochemical analyzer. The measurements were carried out under oxygen free conditions using a three-electrode cell in which a glassy carbon electrode was the working electrode, a saturated Ag/AgCl electrode was the reference electrode and a platinum wire was used as the auxiliary electrode. A ferrocene/ferrocenium (1+) couple was used as an internal standard and $E_{1/2}$ of the ferrocene/ferrocenium (Fc/Fc^+) couple under the experimental conditions was 470 mV. Tetra(*n*-butyl)ammonium perchlorate (TBAP) was used as the supporting electrolyte. The room temperature magnetic moment was measured on a PAR vibrating sample magnetometer Model-155. Variable-temperature magnetic studies were performed on a PAR model 155 vibrating sample magnetometer in the temperature range 77–300 K, and the instrument was calibrated using metallic nickel as supplied with the instrument. The X-band ESR spectra of the Cu(II) complexes were recorded using DMF as a solvent at liquid nitrogen temperature on a Varian EPR-E 112 spectrometer with diphenylpicrylhydrazine (DPPH) as the reference. The catalytic oxidation of catechol to *o*-quinone and the hydrolysis of 4-nitrophenylphosphate by the copper(II) complexes were studied in a 10^{-3} M dimethylformamide solution. The reaction was followed spectrophotometrically by choosing the strongest absorption band of *o*-quinone at 390 nm and monitoring the increase in the absorbance, and the hydrolysis of 4-nitrophenylphosphate was monitored by following the UV absorbance change at 420 nm (assigned to the 4-nitrophenolate anion) as a function of time. A plot of $\log(A_\infty/A_\alpha - A_t)$ versus time was made for each complex and the rate constant for the catalytic oxidation and the hydrolysis of 4-nitrophenylphosphate was calculated.

2.1.1. Chemicals and reagents

5-Methyl salicylaldehyde [21], 3-chloromethyl-5-methyl salicylaldehyde [22], 1,4,8,11-tetraazatricyclo [9.3.1.1^{4,8}] hexadecane [23] and 1,8-[bis(3-formyl-2-hydroxy-5-methyl)benzyl]-4,11-diazaniatricyclo[9.3.1.1^{4,8}]hexadecane dichloride [quaternary ammonium salt] [24] were prepared by following the literature methods. Analytical grade methanol, acetonitrile and dimethylformamide were purchased from Qualigens and were used as such. TBAP, used as a supporting electrolyte in the electrochemical measurements, was purchased from Fluka and recrystallised from hot methanol. **Caution!** TBAP is potentially explosive; hence care should be taken in handling the compound. All other chemicals and solvents were of analytical grade and were used as received without any further purification.

2.2. Synthesis of the ligand (L)

2.2.1. Synthesis of 1,8-[bis(3-formyl-2-hydroxy-5-methyl)benzyl]-l,4,8,11-tetraazacyclotetradecane (L)

The compound 1,8-[bis(3-formyl-2-hydroxy-5-methyl)benzyl]-4,11-diazaniatricyclo[9.3.1.1^{4,8}]hexadecane dichloride (1 g, 0.0017 mol) was dissolved in 200 ml of an aqueous NaOH solution (0.3 M) with stirring. Excess NaOH is used to hydrolyze the methylene bridge inside the cyclam unit. After stirring for 4 h, the solution was extracted with $CHCl_3$ (5 × 30 mL). The combined $CHCl_3$ extracts were dried with anhydrous $MgSO_4$, and then concentrated under vacuum to give the expected compound 1,8-[bis(3-formyl-2-hydroxy-5-methyl)benzyl]-l,4,8,11-tetraazacyclotetradecane. Yield: 72%. M.p.: 282 °C (dec). *Anal.* Calc. for $C_{28}H_{40}N_4O_4$: C, 67.72; H, 8.12; N, 11.28. Found: C, 67.64; H, 8.02; N, 11.17%; IR data (KBr disc, cm^{-1}): 3389, 3285, 1680; ^{1}H NMR, δ (ppm in $CDCl_3$): 1.5 (m, 4H, β-CH_2), 2.32 (m, 18H, α-CH_2), 2.51 (s, 6H Ar-CH_3) 4.1 (s, 4H, N–CH_2-Ar), 7.26 (d, 4H, Ar-H), 9.92 (s, 2H, Ar-CHO), 12.54 (2H, br s, Ar-OH). ^{13}C NMR, δ (ppm in $CDCl_3$): 28.3, 49.4, 51.6, 54.8., 55.2, 55.7, 60.5, 122.4, 126.2, 126.8, 131.0, 136.8, 157.6, 196.0.

2.3. Synthesis of the macrobicyclic binuclear copper(II) complexes

2.3.1. $[Cu_2L^{1a}(ClO_4)](ClO_4)$

A methanolic solution of copper(II) perchlorate hexahydrate (0.74 g, 0.002 mol) was added to a hot solution of ligand L (1.00 g, 0.002 mol) in methanol, followed by the addition of 1,2-diaminoethane (0.12 g, 0.002 mol) and triethylamine (0.41 g, 0.004 mol) in methanol. After an hour, another 1 equiv. of copper(II) perchlorate (0.74 g, 0.002 mol) was added and the solution was refluxed in a water bath for 24 h. A minute quantity of insoluble polymer complexes was formed in the reaction. The resulting solution was filtered whilst hot to remove these insoluble polynuclear complexes, then all the solvents were removed under reduced pressure. After evaporation of the solvent, a dark green compound was collected by filtration, which was recrystallised in acetonitrile, and dried in vacuum.

Yield: 0.92 g (55%). *Anal.* Calc. for $C_{30}H_{42}N_6O_{10}Cl_2Cu_2$: C, 42.66; H, 5.01; N, 9.95; Cu, 15.06. Found: C, 42.62; H, 4.98; N, 9.98; Cu, 15.01%. FAB mass (*m*/*z* (%)): $[Cu_2L^{1a}(ClO_4)–ClO_4]^+$ 745. Conductance (Λ_m, S cm^2 mol^{-1}) in DMF: 77. Selected IR data (KBr, cm^{-1}): 3327, 1618, 1103, 1197, 1088, 626. λ_{max}, nm (ε, M^{-1} cm^{-1}) in DMF: 749 (sh), 555 (184), 357 (10800), 269 (14400). g = 2.10, μ_{eff}: 1.44 B.M.

The complexes $[Cu_2L^{1b}(ClO_4)](ClO_4)$, $[Cu_2L^{1c}(ClO_4)](ClO_4)$, $[Cu_2L^{1d}(ClO_4)](ClO_4)$ and $[Cu_2L^{1e}(ClO_4)](ClO_4)$ were synthesized by following the above procedure using 1,3-diaminopropane (0.15 g, 0.002 mol), 1,4-diaminobutane (0.18 g, 0.002 mol), 1,2-diaminobenzene (0.22 g, 0.002 mol) and 1,8-diaminonaphthalene (0.32 g, 0.002 mol) respectively, instead of using 1,2-diaminoethane.

2.3.2. $[Cu_2L^{1b}(ClO_4)](ClO_4)$

Dark green compound. Yield: 0.94 g (55%). *Anal.* Calc. for $C_{31}H_{44}N_6O_{10}Cl_2Cu_2$: C, 43.36; H, 5.16; N, 9.79; Cu, 14.80. Found: C, 43.32; H, 5.13; N, 9.75; Cu, 14.78%. FAB mass (*m*/*z* (%)): $[Cu_2L^{1b}\text{-}2ClO_4]^+$ 660. Conductance (Λ_m, S cm^2 mol^{-1}) in DMF: 81. Selected IR data (KBr, cm^{-1}): 3349, 1623, 1105, 1091, 1089, 626. λ_{max}, nm (M^{-1} cm^{-1}) in DMF: 751 (sh), 603 (167), 363 (11 400), 271 (14 840). g: 2.09, μ_{eff}: 1.45 B.M.

2.3.3. $[Cu_2L^{1c}(ClO_4)](ClO_4)$

Dark green compound. Yield: 0.90 g (52%). *Anal.* Calc. for $C_{32}H_{46}N_6O_{10}Cl_2Cu_2$: C, 44.02; H, 5.31; N, 9.63; Cu, 14.57. Found: C, 44.00; H, 5.30; N, 9.65; Cu, 14.55%. FAB mass (*m*/*z* (%)): $[Cu_2L^{1c}–2ClO_4]^+$ 673. Conductance (Λ_m, S cm^2 mol^{-1}) in DMF: 83. Selected IR data (KBr, cm^{-1}): 3343, 1620, 1100, 1095, 1090, 627. λ_{max}, nm (ε, M^{-1} cm^{-1}) in DMF: 647 (201), 370 (12100), 273 (15000). *g*: 2.10, μ_{eff}: 1.31 B.M.

2.3.4. $[Cu_2L^{1d}(ClO_4)](ClO_4)$

Dark green compound. Yield: 0.94 g (53%). *Anal.* Calc. for $C_{34}H_{42}N_6O_{10}Cl_2Cu_2$: C, 45.74; H, 4.74; N, 9.41; Cu, 14.24. Found: C, 45.70; H, 4.71; N, 9.39; Cu, 14.21%. FAB mass (*m*/*z* (%)): $[Cu_2L^{1d}$-ClO_4–$ClO_4]^+$ 793. Conductance (Λ_m, S cm^2 mol^{-1}) in DMF: 85. Selected IR data (KBr, cm^{-1}): 3345, 1629, 1103, 1095, 1097, 624. λ_{max}, nm (ε, M^{-1} cm^{-1}) in DMF: 750 (sh), 658 (186), 375 (12800), 277 (17000). *g*: 2.11, μ_{eff}: 1.47 B.M.

2.3.5. $[Cu_2L^{1e}(ClO_4)](ClO_4)$

Dark green compound. Yield: 0.93 g (49%). *Anal.* Calc. for $C_{38}H_{44}N_6O_{10}Cl_2Cu_2$: C, 48.41; H, 4.70; N, 8.91; Cu, 13.48. Found: C, 48.39; H, 4.67; N, 8.94; Cu, 13.46%. FAB mass (*m*/*z* (%)): $[Cu_2L^{1e}$-ClO_4–$ClO_4]^+$ 843. Conductance (Λ_m, S cm^2 mol^{-1}) in DMF: 89. Selected IR data (KBr, cm^{-1}): 3353, 1625, 1110, 1103, 1097, 629. λ_{max}, nm (ε, M^{-1} cm^{-1}) in DMF: 750 (sh), 672 (164) 383 (13600), 277 (17800). *g*: 2.10, μ_{eff}: 1.55 B.M.

3. Results and discussion

A series of macrobicyclic binuclear copper(II) complexes were synthesized by the Schiff's base condensation of the ligand (L) with diamines in the presence of the metal ion. The synthetic pathway for the binuclear complexes is shown in Scheme 1. In all the binuclear copper(II) complexes, one of the copper(II) ions is in the amine compartment and is six coordinated, whilst the other is in the imine compartment and is five coordinated. All attempts to grow single crystals of the complexes (e.g. by the diffusion of diethyl ether vapor into DMF solutions or recrystallisation of the complexes from acetonitrile) failed and only dark green powders or micro crystals were obtained. Spectral, electrochemical, catalytic data and antimicrobial activities of the complexes were recorded.

3.1. Spectral studies

The IR spectra of all the binuclear copper(II) complexes show bands in the region 3327–3353 cm^{-1}, indicating the presence of NH groups in the complexes. The IR spectra of ligand L shows a band at 1680 cm^{-1} due to the presence of a C=O (–CHO) group. All the complexes show a sharp band in the region 1618–1629 cm^{-1} due to the presence of C=N in the complexes. This shows that the aldehyde groups have been completely converted into imine groups, by the disappearance of the aldehydic C=O stretching band at around 1680 cm^{-1} and the appearance of a strong band at around 1618–1629 cm^{-1} assigned to the C=N stretching vibration mode (Schiff-base condensation) [25–27]. All the binuclear copper(II) complexes showed two sharp peaks at near 1100 cm^{-1} and a peak at around 630 cm^{-1}, which are assigned to perchlorate ions [28]. The peak around 1100 cm^{-1} is split, which clearly explains the presence of a coordinated perchlorate ion [29], while the other peak does not show any splitting, indicating the presence of an uncoordinated perchlorate ion. The peak around 630 cm^{-1} belongs to a perchlorate bending vibration and this peak would not show any splitting even if the perchlorate

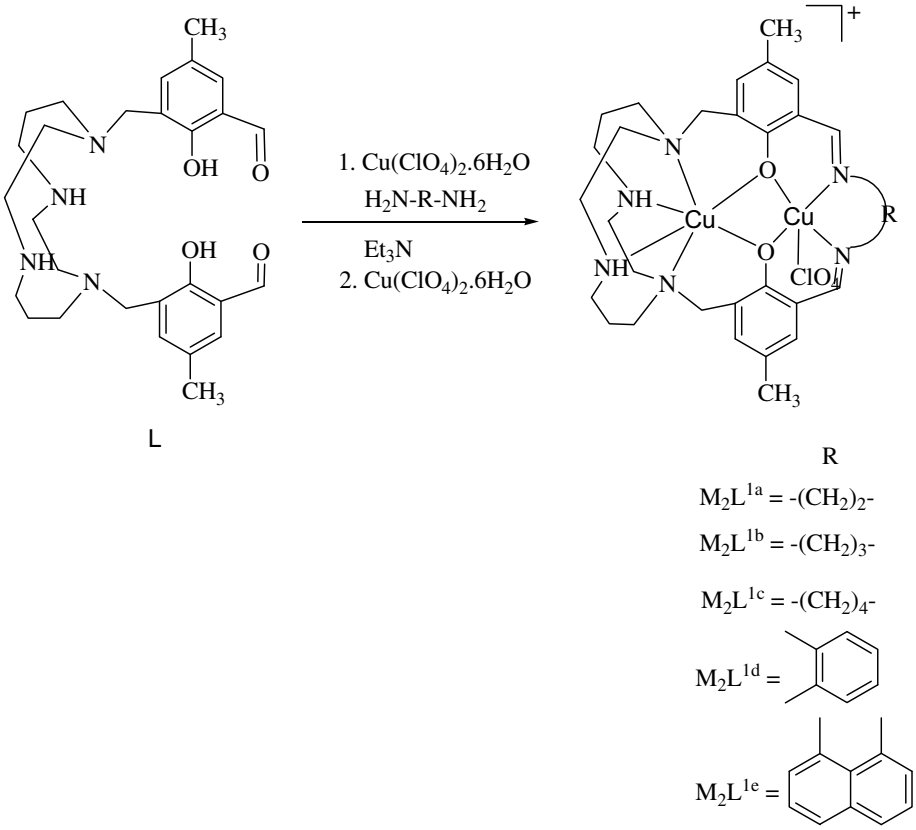

Scheme 1.

coordinates to a metal. The IR spectral data of the complexes clearly shows the presence of two different types of perchlorate ions. Further, the appearance of new bands in the region 1530–1558 cm^{-1} in all the complexes suggests the presence of phenoxide bridging between the metal ions [30].

The electronic spectra of the copper(II) complexes were obtained in DMF medium. The electronic spectra of all the complexes exhibit three main features. One or two peaks in the range 250–300 nm are assigned to the intra ligand charge transfer transition (π–π^*). An intense peak in the range 380–420 nm is due to a ligand-to-metal charge transfer transition, and the d–d transition for the copper(II) complexes shows one peak in the region 555–672 nm and a shoulder at around 750 nm, which are characteristic of Cu^{2+} in a 5/6 coordination environment [31]. The electronic spectral studies inferred that an increase in λ_{max} (red shift) of the d–d transition of the copper(II) ion in the ligand L^{1a} to L^{1c} and L^{1d} to L^{1e} indicates that the coordination geometry around the copper atom of the complexes is more distorted. This is due to the flexibility of the macrocyclic ring upon increasing the chain length of the imine compartment, which causes more distortion of the geometry [32,33].

3.2. ESR spectral analysis

The room temperature solid state X-band ESR spectra of the binuclear copper(II) complexes were obtained. A broad spectrum with no hyperfine splitting was obtained for the binuclear copper(II) complexes with $g = 2.10$ indicating the presence of an antiferromagnetic interaction [34] between the two copper ions.

3.3. Magnetic studies

The room temperature magnetic moment of the binuclear copper(II) complexes is in the range 1.31–1.55 B.M., which are less than the total spin-only values. The lowering of these magnetic moments is due to antiferromagnetic coupling by superexchange through the phenolic oxygen atoms [35–38]. To evaluate the singlet–triplet energy separation ($-2J$), variable temperature magnetic studies for the binuclear copper(II) complexes $[Cu_2L^{1a}(ClO_4)](ClO_4)$, $[Cu_2L^{1c}(ClO_4)](ClO_4)$ and $[Cu_2L^{1e}(ClO_4)](ClO_4)$ were performed in the temperature range 77–298 K, and the experimental magnetic susceptibility values were fitted to the modified Bleaney–Bowers equation [35b].

$$\chi_m = (N_g^2\beta^2/3kT)[3 + exp(-2J/kT)]^{-1}(1 - P) + (0.45P/T) + N_\alpha,$$

where χ_M is the paramagnetic susceptibility per metal atom after the correction for diamagnetism, P is the fraction of monomeric copper(II) impurities, $-2J$ = singlet–triplet energy separation. $N = 120 \times 10^{-6}$ cm^3 mol^{-1} and $g = 2.20$ for all magnetic simulations. The effective magnetic moment was calculated using the relationship $\mu = 2.828\ (\chi_M \times T)^{1/2}$. Plots of χ_{Cu} versus T and μ_{Cu} versus T for the complexes $[Cu_2L^{1c\ and\ e}(ClO_4)](ClO_4)$ are shown in Figs. 1 and 2. The observed $-2J$ value for the binuclear copper(II) complex $[Cu_2L^{1a}(ClO_4)](ClO_4)$ is 172 cm^{-1}, for $[Cu_2L^{1c}(ClO_4)](ClO_4)$ it is $-2J = 154$ cm^{-1}, and for $[Cu_2L^{1e}(ClO_4)](ClO_4)$ it is 236 cm^{-1}.

Since the nature of the donor atoms and endogenous bridging groups in all the complexes are same, it seems very interesting to compare the magnetic properties of the binuclear copper(II) complexes based on the increasing chain length of the imine compartment to discover the possible effects on the spin exchange interactions in the complexes. As observed in the electrochemical studies, here also a smaller $-2J$ value is observed for the complexes $[CuL^{1a\ and\ c}(ClO_4)]ClO_4$ (-$2J$ = 172 and 154) when compared to the complex $[Cu_2L^{1e}(ClO_4)](ClO_4)$, ($-2J = 236$ cm^{-1}). This may be due to the distorted geometry around the copper atoms as a result of the increasing chain length of the imine compartment, which causes more distortion of the geometry [38]. Reports suggest that both distortion from planar geometry [38] and reduction in electron density on the copper atoms [39] are less favorable for effective spin exchange interactions, and hence smaller exchange integral values were observed for the complexes of the ligands L^{1a} and L^{1c} compared to the complex of the ligand L^{1e}. The most probable reason for the strong antiferromagnetic exchange interaction in the L^{1e} complex may be the greater planarity due to the presence of aromatic diimine ($-2J = 236$ cm^{-1}).

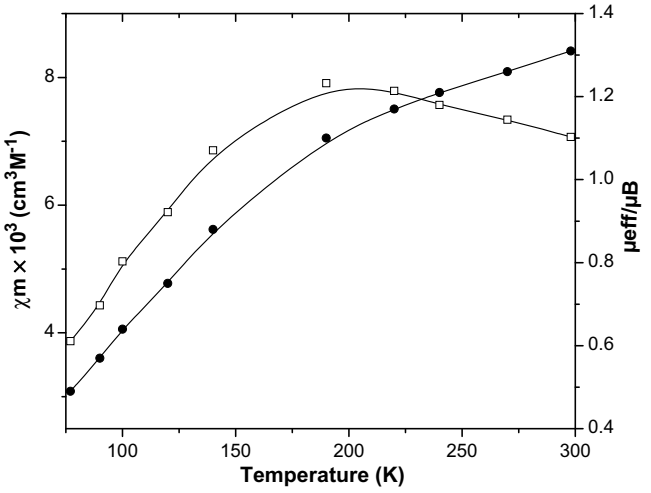

Fig. 1. Temperature-dependence magnetic properties for complex $[Cu_2L^{1c}(ClO_4)](ClO_4)$ where ● is μ_{eff}/μ_B and □ is χ_M.

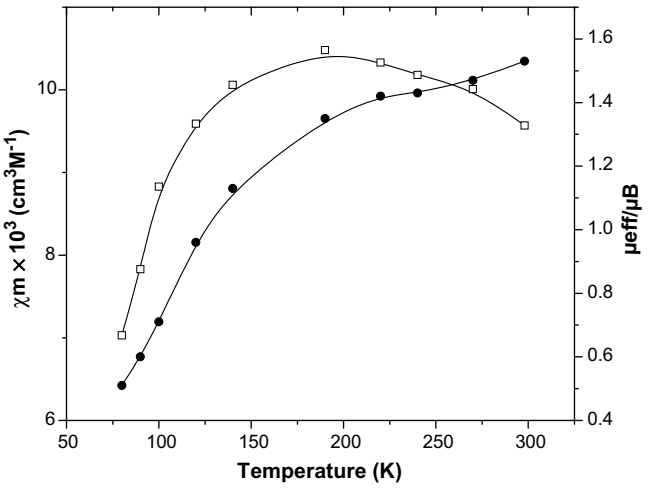

Fig. 2. Temperature-dependence magnetic properties for complex $[Cu_2L^{1e}(ClO_4)](ClO_4)$ where ● is μ_{eff}/μ_B and □ is χ_M.

3.4. Electrochemical properties of the complexes

The electrochemical behavior of the complexes was studied by molar conductance measurements and cyclicvoltammetry in dimethylformamide containing 10^{-1} M tetra(*n*-butyl)ammonium perchlorate. All the complexes show a molar conductance in the range 77–89 Λ_m/S cm^2 mol^{-1} which indicate that the complexes are 1:1 electrolytes [40]. This shows that one of the perchlorates is coordinated to one of the copper atoms. The electrochemical data are summarized in Table 1.

Table 1
Electrochemical[a] (reduction at cathodic potential), hydrolysis of 4-nitrophenylphosphate[b] and catecholase[b] activity data for the complexes

No.	Complexes	E^1_{pc} (V)	E^2_{pc} (V)	Rate constant (k) ($\times 10^{-2}$) min^{-1}	
				NPP	Catecholase
1	$[Cu_2L^{1a}(ClO_4)](ClO_4)$	−0.78	−1.09	7.46	4.81
2	$[Cu_2L^{1b}(ClO_4)](ClO_4)$	−0.64	−1.00	8.43	5.96
3	$[Cu_2L^{1c}(ClO_4)](ClO_4)$	−0.60	−0.94	10.09	7.19
4	$[Cu_2L^{1d}(ClO_4)](ClO_4)$	−1.00	−1.26	4.17	3.13
5	$[Cu_2L^{1e}ClO_4)](ClO_4)$	−0.91	−1.23	2.18	2.09

[a] Measured by CV at 50 mV/s. E vs Ag/AgCl conditions: GC working and Ag/AgCl reference electrodes; supporting electrolyte TBAP; concentration of complex 1×10^{-3} M, concentration of TBAP 1×10^{-1} M.
[b] Measured spectrophotometrically in DMF. Concentration of the complexes: 1×10^{-3} M. Concentration of 4-nitrophenylphosphate: 1×10^{-1} M.

3.5. Reduction process at negative potential

The cyclic voltammograms of the copper(II) complexes were recorded in the potential range 0 to −1.4 V in DMF. The cyclic voltammograms for the copper(II) complexes of the ligands L^{1a-1c} are shown in Fig. 3. The macrocyclic doubly phenoxo-bridged dicopper complexes typically undergo two well-separated one electron reductions [41,42]. It is observed that all the binuclear copper(II) complexes show two irreversible reduction waves in the cathodic potential region. The first reduction potential ranges from −0.60 to −1.00 V and the second reduction potential lies in the range −0.94 to −1.26 V. Controlled potential electrolysis was also carried out and the experiment reports that each couple corresponds to a one-electron transfer process. The two reduction processes are assigned as follows:

$$Cu^{II}Cu^{II} \rightarrow Cu^{II}Cu^{I} \rightarrow Cu^{I}Cu^{I}$$

The first reduction potential of the Cu^{2+}/Cu^{+} couple of the $[CuL^{1a-c}(ClO_4)]ClO_4$ complexes in the range −0.60 to −0.78 (Table 1) is similar to that observed for the [Cu(salen)] complexes, and may suggest that the couples observed for these bimetallic complexes refer to reduction of the copper(II) in the 4-coordinate site (imine compartment). Similarly, the second reduction wave is observed for $[CuL^{1a-c}(ClO_4)]ClO_4$ in the range −0.94 to −1.09 V, which is attributed to the reduction of copper(II) in the amine compartment, and may suggest that the couple observed for the bimetallic complexes refers to the reduction of the copper(II) in the 6-coordinate site. Electrochemical studies of similar type complexes with hexa- and tetra coordination sites reported in the literature [42] suggest that the second reduction potential of the binuclear complexes may be assigned to the metal ion in the hexa coordination site.

It is interesting to compare the reduction potential of the copper(II) complexes. It is apparent that the first and second reduction potentials of the binuclear copper(II) complexes of the ligands L^{1a-c} are shifting towards the anodic direction, from −0.78 to −0.60 V and from −1.09 to −0.94 V, respectively, as the number of methylene groups is increased from 2 to 4 in the side chain [43,44]. For example, the first and second reduction potential for the complex $[Cu_2L^{1c}(ClO_4)](ClO_4)$ has E^1_{pc} −0.60 V and E^2_{pc} −0.94 V, which are less negative in comparison to those of the complex $[Cu_2L^{1b}(ClO_4)](ClO_4)$ (E^1_{pc} −0.64 V and E^2_{pc} −1.00 V), which, in turn, are less negative in comparison to those of the complex $[Cu_2L^{1a}(ClO_4)](ClO_4)$ (E^1_{pc} −0.78 V and E^2_{pc} −1.09 V). This shows that as the number of methylene groups between the imine nitrogen (chain length) increases, the entire macrocyclic ring becomes more flexible, which causes easier reduction. This increase in the flexibility increases the cavity size of the macrocyclic ring. Thus, the large size of the cavity can easily hold the reduced cation and stabilizes the formation of Cu(I) in both the compartments. The observed reduction potentials for $[Cu_2L^{1d}(ClO_4)](ClO_4)$ (E^1_{pc} −1.00 V and E^2_{pc} −1.26 V) and $[Cu_2L^{1e}(ClO_4)](ClO_4)$ (E^1_{pc} −0.91 V and E^2_{pc} −1.23 V) show that the reduction of complexes of the ligands L^{1d} and L^{1e} is rather difficult when compared to the reduction of the complexes of the ligands L^{1a-1c} due to the planarity induced by the aromatic ring, which makes the system more rigid. Whatever the precise interpretation of the bimetallic reduction process, it is clear that their magnitude is subject to variation due to changes caused by the nature of the ligand, geometry and by the presence of the other metal [44c].

3.6. Kinetic studies

3.6.1. Hydrolysis of 4-nitrophenylphosphate

The catalytic activity of the copper(II) complexes for the hydrolysis of 4-nitrophenylphosphate was determined spectrophotometrically, following our earlier reports [45a,b]. Plots of $\log(A_\alpha/A_\alpha - A_t)$ versus time for the hydrolysis of 4-nitrophenylphosphate activity of the binuclear copper(II) complexes were obtained and are shown in Fig. 4. The observed initial rate constant values for all the copper(II) complexes are given in Table 1.

The catalytic activities of the binuclear copper(II) complexes are found to increase as the macrocyclic ring size increases, due to the

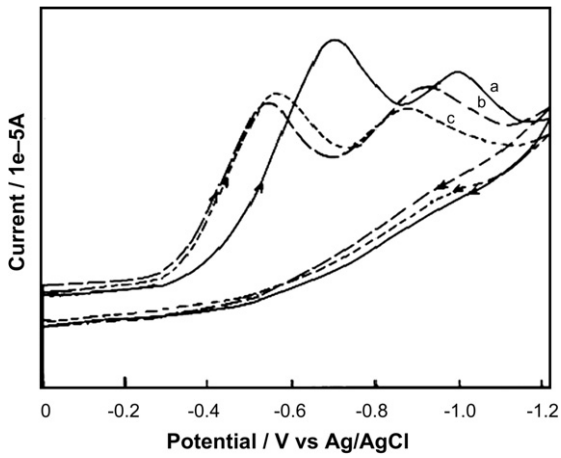

Fig. 3. Cyclic voltammogram of the binuclear copper(II) complexes: (a) $[Cu_2L^{1a}(ClO_4)](ClO_4)$, (b) $[Cu_2L^{1b}(ClO_4)](ClO_4)$, (c) $[Cu_2L^{1c}(ClO_4)](ClO_4)$ (reduction process).

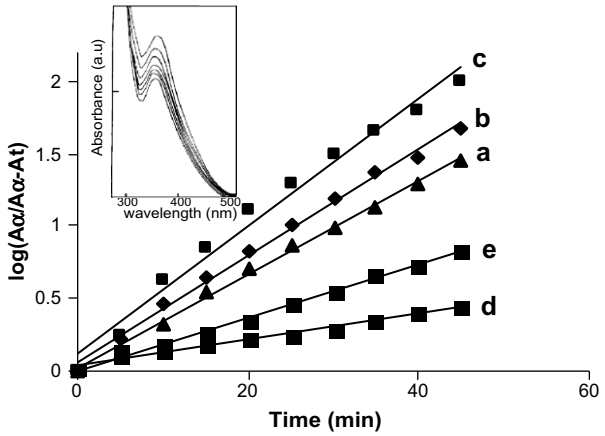

Fig. 4. Hydrolysis of 4-nitrophenylphosphate by binuclear copper(II) complexes: (a) $[Cu_2L^{1a}(ClO_4)](ClO_4)$, (b) $[Cu_2L^{1b}(ClO_4)](ClO_4)$, (c) $[Cu_2L^{1c}(ClO_4)](ClO_4)$, (d) $[Cu_2L^{1d}(ClO_4)](ClO_4)$, (e) $[Cu_2L^{1e}(ClO_4)](ClO_4)$. The inset is the tie dependent growth of the *p*-nitrophenolate chromophore in the presence of $[Cu_2L^{1a}(ClO_4)](ClO_4)$.

intrinsic flexibility, i.e. the increase in the chelate ring size enhances the rate constant of hydrolysis fairly well by producing distortion in the geometry around the metal ion that enhances the accessibility of the metal ion for the bonding of phosphate and OH groups [45c]. The rate constant value for the binuclear copper(II) complex $[Cu_2L^{1c}(ClO_4)](ClO_4)$ is 10.09×10^{-2} min^{-1}, which is higher when compared to complex $[Cu_2L^{1b}(ClO_4)](ClO_4)$ (8.43×10^{-2} min^{-1}), which in turn is more when compared to the complex $[Cu_2L^{1a}(ClO_4)](ClO_4)$ (7.46×10^{-2} min^{-1}). The catalytic activity of the complexes containing aromatic diimines $[Cu_2L^{1d}(ClO_4)](ClO_4)$ and $[Cu_2L^{1e}ClO_4)](ClO_4)$ is found to be less than that of the complexes containing aliphatic diimines. This may be due to the planarity associated with aromatic ring which imparts a lower catalytic efficiency due to the rigidity of the system [46–48].

3.6.2. Oxidation of pyrocatechol (catecholase activity)

The catecholase activity of the copper(II) complexes synthesized in the present work was measured using pyrocatechol as a convenient model substrate for the identification of functional models for the metalloenzymes by following our earlier methods [45a,b].

Plots of $\log(A_\alpha/A_\alpha - A_t)$ versus time for the catecholase activity of the binuclear copper(II) complexes were obtained and are shown in Fig. 5 The observed initial rate constant value for the copper(II) complexes is given in Table 1. The complex $[Cu_2L^{1c}(ClO_4)](ClO_4)$ has higher catalytic activity (7.19×10^{-2} min^{-1}) than the complex $[Cu_2L^{1b}ClO_4)](ClO_4)$ (5.46×10^{-2} min^{-1}), which in turn is more active compared to the $[Cu_2L^{1a}ClO_4)](ClO_4)$ (4.81×10^{-2} min^{-1}) complex. From the results it is observed that the rate

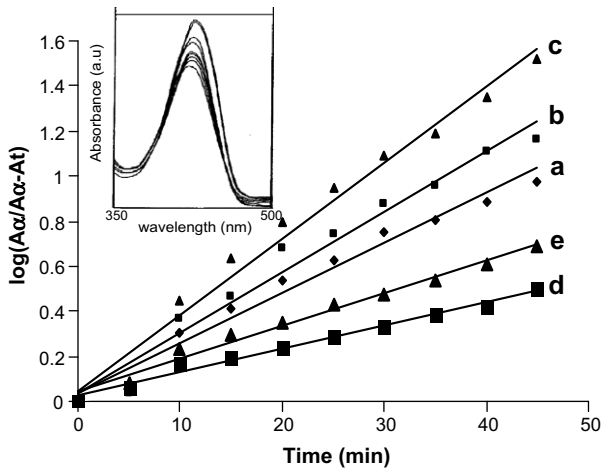

Fig. 5. Catecholase activity of the copper(II) complexes: (a) $[Cu_2L^{1a}(ClO_4)](ClO_4)$, (b) $[Cu_2L^{1b}(ClO_4)](ClO_4)$, (c) $[Cu_2L^{1c}(ClO_4)](ClO_4)$, (d) $[Cu_2L^{1d}(ClO_4)](ClO_4)$, (e) $[Cu_2L^{1e}(ClO_4)](ClO_4)$. The inset is the time dependent growth of the *o*-quinone chromophore in the presence of $[Cu_2L^{1a}(ClO_4)](ClO_4)$.

of oxidation of catechol to *o*-quinone increased as the macrocyclic chain length increased [49a]. The catecholase activity of a highly distorted complex is higher than that of a less distorted complex [49b,c]. It is indeed noteworthy to say that the increase in flexibility due to the increase in the ring size of the macrocycle is a possible reason for the observed higher rate constant value of the complexes.

3.7. Antifungal and antimicrobial activities

Antifungal and antimicrobial activities of the complexes were tested by the cup-plate method using nutrient agar. The radial growth of the colony was recorded on completion of the incubation, and the mean diameter for each complex at a concentration of 100 μg/ml was recorded. The average percentage inhibition of the bactericidal growth medium was compared using the Vincent (Vincent, 1947) equation: $I = 100(C - T)/C$, where I = percentage inhibition, T = average diameter of the bacterial growth on the tested plates and C = average diameter of the growth on the control plates.

3.7.1. Antifungal activity

Studies on the antifungal activity of tetraazamacrocyclic ligands and their complexes are limited in the literature [50–52]. We have evaluated the antifungal activity of all the copper(II) complexes against the phytopathogenic fungus *Candida albicans*. The screening data are reported in Table 2. It is observed from the results that all the tested complexes show some antifungal activity. The activity reported by the present complexes was comparable with the N-substituted tetraazamacrocycles [53,54]. Generally copper(II) and nickel(II) complexes of N-substituted tetraazamacrocycles show higher activity than their corresponding cobalt(III) complexes [55]. Another interesting result observed here is that the complexes of L^{1d} and L^{1e} show higher activity than the complexes of the ligands L^{1a} to L^{1c} which contain aliphatic diimines. It seems from the results that the nature of the ligand and the coordinated metal ion plays a significant role in the inhibition activity. Further the binuclear copper(II) complexes show higher activity than the ligand L.

3.7.2. Antibacterial activity

All the synthesized copper(II) complexes have been screened for their *in vitro* antimicrobial activity against the pathogenic bacteria gram (−) *Escherichia coli* (ATCC 11775), *Pseudomonas aeruginosa* (ATCC 10145), *Bacillus subtilis* (ATCC 6633), *Klebsiella pneumonia* (ATCC 13883) and gram (+) *Staphylococcus aureus* (ATCC 12600) are using the agar dilution method. The screening results are given in Table 2.

All the reported binuclear copper(II) complexes are highly potent against *Pseudomonas aeruginosa*, *Bacillus subtilis*, *Klebsiella pneumonia* and gram (+) *Staphylococcus aureus*. All the tested binuclear copper(II) complexes show moderate activity against gram (−) *Escherichia coli*. All the complexes show superior activity to

Table 2
Antibacterial and antifungal screening data of the complexes

No.	Compound	Representation zone of inhibition					
		Antibacterial (100μg/ml)					Antifungal (100μg/ml)
		Staphylococcus aureus	*Bacillus cearus*	*Klebsiella pneumonia*	*Pseudomonas aureginosa*	*Escherichia coli*	*Candida albicans*
1	$[Cu_2L^{1a}(ClO_4)](ClO_4)$	12	14	14	16	9	12
2	$[Cu_2L^{1b}(ClO_4)](ClO_4)$	12	12	12	14	11	12
3	$[Cu_2L^{1c}(ClO_4)](ClO_4)$	16	18	16	16	11	16
4	$[Cu_2L^{1d}(ClO_4)](ClO_4)$	18	20	22	18	12	22
5	$[Cu_2L^{1e}ClO_4)](ClO_4)$	21	26	24	22	13	21

the ligand L. It is observed from the results that the complexes containing aromatic diimines show higher activity than the complexes containing aliphatic diamines. The observed higher antimicrobial activities of the complexes can be explained on the basis of Tweedy's chelation theory [56]. The lipid membrane that surrounds the cell favors the passage of only lipid soluble materials due to which lipophilicity is an important factor which controls the antimicrobial activity. On chelation, the polarity of the metal ion will be reduced to a greater extent due to the overlap of the ligand orbitals and partial sharing of the positive charge of the metal ion with the donor groups. Further, it increases the delocalization of π-electrons over the whole chelate ring and hence enhances the liposolubility of the complexes. This increased liposolubility enhances the penetration of the complexes into the lipid membrane; the lipophilic group to drive the compound through the semipermeable membrane of the cell; and blocks the metal binding sites in the enzymes of the microorganisms.

The presence of a cyclam unit in the molecule does apparently improve the activity of the complexes. Comparing the activity of the present complexes with the tetraazamacrocyclic copper(II) complexes reported by Roy et al. [57] the present complexes show similar activity. An additional important feature in the biologically active macrocyclic binuclear copper(II) complexes of the present investigation may be imparted by the peculiar nature of the complexes in which the chain length may bring about a change in the coordinating ability. However, further more studies are needed to understand the functions which are responsible for the antifungal and antibacterial activities of the tested complexes.

4. Conclusion

In conclusion, it has been observed that the small variation in the chain length of the imine compartment, (i) causes a red shift in the electronic spectra (ii) shifts the reduction potential anodically on increasing the chain length (iii) shows higher catalytic activity on increasing the chain length. All the complexes show good antimicrobial activity. All these studies of the complexes agree well with the established trends.

Acknowledgements

Financial support from University Grants Commission (RGNF), New Delhi is gratefully acknowledged. We are thankful to CDRI-Lucknow for providing FAB Mass spectral analysis.

References

[1] N.V. Gerbeleu, V.B. Arion, J. Burgess, Template Synthesis of Macrocyclic Compounds, Wiley-VCH, New York, 1999.
[2] P.V. Bernhardt, G.A. Lawrence, Coord. Chem. Rev. 104 (1990) 297.
[3] (a) T.A. Kaden, Pure Appl. Chem. 65 (1993) 1477;
(b) K.P. Wainwright, Coord. Chem. Rev. 166 (1997) 35.
[4] J. Costamagna, G. Ferraudi, B. Matsuhiro, M. Campos-Valette, J. Canales, M. Villagran, J. Vargas, M.J. Aguirre, Coord. Chem. Rev. 196 (2000) 125.
[5] (a) K.P. Wainwright, Adv. Inorg. Chem. 52 (2001) 293;
(b) R.I. Haines, Inorg. Chem. 21 (2002) 165.
[6] P. Guerriero, S. Tamburini, P.A. Vigato, Coord. Chem. Rev. 139 (1995) 17.
[7] C.J. Cairns, D.H. Busch, Coord. Chem. Rev. 69 (1986) 1.
[8] (a) O. Kahn, Molecular Magnetism, VCH: Weinheim, Germany, 1993;
(b) O. Kahn, Struct. Bonding 68 (1987) 89.
[9] H. Golchoubian, E. Baktash, R. Welter, Inorg. Chem. Commun. 10 (2007) 120.
[10] E.V. Rybak-Akimova, N.W. Alcock, D.H. Busch, Inorg. Chem. 37 (1998) 1563.
[11] H. Okawa, H. Furutachi, D.E. Fenton, Coord. Chem. Rev. 51 (1998) 174.
[12] D.G. McCollum, C. Fraser, R. Ostrander, A.L. Rheingold, B. Bosnich, Inorg. Chem. 33 (1994) 2383.
[13] D.G. McCollum, L. Hall, C. White, R. Ostrander, A.L. Rheingold, J. Whelan, B. Bosnich, Inorg. Chem. 33 (1994) 924.
[14] C. Fraser, B. Bosnich, Inorg. Chem. 33 (1994) 338.
[15] C. Fraser, L. Johnston, A.L. Rheingold, B.S. Hagerty, G.K. Williams, L. Whelan, B. Bosnich, Inorg. Chem. 31 (1992) 1835.
[16] (a) H. Golchoubian, W.L. Waltz, Synth. Commun. 28 (1998) 3907;
(b) V. Fusi, A. Llobet, J. Mahia, M. Micheloni, P. Paoli, X. Ribas, P. Rossi, Eur. J. Inorg. Chem. (2002) 987.
[17] M. Rodriguez, A. Liobet, M. Corbella, P. Muller, M.A. Uson, A.E. Martell, J. Reibenspies, J. Chem. Soc., Dalton Trans. (2002) 2900.
[18] (a) W. Kaim, J. Rall, Angew. Chem. 47 (1996) 108;
(b) N. Kitajima, Y. Moro-Oka, Chem. Rev. 94 (1994) 737.
[19] (a) N. Kitajima, Adv. Inorg. Chem. 38 (1992) 1;
(b) J. Reim, R. Werner, W. Haase, B. Krebs, Chem. Eur. J. 4 (1998) 289.
[20] K. Geetha, S.K. Tiwari, A.R. Chakravarthy, G. Ananthakrishnan, J. Chem. Soc., Dalton Trans. (1999) 4463.
[21] J.C. Duff, J. Chem. Soc. (1941) 547.
[22] E. Lambert, B. Chabut, S.C. Noblat, A. Deronzier, G. Chottard, A. Bousseksou, J.-P. Tuchagues, J. Laugier, M. Dardet, J.-M. Latour, J. Am. Chem. Soc. 119 (1997) 9424.
[23] G. Royal, V.D. Gindrey, S. Dahaowi, A. Tabard, R. Guilard, P. Pullumbi, C. Lecomte, Eur. J. Org. Chem. (1998) 1971.
[24] D. Gayathri, D. Velmurugan, K. Ravikumar, S. Sreedaran, V. Narayanan, Acta Cystallogr., Sect. E 62 (2006) o3714.
[25] G. Das, R. Shukala, S. Mandal, R. Singh, P.K. Bharadwaj, J.V. Singh, K.H. Whitemine, Inorg. Chem. 36 (1997) 323.
[26] R.M. Silverstein, G.C. Bassler, Spectrometric Identification of Organic Compounds, John Wiley & Sons, New York, 1991.
[27] C. Fraser, R. Ostrander, A.L. Rheingold, C. White, B. Bosnich, Inorg. Chem. 33 (1994) 324.
[28] M. Lachkar, R. Guilard, A. Attamani, A. De Clan, J. Fisher, R. Weiss, Inorg. Chem. 37 (1997) 1575.
[29] S.S. Tandon, L.K. Thompson, J.N. Bridson, V. Mekee, A.J. Downard, Inorg. Chem. 31 (1992) 4635.
[30] B. Srinivas, N. Arulsamy, P.S. Zacharias, Polyhedron 10 (1991) 731.
[31] (a) D. Volkmer, B. Hommerich, K. Griesar, W. Haase, B. Krebs, Inorg. Chem. 35 (1996) 3792;
(b) M. Ciampolini, Inorg. Chem. 5 (1966) 35;
(c) L. Sacconi, M. Ciampolini, G.P. Speroni, J. Am. Chem. Soc. 87 (1965) 3102;
(d) M. Ciampolini, N. Nardi, Inorg. Chem. 5 (1966) 41.
[32] H. Okawa, S. Kida, Bull. Chem. Soc. Jpn. 45 (1972) 1759.
[33] H. Wada, T. Aono, K. Moodo, M. Ohba, N. Makstumoto, H. Okawa, Inorg. Chem. Acta 246 (1996) 13.
[34] R.C. Agarwal, N.K. Singh, R.P. Singh, Inorg. Chem. 20 (1981) 2794.
[35] (a) H. Okawa, M. Tadokora, T.Y. Aratake, M. Ohba, K. Shindom, M. Mitsumi, M. Koikawa, M. Tomono, D.E. Fenton, J. Chem. Soc., Dalton Trans. (1993) 253;
(b) B. Bleany, K.D. Bowers, Proc. Royal Soc. London Ser. A 214 (1952) 415.
[36] M. Lubben, R. Hage, A. Meetsma, K. Byma, B.L. Fermga, Inorg. Chem. 34 (1995) 2217.
[37] A. Benzekri, P. Dubourdeaux, J.M. Latour, J. Laugier, P. Rey, J. Chem. Soc., Dalton Trans. (1991) 3359.
[38] L.K. Thompson, S.K. Mandal, S.S. Tandon, J.N. Bridson, M.K. Park, Inorg. Chem. 35 (1996) 3117.
[39] K. Brichery, K. Drager, K.T. Jens, M. Tilset, M. Betrem, Chem. Ber. 127 (1994) 465.
[40] J. Geary, Coord. Chem. Rev. 7 (1971) 81.
[41] R.R. Gagne, L.M. Henling, T.J. Kistenmacher, Inorg. Chem. 19 (1980) 1226.
[42] (a) C. Fraser, B. Bosnich, Inorg. Chem. 41 (2002) 1788;
(b) K.R. Krishnapriya, M. Kandaswamy, Polyhedron 24 (2005) 113.
[43] F. Abba, G.D. Santis, L. Fabbrizzi, M. Licchelli, A.M.M. Lanfredi, P. Pallavicini, A. Poggi, F. Ugozzoli, Inorg. Chem. 33 (1994) 1366.
[44] (a) G.A. Bowmaker, J.P. Williams, J. Chem. Soc., Dalton. Trans. (1993) 3593;
(b) G.K. Bareford, G.M. Freeman, D.G. Erver, Inorg. Chem. 86 (1986) 552;
(c) C. Belle, C. Beguin, I. Gautier-luneau, S. Hamman, C. Philouze, J.L. Pierre, F. Thomas, S. Torelli, Inorg. Chem. 41 (2002) 479.
[45] (a) K.S. Bharathi, S. Sreedaran, A.K. Rahiman, K. Rajesh, V. Narayanan, Polyhedron 26 (2007) 3993;
(b) K.S. Bharathi, A.K. Rahiman, K. Rajesh, S. Sreedaran, P.G. Aravindan, D. Velmurugan, V. Narayanan, Polyhedron 25 (2006) 2859;
(c) K. Moore, G.S. Vigee, Inorg. Chim. Acta 66 (1982) 125.
[46] J. Reim, B. Kreks, J. Chem. Soc., Dalton Trans. (1997) 3793.
[47] M.R. Malachowski, H.B. Huynh, L.T. Tomlinson, R.S. Kelly, J.W. Furbeejun, J. Chem. Soc., Dalton Trans. (1995) 31.
[48] P. Akilan, M. Thirumavalan, M. Kandaswamy, Polyhedron 22 (2003) 3483.
[49] (a) H. Kurosaki, C. Bucher, E. Espinosa, J.M. Barbe, G. Guilard, Inorg. Chim. Acta 322 (2001) 145;
(b) M. Thirumavalavan, P. Akilan, M. Kandaswamy, K. Chinnakali, G. Senthil kumar, H.K. Fun, Inorg. Chem. 42 (2003) 3308;
(c) B. Bosnich, Inorg. Chem. 38 (1999) 2554.
[50] (a) T.G. Roy, S.K.S. Hazari, B.K. Dey, S. Chakraborty, E.R.T. Tiekink, Met. Based Drugs 6 (1999) 345;
(b) S.K.S. Hazari, T.G. Roy, B.K. Dey, S.C. Das, E.R.T. Tiekink, Met. Based Drugs 4 (1997) 255.
[51] M.A. Ali, A.H. Mirza, A. Monsur, S. Hossain, M. Nazimuddin, Polyhedron 20 (2001) 1045.
[52] M.E. Hossain, M.N. Alam, J. Begum, M.A. Ali, M. Nazimuddin, E.E. Smith, R.C. Haynes, Inorg. Chim. Acta 249 (1996) 207.
[53] S.K.S. Hazari, T.G. Roy, B.K. Dey, S.C. Das, E.R.T. Tiekink, Met. Based Drugs 4 (1997) 255.

[54] T.G. Roy, S.K.S. Hazari, B.K. Dey, H.A. Miah, C. Bader, D. Rehder, Eur. J. Inorg. Chem. (2004) 4115.
[55] T.G. Roy, S.K.S. Hazari, B.K. Dey, R. Sutradhar, L. Dey, N. Anowar, E.R.T. Tiekink, J. Coord. Chem. Rev. 59 (2006) 351.
[56] B.G. Tweedy, Phytopathology 55 (1964) 910.
[57] (a) T.G. Roy, S.K.S. Hazari, B.K. Dey, H.A. Miah, F.K. Olbrich, D. Rehder, Inorg. Chem. 46 (2007) 5372;
(b) K.B. Shashi, V. Sharma, L. Kamakshi, K. Geetanjli, S. Anuradha, Indian J. Pharm. Sci. 69 (2007) 438.

$C_4H_6CuN_2O_5S$: C, 18.64; H, 2.35; N, 10.87. Found: C, 18.62; H, 2.01; N, 11.00%. IR (KBr, cm^{-1}): 3413 (m), 1435 (s), 1398 (m), 1357 (m), 1255 (m), 1168 (s), 1115 (s), 1026 (s), 966 (m), 831 (m), 764 (m), 748 (m), 701 (m), 642 (m), 627 (m), 594 (m), 490 (s), 476 (s), 435 (m).

2.2.2. $[Cu_2(SO_4)(pyz)_2(H_2O)_2]_n$ (**2**)

An aqua solution (30 mL) of $Cu(SO_4) \cdot 5H_2O$ (0.70 g, 2.8 mmol) was stirred with pyrazine (0.45 g, 5.6 mmol) for 5 min at room temperature. The resulting blue solution was heated to 180 °C in a Teflon autoclave for 48 h to produce dark red single crystals (yield: 56%), which are stable in air. Elemental *Anal.* calc. for $C_8H_{12}Cu_2N_4O_6S$: C, 22.91; H, 2.88; N, 13.36. Found: C, 22.33; H, 2.41; N, 13.18%. IR (KBr, cm^{-1}): 3439 (m), 1648 (s), 1475 (s), 1412 (s), 1359 (m), 1154 (s), 1112 (s), 1046 (s), 974 (m), 813 (m), 799 (m), 617 (m), 445 (s), 421 (m).

2.3. Crystal structure determination

Single crystals of **1** and **2** were mounted on a glass fiber and coated with epoxy resin. X-ray data collection were carried out using a Rigaku Mercury diffractometer (**1**) with a CCD two-dimensional detector and Rigaku R-Axis Rapid II (**2**) with an imaging plate, with graphite monochromated Mo Kα radiation (λ = 0.7107 Å) and at 298(2) K. For **1**, the size of the unit cell was determined from reflections collected on the setting angles of six frames by changing ω by 0.5° for each frame, and intensity data were collected with a ω scan width of 0.5°. For **2**, the size of the unit cell was determined from reflections collected on the setting angles of three frames by changing ω by 3.0° for each frame, and intensity data were collected with a ω scan width of 5.0°. Two different χ settings were used. Empirical absorption correction was performed for all data. The structures were solved by the direct method with subsequent difference Fourier syntheses and the refinement with the SHELXTL (version 5.1) software package [18]. The non-hydrogen atoms were refined anisotropically and hydrogen atoms of pyrazine were placed in calculated positions. The crystal data and structure refinement results are summarized in Table 1. Selected bond lengths and angles are given in Table 2.

Table 1
Crystallographic data and structure refinement for $[Cu(SO_4)(pyz)(H_2O)]_n$ (**1**) and $[Cu_2(SO_4)(pyz)_2(H_2O)_2]_n$ (**2**)

	1	**2**
Empirical formula	$C_4H_4CuN_2O_5S$	$C_8H_{12}Cu_2N_4O_6S$
Formula weight	255.69	419.36
Crystal system	orthorhombic	monoclinic
Space group	$Pmn2_1$	$C2/c$
a (Å)	6.7727(14)	10.979(2)
b (Å)	4.9337(10)	11.850(2)
c (Å)	11.498(2)	11.347(2)
α (°)	90	90
β (°)	90	114.03(3)
γ (°)	90	90
V (Å^3)	384.21(14)	1348.3(5)
Z	2	4
D_{calc} (Mg m^{-3})	2.210	2.066
Absorption coefficient (mm^{-1})	3.104	3.342
F(000)	254	840
Crystal size (mm^3)	0.45 × 0.15 × 0.08	0.45 × 0.10 × 0.10
Measured reflections	2802	6498
Independent reflections (R_{int})	864 (0.0689)	1542 (0.0257)
Data/restraints/parameters	864/1/67	1542/0/104
Goodness-of fit on F^2	1.091	1.119
R [$I > 2\sigma(I)$]	R_1 = 0.0386, wR_2 = 0.0846	R_1 = 0.0252, wR_2 = 0.0585
R (all data)	R_1 = 0.0395, wR_2 = 0.0850	R_1 = 0.0316, wR_2 = 0.0616
Largest difference in peak and hole (e Å^{-3})	0.415 and −0.775	0.331 and −0.485

Table 2
Selected bond lengths (Å) and angles (°) for $[Cu(SO_4)(pyz)(H_2O)]_n$ (**1**) and $[Cu_2(SO_4)(pyz)_2(H_2O)_2]_n$ (**2**)

Complex ***1***			
Cu(1)–N(1)	2.005(3)	Cu(1)–O(1)	1.939(5)
Cu(1)–O(4)	1.966(5)	Cu(1)–O(3*)	2.362(5)
N(1**)–Cu(1)–N(1)	171.30(19)	O(1)–Cu(1)–O(4)	174.3(2)
O(1)–Cu(1)–N(1)	90.10(17)	O(4)–Cu(1)–N(1)	89.46(17)
Complex ***2***			
Cu(1)–N(1)	1.9982(19)	Cu(1)–N(2)	1.9663(17)
Cu(1)–O(1)	2.1112(17)	Cu(1)–O(3)	2.1933(19)
N(1)–Cu(1)–N(2)	125.45(8)	N(1)–Cu(1)–O(1)	102.35(8)
N(1)–Cu(1)–O(3)	108.43(8)	N(2)–Cu(1)–O(1)	118.41(8)
N(2)–Cu(1)–O(3)	104.87(8)	O(1)–Cu(1)–O(3)	92.02(7)

Symmetry code: *: x, y + 1, z; **: −x, y, z.

3. Results and discussion

3.1. Description of the crystal structures

Fig. 1a shows the coordination environment of the copper ion in **1**. In compound **1**, the copper ions adopt a square–pyramidal geometry, defined by trans nitrogen donors from two pyrazine ligands, a sulfate oxygen and an aqua ligand in the equatorial plane and an oxygen atom from the second sulfate group in the axial site, similar to that of $\{[Cu(SO_4)(4,4'\text{-bpy})(H_2O)] \cdot 0.5H_2O\}_n$ [6]. The apical Cu(1)–O(3′) distance of 2.362(5) Å is significantly longer than the equatorial Cu–O distance. In **1**, the Cu(II) ions are linked by pyrazine ligands to form straight one-dimensional chains, and chains in the crystal run parallel along the *a*-axis (Fig. 1b). Each chain is interlinked through sulfate bridges, with axial coordination to Cu(II) ions affording a two-dimensional network (Fig. 1b). The Cu–Cu distance linked by pyz is *ca.* 6.8 Å, and that linked by sulfate ions is *ca.* 4.9 Å. As shown in Fig. 1c, each two-dimensional network is doubly linked by hydrogen bonds of coordinated water molecules with two sulfate oxygen atoms; O(2)···O(4) = 2.67 Å. No solvent molecule other than the coordinated water molecules is contained in the crystal structure of **1**.

Fig. 2a shows the coordination environment of the copper ion in **2**. The copper center is four-coordinated to the two nitrogen atoms of the pyrazine ligands, one water molecule and one oxygen atom of a sulfate ion. The Cu–N bond distances are similar to each other, whereas the Cu–O bond distances are longer, as shown in Table 2. All the bond distances are close to those of typical four-coordinated pyridine complexes [8,19–21], while the geometry around the copper atom is a distorted tetrahedron. Since two protons of coordinated water molecules were determined by X-ray analysis, the oxidation state of copper is +1, considering the stoichiometry in **2**. As shown in Fig. 2b, the pyrazines bridge copper ions to afford zigzag one-dimensional chains. Coordinated water molecules are oriented perpendicular to the chain direction, where each chain is bound by sulfate bridges. The adjacent chains cross at an angle of *ca.* 60°, as shown in Fig. 2c. The Cu–Cu distance of the two copper ions linked by pyz is *ca.* 6.7 Å, and that linked by the sulfate ion is *ca.* 5.8 Å. As in **1**, no solvent molecule other than coordinated water molecules is contained in the crystal structure of **2**.

3.2. Comparison of synthetic conditions for other coordination polymers containing copper and sulfate ions

As mentioned in the experimental section, the significant difference in the synthetic procedure between **1** and **2** is temperature, although the concentrations of the reactant solutions for both compounds are also slightly different. Thus, high temperature (180 °C) probably assists in the reduction of Cu(II) to Cu(I). Table 3 summarizes the synthetic conditions for copper coordination polymers

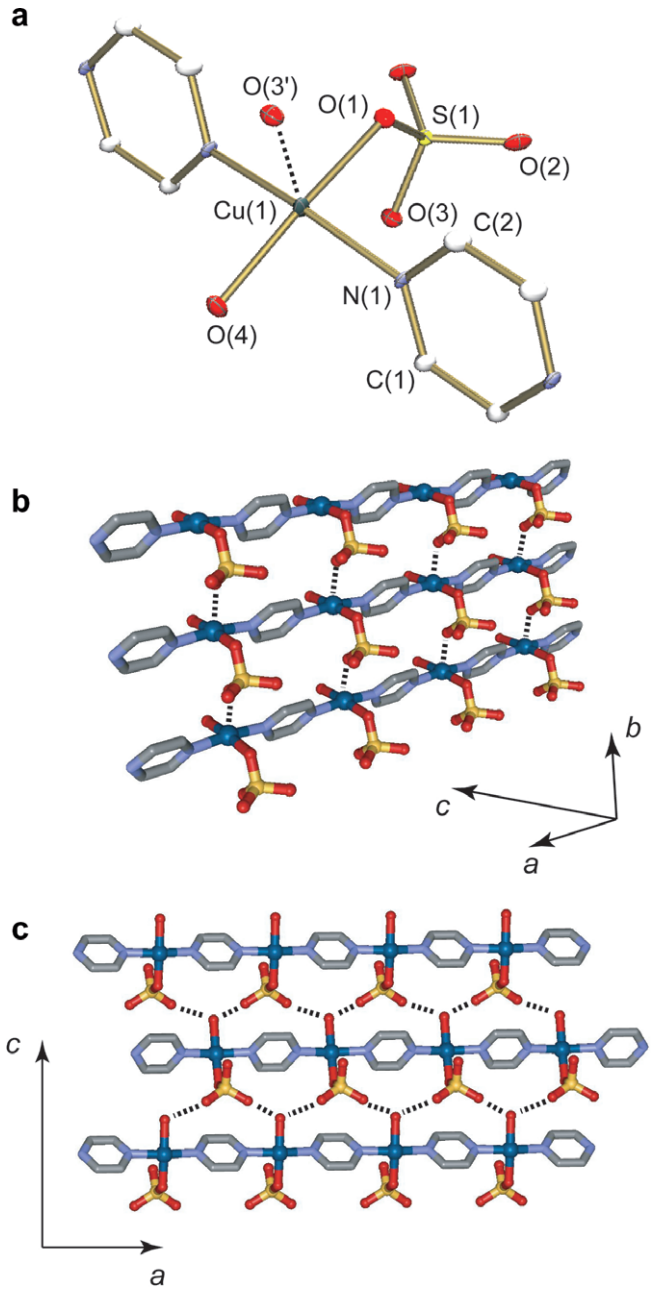

Fig. 1. Crystal structure of $[Cu(SO_4)(pyz)(H_2O)]_n$ (**1**). (a) ORTEP drawing of **1** at the 30% probability level. Hydrogen atoms are omitted for clarity. (b) One-dimensional chains run parallel along the *a*-axis to form a sheet, where SO_4^{2-} anions bridge chains. (c) Overall structure of **1** along the *b*-axis, where each sheet is bound by hydrogen bonds between coordinated water molecules and SO_4^{2-} anions.

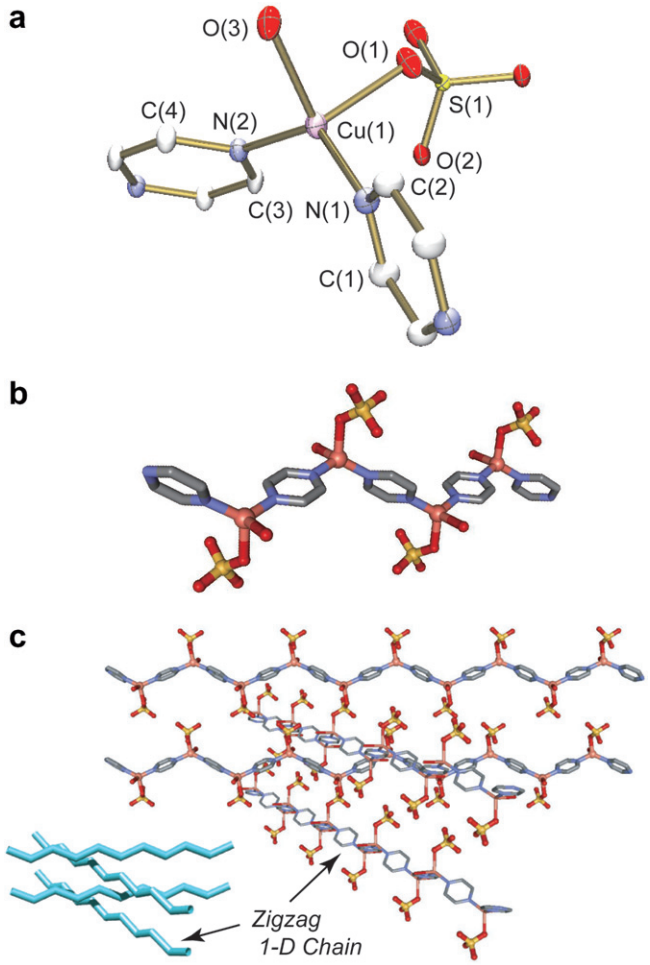

Fig. 2. Crystal structure of $[Cu_2(SO_4)(pyz)_2(H_2O)_2]_n$ (**2**). (a) ORTEP drawing of **2** at the 30% probability level. Hydrogen atoms are omitted for clarity. (b) One-dimensional zigzag chain of $[-Cu-pyz]_n$. (c) Four one-dimensional zigzag chains with the schematic drawing. Each chain is bound with bridging by SO_4^{2-} anions.

comprising sulfate ions and py–X–py type ligands [6,7,22–28], where each compound was synthesized from $Cu(SO_4) \cdot 5H_2O$. The tendency for hot solutions to afford Cu(I) coordination polymers can be seen [6,7]. In addition, room temperature synthesis (namely, self-assembly synthesis) of $Cu(SO_4) \cdot 5H_2O$ and py–X–py-type ligands results in Cu(II) coordination polymers without reduction [22,25–28], although reduction by simple mixing in alcohol at room temperature has been reported several times [19,29].

Taking a previous report into account [4], the reduction of copper ions in **2** would be explained by the Gillard mechanism [30]. This mechanism suggests that attack by nucleophiles occurs at the 2-position of complexed pyridines and induces the reduction of the coordinated metal, releasing H^+ and H_2O_2 species [30]. The

Table 3
Comparison of synthetic conditions (temperature and solvent) for selected coordination polymers comprising copper sulfate and py–X–py type ligands

Compounds	Oxidation state	Synthetic conditions	Ref.
$\{[Cu(SO_4)(4,4'\text{-bpy})(H_2O)] \cdot 0.5H_2O\}_n$	Cu(II)	130 °C (48 h), H_2O	[6]
$\{[Cu_2(SO_4)(4,4'\text{-bpy})_2] \cdot 6H_2O\}_n$	Cu(I)	140 °C (48 h), H_2O/MeOH (v/v = 5:2)	[6]
$\{[Cu_2(SO_4)(4,4'\text{-bpy})_2] \cdot 4H_2O\}_n$	Cu(I)	160 °C (48 h), H_2O	[7]
$\{[Cu(SO_4)(bpe)_2] \cdot 5H_2O\}_n$	Cu(II)	R.T., H_2O/EtOH (v/v = 3:4)	[22]
$[Cu(SO_4)(bpee)(H_2O)]_n$	Cu(II)	120 °C (72 h), H_2O	[23,24]
$\{[Cu(SO_4)(bpee)(H_2O)_3] \cdot 4H_2O]\}_n$	Cu(II)	R.T., MeOH	[25]
$\{[Cu(SO_4)(L_1)(H_2O)] \cdot 2H_2O\}_n$	Cu(II)	R.T., H_2O/MeOH (v/v = 1:1)	[26]
$\{[Cu(SO_4)(L_2)(H_2O)] \cdot 2H_2O\}_n$	Cu(II)	R.T., H_2O/MeOH (v/v = 2:3)	[27]
$\{[Cu(L_3)_2(H_2O)_2](SO_4)\}_n$	Cu(II)	R.T., H_2O	[28]
$[Cu(SO_4)(pyz)(H_2O)]_n$ (**1**)	Cu(II)	R.T., H_2O	this work
$[Cu_2(SO_4)(pyz)_2(H_2O)_2]_n$ (**2**)	Cu(I)	180 °C (48 h), H_2O	this work

4,4′-bpy = 4,4′-Bipyridine, bpe = 1,2-bis(4-pyridyl)ethane, bpee = *trans*-1,2-bis(4-pyridyl)ethylene, L_1 = 2,5-bis(4-pyridyl)-1,3,4-oxadiazole, L_2 = 2,5-bis(4-pyridyl)-1,3,4-thiadiazole, and L_3 = 1,3-bis(pyridin-4-ylmethyl)urea.

pH of the supernatant solution of **2** is 1.8 in our case, suggesting that high temperature promotes this pathway.

3.3. Infrared spectra of *1* and *2*

The use of vibrational spectroscopy to distinguish between terminal and bridging sulfate ions has been a matter of some interest. The IR bands observed, for the most part, can be separated readily into bands arising either from sulfate anion vibrations or pyrazine vibrations (Fig. S1). In both **1** and **2**, broad bands due to SO_4 stretching vibrations [31] around 1100 cm^{-1} are observed. These can be resolved into three bands each, with one additional medium intensity band, as follows: **1**: 1168, 1115, 1026 and 966 cm^{-1}, **2**: 1154, 1112, 1046 and 974 cm^{-1}. According to previous infrared analyses of sulfate ions [32,33], three infrared lines should be observed in the region from 900 to 1300 cm^{-1} for a unidentate ligand and four for a bidentate ligand, which can be explained by assuming a lowering of symmetry from T_d (free ion) to C_{3v} (unidentate coordination) or C_{2v} (bridged bidentate coordination). Although the crystal structures of **1** and **2** clearly show sulfate bridging between two copper ions, the coordination distance in **1** (2.362(5) Å) is slightly longer (Fig. S2). However, the IR results indicate that sulfate ions act as bidentate ligands in **1**.

4. Conclusion

This work was devoted to the synthesis and analysis of two novel coordination polymers prepared using copper sulfate and pyrazine. Single-crystal X-ray analysis revealed that both **1** and **2** form one-dimensional chains, straight and zigzag respectively, with the configuration determined by the coordination environments. Also, in the system of copper(II) and pyrazine, reduction of Cu(II) assisted by high temperature was observed, and we anticipate such a reduction to be applicable in the construction of Cu(I) coordination polymers using other py–X–py-type ligands.

Acknowledgements

This work was supported by the Grants-in-Aid for Scientific Research (Young Scientist (B) No. 19750048) and Mukai Science and Technology Foundation.

Appendix A. Supplementary data

CCDC 681501 and 681502 contain the supplementary crystallographic data for **1** and **2**. These data can be obtained free of charge via http://www.ccdc.cam.ac.uk/conts/retrieving.html, or from the Cambridge Crystallographic Data Centre, 12 Union Road, Cambridge CB2 1EZ, UK; fax: (+44) 1223-336-033; or e-mail: deposit@ccdc.cam.ac.uk. Supplementary data associated with this article can be found, in the online version, at doi:10.1016/j.poly.2008.06.030.

References

[1] B. Moulton, M.J. Zaworotko, Chem. Rev. 101 (2001) 1629.
[2] O.M. Yaghi, M. O'Keeffe, N.W. Ockwig, H.K. Chae, M. Eddaoudi, J. Kim, Nature 423 (2003) 705.
[3] S. Kitagawa, R. Kitaura, S.-i. Noro, Angew. Chem., Int. Ed. 43 (2004) 2334.
[4] X.-M. Zhang, M.-L. Tong, X.-M. Chen, Angew. Chem., Int. Ed. 41 (2002) 1029.
[5] M.-L. Tong, L.-J. Li, K. Mochizuki, H.-C. Chang, X.-M. Chen, Y. Li, S. Kitagawa, Chem. Commun. (2003) 428.
[6] N. Lah, I. Leban, Inorg. Chem. Commun. 9 (2006) 42.
[7] X.-M. Zhang, R.-Q. Fang, H.-S. Wu, S.W. Ng, Acta Crystallogr., Sect. E 60 (2004) m990.
[8] P. Lumme, S. Lindroos, E. Lindell, Acta Crystallogr., Sect. C C43 (1987) 2053.
[9] J.Y. Lu, B.R. Cabrera, R.-J. Wang, J. Li, Inorg. Chem. 38 (1999) 4608.
[10] K. Jin, X. Huang, L. Pang, J. Li, A. Appel, S. Wherland, Chem. Commun. (2002) 2872.
[11] J.-P. Zhang, S.-L. Zheng, X.-C. Huang, X.-M. Chen, Angew. Chem., Int. Ed. 43 (2004) 206.
[12] C.-Z. Xie, Z.-F. Zhang, B.-F. Zhang, X.-Q. Wang, R.-J. Wang, G.-Q. Shen, D.-Z. Shen, B. Ding, Eur. J. Inorg. Chem. (2006) 1337.
[13] J. Tao, Y. Zhang, M.-L. Tong, X.-M. Chen, T. Yuen, C.L. Lin, X. Huangd, J. Li, Chem. Commun. (2002) 1342.
[14] X.-M. Zhang, X.-M. Chen, Eur. J. Inorg. Chem. (2003) 413.
[15] N. Lah, I.K. Cigic, I. Leban, Inorg. Chem. Commun. 6 (2003) 1441.
[16] Y.-Z. Zheng, M.-L. Tong, X.-M. Chen, New J. Chem. (2004) 1412.
[17] F.A. Cotton, G. Wilkinson, Advanced Inorganic Chemistry, fourth ed., Wiley, New York, 1980.
[18] SHELXTL Reference Manual, ver. 5.1, Bruker AXS, Analytical X-Ray Systems, Madison, WI, 1997.
[19] T. Otieno, S.J. Rettig, R.C. Thompson, J. Trotter, Can. J. Chem. 67 (1989) 1964.
[20] S. Kitagawa, M. Munakata, T. Tanimura, Inorg. Chem. 31 (1992) 1714.
[21] C. Inman, J.M. Knaust, S.W. Keller, Chem. Commun. (2002) 156.
[22] L. Carlucci, G. Ciani, D.M. Proserpio, S. Rizzato, J. Chem. Soc., Dalton Trans. (2000) 3821.
[23] D. Hagrman, R.C. Haushalter, J. Zubieta, Chem. Mater. 10 (1998) 361.
[24] D. Hagrman, R.P. Hammond, R. Haushalter, J. Zubieta, Chem. Mater. 10 (1998) 2091.
[25] H.-L. Hu, M.-C. Suen, C.-W. Yeh, J.-D. Chen, Polyhedron 24 (2005) 1497.
[26] Y.-B. Dong, J.-P. Ma, R.-Q. Huang, F.-Z. Liang, M.D. Smith, J. Chem. Soc., Dalton Trans. (2003) 1472.
[27] Z. Huang, H.-B. Song, M. Du, S.-T. Chen, X.-H. Bu, J. Ribas, Inorg. Chem. 43 (2004) 931.
[28] P. Dıaz, J. Benet-Buchholz, R. Vilar, A.J.P. White, Inorg. Chem. 45 (2006) 1617.
[29] T. Otieno, S.J. Rettig, R.C. Thompson, J. Trotter, Inorg. Chem. 32 (1993) 1607.
[30] R.D. Gillard, Coord. Chem. Rev. 16 (1975) 67.
[31] K. Nakamoto, Infrared and Raman Spectra of Inorganic and Coordination Compounds, fifth ed., Wiley, New York, 1997.
[32] K. Nakamoto, J. Fujita, S. Tanaka, M. Kobayashi, J. Am. Chem. Soc. 79 (1957) 4904.
[33] J.E. Finholt, R.W. Anderson, J.A. Fyfe, K.G. Caulton, Inorg. Chem. 4 (1965) 43.

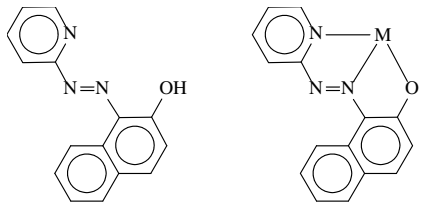

2. Experimental

2.1. Materials

Commercial ruthenium trichloride, was obtained from Arora Matthey, Kolkata, India, was converted to $RuCl_3 \cdot 3H_2O$ by repeated evaporation with concentrated hydrochloric acid. $AgNO_3$ and dimethylsulfoxide were purchased from Merck, India. Triethylamine, 2,2′-bipyridine, 2,2′,2″-terpyridine, and 1-(2′-pyridylazo)-2-naphthol (Hpan) were purchased from Loba Chemie, Mumbai, India. Pyridine and 4-picoline were purchased from Fluka Chemie. $[Ru(dmso)_4Cl_2]$, $[Ru(trpy)Cl_3]$, $[Ru(bpy)Cl_3]$ and $[Ru(PPh_3)_3Cl_2]$ were synthesized by following reported procedures [7]. Calf thymus (CT) DNA and Tris buffer were procured from Sigma Chemical Company. The dry powder of CT DNA was dissolved in 10 mM Tris buffered saline, pH 7.2 (TBS), and dialyzed overnight against the same buffer so that the A_{260}/A_{280} of the dialyzed solution was greater than 1.90. The DNA concentrations were adjusted according to its absorbance at 260 nm using $\varepsilon_{260} = 6.6\ mM^{-1}\ cm^{-1}$. SC pUC18 DNA and agarose were purchased from Bangalore Genei Pvt. Ltd., Bangalore, India. Purification of dichloromethane, acetonitrile and preparation of tetrabutylammonium perchlorate (TBAP) for electrochemical work were performed as reported in the literature [8]. All other chemicals and solvents were reagent grade commercial materials and were used as received.

2.2. Synthesis

2.2.1. $[Ru(pan)_2]$

Hpan (130 mg, 0.52 mmol) was dissolved in ethanol (50 mL) and triethylamine (55 mg, 0.54 mmol) was added to it. Then $[Ru(dmso)_4Cl_2]$ (100 mg, 0.21 mmol) was added and the mixture was refluxed for 24 h to afford a brownish-violet solution. The solvent was then evaporated and the solid mass obtained was purified by preparative thin layer chromatography on a silica plate using 1:10 acetonitrile–benzene as the eluant. A violet band separated, which was extracted with 1:1 acetonitrile–dichloromethane solution and evaporation of the extract afforded $[Ru(pan)_2]$ as a violet crystalline solid. Yield: 49 mg (40%). *Anal.* Calc. for $C_{30}H_{20}N_6O_2Ru$: C, 60.29; H, 3.35; N, 14.07. Found: C, 60.20; H, 3.39; N, 13.95%. ^1H NMR in $CDCl_3$, δ ppm[1]: 6.61 (t, 2H, $J = 6.2$); 6.85 (d, 2H, $J = 9.2$); 7.32 (d, 2H, $J = 5.3$); 7.39 (t, 4H*); 7.49 (d, 2H, $J = 9.2$); 7.64–7.73 (6H*); 10.07 (d, 2H, $J = 8.5$).

2.2.2. $[Ru(trpy)(pan)]ClO_4$

Hpan (57 mg, 0.23 mmol) was dissolved in ethanol (50 mL) and triethylamine (23 mg, 0.23 mmol) was added to it. Then $[Ru(trpy)Cl_3]$ (100 mg, 0.23 mmol) was added and the mixture was refluxed for 5 h to afford a brownish-red solution. It was then concentrated to about 10 mL, and a saturated aqueous solution of $NaClO_4$ (0.5 mL) was added, whereby a brown precipitate is obtained, which was collected by filtration, washed with cold water, and dried in vacuo over P_4O_{10}. Yield: 100 mg (65%). *Anal.* Calc. for $C_{30}H_{21}N_6O_5ClRu$: C, 52.82; H, 3.08; N, 12.32. Found: C, 52.94; H, 3.14; N, 12.25%. ^1H NMR in $CDCl_3$, δ ppm: 6.50–6.72 (2H*); 6.77 (t, 1H, $J = 6.1$); 7.2–8.0 (10H*); 8.08 (d, 2H, $J = 5.5$); 8.31 (t, 1H, $J = 8.0$); 8.47 (d, 2H, $J = 8.0$); 8.72 (d, 2H, $J = 8.0$); 10.14 (d, 1H, $J = 8.6$).

2.2.3. $[Ru(bpy)(pan)Cl]$

Hpan (70 mg, 0.28 mmol) was dissolved in ethanol (30 mL) and to it was added triethylamine (50 mg, 0.50 mmol). Then $[Ru(bpy)Cl_3]$ (100 mg, 0.28 mmol) was added to the mixture and it was refluxed for 6 h to afford a brown solution. The solvent was then evaporated and the solid mass obtained was purified by preparative thin layer chromatography on a silica plate using 1:5 acetonitrile–benzene as the eluant. A brown band separated, which was extracted with acetonitrile and evaporation of the extract afforded $[Ru(bpy)(pan)Cl]$ as a green crystalline solid. Yield: 104 mg (70%). *Anal.* Calc. for $C_{25}H_{18}N_5OClRu$: C, 55.49; H, 3.33; N, 12.95. Found: C, 55.42; H, 3.39; N, 13.02%. ^1H NMR in $CDCl_3$, δ ppm: 6.65 (t, 1H, $J = 6.4$); 6.78 (d, 1H, $J = 4.8$); 6.85 (d, 1H, $J = 9.2$); 7.00 (t, 1H, $J = 6.5$); 7.26–7.41 (2H*); 7.40 (d, 1H, $J = 9.2$); 7.53 (t, 1H, $J = 7.5$); 7.61–7.65 (2H*); 7.70 (d, 1H, $J = 8.4$); 7.80 (t, 1H, $J = 6.6$); 8.00 (t, 2H, $J = 6.9$); 8.30 (d, 1H, $J = 8.1$); 8.47 (d, 1H, $J = 5.7$); 10.07 (d, 1H, $J = 8.5$); 10.46 (d, 1H, $J = 5.7$).

2.2.4. $[Ru(bpy)(pan)(py)]ClO_4$

To a solution of $[Ru(bpy)(pan)Cl]$ (100 mg, 0.19 mmol) in ethanol (30 mL) was added $AgNO_3$ (31 mg, 0.19 mmol). The mixture was warmed and stirred for 30 min, and the deposited AgCl was separated by filtration. To the filtrate was added pyridine (15 mg, 0.19 mmol). The resulting solution was heated at reflux for 4 h. It was then concentrated to about 10 mL, and a saturated aqueous solution of $NaClO_4$ (0.5 mL) was added, whereby a reddish-brown precipitate is obtained, which was collected by filtration, washed with water, and dried in vacuo over P_4O_{10}. It was further purified by preparative thin layer chromatography on a silica plate. Using 1:5 acetonitrile–benzene as the eluant, a reddish-brown band separated, which was extracted with acetonitrile. Evaporation of this extract gave $[Ru(bpy)(pan)(py)]ClO_4$ as a crystalline solid. Yield: 76 mg (60%). *Anal.* Calc. $C_{30}H_{23}N_6O_5ClRu$: C, 52.66; H, 3.36; N, 12.29. Found: C, 51.97; H, 3.41; N, 12.34. ^1H NMR in $CDCl_3$, δ ppm: 6.81 (d, 2H, $J = 9.2$); 7.09 (t, 1H, $J = 6.3$); 7.19–7.26 (3H*); 7.40 (t, 3H*); 7.51 (d, 1H, $J = 9.3$); 7.60–7.70 (3H*); 7.72–7.81 (4H*); 8.18 (t, 1H, $J = 7.7$); 8.25–8.41 (3H*), 8.57 (d, 1H, $J = 8.0$); 9.82 (d, 1H, $J = 8.4$).

2.2.5. $[Ru(bpy)(pan)(4\text{-}pic)]ClO_4$

This complex was synthesized by following the same above procedure using 4-picoline instead of pyridine. Yield: 77 mg 60%. *Anal.* Calc. for $C_{31}H_{25}N_6O_5ClRu$: C, 53.32; H, 3.58; N, 12.04. Found: C, 53.23; H, 3.49; N, 12.10%. ^1H NMR in $CDCl_3$: δ ppm: 2.38 (s, 3H, CH_3); 6.82 (d, 1H, $J = 9.2$); 7.10 (t, 1H, $J = 6.2$); 7.15–7.20 (4H*); 7.37 (t, 1H, $J = 7.5$); 7.51 (d, 1H, $J = 9.2$); 7.55–7.85 (6H*); 8.00–8.12 (2H*); 8.18 (t, 1H, $J = 7.7$); 8.29–8.24 (3H*), 8.56 (d, 1H, $J = 8.1$); 9.83 (d, 1H, $J = 8.4$).

2.2.6. $[Ru(PPh_3)_2(pan)Cl]$

Hpan (26 mg, 0.10 mmol) was dissolved in ethanol (30 mL) and to it was added triethylamine (10 mg, 0.10 mmol). Then $[Ru(PPh_3)_3Cl_2]$ (100 mg, 0.10 mmol) was added to the solution and it was refluxed for 4 h. The $[Ru(PPh_3)_2(pan)Cl]$ complex separated as a brown precipitate, which was collected by filtration, washed with hexane and dried in air. Yield: 70 mg (74%). *Anal.* Calc. for $C_{51}H_{40}N_3OP_2ClRu$: C, 67.36; H, 4.40; N, 4.62. Found: C, 67.25; H,

[1] Chemical shifts are given in ppm and multiplicity of the signals along with the associated coupling constants (J in Hz) are given in parentheses. Overlapping signals are marked with an asterisk.

4.43; N, 4.66%. ^{1}H NMR in $CDCl_3$, δ ppm: 6.29–6.39 (2H*); 6.7–7.5 (36H*); 7.74 (d, 1H, J = 5.4); 9.20 (d, 1H, J = 8.5). ^{31}P NMR in $CDCl_3$, δ ppm: 24.14.

2.3. Physical measurements

Microanalyses (C, H, N) were performed using a Heraeus Carlo Erba 1108 elemental analyzer. Magnetic susceptibilities were measured using a PAR 155 vibrating sample magnetometer fitted with a Walker Scientific L75FBAL magnet. ^{1}H NMR spectra were recorded in $CDCl_3$ solution on a Bruker Avance DPX 300 NMR spectrometer using TMS as the internal standard. ESR spectra were recorded with a JEOL JES-FA200 X-band spectrometer fitted with a quartz Dewar for measurements at 77 K (liquid dinitrogen). All ESR spectra were calibrated with an aid of DPPH (g = 2.0037). IR spectra were obtained on a Shimadzu FTIR-8300 spectrometer with samples prepared as KBR pellets. Electronic spectra were recorded on JASCO V-570 and Shimadzu 2401 spectrophotometers. Electrochemical measurements were made using a CH Instruments model 600A electrochemical analyzer. A platinum disc working electrode, a platinum wire auxiliary electrode and an aqueous saturated calomel reference electrode (SCE) were used in the cyclic voltammetry experiments. All electrochemical experiments were performed under a dinitrogen atmosphere. All electrochemical data were collected at 298 K and are uncorrected for junction potential. Fluorescence studies were performed with a Hitachi F4500 spectrofluorimeter. Electrophoresis experiments were carried out on a BIORAD electrophoretic system using TBS. The DNA binding studies were carried out as follows: (i) Fluorescence studies were performed with the complex and DNA dissolved separately in TBS, and the samples were excited at 480 nm. (ii) For the DNA–agarose gel studies, SC pUC18 DNA was incubated in the presence of different concentrations of the complexes. These solutions were monitored on agarose gel. The DNA was visualized under UV light.

2.4. X-ray crystallography

Single crystals of $[Ru(pan)_2]$ and $[Ru(PPh_3)_2(pan)Cl]$ were obtained by slow diffusion of acetonitrile into dichloromethane solutions of the complexes, followed by evaporation of the resulting solution. Single crystals of $[Ru(trpy)(pan)]ClO_4$ and [Ru(bpy)-(pan)Cl] were obtained by slow evaporation of a solution of the complex in 1:1 dichloromethane–ethanol and acetonitrile, respectively. Selected crystal data and a summary of the data collection parameters appear below, the full details are provided in Table S1. Data on the [Ru(bpy)(pan)Cl] crystal were collected on a Enraf Nonius CAD-4 diffractometer and those for the other three crystals were collected on an Oxford Diffraction X-Calibur CCD system using graphite monochromated Mo Kα radiation (λ = 0.71073 Å). For these three crystals, X-ray data reduction was carried out using the CRYSALIS program [9c]. The structures were solved by direct methods using the SHELXS-97 program [9a]. In the structure of Ru-$(pan)_2$, the data were very weak and all atoms except for Ru were refined isotropically. In the other structures, all non-hydrogen atoms were refined anisotropically. Empirical absorption corrections were carried out using the ABSPACK program [9b]. The structures were refined on F^2 using the SHELXL-97 program [9a].

Crystal data for $C_{30}H_{20}N_6O_2Ru$, M = 597.59, size 0.05 × 0.05 × 0.30 mm^3, triclinic, space group $P\bar{1}$, a = 8.774(9) Å, b = 12.685(12) Å, c = 12.883(13) Å, α = 62.69(10)°, β = 75.07(9)°, γ = 82.15(8)°, U = 1231(2) Å^3, Z = 2, D_{calc} = 1.612 g cm^{-3}, $F(000)$ = 604, λ = 0.71073 Å, T = 150 K, μ = 0.679 mm^{-1}, 7248 reflections collected, 5936 unique (R_{int} = 0.225). Final goodness-of-fit = 0.414, R_1 = 0.0701, wR_2 = 0.0878, R indices based on 630 reflections with [$I > 2\sigma(I)$].

Crystal data for $C_{30}H_{21}N_6O_5ClRu$, M = 680.03, size 0.05 × 0.10 × 0.20 mm^3, monoclinic, space group $C2/c$, a = 30.611(4) Å, b = 11.6611(14) Å, c = 16.491(2) Å, $\alpha = \gamma$ = 90°, β = 114.595(13)°, U = 5352.5(13) Å^3, Z = 8, D_{calc} = 1.688 g cm^{-3}, $F(000)$ = 2736, λ = 0.71073 Å, T = 150 K, μ = 0.741 mm^{-1}, 18729 reflections collected, 7821 unique (R_{int} = 0.109). Final goodness-of-fit = 0.615, R_1 = 0.0486, wR_2 = 0.0790, R indices based on 2125 reflections with [$I > 2\sigma(I)$].

Crystal data for $C_{25}H_{18}N_5OClRu$, M = 540.96, size 0.10 × 0.10 × 0.40 mm^3, orthorhombic, space group $P2_12_12_1$, a = 10.2654(9) Å, b = 13.2256(12) Å, c = 15.7074(14) Å, $\alpha = \beta = \gamma$ = 90°, U = 2132.5(3) Å^3, Z = 4, D_{calc} = 1.685 g cm^{-3}, $F(000)$ = 1088, λ = 0.71073 Å, T = 100 K, μ = 0.890 mm^{-1}, 14079 reflections collected, 5257 unique (R_{int} = 0.045). Final goodness-of-fit = 1.03, R_1 = 0.039, wR_2 = 0.0967, R indices based on 5257 reflections with [$I > 2\sigma(I)$].

Crystal data for $C_{52}H_{42}N_3OP_2Cl_3Ru$, M = 994.25, size 0.10 × 0.20 × 0.30 mm^3, monoclinic, spacegroup Cm, a = 18.325(3) Å, b = 15.2504(12) Å, c = 9.6397(8) Å, $\alpha = \gamma$ = 90°, β = 122.099(5)°, U = 2282.1(5) Å^3, Z = 4, D_{calc} = 1.447 g cm^{-3}, $F(000)$ = 1016, λ = 0.71073 Å, T = 150 K, μ = 0.632 mm^{-1}, 7207 reflections collected, 4280 unique (R_{int} = 0.040). Final goodness-of-fit = 1.007, R_1 = 0.0384, wR_2 = 0.0845, R indices based on 3596 reflections with [$I > 2\sigma(I)$].

3. Results and discussion

3.1. Syntheses and crystal structures

The primary objective of the present study, as already mentioned above, has been to synthesize a series of ruthenium complexes containing 1-(2′-pyridylazo)-2-naphthol (Hpan, **1**), either as the sole ligand or as one of the ligands. For preparing the homoleptic ruthenium complex of Hpan, $[Ru(dmso)_4Cl_2]$ has been selected as the starting material because of its demonstrated ability to undergo displacement of all the six monodentate ligands by chelating ligands [2j,2n]. Reaction of Hpan with $[Ru(dmso)_4Cl_2]$ in refluxing ethanol in the presence of triethylamine has indeed afforded the expected bis-complex, *viz.* $[Ru(pan)_2]$, in a decent yield (Scheme 1). In order to authenticate coordination mode of ligand (**1**) in this complex, its structure has been determined by X-ray crystallography. The structure is shown in Fig. 1 and selected bond parameters are given in Table 1.

The structure shows that in this complex 1-(2′-pyridylazo)-2-naphthol is coordinated to the metal center, via dissociation of the phenolic proton, as a monoanionic N,N,O-donor (**2**, M = Ru),

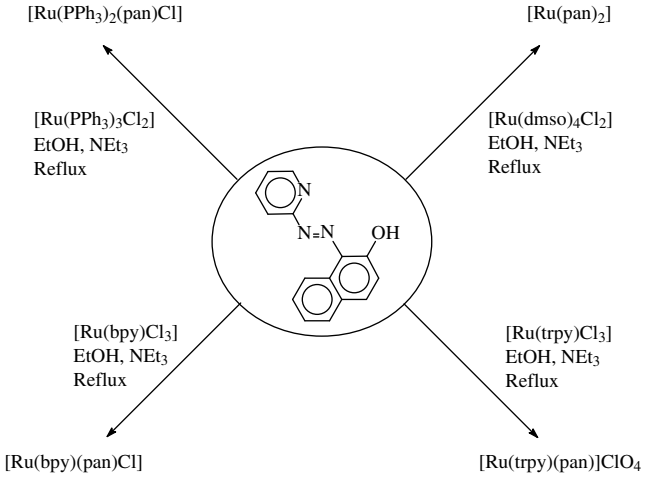

Scheme 1.

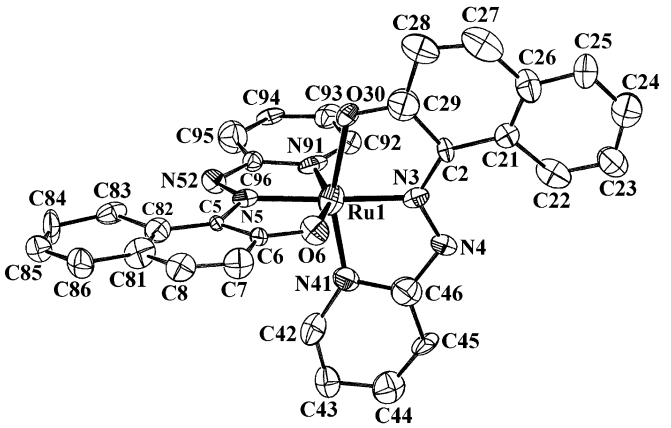

Fig. 1. View of the $[Ru(pan)_2]$ complex (ellipsoids at 25% probability, hydrogens not included for clarity).

Table 1
Selected bond lengths (Å) and bond angles (°) for $[Ru(pan)_2]$, $[Ru(trpy)(pan)]ClO_4$, [Ru(bpy)(pan)Cl] and $[Ru(PPh_3)_2(pan)Cl]$ complexes

$[Ru(pan)_2]$			
Bond distances (Å)			
Ru(1)–N(3)	1.973(10)	Ru(1)–O(6)	2.053(9)
Ru(1)–N(5)	1.965(10)	Ru(1)–O(30)	2.105(8)
Ru(1)–N(41)	1.985(11)	N(3)–N(4)	1.427(13)
Ru(1)–N(91)	2.068(10)	N(5)–N(52)	1.349(11)
Bond angles (°)			
N(3)–Ru(1)–N(5)	177.8(5)	N(3)–Ru(1)–O(30)	78.2(4)
N(41)–Ru(1)–O(30)	160.0(3)	N(5)–Ru(1)–N(91)	77.7(4)
N(91)–Ru(1)–O(6)	157.4(3)	N(5)–Ru(1)–O(6)	79.8(4)
N(3)–Ru(1)–N(41)	81.7(4)		
$[Ru(trpy)(pan)]ClO_4$			
Bond lengths (Å)			
Ru(1)–N(11)	2.049(4)	Ru(1)–N(38)	1.919(4)
Ru(1)–N(22)	1.998(4)	Ru(1)–O(52)	2.077(3)
Ru(1)–N(28)	2.058(4)	N(37)–N(38)	1.337(4)
Ru(1)–N(31)	2.032(4)		
Bond angles (°)			
N(11)–Ru(1)–N(28)	156.43(16)	N(22)–Ru(1)–N(28)	78.55(16)
N(22)–Ru(1)–N(38)	177.82(16)	N(31)–Ru(1)–N(38)	77.49(16)
N(31)–Ru(1)–O(52)	158.65(15)	N(38)–Ru(1)–O(52)	81.18(15)
N(11)–Ru(1)–N(22)	78.09(16)		
[Ru(bpy)(pan)Cl			
Bond lengths (Å)			
Ru–N(1)	1.910(3)	Ru–O	2.102(2)
Ru–N(3)	2.039(3)	Ru–Cl	2.3830(10)
Ru–N(4)	2.042(3)	O–C(1)	1.289(4)
Ru–N(5)	2.093(3)	N(1)–N(2)	1.316(4)
Bond angles (°)			
N(1)–Ru–N(5)	174.92(12)	N(1)–Ru–N(3)	79.23(12)
N(3)–Ru–O	160.94(10)	N(4)–Ru–N(5)	78.03(12)
N(4)–Ru–Cl	172.45(9)	N(1)–Ru–O	81.72(10)
$[Ru(PPh_3)_2(pan)Cl]$			
Bond lengths (Å)			
Ru(1)–N(41)	2.058(4)	Ru(1)–Cl(1)	2.4786(14)
Ru(1)–N(44)	1.916(5)	O(55)–C(54)	1.291(6)
Ru(1)–O(55)	2.130(4)	N(43)–N(44)	1.327(6)
Ru(1)–P(2)	2.3873(9)		
Bond angles (°)			
N(41)–Ru(1)–O(55)	159.50(14)	N(41)–Ru(1)–N(44)	79.5(2)
N(44)–Ru(1)–Cl(1)	173.99(15)	N(44)–Ru(1)–O(55)	80.02(17)
P(2)–Ru(1)–P(2a)	166.74(4)		

with N–Ru–N and N–Ru–O bite angles of ~79°. In this complex ruthenium is thus sitting in a N_4O_2 coordination sphere, which is significantly distorted from ideal octahedral geometry, primarily because of the strain imposed by the two adjacent five-membered chelate rings. The phenolic C–O distance is normal [2n], while the average N–N distance is notably longer than that in uncoordinated azo ligands [10] and the observed elongation is attributable to the metal-to-π^*(azo) back-bonding [11]. The absence of any solvent of crystallization in the crystal lattice of $[Ru(pan)_2]$ indicates the possible existence of non-covalent interactions between the individual complex molecules. To sort this out, packing pattern in the lattice has been examined, which shows that hydrogen-bonding interactions of two types, *viz.* C–H···O and C–H···π interactions, are active in the lattice (Fig. 2). The phenolate-oxygen of each coordinated pan of any complex molecule each coordinated pan of any complex molecule is hydrogen-bonded to two aryl hydrogens of two other pan ligands belonging to two different complex molecules. The δ-hydrogen in the azo-linked phenyl ring of the naphthol fragment of each pan is involved in a C–H···π interaction with the π-cloud over the other ring of the naphthol fragment of another pan of a second neighboring complex molecule. Both of these hydrogen-bonding interactions are extended throughout the entire lattice, and they appear to be responsible for holding the crystal together.

As 1-(2′-pyridylazo)-2-naphthol (**1**) serves as a N,N,O-donor and forms a planar chelate (**2**), in the Ru(pan) fragment only three coordination sites on ruthenium remain accessible. To occupy these three available sites either a planar tridentate ligand, or a combination of a bidentate and a monodentate ligand, or three monodentate ligands can be utilized to obtain the mixed-ligand complexes. Accordingly three different ruthenium starting materials, *viz.* $[Ru(trpy)Cl_3]$ (trpy = 2,2′,2″-terpyridine), $[Ru(bpy)Cl_3]$ (bpy = 2,2′-bipyridine) and $[Ru(PPh_3)_3Cl_2]$, have been chosen. Reactions of ligand (**1**) with these three starting materials in refluxing ethanol in the presence of triethylamine have afforded the targeted mixed-ligand complexes, *viz.* $[Ru(trpy)(pan)]^+$ (isolated as the perchlorate salt), [Ru(bpy)(pan)Cl] and $[Ru(PPh_3)_2(pan)Cl]$, respectively, in good yields (Scheme 1). It is interesting to note here that during synthetic reactions of Hpan with $[Ru(trpy)Cl_3]$ and $[Ru(bpy)Cl_3]$, ruthenium undergoes a one-electron reduction, and either the solvent (ethanol) or the base (NEt_3) might have served as the reducing agent. Structures of these three mixed-ligand complexes have also been determined by X-ray crystallography. Structure of the $[Ru(trpy)(pan)]ClO_4$ complex (Fig. 3) shows that in it the pan ligand is coordinated to ruthenium as before. The remaining three coordination sites on ruthenium are occupied by the three terpyridine-nitrogens in the usual manner. The N_5O coordination sphere around ruthenium is similarly distorted from ideal octahedral geometry as in $[Ru(pan)_2]$, because like the 1-(2′-pyridylazo)-2-naphtholate anion (pan), terpyridine also forms two adjacent five-membered chelate rings. Bond parameters (Table 1) in the Ru(trpy) fragment are found to be normal, as observed in other structurally characterized complexes of ruthenium having this fragment [12]. Bond lengths in the Ru(pan) fragment are comparable to those observed in the $[Ru(pan)_2]$ complex. An examination of the packing pattern in the lattice of the $[Ru(trpy)(pan)]ClO_4$ complex shows the existence of three types of hydrogen-bonding interactions, *viz.* C–H···O, C–H···N and C–H···π interactions (Fig. S1). Two perchlorate-oxygens are hydrogen-bonded to pyridyl-hydrogens of the terpyridine. One pyridyl-hydrogen of the terpyridine is hydrogen-bonded to an azo-nitrogen of the pan ligand of another complex molecule. The γ-hydrogen of the naphthol fragment of pan is involved in a C–H···π interaction with the π-cloud of the pyridine ring of pan of another complex molecule.

Structure of the [Ru(bpy)(pan)Cl] complex (Fig. 4) shows that the pan ligand is coordinated in the expected N,N,O-mode, while the remaining three sites are occupied by a 2,2′-bipyridine, coordinated in the usual N,N-fashion, and a chloride. The observed Ru–Cl length (Table 1) is normal, and so are the bond distances in the Ru(bpy) fragment [13]. The octahedral N_4OCl coordination sphere

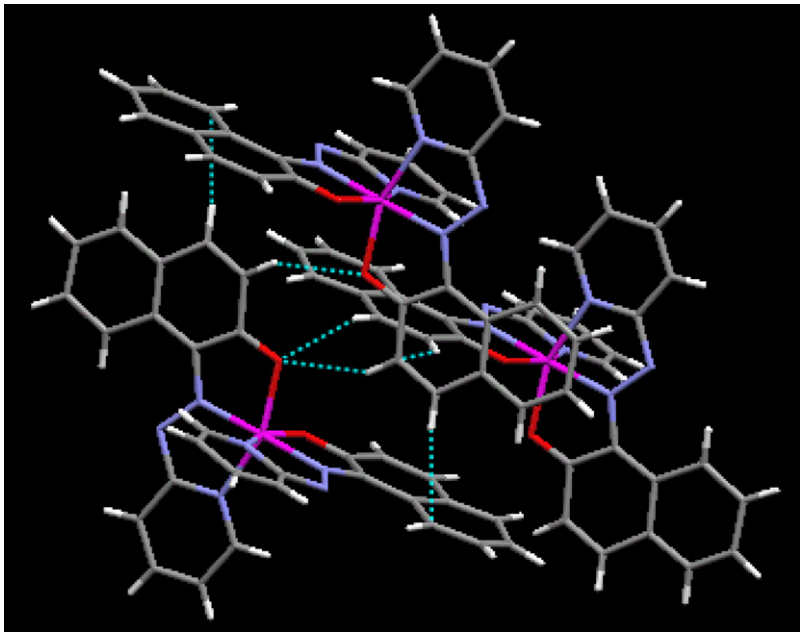

Fig. 2. Packing diagram of $[Ru(pan)_2]$ complex.

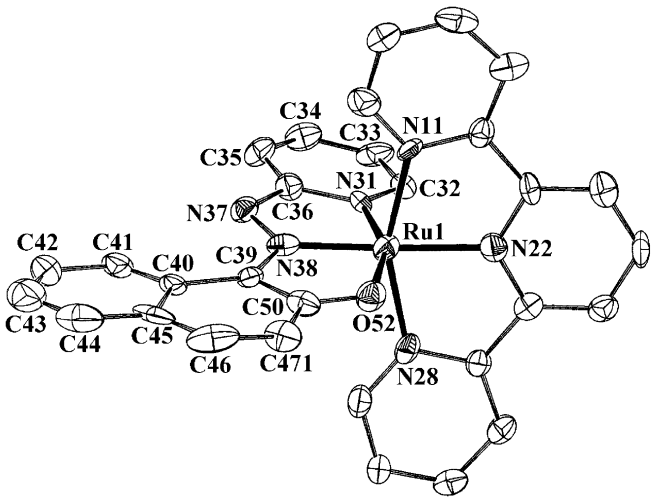

Fig. 3. View of the $[Ru(trpy)(pan)]^+$ complex (ellipsoids at 25% probability, hydrogens not included for clarity).

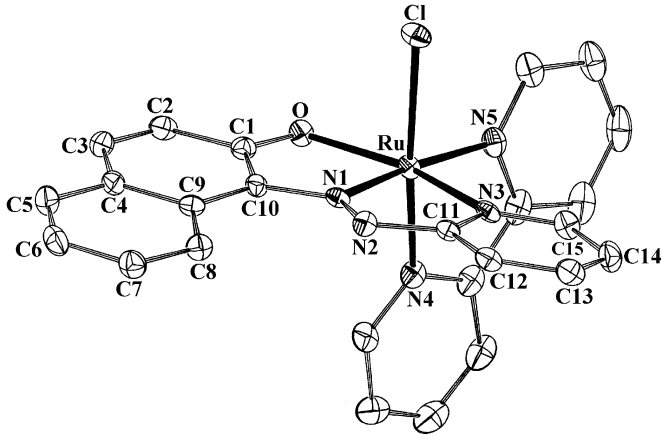

Fig. 4. View of the $[Ru(bpy)(pan)Cl]$ complex (ellipsoids at 25% probability, hydrogens not included for clarity).

in this complex is much less distorted compared to the structures of the $[Ru(pan)_2]$ and $[Ru(trpy)(pan)]^+$ complexes, because of the flexibility associated with a bidentate and a monodentate ligands replacing a tridentate ligand forming two adjacent five-membered chelate rings. An examination of the packing pattern in the lattice of the [Ru(bpy)(pan)Cl] complex shows the existence of three types of non-covalent interactions, *viz.* C–H···O, C–H···Cl and C–H···π interactions (Fig. S2). The phenolate oxygen of pan is hydrogen-bonded to a pyridyl hydrogen of bpy belonging to a neighboring complex molecule. The chloride is hydrogen-bonded to a pyridyl C–H of pan of an adjacent complex molecule. Besides these hydrogen-bonding interactions there are intermolecular C–H···π interactions between two pyridyl C–H's of the bipyridine ligand and naphthyl π-cloud. There is also a C–H···π interaction between a pyridyl C–H of pan ligand of one molecule with a pyridyl π cloud of another.

The structure of the $[Ru(PPh_3)_2(pan)Cl]$ complex (Fig. 5) has mirror symmetry and shows the pan ligand and the chloride sharing an equatorial plane with the metal at the center, where the chloride is obviously trans to the coordinated azo nitrogen, and the two triphenylphosphines occupy the remaining two axial positions and hence they are mutually trans. Compared to the structures of the previous complexes, the N_2OP_2Cl coordination sphere in the present complex is far less distorted, which is attributable to the freedom in disposition of three monodentate ligands. The Ru–P lengths (Table 1) are normal [2i], but the Ru–Cl distance is notably longer than that observed in the [Ru(bpy)(pan)Cl] complex and the observed elongation is attributable to stronger trans effect of the azo-nitrogen than that of the bpy-nitrogen. In the crystal lattice of this complex, there exists one molecule of dichloromethane per molecule of the complex. To find out the non-covalent interaction(s) active in the lattice, particularly between the solvent molecule and the complex molecule, packing pattern in the lattice has been examined (Fig. S3), which reveals that each complex molecule is linked to four surrounding complex molecules through C–H···π interactions. The phenyl C–H of triphenylphosphine is involved in non-covalent interaction with the π cloud on both the pyridyl and naphthyl ring of pan. Each coordinated chloride is engaged in C–H···Cl hydrogen bonding with the hydrogens of the nearest dichloromethane molecule.

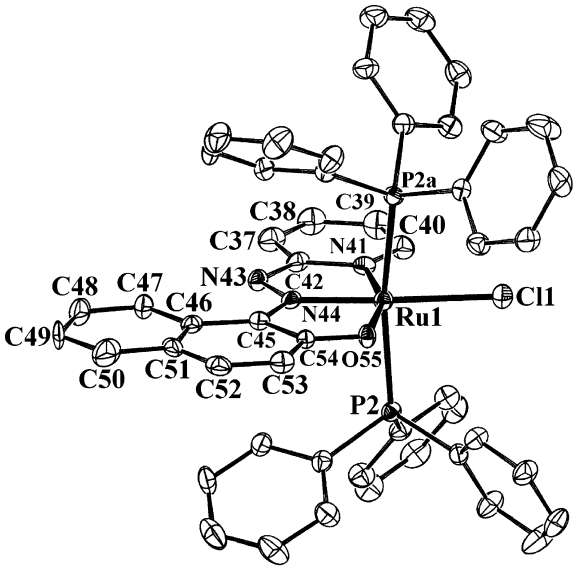

Fig. 5. View of the $[Ru(PPh_3)_2(pan)Cl]$ complex (ellipsoids at 25% probability, hydrogens not included for clarity).

The coordinated chloride in the [Ru(bpy)(pan)Cl] complex has been found to undergo facile displacement by other monodentate ligands under relatively mild condition. This has been manifested in the reactions of [Ru(bpy)(pan)Cl] with pyridine (py) and 4-picoline (pic) carried out in ethanolic medium in the presence of silver ion, for easy removal of the coordinated chloride, which have yielded the desired mixed-ligand complexes, *viz*. $[Ru(bpy)(pan)(py)]^+$ and $[Ru(bpy)(pan)(pic)]^+$, isolated as perchlorate salts in good yields. Composition of these two complexes has been verified by their microanalytical data. Both of these complexes are assumed to have a similar structure as the precursor [Ru(bpy)(pan)Cl] complex, with the chloride replaced by pyridine or 4-picoline.

3.2. Spectral properties

All the six complexes, *viz*. $[Ru(pan)_2]$, $[Ru(trpy)(pan)]ClO_4$, [Ru(bpy)(pan)Cl], $[Ru(PPh_3)_2(pan)Cl]$, $[Ru(bpy)(pan)(py)]ClO_4$ and $[Ru(bpy)(pan)(pic)]ClO_4$, are diamagnetic, which corresponds to the bivalent state of ruthenium (low-spin d^6, $S = 0$) in them. ^1H NMR spectra of these complexes have been recorded in $CDCl_3$ solution and a spectrum has been deposited as supplementary material (Fig. S4). ^1H NMR spectrum of the $[Ru(pan)_2]$ complex shows all the expected signals within 6.5–10.1 ppm, of which the most deshielded doublet at 10.07 ppm is assignable to the proton nearest to the pyridine-nitrogen. Spectra of the other three complexes are complex in nature due to overlap of signals arising from both pan and other organic ligand(s) in the similar region. However, in all these three spectra the isolated doublet near 10.0 ppm, which is diagnostic of coordinated pan, is clearly observed. ^1H NMR spectrum of the $[Ru(bpy)(pan)(py)]ClO_4$ complex shows most of the expected signals clearly, though few signals could not be distinctly identified due to their overlap with other signals. The methyl signal from the 4-picoline fragment of the $[Ru(bpy)(pan)(pic)]ClO_4$ complex is observed at 2.38 ppm, while rest of its ^1H NMR spectrum is very similar to that of the $[Ru(bpy)(pan)(py)]ClO_4$ complex.

Infrared spectra of the complexes show many bands of different intensities within 400–4000 cm^{-1}. Assignment of each individual band to a specific vibration has not been attempted. However, strong bands observed at 1606, 1498, 1199, 1134, 758 cm^{-1} in the spectrum of the $[Ru(pan)_2]$ complex are assignable to the coordinated pan ligand. Such bands are also observed in the other five complexes. In the spectra of the $[Ru(trpy)(pan)]ClO_4$, $[Ru(bpy)(pan)(py)]ClO_4$ and $[Ru(bpy)(pan)(pic)]ClO_4$ complexes two intense bands are observed near 1080 and 620 cm^{-1}, which are attributed to the perchlorate ion. Infrared spectrum of $[Ru(PPh_3)_2(pan)Cl]$ shows sharp bands at 744, 698 and 519 cm^{-1} due to the coordinated PPh_3 ligands.

All the complexes are found to be soluble in ethanol, methanol, acetonitrile, dichloromethane and chloroform, producing reddish-brown solutions. Electronic spectra of the complexes have been recorded in dichloromethane solution. Each complex shows several intense absorptions in the visible and ultraviolet region (Table 2). The absorptions in the ultraviolet region are believed to be due to transitions within the ligand orbitals and those in the visible region are likely to be due to allowed metal-to-ligand charge-transfer transitions. To have a better understanding of the nature of transitions in the visible region, qualitative EHMO calculations have been performed on computer-generated models[2] of all the complexes [14]. Composition of some selected molecular orbitals is given in Table S2 and partial MO diagram of the $[Ru(pan)_2]$ complex is shown in Fig. 6. The top three filled orbitals, *viz*. the highest occupied molecular orbital (HOMO) and the next two filled orbitals (HOMO−1 and HOMO−2), are close in energy and have major contributions from the ruthenium t_2-orbitals and relatively less contributions from the coordinated ligands. The lowest unoccupied molecular orbital (LUMO), though has some contribution from the metal center, is localized mostly on the pan ligand and is concentrated heavily on the azo (-N=N-) fragment. The next couple of vacant orbitals (LUMO + 1, LUMO + 2, etc.) are delocalized over either pan or the co-ligand. The lowest energy absorption in the visible region may therefore be assigned to a transition between the strongly

Table 2
Electronic spectral and cyclic voltammetric data

Compound	Electronic spectral data[a] λ_{max}, nm (ε, M^{-1} cm^{-1})	Cyclic voltammetric data[b]
$[Ru(pan)_2]$	606(11240), 566[c](9370), 548[c](9240), 470(9710), 408(8040), 368(10390), 302(13020)	1.62[d], 0.70[e](80)[f], −0.94[e](89)[f]
$[Ru(trpy)(pan)]ClO_4$	548(16730), 480(24060), 456[c](16070), 376[c]10710), 318(32980), 282(28680), 272(29200), 228(47040)	1.66[d], 0.86[e](69)[f], −0.86[e](90)[f], −1.56[e](60)[f]
[Ru(bpy)(pan)Cl]	610[c](13140), 584[c](12570), 504(36050), 476(22170), 444[c](12360), 368(22290), 296(48210)	1.59[d], 0.44[e](78)[f], −0.88[e](90)[f], −1.58[g]
$[Ru(PPh_3)_2(pan)Cl]$	550(5560), 480(18770), 456(9610)[c], 368(12430), 307(14780)[c], 269(41870)	1.54[d], 0.47[e](67)[f], −1.00[e](96)[f]
$[Ru(bpy)(pan)(py)]ClO_4$	595[c](11250), 572(12800), 555[c](11900), 492(31500), 465(20500), 389[c](16600), 346(19200), 293(43900)	1.69[d], 0.82[e](70)[f], −0.92[e](80)[f], −1.52[g]
$[Ru(bpy)(pan)(pic)]ClO_4$	594[c](7800), 576[c](8400), 492(22100), 464(14000), 388[c](11200), 342(12500), 292(29600)	1.64[d], 0.79[e](71)[f], −0.94[e](83)[f], −1.57[g]

[a] In dichloromethane.
[b] Solvent, 1:9 dichloromethane–acetonitrile; supporting electrolyte, TBAP; reference electrode, SCE; scan rate, 50 mV s^{-1}.
[c] Shoulder.
[d] Anodic peak-potential (E_{pa}) value.
[e] $E_{1/2} = 0.5(E_{pa} + E_{pc})$, where E_{pc} = cathodic peak-potential.
[f] $\Delta E_p = (E_{pa} - E_{pc})$ in mV.
[g] E_{pc} value.

[2] In the $[Ru(PPh_3)_2(pan)Cl]$ complex phenyl rings of the triphenylphosphines are replaced by hydrogen.

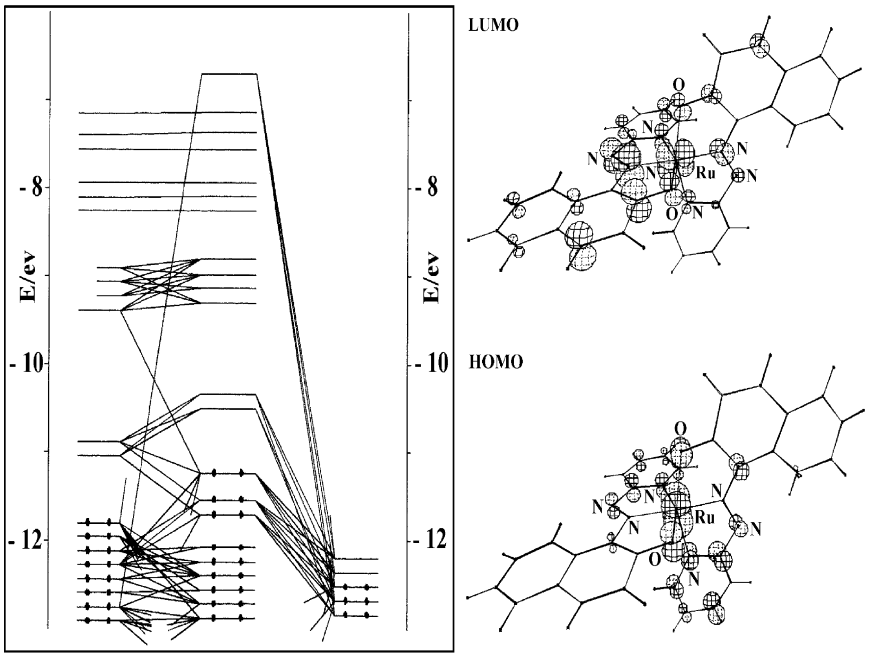

Fig. 6. Partial molecular orbital diagram of [Ru(pan)$_2$]: (a) interaction diagram and (b) highest occupied and lowest unoccupied molecular orbitals.

delocalized HOMO and LUMO with mixed metal-to-ligand charge-transfer (MLCT) and intra-ligand charge-transfer (ILCT) transition.

3.3. Electrochemical properties

Electrochemical properties of all the complexes have been studied by cyclic voltammetry in 1:9 dichloromethane–acetonitrile[3] solution (0.1 M TBAP). The voltammetric data are given in Table 2. All the complexes show two oxidative responses on the positive side of SCE. In view of the composition of the HOMO, the first oxidation is tentatively assigned to the Ru(II)–Ru(III) oxidation. This oxidation is reversible in nature, characterized by a peak-to-peak separation (ΔE_p) of 67–80 mV, which remains unchanged upon changing the scan rate, and the anodic peak-current (i_{pa}) is almost equal to the cathodic peak-current (i_{pc}) as expected for a reversible electron-transfer process. Reversibility of the Ru(II)–Ru(III) oxidation indicates that the one-electron oxidized species might be stable on a time scale much longer than the cyclic voltammetric time scale. To investigate this, as well as to verify assignment of this oxidative response to Ru(II)–Ru(III) oxidation, all the six complexes have been coulometrically oxidized at an appropriate potential[4] in 1:9 dichloromethane–acetonitrile solution (0.1 M TBAP). The oxidations have been smooth and quantitative for each complex. However, the oxidized solutions are found to stable only for the [Ru(bpy)(pan)Cl] and [Ru(PPh$_3$)$_2$(pan)Cl] complexes, which have much less Ru(II)–Ru(III) oxidation potential. For the rest four complexes, color of the solution containing the oxidized species changes rapidly indicating fast decomposition. ESR spectra of solutions containing the [Ru(bpy)(pan)Cl]$^+$ and [Ru(PPh$_3$)$_2$(pan)Cl]$^+$ complexes have been recorded at 77 K. Both the complexes show an axial ESR spectrum with two distinct signals ($g_\perp$ and $g_\parallel$; for the [Ru(bpy)-(pan)Cl]$^+$ complex $g_\perp = 2.28$ and $g_\parallel = 1.90$; for the [Ru(PPh$_3$)$_2$(pan)Cl]$^+$ complex $g_\perp = 2.21$ and $g_\parallel = 1.99$). A selected spectrum is shown in Fig. 7. The observed anisotropic nature of the spectra confirms the +3 oxidation state of ruthenium in the oxidized complexes, which in turn supports assignment of the first oxidative response to Ru(II)–Ru(III) oxidation to be correct. The second oxidative response is irreversible in nature and is tentatively assigned to oxidation of the coordinated pan ligand. A reductive response, quasi-reversible in nature, is displayed by all the complexes near −0.9 V versus SCE, and in view of the composition of the LUMO this reduction is assigned to reduction of the azo (–N=N–) fragment of the coordinated pan ligand. A second irreversible reductive response is observed in the [Ru(trpy)(pan)]ClO$_4$, [Ru(bpy)(pan)Cl],

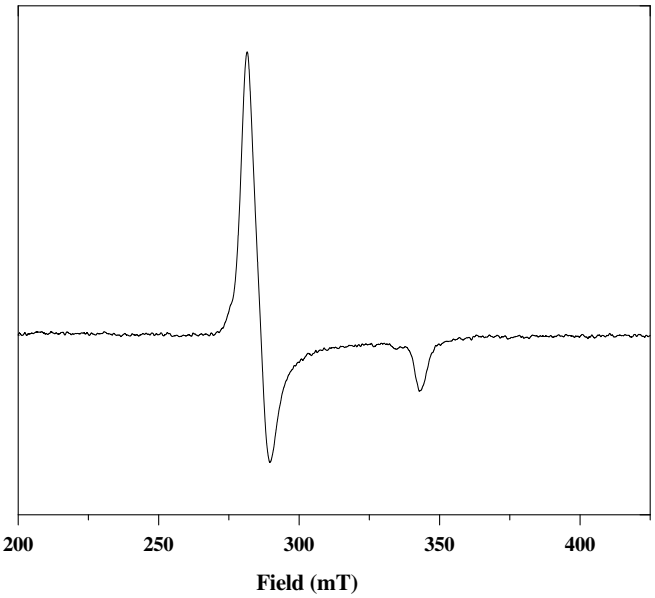

Fig. 7. ESR spectrum of the [Ru^{III}(bpy)(pan)Cl]$^+$ complex in 1:9 dicloromethane–acetonitrile solution at 77 K.

[3] A little dichloromethane was necessary to take the complex into solution. Addition of large excess of acetonitrile was necessary to record the redox responses in proper shape.

[4] Coulometric oxidation has been carried out at a potential 200 mV higher than the anodic peak-potential (E_{pa}).

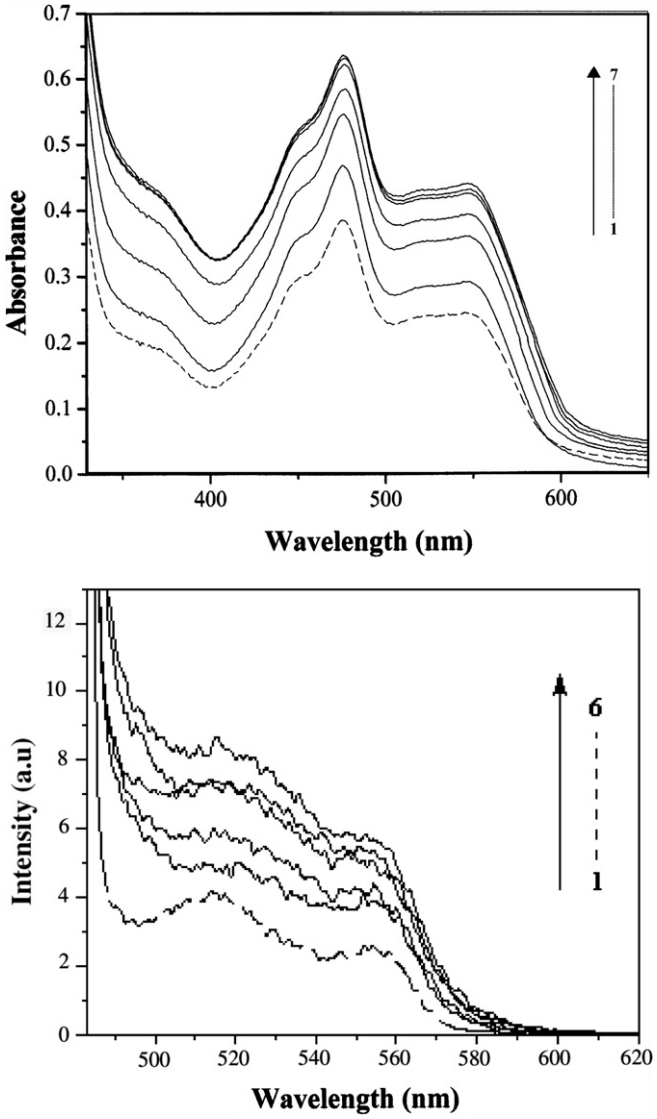

Fig. 8. (a) Absorption spectrum of the [Ru(trpy)(pan)]ClO_4 in Tris–HCl/NaCl buffer (10 mM, pH 7.2) solution in the absence (---) and presence (—) of CT DNA ([DNA]:[complex] = 20:1, 40:1, 50:1, 60:1, 65:1, 70:1; the complex concentration was 30 μM). (b) Fluorescence spectrum of the [Ru(trpy)(pan)]ClO_4 in Tris–HCl/NaCl buffer (10 mM, pH 7.2) solution in the absence (---) and presence (—) of CT DNA ($\lambda_{excitation}$ = 480 nm, [DNA]:[complex] = 40:1, 50:1, 60:1, 65:1, 70:1; the complex concentration was 30 μM).

[Ru(bpy)(pan)(py)]ClO_4 and [Ru(bpy)(pan)(pic)]ClO_4 complexes around −1.6 V versus SCE, which is assigned to reduction of the coordinated polypyridine (trpy or bpy) ligand [13].

3.4. DNA binding properties

As cationic transition metal complexes containing polypyridine ligands are known to display DNA interaction properties [15], we have also explored such possibility in the three such cationic complexes, *viz.* [Ru(trpy)(pan)]ClO_4, [Ru(bpy)(pan)(py)]ClO_4 and [Ru(bpy)(pan)(pic)]ClO_4. These three complexes are fairly soluble in water, another property welcome in DNA binding agents. Interaction of the [Ru(trpy)(pan)]ClO_4 complex with DNA has been monitored initially by absorption and fluorescence spectroscopic studies in Tris–HCl buffer (pH 7.2) solution. In the absorption spectroscopic studies, the maximum at 480 nm, displayed by the complex only, is found to increase in intensity upon addition of DNA. The intensity increases with increasing ratio of [DNA]:[complex] and reaches saturation at [DNA]:[complex] = 70:1 (Fig. 8a). Such increase in intensity of absorption upon interaction with DNA is, though relatively less common, precedent in the literature [16]. In order to explore the interaction one step further, detailed spectrofluorimetric experiments with complex and DNA has also been carried out. The complex shows emission peaks at 515 nm and 554 nm when excited at 480 nm. With the increasing amount of DNA the fluorescence intensity increases for both the peaks (Fig. 8b), and reaches its optimum value in the same ratio (i.e. [DNA]:[complex] = 70:1). Absorption and fluorescence spectroscopic studies in Tris–HCl buffer (pH 7.2) solution in the presence and absence of DNA show that the other two complexes, *viz.* [Ru(bpy)(pan)(py)]ClO_4 and [Ru(bpy)(pan)(pic)]ClO_4, also interact with DNA.

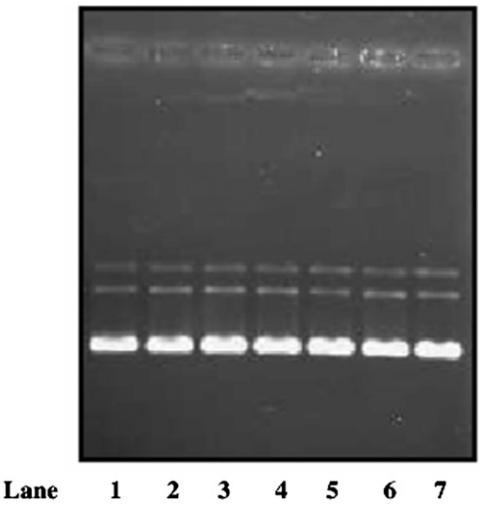

Fig. 9. Results of the gel electrophoresis experiment for [Ru(trpy)(pan)]ClO_4. Lane 1, SC pUC18 DNA control without irradiation. Lane 2, DNA control with irradiation at 254 nm. Lanes 3–7, DNA + complex with [DNA]/[complex] ratio of 1, 20, 40, 60, 70, respectively with irradiation at 254 nm. The complex concentration was 30 μM for Lanes 3–7.

In order to examine whether the above three complexes can also bring about cleavage of DNA upon UV irradiation, a property usually exhibited by such polypyridine complexes [15], interaction of these complexes with a super-coiled DNA, *viz.* SC pUC18 DNA, has been studied by gel electrophoresis. In these experiments SC pUC18 DNA was incubated in the presence of different concentrations of the complexes, followed by irradiation at 254 nm for different time durations. The samples were then analyzed by agarose gel electrophoresis. After the run the DNA was stained with EtBr and visualized by UV transilluminator. A representative picture of EtBr stained DNA is shown in Fig. 9. The extreme left line is for SC pUC18 DNA and in the following five lanes are the bands for increasing DNA complex ratio (i.e. [DNA]/[complex] = 1, 20, 40, 60 and 70. This shows that the complex does not induce any observable conformation changes in SC DNA confirming that they cannot cleave DNA upon UV irradiation. Moreover we could not see any retardation of the SC pUC18 DNA. This is perhaps due to the dissociation of the complex from DNA during the run of gel electrophoresis.

4. Conclusions

The present study shows that 1-(2′-pyridylazo)-2-naphthol (Hpan) can bind strongly to ruthenium as a monoanionic N,N,O-donor affording stable complexes. The mixed-ligand [Ru(bpy)(pan)Cl] complex exhibits interesting reactivity via dissociation of the Ru–Cl bond and such reactions with different bridging and

terminal ligands are currently under exploration. The [Ru(trpy)(pan)]ClO_4, [Ru(bpy)(pan)(py)]ClO_4 and [Ru(bpy)(pan)(pic)]ClO_4 complexes can effectively bind to DNA without causing damage to the DNA double helix.

Acknowledgements

The authors thank the reviewers for their critical comments, which have been useful in revising the manuscript. They also thank Prof. P.K. Bharadwaj, Department of Chemistry, Indian Institute of Technology, Kanpur, for his help with the X-ray diffraction data collection on the crystal of [Ru(bpy)(pan)Cl]. Thanks are also due to Prof. S. Pal of University of Hyderabad (for recording the esr spectra) and, Prof. K.P. Das and Mr. P. Dey of Bose Institute (for their help in recording the fluorescence spectra). Professor Michael G.B. Drew thanks the Engineering and Physical Sciences Research Council, United Kingdom and the University of Reading, for financial help. S. Halder thanks the University Grants Commission, New Delhi [Grant No. 10–2(5)2004(1)-E.U.II] for her fellowship.

Appendix A. Supplementary data

CCDC 644619 and 644622 contains the supplementary crystallographic data for this paper. These data can be obtained free of charge via http://www.ccdc.cam.ac.uk/conts/retrieving.html, or from the Cambridge Crystallographic Data Centre, 12 Union Road, Cambridge CB2 1EZ, UK; fax: (+44) 1223-336-033; or e-mail: deposit@ccdc.cam.ac.uk. Full details of data collection are provided in Table S1and composition of selected molecular orbitals in Table S2. Packing diagrams showing non-covalent interactions in complexes [Ru(trpy)(pan)]ClO_4 (Fig. S1), [Ru(bpy)(pan)Cl] (Fig. S2) and [Ru$(PPh_3)_2$(pan)Cl] (Fig. S3), and ^{1}H NMR spectrum of [Ru$(pan)_2$] (Fig. S4) have been deposited. Supplementary data associated with this article can be found, in the online version, at doi:10.1016/j.poly.2008.05.023.

References

[1] (a) M. Turki, C. Daniel, Coord. Chem. Rev. 216–217 (2001) 31;
(b) V. Balzani, A. Juris, Coord. Chem. Rev. 211 (2001) 97;
(c) B.Z. Shan, Q. Zhao, N. Goswami, D.M. Eichhom, D.P. Rillema, Coord. Chem. Rev. 211 (2001) 117;
(d) N.A.P. Kane-Maguire, J.F. Wheeler, Coord. Chem. Rev. 211 (2001) 145;
(e) L.N. Ji, X.H. Zou, J.G. Liu, Coord. Chem. Rev. 216–217 (2001) 513;
(f) G. Simonneaux, P. Le Maux, Coord. Chem. Rev. 228 (2002) 43;
(g) H. Yersin, C. Kratzer, Coord. Chem. Rev. 229 (2002) 75;
(h) J.F. Endicott, H.B. Schlegel, M.J. Uddin, D.S. Seniveratne, Coord. Chem. Rev. 229 (2002) 95;
(i) I. Gorelsky, A.B.P. Lever, M. Ebadi, Coord. Chem. Rev. 230 (2002) 97;
(j) F. Hartl, M.P. Aarnts, H.A. Nieuwenhuis, J. van Slageren, Coord. Chem. Rev. 230 (2002) 106;
(k) C.M. Che, J.S. Huang, Coord. Chem. Rev. 231 (2002) 151;
(l) M.J. Clarke, Coord. Chem. Rev. 232 (2002) 69;
(m) E. Tfouni, M. Krieger, B.R. McGarvey, D.W. Franco, Coord. Chem. Rev. 236 (2003) 57;
(n) B. Serli, E. Zangrando, T. Gianferrara, L. Yellowless, E. Alessio, Coord. Chem. Rev. 245 (2003) 73;
(o) M.J. Clarke, Coord. Chem. Rev. 236 (2003) 209;
(p) I. Ando, Coord. Chem. Rev. 248 (2004) 185;
(q) M.A.S. Aquino, Coord. Chem. Rev. 248 (2004) 1025;
(r) R.F. Winter, S. Záli, Coord. Chem. Rev. 248 (2004) 1565;
(s) S. Rigaut, D. Touchard, P.H. Dixneuf, Coord. Chem. Rev. 248 (2004) 1585;
(t) M.K. Nazeeruddin, S.M. Zakeeruddin, J.J. Lagref, P. Liska, P. Comte, C. Barolo, G. Viscardi, K. Schenk, M. Graetzel, Coord. Chem. Rev. 248 (2004) 1317;
(u) L. Spiccia, G.B. Deacon, C.M. Kepert, Coord. Chem. Rev. 248 (2004) 1329;
(v) Y. Saito, T. Azechi, T. Kitamura, Y. Hasegawa, Y. Wada, S. Yanagida, Coord. Chem. Rev. 248 (2004) 1469;
(w) Md.K. Nazeeruddin, C. Klein, P. Liska, M. Grätzel, Coord. Chem. Rev. 249 (2005) 1460.
[2] (a) F. Basuli, S.M. Peng, S. Bhattacharya, Inorg. Chem. 36 (1997) 5645;
(b) F. Basuli, M. Ruf, C.G. Pierpont, S. Bhattacharya, Inorg. Chem. 37 (1998) 6113;
(c) A.K. Das, A. Rueda, L.R. Falvello, S.M. Peng, S. Bhattacharya, Inorg. Chem. 38 (1999) 4365;
(d) A.K. Das, S.M. Peng, S. Bhattacharya, J. Chem. Soc., Dalton Trans. (2000) 181;
(e) F. Basuli, S.M. Peng, S. Bhattacharya, Inorg. Chem. 39 (2000) 1120;
(f) F. Basuli, S.M. Peng, S. Bhattacharya, Inorg. Chem. 40 (2001) 1126;
(g) I. Pal, F. Basuli, T.C.W. Mak, S. Bhattacharya, Angew. Chem., Int. Ed. 40 (2001) 2923;
(h) K. Majumder, R.J. Butcher, S. Bhattacharya, Inorg. Chem. 41 (2002) 4605;
(i) R. Acharyya, S.M. Peng, G.H. Lee, S. Bhattacharya, Inorg. Chem. 42 (2003) 7378;
(j) A. Das, S.M. Peng, G.H. Lee, S. Bhattacharya, New J. Chem. 28 (2004) 712;
(k) S. Nag, P. Gupta, R.J. Butcher, S. Bhattacharya, Inorg. Chem. 43 (2004) 4814;
(l) P.K. Sinha, L.R. Falvello, S. Bhattacharya, Indian J. Chem. 43A (2004) 1846;
(m) P. Gupta, S. Dutta, F. Basuli, S.M. Peng, G.H. Lee, S. Bhattacharya, Inorg. Chem. 45 (2006) 460;
(n) S. Halder, R. Acharyya, S.M. Peng, G.H. Lee, M.G.B. Drew, S. Bhattacharya, Inorg. Chem. 45 (2006) 9654;
(o) S. Nag, R.J. Butcher, S. Bhattacharya, Eur. J. Inorg. Chem. (2007) 1251.
[3] (a) C.D. Hubbard, A.D. Pacheco, J. Inorg. Nucl. Chem. 39 (1977) 1373;
(b) M. Katsura, I. Taira, I. Tasuku, F. Masatoshi, Bull. Chem. Soc. Jpn. 51 (1978) 1743;
(c) K. Shigero, M. Yoshiki, A. Kunihiko, Chem. Lett. (1981) 363;
(d) L.M. Rao, D. Satyanarayana, Indian J. Chem. 22A (1983) 455;
(e) H. Akiharu, F. Shigenobu, T. Motoharu, Bull. Chem. Soc. Jpn. 57 (1984) 1255;
(f) P.M. Drozdzewski, Spectrochim. Acta 44A (1988) 1297;
(g) M.A. Taher, S. Puri, R.K. Bansal, B.K. Puri, Talanta 45 (1997) 411;
(h) S. Nabi, A. Alim, A. Islam, M. Amjad, J. Separ. Sci. 28 (2005) 2463.
[4] (a) R.A. Krause, K. Krause, Inorg. Chem. 19 (1980) 2600;
(b) S. Goswami, A.R. Chakravarty, A. Chakravorty, Inorg. Chem. 20 (1981) 2246;
(c) R.A. Krause, K. Krause, Inorg. Chem. 21 (1982) 1774.
[5] (a) S. Bhattacharya, S.R. Boone, G.A. Fox, C.G. Pierpont, J. Am. Chem. Soc. 112 (1990) 1088;
(b) J. Chakravarty, S. Bhattacharya, Polyhedron 15 (1996) 257;
(c) N.C. Pramanik, S. Bhattacharya, Polyhedron 16 (1997) 1755.
[6] (a) E.P. Benson, J.I. Legg, Inorg. Chem. 20 (1981) 2504;
(b) M.S. El-Shahawi, A.Z. Abu Zuhri, M.M. Kamal, Fresen. J. Anal. Chem. 348 (1994) 730.
[7] (a) I.P. Evans, A. Spencer, G. Wilkinson, J. Chem. Soc., Dalton Trans. (1973) 204;
(b) S. Anderson, K.R. Seddon, J. Chem. Res. (S) (1979) 74;
(c) B.P. Sullivan, J.M. Calvert, T.J. Meyer, Inorg. Chem. 19 (1980) 1404;
(d) T.A. Stephenson, G. Wilkinson, J. Inorg. Nucl. Chem. (1996) 945.
[8] (a) M. Walter, L. Ramaley, Anal. Chem. 45 (1973) 165;
(b) D.T. Sawyer, J.L. Roberts Jr., Experimental Electrochemistry for Chemists, Wiley, New York, 1974. p. 167.
[9] (a) G.M. Sheldrick, SHELXS-97 and SHELXL-97, Fortran Programs for Crystal Structure Solution and Refinement, University of Gottingen, Germany, 1997;
(b) ABSPACK, Oxford Diffraction Ltd., Oxford, UK, 2005.;
(c) CRYSALIS, Oxford Diffraction Ltd., Abingdon, UK, 2006.
[10] (a) A. Seal, S. Ray, Acta Crystallogr., Sect. C 40 (1984) 929;
(b) P. Majumdar, S.M. Peng, S. Goswami, J. Chem. Soc., Dalton Trans. (1998) 1569.
[11] A. Das, S.M. Peng, S. Bhattacharya, Polyhedron 19 (2000) 1227.
[12] (a) H.S. Chow, E.C. Constable, C.E. Housecroft, M. Neuburger, S. Schaffner, Polyhedron 25 (2006) 1831;
(b) M. Fabre, J. Jaud, M. Hliwa, J.P. Launay, J. Bonvoisin, Inorg. Chem. 45 (2006) 9332;
(c) E. Lebon, I.M. Dixon, L. Vendier, A. Igau, P. Sutra, Inorg. Chim. Acta 360 (2007) 1235.
[13] (a) M.F. McGuiggan, L.H. Pingnolet, Inorg. Chem. 21 (1982) 2523;
(b) G.A. Eox, S. Bhattacharya, C.G. Pierpont, Inorg. Chem. 30 (1991) 2895.
[14] (a) C. Mealli, D.M. Proserpio, J. Chem. Edu. 67 (1990) 399;
(b) C. Mealli, D.M. Proserpio, CACAO, version 4.0, Italy, 1994.
[15] (a) C.J. Murphy, J.K. Barton, Methods Enzymol. 226 (1993) 576;
(b) D.S. Sigman, A. Mazumder, D.M. Perrin, Chem. Rev. 93 (1993) 2295;
(c) D.B. Hall, R.E. Holmlin, J.K. Barton, Nature 382 (1996) 731;
(d) P.J. Dandlier, R.E. Holmlin, J.K. Barton, Science 274 (1997) 1465;
(e) F.M. O'Reilly, J.M. Kelly, New J. Chem. 22 (1998) 215;
(f) E. Bernal-Mend~ez, J.S. Sun, F. Gonzalez-Vilchez, M. Leng, New J. Chem. 22 (1998) 1479;
(g) B.A. Jackson, V.Y. Alekseyev, J.K. Barton, Biochemistry 38 (1999) 4655;
(h) L. Mishra, S. Srivastava, A.B. Patel, New J. Chem. 24 (2000) 505.
[16] (a) R.J. Morgan, S. Chatterjee, A.D. Baker, T.C. Strekas, Inorg. Chem. 30 (1991) 2687;
(b) W. Lu, D.A. Vicic, J.K. Barton, Inorg. Chem. 44 (2005) 7970;
(c) L.M. Wu, H.B. Teng, X.B. Ke, W.J. Xu, J.T. Su, S.C. Liang, X.M. Hu, Chem. Biodiv. 4 (2007) 2198.

N,*N*,*N*′,*N*″,*N*″-pentamethyldiethylenetriamine (Me_5dien) from Fluka and L-histidine was Merck product. All ligands were used without further purification and their purity was greater than 99%. The exact concentrations of the ligand solutions used for potentiometric measurements were determined by the Gran method [10]. Copper(II) chloride solution was purchased from Merck as a Titrisol concentrate for the preparation of standard solutions. The concentration of the metal ion stock solution was standardized by complexometric ethylenediaminetetraacetate (EDTA) titration. Carbonate-free potassium hydroxide solution (the titrant) was prepared and standardized against a standard potassium hydrogen phthalate solution. All solutions were prepared with deionized water. The formulae of the fully protonated form of the ligands used in this study are shown in Scheme 1.

2.2. Potentiometric measurements

The stability constants of the proton and copper(II) complexes were determined by pH-metric titration of 5 cm^3 samples in aqueous solutions. All the measurements were carried out at 0.2 mol dm^{-3} ionic strength (KCl) and 25.0 ± 0.1 °C using a constant-temperature water-bath. The titrations were performed with carbonate-free KOH solution of known concentration (ca. 0.2 mol dm^{-3}) under argon atmosphere over the pH range 2.0 to ≈11.0. For the binary systems the ligand concentration was 4×10^{-3} or 8×10^{-3} mol dm^{-3}. The metal ion to ligand ratios were 1:1, 1:2, 1:4 and 1:8.

For the ternary systems the ratios of copper(II):en/dien/Me_5dien:His were 1:1:1, 1:1:2, 1:2:1 and 1:2:2. Titrations were made on samples containing the copper(II) ion at 4×10^{-3} mol dm^{-3} prepared from $CuCl_2$ salt. The values of stability constants of the complexes formed in the binary systems were kept constant during calculating the potentiometric data of the ternary systems.

The pH-metric titrations were carried out with a Radelkis Op-208/1 instrument equipped with a combination pH electrode (SINGLE PORE, Hamilton) and an ABU-80 autoburette (Radiometer).The electrode system was calibrated by periodic titrations of HCl solution (7.5×10^{-3} mol dm^{-3} in KCl) against standard KOH solution as described earlier [11]. The pH-metric results were used to establish the stoichiometry of the species and to calculate the stability constants of the species formed in the ternary systems. Calculations were performed with the aid of the HYPERQUAD 2006 computer program [12]. The reported standard deviations were calculated by assuming random errors.

The charges of the complexes have been omitted in the text and tables. However, for clarity, it should be mentioned here that the fully deprotonated form of amino acid (His) is L^- while the amines (en), (dien) or (Me_5dien) are neutral.

2.3. UV–Vis spectroscopy

The electronic absorption spectra in the visible range were measured with a BECKMAN DU68 spectrophotometer using 2-cm quartz cells at room temperature. The spectra were recorded digitally (0.5 nm step) over the range 400–900 nm. The metal ion concentration was 4×10^{-3} mol dm^{-3} prepared from $CuCl_2$ salt. For the ternary systems copper(II):en:His, copper(II):dien:His and copper(II):Me_5dien:His the concentration ratios were 1:2:2, 1:1:2 and 1:2:1, respectively. The net ligand-field absorption band of each mixed-ligand species was extracted from the absorption spectra applying the procedure described in Ref. [13].

2.4. EPR spectroscopy

Electron paramagnetic resonance (EPR) spectra were performed on a Bruker 300E X-band spectrophotometer equipped with a Bruker NMR gaussmeter ER 035 M and a Hewlett–Packard frequency counter HP 5350B at 77 K in water/ethyleneglycol (4:1 v/v) solution. The EPR parameters were calculated by computer simulation of the experimental spectra using Bruker's WIN-EPR SimFonia Software Version 1.25. The metal ion concentration and the metal ion

Ligands	Abreviation
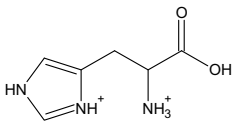 L-histidine	$[H_3L]^{2+}$
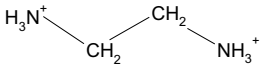 ethylenediamine	$[H_2\text{-en}]^{2+}$
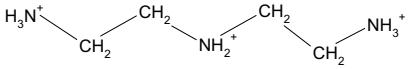 dietylenotriamina	$[H_3\text{-dien}]^{3+}$
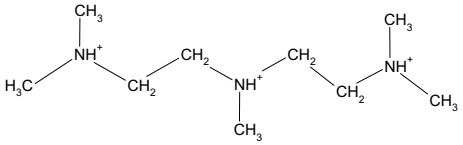 N,N,N',N'',N''-pentamethyldiethylenetriamine	$[H_3\text{-}Me_5\text{dien}]^{3+}$

Scheme 1.

to ligands molar ratios were the same as those used in the electronic absorption spectra.

3. Results and discussion

The values of the protonation constants of the studied ligands were re-determined under the experimental conditions identical to those applied for the ternary systems. The obtained results are in good agreement with the literature data [14–17].

The fully protonated form of the en contains two dissociable protons (H_2L^{2+}), one at each amino group $-NH_3^+$, while dien and Me_5dien (H_3L^{3+}) are able to release three protons in the whole pH range. His (H_3L^{2+}) contains three protons that dissociate off the ligand in the measurable pH range. The carboxylic function is deprotonated in the acidic pH range. The pK_{COOH} value is 1.73 for this ligand and this corresponds well to the characteristic acidity of the carboxylic groups of the amino acids. The next deprotonation corresponds to the imidazole nitrogen ($pK = 6.07$). The most basic donor for His is the amino group with pK values 9.09. The dissociation of the second proton of the imidazole group ($pK_a \sim 14$) is beyond the pH-metric titration range [2]. Thus, it does not participate in the metal coordination equilibria.

3.1. Cu^{2+}-complexation for binary systems

The binary systems of polyamines Cu^{2+}–en [3,18,19], Cu^{2+}–dien [13,15], Cu^{2+}–Me_5dien [3,16,20] were studied previously, however the stability constants were re-determined in the present work under the condition identical to those applied for the ternary systems.

A major effort was made to study the stability, speciation and structure of copper(II)–histidine complexes [2,3,9,21–24]. The composition of the predominant complexes of copper(II) and L-histidine in aqueous solution depends on the metal ion to ligand ratio, temperature and pH [2]. The major species in the basic solution of this binary system is [Cu(L-His)$_2$] (this complex exists in the equilibria with the mixed-ligand complexes in the studied ternary systems (see below)). Deschamps et al. reported the isolation and X-ray structure determination of this species [25]. Structural studies in solution indicate that this species exists in solution as an equilibrium mixture of isomeric structures having three and four N atoms coordinated to the copper(II) in the equatorial plane [21,22,24]. In the 3N isomer of the [Cu(His)$_2$] species, one histidine is bound glycine-like and the other histamine-like, with possible apical binding of the donor atoms of the side chains. The 4N isomer has all nitrogens in equatorial positions with the cis arrangements of the nitrogens of the same kind [22,24].

3.2. Cu^{2+}-complexation for ternary systems

The equilibrium models for ternary systems and corresponding stability constants giving the best fits of the pH-metric titration curves are presented in Table 1.

The general four-component equilibria can be written as:

$$pM + q(A) + r(His) + sH \leftrightharpoons M_p(A)_q(His)_rH_s$$

where p, q, r and s are the stoichiometric coefficients corresponding to the metal ion, M, A (A = en, dien or Me_5dien), His, and H, respectively; charges are omitted for simplicity.

The overall formation constants are defined as:

$$\beta_{pqrs} = [M_p(A)_q(His)_rH_s]/[M]^p[(A)]^q[(His)]^r[H]^s$$

The β_{1111} and β_{1110} constants express the stability of the [Cu(A)(H–His)]$^{2+}$ and [Cu(A)(His)]$^+$ mixed-ligand species, respectively. According to data in Table 1, the mixed-ligand complexes with [Cu(A)(His)]$^+$ stoichiometry are formed in all systems. In addition, [Cu(A)(H–His)]$^{2+}$ species exists in Cu^{2+}–dien–His and Cu^{2+}–Me_5-dien–His systems.

Despite the fact that the β_{1110} constant expresses the stability of the [Cu(A)(His)]$^+$ mixed-ligand species, it does not represent directly the binding strength between His and copper(II) ions in the presence of polyamine. The equilibrium constant, $K_{Cu(A)(His)}$, derived from the computed values of β_{pqrs}, according to equation: $\log K_{Cu(A)(His)} = \log \beta_{Cu(A)(His)} - \log \beta_{Cu(A)}$ (Table 1, row 4), shows how tightly histidine ligand is bound to the simple [Cu(A)]$^{2+}$ complex. The stepwise stability constants of the mixed-ligand species are much lower for the complexes involving tridentate dien and Me_5-dien than the stability constants of species containing bidentate en. In the case of dien and Me_5dien only one position remains available for the coordination of a second ligand.

The relative stability of the mixed-ligand complexes, as compared with the corresponding simple species formed in the binary systems, could be evaluated in different ways. The relative stability of [M(A)(His)]$^+$ can be expressed in terms of $\Delta \log K$ parameter (the constant due to [M(A)] + [M(His)] $\rightleftharpoons$ [M(A)(His)] + M equilibrium). This constant can be calculated from the experimentally measured stability constants according to the equation: $\Delta \log K = \log \beta_{[M(A)(His)]} - (\log \beta_{[M(A)]} + \log \beta_{[M(His)]})$. The statistical value of $\Delta \log K$ depends on the geometry of the complex and for the distorted octahedral coordination sphere of Cu^{2+} with two different bidentate ligands was deduced as -0.9 [26,27]. The calculated $\Delta \log K$ data are listed in Table 1. It can be seen that, $\Delta \log K$ is equal to -1.22 for [Cu(en)(His)]$^+$ and is very low for [Cu(dien)(His)]$^+$ (-5.35) and for [Cu(Me_5dien)(His)]$^+$ (-5.49). This difference is most likely caused by lower than six-coordination number of

Table 1
Cumulative formation constants ($\log \beta$), derived equilibrium constants ($\log K$) and characteristic parameters for the stability of complexes formed in the ternary systems Cu^{2+}–amine (en, dien or Me_5dien)–L-histidine at 25 °C and $I = 0.2$ mol dm^{-3} (KCl)

No.	Assignments	System Cu^{2+}–A–His; (A = en, dien or Me_5dien)		
		Cu^{2+}–en–His	Cu^{2+}–dien–His	Cu^{2+}–Me_5dien–His
1	$\log \beta_{[Cu(A)(H-His)]}$		27.56 (2)	24.43 (9)
2	$\log \beta_{[Cu(A)(His)]}$	19.47 (1)	20.77 (1)	17.09 (1)
3	$pK_{[Cu(A)(H-His)]}$		6.79	7.34
4	$\log K_{[Cu(A)(His)]}$; [Cu(A)]+His = [Cu(A)(His)][a]	8.89	4.76	4.62
5	$\log K_{[Cu(A)(His)]} - pK_{NH_3^+} - pK_{im}$	−6.27	−10.40	
6	χ^2	7.23	10.21	7.01
7	σ	10.54	6.58	8.24
8	$\Delta \log K$	−1.22	−5.35	−5.49
9	$\log X$	1.20	2.77	

Charges are omitted for simplicity.

[a] $\log K_{[Cu(A)(His)]} = \log \beta_{[Cu(A)(His)]} - \log \beta_{[Cu(A)]}$; $\log \beta_{[Cu(en)]} = 10.58$, $\log \beta_{[Cu(en)_2]} = 19.73$ [19]; $\log \beta_{[Cu(dien)]} = 16.01$, $\log \beta_{[Cu(dien)_2]} = 20.76$ [15]; $\log \beta_{[Cu(Me_5dien)]} = 12.47$ [20]; $\log \beta_{[Cu(H-His)]} = 14.14$, $\log \beta_{[Cu(His)]} = 10.11$, $\log \beta_{[Cu(H-His)_2]} = 26.97$, $\log \beta_{[Cu(H-His)(His)]} = 23.73$, $\log \beta_{[Cu(His)_2]} = 18.01$, $\log \beta_{[Cu_2(His)_2H_{-2}]} = 8.07$, $\log \beta_{[Cu(His)H_{-1}]} = 1.97$, $\log \beta_{[Cu(His)_2H_{-1}]} = 6.46$ [29].

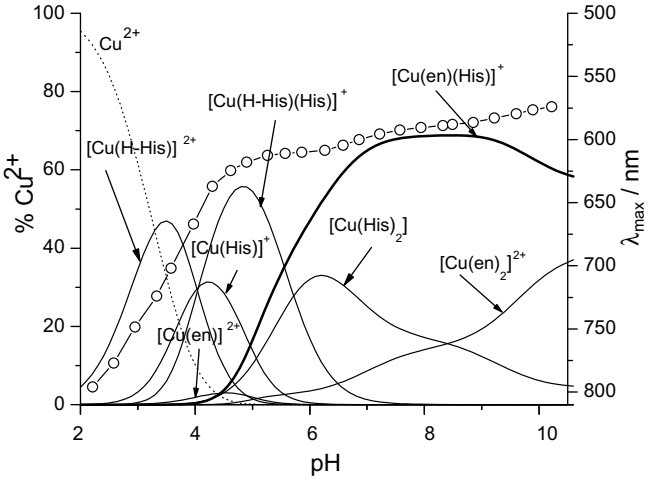

Fig. 1. Species distribution curves as a function of pH and variations of visible absorption maximum wavelength (circle) for the Cu^{2+}–en–His ternary system at 1:2:2 molar ratio; $c_{Cu^{2+}} = 4 \times 10^{-3}$ mol dm^{-3}.

Cu^{2+} in the mixed-ligand complexes formed by dien or Me_5dien [26,27].

It is possible to calculate the $\log X_{M(A)(L)}$ values (the constant due to $[MA_2] + [ML_2] \rightleftharpoons 2[M(A)(L)]$ equilibrium, (Table 1, row 9) which are higher than that expected on a statistical basis (0.6) [28]. This indicates, that the formation of mixed complexes is favoured in the ternary systems of en and dien. For the $[Cu(Me_5\text{-dien})(His)]^+$ mixed-ligand species the $\log X_{M(A)(L)}$ value cannot be calculated, since the complex with 1:2 metal to ligand ratio is not formed in the Cu^{2+}–Me_5dien binary system. It could be noticed that the $\log X_{M(A)(L)}$ value for the system with dien is distinctly higher than that for the system with en. This is a reflection of the ratio of the stepwise formation constants for the binary Cu^{2+}–amine system ($\log(K_{Cu(dien)}/K_{Cu(dien)2}) = 11.26$ is significantly greater than $\log(K_{Cu(en)}/K_{Cu(en)2}) = 1.43$).

Concentration distribution curves for the Cu^{2+}–en–His system at 1:2:2 molar ratio is presented in Fig. 1. It can be seen, that up to pH 4 only a simple species are formed: $[Cu(H–His)]^{2+}$, $[Cu(His)]^+$, $[Cu(H–His)(His)]^+$ and $[Cu(en)]^{2+}$ as a minor one. The EPR parameters of the spectra observed up to pH 4.5 in the liquid solution for the ternary Cu^{2+}–en–His system ($g_{iso} = 2.154$ and $A_{iso} = 59 \times 10^{-4}$ cm^{-1} at pH 3.5 and $g_{iso} = 2.117$ and $A_{iso} = 75 \times 10^{-4}$ cm^{-1} at pH 4.8) are almost identical with those observed for the Cu^{2+}–His

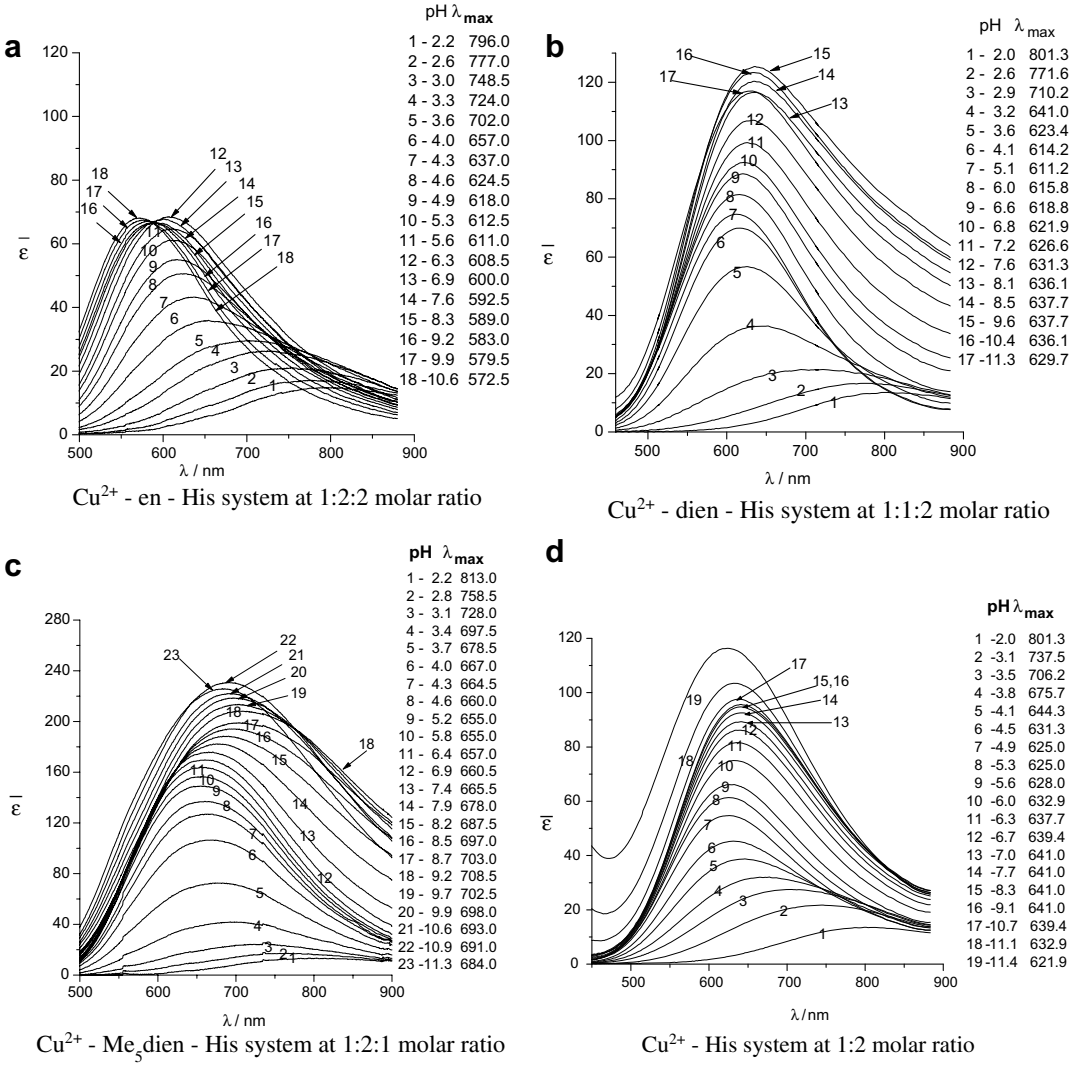

Cu^{2+} - en - His system at 1:2:2 molar ratio

Cu^{2+} - dien - His system at 1:1:2 molar ratio

Cu^{2+} - Me_5dien - His system at 1:2:1 molar ratio

Cu^{2+} - His system at 1:2 molar ratio

Fig. 2. pH-varied absorption spectra of the Cu^{2+}–en–His system at 1:2:2 molar ratio (a), Cu^{2+}–dien–His system at 1:1:2 molar ratio (b), Cu^{2+}–Me_5dien–His system at 1:2:1 molar ratio (c), Cu^{2+}–His system at 1:2 molar ratio (d), ($c_{Cu^{2+}} = 4 \times 10^{-3}$ mol dm^{-3}).

binary system [24], i.e. in this pH range only the simple species of His are formed. Moreover, below pH 4 the absorption spectra exhibit approximately the same changes versus pH for the ternary system with 1:2:2 concentration ratios of Cu^{2+}:en:His as those observed for the binary system with 1:2 concentration ratio of Cu^{2+}:His (Fig. 2a and d). The mixed-ligand species $[Cu(en)(His)]^+$ starts to form at ca. pH 4.5 and dominates in solution above pH 6. In this pH range the absorption spectra for binary and ternary systems are different supporting formation of mixed-ligand complex (Fig. 2). Similarly, the comparison of the EPR spectra for the binary systems with His or en and ternary system allows to detect the formation process of the $[Cu(en)(His)]^+$ mixed-ligand species. The EPR parameters of the liquid and frozen solution observed for Cu–His and Cu–en binary systems (Table 2) are very similar to those reported for $[Cu(His)_2]$ with in-plane coordination mode of the ligands proposed as $\{NH_2, N_{im}, COO^-, NH_2\}$ and $[Cu(en)_2]^{2+}$ with $2\times$ $\{NH_2, NH_2\}$ [17,24,30]. At pH between 8 and 9, when the mixed-ligand species is predicted as predominant in the studied ternary system, the values of the EPR parameters are intermediate between those obtained for the bis(ligand) complexes formed by His or en (Table 2). An apparent decrease of $g_{\|}$ and increase of $A_{\|}$ parameters for $[Cu(en)(His)]^+$ in comparison to the parameters of $[Cu(en)(\alpha\text{-Ala})]^+$ (with $\{NH_2, NH_2, NH_2, COO^-\}$ coordination mode, Table 2) may be unambiguously assigned to 4N donor set and supports the presence of a stronger in-plane ligand field. So, it can be concluded that the coordination in the mixed-ligand species in the studied ternary system is probably realised by amine nitrogens $\{NH_2, NH_2\}$ of en and amine and imidazole nitrogens $\{NH_2, N_{im}\}$ of His in the equatorial plane forming two five-membered chelate rings.

A comparison of relative stability constants for mixed-ligand complexes of His and α-Ala also shows their dissimilarities. The relative stability constants, $\log K_{Cu(en)(\alpha\text{-Ala})} - pK_{NH_3^+} - pK_{COOH}$, which takes into account the difference in the basicity of coordinating amino and carboxylic groups, for the ternary system with α-Ala (−4.96; [29]) is higher than $\log K_{Cu(en)(His)} - pK_{NH_3^+} - pK_{im}$ with His, where coordinating amine and imidazole nitrogens are included (−6.27; Table 1, row 5). This effect may result from the different size of chelate rings formed by amino acids. On the other hand, the comparison of the relative stability constants, $\log K_{Cu(en)(L)} - pK_{NH_3^+} - pK_{NH_{im}^+}$, which takes into account the difference in basicity of the amino group and imidazole nitrogen, for histidine (−6.27; Table 1, row 5) and histamine (−7.97; obtained from data published in [7]) also reveals the stability unlikeness. This fact excludes bidentate, histamine-like $\{N_{am}, N_{im}\}$ coordination mode of His in the mixed-ligand complex strongly suggesting that His coordinates to the metal ion in tridentate manner. Hence, $\{NH_2, NH_2\}$ $\{N_{im}, NH_2, COO^-\}$ groups of the ligands are engaged in copper(II) coordination in the $[Cu(en)(His)]^+$ species, the sixth position is probably occupied by water molecule. The energy of d–d transition for the $[Cu(en)(His)]^+$ species is similar to that stated for $[Cu(en)(\alpha\text{-Ala})]^+$ (Table 2). This is probably the result of the two opposite effects-the involvement of the fourth N-donor into the equatorial position of the metal site and the axial coordination of the carboxylic oxygen.

The calculated concentrations of the copper(II) complex species for the Cu^{2+}–dien–His 1:1:2 molar ratio system as a function of pH presented in Fig. 3a indicate that under these conditions the formation of mixed-ligand species is preceded mainly by the appearance of simple complexes with His and dien. Two patterns of copper hyperfine splitting in EPR spectrum corresponding to equilibrium between $[Cu(dien)]^{2+}$($g_{\|} = 2.234$, $A_{\|} = 194 \times 10^{-4}\ cm^{-1}$) and $[Cu(H\text{–}His)]^{2+}$($g_{\|} = 2.314$, $A_{\|} = 175 \times 10^{-4}\ cm^{-1}$) are observed at pH 3.2 and these EPR parameters are in good agreement with the literature data (Table 2). They are in the equilibrium with Cu_{aqua}^{2+}. The spectrum typical for $[Cu(dien)]^{2+}$ complex is still observed as dominant between pH 4.0 and 5.0 and in a small extent at pH 6.8. At the pH range 6.0–7.0 the spectrum with parameters close to those found for $[Cu(His)_2]$ is also observed in equilibrium with a new spectrum. This new spectrum (obtained by subtraction of the signals due to equilibrial $[Cu(His)_2]$ species from the spectrum observed for the Cu–dien–His system at pH 6.02) should be assigned to the first mixed-ligand species, $[Cu(dien)(H\text{–}His)]^{2+}$, predicted at this pH range (the concentration ca. 18%). Its $A_{\|}$ parameter (Table 2) is greater than for $[Cu(dien)(H\text{-}Asp\text{-}\beta\text{-}ha)]^+$ complex

Table 2
Vis and EPR spectral parameters of the copper(II) complexes

Species	EPR						Coordination mode	Vis
	g_{iso}	A_{iso} ($10^{-4}\ cm^{-1}$)	$g_{\|}$	$A_{\|}$ ($10^{-4}\ cm^{-1}$)	$g_{\perp}$	$A_{\perp}$ ($10^{-4}\ cm^{-1}$)		λ_{max} (nm)[a] ε ($dm^3\ mol^{-1}\ m^{-1}$)
$[Cu(H\text{–}His)]^{2+}$	2.1539 Ref. [24]	56.9	2.305 Ref. [30]	176.6			$\{NH_2, COO^-\}$	750
$[Cu(His)_2]$	2.1223 Ref. [24]	67.2	2.230 Ref. [30]	190.9			$\{N_{im}, NH_2\}$; $\{NH_2, COO^-\}$	641 (90)
$[Cu(en)_2]^{2+}$	2.100	86	2.205	202			$2\times$ $\{NH_2, NH_2\}$	549 (71)
$[Cu(dien)]^{2+}$ Ref. [13]			2.234	192			$\{NH_2, NH, NH_2\}$	614 (78)
$[Cu(en)(His)]^+$	2.111	81	2.218	196			$\{NH_2, NH_2\}$; $\{N_{im}, NH_2\}$ + axial COO^-	581 (69)
$[Cu(en)(\alpha\text{-Ala})]^+$			2.230	190			$\{NH_2, NH_2\}$; $\{NH_2, COO^-\}$	580 (58)
$[Cu(dien)(H\text{–}His)]^{2+}$			2.213	198			$\{NH_2, NH, NH_2\}$; $\{N_{im}, COO^-\}$	
$[Cu(dien)(His)]^+$			2.224	180	2.048	15	$\{NH_2, NH, NH_2\}$; $\{NH_2, N_{im}\}$	640 (132)
	g_z	g_x	g_y	A_z ($10^{-4}\ cm^{-1}$)	A_x ($10^{-4}\ cm^{-1}$)	A_y ($10^{-4}\ cm^{-1}$)		
$[Cu(Me_5dien)]^{2+}$ Ref. [11]	2.240	2.065	2.050	183	29	14	$\{N(CH_3)_2, N(CH_3), N(CH_3)_2\}$	665 (225)
$[Cu(dien)(\alpha\text{-Ala})]^+$	2.217	2.054	2.043	190	30	15	$\{NH_2, NH, NH_2\}$; $\{NH_2, COO^-\}$	635 (106)
	g_1	g_2	g_3	A_1 ($10^{-4}\ cm^{-1}$)	A_2 ($10^{-4}\ cm^{-1}$)	A_3 ($10^{-4}\ cm^{-1}$)		
$[Cu(Me_5dien)(His)]^+$	2.215	2.130	2.010	141	20	61	$\{N(CH_3)_2, N(CH_3), N(CH_3)_2\}$; $\{NH_2, N_{im}\}$ or $\{NH_2, COO^-\}$	772 (286)
$[Cu(Me_5dien)(\alpha\text{-Ala})]^+$	2.208	2.138	2.007	135	20	62	$\{N(CH_3)_2, N(CH_3), N(CH_3)_2\}$; $\{NH_2, COO^-\}$	777 (275)

[a] The Vis absorption bands presented in the table arises from distribution-corrected absorption spectra.

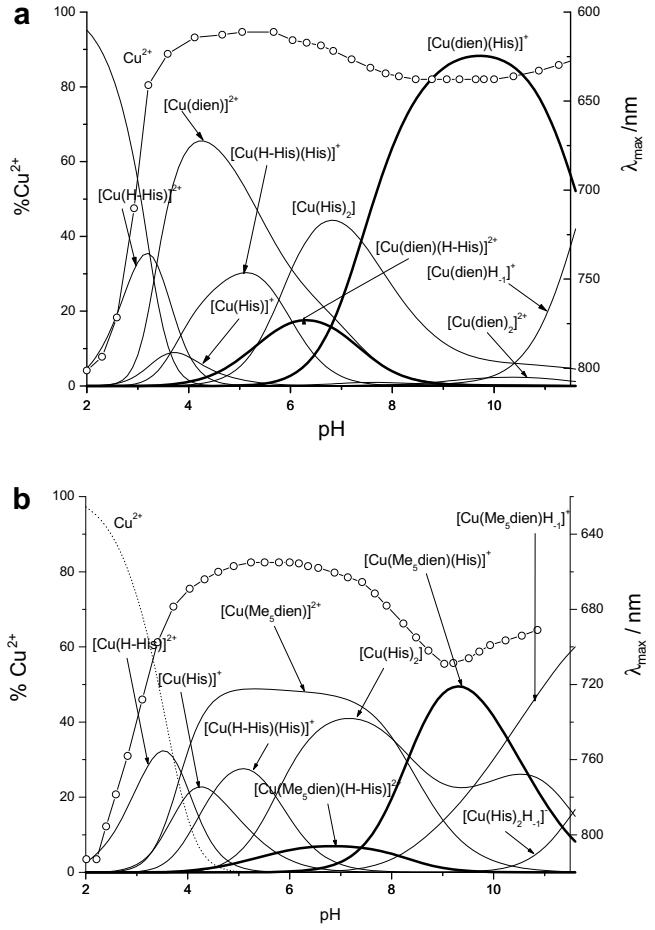

Fig. 3. Species distribution curves as a function of pH and variations of visible absorption maximum wavelength (circle) for the Cu^{2+}–dien–His system at 1:1:2 molar ratio (a) and Cu^{2+}–Me_5dien–His system at 1:2:1 molar ratio (b); $c_{Cu^{2+}} = 4 \times 10^{-3}$ mol dm^{-3}.

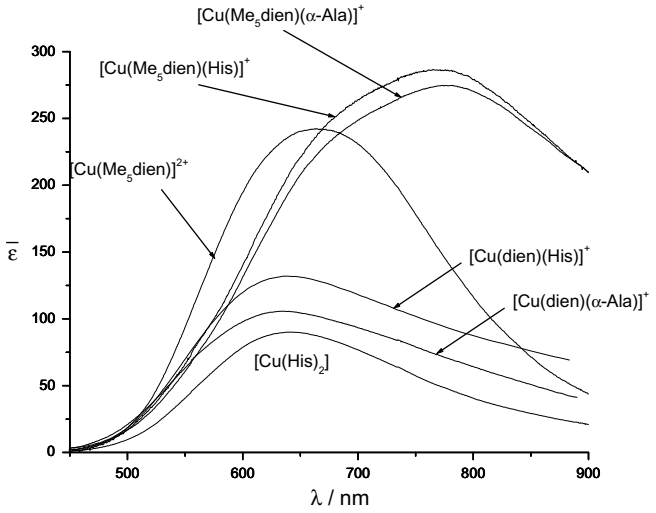

Fig. 4. Distribution-corrected absorption spectra for the $[Cu(dien)(His)]^+$, $[Cu(dien)(\alpha\text{-Ala})]^+$, $[Cu(Me_5dien)(His)]^+$, $[Cu(Me_5dien)(\alpha\text{-Ala})]^+$, $[Cu(Me_5dien)]^{2+}$, $[Cu(His)_2]$ species.

($g_{\|} = 2.218$, $A_{\|} = 190 \times 10^{-4}$ cm^{-1} [16]) with coordination realised by three nitrogens of dien and N_{amino} and $O_{carboxylate}$ of DL-aspartic-β-hydroxamic acid and even greater than for $[Cu(dien)_2]^{2+}$ ($g_{\|} = 2.214$, $A_{\|} = 186 \times 10^{-4}$ cm^{-1} [4]). It strongly suggests that coordination sphere in the Cu^{2+} plane in $[Cu(dien)(H\text{–}His)]^{2+}$ consists of four nitrogen atoms and the carboxylate oxygen of His, which may occupy an axial position, leading to geometry close to square-pyramid. The deprotonation constant, $pK_{[Cu(dien)(H-His)]^{2+}}$, of this mixed-ligand species (Table 1) is higher than that for the imidazole nitrogen atom and lower than that for the amine group in the "free" ligand. This indicates that in $[Cu(dien)(H\text{–}His)]^{2+}$ the amine group of His remains protonated and uncoordinated and deprotonation of this group is promoted by the copper(II) binding in the next mixed-ligand species. In $[Cu(dien)(H\text{–}His)]^{2+}$ the chelate donor system of His consists of $\{N_{im}, COO^-\}$, whereas three nitrogens of dien complete the coordination sphere in the equatorial plane. Above pH 6, due to the loss of one proton, a next $[Cu(dien)(His)]^+$ mixed-ligand species arises and predominates in solution in the pH range 8–11. The effect of this mixed-ligand species formation is observed distinctly in the electronic spectral changes (Figs. 2b and 3a). A comparison between the species distribution curves (Fig. 3a) and pH-varied absorption spectra of the Cu^{2+}–dien–His ternary system (Fig. 2b) clearly indicates that the spectral change, shown as the red shift of visible absorption maximum wavelength (circle in Fig. 3a), is attributable to the formation and decay of the $[Cu(dien)(His)]^+$ mixed-ligand species. From pH 8.5 to 10.5 absorption spectra are very similar ($\lambda_{max} \approx 636$–$637$ nm), what indicates the main contribution of this mixed-ligand complex in this pH range. Additionally, the isolated electronic absorption spectrum for this species at pH 9.6 demonstrates a broad band, asymmetric in the wavelength region 700–900 nm, with poorly noticeable maximum (Fig. 4, Table 2). Such asymmetry is characteristic of the five-coordinate complexes. Moreover, the same spectral behaviour is observed in the Cu^{2+}–dien-α-Ala ternary system what may suggest that the coordination mode in both $[Cu(dien)(His)]^+$ and $[Cu(dien)(\alpha\text{-Ala})]^+$ mixed-ligand species is the same. However, the EPR parameters of the spectra observed within pH range 8–10 for the Cu^{2+}–dien–His ternary system, where $[Cu(dien)(His)]^+$ complex is dominant (Fig. 3a, Table 2), are different to those obtained for $[Cu(dien)(\alpha\text{-Ala})]^+$ (Table 2). The difference between the EPR parameters suggests dissimilar role of the ligands in the complexes; α-Ala completes the coordination number to five by binding Cu^{2+} close to the plane through the amine nitrogen and in an axial position through the carboxylic oxygen. The presence of weak rhombic distortion suggests that the geometry is slightly deviated from square pyramidal towards trigonal bipyramidal [31]. On the other hand smaller $A_{\|}$ and greater $g_{\|}$ for the complex with His as compared to g_z and A_z values for the complex with α-Ala (Table 2) may be treated as indication of weaker in-plane copper–nitrogen bonds (with nitrogen provided by dien and histidine amine) as a result of stronger axial binding through imidazole nitrogen implying displacement Cu^{2+} ion from the plane.

The change of the coordination mode of His in $[Cu(dien)(His)]^+$, $\{NH_2, N_{im}\}$, in the relation to $[Cu(dien)(H\text{–}His)]^{2+}$, $\{N_{im}, COO^-\}$, leads to the formation of a six-membered chelate ring instead of seven-membered in the protonated species. It is interesting to compare the stability of both mixed-ligand species, the deprotonated ($\log K_{[Cu(dien)(His)]} = 4.76$, Table 1) and protonated one ($\log K_{[Cu(dien)(H-His)]} = \log \beta_{[Cu(dien)(H-His)]} - \log \beta_{[Cu(dien)]} - pK_{NH_3^+}) = 2.46$. The higher stability of [Cu(dien)(His)] comparing to [Cu(dien)(H–His)] is probably a result of the formation of a six-membered chelate ring instead of seven-membered.

Concentration distribution curves for the Cu^{2+}–Me_5dien–His system are presented in Fig. 3b. It can be seen, that up to pH 7 simple species with Me_5dien or His, $[Cu(H\text{–}His)]^{2+}$, $[Cu(His)]^+$, $[Cu(Me_5dien)]^{2+}$, $[Cu(H\text{–}His)(His)]^+$, $[Cu(His)_2]$, are mainly formed. The EPR spectrum observed at pH 3.5 in the liquid solution for the ternary Cu^{2+}–Me_5dien–His system ($g_{iso} = 2.155$ and $A_{iso} = 60 \times$

10^{-4} cm^{-1} and g_{iso} = 2.118 and A_{iso} = 73 × 10^{-4} cm^{-1}) is very similar to the spectrum observed for the Cu^{2+}–His binary system [24]. This corresponds to the existence of the equilibrium between the simple species of His in the solution at this pH. The increasing contribution of the $[Cu(Me_5dien)]^{2+}$ complex that is a dominant species between pH 4.0–6.0 is accompanied by a change of EPR spectral feature. The EPR parameters of the spectra observed in the pH range 4.0–5.0 of the liquid and frozen solution are: g_{iso} = 2.120 and A_{iso} = 75 × 10^{-4} cm^{-1} and g_z = 2.238, g_x = 2.060, g_y = 2.050 and A_z = 185, A_x = 24, A_y = 14 × 10^{-4} cm^{-1}, respectively. They are in good agreement with those reported for Cu^{2+} complex with Me_5dien and H_2O molecules [11]. The mixed-ligand species $[Cu(Me_5dien)(H–His)]^{2+}$exists as minor species. The $pK_{[Cu(Me5dien)(H–His)]^{2+}}$ value characteristic of the deprotonation step for the $[Cu(Me_5dien)(H–His)]^{2+}$ complex (Table 1) is higher than the deprotonation constant of the imidazole nitrogen atom and lower than that of the amine group in the "free" ligand. This indicates that in the $[Cu(Me_5dien)(H–His)]^{2+}$ species the amine nitrogen of His is protonated and the imidazole nitrogen and the carboxylic oxygen of His are involved in Cu^{2+} binding, similarly as it is proposed above for $[Cu(dien)(H–His)]^{2+}$. The EPR spectrum of $[Cu(Me_5dien)(H–His)]^{2+}$ species is not identifiable because of its too small contribution in comparison to that for $[Cu(Me_5dien)]^{2+}$ and $[Cu(His)_2]$ in the same pH range.

Above pH 7 the $[Cu(Me_5dien)(His)]^{+}$ species starts to form and reaches a maximum concentration (ca. 50%) at pH ~ 9 (Fig. 3b). The pH varied absorption spectra of Cu^{2+}–Me_5dien–His ternary system are different from those for both Cu^{2+}–Me_5dien [11] and Cu^{2+}–His binary systems (Fig. 2c and d). Furthermore, the pH dependence of λ_{max} in the visible spectra collected on the Cu^{2+}–Me_5dien–His system indicates a significant red shift in the pH region corresponding to the formation of this mixed-ligand species. This is clearly demonstrated in Fig. 3b which shows the λ_{max} versus pH plot together with the species distribution curves. The value of λ_{max} increases from 657 (pH ca. 6.4) to 708 nm (pH ca. 9), but starts to decrease above pH 9.2. Consequently, the red shift which parallels the formation of $[Cu(Me_5dien)(His)]^{+}$ indicates the structural changes around the copper(II) ion and transition from a six to a distorted five-coordination geometry while going from the simple to mixed-ligand species [11,13,15,3,20]. Possible modes of His coordination in the mixed-ligand species are either formation of a $\{NH_2, COO^-\}$ or $\{NH_2, N_{im}\}$ chelate. However, the energy of d–d transition for $[Cu(Me_5dien)(His)]^{+}$ species at around 772 nm (Fig. 4), is similar to those for five-coordinate mixed-ligand species containing Me_5dien and other α-amino acids [3], e.g. $[Cu(Me_5dien)(α\text{-Ala})]^{+}$ (Fig. 4). This fact implies that the coordination modes are similar. On the other hand, the energy of d–d transition for $[Cu(Me_5dien)(His)]^{+}$ species is very close to that for $[Cu(Me_5dien)(α\text{-alaninehydroxamic acid})]$ (790 nm [20]) and $[Cu(Me_5dien)(1,2\text{-diaminopropane})]$ (775 nm [32]) species with 5N coordination. So, the participation of the imidazole nitrogen in coordination in the $[Cu(Me_5dien)(His)]^{+}$ species cannot be excluded. The EPR spectral parameters found for $[Cu(Me_5dien)(His)]^{+}$ species are consistent with those of the five-coordinate mixed-ligand species formed by α-alanine and Me_5dien in copper(II) frozen solution (Table 2) and isolated mixed-ligand complexes $[Cu(Me_5dien)(L\text{-proline})]^{+}$ or $[Cu(Me_5dien)(L\text{-valine})]^{+}$ [3]. Thus, it can be concluded that geometry of the $[Cu(Me_5dien)(His)]^{+}$ species is strongly deviated from square pyramidal towards trigonal bipyramidal, similarly as it was observed for other mixed-ligand species with Me_5dien due to the dominant bulky effect of two methyl substituents at each nitrogen atoms forcing deviation of this *tri*-amine from in-plane coordination.

4. Conclusion

In the studied copper(II)–polyamine–His ternary systems, the potentiometric, VIS and EPR results support the formation of the mixed-ligand complexes with $[Cu(A)(His)]^{+}$ stoichiometry. In the systems with dien and Me_5dien the protonated $[Cu(A)(H–His)]^{2+}$ species also exists in acid solution. The coordination in the $[Cu(en)(His)]^{+}$ species, which dominates in solution above pH 6, is most likely realised by $\{NH_2, NH_2\}$ of en and $\{N_{im}, NH_2, COO^-\}$ of His with sixth coordination position occupied by water molecule. In the protonated $[Cu(dien)(H–His)]^{2+}$ and $[Cu(Me_5dien)(H–His)]^{2+}$ species the Cu^{2+} coordination by three nitrogens of dien or Me_5dien and by $\{N_{im}, COO^-\}$ chelate donor system of His seems to be evident, the amine nitrogen of His is still protonated. For the $[Cu(dien)(His)]^{+}$species, which predominates in basic solution, the geometry slightly deviated from square pyramidal is postulated. In this mixed-ligand species the binding of Cu^{2+} in the equatorial plane is realised by three amine nitrogens of dien and amine nitrogen of His and by imidazole nitrogen at axial position. The change of the coordination mode of His in $[Cu(dien)(His)]^{+}$, $\{NH_2, N_{im}\}$, in the relation to $[Cu(dien)(H–His)]^{2+}$, $\{N_{im}, COO^-\}$, leads to the formation of a six-membered chelate ring instead of seven-membered in the protonated species. However, the geometry of the $[Cu(Me_5dien)(His)]^{+}$ species is strongly deviated from square pyramidal towards trigonal bipyramidal due to the dominant bulky effect of two methyl substituens at each nitrogen atoms.

Acknowledgement

We would like to express our gratitude to Ms. Jadwiga Kędzierska for her technical assistance in the EPR measurements.

References

[1] B. Sarkar, Chem. Rev. 99 (1999) 2535.
[2] P. Deschamps, P.P. Kulkarni, M. Gautam-Basak, B. Sarkar, Coord. Chem. Rev. 249 (2005) 895.
[3] G. Brookes, L.D. Pettit, J. Chem. Soc., Dalton Trans. (1977) 1918.
[4] Y. Altun, F. Koseoglu, J. Solut. Chem. 34 (2005) 213.
[5] H. Hamrit, S. Djebbar-Sid, O. Benali-Baitich, M.A. Khan, G. Bouet, Synth. React. Inorg. Met.-Org. Chem. 30 (2000) 1835.
[6] R.J. Angelici, J.W. Allison, Inorg. Chem. 10 (1971) 2238.
[7] I. Sovago, A. Gergely, Inorg. Chim. Acta 20 (1976) 27.
[8] T. Murakami, K. Murata, Y. Ishikawa, Inorg. Chim. Acta 244 (1996) 51.
[9] I. Sovago, T. Kiss, A. Gergely, J. Chem. Soc., Dalton Trans. (1978) 964.
[10] G. Gran, Acta Chem. Skand. 4 (1950) 559.
[11] B. Kurzak, A. Kamecka, K. Bogusz, J. Jezierska, Polyhedron 26 (2007) 4345.
[12] P. Gans, A. Sabatini, A. Vacca, Talanta 43 (1996) 1739.
[13] B. Kurzak, D. Kroczewska, J. Jezierska, Polyhedron 17 (1998) 11.
[14] J. Urbańska, H. Kozłowski, B. Kurzak, J. Coord. Chem. 25 (1992) 149.
[15] B. Kurzak, K. Bogusz, D. Kroczewska, J. Jezierska, Polyhedron 20 (2001) 2627.
[16] D. Kroczewska, B. Kurzak, J. Jezierska, Polyhedron 25 (2006) 678.
[17] B. Kurzak, A. Kamecka, K. Bogusz, J. Jezierska, Polyhedron 26 (2007) 4223.
[18] A. Odani, O. Yamauchi, Inorg. Chim. Acta 93 (1984) 13.
[19] B. Kurzak, D. Kroczewska, J. Coord. Chem. 34 (1995) 67.
[20] D. Kroczewska, K. Bogusz, B. Kurzak, J. Jezierska, Polyhedron 21 (2002) 295.
[21] B.A. Goodman, D.B. McPhail, H. Kipton, J. Powell, J. Chem. Soc., Dalton Trans. (1981) 822.
[22] L. Casella, M. Gullotti, J. Inorg. Biochem. 18 (1983) 19.
[23] E. Prenesti, G. Daniele, V. Zelano, M. Gulmini, Ann. Chem. (Rome) 89 (1999) 1.
[24] T. Szabo-Planka, A. Rockenbauer, L. Korzec, D. Nagy, Polyhedron 19 (2000) 1123.
[25] P. Deschamps, P.P. Kulkarni, B. Sarkar, Inorg. Chem. 43 (2004) 3338.
[26] H. Sigel, Angew. Chem. 87 (1975) 391.
[27] H. Sigel, Angew. Chem., Int. Ed. Engl. 14 (1975) 394.
[28] H. Sigel, Metal Ions in Biological Systems, vol. 2, Marcel Dekker Inc., New York, 1973.
[29] B. Kurzak, K. Bogusz, unpublished results.
[30] K. Varnagy, E. Garribba, D. Sanna, I. Sovago, G. Micera, Polyhedron 24 (2005) 799.
[31] N. Azuma, Y. Kohno, K. Izshizu, T. Takakuwa, S. Tsuboyama, K. Tsuboyama, K. Kobayashi, T. Sakurai, Inorg. Chim. Acta 215 (1994) 109.
[32] T. Murakami, T. Takei, Y. Ishikawa, S. KitaK, Murata, Y. Ishikawa, Polyhedron 24 (1996) 4391.

IR spectra were recorded on a Nicolet Magna 560 spectrophotometer in the spectral range 4000–400 cm^{-1} with the samples in the form of KBr pellets. Electronic spectra were measured on a spectrophotometer Lab Alliance UV–VIS 8500 in the range 1100–180 nm in methanol solution. Elemental analyses (C H N) were performed on a Perkin–Elmer CHN-2400 analyzer. EPR spectra were recorded at room temperature and 77 K on a Bruker ESP 300 spectrometer operating at X-band equipped with an ER 035M Bruker NMR gaussmeter and HP 5350B Hewlett–Packard microwave frequency counter.

2.2. Preparation of [$CuCl_2$(dppt)] (**1**)

A solution of dppt (0.58 mmol, 0.18 g) in methanol (15 ml) was added to 0.10 g (0.58 mmol) of $CuCl_2 \cdot 2H_2O$ in 10 ml of methanol and stirred for 2 h. The resulting solution was kept for evaporation at room temperature, and after a few days dark red crystals were obtained, filtered off and dried. Yield 75%.

Anal. Calc. for $C_{20}H_{14}N_4Cl_2Cu$: C, 54.01; H, 3.17; N, 12.60. Found: C, 54.70; H, 3.46; N, 12.35%.

IR (KBr; ν/cm^{-1}): 1603(m) and 1515(s), $\nu_{C=N}$ and $\nu_{N=N}$.

UV–Vis (MeOH; λ_{max} [nm] (ε; [$dm^3\ mol^{-1}\ cm^{-1}$])): 775.0 (100), 445.8 (50), 328.4 (36 500), 302.8 (59 750), 242.4 (38 910) and 204.8 (90 870).

2.3. Preparation of [$CuCl_2$(dppt)$_2$] · 2MeOH (**2**)

A procedure similar to that for [$CuCl_2$(dppt)] was used with $CuCl_2 \cdot 2H_2O$ (0.10 g, 0.58 mmol) and dppt (0.36 g, 1.16 mmol). Green crystals of **2** were collected in 80% yield.

Anal. Calc. for $C_{42}H_{36}N_8Cl_2O_2Cu$: C, 61.58; H, 4.43; N, 13.68. Found: C, 60.95; H, 4.68; N, 13.20%.

IR (KBr; ν/cm^{-1}): 3361(br) ν_{O-H}; 1607(m) and 1519(s) ν_{CN} and $\nu_{N=N}$.

UV–Vis (MeOH; λ_{max}[nm] (ε; [$dm^3\ mol^{-1}\ cm^{-1}$])): 769.0 (225), 507.6 (115), 339.4 (22 600), 304.0 (35 770) and 214.0 (68 125).

2.4. Preparation of [Cu(dppt)$_2$(H$_2$O)$_2$](NO$_3$)$_2$ (**3**)

A solution of dppt (0.80 mmol, 0.25 g) in methanol (10 ml) was added to 0.10 g (0.40 mmol) of $Cu(NO_3)_2 \cdot 3H_2O$ in 10 ml of water and stirred for 4 h. The resulting green precipitate was filtered off and recrystallized from methanol. Crystalline precipitate of **3** was collected in 70% yield.

Anal. Calc. for $C_{40}H_{32}N_{10}O_8Cu$: C, 56.90; H, 3.82; N, 16.59. Found: C, 57.35; H, 3.98; N, 16.25%.

IR (KBr; ν/cm^{-1}): 3473(br) ν_{O-H}; 1600 (w), 1530(s) and 1514(m) ν_{CN} and $\nu_{N=N}$; 1384 cm^{-1} (ν_{NO_3}).

UV–Vis (MeOH; λ_{max} [nm] (ε; [$dm^3\ mol^{-1}\ cm^{-1}$])): 676.1 (180), 479.9 (155), 340.1 (26 460), 300.3 (46 590), 240.7 (33 920) and 205.7 (85 180).

2.5. Preparation of [Cu(SO$_4$)(dppt)(H$_2$O)]$_n$ · nH$_2$O (**4**)

A solution of dppt (0.40 mmol, 0.12 g) in methanol (15 ml) was added to 0.10 g (0.40 mmol) of $CuSO_4 \cdot 5H_2O$ in 10 ml of water and stirred for 4 h. The resulting green precipitate was filtered off and recrystallized from methanol. Crystalline precipitate of **4** was collected in 65% yield.

Anal. Calc. for $C_{20}H_{18}N_4O_6SCu$: C, 47.48; H, 3.59; N, 11.07. Found: C, 47.77; H, 3.33; N, 11.85%.

IR (KBr; ν/cm^{-1}): 3650(m) and 3433(br) ν_{O-H}; 1606(br) and 1521(s) $\nu_{C=N}$ and $\nu_{N=N}$; 1196, 1156(sh), 1129, 1021, 934 and 611 cm^{-1} (ν_{SO_4}).

UV–Vis (MeOH; λ_{max} [nm]): 682.3, 464.5, 331.2, 300.9, 240.5 and 202.8.

2.6. Crystal structures determination and refinement

The X-ray intensity data of **1**, **2**, **3** and **4** were collected on a KM-4-CCD automatic diffractometer equipped with CCD detector and graphite monochromated Mo Kα radiation (λ = 0.71073 Å). Details concerning crystal data and refinement are given in Table 1. Lorentz, polarization and numerical absorption correction [10] were applied. The structures were solved by the partial structure expansion method and subsequently completed by the difference Fourier recycling. All the non-hydrogen atoms were refined anisotropically using full-matrix, least-squares technique. The hydrogen atoms were founded from the difference Fourier syntheses and were treated as, "riding" on their adjacent atoms and assigned isotropic temperature factors equal 1.2 times the value of equivalent temperature factor of the aromatic parent atoms and equal 1.5 times the value of equivalent temperature factor of the methyl parent

Table 1
Crystal data and structure refinement for **2**, **3** and **4** complexes

	2	**3**	**4**
Empirical formula	$C_{42}H_{36}Cl_2N_8O_2Cu$	$C_{40}H_{32}N_{10}O_8Cu$	$C_{20}H_{18}N_4O_6SCu$
Formula weight	819.23	844.30	505.98
Temperature (K)	291.0(3)	150(1)	291.0(3)
Wavelength (Å)	0.71073	0.71073	0.71073
Crystal system	monoclinic	monoclinic	triclinic
Space group	*C*2/*c*	$P2_1/n$	$P\bar{1}$
Unit cell dimensions			
a (Å)	15.285(3)	8.4621(6)	7.0084(6)
b (Å)	8.286(2)	6.4346(5)	10.1467(9)
c (Å)	31.414(6)	34.2110(2)	15.2168(14)
α (°)			93.711(7)
β (°)	93.30(3)	93.200(6)	94.531(7)
γ (°)			104.345(7)
Volume (Å^3)	3972.0(14)	1859.9(2)	1041.10(16)
Z	4	2	2
D_{calc} (Mg/m^3)	1.370	1.508	1.614
Absorption coefficient (mm^{-1})	0.731	0.658	1.196
F(000)	1692	870	518
Crystal size (mm)	0.07 × 0.14 × 0.14	0.08 × 0.08 × 0.22	0.199 × 0.027 × 0.024
θ Range for data collection	2.89–25.03	2.92–25.00	2.08–25.05
Index ranges	$-17 \leqslant h \leqslant 18$, $-6 \leqslant k \leqslant 9$, $-35 \leqslant l \leqslant 37$	$-10 \leqslant h \leqslant 6$, $-7 \leqslant k \leqslant 7$, $-40 \leqslant l \leqslant 39$	$-8 \leqslant h \leqslant 8$, $-12 \leqslant k \leqslant 11$, $-18 \leqslant l \leqslant 18$
Reflections collected	12 346	11 201	10 501
Independent reflections (R_{int})	3494 (0.0638)	3254 (0.0450)	3684 (0.0243)
Completeness to 2θ = 50°	99.3%	99.2%	99.9%
Maximum and minimum transmission	0.953 and 0.898	0.937 and 0.953	0.968 and 0.959
Data/restraints/parameters	3494/0/252	3254/0/268	3684/0/289
Goodness-of-fit on F^2	1.144	0.904	1.091
Final *R* indices [$I > 2\sigma(I)$]	R_1 = 0.0679	R_1 = 0.0342,	R_1 = 0.0600
	wR_2 = 0.1678	wR_2 = 0.0914	wR_2 = 0.1863
R indices (all data)	R_1 = 0.1095	R_1 = 0.0595	R_1 = 0.0692
	wR_2 = 0.1920	wR_2 = 0.0977	wR_2 = 0.1935
Largest difference in peak and hole (e Å^{-3})	0.515 and −0.337	0.320 and −0.330	0.671 and −0.493

carbon atom or oxygen atom. All, except water molecule, hydrogen atoms positions were idealised after each cycle of refinement. The methyl and hydroxyl groups were allowed to rotate about theirs local three-fold axes. SHELXS97 [11], SHELXL97 [12] and SHELXTL [13] programs were used for all the calculations. Atomic scattering factors were those incorporated in the computer programs.

2.7. Magnetic measurement

The magnetization of the powdered sample was measured over the temperature range 1.8–300 K at magnetic field 0.5 Tesla, using a Quantum Design SQUID-based MPMSXL-5-type magnetometer. The superconducting magnet was generally operated at a field strength ranging from 0 to 5 Tesla.

The SQUID magnetometer was calibrated with the palladium rod sample. Corrections are based on subtracting the sample-holder signal and contribution χ_D estimated from the Pascal constants [14] and equal $-276 \times 10^{-6}\,cm^3\,mol^{-1}$ for complex. The effective magnetic moment was calculated from the equation, $\mu_{eff} = 2.83(\chi_M T)^{1/2}$ (B.M.).

2.8. Computational details

The geometry of **1** was optimized without any symmetry restrictions in the doublet state using the hybrid B3LYP [15,16] functional of GAUSSIAN-03 [17]. The geometry was fully optimised in methanol utilising IEF-PCM formalism available in GAUSSIAN-03 [18]. The calculations were performed by using the LANL2DZ effective core potential (ECP) set of Hay and Wadt [19] for copper atom and the standard 6-31+G** basis for chloride and nitrogen, 6-31G* for carbon and 6-31G for hydrogen atoms.

Based on the optimized geometry, time-dependent density functional level (TDDFT) calculations were performed at the same B3LYP level and basis sets to calculate the electron transition energies [20].

3. Results and discussion

3.1. Preparation and infrared data

The complexes $[CuCl_2(dppt)]$ (**1**), $[CuCl_2(dppt)_2]\cdot 2MeOH$ (**2**), $[Cu(dppt)_2(H_2O)_2](NO_3)_2$ (**3**) and $[Cu(SO_4)(dppt)(H_2O)]_n\cdot nH_2O$ (**4**) were prepared in good yield by the reaction of 5,6-diphenyl-3-(2-pyridyl)-1,2,4-triazine (dppt) with the appropriate copper salt and molar ratio.

The selected frequencies observed in the IR spectra of $[CuCl_2(dppt)]$ (**1**), $[CuCl_2(dppt)_2]\cdot 2MeOH$ (**2**), $[Cu(dppt)_2(H_2O)_2](NO_3)_2$ (**3**) and $[Cu(SO_4)(dppt)(H_2O)]_n\cdot nH_2O$ (**4**) complexes are given in Section 2. For all the examined complexes the stretching vibrations of the C=N and N=N groups appear at considerable lower values with respect to the ν(C=N) and ν(N=N) of the free 5,6-diphenyl-3-(2-pyridyl)-1,2,4-triazine (dppt) supporting the coordination of the triazine and pyridyl rings to the metal ion [3]. The bands assignable to the bridging sulfate of **4** appear at 934, 1021, 1129, 1156 and 1196 cm^{-1}, whereas the band at 1384 cm^{-1} for **3** suggests the presence of uncoordinated nitrate ion. The broad bands in the range 3650–3100 cm^{-1} in the IR spectra of **2**, **3** and **4** represent the existence of MeOH and H_2O [21].

3.2. Crystal structures

The crystallographic data of **2**, **3** and **4** complexes are summarized in Table 1, The details of hydrogen bonds are given in Table 2, and the molecular structures of **2, 3** and **4** are presented in Figs. 1–3, respectively.

The complex **1** crystallises in the orthorhombic space group *Fdd*2. The coordination geometry about Cu(II) is a *trans* distorted square planar. The Cu ion is coordinated to pyridine and triazine rings of 5,6-diphenyl-3-(2-pyridyl)-1,2,4-triazine ligand and two chloride ions. As the X-ray structure of complex **1** has been recently reported by Eltayeb et al. [22] and quality of our structure is similar, the experimental data for **1** have not been included in the paper.

The copper atom of the compound **2** is located on the inversion centre and occupies special position *a* of the *C*2/*c* space group, thus the asymmetric unit consists of a half of complex molecule and one methanol molecule. By symmetry the environment of copper(II) ion in compound **2** adopts ideal tetragonal bipyramid geometry. The equatorial plane is formed by two pyridine and two triazine nitrogen atoms and the axial sites are occupied by two chloride ions at rather large distances of 2.7062(16), as a consequence of the Jahn–Teller effect. The two dppt ring systems are strictly coplanar and they are bound to central ion in *trans* configuration. Each complex molecule is connected *via* medium strength [23,24] O–H···Cl intermolecular hydrogen bonds with two solvent molecules.

The copper atom of the compound **3** is located on the inversion centre and occupies special position *b* of the $P2_1/n$ space group, thus the asymmetric unit consists of a half of complex cation and one nitrate anion. The overall complex molecule conformation of compound **3** is very similar to these of compound **2**. By symmetry the environment of copper(II) ion adopts ideal tetragonal bipyramid geometry. The equatorial plane is formed by two pyridine and two triazine nitrogen atoms and the axial sites are occupied by two water molecules at rather large distances of 2.3403(19) Å, as a consequence of the Jahn–Teller effect. The two dppt ring systems are strictly coplanar and they are bound to central ion in *trans* configuration. The medium strength O–H···O intermolecular hydrogen bonds of compound **3** joins the molecules to form of hydrogen bonded chain along crystallographic *b*-axis.

All atoms of compound **4** lie in general positions, but the inversion centres located at respectively special positions d and f of the $P\bar{1}$ space group expand the molecule to the one dimensional, ladder type, polymer along crystallographic *a*-axis (the asymmetric unit consists of one Cu^{2+} cation one SO_4^{2-} anion one ligand, one coordinated and one uncoordinated water molecule). Each copper(II) ion is six-coordinate and their coordination geometries are best described as distorted tetragonal bipyramid with the equatorial plane defined by two nitrogen and two oxygen atoms (maximum deviation from the weighted least squares N(2), N(4), O(1), O(2) plane exists for N(4) atom and it is equal to 0.127(2) Å) with copper atom displaced 0.000(2) Å from above mentioned the weighted least squares plane. The Cu(dppt)(H_2O) units are linked by two μ-sulfate-O,O′ bridges forming planar by symmetry Cu_2O_2

Table 2
Hydrogen bonds for **2**, **3** and **4** complexes

D–H···A	H···A (Å)	D···A (Å)	D–H···A (°)	Symmetry code of A
Complex **2**				
O(99)–H(99)···Cl(1)	2.42	3.165(9)	152.5	
Complex **3**				
O(4)–H(4O)···O(1)	1.93	2.783(3)	151.9	$x, y+1, z$
O(4)–H(4P)···O(3)	1.97	2.845(3)	150.7	$-x+1, -y+1, -z$
Complex **4**				
O(1)–H(1O)···O(4)	1.82	2.760(5)	159.2	
O(1)–H(1P)···O(3)	1.63	2.600(5)	164.8	$-x+1, -y+2, -z+1$
O(99)–H(99P)···O(5)	2.08	2.924(8)	179.4	

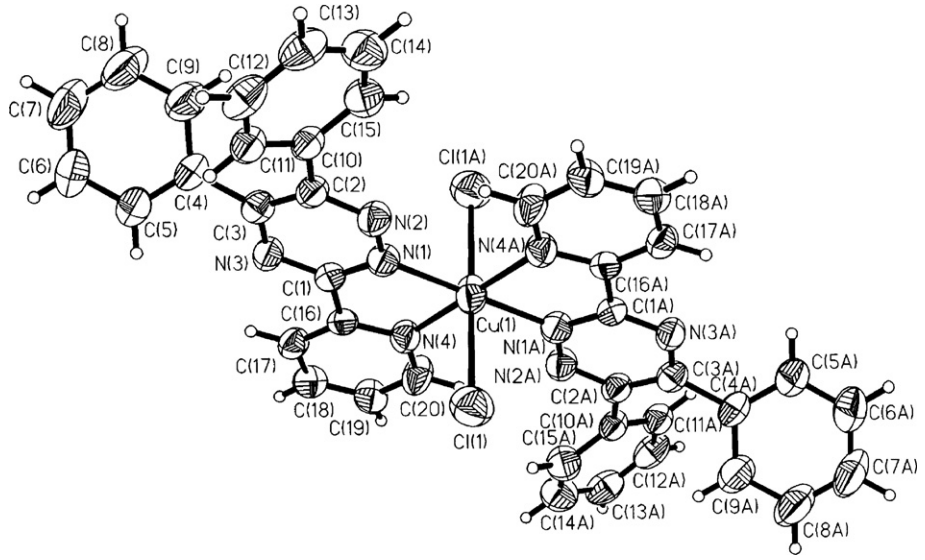

Fig. 1. The molecular structure of **2**. Displacement ellipsoids are drawn at 50% probability.

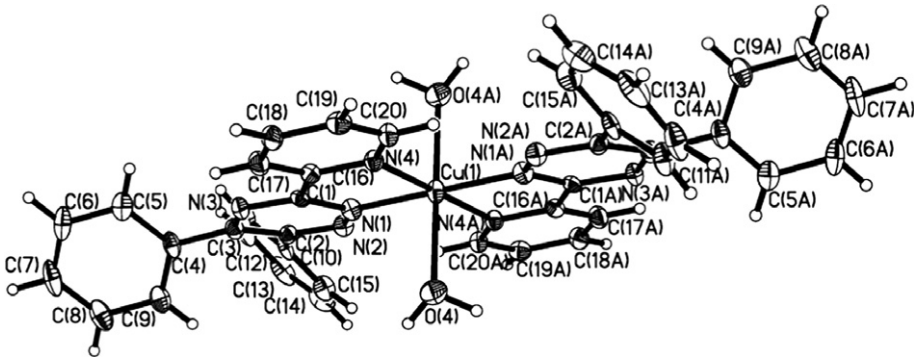

Fig. 2. The molecular structure of the cation $[Cu(dppt)_2(H_2O)_2]^{2+}$ in the structure **3**. Displacement ellipsoids are drawn at 50% probability.

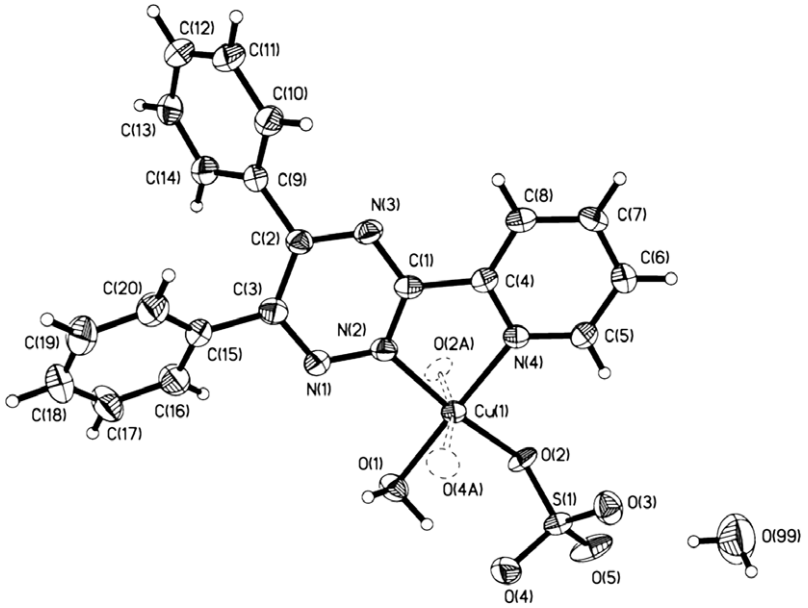

Fig. 3a. Atoms forming asymmetry unit of **4**. Displacement ellipsoids are drawn at 50% probability. The symmetry generated atoms bonded to the asymmetry unit atoms are indicated by dashed lines.

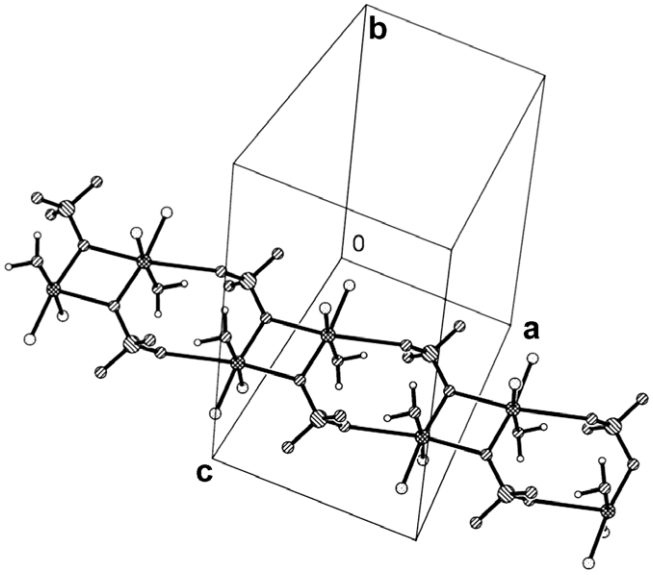

Fig. 3b. The fragment of polymer chain **4**. Atoms not involved in the chain are deleted for clarity. The copper atoms are cross-hatched, the sulphur atoms are backslashed, the oxygen atoms are slashed and nitrogen atoms are dotted.

moiety with two short [1.966(3) Å] and two longer Cu–O distances [2.367(3) Å], two bridging Cu–O–Cu angles of 100.49(12)°, leading to a Cu···Cu separation of 3.3411(11) Å. The sulfate oxygen O(4) is further coordinated to the copper atom of another binuclear unit, resulting in a polymeric structure created by the four-membered Cu_2O_2 and eight-membered $Cu_2O_4S_2$ rings in the spiro arrangement (in the second ring the Cu···Cu distance is 4.8865(11) Å). The structures with two bridging modes for the sulfate groups (μ-O,O′ and μ-O,O), in the same complex are unique. However, a similar arrangement was observed for the $[Cu_4(TPPNOL)_2(\mu\text{-}SO_4)_2](ClO_4)_2$ [HTPPNOL (*N*,*N*,*N*0-tris-(2-pyridylmethyl)-1,3-diaminopropan-2-ol)] complex reported by Fernandes and co-workers [25]. Different bridging modes for the sulfate groups are reflected in the different S–O bond lengths: 1.523(3) Å for S(1)–O(1) and 1.459(4) Å for S(1)–O(4). The solvent water molecule is connected to complex molecule *via* medium strength O–H···O hydrogen bond. The polymer chain is stabilised by medium strength O–H···O intramolecular hydrogen bonds.

The selected bond distances and angles of **2**, **3** and **4** are collected in Tables 3–5. The bite angle of, 6-diphenyl-3-(2-pyridyl)-1,2,4-triazine ranges from 78.99(14)° to 81.19(15)°, and is similar to that reported for the related $[Cu(dppt)_2(H_2O)_2](ClO_4)_2$ complex [79.7(2)°] [6].

For all three complexes, there is no significant difference between Cu–N (pyridine) and Cu–N (triazine) bond lengths, revealing that the two nitrogens are equal in donor strength. The Cu–N bond distances of mononuclear compounds are slightly longer than those in the polymer structure suggesting that the Cu–N bonds in **1**, **2** and **3** complexes are comparatively weaker. However, all the Cu–N bond lengths are consistent with those found in related systems [26].

Table 3
The experimental bond lengths (Å) and angles (°) for **2**

Bond lengths	Experimental	Bond angles	Experimental
Cu(1)–N(1)	2.023(4)	N(1)–Cu(1)–N(4)#1	101.01(14)
Cu(1)–N(4)	2.049(4)	N(1)–Cu(1)–N(4)	78.99(14)
Cu(1)–Cl(1)	2.7062(16)	N(1)–Cu(1)–Cl(1)#1	87.22(11)
		N(1)–Cu(1)–Cl(1)	92.78(11)
		N(4)–Cu(1)–Cl(1)	90.88(11)
		N(4)–Cu(1)–Cl(1)#1	89.12(11)
		N(1)#1–Cu(1)–Cl(1)	87.22(11)

#1: $-x+1, -y, -z$.

Table 4
The experimental bond lengths (Å) and angles (°) for **3**

Bond lengths	Experimental	Bond angles	Experimental
Cu(1)–N(1)	2.028(2)	N(1)–Cu(1)–N(4)	79.84(8)
Cu(1)–N(4)	2.062(2)	N(1)#1–Cu(1)–N(4)	100.16(8)
Cu(1)O(4)	2.3403(19)	N(1)–Cu(1)–O(4)#1	89.30(8)
		N(1)–Cu(1)–O(4)	90.70(8)
		N(4)–Cu(1)–O(4)	84.93(7)
		N(4)–Cu(1)–O(4)#1	95.07(7)

#1: $-x+1, -y+1, -z$.

Table 5
The experimental bond lengths (Å) and angles (°) for **4**

Bond lengths	Experimental	Bond angles	Experimental
Cu(1)–O(1)	1.951(3)	O(1)–Cu(1)–O(2)	88.50(14)
Cu(1)–O(2)	1.966(3)	O(1)–Cu(1)–N(2)	96.97(15)
Cu(1)–O(2)#1	2.367(3)	O(1)–Cu(1)–N(4)	172.52(14)
O(2)–Cu(1)#1	2.367(3)	O(2)–Cu(1)–N(4)	94.23(15)
Cu(1)–N(2)	1.996(4)	O(2)–Cu(1)–N(2)	171.29(14)
Cu(1)–N(4)	1.995(4)	N(4)–Cu(1)–N(2)	81.19(15)
S(1)–O(2)	1.523(3)	O(2)–Cu(1)–O(2)#1	79.51(13)
S(1)–O(3)	1.464(3)	O(1)–Cu(1)–O(2)#1	93.58(12)
S(1)–O(4)	1.459(4)	N(4)–Cu(1)–O(2)#1	93.76(14)
S(1)–O(5)	1.455(4)	N(2)–Cu(1)–O(2)#1	93.34(13)
		Cu(1)–O(2)–Cu(1)#1	100.49(12)

#1: $-x+2, -y+2, -z+1$.

3.3. Magnetic properties

The magnetic properties of the complex **4** were determined over the temperature range 1.8–300 K at magnetic field 0.5 Tesla. The experimental data, plotted as temperature variations of the χ_M^{-1} and $\chi_M T$, are shown in Fig. 4.

The value $\chi_M T$ of at 300 K for complex equals 0.415 $cm^3\ mol^{-1}\ K$ (1.82 B.M.). The value of $\chi_M T$ product increases slightly with temperature lowering and reaches 0.425 $cm^3\ mol^{-1}\ K$ (1.85 B.M.) value at 1.8 K.

The values of the Curie and Weiss constants determined from the relation $1/\chi_M = f(T)$ over temperature range 1.8–300 K are equal

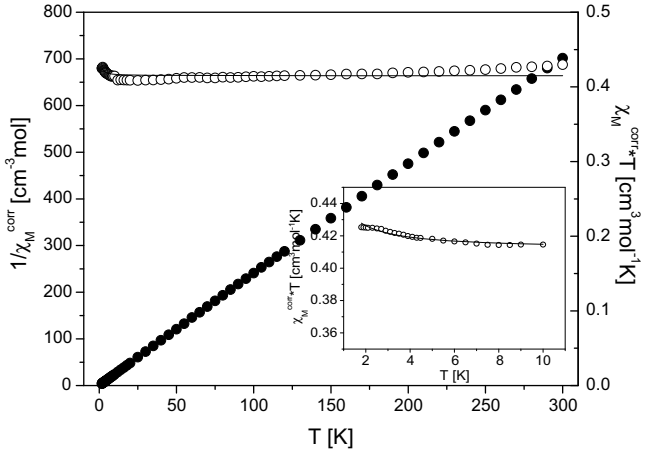

Fig. 4. Temperature dependence of experimental χ_M^{-1} (•) and $\chi_M \cdot T$ (○) for complex **4**. The inset shows dependence $\chi_M T$ vs. T (○) in the lowest temperature range. The solid line is the calculated curve for $\chi_M T$.

to 0.415 $cm^3\ mol^{-1}$ K and 0.04 K, respectively. A very small, positive value of Weiss constant confirms the occurrence of very weak ferromagnetic interactions between the copper centers in the dimer.

The molecular structure of $[Cu(SO_4)(dppt)(H_2O)]_n \cdot nH_2O$ (**4**) (Fig. 4b) suggests the magnetic exchange interactions in alternating chain:

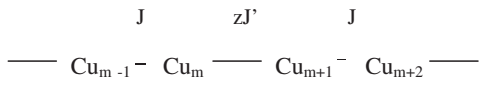

where J and zJ' are the exchange parameters via (–O–) and (–O–S–O–) bridges, respectively.

The path of the magnetic interaction between Cu^{II} centers inside eight-membered ($Cu_2O_4S_2$) ring is considerably longer than inside four-membered (Cu_2O_2) ring. For that reason the dimer model with pairwise interactions may be used as a good approximation [27]. Hamiltonian $H = -2J\vec{S}_1 \cdot \vec{S}_2$ for $S_1 = S_2 = 1/2$ leads to the Bleaney–Bowers expression (1) [28]. To elucidate the significance of exchange between dimeric subunits in the chain, a molecular field correction term was also included (Eq. (2)) [29]

$$\chi_M = \frac{2N\beta^2 g^2}{3kT}\left[1 + \frac{1}{3}\exp(-2J/kT)\right] \quad (1)$$

$$\chi_M^{corr} = \frac{\chi_M}{1 - \frac{2zJ'}{N\beta^2 g^2}\cdot \chi_M} \quad (2)$$

where N is the Avogadro's number, g – the spectroscopic splitting factor, β – the Bohr magneton, k – the Boltzmann constant, J – exchange parameter and zJ' – molecular field correction (interdimer interaction). The least-squares fit of the experimental data using these equations was limited to the temperature range from 1.8 K up to 300 K and leads to singlet–triplet ($2J$) separation value equals 0.20 cm^{-1}, $g = 2.10$ and $zJ' = 0$, as indicated by the solid curve in Fig. 5. The agreement factor R is equal 4.02×10^{-5}. The criterion used in determination of the best fit was based on minimization of the sum of squares of the deviation: $R = \sqrt{\sum_{i=1}^{n} \frac{1}{(\chi_i^{exp})}\left(\chi_i^{exp} - \chi_i^{calc}\right)^2} \Big/ \sqrt{\sum_{i=1}^{n} \frac{1}{(\chi_i^{exp})^2}}$. Magnetic interaction in the dimeric copper compound strongly depends on Cu–O–Cu angle. For angles close to 97° it is possible to found accidental orthogonality and consequently, J values ~0 or positive [30,31]. The weak ferromagnetic interactions between the copper centers in the dimeric subunits (Cu_2O_2) arise from the value of bridging angle Cu(1)–O(2)–Cu(1)#1 (100.49(12)°) [31].

Results of the calculations on the magnetic data indicated only very weak ferromagnetic interaction between copper centers inside four-membered (Cu_2O_2) rings with value of the singlet–triplet separation $2J = +0.2$ cm^{-1}. The value of molecular field corrections ($zJ' = 0$) indicated total magnetic isolation of the four-membered rings in the crystal lattice.

The variation of the magnetization M versus the magnetic field H for complex **4** at 2 K was shown in Fig. 5. As the magnetic field increases, the M versus H curve indicates linear relation up to ~1 T and then shows a sinusoidal variation up to 5 T near saturation value at $M = 0.97$ B.M.

3.4. EPR spectra

The EPR powder spectra of the complex **4** (Fig. 6) recorded in the X-band at room temperature, 77 K and 4.2 K indicate two poorly resolved lines related to $g_\perp = 2.08$ and $g_\perp = 2.21$ parameters. The observed EPR spectrum is the average spectrum of two copper centers in the ligand field of the distorted tetragonal–bipyramidal symmetry $Cu(1)N_2O_4$ and $Cu(2)N_2O_4$, respectively.

3.5. Geometry optimisation

The geometry of **1** was optimised in a doublet state by the DFT method with the B3LYP functional. The optimized geometric parameters of **1** are gathered in Table 6. In general, the predicted bond lengths and angles are in agreement with the values based upon the X-ray crystal structure data, and the general trends observed in the experimental data are well reproduced in the calculations.

3.6. Electronic spectra

The experimental electronic spectra of **1, 2**, **3** and **4** are presented in Fig. 7. The positions of absorption bands and values of molar absorption coefficients for the complexes are given in the Experimental Part. As can be seen from Fig. 7 the UV/Vis spectra are rather indistinctive for molecular structure determination. For all the complexes the visible region exhibit broad poorly resolved absorption bands with maxima at 775.0 and 445.8 nm for **1**, 769.0 and 507.6 nm for **2**, 676.1 and 479.9 nm for **3** and 682.3 and 464.3 nm for **4**. The UV spectra of the **1, 2, 3** and **4** are also very similar in terms of the position, intensity and shape of the bands.

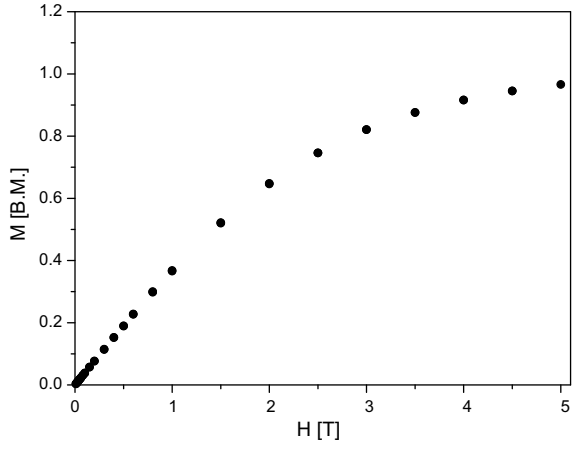

Fig. 5. Field dependence of the magnetization for complex **4**.

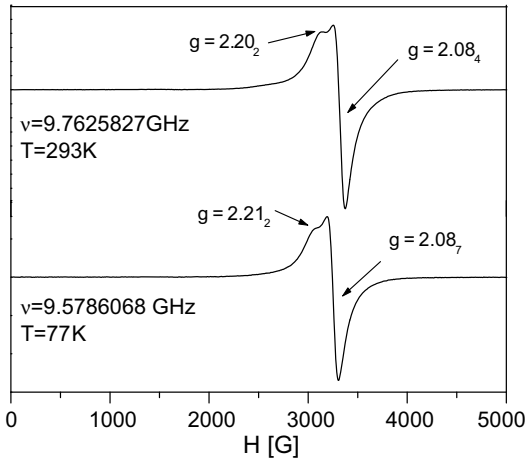

Fig. 6. EPR (X-band) spectrum of powdered **4** at room temperature and 77 K.

Table 6
The optimized bond lengths (Å) and angles (°) for **1**

Bond lengths	Optimized	Bond angles	Optimized
Cu(1)–N(2)	2.067	N(4)–Cu(1)–N(2)	79.47
Cu(1)–N(4)	2.073	N(2)–Cu(1)–Cl(1)	173.71
Cu(1)–Cl(1)	2.344	N(4)–Cu(1)–Cl(1)	94.51
Cu(1)–Cl(2)	2.325	N(2)–Cu(1)–Cl(2)	94.14
		N(4)–Cu(1)–Cl(2)	173.65
		Cl(2)–Cu(1)–Cl(1)	91.82

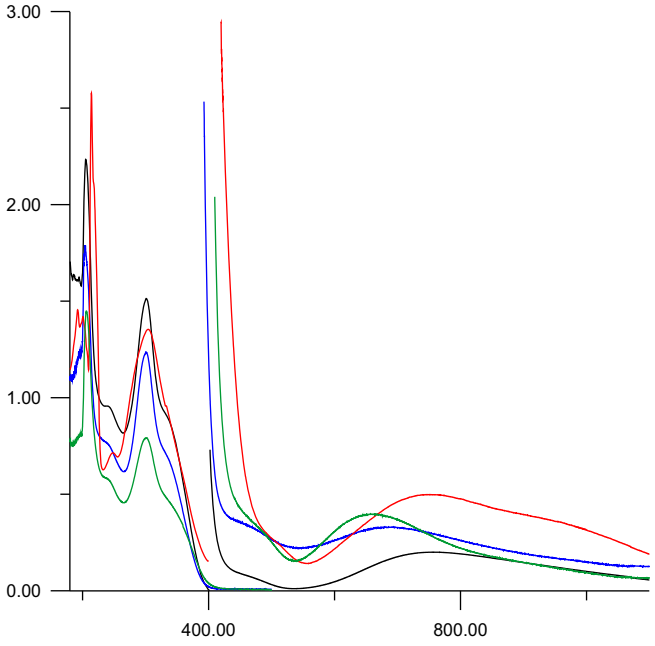

Fig. 7. The experimental electronic absorption spectra of **1** (black), **2** (red), **3** (green) and **4** (blue). (For interpretation of the references to colour in this figure legend, the reader is referred to the web version of this article.)

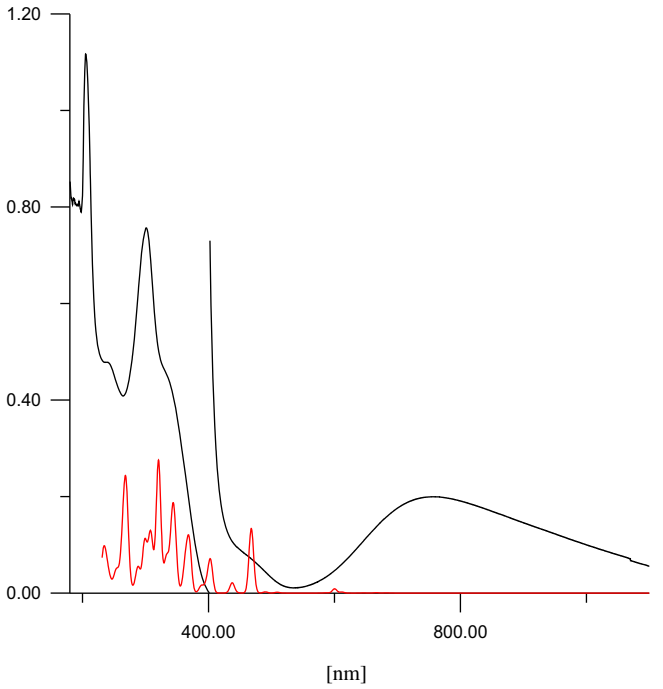

Fig. 8. The experimental (black) and calculated (red) electronic absorption spectra of **1**. (For interpretation of the references to colour in this figure legend, the reader is referred to the web version of this article.)

For complex **1** the nature of the transitions observed in the UV–Vis spectra has been studied by the time-dependent density functional (TDDFT) method. The calculated electronic spectrum of **1** in comparison with the experimental one is presented in Fig. 8. Each calculated transition is represented by a gaussian function $y = ce^{-bx^2}$ with the height (c) equal to the oscillator strength and b equal to 0.04 nm^{-2}.

Table 7
The calculated electronic transitions and their assignments to the experimental absorption bands of **1**

The most important orbital excitations	Character	λ (nm)	E (eV)	f	Experimental λ (nm)
H-5(β) → L(β)	π(Cl)/π(dppt)/d → d	682.2	1.82	0.0004	775.0
H-8(β) → L(β)	π(Cl)/d → d	666.5	1.86	0.0008	
H(β) → L(β)	π(dppt) → d	646.6	1.92	0.0003	
H-14(β) → L(β)	d/π(dppt) → d	611.8	2.03	0.0021	
H-3(β) → L(β)	π(Cl) → d	600.3	2.07	0.0088	
H(β) → L(β)	π(dppt) → d	586.6	2.11	0.0005	
H-2(β) → L(β)	π(dppt) → d	471.1	2.63	0.0144	445.8
H-4(β) → L(β)	π(dppt)/π(Cl) → d	467.6	2.65	0.1251	
H-6(β) → L(β)	π(Cl)/π(dppt)/d → d	437.2	2.84	0.0138	
H-8(β) → L(β)	π(Cl)/π(dppt)/d → d	403.0	3.08	0.0659	
H(α) → L + 1(α) H(β) → L + 2(β)	π(dppt) → π*(dppt)	369.6	3.35	0.0920	328.4
H(β) → L + 2(β)	π(dppt) → π*(dppt)	364.7	3.40	0.0500	
H-1(α) → L(α)	π(dppt) → π*(dppt)	361.9	3.42	0.0212	
H-3(α) → L(α)	π(dppt) → π*(dppt)	347.3	3.57	0.0515	
H-2(β) → L + 1(β)	π(dppt) → π*(dppt)	345.5	3.59	0.0501	
H-11(β) → L(β)	σ(Cl) → d	342.3	3.62	0.1187	
H-1(β) → L + 2(β)	π(dppt) → π*(dppt)	333.1	3.72	0.0489	
H-2(β) → L + 2(β)	π(dppt) → π*(dppt)	320.8	3.86	0.1641	302.8
H-2(β) → L + 2(β)	π(dppt) → π*(dppt)	319.4	3.88	0.0789	
H-12(β) → L(β)	σ(Cl) → d	308.7	4.02	0.0697	
H-5(α) → L + 2(α)	π(Cl)/π(dppt) → π*(dppt)	298.4	4.16	0.0990	
H-7(β) → L + 2(β)	π(Cl)/π(dppt)/d → π*(dppt)	269.6	4.60	0.1032	242.4
H-16(β) → L(β)	n(dppt)/σ(Cl)/d → d	269.4	4.60	0.0626	
H-8(β) → L + 2(β)	π(Cl)/d → π*(dppt)	265.9	4.66	0.0481	
H-8(β) → L + 2(β)	π(Cl)/d → π*(dppt)	264.8	4.68	0.0647	
					204.8

f – oscillator strength; H – highest occupied molecular orbital; L – lowest unoccupied molecular orbital.

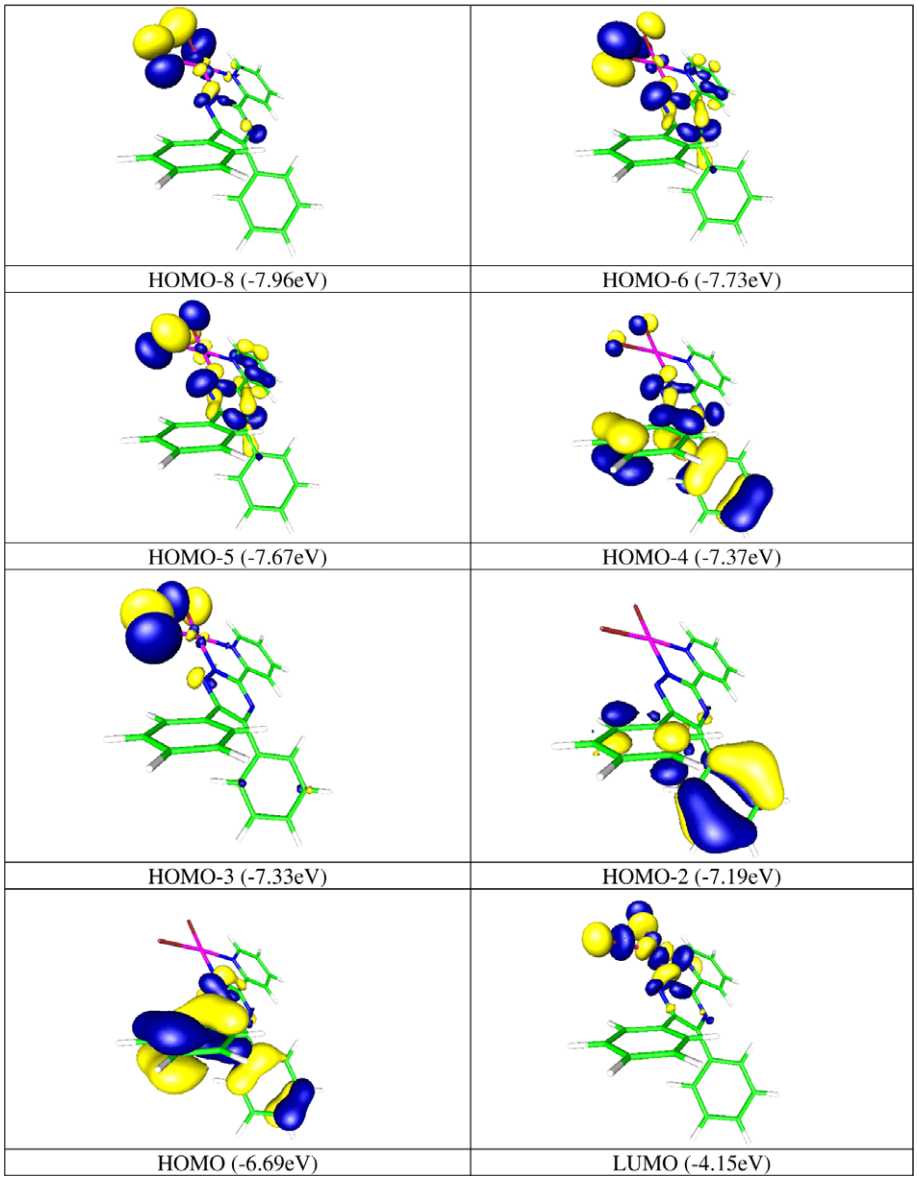

Fig. 9. Contour plots and energy of the selected β-spin HOMO and β-spin LUMO orbitals active in the electronic transitions for complex **1**. The orbitals were plotted with contour values −0.04 (yellow) and 0.04 au (blue). (For interpretation of the references to colour in this figure legend, the reader is referred to the web version of this article.)

Table 7 presents the calculated spin allowed electronic transitions of **1** and their assignments to the experimental bands. For the high energy part of the spectrum, only transitions with oscillator strengths larger than 0.500 are listed in Table 7. The assignment of the calculated orbital excitations to the experimental bands was based on an overview of the contour plots and relative energy to the orbitals HOMO and LUMO involved in the electronic transitions. The several contours of occupied and unoccupied MOs (active in the electronic transitions) of **1** are presented in Fig. 9.

The TDDFT/PCM calculations show that the two longest wavelength experimental bands of **1** at 775.0 and 445.8 nm originate in the transitions between some lowest β-spin HOMO orbitals and β-spin LUMO orbital. As can be seen from the Fig. 9, the LUMO orbital with β-spin is mainly Cu $d_{x^2-y^2}$ orbital in character, the β-spin HOMO and HOMO−1 orbitals are composed of the π-bonding orbitals of 5,6-diphenyl-3-(2-pyridyl)-1,2,4-triazine, and the HOMO−14, HOMO−8, HOMO−5 and HOMO−3 are ligand (Cl or dppt) π-bonding orbitals with some contribution of d_{Cu} orbitals. Accordingly, the transitions assigned to the two longest wavelength experimental bands can be seen as mixed Cl/dppt → Cu (LMCT) and d → d (LF). Thus, no 'clear' d–d transition bands occur in the low-lying energy region for **1**. The reason for this is probably due to the fact that the dppt ligand provides high-lying occupied π-bonding orbitals, and as a result the high-lying occupied orbitals are composed of the π-bonding orbitals of 5,6-diphenyl-3-(2-pyridyl)-1,2,4-triazine.

The experimental bands at 328.4, 302.8, 242.4 and 204.8 nm are attributed to the intraligand (IL) (π(dppt) → π*(dppt)) and ligand–ligand charge transfer (π(Cl) → π*(dppt)) transitions.

4 Supplementary data

CCDC 684890, 684891, 684892 and 684893 contain the supplementary crystallographic data for $C_{20}H_{14}N_4Cl_2Cu$, $C_{42}H_{36}Cl_2N_8O_2Cu$, $C_{40}H_{32}N_{10}O_8Cu$ and $C_{20}H_{18}N_4O_6SCu$. These data can be obtained free of charge via http://www.ccdc.cam.ac.uk/conts/retrieving.html, or from the Cambridge Crystallographic Data Centre, 12 Union Road, Cambridge CB2 1EZ, UK; fax: (+44) 1223-336-033; or e-mail: deposit@ccdc.cam.ac.uk.

Acknowledgements

The GAUSSIAN03 calculations were carried out in the Wrocław Centre for Networking and Supercomputing, WCSS, Wrocław, Poland.

References

[1] G. Garcia, I. Solano, G. Sanchez, G. Lopez, Polyhedron 14 (1995) 1855.
[2] V. Béreau, J. Rey, E. Deydier, J. Marrot, Inorg. Chim. Acta 351 (2003) 389.
[3] V. Béreau, J. Marrot, CR Chim. 8 (2005) 1087.
[4] P.L. Croot, K.A. Hunter, Anal. Chim. Acta 406 (2000) 289.
[5] J. Almog, A. Hirshfeld, B. Glattstein, J. Sterling, Z. Goren, Anal. Chim. Acta 322 (1996) 203.
[6] R. Uma, M. Palaniandavar, R.J. Butcher, J. Chem. Soc., Dalton Trans. (1996) 2061.
[7] H. Chermette, Coord. Chem. Rev. 178–180 (1998) 699.
[8] T.K. Prasad, M.V. Rajasekharan, Polyhedron 26 (2007) 1364.
[9] Y.P. Tong, S.L. Zheng, J. Mol. Struct. 841 (2007) 34.
[10] STOE & Cie, X-RED, Version 1.18. STOE & Cie GmbH, Darmstadt, Germany, 1999.
[11] G.M. Sheldrick, Acta Crystallogr., Sect. A 46 (1990) 467.
[12] G.M. Sheldrick, SHELXL97, Program for the Refinement of Crystal Structures, University of Göottingen, Germany, 1997.
[13] G.M. Sheldrick, SHELXTL: Release 4.1 for Siemens Crystallographic Research Systems, 1990.
[14] E. König, Magnetic Properties of Coordination and Organometallic Transition Metal Compounds, Springer-Verlag, Berlin, 1966.
[15] A.D. Becke, J. Chem. Phys. 98 (1993) 5648.
[16] C. Lee, W. Yang, R.G. Parr, Phys. Rev. B 37 (1988) 785.
[17] M.J. Frisch, G.W. Trucks, H.B. Schlegel, G.E. Scuseria, M.A. Robb, J.R. Cheeseman, J.A. Montgomery Jr., T. Vreven, K.N. Kudin, J.C. Burant, J.M. Millam, S.S. Iyengar, J. Tomasi, V. Barone, B. Mennucci, M. Cossi, G. Scalmani, N. Rega, G.A. Petersson, H. Nakatsuji, M. Hada, M. Ehara, K. Toyota, R. Fukuda, J. Hasegawa, M. Ishida, T. Nakajima, Y. Honda, O. Kitao, H. Nakai, M. Klene, X. Li, J.E. Knox, H.P. Hratchian, J.B. Cross, C. Adamo, J. Jaramillo, R. Gomperts, R.E. Stratmann, O. Yazyev, A.J. Austin, R. Cammi, C. Pomelli, J.W. Ochterski, P.Y. Ayala, K. Morokuma, G.A. Voth, P. Salvador, J.J. Dannenberg, V.G. Zakrzewski, S. Dapprich, A.D. Daniels, M.C. Strain, O. Farkas, D.K. Malick, A.D. Rabuck, K. Raghavachari, J.B. Foresman, J.V. Ortiz, Q. Cui, A.G. Baboul, S. Clifford, J. Cioslowski, B.B. Stefanov, G. Liu, A. Liashenko, P. Piskorz, I. Komaromi, R.L. Martin, D.J. Fox, T. Keith, M.A. Al-Laham, C.Y. Peng, A. Nanayakkara, M. Challacombe, P.M.W. Gill, B. Johnson, W. Chen, M.W. Wong, C. Gonzalez, J.A. Pople, GAUSSIAN 03, Revision B.03, Gaussian, Inc., Pittsburgh, PA, 2003.
[18] M. Cossi, V. Barone, B. Mennucci, J. Tomasi, Chem. Phys. Lett. 286 (1998) 253.
[19] P.J. Hay, W.R. Wadt, J. Chem. Phys. 82 (1985) 299.
[20] M.E. Casida, Recent Developments and Applications in Modern Density Functional Theory, in: J.M. Seminario (Ed.), Theoretical and Computational Chemistry, vol. 4, Elsevier, Amsterdam, 1996.
[21] K. Nakamoto, Infrared and Raman Spectra of Inorganic and Coordination Compounds, 4th ed., Wiley-Interscience, New York, 1986.
[22] N.E. Eltayeb, S.G. Teoh, H.-K. Fun, K. Ibrahim, M.M. Rosli, Acta Crystallogr., Sect. E 63 (2007) m1182.
[23] G.R. Desiraju, T. Steiner, The Weak Hydrogen Bond in Structural Chemistry and Biology, Oxford University Press, 1999.
[24] G.A. Jeffrey, W. Saenger, Hydrogen Bonding in Biological Structures, Springer-Verlag, 1994.
[25] Ch. Fernandes, A.J. Bortoluzzi, B. Szpoganicz, E. Schwingel, A. Neves, Inorg. Chim. Acta 358 (2005) 997.
[26] F.H. Allen, Acta Crystallogr., Sect. B 58 (2002) 380.
[27] A. Cornia, A.C. Fabretti, F. Ferraro, D. Gatteschi, A. Giusti, Chem. Soc., Dalton Trans. 3363 (1993).
[28] B. Bleaney, K.D. Bowers, Proc. R. Soc. London, Ser. A 214 (1952) 451.
[29] J. Samuel Smart, Effective Field Theories of Magnetism, W.B. Saunders Comp., Philadelphia and London, 1966.
[30] O. Kahn, Molecular Magnetism, VCH Publishers, New York, 2003.
[31] W.H. Crawford, H.W. Richardson, J.R. Wasson, D.J. Hadgson, W.E. Hatfield, Inorg. Chem. 15 (1976) 2107.

milli-Q water-methanol mixture (1:1 ratio). To this solution either nickel(II) chloride hexahydrate, zinc(II) chloride dihydrate or copper(II) chloride tetrahydrate (1 mmol) was added. The solution was stirred for 15 min and kept for crystallization. Upon standing the corresponding complexes $[NiL(H_2O)_3]2H_2O$ (**3**) and $\{[ZnL(H_2O)]4H_2O\}_n$ (**4**), crystallized out as single products in each case after one week. The copper complex $[CuL(py)(H_2O)_2]$ (**5**) was crystallized from pyridine.

*2.3.1. Complex $[NiL(H_2O)_3]2H_2O$ (**3**)*

Isolated yield 85%. IR (KBr, cm^{-1}): 3254 (bs), 2930 (w), 2818 (w), 2780 (w), 1598 (s), 1572 (s), 1434 (m), 1421 (m), 1396 (s), 1368 (m), 1351 (m), 1320 (m), 1303 (s), 1226 (w), 1183 (w), 1152 (m), 1092 (m), 968 (m), 935 (s), 818 (w), 765 (w), 718 (s). Elemental *Anal.* Calc. for $C_8H_{18}N_2O_9Sni$: C, 25.48; H, 4.78. Found, C, 25.57; H, 4.84%. Magnetic moment (25 °C): 2.62 BM. Visible (λ_{max}, DMF) 659 nm ($\varepsilon = 20\ M^{-1}\ cm^{-1}$).

*2.3.2. Complex $\{[ZnL(H_2O)]4H_2O\}_n$ (**4**)*

Isolated yield 82%. ^1H NMR (D_2O): 6.69 (s, 1H), 4.36 (s, 2H), 3.1 (s, 2H), 2.16 (s, 3H). IR (KBr, cm^{-1}): 3390 (bs), 2847 (w), 1614 (s), 1564 (s), 1435 (s), 1407 (s), 1368 (s), 1350 (m), 1303 (s), 1229 (m), 1153 (m), 1095 (m), 1025 (w), 937 (w), 809 (w), 724 (s). Elemental *Anal.* Calc. for $C_8H_{18}N_2O_9SZn$: C, 24.83; H, 4.66. Found: C, 25.03; H, 4.82%.

Table 1
Crystallographic parameters for the complexes **3**–**5**

	3	**4**	**5**
Formulae	$C_8H_{18}N_2NiO_9S$	$C_8H_{18}N_2O_9SZn$	$C_{13}H_{17}CuN_3O_6S$
Molecular weight	377.01	383.67	406.90
Crystal system	monoclinic	monoclinic	monoclinic
Space group	$P2_1/c$	$C2/c$	$P2_1/c$
a (Å)	7.9747(3)	20.7062(10)	18.6700(7)
b (Å)	7.6183(3)	7.5190(3)	10.1420(4)
c (Å)	23.8542(9)	19.7050(8)	8.6776(3)
α (°)	90.00	90.00	90.00
β (°)	95.094(2)	101.772(3)	91.757(2)
γ (°)	90.00	90.00	90.00
V (Å^3)	1443.51(10)	3003.3(2)	1642.34(11)
Z	4	8	4
Density (Mg m^{-3})	1.735	1.697	1.646
Absorption coefficient (mm^{-1})	1.534	1.818	1.492
Absorption correction	none	none	none
$F(000)$	784	1584	836
Total number of reflections	2383	3602	3721
Reflections, $I > 2\sigma(I)$	2235	3147	1481
Maximum 2θ (°)	25.00	28.37	28.42
Ranges (h, k, l)	$-8 \leqslant h \leqslant 9$, $-9 \leqslant k \leqslant 9$, $-28 \leqslant l \leqslant 28$	$-21 \leqslant h \leqslant 27$, $-10 \leqslant k \leqslant 9$, $-25 \leqslant l \leqslant 26$	$-24 \leqslant h \leqslant 24$, $-8 \leqslant k \leqslant 13$, $-11 \leqslant l \leqslant 9$
Complete to 2θ (%)	94.1	95.8	99.2
Data/restraints/parameters	2383/0/225	3602/0/228	4096/0/226
Goodness-of-fit (F^2)	1.069	1.019	1.004
R indices [$I > 2\sigma(I)$]	0.0227	0.0262	0.0339
R indices (all data)	0.0242	0.0318	0.0578

*2.3.3. Complex $[CuL(py)(H_2O)_2]$ (**5**)*

Isolated yield 78%. IR (KBr, cm^{-1}): 3428 (bs), 3104 (w), 3065 (w), 3038 (w), 2923 (w), 2851 (w), 1606 (s), 1490 (m), 1450 (s), 1396 (w), 1363 (w), 1237 (w), 1220 (m), 1163 (m), 1080 (s), 1043 (m), 760 (s), 689 (s). Magnetic moment (25 °C): 1.95 BM. Visible (λ_{max}, DMF) 840 nm ($\varepsilon = 15\ M^{-1}\ cm^{-1}$). Elemental *Anal.* Calc. for $C_{13}H_{17}N_3O_6SCu$: C, 38.34; H, 4.18. Found: C, 38.68; H, 4.26%.

The X-ray data were collected at 296 K with Mo Kα radiation ($\lambda = 0.71073$ Å) using a Bruker Nonius SMART CCD diffractometer equipped with a graphite monochromator. The SMART software was used for data collection and also for indexing the reflections and determining the unit cell parameters; the collected data were integrated using SAINT software. The structures were solved by direct methods and refined by full-matrix least-squares calculations using SHELXTL software. All the non-H atoms were refined in the anisotropic approximation against F^2 of all reflections. The H atoms, except those attached to N and O were placed in their calculated positions and refined in the isotropic approximation; those attached to heteroatoms (N, O) were located in the difference Fourier maps, and refined with isotropic displacement coefficients. The crystal data for the complexes are listed in Table 1.

3. Results and discussion

The reaction of 5-methyl-thiazol-2-ylamine with methylbromoacetate gives the di-substituted derivative (2-methoxycarbonylmethylimino-5-methyl-thiazol-3-yl)-acetic acid methyl ester (**1**) (Scheme 1). The important aspect of this reaction is that even when the 5-methyl-thiazol-2-ylamine is reacted with an equimolar amount of methylbromoacetate, the reaction invariably leads to the dialkylated product. Monoalkylated products are not observed in the reaction. This suggests that the second alkylation process on 5-methyl-thiazol-2-ylamine is faster than the first alkylation process (Scheme 1). The dialkylation also takes place with a shift of the endocyclic C=N bond to an exocyclic C=N bond. Compound **1** was characterized by ^1H and ^{13}C NMR spectroscopy, along with other spectroscopic techniques. The formation of the di-substituted product is illustrated in Scheme 2.

The methylester **1** on base hydrolysis (Scheme 1) gives the disodium salt of (2-carboxymethylimino-5-methyl-thiazol-3-yl)acetic acid (Na_2L). The disodium salt (**2**) reacts with nickel(II) chloride, zinc(II) chloride or copper(II) chloride, resulting in mononuclear or polynuclear complexes (Scheme 3). The nickel complex is a mononuclear complex and has the composition $[NiL(H_2O)_3]2H_2O$ (**3**); the zinc complex has the composition $\{[ZnL(H_2O)]4H_2O\}_n$ (**4**), whereas the copper complex crystallized from pyridine (py) and is a mononuclear complex having the composition $[CuL(py)(H_2O)_2]$ (**5**). The crystal structures of all these complexes have been determined.

The nickel complex has a six coordination geometry in which the imine nitrogen and two oxygen atoms of the carboxylate groups coordinate to the nickel, making a five member and seven member cyclic structure (Fig. 1). These three dative bonds along with an aqua ligand occupy the four corners of a plane, and there are two more aqua ligands occupying the axial positions. In

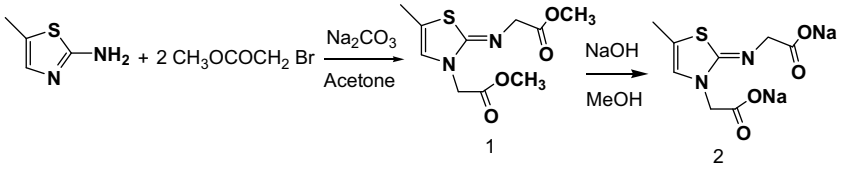

Scheme 1. Dialkylation of 5-methyl-thiazol-2-ylamine.

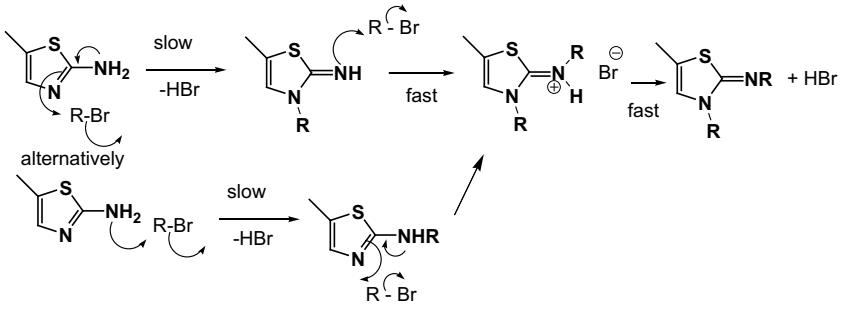

Scheme 2. The possible mechanism of the dialkylation of 5-methyl-thiazol-2-ylamine.

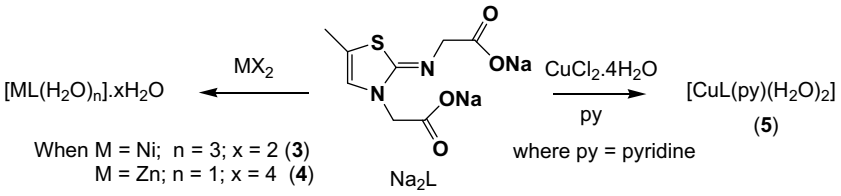

Scheme 3. Preparation of the ligand and its metal complexes.

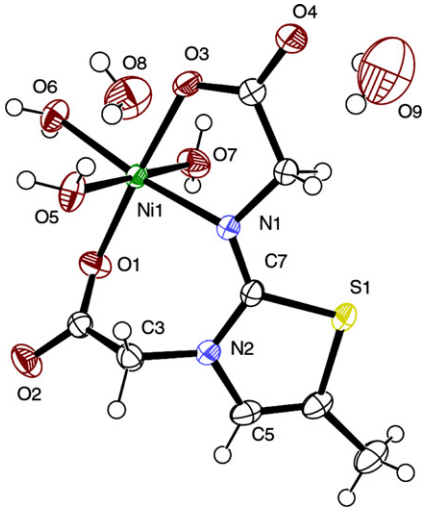

Fig. 1. The structure of the nickel complex **3**. Selected bond distances (Å) and bond angles (°): Ni1–O3, 2.0362(13); Ni1–O6, 2.0472(14); Ni1–O1, 2.0554(13); Ni1–N1, 2.0733(15); Ni1–O5, 2.0775(14); Ni1–O7, 2.1028(15); ∠O3–Ni1–O6, 91.25(7); ∠O3–Ni1–O1, 175.64(5); ∠O6–Ni1–O1, 92.81(6); ∠O3–Ni1–N1, 80.59(5); ∠O6–Ni1–N1, 90.72(6); ∠O1–Ni1–N1, 97.75(6); ∠O3–Ni1–O5, 92.56(5); ∠O6–Ni1–O5, 89.64(6); ∠O1–Ni1–O5, 89.06(6); ∠N1–Ni1–O5, 173.15(6); ∠O3–Ni1–O7, 90.24(6); ∠O6–Ni1–O7, 178.28(7); ∠O1–Ni1–O7, 85.73(6); ∠N1–Ni1–O7, 90.37(6); ∠O5–Ni1–O7, 89.44(6).

addition to these complex **3** has two molecules of water of crystallization. Some of the important bond distances and angles are listed in Fig. 1. The sulfur atom of the ligand does not participate in coordination. The disodium salt Na_2L has a strong absorption at 1590 cm^{-1} arising from carboxylate stretching, whereas the zinc complex has two sharp signals at 1598 and 1572 cm^{-1}, suggesting the two carboxylates are in two different environments; namely one in a five and the other in a seven member ring structure. The compound has a magnetic moment of 2.62 BM which corresponds to a d^8-electronic configuration. The nickel complex absorbs at 659 nm in DMF due to a d–d transition.

The zinc complex (**4**) has a polymeric structure, having pentacoordinated zinc centres, and each zinc center has a distorted square pyramidal geometry. The basal plane is constructed by the coordination of two oxygen atoms and a nitrogen atom to zinc, along with an aqua ligand. The fifth coordination site is completed by an oxygen atom of a carboxylate from another chelating ligand to a neighboring zinc center. The important bond distances and bond angles are listed in Fig. 2. The repeated part of the complex in the crystal lattice is shown in Fig. 2b.

A careful look at the structure suggests that each building block comprises of four coordinated units built from L and an aqua ligand, these units gets connected to each other through the Zn–O bond from the C=O oxygen of a carboxylate group of a neighboring molecule. Thus, a polymeric chain structure is formed in which all the zinc centers have uniformly five coordination. The coordination polymer has a zig–zag structure extending along the crystallographic *b*-axis. Examples of pentacoordination in zinc are lesser in number, but they are biologically important [5a–l] and they are also formed under specific conditions [5m]. The zinc coordination polymer **4** shows IR absorptions at 1614 and 1564 cm^{-1}; this suggests two different environments for the carboxylate groups. The IR stretching of these groups is different from the nickel complex, this difference is attributed to the fact that the two Zn–O bonds arising from the carboxylate groups in the case of the nickel complexes are equivalent, but in the case of the zinc complex they are different. This is also reflected in the bond lengths, namely Zn1–O1 is 2.048 Å, whereas Zn1–O2 is 2.103 Å. The complex in solution shows desirable proton NMR signals for the ligand.

When the product of the reaction of Na_2L with copper(II) chloride is crystallized from pyridine, a mononuclear complex having the composition $[CuL(py)(H_2O)_2]$ (**5**) is obtained. This complex is similar to the nickel complex (**3**) and can be considered as an analogous copper complex in which one of the three aqua ligands is substituted by a pyridine ligand. The complex has a magnetic moment of 1.95 BM, which is generally observed for a d^9-electronic configuration. Complex **5** has a visible absorption at 840 nm for a d–d transition. Apparently the complex has a distorted octahedral geometry around the copper ion, in which two axial bonds, Cu1–

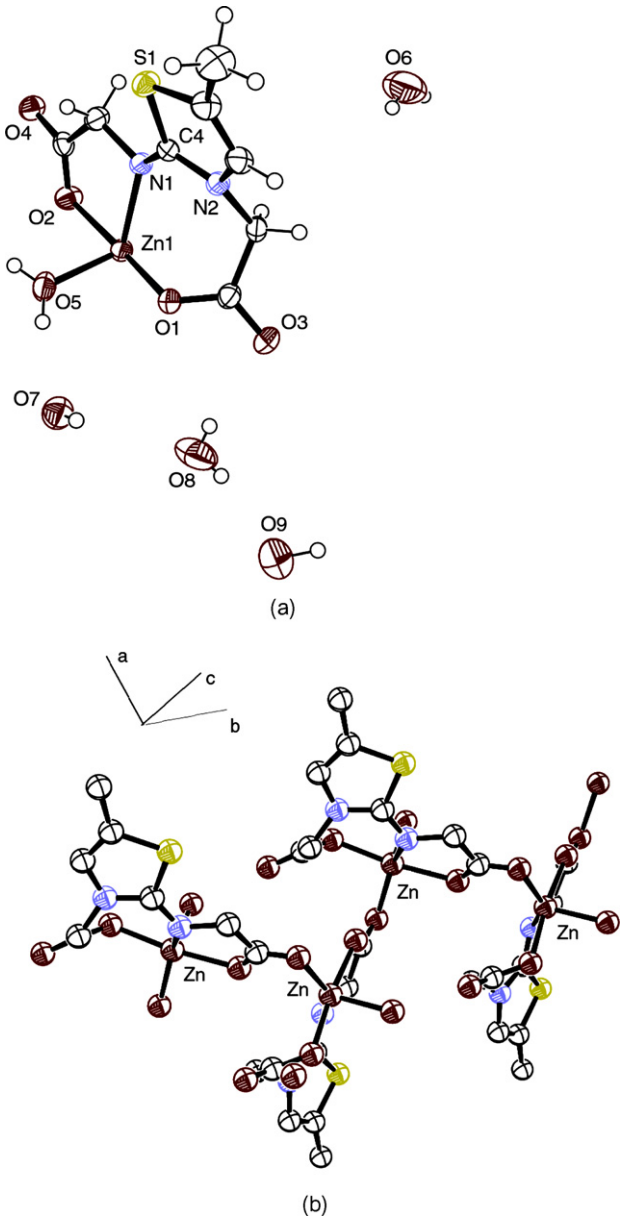

Fig. 2. (a) The repeated units of the coordination polymer **4**. (b) A part of the chain of the coordination polymer **4** (hydrogen atoms are omitted for clarity). Selected bond distances (Å) and bond angles (°): Zn1–O4, 2.0231(12); Zn1–O5, 2.0231(15); Zn1–O1, 2.0479(13); Zn1–N1, 2.0518(14); Zn1–O2, 2.1035(13); ∠O4–Zn1–O5, 110.04(6); ∠O4–Zn1–O1, 93.65(5); ∠O5–Zn1–O1, 84.40(6); ∠O4–Zn1–N1, 138.82(6); ∠O5–Zn1–N1, 110.61(7); ∠O1–Zn1–N1, 96.55(5); ∠O4–Zn1–O2, 92.74(5); ∠O5–Zn1–O2, 90.86(6); ∠O1–Zn1–O2, 173.06(5).

O7, 2.43 Å and Cu1–O8, 2.55 Å, are much longer than the other two Cu–O bonds from the ligand. The Cu1–O8 distance is too long to form a strong Cu–O bond, and thus if this Cu–O interaction is ignored the geometry around copper is distorted square pyramidal (Fig. 3). On the other hand, the pyridine is tightly bound to copper, it has a comparable Cu1–N1 bond distance with the ligand Cu1–N2 distance. Some of the important bond distances and bond angles are listed in Fig. 3. The presence of pyridine as a coordinating ligand in complex **5** suggests that in the case of copper(II) chloride, the reaction with LNa_2 initially forms a tri-aqua complex similar to that of the nickel complex **3**, which then might have undergone a ligand substitution reaction, replacing an aqua ligand by a pyridine, and because of steric congestion in the complex one of the

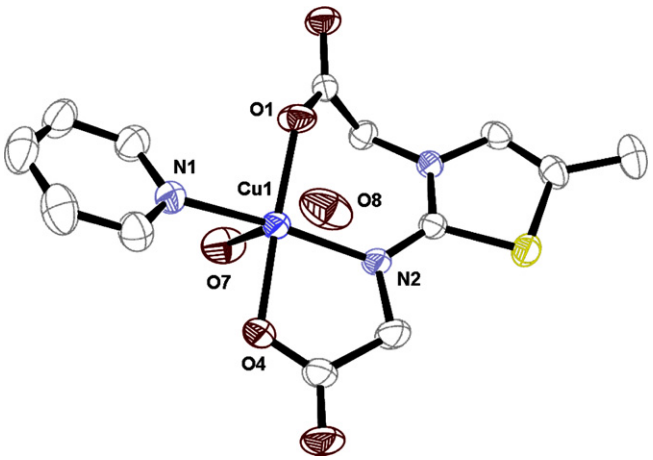

Fig. 3. The structure of complex **5**, the hydrogen atoms are omitted for clarity. Selected bond distances (Å) and bond angles (°): Cu1–O1, 1.967(16); Cu1–O4, 1.960(16); Cu1–N2, 1.981(8); Cu1–N1, 2.015(19); Cu1–O7, 2.430(2); Cu1–O8, 2.555; ∠O4–Cu1–N2, 96.79(7); ∠O4–Cu1–O1, 172.64(8); ∠O1–Cu1–N2, 82.72(7); ∠O4–Cu1–N1, 88.56(8); ∠O1–Cu1–N1, 91.46(8); ∠N2–Cu1–N1, 173.32(8); ∠O4–Cu1–O7, 98.06(8); ∠O1–Cu1–O7, 89.29(8); ∠N2–Cu1–O7, 95.05(8); ∠N1–Cu1–O7, 88.14(8).

aqua ligand remains further away at an axial position of the original six coordinated system.

In conclusion we have synthesized an imine containing flexible dicarboxylic acid through tautomerism in a thiamine derivative and have shown that it can either lead to mononuclear or polynuclear complexes depending on the metals; the hexacoordinated mononuclear nickel complex of L has three aqua ligands on one face leaving scope for further transformations.

4. Supplementary data

CCDC 679648, 679650 and 681972 contain the supplementary crystallographic data for **3**, **4** and **5**. These data can be obtained free of charge via http://www.ccdc.cam.ac.uk/conts/retrieving.html, or from the Cambridge Crystallographic Data Centre, 12 Union Road, Cambridge CB2 1EZ, UK; fax: (+44) 1223-336-033; or e-mail: deposit@ccdc.cam.ac.uk.

Acknowledgements

The authors thank the Council of Scientific and Industrial Research, New-Delhi (India) for financial support. The authors also thank Mr. A. Karmakar for his help.

References

[1] (a) A. Erxleben, Coord. Chem. Rev. 246 (2003) 203;
(b) F.S. Delgado, J. Sanchiz, C. Ruiz-Perez, F. Lloret, M. Julve, CrystEngCommun 6 (2004) 73;
(c) F.S. Delgado, M. Hernandez-Molina, J. Sanchiz, C. Ruiz-Perez, Y. Rodriguez-Martin, T. Lopez, F. Lioret, M. Julve, CrystEngCommun 6 (2004) 929;
(d) I. GildeMuro, L. Lezama, M. Insausti, T. Rojo, Polyhedron 23 (2004) 859;
(e) F.S. Delgado, C. Ruiz-Perez, J. Sanchiz, F. Lloret, M. Julve, CrystEngCommun 8 (2006) 530;
(f) J. Pasan, J. Sanchiz, C. Ruiz-Perez, F. Lloret, M. Julve, Inorg. Chem. 44 (2005) 7794;
(g) P. Lightfoot, A. Snedden, J. Chem. Soc., Dalton Trans. (1999) 3549;
(h) Y. Rodriquez-Martin, J. Sanchiz, C. Ruiz-Perez, F. Lloret, M. Julve, CrystEngCommun 4 (2002) 631.
[2] (a) K. Aoki, M. Nakagawa, K. Ichimura, J. Am. Chem. Soc. 122 (2000) 10997;
(b) W. Schmitt, J.P. Hill, S. Malik, C.A. Volkert, I. Ichinose, C.E. Anson, A.K. Powell, Angew. Chem., Int. Ed. 44 (2005) 7048.
[3] A.M. Baruah, A. Karmakar, J.B. Baruah, Polyhedron 26 (2007) 4518.
[4] M.L. Das, M. Koike, L.J. Reed, Proc. Natl. Acad. Sci. USA 47 (1961) 753.

[5] (a) Y. Yang, M.-H. Zeng, S.-H. Zhang, H. Liang, Wuji Huaxue Xuebao 23 (2007) 1435;
(b) H. Golchoubian, E. Baktash, R. Welter, Inorg. Chem. Commun. 10 (2007) 1035;
(c) H. Nekola, D. Rehder, Inorg. Chim. Acta 337 (2002) 467;
(d) M. Guncheva, P. Dolashka-Angelova, N. Stambolieva, Biochim. Biophys. Acta, Prot. Struct. Mol. Enzymol. 1597 (2002) 335;
(e) F.M. Belicchi, F. Bisceglie, G. Pelosi, T. Pieralberto, R. Albertini, S. Pinelli, J. Inorg. Biochem. 87 (2001) 137;
(f) L. Bresolin, R.A. Burrow, M. Horner, E. Bermejo, A. Castineiras, Polyhedron 16 (1997) 3947.
(g) R. Feldhaus, J. Koeppe, V. Mattes, Z. Naturforsch. B: Chem. Sci. 51 (1996) 1449;
(h) L.X. Chen, Z. Wang, G. Hartwich, I. Katheder, H. Scheer, A. Scherz, P.A. Montano, J.R. Norris, Chem. Phys. Lett. 234 (1995) 437;
(i) Y. Kai, M. Morita, N. Yasuoka, N. Kasai, Bull. Chem. Soc. Jpn. 58 (1985) 1631;
(j) M.W. Makinen, L.C. Kuo, M.B. Yim, W. Maret, G.B. Wells, J. Mol. Catal. 23 (1984) 179;
(k) P. Andersson, J. Kvassman, A. Lindstroem, B. Olden, G.K. Pettersson, Eur. J. Biochem. 108 (1980) 303;
(l) D.P. Madden, M.M. Da Mota, S.M. Nelson, J. Chem. Soc., Sec. A (1970) 790;
(m) A.M. Baruah, R. Sarma, J.B. Baruah, Inorg. Chem. Commun. 11 (2008) 121.

is the sum of the kinetic electron energy density (G_C) and the potential electron energy density (V_C)) derived from the Bader theory also indicate the type of interaction and cooperative effect on the nature of the interactions. The negative value of the Laplacian of the electron density at BCP ($\nabla^2_{\rho BCP} < 0$) designates the concentration of the electron charge in the region between the nuclei of the interacting atoms and is typical of covalent bonds-shared interactions. In the case $\nabla^2_{\rho BCP} > 0$, there is a depletion of the electron charge between atoms, indicating that there is an interaction of closed-shell systems like ions, van der Waals interactions or H-bonds. Hence one can see that the Bader theory arbitrarily provides the characteristics of BCPs based on whether the interaction is covalent in nature. For a negative value of a Laplacian, there is no doubt about its covalency (from the AIM theory point of view). Also, the $-G_C/V_C$ ratio may show the regions belonging to covalent or non-covalent interactions. If such a ratio is greater than 1, then the interaction is non-covalent. In the case of a ratio between 0.5 and 1, the interaction is partly covalent in nature, and where $-G_C/V_C$ is less than 0.5, the interaction is a shared interaction because $\nabla^2_{\rho BCP}$ is smaller than zero [28].

3. Results and discussion

Association of one molecule of cyanic acid with one molecule of water leads to formation of a 1:1 cluster which is denoted as $W1C_H$ (see Table 1, Fig. 1 and S1). C is cyanic acid, W is water and the subscripted letter denotes an atom of HOCN that is incorporated in H-bonding with water, for example $W1C_H$ shows $H_2O\cdots$HOCN. In $W1C_H$, the H of the cyanic acid is connected to the O of water. Our attempts could obtain neither $W1C_O$ nor $W1C_N$ because their starting configurations go to $W1C_H$ upon optimization. In $W1C_O$, the water molecule acts as a hydrogen bond donor (HBD) and the O of the cyanic acid plays the role of a hydrogen bond acceptor (HBA). In the last 1:1 cluster, which was considered to be $W1C_N$, the water molecule acts as the HBD and the N atom of HOCN acts as the HBA.

Since the OCN group is electron deficient, its O and N atoms show a diminished tendency to accept the H atom from a water molecule. In contrast, the electron withdrawing OCN group enhances the positive charge on the H atom of HOCN and improves its HBD capability. In summary, the electron deficiency of OCN enhances the HBD ability of HOCN but is acts against its role as a HBA. Also, the results show that HOCN is a stronger HBD and a weaker HBA than H_2O.

The atoms in the molecules analysis show $\nabla^2_{\rho BCP} > 0$ and $-G_C/V_C < 1$ for $W1C_H$. Thus, it could be mentioned that the HB interactions in $W1C_H$ are partly covalent.

Let us compare the 1:1 cluster studied in the present work at the MP2 level with that which has been reported in our earlier studies for HCNO–H_2O, HNCO–H_2O and HONC–H_2O systems, Table S1 [18–20]. The stabilization energies of $W1C_H$, $W1If_H$ [20], $W1I_H$ [19] and $W1F_H$ [18] are −10.21, −9.99, −5.32 and −4.14 kcal mol^{-1}, respectively. The stabilities of the 1:1 clusters of HOCN and HONC ($W1C_H$ and $W1If_H$) are comparable and are greater than the stabilities of the 1:1 clusters of HNCO and HCNO ($W1I_H$ and $W1F_H$). This is due to the stronger HBD in the former molecules compared to the other two, which arises from greater local charges on the H atoms of the HOCN and HONC molecules.

In addition, the prediction of $W1I_O$, $W1I_N$, $W1If_C$ and $W1F_O$, and failure to predict $W1C_O$ and $W1C_N$ show that HOCN is a poorer HBA than HONC, HNCO and HCNO. Apparently, the group electronegativity depends on the arrangement of the C, N and O atoms in these groups, so that different values of HBA abilities in these isomers lead to the prediction of various stabilities of their 1:1 clusters.

All the starting geometries for the 1:2 clusters of HOCN–HOH–H_2O, H_2O–HOCN–HOH and H_2O–H_2O–HOCN go to a cyclic structure ($W2C_{HN}$) upon optimization. In this structure, the HOCN molecule acts both as a HBD and a HBA. The partly covalent character of the $H_2O\cdots$HOCN bonds and non-covalent character of HOCN$\cdots$HOH could be concluded from the AIM results.

In the 1:2 stoichiometry, upon optimization for HOCN, HONC, HNCO and HCNO, 1, 1, 2 and 4 clusters have been predicted, respectively. The difference in the numbers of 1:2 clusters could be interpreted in term of the HBA ability of these molecules. On the other hand, $W2C_{HN}$ (SE = −21.93 kcal mol^{-1}) has a comparable stability to $W2If_{HC}$ (−20.54), and they are more stable than the 1:2 clusters of the HNCO and HCNO molecules, Table S1.

For 1:3 clusters, the four geometries $W3C_{HO}$, $W3C_{HN(I)}$, $W3C_{HN(II)}$ and $W3C_{HN(III)}$ were obtained. In all of these clusters, the HOCN molecule has both the role of a HBD and a HBA. In the $W3C_{HO}$ cluster, the O atom of HOCN plays the role of a HBA but in $W3C_{HN}$ the N atom of the HOCN molecule has this role. The stabilities of the 1:3 clusters are in the order $W3C_{HO} > W3C_{HN(I)} > W3C_{HN(II)} > W3C_{HN(III)}$. Table 2 shows that the covalent character of the $H_2O\cdots$HOCN bond in the 1:3 clusters has increased with respect to the 1:1 and 1:2 clusters. Like the 1:1 and 1:2 clusters, the stability of the 1:3 cluster of HOCN is slightly greater than the HONC cluster, and in turn they are more stable than the HNCO and HCNO clusters.

In the case of the 1:4 clusters, the starting configurations after optimization go to $W4C_{HO(I)}$, $W4C_{HN(I)}$, $W4C_{HN(II)}$, $W4C_{HNO(I)}$ and $W4C_{HNO(II)}$ as local minima. In all of these structures the HOCN molecule acts both as a HBD and a HBA. The O atom in $W4C_{HO}$, the N atom in $W4C_{HN}$; both N and O atoms in $W4C_{HNO}$ clusters have the role of a HBA in the HOCN molecule. The stabilities of the 1:4 clusters are as follows: $W4C_{HNO(I)} > W4C_{HO(I)} > W4C_{HN(II)} > W4C_{HNO(II)} > W4C_{HN(I)}$.

From a comparison of the AIM results of the 1:4 clusters with the corresponding values for the 1:1, 1:2 and 1:3 clusters in Table 2, it could be concluded that the covalent property of the $H_2O\cdots$HOCN bond is enhanced with the cluster size. It shows that the identity of these interactions depends on the cooperative effect.

Also a comparison of the 1:4 clusters, Table S1, shows that the stabilities of the clusters of HOCN and HONC are close together, and they are more stable than the corresponding 1:4 clusters for HNCO and HCNO. The stabilities of the H_2O–HOCN clusters was predicted as: $W4C_{HN(I)} > W4C_{HNO(II)} > W4C_{HN(II)} > W4C_{HO(I)} > W3C_{HN(III)} > W4C_{HNO(I)} > W3C_{HN(II)} > W3C_{HN(I)} > W3C_{HO} > W2C_{HN} > W1C_H$.

According to the results, clusters with HOCN just as a HBA could not be predicted since they convert to a more stable cluster with HOCN as a HBD during optimization. This is due to the effect of the electron withdrawing character of the OCN groups on the partial charges of the H, N and O atoms. The OCN group, by inducing a greater positive charge on the H of HOCN, enhances its HB interaction with an H_2O molecule. In contrast, the lack of suitable electron

Table 1
BSSE stabilization energy corrected with ZPE, uncorrected stabilization energy, and CE calculated at the MP2/6-311++G(d,p) level

Cluster	BSSE (kcal mol^{-1})	SE(corr.) (kcal mol^{-1})	SE(uncorr.) (kcal mol^{-1})	CE (kcal mol^{-1})
$W1C_H$	2.4	−10.21	−12.48	–
$W2C_{HN}$	5.68	−21.93	−27.2	−6.73
$W3C_{HO}$	8.21	−27.35	−34.9	−8.96
$W3C_{HN(II)}$	7.95	−27.59	−34.88	−8.69
$W3C_{HN(III)}$	7.96	−28.59	−35.51	−9.69
$W3C_{HN(I)}$	8.72	−32.64	−40.5	−13.74
$W4C_{HNO(I)}$	9.12	−31.92	−40.71	−12.23
$W4C_{HO(I)}$	11.18	−35.57	−45.51	−13.49
$W4C_{HN(II)}$	11.15	−36.1	−46.54	−9.81
$W4C_{HNO(II)}$	11.33	−37.57	−47.15	−14.18
$W4C_{HN(I)}$	11.05	−40.37	−50.47	−17.78

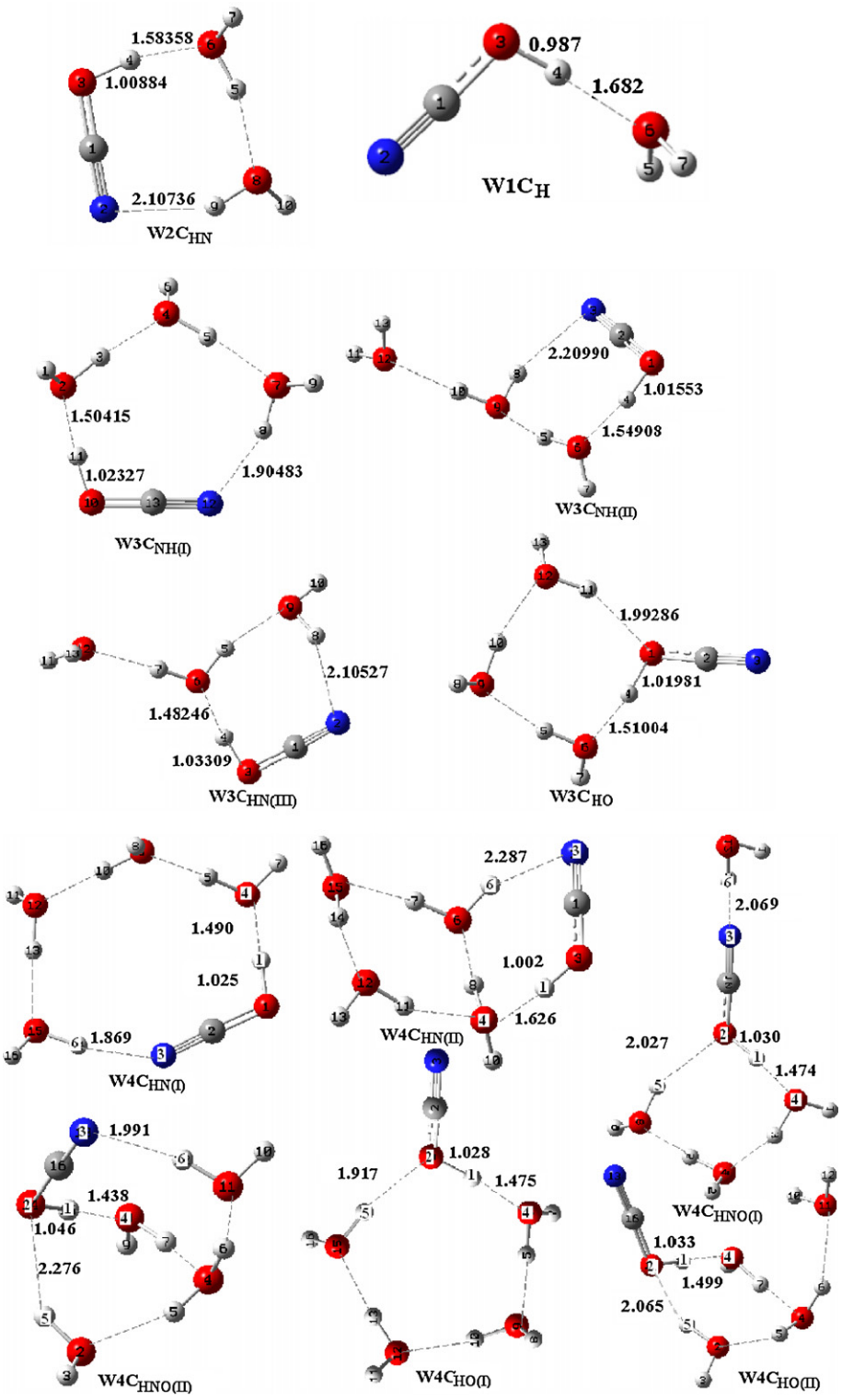

Fig. 1. H-bonded clusters of cyanic acid with water molecules optimized at the MP2/6-311++G(d,p) level, W4C$_{HO(II)}$ at the B3LYP level; some bond distances (Å) have been given.

density on the N and O atoms of HOCN diminish their HBA tendency for a HB interaction with H_2O. The stabilization energies become more negative by increasing the cluster size. This indicates that increasing the number of water molecules in the cluster occurs along with enhancement of its stability.

The results of intermolecular bond lengths and bond angles are given in Table 3. The H_2O···HOCN distance decreases from 1.682 Å in W1C$_H$ to 1.584, 1.504 and 1.490 Å in a series of homologue clusters of W2C$_{HN}$, W3C$_{HN(I)}$ and W4C$_{HN(I)}$. This reduction in the H_2O···HOCN bond length is the result of greater stability of the larger clusters. A similar shortening of the HOH···N distances was found so that the HOH···N bond of 2.107 Å in W2C$_{HN}$ reduced to 1.905 and 1.869 Å in W3C$_{HN(I)}$ and W4C$_{HN(I)}$. These values are in line with the increasing calculated cooperative effects (−6.73,

Table 2
Topological parameters for the fully optimized systems analyzed here at the MP2/6-311++G(d,p) computational level

Cluster	Bond	ρ	Δ^2	G_c	$-V_c$	H_c	$-G_c/V_c$
$W1C_H$	O4–H1	0.0438	0.1435	0.0398	0.0438	−0.0039	0.9099
$W2C_{HN}$	O4–H1	0.0589	0.1535	0.0510	0.0635	−0.0126	0.8019
	H6–N3	0.0172	0.0642	0.0135	0.0110	0.0025	1.2325
$W3C_{HO}$	O4–H1	0.0708	0.1626	0.0607	0.0808	−0.0201	0.7516
	H5–O2	0.0204	0.0828	0.0183	0.0158	0.0024	1.1527
$W3C_{HN(II)}$	O4–H1	0.0647	0.1566	0.0553	0.0716	−0.0162	0.7735
	H6–N3	0.0142	0.0522	0.0108	0.0085	0.0023	1.2637
$W3C_{HN(III)}$	O4–H1	0.0777	0.1560	0.0645	0.0901	−0.0256	0.7164
	H6–N3	0.0174	0.0645	0.0135	0.0110	0.0026	1.2339
$W3C_{HN(I)}$	O4–H1	0.0721	0.1614	0.0615	0.0826	−0.0211	0.7442
	H6–N3	0.0273	0.0941	0.0223	0.0211	0.0012	1.0570
$W4C_{HNO(I)}$	O4–H1	0.0779	0.1614	0.0658	0.0913	−0.0255	0.7209
	H5–O2	0.0189	0.0767	0.0168	0.0144	0.0024	1.1661
	H6–N3	0.0188	0.0710	0.0150	0.0123	0.0027	1.2217
$W4C_{HO(I)}$	O4–H1	0.0773	0.1636	0.0659	0.0908	−0.0250	0.7250
	H5–O2	0.0241	0.0971	0.0219	0.0196	0.0023	1.1178
$W4C_{HN(II)}$	O4–H1	0.0534	0.1475	0.0463	0.0556	−0.0094	0.8314
	H6–N3	0.0122	0.0447	0.0093	0.0074	0.0019	1.2605
$W4C_{HNO(II)}$	O4–H1	0.0870	0.1509	0.0711	0.1044	−0.0333	0.6807
	H5–O2	0.0122	0.0431	0.0096	0.0084	0.0012	1.1445
	H6–N3	0.0221	0.0804	0.0178	0.0155	0.0023	1.1480
$W4C_{HN(I)}$	O4–H1	0.0741	0.1645	0.0636	0.0861	−0.0225	0.7387
	H6–N3	0.0299	0.1005	0.0247	0.0242	0.0005	1.0194
$W4C_{HO(II)}$	O4–H1	0.0751	0.1533	0.0599	0.0815	−0.0216	0.7352
	H5–O2	0.0179	0.0685	0.0147	0.0123	0.0024	1.1981

−13.74 and −17.78 kcal mol^{-1}) for the $W2C_{HN}$, $W3C_{HN(I)}$ and $W4C_{HN(I)}$ clusters. Also the homologue clusters $W3C_{HO}$ and $W4C_{HO(I)}$, with 1.993 and 1.917 Å distances for the H···OC bond and CE values of −8.96 and −13.49, represent an increase of stability with cluster size.

As Table 3 shows, elongation of the H–O bond in HOCN with cluster formation was predicted. For instance, the H–O bond length increases from 0.966 Å in free HOCN to 0.987, 1.009, 1.023 and 1.025 Å in $W1C_H$, $W2C_{HN}$, $W3C_{HN(I)}$ and $W4C_{HN(I)}$ respectively. Also the greatest elongation (1.046 Å) was found for $W4C_{HNO(II)}$. Elongation of the H–O bond results from the contribution of its hydrogen as a HBD in hydrogen bond formation. A higher degree of HB interaction causes more lengthening of this bond.

Elongation of the H–X bonds (Δr_{H-X} X = OCN, ONC, NCO, CNO) in similar clusters shows that Δr_{H-X} in HOCN is greater than in HONC, and in turn both these values are greater than in HNCO and HCNO. In contrast, the $H_2O\cdots HX$ distances for X = OCN is slightly shorter than for X = ONC, and both are shorter than X = NCO or CNO, Tables S2–S4 [18–20]. Greater elongations of the H–X bond along with shorter $H_2O\cdots HX$ distances for HOCN clusters results from the stronger contribution as a HBD toward water molecules.

Similar conclusions could be deduced from the red shift of the H–X stretching frequencies, $\Delta\nu_{H-X}$, for clusters with similar structures, Tables S4 and S5. The larger $\Delta\nu_{H-X}$ value of the H–X stretching mode in HOCN clusters is the result of more SE and stronger $H_2O\cdots HX$ bonds. Also the variation of the H–X bond works against the $H_2O\cdots HX$ interaction, so that stronger $H_2O\cdots HOCN$ bonds have weaker H–OCN bonds with bigger values for Δr_{H-X} and $\Delta\nu_{H-X}$. Thus, it might be concluded that greater values of Δr_{H-X} and $\Delta\nu_{H-X}$ in the HOCN cluster indicate that, in comparison with HONC, HNCO and HCNO, the cluster has a better HBD ability to bond to water molecules.

As Table 3 shows, deviations of the HOC and OCN angles in clusters relative to the values predicted for the free HOCN molecule is evident.

From the results of Table 1, the influence of the cooperative effect (CE) on the stability of the studied complexes can be deduced. The cooperative effect is defined [29] as $\Delta E_{CE} = \Delta E_{cluster} - \sum\Delta E_{dimer}$ where the sum is over the 1:1 clusters that make up

Table 3
Bond lengths (Å) and bond angles (°) of hydrogen bonded clusters at the MP2/6-311++G(d,p) level

Cluster	$r_{O\cdots HOC}$	$r_{OH\cdots N}$	$r_{OH\cdots O}$	r_{NC}	r_{CO}	r_{H-O}	Δr_{H-O}	∠NCO	∠COH
HOCN				1.176	1.304	0.966	–	176.5	108.6
$W1C_H$	1.682			1.178	1.294	0.987	0.021	177.8	107.8
$W2C_{HN}$	1.584	2.107		1.180	1.284	1.009	0.043	179.3	105.4
$W3C_{HO}$	1.510		1.993	1.178	1.294	1.020	0.054	177.1	110.9
$W3C_{HN(I)}$	1.504	1.905		1.180	1.278	1.023	0.057	178.6	107.3
$W3C_{HN(II)}$	1.549	2.210		1.181	1.283	1.016	0.050	179.5	105.8
$W3C_{HN(III)}$	1.482	2.105		1.182	1.279	1.033	0.067	178.9	105.6
$W4C_{HN(I)}$	1.490	1.869		1.179	1.277	1.025	0.059	177.8	108.4
$W4C_{HN(II)}$	1.626	2.287		1.180	1.288	1.002	0.036	179.9	105.8
$W4C_{HO(I)}$	1.475		1.917	1.178	1.294	1.028	0.062	177.0	110.8
$W4C_{HNO(I)}$	1.474	2.069	2.027	1.177	1.288	1.030	0.064	177.0	111.1
$W4C_{HNO(II)}$	1.438	1.991	2.276	1.180	1.281	1.046	0.080	178.1	107.8

Table 4
Unscaled vibrational frequencies (cm^{-1}) with the corresponding intensities (values given in parenthesis, km mol^{-1}) of H-bond clusters calculated at the MP2/6-311++G(d, p) level

Cluster	$\nu_{O\cdots HOH}$	$\nu_{N\cdots H}$	$\nu_{H\cdots OH2}$	ν_{OC}	ν_{CN}	ν_{OH}	$\Delta\nu_{OH}$
HOCN				1079(64)	2254(91)	3844(174)	
W1CH			247(19)	1102(59)	2248(150)	3409(1378)	−435
W2CHN		158(10)	298(10)	1124(53)	2239(216)	3017(1607)	−827
$W3C_{HN(I)}$		187(2)	345(30)	1143(44)	2247(355)	2745(2230)	−1099
$W3C_{HO}$	153(3)		319(30)	1109(54)	2246(231)	2792(2522)	−1052
$W3C_{HN(II)}$		138(6)	320(12)	1125(51)	2233(236)	2887(1811)	−957
$W3C_{HN(III)}$		157(8)	366(34)	1135(54)	2220(464)	2599(2319)	−1245
$W4C_{HN(I)}$		170(1)	378(55)	1152(42)	2260(414)	2713(2511)	−1131
$W4C_{HO(I)}$	153(3)		375(68)	1109(58)	2242(291)	2655(2927)	−1189
$W4C_{HNO(I)}$	156(6)	156(6)	353(31)	1130(48)	2261(394)	2627(2864)	−1217
$W4C_{HNO(II)}$	98(4)	172(3)	300(50)	1134(44)	2210(1017)	2394(1863)	−1450
$W4C_{HN(II)}$		127(3)	262(18)	1114(43)	2239(157)	3034(1048)	−810

the cluster. Thus, for example, $W4C_{HN(I)}$ consists of one 1:1 cluster $W1C_N$, one 1:1 cluster $W1C_H$ and three water dimers with $\Delta E_{CE} = -17.78$ kcal mol^{-1}.

Table 4 gives selected vibrational stretching frequencies (cm^{-1}) with the corresponding intensities (km mol^{-1}) for clusters, along with the H–O frequency shifts in the HOCN subunit.

The greatest change occurs as a large red shift for the H–O stretching frequency (-1450 cm^{-1}) in $W4C_{HNO(II)}$. This red shift gives further evidence about the significant cooperative effect that comes from the greater red shift of H–O with a growing cluster size. For $W1C_H$, $W2C_{HN}$, $W3C_{HN(I)}$ and $W4C_{HN(I)}$, the $H_2O\cdots$HOCN frequencies are 251, 319, 367 and 388 cm^{-1}, and the HOH$\cdots$NCO frequencies are 154, 192 and 222 cm^{-1} for $W2C_{HN}$, $W3C_{HN(I)}$ and $W4C_{HN(I)}$, which confirms an increase in the intermolecular stretching frequencies with an increase in size and consequently stability of the complexes. Also HOH$\cdots$OCN frequencies of 151 and 153 cm^{-1} show a similar trend for the $W3C_{HO}$ and $W4C_{HO(I)}$ clusters.

In general, a comparison of the results in this study with our previous works [18–20] shows that the stability of the clusters is in the order HOCN > HONC > HNCO > HCNO. This arises from the effect of the arrangement of the C, N and O atoms on their group electronegativity towards the H atom. Evidently, a hydrogen attached to a more electronegative O atom has a greater local charge and is better exposed to hydrogen bonding than hydrogens attached to N and C atoms. Therefore, HOCN and HONC are stronger HBDs than HNCO and HCNO. For interpretation of the stronger HBD property of HOCN relative to HONC, it might be mentioned that in OCN the electronegative O and N atoms are on the two sides of the C atom. Thus, the electron releasing vector of the C atom is divided to two smaller vectors between them in opposite directions. Hence, the arrangement of atoms in OCN is such that the N atom cannot compensate for the electron withdrawing effects of the O atom. But in ONC, since the electronegative O and N atoms are on the same side, both the C and N atoms can simultaneously compensate for the electron withdrawing properties of the O atom. Therefore, in HOCN, the H atom has a greater local charge and is a stronger HBD than HONC. Similar discussions and such conclusions could be presented from the B3LYP results, Tables S6–S8.

4. Concluding remarks

The mixed clusters of H_2O and HOCN exhibit clear evidence of cooperative effects of hydrogen bonding in this system. This work discussed hydrogen bonding in terms of the molecular structure for $HX(H_2O)_n$ (X = OCN, ONC, NCO, CNO; n = 1–4) clusters. The results showed that the stability of the hydrogen bonds depends tightly on the arrangement of the C, N and O atoms in the X function. According to our findings for similar structures, the stability of the clusters varies in the order: HOCN > HONC > HNCO > HCNO. This could be interpreted in terms of group electronegativity for the X function in HX, which depends on the order of the C, N and O atoms.

Acknowledgments

We are very grateful to Dr. Mahmood Reza Moradian for reading and corrections of this article.

Appendix A. Supplementary data

Tables of stabilization energies, bond lengths, elongation of H–X, frequency shift of H–X in hydrogen bonded clusters at the MP2/6-311++G(d,p), level of the DFT/B3LYP/6-311++G(d,p) calculations and molecular graphs of the clusters are available. Supplementary data associated with this article can be found, in the online version, at doi:10.1016/j.poly.2008.05.038.

References

[1] G. Winnewisser, C. Kramer, Space Sci. Rev. 90 (1999) 181.
[2] M.S. Lowenthal, R.K. Khanna, M.H. Moore, Spectrochim. Acta Part A 58 (2002) 73.
[3] M.T. Nguyen, D. Sengupta, L. Vereecken, J. Peeters, L.G. Vanquickenborne, J. Phys. Chem. 100 (1996) 1615.
[4] G. Fischer, J. Geith , T.M. Klapotke, B. Krumm, Z. Naturforsch., 57b (2002) 19.
[5] M. Zyrianov, T. Droz-Georget, A. Sanov, H. Reisler, J. Chem. Phys. 105 (1996) 8111.
[6] A. Zabardasti, Chem. Heterocycl. Compd. 43 (2007) 1344.
[7] Z. Qui, Z. Fang, M. Cheng, D. Zhao, J. Shiyou Huagong Xueyuan Xuebao 11 (1999) 56.
[8] D. Conroy, V. Aristov, L. Feng, A. Sanov, H. Reisler, Acc. Chem. Res. 34 (2001) 625.
[9] R.A. Brownsword, M. Hillenkamp, T. Laurent, R.K. Vatsa, H.R. Volppb, J. Chem. Phys. 106 (1997) 4436.
[10] K. Muller-Dethlefs, P. Hobza, Chem. Rev. 100 (2000) 143.
[11] S. Scheiner, Hydrogen Bonding–A Theoretical Perspective, Oxford University Press, Oxford, 1997. and references therein.
[12] P. Hobza, Z. Havlas, Chem. Rev. 100 (2000) 4253.
[13] M. Solimannejad, S. Scheiner, J. Phys. Chem. A 111 (2007) 4431.
[14] P.R. Bangal, J. Phys. Chem. A 111 (2007) 5536.
[15] M. Solimannejad, S. Scheiner, Chem. Phys. Lett. 429 (2006) 38.
[16] M. Solimannejad, S. Scheiner, J. Phys. Chem. A 110 (2006) 5948.
[17] Q. Li, X. An, B. Gong, J. Cheng, J. Phys. Chem. A 111 (2007) 10166.
[18] A. Zabardasti, M. Solimannejad, J. Mol. Struct. (THEOCHEM) 810 (2007) 73.
[19] A. Zabardasti, M. Solimannejad, J. Mol. Struct. (THEOCHEM) 819 (2007) 52.
[20] A. Zabardasti, M. Salehnassaj, A. Kakanejadifard, J. Theor. Comput. Chem., in press.
[21] M.J. Frisch, et al. GAUSSIAN 98, revision A.6, Gaussian, Inc., Pittsburgh, PA, 1998.
[22] R. Barrios, P. Skurski, J. Simon, J. Phys. Chem. A 104 (2000) 10855.
[23] J. Stalrug, M. Schutz, R. Lindh, G. Karlstrom, P.O. Widmark, Mol. Phys. 100 (2002) 3389.
[24] R. Rivelino, P. Chaudhuri, S.J. Canuto, Chem. Phys. 118 (2003) 10593.
[25] S.F. Boys, F. Bernardi, Mol. Phys. 19 (1970) 553.
[26] R.F.W. Bader, Atoms in Molecules: A Quantum Theory, Oxford University Press, Oxford, U.K, 1990.
[27] P.L.A. Popelier, Atoms in Molecules, an Introduction, Prentice Hall, Pearso Education Limited, 2000.
[28] M. Ziółkowski, S.J. Grabowski, J. Leszczynski, J. Phys. Chem. A 110 (2006) 6514.
[29] S.S. Xantheas, C.J. Burnham, R.J. Harrison, J. Chem. Phys. 116 (2002) 1493.

2. Experimental

2.1. Synthesis of **HL**

A solution of diethyl 4-aminobenzylphosphonate (0.243 g, 1 mmol) in CH_2Cl_2 (15 mL) was added dropwise to a solution of $SCNP(S)(OiPr)_2$ (0.263 g, 1.1 mmol) in the same solvent (15 mL). The mixture was stirred at room temperature for 3 h. The solvent was then removed in vacuum. The residue was recrystallized from a dichloromethane–*n*-hexane mixture 1:5 (v/v). The product was obtained as colorless crystals. Yield: 0.429 g (89%). M.p. 73 °C. ^{1}H NMR ($CDCl_3$): δ = 1.26 (t, $^3J_{H,H}$ = 7.1 Hz, 6H, CH_3, EtO), 1.38 (d, $^3J_{H,H}$ = 6.2 Hz, 12H, CH_3, *i*PrO), 3.14 (d, $^2J_{P,H}$ = 21.5 Hz, 2H, CH_2, $P(O)CH_2$), 4.04 (d. quart, $^3J_{H,H}$ = 7.1 Hz, $^3J_{POCH}$ = 8.8 Hz, 4H, OCH_2, EtO), 4.86 (d. sept, $^3J_{H,H}$ = 6.2 Hz, $^3J_{POCH}$ = 10.5 Hz, 2H, OCH, *i*PrO), 7.19 (d, $^2J_{PNH}$ = 10.4 Hz, 1H, NH, P(S)NH), 7.27–7.53 (m, 4H, C_6H_4), 9.66 (s, 1H, NH). $^{31}P\{^1H\}$ NMR ($CDCl_3$): δ = 26.7 (1P, P=O), 53.4 (1P, P=S). IR: ν = 622 (P=S), 968, 992, 1026 (POC), 1207 (P=O), 1559 (S=C–N), 3126, 3272 (NH) cm^{-1}. *Anal.* Calc. for $C_{18}H_{32}N_2O_5P_2S_2$ (482.53): C, 44.80; H, 6.68; N, 5.81. Found: C, 44.68; H, 6.79; N, 5.74.

2.2. Synthesis of **ML_2**

A suspension of **HL** (0.241 g, 0.5 mmol) in aqueous ethanol (20 mL) was mixed with an ethanol solution of potassium hydroxide (0.031 g 0.55 mmol). An aqueous (20 mL) solution of $ZnCl_2$, $Cd(CH_3COO)_2{\cdot}2H_2O$, $Co(NO_3)_2 \cdot 6H_2O$ (0.041, 0.080 or 0.087 g, respectively; 0.3 mmol) was added dropwise under vigorous stirring to the resulting potassium salt. The mixture was stirred at room temperature for a further 3 h and left overnight. The resulting complex was extracted with dichloromethane, washed with water and dried with anhydrous $MgSO_4$. The solvent was then removed in vacuo. The residue was recrystallized from a dichloromethane/*n*-hexane mixture.

ZnL_2. Complex was obtained as colorless crystals. Yield: 0.157 g (61%). M.p. 163 °C. ^{1}H NMR ($CDCl_3$): δ = 1.08–1.47 (m, 36H, CH_3, EtO + *i*PrO), 3.13 (d, $^2J_{P,H}$ = 21.1 Hz, 4H, CH_2, $P(O)CH_2$), 3.93–4.10 (m, 8H, OCH_2, EtO), 4.79 (d. sept, $^3J_{H,H}$ = 6.2 Hz, $^3J_{POCH}$ = 10.1 Hz, 4H, OCH, *i*PrO), 7.25–7.79 (m, 8H, C_6H_4), 6.53 (s, 2H, NH). $^{31}P\{^1H\}$ NMR ($CDCl_3$): δ = 24.9 (2P, P=O), 56.0 (2P, P=S). IR: ν = 603 (P=S), 1008, 1012 (POC), 1263 (P=O), 1547 (S=C–N), 3305 (NH) cm^{-1}. *Anal.* Calc. for $C_{36}H_{62}N_4O_{10}P_4S_4Zn$ (1028.44): C, 42.04; H, 6.08; N, 5.45. Found: C, 42.13; H, 5.91; N, 5.52.

CdL_2. Complex was obtained as colorless crystals. Yield: 0.231 g (86%). M.p. 109 °C. ^{1}H NMR ($CDCl_3$): δ = 1.17–1.51 (m, 36H, CH_3, EtO + *i*PrO), 3.03 (d, $^2J_{P,H}$ = 21.8 Hz, 4H, CH_2, $P(O)CH_2$), 3.85–4.02 (m, 8H, OCH_2, EtO), 4.82 (d. sept, $^3J_{H,H}$ = 6.2 Hz, $^3J_{POCH}$ = 10.3 Hz, 4H, OCH, *i*PrO), 7.27–7.72 (m, 8H, C_6H_4), 6.71 (s, 2H, NH). $^{31}P\{^1H\}$ NMR ($CDCl_3$): δ = 25.2 (2P, P=O), 56.2 (2P, P=S). IR: ν = 607 (P=S), 1007 (POC), 1259 (P=O), 1539 (S=C–N), 3296 (NH) cm^{-1}. *Anal.* Calc. for $C_{36}H_{62}CdN_4O_{10}P_4S_4$ (1075.46): C, 40.20; H, 5.81; N, 5.21. Found: C, 40.39; H, 5.73; N, 5.30.

CoL_2. Complex was obtained as green crystals. Yield: 0.233 g (91%). M.p. 94 °C. IR: ν = 600 (P=S), 1012 (POC), 1260 (P=O), 1551 (S=C–N), 3311 (NH) cm^{-1}. UV–Vis spectra, [λ_{max}, nm (ε, 1 mol^{-1} dm^3cm^{-1})]: 558 (263), 607 (286), 668 (157). *Anal.* Calc. for $C_{36}H_{62}CoN_4O_{10}P_4S_4$ (1021.99): C, 42.31; H, 6.11; N, 5.48. Found: C, 42.47; H, 6.25; N, 5.41.

2.3. Synthesis of **$Cu(PPh_3)L$**

A suspension of **HL** (0.241 g, 0.5 mmol) in aqueous ethanol (15 mL) was mixed with an ethanol solution of KOH (0.031 g 0.55 mmol). A dichloromethane (15 mL) solution of $Cu(PPh_3)_3I$ (0.489 g, 0.5 mmol) was added dropwise under vigorous stirring to the resulting potassium salt. The mixture was stirred at room temperature for a further hour and a precipitate was filtered off. The filtrate was concentrated until the crystallization began. The residue was recrystallized from a dichloromethane–*n*-hexane mixture 1:5 (v/v). Complex was obtained as colorless crystals. Yield: 0.295 g (73%). M.p. 127 °C. ^{1}H NMR ($CDCl_3$): δ = 1.12–1.44 (m, 18H, CH_3, EtO + *i*PrO), 3.10 (d, $^2J_{P,H}$ = 21.3 Hz, 2H, CH_2, $P(O)CH_2$), 3.89–4.08 (m, 4H, OCH, EtO), 4.73 (d. sept, $^3J_{H,H}$ = 6.1 Hz, $^3J_{POCH}$ = 10.4 Hz, 2H, OCH, *i*PrO), 7.13–7.23, 7.28–7.77 (m, 19H, $C_6H_4 + C_6H_5$), 8.47 (s, 1H, NH). $^{31}P\{^1H\}$ NMR ($CDCl_3$): δ = –0.9 (1P, PPh_3), 27.1 (1P, P=O), 55.3 (1P, P=S). IR: ν = 606 (P=S), 962, 974, 998, 1017 (POC), 1252 (P=O), 1530 (S=C–N), 3263 (NH) cm^{-1}. *Anal.* Calc. for $C_{36}H_{46}CuN_2O_5P_3S_2$ (807.36): C, 53.56; H, 5.74; N, 3.47. Found: C, 53.43; H, 5.85; N, 3.34.

2.4. Physical measurements

Infrared spectra (Nujol) were recorded with a Specord M-80 spectrometer in the range 400–3600 cm^{-1}. NMR spectra were obtained on a Varian Unity-300 NMR spectrometer at 25 °C. ^{1}H and $^{31}P\{^1H\}$ spectra were recorded at 299.948 and 75.429 MHz, respectively. Chemical shifts are reported with reference to $SiMe_4$ (^{1}H) and H_3PO_4 ($^{31}P\{^1H\}$). Electronic spectra of absorption in 0.001 M solution of CH_2Cl_2 were measured on a Perkin–Elmer Lambda-35 spectrometer in the range 200–1000 nm. Elemental analyses were performed on a Perkin–Elmer 2400 CHN microanalyser.

2.5. Crystal structure determination and refinement

Crystals of **HL** were obtained by slow evaporation of the solvent from dichloromethane/*n*-hexane solution. $C_{18}H_{32}N_2O_5P_2S_2$, M_r = 482.54 g mol^{-1}, crystal system: monoclinic, space group: $P2_1/c$, a = 7.6294(1), b = 9.3135(2), c = 35.2519(6) Å, β = 94.964 (1)°, V = 2495.48(8) $Å^3$, ρ = 1.284 g cm^{-3}. Cell parameters and intensities of 5931 independent reflections, from which 3689 with $I \geqslant 2\sigma$, were measured (ω-scan, $\theta \leqslant 27.00°$) at 296 K on a Bruker Smart Apex II diffractometer and graphite-monochromatied Mo Kα radiation generated by fine-focus X-ray tube operated at 50 kV and 30 mA. The images were indexed, integrated and scaled using the Apex2 data reduction package [22]. Data were corrected for absorption using SADABS [23] program (μMo 3.71 cm^{-1}). The structure was solved by direct method using SIR-97 [24] program and refined first isotropically and then anisotropically using SHELXL97 [25] and WINGX programs [26]. Hydrogen atoms were revealed from $\Delta\rho$ maps and refined isotropically. The final residuals were R_{ob} = 0.0492, R_{wob} = 0.0903 based on 3689 independent reflections with $F^2 \geqslant 2\sigma$. All figures were made using the program PLATON [27].

Crystals of **$Cu(PPh_3)L$** were obtained by slow evaporation of the solvent from dichloromethane/*n*-hexane solution. $C_{36}H_{46}CuN_2O_5P_3S_2$, M_r = 807.32 g mol^{-1}, crystal system: triclinic, space group: $P\bar{1}$, a = 8.9510(8), b = 11.5966(9), c = 20.0844(16) Å, α = 77.572(6)°, β = 77.538(6)°, γ = 79.331(7)°, V = 1966.8(3) $Å^3$, ρ = 1.363 g cm^{-3}. Cell parameters and intensities of 18274 reflections (7710 unique, R_{int} = 0.0822), from which 4594 had $I \geqslant 2\sigma$, were measured (ω-scan, $\theta \leqslant 25.12°$) at 173 K on a STOE IPDS-II diffractometer and graphite-monochromatied Mo Kα radiation generated by fine-focus X-ray tube operated at 50 kV and 40 mA. The images were indexed, integrated and scaled using the X-Area package [28]. Data were corrected for absorption using PLATON [27] program (μMo 0.826 mm^{-1}). The structure was solved by direct method using SHELXS [29] program and refined first isotropically and then anisotropically using SHELXL97 [25]. Hydrogen atoms were revealed from $\Delta\rho$ maps and refined using a riding model. The final residuals were R_{ob} = 0.0466, R_{wob} = 0.0801 based on

4594 independent reflections with $F^2 \geqslant 2\sigma$. All figures were made using the program PLATON [27].

3. Results and discussion

3.1. Synthesis

N-Thiophosphorylated thiourea **HL** was prepared by the addition of diethyl 4-aminobenzylphosphonate $(EtO)_2P(O)CH_2C_6H_4$-4-NH_2 to *O,O'*-diisopropylthiophosphoric acid isothiocyanate $(i\text{PrO})_2P(S)NCS$ (Scheme 1).

Complexes of **HL** with the Zn(II) (**ZnL_2**), Cd(II) (**CdL_2**) and Co(II) (**CoL_2**) cations were prepared by the following procedure: ligand was converted into potassium salt **KL** and followed by reaction with $ZnCl_2$, $Cd(CH_3COO)_2 \cdot 2H_2O$ or $Co(NO_3)_2 \cdot 6H_2O$ in aqueous EtOH (Scheme 2).

Reaction of the potassium salt of **HL** with $Cu(PPh_3)_3I$ in aqueous $EtOH/CH_2Cl_2$ leads to mononuclear **Cu(PPh$_3$)L** complex (Scheme 2).

The compounds obtained are colorless (**HL**, **ZnL_2** and **CdL_2**) or green (**CoL_2**) crystalline powders, soluble in acetone, benzene, dichloromethane and insoluble in water and *n*-hexane. UV–Vis, ^1H, $^{31}P\{^1H\}$ NMR in solution and IR data indicated that the thiourea **HL** is a 1,5-*S,S'*-ligand.

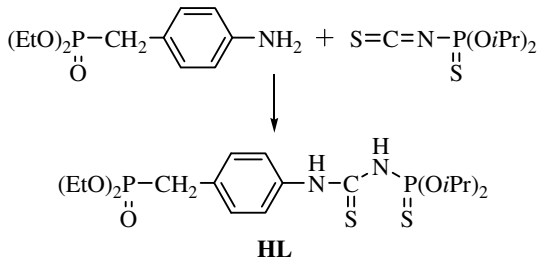

Scheme 1. Preparation of **HL**.

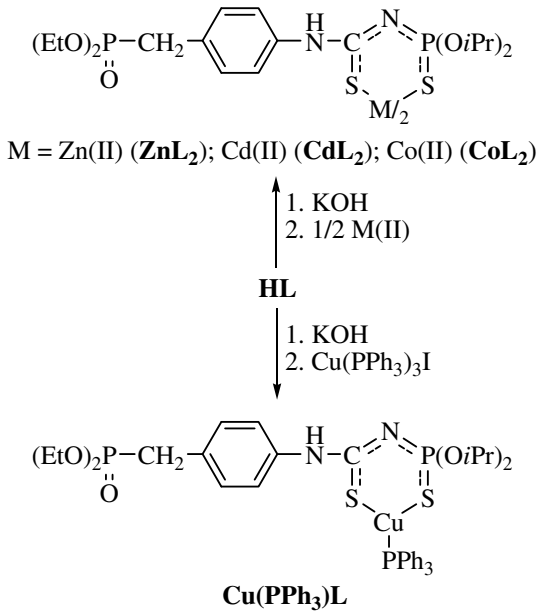

Scheme 2. Preparation of **ZnL_2**, **CdL_2**, **CoL_2** and **Cu(PPh$_3$)L**.

3.2. IR, UV–Vis and NMR spectroscopic data

The IR spectrum of **HL** contains a weak band at 622 cm^{-1} assigned to the P=S group. It is shifted to low frequencies (600–607 cm^{-1}) in the spectra of complexes **ML_2** and **Cu(PPh$_3$)L** due to the coordination with the cation. Occurrence of the new broad and strong absorption peak at 1530–1551 cm^{-1}, related to the conjugated SCN group [30], also proves the formation of 1,5-*S,S'*-chelate. Presence of the substituted POC groups in **HL** and its complexes are seen in the IR spectra by their absorption bands at 962–1026 cm^{-1}.

There are two bands for the ArNH and P(S)NH groups at 3126 and 3272 cm^{-1} in the IR spectrum of **HL**, whereas a unique band at 3296–3311 and 3263 cm^{-1} related to the ArNH group was observed in the spectra of complexes **ML_2** and **Cu(PPh$_3$)L**, respectively. It should be noted that the band for the ArNH group in the IR spectra of **ML_2** is shifted to high frequencies whereas in **Cu(PPh$_3$)L** this band is practically at the same frequencies relative to the band of the parent ligand **HL**. The similar is observed for the P=O absorption band in the IR spectra. The band at 1259–1263 cm^{-1} in the spectra of **ML_2** corresponds to the P=O group and shifted to high frequencies relative to that in **HL**. The P=O band at 1257 cm^{-1} in the IR spectrum of complex **Cu(PPh$_3$)L** is practically at the same area as it was observed in the parent thiourea (1252 cm^{-1}) due to the intermolecular N–H···O=P hydrogen bonds in a crystal (Figs. 1 and 2). This confirms the preservation of the hydrogen bonding in the structure of **Cu(PPh$_3$)L** and absence of it in complexes **ML_2**.

The $^{31}P\{^1H\}$ NMR spectrum of **HL** in a $CDCl_3$ solution shows two single resonances at 26.7 and 53.4 ppm, corresponding to the phosphorus atoms of the P=O and P=S groups, respectively. In the $^{31}P\{^1H\}$ NMR spectra of complexes **ZnL_2**, **CdL_2** and **Cu(PPh$_3$)L**, the resonance for the phosphoryl and thiophosphoryl groups are shown at 24.9–27.1 and 55.3–56.2 ppm, respectively. The signal corresponding to the P=S group is low-field shifted, whereas the singlet for the P=O group is practically at the same region relative to those in the parent ligand for **Cu(PPh$_3$)L** and low-field shifted in the $^{31}P\{^1H\}$ NMR spectra of complexes **ZnL_2** and **CdL_2**. The signal of the triphenylphosphine group in copper(I) complex is shifted downfield relative to the free PPh_3 and exhibit $^{31}P\{^1H\}$ NMR

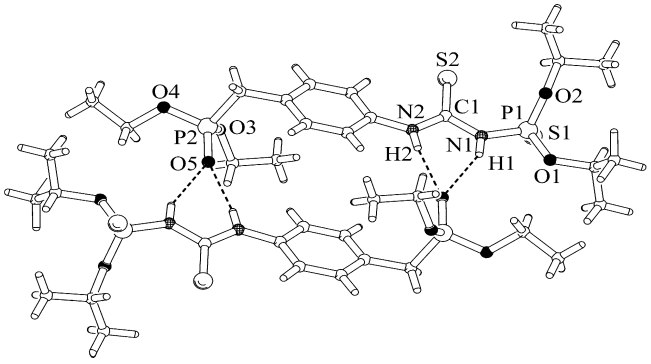

Fig. 1. Molecular structure and hydrogen bonding dimer in crystal of **HL**. Selected bond distances (Å) and angles (°): S(1)–P(1) 1.9166(11), S(2)–C(1) 1.657(3), P(1)–O(1) 1.583(2), P(1)–O(2) 1.561(2), P(1)–N(1) 1.666(2), P(2)–O(3) 1.556(2), P(2)–O(4) 1.570(2), P(2)–O(5) 1.469(2), N(1)–C(1) 1.376(3), N(2)–C(1) 1.346(3); S(1)–P(1)–O(1) 115.73(8), S(1)–P(1)–O(2) 115.57(8), S(1)–P(1)–N(1) 118.90(8), O(1)–P(1)–O(2) 102.92(9), O(1)–P(1)–N(1) 94.11(10), O(2)–P(1)–N(1) 106.58(11), O(3)–P(2)–O(4) 105.24(10), O(3)–P(2)–O(5) 113.44(10), O(4)–P(2)–O(5) 113.67(11), P(1)–N(1)–C(1) 126.8(2), S(2)–C(1)–N(1) 120.3(2), S(2)–C(1)–N(2) 127.1(2), N(1)–C(1)–N(2) 112.6(2). The intermolecular hydrogen bond parameters in the molecule are as follows: N(1)–H(1)···O(5)′(1–x, 1–y, –z): *d*(N–H) 0.81(3), *d*(H···O′) 2.26(3), *d*(N···O′) 2.997(3), ∠(NHO′) 153(3); N(2)–H(2)···O(5)′ (1–x, 1–y, –z): *d*(N–H) 0.79(3), *d*(H···O′) 2.11(3), *d*(N···O′) 2881(3), ∠(NHO′) 167(3).

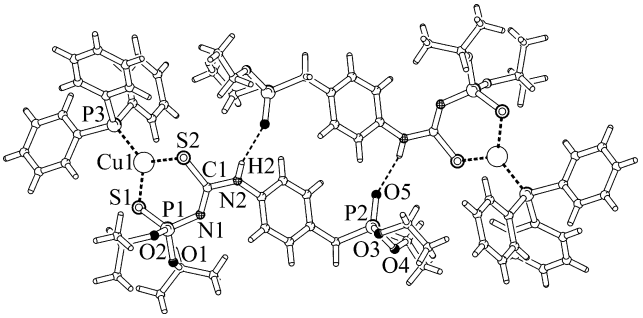

Fig. 2. Molecular structure and hydrogen bonding dimer in crystal of **Cu(PPh$_3$)L**. Selected bond distances (Å) and angles (°): Cu(1)–S(1) 2.2485(11), Cu(1)–S(2) 2.2163(11), Cu(1)–P(3) 2.2142(11), S(1)–P(1) 1.9950(13), S(2)–C(1) 1.754(4), P(1)–O(1) 1.583(3), P(1)–O(2) 1.588(3), P(1)–N(1) 1.600(3), P(2)–O(3) 1.579(4), P(2)–O(4) 1.579(3), P(2)–O(5) 1.474(3), N(1)–C(1) 1.326(5), N(2)–C(1) 1.353(5); S(1)–Cu(1)–S(2) 115.77(4), S(1)–Cu(1)–P(3) 118.63(4), S(2)–Cu(1)–P(3) 124.78(4), Cu(1)–S(1)–P(1) 94.83(5), Cu(1)–S(2)–C(1) 104.63(13), S(1)–P(1)–O(1) 113.38(10), S(1)–P(1)–O(2) 109.24(11), S(1)–P(1)–N(1) 118.28(13), O(1)–P(1)–O(2) 102.08(14), O(1)–P(1)–N(1) 106.69(15), O(2)–P(1)–N(1) 105.71(15), O(3)–P(2)–O(4) 104.27(18), O(3)–P(2)–O(5) 115.38(19), O(4)–P(2)–O(5) 113.47(17), P(1)–N(1)–C(1) 129.1(3), S(2)–C(1)–N(1) 128.4(3), S(2)–C(1)–N(2) 113.9(3), N(1)–C(1)–N(2) 117.6(3). The intermolecular hydrogen bond parameters in the molecule are as follows: N(2)–H(2)···O(5)′ (1–x, 2–y, 1–z): *d*(N–H) 0.84(4), *d*(H···O′) 2.10(4), *d*(N···O′) 2.922(4), ∠(NHO′) 164(4).

chemical shift at −0.9 ppm. In solution, the exchange between free and bound triphenylphosphine group of complex **Cu(PPh$_3$)L** results in a signal broadening of the $^{31}P\{^1H\}$ NMR spectrum, as it was previously observed for the Cu(I) complexes with *N*-thiophosphorylated thioureas and thioamides [31,32].

The ^{1}H NMR spectra of **HL**, **ZnL$_2$**, **CdL$_2$** and **Cu(PPh$_3$)L** contain a set of signals, corresponding to the resulting products. The signals for the CH_3 protons of the $(i\text{PrO})_2\text{P(S)}$ and $(\text{EtO})_2\text{P(O)}$ groups are observed as a doublet, triplet or multiplet at 1.08–1.51 ppm and a doublet of septets, doublet of quartets or multiplet at 3.85–4.86 ppm, corresponding to the OCH and OCH_2 protons. The signals for the C_6H_4 protons in the spectra of **HL**, **ZnL$_2$**, **CdL$_2$** and **Cu(PPh$_3$)L** are shown as a multiplet at 7.25–7.79 ppm. The signals for the C_6H_5 protons in the ^{1}H NMR spectrum of **Cu(PPh$_3$)L** are observed as a multiplet at 7.13–7.23 ppm. The CH_2 protons doublet signals are at 3.03–3.14 ppm. There is a doublet and singlet for the P(S)NH and ArNH protons at 7.19 and 9.66 ppm, respectively, in the spectrum of **HL**, whereas only one singlet signal for the ArNH proton at 6.53–6.71 (**ZnL$_2$** and **CdL$_2$**) and 8.47 [**Cu(PPh$_3$)L**] ppm is observed in the ^{1}H NMR spectra of complexes. This confirms the anionic forms **L** in the structure of complex.

Investigation of complex **CoL$_2$** by NMR spectroscopy was not successful, because of the paramagnetic Co(II) cation presence.

In the UV-spectrum of complex **CoL$_2$** there is an absorption band with peaks at 558 (ε_{max}, 263 mol^{-1} dm^3 cm^{-1}), 607 (ε_{max}, 286 mol^{-1} dm^3 cm^{-1}) and 668 (ε_{max}, 157 mol^{-1} dm^3 cm^{-1}) nm. The specified absorption band corresponds to a transition from the basic state $^4A_2$ to a $^4T_1$(P) state. The thin structure is caused by spin–orbital interaction as a result of which, first, there is a splitting of the state $^4T_1$(P) and, secondly, there are resolved transitions in the next doublet states with the same intensity. Other possible transitions: $^4A_2 \rightarrow {}^4T_2$ and $^4A_2 \rightarrow {}^4T_1$(F) are outside of the visible area. Data of UV-spectroscopy unequivocally confirm the tetrahedral environment of the Co(II) cation in complex **CoL$_2$**.

3.3. Crystal structures

According to the X-ray data, the molecule of **HL** in a crystal is located in a special position at the symmetry centre (Fig. 1).

X-ray analysis of the product **HL** showed that the NC(S)N fragmnet is almost planar, which is evidence of the resonance between the nitrogen lone pair and the double C=S bond. The phosphorus atoms have a distorted tetrahedral configuration typical of phosphates. The conformation of the N–C–N–P fragmnet is almost shielded, torsion angle N(2)–C(1)–N(1)–P(1) is −173.8(2)°. The bonds C(1)–S(2) and P(1)–S(1) are in *anti*-orientation. The molecule of **HL** in the crystal has a *syn*-orientation of the bonds N(1)–H(1) and N(2)–H(2) and an *anti*-orientation of the P(1)–N(1) and N(2)–C(1) bonds. Such arrangement, apparently, is caused by the formation of the intermolecular hydrogen bonds N(1)–H(1)···O(5)′ (1 − *x*, 1 − *y*, −*z*), N(2)–H(2)···O(5)′ (1 − *x*, 1 − *y*, −*z*) and N(1)′–H(1)′···O(5), N(2)′–H′···O(5) (Fig. 1). As a result of the intermolecular interactions, a centosymmetric dimer is formed.

The molecular structure of complex **Cu(PPh$_3$)L** is shown in Fig. 2. The geometry around the Cu atom is trigonal formed by two sulfurs and one PPh_3. S–P and S–C bonds are longer while P–N and N–C are shorter in comparison to those for the free ligand **HL** and have intermediate bond order values between the double and single. The six-membered CuSPNCS metallocyle has the conformation of a distorted boat with the P(1) an S(1) atoms showing the greatest deviation from the least square plane of the CuSPNCS cycle, 0.4260(13) and −0.3256(13) Å, respectively. The fragment NC(S)NP is almost planar, the sulfur of the thiophosphoryl group is significantly deviated from the average plane of this fragment, torsion angle S(1)–P(1)–N(1)–(1) is −57.5(4)°. The phosphorus atoms have a distorted tetrahedral configuration.

In a crystal two molecules of complex **Cu(PPh$_3$)L** also form a centrosymmetric dimer, which is caused by the formation of the intermolecular hydrogen bonds N(2)–H(2)···O(5)′ (1 − *x*, 2 − *y*, 1 − *z*) (Fig. 2). As a result of the intermolecular interactions and steric demanding, only one molecule of PPh_3 is coordinated with the Cu atom. Complex **Cu(PPh$_3$)L** is the first example of copper(I) complexes of *N*-thiophosphorylated thioureas and thioamides of common formula $RC(S)NHP(S)R'_2$ and one molecule of PPh_3.

4. Conclusions

In summary, novel Zn(II), Cd(II), Co(II) and Cu(PPh_3)(I) complexes with *N*-thiophosphorylated thiourea **HL** have been successfully synthesized. Copper(I) complex dissociates in a solution of $CDCl_3$, splitting off a molecule of triphenylphosphine. This process has reversible character.

NMR and UV–Vis experiments in solution and IR have shown that **HL** is a 1,5-*S*,*S*′-ligand in all complexes obtained.

Crystal structures of **HL** and **Cu(PPh$_3$)L** were determined by single crystal X-ray diffraction. According to the X-ray data, both ligand and complex in a crystal form dimer structures by intermolecular hydrogen bonds.

5. Appendix A. Supplementary data

CCDC 680113 and 682359 contain the supplementary crystallographic data for (**HL**) and [**Cu(PPh$_3$)L**]. These data can be obtained free of charge via http://www.ccdc.cam.ac.uk/conts/retrieving.html, or from the Cambridge Crystallographic Data Centre, 12 Union Road, Cambridge CB2 1EZ, UK; fax: (+44) 1223-336-033; or e-mail: deposit@ccdc.cam.ac.uk.

Acknowledgment

This work was supported by the joint program of CRDF and the Russian Ministry of Education and Science (BRHE 2008 Y5-C-07-09); Russian Science Support Foundation.

References

[1] I. Haiduc, Dichalcogenoimidodiphosph(in)ate ligands comprehensive coordination chemistry II. From biology to nanotechnology, in: A.B.P. Lever (Ed.), Fundamentals, Elsevier, 2003, pp. 323–347. (Chapter 1.14).
[2] C. Silvestru, R. RoË sler, I. Haiduc, R. Cea-Olivares, G. Espinosa-Perez, Inorg. Chem. 34 (1995) 3352.
[3] L.M. Gilby, B. Piggott, Polyhedron 18 (1999) 1077.
[4] J. Ellermann, J. Sutter, F.A. Knoch, M. Moll, Chem. Ber. 127 (1994) 1015.
[5] M.C. Aragoni, M. Arca, A. Garau, F. Isaia, V. Lippolis, G.L. Abbati, A.C. Fabretti, Z. Anorg. Allg. Chem. 626 (2000) 1454.
[6] E.A. Bundya, V.M. Amirkhanov, V.A. Ovchynnikov, V.A. Trush, K.V. Domasevitch, J. Sieler, V.V. Skopenko, Z. Naturforsch. B 54 (1999) 1033.
[7] E.A. Trush, V.M. Amirkhanov, V.A. Ovchynnikov, J. Swiatek-Kozlowska, K.A. Lanikina, K.V. Domasevitch, Polyhedron 22 (2003) 1221.
[8] J. Novosad, M. Necas, J. Marek, P. Veltsistas, C. Papadimitriou, I. Haiduc, M. Watanabe, J.D. Woollins, Inorg. Chim. Acta 290 (1999) 256.
[9] D.J. Birdsal, J. Green, T.Q. Ly, J. Novosad, M. Necas, A.M.Z. Slawin, J.D. Woollins, Z. Zak, Eur. J. Inorg. Chem. (1999) 1445.
[10] I. Haiduc, R. Cea-Olivares, R.A. Toscano, C. Silvestru, Polyhedron 14 (1995) 1067.
[11] A. Silvestru, A. Rotar, J.E. Drake, M.B. Hursthouse, M.E. Light, S.I. Farcas, R. Roesler, C. Silvestru, Can. J. Chem. 79 (2001) 983.
[12] N.G. Zabirov, O.K. Pozdeev, F.M. Shamsevaleev, R.A. Cherkasov, G. Kh. Gilmanova, Khim. Farm. Zh. (USSR) 23 (1989) 600.
[13] Z.P. Vetrova, N.G. Zabirov, T.N. Shuvalova, L.S. Smerkovich, L.A. Ivanova, A.K. Golberg, N.T. Karabanov, Zh. Obshch. Khim. (USSR) 62 (1992) 1079.
[14] L.G. Shaidarova, A.V. Gedmina, V.V. Brusko, N.G. Zabirov, N.A. Ulakhovich, G.K. Budnikov, Anal. Sci. 17 (2001) i957.
[15] M.P. Kutyreva, N.G. Zabirov, V.V. Brusko, N.A. Ulakhovich, Anal. Sci. 17 (2001) i1049.
[16] L.G. Shaidarova, A.V. Gedmina, V.V. Brusko, N.G. Zabirov, N.A. Ulakhovich, G.K. Budnikov, Russ. J. Appl. Chem. 75 (2002) 919.
[17] L.G. Shaidarova, A.V. Gedmina, N.A. Ulakhovich, G.K. Budnikov, N.G. Zabirov, Russ. J. Gen. Chem. 72 (2002) 1565.
[18] O. Navratil, E. Herrmann, N.T.T. Chau, Ch. Tea, J. Smola, Collect. Czech. Chem. Commun. 58 (1993) 798.
[19] M.G. Zimin, G.A. Lazareva, N.I. Saveleva, R.G. Islamov, N.G. Zabirov, V.F. Toropova, A.N. Pudovik, Zh. Obshch. Khim. (USSR) 52 (1982) 1776.
[20] M. Bochmann, Chem. Vap. Deposition 2 (1996) 423.
[21] D. Fan, M. Afzaal, M.A. Mallik, C.Q. Nguyen, P.J. Thomas, P. O'Brien, Coord. Chem. Rev. 251 (2007) 1878.
[22] APEX2 (Version 2.1), SAINTPLUS, Data Reduction and Correction Program (Version 7.31A, Bruker Advansed X-ray Solutions, BrukerAXS Inc., Madison, WI, USA, 2006.
[23] G.M. Sheldrick, SADABS, Program for Empirical X-ray Absorption Correction, Bruker-Nonis, 1990–2004.
[24] A. Altomare, G. Cascarano, C. Giacovazzo, D. Viterbo, Acta Crystallogr., Sect. A 47 (1991) 744.
[25] G.M. Sheldrick, SHELXL-97 Program for Crystal Structure Refinement, University of Göttingen, Germany, 1997.
[26] L.J. Farrugia, J. Appl. Crystllogr. 32 (1999) 837.
[27] A.L. Spek, Acta Crystallogr., Sect. A 46 (1990) 34.
[28] X-Area, Diffractometer control program, STOE and Cie, Darmstadt, Germany, 2001.
[29] G.M. Sheldrick, SHELXS, Program for Crystal Structure Solution, University of Göttingen, Germany, 1997.
[30] F.D. Sokolov, V.V. Brusko, N.G. Zabirov, R.A. Cherkasov, Curr. Org. Chem. 10 (2006) 27.
[31] N.G. Zabirov, A.Yu. Verat, F.D. Sokolov, M.G. Babashkina, D.B. Krivolapov, V.V. Brusko, Mendeleev Commun. 13 (2003) 163.
[32] A.Y. Verat, F.D. Skolov, N.G. Zabirov, M.G. Babashkina, D.B. Krivolapov, V.V. Brusko, I.A. Litvinov, Inorg. Chim. Acta 359 (2006) 475.

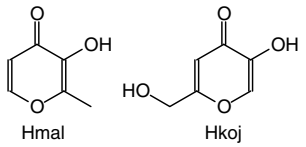

Scheme 1. Structures of the bidentate ligands Hmal and Hkoj.

erenced to TMS and $^{31}P\{^{1}H\}$ spectra were externally referenced to H_3PO_4 (85%, δ 0) with positive chemical shifts downfield the standard. Microanalyses (C, H and N) were obtained on a FISONS EA-1108 elemental analyzer.

2.2. Preparation of complexes

2.2.1. $[ReOCl(mal)_2]$ (**1**)

$(NBu_4)[ReOCl_4]$ (0.117 g, 0.2 mmol) was added to an initially colorless solution of Hmal (0.025 g, 0.2 mmol) in methanol (25 mL). The dark green solution formed was stirred for 1 h at room temperature and then kept at −15 °C for seven days for crystallization. The green crystals obtained were filtered off, washed with a small amount of *n*-hexane and dried under reduced pressure (yield: 0.085 g, 87%). Mp 223–225 °C. *Anal.* Calc. for $C_{12}H_{10}ClO_7Re$: C, 29.54; H, 2.07. Found: C, 29.96; H, 2.44%.

2.2.2. $[ReOCl_2(mal)(PPh_3)]$ (**2**)

A suspension of $[ReOCl_3(PPh_3)_2]$ (0.166 g, 0.2 mmol) and Hmal (0.025 g, 0.2 mmol) in dichloromethane (30 mL) was refluxed for 2 h. After cooling, the homogeneous solution was kept at −15 °C for seven days for crystallization of the product. The green precipitate was filtered off, washed with *n*-hexane and dried under reduced pressure (yield: 0.131 g, 99%). Mp 203–205 °C. *Anal.* Calc. for $C_{24}H_{20}ClO_4PRe$: C, 43.64; H, 3.05. Found: C, 43.67; H, 3.27%.

2.2.3. $[ReOBr_2(mal)(PPh_3)]$ (**3**)

Hmal (0.025 g, 0.2 mmol) was added to a suspension of $[ReOBr_3(PPh_3)_2]$ (0.193 g, 0.2 mmol) in dichloromethane (30 mL). The mixture was refluxed for 4 h. After cooling to room temperature, toluene (10 mL) was added to the solution. Green crystals, obtained by slow evaporation of the resulting solution were filtered off, washed with *n*-hexane and dried under reduced pressure (yield: 0.144 g, 96%). Mp 200–202 °C. *Anal.* Calc. for $C_{24}H_{20}BrO_4PRe$: C, 38.47; H, 2.69. Found: C, 38.76; H, 2.51%.

2.2.4. $[ReOCl_2(koj)(PPh_3)]$ (**4**)

A suspension of $[ReOCl_3(PPh_3)_2]$ (0.167 g, 0.2 mmol) and Hkoj (0.028 g, 0.2 mmol) in methanol (25 mL) was refluxed for 4 h. After cooling to room temperature, *n*-hexane (10 mL) was added to the solution. Green crystals of the complex, formed after 3 days at −15 °C, were filtered off, washed with *n*-hexane and dried under reduced pressure. A second crop of the complex was similarly obtained after four days of a second addition of *n*-hexane (10 mL) (yield: 0.118 g, 87%). Mp 180 °C (dec.). *Anal.* Calc. for $C_{24}H_{20}Cl_2O_5PRe$: C, 42.61; H, 2.98. Found: C, 43.41; H, 3.12%.

2.2.5. $[ReOBr_2(koj)(PPh_3)]$ (**5**)

Hkoj (0.028 g, 0.2 mmol) was added to a suspension of $[ReOBr_3(PPh_3)_2]$ (0.193 g, 0.2 mmol) in methanol (25 mL). The mixture was refluxed for 4 h. After cooling to room temperature, the microcrystalline green solid of the complex, obtained by slow concentration of the resulting solution, was filtered off, washed with *n*-hexane and dried under reduced pressure (yield: 0.142 g, 93%). Mp 210–212 °C. *Anal.* Calc. for $C_{24}H_{20}Br_2O_5PRe$: C, 37.66; H, 2.63. Found: C, 37.55; H, 2.53%.

2.3. Crystallography

The data collection for complex **1** was performed on a Bruker P4 diffractometer. An Enraf-Nonius CAD4 diffractometer was used for the X-ray diffraction measurements on complexes **2**, **3** and **5**. A Nonius KAPPA CCD equipment was used for the data collection for **4**. Standard procedures were applied by the diffractometers, which were equipped with Mo Kα radiation (λ = 0.71073 Å) and graphite monochromators.

Crystals suitable for structure analysis were obtained by crystallization from methanol (**1**), dichloromethane (**2**, **4** and **5**) and 1:1 dichloromethane/*n*-hexane (**3**) solutions of the indicated complexes at −15 °C. The cell constants were calculated from 25 reflections, measured with a wide variation of θ, for complexes **2, 3** and **5**, while 11 909 and 6710 reflections were used by the unit cell calculations for **1** and **4**, respectively. Direct methods [7] were used for the solution of all structures. The hydrogen atoms were found in Fourier-map and refined with isotropic displacement parameter for **1**. They were calculated at idealized positions and refined using the riding model in the structures of **2**, **4** and **5**. For **3**, the free isotropic refinement was combined with the use of the riding model. All non-hydrogen atoms were refined with anisotropic temperature factors, with SHELXL-97 [8]. Additional crystallographic information is given in Table 1.

3. Results and discussion

3.1. Synthesis of the rhenium complexes

The complex **1** was synthesized from $(NBu_4)[ReOCl_4]$ and maltol in methanol, with elimination of 2 equiv. of HCl. Complexes **2–5** were prepared by reacting $[ReOX_3(PPh_3)_2]$ (X = Cl for **2** and **4**; X = Br for **3** and **5**) with Hmal (**2** and **3**) or Hkoj (**4** and **5**) in dichloromethane or methanol, with formation of HX and PPh_3 as by-products. All reactions were carried out in boiling solvents, except the synthesis of **1**, which involved a very reactive starting complex and was performed at room temperature. Pure products were obtained in high yields, as crystalline green solids, directly from the reaction mixtures. Scheme 2 simplifies the synthesis of the complexes presented in the work.

3.2. Crystal structure

3.2.1. Crystal structure of $[ReOCl(mal)_2]$ (**1**)

The structure of the complex **1** is depicted in Fig. 1. The overall geometry around the rhenium atom is best described as highly distorted octahedral, with *cis*-(chloro, oxo) and *cis*-maltolato ligands. One of the monoanionic *O*,*O*-bidentate mal^- ligands occupies two positions in the equatorial plane, while the other bidentate ligand has the keto oxygen positioned equatorially and the alkoxy oxygen situated in axial position, which is *trans* to the oxo ligand. The chlorine atom occupies the remaining equatorial position to form a distorted octahedron. The Re–O(4) distance of 1.678(2) Å is in agreement with its double bond character. The equatorial ClO_3 plane is almost planar with biggest deviation of 0.0554(8) Å observed for O(32). The Re atom is placed 0.2624(7) Å out of this plane toward the oxo ligand. The axial angle O(4)–Re–O(21) = 165.9(7)° also evidences the octahedral distortion. Considering the longer $C(32)–O(22)_{alkoxy}$ and $C(42)–O(32)_{Keto}$ bond lengths as well as the shorter Re–O bond lengths involving the equatorial positioned maltolate versus the axial ligand, it can be stated that the equatorial ligand donates effectively more electron density to the rhenium center than the axial one.

The comparison of the complex **1** with its analog $[ReOBr(mal)_2]$ [4] shows that the Re–X bond distance is elongated by fairly 0.14 Å

Table 1
Crystal data and structure refinement for **1–5**

Complex	**1**	**2**	**3**	**4**	**5**
Empirical formula	$C_{12}H_{10}ClO_7Re$	$C_{24}H_{20}Cl_2O_4PRe$	$C_{24}H_{20}Br_2O_4PRe$	$C_{24}H_{20}Cl_2O_5PRe$	$C_{24}H_{20}Br_2O_5PRe$
Formula weight, *M*	487.85	660.47	749.39	676.47	765.39
Temperature, *T* (°C)	−100(2)	20(2)	20(2)	20(2)	20(2)
Wavelength (Å)/radiation	0.71073/Mo Kα	0.71073/Mo Kα	0.71073/Mo Kα	0.71073/Mo Kα	0.71073/Mo Kα
Crystal system	monoclinic	orthorhombic	orthorhombic	monoclinic	monoclinic
Space group	*C*2/*c*	*Pbca*	*Pbca*	$P2_1/n$	$P2_1/n$
Unit cell dimensions					
a (Å)	12.349(2)	13.524(2)	13.616(1)	14.5554(9)	14.8217(18)
b (Å)	11.448(2)	15.765(1)	15.716(2)	10.1870(8)	10.226(2)
c (Å)	20.287(3)	21.944(3)	22.379(2)	17.3054(10)	17.438(2)
α (°)	90	90	90	90	90
β (°)	90.171(3)	90	90	109.861(3)	110.732(11)
γ (°)	90	90	90	90	90
Volume, *V* (Å^3)	2867.9(8)	4678.5(9)	4788.8(9)	2413.3(3)	2472.0(7)
Z	8	8	8	4	4
Absorption coefficient (mm^{-1})	8.689	5.520	8.508	5.356	8.246
F(000)	1840	2560	2848	1312	1456
Crystal size (mm^3)	0.31 × 0.29 × 0.28	0.3 × 0.2 × 0.2	0.10 × 0.10 × 0.05	0.06 × 0.06 × 0.04	0.24 × 0.22 × 0.21
θ Range for data collection (°)	2.01–30.54	3.01–26.98	3.13–26.98	2.55–26.09	3.11–26.99
Limiting indices (*h*, *k*, *l*)	−17 → 17, −13 → 16, −28 → 28	−1 → 17, 0 → 20, 0 → 28	−1 → 17, 0 → 20, −28 → 28	−17 → 17, −12 → 11, −21 → 21	−1 → 18, 0 → 13, −22 → 21
Reflections collected	17303	5507	11136	12096	5991
Reflections unique/R_{int}	4368/0.0182	5080/0.0322	5203/0.1313	4759/0.0829	5365/0.0273
Completeness to θ (°)	30.54 (99.6%)	26.98 (99.8%)	26.98 (99.9%)	26.09 (99.5%)	26.99 (99.7%)
Data/restraints/parameters	4368/0/208	5080/0/289	5203/0/290	4759/0/299	5365/0/298
Absorption correction	none	ψ-scans [9]	ψ-scans [9]	none	empirical
Minimum and maximum transmission		0.47448/0.98905	0.71785/0.98010		0.460/0.824
Refinement method	full-matrix least-squares on F^2	full-matrix least-squares on F^2	full-matrix least-squares on F^2	full-matrix least-squares on F^2	full-matrix least-squares on F^2
Hydrogen treatment	Fourier-map	calculated	mixed	calculated	calculated
Final *R* indices [$I > 2\sigma(I)$]	R_1 = 0.0157, wR_2 = 0.0370	R_1 = 0.0384, wR_2 = 0.0883	R_1 = 0.0438, wR_2 = 0.0549	R_1 = 0.0444; wR_2 = 0.0981	R_1 = 0.0361; wR_2 = 0.0672
Goodness-of-fit, S	1.138	1.075	0.932	1.020	1.015
Largest peak and hole (e Å^{-3})	0.514 and −0.927	1.057 and −1.265	1.188 and −0.794	1.707 and −1.487	0.808 and −0.879
Programs used	SHELXS-97 [7], SHELXL-97 [8]	SHELXS-97 [7], SHELXL-97 [8]	SHELXS-97 [7], SHELXL-97 [8]	SHELXS]-97 [7], SHELXL-97 [8]	SHELXS-97 [7], SHELXL-97 [8]

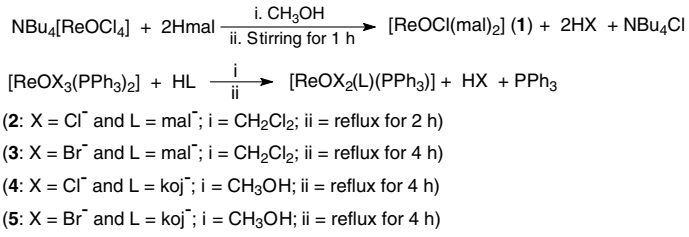

Scheme 2. Synthesis of the complexes **1**–**5**.

by changing the Cl^- ligand to Br^-. This is also observed between the complexes **2–3** and **4–5**. The complex **1**, monoclinic, and [ReOBr(mal)$_2$], triclinic, are not isostructural as are the pairs of compounds **2–3** and **4–5**. The complex [ReOBr(mal)$_2$] shows an elongation for the bonds Re–O(21) and Re–O(22) distances and a shortening for the bonds Re–O(31) and Re–O(32) when compared with the situation in **1**. These are probably results of their different packing modes. The Re–O(4) bond distance and the angles do not suffer considerable variations by changing the chlorine ligand to bromine. Selected bond lengths and angles in complex **1** and in its analogue [ReOBr(mal)$_2$] are given in Table 2.

*3.2.2. Crystal structures of [ReOCl$_2$(mal)(PPh$_3$)] (**2**), [ReOBr$_2$(mal)(PPh$_3$)] (**3**), [ReOCl$_2$(koj)(PPh$_3$)] (**4**) and [ReOBr$_2$(koj)(PPh$_3$)] (**5**)*

The complexes **2** and **3** are isostructural, as are the complexes **4** and **5,** varying only the halogen ligands from chlorine in **2** and **4** to bromine in **3** and **5**. The molecular structures of **2** and **4** are depicted in Figs. 2 and 3, respectively. The molecular structures of **3** and **5** are essentially the same as those of **2** and **4**, respectively, and are therefore not shown here. The molecular labeling schemes of **2** and **4** have also been adopted for the corresponding bromide complexes **3** and **5**. Selected bond lengths and angles for compounds **2–5** are given in Table 3.

The coordination spheres in **2–5** are composed by the oxo ligands, the phosphorus atoms of PPh_3, the halogen ligands, in *cis* arrangement, and the oxygen atoms of the bidentate ligands. It can best be described as a distorted octahedral coordination for the Re(V) central atoms. The alkoxy oxygen atom of the bidentate ligands coordinates in *trans* position to the oxo ligands, while the keto oxygen atoms coordinates *trans* to a halogen ligands. In all complexes, five-membered chelate rings are formed around the Re(V) centers.

The Re–O(4) distances vary between 1.682(4) and 1.661(5) Å in **2–5**, being in the expected range for rhenium(V) monoxo complexes and can be explained by the double bond character of these bonds

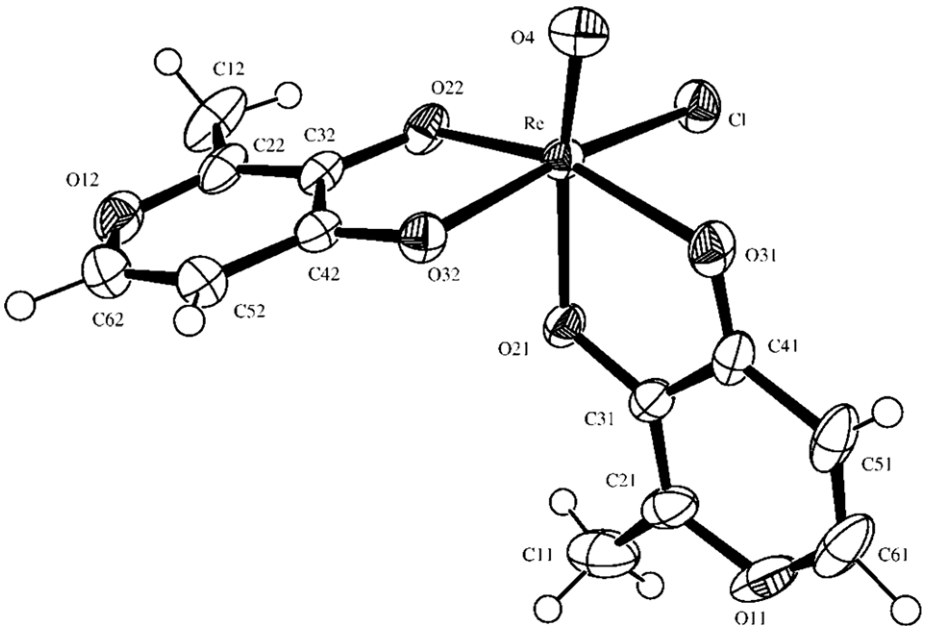

Fig. 1. Molecular structure and labeling scheme of complex [ReOCl(mal)$_2$] (**1**), with thermal ellipsoids drawn at the 50% probability level.

Table 2
Selected bond lengths (Å) and angles (°) for complex **1** and [ReOBr(mal)$_2$] [4]

	1	[ReOBr(mal)$_2$]		**1**	[ReOBr(mal)$_2$]
Bond lengths					
Re–O(4)	1.678(2)	1.673(8)	Re–X[a]	2.368(6)	2.510(1)
Re–O(21)	2.047(2)	2.060(7)	C(31)–O(21)	1.335(2)	1.35(1)
Re–O(22)	1.972(2)	2.114(7)	C(41)–O(31)	1.272(3)	1.27(1)
Re–O(31)	2.097(2)	1.961(7)	C(32)–O(22)	1.352(3)	1.36(1)
Re–O(32)	2.076(2)	2.028(7)	C(42)–O(32)	1.293(3)	1.29(1)
Bond angles					
O(4)–Re–X[a]	98.6(6)	97.4(3)	O(21)–Re–O(22)	85.7(6)	85.2(3)
X–Re–O(32)[a]	168.4(5)	168.8(2)	X–Re–O(22)[a]	92.88(5)	93.7(2)
O(4)–Re–O(21)	165.9(7)	166.8(3)	O(4)–Re–O(31)	90.50(8)	91.5(3)
O(21)–Re–O(31)	76.5(6)	76.1(3)	O(4)–Re–O(22)	107.1(8)	106.9(4)
O(22)–Re–O(32)	81.5(6)	80.7(3)	O(4)–Re–O(32)	92.84(8)	93.5(4)
O(32)–Re–O(21)	82.9(6)	83.2(3)	X–Re–O(31)*	87.40(5)	87.3(2)

[a] X = Cl for **1** and Br for [ReOBr(mal)$_2$].

[1,10]. The interatomic Re–O(2) in the range 2.038(4)–2.017(5) Å are considerably longer than the values observed in other complexes, in which alkoxy donors are bonded in *trans* position to the oxo ligands, whose bond lengths are found between 1.928 and 1.888 Å. The comparably short Re–O bond length in the latter compounds is discussed to be a result of delocalization of π-electron density from the oxo bonds to the *trans* situated ones and has also been found for some chelating ligands with phenoxy or alkoxy functionalities, which direct their oxygen donor atoms to the *trans*-positions of the oxo ligands [1,10]. The values of the axial angle O(4)–Re–O(2) angles are found between 165.2(2)° and 163.3(3)° for **2–5** and describe the distortions from an ideal octahedron.

Intermolecular hydrogen bonds of the type OH···X (X = Cl or Br) involving the methylene hydroxyl group from the kojate moiety and the halogen ligand from independent complex molecules, are found in the crystal structures of **4** and **5**, forming a linear chain of complex molecules (Fig. 4).

3.3. Infrared spectroscopy

The deprotonation of maltol and kojic acid is seen by the disappearance of the typical IR absorption bands ν_{as}(OH), which are observed in the range 3270–3178 cm^{-1} in the spectra of the uncoordinated compounds. For complexes **4** and **5**, the ν_{as}(OH) band referring to the methylene hydroxyl group appears at 3443 cm^{-1} and 3445 cm^{-1}, respectively, [11]. The coordination of these ligands as bidentate *O,O′*-donors is evidenced by a bathochromic shift of the ν_{as}(C=O) band at 1655 cm^{-1} in the spectrum of Hmal and at 1660 cm^{-1} in that of Hkoj. They appear in the IR spectra of the complexes **1–5** in the region between 1619 and 1434 cm^{-1}, typically assigned as ν_{as}(C=O + C=C, chelating ligand) and ν_{as}(C=C, PPh_3) [12,13]. The bands attributed to ν_{as}(Re=O) are found in the range 987–953 cm^{-1} in the products, being in all cases shifted in relation to the starting complexes [14,15]. The coordination of the PPh_3 group to the Re(V) center in **2–5** is observed by the presence of strong bands assigned to ν(PPh) at 1098–1096 cm^{-1}, to out of plane deformation of the phenyl ring hydrogen atoms at 753–748 cm^{-1} and to phenyl ring deformation at 696–692 cm^{-1}, without significant changes when compared to the starting complexes [14,15]. The IR datasets of the uncoordinated Hmal and Hkoj and the complexes can be found in Table 4.

3.4. Multinuclear magnetic resonance

Table 5 lists the $^{13}C\{^1H\}$ and ^1H NMR data for **1**, while ^1H and $^{31}P\{^1H\}$ NMR data for **2–5** are given in Table 6. Due to the lack of

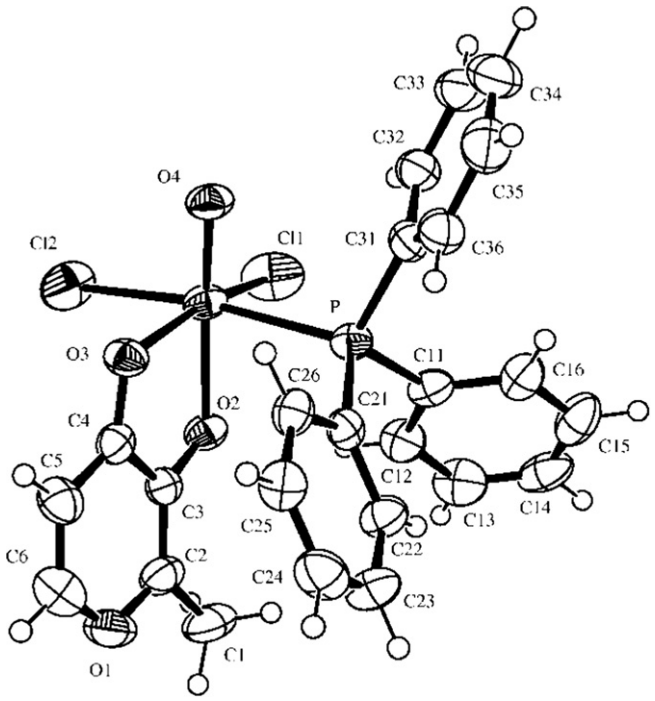

Fig. 2. Molecular structure and labeling scheme of complex $[ReOCl_2(mal)(PPh_3)]$ (**2**), with thermal ellipsoids drawn at the 50% probability level.

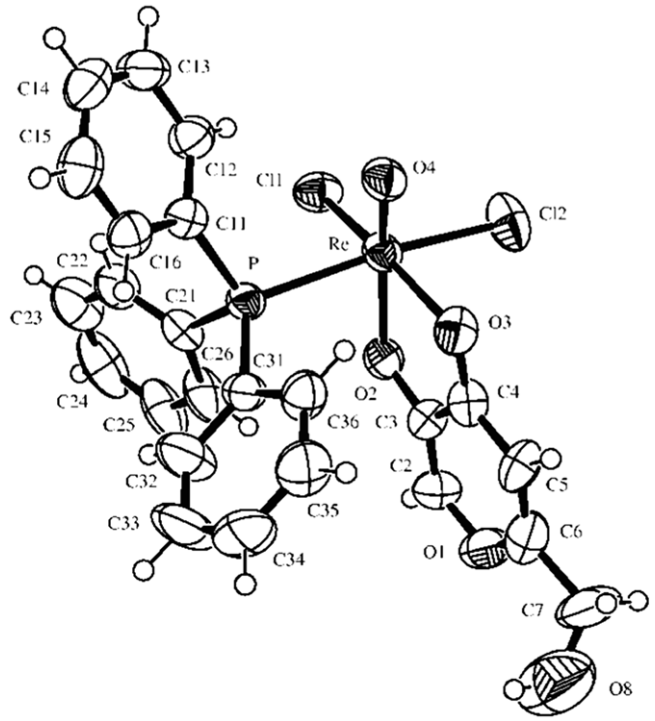

Fig. 3. Molecular structure and labeling scheme of complex $[ReOCl_2(koj)(PPh_3)]$ (**4**), with thermal ellipsoids drawn at the 50% probability level.

solubility, no ^{13}C NMR experiments were carried out for them. Integrations and signal multiplicities are in agreement with all the proposed structures in solution (Scheme 3).

Upon complexation, the resonance of the C7 protons undergo upfield shifts in **1–5**, if compared to the uncoordinated ligands.

Table 3
Selected bond lengths (Å) and angles (°) for complexes **2–5**

Complex	2	3	4	5
Bond lengths				
Re–O(4)	1.672(4)	1.673(5)	1.661(5)	1.682(4)
Re–O(2)	2.038(4)	2.017(5)	2.029(5)	2.018(4)
Re–O(3)	2.109(4)	2.120(5)	2.118(6)	2.115(4)
Re–X(1)[a]	2.3228(2)	2.462(1)	2.337(2)	2.4668(8)
Re–X(2)[a]	2.394(2)	2.545(1)	2.411(2)	2.5584(8)
Re–P	2.461(2)	2.467(2)	2.467(2)	2.458(2)
C(3)–O(2)	1.331(7)	1.336(1)	1.339(1)	1.328(7)
C(4)–O(3)	1.273(7)	1.266(9)	1.265(1)	1.276(7)
Bond angles				
O(4)–Re–O(2)	164.2(2)	165.2(2)	163.3(3)	163.6(2)
O(2)–Re–O(3)	76.3(2)	76.4(2)	76.2(2)	76.1(2)
O(3)–Re–X(1)[a]	164.9(1)	165.4(1)	165.3(1)	166.0(1)
O(3)–Re–P	94.5(1)	94.7(2)	96.4(2)	95.5(1)
X(1)–Re–P	90.1(6)	90.57(6)	88.70(8)	89.28(4)
X(2)–Re–P	172.0(5)	172.2(6)	170.39(8)	170.20(4)
X(1)–Re–X(2)[a]	89.6(8)	89.3(4)	88.27(9)	89.10(3)

[a] X = Cl for **2** and **4** and Br for **3** and **5**.

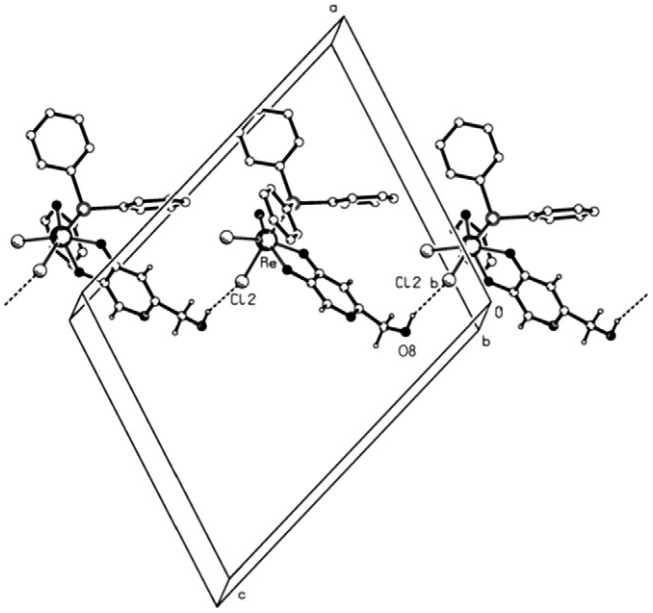

Fig. 4. View of the unit cell of **4** (virtually the same is observed in **5**, in which Cl is changed by Br), showing three complex units interconnected through H-bonds, indicated as dashed lines, forming a linear chain of molecules which is oriented perpendicular to the crystallographic *b*-axis, bisecting the β angle. The H-atoms of the phenyl groups were omitted for clarity. Values found for **4**: O(8)–H(8) = 0.820 Å; H(8)···Cl(2)^b = 2.394 Å, O(8)–H(8)···Cl(2)^b = 159.11°; O(8)···Cl(2)^b = 3.173(1) Å. Values found for **5**: O(8)-H(8) = 0.820 Å; H(8)···Br(2)^b = 2.480 Å, O(8)–H(8)···Br(2)^b = 165.25°; O(8)···Br(2)^b = 3.279 Å. Cl(2)^b and Br(2)^b are generated by using the symmetry operation $-½ + x, ½ - y, -½ + z$.

The protons of hydroxyl groups bounded to C3 in the free ligands are not observed in the spectra of the complexes. This is in agreement with their deprotonation upon the formation of the chelate rings in **1–5**. The resonance of the C(6)–H is overlapped with the PPh_3 protons for most complexes and, therefore, could not be precisely located. The ^1H NMR spectrum of **1** shows two sets of signals in a 1:1 ratio, corresponding to two nonequivalent maltolate units, as has been observed for the analogous complexes $[ReOBr(mal)_2]$ and $[TcOCl(mal)_2]$ [4]. In accord with this study, the ^1H NMR resonances pertaining the maltolate ligand bearing an oxygen atom opposite to the oxo ligand, i.e. axial, are upfield shifted than those

Table 4
Selected IR data for the free ligands and their rhenium complexes (cm^{-1})

Compound	ν(O–H)	ν(C=O)	ν(C=O + C=C, mal or koj; C=C, PPh_3)	ν(P–Ph)	ν(Re=O)	γ(CH, Ph); β(ring, Ph)
Hmal	3254	1655	1621, 1561, 1463			
Hkoj	3270, 3178	1660	1611, 1582, 1472, 1438			
1			1617, 1580, 1566, 1543, 1470		953	
2			1619, 1582, 1563, 1482, 1434	1096	987	753; 697
3			1617, 1580, 1564, 1482, 1435	1096	987	753; 696
4	3443		1611, 1569, 1522, 1483, 1438	1098	981	753; 694
5	3445		1614, 1568, 1526, 1482, 1436	1096	980	748; 694

Table 5
$^{13}C\{^1H\}$ and ^1H NMR data (ppm) for $[ReOCl(mal)_2]$ at room temperature in $CDCl_3$

	Assignments
^{13}C	14.5 (C7), 15.4 (C7′), 110.3 (C5), 111.2 (C5′), 153.4 (C3), 154.2 (C3′), 156.1 (C2), 156.8 (C2′), 159.2 (C6), 160.1 (C6′), 179.8 (C4), 188.5 (C4′).
^1H	2.45 (s, H7), 2.83 (s, H7′), 6.99 (d, J^3 = 5 Hz, H5), 7.12 (d, J^3 = 5 Hz, H5′), 7.52 (d, J^3 = 5 Hz, H6), 8.03 (d, J^3 = 5 Hz, H6′).

Table 6
^1H and $^{31}P\{^1H\}$ NMR data (ppm) for $[ReOX_2(L)(PPh_3)]$ (X = Cl or Br; L = mal or koj) complexes **2–5** at room temperature in CD_2Cl_2

Compound	^1H-Assignments	^{31}P-Assignments
2	2.16 (s, H7), 6.69 (d, J^3 = 5 Hz, H5), 7.32–7.55 (m, H6 overlapped with PPh_3).	−17.71
3	2.16 (s, H7), 6.71 (d, J^3 = 5 Hz, H5), 7.38–7.59 (m, H6 overlapped with PPh_3).	−17.95
4[a]	4.68 (H7), 6.88 (H5), 7.34 (H2), 7.39–7.70 (m)	−16.29
5[a]	4.67 (H7), 6.86 (H5), 7.39–7.68 (m)	−16.51

[a] Resonance of OH not found.

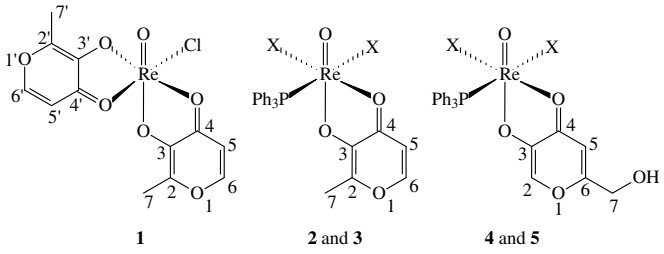

Scheme 3. NMR labeling of the complexes **1–5** (X = Cl for **2** and **4**; X = Br for **3** and **5**).

of the other moiety. Thus, the set of hydrogen signals at 6.99 and 7.52 ppm was assigned to the C5–H and C6–H (axial), respectively, while the set, at 7.12 and 8.03 ppm, was assigned to C5′–H and C6′–H (equatorial), respectively.

The number of observed carbon resonances in complex **1** is in agreement with that expected in the appropriate regions for the proposed structure in solution, which is supposed to be the same as the solid state structure. Like the ^1H NMR spectrum, two sets of signals are observed in the ^{13}C NMR spectrum corresponding to the two nonequivalent mal^- ligands. It is assumed that the ^{13}C NMR signals of the ligand oriented perpendicularly to the octahedral equatorial plane defined in Scheme 3 is upfield shifted with respect to those of the equatorial ligand, which is more strongly bounded to the rhenium center. This assumption is supported by the bond lengths verified in the crystal structure of the complex.

The $^{31}P\{^1H\}$ NMR spectra of **2–5** in CD_2Cl_2 consist of sharp singlets observed in the range between −17.95 and −16.29 ppm, which is consistent with the oxorhenium(V) species given in Scheme 3 [14,15].

4. Conclusions

Five heteroleptic rhenium(V) chelate complexes involving the maltolate or kojate anions acting in the *O,O′*-bidentate mode could be prepared under mild conditions with high yields and were fully characterized both in solution and in the solid state. All complexes are air stable and possess distorted octahedral coordination spheres around the rhenium centers in the solid state, which are retained in the solutions studied.

Acknowledgments

This work was supported by CAPES, CNPq, FAPESP and FINEP (CT Infra 0970/01).

Appendix A. Supplementary data

CCDC 669248, 669249, 669250, 669251 and 669252 contain the supplementary crystallographic data for **1**, **2**, **3**, **4** and **5**, respectively. These data can be obtained free of charge via http://www.ccdc.cam.ac.uk/conts/retrieving.html, or from the Cambridge Crystallographic Data Centre, 12 Union Road, Cambridge CB2 1EZ, UK; fax: (+44) 1223-336-033; or e-mail: deposit@ccdc.cam.ac.uk. Supplementary data associated with this article can be found, in the online version, at doi:10.1016/j.poly.2008.06.022.

References

[1] U. Abram, Comprehensive Coordination Chemistry II, vol. V, Elsevier, 2004. p. 271, and references cited therein.
[2] E. Deutsch, K. Libson, J.L. Vanderheyden, A.R. Ketring, H.R. Maxon, Nucl. Med. Biol. 13 (1986) 465.
[3] V.G. Yuen, P. Caravan, L. Gelmini, N. Glover, J.H. McNeill, I.A. Setyawati, Y. Zbou, C. Orvig, J. Inorg. Biochem. 68 (1997) 109.
[4] H. Luo, S.J. Rettig, C. Orvig, Inorg. Chem. 32 (1993) 4491.

[5] N.P. Johnson, C.J.L. Lock, G. Wilkinson, Inorg. Syn. 9 (1967) 145.
[6] R. Alberto, R. Schibli, A. Egli, P.A. Schubiger, W.A. Hermann, G. Artus, U. Abram, T.A. Kaden, J. Organomet. Chem. 493 (1995) 119.
[7] G.M. Sheldrick, SHELXS97, Program for the Solution of Crystal Structures, University of Göttingen, Germany, 1997.
[8] G.M. Sheldrick, SHELXL97, Program for the Refinement of Crystal Structures, University of Göttingen, Germany, 1997.
[9] A.L. Spek, PLATON, A Multipurpose Crystallographic Toll, University of Utrecht, The Netherlands, 2006.
[10] S. Bolano, J. Bravo, R. Carballo, E. Freijanes, S. Garcia-Fontan, P. Rodriguez-Seoane, Polyhedron 22 (2003) 1711.
[11] O. Vajragupta, P. Boonchoong, Y. Sumanont, H. Watanabe, Y. Wongkrajang, N. Kammasud, Bioorg. Med. Chem. 11 (2003) 2329.
[12] M.C. Barret, M.R. Mahon, K.C. Molloy, J.W. Steed, P. Wright, Inorg. Chem. 40 (2001) 4384.
[13] G. Battistuzzi, M. Cannio, R. Battistuzzi, Polyhedron 19 (2000) 2163.
[14] E.J. Souza, V.M. Deflon, A.G.A. Fernandes, S.S. Lemos, A. Hagenbach, U. Abram, Inorg. Chim. Acta 359 (2006) 1513.
[15] E.J. Souza, A.G.A. Fernandes, V.M. Deflon, K.E. Bessler, S.S. Lemos, A.A. Batista, J. Ellena, E.E. Castellano, U. Abram, A. Hagenbach, J. Brazil Chem. Soc. 17 (2006) 1578.

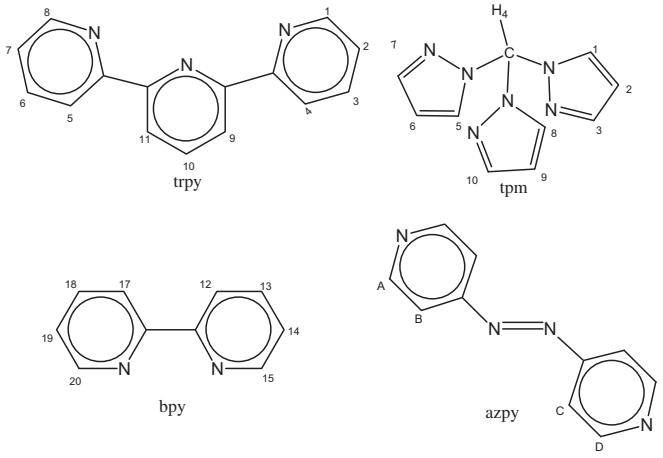

Scheme 1.

electrode, and Ag/AgCl (3 M KCl) as reference electrode. All solutions were prepared in CH_3CN, with 0.1 M TBAH (tetrakis-*n*-butylammonium hexafluorophosphate) as the supporting electrolyte, and thoroughly degassed with argon, prior to each experiment. Cyclic voltammograms were run at a sweep rate of 100 mV s^{-1}. The reported $E_{1/2}$ values were calculated as the average value between the peak values corresponding to the cathodic (E_c) and anodic (E_a) waves: $E_{1/2} = (E_c + E_a)/2$. Controlled potential electrolysis were performed using an OTTLE cell from BAS at a fixed potential of 800 mV, in CH_3CN (0.1 M TBAH), for 10 min. All NMR spectra were obtained in CD_3CN with a Bruker 500 MHz Avance spectrometer. 2D ^1H–^1H COSY and NOESY (mixing time 500 ms) and 2D ^1H–^{13}C HSQC and HMBC experiments were collected in order to unambiguously assign both ^1H and ^{13}C spectra. 2D ^1H–^{15}N HMBC were also recorded to obtain ^{15}N chemical shifts of all ^{15}N non-protonated centers. Chemical analyses were carried out at INQUIMAE, University of Buenos Aires, Buenos Aires, Argentina, with an estimated error of ±0.5%.

2.2. X-ray crystallographic study

Crystal data for $C_{35}H_{27}N_9Ru_1 \cdot 0.85PF_6^- \cdot 0.15CF_3SO_3^- \cdot 0.5CH_3CN$, 987.37 g mol^{-1}, monoclinic, $P2/n$, $a = 14.5890(12)$ Å, $b = 10.7663(9)$ Å, $c = 24.948(2)$ Å, $\beta = 94.491(2)°$, $V = 3906.5(6)$ Å^3, $Z = 2$, $\rho_{calcd} = 1.679$ Mg/m^3, $R_1 = 0.0535$ (0.0794), $wR_2 = 0.1365$ (0.1517), for 14825 reflections with $I > 2\sigma(I)$ (for 19631 reflections [R_{int}: 0.0513] with a total measured of 69467 reflections), goodness-of-fit on $F^2 = 1.081$, largest diff. peak (hole) = 2.277 (−1.790) e Å^{-3}. Measurements were made on a Bruker-Nonius diffractometer equipped with a APPEX 2 4K CCD area detector, a FR591 rotating anode with Mo Kα radiation, Montel mirrors as monochromator and a Kryoflex low temperature device ($T = -173$ °C). Full-sphere data collection was used with ω and φ scans. Programs used: Data collection APEX2 V. 1.0-22 (Bruker-Nonius 2004), data reduction SAINT+ Version 6.22 (Bruker-Nonius 2001), absorption correction SADABS V. 2.10 (2003) and SHELXTL Version 6.10 (Sheldrick, 2000).

2.3. Syntheses

The ligand 4,4′-azo(bis)pyridine was synthesized following a procedure reported in the literature [1]. The precursor [Ru(trpy)(bpy)(H_2O)](PF_6)$_2$ was obtained according to known methods [13].

2.3.1. [Ru(trpy)(bpy)(4,4′-azpy)](PF_6)$_2 \cdot H_2O$, ***1***(PF_6)$_2 \cdot H_2O$

Seventy two milligrams (0.09 mmol) of the known complex [Ru(trpy)(bpy)(H_2O)](PF_6)$_2$ were dissolved in acetone (36 mL), together with 165 mg (0.9 mmol) of 4,4′-azpy. After heating at reflux and stirring for 2 h, the solution was evaporated to *ca.* 10 mL, cooled at room temperature and then diethyl ether (100 mL) was added. The dark red precipitate formed after chilling overnight was removed by filtration, washed with diethyl ether and passed over a Sephadex LH-20 column with a CH_3CN/CH_2Cl_2 (1:1 v/v) mixture. The third eluted red band was rotoevaporated to 5 mL and then precipitated with NH_4PF_6 (2 g/20 mL of H_2O). The obtained red solid was removed by filtration, washed with ether, dried and stored under vacuum over P_4O_{10} for 1 day. Yield: 34 mg (38%). *Anal.* Calc. for $C_{35}H_{29}N_9OP_2F_{12}Ru$ (982.67): C, 42.8; H, 3.0; N, 12.8. Found: C, 42.5; H, 3.0; N, 12.7%. ^1H NMR (CD_3CN, 500.13 MHz): $\delta = 8.86$ (dd, $J = 4.6$ and 1.5 Hz, 2H, H_D), 8.78 (ddd, $J = 5.2$, 1.4 and 0.7 Hz, 1H, H_{15}), 8.71 (ddd, $J = 8.0$, 1.5 and 0.7 Hz, 1H, H_{12}), 8.57 (d, $J = 8.15$ Hz, 2H, H_9 and H_{11}), 8.48 (ddd, $J = 8.1$, 1.3 and 0.7 Hz, 2H, H_4 and H_5), 8.45 (ddd, $J = 8.0$, 1.3 and 0.7 Hz, 1H, H_{17}), 8.36 (dt, $J = 8.0$ and 1.5 Hz, 1H, H_{13}), 8.26 (t, $J = 8.15$, 1H, H_{10}), 8.08 (ddd, $J = 8.1$, 7.5 and 1.4 Hz, 2H, H_3 and H_6), 7.99 (dd, $J = 5.5$ and 1.5 Hz, 2H, H_A), 7.87 (ddd, $J = 8.0$, 5.2 and 1.3 Hz, 1H, H_{14}), 7.86 (ddd, $J = 8.0$, 7.5 and 1.3 Hz, 1H, H_{18}), 7.84 (ddd, $J = 5.5$, 1.4 and 0.7 Hz, 2H, H_1 and H_8), 7.72 (dd, $J = 4.6$ and 1.5 Hz, 2H, H_C), 7.58 (dd, $J = 5.5$ and 1.5 Hz, 2H, H_B), 7.46 (ddd, $J = 7.5$, 5.5 and 1.3 Hz, 2H, H_2 and H_7), 7.31 (ddd, $J = 5.5$, 1.3 and 0.7 Hz, 1H, H_{20}), 7.12 (ddd, $J = 7.3$, 5.5 and 1.3 Hz, 1H, H_{19}) ppm.

^{13}C NMR (CD_3CN, 100.62 MHz) $\delta = 159.1$ (C_{4a} and C_{5a}), 158.5 (C_{9a} and C_{11a}), 158.1 (C_{17a}), 157.8 ($C_{B'}$), 157.4 ($C_{C'}$), 157.2 (C_{12a}), 155.4 (C_A), 154.1 (C_1 and C_8), 152.8 (C_D), 152.7 (C_{15}), 152.2 (C_{20}), 139.7 (C_3 and C_6), 138.8 (C_{13}), 138.5 (C_{18}), 137.3 (C_{10}), 129.6 (C_2 and C_7), 128.6 (C_{14}), 127.7 (C_{19}), 126.0 (C_4 and C_5), 125.5 (C_{12}), 124.9 (C_9 and C_{11}), 124.6 (C_{17}), 119.3 (C_B), 117.0 (C_C) ppm.

2.3.2. [Ru(tpm)(bpy)(4,4′-azpy)](PF_6)$_2 \cdot 3H_2O$, ***2***(PF_6)$_2 \cdot 3H_2O$

Fifty five milligrams (0.07 mmol) of the precursor [Ru(tpm)(bpy)(H_2O)](PF_6)$_2$ were dissolved in acetone (28 mL) together with an excess of 4,4′-azpy (128 mg, 0.7 mmol). After heating under reflux and stirring for 3 h, the solution was evaporated to *ca.* 10 mL, cooled at room temperature and then diethyl ether (100 mL) was added. After keeping in the refrigerator for 24 h, the dark red precipitate was removed by filtration and washed with diethyl ether (2 × 10 mL), dried and stored under vacuum over P_4O_{10} for 1 day. Yield: 62 mg (89%). *Anal.* Calc. for $C_{30}H_{32}N_{12}O_3P_2F_{12}Ru$ (999.66): C, 36.0; H, 3.2; N, 16.8. Found: C, 35.7; H, 2.7; N, 16.6%. ^1H NMR (CD_3CN, 500.13 MHz): $\delta = 9.08$ (s, 1H, H_4), 8.86 (dd, $J = 1.6$ and 4.6 Hz, 2H, H_D), 8.80 (ddd, $J = 8.2$, 1.3, and 0.7 Hz, 2H, H_{12} and H_{17}), 8.65 (ddd, $J = 5.7$, 1.5 and 0.7 Hz, 2H, H_{15} and H_{20}), 8.57 (dd, $J = 2.9$ and 0.5 Hz, 2H, H_1 and H_5), 8.39 (dd, $J = 2.9$ and 0.7 Hz, 1H, H_8), 8.24 (ddd, $J = 8.2$, 7.7, and 1.6 Hz, 2H, H_{13} and H_{18}), 8.00 (dd, $J = 2.3$ and 0.5 Hz, 2H, H_3 and H_7), 7.73 (dd, $J = 4.6$ and 1.6 Hz, 2H, H_C), 7.72 (dd, $J = 5.5$ and 1.6 Hz, 2H, H_A), 7.56 (ddd, $J = 7.7$, 5.6 and 1.3 Hz, 2H, H_{14} and H_{19}), 7.51 (dd, $J = 5.5$ and 1.6 Hz, 2H, H_B), 6.79 (dd, $J = 2.9$ and 2.3 Hz, 2H, H_2 and H_6), 6.61 (dd, $J = 2.3$ and 0.7 Hz, 1H, H_{10}), 6.32 (dd, $J = 2.9$ and 2.3 Hz, 1H, H_9) ppm. ^{13}C NMR (CD_3CN, 100.62 MHz): $\delta = 158.6$ (C_{11} and C_{16}), 157.6 ($C_{C'}$), 157.5 ($C_{B'}$), 156.1 (C_A), 154.0 (C_{15} and C_{20}), 152.7 (C_D), 148.5 (C_3 and C_5), 144.8 (C_{10}), 139.0 (C_{13} and C_{18}), 136.7 (C_1 and C_7), 136.6 (C_8), 127.5 (C_{14} and C_{19}), 126.0 (C_{12} and C_{17}), 118.2 (C_B), 117.0 (C_C), 110.9 (C_2 and C_6), 109.6 (C_9), 77.0 (C_4) ppm.

2.3.3. [(trpy)(bpy)Ru(4,4′-azpy)Ru(NH_3)$_5$](PF_6)$_4 \cdot 10H_2O$, ***3***(PF_6)$_4 \cdot 10H_2O$

A solution of **1** (PF_6)$_2 \cdot H_2O$ (60 mg, 0.062 mmol) in acetone (15 mL) was purged with argon for 30 min. The other precursor [Ru(NH_3)$_5$(H_2O)](PF_6)$_2$ (30 mg, 0.062 mmol), prepared as described before [14], was added to this solution under argon, and the resulting mixture was stirred in darkness, for 2 h, under argon. Deaerated diethyl ether (100 mL) was added and the cloudy solution

was stored in the refrigerator overnight. The red precipitate that formed was removed by filtration, washed with diethyl ether (2×10 mL), sorbed onto a Sephadex LH-20 column and eluted with a CH_3CN/CH_2Cl_2 (1:1 v/v) solution. The second eluted portion (green) was collected, concentrated to *ca.* 5 mL under reduced pressure and precipitated with diethyl ether (50 mL). The dark green solid was removed by filtration, washed with diethyl ether, dried and stored under vacuum over P_4O_{10} for 1 day. Yield: 16 mg (16%). *Anal.* Calc. for $C_{35}H_{62}N_{14}O_{10}P_4F_{24}Ru_2$ (1620.96): C, 25.9; H, 3.9; N, 12.1. Found (mean of several determinations): C, 25.5; H, 3.5; N, 12.8%.

2.3.4. [(trpy)(bpy)Ru(4,4′-azpy)Ru(bpy)(trpy)](PF$_6$)$_4$ · 2H$_2$O, **5**(PF$_6$)$_4$ · 2H$_2$O

211 mg (0.26 mmol) of $[Ru(trpy)(bpy)(H_2O)](PF_6)_2$ were dissolved in acetone (50 mL) together with 4,4′-azpy (24 mg, 0.13 mmol). After heating under reflux and stirring for 15 h, the solution was cooled at room temperature, evaporated to *ca.* 5 mL and precipitated with diethyl ether (50 mL). After keeping in the refrigerator for 24 h, the dark red precipitate was filtered and washed with diethyl ether (2×10 mL). Purification was accomplished by chromatography over Sephadex LH-20, using a CH_3CN/CH_2Cl_2 (1:1 v/v) solution as eluent and collecting only the first of the two obtained fractions. After precipitation with diethyl ether and filtration, the red solid was dried and stored under vacuum over P_4O_{10} for 1 day. Yield: 38 mg (8%). *Anal.* Calc. for $C_{60}H_{50}F_{24}N_{14}O_2P_4Ru_2$ (1781.14): C, 40.5; H, 2.8; N, 11.0. Found: C, 40.7; H, 2.9; N, 10.7%.

3. Results and discussion

3.1. Syntheses and IR spectra

The synthetic procedures used in this work are slight modifications of techniques previously developed in our laboratories [11,12]. The IR spectra of all synthesized complexes display characteristic vibrational modes of the polypyridyl ligands (trpy, tpm, bpy and 4,4′-azpy). Besides, a typical ammonia symmetric deformation mode $\delta_{sym}(NH_3)$ appears in the IR spectrum of the PF_6^- salt of complex **3** at 1270 cm^{-1}, which clearly evidenced a localized oxidation

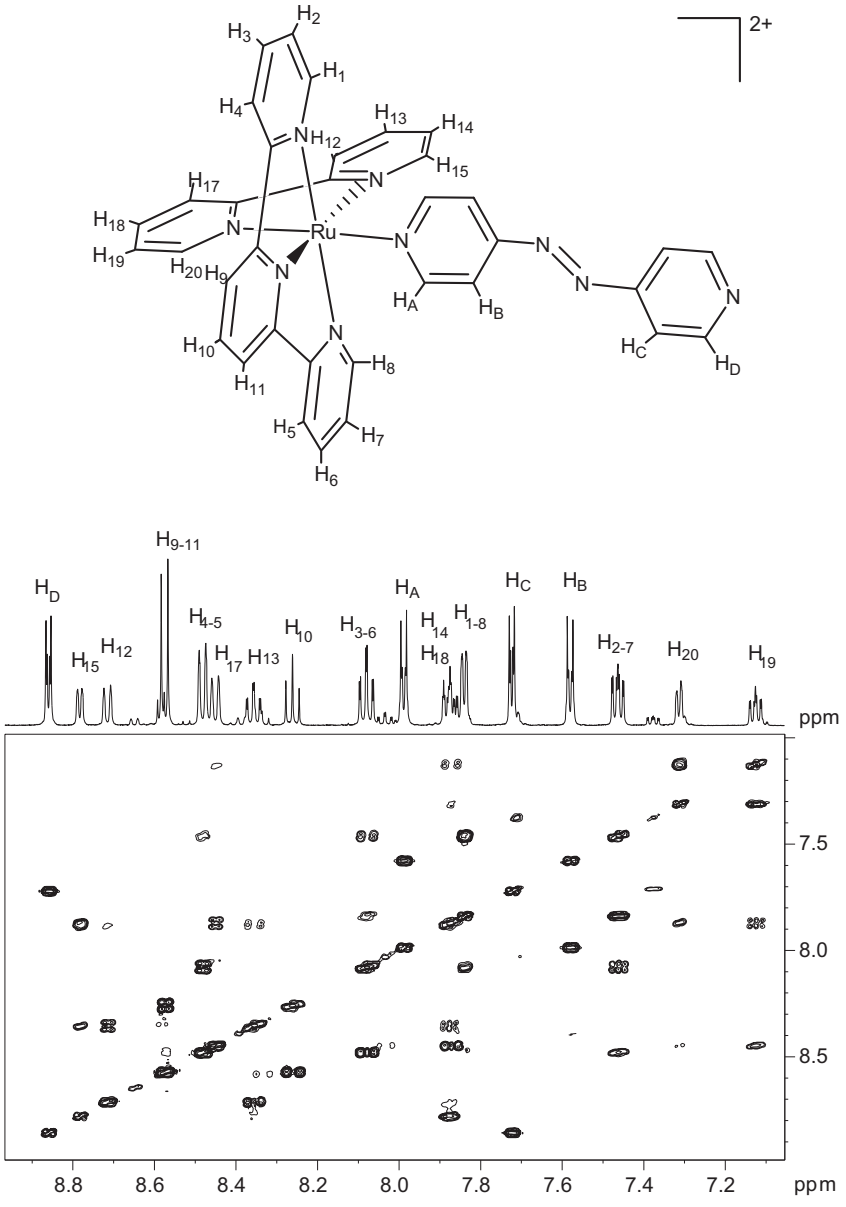

Fig. 1. 2D ^{1}H–^{1}H COSY spectrum of complex **1**.

state (II) for the ammine-bonded Ru atom [10], as shown in Supplementary Fig. 1. The presence of water is also disclosed by the broad band appearing at 1624 cm^{-1} corresponding to H–O–H bending vibrations.

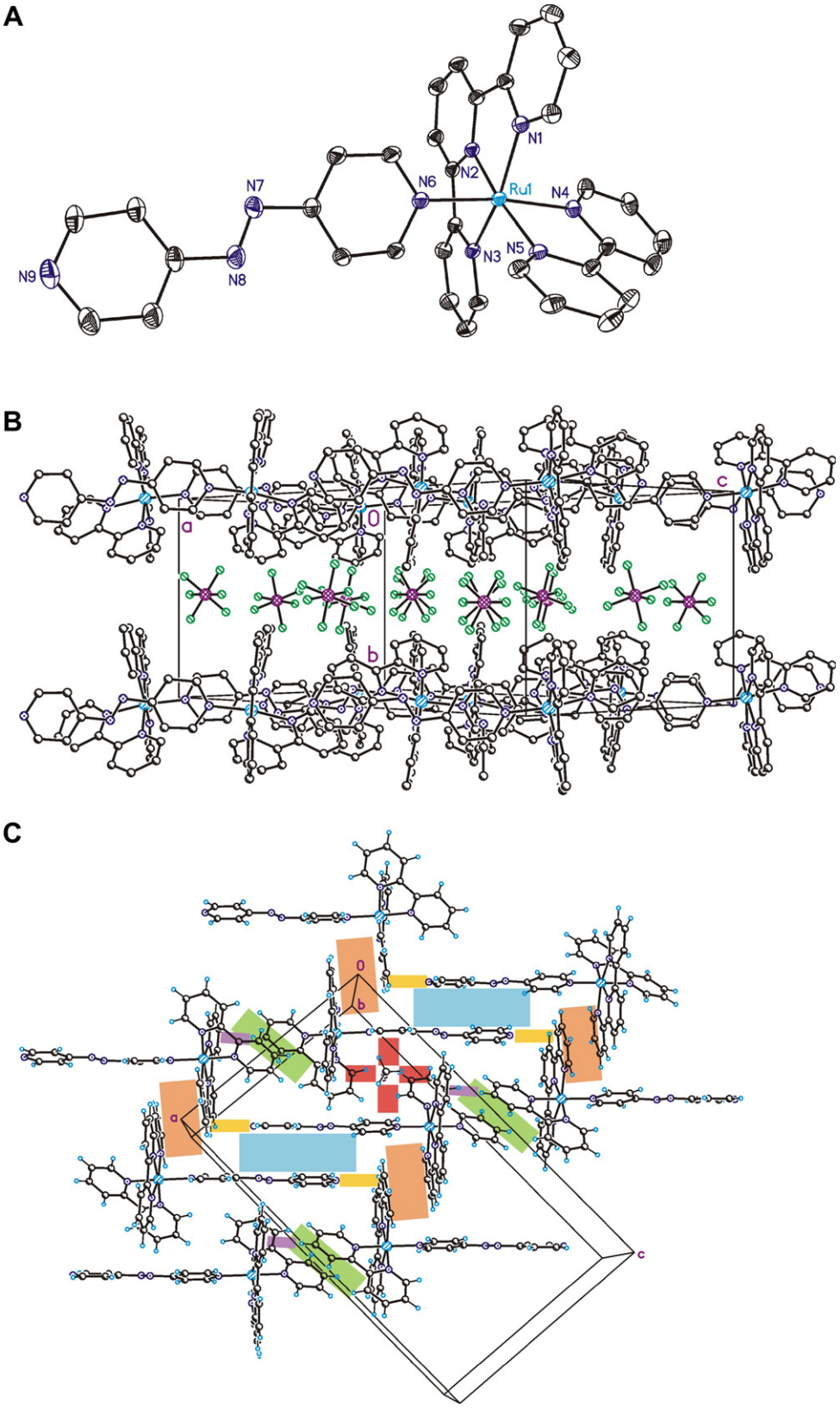

Fig. 2. (A) ORTEP diagram (ellipsoids at 70% probability) for the cationic moiety of **1**, with labelling scheme for N atoms. Hydrogen atoms are omitted in the sake of clarity. (B) View of the crystal packing of **1** showing the cationic and anionic 2D layers. (C) View of the two-dimensional layer formed by the cationic part of the complex showing the intermolecular π interactions marked with colored backgrounds (see text). (For interpretation of the references to colour in this figure legend, the reader is referred to the web version of this article.)

3.2. NMR spectra

Compounds **1** and **2** show well dispersed ^{1}H NMR spectra in the region between 6 and 9 ppm. As an example, Fig. 1 shows the ^{1}H–^{1}H COSY spectra of complex **1** in CD_3CN. Besides, the presence of a symmetry plane simplifies a little bit the NMR spectra: in **1** the plane incorporates the 4,4′-azpy and bpy ligands, whereas in **2** the plane includes the 4,4′-azpy ligand and splits the tmp and bpy ligands in two symmetric moieties. Two-dimensional homonuclear COSY and NOESY spectra, together with ^{13}C and ^{15}N HSQC and HMBC spectra allowed the complete assignment of the signals, as stated in Section 2. The knowledge of the ^{15}N chemical shifts permitted a precise distinction between linked and non-linked connectivities in multicoordinated N-ligands, as discussed before [15].

3.3. Solid state structure

Crystals suitable for X-ray diffraction of $\mathbf{1}(PF_6)_{1.70}(CF_3SO_3)_{0.30}\cdot 0.5CH_3CN$ were obtained by slow diffusion of ether into a concentrated acetone solution of $\mathbf{1}(PF_6)_2$ in the presence of $NaCF_3SO_3$ and a small amount of CH_3CN. An ORTEP diagram of the cation is shown in Fig. 2A. A *trans*-structure of the 4,4′-azpy ligand is disclosed, as already observed in polymeric structures incorporating this ligand [6]. The Ru metal center displays a distorted octahedral coordination with Ru–N bond distances within the range 1.97–2.09 Å (see Table 1), similar to those obtained for related complexes indicating the presence of a strong $d_\pi(Ru) \rightarrow \pi^*(L)$ backbonding [16]. The pyridylic groups of the three ligands are significantly away from planarity with relative rotation angles of 12.6° for bpy, 13.2° for 4,4′-azpy and 15.2° for the peripheral pyridyls of trpy.

In the crystal packing it can be observed that the cationic and anionic parts are forming two-dimensional layers which are contacting through weak interactions (CH-groups with fluorine atoms in the case of PF_6^-, see Fig. 2B). The counter anions are disordered in a proportion 0.85:0.15 (PF_6^- : $CF_3SO_3^-$) occupying exactly the same positions. The cationic part of the crystal has a packing structure that is based on extensive π-interactions within neighboring molecules. In the 3D arrangement represented in Fig. 2C, neighboring azpy ligands are showing a π–π stacking (azo double bond-pyridyl ring with a centroid–centroid distance of 3.5 Å, blue background). Furthermore, this dimer type of arrangement interacts with neighboring dimers via bpy-bpy π–π (shortest distance of 3.6 Å, green background) and bpy-trpy C–H···π ($d_{H\text{-centroid}}$ = 3.3 Å, violet background) contacts. Besides, trpy ligands are having π–π interactions with neighboring trpy ligands (shortest distance 3.6 Å, brown background) and C–H···π interactions with azpy ligands ($d_{H\text{-centroid}}$ = 3.3 Å, yellow background). Finally, the acetonitrile molecules are packing between the metallorganic molecules generating π–π interactions with four pyridyl rings of two trpy and two azpy ligands ($d_{acetonitrile\text{-}trpy}$ = 3.3 Å and $d_{acetonitrile\text{-}azpy}$ = 2.9 Å; red background).

3.4. UV–Vis spectroscopy

The UV–Vis spectra in CH_3CN of all complexes synthesized in this work are shown in Table 2. Fig. 3 shows the UV–Vis spectrum of complex **1** as a representative example. In all cases, the bands between 200 and 300 nm are assigned to intraligand (IL) $\pi \rightarrow \pi^*$ transitions of the polypyridyl ligands (trpy, bpy and 4,4′-azpy). The lowest energy band in complex **1** (λ_{max} = 456 nm) can be assigned to overlapping metal-to-ligand charge transfer (MLCT) transitions $d_\pi(Ru) \rightarrow \pi^*$(trpy), $d_\pi(Ru) \rightarrow \pi^*$(bpy) and $d_\pi(Ru) \rightarrow \pi^*$(4,4′-azpy). In related $[Ru(trpy)(bpy)(L)]^{2+}$ complexes, with L = pz, 4,4′-bpy and BPE (pz = pyrazine; 4,4′-bpy = 4,4′-bipiridine; BPE = *trans*-1,2-bis(4-pyridyl)ethylene), the lowest energy MLCT transitions appear at λ_{max} = 464, 466 and 479 nm, respectively [9,10]. The shift to lower wavelengths detected in **1** points to 4,4′-azpy being the acceptor ligand L with the strongest electron withdrawing effect in the series, similar to that of pz. On the other hand, complex **2** showed two lowest energy bands at λ_{max} = 416 nm and 488 nm, as shown in Table 2, which can be assigned to $d_\pi(Ru) \rightarrow \pi_1^*$(bpy) and overlapping $d_\pi(Ru) \rightarrow \pi_2^*$(bpy) and $d_\pi(Ru) \rightarrow \pi^*$(4,4′-azpy) MLCT transitions, respectively, by comparison to related $[Ru(tpm)(bpy)(L)]^{2+}$ complexes, with L = pz, 4,4′-bpy and BPE [11]. In this case, the strongest electron acceptor character of 4,4′-azpy is evidenced by the highest shift recorded for the lowest energy band.

The dinuclear asymmetric complex **3** revealed two lowest energy bands at λ_{max} = 459 nm and 738 nm, which can be readily assigned to MLCT transitions $d_\pi(Ru_b) \rightarrow \pi^*$(trpy, bpy, 4,4′-azpy) and $d_\pi(Ru_a) \rightarrow \pi^*$(4,4′-azpy), with Ru_b = Ru bonded to bpy and Ru_a = Ru

Table 1
Selected bond distances and angles for cation **1**

Bond distances (Å)	Angles (°)
Ru1 N2 1.9705(14)	N2 Ru1 N4 95.91(6)
Ru1 N4 2.0601(14)	N2 Ru1 N1 79.69(6)
Ru1 N1 2.0751(15)	N4 Ru1 N1 93.18(6)
Ru1 N3 2.0837(14)	N2 Ru1 N3 79.46(6)
Ru1 N5 2.0858(14)	N4 Ru1 N3 85.21(6)
Ru1 N6 2.0910(14)	N1 Ru1 N3 158.81(6)
	N2 Ru1 N5 173.80(6)
	N4 Ru1 N5 78.76(6)
	N1 Ru1 N5 97.34(6)
	N3 Ru1 N5 103.04(6)
	N2 Ru1 N6 90.32(6)
	N4 Ru1 N6 171.95(6)
	N1 Ru1 N6 92.94(5)
	N3 Ru1 N6 90.95(6)
	N5 Ru1 N6 95.28(6)

Table 2
Electronic absorption data of complexes **1**–**5**, in CH_3CN

Complex	λ_{max}, nm (10^{-3} ε_{max}, M^{-1} cm^{-1})
$[Ru(trpy)(bpy)(4,4'\text{-azpy})]^{2+}$	231 (23.8), 242 (23.0), 286 (42.8), 309 (35.7), 456 (12.5)
$[Ru(tpm)(bpy)(4,4'\text{-azpy})]^{2+}$	235 (12.8), 254 (14.4), 286 (31.5), 416 (5.2), 488 (6.8)
$[(trpy)(bpy)Ru(4,4'\text{-azpy})Ru(NH_3)_5]^{4+}$	243 (19.9), 286 (36.4), 309 (30.2), 459 (9.5), 738 (12.6)
$[(trpy)(bpy)Ru(4,4'\text{-azpy})Ru(NH_3)_5]^{5+}$	242 (28.8), 286 (43.8), 309 (37.0), 456 (12.3), 557 (3.1), 670 (1.8)
$[(trpy)(bpy)Ru(4,4'\text{-azpy})Ru(bpy)(trpy)]^{4+}$	242 (27.5), 286 (47.0), 310 (38.6), 458 (13.9), 512 sh

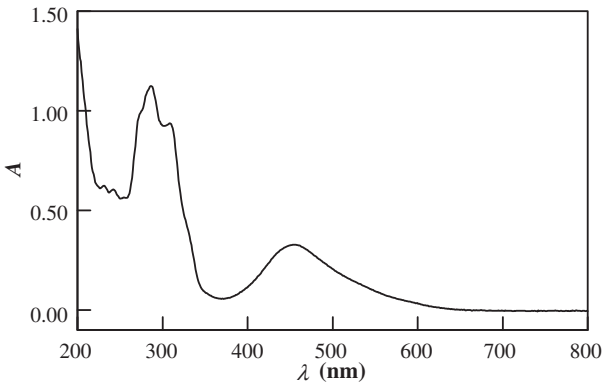

Fig. 3. UV–Vis spectrum of complex **1**, in CH_3CN ($C = 2.6 \times 10^{-5}$ M).

bonded to NH_3, respectively. The previously reported mononuclear species $[Ru(NH_3)_5(4,4'\text{-azpy})]^{+2}$ absorbs at λ_{max} = 645 nm in CH_3CN [1], while the dinuclear species $[(NH_3)_5Ru^{II}(4,4'\text{-azpy})Ru^{II}(NH_3)_5]^{4+}$ has λ_{max} = 710 nm [1], a value similar to that of complex **3**, thus evidencing a comparable electronic distribution. A spectrophotometric titration of **3** was performed by using Br_2 in CH_3CN. After adding a stoichiometric amount of Br_2, the band at λ_{max} = 738 nm disappeared. The same behavior was observed in a controlled potential electrolysis of **3**, as shown in Fig. 4. After applying a potential of 800 mV during 10 min, only the ammine-bonded Ru_a undergoes oxidation to give the mixed-valent species **4**, of formula: $[(trpy)(bpy)Ru^{II}_b(4,4'\text{-azpy})Ru^{III}_a(NH_3)_5]^{5+}$. The reversibility of the process confirms the identity of complex **4**. Gaussian deconvolution of the UV–Vis spectrum of **4** in the region 400–1000 nm, shown as Supplementary Fig. 2, gives λ_{max} = 670 nm for the lowest-energy band, which can be assigned to the intervalence or metal-to-metal charge transfer (MMCT) transition: $[Ru^{II}_b, Ru^{III}_a] \rightarrow [Ru^{III}_b, Ru^{II}_a]$, since the same transition appears at $\lambda_{max} \cong 640$ nm in the corresponding 4,4′-bpy-bridged mixed-valent complex [9].

The dinuclear symmetric complex **5** displays an UV–Vis spectrum very similar to that of the mononuclear species **1**, as shown in Table 2. However, a new shoulder appears at $\lambda_{max} \cong 512$ nm, which can be ascribed to the $d_\pi(Ru) \rightarrow \pi^*(4,4'\text{-azpy})$ MLCT transition, shifted to lower energies as compared to **1**, because of increased electronic delocalization.

3.5. Electrochemistry

The cyclic voltammograms for **1** and **2** display very similar redox potentials associated with the couple Ru^{III}_b/Ru^{II}_b, as displayed in Table 3. Fig. 5 shows the CV of complex **1** as a representative example. In both complexes (**1** and **2**), reversible oxidation wave were observed at $E_{1/2}$ = 1.27 V and $E_{1/2}$ = 1.22 V, respectively (versus SCE). The first one is intermediate between the values obtained for the corresponding Ru couples in the related complexes $[Ru(trpy)(bpy)(pz)]^{2+}$ and $[Ru(trpy)(bpy)(4,4'\text{-bpy})]^{2+}$ ($E_{1/2}$ = 1.34 and 1.23 V, respectively, versus SCE) [9,10], while the second one is intermediate between those of $[Ru(tpm)(bpy)(pz)]^{2+}$ and $[Ru(tpm)(bpy)(4,4'\text{-bpy})]^{2+}$ ($E_{1/2}$ = 1.34 and 1.21 V, respectively, versus SCE) [11].

The dinuclear complex **3** shows two reversible waves in the oxidative range of potentials. The redox potential of the Ru^{III}_b/Ru^{II}_b couple ($E_{1/2}$ = 1.27 V) is the same as that recorded for the mononuclear species **1**, while the redox potential of the Ru^{III}_a/Ru^{II}_a couple ($E_{1/2}$ = 0.45 V), lies again intermediate between the values reported for the related dinuclear complexes $[(trpy)(bpy)Ru^{II}_b(pz)Ru^{II}_a(NH_3)_5]^{4+}$ ($E_{1/2}$ = 0.66 V versus SCE) and $[(trpy)(bpy)Ru^{II}_b(4,4'\text{-bpy})Ru^{II}_a(NH_3)_5]^{4+}$ ($E_{1/2}$ = 0.39 V versus SCE) [9,10]. The difference of redox potential between both Ru couples is therefore: $\Delta E_{1/2} = E_{1/2}(Ru^{III}_b/Ru^{II}_b) - E_{1/2}(Ru^{III}_a/Ru^{II}_a) = 0.82$ V. On the reductive side of the voltammograms, the ligands trpy and bpy display their characteristic reversible waves at $E_{1/2}$ *ca.* −1.3 and −1.6 V, as reported in the literature for similar systems [10]. On the other hand, 4,4′-azpy reductions give rise to one reversible peak at $E_{1/2}$ *ca.* −0.5 V and a quasi-reversible peak at −0.9 V, as expected [1].

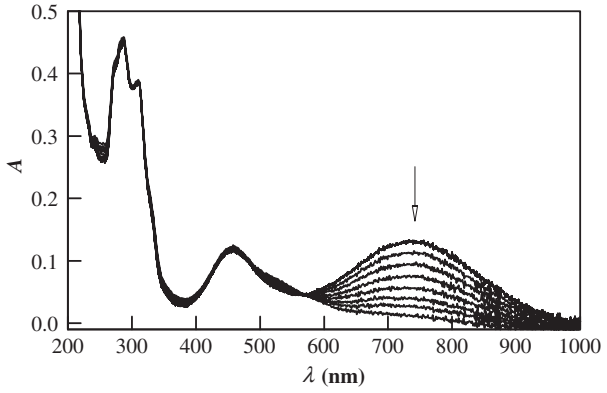

Fig. 4. Controlled potential electrolysis of complex **3**, in CH_3CN ($C = 1.1 \times 10^{-5}$ M), at 800 mV. The arrow indicates increasing times from 0 to 10 min. Each spectrum was taken every minute.

Table 3
Electrochemical data for complexes **1**–**5**, in CH_3CN, at v = 100 mV/s

Complex	Process	$E_{½}$ (V) (ΔE, mV)[a]
$[Ru(trpy)(bpy)(4,4'\text{-azpy})]^{2+}$	$Ru^{3+/2+}$	1.27 (89)
	4,4′-azpy$^{0/-}$	−0.58 (80); −0.98(i)
	trpy$^{0/-}$	−1.36 (83)
	bpy$^{0/-}$	−1.69 (88)
$[Ru(tpm)(bpy)(4,4'\text{-azpy})]^{2+}$	$Ru^{3+/2+}$	1.22 (96)
	4,4′-azpy$^{0/-}$	−0.64 (70); −0.86 (i)
	bpy$^{0/-}$	−1.62 (96)
$[(trpy)(bpy)Ru_b^{II}(4,4'\text{-azpy})Ru_a^{II}(NH_3)_5]^{4+}$	$Ru^{3+/2+}_b$	1.27 (70)
	$Ru^{3+/2+}_a$	0.45 (109)
	4,4′-azpy$^{0/-}$	−0.55 (127); −0.92(i)
	trpy$^{0/-}$	−1.34 (76)
	bpy$^{0/-}$	−1.66 (165)
$[(trpy)(bpy)Ru^{II}(4,4'\text{-azpy})Ru^{II}(bpy)(trpy)]^{4+}$	$Ru^{3+/2+}$	1.27 (127)
	4,4′-azpy$^{0/-}$	−0.39(104); −0.82 (126)
	trpy$^{0/-}$	−1.37(135)
	bpy$^{0/-}$	−1.73(88)

[a] $E_{1/2}$ values are referred to SCE.

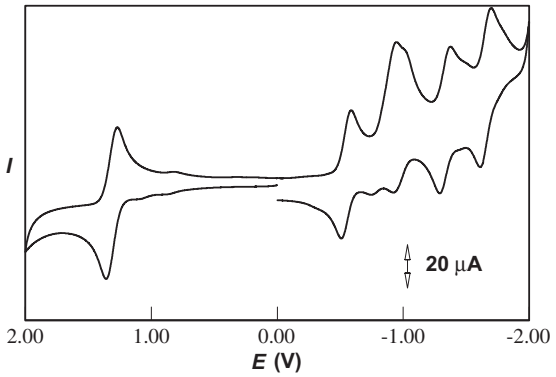

Fig. 5. Cyclic voltammogram of complex **1**, in CH_3CN, 0.1 M TBAH, at v = 100 mV/s. E values are referred to Ag/AgCl.

The cyclic voltammogram of complex **5** is very similar to that of complex **1**, as shown in Table 3. The main distinction is the difference between the cathodic and anodic peaks of the wave corresponding to the redox couple Ru^{III}_b/Ru^{II}_b, which amounts to 127 mV in **5**, pointing to a two-electron process with a comproportionation constant ($K_c \cong 26$) relatively high for weakly coupled mixed-valent complexes [14].

3.6. Intramolecular electron transfer

By using the Marcus–Hush formalism [17], the electronic coupling element can be calculated from the spectral properties of the mixed-valent complex **4**. The parameters $\Delta\tilde{\nu}_{1/2}$ (bandwidth at half-height), ε_{max} (molar absorptivity at the absorption maximum) and $\tilde{\nu}_{max}$ (energy of the intervalence absorption maximum) were obtained after gaussian deconvolution of the visible bands of com-

plex **4** (Supplementary Fig. 2) Using these experimental parameters ($\Delta\tilde{\nu}_{1/2}$ = 4700 cm^{-1}, ε_{max} = 1800 M^{-1} cm^{-1}, $\tilde{\nu}_{max}$=15 000 cm^{-1}) in Eq. (1), where r is the distance (in Å) between both metal centers, estimated as 13.2 Å from the X-ray analysis of complex **1** and the typical Ru_a–N bond length for an aromatic N heterocycle bonded to Ru [16], the electronic coupling was determined to be: H_{AB} = 550 cm^{-1}.

$$H_{AB}\ (cm^{-1}) = 2.06 \times 10^{-2}[(\varepsilon_{max})(\tilde{\nu}_{max})(\Delta\tilde{\nu}_{1/2})]^{1/2}(1/r) \quad (1)$$

H_{AB} is higher by almost a factor of 3 than that determined for the related BPE-bridged mixed-valent species with a similar metal–metal distance (H_{AB} = 189 cm^{-1}), evidencing higher electronic delocalization in the 4,4′-azpy-bridged species. This finding is consistent with previous reports; in effect, Launay et al. have already determined that the comproportionation constant, a measure of the electronic metal–metal interaction, for the mixed-valent species $[(NH_3)_5Ru(4,4'\text{-azpy})Ru(NH_3)_5]^{5+}$ is K_c = 40, a value appreciably higher than that of the isoelectronic BPE complex, for which K_c = 14 [1]. The intermediate value of K_c = 26, determined for the mixed-valent complex [(trpy)(bpy)Ru(4,4′-azpy)Ru(bpy)(trpy)]$^{5+}$, is consistent with the competition between trpy, bpy and 4,4′-azpy for the π-electron density of the metals. Finally, when representing H_{AB} versus r, the slope is increased when including the value for complex **4**, which leads to the conclusion that 4,4′-azpy is a promising ligand for designing "molecular wires", systems in which the electronic transmission is slightly attenuated by the donor–acceptor distance [18].

On the other hand, the reorganization energy λ can be calculated as follows:

$$\lambda = E_{op} - \Delta G^0 - \Delta E_{exc} \quad (2)$$

where ΔG^0 is the free energy difference between both redox centers, assumed as approximately $\Delta E_{1/2}$ = 0.82 V, and ΔE_{exc} is the energy difference between the excited and ground states, estimated as 0.25 eV for several ruthenium complexes in the event that the MMCT transition results in the population of an excited state [19]. Eq. (2) gives a value of λ = 0.79 eV, which is close to the value expected from the slope of the plot of λ versus r calculated for this type of asymmetric mixed-valent complexes [10].

4. Conclusions

New polypyridyl ruthenium mononuclear complexes containing 4,4′-azpy have been prepared and characterized by spectral, diffraction and electrochemical techniques. In complex **1**, extensive π–π interactions within neighboring molecules are disclosed. 4,4′-azpy connects two metal centers in the dinuclear complex **3**, which can be partially oxidized electrochemically to the stable mixed-valent complex **4**. The value of H_{AB} for this latter species is almost 3 times higher than that reported for the related dinuclear complex with BPE, indicating a considerable electronic delocalization in 4,4′-azpy, which confers "molecular wire" properties to complexes with this *N*-heterocycle as a bridging ligand.

Acknowledgments

We thank Universidad Nacional de Tucumán [UNT], Consejo Nacional de Investigaciones Científicas y Técnicas [CONICET] and Agencia Nacional de Promoción Científica y Tecnológica [ANPCyT], all from Argentina, for financial support. Deutscher Akademischer Austauschdienst [DAAD] is gratefully acknowledged for a donation of a Bioanalytical Systems [BAS] equipment. F.F. and N.E.K. are members of the Research Career from CONICET, Argentina. G.P. thanks ANPCyT for a graduate fellowship. We also thank MEC of Spain for projects CSD2006-0003 and CTQ2007-67918.

Appendix A. Supplementary data

CCDC 669446 contains the supplementary crystallographic data for $[Ru(trpy)(bpy)(4,4'\text{-azpy})](PF_6)_{1.70}(CF_3SO_3)_{0.30} \cdot 0.5CH_3CN$. These data can be obtained free of charge via http://www.ccdc.cam.ac.uk/conts/retrieving.html, or from the Cambridge Crystallographic Data Centre, 12 Union Road, Cambridge CB2 1EZ, UK; fax: (+44) 1223-336-033; or e-mail: deposit@ccdc.cam.ac.uk. Supplementary Figs. 1 and 2 show the FTIR spectrum of complex **3** and the Gaussian deconvolution of the visible bands of complex **4**, respectively. Supplementary data associated with this article can be found, in the online version, at doi:10.1016/j.poly.2008.06.014.

References

[1] J.P. Launay, M. Tourrel-Pagis, J.F. Lipskier, V. Marvaud, C. Joachim, Inorg. Chem. 30 (1991) 1033.
[2] V. Marvaud, J.P. Launay, Inorg. Chem. 32 (1993) 1376.
[3] A. Sakamoto, A. Hirooka, K. Namiki, M. Kurihara, M. Murata, M. Sugimoto, H. Nishihara, Inorg. Chem. 44 (2005) 7547.
[4] S. Noro, S. Kitagawa, T. Nakamura, T. Wada, Inorg. Chem. 44 (2005) 3960.
[5] B. Li, H. Liu, Y. Xu, J. Chen, H. Wang, Z. Xu, J. Mol. Struct. 597 (2001) 21.
[6] B. Li, J. Lang, J. Ding, Y. Zhang, Inorg. Chem. Comm. 6 (2003) 141.
[7] B. Li, X. Wang, Y. Zhang, S. Gao, Y. Zhang, Inorg. Chim. Acta 358 (2005) 3519.
[8] Md.K. Nazeeruddin, S.M. Zakeeruddin, J.-J. Lagref, P. Liska, P. Comte, C. Barolo, G. Viscardi, K. Schenk, M. Graetzel, Coord. Chem. Rev. 248 (2004) 1317.
[9] F. Fagalde, N.E. Katz, J. Chem. Soc., Dalton Trans. (1993) 571.
[10] F. Fagalde, N.E. Katz, Polyhedron 14 (1995) 1213.
[11] N.E. Katz, I. Romero, A. Llobet, T. Parella, J. Benet-Buchholz, Eur. J. Inorg. Chem. (2005) 272.
[12] F. Fagalde, M.E. García Posse, M.M. Vergara, M. Cattaneo, N.E. Katz, I. Romero, T. Parella, A. Llobet, Polyhedron 26 (2007) 17.
[13] D.C. Ware, P.A. Lay, H. Taube, M.H. Chou, C. Creutz, in: J.M. Shreeve (Ed.), Inorganic Synthesis, vol. 24, Wiley Interscience, 1986, p. 299.
[14] J.E. Sutton, H. Taube, Inorg. Chem. 20 (1981) 3125.
[15] M. Pérez-Trujillo, P. Nolis, T. Parella, Org. Lett. 9 (2007) 29.
[16] M.E. Gress, C. Creutz, C.O. Quicksall, Inorg. Chem. 20 (1981) 1522.
[17] C. Creutz, Prog. Inorg. Chem. 30 (1983) 1.
[18] J.-P. Launay, C. Crouchet, in: V. Balzani (Ed.), Electron Transfer in Chemistry, vol. 5, VCH, Wiley, 2001, p. 3.
[19] N.E. Katz, C. Creutz, N. Sutin, Inorg. Chem. 27 (1988) 1687.

depending on electronic configuration. [Mn_2(malonate)$_2$(4,4′-bpy)(H_2O)$_2$] exhibits a square-grid manganese malonate layer motif linked into a 3-D net by 4,4′-bpy tethers, with weak antiferromagnetic superexchange operative between manganese ions within the malonate layer [15]. In contrast, [Cu_2(malonate)$_2$(4,4′-bpy)(H_2O)] manifests coordination polymer layers built from [Cu_4(malonate)$_4$] clusters linked into 2-D through 4,4′-bpy ligands; ferromagnetic coupling within the *anti–syn* malonate-bridged tetranuclear kernels was observed [16].

For some time we have been interested in the synthesis and characterization of coordination polymers containing the organodiimine 4,4′-dipyridylamine (dpa). In contrast to 4,4′-bpy, dpa possesses a kinked disposition of its distal nitrogen donor atoms as well as a potential hydrogen bonding donor point, allowing it to aggregate coordination polymer subunits via supramolecular as well as covalent interactions in oxide or carboxylate systems. In our hands, hydrothermal treatment of transition metal precursors with aliphatic α,ω-dicarboxylates and dpa has resulted in the construction of several coordination polymers, some with unprecedented structural motifs [17–19]. For example, [Ni(adipate)(dpa)(H_2O)]$_n$ exhibited the first-ever example of threefold interpenetration within the PtS structure type [17], and {[Ni(dpa)$_2$(succinate)$_{0.5}$]Cl}$_n$ manifested an unprecedented five-connected self-penetrated network with a "regular" 6^{10} topology [18]. {[Cu_2(malonate)$_2$(dpa)(H_2O)$_2$] · H_2O} displayed both *syn–anti* and *anti–anti* 1-D copper malonate chains linked into 2-D via dpa struts, exhibiting net ferromagnetic interactions between malonate-bridged copper ions [19]. We report herein further investigations in this direction with hydrothermal synthesis and structural characterization of a pair of isostructural acentric divalent metal malonate 3-D network coordination polymers incorporating dpa, {[M_2(malonate)$_2$(dpa)(H_2O)$_2$] · 2H_2O}$_n$ (M = Co, **1**; M = Ni, **2**). Thermal and magnetic properties are also discussed; substantial variances in their magnetic properties are observed.

2. Experimental

2.1. 1 General considerations

$CoCl_2 \cdot 6H_2O$, $NiCl_2 \cdot 6H_2O$ and malonic acid were obtained commercially from Fisher. 4,4′-dipyridylamine (dpa) was prepared via a published procedure [20]. Water was deionized above 3 MΩ in-house. Thermogravimetric analysis was performed on a TA Instruments TGA 2050 Thermogravimetric Analyzer with a heating rate of 5 °C/min up to 900 °C. Elemental analysis was carried out using a Perkin Elmer 2400 Series II CHNS/O Analyzer. IR spectra were recorded on a Mattson Galaxy FTIR Series 3000 using KBr pellets. Variable temperature magnetic susceptibility data (2–300 K) was collected on a Quantum Design MPMS SQUID magnetometer at an applied field of 0.1 T. After each temperature change the sample was kept at the new temperature for 5 min before magnetization measurement to ensure thermal equilibrium. The susceptibility data was corrected for diamagnetism using Pascal's constants [21].

2.2. Preparation of {[Co_2(malonate)$_2$(dpa)(H_2O)$_2$] · 2H_2O}$_n$ (**1**)

$CoCl_2 \cdot 6H_2O$ (88 mg, 0.74 mmol), dpa (127 mg, 0.37 mmol), and malonic acid (47 mg, 0.37 mmol), were placed into 10 mL distilled H_2O in a 23 mL Teflon-lined Parr acid digestion bomb, and then 0.5 mL of a 1.0 M NaOH solution was added was added via pipette. The bomb was sealed and heated at 120 °C for 44 h, whereupon it was cooled slowly to 25 °C. Purple crystals of **1** (52 mg, 50 % yield based on malonic acid) were isolated after washing with distilled water, isopropanol and acetone and drying in air. *Anal.* Calc. for $C_{16}H_{21}Co_2N_3O_{12}$ **1**: C, 34.00; H, 3.74; N, 7.43. Found: C, 34.39; H, 3.57; N, 7.46%. IR (KBr, cm^{-1}): 3853 m, 3749 m, 3670 m, 3648 m, 3472 s, 3281 s, 3193 s, 3097 m, 3013 m, 2928 m, 2366 w, 2343 w, 1952 m, 1634 s, 1607 s, 1557 s, 1519 s, 1443 m, 1351 s, 1220 m, 1151 w, 1060 w, 1021 m, 980 w, 952 w, 911 w, 842 w, 822 m, 704, 661 m, 589 m, 531 m.

2.3. Preparation of {[Ni_2(malonate)$_2$(dpa)(H_2O)$_2$] · 2H_2O}$_n$ (**2**)

The preparation for **1** was followed, with the substitution of $NiCl_2 \cdot 6H_2O$ (88 mg, 0.74 mmol) as the metal source. Green crystals of **2** (76 mg, 72% yield based on malonic acid) were isolated after washing with distilled water, isopropanol and acetone and drying in air. *Anal.* Calc. for $C_{16}H_{21}Ni_2N_3O_{12}$ **2**: C, 34.03; H, 3.75; N, 7.44. Found: C, 34.99; H, 3.68; N, 7.89%. IR (KBr, cm^{-1}): 3652 m, 3472 s, 3181 s, 2925 sm, 1600 s, 1569 s, 1520 s, 1443 m, 1358 s, 1266 w, 1224 m, 1153 w, 1061 w, 1025 m, 1061 w, 1025 m, 983 w, 971 w, 911 w, 843 w, 820 w, 710 m, 661 w, 644 w, 608 w, 529 w.

3. X-ray crystallography

A purple block crystal of **1** with dimensions 0.46 mm × 0.28 mm × 0.10 mm and a green block crystal of **2** with dimensions 0.14 mm × 0.12 mm × 0.06 mm were subjected to single-crystal X-ray diffraction at 173 K using a Bruker-AXS SMART 1k CCD instrument. Reflection data were acquired using graphite–monochromated Mo Kα radiation (λ = 0.71073 Å). The data were integrated via SAINT [22]. Lorentz and polarization effect and empirical absorption corrections were applied with SADABS [23]. The structures were solved using direct methods and refined on F^2 using SHELXTL [24]. All non-hydrogen atoms were refined anisotropically, with the exception of the oxygen atoms belonging to the uncoordinated water molecules. Hydrogen atoms bound to carbon atoms were placed in calculated positions and refined isotropically with a riding model. The hydrogen atoms belonging to the coordinated water molecules in **1** and **2** were found via Fourier difference maps, then restrained at fixed positions and refined isotropically. The hydrogen atoms attached to the uncoordinated water molecules (O6 and O7) could not be located. Relevant crystallographic data for **1** and **2** is listed in Table 1.

4. Results and discussion

4.1. Synthesis and spectral analysis

The coordination polymers **1** and **2** were prepared as single phase crystalline products under hydrothermal conditions via combination of the hydrated metal chloride, malonic acid and 4,4′-dipyridylamine in the presence of additional base. Attempts to prepare dpa-containing malonate coordination polymers using zinc chloride and cadmium nitrate resulted in the formation of the 1-D coordination polymer [$ZnCl_2$(dpa)] [25] and the known 3-D quadruply interpenetrated diamondoid network material {[Cd(dpa)$_2$(NO_3)(H_2O)](NO_3)} [26], respectively. The infrared spectra of **1** and **2** were consistent with their formulations. Sharp, medium intensity bands in the range of ~1570–1200 cm^{-1} were ascribed to stretching modes of the pyridyl rings of the dpa moieties [27]. Features corresponding to pyridyl ring puckering mechanisms were evident in the region between 820 cm^{-1} and 600 cm^{-1}. Asymmetric and symmetric C–O stretching modes of the malonate carboxylate moieties were evidenced by very strong, slightly broadened bands at ~1600 cm^{-1} and ~1350 cm^{-1}. Broad bands in the region of ~3800–3200 cm^{-1} in all cases represent N–H stretching modes within the dpa ligands and O–H stretching modes within water molecules of crystallization. The broadness

Table 1
Crystal and structure refinement data for **1** and **2**

Data	1	2
Empirical formula	$C_{16}H_{21}Co_2N_3O_{12}$	$C_{16}H_{21}N_3Ni_2O_{12}$
Formula weight	565.23	564.78
Collection T (K)	173(2)	173(2)
λ (Å)	0.71073	0.71073
Crystal system	orthorhombic	orthorhombic
Space group	*Aba2*	*Aba2*
a (Å)	20.115(3)	20.435(7)
b (Å)	10.1473(12)	10.045(3)
c (Å)	10.4271(13)	10.336(3)
V (Å^3)	2128.3(5)	2121.7(12)
Z	4	4
D_{calc} (g cm^{-3})	1.751	1.759
μ (mm^{-1})	1.628	1.844
Minimum/maximum T	0.699/0.850	0.734/0.895
hkl ranges	$-26 \leqslant h \leqslant 26$, $-13 \leqslant k \leqslant 13$, $-13 \leqslant l \leqslant 13$	$-26 \leqslant h \leqslant 26$, $-13 \leqslant k \leqslant 13$, $-13 \leqslant l \leqslant 13$
Total reflections	12303	12655
Unique reflections	2584	2608
R_{int}	0.0196	0.0877
Parameters/restraints	167/5	167/5
R_1[a] (all data)	0.0194	0.0767
R_1[a] ($I > 2\sigma(I)$)	0.0187	0.0503
wR_2 [b] (all data)	0.0500	0.0904
wR_2 [b] ($I > 2\sigma(I)$)	0.0497	0.0833
Maximum/minimum residual (e$^-$/Å^3)	0.363/−0.332	0.404/−0.619
Goodness-of-fit	1.109	1.076

[a] $R_1 = \Sigma||F_o| - |F_c||/\Sigma|F_o|$.
[b] $wR_2 = \{\Sigma[w(F_o^2 - F_c^2)^2]/\Sigma[wF_o^2]^2\}^{1/2}$.

of these latter spectral features is attributed to supramolecular hydrogen bonding patterns (*vide infra*).

4.2. Structural description of {[M_2(malonate)$_2$(dpa)(H_2O)$_2$] · 2H_2O} (M = Co, **1**; M = Ni, **2**)

X-ray crystallography revealed that **1** and **2** are isomorphous, crystallizing in the non-centrosymmetric space group *Aba2*. The Flack parameters (0.02(1) for **1**, 0.03(3) for **2**) in both cases indicate a high degree of enantiomeric purity [28]. The formation of chiral coordination polymers due to the "double-bladed" nature of the kinked dpa ligand has been previously observed by Hanton and co-workers [29]. While other single crystals were not examined, it is most likely that a racemic mixture exists in the bulk sample. Spontaneous resolution during self-assembly has been observed in other coordination polymer systems [30].

The asymmetric units of **1** and **2** were virtually identical, possessing one divalent metal atom, one fully deprotonated malonate ligand, one-half of a dpa ligand, one coordinated water molecule, and two crystallographically distinct half-occupied unligated water molecule positions (marked by O6 and O7). The N–H bonds of the dpa ligands lie on crystallographic twofold axes along the *c* crystal direction. As seen in Fig. 1 (shown for **1**), the metal atoms display distorted [MO_5N] octahedral coordination spheres. The equatorial plane of the octahedron is comprised of two mutually *cis* oxygen atoms belonging to a 1,3-chelating malonate ligand, and two other mutually *cis* oxygen atoms, each of which is part of two other malonate ligands. The coordinated water molecule and the nitrogen donor from the dpa ligand occupy the *trans* axial positions. Bond lengths and angles within **1** and **2** (Table 2) are consistent with chelated octahedral coordination complexes of Co and Ni. The bond lengths in **2** are slightly shorter than those in **1**, reflective of well-known ionic radius trends [31].

The 1,3-type chelation of the malonate ligand (at O1 and O2) results in {MOC_3O} "boat"-conformation six-membered rings. Each of the other two malonate oxygen atoms not involved in chelation

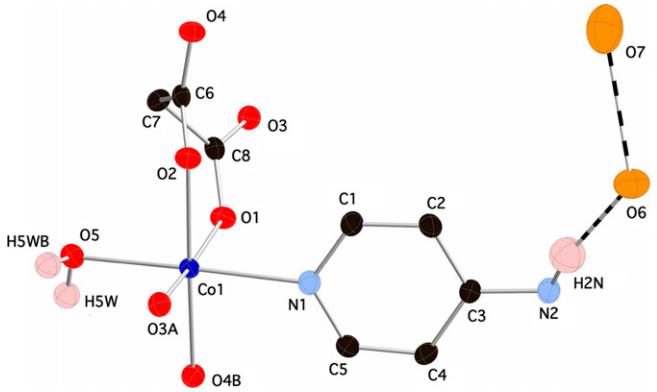

Fig. 1. Coordination environment of **1** with thermal ellipsoids at 50% probability and atom numbering scheme. Most H atoms have been omitted. Hydrogen bonding is indicated as dashed lines. The asymmetric unit of **2** is virtually identical. Symmetry codes A and B are as listed in Table 2.

Table 2
Selected bond lengths (Å) and angles (°) in **1** and **2**

Co1–O3A	2.1125(12)	Ni1–O3A	2.063(3)
Co1–O4B	2.0825(13)	Ni1–O4B	2.086(3)
Co1–O2	2.0842(12)	Ni1–O1	2.047(3)
Co1–O1	2.0919(11)	Ni1–O2	2.046(3)
Co1–O5	2.1531(12)	Ni1–O5	2.103(4)
Co1–N1	2.1553(14)	Ni1–N1	2.106(4)
O1–C8	1.265(2)	O1–C8	1.271(5)
O2–C6	1.271(2)	O2–C6	1.281(6)
O3–C8	1.2663(19)	O3–C6	1.229(6)
O4–C6	1.250(2)	O4–C8	1.267(6)
O4B–Co1–O2	177.13(5)	O2–Ni1–O4B	88.37(12)
O4B–Co1–O1	90.75(5)	O2–Ni1–O3A	178.19(13)
O2–Co1–O1	86.40(5)	O1–Ni1–O3A	89.98(13)
O4B–Co1–O3A	96.92(5)	O2–Ni1–O4B	85.72(12)
O2–Co1–O3A	85.91(5)	O1–Ni1–O4B	173.43(14)
O1–Co1–O3A	172.00(5)	O3A–Ni1–O4B	95.89(12)
O4B–Co1–O5	89.68(5)	O2–Ni1–O5	90.41(13)
O2–Co1–O5	90.63(5)	O1–Ni1–O5	88.38(14)
O1–Co1–O5	88.55(5)	O3A–Ni1–O5	90.29(14)
O3A–Co1–O5	93.72(5)	O4B–Ni1–O5	94.52(13)
O4B–Co1–N1	86.62(5)	O2–Ni1–N1	92.43(15)
O2–Co1–N1	92.82(5)	O1–Ni1–N1	87.01(15)
O1–Co1–N1	86.57(5)	O3A–Ni1–N1	86.73(14)
O3A–Co1–N1	91.63(5)	O4B–Ni1–N1	90.37(14)
O5–Co1–N1	173.83(5)	O5–Ni1–N1	174.52(15)

Symmetry equivalent positions: (A) $-x + 1/2, y, z + 1/2$ (B) $-x + 1/2, y + 1/2, z$.

connects to a different cobalt atom. Therefore each individual malonate ligand is exotridentate, linking three neighboring metal atoms. In turn, each metal atom conjoins to three sets of two others through the carboxylate bridges of the malonate ligands to construct a ruffled two-dimensional (2-D) layer motif coincident with the *bc* crystal plane (Fig. 2). The metal–metal contact distances through the *anti–syn* 1,1-carboxylate linkages in **1** are 5.311(1) Å and 5.445(1) Å; the corresponding distances within **2** are slightly shorter, at 5.247(1) Å and 5.386(1) Å. The metal–metal distances across the bridging 1,3-carboxylate linkages for **1** and **2** are 7.275(1) Å and 7.207(1) Å, respectively. By means of the 1,1-carboxylate and 1,3-carboxylate linkages, each metal atom covalently connects to six others within the 2-D layer motif; thus forming a $3^6.4^6.5^3$ net (**hxl** structure type) as analyzed by TOPOS [32]. However, if only the 1,1-carboxylate linkages are taken into account, a simplified (4,4) rectangular grid network can be invoked for the 2-D [M_2(malonate)$_2$(H_2O)$_2$]$_n$ layers in **1** and **2**; these are similar to those seen in [M_2(malonate)$_2$(4,4′-bpy)(H_2O)$_2$]$_n$ (M = Mn [15], Co [33]; 4,4′-bpy = 4,4′-bipyridine).

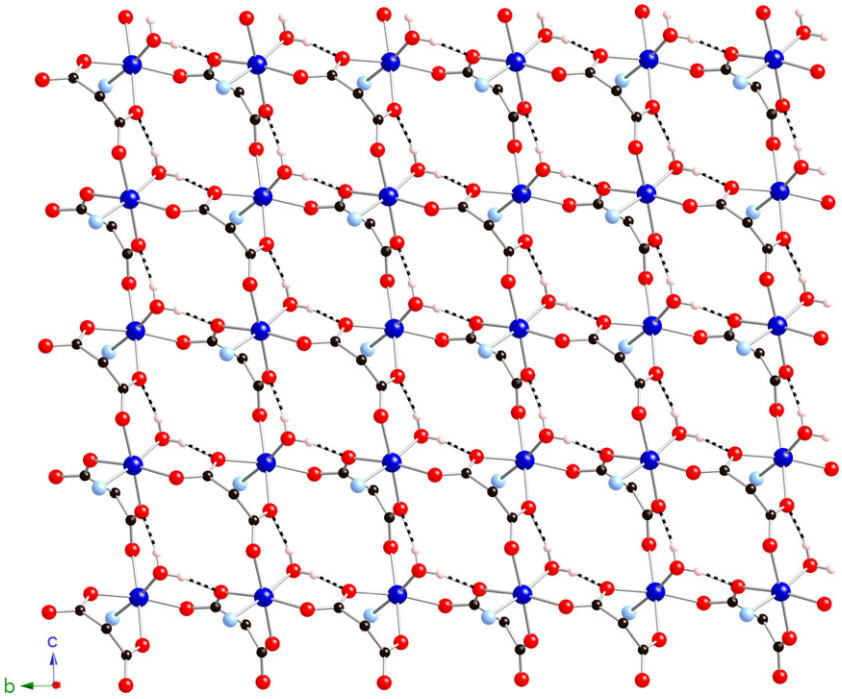

Fig. 2. View down *a* of the six-connected 2-D $[Co_2(malonate)_2(H_2O)]_n$ layer motif in **1**. A similar motif is evident in **2**. Hydrogen bonding is indicated as dashed lines.

Covalent connectivity within the $[M_2(malonate)_2(H_2O)_2]$ layers in **1** and **2** is supplemented by hydrogen bonding pathways between the coordinated water molecules and the malonate oxygen atoms involved in the 1,3-chelating binding pattern. Metrical parameters for these interactions are given in Table 2. In **1**, neighboring coordination octahedra are twisted relative to each other along both the *b* (by ~119.7°) and *c* (by ~102.7°) crystal directions, as measured by O_{aquo}–Co···Co–O_{aquo} torsion angles. The corresponding angles in **2** are extremely similar (~119.8° and ~104.4°). The coordinated water molecules bound to neighboring metal atoms alternate above and below the 2-D layer motifs, as do the nitrogen donor atoms belonging to the dpa ligands.

The 2-D $[M_2(malonate)_2(H_2O)_2]_n$ layers are stacked in an *ABA* pattern along the *a* crystal direction, and covalently linked into 3-D coordination polymer frameworks of formulation $\{[M_2(malonate)_2(dpa)(H_2O)_2]_n$ by means of the dipodal dpa tethering ligands (Fig. 3). The respective through-dpa M–M contact distances for **1** and **2** are 11.674(1) Å and 11.557(1) Å. This Co–Co distance in **1** is ~0.27 Å longer than in its 4,4′-bpy analogue, due to the additional length of the dpa ligand imparted by its central secondary amine subunit. Influenced by the supramolecular environment, the dpa ligands in **1** and **2** adopt somewhat twisted conformations, with inter-ring torsion angles of ~33.2° and ~36.9°, respectively. The linkage of the malonate-based "grid-like" layers through dpa tethers establishes a 3-D coordination polymer framework with $4^4 6^6$ topology (**sqp** lattice) in both **1** and **2** (Fig. 4). In contrast to their previously reported centrosymmetric 4,4′-bpy congeners [15,33], coordination polymers **1** and **2** adopt an acentric space

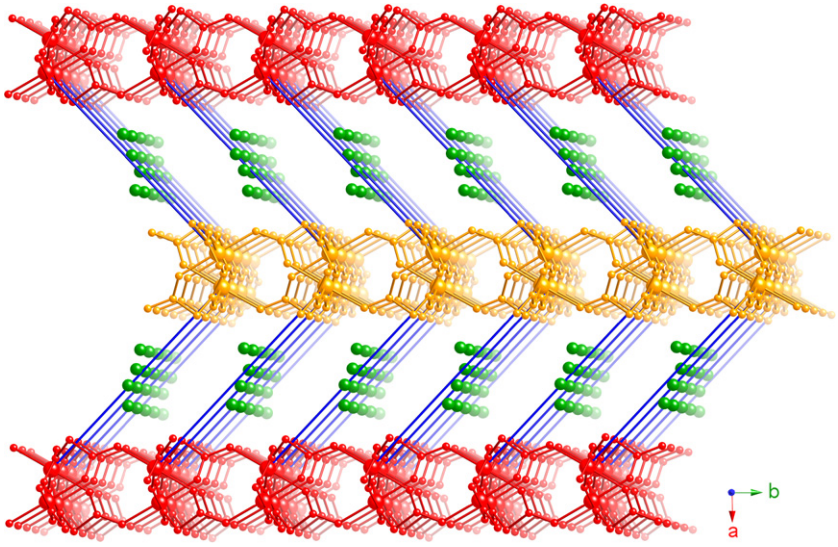

Fig. 3. View down *c* of the 3-D network structure of **1** and **2**. The dpa ligands are shown as rods and the water molecules of crystallization are shown as isolated spheres.

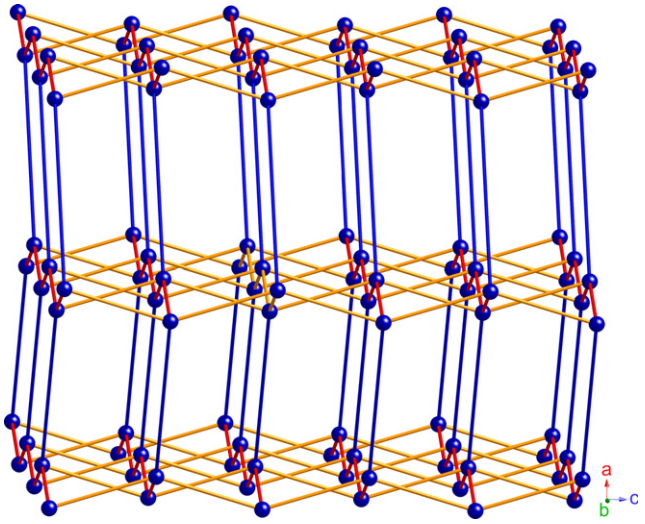

Fig. 4. Simplified network perspective of the 3-D $4^4 6^6$ topology **sqp** coordination polymer connectivity in **1** and **2**.

group due to the central kink and locked inter-ring torsion of their dpa ligands, which possess a local *C*2 point group within their respective crystal structures.

The central N–H subunits of the dpa ligands engage in hydrogen bonding to uncoordinated water molecules (O6) held within interlayer incipient voids. These water molecules in turn hydrogen bond to others (O7), forming discrete water molecule dimers, a commonly observed feature within coordination polymer matrices [34]. Each of the water molecule dimer positions is disordered equally over two symmetry related sets of sites. Distance and angle information for these supramolecular interactions are listed in Table 3. According to calculations performed with PLATON [35], the water molecule-bearing void spaces in **1** and **2** represent 12.9% and 14.0% of their respective unit cell volumes.

4.3. Thermogravimetric analysis

Compounds **1** and **2** were subjected to thermogravimetric analysis to determine the thermal stability of their 3-D coordination polymer frameworks. **1** exhibits dehydration beginning at ~185 °C (13.0% mass loss, 12.7% predicted for four water molecules). It then begins to lose all organic ligands at ~240 °C (56.7% mass loss, 60.2% predicted for one dpa and two malonate ligands), resulting in a CoO remnant (28.1% mass remaining, 26.5% predicted) at ~800 °C. Compound **2** shows a similar pattern of degradation, beginning at ~185 °C with the loss of all coordinated and uncoordinated water molecules (13.2% mass loss, 12.8% predicted). It then loses the rest of its organic ligands beginning at ~270 °C (61.3% mass loss, 66.4% predicted), resulting in the deposition of NiO (25.1% mass remaining, 26.5 % predicted) at ~800 °C. It is possible that the shorter bond lengths in **2** allow its 3-D covalent framework to have a slight enhancement in thermal stability relative to **1**. TGA traces for **1** and **2** are shown in Figs. S1 and S2, respectively.

Table 3
Hydrogen bonding distance (Å) and angle (°) data for **1** and **2**

D–H	d(H···A)	∠DHA	d(D···A)	Symmetry transformation for A
Complex ***1***				
O5–H5WA···O2	1.90(2)	162(2)	2.707(2)	$-x+1/2, y, z+1/2$
O5–H5WB···O1	1.84(2)	158(2)	2.656(2)	$-x+1/2, y+1/2, z$
N2–H2N···O6	2.09(2)	168.3(1)	2.947(4)	
Complex ***2***				
O5–H5WA···O2	1.89(3)	158(5)	2.702(5)	$-x+1/2, y, z+1/2$
O5–H5WB···O1	1.85(3)	154(5)	2.643(5)	$-x+1/2, y+1/2, z$
N2–H2N···O6	2.07(2)	166.0(2)	2.939(10)	

4.4. Variable temperature magnetic susceptibility studies

To investigate the spin communication behavior across the 2-D $[M_2(\text{malonate})_2(H_2O)_2]_n$ layer motifs in **1** and **2**, variable temperature magnetic studies were undertaken. The magnetic susceptibility of **1** followed the Curie–Weiss law ($C = \chi_m/T - \Theta$) acceptably above 75 K (Fig. S3), with $C = 3.63$ cm^3 mol Co^{-1} K and $\Theta = -72$ K. The value of C is comparable to that expected (3.37 cm^3 mol Co^{-1} K, with $C = 0.125\ \mu_{LS}^2$, $\mu_{LS} = [L(L+1) + 4S(S+1)]^{1/2}$ and $L = 3$, $S = 3/2$) when taking both spin and unquenched orbital contributions into effect, relevant for Co^{2+} ions. The negative Weiss constant is indicative of antiferromagnetic spin ordering within the $[Co_2(\text{malonate})_2(H_2O)_2]_n$ layers in **1**, although a reduction in magnetic susceptibility due to spin–orbit coupling cannot be ruled out in this system.

A successful attempt was made to model the magnetic susceptibility behavior of **1** using Lines' high-temperature expansion [36] for a quadratic lattice of $S = 3/2$ spins (Eq. (1)), where the magnetochemical variables have their usual meanings. A temperature-independent paramagnetism term (TIP) was included. Non-linear regression of the data above 50 K resulted in a best fit (Fig. 5) with the following parameters: $g = 2.08(2)$, $J = -1.05(8)$ cm^{-3}, and TIP = 0.0037(2) cm^3 mol^{-1} with $R = 1.83 \times 10^{-3} = \{\Sigma[(\chi_m T)_{obs} - (\chi_m T)_{calc}]^2/[(\chi_m T)_{obs}]^2\}^{1/2}$. The negative value of the exchange integral J corroborates the presence of antiferromagnetic interactions between Co^{2+} ions in **1**. However, the relatively mediocre fit at higher temperature, and significant deviations from the fit at $T < 50$ K indicate the possibility of spin–orbit coupling and/or anisotropy. (It should be noted that Lines' equation neglects single-ion effects.) The lack of any maximum in the $\chi_m(T)$ plot for **1** (Fig. S4) marks the likely absence of any long-range low-temperature antiferromagnetic coupling pathways between layer subunits through the organodiimine tethers. Thus the value of J should be considered a rough estimate of the level of modest intralayer antiferromagnetic interactions in **1**.

$$X_m T = \left(\frac{Ng^2\beta^2 T}{2|J|}\right)\left[3\Theta + \sum_{n=1}^{6}\frac{C_n}{\Theta^{n-1}}\right]^{-1} + \text{TIP}(T) \qquad (1)$$

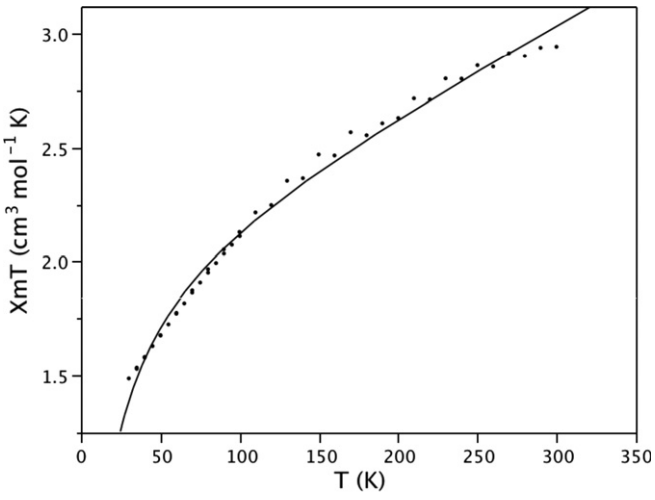

Fig. 5. $\chi_m T$ vs. T plot for **1**. The solid line indicates the best fit to Eq. (1) in the text.

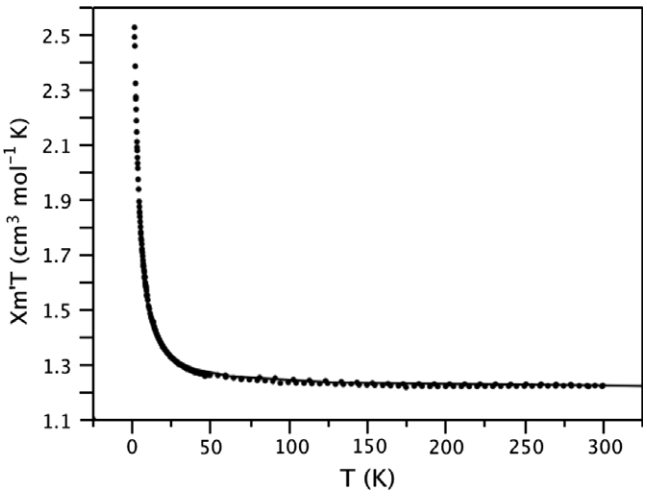

Fig. 6. $\chi_m T$ vs. T plot for **2**. The solid line indicates the best fit to Lines' model for a ferromagnetic square-lattice of $S = 1$ spins.

where $\Theta = kT/(2|J|S(S+1))$ *and* $C_1 = 4$, $C_2 = 1.6$, $C_3 = 0.304$, $C_4 = 0.249$, $C_5 = 0.132$, $C_6 = 0.013$.

The magnetic susceptibility of **2** also follows Curie–Weiss behavior (Fig. S5), but in contrast to **1** does so over the entire temperature range (2–300 K). Parameters C and Θ are 1.21 $cm^3\ mol\ Ni^{-1}\ K$ and 2.0 K, respectively. The value of C is consistent with uncoupled $S = 1$ ions at 300 K (calc. = 1.00 $cm^3\ mol^{-1}\ K$ for $g = 2.0$). In contrast to **1**, ferromagnetic interactions appear to be operative within the 2-D $[M(malonate)_2(H_2O)_2]_n$ subunits in **2** as evidenced by the positive Weiss constant. Weak ferromagnetic interactions in **2** are corroborated by an examination of the $\chi_m T(T)$ plot (Fig. 6). Upon cooling from 300 K and 50 K, a very slow increase in $\chi_m T$ from 1.21 to 1.26 $cm^3\ mol\ Ni^{-1}\ K$, occurs with a more rapid increase at lower temperature. The value of $\chi_m T$ is 2.49 $cm^3\ mol\ Ni^{-1}\ K$ at 2 K, with no sign of a diminution at any point, reflective of a ferromagnetic ground state.

The variable temperature susceptibility of **2** was fit to Lines' square-lattice high-temperature expansion in Eq. (1) (Fig. 6), with different C_n coefficients for $S = 1$ ($C_1 = -4$, $C_2 = 1.834$, $C_3 = -0.445$, $C_4 = 0.224$, $C_5 = -0.132$, $C_6 = 0.019$). No temperature-independent paramagnetism term was necessary for an acceptable fit. The best fit values were $g = 2.201(1)$ and $J = 0.289(1)\ cm^{-3}$ with $R = 1.7 \times 10^{-4}$. The small, yet positive, value of J corroborates the assignment of weak ferromagnetic interactions between the nickel ions in **2**.

Similar divergent magnetic behavior, with carboxylate bridged cobalt 2-D layers exhibiting antiferromagnetism and carboxylate bridged nickel 2-D layers showing ferromagnetism, has been observed in two prior systems, $\{[M(H_2O)_2][M(malonate)_2(H_2O)_2]\}_n$ [14] and $\{M(malate)(4,4'\text{-bpy})_{0.5}] \cdot H_2O\}_n$ (M = Co, Ni) [37]. Differences in the electronic configurations of the *pseudo* octahedrally coordinated high-spin divalent cobalt and nickel ions ($t_{2g}^5 e_g^2$ *versus* $t_{2g}^6 e_g^2$) can give rise to the observed variances in overall magnetic behavior. The greater likelihood of magnetic orbital overlap in **1**, due to the existence of three orbitals with unpaired electrons, can rationalize the greater magnitude of the magnetic interactions in **1**.

5. Conclusions

Hydrothermal synthesis has afforded a pair of isostructural 3-D coordination polymers built from $[M(malonate)_2(H_2O)_2]_n$ layers strutted by the kinked and hydrogen bonding capable tethering organodiimine dpa. While the gross structural features of these compounds resemble those of their previously reported 4,4′-bipyridine congeners, the presence of the dpa ligand enforces acentricity and spontaneous resolution in this coordination polymer system. In addition, the central amine unit of the dpa ligand promotes hydrogen bonding to entrained water molecules of crystallization, resulting in incipient voids of modest volume. The disparate magnetic properties within the square-grid layers of **1** and **2** (moderate antiferromagnetic and weak ferromagnetic, respectively) are reflective of different electronic configurations and magnetic orbital overlap; they reinforce the trends in the magnetic behavior observed in other coordination polymers with divalent cobalt- and nickel-based square-grid layer motifs. The synthetic investigation of other coordination polymer solids based on the underutilized tethering ligand dpa continues in our laboratory.

Acknowledgements

The authors gratefully acknowledge Michigan State University for financial support of this work.

We thank Dr. Rui Huang for elemental analysis and Subhashree Mallika Krishnan for assistance with spectral analysis. M.R.M. thanks the MSU Freshman Chemistry Honors Program for his participation in the work, and Dr. Reza Loloee for the use of the SQUID magnetometer. We thank Mr. Peter Podaras of Cornell University for literature assistance. The thermogravimetric analyzer at King's College was purchased with a grant from the Alden Trust. SDG.

Appendix A. Supplementary data

CCDC 675681 and 675682 contain supplementary crystallographic data for for **1** and **2.** These data can be obtained free of charge via http://www.ccdc.cam.ac.uk/conts/retrieving.html, or from the Cambridge Crystallographic Data Centre, 12 Union Road, Cambridge CB2 1EZ, UK; fax: (+44) 1223-336-033; or e-mail: deposit@ccdc.cam.ac.uk. TGA traces and Curie–Weiss plots for **1** and **2** are also available via the online edition of this journal. Supplementary data associated with this article can be found, in the online version, at doi:10.1016/j.poly.2008.06.010.

References

[1] [a] H. Li, M. Eddaoudi, M. O'Keeffe, O.M. Yaghi, Nature 402 (2005) 276;
[b] R. Matsuda, R. Kitaura, S. Kitagawa, Y. Kubota, R.U. Belosludov, T.C. Kobayashi, H. Sakamoto, T. Chiba, M. Takata, Y. Kawazoe, Y. Mita, Nature 436 (2005) 238;
[c] L. Pan, D. Holson, L.R. Ciemnolonski, R. Heddy, J. Li, Angew. Chem., Int. Ed. 46 (2006) 616;
[d] N.L. Rosi, J. Eckert, M. Eddaoudi, D.J. Vodak, J. Kim, M. O'Keeffe, O.M. Yaghi, Science 300 (2003) 1127;
[e] M. Dinca, A.F. Yu, J.R. Long, J. Am. Chem. Soc. 128 (2006) 8904;
[f] G. Ferey, M. Latroche, C. Serre, F. Millange, T. Loiseau, A. Percheron-Guegan, Chem. Commun. (2003) 2976;
[g] X. Zhao, B. Xiao, A.J. Fletcher, K.M. Thomas, D. Bradshaw, M.J. Rosseinsky, Science 306 (2004) 1012.
[2] [a] J.S. Seo, D. Whang, H. Lee, S.I. Jun, J. Oh, Y.J. Jeon, K. Kim, Nature 404 (2000) 982;
[b] B. Chen, C. Liang, J. Yang, D.S. Contreras, Y.L. Clancy, E.B. Lobkovsky, O.M. Yaghi, S. Dai, Angew. Chem., Int. Ed. 45 (2006) 1390.
[3] [a] Q.-R. Fang, G.-S. Zhu, M. Xue, J.-Y. Sun, S.-L. Qiu, Dalton Trans. (2006) 2399;
[b] X.-M. Zhang, M.-L. Tong, H.K. Lee, X.-M. Chen, J. Solid State Chem. 160 (2001) 118;
[c] O.M. Yaghi, H. Li, T.L. Groy, Inorg. Chem. 36 (1997) 4292.
[4] [a] N. Guillou, P.M. Forster, Q. Gao, J.S. Chang, M. Nogues, S.-E. Park, A.K. Cheetham, G. Ferey, Angew. Chem., Int. Ed. 40 (2001) 2831;
[b] C.-D. Wu, A. Hu, L. Zhang, W. Lin, J. Am. Chem. Soc. 127 (2005) 8940;
[c] H. Han, S. Zhang, H. Hou, Y. Fan, Y. Zhu, Eur. J. Inorg. Chem. (2006) 1594;
[d] W. Mori, S. Takamizawa, C.N. Kato, T. Ohmura, T. Sato, Micropor. Mesopor. Mater. 73 (2004) 15.
[5] [a] S. Zang, Y. Su, Y. Li, Z. Ni, Q. Meng, Inorg. Chem. 45 (2006) 174;
[b] L. Wang, M. Yang, G. Li, Z. Shi, S. Feng, S. Inorg. Chem. 45 (2006) 2474.
[6] [a] S. Wang, Y. Hou, E. Wang, Y. Li, L. Xu, J. Peng, S. Liu, C. Hu, New J. Chem. 27 (2003) 1144;
[b] L.G. Beauvais, M.P. Shores, J.R. Long, J. Am. Chem. Soc. 122 (2000) 2763;

[c] H. Jianghua, Y. Jihong, Z. Yuetao, P. Qinhe, X. Ruren, Inorg. Chem. 44 (2005) 9279.
[7] [a] S.A. Bourne, J.J. Lu, A. Mondal, B. Moulton, M.J. Zaworotko, Angew. Chem., Int. Ed. 40 (2001) 2111;
[b] D.T. Vodak, M.E. Braun, J.H. Kim, M. Eddaoudi, O.M. Yaghi, Chem. Commun. (2001) 2534;
[c] D. Burrows, R.W. Harrington, M.F. Mahon, S.J. Teat, Eur. J. Inorg. Chem. (2003) 766.
[8] [a] Y.-M. Dai, E. Ma, E. Tang, J. Zhang, J.-Z. Li, X.-D. Huang, Y.-G. Yao, Cryst. Growth Des. 5 (2005) 1313;
[b] L. Xu, G.-C. Guo, B. Liu, M.-S. Wang, J.-S. Huang, Inorg. Chem. Commun. 7 (2004) 1145.
[9] Y.-Q. Zheng, Z.-P. Kong, Z. Anorg. Allgem. Chem. 629 (2003) 1469.
[10] S.-M. Ying, J.-G. Mao, Y.-Q. Sun, H.-Y. Zen, Z.-C. Dong, Polyhedron 22 (2003) 3097.
[11] R. Vaidhyanathan, S. Natarajan, C.N.R. Rao, Inorg. Chem. 41 (2002) 5226.
[12] Y.-Q. Zheng, J.-L. Lin, Z.-P. Kong, Inorg. Chem. 43 (2004) 2590.
[13] R.-F. Hu, Y. Kang, J. Zhang, Z.-J. Li, Y.-Y. Qin, Y.-G. Yao, Z. Anorg. Allgem. Chem. 631 (2005) 3053.
[14] F.S. Delgado, M. Hernandez-Molina, J. Sanchiz, C. Ruiz-Perez, Y. Rodriguez-Martin, J. Lopez, F. Lloret, M. Julve, CrystEngComm 6 (2004) 106.
[15] Y. Rodriguez-Martin, M. Hernandez-Molina, J. Sanchiz, C. Ruiz-Perez, F. Lloret, M. Julve, Dalton Trans. (2003) 2359.
[16] Y. Rodriguez-Martin, C. Ruiz-Perez, J. Sanchiz, F. Lloret, M. Julve, Inorg. Chim. Acta 318 (2001) 159.
[17] M.R. Montney, S. Mallika Krishnan, R.M. Supkowski, R.L. LaDuca, Inorg. Chem. 46 (2007) 7362.
[18] M.R. Montney, S. Mallika Krishnan, Niral M. Patel, R.M. Supkowksi, R.L. LaDuca, Cryst. Growth Des. 7 (2007) 1145.
[19] M.R. Montney, R.L. LaDuca, Inorg. Chem. Commun. 10 (2007) 1518.
[20] P.J. Zapf, R.L. LaDuca, R.S. Rarig, K.M. Johnson, J. Zubieta, Inorg. Chem. 37 (1998) 3411.
[21] O. Khan, Molecular Magnetism, VCH Publishers, New York, 1993.
[22] SAINT, Software for Data Extraction and Reduction, Version 6.02, Bruker AXS, Inc., Madison, WI, 2002.
[23] SADABS, Software for Empirical Absorption Correction, Version 2.03, Bruker AXS, Inc., Madison, WI, 2002.
[24] G.M. Sheldrick, SHELXTL, Program for Crystal Structure Refinement, University of Gottingen, Gottingen, Germany, 1997.
[25] S. Mallika Krishnan, R.L. LaDuca, unpublished results.
[26] D.B. Cordes, L.R. Hanton, M.D. Spicer, Cryst. Growth Des. 7 (2007) 328.
[27] M. Kurmoo, C. Estournes, Y. Oka, H. Kumagai, K. Inoue, Inorg. Chem. 44 (2005) 217.
[28] [a] G. Bernardinelli, H.D. Flack, Acta Crystallogr., Sect. A 41 (1985) 500;
[b] H.D. Flack, Acta Crystallogr., Sect. A 29 (1983) 876.
[29] D.B. Cordes, L.R. Hanton, M.D. Spicer, Inorg. Chem. 45 (2006) 7651.
[30] [a] F. Li, T. Li, X. Li, X. Li, Y. Wang, R. Cao, Cryst. Growth Des. 6 (2006) 1458;
[b] M. Sasa, K. Tanaka, X.-H. Bu, M. Shiro, M. Shionoya, J. Am. Chem. Soc. 123 (2001) 10750.
[31] R.D. Shannon, Acta Crystallogr., Sect. A 32 (1976) 751.
[32] V.A. Blatov, A.P. Shevchenko, V.N. Serezhkin, J. Appl. Crystallogr. 33 (2000) 1193.
[33] P. Lightfoot, A. Snedden, J. Chem. Soc., Dalton Trans. (1999) 3549.
[34] L. Infantes, S. Motherwell, CrystEngComm 4 (2002) 454.
[35] A.L. Spek, PLATON, A Multipurpose Crystallographic Tool, Utrecht University, Utrecht, The Netherlands, 1998.
[36] M.E. Lines, J. Phys. Chem. Solids 31 (1970) 101.
[37] L.-M. Duan, F.-T. Xie, X.-Y. Chen, Y. Chen, Y.-K. Lu, P. Cheng, J.-Q. Xu, Cryst. Growth Des. 6 (2006) 1101.

binds to all five ring donors [4], in other cases non-coordination of ether donors was observed [5] with the metal residing either endo or exo with respect to the macrocyclic cavity.

As an extension of the above studies we now report the synthesis and X-ray study of an extended series of new complexes of **L** incorporating the soft metal ions Ag(I), Cd(II), Hg(II) and Pd(II) the results serve to both extend and further exemplify the rich and varied structural chemistry documented so far for complexes of this ligand type.

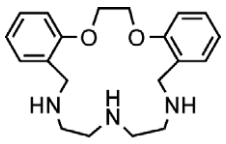

L

2. Experimental

2.1. General comments

All commercial reagents and solvents were of analytical reagent grade where available. Infrared spectra (KBr pellets) were measured on a Mattson Genesis Series FT-IR spectrophotometer. Microanalyses were performed on a LECO CHNS-932 elemental analyser. The mass spectra were obtained on a JEOL JMS-700 spectrometer (FAB) and Applied Biosystems 4000 Q TRAP (ESI) at the Central Instrument Facility of Gyeongsang National University. Melting points are uncorrected. The preparation of **L** has been reported previously [6]. All metal complexes were dried in a vacuum before microanalysis; the complexes were isolated with typical yields of 20–60%.

2.2. Complex synthesis

Caution: the respective perchlorate-containing complexes are potentially explosive and appropriate precautions should be taken during their preparation, handling and storage.

2.2.1. Preparation of $[Ag_2\mathbf{L}_2(NO_3)_2]$ (**1**)

L (20 mg, 0.059 mmol) in warm methanol (2 mL) was added to one equivalent of $AgNO_3$ in a similar volume of warm acetonitrile. Slow evaporation of this solution yielded **1** as a crystalline product that proved suitable for X-ray analysis. Yield: 30%. [*Anal.* Calc. for $C_{40}H_{54}Ag_2N_8O_{10}$: C, 46.98; H, 5.32; N, 10.96. Found: C, 46.66; H, 4.95; N, 11.14%.] IR (KBr, cm^{-1}): 3276, 2909, 2857, 2349, 1590, 1478, 1422, 1374 (s, NO_3^-), 1303, 1239, 1048, 939, 772. MS (FAB) m/z = 448.1 ($[Ag\mathbf{L}]^+$, $[C_{20}H_{27}AgN_3O_2]^+$). Mp 180–182 °C (decomp.).

2.2.2. Preparation of $[Ag_2\mathbf{L}_2](ClO_4)_2 \cdot 2DMF$ (**2**)

A colorless precipitate of **2** was obtained on mixing equimolar amounts of **L** (20 mg, 0.059 mmol) and $AgClO_4$ in warm methanol (5 mL). Yield: 60%. [*Anal.* Calc. for $C_{40}H_{54}Ag_2Cl_2N_6O_{12}$: C, 48.77; H, 4.96; N, 7.66. Found: C, 48.42; H, 5.41; N, 7.72%.] IR (KBr, cm^{-1}): 3282, 2897, 2349, 1592, 1504, 1433, 1235, 1103 (s, ClO_4^-), 933, 774, 603. MS (FAB) m/z = 448.1 ($[Ag\mathbf{L}]^+$, $[C_{20}H_{27}AgN_3O_2]^+$). Mp 220–225 °C. Vapour diffusion of diethyl ether into a DMF solution of this product yielded crystals of **2** that were suitable for X-ray analysis.

2.2.3. Preparation of $[Ag_2\mathbf{L}_2](PF_6)_2 \cdot 2DMF$ (**3**)

A colourless precipitate of **3** was obtained on mixing equimolar amounts of **L** (20 mg, 0.059 mmol) and $AgPF_6$ in warm methanol (5 mL). Yield: 60%. [*Anal.* Calc. for $C_{40}H_{54}Ag_2F_{12}N_6O_4P_2$: C, 40.42; H, 4.58; N, 7.07. Found: C, 40.21; H, 4.59; N, 7.08%.] IR (KBr, cm^{-1}): 3320, 2904, 2349, 1650, 1478, 1434, 1234, 801 (s, PF_6^-), 785, 522. MS (FAB) m/z = 448.1 ($[Ag\mathbf{L}]^+$, $[C_{20}H_{27}AgN_3O_2]^+$). Mp 248–253 °C (decomp.). Vapour diffusion of diethyl ether into a DMF solution of this product afforded **3** as a crystalline product which was suitable for X-ray analysis.

2.2.4. Preparation of $[Ag_2\mathbf{L}_2](OTf)_2$ (**4**)

Slow evaporation a methanol solution (5 mL) of **L** (20 mg, 0.059 mmol) containing one equivalent of AgOTf afforded **4** as a crystalline product that was suitable for X-ray analysis. Yield: 30%. [*Anal.* Calc. for $C_{42}H_{54}Ag_2F_6N_6O_{10}S_2$: C, 42.15; H, 4.55; N, 7.02; S, 5.36. Found: C, 42.24; H, 4.28; N, 6.93; S, 5.82%.] IR (KBr, cm^{-1}): 3321, 2905, 2349, 1658, 1613, 1479, 1268, 1185, 1064, 932, 737 (s, OTf^-), 614. MS (FAB) m/z = 448.1 ($[Ag\mathbf{L}]^+$, $[C_{20}H_{27}AgN_3O_2]^+$). Mp 210–214 °C (decomp.).

2.2.5. Preparation of $[Ag_2\mathbf{L}_2(\mu\text{-}CN)][Ag(CN)_2] \cdot H_2O$ (**5**)

Addition of **L** (20 mg, 0.059 mmol) in warm methanol (2 mL) to one equivalent of $K[Ag(CN)_2]$ in a similar volume of warm water led, on slow evaporation of the solvent mixture, to **5** as a crystalline product that was suitable for X-ray analysis. Yield: 40%. [*Anal.* Calc. for $C_{43}H_{54}Ag_2N_9O_4$: C, 52.88; H, 5.57; N, 12.91. Found: C, 53.10; H, 5.43; N, 13.01%.] IR (KBr, cm^{-1}): 3230, 2947, 2837, 2125 (s, CN^-), 1602, 1589, 1494, 1448, 1384, 1292, 1244, 1062, 952, 763. MS (ESI) m/z = 922, ($[Ag_2\mathbf{L}_2CN]^+$, $[C_{41}H_{54}Ag_2N_7O_4]^+$). Mp 214–215 °C (decomp.).

2.2.6. Preparation of $[Cd\mathbf{L}_2](ClO_4)_2 \cdot CH_3CN$ (**6**)

L (20 mg, 0.059 mmol) in warm methanol (2 mL) was added to one equivalent of $Cd(ClO_4)_2$ in a similar volume of warm methanol to yield a colorless precipitate of **6**. Yield: 60%. [*Anal.* Calc. for $C_{40}H_{54}CdCl_2N_6O_{12}$: C, 48.32; H, 5.47; N, 8.45. Found: C, 47.90; H, 5.33; N, 7.97%.] IR (KBr, cm^{-1}): 3305, 3258, 2987, 2348, 1480, 1241, 1103 (s, ClO_4^-), 932, 854. MS (ESI) m/z = 895.3 ($[Cd\mathbf{L}_2(ClO_4)]^+$, $[C_{40}H_{54}CdClN_6O_8]^+$). Mp 175–177 °C (decomp.). Single crystals of **6** suitable for X-ray analysis were obtained by vapour diffusion of diethyl ether into an acetonitrile solution of this complex.

2.2.7. Preparation of $[Hg\mathbf{L}(ClO_4)_2]$ (**7**)

L (20 mg, 0.059 mmol) in warm dichloromethane (2 mL) was added to one equivalent of $Hg(ClO_4)_2$ in a similar volume of warm methanol to yield a colorless precipitate of **7**. Yield: 50%. [*Anal.* Calc. for $C_{20}H_{27}Cl_2HgN_3O_{10}$: C, 32.42; H, 3.67; N, 5.67. Found: C, 32.18; H, 3.91; N, 5.62%.] IR (KBr, cm^{-1}): 3375, 3285, 2897, 2348, 1480, 1214, 1102 (s, ClO_4^-), 774, 584. MS (FAB): m/z = 642.2 ($[Hg\mathbf{L}(ClO_4)]^+$, $[C_{20}H_{27}ClHgN_3O_6]^+$). Mp 192–198 °C (decomp.). Single crystals of **7** suitable for X-ray analysis were obtained by vapour diffusion of diethyl ether into a DMF solution of this complex.

2.2.8. Preparation of $[Hg\mathbf{L}(SCN)_2] \cdot CH_3CN$ (**8**)

Slow evaporation of a dichloromethane/acetonitrile solution (5 mL) of **L** (20 mg, 0.059 mmol) containing one equivalent of $Hg(SCN)_2$ afforded **8** as a crystalline product that was suitable for X-ray analysis. Yield: 30%. [*Anal.* Calc. for $C_{22}H_{27}HgN_5O_2S_2$: C, 40.15; H, 4.13; N, 10.64; S, 9.74. Found: C, 40.42; H, 4.55; N, 10.25; S, 9.51%.] IR (KBr, cm^{-1}): 3233, 2890, 2100 (s, SCN^-), 1592, 1471, 1269, 934, 734. MS (FAB) m/z = 601.2 ($[Hg\mathbf{L}(SCN)]^+$, $[C_{20}H_{27}HgN_4O_2S]^+$). Mp 170–174 °C (decomp.).

*2.2.9. Preparation of $[Hg_2\mathbf{L}_2](HgI_4)_2 \cdot 2\mathbf{L}$ (**9**)*

Slow evaporation of dichloromethane/acetonitrile solution (5 mL) of **L** (20 mg, 0.059 mmol) containing one equivalent of HgI_2 afforded **9** as a crystalline product that was suitable for X-ray analysis. Yield: 20%. [*Anal.* Calc. for $C_{40}H_{54}Hg_2I_4N_6O_4$: C, 30.18; H, 3.42; N, 5.28. Found: C, 29.87; H, 3.14; N, 5.44%.] IR (KBr, cm^{-1}): 3253, 2930, 2378, 1424, 1204, 943, 752. MS (FAB) m/z = 670.1 ($[Hg\mathbf{L}I]^+$, $[C_{20}H_{27}HgIN_3O_2]^+$). Mp 152–157 °C (decomp.).

*2.2.10. Preparation of $[Hg\mathbf{L}_2](NO_3)_2 \cdot 2CH_3OH$ (**10**)*

Slow evaporation of a dichloromethane/methanol solution (5 mL) containing **L** (20 mg, 0.059 mmol) and one equivalent of $Hg(NO_3)_2$ afforded **10** as a colourless crystalline product that was suitable for X-ray analysis. Yield: 40%. [*Anal.* Calc. for $C_{40}H_{54}HgN_8O_{10}$: C, 47.69; H, 5.40; N, 11.12. Found: C, 47.62; H, 5.34; N, 10.86%.] IR (KBr, cm^{-1}): 3562, 3477, 2839, 2349, 1595, 1479, 1429, 1387 (s, NO_3^-), 1292, 1096, 936, 748. MS (ESI): m/z = 946.8 ($[Hg\mathbf{L}_2(NO_3)]^+$, $[C_{40}H_{54}HgN_7O_7]^+$). Mp 144–145 °C (decomp.).

*2.2.11. Preparation of $[Pd\mathbf{L}Cl]Cl \cdot H_2O$ (**11**)*

A dichloromethane solution (2 mL) of **L** (20 mg, 0.059 mmol) and equal volume of an aqueous solution of K_2PdCl_4 were mixed in a 1:1 molar ratio to yield an orange precipitate of **11**. Yield: 30%. [*Anal.* Calc. for $C_{20}H_{27}Cl_2N_3O_2Pd$: C, 46.30; H, 5.25; N, 8.10. Found: C, 46.21; H, 5.54; N, 7.81%.] IR (KBr, cm^{-1}): 3323, 2842, 2578, 2379, 1568, 1156, 925. MS (FAB) m/z = 484.1 ($[Pd\mathbf{L}Cl]^+$, $[C_{20}H_{27}ClN_3O_2Pd]^+$). Mp 167–168 °C (decomp.). Single crystals of **11** suitable for X-ray analysis were obtained by vapour diffusion of diethyl ether into a methanol solution of this complex.

*2.2.12. Preparation of $[Pd\mathbf{L}(NO_3)]NO_3 \cdot CH_3OH$ (**12**)*

Slow evaporation of a methanol solution (2 mL) of **L** (20 mg, 0.059 mmol) containing one equivalent of $Pd(NO_3)_2$ afforded **12** as orange crystals that was suitable for X-ray analysis. Yield: 30%. [*Anal.* Calc. for $C_{20}H_{27}N_5O_8Pd$: C, 42.00; H, 4.76; N, 12.25. Found: C, 42.31; H, 5.02; N, 12.33%.] IR (KBr, cm^{-1}): 3233, 2956, 2578, 2100, 1424, 1367 (s, NO_3^-), 1156, 925. MS (FAB) m/z = 509.1 ($[Pd\mathbf{L}(NO_3)]^+$, $[C_{20}H_{27}N_4O_5Pd]^+$). Mp 172–173 °C (decomp.).

2.3. X-ray structure determinations

For each determination a suitable crystal was mounted on a Bruker SMART diffractometer equipped with a graphite monochromated Mo Kα (λ = 0.71073 Å) radiation source and a CCD detector and 45 frames of two-dimensional diffraction images were collected and processed to deduce the cell parameters and orientation matrix. A total of 1271 frames of two-dimensional diffraction images were collected. The frame data were processed to give structure factors using the program SAINT [7]. The intensity data were corrected for Lorentz and polarization effects. Empirical absorption corrections were also applied for compounds **2**, **7–8**, **10** and **12** using the program SADABS [8]. The structures were solved by a combination of direct and difference Fourier methods provided by the program package SHELXTL [9], and refined using a full matrix least square against F^2 for all data. All non-H atoms were refined anisotropically. All hydrogen atoms were included in calculated positions with isotropic thermal parameters 1.2 times those of attached atoms. Crystallographic data are summarized in Tables 1–3. Selected geometric parameters for the respective complexes are presented in Tables 4–11.

3. Results and discussion

The following crystalline complexes, $[Ag_2\mathbf{L}_2(NO_3)_2]$ (**1**), $[Ag_2\mathbf{L}_2](ClO_4)_2 \cdot 2DMF$ (**2**), $[Ag_2\mathbf{L}_2](PF_6)_2 \cdot 2DMF$ (**3**), $[Ag_2\mathbf{L}_2](OTf)_2$ (**4**), $[Ag_2\mathbf{L}_2(\mu\text{-}CN)][Ag(CN)_2] \cdot H_2O$ (**5**), $[Cd\mathbf{L}_2](ClO_4)_2 \cdot CH_3CN$ (**6**), $[Hg\mathbf{L}(ClO_4)_2]$ (**7**), $[Hg\mathbf{L}(SCN)_2] \cdot CH_3CN$ (**8**), $[Hg_2\mathbf{L}_2](HgI_4)_2 \cdot 2\mathbf{L}$ (**9**), $[Hg\mathbf{L}_2](NO_3)_2 \cdot 2CH_3OH$ (**10**), $[[Pd\mathbf{L}Cl]Cl \cdot H_2O$ (**11**) and $[Pd\mathbf{L}(NO_3)]NO_3 \cdot CH_3OH$ (**12**) were isolated and characterised using microanalysis, mass spectra, infrared spectroscopy and single-crystal X-ray diffraction. In each case the reaction mixture involved the 1:1 interaction of the corresponding metal salt with **L** in methanol, dichloromethane or acetonitrile (or a mixture of these solvents). Crystals of **1**, **4** and **5**, **8–10** and **12** suitable for X-ray structure determination were obtained on slow evaporation of the corresponding reaction solutions while crystals of the remaining complexes were grown by vapour diffusion of diethyl ether into their DMF (**2**, **3**, **7**), acetonitrile (**6**) or methanol (**11**) solutions.

Table 1
Crystal data and structural refinement for **1–4**

	1	2	3	4
Formula	$C_{20}H_{27}AgN_4O_5$	$C_{23}H_{34}AgClN_4O_6$	$C_{23}H_{33}AgF_6N_4O_3P$	$C_{21}H_{27}AgF_3N_3O_5S$
M	511.33	621.86	666.37	598.39
T (K)	173(2)	173(2)	173(2)	173(2)
Crystal system	triclinic	triclinic	triclinic	orthorhombic
Space group	$P\bar{1}$	$P\bar{1}$	$P\bar{1}$	*Pbca*
a (Å)	9.8528(14)	11.3157(4)	11.2315(6)	18.3409(6)
b (Å)	11.1070(16)	11.3238(4)	11.5622(6)	15.6380(5)
c (Å)	11.5054(16)	11.9184(4)	12.1403(6)	16.2961(5)
α (°)	66.204(2)	113.985(1)	113.651(1)	
β (°)	74.244(2)	106.096(1)	106.073(1)	
γ (°)	68.513(2)	96.665(1)	96.256(1)	
V (Å^3)	1060.6(3)	1294.29(8)	1343.62(12)	4674.0(3)
Z	2	2	2	8
μ(Mo Kα) (mm^{-1})	0.990	0.932	0.884	1.014
Crystal size (mm)	0.20 × 0.05 × 0.05	0.60 × 0.45 × 0.40	0.30 × 0.20 × 0.05	0.30 × 0.20 × 0.20
Absorption correction				
Reflections collected	9242	8060	8409	28560
Independent reflections	4558	5566	5794	5628
Goodness-of-fit on F^2	1.077	1.054	0.965	1.028
Final R_1, wR_2 [$I > 2\sigma(I)$]	0.0388, 0.0803	0.0257, 0.0662	0.0384, 0.0868	0.0398, 0.0832
(all data)	0.0561, 0.0858	0.0291, 0.0684	0.0605, 0.0961	0.0944, 0.1017

Table 2
Crystal data and structural refinement for **5**–**8**

	5	6	7	8
Formula	$C_{21.5}H_{29}Ag_{1.5}N_{4.5}O_3$	$C_{21}H_{28.5}Cd_{0.5}ClN_{3.5}O_6$	$C_{20}H_{27}Cl_2HgN_3O_{10}$	$C_{24}H_{30}HgN_6O_2S_2$
M	560.30	517.62	740.94	699.25
T (K)	173(2)	173(2)	173(2)	173(2)
Crystal system	orthorhombic	orthorhombic	monoclinic	monoclinic
Space group	*Pbcn*	*Aba*2	$P2_1/c$	$P2_1/n$
a (Å)	14.5494(10)	11.4537(4)	9.3323(4)	13.3291(8)
b (Å)	19.4863(13)	16.9810(7)	21.9851(9)	9.8352(6)
c (Å)	15.9080(11)	23.53284(9)	12.7204(6)	21.3585(13)
β (°)			111.410(1)	105.011(1)
V (Å^3)	4510.1(5)	4537.3(3)	2429.76(18)	2704.4(3)
Z	8	8	4	4
μ(Mo Kα) (mm^{-1})	1.346	1.516	6.616	5.878
Absorption correction				
Reflections collected	27309	14032	15457	15861
Independent reflections	5381	5270	5707	6089
Goodness-of-fit on F^2	0.966	1.036	1.056	1.029
Final R_1, wR_2 [$I > 2\sigma(I)$]	0.0644, 0.1369	0.0277, 0.0669	0.0331, 0.0639	0.0384, 0.0949
(all data)	0.1313, 0.1618	0.0340, 0.0699	0.0587, 0.0716	0.0468, 0.0998

Table 3
Crystal data and structural refinement for **9**–**12**

	9	10	11	12
Formula	$C_{20}H_{25.5}HgI_2N_3O_2$	$C_{42}H_{62}HgN_8O_{12}$	$C_{20}H_{29}Cl_2N_3O_3Pd$	$C_{21}H_{31}N_5O_9Pd$
M	794.32	1071.59	536.76	603.91
T (K)	173(2)	173(2)	173(2)	173(2)
Crystal system	monoclinic	orthorhombic	monoclinic	triclinic
Space group	$P2_1/n$	*Pbca*	*C*2/*c*	$P\bar{1}$
a (Å)	11.2126(7)	16.6660(6)	36.8037(16)	8.4606(5)
b (Å)	21.0377(13)	22.6937(8)	6.1245(3)	10.9554(6)
c (Å)	20.4337(12)	23.6807(9)	23.8584(12)	14.1836(8)
α (°)				100.840(1)
β (°)	91.082(1)		123.133(1)	99.559(1)
γ (°)				94.877(1)
V (Å^3)	4819.2(5)	8956.4(6)	4503.4(4)	1264.08(2)
Z	8	8	8	2
μ(Mo Kα) (mm^{-1})	8.969	3.508	1.087	1.587
Absorption correction				
Reflections collected	41078	55515	19211	10940
Independent reflections	10609	10741	5348	5550
Goodness-of-fit on F^2	1.037	1.002	1.042	1.152
Final R_1, wR_2 [$I > 2\sigma(I)$]	0.0501, 0.1271	0.0421, 0.0872	0.0420, 0.0857	0.0270, 0.0624
(all data)	0.0625, 0.1349	0.1165, 0.1143	0.0563, 0.0948	0.0287, 0.0630

Table 4
Selected bond lengths (Å), bond angles (°), torsion angles (°) and interatomic distances (Å) for **1**–**4**

	1	2	3	4
Ag(1)–N(1)	2.267(3)	2.254(2)	2.248(3)	2.235(3)
Ag(1)–N(2)	2.437(3)	2.461(2)	2.443(3)	2.498(3)
Ag(1)–N(3A)	2.195(3)	2.203(2)	2.205(3)	2.193(3)
Ag(1)–Ag(1A)	3.3196(7)	3.2413(3)	3.1962(6)	3.1174(6)
N(1)–Ag(1)–N(3A)	151.26(10)	153.12(6)	152.38(11)	152.39(12)
N(2)–Ag(1)–N(3A)	132.75(10)	126.13(6)	126.22(9)	128.13(10)
N(1)–Ag(1)–N(2)	75.27(9)	75.66(6)	75.89(10)	74.99(10)
N(3A)–Ag(1)–Ag(1A)	76.75(7)	73.29(4)	73.65(7)	77.03(9)
N(1)–Ag(1)–Ag(1A)	120.65(7)	130.03(4)	130.08(7)	126.21(9)
N(2)–Ag(1)–Ag(1A)	80.74(7)	82.47(4)	83.73(7)	81.82(8)
O(1)–C(1)–C(20)–O(2)	72.2(4)	71.5(2)	72.4(4)	−67.3(5)
N(1)–C(9)–C(10)–N(2)	−57.7(4)	−55.9(2)	−55.8(4)	−58.2(4)
N(2)–C(11)–C(12)–N(3)	−50.4(4)	−55.4(3)	−57.0(4)	−52.5(5)
Ag(1)···C(7)		3.185(2)	3.218(3)	3.243(4)
Ag(1)···C(14)		2.984(2)	2.998(3)	2.949(3)
Ag(1)···C(15)		3.313(2)	3.352(3)	3.356(4)

Symmetry code: (A) $-x+1$, $-y+2$, $-z-2$ (**1**), $-x+1$, $-y+1$, $-z$ (**2** and **4**), $-x$, $-y+1$, $-z$ (**3**).

Table 5
Selected bond lengths (Å), bond angles (°) and torsion angles (°) for **5**

Ag(1)–N(1)	2.429(5)	Ag(1)–N(2)	2.394(5)
Ag(1)–N(3)	2.483(5)	Ag(1)–C(21)	2.170(7)
Ag(2)–C(22)	2.045(12)	Ag(2)–C(23)	2.074(12)
Ag(1)–Ag(1A)	2.7437(10)		
N(1)–Ag(1)–N(2)	74.87(17)	N(1)–Ag(1)–N(3)	113.51(17)
N(2)–Ag(1)–N(3)	73.45(17)	N(1)–Ag(1)–C(21)	101.94(19)
N(2)–Ag(1)–C(21)	147.03(14)	N(3)–Ag(1)–C(21)	133.88(16)
Ag(1)–C(21)–Ag(1A)	78.1(3)	N(1)–Ag(1)–Ag(1A)	151.54(12)
N(2)–Ag(1)–Ag(1A)	121.77(13)	N(3)–Ag(1)–Ag(1A)	94.19(12)
C(21)–Ag(1)–Ag(1A)	150.94(15)	N(4)–C(21)–Ag(1A)	140.94(15)
N(4)–C(21)–Ag(1)	140.94(15)		
N(2)–Ag(1)–N(1)	74.90(17)	N(1)–Ag(1)–N(3)	113.41(18)
N(2)–Ag(1)–N(3)	73.43(17)	C(21)–Ag(1)–N(3)	133.75(16)
C(21)–Ag(1)–N(1)	102.1(2)	C(21)–Ag(1)–N(2)	147.12(14)
N(1)–Ag(1)–Ag(1A)	151.59(12)	N(2)–Ag(1)–Ag(1A)	121.78(13)
N(3)–Ag(1)–Ag(1A)	94.21(13)	C(21)–Ag(1)–Ag(1A)	50.79(16)
C(22)–Ag(2)–C(23)	180.00(3)	N(4)–C(21)–Ag(1)	140.79(16)
N(4)–C(21)–Ag(1A)	140.79(16)	Ag(1)–C(21)–Ag(1A)	78.4(3)
O(1)–C(1)–C(20)–O(2)	−69.8(7)		
N(1)–C(9)–C(10)–N(2)	−62.5(7)		
N(2)–C(11)–C(12)–N(3)	−56.7(7)		

Symmetry code: (A) $-x$, y, $-z+3/2$.

Table 6
Selected bond lengths (Å), bond angles (°) and torsion angles (°) for **6**

Cd(1)–N(1)	2.399(2)	Cd(1)–N(2)	2.395(2)
Cd(1)–N(3)	2.465(2)		
N(1)–Cd(1)–N(2)	75.68(8)	N(1)–Cd(1)–N(3)	87.24(7)
N(2)–Cd(1)–N(3)	73.61(8)	N(1)–Cd(1)–N(1A)	90.09(10)
N(1)–Cd(1)–N(2A)	155.04(8)	N(1)–Cd(1)–N(3A)	126.89(7)
N(2)–Cd(1)–N(2A)	124.38(12)	N(2)–Cd(1)–N(3A)	85.27(8)
N(3)–Cd(1)–N(3A)	133.99(11)	N(2)–Cd(1)–N(1)	72.39(17)
N(3)–Cd(1)–N(6)	100.02(17)	N(2)–Cd(1)–N(6)	102.87(19)
N(5)–Cd(1)–N(6)	74.81(18)	N(2)–Cd(1)–N(6)	89.53(17)
N(1)–Cd(1)–N(6)	140.99(16)		
O(1)–C(1)–C(20)–O(2)	66.7(3)		
N(1)–C(9)–C(10)–N(2)	−52.9(3)		
N(2)–C(11)–C(12)–N(3)	53.0(3)		

Symmetry code: (A) $-x, -y, z$.

Table 7
Selected bond lengths (Å), bond angles (°) and torsion angles (°) for **7**

Hg(1)–N(1)	2.275(4)	Hg(1)–N(2)	2.425(4)
Hg(1)–N(3)	2.222(4)	Hg(1)–O(1)	2.537(3)
Hg(1)–O(2)	2.801(3)	Hg(1)–O(3)	2.712(4)
Hg(1)–O(10)	2.843(4)		
N(3)–Hg(1)–N(1)	145.16(16)	N(3)–Hg(1)–N(2)	78.43(15)
N(1)–Hg(1)–N(2)	77.11(15)	N(3)–Hg(1)–O(1)	136.15(13)
N(1)–Hg(1)–O(1)	78.56(13)	N(2)–Hg(1)–O(1)	131.65(13)
N(1)–Hg(1)–O(2)	131.21(13)	N(2)–Hg(1)–O(2)	151.48(13)
N(3)–Hg(1)–O(2)	77.05(13)	O(1)–Hg(1)–O(2)	63.34(10)
N(1)–Hg(1)–O(3)	75.88(14)	N(2)–Hg(1)–O(3)	129.49(13)
N(3)–Hg(1)–O(3)	101.81(13)	O(1)–Hg(1)–O(3)	82.65(11)
O(2)–Hg(1)–O(3)	70.31(12)	N(1)–Hg(1)–O(10)	127.98(13)
N(2)–Hg(1)–O(10)	94.75(12)	N(3)–Hg(1)–O(10)	78.38(13)
O(1)–Hg(1)–O(10)	69.26(11)	O(2)–Hg(1)–O(10)	66.19(10)
O(3)–Hg(1)–O(10)	135.28(12)		
O(1)–C(1)–C(20)–O(2)	−69.5(5)		
N(1)–C(9)–C(10)–N(2)	66.5(5)		
N(2)–C(11)–C(12)–N(3)	−64.4(5)		

Table 8
Selected bond lengths (Å), bond angles (°) and torsion angles (°) for **8**

Hg(1)–N(1)	2.423(4)	Hg(1)–N(2)	2.379(4)
Hg(1)–N(3)	2.467(4)	Hg(1)–S(2)	2.484(1)
Hg(1)–S(1)	2.711(1)		
N(2)–Hg(1)–N(1)	75.89(13)	N(2)–Hg(1)–N(3)	73.00(13)
N(1)–Hg(1)–N(3)	109.62(13)	N(2)–Hg(1)–S(2)	168.57(10)
N(1)–Hg(1)–S(2)	111.33(9)	N(3)–Hg(1)–S(2)	95.92(9)
N(2)–Hg(1)–S(1)	84.52(11)	N(1)–Hg(1)–S(1)	97.56(9)
N(3)–Hg(1)–S(1)	138.52(9)	S(2)–Hg(1)–S(1)	102.78(5)
Hg(1)–S(1)–CN	94.1(2)	Hg(1)–S(2)–CN	102.18(16)
O(1)–C(1)–C(20)–O(2)	67.8(5)		
N(1)–C(9)–C(10)–N(2)	63.3(5)		
N(2)–C(11)–C(12)–N(3)	57.0(5)		

Table 9
Selected bond lengths (Å), bond angles (°) and torsion angles (°) for **9**

Hg(1)–N(1)	2.430(4)	Hg(1)–N(2)	2.412(4)
Hg(1)–N(3)	2.490(4)	Hg(1)–Hg(1A)	2.5529(3)
Hg(2)–I(1)	2.8403(4)	Hg(2)–I(2)	2.7842(4)
Hg(2)–I(3)	2.7813(4)	Hg(2)–I(4)	2.7658(4)
N(2)–Hg(1)–N(1)	74.97(13)	N(2)–Hg(1)–N(3)	73.12(13)
N(1)–Hg(1)–N(3)	95.73(13)	N(2)–Hg(1)–Hg(1A)	137.29(9)
N(1)–Hg(1)–Hg(1A)	133.73(9)	N(3)–Hg(1)–Hg(1A)	122.02(9)
I(4)–Hg(2)–I(3)	113.424(12)	I(4)–Hg(2)–I(2)	108.640(12)
I(3)–Hg(2)–I(2)	115.428(12)	I(4)–Hg(2)–I(1)	113.816(12)
I(3)–Hg(2)–I(1)	102.191(12)	I(2)–Hg(2)–I(1)	102.856(11)
O(1)–C(1)–C(20)–O(2)	−63.8(7)		
N(1)–C(9)–C(10)–N(2)	56.8(8)		
N(2)–C(11)–C(12)–N(3)	−54.2(8)		

Symmetry code: (A) $-x+1, -y+1, -z$.

Table 10
Selected bond lengths (Å), bond angles (°) and torsion angles (°) for **10**

Hg(1)–N(1)	2.414(5)	Hg(1)–N(2)	2.439(5)
Hg(1)–N(3)	2.525(5)	Hg(1)–N(4)	2.503(5)
Hg(1)–N(5)	2.379(5)	Hg(1)–N(6)	2.461(5)
N(1)–Hg(1)–N(2)	75.21(16)	N(1)–Hg(1)–N(3)	98.63(17)
N(1)–Hg(1)–N(4)	86.90(16)	N(1)–Hg(1)–N(5)	159.75(17)
N(5)–Hg(1)–N(6)	74.97(18)	N(1)–Hg(1)–N(6)	115.19(17)
N(2)–Hg(1)–N(3)	72.72(17)	N(2)–Hg(1)–N(4)	160.67(16)
N(2)–Hg(1)–N(5)	124.56(18)	N(2)–Hg(1)–N(6)	83.31(18)
N(3)–Hg(1)–N(4)	118.08(16)	N(3)–Hg(1)–N(5)	84.96(18)
N(3)–Hg(1)–N(6)	131.68(17)	N(4)–Hg(1)–N(5)	73.98(18)
N(4)–Hg(1)–N(6)	98.11(17)		
O(1)–C(1)–C(20)–O(2)	68.8(7)		
O(3)–C(21)–C(40)–O(4)	65.7(7)		
N(1)–C(9)–C(10)–N(2)	−61.7(7)		
N(2)–C(11)–C(12)–N(3)	−61.2(7)		
N(4)–C(11)–C(12)–N(5)	−59.8(7)		
N(5)–C(11)–C(12)–N(6)	−62.0(7)		

Table 11
Selected bond lengths (Å), bond angles (°) and torsion angles (°) for **11** and **12**

	11	**12**
Pd(1)–N(1)	2.087(3)	2.060(2)
Pd(1)–N(2)	2.013(3)	2.001(2)
Pd(1)–N(3)	2.064(3)	2.082(2)
Pd(1)–Cl(1)	2.3333(9)	
Pd(1)–O(3)		2.047(2)
N(2)–Pd(1)–N(3)	83.84(12)	84.38(7)
N(2)–Pd(1)–N(1)	84.04(11)	84.33(7)
N(3)–Pd(1)–N(1)	166.34(11)	166.82(7)
N(2)–Pd(1)–Cl(1)	170.85(9)	
N(3)–Pd(1)–Cl(1)	92.34(8)	
N(1)–Pd(1)–Cl(1)	98.71(8)	
N(2)–Pd(1)–O(3)		176.39(7)
N(3)–Pd(1)–O(3)		97.63(7)
N(1)–Pd(1)–O(3)		93.31(7)
O(1)–C(1)–C(20)–O(2)	−74.0(4)	71.1(2)
N(1)–C(9)–C(10)–N(2)	−54.5(4)	−57.6(2)
N(2)–C(11)–C(12)–N(3)	56.4(4)	56.0(2)

3.1. Silver(I) complexes

The X-ray structure determinations of **1–5** incorporating different anions (Fig. 1) confirm their 2:2:2 (metal:ligand:anion) stoichiometries. For each of **2–4**, the structure consists of a dimeric arrangement in which two macrocycles in a bent arrangement sandwich two silver(I) ions; in these structures the silver ions are shielded from further interaction with solvent or anions by the folded macrocycles (see Fig. 1). Each silver centre is bonded to two N atoms from one **L** and one N atom from a different **L**, with the ether oxygen donors uncoordinated. A weak Ag···Ag contact (double dashed lines) between adjacent silvers is also present. In **2–4** the individual silver centres may be considered to adopt pseudo-four-coordinate (distorted tetrahedral) geometries. However, in the case of $[Ag_2\mathbf{L}_2(NO_3)_2]$ (**1**), each silver centre has an additional bond to a monodentate nitrato ligand, presumably reflecting the latter's relatively smaller size and comparatively higher affinity for this ion.

A range of di- and polymetallic silver(I) complexes have now been documented to exhibit similar Ag···Ag contacts to those mentioned above for the present complexes (with the literature

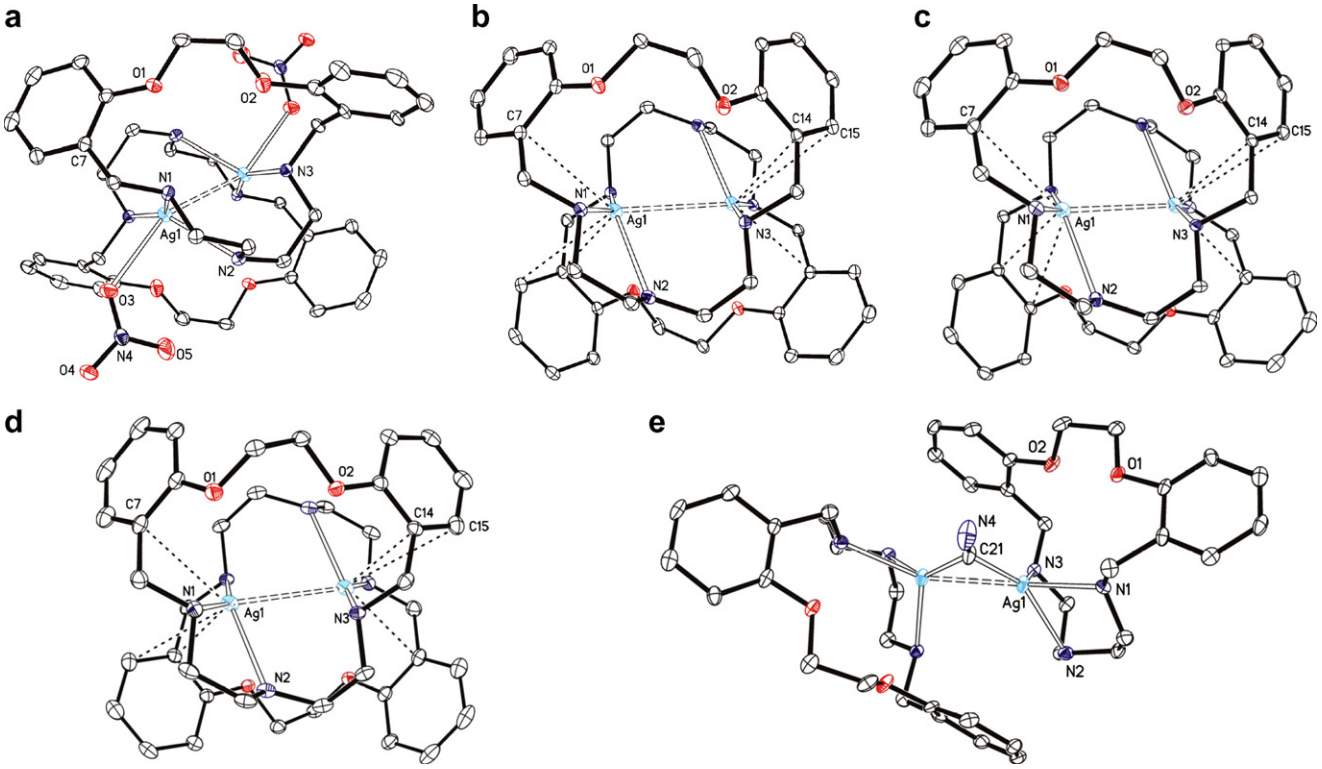

Fig. 1. Dimeric structures of (a) $[Ag_2\mathbf{L}_2(NO_3)_2]$ (**1**), (b) $[Ag_2\mathbf{L}_2](ClO_4)_2 \cdot 2DMF$ (**2**), (c) $[Ag_2\mathbf{L}_2](PF_6)_2 \cdot 2DMF$ (**3**), (d) $[Ag_2\mathbf{L}_2](OTf)_2$ (**4**) and (e) $[Ag_2\mathbf{L}_2(\mu\text{-}CN)][Ag(CN)_2] \cdot H_2O$ (**5**). Hydrogen atoms, non-coordinating anions and non-coordinating solvent molecules are omitted.

internuclear distances falling in the approximate range 2.9–3.3 Å) [10]; the Ag···Ag values are thus significantly shorter than the van der Waals diameter for silver(I) of 3.44 Å [11]. In the present structurally related Ag(I) complexes, **1**–**4**, the internuclear Ag···Ag distances vary with the anion present: [**1** (NO_3^-), 3.3196(7) Å; **2** (ClO_4^-), 3.2413(3) Å; **3** (PF_6^-), 3.1962(6) Å and **4** (OTf^-), 3.1174(6) Å], thus **1** shows the longest contact in keeping with coordination of the nitrate group leading to a weakening of the Ag···Ag interaction through electronic and/or steric effects. In this context it is noted that the closest approach of the remaining anions to a silver centre lies in the range 4.5–5.6 Å.

For the above complexes, the sole coordination of the N_3-donor set of **L** to a single metal centre thus appears to promote both dimerization and formation of a Ag···Ag contact between the respective silver centres in these dinuclear complex species. In addition, some of the relevant silver–aromatic carbon contacts in **2**–**4** are less than the sum of Van der Waals radii (Ag···C 2.9–3.3 Å, dashed lines). Consequently, the preferred anion-free dimerizations of **2**–**4** are due to the weaker affinity of ClO_4^-, PF_6^- and OTf^- than that of NO_3^- (in case of **1**) toward the silver(I) center, allowing the approach of the benzo-group to form such Ag···π interactions.

In the case of $[Ag_2\mathbf{L}_2(\mu\text{-}CN)][Ag(CN)_2]_{\cdot H2}O$ (**5**) a bridging cyano group was observed to link each silver ion in the dinuclear cation [Ag···Ag distance, 2.7437(10) Å; Ag1–C21–Ag1A 78.1(3)°]. The complex adopts a different relative arrangement of the macrocyclic ligands to that present in **1**–**4**, with the macrocyclic ligands orientated away from the dinuclear Ag(I) centres (see Fig. 1e). Once again, the ether oxygens of **L** remaining uncoordinated. The complex is a rare example of a discrete binuclear silver complex incorporating a two-electron μ_2-κC:κC bridging cyanide group, the first compound of this type was reported in 1999 by Schröder et al. [12]. The bridging mode in both these complexes contrasts with the usual linear bridging (μ_2-κC:κN), four-electron-donating CN^- bridges more commonly observed with this anion [13].

3.2. Cadmium complex

The crystal structure of **6** is shown in Fig. 2. The coordination of each **L** to the Cd(II) centre is *via* a facial arrangement of its three nitrogen donors, forming a distorted octahedral array of six N atoms from two **L**, with the ether oxygen donors uncoordinated; the N–Cd–N bite angles vary considerably, ranging from 73° to 155°. Once again, the metal centre is fully shielded by the partially bound macrocycles which surround the cadmium centre in a sandwich-like arrangement. This structure contrasts with that of the related 1:1 complex, $[Cd\mathbf{L}(NO_3)_2]$ reported previously [14] in which all macrocyclic donors coordinate together with two monodentate (O-bound) nitrate ligands such that the Cd(II) centre achieves a seven-coordinate geometry.

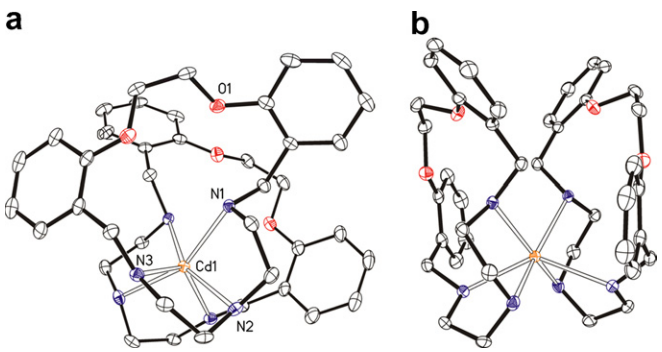

Fig. 2. Molecular structure of $[Cd\mathbf{L}_2](ClO_4)_2 \cdot CH_3CN$ (**6**); (a) top view and (b) side view. Hydrogen atoms and non-coordinating anions are omitted.

3.3. Mercury(II) complexes

The crystal structure of [Hg**L**$(ClO_4)_2$] (**7**) confirms its metal:macrocycle ratio of 1:1. The Hg(II) coordinated to all donors in the macrocyclic N_3O_2-donor set together with two monodentate perchlorato ligands to yield an overall metal coordination geometry of seven (Fig. 3a). The Hg–N bond lengths [Hg–N1 2.275, Hg–N2 2.425 and Hg–N3 2.222 Å] are within the normal literature range for this bond type. Coordination about the Hg(II) centre is not symmetric, with, for example, both ether oxygen atoms being bound asymmetrically; the Hg–O1 bond length is 2.537 Å while that for Hg–O2 is 2.801 Å.

The crystal structure of [Hg**L**$(SCN)_2$] · CH_3CN, **8**, is shown in Fig. 3b. The Hg(II) ion in this complex is five-coordinate, being bound to the three nitrogens of **L** and two sulfur atoms from two thiocyanato ligands; the ether oxygens are not bound. The coordination geometry can best be described as a distorted trigonal bipyramid with two nitrogen donors of **L** and one sulfur atom from a thiocyanato ligand defining the trigonal plane and the axial positions occupied by the remaining ring nitrogen and a sulfur from one of the thiocyanate groups. The S2–Hg1–N2 angle is 168.57°. The latter ions show Hg–S–CN angles of 94.1° and 102.18° in keeping with the usual behaviour of these ions bound to Hg(II) [15].

The structure of **8** contrasts with that of **7**, in that both coordinated anions are located on the same side of the bound macrocycle with the mercury ion positioned ~0.53 Å from the N_3-plane towards the anions, resulting in the metal ion being located well outside the macrocyclic cavity.

The crystal structure of [Hg_2**L**$_2$]$(HgI_4)_2$ · 2**L**, **9**, obtained from the reaction of **L** with one molar equivalent of HgI_2, is shown in Fig. 3c. In this case, the structure consists of a dimeric cation, $[Hg_2\mathbf{L}_2]^{4+}$, and two $(HgI_4)^{2-}$ anions; two non-coordinated macrocycles are also present in the lattice. In the cation, each mercury ion can be described as having a four-coordinate, distorted tetrahedral geometry, being bound to three nitrogens from **L**, with a mercury-mercury bond occupying the fourth position; the bond angles range from 73.1(1)° for N2–Hg1–N3° to 137.3(1)° for N2–Hg1–Hg1A. The Hg–N bond lengths [2.412(4)–2.490(4) Å] are slightly longer than reported previously for such bonds (2.28–2.35 Å) [16]. Both pairs of macrocycle oxygen donors remain uncoordinated (Hg···O distances of 3.59 and 4.06 Å, respectively).

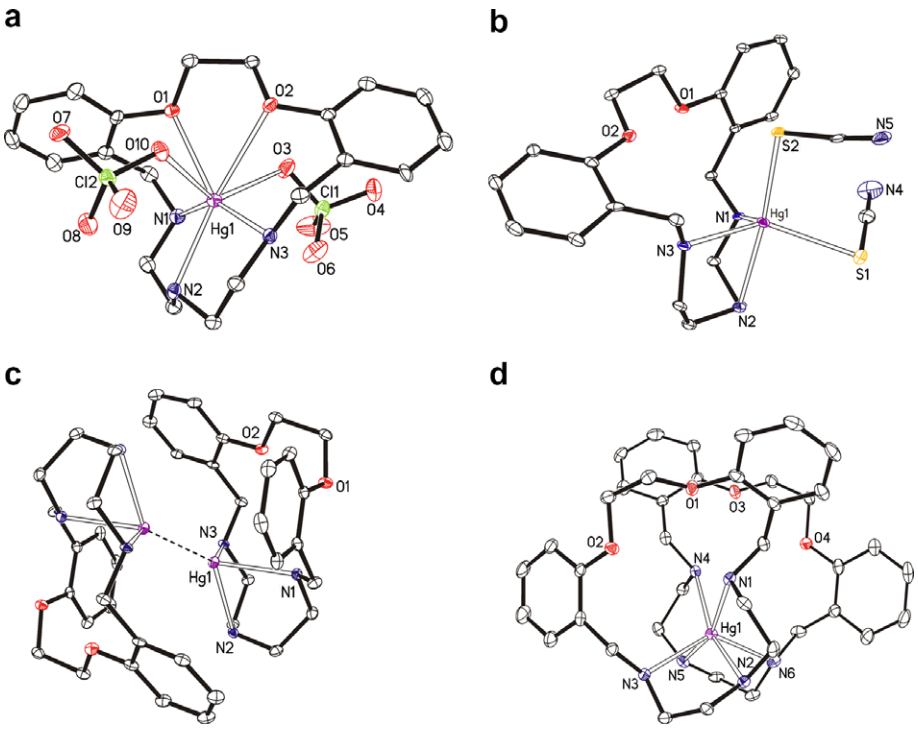

Fig. 3. Molecular structures of (a) [Hg**L**$(ClO_4)_2$] **(7)**, (b) [Hg**L**$(SCN)_2$] · CH_3CN (**8**), (c) [Hg_2**L**$_2$]$(HgI_4)_2$ · 2**L** (**9**) and (d) [Hg**L**$_2$]$(NO_3)_2$ · $2CH_3OH$ (**10**). Hydrogen atoms and non-coordinating solvent and anions are omitted.

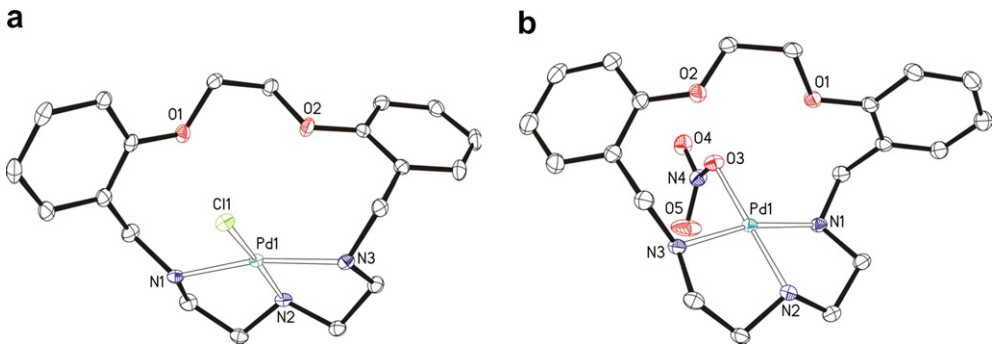

Fig. 4. Molecular structures of (a) [Pd**L**Cl]Cl · H_2O (**11**) and (b) [Pd**L**(NO_3)](NO_3) · CH_3OH (**12**). Hydrogen atoms, non-coordinating anions and solvents are omitted.

Overall, the two macrocycles surround the two mercury centres in a 'twisted' sandwich arrangement. Since there is an imposed inversion at the centre of the Hg(II)–Hg(II) bond, the asymmetric unit contains only half of the structure described above. The mercury atom is located 1.586 Å above the N_3 trigonal plane. The Hg(II)–Hg(II) bond length [2.5459(6) Å] is shorter than reported previously [17]. Only five cases of Hg(II)–Hg(II) bonds (2.7–3.0 Å) [17] were extracted from the CCDC [18] database. We are not aware of any other example of a Hg(II)–Hg(II) bond occurring in a macrocyclic ligand complex that has been characterized by X-ray diffraction. Geometrical parameters for the $[HgI_4]^{2-}$ anion, whose formation apparently aids the stabilization of the $[Hg_2\mathbf{L}_2]^{2+}$ cation in the crystal lattice, are generally similar to those reported previously for this dianion, although some distortion from regular tetrahedral geometry [angles: 102.19(1)–115.43(1)°] is evident in the present case.

When $Hg(NO_3)_2$ was employed in dichloromethane/methanol, $[Hg\mathbf{L}_2](NO_3)_2 \cdot 2CH_3OH$ (**10**), was obtained, which does not contain NO_3^- coordinated to the metal centre. The crystal structure of **10** is shown in Fig. 3d. The coordination of each **L** to the Hg(II) centre is *via* a facial arrangement of its three nitrogen donors, forming a distorted octahedral array of six N atoms from two **L**, with the ether oxygen donors uncoordinated; the N–Hg–N bite angles vary considerably, ranging from 73° to 160°. As occurs for **6**, the metal centre is once again fully shielded by the partially bound macrocycles which surround the mercury centre in a sandwich-like arrangement. Comparing the structures of **7** and **10**, it is noteworthy that two nitrate anions in **10** remain uncoordinated while both perchlorate anions are coordinated to the metal centre in **7** despite the nitrate ion being a stronger ligand than perchlorate ion towards most common metal ions.

3.4. Palladium(II) complexes

Reaction of **L** with K_2PdCl_4 and $Pd(NO_3)_2$ gave the orange complexes $[Pd\mathbf{L}Cl]Cl \cdot H_2O$, **11**, and $[Pd\mathbf{L}(NO_3)](NO_3) \cdot CH_3OH$, **12**. The crystal structures of both products are shown in Fig. 4. As expected for this metal ion, both Pd(II) centres attain a square-planar coordination geometry. Each square plane is somewhat distorted, with the respective coordination sites occupied by three N donors from **L** together with a chloro or nitrato ligand in the remaining site. Once again, the ether oxygens remain uncoordinated in each case. Both structures are analogues of the corresponding acetate-containing complex, $[Pd\mathbf{L}(OAc)]OAc \cdot H_2O$, whose structure was reported in 2004 [5f].

4. Conclusion

From the results presented above, the following observations can be made concerning the influence of the N_3O_2-donor set of **L** (with its three strong binding amine donors and two weaker binding ether oxygen donors) on the nature of its resulting Ag(I), Cd(II), Hg(II) and Pd(II) complexes. Across all four metals, **L** yielded a range of coordination arrangements that included discrete 1:1 (M:**L**) complexation, in which all donor atoms are bound to the central metal (Hg(II)), 1:1 complexation, in which only the N_3-donor set of **L** coordinates to occupy three donor positions of a square-planar (Pd(II)) or trigonal bipyramidal (Hg(II)) arrangement, 1:2 complexation, in which each **L** coordinates only *via* its N_3-donor set to yield a 'sandwich' arrangement with respect to the central metal (Cd(II) and Hg(II)), 2:2 complexation, in which both metal centres are bound to each **L** (Ag(I)) and another 2:2 dinuclear species, in which each **L** binds to a single metal ion, with the respective metal centres linked by a rare [12], two-electron, μ_2-κC:κC cyano bridge (Ag(I)). Finally, Hg(II) also yields a further type of 2:2 dinuclear complex, in which one **L** binds to each Hg(II) metal centre, with these 1:1 subunits then linked by a metal-metal (Hg–Hg) bond.

Based on the present solid state results, the affinity of the ether oxygen donors for Ag(I) and Pd(II) is clearly lower than for Hg(II) across all complexes investigated, with the situation for Cd(II) being unclear since, while non-coordination of ether oxygen occurs in the present 1:2 complex, its coordination is observed in the related 1:1 species, $[Cd\mathbf{L}(NO_3)_2]$, reported previously [14].

Acknowledgments

The support of the Korea Science and Engineering Foundation (R01-2007-000-20245-0) and the Australian Research Council is gratefully acknowledged.

Appendix A. Supplementary data

CCDC 673231, 673232, 673233, 673234, 673235, 673236, 673237, 673238, 673239, 673240, 673241 and 673242 contain the supplementary crystallographic data for **1**, **2**, **3**, **4**, **5**, **6**, **7**, **8**, **9**, **10**, **11** and **12**. These data can be obtained free of charge via http://www.ccdc.cam.ac.uk/conts/retrieving.html, or from the Cambridge Crystallographic Data Centre, 12 Union Road, Cambridge CB2 1EZ, UK; fax: (+44) 1223-336-033; or e-mail: deposit@ccdc.cam.ac.uk. Supplementary data associated with this article can be found, in the online version, at doi:10.1016/j.poly.2008.06.011.

References

[1] (a) K. Gloe, Macrocyclic Chemistry: Current Trends and Future, Springer, Dordrecht, 2005;
(b) N.E. Borisova, E. Nataliya, M.D. Reshetova, Y.A. Ustynyuk, Chem. Rev. 107 (2007) 46.
[2] D.S. Baldwin, P.A. Duckworth, G.R. Erickson, L.F. Lindoy, M. McPartlin, G.M. Mockler, W.E. Moody, P.A. Tasker, Aust. J. Chem. 40 (1987) 1861.
[3] (a) L.F. Lindoy, Pure Appl. Chem. 61 (1989) 1575;
(b) K.R. Adam, S. Donnelly, A.J. Leong, L.F. Lindoy, B.J. McCool, A. Bashall, M.R. Dent, B.P. Murphy, M. McPartlin, D.E. Fenton, P.A. Tasker, J. Chem. Soc., Dalton Trans. (1990) 1635;
(c) K.R. Adam, D.S. Baldwin, P.A. Duckworth, L.F. Lindoy, M. McPartlin, A. Bashall, H.R. Powell, P.A. Tasker, J. Chem. Soc., Dalton Trans. (1995) 1127;
(d) R.R. Fenton, R. Gauci, P.C. Junk, L.F. Lindoy, R.C. Luckay, G.V. Meehan, J.R. Price, P. Turner, G. Wei, J. Chem. Soc., Dalton Trans. (2002) 2185;
(e) Y. Jin, I. Yoon, J. Seo, J.-E. Lee, S.-T. Moon, J. Kim, S.W. Han, K.-M. Park, L.F. Lindoy, S.S. Lee, Dalton Trans. (2005) 788.
[4] (a) K.R. Adam, K.P. Dancey, B.A. Harrison, A.J. Leong, L.F. Lindoy, M. McPartlin, P.A. Tasker, Chem. Commun. (1983) 1351;
(b) K.R. Adam, L.G. Brigden, K. Henrick, L.F. Lindoy, M. McPartlin, B. Mimnagh, P.A. Tasker, Chem. Commun. (1985) 710.
[5] (a) P.A. Harding, K. Henrick, L.F. Lindoy, M. McPartlin, P.A. Tasker, Chem. Commun. (1983) 1300;
(b) K.R. Adam, A.J. Leong, L.F. Lindoy, B.J. McCool, A. Ekstrom, I. Liepa, P.A. Harding, K. Henrick, M. McPartlin, P.A. Tasker, J. Chem. Soc., Dalton Trans. (1987) 2537;
(c) U. Kallert, R. Mattes, Z. Naturforsch. B: Chem. Sci. 47 (1992) 1271;
(d) Y.H. Zhang, H. Vahrenkamp, Inorg. Chim. Acta 351 (2003) 201;
(e) V. Gasperov, S.G. Galbraith, L.F. Lindoy, B.R. Rumbel, B.W. Skelton, P.A. Tasker, A.H. White, Dalton Trans. (2005) 139;
(f) S. Bilge, Z. Kilic, T. Hokelek, B. Erdogan, J. Mol. Struct. 691 (2004) 85.
[6] K.R. Adam, L.F. Lindoy, H.C. Lip, J.H. Rea, B.W. Skelton, A.H. White, J. Chem. Soc., Dalton Trans. (1981) 74.
[7] Bruker, SMART, SAINT and XPREP: Area Detector Control and Integration Software Ver. 5.054; Bruker Analytical X-ray Instruments, Madison, Wisconsin, 2001.
[8] G.M. Sheldrick, SADABS: Empirical Absorption and Correction Software, University of Göttingen, Göttingen, Germany, 1998.
[9] Bruker, SHELXTL: Structure Determination Programs, Ver. 6.12, Bruker Analytical X-ray Instruments, Madison, Wisconsin, 2000.
[10] (a) P. Pyykkö, Chem. Rev. 97 (1997) 597;
(b) C.X. Cui, M. Kertesz, Inorg. Chem. 29 (1990) 2568;
(c) V. McKee, J. Nelson, D.J. Speed, R.M. Town, J. Chem. Soc., Dalton Trans. (2001) 3641;
(d) R.-F. Song, Y.-B. Xie, J.-R. Li, X.-H. Bu, Dalton Trans. (2003) 4742;
(e) O.-S. Jung, Y.J. Kim, Y.-A. Lee, S.W. Kang, S.N. Choi, Cryst. Growth Des. 4

(2004) 23;
(f) M.O. Awaleh, A. Badia, F. Brisse, Cryst. Growth Des. 5 (2004) 1897.
[11] (a) A. Bondi, J. Phys. Chem. 68 (1964) 441;
(b) M. Jansen, Angew. Chem., Int. Ed. Engl. 26 (1987) 1098.
[12] V. Lippolis, A.J. Blake, P.A. Cooke, F. Isaia, W.-S. Li, M. Schröder, Chem. Eur. J. 5 (1999) 1987.
[13] (a) K.R. Dunbar, R.A. Heintz, Prog. Inorg. Chem. 45 (1997) 283;
(b) H. Vahrenkamp, A. Gei, G.N. Richardson, J. Chem. Soc., Dalton Trans. (1997) 3643;
(c) K.K. Klausmeyer, T.B. Rauchfuss, S.R. Wilson, Angew. Chem., Int. Ed. 37 (1998) 1694;
(d) S.W. Lai, K.-K. Cheung, M.C.-W. Chan, C.-M. Che, Angew. Chem., Int. Ed. 37 (1998) 182;
(e) C.J. Shorrock, B.-Y. Xue, P.B. Kim, R.J. Batchelor, B.O. Patrick, D.B. Leznoff, Inorg. Chem. 41 (2002) 6743;
(f) W. Han, L. Yi, Z.-Q. Liu, W. Gu, S.-P. Yan, P. Cheng, D.-Z. Liao, Z.-H. Jiang, Eur. J. Inorg. Chem. (2004) 2130;
(g) Y.-Y. Lin, S.-W. Lai, C.-M. Che, W.-F. Fu, Z.-Y. Zhou, N. Zhu, Inorg. Chem. 44 (2005) 1511;
(h) X. Liu, G.-C. Guo, M.-L. Fu, X.-H. Liu, M.-S. Wang, J.-S. Huang, Inorg. Chem. 45 (2006) 3679.
[14] K.R. Adam, K.P. Dancey, A.J. Leong, L.F. Lindoy, B.J. McCool, M. McPartlin, P.A. Tasker, J. Am. Chem. Soc. 110 (1988) 8471.
[15] (a) M.G.B. Drew, K.C. Lee, K.F. Mok, Inorg. Chim. Acta 155 (1989) 39;
(b) A.M. Costero, M. Pitarch, C. Andreu, L.E. Ochando, J.M. Amigo, T. Debaerdemaeker, Tetrahedron 52 (1996) 669;
(c) Z. Popovic, D. Matkovic-Calogovic, J. Hasic, D. Vikic-Topic, Inorg. Chim. Acta 285 (1999) 208;
(d) Z. Popovic, Z. Soldin, D. Matkovic-Calogovic, G. Pavlovic, M. Rajic, G. Giester, Eur. J. Inorg. Chem. (2002) 171;
(e) A. Morsali, A. Ramazani, A.R. Mahjoub, A.A. Soudi, Z. Anorg. Allg. Chem. 629 (2003) 2058;
(f) A. Morsali, M. Payheghader, M.R. Poorheravi, F. Jamali, Z. Anorg. Allg. Chem. 629 (2003) 1627;
(g) M. Heller, W.S. Sheldrick, Z. Anorg. Allg. Chem. 630 (2004) 1191;
(h) A. Morsali, L.-G. Zhu, Inorg. Chem. Commun. 7 (2004) 1184;
(i) A. Morsali, A.R. Mahjoub, A. Ramazani, J. Coord. Chem. 57 (2004) 347;
(j) G.P.M. van Klink, T. Nomoto, M. Lutz, A.L. Spek, O.S. Akkerman, F. Bickelhaupt, Eur. J. Inorg. Chem. (2004) 254;
(k) J. Dillen, A.T.H. Lenstra, J.G. Haasnoot, J. Reedijk, Polyhedron 2 (1983) 195;
(l) H.-P. Zhou, Y.-P. Tian, J.-Y. Wu, J.-Z. Zhang, D.-M. Li, Y.-M. Zhu, Z.-J. Hu, X.-T. Tao, M.-H. Jiang, Y. Xie, Eur. J. Inorg. Chem. (2005) 4976.
[16] (a) S. Afshar, S.T. Marcus, L.R. Gahan, T.W. Hambley, Aust. J. Chem. 52 (1999) 1;
(b) K.A. Byriel, L.R. Gahan, C.H.L. Kennard, C.T. Sunderland, J. Chem. Soc., Dalton Trans. (1993) 625;
(c) A.P. Marchand, D. Cal, K. Mlinaric-Majerski, K. Ejsmont, W.H. Watson, J. Chem. Cryst. 32 (2002) 447;
(d) C. Caltagirone, A. Bencini, F. Demartin, F.A. Devillanova, A. Garau, F. Isaia, V. Lippolis, P. Mariani, U. Papke, L. Tei, G. Verani, Dalton Trans. (2003) 901.
[17] (a) B. Hammerle, E.P. Muller, D.L. Wilkinson, G. Muller, P. Peringer, Chem. Commun. (1989) 1527;
(b) L.H. Gade, B.F.G. Johnson, J. Lewis, G. Conole, M. McPartlin, J. Chem. Soc., Dalton Trans. (1992) 3249;
(c) A. Muhlecker-Knoepfler, E. Ellmerer-Muller, R. Konrat, K.-H. Ongania, K. Wurst, P. Peringer, J. Chem. Soc., Dalton Trans. (1997) 1607;
(d) A. Knoepfler-Muhlecker, B. Scheffter, H. Kopacka, K. Wurst, P. Peringer, J. Chem. Soc., Dalton Trans. (1999) 2525;
(e) M.L. Cole, G.B. Deacon, P.C. Junk, K. Konstas, P.W. Roesky, Eur. J. Inorg. Chem. (2005) 1090.
[18] Cambridge Crystallographic Centre, Cambridge Structure Database Software CONQUEST 1.9, Cambridge, 2007.

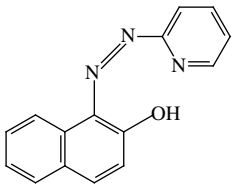

Scheme 1. Structure of HPAN ligand.

basis set, its use with DFT has shown to be sufficient for the geometry optimization and calculation of spectral properties. It gives good agreement with the experimental data and its use is justified in the case of large molecules.

2. Experimental

2.1. General procedure

All the reagents used to the synthesis were commercially available and were used without further purification. The [ReX_3(MeCN)(PPh_3)$_2$] (X = Cl, Br) complexes were prepared according to the literature methods [7].

IR spectra were recorded on a Nicolet Magna 560 spectrophotometer in the spectral range 4000–400 cm^{-1} with the samples in the form of KBr pellets. Electronic spectra were measured on a spectrophotometer Lab Alliance UV–Vis 8500 in the range 1000–200 nm in dichloromethane solution. Elemental analyses (C H N) were performed on a Perkin–Elmer CHN-2400 analyzer.

2.2. Preparation of [ReBr(PAN)$_2$] · 2$CHCl_3$ (**1**)

[Re(MeCN)Br_3(PPh_3)$_2$] (0.5 g, 0.51 mmol) and HPAN (0.28 g, 1.1 mmol) in chloroform (60 cm^3) were refluxed for 4 h. The starting material gradually dissolved and the color of the reaction solution became dark brown. The volume was condensed to 10 cm^3, diethyl ether (50 cm^3) was added and dark green microcrystalline solid was filtered. The product was washed with EtOH and cold ether, and dried *in vacuo*. (Yield 60%). The crystals suitable for X-ray investigation were obtained by recrystallization from a mixture chloroform/ethanol.

IR (KBr): 1613(s), 1587(m), 1556(w) and 1512(s) ν_{CN} and $\nu_{C=C}$; 1278(s), 1237(vs) and 1208(s) $\nu_{N=N}$. *Anal.* Calc. for $C_{32}H_{22}N_6O_2BrCl_6Re$: 38.38; H, 2.21; N, 8.39. Found: C, 38.96; H, 2.28; N, 8.73%.

2.3. Preparation of [ReCl(PAN)$_2$] (**2**)

A procedure similar to those for **1** was used with [Re(MeCN)Cl_3(PPh_3)$_2$] (0.5 g, 0.58 mmol) and HPAN (0.30 g, 1.2 mmol). A dark green crystalline precipitate of [ReOCl(PAN)$_2$] was collected in 65% yield. The crystals suitable for X-ray structure determination were obtained by slow evaporation from an acetonitrile solution of [ReOCl(PAN)$_2$].

IR (KBr): 1613(s), 1587(m), 1557(w) and 1510(s) ν_{CN} and $\nu_{C=C}$; 1278(s), 1235(vs) and 1206(s) $\nu_{N=N}$. *Anal.* Calc. for $C_{30}H_{20}ClN_6O_2Re$: C, 50.17; H, 2.81; N, 11.70. Found: C, 50.88; H, 2.45; N, 11.20%.

2.4. Crystal structures determination and refinement

The X-ray intensities data of **1** and **2** were collected on a KM-4-CCD automatic diffractometer equipped with CCD detector and graphite monochromated Mo Kα radiation (λ = 0.71073 Å) at room temperature. Details concerning crystal data and refinement are given in Table 1. Lorentz, polarization and empirical absorption correction using spherical harmonics implemented in SCALE3 ABSPACK scaling algorithm [24] were applied. The structures were solved by the Patterson method and subsequently completed by the difference Fourier recycling. All the non-hydrogen atoms were refined anisotropically using full-matrix, least-squares technique. The hydrogen atoms were treated as "riding" on their parent carbon atoms and assigned isotropic temperature factors equal 1.2 times the value of equivalent temperature factor of the parent atom. The positions of hydrogen atoms were idealised after each cycle of refinement. SHELXS97 [25], SHELXL97 [26] and SHELXTL [27] programs were used for all the calculations. Atomic scattering factors were those incorporated in the computer programs.

Table 1
Crystal data and structure refinement for **1** and **2** complex

	1	**2**
Empirical formula	$C_{32}H_{22}N_6O_2BrCl_6Re$	$C_{30}H_{20}N_6O_2ClRe$
Formula weight	1001.37	718.17
Temperature (K)	293(2)	293(2)
Wavelength (Å)	0.71073	0.71073
Crystal system	triclinic	orthorhombic
Space group	$P\bar{1}$	*Pbca*
Unit cell dimensions		
a (Å)	9.6460(19)	14.1208(5)
b (Å)	13.208(3)	9.0866(3)
c (Å)	14.071(3)	39.4688(17)
α (°)	93.11(3)	
β (°)	94.88(3)	
γ (°)	102.59(3)	
Volume (Å3)	1738.7(7)	5064.2(3)
Z	2	8
D_{calc} (Mg/m^3)	1.913	1.884
Absorption coefficient (mm^{-1})	5.147	4.947
F(000)	968	2800
Crystal size (mm)	0.04 × 0.14 × 0.18	0.12 × 0.22 × 0.28
θ Range for data collection (°)	2.91–25.00	2.86–25.03
Index ranges	$-11 \leqslant h \leqslant 11$ $15 \leqslant k \leqslant 12$ $-16 \leqslant l \leqslant 16$	$-16 \leqslant h \leqslant 13$ $-10 \leqslant k \leqslant 10$ $-46 \leqslant l \leqslant 46$
Reflections collected	11 065	27 967
Independent reflections (R_{int})	5982 (0.0274)	4453 (0.0366)
Completeness to 2θ (%)	97.5	99.5
Maximum and minimum transmission	0.807 and 0.421	0.557 and 0.280
Data/restraints/parameters	5982/0/433	4453/0/361
Goodness-of-fit on F^2	0.951	1.346
Final *R* indices [$I > 2\sigma(I)$]	R_1 = 0.0322 wR_2 = 0.0739	R_1 = 0.0565 wR_2 = 0.0909
R indices (all data)	R_1 = 0.0443 wR_2 = 0.0767	R_1 = 0.0752 wR_2 = 0.0933
Largest difference in peak and hole (e $Å^{-3}$)	0.848 and −1.029	1.478 and −2.636

2.5. Computational details

The gas phase geometry of [ReOBr(PAN)$_2$] was optimized without any symmetry restrictions in the singlet and triplet states with the DFT method using the hybrid B3LYP functional of GAUSSIAN-03 [28–30]. The calculations were performed by using ECP basis set on the rhenium atom, the standard 6-31+G* basis for bromine, oxygen and nitrogen, 6-31G* for carbon and 6-31G for hydrogen atoms [31,32]. The Xe core electrons of Re were replaced by an effective core potential and DZ quality Hay and Wadt Los Alamos ECP basis set (LANL2DZ) [33] was used for the valence electrons. Additional d function with exponent α = 0.3811 and f function with exponent α = 2.033 on the rhenium atom were added [34]. All vibrations in the calculated vibrational spectrum of [ReOBr(PAN)$_2$] were real thus the calculated geometry corresponds to true energy minimum.

The electronic spectrum of [ReOBr(PAN)$_2$] was calculated with the TDDFT method, and the solvent effect was simulated using the polarizable continuum model with the integral equation formalism (IEF-PCM) [35].

2.6. Magnetic measurements

Magnetization measurements of polycrystalline sample of **1** were carried out with a Quantum Design SQUID magnetometer (MPMSXL-5-type) at a magnetic field of 0.5 T over the temperature range 1.8–300 K. Magnetization measurements versus magnetic field (0–5 T) were made at 2 K.

Corrections are based on subtracting the sample – holder signal and contribution χ_D estimated from the Pascal constants [36] and equal – 486×10^{-6} cm^3 mol^{-1} for complex Re(III). The effective magnetic moment was calculated from the equation, $\mu_{eff} = 2{,}83\ (\chi_M^{corr} \times T)^{1/2}$ B.M.

3. Results and discussion

3.1. Preparation and infrared data

The [ReX(PAN)$_2$] (X = Cl, Br) complexes were prepared in good yield by ligand exchange reaction starting from [ReCl$_3$(MeCN)(PPh$_3$)] and 1-(2-pyridylazo)-2-naphthol (HPAN):

$$[ReX_3(MeCN)(PPh_3)_2] + 2HPAN \rightarrow [ReX(PAN)_2] + 2PPh_3 + 2HX$$

They were isolated as dark green microcrystalline solid, soluble in common organic solvents. Attempts to prepare monosubstituted species in the reaction of [ReCl$_3$(MeCN)(PPh$_3$)] with HPAN in 1:1 molar ratio resulted in isolation of [ReX(PAN)$_2$], but with lower yield. The elemental analyses of the [ReX(PAN)$_2$] complexes are in good agreement with their formulation.

Bands due to N=N vibrations of the azo ligand are observed in the range 1280–1200 cm^{-1} in the IR spectra of the [ReX(PAN)$_2$] (X = Cl, Br) complexes. The peaks corresponding to the ν(C=N) and ν(C=C) modes of the PAN ligand appear in the 1625–1500 cm^{-1} range [37].

The calculated (non-scaled) vibrational spectrum of the [ReOBr(PAN)$_2$] is in a reasonable agreement with the experimental one in terms of the band positions and intensities. The most intense band corresponding N=N vibrations of the azo ligand appears at 1237 cm^{-1} in the experimental spectrum, whereas in the calculated spectrum is shifted to higher energy, and exists at 1376 cm^{-1}. It is higher than the experimental one by 11%, what is usual for such approach. The similar shift values are also observed for the other bands.

Table 2
Hydrogen bonds for **1** and **2** complexes

D–H···A	H···A (Å)	D···A (Å)	D–H···A (°)	Symmetry code of A
Complex ***1***				
C(9)–H(9)···N(2)	2.35	2.937(8)	121.1	
C(24)–H(24)···N(5)	2.37	2.948(8)	119.7	
C(12)–H(12)···O(2)	2.50	3.314(7)	146.3	$-x, -y, -z+1$
Complex ***2***				
C(9)–H(9)···N(2)	2.35	2.952(12)	122.0	
C(24)–H(24)···N(5)	2.35	2.934(12)	120.9	
C(28)–H(28)···O(1)	2.52	3.390(11)	156.9	$-x-0.5, y+0.5, z$

3.2. Crystal structure

The crystallographic data for **1** and **2** complexes are given in Table 1. A summary of bond distances and angles involving hydrogen bonding contacts [38,39] founded in the **1** and **2** structures is given in Table 2. The numbering scheme of [ReOBr(PAN)$_2$] is shown in Fig. 1. The central Re atom of the [ReX(PAN)$_2$] complexes is seven-coordinate, bonding to two nitrogen and one oxygen donors from each of two PAN ligands and having a seventh bond to halide ion. The overall arrangement of the donor atoms around rhenium can be described as slightly distorted capped trigonal prism (Fig. 2), which is one of the three commonly observed geometries for seven-coordinate complexes (capped octahedron, capped trigonal prism and pentagonal bipyramid) [40]. The top and bottom triangle of trigonal prism is constructed of two nitrogen and one oxygen atoms (N4, N6, O1 and N1, N3, O2, respectively) while the halide ion occupies a capping site. The planar in the range of experimental error naphthalene and pyridine rings are inclined at 18.7(2)°, 24.8(2)° (compound **1**) and 20.0(4)°, 22.8(4)° (compound **2**), respectively, for pairs of rings containing C(1)/N(3), C(16)/N(6) atoms.

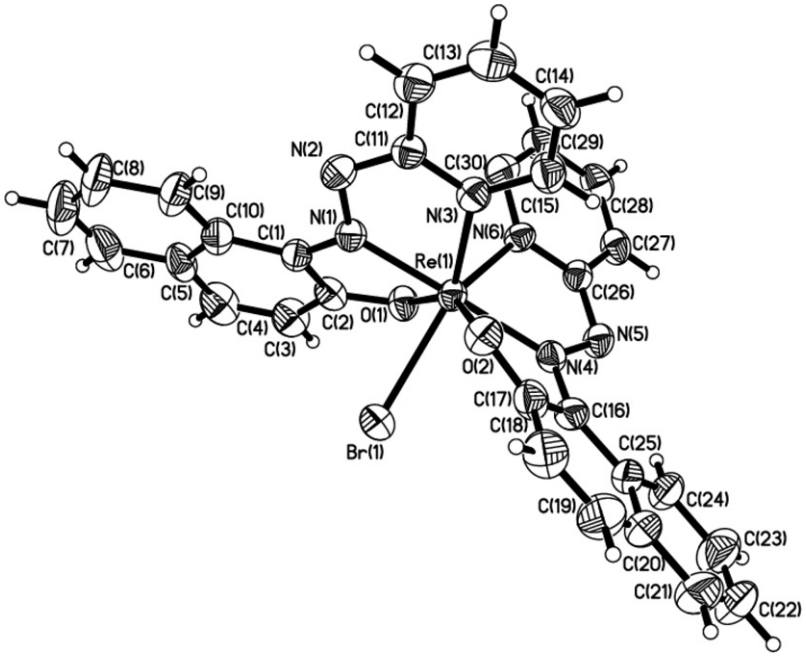

Fig. 1. The molecular structure of [ReBr(PAN)$_2$].

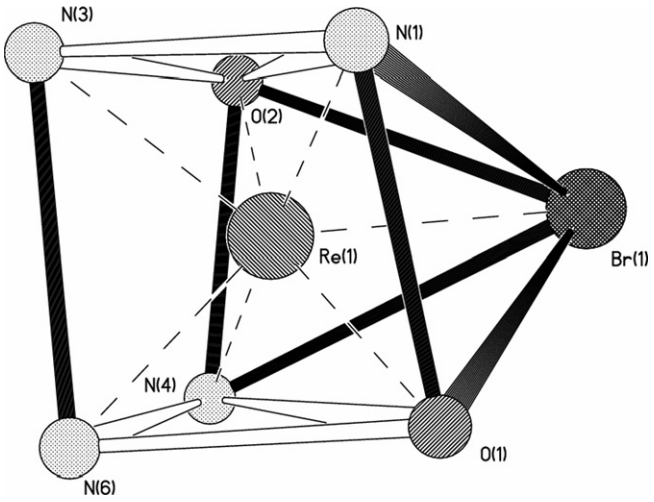

Fig. 2. View of the ReN_4O_2Br coordination polyhedron of $[ReBr(PAN)_2]$.

The selected bond lengths and angles of $[ReX(PAN)_2]$ are given in Tables 3 and 4. For both structures the Re–N_{azo} distances are somewhat shorter than the Re–N_{py} bonds, and the N–N lengths are significantly longer than that (1.25 Å) in uncoordinated azo compounds. The excellent π-acceptor character of azoheterocycles originates from low lying π*(azo) orbitals [41]. The interatomic distances between the rhenium atom and the oxygen atom of PAN ligand are almost equal to an ideal single Re–O bond length. The last one, predicted by the use of Pauling's covalent radius for oxygen and Cotton and Lippard's value for the octahedral covalent radius of rhenium(V), should be *ca.* 2.04 Å [42].

3.3. Magnetic properties

The magnetic properties of complex **1** under the form molar magnetic susceptibility $\chi_M = f(T)$ and $\mu_{eff} = f(T)$ are shown in Fig. 3.

The complex of **1** shows at 0.5 T in the whole temperature range lowering of the magnetic moment is observed, from 2.25 B.M. at 300 K up to 0.18 B.M. at 1.8 K.

This behavior is characteristic of slightly distorted heptanuclear capped trigonal prismatic mononuclear Re(III) complex with d^4 low-spin electron configuration [43,44]. It seems that in the room temperature, in accordance Boltzmann's distribution, are partially populated higher states, which are depopulated with temperature lowering and decreasing of the magnetic moment is observed.

The extended Hückel molecular orbital calculation of Hoffman and al. [45] for capped trigonal prismatic geometry of the coordination sphere of the Re(III) centers results e (xy, $x^2 - y^2$) orbital at low energy and higher energy $a_1(z^2)$ + e (xz,yz) orbitals.

The variation of the magnetization M versus the magnetic field H for complex at 2 K indicates value of the magnetization ~0.0 B.M. for 5 T, confirms totally pairing electrons of the rhenium center and diamagnetic ground state of the complex.

3.4. Geometry optimization and charge distribution

The geometry of $[ReBr(PAN)_2]$ was optimized in triplet and singlet states using the DFT method with the B3LYP functional. The energy of the triplet state is of 20.9 kcal/mol higher. The optimized geometric parameters of the singlet and triplet states are gathered

Table 4
The experimental bond lengths (Å) and angles (°) for **2**

Bond lengths	Experimental	Bond angles	Experimental
Re(1)–N(1)	2.038(7)	N(1)–Re(1)–N(4)	172.0(3)
Re(1)–N(3)	2.066(7)	N(1)–Re(1)–O(1)	74.3(3)
Re(1)–N(4)	2.042(7)	N(4)–Re(1)–O(1)	109.9(3)
Re(1)–N(6)	2.057(7)	N(1)–Re(1)–N(6)	116.2(3)
Re(1)–O(1)	2.061(6)	N(4)–Re(1)–N(6)	71.8(3)
Re(1)–O(2)	2.049(6)	O(1)–Re(1)–N(6)	74.1(3)
Re(1)–Cl(1)	2.393(2)	N(1)–Re(1)–O(2)	97.7(3)
N(1)–N(2)	1.325(9)	N(4)–Re(1)–O(2)	75.6(2)
N(4)–N(5)	1.326(9)	O(1)–Re(1)–O(2)	154.9(2)
		N(6)–Re(1)–O(2)	129.5(3)
		N(1)–Re(1)–N(3)	71.4(3)
		N(4)–Re(1)–N(3)	110.1(3)
		O(1)–Re(1)–N(3)	123.4(3)
		N(6)–Re(1)–N(3)	82.4(3)
		O(2)–Re(1)–N(3)	73.9(3)
		N(1)–Re(1)–Cl(1)	88.7(2)
		N(4)–Re(1)–Cl(1)	85.7(2)
		O(1)–Re(1)–Cl(1)	77.39(18)
		N(6)–Re(1)–Cl(1)	134.4(2)
		O(2)–Re(1)–Cl(1)	78.66(19)
		N(3)–Re(1)–Br(1)	143.2(2)

Table 3
The experimental and optimized bond lengths (Å) and angles (°) for **1**

Bond lengths	Experimental	Optimized		Bond angles	Experimental	Optimized	
		2S + 1 = 1	2S + 1 = 3			2S + 1 = 1	2S + 1 = 3
Re(1)–N(1)	2.040(4)	2.071	2.108	N(1)–Re(1)–N(4)	177.55(17)	176.91	147.23
Re(1)–N(3)	2.055(4)	2.080	2.122	N(1)–Re(1)–O(1)	75.11(15)	74.24	75.21
Re(1)–N(4)	2.043(4)	2.070	2.060	N(4)–Re(1)–O(1)	102.51(15)	104.34	77.35
Re(1)–N(6)	2.051(4)	2.081	2.144	N(1)–Re(1)–N(6)	107.82(16)	109.95	86.64
Re(1)–O(1)	2.047(3)	2.074	2.005	N(4)–Re(1)–N(6)	71.80(17)	72.00	72.11
Re(1)–O(2)	2.055(4)	2.078	2.042	O(1)–Re(1)–N(6)	74.05(16)	73.61	82.11
Re(1)–Br(1)	2.5504(9)	2.633	2.632	N(1)–Re(1)–O(2)	107.23(15)	105.94	139.95
N(1)–N(2)	1.334(6)	1.323	1.339	N(4)–Re(1)–O(2)	74.67(15)	74.14	72.79
N(4)–N(5)	1.329(6)	1.324	1.318	O(1)–Re(1)–O(2)	154.70(15)	155.22	133.95
				N(6)–Re(1)–O(2)	126.43(16)	126.96	119.42
				N(1)–Re(1)–N(3)	71.68(17)	71.97	72.92
				N(4)–Re(1)–N(3)	110.51(17)	110.88	129.25
				O(1)–Re(1)–N(3)	128.91(16)	127.82	147.21
				N(6)–Re(1)–N(3)	80.49(17)	82.00	88.55
				O(2)–Re(1)–N(3)	73.69(16)	73.46	77.66
				N(1)–Re(1)–Br(1)	89.53(12)	88.25	81.50
				N(4)–Re(1)–Br(1)	89.40(12)	88.75	113.67
				O(1)–Re(1)–Br(1)	77.57(11)	77.72	85.13
				N(6)–Re(1)–Br(1)	141.18(11)	139.75	164.44
				O(2)–Re(1)–Br(1)	77.26(11)	77.52	76.00
				N(3)–Re(1)–Br(1)	138.33(12)	138.25	97.50

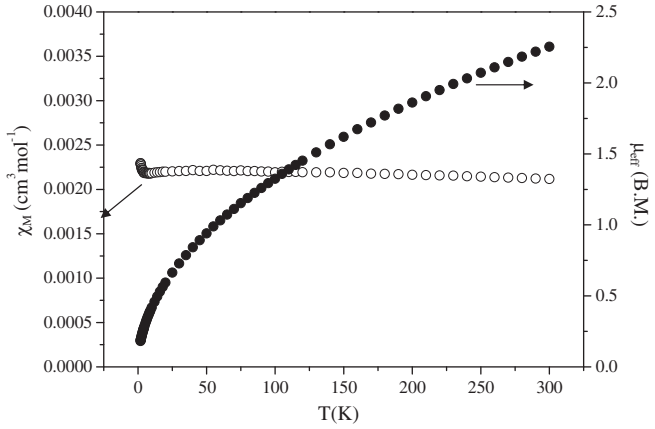

Fig. 3. Experimental magnetic plotted as χ_M (○) and μ_{eff} (●) versus temperature for the complex **1**.

Table 5
The Mulliken atomic charges of [ReBr(PAN)$_2$]

Atom	Atomic charge
Re(1)	0.317
Br(1)	−0.409
N(1)	−0.193
N(2)	−0.372
N(3)	−0.439
N(4)	−0.192
N(5)	−0.374
N(6)	−0.437
O(1)	−0.504
O(2)	−0.504

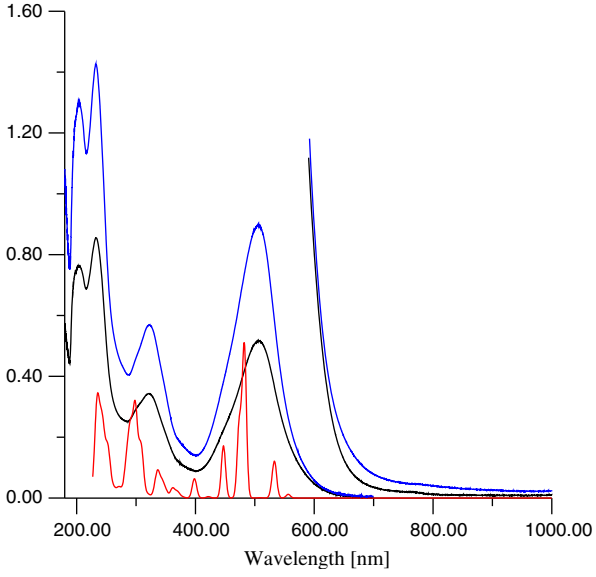

Fig. 4. The experimental electronic absorption spectra of **1** (black) and **2** (blue) complexes and calculated (red) electronic absorption spectrum of **1**. (For interpretation of the references to color in this figure legend, the reader is referred to the web version of this article.)

in Table 3. As can be seen from the Table 3, the predicted bond lengths and angles for the singlet state are definitely better correlated with the values based upon the X-ray crystal structure data than the optimized geometric parameters of the triplet state of [ReBr(PAN)$_2$].

Table 6
The energy and molar absorption coefficients of experimental absorption bands and the electronic transitions calculated with the TDDFT method for [ReBr(PAN)2]

The most important orbital excitations	Character	λ (nm)	E (eV)	f	Experimental Λ [nm] (E [eV]) ε
H − 2 → L	d/π(PAN)/π(Br) → d/π*(PAN)	556.3	2.23	0.0120	515.2 (2.41) 17300
H → L	π(PAN)/π(Br) → d/π*(PAN)	533.7	2.32	0.0965	
H − 3 → L	d/π(PAN)/π(Br) → d/π*(PAN)	530.0	2.34	0.0378	
H → L	π(PAN)/π(Br) → d/π*(PAN)				
H − 1 → L + 1	π(PAN)/d → d/π*(PAN)	482.2	2.57	0.4967	
H − 2 → L	d/π(PAN)/π(Br) → d/π*(PAN)				
H → L + 2	π(PAN)/π(Br) → d/π*(PAN)	473.7	2.62	0.2405	
H − 3 → L + 1	d/π(PAN)/π(Br) → d/π*(PAN)	447.1	2.77	0.1713	
H − 1 → L + 1	π(PAN)/d → d/π*(PAN)				
H − 1 → L + 2	π(PAN)/d → d/π*(PAN)	343.3	3.61	0.0423	323.5 (3.83)
H → L + 3	π(PAN)/π(Br) → d/π*(PAN)	336.6	3.68	0.0721	11870
H − 1 → L + 4	π(PAN)/d → π*(PAN)	310.1	4.00	0.0902	
H → L + 5	π(PAN) → d/π*(PAN)	306.6	4.04	0.0457	
H − 8 → L + 1	π(PAN)/d → d/π*(PAN)	301.8	4.11	0.0411	
H − 1 → L + 5	π(PAN)/d → d/π*(PAN)	298.3	4.16	0.0988	
H − 3 → L + 4	d/π(PAN)/π(Br) → π*(PAN)	298.1	4.16	0.1575	
H − 3 → L + 5	d/π(PAN)/π(Br) → d/π*(PAN)	291.8	4.25	0.1246	
H → L + 6	π(PAN)/π(Br) → d/π*(PAN)	289.1	4.29	0.1069	
H − 3 → L + 2	d/π(PAN)/π(Br) → d/π*(PAN)	284.2	4.36	0.0437	
H − 4 → L + 2	π(PAN)/d → d/π*(PAN)	284.1	4.36	0.0472	
H → L + 8	π(PAN)/d → d/π*(PAN)	255.1	4.86	0.0371	233.0 (5.32)
H − 4 → L + 4	π(PAN)/d → π*(PAN)	252.6	4.91	0.0699	29670
H − 8 → L + 2	π(PAN) → π*(PAN)	245.3	5.05	0.0715	
H − 7 → L + 3	π(PAN)/π(Br) → d/π*(PAN)	242.7	5.11	0.0329	
H − 4 → L + 6	π(PAN)/d → d/π*(PAN)	242.0	5.12	0.0332	
H − 16 → L + 1	π(PAN) → d/π*(PAN)	240.6	5.15	0.0589	
H − 5 → L + 6	π(PAN)/π(Br)/d → d/π*(PAN)				
H − 2 → L + 9	d/π(PAN) → d/π*(PAN)	236.9	5.23	0.0314	
H − 18 → L	π(PAN)/d → d/π*(PAN)	234.5	5.29	0.1888	
H − 5 → L + 6					
H → L + 12	π(PAN)/π(Br) → d	226.8	5.47	0.2869	
					206.3 (6.01) 26330

ε – molar absorption coefficient (dm^3 mol^{-1} cm^{-1}).
f – oscillator strength.
H – highest occupied molecular orbital.
L – lowest unoccupied molecular orbital.

Table 5 presents the Mulliken atomic charges for [ReBr(PAN)$_2$]. The calculated charge on the rhenium atom is considerable lower than the formal charge +3, and the charges on the bromide and oxygen atoms are significantly smaller than expected −1, indicating charge donation from the ligands to the central ion.

3.5. Electronic spectra

The nature of the transitions observed in the UV–Vis spectra of the title complexes has been studied by the time-dependent density functional (TDDFT) method. The calculated electronic spectrum of [ReBr(PAN)$_2$] and experimental electronic spectra of **1** and **2** (in acetonitrile) are presented in Fig. 4. Each calculated

transition is represented by a gaussian function $y = ce^{-b(x-x_0)^2}$ with the height (c) equal to the oscillator strength and b equal to 0.04 nm^{-2}. As seen from the Fig. 4, TDDFT/PCM calculations well reproduce the absorption spectrum of [$ReBr(PAN)_2$].

Table 6 presents the most important electronic transitions calculated with the TDDFT method for [$ReBr(PAN)_2$] and their assignments to the observed absorption bands of the complex. For the high energy part of the spectrum, only transitions with oscillator strengths larger than 0.0300 are listed in Table 6. The assignment of the calculated orbital excitations to the experimental bands was based on an overview of the contour plots and relative energy of occupied and unoccupied molecular orbitals involved in the electronic transitions (Fig. 5).

The TDDFT calculations show that the longest wavelength experimental band of **1** at 515.2 nm originates in the transitions between HOMO, HOMO − 1, HOMO − 2, HOMO − 3 and LUMO, LUMO + 1, LUMO + 2. As can be seen from the Fig. 4, the highest occupied molecular orbital is composed of π-bonding orbitals of the PAN and bromide ligands, whereas the HOMO − 1, HOMO − 2 and HOMO − 3 are delocalized on the whole complex. The LUMO, LUMO + 1 and LUMO + 2 are centered on the π-antibonding orbitals of the PAN ligand and the rhenium center. Accordingly, a delocalized *MLLCT* (metal–ligand-to-ligand CT) description seems to be the most suitable (adequate) for character of the band at 515.2 nm. The similar character can be also assigned to the experimental bands at 323.5 and 233.0 nm.

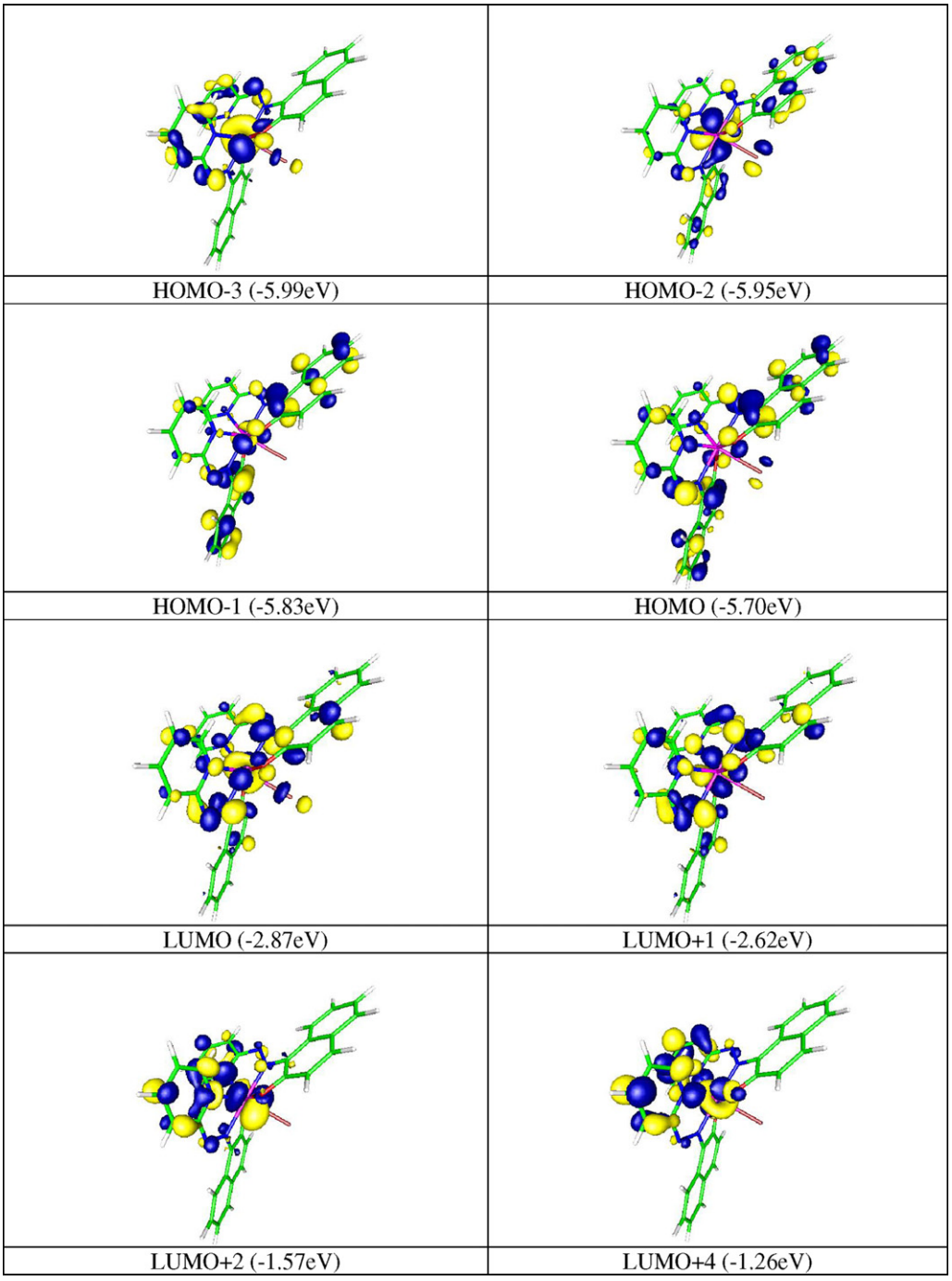

Fig. 5. Contour plots and energy of the selected occupied and unoccupied orbitals active in the electronic transitions. The orbitals were plotted with contour values −0.04 (yellow) and 0.04 au (blue). (For interpretation of the references to color in this figure legend, the reader is referred to the web version of this article.)

To some extent, the electronic absorption spectra of [Re-X(PAN)$_2$] are similar to those observed for *fac*-[ReCl$_3$(L–L)(PPh$_3$)] with bipy-like ligands. The solution spectra of both [ReBr(PAN)$_2$] and *fac*-[ReCl$_3$(L–L)(PPh$_3$)] [46,47] complexes exhibit intense absorption bands in the visible region, which are not observed for Re(III) complexes with chloride ions in a *meridional* fashion: [ReCl$_3$(bpzm)(PPh$_3$)] [10], [ReCl$_3$(pzH)$_2$(PPh$_3$)] and [ReCl$_3$(3,5-Me$_2$pzH)$_2$(PPh$_3$)] [9]. However, in contrast to the *fac*-[ReCl$_3$(L–L)(PPh$_3$)] displaying multiple transitions in the form of peaks and shoulders in the visible region, the solution spectra of the examined complexes show one broad absorption band. Furthermore, in comparison with *fac*-[ReCl$_3$(bipy)(PPh$_3$)], the longest wavelength experimental bands of the [ReX(PAN)$_2$] complexes are significantly more intense. The DFT calculations confirm larger contribution of π-bonding ligand orbitals in the highest occupied molecular orbitals for [ReBr(PAN)$_2$] than *fac*-[ReCl$_3$(bipy)(PPh$_3$)], whereas the lowest unoccupied molecular orbitals of both [Re-Br(PAN)$_2$] and *fac*-[ReCl$_3$(bipy)(PPh$_3$)] are centered on the π-antibonding ligand orbitals. Accordingly, the longest wavelength experimental bands of [ReCl$_3$(bipy)(PPh$_3$)] are mainly attributed to transitions of $d \rightarrow \pi^*_{bipy}$, whereas the experimental band of [Re-Br(PAN)$_2$] at 515.2 nm can be seen as a mixture of MLCT and LLCT transitions.

Supplementary data

CCDC 687571 and 687572 contain the supplementary crystallographic data for $C_{32}H_{22}N_6O_2BrCl_6Re$ and $C_{30}H_{20}N_6O_2ClRe$. These data can be obtained free of charge via http://www.ccdc.cam.ac.uk/conts/retrieving.html, or from the Cambridge Crystallographic Data Centre, 12 Union Road, Cambridge CB2 1EZ, UK; fax: (+44) 1223-336-033; or e-mail: deposit@ccdc.cam.ac.uk.

Acknowledgements

The GAUSSIAN03 calculations were carried out in the Wrocław Centre for Networking and Supercomputing, WCSS, Wrocław, Poland.

References

[1] J.R. Dilworth, S.J. Parrott, Chem. Soc. Rev. 27 (1998) 43.
[2] S.S. Jurisson, J.D. Lydon, Chem. Rev. 99 (1999) 2205.
[3] S. Liu, D.S. Edwards, Chem. Rev. 99 (1999) 2235.
[4] U. Abram, R. Alberto, J. Braz. Chem. Soc. 17 (8) (2006) 1486.
[5] F. Tisato, M. Porchia, C. Bolzati, F. Refosco, A. Vittadini, Coord. Chem. Rev. 250 (2006) 2034.
[6] P. Blower, Dalton Trans. (2006) 1705.
[7] G. Rouschias, G. Wilkinson, J. Chem. Soc. A (1967) 993.
[8] P. Ghosh, A. Pramanik, N. Bag, A. Chakravorty, J. Chem. Soc., Dalton Trans. (1992) 1883.
[9] B. Machura, M. Jaworska, R. Kruszynski, Polyhedron 23 (2004) 1819.
[10] B. Machura, R. Penczek, R. Kruszynski, J. Kłak, J. Mroziński, J. Kusz, Polyhedron 26 (2007) 4833.
[11] S. Chen, D. Lu, Talanta 64 (2004) 140.
[12] A.P. dos Anjos, L. Cornejo-Ponce, S. Cadore, N. Baccan, Talanta 71 (2007) 1252.
[13] A.E. Visser, S.T. Griffin, D.H. Hartman, R.D. Rogers, J. Chromatogr., B 743 (2000) 107.
[14] H. Adams, R.M. Bucknall, D.E. Fenton, M. Garcia, J. Oakes, Polyhedron 17 (1998) 4169.
[15] F.H. Allen, Acta Crystallogr., Sect. B 58 (2002) 380.
[16] H. Chermette, Coord. Chem. Rev. 178–180 (1998) 699.
[17] A. Voigt, U. Abram, R. Böttcher, U. Richter, J. Reinhold, R. Kirmse, Chem. Phys. 253 (2000) 171.
[18] M. Lipowska, L. Hansen, R. Cini, X. Xu, H. Choi, A.T. Taylor, L.G. Marzilli, Inorg. Chim. Acta 339 (2002) 327.
[19] J. Gancheff, C. Kremer, E. Kremer, O.N. Ventura, J. Mol. Struct. (Theochem) 580 (2002) 107.
[20] M.L. Kuznetsov, E.A. Klestova-Nadeeva, A.I. Dement'ev, J. Mol. Struct. (Theochem) 671 (2004) 229.
[21] N. Psaroudakis, K. Mertis, D.G. Liakos, E.D. Simandiras, Chem. Phys. Lett. 369 (2003) 490.
[22] X.-Y. Liu, S. Bouherour, H. Jacobsen, H.W. Schmalle, H. Berke, Inorg. Chim. Acta 330 (2002) 250.
[23] W.-Y. Wong, S.-H. Cheung, X. Huang, Z. Lin, J. Organomet. Chem. 655 (2002) 39.
[24] CRYSALIS RED, Oxford Diffraction Ltd., Version 1.171.29.2, 2000.
[25] G.M. Sheldrick, Acta Crystallogr., Sect. A 46 (1990) 467.
[26] G.M. Sheldrick, SHELXL97. Program for the Solution and Refinement of Crystal Structures, University of Göttingen, Germany, 1997.
[27] G.M. Sheldrick, SHELXTL: Release 4.1 for Siemens Crystallographic Research Systems, 1990.
[28] M.J. Frisch, G.W. Trucks, H.B. Schlegel, G.E. Scuseria, M.A. Robb, J.R. Cheeseman, J.A. Montgomery Jr., T. Vreven, K.N. Kudin, J.C. Burant, J.M. Millam, S.S. Iyengar, J. Tomasi, V. Barone, B. Mennucci, M. Cossi, G. Scalmani, N. Rega, G.A. Petersson, H. Nakatsuji, M. Hada, M. Ehara, K. Toyota, R. Fukuda, J. Hasegawa, M. Ishida, T. Nakajima, Y. Honda, O. Kitao, H. Nakai, M. Klene, X. Li, J.E. Knox, H.P. Hratchian, J.B. Cross, C. Adamo, J. Jaramillo, R. Gomperts, R.E. Stratmann, O. Yazyev, A.J. Austin, R. Cammi, C. Pomelli, J.W. Ochterski, P.Y. Ayala, K. Morokuma, G.A. Voth, P. Salvador, J.J. Dannenberg, V.G. Zakrzewski, S. Dapprich, A.D. Daniels, M.C. Strain, O. Farkas, D.K. Malick, A.D. Rabuck, K. Raghavachari, J.B. Foresman, J.V. Ortiz, Q. Cui, A.G. Baboul, S. Clifford, J. Cioslowski, B.B. Stefanov, G. Liu, A. Liashenko, P. Piskorz, I. Komaromi, R.L. Martin, D.J. Fox, T. Keith, M.A. Al-Laham, C.Y. Peng, A. Nanayakkara, M. Challacombe, P.M.W. Gill, B. Johnson, W. Chen, M.W. Wong, C. Gonzalez, J.A. Pople, GAUSSIAN 03, Revision B.03, Gaussian, Inc., Pittsburgh, 2003.
[29] A.D. Becke, J. Chem. Phys. 98 (1993) 5648.
[30] C. Lee, W. Yang, R.G. Parr, Phys. Rev. B 37 (1988) 785.
[31] T. Clark, J. Chandrasekhar, G.W. Spitznagel, P.v.R. Schleyer, J. Comp. Chem. 4 (1983) 294.
[32] M.J. Frisch, J.A. Pople, J.S. Binkley, J. Chem. Phys. 80 (1984) 3265.
[33] P.J. Hay, W.R. Wadt, J. Chem. Phys. 82 (1985) 299.
[34] H.B. Schlegel, M.J. Frisch, Int. J. Quant. Chem. 54 (1995) 83.
[35] M.E. Casida, Recent developments and applications in modern density functional theory, in: J.M. Seminario (Ed.), Theoretical and Computational Chemistry, vol. 4, Elsevier, Amsterdam, 1996.
[36] E. König, Magnetic Properties of Coordination and Organometallic Transition Metal Compounds, Springer, Berlin, 1966.
[37] K. Nakamoto, Infrared and Raman Spectra of Inorganic and Coordination Compounds, 4th ed., Wiley-Interscience, New York, 1986.
[38] G.R. Desiraju, T. Steiner, The Weak Hydrogen Bond in Structural Chemistry and Biology, Oxford University Press, 1999.
[39] G.A. Jeffrey, W. Saenger, Hydrogen Bonding in Biological Structures, Springer-Verlag, 1994.
[40] S. Alvarez, P. Alemany, D. Casanova, J. Cirera, M. Llunell, D. Avnir, Coord. Chem. Rev. 249 (2005) 1693.
[41] I. Chakraborty, S. Sengupta, Samir Das, S. Banerjee, A. Chakravorty, Dalton Trans. (2003) 134.
[42] S.R. Fletcher, A.C. Skapski, J. Chem. Soc., Dalton Trans. (1972) 1073.
[43] J.U. Abram, Rhenium, in: J.A. McClevery, T.J. Meyer (Eds.), Comprehensive Coordination Chemistry II, vol. 5, Elsevier, Pergamon, 2003, p. 271.
[44] J. Rall, F. Weingart, D.M. Ho, M.J. Heeg, F. Tisato, E. Deutsch, Inorg. Chem. 33 (1994) 3442.
[45] R. Hoffmann, B.F. Beier, E.L. Muetterties, A.R. Rossi, Inorg. Chem. 16 (1977) 551.
[46] B. Machura, R. Kruszynski, M. Jaworska, P. Lodowski, Polyhedron 24 (2005) 701.
[47] S. Sengupta, J. Gangopadhyay, A. Chakravorty, Dalton Trans. (2003) 4635.

2. Results and discussion

2.1. Synthesis and formulation

Reaction of $[Ru(CO)_2Cl_2]_n$ as a methanol suspension with 1-alkyl-2-(phenylazo)imidazole (PaiR) (**1**) or 1-alkyl-2-(*p*-tolylazo)-imidazole (TaiR) (**2**) (where R = Me (**a**), CH_2CH_3 (**b**), CH_2Ph (**c**)) under refluxing conditions in a dinitrogen atmosphere resulted in a brown solution Eq. (1). Upon slow evaporation of the solvent a brown crystalline product was left. The formulation of the complexes, $[Ru(CO)_2Cl_2(PaiR)]$ (**3**) and $[Ru(CO)_2Cl_2(TaiR)]$ (**4**) have been supported by microanalytical data (Section 4). Although three geometrical isomers (**3** and **4**; **3′** and **4′**; **3″** and **4″**) are possible, we have isolated only one isomer, with the CO groups *cis* to each other (**3** and **4**) and two Cl ligands in a *trans* disposition (Scheme 1). The complexes are diamagnetic, indicating the presence of the metal in the +2 oxidation state (d^6). Three stereo-isomers of **3**/**4**, **3′**/**4′** and **3″**/**4″** are possible. The structure has been established by a single crystal X-ray diffraction study in the case of $[Ru(CO)_2Cl_2(PaiEt)]$ and has a *trans*-(Cl,Cl) geometry, abbreviated as *trans*-(Cl)-$[Ru(CO)_2Cl_2$(PaiR/TaiR)] (**3** or **4**). The higher stability of the *trans*-(Cl)-*cis*-(CO) isomer relative to the *cis*-(Cl)-*trans*-(CO) isomer is not surprising due to the *trans* weakening effect of CO. The selectivity of the *trans*-(Cl) configuration has also been supported by DFT calculations (*vide Section* 2.3). Complexes **3** and **4** undergo a selective mono-decarbonylation reaction upon refluxing with Me_3NO in acetonitrile Eq. (2). In this process one CO is released and MeCN is coordinated, *trans*-(Cl)-$[Ru(CO)Cl_2$(PaiR)(NCMe)] (**5**) and *trans*-(Cl)-$[Ru(CO)Cl_2$(TaiR)(NCMe)] (**6**) are formed. The structure of the mono-carbonylated product (**5**, **6**) is supported by a single stretch ν (CO) in the FT-IR spectra (Fig. 1), elemental analysis and ^{1}H NMR spectroscopic measurements. Although isomerisation to give *cis*-(Cl)-$[Ru(CO)Cl_2$(ligand)(NCMe)] is possible, we cannot establish the presence of this isomer, even in the mixed form. The photochemical treatment of the precursor was also unsuccessful for isomerisation and giving the full decarbonylated complexes. The crystals of these complexes are weakly diffracting for X-ray structure determination. The full removal of CO has not been achieved even under drastic reaction conditions in the presence of a large excess of Me_3NO [69,70]. This reaction yielded an intractable brown solid.

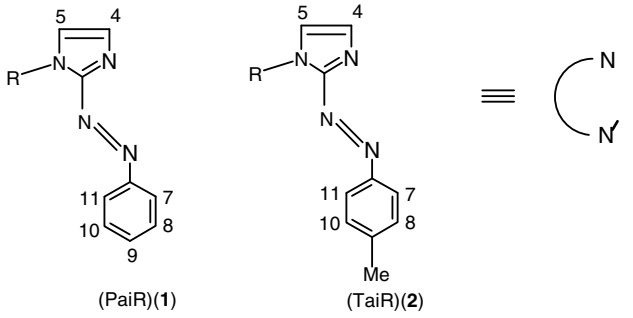

Scheme 1.

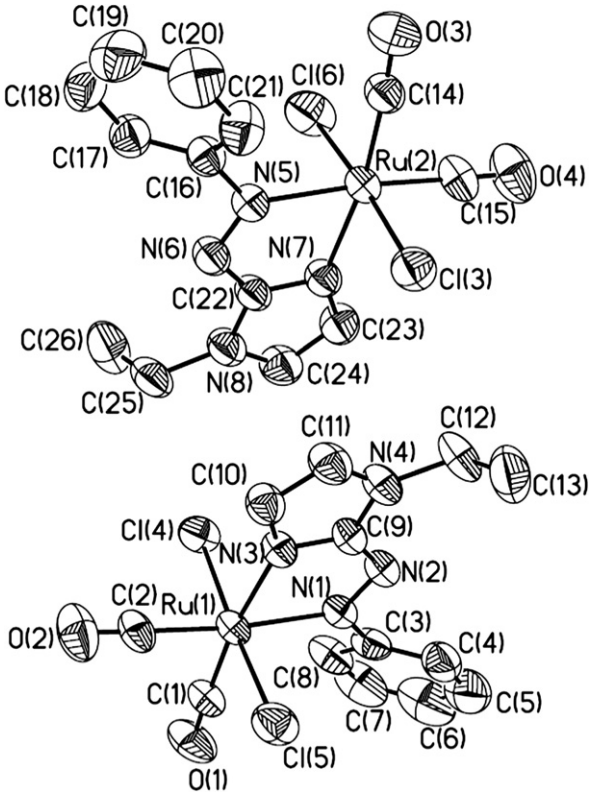

Fig. 1. Molecular structure of two conformers of *trans*-(Cl)-$[Ru(CO)_2Cl_2$(PaiEt)] (**3b**) (30% probability ellipsoids).

2.2. Molecular structure

The X-ray structure of $[Ru(CO)_2Cl_2(PaiEt)]$ (**3b**) is shown in Fig. 1; selected bond parameters are listed in Table 1. The ligands dispositions determine the structure as *trans*-(Cl)-$[Ru(CO)_2Cl_2$(PaiEt)]. The molecule consists of a central Ru surrounded by six donor centers, and the arrangement is distorted octahedral. The atomic arrangement involves two *trans*-chlorine, two *cis*-CO and a chelated 1-ethyl-2-(phenylazo)imidazole (PaiEt) ligand within the $RuCl_2C_2N_2$ coordination sphere. The two CO ligands are *trans* to the azo-N and imidazole-N coordinated centers. The asymmetric unit of the lattice consists of two molecules. A view of the diad, including the atomic numbering scheme, is given in Fig. 1. In terms of bond distances and angles, as well as gross geometry, the two molecules are closely alike to one another. The chelate ring dimensions (∠N(3)–Ru(1)–N(1): 75.13(9) and ∠N(5)–Ru(2)–N(7): 75.28(9)) are comparable with those in other structurally characterized chelates of the azoimine function [26–29,41–44,6,45,7,46–52,12,53–58]. The *trans* chlorine angles, Cl(4)–Ru(1)–Cl(5), 177.14(3) and Cl(3)–Ru(2)–Cl(6), 176.04(3), lie in the range of reported data [51,52,12,53–58]. Other angles about Ru define the distorted octahedral geometry.

The Ru–N(azo) distance (Ru(1)–N(1), 2.132(2); Ru(2)–N(5), 2.123(2) Å) is slightly longer than Ru–N(imidazole) (Ru(1)–N(3), 2.102(2); Ru(2)–N(7), 2.106(2) Å). In general, the Ru–N(azo) bond distance is shorter than the Ru–N(imidazole) bond, which is mainly due to $d\pi(Ru) \rightarrow \pi^*$(azo) back bonding [26–44,6,45,7,46–48]. The –N=N– bond length is 1.275–1.279 Å and is longer than the free ligand azo distance (1.258 Å) [66–68], which supports the $d\pi(Ru)$–π^*(azo) back bonding. Of the Ru–C bond lengths, (Ru(1)–C(1), 1.879(3); Ru(1)–C(2), 1.894(3); Ru(2)–C(14), 1.876(3); Ru(2)–C(15), 1.894(3) Å) the bonds *trans* to Ru–N(imidazole) (Ru(1)–C(1) and Ru(2)–C(14)) are shorter than the bonds

Table 1
Selected bond distances (Å) and bond angles (°) of (**3b**), X-ray and theoretical

Molecule-1		Molecule-2		Calculated structure
C(1)–O(1)	1.133(4)	C(14)–O(3)	1.130(4)	1.139
C(2)–O(2)	1.116(4)	C(15)–O(4)	1.113(4)	1.122
Ru(1)–C(1)	1.879(3)	Ru(2)–C(14)	1.876(3)	1.884
Ru(1)–C(2)	1.894(3)	Ru(2)–C(15)	1.894(3)	1.906
Ru(1)–N(1)	2.132(2)	Ru(2)–N(5)	2.123(2)	2.138
Ru(1)–N(3)	2.102(2)	Ru(2)–N(7)	2.106(2)	2.112
Ru(1)–Cl(4)	2.3798(8)	Ru(2)–Cl(3)	2.3823(8)	2.394
Ru(1)–Cl(5)	2.3852(9)	Ru(2)–Cl(6)	2.3799(9)	2.390
N(1)–N(2)	1.279(3)	N(5)–N(6)	1.275(3)	1.288
O(1)–C(1)–Ru(1)	177.6(3)	O(3)–C(14)–Ru(2)	176.0(3)	178.1
O(2)–C(2)–Ru(1)	177.9(3)	O(4)–C(15)–Ru(2)	178.9(3)	178.2
C(1)–Ru(1)–C(2)	88.34(12)	C(14)–Ru(2)–C(15)	89.08(14)	90.21
C(1)–Ru(1)–N(3)	172.53(12)	C(14)–Ru(2)–N(7)	171.38(12)	174.1
C(2)–Ru(1)–N(3)	98.53(11)	C(15)–Ru(2)–N(7)	98.51(11)	95.06
C(1)–Ru(1)–N(1)	98.13(11)	C(14)–Ru(2)–N(5)	97.11(11)	98.70
C(2)–Ru(1)–N(1)	173.53(11)	C(15)–Ru(2)–N(5)	173.79(11)	170.9
C(1)–Ru(1)–Cl(4)	93.37(10)	C(14)–Ru(2)–Cl(3)	94.00(10)	92.42
C(2)–Ru(1)–Cl(4)	89.77(11)	C(15)–Ru(2)–Cl(3)	90.64(11)	91.64
C(1)–Ru(1)–Cl(5)	88.98(10)	C(14)–Ru(2)–Cl(6)	89.40(10)	89.92
C(2)–Ru(1)–Cl(5)	91.94(11)	C(15)–Ru(2)–Cl(6)	91.44(11)	91.80
N(3)–Ru(1)–N(1)	75.13(9)	N(7)–Ru(2)–N(5)	75.28(9)	75.93
N(1)–Ru(1)–Cl(4)	87.69(7)	N(7)–Ru(2)–Cl(6)	86.35(7)	89.67
N(3)–Ru(1)–Cl(4)	89.61(7)	N(5)–Ru(2)–Cl(6)	88.14(7)	89.88
N(1)–Ru(1)–Cl(5)	90.35(7)	N(7)–Ru(2)–Cl(3)	90.01(7)	86.55
N(3)–Ru(1)–Cl(5)	87.87(7)	N(5)–Ru(2)–Cl(3)	89.43(7)	87.47

that are *trans* to Ru–N(azo) (Ru(1)–C(2) and Ru(2)–C(15)). This is usual due to a better *trans influence* of imidazole-N compared to azo-N donors. The C–O distances (C(1)–O(1), 1.133(4); C(2)–O(2), 1.116(4); C(14)–O(3), 1.130(4); C(15)–O(4), 1.113(4) Å) vary to within 0.01–0.02 Å. The difference between the two molecules in the lattice primarily lies in the detail of the conformation. The pendant phenyl ring is inclined to the mean plane of the chelate ring, and the angles are molecule-1, 36.73(17); molecule-2, 41.99(15). The torsion angles vary in a characteristic manner. Examples from those among the atoms of the chelate ring are: Ru(1)–N(3)–C(9)–N(2): 2.2(4); Ru(2)–N(7)–C(22)–N(6): −3.3(4); C(9)–N(2)–N(1)–Ru(1): −1.3(3); C(22)–N(6)–N(5)–Ru(2): 2.4(3); N(2)–N(1)–Ru(1)–N(3): 1.8(2); N(6)–N(5)–Ru(2)–N(7): −3.2(2). Thus, these two molecules represent a subtle form of conformational isomerism in a metal chelate, sustained by the crystal lattice.

Non-covalent interactions, C–H$\cdots\pi$ and $\pi\cdots\pi$, exist to provide rigidity to the supramolecule. An intermolecular hydrogen bond between one of the coordinated Cl ligands and the H atom of the *ortho* C–H of the pendant azophenyl group of an adjacent molecule constitutes a dimer structure (Fig. 2a). Each dimer interacts with adjacent dimers *via* C–H$\cdots\pi$ and $\pi\cdots\pi$ interactions to generate a supramolecular network (Fig. 2b). The interactions are summarized in Table 2.

2.3. DFT and TD-DFT calculations

DFT and TD-DFT calculations were performed for complexes **3b** and **5b**. All the calculations were performed using the GAUSSIAN03 (G03) [71] software package, running under Windows. The Becke's three-parameter hybrid exchange functional and the Lee–Yang–Parr non-local correlation functional [72] (B3LYP) was used throughout. Elements except ruthenium were assigned a 6-31 G* basis set in our calculations. For ruthenium the Los Alamos effective core potential plus double zeta (LanL2DZ) [73] basis set was employed. Gas and solution-phase geometry optimization was carried out. In all cases, vibrational frequencies were calculated to ensure that the optimized geometries represented local minima. To check the effect of solvation on the calculated optical absorption spectra, we performed TD-DFT calculations of the low lying excitation at the singlet optimized geometry, including the solvation effect by means of the non-equilibrium implementation of the polarizable continuum model [74]; as in the experimental conditions, the chosen solvent was acetonitrile. GaussSum [75] was used to calculate the fractional contributions of various groups to each molecular orbital. This is done using Mulliken population analysis.

The calculated structure of **3b** correlates very well with the results of its X-ray analysis (Fig. 1, Table 1). The theoretical Ru–N bond lengths are about 0.010 Å longer than those observed. Similarly the experimental Ru–Cl distances are shorter by 0.015 Å than the theoretical data. The Ru–C and C–O distances are also reduced by 0.006–0.010 Å in the experimental data compared to the calculated structure. The computation of ν(CO) from the DFT calculation shows a lowering of frequency by 8–10 cm^{-1}.

The DFT calculation shows a lower energy of the HOMO of *trans*-(Cl)-[$Ru(CO)_2Cl_2$(PaiEt)] (**3b**) (E_{HOMO}): −6.17 eV) than that of *cis*-(Cl)-[$Ru(CO)_2Cl_2$(PaiEt)] (**3b′**) (E_{HOMO}): −5.60 eV) and *cis*-(Cl)-*cis*-(CO)-[$Ru(CO)_2Cl_2$(PaiEt)] (**3b″**) (E_{HOMO}): −5.86 eV). This reflects better stability of the *trans*-(Cl,Cl) than *cis*-(Cl,Cl) configuration. An interesting feature of the valence orbitals is that the highest occupied MOs (HOMO, abbreviated as H, H − 1, H − 2, H − 3) contain >65% and >45% of the Cl atomic functions in **3b** and **5b**, respectively. Metal orbitals contribute >20% to H and H − 1. The LUMO (abbreviated L) is mostly characterized by the azoimidazole ligand function (>80%) for both these complexes, while other unoccupied molecular orbitals have CO >20% and Ru contribution varies from 5% to 35%. The results in acetonitrile phase show a significant difference from the gas phase, in particular to the occupied MOs. In the HOMO the contribution of PaiEt (L) is 42% in MeCN and 1% in the gas phase, while the Cl contribution is 28% in MeCN and the gas phase contribution is 67% for **3b**. The situation is different for **5b**: 14% (gas) and 24% (MeCN). H − 1 in the gas and acetonitrile phases remains more or less the same. The HOMO is stabilized by 0.63 eV in **3b** and 0.72 eV in **5b** from the gas to acetonitrile phase. The HOMO is also lowered in energy by 0.54 eV in **3b** compared to **5b** and the HOMO–LUMO energy gaps are 3.04 eV for **3b** and 2.83 eV for **5b** in MeCN (Fig. 3).

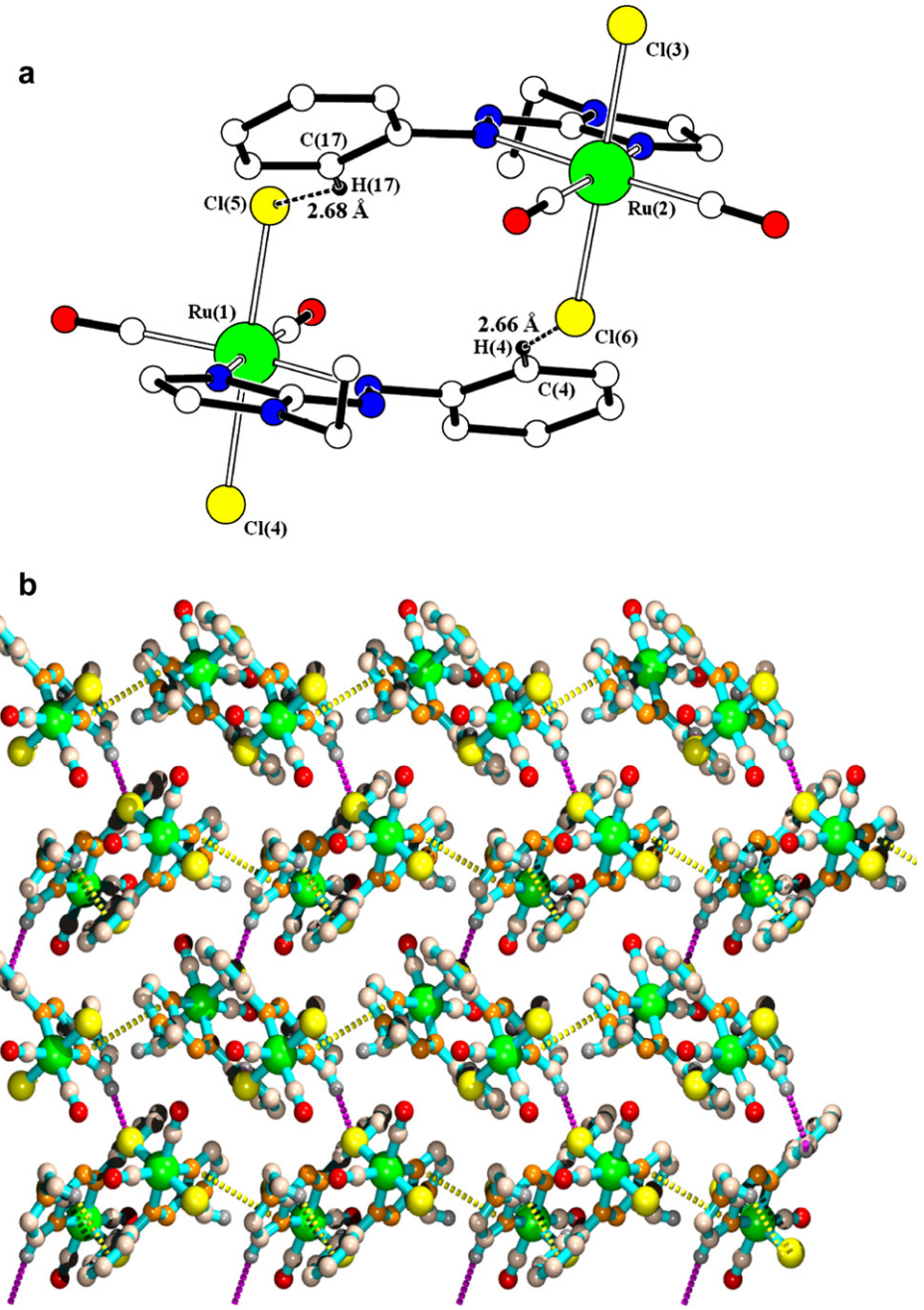

Fig. 2. (a) C–H···Cl hydrogen bonded dimer unit, (b) π···π and CH···π interacted *ab*-plane (π···π; C–H···π in yellow; C–H···Cl in magenta). (For interpretation of the references to color in this figure legend, the reader is referred to the web version of this article.)

Table 2
Distance of non-covalent interactions in **3b**

	d_{C-H} (Å)	$d_{H\cdots Cl}$ (Å)	$d_{C\cdots Cl}$ (Å)	Angle (°)	Symmetry
Hydrogen bonding					
C(4)–H(4)···Cl(6)	0.930	2.680	3.560(4)	157.0	$-1+x, y, z$
C(17)–H(17)···Cl(5)	0.930	2.660	3.456(3)	144.0	$1+x, y, z$
	$d_{H\cdots Cg}$ (Å)	d_{C-Cg} (Å)	Angle (°)	Symmetry	
C–H···π interaction					
C(13)–H(13 C) → Cg(3)	2.984	3.799(8)	143.45	$-1+x, y, z$	
	$d_{Cg\cdots Cg}$ (Å)	Alpha	*d* (perpendicular)	Symmetry	
π···π interaction					
Cg(2) → Cg(5)	3.691(2)	1.02	3.447	*x*, *y*, *z*	

Cg(2): N(7)–C(22)–N(8)–C(24)–C(23); Cg(3): C(16)–C(17)–C(18)–C(19)–C(20)–C(21); Cg(5): N(3)–C(9)–N(4)–C(11)–C(10).

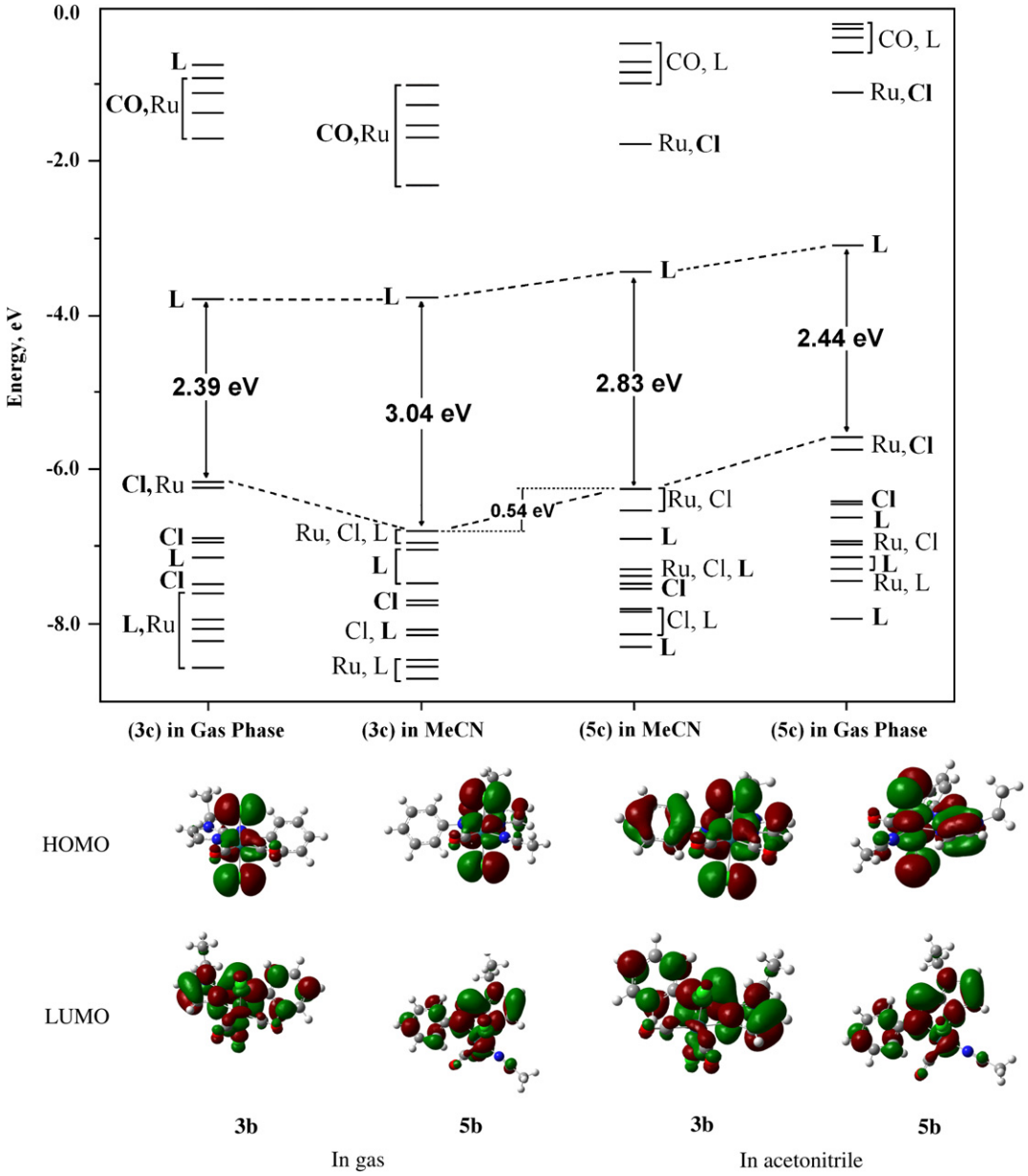

Fig. 3. Energy level correlation diagram of **3b** and **5b** in the gas and acetonitrile phase (top) and HOMO, LUMO picture (bottom).

2.4. Spectra and bonding

The infrared spectra of **3** and **4** show the presence ν (CO) stretching vibrations at 1990–2010 and 2065–2075 cm^{-1} (Table 3) which indicates the *cis* coordination of two CO ligands [67–70,76–78] (Fig. 1.) ν(Ru–Cl) appears at 330–340 cm^{-1}. Other significant peaks appear at 1570–1590 cm^{-1} and 1350–1370 cm^{-1}, corresponding to ν(C=N) and ν(N=N), respectively. The azo stretching is significantly shifted to the lower frequency region compared to the free ligand value (1400–1410 cm^{-1}) [79,80], which supports an efficient back donation, $d\pi(Ru(II)) \rightarrow \pi^*(azo)$. The infrared spectra of **5** and **6** show one ν(CO) at 1980–1985 cm^{-1}, which is in support of mono-carbonyl formulation, and the shifting to the lower frequency region compared to ν(CO) of **3/4** is an indication of better $d\pi(Ru(II)) \rightarrow \pi^*(CO)$ donation in **5/6**. The Mulliken population analysis of **3b** and **5b** show that the positive charge on CO in **5b** (0.18619) is less than that of the CO groups in **3b** (0.21986 and 0.23749). Computation of the major frequencies, ν(C=N), ν(N=N), ν(CO) and ν(Ru–Cl), by the DFT calculation shows a slightly lower frequency (5–10 cm^{-1}) than that of the experimental data, but still being within the reported frequency range.

The electronic spectra of **3** and **4** show an intense broad band at 470–500 nm, and in addition to this the molecules show a more intense and sharp band at 380–400 nm. The lower energy band in the mono-carbonyl complexes (**5** and **6**) has been shifted to a longer wavelength by 15–20 nm compared to the di-carbonyl precursors, **3** and **4** (Fig. 4). Thus, the energy of transition is lowered in **5/6** compared to **3/4**. This is well explained on the basis of the DFT calculation using the optimized geometry of a representative complex. The DFT calculations of **3b** and **5b** show that the HOMO–LUMO energy gap decreased by 0.21 eV in **5b** compared to **3b** in acetonitrile (Fig. 3). The TD-DFT calculations of **3b** and **5b** show that the transition at 470–530 nm (Table 5) could be assigned to $H/H-1 \rightarrow L$. H and H − 1 are localized on parts of the metal and Cl, and L have major ligand character. Thus, the transition is admix-

Table 3
FT-IR[a], UV–Vis spectral[b] and cyclic voltammetric[c] data of the complexes

Complex	IR data ν(CO) (cm^{-1})[a]	UV–Vis spectral data[b] λ_{max} (nm) ($10^{-3} \in M^{-1} cm^{-1}$)	Cyclic voltammetric data[c]	
			$E_{Ru(III)/Ru(II)}$, V (ΔE_p, mV)	Ligand reduction, V (ΔE_p, mV)
trans-(Cl)-[Ru(CO)$_2$Cl$_2$(PaiMe)] (**3a**)	1995, 2068	388(13.76), 500(3.07)	1.35(130)	−0.46(120), −1.30(210)
trans-(Cl)-[Ru(CO)$_2$Cl$_2$(PaiEt)] (**3b**)	2010, 2072	399(12.43), 480(2.88)	1.30(130)	−0.48(120), −1.32(210)
trans-(Cl)-[Ru(CO)$_2$Cl$_2$(PaiBz)] (**3c**)	2000, 2070	390(12.83), 498(3.05)	1.40(140)	−0.50(120), −1.30(210)
trans-(Cl)-[Ru(CO)$_2$Cl$_2$(TaiMe)] (**4a**)	2000, 2068	392(12.84), 498(2.37)	1.36(140)	−0.48(120), −1.25(210)
trans-(Cl)-[Ru(CO)$_2$Cl$_2$(TaiEt)] (**4b**)	2003, 2070	395(13.64), 500(2.82)	1.30(130)	−0.55(120), −1.30(210)
trans-(Cl)-[Ru(CO)$_2$Cl$_2$(TaiBz)] (**4c**)	1990, 2068	390(11.49), 505(2.73)	1.35(140)	−0.53(120), −1.35(210)
trans-(Cl)-[Ru(CO)Cl$_2$(PaiMe)(NCMe)] (**5a**)	1975	369(11.28), 540(3.24)	0.82(110)	−0.53(125), −1.25(220)
trans-(Cl)-[Ru(CO)Cl$_2$(PaiEt)(NCMe)] (**5b**)	1980	386(12.50), 515(2.92)	0.84(110)	−0.58(130), −1.28(220)
trans-(Cl)-[Ru(CO)Cl$_2$(PaiBz)(NCMe)] (**5c**)	1970	382(10.64), 530(4.65)	0.85(110)	−0.60(120), −1.26(220)
trans-(Cl)-[Ru(CO)Cl$_2$(TaiMe)(NCMe)] (**6a**)	1972	383(11.34), 530(3.21)	0.80(110)	−0.57(120), −1.26(220)
trans-(Cl)-[Ru(CO)Cl$_2$(TaiEt)(NCMe)] (**6b**)	1982	383(10.84), 530(4.68)	0.85(100)	−0.62(125), −1.30(220)
trans-(Cl)-[Ru(CO)Cl$_2$(TaiBz)(NCMe)] (**6c**)	1968	378(11.33), 525(2.94)	0.87(100)	−0.65(120), −1.27(220)

[a] KBr disc.
[b] Solvent, dry acetonitrile.
[c] Solvent MeCN, Pt-disk working electrode, Ag/AgCl reference electrode, Pt-wire auxiliary electrode, [nBu$_4$N][ClO$_4$] supporting electrolyte. $E_{Ru(III)/Ru(II)} = 0.5(E_{pa} + E_{pc})$, V for Ru(III)/Ru(II) couple in unit of V, $\Delta E_p = E_{pa} - E_{pc}$, mV where E_{pc} (cathodic-peak-potential), E_{pa} (anodic-peak-potential).

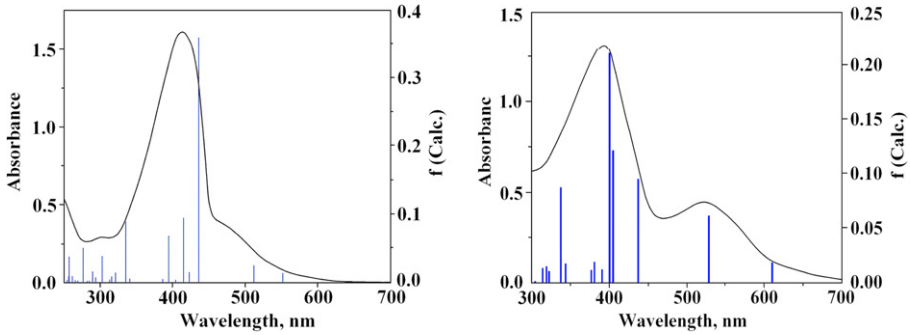

Fig. 4. Experimental UV–Vis spectra and calculated transitions for **3b** (left) and **5b** (right) in acetonitrile.

ture of MLCT and XLCT transitions (X = Cl) [81]. Because of the Cl contribution to H − n (n = 2, 3, 4, 5) (40–80%), the H − n → L transitions may be attributed to XLCT and contribute to the broadening of the band. The transitions H/H − n (n = 1–5) → L + p (p = 1, 2, 3, etc.) may be explained as π(PaiEt) → π^*(CO), an inter-ligand charge transfer transition. This transition is also mixed with π (PaiEt) → π^*(PaiEt) transitions.

The imidazole protons (4- and 5-H) of the coordinated PaiR or TaiR in the complexes *trans*-(Cl)-[Ru(CO)$_2$Cl$_2$(PaiR/TaiR)] (**3**, **4**) show downfield shifting by 0.3–0.4 ppm compared to the free ligand data [75–81] and appear at 7.70–7.85 ppm (4-H) and 7.35–7.50 (5-H) ppm (Table 4). This supports the strong preference of the binding of imidazole-N to Ru(II). 1-Me of the coordinated PaiMe/TaiMe in **3a** or **4a** is singlet at 4.25–4.30 ppm; 1-CH$_2$–CH$_3$ of coordinated PaiEt or TaiEt in **3b** or **4b** appears as a quartet at 4.60–4.65 ppm, (J = 8.0 Hz) and a triplet 1.70–1.72 ppm (J = 7.5 Hz) for –CH$_2$– and –CH$_3$, respectively; 1-CH$_2$–(Ph) in (**3c** and **4c**) is singlet at 5.80–5.90 ppm. The mono-carbonyl complexes, **5** and **6**, in general, show aromatic proton signals at a lower chemical shift position (δ) compare to **3** and **4** (with a difference in chemical shift ($\Delta\delta$) of 0.1–0.3 ppm). This may be due to removal of the strongly π-acidic CO from the Ru(CO)$_2$-motif (**3**, **4**) to prepare the Ru(CO)-motif in **5** and **6**. The coordinated MeCN in **5** and **6** appears as a singlet at 2.07-2.15 ppm for δ (CH$_3$).

2.5. Electrochemistry

The complexes show a Ru(III)/Ru(II) couple (Table 3, Fig. 5) when scanned in the potential range 0.0–2.0 V. The response is quasireversible in nature, as is evident from their peak-to-peak separation (ΔE_p > 100 mV). The nature of the voltammogram does not change with the scan rate (50–250 mV s^{-1}). The Ru(III)/Ru(II) potential, *ca.* 1.35 V, of *trans*-(Cl)-[Ru(CO)$_2$Cl$_2$(PaiR/TaiR)] (**3**, **4**) is significantly shifted to *ca.* 0.85 V for *trans*-(Cl)-[Ru(CO)Cl$_2$(PaiR/TaiR)(NCMe)] (**5**, **6**). This may be due to the better electron withdrawing effect of two CO in **3**, **4** than that of one CO in **5**, **6**. The DFT calculation in acetonitrile also supports the lower energy of the HOMO in **3b** (−6.80 eV) compared to that of **5b** (−6.26 eV). The HOMO is also contributed to by the metal (Ru) orbitals, thus the redox response is assigned to the Ru(III)/Ru(II) couple.

On scanning in the negative direction (0 to −2.0 V), two redox responses are observed. The first response is observed at >−0.70 V, and is quasireversible ($\Delta E_p \geqslant 120$ mV) in nature, while the second one appears at <−1.2 V ($\Delta E_p \geqslant 200$ mV). The chelated ligand belongs to the π-acidic azoimine family and can accommodate two electrons centered at the azo group (–N=N–). The reductive responses are assigned to accommodation of electrons in the azo dominated function [–N=N–]/[–N⋯N–]$^-$ and [–N⋯N]$^-$/[–N–N–]$^{2-}$. Ligand reduction of azoimidazole complexes appear at negative potentials and the present data appear at a less negative value (−0.5 to −0.6 V) than that of *trans*-[Ru(ligand)$_2$Cl$_2$] (−0.7 to −0.8 V). The DFT data have assigned that the LUMO of the complexes are constituted mainly of the azo group of the ligand (>80%) and thus the reduction is considered as electron accommodation at the azo dominated orbitals.

3. Conclusion

A series of di-carbonyl complexes of the formulae *trans*-(Cl)-[Ru(CO)$_2$Cl$_2$(PaiR or TaiR)] (for PaiR: R = Me (**3a**), Et (**3b**), CH$_2$Ph

Table 4
^{1}H NMR spectral data of the complexes in $CDCl_3$ at 298 K

Compound	δ, ppm (J, Hz)						
	4-H[a]	5-H[a]	7, 11-H[b]	8, 10-H	9-H/Me	1-R	CH_3CN
3a	7.78	7.44	8.08 (7.5)	7.52[c]	7.52[c]	4.27[e]	
3b	7.82	7.48	8.08 (7.5)	7.62[c]	7.62[c]	4.65 (8.0)[g], 1.70 (7.5)[h]	
3c	7.84	7.50	8.10 (7.5)	7.60[c]	7.60[c]	5.82[f]	
4[a]	7.76	7.44	7.98 (8.0)	7.36[b] (8.0)	2.50[d]	4.30[e]	
4b	7.78	7.45	8.00 (8.0)	7.40[b] (8.0)	2.50[d]	4.62 (8.0)[g], 1.70 (7.5)[h]	
4c	7.78	7.47	8.05 (8.0)	7.42 (7.8)	2.48[d]	5.94[f]	
5[a]	7.61	7.21	7.80 (7.5)	7.42[c]	7.42[c]	4.20[e]	2.06
5b	7.62	7.28	7.85 (7.5)	7.42[c]	7.42[c]	4.60 (7.5)[g], 1.74 (7.5)[h]	2.07
5c	7.65	7.31	7.83 (7.5)	7.50[c]	7.50[c]	5.90[f]	2.06
6a	7.56	7.30	7.68 (8.0)	7.16[b] (8.0)	2.50[d]	4.18[e]	2.06
6b	7.52	7.25	7.70 (8.0)	7.22[b] (7.5)	2.54[d]	4.60 (7.5)[g], 1.75 (7.5)[h]	2.07
6c	7.48	7.22	7.80 (8.0)	7.22 (8.0)	2.50[d]	5.85[f]	2.07

[a] Broad singlet.
[b] Doublet.
[c] Multiplet.
[d] δ(Ar-Me).
[e] δ(N(1)–Me).
[f] δ(N(1)–CH_2–Ph).
[g] δ(–CH_2–CH_3) quartet for –CH_2–.
[h] Triplet for –CH_3.

Table 5
Selected list of calculated data from TD-DFT excitation energies for **3b** and **5b** in acetonitrile

Excited state	λ, nm($f \times 10^3$)	Major contribution
*Compound **3b***		
1	551.8(10.9)	(79%)HOMO → LUMO (MLCT, IL), (14%)H − 2 → LUMO (IL)
2	512.8(19.2)	(86%)H − 1 → LUMO (MLCT, IL), (10%)H − 2 → LUMO (IL)
3	435.8(358.3)	(49%)H − 2 → LUMO, (18%)H − 4 → LUMO (IL)
5	415(93.7)	(67%)H − 3 → LUMO, (10%)H − 2 → LUMO, (10%)H − 4 → LUMO] (IL)
7	394.7(66.2)	(65%)H − 4 → LUMO, (19%)H − 3 → LUMO] (IL)
*Compound **5b***		
2	528.7(61.2)	(70%)H − 1 → LUMO, (19%)HOMO → LUMO (MLCT, IL)
4	436.7(95.3)	(33%)H − 2 → LUMO, (32%)H − 3 → LUMO, (17%) H − 4 → LUMO (IL)
5	404.2(119.8)	(64%)H − 1 → L + 1, (MLCT, IL), (18%)H − 2 → LUMO (IL)
6	400.4(211.0)	(28%)H − 2 → LUMO, (20%)H − 3 → LUMO, (16%)H − 4 → LUMO (IL), (16%)H − 1 → L + 1 (MLCT, IL)

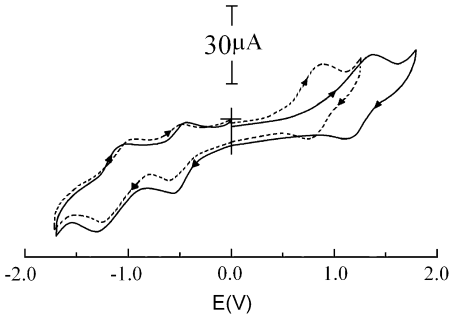

Fig. 5. Cyclic voltammogram of (**3b**) (—) and (**5b**) (– – –) in MeCN using Pt-disk working and Pt-wire auxiliary electrodes and referenced to the Ag/AgCl electrode.

(**3c**); for TaiR: R = Me (**4a**), Et (**4b**), CH_2Ph (**4c**)) has been synthesized by reacting $[Ru(CO)_2Cl_2]_n$ with PaiR or TaiR. The complexes are selectively decarbonylated to isolate *trans*-(Cl)-[$Ru(CO)Cl_2$(PaiR or TaiR)(NCMe)] (**5/6**). However, complete decarbonylation, either by thermal or photochemical methods, has not been possible. The complexes are characterized by spectroscopic data and in one case by an X-ray structure. The computational (DFT) study has discussed the separation of a single isomer on the basis of energy calculation. The electronic structures support metal centered oxidations, and reductions of the chelated ligand.

4. Experimental

4.1. Materials

1-Alkyl-2-(phenylazo)imidazole (**1**) and 1-alkyl-2-(*p*-tolylazo)imidazole (**2**) were synthesized following a previously published procedure [75–81]. $[Ru(CO)_2Cl_2]_n$ was also prepared by the reported method [63,64,76–78]. Imidazole and all other organic chemicals and inorganic salts were available from Sisco Research Lab., Mumbai, India. The purification of acetonitrile and preparation of *n*-tetrabutylammonium perchlorate [nBu$_4$N][ClO_4] for electrochemical work were done as reported before [75–81]. Dinitrogen was purified by bubbling through an alkaline pyrogallol solution. All other chemicals and solvents were of reagent grade and were used without further purification.

4.2. Physical measurements

Microanalytical data (C, H, N) were collected on Perkin–Elmer 2400 CHNS/O elemental analyzer. Spectroscopic data were obtained using the following instruments: UV–Vis spectra, Perkin–Elmer, model Lambda 25; IR spectra (KBr disk, 4000–200 cm^{-1}), Perkin–Elmer, model RX-1; ^{1}H NMR spectra, Bruker (AC) 300 MHz FTNMR spectrometer. Electrochemical measurements were performed using a computer-controlled PAR model 250 VersaStat electrochemical instrument with a Pt-disk electrode. All

Table 6
Summarised crystallographic data for *trans*-(Cl)-[$Ru(CO)_2Cl_2$(PaiEt)](3b)

Empirical formula	$C_{13}H_{12}Cl_2N_4O_2Ru$
Formula weight	428.24
Crystal system	monoclinic
Space group	$P21/c$
a (Å)	10.6772(14)
b (Å)	14.1537(18)
c (Å)	23.074(3)
β (°)	107.173(5)
Size (mm^3)	$0.42 \times 0.19 \times 0.13$
V(Å^3)	3331.5(7)
λ (Å)	0.71073
ρ_{calcd} ($Mg\,m^{-3}$)	1.708
Z	8
T (K)	298(2)
μ(Mo Kα) (mm^{-1})	1.272
Total reflection collected	19700
Unique reflections	6522
Refined parameters	399
Largest difference in peak and hole (e Å^{-3})	0.604 and −0.242
R[a] ($I > 2\sigma(I)$)	0.0330
wR[b]	0.0809
Goodness-of-fit[c]	1.034

[a] $R = \sum||F_o| - |F_c||/\sum|F_o|$.
[b] $wR = [\sum w(F_o^2 - F_c^2)^2/\sum w(F_o^2)^2]^{1/2}$, $w = 1/[s^2(F_o^2) + (0.0417P)^2 + 1.1071P]$, where $P = (F_o^2 + 2F_c^2)/3$.
[c] GOF (Goodness of fit) = $[w(F_o - F_c)/(n_o - n_v)]^{1/2}$, where n_o and n_v denote the number of data and variable.

measurements were carried out under a dinitrogen environment at 298 K with reference to Ag/AgCl in acetonitrile using [nBu_4N][ClO_4] as a supporting electrolyte. The reported potentials are uncorrected for junction potentials.

4.3. Synthesis of trans-(Cl)-[$Ru(CO)_2Cl_2$(PaiEt)] (**3b**)

[$Ru(CO)_2Cl_2$]$_n$ (0.31 g, 1.4 mmol) was dissolved in hot methanol (30 ml). A methanolic solution of PaiEt (0.28 g, 1.4 mmol) was added and the solution was refluxed for 2 h under a dinitrogen atmosphere. The color of the solution changed from orange-red to brown. Under slow evaporation of the solvent, a brown crystalline product was left. The product was further purified from CH2Cl2–MeOH solution. The yield was 0.34 g (58%).

The other complexes were prepared following an identical procedure. The yield varied from 50% to 60%. Microanalytical data: Calc. for $C_{12}H_{10}N_4O_2Cl_2Ru$ (**3a**): C, 34.78; H, 2.41; N, 13.53. Found: C, 34.62; H, 2.38; N, 13.47%. Calc. for $C_{13}H_{12}N_4O_2Cl_2Ru$ (**3b**): C, 36.45; H, 2.80; N, 13.08. Found: C, 36.50; H, 2.81; N, 13.00%. Calc. for $C_{18}H_{14}N_4O_2Cl_2Ru$ (**3c**): C, 44.08; H, 2.86; N, 11.43. Found: C, 43.92; H, 2.81; N, 11.38%. Calc. for $C_{13}H_{12}N_4O_2Cl_2Ru$ (**4a**): C, 36.45; H, 2.80; N, 13.08. Found: C, 36.34; H, 2.78; N, 13.04%. Calc. for $C_{14}H_{14}N_4O_2Cl_2Ru$ (**4b**): C, 38.01; H, 3.17; N, 12.67. Found: C, 37.92; H, 3.23; N, 12.60%. Calc. for $C_{19}H_{16}N_4O_2Cl_2Ru$ (**4c**): C, 45.24; H, 3.17; N, 11.11. Found: C, 45.02; H, 3.21; N, 11.17%.

4.4. Synthesis of trans-(Cl)-[$Ru(CO)Cl_2$(PaiEt)(NCMe)] (5b)

trans-(Cl)-[$Ru(CO)_2Cl_2$(PaiEt)] (**3b**) (0.1 g, 0.24 mmol) was dissolved in dry MeCN and sublimed Me_3NO (0.025 g, 0.33 mmol) was added as a pinch under a dry N_2 environment. The solution was then refluxed for 2 h. The intensity of the bright brown solution was reduced to light brown. The solution was evaporated slowly in air while crystals were deposited on the wall of the beaker. They were collected and dried over a CaCl2 desiccator. These crystals were unstable to X-ray irradiation and we could not perform X-ray diffraction analysis. The yield was 0.087 g (84%).

The other complexes were prepared following an identical procedure. The yield varied from 80% to 90%. Calc. for $C_{13}H_{13}N_5OCl_2Ru$ (**5a**): C, 36.38; H, 2.97; N, 16.30. Found: C, 36.53; H, 3.04; N, 16.39%. Calc. for $C_{14}H_{15}N_5OCl_2Ru$ (**5b**): C, 38.09; H, 3.40; N, 15.87. Found: C, 38.00; H, 3.32; N, 15.83%. Calc. for $C_{19}H_{17}N_5O_2Cl_2$-Ru (**5c**): C, 45.33; H, 3.38; N, 13.92. Found: C, 45.22; H, 3.30; N, 13.98%. Calc. for $C_{14}H_{15}N_5OCl_2Ru$ (**6a**): C, 38.09; H, 3.40; N, 15.87. Found: C, 38.18; H, 3.46; N, 15.82%. Calc. for $C_{15}H_{17}N_5OCl_2Ru$ (**6b**): C, 39.56; H, 3.74; N, 15.38. Found: C, 39.44; H, 3.67; N, 15.30%. Calc. for $C_{20}H_{19}N_5OCl_2Ru$ (**6c**): C, 46.42; H, 3.67; N, 13.54. Found: C, 46.33; H, 3.64; N, 13.48%.

4.5. X-ray crystal structure determination

Crystals of *trans*-(Cl)-[$Ru(CO)_2Cl_2$(PaiEt)] (**3b**) were grown by slow diffusion of a CH_2Cl_2 solution of the complex into hexane. The prismatic red crystal used was of dimensions $0.13 \times 0.19 \times 0.42$ mm. Diffraction data were collected with a Bruker SMART 1 K CCD area-detector diffractometer using fine focused sealed tube graphite-monochromatized Mo Ka radiation (λ = 0.7107 Å). A summary of the crystallographic data and structure refinement parameters are given in Table 6. Data were corrected for Lorentz and polarization effects. Data reduction was carried out using the 'Bruker SAINT' program. The structure was solved by direct methods using SHELXS-97 [82] and successive difference Fourier syntheses. All non-hydrogen atoms were refined anisotropically. Full matrix least squares refinements on F_0^2 were carried out using SHELXL-97 [83] with anisotropic displacement parameters for all non-hydrogen atoms. Hydrogen atoms were constrained to ride on the respective carbon or nitrogen atoms with isotropic displacement parameters equal to 1.2 times the equivalent isotropic displacement of their parent atom in all cases. All calculations were carried out using SHELXS 97 [82] and PLATON 99 [84] programs.

5. Supplementary data

CCDC 645194 contains the supplementary crystallographic data for [$Ru(CO)_2Cl_2$(PaiEt)] (**3b**). These data can be obtained free of charge via http://www.ccdc.cam.ac.uk/conts/retrieving.html, or from the Cambridge Crystallographic Data Centre, 12 Union Road, Cambridge CB2 1EZ, UK; fax: (+44) 1223-336-033; or e-mail: deposit@ccdc.cam.ac.uk.

Acknowledgements

Financial support from DST and UGC, New Delhi are thankfully acknowledged. We thank Dr. A.D. Jana for crystallographic graphics.

References

[1] J. Reedijk, in: G. Willkinson, J.A. Mccleverty (Eds.), Comprehensive Coordination Chemistry, vol. 2, Pergamon, Oxford, UK, 1987, p. 430.
[2] W.T. Wong, Coord. Chem. Rev. 131 (1994) 45.
[3] G. Wilkinson, F.G.A. Stone, E.W. Abel (Eds.), Comprehensive Organometallic Chemistry, Pergamon Press, New York, 1982.
[4] F.A. Cotton, G. Wilkinson, Advanced Inorganic Chemistry, 5th ed., Wiley-Interscience, New York, 1994.
[5] K. Kalyansundaram, Coord. Chem. Rev. 46 (1982) 159.
[6] B.K. Ghosh, A. Chakravorty, Coord. Chem. Rev. 95 (1989) 239.
[7] N. Bag, A. Pramanik, G.K. Lahiri, A. Chakravorty, Inorg. Chem. 31 (1992) 40.
[8] S. Serroni, S. Campagna, F. Puntoriero, C.D. Pietro, N.D. Mcclenaghan, F. Loisean, Chem. Soc. Rev. 30 (2001) 367.
[9] A.C.G. Hotze, H. Kooijman, A.L. Spek, J.G. Haasnoot, J. Reedijk, New J. Chem. 28 (2004) 565.
[10] R.E. Shepherd, Coord. Chem. Rev. 247 (2002) 147.
[11] M.J. Overett, J.R. Moss, Inorg. Chim. Acta 358 (2005) 1715.
[12] S.J. Dougan, M. Melchart, A. Habtemariam, S. Parsons, P.J. Sadler, Inorg. Chem. 45 (2006) 10882.
[13] C.K. Pal, S. Chattopadhyay, C. Sinha, D. Bandhyopadhyay, A. Chakravorty, Polyhedron 13 (1994) 999.
[14] P.K. Santra, R. Roy, C. Sinha, Proc. Indian Acad. Sci. (Chem. Sci.) 112 (2000) 523.
[15] B.K. Santra, P. Munshi, G. Das, P. Bharadwaj, G.K. Lahiri, Polyhedron 18 (1999) 617.
[16] P.K. Santra, P. Byabratta, S. Chattopadhyay, C. Sinha, L.R. Falvello, Eur. J. Inorg. Chem. (2002) 1124.
[17] M. Panda, S. Das, G. Mostafa, A. Castineiras, S. Goswami, J Chem. Soc., Dalton Trans. (2005) 1249.
[18] U.S. Ray, B.K. Ghosh, M. Monfort, J. Ribas, G. Mostafa, T.-H. Lu, C. Sinha, Eur. J. Inorg. Chem. (2004) 250.
[19] U.S. Ray, B.G. Chand, G. Mostafa, J. Cheng, T.-H. Lu, C. Sinha, Polyhedron 22 (2003) 2587.
[20] D. Banerjee, U.S. Ray, J.-C. Liou, C.-N. Lin, T.-H. Lu, C. Sinha, Inorg. Chim. Acta 358 (2005) 1019.
[21] U.S. Ray, D. Banerjee, B.G. Chand, J. Cheng, T. –H. Lu, C. Sinha, J. Coord. Chem. 58 (2005) 1105.
[22] B.G. Chand, U.S. Ray, J. Cheng, T.-H. Lu, C. Sinha, Polyhedron 22 (2003) 1213.
[23] B.G. Chand, U.S. Ray, G. Mostafa, T.-H. Lu, C. Sinha, Polyhedron 23 (2004) 1669.
[24] B.G. Chand, U.S. Ray, G. Mostafa, T.-H. Lu, C. Sinha, J. Coord. Chem. 57 (2004) 627.
[25] B.G. Chand, U.S. Ray, J. Cheng, T.-H. Lu, C. Sinha, Inorg. Chim. Acta 358 (2005) 1927.
[26] T.K. Misra, D. Das, C. Sinha, P.K. Ghosh, C.K. Pal, Inorg. Chem. 37 (1998) 1672.
[27] T.K. Misra, D. Das, C. Sinha, Polyhedron 16 (1997) 4163.
[28] T.K. Misra, D. Das, C. Sinha, Indian J. Chem. A 37 (1998) 741.
[29] S. Pal, T.K. Misra, P. Chattopadhyay, C. Sinha, Proc. Indian Acad. Sci. (Chem. Sci.) 111 (1999) 687.
[30] M.N. Ackermann, C.R. Barton, C.J. Deodene, E.M. Specht, S.C. Keill, W.E. Schreiber, Hiodong. Kim, Inorg. Chem. 28 (1989) 397.
[31] F. Alper, C. Kayram, S. Ozkar, J. Organomet. Chem. 691 (2006) 2734.
[32] W. Kaim, S. Ernst, S. Kohlmann, Polyhedron 5 (1986) 295.
[33] W. Kaim, S. Kohlmann, Inorg. Chem. 25 (1986) 3442.
[34] W. Kaim, S. Kohlmann, Inorg. Chem. 26 (1987) 68.
[35] M.N. Ackermann, W.G. Fairbrother, N.S. Amin, C.J. Deodene, C.M. Lamborg, P.T. Martin, J. Organomet. Chem. 523 (1996) 145.
[36] M.J. Alder, W.I. Cross, K.R. Flower, R.G. Pritchard, J. Organomet. Chem. 568 (1998) 279.
[37] M.N. Ackermann, S.R. Kiihne, P.A. Saunders, C.E. Barnes, S.C. Stalling, H. Kim, C. Woods, M. Lagunoff, Inorg. Chim. Acta 334 (2002) 193.
[38] M.N. Ackermann, M.P. Robinson, I.A. Maher, E.B. LeBlane, R.V. Raz, J. Organomet. Chem. 682 (2003) 248.
[39] P. Datta, P. Gayen, C. Sinha, Polyhedron 25 (2006) 3435.
[40] M.A. Moreno, M. Haukka, A. Turunen, T.A. Pakkanen, J. Mol. Catal. A: Chem. 240 (2005) 7.
[41] E.A. Seddon, K.R. Seddon, The Chemistry of Ruthenium;, Elsevier, Amsterdam, 1984.
[42] S. Goswami, A.R. Chakravarty, A. Chakravorty, Inorg. Chem. 20 (1981) 2246. 21 (1982) 2173; 22 (1983) 602.
[43] S. Goswami, R.N. Mukherjee, A. Chakravorty, Inorg. Chem. 22 (1983) 2825.
[44] P. Ghosh, A. Chakravorty, J. Chem. Soc., Dalton Trans. (1985) 361.
[45] G.K. Lahiri, S. Bhattacharya, S. Goswami, A. Chakravorty, J. Chem. Soc., Dalton Trans. (1990) 561.
[46] G.K. Lahiri, S. Goswami, L.R. Falvello, A. Chakravorty, Inorg. Chem. 26 (1987) 3365.
[47] R. Samanta, P. Munshi, B.K. Santra, N.K. Loknath, M.A. Sridhar, J.S. Prasad, G.K. Lahiri, J. Org. Met. Chem. 579 (1999) 311.
[48] R.A. Krause, K. Krause, Inorg. Chem. 19 (1980) 2600. 1982 (21) 1714; 1984 (23) 219.
[49] A. Bharat, B.K. Santra, P. Munshi, G.K. Lahiri, J. Chem. Soc., Dalton Trans. (1998) 2643.
[50] A. Seal, S. Roy, Acta Crystallogr., Sect C C40 (1984) 929.
[51] A.H. Velders, H. Kooijman, A.L. Spek, J.G. Haasnoot, D. de Vos, J. Reedijk, Inorg. Chem. 39 (2000) 2966.
[52] A.C.G. Hotze, A.H. Velders, F. Ugozzoli, M. Bicingi, A.M. Manotti-Lanfredi, J.G. Haasnoot, J. Reedijk, Inorg. Chem. 39 (2000) 3838.
[53] M. Shivakumar, K. Pramanik, P. Ghosh, A. Chakravorty, Chem. Commun. (1998) 2103.
[54] K.S.Y. Leung, Y. Li, Inorg. Chem. Commun. 2 (1999) 599.
[55] W.Y. Wong, S.H. Cheung, S.M. Lee, S.Y. Leung, J. Org. Chem. 596 (2000) 36.
[56] K. Pramanik, M. Shivakumar, P. Ghosh, A. Chakravorty, Inorg. Chem. 39 (2000) 195.
[57] V.W.W. Yam, V.C.Y. Lan, L.X. Wu, J. Chem. Soc., Dalton Trans. (1998) 1461.
[58] R. Samanta, P. Munshi, B.K. Santra, N.K. Loknath, M.A. Sridhar, J.S. Prasad, G.K. Lahiri, J. Organomet. Chem. 579 (1999) 311.
[59] G. Cripps, A. Pellissier, S. Chardon-Noblat, A. Deronzier, R.J. Haines, J. Organomet. Chem. 689 (2004) 484.
[60] S. Chardon-Noblat, A. Deronzier, R. Ziessel, D. Zsoldos, J. Electroanal. Chem. 444 (1998) 253.
[61] J.-M. Lehn, R. Ziessel, J. Organomet. Chem. 382 (1990) 157.
[62] S. Chardon-Noblat, A. Deronzier, R. Ziessel, Collect. Czech. Chem. Commun. 66 (2001) 207.
[63] J.M. Kelly, C.M. O_Connell, J.G. Vos, Inorg. Chim. Acta 64 (1982) L75.
[64] S. Chardon-Noblat, P. Da Costa, A. Deronzier, M. Haukka, T.A. Pakkanen, R. Ziessel, J. Electroanal. Chem. 490 (2000) 62.
[65] H. Sigel (Ed.), Metal Ions in Biological System, vol. 13, Marcel Dekker, New York, 1981.
[66] J. Otsuki, K. Suwa, K. Narutaki, C. Sinha, I. Yoshikawa, K. Araki, J. Phys. Chem. A 109 (2005) 8064.
[67] J. Otsuki, K. Suwa, K.K. Sarker, C. Sinha, J. Phys. Chem. A 111 (8) (2007) 1403.
[68] P. Bhunia, B. Baruri, U.S. Ray, C. Sinha, S. Das, J. Cheng, T.-H. Lu, Transition Met. Chem. 31 (2006) 310.
[69] E.Y. Li, Y.-M. Cheng, C.-C. Hsu, P.-T. Chou, G.-S. Lee, I.-H. Lin, Y. Chi, C.-S. Liu, Inorg. Chem. 45 (2006) 8041.
[70] E. Eskelinen, M. Haukka, T. Venalainen, T.A. Pakkanen, M. Wasberg, S. Chardon-Noblat, A. Deronzier, Organometallics 19 (2000) 163.
[71] M.J. Frisch, G.W. Trucks, H.B. Schlegel, P.M.W. Gill, B.G. Johnson, M.A. Robb, J.R. Cheeseman, T.A. Keith, G.A. Petersson, J.A. Montgomery, K. Raghavachari, M.A. Al-Laham, V.G. Zakrzewski, J.V. Ortiz, J.B. Foresman, J. Cioslowski, B.B. Stefanov, A. Nanayakkara, M. Challacombe, C.Y. Peng, P.Y. Ayala, W. Chen, M.W. Wong, J.L. Andres, E.S. Replogle, R. Gomperts, R.L. Martin, D.J. Fox, J.S. Binkley, D.J. Defrees, J. Baker, J.P. Stewart, M. Head-Gordon, C. Gonzalez, J.A. Pople, GAUSSIAN98, Gaussian, Inc., Pittsburgh, PA, 1998.
[72] C. Lee, W. Yang, R.G. Parr, Phys. Rev. B 37 (1988) 785.
[73] P.J. Hay, W.R. Wadt, J. Chem. Phys. 82 (1985) 270.
[74] M. Cossi, V.J. Barone, Chem. Phys. 115 (2001) 4708.
[75] N.M. O'Boyle, J.G. Vos, GaussSum 1.0, Dublin City University, Dublin, Ireland, 2005. <http://www.gausssum.sourceforge.net>.
[76] M.I. Bruce, Ruthenium carbonyls and related compounds, in: G. Wilkinson, F.G.A. Stone, E.W. Abel (Eds.), Comprehensive Organometallic Chemistry, vol. 4, Pergamon Press, Oxford, 1982, p. 661.
[77] A.J. Deeming, C. Forth, G. Hogarth, Transition Met. Chem. 31 (2006) 42.
[78] M. Haukka, J. Kiviaho, M. Ahlgren, T.A. Pakkam, Organometallics 14 (1995) 825.
[79] J. Dinda, Ph.D. Thesis, The University of Burdwan, Burdwan, India, 2003.
[80] J. Dinda, K. Bag, C. Sinha, G. Mostafa, T.-H. Lu, Polyhedron 22 (2003) 1367.
[81] A. Gabrielsson, S. Zalis, P. Matousek, M. Towrie, A. Vlcek Jr., Inorg. Chem. 43 (2004) 7380.
[82] G.M. Sheldrick, SHELXS-97, Program for the Solution of Crystal Structure, University of Gottingen, Germany, 1997.
[83] G.M. Sheldrick, SHELXL-97, Program for the Solution of Crystal Structure, University of Gottingen, Germany, 1997.
[84] A.L. Spek, PLATON, Molecular Geometry Program, University of Utrecht, The Netherlands, 1999.

were used as received while pyridine-2-thione, pyrimidine-2-thione and 3,5-dimethyl-pyrimidine-2-thione (Merck or Aldrich) were re-crystallized from hot ethanol prior to their use. All the solvents were purified by respective suitable methods and allowed to stand over molecular sieves. Infra-red spectra in the region of 4000–250 cm^{-1} were obtained in KBr discs with Perkin–Elmer FT-IR Spectrum 1 spectrophotometer. Electronic absorption spectra were measured with a Perkin–Elmer-Hitachi 200 spectrophotometer while a Hitachi F-700 fluorescence spectrophotometer was used to obtain the emission spectra. Melting points were measured in open tubes with a STUART scientific instrument and are uncorrected Scheme 1.

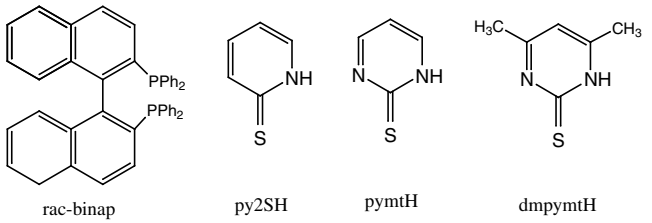

rac-binap py2SH pymtH dmpymtH

Scheme 1. The diphosphane and the heterocyclic thiones used as ligands with their abbreviations.

2.2. Crystal structure determination

Single crystals suitable for crystal structure analysis were obtained by slow evaporation of dichloromethane solutions of the complexes at room temperature. X-ray diffraction data were collected on an Enraf-Nonius Kappa CCD area-detector diffractometer. The programs DENZO [9] and COLLECT [10] were used in data collection and cell refinement. Details of crystal and structure refinement are shown in Table 1. The structures were solved using program SIR97 [11] and refined with program SHELX-97 [12]. Molecular plots were obtained with program ORTEP-3 [13].

2.3. Synthesis of complexes 1–6

Rac-binap (311 mg, 0.5 mmol) was added to a suspension of CuX (0.5 mmol) in 30 cm^3 of dry acetonitrile and the mixture was stirred for 2 h at 50 °C, during which time a white precipitate was formed. A solution of the heterocyclic thione (0.5 mmol) in 20 ml of ethanol was the added slowly, and the reaction mixture was stirred for additional 2 h at 50 °C, whereupon the white precipitate gradually disappeared and the color of the solution turned yellow. The resulting solution was filtered off and left to slowly evaporate at ambient temperature. The microcrystalline solid, which was deposited upon standing for several days, was filtered off and dried *in vacuo*. In some cases major amounts of the product precipitated from the mother-liquid before evaporation. Some of the powder solids were recrystallized from dichloromethane.

Table 1
Crystal data and structure refinement for **2a**, **2** and **8**

	2a	**2**	**8**
Chemical formula	$C_{49}H_{37}BrCuNP_2S \cdot 2CH_2Cl_2$	$C_{49}H_{37}BrCuNP_2S \cdot CH_2Cl_2$	$C_{50}H_{40}BrCuN_2P_2S \cdot CH_2Cl_2$
Formula weight	1047.10	962.17	991.22
Temperature (K)	120(2)	120(2)	120(2)
Wavelength (Å)	0.71073	0.71073	0.71073
Crystal system	monoclinic	monoclinic	monoclinic
Space group	$P2_1$	$P2_1/n$	$P2_1/n$
Unit cell dimensions			
a (Å)	11.2854(4)	11.99580(10)	11.9960(3)
b (Å)	11.2554(5) Å	20.2422(2)	20.5581(5)
c (Å)	36.5426(14)	18.2167(2)	18.2022(5)
α (°)	90	90	90
β (°)	97.6030(10)	105.46	104.074(2)
γ (°)	90	90	90
Volume (Å^3)	4600.9(3)	4263.29(7)	4354.19(19)
Z	4	4	4
D_{calc} (Mg/m^3)	1.512	1.499	1.512
Absorption coefficient (mm^{-1})	1.728	1.736	1.703
F(000)	2128	1960	2024
Crystal size (mm^3)	0.07 × 0.06 × 0.04	0.44 × 0.40 × 0.14	0.60 × 0.46 × 0.20
Theta range for data collection (°)	2.94–25.03	3.07–27.48	3.04–27.51
Index ranges	$-13 \leqslant h \leqslant 13$, $-43 \leqslant k \leqslant 43$, $-27 \leqslant l \leqslant 27$	$-15 \leqslant h \leqslant 15$, $-26 \leqslant k \leqslant 25$, $-23 \leqslant l \leqslant 23$	$-15 \leqslant h \leqslant 15$, $-26 \leqslant k \leqslant 26$, $-23 \leqslant l \leqslant 23$
Reflections collected	26327	58477	39471
Independent reflections	12651 [R(int) = 0.0535]	9753 [R(int) = 0.0349]	9727 [R(int) = 0.0608]
Completeness to theta	91.9% (theta = 25.03°)	99.7% (theta = 27.48°)	97.1% (theta = 27.51°)
Max. and min. transmission	0.9341 and 0.8886	0.7931 and 0.5154	0.7269 and 0.4281
Refinement method	full-matrix 1.s. on F^2	full-matrix l. s. on F^2	full-matrix l. s. on F^2
Data/restraints/parameters	12651/1/980	9753/0/523	9727/0/543
Goodness-of-fit on F^2 (S)	1.152	1.050	1.040
Final R indices [$(I > 2\sigma(I)$]	R_1 = 0.0665, wR_2 = 0.1454	R_1 = 0.0254, wR_2 = 0.0597	R_1 = 0.0413, wR_2 = 0.0955
R indices (all data)	R_1 = 0.0744, wR_2 = 0.1510	R_1 = 0.0275, wR_2 = 0.0607	R_1 = 0.0571, wR_2 = 0.1033
Final weighting scheme	calc w = ([a])	calc w = ([b])	calc w = ([c])
Absolute structure parameter	0.118(12)		
Largest difference in peak and hole (e Å^{-3})	1.429 and −0.677	0.502 and −0.649	0.660 and −0.665

[a] $1/[\sigma^2(F_o^2) + 46.7660P]$ where $P = (F_o^2 + 2F_c^2)/3$.
[b] $1/[\sigma^2(F_o^2) + (0.0209P)^2 + 4.0694P]$ where $P = (F_o^2 + 2F_c^2)/3$.
[c] $1/[\sigma^2(F_o^2) + (0.0427P)^2 + 6.3919P]$ where $P = (F_o^2 + 2F_c^2)/3$.

*2.3.1. [CuCl(binap)(py2SH)] (**1**)*

Yellow powder (242 mg, 58%), m.p. 253–255 °C (decomp.); *Anal.* Calc. for $C_{49}H_{37}NClCuP_2S$: C, 70.67; H, 4.48; N, 1.68. Found: C, 71.13; H, 4.45; N, 1.64%. IR (cm^{-1}): 3165m, 3050w, 2959w, 1585m, 1501s, 1434vs, 1372s, 1131vs, 1096s, 993s, 909, 745vs, 694vs, 508s, 494s. UV–Vis (CH_2Cl_2, λ_{max}, $\log\varepsilon$): 238 (4.92), 291 (4.46). 393 (3.97).

*2.3.2. [CuBr(binap)(py2SH)] (**2**)*

Orange crystals (333 mg, 76%), m.p. 250–252 °C (decomp.); *Anal.* Calc. for $C_{49}H_{37}NBrCuP_2S$: C, 67.09; H, 4.25; N, 1.60. Found: C, 67.19; H, 4.50; N, 1.51%. IR (cm^{-1}): 3048w, 2960w, 1576vs, 1502s, 1477s, 1435vs, 1368s, 1269m, 1131vs, 1097s, 994s, 868m, 818s, 742vs, 696vs, 523s, 507vs, 446m. UV–Vis (CH_2Cl_2, λ_{max}, $\log\varepsilon$): 238 (4.79), 286 (4.47), 387 (3.96).

*2.3.3. [CuI(binap)(py2SH)] (**3**)*

Orange powder (277 mg, 60%), m.p. 280–282 °C (decomp.); *Anal.* Calc. for $C_{49}H_{37}NCuIP_2S$: C, 63.67; H, 4.03; N, 1.51. Found: C, 63.94; H, 4.07; N, 1.45%. IR (cm^{-1}): 3046m, 1584m, 1571m, 1499m, 1490m, 1435vs, 1305m, 1097s, 999m, 817vs, 751vs, 742vs, 694vs, 522s, 509vs, 493vs. UV–Vis (CH_2Cl_2, λ_{max}, $\log\varepsilon$): 246 (4.91), 287 (4.48), 387 (3.69).

*2.3.4. [CuCl(binap)(pymtH)] (**4**)*

Yellow powder (371 mg, 89%), m.p. 265–267 °C (decomp.); *Anal.* Calc. for $C_{48}H_{36}N_2ClCuP_2S$: C, 69.14; H, 4.35; N, 3.36. Found: C, 69.23; H, 4.40; N, 3.28%. IR (cm^{-1}): 3048m, 1568vs, 1529s, 1481s, 1434vs, 1373vs, 1241m, 1172s, 1089m, 1027m, 998m, 888m, 818vs, 749vs, 695vs, 517s, 507vs, 486vs, 458m. UV–Vis (CH_2Cl_2, λ_{max}, $\log\varepsilon$): 235 (4.68), 289 (4.21), 388 (3.27).

*2.3.5. [CuBr(binap)(pymtH)] · CH_2Cl_2 (**5**)*

Orange crystals (334 mg, 76%), m.p. 260–262 °C (decomp.); *Anal.* Calc. for $C_{49}H_{38}N_2BrCl_2CuP_2S$: C, 61.10; H, 3.98; N, 2.91. Found: C, 61.41; H, 4.01; N, 2.94%. IR (cm^{-1}): IR (cm^{-1}): 3050m, 2818w, 1607s, 1566vs, 1471s, 1436s, 1376s, 1217m, 1179vs, 1093s, 977m, 872m, 751s, 740s, 698vs, 508vs, 495m. UV–Vis (CH_2Cl_2, λ_{max}, $\log\varepsilon$): 245 (4.87), 281 (4.53), 389 (3.27).

*2.3.6. [CuI(binap)(pymtH)] (**6**)*

Orange powder (390 mg, 83%), m.p. 265–267 °C (decomp.); *Anal.* Calc. for $C_{48}H_{36}N_2CuIP_2S$: C, 62.31; H, 3.92%; N, 3.02. Found: C, 62.60; H, 4.11; N, 2.96%. IR (cm^{-1}): 3047m, 1566vs, 1543s, 1481s, 1433vs, 1377vs, 1171s, 1089s, 980m, 877m, 818s, 750vs, 740vs, 695vs, 516s, 508vs, 486s. UV–Vis (CH_2Cl_2, λ_{max}, $\log\varepsilon$): 242 (4.74), 286 (4.41), 382 (3.83).

*2.3.7. [CuCl(binap)(dmpymtH)] · 2CH_2Cl_2 (**7**)*

Orange crystals (218 mg, 46%), m.p. 260–262 °C (decomp.); *Anal.* Calc. for $C_{52}H_{44}N_2Cl_5CuP_2S$: C, 60.53; H, 4.30; N, 2.71. Found: C, 60.55; H, 4.27; N, 2.88%. IR (cm^{-1}): 3050m, 2964w, 1617s, 1566vs,1479m, 1435s, 1393m, 1229vs, 1192s, 1096m, 1027m, 980m, 889m, 818s, 745vs, 696vs, 522m, 507s, 495s, 465s. UV–Vis (CH_2Cl_2, λ_{max}, $\log\varepsilon$): 231 (5.04), 291 (4.66).

*2.3.8. [CuBr(binap)(dmpymtH)] · CH_2Cl_2 (**8**)*

Orange crystals (327 mg, 66%), m.p. 269–270 °C (decomp.); *Anal.* Calc. for $C_{51}H_{42}N_2BrCl_2CuP_2S$: C, 61.80; H, 4.27; N, 2.82. Found: C, 61.54; H, 4.34; N, 2.91%. IR (cm^{-1}): 3051m, 2853m, 1614s, 1560vs,1479s, 1436s, 1393m, 1229vs, 1188s, 1093m, 1028m, 978s, 891m, 816s, 749vs, 729s, 696vs, 522s, 506s,496s, 464s. UV–Vis (CH_2Cl_2, λ_{max}, $\log\varepsilon$): 236 (4.99), 288 (4.50), 379 (3.74).

*2.3.9. [CuI(binap)(dmpymtH)] · CH_2Cl_2 (**9**)*

Orange crystals (311 mg, 60%), m.p. 280–282 °C (decomp.); *Anal.* Calc. for $C_{51}H_{42}N_2Cl_2CuIP_2S$: C, 59.00; H, 4.07; N, 2.70. Found: C, 59.06; H, 4.17; N, 2.67%. IR (cm^{-1}): 3036w, 2914w, 1615vs, 1560vs, 1435vs, 1225vs, 1385m, 1187s, 1093m, 1027m, 981s, 892m, 816m, 742s, 695vs, 523m, 507s, 496s, 462s. UV–Vis (CH_2Cl_2, λ_{max}, $\log\varepsilon$): 230 (5.02), 288 (4.65), 380 (3.86).

3. Results and discussion

3.1. Preparative aspects

Previously when we prepared thione/phosphane mixed-ligand mononuclear copper(I) complexes bearing chelating diphosphanes, we used either flexible oligomethylene backboned symmetric diphosphanes of appropriate chain length, or rigid diphosphanes with bite angles suitable to span tetrahedral positions. In this respect, on the basis of its conformational flexibility, binap was anticipated to adopt the same chelating mode upon coordination to Cu^{I}. Considering the vast majority of the binap complexes used in catalytic processes, the ability of this atropisomeric diphosphane to preferably act as a chelating ligand towards many metals, generating mononuclear complexes is already well established. Thus, in order to obtain tetrahedral mixed-ligand complexes of binap, we used once more our approved straightforward synthetic procedure, involving mixing of copper(I) halides with 1 equivalent of rac-binap at 50 °C, followed by addition of 1 equiv. of the thione ligand, and stirring the resulting mixture for 2 h.

All the compounds prepared by this means were air-stable diamagnetic powdery solids, featuring the stoichiometry employed, and were moderately soluble in chloroform and dichloromethane and only sparingly soluble in acetonitrile, ethanol and acetone. Solutions of the new compounds in common organic solvents were non-conducting, and as expected for compounds derived from a racemic precursor, none of them exhibited any optical activity.

In order to obtain single crystals suitable for X-ray analysis, we engaged intensively with re-crystallisation of the complexes from various solvents, whereby we were at first only moderately successful, being able to crystallise a very small amount of compound **2** from dichloromethane, the molecular structure of which was found to correspond to the racemic compound [CuBr(rac-binap)(py2SH)]. However, during our further attempts, crystals separated from one of the samples of compound **2** were of a clearly different morphology and habit (small yellow blocks) than the well-formed orange prisms of [CuBr(rac-binap)(py2SH)], thus we decided also to perform X-ray crystal structure determination on them. In doing so, we surprisingly noticed that these crystals were composed of a mixture of the two possible enantiomers which, however, were not related to each other by a center of symmetry (compound **2a**).

Generally, for a racemic material in solution, there are two possibilities for crystallization. Both enantiomers may crystallise in a nonchiral space group with, e.g., *S*- and *R*- forms related by a center of symmetry in the single crystal, or, spontaneous resolution may provide equal amounts of *S*- and *R*- enantiopure crystals with identical chiral space groups [14]. Unsurprisingly, molecules of **2** crystallized as a racemic mixture in a nonchiral space group but molecules of **2a** crystallized as a racemic mixture in a chiral space group. The latter was possible because the asymmetric unit of the crystal contained both *S*- and *R*- enantiomers ($Z' = 2$) arranged as independent molecules, i.e., not related by a center of symmetry. Apart from the two different molecular arrangements for racemic mixtures in single crystals of **2** and **2a** other possible arrangements for racemic mixtures in a single crystal include enantiomers that may be related by a non-crystallographic center of symmetry

(Z' = 2) [15] and enantiomers that share identical sites throughout the crystal (solid solution) [16].

Unfortunately thermal analysis of crystals was not informative as the crystals decomposed at temperatures below their melting points.

3.2. Spectroscopy

The infrared spectra of compounds **1**–**9**, recorded in the range 4000–250 cm^{-1} display strong vibrational phosphane bands, which remain practically unshifted upon coordination. In addition, the spectra contain the expected four characteristic "thioamide bands" in the ~1570, ~1360, ~980 and ~740 cm^{-1} regions [17], with shifts due to coordination indicative of an exclusive S-coordination mode.

The electronic absorption spectra of the mixed-ligand complexes recorded in dichloromethane at room temperature are dominated by two intense main bands with maxima in the 230–246 nm and 281–291 nm regions, as well as a third weak broad band in the 379–393 nm region. With reference to the absorption spectrum of the uncoordinated binap, which exhibits three bands at λ_{max} = 216 nm, 244 nm and 290 nm, the first two intense bands are attributable to intraligand $\pi^* \leftarrow \pi$ transitions on the phenyl groups of the phosphane ligand, from which the lower energy second one can be considered as to possess some phosphane-originating MLCT transition character involving π^* orbitals of the phosphane ligand [18–19]. Finally, the weak band in the 379–393 nm region can be ascribed to transitions within the thione orbitals.

As many other copper(I) complexes with certain aryl-phosphanes, compounds **1**–**9** are strongly emissive in the solid state, with λ_{max} values of the broad bands in the 526–555 nm range, when excited at λ = 342–375 nm at room temperature. The excitation and emission data of the complexes under investigation are summarized in Table 2 and a representative excitation and emission spectrum of compound **2** is shown in Fig. 1.

Various copper(I) phosphane complexes are luminescent in the solid state at room temperature, and in many cases the luminescence is found to be a phosphorescence, however the nature of the emissive excited states of these compounds has not been yet definitively clarified [20]. In the complexes presented here, a plausible evidence for the presence of phosphorescence is being provided by the fact that the emission spectra do not overlap with the parent excitation spectra (large Stokes shifts). Moreover, recent TD-DFT calculations [21] showed the luminescence in Cu^I arylphosphane complexes to partially originate from MLCT triplets of type Cu(I) → $\pi^*(PPh_2)$, and this applies apparently also to the compounds under investigation. This assignment is reinforced by the fact that the maxima of the emission bands all undergo significant red shifts relative to the solid state r.t. emission spectrum of the free binap, the phosphorescence band of which appears at 490 nm. A further approach to this controversially discussed complex problem has been made by the group of A. Vogler in a series of systematic investigations on the photophysical properties of Au^+, Ag^+, Re^+ and Cu^+ complexes of binap and related phosphanes [22]. In conclusion, the origin of the luminescence can be tentatively assigned as having mixed character between metal–ligand charge transfer (MLCT) of the type Cu(I) → $\pi^*(PPh_2)$ and ligand–ligand charge transfer (LLCT) of the type thione → $\pi^*(PPh_2)$ or/and halide → $\pi^*(PPh_2)$, with an unambiguous prevalence of the MLCT emission.

Table 2
Absorption and emission maxima of [CuX(binap)(thione)] complexes at room temperature

Compound	λ_{exc} [nm] (solid)	λ_{em} [nm] (solid)
1 [CuCl(binap)(py2SH)]	346	553
2 [CuBr(binap)(py2SH)]	350	545
3 [CuI(binap)(py2SH)]	342	526
4 [CuCl(binap)pymtH)]	346	553
5 [CuBr(binap)pymtH)]	355	555
6 [CuI(binap)pymtH)]	356	547
7 [CuCl(binap)(dmpymtH)]	375	543
8 [CuBr(binap)(dmpymtH)]	375	548
9 [CuI(binap)(dmpymtH)]	368	540

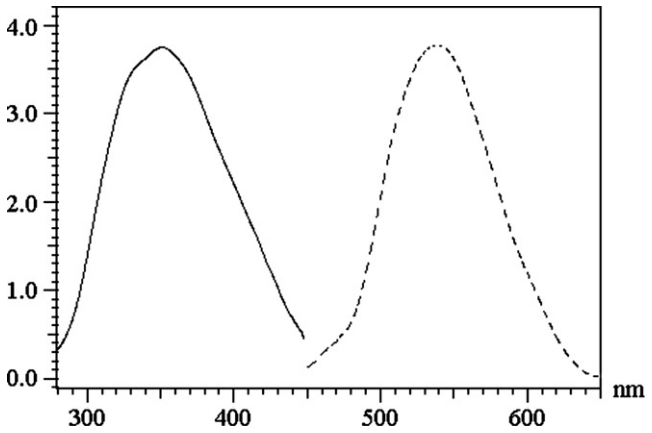

Fig. 1. Room temperature solid state excitation (—) and emission (---) spectrum of [CuBr(binap)(py2SH)] (**2**) (λ_{ex} = 350 nm, λ_{em} = 545 nm).

3.3. X-ray structural investigations

The X-ray crystal structures of [CuBr(rac-binap)(py2SH)] · $2CH_2Cl_2$ (**2a**), [CuBr(rac-binap)(py2SH)] · CH_2Cl_2 (**2**) and [CuBr(S-binap)(dmpmtH)] · CH_2Cl_2 (**8**) (details of crystal and structure refinement are shown in Table 1) corroborate the spectroscopic results discussed above. Tables 3–5 list selected distances and angles of these complexes.

Yellow single crystals of **2a** were grown from a dichloromethane solution upon slow evaporation during several days. The compound crystallizes in the monoclinic space group $P2_1$ with four discrete formula units in the unit cell. Single-crystal analysis of

Table 3
Selected bond lengths (Å) and angles (°) for **2a**

Molecule A		Molecule B	
Br(1)–Cu(1)	2.5192(17)	Br(2)–Cu(2)	2.5205(16)
Cu(1)–P(2)	2.284(3)	Cu(2)–P(3)	2.264(3)
Cu(1)–P(1)	2.310(3)	Cu(2)–P(4)	2.312(3)
Cu(1)–S(1)	2.339(3)	Cu(2)–S(2)	2.312(3)
S(1)–C(1)	1.720(11)	S(2)–C(50)	1.728(10)
P(1)–C(6)	1.832(11)	P(3)–C(67)	1.817(10)
P(1)–C(12)	1.844(11)	P(3)–C(55)	1.826(10)
P(1)–C(18)	1.861(10)	P(3)–C(61)	1.830(11)
P(2)–C(37)	1.830(10)	P(4)–C(93)	1.831(10)
P(2)–C(44)	1.833(10)	P(4)–C(87)	1.846(11)
P(2)–C(38)	1.851(10)	P(4)–C(77)	1.853(10)
P(1)–Cu(1)–P(2)	98.86(10)	P(3)–Cu(2)–P(4)	99.80(10)
P(1)–Cu(1)–S(1)	117.38(10)	P(4)–Cu(2)–S(2)	115.44(10)
P(1)–Cu(1)–Br(1)	114.51(8)	P(3)–Cu(2)–Br(2)	110.55(9)
P(2)–Cu(1)–S(1)	105.84(10)	P(3)–Cu(2)–S(2)	109.95(10)
P(2)–Cu(1)–Br(1)	111.63(9)	P(4)–Cu(2)–Br(2)	111.89(8)
S(1)–Cu(1)–Br(1)	107.98(8)	S(2)–Cu(2)–Br(2)	108.91(8)
C(1)–S(1)–Cu(1)	110.4(4)	C(50)–S(2)–Cu(2)	109.9(3)
C(6)–P(1)–Cu(1)	120.0(3)	C(61)–P(3)–Cu(2)	121.1(3)
C(12)–P(1)–Cu(1)	118.3(4)	C(55)–P(3)–Cu(2)	119.2(4)
C(18)–P(1)–Cu(1)	106.4(3)	C(67)–P(3)–Cu(2)	103.2(3)
C(37)–P(2)–Cu(1)	103.8(3)	C(93)–P(4)–Cu(2)	112.5(3)

Table 4
Selected bond lengths (Å) and angles (°) for [CuBr(S-binap)(py2SH)] · CH_2Cl_2 **(2)**

Bond lengths (Å)		Angles (°)	
Br(1)–Cu(1)	2.4808(2)	P(1)–Cu(1)–P(2)	98.693(15)
Cu(1)–P(1)	2.2944(4)	P(1)–Cu(1)–S(1)	106.225(15)
Cu(1)–P(2)	2.3194(4)	P(1)–Cu(1)–Br(1)	111.718(12)
Cu(1)–S(1)	2.3365(4)	P(2)–Cu(1)–S(1)	118.045(15)
S(1)–C(1)	1.7034(16)	P(2)–Cu(1)–Br(1)	112.415(12)
P(1)–C(6)	1.8359(15)	S(1)–Cu(1)–Br(1)	109.125(12)
P(1)–C(12)	1.8396(15)	C(1)–S(1)–Cu(1)	115.77(6)
P(1)–C(18)	1.8331(15)	C(6)–P(1)–Cu(1)	116.59(5)
P(2)–C(38)	1.8272(15)	C(12)–P(1)–Cu(1)	119.17(5)
P(2)–C(44)	1.8417(15)	C(18)–P(1)–Cu(1)	105.31(5)
P(2)–C(37)	1.8507(15)	C(37)–P(2)–Cu(1)	108.16(5)

Table 5
Selected bond lengths (Å) and angles (°) for [CuBr(S-binap)(dmpmtH). CH_2Cl_2] (**8**)

Bond distances (Å)		Angles (°)	
Br(1)–Cu(1)	2.4690(4)	P(1)–Cu(1)–P(2)	98.91(3)
Cu(1)–P(1)	2.2901(7)	P(1)–Cu(1)–S(1)	106.31(3)
Cu(1)–P(2)	2.3189(8)	P(1)–Cu(1)–Br(1)	111.94(2)
Cu(1)–S(1)	2.3283(8)	P(2)–Cu(1)–S(1)	117.21(3)
S(1)–C(1)	1.699(3)	P(2)–Cu(1)–Br(1)	112.21(2)
P(1)–C(19)	1.831(3)	S(1)–Cu(1)–Br(1)	109.66(2)
P(1)–C(13)	1.836(3)	C(1)–S(1)–Cu(1)	116.99(2)
P(1)–C(7)	1.840(3)	C(7)–P(1)–Cu(1)	120.40(9)
P(2)–C(38)	1.846(3)	C(19)–P(1)–Cu(1)	104.69(9)
P(2)–C(39)	1.821(3)	C(13)–P(1)–Cu(1)	116.42(9)
P(2)–C(45)	1.847(3)	C(38)–P(2)–Cu(1)	109.18(8)

compound **2a** indicates the presence of two solvent (dichloromethane) molecules per formula unit, trapped in the crystal lattice; the latter solvate molecules do not interact specifically with the complex molecules and will not be further discussed Fig. 2

As shown in the ORTEP drawing (Fig. 3) there are two individual molecules in the asymmetric unit, molecule A and molecule B, containing S-binap and R-binap, respectively, thus having different absolute configurations. These two molecules are not related to each other by a center of symmetry and this is a rare example of a racemic mixture in a chiral space group. In each molecule, the copper(I) center is surrounded by the P atoms of the chelating binap, the S atom of the thione and the halide atom, in a highly distorted tetrahedral coordination. This distortion is best displayed by the P–Cu–P angles of 98.86° and 99.80° for molecules A and B, respectively, which are markedly deviating from the ideal tetrahedral geometry.

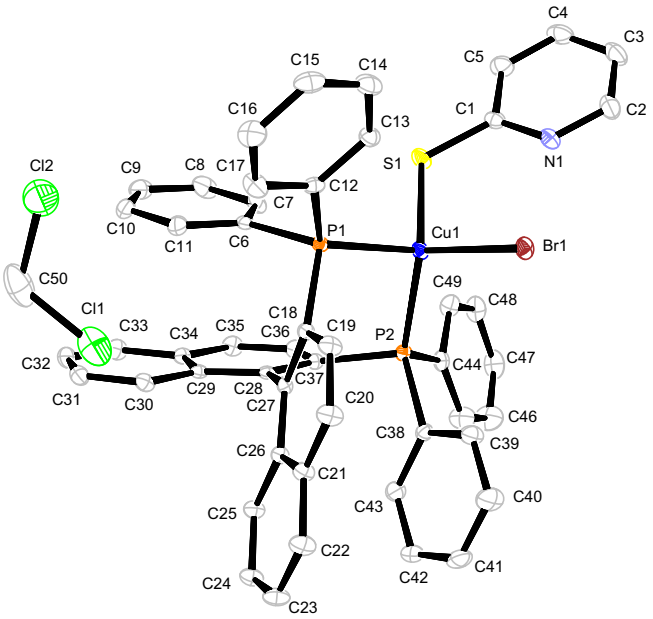

Fig. 3. A view of [CuBr(S-binap)(py2SH)] with displacement ellipsoids shown in the 50% probability level.

With reference to a large number of known tetrahedral mixed-ligand copper(I) complexes with a $CuXSP_2$ core, this P–Cu–P angle, including the two bulkiest ligands, is expected to be the largest one within the tetrahedron, but this is not the case here. However, considering the structural characteristics of the free diphosphane, the steric constrains resulting from this narrow angle seem unavoidable. In fact, the dihedral angle of 88.3° between the two naphthyl groups in free binap, which should provide the ideal situation for the PPh_2 groups to reduce the repulsions between them to a minimum, is narrowed to a value of 73.8(2)° in [CuBr(S-binap)(py2SH)]. On the other hand, the P···P separation of 4.218 Å in

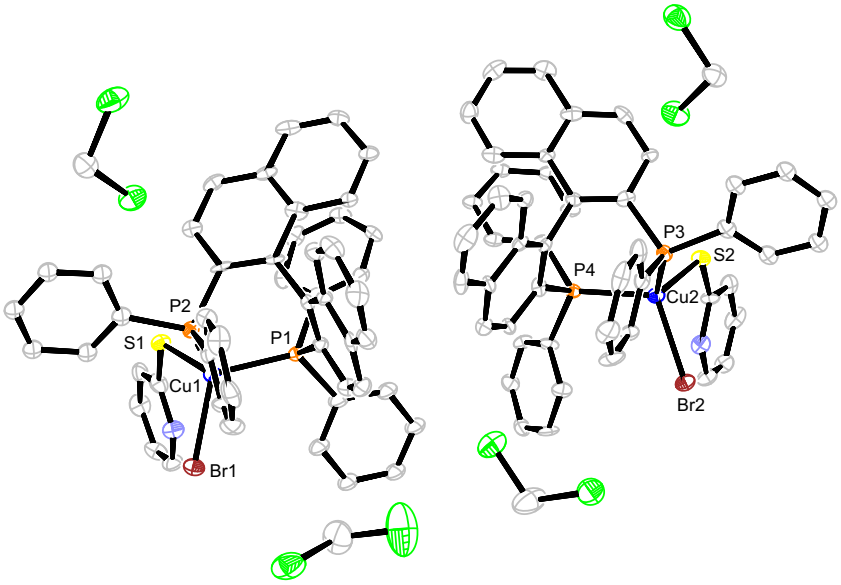

Fig. 2. A view of compound **2a** showing the two enantiomeric molecules with displacement ellipsoids in the 50% probability level.

free binap is shortened to 3.490(3) Å in [CuBr(S-binap)(py2SH)]. This shortening of the P···P distance upon chelation is obviously needed for the formation of Cu–P bonds of appropriate length.

There are only three structurally characterized copper(I) compounds with chelating binap reported so far, namely the cationic complexes [Cu(S-binap)(bpy)]PF_6, and [Cu(S-binap)(dmp)]PF_6 (bpy = 2,2′-bipyridyl and dmp = 2,9-dimethyl-1,10-phenanthroline) [8], as well as [Cu(S-binap)$(CH_3CN)_2$]ClO_4 [7b]. The Cu–P distances in these complexes are clearly shorter than those found in the complexes under investigation. Finally, a comparison of the structural characteristics of [CuBr(rac-binap)(py2SH)] with those of a series of reported monomeric compounds of type [CuX(phosphane)$_2$(S)] or [CuX(diphosphane)(S)], having the same CuP_2SX central core, revealed nearly similar values for the Cu–P, Cu–S and Cu–Br distances [23].

Orange crystals of compounds **2** and **8** were grown upon recrystallization from dichloromethane solutions. Both compounds crystallize in the monoclinic space group $P2_1/n$ with four discrete formula units in the unit cell, as well as one solvent (dichloromethane) molecule per formula unit, trapped in the crystal lattice. Bond lengths and angles around the Cu(I) for **2** and **8** are listed in Tables 3–5, and respective drawings of the molecules with the labeling of the atoms are given in Fig. 3 and 4.

In both cases the content of the asymmetric unit corresponds to a single molecule and the unit cell is comprised of two S- and two R- enantiomers. As it can be seen from the data in Tables 3–5, there are only minor differences in the bond lengths and angles between the three structures under investigation. As in the case of **2**, there is no indication of any specific interaction involving the solvent molecule, but as in many other copper halide complexes containing heterocyclic thione ligands, strong intramolecular hydrogen bridges ([N(1)–H(1) = 0.8800 Å, NH(1)–Br(1) = 2.4000 Å, Br(1)···N(1) = 3.24910(14) Å, Br(1)···H(1)–N(1) = 161.5°] for compound **2** and [N(1)–H(1) = 0.8800 Å, NH(1)–Br(1) = 2.4200 Å, Br(1)···N(1) = 3.28700(2) Å, Br(1)···H(1)–N(1) = 169.0°] for compound **8** contribute to further stabilization of the molecule in the solid state.

Bond lengths and angles involving the metal center are within the range of values found in a large number of complexes with a similar $CuXSP_2$ core. As in the structure of the aforementioned compound **2a**, some conformational adaptation on the part of the diphosphane is required for the benefit of chelation, as it is forced to lose its "relaxed" conformation, suppressing the dihedral angle between the two naphthyl groups by ca. 16 in 2 and ca. 10 in 8, but such a modification of the bite size of the diphosphane may be considered as quite normal. Regarding the geometrical characteristics of the heterocyclic rings in the thione units, coordination to Cu(I) does not causes any significant alterations except for a small lengthening of the C=S bond as a result of charge transfer from the S-atom to the metal.

In summary, we demonstrated the coordination behavior of binap towards copper(I) halides in the presence of heterocyclic thiones. In all the complexes, Cu^I was found to be in a distorted tetrahedral coordination environment with the thione adopting the monodentate-S coordination mode and the diphosphane acting as a chelate. Thus, chelation has been reconfirmed to be the preferred coordination mode for binap, a fact that can be ascribed to its conformational flexibility which allows modifications of the bite angle within a wide range. The new complexes showed interesting luminescent characteristics which will be the object of further prospectively investigations.

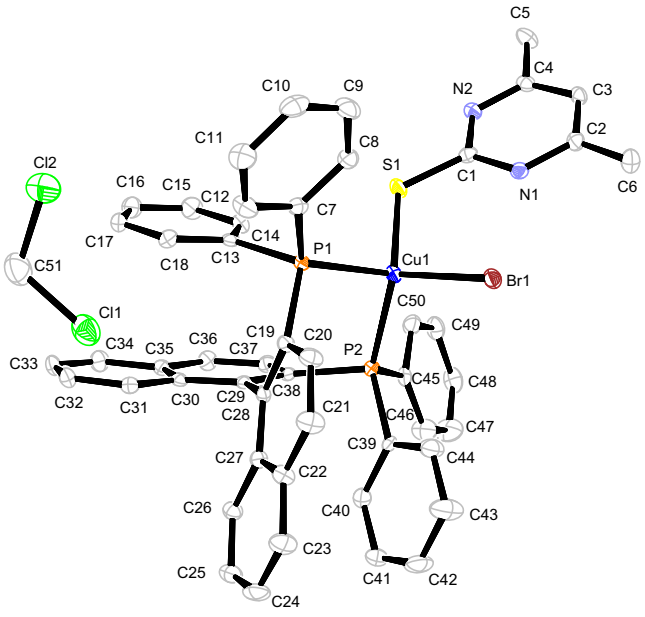

Fig. 4. Ortep view of [CuBr(S-binap)(dmpmtH)] (**8**) with thermal ellipsoids at the 50% probability level.

Acknowledgment

We thank the EPSRC X-ray crystallography service at the University of Southampton for collecting the X-ray data.

References

[1] (a) J.-C. Hierso, R. Amardeil, E. Bentabel, R. Broussier, B. Gautheron, P. Meunier, P. Kalck, Coordin. Chem. Rev. 236 (2003) 143. and references cited therein;
(b) C. Bianchini, A. Meli, M. Peruzzini, F. Vizza, P. Frediani, J.A. Ramirez, Organometallics 9 (1990) 226. and references cited therein.
[2] (a) Effendy, C. Di Nicola, M. Fianchini, C. Pettinari, B.W. Skelton, N. Sommers, A.H. White, Inorg. Chim. Acta 358 (2005) 763;
(b) C. Di Nicola, Effendy, C. Pettinari, B.W. Skelton, N. Somers, A.H. White, Inorg. Chim. Acta 359 (2006) 53;
(c) Effendy, C. Di Nicola, C. Pettinari, A. Pizzabiocca, B.W. Skelton, N. Somers, A.H. White, Inorg. Chim. Acta 359 (2006) 64.
[3] (a) P. Aslanidis, P.J. Cox, P. Karagiannidis, S.K. Hadjikakou, C.D. Antoniadis, Eur. J. Inorg. Chem. (2002) 2216;
(b) P. Aslanidis, P.J. Cox, S. Divanidis, P. Karagiannidis, Inorg. Chim. Acta 357 (2004) 1063;
(c) S.K. Hadjikakou, P. Aslanidis, P.D. Akrivos, P. Karagiannidis, B. Kojic-Prodic, M. Luic, Inorg. Chim. Acta 197 (1992) 31;
(d) A. Kaltzoglou, P.J. Cox, P. Aslanidis, Inorg. Chim. Acta 358 (2005) 3048;
(e) P. Karagiannidis, P. Aslanidis, S. Papastefanou, D. Mentzafos, A. Hountas, A. Terzis, Polyhedron 9 (1990) 2833;
(f) P.J. Cox, P. Aslanidis, P. Karagiannidis, Polyhedron 19 (2000) 1615;
(g) P. Aslanidis, P.J. Cox, A. Kaltzoglou, A.C. Tsipis, Eur. J. Inorg. Chem. (2006) 334.
[4] (a) M. McCarthy, P.J. Guiry, Tetrahedron 57 (2001) 3809. For recent reviews about diphosphanes in asymmetric catalysis, see:;
(b) W. Tang, X. Zhang, Chem. Rev. 103 (2003) 3029.
[5] A. Miyashita, H. Takaya, T. Souchi, R. Noyori, Tetrahedron 40 (1984) 1245.
[6] (a) N. Momiyama, H. Yamamoto, J. Am. Chem. Soc. 126 (2004) 5360;
(b) A.J. Deeming, D.M. Speel, M. Stchedroff, Organometallics 16 (1997) 6004;
(c) F. Prestopino, R. Persson, M. Monari, N. Focci, E. Nordlander, Inorg. Chem. Commun. 1 (1998) 302;
(d) C. Najera, M. de Gracia Retamosa, J.M. Sansano, Organic Lett., 9 (2007) 4025;
(e) H. Kunkely, A. Vogler, Inorg. Chem. Commun. 9 (2006) 866.
[7] (a) D. Ferraris, B. Young, T. Dudding, T. Lectka, J. Am. Chem. Soc. 120 (1998) 4548;
(b) D. Ferraris, B. Young, C. Cox, W.J. Drury, T. Dudding, T. Lectka, J. Org. Chem. 63 (1998) 6090;
(c) S. Yao, M. Johannsen, R.G. Hazell, K.A. Jørgensen, Angew. Chem., Int. Ed. 37 (1998) 3121.
[8] K. Saito, T. Tsukuda, T. Tsubomura, Bull. Chem. Soc. Jpn. 79 (2006) 437.
[9] Z. Otwinowski, W. Minor, in: C.W. Carter Jr., R.M. Sweet (Eds.), Macromolecular Crystallography, Part A, vol. 276, Academic Press, New York, 1997, pp. 307–326.
[10] R. Hooft, COLLECT Data Collection Software. Nonius BV, 1998.
[11] A. Altomare, M.C. Burla, M. Camalli, G.L. Cascarano, C. Giacovazzo, A. Guagliardi, A.G.G. Moliterni, G. Polidori, R. Spagna, J. Appl. Crystallogr. 32 (1999) 115.

[12] G.M. Sheldrick, SHELXL-97. Program for Crystal Strucutre Analysis (Release 97-2), University of Göttingen, Germany, 1997.
[13] L.J. Farrugia, J. Appl. Crystallogr. 30 (1997) 565.
[14] M. Sakamoto, J. Photochem. Photobiol. C: Photochem. Rev. 7 (2006) 183.
[15] M. Lecouvey, C. Barbey, A. Navaza, A. Neuman, T. Pragé, Acta Crystallogr. Sect. C 58 (2002) o521.
[16] P.J. Cox, S. Blaney, S.W. Love, N. Shankland, D.B. Sheen, J. Chem. Crystallogr. 25 (1995) 845.
[17] C.N.R. Rao, P. Vankataraghavan, Spectrochim. Acta 18 (1962) 541.
[18] (a) X. Chen, F.J. Femia, J.W. Babich, J. Zubieta, Inorg. Chim. Acta 315 (2001) 147;
(b) C.P. Lenges, M. Brookhart, P.S. White, Angew. Chem., Int. Ed. 38 (1999) 552;
(c) W.-Y. Yeh, C.-S. Lin, S.-M. Peng, G.-H. Lee, Organometallics 23 (2004) 917;
(d) T.B. Tauchfuss, J. Am. Chem. Soc. 101 (1979) 1045.
[19] M.A. Garralda, C.R. Chimie, 8 (2005) 1413.
[20] (a) C. Koutal, Coordin. Chem. Rev. 99 (1990) 213;
(b) D.R. McMillin, K.M. McNett, Chem. Rev. 98 (1998) 1201;
(c) P.-T. Chou, Y. Chi, Chem. Eur. J. 13 (2007) 380.
[21] V. Pawlowsky, G. Knör, C. Lennarz, A. Vogler, Eur. J. Inorg. Chem. (2005) 3167.
[22] (a) H. Kunkely, A. Vogler, Inorg. Chem. Commun. 2 (1999) 533;
(b) V. Pawlowsky, H. Kunkely, A. Vogler, Inorg. Chim. Acta. 357 (2004) 1309.
[23] (a) S.K. Hadjikakou, C.D. Antoniadis, P. Aslanidis, P.J. Cox, A.C. Tsipis, Eur. J. Inorg. Chem. (2005) 1442;
(b) P. Aslanidis, P.J. Cox, S. Divanidis, P. Karagiannidis, Polyhedron 24 (2005) 351;
(c) A. Kaltzoglou, P.J. Cox, P. Aslanidis, Inorg. Chim. Acta 358 (2005) 3048.

obtained from Fluka were used without further purification. The synthesis of the pbpaen ligand was previously reported in the literature [5].

2.2. Syntheses of the complexes

Reported yields for complexes are based upon metal starting materials. CAUTION: Although we have experienced no problems while handling any of the substances described herein, readers are cautioned to handle these compounds as potentially explosive compounds.

2.2.1. [Ni(pbpaen)](ClO4)2 (1) and [Co(pbpaen)](ClO4)3 (2)

A mixture of sodium acetate trihydrate (0.54 g, 4 mmol) and pbpaen pentahydrochloride monohydrate (0.62 g, 1 mmol), in absolute ethanol (30 mL) was stirred whilst boiling (10 min, water bath), then cooled and the sodium chloride which precipitated was filtered off. Nickel(II) or cobalt(II) perchlorate hexahydrate (0.37 g, 1 mmol) in absolute ethanol (20 mL) was added dropwise to the filtrate and the solution was stirred for 2 h at room temperature. Coloured powder formed which was filtered off, recrystallized from water–ethanol (1:1):

[Ni(pbpaen)](ClO4)2 (**1**): Pink crystals suitable for X-ray diffraction were obtained after one month. Yield: 0.47 g (70%, 0.7 mmol), m.p. 225 °C. *Anal.* Calc. for $C_{24}H_{33}N_7NiCl_2O_8$: C, 42.53; H, 4.87; N, 14.47; Ni, 8.7. Found: C, 42.44; H, 4.93; N, 14.29; Ni, 8.3%. $\chi_M = 4310 \times 10^{-6}$ c.g.s. e.m.u, $\mu_{eff} = 3.18\ \mu_B$. IR (KBr) (cm^{-1}): 3322, 3295 (s, ν_{N-H}); 2945–2860 (m, ν_{C-H}); 1603, 1570, 1483, 1442 (s, $\nu_{pyridine\ ring}$) 1090 (vs, $\nu_{ClO_4^-}$). UV/Vis (solid state): $\lambda_{max} = 520$, 810 nm (DMF or H_2O): λ_{max} (ε) = 520 (12), 810 nm (15 $mol^{-1}\ dm^3\ cm^{-1}$).

[Co(pbpaen)](ClO4)3 (**2**): Light brown crystals unsuitable for X-ray were obtained after six weeks. Yield: 0.435 g (70%, 0.7 mmol), m.p. 218 °C. *Anal.* Calc. for $C_{24}H_{33}N_7CoCl_3O_{12}$: C, 37.07; H, 4.25; N, 12.62; Co, 7.6. Found: C, 37.15; H, 4.38; N, 12.50; Co, 7.9%. IR (KBr) (cm^{-1}): 3320, 3285 (s, ν_{N-H}); 2940–2850 (m, ν_{C-H}); 1600, 1565, 1478, 1442 (s, $\nu_{pyridine\ ring}$) 1090 (vs, $\nu_{ClO_4^-}$). UV/Vis (solid state): $\lambda_{max} = 464$ nm; (H_2O or DMF): λ_{max} (ε) = 355 (215), 462 nm (138 $mol^{-1}\ dm^3\ cm^{-1}$).

2.2.2. [Co(bpaen)](ClO4)3 (3)

To the solution of pbpaen pentahydrochloride monohydrate (0.62 g, 1 mmol) dissolved in water (40 mL) was added dropwise with stirring the solution of cobalt(II) perchlorate hexahydrate (0.37 g, 1 mmol) in water (10 mL). Solid sodium carbonate was added in small portions to the mixture with stirring until the pH reached 4. After stirring at room temperature for 1 h, the solvent was removed by rotavapor. Recrystallization of the crude product obtained from water–acetone (1:1) gave after four months yellow brown crystals suitable for X-ray diffraction. Yield: 0.41 g (60%, 0.6 mmol), m.p. 245 °C. *Anal.* Calc. for $C_{18}H_{28}N_6CoCl_{12}O_{12}$: C, 31.50; H, 4.08; N, 12.25; Co, 8.6. Found: C, 31.60; H, 4.21; N, 12.04; Co, 8.9%. IR (KBr) (cm^{-1}): 3325, 3291 (s, ν_{N-H}); 2940–2850 (m, ν_{C-H}); 1600, 1569, 1480, 1445 (s, $\nu_{pyridine\ ring}$) 1095 (vs, $\nu_{ClO_4^-}$). UV/Vis (solid state): $\lambda_{max} = 461$ nm; (DMF or H_2O): λ_{max} (ε) = 354 (218), 460 nm (140 $mol^{-1}\ dm^3\ cm^{-1}$).

2.3. Physical measurements

Elemental analyses (C, H and N) were carried out on a Perkin–Elmer 2400 C, H, N element analyser in our university. The metal analysis was performed on an ICP AES Liberty Series II Varian apparatus. The UV–Visible spectra in solution were recorded on a Perkin–Elmer Lambda 6 spectrophotometer. In the solid state, visible spectra were obtained on a Beckman 5240 spectrophotometer by depositing the compound on Schleicher and Schul filter paper without ashes, and this paper was used as reference. IR spectra were obtained in KBr pellets with a Nicolet Avatar 320. Magnetic susceptibilities were determined at room temperature (20 °C) using $HgCo(SCN)_4$ as a calibrant; diamagnetic susceptibility corrections were calculated from Pascal's constants [8].

2.4. Crystal structure determination

The crystal data were collected on a Siemens SMART three-circle CCD diffractometer using monochromatic Mo Kα radiation ($\lambda = 0.71073$Å). The structure was solved by the direct method and refined by full matrix least squares, based on F^2 using the SHELX-TL software package [9]. An empirical absorption correction based on symmetric equivalent reflections was applied using the SADABS program [10]. All the hydrogen positions were initially located in the difference map and for the final refinement the hydrogen atoms were placed geometrically and held in the riding mode. The last cycles of the refinement included atomic positions for all the atoms, anisotropic thermal parameters for all non-hydrogen atoms and isotropic thermal parameters for all the hydrogen atoms.

Crystal data and refinement details for [Ni(pbpaen)]$(ClO_4)_2$ (**1**) and [Co(bpaen)]$(ClO_4)_3 \cdot$ (**3**) are shown in Table 1. Additional experimental information, including atomic positional parameters, is supplied in CIF format as described in the Supplementary data.

3. Results and discussion

3.1. Synthesis

New complexes [Ni^{II}(pbpaen)]$(ClO_4)_2$ (**1**) and [Co^{III}(pbpaen)]$(ClO_4)_3$ (**2**) were synthesized by treating an ethanolic suspension of the ligand pentahydrochloride salt and 5 equiv of sodium acetate and the appropriate metal(II) perchlorate hexahydrate. These two compounds were isolated as perchlorate salts, confirmed by the presence of a strong band at ca. 1090 cm^{-1} in the IR spectra. In order to synthesize complexes with protonated forms of the ligand, the reactions between the $M(ClO_4)_2 \cdot 6H_2O$ (M = Ni^{2+} or Co^{2+}) and pentahydrochloride pbpaen ligand were realized in an aqueous medium in acidic conditions using Na_2CO_3 as the base.

Table 1
Crystal data and details of the refinement of the crystal structures of [Ni(pbpaen)]$(ClO_4)_2$ (**1**) and [Co(bpaen)]$(ClO_4)_3 \cdot$ (**3**)

	1	**3**
Formula	$C_{24}H_{33}Cl_2N_7NiO_8$	$C_{18}H_{28}Cl_3CoN_6O_{12}$
M	677.19	685.74
Crystal system	monoclinic	orthorhombic
Crystal size (mm × mm × mm)	0.60 × 0.55 × 0.50	0.35 × 0.20 × 0.06
Space group	$P2_{1/c}$	*Pna*2
a (Å)	9.8539(2)	15.3869(4)
b (Å)	16.2098(2)	14.4225(4)
c (Å)	19.1078(3)	11.6489(2)
α (°)	90.00	90.00
β(°)	103.9620(10)	90.00
γ(°)	90.00	90.00
V (Å^3)	2961.91(8)	2585.10(11)
T (K)	296(2)	293(2)
Z	4	4
μ (Mo Kα) (mm^{-1})	0.894	1.048
Reflections measured	7697	6960
Number of independent reflections [R_{int}]	5818 [0.018]	5186 [0.018]
F(000)	1408	1408
Goodness-of-fit on F^2	1.032	1.052
Final *R* indices	$R_1 = 0.0451$	$R_1 = 0.0461$
[$I > 3\sigma(I)$]	$wR_2 = 0.1310$	$wR_2 = 0.1182$
R indices (all data)	$R_1 = 0.0633$	$R_1 = 0.0758$
	$wR_2 = 0.1457$	$wR_2 = 0.1422$

At pH ≈ 4, the reaction of the Ni^{2+} ion with pbpaen ligand afforded compound **1**, whereas Co^{2+} ion gives $[Co^{III}(bpaen)](ClO_4)_3$ (**3**) compound in which the tripod pbpaen ligand had lost one of the three pyridylmetyl groups procuring then bpaen ligand (bpaen = *N*,*N*-bis{2-[(pyridin-2-ylmethyl)amino]ethyl}ethane-1,2-diamine). At more acidic condition (pH ⩽ 3.5), all our attempts resulted in precipitation of intractable solid. The three complexes were recrystallized from water–ethanol (1:1) (**1** and **2**) or water-acetone (1:1) (**3**) and only compounds **1** and **3** gave suitable crystals for X-ray structure determinations.

3.2. X-ray diffraction studies

3.2.1. $[Ni(pbpaen)](ClO_4)_2$ (**1**)

Complex **1** crystallizes in a monoclinic space group $P2_{1/c}$ with four molecules per unit cell. The molecular structure consists in one $[Ni(pbpaen)]^{2+}$ cation and two ClO_4^- anions. A Platon drawing of the cation $[Ni(pbpaen)]^{2+}$ together with the atoms labelling scheme is shown in Fig. 1, relevant bond lengths and angles in Table 2.

The structure shows the presence of two independent molecules in the crystal lattice. Although pbpaen is a potentially heptadentate ligand, the nickel(II) ion has a coordination number of six in each complex molecule; thus, one of the three pyridyl nitrogen atoms remains uncoordinated. The nickel(II) center is coordinated by the apical nitrogen atom N(3), two aromatic nitrogen atoms [N(1) and N(5)] and three secondary amine nitrogen atoms [N(2), N(4) and N(6)]. The coordination sphere is distorted octahedral with the *trans* angles N(1)–Ni–N(3) = 162.45(9)°, N(2)–Ni–N(5) = 173.72(9)° and N(4)–Ni–N(6) = 160.66(9)°. The bond lengths involving two nitrogen atoms of the same arm (secondary amine and pyridyl) of pbpaen ligand are quite similar [Ni–N(1) = 2.081(2) Å, Ni–N(2) = 2.088(2) Å and Ni–N(4) = 2.171(2) Å, Ni–N(5) = 2.170(2) Å]. The coordination of the apical nitrogen atom induces some strains in the molecule; thus the bond distances of the second coordinated arm of the ligand are increased (≈ +0.086 Å) and the chelate ring formed between pyridyl nitrogen and amine nitrogen is contracted (mean value 78.83°) with respect to an octahedral geometry (90°).

The structure of complex **1** is surprisingly different from hexacoordinated N_6 $[Ni(py)_3tren]^{2+}$ compound [11], with a ligand similar to pbpaen, but containing HC=N bonds instead of H_2C–NH. This latter complex does not exhibit the coordination of the tertiary apical nitrogen atom to the nickel center; Morgenstern and co-workers [12,13] explain this kind of difference by a stronger chelating effect of α-imine linkage present in $(py)_3tren$.

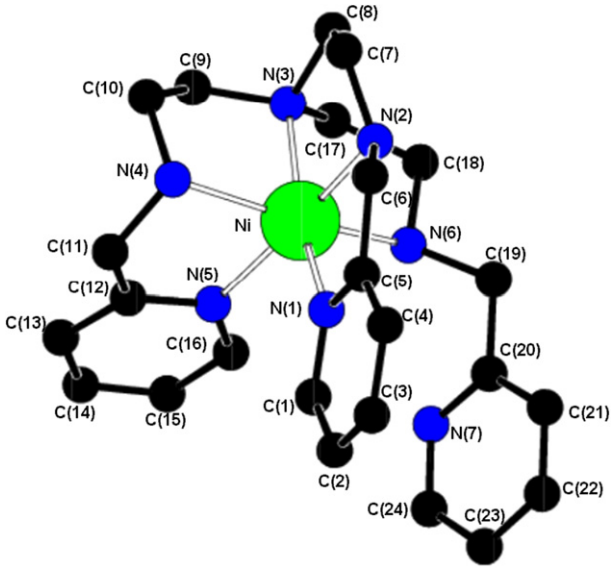

Fig. 1. A Platon drawing of the cation $[Ni(pbpaen)]^{2+}$ and the atoms labelling scheme; hydrogen atoms and perchlorate anions are omitted for clarity.

Table 2
Selected bond lengths (Å) and bond angles (°) for $[Ni(pbpaen)](ClO_4)_2$ (**1**)

Bond lengths			
Ni–N(1)	2.081(2)	Ni–N(4)	2.171(2)
Ni–N(2)	2.088(2)	Ni–N(5)	2.170(2)
Ni–N(3)	2.096(2)	Ni–N(6)	2.162(2)
Bond angles			
N(1)–Ni–N(2)	80.05(9)	N(2)–Ni–N(6)	94.23(9)
N(1)–Ni–N(3)	162.45(9)	N(3)–Ni–N(4)	81.58(9)
N(1)–Ni–N(4)	96.01(8)	N(3)–Ni–N(5)	99.72(9)
N(1)–Ni–N(5)	96.83(8)	N(3)–Ni–N(6)	83.46(10)
N(1)–Ni–N(6)	101.90(9)	N(4)–Ni–N(5)	78.83(9)
N(2)–Ni–N(3)	82.91(9)	N(4)–Ni–N(6)	160.66(9)
N(2)–Ni–N(4)	96.00(9)	N(5)–Ni–N(6)	91.74(8)
N(2)–Ni–N(5)	173.72(9)		

The crystal lattice of complex **1** is stabilized by intra and intermolecular hydrogen bonding systems. One intramolecular H-bond is formed between the hydrogen of the secondary amine nitrogen and the uncoordinated pyridyl nitrogen belonging to the same arm of pbpaen ligand; the distance $NH\cdots N_{pyridyl}$ being 2.761 Å. Two intermolecular H-bonds shows an interesting super-structure based on $O_{ClO_4^-}\cdots HN$ hydrogen interactions between oxygen atoms of one perchlorate anion and the secondary amine groups of the tripod ligand (Fig. 2). The first H-bonds are between two oxygen atoms of ClO_4^- ion and the hydrogen of the secondary amine, forming a two-center chelate H-bonds [14] (average, $O_{ClO_4^-}\cdots HN$ = 3.311 Å). The second hydrogen bond is between the third oxygen atom of the perchlorate anion and the hydrogen of secondary amine of the neighbouring complex; the distance $O_{ClO_4^-}\cdots HN$ being 3.102 Å. The propagation of these hydrogen bonding systems create a polymeric structure giving an interesting one-dimensional sheets like arrays.

3.2.2. $[Co(bpaen)](ClO_4)_3$ (**3**)

Complex **3** crystallizes in an orthorhombic space group *Pna*2 with four molecules per unit cell. The molecular structure consists in one $[Co(bpaen)]^{3+}$ cation (bpaen represents the ligand *N*,*N*-bis{2-[(pyridin-2-ylmethyl)amino]ethyl}ethane-1,2-diamine) and three ClO_4^- anions. Relevant bond lengths and angles are given in Table 3. A Platon drawing of the cation $[Co(bpaen)]^{3+}$ with atoms labelling is illustrated in Fig. 3.

The structure of complex **3** demonstrates that Co^{2+} ion was aerial oxidized to Co(III) in the complex, and one arm of the tripod ligand lost its pyridylmethyl group affording $[Co^{III}(bpaen)](ClO_4)_3$ (**3**) compound. The coordination geometry around the cobalt atom is described as a distorted octahedron with the *cis* bond angles ranging from 82.36(14)° to 86.99(15)° and the *trans* bond angles from 170.67(15)° to 176.84(15)°. As in complex **1**, the strains induced by the coordination of the apical nitrogen atom N(3) of bpaen ligand leads to the difference of the six Co–N bond lengths. The average Co–N distances follow the order $Co{-}N^{amine}_{primary}$ (1.955 Å)≈ $Co{-}N^{amine}_{secondary}$ (1.955 Å) < $Co{-}N^{pyridyl}$ (1.965 Å) expected from the donor capabilities of the lone pairs on the three nitrogen atoms.

The lattice structure of **3** is stabilized by intermolecular hydrogen-bonding network formed by the hydrogen atoms of the primary and secondary amine groups of the bpaen ligand to one oxygen atom of perchlorate anions with the distance of 3.012 Å and 3.045 Å, respectively. Complex cation of **3** is linked into polymers by hydrogen bonds involving the second hydrogen of NH_2 groups and the oxygen atom hydrogen-bonded of the perchlorate

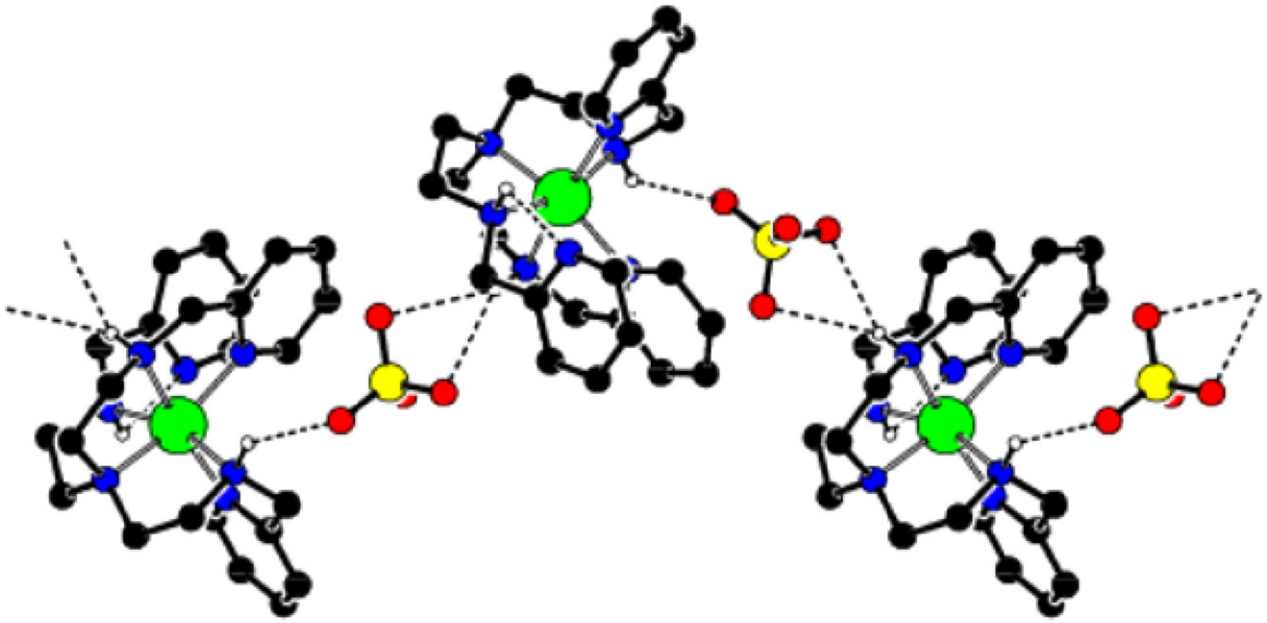

Fig. 2. Extended interactions in **1**, showing the H-bonding contacts.

Table 3
Selected bond lengths (Å) and bond angles (°) for $[Co(bpaen)](ClO_4)_3$ (**3**)

Bond lengths			
Co–N(1)	1.951(3)	Co–N(4)	1.972(3)
Co–N(2)	1.940(4)	Co–N(5)	1.978(3)
Co–N(3)	1.945(3)	Co–N(6)	1.955(3)
Bond angles			
N(1)–Co–N(2)	83.70(16)	N(2)–Co–N(6)	90.13(17)
N(1)–Co–N(3)	170.67(15)	N(3)–Co–N(4)	86.71(13)
N(1)–Co–N(4)	93.50(14)	N(3)–Co–N(5)	94.09(13)
N(1)–Co–N(5)	95.18(14)	N(3)–Co–N(6)	86.79(15)
N(1)–Co–N(6)	93.77(15)	N(4)–Co–N(5)	82.36(14)
N(2)–Co–N(3)	86.99(15)	N(4)–Co–N(6)	171.65(16)
N(2)–Co–N(4)	94.75(16)	N(5)–Co–N(6)	92.89(15)
N(2)–Co–N(5)	176.84(15)		

anion belonging to the neighbouring complex. Propagation of their interaction leads to the formation of two-dimensional layers (Fig. 4). The closest Co···Co separation within the layers is 10.825 Å.

In both compounds, the bond lengths involving pyridine nitrogen atoms are not significantly different from those involving primary or secondary amine nitrogen atoms. All metal–nitrogen bond lengths in the nickel complex (**1**) are longer than those in the cobalt complex (**3**), what is consistent with the larger radius of Ni(II). In each complex, the M–N bond distances of the two pyridylmethylamine groups belonging to the two bound arms of the tripod ligand are different; this difference is more important in the nickel(II) complex [average, 0.086 Å] than the cobalt(III) compound [average, 0.029 Å]. In addition, the five-chelate bond angles of 78.83–83.46° (average, 81.15°) subtended by the ligand at the nickel atom are smaller than their analogues of 82.36–86.79° (average, 84.58°) in the cobalt complex, in agreement with a larger distortion in the nickel compound.

All attempts to isolate the nickel(II) complex with bpaen ligand in acidic medium (pH ≈ 4), as in the compound **3**, have failed. This seems to demonstrate that the oxidation of the metallic ion is necessary to obtain the substitution of the pbpaen ligand giving bpaen complex.

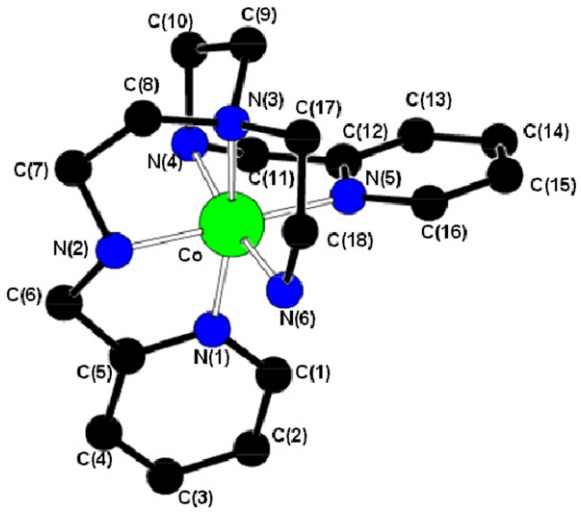

Fig. 3. A Platon drawing of the cation $[Co(bpaen)]^{3+}$ and the atoms labelling scheme; hydrogen atoms and perchlorate anions are omitted for clarity.

3.3. Spectroscopic studies

3.3.1. IR spectra

IR spectra of the nickel(II) and cobalt(III) complexes are similar in pattern to the one of bpbaen. For all the compounds, small shifts are observed for the characteristic secondary amine bands (ca. 3400–3060 cm^{-1}) and those of the pyridyl rings (ca. 1620–1610 cm^{-1}) to lower and higher energies, respectively. These vibrations are similar to those found in the analogous series of complexes with ligands containing pyridyl groups and 5-membered chelate rings [15]. ClO_4^- anions in the three compounds have been characterised by a broad and strong band at 1090–1095 cm^{-1}.

3.3.2. Absorption spectra

The electronic spectra of the three complexes (**1**–**3**) in the solid state are not different from those obtained in H_2O or in DMF solu-

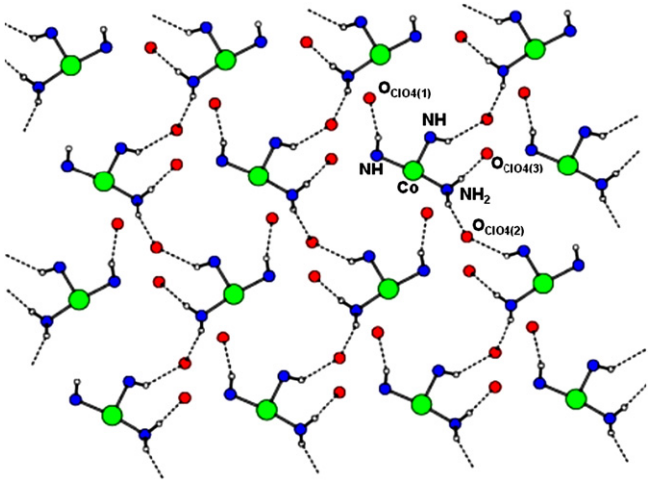

Fig. 4. Part of the lattice structure of $[Co(bpaen)](ClO_4)_3$, showing a two-dimensional layer of cations linked by hydrogen bonding. All atoms not involved in hydrogen-bonding are omitted for clarity.

tion. The absorption spectra of these compounds exhibit essentially similar patterns in the 250–400 nm region, with two strong bands possibly due to intraligand [16,17] and/ or charge transfer transitions.

In the visible region, complex $[Ni(pbpaen)](ClO_4)_2$ (**1**) displays two bands at 890 nm and 560 nm. These two bands arise from $^3A_{2g} \rightarrow {}^3T_{2g}$ and $^3A_{2g} \rightarrow {}^3T_{1g}(^3F)$ transitions. The third band at higher energy is completely obscured by metal–ligand charge-transfer. These observations are consistent with an octahedral geometry around Ni^{2+} ion, and ligand field parameters are calculated using the energy level given by Lever [18]: 10 Dq = 11 270 cm^{-1}, Racah parameter $B = 865\ cm^{-1}$. These parameters, compared to those of octahedral $Ni(pytrien)](ClO_4)_2$ complex (10 Dq = 12 360 cm^{-1}, Racah parameter $B = 826\ cm^{-1}$) [19], are in agreement with NiN_6 chromophores [20,21].

The d–d transitions of complexes **2** and **3** are characteristic of low-spin octahedral cobalt(III) with two spin-allowed absorption bands centred at 462 and 355 nm, and 460 and 354 nm, respectively. The latter bands are almost obscured by the intense low-energy Co–N charge transfer transition. These bands, arising from $^1A_{1g} \rightarrow {}^1T_{1g}$ and $^1A_{1g} \rightarrow {}^1T_{2g}$ d–d transitions, are consistent with those corresponding to $Co^{III}N_6$ chromophore [22–25]. The fact that the two cobalt(III) compounds, **2** and **3**, exhibiting the similar electronic spectra shows that the third uncoordinated pyridyl nitrogen atom of the ligand has no influence on the stereochemistry of these compounds.

Appendix A Supplementary data

CCDC 606972 and 606973 contain the supplementary crystallographic data for $[Ni(pbpaen)](ClO_4)_2$ and $[Co(bpaen)](ClO_4)_3$. These data can be obtained free of charge via http://www.ccdc.cam.ac.uk/conts/retrieving.html, or from the Cambridge Crystallographic Data Centre, 12 Union Road, Cambridge CB2 1EZ, UK; fax: (+44) 1223-336-033; or e-mail: deposit@ccdc.cam.ac.uk. Supplementary data associated with this article can be found, in the online version, at doi:10.1016/j.poly.2008.06.016.

References

[1] D.H. Petering, R.W. Bynes, W.E. Antholine, Chem. Biol. Interact. 73 (1990) 133.
[2] J. Stubbe, J.W. Kozarich, Chem. Rev. 87 (1987) 1107.
[3] S.M. Hecht, Acc. Chem. Res. 19 (1986) 383.
[4] Y. Sigura, T. Takita, H. Umezawa, Met. Ions Biol. Syst. 19 (1985) 81.
[5] C. Gérard, A. Mohamadou, J. Marrot, S. Brandès, A. Tabard, Helv. Chim. Acta 88 (2005) 2397.
[6] A. Mohamadou, C. Gérard, J. Chem. Soc., Dalton Trans. (2001) 3320.
[7] D. Perrin, W.L.F. Armarego, R.D. Perrin, Purification of Laboratory Chemicals, third ed., Pergamon, Oxford, 1988.
[8] A. Earnshaw, Introduction to Magnetochemistry, Academic Press, London, 1968. p.5.
[9] G.M. Sheldrick, SHELXTL NT v 5.10, 1999, Bruker AXS, Inc. Madison, Wisconsin 53719, USA.
[10] (a) G.M. Sheldrick, SADABS, Program for Scalin and Correction of Area Detector Data, University of Göttingen, Germany, 1997;
(b) R. Blessing, Acta Crystallogr. Sect. A 51 (1995) 33.
[11] R.M. Kirchner, C. Mealli, M. Bailey, N. Howe, L.P. Torre, L.J. Wilson, L.C. Andrews, N.J. Rose, E.C. Lingafelter, Coordin. Chem. Rev. 77 (1987) 89.
[12] I. Morgenstern-Baradau, F. Lambert, J.P. Renault, M. Cesario, J.D. Marechal, F. Maseras, Inorg. Chim. Acta 297 (2000) 338.
[13] A. Deroche, I. Morgenstern-Baradau, M. Cesario, J. Gulhem, B. Keita, L. Nadjo, C. Houée-Levin, J. Am. Chem. Soc. 118 (1996) 4567.
[14] H.R. Hoveyda, V. Karunaratne, C.J. Nichols, S.J. Rettig, A.K.W. Stephens, C. Orvig, Can. J. Chem. 76 (1998) 414.
[15] J.R. Hartman, R.W. Vachet, W.H. Pearson, R.J. Wheat, J.H. Callahan, Inorg. Chim. Acta 343 (2003) 119.
[16] M. Ray, S. Mukherjee, R.N. Mukherjee, J. Chem. Soc., Dalton Trans. (1990) 3635.
[17] M. Ray, R.N. Mukherjee, Polyhedron 11 (1992) 2929.
[18] A.B.P. Lever, Inorganic Electronic Spectroscopy, second ed., Elsevier, Amsterdam, 1984. Oxford, New York, Tokyo, p. 126; 517.
[19] C. Jubert, Ph. D. Thesis, University of Reims, 2001, p. 105.
[20] J.R. Hartman, R.W. Vachet, J.H. Callahan, Inorg. Chim. Acta 297 (2000) 79.
[21] N. Arulsamy, J. Glerup, A. Hazell, D.J. Hodgson, C.J. Mc Kenzie, H. Toftlund, Inorg. Chem. 33 (1994) 3023.
[22] C. Jubert, A. Mohamadou, E. Guillon, J.P. Barbier, Polyhedron 19 (2000) 1447.
[23] A. El Dissouky, O.A. Fulij, S.S. Kandil, J. Coordin. Chem. 57 (2004) 605.
[24] M.S. Islam, M. Begum, H.N. Roy, Synth.React. Inorg. Met. Org. Chem. 77 (1995) 89.
[25] I.I. Creaser, R.J. Geue, J. MacB. Harrowfield, A.J. Herlt, A.M. Sargeson, M.R. Snow, J. Springborg, J. Am. Chem. Soc. 104 (1982) 6016.

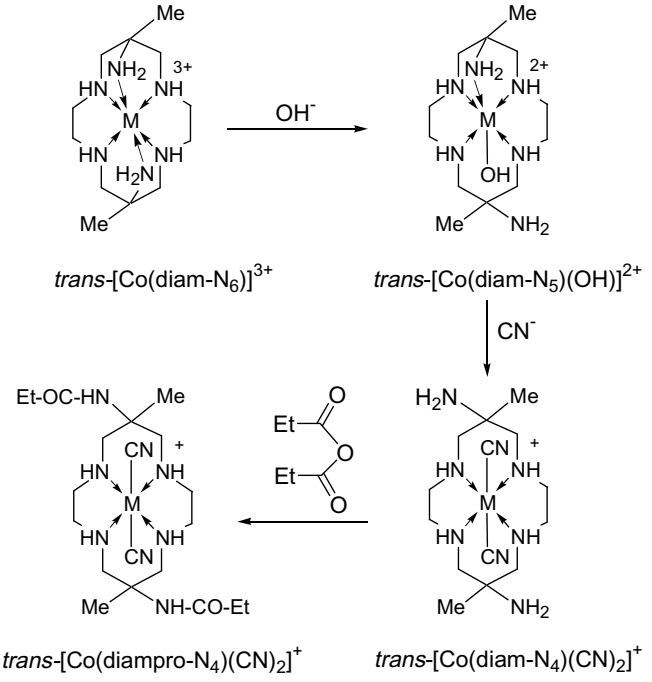

Scheme 1. Showing the preparations of *trans*-$[Co(diam\text{-}N_4)(CN)_2]^+$ and *trans*-$[Co(diampro\text{-}N_4)(CN)_2]^+$.

Table 1
Selected dimensions for *trans*-$[Co(diampro\text{-}N_4)(CN)_2]ClO_4 \cdot 2H_2O$

Atoms	Distance (Å)	Atoms	Angle (°)
Co1–N1	1.979(2)	N1–Co1–N4	87.18(7)
Co1–N4	1.968(2)	N1–Co1–N4[a]	92.82(7)
Co1–C20	1.920(2)	C20–Co1–N4	88.28(9)
C20–N20	1.145(3)	C20–Co1–N4[a]	91.72(9)
N61–C62	1.352(3)	C20–Co1–N1	90.61(8)
C62–O62	1.224(4)	C20–Co1–N1[a]	89.39(8)
		O62–C62–N61	122.4(2)
		O62–C62–C63	122.8(3)
		Co1–C20–N20	175.6(2)

[a] Symmetry operation: $-x, -y, -z$.

Table 2
Hydrogen bonds (Å, °) for *trans*-$[Co(diampro\text{-}N_4)(CN)_2]ClO_4 \cdot 2H_2O$

Atoms	D–H	H···A	D···A	D–H···A	Symmetry operation
N1–H1···O1	0.91	2.09	2.913(2)	149.6	
N4–H4···O62	0.91	2.17	2.912(3)	137.8	$y, -x+y, -z$
N61–H61···O62	0.86	2.25	3.072(3)	158.8	$y, -x+y, -z$
O1–H11···N20	0.83(2)	2.22(3)	2.898(3)	139(3)	$x, x-y+1, z-½$
O1–H12···O12	0.78(2)	2.22(2)	2.986(4)	166(4)	$x, -x+y, -z-½$

with the three other oxygen atom sites generated from sites O12 and O22 by symmetry operations, see Fig. 1.

A hydrogen bonding network links the water O1 to amine N1, cyanide N20 and perchlorate O12, while the amide O62 is linked to amine N4 and amide N61, see Table 2.

2. Discussion

The preparations and structures of cobalt(III) compounds with diam and cyano ligands: *trans*-$[Co(diam\text{-}N_4)(CN)_2] \cdot$ *trans*-$[Co(diamH_2\text{-}N_4)(CN)_2](ClO_4)_4 \cdot 4(H_2O)$ and Na *trans*-$[Co(diam\text{-}N_5)(CN)](ClO_4)_3$ [3] as well as of the related compounds $[Co(L\text{-}N_5)(CN)]ClO_4$, L = 6-amino-6-methyl-1,4,8,11-tetraazacyclotetradecane [4] and *trans*-$[Co(en)_2(CN)_2]ClO_4$ [4] have been reported, as have the structures of *trans*-$[Co(diam\text{-}N_6)]Cl_2(ClO_4)_2$

Table 3
Comparative distances (Å) Co–N and Co–C for *trans*-dicyano(tetraamine)cobalt(III) and related compounds

Cation	Co–N	Co–C	Reference
trans-$[Co(diampro)(CN)_2]^+$	1.97(2)	1.92(2)	This work
trans-$[Co(diam\text{-}N_4)(CN)_2]^+$	1.974(4)	1.926(4)	[3]
trans-$[Co(diamH_2N_4)(CN)_2]^{3+}$	1.980(6)	1.918(4)	[3]
trans-$[Co(en)_2(CN)_2]^+$	1.965(3)	1.917(2)	[7]
trans-$[Co(diam\text{-}N_5)(CN)]^{2+}$	1.964(6)	1.901(3)	[3]
trans-$[Co(L\text{-}N_5)(CN)]^{2+}$[a]	1.954(6)	1.899(3)	[4]
trans-$[Co(diamH_2\text{-}N_4)Cl_2]^+$	1.97(1)		[6]
trans-$[Co(diam\text{-}N_6)]^{3+}$	1.937(2)[b]		[5]

[a] L = 6-amino-6-methyl-1,4,8,11-tetraazacyclotetradecane.
[b] Ring N-atoms.

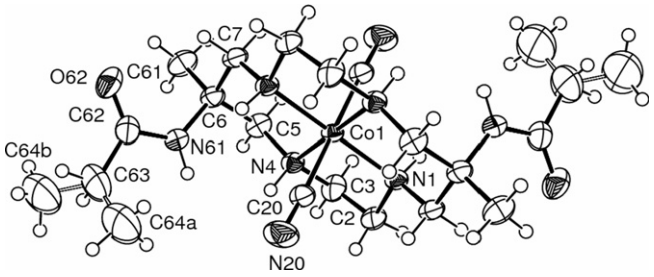

Fig. 1. The cation of *trans*-$[Co(diam\text{-}N_4)(CN)_2]ClO_4 \cdot 2H_2O$ drawn [9] with displacement ellipsoids at 50% confidence, with H-atoms shown as circles of arbitrary radii. Atoms in the asymmetric unit are labeled. The sites C64a and C64b have 0.5 site occupancy.

Table 4
Crystallography details for *trans*-$[Co(diam\text{-}N_4)(CN)_2]ClO_4 \cdot 2H_2O$

Empirical formula	$(C_{20}H_{38}CoN_8O_2)(ClO_4) \cdot 2(H_2O)$
Formula weight	617.0
Temperature (K)	293(2)
Crystal system	trigonal
Space group	$P\bar{3}c1$ (Hall – $P\ 32''c$)
a (Å)	17.403 (2)
b (Å)	17.403 (2)
c (Å)	15.762 (3)
α (°)	90
β (°)	90
γ (°)	120
Volume (Å^3)	4135 (1)
Cell determination (reflections, θ_{min}, θ_{max}) (°)	6595, 1.7, 30.2
Z	6
ρ_{calc} (g/cm^3)	1.443
μ (mm^{-1})	0.773
$F(000)$	1896
Crystallisation	crystal grown from water
Crystal, size (mm)	yellow plate, 0.04 × 0.03 × 0.01
θ Range for data collection	2.67–28.51
Index ranges	$-18 \leqslant h \leqslant 23$, $-22 \leqslant k \leqslant 15$, $-21 \leqslant l \leqslant 10$
Reflections collected (R_{int})	11 004 (0.0189)
Independent reflections	3252
T_{max}, T_{min}	0.997, 0.992
Data/restraints/parameters	3252/4/199
Reflections [$I > 2\sigma(I)$]	2466
Goodness-of-fit on F^2	1.032
Final R indexes [$I > 2\sigma(I)$]	$R_1 = 0.0372$, $wR_2 = 0999$
Final R indexes [all data]	$R_1 = 0.0529$, $wR_2 = 10.1118$

[6], *trans*-[Co(diamH$_2$-N$_4$)Cl$_2$][ZnCl$_4$]Cl · 0.5H$_2$O · 0.5(C$_2$H$_5$OH) [6] and several [Co(diam-N$_5$)X]$^{n+}$ compounds [6]. The Co–N and Co–C distances for the azamacrocycle cyano compounds (Table 3) do not differ significantly from those of the non-cyclic bis(ethane-1,2-diamine) compound [7]. The steric factors leading to the unusually short Co–N$_{secondary}$ bonds observed for hexa-coordinate [Co(diam-N$_6$)]Cl$_2$ · ClO$_4$ [5,8] do not affect the distances for the penta- or tetra-coordinated diam and diampro compounds.

The facile acyclation of diam while coordinated to cobalt(III) provides a mechanism for the incorporation of this azamacrocycle moitey into larger structures.

3. Experimental

3.1. Preparation of compounds

3.1.1. *trans*-Di(cyano-κ^1)-(trans-6,13-dimethyl-6,13-bis(propionylamido)-1,4,8,11-tetraazacyclotetradecane-κ^4)cobalt(III) perchlorate dihydrate, *trans*-[Co(diam-N$_4$)(CN)$_2$]ClO$_4$ · 2H$_2$O

This was prepared by heating [Co(diam-N$_6$)]Cl$_2$ · ClO$_4$ · H$_2$O [5,8] or [Co(diam-N$_6$)](ClO$_4$)$_3$ · ½H$_2$O [8] (1 g) in water (10 cm^3) at c. 80 °C with NaCN (0.5 g) and NaOH (0.2 g). The solution rapidly changed from yellow to orange as [Co(diam-N$_5$)(OH)]$^{2+}$ [8] formed and then more slowly to yellow as the product formed. This was filtered from the cold solution and recrystallized from hot water. The compound can by prepared from [Co(diam-N$_5$)(OH)](ClO$_4$)$_2$ · H$_2$O [8] by similarly heating in aqueous solution with NaCN. *Anal.* calc. for C$_{14}$H$_{34}$ClCoN$_8$O$_8$: C, 33.3; H, 6.8; N, 22.2. Found: C, 33.2; H, 6.7; N, 22.3%. IR spectrum: band maxima/cm^{-1}; *ν* (OH): 3580, 3500, 3431, 3366; ν (NH): 3231, 3173; ν (C≡N): 2132sp; *δ* (HNH, HOH): 1624br.

A preparation of the related compound *trans*-[Co(diam-N$_4$)(CN)$_2$] [Co(diamH$_2$-N$_4$)(CN)$_2$](ClO$_4$)$_4$ · 4(H$_2$O) has been reported [3].

3.1.2. *trans*-Di(cyano-κ^1)-(trans-6,13-dimethyl-6,13-bis(propionylamido)-1,4,8,11-tetraazacyclotetradecane-κ^4)cobalt(III) perchlorate dihydrate, *trans*-[Co(diampro-N$_4$)(CN)$_2$]ClO$_4$ · 2H$_2$O

A solution of *trans*-[Co(diam-N$_4$)(CN)$_2$]ClO$_4$ (1 g) and propionic anhydride (1 g) in DMF (5 cm^3) was heated at 80 °C for 1 h. Propan-2-ol (20 cm^3) was then added. The yellow crystalline product was filtered from the cold solution in near quantitative yield and recrystallized from hot water. The crystal for the structural study was grown by evaporation of an aqueous solution. IR spectrum: band maxima/cm^{-1}; *ν* (OH, NH): 3553, 3429, 3300br, 3259, 3139; *ν (C≡N): 2227w,sp, 2137w,sp; amide: 1653s, 1553.*

The acetylamido homologue can be similarly prepared by using acetic anhydride.

Caution: Although no problems were encountered in this work, perchlorate compounds are potentially explosive. They should be prepared in small amounts and handled with care.

3.2. Crystallography

Diffraction data was collected [Bruker SMART] by using a Bruker CCD diffractometer with Mo Kα radiation (fine focus sealed tube with graphite monochromator, $\lambda = 0.71073$ Å), using omega and epsilon scans [10]. Bruker SAINT was used for cell refinement and data reduction [10]. Absorption corrections were by multi-scan, using Bruker SADABS. See Table 4 for details [10].

The structure was solved by direct methods [SHELXS-97] and full-matrix refined [SHELXL-97] [11]. All H-atoms, other than for the water molecule, were positioned geometrically and refined using a riding model with C–H = 0.97 Å, $U_{iso} = 1.2U_{eq}$ (C) for CH$_2$, 0.96 Å, $U_{iso} = 1.5U_{eq}$ (C) for CH$_3$ atoms and 0.90 Å, $U_{iso} = 1.2U_{eq}$ (N) for the NH groups. The H-atoms of the water were located from difference syntheses and their positions refined, with O–H restrained (0.82 Å) and with $U_{iso} = 1.2U_{iso}$ (O) (see Table 4).

Appendix A. Supplementary data

CCDC 683156 contains the supplementary crystallographic data for this paper. These data can be obtained free of charge via http://www.ccdc.cam.ac.uk/conts/retrieving.html, or from the Cambridge Crystallographic Data Centre, 12 Union Road, Cambridge CB2 1EZ, UK; fax: (+44) 1223-336-033; or e-mail: deposit@ccdc.cam.ac.uk. Supplementary data associated with this article can be found, in the online version, at doi:10.1016/j.poly.2008.06.020.

References

[1] N.F. Curtis, H. Puschmann, Polyhedron 24 (2005) 281.
[2] N.F. Curtis, W.T. Robinson, Polyhedron 24 (2005) 976.
[3] P.V. Bernhardt, N.L. Kilah, Acta Crystallogr., Sect. C 61 (2005) m245.
[4] P.V. Bernhardt, B.P. Macpherson, Acta Crystallogr., Sect. C 59 (2003) m533.
[5] P.V. Bernhardt, G.A. Lawrance, T.W. Hambley, J. Chem. Soc., Dalton Trans. (1989) 1059.
[6] N.F. Curtis, W.T. Robinson, D.C. Weatherburn, Aust. J. Chem. 45 (1992) 1663.
[7] H. Wunderlich, Acta Crystallogr., Sect. C 43 (1987) 1209.
[8] N.F. Curtis, A. Siriwardena, Aust. J. Chem. 44 (1991) 1023.
[9] L.J. Farrugia, J. Appl. Crystallogr. 30 (1997) 565.
[10] Bruker SMART (Version 5.054), SADABS (Version 2.03), SAINT (Version 6.02A), Bruker AXS Inc., Madison, WI, USA, 1997.
[11] G.M. Sheldrick, SHELXS-97, SHELXL-97 and SHELXTL-5.10, Programs for the Solution and Refinement of Crystal Structures, University of Gottingen, Germany, 1997.

Mg, which yields 4 + 1 coordinated complex, and pyridine molecules are linked via O–H···N hydrogen bonds [15,16].

Most of M(II)Pc complexes in the water-free 4-picoline solution form biaxially ligated M(II)Pc(4-picoline)$_2$ complexes [17,18]. However, in the case of BePc and ZnPc in 4-picoline solution monoaxially ligated complexes are formed [18]. In this work, we investigate the products formed in the effect of hydration of M(II)Pc in the solution of 4-picoline/water. In addition, the novel aqua M(II)-phthalocyaninato complexes (M = Be or Mg) isolated in the crystalline form as 4-picoline solvate have been structurally characterised.

2. Experimental

2.1. Synthesis

The BePc and MgPc compounds were obtained as described elsewhere [12,13]. The ZnPc was obtained from Aldrich (purity 97%). Firstly the BePc, MgPc and ZnPc were transferred by the appropriate transformative recrystallisation procedure in dry 4-picoline (4-Mepy) into [BePc(4-Mepy)](4-Mepy) (**I**), MgPc(4-Mepy)$_2$ (**II**) and ZnPc(4-Mepy) (**III**) complexes as described elsewhere [18]. The (**I**), (**II**) and (**III**) complexes obtained in crystalline form were again recrystallised, however now from not dried (containing water) 4-picoline. The suspension consisting appropriately of the crystallites of **I**, **II** or **III** and wet 4-picoline (assigned now as (a), (b) and (c)) were similar thermally processed as in [18]. Elemental analysis of the products was performed on a dispersive energy spectrometer.

(a) In the case of the sample containing compound **I** in wet 4-picoline, which recrystallisation was performed at 80 °C during several hours, the BePcH$_2$O · (4-Mepy) – **Ia** crystals were formed. *Anal.* Calc. for $C_{38}H_{25}N_9OBe$: C, 72.14; Be, 1.42; N, 19.93; O, 2.53. Found: C, 72.25; Be, 1.44; N, 19.85; O, 2.49%.

(b) In the case of **II** in wet 4-picoline, the prolonged recrystallisation process at 140 °C yield to well-developed crystalline product. The analyses performed for the selected single crystal indicates on the presence of the compound with the composition of [MgPcH$_2$O] · (4-Mepy) – **IIa**. If the hot suspension containing **IIa** crystalline product was slowly cooled to room temperature (in days), the crystals **IIa** transform into another crystals containing more 4-picoline moieties – [MgPcH$_2$O-(4-Mepy)$_2$] · (4- Mepy) (**IIb**). The **IIa** crystals could be only separated from hot suspension of 4-picoline. *Anal.* Calc. for $C_{38}H_{25}N_9OMg$ (**IIa**): C, 70.43; Mg, 3.75; N, 19.46; O, 2.47. Found: C, 70.38; Mg, 3.80; N, 19.51; O, 2.44%. *Anal.* Calc. for $C_{50}H_{39}N_{11}OMg$ (**IIb**): C, 71.99; Mg, 2.91; N, 18.47; O, 1.92. Found: C, 72.05; Mg, 2.94; N, 18.42; O, 1.89%.

(c) Several samples containing ZnPc(4-Mepy) in wet 4-picoline were processed at various thermal conditions, however the recrystallisation effect was invariable and lead, as was identified by X-ray powder diffraction, to the ligand free micro crystalline β-ZnPc [19].

2.2. X-ray powder diffraction measurements

The rest of the samples left after thermogravimetric analyses were measured on a STOE powder diffractometer equipped with a linear position detector (PSD) [20] using Cu Kα_1 radiation (λ = 1.540562 Å) at room temperature.

2.3. X-ray crystallography

Suitable single crystals of **Ia**, IIa and **IIb** were used for data collection on a four-circle KUMA KM4 diffractometer equipped with two-dimensional CCD area detector [21]. The graphite monochromatised Mo Kα radiation (λ = 0.71073 Å) and the ω-scan technique ($\Delta\omega$ = 1°) were used for data collection. Data collection and reduction along with absorption correction were performed using CRYSALIS software package [21].

The structures were solved by direct methods using SHELXS-97 giving positions of almost all non-hydrogen atoms. The remaining atoms were located from subsequent difference Fourier syntheses. The structures were refined using SHELXL-97 [22] with the anisotropic thermal displacement parameters. Hydrogen atoms of the phthalocyanine moieties, water and 4-Mepy molecules were located from the difference Fourier maps, but in the final refinement the positions of all hydrogen atoms were constrained: thermal parameters and distances. Details of the data collection parameters, crystallographic data and final agreement parameters are collected in Table 1. Selected geometrical parameters are listed in Table 2.

2.4. Thermal measurements

Thermal analysis was carried out on a Lines L81 thermobalance apparatus with Pt crucibles. Powdered Al_2O_3 has been used as a reference. The measurements have been performed under static air atmosphere on heating from room temperature to 300 °C at the heating rate of 5 °C min^{-1}.

2.5. UV–Vis measurements

The electronic absorption spectra measurements were carried out at room temperature using a CARRY-VARIAN SE UV–Vis–NIR spectrometer. The solid-state spectra of the samples were recorded for thin film nujol mulls as well as in 4-picoline as N-donor solvent and in 2-ethoxyethanol as O-donor solvent.

Table 1
Crystallographic data for **Ia**, **IIa** and **IIb**

	Ia	**IIa**	**IIb**
	(BePc(H$_2$O) · (4-Mepy)	MgPc(H$_2$O) · (4-Mepy)	MgPc(H$_2$O)(4-Mepy)$_2$ · (4-Mepy)
Formula	$C_{38}H_{25}N_9OBe$	$C_{38}H_{25}N_9OMg$	$C_{50}H_{39}N_{11}OMg$
Molecular weight	632.68	647.98	834.23
T (K)	295(2)	295(2)	295(2)
Crystal system	triclinic	monoclinic	monoclinic
Space group	$P\bar{1}$ (no. 2)	$P2_1/n$ (no. 14)	$P2_1/n$ (no. 14)
a (Å)	8.463(2)	12.648(2)	14.228(3)
b (Å)	13.081(2)	28.201(3)	15.267(3)
c (Å)	15.317(3)	17.925(2)	20.875(4)
α (°)	103.99(1)		
β (°)	100.27(1)	107.68(1)	109.09(2)
γ (°)	105.95(1)		
V (Å^3)	1526.6(5)	6091.6(14)	4285.1(15)
Z	2	8	4
D_{Calc}	1.376	1.413	1.293
μ (mm^{-1})	0.090	0.109	0.101
Crystal size (mm^3)	0.38 × 0.27 × 0.21	0.28 × 0.18 × 0.10	0.36 × 0.28 × 0.23
Total/unique reflections [R_{int}]	16972/7693 [0.0510]	56101/13074 [0.0649]	45687/10201 [0.0291]
R [$F^2 > 2\sigma(F^2)$][a]	0.0790	0.0460	0.0590
wR [F^2 all reflections][b]	0.0870	0.0650	0.1590
S	0.990	1.001	1.020
Residual electron density, $\Delta\rho_{max}$, $\Delta\rho_{min}$ (e Å^{-3})	0.24, −0.20	0.33, −0.24	0.22, −0.28

[a] $R = \Sigma||F_o| - |F_c||/\Sigma F_o$.

[b] $wR=\{\Sigma\ [w(F_o^2 - F_c^2)^2]/\Sigma wF_o^4\}^{1/2}$; $w^{-1} = \sigma^2(F_o^2) + (aP)^2 + bP$ where $P = (F_o^2 + 2F_c^2)/3$. The a and b parameters are 0.06 and 0 for compound **Ia**, 0.077 and 0 for **IIa**, 0.0667 and 0.845 for **IIb**.

Table 2
Selected geometrical parameters (Å, °)

$BePcH_2O$(4-Mepy) – ***Ia***			
Be–O	1.683(5)	Be–N1	1.917(6)
Be–N3	1.903(5)	Be–N5	1.908(5)
Be–N7	1.908(5)		
O–Be–N1	100.0(3)	O–Be–N3	99.3(3)
O–Be–N5	98.6(3)	O–Be–N7	89.2(2)
N1–Be–N3	89.3(2)	N1–Be–N7	98.4(2)
N3–Be–N5	87.9(3)	N5–Be–N7	89.2(2)
	Molecule A		Molecule B
$MgPcH_2O \cdot (4\text{-Mepy})$ – ***IIa***			
Mg–O1	2.015(2)		2.009(2)
Mg–N1	2.039(2)		2.037(2)
Mg–N3	2.039(2)		2.039(2)
Mg–N5	2.031(2)		2.040(2)
Mg–N7	2.041(2)		2.035(2)
O1–Mg–N1	102.47(7)		87.47(7)
O1–Mg–N3	104.71(7)		102.76(7)
O1–Mg–N5	104.83(7)		102.61(7)
O1–Mg–N7	102.68(7)		105.19(7)
N1–Mg–N3	89.95(7)		85.62(7)
N3–Mg–N5	87.44(7)		87.56(7)
N5–Mg–N7	86.07(7)		86.12(7)
N1–Mg–N1	87.74(7)		87.47(7)
$[MgPcH_2O \cdot (4\text{-Mepy})_2] \cdot (4\text{-Mepy})$ – ***IIb***			
Mg–O1	1.971(2)	Mg–N1	2.051(2)
Mg–N3	2.052(2)	Mg–N5	2.042(2)
Mg–N7	2.058(2)		
O1–Mg–N1	107.12(7)	O1–Mg–N3	103.99(8)
O1–Mg–N5	102.90(7)	O1–Mg–N7	106.69(8)
N1–Mg–N3	85.80(7)	N1–Mg–N7	86.03(7)
N3–Mg–N5	86.11(7)	N5–Mg–N7	86.33(7)

3. Results and discussion

3.1. Synthesis and equilibrium in solution

The BePc(4-Mepy) (**I**), $MgPc(4\text{-Mepy})_2$ (**II**) and ZnPc(4-Mepy) (**III**) complexes were obtained by recrystallisation of MPc's (M = Be, Mg and Zn) in purified water-free 4-picoline and were characterised by us [18]. Now we used these complexes for recrystallisation procedure in not dried (containing water) 4-picoline as described in Section 2. This procedure gave for each complex **Ia**, **IIa** and **IIb** well-developed crystals suitable for X-ray analysis, showing a typical blue–violet colour for phthalocyanine. As was shown previously [18] the recrystallisation of BePc and ZnPc in water-free 4-picoline yield monoaxially coordinated (4 + 1) complexes, while for MgPc yields biaxially ligated (4 + 2) complex. These complexes when recrystallised from moist 4-picoline (containing water) yield aqua M(II) phthalocyaninato complexes. During recrystallisation process the crystals of BePc(4-Mepy) · 4-Mepy (**I**), as well as the crystals of $MgPc(4\text{-Mepy})_2$ (**II**) interact with water molecules and convert depending on the temperature, into aqua(phthalocyaninato(2-)) complexes **Ia**, **IIa** and **IIb** according to the equation illustrated in Scheme 1.

Recrystallisation of ZnPc(4-Mepy) in wet 4-picoline yields, as was identified by the X-ray powder diffraction experiment, ligand-free microcrystalline β-ZnPc [19]. The crystals of **Ia**, **IIa** and **IIb** are well soluble in 4-picoline, pyridine and other N-donor solvents yield a very intensive green–blue colour, depending on the concentration of the complex. These complexes are also soluble in O-donor solvents like 2-methoxyethanol, 2-ethoxyethanol, ethanol, acetone, etc., yielding blue colour of the solution. However, the solubility of the crystals in O-donor solvents is smaller in comparison to the N-donor solvents. These crystals are insoluble in water.

3.2. Thermal stability

In order to determine the thermal stability of the complexes investigated here, the thermal analyses of **Ia**, **IIa** and **IIb** complexes were carried out on the samples of 40 mg and with the same heating rate of 5 °C/min. The thermogravimetric analyses of the solid-state samples are shown in Fig. 1. Compound **Ia** is stable up to about 150 °C, and at higher temperature loses the 4-Mepy and water molecules in one step (Fig. 1a). The observed weight loss of ~18.5% is equal to the calculated sum of the weight loss of 4-picoline (14.7%) and water (3.83%), (Σ = 18.53%). This value indicates

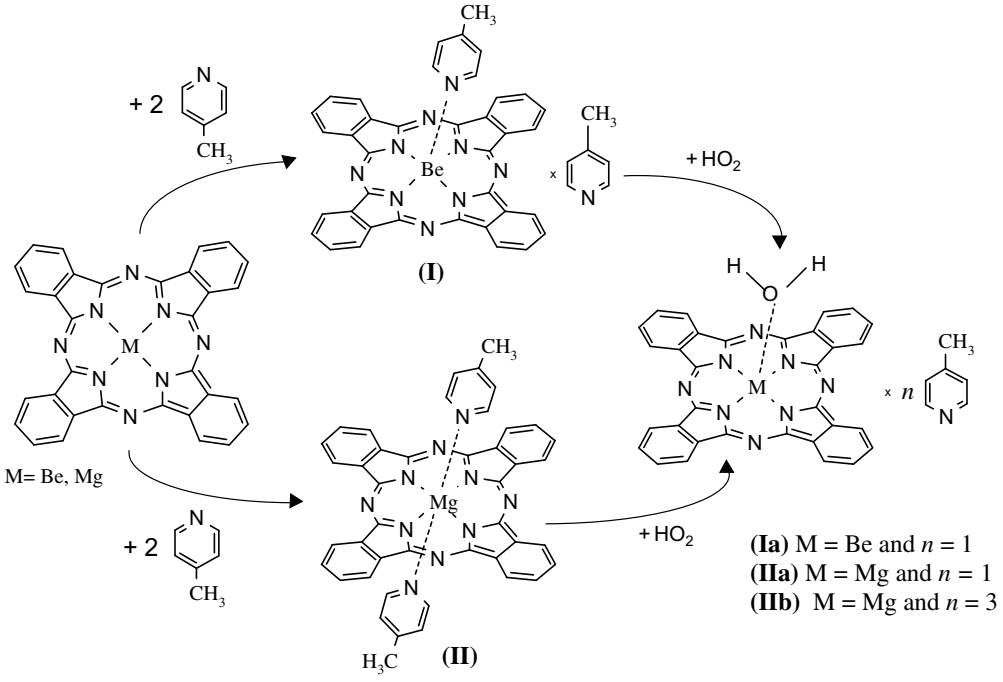

Scheme 1.

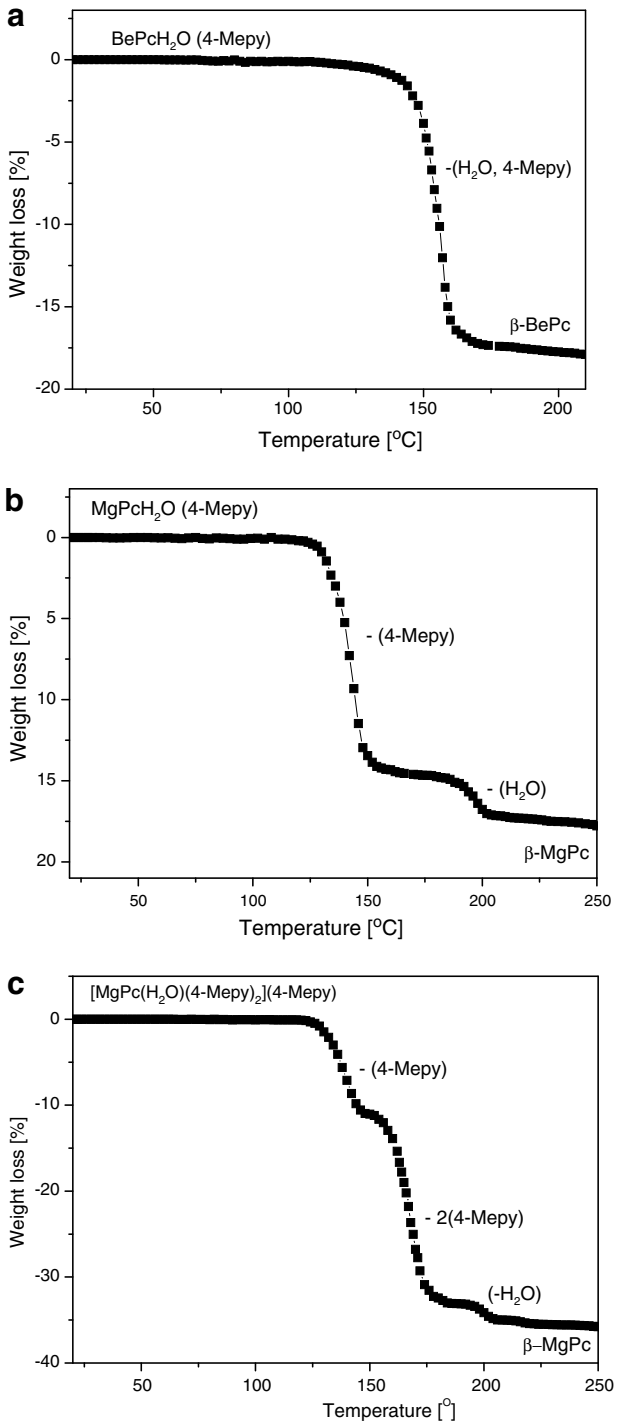

Fig. 1. Thermograms for the solid-state samples of **Ia** (a), **IIa** (b) and **IIb** (c).

that both molecules, 4-Mepy and water, release simultaneously. This result of the thermal analysis is in agreement with the X-ray crystal structure analysis, which shown that 4-picoline and water molecules are joined together by a relatively strong O–H···N hydrogen bond and the Be–O(water) bond of 1.683(5) Å is relatively weak. Quite similar observation was registered in the $(BePcH_2O)\cdot(2\text{-EE})$, where 2-EE = 2-ethoxyethanol, in which the 2-EE and water molecules are released at the same temperature [13].

The complex **IIa** is stable up to ~145 °C (Fig. 1b) at which it loses the 4-picoline molecule and transforms into $MgPcH_2O$ complex. On further heating it loses water molecule (at ~195 °C) and transforms into β-MgPc. This observation is in agreement with the arrangement of molecules in the **IIa** crystal as shown the X-ray structure analysis. In the **IIa** crystal the molecules are arranged in the face-to-face fashion in dimers with the O–H···N interactions between the antiparallel oriented dipole $MgPcH_2O$ molecules with a strong overlap of the π-clouds of the Pc rings. This interactions stabilise the $(MgPcH_2O)_2$ dimeric structure. The 4-picoline molecules are joined to these dimers via O–H···N(4-Mepy) hydrogen bonds, that breaks and the 4-picoline molecules released at ~145 °C (Fig. 1b). The observed weight loss on the heating are ~14.5% (4-Mepy) and 3.2% (water), and are in agreement with the calculated value of 14.35% and 3.24%, respectively.

Compound **IIb** loses it solvent 4-picoline molecules in two steps (Fig. 1c). One of three 4-Mepy molecules is released at ~140 °C, while the other two at ~160 °C. After loss of solvent 4-Mepy molecules the starting compound transforms into $MgPcH_2O$, which during further heating loses water molecule at about 195 °C and finally converts into β-MgPc (which was identified by X-ray powder diffraction technique). The thermogravimetric analysis of the solid-state sample of **IIb** indicates that one 4-Mepy molecule is joined differently than other two 4-Mepy molecules. This observation is in agreement with the X-ray crystal structure analysis, which shown that two 4-Mepy molecules are joined stronger by the O–H···N hydrogen bond than the other one that in the crystal interacts only by van der Waals forces.

Although, in the molecular arrangement in the **Ia** and **IIa** crystals similar $[(M(II)PcH_2O)_2(4\text{-Mepy})_2]$ dimeric aggregates can be found, the thermal stability and decomposition of these solid-state compounds is different. In the Be compound (**Ia**), due to the relatively small radius of Be, the water molecule is weaker joined to the BePc than in Mg complex (**IIa**) and therefore it is released simultaneously together with the 4-Mepy molecule that is joined via O–H···N hydrogen bond with the water. Looking at the molecular arrangement of the Mg complexes (**IIa** and **IIb**), the releasing of 4-Mepy molecules in the two steps in the **IIb** could be understood. The temperature loss of water molecules in both Mg compounds is very similar and comparable with that found in the solid-state sample of aqua magnesium phthalocyanine [23].

All crystals are stable at ambient atmosphere at room temperature. This is in contrast to the pure BePc and MgPc crystals, which especially for MgPc rapidly polycrystallise, because the MgPc molecules interact with the air molecules, O_2 and N_2. The process was confirmed by two separate experiments in pure O_2 and in pure N_2, where MgPc became transformed into complexes with the composition of $(MgPc)_2O_2$ and $(MgPc)_2N_2$, respectively [24]. In the moist atmosphere the MgPc crystals transform rapidly into $MgPc(H_2O)$ complex [25]. This behaviour of MgPc crystals is quite different in relation to the both Mg complexes (**IIa** and **IIb**) investigated here, which are stable under ambient atmosphere and room temperature.

3.3. Stereochemistry and molecular packing

All three crystal structures are built up from $M(II)PcH_2O$ and 4-picoline moieties arranged in different fashions. The independent part of the **Ia** crystal structure consists of $BePcH_2O$ and 4-picoline molecules joined together via almost linear O–H···N hydrogen bond (Fig. 2). The central Be atom of $BePcH_2O$ unit exhibits (4 + 1)-coordination by four equatorial isoindole N atoms of the Pc(2-) macrocyle and by an axial oxygen of water molecule. Owing to the interaction with the axially coordinated oxygen atom, the central Be atom is significantly displaced [0.308(2) Å] from the weighted least-squares plane defined by the four isoindole N atoms. In this complex the shift of Be atom from the N_4-isoindole plane is slightly longer than that found in the crystal of

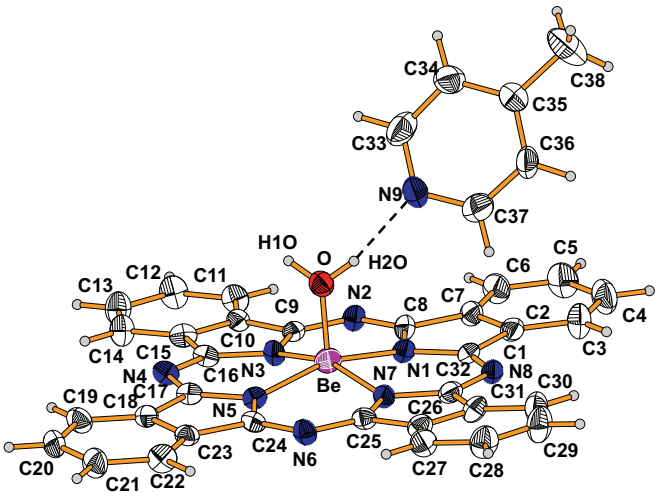

Fig. 2. View of the molecular structure of $BePcH_2O \cdot (4\text{-Mepy})$ with the atom-labelling scheme.

Table 3
Hydrogen-bonding geometry (Å, °)

D–*H*···*A*	*D*–*H*	*H*···*A*	*D*···*A*	*D*–*H*···*A*
Ia				
O–H1O···N4^{i}	0.82	1.99	2.801(4)	167
O–H2O···N9	0.82	1.91	2.713(4)	167
IIa				
O1A–H1OA···N9A	0.82	1.97	2.772(3)	165
O1A–H2OA···N2B	0.82	2.11	2.917(2)	168
O1B–H1OB···N9B	0.82	1.97	2.778(2)	168
O1B–H2OB···N2A	0.82	2.01	2.823(2)	170
IIb				
O1–H1O...N9	0.82	1.93	2.749(3)	177
O1–H2O...N10	0.82	1.88	2.698(3)	175

Symmetry code: (i) $-x, -y, -z$.

$BePcH_2O \cdot 2EE$ (2EE = 2-ethoxyethanol), 0.264(4) Å [13]. The four equatorial Be–N bonds with average distance of 1.905 Å are longer than the axial almost perpendicular to the ring plane Be–O bond [1.683(5) Å]. This correlation between the equatorial and axial bonds is quite similar to that observed in the crystal of $BePcH_2O \cdot 2EE$ [13]. However, according to Bock and Glusker [26], the typical Be–O distance in hydrate lies between 1.60–1.63 Å. Thus, it may be concluded that the cavity formed by $(N_{iso})_4$ is too spacious for the Be(II) ion and despite of its shift from the Pc center, it is submersed between the N_4 isoindole atoms as in square well. The phthalocyaninato(2-) macroring due to the interaction with the oxygen atom of water molecule adopts a saucer-shape form. The most deviated atoms from the N_4-plane are C26–C31 [0.102–0.386 Å], since the C atoms the C26–C31 ring interact with the 4-picoline molecule that is hydrogen bonded to water molecule of $BePcH_2O$. Two $BePcH_2O \cdot 4\text{-Mepy}$ units related by the inversion interact via two additional almost linear O–H···N hydrogen bonds (Table 3) forming a dimeric structure (Fig. 3). In the dimer of $(BePcH_2O)_2$ the phthalocyaninato macrocycles are separated by ~3.46 Å (the distance between the N_4–N_4 planes). In the dimer, one H atom of water molecule acts as a bridge with the N-azamethine atom of the other Pc(2-) macroring, and the second H is an acceptor of a lone-electron pair of the ring N atom of 4-picoline molecule (Fig. 3, Table 3). The coordinated water molecule plays essential role in the formation of a dimeric structure, and additionally links the 4-picoline molecule, that is oriented by its H atom in orto position to the N-ring atom in the direction to the N-azamethine atom (N8) of the Pc-ring. This interaction together with the O–H···N hydrogen bonds in the dimer of $(BePcH_2O)_2$ and with the π–π interactions between the back-to-back oriented dimers (~3.38 Å, Fig. 4) are responsible for the stabilisation and the molecular arrangement in the crystal.

The independent part of the **IIa** crystal structure consists of two $MgPcH_2O \cdot 4\text{-Mepy}$ moieties linked together in non-centrosymmetric dimeric unit (Fig. 5). This unit is built up from two aqua magnesium phthalocyanine molecules (marked as A and B) and two 4-picoline molecules. The geometries of both, A and B, $MgPcH_2O$ molecules are similar. The Pc(2-) macrorings are not planar. The central Mg cations have five-fold (4 + 1) coordination, they coordinate equatorial four N-isoindole atoms of Pc(2-) macrocycles and axially the O atoms of water molecules. The axial Mg–O bond lengths of 2.015(2) and 2.009(2) Å in molecule A and B, respectively, are shorter than four equatorial Mg–N_{iso} bonds with the average distance of 2.039 Å. Owing to the interaction with the axially coordinated O atom of water molecules, the central Mg atom in both $MgPcH_2O$ molecules is significantly displaced [0.482(2) Å in molecule A and 0.490(2) Å in molecule B] from the weighted least-squares planes defined by the four isoindole N atoms of Pc. The geometry of the $(MgPcH_2O)_2$ dimer in **IIa** is similar to that found in the triclinic modification of $MgPcH_2O$ [23]. The face-to-face oriented $MgPcH_2O$ molecules are interconnected by two almost linear O–H···N hydrogen bonds (Table 3). The Pc(2-) rings in the dimer are apart by a distance of 3.231(3) Å, indicating π–π clouds interaction, since the distance between the N_4-planes is shorter than 3.4 Å, the sum of the C-atom van der Waals radii of the π-ring system [27]. The 4-picoline molecules that are located away from the dimer interact only via O–H···N hydrogen bonds,

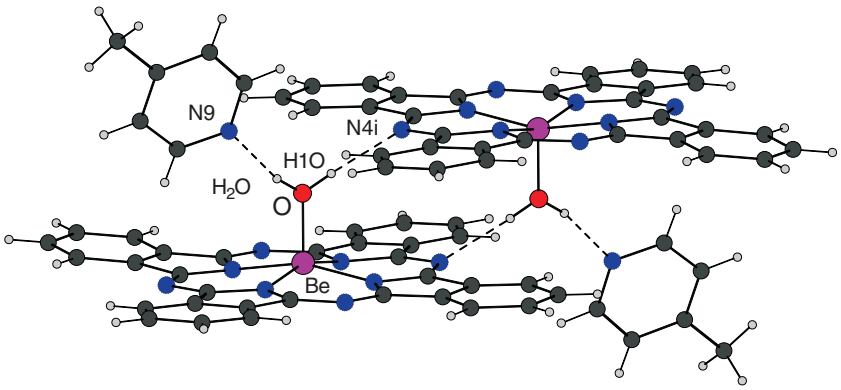

Fig. 3. View of the dimeric structure of **Ia**.

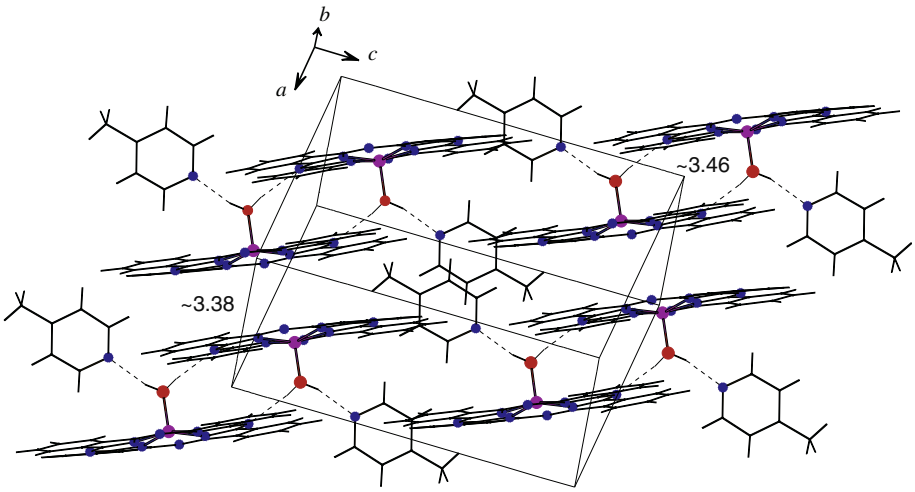

Fig. 4. Arrangement of the $BePcH_2O \cdot (4\text{-Mepy})$ molecules in the unit cell showing π–π interacting back-to-back oriented $(BePcH_2O \cdot (4\text{-Mepy}))_2$ dimeric molecules.

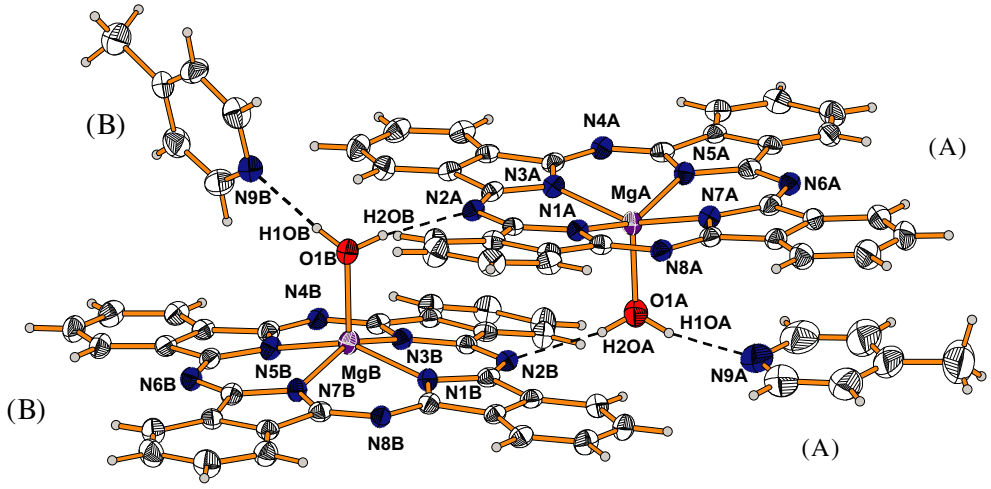

Fig. 5. View of the molecular structure of $(MgPcH_2O \cdot (4\text{-Mepy}))_2$.

in which the 4-picoline molecules act as acceptors by the N-ring atom. This interaction does not disturb the geometry of $(MgPcH_2O)_2$ dimer in relation to the triclinic form of $MgPcH_2O$ that plays an important role in the near-IR spectroscopic properties. The interesting feature of **IIa** crystal structure is the orientation of the 4-picoline molecules in relation to the $(MgPcH_2O)_2$ dimer. The 4-picoline molecule A is almost parallel to the N_4-plane of the $MgPcH_2O$ molecule to which it is linked [4.2(1)°], whereas the molecule B is roughly perpendicular to N_4-plane of $MgPcH_2O$ that join the 4-picoline molecule B [79.2(2)°]. Both O–H···N_{aza} hydrogen bonds linking the $MgPcH_2O$ molecules into a dimer have similar strength and they are weaker than the O–H···N hydrogen bonds joined the 4-picoline molecules into the dimer (Table 3). The difference in the hydrogen bond distances results from the steric interaction between the Pc macrorings in the dimer. The hydrogen bonded $(MgPcH_2O)_2 \cdot 2(4\text{-Mepy})$ aggregates are arranged in a herringbone fashion forming back-to-back stacks along the *c*-axis (Fig. 6). In the stacks the dimers are related by the inversion center. Within the stack the back-to-back distance between the N_4-isoindole planes is equal to ~3.39 Å indicating the π–π interactions between the Pc macrorings.

The asymmetric unit of the **IIb** crystal structure consists of $MgPcH_2O$ unit and three 4-picoline molecules (Fig. 7) The water molecule is directly coordinated to the central Mg cation, which owing to this interaction is shifted out of the N_4-isoindole plane by 0.537(2) Å toward the oxygen atom. Two of three 4-picoline molecules are joined via almost linear O–H···N hydrogen bonds to $MgPcH_2O$ molecule (Table 3), while the third 4-picoline not forms the hydrogen bond. The hydrogen bonded 4-picoline molecules (N9 and N10) to $MgPcH_2O$ are inclined by 63.7(3)° and 61.8(3)° for the 4-picoline molecule containing N9 and N10 atom, respectively. The third 4-picoline molecule is inclined by 73.2(3)° to the N_4-isoindole plane and is roughly parallel to the 4-picoline molecule containing N10 atom, from which it is apart by ~3.51 Å (the dihedral angle between the 4-picoline rings containing N10 and N11 atom is equal to 11.7(3)°). In the crystal the $[MgPcH_2O\text{-}(4\text{-Mepy})_2] \cdot (4\text{-Mepy})$ units related by the inversion center are arranged in the back-to-back fashion with a distance of ~3.613(3) Å between theN_4-isoindole planes of the Pc(2-) ligands. The back-to-back arranged aggregates forming stacks along the *b*-axis (Fig. 8). The face-to-face distance is about twice greater than the back-to-back distance, due to the coordinated water molecules and 4-picoline molecules that are joined via O–H···N hydrogen bonds.

The $MgPcH_2O$ molecule in both crystals (**IIa** and **IIb**) is not planar. The Mg atom is displaced from the N_4-isoindole plane by ~0.5 Å toward the oxygen atom of coordinated water molecule. The displacements observed here are comparable to those

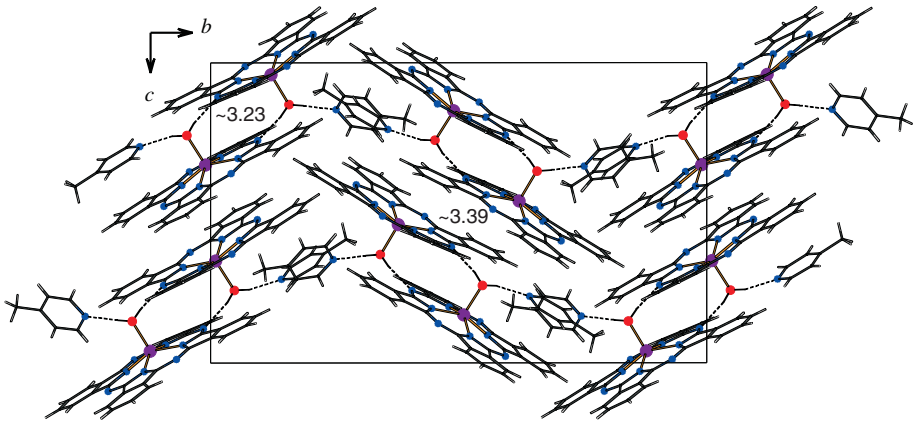

Fig. 6. Arrangement of molecules in the **IIa** crystal showing the π–π interactions in dimers and between the dimers.

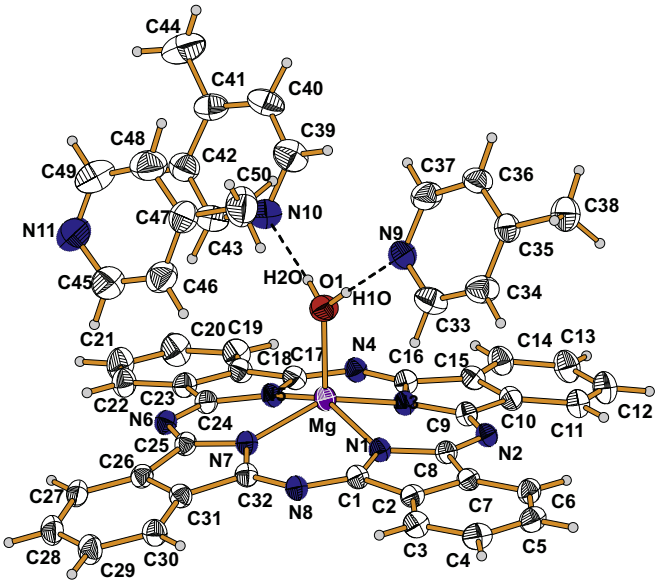

Fig. 7. View of the molecular structure of $(MgPcH_2O \cdot (4\text{-Mepy})_2) \cdot (4\text{-Mepy})$ with the labelling scheme.

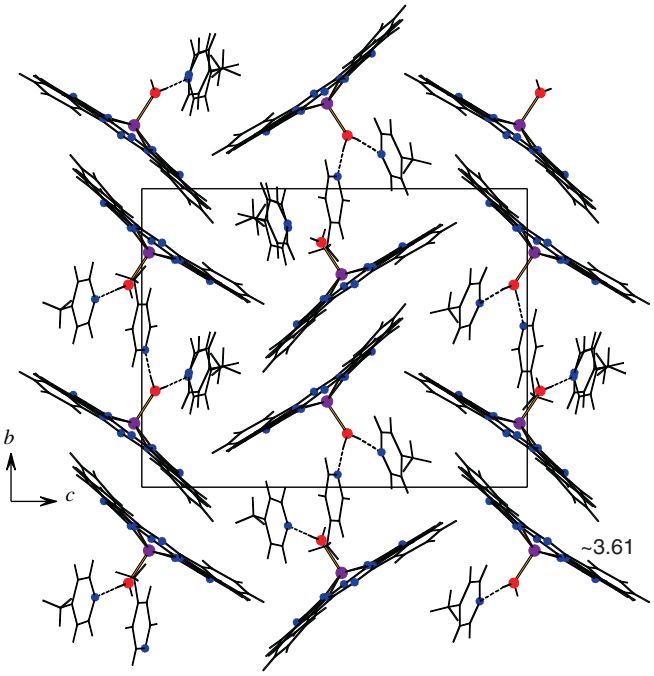

Fig. 8. Arrangement of molecules in the unit cell of **IIb**.

observed in other aqua magnesium phthalocyanine derivatives [28–33]. As can be seen from Table 4 the deviations of the central Mg atom from the N_4-plane in aqua magnesium phthalocyaninato complexes are greater than in aqua magnesium porphyrinato derivatives [34–39] and in chlorophyll derivatives [40–42]. The smaller deviation of Mg from the N_4-plane well correlates with the greater flexibility of the porphyrinato ring and with the larger central hole in relation to the phthalocyaninato macroring. The central Mg atom in both crystals studied here is 4 + 1 coordinated, equatorial by four N-isoindole atoms of Pc(2-) macocycle and axial (almost perpendicular) by oxygen atom of water molecule. The saucer-shape geometry of the Pc(2-) ligand results from the interaction of the positively charged central Mg atom of about +0.5 [43] with the negatively charged oxygen atom of water molecule and is compared to that in the gas-phase structure obtained by molecular orbital calculations [23]. However, the *ab initio* MO calculated axial Mg–O bond [2.142 Å] is significantly longer than that found in both crystals described here (Table 2). Generally the 4 + 1 coordination of Mg is preferred in MgPcL complexes in the case of O-donor ligands (L = O-donor ligands). The axial Mg–O bond length is shorter than the equatorial Mg–N bonds (Table 4). This is quite different in the 4 + 2 coordinated $MgPcL_2$ derivatives in which the axial Mg-N bonds are longer than the equatorial Mg–N bonds [15,18]. Additionally, it can be said, that trans biaxially ligated magnesium phthalocyanine derivatives are known mainly for the N-donor ligands [15,18]. Comparing the molecular arrangement in both Mg complexes studied here can be said, that in **IIa** the molecules are much closely located to each other than in **IIb** (density of the crystals of **IIa** and **IIb** are 1.413 and 1.293 g/cm^3, respectively). The overlap of the Pc ligands and the π–π interactions in **IIa** are greater than in **IIb** (see Figs. 5 and 8). In **IIa** besides the back-to-back interaction the face-to-face overlap in dimer exists. Scheidt and Lee [44] examined the overlap in neutral (structurally characterised) sterically unhindered metal–porphyrinate complexes and discovered trimodal overlapping. According to this rule the π–π interactions in **IIa** are strong, since the interplanar spacing between the Pc-rings is shorter than the sum of the C-atom van der Waals radii of the π-ring system (~3.4 Å) and longer as the distance at which the steric interactions between the π aromatic ring system becomes predominantly repulsive (~3.08 Å). Thus the degree of the π–π stabilisation of the **IIa** structure is greater than in **IIb**.

Table 4
Comparison of the coordination of the central Mg atom in 4 + 1 coordinated magnesium phthalocyaninato and porphyrinato complexes and in chlorophyll derivatives

Complex	Displacement of the Mg atom from the N_4-isoindole plane (Å)	Average Mg–N bond length (Å)	Mg–O bond length (Å)	Ref.
Ia	0.308(2)	1.905	1.683(5)	
IIa (molecula A)	0.482(2)	2.038	2.015(2)	This work
(molecula B)	0.490(2)	2.038	2.009(2)	
IIb	0.537(2)	2.051	1.972(2)	
$MgPc(H_2O)$ (triclinic form)	0.442(3)	2.044	2.008(2)	[16]
$MgPc(H_2O) \times$ (3-Clpy)	0.496(2)	2.031	2.029(2)	[28]
$[MgPc(H_2O)]_2 \times$ MEA	0.498(2)	2.042	2.038(2)	[29]
$[MgPc(H_2O)]_2 \times$ 2MEA	0.491(2)	2.042	2.016(2)	[29]
$[MgPc(H_2O)]_2 \times$ 3MEA	0.493(1)	2.045	2.003(2)	[29]
$MgPc(H_2O) \times$ 2(*n*-propylamine)	0.509(1)	2.038	1.971(2)	[30]
$MgPc(H_2O)$ (monoclinic form)	~0.47	2.045	2.056(3)	[32]
$MgPc(H_2O) \times$ 2py	0.496(4)	2.040	2.022	[16]
$(MgPcH_2O)_2 \times$ 3py	~0.45	2.037	2.013	[31]
$MgPc(H_2O) \cdot 2Et_2NH$	0.492(2)	2.039	1.993(2)	[33]
$MgTPP(H_2O) \times 2(CH_3)_2CO$	0.45	2.083	2.054	[35]
$MgT(OMe)PP(H_2O)$	0.39	2.084	2.078	[36]
$MgTPP(H_2O)$	0.273	2.072	2.099	[37]
Methyl chlorophyllide	0.34	2.078	2.030	[40]
Ethyl chlorophyllide	0.39	2.086	2.035	[41]

3.4. UV–Vis

Since the studied here complexes are moderately temperature stable as shown by the thermogravimetric analyses, the preparation of the solid-state thin films using a standard technique, i.e. thermal evaporation, were impossible due to the loss of 4-picoline as well as the water molecules. Therefore, the solid-state thin films were prepared from nujol mulls. Only compound **IIa** ($MgPcH_2O \cdot$ 4-Mepy) exhibits a broad-band solid-state near-IR absorption (Fig. 9). The solid-state spectrum of **IIa** is very similar to the solid-state spectrum of triclinic modification of $MgPcH_2O$ [23] and to the UV–Vis spectrum of the literature "X-phase" of magnesium phthalocyanine that has been reported many times (for example see Fig. 1 in Ref. [45]). Thus the intense broad-band near-IR absorption is characteristic only for the solid-state of the **IIa**. The other **IIb** complex is not near-IR active. In 4-picoline solution, the spectra of **IIa** and **IIb** are identical and, as expected, show only in this spectral region the characteristic Q band (Fig. 9). This band arises from the exciton between the HOMO ground state (a_2, π, in C_{4v} symmetry in solution) to the LUMO (e, π^*), the first doubly degenerate excited state. This band is typical and characteristic for the phthalocyaninato(2-) macroring. The Q band exhibits characteristic splitting due to the vibronic coupling in the excited state, which is well known in the literature [46,47]. Comparing the molecular architectures of the Mg-complexes (**IIa** and **IIb**) with the architecture of the active near-IR triclinic modification of $MgPcH_2O$ [23], a similar motif can be found in the crystal structure of **IIa**. This motif adopts the face-to-face oriented $(MgPcH_2O)_2$ dimers that in the crystal structure of **IIa** are running in the direction parallel to [001] (see Fig. 6). The geometry of face-to-face oriented $MgPcH_2O$ molecules in $(MgPcH_2O)_2$ dimer (Table 5) in **IIa** crystal is similar to that found in the active triclinic modification of $MgPcH_2O$ [23]. Thus the approximately C_{4v} symmetry in solution and the double degenerate state yields an expected strong Q band as observed in solution. Upon crystallisation the degeneracy of the excited state is lifted due to the molecular distortion and induces a band splitting. However, theoretical calculations shown that the splitting value arises from the molecular distortion is relatively small in relation to the observed broad-band [45,48]. Thus the molecular distortion (reduces the molecular symmetry from C_{4v} to C_1) that lifts the degeneracy of the excited state is necessary, but not sufficient to explain the observed broad-band. For this reason, as has been suggested in [23] the broadening of the band originates, besides the above-mentioned distortion, also from the molecular arrangement and π–π interactions. The $MgPcH_2O$ molecules in **IIa** form dimers via O–H···N hydrogen bonds between the antiparallel oriented dipole $MgPcH_2O$ molecules with the strong overlap of the π-clouds of the Pc rings, quite similar as found in the active form of $MgPcH_2O$ [23], as well as in the triclinic modification of titanyl and vanadyl phthalocyanines (TiOPc and VOPc), both near-IR active [49–53]. Additionally, it should be added that TiOPc and VOPc similar to the $MgPc(H_2O)$, crystallise in two crystallographic modifications, triclinic and monoclinic forms. Only the face-to-face dimeric structure with the strong and π–π interactions between the π-clouds of Pc rings similar as in crystal **IIa** is found in the triclinic (near-IR active) modification of TiOPc and VOPc. The monoclinic modification of TiOPc and VOPc similar to monoclinic modification of $MgPcH_2O$ [32] is not active in the near-IR.

The spectra of **IIa** and **IIb** in N-donor solvents like 4-picoline or pyridine and in O-donor solvents like 2-ethoxyethanol or 2-methoxyethanol are very similar (Fig. 10), however the Q band is blue shifted in the O-donor solvents. The solutions of the complexes IIa or IIb in pyridine or 4-picoline depend on the concentration of the complex are green–blue, while in the O-donor solvent (like 2-ethoxyetanol, 2-methoxyethanol, etc.) are blue. The **IIa** and **IIb** complexes can be used as dyes for colouring cloths or as a pigments.

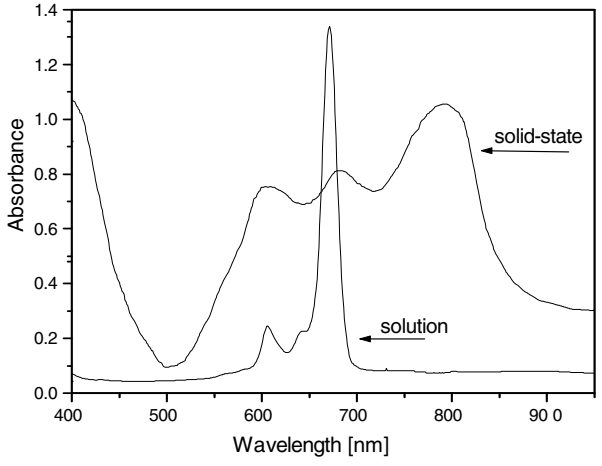

Fig. 9. UV–Vis spectra of IIa in 4-picoline solution and in solid-state.

Table 5
Geometry of the face-to-face oriented $MgPcH_2O$ molecules in the dimer in **IIa** and in triclinic modification of $MgPcH_2O$

	IIa	$(MgPcH_2O)_2$ triclinic form
Deviation of Mg from the N_4-plane (Å)	0.482(2), 0.490(2)	~0.47
Distance between the N_4-planes in the dimer	3.231(3)	3.255(3)
Distance between N_4-plane in back-to-back oriented dimers (Å)	3.391(3)	3.583(3)
Mg···Mg distance in dimer (Å)	6.512(2)	6.588(3)
Mg–O (Å)	2.012(2)	2.022(2)
Donor···Acceptor distance (O···N) in dimer (Å)	2.870	2.850(2)
Ref	This work	[23]

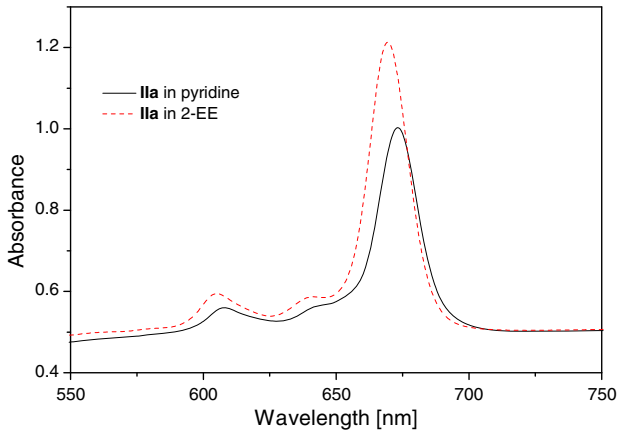

Fig. 10. UV–Vis spectra of **IIa** and **IIb** in pyridine and in 2-ethoxyethanol solutions.

4. Conclusions

Recrystallisation of M(II)Pc (M = Be, Mg and Zn) in water-free 4-picoline solution yields to formation of monoaxially coordinated complexes for Be and Zn (BePc(4-Mepy) – I and ZnPc(4-Mepy) – **III**) and biaxially ligated one for Mg ($MgPc(4\text{-}Mepy)_2$ – **II**), while recrystallisation in not dried 4-picoline (containing water) yields to aqua(phthalocyaninato) complexes for Be and Mg ($BePc(H_2O)\cdot(4\text{-}Mepy)$ – **Ia** and $MgPc(H_2O)\cdot(4\text{-}Mepy)$ – **IIa** or $MgPc(H_2O)\cdot 3(4\text{-}Mepy)$ – **IIb**). In the case of ZnPc(4-Mepy), the recrystallisation in wet 4-picoline yields to the β-ZnPc in the microcrystalline form. The ligated by 4-picoline BePc and MgPc complexes (I and **II**) containing relatively hard Be^{2+} and Mg^{2+} cations in water/4-picoline solution prefer O-donor ligands and replace the 4-picoline molecule by water (hard O-ligand) in the coordination sphere of M forming the aqua(phthalocyaninato) complexes. The 4-picoline molecules can interact by lone-pair of electron at the N atom with coordinated water molecules, and could co-crystallise with the aqua(phthalocyaninato) complexes. The quantity of the solvent 4-picoline molecules depends on the crystallisation conditions. The solubility of the aqua(phthalocyaninato) complexes (**Ia**, IIa and **IIb**) is significantly greater than theirs initial M(II)Pc, due to the decreasing of the π–π stabilisation energy in the solid-state.

Appendix A. Supplementary data

CCDC 687352, 5873534 and 687354 contain the supplementary crystallographic data for **Ia**, IIa and **IIb**. These data can be obtained free of charge via http://www.ccdc.cam.ac.uk/conts/retrieving.html, or from the Cambridge Crystallographic Data Centre, 12 Union Road, Cambridge CB2 1EZ, UK; fax: (+44) 1223-336-033; or e-mail: deposit@ccdc.cam.ac.uk. Supplementary data associated with this article can be found, in the online version, at doi:10.1016/j.poly.2008.06.024.

References

[1] N.B. McKewon, Phthalocyanine Materials: Synthesis, Structure and Function, Cambridge University Press, Cambridge, 1998.
[2] C.C. Leznoff, A.B.P. Lever, Phthalocyanines: Properties and Applications, vol. 2, VCH Publishers, New York, 1993.
[3] C.C. Leznoff, A.B.P. Lever, Phthalocyanines: Properties and Applications, vol. 3, VCH Publishers, New York, 1993.
[4] C.C. Leznoff, A.B.P. Lever, Phthalocyanines: Properties and Applications, vol. 4, VCH Publishers, New York, 1996.
[5] A. Thomas, Phthalocyanine Research and Applications, CRS Press, Boca Raton, 1990.
[6] R.O. Loufty, Macromolecules 14 (1981) 270.
[7] A.K. Ghosh, D.L. Morel, T. Feng, R.F. Shaw, C.A. Rowe, J. App. Phys. 45 (1974) 230.
[8] W. Herbst, K. Hunger, Industrial Organic Pigments, VCH Publishers, New York, 1993.
[9] R.O. Loufty, A.M. Hor, G. DiPaola-Baranyi, C.K. Hesio, J. Imag. Sci. 29 (1985) 116.
[10] P.A. Barrett, C.E. Dent, R.P. Linstead, J. Chem. Soc. (1936) 1719.
[11] J.F. Boas, P.E. Fielding, A.G. MacKay, Aust. J. Chem. 27 (1974) 7.
[12] J. Janczak, R. Kubiak, Polyhedron 20 (2001) 2901.
[13] R. Kubiak, A. Waśkowska, M. Śledź, A. Jezierski, Inorg. Chim. Acta 359 (2006) 1344.
[14] R. Kubiak, A. Waśkowska, A. Pietraszko, E. Bukowska, Inorg. Chim. Acta 358 (2005) 453.
[15] J. Janczak, R. Kubiak, Polyhedron 21 (2002) 265.
[16] M.S. Fischer, D.H. Templeton, A. Zalkin, M. Calvin, J. Am. Chem. Soc. 93 (1971) 2622.
[17] F. Cariati, F. Morazzoni, M. Zocchi, J. Chem. Soc., Dlaton Trans. (1978) 1018.
[18] R. Kubiak, J. Janczak, M. Śledź, E. Bukowska, Polyhedron 26 (2007) 4179.
[19] W.R. Scheidt, W. Dow, J. Am. Chem. Soc. 99 (1977) 1101.
[20] WinXPow Software Manual, STOE & GmbH, Darmstadt, Germany, 1997.
[21] CRYSALIS CCD and CRYSALIS Red program, Ver. 171.31.8, Oxford Diffraction Poland, Wrocław, Poland, 2005.
[22] G.M. Sheldrick, SHELXS-97, SHELXL-97, Programs for Crystal Structure Solution and Refinement, University of Göttingen, Göttingen, Germany, 1997.
[23] J. Janczak, Y.M. Idemori, Polyhedron 22 (2003) 1167.
[24] R. Kubiak, J. Janczak, K. Ejsmont, Chem. Phys. Lett. 245 (1995) 249.
[25] J. Janczak, Y.M. Idemori, Acta Crystallogr. C58 (2002) m549.
[26] C.W. Bock, J.P. Glusker, Inorg. Chem. 32 (1993) 1242.
[27] L. Pauling, The Nature of the Chemical Bond, 3rd ed., Cornell University Press, Ithaca, 1967. p. 260.
[28] V. Kinzhybalo, J. Janczak, Acta Crystallogr. C63 (2007) m357.
[29] V. Kinzhybalo, J. Janczak, Inorg. Chim. Acta 360 (2007) 3314.
[30] V. Kinzhybalo, J. Janczak, Acta Crystallogr. C63 (2007) m105.
[31] J. Mizuguchi, Z. Kristallogr. NCS 217 (2002) 251.
[32] J. Mizuguchi, M. Mochizuki, Z. Kristallogr. NCS 217 (2002) 1267.
[33] V. Kinzhybalo, J. Janczak, J. Mol. Struct. 846 (2007) 134.
[34] O.C. Choon, V. McKee, G.A. Rodley, Inorg. Chim. Acta 123 (1986) L11.
[35] V. McKee, G.A. Rodley, Inorg. Chim. Acta 151 (1988) 233.
[36] S. Yang, R.A. Jacobseon, Inorg. Chim. Acta 190 (1991) 129.
[37] R. Timkovich, A. Tulinsky, J. Am. Chem. Soc. 91 (1969) 4430.
[38] C.S. Velazques, G.A. Fox, W.E. Broderick, K.A. Andersen, O.P. Andersen, G.M. Barrett, B.M. Hoffman, J. Am. Chem. Soc. 114 (1992) 7416.
[39] K.M. Barkigia, L.O. Spaulding, J. Fajer, Inorg. Chim. Acta 122 (1983) 349.
[40] C. Kratky, J.D. Dunitz, Acta Crystallogr. B31 (1975) 1586.
[41] H.C. Chow, R. Serlin, C.E. Stouse, J. Am. Chem. Soc. 97 (1975) 7230.
[42] R. Serlin, H.C. Chow, C.E. Stouse, J. Am. Chem. Soc. 97 (1975) 7237.
[43] M. Zerner, M. Gouterman, H. Kobayshi, Theoret. Chim. Acta 6 (1966) 363.
[44] W.R. Scheidt, Y.J. Lee, Struct. Bond. 64 (1987) 1–70.
[45] A. Endo, S. Matsumoto, J. Mizuguchi, J. Phys. Chem. A103 (1998) 8193.
[46] A. Henriksson, M. Sundbom, Theoret. Chim. Acta 27 (1972) 213.
[47] A. Henriksson, B. Ross, M. Sundbom, Theoret. Chim. Acta 27 (1972) 303.
[48] J. Mizuguchi, J. Phys. Chem. A105 (2001) 1121.
[49] J. Mizuguchi, G. Rihs, H.R. Karfunkel, J. Phys. Chem. 99 (1995) 16217.
[50] T. Saito, W. Sisk, T. Kobayashi, S. Suzuki, T. Iwaynagi, J. Phys. Chem. 97 (1993) 10515.
[51] T. Saito, Y. Iwakabe, T. Kobayashi, S. Suzuki, T. Iwaynagi, J. Phys. Chem. 98 (1994) 2726.
[52] Y. Pan, X. Lia, Y. Wu, L. Chen, Y. Zhao, Y. Shen, F. Li, S. Shen, D. Huang, Thin Solid Films 324 (1998) 209.
[53] N. Nanai, M. Yudasaka, S. Ohki, S. Voskimura, Thin Solid Films 298 (1997) 83.

Table 1
The formulae of the studied ligands

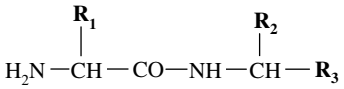

R_1	R_2	R_3	Abbreviation
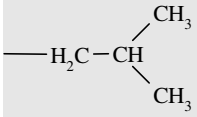	–COOH	–H	Leu-Gly
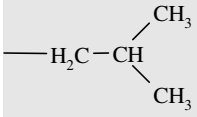	$-PO_3H_2$	–H	Leu-Gly(P)
–H	$-PO_3H_2$	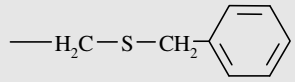	Gly-(Bz)Cys(P), D(−)
			Gly-(Bz)Cys(P), D(+)

solutions. The concentration of nickel(II) chloride stock solution was standardized by complexometric ethylenediaminetetraacetate (EDTA) titration. Carbonate-free potassium hydroxide solution (the titrant) was prepared and standardized against a standard potassium hydrogen phthalate solution.

2.2. Potentiometric measurements

Potentiometric titrations of Leu-Gly, Leu-Gly(P), Gly-(Bz)Cys(P), D(−) and Gly-(Bz)Cys(P), D(+) and complexes with nickel(II) ions in the presence of 0.2 M KCl were performed under purified argon atmosphere at 25 ± 0.5 °C within the pH range of 2.5–10.5 (pH-meter – a Radelkis OP-208/1 instrument and an ABU-80 autoburette (Radiometer)) with CO_2-free ca. 0.13 M KOH as titrant. Changes in pH were monitored with a combined pH electrode SINGLE PORE, Hamilton, calibrated daily in hydrogen-ion concentrations by HCl (7.5×10^{-3} mol dm^{-3} in KCl) against standard KOH solution titrations [8].The resulting titration data were used to calculate the standard electrode potentials, E^0, and the dissociation constant for water ($pK_w = 13.73$). These values were then used to calculate the hydrogen-ion concentration [H^+] from e.m.f. readings. Sample volumes of 5 ml were used. The ligand concentration was 2.5×10^{-3}, 1.9×10^{-3} and 1.8×10^{-3} mol dm^{-3} for Leu-Gly, Leu-Gly(P) and Gly-(Bz)Cys(P), D(−), respectively and the metal ion:ligand ratios were 1:1, 1:2 and 1:6. The data were analyzed using SUPERQUAD program [9]. Standard deviations computed by SUPERQUAD refer to random errors only. The charges of the complexes have been omitted in the figures and tables. For clarity, it should be mentioned that the fully deprotonated forms of the ligands have negative charges L^{2-} and L^- for the monophosphono dipeptides and simple dipeptide, Leu–Gly, respectively.

2.3. NIR–Vis spectroscopy

The absorption spectra were obtained on a Jasco V-570 spectrophotometer using 5 cm and 10 cm quartz cells at room temperature. The spectra were recorded digitally (1.0 nm) over the range 300–1200 nm. The metal ion concentration was 8×10^{-3} mol dm^{-3} for the system with Leu-Gly, 6×10^{-3} mol dm^{-3} for the system with Leu-Gly(P), and concentration ratio of nickel(II):ligand were 1:1 and 1:4. The individual spectra of the nickel(II) complexes were calculated by means of method described in [10]. The absorption bands were fitted to Gaussian components using CFP program [11]. Ligand-field parameters and transition energies were calculated using the LFP program [12]. Both methods were described in detail [11,13,14] (and refs. therein). The assignment of bands is based on fitting the resolved band maxima (deconvolution of spectra) with the calculated transition energies (eigenvectors) using the d^8 quadrate energy levels with full configuration interactions and without spin–orbit coupling.

3. Results and discussion

The fully protonated form (H_3L^+) of Leu-Gly(P), Gly-(Bz)Cys(P), D(−) and Gly-(Bz)Cys(P), D(+) can release three protons. The first proton of the $-PO_3H_2$ group is very acidic (pK ca. 1.0–2.0), and thus this function group is fully deprotonated in the pH range studied in potentiometric titrations (2–10.5) and does not take part in metal coordination equilibria. The second proton comes from the phosphonic function $-PO_3H^-$ and the last one from the amino group $-NH_3^+$. The protonation constants of the studied monophosphono dipeptides together with simple dipeptide, Leu-Gly and the detailed discussion about the acid–base properties of these ligands can be found in our early paper [4].

Nickel(II) complexes of the most common dipeptides have already been studied by several authors and the metal binding modes of the species [NiL]$^+$ and [NiL_2] were described by (NH_2, CO)-coordination of the *N*-terminal [15–18]. Taking into account the octahedral coordination geometry of the metal ion the formation of [NiL_3]$^-$ was also suggested in some cases [17]. The presence of tris(ligand) complexes in well measured concentration requires the application of a high excess of ligand, thus, under our experimental conditions [$Ni(Leu\text{-}Gly)_3$]$^-$ species was not detected. Deprotonation and coordination of the amide functions generally take place at pH ca. 8 and it results in the existence of the species [$NiLH_{-1}$], [NiL_2H_{-1}]$^-$ and [NiL_2H_{-2}]$^{2-}$.

The titrations curves for the systems containing nickel(II) and studied phosphonic ligands were evaluated by assuming the same type of complexes as were determined for the simple aliphatic dipeptides. Due to the higher basicity of $-PO_3^{2-}$, as compared to

Table 2
Logarithmic protonation constants ($\log\beta_n^H$), logarithmic cumulative formation constants ($\log\beta_n$) and derived equilibrium constants ($\log K$) for the complexes formed with Ni^{2+} at 25 °C and I = 0.2 mol dm^{-3} (KCl)

Assignments	Compound						
	Leu-Gly		Leu-Ala(P)	Leu-Gly(P)		Gly-(Bz)Cys(P) D(−)	Gly-(Bz)Cys(P) D(+)
	This work	Ref. [19]	Ref. [23]	This work	Ref. [20]	This work	
[HL]	8.02(1)	8.24	7.814	8.26(1)	8.07	8.35(1)	8.33(1)
[H_2L]	11.11(2)	11.44	14.49	14.71(1)	14.17	14.50(1)	14.46(1)
[H_3L]			16.038	15.95(8)			
[Ni(HL)]			9.60(3)	10.11(4)	9.57(6)	10.88(1)	10.96(1)
[NiL]	3.31(1)	3.39	3.599(3)	3.66(1)	3.79(5)	4.68(1)	4.68(1)
[$NiLH_{-1}$]	−5.31(3)		−5.03(1)	−5.83(4)	−4.68(1)	−4.71(3)	−4.88(4)
[NiL_2]	5.97(3)	6.21	5.92(1)	6.54(4)	6.90(1)	8.48(1)	8.42(2)
[NiL_2H_{-1}]	−2.64(7)	−2.41				−1.76(11)	−1.49(9)
[NiL_2H_{-2}]	−11.77(2)	−12.31					
[NiL_3]		8.46					
$\log K$[NiL_2]	2.66	2.82	2.321	2.88	3.11	3.80	3.74
pK[Ni(HL)]			6.001	6.45	5.78	6.20	6.28
pK[NiL]	8.62		8.629	9.49	8.47	9.39	9.56
pK[NiL_2]	8.61	8.62				10.24	9.91
pK[NiL_2H_{-1}]	9.13	9.90					
$\log\beta$[Ni(HL)] − p$K(PO_3H^-)$			2.924	3.66	3.47	4.73	4.83
$\log(K_1/K_2)$	0.65			0.78		0.88	0.94
$\log K_0$	−4.71			−4.60		−3.67	−3.65
$\log K_1$	−13.33			−13.97		−13.06	−13.21

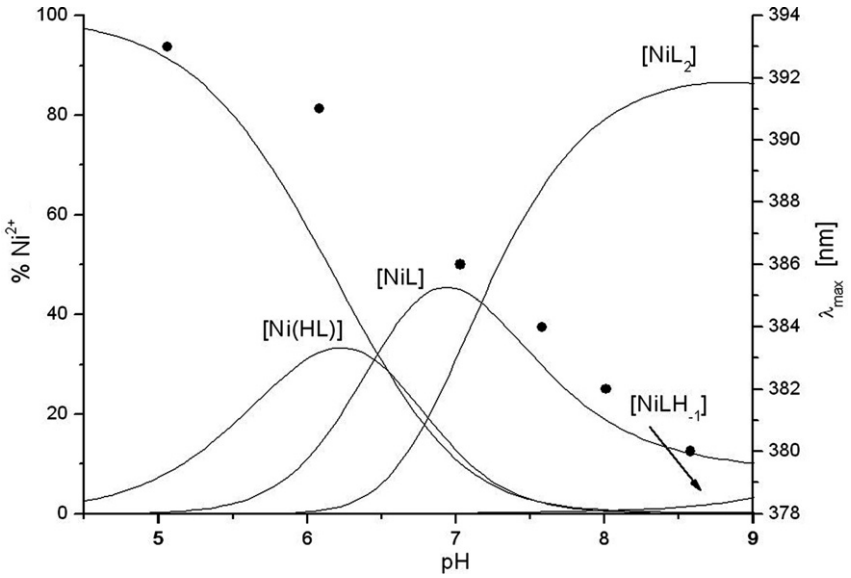

Fig. 1. Distribution diagram of Ni^{2+} complexes with Leu-Gly(P) as a function of pH simulated for conditions used in UV–Vis spectroscopy ($c_{Ni^{2+}}$ = 0.006, c_L = 0.024 mol dm^{-3}). λ_{max} (circle) of UV–Vis spectra recorded in different pH values are overlaid.

that for COO^-, the formation of protonated complexes was also taken into calculations. The best fits between the measured and calculated titration curves were obtained by assuming the species given in Table 2.

As an illustration, the species distribution diagram of Ni^{2+}–Leu-Gly(P) systems is presented in Fig. 1.

In the Ni^{2+}–Leu-Gly(P) system the formation of complexes starts about pH 5 and the precipitation of nickel hydroxide occurs at 9.0. In the acidic region the first protonated species $[Ni(HL)]^+$ is formed and has the maximum concentration at pH 6–6.5. This species is not formed with Leu-Gly because of the lower basicity of the carboxylate group. Taking into account a fact that the values of $\log K_{[Ni(HL)]} = \log\beta_{[Ni(HL)]} - pK_{PO_3H^-}$ of Leu-Gly(P) and $\log\beta_{[NiL]}$ of Leu-Gly are about of the same order of magnitude (Table 2), we can conclude that Leu-Gly(P) is coordinated to the metal ion in the [Ni(HL)] species in the same way as in the simple dipeptides, i.e., *via* the terminal amine and the peptide carbonyl group. This leads to the formation of the thermodynamically stable five-membered chelate ring. The formation of the major species [NiL] begins above pH 5.5 and reaches maximum concentration of ca. 50% at about pH 7. The $pK_{[Ni(HL)]}$ value (6.45) is identical to the value of the free Leu-Gly(P) (6.45) and corresponds to the dissociation constant of the non-coordinated $-PO_3H^-$ group. Because the basicity of Leu-Gly and Leu-Gly(P) is different, the metal binding abilities of the ligands may be estimated by considering the equilibrium constant of the reaction [21,22]: $M^{2+} + HL = [MLH_{-n}]^{(1-n)+} + (n+1)H^+$. The equilibrium constant of the reaction is K_{-n} (where n = 0, 1, 2) and it can be calculated by the equation: $\log K_{-n} = \log\beta_{11(-n)} - pK(HL)$. The $\log K_0$ and $\log K_{-1}$ values are included in Table 2.

The stability constant of [NiL] (K_0 = −4.60) is somewhat higher than that of the same type of the complex with Leu-Gly (K_0 = −4.71), suggesting the type of coordination shown in Scheme

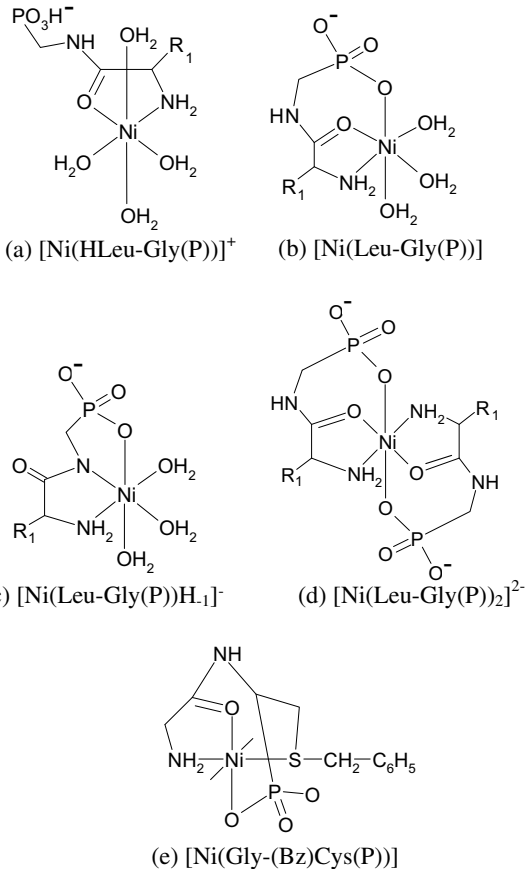

Scheme 1. Tentative structures of the species formed in the Ni^{2+}–phosphonodipeptides systems.

1. This small stabilizing effect is probably derived from the additional coordination of the deprotonated phosphonic group apart from the amine and carbonyl groups to the nickel(II) ion (see below). The similar situation for other phosphonodipeptides was published in paper [23]. The next step in the ligand dissociation and formation of the $[NiLH_{-1}]^-$ species occurs above pH 8.5. The $pK_{[NiL]}$ value is equal 9.49 and presumably can be ascribed to the peptide amide group. For this species the coordination through amine, peptide amide and phosphonic groups is assumed. Precipitation of hydroxo complex(es) of nickel(II) was observed ca. pH 9. This precipitation suggests that the formation of hydroxo species and amide deprotonation takes place in overlapping processes and the $\log K_{-1}$ value (the $\log K_{-1}$ parameter reflects the relative stability of the $[MLH_{-1}]$ complex) cannot be unambiguously assigned to the overall stabilities of the $[MLH_{-1}]$ with (NH_2, N^-, $-PO_3^{2-}$) coordination modes. Possible structures of the discussed complexes are presented in Scheme 1.

In addition to the 1:1 complexes, the nickel(II) ion forms the $[NiL_2]$ complex. According to Kiss et al. [24] and Hermann et al. [23] we assume for this complex coordination to the metal ion *via* the amine, carbonyl and phosphonate groups. The effect of the $[NiL_2]$ species formation is observed in the electronic spectral changes. Fig. 1 presents variations of visible absorption maximum wavelength of the $^3A_{2g} \rightarrow {}^3T_{1g}(P)$ parent octahedral band together with the species distribution as a function of pH. Its shift to higher energies above pH 6 is due to the involvement of nitrogen donors of ligand molecules in Ni^{2+} coordination. The spectra for the Ni^{2+}–Leu-Gly exhibit, approximately the same changes versus pH. The absorption spectra at the pH value where each species exhibit maximal contribution were resolved into the components corresponding to the individual species existing at that pH (as described in Ref. [10]). In general, the Ni^{2+} complexes with studied ligands (Leu-Gly and Leu-Gly(P)) have a distorted octahedral geometry (Fig. 2).

The molar absorptivity for the individual species was then calculated taking into account their distribution. The distribution-corrected curves for these species are shown in Fig. 3 and their parameters are included in Table 3. However, spectroscopic characterization of $[NiLH_{-1}]^-$ species was impossible because of its very low concentration under the applied experimental conditions and too large overlap with other complexes in the pH range 6–9.

The spectra of studied nickel(II) complexes display three absorption bands at ca. 9400–10020 (1063–998), 15333–16000 (576–625) and 25510–26525 cm^{-1} (392–377 nm), and shoulders

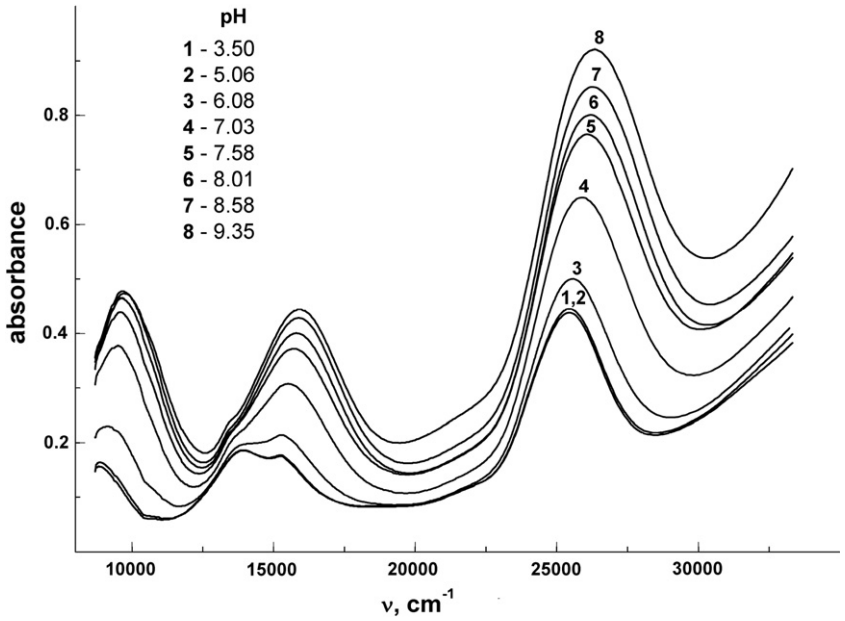

Fig. 2. The pH dependence of the absorption spectra recorded for Ni^{2+}–Leu-Gly(P) system at 1:4 metal:ligand ratio, $c_{Ni^{2+}} = 6.0058 \times 10^{-3}$ mol dm^{-3}.

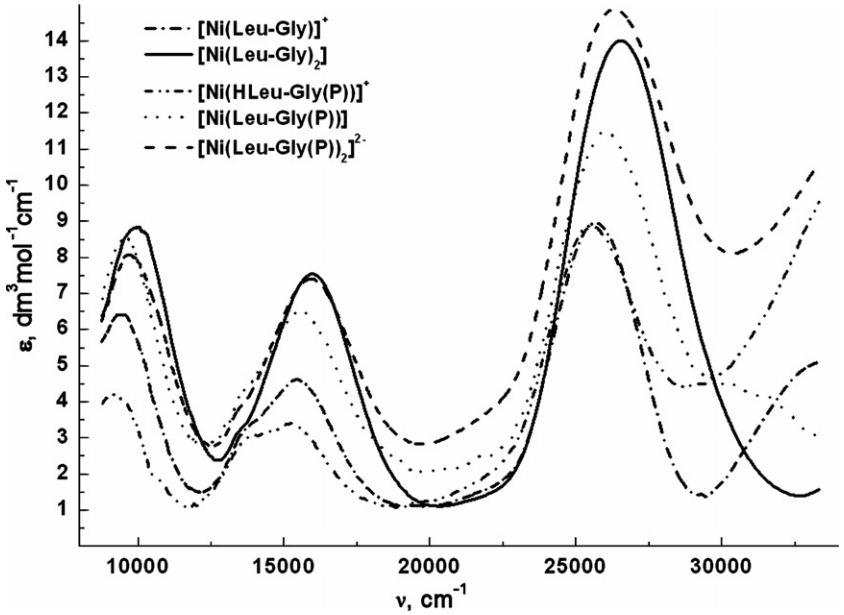

Fig. 3. Comparison of the electronic absorption spectra of nickel(II) complex species studied in aqueous solution at room temperature: $[Ni(Leu\text{-}Gly)]^+$, dash-dot; $[Ni(Leu\text{-}Gly)_2]$, solid; $[Ni(HLeu\text{-}Gly(P))]^+$, dash-dot-dot; $[Ni(Leu\text{-}Gly(P))]$, dot; $[Ni(Leu\text{-}Gly(P))_2]^{2-}$, dash.

at ca. 13 000 cm^{-1} (Fig. 3). The spectra of pseudo-octahedral (e.g., tetragonally distorted) nickel(II) complexes rarely display the lower symmetry components. A few cases are know that the Δ^1_{tetr} tetragonal splitting of $^3T_{2g}[3F]$ parent octahedral state is observed, only. The Δ^2_{tetr} and Δ^3_{tetr} splittings of $^3T_{1g}[^3F]$ and $^3T_{1g}[^3P]$, respectively, are always lower than Δ^1_{tetr}. These resolved tetragonal splittings are considerably lower than 1000 cm^{-1}, from Gaussian analysis of the dihalogenotetrakis(pyridine) nickel(II) complexes [13,25,26]. Whereas, the average band halfwidths of the tetragonal components of all the spectra are not less than 2200 cm^{-1}. This fact explains why the maxima or shoulder are not observed in the experimental solutions spectra, even though the formal symmetry of the complexes is lower. It is immediately evident from Fig. 3 that no tetragonal splitting, even of the first band, is observed. However, the symmetry was assumed to be D_{4h} and the electronic spectra fitted this model.

Fig. 4 shows, as the example, the spectra of the $[Ni(HLeu\text{-}Gly(P)]^+$ and $[Ni(Leu\text{-}Gly(P))_2]^{2-}$ complexes together with Gaussian components. Table 3 presents the ligand-field parameters (crystal field model (CFM) and angular orbital model (AOM)), of some complex species formed with Leu-Gly and Leu-Gly(P) in aqueous solution of nickel(II). Calculated transition energies are compared with those obtained by Gaussian resolution of the experimental spectra. The agreement between experimental and calculated transition energies is satisfactory.

In this and previous papers we used the sign conversion of Perumareddi [27] even though the CFM parameter set was originally introduced by Ballhausen and Moffit [28]. It should be noted that Perumareddi changed the signs of the Ds and Dt parameters. The crystal field parameters (CFM) of the complexes (Table 3) suggest elongation of z axis in pseudo-octahedral complexes, but this affect is lowest for $[Ni(HLeu\text{-}Gly(P))]^+$ species. The symmetry reduction from octahedral to D_{4h}, or C_{4v} (D_{4h} holohedrized symmetry) is due to a weaker donor field along the z axis (i.e., $Dq^{(xy)} > Dq^{(z)}$). The Dq_{xy} values of all the complexes are very close but the lowest for $[Ni(HLeu\text{-}Gly(P))]^+$ complex. Furthermore, the tetragonal Dt parameter values are similar in the errors limit (except $[Ni(HLeu\text{-}Gly(P))]^+$ complex) whilst the $Dq^{(z)}$ parameters are different. This suggests, according to relationship $Dt = (-4/9)(Dq^{(xy)} - Dq^{(z)})$, that influences on the central ion are weaker in the [NiL] species, i.e., both axial and equatorial positions. The greatest differences are observed for the $[Ni(HLeu\text{-}Gly(P))]^+$ species that correspond to the lowest tetragonal distortion, i.e., $Dq^{(xy)} \cong Dq^{(z)}$, and Dt value closes to zero. Thus, in this case axial positions are occupied by water molecules only, whilst equatorial positions are mixed (Scheme 1a). The angular overlap parameters of water molecules are as expected, i.e., $e_\sigma(H_2O) \cong 5000$ and $e_\pi(H_2O) \cong 1500\ cm^{-1}$. In the all other cases AOM parameters are averaged, i.e., for axial and equatorial donors, respectively. Their values confirm also elongation of z axis in pseudo-octahedral complexes. The e_σ and e_π bonding abilities of equatorial donors are stronger then axial.

The stronger effect is observed in the case of the $[NiL_2]$ species. The $Dq^{(xy)}$ is distinctly higher than $Dq^{(z)}$ parameter and Dt parameter is the highest (Table 3). These values clearly indicate that the deprotonated phosphonic groups are involved in the coordination to the metal ions (Scheme 1d). Otherwise, the same tetragonal effects should be observed in the both complex species. A little weaker tetragonal distortion in [NiL] species arises, because of averaged influences of two different groups in an axial positions,

Table 3
Ligand-field parameters, CFM[a] and AOM, of the complex species in aqueous solution, in cm^{-1}

Parameter	$[Ni(Leu\text{-}Gly)]^+$	$[Ni(Leu\text{-}Gly)_2]$	$[Ni(HLeu\text{-}Gly(P))]^+$	$[Ni(Leu\text{-}Gly(P))]$	$[Ni(Leu\text{-}Gly(P))_2]^{2-}$
$Dq^{(z)}$	776	790	879	740	752
$Dq^{(xy)}$	963(24)	1030(22)	945(26)	996(33)	1026(29)
Ds	−236(64)	−388(62)	−391(70)	−260(93)	−289(80)
Dt	−107(38)	−137(35)	−38(39)	−146(52)	−156(45)
B	911(20)	956(23)	868(28)	925(33)	980(28)
β[b]	0.84	0.88	0.83	0.80	0.90
C	3140(46)	2755(101)	3306(121)	2795(145)	2586(127)
C/B	3.5	2.9	3.8	3.0	2.7
$e_\sigma^{(eq)}$	5774(326)	6043(314)	5699(339)	5900(414)	5811(365)
$e_\sigma^{(ax)}$	5039(406)	4927(311)	4829(350)	5019(420)	4846(377)
$e_\pi^{(eq)}$	1920(267)	1955(233)	1910(260)	1934(313)	1793(280)
$e_\pi^{(ax)}$	1841(263)	1723(246)	1427(262)	1915(330)	1756(280)

[a] For Ds and Dt signs formalism of perumareddi was assumed.
[b] B parameter for the ion Ni(II) equals 1084 cm^{-1} (from Ref. [29]).

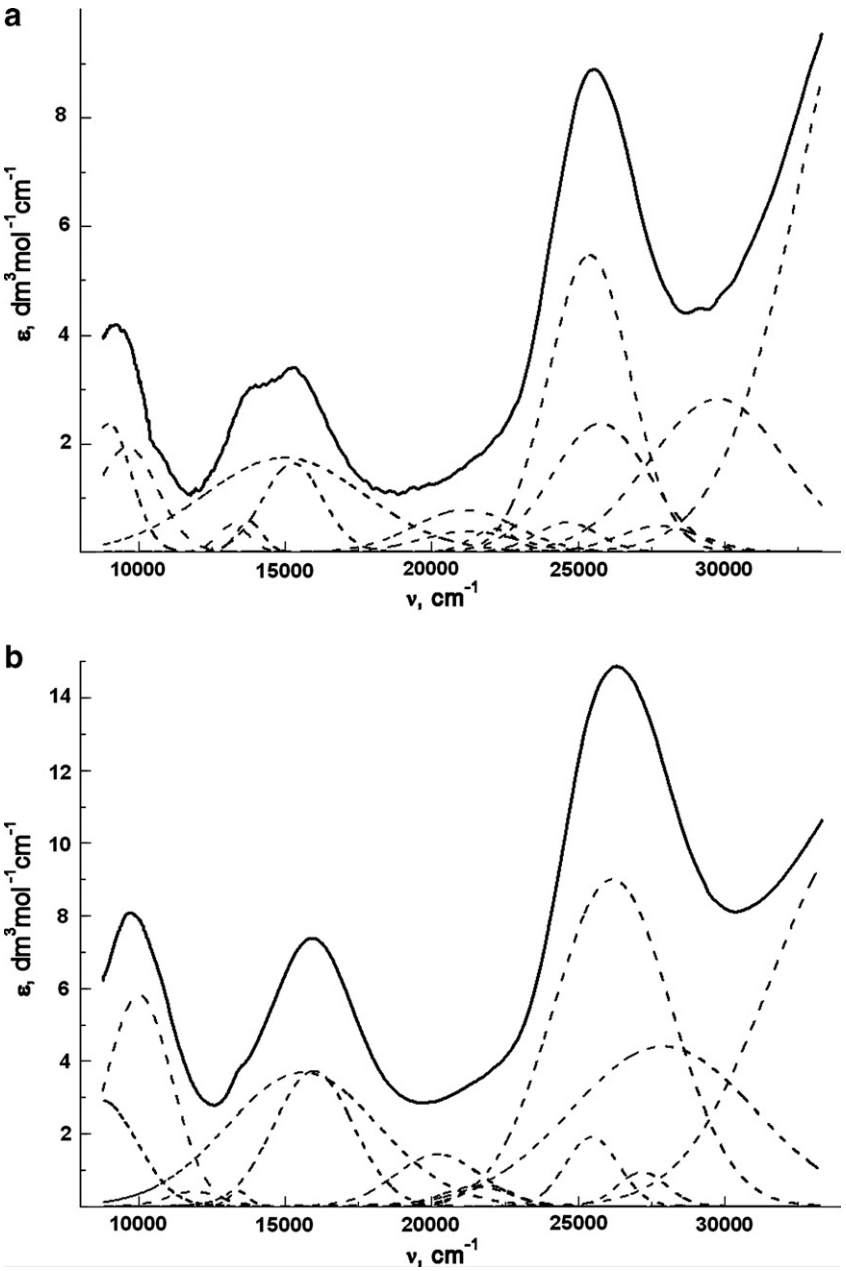

Fig. 4. Electronic absorption spectra in aqueous solution and Gaussian analysis as the example, (a) $[Ni(HLeu\text{-}Gly(P))]^{+}$, (b) $[Ni(Leu\text{-}Gly(P))_2]^{2-}$; experimental spectrum – solid, component bands – dash.

i.e., phosphonic group and water molecule (Scheme 1b). Generally, [NiL] species have somewhat lower Dq values than $[NiL_2]$ species, as well as Racah *B* parameter, for both the ligands analysed. The last shows less covalent character of bonding for $[NiL_2]$ species. The nefeloauxetic β parameters increase in order:

$$[Ni(HLeu\text{-}Gly(P))]^{+} \cong [Ni(Leu\text{-}Gly)]^{+} \cong [Ni(Leu\text{-}Gly(P))] < [Ni(Leu\text{-}Gly)_2] < [Ni(Leu\text{-}Gly(P))_2]^{2-}$$

Due to the fact that in the Ni(II)–Gly-(Bz)Cys(P), D(−) or Ni(II)–Gly-(Bz)Cys(P), D(+) systems the strong tendency to the precipitation was observed, the recording and the detailed analysis of absorption spectra were impossible. Anyway, the equilibrium model for these systems differ if compared with system of Leu-Gly(P) only by the present of an additional $[NiL_2H_{-1}]$ species (Table 2). The overall stability constants can be directly used to compare, because the basicity of these studied phosphonic ligands are almost the same. A comparison of $\log K_n$ of the nickel(II) complexes of Leu-Gly(P) with Gly-(Bz)Cys(P), D(−) or Gly-(Bz)Cys(P), D(+) shows significant differences (Table 2). These values suggest that the thermodynamic stability constants of the species with Gly-(Bz)Cys(P) are higher than with Leu-Gly(P). The differences in $\log K_1$ and $\log K_2$ of ca. 1.0 log units, respectively, suggest additional interaction between sulfur donor atom and nickel(II) in the complex species of Gly-(Bz)Cys(P), D(−) or Gly-(Bz)Cys(P), D(+) (Scheme 1e).

4. Conclusion

Due to the higher basicity of $-PO_3^{2-}$, as compared to that for CO_2^{-}, the formation of 1:1 protonated complexes in nickel(II)-monophosphono dipeptides systems were detected in compared to system with Leu-Gly. From the comparative analysis of the sta-

bility and the NIR–Vis spectroscopy data it has been established that the coordination in [NiHL] species is realised by the terminal amine and the peptide carbonyl group, the axial positions are occupied by water molecules. In this complex species the lowest tetragonal distortion is observed. In the [NiL] species the coordination is through the amine, carbonyl and the deprotonated phosphonic group. The coordination of two different groups in an axial positions (phosphonic group and water molecule) results in a little stronger tetragonal distortion if compare to the protonated species. In the $[NiLH_{-1}]$ species coordination by amine, peptide amide and phosphonic group is assumed. The strongest tetragonal distortion is observed in the case of $[NiL_2]$ species. In this species the deprotonated phosphonic group are involved in the coordination to the metal ions in both axial positions. In the case of nickel(II) complexes with Gly-(Bz)Cys(P), D(−) or Gly-(Bz)Cys(P), D(+) additional interaction between sulfur donor atom and nickel(II) is suggested.

References

[1] M. Lukas, M. Kyvala, P. Hermann, I. Lukes, D. Sanna, G. Micera, J. Chem. Soc., Dalton Trans. (2001) 2850.
[2] J. Gałęzowska, S. Sobek, M. Drąg, A. Much, P. Kafarski, H. Kozłowski, Polish J.Chem. 79 (2005) 603.
[3] J. Gałęzowska, Ł. Szyrwiel, P. Młynarz, S. Śliwińska, P. Kafarski, H. Kozłowski, Polyhedron 26 (2007) 4287.
[4] B. Kurzak, A. Woźna, J. Jezierska, M. Jeżowska-Bojczuk, W. Szczepanik, P. Kafarski, Polyhedron 23 (2004) 1939.
[5] M. Soroka, P. Mastalerz, Polish J. Chem. 50 (1976) 661.
[6] J. Oleksyszyn, E. Gruszecka, P. Kafarski, P. Mastalerz, Monatsh. Chem. 113 (1982) 1138.
[7] G. Gran, Acta Chem. Scand. 4 (1950) 599.
[8] M. Molina, C. Melios, J.O. Tognalli, L.C. Luchiari, M. Jafelicci Jr., J. Electroanal. Chem. 105 (1979) 237.
[9] P. Gans, A. Sabatini, A. Vacca, J. Chem. Soc., Dalton Trans. (1985) 1195.
[10] B. Kurzak, D. Kroczewska, J. Jezierska, Polyhedron 17 (1998) 1831.
[11] K. Kurzak, Ph.D. Thesis, Technical University of Wrocław, 1983.
[12] K. Kurzak, Comput. Biol. Chem. (formerly Computers Chem.) 24 (2001) 519.
[13] K. Kurzak, A. Bartecki, Transition Met. Chem. 13 (1988) 224.
[14] I. Kuźniarska-Biernacka, A. Bartecki, K. Kurzak, Polyhedron 22 (2003) 997.
[15] R.B. Martin, M. Chamberlin, J.T. Edsall, J. Am. Chem. Soc. 82 (1960) 495.
[16] A. Kaneda, A.E. Martell, J. Am. Chem. Soc. 99 (1977) 1586.
[17] G. Brookes, L.D. Petit, J. Chem. Soc., Dalton Trans. (1975) 2106.
[18] H.C. Frejman, J.M. Guss, Acta Crystallogr., Sect. B 34 (1978) 2451.
[19] W.S. Kittl, B.M. Rode, Inorg. Chim. Acta 66 (1982) 105.
[20] P. Herman, I. Lukes, J. Chem. Soc. Dalton Trans. (1995) 2605.
[21] D. Sanna, C.G. Agoston, G. Micera, I. Sovago, Polyhedron 20 (2001) 3079.
[22] H. Sigel, B. Prijs, R.B. Martin, Inorg. Chim. Acta 56 (1981) 45.
[23] P. Hermann, I. Lukes, P. Vojtisek, I. Cisarova, J. Chem. Soc., Dalton Trans. (1995) 2611.
[24] T. Kiss, E. Farkas, H. Kozłowski, Z. Siatecki, P. Kafarski, B. Lejczak, J. Chem. Soc., Dalton Trans. (1989) 1053.
[25] K. Kurzak, A. Kołkowicz, A. Bartecki, Polyhedron 10 (1991) 1759.
[26] K. Kurzak, A. Kołkowicz, A. Bartecki, Transition Met. Chem. 17 (1992) 155.
[27] J.R. Perumareddi, J. Phys. Chem. 71 (1967) 3144.
[28] C.J. Ballhausen, W.E. Moffit, J. Inorg. Nucl. Chem. 3 (1956) 178.
[29] J.S. Griffits, The Theory of Transition Metal Ions, University Press, Cambridge, 1961.

4-nitrobenzophenone thiosemicarbazone ($H4NO_2Bz4M$) (Fig. 1) as well as their ruthenium(II) complexes containing triphenylphosphine or 1,4-bis(diphenylphospine)butane (dppb). A study of the luminescence characteristics of the free thiosemicarbazones and their ruthenium(II) complexes has been performed. X-ray crystal structure of N^4-methyl 4-nitrobenzaldehyde thiosemicarbazone are also reported.

2. Experimental

2.1. Physical measurements

Elemental analyses were performed on a Fison equipment, model EA 1108. A Radiometer Copenhagen Meter Lab., model CDM 230 was employed for molar conductivity measurements. Infrared spectra (KBr pellets) were obtained using a BOMEM MICHELSON instrument, model 102. NMR spectra were obtained at room temperature with a Brucker DRX-400 Avance (400 MHz) spectrometer. For ^1H measurements, $CDCl_3$ was used as solvent and tetramethylsilane (TMS) as internal reference while for $^{31}P\{^1H\}$ (161 MHz), CH_2Cl_2 was used as solvent and H_3PO_4 85% as external reference.

The electrochemical experiments were carried out at room temperature in dichloromethane containing 0.1 mol L^{-1} tetrabutylammonium perchlorate (TBAP) (Fluka Purum) using an electrochemical analyzer from Bioanalytical Systems Inc. (BAS), model 100BW. The working and auxiliary electrodes were stationary Pt foils, and the reference electrode was Ag/AgCl, a medium in which ferrocene is oxidized at 0.48 V (Fc^+/Fc).

Luminescence studies were made on a Perkin–Elmer LS 55 spectrofluorimeter using 10 nm spectral bandpass. Fluorescence measurements were performed in solution using CH_2Cl_2 as solvent conditioned in 1 cm quartz cells. For the phosphorescence measurements, a front solid surface apparatus (Perkin–Elmer) was employed to allow the use of cellulose as the support. The signals were measured directly from the surface dry cellulose substrates (treatment for background reduction [8]) using detector delay and gate times set at 3 ms. Measurements were made in an oxygen free environment established by the use of a purging gas flow (dried nitrogen gas). Solutions (5 μL) of the free thiosemicarbazones and their metal complexes, prepared in CH_2Cl_2, were deposited on the center of the cellulose substrates. These substrates were previously spotted with 5 μL of heavy atom salts solutions which were used as potential heavy atom phosphorescence inducers. Tl(I), Hg(II), Pb(II), Cd(II), Ag(I) and iodine were used as potential heavy atom phosphorescence inducers. Measurements were made after the substrates were dried under vacuum (2 h).

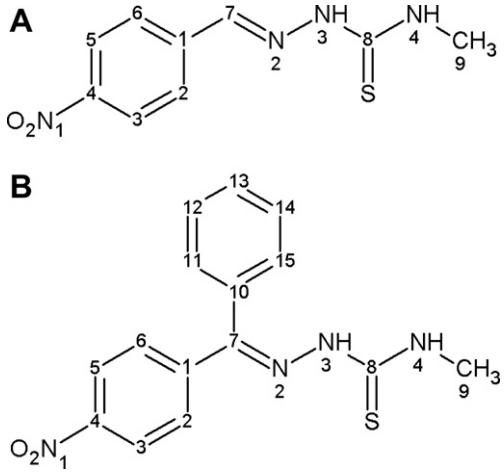

Fig. 1. Structure of (a) N^4-methyl-4-nitrobenzaldehyde thiosemicarbazone ($H4NO_2Fo4M$) and (b) N^4-methyl-4-nitrobenzophenone thiosemicarbazone ($H4NO_2Bz4M$).

2.2. X-ray crystallography

Single crystals of $H4NO_2Fo4M$, adequate for structural X-ray diffraction work, were obtained after slow evaporation of the solvent (ethanol) from the solution. Data were collected with an *Enrof-Nonius Kappa*-CCD [9] diffractometer and graphite-monochromatized Mo Kα radiation. Data were obtained using the PHICHI [10] and EVALCCD [11] software and they were corrected using SADABS [12]. The structure was solved by direct methods and refined on F^2 with anisotropic temperature parameters for all non H atoms [13]. H atoms of the phenyl and methyl groups were positioned geometrically (C–H = 0.93 Å for Csp^2 atoms and C–H = 0.96 Å for Csp^3 atoms) and treated as riding on their respective C atoms, with $U_{iso}(H)$ values set at $1.2U_{eq}Csp^2$ and $1.5U_{eq}Csp^3$.

2.3. Syntheses of $[RuCl_2(PPh_3)_3]$ and $[RuCl_2(dppb)(PPh_3)]$

$[RuCl_2(PPh_3)_3]$ and $[RuCl_2(dppb)(PPh_3)]$ were prepared according to previously described procedures [14,15].

2.4. Synthesis of N^4-methyl 4-nitrobenzaldehyde thiosemicarbazone ($H4NO_2Fo4M$) and N^4-methyl 4-nitrobenzophenone thiosemicarbazone ($H4NO_2Bz4M$)

N^4-Methyl thiosemicarbazide has been purchased from Aldrich and used without further purification. The thiosemicarbazones were obtained by mixing equimolar amounts of 4-nitrobenzaldehyde and 4-nitrobenzophenone (6.6×10^{-3} mol) with N^4-methyl thiosemicarbazide in absolute ethanol (40 mL) with addition of 2–4 drops of concentrated sulfuric acid as catalyst. The reaction mixture was kept under reflux for 6–7 h.

2.4.1. N^4-Methyl 4-nitrobenzaldehyde thiosemicarbazone ($H4NO_2Fo4M$)

Yellow solid. Mp: 225–226 °C. *Anal.* Calc. for $C_9H_{10}N_4O_2S$: C, 45.37; H, 4.23; N, 23.51. Found: C, 45.37; H, 4.20; N, 23.45%. IR (KBr, cm^{-1}): $\nu_{ass}NO_2$ 1528, ν_sNO_2 1342, ν(NH) 3375, ν (C=N) 1599, ν (C=S) 830. ^1H NMR ($CDCl_3$): (δ, ppm) 9.35 (1H, s, N(3)H), 8.27 (2H, d, aryl H(3, 5)), 7.81 (2H, d, aryl H(2, 6)), 7.49 (1H, s, C(7)–H), 2.17 (3H, s, CH_3).

2.4.2. N^4-Methyl 4-nitrobenzophenone thiosemicarbazone ($H4NO_2Bz4M$)

Orange solid. Mp: 210–211 °C. *Anal.* Calc. for $C_{15}H_{14}N_4O_2S$: C, 57.31; H, 4.49; N, 17.82. Found: C, 57.71; H, 4.47; N, 17.19%. IR (KBr, cm^{-1}): $\nu_{ass}NO_2$ 1549, ν_sNO_2 1341, ν (C=N) 1599, ν(C=S) 821. NMR ($CDCl_3$): (δ, ppm) 8.78 (1H, s, N(3)H), 8.37 (2H, d, aryl H(3, 5)), 8.20 (2H, d, aryl H(2, 6)), 7.97 (2H, d, aryl H(11, 15)), 7.97–7.55 (3H, aryl H(12, 13, 14)), 3.34 (3H, s, CH_3).

2.5. Syntheses of $[Ru(4NO_2Fo4\,M)_2(PPh_3)_2]$ and $[Ru(4NO_2Bz4M)_2(PPh_3)_2]$

The complexes were obtained by dissolving the desired thiosemicarbazone (0.200 mmol) in CH_2Cl_2 under argon atmosphere followed by addition of solid $[RuCl_2(PPh_3)_3]$ (0.200 mmol). The reaction mixtures were kept under stirring at room temperature for 5 h. The solids precipitated upon addition of anhydrous hexane and were filtered and washed with diethylether.

2.5.1. $cis[Ru(4NO_2Fo4M)_2(PPh_3)_2] \cdot CH_2Cl_2$ (**1**)

Brown solid. *Anal.* Calc. for $C_{55}H_{50}RuN_8O_4S_2P_2Cl_2$: C, 55.7; H, 4.3; N, 9.5; S, 5.4. Found: C, 55.8; H, 4.1; N, 9.7; S, 5.5%. IR (KBr, cm^{-1}):

$\nu_{ass}NO_2$ 1520, ν_sNO_2 1342, ν(C=N) 1586, ν(C=S) 784, ν(Ru–P) 516, ν(Ru-N) 484, ν(Ru–S) 441. Molar conductivity (1×10^{-3} mol L^{-1} CH_2Cl_2): 3.8 μS cm^{-1}. $^{31}P\{^1H\}$ NMR (CH_2Cl_2 δ/ppm): 38.6 (s).

*2.5.2. trans[Ru(4NO$_2$Bz4M)$_2$(PPh$_3$)$_2$] · 2CH$_2$Cl$_2$ (**2**)*

Brown solid. *Anal.* Calc. ($C_{68}H_{60}RuN_8O_4S_2P_2Cl_4$): C, 57.4; H, 4.3; N, 7.9; S, 4.5. Found: C, 57.6; H, 4.2; N, 7.9; S, 4.6%. IR (KBr, cm^{-1}): $\nu_{ass}NO_2$ 1518, ν_sNO_2 1342, ν(C=N) 1562, ν(C=S) 749, ν(Ru–P) 526, ν(Ru–N) 496, ν(Ru–S) 432. Molar conductivity (1×10^{-3} mol L^{-1} CH_2Cl_2): 5.0 μS cm^{-1}. $^{31}P\{^1H\}$ NMR (CH_2Cl_2 δ/ppm): 29.2 (s).

2.6. Syntheses of [Ru(4NO$_2$Fo4M)$_2$(dppb)] and [Ru(4NO$_2$Bz4M)$_2$-(dppb)]

The complexes were obtained by dissolving the desired thiosemicarbazone (0.120 mmol) in CH_2Cl_2 under argon atmosphere followed by addition of solid [$RuCl_2$(dppb)(PPh_3)] (0.058 mmol). The reaction mixtures were kept under stirring at room temperature for 5 h. The solids precipitated upon addition of anhydrous hexane and were filtered and washed with diethylether.

*2.6.1. [Ru(4NO$_2$Fo4M)$_2$(dppb)] · CH$_2$Cl$_2$ (**3**)*

Brown solid. *Anal.* Calc. ($C_{47}H_{48}RuN_8O_4S_2P_2Cl_2$): C, 51.9; H, 4.5; N, 10.3; S, 5.9. Found: C, 52.0; H, 4.6; N, 9.9; S, 5.8%. IR (KBr, cm^{-1}): $\nu_{ass}NO_2$ 1522, ν_sNO_2 1343, ν(C=N) 1585, ν(C=S) 784, ν(Ru–P) 516, ν(Ru–N) 491, ν(Ru–S) 435. Molar conductivity (1×10^{-3} mol L^{-1} CH_2Cl_2): 1.1 μS cm^{-1}. $^{31}P\{^1H\}$ NMR (CH_2Cl_2 δ/ppm): 38.6(s).

*2.6.2. [Ru(4NO$_2$Bz4M)$_2$(dppb)] · 2CH$_2$Cl$_2$ (**4**)*

Brown solid. *Anal.* Calc. for $C_{60}H_{58}RuN_8O_4S_2P_2Cl_4$: C, 54.4; H, 4.4; N, 8.5; S, 4.8. Found: C, 54.1; H, 4.4; N, 8.3; S, 4.6%. IR (KBr, cm^{-1}): $\nu_{ass}NO_2$ 1539, ν_sNO_2 1342, ν(C=N) 1573, ν(C=S) 743, ν(Ru–P) 515, ν(Ru–N) 486, ν(Ru–S) 420. Molar conductivity (1×10^{-3} mol L^{-1} CH_2Cl_2): 0.42 μS cm^{-1}. $^{31}P\{^1H\}$ NMR (CH_2Cl_2 δ/ppm): 38.6 (s).

3. Results and discussion

3.1. Microanalyses and molar conductivity studies of the ruthenium(II) complexes

Microanalyses and molar conductivity data suggest the formation of [Ru(4NO$_2$Fo4M)$_2$(PPh_3)$_2$] (**1**), [Ru(4NO$_2$Bz4M)$_2$(PPh_3)$_2$] (**2**), [Ru(4NO$_2$Fo4M)$_2$(dppb)] (**3**) and [Ru(4NO$_2$Bz4M)$_2$(dppb)] (**4**). In all complexes CH_2Cl_2 crystallization molecules are present, as confirmed by their ^1H NMR spectra.

3.2. Infrared spectral studies

In the infrared spectra, the ν(C=N) stretching vibration of the thiosemicarbazones at 1599 cm^{-1} shifts to 1586–1562 cm^{-1} in the complexes, indicating coordination of the imine nitrogen [6,16,17]. The absorption at 821–830 cm^{-1} in the spectra of the free bases, attributed to the ν(C=S) vibration, shifts to 743–784 cm^{-1} in the spectra of the complexes, indicating coordination through a thiolate sulfur [6,16,17]. Absorptions at 496–486 cm^{-1} and 441–420 cm^{-1} in the spectra of the complexes were tentatively attributed to the ν(Ru–N) and ν(Ru–S) vibrations [18,19]. Hence the infrared spectra indicate coordination through the N–S chelating system.

3.3. NMR spectral studies

The ^1H NMR spectra of the thiosemicarbazones in $CDCl_3$ show a singlet at δ 9.30 which is attributed to N(3)–H. In the spectra of complexes (**1**)–(**4**) ($CDCl_3$) there are no signals attributable to N(3)–H, indicating coordination of the thiosemicarbazones under the anionic form upon deprotonation at N(3). Moreover the singlet at δ 5.27 is compatible with the presence of CH_2Cl_2 solvation molecule in all cases.

In the $^{31}P\{^1H\}$ NMR spectra of the complexes only one singlet was observed in all cases. For complex (**1**) the singlet at δ 38.6 was attributed to *cis*[Ru(4NO$_2$Fo4M)$_2$(PPh_3)$_2$], in which the two PPh_3 molecules are in *cis* position to each other and probably in *trans* position to the imine nitrogens of the thiosemicarbazone chain. In fact, in previous works $^{31}P\{^1H\}$ NMR signals at ca. δ 38 have been assigned by us to phosphines *trans* to the imine nitrogens of the thiosemicarbazone moiety [19,20]. For complex (**2**) the singlet at δ 29.2 was attributed to *trans*[Ru(4-NO_2Bz4M)$_2$(PPh_3)$_2$] in which the two phosphine ligands are *trans* to each other. For complexes (**3**) and (**4**) the singlet occurs at ca. δ 38, suggesting that the phosphorous atoms of the dppb molecule is *trans* to the imine nitrogen of the thiosemicarbazone chain [19–21].

3.4. Electrochemistry

The voltammograms of the thiosemicarbazones show a quasi-reversible process between −0.91 and 0.93 V, which has been attributed to the formation of the Ar-$NO_2^{\cdot-}$ radical. The second process between −1.11 and −1.21 V has been assigned to the formation of the Ar-NHOH species and the irreversible oxidation at 0.20–0.21 V to the formation of Ar-NO (Fig. 2). The observed signals correspond to the well known mechanism for the nitro aromatic reduction, as previously proposed by us [6] and by other authors [22–25]. Eqs. (1)–(3) describe the suggested electrochemical mechanism.

$$\text{Ar-NO}_2 + e^- \leftrightharpoons \text{Ar-NO}_2^{\cdot-} \quad (1)$$

$$\text{Ar-NO}_2^{\cdot-} + 3e^- + 4H^+ \rightarrow \text{Ar-NHOH} + H_2O \quad (2)$$

$$\text{Ar-NHOH} \leftrightharpoons \text{Ar-NO} + 2e^- + 2H^+ \quad (3)$$

The voltammograms of complexes (**1**)–(**4**) show a quasi-reversible process attributed to the Ru^{II}/Ru^{III} oxidation (between 0.68 V and 0.36 V) followed by the Ru^{III}/Ru^{II} reduction (between 0.49 and 0.28 V) (see Table 1). The formation of the Ar-$NO_2^{\cdot-}$ radical has been observed separately in the voltammograms of the complexes (**1**) and (**4**). In the other cases, this radical has not been observed separately, indicating that once formed it reacts immediately. The process occurring in the −1.05 and −1.19 V

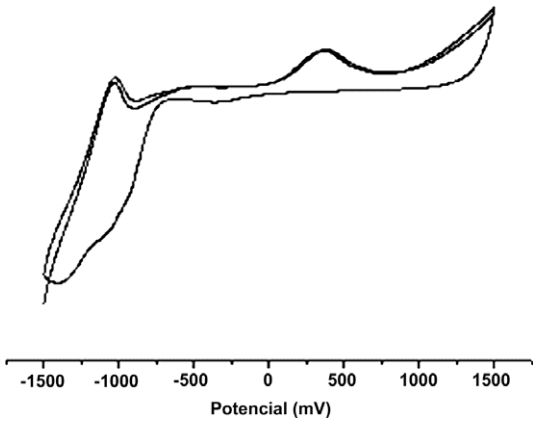

Fig. 2. Cyclic voltammogram of N^4-methyl-4-nitrobenzaldehyde thiosemicarbazone (H4NO$_2$Fo4M) (CH_2Cl_2, 0.1 mol L^{-1} TBAP).

Table 1
Cyclic voltammetry data for the N^4-methyl 4-nitrobenzaldehyde ($H4NO_2Fo4M$) and N^4-methyl 4-nitrobenzophenone thiosemicarbazones ($H4NO_2Bz4M$) (0.100 V s^{-1}, CH_2Cl_2, 0.1 mol L^{-1} TBAP)

Compound	Ar-$NO_2^{\cdot-}$ (V) E_{pc}	Ar-NHOH (V) E_{pc}	Ar-NO (V) E_{pa}
$H4NO_2Fo4M$	−0.93	−1.11	0.21
$H4NO_2Bz4M$	−0.91	−1.21	0.20

range has been attributed to the formation of Ar-NHOH. The remaining processes have been assigned to the thiosemicarbazone moiety, as previously proposed by us [26].

The foregoing results show that the electrochemical behaviors of the two thiosemicarbazones are very similar. Comparison between the values of redox potentials of the two series of complexes (see Table 2) reveal that the complexes with 4-nitrobenzaldehyde thiosemicarbazone undergo oxidation easier than those with 4-nitroacetophenone thiosemicarbazone, probably due to differences in electronic effects of the group attached to C7 (H or C_6H_5). Coordination does not appreciably affect the potential of formation of the Ar-NHOH species, suggesting that its radical precursor must also be formed approximately at the same potential in the free ligands as well as in their corresponding ruthenium(II) complexes.

3.5. Luminescence studies

Similar fluorescence spectra were observed for $H4NO_2Fo4M$, $H4NO_2Bz4M$ and their Ru(II) complexes (Fig. 3). The shapes of the spectral bands of the complexes were characteristic of the thiosemicarbazone ligands with maximum excitation at 214 nm and the respective emission between 293–295 nm. However significantly different fluorescence intensities are observed, which may be explained by the presence of Ru(II) and by the relative rigidity of the molecular structures. When considering $H4NO_2Fo4M$ and its Ru(II) complexes, these effects can be clearly identified. First, the presence of Ru(II) in the molecular structure causes an internal heavy atom effect of transferring electron population from the excited singlet state (S_1) to the excited triplet state (T_1), with a decrease of the population available for the $S_1 \rightarrow S_0$ transition. On the other hand, when the two Ru(II) complexes are compared, the larger fluorescence quantum yield is observed for the more rigid structure, in this case, the $[Ru(4NO_2Fo4M)_2(dppb)]$ (**3**), which is less prone to be affected by radiationless processes caused by the natural vibration of the molecular structure.

For $H4NO_2Bz4M$ and its complexes, the rigidity still explains the higher fluorescence observed for $[Ru(4NO_2Bz4M)_2(dppb)]$ (**4**) comparative to $[Ru(4NO_2Bz4M)_2(PPh_3)_2]$ (**2**). However, fluorescence from (**4**) is also stronger than that characteristic of the $H4NO_2Bz4M$, indicating that the C_6H_5– group of this thiosemicarbazone has a strong contribution to the radiationless loss of energy of the excited state population (through vibrational processes). In this case, the formation of the $[Ru(4NO_2Bz4M)_2(dppb)]$ somehow minimizes vibrational relaxation processes to a point that the fluorescence from $[Ru(4NO_2Bz4M)_2(dppb)]$ is higher than the one from the ligand despite the increase of intercrossing system efficiency caused by Ru(II).

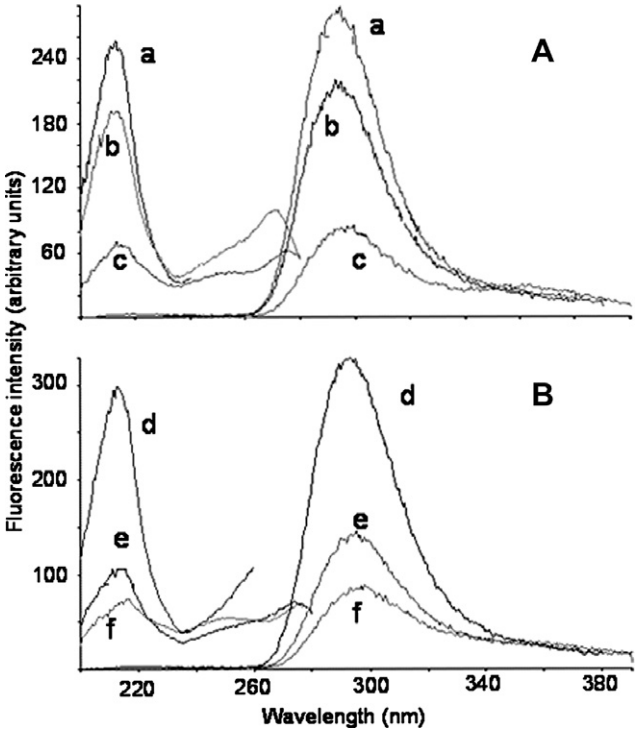

Fig. 3. Emission and excitation fluorescence spectra in CH_2Cl_2 solutions of: A (a) $H4NO_2Fo4M$, (b) $[Ru(4NO_2Fo4M)_2(dppb)]$ (**3**), (c) $[Ru(4NO_2Fo4M)_2(PPh_3)_2]$ (**1**); and B (d) $[Ru(4NO_2Bz4M)_2(dppb)]$ (**4**), (e) $H4NO_2Bz4M$, (f) $[Ru(4NO_2Bz4M)_2(PPh_3)_2]$ (**2**).

No phosphorescence was observed from $H4NO_2Fo4M$, $H4NO_2Bz4M$ and their Ru(II) complexes even if favorable environmental conditions (absence of oxygen, presence of heavy atom enhancers/inducers and in the rigidicity of a dry and solid substrate).

The natural fluorescence from these thiosemicarbazones and their Ru(II) complexes provides a way to identify the presence and to monitor the concentration of these chemical species in biological systems.

3.6. Crystal structure of $H4NO_2Fo4M$

Crystal data and refinement results of $H4NO_2Fo4M$ are shown in Table 3. ORTEP3 view of the structure can be seen in Fig. 4. Table 4 shows selected bond distances [Å] and angles [°]. Hydrogen bonds parameters are shown in Table 5.

$H4NO_2Fo4M$ crystallizes in the triclinic system, P-1 space group with Z = 4 and adopts the *EE* configuration, like N^4-methyl 4-nitroacetophenone thiosemicarbazone ($H4NO_2Ac4M$), the structure of which has been reported previously by us [16].

As expected, the bond distances are very similar in $H4NO_2Fo4M$ and $H4NO_2Ac4M$. However C7–C1 is 1.466(2) in $H4NO_2Fo4M$ and 1.233(4) in $H4NO_2Ac4M$. The C7–N2–N3 and N2–C7–C1 bond angles are 116.70(3)° and 120.77(3)° respectively in $H4NO_2Fo4M$ and 119.6(3)° and 114.6(3)°, respectively, in $H4NO_2Ac4M$, probably due to differences in steric and electronic effects between the group attached to C7 (H or methyl).

The crystal structure of $H4NO_2Fo4M$ is stabilized by N–H···N and C–H···S intra-molecular interactions and by N–H···O, O–H···O, O–H···S and C–H···O intermolecular interactions (Figs. 5a and b). Intra-molecular interactions make both molecules practically planar rigid structures. The angle between the mean plane C1–C2–C3–C4–

Table 2
Cyclic voltammetry data for $[Ru(4NO_2Fo4M)_2(PPh_3)_2]$ (**1**), $[Ru(4NO_2Bz4M)_2(PPh_3)_2]$ (**2**), $[Ru(4NO_2Fo4M)_2(dppb)]$ (**3**) and $[Ru(4NO_2Bz4M)_2(dppb)]$ (**4**) (0.100 V s^{-1}, CH_2Cl_2, 0.1 mol L^{-1} TBAP)

Compound	Ru^{II}/Ru^{III} (V)	Ru^{III}/Ru^{II} (V)	Ar-$NO_2^{\cdot-}$ (V)	Ar-NHOH (V)
$[Ru(4NO_2Fo4M)_2(PPh_3)_2]$ (**1**)	0.36	0.28	−0.99	−1.19
$[Ru(4NO_2Bz4M)_2(PPh_3)_2]$ (**2**)	0.68	0.49	–	−1.12
$[Ru(4NO_2Fo4M)_2(dppb)]$ (**3**)	0.40	0.29	–	−1.05
$[Ru(4NO_2Bz4M)_2(dppb)]$ (**4**)	0.62	0.35	−0.99	−1.18

Table 3
Crystal data for $H4NO_2Fo4M$

Empirical formula	$C_9H_{12}N_4O_3S$
Formula weight	256.29
Temperature (K)	295(2)
Wavelength (Å)	0.71073
Crystal system	triclinic
Space group	$P\bar{1}$
Unit cell dimensions	
a (Å)	7.8686(16)
b (Å)	11.236(2)
c (Å)	13.795(3)
α (°)	83.37(3)
β (°)	81.90(3)
γ (°)	85.10(3)
Volume (Å^3)	1196.4(4)
Z	4
D_{calc} (Mg/m^3)	1.423
Absorption coefficient (mm^{-1})	0.274
$F(000)$	536
Crystal size (mm^3)	0.199 0.543 0.231
Theta range for data collection (°)	3.09–25.00
Index ranges	$-8 \leqslant h \leqslant 9$; $-13 \leqslant k \leqslant 13$; $-16 \leqslant l \leqslant 16$
Reflections collected	28253
Independent reflections	4188 [$R_{(int)}$ = 0.0367]
Completeness to theta = 25.00°	99.5 %
Absorption correction	multi-scan
Refinement method	full-matrix least-squares on F^2
Data/restraints/parameters	4188/0/341
Goodness-of-fit on F^2	1.031
Final R indices [$I > 2$sigma(I)]	R_1 = 0.0365, wR_2 = 0.0875
R indices (all data)	R_1 = 0.0516, wR_2 = 0.0945
Largest difference in peak and hole (e Å^{-3})	0.199 and −0.167

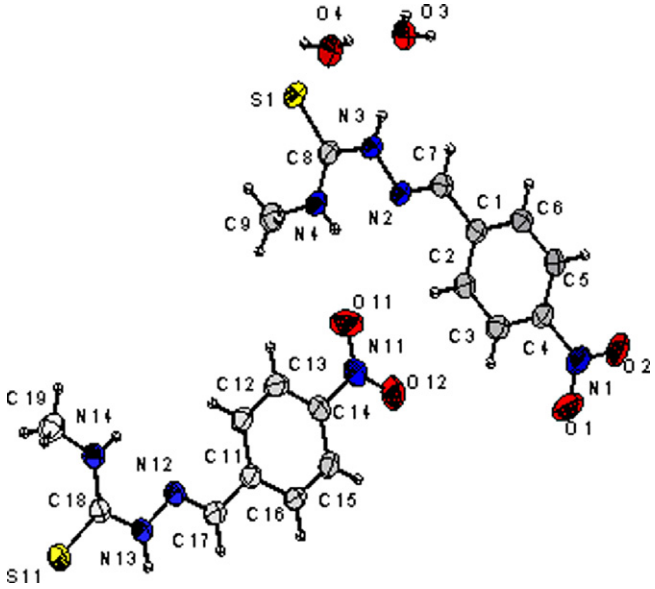

Fig. 4. View of the molecular structure of $H4NO_2Fo4M$ showing the displacement ellipsoids at the 50% probability level.

Table 4
Selected bond lengths (Å) and angles (°) for $H4NO_2Fo4M$

Bond lengths (Å)		Angle (°)	
C(8)–S(1)	1.7000(18)	N(4)–C(8)–S(1)	124.82(14)
C(8)–N(4)	1.323(2)	N(3)–C(8)–S(1)	118.05(14)
C(8)–N(3)	1.354(2)	C(8)–N(3)–N(2)	119.55(16)
N(2)–N(3)	1.374(2)	C(7)–N(2)–N(3)	116.70(16)
C(1)–C(7)	1.466(2)	N(2)–C(7)–H(7)	119.6
N(1)–O(1)	1.228(2)	N(2)–C(7)–C(1)	120.77(16)
N(1)–O(2)	1.223(2)	O(2)–N(1)–O(1)	122.79(18)

Table 5
Geometric parameters for the intra- and intermolecular interactions in $H4NO_2Fo4M$ (Å)

D–H···A (intramolecular)	D–H	H···A	D···A	∠D–H···A
N14–H014···N12	0.86(2)	2.22(2)	2.627(2)	109.0(16)
N^4–H04···N2	0.85(2)	2.236(19)	2.635(2)	108.7(16)
C9–H9C···S1	0.96	2.70	3.141(2)	108
D–H···A (intermolecular)	D–H	H···A	D···A	∠D–H···A
N14–H014···O1^{i}	0.86(2)	2.48(2)	3.174(2)	138.6(18)
N3–H03···O3	0.85(2)	2.13(2)	2.972(2)	176(2)
N^4–H04···O11^{ii}	0.85(2)	2.31(2)	3.018(2)	140.5(18)
O3–H3A···S11^{iii}	0.78(3)	2.45(3)	3.214(2)	168(3)
O3–H3B···S1$^{\#}$	0.90(3)	2.48(3)	3.343(2)	161(3)
N13–H013···O4	0.90(2)	2.11(2)	3.003(3)	169(2)
O4–H4A···O3$^{\#\#}$	0.89(4)	2.04(4)	2.903(3)	164(3)
O4–H4B···S1$^{\#}$	0.76(3)	2.66(3)	3.389(2)	161(3)
C9–H9A···O12	0.96	2.53	3.436(3)	158

Standard deviations in parentheses.
Symmetry operation: i = 1 − x, −y, −z; ii = −x, 1 − y, −z; iii = 1 − x, −y, 1 − z; # = −x, 1 − y, 1 − z; ## = 1 + x, y, z.

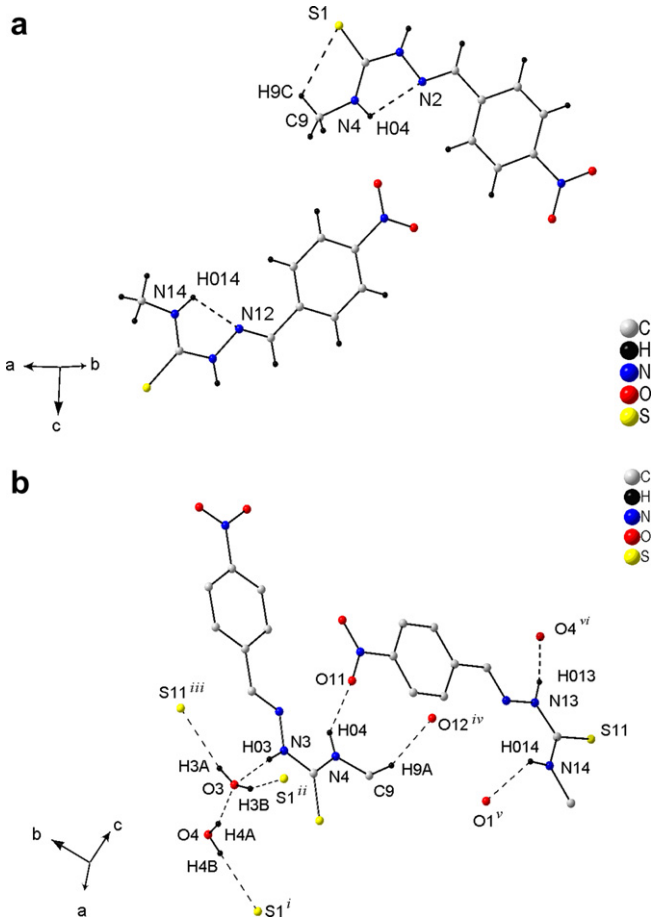

Fig. 5. View of (a) intra-molecular interactions *via* N–H···N classical H-bond and C–H···S non classical H-bond (b) and intermolecular interactions *via* O–H···O, O–H···S, N–H···O classical H-bonds and C–H···O non classical H-bond. Symmetry code (i) 1 − x, 1 − y, 1 − z; (ii) −x, 1 − y, 1 − z; (iii) −1 + x, 1 + y, −1 + z; (iv) −x, 1 − y, 2 − z; (v) 1 + x, −1 + y, z; (vi) 1 − x, 1 − y, −z.

C5–C6 and the plane involving N2–N3–C8–N4 is 3.87(1)° and that between the C11–C12–C13–C14–C15–C16 and N12–N13–C18–N14 planes is 6.35(1)°. In $H4NO_2Ac4M$ this angle is 24.7(2)°. Fig. 6 shows the primitive cell in the [0 0 1] direction.

The values of densities and melting points of $H4NO_2Fo4M$ (1.423 Mg/m^3, 225–226 °C) and $H4NO_2Ac4M$ (1.404 Mg/m^3,

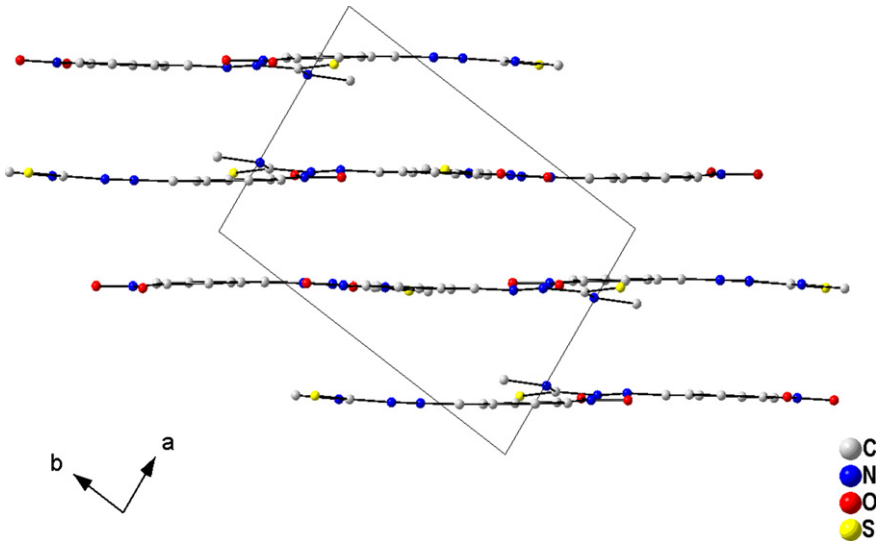

Fig. 6. View of the primitive cell of $H4NO_2Fo4M$ with molecules in a planar arrangement.

216.3–217.6 °C) [16]) are in agreement with a closer packing for the first, as revealed by crystal structure determinations.

4. Conclusions

The above mentioned results suggest that the studied complexes might present anti-trypanosomal activity. Moreover, the intrinsic fluorescence of the thiosemicarbazones and their Ru(II) complexes could be useful for monitoring their uptake into cells and in the investigation of their mechanisms of action.

Acknowledgments

The authors are grateful to Professor R. Guimarães (LDRX), UFF, Brazil, for use of the diffractometer facility. Financial support from CNPq and Fapesp from Brazil is acknowledged.

Appendix A. Supplementary data

CCDC 676878 contains the supplementary crystallographic data for this paper. These data can be obtained free of charge via http://www.ccdc.cam.ac.uk/conts/retrieving.html, or from the Cambridge Crystallographic Data Centre, 12 Union Road, Cambridge CB2 1EZ, UK; fax: (+44) 1223-336-033; or e-mail: deposit@ccdc.cam.ac.uk. Supplementary data associated with this article can be found, in the online version, at doi:10.1016/j.poly.2008.06.002.

References

[1] A. Buschini, F. Giordani, C.N. Albuquerque, C. Pellacani, G. Pelosi, C. Rossi, T.M.A.D. Zucchi, P. Poli, Biochem. Pharmacol. 73 (2007) 1537.
[2] S.N.J. Moreno, R.P. Mason, R. Docampo, J. Biol. Chem. 259 (1984) 6298.
[3] S.N.J. Moreno, R. Docampo, R.P. Mason, W. Leon, A.O.M. Stoppani, Arch. Biochem. Biophys. 218 (1982) 585.
[4] R. Docampo, S.N.J. Moreno, A.O.M. Stoppani, W. Leon, F.S. Cruz, F. Villalta, R.F. Muniz, Biochem. Pharmacol. 30 (1981) 1947.
[5] H. Beraldo, D. Gambino, Mini. Rev. Med. Chem. 4 (2004) 31.
[6] A. Perez-Rebolledo, L.R. Teixeira, A.A. Batista, A.S. Mangrich, G. Aguirre, H. Cerecetto, M. Gonzalez, Paola Hernandez, A.M. Ferreira, N.L. Speziali, Heloisa Beraldo, Eur. J. Med. Chem. 43 (2008) 939.
[7] R.A. Sanchez-Delgado, A. Amzelotti, Mini-Rev. Med. Chem. 4 (2004) 23.
[8] C.E. Cardoso, R.Q. Aucelio, J. Brazil Chem. Soc. 17 (2006) 323.
[9] Nonius. COLLECT. Nonius BV, Delft, The Netherlands, 1998.
[10] A.J.M. Duisenberg, R.W.W. Hooft, A.M.M. Schreurs, J. Kroon, J. Appl. Crystallogr. 33 (2000) 893.
[11] A.J.M. Duisenberg, L.M.J. Kroon-Batenburg, A.M.M. Schreurs, J. Appl. Crystallogr. 36 (2003) 220.
[12] G.M. Sheldrick, SADABS, Program for Empirical Absorption Correction of Area Detector Data, University of Göttingen, Germany, 1996.
[13] G.M. Sheldrick, SHELX97, Program for the Refinement of Crystal Structures, University of Gottingen, Germany, 1997.
[14] D.E. Linn, J. Chem. Educ. 76 (1999) 70.
[15] A.M. Joshi, I.S. Thorburn, S.J. Rettig, B.R. James, Inorg. Chim. Acta 198–200 (1992) 283.
[16] A. Perez-Rebolledo, I.C. Mendes, N.L. Speziali, P. Bertani, J.M. Resende, A.F.C. Alcantara, H. Beraldo, Polyhedron 26 (2007) 1449.
[17] D. Gambino, L. Otero, M. Vieites, M. Boiani, M. González, E.J. Baran, H. Cerecetto, Spectrochim. Acta Part A 68 (2007) 341.
[18] A.E. Graminha, A.A. Batista, I.C. Mendes, L.R. Teixeira, H. Beraldo, Spectrochim. Acta Part A 69 (2008) 1277.
[19] A.E. Graminha, A.A. Batista, J. Ellena, E.E. Castellano, L.R. Teixeira, I.C. Mendes, H. Beraldo, J. Mol. Struct. 875 (2008) 219.
[20] A.E. Graminha, C. Rodrigues, A.A. Batista, L.R. Teixeira, E.S. Fagundes, H. Beraldo, Spectrochim. Acta Part A 69 (2008) 1073.
[21] J. Martinez, L.A. Adrio, J.M. Antelo, M.T. Pereira, J.J. Fernandez, J.M. Vila, Polyhedron 25 (2006) 2848.
[22] S. Bollo, L.J. Nunez-Vergara, M. Bonta, G. Chauviere, J. Perie, J.A. Squella, J. Electroanal. Chem. 511 (2001) 46.
[23] J.C.M. Cavalcanti, N.V. Oliveira, M.A.B.F. de Moura, R. Fruttero, M. Bertinaria, M.O.F. Goulart, J. Electroanal. Chem. 571 (2004) 177.
[24] P.C. Mandal, J. Electroanal. Chem. 570 (2004) 55.
[25] S. Bollo, L.J. Nunez-Vergara, J.A. Squella, J. Electroanal. Chem. 562 (2004) 9.
[26] A. Perez-Rebolledo, O.E. Piro, E.E. Castellano, L.R. Teixeira, A.A. Batista, H. Beraldo, J. Mol. Struct. 794 (2006) 18.

molecules [26]), and the character of ligands (bpy *versus* phen), in terms of inductive and anisotropic effects, caused by LL and Cl groups within a given coordination sphere/geometry. Finally, we have calculated the respective δ^{1H}_{calc}, δ^{13C}_{calc}, δ^{15N}_{calc} parameters by semi-empirical quantum-chemical methods (B3LYP/LanL2DZ+6-31G**// B3LYP/LanL2DZ+6-31G*).

An additional advantage of these multinuclear magnetic resonance studies is the confirmation of N(1),N(1′) chelation mode of bpy and phen {due to the simplicity and easier comparison of the concerned N-donor ligands, also in case of phen we will use its symmetric numbering C(1a)–N(1)···C(5)–C(5′)···N(1′)–C(1a′), instead of the common one C(1a)–N(1)···C(5)–C(6)···N(10)–C(10a)}. In fact, such bidentate coordination was proved till now only for solid *cis*-[Ir(bpy)$_2$Cl$_2$]Cl · 2H$_2$O and *cis*-[Ir(phen)$_2$Cl$_2$]-NO$_3$ · 3H$_2$O (basing on similarity of their X-ray powder diffraction patterns to the respective Co(III), Rh(III) and Cr(III) analogues [29]), as well as for *cis*-[Ir(phen-κ^{2}N(1),N(1′))$_2$Cl$_2$]PF$_6$ (by single crystal X-ray diffraction (AMIPIV) [30]; all reference codes in this paper derive from the Cambridge Structural Database [31]). Especially in case of bpy this problem is worthy to be discussed as its Ir(III) complexes often exhibit alternative complexation types, either in the solid phase ([Ir(bpy)$_2$(bpy*)]$^{3+}$ in [Ir(bpy-κ^{2}N(1),N(1′))$_2$(bpy*-κ^{2}N(1),C(3′))](ClO$_4$)$_3$ · H$_2$O (BARWIA, BARWIA01) [32,33] and [Ir(bpy)$_2$(bpy**)]$^{2+}$ in [Ir(bpy-κ^{2}N(1),N(1′))$_2$(bpy**-κ^{2}N(1),C(3′))](ClO$_4$)$_2$ · 1/3H$_2$O (CEDYOZ) [16] {bpy*, bpy** = the neutral/negatively (−1) charged N(1),C(3′)-coordinated bpy species, deprotonated at C(3′) and protonated/unprotonated at N(1′)}, together with [Ir(bpy)$_3$]$^{3+}$ in [Ir(bpy-κ^{2}N(1),N(1′))$_3$](ClO$_4$)$_3$ · 7/3H$_2$O (CEZMAV) [32]) or in the solution ([Ir(bpy)(bpy**)Cl]$_2^{2+}$ [34], [Ir(bpy)$_2$(bpy*)]$^{3+}$ [35–37], [Ir(bpy)$_2$(bpy**)]$^{2+}$ [16,37,38], [Ir(bpy)$_2$(bpy***)(H$_2$O)]$^{3+}$ {bpy*** = the neutral, monodentately N(1)-coordinated bpy molecule} [15,39,40], [Ir(bpy)$_2$(bpy · H$_2$O)]$^{3+}$ {bpy · H$_2$O = the covalently hydrated, neutral N(1),N(1′)-chelated bpy molecule} [41], [Ir(bpy)$_2$(bpy***)(OH)]$^{2+}$ [15,42,43], together with [Ir(bpy)$_3$]$^{3+}$ [16,24,44,45]).

2. Experimental

2.1. Materials

K$_3$[IrCl$_6$] was purchased from Aldrich, while bpy and phen · H$_2$O (>99% purity) from POCh Gliwice (Poland).

2.2. Syntheses

K$_2$[Ir(H$_2$O)Cl$_5$] was prepared in a way similar to that described by Delepine [46] and Sinitsyn et al. [8]. Fifty-two milligrams of K$_3$[IrCl$_6$] were dissolved in 50 cm^3 of water and left at the room temperature for 1 week (during which the aquation reaction of [IrCl$_6$]$^{3-}$ + H$_2$O → [Ir(H$_2$O)Cl$_5$]$^{2-}$ + Cl$^-$ spontaneously occurred), with slow evaporation to *ca.* 10 cm^3. The yield of the precipitated K$_2$[Ir(H$_2$O)Cl$_5$] green-brown powder was 37 mg (*ca.* 80%).

Both K[Ir(LL)Cl$_4$] coordination compounds were synthesised by the method of Lee et al. [13], *i.e.* by moderate heating (50 °C, 1 h) of water + ethanol (1:1) solutions containing K$_3$[IrCl$_6$] and bpy or phen (at the 1:1 stoichiometric ratios). *cis*-[Ir(bpy)$_2$Cl$_2$]Cl · 2H$_2$O was obtained according to Watts et al. [15], *i.e.* by intense heating (150 °C, 6 h) of K$_3$[IrCl$_6$] and bpy in glycerol, whereas *cis*-[Ir(phen)$_2$Cl$_2$]Cl · 3H$_2$O was prepared following Gillard et al. [14], *i.e.* by stirring K$_3$[IrCl$_6$] in the melted phen · H$_2$O (110 °C; 6 h); in both cases the fivefold excess of the respective azine ligand (K$_3$IrCl$_6$:LL = 1:10) was used. In all preparations the final reaction mixtures were cooled to the room temperature, and the formed ionic complexes were extracted with water (owing to the insolubility of bpy/phen). They were then separated from the simultaneously formed KCl and/or unreacted K$_3$[IrCl$_6$] by precipitation upon cooling to 5 °C. The yields were *ca.* 30–40%.

2.3. Instrumentation

The far-IR spectra were measured in the 100–400 cm^{-1} range with a Perkin–Elmer Spectrum 2000 FT-IR spectrometer, using polyethylene discs. The ^{1}H–^{13}C and ^{1}H–^{15}N HMBC/HSQC/HMQC spectra (^{1}H, ^{13}C referenced to TMS; ^{15}N to external CH$_3$NO$_2$) were measured in saturated D$_2$O (bpy complexes) or DMSO-d_6 (phen complexes) solutions, at 303 K, using a Varian INOVA 500-MHz NMR spectrometer, equipped with an inverse ^{1}H{^{31}P/^{15}N} 5 mm Z-SPEC Nalorac probe with an actively shielded *z*-gradient coil. The pulse sequencies were principally the same as those used during our earlier studies on the coordination compounds with some other transition metals [26,27]. Some additional ^{1}H NMR measurements for K[Ir(bpy)Cl$_4$] in DMSO-d_6 and K[Ir(phen)Cl$_4$] in D$_2$O were performed by a Bruker Avance 300-MHz NMR spectrometer.

2.4. Crystal structure determination

The green-brown single crystals of K$_2$[Ir(H$_2$O)Cl$_5$] (0.22 × 0.16 × 0.09 mm) were obtained by slow evaporation of the aqueous solution. The X-ray diffraction data were measured with an Oxford Sapphire CCD diffractometer using the Mo Kα radiation (λ = 0.71073 Å), at 293(2) K, by the ω–2θ method. The θ range was 2.99–31.47°. The number of reflections was 7610 ($-19 \leqslant h \leqslant 18$, $-13 \leqslant k \leqslant 11$, $-10 \leqslant l \leqslant 9$) with 1494 independent [R_{int} = 0.0480]. The data were numerically corrected for absorption correction with the OXFORD RED 171 program package [47] with the maximum/minimum transmissions of 0.3290/0.1193. The final *R* indices were as follows: R_1 = 0.0259, wR_2 = 0.0537 (for [$I > 2\sigma(I)$] reflections) and R_1 = 0.0285, wR_2 = 0.0548 (for all data). The structure was solved with the Patterson method, using the SHELX97 program package [48].

2.5. Quantum-chemical calculations

The geometry of free bpy and phen was already determined upon our previous studies on some other transition metal complexes [26,27], whereas that for the Ir(III) complexes was primarily constructed by molecular modelling with Hyperchem 5.1, and then optimised with B3LYP/LanL2DZ+6-31G*. The quantum-chemical calculations of the ^{1}H, ^{13}C and ^{15}N NMR shielding constants, allowing to compute the relevant chemical shifts, were performed using B3LYP/LanL2DZ+6-31G**, in two versions: (a) for isolated molecules; (b) for H$_2$O- or DMSO-solvated species. The methodology was generally the same as described in our previous reports for some Pd(II) and Pt(II) complexes with the derivatives of bpy or phen, as well as with quinolines [49,50]. All calculations were done with the GAUSSIAN03 [51] software installed in the supercomputing centres in Brno and Prague (Czech Republic).

3. Results and discussion

3.1. Crystal and molecular structure of potassium aquapentachloroiridate(III) – K$_2$[Ir(H$_2$O)Cl$_5$]

The perspective view of the K$_2$[Ir(H$_2$O)Cl$_5$] ionic molecule is presented at Fig. 1, while its packing in the crystal lattice – at Fig. 2 (PLATON [52]). The crystal structure data are collected in Table 1, whereas the bond lengths and angles within the [Ir(H$_2$O)Cl$_5$]$^{2-}$ anion – in Table 2.

The crystallographic parameters for K$_2$[Ir(H$_2$O)Cl$_5$] are in agreement with those determined by the X-ray powder diffraction

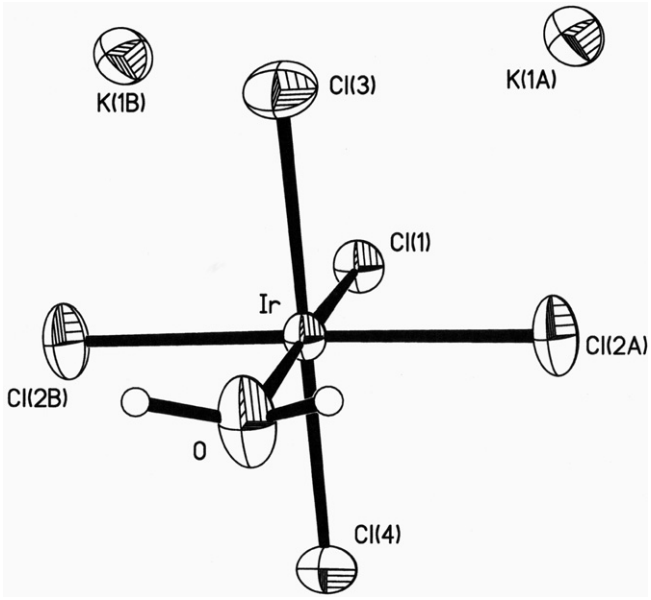

Fig. 1. Molecular structure of $K_2[Ir(H_2O)Cl_5]$.

(orthorhombic; a = 13.58 Å, *b* = 9.26 Å, c = 7.16 Å; *Pnma* space group [8]). They are also very similar to those for $Rb_2[Ir(H_2O)Cl_5]$ (*a* = 13.85(3) Å, *b* = 9.67(2) Å, *c* = 7.23(2) Å, *Pnma* [5]), the respective unit cell dimensions being smaller by only *ca.* 2%. Thus, the increase of the alkali metal ionic radius (from 1.38 Å for K^+ to 1.52 Å for Rb^+ [53]) is insufficient to change the crystal packing of both aquapentachloroiridates(III); however, in case of much larger Cs^+ ions (1.67 Å [53]), *i.e.* for $Cs_2[Ir(H_2O)Cl_5]$, the space group (*Cmcm*) and the unit cell parameters (*a* = 17.283(2) Å, *b* = 8.014(2) Å, *c* = 7.372(1) Å) [5] are different, although the crystal system remains orthorhombic. On the other hand, the replacement of the H_2O ligand by the isoelectronic NH_3 group only slightly affects the crystallization mode, as both potassium and ammonium amminepentachloroiridates(III) are nearly isostructural to $K_2[Ir(H_2O)Cl_5]$ ($K_2[Ir(NH_3)Cl_5]$ – *a* = 13.426(4) Å, *b* = 10.015(2) Å, *c* = 6.8717(7) Å, *Pnma* [7]; $(NH_4)_2[Ir(NH_3)Cl_5]$ – *a* = 13.500(2) Å, *b* = 10.285(3) Å, *c* = 6.896(2) Å, *Pnma* [9]).

Table 1
Crystal structure data for $K_2[Ir(H_2O)Cl_5]$

Compound	$K_2[Ir(H_2O)Cl_5]$
Empirical formula	$Cl_5H_2IrK_2O$
Molecular weight	465.67
Crystal system	orthorhombic
Space group	*Pnma*
a (Å)	13.613(3)
b (Å)	9.391(2)
c (Å)	7.186(1)
α (°)	90
β (°)	90
γ (°)	90
V (Å^3)	918.7(3)
Z	4
Density (Mg/m^3)	3.367
μ (mm^{-1})	16.818
Temperature (K)	293(2)
Wavelength (Å)	0.71073
Reflections collected/unique	7160/1494
Final R_1/wR_2 indices [$I > 2\sigma(I)$] (all data)	0.0285/0.0548

The molecular structure of $K_2[Ir(H_2O)Cl_5]$ (Fig. 1) generally resembles that of $K_2[Ir(NH_3)Cl_5]$ [7], and, besides a various crystal packing, $Cs_2[Ir(H_2O)Cl_5]$ [5]. The Ir–O bond length (2.090(4) Å) is comparable to that in $Cs_2[Ir(H_2O)Cl_5]$ (2.091(2) Å [5]) or $[Pt(NH_3)_4][Ir(H_2O)Cl_5] \cdot 2H_2O$ (2.10(1) Å [6]), while the axial Ir–Cl(1) bond (2.322(1) Å) is slightly shorter than the equatorial Ir–Cl(2a,2b,3,4) ones (2.346(2)–2.360(2) Å). An analogous decrease of the interatomic distance between the Ir(III) central atom and

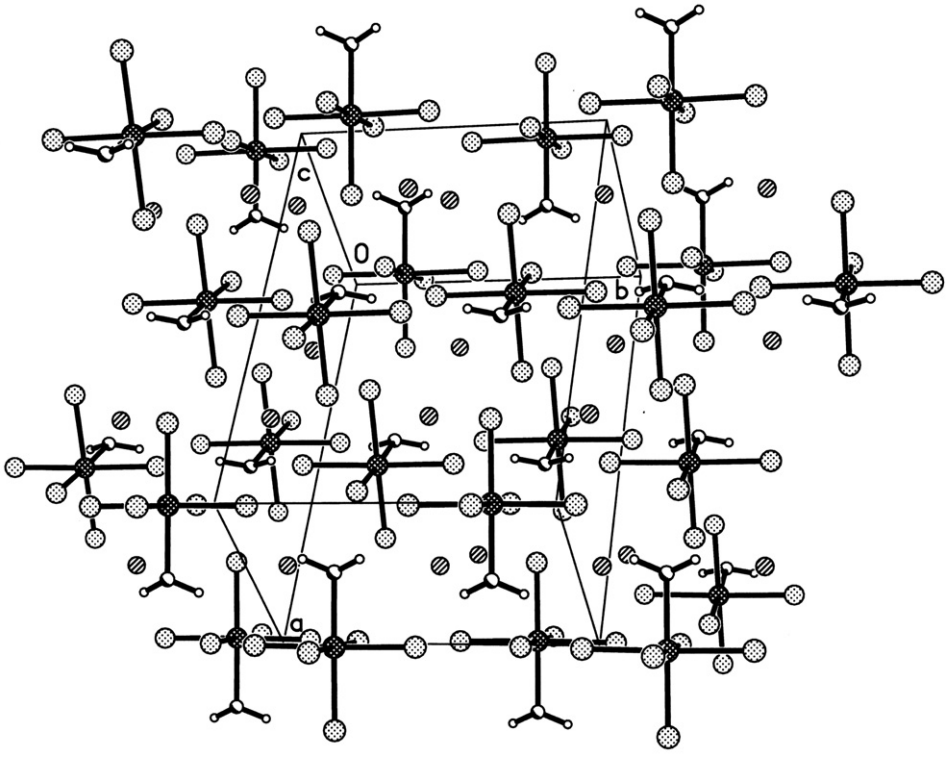

Fig. 2. Crystal packing of $K_2[Ir(H_2O)Cl_5]$.

Table 2
Geometry of $[Ir(H_2O)Cl_5]^{2-}$ in crystalline $K_2[Ir(H_2O)Cl_5]$

Bond length	(Å)	Angle	(°)
Ir–O	2.090(4)	O–Ir–Cl(1)	177.7(2)
Ir–Cl(1)	2.322(1)	Cl(2a)–Ir–Cl(2 b)	178.53(5)
Ir–Cl(2a/2b)	2.347(1)	Cl(3)–Ir–Cl(4)	179.29(6)
Ir–Cl(3)	2.346(2)	O–Ir–Cl(2a/2b)	89.35(3)
Ir–Cl(4)	2.360(2)	O–Ir–Cl(3)	91.4(2)
		O–Ir–Cl(4)	87.9(2)
		Cl(1)–Ir–Cl(2a/2b)	90.64(3)
		Cl(1)–Ir–Cl(3)	90.99(6)
		Cl(1)–Ir–Cl(4)	89.71(5)
		Cl(2a/2b)–Ir–Cl(3)	90.36(3)
		Cl(2a/2b)–Ir–Cl(4)	89.63(3)

Cl(1) is *trans* to O; Cl(2a) is trans to Cl(2b) (both chlorides being related by (x, $-y+3/2$, z) symmetry operation).
Cl(3) is trans to Cl(4) (both chlorides being symmetry-independent).

the chloride anion positioned *trans* to water was noted for $Cs_2[Ir(H_2O)Cl_5]$ ($Ir–Cl_{ax}$ 2.315(1) Å *versus* $Ir–Cl_{eq}$ 2.350(1) Å [5]) and $[Pt(NH_3)_4][Ir(H_2O)Cl_5]\cdot 2H_2O$ ($Ir–Cl_{ax}$ 2.334(4) Å *versus* $Ir–Cl_{eq}$ 2.347(4)–2.373(4) Å [6]), whereas upon the presence of ammonia this effect was opposite (in $K_2[Ir(NH_3)Cl_5]$: $Ir–Cl_{ax}$ 2.365(3) Å *versus* $Ir–Cl_{eq}$ 2.337(3)–2.364(3) Å [7]). An evident elongation of the Ir–Cl(4) bond (2.360(2) Å) comparing to the formally analogous Ir–Cl(2a/2b) and Ir–Cl(3) ones (2.346(2)–2.347(1) Å) reflects a low symmetry of the $[Ir(H_2O)Cl_5]^{2-}$ anion. Nevertheless, the whole range of the Ir–Cl bond lengths in $K_2[Ir(H_2O)Cl_5]$ (2.322(1)–2.360(2) Å) is comparable to that reported for some hexachloroiridate(III) alkali metal salts (2.35(1)–2.37(1) Å for $K_3[IrCl_6]$, $K_3[IrCl_6]\cdot H_2O$ and $(NH_4)_3[IrCl_6]$ [5,54]).

The deviations from an octahedral symmetry concerning the $[Ir(H_2O)Cl_5]^{2-}$ anion can be also characterised by the O–Ir–Cl and Cl–Ir–Cl angles, which are not exactly equal to 180° or 90°, but vary from 177.7(2)° to 179.3(1)°, or from 87.9(2)° to 91.4(2)°. In $Cs_2[Ir(H_2O)Cl_5]$ these parameters were in the 177.3(2)–180.0(0)° or 88.7(1)–91.3(1)° ranges [5], while in $K_2[Ir(NH_3)Cl_5]$ the respective N–Ir–Cl and Cl–Ir–Cl angles ranged from 178.3(1)° to 178.7(1)° or from 88.0(3)° to 90.8(1)° [7]. Generally, such distortions seem to be caused by the replacement of one Cl ligand with a H_2O or NH_3 molecule, as well as by some $K^+\cdots Cl^-$ electrostatic interactions.

In the crystal lattice of $K_2[Ir(H_2O)Cl_5]$, the adjacent $[Ir(H_2O)Cl_5]^-$ anions are positioned in this way that the Cl(1), Cl(3), H_2O, Cl(4) ligands approximately replace each other upon the 90° or 180° rotation around the Cl(2a)–Ir–Cl(2b) axis (Fig. 2). Such a molecular packing is analogous to that described for $K_2[Ir(NH_3)Cl_5]$ [7], what explains the above mentioned crystallographic parameters similarity. All K^+ cations can be generated from one another by several symmetry operations, starting from K(1a) – K(1b) by (x, $-y+3/2$, z); K(1c) by ($-x+1/2$, $y-1/2$, $z-1/2$); K(1d) by ($-x+1/2$, $-y+2$, $z-1/2$); K(1e) by ($x+1/2$, y, $-z+3/2$); K(1f) by ($x+1/2$, $-y+3/2$, $-z+3/2$); K(1g) by ($-x+1/2$, $-y+2$, $z+1/2$); K(1h) by ($-x+1/2$, $y-1/2$, $z+1/2$). Generally, the potassium atoms can be classified into the two categories – distant from Ir(III) by 4.017(2) Å and by 4.067(2) Å. Each of the Cl(1), Cl(3) and Cl(4) chlorides interacts with four K^+ ions (the $Cl\cdots K$ distances varying from 3.241(2) to 3.278(2) Å, from 3.241(2) to 3.412(2) Å, and from 3.229(2) to 3.316(2) Å, respectively), whereas both symmetry-related (x, $-y+3/2$, z) Cl(2a) and Cl(2b) atoms exhibit two relatively short $Cl\cdots K$ contacts (3.247(2) and 3.371(2) Å) and one much longer (3.662(2) Å). The most adjacent potassium cations are distant from one another by 4.521(2) or 4.525(1) Å. No interactions between K^+ and H_2O are present, the shortest $K\cdots O$ distance being as much as 5.619(5) Å.

The similarity of the unit cell parameters for $K_2[Ir(H_2O)Cl_5]$ and $Rb_2[Ir(H_2O)Cl_5]$ [5], as well as of the single crystal X-ray data for $K_2[Ir(H_2O)Cl_5]$ and $Cs_2[Ir(H_2O)Cl_5]$ [5] suggests that all concerned alkali metal salts have analogous molecular structures (despite a variable packing). The same conclusion concerns $(NH_4)_2[Ir(H_2O)Cl_5]$, owing to its analogy with $(NH_4)_2[Ir(NH_3)Cl_5]$ [9] (isostructural to $K_2[Ir(NH_3)Cl_5]$ [7] and $K_2[Ir(H_2O)Cl_5]$ [8]). Hence, the presently described X-ray structure of potassium aquapentachloroiridate(III) can be regarded as typical for the whole class of the $M_2[IrLCl_5]$ compounds (M = K, NH_4, Rb, Cs; L = H_2O, NH_3).

3.2. Far-IR spectroscopy

The far-IR spectra of both $K[Ir(LL)Cl_4]$ complexes reveal four ν_{IrCl} stretching modes, what is consistent with the $2A_1 + B_1 + B_2$ pattern (predicted by the group theory for such a MX_2Y_4 octahedral species of the C_{2v} symmetry [55]) – 334, 315, 310, 299 cm^{-1} (for LL = bpy) and 341, 315, 305, 290 cm^{-1} (for LL = phen). These wave numbers are nearly identical with those reported for $(bpyH)[Ir(bpy)Cl_4]$ (333, 316, 309, 300 cm^{-1}) and $(phenH)[Ir(phen)Cl_4]$ (340, 304, 291 cm^{-1} [10] or 340, 313, 303, 290 cm^{-1} [11]). They are, however, *ca.* 10–25 cm^{-1} smaller comparing to the analogous Ir(IV) species ($[Ir(bpy)Cl_4]$ – 344, 336, 320, 314 cm^{-1}; $[Ir(phen)Cl_4]$ – 365, 338, 330, 318 cm^{-1} [10] or 364, 339, 330, 317 cm^{-1} [11]), what is an obvious consequence of a lower oxidation state [55].

The analogous measurements for both *cis*-$[Ir(LL)_2Cl_2]Cl\cdot nH_2O$ compounds exhibit two ν_{IrCl} vibrations ($A_1 + B_1$ [55]) – 333, 309 cm^{-1} (for LL = bpy) and 337, 313 cm^{-1} (for LL = phen). These values are close to those published for *cis*-$[Ir(phen)_2Cl_2]Cl$ (338, 313 cm^{-1} [11] or 340, 310 cm^{-1} [22]) and *cis*-$[Ir(phen)_2Cl_2]BF_4$ (336, 319 cm^{-1} [10]), as well as for some Ir(III)–chloride–pyridine complexes containing a similar IrN_4Cl_2 chromophore (338 cm^{-1} for *trans*-$[Ir(py)_4Cl_2]Cl$, and 332, 325 cm^{-1} for *cis*-$[Ir(py)_4Cl_2]Cl$] [56]).

3.3. ^1H NMR spectra

The ^1H NMR spectra of $K[Ir(bpy)Cl_4]$ and $K[Ir(phen)Cl_4]$ have been measured in D_2O and DMSO-d_6, *cis*-$[Ir(bpy)_2Cl_2]Cl$ – in D_2O, *cis*-$[Ir(phen)_2Cl_2]Cl$ – in DMSO-d_6. The δ^{1H} chemical shifts and the Δ^{1H}_{coord} coordination shifts (determined in respect to free bpy or phen in DMSO-d_6) are listed in Table 3.

$K[Ir(bpy)Cl_4]$ is well soluble and relatively stable in D_2O, what has allowed to detect also its ^{13}C and ^{15}N NMR spectra (*vide infra*). Nevertheless, in the aqueous medium a slow hydrolysis occurs as gradually some new ^1H signals appear at *ca.* 9.5, 8.5, 8.0, 7.7 ppm (being of *ca.* 20% and *ca.* 50% total intensity, respectively, after 24 and 120 h). Because no liberation of free bpy is observed, one can assume the substitution by the water molecules concerns only the chlorides and not the azine ligands. The solubility of $K[Ir(bpy)Cl_4]$ in DMSO-d_6 is even better but its decomposition, resulting from a well-known ligating ability of this NMR solvent, is much faster; hence, the simple ^1H NMR studies have been done but not the time-consuming $^1H–^{13}C$ or $^1H–^{15}N$ HMBC/HSQC/HMQC experiments.

$K[Ir(phen)Cl_4]$ is more inert and can be studied in both solvents, the content of the formed by-products, after 24 h, not exceeding 5–10%. However, it is sparingly soluble in D_2O and only its ^1H NMR spectrum has been successfully measured, whereas in DMSO-d_6 the ^{13}C and ^{15}N NMR signals have been detected as well using heteronuclear correlation methods (*vide infra*).

cis-$[Ir(bpy)_2Cl_2]Cl$ is easily dissolved in both D_2O and DMSO-d_6, but in the latter solvent it decomposes and thus its ^1H, ^{13}C and ^{15}N NMR measurements have been performed only in the aqueous medium. In contrast, *cis*-$[Ir(phen)_2Cl_2]Cl$ is too weakly soluble in water even for the ^1H NMR studies, while its solubility and stability in DMSO-d_6 has been sufficient to detect all types of the NMR spectra.

Table 3
^{1}H NMR chemical shifts (δ^{1H}, ppm) of Ir(III) chloride complexes with bpy or phen, in D_2O (A) or DMSO-d_6 (B); ^{1}H coordination shifts (Δ^{1H}_{coord}, ppm) are in parentheses

Compound	H(3)	H(4)	H(5)	H(6)
Bpy[B]	8.39	7.95	7.46	8.69
K[Ir(bpy)Cl_4][A,a]	8.47 (+0.08)	8.12 (+0.17)	7.80 (+0.34)	9.60 (+0.91)
K[Ir(bpy)Cl_4][B]	8.50 (+0.11)	8.20 (+0.25)	7.90 (+0.44)	9.70 (+1.01)
cis-[Ir(bpy)$_2Cl_2$]Cl (H)[A,a,b,c,d]	8.53 (+0.14)	8.10 (+0.15)	7.41 (−0.05)	7.72 (−0.97)
cis-[Ir(bpy)$_2Cl_2$]Cl (H′)[A,a,b,c,d]	8.65 (+0.26)	8.43 (+0.48)	8.02 (+0.56)	9.63 (+0.94)
Difference between H′ and H	+0.12	+0.33	+0.61	+1.91
	H(2)	H(3)	H(4)	H(5)
Phen[B]	9.11	7.79	8.50	8.00
K[Ir(phen)Cl_4][A,a]	9.65 (+0.54)	8.02 (+0.23)	8.55 (+0.05)	8.15 (+0.15)
K[Ir(phen)Cl_4][B]	9.88 (+0.77)	8.08 (+0.29)	8.56 (+0.06)	8.23 (+0.23)
cis-[Ir(phen)$_2Cl_2$]Cl (H)[B,d]	8.07 (−1.04)	7.70 (−0.09)	8.75 (+0.25)	8.37 (+0.37)
cis-[Ir(phen)$_2Cl_2$]Cl (H′)[B,d]	9.95 (+0.84)	8.48 (+0.69)	9.15 (+0.65)	8.50 (+0.50)
Difference between H′ and H	+1.88	+0.78	+0.40	+0.13

In the *cis*-[Ir(LL)$_2Cl_2$]$^+$ cations: the protons denoted as H and H′ correspond to these halves of each LL ligand which are positioned *trans* to chlorine and *trans* to another nitrogen, respectively.

[a] Δ^{1H}_{coord} determined for complexes in D_2O *versus* free ligands in DMSO-d_6.

[b] ^{1}H literature data for *cis*-[Ir(bpy)$_2Cl_2$]CF_3SO_3, in CD_3CN: 9.77, 8.56, 2 × 8.42, 8.08, 7.98, 7.72, 7.39 (unassigned) [24]; for *cis*-[Ir(bpy)$_2Cl_2$]PF_6, in DMSO: H(3′) 8.91, H(4′) 8.50, H(5′) 8.15, H(6′) 9.65, H(3) 8.82, H(4) 8.20, H(5) 7.51, H(6) 7.85 [25].

[c] ^{1}H NMR spectrum of [Ir(bpy)(bpy**)Cl]$_2Cl_2$, in unspecified solvent: 15 signals within 7.0–9.7 ppm range [34].

[d] ^{1}H literature data for *cis*-[Ir(bpy)(phen)Cl_2]Cl, in DMSO-d_6: 7.35, 7.70, 7.85, 8.16, 2 × 8.21, 4 × (8.38–8.60), 2 × 8.83, 8.97, 9.14, 9.73, 9.86 (unassigned) [12].

Both K[Ir(LL)Cl_4] coordination compounds exhibit the same orders of the proton signals like the free ligands (H(6) > H(3) > H(4) > H(5) for LL = bpy; H(2) > H(4) > H(5) > H(3) for LL = phen; see also Supplementary Figs. 1S and 3S). So simple spectral patterns unambiguously indicate the symmetric N(1),N(1′) bidentate coordination modes of both azines, excluding either the N(1) monodentate bonding or the N(1),C(3') chelation (possible for bpy). Thus, the [Ir(LL)Cl_4]$^-$ anions have the same structures as assumed by other authors [10,11,13].

All protons in the bpy and phen ligands are noticeably deshielded, the magnitudes of the Δ^{1H}_{coord} parameters decreasing in the orders H(6) > H(5) > H(4) > H(3) for [Ir(bpy)Cl_4]$^-$ and H(2) > H(3) > H(5) > H(4) for [Ir(phen)Cl_4]$^-$. Particularly, the largest Δ^{1H}_{coord} values are noted for H(6) in bpy (*ca.* 0.9 ppm in D_2O, *ca.* 1.0 ppm in DMSO-d_6) and H(2) in phen (*ca.* 0.55 ppm in D_2O, *ca.* 0.75 ppm in DMSO-d_6), *i.e.* in case of the hydrogens mostly adjacent to the N(1) coordination sites. It should be noted here that also for the aqueous solutions the ^{1}H coordination shifts have been determined in respect to the uncoordinated azines in DMSO-d_6; obviously, the ^{1}H chemical shifts of free bpy or phen could not have been measured in D_2O, as these heterocycles are insoluble in water.

The deshielding of the other protons is much smaller (*max. ca.* 0.35–0.45 ppm). Generally, in case of each ^{1}H signal, for both bpy and phen, the shifts to higher frequency are more enhanced in DMSO-d_6 than D_2O; the differences between the respective δ^{1H} parameters, found for the same ^{1}H nucleus but in various solvents, are again mostly expressed for H(6) in bpy (*ca.* 0.1 ppm) and H(2) in phen (*ca.* 0.2 ppm).

The increase of the δ^{1H} values for the [Ir(LL)Cl_4]$^-$ anions is generally similar to that noted upon complexation of the same or derived azines by some other transition metal chlorides, in which this phenomenon also concerned mainly the protons adjacent to the nitrogen [26–28]. Also the fact that in both Ir(III) complexes the deshielding of H(6) in bpy is larger than of H(2) in phen resembles an analogous dependency described for several Au(III), Pd(II), Pt(II) and Pt(IV) chloride coordination compounds having the general [Au(LL)Cl_2]$^+$, [Pd(LL)Cl_2], [Pt(LL)Cl_2] and [Pt(LL)Cl_4] formulae (LL = bpy, phen) [26–28]. However, the magnitude of the Ir(III)-induced ^{1}H high-frequency coordination shifts is even larger: $\Delta^{H(6)}_{coord}$ = 1.01 ppm for [Ir(bpy)Cl_4]$^-$ *versus* 0.43 ppm for [Pd(bpy)Cl_2], 0.81 ppm for [Pt(bpy)Cl_2], 0.82 ppm for [Pt(bpy)Cl_4], 0.70 ppm for [Au(bpy)Cl_2]$^+$; $\Delta^{H(2)}_{coord}$ = 0.77 ppm for [Ir(phen)Cl_4]$^-$ *versus* 0.23 ppm for [Pd(phen)Cl_2], 0.58 ppm for [Pt(phen)Cl_2], 0.63 ppm for [Pt(phen)Cl_4], 0.58 ppm for [Au(phen)Cl_2]$^+$; all data in DMSO-d_6 [26,27]). Furthermore, the large ^{1}H deshielding in the [Ir(LL)Cl_4]$^-$ anions strongly contrasts to a very small effect for the analogous H(2), H(6) nuclei in *cis*-[Pt(py)$_2Cl_4$] ($\Delta^{H(2),H(6)}_{coord}$ = 0.14 ppm [26]), although the geometry of the compared species is quite similar (in both types of such a coordination polyhedron the metallated nitrogen atoms are located *trans*- to chlorides, while the azine rings are *cis*-positioned to each other).

A high similarity of the [Ir(LL)Cl_4]$^-$ and [Pt(LL)Cl_4] species allows for a more detailed comparison. The respective coordination compounds (containing a given azine ligand) are isoelectronic (as the Ir(III) and Pt(IV) central ions have the same 6d^6 electron configuration), reveal a similar geometry (octahedral with the C_{2v} symmetry), and have a nearly identical atomic mass of the platinide (Ir 192.2, Pt 195.1). In fact, the analogous complexes of Ir(III) and Pt(IV) differ only in the overall electric charge, and, apparently, in the metal oxidation state. Thus, it can be seemingly surprising that the corresponding H(6) (in bpy) or H(2) (in phen) protons are more deshielded in the [Ir(LL)Cl_4]$^-$ anions than in the [Pt(LL)Cl_4] neutral molecules, although one could expect a weaker deshielding effect in the former case, owing to the presence of the (−1) negative charge, and, in consequence, a higher electron density within the whole azine ring system.

Such a relation between the $\Delta^{H(6)}_{coord}$ (for bpy) or $\Delta^{H(2)}_{coord}$ (for phen) parameters, in [Ir(LL)Cl_4]$^-$ *versus* [Pt(LL)Cl_4], however, is true for these protons only; in contrast, for all others the ^{1}H deshielding effect decreases upon the Pt(IV) → Ir(III) replacement: $\Delta^{H(3)}_{coord}$ = 0.58 ppm → $\Delta^{H(3)}_{coord}$ = 0.11 ppm; $\Delta^{H(4)}_{coord}$ = 0.65 ppm → $\Delta^{H(4)}_{coord}$ = 0.25 ppm; $\Delta^{H(5)}_{coord}$ = 0.70 ppm → $\Delta^{H(5)}_{coord}$ = 0.44 ppm (for the [Pt(bpy)Cl$_4$] → [Ir(bpy)Cl_4]$^-$ transition), as well as: $\Delta^{H(3)}_{coord}$ = 0.68 ppm → $\Delta^{H(3)}_{coord}$ = 0.29 ppm; $\Delta^{H(4)}_{coord}$ = 0.73 ppm → $\Delta^{H(4)}_{coord}$ = 0.06 ppm, $\Delta^{H(5)}_{coord}$ = 0.54 ppm → $\Delta^{H(5)}_{coord}$ = 0.23 ppm (for the [Pt(phen)Cl_4] → [Ir(phen)Cl$_4$]$^-$ transition) [26]. In our opinion, an overall metal-induced ^{1}H deshielding can be better characterised by a mean value of Δ^{1H}_{coord}, determined for all hydrogen atoms in a given LL ligand: 0.45 ppm for [Ir(bpy)Cl_4]$^-$ *versus* 0.68 ppm for [Pt(bpy)Cl_4], and 0.33 ppm for [Ir(phen)Cl_4]$^-$ *versus* 0.64 ppm for [Pt(phen)Cl_4]. Thus, each [Pt(LL)Cl_4] → [Ir(LL)Cl_4]$^-$ transition weakens an average deshielding effect for the whole set of protons, such a dependency being now consistent with the increased electron density.

The increase of the ^{1}H chemical shifts following Ir(III) chloride complexation seems to be a more general phenomenon, as it was already described for several coordination compounds of some other

azines and azoloazines, being again mostly pronounced for the nitrogen-adjacent protons: $\delta^{H(2)}$ = 8.21 ppm, $\delta^{H(4)}$ = 7.51 ppm, $\delta^{H(5)}$ = 7.20 ppm for *trans*-[Ir(imidazole-N(1))$_2$Cl$_4$]$^-$ in D$_2$O (imidazoleH$^+$ counterions) [57] *versus* $\delta^{H(2)}$ = 7.73 ppm, $\delta^{H(4)/H(5)}$ = 7.13 ppm for free imidazole in CDCl$_3$ [58]; $\delta^{H(6),H(6'')}$ = 9.23 ppm for [Ir(2,2′:6′,2″-terpyridine-N(1),N(1′),N(1″))Cl$_3$] in DMSO-d_6 [59] *versus* $\delta^{H(6),H(6'')}$ = 8.68 ppm for free 2,2′:6′,2″-terpyridine in CDCl$_3$ [58]).

The discussed deshielding phenomenon, in the presently studied [Ir(LL)Cl$_4$]$^-$ anions, seems to be primarily caused by an inductive effect of the electron-acceptor IrCl$_4$ moiety, related to a strongly electronegative character of four chlorine atoms (while iridium is weakly electropositive – 2.20 electronegativity [53]); as already mentioned, the magnitude of this effect is probably partially decreased by the presence of the negative electric charge. Anisotropic phenomena, potentially deriving from the adjacency of some other azine ligands, are principally absent here because both [Ir(LL)Cl$_4$]$^-$ species contain exactly one bpy or phen molecule. Relativistic contributions, characteristic for heavy metal complexes, must be also taken into account. Finally, solvation effects are important, as indicated by the earlier described dependency of the δ^{1H} and Δ^{1H}_{coord} parameters on the solvent type.

The ^{1}H NMR spectra of both *cis*-[Ir(LL)$_2$Cl$_2$]Cl complexes are much more complicated as they reveal a double number of peaks due to the magnetic inequivalency of the two halves of each coordinated azine ligand (although the two bpy or phen molecules, treated as the whole, remain equivalent to each other). Such NMR patterns, consistent with the literature data for *cis*-[Ir(bpy)$_2$Cl$_2$]CF$_3$SO$_3$ or *cis*-[Ir(bpy)$_2$Cl$_2$]PF$_6$ (in CD$_3$CN or DMSO, respectively; 8 signals) [24,25] and *cis*-[Ir(bpy)(phen)Cl$_2$]Cl (in DMSO-d_6; 16 signals) [12] were already described for the analogous *cis*-[Co(LL)$_2$Cl$_2$]Cl and *cis*-[Rh(LL)$_2$Cl$_2$]Cl species [27]. The presence of only eight proton resonances unambiguously proves the symmetric N(1),N(1′) bidentate coordination modes of bpy or phen, excluding the N(1) monodentate bonding or the N(1),C(3′) chelation (possible in case of bpy) for any of the two coordinated molecules; otherwise, we could expect 16 (bpy + bpy* or phen + phen*) or 15 (bpy + bpy**) ^{1}H peaks, by analogy to the spectrum of [Ir(bpy)(bpy**)Cl]$_2$Cl$_2$ [34]). Hence, both *cis*-[Ir(LL)$_2$Cl$_2$]$^+$ cations have, at least in the studied solutions, the analogous structures as in crystalline *cis*-[Ir(phen-κ^2N(1),N(1′))$_2$Cl$_2$]PF$_6$ (AMIPIV) [30], *cis*-[Ir(4,4′-dimethyl-bpy-κ^2N(1),N(1′))$_2$Cl$_2$]PF$_6$ (WABDEJ) [60] and *cis*-[Ir(2,2′-biquinoline-κ^2N(1),N(1′))$_2$Cl$_2$]PF$_6$ (AJUKAR) [61].

Further we will denote as N atoms these positioned (within the IrN$_2$Cl$_4$ chromophore) *trans* to chlorine, while as N′ – those *trans* to another nitrogen – Fig. 3. For each pair of the corresponding protons in the two inequivalent halves of bpy or phen rings, the peak appearing at the higher frequency can be assigned to H′, while that at the lower chemical shift – to H. Such an attribution follows an obvious fact that the former hydrogens (located approximately within the plane determined by the adjacent bpy/phen ring) are more deshielded than the latter ones (far-distanced from that plane), owing to the additional magnetic field generated by the neighbouring heterocyclic molecule.

The orders of the proton signals for *cis*-[Ir(bpy)$_2$Cl$_2$]$^+$ and *cis*-[Ir(phen)$_2$Cl$_2$]$^+$ are H(6′) > H(3′) > H(3) > H(4′) > H(4) > H(5′) > H(6) > H(5) and H(2′) > H(4′) > H(4) > H(5′) > H(3′) > H(5) > H(2) > H(3), respectively (see also Supplementary Figs. 2S and 3S); the former sequence is identical with that suggested for *cis*-[Ir(bpy)$_2$Cl$_2$]PF$_6$ [25]. We observe the highly positive Δ^{1H}_{coord} values for the H′ atoms (*ca.* 0.25–0.95 ppm for bpy, *ca.* 0.5–0.85 ppm for phen) and much smaller (*max ca.* 0.15 ppm for bpy, *max ca.* 0.4 ppm for phen) or even negative (down to *ca.* −1.0 ppm for both ligands) for those of H. The largest absolute magnitudes of the ^{1}H coordination shifts are again noted for H(6)/H(6′) in bpy ($\Delta^{H(6)\prime}_{coord}$ = +0.94 ppm, $\Delta^{H(6)}_{coord}$ = −0.97 ppm) and H(2)/H(2′) in phen ($\Delta^{H(2)\prime}_{coord}$ = +0.84 ppm, $\Delta^{H(2)}_{coord}$ = −1.04 ppm). The same phenomenon

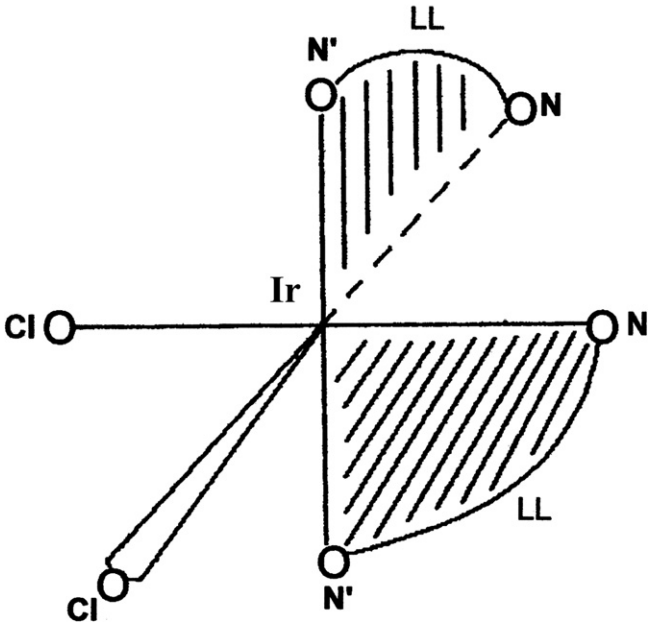

Fig. 3. Geometry of *cis*-[Ir(LL)$_2$Cl$_2$]$^+$ cations (LL = bpy, phen).

was already observed for the *cis*-[Co(LL)$_2$Cl$_2$]$^+$ and *cis*-[Rh(LL)$_2$Cl$_2$]$^+$ cations; however, the Δ^{1H}_{coord} parameters for the Ir(III) complexes are more similar to those for the Rh(III) than Co(III) species (*cis*-[Rh(bpy)$_2$Cl$_2$]$^+$ – $\Delta^{H(6)\prime}_{coord}$ = +0.99 ppm, $\Delta^{H(6)}_{coord}$ = −0.91 ppm and *cis*-[Co(bpy)$_2$Cl$_2$]$^+$ – $\Delta^{H(6)\prime}_{coord}$ = +1.11 ppm, $\Delta^{H(6)}_{coord}$ = −1.36 ppm; *cis*-[Rh(phen)$_2$Cl$_2$]$^+$ – $\Delta^{H(2)\prime}_{coord}$ = +0.88 ppm, $\Delta^{H(2)}_{coord}$ = −1.06 ppm and *cis*-[Co(phen)$_2$Cl$_2$]$^+$ – $\Delta^{H(2)\prime}_{coord}$ = +0.92 ppm, $\Delta^{H(2)}_{coord}$ = −1.56 ppm; all data for the chloride salts in DMSO-d_6 [27]). Most likely, this dependency reflects a larger similarity of the Ir(III) ionic radius to that of Rh(III) than Co(III) (0.68 Å *versus* 0.67 Å and 0.55 Å, respectively [53]), and, in consequence, of the relevant distance between the H(6) (bpy) or H(2) (phen) proton and the metal atom.

The differences between the δ^{1H} parameters for the H′ and H atoms are always positive and increase in the orders H(3) < H(4) < H(5) < H(6) (*cis*-[Ir(bpy)$_2$Cl$_2$]$^+$) or H(5) < H(4) < H(3) < H(2) (*cis*-[Ir(phen)$_2$Cl$_2$]$^+$), having their maxima for the nitrogen-adjacent hydrogens (1.91 ppm for H(6) in bpy, 1.88 ppm for H(2) in phen). Exactly the same dependencies were reported for the respective Co(III) and Rh(III) complexes, the separations between the H(6′) and H(6) (*cis*-[Co(bpy)$_2$Cl$_2$]$^+$: 2.47 ppm, *cis*-[Rh(bpy)$_2$Cl$_2$]$^+$: 1.90 ppm), as well as the H(2′) and H(2) (*cis*-[Co(phen)$_2$Cl$_2$]$^+$: 2.48 ppm, *cis*-[Rh(phen)$_2$Cl$_2$]$^+$: 1.94 ppm) signals being again more similar for Ir(III) and Rh(III) than Co(III) [27].

An overall ^{1}H deshielding, for each of the discussed *cis*-[M(LL)$_2$Cl$_2$]$^+$ cations (M = Ir, Rh, Co; LL = bpy, phen), can be again described by a mean Δ^{1H}_{coord} parameter, determined for all hydrogen atoms in the two coordinated azine molecules: 0.19 ppm in *cis*-[Ir(bpy)$_2$Cl$_2$]$^+$ *versus* 0.37 ppm in *cis*-[Rh(bpy)$_2$Cl$_2$]$^+$ and 0.32 ppm in *cis*-[Co(bpy)$_2$Cl$_2$]$^+$, as well as 0.27 ppm in *cis*-[Ir(phen)$_2$Cl$_2$]$^+$ *versus* 0.32 ppm in *cis*-[Rh(phen)$_2$Cl$_2$]$^+$ and 0.27 ppm in *cis*-[Co(phen)$_2$Cl$_2$]$^+$ [27]. Thus, in both series of the compared complexes we observe the increase of an average ^{1}H deshielding effect from cobalt to rhodium, and then its decrease from rhodium to iridium.

In case of the *cis*-[Ir(LL)$_2$Cl$_2$]$^+$ cations a combination of several factors affects the ^{1}H shielding constants: a general deshielding tendency caused by an inductive effect of the electron-acceptor IrCl$_2$ moiety and the presence of the positive (+1) electric charge; anisotropic phenomena of variable sign and magnitude deriving from the adjacent π-electron ring systems; relativistic contribu-

tions; solvation effects. As all of them are noticeably dependent on the proton position, the ^{1}H resonances appear in the relatively broad spectral ranges (*cis*-[Ir(bpy)$_2$Cl$_2$]Cl: *ca.* 7.4–9.7 ppm; *cis*-[Ir(phen)$_2$Cl$_2$]Cl: *ca.* 7.7–10.0 ppm); quite similar intervals were reported for *cis*-[Ir(bpy)$_2$Cl$_2$]CF$_3$SO$_3$ in CD$_3$CN (*ca.* 7.4–9.8 ppm) [24] and *cis*-[Ir(bpy)$_2$Cl$_2$]PF$_6$ in DMSO (*ca.* 7.5–9.65 ppm) [25]. Comparable or even larger expanses were occupied by the proton peaks in the spectra of *cis*-[Co(bpy)$_2$Cl$_2$]Cl (*ca.* 7.3–9.8 ppm), *cis*-[Rh(bpy)$_2$Cl$_2$]Cl (*ca.* 7.5–9.7 ppm), *cis*-[Co(phen)$_2$Cl$_2$]Cl (*ca.* 7.5–10.1 ppm), *cis*-[Rh(phen)$_2$Cl$_2$]Cl (*ca.* 7.7–10.0 ppm) [27], as well as *cis*-[Ir(bpy)(phen)Cl$_2$]Cl (*ca.* 7.3–9.9 ppm, in DMSO-d_6 [12]) and [Ir(bpy)(bpy**)Cl]$_2$Cl$_2$ (*ca.* 6.9–9.7 ppm, in an unspecified solvent [34]), whereas in case of uncoordinated bpy or phen they were much more narrow (*ca.* 7.4–8.7 ppm and *ca.* 7.8–9.1 ppm).

The other salts containing the *cis*-[Ir(bpy)$_2$Cl$_2$]$^+$ cations exhibits a moderate dependence of the δ^{1H} values on the type of counterions or a solvent. Particularly, for *cis*-[Ir(bpy)$_2$Cl$_2$]CF$_3$SO$_3$ (9.77, 8.56, 2 × 8.42, 8.08, 7.98, 7.72, 7.39 ppm, in CD$_3$CN [24]) and *cis*-[Ir(bpy)$_2$Cl$_2$]PF$_6$ (9.65, 8.91, 8.82, 8.50, 8.20, 8.15, 7.85, 7.51, in DMSO [25]) the ^{1}H chemical shifts differed from ours for *cis*-[Ir(bpy)$_2$Cl$_2$]Cl (in D$_2$O) by *max. ca.* ±0.3 ppm. In contrast, the change of auxiliary ligands within the Ir(III) coordination sphere results in much larger δ^{1H} variations. As an example may serve the replacement of chlorides by trifluoromethylsulfonates (leading to even larger proton deshielding: *cis*-[Ir(bpy)$_2$(OSO$_2$CF$_3$)$_2$]CF$_3$SO$_3$ – 3 × 9.65, 9.52, 9.42, 9.22, 2 × 9.13 ppm, in CD$_3$CN [24]) or hydrides (the majority of protons was shielded: *cis*-[Ir(bpy)$_2$H$_2$]PF$_6$ – 9.37, 2 × 8.34, 8.06, 7.96, 7.76, 7.45, 7.33 ppm, in CD$_3$CN [24]). We do not compare the δ^{1H} parameters of the particular protons in *cis*-[Ir(bpy)$_2$Cl$_2$]$^+$ or *cis*-[Ir(phen)$_2$Cl$_2$]$^+$ to those in *cis*-[Ir(bpy)(phen)Cl$_2$]$^+$, [Ir(bpy)(bpy**)Cl]$_2^{2+}$, *cis*-[Ir(bpy)$_2$(OSO$_2$CF$_3$)$_2$]$^+$ or *cis*-[Ir(bpy)$_2$H$_2$]$^+$ because the ^{1}H signals reported in the literature generally remained unassigned [12,24,34].

The ^{1}H NMR spectral patterns for the Ir(III)-coordinated bpy or phen molecules are also heavily dependent on the presence of another heterocyclic ligand. Particularly, for some mixed Ir(III) chloride complexes with bpy/phen and 2,2′-dipyridylamine ((C$_5$H$_4$N)$_2$NH), a large deshielding of the H(6′)/H(2′) nuclei contrasted to the variable in sign and very slight in magnitude coordination shifts of H(6)/H(2) protons: *cis*-[Ir(bpy)(2,2′-dipyridylamine)Cl$_2$]Cl – $\delta^{H(6')}$ = *9.71 ppm (thus* $\Delta^{H(6')}_{coord} = +1.02$ ppm*) versus* $\delta^{H(6)}$ = 8.73 ppm (thus $\Delta^{H(6)}_{coord}$ = +0.04 ppm); *cis*-[Ir(phen)(2,2′-dipyridylamine)Cl$_2$]Cl – $\delta^{H(2')}$ = 9.95 ppm (thus $\Delta^{H(2')}_{coord} = +0.84$ ppm) *versus* $\delta^{H(2)}$ = 8.76 ppm (thus $\Delta^{H(2)}_{coord}$ = -0.35 ppm); both compounds in DMSO-d_6 [13]. On the other hand, the influence of an additional aromatic ring was sometimes very limited, *e.g.* in some Ir(III) complexes containing one bpy/phen molecule and the pentamethylcyclopentadienyl anion the H(6)/H(2) signals were nearly unaffected: [Ir(bpy)(C$_5$(CH$_3$)$_5$)Cl]ClO$_4$ – $\delta^{H(6)}$ = 8.65 ppm (thus $\Delta^{H(6)}_{coord} = -0.04$ ppm); [Ir(phen)(C$_5$(CH$_3$)$_5$)Cl]ClO$_4$ – $\delta^{H(2)}$ = 9.02 ppm (thus $\Delta^{H(2)}_{coord} = -0.09$ ppm); both compounds in CD$_3$CN [62]. In this case, however, one must take into account the presence of one Cl ligand only, and another character of the pentamethylcyclopentadienyl bonding (ferrocene-like), modifying either inductive or anisotropic effects.

As other examples illustrating the significance of anisotropic phenomena can serve the trischelated [Ir(LL)$_3$]$^{3+}$ cations, which exhibited very low δ^{1H} parameters (unassigned): [Ir(bpy)$_3$](PF$_6$)$_3$ – 8.67, 8.40, 2 × 7.69 ppm, in CD$_3$CN [24]; [Ir(phen)$_3$](ClO$_4$)$_3$ – 9.04, 8.47, 8.16, 7.96 ppm, in CD$_3$OD [63]. In these highly symmetric complexes inductive effects were entirely absent due to the lack of any electronegative elements, while those anisotropic probably balanced one another. In contrast, the unsymmetric [Ir(bpy)$_2$(bpy*)]$^{3+}$ and [Ir(bpy)$_2$(bpy**)]$^{2+}$ cations revealed a much larger variability of the unassigned δ^{1H} values ([Ir(bpy)$_2$(bpy*)](ClO$_4$)$_3$: *ca.* 6.7–9.1 ppm, in DMSO-d_6 [36]; [Ir(bpy)$_2$(bpy**)](ClO$_4$)$_2$: *ca.* 6.7–8.8 ppm, in DMSO-d_6 + D$_2$O (1:1) [16]; [Ir(bpy)$_2$(bpy**)](BF$_4$)$_2$: *ca.* 7.3–9.0 ppm, in CD$_3$OD [38]). A similar situation was in case of [Ir(bpy)$_2$(bpy***)(H$_2$O)]Cl$_3$ and [Ir(bpy)$_2$(bpy · H$_2$O)]Cl$_3$: *ca.* 6.5–9.0 ppm, in DMSO-d_6 [40,41]. So large differences between various types of Ir(III) cations containing three bpy ligands (differing in the complexation mode and/or electric charge) reflect a high dependence of anisotropic effects on the type and orientation of the coordinated heterocycles. Even more complicated and thus unassigned (due to the presence of some other azine ligands) were the ^{1}H NMR patterns reported for [Ir(bpy)$_2$(2-phenylpyridyl)](PF$_6$)$_2$, in DMSO-d_6 [64] and [Ir(bpy)(phen)(9,10-phenanthrenequinonedimine)](CF$_3$SO$_3$)$_3$, in DMSO-d_6 [12].

Mixing of equimolar K[Ir(bpy)Cl$_4$] + *cis*-[Ir(bpy)$_2$Cl$_2$]Cl (in D$_2$O) or K[Ir(phen)Cl$_4$] + *cis*-[Ir(phen)$_2$Cl$_2$]Cl (in DMSO-d_6) solutions results in the appearance of distinct, neither broadened nor averaged, ^{1}H peaks for the cations and the anions (see also Supplementary Fig. 3S). This observation excludes an exchange of the bpy or phen ligands between the coordination spheres of the respective complex ions, reflecting a large strength of the N(1),N(1′)-chelation of both azines, and a well-known kinetic inertness of Ir(III). The formed *cis*-[Ir(bpy)$_2$Cl$_2$][Ir(bpy)Cl$_4$] ionic pair is partially precipitated in D$_2$O, whereas that of *cis*-[Ir(phen)$_2$Cl$_2$][Ir(phen)Cl$_4$] in DMSO-d_6 remains well soluble, allowing for detection also its ^{1}H–^{13}C and ^{1}H–^{15}N NMR spectra (*vide infra*).

3.4. ^{13}C NMR spectra

During the present work, the ^{13}C NMR spectra of both bpy complexes have been measured in D$_2$O, while those of the phen

Table 4
^{13}C NMR chemical shifts (δ^{13C}, ppm) of Ir(III) chloride complexes with bpy or phen, in D$_2$O (A) or DMSO-d_6 (B); ^{13}C coordination shifts (Δ^{13C}_{coord}, ppm) are in parentheses

Compound	C(2)	C(3)	C(4)	C(5)	C(6)
Bpy[B]	155.2	120.4	137.2	124.1	149.2
K[Ir(bpy)Cl$_4$][A,a]	161.9 (+6.2)	126.5 (+5.8)	142.7 (+5.7)	129.9 (+6.0)	154.2 (+5.0)
cis-[Ir(bpy)$_2$Cl$_2$]Cl (C)[A,a]	160.0 (+4.8)	127.7 (+7.3)	143.7 (+6.5)	130.9 (+6.8)	153.1 (+3.9)
cis-[Ir(bpy)$_2$Cl$_2$]Cl (C′)[A,a]	160.1 (+4.9)	127.8 (+7.4)	144.3 (+7.1)	131.5 (+7.4)	153.6 (+4.4)
Average for C and C′	160.05 (+4.85)	127.75 (+7.35)	144.0 (+6.8)	131.2 (+7.1)	153.35 (+4.15)
Difference between C and C	+0.1	+0.1	+0.6	+0.6	+0.5

	C(1a)	C(2)	C(3)	C(4)	C(4a)	C(5)
Phen[B]	145.5	149.9	123.2	136.1	128.4	126.6
K[Ir(phen)Cl$_4$][B]	150.9 (+5.4)	152.1 (+2.2)	124.7 (+1.5)	136.9 (+0.8)	129.8 (+1.4)	127.3 (+0.7)
cis-[Ir(phen)$_2$Cl$_2$]Cl (C)[B]	147.8 (+2.3)	152.1 (+2.2)	126.5 (+3.3)	139.5 (+3.4)	130.7 (+2.3)	128.0 (+1.4)
cis-[Ir(phen)$_2$Cl$_2$]Cl (C′)[B]	148.4 (+2.9)	152.2 (+2.3)	126.9 (+3.7)	140.3 (+4.2)	131.1 (+2.7)	128.2 (+1.6)
Average for C and C′	148.1 (+2.6)	152.15 (+2.25)	126.7 (+3.5)	139.9 (+3.8)	130.9 (+2.5)	128.1 (+1.5)
Difference between C′ and C	+0.6	+0.1	+0.4	+0.8	+0.4	+0.2

In the *cis*-[Ir(LL)$_2$Cl$_2$]$^+$ cations: the carbons denoted as C and C′ correspond to these halves of each LL ligand which are positioned *trans* to chlorine and *trans* to another nitrogen, respectively.

[a] Δ^{13C}_{coord} for bpy complexes determined in D$_2$O *versus* free bpy in DMSO-d_6.

ones – in DMSO-d_6. The respective δ^{13C} chemical shifts and the Δ^{13C}_{coord} coordination shifts are listed in Table 4.

The ^{13}C NMR signal patterns follow those noted upon the ^{1}H measurements, thus in case of the $[Ir(bpy)Cl_4]^-$ and $[Ir(phen)Cl_4]^-$ anions only 5 and 6 peaks are observed, while for the *cis*-$[Ir(bpy)_2Cl_2]^+$ and *cis*-$[Ir(phen)_2Cl_2]^+$ cations their number is again double, being 10 and 12, respectively. It confirms the equivalency of the two bpy or phen molecules (whose halves, however, become inequivalent to each other) in both *cis*-$[Ir(LL)_2Cl_2]^+$ ions, in contrast to the $[Ir(bpy)(bpy^{**})Cl]_2^{2+}$, $[Ir(bpy)_2(bpy^{*})]^{3+}$, $[Ir(bpy)_2(bpy^{**})]^{2+}$ and $[Ir(bpy)_2(bpy^{***})(H_2O)]^{3+}$ species, for which the ^{13}C NMR spectra were more complicated [34,36,38].

The influence of Ir(III) chloride complexation on the δ^{13C} parameters of both azines is relatively limited, the signal orders for the $[Ir(LL)Cl_4]^-$ and *cis*-$[Ir(LL)_2Cl_2]^+$ ions remaining the same like for uncoordinated bpy (C(2) > C(6) > C(4) > C(5) > C(3)) or phen (C(2) > C(1a) > C(4) > C(4a) > C(5) > C(3)). Comparing to the free ligands, all ^{13}C nuclei are moderately deshielded. This phenomenon is more pronounced for bpy (*ca.* 4–7 ppm) than phen (*ca.* 1–5 ppm), with no clear correlation to the carbon position. In contrast to ^{1}H NMR, the Δ^{13C}_{coord} parameters for the $[Ir(LL)Cl_4]^-$ and *cis*-$[Ir(LL)_2Cl_2]^+$ ions containing the same azine ligand are comparable (the variations up to ±2 ppm), with very small differences (always positive: *ca.* 0.1–0.8 ppm) between the C′ and C atoms in the latter species. So slight dependencies, similar in sign and magnitude to those for the analogous Co(III) and Rh(III) complexes [27], allow for a general conclusion that a high invariability of the δ^{13C} parameters on the affiliation of a carbon atom to one of the two halves of the bpy or phen ring systems (C′ *versus* C) reflects, unlike in ^{1}H NMR, a negligible contribution of anisotropic phenomena into the ^{13}C shielding constants.

3.5. ^{15}N NMR spectra

Like during the ^{13}C NMR measurements, the ^{15}N NMR spectra of both bpy complexes have been recorded in D_2O, while those of the phen ones and of the free ligands – in DMSO-d_6. The respective δ^{15N} chemical shifts and the Δ^{15N}_{coord} coordination shifts are listed in Table 5.

Generally, Ir(III) chloride complexation of both azines results in *ca.* 105–120 ppm low-frequency shifts of the ^{15}N signals of the pyridine-like nitrogens, thus the $\Delta^{N(1)}_{coord}$ parameters are strongly negative. No really significant differences are observed between the $[Ir(LL)Cl_4]^-$ and *cis*-$[Ir(LL)_2Cl_2]^+$ ions ($\Delta^{N(1)}_{coord}$ varying from *ca.* −107 ppm to *ca.* −116 ppm, and from *ca.* −111 ppm to *ca.* −120 ppm, respectively) although these species differ in such important structural features as the number of chloride and azine ligands, and the electric charge. Hence, neither inductive effects nor anisotropic phenomena, important in case of ^{1}H NMR, have a noticeable influence on the ^{15}N chemical shift. This is consistent with a well-known fact that the above factors determine rather the diamagnetic and not the paramagnetic contribution in a given shielding constant, while for the ^{15}N nuclei the former term is less significant than the latter one.

Table 5
^{15}N NMR chemical and coordination shifts (δ^{15N}, Δ^{15N}_{coord}; ppm) of Ir(III) chloride complexes with bpy or phen, in D_2O (A) or DMSO-d_6 (B).

Compound	$\delta^{N(1)}$	$\Delta^{N(1)}_{coord}$
Bpy[B]	−72.6	
K[Ir(bpy)Cl$_4$][A]	−189.0	−116.4[a]
cis-[Ir(bpy)$_2$Cl$_2$]Cl (N)[A]	−192.2	−119.6[a]
cis-[Ir(bpy)$_2$Cl$_2$]Cl (N′)[A]	−183.9	−111.3[a]
Average for N and N′	−188.0	−115.4[a]
Difference between N′ and N	+8.3	+8.3
Phen[B]	−69.3	
K[Ir(phen)Cl$_4$][B]	−176.1	−106.8
cis-[Ir(phen)$_2$Cl$_2$]Cl (N)[B]	−188.2	−118.9
cis-[Ir(phen)$_2$Cl$_2$]Cl (N′)[B]	−185.5	−116.2
Average for N and N′	−186.85	−117.55
Difference between N′ and N	+2.7	+2.7

In the *cis*-$[Ir(LL)_2Cl_2]^+$ cations: the nitrogens denoted as N and N′ are positioned *trans* to chlorine and *trans* to another nitrogen, respectively.

[a] $\Delta^{N(1)}_{coord}$ for bpy complexes determined in D_2O *versus* free bpy in DMSO-d_6.

The $|\Delta^{N(1)}_{coord}|$ absolute magnitudes for the $[Ir(LL)Cl_4]^-$ anions (*ca.* 107–116 ppm) are larger than those previously reported for the $[Au(LL)Cl_2]^+$ cations (*ca.* 78–82 ppm) [27] and the $[Pd(LL)Cl_2]$ (*ca.* 90–95 ppm), $[Pt(LL)Cl_2]$ (*ca.* 105–111 ppm), $[Pt(LL)Cl_4]$ (*ca.* 99–105 ppm) neutral molecules [26] (all data in DMSO-d_6). They are also much higher than the relevant $|\Delta^{N(1)}_{coord}|$ absolute values found in case of some Ge(IV) compounds having the general $[Ge(bpy)Cl_x(NCS)_{4-x}]$ (x = 0–4) formulae, for which $\delta^{N(1)}$ ranged from *ca.* −123 to *ca.* −130 ppm (in DMSO-d_6) [65], and thus $\Delta^{N(1)}_{coord}$ varied from *ca.* −50 ppm to *ca.* −57 ppm. So a huge difference between the ^{15}N shielding effects may result from the fact that, in contrast to iridium, gold, palladium and platinum, the germanium element is not a transition metal and has only semi-metallic properties.

The detailed comparison of the $\Delta^{N(1)}_{coord}$ parameters for $[Ir(bpy)Cl_4]^-$ and $[Pt(bpy)Cl_4]$ (−116.4 ppm *versus* −99.5 ppm [26]), as well as for $[Ir(phen)Cl_4]^-$ and $[Pt(phen)Cl_4]$ (−106.8 ppm *versus* −105.1 ppm [26]) exhibits a more enhanced ^{15}N shielding effect in case of the Ir(III) than Pt(IV) complexes, although, as we have mentioned upon the ^{1}H NMR discussion, both types of compounds have quite similar molecular structures. In our opinion, the negative differences between the δ^{15N} (or Δ^{15N}_{coord}) values for the $[Ir(LL)Cl_4]^-$ and $[Pt(LL)Cl_4]$ species (which are, however, of a variable magnitude: *ca.* −17 ppm for LL = bpy and *ca.* −2 ppm for LL = phen) may reflect another scale of the diamagnetic contribution in the relevant ^{15}N shielding constants; since this factor is related mainly to the electron density at the nitrogen, it should be larger for anions than neutral molecules, *i.e.* it must increase upon the $[Pt(LL)Cl_4] \rightarrow [Ir(LL)Cl_4]^-$ transitions. Obviously, the major part of the ^{15}N shielding effect results, most likely, from the decrease of the paramagnetic contribution (*via* the replacement of the main $n_N \rightarrow \pi^*$ electronic transition by a more energetic $\sigma_{N-M} \rightarrow \pi^*$ [26–28]) and from the appearance of relativistic phenomena (associated to the presence of the heavy metal ions); nevertheless, these factors are probably of a comparable magnitude in the corresponding Ir(III) and Pt(IV) complexes, due to their structural similarity.

Such a hypothesis, *i.e.* that the variations in the diamagnetic contribution (which itself is, principally, of a minor significance in determining the ^{15}N shielding constants) are mainly responsible for the final differences in the Δ^{15N}_{coord} values, noted for analogous coordination compounds having nearly the same structure but another electric charge, is supported by the fact that a similar enhancement of the ^{15}N low-frequency coordination shifts was observed upon the $[Au(LL)Cl_2]^+ \rightarrow [Pt(LL)Cl_2]$ transitions (for LL = bpy: $\Delta^{N(1)}_{coord}$ = −78.1 ppm → −105.3 ppm; for LL = phen: $\Delta^{N(1)}_{coord}$ = −81.8 ppm → −110.7 ppm [26,27]). In fact, the corresponding cationic Au(III) and neutral Pt(II) species were also very similar to each other, as they had the same $6d^8$ electron configuration of the central atom and the square-planar *cis*-geometry, as well as a very close metal atomic mass (Au 197.0, Pt 195.1), again differing mainly in the electron densities within the whole azine ring systems, and, in consequence, around the nitrogen atoms. Hence, the relation between $[Au(LL)Cl_2]^+$ and $[Pt(LL)Cl_2]$ is more or less like between $[Pt(LL)Cl_4]$ and $[Ir(LL)Cl_4]^-$. In our opinion, both comparisons lead to the same dependencies: the decrease of the central atom oxidation number and the overall electric charge by +1 results in the increase of the diamagnetic term in the expression for the ^{15}N shielding constant, what, owing to comparable magnitudes of the paramagnetic contributions, finally diminishes the respective δ^{15N} (or Δ^{15N}_{coord}) parameter.

Surprisingly, the ^{15}N shielding effect is *ca.* 9 ppm more pronounced for $[Ir(bpy)Cl_4]^-$ than $[Ir(phen)Cl_4]^-$ ($|\Delta^{N(1)}_{coord}|$ being *ca.* 116 ppm and *ca.* 109 ppm, respectively), although for the analogous Au(III), Pd(II), Pt(II) and Pt(IV) complexes the opposite relation was observed (with *ca.* 4–6 ppm smaller $|\Delta^{N(1)}_{coord}|$ parameters for LL = bpy than LL = phen [26,27]). This anomaly may be partially caused by the fact that the ^{15}N signals of $K[Ir(bpy)Cl_4]$ and bpy have been detected in various solvents (D_2O *versus* DMSO-d_6), so the difference between their $\delta^{N(1)}$ chemical shifts cannot be regarded as an accurate $\Delta^{N(1)}_{coord}$ coordination shift.

The comparison of the ^{15}N NMR spectra for *cis*-$[Ir(LL)_2Cl_2]^+$ to *cis*-$[Co(LL)_2Cl_2]^+$ and *cis*-$[Rh(LL)_2Cl_2]^+$ exhibits the increase of the mean $|\Delta^{N(1)N(1')}_{coord}|$ absolute magnitude (we have averaged it for N(1) and N(1′)) in the order: Rh(III) (*ca.* 88–95 ppm) < Co(III) (*ca.* 95–103 ppm) < Ir(III) (*ca.* 115–118 ppm). The enhancement of the ^{15}N shielding effect following the Rh → Co transition (by *ca.* 7–8 ppm) probably results from the shortening of the respective metal–nitrogen bonds, as usually Rh–N > Co–N: 2.011(5)–2.037(6) Å in *cis*-$[Rh(bpy\text{-}\kappa^2N(1),N(1'))_2Cl_2]Cl \cdot 2H_2O$ (KIKPEZ) [66] *versus* 1.933(3)–1.940(3) Å in *cis*-$[Co(bpy\text{-}\kappa^2N(1),N(1'))_2Cl_2]Cl \cdot 2H_2O$ (QQQEQG01) [67], and 2.022(8)–2.049(7) Å in *cis*-$[Rh(phen\text{-}\kappa^2N(1),N(1'))_2Cl_2]ClO_4$ (GOLHOE) [68] *versus* 1.94–2.03 Å in *cis*-$[Co(phen\text{-}\kappa^2N(1),N(1'))_2Cl_2]Cl \cdot 3H_2O$ (CPHCOC) [69], what is again a consequence of the smaller ionic radius of Co(III) than Rh(III). In contrast, a further increase of the mean $|\Delta^{N(1)N(1')}_{coord}|$ absolute value upon the Rh(III) → Ir(III) replacement (by *ca.* 23–27 ppm), analogous to that reported during the Pd(II) → Pt(II) change (by *ca.* 15–16 ppm [26]) cannot be explained in this way, because the typical Ir–N bond lengths (*e.g.* 2.046(4)–2.053(5) Å in *cis*-$[Ir(phen\text{-}\kappa^2N(1),N(1'))_2Cl_2]PF_6$ (AMIPIV) [30]; 2.015(5)–2.131(5) Å in *cis*-$[Ir(4,4'\text{-dimethyl-bpy-}\kappa^2N(1),N(1'))_2Cl_2]PF_6$ (WABDEJ) [60]; 2.058(4)–2.070(4) in *cis*-$[Ir(2,2'\text{-biquinoline-}\kappa^2N(1),N(1'))_2Cl_2]PF_6$ (AJUKAR) [61]) are usually very close to the corresponding Rh–N ones, due to nearly the same ionic radii of Rh(III) and Ir(III). As also the other atomic properties of the rhodium and iridium elements are comparable (their electronegativities being 2.28 and 2.2; the electronic polarisabilities being 8.6±25% and 7.6±25%, respectively [53]), most likely relativistic phenomena (much more pronounced for Ir than Rh) may be of a major significance.

In both *cis*-$[Ir(LL)_2Cl_2]^+$ cations the N(1) atoms are more shielded than N(1′) ($\delta^{N(1')} > \delta^{N(1)}$; the $\delta^{N(1')} - \delta^{N(1)}$ difference being *ca.* +8 ppm for LL = bpy, and *ca.* +3 ppm for LL = phen). The same dependency (but with smaller separations of the N(1′) and N(1) signals: $\delta^{N(1')} - \delta^{N(1)}$ = *ca.* +3 ppm for LL = bpy, $\delta^{N(1')} - \delta^{N(1)}$ = *ca.* +1 ppm for LL = phen) was noted for the similar *cis*-$[Rh(LL)_2Cl_2]^+$ ions [27]. A more expressed ^{15}N shielding effect for the nitrogens *trans* to chlorine (N(1)) comparing to those *trans* to another nitrogen (N(1′)) can be again related to the fact that the Ir–N(1) or Rh–N(1) bonds are shorter than Ir–N(1′) or Rh–N(1′) (*cis*-$[Ir(phen\text{-}\kappa^2N(1),N(1'))_2Cl_2]PF_6$ (AMIPIV) – 2.046(4) Å *versus* 2.053(5) Å [30]; *cis*-$[Rh(bpy)_2Cl_2]Cl \cdot 2H_2O$ (KIKPEZ) – 2.016(5) Å *versus* 2.032(6) Å [66]; *cis*-$[Rh(phen)_2Cl_2]ClO_4$ (GOLHOE) – 2.036(8) Å *versus* 2.044(8) Å [68]; the mean lengths for both coordinated azine molecules). This hypothesis can also explain the opposite order of the N(1) and N(1′) peaks in the *cis*-$[Co(LL)_2Cl_2]^+$ cations ($\delta^{N(1')} - \delta^{N(1)}$ = *ca.* −0.1 ppm for LL = bpy, $\delta^{N(1')} - \delta^{N(1)}$ = *ca.* −2 ppm for LL = phen [27]), because, in contrast to the corresponding Rh(III) and Ir(III) complexes, in both Co(III) species the Co–N(1) bonds are longer than Co–N(1′) (*cis*-$[Co(bpy)_2Cl_2]Cl \cdot 2H_2O$ (QQQEQG01) – 1.939(3) Å *versus* 1.936(3) Å [67]; *cis*-$[Co(phen)_2Cl_2]Cl \cdot 3H_2O$ (CPHCOC) – 2.00 Å *versus* 1.96 Å [69]; the mean lengths for both coordinated azine molecules). Summing up, the interatomic metal-nitrogen distance seems to be an important factor determining the $\Delta^{N(1)}_{coord}$ parameter.

The ^{15}N NMR low-frequency coordination shifts, observed for the sp^2-hybridised pyridine-like nitrogens in bpy or phen, are analogous to those reported for some anionic (deprotonated) ligands deriving from pyrazole. Particularly, in the mixed Ir(III)–pyrazolate–pentamethylcyclopentadienyl-triphenylphosphine complex of the $[Ir(pyrazolate\text{-}N(1))_2(C_5(CH_3)_5)(P(C_6H_5)_3)]$ formula, the signal of the iridium-bonded N(1) atom was shifted to the lower frequency by as much as *ca.* 150 ppm, comparing to the uncoordinated N(2) nitrogen ($\delta^{N(1)-Ir}$ = −203.5 ppm *versus* $\delta^{N(2)}$ = −53.7 ppm; in $CDCl_3$ at −80 °C [70]). Furthermore, in the mixed triphenylphosphine–chloride–hydride Ir(III) complexes with L = pyridine, benzoimidazole, purine or adenine (*trans*(H,N)(H,Cl)–$[IrL(P(C_6H_5)_3)_2Cl(H)_2]$) the ^{15}N signals were also noticeably low-frequency shifted (*e.g.* for py from $\delta^{N(1)}$ = −60.6 ppm to $\delta^{N(1)-Ir}$ = *ca.* −131 ppm, in toluene-d_8; those of benzoimidazole, purine and adenine complexes appeared at *ca.* −137 ppm, *ca.* −177 ppm and *ca.* −105 ppm, respectively, all in toluene-d_8) [71]. For *trans*(H,N)(H,Cl)–$[Ir(py)(P(C_6H_5)_3)_2Cl(H)_2]$ such relatively small *ca.* 70 ppm ^{15}N shift probably reflected a smaller *trans* influence of H than N or Cl atoms; for the other cases some equilibria between the coordination species containing variously coordinated ligands (being ambidentate N-donors) must be considered.

Negative in sign (although smaller in the absolute magnitude) were also the Δ^{15N}_{coord} parameters for the sp^3 nitrogens in the NH_3 molecules, present in several Ir(III) complexes with such auxiliary groups as hydrides, chlorides, triethylphosphine or cyclooctene. Comparing to the liquid ammonia (δ^{NH3} = −381.7 ppm [72]), the ^{15}N signals were *ca.* 20–90 ppm low-frequency shifted as their δ^{Ir-NH3} values ranged from −403 ppm to −473 ppm [73,74]. This ^{15}N shielding effect was surprisingly opposite to the well-known *ca.* 20–25 ppm deshielding caused by ammonia protonation (as for NH_4^+: $\delta^{NH_4^+}$ = *ca.* − 358 ppm to *ca.* −361 ppm [72]), being noticeably dependent on the type of auxiliary ligands and the arrangement of the NH_3 molecules within the Ir(III) coordination sphere. Particularly, the ^{15}N low-frequency coordination shifts were more expressed for the ammonia ligands positioned *trans* to each other than for those *trans* to some other groups, as illustrated by the following δ^{15N} parameters: $[Ir(C_8H_{14})(NH_3)_4H]^{2+}$ – δ^{Ir-NH3} = −447.2 ppm (2 × N *trans* to NH_3) *versus* −420.0 ppm and −403.2 ppm (1 × N + 1 × N *trans* to H or cyclooctene); $[Ir(C_8H_{14})(NH_3)_3HCl]^+$ – δ^{Ir-NH3} = -442.8 ppm (2 × N *trans* to NH_3) *versus* -411.8 ppm (1 × N *trans* to cyclooctene); $[Ir(P(C_2H_5)_3)_3(NH_3)_2H]^{2+}$ – δ^{Ir-NH3} = -473.0 ppm (2 × N *trans* to NH_3); $[Ir(P(C_2H_5)_3)_2(NH_3)_3H]^{2+}$ – δ^{Ir-NH3} = −466.1 ppm (2 × N *trans* to NH_3) *versus* −425.3 ppm (1 × N *trans* to H); $[Ir(P(C_2H_5)_3)_2(NH_3)_2HCl]^+$ – δ^{Ir-NH3} = −461.2 ppm (2 × N *trans* to NH_3); PF_6^- salts in THF/THF-d_8 [73,74]. Such a dependency reflects the importance of some geometric factors in determining the ^{15}N coordination shielding effect.

The ^{15}N shielding phenomenon was described as well for the sp^3 nitrogens in the Ir(III)-coordinated –NH_2 and –NH–CO– moieties, present in 8-aminoquinoline and its trimethylacetamide. In the $[Ir(quinoline\text{-}8\text{-}NH_2)(P(C_6H_5)_3)_2H_2]^+$ and $[Ir(quinoline\text{-}8\text{-}NHCOC(CH_3)_3)(P(C_6H_5)_3)_2H_2]^+$ cations (SbF_6^- salts in CD_2Cl_2), the ^{15}N resonances were *ca.* 40 ppm low-frequency shifted, comparing to the free ligands: δ^{Ir-NH2} in quinoline-8-NH_2 – from −329.2 to −372.6 ppm, δ^{Ir-NH} in quinoline-8-$NHCOC(CH_3)_3$ – from −263.2 to −304.6 ppm [75].

The Ir(III)-induced ^{15}N low-frequency coordination shifts were reported also for many other types of nitrogen atoms, *e.g.* for nitro groups (sp^2) and cyanides (sp). As examples may serve: (a) *ca.* 180–220 ppm decrease of the δ^{15N} values in various nitro-, nitro-chloride- and nitro-aqua-iridate(III) anions ($[Ir(NO_2)_6]^{3-} - \delta^{Ir-NO2}$ = *ca.* +52 ppm, *trans*-$[Ir(NO_2)_4Cl_2]^{3-} - \delta^{Ir-NO2}$ = *ca.* +50 ppm, *fac*-$[Ir(NO_2)_3Cl_3]^{3-} - \delta^{Ir-NO2}$ = *ca.* +32 ppm, *fac*-$[Ir(NO_2)_3(H_2O)_3] - \delta^{Ir-NO2}$ = *ca.* +11 ppm (in 2 M NaCl aqueous solutions) comparing to free NO_2^- ($\delta^{NO2(-)}$= *ca.* +230 ppm) [76,77]); the original ^{15}N chemical shifts were primarily referenced to 1 M $NaNO_3$ and then recalculated by us to the neat nitromethane by adding *ca.* −4 ppm [78];

(b) *ca.* 110 ppm lower δ^{15N} parameters for the bridged –CN– than terminal –CN ligands in the two Ir(III) cyanide–chloride–dimethylphenylphosphine complexes ($\delta^{Ir-CN-Ir}$ = −204.6 ppm in [(P(C$_6$H$_5$)-(CH$_3$)$_2$)$_3$Cl$_2$Ir(μ-CN)IrCl$_2$(P(C$_6$H$_5$)(CH$_3$)$_2$)$_3$]ClO$_4$ *versus* δ^{Ir-CN} = −95.9 ppm in [Ir(P(C$_6$H$_5$)(CH$_3$)$_2$)$_3$Cl$_2$(CN)] (both in CD$_2$Cl$_2$) [79]).

Summing up, this short review exhibits that generally the formation of the iridium-nitrogen coordination bonds results in the ^{15}N shielding effect (*i.e.* in the low-frequency shifts of the ^{15}N resonances), such a phenomenon being observed for a large variety of N atoms.

The presently studied Ir(III) complexes reveal no ^{15}N chemical shift isotopomerism associated with the natural abundance of the ^{191}Ir (37.3%) and ^{193}Ir (62.7%) nuclei [53]. Furthermore, all ^{15}N signals appear as singlets, the absence of ^{15}N–^{191}Ir or ^{15}N–^{193}Ir couplings being probably caused by a quadrupolar character of both iridium isotopes (their spin numbers are 3/2, their electric quadrupol moments are +0.82 and +0.75 barn (10^{-28} m^2) [53]). Such a behaviour is analogous to that noted for the respective Co(III) species [27,80] (the 100% abundant ^{59}Co nucleus has the 7/2 spin number and the electric quadrupol moment of +0.41 barn [53]) but entirely different from the one observed for similar Rh(III) compounds (the only ^{103}Rh isotope has the 1/2 spin number [53]), where the intense ^{15}N–^{103}Rh spin–spin interactions were detected [27].

3.6. Calculated ^{1}H NMR chemical shifts

The δ^{1H}_{calc} parameters, calculated for free bpy and phen, as well as for the [Ir(LL)Cl$_4$]$^-$ and *cis*-[Ir(LL)$_2$Cl$_2$]$^+$ ions, by B3LYP/LanL2DZ+6-31G**//B3LYP/LanL2DZ+6-31G* (as isolated species, *i.e. in vacuo*; method (a)) or by B3LYP/LanL2DZ+6-31G**(PCM)//B3LYP/LanL2DZ+6-31G* (as solvated species, assuming as medium: H$_2$O for the bpy complexes, DMSO for the free ligands and the phen complexes; method (b)), are listed in Table 6.

The reproducibility of the calculated ^{1}H chemical shifts has been significantly improved after the inclusion of solvation effects, as exhibited by the large decrease of the rmsd values, observed for each studied compound (for all species: 0.51→0.11); this is why we will focus at the results obtained by the method (b). Upon its application, the respective rmsd parameters for the complexes are comparable or even smaller than those in case of the free ligands.

For both [Ir(LL)Cl$_4$]$^-$ anions the order of the ^{1}H resonances has been correctly predicted: H(6) > H(3) > H(4) > H(5) for LL = bpy, H(2) > H(4) > H(5) > H(3) for LL = phen. Furthermore, the most expressed deshielding effects of *ca.* 0.6–0.9 ppm have been forecasted for H(6) in bpy and H(2) in phen, *i.e.* in accordance with the actual NMR measurements.

For both *cis*-[Ir(LL)$_2$Cl$_2$]$^+$ cations a larger deshielding of the corresponding H′ than H atom has been reproduced for all protons; moreover, the separation of these signals (*i.e.* the $\delta^{H'}_{calc} - \delta^{H}_{calc}$ difference) increases in the same order like in the real NMR spectra: H(3) < H(4) < H(5) < H(6) for LL = bpy, H(5) < H(4) < H(3) < H(2) for LL = phen, reaching *ca.* 2.0–2.1 ppm for the nitrogen-adjacent protons. In consequence, H(6′) in bpy and H(2′) in phen are predicted to be deshielded by *ca.* 0.9–1.1 ppm, whereas those of H(6) in bpy and H(2) in phen – to be shielded by *ca.* 1.0–1.3 ppm, comparing to the same protons in the free ligands, also in a qualitative agreement with the experimental results.

Table 6
Quantum-chemically calculated, by B3LYP/LanL2DZ+6-31G**//B3LYP/LanL2DZ+6-31G* – (a), or B3LYP/LanL2DZ+6-31G** (PCM)//B3LYP/LanL2DZ+6-31G* – (b), ^{1}H NMR chemical shifts (δ^{1H}_{calc}, ppm) for bpy, phen and their Ir(III) chloride complexes

Compound	H(3)	H(4)	H(5)	H(6)	rmsd
Bpy (a)[C]	9.06	7.87	7.32	8.93	0.32
Bpy (b)[B]	8.72	7.89	7.38	8.70	0.17
[Ir(bpy)Cl$_4$] - (a)[C]	7.56	7.22	7.13	10.70	0.84
[Ir(bpy)Cl$_4$]$^-$ (b)[A]	8.29	8.08	7.66	9.64	0.09
cis-[Ir(bpy)$_2$Cl$_2$]$^+$ (H) (a)[C]	8.41	8.21	7.55	7.87	0.30
cis-[Ir(bpy)$_2$Cl$_2$]$^+$ (H′) (a)[C]	8.47	8.49	8.19	10.51	
cis-[Ir(bpy)$_2$Cl$_2$]$^+$ (H) (b)[A]	8.54	8.20	7.58	7.74	0.07
cis-[Ir(bpy)$_2$Cl$_2$]$^+$ (H′) (b)[A]	8.63	8.43	8.02	9.79	
	H(2)	H(3)	H(4)	H(5)	rmsd
Phen (a)[C]	9.55	7.73	8.21	7.89	0.27
Phen (b)[B]	9.21	7.81	8.36	7.95	0.09
[Ir(phen)Cl$_4$]$^-$ (a)[C]	10.75	7.56	7.63	7.55	0.70
[Ir(phen)Cl$_4$]$^-$ (b)[B]	9.81	8.03	8.55	8.15	0.03
cis-[Ir(phen)$_2$Cl$_2$]$^+$ (H) (a)[C]	8.06	7.81	8.61	8.37	0.30
cis-[Ir(phen)$_2$Cl$_2$]$^+$ (H′) (a)[C]	10.80	8.59	8.94	8.53	
cis-[Ir(phen)$_2$Cl$_2$]$^+$ (H) (b)[B]	7.91	7.86	8.70	8.36	0.11
cis-[Ir(phen)$_2$Cl$_2$]+ (H′) (b)[B]	10.11	8.46	8.99	8.46	

The overall rmsd value is 0.51 (method (a)) and 0.11 (method (b)).
In the *cis*-[Ir(LL)$_2$Cl$_2$]$^+$ cations: the protons denoted as H and H′ correspond to these halves of each LL ligand which are positioned *trans* to chlorine and *trans* to another nitrogen, respectively.
[A] Calculated in H$_2$O.
[B] Calculated in DMSO.
[C] Calculated *in vacuo*.

3.7. Calculated ^{13}C NMR chemical shifts

The δ^{13C}_{calc} parameters, calculated for free bpy and phen, as well as for the [Ir(LL)Cl$_4$]$^-$ and *cis*-[Ir(LL)$_2$Cl$_2$]$^+$ ions, by B3LYP/LanL2DZ+6-31G**//B3LYP/LanL2DZ+6-31G* (as isolated species, *i.e. in vacuo*; method (a)) or by B3LYP/LanL2DZ+6-31G**(PCM)//B3LYP/LanL2DZ+6-31G* (as solvated species, assuming as medium: H$_2$O for the bpy complexes, DMSO for the free ligands and the phen complexes; method (b)), are listed in Table 7.

The quality of these ^{13}C NMR calculations is again better in case of the method (b) than (a), although the decrease of the rmsd parameters is much less pronounced than in case of ^{1}H NMR (3.5→2.6, for all species), probably due to a smaller impact of solvation effects on the δ^{13C} parameters. The rmsd values for the complexes are always larger than in case of the free ligands. Nevertheless, the orders of the ^{13}C signals have been correctly predicted: C(2) > C(6) > C(4) > C(5) > C(3) for LL = bpy, C(2) > C(1a) > C(4) > C(4a) > C(5) > C(3) for LL = phen, with rather slight differences (being, however, of variable sign) between the corresponding C′ and C carbons in both *cis*-[Ir(LL)$_2$Cl$_2$]$^+$ cations.

3.8. Calculated ^{15}N NMR chemical shifts

The δ^{15N}_{calc} parameters, calculated for all [Ir(LL)Cl$_4$]$^-$ and *cis*-[Ir(LL)$_2$Cl$_2$]$^+$ ions by B3LYP/LanL2DZ+6-31G**//B3LYP/LanL2DZ+6-31G* (as isolated species, *i.e. in vacuo*; method (a)) or by B3LYP/LanL2DZ+6-31G**(PCM)//B3LYP/LanL2DZ+6-31G* (as solvated species, assuming as medium: H$_2$O for the bpy complexes, DMSO for the phen ones; method (b)), are listed in Table 8.

The introduction of solvation effects has generally improved the quality of the ^{15}N NMR calculations (rmsd for all complexes: 13.6→5.7). Nevertheless, in contrast to the actual experiments, the calculated ^{15}N chemical shifts are noticeably lower for *cis*-[Ir(LL)$_2$Cl$_2$]$^+$ than [Ir(LL)Cl$_4$]$^-$ (by *ca.* 10 ppm for LL = bpy and by *ca.* 12 ppm for LL = phen). Furthermore, the δ^{15N}_{calc} parameters are smaller for the nitrogen atoms in bpy than phen, differing by *ca.* 1 ppm for [Ir(LL)Cl$_4$]$^-$ and by *ca.* 3 ppm for *cis*-[Ir(LL)$_2$Cl$_2$]$^+$, what is again inconsistent with the experimental dependencies. On the other hand, a more pronounced shielding of the nitrogens *trans* to chlorine (N(1)) comparing to those *trans* to another nitrogen (N(1′)) has been well reproduced by the method (b), although the computed $\delta^{N(1')}_{calc} - \delta^{N(1)}_{calc}$ differences are slight (*ca.* 1–2 ppm). It is worth noting that analogous calculations performed by the method

Table 7
Quantum-chemically calculated, by B3LYP/LanL2DZ+6-31G**//B3LYP/LanL2DZ+6-31G* – (a), or B3LYP/LanL2DZ+6-31G** (PCM)//B3LYP/LanL2DZ+6-31G* – (b), ^{13}C NMR chemical shifts (δ^{13C}_{calc}, ppm) for bpy, phen and their Ir(III) chloride complexes

Compound	C(2)	C(3)	C(4)	C(5)	C(6)	rmsd
Bpy (a)[C]	159.4	124.2	137.7	125.3	150.9	1.5
Bpy (b)[B]	157.0	122.5	138.1	125.6	150.1	0.5
$[Ir(bpy)Cl_4]^-$ (a)[C]	157.9	120.5	130.3	123.9	157.1	4.9
$[Ir(bpy)Cl_4]^-$ (b)[A]	155.5	125.5	139.4	128.2	152.0	1.9
cis-$[Ir(bpy)_2Cl_2]^+$ (C) (a)[C]	156.3	126.2	140.9	129.6	151.1	1.8
cis-$[Ir(bpy)_2Cl_2]^+$ (C′) (a)[C]	155.2	125.6	141.6	130.9	155.6	
cis-$[Ir(bpy)_2Cl_2]^+$ (C) (b)[A]	154.8	127.0	142.2	129.9	150.6	1.6
cis-$[Ir(bpy)_2Cl_2]^+$ (C′) (b)[A]	154.7	126.7	142.3	130.0	152.1	
	C(1a)	C(2)	C(3)	C(4)	C(4a)	C(5)	rmsd
Phen (a)[C]	151.4	151.8	124.2	136.9	132.1	130.0	1.8
Phen (b)[B]	148.4	150.6	124.6	138.1	131.7	129.6	0.9
$[Ir(phen)Cl_4]^-$ (a)[C]	150.1	156.5	124.5	129.5	130.9	127.6	3.5
$[Ir(phen)Cl_4]^-$ (b)[B]	146.2	151.9	126.9	138.6	132.4	130.1	2.6
cis-$[Ir(phen)_2Cl_2]^+$ (C) (a)[C]	146.9	150.2	128.0	140.5	134.2	131.2	2.0
cis-$[Ir(phen)_2Cl_2]^+$ (C′) (a)[C]	147.0	155.5	129.4	141.2	133.9	132.5	
cis-$[Ir(phen)_2Cl_2]^+$ (C) (b)[B]	144.9	150.5	128.2	142.1	133.7	131.1	2.2
cis-$[Ir(phen)_2Cl_2]^+$ (C′) (b)[B]	145.3	152.3	128.5	142.2	133.5	131.5	

The overall rmsd value is 3.5 (method (a)) and 2.6 (method (b)).
In the *cis*-$[Ir(LL)_2Cl_2]^+$ cations: the carbons denoted as C and C′ correspond to these halves of each LL ligand which are positioned *trans* to chlorine and *trans* to another nitrogen, respectively.
[A] Calculated in H_2O.
[B] Calculated in DMSO.
[C] Calculated *in vacuo*.

Table 8
Quantum-chemically calculated, by B3LYP/LanL2DZ+6-31G**//B3LYP/LanL2DZ+6-31G* – (a), or B3LYP/LanL2DZ+6-31G** (PCM)//B3LYP/LanL2DZ+6-31G* – (b), ^{15}N NMR chemical shifts (δ^{15N}_{calc}, ppm) for Ir(III) chloride complexes with bpy and phen

Compound	$\delta^{N(1)(a)}_{calc}$	$\delta^{N(1)(b)}_{calc}$
$[Ir(bpy)Cl_4]^-$	−164.3 [C]	−177.7 [A]
cis-$[Ir(bpy)_2Cl_2]^+$ (N)	−192.9 [C]	−188.8 [A]
cis-$[Ir(bpy)_2Cl_2]^+$ (N′)	−195.5 [C]	−186.5 [A]
Average for N and N′	−194.2	−187.65
Difference between N′ and N	−2.6	+2.3
$[Ir(phen)Cl_4]^-$	−166.5 [C]	−179.1 [B]
cis-$[Ir(phen)_2Cl_2]^+$ (N)	−196.0 [C]	−191.9 [B]
cis-$[Ir(phen)_2Cl_2]^+$ (N′)	−199.8 [C]	−190.8 [B]
Average for N and N′	−197.9	−191.35
Difference between N′ and N	−3.8	+1.1
Rmsd for all Ir(III) species	13.6	5.7

In the *cis*-$[Ir(LL)_2Cl_2]^+$ cations: the nitrogens denoted as N and N′ are positioned *trans* to chlorine and *trans* to another nitrogen, respectively.
[A] Calculated in H_2O.
[B] Calculated in DMSO.
[C] Calculated *in vacuo*.

(a) have lead to the opposite, erroneous relations, *i.e.* to negative $\delta^{N(1')}_{calc} - \delta^{N(1)}_{calc}$ differences. The change of sign of such $\delta^{N(1')}_{calc} - \delta^{N(1)}_{calc}$ expressions upon the solvent introduction may suggest an importance of solvation effects in determining the δ^{15N} chemical shifts.

4. Conclusions

The molecular structure of potassium aquapentachloroiridate(III) is typical for the whole class of the $M_2[IrLCl_5]$ compounds (M = K, NH_4, Rb, Cs; L = H_2O, NH_3), although the crystal packing of these inorganic salts is variable. Particularly, $K_2[Ir(H_2O)Cl_5]$ is crystallographically nearly isostructural with $K_2[Ir(NH_3)Cl_5]$, a distorted octahedral geometry of the $[Ir(H_2O)Cl_5]^{2-}$ anions being similar to those in $Cs_2[Ir(H_2O)Cl_5]$ and $[Pt(NH_3)_4][Ir(H_2O)Cl_5] \cdot 2H_2O$.

The ^1H, ^{13}C, ^{15}N NMR spectral patterns correspond well to the assumed structures of the $[Ir(LL)Cl_4]^-$ and *cis*-$[Ir(LL)_2Cl_2]^+$ ions. They confirm the N(1),N(1′)-chelation of both azines, excluding either the monodentate N(1)-bonding or the unsymmetric N(1), C(3′)-coordination.

The ^1H NMR spectra are heavily affected by Ir(III) chloride complexation, this effect being noticeably dependent on the composition and geometry of the coordination sphere, as well as on the proton position. In the $[Ir(LL)Cl_4]^-$ anions, the ^1H signals are high-frequency shifted, the Δ^{1H}_{coord} parameters decreasing in the orders H(6) > H(5) > H(4) > H(3) for LL = bpy, and H(2) > H(3) > H(5) > H(4) for LL = phen; the largest values are noted for the hydrogens directly adjacent to the coordination sites, *i.e.* H(6) in bpy (*ca.* 0.9–1.0 ppm) and H(2) in phen (*ca.* 0.5–0.8 ppm). In the *cis*-$[Ir(LL)_2Cl_2]^+$ cations, the magnetic inequivalency of the two halves of each coordinated azine molecule results in a double number of the ^1H resonances; for each pair of the corresponding protons, the peak appearing at the higher frequency (H′) can be assigned to the ligand moiety positioned *trans* to N, while its counterpart at the lower frequency (H) – to that *trans* to Cl. In consequence, the highly positive Δ^{1H}_{coord} parameters (*ca.* 0.2–1.0 ppm) are noted for H′ protons, whereas much smaller (up to *ca.* 0.4 ppm) or even negative (down to *ca.* −1.0 ppm) for the H ones; the respective absolute values ($|\Delta^{1H}_{coord}|$) as well as the separations of the corresponding H′ and H signals ($\delta^{(H')} - \delta^{(H)}$) are again the largest for H(6)/H(6′) in bpy and H(2)/H(2′) in phen. This δ^{1H} patterns variability reflects an importance of several factors influencing the σ^{1H} shielding constants: an inductive effect of the electron-acceptor $IrCl_4$ or $IrCl_2$ moiety, anisotropic phenomena deriving from the adjacency of some additional π-electron ring systems and relativistic contributions.

The ^{13}C NMR spectra are only moderately influenced, the orders of resonances remaining the same like in the free ligands. The carbon deshielding is generally observed, the Δ^{13C}_{coord} parameters not exceeding 8 ppm. In contrast, the formation of Ir–N bonds results in the large ^{15}N low-frequency shifts (the Δ^{15N}_{coord} values ranging from *ca.* −105 ppm to *ca.* −120 ppm), even more expressed than in the similar Pd(II), Pt(II), Pt(IV), Au(III), Co(III) and Rh(III) species. In the *cis*-$[Ir(LL)_2Cl_2]^+$ cations the nitrogens positioned *trans* to chlorine (N(1)) are *ca.* 3–8 ppm more shielded than those *trans* to another nitrogen (N(1′)), this relation being the same as in the analogous Rh(III) complexes, but opposite to that in the relevant Co(III) species.

Acknowledgements

This work was supported by the Ministry of Education of the Czech Republic (MSM0021622413) as well as by the bilateral PL-CZ cooperation project (11/2006/PL/CZ). We express our gratitude to the staff of the supercomputing centres in Brno and Prague for CPU time.

Appendix A. Supplementary data

Crystallographic data for structural analysis of K2[Ir(H2O)Cl5]) have been deposited in the Inorganic Crystal Structure Database at the Fachinformationszentrum Karlsruhe, the ICSD Deposition Number being 419168. Some representative ^1H–^{15}N HMQC–NMR spectra of the ionic species containing $[Ir(LL)Cl4]^-$ and *cis*-$[Ir(LL)_2Cl_2]^+$ have been shown as supplementary figures (Fig. 1S–3S). Supplementary data associated with this article can be found, in the online version, at doi:10.1016/j.poly.2008.06.040.

References

[1] I.I. Alekseeva, L.E. Romanovskaya, A.S. Kozlov, Zh. Neorg. Khim. 32 (1987) 2737.
[2] I.B. Usmanov, V.S. Bondarenko, V.I. Kazbanov, Zh. Neorg. Khim. 32 (1987) 2306.
[3] V.S. Bondarenko, I.B. Usmanov, V.I. Kazbanov, Zh. Neorg. Khim. 33 (1988) 2138.

[4] J.E. Fergusson, D.A. Rankin, Aust. J. Chem. 36 (1983) 863.
[5] R.K. Coll, J.E. Fergusson, B.R. Penfold, D.A. Rankin, W.T. Robinson, Aust. J. Chem. 40 (1987) 2115.
[6] E. Garnier, M. Bele, Acta Crystallogr., Sect. C 50 (1994) 994.
[7] E. Bernhardt, W. Preetz, Z. Anorg. Allg. Chem. 623 (1997) 1389.
[8] N.M. Sinitsyn, V.V. Borisov, A.S. Kozlov, V.V. Kravchenko, L.I. Prokhodtseva, Zh. Neorg. Khim. 27 (1982) 164.
[9] V.M. Deflon, C.M. Mössmer, J. Strähle, Z. Anorg. Allg. Chem. 625 (1999) 2186.
[10] R.A. Cipriano, L.R. Hanton, W. Levason, D. Pletcher, N.A. Powell, M. Webster, J. Chem. Soc., Dalton Trans. (1988) 2483.
[11] J.A. Broomhead, W. Grumley, Inorg. Chem. 10 (1971) 2002.
[12] C. Stinner, M.D. Wightman, S.E. Kelley, M.G. Hill, J.K. Barton, Inorg. Chem. 40 (2001) 5245.
[13] J.R. Lee, Y.R. Liou, W.L. Huang, Inorg. Chim. Acta 319 (2001) 83.
[14] R.D. Gillard, B.T. Heaton, J. Chem. Soc. A (1969) 451.
[15] R.J. Watts, J.S. Harrington, J. van Houten, J. Am. Chem. Soc. 99 (1977) 2179.
[16] G. Nord, A.C. Hazell, R.G. Hazell, O. Farver, Inorg. Chem. 22 (1983) 3429.
[17] L. Wallace, G.A. Heath, E. Krausz, G. Moran, Inorg. Chem. 30 (1991) 347.
[18] B. Divisia-Blohorn, Inorg. Chim. Acta 117 (1986) 97.
[19] B. Chiswell, S.E. Livingstone, J. Inorg. Nucl. Chem. 26 (1964) 47.
[20] Y. Ohashi, Bull. Chem. Soc. Jpn. 54 (1981) 3673.
[21] T. Kobayashi, Y. Ohashi, Chem. Phys. Lett. 86 (1982) 289.
[22] K. Burger, F.E. Wagner, A. Vertes, E. Bencze, J. Mink, I. Labadi, Z. Nemes-Vetessy, J. Phys. Chem. Solids 62 (2001) 2059.
[23] T.L. Cremers, G.A. Crosby, Chem. Phys. Lett. 73 (1980) 541.
[24] C.M. Bolinger, N. Story, B.P. Sullivan, T.J. Meyer, Inorg. Chem. 27 (1988) 4582.
[25] R.E. De Simone, R.S. Drago, Inorg. Chem. 8 (1969) 2517.
[26] L. Pazderski, E. Szłyk, J. Sitkowski, B. Kamieński, L. Kozerski, J. Toušek, R. Marek, Magn. Reson. Chem. 44 (2006) 163.
[27] L. Pazderski, J. Toušek, J. Sitkowski, L. Kozerski, R. Marek, E. Szłyk, Magn. Reson. Chem. 45 (2007) 24.
[28] L. Pazderski, Polish J. Chem. 80 (2006) 1083.
[29] P. Andersen, J. Josephsen, Acta Chem. Scand. 25 (1971) 3255.
[30] N. Yoshikawa, J. Sakamoto, N. Kanehisa, Y. Kai, K. Matsumura, H. Takashima, K. Tsukahara, Acta Crystallogr., Sect. E 59 (2003) m972.
[31] Cambridge Structure Database, Cambridge Crystallographic Data Centre, Cambridge, UK, 2008.
[32] A.C. Hazell, R.G. Hazell, Acta Crystallogr., Sect. C 40 (1984) 806.
[33] W.A. Wickramasinghe, P.H. Bird, N. Serpone, J. Chem. Soc., Chem. Commun. (1981) 1284.
[34] F.O. Garces, R.J. Watts, Inorg. Chem. 29 (1990) 582.
[35] A. Slama-Schwok, D. Avnir, M. Ottolenghi, J. Phys. Chem. 93 (1989) 7544.
[36] P.J. Spellane, R.J. Watts, C.J. Curtis, Inorg. Chem. 22 (1983) 4060.
[37] M.F. Finlayson, P.C. Ford, R.J. Watts, J. Phys. Chem. 90 (1986) 3916.
[38] P.S. Braterman, G.A. Heath, A.J. MacKenzie, B.C. Noble, R.D. Peacock, L.J. Yellowlees, Inorg. Chem. 23 (1984) 3425.
[39] R.J. Watts, S.F. Bergeron, J. Phys. Chem. 83 (1979) 424.
[40] P.J. Spellane, R.J. Watts, Inorg. Chem. 20 (1981) 3561.
[41] R.D. Gillard, R.J. Lancashire, P.A. Williams, J. Chem. Soc., Dalton Trans. (1979) 190.
[42] J.L. Kahl, K. Hanck, K. de Armond, J. Inorg. Nucl. Chem. 41 (1979) 495.
[43] P.A. Grutsch, C. Kutal, J. Chem. Soc., Chem. Commun. (1982) 893.
[44] V.T. Coombe, G.A. Heath, A.J. MacKenzie, L.J. Yellowlees, Inorg. Chem. 23 (1984) 3423.
[45] N. Yoshikawa, Y. Masuda, T. Matsumura-Inoue, Chem. Lett. (2000) 1206.
[46] M. Delepine, Bull. Soc. Chim. Fr. 3 (1908) 906.
[47] CRYSALIS CCD and CRYSALIS RED, Oxford Diffraction, Abingdon, 2000.
[48] G.M. Sheldrick, SHELXS97 and SHELXL97, University of Göttingen, 1997.
[49] L. Pazderski, J. Toušek, J. Sitkowski, L. Kozerski, E. Szłyk, Magn. Reson. Chem. 45 (2007) 1045.
[50] L. Pazderski, J. Toušek, J. Sitkowski, L. Kozerski, E. Szłyk, Magn. Reson. Chem. 45 (2007) 1059.
[51] M.J. Frisch, G.W. Trucks, H.B. Schlegel, G.E. Scuseria, M.A. Robb, J.R. Cheeseman, J.A. Montgomery, Jr., T. Vreven, K.N. Kudin, J.C. Burant, J.M. Millam, S.S. Iyengar, J. Tomasi, V. Barone, B. Mennucci, M. Cossi, G. Scalmani, N. Rega, G.A. Petersson, H. Nakatsuji, M. Hada, M. Ehara, K. Toyota, R. Fukuda, J. Hasegawa, M. Ishida, T. Nakajima, Y. Honda, O. Kitao, H. Nakai, M. Klene, X. Li, J.E. Knox, H.P. Hratchian, J.B. Cross, C. Adamo, J. Jaramillo, R. Gomperts, R.E. Stratmann, O. Yazyev, A.J. Austin, R. Cammi, C. Pomelli, J.W. Ochterski, P.Y. Ayala, K. Morokuma, G.A. Voth, P. Salvador, J.J. Dannenberg, V.G. Zakrzewski, S. Dapprich, A.D. Daniels, M.C. Strain, O. Farkas, D.K. Malick, A.D. Rabuck, K. Raghavachari, J.B. Foresman, J.V. Ortiz, Q. Cui, A.G. Baboul, S. Clifford, J. Cioslowski, B.B. Stefanov, G. Liu, A. Liashenko, P. Piskorz, I. Komaromi, R.L. Martin, D.J. Fox, T. Keith, M.A. Al-Laham, C.Y. Peng, A. Nanayakkara, M. Challacombe, P.M.W. Gill, B. Johnson, W. Chen, M.W. Wong,. C. Gonzalez, J.A. Pople, GAUSSIAN 03, Revision B.05, Gaussian, Pittsburgh, 2003.
[52] A.L. Spek, J. Appl. Crystallogr. 36 (2003) 7.
[53] Handbook of Chemistry and Physics, 85th ed., CRC Press, Boca-Raton, 2004–2005 (Sect. 9, p. 76; Sect. 10, p. 168; Sect. 11, p. 50, Sect. 12, p. 14).
[54] D.A. Rankin, B.R. Penfold, J.E. Fergusson, Aust. J. Chem. 36 (1983) 871.
[55] K. Nakamoto, Infrared and Raman Spectra of Inorganic and Coordination Compounds. Part A: Theory and Applications in Inorganic Chemistry, 5th ed., Wiley, New York, 1997. p. 346.
[56] H.H. Schmidtke, A. Wolf, Inorg. Chim. Acta 29 (1978) 11.
[57] P. Mura, A. Casini, G. Marcon, L. Mesori, Inorg. Chim. Acta 312 (2001) 74.
[58] SDBS – Spectral Database for Organic Compounds, National Institute of Advanced Industrial Science and Technology, Japan, <http://www.aist.go.jp/RIODB/SDBS/2007>.
[59] J.P. Collin, I.M. Dixon, J.P. Sauvage, J.A.G. Williams, F. Barigeletti, L. Flamigni, J. Am. Chem. Soc. 121 (1999) 5009.
[60] N. Yoshikawa, J. Sakamoto, N. Kanehisa, Y. Kai, T. Matsumura-Inoue, Acta Crystallogr., Sect. E 59 (2003) m155.
[61] N. Yoshikawa, J. Sakamoto, N. Kanehisa, Y. Kai, T. Matsumura-Inoue, H. Takashima, K. Tsukahara, Acta Crystallogr., Sect. E 59 (2003) m551.
[62] M.T. Youinou, R. Ziessel, J. Organomet. Chem. 363 (1989) 197.
[63] N.P. Ayala, C.M. Flynn, L.A. Sacksteder, J.N. Demas, B.A. de Graff, J. Am. Chem. Soc. 112 (1990) 3837.
[64] E.C. Constable, T.A. Leese, J. Organomet. Chem. 335 (1987) 293.
[65] E. Kupce, L.M. Ignatovich, E. Lukevics, J. Organomet. Chem. 372 (1989) 189.
[66] P. Lahuerta, J. Latorre, R. Martinez-Manez, S. Garcia-Granda, F. Gomez-Beltran, Acta Crystallogr., Sect. C 47 (1991) 519.
[67] I. Strenger, T. Rosu, M. Negoiu, Z. Kristallogr.-New Cryst. Struct. 215 (2000) 489.
[68] Z. Ji, Y. Shan, A.R. Guadalupe, S.D. Huang, Z. Kristallogr-New Cryst. Struct. 214 (1999) 387.
[69] A.V. Ablov, A.Y. Kon, T.I. Malinovskii, Dokl. Akad. Nauk. SSSR 167 (1966) 1051.
[70] D. Carmona, L.A. Oro, M.P. Lamata, M.L. Jimeno, J. Elguero, A. Belguise, P. Lux, Inorg. Chem. 33 (1994) 2196.
[71] N.J. Wood, J.A. Brannigan, S.B. Duckett, S.L. Heath, J. Wagstaff, J. Am. Chem. Soc. 129 (2007) 11012.
[72] R. Marek, A. Lyčka, Curr. Org. Chem. 6 (2002) 35.
[73] R. Koelliker, D. Milstein, Angew. Chem. 103 (1991) 724.
[74] R. Koelliker, D. Milstein, J. Am. Chem. Soc. 113 (1991) 8524.
[75] J.C. Lee, B. Müller, P. Pregosin, G.P.A. Yap, A.L. Rheingold, R.H. Crabtree, Inorg. Chem. 34 (1995) 6295.
[76] A.B. Venediktov, M.A. Fedotov, S.V. Korenev, Koord. Khim. 25 (1999) 285.
[77] S.V. Korenev, A.B. Venediktov, V.I. Malkova, M.A. Fedotov, Koord. Khim. 25 (1999) 696.
[78] M. Witanowski, L. Stefaniak, G.A. Webb, Annu. Rep. NMR Spectrosc. 25 (1993) 86.
[79] A.J. Deeming, G.P. Proud, H.M. Dawes, M.B. Hursthouse, J. Chem. Soc., Dalton Trans. (1988) 2475.
[80] L. Pazderski, A. Surdykowski, M. Pazderska-Szabłowicz, J. Sitkowski, L. Kozerski, B. Kamieński, E. Szłyk, Cent. Eur. J. Chem. 6 (2008) 55.

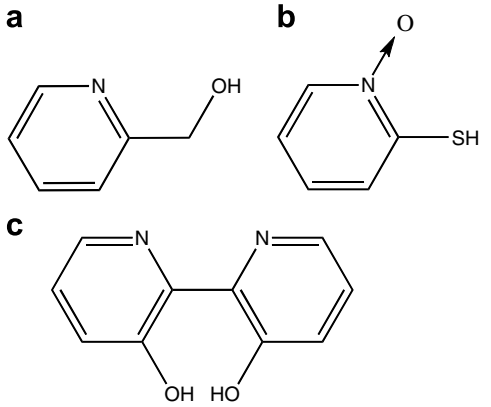

Fig. 1. Schematic of ligands (a) H-OPy, (b) H-2MPO, and (c) H_2-OBPy.

2. Experimental

All compounds described below were handled under an argon atmosphere with rigorous exclusion of air and water using standard Schlenk line and glove box techniques. All solvents were stored under argon and used as received (Aldrich) in Sure/Seal™ bottles, including toluene (tol) and pyridine (py). The following chemicals were used as received (Aldrich and Alfa Aesar): $Ti(OPr^i)_4$, $Zr(OBu^t)_4$, H-ONep, H-2MPO, and (*R*,*S*) H_2-OBPy. [Ti(μ-ONep)(O-Nep)$_3$]$_2$was prepared according to the literature procedure [7].

FT-IR data were obtained on a Bruker Vector 22 Instrument using KBr pellets under an atmosphere of flowing nitrogen. Elemental analysis was performed on a Perkin–Elmer 2400 CHN–S/O Elemental Analyzer. All NMR samples were prepared from dried crystalline materials that were handled and stored under an argon atmosphere and redissolved in toluene-d_8.

2.1. General synthesis

Due to the similarity of synthesis of **1**–**5**, a general description is supplied with specific details listed for each compound below. The desired ligand was slowly added to a stirring solution of the $M(OR)_4$ dissolved in toluene (~5 mL). After 12 h, the resultant clear reaction mixtures were concentrated by rotary evaporation and then either cooled at −35 °C or left at room temperature uncapped until X-ray quality crystals formed.

2.1.1. $(2MPO)_2Ti(OCHMe_2)_2$ (**1**)

Used $Ti(OCHMe_2)_4$ (1.00 g, 3.52 mmol), H-2MPO (0.895 g, 7.04 mmol), and tol (~10 mL). Yield 1.26 g (85.7%). FT-IR (KBr, cm^{-1}) 3081(w), 3053(w), 2966(s), 2926(s), 2855(s), 1595(m), 1546(m), 1461(s), 1419(m), 1372(m), 1324(m), 1255(m), 1208(s), 1162(s), 1116(s), 983(s), 850(s), 764(s), 713(s), 608(s), 488(m). ^{1}H NMR (399.9 MHz, tol-d_8) δ 8.01–7.99 (4H, mult, ONC_5H_4S, J_{H-H} = 6.0 Hz), 5.04 (0.97H, $OCH(CH_3)_2$, J_{H-H} = 6.2 Hz), 1.23 (8.8H, d, $OCH(CH_3)_3$, J_{H-H} = 8.0 Hz). Elemental *Anal.* Calc. for $C_{16}H_{22}N_2O_4S_2Ti$: C, 45.93; H, 5.30; N, 6.70. Found: C, 45.85; H, 5.31; N, 6.30%.

2.1.2. $(2MPO)_2Ti(OCH_2CMe_3)_2$ (**2**)

Used $Ti(OCH_2CMe_3)_4$ (1.00 g, 2.52 mmol), H-2MPO (0.642 g, 5.05 mmol), and tol (~10 mL). Yield 1.14 g (95.2%). FT-IR (KBr, cm^{-1}) 3105(w), 2950(s), 2903(m), 2865(s), 2828(s), 2687(w), 1601(m), 1543(m), 1460(s), 1419(m), 1395(m), 1375(m), 1207(s), 1142(s), 1090(s), 1059(s), 1023(s), 812 (m), 800(w), 755(m), 710(w), 670(s), 612(m), 578(m), 480(m). ^{1}H NMR (399.9 MHz, $CDCl_3$) δ 8.01 (1H, d, ONC_5H_4S, J_{H-H} = 6.8 Hz), 7.45 (1.1H, d, ONC_5H_4S, J_{H-H} = 6.8 Hz), 7.21 (1.3H, t, ONC_5H_4S, J_{H-H} = 7.6 Hz), 6.81 (1.1 H, t, ONC_5H_4S, J_{H-H} = 6.8 Hz) 4.34 (2.2H, s, $OCH_2C(CH_3)_3$), 0.86 (13.2H, s, $OCH_2C(CH_3)_3$). Elemental *Anal.* Calc. for $C_{20}H_{30}N_2O_4S_2Ti$: C, 50.60; H, 6.37; N, 5.90. Found: C, 51.31; H, 6.64; N, 5.69%.

2.1.3. $(2MPO)_2Ti(OCMe_3)_2$ (**3**)

Used $Ti(OCMe_3)_4$ (1.00 g, 2.94 mmol), H-2MPO (0.747 g, 5.88 mmol), and tol (~10 mL). Yield 1.22 g (93.1%). FT-IR (KBr, cm^{-1}) 3078(m), 3032(w), 2972(s), 2924(s), 2859(m), 1595(m), 1545(m), 1460(s), 1418(m), 1389(w), 1354(m), 1257(m), 1188(m), 1167(m), 1139(m), 1091(m), 1015(s), 983(s), 840(m), 782(m), 736(m), 708(m), 602(m), 583(m). ^{1}H NMR (399.9 MHz, tol-d_8) δ 7.99 (1H, d, ONC_5H_4S, J_{H-H} = 6.4 Hz), 7.43 (1H, d, ONC_5H_4S, J_{H-H} = 6.8 Hz), 7.15 (1.2H, t, ONC_5H_4S, J_{H-H} = 7.8 Hz), 6.77 (1H, t, ONC_5H_4S, J_{H-H} = 7.0 Hz), 1.31 (11H, s, $OC(CH_3)_3$). Elemental *Anal.* Calc. for $C_{18}H_{26}N_2O_4S_2Ti$: C, 48.43; H, 5.87; N, 6.28. Found: C, 48.19; H, 5.87; N, 6.26%.

2.1.4. $[(ONep)_2Ti(\mu_c\text{-}OBPy)]_3$ (**4**)

Used $Ti(ONep)_4$ (0.11 g, 0.27 mmol) and H_2-OBPy (0.05 g, 0.27 mmol). FT-IR: (KBr, cm^{-1}) 2952(s), 2865(s), 2829(m), 1574(m), 1442(m), 1411 (s), 1362(w), 1316(s), 1261(w), 1227(w), 1206(w), 1098(s), 1074(s), 1024(s), 871(m), 805(m), 731(m), 659(s), 490(w), 471(w). ^{1}H NMR (400.1 MHz, tol-d_8) δ 8.27 (1.0H, dd, $(NC_5H_3O)_2$), 6.82 (1.1H, dd, $(NC_5H_3O)_2$), 6.55 (1.1H, mult, $(NC_5H_3O)_2$), 4.29 4.16 (1.8H, dd, $OCH_2(CH_3)_3$), 0.95 (9H, s, $OCH_2(CH_3)_3$). Elemental *Anal.* Calc. for $C_{60}H_{84}N_6O_{12}Ti_3$: C, 58.87; H, 6.83; N, 6.86. Found: C, 58.79; H, 6.58; N, 6.79%.

2.1.5. $[(OBu^t)_2Zr(\mu_c\text{-}OBPy)]_3$ (**5**)

Used $Zr(OBu^t)_4$ (0.075 g, 0.27 mmol) and H_2-OBPy (0.05 g, 0.27 mmol). FT-IR: (KBr, cm^{-1}) 2968(s), 2928(m, sh), 2866(m, sh), 2813(w, sh), 1577(m), 1449(s), 1413(s), 1359(m), 1322(s), 1260(w), 1227(m, sh), 1198(s), 1115(m), 1073(w), 1024(s, br), 906(m), 869(s), 787(m, sh), 752(m, sh), 733(m), 647(s), 623(s), 538(m, br), 480(m,br). ^{1}H NMR (400.1 MHz, tol-d_8) δ 8.23 (1.0H, dd, $(NC_5H_3O)_2$), 6.91 (1.0H, dd, $(NC_5H_3O)_2$), 6.58 (1.0H, mult, $(NC_5H_3O)_2$) 1.31 (9.4H, s, $OC(CH_3)_3$). Elemental *Anal.* Calc. for $C_{68}H_{89}N_6O_{12}Zr_3$: C, 56.09; H, 6.16; N, 5.77. Found: C, 52.25; H, 6.53; N, 4.48%.

2.2. General X-ray crystal structure information [8,9]

Crystals were mounted onto a glass fiber from a pool of Fluorolube™ and immediately placed in a cold N_2 vapor stream, on a Bruker AXS diffractometer equipped with a SMART 1000 CCD detector using graphite monochromatized Mo Kα radiation (λ = 0.7107 Å). Lattice determination and data collection were carried out using SMART Version 5.054 software. Data reduction was performed using SAINTPLUS Version 6.01 software and corrected for absorption using the SADABS program within the SAINT software package.

Structures were solved by direct methods that yielded the heavy atoms, along with a number of the lighter atoms or by using the PATTERSON method, which yielded the heavy atoms. Subsequent Fourier syntheses yielded the remaining light-atom positions. The hydrogen atoms were fixed in positions of ideal geometry and refined using SHELXS software. The final refinement of each compound included anisotropic thermal parameters for all non-hydrogen atoms. It is of note that crystal structures of $M(OR)_x$ often contain disorder within the atoms of the ligand chain causing higher than normal final correlations [10–15]. All final CIF files were checked at http://www.iucr.org/. Additional information concerning the data collection and final structural solutions can be found in the Supplementary data or by accessing CIF files through the Cambridge Crystallographic Data Base [8]. Data collection parameters for **1**–**6** are

given in Table 1. The problems associated with particular crystal structures are listed below.

*2.2.1. Compound **2***

For **2**, the 2MPO ring was found to be distorted away from normal in the final refinement efforts due to disordering which was successfully modeled as two environments based on the coordination of the ring (see Fig. 2). The modeling of the disordered 2MPO ligand proceeded first by locating sites for both the O and S atoms for each of the octahedral positions about the Ti atom (4 sites total). These sites were assigned as S(2), O(2), S(2′), or O(2′) based on the approximate bond distance from the Ti atom. Each of the S and O sites were assigned 0.5 occupancy and their positional and thermal ellipsoid parameters were refined. In similar fashion, N and C atoms in the 2MPO ring also required partial occupancy assignment and refinement. Finally, all similar bonds (i.e., S(1)–Ti(1) bond equal to S(1′)–Ti(1) bond, etc.) for the disordered configurations of the 2MPO ligand were restrained to be equivalent at appropriate bond lengths. The final refinement revealed stable atom positions and reasonable thermal ellipsoids for all of the disordered 2MPO sites. Due to the disorder, H atoms were not modeled on this ligand, but were added to the chemical formula during the final refinement to generate appropriate crystal data values.

*2.2.2. Compound **4***

In the host lattice of structure **4** several disordered toluene (tol) solvent molecules were observed. These were modeled using the PLATON/SQUEEZE program (Ver. 251005) and were located at: (1/2,0,0) (0,1/2,0) (0,0,0) (0.663,0.127,1/2) (0.337,0.873,1/2) (0.151,0.261,0.881) (0.849,0.739,0.119) (0,0.280,0.859) (0,0.720,0.141). The SQUEEZE program calculated a potential volume of 1405.4 Å^3 and an electron count of 266 electrons/cell, consistent with ~6 toluene molecules/unit cell which implied partial occupancy for most of the toluene solvent molecules. Based on the determined electron density obtained via SQUEEZE, 6 tol molecules were added to the contents of the unit cell during the final refinement series so that the proper crystal data could be calculated. In addition, a number of the terminal ONep groups were found to display rotational and/or displacement disorder, which is often noted for metal alkoxides [10–15]. For the dominant configuration, the C atoms were refined with anisotropic atomic displacement parameters, whereas for the minor orientation, the ONep group was refined using isotropic atomic displacement parameters. The disordered ONep groups were restrained (37 restraints total) to have equivalent C–C bond lengths for the two differing orientations (e.g., all C–CH_3 bond lengths for both ONep orientations were restrained to be equal). This aided in convergence of the refinement. Disordered C atoms on ONep ligands were refined without H atoms; however, the H

Table 1
Data collection parameters for **1**–**5**

Compound	**1**	**2**	**3**	**4** · 6 tol	**5**
Chemical formula	$C_{16}H_{22}N_2O_4S_2Ti$	$C_{20}H_{30}N_2O_4S_2Ti$	$C_{18}H_{26}N_2O_4S_2Ti$	$C_{60}H_{84}N_6O_{12}Ti_3$	$C_{54}H_{72}N_6O_{12}Zr_3$
Formula weight	418.38	474.48	446.42	1497.40	1270.84
Temperature (K)	173(2)	173(2)	173(2)	173(2)	273(2)
Space group	monoclinic, *C*2/*c*	triclinic, *P*$\bar{1}$	monoclinic, *c*2/*c*	triclinic, *P*$\bar{1}$	orthorhombic, *P*2(1)2(1)2(1)
a (Å)	11.070(7)	9.8761(14)	13.319(3)	11.241(3)	15.800(2)
b (Å)	15.828(10)	10.5179(15)	14.978(3)	18.098(5)	16.544(2)
c (Å)	10.706(7)	12.7351(18)	10.685(2)	21.567(6)	27.596(4)
α (°)		95.878(3)		86.300(4)	
β (°)	95.333(10)	104.109(2)	95.781(3)	89.248(4)	
γ (°)		105.309(2)		75.033(4)	
V (Å^3)	1868(2)	1217.6(3)	2120.9(7)	4230(2)	7213.1(16)
Z	4	2	4	2	4
D_{calc} (Mg/m^3)	1.488	1.294	1.398	1.176	1.170
μ (Mo Kα) (mm^{-1})	0.705	0.549	0.626	0.335	0.476
R_1[a] (%) (all data)	3.25 (3.66)	5.75 (7.30)	5.16 (5.65)	7.48 (9.18)	3.24 (3.54)
wR_2[b] (%) (all data)	8.00 (8.24)	15.58 (16.91)	15.57 (16.11)	21.56 (22.86)	7.99(8.16)

[a] $R_1 = \sum ||F_o| - |F_c|| / \sum |F_o| \times 100$.
[b] $wR_2 = [\sum w(F_o^2 - F_c^2)^2 / \sum (w|F_o|^2)^2]^{1/2} \times 100$.

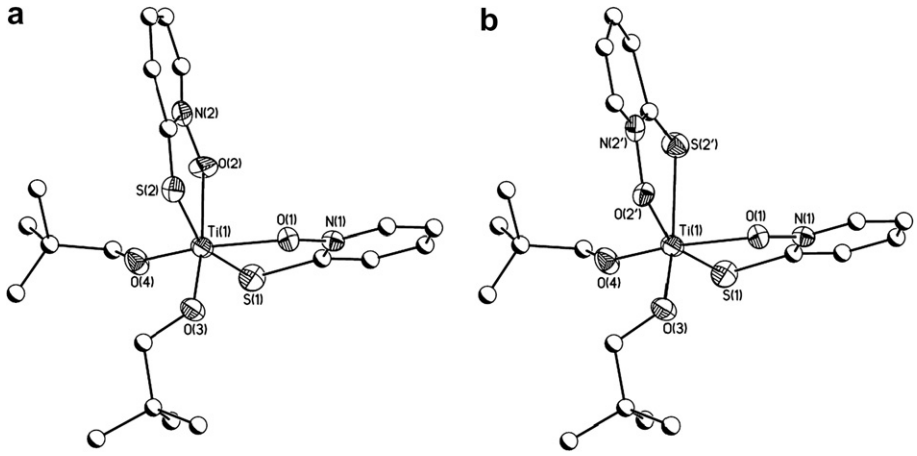

Fig. 2. Structure plot of **2**. Heavy atom thermal ellipsoids drawn at 30% level and carbon atoms drawn as ball and stick for simplicity. Two orientations are available (a) *trans* and (b) *cis*.

atoms were included in the formula unit during the final refinement for proper crystal data calculation.

3. Results and discussion

A search of the literature reveals that the 2MPO ligand (or derivatives) will bind to numerous metal centers (46 by CDCC search V 1.7), [8,9] with the late transition metals Co (13 derivatives) [16–23] or Zn (6 derivatives) being the most common metals [16,24–27]. For these compounds, the 2MPO acts in a chelating mode to form disubstituted monomers [16,26,27] or chelating unidentate bridged dinuclear [24,25] species. There are no reports of group 4 2MPO derivatives or OR/2MPO systems. For the OBPy ligand, only a single Ru species, $[(bipy)_2Ru(\mu\text{-}OBPy)]_2[PF_6]$ [28] has been reported wherein the OBPy moiety acts as a bridge in a twist conformation where the N atom on one ring and the O on the other bind to the same metal. As can be determined, these ligands offer the potential to generate controlled structures acting as chelates in the case of the 2MPO or as bridges as observed for the OBPy ligand. Since there were no group 4 cations that employ these ligand, we initiated our investigation with $Ti(OR)_4$ (Eqs. (1) and (2)).

3.1. Synthesis

Whether using the 2MPO or OBPy ligand, the alcohol exchange proceeds smoothly with toluene as a solvent. For each reaction, there is a significant intense color change associated with the binding of the ligand, turning from colorless to intense yellow-orange colors. Due to the minimum amount of solvent used, several of the reactions precipitated after stirring but a clear solution was easily produced upon heating. X-ray quality crystals were isolated upon cooling of the reaction mixture to room temperature or through slow evaporation of the volatile component. Dried crystalline materials were used for all remaining analyses.

The FT-IR spectrum of the H-2MPO ligand has a sharp stretch at 754 cm^{-1}, which is consistent with the N–O interaction. After binding to the $Ti(OR)_4$ (**1**–**3**, Eq. (1)), the N–O stretch of the 2MPO has been significantly reduced in intensity and slightly shifted for each of the compounds (**1**, 764; **2**, 755; **3** 782 cm^{-1}). Interestingly, the SH stretch (reportedly present at 2600–2550 cm^{-1}) is not observed with any intensity in the IR spectrum of the free ligand and therefore, not unexpectedly it was not found in the spectra of **1**–**3**. For each compound a stretch around 3100 cm^{-1} is observed which may represent the C–S stretch of the 2MPO ligand which is much more intense in **1**–**3** versus the free ligand. The remainder of the stretches and bends are associated with the 2MPO ligand or the OR ligands of **1**–**3**. Combined, these data indicate that the 2MPO has reacted and bound through the S and O atoms of the ligand.

The FT-IR spectrum of the H_2-OBPy ligand displays a broad OH stretch around 3000 cm^{-1} with the majority of stretches and bends of the py ring below 1500 cm^{-1}. Upon reacting, the spectrum of **4** or **5** (Eq. (2)) no longer displays an OH stretch but does show stretches below 1500 cm^{-1} similar to those noted for the free ligand. In addition, there are a number of stretches and bends from 3000 to 2700 cm^{-1} that represent the aliphatic pendant chains of the OBu^t and ONep ligands of **4** and **5**, respectively. Again, it appears the alcoholysis exchange had successfully occurred for Eq. (2).

3.2. Structures

Single crystal X-ray diffraction studies were undertaken to assist in identifying the structure of the final products of Eq. (1) (**1**–**3**) and Eq. (2) (**4**–**5**). The structures of **1**–**3** were found to be similar in constructs where Fig. 2 is the representative structure plot of **2**. Table 2 lists the selected average metrical data for **1**–**3**. For each of these compounds, two bidentate 2MPO ligands use their O and S atoms to fill 4 of the octahedrally (Oh) bound Ti metal center. The final 2 sites are filled by two parent alkoxides. Due to the bidentate nature of the 2MPO ligand two binding modes are available however, this only led to disorder in the final structure of **2**. Fig. 2 shows the *trans* S and Fig. 2b shows the *cis* S arrangement that were successfully modeled for **2**. The Ti–O and Ti–S distance for **1**–**3** are self-consistent (av 1.80 Å and 2.46 Å, respectively) and are in agreement with literature reported distances [16,24–27]. The bite angle of the 2MPO ligand was found to be av 78.2 ° which is on the short end of the range (72.8–89.7°) noted for 2MPO ligated compounds [29,30]. This imparts a slight distortion to the semi-regular Oh geometry around each of the Ti metal. The av Ti–O–N angle (118.8°) is significantly larger in comparison to the Ti–S–C angle (98.4°). The remainder of angles and distances are consistent with each other and literature model compounds [16,24–27].

Table 2
Selected averaged metrical data for **1**–**3**

	1	2	3
Distances (Å)			
Ti–OR	1.80	1.81	1.79
$Ti–O_{2MPO}$	2.05	2.22	2.07
Ti–S	2.48	2.43	2.47
C–S	1.72	1.64	1.72
N–O	1.34	1.40	1.34
Angles (°)			
OR–Ti–OR	98.1	94.8	98.8
$S_{2MPO}–Ti–O_{2MPO}$	77.4	79.8	77.4
$RO–Ti–O_{2MPO}$	92.1, 162.5	90.2, 163.7	91.3, 164.8
RO–Ti–S	85.8, 108.6	83.9, 108.5	88.9, 105.6
S–Ti–S	158.3	161.9	157.9
Ti–O–N	121.3	113.6	121.4
Ti–S–C	97.3	100.2	97.8
N–C–S	118.1	121.1	188.1

Switching to the heterocyclic OBPy ligand, compounds **4** (see Graphical Abstract) and **5** (Fig. 3) were isolated. The μ_c-OBPy ligand is found to act in a tetradentate chelating bridging manner, forming a trinuclear species with C_{3v} symmetry wherein each metal center adopts an Oh geometry with two terminal OR, two O and two N from the three bridging OBPy ligand. While the OBPy ligands use both the N and O to bind to the metal centers, due to the free

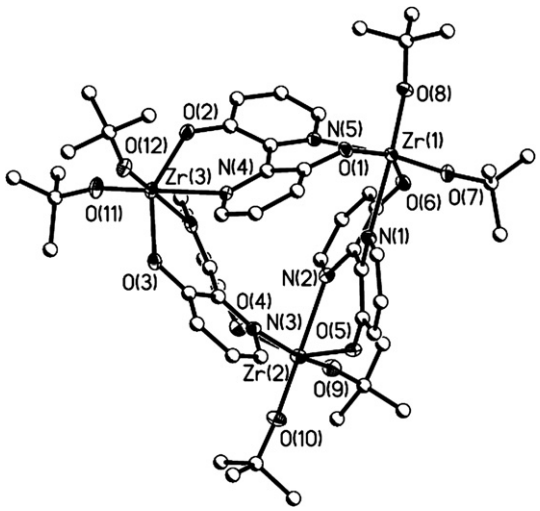

Fig. 3. Structure plot of **5**. Heavy atom thermal ellipsoids drawn at 30% level and carbon and hydrogen atoms drawn as ball and stick for simplicity.

rotation of the rings, the N and O atoms of one ring bind to different metal centers. This structure forms independent of the metal or pendant hydrocarbon chain. The metrical data for **4** and **5** are listed in Table 3. For 4, the av Ti–O distance was found to be 1.86 Å from a range of 1.78–1.92 Å and an av Ti–N distance of 2.31 Å with a range of (2.30–2.33 Å). The Ti–N distance for **4** are long in comparison to other $Ti(OR)_4$ that possess a bound py (range 2.17–2.34 Å; av 2.26 Å) [5,31–33]. The forced interaction by the OBPy constructs may account for the longer interaction. In comparison, the av Zr–O distances of **5** were found to be 1.99 Å and Zr–N av distance of 2.44 Å. In contrast to the Ti system, the Zr–N distances are in agreement with the few zirconium alkoxy pyridine compounds present in the literature (range 2.34–2.53 Å; av 2.44 Å) [5,34–37]. The larger Zr cation may allow for a less forced interaction with the distance variations between 4 and 5 being attributed to the size change from 6-coordinated Ti (0.745 Å) to Zr (0.86 Å) [38]. Not surprisingly, the geometries noted around the metals are distorted octahedrons.

Elemental analyses of the bulk powder of **1**–**5** were found to be in agreement with the solved crystal structures. The analyses of the 2MPO species are surprisingly accurate even though $M(OR)_x$ often give unreliable elemental analyses due to ligand decomposition, volatility, or high reactivity with the circumjacent atmosphere. The reproducibility of **1**–**3** indicates the stability of these compounds. In fact, air exposed samples unexpectedly also had acceptable elemental analysis consistent with the single crystal structures. For **4**, the elemental analysis is within agreement but **5** differs slightly from expected values. This may be attributed to the problems discussed above with a slightly reduced stability of the larger congener.

3.2.1. Solution behavior

In order to determine if the structures were retained in solution, the crystals of **1**–**5** were individually dissolved in tol-d_8 at as concentrated levels as possible. The ^{1}H NMR spectra were collected at room temperature and are discussed in terms of the different alkoxides below.

For **1**–**3**, the spectra in tol-d_8 showed the expected 4 resonances for the 2MPO ligand and the respective alkoxide ligands. However, the expected doublets and triplets of the 2MPO were further complicated by additional H–H splittings. In order to investigate solvent interaction effects, the samples were redissolved in $CDCl_3$ and the NMR spectra collected with no change in the multiple resonances noted. Variable temperature NMR (−40 to +45 °C) investigations also showed no change in the alkoxide resonances and only a slight decrease in the splittings noted previously. This eliminates the idea that the bidentate ligand is reversibly binding/unbinding to the metal center; however, cross-ligand H interactions or isolation of diastereomers based on the binding nature of the 2MPO ligand with four potential arrangements of the 2MPO ligand around the metal center (2 meso and 2 enantiomers) may result. Computational simulation of the expected spectra and the experimentally observed samples were identical. This indicates that the multiplet and fine structure observed in ^{1}H NMR of **1**–**3** and the H-2MPO ligand itself, result from the ^{1}H–^{1}H *J* couplings which ranged from 6.8 to 8.5 Hz, 1.3 to 1.6 Hz and 0.3 to 0.5 Hz for the ^1J, ^2J and ^3J couplings, respectively. Therefore, it can be concluded that the solid-state constructs of **1**–**3** are retained in solution.

The OBPy ligand is sold as a mixture of *R* and *S* due to the hindered rotation of the OH moieties. Therefore the ^{1}H NMR spectrum of the ligand reflects two complete sets of resonances for the *R* and *S* derivatives with significant overlap occurring. Upon binding to form either **4** or **5**, the ^{1}H NMR spectra revealed a significant change in the chemical shift but not the splittings. In comparison to the bound species, compound **5** displays greater resolution of the peaks than what was observed for **4**. The simplicity of these spectra and similarity to starting racemic mixture indicates that there is a handedness to the binding of the OBPy ligand to the metal centers. If there was a mixture of *R* and *S* to each metal center, more diastereomers would be observed, the OBPy resonances would therefore would be much more complex since the *R*/*S* ratio would range from 3:0, 2:1, 1:2 and 0:3 and each would be present in the NMR. Consequently, each molecule of **4** or **5** is either completely bound by *R* or *S* OBPy ligand which is has been observed previously for chiral alkoxide ligands [39]. For 4 and **5**, only one Bu^t resonance is observed for either compound; however, for the aromatic protons, doublets of the expected resonances are observed since these protons are now diastereotopic due to the handedness of the central core induced by the OBPy ligand.

Table 3
Selected averaged metrical data for **4**–**5**

Compound	M–OR (Å)	$M–O_{OBPy}$ (Å)	M–N (Å)
4	1.82	1.90	2.31
5	1.93	2.05	2.44
	O–M–O (°)	N–M–N (°)	$N–M–O_{OBPy}$ (°)
4	98.8, 152.3	91.5	82.1, 176.5
5	100.6, 146.3	87.4	80.7, 172.6

4. Summary and conclusion

We have continued our exploration of potential ceramic materials precursors using group 4 $M(OR)_x$ and the heterocyclic modifying ligands H-2MPO and H_2-OBPy which have led to the isolation of **1**–**3** and **4**–**5**, respectively. The products were isolated and characterized by single crystal X-ray diffraction as the first examples of these ligands and group 4 $M(OR)_x$. The 2MPO ligand was found to chelate to the Ti metal center through the N and the S forming $(2MPO)_2Ti(OR)_2$ independent of the hydrocarbon chain present. This species is reminiscent of '$(OPy)_2$Ti' [6] and '$(CP)_2$Ti' species and the potential rich chemistry associated with the '$(2MPO)_2$Ti' system is being explored. In contrast, the OBPy ligand was found to act as a tetradentate chelating bridging ligand only forming $[(\mu_c\text{-OBPy})M(OR)_2]_3$. With the unique trinuclear constructs, controlled manipulation of the terminal alkoxides is possible and is currently under exploration. Combined, these new N-based heterocycles motifs allow for controlled construction of $M(OR)_x$ and their utility in materials applications are also being explored.

Appendix A. Supplementary data

CCDC 683997, 683998, 683999, 6834000 and 684001 contain the supplementary crystallographic data for **1**–**5**. These data can be obtained free of charge via http://www.ccdc.cam.ac.uk/conts/retrieving.html, or from the Cambridge Crystallographic Data Centre, 12 Union Road, Cambridge CB2 1EZ, UK; fax: (+44) 1223-336-033; or e-mail: deposit@ccdc.cam.ac.uk.

Acknowledgements

The authors would like to thank Dr. Todd M. Alam for his simulation of the NMR data. For support of this research, the authors thank the Office of Basic Energy Science and the US Department of Energy under Contract DE-AC04-94AL85000. Sandia is a multiprogram laboratory operated by Sandia Corporation, a Lockheed Martin Company, for the United States Department of Energy.

References

[1] T.J. Boyle, S.D. Bunge, N.L. Andrews, L.E. Matzen, K. Sieg, M.A. Rodriguez, T.J. Headley, Chem. Mater. 16 (2004) 3279.

[2] T.J. Boyle, B.A. Hernandez-Sanchez, C.M. Baros, L.N. Brewer, M.A. Rodriguez, Chem. Mater. 19 (2007) 2016.
[3] T.J. Boyle, S.D. Bunge, T.M. Alam, G.P. Holland, T.J. Headley, G.R. Avilucea, Inorg. Chem. 44 (2005) 1309.
[4] H. Gerung, T.J. Boyle, L.J. Tribby, S.D. Bunge, C.J. Brinker, S.M. Han, J. Am. Chem. Soc. 128 (2006) 5244.
[5] T.J. Boyle, M.A. Rodriguez, T.M. Alam, Dalton Trans. 24 (2003) 4598.
[6] T.J. Boyle, R.M. Sewell, L.A.M. Ottley, H.D. Pratt, C.J. Quintana, S.D. Bunge, Inorg. Chem. 46 (2007) 1825.
[7] T.J. Boyle, T.M. Alam, E.R. Mechenbier, B.L. Scott, J.W. Ziller, Inorg. Chem. 36 (1997) 3293.
[8] Conquest Version 1.10, Cambridge Crystallographic Data Centre:support@ccdc.cam.ac.uk or www.ccdc.cam.ac.uk [CSD version 5.29 (November 2007)].
[9] F.H. Allen, Acta Crystallogr., Sect. B 58 (2002) 380.
[10] D.C. Bradley, Chem. Rev. 89 (1989) 1317.
[11] D.C. Bradley, R.C. Mehrotra, D.P. Gaur, Metal Alkoxides, Academic Press, New York, 1978.
[12] K.G. Caulton, L.G. Hubert-Pfalzgraf, Chem. Rev. 90 (1990) 969.
[13] C.D. Chandler, C. Roger, M.J. Hampden-Smith, Chem. Rev. 93 (1993) 1205.
[14] L.G. Hubert-Pfalzgraf, New J. Chem. 11 (1987) 663.
[15] N.Y. Turova, E.P. Turevskaya, V.G. Kessler, M.I. Yanovskaya, The Chemistry of Metal Alkoxides, Kluwer Academic Publishers, Boston, 2002.
[16] D.X. West, C.A. Brown, J.P. Jasinski, J.M. Jasinski, R.M. Heathwaite, D.G. Fortier, R.J. Staples, R.J. Butcher, J. Chem. Cryst. 28 (1998) 853.
[17] Y.X. Tong, y.P. Cai, H.X. Zhang, L.R. Deng, X.L. Yi, X.M. Chen, B.S. Kang, Pol. J. Chem. 75 (2001) 1219.
[18] B.-S. Kang, Y.J. Xu, J.-H. Peng, D.-S. Wu, X.-T. Chen, Y.-H. Hu, M.-C. Hong, J.X. Lu, Polyhedron 12 (1993) 871.
[19] Y.-J. Xu, B.-S. Kang, X.-T. Chen, L.-R. Huang, Acta Crystallogr., Sect C.: Cryst. Struct. Commun. 51 (1995) 370.
[20] H.-W. Xu, Z.-N. Chen, J.-G. Wu, Acta Crystallogr., Sect E.: Struct. Rep. Online 58 (2002) M672.
[21] V. Manivannan, S. Dutta, P. Basu, A. Chakravoty, Inorg. Chem. 32 (1993) 769.
[22] Y.-P. Fang, C.-L. Chen, X.-J. Wang, B.-S. Kang, K. Yu, C.-Y. Su, Acta Crystallogr., Sect E.: Struct. Rep. Online 58 (2002) M480.
[23] Y. Hu, L. Weng, L.-R. Huang, X. Chen, D. Wu, B. Kang, Acta Crystallogr., Sect C.: Cryst. Struct. Commun. 47 (1991) 2655.
[24] D.-Z. Niu, B.-W. Sun, Z.-S. Lu, B.-L. Song, Chin. J. Struct. Chem. 20 (2001) 108.
[25] B.L. Barnett, H.C. Kretschmar, F.A. Hartman, Inorg. Chem. 16 (1977) 1834.
[26] R.-G. Xiong, B.-L. Song, X.-Z. You, T.C.W. Mak, Z.-Y. Zhou, Polyhedron 15 (1996) 991.
[27] A.D. Bond, F. Benevelli, W. Jones, J. Mater. Chem. 12 (2002) 324.
[28] A.M.W. Thompson, J.C. Jeffery, D.J. Liard, M.D. Ward, J. Chem. Soc., Dalton Trans. (1996) 879.
[29] T.S. Lobana, S. Paul, A. Castineiras, J. Chem. Soc., Dalton Trans. (1999) 1819.
[30] X. Chen, Y. Hu, D. Wu, L. Weng, B. Kang, Polyhedron (1991) 2651.
[31] J.M. Tanski, T.P. Vaid, E.B. Lobokovsky, P.T. Wolczanski, Inorg. Chem. 39 (2000) 4756.
[32] L.D. Durfee, P.E. Fanwick, I.P. Rothwell, Angew. Chem., Int. Ed. 27 (1988) 1181.
[33] L.T. Armistead, P.S. White, M.R. Gagne, Organometallics 17 (1998) 4232.
[34] P.E. Fanwick, L.M. Kobriger, A.K. McMullen, I.P. Rothwell, J. Am. Chem. Soc. 108 (1986) 8095.
[35] C.H. Zambrano, A.K. McMullen, L.M. Kobriger, P.E. Fanwick, I.P. Rothwell, J. Am. Chem. Soc. 112 (1990) 6565.
[36] D.N. Williams, U. Piarulli, C. Floriani, A. Chiesi-Villa, C. Rizzoli, J. Chem. Soc., Dalton Trans. (1994) 1243.
[37] T.J. Boyle, L.J. Tribby, T.M. Alam, S.D. Bunge, G.P. Holland, Polyhedron 24 (2005) 1143.
[38] R.D. Shannon, Acta Crystallogr., Sect. A 32 (1976) 751.
[39] T.J. Boyle, D.L. Barnes, J.A. Heppert, L. Morales, F. Takusagawa, J.W. Connolly, Organometallics 11 (1992) 1112.

reducing $HAuCl_4$ self-assembled into uniform spherical aggregates when a low concentration of compound **1** is used, but spherical Au nanoparticles are obtained with relatively higher concentration of the reducing agent. The suitable chemical environment permits reduction at more moderate conditions and results in higher colloid uniformity than the usual methods. It is noteworthy that Au nanoparticles have been prepared earlier by using many benzenethiol-derivatives [18,19]. Our objective is to synthesize such nanoparticles of varied morphologies by using a benzene diol derivative.

2. Experimental

2.1. Materials and physical methods

All aqueous solutions were prepared from Millipore water (resistivity, 18 MΩ; Millipore Systems). Gold chloride trihydrate ($HAuCl_4 \cdot 3H_2O$) was purchased from Aldrich and used without purification. Other reagents were purchased from commercial sources and used without further purification. Solvents used for spectroscopic studies were purified and dried by standard procedures before use [20]. Elemental analysis was carried out in a 2400 Series-II CHN analyzer, Perkin Elmer, USA. FT-IR spectra were obtained on a Nicolet MAGNA-IR 750 spectrometer with samples prepared as KBr pellets. Absorption spectra were studied on a Shimadzu UV2100 UV–Vis recording spectrophotometer. The ESI-MS was recorded on Qtof Micro YA263 mass spectrometer. Morphology of all the samples was investigated by Transmission Electron Microscope (TEM). TEM images were recorded in a Jeol JEM 2010 transmission electron microscope operated at an accelerated voltage of 200 kV. A drop of dilute solution of the sample in water–methanol on a 300 mesh carbon coated copper grids was dried in vacuum and directly observed in the TEM.

2.2. Synthesis of 2,3,5,6-tetrakis(morpholinomethyl)hydroquinone (*1*)

The mixture of hydroquinone (1.1 g, 10 mmol), morpholine (3.48 g, 40 mmol) and paraformaldehyde (2 g, 66.67 mmol) in 1,4-dioxane (20 mL) was heated to reflux and kept at this temperature for 24 h. The resulting solution was cooled to room temperature. The solution was filtered, concentrated on a rotary evaporator to dryness and kept overnight at 4 °C. The resulting compound is solid. Colorless prismatic single crystals of **1** suitable for X-ray crystallography were obtained on recrystallization with toluene (yield = 0.58 g, 65%). Data for **1**: *Anal.* Calc. for $C_{26}H_{42}N_4O_6$: C, 61.66; H, 6.94; N, 11.06. Found: C, 61.54; H, 6.81; N, 10.93%. FT-IR (KBr phase) ν/cm^{-1} 3433, 2852, 1650. ^1H NMR ($CDCl_3$, 300 MHz), δ = 10.4 (br s, 2H), 3.68 (s, 16H), 2.51 (s, 8H), 1.58 (s, 16H). ^{13}C NMR ($CDCl_3$, 75 MHz), δ = 149.7 (2C), 121.5 (4C), 67.0 (8C), 54.7 (4C), 52.9 (8C). HR-MS (ESI): ($C_{26}H_{42}N_4O_6 + H^+$) Calc. 507.64, found 507.64.

2.3. Synthesis of gold nanoparticle

The synthesis of Au nanoparticles was achieved by the chemical reduction of $HAuCl_4$ in methanol–water medium with compound **1** without using any stabilizer. The following reduction methods with different concentrations of compound **1** were employed.

2.3.1. Method I

To 20 mL of a 10^{-3} M methanolic solution of compound **1**, a total of 1 mL of a 2.23×10^{-5} M $HAuCl_4$ aqueous solution was added dropwise over a period of 60 s at room temperature. Stirring was stopped 20 s after the addition was completed. During this period, the color of the solution changed from pale yellow to purple.

Table 1
Crystallographic information for **1**

Empirical formula	$C_{26}H_{42}N_4O_6$
Formula weight	506.64
Crystal system	monoclinic
Space group	$C2/c$ (No. 15)
a (Å)	26.763(2)
b (Å)	6.0023(6)
c (Å)	17.8750(10)
α (°)	90
β (°)	114.360(10)
γ (°)	90
V (Å^3)	2615.8(4)
Z	4
D_{calc} (g cm^{-3})	1.286
μ (Mo Kα) (mm^{-1})	0.092
F(000)	1096
T (K)	150
λ (Mo Kα)	0.71073
Maximum and minimum θ range (°)	28.0, 3.0
Total data, unique data	14222, 3411
R_{int}	0.0244
Final R indices (R_1, wR_2)	0.055, 0.092
Goodness-of-fit	1.056

2.3.2. Method II

The method is similar to method I except that 60 mL of compound **1** was used and the color of the solution changed from pale yellow to blue.

2.4. X-ray data collection and structure determination

Crystal data of **1** are summarized in Table 1. The diffraction experiment was carried out on a Bruker SMART CCD area-detector diffractometer at 150 K. No crystal decay was observed, so that no time-decay correction was needed. The collected frames were processed with the software SAINT [21], and an empirical absorption correction was applied (SADABS) [22] to the collected reflections. The calculations were performed using the Personal Structure Determination Package [23] and the physical constants tabulated therein [24]. The structure was solved by direct methods (SHELXS) [25] and refined by full-matrix least-squares using all reflections and minimizing the function $\sum w(F_o^2 - kF_c^2)^2$ (refinement on F^2). All the non-hydrogen atoms were refined with anisotropic thermal factors. All the other hydrogen atoms were placed in their ideal positions (C–H or O–H = 0.97 Å), with the thermal parameter U 1.10 times that of the atom to which they are attached, and not refined.

3. Results and discussion

3.1. Description of the structure of 2,3,5,6-tetrakis(morpholinomethyl)-hydroquinone (*1*)

2,3,5,6-Tetrakis(morpholinomethyl)hydroquinone (**1**) has been synthesized by the aminomethylation of hydroquinone with morpholine. An ORTEP view of **1** is shown in Fig. 1. Selected bond lengths and bond angles are listed in Table 2. As shown in Fig. 1, the asymmetric unit of **1** contains one-half molecule with the other half generated by a center of inversion which lies at the center of the benzene ring. The benzene rings in the molecules do not show any unusual features, and the bond lengths and bond angles are within the normal ranges. The shorter bond distance O1–C1 of 1.3763(14) Å [26] in the molecular unit indicates the p–π conjugation of O1 with the benzene ring. The morpholino rings adopt the usual chair conformation similar to those of 2,6-bis-(*N*-methylenemorpholino)-4-methylphenol [27] and 2,5-bis(morpholinomethyl) hydroquinone [26], but the two morpholine pendant arms in *para*

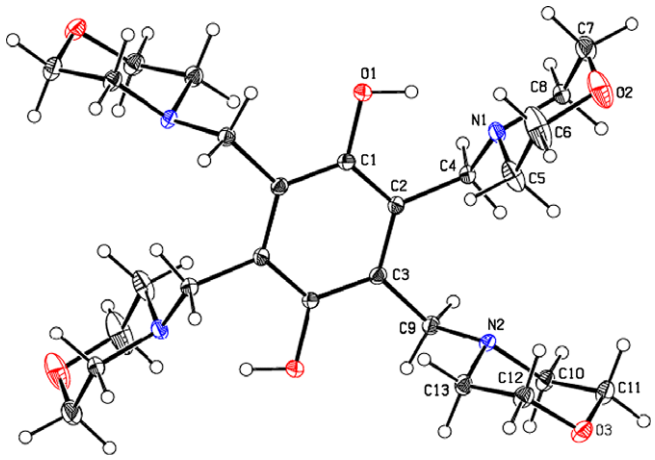

Fig. 1. ORTEP drawing and atom numbering scheme for compound (**1**).

positions display *trans*-configuration as regards the parent phenol ring with atoms N1, O2, N2 and O3 deviating from the phenol moiety by 0.897, 3.029, 1.343 and 3.753 Å, respectively. The bond distances N1–C5 (1.4610(14) Å) and N2–C9 (1.4673(13) Å) are in accordance with that of reported one [26]. There exists the intramolecular O1–H ··· N1 hydrogen bond between the phenolic O atom and the morpholine N donor, and the distance (1.811(13) Å) between the proton and acceptor nitrogen atom is obviously shorter than the sum of their Van der Waals' radii (2.6615(11) Å), all being normal weak hydrogen bond interactions [28]. It is worthy of being noted that the two six-membered hydrogen-bonded rings in one unit can stabilize the crystal structure. No significant π–π interaction between the phenyl rings of the molecules packing together in the solid state exists.

3.2. Preparation and characterization of gold nanoparticles by method I

Au colloids have been obtained through reduction of $HAuCl_4$ by 2,3,5,6-tetrakis-(morpholinomethyl)hydroquinone at room temperature. The characteristic UV–Vis absorption spectrum of the Au nanoparticles prepared by this method is shown in Fig. 2. On mixing $HAuCl_4$ and **1**, the plasmon band of gold nanoparticles at 535 nm is observed. This indicates that the reduction of $AuCl_4^-$ occurs by compound **1** to produce the nanoparticles. A broad and well defined absorption band at 744 nm is also found, and could be assigned to the aggregative states of gold nanoparticles [29]. The coupling of the plasma resonance modes of the Au nanoparticles is caused by aggregation, and this is reflected in the red shift of

Table 2
Selected bond lengths (Å) and bond angles (°)

O1–C1	1.3763(14)	N2–C9	1.4673(13)
O2–C6	1.4329(18)	N2–C10	1.4609(13)
O2–C7	1.4220(17)	N2–C13	1.4645(14)
O3–C11	1.4273(13)	C5–C6	1.5042(18)
O3–C12	1.4279(13)	C7–C8	1.4997(17)
N1–C4	1.4760(14)	C10–C11	1.5078(15)
N1–C5	1.4610(14)	C12–C13	1.5081(15)
N1–C8	1.4643(14)		
C6–O2–C7	109.45(10)	C11 – O3–C12	110.57(8)
C4–N1–C5	112.04(8)	C9–N2–C10	112.01(8)
C4–N1–C8	112.48(8)	C9–N2–C13	112.33(8)
C5 –N1–C8	108.08(8)	C10–N2–C13	108.28(8)
N1–C4–C2	111.03(9)	N2–C9–C3	110.85(9)
N1–C5–C6	108.83(10)	N2–C10–C11	109.47(9)
N1–C8–C7	109.43(9)	N2–C13–C12	109.43(9)
O2–C6–C5	111.27(10)	O3–C11–C10	111.54(9)
O2–C7–C8	111.69(10)	O3–C12–C13	111.67(9)

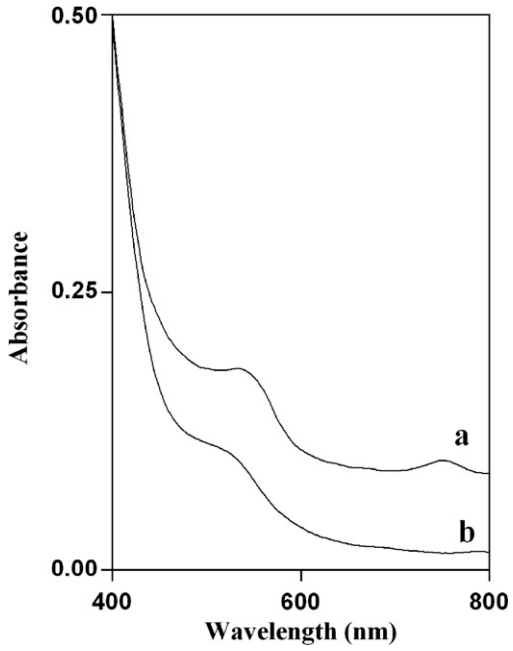

Fig. 2. UV–Vis spectra for the gold nanoparticles synthesized by method I before (a) and after (b) ultrasonic treatment.

the surface plasma resonance in the optical spectrum. Such red shift is supported by the well-known Mie scattering theory [30]. The essence of this theory is that a shift in surface plasma resonance is caused by deviation of the particles from the spherical geometry, such as that occurring in aggregates. In the circumstances, equivalent resonances are no longer produced by transverse and longitudinal dipole polarizability. As a result, there appear two plasma resonances: (i) a broadened and red-shift longitudinal plasma resonance and (ii) a transverse plasma resonance whose absorbance remains centered at *ca.* 540 nm. The electron spray ionization mass spectrum of the mixture of compound **1** and $HAuCl_4$ shows a peak at $m/z = 527.62$ along with the peak at $m/z = 507.64$ (for compound **1**) that can be assigned to the formation of 2,3,5,6-tetrakis-(morpholinomethyl)quinone ($C_{26}H_{40}N_4O_6$). The isotropic distributions for the above molecular species obtained experimentally (at $m/z = 527.62$) correspond to the simulated patterns (see Supplementary data, Fig. S1). In this spectrum the peak at $m/z = 527.62$ assigned to ($C_{26}H_{40}N_4O_6 + Na^+$) species corroborate the presence of 2,3,5,6-tetrakis-(morpholinomethyl)quinone, the oxidized product of **1**.

We have then characterized the gold colloids by transmission electron microscopy (TEM). A representative one is shown in Fig. 3. Spherical aggregates having diameter of *ca.* 170 ± 17 nm were observed. The enlarged view (Fig. 3, inset) clearly shows the edge of a randomly selected spherical aggregate which consists of individual particles with a size of *ca.* 10 nm. It should be noted that the interaction between individual particles is relatively weak and the spherical aggregates could be destroyed by ultrasonic treatment. The spherical aggregates disappeared and individual nanoparticles were monodispersed after ultrasonic treatment (30 min at 10 kHz), as shown in Fig. 4. The results indicate that the spherical aggregates might be formed through intermolecular interaction between nanoparticles. Fig. 2 shows the UV–Vis absorption spectra of the spherical aggregates before and after ultrasonic treatment. The plasmon absorption band of the gold nanoparticles at 535 nm is retained, but the absorption of the spherical aggregates at 744 nm disappears on ultrasonic treatment. These results also indicate that the spherical aggregates are composed of individual nanoparticles [31].

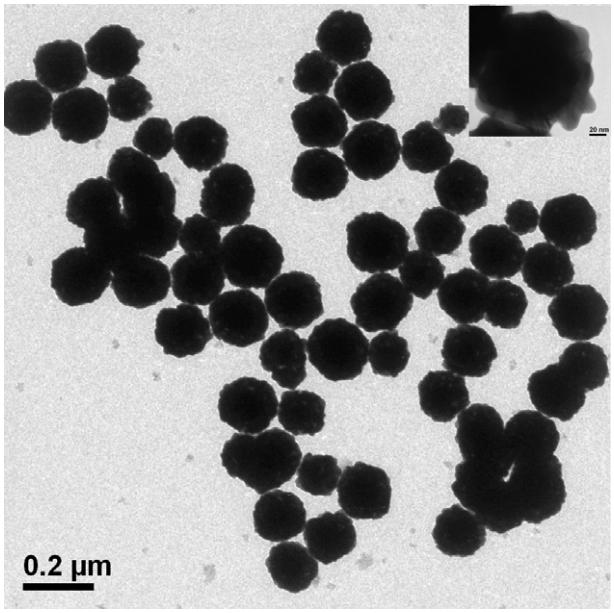

Fig. 3. Representative TEM image of gold nanoparticles prepared by method I.

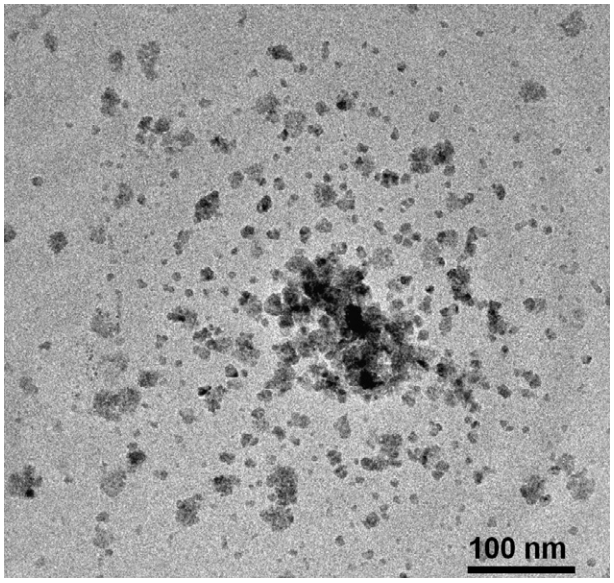

Fig. 4. TEM image of gold nanoparticles synthesized by method I after ultrasonic treatment.

In order to confirm the formation of a crystal phase and calculate the mean size of the nanoparticles, X-ray diffraction (XRD) analysis was performed. Fig. 5 shows the XRD pattern of the nanoparticles obtained by method I. The diffraction features appearing at $2\theta = 38.37°$, 44.49°, 64.62°, 77.72° and 81.52° correspond to the (111), (200), (220), (311) and (222) planes of the standard cubic phase of Au, respectively. As expected, the XRD peaks of the nanocrystallites were considerably broadened compared to those of the bulk Au because of the finite size of these crystallites.

3.3. Preparation and characterization of gold nanoparticles by method II

Au colloids were obtained through the reduction of $HAuCl_4$ by compound **1** under similar condition as that for Method I. Aqueous $HAuCl_4$ solution showed a very pale yellow color. Reduction of

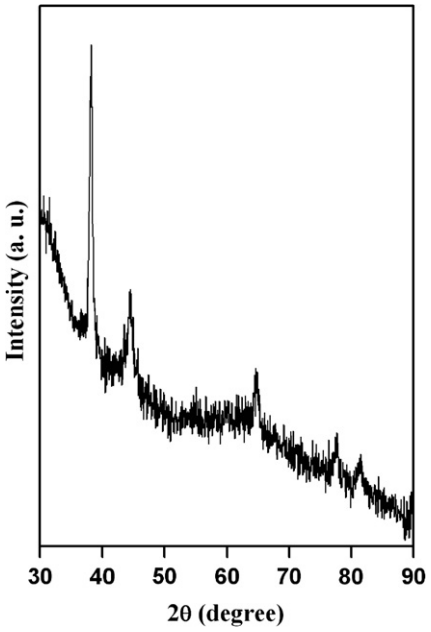

Fig. 5. XRD pattern of aggregate of gold nanoparticles.

$HAuCl_4$by compound 1 in methanol changed the color of the solution to blue. Gold nanoparticles exhibit strong plasmon resonance absorption that is dependent on the particle size and shape. For roughly spherical gold nanoparticles, the plasmon band maximum falls between 520 and 530 nm [32]. Fig. 6 shows the UV–Vis absorption spectrum of gold nanoparticles generated by method II. The spectrum was taken for freshly prepared samples. The absorption band for the nanoparticles is centered at 527 nm.

Fig. 7 shows the TEM image of prepared gold nanoparticles following method II in methanol–water medium. The micrograph clearly indicates the formation of nearly spherical nanoparticles with an average diameter of 12 nm. The diameter of these nanoparticles is shorter than those prepared by method I. The particles

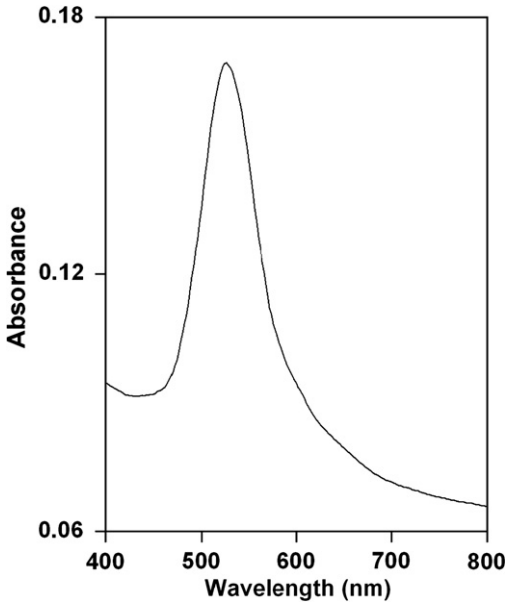

Fig. 6. UV–Vis spectrum of the spherical gold nanoparticles prepared by method II.

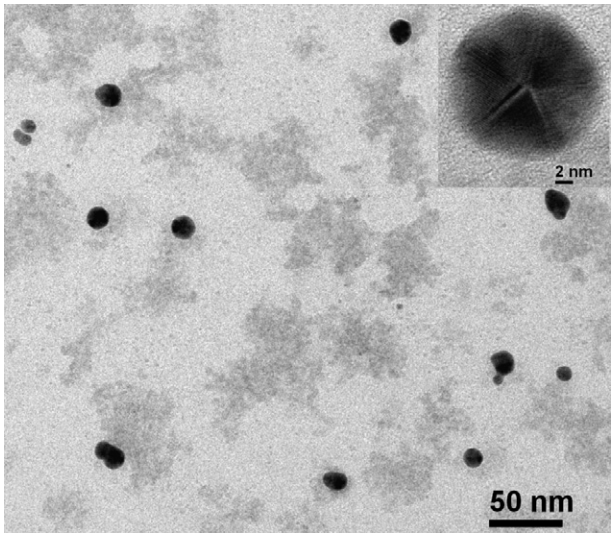

Fig. 7. Representative TEM image of spherical gold nanoparticles prepared by method II.

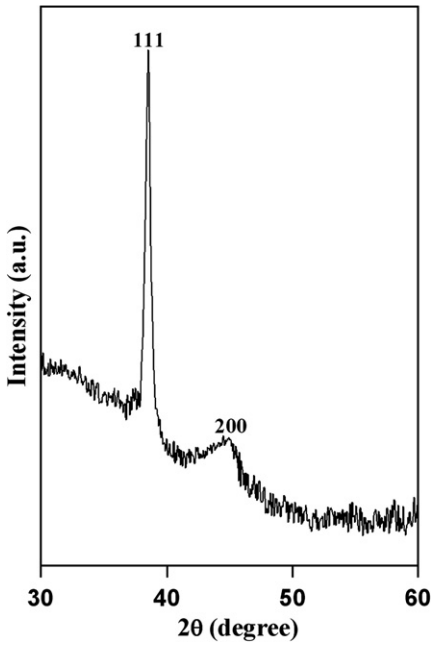

Fig. 8. XRD pattern of spherical gold nanoparticles.

do not get self-assembled unlike that of method I where compound **1** acting as a capping agent too was lesser in amount compared to that in method II. Thus self-assembly can be regulated smoothly, and the growth is limited to the aforementioned sizes by controlling the critical $AuCl_4^-$/compound **1** ratio. However, the TEM micrograph shows randomness of the particles, depicting crystalline assembly with the individual clusters placed in random locations. The high-resolution TEM image of these nanoparticles has been shown in the inset given in Fig. 7. The inset of the figure clearly indicates the presence of twin boundaries [33]. Further, the crystalline nature of these particles has been confirmed from the XRD analysis. XRD pattern of the gold nanoparticles prepared by method II is given in Fig. 8. Fig. 8 shows the peaks at 38.51° and 44.85° corresponding to (111) and (200) planes.

4. Conclusion

We have prepared a new compound, 2,3,5,6-tetrakis-(morpholinomethyl) hydroquinone, which can form gold nanoparticles from Au(III) solution. This compound also behaves as the capping agent for the nanoparticles synthesis. Gold nanoparticles with two different shapes and sizes have been prepared by simply altering the ratio of $AuCl_4^-$ and compound **1** which has been prepared by Mannich-type aminomethylation of hydroquinone with morpholine and characterized by single crystal X-ray diffraction analysis. These nanoparticles are stable and remain suspended for about three months, and may find potential applications such as catalysis, optical coatings.

Acknowledgement

K.D. acknowledges the Council of Scientific and Industrial Research, New Delhi, India, for financial support.

Appendix A. Supplementary data

CCDC 680253 contains the supplementary crystallographic data for **1**. These data can be obtained free of charge via http://www.ccdc.cam.ac.uk/conts/retrieving.html, or from the Cambridge Crystallographic Data Centre, 12 Union Road, Cambridge CB2 1EZ, UK; fax: (+44) 1223-336-033; or e-mail: deposit@ccdc.cam.ac.uk. Supplementary data associated with this article can be found, in the online version, at doi:10.1016/j.poly.2008.07.002.

References

[1] K.L. Kelly, E. Coronado, L.L. Zhao, G.C. Schatz, J. Phys. Chem. B 107 (2003) 668.
[2] (a) P.R. Selvakannan, S. Mandal, S. Phadtare, R. Pasricha, M. Sastry, Langmuir 19 (2003) 3545;
(b) A. Swami, A. Kumar, M. D'Costa, R. Pasricha, M. Sastry, J. Mater. Chem. 14 (2004) 1;
(c) Y. Shao, Y. Jin, S. Dong, Chem. Commun. 1104 (2004);
(d) M. Han, X. Gao, J.Z. Su, S. Nie, Nat. Biotechnol. 19 (2001) 631.
[3] R. Narayanan, M.A. El-Sayed, J. Phys. Chem. B 109 (2005) 12663.
[4] V.M. Rotello, Nanoparticles: Building Blocks for Nanotechnology, Kluwer Academic/Plenum Publishers, New York, 2004.
[5] T. Hassenkam, K. Moth-Poulsen, N. Stuhr-Hansen, K. Norgaard, M.S. Kabir, T. Bjornholm, Nano Lett. 4 (2004) 9.
[6] (a) D.P. Yu, Z.G. Bai, Y. Ding, Q.L. Hang, H.Z. Zhang, J.J. Wang, Y.H. Zou, W. Qian, G.C. Xiong, H.T. Zhou, S.Q. Fang, Appl. Phys. Lett. 72 (1995) 3458;
(b) S.-W. Chung, J.-Y. Yu, J.R. Heath, Appl. Phys. Lett. 76 (2000) 2068.
[7] (a) B. Nikoobakht, M.A. El-Sayed, Chem. Mater. 15 (2003) 1957;
(b) F. Kim, J.H. Song, P. Yang, J. Am. Chem. Soc. 124 (2002) 14316;
(c) N.R. Jana, L. Gearheart, C.J. Murphy, Adv. Mater. 13 (2001) 1389.
[8] (a) G.S. Metraux, Y.C. Cao, R. Jin, C.A. Mirkin, Nano Lett. 3 (2003) 519;
(b) Y. Zhou, C.Y. Wang, Y.R. Zhu, Z.Y. Chen, Chem. Mater. 11 (1999) 2310.
[9] Y. Sun, Y. Xia, Science 298 (2002) 2176.
[10] (a) E. Hao, R.C. Bailey, G.C. Schatz, J.T. Hupp, S. Li, Nano Lett. 4 (2004) 327;
(b) S. Chen, Z.L. Wang, J. Ballato, S.H. Foulger, D.L. Carroll, J. Am. Chem. Soc. 125 (2003) 16186.
[11] (a) J. Turkevich, P.C. Stevenson, J. Hiller, Discuss. Faraday Soc. 11 (1951) 55;
(b) B. Enustun, J. Turkevich, J. Am. Chem. Soc. 85 (1963) 3317.
[12] Q.F. Zhou, J.C. Bao, Z. Xu, J. Mater. Chem. 12 (2002) 384.
[13] (a) M. Horrisberger, in: J.A. Murphy, G.M. Roomans (Eds.), Preparation of Biological Specimens for Scanning Electron Microscopy, Scanning Electron Microscopy, Inc., Chicago, IL, 1984, p. 315;
(b) J. DeMey, EMSA Bull. 14 (1984) 54;
(c) M.P. Pileni, J. Phys. Chem. 97 (1993) 6961;
(d) M.P. Pileni, A. Taleb, C. Petit, J. Dispersion Sci. Technol. 19 (1998) 185;
(e) Z. Zhang, R.C. Patel, R. Kothari, C.P. Johnson, S.E. Friberg, P.A. Aikens, J. Phys. Chem. B 104 (2000) 1176;
(f) C.L. Chiang, J. Colloid Interf. Sci. 239 (2001) 334;
(g) M.P. Pileni, J. Phys. Chem. B 105 (2001) 3358. and references cited therein;
(h) M.P. Pileni, Langmuir 17 (2001) 7476. and references cited therein;
(i) M.A. López-Quintela, J. Rivas, J. Colloid Interf. Sci. 158 (1993) 446;
(j) C.L. Chang, H.S. Fogler, Langmuir 13 (1997) 3295.
[14] (a) J.R. Heath, C.M. Knobler, D.V. Leff, J. Phys. Chem. B 101 (1997) 189;
(b) S. Chen, Langmuir 17 (2001) 2878.
[15] (a) J. Hambrock, R. Becker, A. Birkner, J. Weib, R.A. Fischer, Chem. Commun. (2002) 68;

(b) T. Hyeon, S.S. Lee, J. Park, Y. Chung, H.B. Na, J. Am. Chem. Soc. 123 (2001) 12798;
(c) Y. Li, J. Liu, Y. Wang, Z.L. Wang, Chem. Mater. 13 (2001) 1008.
[16] (a) X.M. Lin, M.H. Jaeger, C.M. Sorensen, K.J. Klabunde, J. Phys. Chem. B 105 (2001) 3353;
(b) N.K. Chaki, S.G. Sudrik, H.R. Sonawane, K. Vijayamohanan, Chem. Commun. (2002) 76;
(c) B.V. Enustun, J. Turkevich, J. Am. Chem. Soc. 85 (1963) 3317;
(d) M. Brust, M. Walker, D. Bethell, D.J. Schiffrin, R.J. Whyman, Chem. Commun. (1994) 801;
(e) K.V. Sarathy, G. Raina, R.T. Yadav, G.U. Kulkarni, C.N.R. Rao, J. Phys. Chem. B 101 (1997) 9876;
(f) S. Chen, K. Huang, J.A. Stearns, Chem. Mater. 12 (2000) 540;
(g) C.H. Walker, J.V. St. John, P.W. Neilson, J. Am. Chem. Soc. 123 (2001) 3846.
[17] S. Yang, T. Zhang, L. Zhang, Q. Wang, R. Zhang, B. Ding, Nanotechnology 17 (2006) 5639.
[18] J. Sharma, S. Mahima, B.A. Kakade, R. Pasricha, A.B. Mandale, K. Vijayamohanan, J. Phys. Chem. B 108 (2004) 13280.
[19] (a) S. Chen, Langmuir 15 (1999) 7551;
(b) M. Brust, M. Walker, D. Bethell, D.J. Schiffrin, R. Whyman, J. Chem. Soc., Chem. Commun. (1994) 801;
(c) S. Chen, R.W. Murray, Langmuir 15 (1999) 682.
[20] D.D. Perrin, W.L. Armarego, D.R. Perrin, Purification of Laboratory Chemicals, second ed., Pergamon, Oxford, UK, 1980.
[21] SAINT Reference Manual, Siemens Energy and Automation, Madison, W1, 1994–1996.
[22] G.M. Sheldrick, SADABS, Empirical Absorption Correction Program, University of Gottingen, 1997.
[23] B.A. Frenz, Comput. Phys. 2 (1988) 42.
[24] Crystallographic Computing, vol. 5, Oxford University Press, Oxford, UK, 1991, Chapter 11, p. 126.
[25] G.M. Sheldrick, SHELXS 86 Program for the Solution of Crystal Structures, University of Gottingen, Germany, 1985.
[26] M.A. Peng-Gao, Z. Ming-Jie, Y. Qi-Cha, Y. Jiu-Gao, Chin. J. Struct. Chem. 24 (2005) 311.
[27] S.S.S. Raj, M.N. Ponnyswamy, G. Shanmugam, M. Kandaswamy, J. Chem. Crystallogr. 24 (1994) 83.
[28] (a) Y.M. Guo, M. Du, X.H. Bu, J. Mol. Struct. 646 (2003) 191;
(b) R. Taylor, O. Kennard, J. Am. Chem. Soc. 104 (1982) 5063.
[29] A.N. Shipway, M. Lahav, R. Gabai, I. Willner, Langmuir 16 (2000) 8789.
[30] (a) G. Mie, Ann. Physik 25 (1908) 377;
(b) U. Kreibig, L. Genzel, Surf. Sci. 156 (1985) 678;
(c) T.J. Norman Jr., C.D. Grant, D. Magana, J. Zhang, J. Liu, D. Cao, F. Bridges, A. Van Buuren, J. Phys. Chem. B 106 (2002) 7005;
(d) X. Li, Y. Li, Y. Tan, C. Yang, Y. Li, J. Phys. Chem. B 108 (2004) 5192.
[31] J. Jin, T. Iyoda, C. Cao, Y. Song, L. Jiang, T.J. Li, D.B. Zhu, Angew. Chem., Int. Ed. 40 (2001) 2135.
[32] (a) T. Shimizu, T. Teranishi, S. Hasegawa, M. Miyake, J. Phys. Chem. B 107 (2003) 2719;
(b) N.R. Jana, L. Gearheart, C.J. Murphy, Langmuir 17 (2001) 6782;
(c) N.R. Jana, L. Gearheart, C.J. Murphy, Chem. Mater. 13 (2001) 2313.
[33] C.-H. Kuo, T.-F. Chiang, L.-J. Chen, M.H. Huang, Langmuir 18 (2004) 7820.

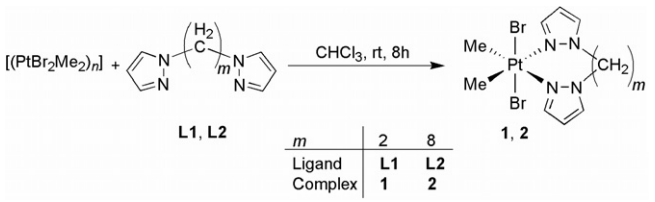

Scheme 1.

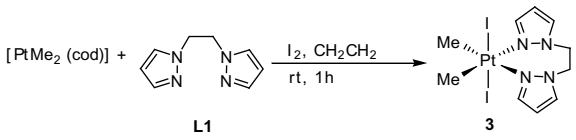

Scheme 2.

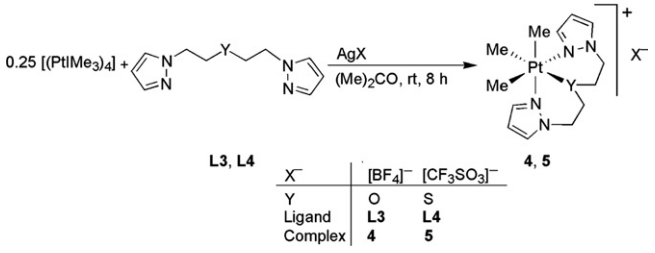

Scheme 3.

the presence of minor impurities but was fully characterized in solution as an analogue of **4**, with a triflate rather than tetrafluoroborate counterion, as discussed below.

2.2. Characterization

Complexes **1**–**5** have good solubility in common organic solvents such as acetone and chloroform and were characterized by NMR spectroscopy. As can be seen from the data given in Table 1, the ^{195}Pt NMR spectra contain a single resonance between −3409 and −2195 ppm with the diiodo substituted complex **3** the most high-field shifted, as may be expected [11]. A single resonance is found for the methyl ligands in the ^{1}H and ^{13}C NMR spectra of **1**–**3**. The $^{2}J_{Pt,H}$ (70–75 Hz) and $^{1}J_{Pt,C}$ (526.6 and 543.7 Hz) coupling constants confirm the *trans* coordination of the nitrogen donor ligands to the methyl ligands with the halo ligands occupying mutually *trans* positions (configuration index: *OC*-6-13), as may be expected [10,12]. In addition, the ^{1}H NMR spectrum of **2** shows a broadening of the signals assignable to the CH_2 groups of the spacer, relative to those of the free ligand, whereas the resonance of the methyl ligands are sharp.

The ^{1}H and ^{13}C NMR spectra of **4** and **5** share a number of similarities. Comparing the ^{1}H NMR spectrum of **4** to that of the corresponding free ligand **L3** (Fig. 1), the AA′XX′ spin system of the protons on the **L3** backbone ($C^6H_2C^7H_2$) becomes an ABCD spin system in **4** (δ_H 4.2–4.6 ppm; assignment by correlation spectroscopy). The three methyl ligands have two sets of resonances in a 2:1 intensity ratio and the corresponding $^{2}J_{Pt,H}$ (69.9 and 80.7 Hz) and $^{1}J_{Pt,C}$ (692.5 and 773.3 Hz) coupling constants confirm the coordination of two of the methyl ligands *trans* configured to the ligating nitrogen atoms and the third methyl ligand *trans* configured to the ligating oxygen atom (sulfur atom in **5**) giving a configuration index of *OC*-6-33. Due to the C_s point group symmetry of **4**, one resonance for C^6 atoms and one resonance for C^7 atoms are observed in the ^{13}C NMR spectrum. Similar findings are observed in the ^{1}H and ^{13}C NMR spectra of **5** (see Section 4).

Complexes **4** and **5** were also characterized by high resolution ESI-MS. The $[PtMe_3(pzCH_2CH_2OCH_2CH_2pz)]^+$ ($[M]^+$) cation at *m*/*z* 446.15124 is the only peak observed in the positive mode spectrum of **4** and the isotopic pattern is in satisfactory agreement with the calculated values (see Section 4). The most intensive peak in the positive mode spectrum of **5** is found to be the $[PtMe_3(pzCH_2CH_2SCH_2CH_2pz)]^+$ ($[M]^+$) cation at *m*/*z* 462.12835 (Fig. 2a). Enlargement of the peak assignable to $[M]^+$ shows an isotopic pattern consistent with the calculated values expected for a cation of this composition (Fig. 2b and Section 4). The second most intensive peak in the spectrum at *m*/*z* 1071.19950 is attributed to the dication + anion cluster ($[2M+CF_3SO_3]^+$). The signal at *m*/*z* 431.07891 agrees with the elimination of two methyl fragments from $[M]^+$.

2.3. Crystal structures

Complex **1** crystallized as **1** · $CHCl_3$ in the monoclinic space group $P2_1/c$ (Fig. 3). As the data collected in Table 2 confirm, the molecule has a distorted octahedral geometry. There is no evidence of any unusual intra- or intermolecular interactions.

The chelating ligand **L1** is *trans* configured to the methyl ligands. A large N1–Pt–N3 bite angle (97.3(1)°) is created by the chelating ligand due to geometrical constraints and is a common feature in the small number of reported platinum(IV) complexes with N,N′-bidentate ligands giving seven-membered chelate rings [13]. Although the C1–Pt–C2 bond angle is 86.4(2)° it is similar to other C–Pt–C bond angles observed for related dihalodimethylplatinum(IV) structures (86.8(4)–96.6(3)°) [10,14]. Other than the Pt–N3 bond length (2.235(3) Å) which is longer than expected for a Pt(IV)–N bond *trans* to a carbon ligator atom (median 2.163 Å; lower/upper quartile 2.142/2.198 Å; *n* = 351; *n* = number of observations) no peculiarities are found for the bond lengths of **1** [15]. Both pyrazolyl rings are twisted out of the $[PtC_2N_2]$ coordination plane (γ = 8.9(2)° and 34.5(2)°). The C6 and C7 atoms of the

Table 1
Selected ^{1}H, ^{13}C and ^{195}Pt NMR data for **1**–**5** (δ in ppm, *J* in Hz)

Complex	Solvent	δ (Pt–CH_3) ($^{2}J_{Pt,H}$)	δ (Pt–CH_3) ($^{1}J_{Pt,C}$)	δ_{Pt}
1	$CDCl_3$	2.31 (73.3)	−3.8 (543.7)	−2319
2	$CDCl_3$	2.31 (73.3)	−5.9 (526.6)	−2320
3	$(CD_3)_2CO$	2.66 (75.5)	−13.5[a]	−3409
4	$(CD_3)_2CO$	1.02 (69.9) (H_3C–Pt–N)	−7.1 (773.3) (H_3C–Pt–O)	−2195
		1.50 (80.7) (H_3C–Pt–O)	−6.7 (692.5) (H_3C–Pt–N)	
5	$(CD_3)_2CO$	0.95 (70.9) (H_3C–Pt–N)	−7.8 (669.5) (H_3C–Pt–N)	−2874[b]
		1.33 (66.8) (H_3C–Pt–S)	9.3 (662.0) (H_3C–Pt–S)	

[a] Coupling not observed.
[b] Measured in $CDCl_3$.

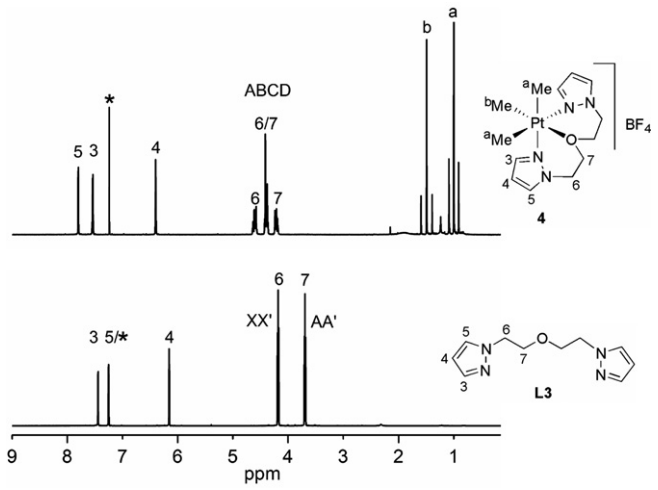

Fig. 1. ^{1}H NMR spectra of complex **4** and its free ligand **L3** measured in $CDCl_3$; "*" indicates $CHCl_3$.

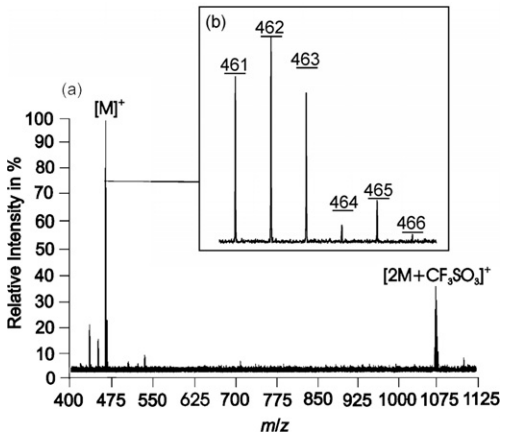

Fig. 2. (a) Positive mode HR-ESI-MS of **5**. (b) Isotopic pattern of cation $[PtMe_3(pzCH_2CH_2SCH_2CH_2pz)]^+$ ($[M]^+$) at *m*/*z* 462 (exact *m*/*z* 462.12835) showing the experimentally obtained pattern due to isotopic composition (calculated values are shown by horizontal bars).

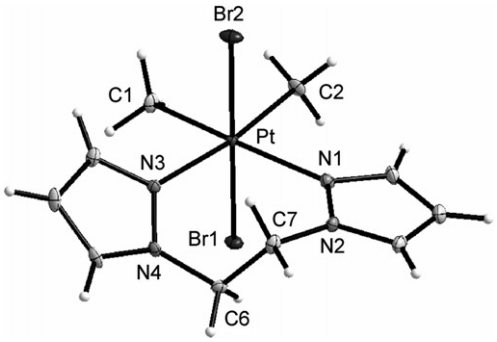

Fig. 3. Molecular structure of **1** · $CHCl_3$, $CHCl_3$ omitted. Displacement ellipsoids at 30% probability.

ethylene spacer are positioned to either side (0.04 and 1.10 Å, respectively) of the $[PtC_2N_2]$ plane.

Complex **4** crystallized in the monoclinic space group $P2_1/c$ and is the first structure of this type with platinum(IV) coordinated to a neutral chelating tridentate $\kappa^2N,N',\kappa O$ ligand while subsequently

Table 2
Selected angles and bond lengths of **1**·$CHCl_3$ and **4**

1 · $CHCl_3$		**4**	
Bond lengths [Å]			
Pt–C1	2.044(3)	Pt–C1	2.054(7)
Pt–C2	2.050(3)	Pt–C2	2.051(5)
Pt–N1	2.235(3)	Pt–C3	2.026(6)
Pt–N3	2.207(3)	Pt–N1	2.178(4)
Pt–Br1	2.436(1)	Pt–N3	2.150(4)
Pt–Br2	2.450(1)	Pt–O	2.265(4)
Bond Angles [°]			
C1–Pt–N1	174.1(1)	C2–Pt–N3	178.7(2)
C2–Pt–N3	173.0(1)	C3–Pt–N1	175.0(2)
Br1–Pt–Br2	178.1(1)	C1–Pt–O	177.0(2)
C1–Pt–C2	86.4(2)	C3–Pt–C2	85.7(2)
N3–Pt–N1	97.3(1)	N3–Pt–O	85.8(2)
		N1–Pt–O	87.9(2)
γ:N1	8.9(2)	γ:N1	88.2(3)
γ:N3	35.8(2)	γ:N3	59.9(3)

γ: Interplanar angle between least squares planes of the $[PtC_2N_2]$ atoms (carbon atoms *trans* to *N*-donors) and the pyrazolyl rings (coordinating *N*-donor atom specifies the pyrazolyl ring).

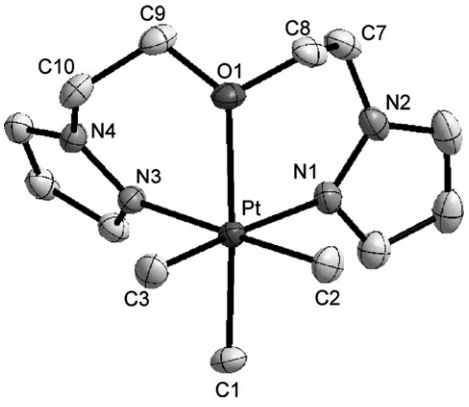

Fig. 4. Molecular structure **4**, $[BF_4]^-$ counterion and hydrogen atoms omitted. Displacement ellipsoids at 30% probability.

forming two six-membered chelate rings (Fig. 4). The ligand **L3** adopts a facial arrangement with the methyl ligands occupying the three remaining coordination sites resulting overall in an approximate octahedral arrangement of the ligator atoms around the platinum atom. Thus two diazaoxaplatina six-membered chelate rings result form the tridentate coordination of **L3**.

The Pt–C bond lengths of **4** do not differ significantly from one another or indeed from the range typical for Pt(IV)–C bond lengths *trans* to nitrogen (median 2.053 Å; lower/upper quartile 2.040/2.069 Å; $n = 351$) or oxygen donor atoms (median 2.024 Å; lower/upper quartile 2.003/2.044 Å; $n = 109$), respectively. As seen from the Pt(IV)–N range given above in the discussion of **1** · $CHCl_3$ the Pt(IV)–N bond length values are within the expected range. A very small number of structures have been reported with Pt(IV)–O bonds in which the oxygen atom is part of a C–O–C fragment and the equivalent bond length in **4** compares well with these [16]. Several of the angles around the platinum atom deviate from the ideal values; the greatest deviation is found for the C3–Pt–N1 bond angle (175.0(2)°). Two other trimethylplatinum(IV) structures with tridentate $\kappa^2N,N',\kappa O$ ligands are known [14a,17]. While the respective bond lengths in all three structures are similar, the arrangement of the ligating atoms around the platinum atom in **4** is closer to the ideal geometry as demonstrated by comparison of the most distorted angle in each of the three structures (C–Pt–O: 168.8 and C–Pt–O: 172.2, [14a,17] respectively). A further

feature of **4** is the twisting of the pyrazolyl ring coordinated via N3 relative to the $[PtC_2N_2]$ plane as given by the interplanar angle $\gamma = 59.9(3)°$. In contrast, the pyrazolyl ring coordinated via N1 is approximately perpendicular ($\gamma = 88.2(3)°$) to the $[PtC_2N_2]$ plane. Although three of the four fluorine atoms of the $[BF_4]^-$ anion of **4** are disordered, a number of short C···F distances (3.01–3.29 Å) and F···H contacts (2.37–2.40 Å; hydrogen atoms calculated) indicate the formation of weak hydrogen bonding interactions between each cation and three of the surrounding tetrafluoroborate anions [18].

3. Summary and conclusions

The preparation of several platinum(IV) complexes with simple α,ω-bis(pyrazol-1-yl) alkanediyl and diethyl ether/thioether ligands was described. The ethylene linked bis(pyrazol-1-yl) **L1** yielded platinum(IV) complexes with seven-membered chelate rings. Bis[2-(pyrazol-1-yl)ethyl]ether (**L3**) can behave as a tridentate ligand, as can bis[2-(pyrazol-1-yl)ethyl]thioether (**L4**), thus being $\kappa^2N,N',\kappa O$ and $\kappa^2N,N',\kappa S$ ligands respectively. The solid state structures of **1** · $CHCl_3$ and **4** reveal in each case a distorted octahedral arrangement adopted by the ligating atoms around the platinum atom, owing to geometrical constraints of the respective ligands, **L1** and **L3**. Furthermore, a small number of structures with substituted bis[2-(pyrazol-1-yl)ethyl]ether ligands are reported for Rh(I) [8a], Cu(I)/(II) [8c,19] Zn(II), Co(II) [8b] and Cd (II) [8d] complexes. In addition, only one of these structures (Rh(I) complex) demonstrates a facial binding mode of the bis[2-(3,5-dimethylpyrazol-1-yl)ethyl]ether ligand [8a]. The structure of **4** with a facial arrangement of the tridentate **L3** is of interest since structures of any *d*-block element hexacoordinated with a neutral $\kappa^2N,N',\kappa O$ ligand are unknown. The structure of **4** verifies the applicability of **L3** as new neutral κ^2N,N', κO type ligand for hexacoordinated complexes.

4. Experimental

4.1. General comments

Preparative centrifugal thin layer chromatography was performed using a Chromatotron (Harrison Research). ^1H and ^{13}C NMR spectra were recorded on Varian Gemini 2000 (200 and 400 MHz) and Varian Unity 500 (500 MHz) spectrometers. Chemical shifts are relative to solvent signals ($CDCl_3$ δ_H 7.24, δ_C 77.0; $(CD_3)_2CO$ δ_H 2.04, δ_C 29.8). ^{195}Pt NMR data were referenced to $H_2[PtCl_6]$ in D_2O (δ_{Pt} 0). Assignment of NMR signals was revealed by COSY and HMBC experiments. IR spectra were recorded on a Galaxy Mattson 5000 FT-IR spectrometer using KBr pellets. Microanalyses were performed at the microanalytical laboratory of Martin-Luther-Universität Halle-Wittenberg using CHNS-932 (LECO) and Vario EL (Elementaranalysensysteme) elemental analyzers. EI-MS was determined by slow heating of **L4** to a maximum of 350 °C and application of an ionization energy of 70 eV on an AMD 402 (AMD Intectra GmbH). GC-EI-MS for **L2** was preformed using an HP 5890 Series II/HP-5972 MSD (Hewlett–Packard) (column: HP5-MS 30 m). The method used: injector port 250 °C; helium flow rate 1.10 ml/min; oven temperature was 70 °C for 1 min and ramped to 250 °C over 10 min. High resolution (HR) positive mode ESI-MS were obtained using a Bruker Apex III Fourier transform ion cyclotron resonance (FT-ICR) mass spectrometer (Bruker Daltonics, Billerica, USA) equipped with an Infinity™ cell, a 7.0 T superconducting magnet (Bruker, Karlsruhe, Germany), an RF-only hexapole ion guide and an external electrospray ion source (Agilent, off axis spray, voltages for positive ion: endplate, −3.700 V; capillary, −4.200 V; capillary exit, +100 V; skimmer 1, +15.0 V; skimmer 2, +6.0 V). Nitrogen was used as drying gas at 150 °C. The sample solution were introduced continuously via a syringe pump at a flow rate of 120 μl h^{-1}. The data were acquired with 512 k data points and zero filled to 2048 k by averaging 32 scans. All starting materials necessary for the preparation of the ligands were obtained commercially (Acro, Fluka and Aldrich) and were used as received. The ligands **L1**–**L4** were prepared by analogy to a known procedure [7]. Characterization of **L1** and **L3** agreed with reported data [20,9]. $[(PtBr_2Me_2)_n]$, $[PtMe_2(cod)]$ and $[(PtIMe_3)_4]$ were prepared according to reported procedures [21–23].

4.2. General procedure for the synthesis of L2 and L4

As per [7]. In brief, pyrazole (1.50 g, 22 mmol) and NaH (37 mmol) suspended in paraffin were added to a flask fitted with a reflux condenser. At 0 °C under anaerobic conditions DMF (15 ml) was slowly added and the reagents were stirred until no further H_2 evolved. A DMF solution (ca. 15 ml) of the appropriate glycol ditosylate (11 mmol) was added over 4–5 min and allowed to stir for 15 min at ambient temperature before stirring at 82 °C for ca. 12 h. The reaction was then stopped and the solvent was removed under vacuum. The crude product was washed from reaction residue with ether (100 ml). **L2** was purified by preparative centrifugal thin layer chromatography using *n*-pentane, *n*-pentane/ether 90/10 and finally *n*-pentane/ether 50/50 to elute the product. **L4** was used without further purification.

4.2.1. $pzC^6H_2C^7H_2C^8H_2C^9H_2CH_2CH_2CH_2CH_2pz$ (**L2**)

Yellow oil/crystalline mix 1.89 g (70%). ^1H NMR (400 MHz, $CDCl_3$): δ 1.22 (m(br), 8H, $C^{8,9}H_2$), 1.82 (m, 4H, C^7H_2), 4.08 ('t', 4H, C^6H_2), 6.20 ('t', $^3J_{H,H}$ = 2.1 Hz, 2H, C^4H), 7.32 (d(br), 2H, C^5H), 7.46 (d(br), 2H, C^3H). ^{13}C NMR (101 MHz, $CDCl_3$): δ 26.5 (s, C^9H_2), 28.9 (s, C^8H_2), 30.3 (s, C^7H_2), 52.0 (s, C^6H_2), 105.1 (s, C^4H), 128.6 (s, C^5H), 138.9 (s, C^3H). RT = 16.91 min; EI-MS (*m*/*z*, rel. int. (%)): 246 ($M^{+\cdot}$, 23), 179 (7), 165 (53), 151 (23), 137 (30), 123 (28), 109 (13), 96 (17), 81 (100), 69 (41).

4.2.2. $pzC^6H_2C^7H_2SCH_2CH_2pz$ (**L4**)

Viscous orange oil. Yield 50% (0.80 g) ^1H NMR (400 MHz, $CDCl_3$): δ 2.79 ('t', 4H, C^7H_2), 4.21 ('t', 4H, C^6H_2), 6.22 ('t', $^3J_{H,H}$ = 2.1 Hz, 2H, C^4H), 7.36 (d(br), 2H, C^5H), 7.45 (d(br), 2H, C^3H). ^{13}C NMR (125 MHz, $CDCl_3$): δ 32.4 (s, C^6H_2), 52.2 (s, C^7H_2), 105.4 (s, C^4H), 129.6 (s, C^5H), 139.7 (s, C^3H). EI-MS (*m*/*z* (rel. int. (%)): 222 ($M^{+\cdot}$, 2), 154 (100), 141 (4), 127 (17), 95 (13), 86 (96), 81 (36), 68 (32).

4.3. Synthesis of 1–5

4.3.1. $[PtBr_2Me_2(pzC^6H_2CH_2pz)]$ (**1**)

As per [12a,b]. In brief, using standard Schlenk techniques $[(PtBr_2Me_2)_n]$ (30 mg, 0.08 mmol) and **L1** (13 mg, 0.08 mmol) were stirred in $CHCl_3$ (5 ml) for ca. 8 h after which time the solution became transparent yellow. The solvent was removed under vacuum. The residue was taken up in $CHCl_3$ (2 ml) and the product, a yellow powder, precipitated upon addition of pentane (10 ml). Yield: 40 mg (98%). T_{dec}: 125 °C. *Anal.* Calc. for $C_{10}H_{16}Br_2N_4Pt$ (547.15): C, 21.95; H, 2.95; N, 10.24. Found: C, 22.32; H, 3.17; N, 10.14%. IR [cm^{-1}]: *ν* 3429 (s), 2915 (m), 1560 (w), 1508 (w), 1448 (s), 1449 (s), 1275 (m), 1227 (w), 1165 (w), 1072 (m), 760 (s), 669 (m), 619 (w). ^1H NMR (400 MHz, $CDCl_3$): δ 2.31 (s + d, $^2J_{Pt,H}$ = 73.3 Hz, 6H, CH_3), 4.82 (s, 4H, C^6H_2), 6.40 (m, 2H, C^4H), 7.49 (m, 2H, C^5H), 7.98 (m, 2H, C^3H). ^{13}C NMR (125 MHz, $CDCl_3$): δ −3.8 (s + d, $^1J_{Pt,C}$ = 543.7 Hz, CH_3), 51.5 (s, C^6H_2), 107.1 (s, C^4H), 133.8 (s, C^5H), 142.8 (s + d, $^2J_{Pt,C}$ = 73.3 Hz, C^3H). ^{195}Pt NMR (107 MHz, $CDCl_3$): δ −2319 (s).

4.3.2. [PtBr$_2$Me$_2$(pzC^{6}H$_2$C^{7}H$_2$C^{8}H$_2$C^{9}H$_2$CH$_2$CH$_2$CH$_2$CH$_2$pz)] (**2**)

As for **1** except **L2** instead of **L1** and the final product was isolated after the solvent was removed. Bright yellow residue. T_{dec}: 110 °C. IR [cm^{-1}]: *ν* 3997 (m), 3103 (m), 2920 (s), 2854 (s), 1625 (w), 1458 (w), 1420 (m), 1275 (w), 1215 (w), 1105 (w), 1065 (m), 985 (w), 889 (w), 755 (s), 616 (w). ^{1}H NMR (400 MHz, $CDCl_3$): *δ* 1.26 (m(br), 8H, C^{8,9}H$_2$), 1.77 (s(br), 4H, C^{7}H$_2$), 2.31 (s + d, $^2J_{Pt,H}$ = 73.3 Hz, 6H, C*H*$_3$), 4.13 (m(br), 4H, C^{6}H$_2$), 6.40 (s, 2H, C^4*H*), 7.48 (s(br), 2H, C^5*H*), 7.84 (s(br), 2H, C^3*H*). ^{13}C NMR (101 MHz, $CDCl_3$): *δ* −5.8 (s + d, $^1J_{Pt,C}$ = 526.6 Hz, *C*H$_3$), 26.3 (s, *C*^{9}H$_2$), 28.8 (s, *C*^{8}H$_2$), 30.6 (s, *C*^{7}H$_2$), 51.6 (s, *C*^{6}H$_2$), 106.7 (s(br), *C*^{4}H), 131.2 (s(br), *C*^{5}H), 142.9 (s(br), *C*^{3}H). ^{195}Pt NMR (107 MHz, $CDCl_3$): *δ* −2320 (s).

4.3.3. [PtI$_2$Me$_2$(pzCH$_2$CH$_2$pz)] (**3**)

By analogy to a known procedure [10]. In brief, to a stirring solution of [PtMe$_2$(cod)] (33 mg, 0.10 mmol) and **L1** (16 mg, 0.10 mmol) in CH_2Cl_2 (10 ml) a solution of I_2 (ca. 50 mg in 5 ml) was added dropwise until the red-purple color of the I_2 persisted. After stirring for ca. 1 h the solvent was removed under vacuum. The residue was washed with small portions of CH_2Cl_2 (5 × 2 ml) and decanted to a separate flask. The solvent was removed. The residue was taken up in CH_2Cl_2 (4 ml) and the product precipitated upon addition of pentane (10 ml) at −18 °C. The latter step was repeated three times to afford the product, an orange powder. Yield 51 mg (81%). T_{dec}: 133 °C. *Anal.* Calc. for [C$_{10}$H$_{16}$I$_2$N$_4$Pt] (641.15): C, 18.73; H, 2.52; N, 8.74. Found: C, 18.96; H, 2.90; N, 8.29%. IR [cm^{-1}]: *ν* 3404 (m), 3108 (w), 2915 (m), 1521 (w), 1419 (s), 1281 (m), 1165 (w), 1111 (m), 1074 (m), 1005 (w), 984 (w), 758 (s), 613 (m). ^{1}H NMR (400 MHz, $CDCl_3$): *δ* 2.66 (s + d, $^2J_{Pt,H}$ = 75.5 Hz, 6H, C*H*$_3$), 4.76 (s, 4H, C^6*H*$_2$), 6.40 (t, $^3J_{H,H}$ = 2.4 Hz, 2H, C^4*H*), 7.47 (d, $^3J_{H,H}$ = 2.1 Hz, 2H, C^5*H*), 7.98 (d, $^3J_{H,H}$ = 2.5 Hz, 2H, C^3*H*). ^{13}C NMR (100 MHz, $(CD_3)_2CO$): *δ* −13.5 (s, *C*H$_3$), 51.9 (s, *C*^{6}H$_2$), 106.3 (s, *C*^{4}H), 135.1 (s, *C*^{5}H), 142.5 (s, *C*^{3}H). ^{195}Pt NMR (107 MHz, $(CD_3)_2CO$): *δ* −3409 (s).

4.3.4. [PtMe$_3$(pzC^{6}H$_2$C^{7}H$_2$OCH$_2$CH$_2$pz)][BF$_4$] (**4**)

To a flask **L3** (36 mg, 0.18 mmol), [(PtIMe$_3$)$_4$] (64 mg, 0.18 mmol), an excess of $AgBF_4$ (ca. 49 mg, 0.25 mmol) and acetone (10 ml) were added. The reagents were stirred 24 h in darkness before the reaction mixture was filtered and the transparent filtrate was evaporated to dryness. The residue was taken up in $CHCl_3$ (ca. 2 ml) and **4** precipitated upon addition of pentane (10 ml). White microcrystalline solid. Yield: 84 mg (90%). T_{dec}: 192 °C. IR [cm^{-1}]: ν 3441 (s), 3148 (m), 2970 (s), 2901 (s), 2819 (w), 1636 (w), 1520 (w), 1415 (s), 1299 (m), 1237 (m), 1190 (m), 1054 (s), 787 (s), 618 (m), 522 (w). ^{1}H NMR (400 MHz, $(CD_3)_2CO$): *δ* 1.02 (s + d, $^2J_{Pt,H}$ = 69.9 Hz, 6H, C*H*$_3$–Pt–N), 1.50 (s + d, $^2J_{Pt,H}$ = 80.7 Hz, 3H, C*H*$_3$–Pt–O), 4.31 (m, 2H, C^7*H*$_2$), 4.40 (m, 4H, C^{6,7}*H*$_2$), 4.59 (m, 2H, C^6*H*$_2$), 6.42 (m, 2H C^4*H*), 7.50 (m, 2H, C^3*H*), 7.76 (m, 2H, C^5*H*). ^{13}C NMR (125 MHz, $(CD_3)_2CO$): *δ* −7.1 (s + d, $^1J_{Pt,C}$ = 773.3 Hz *C*H$_3$–Pt–O), −6.7 (s + d, $^1J_{Pt,C}$ = 692.5 Hz, *C*H$_3$–Pt–N), 49.6 (s, C^{6}H$_2$), 53.0 (s, C^{7}H$_2$), 107.0 (s + d, $^3J_{Pt,C}$ = 12.4 Hz, C^{4}H), 135.2 (m, C^{5}H), 139.3 (m, CH^3). ^{195}Pt NMR (107 MHz, $(CD_3)_2CO$): *δ* −2195 (s). Positive mode ESI-FTICR-MS (MeOH): *m*/*z* 446.15124, calc. for [C$_{13}$H$_{23}$N$_4$O^{195}Pt]$^+$ 446.15141; *m*/*z* (intensity calc./found for cation [C$_{13}$H$_{23}$N$_4$OPt]$^+$, %) 445 (85/75), 446 (100/100), 447 (79/87), 448 (12/12), 449 (19/25), 450 (3/3).

4.3.5. [PtMe$_3$(pzC^{6}H$_2$C^{7}H$_2$SCH$_2$CH$_2$pz)][CF$_3$SO$_3$] (**5**)

As for **4** except **L4** instead of **L3**, $AgCF_3SO_3$ instead of $AgBF_4$ and the final product was isolated in the presence of minor impurities after evaporation of the filtrate. A clear residue. Yield (crude, ca. 10% impurities): 82 mg. ^{1}H NMR (400 MHz, $(CD_3)_2CO$): *δ* 0.95 (s + d, $^2J_{Pt,H}$ = 70.9 Hz, 6H, C*H*$_3$–Pt–N), 1.38 (s + d, $^2J_{Pt,H}$ = 66.8 Hz, 3H, C*H*$_3$–Pt–S), 3.54 (m, 4H, C^{7}H$_2$), 4.14 (m, 2H, C^{6}H$_2$), 4.70 (m, 2H, C^{6}H$_2$), 6.39 (t, $^3J_{H,H}$ = 2.4 Hz, 2H, C^4*H*), 7.42 (d, $^3J_{H,H}$ = 2.4 Hz, 2H, C^3*H*), 7.70 (d, $^3J_{H,H}$ = 2.5 Hz, 2H, C^5*H*). ^{13}C NMR (125 MHz, $(CD_3)_2CO$): *δ* −7.8 (s + d, $^1J_{Pt,C}$ = 669.5 Hz, *C*H$_3$–Pt–N), 9.3 (s + d, $^1J_{Pt,C}$ = 662.0 Hz, *C*H$_3$–Pt–S), 34.1 (s, *C*^{7}H$_2$), 50.2 (s + d, $^3J_{Pt,C}$ = 13.1 Hz, C^{6}H$_2$), 107.7 (s + d, $^3J_{Pt,C}$ = 12.4 Hz, C^{4}H), 135.8 (s, *C*^{5}H), 140.9 (s + d, $^2J_{Pt,C}$ = 12.4 Hz, *C*^{3}H) 160.5 ('m', *C*F$_3$). ^{195}Pt NMR (107 MHz, $CDCl_3$): *δ* −2874 (s). Positive mode ESI-FTICR-MS (MeOH): *m*/*z* 431.07891, calc. for [C$_1$^{1}H$_{17}$N$_4$^{194}Pt^{32}S]$^+$ 431.07951; *m*/*z* 461.12599, calc. for [C$_{13}$H$_{23}$N$_4$^{194}Pt^{32}S]$^+$ 461.12646; *m*/*z* 462.12835, calc. for [C$_{13}$H$_{23}$N$_4$^{195}Pt^{32}S]$^+$ 462.12857; *m*/*z* 1071.19950, calc. for [C$_{27}$H$_{46}$F$_3$N$_8$O$_3$^{194}Pt$_2$^{32}S$_3$]$^+$ 1071.20549; *m*/*z* (intensity calc./found for cation [C$_{13}$H$_{23}$N$_4$PtS]$^+$, %) 461 (84/82), 462 (100/100), 463 (83/73), 464 (16/9), 465 (23/21), 466 (4/4).

4.4. X-ray crystal structure determination

Single crystals of **1** · $CHCl_3$ and **4** were obtained by slow evaporation of a chloroform solution of the respective compound at room temperature. Table 3 shows crystallographic and data collection parameters. Intensity data were collected on either a CCD Xcalibur S diffractometer (**1** · $CHCl_3$) at 130(2) K or a Stoe-IPDS (**4**) at 293(2) K both with Mo Kα radiation (*λ* = 0.7103 Å, graphite monochromator). The absorption correction for **4** was made using the IPDS software package and a semi-empirical correction was made for **1** · $CHCl_3$ with SCALE3 ABSPACK [24]. Both structures were solved by direct methods using SHELXS-97 and refined using full-matrix least-squares routines against F^2 with SHELXL-97 [25]. Non-hydrogen atoms were refined with anisotropic displacement parameters. Three of the four fluorine atoms of $[BF_4]^-$ in the structure of **4** (F2, F3 and F4) are disordered with refined occupancy factors (70/30%). Hydrogen atoms were included in the models by calculating the positions using the riding model and refined with isotropic displacement parameters. Illustrations were generated using DIAMOND 3.0 software [26].

5. Supplementary data

CCDC 684953 and 684952 contain the supplementary crystallographic data for **1** · $CHCl_3$ and **4**. These data can be obtained free of charge via http://www.ccdc.cam.ac.uk/conts/retrieving.html, or from the Cambridge Crystallographic Data Centre, 12 Union Road, Cambridge CB2 1EZ, UK; fax: (+44) 1223-336-033; or e-mail: deposit@ccdc.cam.ac.uk.

Table 3
Crystallographic and data collection parameters for **1** · $CHCl_3$ and **4**

	1 · $CHCl_3$	**4**
Empirical formula	$C_{11}H_{17}Br_2Cl_3N_4Pt$	$C_{13}H_{23}BF_4N_4OPt$
M_r	666.55	533.25
Crystal system	monoclinic	monoclinic
Space group	$P2_1/c$	$P2_1/n$
a (Å)	9.557(1)	12.530(3)
b (Å)	8.318(1)	9.624(2)
c (Å)	22.696(1)	15.710(4)
β (°)	94.970(1)	108.30(3)
V (Å^3)	1797(1)	1798(1)
Z	4	4
D_{calc} (g/cm)	2.463	1.969
μ (mm^{-1})	12.697	7.848
F(000)	1240	1024
Independent reflections	5480	3421
Number of observed reflections	4991	2747
Data/restraints/parameters	5480/0/192	3421/0/249
Goodness-of-fit F^2	1.310	1.071
R_1 [$I>2\sigma(I)$], R_1 (all data)	0.0226, 0.0267	0.0381, 0.0464
wR_2 [$I>2\sigma(I)$], wR_2 (all data)	0.0518, 0.0533	0.0908, 0.0958
T_{min}/T_{max}	0.45/1.00	0.06/0.20

Acknowledgement

The authors wish to acknowledge the Deutsche Forschungsgemeinschaft for financial support and Merck for gifts of chemicals.

References

[1] (a) S. Trofimenko, Chem. Rev. 72 (1972) 497;
(b) S. Trofimenko, Chem. Rev. 93 (1993) 943;
(c) H.R. Bigmore, S.C. Lawerence, P. Mountford, C.S. Tredget, Dalton Trans. (2005) 635;
(d) S. Trofimenko, Scorpionates: The Coordination Chemistry of Polypyrazolborate Ligands, Imperial College Press, River Edge, New Jersey, 1999.
[2] A.M. Schuitema, M. Engelen, I.A. Koval, S. Gorter, W.L. Driessen, J. Reedijk, Inorg. Chim. Acta 324 (2001) 57.
[3] A.J. Canty, J. Patel, B.W. Skelton, A.H. White, J. Organomet. Chem. 607 (2000) 194.
[4] A. Lorenzotti, P. Cecchi, C. Pettinari, D. Leonesi, F. Bonati, Gazz. Chim. Ital. 121 (2) (1991) 89.
[5] C. Pettinari, A. Lorenzotti, A. Cingolani, D. Leonesi, M. Marra, F. Marchetti, Gazz. Chim. Ital. 123 (9) (1993) 481.
[6] C. Pettinari, A. Lorenzotti, G. Sclavi, A. Cingolani, E. Rivarola, M. Colapietro, A. Cassetta, J. Organomet. Chem. 496 (1995) 69.
[7] P. Grosshans, A. Jouaiti, M.W. Hosseini, A. De Cian, N. Kyritsakas-Gruber, Tetrahedron Lett. 44 (2003) 1457.
[8] (a) A. Boixassa, J. Pons, J. Ros, R. Mathieu, N. Lugan, J. Organomet. Chem. 682 (2003) 233;
(b) C. Dowling, V.J. Murphy, G. Parkin, Inorg. Chem. 35 (1996) 2415;
(c) T.N. Sorrell, M.R. Malachowski, Inorg. Chem. 22 (1983) 1883;
(d) E.A.H. Griffith, N.G. Charles, K. Lewinski, E.L. Amma, P.F. Rodesilers, Inorg. Chem. 26 (1987) 3983.
[9] A.S. Potapov, G.A. Domina, A.I. Khlebnikov, V.D. Ogorodnikov, Eur. J. Org. Chem. (2007) 5112.
[10] H.C. Clark, G. Ferguson, V.K. Jain, M. Parvez, Organometallics 2 (1983) 806.
[11] P.S. Pergosin, Transition Metal Nuclear Magnetic Resonance, Elsevier, Amsterdam, The Netherlands, 1991.
[12] (a) M.E. Kelly, S. Gómez-Ruiz, R. Kluge, K. Merzweiler, D. Steinborn, Ch. Wagner, H. Schmidt, Inorg. Chim. Acta, accepted for publication, doi:10.1016/j.ica.2008.06.025;
(b) J.R. Hall, G.A. Swile, J. Organomet. Chem. 56 (1973) 419;
(c) J.R. Hall, G.A. Swile, J. Organomet. Chem. 56 (1973) 419.
[13] (a) Y.-E. Kwon, K.-J. Whang, Y.-J. Park, K.H. Kim, Bioorg. Med. Chem. 11 (2003) 1669;
(b) S. Shamsuddin, C.C. Santillan, J.L. Stark, K.H. Whitmire, Z.H. Siddik, A.R. Khokhar, J. Inorg. Biochem. 71 (1998) 29;
(c) A.R. Khokhar, S. Shamsuddin, Q. Xu, Inorg. Chim. Acta 219 (1994) 193;
(d) S. Shamsuddin, J.W. van Hal, J.L. Stark, K.H. Whitmire, A.R. Khokhar, Inorg. Chem. 36 (1997) 5969.
[14] (a) F. Zhang, M.E. Broczkowski, M.C. Jennings, R.J. Puddephatt, Can. J. Chem. 83 (2005) 595;
(b) A. Canty, R.T. Honeyman, B.W. Skelton, A.H. White, J. Organomet. Chem. 396 (1990) 105;
(c) G.N. Kaluderović, H. Schmidt, Ch. Wagner, D. Steinborn, Acta Crystallogr., Sect. E 63 (8) (2007) m1985;
(d) R.P. Hughes, J.T. Sweetser, M.D. Tawa, A. Williamson, C.D. Incarvito, B. Rhatigan, A.L. Rheingold, G. Rossi, Organometallics 20 (2001) 3800.
[15] Cambridge Structural Database (CSD), University Chemical Laboratory, Cambridge.
[16] (a) V. Ananikov, S.A. Mitchenko, I.P. Beletskaya, S.E. Nefedov, I.L. Eremenko, Inorg. Chem. Commun. 1 (1998) 411;
(b) H. Junicke, C. Bruhn, R. Kluge, A.S. Serianni, D. Steinborn, J. Am. Chem. Soc. 121 (1999) 6232;
(c) H. Junicke, C. Bruhn, D. Ströhl, R. Kluge, D. Steinborn, Inorg. Chem. 37 (1998) 4603;
(d) S. Schlecht, K. Dehnicke, J. Magull, D. Fenske, Angew. Chem., Int. Ed. 36 (1997) 1994;
(e) E. Wehman, G. van Koten, C.T. Knapp, H. Ossor, M. Pfeffer, A.L. Spek, Inorg. Chem. 27 (1988) 4409;
(f) M.L. Creber, K.G. Orrell, A.G. Osborne, V. Sik, M.B. Hursthouse, K.M.A. Malik, J. Chem. Soc., Dalton Trans. (2000) 4218.
[17] E. Khaskin, P.Y. Zavalij, A.N. Vedernikov, Angew. Chem., Int. Ed. 46 (2007) 6309.
[18] F. Grepioni, G. Cojazzi, S.M. Draper, N. Scully, D. Braga, Organometallics 17 (1998) 296.
[19] S.V. Voitekhovich, P.N. Gaponik, D.S. Pytleva, A.S. Lyakhov, O.A. Ivashkevich, Pol. J. Chem. 76 (2002) 1371.
[20] (a) E. Díez-Barra, A. de la Hoz, A. Sánchez-Migallón, J. Tajeda, Heterocycles 34 (7) (1992) 1365;
(b) J. Torres, J.L. Lavandera, P. Cabildo, R.M. Claramunt, J. Elguero, J. Heterocycl. Chem. 25 (1988) 771.
[21] T.G. Appleton, C.J. D'Alton, J.R. Hall, M.T. Mathieson, M.A. Williams, Can. J. Chem. 74 (1996) 2008.
[22] T.G. Appleton, J.R. Hall, M.A. Williams, J. Organomet. Chem. 303 (1) (1986) 139.
[23] (a) W.J. Pope, S.J. Peachey, Proc. Chem. Soc. 23 (1907) 86;
(b) J.C. Baldwin, W.C. Kaska, Inorg. Chem. 14 (1975) 2020.
[24] (a) IPDS–Software Package, Stoe & Cie, 1999.;
(b) SCALE3 ABSPACK: Empirical Absorption Correction, CRYSALIS – Software Package, Oxford Diffraction Ltd., 2006.
[25] G.M. Sheldrick, Acta Crystallogr., Sect. A 64 (2008) 112.
[26] K. Branderburg, Diamond, Release 2, Crystal Impact GmbR, Bonn (1997).

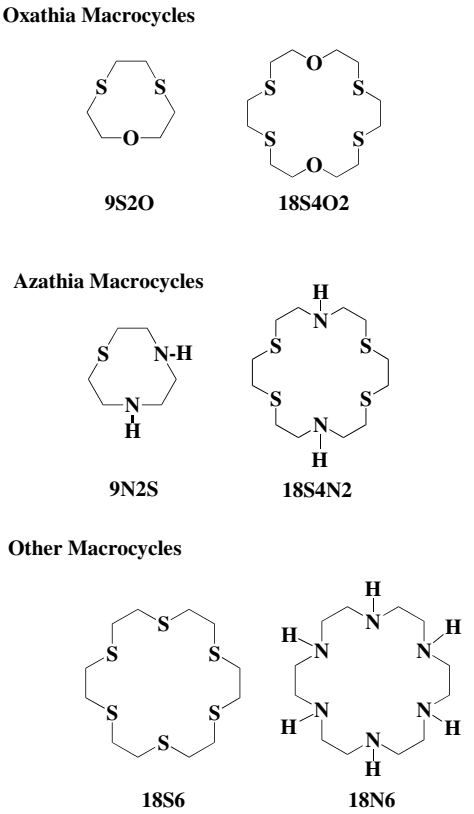

Scheme 1. Macrocyclic ligands discussed in this report.

2. Experimental

2.1. Materials and measurements

The ligands 9S2O, 18S4O2, and 9N2S were prepared by their respective literature methods [21–24]. All other reagents and solvents were purchased commercially and used as received. An aqueous solution containing 45% by weight of $Cd(BF_4)_2$ was used as the source of that reagent in aqueous syntheses. *Caution!!! Although the perchlorate salts prepared in this report do not appear to be shock-sensitive, they should be handled with caution and only in very small quantities.* Mercury and cadmium are toxic metals, and their compounds should be handled accordingly.

Elemental analyses were performed by Atlantic Microlab, Inc., of Atlanta, Georgia. Fourier Transform Infrared spectra were obtained on a Nicolet FT-IR using dry pre-weighed KBr powder and an ATR accessory. All $^{13}C\{^1H\}$ and ^1H NMR spectra were recorded on a JEOL ECX-400 NMR spectrometer using either the residual deuterated organic solvent (CD_3NO_2, CD_3CN, etc.) peaks for the internal reference or an internal reference of d-6-acetone for $^{13}C\{^1H\}$ NMR spectra obtained in D_2O. The $^{113}Cd\{^1H\}$ NMR spectra were collected at 25 °C and 88.66726 MHz using a 75° pulse, a 0.5 s acquisition time, and a relaxation delay time of 5.0 s. Referencing was done using a 0.10 M solution of $Cd(ClO_4)_2$ in D_2O at 0 ppm. The $^{113}Cd\{^1H\}$ NMR spectra were collected until a minimum signal/noise ratio of 20/1 was obtained. Data collection on one sample typically required 10 000–12 000 transients and took 24–30 h to complete.

2.2. Complexes with oxathiacrown ligands

2.2.1. Synthesis of $[Hg(9S2O)_2](ClO_4)_2$

A solution containing 107 mg of $Hg(ClO_4)_2 \cdot 3H_2O$ (0.236 mmol) and 10 drops of acetic anhydride in 10 mL of CH_3NO_2 was added dropwise to a solution containing a mass of 76.9 mg of 9S2O (0.468 mmol) in 5 mL of CH_3NO_2 and cooled at 0°C for about 15 min. A volume of 40 mL of diethyl ether was added dropwise to the cold solution which was left at 0° overnight. White crystals of $[Hg(9S2O)_2](ClO_4)_2$ had formed which were filtered, washed with diethyl ether (3×15 mL) to yield 126 mg of product (73.9%). *Anal.* calc. for $C_{12}H_{24}Cl_2HgO_{10}S_4$: C, 19.80; H, 3.32; S, 17.62; Cl, 9.74. Found: C, 19.63; H, 3.27; S, 17.34, Cl, 9.73%. FT-IR (cm^{-1}): 2991 (C–H), 2939 (C–H), 2904(C–H), 2866 (C–H), 1628, 1543, 1469, 1409, 1297, 1111–1081 s, (ClO_4^-), 904, 813, 624, 409. ^1H NMR (CD_3NO_2) δ (ppm): complex AA′BB′ symmetrical pattern at 4.09–4.01 (4H) and 3.86–3.78 (4H) (–O–C*H*$_2$–CH$_2$–S–); broad, overlapping multiplets at 3.49–3.26 (16H, –O–CH$_2$–C*H*$_2$–S– and –S–C*H*$_2$–C*H*$_2$–S–). $^{13}C\{^1H\}$ NMR (CD_3CN) δ (ppm): 62.11 (4C, –O–*C*H$_2$–CH$_2$–S–), 32.94 (4C, –O–CH$_2$–*C*H$_2$–S–), 29.87 (–S-(*C*H$_2$)$_2$–S–). No ^{199}Hg NMR signal in CD_3NO_2 was observed after 12 000 transients. Slow evaporation of a nitromethane solution produced large rods suitable for single crystal X-ray analysis.

2.2.2. Synthesis of $[Hg(18S4O2)](ClO_4)_2$

A mixture containing 88.8 mg of $Hg(ClO_4)_2 \cdot 3H_2O$ (0.196 mmol), 10 drops of acetic anhydride, and 57.5 mg of 18S4O2 (0.175 mmol) in 15 mL of CH_3NO_2 was refluxed for 1.5 h. After cooling in an ice bath, 20 mL of diethyl ether was slowly added to precipitate a white crystalline solid. The solid was isolated by filtration and washed with diethyl ether (3×15 mL) to yield 57.7 mg (45.3%) of $[Hg(18S4O2)](ClO_4)_2$. *Anal.* calc. for $C_{12}H_{24}Cl_2HgO_{10}S_4$: C, 19.80; H, 3.32; S, 17.62; Cl, 9.74. Found: C, 19.78; H, 3.29; S, 17.40; Cl, 9.59%. FT-IR (cm^{-1}): 2987 (C–H), 2939 (C–H), 2870 (C–H), 2793 (C–H), 1559, 1464, 1409, 1357, 1271, 1111–1081 s, (ClO_4^-), 1020, 913, 775, 693, 624. ^1H NMR (CD_3CN) δ (ppm): sharp multiplet at 3.73 (8H, –O–C*H*$_2$–CH$_2$–S–), broad mutliplet at 3.33–3.05 (16H, –O–CH$_2$–C*H*$_2$–S– and –S–C*H*$_2$–C*H*$_2$–S–). $^{13}C\{^1H\}$ NMR (CD_3CN) δ (ppm): 66.21 (4C, –O–*C*H$_2$–CH$_2$–S–), 34.24 (4C, –O–CH$_2$–*C*H$_2$–S–), 31.76 (4C, –S-(*C*H$_2$)$_2$–S–). No ^{199}Hg NMR signal in CD_3CN was observed after 40 000 transients. Two consecutive crystallizations using diethyl ether diffusion into acetonitrile resulted in X-ray quality colorless prisms.

2.2.3. Synthesis of $[Cd(9S2O)_2](ClO_4)_2$ and $[Cd(18S4O2)](ClO_4)_2$

The two known Cd(II) complexes $[Cd(9S2O)_2](ClO_4)_2$ and $[Cd(18S4O2)](ClO_4)_2$ were prepared by the published methods [25]. Verification of complex formation was accomplished by ^1H and $^{13}C\{^1H\}$ NMR spectra which matched the prior results.

For $[Cd(9S2O)_2](ClO_4)_2$: ^1H NMR (CD_3NO_2), δ (ppm): multiplet at 3.99 (8H, –OC*H*$_2$–CH$_2$S–), singlet at 3.29 (8H, –SC*H*$_2$–C*H*$_2$S–), multiplet at 3.24 (8H, –OCH$_2$–C*H*$_2$S–). $^{13}C\{^1H\}$ NMR (CD_3NO_2) δ (ppm): 63.91, 31.37, 29.52. Data collection for the $^{113}Cd\{^1H\}$ NMR spectrum of the complex was attempted, but no ^{13}Cd NMR peak was observed. Data collection on one sample typically required 10 000–12 000 transients and 24–30 h to complete. Colorless plates of the complex, suitable for X-ray diffraction studies, were obtained from diethyl ether diffusion into a nitromethane solution.

For $[Cd(18S4O2)](ClO_4)_2$: ^1H NMR (CD_3NO_2), δ (ppm): multiplets at 3.97 (8H, –OC*H*$_2$–CH$_2$S–), 3.41 (8H, –OCH$_2$–C*H*$_2$S–), 3.28 (8H, –SC*H*$_2$–C*H*$_2$S–). $^{13}C\{^1H\}$ NMR (CD_3NO_2) δ (ppm): 66.89, 32.79, 31.28. The $^{113}Cd\{^1H\}$ NMR spectra were collected, but again no ^{113}Cd NMR peak for the complex was observed. Data collection on one sample typically required 10 000–12 000 transients and 24–30 h to complete. Colorless plates of the complex were obtained from diethyl ether diffusion into a nitromethane solution.

2.3. Complexes with azathiacrown ligands

2.3.1. Synthesis of $[Cd(9N2S)_2](ClO_4)_2$

A solution containing 91.0 mg of $Cd(ClO_4)_2 \cdot 6H_2O$ (0.217 mmol) dissolved in 10 mL of MeOH was slowly added to a stirred solution

containing 65.9 mg of 9N2 S (0.451 mmol) in 5 mL of MeOH. A white precipitate formed immediately. The precipitate was filtered, washed with cold MeOH (3 × 15 mL), diethyl ether (3 × 15 mL), and air-dried. A mass of 58.0 mg of $[Cd(9N2S)_2](ClO_4)_2 \cdot 3H_2O$ was obtained in a 40.7% yield. *Anal.* calc. for $C_{12}H_{36}Cl_2CdN_4O_{11}S_2$: C, 21.98; H, 4.92; S, 9.78; Cl, 10.81; N, 8.54. Found: C, 21.73; H, 5.26; S, 9.55; Cl, 10.45; N, 8.44%. FT-IR (KBr, cm^{-1}): 3283 (N–H), 2938 (C–H), 2876 (C–H), 1462, 1414, 1359, 1290, 1228, 1117 (ClO_4^-), 917, 779, 634. ^1H NMR (CD_3NO_2) δ (ppm): broad singlet at 3.49–3.40 (4H, –N*H*–CH_2CH_2–), multiplet at 3.27–3.15 (8H, –N–CH_2CH_2-N–), multiplet at 3.07–2.95 (8H, –N–CH_2CH_2–S), and multiplet at 2.91–2.77 (8H, –N–CH_2CH_2–S–). $^{13}C\{^1H\}$ NMR (CD_3NO_2) δ (ppm): 44.69 (2C, –N–CH_2CH_2-N–), 44.58 (2C, –N–CH_2CH_2-N–), 43.56 (2C, –N–CH_2CH_2–S–), 43.46 (2C, –N–CH_2CH_2–S–), 30.59 (4C, -CH_2–S–CH_2–). ^{113}Cd NMR (CD_3NO_2): δ ($\nu_{1/2}$) 521 ppm (34 Hz). Colorless rods suitable for X-ray diffraction were obtained by slow evaporation of a nitromethane solution.

2.4. Preparation of Cd(II) complexes with other macrocyclic ligands

2.4.1. Synthesis of $[Cd(18N6)](BF_4)_2$

A mass of 18N6 · $3H_2SO_4$ (151 mg, 0.273 mmol) was placed in 15 mL of H_2O and heated to 60 °C to completely dissolve the ligand. A mass of $BaCO_3$ (162 mg, 0.821 mmol) was added, and the reaction mixture was then heated to 75 °C and stirred for 1.5 h. The reaction solution was filtered to remove the white solid of precipitated $BaSO_4$. A mass of $Cd(BF_4)_2$ (77.9 mg, 0.272 mmol) was then added to the filtrate, and the reaction heated to 75 °C and stirred for 2 h. The solution was evaporated to dryness giving an off-white solid. The solid was crystallized from water to yield colorless, hygroscopic crystals. These were dried *in vacuo* to produce 50.2 mg (33.9% yield) of $[Cd(18N6)](BF_4)_2$. *Anal.* calc. for $C_{12}H_{30}B_2CdN_6F_8$: C, 26.46; H, 5.55; N, 15.44. Found: C, 26.73; H, 5.26; N, 15.44%. FT-IR (KBr, cm^{-1}): 3428 (b, N–H), 3235(b, N–H), 2910 (C–H), 2855 (C–H), 2076, 1621, 1455, 1366, 1338, 1283, 1214, 1083 s, (BF_4^-), 1028, 938, 821, 621, 517. ^1H NMR (CD_3OD) δ (ppm): 4.86 (b, s, N*H*, 6H), 2.99 (m, 8H), 2.69 (m, 8H). 2.57 (m, 8H). $^{13}C\{^1H\}$ NMR (D_2O) δ (ppm): approximately equal intensity singlets at 45.82, 45.65, 44.96. ^{113}Cd NMR (D_2O): δ ($\nu_{1/2}$) 277 ppm (57 Hz).

2.4.2. Synthesis of $[Cd(18S6)](BF_4)_2$

A mass of 18S6 (53.1 mg, 0.147 mmol) was added to 10 mL of CH_3NO_2. Solid $Cd(BF_4)_2 \cdot 6H_2O$ (57.7 mg, 0.146 mmol) followed by 5 drops of acetic anhydride was then added, and the mixture was stirred at room temperature for 30 min. A white precipitate had formed which was filtered and washed with CH_3NO_2 (3 × 25 mL) and $CHCl_3$ (3 × 25 mL) to remove any unreacted ligand and starting Cd(II). The product was air dried to yield 71 mg (75% yield) of $[Cd(18S6)](BF_4)_2$. *Anal.* calc. for $C_{12}H_{24}B_2CdF_8S_6$: C, 22.29; H, 3.74; S, 29.74. Found: C, 22.39; H, 3.82; S, 29.55%. FT-IR (cm^{-1}): 2979 (C–H), 2938 (C–H), 1421, 1276, 1097, 1062 (ClO_4^-), 1028, 931, 903, 855, 710, 676 (C–S), 524. ^1H NMR (DMSO-d_6) δ (ppm): 2.80(s). $^{13}C\{^1H\}$ NMR (DMSO-d_6) δ (ppm): 31.56(s). The $^{113}Cd\{^1H\}$ NMR spectra were collected on a solution in DMSO-d_6, but no ^{113}Cd NMR peak for the complex was observed. Data collection on one sample typically required 10 000–12 000 transients and took 24–30 h to complete.

2.5. Data collection and processing

Table 1 contains crystal data, collection parameters, and refinement criteria for the structures of all four compounds. For all structures, X-ray intensity data were measured at low temperature (153(2) K) with graphite-monochromated radiation (λ = 0.71073 Å) on a Rigaku AFC8S diffractometer equipped with a 1 K Mercury CCD detector [26]. The structure was solved using direct methods and refinement was done using full-matrix least-squares techniques (on F^2). Data were corrected for absorption, using semi-empirical methods. Structure solution, refinement and the calculation of derived results were performed with the SHELXTL package of computer programs [27]. All H atoms were geometrically fixed and allowed to ride on the corresponding non-H atom with C–H = 0.96 Å and $U_{iso}(H) = 1.5U_{eq}(C)$ of the attached C atom for methyl H atoms and $1.2U_{eq}(C)$ for other H atoms. Larger

Table 1
Crystal data, data collection, and refinement parameters for $[Hg(9S2O)_2](ClO_4)_2 \cdot 2CH_3NO_2$ (**1**), $[Hg(18S4O2)](ClO_4)_2$ (**2**), $[Cd(9S2O)_2](ClO_4)_2 \cdot 2CH_3NO_2$ (**3**), and $[Cd(9N2S)_2](ClO_4)_2$ (**4**)

Compound	**1**	**2**	**3**	**4**
Formula	$C_{14}H_{30}Cl_2HgN_2O_{14}S_4$	$C_{12}H_{24}Cl_2HgO_{10}S_4$	$C_{14}H_{30}Cl_2CdN_2O_{14}S_4$	$C_{12}H_{28}Cl_2CdN_4O_8S_2$
Habit, color	rod, colorless	prism, colorless	plate, colorless	rod, colorless
Lattice type	monoclinic	monoclinic	triclinic	monoclinic
Space group	$P2_1/n$	$P2_1/c$	P-1	$P2_1/c$
a (Å)	7.7987(16)	12.642(3)	9.9356(5)	7.6549(15)
b (Å)	37.911(8)	10.519(2)	10.4558(5)	15.765(3)
c (Å)	9.3968(19)	16.272(3)	15.0518(12)	8.8375(18)
α (°)	90	90	95.109(13)	90
β (°)	91.90(3)	97.44(3)	104.871(13)	92.45(3)
γ (°)	90	90	111.954(13)	90
V (Å^3)	2776.7(10)	2145.6(7)	1371.5(2)	1065.5(4)
Z	4	4	2	2
Temperature (K)	153(2)	153(2)	153(2)	153(2)
Fw (g mol^{-1})	850.13	728.04	761.94	603.80
D_c (Mg m^{-3})	2.034	2.254	1.845	1.882
μ (mm^{-1})	6.102	7.860	1.362	1.519
Reflections collected	8143	12 513	12 357	7523
Unique reflections (R_{int})	3824 (0.0492)	3728 (0.0941)	5335 (0.0289)	1885 (0.0586)
Maximum, minimum transmission	0.5280, 0.1577	0.950, 0.603	0.9107, 0.7358	0.9279, 0.4627
Data/restraints/parameters	3686/0/257	3684/1/287	5335/0/336	1885/0/133
R_1, wR_2 ($I > 2\sigma(I)$)	0.0577, 0.1388	0.0839, 0.1311	0.0337, 0.0785	0.0586, 0.1444
R_1, wR_2 (all data)	0.0736, 0.1513	0.2051, 0.2503	0.0438, 0.0823	0.0699, 0.1545
Goodness-of-fit (F^2)	1.130	1.044	1.039	1.106
Largest difference in peak, hole (e Å^{-3})	1.911, −1.339	3.070, −2.373	0.732, −0.517	1.780, −0.980

$R_1 = \sum||F_o| - |F_c||/\sum|F_o|$ for observed data ($I > 2\sigma I$).
$wR_2 = \{\sum[w(F_o^2 - F_c^2)^2]/\sum[w(F_o^2)^2]\}^{1/2}$ for all data.

than expected residual peaks of electron density were observed in the Compounds **1**, **2**, and **4**. This arises due to the presence of the large Hg and Cd ions, and the remaining electron peak density ranges from 1.78 to 3.07 in Compounds **1**, **2** and **4**. The location of the peak density in these three structures is as follows: Compound **1**, 1.39 Å from S16; Compound **2**, 1.39 Å from O10; Compound **4**, 1.51 Å from H3B.

We have isolated single crystals of $[Cd(18S4O2)](ClO_4)_2$ and obtained a partial structure of the complex. Using Space Group *P1* yielded a structure with $R_1 = 0.119$ and GOF = 1.08. However, there were disorder problems within the macrocycle for the thioether(S) and ether(O) positions as well as the perchlorate ion. Nevertheless, the structure clearly shows a six-coordinate environment around the Cd(II) center involving the hexadentate 18S4O2 ligand.

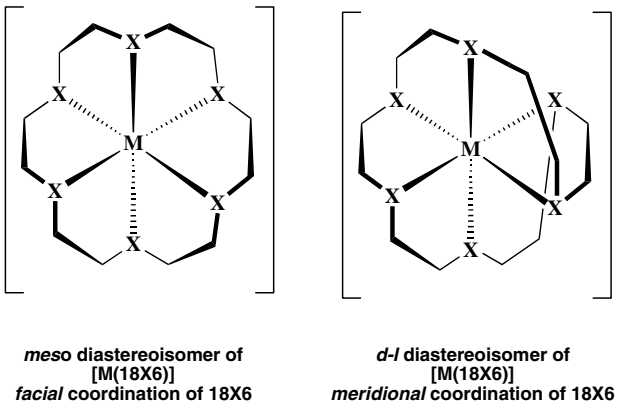

Scheme 2. Possible diastereoisomers of hexacoordinate macrocycles.

3. Results and discussion

3.1. Synthesis and spectra

The homoleptic macrocyclic complexes of Cd(II) and Hg(II) are prepared by substitution of the macrocyclic ligand on the metal ion in the presence of a non-coordinating anion. The formulae of all five new complexes have been confirmed by elemental analyses. Infrared spectra of the complexes show the presence of bands associated with the particular macrocyclic ligand and non-coordinating anion. The proton and ^{13}C NMR spectra for the complexes show all methylene resonances and NH peaks (if present) in the correct ratios, chemical shifts, and splittings. Four new X-ray crystal structures further characterize several of the complexes.

As expected in both the proton and ^{13}C NMR spectra, the methylene groups within the macrocyclic ring that are closer to the more electronegative oxygen or nitrogen appear more downfield compared to the methylene groups attached to the sulfur. In the proton spectrum of $[Hg(9S2O)_2](ClO_4)_2$ we observe a characteristic AA′BB′ splitting pattern of the four methylene protons adjacent to the oxygen donor which split into a symmetrical pattern with a dispersion of 0.2 ppm (see Experimental Supplementary data). This is commonly observed in related 9S3 complexes of transition metals and arises from the non-equivalency of the methylene protons upon complexation [28]. Curiously, none of the other oxa thioether macrocyclic complexes exhibit this distinctive feature, but rather they show other non-first order couplings (see Experimental Supplementary data). As we have noted previously for other Hg(II) and Cd(II) complexes involving thiacrown ligands, all ^{13}C NMR methylene resonances in the ligand show unusual upfield chemical shifts (over 10 ppm in some cases) upon complexation rather than the expected downfield ones [6]. For all Hg(II) and Cd(II) complexes with the two cyclononane macrocycles, we again observe these upfield chemical shifts for several methylene resonances, in some cases 10 ppm relative to free ligand. The methylene resonances in both 18S4O2 complexes also show upfield ^{13}C NMR chemical shifts, but not to the same degree. We have argued that these arise from distortions of the methylene carbons from tetrahedral environments, and again, a similar trend is seen. All four of the structurally characterized complexes show X–C–C angles that average 112°, larger than an ideal tetrahedral value.

For homoleptic hexathia or hexaaza 18X6 complexes (X = S or N–H), two possible diastereoisomers are possible as seen in Scheme 2, a *meso* and a *d-l racemic (*rac) isomer. Based upon the known preference of C–S bonds to adopt *gauche* conformations, the *meso* is the preferred stereoisomer in octahedral 18S6 complexes [29]. A single resonance in the ^{13}C NMR spectrum for the Cd(II) of 18S6 complex is consistent with exclusive presence of the *meso* diastereoisomer. In that regard, we also note our prior work with the related complex $[Hg(18S6)](PF_6)_2$ whose multinuclear NMR spectra as well as its X-ray crystal structure show exclusive *meso* formation [6]. In contrast, the ^{13}C NMR spectrum for the Cd(II) complex with 18N6 shows three equal intensity resonances. This again is consistent with the known contrasting preference of C–N bonds to adopt *anti* conformations, resulting in a preferred *rac* stereoisomer for the azacrown [7,15,30]. Thus, ^{13}C NMR spectroscopy provides an effective tool for diastereoisomer identification for octahedral complexes involving hexadentate macrocycles.

For the *trans* diastereoisomer of $[Cd(9N2S)_2]^{2+}$, a three-line carbon ^{13}C NMR spectrum would be anticipated. In contrast, the *cis* stereoisomer would yield an equal intensity six-line ^{13}C NMR spectrum [31]. For the aza thiacrown complex in CD_3NO_2, we obtain a ^{13}C NMR spectrum best described as a three-line spectrum which is consistent with the crystal structure which shows the *trans* stereoisomer. However, there is an unusual feature. Two near equal intensity singlets appear for the methylene carbons adjacent to each of the two nitrogen donors while the methylene carbons next to the sulfur show a single, more intense peak (see Experimental Supplementary data). As the temperature is raised from 25° to 75°, the peaks broaden resulting in a three-line carbon spectrum and suggesting some type of exchange process involving the ligand is occurring. We propose that there is a modification in the Cd–N bond (possibly through bond rupture and reformation), resulting in a more complex spectrum than would normally be anticipated based upon a simple *trans* positioning of the two sulfur donors. However, an exchange involving the secondary amine protons is also a possible source of the complex NMR pattern.

We have been unsuccessful in our attempts to observe a ^{199}Hg NMR signal in either Hg(II) complex. This failure occurs despite long acquisition times, and our prior experience in making successful ^{199}Hg NMR measurements for these types of complexes [6]. We suggest that ligand exchange of the 9S2O and 18S4O2 macrocycles is the source of the problem. Similarly, we cannot observe a ^{113}Cd NMR signal for either of the two related Cd complexes with oxathia macrocycles, again despite long acquisition times and successful prior measurements [7]. We also do not observe a ^{113}Cd NMR signal for the 18S6 complex. Low solubility might be a possible cause although we would also note our inability to observe a ^{199}Hg NMR signal for the mercury(II) analog [6]. In that case, we proposed that the unusual hexagonal structure of the ligand binding (all six Hg–S bond distances are identical by symmetry restrictions) was the source of the lack of an NMR signal. It is possible that a similar situation may be occurring with the Cd(II) 18S6 complex, but this cannot be confirmed until a crystal structure is obtained. In contrast, we readily were able to measure ^{113}Cd NMR resonances for the two Cd(II) complexes involving amine donors, $[Cd(9N2S)_2]^{2+}$ and $[Cd(18N6)]^{2+}$. These show single peaks with chemical shifts at 521 ppm and 277 ppm, respectively. Combined with our prior

^{113}Cd NMR data for $[Cd(9S3)_2]^{2+}$ (731 ppm, S6 environment) and $[Cd(18S4N2)]^{2+}$ (560 ppm, S4N2 environment), a discernible trend emerges. Each time a secondary amine donor replaces a thioether sulfur donor, there is a progressive upfield chemical shift. Thus, ^{113}Cd NMR can be used as a powerful probe in elucidating coordination environment around a cadmium center.

3.2. X-ray crystal structures

Crystallographic data for the four complexes are presented in Table 1, selected bond distances and angles appear in Table 2, and thermal ellipsoid plots of all four structures are presented in Figs. 1–4.

3.2.1. $[Hg(9S2O)_2](ClO_4)_2 \cdot 2CH_3NO_2$ (**1**)

The complex $[Hg(9S2O)_2](ClO_4)_2 \cdot 2CH_3NO_2$ crystallizes in the monoclinic space group $P2_1/n$ and contains four complex formula units per unit cell which also includes eight perchlorate counter anions and eight nitromethane solvate molecules. The asymmetric unit consists of the mercury(II) ion, situated at an inversion center,

Table 2
Selected lengths (Å)[a] and angles (°)[a] for $[Hg(9S2O)_2](ClO_4)_2 \cdot 2CH_3NO_2$ (**1**), $[Hg(18S4O2)](ClO_4)_2$ (**2**), $[Cd(9S2O)_2](ClO_4)_2 \cdot 2CH_3NO_2$ (**3**), and $[Cd(9N2S)_2](ClO_4)_2$ (**4**)

	1	2	3	4
M–S[b]	2.547(3)	2.558(6)	2.6036(9)	2.6994(17)
	2.551(3)	2.568(6)	2.6063(9)	
	2.635(3)	2.602(4)	2.6223(9)	
	2.649(3)	2.605(4)	2.6370(11)	
M–O[b]	2.733(3)	2.872(6)	2.420(2)	NA
	2.705(3)	2.770(6)	2.433(2)	
Cd–N	NA	NA	NA	2.342(6)
				2.371(6)
S–M–S[b]	134.73(11)	134.00(19)	84.62(3)	180
	106.87(11)	108.08(15)	109.94(3)	
	85.90(10)	86.09(14)	122.06(3)	
	85.27(10)	85.96(15)	106.63(3)	
	111.51(10)	111.99(15)	85.12(3)	
	141.68(10)	138.96(14)	153.12(3)	
O–M–O[b]	77.68(10)	174.41(15)	84.78(8)	NA
N–Cd–N	NA	Na	NA	180
				74.9(2)

[a] Estimated standard deviations are given in parentheses.
[b] M = Hg or Cd.

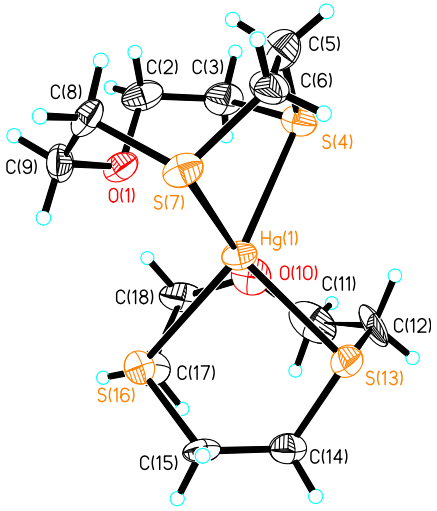

Fig. 1. Thermal ellipsoid perspective (50% probability) of cation in $[Hg(9S2O)_2](ClO_4)_2 \cdot 2CH_3NO_2$ (**1**).

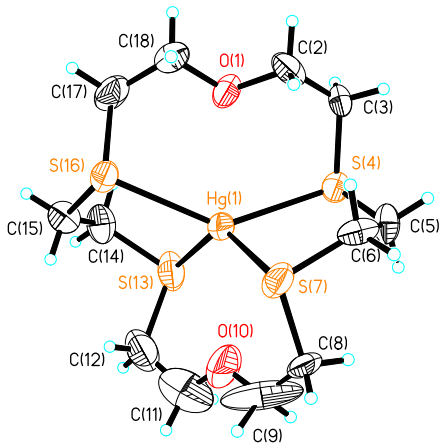

Fig. 2. Thermal ellipsoid perspective (50% probability) of cation in $[Hg(18S4O2)](ClO_4)_2$ (**2**).

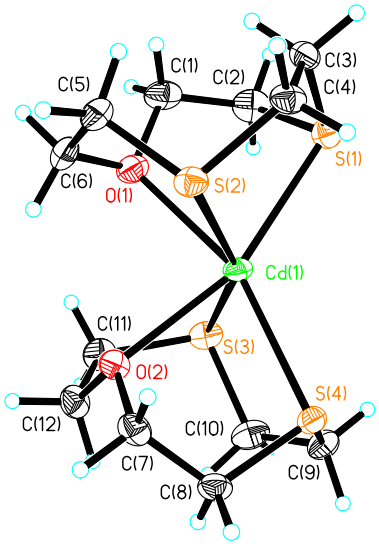

Fig. 3. Thermal ellipsoid perspective (50% probability) of cation in $[Cd(9S2O)_2](ClO_4)_2 \cdot 2CH_3NO_2$ (**3**).

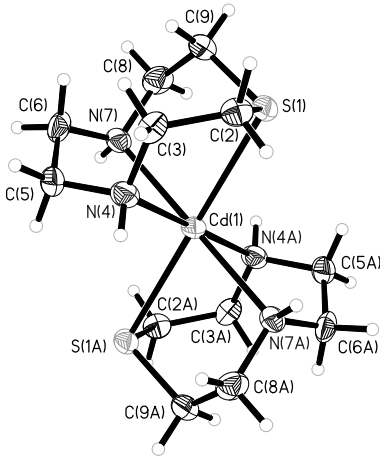

Fig. 4. Thermal ellipsoid perspective (50% probability) of cation in $[Cd(9N2S)_2](ClO_4)_2$ (**4**).

one 9S2O ligand, one anion, and one nitromethane, each occupying general positions within the cell. The four sulfur donors (two each

per macrocycle) form a distorted tetrahedral environment around the four-coordinate mercury center. The Hg–S bond distances range from 2.547(3) Å to 2.649(3) Å with an average of 2.596(3) Å. These are typical bond lengths for a mercury-thioether sulfur in a four-coordinate complex [32,33]. For higher coordination number complexes, longer Hg–S bonds are observed. For example, in the octahedral $[Hg(9S3)_2]^{2+}$ complexes, the Hg–S bond distances average 2.68 Å [34–37]. The two Hg–O distances (2.705(3) and 2.733(3) Å) are longer than any of these Hg–S bonds indicating the lack of oxygen coordination to the Hg center. Indeed, the mean Hg–O bond distance in six-coordinate mercury complexes is reported at 2.39 Å, significantly shorter than what we observe in the complex [32]. Our structural data are also consistent with other reported crystal structures involving oxathia crown complexes with a variety of soft metal ions including Hg(II) [38–40], Ru(II) [41], Pd(II) [42,43], and Ag(I) [44]. Coordination by the ether oxygens to the metal center is never observed in any of these cases. Although the two oxygen atoms are oriented in an *endodentate* fashion in the Hg(II) 9S2O structure, we believe that this a consequence of the ligand conformation and not due to bond formation between the mercury(II) and the hard oxygen donor. The 9S2O ligand adopts the [333] conformation [45], and this particular conformation of the ligand had only been observed previously in the Jahn–Teller distorted bis Cu(II) complex [25]. Interestingly, molecular mechanics calculations on mixed donor tridentate cyclononane ligands have suggested that the [333] conformation is less strained than the [234] conformation by 12–20 kJ/mol [46].

The tetrahedral environment is further demonstrated through the S–Hg–S bond angles (six total). Although these angles range widely from 85.27(10)° to 141.68(10)°, the median of the six is 109.19(10)°, very close to an ideal tetrahedral value. Sulfur atoms S4 and S16 are located 0.928 Å and 0.892 Å, respectively, above the mean tetrahedral plane (defined by the mercury and four sulfur donors) while S7 and S13 lie 0.902 Å and 0.964 Å, respectively, below the plane. Consistent with the difference in complexation behavior between 9S2O and the trithiacrown 9S3, octahedral complexes of $[Hg(9S3)_2]^{2+}$ show S–Hg–S chelate angles no larger than 83°, smaller than the values exhibited here [35]. The O–Hg–O angle is 77.68(10)° which is closer to a *cis* positioning of the oxygen donors and would result in a six line ^{13}C NMR spectrum. However, we obtain a three line ^{13}C NMR spectrum for the complex. The simplicity of that spectrum would be expected only with an exclusive *trans* positioning of the two O donors unless a ligand exchange process were occurring. The combination of the NMR data and the X-ray structure suggest that a ligand exchange of the 9S2O in the mercury complex is indeed occurring in solution.

3.2.2. [Hg(18S4O2)](ClO4)2 (2)

The complex $[Hg(18S4O2)](ClO_4)_2$ crystallizes in the monoclinic space group $P2_1/c$ and contains four complex formula units including eight perchlorate anions, but unlike **(1)**, without any solvate molecules. The asymmetric unit consists of one entire complex along with two anions, occupying general positions within the unit cell. The overall structure is similar to the above bis 9S2O complex in that the four sulfur donors from the macrocycle again form a distorted tetrahedral S4 environment around the Hg(II). The two oxygen donors are at too great of a distance (2.872(6) Å, 2.770(6) Å) to bond with the mercury. The Hg–S bond distances are essentially the same as in the 9S2O complex, ranging from 2.558(6) Å to 2.605(4) Å with an average of 2.596(5) Å. These Hg–S bond distances are again consistent with an S4 mercury(II) coordination environment. Sulfur atoms S4 and S16 lie 0.966 Å and 0.928 Å, respectively, above the mean tetrahedral plane (defined by the mercury and four sulfur donors) while S7 and S13 lie 0.947 Å and 0.987 Å, respectively, below the plane. The tetrahedral structure around the Hg center is best seen in the S–Hg–S angles which range widely from 85.96(15)° to 138.96(14)°, but again show a median value close to an ideal tetrahedral value at 110.04(14)°. The angles again contrast those found in the related octahedral $[Hg(18S6)]^{2+}$ structure where the S–Hg–S angle is 82.21(6)° [6]. It is interesting to note that the *trans* annular oxygen–oxygen distance within the 18S4O2 macrocyclic ring has increased upon complexation, from 5.294 Å in the reported structure of the free ligand to 5.638(9) Å in the Hg(II) structure [21]. We believe that the increase is a consequence of coordination by the macrocycle to the mercury through all four sulfur donors which pushes the oxygen donors further apart. Unlike the bis 9S2O Hg(II) complex which showed *cis* positioning of the two oxygen atoms, the O–Hg–O angle here is *trans* at 174.41(15)° due to the rigid environment of the larger 18-membered ring macrocycle,

3.2.3. [Cd(9S2O)2](ClO4)2 · 2CH3NO2 (3)

The complex $[Cd(9S2O)_2](ClO_4)_2 \cdot 2CH_3NO_2$ crystallizes in the triclinic space group *P-1* and contains two complex formula units per unit cell with four perchlorate anions and four nitromethane solvate molecules. The structure consists of two 9S2O macrocyclic ligands bonded to a Cd^{2+} center, and the asymmetric unit consists of one entire $[Cd(9S2O)_2]^{2+}$ cation, two perchlorates, and two nitromethanes. Unlike the above Hg(II) analog (**1**) or the 18S4O2 Hg complex (**2**), all six donor atoms, four sulfur and two oxygen donors from both 9S2O ligands, are coordinated to the Cd(II) in a highly distorted octahedral structure. To our knowledge, this is the first example of a crystal structure involving a neutral S4O2 environment around a Cd(II) center [47]. The Cd–O bond distances average 2.427(2) Å, significantly shorter than the Hg–O distances in (**1**) and (**2**), respectively. The Cd–S distances do not show large differences, ranging from 2.6039(9) to 2.6370(11) Å, and are slightly longer than the Hg–S distances in the two mercury structures, consistent with a higher coordination number. Thus, there is an interesting contrast between Hg(II) and Cd(II) with regards to how these oxathia ligands are complexing the two heavy metal ions.

The orientation of the coordinated oxygen atoms lies closer to *cis* and not *trans*, but the O1-Cd1-O2 angle is significantly less than 90° (84.78(8)°). There are also other significant deviations overall from an octahedral geometry as pronounced through certain *cis* S–Cd–S angles (S1-Cd1-S4 122.06(3)°, S1–Cd1–S3 106.63(3)°, S2–Cd1–S4 109.94(3)°) as well as the difference in the least-squares planes formed by the ligating atoms of each 9S2O ligand (25.05°). The distortions of the Cd–S4 environment are towards a tetrahedral structure, similar to those observed previously in the six-coordinate Cd(II) 18N2S4 complex [7]. The cyclononane macrocycle adopts the [333] conformation which now appears to be the more common one for 9S2O complexes structures and consistent with the prior molecular mechanics calculations. The open face of the Cd coordination sphere has an interesting approach of a perchlorate (Cl2, O7-O10). This perchlorate is 3.595 Å from Cd center (Cd1-O9), which is the sum of the van der Waals radii plus 0.495 Å. While the perchlorate and Cd obviously do not form a Cd–O bond, a perchlorate–Cd interaction may be important in solution. We have also isolated single crystals of $[Cd(18S4O2)](ClO_4)_2$, but disorder problems prevented a full structural solution. Although not crystallographically acceptable, the partial structure shows a six-coordinate S4O2 environment around the Cd(II) center containing a hexadentate 18S4O24 ligand. This is consistent with the complexation behavior of the 9S2O macrocycle towards Cd(II).

3.2.4. [Cd(9N2S)2](ClO4)2 (4)

The complex $[Cd(9N2S)_2](ClO_4)_2$ crystallizes in the monoclinic space group $P2_1/c$ and contains two complex formula units including four perchlorate anions. No solvent molecules are present, and the two tridentate 9N2S macrocycles are centrosymmetrically oriented around the octahedral Cd center. The asymmetric unit con-

sists of the cadmium(II) ion, situated at an inversion center, one 9N2S ligand and one anion, each occupying general positions within the cell. In contrast to the previous three structures, the complex is octahedral with only a small degree of distortion. Several crystal structures for homoleptic bis complexes with this ligand have been reported including Ni(II) [48], Zn(II) [49], Hg(II) [12], Mn(II) [50], Fe(II) [49,51], and Co(III) [52]. These are generally octahedral as we observe here for Cd(II). However, metal ions such as Cu(II) [53], Pd(II) [54], and Pt(II) [55], which have electronic preferences for other geometries, exhibit bis 9N2S structures which are not octahedral. The 9N2S ligand adopts the [333] conformation, the predominate one that is seen in its complexes. Unlike other tridentate cyclononane ligands such as 9S3 and 9N3, the 9N2S macrocycle is not sufficiently rigid to force a particular stereochemistry on the metal ion, but nevertheless Cd(II) forms an octahedral structure.

The four nitrogen donors and the Cd ion are co-planar, and the *trans* N–Cd–N and S–Cd–S angles are 180° due to symmetry requirements. The *cis* N–Cd–N angle is 74.9(2) ° which is comparable to the N–Cd–N values (75.7(4)°) seen in the structure of the bis Cd(II) complex for the triazacyclononane macrocycle 9N3 [56]. The Cd–S distance is 2.6994(17) Å, the longest metal-sulfur distance among the four structures in our report. The Cd–N distances average 2.356(6) Å, but vary by over 0.03 Å. The longer Cd–N bond (2.371(6) Å) involves the smaller S–Cd–N chelate angle (78.261(14)° versus 79.641(14)°). We believe that the less distorted octahedral structure obtained for the azathia crown is a reflection of the donor properties of the ligand, in particular the Cd–N bond. The weaker Cd–O bonds for the oxathiacrown complex are seen in the distortions as well as in the exchange seen in solution NMR. To our knowledge, this is only the second reported Cd(II) structure containing a N4S2(thioether) coordination environment [47]. Bebout and co-workers have recently reported the structure for the bis Cd(II) complex of bis(2-methylpyridyl)sulfide [57]. Their structure also shows a six-coordinate Cd(II), but it is much more distorted with the two thioether sulfur atoms (from two different ligands) arranged in a *cis*, not *trans* orientation, with a S–Cd–S angle of 126.264(19)°. We propose that the difference in complexation behavior between the two ligands arises from the different types of nitrogen donors (sp^2 N in the pyridyl ligands versus sp^3 N in 9N2S) as well as the rigidity of the cyclononane macrocycle.

4. Conclusions

The mixed oxathia macrocycles 9S2O and 18S4O2 complex Hg(II) and Cd(II) to form homoleptic complexes, but different coordination behavior is seen between the two heavy metals. For Hg(II), S4 tetrahedral structures are obtained which do not involve oxygen coordination, but for Cd(II), all six donor atoms coordinate in highly distorted structures. All four of the heavy metal complexes with oxathia macrocycles exhibit fluxional ligands in solution. We also report the structure of bis(9N2S (1,4-diaza-7-thiacyclononane))cadmium(II) which shows octahedral coordination in a *trans*-N4S2 environment. The macrocycles 18N6 and 18S6 show hexadentate coordination to Cd(II) with stereoisomer preference determined by the conformations of the individual C–X bonds for the ligand. Lastly, we note a trend in ^{113}Cd NMR chemical shifts that shows progressive upfield shifts as secondary amine N donors replace thioether S donors.

Acknowledgements

This research was generously supported by grants from the Petroleum Research Fund, administered by the American Chemical Society, the Grote Chemistry Fund, the National Science Foundation RUI Program, and the Research Corporation.

Appendix A. Supplementary data

CCDC 686739, 686740, 686741 and 686742 contain the supplementary crystallographic data for $Hg(9S2O)_2](ClO_4)_2 \cdot 2CH_3NO_2$ (**1**), $[Hg(18S4O2)](ClO_4)_2$ (**2**), $[Cd(9S2O)_2](ClO_4)_2 \cdot 2CH_3NO_2$ (**3**), and $[Cd(9N2S)_2](ClO_4)_2$ (**4**). These data can be obtained free of charge via http://www.ccdc.cam.ac.uk/conts/retrieving.html, or from the Cambridge Crystallographic Data Centre, 12 Union Road, Cambridge CB2 1EZ, UK; fax: (+44) 1223-336-033; or e-mail: deposit@ccdc.cam.ac.uk. Supplementary data associated with this article can be found, in the online version, at doi:10.1016/j.poly.2008.07.005.

References

[1] P. Vernet, Heavy Metals in the Environment, Elsevier Science, New York, 1991.
[2] M. Borsari, in: R.B. King (Ed.), Encyclopedia of Inorganic Chemistry, Wiley, New York, 1994, p. 455.
[3] T.F. Baumann, J.G. Reynolds, G.A. Fox, J. Chem. Soc., Chem. Commun. (1998) 1637.
[4] The use of this polystyrene-linked pentathiacrown for the removal of Hg(II) was subsequently patented: T.F. Baumann, J.G. Reynolds, G.A. Fox, PCT Int. Appl. WO 2000052004, 2000.
[5] L. Prodi, C. Bargossi, M. Montalti, N. Zaccheroni, N. Su, J.S. Bradshaw, R.M. Izatt, P.B. Savage, J. Am. Chem. Soc. 122 (2000) 6769.
[6] M.L. Helm, G.H. Helton, D.G. VanDerveer, G.J. Grant, Inorg. Chem. 44 (2005) 5696.
[7] M.L. Helm, J.P. Lee, L.L. Hill, D.G. VanDerveer, G.J. Grant, J. Chem. Soc., Dalton Trans. (2006) 3534.
[8] P.S. Pregosin, in: P.S. Pregosin (Ed.), Transition Metal Nuclear Magnetic Resonance, Elsevier, New York, 1991, p. 293. p. 306 and references cited therein.
[9] M.F. Summers, Coord. Chem. Rev. 86 (1988) 43.
[10] P.D. Ellis, Science 221 (1983) 1141.
[11] G.J. Grant, in: D.A. Atwood (Ed.), Structure and Bonding, Recent Developments in Mercury Science, Springer, Berlin, 2006, pp. 107–142.
[12] J.P. Danks, N.R. Champness, M. Schröder, Coord. Chem. Rev. 174 (1998) 417.
[13] M.W. Glenny, L.G.A. van de Water, W.L. Dreissen, J. Reedijk, A.J. Blake, C. Wilson, M. Schröder, J. Chem. Soc, Dalton Trans. (2004) 1953.
[14] U. Heinzel, R. Mattes, Polyhedron 11 (1992) 597.
[15] A.J. Blake, G. Reid, M.M. Schröder, Polyhedron 9 (1990) 2931.
[16] A. Tamayo, B. Pedras, C. Lodeiro, L. Escriche, J. Casabó, J.L. Capelo, B. Covelo, R. Kikekâs, R. Sillianpaa, Inorg. Chem. 46 (2007) 7818.
[17] S. Yoon, A.E. Albers, A.P. Wong, C.J. Chang, J. Am. Chem. Soc. 127 (2005) 16030.
[18] M. Kadarkaraisamy, A.G. Sykes, Polyhedron 26 (2007).
[19] A. Coskun, E.U. Akkaya, J. Am. Chem. Soc. 128 (2006) 144474.
[20] H.G. Lee, J.-E. Lee, K.S. Choi, Inorg. Chem. Commun. 9 (2006) 582.
[21] G.J. Grant, D.F. Galas, M.W. Jones, K.D. Loveday, W.T. Pennington, G.S. Schimek, C.T. Eagle, D.G. VanDerveer, Inorg. Chem. 37 (1998) 5299.
[22] C.R. Lucas, W. Liang, D. O Miller, J.N. Bridson, Inorg. Chem. 36 (1997) 4508.
[23] C.A. Grapperhaus, M. Li, E.R. Gibson, M.S. Mashuta, J. Chem. Cryst. 34 (2004) 5.
[24] P. Hoffmann, A. Steinhoff, R. Mattes, Z. Nautrforsch. B, Chem. Sci. 42b (1987) 867.
[25] G.J. Grant, M.W. Jones, D.G. VanDerveer, W.T. Pennington, L.F. Mehne, Inorg. Chim. Acta 300 (2000) 250.
[26] The programs used for data collection, solution and refinement of this structure were: CRYSTALCLEAR 1.3, Rigaku/MSC. The Wooddlands, TX, USA, 1998–2006.
[27] SHELXTL 6.10, Bruker-AXS, Madison, WI, USA, 2000.
[28] A.J. Blake, Y.V. Roberts, M. Schröder, J. Chem. Soc., Dalton Trans. (1996) 1885.
[29] R.E. Wolf, J.A.R. Hartman, J.M.E. Storey, B.M. Foxman, S.R. Cooper, J. Am. Chem. Soc. 109 (1987) 4328.
[30] D.J. Royer, G.J. Grant, D.G. VanDerveer, M.J. Castillo, Inorg. Chem. 21 (1982) 1902.
[31] L.R. Gahan, T.W. Hambley, G.H. Searle, M.J. Bjerrum, E. Larsen, Inorg. Chim. Acta 147 (1988) 17.
[32] C.E. Holloway, M. Melnik, Main Group Met. Chem. 11–12 (1994) 99.
[33] W.N. Setzer, Y. Tang, G.J. Grant, D.G. VanDerveer, Inorg. Chem. 30 (1991) 3652.
[34] A.J. Blake, A.J. Holder, T.I. Hyde, G. Reid, M. Schröder, Polyhedron 8 (1989) 2041.
[35] W.N. Setzer, Q. Guo, G.J. Grant, J.L. Hubbard, R.S. Glass, D.G. VanDerveer, Heteroat. Chem. 1 (1990) 317.
[36] J. Pickardt, J. Shen, Z. Naturforsch. B 48 (1993) 969.
[37] W. Wilhelm, S. Deeken, E. Berseen, W. Saak, A. Lützen, A. Kock, H. Strasdeit, Eur. J. Inorg. Chem. (2004) 2301.
[38] K.N. Dalley, S.B. Larson, Acta Crystallogr., Sect. B 37 (1981) 2225.
[39] S.Y. Lee, S. Park, H.J. Kim, H.H. Jung, S.S. Lee, Inorg. Chem. 47 (2008), published online, 02/14/2008.
[40] A.J. Blake, S. Parsons, C. Radek, M. Schröder, Acta Crystallogr., Sect. C C52 (1996) 21.
[41] A.J. Blake, C. Radek, M. Schröder, Acta Crystallogr., Sect. C 52 (1996) 1401.

[42] A.J. Blake, G. Reid, M. Schröder, J. Chem. Soc., Dalton Trans. (1990) 3849.
[43] A.J. Blake, R.O. Gould, C. Radek, M. Schröder, J. Chem. Soc., Dalton Trans. (1995) 4046.
[44] C.R. Lucas, S. Liu, Inorg. Chim. Acta 230 (1995) 133.
[45] For a definition of this nomenclature, see: J. Dale, Acta Chem. Scand. 27 (1973) 1115.
[46] R.D. Hancock, S.M. Dobson, J.C.A. Boeyens, Inorg. Chim. Acta 133 (1987) 221.
[47] The Cambridge Structural Database Version 5.29, 2008 release. There are five reported structures which contain S4O2 ligand donor environments around Cd(II). However, all of these involve oxoanion ligand donors, and not neutral oxygen donors as described here.
[48] S.M. Hart, J.C.A. Boeyens, J.P. Michael, R.D. Hancock, J. Chem. Soc., Dalton Trans. (1983) 1601.
[49] U. Heinzel, A. Henke, R. Mattes, J. Chem. Soc., Dalton Trans. (1997) 501.
[50] L.R. Gahan, V.A. Grillo, T.W. Hambley, G.R. Hanson, C.J. Hawkins, E.M. Proudfoot, B. Moubaraki, K.S. Murary, D. Wang, Inorg. Chem. 35 (1996) 1039.
[51] V.A. Grillo, L.R. Gahan, G.R. Hanson, R. Stranger, T.W. Hambley, K.S. Murray, B. Moubaraki, J.D. Cashion, J. Chem. Soc., Dalton Trans. (1998) 2341.
[52] T.W. Hambley, L.R. Gahan, G.H. Searle, Acta Crystallogr., Sect. C 45 (1989) 864.
[53] J.C.A. Boeyens, S.M. Dobson, R.D. Hancock, Inorg. Chem. 24 (1985) 3073.
[54] P. Hoffmann, R. Mattes, Z. Naturforsch. 43b (1988) 261.
[55] U. Heinzel, R. Mattes, Inorg. Chim. Acta 194 (1992) 157.
[56] H. Strasdeit, A.-K. Duhme, M. Weber, S. Pohl, Acta Crystallogr., Sect. C 48 (1992) 437.
[57] S.M. Berry, D.C. Bebout, R.J. Butcher, Inorg. Chem. 44 (2005) 27.

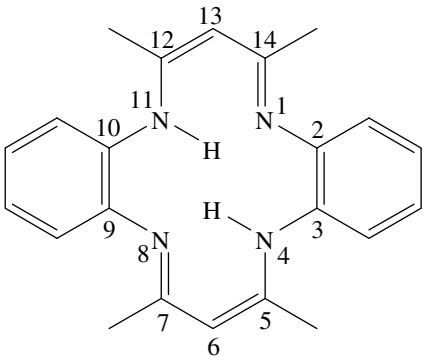

Fig. 1. Suggested structure of H_2tmtaa.

groups through such substitution reactions, this offers an attractive method for the synthesis of novel receptors of higher complexity.

The "sandwich compound", ferrocene (Fc), and its derivatives are today universally being studied in the fields of medicine [35], biosensors [36], asymmetric catalysts [37], redox agents [38], photoactive agents [39] and so on for their favorable electrochemical properties. Our attention has been directed towards the synthesis of ferrocene derivatives of Nitmtaa for the addition of extended functionality. In order to study the electrochemistry behaviors between the completely conjugated system of tmtaa and electroactive ferrocene, we grafted one and two ferrocenes on the γ,γ' positions of Nitmtaa through carbonyl groups to acquire two complexes {[(η-C_5H_5)Fe(η-C_5H_4)(CO)](\(C_{22}H_{21}N_4\))Ni} (**1**) and {[(η-C_5H_5)Fe(η-C_5H_4)(CO)]$_2$-(\(C_{22}H_{20}N_4\))Ni} (**2**), respectively (Fig. 2). The electrochemical properties of complexes **1** and **2** have been studied using cyclic voltammetry (CV). The X-ray crystal structure of **1** is also presented here.

2. Experimental

2.1. Reagents and physical measurements

All solvents were distilled and all chemicals were of reagent grade. Nitmtaa [3] and ferrocenoyl chloride (FcCOCl) [40] were prepared according to the literature methods. Thin-layer chromatography (TLC) was performed on commercial Merck plates coated with a 0.20 mm layer of an alumina gel (Wako Pure Chemical Industries Ltd.: B-10) to separate and purify the products.

Elemental analyses were performed on a Yanaco CHN corder MT-3. IR spectra (4000–400 cm^{-1}) were recorded on a JASCO FT/IR-400 spectrophotometer in KBr pellets at room temperature (r.t.). FAB^+ mass spectra were carried out with a JEOL JMSSX102A gas chromatograph–mass spectrometer in a 2-nitrophenyloctylether matrix. Ultraviolet and visible spectra were recorded on a Shimadzu UV-200S double beam spectrophotometer in chloroform at r.t. DSC data were obtained using a Shimadzu DSC-50 differential calorimeter. ^{1}H NMR measurements were taken on a BRUKER AVANCE-400 in chloroform-*d* and chemical shifts are given in ppm relative to tetramethylsilane as an internal reference standard.

2.2. Syntheses of complexes *1* and *2*

After the solution of Nitmtaa (0.626 g, 1.56 mmol) and triethylamine (2 mL) in dry toluene (50 mL) was stirred at r.t. under nitrogen atmosphere for 10 min, a solution of FcCOCl (0.384 g, 1.55 mmol) in dry toluene (50 mL) was slowly added dropwise and the reaction mixture was further stirred at 80 °C for 12 h. After being cooled to r.t., the solution was filtered to eliminate the hydrochloride of triethylamine. Evaporating the filtrate resulted in a dark green powder. The powder was purified and separated on a large-scale alumina gel TLC using dichloromethane–hexane (4:1 v/v) as the developing solution. The products were recrystallized from dichloromethane and hexane to give green micro-crystals of **1** and **2**, respectively.

Complex **1**, yield: 0.213 g (22.3%). *Anal.* Calc. for \(C_{33}H_{30}FeN_4NiO\) (613.16): C, 64.64; H, 4.93; N, 9.14. Found: C, 64.58; H, 4.88; N, 9.19%. M.p.: 333–336 °C (DSC). UV ($CHCl_3$, r.t., λ_{max}/nm): 390, 583. IR (KBr, cm^{-1}): ν(C=O) 1635; ν(C=C, C=N) 1527, 1386. FAB^+ MS: $m/z = 612$ (M), 399 (M−FcCO). ^{1}H NMR ($CDCl_3$, ppm): δ 2.01 (s, 6H, CH_3-γ), 2.13 (s, 6H, CH_3-γ'), 4.26 (s, 5H, η-C_5H_5), 4.55 (t, $J = 2.0$ Hz, 2H, η-C_5H_4), 4.91 (t, $J = 2.0$ Hz, 2H, η-C_5H_4), 6.57 (t, $J = 7.2$ Hz, 2H, C_6H_4), 6.61 (t, $J = 7.3$ Hz, 2H, C_6H_4), 6.67 (d, $J = 7.2$ Hz, 2H, C_6H_4), 6.71 (d, $J = 7.3$ Hz, 2H, C_6H_4).

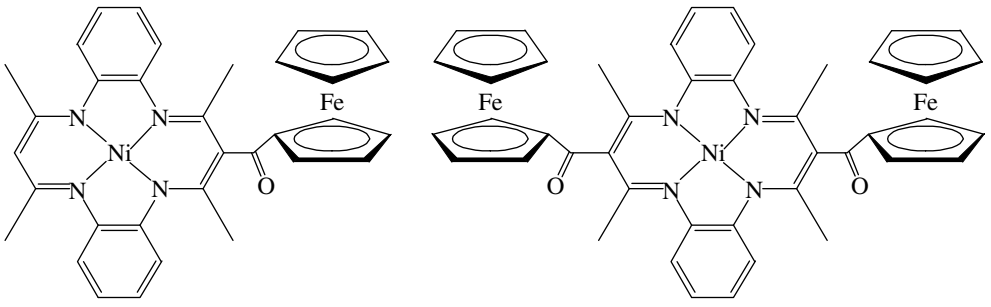

1 **2**

Fig. 2. Complexes **1** and **2**.

Complex **2**, yield: 0.230 g (17.9%). *Anal.* Calc. for $C_{44}H_{38}Fe_2N_4NiO_2$ (825.18): C, 64.04; H, 4.64; N, 6.79. Found: C, 64.18; H, 4.53; N, 6.75%. M.p.: 340–343 °C (DSC). UV ($CHCl_3$, r.t., λ_{max}/nm): 391, 585. IR (KBr, cm^{-1}): ν(C=O) 1628; ν(C=C, C=N) 1525, 1374. FAB^+ MS: $m/z = 824$ (M), 611 (M−FcCO), 399 (M−2FcCO). ^1H NMR ($CDCl_3$, ppm): δ 2.13 (s, 12H, CH_3), 4.30 (s, 10H, η-C_5H_5), 4.59 (t, $J = 2.0$ Hz, 4H, η-C_5H_4), 4.94 (br, 4H, η-C_5H_4), 6.60–6.72 (m, 8H, C_6H_4).

2.3. Electrochemical measurements

Cyclic voltammograms were collected using a Yanaco POLAROGRAPHIC ANALYZER P-1100 potentiostat at r.t. A typical three-electrode configuration was used, where the working electrode was glass carbon, a platinum wire was used as the counter electrode and a Saturated Calomel Electrode (SCE, Hg/Hg_2Cl_2, KCl-saturated) was the reference electrode. All samples for electrochemical analysis were prepared in CH_2Cl_2 (being refined in accordance with the standard method) at a concentration of 2×10^{-4} M. The supporting electrolyte was tetra-*n*-butylammonium perchlorate (*n*-Bu_4NClO_4) and its concentration was 1×10^{-1} M. The scan rate was 200 mV s^{-1} and the scanning scope was from 0 to 1.6 V.

Table 1
Details of the crystal data, data collection and refinement for **1**

Empirical formula	$C_{33}H_{30}FeN_4NiO$
Formula weight	613.17
Crystal color	green
Habit	chunk
Crystal dimensions (mm^3)	0.30 × 0.20 × 0.20
Crystal system	triclinic
Space group	$P\bar{1}$
No. of reflections used for unit cell determination (2θ range)	25 (20.4–26.0°)
Lattice parameters	
a (Å)	10.904(2)
b (Å)	11.512(2)
c (Å)	12.488(2)
α (°)	100.57(1)
β (°)	105.19(1)
γ (°)	111.66(1)
Cell volume ($Å^3$)	1335.7(4)
Z	2
T (K)	273(2)
F(000)	636
D_{calc} (g cm^{-3})	1.524
Diffractometer	Rigaku AFC-7R
Radiation	Mo Kα ($\lambda = 0.71069$ Å) graphite monochromated
Scan type	ω–2θ
$2\theta_{max}$ (°)	56.0
μ (mm^{-1})	1.28
Reflections collected	6768
Independent reflections	6451
Observed reflections	4517 [$F^2 > 2.0\sigma(F^2)$]
No. of refined parameters	482
$R(F)$	0.0366
$\omega R(F^2)$	0.1095
Goodness of fit indicator	1.038
Max shift/error in final cycle	0.003
Δ/σ_{max}	0.0027
$\Delta\rho_{max}, \Delta\rho_{max}$ (e $Å^{-3}$)	0.55, −0.56

2.4. X-ray crystal structure analysis

Crystals of **1** are stable in air. A dark green crystal of **1** was measured on a Rigaku AFC7R diffractometer equipped with a rotating anode generator using monochromated Mo Kα radiation ($\lambda = 0.71069$ Å). The structure of **1** was solved by direct methods [41] and expanded using the Fourier technique [42]. The non-hydrogen atoms were refined with anisotropic thermal parameters. Crystal data and details associated with data collection of **1** are summarized in Table 1.

3. Results and discussion

3.1. Syntheses and spectra

One and two [(η-C_5H_5)Fe(η-C_5H_4)(CO)] grafted tmtaa Ni(II) complexes **1** and **2** were simultaneously synthesized from the reaction of FcCOCl and Nitmtaa in a 1:1 molar ratio and the yields were 22.3% and 17.9%, respectively. In order to obtain the one [(η-C_5H_5)Fe(η-C_5H_4)(CO)] substituted complex **1** in a higher yield, the reaction was performed with a 1:2 molar ratio of FcCOCl and Nitmtaa, in which the yield of **1** increased to 30.3%. Since the spots of the products and the starting reactant, Nitmtaa, were very close in the column chromatography, purification of **1** and **2** could not be achieved favorably by using column chromatograph. Thus, the purification was carried out by large-scale TLC. However, if the molar ratio of the reactants, FcCOCl and Nitmtaa, was changed to 4:1, the two [(η-C_5H_5)Fe(η-C_5H_4)(CO)] substituted complex **2** could be obtained separately in a higher yield and the purification could be achieved by short column chromatography. Crystals of **1** suitable for X-ray structure analysis were grown in a dichloromethane–hexane (1:1 v/v) solution at r.t. Unfortunately a single crystal of **2** was not obtained.

Complexes **1** and **2** were characterized by ^1H NMR, IR, MS spectra, element analyses and DSC measurements. The electronic absorption spectra for Nitmtaa, **1** and **2** were measured in chloroform solution at r.t. The spectrum of Nitmtaa showed two absorption bands at ca. 393 and 581 nm (shoulder), attributed to a $\pi \rightarrow \pi^*$ transition within the ligand and a $d \rightarrow d^*$ transition from the central metal to the ligand, respectively. After the Fc groups were introduced to Nitmtaa, great changes of the electronic absorption spectra should be observed because of the distinctive electronic characteristics of Fc. Nevertheless, comparing the electronic absorption spectra of **1** [ca. 390 and 583 nm (shoulder)] and **2** [ca. 391 and 584 nm (shoulder)] with that of Nitmtaa, almost no changes were observed. Hence, only judging from the electronic absorption spectra, there was almost no influence to the ligand and the central metal when the Fc groups were introduced to Nitmtaa.

This may be due to the spatial structures of complexes **1** and **2**. In complex **1**, the symmetry axis of ferrocene is almost parallel to the cyclic tmtaa (see Section 3.2) and the impact to this conjugated system is extraordinarily small. Because almost no new charge transition bands were observed, it is difficult to appraise the interaction of Fc and the tmtaa ring or central metal from the electronic absorption spectra.

3.2. Crystal structure of complex 1

A structural representation of **1** is shown in Fig. 3. Selected bond lengths and bond angles are given in Table 2. In the molecular structure of **1**, the non-planar, saddle-shaped geometry reported for the free ligand, H_2tmtaa, is almost retained in the tmtaa moiety of the complex. Ni(II) coordinates to four nitrogen atoms of tmtaa to form a four-coordinated complex. The N1–Ni1–N3 and N2–Ni1–N4 angles are 176.34(10)° and 178.06(9)°, respectively, showing that the Ni atom is almost in the same plane as that of N_4. The displacement of the nickel center out of the N_4 plane is only 0.061(5) Å. The mean Ni–N bond distance is 1.866 Å. In **1**, the C–N and C–C bond distances in the chelate ring are from 1.336(4) to 1.419(4) Å and from 1.400(5) to 1.416(4) Å, respectively, showing obvious differences from those in Nitmtaa, in which the C–N and C–C bond distances range from 1.324 to 1.342 Å and from 1.394 to 1.408 Å, respectively [43]. This may be due to the spatial interaction between the nickel complex and ferrocene.

Ferrocene was grafted onto the methine of the tmtaa nickel complex through a carbonyl group. The two cyclopentadieny (Cp) rings are virtually parallel to each other. The average distances of Fe to the C atoms of the Cp rings (2.041(4) Å in the substituted Cp ring and 2.043(4) Å in the unsubstituted Cp ring) are normal and compare well with those of other ferrocenoyl structures [44]. The average C–C–C angles in two Cp rings are the same (108.0(3)°). Interestingly, the Cp internal average C–C bond distance in the substituted Cp ring (1.417(5) Å) is longer than that in the unsubstituted Cp ring (1.407(5) Å). The distance of the carbonyl carbon to the Cp ring (C(23)–C(24): 1.479(4) Å) is a normal C–C single bond distance. The carbonyl C═O distance (1.220(4) Å) compares well with those of other ferrocenoyl structures. The symmetry axis of the ferrocene is almost parallel to the nickel tmtaa complex moiety. The dihedral angle between the N_4 plane in the nickel complex and the grafted Cp ring (C24–C25–C26–C27–C28) in the ferrocene is 98.5°, while the dihedral angle between the iminato fragment in the Nitmtaa moiety and the Cp ring is 71.6°. Apparently, this difference is caused by the non-planar, saddle-shaped geometry of the Nitmtaa moiety.

Table 2
Selected geometric parameters (Å, °) for **1**

Ni1–N1	1.859(2)	C1–C23	1.515(4)
Ni1–N2	1.862(3)	O1–C23	1.220(4)
Ni1–N3	1.873(2)	C23–C24	1.479(4)
Ni1–N4	1.870(3)		
av Fe1–C for CpR	2.041(4)	av Fe1–C for Cp	2.043(4)
av C–C for CpR	1.417(5)	av C–C for Cp	1.407(5)
N1–Ni1–N2	92.96(10)	N1–Ni1–N3	176.34(10)
N2–Ni1–N3	85.61(10)	N2–Ni1–N4	178.06(9)
N3–Ni1–N4	95.79(10)	C1–C23–O1	121.8(3)
N4–Ni1–N1	85.56(10)	C24–C23–O1	120.3(3)
		C1–C23–C24	117.9(2)
av C–C–C for CpR	108.0(3)	av C–C–C for Cp	108.0(3)

3.3. Electrochemical properties of complexes *1* and *2*

The electrochemical behaviors of related compounds including **1** and **2** were investigated by the cyclic voltammetric technique in $CH_2Cl_2/1 \times 10^{-1}$ M n-Bu_4NClO_4 using a glass carbon working electrode. The scan rate

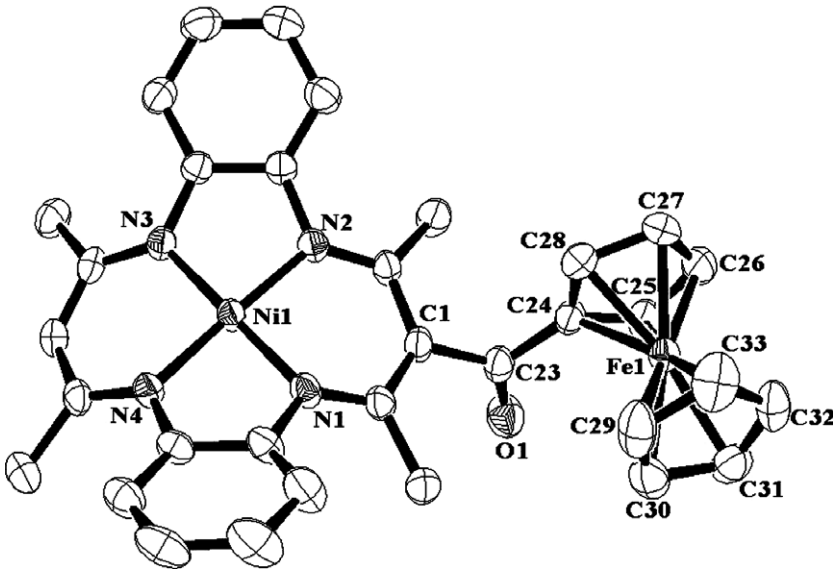

Fig. 3. ORTEP drawing of **1**. The thermal ellipsoids are drawn at the 50% probability level. The H atoms are omitted for clarity.

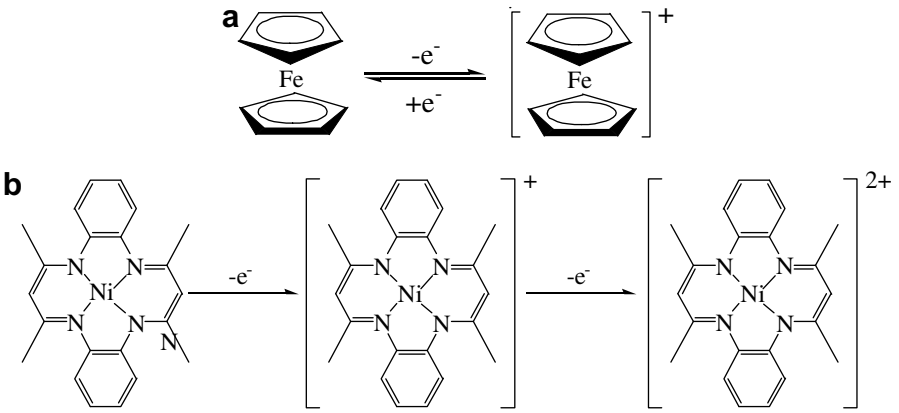

Scheme 1. The redox processes with a scanning scope from 0 to 1.6 V in the CV experiments. (a) The redox process of Fc. (b) The oxidation process of Nitmtaa.

was 200 mV s^{-1} and the scanning scope was from 0 to 1.6 V. As a contrast, cyclic voltammetries of the free Fc and Nitmtaa were also carried out under similar conditions. The CV experiments in CH_2Cl_2/*n*-Bu_4NClO_4 indicate a totally reversible one-electron oxidation–reduction of Fc ($E_{Pa} = 0.61$ V, $E_{Pc} = 0.38$ V versus SCE, $\Delta E_p = 0.23$ V). While the cyclic voltammogram of Nitmtaa shows an irreversible two-electron oxidation. The first and second oxidation potentials are 0.61 and 1.20 V versus SCE, respectively. The oxidation–reduction process of Fc and the oxidation process of Nitmtaa are shown in Scheme 1. Under our experiment conditions, free Fc shows a good reversible one-electron oxidation–reduction process. The oxidation wave corresponds to the Fe(II) → Fe(III) process and the reduction wave corresponds to the Fe(III) → Fe(II) process. However, in the cyclic voltammogram of free Nitmtaa, two oxidation potential peaks ($E^1_{Pa} = 0.61$ V, $E^2_{Pa} = 1.20$ V) were observed, while no reduction potential peaks were observed. To the best of our knowledge, central metals in tmtaa complexes may not be oxidized or reduced easily because of the π electron conjugated system of tmtaa ring. Up until now, no literature has conclusively proved that the central metals in tmtaa complexes can be oxidized or reduced. Thus, we consider that the π electron conjugated system of the tmtaa ring is oxidized in the CV experiments. The oxidation waves correspond to $tmtaa^{2-} \rightarrow tmtaa^{-}$ and $tmtaa^{-} \rightarrow tmtaa$ processes, respectively.

Table 3
Electrochemical parameters[a] of **1**, **2** and CH_3COFc at r.t. in CH_2Cl_2 with a concentration of 2×10^{-4} M, supporting electrolyte *n*-Bu_4NClO_4 with a concentration of 1×10^{-1} M

Compound	E_{Pa}		E_{Pc}		ΔE^1_{Pa} (V)[c]
	E^1_{Pa} (V)	E^2_{Pa} (V)	E^1_{Pc} (V)	E^2_{Pc} (V)	
1	0.85	1.50	0.63	1.20	−0.05
2	0.84	1.33	0.62	1.14	−0.06
CH_3COFc	0.90[b]		0.60[b]		

[a] Maximum error ±6%; all potentials are measured against SCE reference electrode.
[b] The cyclic voltammogram of CH_3COFc shows a reversible one-electron oxidation reduction, thus, only E_{Pa} and E_{Pc} data are listed in the table.
[c] $\Delta E^1_{Pa} = E^1_{Pa,complex} - E_{Pa,CH_3COFc}$.

In **1** and **2**, one and two ferrocenes connect with Nitmtaa through carbonyl groups, respectively. In order to investigate the electrochemical behaviors between the completely conjugated system of Nitmtaa and ferrocene-containing substituted groups in **1** and **2**, cyclic voltammetries of **1**, **2** and acetylferrocene (CH_3COFc), an analogue of the substituted groups (–COFc) in **1** and **2**, were carried out under similar conditions. Because CH_3COFc and the

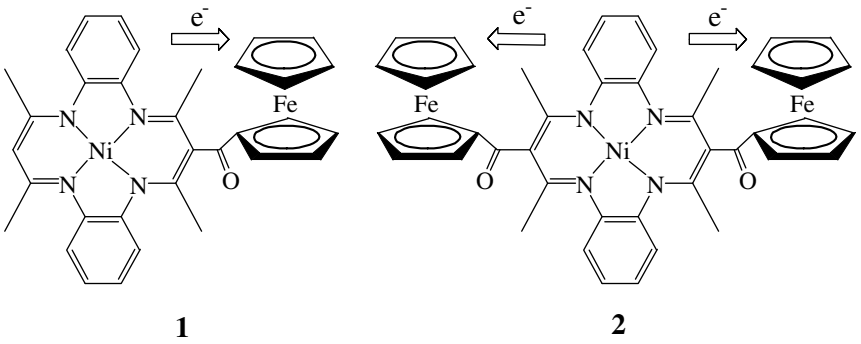

Fig. 4. The proposed electron flows in **1** and **2**.

substituted groups (–COFc) in **1** and **2** all contain electron withdrawing carbonyl groups and electroactive Fc, we consider it is significant to investigate the electrochemical property of CH_3COFc instead of the –COFc groups in **1** and **2**. All the electrochemical data are summarized in Table 3. Both **1** and **2** show a reversible two-electron oxidation–reduction, which is different from those of free Nitmtaa and Fc. Furthermore, the cyclic voltammogram of CH_3COFc shows a totally reversible one-electron oxidation–reduction, which is similar to that of free Fc. However, its oxidation and reduction potentials are higher than those of free Fc. The differences of the first oxidation potentials of **1** and **2** to the oxidation potential of CH_3COFc are −0.05 and −0.06 V, respectively. Although these potential differences are very tiny, the minus values still hint that electrons flow from the π electron conjugated system of the tmtaa ring to the ferrocenes in **1** and **2** (Fig. 4), which means that the ferrocenes act as electron acceptors in **1** and **2**. This is reverse to the fact that Fc is often used as an electron donator. In **1** and **2**, Nitmtaa and Fc are connected through carbonyl groups. The carbonyl group is an electron withdrawing group and perhaps it facilitates electrons flowing from Nitmtaa to Fc.

4. Conclusions

In summary, two ferrocene-containing tmtaa nickel complexes, $\{[(\eta\text{-}C_5H_5)Fe(\eta\text{-}C_5H_4)(CO)](C_{22}H_{21}N_4)Ni\}$ (**1**) and $\{[(\eta\text{-}C_5H_5)Fe(\eta\text{-}C_5H_4)(CO)]_2(C_{22}H_{20}N_4)Ni\}$ (**2**), were simultaneously synthesized from the reaction of FcCOCl and Nitmtaa in a 1:1 molar ratio. **1** and **2** are the first examples of tmtaa complexes in which ferrocenes are introduced. The single crystal structure of **1** was determined. In **1**, the symmetry axis of ferrocene is almost parallel to the tmtaa nickel complex moiety. The electrochemical properties of **1** and **2** were investigated using the cyclic voltammetric technique and the results suggest that the ferrocenes act as electron acceptors in the complexes.

Acknowledgements

This work was sponsored by the Scientific Research Foundation for the Returned Overseas Chinese Scholars, State Education Ministry (51101024) and the National Natural Science Foundation of China (20771059). We are also grateful to the Center for Instrumental Analysis, Kyushu Institute of Technology, Japan for the X-ray structure determination.

Appendix A. Supplementary data

CCDC 287154 contains the supplementary crystallographic data for **1**. These data can be obtained free of charge via http://www.ccdc.cam.ac.uk/conts/retrieving.html, or from the Cambridge Crystallographic Data Centre, 12 Union Road, Cambridge CB2 1EZ, UK; fax: (+44) 1223-336-033; or e-mail:deposit@ccdc.cam.ac.uk. Supplementary data associated with this article can be found, in the online version, at doi:10.1016/j.poly.2008.01.034.

References

[1] F.A. Cotton, J. Czuchajowska, Polyhedron 9 (1990) 2553.
[2] P. Mountford, Chem. Soc. Rev. 27 (1998) 105.
[3] E.G. Jäger, Z. Anorg. Chem. 364 (1969) 177.
[4] P.J. Lukes, A.C. McGregor, T. Clifford, J.A. Crayston, Inorg. Chem. 31 (1992) 4697.
[5] D.A. Atwood, V.O. Atwood, A.H. Cowley, H.R. Gobran, J.L. Atwood, Inorg. Chem. 32 (1993) 4671.
[6] Z. Wang, K. Sakata, M. Hashimoto, T. Moriguchi, A. Tsuge, Synth. React. Inorg. Met.-Org. Chem. 30 (2000) 73.
[7] X. Shen, K. Sakata, M. Hashimoto, Polyhedron 21 (2002) 969.
[8] X. Shen, A. Nakashima, K. Sakata, M. Hashimoto, Inorg. Chim. Acta 375 (2004) 3510.
[9] D. Mandon, J. Giraudon, L. Toupet, J. Sala-Pala, J.E. Guerchais, J. Am. Chem. Soc. 109 (1987) 3490.
[10] P. Berno, C. Floriani, A. Chiesi-Villa, C. Guastini, J. Chem. Soc., Dalton Trans. (1989) 551.
[11] F.A. Cotton, J. Czuchajowska, X. Feng, Inorg. Chem. 29 (1990) 4329.
[12] S.D. Angelis, E. Solari, E. Gallo, C. Floriani, A. Chiesi-Villa, C. Rizzoli, Inorg. Chem. 31 (1992) 2520.
[13] J. Magull, A. Simon, Z. Anorg. Allg. Chem. 615 (1992) 77.
[14] C.E. Housmekerides, D.L. Ramage, C.M. Kretz, J.T. Shontz, R.S. Pilato, G.L. Geoffroy, A.L. Rheingold, B.S. Haggerty, Inorg. Chem. 31 (1992) 4453.
[15] Z. Wang, N. Hu, K. Sakata, M. Hashimoto, J. Chem. Soc., Dalton Trans. (1999) 1695.
[16] W.J. Belcher, P.J. Brothers, A.P. Meredith, C.E.F. Rickard, D.C. Ware, J. Chem. Soc., Dalton Trans. (1999) 2833.
[17] J. Hesschenbrouck, E. Solari, R. Scopelliti, C. Floriani, N. Re, J. Organomet. Chem. 596 (2000) 77.
[18] X. Shen, K. Sakata, M. Hashimoto, Chem. Lett. 12 (2001) 1326.
[19] X. Shen, D. Hirayama, K. Sakata, M. Hashimoto, Polyhedron 22 (2003) 529.
[20] X. Shen, A. Nakashima, K. Sakata, M. Hashimoto, Inorg. Chem. Commun. 7 (2004) 621.
[21] D.A. Issahary, G. Ginzburg, M. Polka, B. Meyerstein, J. Chem. Soc., Chem. Commun. (1982) 441.
[22] C.L. Bailey, R.D. Bereman, D.P. Rillema, R. Nowak, Inorg. Chem. 23 (1984) 3956.
[23] C.L. Bailey, R.D. Bereman, Inorg. Chim. Acta 116 (1986) L45.
[24] B.W. Clauberg, G. Sandstede, J. Electroanal. Chem. 74 (1976) 393.
[25] K. Sakata, M. Hashimoto, T. Hamada, S. Matsuno, Polyhedron 15 (1996) 967.
[26] Y.-H. Tsai, Y.-L. Sun, C.-C. Lin, C.-Y. Kuo, Polyhedron 16 (1997) 2599.
[27] K. Sakata, M. Itoh, J. Heterocycl. Chem. 29 (1992) 921.
[28] K. Sakata, M. Shimoda, M. Hashimoto, J. Heterocycl. Chem. 33 (1996) 1593.
[29] K. Sakata, K. Koyanagi, M. Hashimoto, J. Heterocycl. Chem. 32 (1995) 329.
[30] J. Eilmes, Polyhedron 6 (1987) 423.
[31] J. Eilmes, Polyhedron 7 (1988) 2197.
[32] J. Eilmes, Polyhedron 8 (1989) 1243.
[33] J. Eilmes, M. Ptaszek, K. Zielinska, Polyhedron 20 (2001) 143.
[34] J. Eilmes, O. Michalski, K. Wozniak, Inorg. Chim. Acta 317 (2001) 103.
[35] D.R. van Staveren, N. Metzler-Nolte, Chem. Rev. 104 (2004) 5931.
[36] C.G. Tsiafoulis, A.B. Florou, P.N. Trikalitis, T. Bakas, M.I. Prodromidis, Electrochem. Commun. 7 (2005) 781.
[37] T.T. Co, S.C. Shim, C.S. Cho, T.-J. Kim, S.O. Kang, W.-S. Han, J. Ko, C.-K. Kim, Organometallics 24 (2005) 4824.

[38] S. Yoshimoto, A. Saito, E. Tsutsumi, F. D'Souza, O. Ito, K. Itaya, Langmuir 20 (2004) 11046.
[39] H. Kanato, K. Takimiya, T. Otsubo, Y. Aso, T. Nakamura, Y. Araki, O. Ito, J. Org. Chem. 69 (2004) 7183.
[40] F.S. Arimoto, A.C. Haven, J. Am. Chem. Soc. 77 (1955) 6295.
[41] SIR92: A. Altomare, M.C. Burla, M. Camalli, M. Cascarano, C. Giacovazzo, A. Guagliardi, G. Polidori, J. Appl. Cryst. 27 (1994) 435.
[42] DIRDIF94: P.T. Beurskens, G. Admiraal, G. Beurskens, W.P. Bosman, R. de Gelder, R. Israel, J.M.M. Smits, The DIRDIF-94 Program System, Technical Report of the Crystallography Laboratory, University of Nijmegen, The Netherlands, 1994.
[43] G. Ricciardi, A. Bavoso, A. Rosa, F. Lelj, Y. Gizov, J. Chem. Soc., Dalton Trans. (1995) 2385.
[44] H.B. Kraatz, J. Lusztyk, G.D. Enright, Inorg. Chem. 36 (1997) 2400.

planar moiety and also the reluctance to axial binding arising out of the Jahn–Teller effect.

In a continuation of our studies in this field [7], here we have strategically selected an N_4-donor copper(II) synthon, [Cu(nelin)]-$(ClO_4)_2$ (**1**) (nelin = 1,9-diamino-5-methyl-5-nitro-3,7-diazanonane) with a nitroalkyl pendant attached to the main ligand frame.

The utilization of such a precursor deserves special attention since nitro compounds are used extensively as antibacterial, antiprotozoal and anticancer agents [8]. Again, such compounds in metabolic pathways undergo a one-electron reduction to generate nitro-radical anions that exhibit cytotoxicity towards cellular systems [9], causing DNA damage within the cell. Furthermore, several nitro compounds [10] and some of their metal complexes [11] are potent radio-sensitizers towards hypoxic tumour cells, and the efficiency of these drugs is related to the one-electron reduction potential of these compounds [12]. It is therefore important to study the redox behavior of these nitro compounds and the reactivity of the corresponding one-electron reduced nitro-radical anions. So far, the reactivity of these nitro-radical anions has been studied mainly by pulse radiolysis [13] and in few cases by cyclic voltammetry [14], mostly in a mixed solvent medium. The cyclic voltammetric reduction of **1** [15] and other nitro compounds [16] in protic solvents at neutral pH resulted in a single irreversible cathodic wave corresponding to the four-electron reduction of the nitro group to the hydroxylamine derivative. Recently, cyclic voltammetric reduction of a heterocyclic drug, metronidazole, in aqueous solution and aqueous DMF [17] produced the nitro-radical anion successfully. However, monitoring of the redox behavior of copper(II) complexes containing a nitro group on a ligand fragment in vivo-friendly pure aqueous medium is absolutely a new era in this dimension.

In this paper attempts have been made to highlight two relevant aspects in a justified way. First we report the syntheses, crystal structures and other physical characterizations of two new cyano complexes viz. ionic $[Cu(nelin)(H_2O)_2]_2[Fe(CN)_6]\cdot 6H_2O$ (**2**) and bridged $[\{Cu(nelin)\}_2Ni(CN)_4](ClO_4)_2\cdot 2H_2O$ (**3**), by taking $[Cu(nelin)]^{2+}$ as the strategically starting synthon. It is noteworthy to mention here that cyanometallate incorporated copper(II) complexes in an N_4-donor diaza-diamine environment containing an $-NO_2$ pendant group has been scarcely studied [6e]. Here, the supramolecular view not only provides an aesthetically pleasing architecture, the simultaneous transformation of **2** to a quasi-glass phase on dehydration warrants special attention in material science. In the next part, we report the detailed comparative cyclic voltammetric studies of these compounds as well as the parent complex $[Cu(nelin)](ClO_4)_2$ (**1**), especially giving emphasis on the generation of the nitro-radical anion and its effects on the subsequent redox processes in pure aqueous and in MeCN media. In this regard, it is mentionable that the nitroalkyl-substituted $Cu^{II}N_4$ precursor and the cyanometallate incorporated complexes deserve further exploration in the context of the possibility of their potential application as radio-sensitizers in the treatment of cancer, as they are expected to serve in a better way than other organic drugs having poor solubility and high toxicity in physiological conditions compared to the macro-cyclic and acyclic complexes.

2. Experimental

2.1. Materials and methods

Materials such as aqueous formaldehyde (37%) (E-Merck, India), nitroethane (Aldrich), $HClO_4$, and $K_4[Fe(CN)_6]$ (E-Merck, India) were of reagent grade and were used as received. Ethylenediamine (E-Merck, India) and triethylamine (Ranbaxy, India) were distilled over sodium metal before use. Single distilled HPLC grade MeCN (Merck Germany) was used for the electrochemical studies. All the solutions of the complexes for the electrochemical studies were prepared freshly with double distilled water.

Elemental analyses were carried out using a Perkin–Elmer 240 elemental analyzer. Infrared spectra (400–4000 cm^{-1}) were recorded from KBr pellets on a Nicolet Magna IR 750 series-II FTIR spectrophotometer. EPR spectra of polycrystalline samples were recorded using a Varian Century Series X-band EPR spectrophotometer having 100 KHz magnetic field modulation (model E 109) and equipped with a low-temperature quartz Dewar for low-temperature measurements. Room temperature magnetic susceptibilities were recorded on a PAR vibrating sample magnetometer using $Hg[Co(NCS)_4]$ as the calibrant. Diamagnetic corrections were estimated from Pascal's constants. TGA and DTA curves were recorded simultaneously on a Perkin–Elmer, Model Pyris Dimond TG/DTA in static dry nitrogen at a heating rate of 5 °C min^{-1}. Electrochemical measurements were carried out using a computer controlled PAR model 263A VERSASTAT electrochemical instrument with a glassy carbon disk (4 mm diameter, EG&G instrument) as the working electrode. All the results were collected at 25 ± 0.5 °C with reference to the Ag/AgCl electrode. All the solutions were purged with pure argon gas for at least 10 min prior to each experiment. Junction potentials were not corrected. Electronic spectra was recorded on an Agilent 8453 UV–Vis diode array spectrophotometer with a Peltier thermostatic temperature control facility at 25 ± 0.10 °C.

2.2. Syntheses

Caution! Since perchlorate salts are potentially explosive, only small amounts of the materials should be handled with care.

Preparation of $Cu(ClO_4)_2\cdot 6H_2O$, $[Cu(en)_2](ClO_4)_2$, $Na_2[Ni(CN)_4]\cdot 3H_2O$ and the starting material $[Cu(nelin)](ClO_4)_2$ (**1**) have been mentioned elsewhere [7,18] and the purity of each was checked by CHN analysis.

2.2.1. Synthesis of $[Cu(nelin)(H_2O)_2]_2[Fe(CN)_6]\cdot 6H_2O$ (*2*)

To an aqueous solution of $[Cu(nelin)](ClO_4)_2$ (0.576 g, 1.0 mmol), $K_4[Fe(CN)_6]$ (0.375 g, 1.0 mmol) dissolved in a minimum volume of water was added dropwise with constant stirring over 5 min. The precipitate that appeared initially was filtered off and the deep blue filtrate was kept in a refrigerator at 4 °C for several weeks, during which time dark brown block shaped crystals of **2** suitable for X-ray study were obtained. These were washed with cold water and dried in air at room temperature. Yield: 62% based on $[Cu(nelin)](ClO_4)_2$. *Anal.* Calc. for $C_{22}H_{62}Cu_2FeN_{16}O_{14}$: C, 27.56; H, 6.47; N, 23.39. Found: C, 27.92; H, 6.88; N, 23.06%.

IR in cm^{-1} (KBr): 3582 (s,br), 3495 (w,br), 3287 (w), 3227 (w,m), 3173 (w,sh), 2959 (w), 2886 (w), 2045 (vs), 1604 (s), 1548 (s), 1346 (s). μ_{eff} (per monomer): 1.67 μ_B at 27 °C. Electronic spectrum (water): λ_{max} = 532 nm (ε: 61.2 M^{-1} cm^{-1}).

2.2.2. Synthesis of $[\{Cu(nelin)\}_2Ni(CN)_4](ClO_4)_2\cdot 2H_2O$ (*3*)

To an aqueous solution of $[Cu(nelin)](ClO_4)_2$ (0.576 g, 1.0 mmol), $Na_2[Ni(CN)_4]\cdot 3H_2O$ (0.158 g, 0.6 mmol) dissolved in a minimum volume of water was added dropwise with constant stirring over 5 min. The precipitate that appeared initially was filtered off and the deep blue colored filtrate was allowed to undergo slow evaporation at ambient temperature in the open air. After several weeks, dark blue needle shape shiny crystals of **3** suitable for an X-ray study were obtained from the filtrate, which were filtered and washed with cold water followed by diethyl ether and dried in air at room temperature. Yield: 49%. based on $[Cu(nelin)](ClO_4)_2$. *Anal.* Calc. for $C_{20}H_{46}Cl_2Cu_2N_{14}NiO_{14}$: C, 24.91; H, 4.77; N, 20.34. Found: C, 25.01; H, 4.41; N, 20.06%.

IR in cm^{-1} (KBr): 3609 (w), 3383 (w), 3287 (w), 3225 (w), 3151 (w), 2959 (w), 2923 (w), 2893 (w), 2141 (vs), 2124 (s), 1604 (s),

1556 (s), 1444 (s), 1350 (w), 1115 (vs), 1087 (s), 1022 (s), 978 (s), 910 (vw), 711 (w), 630 (s). μ_{eff} (per monomer): 1.76 μ_B at 25 °C. Electronic spectrum (MeCN): λ_{max} = 581 nm (ε: 73.6 M^{-1} cm^{-1}).

2.3. Crystal data collection and refinement

Intensity data for **2** and **3** were collected at 293(2) K on a Siemens P4 diffractometer using graphite monochromatized Mo Kα radiation (λ = 0.71073 Å) and the ω–2θ scan mode in the range $2.44 \leqslant \theta \leqslant 26.47^{o}$ and $2.47 \leqslant \theta \leqslant 24.00^{\circ}$, respectively. The intensities were corrected for Lorentz-polarization effects and for absorption using ψ-scans. The minimum and maximum transmission factors were 0.357 and 0.596 for **2** and 0.122 and 0.142 for **3**. The structures were solved by direct methods and all non-hydrogen atoms refined anisotropically by full matrix least squares on F^2 using the SHELXTL PLUS-PC version [25,19] and hydrogen atoms were included geometrically and refined isotropically except those of water hydrogens. Other additional information concerning the data collection and refinement of the structure are compiled in Table 1.

Table 1
Crystal data and structure refinement for **2** and **3**

Complex	2	3
Molecular formula	$C_{22}H_{62}Cu_2FeN_{16}O_{14}$	$C_{20}H_{46}Cl_2Cu_2N_{14}NiO_{14}$
Formula weight	957.76	963.40
Crystal system	Monoclinic	Monoclinic
Space group	$P2_1/n$	$P2_1/n$
Unit cell dimensions		
a (Å)	9.300(2)	8.000(2)
b (Å)	15.510(3)	16.505(3)
c (Å)	14.325(3)	13.977(3)
β (°)	99.25(3)	90.98(3)
V (Å^3)	2039.4(7)	1845.3(6)
Z	4	2
μ (mm^{-1})	1.46	1.87
Reflections collected	4435	3086
Independent reflections (R_{int})	4180 (0.0202)	2866 (0.1085)
Goodness-of-fit on F^2	1.039	1.021
Final *R* indices [$I > 2\sigma(I)$]	R_1 = 0.0388	R_1 = 0.0650
	wR_2 = 0.0961	wR_2 = 0.1609
R indices (all data)	R_1 = 0.0548	R_1 = 0.1015
	wR_2 = 0.1037	wR_2 = 0.1837

2.4. PXRD data collection

Powder X-ray diffraction data were collected on a Bruker D8 Advance powder diffractometer in the Bragg-Brentano geometry using monochromatic Cu Kα1 radiation (λ = 1.5406 Å) selected with an incident beam germanium monochromator.

3. Results and discussion

Description of the structure of $[Cu(nelin)(H_2O)_2]_2[Fe^{II}(CN)_6] \cdot 6H_2O$ (**2**). Complex **2** crystallizes in the monoclinic space group $P2_1/n$. The asymmetric unit contains half of the formula unit along with three water molecules (Fig. 1). The molecular structure of complex **2** consists of two cationic $[Cu(nelin)(H_2O)_2]^{2+}$ fragments

Table 2
Selected bond distances (Å) and bond angles (°) for **2**[*] and **3**[*]

2		3	
Cu–N(1)	2.017(3)	Cu–N(1)	2.032(6)
Cu–N(2)	2.017(2)	Cu–N(2)	2.020(7)
Cu–N(3)	2.027(2)	Cu–N(3)	2.012(7)
Cu–N(4)	2.009(2)	Cu–N(4)	2.024(7)
Cu–OW1	2.413(2)	Cu–N(6)	2.294(6)
Cu–OW2	2.722(2)	Cu–O(1′)	2.936(15)
Fe′–C(2′)	1.927(3)	Ni–C(6)	1.870(7)
Fe′–C(3′)	1.923(3)	Ni–C(7)	1.875(8)
Fe′–C(4′)	1.917(3)	N(6)–C(6)	1.143(9)
N(2′)–C(2′)	1.161(4)	N(7)–C(7)	1.136(10)
N(5)–O(1)	1.206(4)	N(21)–O(21)	1.181(11)
N(5)–O(2)	1.223(4)	N(21)–O(22)	1.181(10)
N(2)–Cu–N(1)	85.3(1)	N(2)–Cu–N(1)	91.9(3)
N(2)–Cu–N(3)	94.0 (1)	N(2)–Cu–N(3)	85.8 (3)
N(1)–Cu–N(3)	174.2(1)	N(1)–Cu–N(3)	169.4(2)
N(2)–Cu–N(4)	177.3(1)	N(2)–Cu–N(4)	167.8(3)
N(1)–Cu–N(4)	95.1(1)	N(1)–Cu–N(4)	85.4(3)
N(3)–Cu–N(4)	85.3(9)	N(3)–Cu–N(4)	94.6(3)
N(4)–Cu–OW1	93.7(1)	N(2)–Cu–N(6)	92.9(3)
N(2)–Cu–OW1	88.9(1)	N(1)–Cu–N(6)	93.8(2)
N(1)–Cu–OW1	91.9(1)	N(3)–Cu–N(6)	96.7(3)
N(3)–Cu–OW1	93.7(1)	Ni–C(7)–N(7)	176.9(7)
OW1–Cu–OW2	174.6(6)	Ni–C(6)–N(6)	176.2(7)
Fe′–C(2′)–N(2′)	179.1(3)	C(6)–Ni–C(6)#2	180.0(6)
C(2′)–Fe′–C(2′)#1	180.0(5)	C(7)–Ni–C(7)#2	180.0(5)

[*] Symmetry transformation used to generate equivalent atoms: #1 $-x, -y, -z$; #2 $-x+1, -y, -z$.

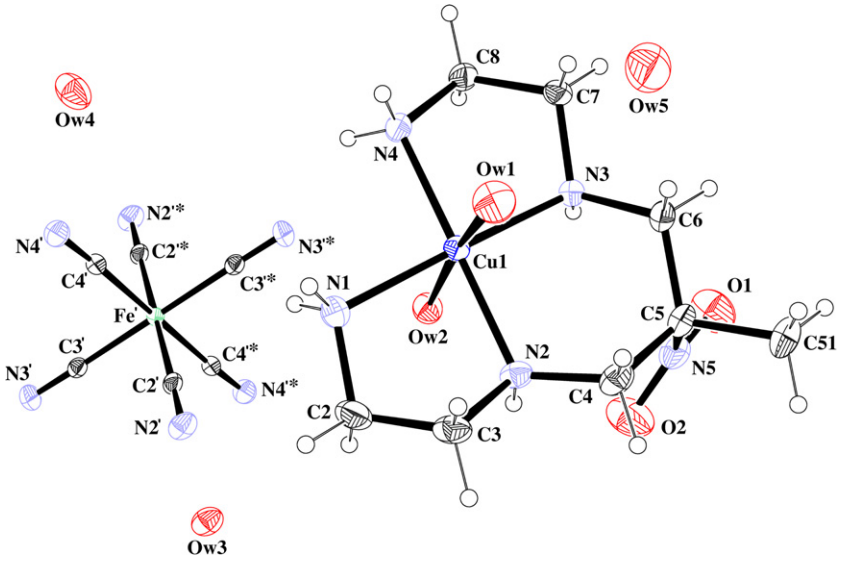

Fig. 1. ORTEP diagram (30% ellipsoidal probability) with the atom numbering scheme for complex **2** ([*] = $-x+1, -y, -z$).

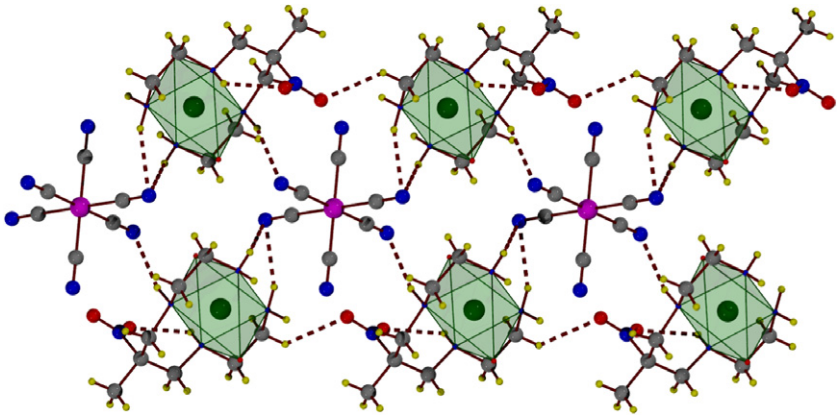

Fig. 2. H-bonded supramolecular 1D chain of anions and cations for complex **2** along the *a*-axis.

the charges of which are counter-balanced by the $[Fe^{II}(CN)_6]^{4-}$ anion along with six water molecules. The coordination geometry of each copper(II) atom is best described as distorted octahedral. The square plane is constructed by the four nitrogen atoms (N1, N2, N3 and N4) of the diaza-diamine ligand and the axial sites are occupied by two more distant oxygen atoms of two water molecules. The N(4)–Cu–N(2) (177.3(1)°) and N(1)–Cu–N(3) (174.2(1)°) angles in the equatorial plane slightly deviate from 180° and the average of the four OW_1–Cu–N angles (92.1°) (Table 2) is slightly higher than 90°. All these indicate a slight distortion from a regular octahedral geometry with the copper center situated at 0.100(4) Å above the mean plane towards the axial OW1 water molecule. In the equatorial plane, the Cu–N bond distances vary from 2.009(2) to 2.027(2) Å (avg. 2.017(2) Å) and are comparable with the previously reported values [18]. It is noteworthy that the two axial Cu–OW bond distances are not identical; Cu–OW_1 2.413(2) and Cu–OW_2 2.722(2) Å; probably due to a different extent of H-bonding. On the other hand, $[Fe^{II}(CN)_6]^{4-}$ retains its perfect octahedral geometry (Table 2).

Hydrogen bonds play a pivotal role in assembling the discrete cationic and anionic entities towards higher dimensionality. The packing diagram clearly indicates that all the ferrocyanide ions occupy special positions and the participation of the cyano nitrogen in extensive intermolecular H-bonding. The $[Fe(CN)_6]^{4-}$ unit act as a template for the organization of four $[Cu(nelin)]^{2+}$ units around it and due to successive hydrogen bonding this gives rise to a supramolecular chain along the crystallographic *a*-axis (Fig. 2, Table 3). The H-bonded polymeric chains are three dimensionally interlinked through hydrogen bonding (N4–H44···O2) to form irregular honeycomb-like channels (Fig. 3), which accommodate a one dimensional helical water chain as shown in Fig. 4. Three lattice water molecules (OW3, OW4, OW5), by hydrogen bonding association with themselves together with the coordinated water molecule (OW1), give rise to this helical assembly. The hydrogen bonding distances are OW1···OW3 = 2.818(4) Å; OW3···OW4 = 2.889(4) Å; OW4···OW5 = 2.807(4) Å; OW5···OW1 = 2.724(4) Å. The pitch of the helical water chain is 9.3 Å and it is supported within the channel by three more hydrogen bonding contacts OW3···OW2 = 2.804(4) Å; OW3···N2′ = 2.729(4) Å and OW3···N4′ = 2.887(4) with the wall as it propagates along the *a*-axis. Each of the channels is symmetric and it is divided

Table 3
Important H-bonding parameters for **2** and **3**

D–H···A	D–H (Å)	H···A (Å)	D–A (Å)	∠D–H···A (°)	Symmetry[a]
Complex ***2***					
N2–H2···O2	0.910	2.230	2.835(4)	123.0	
N3–H3···N5	0.910	2.620	2.947(4)	102.0	
N3–H3···N3′	0.910	2.350	3.222(4)	161.0	2a
N1–H12···N4′	0.900	2.450	3.279(4)	154.0	2b
N4–H43···N4′	0.900	2.610	3.410(4)	149.0	2b
N4–H44···O2	0.900	2.380	3.128(4)	140.0	2c
Complex ***3***					
N1–H1···O3′	0.910	2.200	3.061(14)	157.0	
N2–H1···O3′	0.910	2.250	3.078(14)	151.0	
N2–H1···O21	0.910	2.490	3.032(13)	119.0	
N2–H31···N7	0.900	2.200	3.091(10)	171.0	3a
N3–H32···O2′	0.900	2.350	3.057(14)	135.0	3b
N4–H41···O4′	0.900	2.560	3.304(17)	141.0	3c
N4–H42···N7	0.900	2.620	3.441(10)	151.0	3a

[a] 2a: 1/2 + *x*, 1/2 − *y*, 1/2 + *z*; 2b: 1/2 − *x*, 1/2 + *y*, 1/2 − *z*; 2c: 1/2 + *x*, 3/2 − *y*, 1/2 + *z*. 3a: 1/2 − *x*, 1/2 + *y*, 1/2 − *z*; 3b: 1/2 + *x*, 1/2 − *y*, −1/2 + *z*; 3c: 1 + *x*, *y*, *z*.

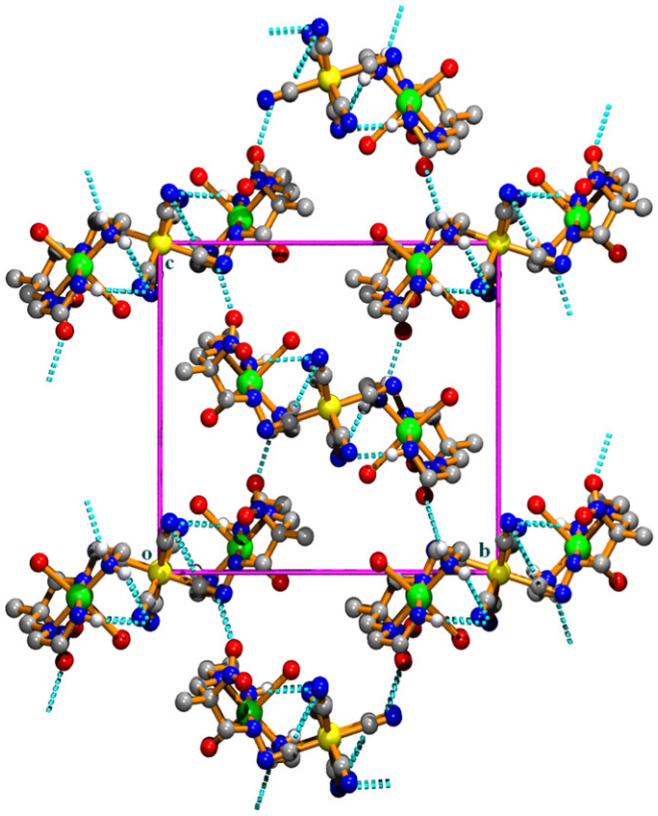

Fig. 3. Formation of supramolecular channels along the *a*-axis through interlinking of nearby chains for complex **2**.

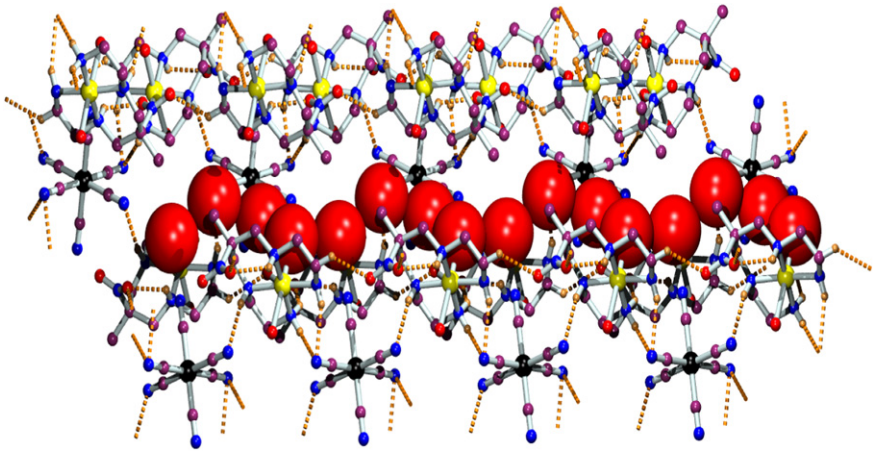

Fig. 4. Helical water chain comprising of three lattice water molecules and one coordinated water molecule (OW1) within one half of the channel for complex **2**.

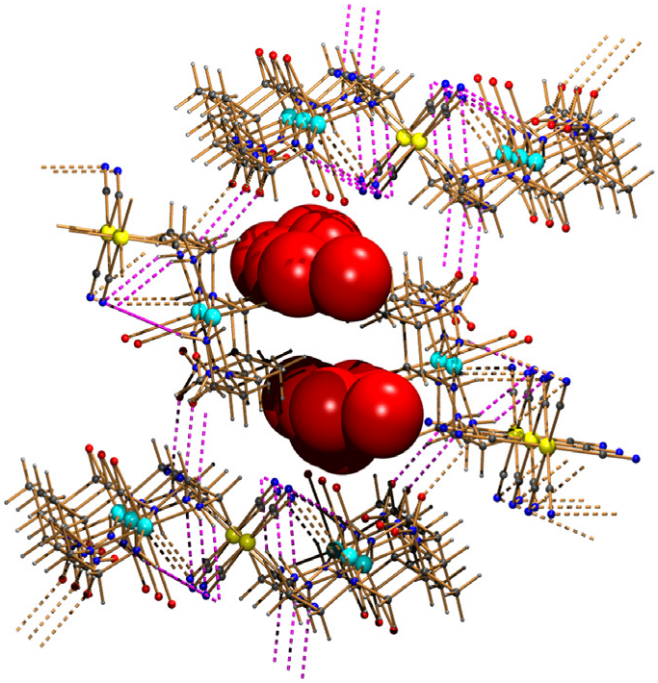

Fig. 5. The symmetric channels accommodate helical water chains in either half. Helical water chains in either half run in opposite directions to each other for complex **2**.

into two halves. Each half accomodates a helical water chain which run in opposite directions to each other (Fig. 5).

3.1. Description of structure of $[\{Cu(nelin)\}_2Ni(CN)_4](ClO_4)_2.2H_2O$ (3)

The molecular structure of **3** consists of a trinuclear $[\{Cu(nelin)\}_2Ni(CN)_4]^{2+}$ cation, two perchlorate anions and two water molecules (Fig. 6). The asymmetric unit consists of one half of the formula unit with the inversion center located at the nickel atom. The $[Ni(CN)_4]^{2-}$ anion is coordinated to two $[Cu(nelin)]^{2+}$ cations through two cyano groups bridging in a di-*trans* fashion, leaving the two other *trans*-CN groups uncoordinated, and complex **3** in this sense is comparable to $[Cu(HL)]_2[Ni(CN)_4]\cdot 4H_2O$ [7b] (H_2L = 3,9-dimethyl-4,8-diazaundec-3,8-diene-2,10-dione-dioxime). The bonding arrangement of this trinuclear unit is shown in Fig. 6 and selected bond distances and angles are given in Table 2.

The coordination geometry around the copper center is best described by a square pyramid with the geometrical factor $\tau = 0.03$ [7a]. The basal plane is constructed by the four nitrogen atoms of the diaza-diamine ligand and the apical position is occupied by the nitrogen atom of the bridging cyanide. In the basal plane the Cu–N bond distances vary from 2.012(7) to 2.032(6) Å, whilst that of the apical Cu–N(6) is 2.294(6) Å, which is significantly longer than the basal Cu–N bond lengths. The N(1)–Cu–N(3), 169.4(2)° and N(2)–Cu–N(4), 167.8(3)° angles in the basal plane deviate significantly from 180° and the four N(6)–Cu–N(x) [x = 1, 2, 3 and 4] angles are larger than 90° (avg. 95.6(3)°), indicating that the coordination geometry around each copper(II) center is a distorted square pyramid. The copper center is situated 0.199 Å above the plane towards the apical direction. It is interesting to mention here that one oxygen atom from the perchlorate anion, O(1′), is at an elongated contact distance 2.936(15) Å to the copper(II) center. The bridging cyanide coordinates to the copper ion in a bent fashion with a C(6)–N(6)–Cu bond angle of 165.3(6)°. The intramolecular Cu···Cu separation is 10.497 Å. Like the earlier trends [7b] no significant difference has been observed here between the bridging (C(6)–N(6) = 1.143(9) Å) and terminal (C(7)–N(7) = 1.136(10) Å) cyano groups and $[Ni(CN)_4]^{2-}$ retains its square planer(SP) geometry (Table 2).

As shown in Fig. 7, the trinuclear units are arranged in successive rows in a herringbone fashion and the bifurcated hydrogen bonding (N3–H31···N7 and N4–H42···N7) (Table 3) through the uncoordinated terminals of the $[Ni(CN)_4]^{2-}$ units give rise to a supramolecular (4,4) network in the (202) plane. In this arrangement the $[Ni(CN)_4]^{2-}$ units act as a template for a (4,4) net architecture. Perchlorate anions and lattice water molecules occupy the void spaces within this network and bind to the cationic part of the trinuclear units through hydrogen bonding (Table 3). Successive (202) planes are stacked along the [101] direction through C–H···O hydrogen bonding (Fig. 8).

3.2. IR study

The positions of the relevant IR bands of complexes **2** and **3** are given in Section 2. The IR active bands fall in the region of *ca.* 3151–3600 cm^{-1} for both complexes which is characteristic for ν(O–H) and ν(N–H) groups. For cyano complexes, absorption bands due to ν_{CN} stretching vibrations are very characteristic. In $K_4[Fe^{II}(CN)_6]$ the ν_{CN} band appears at 2042 cm^{-1} [20] and in complex **2** a sharp peak at *ca.* 2045 cm^{-1} clearly indicates that all the cyano groups of the ferrocyanide ion are terminal. For the tetracyanonickelate anion this absorption band appears at 2128 cm^{-1} [20]. On bridging

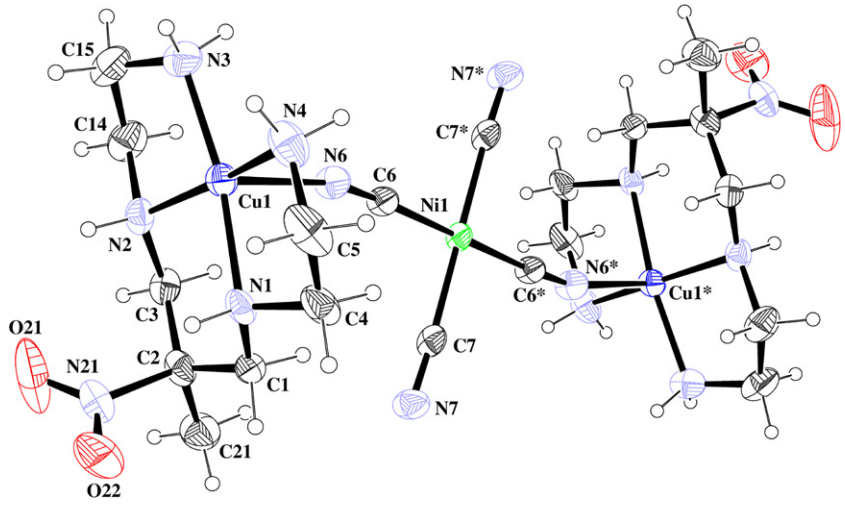

Fig. 6. ORTEP view (30% ellipsoidal probability) of the trinuclear unit of **3** with the atom numbering scheme. Perchlorate ions and water molecules are omitted for clarity (* = $-x$, $-y$, $-z$).

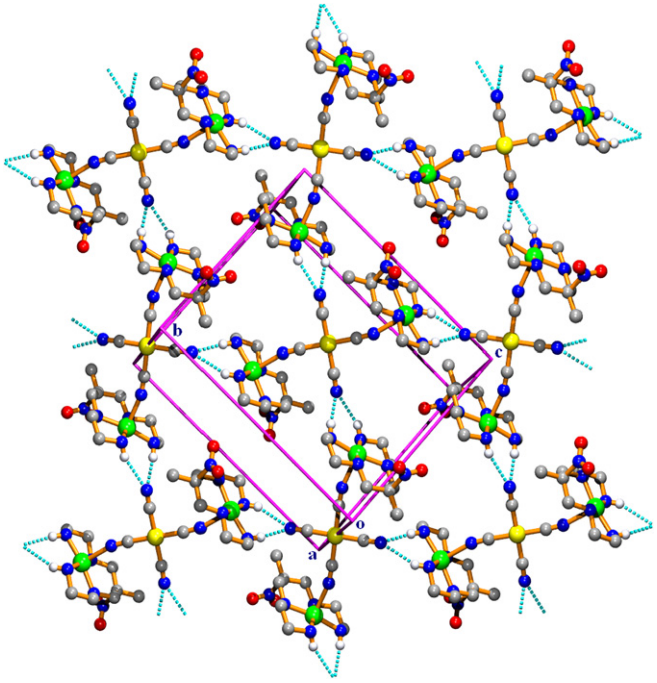

Fig. 7. The (4,4) supramolecular network in the (202) plane of complex **3**. $[Ni(CN)_4]^{2-}$ units act as a template for this network. Perchlorate ions and water molecules, which are omitted for clarity, occupy the void space within the network.

via N atoms this band shifts to a higher wave number. The two ν_{CN} IR bands appearing at 2124 (vs) and 2141 (s) cm^{-1} for **3** can be assigned to the terminal and bridging cyanide groups, respectively [20a]. The characteristic IR bands corresponding to the nitro group appear for **2** at 1548 cm^{-1} (s, ν_{as}) and 1346 cm^{-1} (m, ν_s) and that for **3** at 1556 cm^{-1} (s, ν_{as}) and 1350 cm^{-1} (w, ν_s) [1g]. Additionally, a strong band near 1115 cm^{-1} and a sharp band near 623 cm^{-1} indicate the presence of an uncoordinated perchlorate anion for complex **3** [20b]. All other bands appear at their usual positions.

3.3. Thermal analyses

Complex **2** remains unchanged at room temperature (27 °C) for an indefinite period. TGA studies show that total water loss occurs in two narrow temperature regions: an 8.57% weight loss was observed in between 40 and 90 °C, which is almost equivalent to a loss of 4.5 water molecules. This is accompanied by a small *endo*-effect on the DTA curve at *ca.* 80 °C. Obviously these are due to non-coordinated lattice water molecules present in the cavities. On gradual heating a further 8.51% weight loss was monitored in between 100 and 130 °C and the total weight loss is equivalent to 4.46 water molecules. These are partially lattice as well as coordinated water molecules. The corresponding endo-therm was observed at *ca.* 122 °C. The remaining water molecules are retained up to 140 °C, after which the complex undergoes an immediate decomposition with a large exothermal peak at *ca.* 145 °C in the DTA curve. Losses of water molecules in different stages are due to the different extent of H-bonding. For example, some water mol-

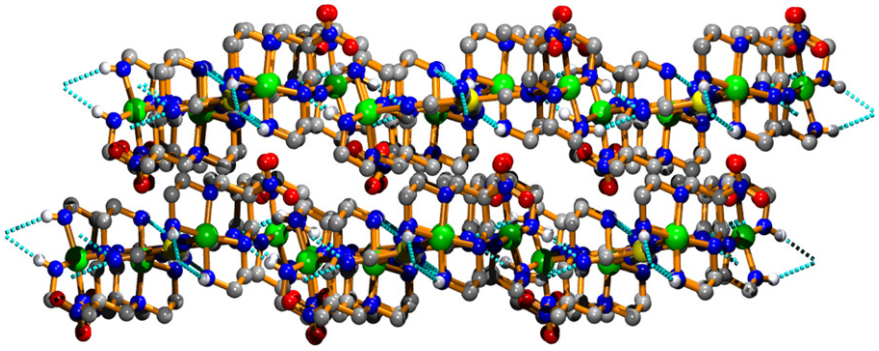

Fig. 8. The disposition of successive (202) layers in complex **3**.

ecules are doubly H-bonded with two neighbouring water molecules while some water molecules are triply H-bonded with an additional H-bond to a cyano nitrogen atom. As it is envisaged that the network is purely built up of strong H-bonding, complete removal of all the water molecules ultimately results in collapse of the structural morphology. This is evident from the powder X-ray diffraction (PXRD) pattern (Fig. 9).

Thermal decomposition of complex **3** starts at *ca.* 65 °C and consequently the complex eliminates its two uncoordinated water molecules, and the process continues up to *ca.* 100 °C (found/calc.: 3.70%/3.74% with respect to loss of weight%). This is accompanied by a small *endo*-effect on the DTA curve at *ca.* 90 °C. The anhydrous complex, having the formula $[\{Cu(nelin)\}_2Ni(CN)_4](ClO_4)_2$, maintains its thermal stability up to *ca.* 180 °C. After that the complex undergoes an immediate decomposition with a small exothermal peak at *ca.* 190 °C in the DTA curve. Since the complex contains the perchlorate anion, we have not carried out the experiment beyond 200 °C.

3.4. PXRD analysis

To study the effect of dehydration on the structure, a PXRD pattern of complex **2** was recorded at 27 °C (Fig. 9a). It was then heated to (130 ± 2) °C in a stream of nitrogen and was kept at this temperature for 30 min. An X-ray powder diffraction pattern (Fig. 9b) was recorded almost immediately on cooling the compound to room temperature (27 °C), which showed marked changes in the diffraction pattern compare to that of the original phase (Fig. 9a). The PXRD pattern of the dehydrated species clearly indicates that in addition to water removal from the original crystalline structure, it has transformed into a quasi glassy material. Dehydration of the hydrated species to generate a glassy state is most unusual, since up until now only hydrated trehalose [21], raffinose [22] and magnesium acetate [23] have been reported to have this property. Such a finding may be explored by crystal engineers in a more applied way.

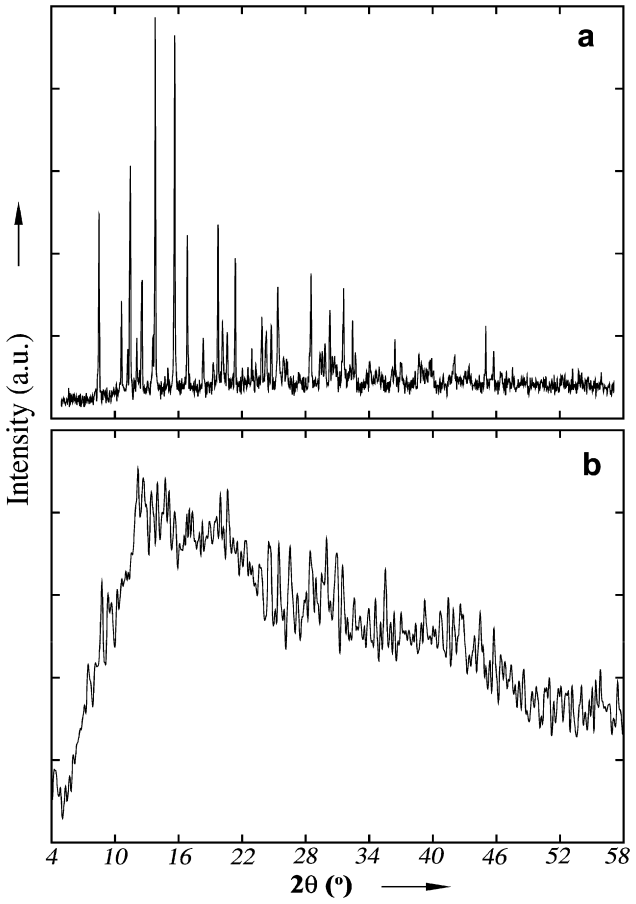

Fig. 9. (a) PXRD pattern (complex **2**); (b) PXRD patten (complex **2** after heating).

3.5. EPR studies

Room temperature solid state EPR of a polycrystalline sample of **2** is typical for a mononuclear copper(II) complex with axial distortion, and the elongation of the axis is characterized by $g_{||} = 2.21$ and $g_{\perp} = 2.01$. An almost identical spectrum for **3** is characterized by $g_{||} = 2.11$ and $g_{\perp} = 2.04$. The observed values ($g_{||} > g_{\perp}$) confirm that the unpaired electron resides in the $d_{x^2-y^2}$ orbital. In the water–alcohol glass phase at 77 K complex 2 exhibits a typical four-line hyperfine spectra with $g_{||} = 2.11$, $g_{\perp} = 2.02$, $A_{||} = 150$ Oe and $A_{\perp} = 5$ Oe at $V = 9.45$ MHz. On standing the solution for 2–5 days a moderately strong signal at $g = 4.3$ indicates the presence of Fe^{III} species in the system [24]. This may be attributed to the oxidation of a portion of $[Fe^{II}(CN)_6]^{4-}$ to $[Fe^{III}(CN)_6]^{3-}$ in aqueous solution, as indicated by the slow disappearance of the color of the complex with time.

3.6. Electrochemical studies

The electrochemical properties of the complexes $[Cu(nelin)(H_2O)_2]_2[Fe^{II}(CN)_6] \cdot 6H_2O$ (**2**) and $[\{Cu(nelin)\}_2Ni(CN)_4](ClO_4)_2 \cdot 2H_2O$ (**3**) were investigated using the cyclic voltammetric technique in aqueous and in MeCN solutions, respectively, with Ag/AgCl as the reference electrode. The cyclic voltammetric behavior of the parent complex $[Cu(nelin)](ClO_4)_2$ (**1**) was also studied under similar conditions in aqueous and in MeCN media to compare the results. All the electrochemical data are summarized in Table 4.

The electrochemical responses of complex **1** in aqueous solution were found to be highly influenced by the scan rate. At a scan rate of $\sim$1.0 V s^{-1}, a single irreversible reduction peak at a potential of *ca.* −0.94 V was found and attributed to a four-electron reduction process (Eq. (1)), as generally observed for nitro compounds in protic solvents [15,16]:

$$-NO_2 + 4H^+ + 4e^- \rightarrow -NHOH + H_2O \quad (1)$$

At appreciably lower scan rates, the situation is quite different. Thus, at a scan rate of 0.05 V s^{-1}, two irreversible reduction waves having peaks *viz.* A and B at potentials of *ca.* −0.69 V and −1.0 V, respectively, were observed, and on the reverse sweep an anodic peak (D) at *ca.* −0.31 V was monitored. After a second sweep, another reduction peak C at *ca.* −0.49 V in addition to peaks A and B appeared, while the anodic peak D remained invariant with respect to its position (Fig. 10). However, it is important to note that after the first sweep the peak intensities for A and B were greatly diminished while that of D remained almost unchanged. In order to assess the number of electron transfers involved in these processes, peak A was assigned to be a one-electron reduction of a nitro group to a nitro-radical anion followed by a three-electron reduction of the nitro-radical anion (peak B) to the hydroxylamine derivative (Scheme 1). These are comparable with the nitro-containing heterocyclic drug metronidazole [17].

Surprisingly, no cathodic wave (peak C), for a $Cu^{II} \rightarrow Cu^{I}$ reduction was observed during the first scan. However, if we assume that the anodic oxidation peak D observed in the reverse sweep in the first scan is due to oxidation of $Cu^{I} \rightarrow Cu^{II}$, then it is likely to assume that the nitro-radical anion generated in the first sweep is responsible for initiation of the reduction of the Cu^{II} center, which in the reverse sweep undergoes oxidation. Thus keeping

Table 4
Electrochemical parameters[a]

Complex (1.0×10^{-3} M)	Solvent	Supporting electrolyte (0.1 M)	E_{pc} (V)	E_{pa} (V)	ΔE_p (V)	$E_{1/2}$ (V)	Redox couple and reaction
$[Cu(nelin)](ClO_4)_2$ **(1)**	Water	$NaClO_4$	−1.06				$-NO_2 \rightarrow -NHOH$[b]
(Reported)	pH ~ 6				0.08	−0.59	Cu^{II}/Cu^{I}[b]
$[Cu(nelin)](ClO_4)_2$ (**1**) (Our Investigation)	Water	$NaClO_4$	−0.69				$-NO_2 \rightarrow NO_2^-$
			−1.05				$-NO_2^- \rightarrow -NHOH$
	pH 6.4		−0.49	−0.31	0.18	−0.40	Cu^{II}/Cu^{I}
	MeCN	TBAP	−0.96				Cu^{I}/Cu^{0}
			−1.65				$-NO_2 \rightarrow NO_2^-$
			−0.62	−0.36	0.26	−0.49	Cu^{II}/Cu^{I}
$[Cu(nelin)(H_2O)_2]_2$. $[Fe(CN)_6].6H_2O$ (**2**)	Water pH 6.8	$NaClO_4$	−0.64				$-NO_2 \rightarrow NO_2^-$
			−0.87				$-NO_2^- \rightarrow -NHOH$
			0.22	0.40	0.18	0.31	Fe^{III}/Fe^{II}
$[\{Cu(nelin)\}_2Ni(CN)_4](ClO_4)_2 \cdot 2H_2O$ **(3)**	MeCN	TBAP	−0.99				Cu^{I}/Cu^{0}
			−1.63				$-NO_2 \rightarrow -NO_2^-$
			−0.58	−0.32	0.26	−0.45	Cu^{II}/Cu^{I}
Ferrocene	MeCN	TBAP	0.36	0.52	0.16	0.44	Fe^{III}/Fe^{II}

[a] Maximum error ±5%; all potentials are measured against the Ag/AgCl reference electrode; $E_{1/2}$ is determined as 1/2 ($E_{pc} + E_{pa}$).
[b] Reported values (Ref. [15]): measured for DME *vs.* Ag/Ag^+.

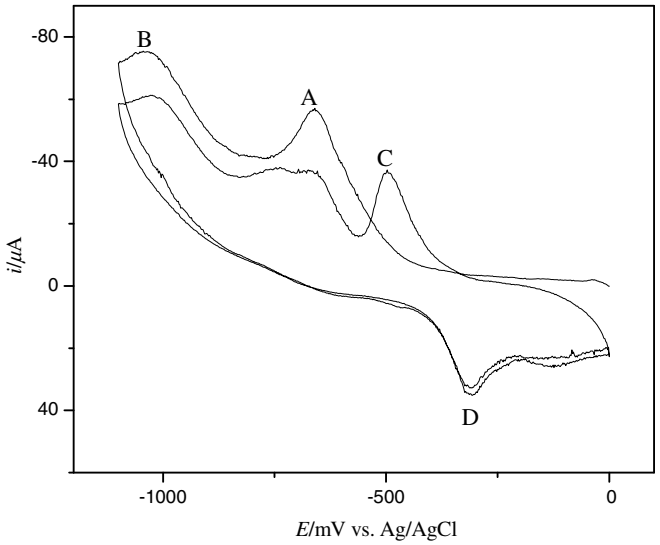

Fig. 10. Two successive cyclic voltammograms of **1** in water at a scan rate of 0.05 V s^{-1}.

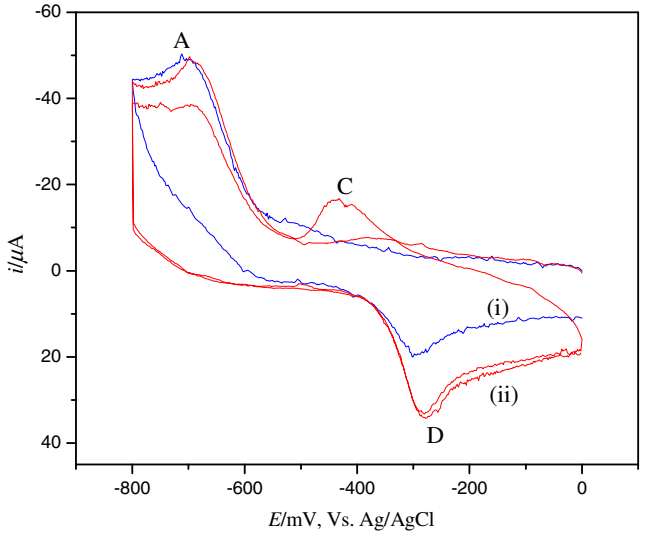

Fig. 11. Comparative cyclic voltammograms of **1** in water at a scan rate of 0.05 V s^{-1}: (i) The sweep is reversed just after formation of the nitro-radical anion (A), (ii) the sweep is reversed just after formation of the nitro-radical anion (A) but is delayed for 5 min.

$$Cu^{II}R - NO_2 + e^- \rightarrow Cu^{II}R - NO_2^{\cdot -} \qquad (2)$$

$$Cu^{II}R - NO_2^{\cdot -} + 3e^- + 4H^+ \rightarrow Cu^{II}R\text{-}NHOH + H_2O \qquad (3)$$

Scheme 1.

the copper(II) to copper(I) reduction silent in the first scan and its appearance from the second scan (peak C) may be thought of that the original Cu^{II} complex remains silent towards the redox transformation. The above proposition is supported by the following observations:

(1) When the scan was reversed just before the generation of the nitro-radical anion (peak A), the anodic peak D was absent.
(2) When the scan was reversed just after the appearance of peak A, the anodic peak D was observed.
(3) If the scan is reversed just after the appearance of peak A and is delayed for 5 min at the same potential the intensity of the anodic peak (D) is increased (Fig. 11).

Thus the copper(II) center in complex **1** is found to be silent towards redox transformation in the experimental scan rate at the first scan. Now the question arises, why is the copper(II) center in **1** silent towards this redox process. A reasonable argument can be made as follows: the copper(II) center is deeply buried in the ligand environment while the NO_2 group on the ligand fragment is well exposed in space for redox processes. Thus, it is the NO_2 group which first undergoes reduction to give the nitro-radical anion $Cu^{II}RNO_2^-$. The highly reactive nitro-radical anion thus generated electrochemically from the nitro group, in close proximity towards the metal center due to conformational puckering, [15] immediately transmits its electron to facilitate the copper(II) reduction to copper(I), which concomitantly undergoes some kind of structural modification to give $Cu^{I}R^{*}NO_2$. This modified species, only after oxidation to $Cu^{II}R^{*}NO_2$, can initiate its second time reduction without the assistance from a nitro-radical anion; and by this way $E_{1/2}$ for Cu^{II}/Cu^{I} was estimated as −0.40 V. All these transformations are given in Scheme 2.

Considering the overall cyclic voltammetric pattern of **1** in aqueous solution in the above mentioned slow scan rate, a

$$Cu^{II}(R\text{-}NO_2)^{+} \xrightarrow{e^-} Cu^{II}(R\text{-}NO_2^{\bullet-}) \xrightarrow{iet} Cu^{I}(R\text{-}NO_2) \xrightarrow{cm} Cu^{I}(R^{*}\text{-}NO_2)$$

$$\xrightarrow{-e^-} Cu^{II}(R^{*-}NO_2) \longrightarrow Cu^{I}(R^{*}\text{-}NO_2)$$

iet = intramolecular electron transfer; cm = conformational modification

Scheme 2.

speculative explanation may be furnished: peak A is just due to the irreversible reduction of $[Cu^{II}(nelin)]^{2+}$ to $[Cu^{I}(nelin)]^{+}$; which subsequently undergoes decomposition to generate the free Cu^{+} ion, which in turn is reoxidized to the Cu^{2+} ion (peak D) and re-reduced to the bare Cu^{+} ion (peak C). However, a serious problem for such a proposition arises from the $E_{1/2}$ value for the Cu^{II}/Cu^{I} couple (−0.40 V *versus* Ag/AgCl). The observed potential (−0.18 V *versus* NHE) is much more negative than the corresponding standard electrode potential for the free Cu^{II}/Cu^{I} couple (0.15 V). Moreover, the free Cu^{+} ion is too susceptible for disproportionation in aqueous solution, but no such indication was observed in the back scan, either through the appearance of an anodic stripping peak or through elemental copper deposition in the experimental solution during and after the completion of the cyclic voltammetric process. Thus the speculation of the transformation of $[Cu^{I}(nelin)]^{+}$ to $[Cu^{0}$-$(nelin)]^{0}$, or put in a better way Cu^{0}, (peak B) can be discarded safely.

The electrochemical behavior of complex **1** at the same scan rate (0.05 V s^{-1}) in MeCN (Fig. 12) was completely different from that which was observed in aqueous solution. Here, from the beginning a cathodic peak (E) for $Cu^{II} \rightarrow Cu^{I}$ reduction was observed at a potential of *ca.* −0.62 V; for which the reverse scan showed an anodic wave (H) at *ca.* −0.36 V and the corresponding $E_{1/2}$ was estimated as −0.49 V *versus* Ag/AgCl. It is important to note that after formation of the Cu^{I} complex (peak E), it subsequently undergoes slow disproportionation to Cu^{II} and Cu^{0}, and a well defined anodic stripping peak at *ca.* −0.16 V was observed for Cu^{0}. As a consequence the anodic peak (peak H) for oxidation of $Cu^{I} \rightarrow Cu^{II}$ was greatly diminished. To support this proposition two separate CV profiles were recorded, inverting the scan immediately after traversing peak E and peak F, respectively, under same scan rate (0.05 V s^{-1}). The great increment of the anodic stripping peak after traversing peak F compare to peak E, not only certified the disproportionation of the $[Cu^{I}(nelin)]^{+}$ complex but simultaneously helped to assign peak F as $Cu^{I} \rightarrow Cu^{0}$. At a comparatively higher scan rate (0.8 V s^{-1}) no such anodic stripping peak in the back scan after traversing peak E indicates the slower nature of the disproportionation reaction. Here peak G is conceivably assign to the irreversible $NO_2/-NO_2^{-}$ reduction. The cathodical fluctuation of the nitro-radical anion peak from solvent to solvent is a common feature for nitro-containing compounds [25].

In conclusion, it is clear that the nitro-radical induced reduction of $[Cu^{II}(nelin)]^{2+}$ and the reluctancy of the disproportionation reaction of the modified $Cu^{I}R^{*}NO_2$ is the main feature in aqueous medium, while the normal reduction (without any assistance of a nitro group) of $[Cu^{II}(nelin)]^{2+}$ to $[Cu^{I}(nelin)]^{+}$ followed by slow disproportionation to Cu^{II} and Cu^{0} are the mentionable characteristics in MeCN for complex 1. It also further indicates that the initial environment of $[Cu^{II}(nelin)]^{2+}$ in aqueous and in MeCN solution are to some extent different.

The electrochemical behavior of complex **2** was monitored at a slow scan rate (0.05 V s^{-1}) in aqueous medium (Fig. 13). A well defined anodic wave at *ca.* 0.40 V and a corresponding cathodic wave at *ca.* 0.22 V appeared. It was assigned to the $[Fe^{III}(CN)_6]^{3-}/[Fe^{II}(CN)_6]^{4-}$ couple and the corresponding $E_{1/2}$ was estimated as 0.31 V *versus* Ag/AgCl. From the peak height and intensity it is evident that the concentration of iron(II) is higher than that of the iron(III) species. When the scan was continued further to negative potential, two irreversible reduction peaks at potentials of *ca.* −0.72 V and −0.95 V were observed, and these are assigned to the corresponding nitro group reduction (*vide infra*). It is surprising that no Cu^{II}/Cu^{I} couple was observed even after a second sweep, as compared to that observed in the parent complex **1**. On the

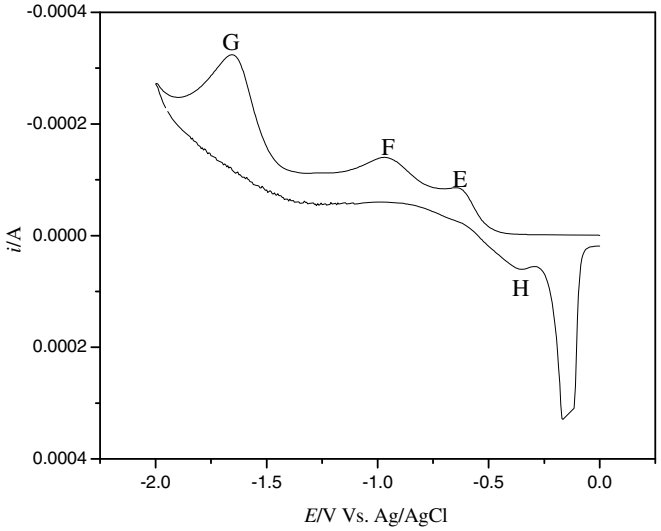

Fig. 12. Cyclic voltammogram of **1** in MeCN at a scan rate of 0.05 V s^{-1}.

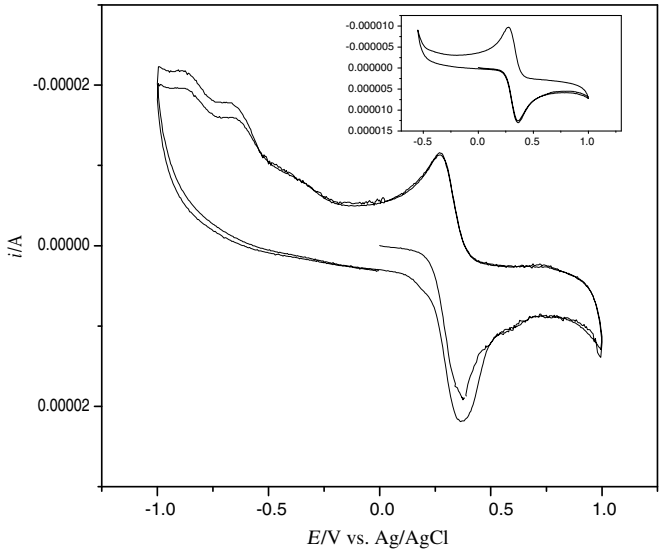

Fig. 13. Cyclic voltammograms of **2** in water at a scan rate of 0.05 V s^{-1}. The scan is reversed before nitro-radical anion formation (inset).

other hand, on the reverse sweep, the peak height of the anodic wave was markedly enhanced in comparison to that of the cathodic wave in the positive potential range, indicating the conversion of $Fe^{II} \rightarrow Fe^{III}$ increases after the nitro group reduction. Since the reduction potential of the $[Fe^{III}(CN)_6]^{3-}/[Fe^{II}(CN)_6]^{4-}$ couple is much more than that of Cu^{II}/Cu^{I} (−0.40 V *versus* Ag/AgCl for complex **1**), most probably the nitro-radical anion transfers its electron to the Fe^{III} instead of the Cu^{II} center and that is why nitro-radical induced copper(II) reduction does not take place as observed in complex **1**. Consequently the Cu^{II}/Cu^{I} couple remains silent towards redox transformation. To check whether the nitro group has any influence upon the iron center, a number of CV profiles were recorded starting from 0.0 V to 1.0 V, 1.0 V to −0.60 V (*i.e.* before nitro-radical anion generation) (Fig. 13, inset) under the same scan rate and it was observed that the peak height and intensity for the anodic and cathodic waves responsible for the $[Fe^{III}(CN)_6]^{3-}/[Fe^{II}(CN)_6]^{4-}$ couple remain invariant even after a second successive sweep. It is well known [25] that the nitro-radical anion is not generated particularly with a platinum working electrode. To confirm whether the reduction peaks arise due to nitro group reduction or for copper (II) reduction, a cathodic CV profile starting from 0.0 V to −1.2 V was recorded using platinum working electrode under same scan rate, but no peak responsible for the nitro-radical anion was observed. In conclusion, it may be assumed that only a portion of the ferrocyanide ion may coordinate to the copper(II) center, facilitating a lower energy pathway for electron transfer. This chemically generated ferricyanide ion on electrochemical processing is reduced to the ferrocyanide by capturing the electron from the nitro-radical anion. In cyclic voltammetry, such a coordinated ferrocyanide ion reduced by a generated nitro-radical, as well as the non-coordinated ferrocyanide ion, enhances the peak height for the $Fe^{II} \rightarrow Fe^{III}$ conversion in the reverse sweep.

The electrochemical behavior of complex **3** warrants special features in comparison to that of the parent complex **1** in MeCN (Fig. 14). The quasi-reversible reduction process for $Cu^{II} \rightarrow Cu^{I}$ (peak I/L) appeared at a slightly more positive potential than that in complex **1** under similar conditions and the corresponding $E_{1/2}$ was estimated as −0.45 V *versus* Ag/AgCl. It is noteworthy that compared to complex **1**, both electrochemical reduction and oxidation for the Cu^{II}/Cu^{I} couple in complex **3** are more facile and this is attributed to the axial ligation of $[Ni(CN)_4]^{2-}$ to the $[Cu(nelin)]^{2+}$ precursor [7b]. Another interesting aspect of complex **3** compared to **1** is that after formation of the Cu^{I} complex (peak I) it does not undergo any disproportionation reaction like 1 at either high or slow scan rates. This is also due to the axial attachment of $[Ni(CN)_4]^{2-}$ to the $[Cu^{II}(nelin)]^{+2}$ moiety which ultimately stabilizes the $[Cu^{I}(nelin)]^{+}$ species. No anodic stripping peak was observed during the back scan after traversing from peak I. Peak J is certainly for $[Cu^{0}(nelin)]^{0}$, or put in better way Cu^{0}, which on back scanning produces an anodic stripping peak at *ca.* 0.0 V.

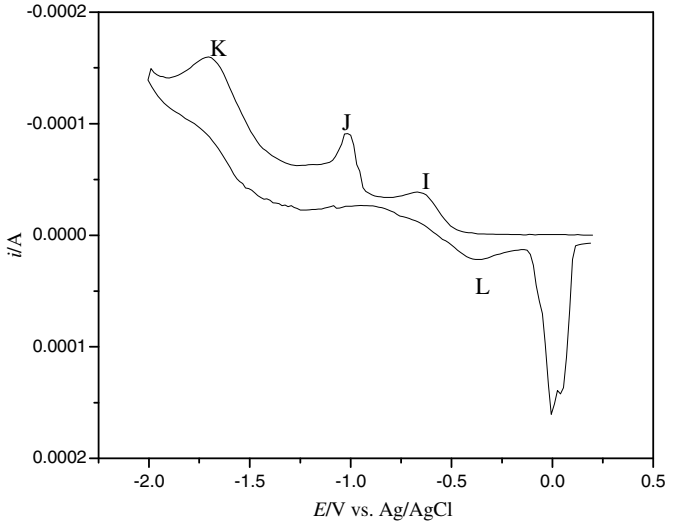

Fig. 14. Cyclic voltammogram of **3** in MeCN at a scan rate of 0.05 V s^{-1}.

4. Conclusions

Two new complexes, $[Cu(nelin)(H_2O)_2]_2[Fe(CN)_6] \cdot 6H_2O$ (**2**) and $[\{Cu(nelin)\}_2Ni(CN)_4](ClO_4)_2 \cdot 2H_2O$ (**3**), have been synthesized using a nitroalkyl-substituted $Cu^{II}N_4$ precursor and have been characterized using the single crystal X-ray diffraction technique. The H-bonded 1D chains of 2 along the *a*-axis, generated from supramolecular synthons using cations and anions, are further propagated into a 3D array to form irregular honeycomb-like channels which are divided into two halves, in each half there is a helical water chain which runs in opposite directions to each other. In complex **3** trinuclear units are arranged in successive rows in a herringbone fashion and bifurcated hydrogen bonding through the uncoordinated terminals of the $[Ni(CN)_4]^{2-}$ units give rise to a supramolecular (4,4) network. Complex **2** exhibits a quasi-glass nature on dehydration, which is important in material science. The electrochemical properties of **1**, 2 and **3** have been investigated in comparative ways using the cyclic voltammetric technique in aqueous and in MeCN solutions with Ag/AgCl as the reference electrode. Electrochemical studies in aqueous medium generate the one-electron reduced nitro-radical anion which is highly important and may find application as a radio-sensitized drug in cancer treatment. Although organic, especially aromatic, nitro compounds have widespread application in medicine and cancer therapy, there is direct proof that nitro-radical anions are involved as an obligate intermediate but in many cases they act as a direct damaging toxin. The corresponding use of coordination complexes bearing a nitro group on a side arm of a ligand fragment has not yet been reported. Inorganic macrocyclic or macrocyclic complexes of transition metals may serve in a better way than the aromatic nitro compounds as drugs, as they may have comparatively better solubility and show a lesser toxic effect.

Acknowledgements

Financial support from the Council for CSIR (Ref. No. 01(7329)/07/EMR-II) and DST (Ref. No. SR/S1/IC-35/2006), New Delhi, India is gratefully acknowledged.

Appendix A. Supplementary data

CCDC 278587 and 278586 contain supplementary crystallographic data for **2** and **3**. These data can be obtained free of charge via http://www.ccdc.cam.ac.uk/conts/retrieving.html, or from the Cambridge Crystallographic Data Centre, 12 Union Road, Cambridge CB2 1EZ, UK; fax: (+44) 1223-336-033; or e-mail: deposit@ccdc.cam.ac.uk. Supplementary data associated with this article can be found, in the online version, at doi:10.1016/j.poly.2008.06.035.

References

[1] (a) J.M. Lehn, Supramolecular Chemistry, VCH, Weinheim, Germany, 1995;
(b) T. Iwamoto, D.D. MacNicol, F. Tod, R. Bishop (Eds.), Comprehensive Supramolecular Chemistry, Pergamon Press, Oxford, 1996, p. 6. (Chapter 19);
(c) G.R. Desiraju, Nature 412 (2001) 397;
(d) M. Kawahara, M.K. Kabir, K. Yamada, K. Adachi, H. Kumagai, Y. Narumi, K.

Kindo, S. Kitagawa, S. Kawata, Inorg. Chem. 43 (2004) 92;
(e) B.H. Ye, M.L. Tong, X.M. Chen, Coord. Chem. Rev. 249 (2005) 545;
(f) A. Ray, D. Maiti, M. Ali, W.S. Sheldrick, H. Meyer-Figge, Indian J. Chem. A 44 (2005) 261 and references cited therein;
(g) A. Ray, M. Mijanuddin, R. Chatterjee, J. Marek, S. Mondal, M. Ali, Inorg. Chem. Commun. 9 (2006) 167 and references cited therein.

[2] (a) O. Kahn (Ed.), Magnetism: A Supramolecular Function, Kluwer, Dordrecht, 1996;
(b) M. Eddaoudi, D.B. Moler, H. Li, B. Chen, T.M. Reineke, M. O'Keeffe, O.M. Yaghi, Acc. Chem. Res. 34 (2001) 319;
(c) Y.R. Martin, M.H. Molina, F.S. Delgado, J. Pasan, C.R. Perez, J. Sanchiz, F. Lloret, M. Julve, Cryst. Eng. Commun. 4 (2002) 522;
(d) A. Ray, C.S. Hong, S. Mondal, M. Mukherjee, M. Ali, Inorg. Chem. Commun. 10 (2007) 527 and references cited therein.

[3] J. Černák, M. Orendáč, I. Potočňák, J. Chomič, A. Orendáčová, J. Skoršepa, A. Feher, Coord. Chem. Rev. 224 (2002) 51.

[4] (a) M. Verdaguer, A. Bleuzen, V. Marvaud, J. Vaissermann, M. Seuleiman, C. Desplanches, A. Scuiller, C. Train, R. Garde, G. Gelly, C. Lomenech, I. Rosenman, P. Veillet, C. Cartier, F. Villain, Coord. Chem. Rev. 190–192 (1999) 1023;
(b) D.H. Kim, J.E. Koo, C.S. Hong, S. Oh, Y. Do, Inorg. Chem. 44 (2005) 4383. and references cited therein.

[5] (a) H.Z. Kou, D.Z. Liao, P. Cheng, Z.H. Jiang, S.P. Yan, G.L. Wang, X.K. Yao, H.G. Wang, J. Chem. Soc., Dalton Trans. (1997) 1503;
(b) D.G. Fu, J. Chen, X.S. Tan, L.J. Jiang, S.W. Zhang, P.J. Zheng, W.X. Tang, Inorg. Chem. 36 (1997) 220;
(c) D. Ghoshal, A.K. Ghosh, T.K. Maji, J. Ribas, G. Mostafa, E. Zangrando, N. Ray Chaudhuri, Inorg. Chim. Acta 359 (2006) 593;
(d) D.J. Chesnut, J. Zubieta, Chem. Commun. (1998) 1707.

[6] (a) E. Colacio, J.M. Domínguez-Vera, M. Gazi, R. Kivekäs, J.M. Moreno, A. Pajunen, J. Chem. Soc., Dalton Trans. (2000) 505;
(b) M. Salah El Fallah, J. Ribas, X. Solans, M. Font-Bardia, J. Chem. Soc., Dalton Trans. (2001) 247;
(c) Z. Smékal, Z. Trávníček, J. Mroziński, J. Marek, Inorg. Chem. Commun. 6 (2003) 1395;
(d) Y.S. You, D. Kim, Y. Do, S.J. Oh, C.S. Hong, Inorg. Chem. 43 (2004) 6899;
(e) N.F. Curtis, H. Puschmann, Acta Crystallogr., Sect. C 60 (2004) m410.

[7] (a) M. Ali, A. Ray, W.S. Sheldrick, H. Mayer-Figge, S. Gao, A.I. Sahmes, New. J. Chem. 28 (2004) 412;
(b) A. Ray, D. Dutta, P.C. Mondal, W.S. Sheldrick, H. Meyer-Figge, M. Ali, Polyhedron 26 (2007) 1012.

[8] (a) D.I. Edwards, M. Dye, H. Crane, J. Gen. Microbiol. 76 (1973) 135;
(b) D.I. Edwards, in: C. Hansch (Ed.), Comprehensive Medicinal Chemistry, fifth 5th ed., vol. 2, Pergamon Press, New York, 1990, p. 725;
(c) D. Greenwood, Antimicrobial Chemotherapy, 13th ed., Oxford University Press, Oxford, UK, 1995;
(d) N.S. Guenay, G. Capau, N. Ulusoy, N. Ergene, G. Oetuek, D. Kaya, Farmaco 54 (1999) 826;
(e) S. Kasai, H. Nagasawa, M. Yamashita, M. Masui, H. Kuwasaka, T. Oshodani, Y. Uto, T. Inomata, S. Oka, S. Inayama, H. Hori, Bioinorg. Med. Chem. 9 (2001) 453;
(f) J.D. Maya, S. Bollo, L.J. Núñez-Vergara, J.A. Squella, Y. Repetto, A. Morello, J. Perie, G. Gauviere, Biochem. Pharmacol. 65 (2003) 999.

[9] (a) J.E. Biaglow, B. Jarabson, C.L. Greenstock, J. Raleigh Mol. Pharmacol. 13 (1977) 269;
(b) C. Viode, N. Bettache, N. Cenas, R. Luise Krauth-Siegel, G. Chauviere, N. Bakalara, J. Perie. Biochem. Pharmacol. 57 (1999) 549;
(c) S. Trinh, G. Reysset, Mutat. Res. 398 (1998) 55.

[10] (a) P.B. Roberts, W.A. Denny, B.F. Cain, Br. J. Cancer 40 (1979) 641;
(b) P.B. Roberts, R.F. Anderson, W.R. Wilson, Int. J. Radiat. Biol. 51 (1987) 641;
(c) W.R. Wilson, B.G. Siim, W.A. Denny, P.L. van Zijl, M.L. Taylor, D.M. Chambers, P.B. Roberts, Radiat. Res. 131 (1992) 257;
(d) T. Sugita, M. Masuoka, Y. Nishikawa, S. Nishimoto, L. Jhou, K. Sasai, T. Kagiya, Anticancer Drug Des. 7 (1992) 277.

[11] (a) K.A. Skov, N.P. Farrell, Int. Radiat. Biol. 52 (1987) 289;
(b) K.A. Skov, Radiat. Res. 112 (1987) 217;
(c) K.A. Skov, N.P. Farrell, Int. J. Radiat. Biol. 57 (1990) 947.

[12] G.E. Adams, I.R. Flockhart, C.E. Smithen, I.J. Stratford, P. Wardman, M.E. Watts, Radiat. Res. 67 (1976) 9.

[13] (a) R.P. Mason, in: W.A. Pryor (Ed.), Free Radicals in Biology, vol. V, Academic Press, New York, 1982, p. 161;
(b) P. Wardman, M.F. Dennis, S.A. Everette, K.B. Patel, M.R.L. Stratford, M. Tracy, in: C.C. Rice-Evans, B.B. Halliwell (Eds.), Biochemical Society Symposium, vol. 61, Portland Press, 1985, p. 171;
(c) P. Wardman, Environ. Health Persp. 64 (1985) 309.

[14] (a) J.H. Tocher, D.I. Edwards, Free Radical Res. Commun. 6 (1989) 39;
(b) J.H. Tocher, D.I. Edwards, Free Radical Res. Commun. 16 (1992) 19;
(c) J. Carbajo, S. Bollo, L.J. Núñez-Vergara, P.A. Navarrete-Encina, J.A. Squella, J. Electroanal. Chem. 494 (2000) 69;
(d) L.J. Núñez-Vergara, D. Farias, S. Bollo, J.A. Squella, Bioelectrochemistry 53 (2000) 103;
(e) J. Carbajo, S. Bollo, L.J. Núñez-Vergara, A. Campero, J.A. Squella, J. Electroanal. Chem. 531 (2002) 187.

[15] P. Comba, N.F. Curtis, G.A. Lawrance, A.M. Sargeson, B.W. Skelton, A.H. White, Inorg. Chem. 25 (1986) 4260.

[16] H. Lund, Cathodic reduction of nitro and related compounds, in: H. Lund, O. Hammerich (Eds.), Organic Electrochemistry, 4th ed., Marcel Dekker, New York, 2001, p. 379.

[17] P.C. Mondal, J. Electroanal. Chem. 570 (2004) 55.

[18] A. Ray, D. Maiti, W.S. Sheldrick, H. Meyer-Figge, S. Mondal, M. Mukherjee, M. Ali, Inorg. Chim. Acta 358 (2005) 3471.

[19] G. M. Sheldrick, SHELXL'97, Program for Crystal Structure Refinement, University of Gottingen, Germany, 1997.

[20] (a) A.G. Sharpe, The Chemistry of the Cyano Complexes of Transition Metals, Academic Press, London, 1976;
(b) K. Nakamoto, Infrared and Raman Spectra of Inorganic and Coordination Compounds, 4th ed., Wiley Interscience, New York, 1987.

[21] J.F. Willart, A. De Gusseme, S. Hemon, G. Odou, F. Danede, M. Descamps, Solid State Commun. 119 (2001) 501.

[22] A. Saleki-Gerhardt, J.G. Stowell, S.R. Byrn, G. Zografi, J. Pharm. Sci. 84 (1996) 318.

[23] N. Onodera, H. Suga, S. Seki, Bull. Chem. Soc. Jpn. 41 (1968) 2222.

[24] N. Shaikh, S. Goswami, A. Panja, X.Y. Wang, S. Gao, R.J. Butcher, P. Banerjee, Inorg. Chem. 43 (2004) 5908.

[25] M. Noel, K.I. Vasu, in: Mohan Primlani (Ed.), Cyclic Voltammetry and the Frontiers of Electrochemistry, Oxford & IBH Publishing Co. Pvt. Ltd., New Delhi, 1990.

meso-cis-1,3-cyclohexanedicarboxylic acid and chiral *cis*-(1*R*,3*S*)-(+)-camphoric acid with trimethyltin chloride under hydrothermal conditions.

2. Results and discussion

2.1. Syntheses

Reactions of 5-nitroisophthalic acid, 4-cyclohexene-1,2-dicarboxylic acid, 1,4-cyclohexanedicarboxylic acid, 1,3-cyclohexanedicarboxylic acid, and camphoric acid with trimethyltin chloride in 1:2 stoichiometry afford air-stable complexes **1**–**5**. The syntheses procedures are shown in Scheme 1a–e.

2.2. Spectroscopic studies

The stretching frequencies of interest are those associated with the acid COO, Sn–C and Sn–O groups. The strong absorption appearing at 442–454 cm^{-1} in the respective IR spectra of the complexes **1–5**, which is absent in the spectra of the free ligand, is assigned to the Sn–O stretching mode of vibration. Also strong absorption appearing at 1574–1615 and 1433–1469 cm^{-1} in the respective spectra of complexes **1–5** is assigned to the asymmetric and symmetric vibrations, respectively, of the COO moiety; moreover, the strong peaks at 649–669 cm^{-1} are assigned to *ν(O–Sn–O)*, indicating O–Sn–O bridging structures. All these values are consistent with that detected in a number of organotin(IV) derivatives [7].

The ^{1}H NMR spectra show the expected integration and peak multiplicities. The single resonance of –OH in the spectra of the free ligands are absent in the spectra of complexes **1–5** indicating the replacement of the carboxylic acid protons by a dimethyltin moiety on the complexes formation. The ^{13}C NMR spectra of all complexes show a significant downfield shift of all carbon resonances compared with the free ligands, the shift is a consequence of an electron density transfer from the ligand to the acceptor. The single resonances at 167.3–171.4 are attributed to the COO groups in complexes **1–5**. The ^{119}Sn NMR spectra of complexes **1–5** show resonances between –116.9 and –259.3 ppm. As reported in the literature [8], values of δ (^{119}Sn) in the ranges −210 to −400, −90 to −190 and 200 to −60 ppm have been associated with six-, five-, and four-coordinated tin centers, respectively. On this basis we can conclude that complexes **1, 2** and **4** have two different coordination environments around the tin atoms, these are confirmed by the X-ray crystal structures of complexes **1, 2** and **4**. Complex **3** as well as complex **5** has only one signal in −138.7 and −116.9 ppm, respectively, thus indicating only existence of five-coordinated atoms for complexes **3** and **5**, which are not completely accordance with the structure in the solid state. Some Sn–O bonds about the six-coordinated tin atoms in complexes **3** and **5** are much longer than the covalent radii of tin and oxygen, maybe these weak Sn–O bonds rupture in solution and the six-coordinated tin atoms become five-coordinated, so only the five-coordinated tin atoms are found in the ^{119}Sn NMR spectra.

2.3. Description of crystal structures

2.3.1. $\{(Me_2Sn)_2[\mu_4\text{-}(C_8H_3NO_6)](\mu_3\text{-}O)\}_n$ (**1**)

The repeating unit and 1D infinite chain structure of complex **1** are illustrated in Figs. 1 and 2, respectively, and selected bond lengths and bond angles are given in Table 2. As shown in Fig. 1, the predominant structural form of complex **1** is dimeric dicarboxylatotetraorganodistannoxane which consists of a central planar $(Me_2Sn)_2O_2$ four-membered ring and two peripheral Me_2Sn units, each bridging oxygen atom in the Sn_2O_2 ring is attached to three Me_2Sn units and as a result these oxygen atoms are three-coordinated. The geometries of all the tin atoms in complex **1** can be classified into two types: pentacoordinated tin (Sn1), and hexacoordinated tin (Sn2). Each of the pentacoordinated tin atoms – Sn1, for example – forms three short Sn–O bonds with three oxygen atoms: one from the Sn_2O_2 moiety and the other two from two different carboxylate groups. Together with the two bonds to methyltin groups, the Sn1 atom may be viewed as a slightly distorted trigonal bipyramid with the axial site occupied by the O(1)#1 and O(1) atoms O(1)#1–Sn(1)–O(1) 168.2(4)). Each of the hexacoordinated tin atoms – Sn2, for example – has an octahedral geometry with four equatorial oxygen atoms and two axial carbon atoms, the geometry being somewhat distorted by the small angles in the stannoxane rings, affecting the equatorial angles. Steric effects between the methyl groups across the stannoxane ring cause the rings to bend away from the center of molecule C(7)–Sn(2)–C(7)#2 154.0(7)°) and also to twist relative to each other.

As shown in Fig. 2, complex **1** has a one-dimensional infinite chain structure constructed from approximately hexagon rings. Each ring is composed of two deprotoned 5-nitroisophthalic acid ligands and two dimeric tetraorganodistannoxane units. 5-Nitroisophthalic acid in a μ_4-bridging mode links two dimeric tetraorganodistannoxane units are shared by the approximately hexagon rings to form a one-dimensional chain coordination polymer. This structural feature of **1** is quite different from that of $\{(Me_2Sn(OAc)_2O)_2\}_n$, a one-dimensional organotin polymer; in which the acetate links the dimeric tetraorganodistannoxane units in a tetradentate mode [9].

2.3.2. $\{(Me_2Sn)_2[\mu_3\text{-}(C_8H_8O_4)](\mu_3\text{-}O)\}_n$ (**2**), $\{(Me_2Sn)_2[\mu_4\text{-}(C_8H_{10}O_4)](\mu_3\text{-}O)\}_n$ (**3**) and $\{(Me_2Sn)_2[\mu_4\text{-}(C_8H_{10}O_4)](\mu_3\text{-}O)\}_n$ (**4**)

The repeating units and 2D polymeric structures of complexes **2, 3** and **4** are illustrated in Figs. 3–8, respectively, and selected bond lengths and bond angles are given in Tables 3–5, respectively. Complexes **2–4** are all 2D organotin polymers made up of the dimeric tetraorganodistannoxane and bridging dicarboxylate units. Complex **2** is a 2D corrugated sheet polymer made up of two types of typical ladder tetraorganodistannoxane units and bridging deprotoned 4-cyclohexene-1,2-dicarboxylic acid ligands. In the first type of the ladder tetraorganodistannoxane units each Sn atom is a five-coordinate geometry, it consists of a central planar $(Me_2Sn)_2O_2$ four-membered ring and two peripheral Me_2Sn units attached to two μ_3-oxygen atoms. Deprotoned 4-cyclohexene-1,2-dicarboxylic acid acts as a tridentate ligand which coordinates to an outer Sn atom through an oxygen atom of the carboxylate and chelates between exocyclic and endocyclic Sn atoms forming a stable six-membered ring through the other carboxylate oxygen atoms. Thus, all the Sn atoms adopt distorted trigonal bipyramidal geometry. The exocyclic and endocyclic Sn atoms lie 0.2539 and 0.0789 Å out of the plane defined by the three-coordinated oxygen atoms, respectively. In the second type of the ladder tetraorganodistannoxane units all the tin atoms can be classified into two types: pentacoordinated tin (Sn4), and hexacoordinated tin (Sn3). Each of the pentacoordinated tin atoms – Sn4, for example – in this complex each have five primary bonds, two to the methyl groups and the others to the μ_3-oxygen atoms, thus adopting a distorted trigonal bipyramid geometry similar to that found in $[(n\text{-BuSn(O)}O_2CR)_2\text{-}n\text{-BuSn}(O_2CR)_3]_2$ (R = Ph and Me) [10]. Each of the hexacoordinated tin atoms – Sn3, for example – forms six primary bonds: two to the methyl groups, two to the μ_3- oxygen atoms and the others to the bidentate carboxylate groups, and the geometry around Sn2 is similar to that found in $\{([Me_2Sn(VA)_{0.5}]_2O)_2{\cdot}2H_2O\}_n$ [VA = 4-hydroxy-3-methoxybenzoic acid] [11] The ladder core can be viewed as four-rung ladder frameworks have found in $[(n\text{-Bu–Sn(O)}O_2CC_6H_{11})_3]_2$ [10], the central Sn(4)–O(10)–Sn(4)#2–O(10)#2 ring is strictly planar, with the terminal tins and terminal oxygen atoms have no deviation out of the ladder plane, the ladder

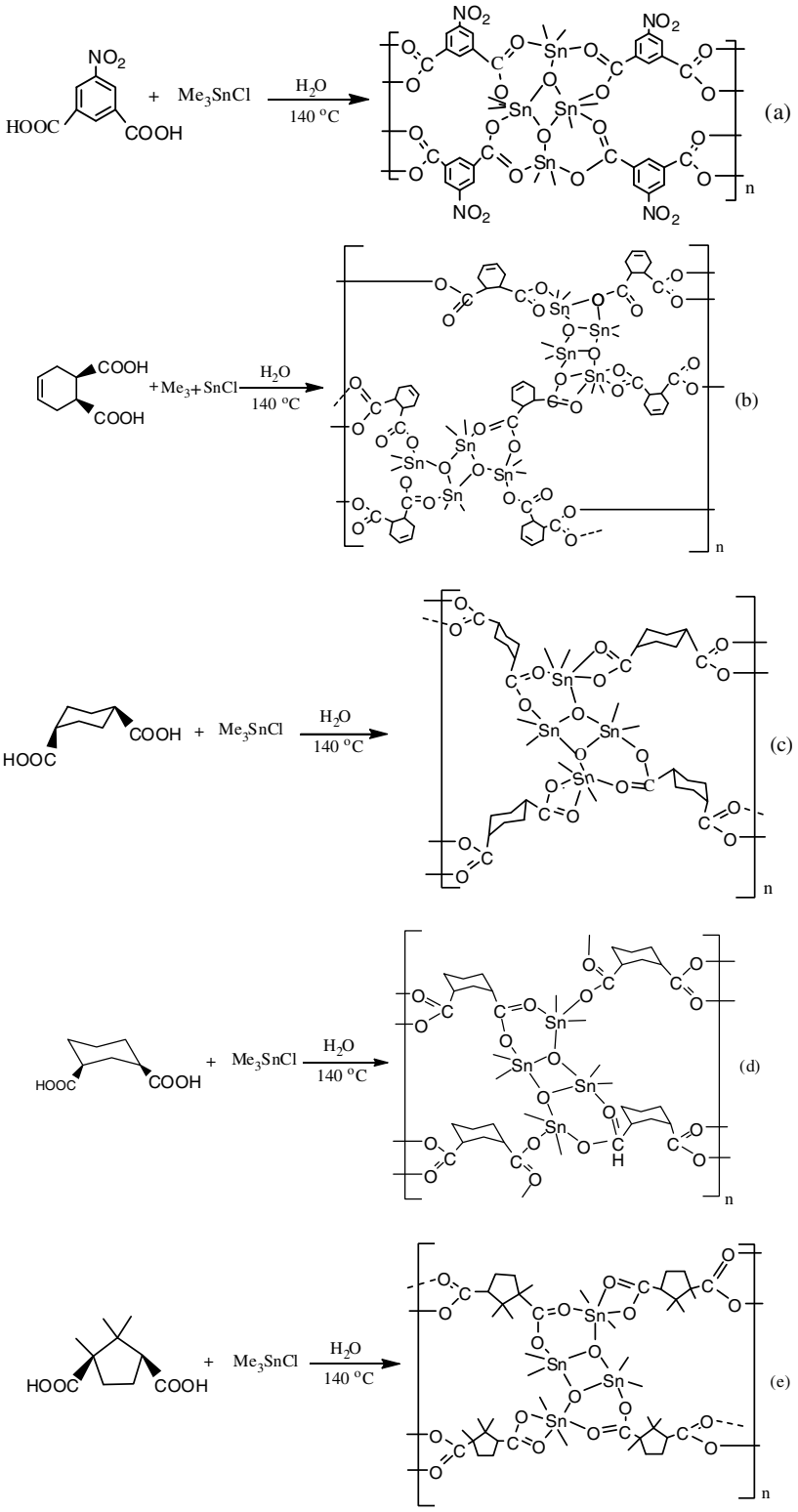

Scheme 1.

does not have linear sides but is bent, with the angles Sn(3)–O(10)–Sn(4)#2 and O(3)–Sn(4)–O(10)#2 being 130.7° and 149.7°, respectively. As shown in Fig. 4, each deprotoned 4-cyclohexene-1,2-dicarboxylic acid as a tridentate ligand connecting two different ladders to give rise to a 2D corrugated structure which consists of 28-membered organotin rings, and the width of 28-ring channel is 10.71 × 9.52 Å (transannular Sn3···Sn3′ and Sn1···Sn1′), the structure is similar to that found in $[(Me_2Sn)_4(\mu_3\text{-DPA})(\mu_4\text{-DPA})(\mu_3\text{-O})_2]_n$ [12], which also was a 2D corrugated sheet polymer made up of the dimeric tetraorganodistannoxane units and bridging DPA ligands (Table 6).

Different from complex **2**, complex **3** is a 2D network polymer made up of only one type of typical ladder tetraorganodistannoxane units and bridging deprotoned 1,4-cyclohexanedicarboxylic

Table 1
Crystal, data collection and structure refinement parameters for **1–5**

Complex	1	2	3	4	5
Empirical formula	$C_{12}H_{15}NO_7Sn_2$	$C_{24}H_{40}O_{10}Sn_4$	$C_{12}H_{22}O_5Sn_2$	$C_{12}H_{22}O_5Sn_2$	$C_{14}H_{26}O_6Sn_2$
M	522.63	963.32	483.68	483.68	527.73
Crystal system	orthorhombic	triclinic	orthorhombic	monoclinic	tetragonal
Space group	*Ibam*	$P\bar{1}$	*Pbca*	*P*2/*c*	*P*4(3)2(1)2
a (Å)	11.3130(16)	9.541(6)	18.596(6)	11.343(2)	9.5136(10)
b (Å)	13.5760(18)	13.119(8)	9.476(3)	7.3614(19)	9.5136(10)
c (Å)	22.030(2)	13.292(8)	19.051(6)	21.191(3)	42.072(3)
α (°)	90	96.377(7)	90	90	90
β (°)	90	96.457(6)	90	103.313(3)	90
γ (°)	90	99.000(7)	90	90	90
V (Å^3)	3383.5(7)	1618.7(16)	3357.0(19)	1721.8(6)	3807.9(6)
Z	8	2	8	4	8
μ (mm^{-1})	2.983	3.097	2.987	2.912	2.646
Reflections collected	6710	10208	15588	7369	23592
Independent reflections	1524	7155	2923	2887	4500
R_{int}	0.0808	0.0607	0.0956	0.0756	0.0704
R_1 [$I > 2\sigma(I)$]/R_1 (all data)	0.0423, 0.1057	0.0668, 0.1555	0.0586, 0.1320	0.0872, 0.2144	0.0652, 0.1627
wR_1[$I > 2\sigma(I)$]]/wR_1 (all data)	0.0923, 0.1594	0.1222, 0.1970	0.1040, 0.1612	0.1323, 0.2433	0.0856, 0.1733

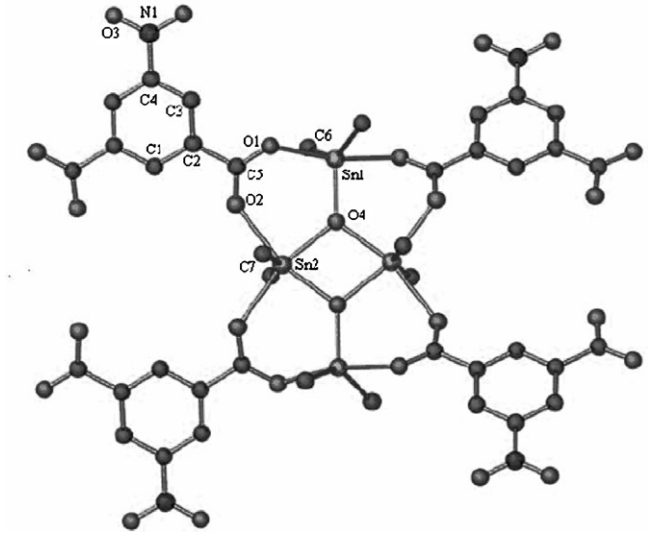

Fig. 1. The repeating unit of complex **1**.

Table 2
Selected bond lengths and bond angels for complex **1**

Bond	Distance (Å)	Bond	Distance (Å)
Sn(1)–O(4)	1.990(9)	Sn(2)–C(7)	2.107(10)
Sn(1)–C(6)	2.096(12)	Sn(2)–O(4)	2.125(5)
Sn(1)–O(1)	2.239(7)	Sn(2)-O(2)	2.385(6)
Angle	**Amplitude (°)**	**Angle**	**Amplitude (°)**
O(4)–Sn(1)–C(6)	110.7(3)	C(7)–Sn(2)–O(4)#2	99.0(3)
C(6)–Sn(1)–C(6)#1	138.5(7)	C(7)#2–Sn(2)–O(4)#2	101.5(3)
C(6)–Sn(1)–O(1)#1	86.1(4)	O(4)–Sn(2)–O(4)#2	76.0(4)
O(4)–Sn(1)–O(1)	95.9(2)	C(7)–Sn(2)–O(2)#	81.6(4)
C(6)–Sn(1)–O(1)	89.7(4)	O(4)–Sn(2)–O(2)#2	163.9(3)
O(1)#1–Sn(1)–O(1)	168.2(4)	C(7)–Sn(2)–O(2)	83.2(4)
C(7)–Sn(2)–C(7)#2	154.0(7)	O(4)–Sn(2)–O(2)	87.9(2)
C(7)–Sn(2)–O(4)	101.5(3)	O(2)#2–Sn(2)–O(2)	108.2(4)
C(7)#2–Sn(2)–O(4)	99.0(3)		

#1: $x, -y+1, -z+3/2$; #2: $-x+1, -y+1, z$.

acid ligands. This ladder tetraorganodistannoxane units is a tetranuclear centrosymmetric dimeric structure with one four-membered planar Sn(2)–O(1)–Sn(2)#1–O(1)#1 ring and two six-membered planar Sn(1)–O(1)–Sn(2)–O(3)–C(7)–O(2) and Sn(1)#1–O(1)#1–Sn(2)#1–O(3)#1–C(7)#1–O(2)#1 rings. The four Me_2Sn moieties are linked by two bridging carboxylate groups, while the remaining two carboxylate groups are attached to each of the exocyclic Me_2Sn moieties. Similar tetraorganodistannoxane units have been documented in the arrangement of $[Bu_2SnLOLSnBu_2]_2$ (L = *o*-methylbenzoic acid) and $[(n\text{-}Bu_2SnO_2CC_6H_4\text{–}o\text{-}Cl)_2O]_2$ [13]. The geometries of all the tin atoms in complex **3** can also be classified into two types: pentacoordinated tin (Sn2), and hexa-

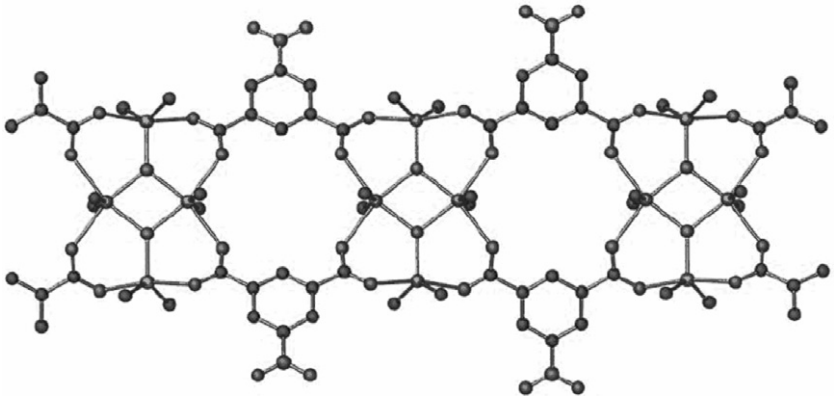

Fig. 2. The 1D infinite polymeric chain structure of complex **1**.

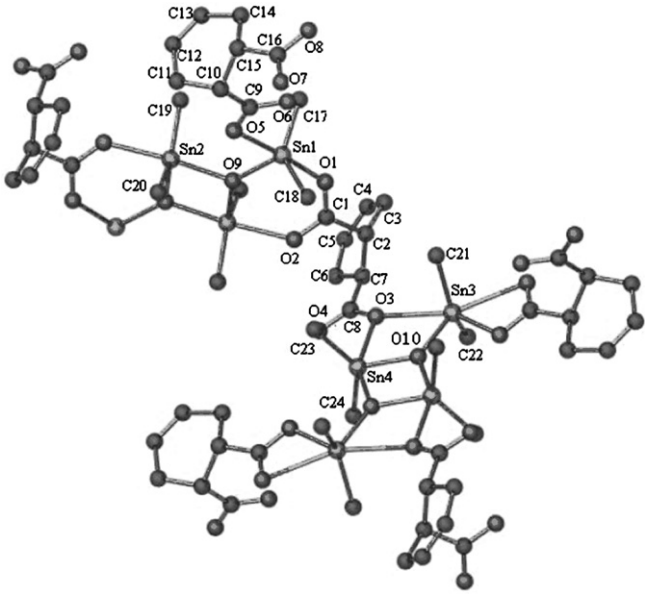

Fig. 3. The repeating unit of complex **2**.

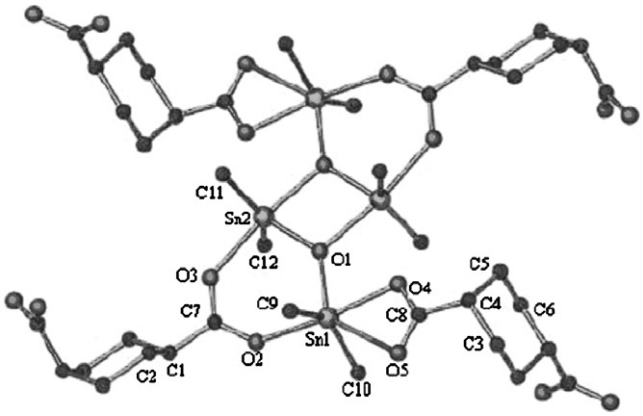

Fig. 5. The repeating unit of complex **3**.

coordinated tin (Sn1). The pentacoordinated tin atoms –Sn2, for example, also form three short Sn–O bonds with three oxygen atoms: two from the Sn_2O_2 moiety and the other one from the carboxylate group, together with the two bonds to methyltin groups, the Sn2 atom may be viewed as slightly distorted trigonal bipyramid with the axial site occupied by the O(1)#1 and O(3) atoms ((O1)#1–Sn(2)–O(3) 166.8(3)°). Each of the hexacoordinated tin atoms – Sn1, for example – forms four short Sn–O bonds with four oxygen atoms: one from the Sn_2O_2 moiety and the other three from two different carboxylate groups. Together with the two bonds to methyltin groups, the Sn1 atom may be viewed as distorted octahedral geometry. Thus, each deprotoned 1,4-cyclohexanedicarboxylic acid affords its four O atoms as a tetradentate ligand connecting two adjacent ladders to give rise to a 2D network polymer (Fig. 7), which is different from that found in other related organotin complexes [14].

Similar to complex **3**, complex **4** is also a 2D network polymer made up of only one type of typical ladder tetraorganodistannoxane units and bridging deprotoned 1,3-cyclohexanedicarboxylic acid ligands. This ladder tetraorganodistannoxane units is also a tetranuclear centrosymmetric dimeric structure with a central planar $(Me_2Sn)_2O_2$ four-membered ring and two peripheral Me_2Sn units. each bridging oxygen atom in the Sn_2O_2 ring is attached to three Me_2Sn units and as a result these oxygen atoms are three-coordinated. The geometries of all the tin atoms in complex **4** can also be classified into two types: pentacoordinated tin (Sn2), and hexacoordinated tin (Sn1). Each of the pentacoordinated tin atoms – Sn2, for example – forms three short Sn–O bonds with three oxygen atoms: two from the Sn_2O_2 moiety and the other two from dicarboxylate groups. Together with the two bonds to methyltin groups, the Sn2 atom may be viewed as a slightly distorted trigonal bipyramid with the axial site occupied by the O(5A) and O(2) atoms O(5)#1–Sn(2)–O(2) 168.2(4)°). Each of the hexacoordinated tin atoms – Sn1, for example – forms four short Sn–O bonds with four oxygen atoms: one from the Sn_2O_2 moiety and the other three from three different dicarboxylate groups. Together with the two bonds to methyltin groups Sn1 forms an octahedral geometry. The geometry being somewhat distorted by the small angles in the stannoxane rings, affecting the equatorial angles. Steric effects between the methyl groups across the center of the molecule ((C(10)–Sn(1)–C(9) = 148.8(10)°) and also to twist relative to each other. As shown in Fig. 9, each deprotoned 1,3-cyclohexanedicarboxylic acid as a tetradentate ligand connecting two adjacent ladders to give rise to a 2D network polymer which consists of 20-membered organotin rings, and the width of 20-ring channel is 12.429×7.439 Å (transannular Sn1···Sn1′and Sn2···Sn2′), which is larger than other organotin complexes we have been reported [15] (Fig. 10).

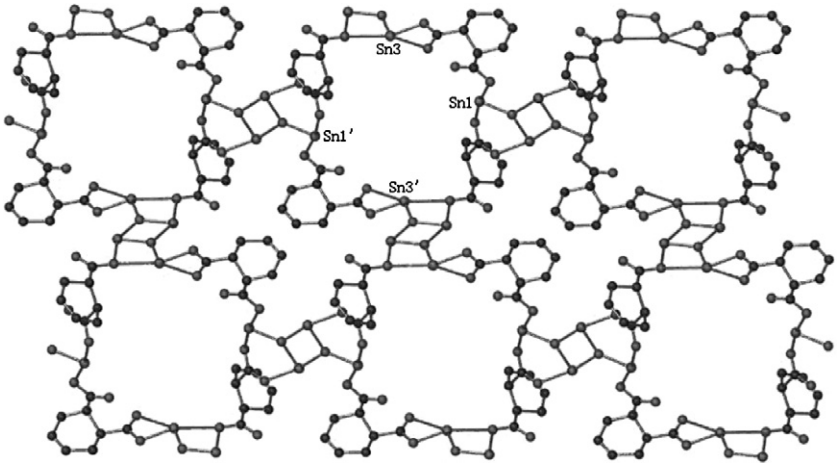

Fig. 4. The 2D corrugated polymer of complex **2** (the methyl groups are omitted for clarity).

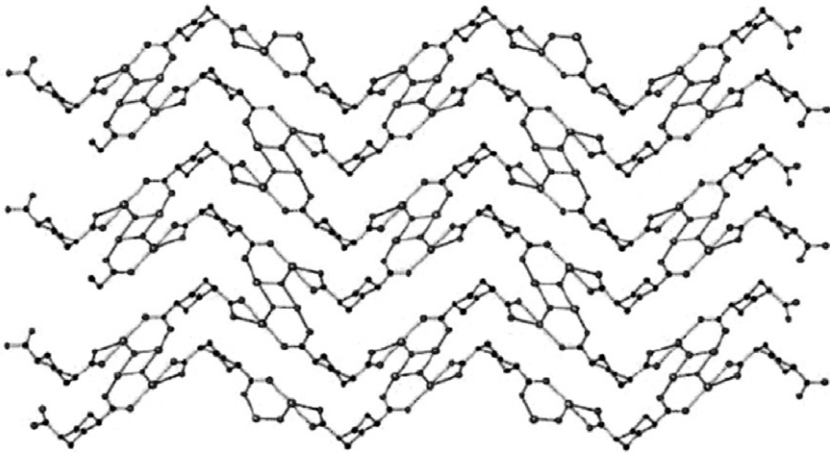

Fig. 6. The 2D network structure of complex **3** (the methyl groups are omitted for clarity).

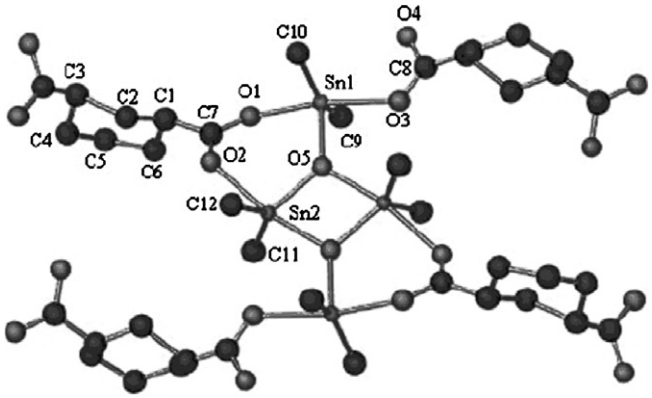

Fig. 7. The repeating unit of complex **4**.

*2.3.3. {(Me_2Sn)$_2$[μ_3-($C_8H_8O_4$)](μ_3-O)}$_n$ (**5**)*

X-ray diffraction study reveals that complex **5** crystallizes in the tetragonal chiral space group *P*4(3)2(1)2. the molecular of complex **5** also is a tetranuclear centrosymmetric dimeric structure with one four-membered planar Sn(2)–O(5)–Sn(2)#2–O(5)#2 ring and two six-membered planar Sn(2)–O(4C)–C(7C)–O(3C)–Sn(1)#2–O(5)#2 and Sn(1)–O(5)–Sn(2)#2–O(4)#1–C(7)#1–O(3)#1 rings, The four Me_2Sn moieties are linked by two bridging carboxylate groups, while the remaining two carboxylate groups are attached to each of the exocyclic Me_2Sn moieties, the central Sn(2)–O(5)–Sn(2)#2–O(5)#2 ring is strictly planar, with the terminal tins being 0.0013 Å out of the ladder planar. The geometries of all the tin atoms in complex **5** can also be classified into pentacoordinated tin (Sn2) and hexacoordinated tin (Sn1). Each of the pentacoordinated tin atoms – Sn2, for example – forms five primary bonds, and the geometry around Sn2 is similar to that in complexes **1–4**, Each of the hexacoordinated tin atoms – Sn1, for example – forms six primary bonds and its coordinate environment is essentially the same as its counterpart in complex **3** except for little short of the O(1)–Sn(1) distance (2.152 Å) and O(2)–Sn(1) distance (2.717 Å). The polymeric structure of complex **5** is different from complexes **1–4**. Each deprotoned camphoric acid affords its four carboxylate O atoms as a tetradentate ligand connecting two adjacent ladders to give rise to a 3D organotin framework, which is an irregular 3D polymer and to the best of our knowledge, similar organotin structures have so far not been reported by any other people.

In summary, through the hydrothermal reaction, we have obtained five new organotin polymers consisting of dimeric dicarboxylatotetraorganodistannoxane derived from the trimethyltin chloride and dicarboxylate acids, in all complexes **1–5** the trimethyltin groups became dimethyltin groups due to the Sn–C cleavage on the condition of high temperature. The results suggest that hydrothermal reaction is a potent synthetic route to prepare

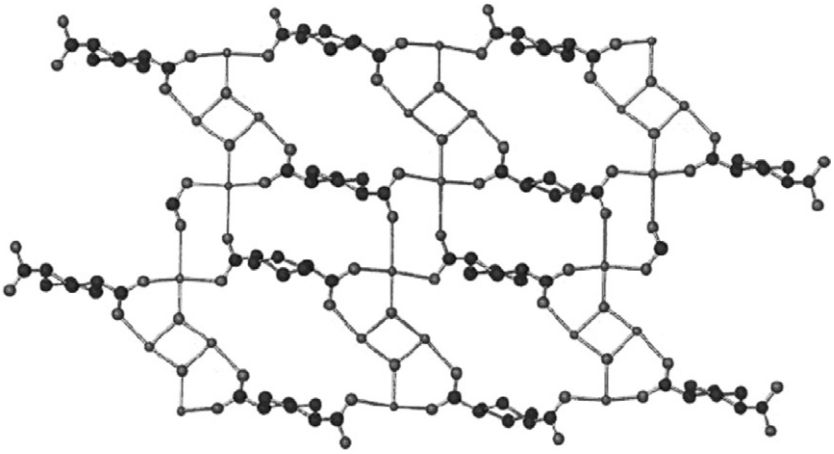

Fig. 8. The 2D network structure of complex **4** (the methyl groups are omitted for clarity).

Table 3
Selected bond lengths and bond angels for complex **2**

Bond	Distance (Å)	Bond	Distance (Å)
Sn(1)–O(9)	1.999(7)	Sn(3)–O(10)	1.992(8)
Sn(1)–C(17)	2.073(15)	Sn(3)–O(8)#2	2.064(8)
Sn(1)–C(18)	2.088(2)	Sn(3)–C(22)	2.083(12)
Sn(1)–O(5)	2.149(9)	Sn(3)–C(21)	2.092(14)
Sn(1)–O(1)	2.292(10)	Sn(3)–O(3)	2.633(8)
Sn(2)–O(9)#1	2.028(7)	Sn(4)–O(10)	2.028(8)
Sn(2)–C(19)	2.074(15)	Sn(4)–C(23)	2.101(12)
Sn(2)–C(20)	2.097(17)	Sn(4)–C(24)	2.102(12)
Sn(2)–O(9)	2.131(8)	Sn(4)–O(10)#3	2.135(7)
Sn(2)–O(2)#1	2.233(10)	Sn(4)–O(3)	2.193(8)
Sn(2)–O(5)	2.896(8)		
Angle	Amplitude (°)	Angle	Amplitude (°)
O(9)–Sn(1)–C(17)	111.9(5)	O(10)–Sn(3)–O(8)#2	84.5(3)
C(17)–Sn(1)–C(18)	137.8(8)	O(10)–Sn(3)–C(21)	107.1(6)
O(9)–Sn(1)–O(5)	116.6(5)	O(10)–Sn(3)–O(3)	67.5(3)
O(9)–Sn(1)–O(1)	90.4(3)	O(8)#2–Sn(3)–O(3)	151.8(3)
O(5)–Sn(1)–O(1)	170.4(4)	C(21)–Sn(3)–O(3)	87.4(5)
O(9)#1–Sn(2)–C(19)	110.8(5)	O(10)–Sn(4)–C(23)	114.6(5)
O(9)#1–Sn(2)–O(9)	75.9(3)	O(10)–Sn(4)–C(24)	110.7(5)
C(19)–Sn(2)–O(9)	95.9(5)	O(10)–Sn(4)–O(10)#3	73.3(3)
O(9)#1–Sn(2)–O(2)#1	89.0(3)	O(10)–Sn(4)–O(3)	76.8(3)
O(9)–Sn(2)–O(2)#1	163.4(3)	C(23)–Sn(4)–O(3)	92.0(5)
O(9)#1–Sn(2)–O(5)	138.1(3)	C(24)–Sn(4)–O(3)	99.7(4)
O(9)–Sn(2)–O(5)	62.7(3)	O(10)#3–Sn(4)–O(3)	149.7(3)
O(2)#1–Sn(2)–O(5)	132.9(3)		

#1: $-x$, $-y+1$, $-z$; #2: $-x+1$, $-y+1$, $-z+1$; #3: $-x+1$, $-y+2$, $-z+1$.

Table 4
Selected bond lengths and bond angels for complex **3**

Bond	Distance (Å)	Bond	Distance (Å)
Sn(1)–O(1)	2.013(8)	Sn(2)–C(12)	2.103(16)
Sn(1)–C(9)	2.079(14)	Sn(2)–C(11)	2.109(13)
Sn(1)–C(10)	2.122(15)	Sn(2)–O(1)#1	2.163(8)
Sn(1)–O(4)	2.179(9)	Sn(2)–O(3)	2.252(10)
Sn(1)–O(2)	2.261(10)	Sn(2)–O(1)	2.034(8)
Angle	Amplitude (°)	Angle	Amplitude (°)
O(1)–Sn(1)–C(9)	104.9(5)	O(1)–Sn(2)–C(12)	106.2(5)
O(1)–Sn(1)–C(10)	114.0(5)	O(1)–Sn(2)–C(11)	109.4(5)
C(9)–Sn(1)–C(10)	140.0(7)	C(12)–Sn(2)–C(11)	143.9(6)
O(1)–Sn(1)–O(4)	80.3(3)	O(1)–Sn(2)–O(1)#1	76.3(3)
C(9)–Sn(1)–O(4)	100.1(5)	C(12)–Sn(2)–O(1)#1	99.0(5)
C(10)–Sn(1)–O(4)	95.2(5)	C(11)–Sn(2)–O(1)#1	95.3(5)
O(1)–Sn(1)–O(2)	89.0(3)	O(1)–Sn(2)–O(3)	91.4(3)
C(9)–Sn(1)-O(2)	89.1(6)	C(12)–-Sn(2)–O(3)	88.9(5)
C(10)–Sn(1)–O(2)	83.0(5)	C(11)–Sn(2)–O(3)	84.2(5)
O(4)–Sn(1)–O(2)	167.3(3)	O(1)#1–Sn(2)–O(3)	166.8(3)

#1: $-x$, $-y+1$, $-z+1$.

discrete dimeric dicarboxylatotetraorgandistannoxane that hardly arise from the common synthetic methods.

3. Experimental details

3.1. Materials and methods

Trimethyltin chloride, 5-nitroisophthalic acid, 4-cyclohexene-1,2-dicarboxylic acid, 1,4-cyclohexanedicarboxylic, 1,3-cyclohexanedicarboxylic acid and camphoric acid are commercially available and they are used without further purification. The melting points were obtained with an X-4 digital micro melting-point apparatus and were uncorrected. Infrared-spectra were recorded on a Nicolet-5700 spectrophotometer using KBr discs and sodium chloride optics. ^{1}H and ^{13}C NMR spectra were recorded on Varian Mercury Plus 400 spectrometer operating at 400, 100.6 and 149.2 MHz, respectively. The spectra were acquired at room temperature (298 K) unless otherwise specified; ^{13}C NMR spectra are broadband proton decoupled. The chemical shifts were reported in ppm with respect to the references and were stated relative to external tetramethylsilane (TMS) for ^{1}H and ^{13}C NMR and Me_4Sn for ^{119}Sn NMR. Elemental analyses (C, H, N) were performed with a PE-2400II apparatus.

Table 5
Selected bond lengths and bond angels for complex **4**

Bond	Distance (Å)	Bond	Distance (Å)
Sn(1)–O(5)	2.031(14)	Sn(2)–O(5)	2.034(13)
Sn(1)–C(10)	2.11(2))	Sn(2)–C(11)	2.08(2)
Sn(1)–C(9)	2.11(2)	Sn(2)–O(5)#1	2.125(12)
Sn(1)–O(1)	2.147(13)	Sn(2)–C(12)	2.21(2)
Sn(1)–O(3)	2.287(14)	Sn(2)–O(2)	2.272(14)
Angle	Amplitude (°)	Angle	Amplitude (°)
O(5)–Sn(1)–C(10)	104.9(7)	O(5)–Sn(2)–C(12)	115.6(7)
O(5)–Sn(1)–C(9)	106.3(7)	C(11)–Sn(2)–C(12)	134.3(8)
C(10)–Sn(1)–C(9)	148.8(10)	O(5)#1–Sn(2)–C(12)	99.0(7)
O(5)–Sn(1)–O(1)	91.2(5)	O(5)–Sn(2)–O(2)	93.4(5)
C(10)–Sn(1)–O(1)	94.1(7)	C(11)–Sn(2)–O(2)	86.3(7)
C(9)–Sn(1)–O(1)	83.6(7)	O(5)#1–Sn(2)–O(2)	169.0(5)
O(5)–Sn(1)–O(3)	82.6(5)	C(12)–Sn(2)–O(2)	81.7(7)
C(10)–Sn(1)–O(3)	95.2(7)	C(9)–Sn(1)–O(3)	90.5(7)
O(1)–Sn(1)–O(3)	169.9(5)	O(5)–Sn(2)–C(11)	108.9(7)
O(5)–Sn(2)–O(5)#1	76.3(6)	C(11)–Sn(2)–O(5)#1	100.6(7)

#1: $-x$, $-y$, $-z+1$.

Table 6
Selected bond lengths and bond angels for complex **5**

Bond	Distance (Å)	Bond	Distance (Å)
Sn(1)–O(5)	2.026(7)	Sn(2)–C(14)	2.051(17)
Sn(1)–C(12)	2.079(15)	Sn(2)–C(13)	2.119(18)
Sn(1)–C(11)	2.102(17))	Sn(2)–O(5)	2.165(7)
Sn(1)–O(1)	2.152(7)	Sn(2)–O(4)#3	2.216(10)
Sn(1)–O(3)#1	2.313(11)	Sn(2)–O(5)#2	2.018(7)
Angle	Amplitude (°)	Angle	Amplitude (°)
O(5)–Sn(1)–C(12)	106.5(6)	O(5)#2–Sn(2)–O(5)	76.5(3)
O(5)–Sn(1)–C(11)	111.1(6)	C(14)–Sn(2)–O(5)	96.2(6)
C(12)–Sn(1)–C(11)	140.3(8)	C(13)–Sn(2)–O(5)	95.3(6)
O(5)–Sn(1)–O(1)	82.7(3)	O(5)#2–Sn(2)–O(4)#3	90.4(3)
C(12)–Sn(1)–O(1)	103.0(6)	C(14)–Sn(2)–O(4)#3	95.1(7)
C(11)–Sn(1)–O(1)	94.1(6)	C(13)–Sn(2)–O(4)#3	81.2(6)
O(5)–Sn(1)–O(3)#1	89.7(4)	O(5)–Sn(2)–O(4)#3	164.7(4)
C(12)–Sn(1)–O(3)#1	90.1(6)	C(11)–Sn(1)–O(3)#1	78.0(6)
O(1)–Sn(1)–O(3)#1	166.3(4)	O(5)#2–Sn(2)–C(14)	107.0(5)
O(5)#2–Sn(2)–C(13)	108.1(6)	C(14)–Sn(2)–C(13)	144.7(7)

#1: $-y+3/2$, $x+1/2$, $z-1/4$; #2: y, x, $-z$; #3: $x+1/2$, $-y+3/2$, $-z+1/4$.

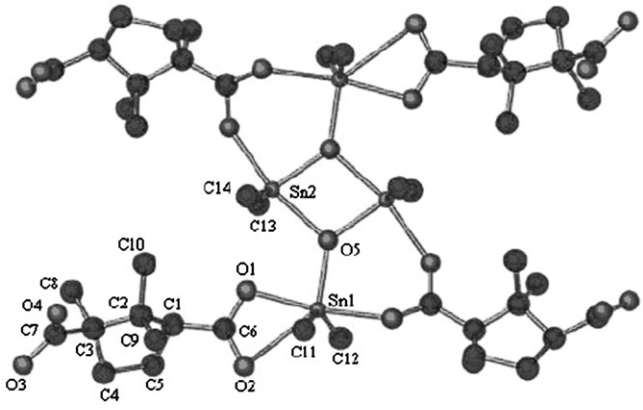

Fig. 9. The repeating unit of complex **5**.

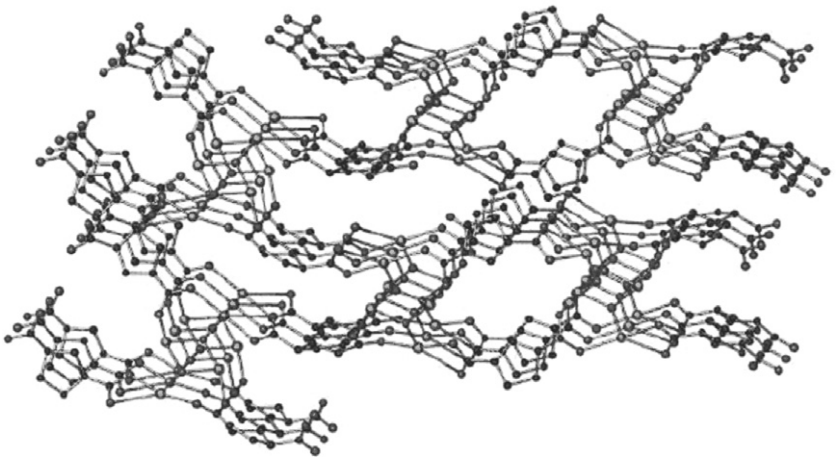

Fig. 10. The 3D polymeric structure of complex **5** (the methyl groups are omitted for clarity).

3.2. Syntheses of complexes **1–6**

3.2.1. $\{(Me_2Sn)_2[\mu_4\text{-}(C_8H_3NO_6)](\mu_3\text{-}O)\}_n$ (**1**)

Complex **1** was synthesized by the hydrothermal reaction of 5-nitroisophthalic acid (0.211 g, 1 mmol), trimethyltin chloride (0.398 g, 2 mmol) and H_2O (20 ml) in a Teflon-lined autoclave at 140 °C for 3 days. After the reaction autoclave was cooled to room temperature for 24 h, colorless crystals of complex **1** were collected and washed with hexane. Yield: 82%. M.p. 178–181 °C. *Anal.* Calc. for $C_{12}H_{15}NO_7Sn_2$: C, 27.58; H, 2.89, N, 2.68. Found: C, 27.76; H, 2.67; N, 2.88%. IR (KBr, cm^{-1}): ν_{as}(COO), 1574; ν_s(COO), 1469; ν(Sn–C), 555; ν(Sn–O), 442; ν(O–Sn–O), 668. ^{1}H NMR [$(CD_3)_2SO$, ppm]: δ 0.82 (12H, Sn–CH_3, $^2J_{Sn,H}$ = 88 Hz), 7.52–7.63 (3H, Ar-H). ^{13}C NMR [$(CD_3)_2SO$, ppm]: 169.2, 128.3–141.6, 8.35 ($^1J_{Sn,C}$ = 784 Hz). ^{119}Sn NMR: −259.3 ($^2J_{Sn,Sn}$ = 96 Hz), −124.4 ($^2J_{Sn,Sn}$ = 101 Hz).

3.2.2. $\{(Me_2Sn)_2[\mu_4\text{-}(C_8H_3NO_6)](\mu_3\text{-}O)\}_n$ (**2**)

Complex **2** was synthesized by the hydrothermal reaction of 4-cyclohexene-1,2-dicarboxylic acid (0.170 g, 1 mmol), trimethyltin chloride (0.398 g, 2 mmol) and H_2O (20 ml) in a Teflon-lined autoclave at 140 °C for 3 days. Yield: 77%. M.p. 197–199 °C. *Anal.* Calc. for $C_{24}H_{40}O_{10}Sn_4$: C, 29.92; H, 4.18. Found: C, 29.70; H, 4.37%. IR (KBr, cm^{-1}): ν_{as}(COO), 1580; ν_s(COO), 1433; ν(Sn–C), 547; ν(Sn–O), 446; ν(O–Sn–O), 669. ^{1}H NMR [$(CD_3)_2SO$, ppm]: δ 0.79 (24H, Sn–CH_3, (12H, Sn–CH_3, $^2J_{Sn,H}$ = 92 Hz), 5.46 (4H, γH), 2.01 (8H, βH), 2.68 (4H, αH). ^{13}C NMR [$(CD_3)_2SO$, ppm]: 167.3, 129.7, 26.8, 22.3, 8.67 ($^1J_{Sn,C}$ = 796 Hz). ^{119}Sn NMR: −247.1 ($^2J_{Sn,Sn}$ = 108 Hz), −144.3.

3.2.3. $\{(Me_2Sn)_2[\mu_4\text{-}(C_8H_{10}O_4)](\mu_3\text{-}O)\}_n$ (**3**)

Complex **3** was synthesized by the hydrothermal reaction of 1,4-cyclohexanedicarboxylic acid (0.172 g, 1 mmol), trimethyltin chloride (0.398 g, 2 mmol) and H_2O (20 ml) in a Teflon-lined autoclave at 140 °C for 3 days. Yield: 74%. M.p. 161–163 °C. *Anal.* Calc. for $C_{12}H_{22}O_5Sn_2$: C, 29.80; H, 4.58. Found: C, 29.51; H, 4.81%. IR (KBr, cm^{-1}): ν_{as}(COO), 1583; ν_s(COO), 1461; ν(Sn–C), 552; ν(Sn–O), 449; ν(O–Sn–O), 664. ^{1}H NMR [$(CD_3)_2SO$, ppm]: δ 0.82 (12H, Sn–CH_3), 4.15–4.18 (8H, CH_2), 4.86 (2H, CH, $^2J_{Sn,H}$ = 84 Hz). ^{13}C NMR [$(CD_3)_2SO$, ppm]: 168.7, 46.6, 28.4, 8.17 ($^1J_{Sn,C}$ = 820 Hz). ^{119}Sn NMR: −138.7 ($^2J_{Sn,Sn}$ = 125 Hz).

3.2.4. $\{(Me_2Sn)_2[\mu_4\text{-}(C_8H_{10}O_4)](\mu_3\text{-}O)\}_n$ (**4**)

Complex **4** was synthesized by the hydrothermal reaction of 1,3-cyclohexanedicarboxylic acid (0.172 g, 1 mmol), trimethyltin chloride (0.398 g, 2 mmol) and H_2O (20 ml) in a Teflon-lined autoclave at 140 °C for 3 days. Yield: 81%. M.p. 182–184 °C. *Anal.* Calc. for $C_{12}H_{22}O_5Sn_2$: C, 29.80; H, 4.58. Found: C, 29.55; H, 4.32%. IR (KBr, cm^{-1}): ν_{as}(COO), 1597; ν_s(COO), 1468; ν(Sn–C), 549; ν(Sn–O), 452; ν(O–Sn–O), 653. ^{1}H NMR [$(CD_3)_2SO$, ppm]: δ 0.81 (12H, Sn–CH_3, $^2J_{Sn,H}$ = 86 Hz), 4.01–4.32 (8H, CH_2), 4.94 (2H, CH). ^{13}C NMR [$(CD_3)_2SO$, ppm]: 170.3, 47.6, 29.7, 8.36 ($^1J_{Sn,C}$ = 812 Hz). ^{119}Sn NMR: −235.6, −117.8 ($^2J_{Sn,Sn}$ = 108 Hz).

3.2.5. $\{(Me_2Sn)_2[\mu_4\text{-}(C_{10}H_{14}O_4)](\mu_3\text{-}O)\}_n$ (**5**)

Complex **5** was synthesized by the hydrothermal reaction of camphoric acid (0.200 g, 1 mmol), trimethyltin chloride (0.398 g, 2 mmol) and H_2O (20 ml) in a Teflon-lined autoclave at 140 °C for 3 days. Yield: 80%. M.p. 201–202 °C. *Anal.* Calc. for $C_{14}H_{26}O_6Sn_2$: C, 31.86; H, 4.97. Found: C, 31.61; H, 4.78%. IR (KBr, cm^{-1}): ν_{as}(COO), 1615; ν_s(COO), 1460; ν(Sn–C), 574; ν(Sn–O), 454; ν(O–Sn–O), 649. ^{1}H NMR [$(CD_3)_2SO$, ppm]: δ 0.80 (12H, Sn–CH_3, $^2J_{Sn,H}$ = 89 Hz), 4.01–4.18 (4H, CH_2), 4.46 (1H, CH) 1.37 (9H, ring-CH_3). ^{13}C NMR [$(CD_3)_2SO$, ppm]: δ 176.8, 174.4, 57.5, 52.7, 41.1, 39.8, 34.9, 22.3–23.7, 12.3 ($^1J_{Sn,C}$ = 748 Hz). ^{119}Sn NMR: −116.9 ($^2J_{Sn,Sn}$ = 114 Hz).

3.3. X-ray structure analyses of **1–5**

Diffraction data were collected on a Smart CCD area-detector with graphite monochromated Mo Kα radiation (λ = 0.71073 Å). A semiempirical absorption correction was applied to the data. The structure was solved by direct methods using SHELXS-97 and refined against F^2 by full matrix least-squares using SHELXL-97. Hydrogen atoms were placed in calculated positions. Crystal data and experimental details of the structure determinations are listed in Table 1.

Acknowledgment

We thank the National Nature Science Foundation of China (20271025) for financial support.

Appendix A. Supplementary data

CCDC 640900, 654376, 654378, 659335 and 654377 contain the supplementary crystallographic data for complexes **1, 2, 3, 4 and 5**. These data can be obtained free of charge via http://www.ccdc.cam.ac.uk/conts/retrieving.html, or from the Cambridge Crystallographic Data Centre, 12 Union Road, Cambridge CB2 1EZ, UK;

fax: (+44) 1223-336-033; or e-mail: deposit@ccdc.cam.ac.uk. Supplementary data associated with this article can be found, in the online version, at doi:10.1016/j.poly.2008.06.039.

References

[1] (a) V. Chandrasekhar, S. Nagen, V. Baskar, Coord. Chem. Rev. 1 (2002) 235;
(b) P.J. Hagrman, D. Hagrman, J. Zubieta, Angew. Chem. 111 (1999) 2798 Angew. Chem., Int. Ed. 38 (1999) 2638;
(c) P.J. Langley, J. Hulliger, Chem. Soc. Rev. 28 (1999) 279;
(d) P.J. Stang, Chem. Eur. J. 4 (1998) 19;
(e) M. Fujita, Struct. Bond. (Berlin) 96 (2000) 177;
(f) R.W. Saalfrank, E. Uller, B. Demleitner, I. Bernt, Struct. Bond. (Berlin) 96 (2000) 1749;
(g) G.F. Swiegers, T.J. Malefetse, Chem. Rev. 100 (2000) 3483;
(h) B.J. Holliday, C.A. Mirkin, Angew. Chem. 113 (2001) 2076;
(j) B.J. Holliday, C.A. Mirkin, Angew. Chem., Int. Ed. 40 (2001) 2022.

[2] (a) R. García-Zarracino, H. Höpfl, Angew. Chem. 116 (2004) 1533 Angew. Chem., Int. Ed. Engl. 43 (2004) 1507;
(b) R. García-Zarracino, H. Höpfl, J. Am. Chem. Soc. 127 (2005) 3120;
(c) R. García-Zarracino, J. Ramos-Quiñones, H. Höpfl, Inorg. Chem. 42 (2003) 3835;
(d) T.P. Lockhart, Organometallics 7 (1988) 1438;
(e) G. Prabusankar, R. Murugavel, Organometallics 23 (2004) 5644;
(f) S.W. Ng, V.G.K. Das, G. Pelizzi, F. Vitali, Heteroatom Chem. 1 (1990) 433;
(g) J. Meunier-Piret, M. Boualam, R. Willem, M. Gielen, Main Group Met. Chem. 16 (1993) 329.

[3] (a) R.R. Holmes, Acc Chem. Res. 22 (1989) 190;
(b) E.R.T. Tiekink, Trends Organomet. Chem. 1 (1994) 71;
(c) E.R.T. Tiekink, Appl. Organomet. Chem. 5 (1991) 7;
(d) J. Beckmann, D. Dakternieks, A. Duthie, F.S. Kuan, K. Jurkschat, M. Schürmann, E.R.T. Tiekink, New J. Chem. 28 (2004) 1268;
(e) M. Mehring, G. Gabriele, S. Hadjikakou, M. schürmann, D. Dakternieks, K. Jurkschat, Chem. Commun. (2002) 834;
(f) M. Mehring, I. Paulus, B. Zobel, M. schürmann, K. Jurkschat, A. Duthie, D. Dakternieks, Eur. J. Inorg. Chem. (2001) 153.

[4] V. Chandrasekhar, S. Nagendran, R. Azhakar, M.R. Kumar, A. Srinivasan, K. Ray, T.K. Chandrashekar, C. Madhavaiah, S. Verma, U.D. Priyakumar, G.N. Sastry, J. Am. Chem. Soc. 127 (2005) 2410.

[5] (a) D.M. Low, L.F. Jones, A. Bell, E.K. Brechin, T. Mallah, E. Rivière, S.J. Teat, E.J.L. McInnes, Angew. Chem., Int. Ed. 42 (2003) 3781;
(b) J. Spandl, I. Brüdgam, H. Hartl, Angew. Chem., Int. Ed. 40 (2001) 4081;
(c) S.O.H. Gutschke, D.J. Price, A.K. Powell, P.T. Wood, Angew. Chem., Int. Ed. 38 (1999) 1088;
(d) G.L. Zheng, J.F. Ma, Z.M. Su, L.K. Yan, J. Yang, Y.Y. Li, J.F. Liu, Angew. Chem., Int. Ed. 43 (2004) 2409.

[6] (a) C.L. Ma, J.K. Li, R.F. Zhang, D.Q. Wang, Inorg. Chim. Acta 358 (2005) 4575;
(b) C.L. Ma, G.R. Tian, R.F. Zhang, Inorg. Chem. Commun. 9 (2006) 882.

[7] (a) V. Chandrasekhar, P. Thilagar, J.F. Bickley, A. Steiner, J. Am. Chem. Soc. 127 (2005) 11556;
(b) V. Chandrasekhar, P. Thilagar, P. Sasikumar, J. Organomet. Chem. 691 (2006) 961.

[8] J. Holecek, M. Nadvornik, K. Handlir, A. Lycka, J. Organomet. Chem. 315 (1986) 299.

[9] T.P. Lockhart, W.F. Manders, E.M. Holt, J. Am. Chem. Soc. 108 (1986) 6611.

[10] (a) R.R. Holmes, Acc. Chem. Res. 22 (1989) 190;
(b) R.R. Holmes, Phosphorus, Sulfur Silicon 1 (1999) 150.

[11] R.G. Xiong, J.L. Zuo, X.Z. You, H.K. Fun, S.S. Raj, Organometallics 19 (2000) 4183.

[12] R.H. Wang, M.C. Hong, J.H. Luo, R. Cao, J.B. Weng, Eur. J. Inorg. Chem. (2002) 2082.

[13] (a) S.P. Narula, S. Kaur, R. Shankar, S.K. Bharadwaj, R.K. Chadha, J. Organomet. Chem. 506 (1996) 181;
(b) J. Bechmann, M. Biesemans, K. Hassler, K. Jurkschat, J.C. Marrtins, M. Schurmann, R. Willem, Inorg. Chem. 37 (1998) 4891.

[14] (a) J.X. Tao, W.J. Xiao, Q.C. Yang, J. Organomet. Chem. 531 (1997) 223;
(b) H.D. Yin, Q.B. Wang, S.C. Xue, J. Organomet. Chem. 690 (2005) 435.

[15] (a) C.L. Ma, Y.F. Han, R.F. Zhang, D.Q. Wang, Eur. J. Inorg. 15 (2005) 3024;
(b) C.L. Ma, J.K. Li, R.F. Zhang, D.Q. Wang, J. Organomet. Chem. 691 (2006) 1713.

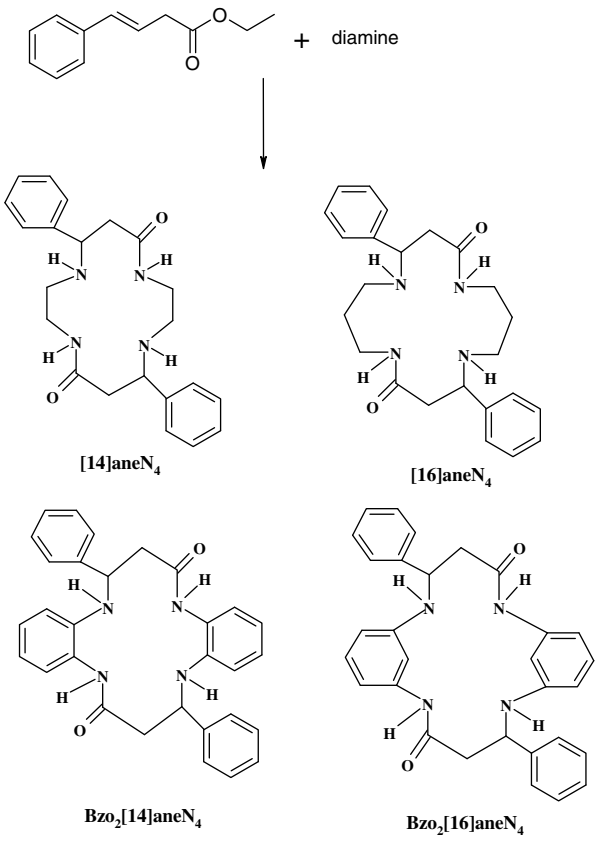

Scheme 1.

both the reactants and products when involved in chemical reactions and processes. The large internal surface area and void volumes with extremely narrow pore size distribution as well as functional centers homogeneously dispersed over the surface make nanoporous solids highly active materials. Over the last decade, there has been a dramatic increase in the synthesis, characterization and application of novel nanoporous materials [1–15].

In this work tetraaza dioxo diphenyl ligands and their encapsulated complexes were chosen (Schemes 1 and 2) for the oxidation reaction because, so far, encapsulated tetraaza dioxo diphenyl nickel(II) complexes have not been used within the nanopores of zeolite-Y for the oxidation of cyclohexene. The use of these encapsulated complexes as nanocatalysts can enhance and increase the selectivity in the oxidation reaction. The HGNM can act as windows for the selection of a suitable nanocatalyst for the oxidation reaction. In this paper the synthesis and characterization of nickel(II) complexes of 14- and 16-membered tetraaza dioxo diphenyl macrocyclic ligands, [14]aneN$_4$: 1,5,8,12-tetraaza-2,9-dioxo-4,11-diphenylcyclotetradecane; [16]aneN$_4$: 1,5,9,13-tetraaza-2,10-dioxo-4,12-diphenylcyclohexadecane; Bzo$_2$[14]aneN$_4$: dibenzo-1,5,8,12-tetraaza-2,9-dioxo-4,11-diphenylcyclotetradecane and Bzo$_2$[16]aneN$_4$: dibenzo-1,5,9,13-tetraaza-2,10-dioxo-4,12-diphenylcyclohexadecane, are reported and these complexes are encapsulated within the nanopores of zeolite-Y by the template condensation of ethylcinnamate and [bis(diamine)nickel(II)], producing [Ni([14]aneN$_4$)]$^{2+}$–NaY, [Ni([16]aneN$_4$)]$^{2+}$–NaY, [Ni(Bzo$_2$[14]aneN$_4$)]$^{2+}$–NaY and [Ni(Bzo$_2$[16]aneN$_4$)]$^{2+}$–NaY, as shown in Schemes 1 and 2 and used in the oxidation of cyclohexene with molecular oxygen.

2. Experimental

2.1. Materials and physical measurements

Cyclohexene was distilled under nitrogen and stored over molecular sieves (4 Å). Cyclohexanone was used as an internal standard for the quantitative analysis of the product using gas chromatography. Reference samples of 2-cyclohexene-1-ol and 2-cyclohexene-1-one

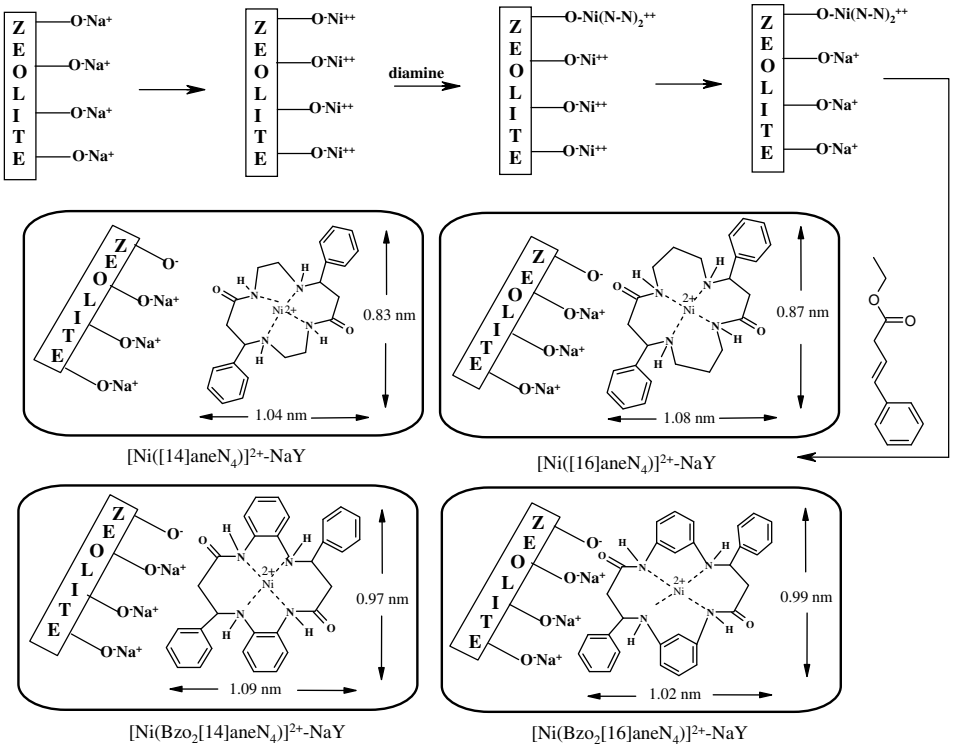

Scheme 2.

(Aldrich) were distilled and stored in a refrigerator. NaY with a Si:Al ratio of 2.53 was purchased from Aldrich (Lot No. 67812). The complex $[Ni(N–N)_2](ClO_4)_2$ was prepared according to the published procedures [16]. FAB mass spectra were recorded on a Kratos MS50TC spectrometer. FT-IR spectra were recorded on a Shimadzu Varian 4300 spectrophotometer in KBr pellets. The electronic spectra of the neat complexes were taken on a Shimadzu UV–Vis scanning spectrometer (Model 2101 PC). The stability of the encapsulated catalyst was checked after the reaction by UV–Vis spectroscopy, as was the possible leaching of the complex in the reaction solution after filtration of the zeolite. The amounts of metallocomplexes encapsulated in the zeolite matrix were determined by elemental analysis and by subtracting the amount of metallocomplex left in the solution after the synthesis of the catalysts, as determined by UV–Vis spectroscopy, from the amount taken for the synthesis. Atomic absorption spectra (AAS) were recorded on a Perkin–Elmer 4100–1319 spectrophotometer using a flame approach, after acid (HF) dissolution of known amounts of the zeolitic material, and SiO_2 was determined by gravimetric analysis. Diffuse reflectance spectra (DRS) were registered on a Shimadzu UV/3101 PC spectrophotometer the range 1500–200 nm, using MgO as a reference. The elemental analysis (carbon, hydrogen and nitrogen) of the materials was obtained from a Carlo ERBA Model EA 1108 analyzer. XRD patterns were recorded by a Rigaku D-max C III, X-ray diffractometer using Ni-filtered Cu Kα radiation. Nitrogen adsorption measurements were performed at 77 K using a Coulter Ofeisorb 100CX instrument. The samples were degassed at 150 °C until a vacuum better than 10^{-3} Pa was obtained. Micropore volumes were determined by the *t*-method, a "monolayer equivalent area" was calculated from the micropore volume [17,18]. The electrochemical data was obtained in acetonitrile with 0.1 M $(n\text{-}Bu)_4NClO_4$ as the supporting electrolyte. The working electrode was a platinum disk, the auxiliary electrode was a coiled platinum wire and the reference electrode was $Ag/AgClO_4$ (0.1 M in CH_3CN), which showed +0.24 V versus SCE.

2.2. Synthesis of the 14-, and 16-membered tetraaza dioxo diphenyl macrocyclic ligands

The tetraaza dioxo diphenyl macrocyclic ligands ([14]aneN$_4$, [16]aneN$_4$, Bzo$_2$[14]aneN$_4$ or Bzo$_2$[16]aneN$_4$) were prepared by following the procedures reported in Ref. [19]. A hot ethanolic solution (20 ml) of ethylcinnamate (3.52 g, 0.02 mol) and a hot ethanolic solution (20 ml) of diamine (0.02 mol), 1,2-diaminoethane (1.20 g), 1,3-diaminopropane (1.48 g), 1,2-diaminobenzene (2.16 g) or 1,3-diaminobenzene (2.16 g) were mixed slowly with constant stirring. This mixture was refluxed at 80 °C for 12 h in the presence of a few drops of concentrated hydrochloric acid. On cooling, a white precipitate was formed which was filtered, washed with cold ethanol, and dried under vacuum over P_4O_{10}. The purity was checked by the HPLC technique.

2.3. Preparation of the [Ni([14 or 16]aneN$_4$)](ClO$_4$)$_2$ and [Ni(Bzo$_2$[14 or 16]aneN$_4$)](ClO$_4$)$_2$complexes

Nickel(II) perchlorate hexahydrate (0.01 mol) dissolved in ethanol (20 ml) was reacted with an ethanolic (20 ml) solution of the tetraaza dioxo diphenyl ligands ([14]aneN$_4$, [16]aneN$_4$, Bzo$_2$[14]aneN$_4$ or Bzo$_2$[16]aneN$_4$) (0.01 mol) by refluxing for 4 h under a nitrogen atmosphere. The mixture was heated at reflux for 6 h until an orange solution resulted. The solution was cooled to room temperature and filtered to remove nickel hydroxide. Excess lithium perchlorate dissolved in methanol was added to the filtrate, and the mixture was kept in the refrigerator until an orange solid formed. The solids were filtered, washed thoroughly with cold ethanol and dried in vacuum.

2.4. Preparation of Ni(II)–NaY

Two grams of NaY zeolite were suspended in 100 ml distilled water, which contained nickel(II) nitrate (0.025 M). The mixture was then heated while stirring at 90 °C for 24 h. The solid was filtered, washed with hot distilled water until the filtrate was free from any nickel(II) ion (by AAS of filtrate) content and dried for 10 h at 80 °C under vacuum. The ionic exchange degree was determined by atomic absorption spectrophotometry.

2.5. Preparation of [Ni(N–N)$_2$]$^{2+}$–NaY

Typically a 4 g sample of NaY zeolite was mixed with 0.37 g of [bis(diamine)nickel(II)] perchlorate, the diamine 1,2-diaminopropane, 1,3-diaminopropane, 1,2-diaminobenzene or 1,3-diaminobenzene suspended in 100 ml of methanol, and then refluxed for 8 h. The pale yellow solid consisting of $[Ni(N–N)_2]^{2+}$, exchanged with Na^+ in NaY and denoted as $[Ni(N–N)_2]^{2+}$–NaY, was collected by filtration, and then washed with ethanol. The resulted zeolites, were Soxhlet extracted with *N*,*N*′-dimethylformamide (for 4 h) and then with ethanol (for 3 h) to remove excess unreacted diamine and any Ni(II) complexes adsorbed onto the external surface of the crystalline zeolite. The resulting light blue solids were dried at 60 °C under vacuum for 24 h.

2.6. Preparation of host–guest nanocomposite materials, [Ni([14 or 16]aneN$_4$)]$^{2+}$–NaY and [Ni(Bzo$_2$ [14 or 16]aneN$_4$)]$^{2+}$–NaY

To a stirred methanol suspension (100 ml) of $[Ni(N–N)_2]^{2+}$–NaY (2 g) was slowly added ethylcinnamate (under N_2 atmosphere). The mixture was heated under reflux conditions for 24 h until a pale yellow suspension resulted. The solution was filtered and the resulting zeolites, were Soxhlet extracted with *N*,*N*′-dimethylformamide (for 6 h) and then with ethanol (for 5 h) to remove excess unreacted products from the amine-ester condensation and any nickel(II) complexes adsorbed onto the external surface of the crystalline zeolite. The resulting pale yellow solids were dried at 70 °C under vacuum for 12 h. The remaining [bis(diamine)nickel(II)] ions in the zeolite were removed by exchanging with aqueous 0.1 M NaCl solution. The stability of the encapsulated catalyst was checked after the reaction by UV–Vis spectroscopy, as was the possible leaching of the complex into the reaction solution after filtration of the zeolite.

2.7. Oxidation of cyclohexene, general procedure

General procedure for oxidation of cyclohexene with molecular oxygen: 10 ml of cyclohexene and 1.2×10^{-5} mol of heterogeneous catalyst were added to a glass reactor with a gas inlet tube connected to a gas burette and an oxygen storage bottle. The mixture was heated to 70 °C in a water bath and stirred with a magnetic stirring bar. The oxidation reactions were performed under atmospheric pressure of molecular oxygen in the absence of solvent, and 2-cyclohexene-1-ol and 2-cyclohexene-1-one were the major products.

3. Results and discussion

3.1. Synthesis of [Ni([14 or 16]aneN$_4$)] (ClO$_4$)$_2$ and [Ni(Bzo$_2$ [14 or 16]aneN$_4$)](ClO$_4$)$_2$

The deep yellow complexes [Ni([14 or 16]aneN$_4$)](ClO$_4$)$_2$ and [Ni(Bzo$_2$[14 or 16]aneN$_4$)](ClO$_4$)$_2$ readily dissolve in polar solvents such as H_2O, CH_3CN, CH_3NO_2 and Me_2SO_2. The nickel(II) complexes are extremely stable in the solid state and in solution and are

Table 1
Elemental analysis, vibrational parameters and molecular ion peaks for the ligands and the tetraaza dioxo diphenyl macrocyclic nickel(II) complexes

Complex	Calculated (found)					IR (KBr, cm^{-1})						FAB mass (m/z)	
	C (%)	H (%)	N (%)	C/N	Ni (%)	**I**	**II**	**III**	**IV**	ν_{N-H}	ν_{M-N}	$[M-ClO_4]^+$	$[M-2ClO_4]^{2+}$
$[14]aneN_4$	69.45 (69.28)	7.42 (7.30)	14.72 (14.90)	4.72 (4.65)		1624	1593	1249	780	3286			
$[Ni([14]aneN_4)](ClO_4)_2$	41.41 (41.20)	4.42 (4.31)	8.78 (8.92)	4.72 (4.62)	9.20 (9.03)	1623	1590	1247	778	3255	345	538	439
$[16]aneN_4$	70.56 (70.33)	7.89 (7.74)	13.71 (13.88)	5.15 (5.07)		1620	1590	1248	780	3280			
$[Ni([16]aneN_4)](ClO_4)_2$	43.27 (43.02)	4.84 (4.65)	8.41 (8.56)	5.15 (5.03)	8.81 (8.64)	1620	1590	1246	780	3250	340	566	467
$Bzo_2[14]aneN_4$	75.61 (75.40)	5.92 (5.73)	11.76 (11.84)	6.43 (6.37)		1630	1596	1252	782	3290			
$[Ni(Bzo_2[14]aneN_4)](ClO_4)_2$	49.08 (48.83)	3.84 (3.69)	7.63 (7.82)	6.43 (6.24)	8.00 (7.82)	1632	1594	1250	782	3260	350	635	535
$Bzo_2[16]aneN_4$	75.61 (75.43)	5.92 (5.71)	11.76 (11.88)	6.43 (6.35)		1627	1594	1250	782	3288			
$[Ni(Bzo_2[16]aneN_4)](ClO_4)_2$	49.08 (48.80)	3.84 (3.72)	7.63 (7.79)	6.43 (6.26)	8.00 (7.79)	1628	1592	1253	781	3257	346	635	535

relatively stable against ligand dissociation even in highly acidic solutions. The molecular formulae of the complexes have been assigned on the basis of the results of their elemental analyses and the molecular ion peaks in the mass spectra (Table 1). All the mass spectra showed molecular ion peaks for the 1:1 metal-to-ligand stoichiometry, with no further peaks above them. A preliminary identification of the metal complexes was made on the basis of their IR spectra, which exhibited no bands characteristic of free primary amine, thus supporting the proposed macrocyclic skeleton (Scheme 1). The EI mass spectra of the free ligands confirm the proposed formula by showing a peak at 381 amu ($C_{22}H_{28}N_4O_2$), 409 amu ($C_{24}H_{32}N_4O_2$) and 477 amu ($C_{30}H_{28}N_4O_2$) corresponding to the macrocyclic moiety.

The molar conductance values of the complexes (~220 Ω^{-1} mol^{-1} cm^2), measured in nitromethane, correspond to 1:2 electrolytes. The overall geometries of all the macrocycles have been deduced on the basis of the observed values of the magnetic moments and the band positions in the electronic spectra. The magnetic moments (−0.08 to −0.12 μ_B) of the nickel(II) complexes measured in the solid state correspond to the square-planar coordination geometry of the complexes (Table 2).

The 14- and 16-membered tetraaza dioxo diphenyl macrocyclic nickel(II) complexes undergo intense color changes due to deprotonation of the macrocyclic ligand in the presence of amine bases such as pyridine and Et_3N. Similar N–H deprotonations have been observed with other metal complexes containing N–H linkages. For the nickel(II) complexes, Et_3N is sufficiently basic to facilitate formation of the molecular complexes. For the preparation of the deprotonated form of $[Ni(Bzo_2[14]aneN_6)](ClO_4)_2$, Et_3N (0.5 ml) was added to a solution of 200 mg of $[Ni(Bzo_2[14]aneN_6)](ClO_4)_2$ in 15 ml of CH_3CN. The shiny-brown product, which began precipitating within minutes, was filtered after 0.5 h under a N_2 atmosphere, washed with anhydrous EtOH, and dried in a vacuum. The product was characterized by elemental analysis and IR spectroscopy. The elemental analysis data support formula (I). IR (KBr, cm^{-1}): 3204 (ν_{N-H}). *Anal.* Calc. for $[Ni(C_{30}H_{26}N_4)]$: Ni, 11.00; C, 67.58; H, 4.92; N, 10.50. Found: Ni, 10.82; C, 67.39; H, 4.80; N, 10.63%. The N–H stretching frequency of this compound $[Ni(C_{30}H_{26}N_4)]$, 3204 cm^{-1}, is reduced significantly from its dicationic precursor, $[Ni(Bzo_2[14]aneN_4)](ClO_4)_2$, 3260 cm^{-1}.

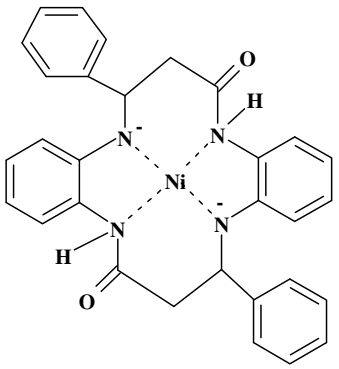

(I)

3.2. ^{1} H NMR spectral study

The ^{1}H NMR spectra of the tetraaza dioxo diphenyl ligands ([14]$aneN_4$, [16]$aneN_4$, Bzo_2[14]$aneN_4$, Bzo_2[16]$aneN_4$) do not give any signal corresponding to primary amine and alcoholic protons. They give a doublet in the region 8.60–8.73 ppm, which is due to

Table 2
Magnetic moment, electronic spectral (cm^{-1}; ε, $dm^3\ mol^{-1}\ cm^{-1}$) and molar conductance (in $MeNO_2$ solutions) values of the tetraaza dioxo diphenyl macrocyclic nickel(II) complexes

Sample	Solvent	$1A_{1g}$ (D) → $1A_{2g}$(G)	$1A_{1g}$ (D) → $1B_{2g}$(G)	$1A_{1g}$ (D) → $1E_g$(G)	μ_{eff} (MB)	Λ_M[a] ($\Omega^{-1}\ cm^2\ M^{-1}$)
$[Ni([14]aneN_4)](ClO_4)_2$	DMSO	13800 (56)	21360 (95)	24970 (136)	−0.08	230
	$MeNO_2$	14150 (75)	21640 (114)	25200 (153)		
	H_2O	13900 (67)	22400 (107)	25030 (146)		
	In 3.0 M NaCl	13930 (70)	22480 (109)	25090 (148)		
$[Ni([16]aneN_4)](ClO_4)_2$	DMSO	13640 (58)	21200 (97)	24800 (140)	−0.09	225
	$MeNO_2$	13840 (78)	21480 (116)	25000 (154)		
	H_2O	13700 (72)	21220 (110)	24830 (148)		
	In 3.0 M NaCl	13750 (74)	21280 (114)	24860 (150)		
$[Ni(Bzo_2[14]aneN_4)](ClO_4)_2$	DMSO	14050 (53)	21640 (88)	25190 (130)	−0.11	210
	$MeNO_2$	14320 (72)	21930 (108)	25440 (150)		
	H_2O	14100 (66)	21700 (103)	25230 (144)		
	In 3.0 M NaCl	14130 (68)	21740 (104)	25280 (146)		
$[Ni(Bzo_2[16]aneN_4)](ClO_4)_2$	DMSO	13980 (54)	21570 (90)	25040 (133)	0.12	206
	$MeNO_2$	14200 (73)	21860 (110)	25320 (155)		
	H_2O	14000 (67)	21590 (103)	25100 (145)		
	In 3.0 M NaCl	14010 (69)	21630 (105)	25110 (148)		

[a] In nitromethane.

the amide group (–NH–CO–, 4H) protons [20]. Signals appear in the region ~1.57, ~2.38 and ~7.26 ppm, which correspond to methyne (–CH–CH_2–), methylene (–CH_2–CO–) and benzenoid protons, respectively. The presence of another signal at δ5.17–5.22 ppm is due to the protons of the –NH group (Table 3). The diamagnetic nature of the Ni(II) complexes of $[Ni(Bzo_2[14\ or\ 16]aneN_6)](ClO_4)_2$ has allowed their characterization by NMR spectrometry. ^1H NMR spectra of the Ni(II) complexes exhibit very broad peaks in D_2O, CH_3CN-d_3 and Me_2SO-d_6 but sharp resolvable peaks in CH_3NO_2-d_3. This indicates that a considerable amount of paramagnetic octahedral species of $[Ni(Bzo_2[14]aneN_4)(Solvent)_2]^{2+}$ exists in donating solvents, where as the Ni(II) complexes of $Bzo_2[14]aneN_4$ exist primarily as diamagnetic square-planar species in CH_3NO_2-d_3. The ^1H NMR spectra of the nickel complex $[Ni(Bzo_2[14]aneN_4)](ClO_4)_2$ gave a singlet at 7.27 ppm corresponding to the C_6H_5 (10H) protons. However, the ^1H NMR spectra of the complexes $[Ni(Bzo_2[14\ or\ 16]aneN_4)](ClO_4)_2$ showed a multiplet in the region 7.35–7.45 ppm, corresponding to the –C_6H_4– ring protons (8H). The ^1H NMR spectra of all the complexes showed a broad signal at ~6.95 ppm which can be assigned to secondary amine protons (4H). A singlet for the complexes at 2.38 ppm corresponds to the CH_2 (4H) protons adjacent to nitrogen. However, none of the spectra show any signal corresponding to free primary amine protons for any of the complexes.

Table 3
^1H NMR data for the complexes in CD_3NO_2 solvent

	–N–H, 4H	–CH_2–CO	–C_6H_5	–C_6H_4–
$[14]aneN_4$	8.66	2.37	7.26	
$[Ni([14]aneN_4)](ClO_4)_2$	8.85	2.38	7.28	
$[16]aneN_4$	8.60	2.38	7.25	
$[Ni([16]aneN_4)](ClO_4)_2$	8.79	2.39	7.28	
$Bzo_2[14]aneN_4$	8.73	2.39	7.27	7.36–7.45
$[Ni(Bzo_2[14]aneN_4)](ClO_4)_2$	8.91	2.40	7.27	7.40–7.50
$Bzo_2[16]aneN_4$	8.70	2.39	7.27	7.35–7.44
$[Ni(Bzo_2[16]aneN_4)](ClO_4)_2$	8.88	2.39	7.29	7.41–7.49

3.3. Synthesis of host–guest nanocomposite materials

The synthesis of tetraaza dioxo diphenyl nickel(II) complexes encapsulated in the nanocavity of zeolite-Y involves two steps: (i) exchange of $[Ni(N–N)_2]^{2+}$ (diamine = 1,2-diaminopropane, 1,3-diaminopropane, 1,2-diaminobenzene or 1,3-diaminobenzene) ions with NaY in methanol solution and (ii) reaction of $[Ni(N–N)_2]^{2+}$–NaY with excess ethylcinnamate in methanol where ethylcinnamate slowly enters into the nanocavity of zeolite-Y due to its template nature and interacts with [bis(diamine)nickel(II)] ions. Soxhlet extraction using methanol finally purified the impure complexes. The remaining uncomplexed metal ions in the zeolite were removed by exchange with aqueous 0.01 M NaCl solution. As one extra anionic ligand would be required to balance the overall charge on the Ni(II), Cl^- of NaCl used during the exchange process fulfills this requirement. Thus, the formula of the nickel(II) complexes may be written as $[Ni([14]aneN_4)]^{2+}$–NaY, $[Ni([16]aneN_4)]^{2+}$–NaY, $[Ni(Bzo_2[14]aneN_4)]^{2+}$–NaY and $[Ni(Bzo_2[16]aneN_4)]^{2+}$–NaY. The percentage metal content determined before and after encapsulation by inductively coupled plasma (ICP), along with their expected formula, is presented in Table 4. As crude mass was extracted with methanol, the metal ion content found after encapsulation is only due to the presence of metal complexes in the nanopores of the zeolite-Y. The molecular formula of the complexes are based on the neat complexes $[Ni([14]aneN_4)]^{2+}$,

Table 4
Chemical composition and IR stretching frequencies (as KBr pellets, cm^{-1}) of host (nanopores of zeolite) guest (tetraaza dioxo diphenyl macrocyclic nickel(II) complexes) nanocomposite materials

Sample	C (%)	H (%)	N (%)	C/N	Si (%)	Al (%)	Na (%)	Ni (%)	Si/Al	ν_{N-H}	$\nu_{C=O}$	d ↔ d (cm^{-1})
NaY					21.76	8.60	7.50		2.53			
Ni(II)–NaY					21.79	8.62	3.28	3.72	2.53			
$[Ni([14]aneN_4)]^{2+}$–NaY	4.25	1.60	0.95	4.49	21.10	8.34	5.23	2.60	2.53	3255	1625	21700, 25250
$[Ni([16]aneN_4)]^{2+}$–NaY	4.29	1.62	0.87	4.93	21.09	8.34	5.21	2.58	2.53	3250	1622	21520, 25100
$[Ni(Bzo_2[14]aneN_4)]^{2+}$–NaY	4.34	1.64	0.70	6.22	21.06	8.32	5.19	2.55	2.53	3260	1632	22030, 25510
$[Ni(Bzo_2[16]aneN_4)]^{2+}$–NaY	4.35	1.65	0.70	6.24	21.05	8.32	5.20	2.55	2.53	3257	1630	21900, 25380

$[Ni([16]aneN_4)]^{2+}$, $[Ni(Bzo_2[14]aneN_4)]^{2+}$ and $[Ni(Bzo_2[16]aneN_4)]^{2+}$ that have also been prepared and characterized.

3.4. IR spectral study

The IR spectra of the ligands do not exhibit any band corresponding to the free primary diamine and hydroxyl group. The absorption in IR spectra of the tetraaza dioxo diphenyl ligands in the range 730–770 and 1415–1645 cm^{-1} [21] is due to the presence of the phenyl groups. Four new bands appear in the spectra of the free ligands in the regions ~1620, ~1590, ~1248 and ~780 cm^{-1}, corresponding to amide I [ν(C=O)], amide II [ν(C–N) + δ(N–H)], amide III [δ(N–H)] and amide IV [ϕ(C=O)] bands, respectively, [22]. A sharp band observed at ~3287 cm^{-1}, may be due to [ν(N–H)] of the secondary amino group [23]. The IR spectra of all the complexes (Table 1) showed a single sharp absorption around ~3250 cm^{-1} which may possibly arise from a secondary amine, ν_{N-H}, although its position has been found to be lower by ~30 cm^{-1} than the analogous metal-free tetraaza ligands [24]. This suggests that the secondary amine nitrogens take part in coordination to the metal ions, which has been further confirmed by the appearance of bands in the 340–350 cm^{-1} region in all the complexes, corresponding to ν_{M-N} vibrations. The absorption bands in the 2850–3050 and 1400–1450 cm^{-1} regions observed in the complexes may reasonably correspond to CH stretching and CH bending vibrational modes. The IR bands of all the encapsulated complexes are weak in comparison with the neat complexes due to their low concentrations in zeolite nanocages. The four entrapped complexes exhibit very similar IR spectra, with bands in all regions that are shifted by ~10 cm^{-1} relative to those of the corresponding free complexes (Table 4).

3.5. Elemental analyses of neat and HGNM

The C, H, N analysis results of the neat nickel(II) complexes show close similarity to the theoretical values. The molecular formulae of the tetraaza dioxo diphenyl complexes have been assigned on the basis of the results of their elemental analyses. A preliminary identification of the metal complexes was made on the basis of their IR spectra, which exhibited no bands characteristic of free primary amine, thus supporting the proposed macrocyclic skeleton (Scheme 1). The nickel contents of the HGNM catalysts were estimated by dissolving known amounts of the catalyst in *conc*. HCl and from these solutions, the nickel contents were estimated by using atomic absorption spectrometry (AAS). The chemical compositions (Tables 1 and 4) confirm the purity and stoichiometry of the neat and encapsulated complexes. The chemical analyses of the samples revealed the presence of organic matter with a C/N ratio roughly similar to that for the neat complexes. In Table 5 the molar ratios Si/Al obtained by chemical analysis for the zeolites have been presented. The Si and Al contents in Ni(II)–NaY and the zeolite complexes were almost in the same ratio as in the parent zeolite. This indicates little change in the zeolite framework due to the absence of de-alumination in the metal ion exchange. The parent NaY zeolite has Si/Al molar ratio of 2.53 which corresponds to a unit cell formula $[Na_{56}[(AlO_2)_{56}(SiO_2)_{136}]$. The unit cell formula of metal-exchanged zeolites showed a nickel dispersion of 11.2 moles per unit cell $[(Na_{33.8}Ni_{11.2}[(AlO_2)_{56}(SiO_2)_{136}] \cdot nH_2O)$. The analytical data of each complex indicated Ni:C:N molar ratios very close to those calculated for the mononuclear structure. However, the presence of minute traces of free $[Ni(N–N)_2]^{2+}$ in the lattice can be assumed as the $[Ni(N–N)_2]^{2+}$ content, which is slightly higher than the stoichiometric requirement, only a portion of $[Ni(N–N)_2]^{2+}$ in the exchanged zeolite has undergone complexation and the rest is expected to be removed on re-exchange with NaCl solution.

3.6. Electronic spectral studies

Nickel(II) complexes with 14- and 16-membered tetraaza dioxo macrocyclic ligands exist in aqueous solution as an equilibrium mixture of a yellow, square-planar, diamagnetic, low-spin species and a blue, octahedral, paramagnetic, high-spin species. Solutions of the tetraaza dioxo macrocyclic nickel(II) complexes in non-coordinating solvents show an absorption maximum at 14320, 21930 and 25440 cm^{-1}, characteristic for square-planar yellow species, and at 14050, 21640 and 25190 cm^{-1}, characteristic for blue octahedral species. Table 2 shows that the molar absorption coefficient of the ligand field transition band for the complexes measured in a coordinating solvent is smaller than that in nitromethane, a non-coordinating solvent. These results are quite similar to those reported for other related polyaza macrocyclic complexes, indicating that the complexes dissolve in water or acetonitrile to produce an equilibrium mixture of square-planar $[Ni(Bzo_2[14]aneN_4)]^{2+}$ and octahedral *trans*-$[Ni(Bzo_2[14]aneN_4)(solvent)_2]^{2+}$ [25,26]. Generally, the ligand structure, the nature of the solvent and the concentration of added electrolyte affect the equilibrium. The molar absorption coefficient of the ligand field transition band for $[Ni(Bzo_2[14]aneN_4)]^{2+}$ measured in 3.0 M NaCl aqueous solution is somewhat higher than that in pure water (Table 2). A similar result was also observed in the solutions containing NaBr, $NaNO_3$ or $NaClO_4$. This corresponds to the generally observed trend that neutral salts such as NaCl dissolved in water from their hydrate, reduce the effective concentration of free water, and then increase the concentration of the square-planar species [27]. The electronic spectra (Table 2) of the Ni(II) complexes are comparable to other square-planar tetraaza macrocyclic nickel(II) complexes, indicating that the tetraaza ligands of this study do not differ significantly from these other tetraaza ligands with respect to the ligand field strength [25–32].

At room temperature these complexes show a diamagnetic behavior, indicating the square-planar environment around the Ni(II) ion (Scheme 2). The electronic spectra of the Ni(II) complexes in Table 2 exhibit three absorption bands in the range 13640–13980 (ε = 53–58 l mol^{-1} cm^{-1}), 21200–21640 (ε = 88–97 l mol^{-1} cm^{-1}), and 24800–25190 cm^{-1} (ε = 130–140 l mol^{-1} cm^{-1}), corresponding to a square-planar geometry. These bands may be assigned to the three spin allowed transitions: $1A_{1g}(D) \rightarrow 1A_{2g}(G)$ (ν_1), $1A_{1g}(D) \rightarrow 1B_{2g}(G)$ (ν_2) and $1A_{1g}(D) \rightarrow 1E_g(G)$ (ν_3), respectively, [33]. When the complexes were encapsulated in zeolite-Y, the d ↔ d band shifted again to the higher energy side. The stability of the complexes apparently increases when they are encapsulated in zeolite-Y. The position of the d ↔ d band corresponds to a square-planar geometry for the tetraaza macrocyclic nickel(II) complexes [25–32].

3.7. Cyclic voltammetry studies

Cyclic voltammetric data are summarized in Table 4. Table 4 shows that the oxidation and reduction potentials of the Ni(II) complexes of tetraaza dioxo diphenyl do not differ significantly from other $[14]aneN_4$ complexes. This suggests that the tetraaza dioxo diphenyl macrocycles have Lewis basicities and hole sizes similar to the $[14]aneN_4$ ligand, in spite of the structural differences. A pronounced shift in the oxidation state stability occurs when there is a change in the macrocyclic ring size. An increase in ring size promotes the ease of formation of Ni(I), whilst rendering the oxidation to Ni(III) more difficult. The difference in potential between the $[Ni([14]aneN_4)]^{2+}$ and $[Ni((CH_3)_6[16]1,4,12\text{-}trieneN_4)]^{2+}$ complexes is 0.3 V. Busch and co-workers suggested that this difference is primarily due to deviations from the ideal metal-donor atom distances accompanying the redox changes [34]. This concept of an optimum fit between the coordi-

Table 5
Cyclic voltammetric data for Ni(II) complexes with 14- and 16-membered tetraaza macrocycles[a,b]

Complexes	Oxidation potential (V), $[Ni(polyaza)]^{2+}/[Ni(polyaza)]^{3+}$	Reduction potential (V) $[Ni(polyaza)]^{2+}/[Ni(polyaza)]^{+}$	Ref.
$[Ni([14]aneN_4)](ClO_4)_2$	1.23	−1.40	This work
$[Ni([16]aneN_4)](ClO_4)_2$	1.19	−1.38	This work
$[Ni(Bzo_2[14]aneN_4)](ClO_4)_2$	1.27	−1.46	This work
$[Ni(Bzo_2[16]aneN_6)](ClO_4)_2$	1.25	−1.43	This work
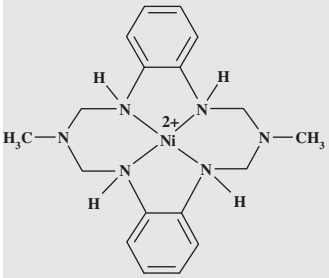	1.07	−1.47	[24g]
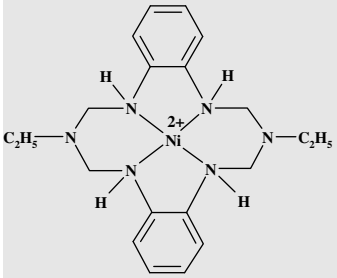	1.07	−1.47	[24f]
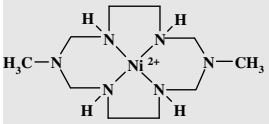	+0.93	−1.55	[25]
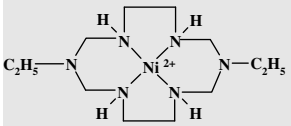	+0.90	−1.47	[25]
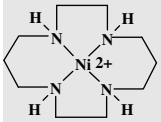	+0.91	−1.46	[25]
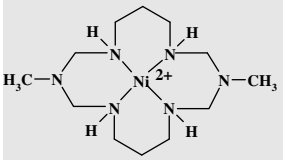	+0.94	−1.57	[24c]
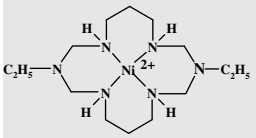	+0.93	−1.47	[24c]
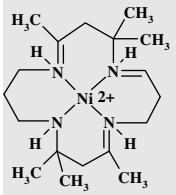	1.30	−1.30	[25]

[a] Measured in acetonitrile solutions; 0.1 M $(n\text{-}Bu)_4NClO_4$; vs. SCE.
[b] Redox potentials of this work and Ref. [25] were measured against a Ag/Ag^+ (0.1 M) reference electrode and were converted to the values measured against the SCE by adding +0.24 V.

Table 6
Surface area and pore volume data of host (nanopores of zeolite-Y) guest (tetraaza dioxo diphenyl macrocyclic nickel(II) complexes) nanocomposite materials

Sample	Surface area [a] (m^2/g)	Pore volume[b] (ml/g)
NaY	545	0.31
Ni(II)–NaY	528	0.31
$[Ni([4]aneN_4)]^{2+}$–NaY	430	0.18
$[Ni([16]aneN_4)]^{2+}$–NaY	422	0.16
$[Ni(Bzo_2[14]aneN_4)]^{2+}$–NaY	386	0.14
$[Ni(Bzo_2[16]aneN_4)]^{2+}$–NaY	370	0.13

[a] Surface area is the "monolayer equivalent area" calculated as explained in Refs. [17,18].
[b] Calculated by the *t*-method.

nated metal ion and the "hole size" provided by the macrocyclic ligand is also in accord with theoretical conclusions and electronic spectral studies. The more common effect of ligand unsaturation also favors the formation of the lower valent states of the complexes and causes the Ni(II) to Ni(III) process to occur at higher energy. The effect of the Bzo function on the reduction reactions of the nickel macrocycles is very pronounced and the structures containing this moiety form the stable complexes in the lower valence states under the influence of relatively mild potentials.

3.8. X-ray diffraction

The X-ray powder diffraction (XRD) patterns of NaY, Ni(II)NaY and the encapsulated metal complexes along with the simple complexes $[Ni(Bzo_2[14]aneN_4)]^{2+}$ were recorded at 2θ values between 5° and 70° to study the crystallinity and to ensure encapsulation. The XRD patterns of the nickel exchanged zeolite and the respective encapsulated complexes are essentially similar to that of NaY, though a slight change in the intensity of the bands has been noticed. These observations indicate that the framework of the zeolite has not undergone any significant structural changes during incorporation of the catalysts i.e. the crystallinity of zeolite-Y is preserved during the encapsulation. A new band with a 2θ value of 25.3° was located in Ni(II)NaY, $[Ni([14]aneN_4)]^{2+}$–NaY, $[Ni([16]aneN_4)]^{2+}$–NaY, $[Ni(Bzo_2[14]aneN_4)]^{2+}$–NaY and $[Ni(Bzo_2[16]aneN_4)]^{2+}$–NaY while another band with a 2θ value of 17.3° could be located only in Ni(II)NaY and $[Ni(Bzo_2[14]aneN_4)]^{2+}$–NaY. This clearly suggests the presence of metal complexes in the zeolite matrix.

3.9. Surface area and pore volume studies

The surface area and pore volume of the catalysts is presented in Table 6. The encapsulation of $[Ni([14]aneN_4)]^{2+}$–NaY, $[Ni([16]aneN_4)]^{2+}$–NaY, $[Ni(Bzo_2[14]aneN_4)]^{2+}$–NaY and $[Ni(Bzo_2[16]aneN_4)]^{2+}$–NaY complexes in zeolite reduced the adsorption capacity and the surface area of the zeolite. The lowering of the pore volume and surface area indicated the presence of complexes $(Ni([14]aneN_4)]^{2+}$, $[Ni([16]aneN_4)]^{2+}$, $[Ni(Bzo_2[14]aneN_4)]^{2+}$ and $[Ni(Bzo_2[16]aneN_4)]^{2+})$ within the zeolite nanocages and not on the external surface.

3.10. Catalytic activity

The tetraaza dioxo diphenyl macrocyclic nickel(II) complexes exhibited good activity in the oxidation of cyclohexene using molecular oxygen (Table 7). Blank reactions performed over NaY zeolite under identical conditions show only negligible conversion indicating that the zeolite host is inactive for oxidation. Furthermore, O_2 alone is unable to oxidize the substrates in the absence of any catalyst. In representative tests, HGNM was filtered out

Table 7
Oxidation of cyclohexene with molecular oxygen catalyzed by "neat" 14- and 16-membered tetraaza dioxo diphenyl macrocyclic nickel(II) complexes (reaction conditions: 1 atm of O_2; time 8 h; catalyst 1.2×10^{-5} mol; substrate, cyclohexene 10 ml, temperature (70° C))

Catalyst	Conversion (%)	Selectivity (%)	
		2-Cyclohexene-1-ol	2-Cyclohexene-1-one
$[Ni([14]aneN_4)](ClO_4)_2$	44.7	52.5	47.5
$[Ni([16]aneN_4)](ClO_4)_2$	40.3	54.8	45.2
$[Ni(Bzo_2[14]aneN_4)](ClO_4)_2$	53.8	61.5	38.5
$[Ni(Bzo_2[14]aneN_4)](ClO_4)_2$[a]	30.4	70.2	29.8
$[Ni(Bzo_2[14]aneN_4)](ClO_4)_2$[b]	50.1	58.4	41.6
$[Ni(Bzo_2[14]aneN_4)](ClO_4)_2$[c]	39.6	51.3	48.7
$[Ni(Bzo_2[16]aneN_4)](ClO_4)_2$	42.1	64.7	35.3

[a] Catalyst = 0.5×10^{-5} mol.
[b] Catalyst = 2.04×10^{-5} mol.
[c] Catalyst = 4.08×10^{-5} mol.

and the filtrate was analyzed for nickel content. The absence of nickel ions in the solution phase indicates that no leaching of the complexes occurred during the reaction, as they are too intact in the nanopores. These observations suggest that the oxidations occur due to the catalytic nature of the encapsulated macrocyclic complexes and no significant role is played by either the zeolite support or the free complexes.

2-Cyclohexene-1-ol is the major product and 2-cyclohexene-1-one is also formed in small quantities (Table 7). The type of macrocyclic ring and encapsulation affected the activity and product selectivity. Conversion for the nickel(II) complexes with different macrocyclic ligands decreased in the order: $Bzo_2[16]\ aneN_4 > Bzo_2[14]aneN_4 > [16]aneN_4 > [14]aneN_4$ (for "neat" and encapsulated complexes) (Tables 7 and 8).

A comparison between the "neat complexes" and "HGNM" as catalysts evidenced that the "neat complexes" gave higher conversion of cyclohexene than their corresponding HGNM. For homogeneously catalysis reactions, the termination of a catalytic cycle may occur because of two factors, due to the formation of Ni–O–Ni species, which have poor catalytic activity, or due to the oxidative degradation of the metal complexes (Tables 7, 8 and Schemes 1 and 2). This was confirmed by taking the IR spectra of the solid after the catalytic reaction. The IR spectra of these solids are very different from the IR spectra of the parent compounds. To improve the stability of the metal complexes under the reaction conditions we have heterogenized the complexes by preventing the catalytic species from dimerizing or aggregating, and to tune the selectivity of the reaction using the walls of the nanopores of the solid via steric effects.

As mentioned before [6,23,31,32], the higher activity of the $[Ni(Bzo_2[14]aneN_4)]^{2+}$–NaY complex might be attributed to the

Table 8
Oxidation of cyclohexene with molecular oxygen catalyzed by host/guest nanocomposite materials (reaction conditions: 1 atm of O_2; time 8 h; catalyst 1.2×10^{-5} mol; substrate, cyclohexene 10 ml, temperature (70 °C))

Catalyst	Conversion (%)	Selectivity (%)	
		2-cyclohexene-1-ol	2-cyclohexene-1-one
$[Ni([14]aneN_4)]^{2+}$-NaY	40.3	54.3	45.7
$[Ni([16]aneN_4)]^{2+}$-NaY	35.1	58.6	41.4
$[Ni(Bzo_2[14]aneN_4)]^{2+}$-NaY	49.6	75.4	24.6
$[Ni(Bzo_2[14]aneN_4)]^{2+}$-NaY[a]	49.1	74.3	25.7
$[Ni(Bzo_2[14]aneN_4)]^{2+}$-NaY[b]	48.2	73.8	26.2
$[Ni(Bzo_2[14]aneN_4)]^{2+}$-NaY[c]	47.9	78.9	26.9
$[Ni(Bzo_2[16]aneN_4)]^{2+}$-NaY	38.2	78.9	21.1

[a] First reuse.
[b] Second reuse.
[c] Third reuse.

higher activity of the aromatic ligand and its more active cation radical intermediate with respect to the aliphatic ligand system. Lower activity (35.1%) of $[Ni([16]aneN_4)]^{2+}$–NaY and can be accounted for by the substantial steric hindrance of the propylene groups that prevent the approaching oxidant from reaching the central metal of the catalyst.

Homogeneous catalysts are more prone to deactivation by dimerization of the active centers, which is expected to be reduced by encapsulating them in zeolites. $[Ni(Bzo_2[14]aneN_4)]^{2+}$–NaY was recycled for the oxidation of cyclohexene with molecular oxygen with a view to establish the effect of encapsulation on stability. The initial run showed a conversion of 49.6% and it is only marginally reduced to 49.1% on recycling the catalyst. These results indicate that the $[Ni(Bzo_2[14]aneN_4)]^{2+}$–NaY complex is almost stable enough to be recycled for the oxidation of cyclohexene without much loss in activity. Thus, the encapsulation of the complexes in zeolites is found to increase the life of the catalyst by reducing dimerization due to the restriction of the internal framework structure. The IR spectrum of the recycled sample is quite similar to that of the fresh sample, indicating little change in the coordination of $Bzo_2[14]aneN_4$ after the oxidation reactions.

The results clearly suggest that $[Ni(Bzo_2[14]aneN_4)]^{2+}$–NaY efficiently catalyses the conversion of cyclohexene to 2-cyclohexene-1-ol with 75.4% selectivity. Greater activity of the $Bzo_2[14]aneN_4$ system has clearly arisen from the existence of the electron donating ligand which facilitates the electron transfer rate, a process that has previously been observed by us in other oxidation reactions [31,32]. All conversion efficiencies with high selectivity obtained in this study are significantly higher than those obtained using metal containing porous and non-porous materials [31,32].

4. Conclusion

In summary, the results show that the "neat" complexes can be encapsulated in the nanopores of zeolite by a template condensation between the pre-entrapped $[Ni(N–N)_2]^{2+}$ complexes and ethylcinnamate. The "neat" and zeolite-Y-encapsulated nickel(II) tetraaza dioxo diphenyl macrocyclic complexes exhibit efficient catalytic activity in the oxidation of cyclohexene using O_2. The encapsulated complexes exhibit enhanced selectivity in the oxidation reaction. The size of the macrocyclic ring and substitution also influence the catalytic activity. These encapsulated systems offer structural integrity by having a uniform distribution of the metal complex in the pore structure of the support. The zeolite framework keeps the guest complexes dispersed and prevents their dimerization leading to retention of the catalytic activity. Future work on this system is expected to envisage its industrial applications for partial oxidation reactions.

Acknowledgment

The author is grateful to the Council of the University of Kashan for providing financial support to undertake this work.

References

[1] P.P. Knops-Gerrits, F. Thibault-Starzyk, P.A. Jacobs, Stud. Surf. Sci. Catal. 84 (1994) 1411.
[2] K.J. Balkus Jr., A.K. Khanrnamedova, K.M. Dixon, F. Bedioui, Appl. Catal. A: Gen. 143 (1996).
[3] M.R. Maurya, S.J.J. Titinchi, S. Chand, J. Mol. Catal. A: Chem. 214 (2004) 257.
[4] I.W.C.E. Arends, R.A. Sheldon, Appl. Catal. A: Gen. 212 (2001) 175.
[5] D. Chatterjee, A. Mitr, J. Mol. Catal. A: Chem. 144 (1999) 363.
[6] (a) M. Salavati-Niasari, J. Mol. Catal. A: Chem. 245 (2006) 192;
(b) M. Salavati-Niasari, J. Mol. Catal. A: Chem. 229 (2005) 159;
(c) M. Salavati-Niasari, J. Mol. Catal. A: Chem. 217 (2004) 87;
(d) M. Salavati-Niasari, A. Amiri, J. Mol. Catal. A: Chem. 235 (2005) 114.
[7] M. Hartman, Angew. Chem., Int. Ed. 39 (2000) 888.
[8] (a) M. Salavati-Niasari, Chem. Lett. 34 (2005) 244;
(b) M. Salavati-Niasari, Chem. Lett. 34 (2005) 1444;
(c) M. Salavati-Niasari, Micropor. Mesopor. Mater. 92 (2006) 173;
(d) M. Salavati-Niasari, Micropor. Mesopor. Mater. 95 (2006) 248.
[9] C.R. Jacob, S.P. Varkey, P. Ratnasamy, Appl. Catal. A: Gen. 168 (1998) 353.
[10] P.C.H. Mitchel, Chem. Ind. 6 (1991) 308.
[11] C. Bowers, P.K. Dutta, J. Catal. 122 (1990) 271.
[12] P.K. Dutta, M. Ledney, Prog. Inorg. Chem. 44 (1997) 209.
[13] Q. Zhang, Q. Xia, X. Lu, H. Zhan, G. Xu, Indian J. Chem. 64A (2007) 909.
[14] (a) B. Grzybowska-Swierkosz, Catal. Today 112 (2006) 3;
(b) F.F. Sun, S.H. Zhang, Chinese J. Catal. 24 (2003) 600;
(c) B.S. Uphad, Y. Yamada, T. Akita, M. Haruta, App. Catal. A. Gen. 215 (2001).
[15] D. Kaucky, A. Vondrova, J. Dedecek, B. Wichterlova, J. Catal. 194 (2000) 318.
[16] J. Basset, G.H. Denney, G.H. Jeffery, J. Mendham, Vogel's Textbook of Quantitative Inorganic Analysis, Wiley, New York, 1987.
[17] S.W. Wang, H. Everett, R.A.W. Haul, L. Moscou, R.A. Pierotti, J. Rouquerol, T. Siemieniewska, Pure Appl. Chem. 57 (1985) 603.
[18] A. Lineares-Solano, Textural characterization of porous carbons by physical adsorption of gases, in: J.L. Figueiredo, J.A. Moulijn (Eds.), Carbon and Coal Gasification, M. Nijhoff, M.A. Dordrecht, 1986, p. 137.
[19] S. Chandra, L.K. Gupta, D. Jain, Spectrochim. Acta Part A 60 (2004) 2411.
[20] E. Franco, E.L. Torres, M.A. Mandiola, M.T. Sevilla, Polyhedron 19 (2000) 447.
[21] S. Chandra, K. Gupta, Trans. Met. Chem. 27 (2002) 329.
[22] S. Chandra, L.K. Gupta, J. Saudi Chem. Soc. 7 (2003) 243.
[23] (a) M. Salavati-Niasari, Inorg. Chem. Commun. 9 (2006) 628;
(b) M. Salavati-Niasari, F. Davar, Inorg. Chem. Commun. 9 (2006) 263;
(c) M. Salavati-Niasari, F. Davar, Inorg. Chem. Commun. 9 (2006) 304;
(d) M. Salavati-Niasari, Inorg. Chem. Commun. 8 (2005) 174;
(e) M. Salavati-Niasari, Inorg. Chem. Commun. 7 (2004) 963;
(f) M. Salavati-Niasari, Inorg. Chem. Commun. 7 (2004) 698;
(g) M. Salavati-Niasari, F. Davar, Inorg. Chem. Commun. 9 (2005) 175.
[24] (a) M. Shakir, S.P. Varkey, P.S. Hameed, Polyhedron 12 (1993) 2775;
(b) D.H. Cook, D.E. Fenton, Znorg. Chim. Acta 25 (1977) L95;
(c) M. Salavati-Niasari, H. Najafian, Polyhedron 22 (2003) 2633;
(d) M. Salavati-Niasari, M. Rezai-Adaryani, Polyhedron 23 (2004) 1325;
(e) M. Salavati-Niasari, Polyhedron 24 (2005) 1405;
(f) M. Salavati-Niasari, A. Amiri, Trans. Met. Chem. 30 (2005) 720;
(g) M. Salavati-Niasari, F. Davar, Polyhedron 25 (2006) 2127.
[25] (a) R.W. Hay, B. Jeragh, G. Ferguson, B. Kaiter, B.L. Rule, J. Chem. Soc., Dalton Trans. (1982) 1531;
(b) M.P. Suh, S.-G. Kang, Inorg. Chem. 27 (1988) 2544.
[26] M.P. Suh, B.Y. Shim, T.-S. Yoon, Inorg. Chem. 33 (1994) 5509.
[27] L. Fabbrizzi, A.M.M. Lanfredi, P. Pallavicini, A. Perotti, A. Taglietti, F. Ugozzoli, J. Chem. Soc., Dalton Trans. (1991) 3263.
[28] (a) N.F. Curtis, Coord. Chem. Rev. 3 (1968) 3;
(b) M. Shakir, S.P. Varkey, O.S.M. Nasman, Polyhedron 14 (1995) 1283;
(c) V. Goedken, S. Peng, J. Chem. Soc., Chem. Commun. (1973) 62;
(d) M. Shakir, M. Azam, Y. Azim, S. Parveen, A. Ullah Khan, Polyhedron 26 (2007) 5513.
[29] (a) D.E. Fenton, P.A. Vigato, Chem. Soc. Rev. 17 (1988) 69;
(b) B.Z. Shan, X.Z. Yu, H.K. Fun, K. Sivakumar, Acta Crystallogr., Sect. C 52 (1996) 3035;
(c) R.W. Hay, J.A. Crayston, T.J. Cromie, P. Lightfoot, D.C. L Dealwis, Polyhedron 16 (1997) 3557.
[30] (a) R.M. Izatt, J.J. Christensen, Synthetic Multidentate Macrocyclic Compounds, Academic Press, New York, 1987;
(b) M.P. Suh, S. Kim, Inorg. Chem. 32 (1993) 3562.
[31] (a) S.-G. Kang, K. Ryu, S.-K. Jung, J. Kim, Inorg. Chim. Acta 293 (1999) 140;
(b) M. Shakir, S.P. Varkey, Polyhedron 14 (1995) 1117.
[32] (a) H.-Z. Kou, S. Gao, B.-Q. Ma, D.-Z. Liao, Chem. Commun. (2000) 713;
(b) T.-B. Lu, H. Xiang, R.L. Luck, L. Jiang, Z.-W. Mao, L.-N. Ji, New J. Chem. 26 (2002) 969.
[33] A.B.P. Lever, Crystal field spectra, in: Inorganic Electronic Spectroscopy, first ed., Elsevier, Amsterdam, 1968, pp. 249–360.
[34] F.V. Lovecchio, E.S. Gore, D.H. Busch, J. Am. Chem. Soc. 96 (1974) 3109.

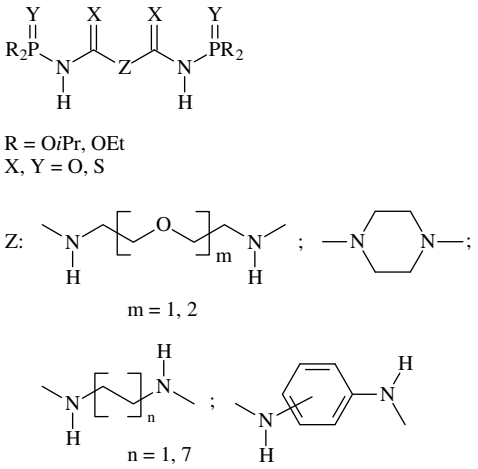

Scheme 1.

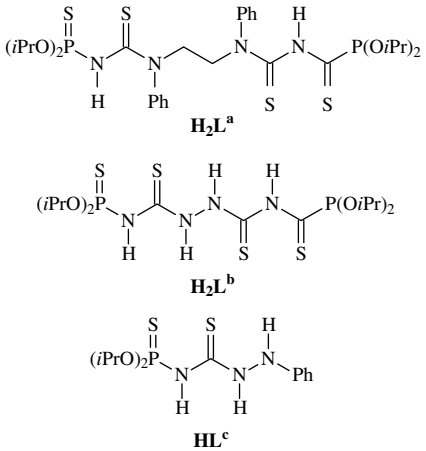

Scheme 2.

PNH, minor form), 9.11 (d, $^2J_{PNH}$ = 11.7 Hz, PNH, major form), 9.72 (br. s, NHNH, minor form), 11.22 (br. s, NHNH, major form). ^{31}P NMR ($CDCl_3$): δ = 54.1 (t, $^3J_{POCH}$ = 10.4 Hz, 3.9P, major form), 66.2 (m, 1P, minor form) ppm. ^{31}P NMR (acetone-d_6): δ = 56.3 (m, 1.9P, major form), 59.6 (m, 1P, minor form) ppm. IR: ν = 653 (P═S), 971, 988, 1009 (POC), 1516 (S═C–N), 3102, 3155, 3316 (NH) cm^{-1}. Calc. for $C_{14}H_{32}N_4O_4P_2S_4$ (510.64): C, 32.93; H, 6.32; N, 10.97. Found: C, 33.02; H, 6.28; N, 11.03%.

HL[c]: Yield: 1.61 g (93%). M.p. 117 °C. ^{1}H NMR ($CDCl_3$): δ = 1.35–1.40 (m, 12H, CH_3), 4.92 (d, sept, $^3J_{POCH}$ = 10.6 Hz, $^3J_{H,H}$ = 6.2 Hz, 2H, OCH), 6.34 (s, 1H, PhNH), 6.84–6.92 (m, 2H, *o*-H, Ph), 6.96–7.05 (m, 1H, *p*-H, Ph), 7.24–7.32 (m, overlapped with the solvent signal, *m*-H, Ph), 8.00 (s, 1H, C(S)NHN), 8.23 (d, 1H, $^2J_{PNH}$ = 13.9 Hz, P(S)NH), 9.44 (d, $^4J_{PNH}$ = 5.6 Hz, C(S)NHN, minor form) ppm. ^{31}P NMR ($CDCl_3$, 20 °C): δ = 53.5 (br. t, $^3J_{POCH}$ = 9.8 Hz, 1P), 58.5 (q, $^2J_{PNH}$ = $^3J_{POCH}$ = 12.2 Hz, 1.9P) ppm. ^{31}P NMR ($CDCl_3$, −50 °C): δ = 53.7 (q, $^2J_{PNH}$ = $^3J_{POCH}$ = 11.0 Hz, 1P), 58.4 (q, $^2J_{PNH}$ = $^3J_{POCH}$ = 11.2 Hz, 6.7P) ppm. ^{31}P NMR (acetone-d_6, 20 °C): δ = 56.8 (br. q, $^2J_{PNH}$ = $^3J_{POCH}$ = 9.8 Hz, 1P), 60.0 (q, $^2J_{PNH}$ = $^3J_{POCH}$ = 12.2 Hz, 6.1P) ppm. IR: ν = 624 (P═S), 1000, 1010 (POC), 1528 (S═C–N), 3224, 3288 (NH) cm^{-1}. Calc. for $C_{13}H_{22}N_3O_2PS_2$ (347.44): C, 44.94; H, 6.38; N, 12.09. Found: C, 44.91; H, 6.41; N, 12.07%.

2.2. Physical measurements

Infrared spectra (Nujol) were recorded with a Specord M-80 spectrometer in the range 400–3600 cm^{-1}. NMR spectra were obtained on a Varian Unity-300 NMR spectrometer at 25 °C. ^{1}H and ^{31}P NMR spectra were recorded at 299.948 and 121.420 MHz, respectively. Chemical shifts are reported with reference to $SiMe_4$ (^{1}H) and H_3PO_4 (^{31}P). Elemental analyses were performed on a Perkin–Elmer 2400 CHN microanalyser.

2.3. Crystal structure determination and refinement

Data for both structures were collected on a STOE IPDS-II diffractometer with graphite-monochromated Mo Kα radiation. The images were indexed, integrated and scaled using the X-AREA package [11]. Data were corrected for absorption using the PLATON [12] program. The structures were solved by direct methods using the SHELXS [13] program and refined first isotropically and then anisotropically using SHELXL97 [14]. Hydrogen atoms were revealed from $\Delta\rho$ maps and refined using a riding model. All figures were made using the program XP [15].

3. Results and discussion

The thioureas $\mathbf{H_2L}^a$ and $\mathbf{H_2L}^b$ were synthesized by the treatment of *N,N'*-diphenyl-1,2-diaminoethylene or hydrazine hydrate with the isothiocyanate $(i\text{PrO})_2\text{P(S)NCS}$. Their compositions were successfully proved by the microanalysis data.

The ^{31}P NMR spectrum of $\mathbf{H_2L}^a$ in $CDCl_3$ contained a singlet at 58.8 ppm, which is typical for *N*-thiophosphoryl thioureas with a *tert*-nitrogen group $R_2NC(S)$ [7]. The IR and ^{1}H NMR spectra confirm the structure.

Surprisingly, there are two signals in the ^{31}P NMR spectrum of $\mathbf{H_2L}^b$: a major signal at 54.1 and a minor low-field peak at 66.2 ppm in $CDCl_3$ solution. A similar picture was observed in acetone-d_6 solution: the peaks appeared at 56.3 (major form) and 58.6 ppm. The integral intensity ratio changes from 3.9:1 to 1.9:1 for the high- and low-field signals, respectively.

Doubling of signals is also observed in the ^{1}H NMR spectra. The signals of the alkyl protons are overlapped, but the NH-groups show independent sets of different intensities. Phosphorus–proton coupling, $^2J_{PNH}$, allows the separation of the signals of the PNH groups and the NHNH moiety.

It is known that in these compounds processes of complicated rotation along the CN bond in the fragment CNP may show an essential influence on the chemical shifts of the phosphorus signals [7,16–18]. It was established that for compounds of the common formula $RC(S)NHP(S)(OR')_2$ (R = Ar, Me, NR^1R^2) in solutions the formation of conformers, caused by a complicated rotation along the C–N(P) bond, is observed (Scheme 3). The chemical shifts in the ^{31}P NMR spectra depend on the conformation balance in solutions. The activation energy of the rotation around the CN bond, established on the basis of the NMR data, is $\Delta G^{\neq}$ = 49–60 kJ/mol [17]. For example, in the case of *N*-phosphorylated thioacetamide $CH_3C(S)NHP(O)(O\text{i}Pr)_2$ there is a rather slow conformation exchange between the *Z*- and *E*-rotamers in solutions, whose signals

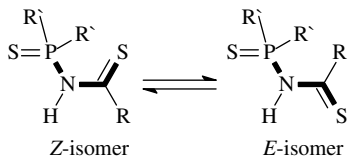

Scheme 3.

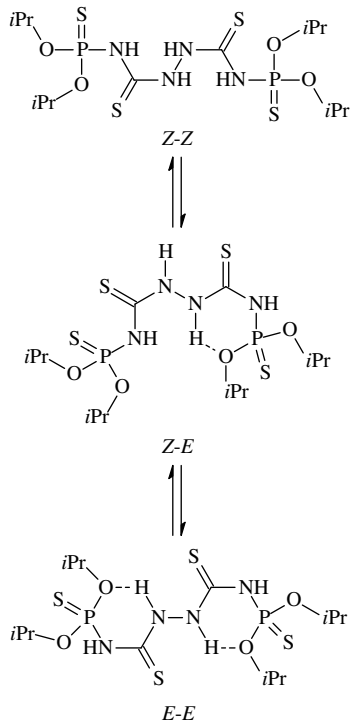

Scheme 4.

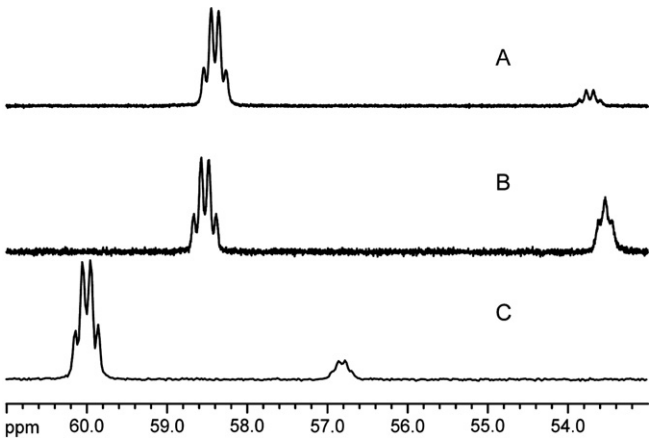

Fig. 1. ^{31}P NMR spectra of **HL**^{c} in $CDCl_3$ (−50 °C, A; 25 °C, B) and in acetone-d_6 (25 °C, C).

are managed to be observed at room temperature by ^{31}P NMR spectroscopy [18].

The conformation describing a *Z*-arrangement of the N–P and C=S bonds (Scheme 3), is prevailing for the majority of *N*-thiophosphorylated thioamides and *N*-thiophosphorylated thioureas of the common formula $Alk_2NC(S)NHP(S)(OAlk)_2$, containing a tertiary nitrogen atom of the $R_2NC(S)$ fragment [7]. As well as for **H$_2$L**^{a}, they show chemical shifts in the range 57–60 ppm in the ^{31}P NMR spectra.

The ^{31}P NMR spectra of the compounds $RNHC(S)NHP(S)(OiPr)_2$ in non-polar solvents contain signals in the characteristic area of 52–54 ppm [7]. This is caused by the formation of intramolecular hydrogen bonds between the RNH fragment and the oxygen or sulfur atoms of the (thio)phosphoryl group [7]. Formation of these bonds stabilizes the *E*-conformer (Scheme 3). In polar solvents (acetone-d_6) the signals in the ^{31}P NMR spectra are shifted by up to 60 ppm [16].

The doubling of signals in the NMR spectra of **H$_2$L**^{b} could be explained by the similar *E*-, *Z*-conformation isomerism or by the unequivalence of the two $-C(S)NHP(S)(OR)_2$ moieties in the bifunctional molecule. To eliminate the latter reason we decided to compare the obtained data to the simpler monofunctional analogue. This allowed us to avoid the complication caused by the multiple isomeric forms in the bifunctional 2,5-dithiobiurea (Scheme 4) and gives evidence that the observed signals are provided by the conformation isomers of the $RC(S)NHP(S)(OR)_2$ moiety.

The thiophosphorylated thiosemicarbazide **HL**^{c} was synthesized by the addition of phenylhydrazine to the isothiocyanate $(iPrO)_2P(S)NCS$. There are no absorption bands for the NH_2 group in the IR spectrum of **HL**^{c}. This confirms the isothiocyanate addition to the non-substituted nitrogen atom of the parent hydrazine. The ^{31}P NMR spectra of **HL**^{c} contain two signals (Fig. 1). The ratio of the integrated intensities depends on the temperature. At 25 °C (Fig. 1 B) this ratio is approximately 1:2, whereas at −50 °C (Fig. 1 A) it is 1:7 for the high-field and low-field signals, respectively. In the acetone-d_6 medium (25 °C), the integrated intensities ratio is 6.4:1 in favour of the high-field signal (Fig. 1 C). Thus, in contrast to **H$_2$L**^{b}, the ^{31}P spectra of **HL**^{c} shows the superiority of the low-field signal.

We suppose that in solution, both *Z*- and *E*-forms of **HL**^{c} are present, and they are stabilized by the intramolecular hydrogen bonds (Scheme 5). The bond of the basic nitrogen atom of the PhNH group should surpass on durability the bond in the *E*-isomer, which is in agreement with the ^{31}P NMR spectroscopy data. The chemical shifts of phosphorus are in the area which is characteristic for the *Z*- and *E*-isomers of *N*-thiophosphorylthioureas, which are related by structure to the investigated compounds [7].

The signals in the ^{31}P NMR spectrum of **HL**^{c} at −50 °C (Fig. 1A) are shown as quartets. This spin–spin coupling is typical for the $NHP(S)(OiPr)_2$ group. The phosphorus spectrum at 25 °C (Fig. 1B) shows less coupling, with $^{2}J_{PNH}$ being constant for the labile proton of the PNH group. The data obtained show that the speed of the proton exchange in the *E*-isomer (high-field signal) is higher than for the *Z*-form, in which the PNH proton participates in the intramolecular hydrogen bond formation.

In the acetone medium, the picture changes again (Fig. 1C). A significant low-field shift and increasing in intensity for the *E*-isomer is observed at 25 °C. This is in agreement with the assumption of the weak hydrogen bonds destruction in the *E*-form. Suppression of a proton exchange in the acetone medium leads to the appearance of the $^{2}J_{PNH}$ constant. A similar shift is also observed for the signal of the *Z*-form.

In the compound **H$_2$L**^{b}, the nitrogen atoms of the NHNH group are not basic, which makes the stabilization of the *Z*-isomer impossible by an intramolecular hydrogen bond (Scheme 5). As a result the accumulation of the *E,E*-isomer (high-field signal) is observed in solution.

Crystals of **H$_2$L**^{a} and **H$_2$L**^{b} were obtained by recrystallization from a 1:5 (v/v) mixture of methylene chloride and *n*-hexane (Table 1). The NMR probes and the crystals for the X-ray

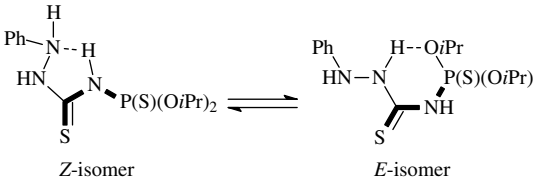

Scheme 5.

Table 1
Crystal data, data collection and refinement details for $\mathbf{H_2L}^a$ and $\mathbf{H_2L}^b$

	$\mathbf{H_2L}^a$	$\mathbf{H_2L}^b$
Empirical formula	$C_{28}H_{44}N_4O_4P_2S_4$	$C_{14}H_{32}N_4O_4P_2S_4$
Formula weight	690.85	510.62
Temperature (K)	173(2)	173(2)
Radiation (Å)	0.71073	0.71073
Crystal form	triclinic	triclinic
Space group	$P\bar{1}$	$P\bar{1}$
a (Å)	6.0698(7)	11.0277(10)
b (Å)	9.2882(12)	11.4439(9)
c (Å)	15.971(2)	11.9212(10)
α (°)	94.288(10)	90.850(7)
β (°)	96.636(10)	113.448(6)
γ (°)	100.695(10)	102.697(7)
V (Å^3)	874.56(19)	1337.6(2)
Z	1	2
D_{calc} (Mg m^{-3})	1.312	1.268
Absorption correction, μ (cm^{-1})	4.01	4.99
$F(000)$	366	540
Crystal size (mm^3)	0.33 × 0.21 × 0.08	0.29 × 0.27 × 0.26
Recording range, θ_{max} (°)	3.52–25.62	3.46–27.55
Number of recorded reflections	7531	16442
Number of recorded independent reflections (R_{int})	3257 (0.0539)	6129 (0.0303)
Final R indices [$I > 2\sigma(I)$]	R_1 = 0.0378, wR_2 = 0.0958	R_1 = 0.0345, wR_2 = 0.0913
R indices (all data)	R_1 = 0.0471, wR_2 = 0.0992	R_1 = 0.0441, wR_2 = 0.0957
S	1.045	1.031

Table 2
Selected bond lengths (Å), and bond and torsion angles (°) for $\mathbf{H_2L}^a$

Bond lengths			
P(1)–N(1)	1.6838(18)	N(2)–C(1)	1.353(3)
P(1)–S(1)	1.9194(8)	N(2)–C(11)	1.446(3)
S(2)–C(1)	1.676(2)	N(2)–C(2)	1.479(3)
N(1)–C(1)	1.381(3)		
Bond angles			
N(1)–P(1)–S(1)	118.65(8)	C(1)–N(2)–C(2)	120.67(18)
C(1)–N(1)–P(1)	127.32(16)	C(11)–N(2)–C(2)	117.58(16)
C(1)–N(2)–C(11)	121.72(17)		
Torsion angles			
P(1)–N(1)–C(1)–N(2)	174.87(15)	C(1)–N(2)–C(2)–C(2)#1[a]	−86.2(3)
P(1)–N(1)–C(1)–S(2)	−4.9(3)	C(11)–N(2)–C(2)–C(2)#1[a]	95.5(3)

[a] Symmetry transformations used to generate equivalent atoms: #1 $-x$, $-y+1$, $-z+1$.

Table 3
Selected bond lengths (Å), and bond and torsion angles (°) for $\mathbf{H_2L}^b$

Bond lengths			
P(1)–N(1)	1.6812(13)	P(11)–N(11)	1.6821(14)
P(1)–S(1)	1.9189(6)	P(11)–S(11)	1.9154(6)
S(2)–C(1)	1.6778(15)	S(12)–C(11)	1.6829(16)
N(1)–C(1)	1.3832(18)	N(11)–C(11)	1.3794(18)
N(2)–C(1)	1.3371(18)	N(12)–C(11)	1.3376(19)
N(2)–N(12)	1.3857(17)		
Bond angles			
C(1)–N(1)–P(1)	129.95(11)	N(2)–C(1)–S(2)	122.10(11)
C(1)–N(2)–N(12)	119.77(13)	N(1)–C(1)–S(2)	122.50(11)
N(2)–C(1)–N(1)	115.39(13)		
Torsion angles			
N(12)–N(2)–C(1)–N(1)	−178.27(14)	C(1)–N(2)–N(12)–C(11)	178.74(14)
N(12)–N(2)–C(1)–S(2)	0.7(2)	N(2)–N(12)–C(11)–N(11)	−178.46(14)
P(1)–N(1)–C(1)–N(2)	−20.7(2)	N(2)–N(12)–C(11)–S(12)	3.0(2)
P(1)–N(1)–C(1)–S(2)	160.26(9)	P(11)–N(11)–C(11)–N(12)	28.2(2)
P(11)–N(11)–C(11)–S(12)	−153.23(10)		

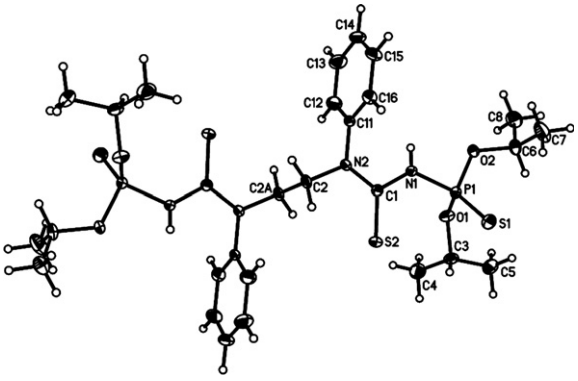

Fig. 2. Molecular structure of $\mathbf{H_2L}^a$.

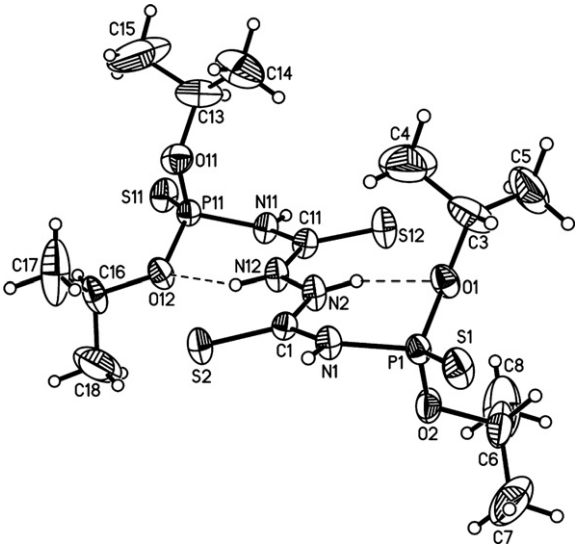

Fig. 3. Molecular structure of $\mathbf{H_2L}^b$.

determination were taken from the same samples. The parameters of the C=S, C–N, P–N and P=S bonds observed for both compounds (Tables 2 and 3) are in the typical range for *N*-thiophosphorylated thiourea derivatives [7,19].

The bifunctional thiourea $\mathbf{H_2L}^a$ has a centrosymmetrical conformation in the crystal (Fig. 2). Two N2–C1(S2)–N1–P1–O2 moieties are significantly flattened. These planes are placed orthogonal to the 1,2-diaminoethylene spacer backbone N2–C2–C2#1–N2#1 which possesses an anti-planar conformation (Table 2). As expected, the S2–C1–N1–P1 moieties in the crystal phase have a *Z*-conformation (Scheme 3), typical for *N*-thiophosphoryl thioureas with a *tert*-amide group $R_2NC(S)$.

The 2,5-dithiobiurea $\mathbf{H_2L}^b$ molecules consist of two independent NHC(S)NHP(S)(O*i*Pr)$_2$ groups with a similar conformation (Fig. 3). The 2,5-dithiobiurea backbone together with the thiophosphoryl substituents are in an anti-planar displacement (Table 3). Contrary to the thiourea $\mathbf{H_2L}^a$, the 2,5-dithiobiurea $\mathbf{H_2L}^b$ has an *E*,*E*-conformation of the S–C–N–P backbones. The conformation is supported by intramolecular H-bonding of the type C(S)NH···O(*i*Pr)P. The

Table 4
Hydrogen bond lengths (Å) and angles (°) for $\mathbf{H_2L}^b$

D–H···A[a]	*d*(D–H)	*d*(H···A)	*d*(D···A)	∠(DHA)
N(1)–H(1)···S(2)#1	0.864(9)	2.511(10)	3.3611(13)	168(2)
N(2)–H(2)···O(1)	0.867(9)	2.164(16)	2.8577(17)	136.7(18)
N(11)–H(11)···S(12)#2	0.858(9)	2.459(11)	3.2957(13)	165(2)
N(12)–H(12)···O(12)	0.864(9)	2.120(16)	2.7816(17)	133.0(17)

[a] Symmetry transformations used to generate equivalent atoms: #1 $-x+1$, $-y+2$, $-z+2$; #2 $-x+1$, $-y+1$, $-z+1$.

molecules in the crystal are paired by two weak intermolecular NH···S=C hydrogen bonds (Table 4).

4. Conclusions

A *Z,Z*-arrangement of the C=S and P–N bonds in the SCNPS backbone was found both in the crystal phase and in $CDCl_3$ solution for the bis-thiourea $\mathbf{H_2L}^a$. The 2,5-dithiobiurea $\mathbf{H_2L}^b$ and the thiosemicarbazide $\mathbf{HL}^c$ are presence as a mixture of *E*- and *Z*-conformation isomers, stabilized by H-bonds in acetone-d_6 and $CDCl_3$ solutions. Comparison of the ^{31}P NMR data allows the superiority of the *Z*-isomer for the thiosemicarbazide $\mathbf{HL}^c$, which is stabilized by the H-bond PhN···H–NP, to be determined. The superiority of the *E,E*-isomer of the 2,5-dithiobiurea $\mathbf{H_2L}^b$ was found both in the crystal phase and in solution.

Acknowledgments

This work was supported by the joint program of CRDF and the Russian Ministry of Education and Science (BRHE 2008 Y5-C-07-09); Russian Science Support Foundation.

Appendix A. Supplementary data

CCDC 686895 and 686896 contain the supplementary crystallographic data for $\mathbf{H_2L}^a$ and $\mathbf{H_2L}^b$. These data can be obtained free of charge via http://www.ccdc.cam.ac.uk/conts/retrieving.html, or from the Cambridge Crystallographic Data Centre, 12 Union Road, Cambridge CB2 1EZ, UK; fax: (+44) 1223-336-033; or e-mail: deposit@ccdc.cam.ac.uk. Supplementary data associated with this article can be found, in the online version, at doi:10.1016/j.poly.2008.06.034.

References

[1] J.K. Clegg, L.F. Lindoy, J.C. McMurtrie, D. Schilter, J. Chem. Soc., Dalton Trans. (2006) 3114.
[2] J.K. Clegg, K. Gloe, M.J. Hayter, O. Kataeva, L.F. Lindoy, B. Moubaraki, J.C. McMurtrie, K.S. Murray, D. Schilter, J. Chem. Soc., Dalton Trans. (2006) 3977.
[3] S.A. Bourne, O. Hallale, K.R. Koch, Cryst. Growth Des. 5 (2005) 307.
[4] K.R. Koch, O. Hallale, S.A. Bourne, J. Miller, J. Bacsa, J. Mol. Struct. 561 (2001) 185.
[5] O. Hallale, S.A. Bourne, K.R. Koch, Cryst. Eng. Commun. 25 (2005) 161.
[6] K.R. Koch, S.A. Bourne, A. Coetzee, J. Miller, J. Chem. Soc., Dalton Trans. 18 (1999) 3157.
[7] F.D. Sokolov, V.V. Brusko, N.G. Zabirov, R.A. Cherkasov, Curr. Org. Chem. 10 (2006) 27.
[8] N.G. Zabirov, V.V. Brusko, S.V. Kashevarov, F.D. Sokolov, V.A. Shcherbakova, A.Yu. Verat, R.A. Cherkasov, Russ. J. Gen. Chem. 70 (2000) 1214.
[9] N.G. Zabirov, V.V. Brusko, A.Yu. Verat, D.B. Krivolapov, I.A. Litvinov, R.A. Cherkasov, Polyhedron 23 (2004) 2243.
[10] A.Y. Verat, F.D. Sokolov, N.G. Zabirov, M.G. Babashkina, D.B. Krivolapov, V.V. Brusko, I.A. Litvinov, Inorg. Chim. Acta 359 (2006) 475.
[11] X-AREA, Diffractometer Control Program, STOE and Cie, Darmstadt, Germany, 2001.
[12] A.L. Spek, Acta Crystallogr., Sect. A 46 (1990) 34.
[13] G.M. Sheldrick, SHELXS, Program for Crystal Structure Solution, University of Göttingen, Germany, 1997.
[14] G.M. Sheldrick, SHELXL-97 Program for Crystal Structure Refinement, University of Göttingen, Germany, 1997.
[15] G.M. Sheldrick, XP Version 4.1, Program for Molecular Graphics, Siemens Analytical X-ray Instruments Inc., Madison, Wisconsin, USA, 1991.
[16] F.Kh. Karataeva, A.R. Yulmetov, N.G. Zabirov, A.V. Aganov, V.V. Klochkov, Russ. J. Gen. Chem. 75 (2005) 856.
[17] F.Kh. Karatayeva, A.V. Aganov, V.V. Klochkov, Appl. Magn. Res. 14 (1998) 545.
[18] F.Kh. Karataeva, Russ. J. Gen. Chem. 70 (2000) 1062.
[19] F.D. Sokolov, D.A. Safin, M.G. Babashkina, N.G. Zabirov, V.V. Brusko, N.A. Mironov, D.B. Krivolapov, I.A. Litvinov, R.A. Cherkasov, B.N. Solomonov, Polyhedron 26 (2007) 1550.

$$\sigma = -\frac{8}{3}\mathrm{Im}\left\{\sum_{L,L',m_c} \mathrm{i}^{l-l'} \exp\{\mathrm{i}(\delta_l^A + \delta_{l'}^A)\}\rho_c(l)\rho_c(l') \times G(L_c 10|L)G(L_c 10|L')(t^{-1})_{LL}^{AA}[(1-X)^{-1}]_{LL'}^{AA}\right\},$$

where $G(LL'|L'')$ is Gaunt's integral and $\rho_c(l)$ is the radial dipole integral between the radial part of $\phi_c(\mathbf{r})$ and the lth partial wave of photoelectrons $R_l(r)$ at site A. The phase shift of the lth partial wave at site A is represented by δ_l^A. We introduce the matrix X specified with site index α and angular momentum L and so on; it is defined as

$$X_{LL'}^{\alpha\beta} = t_l^{\alpha} G_{LL'}(\mathbf{R}_\alpha - \mathbf{R}_\beta)(1-\delta_{\alpha\beta}), \quad (2)$$

where t_l^{α} and $G_{LL'}$ represent the T-matrix at site α and the Green's function in an angular momentum representation. The inverse matrix $(1-X)^{-1}$ includes an infinite order of the full multiple-scattering inside the cluster we are considering. The phase shifts in $t_l^{\alpha}(= -[\exp(2\mathrm{i}\delta_l^{\alpha}) - 1]/2\mathrm{i}k)$ are one of the most important features and reflect the electronic structure of the surrounding atoms, which are calculated within the Hartree–Fock approximation. The Green's function $G_{LL'}$ reflects the geometrical structure.

3. Results and discussion

3.1. Experimental results

Figs. 1–3 show the observed Sn L_3-edge XANES spectra for methyl (Fig. 1), butyl (Fig. 2) and phenyl (Fig. 3) compounds measured by Takahashi et al. [6]. The XANES spectra depend on the organic extent. The white-line region sometimes reflects bound unoccupied levels localized on Sn in addition to the transition to continuum: the latter is sensitive to the local structures. We rather pay attention to the region A (well above the edge, 3940–3980 eV) which mainly reflects the local structure. In recent study of Sn L_3-edge XANES of gas-phase $SnCl_4$ molecule, the continuum edge is observed at 3940 eV [7]. The extended spectra are also shown in Figs. 1–3b, which show the systematic change depending on the

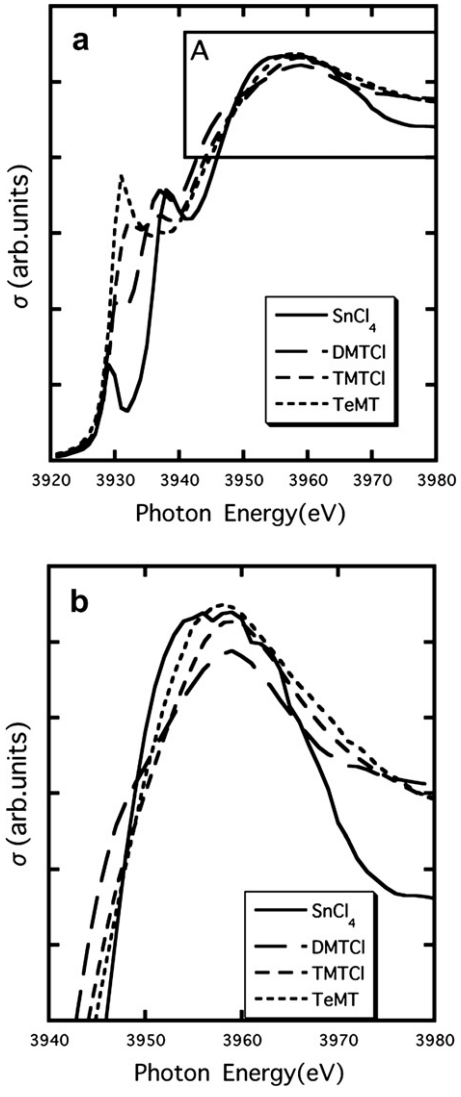

Fig. 1. (a) The observed Sn L_3-edge XANES spectra of methyl compounds (b) Extended spectra in the region A. DMTCl is dimethyltin chloride (n = 2), TMTCl is trimethyltin chloride (n = 3), TeMT is tetramethyltin (n = 4), respectively.

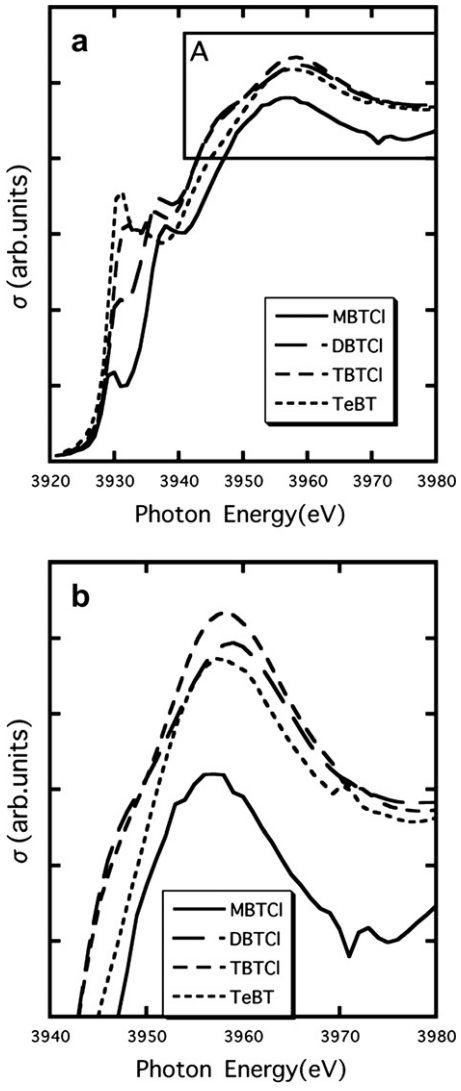

Fig. 2. (a) The observed Sn L_3-edge XANES spectra of butyl compounds. (b) Extended spectra in the region A. MBTCl is monobutyltin chloride (n = 1), DBTCl is dibutyltin chloride (n = 2), TBTCl is tributyltin chloride (n = 3), TeBT is tetrabutyltin (n = 4), respectively.

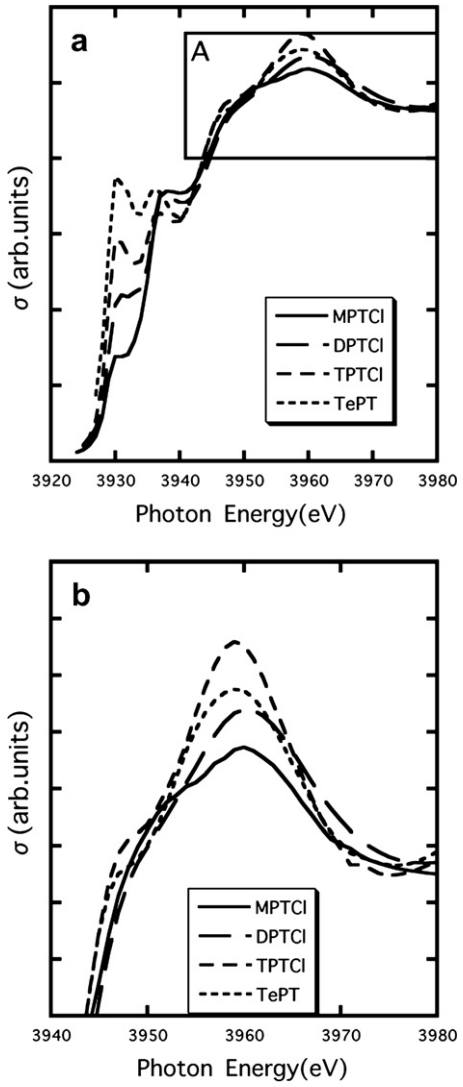

Fig. 3. (a) The observed Sn L_3-edge XANES spectra of phenyl compounds. (b) Extended spectra in the region A. MPTCl is monophenyltin chloride ($n = 1$), DPTCl is diphenyltin chloride ($n = 2$), TPTCl is triphenyltin chloride ($n = 3$), TePT is tetraphenyltin ($n = 4$), respectively.

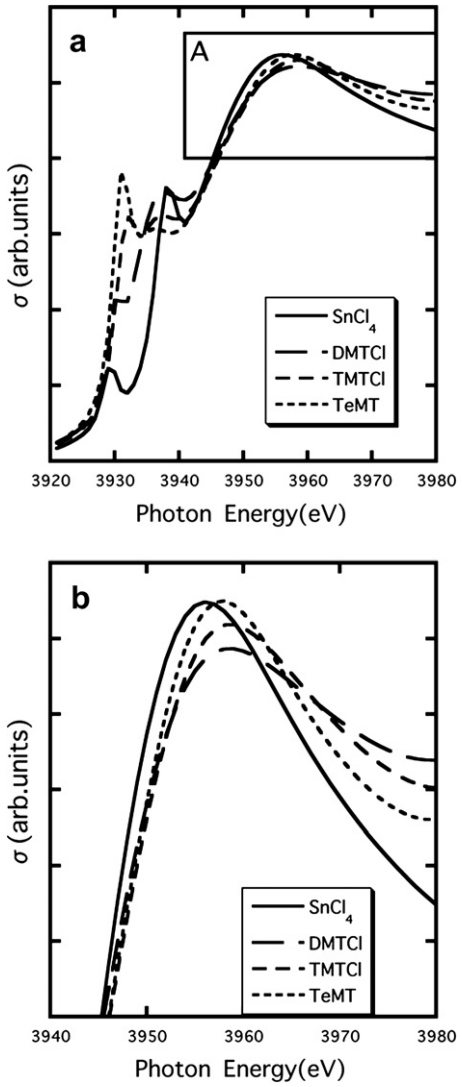

Fig. 4. (a) The calculated Sn L_3-edge XANES spectra of methyl compounds. (b) Extended spectra in the region A. DMTCl is dimethyltin chloride ($n = 2$), TMTCl is trimethyltin chloride ($n = 3$), TeMT is tetramethyltin ($n = 4$), respectively.

organic extent n, $SnCl_{4-n}X_n$ (X = Me, Bt, Ph). The peak position shifts to left and its intensity grows with the organic extent n. We thus expect that these systematic changes can be related to the structural changes, which of course cause changes in electronic structures.

3.2. Structural models and DF calculations

No experimental attempt to obtain structural information has been undertaken except $SnCl_4$ for which electron diffraction measurement gives the information on the Sn–Cl distance, Sn–Cl = 2.31 Å [13].

In order to obtain useful information about the electronic and geometric structures, we thus apply *ab initio* molecular-orbital approaches to these organotin compounds [14], where a density functional theory employs the B3LYP type exchange-correlation potential with LanL2DZ basis set. All the optimized structures are tetrahedral whose Sn–C and –Cl distances are shown in Table 1. The optimized Sn–Cl distance 2.37 Å is quite close to the observed one 2.31 Å. We thus can put trust in the calculated results. The Sn–Cl distance increases with the organic extent n, while Sn–C distances are nearly constant. These structural changes are related to the changes in bond order. The Sn–C bond order is nearly constant, whereas the Sn–Cl bond order decreases with n.

Table 1
Calculated Sn–C, Sn–Cl distances in organic tin molecules

	Sn–C/Å	Sn–Cl/Å		Sn–C/Å	Sn–Cl/Å		Sn–C/Å	Sn–Cl/Å
$SnCl_4$		2.37	MBTCl	2.13	2.39	MPTCl	2.10	2.39
DMTCl	2.12	2.41	DBTCl	2.13	2.42	DPTCl	2.11	2.41
TMTCl	2.13	2.45	TBTCl	2.15	2.45	TPTCl	2.12	2.44
TeMT	2.15		TeBT	2.16		TePT	2.14	

3.3. Sn L_3-edge XANES analyses

Our multiple-scattering calculations describe core to continuum transitions, so that purely core to localized bound state transitions are taken into account by use of several Voigt functions. Fig. 4 shows the calculated Sn L_3-edge XANES spectra for $SnCl_{4-n}Me_n$ (n = 0–4). The calculated results also show that the specific peak shifts to high-energy side in the region A with n from $SnCl_4$ to $SnClMe_3$. The peak A is caused by the multiple-scattering, which suggests that the peak shift can be explained on the basis of Natoli's rule [15],

$$(E_p - E_0)R^2 = \text{const.}, \quad (3)$$

where $E_p - E_0$ is the energy of the peak A measured from E_0 (muffin-tin constant), and R is Sn–Cl distance. Of course Sn → C scattering paths contribute to the XANES spectra, but Cl is stronger scatterer than C. With increase of n the Sn–Cl distance gets shorter, which gives rise to the energy shift to low energy side. Both the observed and the calculated results support this rule. The calculated results also explain the intensity change depending on the organic extent n, which cannot be explained on the basis of the Natoli's rule.

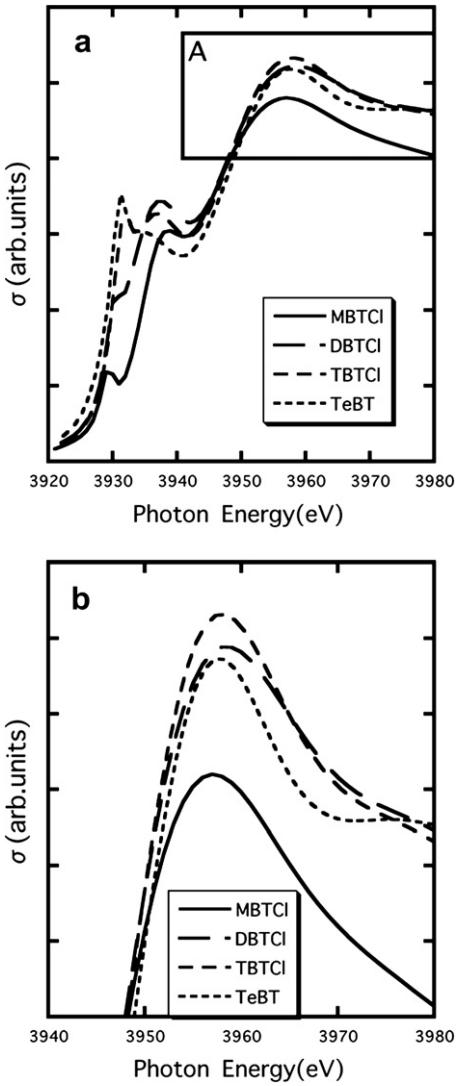

Fig. 5. (a) The calculated Sn L_3-edge XANES spectra of butyl compounds. (b) Extended spectra in the region A. MBTCl is monobutyltin chloride (n = 1), DBTCl is dibutyltin chloride (n = 2), TBTCl is tributyltin chloride (n = 3), TeBT is tetrabutyltin (n = 4), respectively.

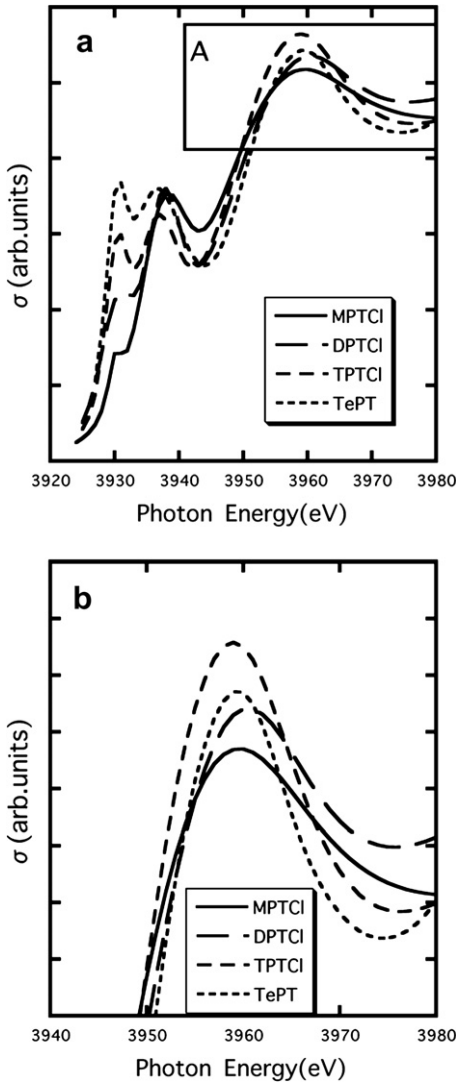

Fig. 6. (a) The calculated Sn L_3-edge XANES spectra of phenyl compounds. (b) Extended spectra in the region A. MPTCl is monophenyltin chloride (n = 1), DPTCl is diphenyltin chloride (n = 2), TPTCl is triphenyltin chloride (n = 3), TePT is tetraphenyltin (n = 4), respectively.

Fig. 5 shows the calculated Sn L_3-edge XANES spectra for $SnCl_{4-n}Bt_n$ (n = 0–4), which are quite similar to the previous results. The peak shifts again follow the Natoli's rule, and the calculated peak intensities well explain the observed result. Fig. 6 shows the same ones for $SnCl_{4-n}Ph_n$. In contrast to the previous results, the observed peak shifts and the intensity changes cannot be explained by the present calculations. This should be due to the difficulty in optimizing the structures by DFT calculations because large phenyl groups can easily rotate around Sn–C bonds.

Fig. 7 shows the calculated Sn L_3-edge XANES spectra for different Sn–Cl distances in $SnCl_4$ (a) and Sn–C distances in $SnMe_4$ (b). For the larger Sn–Cl or Sn–C distance we observe the energy shift of the peak A to low energy side in consistent with the Natoli's rule [15]. For $SnCl_4$, $(E_p - E_0)R^2$ = 204 eV Å^2 at R = 2.27 Å, 202 eV Å^2 at 2.37 Å whereas 180 eV Å^2 at 2.47 Å: the peak at 3938 eV is lost because of the XANES peak at ~3940 eV shifts to low energy side. For $SnMe_4$ we find similar behavior, 183 eV Å^2 at R = 2.05 Å, 174 eV Å^2 at 2.15 Å and 162 eV Å^2 at 2.25 Å. We thus find that Natoli's rule is not quantitative but qualitative.

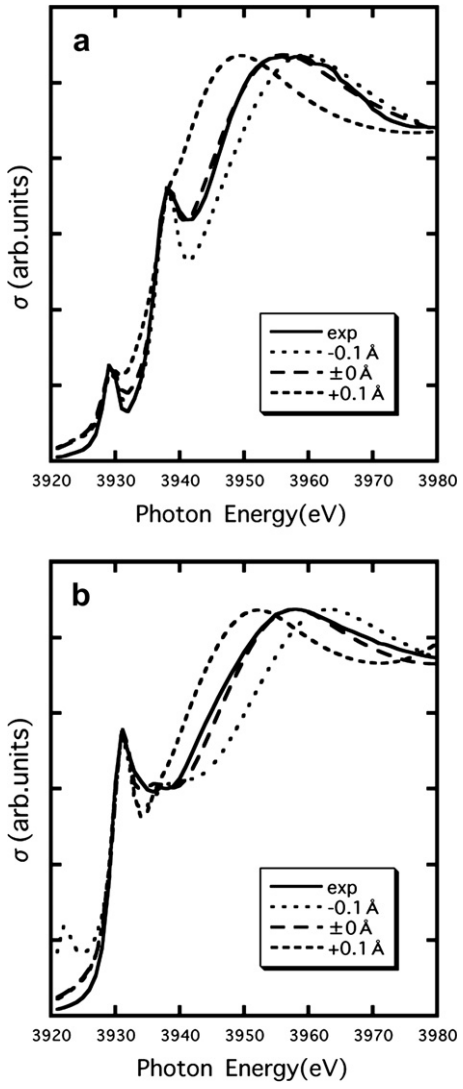

Fig. 7. The calculated Sn L_3-edge XANES spectra for different Sn–Cl distances in $SnCl_4$ (a), and Sn–C distances in $SnMe_4$(TeMT) (b).

4. Concluding remarks

The multiple-scattering XANES analyses for Sn L_3-edge spectra have been applied to organotin compounds $SnCl_{4-n}Me_n$, $SnCl_{4-n}Bt_n$, and $SnCl_{4-n}Ph_n$ (n = 0–4). The white-lines are ascribed to $2p_{3/2} \rightarrow$ bound unoccupied state transitions, which are sensitive to the electronic structure on Sn. The spectral changes are clearly related to the changes in electronic structures. On the other hand, the peak A at ~3960 eV is sensitive to the local geometry around the central Sn. With aid of Natoli's rule we can easily obtain qualitative structural information. The present XANES analyses support the optimized structures obtained on the basis of DFT calculations.

References

[1] Y. Takahashi, A. Usui, K. Okumura, T. Uruga, M. Nomura, H. Shimizu, Chem. Lett. (2002) 366.
[2] M. Sakamaki, H. Takahashi, T. Konishi, A. Inoue, T. Fujikawa, AIP Conf. Proc. 882 (2007) 271.
[3] M. Abalos, J.M. Bayona, R. Compano, M. Granados, C. Leal, M.D. Part, J. Chromatogr. A 788 (1997) 1.
[4] G.E. Brown, J.G. Catalano, A.S. Templeton, T.P. Trainor, F. Farges, B.C. Bostick, T. Kendelewicz, C.S. Doyle, A.M. Spormann, K. Revill, G. Morin, F. Juillot, G. Calas, Phys. Scripta T 115 (2005) 80.
[5] N. Sakakibara, Y. Takahashi, Y. Yamaguchi, K. Shibata, T. Uruga, Chem. Lett. 33 (2004) 264.
[6] Y. Takahashi, N. Sakakibara, M. Nomura, Anal. Chem. 76 (2004) 4307.
[7] F. Guillot, C. Dézarnaud-Dandine, M. Tronc, Chem. Phys. 224 (1997) 281.
[8] T. Fujikawa, T. Matsuura, H. Kuroda, J. Phys. Soc. Jpn. 52 (1983) 905.
[9] T. Fujikawa, J. Phys. Soc. Jpn. 62 (1993) 2155.
[10] T. Fujikawa, N. Yiwata, Surf. Sci. 357 (1996) 60.
[11] T. Fujikawa, R. Yanagisawa, N. Yiwata, K. Ohtani, J. Phys. Soc. Jpn. 66 (1997) 257.
[12] T. Fujikawa, K. Nakamura, S. Nagamatsu, J.J. Rehr, J. Phys. Soc. Jpn. 71 (2002) 357.
[13] A.M. Domingos, G.M. Sheldrick, J. Chem. Soc., Dalton Trans. 1 (1974) 475.
[14] M.J. Frisch, G.W. Trucks, H.B. Schlegel, G.E. Scuseria, M.A. Robb, J.R. Cheeseman, J.A. Montgomery Jr., T. Vreven, K.N. Kudin, J.C. Burant, J.M. Millam, S.S. Iyengar, J. Tomasi, V. Barone, B. Mennucci, M. Cossi, G. Scalmani, N. Rega, G.A. Petersson, H. Nakatsuji, M. Hada, M. Ehara, K. Toyota, R. Fukuda, J. Hasegawa, M. Ishida, T. Nakajima, Y. Honda, O. Kitao, H. Nakai, M. Klene, X. Li, J.E. Knox, H.P. Hratchian, J.B. Cross, V. Bakken, C. Adamo, J. Jaramillo, R. Gomperts, R.E. Stratmann, O. Yazyev, A.J. Austin, R. Cammi, C. Pomelli, J.W. Ochterski, P.Y. Ayala, K. Morokuma, G.A. Voth, P. Salvador, J.J. Dannenberg, V.G. Zakrzewski, S. Dapprich, A.D. Daniels, M.C. Strain, O. Farkas, D.K. Malick, A.D. Rabuck, K. Raghavachari, J.B. Foresman, J.V. Ortiz, Q. Cui, A.G. Baboul, S. Clifford, J. Cioslowski, B.B. Stefanov, G. Liu, A. Liashenko, P. Piskorz, I. Komaromi, R.L. Martin, D.J. Fox, T. Keith, M.A. Al-Laham, C.Y. Peng, A. Nanayakkara, M. Challacombe, P.M.W. Gill, B. Johnson, W. Chen, M.W. Wong, C. Gonzalez, J.A. Pople, GAUSSIAN 03, Revision C.02 Gaussian, Inc., Wallingford, CT, 2004.
[15] C.R. Natoli, in: A. Bianconi, L. Incoccia, S. Stipcich (Eds.), EXAFS and Near Edge Structure, 1983, p. 43.

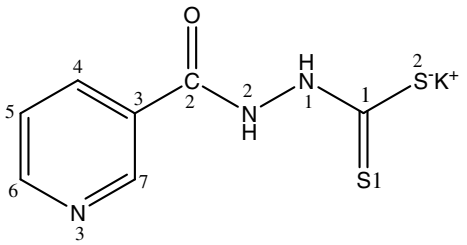

Fig. 1. [N′-(pyridine-3-carbonyl)- hydrazine]-carbodithioate $[K^+(H_2L)^-]$.

691. ^{1}H NMR (DMSO-d_6; δ ppm): 10.01 (m, 2H, –NH), 9.05, 8.73, 7.51, 8.23 (4H, pyridine ring). ^{13}C NMR (DMSO-d_6, δ ppm): 214.76 (>C=S), 161.99 (>C=O), 128.96 (C3), 151.99 (C7), 148.45 (C6), 123.52 (C5), 135.06 (C4). Based on the above physico-chemical studies the tentative structure of the ligand is depicted in Fig. 1.

2.3. Synthesis of the complexes

2.3.1. $[Ni(en)_2(3\text{-}pyt)_2]$ (**1**)

A methanolic solution (10 ml) of $[Ni(en)_2(NCS)_2]$ (1 mmol) was mixed with an aqueous methanolic solution (50:50 v/v) (10 ml) of $[K^+(H_2L)^-]$ (2 mmol). The resulting solution was filtered off and kept for crystallization. After 20 days, reddish crystals of **2** suitable for an X-ray crystallographic study were obtained.

Anal. Calc. for $C_{18}H_{24}N_{10}NiO_2S_2$ (535.26): C, 40.39; H, 4.52; N, 26.17; S, 11.98; Ni, 10.96. Found: C, 40.42; H, 4.50; N, 26.17; S, 11.90; Ni, 10.80%. μ_B = 2.83 B.M. M.p.: 240 °C (dec.). IR data (ν, KBr, cm^{-1}); ν(NH of en) 3247; ν(C=N) 1584; ν_{as}(C–O–C) 1273; ν_s(C–O–C) 1190; ν(N–N) 1080; ν(C=S) 947; ν(Ni–N) 426; pyridine ring 689. UV–Vis [λ_{max}, MeOH, nm]: 670, 450, 299, 226.

2.3.2. $[Cu(en)_2](3\text{-}pyt)_2$ (**2**)

A methanolic solution (10 ml) of $CuCl_2 \cdot 2H_2O$ (1 mmol) was stirred with an aqueous methanolic solution (50:50 v/v) (10 ml) of $[K^+(H_2L)^-]$ (2 mmol), the precipitated green product was filtered off and washed twice with cold water. The above precipitate was added to a MeOH solution of en and shaken for a few minutes; the resulting solution of **2** was filtered off and on keeping this solution for 15 days, purple crystals of **2** suitable for an X-ray crystallography study were obtained.

Anal. Calcd.(%) for $C_{18}H_{24}N_{10}CuO_2S_2$ (540.12): C, 40.03; H, 4.48; N, 25.93; S, 11.87; Cu, 11.77. Found: C, 40.10; H, 4.46; N, 25.86; S, 11.85; Cu, 11.95%. μ_B = 1.78 B.M. M.p.: >300 °C. IR data (KBr, cm^{-1}); ν(NH of en) 3284m; ν(C=N) 1604s; ν_{as}(C–O–C) 1277; ν_s(C–O–C)

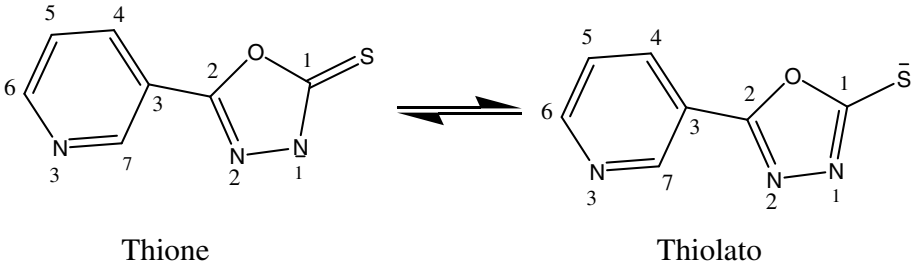

Fig. 2. Thione-thiolato forms of 5-(3-pyridyl)-1,3,4-oxadiazole-2-thione $(3\text{-pyt})^-$.

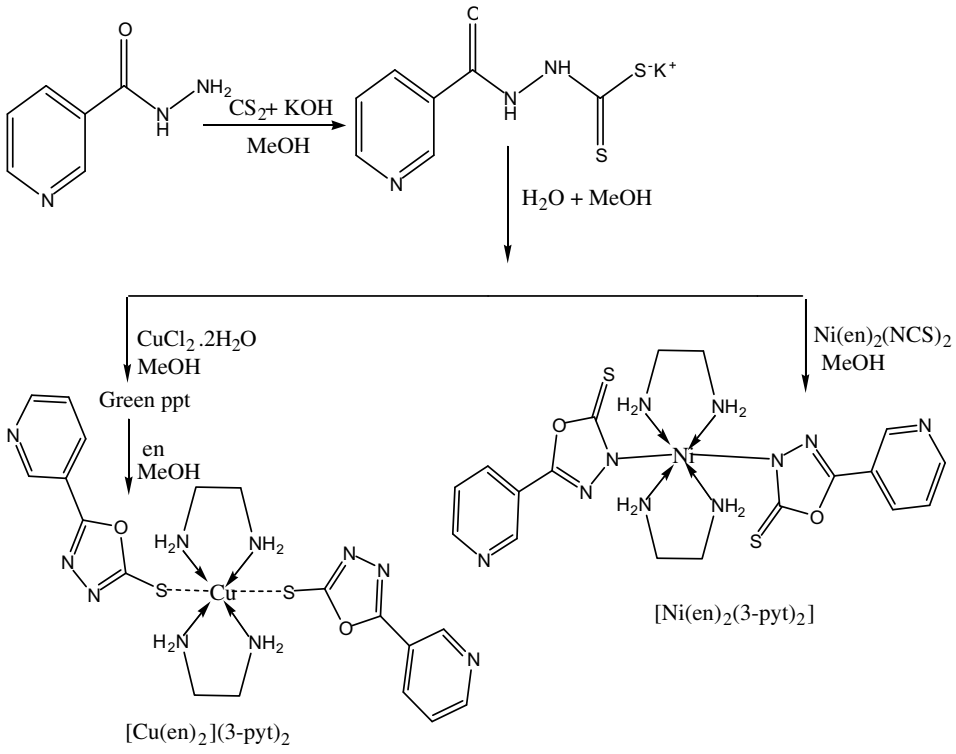

Scheme 1. Preparation of $[K^+(H_2L)^-]$ and its Ni(II) and Cu(II) complexes.

Table 1
Crystallographic data and structure refinement for $[Ni(en)_2(3\text{-pyt})_2]$ (**1**) and $[Cu(en)_2](3\text{-pyt})$ (**2**)

Parameters	1	2
Empirical formula	$C_{18}H_{24}N_{10}NiO_2S_2$	$C_{18}H_{24}N_{10}CuO_2S_2$
Formula weight	535.30	540.13
Crystal system	orthorhombic	monoclinic
Space group	*Pca*2(1)	*C*2/*c*
T (K)	173(2)	173(2)
λ, Mo Kα (Å)	0.71073	0.71073
a (Å)	12.4742(12)	21.803(3)
b (Å)	10.0791(10)	8.7360(12)
c (Å)	18.8499(18)	12.9903(18)
α (°)	90	90
β (°)	90	111.810 (2)
γ (°)	90	90
V (Å^3)	2370.0(4)	2297.2(5)
Z	4	4
ρ_{calc} (Mg/m^3)	1.500	1.562
μ (mm^{-1})	1.032	1.171
F(000)	1112	1116
Crystal size (mm)	0.28 × 0.31 × 0.49	0.61 × 0.39 × 0.17
θ Range for data collection, °	2.60–29.59	2.54–29.61
Index ranges	$-17 \leqslant h \leqslant 14$, $-13 \leqslant k \leqslant 10$, $-25 \leqslant l \leqslant 25$	$-29 \leqslant h \leqslant 30$, $-12 \leqslant k \leqslant 12$, $-15 \leqslant l \leqslant 18$
Reflections collected	20583	12490
Independent reflections	6518	3188
Data/restraints/parameters	6518/1/301	3188/0/151
Goodness-of-fit on F^2	1.042	1.053
R_1[a], wR_2[b] [$I > 2\sigma(I)$]	0.0242, 0.0587	0.0254, 0.0666
R_1[a], wR_2 [b](all data)	0.0267, 0.0596	0.0287, 0.0681
Largest difference in peak/hole (e Å^{-3})	0.297/−0.401	0.387/−0.336

[a] $R_1 = \sum||F_o| - |F_c||/\sum|F_o|$.
[b] $R_2 = [\sum w(|F_o^2| - |F^{2c}|)^2/\sum wIF_o^2|^2]^{1/2}$.

1187; ν(N–N) 1067s; ν(C–S) 896m; ν(Cu–N) 470; pyridine ring 698. UV–Vis [λ_{max}, MeOH, nm]: 645, 305, 268.

3. Analyses and physical measurements

Carbon, hydrogen, nitrogen and sulfur contents were estimated on a CHN Model CE-440 Analyser and on an Elementar Vario EL III Carlo Erbo 1108. By following standard procedures, the complexes were analyzed for their metal content, after decomposition with a mixture of conc. HNO_3 and HCl, followed by conc. H_2SO_4 [20]. Magnetic susceptibility measurements were performed at room temperature on a Cahn Faraday balance using $Hg[Co(NCS)_4]$ as the calibrant and electronic spectra were recorded on an UV-1700 Pharmaspec spectrophotometer. IR spectra were recorded in the 4000–400 cm^{-1} region as KBr pellets on a Varian Excalibur 3100 FT-IR spectrophotometer. ^{1}H and ^{13}C NMR spectra were recorded in DMSO-d_6 on a JEOL AL300 FT NMR spectrometer using TMS as an internal reference.

4. Crystal structure determination and structure refinement

Data for the structures were obtained at 173(2) K on a Bruker three-circle diffractometer equipped with a SMART 6000 CCD diffractometer using a graphite monochromated Mo Kα (0.71073 Å) radiation source. Intensity measurements were performed on a rapidly cooled crystal. The spectra were solved by direct methods (SHELXL-97) and refined against all data by full matrix least-squares on F^2 using anisotropic displacement parameters for all non-hydrogen atoms. All the hydrogen atoms were included in the refinement at geometrically ideal positions and refined with a riding model [21,22]. The MERCURY package was used for molecular graphics [23]. Crystal structure diagrams were generated by use of the ORTEP-3 for windows program [24].

Table 2
Interatomic distances (Å) and angles (°) for $[Ni(en)_2(3\text{-pyt})_2]$ (**1**)

Nickel coordination sphere			
Ni–N(11A)	2.0930(14)	N(11B)–Ni–N(11A)	179.57(7)
Ni–N(12A)	2.1127(13)	N(11B)–Ni–N(12B)	83.06(5)
Ni–N(11B)	2.0918(14)	N(11A)–Ni–N(12B)	96.58(5)
Ni–N(12B)	2.1059(13)	N(11B)–Ni–N(12A)	97.10(5)
Ni–N(1A)	2.1090(14)	N(11A)–Ni–N(12A)	83.27(5)
Ni–N(1B)	2.1150(14)	N(12B)–Ni–N(12A)	179.32(6)
		N(1A)–Ni–N(1B)	179.63(6)
		N(1A)–Ni–N(12A)	90.18(5)
		N(11B)–Ni–N(1B)	90.07(5)
		N(11A)–Ni–N(1B)	90.15(5)
		N(12B)–Ni–N(1B)	89.14(5)
		N(1A)–Ni–N(1B)	179.63(6)
		N(12A)–Ni–N(1B)	90.19(5)
Ethylenediamine			
N(11A)–C(11A)	1.476(2)	C(11A)–N(11A)–Ni	107.58(10)
N(12A)–C(12A)	1.479(2)	C(12A)–N(12A)–Ni	106.46(10)
N(11B)–C(11B)	1.485(2)	C(11B)–N(11B)–Ni	107.74(10)
N(12B)–C(12B)	1.470(2)	C(12B)–N(12B)–Ni	107.38(10)
C(11A)–C(12A)	1.517(2)	N(11A)–C(11A)–C(12A)	108.11(14)
C(11B)–C(12B)	1.522(2)	N(12A)–C(12A)–C(11A)	108.58(13)
		N(11B)–C(11B)–C(12B)	107.61(13)
		N(12B)–C(12B)–C(11B)	108.76(13)
Oxadiazole ring			
S(1A)–C(1A)	1.685(2)	C(2A)–O(1A)–C(1A)	103.81(13)
S(1B)–C(1B)	1.687(2)	C(2B)–O(1B)–C(1B)	103.93(12)
O(1A)–C(1A)	1.391(2)	C(1A)–N(1A)–N(2A)	108.48(14)
O(1B)–C(1B)	1.388(2)	C(1A)–N(1A)–Ni	132.97(13)
O(1A)–C(2A)	1.3585(19)	N(2A)–N(1A)–Ni C(2A)	117.99(10)
O(1B)–C(2B)	1.3708(18)	N(2A)–N(1A)	105.52(13)
N(1A)–C(1A)	1.317(2)	C(1B)–N(1B)–N(2B)	108.58(14)
N(2A)–C(2A)	1.284(2)	C(1B)–N(1B)–Ni	133.12(12)
N(1B)–C(1B)	1.318(2)	N(2B)–N(1B)–Ni	118.17(10)
N(2B)–C(2B)	1.285(2)	C(2B)–N(2B)–N(1B)	105.86(13)
N(1A)–N(2A)	1.4029(19)	N(1A)–C(1A)–O(1A)	108.75(18)
N(1B)–N(2B)	1.4018(19)	N(1A)–C(1A)-S(1A)	131.14(14)
		O(1A)–C(1A)-S(1A)	120.10(12)
		N(2A)–C(2A)–O(1A)	113.43(14)
		N(2A)–C(2A)–C(3A)	128.37(14)
		O(1A)–C(2A)–C(3A)	118.16(13)
		N(1B)–C(1B)–O(1B)	108.82(16)
		N(1B)–C(1B)-S(1B)	130.60(13)
		O(1B)–C(1B)-S(1B)	120.58(11)
		N(2B)–C(2B)–O(1B)	112.80(13)
		N(2B)–C(2B)–C(3B)	128.53(14)
		O(1B)–C(2B)–C(3B)	118.65(13)

5. Results and discussion

As a part of our study on metal complexes of pyridyl-1,3,4-oxadiazole-2-thione and 5-phenyl-1,3,4-oxadiazole-2-thiol [10,13], we report herein the preparation, spectroscopic and X-ray studies of two new Ni(II) and Cu(II) complexes based on 5-(3-pyridyl)-1,3,4-oxadiazole-2-thione $(3\text{-pyt})^-$. A methanol solution of $Ni(en)_2(NCS)_2$ reacts with $[K^+(H_2L)^-]$ to produce $[Ni(en)_2(3\text{-pyt})_2]$ (**1**). $[K^+(H_2L)^-]$ reacts with $CuCl_2 \cdot 2H_2O$ to give a green precipitate which dissolves in methanolic en to form $[Cu(en)2](3\text{-pyt})_2$ (**2**). The single crystal X-ray diffraction studies indicate that the ligand $(3\text{-pyt})^-$ adopts the thione form in **1** but is present as the thiolato form in **2** (as shown in Fig. 2). The complexes are stable towards air and moisture for several days. Scheme 1 shows the formation of the Ni(II) and Cu(II) complexes with $[K^+(H_2L)^-]$ as the ligand and en as a co-ligand. Both complexes are soluble in MeOH and other polar solvents such as DMF and DMSO.

5.1. ^{1}H and ^{13}C NMR spectra

The ^{1}H NMR spectrum of $[K^+(H_2L)^-]$ in DMSO-d_6 shows a signal at δ 10.01 ppm for the two NH protons. The pyridine ring protons

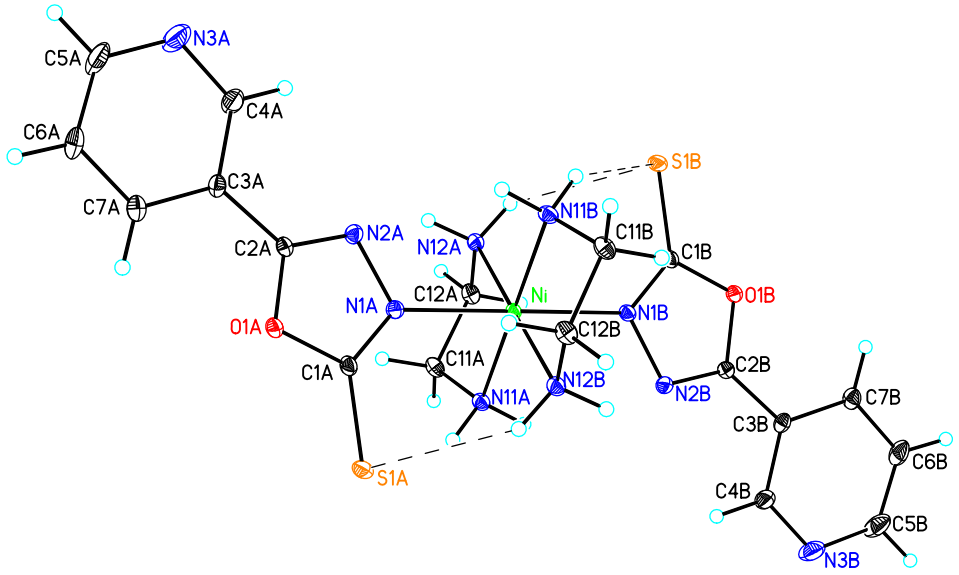

Fig. 3. Molecular structure of $[Ni(en)_2(3\text{-pyt})_2]$ with the atomic labelling scheme, showing N–H···S hydrogen bonding.

Table 3
Hydrogen bonds for $[Ni(en)_2(3\text{-pyt})_2]$ (Å and °)

D–H···A	d(D–H)	d(H···A)	d(D···A)	∠(DHA)
N(11A)–H(11D)···N(2B)	0.92	2.60	3.184(2)	122.2
N(11A)–H(11D)···S(1A)#1	0.92	2.98	3.7566(15)	143.7
N(11A)–H(11F)···S(1A)	0.92	2.86	3.6164(15)	140.5
N(12A)–H(12D)···N(2A)	0.92	2.59	3.1751(19)	121.7
N(12A)–H(12F)···S(1B)	0.92	2.68	3.4572(14)	142.6
N(11B)–H(11G)···S(1B)	0.92	2.73	3.5011(15)	141.9
N(11B)–H(11H)···N(2A)	0.92	2.63	3.204(2)	121.4
N(11B)–H(11H)···S(1B)#2	0.92	2.97	3.7518(15)	143.9
N(12B)–H(12G)···S(1A)	0.92	2.58	3.3662(15)	144.4
N(12B)–H(12H)···N(2B)	0.92	2.59	3.178(2)	122.2

#1: $x-1, -y+2, z$; #2: $x+1/2, -y+1, z$.

appear at δ 9.05, 8.73, 7.51 and 8.23 ppm. ^{13}C NMR signals at δ 214.76 (>C=S), 161.99 (>C=O), 128.96 (C3), 151.99 (C7), 148.45 (C6), 123.52 (C5) and 135.06(C4) ppm suggest the presence of a dithiocarbazate moiety in the potassium salt. We were unable to record the NMR spectra of the Ni(II) and Cu(II) complexes due to their paramagnetic nature.

5.2. IR spectra

The IR spectrum of $[K^+(H_2L)^-]$ is expected to give rise to characteristic bands due to ν(NH), ν(C=O), thioamide I, thioamide II, ν(C=S) and ν(N–N), which occur at 3218, 3148, 1665, 1470, 1329, 989 and 1087 cm^{-1}, respectively. The band at 691 cm^{-1} is due to the pyridine ring.

A comparative study of the IR spectra of complexes **1** and **2** with that of $[K^+(H_2L)^-]$ indicate very surprising results, the bands due to the –C(O)NHNHC(S)– moiety i.e. ν(C=O), thioamide I, thioamide II and ν(C=S) are found to be absent. In addition to this, the IR spectra of both complexes are devoid of any peak due to ν(NH), which

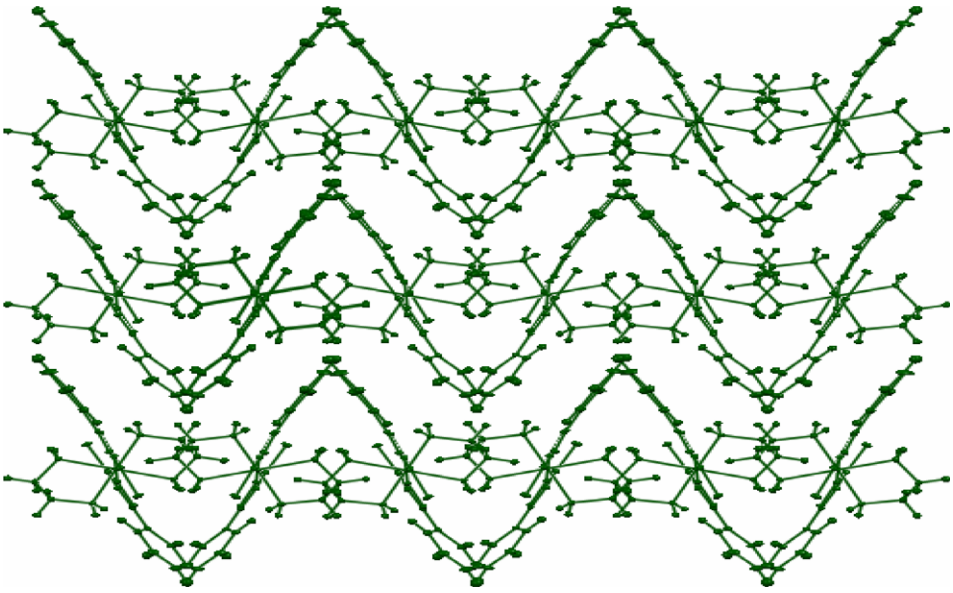

Fig. 4. The metal–organic framework of $[Ni(en)_2(3\text{-pyt})_2]$ along the a axis leading to a wave-like supramolecular architecture.

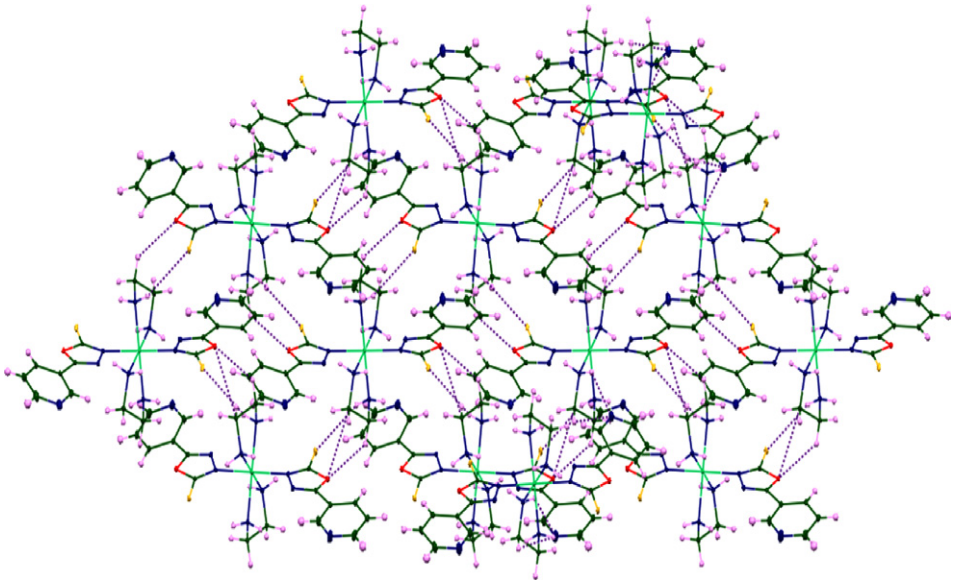

Fig. 5. Perspective view of the crystal packing of $[Ni(en)_2(3\text{-pyt})_2]$ along the b axis showing N···H, O···H, S···H intermolecular hydrogen bonding.

Table 4
Interatomic distances (Å) and angles (°) for $[Cu(en)_2](3\text{-pyt})_2$ (**2**)

Cu coordination sphere			
Cu–N(11)	2.0145(11)	N(11)#1–Cu–N(11)	180.00(3)
Cu–N(11)#1	2.0144(11)	N(11)#1–Cu–N(12)#1	84.18(4)
Cu–N(12)	2.0327(11)	N(11)–Cu–N(12)#1	95.82(4)
Cu–N(12)#1	2.0327(11)	N(11)#1–Cu–N(12)	95.82(4)
		N(11)–Cu–N(12)	84.18(4)
		N(12)#1–Cu–N(12)	180.0
Ionic distances			
Cu–S#1	3.0585(5)	S#1-Cu–S	180.00(2)
Cu–S	3.0585(5)		
Ethylenediamine			
N(11)–C(11)	1.4759(17)	C(11)–N(11)–Cu	108.56(8)
N(12)–C(12)	1.4800(16)	C(12)–N(12)–Cu	108.16(8)
C(11)–C(12)	1.511(2)	N(11)–C(11)–C(12)	107.19(10)
		N(12)–C(12)–C(11)	107.02(10)
Oxadiazole ring			
S–C(1)	1.6882(13)	C(2)–O–C(1)	103.60(9)
O–C(2)	1.3584(14)	C(1)–N(1)–N(2)	107.40(10)
O–C(1)	1.4014(15)	C(2)–N(2)–N(1)	106.58(10)
N(1)–C(1)	1.3138(16)	N(1)–C(1)–O	109.58(11)
N(1)–N(2)	1.4084(16)	N(1)–C(1)–S	131.11(10)
N(2)–C(2)	1.2875(16)	O–C(1)–S	119.30(9)
N(2)–C(2)-O	112.84(11)	N(2)–C(2)–C(3)	128.15(11)
O–C(2)–C(3)	119.01(10)		
Some other important bond angles			
N(11)#1–Cu–S#1	88.26(3)	N(12)#1–Cu–S#1	92.15(3)
N(11)–Cu–S#1	91.74(3)	N(11)#1–Cu–S	91.74(3)
N(12)–Cu–S#1	87.85(3)	N(12)#1–Cu–S	87.85(3)
N(11)–Cu–S	88.26(3)	N(12)-Cu–S	92.15(3)
C(1)–S–Cu	102.66(4)		

is present in the ligand. Further, the disappearance of bands related to ν(C=O) and ν(C=S) and the appearance of new bands at 1584 and 1604 cm^{-1} (endocyclic C=N), 1273–1277 for ν_{as}(C–O–C) and 1187–1190 for ν_s(C–O–C) cm^{-1}, suggest cyclization of the acyclic dithiocarbazate moiety. The IR data are thus consistent with the presence of a 1,3,4-oxadiazole moiety [25]. The slight negative shift in the ν(C=S) band in complex **1** may be due to the presence of N–H···S bonding. The absorption appearing in the region 3247–3284 cm^{-1} due to NH stretching vibrations of en is found to be shifted to lower frequency than those encountered in free en due to the presence of N–H···S and N–H···O hydrogen bonding in **1** and **2** [26]. The appearance of new bands at 426 and 470 cm^{-1} for complexes **1** and **2**, respectively, suggests the formation of a chelate ring in both complexes.

5.3. Electronic spectra and magnetic moment

The magnetic moment of 2.83 B.M. for $[Ni(en)_2(3\text{-pyt})_2]$ and the presence of two d–d bands at 670 and 450 nm assigned to the $^3A_{2g}(F) \rightarrow {}^3T_{1g}(F)$ and $^3T_{1g}(P)$ transitions, respectively, suggest an octahedral geometry around Ni(II) in the complex [27]. Another two bands at 299 and 226 nm may be due to charge transfer/intraligand transitions.

$[Cu(en)_2](3\text{-pyt})_2$ shows a magnetic moment of 1.78 B.M., which indicates the presence of one unpaired electron. The presence of a broad band around 645 nm assigned to the envelope of the $^2B_{1g} \rightarrow {}^2A_{1g}$, $^2B_{2g}$, ^2E_g transitions suggests a square planar geometry for the complex [27]. Two other high energy bands observed at 305 and 268 nm may be due to charge transfer/intraligand transitions.

5.4. Crystal structure description of $[Ni(en)_2(3\text{-pyt})_2]$ (**1**)

The crystal structure refinement data related to complex **1** are given in Table 1 and selected bond length and angles are given in Table 2. The X-ray crystal structure of **1** shows the presence of two bidentate ethylenediamines as a co-ligand and two $(3\text{-pyt})^-$ as ligands coordinated to Ni(II), resulting in a somewhat distorted NiN_6 octahedral geometry (Fig. 3). The monomeric unit $[Ni(en)_2(3\text{-pyt})_2]$ possesses a centrosymmetry nickel at the inversion center. Its coordination environment is fulfilled by two axial $(3\text{-pyt})^-$ anions at trans positions, bonded through nitrogen atoms at distances of 2.1090(14) and 2.1150(14) Å, and the four equatorial sites are occupied by the two bidentate *N,N′* ethylenediamine co-ligands. The binding of the en co-ligands, Ni–N(11A), Ni–N(11B) with a distance of 2.0930(14) and 2.0918(14) Å and Ni–N(12A), Ni–N(12B) with a distance of 2.1127(13) and 2.1059(13) Å, involves two five-membered chelate rings Ni–N12A–C12A–C11A–N11A and Ni–N11B–C12B–N11B with bite angles of 83.27(5)° and 83.06 (5)°, which represent a major deviation from the octahedral geometry. Although all the N(11A), N(11B), N(12A) and N(12B) atoms of

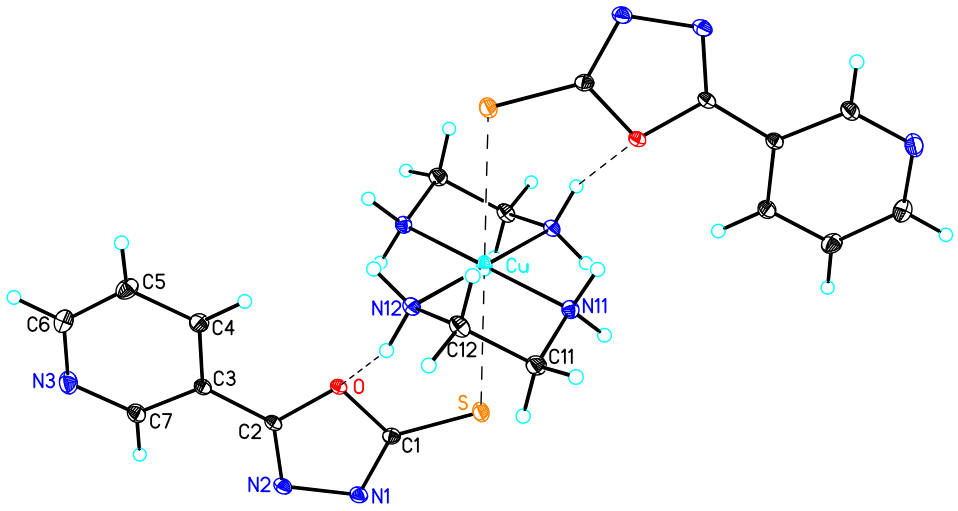

Fig. 6. Molecular structure of $[Cu(en)_2](3\text{-pyt})_2$ with the atomic labelling scheme and showing weak Cu···S interactions.

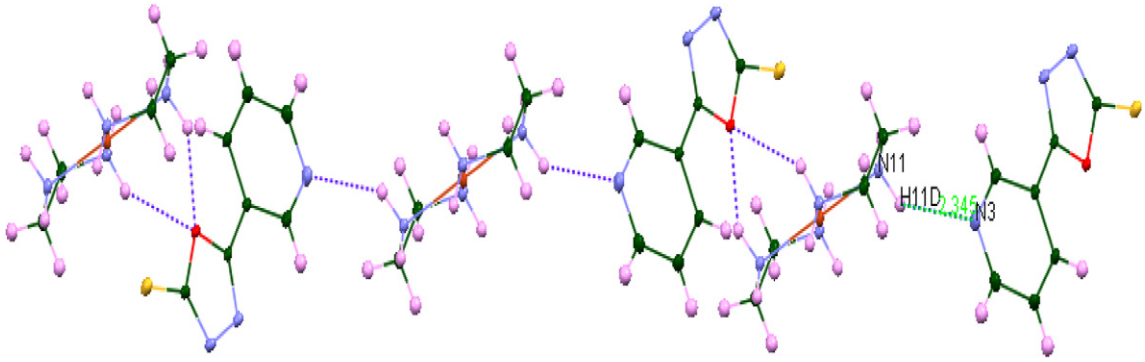

Fig. 7a. One-dimensional chain due to N–H···N hydrogen bonding.

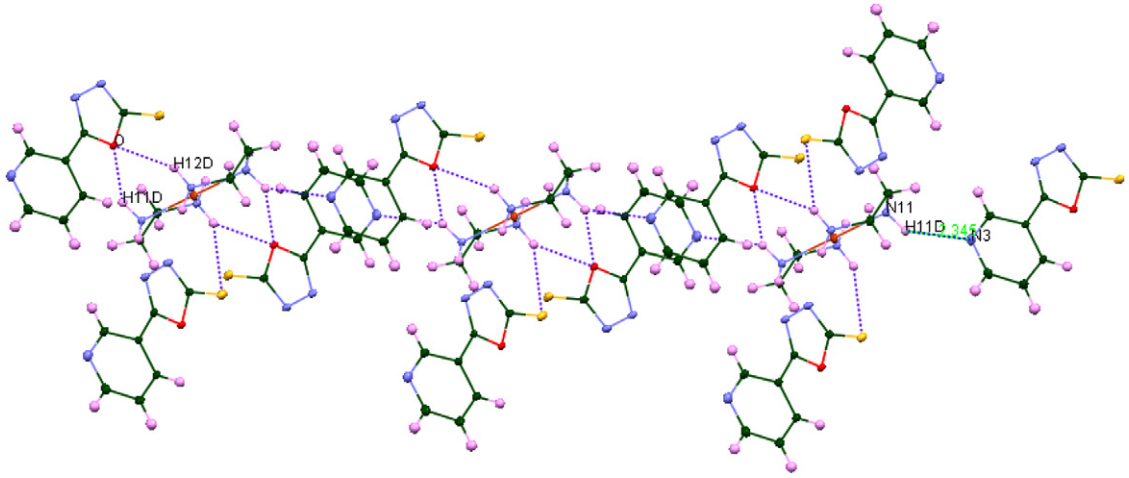

Fig. 7b. Two-dimensional network via N–H···O hydrogen bonding and face to face (π···π) interactions between two pyridine rings ($Cg_{py}\cdots Cg_{py}$).

en involved in bonding lie in a plane, the $Ni(en)_2^{2+}$ core is non-planar due to typical out of plane deviation of the methylene groups.

The geometry and bonding parameters within the en molecule agree with those of related compounds, e.g. $[Ni\{trans\text{-}(L)_2(en)_2\}${L = N-(5-chlorouracilato) [28], isothiocyanato [29] and salicylato [30]}. Similarly, the almost planar $(3\text{-pyt})^-$ ligands in **1**, bound via Ni–N(1A) = 2.1090(14) and Ni–N(1B) = 2.1150(14) Å, are significantly lengthened in comparison to the corresponding

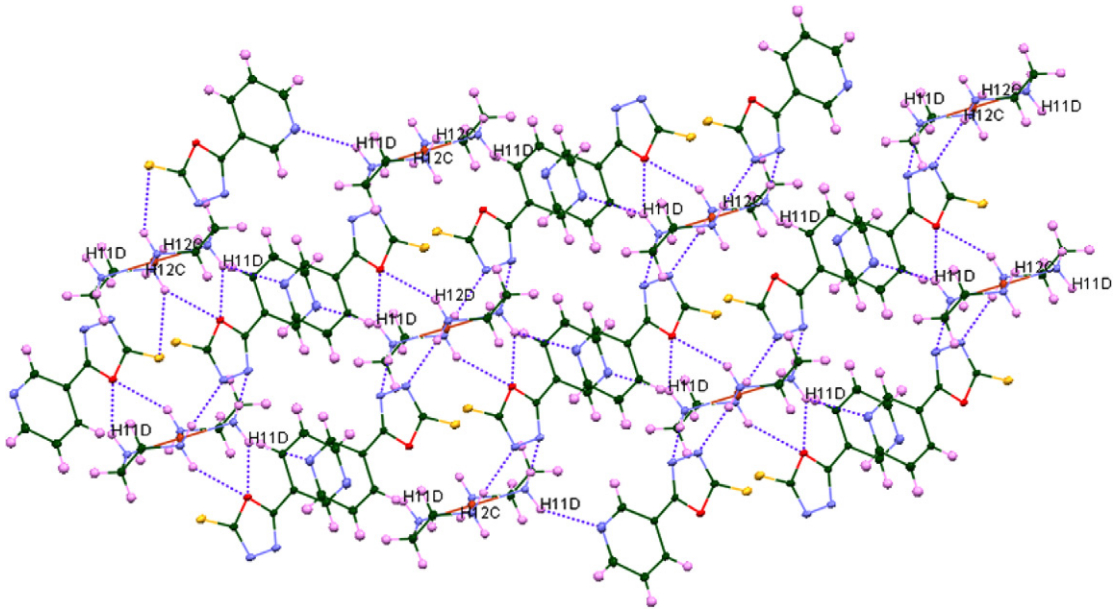

Fig. 7c. Three-dimensional frameworks originating through N–H···N, N–H···O, N- H···S hydrogen bonding and π···π interactions giving a supramolecular structure.

Table 5
Hydrogen bonds for $[Cu(en)_2](3\text{-pyt})_2$ (Å and °)

D–H···A	*d*(D–H)	*d*(H···A)	*d*(D···A)	∠(DHA)
N(11)–H(11C)···N(2)$^{\#2}$	0.92	2.11	3.0307(15)	174.5
N(11)–H(11D)···O$^{\#1}$	0.92	2.46	3.1623(14)	133.5
N(12)–H(12C)···N(1)$^{\#3}$	0.92	2.18	3.0954(16)	173.6
N(12)–H(12D)···O	0.92	2.40	3.1238(14)	135.2
N(12)–H(12D)···S$^{\#4}$	0.92	2.97	3.7434(12)	143.2

#1: $-x+1/2, -y+1/2, -z$; #2: $-x+1/2, y-1/2, -z+1/2$; #3: $x, -y+1, z-1/2$; #4: $-x+1/2, y+1/2, -z+1/2$.

bonds of 1.907(3) and 1.895(4) Å in [Ni{^{5}-(2-dimethylaminoethyl)cyclopentadienyl}(pti)]0.5(C_7H_8) [31] and [Ni{^{5}-(1-methylindene)(pti)(PPh_3)] [32], respectively, but are comparable to that of ca. 2.102 Å encountered in the related *N*-succinimido compound [Ni(succinimido)$(H_2O)_4$] · $2H_2O$[33]. The binding of en and (3-pyt)$^-$ in **1** is further stabilized by extensive intramolecular hydrogen bonding interactions (Fig. 5). The remaining atoms of the (3-pyt)$^-$ groups participate in hydrogen bonding interactions with the ethylenediamine present as a co-ligand. Hence, all the hydrogens of the NH_2 groups are involved in H-bonding to the oxygen, nitrogen and sulfur atoms of the oxadiazole ring of (3-pyt)$^-$, thus providing multiple N–H···O, linkages with D···A distances ranging from 2.578 to 2.634 Å and ∠DHA angles of 128.36–129.27° (Fig. 5). In addition, the monomeric $[Ni(en)_2(3\text{-pyt})_2]$ units are held together through N–H···S/N intermolecular hydrogen bonding, listed in Table 3, leading to the formation of wave-like metal–organic chains along the *a*-axis (Fig. 4). The shortest intra and inter chain Ni···Ni separations within these chains are 8.095 and 9.896 Å, respectively (Fig. 4). The arrangement of the monomeric $[Ni(en)_2(3\text{-pyt})_2]$ units

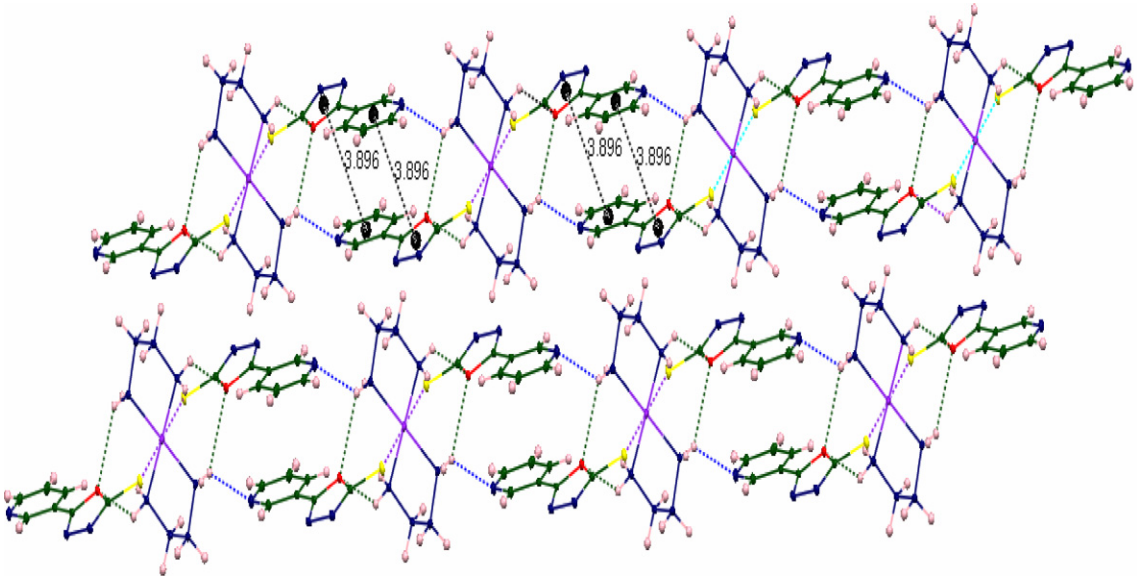

Fig. 8. MERCURY view of the crystal packing of $[Cu(en)_2](3\text{-pyt})_2$ showing face to face (π···π) interactions between the pyridine ring (Cg_{py}) and the oxadiazole ring (Cg_{oxa}).

in the three-dimensional architecture along the *a*-axis provide a supramolecular network.

5.5. Crystal structure description of $[Cu(en)_2](3\text{-pyt})_2$ (**2**)

The crystal structure refinement data related to complex **2** are given in Table 1 and selected bond length and angles are given in Table 4. The structure of complex **2** is presented in Fig. 6 and packing diagrams are presented in Fig. 7. The X-ray crystal structure analysis of **2** has a composition $[Cu(en)_2]^{2+}$ cation surrounded by two $(3\text{-pyt})^-$ anions. In the centrosymmetric unit of $[Cu(en)_2](3\text{-pyt})_2$ the metal ion has a square planar geometry where Cu(II) is bonded with four symmetry related N-atoms of two en molecules and is ionically bonded with two $(3\text{-pyt})^-$ anions. The complex cation consists of two en molecules which chelate Cu(II) in equatorial positions and two $(3\text{-pyt})^-$ occupy apical positions in a trans manner (Fig. 6). The Cu–N distances in complex **2** are in the range 2.0144(11)–2.0327(11) Å, which is almost normal for Cu–N (amine) bonds. The bite angles for the CuN_4 core are 84.18(4)° and 95.82(4)°, indicating a substantial distortion in the molecule with two five-membered CuC_2N_2 chelate rings around the Cu(II) ion. Similar geometrical parameters for the coordination sphere have been reported for diaquao-bis(ethylenediamine)copper(II) salts [34–37]. In $[Cu(en)_2]^{2+}$, the copper(II) and ethylenediamine lie in the same plane. Each $[Cu(en)_2]^{2+}$ forms a pair of weak intermolecular Cu···S interactions with a distance of 3.0585(5) Å. This distance is well within the distance of 3.2 Å, the sum of van der Waals' radii of Cu and S [38], and suggests a comparatively strong interaction. The propensity towards such an interaction is probably due to the tendency of Cu(II) to increase its coordination number. The Cu(II) in D_{4h} symmetry is bonded to four nitrogen atoms of en groups which offer interesting hydrogen bonding packing. The elements of the structure are joined to each other in the crystal packing by means of an extended system of hydrogen bonding and weak π···π interactions present (i) between the adjacent pyridine ring (Cg_{py}) and oxadiazole ring (Cg_{oxa}) with a distance of 3.896 Å (ii) between two adjacent pyridine rings (Cg_{py}) with a distance of 4.029 Å (Fig. 7b and Fig. 8).

In the molecular packing of complex **2**, the ligand $(3\text{-pyt})^-$ has formed one-dimensional chains via intermolecular N11–H11D···N3 (2.345 Å) hydrogen bonding along the *b*-axis (Fig. 7a). The π···π stacking interactions between two adjacent pyridine rings of $(3\text{-pyt})^-$ and intermolecular N11–H11D···O and N12–H12D···O hydrogen bonding connect the one-dimensional chains into a two-dimensional network (Fig. 7b). Further, $(3\text{-pyt})^-$ has formed intermolecular hydrogen bonding with the hydrogen atoms of en, viz. N(11)–H(11C)···N1#3 and N(12)–H(12D)···S#4. All these hydrogen bondings, together with weak π···π interactions, grow the chains into a three-dimensional framework (Fig. 7c). The hydrogen bonding parameters are listed in Table 5. The arrangement of $[Cu(en)_2]^{2+}$ at a dihedral angle of 84.44° with respect to $(3\text{-pyt})^-$ provides a network of intermingled chains giving the shortest intra and inter chain Cu···Cu separations within these chains of 11.744 and 12.990 Å, respectively (Fig. 8).

6. Conclusion

This paper reports the $[Ni(en)_2(3\text{-pyt})_2]$ and $[Cu(en)_2](3\text{-pyt})_2$ complexes of 5-(3-pyridyl)-1,3,4-oxadiazole-2-thione/thiol $(3\text{-pyt})^-$, containing en as a co-ligand. Both complexes contain extended hydrogen bonding, providing a three-dimensional supramolecular framework. $[Cu(en)_2](3\text{-pyt})_2$ shows weak π···π interactions.

7 Supplementary data

CCDC 656004 and 656003 contain the supplementary crystallographic data for **1** and **2**. These data can be obtained free of charge via http://www.ccdc.cam.ac.uk/conts/retrieving.html, or from the Cambridge Crystallographic Data Centre, 12 Union Road, Cambridge CB2 1EZ, UK; fax: (+44) 1223-336-033; or e-mail: deposit@ccdc.cam.ac.uk.

Acknowledgement

This work was supported by CSIR Grant No. 01(2152)07/EMR-II.

References

[1] (a) I.R. Baxendale, S.V. Ley, M. Martinelli, Tetrahedron 61 (2005) 5323;
(b) L. Spiros, M.P. Allen, B.E. Segelstein, Synth. Commun. 30 (2000) 437;
(c) B. Brown, I. Clemens, J.K. Neesom, Synlett 1 (2000) 131;
(d) F.T. Coppo, K.A. Evans, T.L. Graybill, G. Burton, Tetrahedron Lett. 45 (2004) 3257.
[2] (a) C.T. Brain, J.M. Paul, Y. Loong, P.J. Oakley, Tetrahedron Lett. 40 (1999) 3275;
(b) C.T. Brain, S.A. Brunton, Synlett 3 (2001) 382;
(c) V.K. Tandon, R.B. Chhor, Synth. Commun. 31 (2001) 1727;
(d) S.H. Mashraqui, Sh. G. Ghadigaonkar, R.S. Kenny, Synth. Commun. 33 (2003) 2541.
[3] (a) F. Bentiss, M. Lagrenee, D. Barbry, Synth. Commun. 31 (2001) 935;
(b) E. Jedlovska, J. Lesko, Synth. Commun. 24 (1994) 1879;
(c) Y. Wang, D.R. Sauer, S.W. Djuric, Tetrahedron Lett. 47 (2006) 105.
[4] (a) N.K. Singh, R.J. Butcher, P. Tripathi, A.K. Srivastava, M.K. Bharty, Acta Crystallogr., Sect. E 63 (2007) o782;
(b) N.K. Singh, R.J. Butcher, M.K. Bharty, A.K. Srivastava, P. Tripathi, Acta Crystallogr., Sect. E 62 (2006) o3473;
(c) N.K. Singh, R.J. Butcher, A.K. Pandey, M. Singh, M.K. Bharty, Acta Crystallogr., Sect. E 63 (2007) o4327.
[5] (a) Z.-B. Zheng, R.-T. Wu, J.-K. Li, Y.-F. Sun, Acta Crystallogr., Sect. E 63 (2007) o1586;
(b) Y.-T. Wang, Z.-W. Qiang, W.-Z. Wan, G.-M. Tang, Acta Crystallogr., Sect. E 62 (2006) o5585.
[6] K. Potts, A.R. Katritzky (Eds.), Comprehensive Heterocyclic Chemistry, vol. 6, Pergamon Press, 1984, p. 427.
[7] Y.D. Kulkarni, A. Rowhani, J. Indian Chem. Soc. 66 (1989) 492.
[8] K.Obi.A. Kojima, H. Fukuda, K. Hirai, Bioorg. Med. Chem. Lett. 5 (1995) 2777.
[9] (a) W.R. Tully, C.R. Gardner, R.J. Gillespie, R.J. Westwood, J. Med. Chem. 34 (1991) 2060;
(b) J. Saunders, M. Cassidy, S.B. Freedmen, E.A. Harley, L.L. Iversen, C. Kneen, A.M. MacLeod, K.J. Merchant, R.J. Snow, R.J. Baker, Med. Chem. 33 (1990) 1128;
(c) F.A. Omar, N.M. Mahfouz, M.A. Rahman, Eur. J. Med. Chem. 37 (1996) 2421;
(d) L. Mishra, M.K. Said, H. Itokawa, K. Takeya, Bioorg. Med. Chem. 3 (1995) 1241;
(e) S.P. Suman, S.C. Bahel, J. Indian Chem. Soc. 75 (1998) 53.
[10] N.K. Singh, M.K. Bharty, R.J. Butcher, Polyhedron (2008).
[11] R.W. Young, K.H. Wood, J. Am. Soc. 77 (1955) 400.
[12] (a) J.R. Reid, N.D. Heindel, J. Heterocycl. Chem. 13 (1976) 925;
(b) H. Foks, J. Mieczkowska, M. Janowiec, Z. Zwolska, Z. Andrzejczyk, Chem. Heterocycl. Comp. 38 (2002) 810;
(c) E. Hoggarth, J. Chem. Soc. (1952) 4811;
(d) C. Ainsworth, J. Am. Soc. 78 (1956) 4475.
[13] P. Tripathi, A. Pal, V. Jancik, A.K. Pandey, J. Singh, N.K. Singh, Polyhedron 26 (2007) 2597.
[14] (a) Z.-H. Zhang, Y.-L. Tian, Y.-M. Guo, Inorg. Chim. Acta 360 (2007) 2783;
(b) Z.-H. Zhang, C.-P. Li, G.-M. Tang, Y.-L. Tian, Y.-M. Guo, Inorg. Chem. Commun. 11 (2008) 326;
(c) Y.-T. Wang, G.-M. Tang, W.-Y. Ma, W.-Z. Wan, Polyhedron 26 (2007) 782.
[15] (a) M. Du, Z.-H. Zhang, X.-J. Zhao, Q. Xu, Inorg. Chem. 45 (2006) 5785;
(b) Y.-T. Wang, G.-M. Tang, Inorg. Chem. Commun. 10 (2007) 53.
[16] Y.-T. Wang, G.-M. Tang, Z.-W. Qiang, Polyhedron 26 (2007) 4542.
[17] (a) O.H. Amin, L.J. Al-Hayaly, S.A. Al-Jibori, T.A.K. Al-Allaf, Polyhedron 23 (2004) 2013;
(b) C.-L. Ma, G.-R. Tian, R.-F. Zhang, Polyhedron 24 (2005) 1773.
[18] T. Curtius, J. Prakt. Chem. 50 (1984) 278.
[19] B.W. Brown, E.C. Lingafelter, Acta Crystallogr. 16 (1963) 753.
[20] A.I. Vogel, A. Text Book of Quantitative Inorganic Analysis, 3rd ed., ELBS, Longman, London, 1969.
[21] G.M. Sheldrick, Acta Crystallogr., Sect. A 46 (1990) 467.
[22] G.M. Sheldrick, SHELXL-97, Program for Crystal Structure Refinement, University of Göttingen, Germany, 1997.
[23] I.J. Bruno, J.C. Cole, P.R. Edgington, M. Kessler, C.F. Macrae, P. McCabe, J. Pearson, R. Taylor, Acta Crystallogr., Sect. B 58 (2002) 389.
[24] L.J. Farrugia, J. Appl. Crystallogr. 30 (1997) 565.

[25] G.-S. Patricia, G.-T. Javier, A.M. Miguel, J. Arnaiz Francisco, R. Teo'filo, Inorg. Chem. 41 (2002) 1345.
[26] P. Molina, A. Tarraaga, A. Espinosa, Synthesis (1998) 565.
[27] A.B.P. Lever, Inorganic Electronic Spectroscopy, 2nd ed., Elsevier, Amsterdam, 1984.
[28] A. Terron, A.G. Raso, J.J. Fiol, S. Amengual, M.B. Oliver, R.M. Totaro, M.C. Apella, E. Molins, I. Mata, J. Inorg. Biochem. 98 (2004) 632.
[29] P.J. Squattrito, T. Iwamoto, S.-I. Nishikiori, Chem. Commun. (1996) 2665.
[30] H. Icbudak, H. Olmez, O.Z. Yesilel, F. Arslan, P. Naumov, G. Jovanovski, A.R. Ibrahim, A. Usman, H.-K. Fun, S. Chantrapromma, S.W. Ng, J. Mol. Struct. 657 (2003) 255.
[31] O. Segnitz, M. Winter, R.A. Fischer, J. Organomet. Chem. 691 (2006) 4733.
[32] I. Dubuc, M.-A. Dubois, F.B. Gariepy, D. Zargarian, Organometallics 18 (1999) 30.
[33] H.J. Cumming, D. Hall, Acta Crystallogr., Sect. B 32 (1976) 1281.
[34] A.Y. Fridman, N.M. Dyatlova, V.K. Trunov, V.M. Agre, N.N. Borkhanova, T.F. Sisoeva, Koord. Khim. 7 (1981) 1638.
[35] J. Emsely, M. Arif, P.A. Bates, M.H. Hursthouse, Chem. Commun. (1998) 1387.
[36] P.G. Romero, G.B. Jameson, J.J.B. Almenar, E. Escriva, E. Coronado, D. Beltran, J. Chem. Soc., Dalton Trans. (1988) 274.
[37] M.S. Moghadam, U. Timper, G.Z. Heller, Natureforsch 49 (1994) 627.
[38] A.J. Bondi, Phys. Chem. 68 (1964) 441.

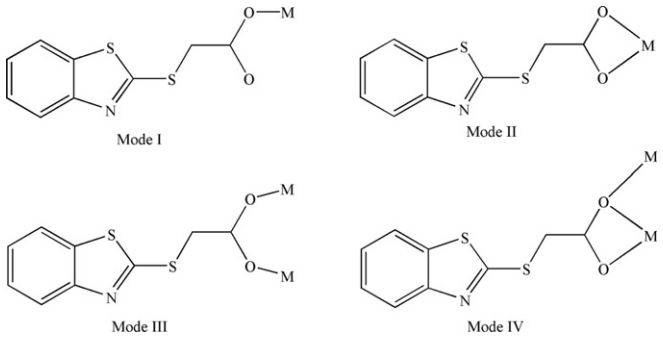

Scheme 1. Different coordination modes of the BTTAA ligand in the six complexes.

2.2. Syntheses of the complexes

2.2.1. Synthesis of **1**

A mixture of HBTTAA (225 mg, 1.00 mmol), $Mn(ClO_4)_2 \cdot 6H_2O$ (362 mg, 1.00 mmol) and 4,4′-bipyridine (312 mg, 2.00 mmol) were dissolved in an ethanol solution (15 mL) and the solution was stirred for 3 h at room temperature and then filtered. Orange block-shaped crystals of **1** were obtained from the filtrate after several days. Yield: 30% (on the basis of HBTTAA). *Anal.* Calc. for $C_{76}H_{60}Cl_2Mn_3N_{12}O_{18}S_8$: C, 47.50; H, 3.15; N, 8.75; S, 13.35. Found: C, 47.23; H, 3.12; N, 8.58; S, 13.58%. IR (KBr, cm^{-1}): 3460w, 1606s, 1591s, 1560s, 1536m, 1519w, 1490m, 1457m, 1421s, 1392s, 1221m, 1108s, 994s, 807m, 722w.

2.2.2. Synthesis of **2**

This complex was prepared by a similar procedure as that for **1**, but with a higher molar ratio (2:1:2) of HBTTAA to $Mn(ClO_4)_2 \cdot 6H_2O$ and 4,4′-bipyridine. Yield: 70% (on the basis of HBTTAA). *Anal.* Calc. for $C_{28}H_{20}MnN_4O_4S_4$: C, 55.94; H, 3.46; N, 10.30; S, 15.72. Found: C, 55.69; H, 3.12; N, 10.58; S, 5.58%. IR (KBr, cm^{-1}): 3445w, 1581s, 1530m, 1489w, 1462m, 1427s, 1385s, 1222m, 995s, 807w, 723w.

2.2.3. Synthesis of **3**

A mixture of HBTTAA (450 mg, 2.00 mmol), NaOH (80 mg, 2.00 mmol), $Cd(NO_3)_2 \cdot 4H_2O$ (309 mg, 1.00 mmol), 4,4′-bipyridine (156 mg, 1.00 mmol) and water (17 mL) was placed in a 25 mL Teflon-lined stainless autoclave and heated under autogenous pressure at 100 °C for 5 days. It was then slowly cooled to room temperature over 24 h. Colorless block-like crystals of **3** were separated from the reaction mixture in about 54% yield (on the basis of HBTTAA). *Anal.* Calc. for $C_{28}H_{20}CdN_4O_4S_4$: C, 46.89; H, 2.81; N, 7.81; S, 17.88. Found: C, 46.57; H, 3.12; N, 7.58; S, 17.58%. IR (KBr, cm^{-1}): 3444w, 1584s, 1532m, 1490w, 1460m, 1426s, 1401s, 1220m, 994m, 806m, 728w.

2.2.4. Synthesis of **4**

A mixture of HBTTAA (255 mg, 1.00 mmol), $Cd(NO_3)_2 \cdot 4H_2O$ (309 mg, 1.00 mmol) and 4,4′-bipyridine (156 mg, 1.00 mmol) were dissolved in methanol (15 mL) and the solution was stirred for 3 h at room temperature and filtered. Colorless block-shaped crystals of **4** were obtained from the filtrate after several days. Yield: 37% (on the basis of HBTTAA). *Anal.* Calc. for $C_{19}H_{16}CdN_4O_6S_2$: C, 39.83; H, 2.81; N, 9.78; S, 11.19. Found: C, 39.56; H, 3.17; N, 9.58; S, 11.58%. IR (KBr, cm^{-1}): 3436w, 1602m, 1585s, 1534w, 1489w, 1454m, 1426m, 1384vs, 1220w, 1006m, 806m, 727w.

2.2.5. Synthesis of **5**

A mixture of HBTTAA (450 mg, 2.00 mmol), NaOH (80 mg, 2.00 mmol), $Co(NO_3)_2 \cdot 6H_2O$ (291 mg, 1.00 mmol), 4,4′-bipyridine (312 mg, 2.00 mmol) and ethanol (15 mL) was placed in a 25 mL Teflon-lined stainless autoclave and heated under autogenous pressure at 100 °C for 5 days. It was then slowly cooled to room temperature over 24 h. Red block-like crystals of **5** were separated from the reaction mixture. Yield: 11% (on the basis of HBTTAA). *Anal.* Calc. for $C_{28}H_{24}CoN_4O_6S_4$: C, 48.06; H, 3.46; N, 8.01; S, 18.33. Found: C, 48.23; H, 3.17; N, 8.38; S, 18.47%. IR (KBr, cm^{-1}): 3405s, 1607s, 1577s, 1491w, 1450m, 1423s, 1374s, 1222m, 1008m, 811m, 752m.

2.2.6. Synthesis of **6**

A mixture of HBTTAA (450 mg, 2.00 mmol), NaOH (80 mg, 2.00 mmol), $CuCl_2 \cdot 2H_2O$ (171 mg, 1.00 mmol), 4,4′-bipyridine (312 mg, 2.00 mmol) and ethanol (15 mL) was placed in a 25 mL Teflon-lined stainless autoclave and heated under autogenous pressure at 110 °C for 5 days. It was then slowly cooled to room temperature over 24 h. Blue block-like crystals of **6** were separated from the reaction mixture. Yield: 70% (on the basis of HBTTAA). *Anal.* Calc. for $C_{28}H_{20}CuN_4O_4S_4$: C, 50.32; H, 3.02; N, 8.38; S, 19.19. Found: C, 50.49; H, 3.23; N, 8.57; S, 19.48%. IR (KBr, cm^{-1}): 3443w, 1611s, 1598s, 1495w, 1454m, 1424s, 1385m, 1222w, 1009m, 758w.

CAUTION! Although we have experienced no problems in handling perchlorate compounds, these should be handled with great caution due to the potential for explosion.

2.3. Crystal structure determination

X-ray crystal data collection for the six complexes was performed on a Bruker Smart 1000 CCD diffractometer with monochromated Mo-Kα radiation ($\lambda = 0.71073$ Å) at 298 K (Table 1). Semi-empirical absorption corrections were applied using the SADABS program. All calculations were carried out with SHELXS-97 and SHELXL-97 [10,11]. The structures were solved by direct methods and refined on $|F|^2$ by full-matrix least squares methods.

3. Results and discussion

3.1. Description of the crystal structures

The X-ray diffraction analysis of **1** reveals a novel 2D coordination polymer with a linear trinuclear manganese(II) unit bridged by 4,4′-bipy ligands (Fig. 1a). In the trinuclear unit, the Mn2 atom is located on a crystallographic inversion center and is coordinated octahedrally by two 4,4′-bipy nitrogen atoms and four BTTAA carboxylato oxygen atoms (Table 2). Mn2 is bridged to Mn1 through the two BTTA anions. One is in a *syn–syn* mode (μ_2,η_2-carboxylato), and the other coordinates through one oxygen atom (μ_2,η_1-carboxylato). In short, BTTAA links the metal centers in two different coordinated modes (III and IV). The coordination environment of Mn1 is completed by three carboxylato oxygen atoms and three N atoms from three 4,4′-bipy ligands to form a distorted MnN_3O_3 octahedron while Mn2 has a distorted MnN_2O_4 octahedral geometry. The $Mn_3(BTTAA)_4$ core is similar to those found in Refs. [12–18]. The Mn···Mn distance (3.853(2) Å) linked by the carboxylato group in the Mn_3 core is slightly longer than those observed in $[Mn_3(bipy)_2(O_2CPh)_6]$ (3.588 Å) [12] and $[Mn_3(bipy)_2(OAc)_6]$ (3.614 Å) [16]. Interestingly, these Mn_3 subunits are linked via 4,4′-bipy ligands with Mn···Mn separations of 11.462(2) and 11.632(2) Å, respectively, to form a novel two-dimensional network in the *ab* plane, as well as uncoordinated ClO_4^- anions and water molecules that fill in the network (Fig. 1b). The 4,4′-bipy ligands act as bridges between the trimers such that the structure forms two different perfect 4^4 square grid networks [19] and adjacent layers are packed with an ABAB mode as shown in Fig. 1c.

When we change the molar ratio of HBTTAA to 4,4′-bipy and metal salt, compound 2, with a layered structure, was isolated. Compounds **2** and **3** are isostructural, so only the structure of **2** will

Table 1
Crystallographic data for complexes **1–6**

Complex	**1**	**2**	**3**	**4**	**5**	**6**
Empirical formula	$C_{76}H_{60}Cl_2Mn_3N_{12}O_{18}S_8$	$C_{28}H_{20}MnN_4O_4S_4$	$C_{28}H_{20}CdN_4O_4S_4$	$C_{19}H_{16}CdN_4O_6S_2$	$C_{28}H_{24}CoN_4O_6S_4$	$C_{28}H_{20}CuN_4O_4S_4$
Formula weight	1921.56	659.66	717.12	572.91	699.68	668.26
Crystal system	monoclinic	monoclinic	monoclinic	orthorhombic	triclinic	triclinic
Space group	*P*2(1)/*c*	*P*2(1)/*c*	*P*2(1)/*c*	*Pbca*	$P\bar{1}$	$P\bar{1}$
a (Å)	11.632(3)	4.985(5)	5.0627(10)	17.319(2)	5.678(6)	10.822(3)
b (Å)	19.152(4)	23.18(2)	22.815(4)	10.3336(14)	11.437(12)	11.061(3)
c (Å)	18.811(4)	11.763(11)	11.833(2)	123.457(3)	11.623(12)	12.269(4)
α (°)	90	90	90	90	71.699(12)	112.081(3)
β (°)	104.860(4)	100.082(11)	100.204(2)	90	85.635(13)	98.364(3)
γ (°)	90	90	90	90	77.478(13)	90.700(3)
V (Å^3)	4050.5(16)	1338(2)	1345.1(5)	4198.3(10)	699.5(13)	1342.8(7)
Z	4	4	4	8	1	2
D_{calc} [g cm^{-3}]	1.576	1.637	1.771	1.816	1.661	1.653
F(000)	1962	674	720	2304	359	682
Reflections collected	20882	6630	6796	24916	3531	6962
Independent reflections (R_{int})	7124 (0.0850)	2325(0.1469)	2352 (0.0257)	5076 (0.0543)	2406 (0.0363)	4641 (0.0190)
Data/restraints/parameters	7124/73/538	2325/0/224	2352/0/187	5076/3/289	2406/0/196	4641/0/370
Goodness-of-fit on F^2	1.000	0.990	1.009	0.978	0.993	1.036
Final *R* indices	R_1 = 0.0600	R_1 = 0.0596	R_1 = 0.0324	R_1 = 0.0371	R_1 = 0.0652	R_1 = 0.0376
[$I > 2\sigma(I)$]	wR_2 = 0.1366	wR_2 = 0.1214	wR_2 = 0.0848	wR_2 = 0.0758	wR_2 = 0.1561	wR_2 = 0.0856
R indices (all data)	R_1 = 0.1281	R_1 = 0.0824	R_1 = 0.0382	R_1 = 0.0852	R_1 = 0.1036	R_1 = 0.0591
	wR_2 = 0.1654	wR_2 = 0.1340	wR_2 = 0.0886	wR_2 = 0.0969	wR_2 = 0.1829	wR_2 = 0.0940

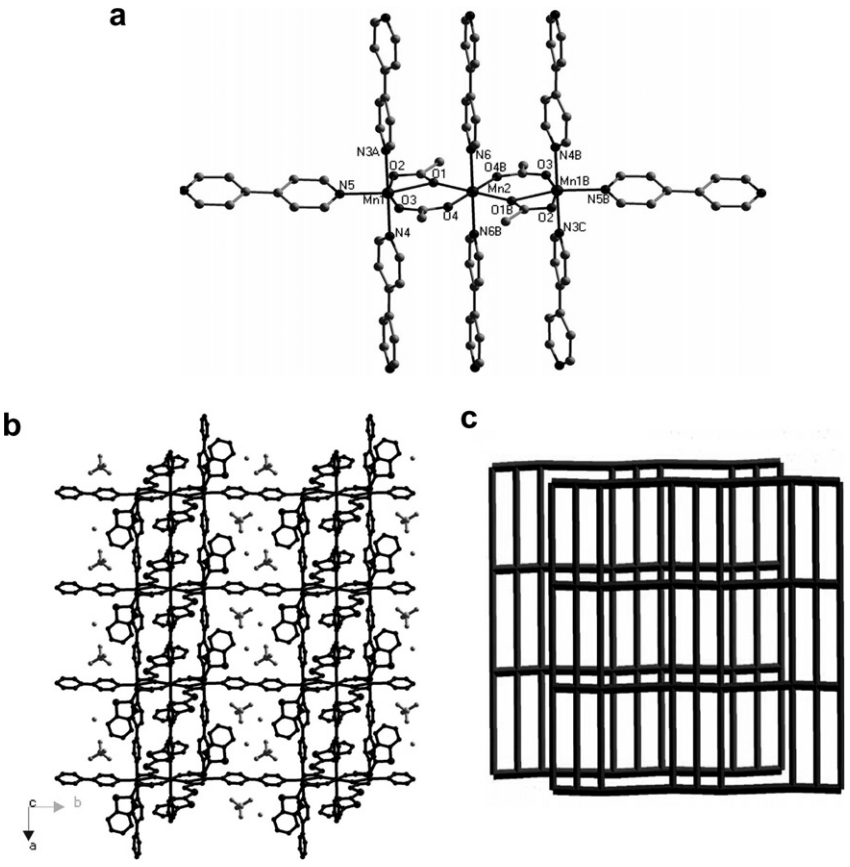

Fig. 1. (a) The asymmetric unit of **1**, the BTTAA ligands are reduced to the acetic ligand for clarity. (b) The two different 4^4 grid networks. (c) Schematic representation of the mode of ABAB packing.

be discussed in detail as a representative example. The Mn(II) atoms in **2** lie at a crystallographic inversion center and each of them is six-coordinated by four carboxylato oxygen atoms in the equatorial plane and two N atoms from two disordered 4,4′-bipy ligands (a similar "disordered" phenomenon appears in **3**) at axial sites, as shown in Fig. 2a (Table 2). Each Mn(II) is connected by two *syn–anti* (μ_2,η_2-BTTAA) carboxylato bridges (mode III) with a Mn···Mn separation of 4.985(5) Å, and Cd···Cd separation of 5.063(1) Å for **3**. This leads to the formation of an infinite 1D chain which is further connected by the coordination of 4,4′-bipy molecules to adjacent chains with an interchain Mn···Mn separation of 11.763(3) Å (interchain Cd···Cd separation of 11.833(2) Å for **3**),

Table 2
Selected bond lengths (Å) and angles (°) for complexes **1**–**6**

Compound ***1***					
Mn1–O3	2.060(4)	Mn1–N5	2.193(5)	Mn1–O2	2.247(4)
Mn1–N4	2.272(4)	Mn1–N3A	2.278(4)	Mn1–O1	2.309(4)
Mn2–O4	2.156(4)	Mn2–N6	2.261(4)	Mn2–O1	2.198(4)
O3–Mn1–N5	105.6(2)	O3–Mn1–O2	159.4(2)	N5–Mn1–O2	95.0(2)
O3–Mn1–N4	88.3(2)	N5–Mn1–N4	90.1(2)	O2–Mn1–N4	91.3(2)
O3–Mn1–N3A	89.6(2)	N5–Mn1–N3A	89.6(2)	O2–Mn1–N3A	91.1(2)
N4–Mn1–N3A	177.6(2)	N5–Mn1–O1	152.2(2)	N4–Mn1–O1	92.1(2)
O3–Mn1–O1	102.2(2)	O2–Mn1–O1	57.2(2)	N3A–Mn1–O1	89.3(2)
O1–Mn2–N6	90.2(2)	O4–Mn2–O1	95.2(2)	O4–Mn2–N6	89.6(2)
Compound ***2***					
Mn1–O2B	2.153(3)	Mn1–O1	2.210(3)	Mn1–N2	2.323(4)
O1–Mn1–N2	94.0(1)	O2B–Mn1–O1	90.9(1)	O2B–Mn1–N2	88.9(1)
Compound ***3***					
Cd1–O1	2.318(2)	Cd1–N2	2.323(4)	Cd1–O2B	2.297(2)
O1– Cd1–N2	84.0(1)	O2B– Cd1–O1	89.0(1)	O2B– Cd1–N2	88.6(1)
Compound ***4***					
Cd1–N2	2.309(3)	Cd1–O4	2.440(3)	Cd1–O2	2.331(3)
Cd1–O6	2.324(3)	Cd1–O1	2.467(3)	Cd1–O3	2.480(3)
Cd1–N1	2.349(3)				
N2–Cd1–O6	91.0(1)	O6–Cd1–O1	86.2(1)	N2–Cd1–O4	89.5(1)
N2–Cd1–O2	100.1(1)	O2–Cd1–O1	54.4(1)	O6–Cd1–O4	86.4(1)
O6–Cd1–O2	137.2(1)	N1–Cd1–O1	98.6(1)	O2–Cd1–O4	134.4(1)
N2–Cd1–N1	176.1(1)	O4–Cd1–O1	170.4(1)	N1–Cd1–O4	87.1(1)
O6–Cd1–N1	86.9(1)	N2–Cd1–O3	93.6(1)	N2–Cd1–O1	84.5(1)
O2–Cd1–N1	83.6(1)	O6–Cd1–O3	137.5(1)	O2–Cd1–O3	83.4(1)
O1–Cd1–O3	136.4(1)	O4–Cd1–O3	51.4(1)	N1–Cd1–O3	85.8(1)
Compound ***5***					
Co1–O3	2.093(4)	Co1–O1	2.120(4)	Co1–N2	2.163(5)
O3–Co1–O1	92.2(2)	O1–Co1–N2A	90.4(2)	O3–Co1–N2	91.4(2)
Compound ***6***					
Cu1–O3	1.966(2)	Cu1–N4A	1.980(2)	Cu1–O1	1.970(2)
Cu1–N3	1.995(2)				
O3–Cu1–O1	177.2(1)	O3–Cu1–N3	88.8(1)	O1–Cu1–N4A	91.5(1)
O3–Cu1–N4A	91.3(1)	O1–Cu1–N3	88.4(1)	N4A–Cu1–N3	179.6(1)

Symmetry codes for **1**: A $x+1, y, z$; B $-x+1, -y+1, -z+1$; for **2**: A $-x+1, -y+1, -z+1$; B $x+1, y, z$; C $-x, -y+1, -z+1$; for **3**: A $-x+1, -y+1, -z+1$; B $x+1, y, z$; C $-x, -y+1, -z+1$; for **5**: A $-x+1, -y+1, -z+1$; for **6**: A $x, y+1, z$.

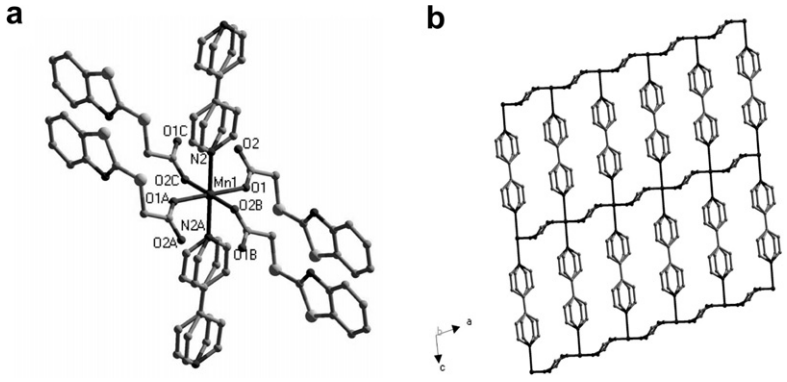

Fig. 2. (a) The coordination environment of the Mn(II) ion in **2**. (b) The 4^4 grid network, the BTTAA ligands are reduced to the acetic ligand for clarity.

resulting in the construction of a 2D 4^4 grid network in the ac plane, as shown in Fig. 2b.

Compounds **4**, **5** and **6** all have a one-dimensional polymeric structure with neutral $[Cd(BTTAA)(4,4'\text{-bipy})(NO_3)(H_2O)]$, $[Co(BTTAA)_2(4,4'\text{-bipy})(H_2O)_2]$ and $[Cu(BTTAA)_2(4,4'\text{-bipy})]$ as repeating units, respectively. In **4**, the Cd(II) atom is coordinated by two carboxylato O atoms (O1, O2) from a BTTAA ion (in mode II), two O atoms (O3, O4) from NO_3^-, two N atoms (N1, N2) from two different 4,4′-bipy ligands and one water molecule (Fig. 3a). The geometry around the metal center is a slightly distorted pentagonal-bipyramidal, with two N atoms lying in the axial positions. The Cd–O bond distances lie in the 2.324(3)–2.480(3) Å range, and Cd–N distances are between 2.309(3) and 2.349(3) Å, which is similar to that observed in the complex we reported previously [20]: $[Cd(BTTAA)(phen)_2(H_2O)] \cdot NO_3 \cdot H_2O$. The 4,4′-bipy spacers bridge the Cd(II) atoms with a Cd···Cd separation of 11.729(5) Å, leading to a 1D chain along the crystallographic *c* axis. The most important interchain interaction in the crystal packing is hydrogen bonds (O6–H6A···O1^{i}, O6–H6B···O5^{ii}, Symmetry codes: i $-x+2, -y, -z+1$; ii $x+2, -y-3/2, z-1/2$) among the coordinated carboxylate oxygen atoms, the uncoordinated NO_3^- oxygen atoms and coordinated water molecules. The hydrogen bonds in the structure

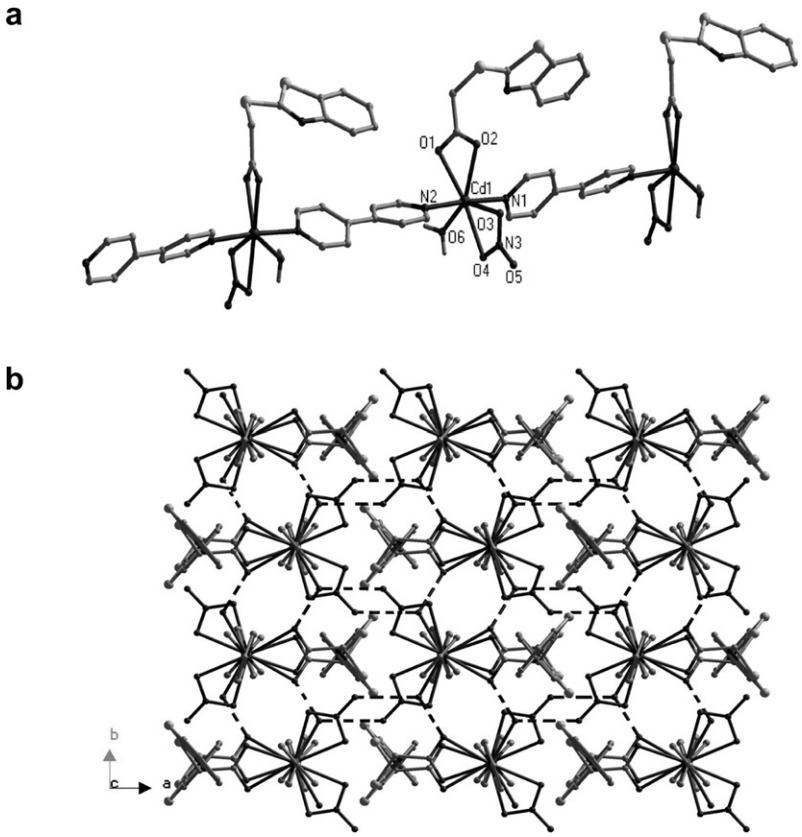

Fig. 3. (a) The coordination environment of the Cd(II) ion in **4**. (b) The 3D supramolecular structure of **4**.

allow the formation of an extended 3D supramolecular framework as shown in Fig. 3b.

As shown in Fig. 4, Co1 in **5** was located on a crystallographic inversion center and coordinated octahedrally by two 4,4′-bipy nitrogen atoms, two BTTAA carboxylato oxygen atoms and two water molecules, giving a CoN_2O_4 octahedron. The 4,4′-bipy spacers bridge adjacent Co(II) atoms with a Co···Co separation of 11.437(3) Å, leading to a 1D chain along the crystallographic *c* axis.

In **6** (Fig. 5), the Cu(II) center is coordinated by two carboxylato O atoms (O1, O3) from two different BTTAA ions and two N atoms (N3, N4) from two 4,4′-bipy ligands. The geometry around the metal center is a slightly distorted square. The 4,4′-bipy spacers bridge adjacent Cu(II) atoms with a Cu···Cu separation of 11.061(1) Å, leading to a 1D chain along the crystallographic c axis. It should be summarized that the carboxylato groups coordinating to the metal atoms in **5** and **6** are all in mode I.

3.2. Magnetic properties

The magnetic properties of the complexes **1**, **2**, 5 and **6** were investigated over the temperature range 2.0–300.0 K and the

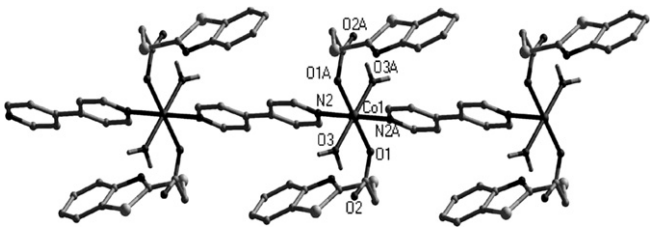

Fig. 4. The coordination environment of Co(II) in **5**.

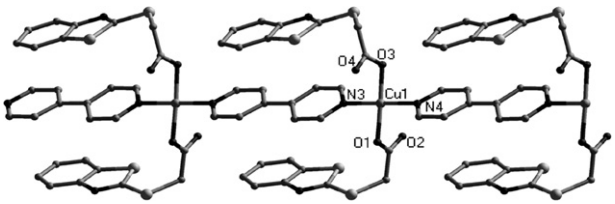

Fig. 5. The coordination environment of the Cu(II) ion in **6**.

resulting data are shown in Fig. 6. For **1**, the μ_{eff} value at 300.0 K is 10.18 B.M., which is characteristic of three independent d^5 ions. As the temperature decreases, μ_{eff} decreases continuously to a value of 5.03 B.M. at 2.0 K (Fig. 6a). This behavior indicates a dominant antiferromagnetic interaction between the Mn(II) ions. As the shortest Mn···Mn distance across the 4,4′-bipy bridge is 11.462(2) Å in **1**, the magnetic exchange coupling through the bridge is expected to be very weak [21]. The observed antiferromagnetic interaction, therefore, should mainly arise from the magnetic superexchange through the carboxylato bridges in the linear trinuclear subunit. For a linear trinuclear compound, the magnetic susceptibility can be calculated using the Hamiltonian $H = -2J(S_1S_2 + S_2S_3) - 2J_{13}S_1S_3$, where J and J_{13} represent the exchange constants between neighboring metal ions bridged by carboxylato groups and between the terminal metal ions, respectively. In the absence of a clearly defined exchange pathway between the terminal metal ions, J_{13} was taken as zero [22]. The best fit to the magnetic susceptibility data yielded $g = 2.02$, $J = -1.33\ cm^{-1}$, $zJ' = -0.08\ cm^{-1}$ and agreement factor $R = 8.77 \times 10^{-4}$.

For **2** (Fig. 6b), when the temperature decreases, μ_{eff} decreases slightly from a value close to 5.88 B.M. at 300.0 K, which is close to the spin-only value for two magnetically isolated high-spin

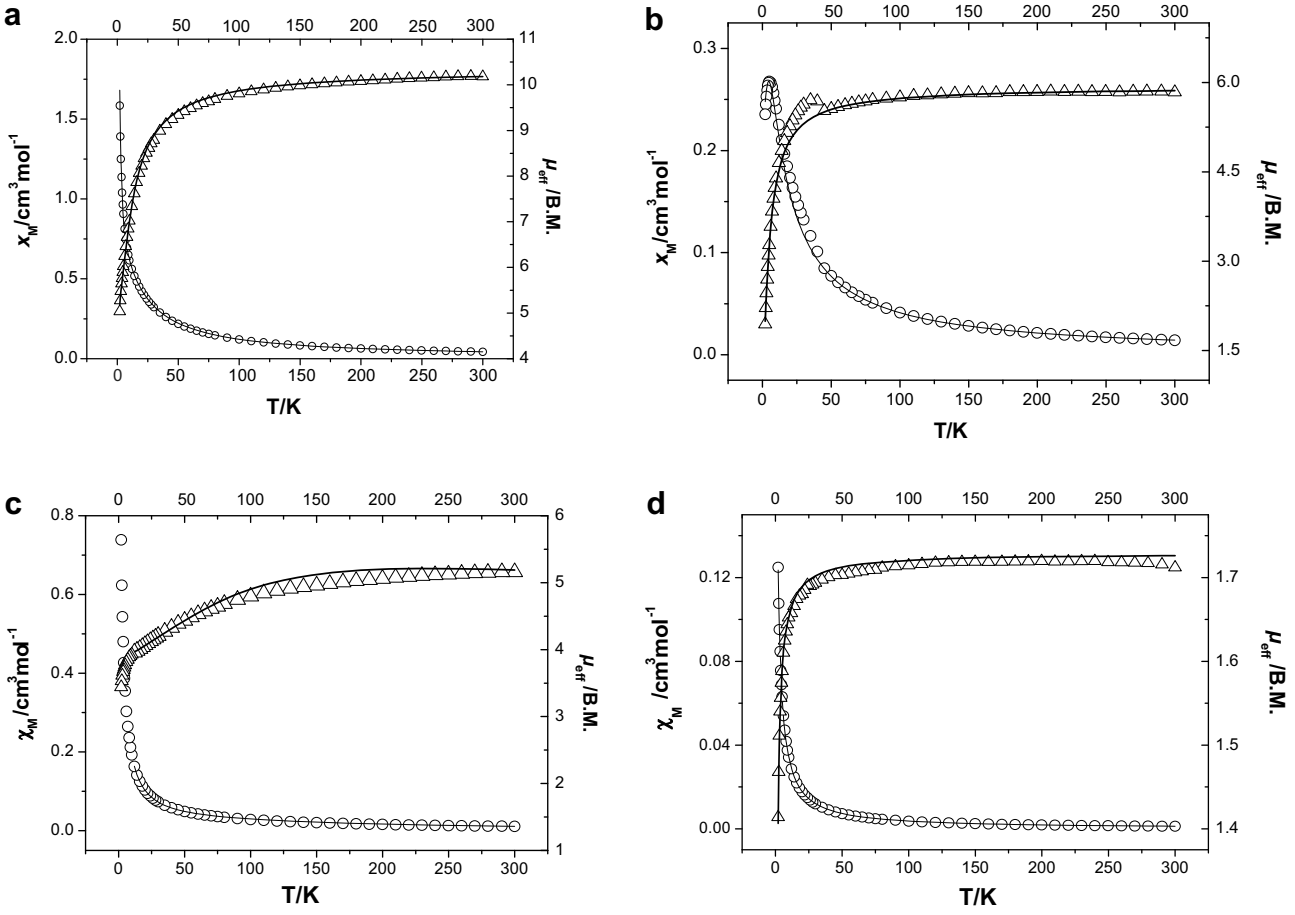

Fig. 6. Plots of the μ_{eff} product (Δ) and χ_M (○) vs. T for the complexes: (a) **1**, (b) **2**, (c) **5** and (d) **6**. The solid lines show the best fit of the data (see text).

Mn(II) ions (μ_{eff} = 5.86 B.M.), to 5.52 B.M. at 47.3 K, indicating a weak antiferromagnetic exchange interaction. From 47.3 to 34.7 K, there is a slight increase in μ_{eff}, with a maximum at 5.71 B.M. [23,24], then μ_{eff} decreases steeply below 34.7 K to a value of 1.94 B.M. at 2.0 K. In **2**, it can be considered that chains, made by the Mn(II) ions bridged by carboxylato bridging ligands, link to each other through 4,4′-bipy ligands. To simulate the experimental magnetic behavior, we used the expression derived by Fisher [25] with an interchain interaction (zJ'). The best fit parameters to reproduce satisfactorily the experimental data are g = 2.00, $J = -0.77$ cm^{-1}, $zJ' = -0.05$ cm^{-1}, $R = 2.6 \times 10^{-3}$.

In the previous literatures, polynuclear Mn(II) complexes bridged by carboxylato groups show weak coupling which is usually antiferromagnetic. In general, the magnitude of $|J|$ increases with the number of carboxylato bridges [26]. In addition, the exchange coupling is highly dependent on the conformation modes of the bridge between the metal centers. The *syn–syn* mode causes the larger $|J|$ value than other tri-atomic carboxylato bridges. In our case, complex **1** shows one *syn–syn* and one μ_2,η_1-carboxylato bridge. Thus the exchange ($J = -1.44$ cm^{-1}) is smaller than that of complexes with double *syn–syn* bridges [27] ($J = -3.5$ to -4.4 cm^{-1}), while it is larger than the values of complexes with double μ_2,η_1-carboxylato bridges [26]. In **2**, the Mn(II) ions are linked through double *syn–anti* mode bridges. The exchange ($J = -0.77$ cm^{-1}) is comparable to those reported for other similar Mn(II) complexes [28].

For **5**, the μ_{eff} value is close to 5.07 B.M. at 300.0 K, which is much larger than the expected spin-only value (3.87 B.M.) of one magnetically isolated high-spin Co(II) ion (S = 3/2). Upon cooling, the μ_{eff} value decreases slightly to 3.44 B.M. at 2 K (Fig. 6c). As the Co···Co distance through the 4,4′-bipy bridge is 11.437(3) Å in **5**, the magnetic exchange coupling through the bridge is expected to be very weak. Therefore, the magnetic behavior should be due to a larger orbital contribution arising from the $^4T_{1g}$ ground state of Co(II) [29]. Taking into account the contribution of the orbital momentum of the Co(II) ion, and considering the very weak magnetic interactions between the paramagnetic ions through 4,4′-bipy bridges, we tried to analyze the experimental data using a magnetic susceptibility equation derived by Miller [30]. The best fit parameters for reproducing satisfactorily the experimental data are g = 2.21, $zJ' = -0.08$ cm^{-1}, $\lambda = -115.6$ cm^{-1} and $R = 1.83 \times 10^{-4}$, where λ is the spin–orbit coupling constant ($\lambda = -176$ cm^{-1} is the free-ion value for Co(II)). The value of zJ' indicates a very weak antiferromagnetic exchange interaction between the metal ions through the 4,4′-bipy bridges.

As shown in Fig. 6d, for **6**, when the temperature decreases, μ_{eff} decreases slightly from a value close to 1.71 B.M. at 300.0 K, which is close to the spin-only value (μ_{eff} = 1.73 B.M.) for one magnetically isolated Cu(II) ion (S = 1/2), to 1.41 B.M. at 2.0 K. This behavior indicates a very weak antiferromagnetic interaction between the Cu(II) ions through the 4,4′-bipy bridges in the structure [31]. Keeping in mind the structure of 6 we have analyzed its magnetic data through the expression derived by Hall [32], which describes well the results of Niclós-Gutiérrez and coworkers [33] on a uniformly-spaced linear chain of local spin S = 1/2. The best fit parameters for reproducing satisfactorily the experimental data are g = 2.00, $J = -0.99$ cm^{-1} and $R = 3.3 \times 10^{-5}$. The value of J is small, as expected for this type of compound, indicating a weak antiferro-

magnetic exchange interaction between the metal ions through the 4,4′-bipy bridges.

4. Conclusion

In this paper, we have presented the synthesis and crystal structures of six low-dimensional coordination polymers using 2-benzothiazolylthioacetic acid and 4,4′-bipyridine as mixed ligands, reacted with Mn(II), Cd(II), Co(II) and Cu(II) ions. There are four coordination modes (monodentate, chelating, bridging and bridging-chelating) in the six complexes. As a result of different reaction conditions, Mn(II) and Cd(II) coordinate with the ligands to form two different complexes. The metal centers are bridged by carboxylato groups as well as 4,4′-bipy molecules in the 2D complexes **1**–**3**. However, only 4,4′-bipy ligands link the metal centers to form 1D complexes in **4**–**6**. Weak antiferromagnetic interactions were observed between the Mn(II) atoms bridged by μ_2,η_2-carboxylato and μ_2,η_1-carboxylato groups in **1** and by μ_2,η_2-carboxylato groups in **2**. There are weak antiferromagnetic interactions between the metal centers bridged by 4,4′-bipy in **1**, **2**, 5 and **6**.

5 Supplementary data

CCDC 665657, 665658, 680195, 680201, 680196 and 680202 contain the supplementary crystallographic data for **1**–**6**. These data can be obtained free of charge via http://www.ccdc.cam.ac.uk/conts/retrieving.html, or from the Cambridge Crystallographic Data Centre, 12 Union Road, Cambridge CB2 1EZ, UK; fax: (+44) 1223-336-033; or e-mail: deposit@ccdc.cam.ac.uk.

Acknowledgments

We gratefully acknowledge the Teaching and Research Program for Outstanding Young Teachers in the Higher Education Institutions of the Ministry of Education, the Nature Science Foundation of Guangxi Province, the Nature Science Foundation of Guangxi Normal University, the foundation of Key Laboratory of Medicinal Chemical Resources and Molecular Engineering, Guangxi Normal University, China.

References

[1] (a) S. Leininger, B. Olenyuk, P.J. Stang, Chem. Rev. 100 (2000) 853;
(b) M. Eddaoudi, D.B. Moler, H.-L. Li, B.-L. Chen, T.M. Reineke, M. O'Keeffe, O.M. Yaghi, Acc. Chem. Res. 34 (2001) 319;
(c) D.N. Dybtsev, H. Chun, S.H. Yoon, D. Kim, K. Kim, J. Am. Chem. Soc. 126 (2004) 32;
(d) S. Kitagawa, R. Kitaura, S. Noro, Angew. Chem., Int. Ed. 43 (2004) 2334.
[2] (a) S.L. James, Chem. Soc. Rev. 32 (2003) 276;
(b) D. Maspoch, D. Ruiz-Molina, J. Veciana, J. Mater. Chem. 14 (2004) 2713.
[3] (a) O. Evans, R.–G. Xiong, Z. Wang, G.–K. Wong, W. Lin, Angew. Chem., Int. Ed. 38 (1999) 536;
(b) O.R. Evans, W. Lin, Acc. Chem. Res. 35 (2002) 511.
[4] (a) B.F. Abrahams, M. Moylan, S.D. Orchard, R. Robson, Angew. Chem., Int. Ed. 42 (2003) 1848I;
(b) R.G. Xiong, X. Xue, H. Zhao, B.F. Abrahams, X.Z. You, Z. Xue, Angew. Chem., Int. Ed. 41 (2002) 3800.
[5] (a) A.F. Wells, Three-Dimensional Nets and Polyhedra, Wiley-Interscience, New York, 1977;
(b) R. Robson, J. Chem. Soc., Dalton Trans. (2000) 3735;
(c) L. Carlucci, G. Ciani, D.M. Proserpio, Coord. Chem. Rev. 246 (2003) 247;
(d) V.A. Blatov, L. Carlucci, G. Cianib, D.M. Proserpio, CrystEngComm 6 (2004) 378.
[6] (a) D. Bradshaw, J.B. Claridge, E.J. Cussen, T.J. Prior, M.J. Rosseinsky, Acc. Chem. Res. 38 (2005) 273;
(b) J.H. Chou, M.E. Kosal, S. Nakagaki, D.W. Smithenry, S.R. Wilson, Acc. Chem. Res. 38 (2005) 283;
(c) N.W. Ockwig, O. Delgado-Friedrichs, M. O'Keefee, O.M. Yaghi, Acc. Chem. Res. 38 (2005) 176;
(d) R.J. Hill, D.L. Long, N.R. Champness, P. Hubberstey, M. Schröder, Acc. Chem. Res. 38 (2005) 335.
[7] (a) R. Robson, Comprehensive Supramolecular Chemistry, Pergamon, New York, 1996;
(b) J. Tao, M.L. Tong, X.M. Chen, J. Chem. Soc., Dalton Trans. (2000) 3669;
(c) X. Li, Z.Y. Zhang, Y.Q. Zou, Eur. J. Inorg. Chem. (2005) 2909.
[8] C.N.R. Rao, S. Natarajan, R. Vaidhyanathan, Angew. Chem., Int. Ed. 43 (2004) 1466.
[9] H.M. Mei, H.P. Li, H.T. Zhao, S.P. Liu, D.T. Guo, J. HuNan Univ. 25 (1998) 33.
[10] G.M. Sheldrick, Phase annealing in SHELX-90: direct methods for larger structures, Acta Crystallogr., Sect. A. 46 (1990) 467.
[11] G.M. Sheldrick, SHELXL97, Program for X-ray Crystal Structure Solution, University of Göttingen, Germany, 1997.
[12] G. Christou, Acc. Chem. Res. 22 (1989) 328. and references therein.
[13] J.C. Burley, T.J. Prior, Acta Crystallogr., Sect. C 62 (2006) m63.
[14] B.W. Sun, S. Gao, Chem. Lett. (2001) 2.
[15] R.A. Reynolds III, W.R. Dunham, D. Coucouvanis, Inorg. Chem. 37 (1998) 1232.
[16] B.H. Ye, X.M. Chen, F. Xue, L.N. Ji, C.W. Mak, Inorg. Chim. Acta 299 (2000) 1.
[17] W.X. Zhang, C.Q. Ma, J.L.X. Ni Wang, Z.G. Yu, D.H. Jiang, Chinese J. Struct. Chem. 17 (1998) 57.
[18] S.G. Baca, Y. Sevryugina, R. Clrac, I. Malaestean, N. Gerbeleu, M.A. Petrukhina, Inorg. Chem. Commun. 8 (2005) 474 and references therein.
[19] O.V. Dolomanov, A.J. Blake, N.R. Champness, M. Schröder, J. Appl. Crystallogr. 36 (2003) 1283.
[20] H.D. Bian, F.P. Huang, Q. Yu, H. Liang, Acta Crystallogr., Sect. E 63 (2007) m369.
[21] (a) T.K. Maji, S. Sain, G. Mostafa, T.H. Lu, J. Ribas, M. Monfort, N.R. Chaudhuri, Inorg. Chem. 42 (2003) 709;
(b) Z.L. Chen, Y.S. Ma, F.P. Liang, Z.H. Zhou, Eur. J. Inorg. Chem. (2007) 2040.
[22] (a) S. Ménage, S.E. Vitols, P. Bergerat, E. Codjov, O. Kahn, J.J. Girerd, M. Guillot, X. Solans, T. Calvet, Inorg. Chem. 30 (1991) 2666;
(b) B. Albela, M. Corbella, J. Ribas, I. Castro, J. Sletten, H. Stoeckli-Evans, Inorg. Chem. 37 (1998) 788.
[23] W. Gu, H.D. Bian, J.Y. Xu, S.P. Yan, D.Z. Liao, Z.H. Jiang, Inorg. Chem. Commun. 6 (2003) 217.
[24] T. Vasilis, P. George, D.S. Catherine, P.R. Catherine, T. Aris, P.K. Dimitris, Inorg. Chem. 35 (1996) 7655.
[25] M.E. Fisher, Am. J. Phys. 32 (1964) 343.
[26] (a) H. Iikura, T. Nagata, Inorg. Chem. 37 (1998) 4702;
(b) R. Wang, E. Gao, M. Hong, S. Gao, J. Luo, Z. Lin, L. Han, R. Cao, Inorg. Chem. 42 (2003) 5486.
[27] (a) K. Wieghardt, U. Bossek, B. Nuber, J. Weiss, J. Bonvoisin, M. Corbella, S.E. Vitols, J.J. Girerd, J. Am. Chem. Soc. 110 (1988) 7398;
(b) U. Bossek, K. Wieghardt, B. Nuber, J. Weiss, Inorg. Chim. Acta 165 (1989) 123;
(c) D.P. Goldberg, A. Caneschi, C.D. Delfs, R. Sessoli, S.J. Lippard, J. Am. Chem. Soc. 117 (1995) 5789;
(d) T. Tanase, S.J. Lippard, Inorg. Chem. 34 (1995) 4682.
[28] (a) G. Fernández, M. Corbella, J. Mahía, M.A. Maestro, Eur. J. Inorg. Chem. (2002) 2502;
(b) H. Oshio, E. Ino, I. Mogi, T. Ito, Inorg. Chem. 32 (1993) 5697;
(c) A.K. Ghosh, D. Ghoshal, E. Zangrando, J. Ribas, N.R. Chaudhuri, Inorg. Chem. 44 (2005) 1786;
(d) M.A.M. Abu-Youssef, A. Escuer, F.A. Mautner, G.J. Reiss, R. Vicente, Angew. Chem., Int. Ed. 39 (2000) 1624.
[29] L.N. Zhu, Q.L. Wang, W.Z. Wang, D.Z. Liao, Z.H. Jiang, S.P. Yan, J. Mol. Struct. 649 (2003) 111.
[30] J.W. Raebiger, J.L. Manson, R.D. Sommer, U. Geiser, A.L. Rheingold, J.S. Miller, Inorg. Chem. 40 (2001) 2578.
[31] L.M. Zheng, X.Q. Wang, Y.S. Wang, A.J. Jacobson, J. Mater. Chem. 11 (2001) 1100.
[32] J.W. Hall, PhD dissertation, University of North Carolina, 1977.
[33] M.J. Román-Alpiste, J.D. Martín-Ramos, A. Castiñeiras-Campos, E. Bugella-Altamirano, A.G. Sicilia-Zafra, J.M. González-Perez, J. Niclós-Gutiérrez, Polyhedron 18 (1999) 3341.

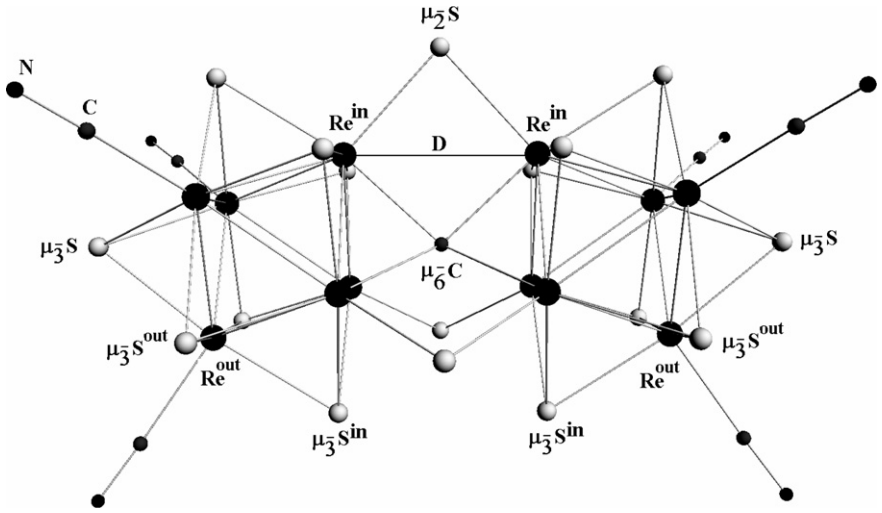

Fig. 1. The structure of $[Re_{12}CS_{17}(CN)_6]^{n-}$ (n = 6,8) clusters [5]. The distance (D) between rheniums is 2.90 Å at n = 6, and 3.17 Å for n = 8.

Table 1
Experimental and calculated interatomic distances, their differences (δ, Δ) in cluster units $[Re_{12}CS_{17}(CN)_6]^{n-}$. $\delta = R_{cal} - R_{exp}$ signifies intramolecular distances, $\Delta = R_{(n=8)} - R_{(n=6)}$ signifies intermolecular calculated and experimental distances

Complexbond length, Å	$[Re_{12}CS_{17}(CN)_6]^{8-}$			$[Re_{12}CS_{17}(CN)_6]^{6-}$			Δ	
	Cal	Exp[a]	δ	Cal	Exp[a]	δ	Cal	Exp
Re^{in}–Re^{in}, in prism	3.273	3.168	0.105	2.974	2.901	0.073	**0.299**	**0.267**
μ_6-C–μ_2-S	3.330	3.332	-0.002	3.454	3.438	0.016	**−0.124**	**−0.106**
Re^{in}–Re^{in}	2.628	2.591	0.037	2.739	2.692	0.047	**−0.111**	**−0.101**
Re^{in}–μ_6-C	2.231	2.179	0.052	2.171	2.126	0.045	**0.060**	**0.053**
Re^{in}–μ_2-S	2.442	2.425	0.017	2.391	2.378	0.013	**0.051**	**0.047**
Re^{out}–Re^{out}	2.669	2.595	0.074	2.664	2.600	0.064	0.069	−0.005
Re^{in}–Re^{out}	2.686	2.622	0.064	2.687	2.630	0.057	−0.001	−0.008
Re^{out}-μ_3-S^{top}	2.461	2.420	0.041	2.460	2.424	0.036	0.001	−0.004
Re^{in}–μ_3-S^{in}	2.466	2.425	0.041	2.464	2.422	0.042	0.002	0.003
Re^{out}–μ_3-S^{out}	2.457	2.428	0.029	2.448	2.405	0.043	0.009	0.023

[a] Since the complexes $[Re_{12}CS_{17}(CN)_6]^{n-}$ in the synthesized compound $Cs_6[Re_{12}CS_{17}(CN)_6] \cdot 20H_2O$ and $K_8[Re_{12}CS_{17}(CN)_6]$ are not of the ideal point symmetry D_{3h}, we cite only average characteristic interatomic distances [5].

3. Results

Table 1 shows interatomic distances of the complexes. As is seen, both computed and experimental distances change strongly as functions of the redox state. Table 2 lists predicted charges on the atoms of complexes $[Re_{12}CS_{17}(CN)_6]^{n-}$. Note that the effective charge on the μ_6-C atoms remains almost invariable when the redox state changes. $[Re_{12}CS_{17}(CN)_6]^{6-}$ has a larger absolute bond energy (−309.1 eV) than $[Re_{12}CS_{17}(CN)_6]^{8-}$ (−285.0 eV) and is thus more stable. This result is in a good accordance with experimental data which show that $K_8[Re_{12}CS_{17}(CN)_6]$ is not stable in aqueous solutions and rapidly transforms into $[Re_{12}CS_{17}(CN)_6]^{6-}$ anion [5].

Table 2
Calculated atomic charges in cluster units $[Re_{12}CS_{17}(CN)_6]^{n-}$

Complex	$[Re_{12}CS_{17}(CN)_6]^{8-}$	$[Re_{12}CS_{17}(CN)_6]^{6-}$
Re^{in}	0.069	0.076
Re^{out}	0.026	0.042
μ_6-C	−0.201	−0.201
μ_2-S	−0.427	−0.306
μ_3-S^{top}	−0.255	−0.171
μ_3-S^{in}	−0.187	−0.147
μ_3-S^{out}	−0.264	−0.164
C	−0.138	−0.127
N	−0.508	−0.438

The electronic structure of the studied systems stands out by strong redox dependence of the energy level of MO 77a″2 (fig. 2). The splitting ΔE between 30a′2 and 77a″2 is ∼1.07 eV for n = 6 and ∼0.06 eV for n = 8. The molecular orbital 30a′2 consists of 5d

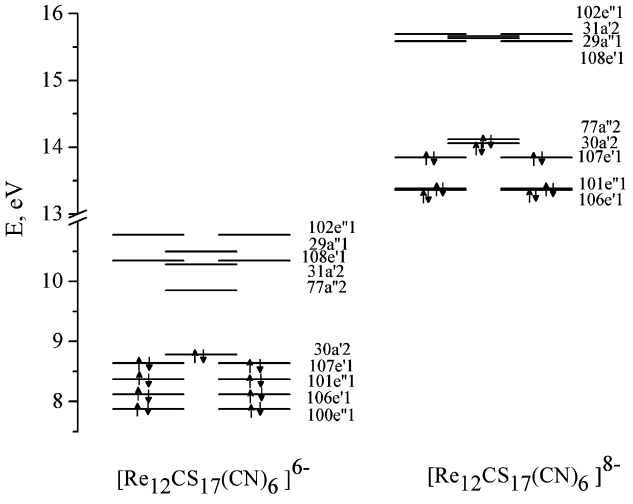

Fig. 2. Energy levels of molecular orbitals for $[Re_{12}CS_{17}(CN)_6]^{n-}$ (n = 6, 8).

valence orbitals of Re (~20%) and 3p orbitals of μ_2-S (~50%) 3p orbitals of μ_3-S^{in} (~30%) with no contribution from the carbon μ_6-C. d-Orbitals of Re^{in} atoms and 3p orbitals of μ_3-S^{in} show a weak bonding interaction between two symmetric groups $\{Re_6S_7\}$. MO 77a″2 consists of valence 5d- and vacant 6d-orbitals of Re (~45%), valence 3p- and vacant 4p-orbitals of μ_2-S (~25%), valence 3p- and vacant 4p-orbitals of μ_3-S^{out} (~17%) and with considerable contribution (~10%) of 2p and 3p orbitals from μ_6-C, but no direct overlap of atomic shells between Re^{in} in two symmetrical groups $\{Re_6S_7\}$ (fig. 3). Comparison of measured and computed interatomic distances suggests that the singularity in interatomic interactions on the redox state changes is "localized" in the vicinity of μ_6-C (Table 1). However, the structure of the molecular orbitals alone cannot clarify the behaviour of interatomic interactions with μ_6-C. Therefore we studied the electronic density in $[Re_{12}CS_{17}(CN)_6]^{n-}$ (n = 6, 8) by the method of electron localisation function.

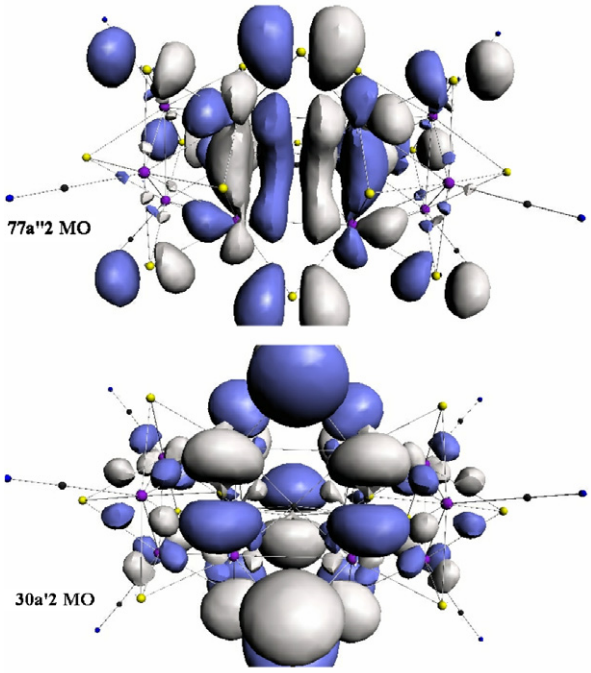

Fig. 3. Schematic 77a″2 and 30a′2 molecular orbitals for $[Re_{12}CS_{17}(CN)_6]^{n-}$ (n = 6, 8).

Figs. 4 and 5 show the results of the topological analysis of the electron density in $[Re_{12}CS_{17}(CN)_6]^{n-}$ (n = 6, 8) in the vicinity of μ_6-C. At ELF ≈ 0.78, the μ_6-C atom has three identical attractors (lone pairs) in the $[(\mu_6\text{-C})(\mu_2\text{-S})_3]$ plane for both complexes $[Re_{12}CS_{17}(CN)_6]^{n-}$ (n = 6, 8). The monosynaptic attractors are directed from the centre μ_6-C of the triangle towards its apexes made by μ_2-S atoms to form the angles 120°. In the vicinity of μ_6-C along the triad axis in the plane perpendicular to the $[(\mu_6\text{-C})(\mu_2\text{-S})_3]$ plane there is yet another region of electron localization (ELF ≈ 0.78) that can be also interpreted as a lone pair. The observed pattern of electron localization suggests that the electron configuration of μ_6-C is made by sp^2-hybrids. Since ELF is close to 0.8 at each of the four attractors corresponding to the three sp^2 hybrid orbitals and the remaining nonhybrid p orbital, the redox state is close to −4 in both complexes (this is in general agreement with the invariant charges of μ_6-C, Table 2).

When the redox state of $[Re_{12}CS_{17}(CN)_6]^{n-}$ changes, the only result is the change in interaction within the systems $[(\mu_6\text{-C})(\mu_2\text{-S})_3]$ and $[(\mu_6\text{-C})\{Re_6\}_2]$. A bonding attractor, or V(Re,Re) disynaptic basin, is seen between each pair of Re atoms at ELF ≈ 0.5. Though ELF is not so high here, it is known that low ELF values associated with covalent bonding between d elements are explained by the fact that electron localization is greatly reduced due the Pauli repulsion exerted by the electron density concentrated in core

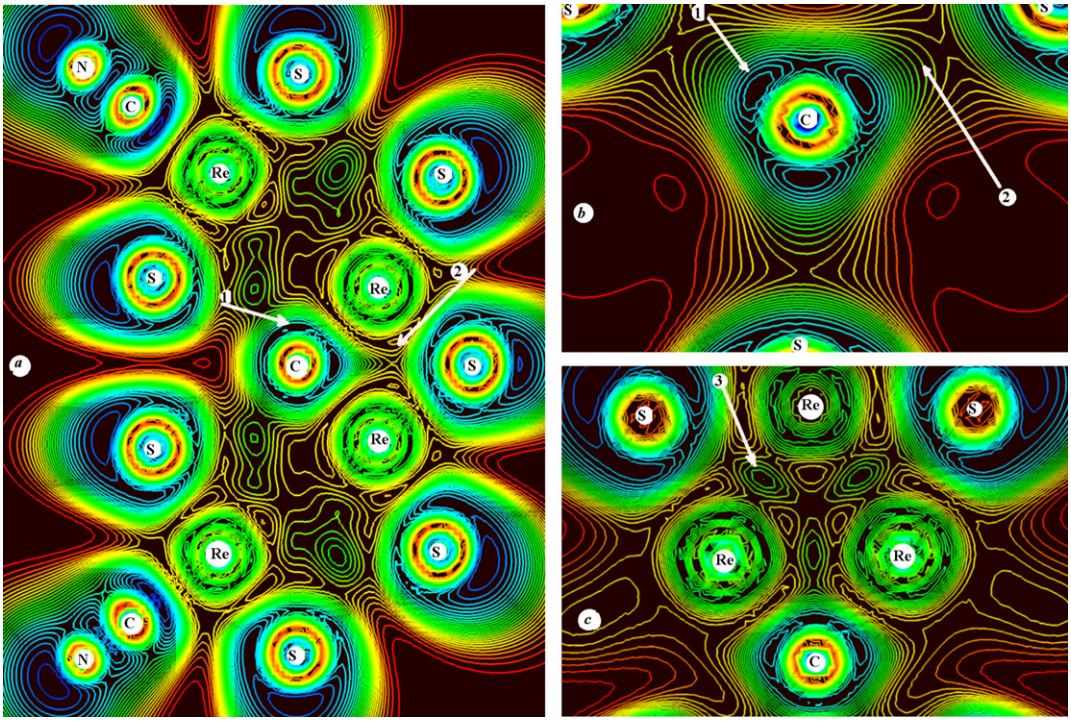

Fig. 4. ELF distribution maps for $[Re_6CS_{17}(CN)_6]^{6-}$ complex: (a) cutting plane Re–(μ_2-S)–Re–(μ_6-C), the Re atoms belong to different symmetry groups $\{Re_6S_7\}$; (b) cutting plane through three atoms μ_2-S and the atom μ_6-C; (c) cutting plane through the atoms Re–(μ_6-C)–Re (the rheniums belong to the same group $\{Re_6S_7\}$). Arrows 1 point to the attractors of sp^2-hybridization, arrows 2 point to the bonding between μ_6-C and μ_2-S, arrows 3 point to the disynaptic V(Re,Re) basins of covalent bond Re–Re.

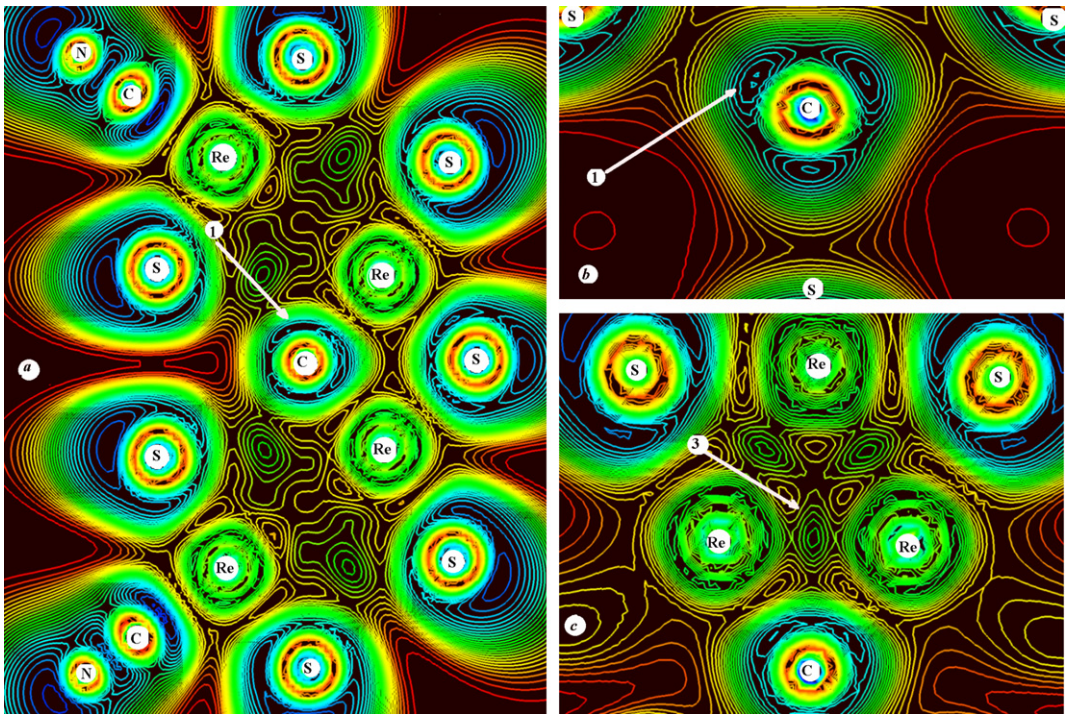

Fig. 5. ELF distribution maps for $[Re_6CS_{17}(CN)_6]^{8-}$ complex: (a) the plane crossing the atoms Re–(μ_2-S)–Re–(μ_6-C), the Re atoms belong to different symmetric groups $\{Re_6S_7\}$; (b) the plane crossing three atoms μ_2-S and the atom μ_6-C; (c) the plane crossing the atoms Re–(μ_6-C)–Re (the rheniums belong to the same group $\{Re_6S_7\}$). Arrows 1 point to the attractors of sp^2-hybridization, arrow 3 point to the disynaptic V(Re,Re) basins of covalent bond Re–Re.

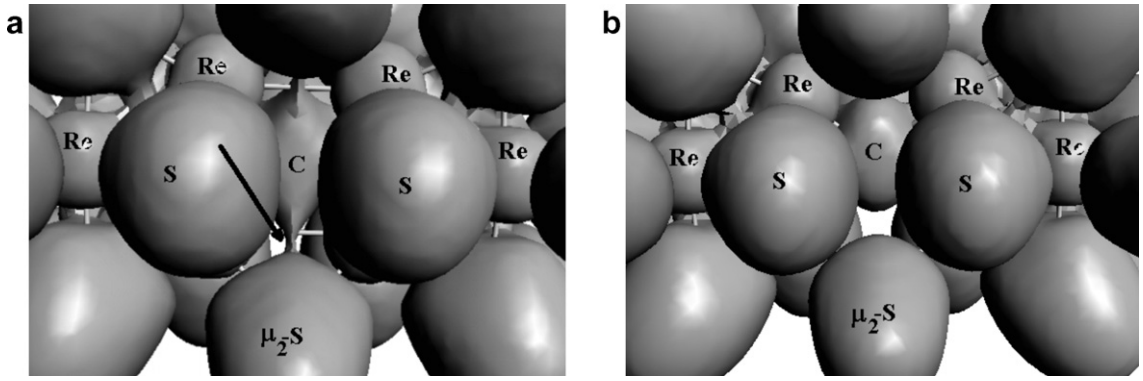

Fig. 6. Isosurfaces ELF = 0.3 for $[Re_{12}CS_{17}(CN)_6]^{6-}$ (a) and $[Re_{12}CS_{17}(CN)_6]^{8-}$ (b). The arrow depicts the bonding between μ_6-C and μ_2-S in $[Re_{12}CS_{17}(CN)_6]^{6-}$, the bonding disappears in $[Re_{12}CS_{17}(CN)_6]^{8-}$.

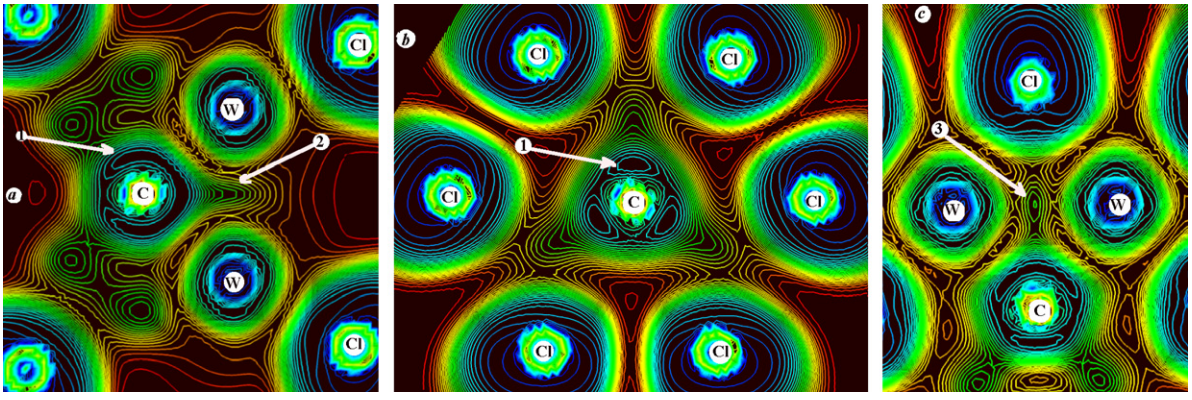

Fig. 7. ELF distribution maps for W_6CCl_{18} molecule: (a) cutting plane through W–(μ_6-C)–W atoms; (b) cutting plane through Cl atoms and the atom μ_6-C; (c) cutting plane crossing the atoms W–(μ_6-C)–W (the W belong to the same fragment $[W_3]$). Arrows 1 point to the attractors of sp^2-hybridization, arrows 2 point to the region between W, arrow 3 points to the disynaptic V(W,W) basins of the covalent bond W–W.

regions [16,18]. The bonding between μ_6-C and Re^{in} in the fragments $[(\mu_6\text{-C})\{Re_6\}_2]$ results from electron exchange that binds the valent area μ_6-C with the V(Re,Re) associated with different levels of electron density localization (ELF ≈ 0.36 for $[Re_{12}CS_{17}(CN)_6]^{6-}$ and ELF ≈ 0.32 for $[Re_{12}CS_{17}(CN)_6]^{8-}$). We characterize this interaction as a multicentered shared electron interaction. At $[Re_{12}CS_{17}(CN)_6]^{6-}$ an unexpected bonding (ELF ≈ 0.3) is seen between μ_6-C and μ_2-S in the group $[(\mu_6\text{-C})(\mu_2\text{-S})_3]$ which is not observed in $[Re_{12}CS_{17}(CN)_6]^{8-}$ (Figs. 4–6).

To compare our results for $[Re_{12}CS_{17}(CN)_6]^{n-}$ with the analysis of the carbon μ_6-C in trigonal prismatic environment of tungsten atoms in $[W_6CCl_{18}]^{n-}$ [3], we studied the electron localization function in diamagnetic W_6CCl_{18} ($n = 0$ and $2S + 1 = 1$) in the vicinity of μ_6-C with ELF function (all quantum-chemical calculations were made in the same manner as for $[Re_{12}CS_{17}(CN)_6]^{n-}$). In isolated molecular clusters W_6CCl_{18}, the atom C was hypothesized to be characterized by sp^2p_z-state with the sp^2 lobes directed to the prism edges, increasing the Cl–Cl distances of the bridges [3]. As is seen in Fig. 7 of the ELF distribution map, the attractors of the lone pairs of μ_6-C atom are indeed directed to the prism edges.

4. Conclusion

The obtained results indicate that the electronic state of μ_6-C in the trigonal-prismatic environment can be interpreted as the one formed by filled sp^2 hybrid orbitals and having the oxidation state ~−4 independently on the redox state of the complexes. It is thus shown that C^{4-} carbide anion can be viewed as a strong electron donor ligand in the trigonal prismatic environment of transition metals, which is in agreement with [3]. The obtained evidence of very weak long-distant (3.454 Å) interactions between μ_6-C and μ_2-S (ELF ≈ 0.3) in the $[(\mu_6\text{-C})(\mu_2\text{-S})_3]$ of $[Re_{12}CS_{17}(CN)_6]^{6-}$ and the absence of such interactions in $[Re_{12}CS_{17}(CN)_6]^{8-}$ is an unexpected result. The discovered interaction between μ_6-C and μ_2-S cannot be of covalent nature since it occurs at the distance ~3.454 Å in complex $[Re_{12}CS_{17}(CN)_6]^{6-}$ and disappears at shorter distances ~3.330 Å in $[Re_{12}CS_{17}(CN)_6]^{8-}$ (a disynaptic attractor could be expected to appear at a covalent bonding when the interatomic distance decreases). According to the classification [13] the observed bonding belongs to the unshared electron interaction. Since the charges on μ_6-C and μ_2-S are negative (Table 2), the interaction between them can be characterized only as an exchange-correlation interaction between closed-shell atoms [20]. We think that the weak electron bonding between μ_6-C and μ_2-S is responsible for shortened Re^{in}–Re^{in} distances in the system $[Re_{12}CS_{17}(CN)_6]^{6-}$. This interaction seems to be substantially weakened when the antibonding MO 77a″2 in $[Re_{12}CS_{17}(CN)_6]^{8-}$ is filled by two electrons and is absent at ELF = 0.3 (Fig. 6) which results in a strong increase of interatomic distances Re^{in}–Re^{in} and a significant change in MO 77a″2 energy (Fig. 2).

The obtained results appear to have important implications for the carbon coordination behaviour in the complexes of transition metals.

Acknowledgements

The study was supported by Russian Foundation for Basic Research (Grants 07-03-00912 and 08-03-00826).

References

[1] P. Chini, J. Organomet. Chem. 2000 (1) (1980) 37.
[2] V.I. Minkin, R.M. Minyaev, Mendeleev Commun. 2 (2004) 43.
[3] Y.-Q. Zheng, H.G. von Schnering, J.-H. Chang, Y. Grin, G. Engelhardt, G. Heckmann, Z. Anorg. Allg. Chem. 629 (2003) 1256.
[4] E.J. Welch, N.R.M. Crawford, R.G. Bergman, J.R. Long, J. Am. Chem. Soc. 125 (2003) 11464.
[5] Yu.V. Mironov, N.G. Naumov, S.G. Kozlova, S.G. Sung-Jin Kim, V.E. Fedorov, Angew. Chem., Int. Ed. 44 (2005) 6867.
[6] Amsterdam Density Functional (ADF) Program, Release 2006.02; Vrije Universteit: Amsterdam, The Netherlands, 2006.
[7] S.H. Vosko, L. Wilk, M. Nusair. Can. J. Phys. 58 (1980) 1200.
[8] A.D. Becke, Phys. Rev. A 38 (1988) 3098.
[9] J.P. Perdew, Phys. Rev. B 33 (N12) (1986) 8822.
[10] L. Versluis, T. Ziegler, J. Chem. Phys. 88 (1988) 322.
[11] E. Van Lenthe, A.E. Ehlers, E.J. Baerends, J. Chem. Phys. 110 (1999) 8943.
[12] F.L. Hirshfeld, Theor. Chim. Acta 44 (1977) 129.
[13] A.D. Becke, K.E. Edgecombe, J. Chem. Phys. 92 (1990) 5387.
[14] A. Savin, O. Jepsen, J. Flad, O.K. Andersen, H. Preuss, H.G. von Schnering, Angew. Chem. 31 (1992) 187.
[15] B. Silvi, A. Savin, Nature 371 (1994) 683.
[16] S. Berski, G.L. Gutsev, M.D. Mochena, J. Andrés, J. Phys. Chem. A 108 (2004) 6025.
[17] S. Noury, B. Silvi, R.J. Gillespie, Inorg. Chem. 41 (8) (2002) 2164–2172.
[18] B. Silvi, C. Gatti, J. Phys. Chem. A 104 (2000) 947.
[19] M. Kohout, A. Savin, Int. J. Quant. Chem. 60 (1996) 875.
[20] P. Pyykko, Chem. Rev. 97 (1997) 597.

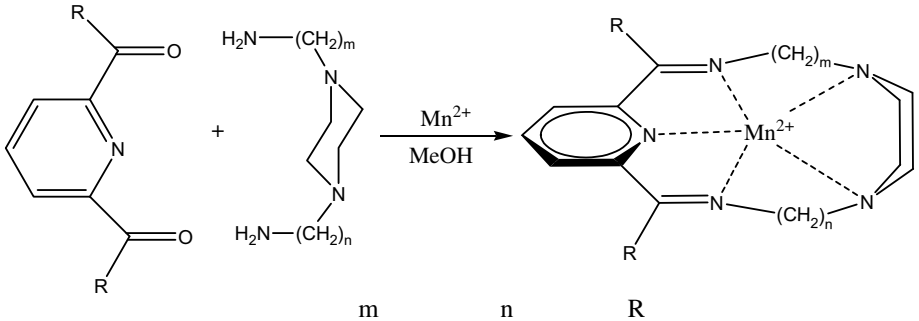

	m	n	R
L^1	2	3	H
L^2	2	3	CH_3
L^3	3	3	H
L^4	3	3	CH_3

Scheme 1. The template condensation between 2,6-diacetylpyridine or 2,6-pyridinedicarbaldehyde and two linear tetraamines with piperazine moiety in the presence of Mn(II).

In all cases, the [1+1] template cyclocondensation occurs and the metal complexes of the 16-, and 17-membered pentaaza macrocycles L^1–L^4 were obtained.

The template cyclocondensation involving the *N,N′*(2-aminoethyl)(3-aminopropyl)piperazine precursor give rise to Mn(II) complexes of the asymmetrical macrocycles L^1 and L^2, whilst with the 1,4-bis(3-aminopropyl)piperazine amine, the Mn(II) complexes of L^3 and L^4 were obtained. The Mn(II) complexes recorded in Scheme 1 have been obtained. The crystal structures of $[MnL^2Cl(CH_3OH)](ClO_4)$ and $[MnL^4Cl](PF_6)$ are also reported.

2. Experimental

2.1. Chemical and starting materials

2,6-Pyridinedicarbaldehyde was prepared according to the literature method [27]. 2,6-Diacetylpyridine, 1,4-bis(3-aminopropyl)piperazine and the metal salts were commercial products (from Merck, Aldrich and Fluka, respectively) and were used without further purification. Solvents were of reagent grade purified by the usual methods.

Caution: Perchlorate salts are potentially explosive. While we have not experienced any problems with the compounds described, they should be treated with caution and handled in small quantities.

2.2. Synthesis of N,N′(2-aminoethyl)(3-aminopropyl)piperazine

2-Aminoethylpiperazine (2.58 g, 20 mmol) and phthalic anhydride (2.96 g, 20 mmol) were mixed in appropriate beaker and fused at 180 °C with constant stirring for 15 min. After lowering the temperature (at about 160 °C), *N*-(3-bromopropyl) phthalimide (5.36 g , 20 mmol) was also added and fused together at with constant stirring for 30 min. The resulting solid was washed two steps with hot ethanol, pulverized and heated under reflux with HCl (300 ml, 25%) for 12 h. The phthalic acid which formed on cooling was filtered off and the filtrate evaporated to small bulk and poured into absolute ethanol. The resulting viscous precipitate was recrystallized from $EtOH/H_2O$, washed with a small amount of cooled absolute ethanol and diethyl ether, and the resulting yellow powder was dried and characterized as the pure compound (Scheme 2). Yield: 3.15 g (45%). *Anal.* Calc. for $C_9H_{28}Cl_4N_4O$ (MW: 348.1): C, 30.9; H, 8.1; N, 16.0. Found: C, 30.7; H, 8.2; N, 16.1%. FAB-MS (*m/z*): 187 $[M+1]^+$.

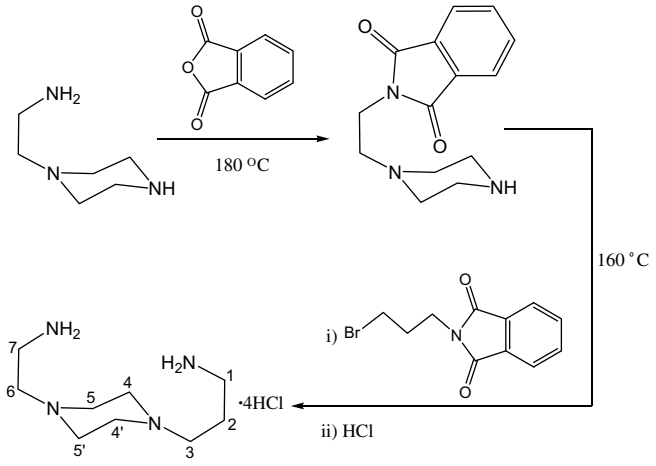

Scheme 2. The processes of synthesis of *N,N′*(2-aminoethyl)(3-aminopropyl)-piperazine.

^1H NMR (D_2O, ppm) δ = 2.26 (m, 2H, 2-H); 3.18 (t, 2H, 3-H); 3.50 (t, 2H, 1-H); 3.58 (t, 2H, 6-H); 3.73 (t, 2H, 7-H); 3.85 (br, 8H, 4,4′ and 5,5′-H). ^{13}C NMR (D_2O, ppm) δ = 21.75 (C-2); 33.8 (C-6); 36.40 (C-3); 49.01, 49.35 (C-4,4′ and 5,5′); 52.81 (C-7); 53.64 (C-1).

2.3. Synthesis of the metal complexes – general procedure

All macrocyclic complexes were prepared according to the literature method [28]. A solution of NaOH (2 mmol) in absolute ethanol (10 ml) was added to a suspension of the appropriate tetramine salt (0.5 mmol) in absolute ethanol (10 ml). The mixture was stirred at room temperature for a few minutes then filtered, and the precipitate was washed well with absolute ethanol (10 ml). The washings and the filtrate were combined and this solution was added dropwise to a hot solution of $Mn(ClO_4)_2 \cdot xH_2O$ (0.5 mmol) and 2,6-diacetylpyridine or 2,6-pyridinedicarbaldehyde (0.5 mmol) in absolute methanol (20 ml), over a period of 2 h. After refluxing the solution for 24 h it was filtered. Crystalline compound was obtained by slow diffusion of diethyl ether vapour into the MeOH/MeCN solution of the above solid.

2.3.1. $[MnL^1Cl\ (CH_3OH)](ClO_4)$

Anal. Calc. for $C_{16}H_{25}Cl_2MnN_5O_5$ (MW: 492.06): C, 39.0; H, 5.1; N, 14.2. Found: C, 39.2; H, 5.0; N, 14.1%. Yield: 45%. IR (KBr,

cm^{-1}) 3444, 1650, 1632 [ν(C=N)], 1588, 1465 [ν(C=C) and ν(C=N)]$_{py}$, 1107, 625 $\nu(ClO_4^-)$. FAB-MS (*m/z*, %): 375 (100%), $[MnL^1Cl]^+$. Λ_M/Ω^{-1} cm^2 mol^{-1} (in DMF): 157 (2:1).

2.3.2. [MnL²Cl(CH₃OH)](ClO₄)

Anal. Calc. for $C_{18}H_{29}Cl_2MnN_5O_5$ (MW: 520.09): C, 41.5; H, 5.6; N, 13.5. Found: C, 41.2; H, 5.5; N, 13.3%. Yield: 50%. IR (KBr, cm^{-1}) 3463, 1648, 1633 [ν(C=N)], 1585, 1487 [ν(C=C) and ν(C=N)]$_{py}$, 1110, 625 $\nu(ClO_4^-)$. FAB-MS (*m/z*, %): 403(100%), $[MnL^2Cl]^+$. Λ_M/Ω^{-1} cm^2 mol^{-1} (in DMF): 172 (2:1).

2.3.3. [MnL³Cl](ClO₄)

Anal. Calc. for $C_{17}H_{25}Cl_2MnN_5O_4$ (MW: 488.07): C, 41.7; H, 5.1; N, 14.3. Found: C, 41.3; H, 5.2; N, 14.1%. Yield: 47%. IR (KBr, cm^{-1}) 3418, 1643 [ν(C=N)], 1592, 1462 [ν(C=C) and ν(C=N)]$_{py}$, 1110, 625 $\nu(ClO_4^-)$. FAB-MS (*m/z*, %): 389(100%), $[MnL^3Cl]^+$. Λ_M/Ω^{-1} cm^2 mol^{-1} (in DMF): 120 (2:1).

2.3.4. [MnL⁴Cl](ClO₄) · 2H₂O, [MnL⁴Cl](PF₆)

Anal. Calc. for $C_{19}H_{33}Cl_2MnN_5O_6$ (MW: 552.12): C, 41.3; H, 6.0; N, 12.7. Found: C, 41.4; H, 5.9; N, 12.7%. Yield: 40%. IR (KBr, cm^{-1}) 3441, 1634 [ν(C=N)], 1589, 1451 [ν(C=C) and ν(C=N)]$_{py}$, 1089, 624 $\nu(ClO_4^-)$. FAB-MS (*m/z*, %): 477(100%), $[MnL^4Cl]^+$. Λ_M/Ω^{-1} cm^2 mol^{-1} (in DMF): 143 (2:1).

Recrystallization of 0.5 g of the above compound in methanol in the presence of an excess of NH_4PF_6 gave brown needle orange crystals of $[MnL^4Cl](PF_6)$. *Anal.* Calc. for $C_{19}H_{31}ClF_6MnN_5OP$ (MW: 580.12): C, 39.3; H, 5.4; N, 12.1. Found: C, 39.5; H, 5.3; N, 11.9%. Yield: 75%.

2.4. Physical measurements

Elemental analyses were performed in a Carlo-Erba EA microanalyser. FT-IR spectra in the 4000–400 cm^{-1} region were recorded from KBr pellets on Bruker VECTOR 22 and Perkin–Elmer GX spectrophotometers. FAB mass spectra were recorded using a Kratos-MS-50T spectrometer connected to a DS90 data system using 3-nitrobenzyl alcohol as the matrix. Magnetic susceptibility measurements were performed at 25 °C using a Johnson Matthey Alfa MSBMKI Gouy balance. Conductivity measurements were carried out in 10^{-3} mol dm^{-3} dimethylformamide solutions at 20 °C using a CARISON GLP32 conductivimeter. ^1H and ^{13}C NMR spectra were recorded on a Bruker 500 MHz using D_2O as solvent.

2.5. X-ray crystal structure determination

Vapour diffusion of diethyl ether into a solution of $[MnL^nCl]^+$ (n = 2 and 4) in mixture of acetonitrile and methanol, afforded crystal suitable for study by X-ray crystallography. The details of the X-ray crystal data, and of the structure resolution and refinement, are given in Table 1. Measurements were made on a Bruker SMART CCD area diffractometer. All data were corrected for Lorentz and polarization effects. Empirical absorption corrections were also applied for all the crystal structures obtained [29]. Complex scattering factors were taken from the program package SHELXTL [30]. The structures were solved by direct methods which revealed the position of all non-hydrogen atoms. All the structures were refined on F^2 by a full-matrix least-squares procedure using anisotropic displacement parameters for all non-hydrogen atoms. The hydrogen atoms were located in their calculated positions and refined using a riding model. Molecular graphics were generated using ORTEP-3 [31].

Table 1
Crystal data and structure refinement for $[MnL^2Cl(CH_3OH)](ClO_4)$ and $[MnL^4Cl]PF_6$

	$[MnL^2Cl(CH_3OH)]ClO_4$	$[MnL^4Cl]PF_6$
Empirical formula	$C_{19}H_{30}N_5O_5Cl_2Mn$	$C_{19}H_{29}N_5PF_6ClMn$
Formula weight	534.32	562.83
Temperature (K)	293(2)	293(2)
Wavelength (Å)	0.71073	0.71073
Crystal system	triclinic	monoclinic
Space group	$P\bar{1}$	$P21/c$
Unit cell dimensions		
a (Å)	7.1963(15)	12.6286(15)
b (Å)	11.437(2)	15.4112(19)
c (Å)	14.829(3)	12.5828(16)
α (°)	79.894(4)	
β (°)	83.110(4)	103.797(3)
γ (°)	81.545(4)	
V (Å^3)	1182.9(4)	2378.2(5)
Z	2	4
D_{calc} (Mg/m^3)	1.500	1.572
Absorption coefficient (mm^{-1})	0.824	0.799
F(000)	556	1156
Crystal size (mm^3)	0.43 × 0.36 × 0.19	0.37 × 0.35 × 0.30
θ Range for data collection (°)	1.40–28.06	1.66–28.03
Index ranges	$-9 \leqslant h \leqslant 5$, $-14 \leqslant k \leqslant 14$, $-18 \leqslant l \leqslant 19$	$-16 \leqslant h \leqslant 12$, $-18 \leqslant k \leqslant 20$, $-11 \leqslant l \leqslant 16$
Reflections collected	7812	15 349
Independent reflections (R_{int})	5445 (0.0308)	5648 (0.0579)
Completeness to θ	94.7% (28.06°)	98.0% (28.03°)
Absorption correction	SADABS	SADABS
Maximum and minimum transmission	0.8592 and 0.7183	0.7955 and 0.7564
Refinement method	full-matrix least-squares on F^2	full-matrix least-squares on F^2
Data/restraints/parameters	5445/0/292	5648/24/340
Goodness-of-fit on F^2	1.024	1.005
Final R indices [$I > 2\sigma(I)$]	R_1 = 0.0808, wR_2 = 0.2269	R_1 = 0.0487, wR_2 = 0.1115
R indices (all data)	R_1 = 0.1458, wR_2 = 0.2780	R_1 = 0.1379, wR_2 = 0.1482
Largest difference in peak and hole (e Å^{-3})	1.386 and −0.998	0.426 and −0.307

3. Results and discussion

The new asymmetric amine *N*,*N*′(2-aminoethyl)(3-aminopropyl)piperazine was readily prepared starting from *2*-aminoethylpiperazine, phthalic anhydride and *N*-(3-bromopropyl) phthalimide in a 45% yield.

The FAB mass spectra confirm the presence of the desired final product as it shows a peack at *m/z* 187 belonging to the protonated amine.

The Schiff-base macrocyclic complexes $[MnL^nCl]^+$ (n = 1–4) were prepared from [1+1] cyclocondensation of 2,6-diacetypyridine or 2,6-pyridinedicarbaldehyde and the amine salts of 1,4-bis(3-aminopropyl)piperazine or *N*,*N*′(2-aminoethyl)(3-aminopropyl)piperazine. The complexes were characterised by elemental analyses, IR, FAB-MS, magnetic properties and conductivimetry measurements. The solid compounds are air stable and elemental analyses are consistent with the formulations given in Section 2.

All of the complexes exhibit a ν(C=N) vibration in the range 1633–1650 cm^{-1} and also bands at approximately 1600 and 1450 cm^{-1} associated with $\nu(C=N)_{py}$ and ν(C=C) vibrations from the pyridine and phenyl rings [32]. However no bands are observed for the free carbonyls or primary diamines, indicating that complete condensation has occurred. The IR spectrum of $[MnL^4Cl](ClO_4) \cdot 2H_2O$ is consistent with the presence of water molecules accordingly with the microanalytical data. For the perchlorate complexes, absorptions attributable to perchlorate ions were found at approximately 1100 and 625 cm^{-1} [33]. The lack of splitting of these bands suggests that the perchlorate anions are not coordinated [34].

The molar conductance values of the complexes measured in dimethylformamide lie in the range reported for 2:1 electrolytes in this solvent [35].

Positive-ion FAB mass spectrometry provided further evidence for cyclocondensation and the formation of di-imine complexes. The spectra show that most intense peaks are observed at *m/z* 375, 403, 389 and 477 a.m.u. corresponding to $[MnL^n(Cl)]^+$ (n = 1–4), respectively.

The values of the room temperature magnetic moment of the complexes, 5.44, 5.53, 5.59 and 5.54 BM for $[MnL^1Cl]^+$, $[MnL^2Cl]^+$, $[MnL^3Cl]^+$and $[MnL^4Cl]^+$, respectively are indicative of high-spin Mn(II) in all cases [36]. The high-spin Mn(II) ion possesses a half-filled 3d-shell and thus the coordination geometries of its complexes are not subject to ligand field effects and are determined mainly by the chelating power and geometrical arrangement of the ligands.

3.1. Crystal structures

The crystal structure of the two Mn(II) complexes with formula $[MnL^2Cl(CH_3OH)](ClO_4)$ and $[MnL^4Cl](PF_6)$ have been determined by X-ray diffraction. The projection view of the molecular structures of the cationic unit present in the complexes with non-hydrogen atoms represented by 50% thermal ellipsoids are shown in Figs. 1 and 2, respectively, together with selected bond lengths and angles relating to the coordination environment of the metal (Table 2).

The $[MnL^2Cl(CH_3OH)](ClO_4)$ complex crystallizes in the triclinic $P\bar{1}$ space group and shows that the metal atom is seven coordinated in a pentagonal bipyramidal geometry, arising from coordination by the five N atoms of the macrocycle, one chloride ion and one oxygen atom from a methanol molecule. A similar seven coordinate geometry has been found for other Mn(II) complexes with N5 macrocyclic ligands [37,38]. The ligand shows a nearly plane conformation, and the rms of the plane formed by the five N atoms is 0.0756, showing that these atoms are almost coplanar, with the Mn(II) ion 0.0942 Å out of this plane. The sum of the five N–Mn–N chelate angles (359.96°) is almost 360° for an ideal planar structure. The Cl and O donor atoms are sited *trans* to the macrocyclic plane, with an angle Cl–Mn–O of 170.19(13)°, near to 180°. The five Mn–N bond lengths are in the range 2.246–2.346 Å, affording an average Mn–N bond distance of 2.321 Å. The Mn–Cl and Mn–O distances of 2.5214 and 2.332 Å, respectively, are within the range observed previously for this sort of complexes.

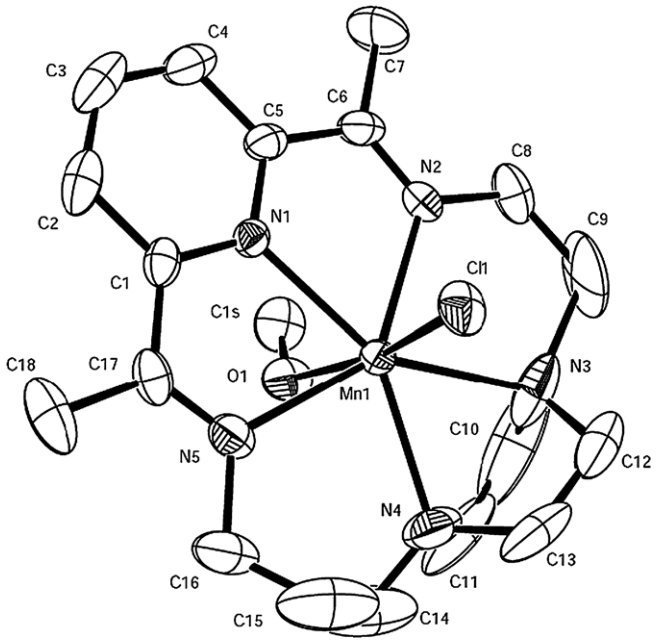

Fig. 1. Crystal structure of the cation $[MnL^2Cl(CH_3OH)]^+$.

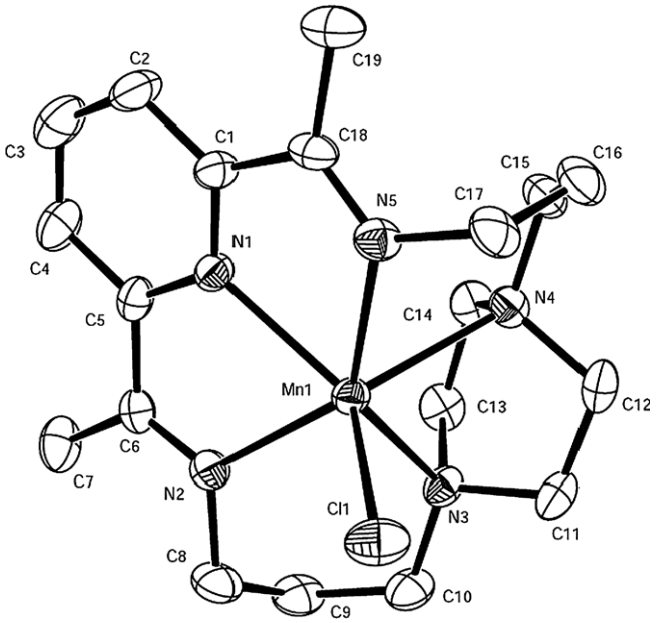

Fig. 2. Crystal structure of the cation $[MnL^4Cl]^+$.

Table 2
Selected bond lengths (Å) and bond angles (°) for $[MnL^2Cl(CH_3OH)]^+$ (**1**) and $[MnL^4Cl]^+$ (**2**)

Bond lengths (Å)	**1**	Bond lengths (Å)	**2**
Mn(1)–N(1)	2.246(4)	Mn(1)–N(1)	2.250(3)
Mn(1)–N(2)	2.337(5)	Mn(1)–N(2)	2.276(3)
Mn(1)–N(3)	2.346(6)	Mn(1)–N(3)	2.352(3)
Mn(1)–N(4)	2.334(6)	Mn(1)–N(4)	2.387(3)
Mn(1)–N(5)	2.344(5)	Mn(1)–N(5)	2.286(3)
Mn(1)–O(1)	2.332(4)	Mn(1)–Cl(1)	2.364(11)
Mn(1)–Cl(1)	2.521(17)		
Bond angle (°)		*Bond angle (°)*	
N(1)–Mn(1)–N(2)	69.92(16)	N(1)–Mn(1)–N(2)	69.51(11)
N(1)–Mn(1)–N(3)	147.2(3)	N(1)–Mn(1)–N(3)	127.48(10)
N(1)–Mn(1)–N(4)	150.0(2)	N(1)–Mn(1)–N(4)	104.53(10)
N(1)–Mn(1)–N(5)	139.29(19)	N(1)–Mn(1)–N(5)	68.94(11)
N(2)–Mn(1)–N(3)	77.3(3)	N(2)–Mn(1)–N(3)	80.23(10)
N(2)–Mn(1)–N(4)	138.4(2)	N(2)–Mn(1)–N(4)	130.03(11)
N(2)–Mn(1)–N(5)	139.29(19)	N(2)–Mn(1)–N(5)	136.04(11)
N(3)–Mn(1)–N(4)	62.1(3)	N(3)–Mn(1)–N(4)	64.47(10)
N(3)–Mn(1)–N(5)	143.2(3)	N(3)–Mn(1)–N(5)	138.46(11)
N(4)–Mn(1)–N(5)	81.1(2)	N(4)–Mn(1)–N(5)	740.70(10)
O(1)–Mn(1)–N(1)	81.45(15)	N(1)–Mn(1)–Cl(1)	129.62(8)
O(1)–Mn(1)–N(2)	85.34(17)	N(2)–Mn(1)–Cl(1)	99.71(8)
O(1)–Mn(1)–N(3)	96.6(2)	N(3)–Mn(1)–Cl(1)	96.36(8)
O(1)–Mn(1)–N(4)	90.1(2)	N(4)–Mn(1)–Cl(1)	117.53(8)
O(1)–Mn(1)–N(5)	85.12(18)	N(5)–Mn(1)–Cl(1)	95.73(8)
O(1)–Mn(1)–Cl(1)	170.19(13)		
N(1)–Mn(1)–Cl(1)	88.84(11)		
N(2)–Mn(1)–Cl(1)	92.69(12)		
N(3)–Mn(1)–Cl(1)	92.3(2)		
N(4)–Mn(1)–Cl(1)	97.70(19)		
N(5)–Mn(1)–Cl(1)	90.18(13)		

The perchlorate ion is non-coordinating reflecting the low coordination ability of this anion.

No intra- or intermolecular π,π-interactions have been observed in the net.

The $[MnL^4Cl](PF_6)$ complex crystallizes in the monoclinic $P2(1)/c$ space group, and the $[MnL^4Cl]^+$ cation shows the Mn(II) ion in a six coordinated environment into the macrocycle hole interacting

with the five N donor atom of the ligand, whilst the sixth coordination position is occupied by one chloride ion. The geometry can be described as highly distorted octahedral, where the equatorial plane is comprised by N(1) N(2) N(3) N(5) donor atoms, being the apical positions occupied by the chloride ion and the N(4) donor atom. In this case, the $[MnL^4Cl]^+$ cation shows that the ligand is folded due to the presence of two propylene chains between the tertiary amine groups of the molecule, which give rise to a higher flexibility of L^4 compared with L^2. The rms of the equatorial plane is 0.4716 and the Mn(II) ion is 0.6838 Å out of this plane. The five Mn–N bond lengths vary from 2.250 to 2.286 Å, with average Mn-N bond distance of 2.310 Å, similar to previously reported six-coordinate manganese(II) complexes with this kind of ligands, and only 0.01 Å shorter than the average distance in the seven-coordinate complex [39].

The Mn(II) to chlorine distance [Mn(1)–Cl(1) 2.3646 Å], is slightly shorter than the Mn–Cl distances found previously in this sort of complex. The PF_6^- anion is disordered in four of the six fluoride ions of the counter ion with occupancies of 65% and 35% for the two components present.

As in the previous complex no intra- or intermolecular π,π-interactions have been observed.

4. Conclusion

The Mn(II) ion is effective as a template for the Schiff-base condensation of 2,6-diacetylpyridine or 2,6-pyridinedicarbaldehyde with two different tetraamines having a piperazine moiety. In spite of presence of steric hindrance due to structural restriction of piperazine, cyclocondensation has occurred and pentaaza macrocyclic complexes based on the [*X*]piperazine N_5 rings (*X* = 16 and 17) were obtained. The crystal structures of $[MnL^2Cl(CH_3OH)](ClO_4)$ and $[MnL^4Cl](PF_6)$ were determined and indicate that in the solid state the complexes adopt a pentagonal bipyramidal and a highly distorted octahedral geometry, respectively.

5 Supplementary data

CCDC 649842 and 686394 contain the supplementary crystallographic data for $[MnL^2Cl(CH_3OH)](ClO_4)$ and $[MnL^4Cl](PF_6)$. These data can be obtained free of charge via http://www.ccdc.cam.ac.uk/conts/retrieving.html, or from the Cambridge Crystallographic Data Centre, 12 Union Road, Cambridge CB2 1EZ, UK; fax: (+44) 1223-336-033; or e-mail: deposit@ccdc.cam.ac.uk.

Acknowledgements

We are grateful to the Faculty of Chemistry of Bu-Ali Sina University, Ministry of Science, Research and Technology of Iran, for financial support and to The University of Vigo for a Visiting Fellowship to M.R.

References

[1] D.S.C. Black, E. Markham, Rev. Pure Appl. Chem. 15 (1965) 109.
[2] L.F. Lindoy, The Chemistry of Macrocyclic Ligand Complexes, Cambridge University Press, Cambridge, 1989.
[3] D.C. Weatherburn, S. Mandal, S. Mukhopadhyay, S. Bhaduri, L.F. Lindoy, in: J.A. McCleverty, T.J. Meyer (Eds.), Comprehensive Coordination Chemistry II, vol. 5, Elsevier, 2004, pp. 1–125.
[4] H. Okawa, H. Furatachi, D.E. Fenton, Coord. Chem. Rev. 174 (1998) 51.
[5] O. Khan, Struct. Bond. 68 (1987) 89.
[6] K.O.A. Chin, J.R. Morrow, C.H. Lake, M.R. Churchill, Inorg. Chem. 33 (1994) 656.
[7] H. Adams, R. Bastida, A. de Blas, M. Carnota, D.E. Fenton, A. Macias, A. Rodriguez, T. Rodriguez-Blas, Polyhedron 16 (1997) 567.
[8] G.L. Eichhorn, Ed., I k g . Bioccem. 1973.
[9] M.W. Lynch, D.N. Hendrckson, B.J. Fitzgerald, C.G. Pierpont, J. Am. Chem. Soc. 106 (1984) 2041.
[10] D.P. Kessissoglou, X. Li, W.M. Butler, V.L. Pecorato, Inorg. Chem. 26 (1987) 2487.
[11] K. Rissanen, J. Huuskonen, A. Koskinen, J. Chem. Soc., Chem. Commun. (1993) 771.
[12] K. Rissanen, J. Breitenbach, J. Huuskonen, J. Chem. Soc., Chem. Commun. (1994) 1265.
[13] J. Huuskonen, J. Schulz, E. Kolehmainen, K. Rissanen, Chem. Ber. 127 (1994) 2267.
[14] J. Huuskonen, J. Schulz, K. Rissanen, Liebigs Annalen. (1995) 1515.
[15] J. Huuskonen, K. Rissanen, Liebigs Annalen. (1995) 1611.
[16] J. Ratilainen, K. Airola, E. Kolehmainen, K. Rissanen, Chem. Ber. 130 (1997) 1353.
[17] S. Loukiala, J. Ratilainen, J. Valkonen, K. Rissanen, Acta Chem. Scand. 51 (1997) 1162.
[18] K. Airola, J. Ratilainen, T. Nyrönen, K. Rissanen, Inorg. Chim. Acta 277 (1998) 55.
[19] S. Loukiala, J. Ratilainen, K. Airola, J. Valkonen, K. Rissanen, Acta Chem. Scand. 52 (1998) 593.
[20] H.J. Schneider, Angew. Chem., Int. Ed. Engl. 30 (1991) 1417.
[21] J.D. Curry, D.H. Busch, J. Am. Chem. Soc. 86 (1964) 592.
[22] R.H. Prince, D.A. Stotter, P.R. Woolley, Inorg. Chim. Acta 9 (1974) 51.
[23] H. Keypour, D.A. Stotter, Inorg. Chim. Acta 19 (1976) L48.
[24] H. Keypour, D.A. Stotter, Inorg. Chim. Acta 33 (1979) L149.
[25] H. Keypour, S. Salehzadeh, R.G. Pritchard, R.V. Parish, Inorg. Chem. 9 (2000) 5787.
[26] H. Keypour, H. Goudarziafshar, A.K. Brisdon, R.G. Pritchard, M. Rezaeivala, Inorg. Chim. Acta 361 (2008) 1415–1420.
[27] D. Jerchel, J. Heider, H. Wagner, Leibig Ann. Chem. 613 (1958) 153.
[28] H. Keypour, H. Khanmohammadi, K.P. Wainwright, Max R. Taylor, Inorg. Chim. Acta 358 (2005) 247–256.
[29] G.M. Sheldrick, SADABS, Program for Empirical Absorption Correction of Area Detector Data, University of Göttingen, Germany, 1996.
[30] SHELXTL version, an integrated system for solving and refining crystal structures from diffraction data (Revision 5.1), Bruker AXS LTD., Madison, WI, USA, 1997.
[31] L. Farrugia, J. J. Appl. Crystallogr. 30 (1997) 565.
[32] N.S. Gill, R.H. Nutall, D.E. Scaife, J. Inorg. Nucl. Chem. 18 (1961) 79.
[33] A.J. Hataway, D.E. Underhill, J. Chem. Soc. (1961) 3091.
[34] M.F. Rosenthal, J. Chem. Educ. 50 (1973) 331.
[35] W.J. Geary, Coord. Chem. Rev. 7 (1971) 81.
[36] S.F.A. Kettle, Physical Inorganic Chemistry Approach, Oxford University Press, 1998.
[37] W. Park, M.H. Shin, J.H. Chung, J.P. Lah, D. Lim, Tetrahedron Lett. 47 (2006) 8841.
[38] W.L. Newmann, G. Franklin, K. Sample, Aston, R. Weiss, D.P. Riley, Tetrahedron Lett. 38 (1997) 779.
[39] K. Aston, N. Rath, A. Naik, U. Slomezynska, O.F. Schall, Inorg. Chem. 40 (2001) 1779.

(aldehyde/alcohol) and potentially stereoselectivity of the products. Carbon monoxide is a competing ligand in hydroformylation reactions and, since CO is present in high concentration, excess phosphine is often required to avoid the formation of species such as **A** in Scheme 1. An example of this phenomenon was presented by Pruett and Smith [43]. They showed that the yield of the linear aldehyde product increased from 31% to 89% when the number of equivalents of triphenylphosphite was increased from 0 to 60 during the rhodium catalyzed hydroformylation of 1-pentene. The goal is to manipulate the equilibrium in Scheme 1 such that the predominant species is **D**. To this end, CO concentration, ligand concentration, and the nature of PR_3 can be varied. A logical extension is that if the correct NHC is chosen to stabilize **D**-type intermediates, then high selectivities should be achievable without excess ligand.

In a 1997 patent, Herrmann et al. [44] claimed catalytic hydroformylation activity using (COD)RhCl(NHC) (where NHC = 1,3-dimethylimidazolin-2-ylidine) as the catalyst. With 1-hexene as substrate 33.8% *n*-heptanal and 66.2% 2-methylhexanal were formed. Crudden and coworkers [45] followed this patent in the chemistry literature in 2000. Scheme 2 depicts the synthesis of two precatalysts (**1** and **2**) Crudden used in the hydroformylation of styrene derivatives. To form complex **1**, PPh_3 is displaced from Wilkinson's complex with 1,3-bis(2,4,6-trimethylphenyl)imidazol-2-ylidene (**IMes**). Conversion to complex **2** demonstrates the lability of phosphines towards substitution with CO, and is the primary reason for the need for excess phosphine. Once CO is installed, complex **2** is rendered stable to oxygen, but **1** decomposes and must be manipulated under inert conditions. Presumably the first step under hydroformylation conditions (CO atmosphere) is to convert **1** into **2**. The expectation then is **1** and **2** should perform uniformly in hydroformylation reactions but that is not the case; compare entries 1 and 2 in Table 1. Instead, **1** is twice as reactive as **2**. Surprisingly, if one equivalent of PPh_3 is added to **2** then the activity is again equal to **1** (entry 3). This raises questions as to the true identity of the catalytically active species. If the NHC ligand is displaced during hydroformylation then $Rh(CO)Cl(PPh_3)_2$ could be formed, but when tested under similar conditions, the branched to linear ratio was much different (88:12 compared to 96:4 for **2**).

It is still unclear what role the additional phosphine plays, but regardless of the conditions, the precatalyst, or the substrate used, the branched to linear ratio is consistently very high 95:5 (±2).

A report by Crudden and coworkers [46] that describes the clean displacement of **IMes** from complex **1** further complicates the question of active catalyst identity. The implication is the NHC ligands used in hydroformylation reactions are not substitutionally inert. Treating complex **1** with one equivalent of PPh_3 cleanly forms Wilkinson's complex at 60 °C in dichloroethane (Scheme 3). The carbonyl substituted derivative **2** depicted is less reactive towards NHC displacement but eventually loses **IMes** at 80 °C with a $t_{1/2}$ of three weeks. In hydroformylation studies performed by Crudden, the most efficient reactions always have at least one equivalent of PPh_3. Confirmation of detrimental solvent reactivity was demonstrated by simply dissolving **IMes** in dichloroethane to irreversibly form the diimidazolium salt (77% yield), which was characterized by single-crystal X-ray diffraction, and IMesHCl (18%).

The consistent b:l ratios are strikingly similar to those originally obtained by simply using hydridocarbonyltris(triphenylphosphine)rhodium(I) $RhH(CO)(PPh_3)_3$, studied extensively by Wilkinson [47–53]. Under CO atmosphere at 273 K, $RhH(CO)(PPh_3)_3$ quickly converts to the hydridodicarbonylbistriphenylphospine-rhodium(I) complex $RhH(PPh_3)_2(CO)_2$. Addition of one equivalent of styrene results in the detectable formation of two distinct acyl b:l isomers in a 91:9 ratio, which is similar to the ratios of aldehyde products obtained under catalytic conditions [54].

Crudden and coworkers [55] continued to explore hydroformylation, and reported the synthesis of complexes bearing the saturated carbene 1,3-dimesitylimidazolium-2-ylidene (**SIMes**) and various trialkyl phosphines (**3-R**, Scheme 4). Entries 16 and 17 (Table 1) provide a direct comparison of two different NHCs while retaining the same phosphine, namely PPh_3. The catalyst **3-Ph** (TOf = 14) has a TOF twice that of **1** (TON = 8) and the b:l ratios of the resulting styrenic aldehydes are statistically identical. Certainly this rate difference, though small, suggests the active species retains the NHC ligand. A greater spread of steric and electronically adjusted NHCs will provide conclusive evidence.

Clear evidence is presented that the trialkyl phosphine is important during the rate determining step. A one order of magnitude dif-

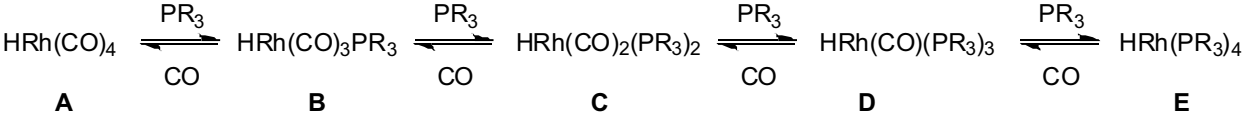

Scheme 1. PR_3/CO competing intermediates in Rh-modified hydroformylation.

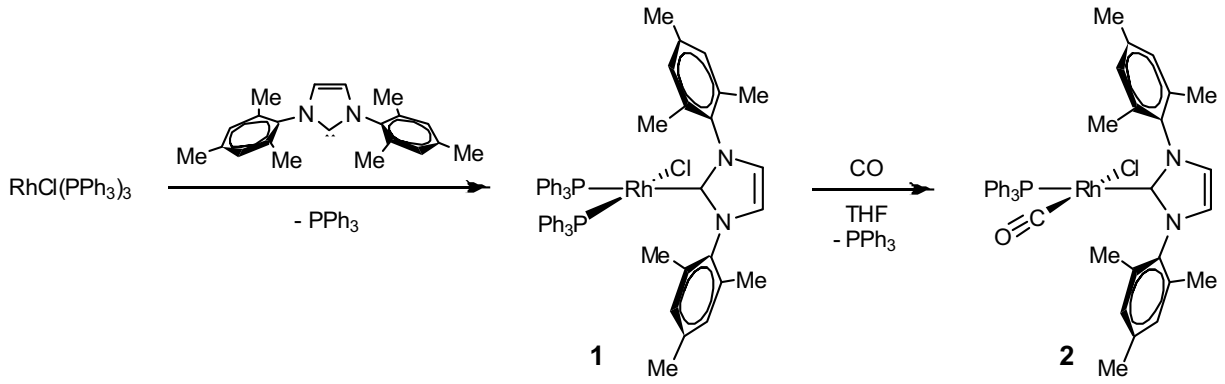

Scheme 2.

Table 1
Hydroformylation of vinylarenes[a]

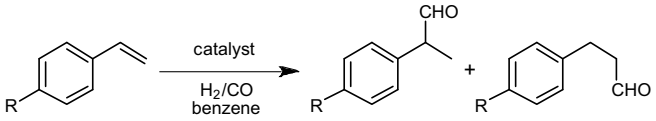

Entry	Catalysts	R	Load (%)	Additive	Time (h)	Conversion (%)	TOF	Yield (%)	b:l
1	**1**	H	0.5		20	78	7		95:5
2	**2**	H	0.5		19	38	4		94:6
3	**2**	H	0.5	1 PPh_3	19	74	8		96:4
4	**2**	H	0.5	2 PPh_3	19	79	8		96:4
5	**2**	H	0.5	10 PPh_3	19	80	8		96:4
6	**1**	H	1.0		20–22			85	96:4
7	**1**	Me	1.0		20–22			88	94:6
8	**1**	Cl	0.8		20–22			94	98:2
9	**1**	MeO	1.0		20–22			91	95:5
10	**1**	^{i}Bu	1.1		16			95	97:3
11	**2**	H	0.5	2% PPh_3	22				96:4
12	**2**	Me	1	2% PPh_3	22			96	96:4
13	**2**	Cl	1	2% PPh_3	22			94	97:3
14	**2**	MeO	1	2% PPh_3	22			98	95:5
15	**2**	^{i}Bu	2.0	2% PPh_3	22			93	96:4
16	**1**	H	0.5	1% PPh_3	19		8		96:4
17	**3-Ph**	H	0.5	1% PPh_3	19		14		94:6
18	**3-OPh**	H	0.5	1% PPh_3	19		0.5		65:35
19	**3-*p*-OMePh**	H	0.5	1% PPh_3	19		13		96:4
20	**3-*p*-FPh**	H	0.5	1% PPh_3	19		31		95:5
21	**3-DBP**[b]	H	0.5	1% PPh_3	19		3		93:7
22	**3-Furyl**	H	0.5	1% PPh_3	19		44		91:9
23	**3-Cy**	H	0.5	1% PPh_3	19		2		84:16
24	**3-*o*-Tolyl**	H	0.5	1% PPh_3	19		3		91:9
25	[c]	H	0.5	2 PPh_3	19	27	3		88:12

[a] Reaction conditions: substrate (0.8 mmol) in 5 mL benzene under 1000 psi H_2/CO at 60 °C.
[b] DBP = phenyldibenzophosphole.
[c] Catalyst = $Rh(CO)Cl(PPh_3)_2$.

ference in TOF is reported between the electron-withdrawing substituted **3-*p*-FPh** catalyst and the bulky orthomethyltolyl derivative **3-*o*-tolyl**. Switching the *para*-substituent to electron-donating –OMe (**3-*p*-OMePh**) resulted in a less reactive species (compare entries 19 and 20). A peculiar result was observed when **3-OPh** featuring a trialkylphosphite $P(OPh)_3$ was used: the branched to linear ratio dropped to 65:35, though no explanation was provided. Though Crudden et al. state preparation of asymmetric versions of their Rh–NHC complexes is underway, no report of enantioselective hydroformylation has emerged since 2000. This is odd considering the availability of chiral NHCs and chiral Rh–NHC complexes [4,8,10,56]. Surely any amount of enantioselectivity obtained would be conclusive evidence that the NHC remains bound.

The authors were able to drastically increase the TOF for styrene hydroformylation using the carboxylato derivative **7** described in Scheme 5 [57]. Complex **7** contains one NHC and can be converted to the *bis*-NHC complex **8** by adding an additional equivalent of IPr. Both **7** and **8** were characterized by X-ray crystallography. In this case, when **7** is used as the catalyst under a variety of conditions, a distribution of b:l ratios is observed instead of the consistent 95:5 (±2) discussed above. The authors were able to optimize the conditions for which benzene was solvent: 80 °C, 0.5 mol% **7**, 0.5 mol% PPh_3, and 1000 psi H_2/CO. Again, excellent branched to linear ratios were obtained, but in this case the TOF's were much higher, the best being 515 h^{-1} in the case of 4-chlorostyrene. The authors also examined hydroformylation of the α-olefins 4-phenyl-1-butene and 1-decene and observed b:l ratios of 30:70 and 25:75, respectively (Table 2).

Catalyst **7** is touted as the first example of a square-planar catalytically active rhodium carboxylato complex bearing an NHC ligand. The analogous acetylacetonate complexes **9** and **10** displayed in Fig. 1 do not exhibit hydroformylation activity. Instead, Otto and coworkers [58] tested the stability of **10** using high pressure ^{31}P NMR spectroscopy to simulate real hydroformylation conditions. ^{31}P resonances attributed to **10** quickly disappear under 20 bar CO/H_2 gas and are replaced with two new doublets at 36.9 ppm ($^{1}J_{Rh-P}$ = 140 Hz) and 44.3 ppm ($^{1}J_{Rh-P}$ = 151 Hz), respectively. The authors attribute the resonances at 36.9 and 44.3 ppm to the well-known hydroformylation catalyst precursor $[HRh(CO)_2(PPh_3)]$ and the non-active compound $[Rh(CO)_3(L_2)(PPh_3)]^+$, [59], respectively. The key finding is that complex **10** does not exhibit any hydroformylation activity. However, if PPh_3 is added, then the hydroformylation activity is turned on. The resultant activity is identical to simply using $[Rh(acac)(CO)_2]$ with PPh_3, and no benefit was realized by the preinstalled NHC ligand. Is Crudden's catalyst retaining the NHC ligand? Crudden admits they cannot rule out NHC-free catalytically active species, but also note their yields and selectivities do not match those for $Rh(CO)(acac)(PPh_3)/PPh_3$ mixtures reported by Trzeciak and coworkers [60].

If keeping the NHC ligand bound to the metal center is problematic, then a multidentate NHC ligand may be a solution. Crabtree and coworkers [61–63] synthesized the pincer-type diimidizolium salt **11** (Scheme 6). The dinuclear complex **12** is easily prepared by deprotonating **11** with a mild base (NEt_3) followed by addition of $[Rh(COD)Cl]_2$ at 40 °C. The tridentate Rh(III) complex **13** can be prepared either from **12** by adding an additional equivalent of **11**, or by simply refluxing the initial reaction mixture in aerated CH_3CN in the presence of excess KBr. Additionally, the authors report the synthesis of the chelating bis-NHC rhodium complex **14**. These complexes exhibited high activity for the hydrosilylation of alkynes and olefins, and in the hydrogen transfer from alcohols to ketones. Subsequently, Peris and coworkers [63] tested **12** and

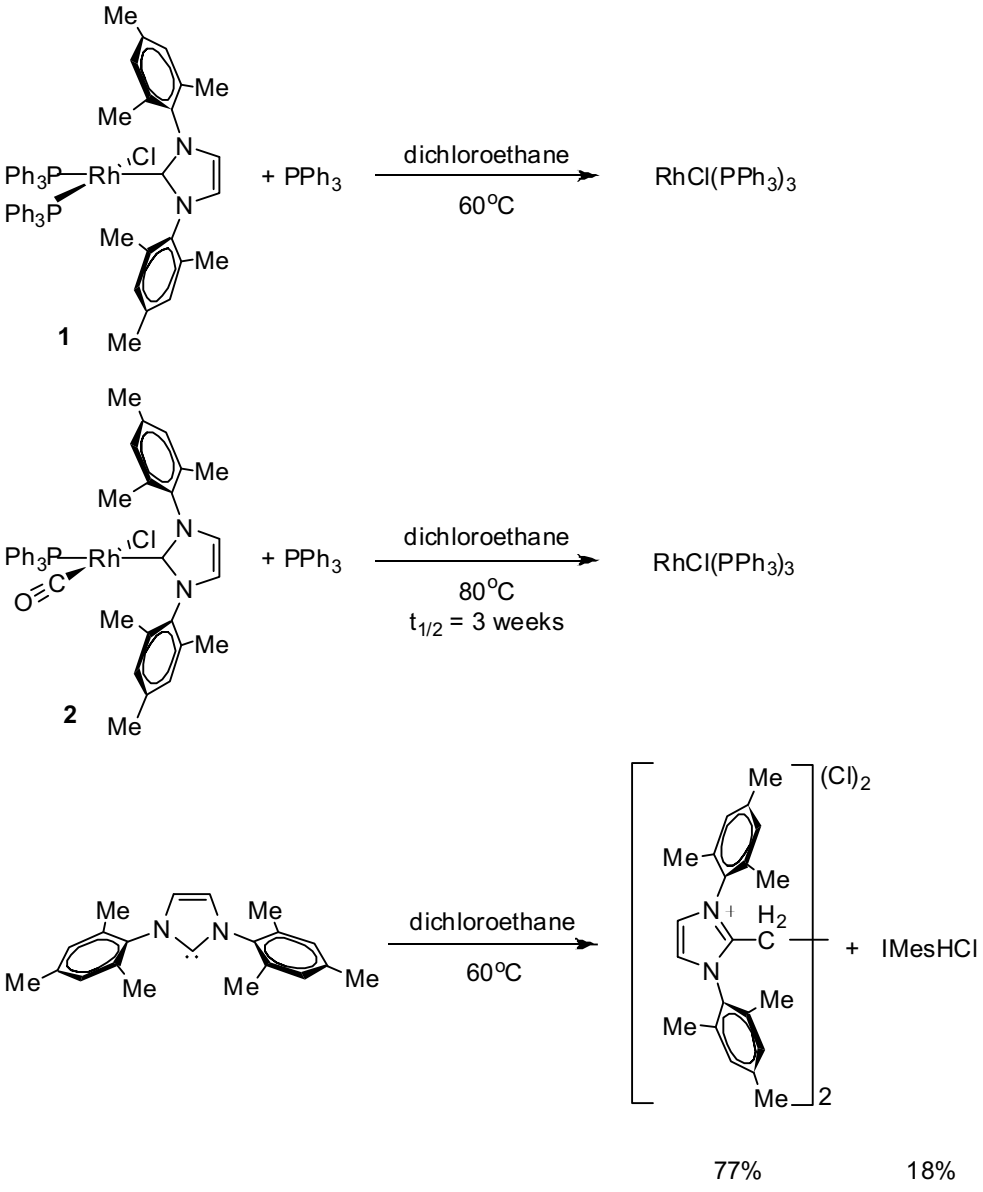

Scheme 3.

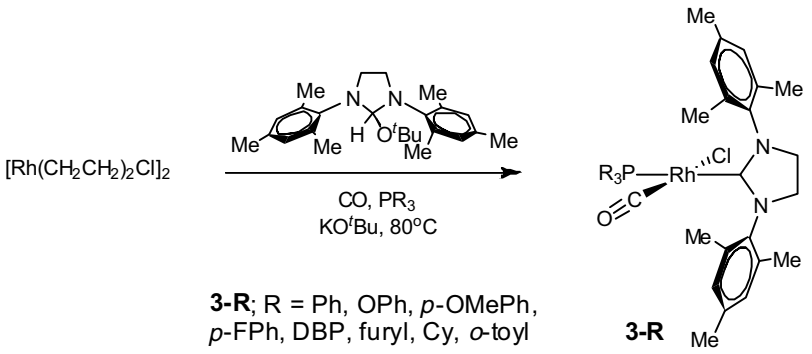

Scheme 4.

14 as hydroformylation precatalysts and obtained branched aldehyde in quantitative yield when complex **12** was used. Boosting the temperature and pressure to 40 °C and 80 atm provided 100% conversion and maintained a very high b:l ratio of 97:3 (Table 3, entry 5). Catalyst **12** is not particularly selective for linear alkenes and only provided 43% branched aldehyde for 1-octene.

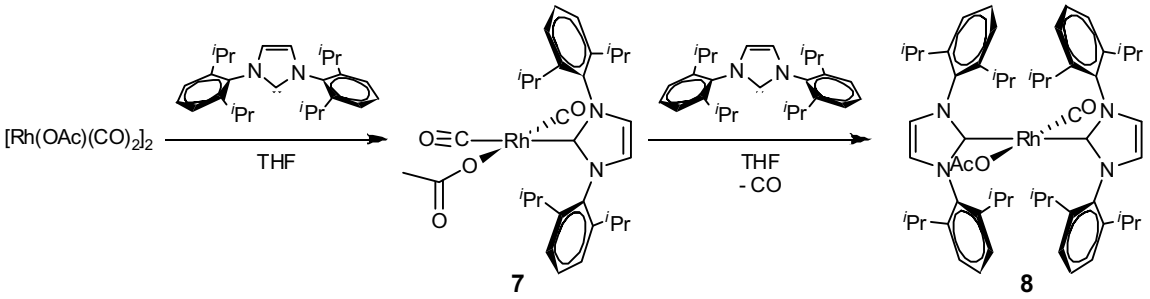

Scheme 5.

Table 2
Hydroformylation of alkenes catalyzed by **7**[a]

Entry	Alkene	TOF (h^{-1})[b]	b:l
1	Styrene	338	96:4
2	4-Chlorostyrene	515	96:4
3	4-Methoxystyrene	334	90:10
4	4-Methylstyrene	426	92:8
5	4-Acetoxystyrene	282	94:6
6	4-Phenyl-1-butene	725	30:70
7	1-Decene	345	25:75

[a] Reaction conditions: 0.5 mol% of 7, 0.05 mol% of PPh_3 in ca. 1.0–1.2 M benzene solution of substrate under 1000 psi (CO/H_2).
[b] TOF's determined after 1 h by ^1H NMR using an internal standard.

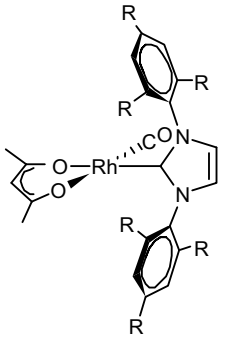

Fig. 1.

Surprisingly, the bis-NHC complex **14** showed zero activity towards hydroformylation of styrene even under harsh reaction conditions (80 °C and 80 atm).

Another approach to stabilizing active Rh(I) hydroformylation catalysts is to use a hemilabile ligand. Green and coworkers [64,65] prepared the first example of a stable crystalline noncyclic imino NHC according to Scheme 7. The stable carbene was structurally characterized and is a significant achievement, considering an earlier report indicated these ligands can undergo [1,2]-rearrangement prior to metallation [66,67]. Access to the free carbene enabled the synthesis of complex **17** according to Scheme 6. Complex **17** was tested for activity in the hydroformylation of 1-octene. The yields of aldehydes reached >99% but l:b ratios were unremarkable (1.2) at high pressure and temperature. Under milder conditions (60 °C, 10 bar) a l:b ratio of 2.5 was observed but only 30% of the olefin was converted to aldehyde products.

Raubenheimer and coworkers [68] pursued the hydroformylation of 1-hexene using Rh(I) precursors with particular focus on the potential activity when thione ligands (C = S, Chart 1) were employed. The authors prepared numerous complexes by varying the combinations of ligands presented in Chart 1. Several of the combinations included either monodentate NHC_R (R = Me, ^{i}Pr) or bidentate NHC–NHC ligands. The composition of Rh catalysts containing at least one NHC ligand combination are as follows: $Rh(COD)NHC_{Me}Cl$, $[Rh(NHC_{Me})_2]Cl$, *cis*-$Rh(CO)_2NHC_{Me}Cl$, *trans*-$Rh(CO)(NHC_{Me})_2Cl$, $[Rh(COD)(NHC–NHC)]PF_6$, $[Rh(CO)_2(NHC–NHC)]PF_6$, $Rh(CO)(C=S)NHC_{Me}Cl$, $[Rh(COD)(thione)NHC_{iPr}]BF_4$, $[Rh(CO)_2(thione)NHC_{iPr}]BF_4$, $Rh(CO)(PPh_3)NHC_{iPr}Cl$, $Rh(CO)[P(thiazole)_3]NHC_{iPr}Cl$. The authors present hydroformylation results obtained under a variety of conditions, but it is apparent that no benefit is obtained by including the NHC ligand in the catalyst precursor. The percent conversion, yield of aldehyde, and b:l ratio are all similar to those obtained by simply using Wilkinson's complex.

Buchmeiser, Nuyken, Weberskirch and coworkers [69,70] examined the hydroformylation activity of a series of compounds in which the NHC heterocycle is 1,3-R-3,4,5,6-tetrahydropyrimidin-2-ylidene (R = ^{i}Pr, and Mes; see Fig. 2.). Not surprisingly, the chloro (**18-Cl, 19-Cl**) and bromo (**18-Br, 19-Br**) derivatives displayed identical reactivity, implying an active catalyst of the general formula $Rh(CO)_2(H)NHC$. Gratifyingly, significant differences were observed in the initial TOF between catalyst **18-Cl** and **19-Cl** bearing *N*-^{i}Pr and *N*-Mes groups, respectively. Complex **19-Cl** exhibited a TOF of 1500 h^{-1}, whereas under identical conditions **18-Cl** only turned over at a pace of 520 h^{-1}. None of the catalysts were particularly selective for the formation of aldehydes, but convincing evidence for an NHC-bound active catalyst was finally realized.

Immobilization of well-defined, air-stable, and recyclable polymer-supported NHC catalysts and their application in Heck reactions was first reported in 2000 [71]. Following this approach, Weberskirch and coworkers [72] synthesized the unsymmetrical, monohydroxy-functionalized rhodium NHC complex **20** with the intent to attach an amphiphilic polymer to enable biphasic hydroformylation catalysis (Scheme 8). Complex **20** catalyzes the hydroformylation of 1-octene in benzene with a inspiring TOF of 2400 h^{-1}, the fastest to date, however selectivity was unremarkable (l:b = 0.67). However, when the supported complex **21** is employed under biphasic conditions (water/1-octene) the ratio increases to 2.6 and the initial TOF is 1100 h^{-1}, which indicates a definite change in the steric environment of the active metal center once supported. The authors demonstrated that **21** was easily recyclable and the TOF increased to 2320–2360 h^{-1} after recycling twice, identical to the unbound catalyst, but the l:b ratio declined to 1.2 and then remained constant. The pronounced increase in TOF was attributed to slow catalyst activation which requires approximately 4 h to fully activate each metal center. To summarize this work, NHC–Rh(I) precatalysts can be attached to polymer supports and retain their activity. More importantly, the supported Rh(I) catalyst is *air* and *water* stable, thereby enabling catalysis under biphasic conditions to facilitate product separation and catalyst recycling.

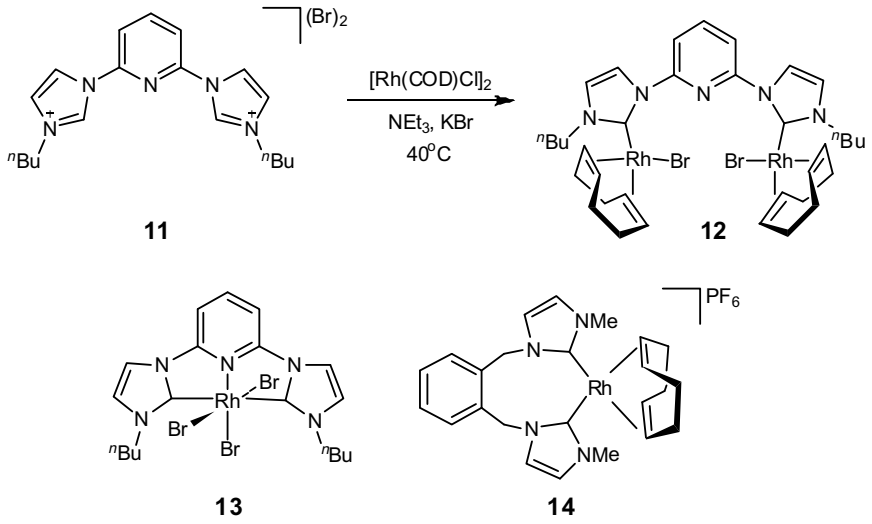

Scheme 6.

Table 3
Hydroformylation of alkenes catalyzed by **12**

Entry	Alkene	Solvent	Load (%)	*T* (°C)	*P* (atm)	Conversion (%)	TOF	Ald (%)	b:l
1	Styrene	Toluene	0.14	25	30	4	1.2	96	100:1
2	Styrene	Toluene	0.14	40	30	11	3.2	99	98:2
3	Styrene	Toluene	0.14	40	80	30	8.7	98	98:2
4	Styrene	Toluene	0.14	80	80	100	29.1	99	86:14
5	Styrene	Toluene	0.25	40	80	100	16.7	99	97:3
6	Styrene	CH_2Cl_2	0.25	40	80	94	15.7	100	97:3
7	*p*-MeOPh	Toluene	0.25	40	50	74	12.3	100	96:4
8	*p*-FPh	Toluene	0.25	40	50	69	11.5	100	96:4
9	1-Octene	Toluene	0.25	40	50	70	11.6	92	43:57
10	2,5-Dihydrofuran	Toluene	0.25	40	50	90	15	98	63[a]:47

[a] Tetrahydrofuran-3-carbaldehyde.

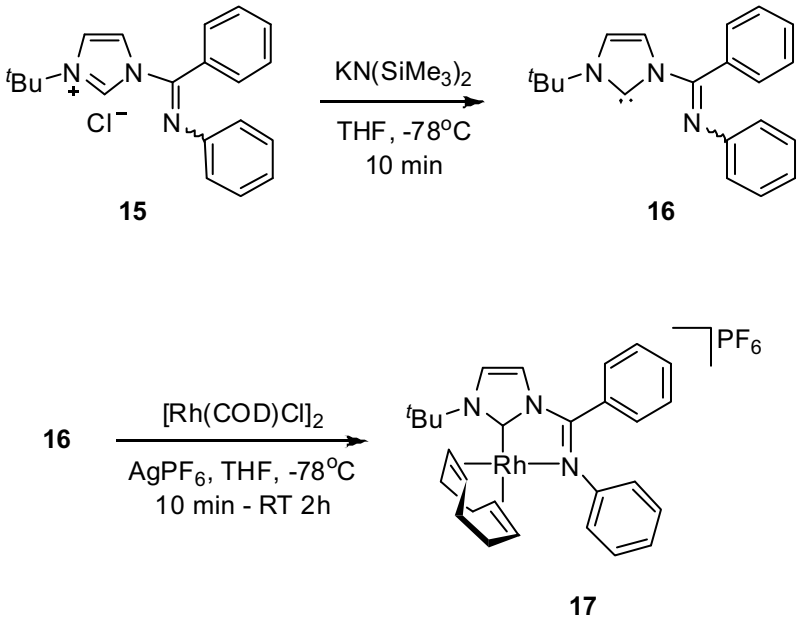

Scheme 7.

Co–NHC complexes have received considerably less attention than Rh–NHCs despite the fact NHCs may actually be better suited to cobalt. That is, basic phosphines work well with Co whereas less basic phosphines and phosphites provide the best Rh catalysts [38]. If the purported electronic correlation between NHCs and trialkylphoshines is true, then Co–NHC catalysts should prove effec-

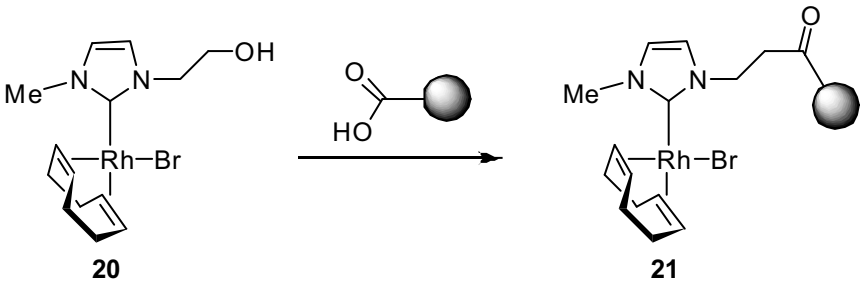

Scheme 8.

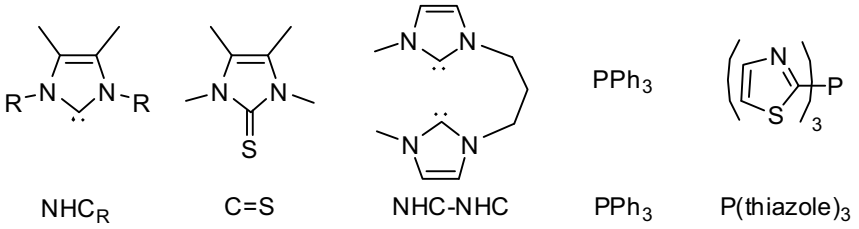

Chart 1.

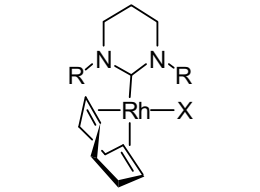

18-X: R = ^{i}Pr, X = Cl, Br
19-X: R = Mes, X= Cl, Br

Fig. 2.

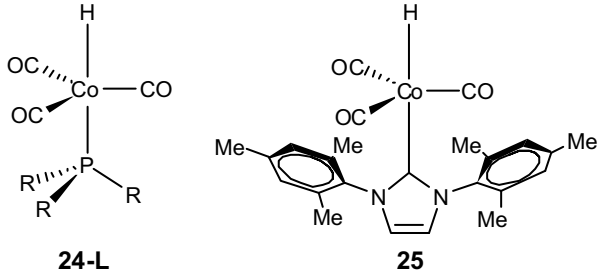

Fig. 3.

tive as hydroformylation catalysts. van Rensburg et al. [73,74] synthesized the disproportionation salt **22** by treating Co_2CO_8 with two equivalents of **IMes** (Scheme 9). The salt is surprisingly stable and does not spontaneously convert to dimer **23**, as do the phosphine derivatives $[Co(CO)_3P_2][Co(CO)_4]$. The authors note the strong σ-donor phosphine derivative, where P = P^{n}Bu$_3$, converts to the dimer much more slowly than when P = PPh$_3$. Thus, the apparent stability of **22** may be due to the exceptionally strong σ-donor capability of **IMes**. Regardless, the dimer can be synthesized by treating $Co_2CO_6(PCyPh_2)_2$ with two equivalents of **IMes**. However, when **23** is treated with 1-octene and syngas (H_2:CO = 2:1) at 60 bar and 170 °C, a dark brown oily compound precipitated which was identified as the imidazolium salt [1,3-bis(2,4,6-trimethylphenyl)imidazolium][$Co(CO)_4$].

Despite detrimental decomposition Llewellyn, Green, and Cowley [75] were able to isolate the Co–H complex $Co(CO)_3$HIMes (**25**) by treating the corresponding acyl species $Co(CO)_3$(COMe)IMes with hydrogen (Fig. 3). The authors note **25** is solid-state stable in the absence of oxygen and moisture and only 15% decomposition occurs after 7 d in solution. This is in contrast to the phosphine versions Co(L)$(CO)_3$H (**24-L**; L = P^{n}Bu$_3$, PPh$_3$, P(OPh)$_3$, and PF$_3$) which dimerize at room temperature. The Co-hydride complex **25** was examined for activity in the hydroformylation of 1-octene. With 8 atm of syngas (H_2/CO) at 50 °C for 17 h and 1 mol% **25**, 47% conversion to aldehyde products was achieved. Surprisingly 83% of the product was the internal aldehyde 2-methyl-octanal. Presumably 1-octene is rapidly isomerized to 2-octene followed by hydroformylation. The authors only present one catalytic result, but if the improved stabilization is indeed due to better σ-donation of NHCs over phosphines, then more Co–NHC catalysts should be forthcoming.

3. Hydroaminomethylation

Hydroaminomethylation is a direct and efficient method of generating higher value amines from inexpensive feedstock alkenes and syngas [76–78] (Scheme 10). Application of this reaction has procured key pharmaceuticals, agrochemicals, and natural products, most notably the 3,3-diarylpropylamines depicted in Fig. 4 [79–86]. Hydroaminomethylation is essentially hydroformylation coupled to amine-aldehyde condensation followed by hydrogenation. The key reaction is hydroformylation, since this reaction establishes the regiochemistry, and the hydrogenation step determines the chemoselectivity between amine and eneamine products. Once the aldehyde is formed and as long as the catalyst can serve a dual role to catalyze hydrogenation, the amine product forms. Considering the discussion above regarding hydroformylation, hydroaminomethylation is a logical reaction to try with Rh and Co based NHC complexes.

Beller and coworkers [87,88] are the first to report hydroaminomethylation with an NHC supported catalyst. The authors screened a series of catalysts depicted in Fig. 5. Initially catalyst **26** was used in the hydroaminomethylation of 1- and 2-pentene with piperidine. The results varied dramatically with changes in

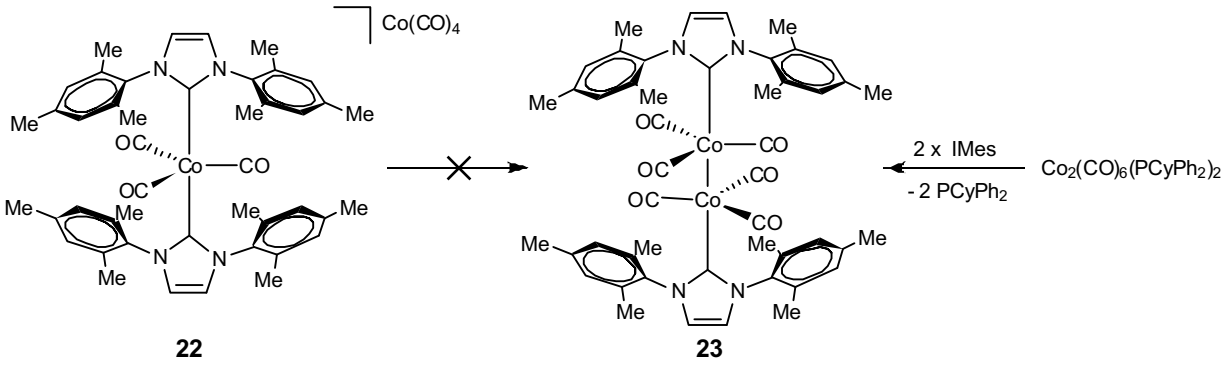

Scheme 9.

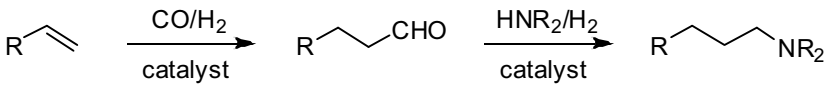

Scheme 10.

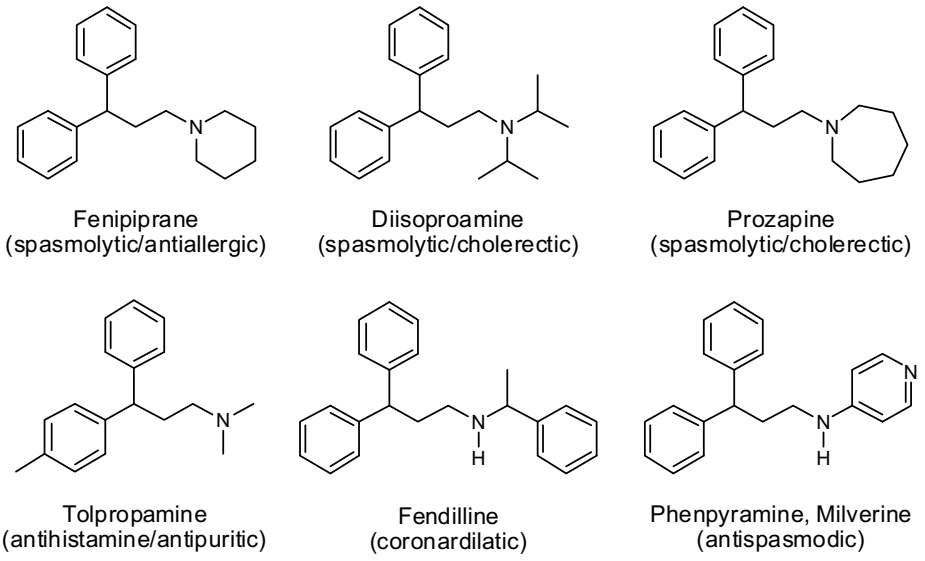

Fig. 4. Pharmaceutically active 3,3-diarylpropylamines (pheniramines) [87].

pressure of H_2/CO, temperature, and solvent. The best result obtained converted 99% of 1-pentene into 99% amine with a l:b ratio of 62:38, which is fairly typical for the Rh-NHC hydroformylation catalysts discussed above. $[Rh(COD)Cl]_2$ will catalyze the reaction faster, but unselectively, and decomposes to Rh(0) during catalysis.

When 1,1-diarlyethylenes are used, only linear products are formed due to the sterics of the substrate, not the catalyst. The authors optimized conditions for the general reaction of 1,1-diphenylethylene and piperidine displayed in Scheme 11 and note that the highest TOF (288 h^{-1}) for this specific reaction is obtained using complex **29**, syngas (H_2:CO = 5:1), at 125 °C for 24 h. Similarly, prozapine, fendilline, and diisopromine were obtained in 85%, 91%, and 88% yield, respectively, using the one-pot method. The authors were able to demonstrate that Rh–NHC-catalyst activities compare favorably with the established the Rh-Xantphos system [89]. The authors also note the first one-step synthesis of Milverine (an important antispasmodic agent) was achieved, which was previously unattainable since the aldehyde intermediate is susceptible to reduction [90]. This represents a clear example of the potential benefit of Rh–NHC catalysts over Rh-PR_3 complexes.

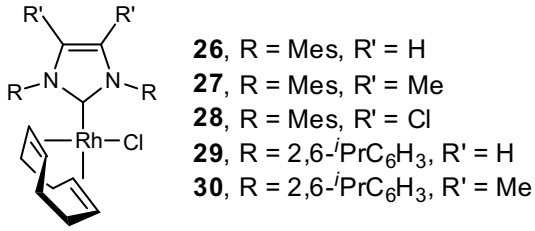

Fig. 5.

4. Carbonylation of aryl halides

Incorporating CO as a one-carbon synthon to form organic acids from organic halides is routinely catalyzed by Pd catalysts bearing

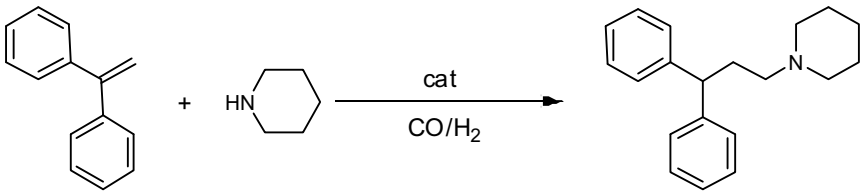

Scheme 11.

ubiquitous trialkylphosphine ligands [91–95]. The problem, or opportunity to improve, occurs when harsh conditions are required to carbonylate less reactive C–X bonds such as aryl-chlorides. Catalyst degradation via P–C [39–42] bond cleavage typifies the need for more robust ligands. Benzothiazole carbene ligated Pd complexes are stable to high temperatures, oxygen and moisture and exhibit activity in C–C coupling reactions. Complex **31** was first reported in 2000 [96] and was subsequently tested as a catalyst in the carbonylation of aryl halides [97]. When complex **31** is used as the precatalyst, activated aryl halides are carbonylated in good yield under 1 atm pressure of CO (Table 4). The less reactive bromobenzene required additional additives to achieve reasonable conversion (Fig. 6).

Some questions regarding the identity of the active catalyst remain. That is, the best results are always obtained when PPh_3 is present during catalysis, suggesting the benzothiazole carbene may be substituted. However, when just $Pd(OAc)_2$ and PPh_3 are used, the system loses reactivity when recycled, and Pd(0) forms. In contrast, complex **31** can be recycled seven times with only a 10% drop in product yield, and no Pd(0) is observed. In addition to the above study, a few reports have appeared describing the Pd catalyzed methoxycarbonylation of aryl and alkyl iodides in ionic liquids (IL). The ionic liquids are imidazolium salts, and NHC–Pd species have been proposed as the active species, though conclusive evidence remains elusive [98,99].

5. Oxidative carbonylation of amino compounds

The formation of *N*-containing carbonyl compounds such as ureas, carbamates, and 2-oxazolidinones (Scheme 12) traditionally requires the use of phosgene or its derivatives [100]. These toxic pollutants have been replaced by the direct metal-catalyzed carbonylation of amino compounds, most notably $W(CO)_6$ [101]. Some of the catalytic reactions require harsh conditions to obtain reasonable yields and often require the additives KI or I_2. If high pressures of CO are required and water is a byproduct, then strong σ-donating NHCs may be well-suited ancillary ligands.

The NHC–Cu complexes **31-X** (X = Cl, Br, I) [102] were tested as catalysts for the oxidative carbonylation of amino alcohols (Fig. 7). The authors note that **31-I** is the first catalyst to selectively prepare the three different *N*-containing carbonyl derivative types displayed in Scheme 12, and furthermore, no additive was required. Table 5 shows the counterion is critical to achieving complete conversion and the NHC ligand improves upon the use of CuI alone. **31-I** will also catalyze the oxidative carbonylation of primary amines to yield ureas and carbamates. *N*-Propylamine, *n*-butylamine, and *t*-butylamine were transformed to the corresponding ureas, and when CH_3OH was used, the carbamates were isolated in yields ranging from 86% to 98%. **31-I** will not convert aromatic amines, presumably due to their lower basicity.

Subsequently, the authors prepared the series of Pd(II)–NHC complexes depicted in Fig. 8 [103]. These complexes also catalyze the oxidative carbonylation of amino compounds and exhibit high TOFs (Table 6). Unlike the Cu–NHC-catalyst **31-X**, **32-L** will catalyze the oxidative carbonylation of a variety aromatic amines. For example, 4-Me–C_6H_4–NH_2, 4-Cl–C_6H_4–NH_2, 4-Me–C_6H_4–NH_2, 2,4-Me_2–C_6H_3–NH_2, 2,6-Me_2–C_6H_3–NH_2, and 4-Ac–$C_6H_3NH_2$ are converted to the corresponding ureas after 1 h at 150 °C, with only 0.02 mol% **32-an** in 99%, 87%, 85%, 72%, and 60% isolated yields, respectively (P_{CO/O_2} = 3.2/0.8 MPa).

6. Oxidative carbonylation of phenolic compounds

Metal catalyzed oxidative carbonylation can also be used to synthesize aromatic polycarbonates (PCs) which are desirable materials [104]. The motivation in PC synthesis is to avoid the

Table 4
Select data for the carbonylation of arylhalides with **31** [97][a]

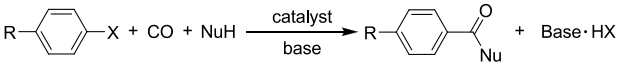

Entry	Catalysts	X	R	NuH	Base	Time (h)	*T* (°C)	P_{CO} (atm)	Yield (%)
1	31	I	H	MeOH	Et_3N	2	80	1	>99
2	31	I	H	H_2O	AcONa	7	90	1	>99
3	31	I	H	OH^-	NaOH	5	100	1	90
4	31	Br	COMe	H_2O	AcONa	10	130	1	95
5	31	Br	COMe	MeOH	Et_3N	5	130	1	91
6	31	Br	COMe	Et_2NH	Et_3N	6	130	1	95
7	31	Br	H	MeOH	Et_3N	14	150	1	Trace
8	31	Br	H	MeOH	Et_3N	14	130	1	35
9	31	Br	H	MeOH	Et_3N	14	130	1	85
10	31	I	H	BuOH	Et_3N	14	100	1	85
11	31	Br	COMe	BuOH	Et_3N	14	130	1	3
12	31	Br	COMe	BuOH	Et_3N	14	130	4	22
13	31	Br	COMe	BuOH	Et_3N	14	130	8	76
14	$Pd(OAc)_2$[b]	Br	COMe	BuOH	Et_3N	14	130	8	78
15	31	Br	H	BuOH	Et_3N	14	130	8	27
16	20/PPh_3[b]	Br	H	BuOH	Et_3N	14	130	8	85

[a] See Ref. [97] for complete details.
[b] PPh_3 (3 mol%) used.

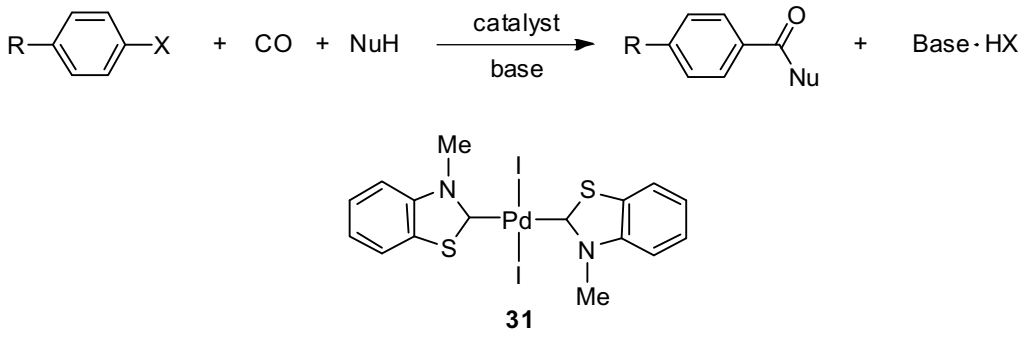

Fig. 6. General reaction scheme for the carbonylation of aryl halides catalyzed by complex 31.

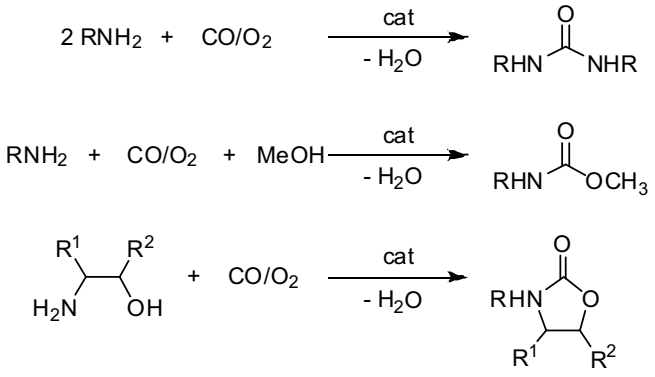

Scheme 12.

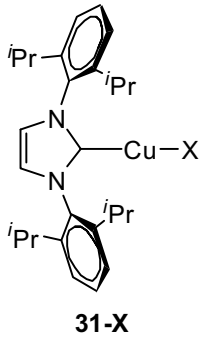

31-X

Fig. 7.

Table 5
Oxidative cyclocarbonylation of 1-amino-2-propanol catalyzed by **31-X**[a]

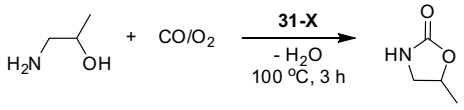

Entry	Catalyst	Solvent	Conversion (%)	Selectivity (%)
1	**31–I**	Dioxane	100	99(96)[b]
2	**31–Br**	Dioxane	8	87
3	**31–Cl**	Dioxane		
4	**Cu–I**	Dioxane	53	96

[a] Reaction conditions: 0.01 mmol of catalyst, 1 mmol of 1-amino-2-propanol, solvent (4 ml), P_{CO} = 4.8 MPa, P_{O_2} = 0.2 MPa, 100 °C for 3 h.
[b] Isolated yield.

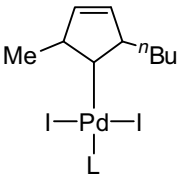

32-L

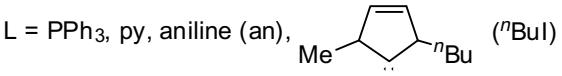

Fig. 8.

Table 6
Oxidative carbonylation of aniline by **32-L**[a]

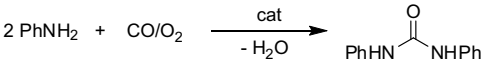

Entry	Catalyst	Conversion (%)	Selectivity (%)[b]	TOF (h^{-1})[c]
1	**32-PPh_3**	93	98	4200
2	**32-py**	86	99	4200
3	**32-an**	99	99	4900
4	**32-^{n}BuI**	70	99	3400

[a] Reaction conditions: 0.0044 mmol of catalyst, aniline (22 mmol), solvent (6 ml); P_{CO} = 3.2 MPa, P_{O_2} = 0.8 MPa, 150 °C for 1 h.
[b] Determined by HPLC.
[c] Mol of amine converted per mol of catalyst per hour.

conventional employment of phosgene, which is normally treated with bisphenol A under interfacial polycondesation conditions. Transesterification from diphenyl carbonate (DPC) is advantageous but DPC is itself synthesized using phosgene and sodium phenolate or dimethyl carbonate with phenol. Catalysts that can directly car-

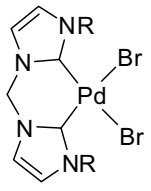

33-R

R = Me, Et, ^{n}Bu, ^{t}Bu, ^{c}Hex, Ph, Mes

Fig. 9.

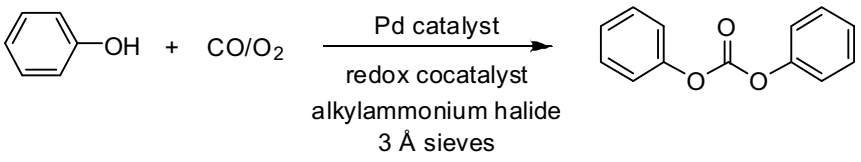

Scheme 13.

bonylate bisphenol A to efficiently provide DPC or PCs with high molecular weights would be advantageous. Simple metal salts such as PdX_2 (X = Cl, Br) produce PCs with low molecular weights, and some improvements are made by utilizing bipyridyl ancillary ligands, but none provide materials deemed useful for industry.

Sugiyama and coworkers [105] explored the synthesis of DPC using the catalysts in Fig. 9 which were synthesized according to or adapted from known procedures. The premise for using NHCs is to take advantage of their strong σ-donation capability to create longer-lived catalysts which may lead to longer chained polymers. The authors attempted to directly carbonylate phenol to form DPC which is then converted to PCs, without phosgene. The catalyst system is complicated and requires an inorganic redox active cocatalyst, alkylammonium halide, sieves and the NHC-catalyst **33-R** (Scheme 13). The best results were obtained with **33-^{t}Bu**, $Ce(TMHD)_4$ (TMHD = 2,26,6-tetramethyl-3,5-heptanedionate), hydroquinione, $^n Bu_4NBr$ and 3 Å molecular sieves which provided DPC in 45% yield with a TOF of 50.7 (mol-DPC/mol-Pd h).

Eventually the authors discovered they could catalyze the formation of polycarbonate with **33-R** via oxidative carbonylation of bisphenol A [106]. Using similar conditions and **33-^{t}Bu** a polycarbonate with M_w = 24 000 and M_n = 9400 was obtained in 80% yield. The authors note the polymer obtained has the highest molecular weight synthesized directly from PC via oxidative carbonylation of bisphenol A and is comparable to commercially available PC.

The properties and yield of the polymer product are directly related to the NHC used, providing clear evidence the NHC ligand is bound and influencing the reaction. Smaller R groups (Me, Et) on **33-R** provided low molecular weights and yields, and detectable amounts of cross-linked salicylate byproduct were observed. The above study only examined the influence of sterics on the formation of polycarbonate. Considering the copious NHCs now available and the ability to dramatically change their electronic and steric properties, this reaction is ripe for further optimization. Clearly this reaction exemplifies the general thought that creating a stable catalyst by incorporating an NHC ligand will lead to longer catalyst lifetimes. Extension of this technology has already been applied to NHC ligands tethered to a styrene bead [107].

7. Copolymerization of alkenes and CO

Guided by the principle that switching to NHC ligands may improve catalyst lifetimes and enhance reactivity, Herrmann and coworkers [108,109] examined the copolymerization of CO and ethylene. Their catalyst design was based upon the exceptional work by Drent and Budzelaar who demonstrated monocationic and dicationic *cis*-chelating phosphine complexes of the general formula $[L_2Pd(solvent)Me]^+$ and $[L_2Pd(solvent)_2]^{2+}$ are active catalysts for copolymerization [110]. By analogy then, a *cis*-chelating NHC complex of the form $[NHC_2Pd(solvent)Me]^+$ or $[NHC_2Pd(solvent)_2]^{2+}$ should also catalyze this polymerization. Accordingly, the complexes **36-R$_X$** (R = Me, X = BF_4, and R = Mes, X = PF_6) were synthesized using standard procedures in CH_3CN (Scheme 15). Table 7 highlights some of the results from the study and entry 2 in particular, shows the best conditions. Under identical conditions (entries 2 and 6) catalyst **36-Mes$_{PF6}$** performed better than **36-Mes$_{BF4}$** by providing 810 and 324 g polymer/g Pd, respectively. Apparently three equivalents of *p*-benzoquinone was the ideal amount of oxidant required as any more or less was detrimental. The authors were unable to determine the identity of the active catalyst but did note that not all of the Pd metal centers were activated. The polymer obtained melted between 250 and 260 °C indicating high purity. The estimated average molecular weight of the copolymer is exceedingly high, even higher than that obtained by Drent. The catalysts are inactive for CO/propene and CO/styrene copolymerization.

Surprisingly, only one other report has surfaced for M–NHC catalyzed copolymerization of CO/alkenes since 1999. Again, by analogy to known pyridylphosphine hemilabile ligands, Chen and Lin [111] synthesized the imidizaolium salt **37**. Subsequent metallation with $Pd(OAc)_2$ generated the bis-NHC dication **38** that features a hemilabile pyridyl-NHC ligand (Scheme 16). Indeed, spectroscopic and reactivity studies indicate the pyridyl arms are fluxional and labile enabling the catalyst to copolymerize CO and norbornene. The copolymer can be synthesized in 87% yield by employing 0.5 mol%

Table 7
Copolymerization of CO/ethane catalyzed by **36-R$_X$**[a]

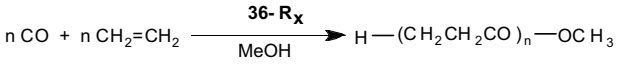

Entry	T (°C)	$P_{ethene/CO}$ (bar)	p-$C_6H_4O_2$ (mg)	Time (min)	Yield (g polymer/g Pd)
1	50	40/40	3	90	210
1	50	50/20		90	256
2	50	50/20	3	240	810
3	50	50/20	20	90	200
4	50	50/20	40	60	62
5	r.t.	50/20	3	600	162
6[b]	50	50/20	3	90	324

[a] 20 mg of **36-Mes$_{PF6}$**.
[b] 10 mg of **36-Me$_{BF4}$**.

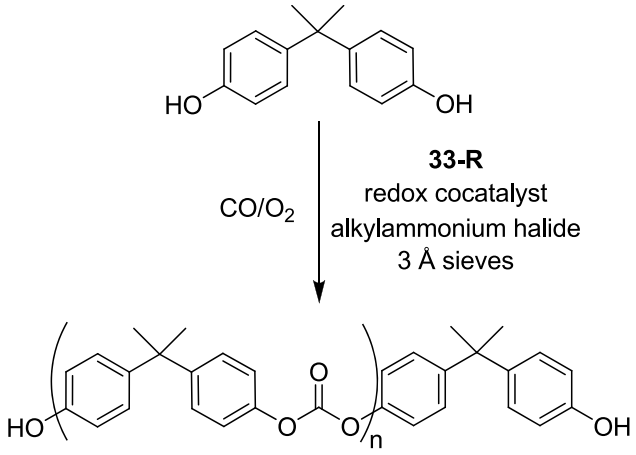

Scheme 14.

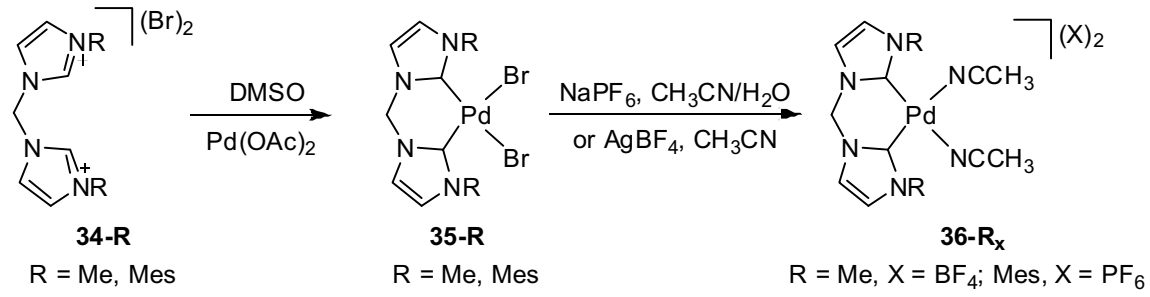

Scheme 15.

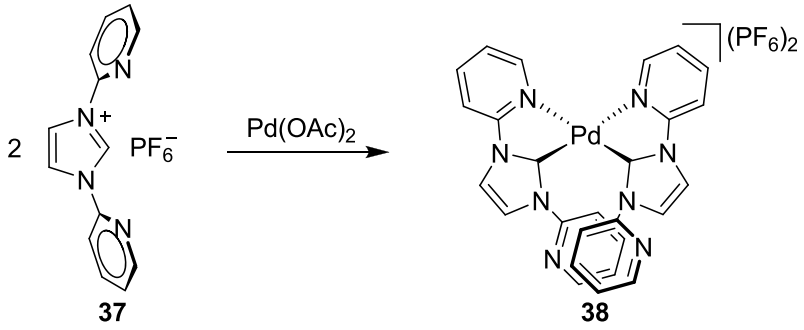

Scheme 16.

38, and 750 psi CO gas after 3 d at 60 °C. The polymer formed contained ~37 repeat units and M_w = 4660 and M_n = 3790.

8. Conclusions

Tremendous economic and environmental benefit can be realized if CO is efficiently and catalytically incorporated into organic substrates to create higher value products. Exemplary cases presented herein include the hydroaminomethylation of simple vinylic arenes to produce a variety of useful pharmaceuticals in a one-pot reaction (Fig. 4), and the phosgene-free carbonylation of amino and phenolic compounds (Schemes 12 and 14). The purpose of this review was to examine the extent M–NHC catalysts will promote reactions that use CO as a C1-carbon source. Though the first catalytic reaction incorporating CO by a M–NHC was reported in 1997, only a small set of reactions have emerged that clearly benefit from the presence of a NHC ligand. Certainly, a case can be made that M–NHCs can compete with traditional M–PR_3 catalysts, and can in some instances out-perform them. However, this review reveals, or at least adds to, growing evidence that NHCs are not substitutionally inert. The notion that NHCs are stronger σ-donors than even the most basic phosphine does not, in all cases, translate into better catalysts. Hydroformylation is the most extensively studied reaction involving CO, and the results are somewhat mixed. Exceptionally high b:l ratios for vinylic arenes are achieved for a variety of M–NHC precatalysts but the identity of the active species is still unclear. Non-aromatic 1-alkenes are hydroformylated with only average b:l ratios, and no clear benefit is obtained by the presence of an ancillary NHC. Surprisingly, after nearly one decade, no enantioselective hydroformylation has been achieved by M–NHCs. These results are perhaps symptomatic of the glaring omission of a singular experimental mechanistic investigation. The activity of NHC versus PR_3 ligands in metal-catalyzed hydroformylation has been explored by computation [112] but focused mechanistic work is sadly absent.

Acknowledgments

I thank my coworkers Matthew S. Jeletic and Roxy J. Lowry for their valuable discussions and comments and Melanie K. Veige for editing this document.

References

[1] R.H. Crabtree, J. Organomet. Chem. 690 (2005) 5451.
[2] P.L. Arnold, S. Pearson, Coord. Chem. Rev. 251 (2007) 596.
[3] K.J. Cavell, D.S. McGuinness, Coord. Chem. Rev. 248 (2004) 671.
[4] V. Cesar, S. Bellemin-Laponnaz, L.H. Gade, Chem. Soc. Rev. 33 (2004) 619.
[5] E. Colacino, J. Martinez, F. Lamaty, Coord. Chem. Rev. 251 (2007) 726.
[6] C.M. Crudden, D.P. Allen, Coord. Chem. Rev. 248 (2004) 2247.
[7] S. Diez-Gonzalez, S.P. Nolan, Coord. Chem. Rev. 251 (2007) 874.
[8] R.E. Douthwaite, Coord. Chem. Rev. 251 (2007) 702.
[9] V. Dragutan, I. Dragutan, L. Delaude, A. Demonceau, Coord. Chem. Rev. 251 (2007) 765.
[10] L.H. Gade, S. Bellemin-Laponnaz, Coord. Chem. Rev. 251 (2007) 718.
[11] W.A. Herrmann, Angew. Chem., Int. Ed. 41 (2002) 1291.
[12] A. Kascatan-Nebioglu, M.J. Panzner, C.A. Tessier, C.L. Cannon, W.J. Youngs, Coord. Chem. Rev. 251 (2007) 884.
[13] O. Kuhl, Chem. Soc. Rev. 36 (2007) 592.
[14] H.M. Lee, C.C. Lee, P.Y. Cheng, Curr. Org. Chem. 11 (2007) 1491.
[15] S.T. Liddle, I.S. Edworthy, P.L. Arnold, Chem. Soc. Rev. 36 (2007) 1732.
[16] I.J.B. Lin, C.S. Vasam, Comm. Inorg. Chem. 25 (2004) 75.
[17] I.J.B. Lin, C.S. Vasam, Can. J. Chem. 83 (2005) 812.
[18] I.J.B. Lin, C.S. Vasam, Coord. Chem. Rev. 251 (2007) 642.
[19] J.A. Mata, M. Poyatos, E. Peris, Coord. Chem. Rev. 251 (2007) 841.
[20] E. Peris, R.H. Crabtree, Coord. Chem. Rev. 248 (2004) 2239.
[21] N.M. Scott, S.P. Nolan, Eur. J. Inorg. Chem. (2005) 1815.
[22] W.J. Sommer, M. Weck, Coord. Chem. Rev. 251 (2007) 860.
[23] T. Weskamp, V.P.W. Bohm, W.A. Herrmann, J. Organomet. Chem. 600 (2000) 12.
[24] K. Öfele, J. Organomet. Chem. 12 (1968) P42.
[25] K. Öfele, Angew. Chem., Int. Ed. 8 (1969) 916.
[26] K. Öfele, H. M, Angew. Chem., Int. Ed. 9 (1970) 739.
[27] H.-W. Wanzlick, H.J. Schonherr, Angew. Chem., Int. Ed. 7 (1968) 141.
[28] H.-W. Wanzlick, Angew. Chem., Int. Ed. 1 (1962) 75.
[29] A.J. Arduengo, Acc. Chem. Res. 32 (1999) 913.
[30] A.J. Arduengo, H.V.R. Dias, J.C. Calabrese, F. Davidson, J. Am. Chem. Soc. 114 (1992) 9724.
[31] A.J. Arduengo, J.R. Goerlich, W.J. Marshall, J. Am. Chem. Soc. 117 (1995) 11027.
[32] A.J. Arduengo, R.L. Harlow, M. Kline, J. Am. Chem. Soc. 113 (1991) 361.
[33] M.F. Lappert, J. Organomet. Chem. 690 (2005) 5467.

[34] M.F. Lappert, J. Organomet. Chem. 358 (1988) 185.
[35] D.J. Cardin, B. Cetinkay, M.F. Lappert, Chem. Rev. 72 (1972) 545.
[36] F. Glorius (Ed.), *N*-Heterocyclic Carbenes in Transition Metal Catalysis: Topics in Organometallic Chemistry, Springer, Berlin, 2007.
[37] D.S. McGuinness, K.J. Cavell, Organometallics 19 (2000) 4918.
[38] P.W.N.M. van Leeuwen, C. Carman, Rhodium Catalyzed Hydroformylation, Kluwer, New York, 2002.
[39] A.G. Abatjoglou, D.R. Bryant, Organometallics 3 (1984) 932.
[40] M. Lewin, Z. Aizenshtat, J. Blum, J. Organomet. Chem. 184 (1980) 255.
[41] P.E. Garrou, Chem. Rev. 85 (1985) 171.
[42] W.A. Herrmann, C. Brossmer, K. Ofele, M. Beller, H. Fischer, J. Organomet. Chem. 491 (1995) C1.
[43] R.L. Pruett, J.A. Smith, J. Org. Chem. 34 (1969) 327.
[44] W.A. Herrmann, J. Fischer, M. Elison, C. Köcher, (Hoechst AG), DE 4447068.1 A1, 1994; EP 0719758 A1; US 5.703.269, 1997 (Chem. Abstr. 125 (1996) 167571y).
[45] A.C. Chen, L. Ren, A. Decken, C.M. Crudden, Organometallics 19 (2000) 3459.
[46] D.P. Allen, C.M. Crudden, L.A. Calhoun, R.Y. Wang, J. Organomet. Chem. 689 (2004) 3203.
[47] C.K. Brown, G. Wilkinson, Tetrahedron Lett. (1969) 1725.
[48] C.K. Brown, G. Wilkinson, J. Chem. Soc. (A) (1970) 2753.
[49] D. Evans, J.A. Osborn, G. Wilkinson, J. Chem. Soc. (A) (1968) 3133.
[50] D. Evans, G. Yagupsky, G. Wilkinson, J. Chem. Soc. (A) (1968) 2660.
[51] G. Yagupsky, C.K. Brown, G. Wilkinson, J. Chem. Soc., Chem. Commun. (1969) 1244.
[52] G. Yagupsky, C.K. Brown, G. Wilkinson, J. Chem. Soc. (A) (1970) 1392.
[53] M. Yagupsky, C.K. Brown, G. Yagupsky, G. Wilkinson, J. Chem. Soc. (A) (1970) 937.
[54] J.M. Brown, A.G. Kent, J. Chem. Soc., Chem. Commun. (1982) 723.
[55] A.C. Chen, D.P. Allen, C.M. Crudden, R.Y. Wang, A. Decken, Can. J. Chem. 83 (2005) 943.
[56] M.C. Perry, K. Burgess, Tetrahedron: Asymmetry 14 (2003) 951–961.
[57] J.M. Praetorius, M.W. Kotyk, J.D. Webb, R.Y. Wang, C.M. Crudden, Organometallics 26 (2007) 1057.
[58] M.S. Datt, J.J. Nair, S. Otto, J. Organomet. Chem. 690 (2005) 3422.
[59] C. Bianchini, H.M. Lee, A. Meli, F. Vizza, Organometallics 19 (2000) 849.
[60] E. Mieczynska, A.M. Trzeciak, J.J. Ziolkowski, J. Mol. Catal. 73 (1992) 1.
[61] J.A. Loch, M. Albrecht, E. Peris, J. Mata, J.W. Faller, R.H. Crabtree, Organometallics 21 (2002) 7006.
[62] M. Poyatos, E. Mas-Marza, J.A. Mata, M. Sanau, E. Peris, Eur. J. Inorg. Chem. (2003) 1215.
[63] M. Poyatos, P. Uriz, J.A. Mata, C. Claver, E. Fernandez, E. Peris, Organometallics 22 (2003) 440.
[64] K.S. Coleman, S. Dastgir, G. Barnett, M.J.P. Alvite, A.R. Cowley, M.L.H. Green, J. Organomet. Chem. 690 (2005) 5591.
[65] S. Dastgir, K.S. Coleman, A.R. Cowley, M.L.H. Green, Organometallics 25 (2006) 300.
[66] G. Steiner, H. Kopacka, K.H. Ongania, K. Wurst, P. Preishuber-Pflugl, B. Bildstein, Eur. J. Inorg. Chem. (2005) 1325.
[67] G. Steiner, A. Krajete, H. Kopacka, K.H. Ongania, K. Wurst, P. Preishuber-Pflugl, B. Bildstein, Eur. J. Inorg. Chem. (2004) 2827.
[68] A. Neveling, G.R. Julius, S. Cronje, C. Esterhuysen, H.G. Raubenheimer, Dalton Trans. (2005) 181.
[69] M. Bortenschlager, M. Mayr, O. Nuyken, M.R. Buchmeiser, J. Mol. Catal. A: Chem. 233 (2005) 67.
[70] M. Bortenschlager, J. Schutz, D. von Preysing, O. Nuyken, W.A. Herrmann, R. Weberskirch, J. Organomet. Chem. 690 (2005) 6233.
[71] J. Schwarz, V.P.W. Bohm, M.G. Gardiner, M. Grosche, W.A. Herrmann, W. Hieringer, G. Raudaschl-Sieber, Chem. Eur. J. 6 (2000) 1773.
[72] M.T. Zarka, M. Bortenschlager, K. Wurst, O. Nuyken, R. Weberskirch, Organometallics 23 (2004) 4817.
[73] H. van Rensburg, R.P. Tooze, D.F. Foster, A.M.Z. Slawin, Inorg. Chem. 43 (2004) 2468.
[74] H. van Rensburg, R.P. Tooze, D.F. Foster, S. Otto, Inorg. Chem. 46 (2007) 1963.
[75] S.A. Llewellyn, M.L.H. Green, A.R. Cowley, Dalton Trans. (2006) 4164.
[76] P. Eilbracht, L. Barfacker, C. Buss, C. Hollmann, B.E. Kitsos-Rzychon, C.L. Kranemann, T. Rische, R. Roggenbuck, A. Schmidt, Chem. Rev. 99 (1999) 3329.
[77] T. Rische, K.S. Muller, P. Eilbracht, Tetrahedron 55 (1999) 9801.
[78] T. Rische, P. Eilbracht, Synthesis – Stuttgart (1997) 1331.
[79] J. Seayad, A. Tillack, C.G. Hartung, M. Beller, Adv. Synth. Catal. 344 (2002) 795.
[80] A. Seayad, M. Ahmed, H. Klein, R. Jackstell, T. Gross, M. Beller, Science 297 (2002) 1676.
[81] T. Gross, A.M. Seayad, M. Ahmad, M. Beller, Org. Lett. 4 (2002) 2055.
[82] M. Beller, C. Breindl, M. Eichberger, C.G. Hartung, J. Seayad, O.R. Thiel, A. Tillack, H. Trauthwein, Synlett (2002) 1579.
[83] M. Ahmed, A.M. Seayad, R. Jackstell, M. Beller, Angew. Chem., Int. Ed. 42 (2003) 5615.
[84] M. Ahmed, R. Jackstell, A.M. Seayad, H. Klein, M. Beller, Tetrahedron Lett. 45 (2004) 869.
[85] M. Beller, J. Seayad, A. Tillack, H. Jiao, Angew. Chem., Int. Ed. 43 (2004) 3368.
[86] L. Routaboul, C. Buch, H. Klein, R. Jackstell, M. Beller, Tetrahedron Lett. 46 (2005) 7401.
[87] A.M. Seayad, K. Selvakumar, M. Ahmed, M. Beller, Tetrahedron Lett. 44 (2003) 1679.
[88] M. Ahmed, C. Buch, L. Routaboul, R. Jackstell, H. Klein, A. Spannenberg, M. Beller, Chem. Eur. J. 13 (2007) 1594.
[89] M. Ahmed, A.M. Seayad, R. Jackstell, M. Beller, J. Am. Chem. Soc. 125 (2003) 10311.
[90] T. Mizoroki, M. Kioka, M. Suzuki, S. Sakatani, A. Okumura, K. Maruya, Bull. Chem. Soc. Jpn. 57 (1984) 577.
[91] V.V. Grushin, H. Alper, J. Am. Chem. Soc. 117 (1995) 4305.
[92] W. Magerlein, A.F. Indolese, M. Beller, J. Organomet. Chem. 641 (2002) 30.
[93] W. Magerlein, A.F. Indolese, M. Beller, Angew. Chem., Int. Ed. 40 (2001) 2856.
[94] M. Beller, W. Magerlein, A.F. Indolese, C. Fischer, Synthesis – Stuttgart (2001) 1098.
[95] A. Yamamoto, Bull. Chem. Soc. Jpn. 68 (1995) 433.
[96] V. Calo, R. Del Sole, A. Nacci, E. Schingaro, F. Scordari, Eur. J. Org. Chem. (2000) 869.
[97] V. Calo, P. Giannoccaro, A. Nacci, A. Monopoli, J. Organomet. Chem. 645 (2002) 152.
[98] T. Fukuyama, T. Inouye, I. Ryu, J. Organomet. Chem. 692 (2007) 685.
[99] W. Zawartka, A.M. Trzeciak, J.J. Ziolkowski, T. Lis, Z. Ciunik, J. Pernak, Adv. Synth. Catal. 348 (2006) 1689.
[100] A.F. Hegarty, L.J. Drennan, in: A.R. Katritzky, O. Meth-Cohn, C.W. Rees (Eds.), Comprehensive Organic Functional Group Transformations, Pergamon, Oxford, 1995, p. 499.
[101] D.J. Diaz, A.K. Darko, L. McElwee-White, Eur. J. Org. Chem. (2007) 4453.
[102] S.Z. Zheng, F.W. Li, J.M. Liu, C.G. Xia, Tetrahedron Lett. 48 (2007) 5883.
[103] S.Z. Zheng, X.G. Peng, J.M. Liu, W. Sun, C.G. Xia, Helv. Chim. Acta 90 (2007) 1471.
[104] D. Freitag, U. Grigo, P.R. Muller, W. Nouvertne, Encyclopedia of Polymer Science and Engineering, Wiley, New York, 1988.
[105] K. Okuyama, J. Sugiyama, R. Nagahata, M. Asai, M. Ueda, K. Takeuchi, J. Mol. Catal. A: Chem. 203 (2003) 21.
[106] K. Okuyama, J. Sugiyama, R. Nagahata, M. Asai, M. Ueda, K. Takeuchi, Macromolecules 36 (2003) 6953.
[107] K. Okuyam, J. Sugiyama, R. Nagahata, M. Asai, M. Ueda, K. Takeuchi, Green Chem. 5 (2003) 563.
[108] M.G. Gardiner, W.A. Herrmann, C.P. Reisinger, J. Schwarz, M. Spiegler, J. Organomet. Chem. 572 (1999) 239.
[109] W.A. Herrmann, J. Schwarz, M.G. Gardiner, M. Spiegler, J. Organomet. Chem. 575 (1999) 80.
[110] E. Drent, P.H.M. Budzelaar, Chem. Rev. 96 (1996) 663.
[111] J.C.C. Chen, I.J.B. Lin, Organometallics 19 (2000) 5113.
[112] M. Sparta, K.J. Borve, V.R. Jensen, J. Am. Chem. Soc. 129 (2007) 8487.

collected at 298 K. The reported results are referenced to SCE in MeCN and are uncorrected for junction potential. [*n*-Bu_4N][ClO_4] was used as supporting electrolyte.

2.3. Synthesis of [Ni(β-NaiEt)$_2$(NCS)$_2$] (**6b**)

In methanolic solution of $Ni(ClO_4)_2 \cdot 6H_2O$ (0.25 g, 0.68 mmol) (10 ml) solid ammonium thiocyanate (NH_4SCN) (1.04 g, 1.38 mmol) was added under stirring at 298 K. To this solution 1-ethyl-2-(naphthyl-β-azo)imidazole (β-NaiEt) (**2b**) (0.37 g, 1.48 mmol) in the same solvent (20 ml MeOH) was added dropwise. The resulting brown solution was stirred for 15 min. The solid product was separated from the solution. The orange crystalline products were collected, washed with aqueous methanol and finally with ether. It was dried in vacuo. Yield was 0.19 g (54%).

All other complexes were prepared by the same procedure. Crystalline products were obtained in the yield of 50–70%.

Elemental analysis data were as follows: [Ni(α-NaiMe)$_2$(N_3)$_2$], **3a**: $C_{28}H_{24}N_{14}Ni$: *Anal.* Calc.: C, 54.65; H, 3.94; N, 31.87. Found: C, 54.73; H, 3.90; N, 31.77%. [Ni(β-NaiMe)$_2$(N_3)$_2$], **3b**: $C_{28}H_{24}N_{14}Ni$: *Anal.* Calc.: C, 54.65; H, 3.94; N, 31.87. Found: C, 54.60; H, 4.01; N, 31.92%. [Ni(α-NaiEt)$_2$(N_3)$_2$], **4a**: $C_{30}H_{28}N_{14}Ni$: *Anal.* Calc.: C, 56.00; H, 4.38; N, 30.48. Found: C, 56.04; H, 4.44; N, 30.52%. [Ni(β-NaiEt)$_2$(N_3)$_2$], **4b**: $C_{30}H_{28}N_{14}Ni$: Calc: C, 56.00; H, 4.38; N, 30.48. Found: C, 56.07; H, 4.44; N, 30.40%. [Ni(α-NaiMe)$_2$(NCS)$_2$], **5a**: $C_{30}H_{24}N_{10}S_2Ni$: *Anal.* Calc: C, 55.65; H, 3.73; N, 21.63. Found: C,

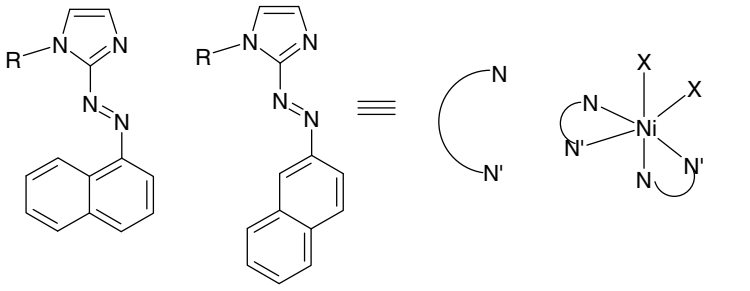

α-NaiR (**1**) β-NaiR (**2**) [Ni(NaiR)$_2$(X)$_2$] (**3**-**6**)

[Ni(α-Nai-Me)$_2$(N_3)$_2$], **3a**; [Ni(α-Nai-Et)$_2$(N_3)$_2$], **4a**; [Ni(β-Nai-Me)$_2$(N_3)$_2$], **3b**; [Ni(β-Nai-Et)$_2$(N_3)$_2$], **4b**; [Ni(α-Nai-Me)$_2$(NCS)$_2$], **5a**; [Ni(α-Nai-Et)$_2$(NCS)$_2$], **6a**; [Ni(β-Nai-Me)$_2$(NCS)$_2$], **5b**; [Ni(β-Nai-Et)$_2$(NCS)$_2$], **6b**

Scheme 1.

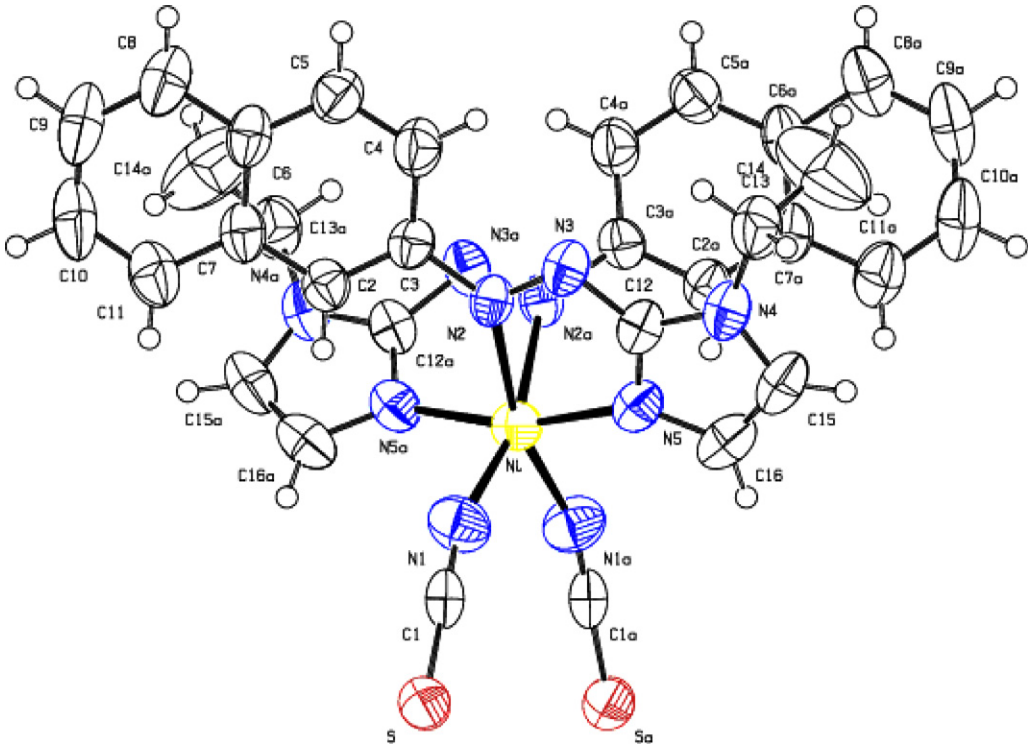

Fig. 1. ORTEP of *cis–cis–trans*-[Ni(β-NaiEt)$_2$(NCS)$_2$] (30% probability ellipsoid).

55.74; H, 3.70; N, 21.69%. [Ni(β-NaiMe)$_2$(NCS)$_2$], **5b**: $C_{30}H_{24}N_{10}S_2Ni$: *Anal.* Calc.: C, 55.65; H, 3.73; N, 21.63. Found: C, 55.72; H, 3.70; N, 21.57%. [Ni(α-NaiEt)$_2$(NCS)$_2$], **6a**: $C_{32}H_{28}N_{10}S_2Ni$: *Anal.* Calc.: C, 56.90; H, 4.17; N, 20.73. Found: C, 56.96; H, 4.23; N, 20.83%. [Ni(β-NaiEt)$_2$(NCS)$_2$], **6b**: $C_{32}H_{28}N_{10}S_2Ni$: *Anal.* Calc: C, 56.90; H, 4.17; N, 20.73. Found: C, 56.86; H, 4.22; N, 20.83%.

2.4. X-ray crystal structure analysis

X-ray quality red colored cubic crystals of [Ni(β-NaiEt)$_2$(NCS)$_2$] (**6b**) were isolated by diffusion of 2-methoxy-ethanol solution of the complex to methanol at room temperature. Data were collected (Table 1) with Siemens SMART CCD diffractometer using graphite-monochromatized Mo Kα radiation ($\lambda = 0.71073$ Å) at 293 (2) K. Unit cell parameters were determined from least-squares refinement of setting angles of 3810 reflections ($I > 2\sigma(I)$) out of 10336 collected data with 2θ in the range $3.88° \leqslant 2\theta \leqslant 56.64°$. A summary of the results were recorded using the ω scan technique in the *hkl* range of $-22 \leqslant h \leqslant 26$, $-18 \leqslant k \leqslant 18$, $-19 \leqslant l \leqslant 11$. Data were corrected for Lorentz polarization effects and for linear decay. Semi-empirical absorption corrections were applied using SADABS programme. The structure was solved by direct method and successive difference Fourier syntheses. All non-hydrogen atoms were refined anisotropically. The hydrogen atoms were fixed geometrically and refined using the riding model. In the final difference Fourier map the residual minima and maxima were −0.195 and 0.604 (e/Å^3) respectively, carried out using SHELXL-97. All calculations were carried out using SHELXL-97 [33], ORTEP-32 [34], PLATON-99 [35] programs.

3. Results and discussion

3.1. Synthesis and formulation

1-Methyl-2-(naphthyl-α-azo)imidazole (α-NaiMe, **1a**), 1-ethyl-2-(naphthyl-α-azo)imidazole (α-NaiEt, **2a**), 1-methyl-2-(naphthyl-β-azo)imidazole (β-NaiMe, **1b**), 1-ethyl-2-(naphthyl-β-azo)imidazole (β-NaiEt, **2b**) are used as bidentate N, N′ (where N and N′ refer to N(imidazole) and N(azo) centres) (Scheme 1). Pseudohalides, azide (N_3^-) and thiocyanate (SCN^-), are used to balance charge of the complexes. To methanolic solution of $Ni(ClO_4)_2 \cdot 6H_2O$ solid NaN_3 or NH_4NCS (2 equiv) was added under stirring at 298 K. To this solution α/β-NaiR in methanol in 1:2 mole ratio of Ni:ligand was added. Solution colour immediately turned to brown red and orange precipitate slowly separated from the solution. The product was isolated by filtration in the yield of >50%. The composition of the complex, [Ni(α/β-NaiR)$_2$(X)$_2$] (**3–6**) was supported by microanalytical data.

The complexes in this paper are non-electrolyte in MeCN solution. The are soluble in common organic solvents like $CHCl_3$, CH_2Cl_2. Bulk room temperature magnetic moment with correction incorporating Pascal's diamagnetic constant show two electron paramagnetic nature of Ni(II) ($\mu_{av} = 2.6–2.8$ B.M.) suggesting $t_{2g}^6e_g^2$ electronic configuration in octahedral geometry.

Table 1
Summarised crystallographic data for [Ni(β-NaiEt)$_2$(NCS)$_2$] (**6b**)

Empirical formula	$C_{32}H_{28}N_{10}S_2Ni$
Formula weight	675.47
Temperature (K)	295 (2)
Crystal system	monoclinic
Space group	*C*2/*c*
Crystal size (mm)^3	0. 25 × 0.20 × 0.20
Unit cell dimensions	
a (Å)	19.863(4)
b (Å)	13.847(3)
c (Å)	14.237(3)
β (°)	125.47(3)
V (Å)^3	3189.3(11)
Z	4
λ (Å)	0.71073
μ (Mo Kα) (mm^{-1})	0.780
D_{calc} (mg m^{-3})	1.407
Refine parameters	204
Reflection number total	10336
Reflection number get	3810
R_1[a] [$I > 2\sigma(I)$]	0.0522
wR_2[b]	0.0687
Goodness-of-fit	0.971

[a] $R = \sum|F_o - F_c|/\sum F_o$.
[b] $wR = [\sum w(F_o^2 - F_c^2)/\sum wF_o^4]^{1/2}$ $w = 1/[\sigma^2(F_o^2) + (0.0250P)^2]$ where $P = (F_o^2 + 2F_c^2)/3$.

Table 2
Bond distance and bond angle of [Ni(β-Nai-Et)$_2$(NCS)$_2$] (**6b**)

Bond distance	(Å)	Bond angle	(°)
Ni–N(1)	2.0181(19)	N(2)–Ni –N(1*)[a]	91.82(11)
Ni–N(2)	2.3109(15)	N(1)–Ni–N(2)	96.39(7)
Ni–N(5)	2.0401(17)	N(1)–Ni–N(5)	98.07(7)
N(1)–C(1)	1.149(2)	N(2)–Ni–N(5)	73.08(6)
N(2)–N(3)	1.2671(19)	N(2)–Ni–N(1*)[a]	164.78(6)
N(2)–C(3)	1.418(2)	N(5)–Ni–N(1*)[a]	93.13(7)
N(3)–C(12)	1.375(2)	N(5)–Ni–N(5*)[a]	163.89(9)
C(1)–S(1)	1.626(2)	N(5)–Ni–N(2)	94.26(6)
		N(2)–Ni–N(2*)[a]	78.68(7).

[a] Symmetry: $-x, y, 1/2 - z$.

3.2. Molecular structure of [Ni(β-Nai-Et)$_2$(NCS)$_2$] (**6b**)

The molecular structureof [Ni(β-Nai-Et)$_2$(NCS)$_2$] (**6b**) is shown in Fig. 1. In this molecule Ni(II) is surrounded by two β-Nai-Et and two thiocyanates. β-NaiEt serves as unsymmetric N,N′-chelat-

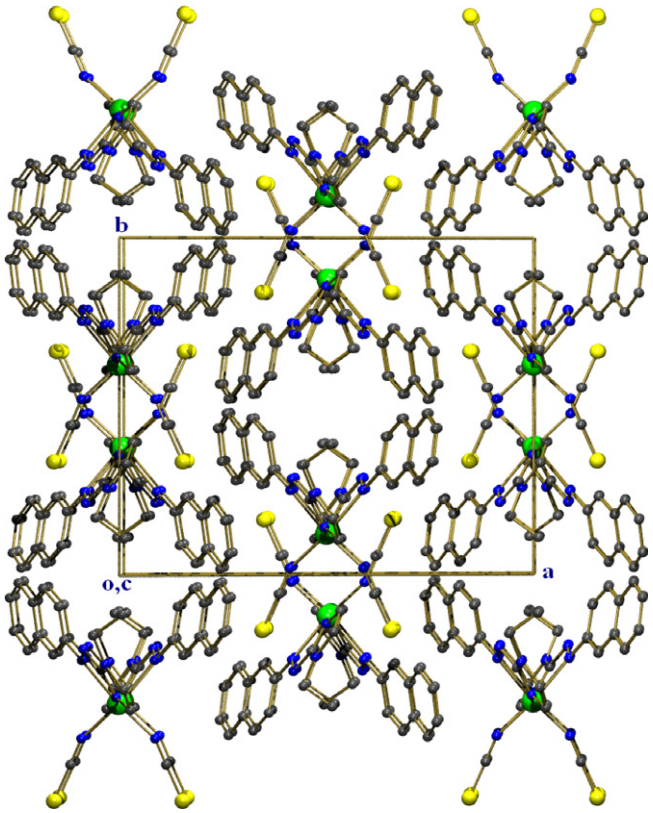

Fig. 2. Packing viewed along *c*-axis of [Ni(β-Nai-Et)$_2$(NCS)$_2$] (**6b**).

ing agent (N refers to imidazole-N and N/ refers to azo-N donor centres) and the coordination disposition of N and N/ has identified an arrangement of *trans*-N,N and *cis*-N/,N/ stereochemistry. Pseudooctahedral complexes of formula, $M(N,N^{/})_2X_2$ may exist in five stereoisomeric forms referring to sequence of the coordination pairs of X,X; N,N; N/, N/; the isomers are abbreviated as *trans–cis–cis* (*tcc*); *trans–trans–trans* (*ttt*); *cis–trans–trans* (*ctc*); *cis–cis–trans* (*cct*) and *cis–cis–cis* (*ccc*) (see Table 1).

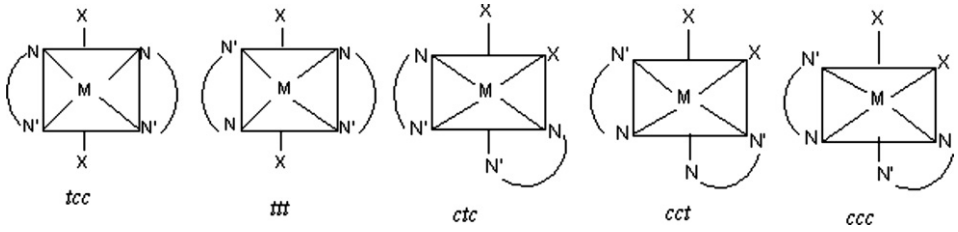

In these complexes NCS^- is N-donor ligand and two NCS^- coordinate in a *cis*-fashion around Ni(II). Thus, coordination sequence of thiocyanato-N, imidazole-N(N) and azo-N(N/) describe *cis–trans–cis* (ctc) stereochemical orientation [7–10]. Selected bond lengths and angles are given in Table 2. The N–Ni–N/ bond angles subtended by the chelating ligand is N(2)–Ni–N(5), 73.08(6)°. The deviation of the angle from ideal 90° for a regular octahedron is the result of steric requirements of the ligand [36–41]. Other angles in the chelated motif are also deviated in either direction from the regular five member ring. The pendant naphthyl ring makes dihedral 27.84(8)° with chelate plane. Out of N(imidazole), N(azo) and N(thiocyanato) donor centres the N(azo) requires considerably more space than other two types N-donors. The N(azo) is exocyclic N=N in a pendant naphthyl group; thus the van der Waals repulsion will be greater than N(imidazole) and thus N(azo) is more space demanding. The Ni–N(azo) distance, 2.3109(15) Å is less than that of the sum of the van der Waals radii of Ni(II) (1.63 Å) and N(azo) (1.55 Å) [42]. This implies covalent interaction of N(azo) and Ni(II).

In the equatorial plane the trans angle is 164.78(6)° [N(1*)–Ni–N(2)]. The large deviation (~15°) from 180° is undoubtedly from the combined contribution of short chelate angle and steric

Table 3
UV–Vis[a], IR spectral and cyclic voltammetric data

Compound	UV–Vis spectral data (λ_{max}/nm) (10^{-3} ε M^{-1} cm^{-1})	IR data (KBr disk), cm^{-1}			Cyclic voltammetric data[b] V (ΔEp, mV)		
		(N_3)/(NCS)	(C=N)	(N=N)	E_M	E_L^I	E_L^{II}
[Ni(α-Nai-Me)$_2$(N_3)$_2$] (**3a**)	396(2.00), 417 (1.99), 445 (1.63), 635 (0.19), 713 (0.13)	2061	1585	1424	0.34	−0.44 (130)	−1.05 (160)
[Ni(α-Nai-Et)$_2$(N_3)$_2$] (**4a**)	391(2.23), 420 (1.66), 442 (2.32), 633 (0.13), 712 (0.09)	2063	1580	1431	0.30	−0.47 (140)	−1.12 (200)
[Ni(β-Nai-Me)$_2$(N_3)$_2$] (**3b**)	389 (3.42), 424 (3.47), 447 (2.88), 630 (0.14), 715 (0.07)	2058	1590	1420	0.37	−0.41 (130)	−1.04 (170)
[Ni(β-Nai-Et)$_2$(N_3)$_2$] (**4b**)	393 (3.02), 419 (2.17), 439 (1.49), 637 (0.20), 718 (0.06)	2060	1583	1430	0.34	−0.45 (130)	−1.05 (150)
[Ni(α-Nai-Me)$_2$(NCS)$_2$] (**5a**)	352 (2.08), 395 (1.88), 446 (1.96), 647 (0.12), 730 (0.07)	2082	1590	1415	0.40	−0.40 (120)	−1.24 (140)
[Ni(α-Nai-Et)$_2$(NCS)$_2$] (**5b**)	356 (0.81), 397 (2.03), 439 (0.74), 641 (0.17), 733 (0.04)	2093	1595	1428	0.35	−0.55 (140)	−1.20 (210)
[Ni(β-Nai-Me)$_2$(NCS)$_2$] (**6a**)	358 (1.45), 409 (2.78), 433 (2.77), 637 (0.18), 732 (0.09)	2091	1580	1432	0.30	−0.48 (120)	−1.16 (140)
[Ni(β-Nai-Et)$_2$(NCS)$_2$] (**6b**)	362 (1.23), 401 (2.82), 438 (2.68), 627 (0.11), 728 (0.05)	2090	1587	1429	0.36	−0.56 (130)	−1.25 (180)

[a] Solvent: acetonitrile (MeCN).
[b] Solvent: acetonitrile (MeCN), Pt-disk working electrode, reference SCE, supporting electrolyte [nBu$_4$N][ClO_4], $E_{1/2}$ = 0.5(Ep_a + Ep_c), V; ΔEp = | Ep_a − Ep_c|, mV; Ep_a = anodic peak potential, Ep_c = cathodic peak potential; E_M = Ni(III)/Ni(II) anodic peak (Ep_a), E_L = ligand reductions.

HOMO	HOMO-1	LUMO	LUMO+1
Energy (eV): -3.96 Ni, 4 %; β-Nai-Et 1%; NCS, 95 %	Energy (eV): -4.19 Ni, 1 %; β-Nai-Et, 1 %; NCS, 98 %	Energy (eV): -3.52 Ni, 3 %; β-Nai-Et, 95 %; NCS, 2 %	Energy (eV): -3.42; β-Nai-Et -98 %; NCS, 2 %

Scheme 2. Composition and drawing of HOMO, HOMO − 1, LUMO and LUMO + 1 of [Ni(β-Nai-Et)$_2$(NCS)$_2$] (**6b**).

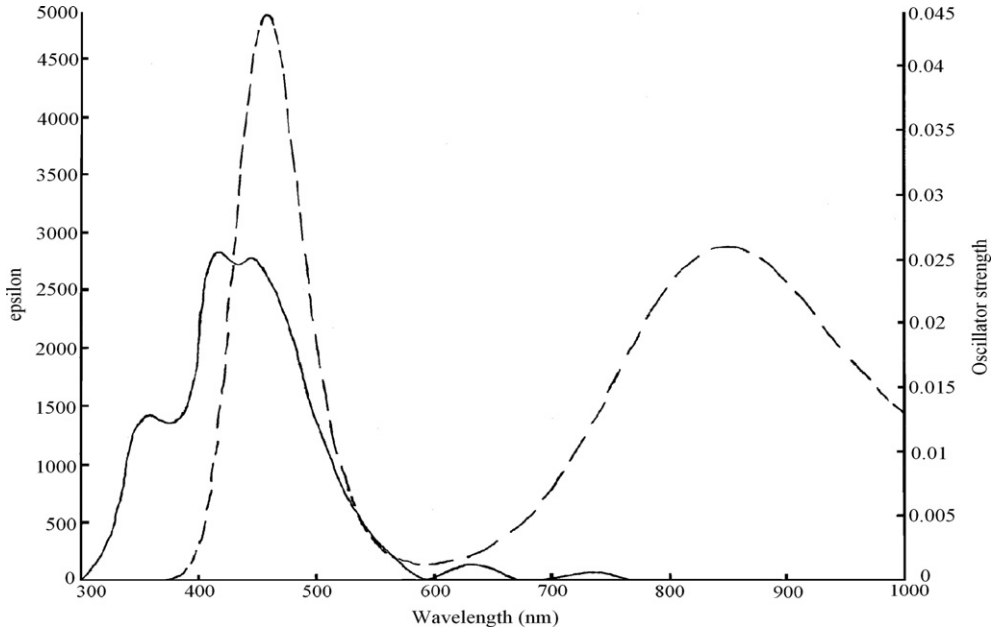

Fig. 3. UV–Vis spectra of [Ni(β-Nai-Et)$_2$(NCS)$_2$] (**6b**) in MeCN (—) and theoretically calculated (DFT) transitions (---) in gas phase.

requirement of azo-N centres. The azo, N=N, distances is 1.2671(19) Å which is longer than the free ligand value (1.250(1) Å) [18]. A small extension of azo bond may come from the structural strain arises out of small chelate bite angle and steric requirement of the chelated azoimine fragment. Packing viewed along *c*-axis (or along *a*- or *b*-axes) does not show any reasonable noncovalent interaction; however, the packing shows proper disposition of naphthyl groups so that they may have a trend of noncovalent interaction. Packing structure along *c*-axis is shown in Fig. 2.

3.3. Spectral studies

[Ni(α/β-Nai-R)$_2$(N$_3$)$_2$] show characteristic strong transmission at 2118–2042 cm^{-1} along with a weak band at 2045–2047 cm^{-1} in infrared spectra. These are corresponding to $\nu_{asym}(N_3)$. This supports mononuclear mono-dentate N_3^- bonding in **3** and **4**. The [Ni(α/β-Nai-R)$_2$(NCS)$_2$] (**5** and **6**) complexes show band at 2098–2105 cm^{-1} along with a weak band at 2090–2093 which correspond to ν(CN) of bounded NCS. Medium to strong bands observe at 760–770 and 680–695 cm^{-1} have been assigned to ν(CS) for [Ni(α/β-NaiR)$_2$(NCS)$_2$]. The chelated ligand α/β-Nai-R shows characteristic transmission at 1600–1200 cm^{-1}. Moderately intense stretching at 1585–1600 and 1435–1440 cm^{-1} are due to ν(C=N) and ν(N=N), respectively.

The absorption spectrum of free ligands show characteristics structured absorption band around 350–370 nm with a molar absorption coefficient on the order of 10^4 M^{-1} cm^{-1} and a tail extending into 400–420 nm. The large absorption band around below 400 nm corresponds to $\pi \rightarrow \pi^*$ transitions, while the tail corresponds to $n \rightarrow \pi^*$ transition [18]. These bands suffer marginal shifts to longer wavelength region on complexation. The solution spectra were recorded in MeCN and data are listed in Table 3. Intense band ($(\varepsilon \sim 10^4$ dm^3 mol^{-1} cm^{-1}) appear in the range 430–445 nm may be assigned to $d\pi(Ni) \rightarrow \pi^*$ (ligand) charge transfer transitions. Two broad bands at longer wavelengths (710–730 and 620–650 nm) are observed and the molar extinction coefficient data warrant to consider them not only d–d bands rather admixture of d–d and MLCT transitions. The azoimine (–N=N–C=N–) function is π-acidic enough to insist such MLCT transitions. The assignment is also supported by theoretical calculations [18]. DFT analyses show that HOMO, HOMO − 1 of [Ni(β-Nai-Et)$_2$(NCS)$_2$] (**6b**) have small contribution from Ni (Scheme 2) (HOMO, 4% (Ni); HOMO-1, 1% (Ni)) and also the LUMO (3% Ni) and LUMO + 1 (nil, Ni) while HOMO, HOMO-1 bear ⩾95% contribution from NCS group. β-Nai-Et dominates (⩾95%) in LUMO and LUMO+1. The calculated transitions are (wavelength λ, nm and oscillator strength, $f \times 10^3$), (% contribution) recommended transition (assignment): (855 (0.0367), (46%) H-3 → L + 2 (XLCT); 509 (0.0046), (62%) H-6 → LUMO (MLCT).; 461 (0.0444), (20%) H-7 → L + 1, (61%) H-5 → LUMO (LLCT) (where XLCT: NCS to β-Nai-Et charge transfer; MLCT: Ni(II) to β-Nai-Et charge transfer; LLCT: β-Nai-Et to β-Nai-Et charge transfer). A plot of oscillator strength (*f*) *versus wavelength* (λ) is given in Fig. 3. The correlation between theoretical and experimental spectra exhibit widely different transition region which may be due to influence of solvent polarity on the stabilization of polar ground and excited states. Calculation is carried out in gas phase while spectra are recorded in MeCN solution. We cannot perform calculation using solvent system due to some infrastructural problem with computational facilities.

3.4. Cyclic voltammetry

During voltammetric study the anodic current increases progressively above 0.5 V and ill-defined anodic response is observed in the potential range 0.3–0.4 V but no cathodic counterpart is observed on scan reversal. The anodic response may be assigned to unstable oxidized Ni(III) species [43,44]. Redox couples negative to SCE are reductive in nature and have been assigned to reductions of chelated azo-ligand. Arylazoheterocycles accommodate two electrons at LUMO which is mostly azo in character: [–N=N]/[–N⁻⁻⁻⁻N–]$^-$ and [–N⁻⁻⁻⁻N]$^-$/[–N–N–]$^{2-}$. Voltammetric data are set out in Table 3 and a representative figure is shown in Fig. 4. The DFT calculation suggests 95% contribution of β-Nai-Et to LUMO and thus the reduction is explained as electron feeding into the azo-dominated LUMO. We find that the HOMO has 4% from Ni and 95% from thiocyanate group. It is not expected that the oxidation of coordinated NCS at 0.3–0.4 V [45] and Ni(II) → Ni(III) oxidation is recommended.

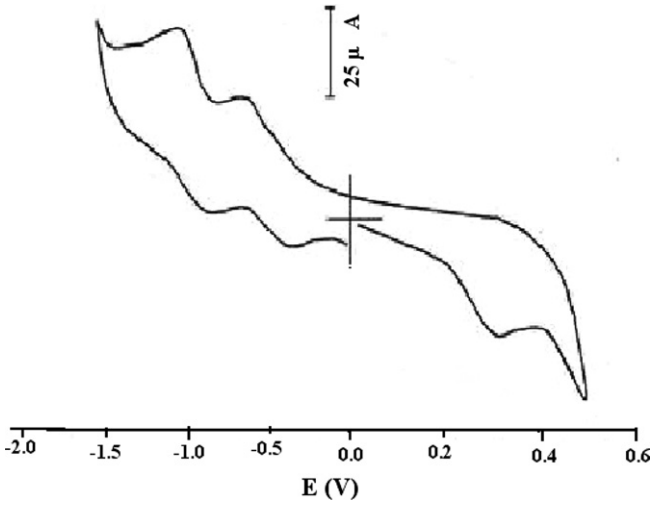

Fig. 4. Cyclic voltammogram of [Ni(β-Nai-Et)$_2$(SCN)$_2$] (**6b**) in MeCN using Pt working electrode, SCE reference and [nBu$_4$N][ClO$_4$] supporting electrolyte.

4. Conclusion

Ni(β-NaiR)$_2$(X)$_2$ (X = N$_3$, NCS) complexes are reported in this work. The structure supports this composition. Distorted octahedral geometry supports mixed electronic transition of MLCT, LLCT, XLCT type. Electrochemistry of the complexes show irreversible Ni(III)/Ni(II) response with azo reduction of coordinated azoimine function. The electronic configuration, spectra and redox property have been attempted to explain by DFT calculation.

Acknowledgements

Financial support from University Grants Commission, New Delhi is gratefully acknowledged.

Appendix A. Supplementary data

CCDC 654277 contains the supplementary crystallographic data for [Ni(β-Nai-Et)$_2$(SCN)$_2$] (**6b**). These data can be obtained free of charge via http://www.ccdc.cam.ac.uk/conts/retrieving.html, or from the Cambridge Crystallographic Data Centre, 12 Union Road, Cambridge CB2 1EZ, UK; fax: (+44) 1223-336-033; or e-mail: deposit@ccdc.cam.ac.uk. Supplementary data associated with this article can be found, in the online version, at doi:10.1016/j.poly.2008.04.045.

References

[1] J. Reedijk, in: G. Wilkinson, R.D. Gillard, J.A. McCleverty (Eds.), Comprehensive Coordination Chemistry, vol. 2, Pergamon Press, Oxford, 1987.
[2] G.R. Newkome, A.R. Katritzky (Ed.), Comprehensive Heterocyclic Chemistry, vol. 3, 1984.
[3] A.R. Katritzky, C.W. Rees, A.J. Boulton, A. Mckillop (Eds.), Comprehensive Heterocyclic Chemistry, vol. 33, 1984, p. 57.
[4] F.A. Cotton, G. Wilkinson, Advanced Inorganic Chemistry, fifth ed., John Wiley & Sons, New York, 1988.
[5] W. Kaim, B. Schwederski, Bioinorganic Chemistry: Inorganic Elements in the Chemistry of Life, J. Wiley & Sons, Chichester-New York-Brisbane-Toronto-Singapore, 1994.
[6] S.J. Lippard, J.M. Berg, Principles of Bioinorganic Chemistry, University Science Books, Mill Valley, CA, 1994.
[7] T.K. Misra, D. Das, C. Sinha, P. Ghosh, C.K. Pal, Inorg. Chem. 37 (1998) 1672.
[8] P. Byabartta, J. Dinda, P.K. Santra, C. Sinha, K. Panneerselvam, F.–L. Liao, T.-H. Lu, J. Chem. Soc., Dalton Trans. (2001) 2825.
[9] P. Byabartta, Sk. Jasimuddin, B.K. Ghosh, C. Sinha, A.M.Z. Slawin, J.D. Woollins, New. J. Chem. 26 (2002) 1415.
[10] U.S. Ray, B.K. Ghosh, M. Monfort, J. Ribas, G. Mostafa, T. –H.T.-H. Lu, C. Sinha, Eur. J. Inorg. Chem. (2004) 250.
[11] S. Bhattacharya, I. Chakrabarty, B.K. Dirghangi, A. Chakravorty, Chem. Commun. (2000) 1813.
[12] M. Shivakumar, K. Pramanik, P. Ghosh, A. Chakravorty, Chem. Commun. (1998) 2103.
[13] M. Shivakumar, K. Pramanik, P. Ghosh, A. Chakravorty, Inorg. Chem. 39 (2000) 4332.
[14] M. Shivakumar, K. Pramanik, P. Ghosh, A. Chakravorty, Inorg. Chem. 37 (1998) 5968.
[15] P.K. Santra, P. Byabartta, S. Chattopadhyay, L.R. Falvello, C. Sinha, Eur. J. Inorg. Chem. (2002) 1124.
[16] S. Pal, D. Das, C. Sinha, C.H.L. Kennard, Inorg. Chim. Acta 313 (2001) 21.
[17] J. Dinda, D. Das, P.K. Santra, C. Sinha, L.R. Falvello, J. Organomet. Chem. 629 (2001) 28.
[18] J. Otsuki, K. Suwa, K. Narutaki, C. Sinha, I. Yoshikawa, K. Araki, J Phys. Chem. A 109 (2005) 8064.
[19] I. Chakraborty, S. Bhattacharya, S. Banergee, B.K. Dirghangi, A. Chakrovorty, J. Chem. Soc., Dalton Trans. (1999) 3747.
[20] I. Chakraborty, S. Sengupta, S. Das, S. Banerjee, A. Chakarvorty, J. Chem. Soc., Dalton Trans. (2003) 134.
[21] M.N. Ackermann, M.P. Robinson, I.A. Mather, E.B. LeBlanc, R.V. Raz, J. Organomet. Chem. 682 (2003) 248.
[22] M. Nakagawa, M. Rikukawa, M. Watanable, K. Sanui, N. Ogata, Bull. Chem. Soc. Jpn. 70 (1997) 737. and reference therein.
[23] J. Otsuki, K. Sato, M. Tsujino, N. Okuda, K. Araki, M. Seno, Chem. Lett. (1996) 847.
[24] V.W.-W. Yan, V.C.-Y. Lan, K. –K. Cheung, J. Chem. Soc., Chem. Commun. (1995) 259.
[25] V. Marvand, J.P. Launary, Inorg. Chem. 32 (1993) 1376.
[26] A. Das, J.P. Mather, J.A. Acclavery, J.A.N. Bodiola, M.D. Ward, J. Chem. Soc., Dalton Trans. (1993) 681.
[27] P.G. Lacroix, I. Malfant, G. Iftime, A. Razus, K. Naratani, J.A. Delaria, Chem. Eur. J. 6 (2000) 2599.
[28] J.S. Kong, H.T. Hong, D.H. Chy, Mol. Cryst. Liq. Cryst. Sci. Technol. 327A (1999) 1.
[29] D. Zanette, S.J. Frochnev, E. Minatti, A.A. Ruzza, Langmuir 13 (1997) 659.
[30] D.H. Gold, H.P. Gregar, J. Phys. Chem. 64 (1960) 1464.
[31] P. Chattopadhyay, C. Sinha, D.K. Pal, Fresnius J. Anal. Chem. 357 (1997) 368.
[32] A.I. Vogel, A Text Book of Practical Organic Chemistry, second ed., Longman, London, 1959.
[33] G.M. Sheldrick, Acta Crystallogr., Sect. A 64 (2008) 112.
[34] L.J. Farrugia, J. Appl. Crystallogr. 30 (1997) 565.
[35] A.L. Spek, PLATON, Molecular Geometry Program, University of Utrecht, The Netherlands, 1999.
[36] J. Dinda, S. Senapoti, T. Mondal, A.D. Jana, M. Chiang, T.-H. Lu, C. Sinha, Polyhedron 25 (2006) 1125.
[37] D. Banerjee, U.S. Ray, J.-S. Wu, T.-H. Lu, C. Sinha, Polyhedron 25 (2006) 3077.
[38] D. Das, J. Dinda, T. Mondal, K.K. Sarker, C. Sinha, J. Indian Chem. Soc. 83 (2006) 861.
[39] D. Banerjee, C. Sinha, Indian J. Chem. A 45A (2006) 2224.
[40] P. Bhunia, K.K. Sarker, C.-N. Lin, T.-H. Lu, C. Sinha, Indian J. Chem. 46A (2007) 576.
[41] D. Das, B.G. Chand, J.-S. Wu, T.-H. Lu, C. Sinha, J. Mol. Struct. 842 (2007) 17.
[42] A.G. Orpen, L. Brammer, F.H. Allen, O. Kennard, D.G. Waston, R. Taylor, J. Chem. Soc., Dalton Trans. SI (1999).
[43] S. Karmakar, S.B. Choudhury, D. Ray, A. Chakravorty, Polyhedron 12 (1993) 291.
[44] S. Mukhopadhyay, D. Ray, J. Chem. Soc., Dalton Trans. 265 (1995).
[45] N.K. Soni, M. Bhasin, P.D. Sharma, Oxid. Commun. 30 (2007) 641.

dinated by the incorporation of one methanol (solvent) molecule [7,10–12] in its coordination sphere or remains penta-coordinated [8,12] (where the coordination of the solvent molecule is inhibited probably due to steric repulsion between the methyl group attached to the carbonyl carbon instead of a hydrogen atom in the aryloxy ring of the hydrazone ligand and the OH group of the solvent alcohol).

Such an observation indicates that there should be ligands of intermediate basicity, which would be able to form both the penta-coordinated monomeric and the hexa-coordinated methoxy-bridged dimeric complexes. For this purpose, a family of tridentate ligands with varying basicity will be ideal and on this ground, the hydrazone ligands derived from the condensation of aliphatic/aromatic acid hydrazide with aromatic 2-hydroxycarbonyl compound containing a substitution in the aromatic ring may be suitable, where, the basic property of the ligands can be finely tuned through the incorporation of suitable substituent. With a view to searching for suitable ligand(s) of borderline basicity, we have chosen the benzoyl hydrazones of 2-hydroxyacetophenone and its 5-substituted derivatives (H_2L^{1-4}, general abbreviation H_2L, Scheme 1) for this study. There are two reasons behind the selection of this family of ligands: (i) these hydrazone ligands contain two intermediate basic phenolic and amide (which binds through their enol forms) groups, which are very suitable for the stabilization of +V state of vanadium [13–15] and (ii) due to presence of one methyl group with the carbonyl carbon (in stead of hydrogen in 2-hydroxybenzaldehyde), the coordination of solvent molecule is inhibited for steric reason. Utilizing this family of ligands we have been able to identify three suitable hydrazone ligands which are able to form both the methoxy bonded monomeric complexes and their dimethoxy-bridged dimeric analogues, which, to the best of our knowledge, represent the first report in this area. We also report the procedure for the transformation of these complexes to the corresponding complexes with $V_2O_3^{4+}$ and VO_2^+ motifs, which is important in connection with their catalytic activities. Such type of oxidovanadium(V)–alkoxide complexes are important due to their biological relevance [16] and also for their catalytic activities [17,18].

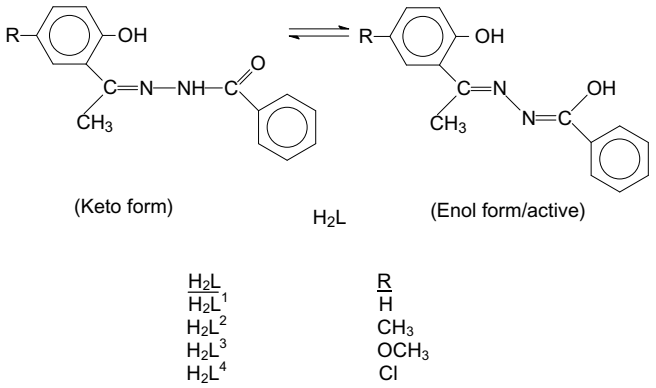

H_2L	R
H_2L^1	H
H_2L^2	CH_3
H_2L^3	OCH_3
H_2L^4	Cl

Scheme 1.

2. Experimental

2.1. Materials

$[V^{IV}O(acac)_2]$ [19] and the hydrazone ligands (H_2L^{1-4}) [20] (Scheme 1) were prepared by the reported methods. Reagent grade solvents were dried and distilled prior to use. All other chemicals were reagent grade, obtained from commercial sources and used without further purification. Spectroscopic grade solvents were used for spectral measurements.

2.2. Synthesis of the complexes $[VO(L)(OCH_3)]$, (**1**)–(**4**)

All these complexes except **3** were synthesized by a simple general method using $[V^{IV}O(acac)_2]$ (where $acac^-$ represents the acetyl acetonate ion) as the starting material (Scheme 2).

2.2.1. $[VO(L^1)(OCH_3)]$ (**1**)

A total of 0.254 g (1.0 mmol) of H_2L^1 was dissolved in 30 ml of methanol and 0.265 g (1.0 mmol) of $[V^{IV}O(acac)_2]$ was added to the ligand solution. The mixture was then heated under reflux for 2 h. A reddish brown solution was obtained which was kept

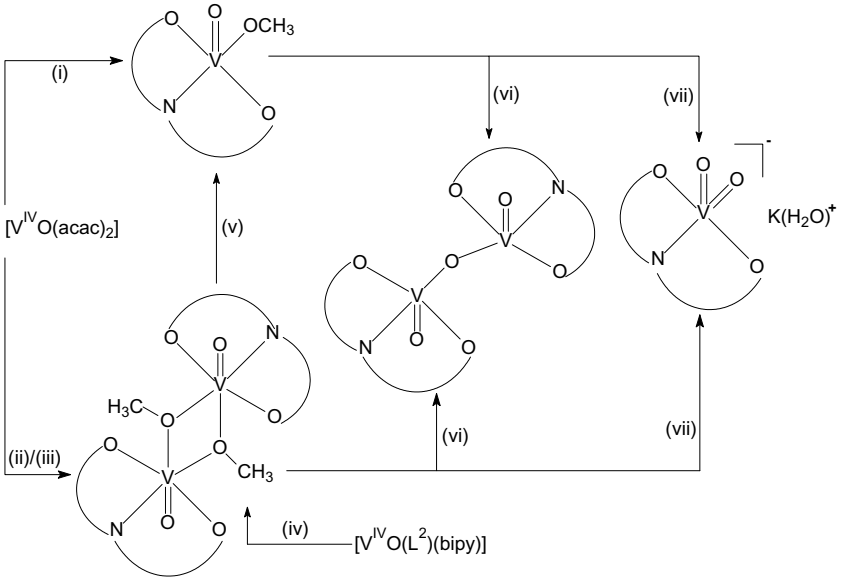

Scheme 2. (i) Heated under reflux in methanol with one equivalent H_2L^1 or H_2L^2 or H_2L^4; (ii) on heating under reflux in methanol with one equivalent H_2L^3; (iii) on heating under reflux in methanol with one equivalent H_2L^1 in presence of half-equivalent 4,4′-bipyridine; (iv) on keeping its methanol solution for ~7 days; (v) heated under reflux with the excess amount of imidazole in methanol; (vi) on heating under reflux in acetone; (vii) on reaction with the methanolic solution of KOH at slightly warm condition.

for slow evaporation at room temperature. Shiny black crystalline compound, suitable for X-ray diffraction analysis were obtained after one week. Yield: 0.30 g (86%). *Anal.* Calc. for $C_{16}H_{15}N_2O_4V$: C, 54.82; H, 4.28; N, 7.99. Found: C, 54.79; H, 4.25; N, 7.97%. Selected IR data (cm^{-1}): ν = 1590 (s, C=$N_{azomethine}$); 1238 (s, C–$O_{enolate}$); 1041 (m, N–N); 992 (s, V=O). ^1H NMR (300 MHz; $CDCl_3$): δ = 7.28–7.32 (m, 2H, H-3, H-13); 7.36 (dd, 1H, H-4, J = 8.4, 0.8 Hz); 7.16–7.21 (m, 1H, H-5); 7.75 (dd, 1H, H-6, J = 8.2, 0.8 Hz); 2.26 (s, 3H, 3 × H-8); 7.66 (dd, 2H, H-11, H-15, J = 7.9, 1.0 Hz); 7.05 (t, 2H, H-12, H-14, J = 7.8 Hz); 3.49 (s, 3H, 3 × H-16) ppm. λ_{max} (ε, $dm^3\ mol^{-1}\ cm^{-1}$) = 384^{sh} nm (10845), 323 nm (26228).

2.2.2. $[VO(L^2)(OCH_3)]$ (**2**)

Compound **2** was also prepared analogously to **1** and was obtained as shiny black crystalline solid (suitable for X-ray diffraction analysis). Yield: 0.30 g (82%). *Anal.* Calc. for $C_{17}H_{17}N_2O_4V$: C, 56.00; H, 4.67; N, 7.69. Found: C, 55.97; H, 4,64; N, 7.68%. Selected IR data (cm^{-1}): ν = 1585 (s, C=$N_{azomethine}$); 1237 (s, C–$O_{enolate}$); 1031 (m, N–N); 1000 (s, V=O). ^1H NMR (300 MHz; $CDCl_3$): δ = 7.25 (d, 1H, H-3, J = 8.3 Hz); 7.50 (dd, 1H, H-4, J = 8.3, 0.8 Hz); 7.52 (d, 1H, H-6, J = 0.8 Hz); 2.26 (s, 3H, 3 × H-8); 7.65 (dd, 2H, H-11, H-15, J = 7.6, 0.7 Hz); 7.06 (dt, 2H, H-12, H-14, J = 7.6, 7.4 Hz); 7.32 (dt, 1H, H-13, J = 7.4, 0.8 Hz); 3.49 (s, 3H, 3 × H-16); 2.46 (s, 3H, 3 × H-17) ppm. λ_{max} (ε, $dm^3\ mol^{-1}\ cm^{-1}$) = 380^{sh} nm (10523), 323 nm (19636).

2.2.3. $[VO(L^3)(OCH_3)]$ (**3**)

Compound **3** was obtained as shiny black crystalline solid (suitable for X-ray diffraction analysis) by the reaction with **3A** (vide infra) with an excess (~3 times) amount of imidazole in methanol. A total of 0.200 g of $[V^{V}O(L^3)(OCH_3)]_2$ **(3A)** and 0.05 g of imidazole were dissolved in 40 ml methanol on warming. The resulting mixture was heated under reflux for ½ h and then kept for slow evaporation at room temperature. A shiny black crystalline compound was obtained after 3 days. Yield: 0.18 g (90%). *Anal.* Calc. for $C_{17}H_{17}N_2O_5V$: C, 53.68; H, 4.47; N, 7.37. Found: C, 53.63; H, 4.45; N, 7.36%. Selected IR data (cm^{-1}): ν = 1588 (s, C=$N_{azomethine}$); 1228 (s, C–$O_{enolate}$); 1034 (m, N–N); 995 (s, V=O). ^1H NMR (300 MHz; $CDCl_3$): δ = 7.30–7.33 (m, 3H, H-3, H-4, H-13); 7.19 (d, 1H, H-6, J = 0.7 Hz); 2.26 (s, 3H, 3 × H-8); 7.65 (dd, 2H, H-11, H-15, J = 7.3, 0.5 Hz); 7.07 (dt, 2H, H-12, H-14, J = 7.3, 7.7 Hz); 3.49 (s, 3H, 3 × H-16); 3.91 (s, 3H, 3 × H-17) ppm. λ_{max} (ε, $dm^3\ mol^{-1}\ cm^{-1}$) = 378^{sh} nm (14766), 324 nm (26502).

2.2.4. $[VO(L^4)(OCH_3)]$ (**4**)

Compound **4** was obtained as microcrystalline shiny black solid by using a protocol very similar to that for **1**. Yield: 0.35 g (91%). *Anal.* Calc. for $C_{16}H_{14}N_2O_4ClV$: C, 49.93; H, 3.64; N, 7.28. Found: C, 49.90; H, 3.61; N, 7.26%. Selected IR data (cm^{-1}): ν = 1580 (s, C=$N_{azomethine}$); 1236 (s, C–$O_{enolate}$); 1025 (m, N–N); 997 (s, V=O). ^1H NMR (300 MHz; $CDCl_3$): δ = 7.31 (d, 1H, H-3, J = 8.9 Hz); 7.44 (dd, 1H, H-4, J = 8.9, 1.5 Hz); 7.70 (d, 1H, H-6, J = 1.5 Hz); 2.25 (s, 3H, 3 × H-8); 7.64 (dd, 2H, H-11, H-15, J = 7.4, 0.6 Hz); 7.10 (dt, 2H, H-12, H-14, J = 7.4 Hz); 7.37 (dt, 1H, H-13, 7.4, 7.2 Hz); 3.49 (s, 3 × H-16) ppm. λ_{max} (ε, $dm^3\ mol^{-1}\ cm^{-1}$) = 388^{sh} nm (6465), 321 nm (15043).

2.3. Synthesis of the complexes $[VO(L)(OCH_3)]_2$, (**1A**)–(**3A**)

2.3.1. $[VO(L^1)(OCH_3)]_2$ (**1A**)

A total of 0.254 g (1.0 mmol) of H_2L^1 and 0.08 g (~0.5 mmol) of 4,4′-bipyridine were dissolved in 30 ml of methanol and 0.265 g (1.0 mmol) of $[V^{IV}O(acac)_2]$ was added to this solution. The mixture was then heated under reflux for 2 h. A reddish brown solution was obtained which was kept for slow evaporation at room temperature. Shiny black crystalline compound, suitable for X-ray diffraction analysis were obtained after one week. Yield: 0.32 g (91%). *Anal.* Calc. for $C_{16}H_{15}N_2O_4V$: C, 54.82; H, 4.28; N, 7.99. Found: C, 54.79; H, 4.25; N, 7.97%. Selected IR data (cm^{-1}): ν = 1597 (s, C=$N_{azomethine}$); 1244 (s, C–$O_{enolate}$); 1040 (m, N–N); 982 (s, V=O). ^1H NMR (300 MHz; $CDCl_3$): δ = 7.28–7.37 (m, 2H, H-3, H-13); 7.45 (dd, 1H, H-4, J = 7.6, 1.0 Hz); 7.15–7.22 (m, 1H, H-5); 7.90 (dd, 1H, H-6, J = 8.1, 0.9 Hz); 2.26 (s, 3H, 3 × H-8); 7.73 (dd, 2H, H-11, H-15, J = 8.2, 0.9 Hz); 7.04 (t, 2H, H-12, H-14, J = 7.6 Hz); 3.48 (s, 3H, 3 × H-16); 5.20 (s, 3H, 3 × H-16(bridged)) ppm. λ_{max} (ε, $dm^3\ mol^{-1}\ cm^{-1}$) = 381^{sh} nm (11550), 323 nm (28240).

2.3.2. $[VO(L^2)(OCH_3)]_2$ (**2A**)

0.100 g of $[V^{IV}O(L^2)(bipy)]$ [21] was dissolved in 40 ml methanol on warming. The resulting orange red solution was kept at room temperature for slow evaporation. A black crystalline compound of **2A** (suitable for X-ray diffraction analysis) was obtained after 7 days. Yield: 0.063 g (85%). *Anal.* Calc. for $C_{34}H_{34}N_4O_8V_2$: C, 56.00; H, 4.67; N, 7.69. Found: C, 55.96; H, 4.64; N, 7.67%. Selected IR data (cm^{-1}): ν = 1582 (s, C=$N_{azomethine}$); 1239 (s, C–$O_{enolate}$); 1026 (m, N–N); 976 (s, V=O). ^1H NMR (300 MHz; $CDCl_3$): δ = 7.24 (d, 1H, H-3, J = 8.1 Hz), 7.39 (dd, 1H, H-4, J = 8.1, 0.7 Hz), 7.51 (d, 1H, H-6, J = 0.7 Hz), 2.25 (s, 3H, 3 × H-8), 7.64 (dd, 2H, H-11, H-15, J = 7.6, 1.0 Hz), 7.05 (dt, 2H, H-12, H-14, J = 7.6, 7.3 Hz), 7.31 (dt, 1H, H-13, J = 7.3, 1.0 Hz), 3.48 (s, 3H, 3 × H-16), 5.18 (s, 3H, 3 × H-16(bridged)), 2.45 (s, 3H, 3 × H-17) ppm. λ_{max} (ε, $dm^3\ mol^{-1}\ cm^{-1}$) = 378^{sh} nm (25115), 324 nm (46476).

2.3.3. $[VO(L^3)(OCH_3)]_2$ (**3A**)

Compound **3A** was also obtained as shiny black crystalline solid (suitable for X-ray diffraction analysis) by using the same method as that of **1**. Yield: 0.33 g (87%). *Anal.* Calc. for $C_{34}H_{34}N_4O_{10}V_2$: C, 53.68; H, 4.47; N, 7.37. Found: C, 53.64; H, 4.44; N, 7.36%. Selected IR data (cm^{-1}): ν = 1588 (s, C=$N_{azomethine}$); 1235 (s, C–O_{enolic}), 1032 (m, N–N), 974 (s, V=O). ^1H NMR (300 MHz; $CDCl_3$): δ = 7.12–7.20 (m, 2H, H-3, H-4); 7.28 (d, 1H, H-6, J = 0.8 Hz); 2.25 (s, 3H, 3 × H-8); 7.65 (dd, 2H, H-11, H-15, J = 7.5, 0.6 Hz); 7.06 (dt, 2H, H-12, H-14, J = 7.5, 7.4 Hz); 7.47 (dt, 1H, H-13, J = 7.4, 0.6 Hz); 3.47 (s, 3H, 3 × H-16); 5.18 (s, 3H, 3 × H-16(bridged)); 3.88 (s, 3H, 3 × H-17) ppm. λ_{max} (ε, $dm^3\ mol^{-1}\ cm^{-1}$) = 376^{sh} nm (23272), 325 nm (41066).

2.4. Conversion of these VO^{3+} complexes to the complexes with $V_2O_2^{4+}$ motif

The conversion of these VO^{3+} complexes to the complexes with $V_2O_3^{4+}$ motif can be done by a simple general method and for this reason only one representative method is described here.

2.4.1. Conversion to $[V_2O_3(L^1)_2]$

0.100 g of $[VO(L^1)(OCH_3)]$ (**1**) was dissolved in 40 ml acetone on warming. The solution was then heated under reflux for 2 h and the resulting red-brown solution was then kept for slow evaporation at room temperature. A deep brown microcrystalline compound was obtained. Yield: 89%. This compound was found to be identical in all respects with the $[V_2O_3(L^1)_2]$ complex reported earlier [15].

2.5. Conversion of these VO^{3+} complexes to the complexes with VO_2^+ motif

This conversion has also been done by a simple general method. So, one representative method is described here.

2.5.1. Conversion to $K^+(H_2O)[VO_2(L^1)]^-$

To a methanol solution (30 ml) of KOH (0.025 g), a total of 0.150 g of $[VO(L^1)(OCH_3)]$ (**1**) was added and dissolved on warming. The reddish-yellow solution was then stirred at room temperature for 2 h and the resulting solution was then kept for slow evaporation at room temperature. A yellow crystalline compound was obtained. Yield: 72%. This compound was found to be identical in all respects with the $K^+(H_2O)[VO_2(L^1)]^-$ complex reported earlier [15].

2.6. Physical measurements

Elemental analyses were performed on a Perkin-Elmer 2400 CHNS/O analyzer. Electronic spectra (in CH_2Cl_2) were recorded on a Hitachi U-3501 spectrophotometer and IR spectra (as KBr pellets) were taken on a Perkin-Elmer 782 spectrophotometer. The ^1H NMR spectra were recorded in $CDCl_3$ on a Bruker AM 300L (300 MHz) superconducting FT NMR spectrophotometer. Electrochemical measurements were performed at 298 K in CH_2Cl_2 solution for *ca.* 10^{-3} M using Et_4NClO_4 as supporting electrolyte under a dry N_2 atmosphere on a PC controlled PAR model 273 A electrochemistry system. A Pt disk, a Pt wire auxiliary electrode and an aqueous saturated calomel electrode (SCE) were used in a three-electrode configuration. All the potential values reported here are uncorrected for junction contribution. The ferrocene/ferrocinium (Fc/Fc^+) couple was used as the internal standard.

2.7. Crystallographic data collection and refinement

Data were measured with Mo Kα radiation at 150 K using the Oxford Diffraction X-Calibur CCD System. Data analysis was carried out with the Crysalis [22] program and the structures were solved with the SHELXS97 program [23]. For all six structures, the non-hydrogen atoms were refined with anisotropic thermal parameters. The hydrogen atoms bonded to carbon were included in geometric positions and given thermal parameters equivalent to 1.2 times those of the atom to which they were attached. Absorption corrections were carried out with the ABSPACK program [24]. The structures were refined on F^2 using SHELXL-97 program [23] and molecular graphics were computed using PLATON [25]. Crystallographic data are given in Tables 1 and 2. The somewhat high R values obtained, particularly for structure **1A**, from the refinements are due to the poor quality of the crystals and resulting diffraction data.

3. Results and discussion

3.1. Synthesis of methoxy bonded monomeric and methoxy-bridged dimeric VO^{3+}-hydrazone complexes and their conversion into the complexes with $V_2O_3^{4+}$ and VO_2^+ motifs

In the attempt to prepare the methoxy bonded mixed-ligand oxidovanadium(V)-hydrazone complexes of the type $[V^VO(L)(OCH_3)]$ [where L^{2-} is the general abbreviation of the deprotonated form of tridentate dinegative hydrazone ligands (H_2L^{1-4}) derived from the condensation of benzoyl hydrazine with 2-hydroxyacetophenone and its five-substituted derivatives] led to an interesting observation which encouraged us to make a systematic study on the role of ligands' basicity (as the steric factor is almost constant) regarding the structure of these complexes. It was found that the methanol solution of $[V^{IV}O(acac)_2]$ on reaction with H_2L^1, H_2L^2 (containing an electron donor methyl group at the 5-position of the aryloxy ring with σ (Hammett parameter [26]) = −0.17) and H_2L^4 (containing an electron withdrawing chlorine atom at the 5-position with σ = +0.23) produced only the monomeric complexes $[V^VO(L^1)(OCH_3)]$ (**1**), $[V^VO(L^2)(OCH_3)]$ (**2**) and $[V^VO(L^4)(OCH_3)]$ (**4**), respectively, while the similar reaction with H_2L^3 (containing a relatively stronger electron donor OCH_3 group at the 5-position with σ = −0.27) ligand yielded only the dimethoxy-bridged dimeric $[V^VO(L^3)(OCH_3)]_2$ (**3A**) complex. Such observations suggest that the basicity of H_2L^1 and H_2L^2 ligands should be of borderline nature and they should also form the dimethoxy-bridged dimeric analogue of, respectively, **1** and **2** and ultimately we have been able to synthesize the desired dimeric forms **1A** and **2A** from the reaction of $[V^{IV}O(acac)_2]$ with the H_2L^1 ligand in presence of half-equivalent 4,4′-bipyridine in methanol and from the decomposition of $[V^{IV}O(L^2)(bipy)]$ complex [21] in methanol, respectively, though the specific role of 4,4′-bipyridine and 2,2′-bipyridine (bipy) is not clear. But such type of dimeric complex with H_2L^4 ligand was not obtained by any of these methods indicating the borderline basicity of H_2L^1 and H_2L^2 ligands. Interestingly, when these dimeric compounds **1A**–**3A** were allowed to react with an excess (~3 times) amount of imidazole in methanol the respective monomeric form **1**–**3** was obtained. The oxidizing agent for the formation of pentavalent state of vanadium is the

Table 1
Crystal data and structure determination summary of the complexes **1**, **1A**, **2**, **2A**, **3** and **3A**

	1	1A	2	2A	3	3A
Empirical formula	$C_{16}H_{15}N_2O_4V$	$C_{16}H_{15}N_2O_4V$	$C_{17}H_{17}N_2O_4V$	$C_{34}H_{34}N_4O_8V_2$	$C_{17}H_{17}N_2O_5V$	$C_{17}H_{17}N_2O_5V$
Formula weight	350.24	350.24	364.27	728.53	380.27	380.27
Crystal colour	black	black	black	black	black	black
Crystal system	orthorhombic	orthorhombic	monoclinic	monoclinic	monoclinic	triclinic
Space group	$P2_1ab$	$Pbca$	$P2_1/c$	$C2/c$	$P2_1/c$	$P\bar{1}$
a (Å)	14.7377(13)	15.0154(19)	8.1336(9)	20.897(10)	8.7116(8)	7.286(2)
b (Å)	15.3060(11)	13.1115(16)	18.7192(18)	7.583(4)	10.2097(8)	9.696(3)
c (Å)	6.7572(4)	15.4949(19)	11.3647(11)	21.696(10)	19.1442(18)	13.052
α (°)	90	90	90.00	90	90	77.66(4)
β (°)	90	90	108.040(9)	94.542(6)	93.161(11)	74.292(16)
γ (°)	90	90	90.00	90	90	72.70(3)
V (Å^3)	1524.3(2)	3050.5(7)	1645.3(3)	3427(3)	1700.1(3)	838.5(4)
Z	4	8	4	4	4	2
ρ_{calc} (g cm^{-3})	1.526	1.525	1.471	1.412	1.486	1.506
μ (mm)	0.672	0.672	0.626	0.601	0.614	0.622
$F(000)$	720	1440	752	1504	784	392
Data/restraints/parameters	3854/1/210	4412/0/210	4786/0/220	3017/0/220	4897/0/229	4458/0/224
Goodness-of-fit on F^2	1.010	1.333	0.844	1.091	1.042	0.852
R indices [$I > 2\sigma(I_0)$] R_1, wR_2	0.0827, 0.1702	0.1163, 0.3754	0.0518, 0.1279	0.0467, 0.1200	0.0900, 0.2467	0.0751, 0.1772
R indices (all data) R_1, wR_2	0.1304, 0.2007	0.1634, 0.3934	0.0766, 0.1332	0.0560, 0.1267	0.1851, 0.3207	0.1435, 0.2097

Table 2
Selected bond distances (Å) and angles (°) for complexes **1**, **1A**, **2**, **2A**, **3** and **3A**

	1	1A	2	2A	3	3A
V–O1	1.580(4)	1.569(5)	1.5847(17)	1.584(2)	1.604(3)	1.558(3)
V–O2	1.844(4)	1.819(5)	1.8222(16)	1.8127(19)	1.837(3)	1.841(3)
V–O3	1.938(4)	1.948(5)	1.9098(16)	1.922(2)	1.927(4)	1.932(3)
V–O4	1.757(5)	1.838(5)	1.7688(16)	1.8248(18)	1.790(3)	1.838(3)
V–Nl	2.112(6)	2.107(6)	2.1135(19)	2.104(2)	2.154(4)	2.126(4)
V–O4$l/$2/$3		2.400(5)$1		2.311(2)$2		2.282(3)$3
V–V		3.373(2)		3.329(1)		3.309(1)
O1 V O4	105.2(2)	103.2(2)	106.66(8)	102.42(9)	106.53(18)	101.52(15)
O1 V O2	106.7(2)	99.9(3)	100.34(11)	100.34(11)	100.33(16)	
O4 V O2	100.3(2)	105.8(2)	98.17(7)	105.53(8)	97.40(14)	104.71(14)
O1 V O3	112.0(2)	99.0(2)	111.23(8)	100.99(10)	104.55(15)	99.45(15)
O4 V O3	88.4(2)	88.0(2)	89.37(7)	90.42(8)	91.60(15)	91.12(13)
O2 V O3	136.4(2)	153.2(2)	136.79(7)	149.81(9)	142.84(17)	151.52(14)
O1 V N1	94.5(2)	99.2(2)	96.18(8)	95.18(10)	98.24(16)	96.48(16)
O4 V N1	157.9(2)	154.1(2)	155.76(8)	158.98(9)	153.99(16)	158.71(15)
O2 V N1	83.1(2)	82.8(2)	82.36(7)	82.18(9)	82.40(14)	82.90(14)
O3 V N1	74.7(2)	75.7(2)	74.59(7)	74.86(8)	74.34(15)	74.67(13)
N2 N1 V	115.9(4)	115.0(4)	115.71(13)	115.03(15)	113.6(3)	115.7(3)
O1 V O4$l/$2/$3		178.3(2)$1		175.68(8)$2		175.04(13)$3
O2 V O4$l/$2/$3		81.34(19)$1		80.11(8)$2		82.20(13)$3
O4 V O4$l/$2/$3		75.3 (2)$1		73.37(8)$2		73.65(13)$3
O3 V O4$l/$2/$3		80.15(18)$1		80.22(8)$2		79.75(12)$3
N1 V O4$l/$2/$3		82.13(19)$1		89.14(8)$2		88.04(13)$3
V O4 V$l/$2/$3		104.7(2)$1		106.63(8)$2		106.35(13)$3

$1 = 1 − x, −y, 1 − z; $2 = −x + ½, −y + ½, −z; $3 = −x, −y, −z.

aerial oxygen and all the stated reactions can be represented as

$$2[V^{IV}O(acac)_2] + 2H_2L + 2CH_3OH + 1/2O_2 \rightarrow 2[V^{V}O(L)(OCH_3)] + 4Hacac + H_2O \quad (1)$$

where $H_2L = H_2L^1$ (for **1**) or H_2L^2 (for **2**) or H_2L^4 (for **4**).

$$2[V^{IV}O(acac)_2] + 2H_2L^3 + 2CH_3OH + 1/2O_2 \rightarrow [V^{V}O(L^3)(OCH_3)]_2\ (\mathbf{3A}) + 4Hacac + H_2O \quad (2)$$

$$2[V^{IV}O(acac)_2] + 2H_2L^1 + 2CH_3OH + 1/2O_2 + 4,4'\text{-bipy} \rightarrow 2[V^{V}O(L^1)(OCH_3)]_2\ (\mathbf{1A}) + 4Hacac + H_2O + 4,4'\text{-bipy} \quad (3)$$

$$2[V^{IV}O(L^2)(bipy)] + 2CH_3OH + 1/2O_2 \rightarrow [V^{V}O(L^2)(OCH_3)]_2\ (\mathbf{2A}) + 2bipy + H_2O \quad (4)$$

$$[V^{V}O(L)(OCH_3)]_2 + 3Im \rightarrow 2[V^{V}O(L)(OCH_3)] + 3Im \quad (5)$$

where $H_2L = H_2L^1$ (for **1A**) or H_2L^2 (for **2A**) or H_2L^3 (for **4A**).

Where Hacac, 4,4′-bipy, bipy and Im represent the acetyl acetone, 4,4′-bipyridine, 2,2′-bipyridine and imidazole molecule, respectively.

These complexes can be easily transformed into the corresponding complexes with $V_2O_3^{4+}$ motif simply on refluxing them in wet acetone and to the corresponding complexes with VO_2^+ motif by the reaction with one equivalent KOH in methanol at slightly warm (∼60 °C) condition. These conversions can be represented as

$$2[VO(L)(OCH_3)] + H_2O \xrightarrow{\text{wet acetone}} [V_2O_3(L)_2] + 2CH_3OH \quad (6)$$

$$[VO(L)(OCH_3)] + KOH \xrightarrow{\text{wet acetone}} K^+(H_2O)[VO_2(L)]^- + CH_3OH \quad (7)$$

The properties of these complexes are very much identical with the reported complexes, which we have synthesized by other methods and reported [15] very recently.

3.2. IR spectra of the complexes

IR spectra of the complexes exhibit all the characteristic bands of the enol forms of the coordinated tridentate dianionic ligands and these are described in Section 2. In addition, the monomeric complexes **1–4** exhibited a strong band near 1000 cm^{-1} which are attributed to ν(V=O) band and for the dimeric complexes **1A**, **2A** and **3A**, this band was observed near 975 cm^{-1} (which is significantly lower than **1–4**) indicating, respectively, the penta- and hexa-coordinated environment around the vanadium center [10–14,20].

3.3. Structure of the complexes

3.3.1. Structure of $[VO(L^1)(OCH_3)]$ (**1**)

The crystals of complex **1** belong to the orthorhombic crystal system with $P2_1ab$ space group. Fig. 1 displays a perspective view of the complex **1** and the bond parameters are collected in Table 2. The vanadium atom in the molecule is penta-coordinated existing in a distorted square-pyramidal environment in which the basal plane consists of a phenolic oxygen O(2), an enolic oxygen O(3)

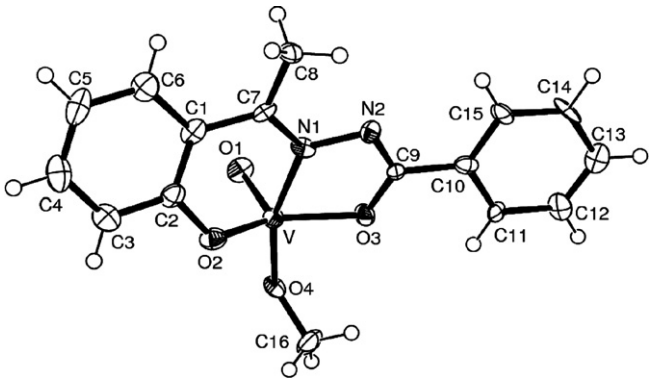

Fig. 1. Molecular structure of **1** showing the atom-numbering scheme with ellipsoid at 50% probability.

and an imine nitrogen N(1) from the fully deprotonated H_2L^1 ligand in its enol form and O(4) from the methoxide oxygen. The r.m.s. deviation of the four contributing atoms is 0.08 Å. The vanadium atom is displaced from this plane by 0.548 Å towards the axial oxido oxygen O(1). The unequal bond lengths of V–O(1), V–O(2), V–O(3), V–O(4) and V–N(1) bonds as well as unequal bond angles generated by these bonds at the V-acceptor center indicate a significant distortion from the perfect square-pyramidal geometry. The amount of distortion can be quantitatively estimated from the average O(axial)–V–O/N(basal) angle [27] and also from the τ parameter [28] (equal to $\Delta/60$, where Δ is the difference between the largest and next-to-largest ligand–metal–ligand angles). These values are, respectively, 104.6° (for idealized square-pyramid this value is 102°) and 0.358 ($\Delta = 0$, $\tau = 0$, for idealized square-pyramid) indicating appreciable distortion.

In this molecule, the H_2L^1 hydrazone ligand in its dinegative form $(L^1)^{2-}$, forms one six-membered and one five-membered chelate ring at the V(V) acceptor center with the corresponding bite angles being 83.1(2)° and 74.7(2)°. The atoms in the five-membered ring are coplanar with an r.m.s. deviation of 0.03 Å and the six-membered ring is folded. The C–O, C–N and N-N distances of the five-membered chelate ring are consistent with the enolate form of the amide. The four V–O bond lengths present in the molecule are unequal and follow the order: V–O(oxido) < V–O(alkoxide) < V–O(phenoxide) < V–O(enolate), which can be explained on the basis of π-bonding ability and the basicity of the O-donor moieties. The short V–O(1) distance of 1.580(4) Å indicates the presence of a vanadium-oxygen double bond which is commonly found in the VO^{3+} complexes.

3.3.2. Structure of $[VO(L^1)(OCH_3)]_2$ (**1A**)

Like the complex **1**, the crystals of complex **1A** also belong to the orthorhombic crystal system but with *Pbca* space group. The dimeric structure of **1A** is illustrated in Fig. 2. The dimensions in the metal coordination sphere are collected in Table 2. The dimer, which lies on a crystallographic center of symmetry is formed by two bridging methoxide-O atoms with V–O(4) and V–O(4)$1 [Symmetry code $1 = 1 − x, −y, 1 − z] bond lengths of 1.838(5) and 2.400(5) Å, respectively. This symmetry is also reflected in its electrochemical behaviour. The V···V separation is 3.373(2) Å and the V–O(4)–V$1 angle is 104.7(2)° which is very similar with the other hydrazone complexes [8,9]. The V···V separation is longer than in **2A** (by ~0.04 Å) and **3A** (by ~0.06 Å) indicating less effective bridging which is expected from the ligand's basicity point of view. Like **1**, the H_2L^1 ligand also binds the vanadium meridionally in its fully deprotonated $(L^1)^{2-}$ form through the phenolate-O, imine-N and deprotonated amide-O in its enol form generating a folded six-membered and an almost planar (with an r.m.s. deviation of 0.0735 Å) five-membered chelate ring. The corresponding bite angles are 82.8(2)° and 75.7(2)° which are very similar with the other four complexes and also other reported hydrazone complexes [7–10,12]. So, the phenolate-O, enolate-O and the imine-N atoms of $(L^1)^{2-}$ species and the methoxide-O atom (lying *trans* to the imine-N) form the square plane with an r.m.s. deviation of 0.0324 Å. Two axial positions are occupied by the oxido-O(1) atom and a bridging methoxide-O(4$1) atom of the neighbouring molecule. The displacement of the V(V) center towards the O(1) atom from the square plane is 0.349(3) Å which is significantly lower than the complex **1** (*vide supra*) and the atoms of the ligands are also symmetrically disposed relative to the center of the $[VO(\mu_2\text{-}OCH_3)_2VO]^{4+}$ core and the disposition of the oxidovanadium groups is anti-coplanar which is also observed in other dimeric oxidovanadium complexes [7–9]. The V=O distance is only 1.569(5) Å which is very closed to **3A** (*vide infra*) and another complex reported by Moon et al. [29] (in a pentacoordinated ethoxy bonded oxidovanadium(V)-hydrazone complex derived from salicyl hydrazide and acetyl acetone) but shorter than the other four complexes and also other similar type of reported complexes (~1.580 Å) [7–10,12]. Due to the formation of bridge, the V–O(4) (methoxide) bond increases significantly (by ~0.08 Å) in comparison to its monomer **1** and it becomes longer than the V–O(2) (phenolate) bond. The five V–O bond lengths follow the order: V–O(oxido) < V–O(phenoxide) < V–O(methoxide)^e (e = equatorial) < V–O(enolate) < V–O(methoxide)^a (a = axial).

3.3.3. Structure of $[VO(L^2)(OCH_3)]$ (**2**)

The molecular structure of **2** is very similar to the structure of **1** with the hydrogen atom at the 5-position of the aryloxy ring replaced by a methyl group and its crystals belong to the monoclinic crystal system with $P2_1ab$ space group. The molecular structure and the atom-numbering scheme are illustrated in Fig. 3 and the dimensions are provided in Table 2.

In **2**, the equatorial positions of vanadium atom are occupied by phenolate-O, imine-N and the enolate-O atoms of the fully deprotonated H_2L^2 ligand in its enol form along with a methoxy oxygen (with an r.m.s. deviation of 0.13 Å) and one axial position is occupied by the oxido oxygen atom. Thus, a distorted square-pyramidal geometry is formed at the vanadium center. The vanadium atom is 0.504 Å from the mean equatorial plane towards the oxido oxygen atom O(1). The $(L^2)^{2-}$ species binds meridionally generating a six-membered ring (which is folded) and a almost planar five-membered ring (with an r.m.s. deviation of 0.04 Å), the corresponding bite angles being 82.36(7)° and 74.59(7)°. Significant distortion from the perfect square-pyramidal geometry can be estimated from the value of average O(axial)–V–O/N(basal) angle (105.3°)

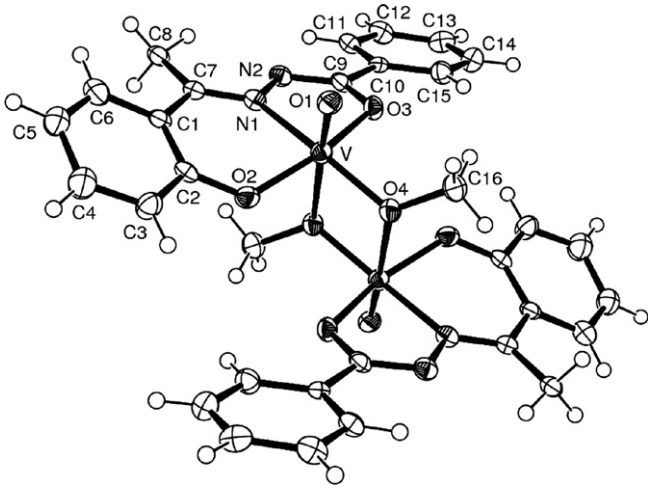

Fig. 2. Molecular structure of **1A** showing the atom-numbering scheme with ellipsoid at 50% probability.

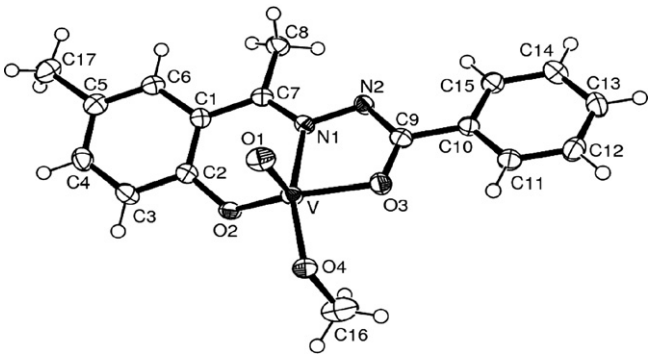

Fig. 3. Molecular structure of **2** showing the atom-numbering scheme with ellipsoid at 50% probability.

and also from the τ value (0.316). The four bond lengths follow the similar order as that in **1**.

3.3.4. Structure of $[VO(L^2)(OCH_3)]_2$ (**2A**)

Like **2**, the crystals of complex **2A** also belong to the monoclinic crystal system but with *C2/c* space group. The molecular structure of **2A** is illustrated in Fig. 4 and the bond parameters are listed in Table 2. The dimer, which lies on a crystallographic center of symmetry is formed by two bridging methoxide-O atoms with V–O(4) and V–O(4)$2 [Symmetry code $2 = $-x + ½, -y + ½, -z$] bond lengths of 1.8248(18) and 2.311(2) Å, respectively. The V···V separation is 3.329(1) Å and the angle V–O(4)–V$2 is 106.35(13)° which is very similar to **1A** and **3A** (*vide infra*) and also other reported dimethoxy-bridged hydrazone complexes [8,9]. The V···V separation is shorter (by ~0.04 angle Å) than **1A** indicating more effective bridging due to the higher basic property of $(L^2)^{2-}$ ligand in comparison to $(L^1)^{2-}$ ligand but it is longer (by ~0.02 Å) than **3A** indicating less effective bridging arising from lower basic property of $(L^2)^{2-}$ ligand in comparison to $(L^3)^{2-}$ ligand. The binding nature of $(L^2)^{2-}$ ligand in this complex is very similar to **2** forming a folded six-membered and an almost planar five-membered chelate ring with the corresponding bite angles being 82.19(9)° and 74.86(8)°. The displacement of the V atom towards the O(1) atom from the mean square plane [formed by O(2), N(1), O(3) and O(4) atoms] is 0.330 Å, which is lower than **1**, **1A**, **2** and **3** but higher than **3A**. Due to hexa-coordination, there is a significant change in equatorial V–O/N bond lengths in comparison to its monomeric analogue **2**: V–O(2) and V–N(1) bonds are shortened by ~0.01 Å while V–O(3) and V–O(4) bonds are lengthened by ~0.02 and ~0.06 Å, respectively. Like **1A**, the V–O(4) (methoxide) bond in this complex, is also longer than V–O(2) (phenolate) bond by ~0.01 Å, which is not usual. Hence, the five V–O bond lengths follow the similar order to **1A**.

3.3.5. Structure of $[VO(L^3)(OCH_3)]$ (**3**)

The crystals of complex **3** belong to the monoclinic crystal system with $P2_1/c$ space group and its crystallographic data are collected in Table 1. Fig. 5 displays a perspective view of this complex and the bond parameters are listed in Table 2. The molecular structure of **3** is also very much similar to **1** and **2** with the 5-position occupied by a methoxy group and the geometry around the vanadium center is also distorted square-pyramidal. The basal plane is occupied by the phenolate-O, enolate-O and the imine-N atoms of the meridionally disposed $(L^3)^{2-}$ ligand [forming one six-membered (folded) and one five-membered (atoms are coplanar with an r.m.s. deviation of 0.080 Å) chelate ring at the V(V) acceptor center with the corresponding bite angles being 82.40(14)° and 74.34(15)°] together with a methoxy oxygen atom. The r.m.s. deviation of the four contributing atoms of the basal plane is 0.054 Å. The vanadium atom is displaced from this plane by 0.475(2) Å towards the axial oxido oxygen O(1). The values of average O(axial)–V–O/N(basal) angle and τ parameter are, respectively, 104.1° and 0.186 indicating appreciable distortion but to a lesser extent than the complexes **1** and **2**. The four V–O bond lengths present in the molecule are unequal and also follow the similar order as that in **1** and **2**.

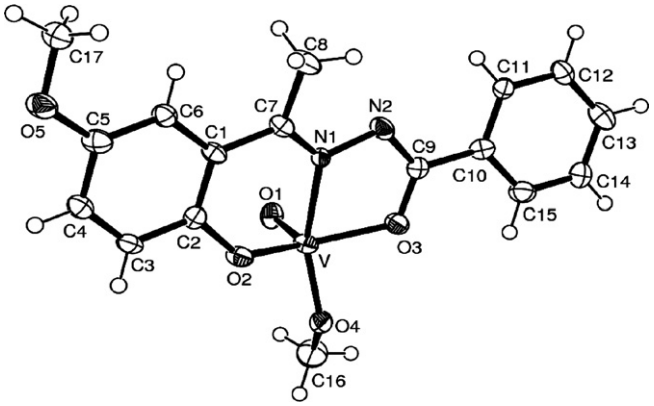

Fig. 5. Molecular structure of **3** showing the atom-numbering scheme with ellipsoid at 50% probability.

3.3.6. Structure of $[VO(L^3)(OCH_3)]_2$ (**3A**)

The crystals of complex **3A** belong to the triclinic crystal system with $P\bar{1}$ space group. The molecular structure of **3A** is illustrated in Fig. 6, which is very similar to the structure of **1A** and **2A** with the hydrogen atom and the methyl group, respectively, at the 5-position in the aryloxy ring replaced by a methoxy group. The molecular dimensions in the coordination sphere are collected in Table 2. Like **1A** and **2A**, this dimer also lies on a crystallographic center of symmetry, formed by two methoxide-O atoms with V–O(4) and V–O(4)$3 [Symmetry code $3 = $-x, -y, -z$] bond lengths of 1.838(3) and 2.282(3) Å, respectively. The V···V separation is 3.309(1) Å and the angle V–O(4)–V$3 is 106.35(13)° which is very similar with

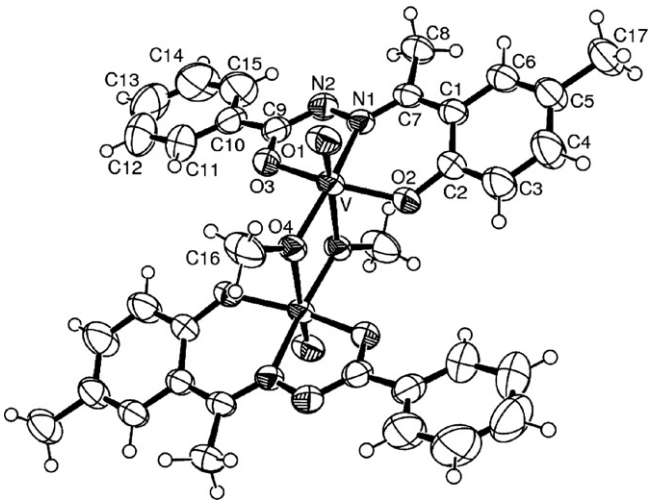

Fig. 4. Molecular structure of **2A** showing the atom-numbering scheme with ellipsoid at 50% probability.

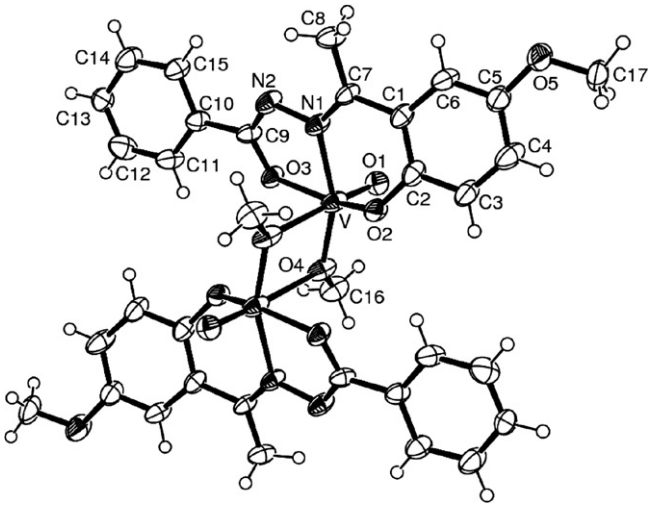

Fig. 6. Molecular structure of **3A** showing the atom-numbering scheme with ellipsoid at 50% probability.

the other two dimeric hydrazone complexes reported here The V···V separation is shorter than in **1A** and **2A**, respectively, by 0.06 Å and 0.02 Å, indicating more effective bridging which is expected from the ligand's basicity point of view. Like **3**, the H_2L^3 ligand binds the vanadium meridionally through the phenolate-O, imine-N and deprotonated amide-O in its enol form generating a folded six-membered and an almost planar (with an r.m.s. deviation of 0.05 Å) five-membered chelate ring with the corresponding bite angles being 82.90(14)° and 74.67(13)°. So, the fully deprotonated ONO donor moieties of the $(L^3)^{2-}$ species and the methoxide-O (lying *trans* to the imine-N) form the square plane with an r.m.s. deviation of 0.01 Å. Two axial positions are occupied by the oxido-O(1) atom and a bridging methoxide-O(4$3) atom of the neighbouring molecule. The displacement of the V(V) center towards the O(1) atom from the square plane is 0.322 Å which is significantly lower than the complexes **1**, **1A**, **2**, **2A** and **3** (*vide infra*). Like **1A** and **2A**, the atoms of the ligands are also symmetrically disposed relative to the center of the $[VO(\mu_2\text{-}OCH_3)_2VO]^{4+}$ core and the disposition of the oxidovanadium groups is anti-coplanar. The V=O distance is only 1.558(3) Å which is very closed to **1A** and shorter than the other four complexes and also other similar type of reported complexes (~1.580 Å) [7–10,12]. To the best of our knowledge, this V=O bond length represents the shortest V=O distance in the family of complexes with VO^{3+} motif both in penta- and hexa-coordinated environment. Due to the formation of bridge, the V–O(4) (methoxide) bond increases significantly in comparison to its monomeric form **3** and is almost equal in length to the V–O(2) (phenolate) bond and hence, the five V–O bond lengths follow the order: V–O(oxido) < V–O(methoxide)^e (e = equatorial) ≈ V–O(phenoxide) < V–O(enolate) < V–O(methoxide)^a (a = axial).

From the structural analysis discussed above, it is evident that the extent of displacement of the vanadium atom from the mean square plane decreases with the increase of electron donating property of the substituent in both the monomeric and dimeric complexes. Furthermore, the V=O bond distance in **3A** represents the shortest V=O bond in the complexes with VO^{3+} motif present in either penta- or hexa-coordinated environment while in the complexes **1A** and **2A**, the V–O(methoxide) bond represents the unusually long bond which is even longer than V–O(phenolate) bond.

3.4. Proton NMR spectra of the complexes

^{1}H NMR data of all the complexes are given in Section 2. Complex $[VO(L^4)(OCH_3)]$ (**4**) was identified by its NMR spectra in $CDCl_3$ solution. Apart from all the proton signals of the coordinated ligand $(L^1)^{2-}$, $(L^2)^{2-}$ and $(L^3)^{2-}$, the spectrum of **1A**, **2A** and **3A** exhibited one singlet at ~5.18 ppm corresponds to protons of the bridging OCH_3 group in addition to another singlet (with different intensity) at 3.48 ppm attributed to the coordinated terminal OCH_3 group (observed in the NMR spectra of monomeric **1**–**4** complexes). These two peaks indicate that these dimeric species **1A**, **2A** and **3A** are decomposed to the corresponding monomeric species significantly (the ratio of dimeric species to monomeric being ~1:1 for **1A** and **2A** and ~10:7 for complex **3A**) in $CDCl_3$ solution.

3.5. Electronic spectra of the complexes

The electronic spectral data of all the complexes are described in the Section 2. The electronic spectra of the monomeric complexes **1**–**4** in CH_2Cl_2 solution exhibit two intense absorption bands: one in the 378–388 nm region, which is assigned to L→V(dπ) LMCT transition and another in the 321-326 nm region attributed to intra-ligand π→π* transition of C≡N bond. Such type of LMCT transition band for the complexes **1A**, **2A** and **3A** was observed at 381 nm, 378 nm and 376 nm, respectively, and the intra-ligand π→π* transition at *ca.* 325 nm.

3.6. Electrochemistry of the complexes

All the complexes exhibit one quasi-reversible reduction peak in the +0.19 V to +0.31 V versus SCE region in CH_2Cl_2 solution due to VO^{3+}/VO^{2+} couple. Cyclic voltammetric data for all the complexes are collected in Table 3 and the Fig. 7 displays a representative cyclic voltammogram of **2**. The dinuclear V(V) complexes are usually expected to undergo a two step one electron reduction, with the first step leading to the formation of mixed-valence V(V)–V(IV) species. But contrary to such an expectation, all the dinuclear complexes **1A**, **2A** and **3A** were found to undergo only one-step quasi-reversible reduction in CH_2Cl_2 solution in the potential +0.19–0.25 V region. On changing from the penta- to hexa-coordinated environment around the vanadium in the respective dimeric form, the redox potential value is decreased by only 0.01 V. The appearance of one reduction peak for these dinuclear complexes is probably due to their conversion to the monomeric species in solution (which have almost identical redox potential value) to a significant extent as evident in their ^{1}H NMR specta. The $E_{½}$ values of the complexes have been found to follow a linear trend with the Hammett parameter (σ) of the substituent in the ligands (*vide supra*).

Table 3
Electrochemical[a] data of the complexes **1**–**4** in CH_2Cl_2 solution at 298 K

Compound	E_p^c (V)	E_p^a (V)	$E_{½}$[b]/V (ΔE_P/mV)
$[VO(L^1)(OCH_3)]$ (**1**)	+0.215	+0.305	+0.26(90)
$[VO(L^1)(OCH_3)]_2$ (**1A**)	+0.21	+0.29	+0.25(80)
$[VO(L^2)(OCH_3)]$ (**2**)	+0.17	+0.27	+0.22(100)
$[VO(L^2)(OCH_3)]_2$ (**2A**)	+0.16	+0.26	+0.21(100)
$[VO(L^3)(OCH_3)]$ (**3**)	+0.15	+0.25	+0.20(100)
$[VO(L^3)(OCH_3)]_2$ (**3A**)	+0.14	+0.24	+0.19(100)
$[VO(L^4)(OCH_3)]$ (**4**)	+0.27	+0.35	+0.31(80)

[a] At a Pt disk electrode; supporting electrolyte: Et_4NClO_4 (TEAP, 0.1 M), scan rate 50 mV s^{-1}, reference electrode SCE, solute concentration ~10^{-3} M.
[b] $E_{½}$ is calculated as the average of anodic (E_p^a) and cathodic (E_p^c) peak potential values; ΔE_p = difference of cathodic and anodic peak potential values.

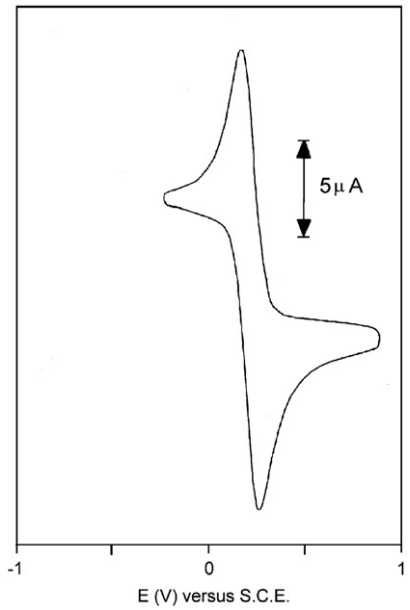

Fig. 7. Cyclic voltammogram of **2** in CH_2Cl_2 solution.

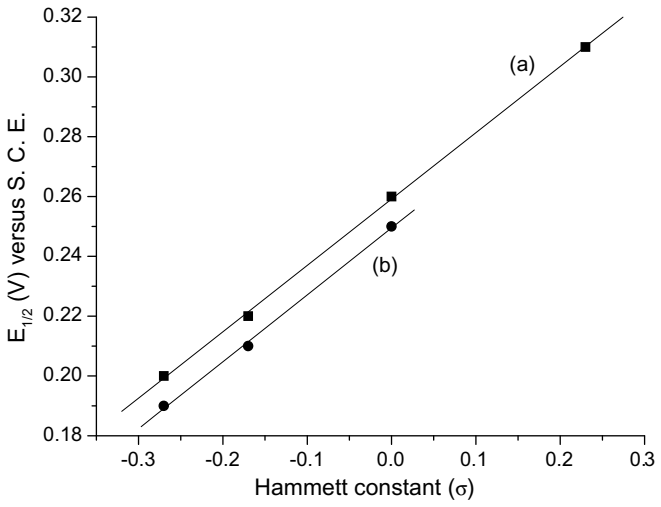

Fig. 8. (a) Plot of $E_{½}$ vs. Hammett constant (σ) of the monomeric complexes **1**–**4**; (b) Plot of $E_{½}$ vs. Hammett constant (σ) of the dimeric complexes **1A**–**3A**.

3.7. Influence of ligand substituents on $E_{½}$ values of the complexes

An analysis of the $E_{½}$ values of the complexes **2**, **2A**, **3** and **3A** indicate that for the complexes with an electron donating substituent at 5-position, a decrease in $E_{½}$ values occurs compared to complex **1** and **1A** while, for the complex **4** with an electron withdrawing substituent, the opposite is true. For finding out the quantitative relation with the electronic effect of the substituent at the 5-position on the vanadium center, the redox potential ($E_{½}$) value of both monomeric and dimeric complexes are plotted against the respective Hammett constant (σ) (Fig. 8a and b, respectively).

These two plots show linear relations [20,21,30–32] and statistical analysis gives the following relations describing the dependence on σ:

For monomeric complexes:

$$E_{1/2}\ (\mathrm{V}) = 0.26 + 0.22 \times \sigma \quad (8)$$

For dimeric complexes:

$$E_{1/2}\ (\mathrm{V}) = 0.25 + 0.22 \times \sigma \quad (9)$$

These correlations have r-values of ~1.00 with a standard deviation 0.0013 and 0.0018, respectively, for monomeric and dimeric complexes. The estimated error in the intercept of Fig. 8a is 6.74×10^{-4} and in the $dE_{½}/d\sigma$ value is 3.43×10^{-3} while those of Fig. 8b are, respectively, 0.0017 and 0.0093.

4. Conclusion

The basic property of a family of hydrazone ligands has been nicely exploited in the syntheses of mixed-ligand methoxy bonded monomeric and methoxy-bridged dimeric oxidovanadium(V)-hydrazone complexes. Six of the seven complexes (except **4**) reported here, have been structurally characterized. This study indicates that the lower basic hydrazone ligands (e.g., H_2L^1, H_2L^2 and H_2L^4) have the normal tendency to form monomeric complex (**1**, **2** and **4**, respectively), while the higher basic ligand (e.g., H_2L^3) has a tendency to form methoxy-bridged dimeric complexes **3A**. The intermediate basic H_2L^1 and H_2L^2 ligands can form the dimeric species **1A** and **2A** in the presence of 4,4′-bipyridine and 2,2′-bipyridine, respectively, while the strong basic H_2L^3 ligand can form the monomeric species **3** only by the decomposition of **3A** with the influence of imidazole (a monodentate intermediate basic N-donor ligand). These VO^{3+} complexes are easily interconvertible to the complexes with $V_2O_3^{4+}$ and VO_2^{+} motifs.

5. Supplementary data

CCDC 681054, 689347, 681055, 681056, 681057 and 681058 contain the supplementary crystallographic data for **1**, **1A**, **2**, **2A**, **3** and **3A**. These data can be obtained free of charge via http://www.ccdc.cam.ac.uk/conts/retrieving.html, or from the Cambridge Crystallographic Data Centre, 12 Union Road, Cambridge CB2 1EZ, UK; fax: (+44) 1223-336-033; or e-mail: deposit@ccdc.cam.ac.uk.

Acknowledgements

Our sincere thanks are due to the University Grants Commission (New Delhi, India) for financial assistance. We are grateful to our College authorities for providing research facilities. We are also grateful to Dr. S. Chattopadhyay, Department of Inorganic Chemistry, University of Kalyani, India for electrochemical measurements.

References

[1] (a) R. Liasko, T.A. Kabanos, S. Karkabounus, M. Malamas, J.A. Tasiopoulos, D. Stefanou, P. Collery, A. Evangelou, Anticancer Res. 18 (1998) 3609;
(b) A. Evangelou, Crit. Rev. Oncol. Hematol. 42 (2002) 249.
[2] (a) H. Sakurai, K. Tsuchiya, M. Nukatsuka, J. Kawada, S. Ishikawa, H. Yoshida, M. Komatsu, J. Clin. Biochem. Nutr. 8 (1990) 193;
(b) R.E. Tapscott, R.L. Belford, Inorg. Chem. 6 (1967) 735;
(c) J.H. McNeill, V.G. Yuen, H.R. Hoveyada, C. Orvig, J. Med. Chem. 35 (1992) 1489;
(d) D.C. Crans, M. Mahroof-Tahir, P.K. Shin, A.D. Keramidas, Mol. Cell. Biochem. 153 (1995) 17;
(e) K.H. Thompson, C. Orvig, Coord. Chem. Rev. 219–221 (2001) 1033;
(f) H. Sakurai, Y. Kojima, Y. Yoshikawa, J. Kawada, H. Yasui, Coord. Chem. Rev. 226 (2002) 187;
(g) S.A. Dikanov, B.D. Liboiron, C. Orvig, J. Am. Chem. Soc. 124 (2002) 2969;
(h) B. Song, N. Aebischer, C. Orvig, Inorg. Chem. 41 (2002) 1357;
(i) D. Rehder, J.C. Pessoa, C.F. Geraldes, J. Biol. Inorg. Chem. 7 (2002) 675;
(j) D.C. Crans, L. Yang, J.A. Alfamo, L.H. Chi, W. Jin, M. Mahroof-Tahir, K. Robbins, M.M. Tolloue, L.K. Chan, A.J. Plante, R.Z. Grayson, G.R. Willsky, Coord. Chem. Rev. 237 (2003) 13.
[3] (a) M. Weyand, H.-J. Hecht, M. Kiess, M.-F. Liaud, H. Vitler, D. Scomburg, J. Mol. Biol. 293 (1999) 595;
(b) J.N. Carter-Franklin, J.D. Parrish, R.A. Tchirret-Guth, R.D. Little, A. Butler, J. Am. Chem. Soc. 125 (2003) 3688;
(c) D. Rehder, G. Santoni, G.M. Licini, C. Schulzke, B. Meier, Coord. Chem. Rev. 237 (2003) 63.
[4] P.J. Stankicwicz, A.S. Tracey, D.C. Crans, in: H. Sigel, A. Sigel (Eds.), Vanadium and its Role in life, Metal Ions in Biological Systems, vol. 31, Marcel Dekker, New York, 1995 (Chapter 9).
[5] G.L. Mendz, Arch. Biochem. Biophys. 291 (1991) 201.
[6] (a) F. Wolff, C. Lorber, R. Choukroun, B. Donnadieu, Inorg. Chem. 42 (2003) 7839;
(b) G.W. Coates, P.D. Hustad, S. Reinartz, Angew. Chem., Int. Ed. 41 (2002) 2236;
(c) H. Hagen, J. Boerrsma, G. van Koten, Chem. Soc. Rev. 31 (2002) 357;
(d) S. Gambarotta, Coord. Chem. Rev. 237 (2003) 229;
(e) C. Lorber, R. Choukroun, B. Donnadieu, Inorg. Chem. 42 (2003) 673.
[7] N.R. Sangeetha, V. Kavita, S. Wocadto, A.K. Powell, S. Pal, J. Coord. Chem. 51 (2000) 55.
[8] C. Tsiamis, B. Voulgaropoulos, D. Charistos, G.P. Voutsas, C.A. Kavounis, Polyhedron 19 (2000) 2003.
[9] Z.-P. Deng, S. Gao, L.H. Huo, H. Zhao, Acta Crystallogr., Sect. E 61 (2005) m2214.
[10] M.R. Maurya, S. Agarwal, C. Bader, M. Ebel, D. Rehder, Dalton Trans. (2005) 537.
[11] M.R. Maurya, S. Khurana, C. Schulzke, D. Rehder, Eur. J. Inorg. Chem. (2001) 779.
[12] S.P. Rath, S. Mondal, A. Chakravorty, Inorg. Chim. Acta 263 (1997) 247.
[13] N.R. Sangeetha, S. Pal, Bull. Chem. Soc. Jpn. 73 (2000) 357.
[14] R. Dinda, P. Sengupta, S. Ghosh, T.C.W. Mak, Inorg. Chem. 41 (2002) 1684.
[15] (a) B. Mondal, T. Ghosh, M. Sutradhar, G. Mukherjee, M.G.B. Drew, T. Ghosh, Polyhedron 27 (2008) 2193;
(b) B. Mondal, M.G.B. Drew, T. Ghosh, Ind. J. Chem. A 47 (2008).
[16] H. Sigel, A. Sigel (Eds.), Metal Ions in Biological Systems, vol. 31, Marcel Dekker, New York, 1995.
[17] D. Rehder, Angew. Chem., Int. Ed. 30 (1991) 148.
[18] Q. Chen, J. Zubieta, Coord. Chem. Rev. 114 (1992) 107.

[19] R.A. Rowe, M.M. Jones, Inorg. Synth. 5 (1957) 113.
[20] T. Ghosh, B. Mondal, T. Ghosh, M. Sutradhar, G. Mukherjee, M.G.B. Drew, Inorg. Chim. Acta 360 (2007) 1753.
[21] T. Ghosh, B. Mondal, J. Chem. Res. (2007) 407.
[22] CRYSALIS Program, Oxford Diffraction Ltd., 2005.
[23] G.M. Sheldrick, SHELXS-97 and SHELXL-97 Programs for Crystallography Structure Solution and Refinement, University of Göttingen, Germany, 1997.
[24] ABSPACK Program, Oxford Diffraction Ltd., 2005.
[25] A.L. Spek, PLATON-94 Program, Utrecht University, The Netherlands, 2004.
[26] L.P. Hammett, Physical Organic Chemistry, second ed., McGraw-Hill, New York, 1970.
[27] E.L. Muetterties, L.J. Guggenberger, J. Am. Chem. Soc. 96 (1974) 1748.
[28] A.W. Addison, T.N. Rao, J. Reedjik, J. Rijn, G.C. van Verschoor, J. Chem. Soc., Dalton Trans. (1984) 1349.
[29] M. Moon, M. Pyo, Y.C. Myoung, C.I. Ahn, M.S. Lah, Inorg. Chem. 40 (2001) 554.
[30] T. Ghosh, B. Mondal, R. Patra, Transition Met. Chem. 32 (2007) 468.
[31] T. Ghosh, B. Mondal, Ind. J. Chem. A 47 (2008) 361.
[32] H. Hagen, A. Barbon, E.E. van Faassen, B.T.G. Lutz, J. Boersma, A.L. Spek, G. van Koten, Inorg. Chem. 38 (1999) 4079.

2. Experimental

2.1. Materials

Safety note: cobalt perchlorate salt with organic ligands is often explosive and should be handled with caution.

All other reagents and solvent were purchased from Merck (pro-analysis) and dried using molecular sieves (Linde 4 Å). NaY with the Si:Al ratio of 2.53 was purchased from Aldrich (Lot No. 67812). Thiodiglycolic acid also obtained from Aldrich. 1,2-Diaminoethane, 1,3-diaminopropane, 1,2-diaminobenzene, 1,3-diaminobenzene was obtained from Merck. Solvents were dried before used.

2.2. Physical measurements

The elemental analysis (CHN) of the materials was obtained from Carlo ERBA Model EA 1108 analyzer. XRD patterns were recorded by a Rigaku D-max C III, X-ray diffractometer using Ni-filtered Cu Kα radiation. Nitrogen adsorption measurements were performed at 77 K using a Coulter Ofeisorb 100CX instrument. The samples were degassed at 150 °C until a vacuum more than 10^{-3} Pa was obtained. Micropore volumes were determined by the *t*-method, a "monolayer equivalent area" was calculated from the micropore volume [22,23]. The stability of the encapsulated complexes was checked after the reaction by UV–Vis and possible leaching of the complex was investigated by UV–Vis in the reaction solution after filtration of the zeolite. The amounts of metallocomplexes encapsulated in zeolite matrix were determined by the elemental analysis and followed by subtracting the amount of metallocomplex left from the solutions after the synthesis of the complexes as determined by UV–Vis spectroscopy, from the amount taken for the synthesis. Atomic absorption spectra (AAS) were recorded on a Perkin–Elmer 4100-1319 Spectrophotometer using a flame approach, after the acid (HF) dissolves the known amounts of the zeolitic material. SiO_2 was determined by gravimetric analysis. Magnetic moments were calculated from magnetic susceptibility data obtained using a Johnson Matthey MK-1 magnetic susceptibility balance and conductance measurements with a Metrohm Herisau conductometer E 518. FT-IR spectra were recorded on Shimadzu Varian 4300 spectrophotometer in KBr pellets. The electronic spectra of the neat complexes were taken on a Shimadzu UV–Vis scanning spectrometer (Model 2101 PC). Diffuse reflectance spectra (DRS) were registered on a Shimadzu UV/3101 PC spectrophotometer over the range 1500–200 nm, using MgO as reference. FAB mass spectra were recorded on a Kratos MS50TC spectrometer.

2.3. Synthesis of tetraoxodithiatetraaza macrocyclic ligand

Tetraoxodithiatetraaza macrocyclic ligands ([18]aneN$_4$S$_2$, [20]aneN$_4$S$_2$, Bzo$_2$[18]aneN$_4$S$_2$ or Bzo$_2$[20]aneN$_4$S$_2$) were prepared by following the procedures reported in Ref. [24]. The ligand has been synthesized by the condensation reaction of the thiodiglycolic acid (0.02 mol) and diamine (0.02 mol); diamine = 1,2-diaminoethane (1.20 g), 1,3-diaminopropane (1.48 g), 1,2-diaminobenzene (2.16 g), 1,3-diaminobenzene (2.16 g). Both reagents were taken in equimolar ratio in a round bottom flask, in the presence of few drops of concentrated hydrochloric acid (∼pH 4–5) and were refluxed on a water bath up to the completion of reaction. After completion of the reaction mixture was kept in a refrigerator at 0 °C, over night. The cream colored crystals separated out, which were filtered, washed with cold EtOH and dried in vacuum over P_4O_{10}. The purity was checked by HPLC technique.

2.4. Preparation of [Co([18 or 20]aneN$_4$S$_2$)](ClO$_4$)$_2$ and [Co(Bzo$_2$[18 or 20]aneN$_4$S$_2$)](ClO$_4$)$_2$ complexes

Cobalt(II) perchlorate hexahydrate (3.66 g, 0.01 mol) dissolved in ethanol (20 ml) was reacted with an ethanolic (20 ml) solution of tetraoxodithiatetraaza ligands ([18]aneN$_4$S$_2$, [20]aneN$_4$S$_2$, Bzo$_2$[18]aneN$_4$S$_2$ or Bzo$_2$[20]aneN$_4$S$_2$) (0.01 mol) by refluxing for 1 h under nitrogen atmosphere. The mixture was heated at reflux for 6 h until an orange solution resulted. The solution was cooled to room temperature and filtered to remove cobalt hydroxide. Excess lithium perchlorate dissolved in methanol was added to the filtrate, and the mixture was kept in the refrigerator until orange solid formed. The solids were filtered, washed thoroughly with cold ethanol and dried in vacuum.

2.5. Preparation of [Co(N–N)$_2$]$^{2+}$–NaY

Typically a 4 g sample of NaY zeolite was mixed with 0.37 g of bis(diamine)cobalt(II) perchlorate; diamine = 1,2-diaminopropane, 1,3-diaminopropane, 1,2-diaminobenzene or 1,3-diaminobenzene; suspended in 100 ml of methanol and then refluxed for 8 h. The pale orange solid consisting of [Co(N–N)$_2$]$^{2+}$ exchanged with Na^+ in NaY and denoted as [Co(N–N)$_2$]$^{2+}$–NaY was collected by filtration, washed with ethanol. The resulted zeolites, were Soxhlet extracted with *N*,*N*′-dimethylformamide (for 4 h) and then with ethanol (for 3 h) to remove excess unreacted diamine and any Co(II) complexes adsorbed onto the external surface of the zeolite crystallines. The resulting light orange solids were dried at 60 °C under vacuum for 24 h.

2.6. Preparation of [Co([18 or 20]aneN$_4$S$_2$)]$^{2+}$–NaY and [Co(Bzo$_2$[18 or 20]aneN$_4$S$_2$)]$^{2+}$–NaY

To a stirred methanol suspension (100 ml) of [Co(N–N)$_2$]$^{2+}$–NaY (2 g) was slowly added thiodiglycolic acid (under N_2 atmosphere). The mixture was heated under reflux condition for 24 h until a pale pink suspension resulted. The solution was filtered and the resulting zeolites, were Soxhlet extracted with *N*,*N*′-dimethylformamide (for 6 h) and then with ethanol (for 5 h) to remove excess unreacted products from amine-ester condensation and any cobalt(II) complexes adsorbed onto the external surface of the zeolite crystallines. The resulting pale pink solids were dried at 70 °C under vacuum for 12 h. The remaining [bis(diamine)cobalt(II)] ions in zeolite were removed by exchanging with aqueous 0.1 M $NaNO_3$ solutions. The stability of the encapsulated complexes was checked after the reaction by UV–Vis and possible leaching of the complex was investigated by UV–Vis in the reaction solution after filtration of the zeolite. The amount of cobalt(II) complexes encapsulated in zeolite matrix were determined by the elemental analysis and subtracting the amount of Co(II) complex left from the solutions after the synthesis of the complexes is determined by UV–Vis spectroscopy, from the amount taken for the synthesis.

3. Results and discussion

Cobalt(II) reacted with 18- and 20-membered tetraoxodithiatetraaza macrocyclic ligands ([18]aneN$_4$S$_2$, [20]aneN$_4$S$_2$, Bzo$_2$[18]aneN$_4$S$_2$ and Bzo$_2$[20]aneN$_4$S$_2$) in presence of $LiClO_4$ to yield the cationic complexes; [Co([18]aneN$_4$S$_2$)](ClO$_4$)$_2$, [Co([20]aneN$_4$S$_2$)](ClO$_4$)$_2$, [Co(Bzo$_2$[18]aneN$_4$S$_2$)](ClO$_4$)$_2$ and [Co(Bzo$_2$[20]aneN$_4$S$_2$)](ClO$_4$)$_2$ (Scheme 1).

3.1. ^{1}H NMR studies

The ^{1}H NMR a spectrum of all tetraoxodithiatetraaza macrocyclic ligands in $CDCl_3$ does not give any signal corresponding to primary amine and alcoholic protons. It shows a multiplet at

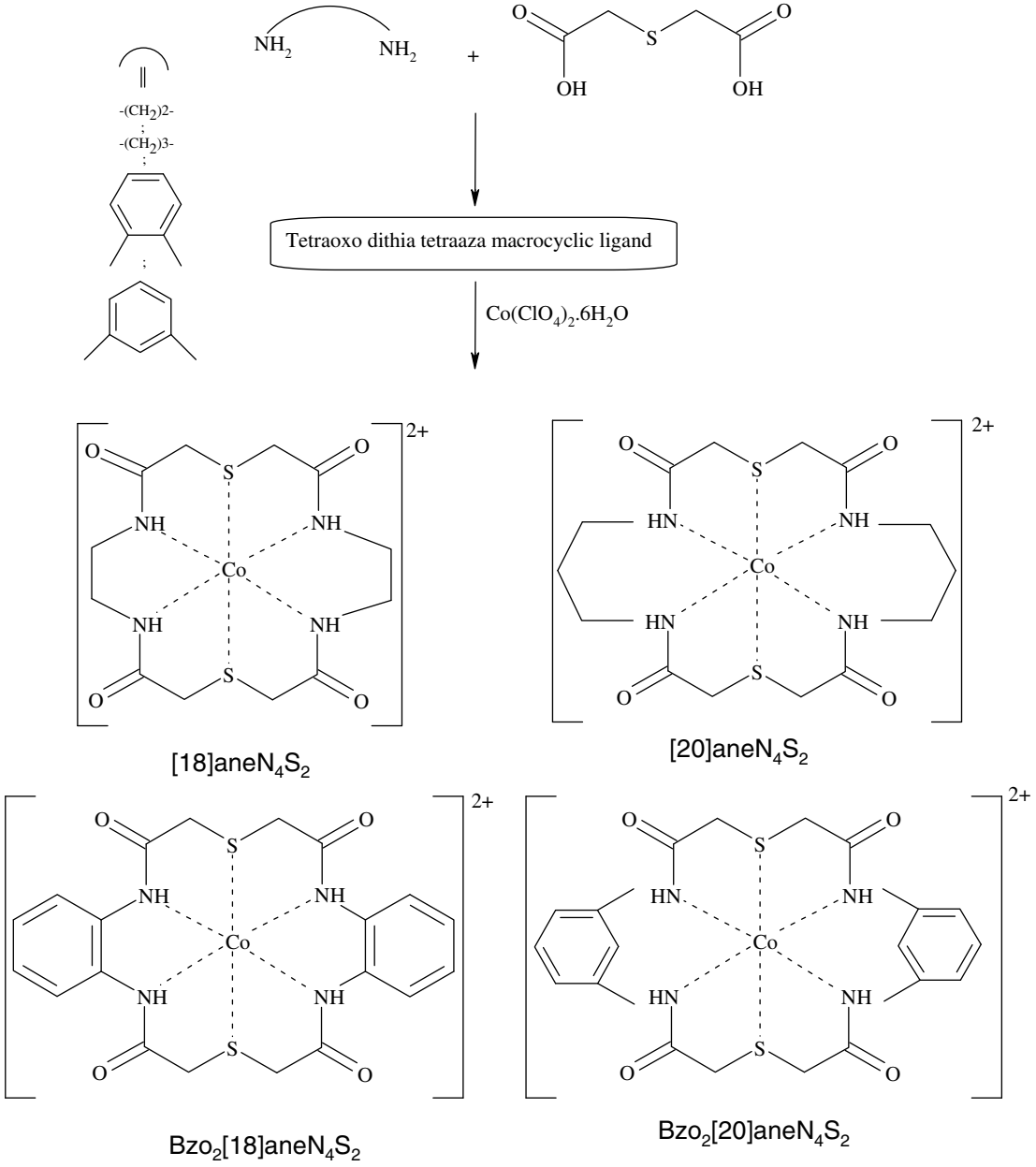

Scheme 1.

~8.60 ppm corresponding to amide CO–NH (4H) protons and does not show any signal corresponding to primary amine and alcoholic protons. A multiplet signal corresponding to methylene proton CO–N–CH_2 (8H) that are adjacent to the nitrogen atom appeared at ~3.40 ppm. NMR spectrum also shows a singlet at ~2.35 ppm corresponding to CO–CH_2–S (8H) that is close to sulphur atom.

For more investigation of structure, were synthesized the diamagnetic zinc(II) complexes (Table 1). The diamagnetic nature of the zinc(II) complexes has allowed its characterization by NMR spectrometry. The ^{1}H NMR spectrum of zinc complexes has been recorded in DMSO-d_6 as it is insoluble in $CHCl_3$-*d*. The ^{1}H NMR spectra of all the zinc(II) complexes does not show any signal corresponding to primary amino and alcoholic protons. However, show multiplet in the region 8.50–8.68 ppm, which is assigned to amide (HN–CO, 4H) protons [25]. Another multiplet appeared in the region 3.37 ppm ($[Zn([18]aneN_4S_2)]^{2+}$) and 3.35 ppm ($[Zn([20]aneN_4S_2)]^{2+}$), corresponding to the methylene protons [26] (CO–N–CH_2, 8H) which are adjacent to the nitrogen atoms. The multiplet appearing in the region δ 7.1–7.6 ppm has been assigned to phenyl protons ($[Zn(Bzo_2[18]aneN_4S_2)]^{2+}$ and $[Zn(Bzo_2[20]aneN_4S_2)^{2+}$). Furthermore, a singlet in the region 2.43–2.46 ppm was observed assignable to methylene protons (CO–CH_2–S, 8H) which are adjacent to the sulfur atom.

3.2. Co content and textural analysis

The molecular formulae of the complexes "$[Co([18]aneN_4S_2)](ClO_4)_2$, $[Co([20]aneN_4S_2)](ClO_4)_2$, $[Co(Bzo_2[18]aneN_4S_2)](ClO_4)_2$ and $[Co(Bzo_2[20]aneN_4S_2)](ClO_4)_2$" have been assigned on the basis of the results of their elemental analysis and the molecular ion peaks in the mass spectra. All mass spectra showed molecular ion peaks for the 1:1 metal-to-ligand stoichiometry with no further peaks above them. A preliminary identification of the metal complexes was made on the basis of their IR spectra, which exhibited no bands characteristic of free primary amine, thus supporting the proposed macrocyclic skeleton (Scheme 1).

DMSO solutions of these complexes were conductive (Table 2). Unfortunately, I could not grow any single crystals suitable for

Table 1
Elemental analysis, vibrations parameters and molecular ion peaks for ligands and tetraoxodithiatetraaza macrocyclic cobalt(II) and zinc(II) complexes

Complex	Elemental analysis data calculated (found)					IR (KBr, cm^{-1})						FAB mass (m/z)	
	C (%)	H (%)	N (%)	C/N	Co (%)	I	II	III	IV	ν_{N-H}	ν_{M-N}	$[M-ClO_4]^+$	$[M-2ClO_4]^{2+}$
$[18]aneN_4S_2$	41.37 (41.13)	5.79 (5.60)	16.08 (16.20)	2.57 (2.54)		1645	1572	1246	662	3205			
$[Co([18]aneN_4S_2)](ClO_4)_2$	23.77 (23.52)	3.32 (3.20)	9.24 (9.37)	2.57 (2.51)	9.72 (9.55)	1642	1570	1243	662	3200	411	506	407
$[20]aneN_4S_2$	44.66 (44.42)	6.43 (6.25)	14.88 (14.96)	3.00 (2.97)		1641	1570	1244	662	3200			
$[Co([20]aneN_4S_2)](ClO_4)_2$	26.51 (26.34)	3.81 (3.70)	8.83 (8.98)	3.00 (2.93)	9.29 (9.10)	1639	1568	1240	661	3195	410	534	435
$Bzo_2[18]aneN_4S_2$	54.04 (53.88)	4.53 (4.37)	12.60 (12.75)	4.29 (4.23)		1650	1571	1248	661	3286			
$[Co(Bzo_2[18]aneN_4S_2)](ClO_4)_2$	34.20 (34.01)	2.87 (2.69)	7.98 (8.12)	4.29 (4.19)	8.39 (8.14)	1648	1573	1245	664	3280	414	602	503
$Bzo_2[20]aneN_4S_2$	54.04 (53.86)	4.53 (4.40)	12.60 (12.72)	4.29 (4.23)		1648	1571	1248	662	3284			
$[Co(Bzo_2[20]aneN_4S_2)](ClO_4)_2$	34.20 (34.02)	2.87 (2.73)	7.98 (8.14)	4.29 (4.18)	8.39 (8.13)	1645	1573	1246	663	3280	413	602	503
$[Zn([18]aneN_4S_2)](ClO_4)_2$	23.52 (23.35)	3.29 (3.17)	9.14 (9.25)	2.57 (2.52)	10.67 (10.42)	1640	1567	1244	660	3160	403		
$[Zn([20]aneN_4S_2)](ClO_4)_2$	26.24 (26.11)	3.78 (3.57)	8.74 (8.87)	3.00 (2.94)	10.20 (10.04)	1637	1570	1245	662	3150	405		
$[Zn(Bzo_2[18]aneN_4S_2)](ClO_4)_2$	33.89 (33.72)	2.84 (2.69)	7.90 (8.06)	4.29 (4.20)	9.22 (9.08)	1645	1571	1243	663	3100	407		
$[Zn(Bzo_2[20]aneN_4S_2)](ClO_4)_2$	33.89 (33.70)	2.84 (2.70)	7.90 (8.03)	4.29 (4.20)	9.22 (9.10)	1640	1570	1244	664	3100	409		

Table 2
Magnetic moment, electronic spectral and molar conductance values of the tetraoxodithiatetraaza macrocyclic cobalt(II) complexes

Sample	$4T_{1g}(F) \rightarrow 4T_{2g}(F)$ (cm^{-1})	$4T_{1g}(F) \rightarrow 4T_{1g}(P)$ (cm^{-1})	μ_{eff} (MB)	Λ_M[a] (Ω^{-1} cm^2 M^{-1})
$[Co([18]aneN_4S_2)](ClO_4)_2$	15620	19100	4.90	174
$[Co([20]aneN_4S_2)](ClO_4)_2$	15580	19050	4.93	168
$[Co(Bzo_2[18]aneN_4S_2)](ClO_4)_2$	15800	19700	4.89	164
$[Co(Bzo_2[20]aneN_4S_2)](ClO_4)_2$	15760	19620	4.87	160

[a] In DMSO solutions.

X-ray crystallographic studies. The molar conductance values ($\sim$170 Ω^{-1} mol^{-1} cm^2) and measured of tetraoxodithiatetraaza macrocyclic complexes correspond to 1:2 electrolytes. Comparing the obtained magnetic measurement at room temperature and the results of electronic spectra (Table 2) of metal complexes with octahedral Co(II) tetraoxodithiatetraaza macrocycle complexes indicated that the tetraoxodithiatetraaza ligands of this study do not differ significantly from the dithiatetraaza ligands respect to the ligand field strength. The results of elemental analysis (Table 1) support the proposed macrocyclic structure.

The 18- and 20-membered tetraoxodithiatetraaza macrocyclic cobalt(II) complexes undergo intense color changes due to deprotonation of the macrocyclic ligand in the presence of amine bases such as pyridine and Et_3N. Similar N–H deprotonations have been observed with other metal complexes containing N–H linkages. For the cobalt(II) complex, Et_3N is sufficiently basic to facilitate formation of the molecular complex. For preparation of the deprotonation form of $[Co([18]aneN_4S_2)](ClO_4)_2$; triethyleneamine (0.5 ml) was added to a deaerated solution of 200 mg of $[Co([18]aneN_4S_2)](ClO_4)_2$in 15 ml of MeCN. The deep-pink product, which began precipitating within minutes, was filtered after 0.5 h under a N_2 atmosphere, washed with anhydrous EtOH, and dried in a vacuum. IR (KBr, cm^{-1}): 3120 (ν_{N-H}). *Anal.* Calc. for $[Co(C_{12}H_{18}O_4N_4S_2)]$ (I): Co, 14.33; C, 35.40; H, 4.25; N, 13.94. Found: Co, 14.55; C, 35.57; H, 4.48; N, 13.82%. The N–H stretching frequency of this compound $[Co(C_{12}H_{18}O_4N_4S_2)]$, 3120 cm^{-1}, is reduced significantly from its dicationic precursor, $[Co([18]aneN_4S_2)](ClO_4)_2$, 3200 cm^{-1}.

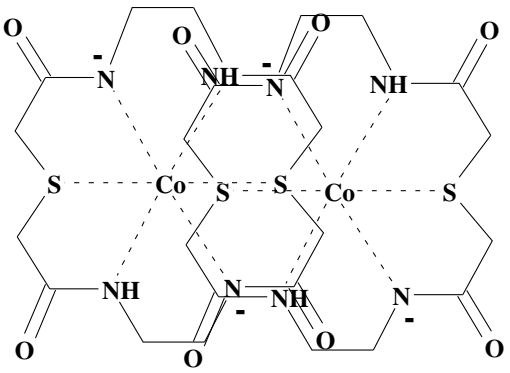

The CHN analysis results of the neat cobalt complexes showed near similarity to the theoretical values. The cobalt contents of the zeolite encapsulated complexes were estimated by dissolving known amounts of the complex in concentric HCl and using AAS. The analytical data of each complex indicate molar ratios of Co:C:H almost close to those calculated for the mononuclear structure (Table 1). However, the presence of minute traces of free metal ions in the lattice could be assumed as the metal content which is slightly higher than the stoichiometric requirement. Only a portion of metal ions in metal-exchanged zeolite has undergone complexation and the rest is expected to be removed on re-exchange with sodium nitrate solution. The Si and Al contents in the metal-exchanged zeolites and the zeolite complexes are almost the same ratio as in the parent zeolite (Table 3). This indicates little changes in the zeolite framework due to the absence of dealumination in metal ion exchange.

The flexible ligand synthesis scheme leads to the encapsulation of Co(II) complexes of tetraoxodithiatetraaza macrocyclic ligands ($[18]aneN_4S_2$, $[20]aneN_4S_2$, $Bzo_2[18]aneN_4S_2$ and $Bzo_2[20]aneN_4S_2$) inside the nanopores of zeolite (Scheme 2). The results of chemical analysis of the samples are given in Table 3. The parent NaY zeolite has Si/Al molar ratio of 2.53 which corresponds to a unit cell formula $Na_{56}[(AlO_2)_{56}(SiO_2)_{136}]$. The unit cell formula of metal-exchanged zeolites shows 11 moles of cobalt dispersion per unit cell ($Na_{34}Co_{11}[(AlO_2)_{56}(SiO_2)_{136}] \cdot nH_2O$). The cobalt contents of all the encapsulated samples very little in the range of 2.5–2.6 wt%. On that basis of these results, along with elemental analysis, the average number of encapsulated Co complexes per nanocavity was determined to be 0.33 for the Co complexes–NaY.

3.3. Powder X-ray diffraction studies

The X-ray diffraction (XRD) patterns of encapsulated complexes are shown in Fig. 1. The encapsulated complex exhibit similar peaks to those of zeolite Y; except for a slight change in the intensity of the peaks, no new crystalline pattern emerges. These facts confirmed that the framework and crystallinity of zeolite were not destroyed during the preparation, and that the complexes were well distributed in the cages. The relative peak intensities of the 220, 311 and 331 reflections have been thought to be correlated to the locations of cations. In zeolite Y, the order of peak intensity is

Table 3
Chemical composition and IR stretching frequencies (as KBr pellets, cm^{-1}) of host (nanopores of zeolite) guest (tetraoxodithiatetraaza macrocyclic cobalt(II) complexes) nanocomposite materials

Sample	C (%)	H (%)	N (%)	C/N	Si (%)	Al (%)	Na (%)	Co (%)	Si/Al	I	II	III	d ↔ d (cm^{-1})
NaY					21.76	8.60	7.50		2.53				
Co(II)–NaY					21.53	8.53	3.36	3.71	2.53				
$[Co([18]aneN_4S_2)]^{2+}$–NaY	4.12	1.73	1.79	2.30	20.92	8.27	5.14	2.68	2.53	1640	1570	3195	15630, 19154
$[Co([20]aneN_4S_2)]^{2+}$–NaY	4.20	1.78	1.57	2.67	20.88	8.25	5.10	2.64	2.53	1634	1566	3190	15603, 19073
$[Co(Bzo_2[18]aneN_4S_2)]^{2+}$–NaY	4.37	1.84	1.08	4.03	20.80	8.22	5.01	2.58	2.53	1645	1571	3276	15830, 19742
$[Co(Bzo_2[20]aneN_4S_2)]^{2+}$–NaY	4.35	1.85	1.06	4.10	20.82	8.23	5.03	2.60	2.53	1643	1572	3275	15781, 19643

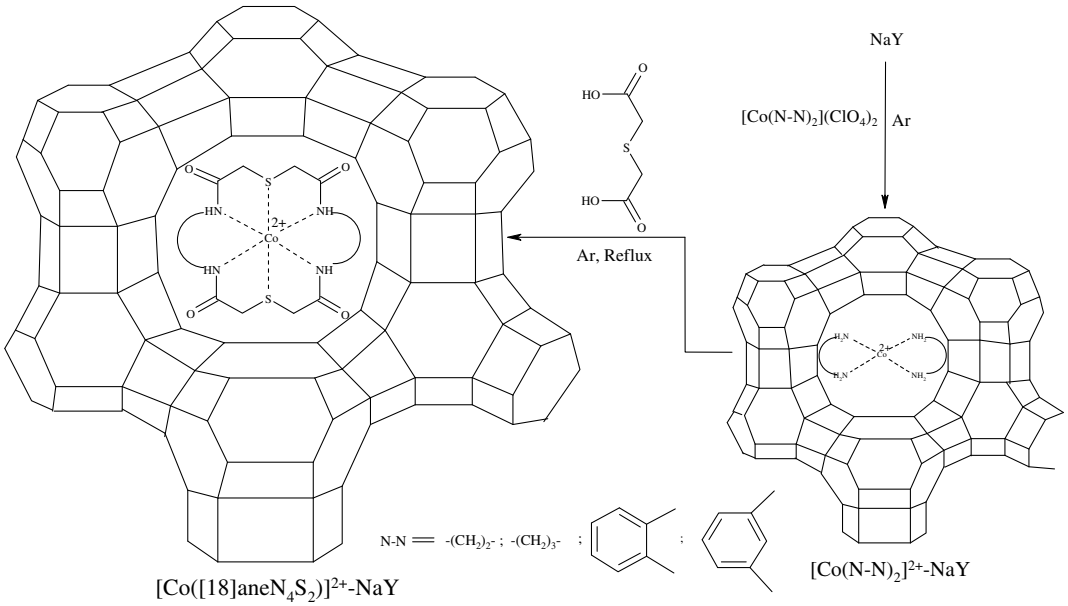

$[Co([18]aneN_4S_2)]^{2+}$-NaY
$[Co([208]aneN_4S_2)]^{2+}$-NaY
$[Co(Bzo_2[18]aneN_4S_2)]^{2+}$-NaY
$[Co(Bzo_2[18]aneN_4S_2)]^{2+}$-NaY

Scheme 2.

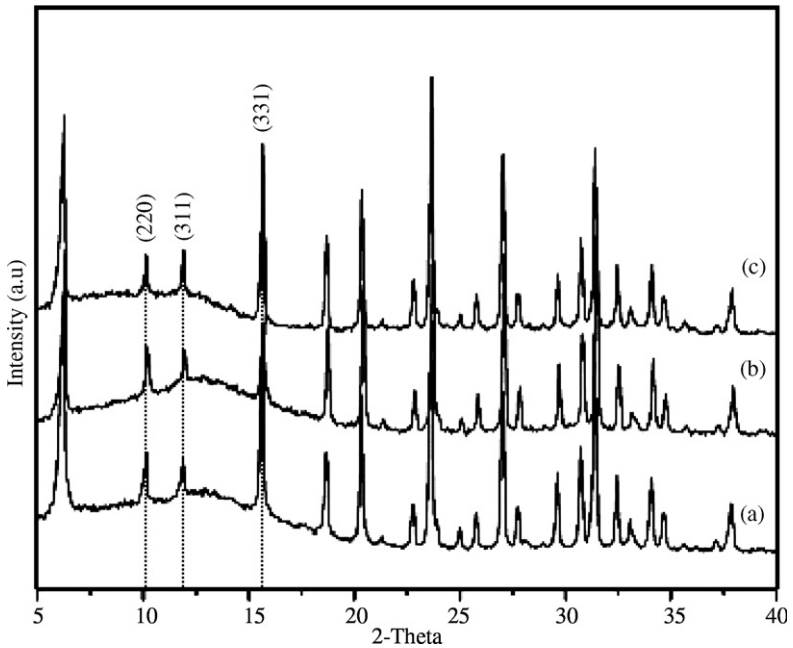

Fig. 1. XRD pattern of (a) zeolite Y, (b) Co–NaY and (c) $[Co([18]aneN_4S_2)]^{+2}$–NaY.

in the order: $I_{331} > I_{220} > I_{311}$, while in encapsulated complexes, the order of peak intensity became $I_{331} > I_{311} > I_{220}$. The difference indicates that the ion-exchanged Co^{2+}, which substitutes at the location of Na+, undergoes rearrangement during complexation.

3.4. Scanning electron micrograph study

The SEM photographs of the samples taken before Soxhlet extraction show the deposition of complexes on the external surface. However, the absence of extraneous materials in the SEM photographs of finished products indicates the complete removal of complexes surface which could be accomplished by extended extraction procedures.

3.5. Electronic spectral studies

The electronic spectra of all tetraoxodithiatetraaza macrocyclic cobalt(II) complexes exhibit absorption in the region 15580–15800 and 19050–19700 cm^{-1} which may be assigned to the $4T_{1g}(F) \rightarrow 4A_{2g}(F)$ and $4T_{1g}(F) \rightarrow 4T_{1g}(P)$ transitions, respectively [27], suggesting an octahedral environment around the cobalt ions in these complexes. Furthermore, magnetic moments measurements in the range 4.87–4.93 BM (Table 2) support the above octahedral geometry [28]. Comparing the obtained magnetic measurement and the results of electronic spectra (Table 1) of metal complexes with octahedral Co(II) macrocycle complexes indicated that the N_4S_2 ligands of this study do not differ significantly from the tetraoxodithiatetraaza ligands respect to the ligand field strength. The diffuse reflectance spectra of Co(II) complexes contain dithiatetraaza macrocycle were almost identical before and after encapsulation, indicating the complexes maintain their geometry even after supported without significant distortion. The UV–Vis spectrum of Co(II)–NaY does not show any absorption band appear in the near-UV region, while spectrum of encapsulated complexes display two broad band at near-UV region, which is probably due to a symmetry forbidden ligand to metal charge transfer transition (Fig. 2). These data compare closely with that of pure complexes as well as of encapsulated complexes and are indicative of an octahedral structure present within the nanodimensional pores of zeolite. Bands due to zeolite encapsulated Co(II) complex appeared in the visible, and charge transfer bands appeared in the near-UV region; these values were very similar to the obtained values for the discrete neat complex [27,28].

3.6. IR spectral study

The infrared spectra of the complexes (Table 1) does not exhibit any band corresponding for the free –NH and –OH groups. Four new bands appear in the spectrum of free ligand in the regions 1637–1650, 1567–1573, 1243–1248 and 660–664 cm^{-1}, assignable to amide **I** [ν(C=O)], amide **II** [ν(C–N)+δ(N–H)], amide **III** [δ(N–H)], and amide **IV** [ϕ(C=O)] bands, respectively, which support the

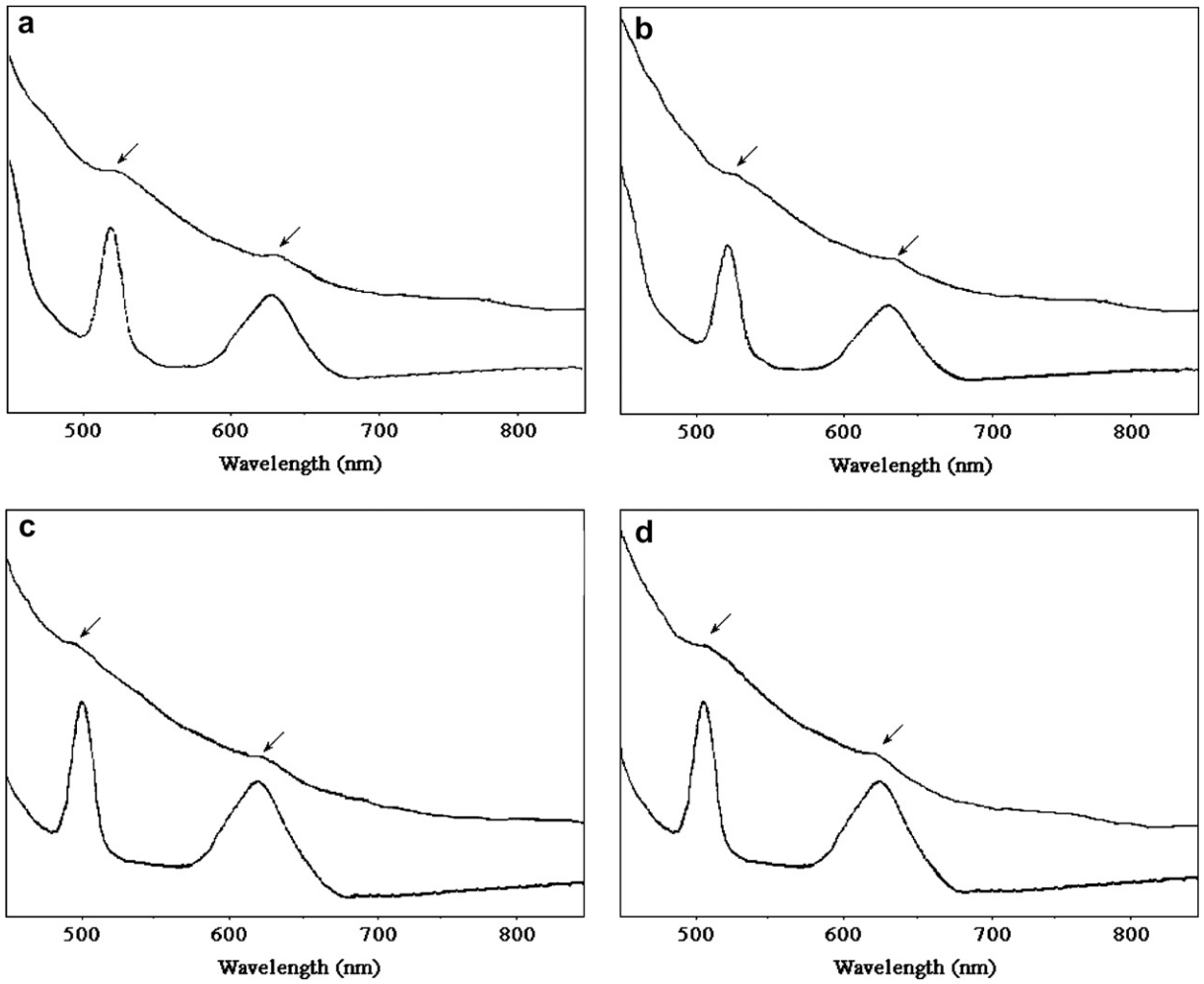

Fig. 2. UV–Vis and DRS spectra of (a) $[Co([18]aneN_4S_2)](ClO_4)_2$, $[Co([18]aneN_4S_2)]^{2+}$–NaY; (b) $[Co([20]aneN_4S_2)](ClO_4)_2$, $[Co([20]aneN_4S_2)]^{2+}$–NaY; (c) $[Co(Bzo_2[18]aneN_4S_2)](ClO_4)_2$, $[Co(Bzo_2[18]aneN_4S_2)]^{2+}$–NaY and (d) $Co(Bzo_2[20]aneN_4S_2)](ClO_4)_2$, $[Co(Bzo_2[20]aneN_4S_2)]^{2+}$–NaY.

macrocyclic structure. A single sharp band observed in the region 3100–3295 cm^{-1}may be assigned to ν(N–H) of the secondary amino group [29,30]. An important feature is the appearance of a new medium intensity band at 403–414 cm^{-1}attributable to ν(M–N) which provide strong evidence for the involvement of nitrogen in coordination [31].

IR spectra of the encapsulated complexes were obtained (Table 3). The intensity of the peaks of encapsulated complex is, though, weak due to low concentration of the complex in zeolite, the IR spectrum of encapsulated complex is essentially similar to that of the free metal complex. No significant broadening or shift of the structure-sensitive zeolite vibrations at 1130 cm^{-1} (due to asymmetric T–O stretch) on encapsulation indicates that there is no significant expansion of the zeolite cavity or dealumination during the encapsulation process. This further indicates that structure of metal complex fit nicely within the nanocavity of the zeolite. The entrapped complexes exhibit very similar IR data that are shifted 2–4 cm^{-1} relative to those of the corresponding free complexes (Table 1). These variations in band frequency can also be attributed to (i) distortions of the complexes, or to (ii) interactions with the zeolitic matrix (by electrostatic effects or co-ordination-the higher negative charge of the zeolite host makes it a stronger ligand). Thus, IR and UV–Vis data indicates the encapsulation of tetraoxodithiatetraaza macrocyclic complexes in the zeolite nanocavity.

3.7. Surface area and pore volume studies

The surface area and nanopore volume of the host–guest nanocomposite materials are presented in Table 4. The encapsulation of cobalt ions and cobalt tetraoxodithiatetraaza macrocyclic complexes reduced the surface area and adsorption capacity of nanopores of zeolite. The lowering of the nanopore volume and surface area supported the fact that cobalt(II) tetraoxodithiatetraaza macrocyclic complexes are present within the zeolite cages and not on the external surface.

3.8. XPS studies

The Co ($2p_{3/2}$) binding energy (E_b) is 857.7 and 856.3 eV in the Co complex in cobalt(II) perchlorate, respectively. The Co ($2p_{3/2}$) binding energy of the cobalt(II) complex has been increased 1.5 eV compared with that of the cobalt(II) chloride. The results indicate that the charge on the metals decreases when complexes were formed. The encapsulated complexes are referenced to the binding energy of 102.7 eV for the Si 2p core level due to its extensive use of this binding energy in NaY system [32–34]. However, the neat complexes are referenced to the binding energy of 292.7 eV for the K $2p_{3/2}$ core level. Table 5 shows the Co 2p core levels of the neat and the encapsulated complexes. Cobalt remains in the +2 oxidation states in both the neat and the encapsulated complexes and it matches well with the reported values for similar systems [35]. There is a high increase in satellite intensity for Co 2p levels and a large energy gap (~16.0 eV) in the encapsulated complex which show the higher stability than the neat complex.

Table 4
Surface area and pore volume data of host (nanopores of zeolite Y) guest (tetraoxodithiatetraaza macrocyclic cobalt(II) complexes) nanocomposite materials

Sample	Surface area[a] (m^2/g)	Pore volume[b] (ml/g)
NaY	545	0.31
Co(II)–NaY	532	0.30
$[Co([18]aneN_4S_2)]^{2+}$–NaY	395	0.18
$[Co([20]aneN_4S_2)]^{2+}$–NaY	388	0.17
$[Co(Bzo_2[18]aneN_4S_2)]^{2+}$–NaY	367	0.14
$[Co(Bzo_2[20]aneN_4S_2)]^{2+}$–NaY	355	0.12

[a] Surface area is the "monolayer equivalent area" calculated as explained in Ref. [22,23].
[b] Calculated by the *t*-method.

Table 5
XPS data of neat and host (nanopores of zeolite Y) guest (tetraoxodithiatetraaza macrocyclic cobalt(II) complexes) nanocomposite materials

Sample	BE, Co $2p_{3/2}$ (eV)	$2p_{3/2}$ and $2p_{1/2}$ separation (eV)
$[Co([18]aneN_4S_2)](ClO_4)_2$	782.1	15.5
$[Co([18]aneN_4S_2)]^{2+}$–NaY	782.9	16.8
$[Co([20]aneN_4S_2)](ClO_4)_2$	782.0	15.4
$[Co([20]aneN_4S_2)]^{2+}$–NaY	782.7	16.7
$[Co(Bzo_2[18]aneN_4S_2)](ClO_4)_2$	782.8	15.8
$[Co(Bzo_2[18]aneN_4S_2)]^{2+}$–NaY	783.4	17.3
$[Co(Bzo_2[20]aneN_4S_2)](ClO_4)_2$	782.6	15.6
$[Co(Bzo_2[20]aneN_4S_2)]^{2+}$–NaY	783.2	17.4

4. Conclusions

By combining surface analysis and spectroscopic data, it was possible to prove that $[Co([18]aneN_4S_2)]^{2+}$, $[Co([20]aneN_4S_2)]^{2+}$, $[Co(Bzo_2[18]aneN_4S_2)]^{2+}$ and $[Co(Bzo_2[20]aneN_4S_2)^{2+}$ can be encapsulated in the FAU nanopores of zeolite NaY by template condensation between preadsorbed; [bis(diamine)cobalt(II)]; (diamine = 1,2-diaminoethane, 1,3-diaminopropane, 1,2-diaminobenzene, 1,3-diaminobenzene); $[Co(N–N)_2]^{2+}$–NaY; and the corresponding thiodiglycolic acid, without damage of the main framework of the zeolite or loss of its crystallinity. The data indicate that all cobalt(II) complexes in NaY zeolite exhibit structural and electronic properties that are different from those of the same complexes encapsulated in NaY, which have been shown to be mainly physically entrapped in the FAU supercages, with no significant interaction with the zeolite matrix. Spectroscopic data (FT-IR, XRD, XPS and DRS) and BET technique for the encapsulated complexes in NaY suggest host/guest interactions within the zeolite.

Acknowledgement

Author is grateful to Council of University of Kashan for providing financial support to undertake this work.

References

[1] S.R. Cooper, Acc. Chem. Res. 21 (1988) 141.
[2] S.C. Rawle, S.R. Cooper, Struct. Bond. 72 (1991) 1.
[3] K. Wieghardt, P. Chaudhuri, Prog. Inorg. Chem. 35 (1987) 329.
[4] R. Bhula, P. Osvath, D.C. Weatherburn, Coord. Chem. Rev. 91 (1988) 89.
[5] S. Chandrasekhar, A. McAuley, Inorg. Chem. 31 (1992) 2234.
[6] K. Brand, W.S. Sheldrick, J. Chem. Soc., Dalton Trans. (1996) 1237.
[7] C. Landgrafe, W.S. Sheldrick, J. Chem. Soc., Dalton Trans. (1996) 989.
[8] G.J. Grant, K.E. Rogers, W.N. Setzer, D.G. Van Derveer, Inorg. Chim. Acta 234 (1995) 35.
[9] P.R. Ashton, A.L. Burns, C.G. Claessens, G.K. Shimizu, K. Small, J.F. Stoddart, A.P.J. White, D.J. Williams, J. Chem. Soc., Dalton Trans. (1997) 1493.
[10] J. Casabo, L. Escriche, S. Alegret, C. Jaime, C.P. Jimenez, L. Mestres, J. Rius, E. Molind, C. Miravitlles, F. Teixidor, Inorg. Chem. 30 (1991) 1893.
[11] M.P. Suh, K.Y. Oh, J.W. Lee, Y.Y. Boe, J. Am. Chem. Soc. 118 (1996) 777.
[12] L. Fabrizzi, T.A. Kaden, A. Perotti, B. Seghi, L. Siegfried, Inorg. Chem. 25 (1986) 321.
[13] A.J. Blake, R.O. Gould, A.J. Holder, T.I. Hyde, A.J. Lavery, M.O. Odulate, M. Schröder, J. Chem. Soc., Chem. Commun. (1987) 118.
[14] J.D. Woollins, P.F. Kelly, Coord. Chem. Rev. 65 (1985) 115.
[15] S. Ray, S. Vasudevan, Inorg. Chem. 42 (2003) 1711.
[16] M.A. Zanjanchi, K. Tabatabaeian, M. Moosavifar, J. Inclusion Phenom. Macrocycle Chem. 40 (2001) 193.
[17] M. Salavati-Niasari, Chem. Lett. 34 (2005) 1444.
[18] (a) K.O. Xavier, J. Chacko, K.K. Mohammed Yusuff, J. Mol. Catal. A: Chem. 178 (2002) 275;
(b) A. Kumar, G.S. Mishra, A. Kumar, J. Mol. Catal. A: Chem. 201 (2003) 179.
[19] (a) F. Schüth, W. Schmidt, Adv. Mater. 14 (2002) 629;
(b) F. Schuth, K. Sing, J. Weitkamp (Eds.), Handbook of Porous Solids, vol. I–V, Wiley-VCH, Weinheim, 2002.

[20] (a) I.F.J. Vankelecom, R.F. Parton, M.J.A. Casselman, J.B. Uytterhoeven, P.A. Jacobs, J. Catal. 163 (1996) 457;
(b) P.G.N. Mertens, H. Poelman, X. Ye, I.F.J. Vankelecom, P.A. Jacobs, D.E. De Vos, Catal. Today 122 (2007) 352;
(c) N. Herron, J. Coord. Chem. 19 (1988) 25;
(d) D.E. de Vos, P.P. Knops-Gerrits, D.L. Vanoppen, P.A. Jacobs, Supramol. Chem. 6 (1995) 49;
(e) P.P. Knops-Gerrits, D.E. de Vos, P.A. Jacobs, J. Mol. Catal. A: Chem. 117 (1997) 57;
(f) M.R. Maurya, S.J.J. Titinchi, S. Chand, J. Mol. Catal. A: Chem. 214 (2004) 257;
(g) D. Chatterjee, H.C. Bajaj, A. Das, K. Bhatt, J. Mol. Catal. 92 (1994) L235;
(h) R. Raja, P. Ratnaswamy, J. Catal. 170 (1997) 244;
(i) M.L. Kantam, K.V.S. Ranganath, M. Sateesh, K.B.S. Kumar, B. Manoranjan, J. Mol. Catal. A: Chem. 225 (2005) 15;
(j) C. Hardacre, S.P. Katdare, D. Milroy, P. Nancarrow, D.W. Rooney, J.M. Thompson, J. Catal. 227 (2004) 44;
(k) V.R. Choudhary, S.K. Jana, N.S. Patil, S.K. Bhargava, Micropor. Mesopor. Mater. 57 (2003) 21;
(l) P.K. Dutta, J. Inclusion Phenom. Mol. Recog. Chem. 21 (1995) 215.
[21] (a) M. Hartman, Angew. Chem., Int. Ed. 39 (2000) 888;
(b) M. Salavati-Niasari, Inorg. Chem. Commun. 9 (2006) 628;
(c) M. Salavati-Niasari, F. Davar, Inorg. Chem. Commun. 9 (2006) 263;
(d) M. Salavati-Niasari, F. Davar, Inorg. Chem. Commun. 9 (2006) 304;
(e) M. Salavati-Niasari, J. Mol. Catal. A: Chem. 245 (2006) 192;
(f) M. Salavati-Niasari, J. Mol. Catal. A: Chem. 229 (2005) 159;
(g) M. Salavati-Niasari, Chem. Lett. 34 (2005) 244;
(h) M. Salavati-Niasari, Inorg. Chem. Commun. 8 (2005) 174;
(i) M. Salavati-Niasari, Inorg. Chem. Commun. 7 (2004) 963;
(j) M. Salavati-Niasari, J. Mol. Catal. A: Chem. 217 (2004) 87.
[22] S.W. Wang, H. Everett, R.A.W. Haul, L. Moscou, R.A. Pierotti, J. Rouquerol, T. Siemieniewska, Pure Appl. Chem. 57 (1985) 603.
[23] A. Lineares-Solano, Textural characterization of porous carbons by physical adsorption of gases, in: J.L. Figueiredo, J.A. Moulijn (Eds.), Carbon and Coal Gasification, M. Nijhoff, M.A. Dordrecht, 1986, p. 137.
[24] S. Chandra, L.K. Gupta, Spectrochim. Acta, Part A 62 (2005) 1102.
[25] S.C. Rawle, A.J. Clarke, P. Moore, N.W. Alcock, J. Chem. Soc., Dalton Trans. (1992) 2755.
[26] I. Tabushi, Y. Taniguchi, H. Kato, Tetrahedron Lett. 12 (1977) 1049.
[27] A.B.P. Lever, Inorganic Electronic Spectroscopy, Elsevier, Amsterdam, 1984.
[28] F.A. Cotton, G. Wilkinson, Advanced Inorganic Chemistry, 5th ed., Wiley, New York, 1988.
[29] M. Shakir, S.P. Varkey, P.S. Hameed, Polyhedron 12 (1993) 2775.
[30] S. Chandra, L.K. Gupta, Spectrochim. Acta, Part A 60 (2004) 1751.
[31] K. Nakamoto, Infrared Spectra of Inorganic and Coordination Compounds, Wiley Interscience, New York, 1970.
[32] E.E. Mercer, R.R. Buckley, Inorg. Chem. 4 (1981) 1692.
[33] L.A. Pederson, J.H. Lunsford, J. Catal. 61 (1980) 39.
[34] T.L. Barr, in: D. Briggs, M.P. Seah (Eds.), Practical Surface Analysis, Wiley, New York, 1980.
[35] L. Guczi, R. Sundararajan, Zs. Koppany, Z. Zsoldos, Z. Schay, F. Mizukami, S. Niwa, J. Catal. 167 (1997) 482.

Although the coordination chemistry of *S*-alkyl and *S*-benzyldithiocarbazate Schiff bases derived from orthohydroxy aldehydes and ketones [16–18], β-diketones [19–21] as well as β-*N*-heterocyclic aldehydes and ketones [22–25] have been extensively studied, less attention, however, was paid for Schiff bases obtained from the condensation of *S*-methyl and *S*-benzyldithiocarbazate with diacetylmonoxime (**1**) [26]. In the present work, the synthesis, characterization and X-ray crystal and molecular structures of some nickel(II) complexes derived from diacetylmonoxime *S*-benzyldithiocarbazonate have been studied aiming to search for new building blocks capable to form extended supramolecular assemblies via interligand or ligand–solvent hydrogen bonding.

2. Experimental

2.1. Materials

Diacetylmonoxime was obtained from Sigma, while pyrazole and imidazole were obtained from Aldrich and used without further purification.

2.2. Preparation of diacetylmonoxime S-benzyldithiocarbazonate (H_2L) (**1**)

A solution of *S*-benzyldithiocarbazate (1.98 g, 10 mmol) in ethanol (50 ml) was added to a solution of diacetylmonoxime (1.01 g, 10 mmol) in the same solvent (50 ml). The reaction mixture was heated under reflux for 2 h during which a white precipitate was formed. After cooling to room temperature, the solid product was isolated by filtration. The crude product was crystallized from ethanol then dried in vacuo. Yield: 75%. M.p. 210 °C, *Anal.* Calc. for $C_{12}H_{15}N_3OS_2$: C, 51.22; H, 5.37; N, 14.93, Found: C, 51.34; H, 5.42; N, 14.85%. IR (KBr) (cm^{-1}): 3412m ν(O–H); 3288m ν(N–H); [3155m, 2924m ν(C–H)]; 1641m,1606m $\nu(C{=}N)_{hy}$; 1485s,1449m,1419s, 1366m, 1281s, 1232m, 1140m, 1072s, 975m, 928m, 714m, 702m. UV–Vis (EtOH, λ_{max}/nm ($\log\varepsilon$)): 289(4.10); 322(4.50); 0.007 M KOH (EtOH): 273(4.06); 325(4.04); 370sh. ^{1}H NMR (DMSO-d_6, TMS, ppm): 12.47 (1H, oxime OH); 11.79 (1H, CONH); 7.40 (2H, m, aromatic); 7.30 (2H, m, aromatic); 7.24 (1H, m, aromatic); 4.46 (2H, s, SCH_2); 2.19 (3H, s, $CH_3C{=}NN$), 1.95 (3H, s, $CH_3C{=}NO$). $^{13}C\{^1H\}$ NMR (DMSO-d_6, TMS, δ): 198.68 (C=S); 154.11 (C=N-OH); 150.76 (C=N–NH); 136.77, 129.13, 128.38, 127.08 (CH- aromatic); 12.23 (CH_3–C=NOH); 9.16 (CH_3–C=N · N).

2.3. Preparation of nickel(II) complexes

2.3.1. Preparation of $[Ni(L)]_2$ (**2**)

A solution of nickel(II) acetate tetrahydrate (1.0 mmol, 0.281 g) in ethanol (30 ml) was added to a suspension of diacetylmonoxime-*S*-benzyldithiocarbazonate (1.0 mmol, 0.248 g) in ethanol (50 ml). The resulting mixture was treated with a solution of KOH (0.02 mol) in ethanol (20 ml). On refluxing the reaction mixture with stirring for 1 h a red precipitate was formed. It was then filtered, washed with hot ethanol (3 × 5 ml) and dried in vacuo, over anhydrous calcium chloride. *Anal.* Calc. for $C_{24}H_{26}N_6O_2S_4Ni_2$: C, 42.63; H, 3.88; N, 12.34, Found: C, 42.33; H, 3.85; N, 21.46%. IR (KBr) (cm^{-1}): 3059m, 3027m, 2915m, 1644m, 1627m,1600m $\nu(C{=}N)_{hy}$; 1571m, 1522m, 1535m, 1518m $\nu(C{=}N)_{ox}$; 1458s, 1429s, 1386s, 1350m, 1255m, 1214vs, 1186s, 1136s, 1136s, 1099s, 1070m, 1039vs, 990m, 940m, 787m, 769m, 720. Electronic spectrum ($CHCl_3$, λ_{max}/nm ($\log\varepsilon$)): 271(4.16), 315(4.22), 350(4.06), 366sh, 425sh, 445sh, 615sh, 660(2.47). ^{1}H NMR (DMSO-d_6, TMS, ppm), 7.10–7.30 (5H, m, aromatic), 4.20 (2H, s, SCH_2), 1.90 (3H, s, $CH_3C{=}NN$), 1.72 (3H, s, $CH_3C{=}NO$). FD MS, m/z = 674 (100%).

2.3.2. Preparation of [NiL · HPyr] (**3**)

To a suspension of dimeric $[Ni(L)]_2$ complex (1.0 mmol, 0.338 g) in ethanol (50 ml), a sufficient amount of solid pyrazole (5.0 mmol, 0.34 g) was added and the reaction mixture was heated under reflux until complete dissolution. The reaction mixture was filtered to remove any unreacted starting material and the filtrate was evaporated to half its volume. On cooling, the pyrazole nickel complex which separated out was filtered, washed with diethyl ether (3 × 5 ml) and dried in vacuo over anhydrous calcium chloride.

Anal. Calc. for $C_{15}H_{17}N_5OS_2Ni$: C, 44.36; H, 4.22; N, 17.24, Found: C, 44.78; H, 4.35; N, 16.45%. IR (KBr) (cm^{-1}): 3145w ν(N–H), 3119s, 3060, 3033w, 3007w, 2928m, 2851w [ν(N–H) + ν(C–H)]; 1642m, 1624m, 1598w; 1570m; 1450s, 1390m, 1342s, $NCSSCH_2C_6H_5$: 1220s, 1174s, 1130vs, 1067s, 1040vs, 945m, 925m, 850m, 815m, 777s, 759s, 710m. Electronic spectrum ($CHCl_3$, λ_{max}/nm ($\log\varepsilon$)): 310(4.31), 375(3.87), 385(3.90), 440sh, 445sh 552(2.69), 625sh. ^{1}H NMR ($CDCl_3$, TMS, ppm), 7.26–7.34(8H, m, aromatic + pyrazole), 6.22 (1H, CONH), 4.32 (2H, s, SCH_2), 2.18 (3H, s, $CH_3C{=}NN$), 2.00 (3H, s, $CH_3C{=}NO$). FD MS, m/z = 676 (100%).

2.3.3. Preparation of [NiL · HIm] (**4**)

The imidazole complex [NiL · HIm] was prepared from the reaction of $[Ni(L)]_2$ complex with excess imidazole using the same procedure described for the corresponding pyrazole complex.

Anal. Calc. for $C_{15}H_{17}N_5OS_2Ni$: C, 44.36; H, 4.22; N, 17.24, Found: C, 44.04; H, 4.24; N, 17.45%. IR (KBr) (cm^{-1}): 3100s ν(N–H), 3026s, 2929s, 2847s [ν(N–H)+ν(C–H)]; 1598w; 1570w, 1537w, 1490m; 1475s, 1446vs, 1383m, 1327m, 1260vs, 1193m, 1148s, 1095s, 1070s, 1038vs, 939m, 910m, 846m, 769m, 742s, 699s. Electronic spectrum (saturated solution in $CHCl_3$, λ_{max}/nm): 322, 380, 600sh, 650sh. ^{1}H NMR (DMSO-d_6, TMS, ppm), 12.60 (1H, CONH), 7.87 (1H, N=C*H*–NH, imidazole), 7.28–7.31(5H, m, aromatic), 7.0 (2H, CH=CH, imidazole) 4.27 (2H, s, SCH_2), 2.17 (3H, s, $CH_3C{=}NN$), 1.70 (3H, s, $CH_3C{=}NO$). FD MS, m/z = 674 (100 %).

2.3.4. Preparation of $[Ni(HL)_2] \cdot H_2O$ (**5**)

A solution of nickel(II) acetate tetrahydrate (1.0 mmol, 0.248 g) in ethanol (30 ml) was added dropwise, with constant stirring, to a suspension of diacetyl-*S*-benzyldithiocarbazonate (2.0 mmol, 0.562 g) in ethanol (50 ml). The reaction mixture was then refluxed with constant stirring for 30 min. The dark green crystals which were separated on cooling were filtered off, washed several times with hot ethanol (3 × 5 ml) then dried over anhydrous calcium chloride. *Anal.* Calc. for $C_{24}H_{30}N_6O_3S_4Ni$: C, 44.98; H, 4.92; N, 12.82, Found: C, 44.66; H, 4.43; N, 12.76%. IR (KBr) (cm^{-1}): 3175m, 3060m, 3029m, 2970m, 2923m, 2848m, 1624m, 1600m, 1535m, 1491m, 1448s, 1407vs, 1371vs, 1292vs,1233m, 1180s, 1158m, 1060s, 1017vs, 981s, 928m, 822m, 769m, 706m. Electronic spectrum (in $CHCl_3$, λ_{max}/nm ($\log\varepsilon$)): 325 (4.49), 375 (4.21), 466sh,565 (1.1) 655sh, 750 (0.70), 890 (0.50).

2.4. Physical measurements

The infrared spectra were recorded on a Perkin–Elmer 1430 Data system and/or a Perkin–Elmer (FT-IR) Paragon 1000 PC spectrophotometer. Calibrations of frequency reading were made with polystyrene film. Solid samples were examined as KBr discs. The ultraviolet and visible absorption spectra were recorded on double beam ratio recording Lambada 4B Perkin–Elmer spectrophotometers. ^{1}H NMR and ^{13}C NMR were recorded on Brucker WM 300 (300 MHz) instrument. Mass spectra were recorded on Esquire-LC from Bruker Daltonic Nebulizer 10 psi (dry gas 8 L/min., dry temp. 250 °C). Magnetic susceptibilities of powdered dried samples were recorded on a Faraday-type magnetometer using a sensitive computer controlled D-200 Cahn RG microbalance. The magnetic field applied was ~1.5 T. Experimental susceptibility

data were corrected for the underlying diamagnetism using Pascal's constants.

X-ray diffraction data were collected on CRYSALIS CCD, Oxford Diffraction limited, version 1.70.14 (2002), using graphite monochromated Mo Kα radiation ($\lambda = 0.71013$ Å). The structures were solved by direct method with SHELXS-97 [27]; refinement was done by full-matrix least squares on F^2 using the SHEXL-97 [27]. Drawings of the molecules were produced with ORTEP 3 [28] or PLATON [29].

3. Results and discussion

3.1. Synthesis and characterization

Similar to other NNO and NNS tridentate hydrazoneoximes [13–15,30], the reaction of diacetylmonoxime-*S*-benzyldithiocarbazonate (H_2L) (**1**) with nickel(II) acetate tetrahydrate, using 1:1 molar ratio, in presence of KOH proceeded with the deprotonation of both oxime and thiolimine residues and eventually gave the dinuclear complex [{NiL}$_2$] (**2**). Both electron impact and field desorption mass spectra of [{NiL}$_2$] show a base peak at $m/z = 676$, confirming dimerization via oximate bridges [31]. The absence of both oxime ν(O–H) and hydrazone ν(N–H) from the IR spectrum of **2** is in agreement with this assignment. The dinuclear [{NiL}$_2$] was found to be diamagnetic indicating square planar arrangement with $^1A_{1g}$ ground state. The solution absorption electronic spectrum in $CHCl_3$ is also diagnostic of square planar environment around each Ni(II) ion. The spectrum shows absorptions at 270, 315 and 350 nm originated from different L–L* transitions of the dinegative hydrazoneoxime ligand, while absorptions at 360 and 400 nm can be assigned to LMCT transitions. The d–d transitions ($^1A_{1g}$–$^1B_{1g}$, $^1B_{3g}$) appear at 425 and 445 nm. The absorptions at low energy side at 615sh and 660sh nm can be safely related to MLCT transitions [32–34]. The ^{1}H NMR spectrum of **2** in DMSO-d_6 displays two singlets at 1.72 and 1.90 ppm, respectively, due to two non-equivalent (CH_3–C=N) and (CH_3–C=NO) methyl groups, in addition to a CH_2 singlet at 4.21 ppm. The NH and OH singlets, which appear at 11.798 and 12.47 ppm in the spectrum of the metal free ligand, disappeared from the spectrum of the **2**, confirming the deprotonation of both oxime and enolimine groups.

Reaction of [{NiL}$_2$] (**2**) with excess pyrazole (HPyr) or imidazole (HIm) in methanol proceeds with the rupture of the oximate bridges and eventually gives the monomeric [NiL · HPyr] (**3**) or [NiL · HIm] (**4**) complexes. The IR spectra of both **3** and **4** lack absorptions attributable to oxime ν(O–H) and hydrazone ν(N–H) but show a medium absorption at 3145 and 3100 cm^{-1}, respectively, due to pyrazole and imidazole ν(N–H), implying the deprotonation of both oxime (O–H) and thiol SH of the thiolimine tautomer. Both **3** and **4** were found to be dia-

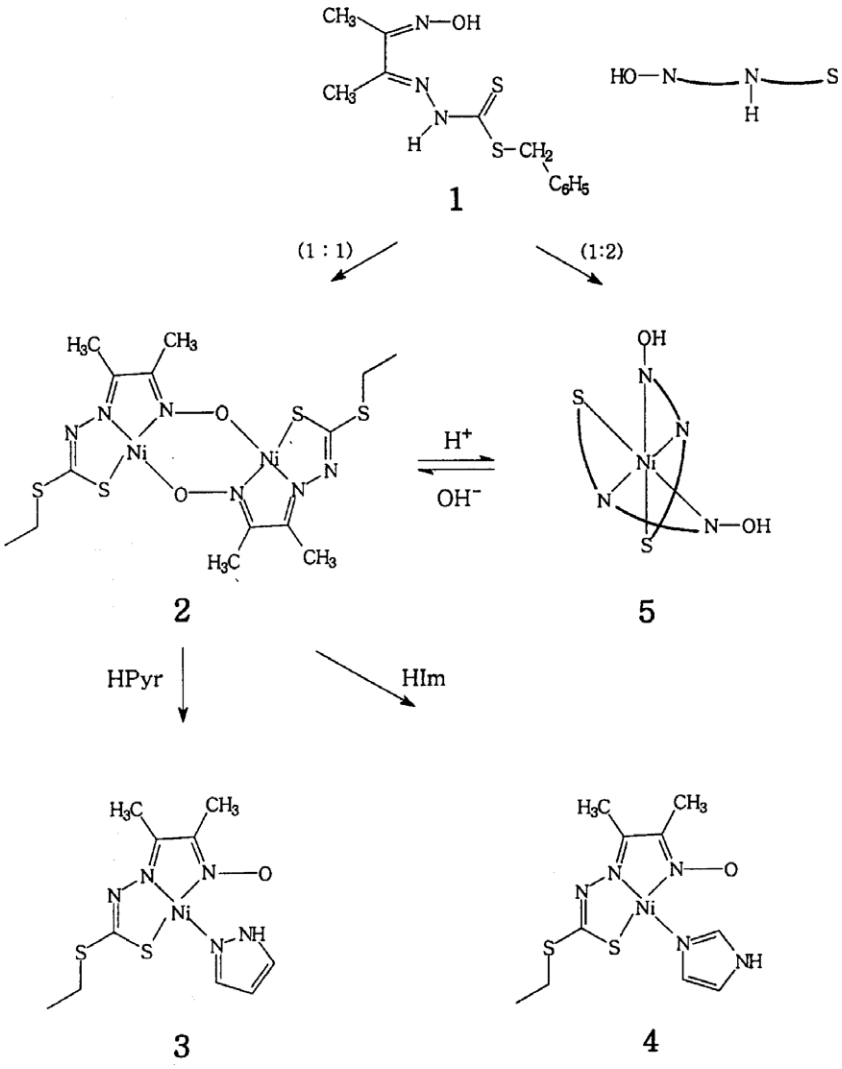

magnetic, implying square planar arrangement around the Ni(II) ion. The electronic absorption spectrum of **3**, in $CHCl_3$, shows absorptions at 315 and 370 nm originating from different L–L* transitions, besides relatively lower intense absorption at 385 nm due to LMCT transition. The d–d* transitions ($^1A_{1g} \rightarrow {}^1B_{1g}$, $^1B_{3g}$) appears at 440 and 445 nm. The two broad unresolved bands at lower energies 552 and 625 nm can be related to MLCT transitions usually observed in the spectra of square planar Ni(II) complexes with sulphur containing ligands [35]. The spectrum of **4** also displays the L–L* and MLCT bands at 322 and 380 nm, respectively. The d–d transitions cannot be observed, most probably hidden under the relatively intense LMCT band at 380 nm. Here again, the spectrum displays the MLCT transitions at 600 and 650 nm. The ^1H NMR spectra of both **3** and **4** are more or less similar and display the two non-equivalent methyl signals at *ca* 2.00 and 2.18 ppm, besides the methylene protons at *ca* 4.30 ppm. The pyrazole and imidazole N–H protons appear at 6.22 and 6.29 ppm, respectively.

Careful acidification of the dimeric $[\{NiL\}_2]$ resulted in the formation of bisligand complex $[Ni(HL)_2]\cdot H_2O$ (**5**). This bisligand complex can be also prepared by reacting the hydrazoneoxime (H_2L) (**1**) with nickel(II) acetate tetrahydrate in methanol, using (2:1) molar ratio. Deprotonation of $[Ni(HL)_2]$ (**5**) with KOH in methanol afforded the dimeric $[\{NiL\}_2]$ (**2**) complex. The prepared bisligand Ni(II) complex is paramagnetic with $\mu = 3.32\ \mu_\beta$ suggesting octahedral structure. The electronic absorption spectrum is in agreement with this assignment. In $CHCl_3$ the spectrum shows the L–L* absorptions at 325 and 375 (sh) nm, besides a broad band centered at 560 nm, most probably, due to MLCT transitions. The spectrum also shows a series of weak broad absorptions at *ca* 750 and 890 nm corresponding to $^3A_{2g}$–$^3T_{1g}$(F), $^3T_{2g}$ transitions in octahedral symmetry [34].

3.2. Electrospray ionization mass spectra (ESI MS)

The positive mode ESI MS of the prepared nickel(II) complexes can assist for better understanding the behaviour of these complexes in solutions, since the generated ions in the gas phase closely reflect those in solution [36,37]. The cations displayed in the recorded ESI MS of $[\{Ni(L)\}_2]$, $[Ni(HL)_2]$, [NiL · HPyr] and [NiL · HIm] together with their assignments are listed in Table 1. The *m*/*z* values are given for the most intense peak in the isotope mass distribution. In all cases the observed isotope distribution patterns are well matched with the simulated patterns [38]. The observed association of Na^+ with many cations came from traces of Na^+ often present even in HPLC grade solvents or from the instrument [37].

The ESI mass spectrum of $[\{NiL\}_2]$ (**2**) display peaks at *m*/*z* = 339, 677 and 698, corresponding to $[\{NiL\}_2 + 2H]^{2+}$, $[\{NiL\}_2 + H]^{1+}$ and $[\{NiL\}_2 + Na]^{1+}$ species, confirming the dimeric structure (**2**). The spectrum also shows a peak at *m*/*z* = 412 attributed to the presence of a solvated cation $[NiL \cdot DMF + H]^{1+}$ originating from the rupture of the oximate bridges in the coordinating solvent DMF.

The positive ion ESI MS spectrum of [NiL · HPyr] (**3**) lacks any peak attributable to the monomeric $[NiL \cdot HPyr + H]^{1+}$ cation. The spectrum, however, shows a base peak at *m*/*z* = 643 corresponding to the dipositive cyclic trimeric cation, $[Ni_3L_3Pyr_3 + 2H + 3Na]^{2+}$ ($[\mathbf{6} + 2H]^{2+}$). The formation of ($[\mathbf{6} + 2H]^{2+}$) may initially proceed by the deprotonation of the pyrazole NH proton followed by self assembly which ultimately gives the cyclic trimeric species where the oximate groups are associated with protons or Na^+ ions. This is in quite agreement with the coordination chemistry of metal(II) complexes with pyrazole and pyrazole containing ligands [7,15,39–42]. The spectrum also displays two peaks at *m*/*z* = 677 and 699 which can be assigned as $[\{NiL\}_2 + H]^{1+}$ and $[\{NiL\}_2 + Na]^{1+}$, respectively. The formation of these dinuclear cations initially pro-

Table 1
Positive mode ESI mass spectra of $[\{NiL\}_2]$, [NiL · HPyr], [NiL · HIm] and $[Ni(L)_2]\cdot H_2O$

Complex	Solvent	*m*/*z* Found (calc.)	RA (%)	Assignment
$[\{NiL\}_2]$ (**2**)	DMF/CH_3OH	339.0 (339.0842)	15.0	$[\{NiL\}_2 + 2H]^{2+}$
		413.2 (412.1785)	29.0	$[NiL \cdot DMF + H]^{1+}$
		677.0 (677.1603)	8.0	$[\{NiL\}_2 + H]^{1+}$
		698.0 (699.1422)	100.0	$[\{NiL\}_2 + Na]^{1+}$
[NiL · HPyr] (**3**)	THF/DMSO	644.1(643.2115)	100.0	$[Ni_3L_3Pyr_3 + 2H + 3Na]^{2+}$ $[\mathbf{6} + 2H]^{2+}$
		677.0 (677.1603)	56.5	$[\{NiL\}_2 + H]^{1+}$
		698.0 (699.1422)	25.0	$[\{NiL\}_2 + Na]^{1+}$
		981.0 (980.5443)	15.0	$[Ni_2(HL)_2L + Na]^{1+}$ $[\mathbf{7} + Na]^{1+}$
		1036.0 (1036.6971)	4.0	$[Ni_2(HL)_2L + DMSO + H]^{1+}$ $[\mathbf{7} + H]^{1+}$
[NiL · HIm] (**4**)	DMF/CH_3OH	338.0 (339.0842)	33.0	$[\{NiL\}_2 + 2H]^{2+}$
		356.0 (357.3577)	30.7	$[\{NiL\}_4 \cdot DMF + 4H]^{4+}$ $[\mathbf{11} + DMF + 4H]^{4+}$
		(368.3487)	19.2	$[\{NiL\}_4 \cdot DMF + 2H + 2Na]^{4+}$ $[\mathbf{11} + DMF + 2H + 2Na]^{4+}$
		396.0 (395.1050)	100.0	$[\{NiL\}_2 \cdot HIm + 2Na]^{2+}$
		424.0 (425.8707)	15.4	$[\{Ni(HL)Im\}_4 \cdot DMF + 4H]^{4+}$ $[\mathbf{10} + DMF + 4H]^{4+}$
		677.0 (677.1603)	8.0	$[\{NiL\}_2 + H]^{1+}$
		763.0 (768.2282)	14.6	$[Ni_2L_2Im + H + Na]^{1+}$
		791.2 (789.2022)	34.6	$[Ni_2L_2Im + 2Na]^{1+}$
$[Ni(HL)_2]\cdot H_2O$ (**5**)	DMF/CH_3OH	338.0 (339.0842)	12.5	$[\{NiL\}_2 + 2H]^{2+}$
		620.1 (620.4862)	15.0	$[Ni(HL)_2 + H]^{1+}$
		659.0 (659.8142)	29.0	$[Ni_3(HL)_2L_2 + H + Na]^{2+}$ $[\mathbf{8} + H + Na]^{2+}$
		677.0 (677.1603)	100.0	$[\{NiL\}_2 + H]^{1+}$
		958.0 (958.5624)	6.6	$[Ni_2L_3 + H]^{1+}$ $[\mathbf{7} + H]^{1+}$
		1298.0 (1296.63861)	6.0	$[Ni_3(HL)_2L_2 + H]^{1+}$ $[\mathbf{8} + H]$

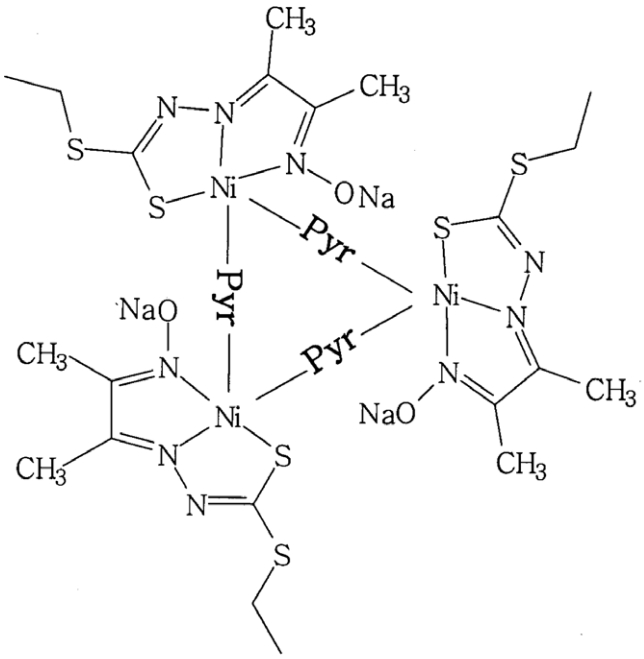

6

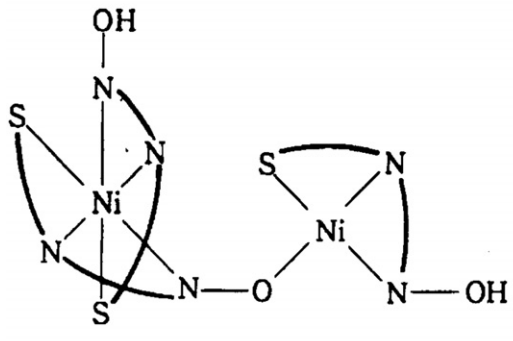

7

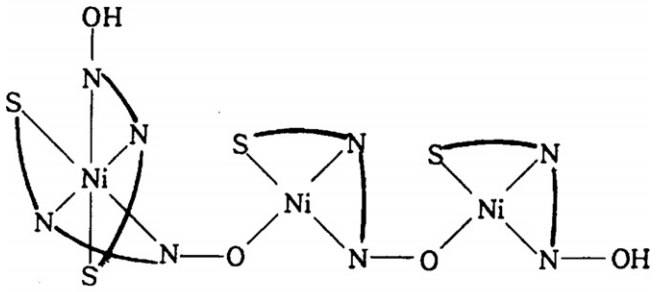

8

Table 2
Crystal data and structure refinement for [NiL · Hpyr], [NiL · HIm] and $[Ni(HL)_2] \cdot H_2O$

	[NiL · Hpyr] (**3**)	[NiL · HIm] (**4**)	$[Ni_2(HL)_4] \cdot H_2O$ (**5**)
Empirical formula	$C_{15}H_{17}N_5NiOS_2$	$C_{15}H_{17}N_5NiOS_2$	$C_{48}H_{58}N_{12}Ni_2O_5S_8$
Formula weight	406.17	406.17	628.48
Temperature (K)	293(2)	299(2)	293(2)
Wavelength (Å)	0.71073	0.71073	0.71073
Crystal system	monoclinic	monoclinic	monoclinic
Space group	*P*21	*P*21/*c*	*C*2/*c*
Unit cell dimensions			
a (Å)	8.2173(8)	10.8760(10)	26.385(2)
b (Å)	5.7493(7)	19.943(2)	7.913(2)
c (Å)	18.602(2)	16.852(2)	29.544(5)
α (°)	90	90	90
β (°)	91.543(8)	102.919(8)	112.71(2)
γ (°)	90	90	90
Volume (Å^3)	878.51(17)	3562.7(6)	5690.1(18)
Z	2	8	4
D_{calc} (Mg m^{-3})	1.535	1.514	1.467
Absorption coefficient (mm^{-1})	1.354	1.336	1.011
F(000)	420	1680	2616
Crystal size (mm)	0.60 × 0.06 × 0.04	0.20 × 0.16 × 0.12	0.80 × 0.06 × 0.04
θ Range for data collection (°)	4.17–26.36	4.57–26.37	2.72–28.05
Limiting indices	$-10 \leqslant h \leqslant 10$, $-4 \leqslant k \leqslant 7$, $-23 \leqslant l \leqslant 23$	$-13 \leqslant h \leqslant 12$, $-23 \leqslant k \leqslant 23$, $-21 \leqslant l \leqslant 21$	$-34 \leqslant h \leqslant 34$, $-10 \leqslant k \leqslant 10$, $-37 \leqslant l \leqslant 38$
Reflections collected	5884	15230	25918
Independent reflections (R_{int})	2256 (0.0495)	6730 (0.0984)	6306 (0.0905)
Completeness to θ (%)	26.36 (97.4)	26.37 (92.3)	28.05 (91.0)
Absorption correction	empirical	empirical	empirical
Maximum and minimum transmission	0.999 and 0.960	0.8562 and 0.7760	0.989 and 0.953
Refinement method	full-matrix least-squares on F^2	full-matrix least-squares on F^2	full-matrix least-squares on F^2
Data/restraints/parameters	2256/1/217	6730/0/433	6306/0/343
Goodness-of-fit on F^2	1.115	0.855	0.931
Final *R* indices ($I > 2\sigma(I)$)	$R_1 = 0.0577$, $wR_2 = 0.1305$	$R_1 = 0.0601$, $wR_2 = 0.0480$	$R_1 = 0.0551$, $wR_2 = 0.1041$
R indices (all data)	$R_1 = 0.0684$, $wR_2 = 0.1366$	$R_1 = 0.1923$, $wR_2 = 0.0658$	$R_1 = 0.1773$, $wR_2 = 0.1347$
Largest difference in peak and hole (e Å^{-3})	0.343 and −0.336	0.387 and −0.314	0.491 and −0.547

ceeds by the expulsion of the pyrazole from **3** followed by dimerization. Furthermore, expulsion of pyrazolate anion from **4** followed by the disproportionation of the generated $[Ni(HL).solvent]^{1+}$ or $[Ni(HL)]^{1+}$ gives rise to the partially deprotonated [Ni(HL)(L)]

species which readily recombine with either $[Ni(HL).solvent]^{1+}$ or $[Ni(HL)]^{1+}$ giving ultimately the dinuclear $[Ni_2(HL)_2L + Na]^{1+}$ ($[\mathbf{7} + Na]^{1+}$) and $[Ni_2(HL)_2L + DMSO + H]^{1+}$ ($[\mathbf{7} + DMSO + H]^{1+}$), which appear at $m/z = 980$ and 1036, respectively.

The ESI mass spectrum of **4**, Table 1, displays a series of peaks at $m/z = 396$ (base peak), 763 and 791, respectively, due to the dinuclear imidazole containing cations, $[Ni_2L_2 \cdot Im + 2Na + H]^{2+}$ ($[\mathbf{9} + H]^{2+}$), $[Ni_2L_2 \cdot Im + Na + H]^{1+}$ and $[Ni_2L_2.Im + 2Na]^{1+}$, besides a less intense peak at $m/z = 424$ due to the tetranuclear cation $[\{Ni(HL) \cdot Im\}_4 + DMF + 4H]^{4+}$ ($[\mathbf{10} + DMF + 4H]^{4+}$). The formation of these dinuclear or tetranuclear cations may proceed via the initial deprotonation of the imidazole N–H proton followed by self-assembly. It is not uncommon that self assembly of deprotonated imidazolate complexes leads to the formation of either linear or cyclic polynuclear imidazolate species, where the imidazolate anion acts as a bridge [6,8,43]. On the other hand, expulsion of imidazole from **4**, followed by self-assembly also gives rise to the dinuclear, $[\{NiL\}_2 + 2H]^{2+}$ and $[\{NiL\}_2 + H]^{1+}$, as well as the tetranuclear $[\{NiL\}_4 + DMF + 4H]^{4+}$ ($[\mathbf{11} + DMF]^{4+}$) and $[\{NiL\}_4 + DMF + 2H + 2Na]^{4+}$ imidazole free cations. In these cations, the oximate N–O acts as a bridge between the Ni(II) ions. The generation of di-, tri, and tetranuclear cation during electro spray ionization was also reported for other hydrazoneoxime copper(II) and nickel (II) complexes [13–15].

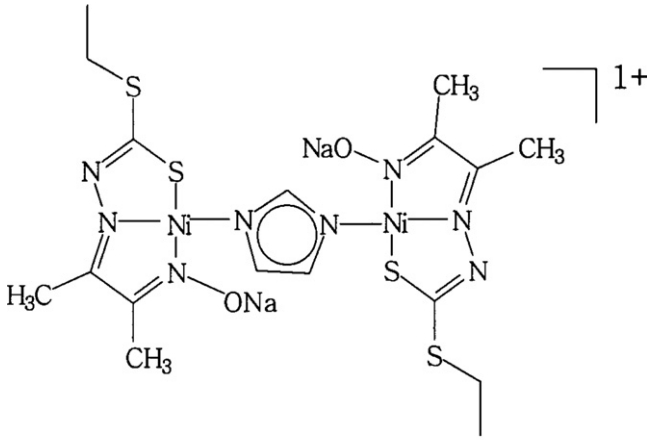

9

The spectrum of the bisligand complex $[Ni(HL)_2] \cdot H_2O$ (**5**) shows the parent cationic species $[Ni(HL)_2 + H]^{1+}$ ($m/z = 620$) which is transformed from the solution to the gas phase. The spectrum also displays the dimeric cation $[\{NiL\}_2 + H]^{1+}$ ($m/z = 677$) besides other polynuclear cations $[Ni_3(HL)_2L_2 + H + Na\ ]^{2+}$ ($m/z = 659$), $[Ni_2(HL)_2L + H]^{1+}$ ($m/z = 958$) and $[Ni_3(HL)_2L_2 + H]^{1+}$ ($m/z = 1296$). The formation of $[\{NiL\}_2 + H]^{1+}$ is suggested to occur in the electro spray ion source via complete deprotonation of the two oxime groups of $[Ni(HL)_2]$ (**5**). This is in agreement with the observed chemical deprotonation of **5** (using methanolic KOH) which eventually gives the dimeric complex (**2**). The formation of the other polynuclear cations proceeds by the initial partial deprotonation of $[Ni(HL)_2]$ to give $[Ni(HL)(L)]$ which readily reacts with one or two solvated mononuclear $[NiL \cdot DMF + H]^{1+}$, generated from the dissociation of $[\{NiL\}_2]$ in DMF, giving ultimately $[Ni_2(HL)_2L + H]^{1+}$ ($[\mathbf{7} + H]^{1+}$) and $[Ni_3(HL)_2L_2 + H]^{1+}$ ($[\mathbf{8} + H]^{1+}$), respectively.

3.3. X-ray crystal and molecular structures of *3*, *4* and *5*

The crystal data and structural refinement parameters for **3**, **4** and **5** are listed in Table 2. Selected bond distances (Å) and bond angles (°) for **3** and **4** are collected in Table 3, while those of **5** are listed in Table 4. The structures of **3** and **4** together with the atomic numbering scheme are, respectively, shown in Figs. 1 and 2. The crystal structure of **3** consists of one type of discrete molecular units, while that of **4** consists of two molecular units, namely Ni1 and Ni2 molecular units which are crystallographically independent but chemically similar. In either **3** or **4**, the Ni(II) is in a distorted square planar environment and is coordinated to the dianionic NNS tridentate hydrazoneoxime ligand via deprotonated oximate nitrogen N2, hydrazone imine nitrogen N1, and thiolate sulphur S1. The fourth coordination sites in **3** and **4** are occupied, respectively, by the pyrazole N3 and imidazole N3 or N8 nitrogens. Deviation from idealized square planar arrangement in either **3** or **4** is evident from the values, Table 3, of both cis- and trans bond angles around the central Ni(II). The pyrazole plane (C4, C5, C6, N4, N3) in **3** is almost coplanar with the nickel coordination plane (N1, N2, N3, S1, Ni1) as the dihedral angle between these two planes is only 3.15°. However, in **4** the imidazole planes (N3, C4, N4, C5, C6) and (N8, C19, N9,C20, C21) deviate from the Ni1(N1, N2, N3, S1, Ni1) and Ni2 (N6, N7, N8, S3, Ni2) coordination planes by 52.30° and 50.47° angles, respectively. The phenyl plane in **3**

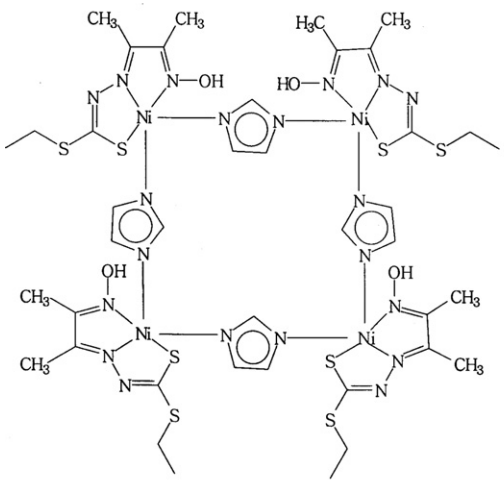

10

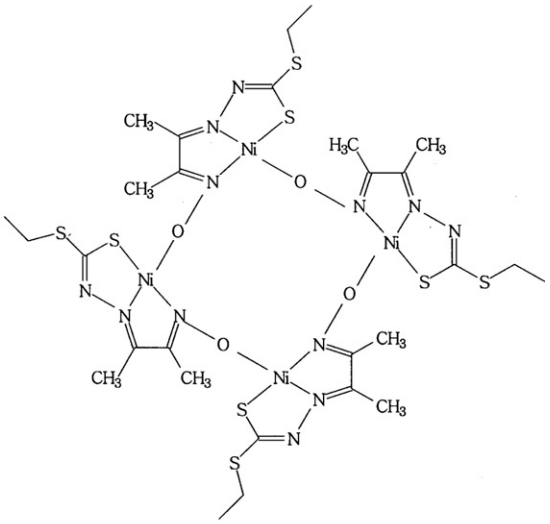

11

Table 3
Selected bond distances (Å) and bond angles (°) for [NiL · HPyr] (**3**) and [NiL · HIm] (**4**)

[NiL · HPyr] (**3**)		[NiL · HIm] (**4**)			
		Ni1 molecular unit		Ni2 molecular unit	
Ni–S1	2.1740(17)	Ni–S1	2.1665(16)	Ni–S3	2.1795(16)
Ni–N1	1.836(6)	Ni–N1	1.843(4)	Ni–N6	1.831(4)
Ni–N2	1.923(5)	Ni–N2	1.906(4)	Ni–N7	1.900(4)
Ni–N3	1.893(6)	Ni–N3	1.885(4)	Ni–N8	1.891(4)
O1–N2	1.306(7)	O1–N2	1.297(4)	O2–N7	1.299(4)
C3–N2	1.306(9)	C3–N2	1.327(5)	C18–N7	1.313(6)
C2–C3	1.427(10)	C2–C3	1.424(7)	C17–C18	1.450(7)
C2–N1	1.306(8)	C2–N1	1.301(6)	C17–N6	1.289(6)
N1–N5	1.397(8)	N1–N5	1.389(5)	N6–N10	1.409(5)
C1–N5	1.253(9)	C1–N5	1.284(5)	C16–N10	1.289(6)
C1–S1	1.743(8)	C1–S1	1.753(5)	C16–S3	1.748(5)
C1–S2	1.761(7)	C1–S2	1.725(6)	C16–S4	1.754(5)
C7–S2	1.819(9)	C7–S2	1.807(5)	C22–S4	1.816(5)
C7–C8	1.508(9)	C7–C8	1.479(7)	C22–C23	1.511(7)
N1–Ni–S1	86.29(17)	N1–Ni–S1	86.52(16)	N6–Ni–S3	87.03(16)
N1–Ni–N2	81.9(2)	N1–Ni–N2	82.7(2)	N6–Ni–N7	82.4(2)
N2–Ni–N3	98.1(2)	N2–Ni–N3	98.0(2)	N7–Ni–N8	97.6(2)
S1–Ni–N3	93.69(17)	S1–Ni–N3	92.83(14)	S3–Ni–N8	93.06(13)
N3–Ni–N1	178.1(3)	N3–Ni–N1	179.0(2)	N8–Ni–N6	178.6(2)
N2–Ni–S1	168.2(2)	N2–Ni–S1	168.94(15)	N7–Ni–S3	168.95(15)
O1–N2–C3	121.3(5)	O1–N2–C3	121.3(5)	O2–N7–C18	119.5(5)
N2–C3–C2	112.8(5)	N2–C3–C2	112.8(5)	N7–C18–C17	112.0(5)
N1–C2–C3	114.5(5)	N1–C2–C3	114.5(5)	N6–C17–C18	113.6(5)
C2–N1–N5	119.5(5)	C2–N1–N5	119.5(5)	C17–N6–N10	118.3(5)
C1–N5–N1	110.4(4)	C1–N5–N1	110.4(4)	C16–N10–N6	109.1(4)
N5–C1–S1	124.2(4)	N5–C1–S1	124.2(4)	N10–C16–S3	125.7(4)
N5–C1–S2	121.5(4)	N5–C1–S2	121.5(4)	N10–C16–S4	121.8(4)
C1–S2–C7	102.9(3)	C1–S2–C7	102.9(3)	C16–S4–C22	103.6(3)
S2–C7–C8	114.5(4)	S2–C7–C8	114.5(4)	S4–C22–C23	109.0(4)

Table 4
Selected bond distances (Å) and bond angles (°) for [Ni(L)$_2$] (**5**)

Bond distance		Bond angels	
Ni–S1	2.3034(14)	N1–Ni–S1	83.96(12)
Ni–N1	1.934(4)	N1–Ni–N3	79.87(18)
Ni–N3	1.987(4)	N1–Ni–N4	178.04(16)
Ni–S2	2.3877(16)	S1–Ni–S2	93.30(5)
Ni–N4	1.958(4)	N4–Ni–N6	77.35(16)
Ni–N6	2.143(4)	N6–Ni–S2	158.95(12)
O1–N3	1.299(5)	N3–Ni–N6	88.00(15)
C3–N3	1.306(6)	S1–Ni–N6	95.97(11)
C2–C3	1.450(6)	S1–Ni–N3	163.83(16)
C2–N1	1.306(5)	N4–Ni–S2	82.72(12)
N1–N2	1.392(5)	O1–N3–C3	122.5(5)
C1–N2	1.317(5)	C3–C2–N1	113.9(4)
C1–S1	1.714(5)	C2–N1–N2	119.1(4)
C1–S3	1.744(5)	N2–C1–S1	126.1(4)
C7–S3	1.814(5)	N2–C1–S3	122.0(3)
C7–C8	1.497(7)	S3–C1–S1	121.9(3)
O2–N6	1.371(4)	C1–S3–C7	104.7(2)
N6–C6	1.288(5)	S3–C7–C8	108.2(4)
C6–C5	1.468(6)	O2–N6–C6	113.7(4)
C5–N4	1.300(6)	C6–C5–N4	115.2(5)
N4–N5	1.387(5)	C5–N4–N5	117.8(4)
N5–C4	1.297(5)	N5–C4–S2	127.9(4)
C4–S2	1.713(5)	N5–C4–S4	118.2(4)
C4–S4	1.748(5)	S2–C4–S4	113.9(3)
S4–C14	1.820(5)	C4–S4–C14	104.5(2)
C14–C15	1.478(7)	S4–C14–C15	114.6(4)

also forms a dihedral angle of 74.73° with the Ni coordination plane while the Ni1 and Ni2 coordination planes of **4** form 78.14° and 79.21° angles with the corresponding phenyl planes.

The Ni–N (oximate) bond distances in both **3**[Ni1–N2 = 1.923(5) Å] and **4**[Ni1–N2 = 1.906(4) Å, Ni2–N7 = 1.900(4) Å], are within the range (1.93–1.87 Å) reported for other Ni(II) hydrazoneoxime complexes [15,30]. The Ni–N (hydrazone imine) bond distances of **3** [Ni1–N1 = 1.836(6) Å] and **4** [Ni1–N1 = 1.843(4) Å, Ni2–N6 = 1.831(4) Å] are shorter than the Ni–N (oximate), but still within the normal range (1.84–1.88 Å) reported for other Ni(II) complexes derived from dianionic NNS [44–47] and ONS tridentate hydrazones [48–54]. The Ni–S bond distances in the pyrazole complex **3** [Ni1–S1 = 2.1740(17) Å] and imidazole complex **4** [Ni1–S1 = 2.1665(16) Å, Ni2–S3 = 2.1795 Å] are also comparable with those reported for square planar Ni(II) complexes derived of NNS- and ONS-tridentate thiosemicarbazonates [44–54] and dithiocarbazates [55,56].

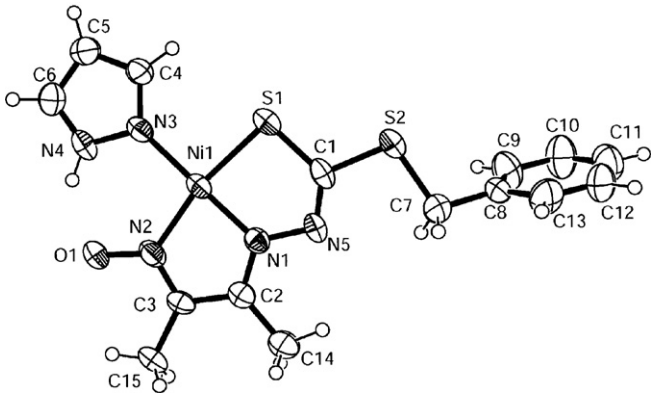

Fig. 1. ORTEP representation of [NiL · HPyr] (**3**) with labeling atoms.

The oximate O1 of **3** is involved in intramolecular hydrogen bond with the pyrazole N4H proton (N4···O1 = 2.557(9) Å). This hydrogen bond motif of graph set descriptor **S**(**6**) [57,58], Fig. 3, forms a six membered ring which is almost coplanar with the two five membered chelate rings as well as the pyrazole ring.

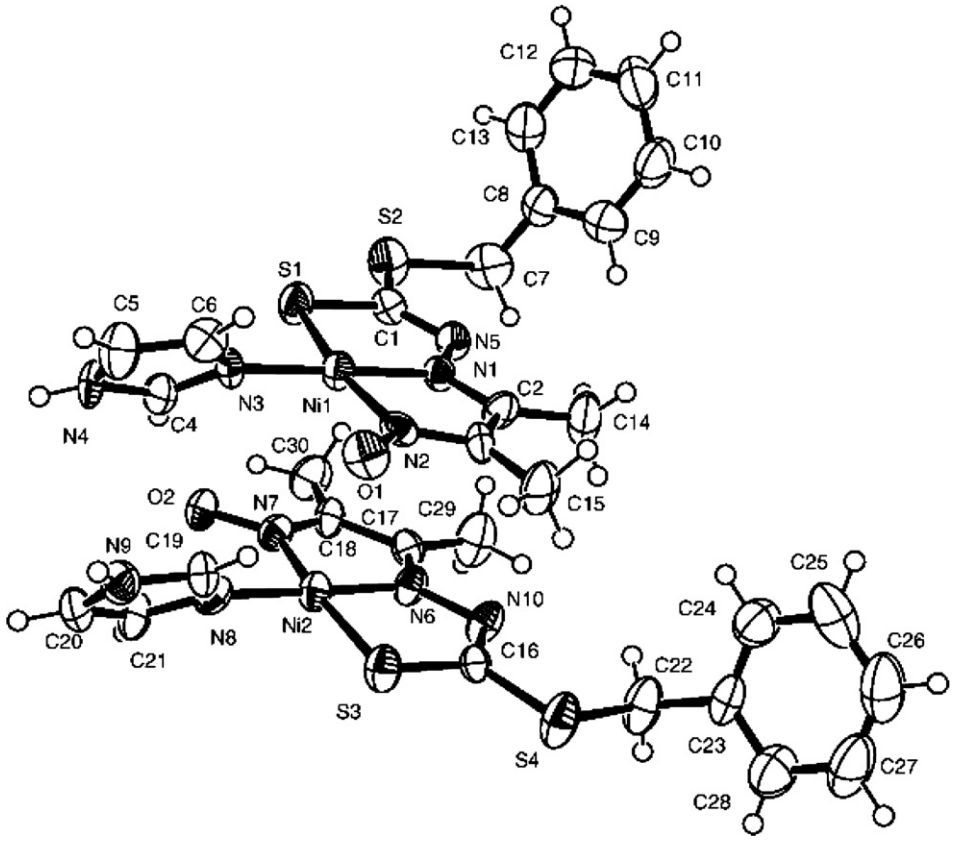

Fig. 2. ORTEP representation of [NiL · HIm] (**4**) with labeling atoms.

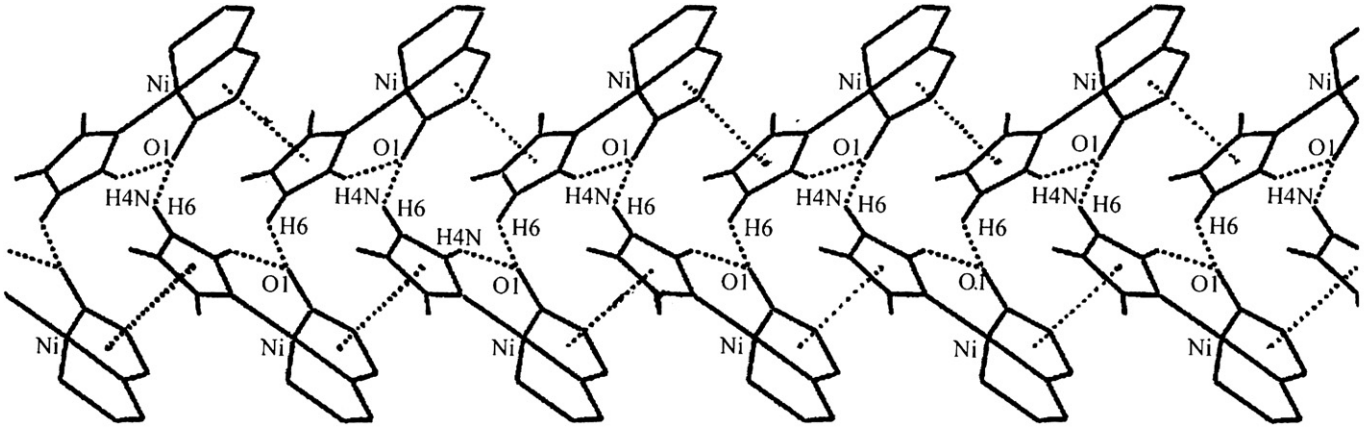

Fig. 3. Intramolecular N4H···O1, C6H···O1 and π···π non-covalent bond interactions in helical chains of [NiL · HPyr] (**3**), Methyl and *S*-benzyl groups are omitted for clarity.

The oximate O1 is also involved in weak (CH···O) intermolecular hydrogen bond formation with the pyrazole H6 proton of the neighboring molecular unit. This hydrogen bond of the graph set descriptor **C7** [57,58] forms a helical chain propagating along the *b*-axis as shown in Fig. 3. The existence and structural importance of weak CH···O hydrogen bonding interactions are now well established and are observed in other metal complexes [59,60]. The Ni coordination planes on each side of the helical chain are arranged parallel to each other, but make an angle of 71.53° with the corresponding Ni coordination plane on the other side. The parallel arrangement of the molecular units on both sides of the helical chain is stabilized by π···π interactions between the delocalized diimine chelate ring, which acts as an aromatic ring [61,62], and the aromatic heterocyclic pyrazole ring of the adjacent molecular unit (Cg1···Cg2 = 3.330 Å). The mean plane of the diimine ring is almost parallel to that of the pyrazole plane and the dihedral angle between these planes is 3.89°. The intra and intermolecular non-covalent bond interactions within the helical chain are listed in Table 5. The pyrazole rings of each chain are interconnected to the pyrazole rings of two neighboring chains by two reciprocal edge to face CH···π interactions (H5···Cg1 = 2.768 Å) [63,64], where Cg1 refers to pyrazole ring centroid. Such interactions give rise to short contacts between the pyrazole H4 and methyl C15 carbon. Similarly, the phenyl rings of the benzyl residues in this chain

Table 5
Non-covalent bond interactions of **3**, **4** and **5**

D–H···A	Symmetry	*d*(D–H) (Å)	*d*(H···A) (Å)	*d*(D···A) (Å)	∠DHA°
[NiL · HPyr] (**3**)					
N4H···O1	*x*, *y*, *z*	0.860	1.817	2.556	142.83
CH6···O1	1 − x, −1/2 + *y*, 1 − *z*	0.930	2.492	3.174	130.36
Cg1···Cg2	−*x*, 1/2 + *y*, −*z*	Cg1···Cg2 = 3.330Å, N4–Cg1–Cg2 = 91.57° Ni–Cg2–Cg1 = 91.55°			
CH5···Cg1	−*x*, 1/2 + *y*, −*z*	0.93	2.768	3.524	139.01
CH9···Cg3	−*x*, 1/2 + *y*, −*z*	0.93	3.303	4.099	144.87
CH4···C15	−1 + *x*, −1 + *y*, *z*	0.93	2.858	3.575	134.87
[NiL · HIm] (**4**)					
N4H···O2	2 − *x*, −*y*, 1−*z*	0.859	1.918	2.735	158.35
N9H···O1	1 − *x*, −*y*, 1 − *z*	0.860	1.891	2.687	153.42
Cg4···Cg5	−*x*, 1/2 + *y*, 1/2 − *z*	Cg4···Cg4 = 3.586 Å, N3–Cg4–Cg4 = 90.87° N8–Cg4–Cg4 = 91.42°			
CH4···O2	*x*, *y*, *z*	0.930	2.446	3.302	152.93
CH9···O1	*x*, *y*, *z*	0.930	2.416	3.252	149.38
CH29C···S1	*x*, 1/2 − *y*, 1/2 + *z*	0.959	2.997	3.796	141.63
CH7B···S3	2 − *x*, 1/2 − *y*, 1/2 + *z*	0.970	2.820	3.761	163.96
[Ni(L)$_2$] · H$_2$O (**5**)					
O2H···N2	−*x*, 2 − *y*, −*z*	0.920	2.009	2.784	157.42
O2H···S3	−*x*, 2 − *y*, −*z*	0.820	2.840	3.307	118.16
O2H···C1	−*x*, 2 − *y*, −*z*	0.820	2.814	3.553	151.01
CH21C···O2	−*x*, 2 − *y*, −*z*	0.960	2.394	3.349	173.14
O3H···O1	−*x*, *y*, 1/2 − *z*	1.105	2.527	3.175	116.30
CH7A···Cg2	1/2 + *x*, 1/2 + *y*, *z*	0.971	2.824	3.611	138.82
CH17···Cg2	1/2 + *x*, 1/2 + *y*, *z*	0.928	2.632	4.347	163.87
CH22C···Cg6	1/2 + *x*, 1/2 + *y*, *z*	0.960	3.663	4.468	143.05
CH23B···Cg6	1/2 + *x*, 1/2 + *y*, *z*	0.960	2.850	3.529	128.63
CH11···S2	1/2 − *x*, 1.5*y*, −*z*	0.932	2.945	3.686	137.54

Cg1 pyrazole ring (C4, C5, C6, N3, N4) centroid.
Cg2 diimine chelate ring (C2, C3, N2, Ni, N1) centroid.
Cg3 phenyl ring (C8, C9, C10, C11, C12, C13) centroid.
Cg4 imidazole ring (N3, C4, N4, C5, C6) centroid.
Cg5 imidazole ring (N8, C19, N9, C20, C21) centroid.
Cg6 phenyl ring (C15, C16, C17, C18, C19, C20) centroid.

are also interconnected to the phenyl rings of other two helical chains via a pair of reciprocal edge to face CH···π interactions (CH9···Cg3 = 3.303 Å). In these interactions, both pyrazole and phenyl rings act as proton donor as well as π acceptor. Thus each helical chain is interconnected to four different chains giving rise to two dimensional arrays of helical chains.

Each Ni1 molecular unit in **4** are linked to the two adjacent Ni2 molecular units via N4H···O2 (N4···O2 = 2.735 Å) and O1···H9N

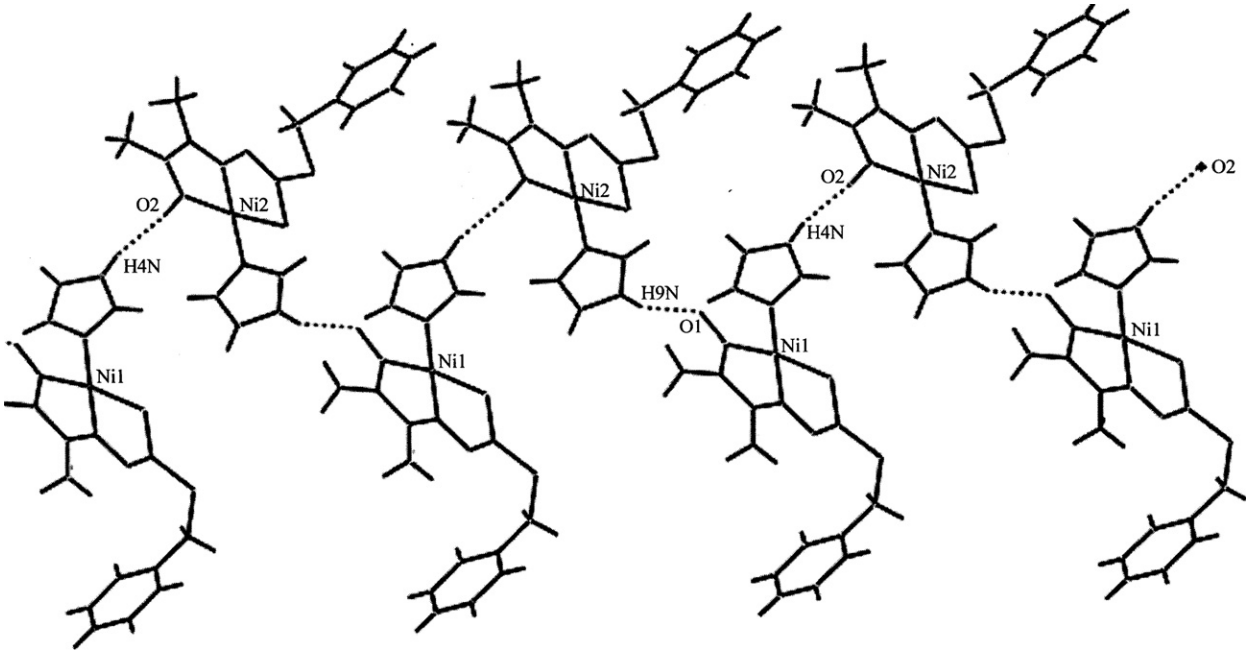

Fig. 4. Intermolecular N4H···O2 hydrogen bonding in the zigzag chain of [NiL · HIm] (**4**) extending along *a*-axis.

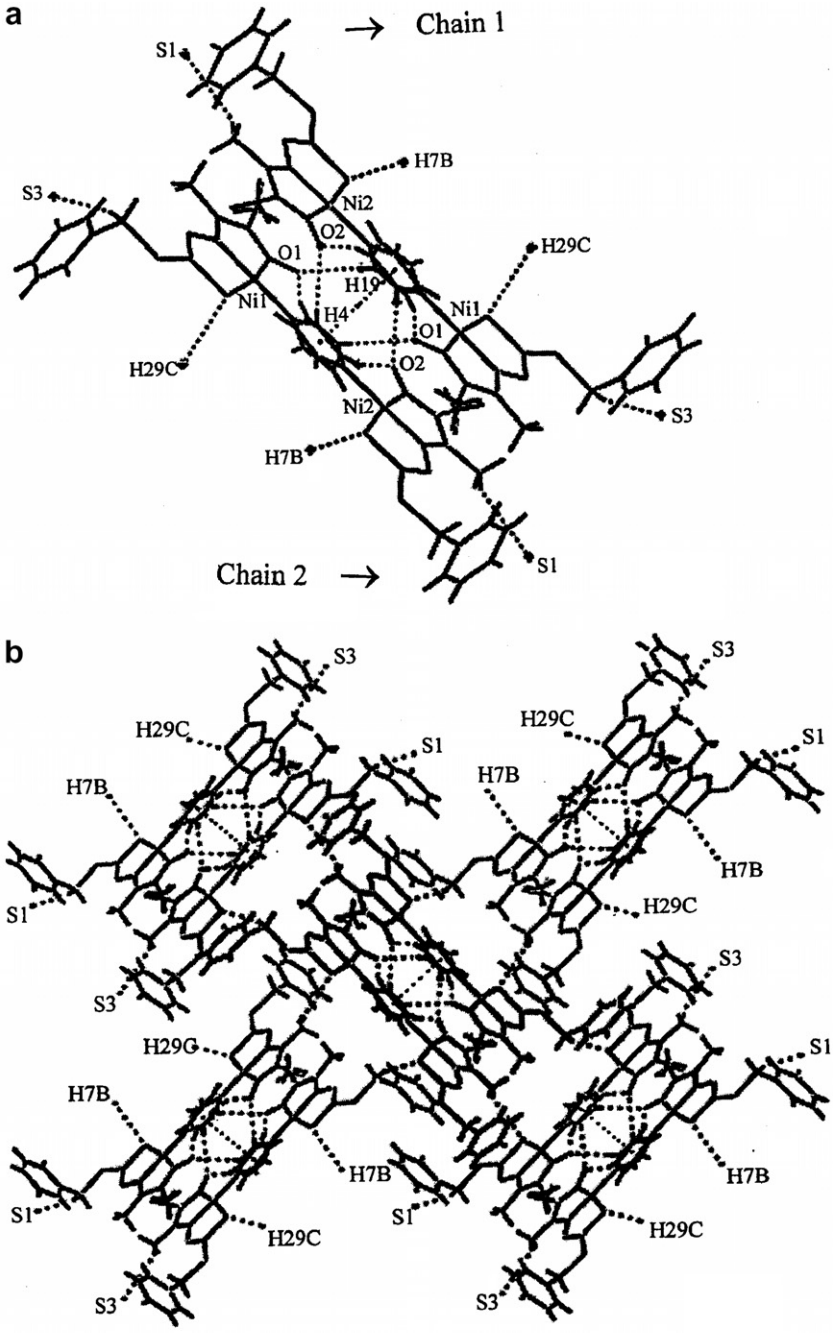

Fig. 5. Diagrammatic representation of (a) the double chain of [NiL · HIm] (**4**) viewed along *a*-axis and (b) the interaction a double chain with four neighboring chains via C29H···S1 and C7H···S3 interactions.

(N9···O1 = 2.687 Å) hydrogen bonds of graph set descriptor **C7**, forming an infinite zigzag chain (chain 1) extended along the *a*-axis as shown in Fig. 4. Similarly, the other crystallographically independent Ni2 molecular unit also forms another chain (chain 2) which propagates parallel to chain1. The two chains are interconnected by π···π and CH···O non-covalent bond interactions, Table 5, forming a double chain structure as shown in Fig. 5. The π···π interactions involve the imidazole rings [N8, C19,N9, C20, C21 (Cg5)] of Ni2 molecular units in Chain 1 and the imidazole rings Ni1 [N3, C4, N4, C5, C6 (Cg4)] of molecular units in chain 2 where Cg4–Cg5 = 3.586 Å. Both O1 and O2 oximate oxygens are also involved in two CH···O weak hydrogen bond formation with the imidazole C19H and C4H protons, respectively. Each double chain is interconnected to four neighboring double chains via four pairs of reciprocal S1···H29C and S3···H7C [S1···H29 = 3.796 Å and S3···H7 = 3.761 Å] interactions, Fig. 5a and b, giving rise to two dimensional arrays of double chains.

Selected bond distances and bond angles for **5** are given in Table 4. The crystal structure of **5**, Fig. 6, shows that the Ni(II) is in a distorted octahedral environment. The two mononegative hydrazoneoxime ligands are coordinated in the meridional configuration where the two thiol sulphur atoms (S1 and S2) and the two oxime nitrogen atoms (N3 and N6) are cis to each other, while the imine nitrogen atoms (N1 and N4) are trans. Similar

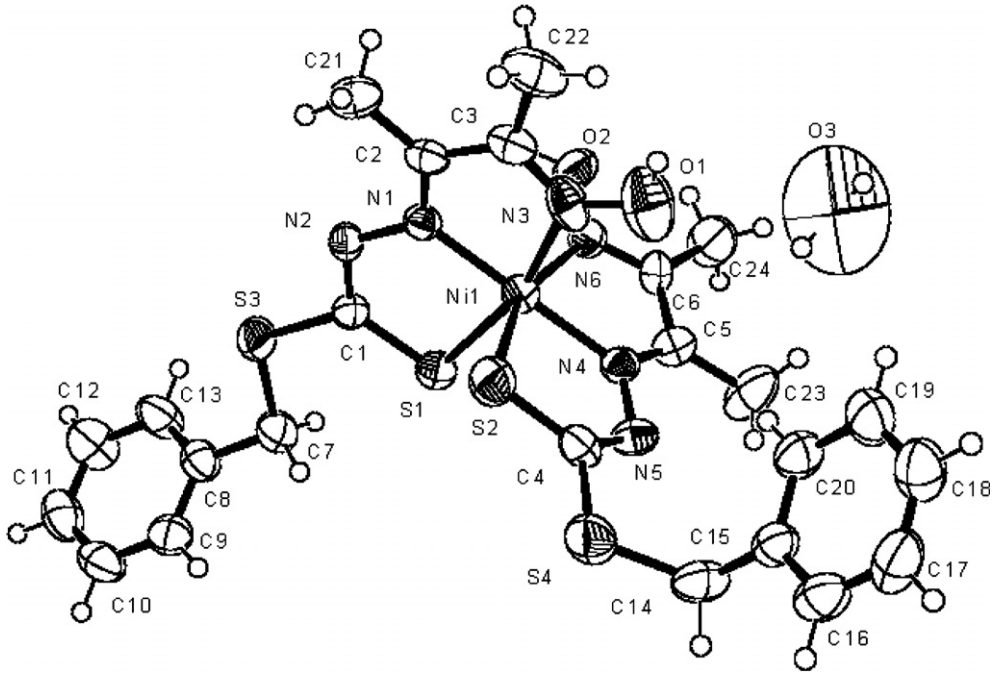

Fig. 6. ORTEP representation of $[Ni(HL)_2] \cdot 1/2H_2O$ (**5**) with labeling atoms.

meridional configurations have also been reported for other octahedral Ni(II) complexes with NNS tridentate ligands [65–71]. Each ligand is bounded to the Ni(II) via oxime nitrogen [Ni1–N3 = 1.987 Å, Ni1–N6 = 2.142 Å], imine nitrogen [Ni1–N1 = 1.9341 Å, Ni1–N4 = 1.959 Å] and deprotonated thiol sulphur [Ni1–S1 = 2.3034 Å, Ni–S2 = 2.3883 Å]. The bond distances between the Ni and the set of ligand donor atoms are within the range reported for other octahedral Ni(II) complexes with NNS tridentate thiosemicarbazones [65–67], dithiocarbazonates [68–70] and thiosemicarbazoneoximes [71].

The oxime proton O2H is involved in a reciprocal bifurcated hydrogen bond formation with both N2 and S3 of the adjacent molecule giving rise to hydrogen bonded dimer. This dimeric structure is further stabilized by a pair of reciprocal C21H···O2 and O2H···C interactions. A one dimensional chain of alternating dimeric unit and water molecule propagating along the *c*-axis is formed via hydrogen bond formation between the oxime O1 oxygen and the bridged water molecule proton O3H (O1···O3 = 3.175 Å).

The chains are packed together through a combination of several CH···π interactions involving the (C8–C13) and (C15–C20) phenyl rings of the benzyl residues. The acidic methylene H7A protons of the molecular units of one chain are involved in reciprocal CH···π interactions with the (C8– C13) phenyl rings of the adjacent chain (C7H···Cg6 = 2.824 Å). The (C8–C13) phenyl rings are also involved in an edge to face interactions with the H17 proton of (C15–C20) phenyl rings of another adjacent chain (C17H···Cg6 = 4.347). Both H22C and H23B methyl proton of two different chains are directed towards the (C15–C20) phenyl ring centroid, thus forming two non-equivalent CH···π interactions. Reciprocal CH21···C2 interactions connecting two neighboring chains are also observed. Moreover, the two dithiocarboxylate S2 sulphur atoms of each hydrogen bonded dimeric unit are involved in weak hydrogen bond formation with phenyl C11H protons of two neighboring dimers, thus each chain is interconnected by two other neighboring chains via C11H···S2 hydrogen bonds (C11···S2 = 3.686 Å). These non-covalent bond interactions, Table 5, combine to form an entangled multidimensional supramolecular network.

4. Supplementary data

CCDC 684840, 684841 and 684842 contain the supplementary crystallographic data for [NiL · HPyr], [NiL · HIm] and $[Ni(HL)_2] \cdot H_2O$. These data can be obtained free of charge via http://www.ccdc.cam.ac.uk/conts/retrieving.html, or from the Cambridge Crystallographic Data Centre, 12 Union Road, Cambridge CB2 1EZ, UK; fax: (+44) 1223-336-033; or e-mail: deposit@ccdc.cam.ac.uk.

Acknowledgement

Thanks are due to BMBF/Forschungszentrm, Jüelich, ÖA-IB/Wo WTZ for supporting this bilateral project.

References

[1] J.-M. Lehn, Supramolecular Chemistry, Concepts and perspectives, VCH, 1995.
[2] J.W. Steed, J.L. Atwood, Supramolecular Chemistry, John Wiley and Sons, Ltd., 2000.
[3] A.M. Beatty, Coord. Chem. Rev. 246 (2003) 131.
[4] H.W. Roesky, M. Andruh, Coord. Chem. Rev. 236 (2003) 91.
[5] B.J. Holliday, C.A. Mirkim, Angew. Chem., Int. Ed. Engl. 40 (2001) 2022.
[6] M.F. Iskander, T.E. Khalil, R. Werner, W. Haase, I. Svoboda, H. Fuess, Polyhedron 19 (2000) 1181.
[7] M.F. Iskander, T.E. Khalil, R. Werner, W. Haase, I. Svoboda, H. Fuess, Polyhedron 20 (2001) 2787.
[8] M.F. Iskander, T.E. Khalil, W. Haase, S. Faro, H.J. Lindner, J. Coord. Chem. 58 (2005) 111.
[9] S. Das, G.P. Muthakumaragopal, S. Pal, S. Pal, New J. Chem. 27 (2003) 1102.
[10] A. Mukhopadhyay, G. Padmaja, S. Pal, S. Pal, Inorg. Chem. Commun. 6 (2003) 381.
[11] S. Das, S. Pal, J. Mol. Struct. 741 (2005) 183.
[12] S. Das, S. pal, J. Mol. Struct. 753 (2005) 68.
[13] M.F. Iskander, L. El-Sayed, N.M.H. Salem, R. Werner, H. Haase, J. Coord. Chem. 56 (2003) 1075.
[14] N.M.H. Salem, L. El-Sayed, W. Haase, M.F. Iskander, J. Coord. Chem. 58 (2005) 1327.
[15] N.M.H. Salem, L. El-Sayed, S. Fro, W. Haase, M.F. Iskander, Polyhedron 261 (2007) 4161.
[16] M.A. Ali, T.S. Guan, P. Bhattacharjee, R.J. Butcher, T.P. Jasinski, Y. Li, Transition Met. Chem. 17 (1992) 74. and references cited therein.
[17] F. Mevellec, A. Roucoux, N. Noiret, H. Patin, J. Chem. Soc., Dalton Trans. (2001) 3603.

[18] M.R. Maurya, S. Khurara, Shailendra, A. Azam, W. Zhang, D. Rehder, Eur. J. Inorg. Chem. (2003) 1966.
[19] Y.-C. Shi, H.-M. Yang, H.-B. Song, C.-G. Yan, X.-Y. Hu, Polyhedron 23 (2004) 567.
[20] M. Nazimuddin, M.A. Ali, F.E. Smith, M.A. Mridha, Transition Met. Chem. 17 (1992) 74.
[21] M.F. Iskander, L. El-Sayed, A. El Toukhy, M. Tawfik, Transition Met. Chem. 7 (1982) 135.
[22] S. Roy, T.N. Mandal, A.K. Barik, S. Pal, S. Gupta, A. Hazra, R.J. Butcher, A.D. Hunter, M. Zeller, S.K. Kar, Polyhedron 26 (2007) 2603.
[23] A.K. Ali, A.H. Mirza, F.H. Bujang, M.H.S.A. Hamid, P.V. Bernhardt, Polyhedron 25 (2006) 3245. and references cited therein.
[24] M.R. Maurya, S. Khurana, W. Zhang, D. Rehder, Eur. J. Inorg. Chem. (2002) 1749.
[25] P. Bera, R.J. Butcher, S. Chaudhuri, N. Saha, Polyhedron 21 (2002) 1.
[26] V.N. Kaftanat, N.I. Belichuk, V.V. Zelenstov, Russ. J. Inorg. Chem. (1978).
[27] G.M. Sheldrick, SHELXS-97, SHELXL-97: Programs for Crystal Structure Analysis, University of Göttingen, Göttingen, Germany, 1998.
[28] C.K. Johnson, M.N. Burnett, ORTEPIII. Report ORNL-6895, Oak Ridge National Laboratory, Tennessee, USA,1996.
[29] A.L. Spek, PLATON, A multipurpose Crystallographic Tool, Utrecht University, Utrecht, The Netherlands, 2002.
[30] W. Kaminsky, J.P. Jasinski, R. Woudenberg, K.I. Goldberg, D.X. West, J. Mol. Struct. 608 (2002) 135.
[31] M. Maekawa, S. Kitagawa, Y. Nakao, S. Sakamoto, A. Yatani, W. Mori, S. Koshino, M. Munakata, Inorg. Chim. Acta 293 (1999) 20. and references cited therein.
[32] A.B.P. Lever, Inorganic Electronic Spectroscopy, 2nd ed., Elsevier, Amsterdam, 1984.
[33] H.B. Gray, Electronic structures of square planar metal complexes, in: R.L. Carlin (Ed.), Transition Metal Chemistry, vol. 1, Marcel Dekker, Inc., New York, 1965.
[34] L. Sacconi, Electronic structure and Stereochemistry of Nickel(II), in: R.L. Carlin (Ed.), Transition Metal Chemistry, vol. 4, Marcel Dekker, Inc., New York, 1968.
[35] M.A. Abou Taleb, L. Labib, M.F. Iskander, Polyhedron 13 (1994) 3015.
[36] R. Colton, A. D'Agostino, J.C. Traeger, Mass Spectrom. Rev. 14 (1995) 79.
[37] W. Henderson, B.K. Nicholson, L.J. McCaffrey, Polyhedron 17 (1998) 4291.
[38] Sheffield Chemputer, Isotope Pattern. <www.shef.ac.uk/chemistry/isotopes.htm>.
[39] E. Kavlakoglu, A. Elmali, Y. Elerman, I. Svoboda, Polyhedron 21 (2002) 1539.
[40] H. Matsushima, H. Hamada, K. Watanabe, M. Koikawa, T. Tokii, J. Chem. Soc. (1999) 971.
[41] T. Kogane, T. Yammaoto, M. Hayashi, R. Hirota, C.A. Horiuchi, Polyhedron 14 (1995) 2475.
[42] G.A. Ardizzoia, M.A. Angaroni, G. la Monica, F. Cariati, S. Cenini, Massimo Moret, N. Masciocchi, Inorg. Chem. 30 (1991) 4347.
[43] Y. Sunatsuki, Y. Motoda, N. Matsumoto, Coord. Chem. Rev. 226 (2002) 199.
[44] D.X. West, G.A. Bain, R.J. Butcher, J.P. Jasinski, Yu Li, R.Y. Pozdniakiv, J. Vales-Martinez, R.A. Toscano, S. Hernandez-Ortega, Polyhedron 15 (1996) 665.
[45] D.X. West, H. Gebremedhin, R.J. Butcher, J.P. Jasinski, A.E. Libert, Polyhedron 12 (1993) 2489.
[46] D.X. West, M.A. Lockwood, A.E. Liberta, X. Chen, R.D. Willett, Transition Met. Chem. 18 (1993) 221.
[47] D.X. West, J.P. Scovill, J.V. Silverton, A. Bavoso, Transition Met. Chem. 11 (1986) 123.
[48] V.M. Leovac, L.S. Jovanovic, V. Divjakovic, A. Pevec, Ivan Leban, T. Armbruster, Polyhedron 26 (2007) 49.
[49] Z.-Y. Cao, Z.-P. Deng, S. Gao, Acta Crystallogr., Sect. E 63 (2007) m1961.
[50] P.X. Grcia-Reynaldos, S. Hernandez-Ortega, J. Valdes-Martinez, Acta Crystallogr., Sect. E 62 (2006) m3410.
[51] R. Prabhakaran, R. Karvembu, T. Hashimoto, K. Shimiza, K. Natarajan, Inorg. Chim. Acta 358 (2005) 2093.
[52] J. Valdes-Martinez, S. Hernandez-Ortega, V.B. Jimenez, Acta Crystallogr., Sect. E 60 (2004) m42.
[53] J. Valdes-Martinez, S. Hernandez-Ortega, V.B. Jimenez, Acta Crystallogr., Sect. E 58 (2002) m710.
[54] M. Soriano-Garcia, R.A. Toscano, J. Valdes-Martinez, J.M. Fernandez, Acta Crystallogr., Sect. C C41 (1985) 498.
[55] M.A. Ali, A.H. Mirza, M. Nazimuddin, P.K. Dhar, R.J. Butcher, Transition Met. Chem. 28 (2000) 27.
[56] M.A. Ali, T.S. Guan, P. Bhaltcharjee, R.J. Butcher, J.P. Jasinski, Y. Li, Transition Met. Chem. 21 (1996) 351.
[57] M.C. Etter, Acc. Chem. Res. 23 (1990) 120.
[58] J. Bernstein, R.E. Davis, L. Shimoni, N.-L. Chang, Angew. Chem., Int. Ed. Engl. 34 (1995) 1555.
[59] G.R. Desiraju, Acc. Chem. Res. 29 (1996) 441.
[60] G.R. Desiraju, Acc. Chem. Res. 24 (1991) 290.
[61] Z.D. Tomic, S.B. Novakovic, S.D. Zaric, Eur. J. Inorg. Chem. (2004) 2215.
[62] Z.D. Tomic, V.M. Leovac, S.V. Pokorni, D. Zobel, S.D. Zaric, Eur. J. Inorg. Chem. (2003) 1222.
[63] G.R. Desiraju, T. Steiner, The Weak Hydrogen Bonds in Structural Chemistry and Biology, Oxford University Press, 1999.
[64] M. Nishio, M. Hirota, Y. Umezawa, The CH/π Interaction, Evidence, Nature and Consequences, John Wiley and Sons, Inc., New York, 1998.
[65] M. Mathew, G.J. Palenik, J. Am. Chem. Soc. 91 (1961) 6310.
[66] G.R. Clark, G.J. Palenik, Cryst. Struct. Commun. 9 (1980) 449.
[67] D.X. West, M.A. Lockwood, H. Gebermedhin, A. Castieiras, A.E. Liberta, Polyhedron 12 (1993) 1887.
[68] G.-B. Li, M.-S. Liu, Q.-Y. Yu, H.-P. Zeng, Y.-P. Cai, Acta Crystallogr., Sect. E 62 (2006) m3113.
[69] M.A. Ali, A.H. Mirza, F.H. Bujang, M. Haniti, S.A. Hamid, P.V. Berhardt, Polyhedron 25 (2006) 3245.
[70] M.A. Ali, A.H. Mirza, M. Nazimuddin, H. Rahman, R.J. Butcher, Polyhedron 20 (2001) 2431.
[71] E. Bermejo, A. Castineiras, D.X. West, Z. Naturforsch. 56b (2001) 369.

determined by HPLC analysis using a chiralcel OD-H column. Optical rotation was measured on JASCO polarimeter. Elemental analyses were carried on EA 1108-Elemental Analyzer at the Chemical Analysis Laboratory of the Center for Scientific Instruments of Kyungpook National University.

2.2. Syntheses of Cu(**L**)Cl_2 and Zn(**L**)Cl_2

A solution of **L** (1.0 g, 3.40 mmol) in methanol (5 ml) was added dropwise to a solution of $CuCl_2 \cdot 2H_2O$ (0.58 g, 3.37 mmol) or $ZnCl_2$ (0.46 g, 3.37 mmol) in methanol (10 ml). The mixture was stirred overnight at ambient temperature. The solvent was removed to yield blue or white solid, respectively. The yield of blue solid was 87% (1.26 g). *Anal.* Calc. for $C_{20}H_{26}Cl_2N_2Cu$: C, 56.01; H, 6.11; N, 6.53. Found: C, 55.90; H, 6.21; N, 6.51%.

The yield of white solid was 85% (1.23 g). *Anal.* Calc. for $C_{20}H_{26}Cl_2N_2Zn$: C, 55.77; H, 6.08; N, 6.50. Found: C, 55.67; H, 6.02; N, 6.52%. ^{1}H NMR (400 Hz, CD_3CN) δ 7.54 (t, 4H, Ph), 7.36 (m, 6H, Ph), 4.06 (dd, 2H, CH_2), 3.92 (t, 2H, CH_2), 2.86 (m, 2H, CHA), 2.58 (s, 2H, NH), 2.52 (m, 2H, CHA), 1.83 (m, 2H, CHA), 1.32 (m, 4H, CHA).

2.3. Crystal structures of Cu(**L**)$Cl_2 \cdot 2CH_3OH$ and Zn(**L**)Cl_2

Single crystals suitable for X-ray analysis were grown from methanol solutions and sealed in thin walled glass capillaries and mounted on an Enraf-Nonius CAD-4 diffractometer equipped with monochromated Mo Kα radiation (λ = 0.71073 Å) at room temperature. The intensity data were corrected for Lorentz-polarization effect. Data reductions were carried out using an XCAD program package and empirical absorption corrections with ABSCAL program were applied based on ψ scans [22]. Crystal data and structure refinement for these complexes are listed in Table 1. The structures were determined by direct methods and refined by full-matrix least-squares using SHELXS-97 and SHELXL-97 program packages [23]. All non-hydrogen atoms were refined anisotropically. Hydrogen atoms were constrained by riding models except H atoms at OH of solvated molecules in Cu(**L**)Cl_2. Selected bond lengths and bond angles are given in Table 2.

Table 1
Crystal data and structure refinement for Cu(**L**)$Cl_2 \cdot 2$MeOH and Zn(**L**)Cl_2

Compound	Cu(**L**)$Cl_2 \cdot 2$MeOH	Zn(**L**)Cl_2
Empirical formula	$C_{22}H_{34}Cl_2CuN_2O_2$	$C_{20}H_{26}Cl_2N_2Zn$
Formula weight	492.95	430.70
Crystal system	tetragonal	triclinic
Space group	$P4_32_12$	$P1$
Unit cell dimensions		
a (Å)	9.4141(7)	9.0699(9)
b (Å)	9.4141(7)	10.2096(8)
c (Å)	28.178(2)	11.7756(9)
α (°)		96.854(7)
β (°)		103.066(8)
γ (°)		103.935(7)
V (Å^3)	2497.3(3)	1013.4(2)
Z	4	2
D_{calc} (Mg/m^3)	1.311	1.412
Absorption coefficient (mm^{-1})	1.108	1.481
F(000)	1036	448
Crystal size	0.40 × 0.40 × 0.40	0.35 × 0.40 × 0.45
θ Range for data collection (°)	2.28–25.46	1.81–25.47
Index ranges	$0 \leqslant h \leqslant 11$; $-11 \leqslant k \leqslant 0$; $-34 \leqslant l \leqslant 0$	$-10 \leqslant h \leqslant 10$; $-12 \leqslant k \leqslant 12$; $0 \leqslant l \leqslant 14$
Reflections collected	2742	4068
Independent reflections (R_{int})	2322 (0.0186)	3959 (0.0083)
Reflections observed (>2σ)	1429	3713
Refinement method	full-matrix l.s. on F^2	full-matrix l.s. on F^2
Data/restraints/parameters	2322/0/134	3959/3/284
Goodness-of-fit on F^2	0.999	1.067
Final R indices [$I > 2\sigma(I)$]	R_1 = 0.027, wR_2 = 0.062	R_1 = 0.025, wR_2 = 0.066
R indices (all data)	R_1 = 0.049, wR_2 = 0.065	R_1 = 0.028, wR_2 = 0.067
Absolute structure parameter	−0.04(2)	0.005(9)
Largest difference in peak/hole (e Å^{-3})	0.156/−0.135	0.442/−0.293

Table 2
Selected bond lengths (Å) and angles (°) for Cu(**L**)$Cl_2 \cdot 2$MeOH and Zn(**L**)Cl_2

Cu(**L**)Cl_2		Zn(**L**)Cl_2	
Bond lengths		*Bond lengths*	
Cu–N	2.017(2)	Zn(1)–N(1)	2.090(3)
Cu–Cl	2.2448(7)	Zn(1)–N(2)	2.090(3)
N–C(1)	1.492(3)	Zn(1)–Cl(1)	2.197(1)
N–C(5)	1.486(3)	Zn(1)–Cl(2)	2.222(1)
		Zn(2)–N(3)	2.086(3)
		Zn(2)–N(4)	2.073(3)
		Zn(2)–Cl(3)	2.212(1)
		Zn(2)–Cl(4)	2.234(1)
Bond angles		*Bond angles*	
N–Cu–N$^{\#1}$	84.77(6)	N(1)–Zn(1)–N(2)	86.0(1)
N–Cu–Cl	93.35(6)	N(1)–Zn(1)–Cl(1)	111.97(8)
N–Cu–Cl$^{\#1}$	155.82(6)	N(2)–Zn(1)–Cl(1)	112.24(9)
Cl–Cu–Cl$^{\#1}$	97.84(4)	N(1)–Zn(1)–Cl(2)	105.97(8)
C(1)–N–Cu	107.9(1)	N(2)–Zn(1)–Cl(2)	108.26(8)
C(5)–N–Cu	115.3(2)	Cl(1)–Zn(1)–Cl(2)	125.29(5)
		N(3)–Zn(2)–N(4)	87.3(1)
		N(3)–Zn(2)–Cl(3)	113.20(9)
		N(4)–Zn(2)–Cl(3)	113.09(9)
		N(3)–Zn(2)–Cl(4)	105.22(9)
		N(4)–Zn(2)–Cl(4)	106.94(8)
		Cl(3)–Zn(2)–Cl(4)	124.57(4)

Symmetry transformations used to generate equivalent atoms: #1 y, x, $-z$.

Table 3
Asymmetric nitroaldol reactions of nitromethane and benzaldehyde

Entry	Catalyst (10%)	Base (6%)	Yield (%)[a]	$[\alpha]_D$ (°)	Ee (%)
1	Cu(**L**)Cl_2	(i-Pr)$_2$NEt	57	(+)9.5	23
2	Cu(**L**)Cl_2	Et_3N	53	(+)24	39
3	Zn(**L**)Cl_2	(i-Pr)$_2$NEt	55	(−)1.5	5
4	Zn(**L**)Cl_2	Et_3N	51	(−)1.1	3
5	**L**	(i-Pr)$_2$NEt	70	~0	~0

[a] Values are isolated yields after chromatographic purification.

2.4. Asymmetric nitroaldol reactions

Reactions were carried out at room temperature. At first 10% equivalent of Cu(**L**)Cl_2 or Zn(**L**)Cl_2 was dissolved in 25 ml methanol. Then 6% equivalent of diisopropylethylamine or triethylamine was added after the addition of 1.1 ml nitromethane (2 equiv.) and 1.0 ml benzaldehyde. Reactions were monitored by TLC. After stirring for a week at room temperature, reaction was quenched with 1 ml of 1 N HCl solution and then evaporated. The mixture was extracted by CH_2Cl_2 (3 times × 20 ml) and dried with anhydrous $MgSO_4$, then filtered and the solvent was removed by evaporation. The crude product was purified by column chromatography to afford 1-phenyl-2-nitroethanol with yields of 51–57% (Table 3). Ee was determined by HPLC with a Chiralcel OD-H column at 20 °C, 15% isopropyl alcohol in hexane, flow rate 0.5 ml/min, *R* enantiomer t_r = 18.3 min, *S* enantiomer t_r = 22.1 min. $[\alpha]_D$ = (−)1.5–(+)24 (c = 1, CH_2Cl_2, at 25 °C) (Table 3).

3. Results and discussion

3.1. Syntheses and X-ray crystal structures of Cu(**L**)Cl_2 and Zn(**L**)Cl_2

The complexes were obtained from the reaction of the ligand with $ZnCl_2$ and $CuCl_2 \cdot 2H_2O$ using methanol as solvent. Zn(II) or

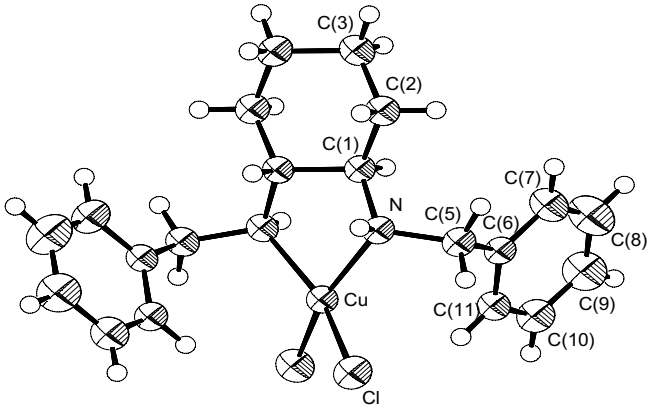

Fig. 1. An ORTEP drawing of Cu(***L***)Cl_2. Displacement ellipsoids are shown at the 40% probability level.

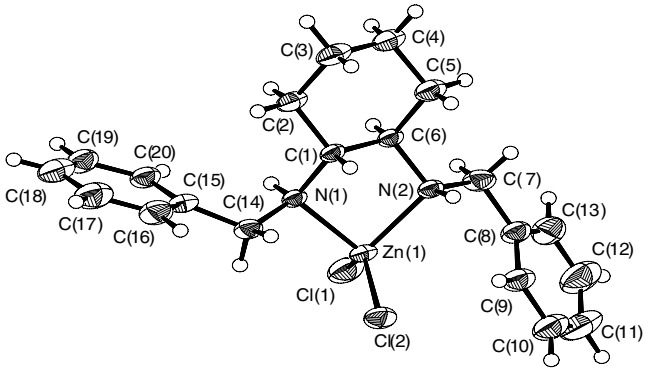

Fig. 2. An ORTEP drawing of Zn(***L***)Cl_2. Displacement ellipsoids are shown at the 40% probability level.

Cu(II) complex is soluble in polar organic solvents such as acetonitrile, methanol and dichloromethane. The crystal structures of the chiral Cu(***L***)Cl_2 and Zn(***L***)Cl_2 are shown in Figs. 1 and 2, respectively. The central Cu ion is coordinated by two nitrogen atoms of ***L*** and two chlorine atoms in distorted square-planar geometry while Zn ion is also coordinated by two nitrogen atoms of ***L*** and two chlorine atoms in a nearly tetrahedral arrangement. The average bond distance of Zn–N is 2.085(3) Å, which are close to those in a similar complex of Zn(*R,R*-bmbcd)Cl_2 [bmbcd: *N,N′*-bis(4-methoxy-benzyl)-cyclohexane-1,2-diamine] [8], but longer than Cu–N 2.017(2) Å. The mean bond distances of Zn–Cl is 2.216(1) Å, also close to those in the similar complex of Zn(*R,R*-bmbcd)Cl_2, 2.2289(2) and 2.2036(8) Å, respectively, but shorter than Cu–Cl 2.2448(7) Å. The bond angle of N–Cu–$N^{\#1}$ is 84.77(6)° similar to N(1)–Pd–N(2), 84.8(1)° [25]. However, Cl–Cu–$Cl^{\#1}$ is 97.84(4)° larger than Cl(1)–Pd–Cl(2), 92.95(4)°. The bond angles of N–Zn–N and Cl–Zn–Cl are similar to those in Zn(*R,R*-bmbcd)Cl_2, respectively. The coordination of ligand to Cu or Zn leads to 5-membered heterocyclic rings which block nitrogen atoms and induces chirality in (*S,S*)-configuration which is similar to the coordination in the compounds of Zn(*R,R*-bmbcd)Cl_2 and Ni-complex [9], but entirely different from that in Pd-complex [24] of (*R,S*)-configuration.

3.2. Asymmetric nitroaldol reaction

10 mol% of Cu(***L***)Cl_2 or Zn(***L***)Cl_2 as the chiral Lewis acid and 6 mol% of bases as promoters were used for nitroaldol reaction at room temperature, (Scheme 1), herein methanol used as the solvent.

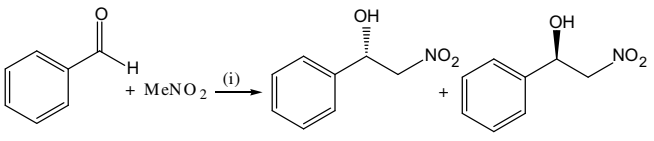

Scheme 1. (i) Cu(***L***)Cl_2 or Zn(***L***)Cl_2 10 mol%, (*i*-Pr)$_2$Net or Et_3N 6 mol%, MeOH.

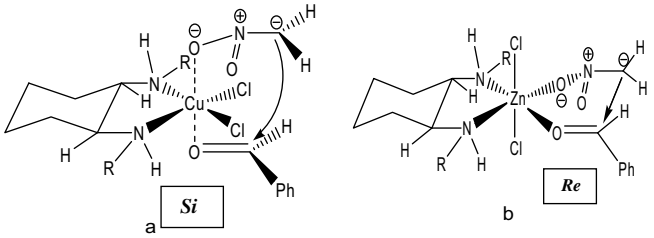

Fig. 3. Proposed transition states for the catalyzed enantioselective nitroaldol reactions with Cu and Zn complexes.

The reaction took place in a slow rate in the case of both conditions. After a week, the conversion was in the range of 51–57% (Table 3). However, in the case of the Zn-complex as chiral catalyst, ee(s) are low, 3% for Et_3N and 5% for (*i*-Pr)$_2$NEt and (*R*)-enantiomer is preferential. Ee(s) in the case of Cu-complex as catalyst are 39% for Et_3N and 23% for (*i*-Pr)$_2$NEt and (*S*)-enantiomer is preferential. In addition, a sample without chiral complex was also carried out (Table 3, entry 5). Although a higher conversion obtained because of organic base catalyst the selectivity is almost zero. So the selectivity observed (entries 1–4) clearly thanks to the chiral complexes. The reason of (*R*) or (*S*) selectivity may be the geometrical difference around the metals, distorted square-planar for Cu whereas nearly tetrahedral for Zn.

As we have seen, these complexes have the same ligand however in different stereochemical patterns so they lead to different major enantiomers. Based on our experimental observation, X-ray structure data and the previous reported steric and electronic considerations [11b,13b,19,25], we propose two transition states, which can account for the absolute configuration of the products obtained with the chiral Cu and Zn complexes. Because the metal center geometry of Cu complex is distorted square-planar therefore in the transition state for nitroaldol reaction oxygen atoms of the two reactants may be coordinated to Cu complex at axial positions of the distorted octahedron (Fig. 3a). The attack of the nitronate would take place preferentially to *si*-face of carbonyl group giving the nitroaldol product with the (*S*)-configuration. In the case of Zn complex, the metal center geometry of Zn complex is nearly tetrahedral so in the transition state for nitroaldol reaction oxygen atoms of the substrates may be coordinated to Zn at equatorial positions resulted the distorted octahedron (Fig. 3b). The attack of the nitronate would take place preferentially to *re*-face of carbonyl group giving the nitroaldol with (*R*)-configuration, respectively.

4. Conclusions

We have synthesized and determined X-ray crystal structures of chiral Lewis acids, Cu(***L***)Cl_2 and Zn(***L***)Cl_2, successfully. Zn(II) was in a nearly tetrahedral geometry while Cu was coordinated in distorted square-planar. In both cases, (*S,S*)-coordination of nitrogen atoms was induced. Application as enantioselective catalysts to nitroaldol reaction was carried out. Although the enantioselectivities are low, the geometrical difference between Cu and

Zn may be the main reason for (*S*) or (*R*) enantiomer selectivity, respectively.

5. Supplementary data

CCDC 682511 and 682512 contains the supplementary crystallographic data for Cu(***L***)$Cl_2 \cdot 2CH_3OH$ and Zn(***L***)Cl_2. These data can be obtained free of charge via http://www.ccdc.cam.ac.uk/conts/retrieving.html, or from the Cambridge Crystallographic Data Centre, 12 Union Road, Cambridge CB2 1EZ, UK; fax: (+44) 1223-336-033; or e-mail: deposit@ccdc.cam.ac.uk.

References

[1] C.A. Caputo, N.D. Jones, Dalton Trans. (2007) 4627.
[2] Y. Bennani, S. Hanessian, Chem. Rev. 97 (1997) 3161.
[3] (a) K. Püntener, L. Schwink, P. Knochel, Tetrahedron Lett. 37 (1996) 8165;
(b) J. Balsells, L. Mejorado, M. Phillips, F. Ortega, G. Aguirre, R. Somanathan, P.J. Walsh, Tetrahedron: Asymmetry 9 (1998) 4135;
(c) C.G. Frost, P. Mendonça, Tetrahedron: Asymmetry 10 (1999) 1831;
(d) C. Bied, J.J.E. Moreau, M.W.C. Man, Tetrahedron: Asymmetry 12 (2001) 329.
[4] (a) J. Lopez, E.A. Mintz, F.L. Hsu, X.R. Bu, Tetrahedron: Asymmetry 9 (1998) 3741;
(b) J.M. Mitchell, N.S. Finney, Tetrahedron Lett. 41 (2000) 8431;
(c) A. Alexakis, A.S. Chauvin, R. Stouvenel, E. Vrancken, S. Mutti, P. Mangeney, Tetrahedron: Asymmetry 12 (2001) 1171;
(d) H. Tye, C. Eldred, M. Wills, Tetrahedron Lett. 43 (2002) 155;
(e) A. Brethon, J.J.E. Moreau, M.W.C. Man, Tetrahedron: Asymmetry 15 (2004) 495;
(f) J. Bayardon, D. Sinou, O. Holczknecht, L. Mercs, G. Pozzi, Tetrahedron: Asymmetry 16 (2005) 2319.
[5] (a) E. Boyd, G.S. Coumbarides, J. Eames, R.V.H. Jones, R.A. Stenson, M.J. Suggate, Tetrahedron Lett. 46 (2005) 3479;
(b) E. Boyd, G.S. Coumbarides, J. Eames, R.V.H. Jones, M. Motevalli, R.A. Stenson, M.J. Suggate, Tetrahedron Lett. 46 (2005) 3473;
(c) H. Arjan, E. Boyd, G.S. Coumbarides, J. Eames, R.V.H. Jones, R.A. Stenson, M.J. Suggate, Tetrahedron Lett. 46 (2005) 1921.
[6] (a) S. Goumain, H. Oulyadi, P. Jubault, C. Feasson, J.C. Quirion, J. Chem. Soc., Perkin Trans. 1 (2001) 701;
(b) J.P.L. Porte, J.J.E. Moreau, F.S. Spirau, S. Wakim, Tetrahedron Lett. 42 (2001) 3073;
(c) R. Attrill, H. Tye, L.R. Cox, Tetrahedron: Asymmetry 15 (2004) 1681;
(d) S.E. Denmark, J. Fu, D.M. Coe, X. Su, N.E. Pratt, B.D. Griedel, J. Org. Chem. 71 (2006) 1513;
(e) M. Bandini, F. Piccinelli, S. Tommasi, A.U. Ronchi, C. Ventrici, Chem. Commun. (2007) 616.
[7] K. Kubota, L. Leighton, Angew. Chem., Int. Ed. 42 (2003) 946.
[8] S.G. Roh, J.U. Yoon, J.H. Jeong, Polyhedron 23 (2004) 2063.
[9] (a) D.A. Evans, D. Seidel, J. Am. Chem. Soc. 127 (2005) 9958;
(b) D.A. Evans, S. Mito, D. Seidel, J. Am. Chem. Soc. 129 (2007) 11583.
[10] M. Kwit, J. Gawronski, Tetrahedron 59 (2003) 9323.
[11] (a) C. Christensen, K. Juhl, K.A. Jørgensen, Chem. Commun. (2001) 2222;
(b) C. Christensen, K. Juhl, R.G. Hazell, K.A. Jørgensen, J. Org. Chem. 67 (2002) 4875.
[12] K. Ma, J. You, Chem. Eur. J. 13 (2007) 1863.
[13] (a) G. Blay, E. Climent, I. Fernández, V.H. Olmos, J.R. Pedro, Tetrahedron: Asymmetry 17 (2006) 2046;
(b) G. Blay, E. Climent, I. Fernández, V.H. Olmos, J.R. Pedro, Tetrahedron: Asymmetry 18 (2007) 1603.
[14] H. Maheswaran, K.L. Prasanth, G.G. Krishna, K. Ravikumar, B. Sridhar, M.L. Kantam, Chem. Commun. (2006) 4066.
[15] (a) T. Arai, M. Watanabe, A. Fujiwara, N. Yokoyama, A. Yanagisawa, Angew. Chem., Int. Ed. 45 (2006) 5978;
(b) T. Arai, M. Watanabe, A. Yanagisawa, Org. Lett. 9 (2007) 3595.
[16] B. Qin, X. Xiao, X. Liu, J. Huang, Y. Wen, X. Feng, J. Org. Chem. 72 (2007) 9323.
[17] (a) B.M. Trost, V.S.C. Yeh, Angew. Chem., Int. Ed. 41 (2002) 861;
(b) B.M. Trost, V.S.C. Yeh, H. Ito, N. Bremeyer, Org. Lett. 4 (2002) 2621.
[18] J. Gao, A.K. Martell, Org. Biomol. Chem. 1 (2003) 2801.
[19] C. Palomo, M. Oiarbide, A. Laso, Angew. Chem., Int. Ed. 44 (2005) 3881.
[20] M. Çolak, T. Aral, H. Hoşgören, N. Demirel, Tetrahedron: Asymmetry 18 (2007) 1129.
[21] D.M. Du, S.F. Lu, T. Fang, J. Xu, J. Org. Chem. 70 (2005) 3712.
[22] P. McArdle, XCAD, ABSCAL, Data Reduction and Absorption Correction Programs for CAD4 Data, National University of Ireland, Galway Ireland, 2000.
[23] G.M. Sheldrick, Acta Crystallogr., Sect. A 64 (2008) 112.
[24] E. Rafii, B. Dassonneville, A. Heumann, Chem. Commun. (2007) 583.
[25] S. Liu, C. Wolf, Org. Lett. 10 (2008) 1831.

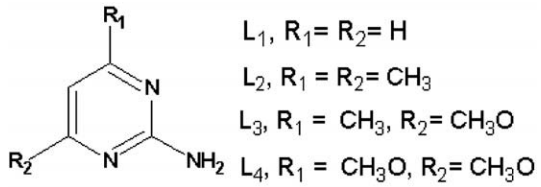

Chart 1. Structural drawings of ligand L_1–L_4.

6-methylpyrimidine; L_4 = 2-amino-4,6-dimethoxypyrimidine]. The research results indicate that difference of steric hindrance from substituted groups in ligands and the choice of solvent all have great impact on the structure of the complexes.

2. Experimental

2.1. Materials

All reagents and solvents in the synthesis were of reagent grade, and they were used without further purification. Infrared spectra were recorded on a Nicolet AVATAT FT-IR360 spectrometer as KBr pellets in the frequency range 4000–400 cm^{-1}. The elemental analyses (C, H, N contents) were determined on a CE instruments EA 1110 analyzer. Photoluminescence measurements were performed on a Hitachi F-4500 fluorescence spectrophotometer with solid powder on a 1 cm quartz round plate at room temperature.

2.2. Synthesis of complexes

2.2.1. Synthesis of complex $[Ag(L_1)(NO_3)]_n$ (**1**)

To a solution of $AgNO_3$ (170 mg, 1 mmol) in distilled water (3 ml) was added a solution of L_1 (94 mg, 1 mmol) of in distilled water–CH_3OH (5:5 v/v, 10 mL) at 60 °C. A small amount of white precipitate was removed from the resulting solution. Colorless crystals of **1** were obtained in 50% yield by slow evaporation at room temperature after one week. They were washed with a small volume of cold CH_3OH and diethyl ether. *Anal.* Calc. for $AgC_4H_5N_4O_3$: C, 18.13; H, 1.90; N, 21.14. Found: C, 18.20; H, 1.86; N, 21.18%. IR (cm^{-1}): 3396 (s), 3302 (m), 3188 (m), 1762 (m), 1625 (s), 1570 (s), 1529 (m), 1477 (s), 1459 (m), 1384 (s), 1223 (m), 1187 (m), 976 (w), 871 (m), 825 (m), 788 (m), 658 (m), 515 (m), 465 (m).

2.2.2. Synthesis of complex $[Ag_4(L_2)_6(NO_3)_4]$ (**2**)

The synthesis of **2** was similar to that of **1**, but with ligand L_2 (123 mg, 1 mmol) in place of ligand L_1. Colorless crystals were obtained in 66% yield. *Anal.* Calc. for $Ag_4C_{36}N_{22}H_{54}O_{12}$: C, 30.48; H, 3.84; N, 21.72. Found: C, 30.47; H, 3.81; N, 21.78%. IR (cm^{-1}): 3396 (s), 3313 (m), 3138 (br), 1654 (s), 1594 (m), 1568 (m), 1475 (m), 1453 (m), 1384 (s), 1233 (m), 1026 (m), 961(m), 834 (m), 825 (m), 788 (m), 729 (m), 567 (m), 547 (m), 474 (m).

2.2.3. Synthesis of complex $[Ag(L_3)(NO_3)]_n$ (**3**)

The synthesis of **3** was similar to that of **1**, but with ligand L_3 (139 mg, 1 mmol) in place of ligand L_1. Colorless crystals were obtained in 60% yield. *Anal.* Calc. for $AgC_6H_9N_4O_4$: C, 23.32; H, 2.94; N, 18.13. Found: C, 23.35; H, 2.90; N, 18.09%. IR (cm^{-1}): 3367 (s), 3314 (w), 3183 (m), 3023 (m), 1637 (s), 1585 (s), 1458 (m), 1384 (s), 1346 (m), 1204 (m), 1152 (m), 1023 (m), 938(m), 839 (w), 798(m), 782 (m), 646(m), 585 (w), 546 (w).

2.2.4. Synthesis of complex $[Ag_3(L_4)_3(NO_3)_3]_n$ (**4**)

The synthesis of **4** was similar to that of **1**, but with ligand L_4 (155 mg, 1 mmol) in place of ligand L_1. Colorless crystals were obtained in 55% yield by the slow evaporation at room temperature after one week. They were washed with a small volume of cold CH_3OH and diethyl ether. *Anal.* Calc. for $Ag_3C_{18}H_{27}N_{12}O_{15}$: C, 22.17; H, 2.79; N, 17.24. Found: C, 22.07; H, 2.65; N, 17.30%. IR (cm^{-1}): 3413 (m), 3312 (m), 3192 (m), 3025 (m), 1637 (s), 1581 (s), 1452 (m), 1384 (s), 1215 (m), 1151 (m), 1102 (m), 1047 (m), 928(m), 794(m), 786 (m), 671(m), 564 (w), 512 (w).

2.2.5. Synthesis of complex $[Ag(L_4)(NO_3)]_n$ (**5**)

To a solution of $AgNO_3$ (170 mg, 1 mmol) in distilled water (3 ml) was added a solution of L_4 (155 mg, 1 mmol) of in distilled water–CH_3CH_2OH (5:5 v/v, 10 mL) at 60 °C. A small amount of white precipitate was removed from the resulting solution.

Table 1
Crystallographic data for complexes **1**–**5**

Complexes	**1**	**2**	**3**	**4**	**5**
Formula	$AgC_4H_5N_4O_3$	$Ag_4C_{36}H_{54}N_{22}O_{12}$	$AgC_6H_9N_4O_4$	$Ag_3C_{18}H_{27}N_{12}O_{15}$	$AgC_6H_9N_4O_5$
M_r	264.99	1418.49	309.04	975.13	325.04
Crystal system	monoclinic	triclinic	monoclinic	monoclinic	monoclinic
Space group	$P2_1/n$	$P\bar{1}$	$P2_1/c$	$P2_1/c$	$C2/c$
a (Å)	6.997(2)	10.309(3)	9.2083(4)	11.3311(2)	15.0128(8)
b (Å)	10.581(3)	10.309(3)	12.2396(5)	12.3445(3)	11.3189(3)
c (Å)	9.553(2)	13.410(3)	8.8356(4)	20.9588(6)	12.3862(5)
α (°)	90	95.582(4)	90	90	90
β (°)	90.332(4)	95.582(4)	106.978(5)	96.389(2)	117.096(5)
γ (°)	90	115.67	90	90	90
Z	4	1	4	4	8
V (Å^3)	705.8(3)	1262.9(7)	952.42(7)	2913.4(1)	1873.7(1)
D_{calc} (g cm^{-3})	2.494	1.865	2.155	2.223	2.304
μ(mm^{-1})	2.825	1.608	2.118	2.091	2.167
F(000)	512	708	608	1920	1280
Number of unique reflections	1385	4774	2051	5541	1823
Number of observed reflections [$I > 2\sigma(I)$]	1314	4631	1662	3563	1422
Parameters	109	334	136	433	1280
Goodness-of-fit	1.005	1.190	1.022	1.011	1.023
Final R indices [$I > 2\sigma(I)$]	R_1 = 0.0388, wR_2 = 0.0931	R_1 = 0.0387, wR_2 = 0.0964	R_1 = 0.0192, wR_2 = 0.0429	R_1 = 0.0478, wR_2 = 0.0942	R_1 = 0.0215, wR_2 = 0.0508
R indices (all data)	R_1 = 0.0408, wR_2 = 0.0951	R_1 = 0.0399, wR_2 = 0.0973	R_1 = 0.0264, wR_2 = 0.0437	R_1 = 0.0862, wR_2 = 0.1044	R_1 = 0.0309, wR_2 = 0.0525
Largest difference in peak and hole (e Å^{-3})	0.993 and −0.946	0.748 and −0.388	0.295 and −0.365	1.771 and −1.207	0.667 and −0.415

Table 2
Selected bond distances (Å) and angles (°) for **1**–**5**

Complex ***1***					
Ag(1)–N(3)	2.281(3)	Ag(1)–N(1A)	2.276(3)	Ag(1B)–N(1)	2.276(4)
Ag(1)–O(1)	2.581(4)	Ag(1)–O(2)	2.680(4)		
N(3)–Ag(1)–N(1A)	136.6(1)	N(3)–Ag(1)–O(1)	120.7(1)		
N(1A)–Ag(1)–O(1)	90.4(1)	O(1)–Ag(1)–O(2)	47.9(1)		
Complex ***2***					
Ag(1)–N(8)	2.182(3)	Ag(1)–N(11A)	2.209(3)	Ag(1)–O(3)	2.529(3)
Ag(1)–O(4)	2.520(3)	Ag(2)–N(3)	2.156(3)	Ag(2)–N(9)	2.175(3)
Ag(1A)–N(11)	2.209(3)	Ag(2)–O(3)	2.531(3)	Ag(2)–O(4)	2.640(3)
N(8)–Ag(1)–N(11A)	152.1(1)	N(8)–Ag(1)–O(4)	115.4(1)		
N(11A)–Ag(1)–O(4)	83.4(1)	N(8)–Ag(1)–O(3)	100.00(2)		
N(11A)–Ag(1)–O(3)	106.2(1)	O(4)–Ag(1)–O(3)	69.4(1)		
N(3)–Ag(2)–N(9)	162.1(1)	N(3)–Ag(2)–O(3)	104.7(1)		
N(9)–Ag(2)–O(3)	89.8(1)	O(3)–Ag(2)–O(4)	67.5(1)		
Complex ***3***					
Ag(1)–N(1)	2.274(2)	Ag(1)–N(3)	2.287(2)	Ag(1)–O(2)	2.597(2)
Ag(1)–O(2B)	2.664(2)	Ag(1)–O(3B)	2.657(2)	Ag(1)–O(1)	3.014(2)
N(1)–Ag(1)–N(3)	149.77(6)	N(1)–Ag(1)–O(2)	111.74(5)		
N(3)–Ag(1)–O(2)	93.00(5)	O(2B)–Ag(1)–O(3B)	47.82(5)		
Complex ***4***					
Ag(1)–N(1)	2.249(5)	Ag(1)–N(3)	2.213(5)	Ag(2)–N(4)	2.261(5)
Ag(2)–N(5)	2.266(5)	Ag(3)–N(9)	2.241(5)	Ag(3)–N(7)	2.273(5)
Ag(2)–O(10)	2.746(4)	Ag(2)–O(9)	2.618(4)	Ag(3)–O(9)	2.540(4)
Ag(3)–O(13B)	2.686(4)	Ag(3)–O(14B)	2.639(4)	Ag(1)–O(13A)	2.643(4)
N(3)–Ag(1)–N(1)	152.2(2)	N(4)–Ag(2)–N(5)	146.2(2)		
N(7)–Ag(3)–N(9)	148.1(2)	N(7)–Ag(3)–O(9)	112.1(2)		
N(9)–Ag(3)–O(9)	94.7(2)	O(13B)–Ag(3)–O(14B)	47.8(2)		
Ag(2)–O(9)–Ag(3)	112.9(2)				
Complex ***5***					
Ag(1)–N(1)	2.250(2)	Ag(1)–N(2A)	2.256(2)	Ag(1)–O(1)	2.459(2)
N(2)–Ag(1B)	2.256(2)	Ag(1)–O(2B)	2.650(2)		
N(1)–Ag(1)–N(2A)	147.16(8)	N(1)–Ag(1)–O(1)	107.70(8)		
N(2A)–Ag(1)–O(1)	92.85(8)	O(1)–Ag(1)–O(2B)	82.53(8)		

Symmetry transformations used to generate equivalent atoms: (A) $x + 1/2, -y + 1/2, z - 1/2$; (B) $x - 1/2, -y + 1/2, z + 1/2$ for **1**. (A) $-x + 1, -y + 1, -z + 1$ for **2**. (B) $-x, y - 1/2, -z + 3/2$ for **3**. (B) $x, y + 1, z$ for **4**. (A) $x, -y + 1, z + 1/2$; (B) $x, -y + 1, z - 1/2$ for **5**.

Colorless crystals of **5** were obtained in 45% yield by slow evaporation at room temperature after one week. They were washed with a small volume of cold CH_3CH_2OH and diethyl ether. *Anal.* Calc. for $AgC_6H_9N_4O_5$: C, 22.17; H, 2.79; N, 17.24%. Found: C, 22.10; H, 2.70; N, 17.14%. IR (cm^{-1}): 3416 (m), 3308 (m), 3201 (m), 3027 (m), 1644 (s), 1583 (s), 1450 (m), 1378 (s), 1209 (m), 1142 (m), 1101 (m), 1040 (m), 1004 (w), 923(m), 840 (w), 820(m), 784 (m), 676(w), 656(w), 554 (w), 507 (w).

2.3. X-ray crystallography

Single crystals of these complexes with appropriate dimensions were mounted on a glass fiber and used for data collection. Data were collected on a Bruker-AXS CCD diffractometer equipped with a graphite-monochromated Mo Kα radiation source ($\lambda = 0.71073$ Å) at 298 K for **1**–**5**. All absorption corrections were performed with the SADABS program [26a]. All the structures were solved by direct methods using SHELXS-97 [26b] and refined by full-matrix least-squares techniques using SHELXL-97 [26c]. All the non-hydrogen atoms were treated anisotropically. The positions of hydrogen atoms were generated geometrically. The crystallographic details of **1**–**5** are summarized in Table 1. Selected bond lengths and bond angles of **1**–**5** are displayed in Table 2.

3. Results and discussion

3.1. Synthesis of the complexes

The synthesis of complexes **1–5** is readily prepared by the reactions of $AgNO_3$ with a family of 2-aminopyrimidyl ligands and is

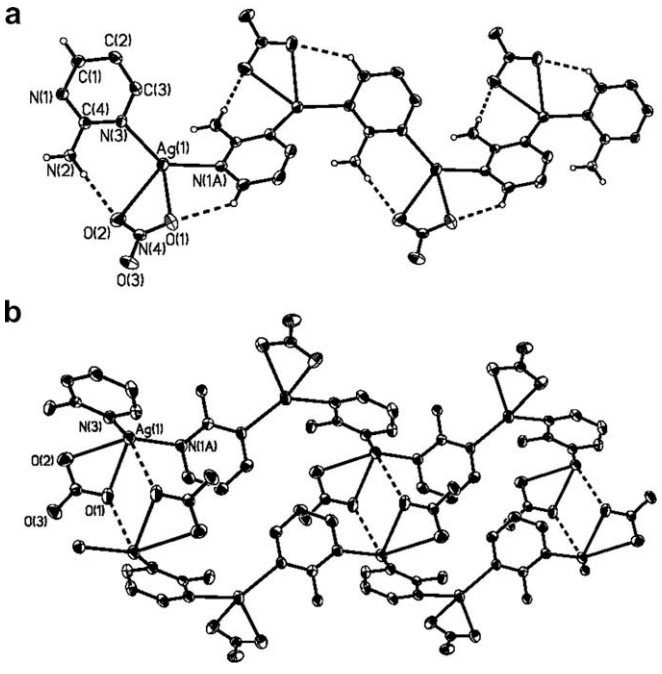

Fig. 1. (a) Perspective drawing of a fragment of the chain of **1** growing along the *a* axis. The dashed lines correspond to the hydrogen bonds. The thermal ellipsoids are drawn at the 35% probability level. Hydrogen atoms in pyrimidyl groups partially omitted for clarity. (b) The 1-D ladder structure formed through Ag···O weak interactions (indicated by dashed lines) between the adjacent chains. All hydrogen atoms omitted for clarity.

summarized in the Supplementary data. The formation of the products is not significantly affected by changes of the reaction mole ratio of ligands to metal ions, and the resultant crystals are insoluble in water and common organic solvents. Three complexes (**1** with 1-D zigzag chain, **2** with 0-D tetramer, and **3** with 2-D grid network) are obtained by using the same silver(I) nitrate but different ligands to investigate the effect of substituted groups of ligands on the structure of the complexes. On the other hand, **4** and **5** are isolated by using the same silver salt and ligand but different solvent systems to investigate the influence of reaction solvents on the structure of the complexes. Complex **4** has a 1-D polymeric ribbon further connected by hydrogen bonds to generate a 2-D layer structure. While Complex **5** shows a 2-D honeycomb-like layer consisting of 24-membered metallocycles. In **1**–**5**, 2-aminopyrimidine and its derivatives adopt similar coordination modes, bidentate N,N′-donor ligands binding with silver atoms, while the different substitutions of 2-aminopyrimidyl ligands in the same substitutional positions in these complexes result in distinct structural motifs. Thus, we have reason to believe that subtle structural changes of ligands might create a tuning effect on the formation of crystal structures. Additionally, as far as certain ligand such as L_4 concerned, the structure of complexes (**4**–**5**) can be controlled by choosing different solvent systems. In addition, the secondary forces such as intramolecular and intermolecular hydrogen bonds also play important role in the overall architecture and stabilization of the complexes. The hydrogen bond geometries **1**–**5** are summarized in Table S1.

3.2. Description of the crystal structures of *1*–*5*

3.2.1. Crystal structure of $[Ag(L_1)(NO_3)]_n$ (*1*)

X-ray analysis reveals that **1** has an infinite 1-D zigzag chain structure. As depicted in Fig. 1a, the basic repeat is a distorted tetragonal four-coordinate AgO_2N_2 unit, which comprises two oxygen atoms from one nitrate anion and two independent pyrimidine hetero-nitrogens in a distinctly nonlinear geometry forming zigzag chains. The average Ag–N distance in **1** is agreement with those reported in the literature, such as $[\{Ag(pts)\}_2(L_2)_3]_n$ [24b] and $[Ag(L_2)(NO_3)]_n$ [24h] (pts = *p*-toluenesulfonate; L_2 = 2-amino-4,6-dimethylpyrimidine). The acute angle at the chelate site of nitrate [47.9(1)° for O(1)–Ag(1)–O(2)] accounts for the obviously distorted surrounding of silver ions. In **1**, each ligand L_1 links two Ag atoms to form a 1-D zigzag chain. In the 1-D chain, two kinds of intramolecular hydrogen bonds are observed including $C_{(pyrimidyl)}$–H···O and N–H···O [3.238(4) and 2.979(4) Å for C(1A)···O(1) and N(2)···O(2), respectively, symmetry code: (A) = $x + 1/2$, $-y + 1/2$, $z - 1/2$], which contribute to the stabilization of the crystal packing. The adjacent chains in **1** are further interlinked by means of Ag···O weak interactions with Ag–O distance of 2.832 Å to generate 1-D ladder structure (Fig. 1b). In the 1-D ladder, the value of

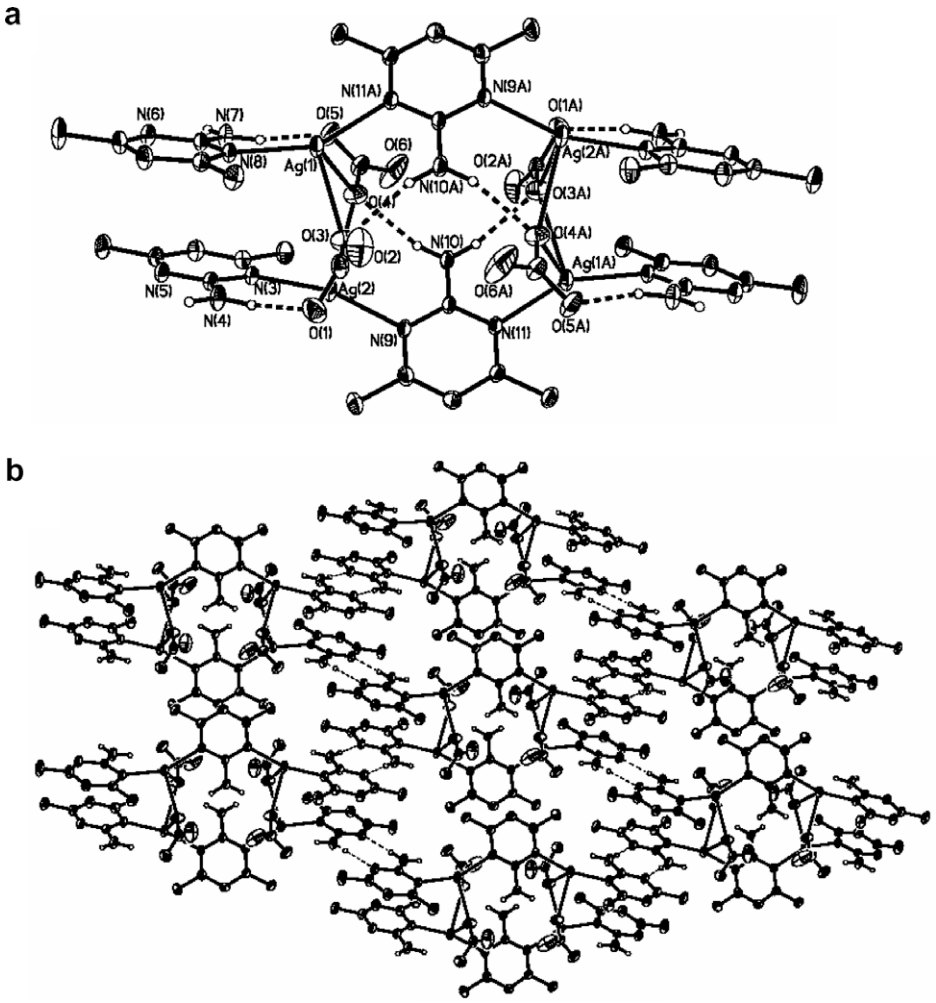

Fig. 2. (a) ORTEP drawing of **2** showing the coordination environment around Ag(I) centers at 30% probability level. The hydrogen atoms in pyrimidyl groups were omitted for clarity. (b) Hydrogen-bonding indicated by dashed lines in crystals of **2** showing tetramers further linked into layers. The hydrogen atoms in pyrimidyl groups were omitted for clarity.

the intrachain silver–silver separation is 6.463 Å whereas that of the shortest interchain distance is 4.394 Å.

3.2.2. Crystal structure of $[Ag_4(L_2)_6(NO_3)_4]$ (**2**)

When the L_2 ligand reacts with $AgNO_3$ under the same reaction conditions, a new complex **2** is obtained. X-ray analysis shows that **2** consists of the neutral tetranuclear $[Ag_4(L_2)_6(NO_3)_4]$ unit. As depicted in Fig. 2a, the overall molecular structure of **2** is centrosymmetric, having two independent Ag^I ions with similar coordination environments linked together through nitrate groups and N donors of L_2. Each Ag center is four-coordinate by two N atoms from two different L_2 ligands and two O atoms form two bridging ONO_2^- anions. The Ag–N and Ag–O bond distances are all within normal range. In tetramer **2**, four Ag atoms (Ag1, Ag2, Ag1A and Ag2A) are approximately coplanar with the average Ag–Ag separation is 5.076 Å, preclusive of any direct metal–metal interaction.

Hydrogen bonds play a key role in stabilizing and assembling 2-D supramolecular architectures in **2**. Intramolecular N–H···O hydrogen bonds in the tetramer occur where oxygen atoms of nitrate anions serve as acceptors while the uncoordinated amino group of the L_3 ligand act as donors [H···O, 2.13 to 2.60 Å, N···O, 2.932(5) to 3.361(6) Å, ∠N–H···O, 147.0–155.0°]. Interestingly, an extended 2-D supramolecular network arises from self-complementary intermolecular N–H···N hydrogen bonds from the syn-amino proton to a nitrogen atom of the pyrimidine ring [H···N, 2.14–2.17 Å, N···N, 2.997(5)–3.029(5) Å, ∠N–H···N, 176.5–178.5°] (see Fig. 2b).

3.2.3. Crystal structure of $[Ag(L_3)(NO_3)]_n$ (**3**)

To evaluate the effect of the substituting group of the 2-aminopyrimidyl ligands on the framework formation of their complexes, the L_3 ligand is chosen to react with $AgNO_3$ under the same reaction conditions and a new complex **3** is obtained. X-ray analysis shows that **3** features a 2-D grid structure. As shown in Fig. 3a, the central Ag atom has distorted trigonal-bipyramidal geometry, and is confined by two N atoms from two pyrimidine rings, three O atoms from two individual nitrate groups. N1 and N3 and O2 define the trigonal equatorial plane, while O2B and O3B occupy the axial positions. The average Ag–N distance in **3** is in agreement with that of **1**. Additionally, the distance between the silver atom and the oxygen atom from methoxy group in pyrimidyl ring is 3.014(2) Å, a value which is smaller than the sum of the van der Walls radii [27,28], revealing the weak interaction of the silver(I) ions with CH_3O groups. As shown in Fig. 3b, each L_3 ligand as a bidentate ligand links two Ag atoms to form a 1-D zigzag chain and the adjacent chains are further connected by the atoms from nitrate anions to generate a 2-D grid structure in the *ac* plane. The intramolecular nonbonding metal–metal distances of Ag1···Ag1A and Ag1···Ag1B in **3** are 6.373 and 4.559 Å, which are longer than those in **2**. It is noticeable that the 2-D grid network is further stabilized by two kinds of intermolecular N–H···O hydrogen bonds where oxygen atoms of nitrate anions and CH_3O groups serve as acceptors while hydrogen atoms of the uncoordinated amino group of the L_3 ligand act as donors [N(2)–H(2A)···O(2), 2.846 Å, N–H···O, 156.2°; N(2)–H(2B)···O(1), 2.976 Å, N–H···O, 159.4°]. Obvious changes are observed from the structures of **2** and **3**, and the dimension of the complexes increase from 0-D (**2**) to 2-D (**3**). Striking structural difference between **2** and **3** simply is caused by a subtle difference in the ligand structure, *i.e.*, the replacement of 4-position of methyl group by methoxy group. On the basis of the above results, it may be concluded that structural major transformation between **2** and **3** may partially be attributed to steric effect of substituted groups of ligands.

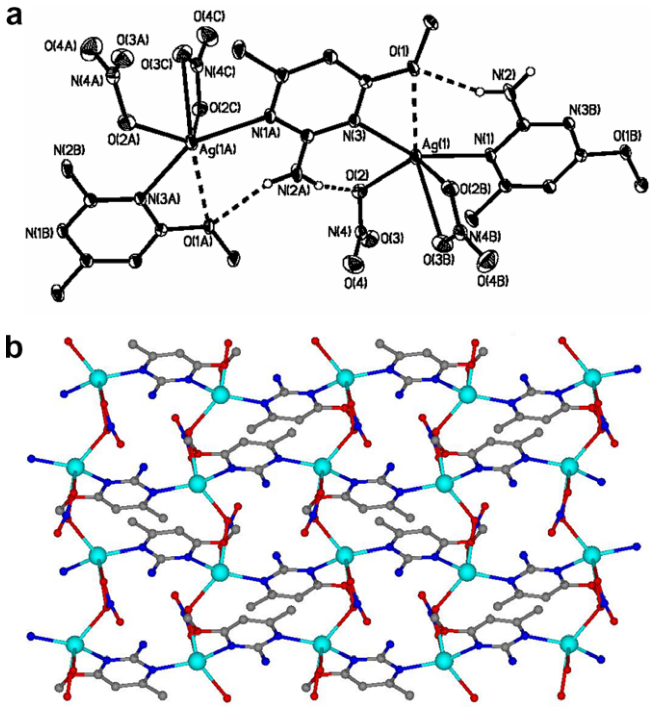

Fig. 3. (a) ORTEP drawing of **3** showing the coordination environment around Ag(I) centers at 30% probability level. The hydrogen atoms in pyrimidyl, methyl, and methoxy groups were omitted for clarity. (b) A view along the *a* axis of 2-D grid network structure in **3**. Hydrogen atoms are omitted for clarity. Ag stressed in bigger ball.

3.2.4. Crystal structure of $[Ag_3(L_4)_3(NO_3)_3]_n$ (**4**)

To evaluate the effect of the reaction solvent systems on the structure of the complexes, reactions of ligand L_4 with $AgNO_3$ are carried out under different mixed solvents (methanol–water and ethanol–water, respectively) and complexes **4** and **5** are successfully isolated. X-ray analysis shows the asymmetric unit in **4** contains three Ag^I atoms, three L_4 ligands and three nitrate anions. As depicted in Fig. 4a, there are three metal atoms with different coordination environments in **4**. The Ag(1) atom adopts the distorted triangular geometry, in which the metal is coordinated by the nitrogen atoms of two L_4 ligands and one oxygen atom of the nitrate anion. The Ag(2) atom displays a distorted tetrahedral geometry, being coordinated by two nitrogen atoms from two different L_4 ligands, one μ_2-O atom from one bridging nitrate anion, and one terminated μ_1-O atom from another nitrate anion. The Ag(3) atom adopts the distorted trigonal-bipyramidal geometry in which two nitrogen atoms of two L_4 and three O atoms of separate nitrate anions coordinate the metal silver center. Three types of NO_3^- anions are found in **4**. The first type adopts the μ_1-O, μ_2-O′ bonding mode to bridge two Ag(I) ions. The second adopts the μ_1-O bonding mode to coordinate weakly to one Ag(I) ion. While the third type adopts the μ_2-O bonding mode to bridge two Ag(I) atoms. Fig. 4b shows that **4** forms a 1-D polymeric ribbon arrangement by the continual symmetry operations including twofold screw axis and inversion center. In the 1-D ribbon, intramolecular hydrogen bonds are observed involving the free amino group of the L_4 with the oxygen atoms on the mono-coordinated NO_3^- anion and on the methoxy groups, respectively [2.996(7) and 3.172(7) Å for N(2)···O(10) and N(2)···O(1)], and one kind of non-classical hydrogen bonds where oxygen atoms of NO_3^- anions serve as acceptors while hydrogen atoms of methoxy groups of the pyrimidine rings act as donors [3.339(9) Å for C(8)···O(12)]. The adjacent ribbons in **4** are interlinked to form 2-D layer structure by means of intermolecular hydrogen bonds in which oxygen atoms of nitrate anions serve as acceptors while hydrogen atoms of NH_2 groups of the pyrimidine rings act as donors [H···O = 2.06–2.64 Å, N···O = 2.883(7)–3.172(7) Å, ∠N–H···O = 123.2–170.3°] (Fig. 4b).

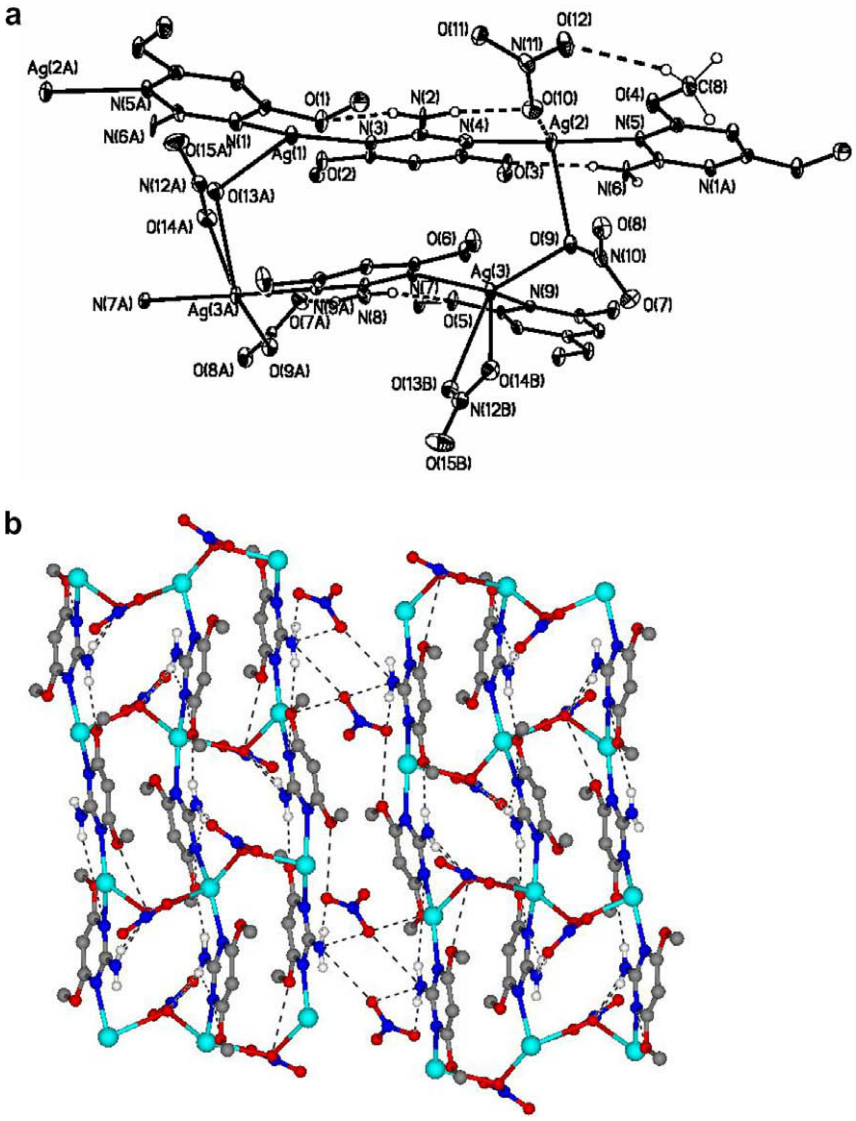

Fig. 4. (a) ORTEP drawing of **4** showing the coordination environment around Ag(I) centers at 30% probability level. Hydrogen atoms in pyrimidyl and methoxy groups were omitted for clarity. (b) A view along the *a* axis of 2-D layer structure in **4**. The dashed lines correspond to the hydrogen bonds. Ag stressed in bigger ball.

*3.2.5. Crystal structure of $[Ag(L_4)(NO_3)]_n$ (**5**)*

It is interesting that complex **5** has a different space group *C*2/*c* and structure from that of **4**, caused by different mixed solvent. The repeat unit of **5** consists of one Ag^I atoms, one L_4 ligands, and one nitrate anion. It is clear that the metal-to-ligand ration is 1 in **5**, which is the same as **4** or **3**. As shown in Fig. 5a, the silver metal centers only possess one type of geometry different from that of **4**. Each four-coordinate Ag which adopts a distorted tetrahedral geometry is coordinated by two μ_1-O donors from two individual nitrate anions, and two bridging L_4 pyrimidine nitrogen atoms. The angle of O–Ag–O [82.53(8)° for O(1)–Ag(1)–O(2B)] is responsible for the distorted tetrahedral geometry of Ag^+ ions. The average Ag–O distance in **5** is slightly shorter than that of **4**. X-ray analysis shows that **5** is a 2-D honeycomb-like layer consisting of 24-membered metallocycles different from 1-D ribbon of **4**, implying that the choice of solvent has a great influence on the overall structure of the complexes in this system (Fig. 5b). The metallocycles involve two sorts of Ag(I) ions. One type Ag(I) ions are bridged by four L_4 ligands through the pyrimidyl nitrogen atoms, while the other Ag(I) ions are not only bridged by four L_4 ligands *via* the pyrimidyl nitrogen atoms, but by four NO_3^- anions by μ_1-O, μ_1-O′ bonding modes (Fig. 5b). It is noteworthy that inside the 24-membered metallocycles, intramolecular hydrogen bonds are observed between bridging nitrate anions, methoxy groups and NH_2 groups of the pyrimidyl rings, respectively: N(3)···O(5A) = 3.050(3), N(3)···O(2B) = 2.932(3) Å [symmetry codes: (A), x, $-y+1$, $z-1/2$; (B), $-x+1/2$, $-y+3/2$, $-z+1$].

3.3. Photoluminescence properties

The mixed inorganic–organic hybrid coordination polymers have been investigated for fluorescence properties and for potential applications. However, owing to the intense spin–orbital coupling of Ag(I), most of luminescent Ag(I) complexes exhibit luminescence at low temperature [29] and Ag(I) complexes which exhibit luminescence at room temperature are few [30]. The complexes **1**–**5** reported herein represent room temperature luminescent Ag-containing polymeric complexes [31].

The solid-state fluorescence data for both free ligands and the complexes **1–5** at room temperature are shown in Table 3. As

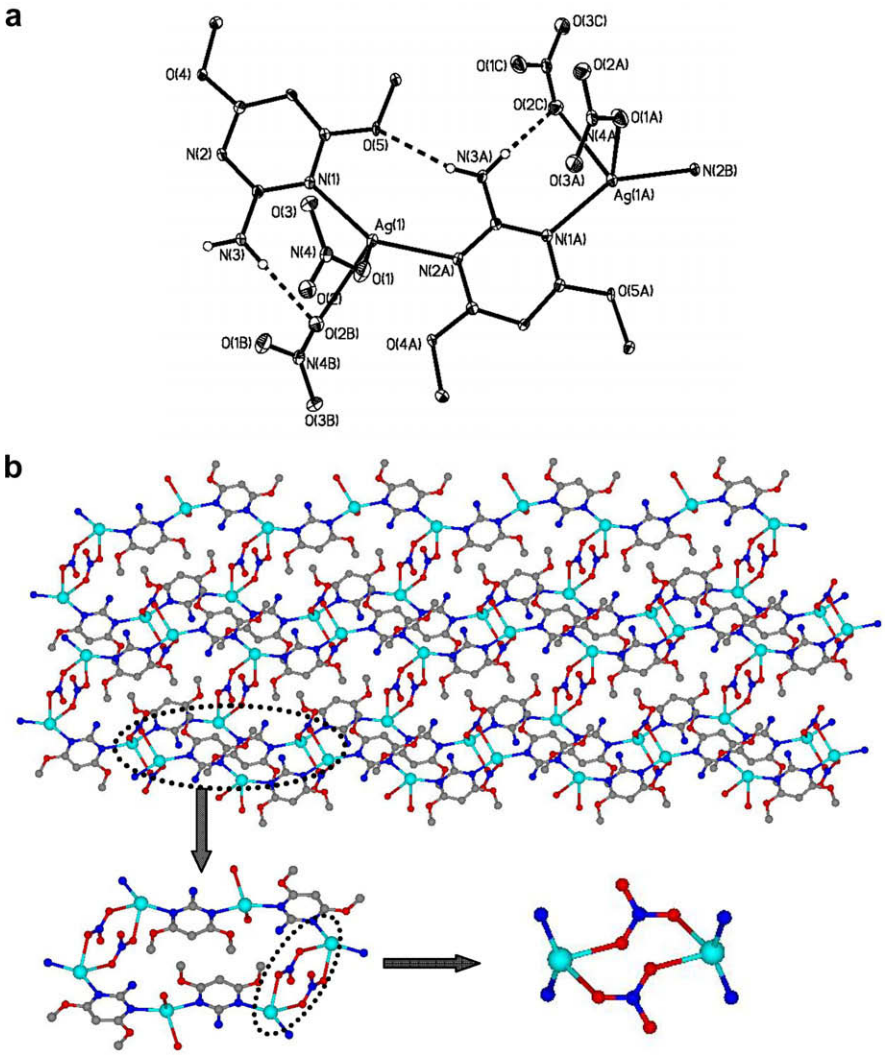

Fig. 5. (a) ORTEP drawing of **5** showing the coordination environment around Ag(I) centers at 30% probability level. Hydrogen atoms in pyrimidyl and methoxy groups were omitted for clarity. (b) A view along the *a* axis of 2-D honeycomb structure in **5**. Hydrogen atoms are omitted for clarity. Ag stressed in bigger ball.

Table 3
Comparison of emission peaks between the complexes and free ligands

Ligands	$\lambda_{em\ (ligand)}$ (nm)	Complexes	$\lambda_{em\ (complex)}$ (nm)	Red-shifted wavelength comparable with ligands (nm)
L_1	345	1	360	15
L_2	340	2	352	12
L_3	331	3	338	7
L_4	327	4	336	9
L_4	327	5	335	8

can be seen, **1** shows a main peak at 360 nm upon photo-excitation at 280 nm. And **2** and **3** exhibit an intense emission band with the maximum intensity at 352 nm and 338 nm, respectively. Here the presence of the silver only causes minor change in the emission spectra of the ligands. The emission spectrum of L_4 shows a peak at 327 nm upon excitation at 280 nm, and this emission is probably attributed to the aromatic π–π^* transition of L_4. By comparison, both of complexes **4** and **5** exhibit similar red-shift values for emission maxima as compared to the corresponding free ligand values. All the complexes **1**–**5** exhibit some low-energy emission bands, which have shapes and positions similar to the free ligands L_1–L_4. The emissions are neither metal-to-ligand charge (MLCT) nor ligand-to-metal charge transfer (LMCT) in nature and probably can be assigned to the intraligand π_L—π_L^* transitions fluorescent emission (LLCT) because very similar emissions are also observed for the free ligands.

4. Conclusions

In this study, five new silver(I) complexes with interesting structural motifs have been successfully synthesized from the various rigid ligands L_1, L_2, L_3 and L_4 with silver(I) nitrate. The analysis of the crystallographic data of **1–5** clearly shows that the overall architecture of the crystals is not only controlled by the nature of the rigid ligands present in the moiety, but by different solvent systems. Table S2 shows the cation–anion interaction, metal geometry and structure in complexes **1–5**. Moreover, the photoluminescent properties of free ligands L_1–L_3, and complexes **1**–**5** have been examined.

Acknowledgments

This work was financially supported by the National Natural Science Foundation of China (Nos. 20571062 and 20721001) and the National Basic Research Program of China (2007CB815301).

Appendix A. Supplementary data

CCDC 652463, 646314, 652465, 665093 and 665092 contain the supplementary crystallographic data for **1**, **2**, **3**, **4** and **5**. These data can be obtained free of charge via http://www.ccdc.cam.ac.uk/conts/retrieving.html, or from the Cambridge Crystallographic Data Centre, 12 Union Road, Cambridge CB2 1EZ, UK; fax: (+44) 1223-336-033; or e-mail: deposit@ccdc.cam.ac.uk. Supplementary data associated with this article can be found, in the online version, at doi:10.1016/j.poly.2008.07.013.

References

[1] (a) M. Fujita, M. Tominaga, K. Suzuki, M. Kawano, T. Kusukawa, Angew. Chem., Int. Ed. 43 (2004) 5621;
(b) A.K. Cheetham, G. Ferey, T. Loiseau, Angew. Chem., Int. Ed. 38 (1999) 3268.
[2] (a) X.-Y. Wang, L. Wang, Z.-M. Wang, S. Gao, J. Am. Chem. Soc. 128 (2006) 674;
(b) X.-L. Wang, C. Qin, N.-B. Wang, Angew. Chem., Int. Ed. 44 (2005) 5824.
[3] (a) O.R. Evans, W. Lin, Acc. Chem. Res. 35 (2002) 511;
(b) M. Eddaoudi, D.B. Moler, H.-L. Li, B.-L. Chen, T.M. Reineke, M. O'Keeffe, O.M. Yaghi, Acc. Chem. Res. 34 (2001) 319.
[4] S.R. Batten, R. Robson, Angew. Chem., Int. Ed. 37 (1998) 1460.
[5] S.L. James, Chem. Soc. Rev. 32 (2003) 276.
[6] C.N.R. Rao, S. Natarajan, R. Vaidhyanathan, Angew. Chem., Int. Ed. 43 (2004) 1466.
[7] S. Kitagawa, R. Kitaura, S. Noro, Angew. Chem., Int. Ed. 43 (2004) 2334.
[8] M.J. Rosseinsky, Micropor. Mesopor. Mater. 73 (2004) 15.
[9] J.L.C. Rowsell, O.M. Yaghi, Micropor. Mesopor. Mater. 73 (2004) 3.
[10] A.K. Cheetham, C.N.R. Rao, R.K. Feller, Chem. Commun. (2006) 4780.
[11] O.M. Yaghi, M. O'Keeffe, N.W. Ockwig, H.K. Chae, M. Eddaoudi, J. Kim, Nature 423 (2003) 705.
[12] (a) C. Janiak, Dalton Trans. (2003) 2781;
(b) U. Mueller, M. Schubert, F. Teich, H. Puetter, K.S. Arndt, J. Pastré, J. Mater. Chem. 16 (2006) 626;
(c) N.R. Champness, Dalton Trans. (2006) 877;
(d) X. Lin, J.-H. Jia, P. Hubberstey, M. Schröder, N.R. Champness, CrystEngComm 9 (2007) 438;
(e) C.-L. Chen, B.-S. Kang, C.-Y. Su, Aust. J. Chem. 59 (2006) 3;
(f) S.-L. Zheng, X.-M. Chen, Aust. J. Chem. 57 (2004) 703.
[13] (a) C.K.V. Sharma, R.D. Rogers, Chem. Commun. (2003) 1808;
(b) E.-Q. Gao, A.-L. Cheng, Y.-X. Xu, C.-H. Yan, M.-H. He, Cryst. Growth Des. 5 (2005) 1005;
(c) N.S. Oxtoby, N.R. Champness, CrystEngComm 7 (2005) 284.
[14] (a) M.-L. Tong, B.-H. Ye, J.-W. Cai, X.-M. Chen, S.W. Ng, Inorg. Chem. 37 (1998) 2645;
(b) M. Oh, C.L. Stern, C.A. Mirkin, Inorg. Chem. 44 (2005) 2647;
(c) M.B. Zaman, K. Udachin, J.A. Ripmeester, Inorg. Chem. 44 (2005) 5047;
(d) A.N. Khlobystov, N.R. Champness, M. Schroder, J. Am. Chem. Soc. 125 (2003) 6753.
[15] (a) R.P. Feazell, C.E. Carson, K.K. Klausmeyer, Eur. J. Inorg. Chem. (2005) 3287;
(b) R.P. Feazell, C.E. Carson, K.K. Klausmeyer, Inorg. Chem. 45 (2006) 2627;
(c) R.P. Feazell, C.E. Carson, K.K. Klausmeyer, Inorg. Chem. 45 (2006) 2635;
(d) R.P. Feazell, C.E. Carson, K.K. Klausmeyer, Inorg. Chem. 45 (2006) 935.
[16] A.J. Blake, N.R. Champness, P. Hubberstey, W.-S. Li, M.A. Withersby, M. Schröder, Coord. Chem. Rev. 183 (1999) 117.
[17] D.B. Leznoff, B.Y. Xue, R.J. Batchelor, F.W.B. Einstein, B. Patrick, Inorg. Chem. 40 (2001) 6026.
[18] M. Munakata, L.P. Wu, T. Kuroda-Sowa, Adv. Inorg. Chem. 46 (1999) 173.
[19] (a) C.M. Fitchett, P.J. Steel, Aust. J. Chem. 59 (2006) 19;
(b) T. Dorn, K.M. Fromm, C. Janiak, Aust. J. Chem. 59 (2006) 22;
(c) M.B. Duriska, S.R. Batten, D.J. Price, Aust. J. Chem. 59 (2006) 26;
(d) Y.-B. Xie, J.-R. Li, X.-H. Bu, Aust. J. Chem. 59 (2006) 34;
(e) L.C. Silva, R. Ahmad, M.J. Hardie, Aust. J. Chem. 59 (2006) 40.
[20] (a) L. Carlucci, G. Ciani, D.M. Proserpio, A. Sironi, Angew. Chem., Int. Ed. Engl. 34 (1995) 1895;
(b) G.K.H. Shimizu, G.D. Enright, C.I. Ratcliffe, J.A. Ripmeester, D.D.M. Wayner, Angew. Chem., Int. Ed. Engl. 37 (1998) 1407;
(c) G.K.H. Shimizu, G.D. Enright, C.I. Ratcliffe, K.F. Preston, J.L. Reid, J.A. Ripmeester, Chem. Commun. (1999) 1485.
[21] (a) R. Lescouezec, F. Lloret, M. Julve, M. Verdaguer, Inorg. Chem. 41 (2002) 818;
(b) A.-Q. Wu, F.-K. Zheng, G.-C. Guo, Inorg. Chem. 43 (2004) 4839.
[22] (a) E. Tynan, P. Jensen, P.E. Kruger, CrystEngComm 7 (2005) 90;
(b) E. Tynan, P. Jensen, P.E. Kruger, Chem. Commun. (2004) 776.
[23] C. Seward, W.L. Jia, R.Y. Wang, G.D. Enright, S. Wang, Angew. Chem., Int. Ed. Engl. 43 (2004) 2933.
[24] (a) K. Aoki, M. Inaba, S. Teratani, H. Yamazaki, Y. Miyashita, Inorg. Chem. 33 (1994) 3018;
(b) G. Smith, B.A. Cloutt, D.E. Lynch, K.A. Byriel, C.H.L. Kennard, Inorg. Chem. 37 (1998) 3236;
(c) C.V.K. Sharma, S.T. Griffin, R.D. Rogers, Chem. Commun. (1998) 215;
(d) C.V.K. Sharma, R.D. Rogers, Cryst. Eng. 1 (1998) 18;
(e) H. Cai, H.-M. Hu, W.-Z. Chen, H.-G. Zhu, X.-Z. You, Chem. Lett. (1999) 221;
(f) D.R. Armstrong, F. Benevelli, A.D. Bond, N. Feeder, E.A. Harron, A.D. Hopkins, M. Mcpartlin, D. Moncrieff, D. Saez, E.A. Quadrelli, A.D. Woods, D.S. Wright, Inorg. Chem. 41 (2002) 1492;
(g) C.K. Terajima, H. Miyasaka, T. Ishii, K. Sugiura, M. Yamashita, Inorg. Chim. Acta 332 (2002) 210;
(h) Y.-H. Wang, K.-L. Chu, H.-C. Chen, C.W. Yeh, Z.-K. Chan, M.-C. Suen, J.-D. Chen, J.-C. Wang, CrystEngComm 8 (2006) 84.
[25] (a) Y.-N. Chi, K.-L. Huang, F.-Y. Cui, Y.-Q. Xu, C.-W. Hu, Inorg. Chem. 45 (2006) 10605;
(b) H.-P. Wu, C. Janiak, G. Rheinwald, H. Lang, J. Chem. Soc., Dalton Trans. (1999) 183;
(c) C. Janiak, L. Uehlin, H.-P. Wu, P. Klufers, H. Piotrowski, T.G. Scharmann, J. Chem. Soc., Dalton Trans. (1999) 3121.
[26] (a) R.H. Blessing, Acta. Crystallogr., Sect. A 51 (1995) 33;
(b) G.M. Sheldrick, SHELXS 97: Program for Crystal Structure Solution, University of Göttingen, Göttingen, Germany, 1997;
(c) G.M. Sheldrick, SHELXL 97: Program for Crystal Structure Refinement, University of Göttingen, Göttingen, Germany, 1997.
[27] A. Bondi, J. Phys. Chem. 68 (1964) 441.
[28] (a) O.M. Yaghi, H. Li, J. Am. Chem. Soc. 118 (1996) 295;
(b) M.A. Withersby, A.J. Blake, N.R. Champness, P. Hubberstey, W.-S. Li, M. Schroder, Angew. Chem., Int. Ed. Engl. 36 (1997) 2327;
(c) P. Lin, R.A. Henderson, R.W. Harrington, W. Clegg, C.-D. Wu, X.-T. Wu, Inorg. Chem. 43 (2004) 181.
[29] (a) V.W.W. Yam, K.K.W. Lo, W.K.M. Fung, C.-R. Wang, Coord. Chem. Rev. 171 (1998) 17;
(b) P.D. Harvey, D. Fortin, Coord. Chem. Rev. 171 (1998) 351.
[30] (a) M.-L. Tong, X.-M. Chen, B.-H. Ye, L.-N. Ji, Angew. Chem., Int. Ed. 38 (1999) 2237;
(b) S.-L. Zheng, M.-L. Tong, S.-D. Tan, Y. Wang, J.-X. Shi, Y.-X. Tong, H.-K. Lee, X.-M. Chen, Organometallics 20 (2001) 5319;
(c) V.W.W. Yam, K.K.W. Lo, C.-R. Wang, K.K. Cheng, Inorg. Chem. 35 (1996) 5116;
(d) X.-C. Huang, S.-L. Zheng, J.-P. Zhang, X.-M. Chen, Eur. J. Inorg. Chem. (2004) 1024;
(e) V.J. Catalano, H.M. Kar, J. Garnas, Angew. Chem., Int. Ed. 38 (1999) 1979;
(f) D. Fortin, M. Drouin, M. Turcotte, P.D. Harvey, J. Am. Chem. Soc. 119 (1997) 531;
(g) Y.-Q. Wei, K.-C. Wu, B.-T. Zhuang, Z.-F. Zhou, J. Mol. Struct. 751 (2005) 143;
(h) Y.-Q. Wei, K.-C. Wu, B.-T. Zhuang, Z.-F. Zhou, M.-X. Zhang, C.-P. Liu, Z. Anorg. Allg. Chem. 631 (2005) 1532.
[31] (a) Y.-B. Dong, G.-X. Jin, M.D. Smith, R.-Q. Huang, B. Tang, H.C. Zur Loye, Inorg. Chem. 41 (2002) 4909;
(b) Q.-X. Liu, F.-B. Xu, Q.-S. Li, X.-S. Zeng, X.-B. Leng, Y.-L. Chou, Z.-Z. Zhang, Organometallics 22 (2003) 309.

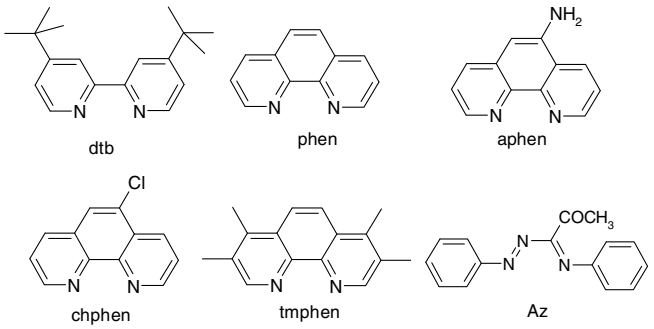

The spectral studies, redox properties and single crystal X-ray structures (for two representative examples) of this family are described in this work. The electrochemical parameters (E_L(L)) of the substituted diimine ligands (L) are reported. These values have broad utilization across both organometallic and coordination chemistry and can be used to predict M^n/M^{n-1} redox potentials by assuming that all ligand contributions are additive.

2. Experimental

2.1. Materials

The reagents: aniline-, bipyridine- and phenanthroline-derivatives, lithium chloride and ruthenium trichloride hydrate, and solvents (reagent grade) were purchased from Aldrich and were used as received. Tetrabutylammonium hexafluorophosphate (TBAH), was recrystallized twice from 1:1 ethanol/water solution and then vacuum dried at 110 °C. The synthesis and the physical characterization of the ligand, 1-(4-phenylimino)-1-(phenylhydrazono)-propan-2-one (Az) and the complex *trans*-[Ru(bpy)(L)Cl_2] have been prepared as described in the literature [6].

2.2. General procedure for the preparation of trans-[Ru(Az)(L)Cl_2] **2–8**

A suspension of ruthenium trichloride trihydrate (0.26 g, 1.00 mmol) and the 1-(4-phenylimino)-1-(phenylhydrazono)-propan-2-one (Az) (0.023 mmol) in 100 mL absolute ethanol were reacted under reflux conditions. After 1 h, 1.0 mmol of the corresponding ligand and excess amount of LiCl (0.50 g, 11.8 mmol) were added. The reaction was heated for an additional 3 h, after which the solvent was removed by using a rotary evaporator. The crude product was dissolved in dichloromethane, filtered and washed with water to remove the unreacted ruthenium trichloride and lithium chloride. The filtrate was reduced to 20 mL and purified by chromatography (50 × 3 cm) on alumina grade (III). Elution with acetone gave a yellow band which was discarded followed by a dark-red band of the product. The products were recrystallized from slowly evaporating solution of dichloromethane.

2.2.1. trans-[Ru(Az)(dmb)Cl_2] (**2**)

Yield (0.28 g, 46%). *Anal.* Calc. for $C_{27}H_{25}N_5ORuCl_2$: C, 53.38; H, 4.15; N, 11.53. Found: C, 53.70; H, 4.27; N, 11.47%. UV–Vis in acetonitrile: λ_{max} ($\varepsilon_{max}/M^{-1}\,cm^{-1}$): 370 ($6.688 \times 10^3$), 504 ($5.146 \times 10^3$). IR: ν(N=N) 1486, ν(C=N) 1616, ν(C=O) 1717 cm^{-1}. ^{1}H NMR (DMSO-d_6): δ 2.44 (6H, s, dmb), 2.73 (3H, s, $COCH_3$), 6.71 (1H, d, dmb), 7.05 (2H, d, H4), 7.31 (1H, d, dmb), 7.48 (1H, t, H6), 7.52 (2H, t, H5), 7.57 (1H, t, dmb), 7.62 (2H, t, H2), 7.80 (1H, t, H3), 7.95 (2H, d, H1), 8.30 (1H, s, dmb), 8.40 (1H, s, dmb).

2.2.2. trans-[Ru(Az)(dmeb)Cl_2] (**3**)

Yield (0.31 g, 47%). *Anal.* Calc. for $C_{27}H_{25}N_5O_3RuCl_2 \cdot H_2O$: C, 49.32; H, 4.14; N, 10.65. Found: C, 49.41; H, 4.18; N, 10.51%. UV–Vis in acetonitrile: λ_{max} ($\varepsilon_{max}/M^{-1}\,cm^{-1}$): 378 ($7.449 \times 10^3$), 500 ($6.55 \times 10^3$). IR: ν(N=N) 1490, ν(C=N) 1612, ν(C=O) 1705 cm^{-1}. ^{1}H NMR (DMSO-d_6): δ 2.66 (3H, s, $COCH_3$), 3.97 (6H, s, dmeb), 6.67 (1H, d, dmeb), 6.75 (1H, d, dmeb), 6.83 (1H, d, dmeb), 7.30 (1H, t, H6), 7.34 (2H, d, H4), 7.45 (2H, t, H5), 7.49 (1H, d, dmeb), 7.59 (2H, t, H2), 7.80 (1H, t, H3), 8.96 (2H, d, H1), 8.09 (1H, s, dmeb), 8.16 (1H, s, dmeb).

2.2.3. trans-[Ru(Az)(dtb)Cl_2] (**4**)

Yield (0.36 g, 55%). *Anal.* Calc. for $C_{33}H_{37}Cl_2N_3ORu \cdot CH_2Cl_2$: C, 63.07; H, 6.07; N, 6.49. Found: C, 63.29; H, 6.39; N, 6.56%. UV–Vis in acetonitrile: λ_{max} ($\varepsilon_{max}/M^{-1}\,cm^{-1}$): 368 ($6.40 \times 10^3$), 506 ($5.684 \times 10^3$). IR: ν(N=N) 1480, ν(C=N) 1611, ν(C=O) 1701 cm^{-1}. ^{1}H NMR (DMSO-d_6): δ 1.34 (18H, s, dtb), 2.73 (3H, s, $COCH_3$), 6.84 (1H, d, dtb), 7.12 (1H, d, dtb), 7.17 (1H, d, dtb), 7.32 (2H, d, H4), 7.49 (1H, d, dtb), 7.50 (2H, t, H5), 7.54 (1H, t, H3), 7.61 (2H, t, H2), 7.83 (1H, t, H6), 7.96 (2H, d, H1), 8.47 (1H, s, dtb), 8.40 (1H, s, dt*b*).

2.2.4. trans-[Ru(Az)(phen)Cl_2] (**5**)

Yield (0.23 g, 40%). *Anal.* Calc. for $C_{27}H_{21}Cl_2N_3ORu$: C, 56.35; H, 3.68; N, 7.30. Found: C, 56.51; H, 3.87; N, 7.48%. UV–Vis in acetonitrile: λ_{max} ($\varepsilon_{max}/M^{-1}\,cm^{-1}$): 372 ($9.015 \times 10^3$), 505 ($6.321 \times 10^3$). IR: ν(N=N) 1495, ν(C=N) 1606, ν(C=O) 1711 cm^{-1}. ^{1}H NMR (DMSO-d_6): δ 2.83 (3H, s, $COCH_3$), 7.24 (1H, d, phen), 7.33 (1H, dd, phen), 7.38 (1H, dd, phen), 7.53 (1H, t, H6), 7.58 (2H, d, H2), 7.50 (2H, t, H5), 7.75 (1H, t, H3), 7.84 (2H, d, H4), 7.95 (1H, d, phen), 8.12 (2H, d, H1), 8.25 (1H, d, phen), 8.29 (1H, d, phen),

2.2.5. trans-[Ru(Az)(aphen)Cl_2] (**6**)

Yield (0.30 g, 48%). *Anal.* Calc. for $C_{27}H_{22}Cl_2N_6ORu \cdot 0.5H_2O$: C, 51.68; H, 3.69; N, 13.39. Found: C, 51.34; H, 3.63; N, 13.70%. UV–Vis in acetonitrile: λ_{max} ($\varepsilon_{max}/M^{-1}\,cm^{-1}$): 378 ($7.343 \times 10^3$), 507 ($6.464 \times 10^3$). IR: ν(N=N) 1490, ν(C=N) 1637, ν(C=O) 1705 cm^{-1}. ^{1}H NMR (DMSO-d_6): δ 2.70 (3H, s, $COCH_3$), 5.76 (2H, s, NH_2), 6.73 (1H, s, aphen), 6.94 (1H, d, aphen), 7.14 (1H, d, aphen), 7.29 (1H, t, H6), 7.42 (2H, t, H5), 7.58 (2H, d, H4), 7.63 (1H, d, aphen), 7.65 (1H, t, aphen), 7.77 (2H, t, H2), 7.86 (1H, t, H3), 8.06 (2H, d, H1), 8.21 (1H, d, aphen), 8.80 (1H, d, aphen).

2.2.6. trans-[Ru(Az)(chphen)Cl_2] (**7**)

Yield (0.36 g, 50%). *Anal.* Calc. for $C_{27}H_{20}Cl_3N_5ORu \cdot CH_2Cl_2$: C, 46.53; H, 3.07; N, 9.69. Found: C, 46.82; H, 3.19; N, 9.92%. UV–Vis in acetonitrile: λ_{max} ($\varepsilon_{max}/M^{-1}\,cm^{-1}$): 374 ($9.277 \times 10^3$), 500 ($8.62 \times 10^3$). IR: ν(N=N) 1487, ν(C=N) 1632, ν(C=O) 1704 cm^{-1}. ^{1}H NMR (DMSO-d_6): δ 2.73 (3H, s, $COCH_3$), 7.13 (1H, d, chphen), 7.43 (2H, d, H4), 7.59 (2H, t, H5), 7.60 (1H, t, chphen), 7.68 (2H, d, H2), 7.73 (1H, t, chphen), 7.74 (1H, d, chphen), 7.76 (1H, t, H6), 7.88 (1H, t, H3), 7.99 (2H, d, H1), 8.50 (1H, s, chphen), 8.65 (1H, d, chphen) , 8.90 (1H, d, chphen).

2.2.7. trans-[Ru(Az)(tmphen)Cl_2] (**8**)

Yield (0.30 g, 46%). *Anal.* Calc. for $C_{31}H_{29}Cl_2N_5ORu$: C, 56.45; H, 4.43; N, 10.62. Found: C, 56.61; H, 4.10; N,10.87%. UV–Vis in acetonitrile: λ_{max} ($\varepsilon_{max}/M^{-1}\,cm^{-1}$): 372 ($8.343 \times 10^3$), 509 ($6.195 \times 10^3$). IR: ν(N=N) 1443, ν(C=N) 1623, ν(C=O) 1702 cm^{-1}. ^{1}H NMR (DMSO-d_6): δ 2.04 (3H, s, tmphen), 2.10 (3H, s, tmphen), 2.70(3H, s, $COCH_3$), 6.69 (2H, s, tmphen), 7.40 (1H, t, H6), 7.45 (2H, d, H4), 7.59 (2H, t, H5), 7.72 (2H, t, H2), 7.89 (1H, t, H3), 7.97 (2H, d, H1), 8.3 (1H, d, tmphen).

2.3. Instrumentation

Cyclic voltammetric studies were performed in acetonitrile (Aldrich, HPLC grade) using a voltalab 21 (PGP201). Three electrodes were utilized in this system, two platinum-disk working and counter (auxiliary) electrodes (platinum electrode, 2-mm diameter),

and a silver wire pseudo-reference electrode with ferrocene (0.665 V versus NHE) as an internal reference [7]. To maintain the cell temperature at 25.0 ± 0.1 °C, a Haake D8-G refrigerated bath and circulator was used. Tetrabutylammonium hexafluorophosphate was twice recrystallized and vacuum dried at 120 °C, and used as the supporting electrolyte. Spectroscopic data were obtained using Cary 5 spectrophotometer. IR spectra were measured by FT-IR JASCO model 420. Nuclear magnetic resonances (^{1}H NMR) spectra were measured on a Bruker-Avance 400 MHz spectrometer. Elemental analyses were carried out on an Eurovector E.A.3000 instrument using copper sample-tubes.

Table 1
Crystallographic data and structure refinement parameters for **2** and **5**

	Complex **2**	Complex **5**
Empirical formula	$C_{27}H_{25}Cl_2N_5ORu$	$C_{27}H_{21}Cl_2N_5ORu$
Formula weight	607.49	603.46
Temperature (K)	90(2)	90(2)
Wavelength (Å)	0.71073	0.71073
Crystal system	triclinic	monoclinic
Space group	$P\bar{1}$	$P2(1)/n$
Unit cell dimensions		
a (Å)	9.2166(3)	9.7453(4)
b (Å)	12.3156(5)	13.6453(5)
c (Å)	12.6505(5)	18.4318(7)
α (°)	95.1135(6)	90
β (°)	99.5710(6)	90.079(1)
γ (°)	109.8525(5)	90
V (Å^3)	1315.28(9)	2451.01(16)
Z	2	4
D_{calc} (Mg/m^3)	1.534	1.635
Absorption coefficient (mm^{-1})	0.829	0.889
$F(000)$	616	1216
Crystal size (mm^3)	0.28 × 0.21 × 0.12	0.19 × 0.17 × 0.04
Crystal color and habit	red plate	red fragment
θ Range for data collection (°)	1.65–27.50	1.86–27.50
Index ranges	$-11 \le h \le 11$ $-15 \le k \le 15$ $-16 \le l \le 16$	$-12 \le h \le 12$ $-17 \le k \le 17$ $-23 \le l \le 23$
Reflections collected	19611	36655
Independent reflections (R_{int})	6020 (0.0268)	5625 (0.0429)
Completeness to θ = 27.50°	99.9%	100.0%
Absorption correction	semi-empirical from equivalents	semi-empirical from equivalents
Maximum and minimum transmission	0.9071 and 0.8010	0.9653 and 0.8492
Goodness-of-fit on F^2	1.050	1.035
Final R indices [$I > 2\sigma(I)$]	R_1 = 0.0317, wR_2 = 0.0714	R_1 = 0.0302, wR_2 = 0.0703
R indices (all data)	R_1 = 0.0380, wR_2 = 0.0752	R_1 = 0.0403, wR_2 = 0.0751
Largest difference in peak and hole (e Å^{-3})	1.305 and −0.889	0.732 and −0.289

2.4. Computational methods

The crystallographic geometries of **2** and **5** were used as examples for our calculations. All theoretical calculations were carried out using a Becke's three-parameter hybrid function [8] with LYP correlation function [9] (B3LYP), as implemented in the GAUSSIAN 03 program package [10]. LanL2DZ effective core potential basis set was employed for all atoms in acetonitrile solution [11]. The theoretical electronic spectra were simulated from the energy of the excited states and transition oscillator strengths calculated by the TD-DFT formalism as implemented in the GAUSSIAN 93 program [10]. A value equal to 3000 cm^{-1} for the bandwidth at half height has been used in these simulations with Gaussian line shapes because this value often provides us with molar extinction coefficient values close to experimental data.

2.5. Crystallography

Crystals of compounds **2** and **5** were removed from the flask, a suitable crystal was selected, attached to a glass fiber and data were collected at 90(2) K using a Bruker/Siemens SMART APEX instrument (Mo Kα radiation, λ = 0.71073 Å) equipped with a Cryocool NeverIce low temperature device. Data were measured using omega scans 0.3° per frame for 5 s, and a full sphere of data was collected. A total of 2400 frames were collected with a final resolution of 0.77 Å. Cell parameters were retrieved using SMART [12] software and refined using SAINTPLUS on all observed reflections [13]. Data reduction and correction for Lp and decay were performed using the SAINTPLUS software. Absorption corrections were applied using SADABS [14]. The structure was solved by direct methods and refined by least squares method on F^2 using the SHELXTL program package [15]. The structure was solved in the space group $P\bar{1}$ for complex **5** and $P21/n$ for complex **2** by analysis of systematic absences. The ketone group was disordered in two positions with occupancies of 84:16% and all non-hydrogen atoms were refined anisotropically. No decomposition was observed during data collection. Details of the data collection and refinement are given in Table 1. Further details are provided in the Supporting Information.

3. Results and discussion

3.1. Synthesis

The new complexes *trans*-[Ru(Az)(L)Cl$_2$] **(2–8)** used in this study were prepared by stepwise equimolar addition of RuCl$_3$, 1-(phenylimino)-1-(phenylhydrazono)-propan-2-one (Az), substi-

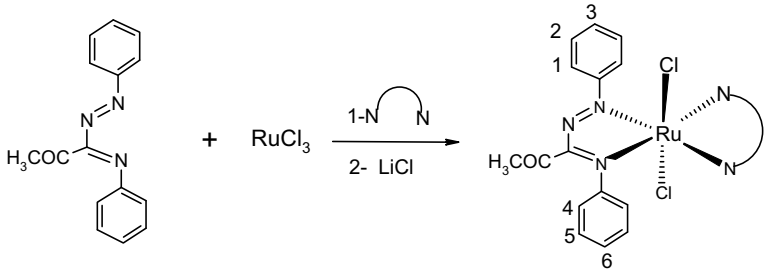

Ligand	bpy	dmb	dmeb	dtb	phen	aphen	chphen	tmphen
L	**L$_1$**	**L$_2$**	**L$_3$**	**L$_4$**	**L$_5$**	**L$_6$**	**L$_7$**	**L$_8$**
Complex	1	2	3	4	5	6	7	8

Scheme 1.

tuted bipyridine or phenanthroline ligands ($\mathbf{L_1}$–$\mathbf{L_8}$) and then an excess of lithium chloride according to Scheme 1.

These neutral complexes are air stable, diamagnetic and their structures were confirmed by ^{1}H NMR spectra and X-ray diffraction for complexes **2** and **5**. The ^{1}H NMR spectra of complexes **2–8** show featureless multiplets due to aromatic protons of the phenyl rings of the ligands. In their IR-spectra, all complexes show bands in the range of 1660–1712 cm^{-1} assignable to C=O stretching frequency of the acetyl group and intense bands in the ranges of 1560–1590 and 1430–1500 cm^{-1} which are assigned to the C=N and N=N stretching bands of azoimine ligands, respectively.

3.2. Crystal structures

The X-ray structures of (**2**) and (**5**) were determined and the perspective molecular views for the asymmetric units are shown in Figs. 1 and 2, respectively. The selected bond parameters are listed in Table 2. The ORTEP geometry of complex **5** as representative example for phenanthroline family is shown in Fig. 2. This complex crystallizes in the $P\bar{1}$ space group, which is different from $P21/n$ of complex **2**. The coordination geometry of the complexes is distorted from regular octahedral as a consequence of the small bite angles of bidentate phen (77.31°) and bpy ligands (78.9°), which deviate very much from the ideal octahedral angle of 90°. For both complexes (**2** and **5**) the chloride ligands are *trans* to each other and the azomethine and diimine nitrogen donor atoms are equatorially coordinated. Most bis bipyridine or phenanthroline complexes prefer a *cis* geometry because of steric hindrance between α protons in the *trans* geometry [16]. Steric hindrance is evidently not as great for the complexes of this study because the Az ligand phenyl rings can twist away from the α protons as shown in Figs. 1 and 2. The *trans* complexes of this study appear to be thermally stable in solution and we hope to explore their photochemical properties in the future. For complex **5**, the N(7)–Ru(1)–N(13) angle of the azomethine ligand has a value of 76.33. The azomethine ligand is known to participate strongly in dπ–π^* interactions with Ru(II). This has been reflected in the Ru–N(bpy), Ru–N(phen) and Ru–N(Az) bond distance data. The Ru–N(py) bond distances for complex **5** and **2** fall within a narrow range of 2.121–2.146 Å. The Ru–N(bpy) and Ru–N(phen) distances are longer than those in the

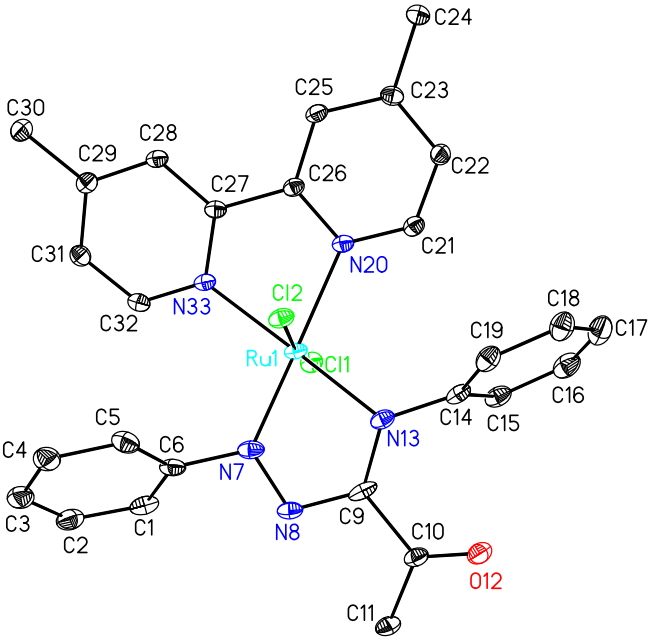

Fig. 1. Thermal ellipsoid plot (30%) of **2**. Hydrogen atoms omitted for clarity.

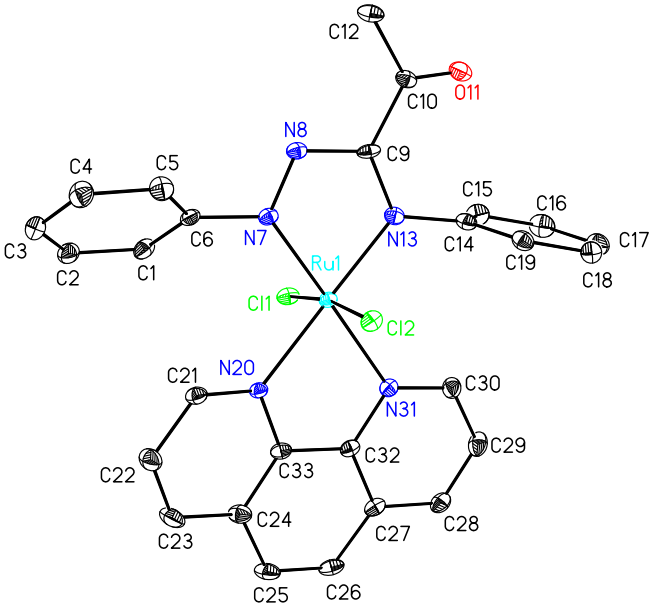

Fig. 2. Thermal ellipsoid plot (30%) of **5**. Hydrogen atoms omitted for clarity.

Table 2
Bond lengths [Å] and angles [°] for complex **2** and **5**

Bond lengths [Å]		Bond angles [°]	
*Complex **5***			
N(7)–Ru(1)	1.9498(19)	N(20)–Ru(1)–N(31)	77.31(7)
C(9)–N(13)	1.361(4)	N(13)–Ru(1)–N(31)	104.23(8)
N(20)–Ru(1)	2.1200(19)	N(7)–Ru(1)–N(31)	176.80(7)
N(31)–Ru(1)	2.1610(19)	N(13)–Ru(1)–N(20)	174.25(7)
Cl(1)–Ru(1)	2.3714(6)	N(7)–Ru(1)–N(20)	102.44(8)
Cl(2)–Ru(1)	2.3564(6)	N(7)–Ru(1)–N(13)	76.33(8)
N(13)–Ru(1)	1.9919(19)	N(20)–Ru(1)–N(31)	77.31(7)
N(8)–C(9)	1.370(4)	N(13)–Ru(1)–N(31)	104.23(8)
N(7)–N(8)	1.301(4)	N(7)–Ru(1)–N(31)	176.80(7)
		Cl(2)–Ru(1)–Cl(1)	172.68(2)
*Complex **2***			
N(7)–N(8)	1.302(3)	N(13)–Ru(1)–N(20)	104.80(8)
N(7)–Ru(1)	1.9517(19)	N(13)–Ru(1)–N(33)	178.09(8)
N(13)–N(9B)	1.293(10)	Cl(1)–Ru(1)–Cl(2)	171.76(2)
N(13)–Ru(1)	1.9986(19)	N(8)–N(7)–Ru(1)	122.65(19)
N(20)–Ru(1)	1.362(3)	N(33)–Ru(1)–N(20)	76.27(7)
N(33)–Ru(1)	2.1119(18)	N(7)–Ru(1)–N(20)	179.30(8)
Cl(1)–Ru(1)	2.3443(6)	N(7)–Ru(1)–N(33)	103.13(8)
Cl(2)–Ru(1)	2.3780(6)	N(7)–Ru(1)–N(13)	75.81(8)

corresponding $[Ru(bpy)_3]^{2+}$ and $[Ru(phen)_3]^{2+}$ complexes, respectively [17]. For complex **2,** the Ru–N(bpy) distances (average, 2.121(3) Å) are shorter than Ru–N(phen) distances (average, 2.146(3) Å) revealing that bpy is more strongly coordinated than phen. For complex **5**, the average Ru–N(azo) and Ru–N(methine) distances of the azoimethine ligand is 1.971(3) Å which is shorter than Ru–N(phen) lengths (average, 2.146(3) Å). This shortening may be due to greater π-back donation from Ru-d orbital to the empty π^* orbital of the azoimine ligand, and this comes as an indication that the M–(Az) π interaction is localized in the M–azo fragment [18]. Reported Ru–Cl distances in chloro-Ru(II) complexes lie in the range 2.389–2.401 Å [19]. The average Ru–Cl bond lengths in **5** (2.364) is comparable to similar reported systems [19].

3.3. Electrochemistry

Formal oxidation and reduction potentials versus NHE were obtained from cyclic voltammograms recorded at a platinum elec-

trode in acetonitrile containing 0.1 M tetrabutylammonium hexafluorophospate. These data are listed in Table 3. Ru(III/II) values were obtained from an average of anodic and cathodic peak potentials. Complex **5**, as a representative example (Fig. 3), displays a reversible oxidation peak at 1.18 V, being attributed to the metal-centered Ru(III/II) couple. The two reduction waves at −0.43 and −0.77V are assigned to azo(0/−) and azo(−/−2) ligand-centered processes. This reduction couples are shifted to more positive potentials by the electron withdrawing group attached to bipyridine and phenanthroline ligands. The electrochemical properties of Ru(II) complexes containing substituted phenanthroline ligand were quite similar to those of substituted bipyridine complexes. However, the half-wave potential of earlier complex was shifted anodically by 20 mV compared to those observed with later complexes. This relationship indicates that the donor ability of the phenanthroline ligand is slightly weaker than that of the bipyridine ligand [19]. The Ru(III/II) couple is slightly affected by changing the substituent on the phenanthroline ligand and is shifted to more positive potentials upon replacing the donating methyl group with the more withdrawing chloro group. Lever has developed an electrochemical parameterization method to calculate ruthenium(III/II) couples of complexes with octahedral geometry as shown in Eq. (1) [4].

$$E_{\mathrm{Ru(III/II)}} = 0.97\left[\sum E_{\mathrm{L}}\right] + 0.04 \text{ in V versus NHE} \quad (1)$$

where $\sum E_{\mathrm{L}}$ is the sum of electrochemical parameters for each ligand in the complex. The parameter E_{L} is a measure of the stabilizing effect a ligand has on the Ru(II) state and so the greater the magnitude of positive E_{L} the more positive the Ru(III/II) couple. Based on the previously found (E_{L}(Az) = 0.42) [6], E_{L}(Cl) = −0.24 [4]) and assuming ligand additivity, the Ru(III/II) couple for these octahedral complexes was used to find the ligand electrochemical parameters (E_{L}(L)) for unreported diimine ligands (L) using Eq. (1) and the data are listed in Table 3.

Table 3
Cyclic voltammetry and electronic spectroscopy data of *trans*-[Ru(II)(Az)(L)Cl_2][a]

Complex	Calculated E_{L}(L) for ligand L[b]	$(E^{\circ}_{1/2M})$[c]	Azo (0/−)[d]	(ΔE°)[e]	λ_{max} (nm) (E_{MLCT}))[f]
1	0.25	1.16	−0.48	1.64	(510) (2.43)
2	0.23	1.14	−0.50	1.64	(504) (2.46)
3	0.23	1.14	−0.52	1.66	(500) (2.48)
4	0.22	1.13	−0.45	1.58	(506) (2.45)
5	0.28	1.18	−0.43	1.61	(505) (2.45)
6	0.22	1.13	−0.44	1.57	(507) (2.44)
7	0.30	1.20	−0.45	1.65	(500) (2.48)
8	0.21	1.12	−0.44	1.56	(509) (2.44)

[a] Solvent MeCN, supporting electrolyte Bu_4NPF_6 (0.1 M), scan rate 0.1 V s), Pt-disk working electrode, Pt-wire auxiliary electrode, reference electrode Ag at 25 °C.
[b] Calculated using $E_{\mathrm{Ru(III/II)}} = 0.97[\sum E_{\mathrm{L}}] + 0.04$ in V vs. NHE, (E_{L} for Az = 0.42 and for chloride = −0.24) [29].
[c] $E^{\circ}_{1/2M} = (E^{\circ}_{pa} - E^{\circ}_{pc})/2$.
[d] The cathodic peak maximum.
[e] ΔE° = Ru(III/II) − Azo(0/−).
[f] MLCT = [1239.8/λ_{max} (nm)] eV.

3.4. Electronic structure

Theoretical calculations were performed on **5**; relative percentages of atomic contributions to the lowest unoccupied and highest occupied molecular orbitals have been placed in Table 4. Moreover, the isodensity plots for the HOMOs and LUMOs orbitals are shown in Fig. 4. The lower unoccupied molecular orbitals (LUMOs) consists

Table 4
Relative percentages of atomic contributions to the lowest unoccupied and highest occupied molecular orbitals (LUMO and HOMO) of **5**

MO	Energy (ev)	Ru	phen	Azo-imine ring	Cl
HOMO − 6	−7.27	5	4	84	8
HOMO − 5	−7.15	2	14	80	3
HOMO − 4	−6.98	1	67	28	5
HOMO − 3	−6.78	16	8	74	2
HOMO − 2	−6.37	63	3	33	1
HOMO − 1	−6.16	30	1	29	40
HOMO	−5.53	61	2	7	29
LUMO	−3.41	26	9	60	5
LUMO + 1	−2.21	5	90	4	0
LUMO + 2	−2.11	0	95	5	0
LUMO + 3	−1.67	3	4	93	0
LUMO + 4	−0.92	1	86	12	0
LUMO + 5	−0.72	45	5	28	23
LUMO + 6	−0.57	20	8	70	2

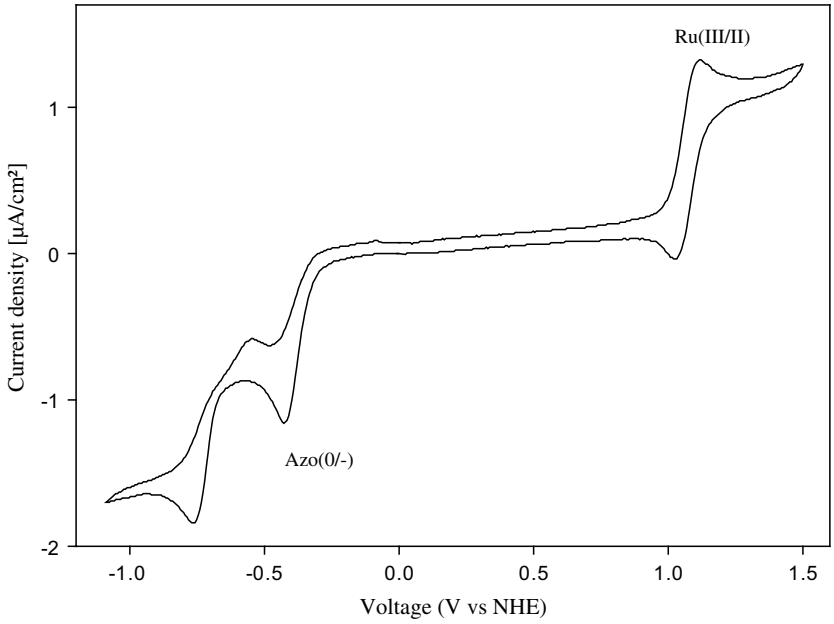

Fig. 3. Cyclic voltammogram for **5** in acetonitrile 0.1 M TBAH at 25 °C, data reported in V vs. NHE with scan rate of 0.1 V/s.

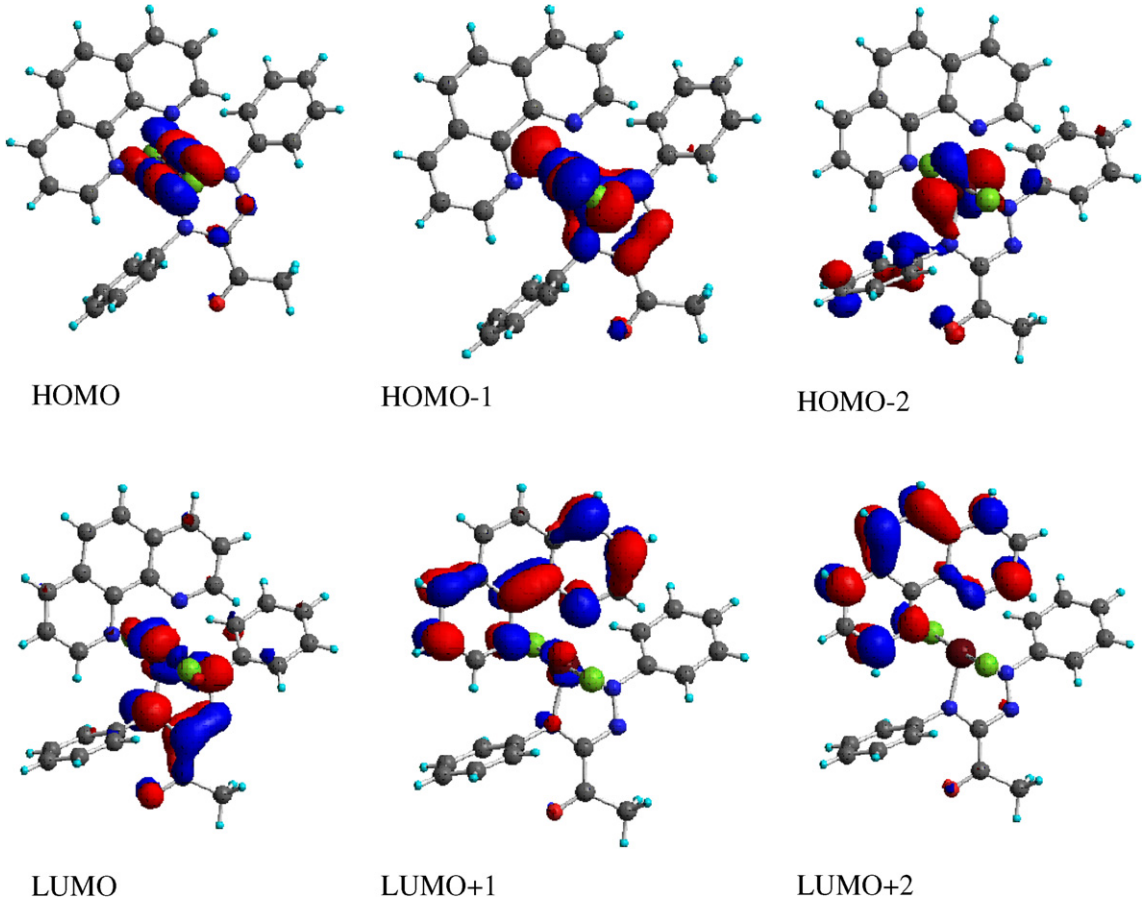

Fig. 4. Isodensity plots of the HOMO and LUMO orbitals of **5**.

mostly of a series of antibonding π^* orbital of azoimine together with a small contribution from π^* orbital of phenanthroline. Results indicate that the LUMO is constructed mainly from the π^* orbital of azoimine (60%) and has 26% metal d-orbital character which suggests significant back donation [20]. The other group of HOMOs, can be described as t_2g Ru orbitals (HOMO to HOMO − 2) with small contributions from the azomethine ligands. Moreover, results indicate that π orbital of azoimine ligand contributes significantly to HOMO − 3.

The lowest 20 singlet-to-singlet spin-allowed excitation states were taken into account for the calculation of the electronic absorption spectrum of complex **5** using TD-DFT method. Excitation energies, oscillator strengths and corresponding transitions compositions for the simulated absorption bands in acetonitrile solution are listed in Table 5. Each excited state was interpolated by a Gaussian convolution with the full width at half-maximum (fwhm) of 3000 cm^{-1}. Both the experimental UV–Vis spectrum for complex **5** (as a representative example) and its simulated absorption spectrum reported in acetonitrile, shown in Fig. 5, were in good agreement. Experimentally, complex **5** has a maximum centered at 504 nm and a shoulder peak at 390 nm. Contrary to the experimental information, the simulated near-UV band is much higher than the visible one. Assuming that the appropriate fwhm values are chosen, the molar absorptivity of the band maximum in visible region is slightly underestimated, while the one in the near-UV region is significantly overestimated. Similar results in simulation of N3-type dye also exist [21]. The study of Tozer et al. also revealed that TD-DFT has difficulty in distributing intensity properly [22]. For the absorption band in visible region, TD-DFT calculations shows that the band centered at λ_{max} = 504 nm (≈550 nm (calculated)) resulted from HOMO − 1 orbital, which have sizable contributions of Ru(dπ) orbitals mixed with azomethine to LUMO which has a significant contribution from the π^* orbital of azomethine. Thus this band is assigned to MLCT (Ru(dπ) → π^* azomethine). For the band in the near-UV region, the band centered at 390 nm (≈388 nm (calculated)) arises from the overlap of several transitions, MLCT and $\pi \rightarrow \pi^*$. The MLCT band centered at 395 resulted from HOMO (mainly Ru) → LUMO + 3 (azomethine in character), while the $\pi \rightarrow \pi^*$ transition is at centered 388 nm and resulted from the HOMO − 6 (azomethine

Table 5
Computed excitation energies (eV), electronic transition configurations and oscillator strengths (*f*) for the optical transitions in the visible region of **5** (transitions with $f > 0.01$ are listed)

Wavelength nm (eV)	Oscillator strengths (*f*)	Contribution
550 (2.258)	0.0815	81.1% HOMO − 1 → LUMO
453 (2.742)	0.0221	97.38% HOMO → LUMO + 2
420 (2.9586)	0.0171	18.27% HOMO − 7 → LUMO, 61.42% HOMO − 4 → LUMO
405 (3.069)	0.0115	91.04% HOMO − 5 → LUMO
395 (3.146)	0.0374	26.44% HOMO − 1 → LUMO + 1, 61.72% HOMO → LUMO + 3
388 (3.204)	0.0624	67.50% HOMO − 6 → LUMO, 10.06% HOMO − 2 → LUMO + 1,
381 (3.257)	0.0292	20.08% HOMO − 6 → LUMO, 21.40% HOMO − 2 → LUMO + 1, 28.61% HOMO − 1 → LUMO + 1, 11.06% HOMO → LUMO + 3
375 (3.313)	0.0111	78.1% HOMO − 10 → LUMO

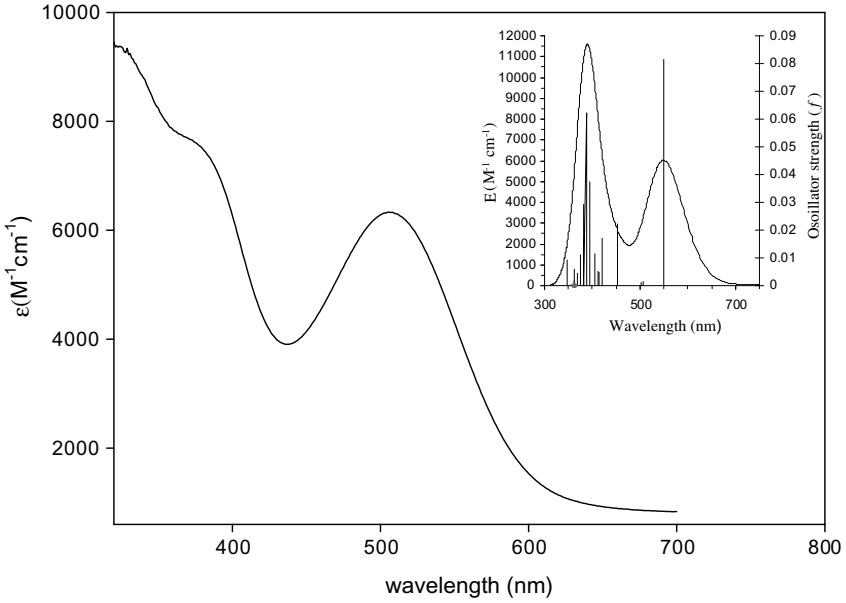

Fig. 5. UV–Vis spectrum for **5** in acetonitrile. Inset shows simulated absorption spectrum. (black line) based on TD-DFT calculations, compared to excitation energies and oscillator strengths.

in character) → LUMO. The observation of two MLCT transition may be explained by the low symmetry of this distorted octahedral Ru complexes [23–25].

The difference in the two successive redox responses at potentials positive and negative to NHE [$\Delta E^\circ = E^\circ_{1/2M} - E^\circ_{L^*}(0/-)$] may be correlated with the low energy MLCT [t(Ru) → π*(azomethine)] transition [25]. Charge transfer transitions may be considered an intramolecular redox process [26–29] and the intense spin-allowed MLCT transition is expected to be linearly related to ΔE° with slope equal to unity. A least-squares plot of ΔE° versus lower energy MLCT (Fig. 6) gave a linear correlation ($E_{MLCT} = 0.39\ \Delta E^\circ + 1.829$) however the slope of the line is only 0.39. This may result from solvent effects that become important for the small changes in energy that are seen in this group of complexes [26].

4. Conclusions

A series of complexes of general formula *trans*-[Ru(II)(Az)(L)Cl_2] where Az = $C_6H_5N{=}NC(COCH_3){=}NC_6H_5$, and L is nitrogen substituted bipyridine and phenanthroline ligands have been prepared and their redox chemistry and UV–Vis spectroscopy examined. The structures for complex **2** and **5** have been further characterized by X-ray diffraction analysis. Crystallographic studies shows that bidentate azomethine ligands are strong π-acceptor that coordinate via imine and azo nitrogens. Electrochemical and photophysical data in acetonitrile showed that electron-donating groups in the bipyridine and phenanthroline ligands shifts the redox potentials to more negative values than those observed for the parent ligands. Assuming ligand additivity, the Ru(III/II) couple for these octahedral complexes was used to find the ligand electrochemical

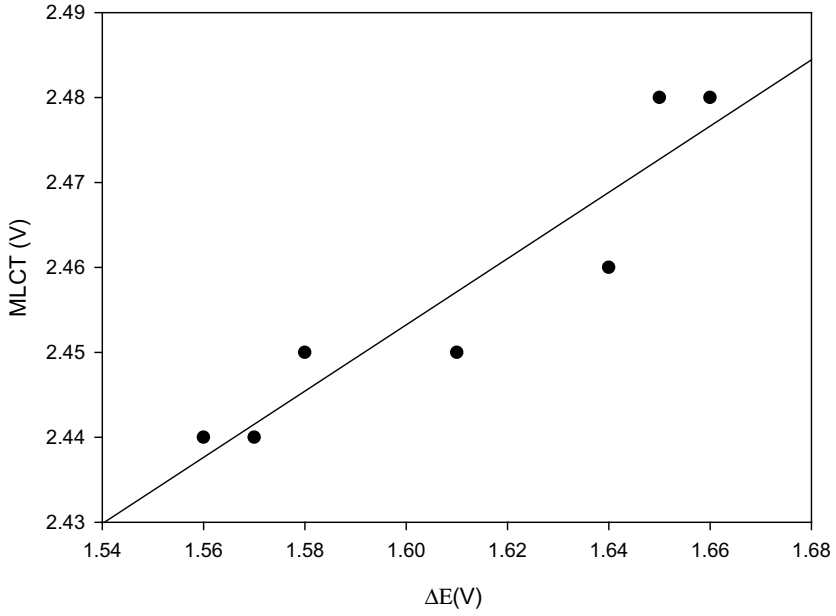

Fig. 6. Linear correlation between MLCT band energies and ΔE° (ΔE° = Ru(III/II) − Azo(0/−)) in volts. The equation of the line is ($E_{MLCT} = 0.39\Delta E^\circ + 1.829$).

parameter (E_L(L)) for unreported diimine ligands (L). The electronic absorption spectra of these complexes show two strong MLCT band in the visible region and near UV–Vis region in acetonitrile solution. These two bands are assigned to a (Ru(II)-to-azomethine) MLCT transition based on TD-DFT calculations. Good agreement between computed and experimental absorption spectra was obtained.

5 Supplementary data

CCDC 690081 and 690082 contain the supplementary crystallographic data for **2** and **5**. These data can be obtained free of charge via http://www.ccdc.cam.ac.uk/conts/retrieving.html, or from the Cambridge Crystallographic Data Centre, 12 Union Road, Cambridge CB2 1EZ, UK; fax: (+44) 1223-336-033; or e-mail: deposit@ccdc.cam.ac.uk.

Acknowledgements

Authors would like to thank the Hashemite University (Jordan) for their research support. R.J.C. would like to thank the Natural Sciences and Engineering Council of Canada for its support. This work is supported in part by the Deanship of Academic Research. The University of Jordan, Amman 11942, Jordan.

References

[1] (a) B. O'Reagan, M. Grätzel, Nature (London) 353 (1991) 737;
(b) F.G. Gao, A.J. Bard, J. Am. Chem. Soc. 122 (2000) 7426;
(c) H. Rudmann, S. Shimada, M.F. Rubner, J. Am. Chem. Soc. 124 (2002) 4918.
[2] (a) H.P. Ross, M. Boldaji, D.P. Rillema, C.B. Blanton, R.P. White, Inorg. Chem. 28 (1989) 1013;
(b) K. Haarmann, Master Thesis, University Fribourg, 1986.;
(c) D.P. Rillema, G. Allen, T.J. Meyer, D. Conrad, Inorg. Chem. 22 (1983) 1617;
(d) J.C. Curtis, B.P. Sullivan, T.J. Meyer, Inorg. Chem. 22 (1983) 224.
[3] (a) R. Languri, J.J. Morris, W.C. Stanley, E.T. Bell-Loncella, M. Turner, W.J. Boyko, C.A. Bessel, Inorg. Chim. Acta 315 (2001) 53;
(b) X.-J. Yang, C. Janiak, J. Heinze, F. Drepper, P. Mayer, H. Piotrowski, P. Klüfers, Inorg. Chim. Acta 318 (2001) 103.
[4] (a) W. Kaim, Coord. Chem. Rev. 219–221 (2001) 463;
(b) T.K. Misra, D. Das, C. Sinha, P. Ghosh, C.K. Pal, Inorg. Chem. 37 (1998) 1672.
[5] A.B.P. Lever, Inorg. Chem. 29 (1990) 1271.
[6] M. Al-Noaimi, H. Saadeh, S. Haddad, M. El-Barghouthi, M. El-khateeb, R. Crutchley, Polyhedron 26 (2007) 3675.
[7] T. Gennett, D.F. Milner, M.J. Weaver, J. Phys. Chem. 89 (1985) 2787.
[8] A.D. Becke, J. Chem. Phys. 98 (1993) 5648.
[9] C. Lee, W. Yang, R.G. Parr, Phys. Rev. B 37 (1988) 785.
[10] M.J. Frisch et al., GAUSSIAN 03, Revision B.03, Gaussian Inc., Pittsburgh, PA, 2003.
[11] (a) T.H. Dunning, P.J. Hay, in: H.F. Schaefer (Ed.), Modern Theoretical Chemistry, vol. 3, Plenum Press, 1977, p. 1;
(b) P.J. Hay, W.R. Wadt, J. Chem. Phys. 82 (1985) 284;
(c) P.J. Hay, W.R. Wadt, J. Chem. Phys. 82 (1985) 270;
(d) P.J. Hay, W.R. Wadt, J. Chem. Phys. 82 (1985) 299.
[12] SMART: v. 5.632, Bruker AXS, Madison, WI, 2005.
[13] SAINTPLUS: v. 7.23a, Data Reduction and Correction Program, Bruker AXS, Madison, WI, 2004.
[14] SADABS: v.2007/4, an empirical absorption correction program, Bruker AXS Inc., Madison, WI, 2007.
[15] G.M. Sheldrick, SHELXTL: v. 6.14, Structure Determination Software Suite, Bruker AXS Inc., Madison, WI, 2004.
[16] Bill Durham, Scott R. Wilson, Derek J. Hodgson, Thomas J. Meyer, J Am. Chem. Soc. 102 (1980) 600.
[17] (a) M. Biner, H.-B. Bürgi, A. Ludi, C. Röhr, J. Am. Chem. Soc. 114 (1992) 5197;
(b) E. Krausz, H. Riesen, A.D. Rae, Aust. J. Chem. 48 (1995) 929;
(c) D.J. Maloney, F.M. MacDonnell, Acta Crystallogr., Sect. C 53 (1997) 705;
(d) T.J. Rutherford, P.A. Pellegrini, J. Aldrich-Wright, P.C. Junk, F.R. Keene, Eur. J. Chem. (1998) 1677.
[18] S. Goswami, L.F. Falvello, A. Chakravorty, Inorg. Chem. 26 (1987) 3365.
[19] (a) R. Lalrempuia, K.M. Rao, P.J. Carroll, Polyhedron 22 (2003) 605;
(b) S.K. Mandal, A.R. Chakravarty, Polyhedron 11 (1992) 823.
[20] S.I. Gorelsky, A.B.P. Lever, M. Ebadi, Coord. Chem. Rev. 230 (2002) 97.
[21] (a) J.E. Monat, J.H. Rodriguez, J.K. McCusker, J. Phys. Chem. A 106 (2002) 7399;
(b) F.D. Angelis, S. Fantacci, A. Selloni, M.K. Nazeeruddin, Chem. Phys. Lett. 415 (2005) 115;
(c) F.D. Angelis, S. Fantacci, A. Selloni, Chem. Phys. Lett. 389 (2004) 204.
[22] D.J. Tozer, R.D. Amos, N.C. Handy, B.O. Roos, L. Serrano-Andres, Mol. Phys. 97 (1999) 859.
[23] (a) H. Zabri, I. Gillaizeau, C.A. Bignozzi, S. Caramori, M.-F. Charlot, J. Cano-Boquera, F. Odobel, Inorg. Chem. 42 (2003) 6655;
(b) M.K. Nazeeruddin, S.M. Zakeeruddin, R. Humpry-Baker, S.I. Gorelsky, A.B.P. Lever, M. Grätzel, Coord. Chem. Rev. 208 (2000) 213.
[24] E.R. Batista, R.L. Martin, J. Phys. Chem. A 109 (2005) 3128.
[25] (a) C. Barolo, M.K. Nazeeruddin, S. Fantacci, D.D. Censo, P. Comte, P. Liska, G. Viscardi, P. Quagliotto, F.D. Angelis, S. Ito, M. Grätzel, Inorg. Chem. 45 (2006) 4642;
(b) M.K. Nazeeruddin, F.D. Angelis, S. Fantacci, A. Selloni, G. Viscardi, P. Liska, S. Ito, B. Takeru, M. Grätzel, J. Am. Chem. Soc. 127 (2005) 16835;
(c) F.D. Angelis, S. Fantacci, A. Selloni, Chem. Phys. Lett. 389 (2004) 204;
(d) S. Fantacci, F.D. Angelis, A. Selloni, J. Am. Chem. Soc. 125 (2003) 4381.
[26] A.B.P. Lever Electronic Absorption Spectroscopy, 2nd ed., Elsevier Publishing Co.; Amsterdam, 1985.
[27] Tarun Kumar Misra, Chittaranjan Sinha, Trans. Met. Chem. 24 (1999) 467.
[28] P. Mosher, G. Yap, R. Crutchley, Inorg. Chem. 40 (2001) 550.
[29] (a) R. Crutchley, B. Lever, Inorg. Chem. 21 (1982) 2276;
(b) R.J. Crutchley, K. McCaw, F.L. Lee, E.J. Gabe, Inorg. Chem. 29 (1990) 2576.

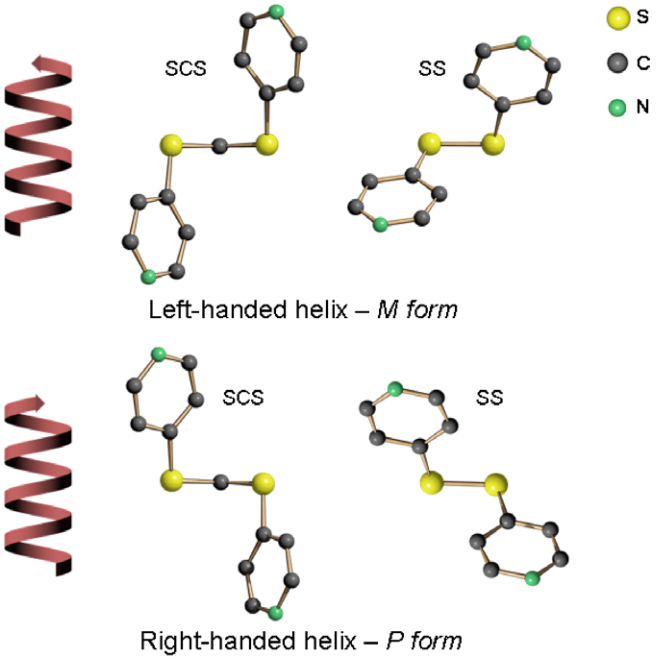

Scheme 1.

Vector 22 spectrophotometer. A Shimadzu UV-3101PC spectrophotometer was used to obtain electronic spectra in the solid state. Magnetic susceptibility measurements were performed at room temperature using a Johnson-Matthey Alfa MSB-MK1 Gouy balance. TGA analysis was carried out using a TA Instruments Hi-Res TGA2950 Thermobalance coupled to an FT-IR Bruker Tensor 27 apparatus.

2.2. Synthesis of the complexes

2.2.1. $[Cu(SO_4)(4\text{-bpytm})(H_2O)_3] \cdot H_2O$ (**1** · **H_2O**)

Compound **1** · **H_2O** was obtained by reaction of bis(4-pyridylthio)methane (4-bpytm) (0.86 mmol) in EtOH (10 mL) and $CuSO_4 \cdot 5H_2O$ (0.86 mmol) in a 1:1 mixture EtOH:H_2O (20 mL). The resulting mixture was heated under reflux for 48 h and was left to cool down to room temperature. The resulting blue precipitate was filtered off, washed with EtOH and dried under vacuum. Single crystals were obtained by recrystallization of the precipitate from water.

Data: Yield: 73%. *Anal.* Calc. for $C_{11}H_{18}N_2O_8S_3Cu$: C, 28.3; H, 3.9; N, 6.0. Found: C, 28.8; H, 3.9; N, 5.9%. IR (KBr, cm^{-1}): 3500–2959s,b, 1597s, 1541m, 1484m, 1421s, 1232m, 1167s, 1112s, 1065m, 1032m, 970m, 800m, 732m, 463m, 657w, 618s. UV–Vis (λ_{max}, cm^{-1}): 14500. μ (R.T.): 2.0 B.M.

2.2.2. $[Cu(NO_3)_2(4\text{-bpytm})_2] \cdot H_2O$ (**2** · **H_2O**)

A solution of bis(4-pyridylthio)methane (4-bpytm) (0.92 mmol) in EtOH (10 mL) was slowly added to a solution of $Cu(NO_3)_2 \cdot 3H_2O$ (0.46 mmol) in EtOH (10 mL). The resulting mixture was heated under reflux for 21 h and was left to cool down to room temperature. The resulting blue-lilac precipitate was filtered off, washed with EtOH and dried under vacuum. Single crystals of **2** · **H_2O** were obtained by slow diffusion of $Cu(NO_3)_2 \cdot 3H_2O$ (2.25 mmol) in water into a solution of 4-bpytm (0.25 mmol) in CH_3CN. The elemental analysis and the spectroscopic data for the single crystal and the powder phase were coincident.

Data: Yield: 98%. *Anal.* Calc. for $C_{22}H_{20}S_4O_7N_6Cu$: C, 39.2; H, 3.3; N, 12.5. Found: C, 39.9; H, 3.1; N, 12.8%. IR (KBr, cm^{-1}): 3446m, 1597s, 1536m, 1487m, 1385s, 1311m, 1223m, 1064m, 1023w, 810m, 733m, 501m. UV–Vis (λ_{max}, cm^{-1}): 17700. μ (R.T.): 1.7 B.M.

2.2.3. $[Cu(NO_3)2(4\text{-bpytm})_2] \cdot Solv$ (2 · ***Solv***)

4-bpytm (0.213 mmol), $Cu(NO_3)_2 \cdot 3H_2O$ (0.107 mmol), dmf (4 mL) and EtOH (2 mL) were added to a Schlenk tube, which was then placed in a microwave oven. The mixture was irradiated for 90 s at 700 W. The resulting blue solution was allowed to cool down to room temperature and immediately yielded blue crystals of **2** · **Solv**.

Data: Yield: 69%. *Anal.* Calc. for $C_{25}H_{31}S_4O_{10}N_7Cu$ (781.4; Solv = $2H_2O$ + dmf): C, 38.4; H, 4.0; N, 12.6. Found: C, 38.0; H, 3.8, N, 12.3%. IR (KBr, cm^{-1}): 3443m, 1658s, 1595s, 1485m, 1421m, 1385m, 1290m, 1219m, 1110m, 1066m, 1026w, 810m, 732m, 664m, 503m. μ (R.T.): 1.6 B.M.

2.3. Crystallography

Crystallographic data were collected on a Bruker Smart 1000 CCD diffractometer at 293 K using graphite monochromated Mo K_α radiation (λ = 0.71073 Å) and were corrected for Lorentz and polarisation effects. The frames were integrated with the Bruker SAINT [20] software package and the data were corrected for absorption using the program SADABS [21]. The structures were solved by direct methods using the program SHELXS97 [22]. All non-hydrogen atoms were refined with anisotropic thermal parameters by full-matrix least-squares calculations on F^2 using the program SHELXL97 [23]. Hydrogen atoms were inserted at calculated positions and constrained with isotropic thermal parameters, except for the hydrogen atoms of the water molecules in **1**, which were located from a difference Fourier map and refined isotropically. For **2** · **H_2O** disorder was observed in nitrate ions and in the refinement the N–O distance was restrained to values around 1.2 Å (DFIX 1.2). In the structures of **2** · **H_2O** and **2** · **Solv** the contribution of the disordered solvents to the diffraction pattern could not be rigorously included in the crystallographic calculations and these were consequently removed by the SQUEEZE routine of PLATON [24]. The *R* values before SQUEEZE application were 0.1128 [$I > 2\sigma(I)$] and 0.3030 (all data) for **2** · **H_2O** and 0.1770 [$I > 2\sigma(I)$] and 0.4876 (all data) for **2** · **Solv**. Drawings were produced with MERCURY [25] and special computations for the crystal structure discussions were carried out with PLATON. Crystal data and structure refinement data are listed in Table 1.

3. Results and discussion

The reaction of 4-bpytm with $CuSO_4 \cdot 5H_2O$ and $Cu(NO_3)_2 \cdot 3H_2O$ in metal/ligand molar ratios of 1:1 and 1:2, respectively, under reflux conditions yielded the polymeric compounds **1** · **H_2O** and **2** · **H_2O** (Scheme 2). Single crystals of **1** · **H_2O** and **2** · **H_2O** were obtained by recrystallization from EtOH and by diffusion, respectively. The microwave synthesis was an interesting method due to its high efficiency, leading to a reduction in reaction times, purer products and also acceleration of the crystallization process. As a result, we performed the synthesis with $Cu(NO_3)_2 \cdot 3H_2O$ using dmf and EtOH under microwave irradiation. In this way we isolated the pseudo-polymorph **2** · **Solv**.

Compounds **1** · **H_2O** and **2** · **H_2O** proved to be stable in air but this was not the case for **2** · **Solv**, which slowly loses the solvent component in air, leading to slight changes in the initial blue colour. The solvent component of **2** · **Solv** could not be accurately determined; the analytical data agree with the solvent component being $2H_2O$ and dmf but the X-ray structural resolution shows a highly disordered solvent area, which seems to contain dmf, H_2O and probably also EtOH.

The IR spectrum of **1** · **H_2O** exhibit a medium intensity, very broad band centred at 3230 cm^{-1} assignable to ν(OH) vibrations of the coordinated and lattice water molecules. The broadness

Table 1
Crystal and structure refinement data

Compound	**1 · H_2O**	**2 · H_2O**	**2 · Solv**
Empirical formula	$C_{11}H_{18}N_2O_8S_3Cu$	$C_{22}H_{20}N_6O_6S_4Cu$	$C_{22}H_{20}N_6O_6S_4Cu$
Formula weight	465.99	656.22	656.22
Crystal system	orthorhombic	monoclinic	monoclinic
Space group	*Pbca*	*C*2/*c*	$P2_1/c$
Unit cell dimensions			
a (Å)	8.9373(7)	8.553(2)	16.130(3)
b (Å)	12.8647(11)	20.449(5)	17.431(3)
c (Å)	31.145(3)	16.694(4)	16.333(3)
β (°)		96.372(5)	111.758(3)
V (Å^3)	3581.0(5)	2901.7(12)	4265.0(12)
Z	8	4	4
°ρ_{calc} (g cm^{-3})	1.729	1.502	1.022
Absorption coefficient (mm^{-1})	1.611	1.087	0.740
F(000)	1912	1340	1340
Crystal size (mm)	0.06 × 0.12 × 0.15	0.23 × 0.24 × 0.27	0.33 × 0.41 × 0.44
θ Range (°)	1.31–8.03	1.99–8.13	1.78–8.05
Reflections collected	18513	7711	17780
Independent reflections (R_{int})	4261 (0.0972)	3254 (0.0889)	7924 (0.0846)
Maximum/minimum transmission	0.9080/0.8120	1.0000/0.3400	0.7830/0.5340
Goodness-of-fit on F^2	0.865	0.857	0.863
Final *R* indices [$I>2\sigma(I)$]	R_1 = 0.0509	R_1 = 0.0991	R_1 = 0.0683
	wR_2 = 0.0901	wR_2 = 0.2581	wR_2 = 0.1661

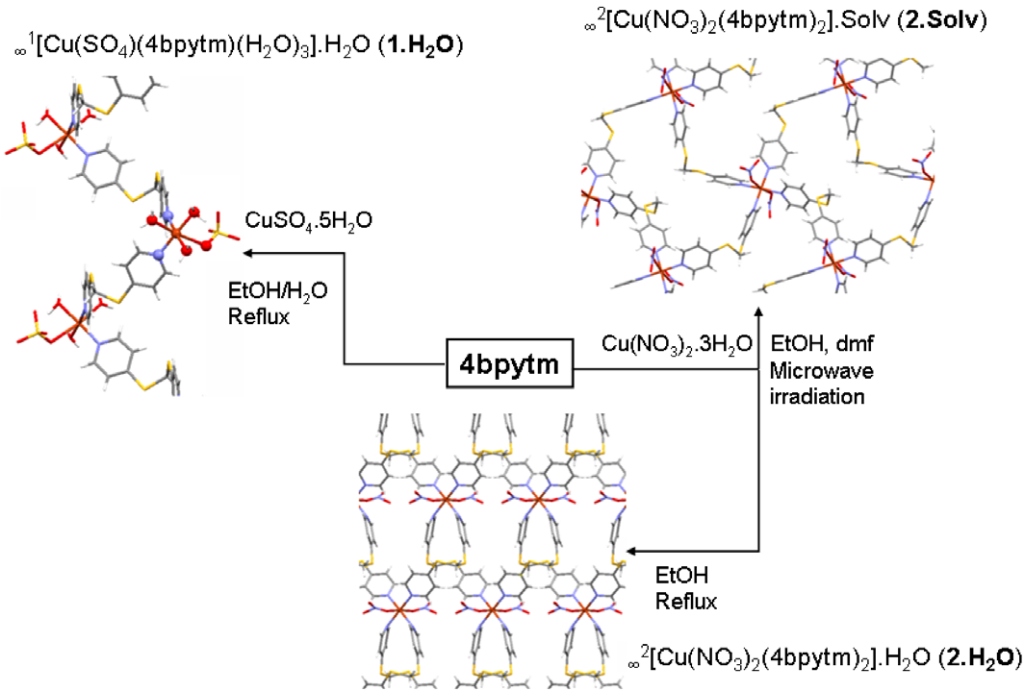

Scheme 2.

and relatively low frequency of this band are indicative of extensive hydrogen bonding. In **2 · H$_2$O** and **2 · Solv** the bands corresponding to the ν(OH) vibrations are located at about 3440 cm^{-1} and are narrow, suggesting that the water lattice molecules are weakly involved in hydrogen bonding. The IR spectrum of **1 · H$_2$O** exhibits two strong peaks at 1112 and 618 cm^{-1}, indicating the implication of the SO_4^{2-} group in the coordination to the Cu(II) centre. Compounds **2 · H$_2$O** and **2 · Solv** shows bands corresponding to the NO_3^- anions at 1311 cm^{-1} (**2 · H$_2$O**) and 1219 cm^{-1} (**2 · Solv**) for $\nu_a(NO_2)$ and at 1023 cm^{-1} (**2 · H$_2$O**) and 1026 cm^{-1} (**2 · Solv**) for $\nu_s(NO_2)$. Also in the spectrum of **2 · Solv** a strong peak at 1658 cm^{-1} is attributed to the amide I band of the dmf solvent.

The thermal decomposition of the complexes was studied using thermogravimetric analysis. In compound **1 · H$_2$O**, an initial mass loss of 15.2% was observed between room temperature and 109 °C, which corresponds to the release of the lattice H_2O molecule and the three aqua ligands (calc. 15.4%). A plateau was then reached up to 244 °C, suggesting that the anhydrous species is thermally stable. The second weight loss of 52%, between 244 and 270 °C, corresponds to the escape of the 4-bpytm ligand (calc. 50%). For compound **1 · H$_2$O** the release of the water lattice molecule occurs between RT and 58 °C and in the two following steps, between 58 and 393 °C, a complicated degradation occurs with a total weight loss of 72%. In **2 · Solv**, an initial step with a loss of about 1.5%, between R.T. and 120 °C, is consistent with the escape

of 0.7 water molecules and a second release of about 7.9%, in the range 120–220 °C, could corresponds to the loss of one dmf molecule (calc. 8.4%) and the final release, in the range 220–340 °C, corresponds to the total decomposition of the sample.

3.1. Structure of $[Cu(SO_4)(4\text{-bpytm})(H_2O)_3] \cdot H_2O$ (**1** · **H_2O**)

The coordination environment of the copper atom in **1** · **H_2O** is represented in Fig. 1, together with the atom numbering scheme for coordinating atoms, and selected bond distances and angles are listed in Table 2. The structure is based on 1D helical chains and water of crystallization. The metal centre adopts a distorted octahedral coordination geometry that can be described as a 4 + 1 + 1′ type, with two *cis* pyridyl nitrogen atoms and two *cis* oxygen atoms of aqua molecules in the equatorial plane (Cu–N = 2.020; 1.987 and Cu–O = 1.976; 1.965 Å). The copper atom is also bonded to one oxygen atom of an aqua molecule (Cu–O3 = 2.305 Å) and one oxygen atom of the sulfate ion (Cu–O11 = 2.635 Å) in the axial positions. The Cu···Cu distance in the chain separated by the bridging 4-bpytm is 13.0098(14) Å. The helices run along the *b* axis and in the 4-bpytm ligand the C–S–C–S torsion angles are 75.5(4)° and 74.4(4)°, which are in the range reported for other polymeric metal complexes [15]. The data for some very similar one-dimensional copper(II) polymers containing different N,N′-bridging ligands [26–29] are listed in Table 3 for the sake of comparison. In all cases the equatorial Cu–N and Cu–Ow distances are around 2 Å, but the axial Cu–Ow and Cu–OSO_3 distances have values in the ranges 2.207–2.594 and 2.378–2.673 Å, respectively. When a rigid N,N′-ligand is used the N *trans* disposition is obtained, but when the ligand has some degree of flexibility the N *cis* arrangement is preferred. Some other similar 1D metal polymers, such as $[M(SO_4)(44bipy)(H_2O)_3] \cdot C_2H_6O_2$, M = Co(II) [30] and M = Zn(II) [31], also show an N *trans* disposition for the rigid ligand 4,4′-bipyridine.

Table 2
Selected interatomic bond lengths (Å) and angles (°)

	Bond lengths		Angles	
1 · **H_2O**	Cu–O1	1.965(3)	O1–Cu–O2	91.22(14)
	Cu–O2	1.976(3)	O1–Cu–N11	175.89(16)
	Cu–O3	2.305(3)	O2–Cu–N11	90.80(16)
	Cu–N1	2.020(4)	O1–Cu–N1	86.30(15)
	Cu–N11	1.987(4)	O2–Cu–N1	174.38(16)
	Cu–O11^{iii}	2.635(4)	N11–Cu–N1	91.38(16)
			O1–Cu–O3	90.23(13)
			O2–Cu–O3	93.17(14)
			N11–Cu–O3	93.24(15)
			N1–Cu–O3	91.89(15)
iii = $-x + 1/2, y - 1/2, z$				
2 · **H_2O**	Cu–N1	1.999(7)	N1–Cu–N1^{i}	93.8(4)
	Cu–N2^{ii}	2.059(7)	N1–Cu–N2^{ii}	170.5(3)
	Cu–O1^{iv}	2.6735(5)	N1–Cu–N2^{iii}	91.8(3)
			N2^{ii}–Cu–N2^{iii}	83.7(4)
i = $-x, y, -z + 1/2$, ii = $-x + 1/2, y + 1/2, -z + 1/2$, iii = $x-1/2, y + 1/2, z$, iv = $x-1, y, z$				
2 · **Solv**	Cu–N1	2.034(5)	N11–Cu–N2	176.1(2)
	Cu–N11	2.212(5)	N11–Cu–N12	90.27(18)
	Cu–N2	2.017(5)	N2–Cu–N12	89.03(18)
	Cu–N12	2.020(5)	N11–Cu–N1	91.69(19)
	Cu–O11	2.367(6)	N2–Cu–N1	89.16(18)
	Cu–O1	2.604(5)	N12–Cu–N1	177.14(19)
			N11–Cu–O11	88.6(2)
			N2–Cu–O11	95.1(2)
			N12–Cu–O11	84.2(2)
			N1–Cu–O11	93.8(2)

As depicted in Fig. 1 (right) the homochiral chains interact through hydrogen bonding to give rise to the formation of a 2D homochiral layer parallel to the *ac* plane. The H-bonds (Table 4)

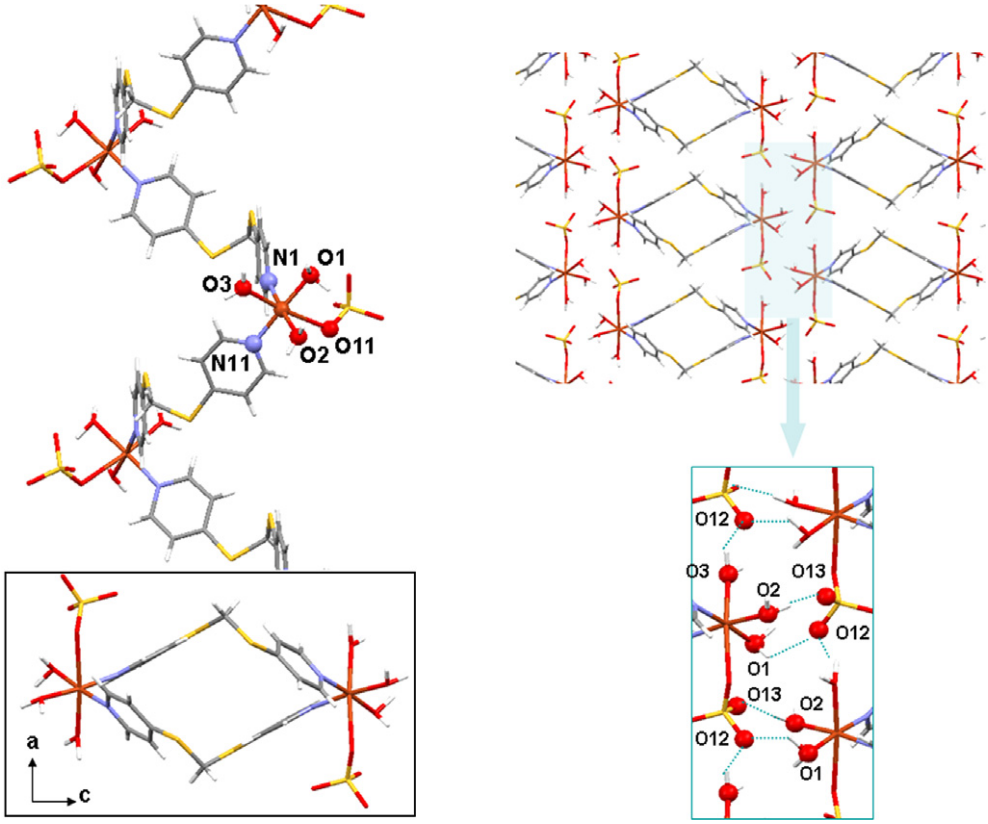

Fig. 1. Structure of $[Cu(SO_4)(4\text{-bpytm})(H_2O)_3] \cdot H_2O$ (**1** · **H_2O**). Left: 1D helical chain that runs along the *b* axis. Right: 2D homochiral association through hydrogen bonding.

Table 3
Structural parameters (Å) for closely related 1D copper(II) complexes

Compound	Cu–N (Å)	Cu–Ow (Å)	Cu–OSO_3	Coord.	Description	Ref.
$[Cu(SO_4)(bix)(H_2O)_3]\cdot H_2O$	N *cis*	1.975	2.378	4 + 1 + 1′	Undulated chains	26
	1.987	1.982				
	2.003	2.594 (Axial)				
$[Cu(SO_4)(44bipy)(H_2O)_3]\cdot 2H_2O$	N *trans*	1.952	2.673	5 + 1	Linear chains	27
	2.049	1.976				
	2.044	2.207 (Axial)				
$[Cu(SO_4)(bpz)(H_2O)_3]\cdot H_2O$	N *trans*	2.002	2.528	4 + 1 + 1’	Linear chains	28
	1.966	2.019				
	1.975	2.329 (Axial)				
$[Cu(SO_4)(bpen)(H_2O)_3]\cdot 4H_2O$	N *trans*	1.969	2.471	4 + 2	Linear chains	29
	2.028	2.005				
	2.031	2.405 (Axial)				
$[Cu(SO_4)(4\text{-}bpytm)(H_2O)_3]\cdot H_2O$	N *cis*	1.965	2.635	4 + 1 + 1′	Helical chains	This work
	1.987	1.976				
	2.020	2.305 (Axial)				

Bix = 1,4-bis(imidazol-1-ylmethyl)benzene; 44bipy = 4,4′-bipyridine.
bpz = 4,4′-bipyrazolyl; bpen = *trans*-bis(4-pyridyl)ethene.

Table 4
Main hydrogen bond distances (Å) and angles (°)

Compound	D–H···A	*d*(D–H)	*d*(H···A)	*d*(D···A)	∠(DHA)
1 · H_2O	O1–H1B···O12^{iv}	1.082(3)	1.775(4)	2.644(5)	134.0(2)
	O2–H2A···O4^{v}	0.846(3)	1.923(3)	2.758(5)	169.3(3)
	O2–H2B···O13^{iv}	0.966(3)	1.736(3)	2.696(5)	171.7(2)
	O3–H3A···O4^{vi}	0.888(3)	1.987(3)	2.830(5)	158.2(2)
	O3–H3B···O12^{viii}	0.944(3)	2.188(4)	2.994(6)	142.7(2)
	O4–H4A···O11^{vii}	0.961(3)	2.027(4)	2.903(5)	150.5(2)
	O4–H4B···O12^{iv}	0.906(3)	1.959(4)	2.781(5)	150.2(3)
	C3–H3···O14^{vii}	0.93	2.37	3.231(7)	154.0
	C13–H13···O14	0.93	2.34	3.240(6)	163.6
iv = $-x, -y, -z+1$, v = $x-1/2, -y+1/2, -z+1$, vi = $-x, -y+1, -z+1$, vii = $x, y+1, z$, viii = $-x-1/2, y+1/2, z$					
2 · H_2O	C11–H11A···O1^{vi}	0.97	2.42	3.368(9)	164.5
	C11–H11A···O3^{vi}	0.97	2.57	3.345(9)	136.9
	C2–H2···O3^{vii}	0.93	2.63	3.390(8)	139.3
vi = $-x+3/2, -y+1/2, -z$, vii = $-x+1/2, -y+1/2, -z$					
2 · Solv	C9–H9···O2^{v}	0.93	2.79	3.198(8)	107.9
	C20–H20···O3^{v}	0.93	2.58	3.329(8)	138.3
	C22–H22···O13^{vi}	0.93	2.57	3.291(12)	134.8
v = $x, -y+3/2, z-1/2$, vi = $x, -y+3/2, z+1/2$					

involving the coordinated water molecules and the sulfate anions are responsible for the association of the chains to form this layer.

The layers with opposite helicity are connected to give a 3D architecture (Fig. 2, left) through hydrogen bonding involving the water molecule of crystallization, one oxygen (O14) of the sulfate anion and two –CH (C3 and C13) units of the two pyridine rings (Table 4). So, each unit, by means of two $CH_{py}\cdots OSO_3$ hydrogen bonds, connects along the *b* axis each helix with two others of opposite helicity (Fig. 2, right top) and the hydrogen bonds involving the water of crystallization and the coordinated oxygen atom (O11) of the sulfate connect the helices along the *a* axis (Fig. 2, right bottom). The final 3D supramolecular architecture is racemic due to the existence of equal amounts of P- and M-helices. The crystallization water (O4) is involved in four hydrogen bonds: as an acceptor with two coordinated water molecules (O2 and O3) from two different chains and as a donor with two of the oxygen atoms (O11 and O12) of the sulfate anions of another two chains.

*3.2. Structure of $[Cu(NO_3)_2(4\text{-}bpytm)_2]\cdot H_2O$ (**2 · H_2O**) and $[Cu(NO_3)_2(4\text{-}bpytm)_2]\cdot Solv$ (2 · **Solv**)*

The 2D coordination polymers **2 · H_2O** and **2 · Solv** are pseudo-polymorphs. The different solvents and probably the different synthetic methodologies used play a determinant role in the formation of the 2D coordination network and also, consequently, in the supramolecular organization in both compounds. The 2D coordination networks are represented in Figs. 3 and 4 together with the atom numbering scheme for coordinating atoms and a schematic representation showing the different patterns of the layers of **2 · H_2O** and **2 · Solv**, respectively. Selected interatomic distances and angles and the main hydrogen bonds are listed in Tables 2 and 4, respectively.

In both compounds, as in other tetrakis-bipyridyl based structures with $M(NO_3)_2$ [32], the four bridging bipyridyl ligands occupy equatorial coordination sites of the metal centre, leading to the propagation of a 2D sheet structure. The Cu–N distances are all about 2 Å but in **2 · Solv** one of the Cu–N distances has a value of 2.212 Å, which is clearly longer than the others.

The remaining axial sites are occupied by the monodentate nitrate ions. In **2 · H_2O**, the Cu–O distance of 2.765 Å is indicative of a very weak coordination so the coordination geometry around the copper centre corresponds to an elongated octahedron (4+2 type). In **2 · Solv** there are two different Cu–O distances, one short (2.367 Å) and one long (2.604 Å), although both of these are shorter than those observed in **2 · H_2O**. The 2D layer in **2 · H_2O** can be described as a rhombic-grid with a Cu···Cu distance of 11.08 Å through the bridging ligand, a major diagonal Cu···Cu distance of 20.44 Å and a minor diagonal Cu···Cu distance of 8.55 Å (Fig. 3).

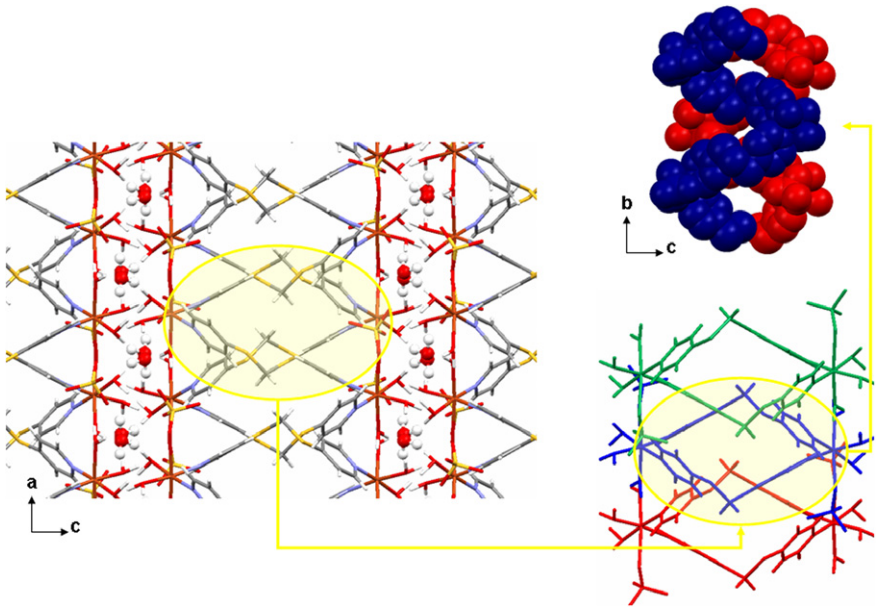

Fig. 2. View in the *ac* plane of the 3D organization in **1** · **H_2O**, showing details of the arrangement of the helices with different handedness (right) marked with different colours.

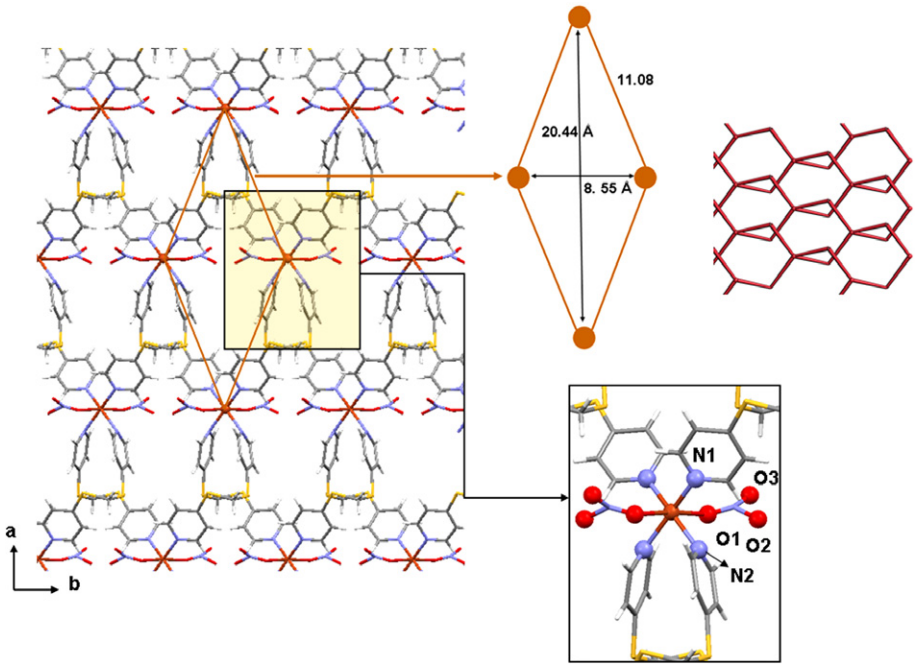

Fig. 3. View of the 2D coordination polymer $[Cu(NO_3)_2(4\text{-bpytm})_2] \cdot H_2O$ (**2** · **H_2O**) together with the coordination environment of copper ions, a topological representation of the layer and a metrical representation of the rhombic-grid showing the Cu···Cu distances.

The 2D layer in **2.Solv** presents a parquet motif with Cu···Cu distances through the bridging ligands of about 12 Å and diagonal Cu···Cu distances of 16.13 and 17.43 Å (Fig. 4).

In the 4-bpytm ligands the values for the C–S–C–S torsion angles of 73.3(6)/62.8(6)° in **2** · **H_2O** and 67.1(4)/63.3(4)° and 69.2(4)/67.3(4)° in **2** · **Solv** are lower than those found in **1** · **H_2O**, but all fall within the range 63.2–76.9° observed in the free 4-bpytm ligand and in the 2D polymeric complexes $[CuX_2(4\text{-bpytm})_2]$ (X = Cl, Br) [15]. However, all of these values are lower than 82.4°, which was recently observed in the 1D compound $[Cu(HCOO)_2(4\text{-bpytm})]$ [16]. An interesting point is that in both compounds each sheet incorporates molecules of the 4-bpytm with the same helicity, and then each sheet is homochiral and connects through weak interactions to sheets of opposite chirality to generate racemic supramolecular arrays.

Both compounds exhibit an AB stacking mode of the layers (Figs. 5 and 6) with a linkage by means of weak CH···O hydrogen bonds (Table 4) between layers of opposite chirality. The shorter Cu···Cu distances between adjacent layers are 9.61 Å in **2** · **H_2O** and 8.61 Å in **2** · **Solv**, with the latter value lower than all the intralayer Cu···Cu distances.

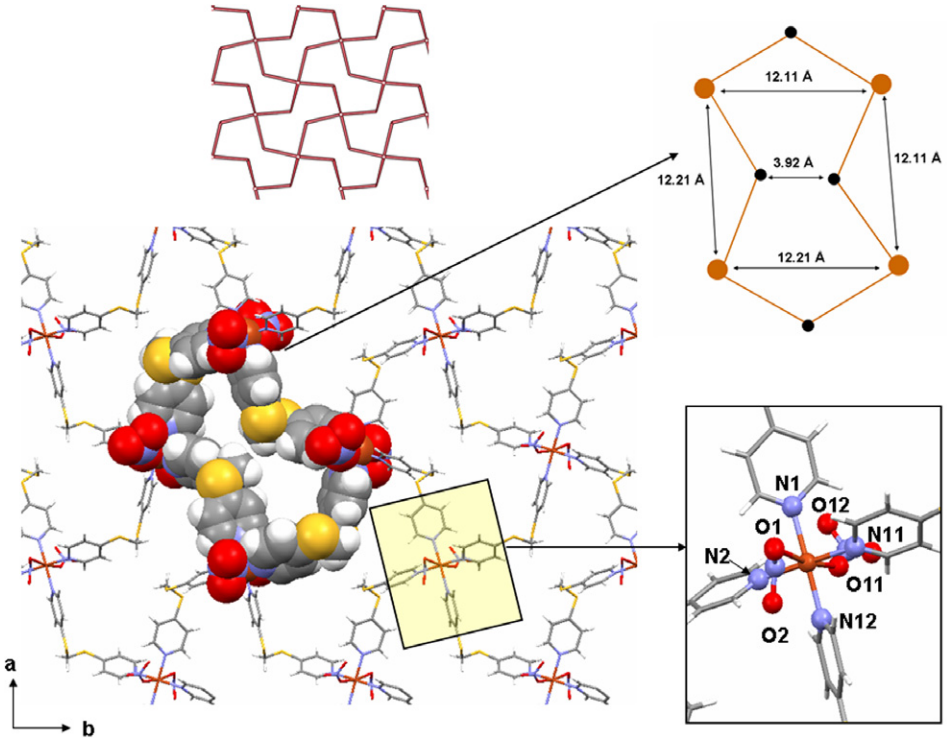

Fig. 4. View of the 2D coordination polymer $[Cu(NO_3)_2(4\text{-bpytm})_2]$ · Solv (**2** · **Solv**) together with the coordination environment of copper ions, a topological representation of the layer and a metrical representation (black circle represents the $-CH_2$ groups of the ligands) of the hole showed also as space filling representation.

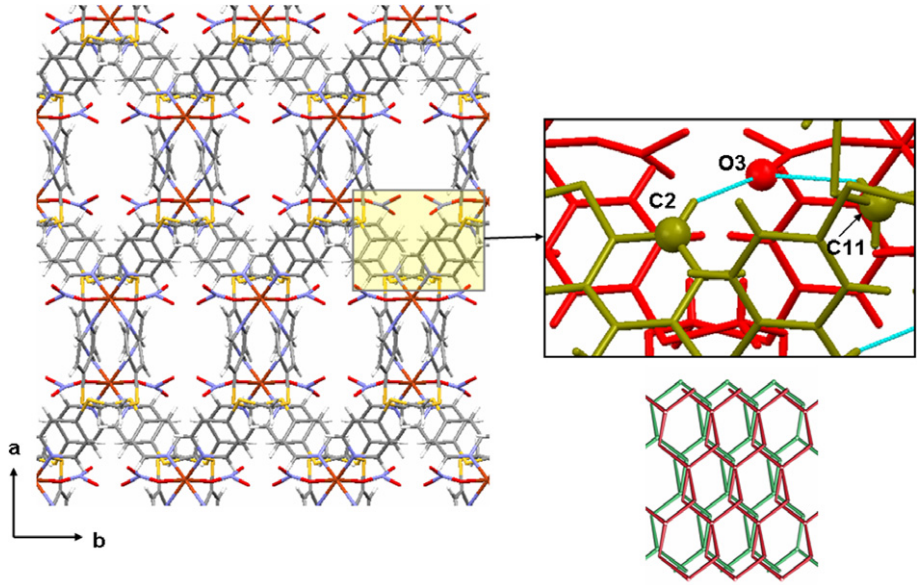

Fig. 5. View of the 3D supramolecular structure and 3D topological representation of **2** · $\mathbf{H_2O}$ showing detail of the CH···O linkage between sheets of opposite chirality.

Since the solvent component for both structures could not be successfully determined in the crystallographic calculations, the analysis of the supramolecular organization is based on the study of the weak interactions in the metal-organic framework. However, the analysis of the corresponding solvent areas showed marked differences between the two compounds. For **2** · $\mathbf{H_2O}$ the solvent area corresponds to a volume of 370.5 $Å^3$, which represents 12.8% of the unit cell, and corresponds to a total of 64 electrons per unit cell which is assigned to 6.4 molecules of water. In **2** · **Solv** the situation is clearly different with a solvent area volume of 1978 $Å^3$ (46.4% of the unit cell) and a total of 470 electrons per unit cell, assigned to two water, one dmf and two ethanol molecules. These differences are also evident in the corresponding values for the Kitaigorodskii packing index [33]: 64.7% for **2** · $\mathbf{H_2O}$ and 44% for **2** · **Solv**. This analysis suggests that the solvent mixture used (dmf + EtOH) under microwave irradiation plays a key role in the preparation and crystallization of **2** · **Solv**, meaning that it is not unreasonable to consider a template function of the solvent mixture.

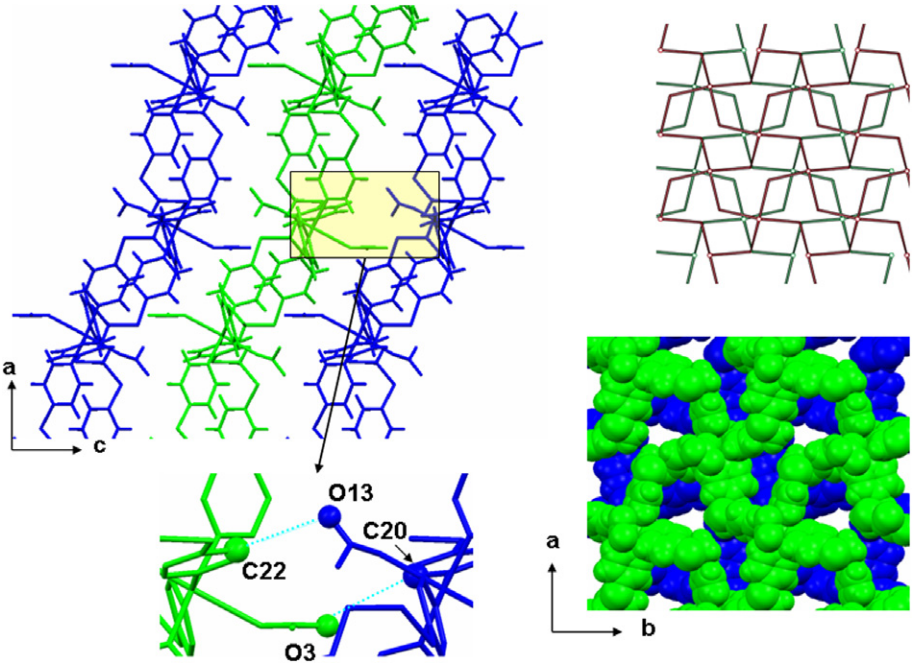

Fig. 6. View of the 3D supramolecular structure and 3D topological representation of **2** · **Solv** showing detail of the CH···O linkage between sheets of opposite chirality and a space filling representation.

4. Conclusions

The reaction of 4-bpytm with $CuSO_4 \cdot H_2O$ afforded a helical chain for **1** · **H_2O**. The reaction with $Cu(NO_3)_2 \cdot 3H_2O$ under different synthetic conditions afforded two 2D pseudo-polymorphs with different (4,4) topology: the rhombic-grid in **2** · **H_2O** and the parquet motif in **2** · **Solv**. The non-rigid 4-bpytm spacer is responsive to the nature of the anion, so that the anion effect seems to control the dimensionality and topology of the resulting coordination polymer. The microwave synthesis has proven to be very efficient for the preparation and crystallization of **2** · **Solv** and the mixture of solvents used seem to play a template role.

5. Supplementary data

CCDC 675465, 675466 and 675467 contains the supplementary crystallographic data for **1** · **H_2O**, **2** · **H_2O** and **2** · **Solv**. These data can be obtained free of charge via http://www.ccdc.cam.ac.uk/conts/retrieving.html, or from the Cambridge Crystallographic Data Centre, 12 Union Road, Cambridge CB2 1EZ, UK; fax: (+44) 1223-336-033; or e-mail: deposit@ccdc.cam.ac.uk.

Acknowledgements

Financial support from ERDF (EU), MEC (Spain) and Xunta de Galicia (Spain) (research Projects CTQ2006-05642/BQU and PGIDIT06-PXIB314373PR) are gratefully acknowledged.

References

[1] J.M. Lehn, Supramolecular Chemistry: Concepts and Perspectives, VCH, Weinheim, Germany, 1995.
[2] R. Robson, J. Chem. Soc., Dalton Trans. (2000) 3735.
[3] Y. Rodríguez-Martín, M. Hernández-Molina, F.S. Delgado, J. Pasán, C. Ruíz-Pérez, J. Sanchiz, F. Lloret, M. Julve, CrystEngCommun. 4 (2002) 522.
[4] C. Janiak, Dalton Trans. (2003) 2781.
[5] L. Carlucci, G. Ciani, D.M. Proserpio, CrystEngCommun. 5 (2003) 269.
[6] K. Biradha, CrystEngCommun. 5 (2003) 374.
[7] S. Kitagawa, R. Kitaura, S. Noro, Angew. Chem., Int. Ed. 43 (2004) 2334.
[8] M. Du, C-P. Li, X-J. Zhao, Cryst. Growth Des. 6 (2006) 335.
[9] T.-T. Luo, H.-L. Tsai, S.-L. Yang, Y.-H. Liu, R.D. Yadav, C.-C. Su, C.-H. Ueng, L.-G. Lin, K.-L. Lu, Angew. Chem., Int. Ed. 44 (2005) 6063.
[10] G. Peli, S. Rizzato, S. Cassesse, L. Garlaschelli, M. Manassero, CrystEngCommun 7 (2005) 575.
[11] J.K. Clegg, L.F. Lindoy, B. Moubaraki, K.S. Murray, J.C. McMurtrie, Dalton Trans. (2004) 2417.
[12] M. Albrecht, I. Janser, S. Kamptmann, P. Weis, B. Wibbeling, R. Fröhlich, Dalton Trans. (2004) 37.
[13] J.D. Dunitz, Chem. Commun. (2003) 545.
[14] R. Custelcean, B.A. Moyer, Eur. J. Inorg. Chem. (2007) 1321.
[15] A. Amoedo-Portela, R. Carballo, J.S. Casas, E. García-Martínez, A.B. Lago-Blanco, A. Sánchez-González, J. Sordo, E.M. Vázquez-López, Z. Anorg. Allg. Chem. 631 (2005) 2241.
[16] R. Carballo, B. Covelo, E. García-Martínez, A.B. Lago, E.M. Vázquez-López, Z. Anorg. Allg. Chem. 633 (2007) 780.
[17] M. Korn, A. Haas, H. Oberhammer, Chem. Ber. 128 (1995) 461.
[18] E.M. Page, D.A. Rice, K. Aerset, K. Hagen, A.R.J. Genge, J. Phys. Chem. A 104 (2000) 6672.
[19] S.H. Jhung, J.-H. Lee, P.M. Forster, G. Férey, A.K. Cheetham, J.-S. Chang, Chem. Eur. J. 12 (2006) 7899.
[20] Siemens SAINT, Version 4, Software Reference Manual, Siemens Analytical X-ray Systems, Inc., Madison, WI, USA, 1996.
[21] G.M. Sheldrick, SADABS, Program for Empirical Absorption Correction of Area Detector Data, University of Göttingen, Germany, 1996.
[22] G.M. Sheldrick, SHELXS-97, Program for the Solution of Crystal Structures from X-ray Data, University of Göttingen, Germany, 1997.
[23] G.M. Sheldrick, SHELXL-97, Program for the Refinement of Crystal Structures from X-ray Data, University of Göttingen, Germany, 1997.
[24] A.L. Spek, PLATON, A Multipurpose Crystallographic Tool, Utrecht University, Utrecht, The Netherlands, 2001.
[25] I.J. Bruno, J.C. Cole, P.R. Edgington, M.K. Kessler, C.F. Macrae, P. McCabe, J. Pearson, R. Taylor, MERCURY. New Software for Visualizing Crystal Structures, Acta Crystallogr., Sect. B 58 (2002) 389.
[26] L. Carlucci, G. Ciani, D.M. Proserpio, L. Spadacini, CrystEngCommun. 6 (2004) 96.
[27] D. Hagrman, R.P. Hammond, R. Haushalter, J. Zubieta, Chem. Mater. 10 (1998) 2091.
[28] I. Boldog, J. Sieler, A.N. Chernega, K.V. Domasevitch, Inorg. Chim. Acta 338 (2002) 69.
[29] H-L. Hu, M.-C. Suen, C.-W. Yeh, J.-D. Chen, Polyhedron 24 (2005) 1497.
[30] W.-J. Lu, Y.-M. Zhu, K.-L. Zhong, Acta Crystallogr., Sect. C 62 (2006) m448.
[31] W.-J. Lu, Y.-M. Zhu, K.-L. Zhong, Acta Crystallogr., Sect. E 62 (2006) m3036.
[32] S.A. Barnett, N.R. Champness, Coord. Chem. Rev. 246 (2003) 145.
[33] A.I. Kitaigorodskii, Molecular Crystals and Molecules, Academic Press, New York, 1973.

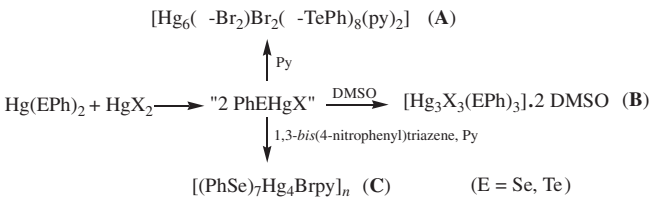

Scheme 1. Reactions attained from the intermediary PhTeHgX (X = halogenide).

and of the cluster $[(PhTe)_{16}Ag_4Hg_6Py_4] \cdot H_2O$ (**2**) are given in Table 1. The polymeric structure of **1** is represented in Fig. 1, and the high symmetric structure of **2** is shown in Fig. 2, for clarity, without the H_2O solvate molecule.

The asymmetric unit of **1** corresponds to its empirical formula, $[(PhTe)_4Ag_2Hg_2(Cl)_2]$. The association of the asymmetric units through "intermolecular" Ag–Te, Hg–Te, Hg–Cl, and Ag–Cl bonds leads to the assembly of polymeric, bidimensional and polycyclic layers in the *ab*-plane. The mean Hg–Cl bond distance within the monomeric unit is 2.66 Å, but this bond becomes noticeably longer (2.95 Å) for Hg and Cl atoms belonging to different units. The layers of the coordination polymer **1** stack in the *c*-plane at a distance of 9.6 Å from each other (distance between the closest Te atoms belonging to vicinal layers).

Cluster **2** stands in bold relief due to two main characteristics: first, its high symmetry; and second, the occupational disorder related to the Hg and Ag atoms [5,25]. A minor, but also interesting feature is the coordination of pyridine molecules to the terminal Hg atoms. The occupational relationship was set up in 40%/60%

Table 1
Crystal data and structure refinement for **1** and **2**

	1	**2**
Empirical formula	$C_{24}H_{20}Ag_2Cl_2Hg_2Te_4$	$C_{116}H_{102}Ag_4Hg_6N_4OTe_{16}$
Formula weight	1506.62	5244.64
T (K)	293(2)	293(2)
Radiation, λ (Å)	0.71073	0.71073
Crystal system, space group	triclinic, $P\bar{1}$	cubic, $1a\bar{3}d$
Unit cell dimensions		
a (Å)	6.332	46.7417(7)
b (Å)	8.021	46.7417(7)
c (Å)	29.156	46.7417(7)
α (°)	82.56	90
β (°)	89.52	90
γ (°)	85.19	90
V (Å^3)	1463.2	102121(3)
Z, D_{calc} (g cm^{-3})	2, 3.420	24, 2.047
Absorption coefficient (mm^{-1})	15.884	8.562
F(000)	1320	56016
Crystal size (mm)	0.194 × 0.100 × 0.07	0.171 × 0.168 × 0.161
θ Range (°)	1.41–30.72	2.39–30.58
Index ranges	$-8 \leqslant h \leqslant 9$, $-11 \leqslant k \leqslant 11$, $-41 \leqslant l \leqslant 40$	$-66 \leqslant h \leqslant 64$, $-66 \leqslant k \leqslant 66$, $-54 \leqslant l \leqslant 65$
Reflections collected	36692	622848
Reflections unique (R_{int})	9004 (0.0315)	13044 (0.0629)
Completeness to θ_{max} (%)	99.1	99.6
Absorption correction	GAUSSIAN	GAUSSIAN
Maximum and minimum transmission	1 and 0.901050	1 and 0.548122
Refinement method	full-matrix least-squares on F^2	full-matrix least-squares on F^2
Data/restraints/parameters	9004/0/307	13044/0/122
Goodness-of-fit on F^2	1.227	1.061
Final R indices [$I > 2\sigma(I)$]	$R_1 = 0.0269$, $wR_2 = 0.0729$	$R_1 = 0.0892$, $wR_2 = 0.2196$
R indices (all data)	$R_1 = 0.0345$, $wR_2 = 0.0911$	$R_1 = 0.1116$, $wR_2 = 0.2396$
Largest difference in peak and hole (e Å^{-3})	1.515 and −1.897	5.797 and −3.666

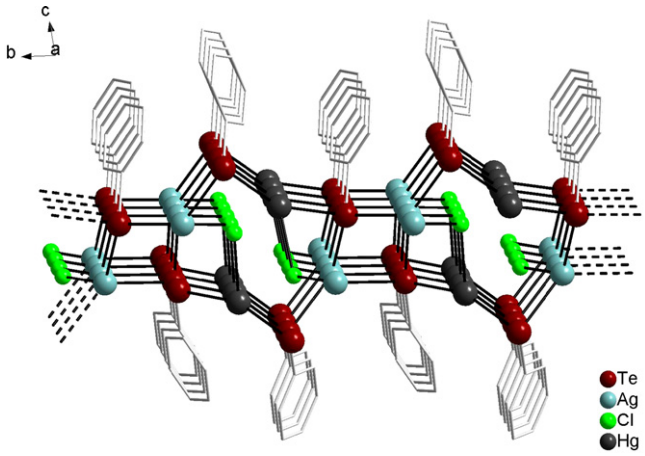

Fig. 1. Polymeric, bidimensional structure of $[(PhTe)_4Ag_2Hg_2(Cl)_2]_n$ (**1**).

for Ag and Hg, respectively. Occupational relationships define the rate of occupation of the same spatial position by two different atoms.

The occupational disorder of the metal ions in cluster **2** was calculated by restraints on the linear combinations of free variables [26],[1] which provide a way of restraining the sum of the occupancies of a multi-component disorder to be unity, also in order to fit the charge balances and chemical analysis of a mineral with several sites occupied by a mixture of cations. Occupation disorders, which occur with the ions with different charges (as in the case of compound **2**), have been reported also in high symmetric compounds, for example, supertetrahedral clusters [27].

The asymmetric unit of the cluster **2** represents 1/4 of the empirical formula. The other ¾ are generated by the symmetry operations $z + 3/4$, $-y + 1/4$, $-x + 3/4$; $-z + 3/4$, $-y + 1/4$, $x - 3/4$; $x + 3/2$, $y + 0$, $-z + 0$. The cluster is composed overall by 10 metal atoms (with an occupational relationship of 40%/60% for Ag and Hg, respectively), which are connected through PhTe groups attaining μ_2 bridges. The Te–metal bond distances are situated between 2.739(0) and 2.819(0) Å, which are the standard values for these compound types [5,24,25,28].

2.2. Synthetic considerations and inherent possibilities

In an early report, we have pointed out that the reaction of $[Hg(TePh)_2]$ and metal salts stabilized by different phosphine ligands and (coordinative) solvent molecules should lead to different redistribution reactions [24]. In the present case, these reactions would comprise the simultaneous formation of PhTeHgX, $[(TePh)_2HgX]^-$, and $(TePh)[M(L)_n]$ (M = Ag; L = PMe_2Ph, PPh_3, DMSO, pyridine; X = Cl^-) moieties [17,20,22].

The symmetric structures of the clusters $[Hg_6Ag_4(TePh)_{16}]$ and $[Hg_6Ag_4Te(TePh)_{14}]_n$ [24] obtained through the reaction of $[Hg(TePh)_2]$ with AgCl or $AgNO_3$ in the presence of $PMePh_2$, PPh_3, or DMF – arising actually from the correspondent adducts $[Ag(L)_n]X$ (X = Cl^-, NO_3^-; L = $PMePh_2$, PPh_3, DMF) – can also be attributed to the prevalence of some order of aggregation of the Ag^+ ions into the cluster frame, since this metal occupies very symmetrical equatorial positions, practically dividing the clusters into two halves. We think that this "entry selectivity" is highly dependent on the coordinative character of the counterion of the silver salt. Both ions Cl^- and NO_3^- have good coordinative characters, although Cl^- is somewhat better. In the presence of other ligands such as phosphines, or coordinative solvents such as DMF, DMSO

[1] The SHELX-97 Manual, p. 5-4.

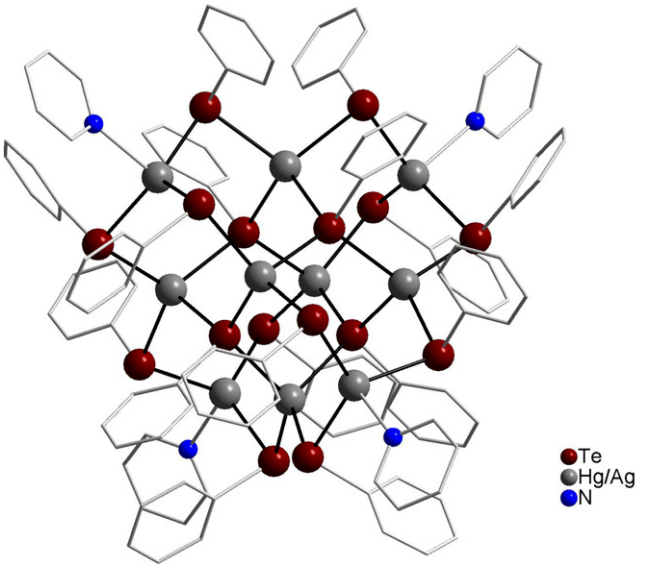

Fig. 2. Structure of $[(PhTe)_{16}Ag_4Hg_6Py_4] \cdot H_2O$ (**2**). For clarity the solvate molecule is not displayed.

or pyridine, an exchange should occur between the more or less coordinative counterion and solvent/ligand molecules. We believe that the lower the exchange velocities (for good coordinating counterions), the better the entry selectivity of the silver ions in the assembling process of the cluster.

One of the differences in the synthesis of clusters **1** and **2**, in the present work, is the use of different silver salts, AgCl (**1**) and $AgClO_4$ (**2**). It is known that the perchlorate anion is a very poor coordinative species, and when we assume that the entry selectivity of the silver ion into the skeleton of a cluster is proportional to the coordinative character of the counterion of the salt, this selectivity should increase in the series $ClO_4^- < NO_3^- < Cl^-$. This should mean that for the perchlorate salt the entry selectivity of the silver ion is practically null, and this can be related to the occupational disorder of the metal ions in the frame of cluster **2**: the – very probable – high velocity of formation of **2** allows inferring that the relatively "free" metal ions are also free to occupy any space in any point thermodynamically possible, during the cluster formation.

However, since the synthesis of **2** was carried out with the initial addition of an excess of triphenylphosphine to $AgClO_4$, our assumption that the failed coordinative character of the ClO_4^- ion would determine the low entry selectivity of the silver ions into the cluster could be a *nonsense*, because the Ag^+ species should be coordinated to the PPh_3 molecules (thus, with less freedom degrees). The evident autonomy of the silver ions in solution, together with the absence of triphenylphosphine in the cluster, leads us to consider the selective oxidation of the Lewis π-acid triphenylphosphine to triphenylphosphine oxide by the perchlorate anions.

3. Experimental

3.1. Synthesis of $[(PhTe)_4Ag_2Hg_2(Cl)_2]_n$ (**1**)

To a mixture of AgCl (0.036 g, 0.25 mmol) and dimethylphenylphosphine (0.070 g, 0.5 mmol) in 10 mL of dimethyl sulfoxide (DMSO), $Hg(TePh)_2$ (0.158 g, 0.26 mmol) was added. The solution was warmed up at 75 °C under stirring for 1 h, and then was kept still for one month at room temperature. Thereafter, yellow crystals were formed, and were washed with anhydrous ethanol. Yield: 56.3% based on $Hg(TePh)_2$.

Properties: yellow, tabular crystals. *Anal.* Calc. for $C_{24}H_{20}Ag_2Cl_2Hg_2Te_4$ (1506.62): C, 19.13; H, 1.32. Found: C, 19.2; H, 1.29%. Melting point: 165 °C.

3.2. Synthesis of $[(PhTe)_{16}Ag_4Hg_6Py_4] \cdot H_2O$ (**2**)

To a mixture of $AgClO_4$ (0.025 g, 0.125 mmol) and triphenylphosphine (0.066 g, 0.25 mmol) in 10 mL of CH_2Cl_2, $Hg(TePh)_2$ (0.182 g, 0.3 mmol) was added. After 1 h stirring at room temperature, 0.5 mL pyridine was added. In the solution which was kept still, after one week red crystals were formed. Yield: 71% based on $Hg(TePh)_2$.

Properties: red, cubic crystals. *Anal.* Calc. for $C_{116}H_{102}Ag_4Hg_6N_4OTe_{16}$ (5244.64): C, 26.58; H, 1.94; N, 1.04. Found: C, 26.3; H, 1.92; N, 0.09%. Melting point: 127.5 °C.

3.3. X-ray structure determinations

Data were collected with a Bruker APEX II CCD area-detector diffractometer and graphite-monochromatized Mo Kα radiation. The structures were solved by direct methods using SHELXS [26]. Subsequent Fourier-difference map analyses yielded the positions of the non-hydrogen atoms. Refinements were carried out with the SHELXL package [26]. All refinements were made by full-matrix least-squares on F^2 with anisotropic displacement parameters for all non-hydrogen atoms. Hydrogen atoms were included in the refinement in the calculated positions. Crystal data and more details of the data collections and refinements are given in Table 1.

4. Supplementary data

CCDC 685648 and 685649 contains the supplementary crystallographic data for **1** and **2**. These data can be obtained free of charge via http://www.ccdc.cam.ac.uk/conts/retrieving.html, or from the Cambridge Crystallographic Data Centre, 12 Union Road, Cambridge CB2 1EZ, UK; fax: (+44) 1223-336-033; or e-mail: deposit@ccdc.cam.ac.uk.

Acknowledgment

This work was supported with funds from PRONEX-CNPq/FAPERGS (Brazil).

References

[1] D.L. Klein, R. Roth, A.K.L. Lim, A.P. Alivisatos, P.L. McEuen, Nature 389 (1997) 699.
[2] C. Radloff, C.E. Moran, J.B. Jackson, N.J. Halas, in: M.A. Reed, T. Lee (Eds.), Molecular Nanoelectronics, ISBN: 1-58883-006-3, 2003, p. 229.
[3] X. Michalet, A.N. Kapanidis, T. Laurence, F. Pinaud, S. Doose, M. Pflughoefft, S. Weiss, Ann. Rev. Biophys. Biomol. Struct. 32 (2003) 161.
[4] M. Bruchez, M. Moronne, P. Gin, S. Weiss, A. Alivisatos, Science 281 (1998) 2013.
[5] M.W. DeGroot, N.J. Taylor, J.F. Corrigan, Inorg. Chem. 44 (2005) 5447.
[6] A.P. Alivisatos, J. Phys. Chem. 100 (1996) 13226.
[7] A.L. Efros, M. Rosen, Annu. Rev. Mater. Sci. 30 (2000) 475.
[8] M.W. DeGroot, M.W. Cockburn, M.S. Workentin, J.F. Corrigan, Inorg. Chem. 40 (2001) 4678. and references therein.
[9] M.L. Steigerwald, Polyhedron 13 (1994) 1245.
[10] M.L. Steigerwald, T. Siegrist, S.M. Stuczynski, Inorg. Chem. 30 (1991) 4940.
[11] J.G. Brennan, T. Siegrist, S.M. Stuczynski, M.L. Steigerwald, J. Am. Chem. Soc. 112 (1990) 9233.
[12] J.G. Brennan, T. Siegrist, S.M. Stuczynski, M.L. Steigerwald, J. Am. Chem. Soc. 111 (1989) 9240.
[13] J.F. Corrigan, D. Fenske, Angew. Chem., Int Ed. Engl. 36 (1997) 1981.
[14] M. Bettenhausen, A. Eichöfer, D. Fenske, M.Z. Semmelmann, Z. Anorg. Allg. Chem. 625 (1999) 593.
[15] N. Zhu, D. Fenske, J. Chem. Soc., Dalton Trans. (1999) 1067.
[16] D. Fenske, N. Zhu, T. Langetepe, Angew. Chem., Int. Ed. Engl. 37 (1998) 2640.
[17] E. Schulz Lang, M.M. Dias, S.S. Santos, E.M. Vázquez-López, U. Abram, Z. Anorg. Allg. Chem. 630 (2004) 462.
[18] I.D. Sadekov, A.V. Zakharov, Russ. Chem. Rev. 68 (1999) 909.

[19] Y. Okamoto, T. Yano, J. Organomet. Chem. 29 (1971) 99.
[20] E. Schulz Lang, R.A. Zan, C.C. Gatto, R.A. Burrow, E.M. Vázquez-López, Eur. J. Inorg. Chem. 2 (2002) 331.
[21] G.A. Casagrande, E. Schulz Lang, G. Manzoni de Oliveira, M. Hörner, F. Broch, Inorg. Chim. Acta 360 (2007) 1776.
[22] E. Schulz Lang, C. Peppe, R.A. Zan, U. Abram, E.M. Vázquez-López, B. Krumm, O.P. Ruscitti, Z. Anorg. Allg. Chem. 628 (2002) 2815.
[23] E. Schulz Lang, G. Manzoni de Oliveira, D.F. Back, S.S. Santos, Z. Anorg. Allg. Chem. 630 (2004) 730.
[24] D.F. Back, G. Manzoni de Oliveira, R.A. Burrow, E.E. Castellano, U. Abram, E. Schulz Lang, Inorg. Chem. 46 (2007) 2356.
[25] A. Eichhöfer, P. Deglmann, Eur. J. Inorg. Chem. (2004) 349.
[26] G.M. Sheldrick, Acta Crystallogr., Sect. A 64 (2008) 112.
[27] C. Wang, Y. Li, X. Bu, N. Zheng, O. Zivcovic, C.-S. Yang, P. Feng, J. Am. Chem. Soc. 123 (2001) 11506.
[28] M.C. Copsey, A. Panneerselvam, M. Afzaal, T. Chivers, P. O'brien, J. Chem. Soc., Dalton Trans. (2007) 1528.

Table 1
Crystallographic data for **1**, **2** and **2** · CH_2Cl_2

Compound	**1**	**2**	**2** · CH_2Cl_2
Formula	$C_{21}H_6O_{24}Re_6Se_6$	$C_{14}O_{14}Re_4Se_7$	$C_{14}O_{14}Re_4Se_7$, CH_2Cl_2
Formula weight	2233.3	1689.7	1774.6
Wavelength (Å)	0.71073 (Mo Kα)	0.71073 (Mo Kα)	0.71073 (Mo Kα)
Temperature (K)	90.0(2)	296(2)	100.0(2)
Space group	$P6_322$	$P\bar{1}$	$P\bar{1}$
a (Å)	12.70850(10)	9.8896(3)	9.8304(2)
b (Å)	12.70850(10)	12.5609(5)	12.8716(3)
c (Å)	16.4566(3)	12.8091(5)	13.1663(3)
α (°)	90	99.7320(10)	106.7530(10)
β (°)	90	94.4650(10)	97.3490(10)
γ (°)	120	96.2150(10)	93.8380(10)
V (Å^3)	2301.76(5)	1551.53(10)	1572.68(6)
Z	2	2	2
F(000)	1956	1468	1552
D_{calc} (g cm^{-1})	3.222	3.617	3.747
Crystal form, colour	prism, red	plate, red	block, dark red
Crystal size (mm)	0.13 × 0.13 × 0.11	0.06 × 0.06 × 0.02	0.14 × 0.08 × 0.06
μ (cm^{-1})	20.531	23.820	23.674
Diffractometer	Bruker X8Apex CCD	Bruker X8Apex CCD	Bruker X8Apex CCD
Data collection range (°)	1.85–31.38	1.62–27.5	1.95–33.15
	$-16 \rightarrow h \rightarrow 10$	$-9 \rightarrow h \rightarrow 12$	$-14 \rightarrow h \rightarrow 12$
Range of h, k, l	$-13 \rightarrow k \rightarrow 6$	$-16 \rightarrow k \rightarrow 16$	$-19 \rightarrow k \rightarrow 17$
	$-13 \rightarrow l \rightarrow 23$	$-15 \rightarrow l \rightarrow 16$	$-18 \rightarrow l \rightarrow 18$
Number of measured, independent and observed reflections	9894/2191/2080	12073/6956/5315	21024/9015/7671
Criterion for observed reflections	$I > 2\sigma(I)$	$I > 2\sigma(I)$	$I > 2\sigma(I)$
R_{int}	0.0270	0.0246	0.0202
Number of parameters	87	352	379
R	0.0512	0.0280	0.0275
Rw	0.1167	0.0552	0.0683
Weighting scheme	$w = 1/[\sigma^2F_o^2 + 148.1959P]$, where $P = (F_o^2 + 2F_c^2)/3$	$w = 1/[\sigma^2F_o^2 + (0.0179P)^2]$, where $P = (F_o^2 + 2F_c^2)/3$	$w = 1/[\sigma^2F_o^2 + (0.0235P)^2 + 19.3023P]$, where $P = (F_o^2 + 2F_c^2)/3$
Largest peak (e Å^{-3})	4.231	0.946	2.345
Flack parameter	0.05(5)		

solvated 2 · CH_2Cl_2 (first fraction, 12 mg) and of $[Re(CO)_3(H_2O)_3][Re_5(CO)_{18}(Se_2)_3]$ (**1**) (second fraction, 30 mg). IR (ν (CO), CH_2Cl_2): 2108, 2098, 2055, 2035, 2012, 1967 cm^{-1} (**1**) and 2129, 2089, 2022, 1949, 1922 cm^{-1} (**2**).

2.2. X-ray crystallography

Slow evaporation of the respective solutions in dichloromethane yielded red-orange crystals of **1**, and a mixture of **2** and **2** · CH_2Cl_2, suitable for X-ray analysis. Crystallographic data and structure refinement details for the compounds are given in Table 1. All diffraction data were collected on a Bruker X8Apex CCD diffractometer with Mo Kα radiation (λ = 0.71073 Å) using φ and ω scans of narrow (0.5°) frames. All structures were solved by direct methods and refined by full-matrix least-squares method against $|F|^2$ in anisotropic approximation using SHELXTL programs set [12]. Absorption corrections were applied empirically using SADABS program [13]. All non-hydrogen atoms were refined anisotropically.

3. Results and discussion

Hydrogen selenide H_2Se (pK_{a1} = 3.89; pK_{a2} = 11.0 at 25 °C) is a very reactive compound used for dosage of semiconductors with Se and in the synthesis of organoselenium compounds, which is, however, usually avoided by the synthetic inorganic chemists because of its well-known disadvantages including the nasty smell, a high toxicity (exposure limit 0.3 ppm over an 8 h period) and low stability [14]. The dosage of H_2Se in an open-flow system is difficult. To avoid the use of free H_2Se in an open system, we used in situ generated H_2Se, which is quantitatively generated from ZnSe powder with 4 M HCl. As the reaction of ZnSe with HCl of this concentration takes place only at high temperature, a mixture of a reagent, ZnSe and 4 M HCl can be safely placed in a glass tube at room temperature. The tube is then evacuated and sealed, and exactly known amount of H_2Se is then released upon heating. In this way the problem of dosage and disposal of unreacted H_2Se is circumvented [15]. The reaction gives two products, a pentanuclear complex $[Re(CO)_3(H_2O)_3][Re_5(CO)_{18}(Se_2)_3]$ (**1**) (Fig. 1) and a tetranuclear complex $[Re_4(CO)_{14}(Se_2)(Se_5)]$ (**2**) (Fig. 2), which are structurally related. Increasing the Re/Se ratio from 2/3 to 1/3 does

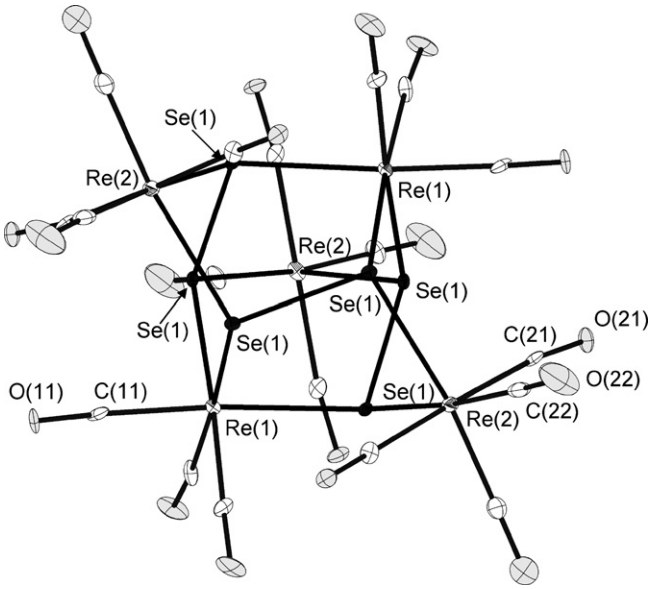

Fig. 1. The anion $[Re_5(Se_2)_3(CO)_{18}]^-$ in crystal structure of **1**, a.d.p. ellipsoids (50% probability). The distances (Å) in Re/Se core are (at 90 K): Re(1)–Se(1) 2.5842(14), Re(2)–Se(1) 2.6206(14), Se(1)–Se(1) 2.430(3).

not influence the yields in this reaction and does not lead to new products.

The first step in the formation of both **1** and **2** is probably substitution of water ligands in $[Re(CO)_3(H_2O)_3]^+$ with H_2Se, followed by deprotonation of coordinated H_2Se to give transient $[Re(CO)_3(SeH)_3]^{2-}$ species. Taking into account that Se^{2-} is strongly reducing even toward protons (E^0 for the Se/H_2Se couple is –0.399 V) [27], it is not difficult to explain oxidative dimerization of two such species into the $[Re_2(CO)_6(Se_2)_3]^{4-}$ central unit, which then acts as centre of coordination for three *cis*-$\{Re(CO)_4\}^+$ groups to give **1**. A deviation from this route gives **2** by incorporation of liberated Se between two of the three Se_2 bridges. Fig. 3 illustrates this putative reaction route. Reaction of $Re_2(CO)_{10}$ with K_2Se_3 was reported to yield a binuclear tetraselenide complex, $[Re_2(CO)_6(Se_4)_2]^{2-}$, where each bridging Se_4^{2-} ligand is chelating bidentate toward one Re and monodentate to the other [28].

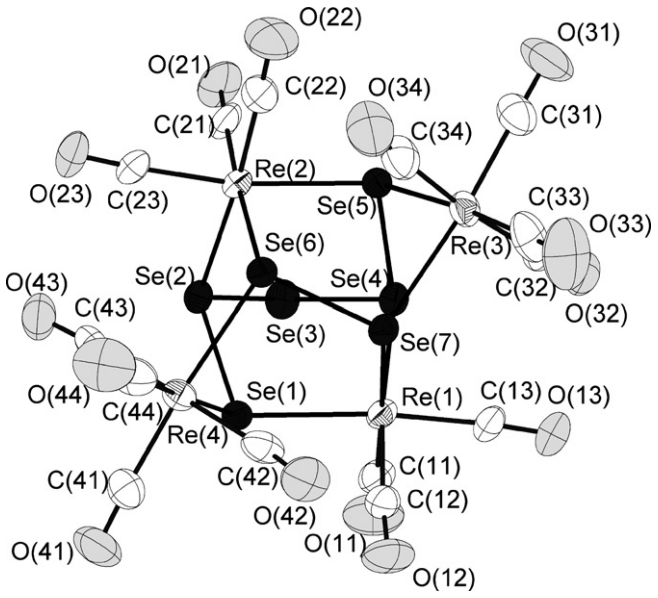

Fig. 2. Molecular fragment $[Re_4(Se_5)(Se_2)(CO)_{14}]$ in crystal structure of **2** · CH_2Cl_2, a.d.p. ellipsoids (50% probability). The numeration scheme is the same in **2** and **2** · CH_2Cl_2. The distances (Å) in Re/Se core are listed for **2** · CH_2Cl_2 (at 100 K): Re(1)–Se(4) 2.5360(6), Re(1)–Se(1) 2.5701(7), Re(1)–Se(7) 2.5888(6), Re(2)–Se(2) 2.5566(7), Re(2)–Se(5) 2.5734(7), Re(2)–Se(6) 2.5863(7), Re(3)–Se(5) 2.6085(6), Re(3)–Se(7) 2.6183(7), Re(4)–Se(6) 2.6002(8), Re(4)–Se(1) 2.6130(7), Se(3)–Se(4) 2.3332(8) Se(3)–Se(2) 2.3463(8) Se(6)–Se(7) 2.4125(8) Se(2)–Se(1) 2.4388(9) Se(5)–Se(4) 2.4430(8).

The structure of **1** contains the well-known *fac*-$[Re(CO)_3(H_2O)_3]^+$ cations [16] (disordered over two positions) and unusual pentanuclear anions $[Re_5(CO)_{18}(Se_2)_3]^-$ (Fig. 1), which can be represented as a distorted trigonal bipyramid of five Re atoms as *fac*-$\{Re(CO)_3\}^+$ and $\{cis$–$Re(CO)_4\}^+$ groups, connected together by three μ_4-Se_2^{2-} bridges (Re(CO)$_3$–Se 2.584 Å, Re(CO)$_4$–Se 2.621 Å, Se–Se 2.430 Å). In $[Cp^*Re(Se_3)(\mu\text{-}Se_2)]_8$ the Se–Se distance in the Re–Se–Se–Re unit is shorter, 2.36–2.38 Å. The difference may reflect the increasing population of the π^*–Se_2 orbital through increasing back donation in the case of the μ_4-Se_2^{2-} binding mode. The 18-electrons rule is satisfied at each Re atom without involving metal-metal bonding, and Re···Re distance are large, about 6 Å between the equatorial atoms, and 4 Å between polar and equatorial Re atoms. The structure of the other product, tetranuclear complex **2** is very similar (the geometrical parameters of the complex in the unsolvated crystal (**2**) and in the solvate (**2** · CH_2Cl_2) is virtually identical), except that one of the $\{Re(CO)_4\}$ groups is replaced with a Se^{2+} so that a pentaselenide Se_5^{2-} ligand results (Fig. 2). In this ligand the two peripheral Se–Se bonds are much longer than the two central ones (2.41, 2.44 Å vs. 2.33, 2.34 Å). While this situation is typical for the coordinated Se_5^{2-} ligand (as, for example, in $[V_2Se_{13}]^{2-}$ [17]), in free Se_5^{2-} the reverse is true: the two central Se–Se bonds are longer than the two peripheral ones [18–20]. This is the first example of a Se_5^{2-} ligand bridging four metal centers.

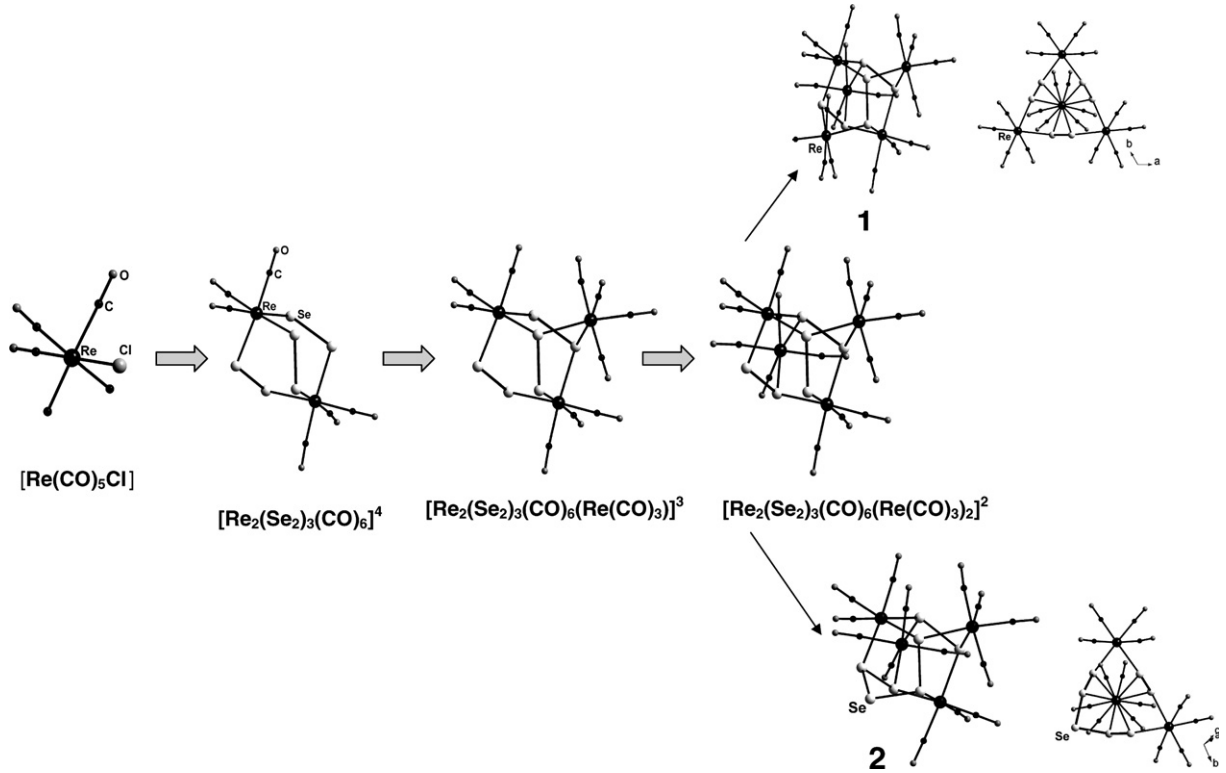

Fig. 3. Tentative scheme fro the formation of $[Re_5(Se_2)_3(CO)_{18}]^-$.

Bridging of three metal atoms is achieved in $[Cu_4Se_{13}]^{2-}$ [20,21]. A similar way of coordination is found, however, for S_5^{2-} in the copper clusters $[Cu_4(\mu_4\text{-}S_5)_2(L)_4]$ (L = Py, 4-Mepy) [22,23]. The Se–Se distance in the diselenide ligand in **2** is also long, 2.41 Å. It is remarkable that the Re and Se framework of **1** and **2**, taken as whole, has exactly the same geometry and connectivity as Zintl anions E_{11}^{3-} (E = As, Sb) which can be explained by taking into account equal number of the cluster skeletal electrons (30) in these species (electronic contributions are zero for $\{Re(CO)_3\}^+$, two for both $\{Re(CO)_4\}^+$ and Se^{2+}, four for E^- and E_2 units in the Zintl anion, and six for Se_2^{2-} [24,25]. Cluster $[Cp_2Ni_2Mn_2(CO)_6(\mu_4\text{-}S_2)(\mu_4\text{-}S_5)]$ has similar structure because the $\{Re(CO)_4\}$ and $\{CpNi\}$ groups contribute the same number of electrons [26].

Thus, a new method of self-assembly of polynuclear selenides based on reaction with in situ generated H_2Se has been introduced. Testing its applicability to other metal carbonyls is under way.

Acknowledgement

The work was supported by the Praesidium of Siberian Branch of Russian Academy of Sciences (Lavrentyev Grant for Young Scientists to EVP).

Appendix A. Supplementary data

CCDC 674976, 674977 and 674978 contain the supplementary crystallographic data for **1**, **2** and **2** · CH_2Cl_2. These data can be obtained free of charge via http://www.ccdc.cam.ac.uk/conts/retrieving.html, or from the Cambridge Crystallographic Data Centre, 12 Union Road, Cambridge CB2 1EZ, UK; fax: (+44) 1223-336-033; or e-mail: deposit@ccdc.cam.ac.uk. Supplementary data associated with this article can be found, in the online version, at doi:10.1016/j.poly.2008.07.021.

References

[1] H.W. Roesky, I. Haiduc, J. Chem. Soc., Dalton Trans. (1999) 2249.
[2] J.W. Gilje, H.W. Roesky, Chem. Rev. 94 (1994) 895.
[3] O.A. Gerasko, E.A. Mainicheva, D.Yu. Naumov, N.V. Kuratieva, M.N. Sokolov, V.P. Fedin, Inorg. Chem. 44 (2005) 4133.
[4] D. Fenske, C.E. Anson, A. Eichhöfer, O. Fuhr, A. Ingendoh, C. Persau, C. Richert, Angew. Chem., Int. Ed. 44 (2005) 5242.
[5] X.-T. Wu, B. Wang, Y.-F. Zhang, J.-X. Liu, Chin. J. Struct. Chem. (Jiegou Huaxue) 7 (1988) 47.
[6] G.-X. Jin, Y. Arikawa, K. Tatsumi, J. Am. Chem. Soc. 123 (2001) 735.
[7] C.G. Pernin, J.A. Ibers, Inorg. Chem. 36 (1997) 3802.
[8] S. Eijsbouts, V.H. de Beer, R. Prins, J. Catal. 109 (1988) 217.
[9] M. Ledoux, O. Michaux, G. Agostina, P. Panissod, J. Catal. 102 (1986) 275.
[10] J.K. Norskov, B.S. Clausen, H. Topsoe, Catal. Lett. 13 (1992) 1.
[11] M. Rakowski DuBois, B. Jagirdar, B. Noll, S. Dietz, in: E.I. Stiefel, K. Matsumoto (Eds.), Transition Metal Sulfur Chemistry, ACS Ser. 653, Oxford University Press, Washington, DC, 1996.
[12] APEX2 (Version 1.08), SAINT (Version 7.03), and SADABS (Version 2.11), Bruker Advanced X-ray Solutions, Bruker AXS Inc., Madison, WI, USA, 2004.
[13] SHELXTL (Version 6.12), Bruker Advanced X-ray Solutions, Bruker AXS Inc., Madison, WI, USA, 2004.
[14] http://www.hse.gov.uk/ria/chemical/h-selen.htm.
[15] P.A. Abramov, M.N. Sokolov, A.V. Virovets, E.V. Peresypkina, V.P. Fedin, J. Clust. Sci. 18 (2007) 597.
[16] H. He, M. Lipowska, X. Xu, A.T. Taylor, M. Carlone, L.G. Marzilli, Inorg. Chem. 44 (2005) 5437.
[17] C.-N. Chau, R.W.M. Wardle, J.A. Ibers, Inorg. Chem. 26 (1987) 2740.
[18] N.E. Brese, C.R. Raundall, J.A. Ibers, Inorg. Chem. 27 (1988) 940.
[19] C.-N. Chau, R.W.M. Wardle, J.A. Ibers, Acta Crystallogr., Sect. C 44 (1988) 803.
[20] P.J. Barrie, R.J.H. Clark, D.-Y. Chung, D. Chakrabarty, M.G. Kanatzidis, Inorg. Chem. 34 (1995) 4299.
[21] J. Cusick, M.L. Scudder, D.C. Craig, I.G. Dance, Polyhedron 8 (1989) 1139.
[22] E. Ramli, T. Rauchfuss, C.L. Stern, J. Am. Chem. Soc. 112 (1990) 4043.
[23] A.F. Hepp, R.M. Richman, S.A. Duraj, M.T. Andras, H.L. Moore, M. Sabat, W.E. Eckles, R.M. Martuch, J. Clust. Sci. 7 (1996) 199.
[24] C. Housecroft, Metal–Metal Bonded Carbonyl Dimers and Clusters, Oxford University Press, 1996.
[25] C. Housecroft, Cluster Molecules of the p-Block Elements, Oxford University Press, 1994.
[26] R.D. Adams, S. Miao, M.D. Smith, H. Farach, C.E. Webster, J. Manson, M.B. Hall, Inorg. Chem. 43 (2004) 2515.
[27] N.N. Greenwood, A. Earnshaw, Chemistry of Elements (1997).
[28] S. O'Neal, W. Pennington, J.W. Kolis, Can. J. Chem. 67 (1989) 1980.

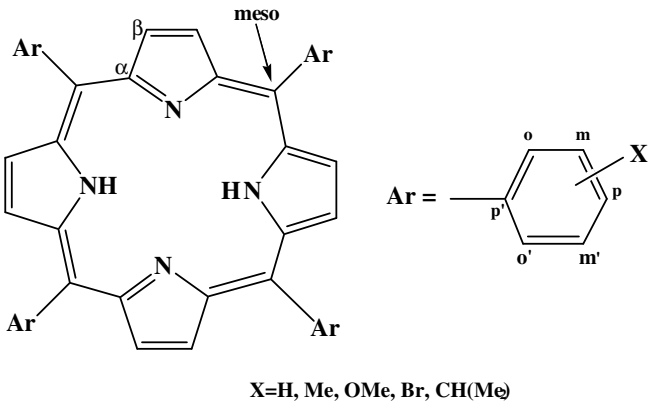

Fig. 1. *Meso*-tetraarylporphyrins, H_2tap.

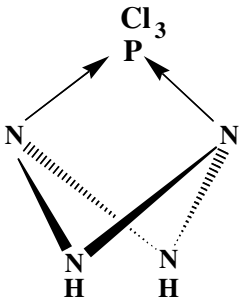

Fig. 2. Only the nitrogens of the distorted porphyrin core are shown.

2.2. Physical measurements

The NMR spectra (^{1}H, ^{13}C) were recorded on a Bruker 400 Ultrashield spectrometer in $CDCl_3$. The ^{31}P NMR spectra were recorded on a Bruker 250 Ultrashield spectrometer in $CDCl_3$ with H_3PO_4 as the reference. The residual $CHCl_3$ in the conventional 99.8% atom $CDCl_3$ gives a signal at δ = 7.26 ppm, which was used for calibration of the chemical shift scale. The UV–Vis measurements were obtained with a GBC cintra 6 UV–Vis spectrophotometer. FT-IR spectra were recorded on a Magna 550 Nicolet spectrometer using KBr pellets. The molar conductance of the complexes and the diprotonated species were measured on a METROHM 644 conductometer.

2.3. Preparation of the i-SAT complexes

To H_2tap (1 mmol) in a mortar, PCl_3 (1 mmol) was added with grinding at ambient temperature for 20 min, without addition of any solvent until complexation was completed. The porphyrins were completely converted to the i-SAT complexes. The completion of the reactions was determined by UV–Vis and ^{1}H NMR spectroscopies. The 1:1 mixture of the porphyrins with PCl_3 did not show the absorption bands or ^{1}H NMR signals due to the free base porphyrins. The results of elemental analysis for the i-SAT complexes are presented in Table 1.

Table 1
The results of elemental analyses for the i-SAT complexes

i-SAT complexes	Found (calculated)		
	%C	%H	%N
[PCl_3(H_2tpp)]	69.9 (70.3)	3.8 (3.4)	7.4 (7.4)
[PCl_3(H_2t(4-OMep)p)]	65.7 (66.1)	4.3 (4.4)	6.4 (6.4)
[PCl_3(H_2t(4-Mep)p)]	71.0 (71.4)	4.5 (4.7)	6.9 (6.9)
[PCl_3(H_2t(4-Brp)p)]	61.2 (61.5)	2.8 (3.0)	6.3 (6.5)
[PCl_3(H_2t(4-CH(Me)$_2$p)p)]	72.6 (73.1)	5.6 (5.9)	5.9 (6.1)
[PCl_3(H_2t(3-OMep)p)]	65.8 (66.1)	4.1 (4.4)	6.3 (6.4)
[PCl_3(H_2t(3-Mep)p)]	70.9 (71.3)	4.5 (4.7)	6.7 (6.9)
[PCl_3(H_2t(3-Brp)p)]	61.1 (61.5)	2.8 (3.0)	6.4 (6.5)

3. Results and discussion

The SAT complexation was followed by monitoring the changes in the ^{1}H NMR and UV–Vis spectra. These changes are due to adduct formation between different equivalents (0.25, 0.5, 0.75, 1.0, 1.5 and 2.0) of PCl_3 and H_2tpp until a 1:1 (PCl_3:H_2tpp) molar ratio, where addition of an excess amount of PCl_3 caused no changes in the spectra of the [PCl_3(H_2tpp)] complex. Consequently the reactants have a 1:1 molar ratio in the i-SAT complexes. This subject also was confirmed by elemental analysis.

In the free base H_2tap, the N–H protons are upfield (−2.74 to −2.82 ppm, singlet) and the β-protons appear in the range of 8.85–8.90 ppm (singlet) (Table 2). The i-SAT complexation of *meso*-tetraarylporphyrins with PCl_3, similar to the molecular complexation of the porphyrins with various acceptors, caused downfield shifts for the proton signals of N−H and the aryl rings, and an upfield shift of the β-hydrogens [16–23]. These observations indicate that binding of phosphorus(III) to the pyrrolenine nitrogen atoms distorts the porphyrin ring and as a result the ring current is lost in the i-SAT complexes. Distortion of the porphyrin ring leads to an extension of the aryl π-system whereupon there are downfield shifts of the proton signals of the aryl rings. The presence of a singlet signal for the β-protons in the ^{1}H NMR spectra of the complexes do not corresponded the unsymmetrical pyrrole rings in the proposed structure. This shows that ring inversion of the tilted core conformation of the porphyrin is probably fast on the NMR timescale [16,17,23]. The results of the ^{1}H NMR spectral data for NH and H_β of the *meso*-tetraarylporphyrins and the complexes are listed in Table 2.

In the ^{13}C NMR spectrum of H_2tpp six sharp signals for the porphine core and aryl rings are observed (120.5 (C_{meso}), 127.1 ($C_{m,m'}$), 128.1 (C_p), 131.5 (C_β), 135.0 ($C_{o,o'}$), *142.6* ($C_{p'}$) ppm), along with very broad signal (145 ppm) for the α-carbon [20,21]. The i-SAT complexation of H_2tpp with PCl_3 leads to changes in the ^{13}C NMR spectrum of the porphyrin. After complexation peaks were revealed at 122.6 (C_{meso}), 128.0 (C_β), 128.4 ($C_{m,m'}$), 130.0 (C_p), 139.0 ($C_{o,o'}$), *139.9* ($C_{p'}$) and 146.0 (C_α) ppm. The observed changes upon the i-SAT complexation of the *meso*-tetraarylporphyrins with PCl_3 are very similar to the molecular complexation of the porphyrins with different acceptors [16,17,20,21].

The UV–Vis spectrum of H_2tpp has absorption bands at 416.7(S), 516.8, 551.5, 592.0, 648.0 nm, whereas the related complex with PCl_3 shows two new absorption bands at 444.5 (soret) and 660.0 nm. Upon addition of PCl_3 to the free base H_2tpp, the UV–Vis spectrum of the porphyrin is 12–28 nm red shifted. This is interpreted as evidence for the increased resonance interaction of the aryl rings with the porphyrin nucleus in going from the free base to the i-SAT complex, which would be allowed by the deformation of the pyrroles [16,17]. The results of UV–Vis spectra for the other complexes are shown in Table 3.

UV–Vis, ^{1}H NMR and ^{13}C NMR correspondences between spectral data of the molecular complexes of σ- or π-acceptors with *meso*-tetraarylporphyrins and [PCl_3(H_2tap)] complexes suggest similar structures for the porphyrin core in all of the species [16–23]. In this conformation the lone pairs of two pyrrolenine nitrogens act as electron donors to the phosphorus atom of PCl_3, and so two hydrogen atoms of the pyrrole groups (N–H) still remain on the macrocycle (Fig. 2).

The UV–Vis and ^{1}H NMR spectral data of the complexation of substituted *meso*-tetraarylporphyrins with PCl_3 (Tables 2 and 3) showed that the π-resonance is greater than σ-induction effects,

Table 2
^{1}H NMR spectral data of different *meso*-tetraarylporphyrins and [PCl_3(H_2tap)] complexes

i-SAT complexes	N–H	H_β	H_o	$H_{o'}$	H_m	$H_{m'}$	H_p	X
H_2tpp	−2.76	8.85	8.21, 8.24		7.75–7.77		7.75–7.77	
[PCl_3(H_2tpp)]	0.29	8.59	8.61, 8.63		7.97–8.04		7.97–8.04	
$\Delta\delta$	3.05	−0.26	0.40		0.22		0.22	
H_2t(4-OMep)p	−2.75	8.86	8.11, 8.14		7.27, 7.31			4.10
[PCl_3(H_2t(4-OMep)p)]	0.40	8.50	8.53, 8.55		7.54, 7.56			4.18
$\Delta\delta$	3.15	−0.36	0.42		0.27			0.08
H_2t(4-Mep)p	−2.77	8.85	8.08, 811		7.54, 7.56			2.70
[PCl_3(H_2t(4-Mep)p)]	0.32	8.55	8.48, 8.50		7.81, 7.83			2.78
$\Delta\delta$	3.09	−0.30	0.40		0.27			0.08
H_2t(4-Brp)p	−2.82	8.89	8.11, 8.14		7.74			
[PCl_3(H_2t(4-Brp)p)]	0.40	8.62	8.47, 8.49		8.12, 8.17			
$\Delta\delta$	3.22	−0.27	0.36		0.38			
H_2t(4-CH(Me)$_2$p)p	−2.74	8.87	8.12, 8.15		7.59, 7.62			CH = 3.20–3.32, Me = 1.54, 1.57
[PCl_3(H_2t(4-CH(Me)$_2$p)p)]	0.06	8.55	8.49, 8.51		7.83, 7.85			CH = 3.29–3.34, Me = 1.57, 1.59
$\Delta\delta$	2.80	−0.32	0.37		0.24			0.09 0.03
H_2t(3-OMep)p	−2.75	8.90	7.80–7.85			7.65-7.70	7.35–7.37	4.10
[PCl_3(H_2t(3-OMep)p)]	0.22	8.62	8.17			7.90	7.52	4.16
$\Delta\delta$	2.97	−0.28	0.37			0.25	0.17	0.06
H_2t(3-Mep)p	−2.75	8.88	8.06–8.10			7.64-7.67	7.60–7.62	2.67
[PCl_3(H_2t(3-Mep)p)]	0.15	8.61	8.42			7.77	7.89	2.85
$\Delta\delta$	2.90	0.27	0.36			0.13	0.29	0.18
H_2t(3-Brp)p	−2.80	8.87	8.38	8.14, 8.16		7.65	7.95	
[PCl_3(H_2t(3-Brp)p)]	0.31	8.63	8.85	8.52, 8.53		7.91	8.12, 8.14	
$\Delta\delta$	3.11	0.24	0.47	0.38		0.26	0.17	

$\Delta\delta$: chemical shifts of the proton signals for the porphyrins upon i-SAT complexation with PCl_3.

Table 3
UV–Vis spectral data of the different *meso*-tetraarylporphyrins and [PCl_3(H_2tap)] complexes in $CHCl_3$

i-SAT complexes	λ_{max} (nm)	
H_2tpp	416.7(S), 516.8, 551.5, 592.0, 648.0	
[PCl_3(H_2tpp)]	444.5	660.0
$\Delta\lambda$[a]	27.8	12.0
H_2t(4-OMep)p	419.5(S), 520.5, 557.1, 596.0, 653.0	
[PCl_3(H_2t(4-OMep)p)]	453.5(S)	687.7
$\Delta\lambda$[a]	34.0	34.7
H_2t(4-Mep)p	418.3(S), 518.4, 554.0, 593.0, 649.0	
[PCl_3(H_2t(4-Mep)p)]	447.1(S)	670.2
$\Delta\lambda$[a]	28.8	21.2
H_2t(4-Brp)p	418.1(S), 514.3, 550.1, 590.5, 646.5	
[PCl_3(H_2t(4-Brp)p)]	449.2(S)	665.1
$\Delta\lambda$[a]	31.1	18.6
H_2t(4-CH(Me)$_2$p)p	419.7(S), 519.2, 555.1, 594.4, 650.4	
[PCl_3(H_2t(4-CH(Me)$_2$p)p)]	448.3(S)	670.2
$\Delta\lambda$[a]	28.6	19.8
H_2t(3-OMep)p	418.9(S), 517.0, 550.3, 590.3, 646.6	
[PCl_3(H_2t(3-OMep)p)]	450.9(S)	660.8
$\Delta\lambda$[a]	32.0	14.2
H_2t(3-Mep)p	418.2(S), 517.5, 550.6, 590.0, 647.2	
[PCl_3(H_2t(3-Mep)p)]	445.4(S)	661.7
$\Delta\lambda$[a]	27.2	14.5
H_2t(3-Brp)p	418.3(S), 514.4, 548.2, 590.1, 647.3	
[PCl_3(H_2t(3-Brp)p)]	447.1(S)	655.7
$\Delta\lambda$[a]	28.8	8.4

(S): soret band.
[a] $\Delta\lambda$: red shifts for the bands of the porphyrins upon i-SAT complexation.

and so the trend in electron donating ability for the substituted *meso*-tetraarylporphyrins is *para* > *meta*. This trend corresponds to lower steric hindrance from the *meta* substituents compared to the *para* substituents. On the other hand, halogens are σ-electron withdrawing and π-donor groups. With these substituents the π-effect is more efficacious than the σ-effect. Further, the 4-isopropyl group is a greater electron donor than the 4-methyl group.

The ^{31}P NMR spectra were used to confirm the coordination of phosphorus(III) chloride to the porphyrins. The proton-decoupled ^{31}P NMR spectra (85% H_3PO_4 external reference) gave signals at 220 ppm and 5.5 ppm for PCl_3 and the [PCl_3(H_2t(4-Mep)p)] complex, respectively. The produced upfield shift upon the i-SAT complexation of PCl_3 with H_2t(4-Mep)p demonstrates the proposed structure for the new complex (a five-coordination number for the phosphorus atom), (Fig. 2).

The FT-IR spectrum of the free base (H_2tap) shows an N–H stretching band at 3320 cm^{-1} [24], that upon i-SAT complexation with PCl_3 does not shift considerably. This indicates that two protons remain on the complexed porphyrins and this completely corresponds to the proposed structure, (Fig. 2).

The UV–Vis and (^{1}H, ^{13}C) NMR spectra of the i-SAT complexes of *meso*-tetraarylporphyrins with PCl_3 are similar to those of the related porphyrin diprotonated species [16,17,25–27]. However, the molar conductivity results for the i-SAT complexes and those diprotonated species were completely different. For example, the molar conductance of [PCl_3(H_2tpp)] (in acetone) shows that the complex is not an electrolyte, whereas the molar conductance of [H_4tpp]Cl_2 is in accord with a 1:2 electrolyte (Λ (in methanol) = 213.3 Ω^{-1} cm^2 mol^{-1}) [28]. The remarkable spectral correspondence between the i-SAT complexes and the diprotonated species thus suggest only an analogous tilted porphyrin core structure in these species.

4. Conclusion

An investigation of the sitting-atop complexation between *meso*-tetraarylporphyrins and phosphorus(III) chloride has been carried out in this study. Using phosphorus(III) chloride and free solvent conditions has led to the formation of i-SAT complexes, $[PCl_3(H_2tap)]$. Two pyrrolic protons of the porphyrins prohibit the phosphorus atom from going into the centre of the porphyrin plane and in result it resides above the ring plane.

Acknowledgment

This work was partly supported by the Kashan University Research Council.

References

[1] E.I. Sagun, E.I. Zenkevich, V.N. Knyukshto, A.M. Shulga, D.A. Starukhin, C. von Borczyskowski, Chem. Phys. 275 (2002) 211.
[2] F. Lu, Polyhedron 26 (2007) 3939.
[3] Z. Valicsek, O. Horvath, J. Photochem. Photobiol. 186 (2007) 1.
[4] E.B. Fleischer, J.H. Wang, J. Am. Chem. Soc. 82 (1960) 3498.
[5] J.P. Macquet, T. Theophahanides, Can. J. Chem. 51 (1973) 219.
[6] K. Letts, R.A. Mackay, Inorg. Chem. 14 (1975) 2993.
[7] E.B. Fleischer, F. Dioxn, Bioinorg. Chem. 7 (1977) 129.
[8] Y. Shen, U. Ryde, Inorg. Biochem. 98 (2004) 878.
[9] Y. Hsiao, U. Ryde, Inorgan. Chim. Acta 359 (2006) 1081.
[10] Y. Inada, Y. Sugimoto, Y. Nakano, Y. Itoh, S. Funahashi, Inorg. Chem. 37 (1998) 5519.
[11] H. Dehghani, M.R. Mansournia, Polyhedron 27 (2008) 849.
[12] H. Dehghani, M. Payam, M.R. Mansournia, Polyhedron 27 (2008) 2416.
[13] M. Gouterman, H. Sayer, E. Shankl, J.P. Smith, Inorg. Chem. 20 (1981) 87.
[14] A.M.d'A.R. Gonsalves, J.M.T.B. Varejao, M.M. Pereira, J. Heterocycl. Chem. 28 (1991) 635.
[15] A.D. Adler, F.R. Longo, J.H. Finarelli, J. Goldmacher, J. Assour, L. Korsakoff, J. Org. Chem. 32 (1967) 476.
[16] H. Dehghani, A.R. Ansari Sardrood, Polyhedron 26 (2007) 4263.
[17] H. Dehghani, A.R. Ansari Sardrood, Bull. Chem. Soc. Jpn. 80 (2007) 518.
[18] H. Dehghani, F. Fathi, Dyes Pigments 77 (2008) 323.
[19] H. Dehghani, F. Fathi, J. Porphyrins Phthalocyanines 11 (2007) 742.
[20] D. Mohajer, H. Dehghani, J. Chem. Soc., Perkin Trans. 2 (2000) 199.
[21] D. Mohajer, H. Dehghani, Bull. Chem. Soc. Jpn. 73 (2000) 1477.
[22] D. Mohajer, S. Rayati, New J. Chem. 27 (2003) 242.
[23] D. Mohajer, S. Zakavi, S. Rayati, M. Zahedi, N. Safari, H.R. Khavasi, S. Shahbazian, New J. Chem. 28 (2004) 1600.
[24] H.H. Limbach, J. Henning, J. Stulz, J. Chem. Phys. 78 (1983) 5432.
[25] R.I. Walter, E.C.A. Ojadi, H. Linschitz, J. Phys. Chem. 97 (1993) 13308.
[26] M. Meot-Ner, A.D. Adler, J. Am. Chem. Soc. 97 (1975) 5107.
[27] A. Stone, E.B. Fleischer, J. Am. Chem. Soc. 90 (1968) 2735.
[28] W.J. Geary, Coord. Chem. Rev. 7 (1971) 81.

as well as in their conformations. It is important to note that in 'unit A' V(V) is hexa-coordinated, while in 'unit B' it is penta-coordinated. Again, when HL_2 reacts with $Cu(ClO_4)_2 \cdot 6H_2O$ in 1:1 molar ratio, complex $[Cu(L_2)ClO_4]$ (**3**) is formed. All attempts to prepare X-ray quality crystals produced micro crystals which were not suitable for X-ray diffraction. The elemental analyses and spectral data fit with the composition $[Cu(L_2)ClO_4]$ (**3**). Upon reaction with $VO(acac)_2$ in 1:1 molar ratio HL_2 produced the hexa-coordinated V(V) $[VO(L_2)(OCH_3)(CH_3OH)]$ (**4**) complex.

2. Experimental

2.1. Materials

All chemicals were of reagent grade, purchased from commercial sources and used without further purification. Tetraethyl ammonium perchlorate (TEAP) used for electrochemical work was prepared as reported in the literature [23]. Salicylaldehyde was purchased from Aldrich Chemical Company, USA and used without further purification.

Caution! Although we have not encountered any problem, it should be kept in mind that perchlorate compounds of metal ions are potentially explosive especially in the presence of organic ligands. Only a small amount of the material should be prepared and it should be handled with care.

2.2. Physical measurement

Elemental analyses (carbon, hydrogen and nitrogen) of the ligand and the metal complexes were determined with a Perkin–Elmer CHN analyzer 2400 at the Indian Association for the Cultivation of Science, Kolkata. The molar conductance values of the complexes were measured in purified CH_3OH with a Systronic model 304 digital conductivity meter. The electronic spectra of the complexes in methanolic solution were recorded on a Hitachi model U-3501 spectrophotometer. IR spectra (KBr pellet, 400–4000 cm^{-1}) were recorded on a Perkin–Elmer model 883 infrared spectrophotometer. ^1H NMR spectra of the ligands were recorded in $CDCl_3$ with a Bruker AM 300L (300 MHz) superconducting FTNMR. Cyclic voltammetry was carried out with a Sycopel model AEW2 1820F/L instrument. The measurements were carried out at 293 K in CH_3OH solution containing 0.2 M TEAP as supporting electrolyte and 10^{-3}–10^{-4} M solution of the respective complexes deoxygenated by bubbling with nitrogen. The working, counter and reference electrodes used were a Pt wire, platinum coil and an SCE, respectively.

2.3. Synthesis of ligands

Ethyl-5-methyl-1-(2-pyridyl)pyrazole-3-carboxylate was prepared following a literature method [24]. Methyl-5-methyl-1-(4,6-dimethyl-2-pyrimidyl)pyrazole-3-carboxylate has been synthesized by passing dry HCl gas into the solution of 5-methyl-1-(4,6-dimethyl-2-pyrimidyl)pyrazole-3-carboxylic acid [25] in dry methanol following the usual procedure. The corresponding carbohydrazides were prepared by the reaction between hydrazine hydrate and the respective ester in methanol taken in a 1:1 molar ratio. Salicylaldehyde was condensed with the synthesised carbohydrazides taken in 1:1 molar ratio (Scheme 1). Details are described below.

The two ligands HL_1 and HL_2 were synthesized in a similar way by refluxing a methanolic solution (30 cm^3) of ethyl-5-methyl-1-(2-pyridyl)pyrazole-3-carbohydrazide (2.17 g, 10 mmol) and methyl-5-methyl-1-(4,6-dimethyl-2-pyrimidyl)pyrazole-3-carbohydrazide (2.46 g, 10 mmol), respectively, with salicylaldehyde (1.22 g, 10 mmol), also taken in methanol (10 cm^3). Reflux was continued for ca. 30 min at water bath temperature. After slow evaporation of the respective reaction mixture a solid microcrystalline compound separated. It was filtered off, washed several times with cold methanol and dried in vacuo over fused $CaCl_2$.

Single crystals of HL_1 and HL_2, suitable for X-ray diffraction were obtained by slow evaporation of the respective methanolic solution of the ligands.

HL_1: Yield: 2.71 g (80%); M.p. (°C) 140; *m*/*z* 321 (M^+, 100%); *Anal.* Calc. for $C_{17}H_{15}N_5O_2$: C, 63.50; H, 4.67; N, 21.80. Found: C, 63.40; H, 4.64; N, 21.78%. ^1H NMR ($CDCl_3$, δ): 7.27–8.48 (m, 4H, $-C_5H_4N$), 6.72 (s, 1H, ring pz-H), 2.67(s, 3H, ring pz-CH_3), 8.67 (s, 1H, –CH=N–), 6.89–7.41 (m, 4H, $-C_6H_4$), 12.01 (s, 1H, aromatic-OH). IR (KBr, cm^{-1}): 1570 (py $\nu_{C=N}$), 1470 (pz $\nu_{C=N}$), 3175 (ν_{OH}), 1648 ($\nu_{C=O}$), 1546 ($\nu_{C=C}$).

HL_2: Yield: 3.13 g (85%); M.p. (°C) 152; *m*/*z* 350 (M^+, 100%); *Anal.* Calc. for $C_{18}H_{18}N_6O_2$: C, 61.71; H, 5.14; N, 24. Found: C, 61.50; H, 5.02; N, 23.85.78%. ^1H NMR ($CDCl_3$, δ): 2.49 (s, 6H, pym-CH_3), 2.59 (s, 3H, ring pz-CH_3), 6.69 (s, 1H, ring pz-H), 7.30

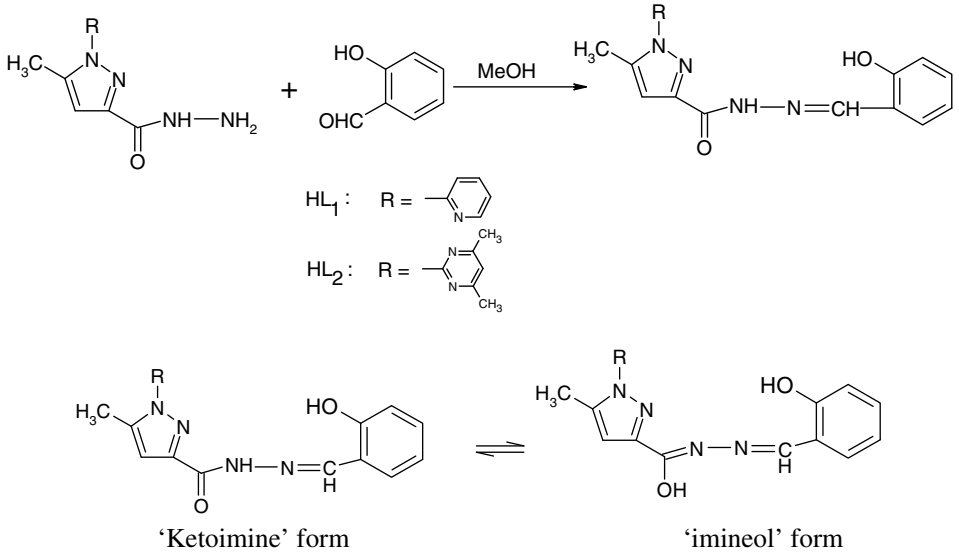

Scheme 1.

(s, 1H, ring pym-H), 8.69 (s, 1H, –CH=N–), 12.15 (s, 1H, aromatic-OH). IR (KBr, cm^{-1}): 1606 (pym $\nu_{C=N}$), 1460 (pz $\nu_{C=N}$), 3175 (ν_{OH}), 1650 ($\nu_{C=O}$), 1546 ($\nu_{C=C}$).

2.4. Preparation of the complexes

2.4.1. Preparation of complex **1**

To a solution of HL_1 (0.321 g, 1 mmol) in methanol (10 cm^3), $Cu(ClO_4)_2 \cdot 6H_2O$ (0.371 g, 1 mmol) taken in the same solvent was added dropwise with constant stirring. Immediately, the solution turned deep green and stirring was continued for ca. 15 min. A green coloured compound separated out from the reaction mixture. This was filtered under suction, washed with methanol and dried over fused $CaCl_2$. X-ray quality crystals were obtained by slow evaporation of acetonitrile solution of the complex. Yield, 0.484 g (70%). *Anal.* Calc. for $C_{19}H_{17}N_6O_6ClCu$: C, 43.48; H, 3.24; N, 16.02. Found: C, 43.50; H, 3.19; N, 16.01%. IR (KBr, cm^{-1}): 1567 (py $\nu_{C=N}$), 1465 (pz $\nu_{C=N}$), 1660 ($\nu_{C=O}$), 1540 ($\nu_{C=C}$), 1092 ($\nu_{ClO_4^-\ coordinated}$). UV–Vis ($CH_3OH$): $\lambda_{max/nm}$: 406, 669. λM (MeOH, $ohm^{-1}\ cm^2\ mol^{-1}$): 22. μ_{eff} (at 298 K): 1.70 B.M.

2.4.2. Preparation of complex **2**

To a solution of HL_1 (0.321 g, 1 mmol) in methanol (10 cm^3), $VO(acac)_2$ (0.265 g, 1 mmol) taken in the same solvent was added with continuous stirring. The resulting colour of the solution was violet and stirring was continued for ca. 1 h. The solution was filtered and the filtrate was kept for slow evaporation. After two days, X-ray quality crystals of the complex were separated and they are collected by usual technique. Yield: 0.381 g (65%). *Anal.* Calc. for $C_{37}H_{36}N_{10}O_9V_2$: C, 51.23; H, 4.15; N, 16.15. Found: C, 51.15; H, 4.01; N, 16.12%. IR (KBr, cm^{-1}): 1560 (py $\nu_{C=N}$), 1463 (pz $\nu_{C=N}$), 970 ($\nu_{V=O}$). UV–Vis (CH_3OH): $\lambda_{max/nm}$: 398. λM (MeOH, $ohm^{-1}\ cm^2\ mol^{-1}$): 20. μ_{eff} (at 298 K): 0 B.M.

2.4.3. Preparation of complex **3**

A methanolic solution of (5 cm^3) of $Cu(ClO_4)_2 \cdot 6H_2O$ (0.371 g, 1 mmol) was added dropwise to a solution of HL_2 (0.350 g, 1 mmol) in the same solvent (10 cm^3) with constant stirring. The solution became deep green and it was filtered and the filtrate was kept for slow evaporation. After a few days a green microcrystalline compound was isolated. All attempts to prepare X-ray quality crystals were futile. Yield: 0.484 g (70%). *Anal.* Calc. for $C_{18}H_{17}N_6O_6ClCu$: C, 42.10; H, 3.50; N, 16.37. Found: C, 42.15; H, 3.58; N, 16.35%. IR (KBr, cm^{-1}): 1611 (pym $\nu_{C=N}$), 1535 (pz $\nu_{C=N}$), 1650 ($\nu_{C=O}$), 1095 ($\nu_{ClO_4^-\ coordinated}$). UV–Vis ($CH_3OH$): $\lambda_{max/nm}$: 398. λM (MeOH, $ohm^{-1}\ cm^2\ mol^{-1}$): 25. μ_{eff} (at 298 K): 1.72 B.M.

2.4.4. Preparation of complex **4**

To a solution of HL_2 (0.350 g, 1 mmol) in methanol (10 cm^3), $VO(acac)_2$ (0.265 g, 1 mmol) taken in the same solvent was added with stirring. A deep violet solution was obtained and stirring was continued for ca. 1 h. The solution was filtered and kept for slow evaporation. After a few days, crystals suitable for X-ray diffraction were obtained. Yield: 0.461 g (75%). *Anal.* Calc. for $C_{20}H_{23}N_6O_5V$: C, 50.17; H, 4.81; N, 17.56. Found: C, 50.10; H, 4.75; N, 17.58%. IR (KBr, cm^{-1}): 1610 (pym $\nu_{C=N}$), 1547 (pz $\nu_{C=N}$), 970 ($\nu_{V=O}$). UV–Vis (CH_3OH): $\lambda_{max/nm}$: 399. λM (MeOH, $ohm^{-1}\ cm^2\ mol^{-1}$): 21. μ_{eff} (at 298 K): 0 B.M.

2.5. Single crystal X-ray crystallography

Crystal data of HL_1, HL_2, **1**, **2** and **4** have been deposited in CCDC. Selected crystal data for HL_1, HL_2, **1**, **2** and **4** are given in Table 1 and selected metrical parameters of these complexes are given in Table 2. Oxford Diffraction Gemini (for HL_1, **1** and **2**) and CCD area detector (for HL_2, **4**) equipped with graphite monochromated Mo Kα radiation (λ = 0.71073 Å) source in φ and ω scan mode were

Table 1
Experimental data for crystallographic analysis

Compound	Ligand HL_1	Ligand HL_2	Complex **1**	Complex **2**	Complex **4**
Empirical formula	$C_{17}H_{15}N_5O_2$	$C_{19}H_{22}N_6O_3$	$C_{19}H_{17}ClCuN_6O_6$	$C_{37}H_{36}N_{10}O_9V_2$	$C_{20}H_{23}N_6O_5V$
Formula weight	321.34	382.43	524.38	866.64	478.38
Temperature (K)	200 (2)	100(2)	296(2)	296(2)	103(2)
Wavelength (Å)	0.71073	0.71073	0.71073	0.71073	0.71073
Crystal system	tetragonal	monoclinic	triclinic	triclinic	monoclinic
Space group	$I4_1/a$	$P2_1/c$	$P\bar{1}$	$P\bar{1}$	$P2_1/n$
Unit cell dimensions					
a (Å)	19.4328(7)	7.0441(6)	8.1028(7)	11.5894(16)	7.6194(12)
b (Å)	19.4328(7)	15.9399(14)	9.996(4)	12.8800(19)	26.049(4)
c (Å)	17.0010(9)	16.7412(15)	13.0421(9)	14.5735(12)	10.9363(17)
α (°)			82.705(15	88.370(9)	
β (°)		90.716(2)	82.601(7)	70.701(10)	101.353(2)
γ (°)			89.656(15)	68.940(13)	
Volume (Å^3)	6420.2(5)	1879.6(3)	1039.0(4)	1905.9(4)	2128.1(6)
Z	16	4	2	2	4
D_{calc} (Mg/m^3)	1.330	1.351	1.676	1.510	1.493
Absorption coefficient (mm^{-1})	0.092	0.095	1.232	0.560	0.512
$F(000)$	2688	808	534	892	992
Crystal size (mm^3)	0.41 × 0.32 × 0.30	0.70 × 0.28 × 0.28	0.44 × 0.41 × 0.35	0.49 × 0.41 × 0.27	0.56 × 0.46 × 0.20
θ Range (°) for data collection	4.69–32.56	1.76–30.59	4.59–32.55	4.63–32.57	1.56–30.82
Index ranges	$-29 \leqslant h \leqslant 24$	$-9 \leqslant h \leqslant 10$	$-12 \leqslant h \leqslant 12$	$-17 \leqslant h \leqslant 17$	$-10 \leqslant h \leqslant 10$
	$-24 \leqslant k \leqslant 29$	$-22 \leqslant k \leqslant 21$	$-15 \leqslant k \leqslant 14$	$-18 \leqslant k \leqslant 19$	$-35 \leqslant k \leqslant 35$
	$-25 \leqslant k \leqslant 24$	$-23 \leqslant k \leqslant 23$	$-18 \leqslant k \leqslant 19$	$-20 \leqslant k \leqslant 21$	$-15 \leqslant k \leqslant 15$
Goodness-of-fit on F^2	0.766	1.068	0.848	1.075	1.138
Completeness to θ = 25.00° (%)	99.3	99.5	99.1	98.6	98.7
Independent reflections (R_{int})	5432 (0.0499)	5671 (0.0305)	6917 (0.0410)	12345 (0.0236)	6084 (0.0578)
Data/restraints/parameters	5432/0/219	5671/0/256	6917/20/337	12345/0/529	6084/0/297
Reflections collected	19787	21304	16065	26265	22714
Final R indices [$I > 2\sigma(I)$]	R_1 = 0.0402,	R_1 = 0.0700,	R_1 = 0.0397,	R_1 = 0.0394,	R_1 = 0.0868,
	wR_2 = 0.0861	wR_2 = 0.1855	wR_2 = 0.0890	wR_2 = 0.0954	wR_2 = 0.2168
R indices (all data)	R_1 = 0.1667,	R_1 = 0.0873,	R_1 = 0.1078,	R_1 = 0.0762,	R_1 = 0.0992,
	wR_2 = 0.1068	wR_2 = 0.1964	wR_2 = 0.1013	wR_2 = 0.1175	wR_2 = 0.2229
Largest difference peak and hole (e Å^{-3})	0.145 and −0.152	0.581 and −0.531	0.493 and −0.338	0.399 and −0.415	2.059 and −1.228

Table 2
Selected bond distances (Å) and angles (°) involving HL_1, HL_2 **1**, **2** and **4**

Selected bonds (Å)		Values	Selected angles (°)	Values
HL_1	O(2)–C(8)	1.2272(14)		
	O(1)–C(2)	1.3567(16)		
	N(2)–H(2A)	0.88		
	N(1)–N(2)	1.3714(14)		
	N(5)–C(13)	1.3125(15)		
	N(4)–C(13)	1.4248(15)		
	N(3)–N(4)	1.3578(13)		
	N(1)–C(7)	1.2762(17)		
HL_2	O(2)–C(8)	1.217(2)		
	O(1)–C(1)	1.361(2)		
	N(2)–H(2B)	0.88		
	N(1)–N(2)	1.373(2)		
	N(5)–C(13)	1.333(2)		
	N(6)–C(13)	1.330(2)		
	N(3)–N(4)	1.357(2)		
	N(1)–C(7)	1.282(3)		
1	Cu–O(1)	1.8462(10)	O(1)–Cu–N(1)	96.66(5)
	Cu–N(3)	1.8942(12)	N(3)–Cu–N(1)	89.69(5)
	Cu–N(1)	1.9642(14)	N(3)–Cu–N(5)	78.76(5)
	Cu–N(5)	2.0246(14)	O(1)–Cu–N(5)	94.73(5)
2	V(1)–O(2A)	1.5856(14)	O(1A)–V(1)–N(1A)	83.18(6)
	V(1)–O(3A)	1.7630(12)	O(5A)–V(1)–N(1A)	73.82(5)
	V(1)–O(1A)	1.8481(14)	O(3A)–V(1)–O(5A)	95.58(6)
	V(1)–O(5A)	1.9645(13)	O(3A)–V(1)–O(1A)	102.00(6)
	V(1)–N(1A)	2.1435(13)	O(2A)–V(1)–O(4A)	175.13(7)
	V(1)–O(4A)	2.3140(13)	O(3B)–V(2)–N(1B)	74.44(5)
	V(2)–O(2B)	1.5762(15)	O(1B)–V(2)–N(1B)	82.83(5)
	V(2)–O(4B)	1.7660(13)	O(4B)–V(2)–O(1B)	95.76(6)
	V(2)–O(1B)	1.8390(12)	O(2B)–V(2)–N(1B)	95.61(7)
	V(2)–O(3B)	1.9319(12)	O(2B)–V(2)–O(3B)	110.93(7)
	V(2)–N(1B)	2.0860(14)	O(2B)–V(2)–O(4B)	106.45(8)
			O(2B)–V(2)–O(1B)	108.34(7)
4	V–O	1.600(3)	O(1)–V–N(1)	84.64(12)
	V–O(1M)	1.800(3)	O(2)–V–N(1)	75.12(11)
	V–O(1)	1.876(3)	O–V–O(2M)	172.92(13)
	V–O(2)	1.967(3)	O(1M)–V–O(2)	92.32(12)
	V–N(1)	2.113(3)	O(1M)–V–O(1)	102.83(13)
	V–O(2M)	2.331(3)		

used for data collection. Cell parameters refinement and data reduction were carried out using the CRYSALIS RED, Oxford Diffraction Ltd., [Version 1.171.32.5 (release 08-05-2007 CRYSALIS171 .NET) and Version 1.171.31.8 (release 12-01-2007 CrysAlis171.NET)] [26a] for HL_1, **1** and **2**, respectively. Bruker SMART [26b] and Bruker SAINT softwares [27] were used for cell parameters refinement and data reduction of HL_2 and complex **4**. All the structures were solved by conventional direct methods and refined by full-matrix least square methods using F^2 data. SHELXS-97 and SHELXL-97 programs [28] were used for structure solution and refinement, respectively. Positions of H-atoms were treated as riding on their parent atoms.

3. Results and discussion

3.1. Syntheses

Two new ligands HL_1 and HL_2 were synthesized by the 1:1 condensation reaction of Salicylaldehyde with ethyl-5-methyl-1-(2-pyridyl)pyrazole-3-carbohydrazide/methyl-5-methyl-1-(4,6-dimethyl-2-pyrimidyl)pyrazole-3-carbohydrazide in methanol, respectively. The complexation behaviour of these ligands towards Cu(II) and V(V) were investigated. All the complexes (**1**–**4**) of these ligands were obtained from a refluxing mixture of the respective ligand and the appropriate metal salts, taken in a 1:1 molar proportion in methanol. X-ray quality crystals of these complexes (**1**, **2** and **4**) were obtained upon slow evaporation of the respective reaction mixture at room temperature. The ligands were characterized primarily by X-ray crystallography along with the elemental analyses, IR and ^{1}H NMR spectroscopy. The metal complexes were characterized by elemental analyses, solution electrical conductivity, magnetic susceptibility, IR, UV–Vis spectroscopy. X-ray crystallographic studies are made for **1**, **2** and **4**. The results are consistent with the proposed mononuclear formulations. The complexes were found to be fairly soluble in most common organic solvents. Molar conductivity values of the complexes are in accord with non-electrolytic behaviour of the complex species.

3.2. Description of crystal structure

3.2.1. Structural descriptions of HL_1 and HL_2

Perspective view of the asymmetric units of the ligands HL_1, HL_2 and the complexes **1**, **2** and **4** with the atom numbering schemes are shown in Figs. 1–5, respectively. Selected metrical parameters are listed in Table 2. The ligands HL_1 and HL_2 crystallize with the space groups $I4_1/a$ and $P2_1/c$, respectively. In the molecular structure, pyridyl/pyrimidyl–pyrazole and salicylaldehyde moieties adopt a trans orientation to each other leaving the O2 and O1 atoms in cis position. In the free ligand moiety HL_1, pyridine nitrogen (N5) and pyrazole nitrogen (N3) are trans to each other. During chelation, they rearrange to cis fashion in complex **1**. In HL_1 the dihedral angle between pyridine and pyrazole plane is 4.93°, whereas in HL_2 that between pyrimidine and pyrazole plane is 4.60° showing that the pyridyl–pyrazole part in HL_1 and pyrimidyl–pyrazole part in HL_2 are almost planar. The planarity is almost retained after complexation in the 'unit B' of complex **2** (dihedral angle 10.16°) and in complex **4** (dihedral angle 10.75°). However, in the 'unit A' of complex **2** a marked deviation from planarity (dihedral angle 33.56°) in the same portion of the ligand is noted.

Both HL_1 and HL_2 are stabilized through a network of weak H-bond interactions (Figs. 6 and 7, respectively). Relevant H-bond parameters are listed in Table 3.

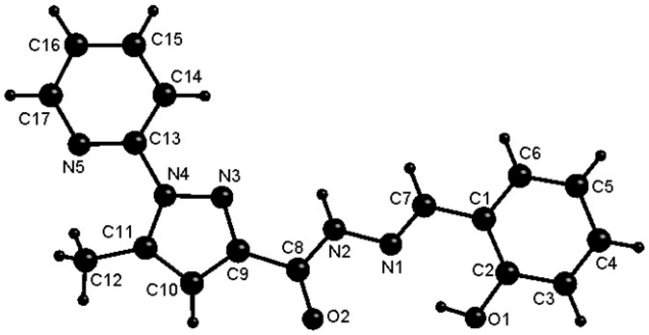

Fig. 1. Structural representation with atom numbering scheme of HL_1.

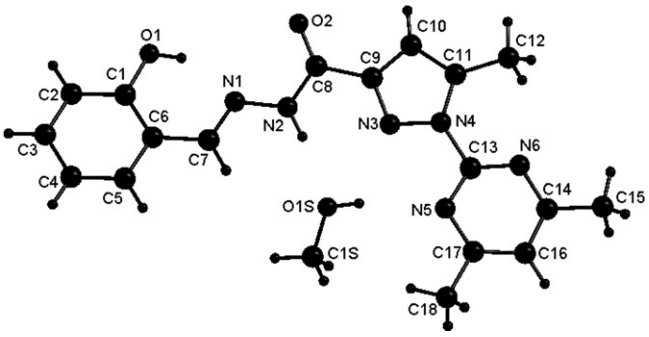

Fig. 2. Structural representation with atom numbering scheme of HL_2.

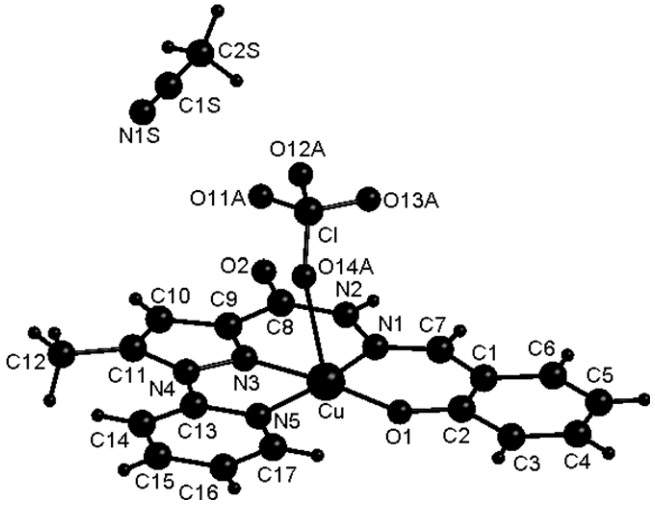

Fig. 3. Structural representation with atom numbering scheme of **1**.

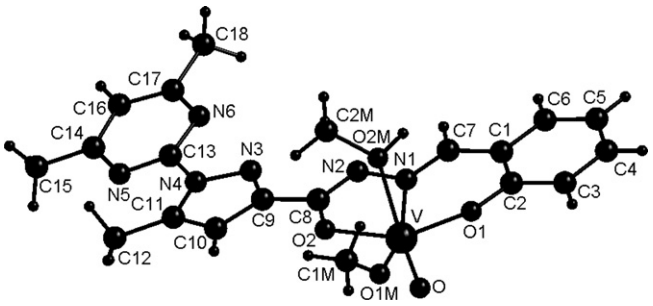

Fig. 5. Structural representation with atom numbering scheme of **4**.

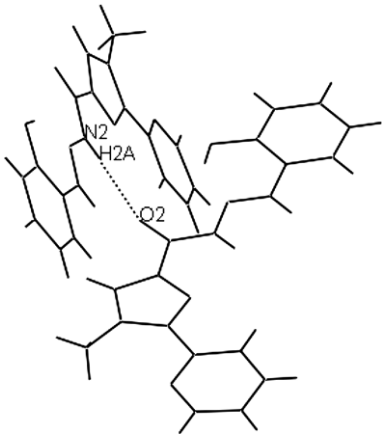

Fig. 6. H-bonding in HL_1.

3.2.2. Structural description of ***1***

Complex **1** crystallizes in space group $P\bar{1}$. The coordination geometry around Cu(II) atom is slightly distorted square pyramidal, where four equatorial positions are occupied by three nitrogen atoms (N5 of pyridine, N3 of pyrazole and N1 of azomethine nitrogen) and one phenoxide oxygen (O1) of salicylaldehyde part while the axial position is occupied by one oxygen atom (O14A) of perchlorate anion. The unit cell of **1** comprises of two molecules. HL_1 ligand forms one five membered and two six membered chelate rings with the Cu(II) metal centre. The bond angle of N3–Cu–N5 deviates maximum [78.76(5)°] from the ideal bond angle of 90°, due to formation of five membered chelate ring, where as least deviation is observed for the angle N3–Cu–N1 [89.69(5)°]. Among the four equatorial bonds Cu–O1 is the shortest [1.8462(10) Å] whereas Cu–N5 is the longest [2.0246(14) Å]. The shortest distance is due to the formation of strong bond between Cu(II) and negatively charged oxygen atom. The axial Cu–O14A bond is 2.606 Å which is much longer than the Cu–O1 equatorial bonds although both oxygen atoms are uninegative. This proves that the phenoxide oxygen is stronger donor centre than the perchlorate oxygen. The Cu-atom is shifted through a distance of 0.052 Å upward beyond the basal plane towards the ClO_4^- unit. The τ-value (0.08) [29] for complex **1** implies that the central copper atom sits in an almost square pyramidal geometry.

The complex **1** is stabilized through a network of hydrogen bonding (Fig. 8). It shows that there is a weak H-bond interaction between H2A and O2 atoms [d(D···A) 2.8012(19) Å] of the two adjacent molecules lying parallel.

3.2.3. Structural descriptions of ***2*** and ***4***

Complex **2** crystallizes in space group $P\bar{1}$ while **4** in space group $P2_1/c$. Unit cells of both **2** and **4** comprise of four molecules. The

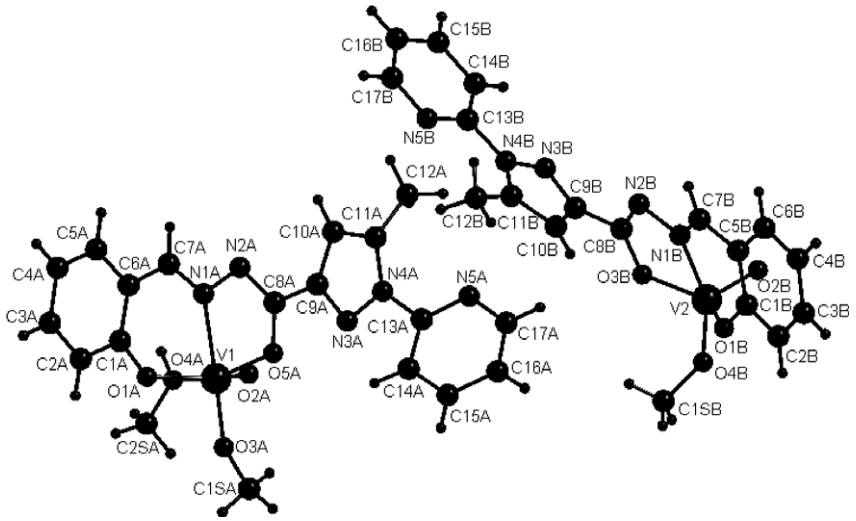

Fig. 4. Structural representation with atom numbering scheme of **2**.

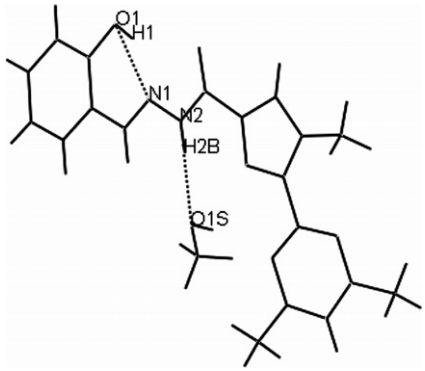

Fig. 7. H-bonding in HL_2.

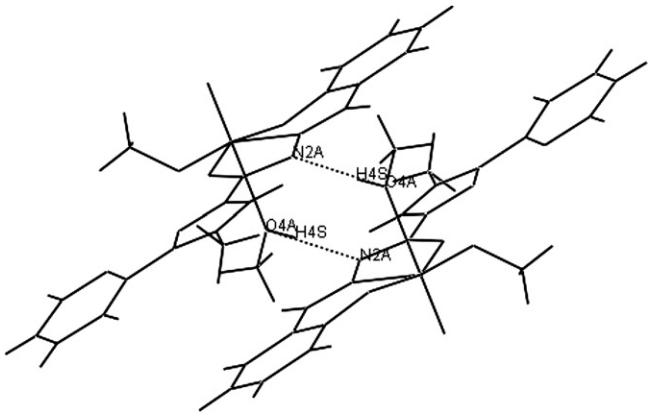

Fig. 9. H-bonding in **2**.

Table 3
Details of hydrogen bond distances (Å) and angles (°)

D–H···A		d(D–H)	d(H···A)	d(D···A)	∠(DHA)
HL_1	O(1)–H(1)···N(1)	0.84	1.87	2.6033(13)	145.4
	N(2)–H(2A)···O(2)#1	0.88	2.14	2.9568(14)	153.8
HL_2	O(1)–H(1)···N(1)	0.84	1.88	2.613(2)	145.6
	O(1S)–H(1S)···N(3)	0.84	2.32	2.835(2)	119.9
	N(2)–H(2B)···O(1S)	0.88	1.97	2.850(2)	172.9
1	N(2)–H(2A)···O(2)#1	0.86	1.95	2.8012(19)	173.4
2	O(4A)–H(4S)···N(2[a])#1	0.82	1.95	2.7670(18)	174.3
4	O(2M)–H(2M)···N(6)#1	0.86(6)	2.04(6)	2.883(4)	164(5)

Symmetry transformations used to generate equivalent atoms:
#1: $y + 3/4, -x + 3/4, z - 1/4$ for HL_1.
#1: $-x + 2, -y + 1, -z - 1$ for **1**.
#1: $-x, -y + 1, -z + 1$ for **2**.
#1: $-x, -y, -z + 1$ for **4**.

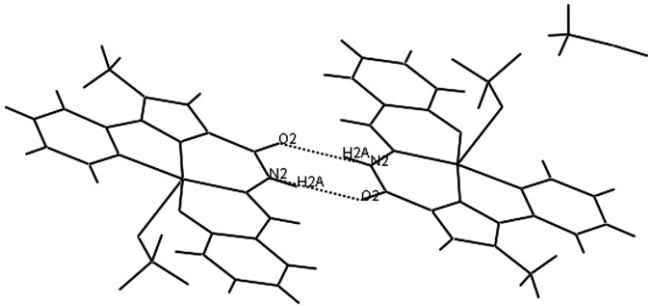

Fig. 8. H-bonding in **1**.

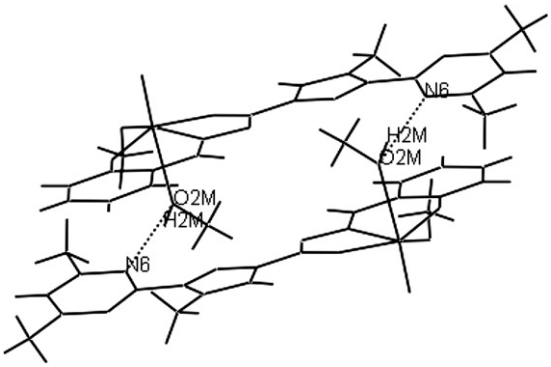

Fig. 10. H-bonding in **4**.

asymmetric unit of **2** contains two independent molecules. Here it is interesting to note that in 'unit A', V(V) is hexa-coordinated while in 'unit B', it is penta-coordinated. The vanadium atoms in the two units (A and B) are separated by a distance of 13.632 Å. For 'unit A', the vanadium atom is in distorted octahedral geometry, where four equatorial positions are satisfied by three oxygen atoms (deprotonated enol oxygen O5A, phenoxide oxygen O1A and methoxy oxygen O3A) and one azomethine nitrogen (N1A) atom, while two axial positions are occupied by two oxygen atoms (one terminal oxo group (O2A) and one methanol oxygen atom (O4A)). In 'unit B', the vanadium atom like copper atom in **1** is also in distorted square pyramidal geometry. Here four equatorial positions are occupied by three oxygen atoms (deprotonated enol oxygen O3B, phenoxide oxygen O1B and methoxy oxygen O4B) and one azomethine nitrogen (N1B) and the axial coordination is completed by one terminal oxo group (O2B). Thus the two vanadium atoms in the same asymmetric unit face the same donor environment with the exception of one extra coordinated methanol moiety in 'unit A' which is absent in 'unit B'. The methanol moiety accounts for the different coordination geometry around the two vanadium atoms. However, compared to penta-coordinated copper atom in **1**, the penta-coordinated V-atom in 'unit B' of **2** experiences a greater extent of deviation from the ideal square pyramidal geometry. This is evidenced by the calculation of τ-value ($\tau = 0.35$ compared to 0.08 in **1**). In complex **4**, vanadium(V) atom is in distorted octahedral environment similar to that in 'unit A' of **2**. The vanadium atom is displaced almost equally out of the mean basal plane in 'unit A' of **2** and in **4** (0.290 Å for 'unit A' of **2** and 0.285 Å for **4**) but the displacement is almost doubled for 'unit B' of **2** (0.508 Å). The V=O distances are 1.5856(14) Å for 'unit A', 1.5762(15) Å for 'unit B' of **2** and 1.600(3) Å for **4**, which are same as normal V=O distance of 1.595 Å. The V1–N1A distance 2.1435(13) Å in 'unit A' and V2–N1B distance 2.0860(14) Å in 'unit B' of **2** and V–N1 distance 2.113(3) Å in **4** are in accordance with literature values for V–N distances [30,31].

In 'unit A' of **2** there is a weak intermolecular H-bond interaction through H(4S) and N(2A) between two molecules (Fig. 9). In complex **4**, a weak intermolecular H-bond exists between H(2M) atom of one molecule and N(6) of another (Fig. 10). The details are presented in Table 3.

4. Characterization of the complex species

The V(V) complexes have been prepared employing a V(IV) starting material such as $VO(acac)_2$. Molecular dioxygen from air serves as the oxidant during the course of the reaction. The V-complexes (**2** and **4**) are diamagnetic in nature.

Table 4
Summary of electrochemical data for complexes **1**, **2**, **3** and **4**

Complex	E_{pc} (V) (Cu^{II}/Cu^{I})	E_{pa} (V) (Cu^{II}/Cu^{III})	E_{pc} (V) (Cu^{III}/Cu^{II})	ΔE (V)	E_{pc} (V) (V^{V}/V^{IV})	E_{pa} (V) (V^{V}/V^{IV})
1	−0.467	0.480	0.367	0.113		
2				0.196	−0.172	−0.024
3	−0.623	0.466	0.291	0.175		
4				0.394	−0.302	−0.092

4.1. Electronic spectra

The electronic solution spectra of the complexes were recorded in CH_3OH solution. Complex **1** shows a pyridine → Cu charge transfer band at 406 nm. A broad characteristic band at 669 nm may be due to the slightly distorted square pyramidal environment around Cu(II) centre [32]. Complex **3** shows $N_{(pym)}$ → Cu charge transfer band at 398 nm. The spectral feature of **3** is quite similar to that of **1**. This implies that like **1**, **3** also bear the central Cu atom in almost square pyramidal geometry. The electronic spectra of the vanadium complexes (**2** and **4**) exhibit one intense band near 400 nm, which is assigned to L–V(dπ) LMCT transition [33].

5. Electrochemistry

The cyclic voltammetry of the Cu(II) complexes **1** and **3** are studied in CH_3OH solution in the potential range −1.5 to +1.5 V. For all the complexes, the most important electrochemical data associated with the metal centres are listed in the Table 4. Complex **1** shows an irreversible reductive response associated with Cu(II)/Cu(I) at −0.46 V. In case of complex **3** the same peak is obtained at −0.62 V. None of the complexes shows the characteristic reduction peak for Cu(I)/Cu(0) in the same potential window. In the anodic scan of complex **1**, couple of quasireversible nature is obtained for Cu(II)/Cu(III) process at 0.42 V. For complex **3**, the irreversible peak for Cu(II)/Cu(III) is obtained at 0.38 V (for complex **1** ΔE = 0.113 V and for complex **3** ΔE = 0.175 V). Complex **2** shows an irreversible one-step, one-electron response at −0.098 V (ΔE = 0.196V), corresponding to V(V)/V(IV) reduction. Although two different peaks are expected in the same direction of the scan due to the different coordination environment around the two V(V) centres, the appearance of only one cathodic peak and one anodic peak infer that $E_{1/2}$ value is coordination insensitive. The mono oxo alkoxo V(V) complex **4** shows an irreversible one electron reductive response at −0.197 V (ΔE = 0.394 V).

6. Concluding remarks

We have prepared Cu(II) and V(V) complexes of HL_1 and HL_2 where HL_1 and HL_2 are pyridyl/pyrimidyl–pyrazole derived Schiff base ligands, respectively. In complex **1** the HL_1 ligand in its 'keto-imine' form behaves as mononegative NNNO tetradentate one utilizing all the possible nitrogen donor centres (pyridine N, pyrazole N and azomethine N). In complex **2**, HL_1 ligand in its 'imineol' form acts as tridentate dianionic ONO donor where the heterocyclic nitrogen atoms remain non-coordinated, instead the deprotonated enol oxygen atom participates in the game. This is to fulfill the differential preference for donor sites by the two different metal atoms. Cu(II) being a borderline acid prefers relatively less harder N-donor centre while O-donor centre being the harder one is preferred by hard V(V) cation. Thus to avail the oxygen as donor centre, HL_1 undergoes tautomerisation to its 'imineol' form followed by deprotonation during complexation with V(V). Further, in the asymmetric unit of complex **2**, two different coordination geometry around two V(V) centres have been observed with the same ligand HL_1. In 'unit A', V(V) is hexa-coordinated employing a methanoate species, a methanol moiety and one oxo group apart from the tridentate ligand unit, whereas in 'unit B' the same metal atom is penta-coordinated using the same donor environment except the coordinated methanol moiety. In **4**, the vanadium(V) atom sits in the distorted octahedral coordination pocket formed by one tridentate ONO binegative ligand molecule (HL_2), one oxo group, one methoxy group and one methanol moiety. Likewise HL_1, the HL_2 ligand is expected to behave similarly regarding its donor sites towards Cu(II) centre in **3** which is concluded from the similar spectral features of **1** and **3**. As a concluding remark, it is stated that the two similar ligands produce the identical coordination environment towards Cu or V, but these similar environments for these two different metal atoms differ from each other.

Acknowledgements

The authors thank to University Grants Commission, New Delhi, India, for financial assistance (JRF to T.N.M.). S.R. also thanks to CSIR for awarding SRF (Sanc. No. 09/028 (0698)/2008-EMR-1, dated 14.03.2008).

Appendix A. Supplementary data

CCDC 692613, 692614, 692615, 692616 and 692617 contain the supplementary crystallographic data for HL_1, HL_2, **1**, **2** and **4**. These data can be obtained free of charge via http://www.ccdc.cam.ac.uk/conts/retrieving.html, or from the Cambridge Crystallographic Data Centre, 12 Union Road, Cambridge CB2 1EZ, UK; fax: (+44) 1223-336-033; or e-mail: deposit@ccdc.cam.ac.uk. Supplementary data associated with this article can be found, in the online version, at doi:10.1016/j.poly.2008.07.024.

References

[1] (a) M.B. Davies, Coord. Chem. Rev. 164 (1997) 27;
(b) D.R. Smith, Coord. Chem. Rev. 172 (1998) 457.
[2] W. Zieshen, L. Zhiping, Y. Zhenhaun, Transition Met. Chem. 18 (1993) 291.
[3] B.G. Malmstrom, J. Leckner, J. Curr. Opin. Chem. Biol. 2 (1998) 286.
[4] E.I. Solomon, U.M. Sundaram, T.E. Machonkin, Chem. Rev. 96 (1996) 2563.
[5] E.I. Solomon, P. Chen, M. Metz, S.K. Lee, A.E. Palmer, Angew. Chem., Int. Ed. 40 (2001) 4570.
[6] E.I. Solomon, F. Tuczek, D.E. Root, C.A. Brown, Chem. Rev. 94 (1994) 827.
[7] P.M. Colman, H.C. Freeman, J.M. Guss, M. Murata, V.A. Norris, J.A.M. Ramshaw, M.P. Venkatappa, Nature 272 (1978) 319.
[8] R. Durley, L.Y. Chen, F.S. Mathews, V.L. Davidson, Protein Sci. 2 (1993) 739.
[9] P.J. Hart, A.M. Nersissian, R.G. Herrmann, R.M. Nalbandyan, J.S. Valentine, D. Eisenberg, Protein Sci. 5 (1996) 2175.
[10] N. Shibata, T. Inoue, C. Nagano, N. Nishio, T. Kohzuma, K. Onodera, F. Yoshizaki, Y. Sugimura, Y. Kai, J. Biol. Chem. 274 (1999) 4225.
[11] J.N. Chan, Z.Y. Huang, M.E. Merrifield, M.T. Salgado, M. Stillman, J. Coord. Chem. Rev. 233 (2002) 319.
[12] D. Rehder, Angew. Chem., Int. Ed. 30 (1991) 148.
[13] A. Butler, C.J. Carrano, Coord. Chem. Rev. 109 (1991) 61.
[14] R.R. Eady, Coord. Chem. Rev. 237 (2003) 23. and references cited therein.
[15] (a) M. Weyand, H.J. Heeht, M. Kiess, M.F. Liaud, H. Vilter, D.J. Schomburg, Mol. Biol. 293 (1999) 595;
(b) J.N. Carter-Franklin, J.D. Parrish, R.A. Tehirret-Guth, R.D. Little, A. Butler, J. Am. Chem. Soc. 125 (2003) 3688;
(c) D. Rehder, G. Santoni, G.M. Licini, C. Schulzke, B. Meier, Coord. Chem. Rev. 237 (2003) 53.
[16] (a) D. Rehder, J.C. Pessoa, C.F. Geraldes, J. Biol. Inorg. Chem. 7 (2002) 675;
(b) D.C. Crans, L. Yang, J.A. Alfano, L.H. Chi, W. Jin, M. Mahroof-Tahir, K. Robbins, M.M. Toloue, L.K. Chan, A.J. Plante, R.Z. Grayson, G.R. Willsky, Coord. Chem. Rev. 237 (2003) 13;
(c) S.A. Dikanov, B.D. Liboiron, C. Orvig, J. Am. Chem. Soc. 124 (2002) 2969;
(d) H. Sakurai, Y. Kojima, Y. Yoshikawa, K. Kawabe, H. Yasui, Coord. Chem. Rev. 226 (2002) 187.
[17] (a) D.C. Crans, J.J. Smee, in: J.A. McCleverty, T.J. Meyer (Eds.), Comprehensive Coordination Chemistry II, vol. 4, Elsevier, New York, 2004, p. 175;
(b) C.J. Carranon, C.M. Nunn, R. Quan, J.A. Bonadies, V.L. Pecoraro, Inorg. Chem. 29 (1990) 944–951;
(c) M. Moon, M. Pyo, Y.C. Myoung, C. Ahn, M.S. Lah, Inorg. Chem. 40 (2001) 554.

[18] (a) C. Grüning, H. Schmidt, D. Rehder, Inorg. Chem. Commun. 2 (1999) 57;
(b) M.R. Maurya, S. Khurana, C. Schulzke, D. Rehder, Eur. J. Inorg. Chem. (2001) 779;
(c) C. Kimblin, X. Bu, A. Butler, Inorg. Chem. 41 (2002) 161.
[19] W. Wei, Z. Fu-Li, W. Xin, T. Min-Yu, Polyhedron 15 (1996) 1699.
[20] M.R. Maurya, Coord. Chem. Rev. 237 (2003) 163.
[21] (a) S. Roy, T.N. Mandal, A.K. Barik, S. Pal, S. Gupta, A. Hazra, R.J. Butcher, A.D. Hunter, M. Zeller, S.K. Kar, Polyhedron 26 (2007) 2603;
(b) S. Roy, T.N. Mandal, A.K. Barik, S. Pal, R.J. Butcher, M.S. El Fallah, J. Tercero, S.K. Kar, Dalton Trans. (2007) 1229.
[22] (a) S. Roy, T.N. Mandal, A.K. Barik, S. Gupta, R.J. Butcher, M. Nethaji, S.K. Kar, Polyhedron 27 (2008) 593;
(b) A. Hazra, A.K. Barik, S. Pal, S. Gupta, S. Roy, R.J. Butcher, S.M. Peng, G.H. Lee, S.K. Kar, Polyhedron 26 (2007) 773;
(c) S. Gupta, A.K. Barik, S. Pal, A. Hazra, S. Roy, R.J. Butcher, S.K. Kar, Polyhedron 26 (2007) 133.
[23] D.T. Sawyer, J.L. Roberts, Experimental Electrochemistry for Chemists, Wiley, New York, 1974. p. 212.
[24] N. Adhikari, S. Chowdhury, R.J. Butcher, N. Saha, Polyhedron 18 (1999) 1323.
[25] N. Adhikari, N. Saha, J. Indian Chem. Soc. 83 (2006) 427.
[26] (a) Oxford Diffraction, CRYSALIS CCD and CRYSALIS RED. Versions 1.171.32. Oxford Diffraction Ltd, Abingdon, Oxfordshire, England, 2007.;
(b) Bruker, SMART v 5.631, Bruker AXS Inc., Madison, WI, 2001.
[27] Bruker, SAINT v7.34A, Bruker AXS Inc., Madison, WI, 2005.
[28] G.M. Sheldrick, SHELXS-97 and SHELXL-9, University of Göttingen, Göttingen, 1997.
[29] A.W. Addison, T.N. Rao, J. Reedijk, J. Rijn, G.C. van Verschoor, J. Chem. Soc., Dalton Trans. (1984) 1349.
[30] H. Schmidt, M. Bashirpoor, D. Rehder, J. Chem. Soc., Dalton Trans. (1996) 865.
[31] G. Asgedom, A. Sreedhara, J. Kivikoski, E. Kolehmainen, C.P. Rao, J. Chem. Soc., Dalton Trans. (1996) 93.
[32] S. Gupta, S. Pal, A.K. Barik, A. Hazra, S. Roy, T.N. Mandal, S.-M. Peng, G.-H. Lee, M.S.E. Fallah, J. Tercero, S.K. Kar, Polyhedron 27 (2008) 2519.
[33] R. Dinda, P. Sengupta, S. Ghosh, T.C.W. Mak, Inorg. Chem. 41 (2002) 1684.

*2.2.1. Synthesis of [$PdCl_2(Y^1)_2$] (**1a**) general procedure*

To a saturated solution of $PdCl_2$ (0.049 g, 0.28 mmol) in acetonitrile (10 ml) was added solid Y^1 (0.198 g, 0.55 mmol), and the suspension was stirred for 15 min. The resulting brown solution was concentrated (2 ml) and diethyl ether (10 ml) was added to precipitate the brown solid **1a**. *Anal.* Calc. for $C_{48}H_{50}Cl_2O_2P_2Pd$: C, 64.19; H, 5.61. Found: C, 64.0; H, 5.79%. Yield 0.185 g (75%), m.p. 170–172 °C. IR (KBr disk) ν (cm^{-1}): 1643 (C=O), 1599, 1498, 1399, 1347, 1293, 1191, 1147, 1104, 1020, 966, 873, 806 (P–C), 763, 658. ^1H NMR ($CDCl_3$) δ_H (ppm): 2.25 (3H, s, $COCH_3$), 2.39 (9H, s, $3CH_3$), 5.09 (br, *CH*), 7.26–7.66 (12H, m, arom.). ^{31}P NMR ($CDCl_3$) δ_P (ppm): 23.52 and 23.38 (2s, at 25 °C), 23.50 (1s, at 55 °C). ^{13}C NMR ($CDCl_3$) δ_C (ppm): 22.13 (s, $3CH_3$), 32.63 (d, $^3J_{PC}$ = 16.38 Hz, $COCH_3$), 119.28 (d, $^1J_{PC}$ = 149.8 Hz, *p*-tolyl, (*ipso*)), 135.04 (d, $^2J_{PC}$ = 7.35 Hz, *p*-tolyl, (*ortho*)), 130.15 (d, $^3J_{PC}$ = 21.64 Hz, *p*-tolyl, (*meta*)), 135.12 (d, $^4J_{PC}$ = 7.35 Hz, *p*-tolyl, (*para*)), 205.16 (*CO*).

*2.2.2. Data for [$PdCl_2(Y^2)_2$] (**1b**)*

Orange solid. *Anal.* Calc. for $C_{54}H_{46}Cl_2O_4P_2Pd$: C, 64.11; H, 4.89. Found: C, 64.97; H, 4.64%. Yield 0.217 g (78%), m.p. 184–186 °C. IR (KBr disk) ν (cm^{-1}): 1683 (C=O), 1435, 1285, 1128, 1106, 836 (P–C), 801, 741, 688. ^1H NMR (DMSO-d_6) δ_H (ppm): 4.95 (s, CH_2, minor diastereoisomer) 5.10 (s, CH_2, major diastereoisomer) 5.36 (bd, $^2J_{PH}$ = 14.33 HZ, *CH*, two diastereoisomers), 7.22–7.81 (20H, m, arom.). ^{31}P NMR (DMSO-d_6) δ_P (ppm): 19.83 (trans, minor diastereoisomer), 20.80 (trans, major diastereoisomer), 27.84 (cis, minor diastereoisomer), 28.09 (cis, major diastereoisomer). ^{13}C NMR (DMSO-d_6) δ_C (ppm): 28.61 (d, $^1J_{PC}$ = 52.24 Hz, *CH*, minor diastereoisomer), 29.38 (d, $^1J_{PC}$ = 56.75 Hz, CH, major diastereoisomer), 64.94 (s, CH_2, minor diastereoisomer), 67.62 (s, CH_2, major diastereoisomer), 115.79–136.05 (arom.), 164.19 (*CO*, minor diastereoisomer), 170.45 (*CO*, major diastereoisomer).

*2.2.3. Synthesis of [Pd{CH{P(C_7H_6)(p-tolyl)$_2$}$COCH_3$}(μ-Cl)]$_2$ (**2a**) general procedure*

To a suspension of $PdCl_2$ (0.090 g, 0.51 mmol) in acetonitrile (20 ml) was added solid Y^1 (0.376 g, 1.02 mmol). The mixture was refluxed for 8 h and then allowed to cool to room temperature. The suspension was filtered and the solid was washed with diethyl ether (10 ml) to give a greenish-yellow solid as product **2a**. The phosphonium salt [(*p*-tolyl)$_3$PCH_2COCH_3]Cl separated, as a by-product, via the mother liquor by washing solid **2a**. *Anal.* Calc. for $C_{48}H_{48}Cl_2O_2P_2Pd_2$: C, 57.50; H, 4.83. Found: C, 57.0; H, 5.06%. Yield 0.356 g (78%), m.p. 316–319 °C. IR (KBr disk) ν (cm^{-1}): 1645, 1599, 1441, 1292, 1193, 1152, 1108, 1030, 805 (P–C), 656.

*2.2.4. Data for [Pd{CHP(C_6H_4)$Ph_2CO_2CH_2Ph$}(μ-Cl)]$_2$ (**2b**)*

Greenish-yellow solid. *Anal.* Calc. for $C_{54}H_{44}Cl_2O_4P_2Pd_2$: C, 58.82; H, 4.02. Found: C, 58.76; H, 4.40%. Yield 0.210 g (75%), m.p. 283–285 °C. IR (KBr disk) ν (cm^{-1}): 1695 (C=O), 1435, 1284, 1126, 1106, 836 (P–C), 734, 689.

*2.2.5. Synthesis of [Pd{CH{P(C_7H_6)(p-tolyl)$_2$}$COCH_3$}Cl(PPh_3)] (**3a**) general procedure*

To a suspension of complex **2a** (0.046 g, 0.06 mmol) in CH_2Cl_2 (20 ml) was added solid PPh_3 (0.033 g, 0.13 mmol). The mixture was stirred for 30 min. The resulting colorless solution was concentrated (2 ml) and diethyl ether (30 ml) was added to precipitate the white solid **3a**. *Anal.* Calc. for $C_{42}H_{39}ClOP_2Pd$: C, 66.06; H, 5.15. Found: C, 65.89; H, 5.35%. Yield 0.064 g (82%), m.p. 246–248 °C. IR (KBr disk) ν (cm^{-1}): 1639, 1594, 1572, 1475, 1433, 1351, 1302, 1180, 1154, 1103, 803 (P–C), 747, 692, 556. ^1H NMR ($CDCl_3$) δ_H (ppm): 1.66 (3H, s, $COCH_3$), 2.37 and 2.42 (9H, 2s, $3CH_3$), 4.90 (dd, $^2J_{PH}$ = 8.96 Hz, $^3J_{PH}$ = 8.87 Hz, 1H, *CH*), 6.66–7.78 (26H, m, arom.). ^{31}P NMR ($CDCl_3$) δ_P (ppm): 12.00 (PPh_3) and 28.49 (P(*p*-tolyl)$_2$) (2d, $^3J_{PP}$ = 19.0 Hz). ^{13}C NMR ($CDCl_3$) δ_C (ppm): 21.65 (s, $3CH_3$), 31.45 (d, $^3J_{PC}$ = 11.30 Hz, $COCH_3$), 50.09 (d, $^1J_{PC}$ = 63.64 Hz, *CH*), 124.02–142.96 (m, arom.), 201.68 (*CO*).

*2.2.6. Data for [Pd{CH{P(C_7H_6)(p-tolyl)$_2$}$COCH_3$}Cl(PPh_3)] (**3b**)*

White solid. *Anal.* Calc. for $C_{45}H_{37}ClO_2P_2Pd$: C, 66.43; H, 4.58. Found: C, 66.09; H, 4.93%. Yield 0.079 g (81%), m.p. 222–224 °C. IR (KBr disk) ν (cm^{-1}): 1677 (C=O), 1434, 1303, 1132, 1109, 855 (P–C), 751, 690. ^1H NMR ($CDCl_3$) δ_H (ppm): 4.19 (dd, $^2J_{PH}$ = 9.02 Hz, $^3J_{PH}$ = 5.82 Hz, 1H, *CH*), 5.15 (s, CH_2), 6.9–7.8 (m, arom.). ^{31}P NMR ($CDCl_3$) δ_P (ppm): 13.70 (PPh_3) and 27.86 (P(*p*-tolyl)$_2$) (2d, $^3J_{PP}$ = 19.21 Hz). ^{13}C NMR ($CDCl_3$) δ_C (ppm): 35.55 (dd, $^1J_{PC}$ = 70.69 Hz, $^2J_{PC}$ = 61.25 Hz, *CH*), 65.31 (s, CH_2), 122.82–139.81 (m, arom.), 172.16 (s, *CO*).

*2.2.7. Synthesis of [Pd{CH{P(C_7H_6)(p-tolyl)$_2$}$COCH_3$}Cl{P(p-tolyl)$_3$}] (**4a**) general procedure*

To a suspension of complex **2a** (0.046 g, 0.06 mmol) in CH_2Cl_2 (20 ml) was added solid P(*p*-tolyl)$_3$ (0.039 g, 0.13 mmol). The mixture was stirred for 30 min. The resulting colorless solution was concentrated (2 ml) and diethyl ether (30 ml) was added to precipitate the white solid **4a**. *Anal.* Calc. for $C_{45}H_{45}ClOP_2Pd$: C, 67.09; H, 5.63. Found: C, 67.22; H, 5.89%. Yield 0.071 g (84%), m.p. 252–254 °C. IR (KBr disk) ν (cm^{-1}): 1641 (C=O), 1598, 1497, 1444, 1396, 1295, 1189, 1152, 1104, 1027, 802 (P–C), 649, 511 ^1H NMR ($CDCl_3$) δ_H (ppm): 1.67 (3H, s, $COCH_3$), 2.31 and 2.43 (9H, 2s, $3CH_3$), 4.88 (dd, $^2J_{PH}$ = 9.85 Hz, $^3J_{PH}$ = 9.22 Hz, 1H, *CH*), 7.03–7.62 (23H, m, arom.). ^{31}P NMR ($CDCl_3$) δ_P (ppm): 11.56 (P(*p*-tolyl)$_3$) and 26.97 (P(*p*-tolyl)$_2$) (2d, $^3J_{PP}$ = 18.5 Hz). ^{13}C NMR ($CDCl_3$) δ_C (ppm): 21.43 (s, $3CH_3$), 31.24 (d, $^3J_{PC}$ = 11.06 Hz, $COCH_3$), 49.90 (d, $^1J_{PC}$ = 60.71 Hz, *CH*), 122.02–165.18 (m, arom.), 201.31 (*CO*).

*2.2.8. Data for [Pd{CH{P(C_6H_4)Ph_2}CO_2CH_2Ph}Cl{P(p-tolyl)$_3$}] (**4b**)*

White solid. *Anal.* Calc. for $C_{48}H_{46}ClO_2P_2Pd$: C, 67.14; H, 5.40. Found: C, 66.27; H, 5.31%. Yield 0.087 g (85%); m.p. 234–236 °C. IR (KBr disk): ν (cm^{-1}): 1688 (C=O), 1436, 1294, 1128, 844 (P–C), 806, 734, 692. ^1H NMR ($CDCl_3$) δ_H (ppm): 4.18 (dd, $^2J_{PH}$ = 9.05 Hz, $^3J_{PH}$ = 5.31 Hz, 1H, CH), 5.156 (s, 2H, CH_2), 2.30 (s, 9H, $3CH_3$), 6.9–8 (m, 31H, arom). ^{31}P NMR ($CDCl_3$) δ_P (ppm): 13.51 (P(*p*-tolyl)$_3$), 26.47 (PPh_2), (2d, $^3J_{PP}$ = 18.5 Hz). ^{13}C NMR ($CDCl_3$) δ_C (ppm): 35.27 (dd, $^1J_{PC}$ = 69.3 Hz, $^2J_{PC}$ = 61.02 Hz, *CH*), 65.12 (s, CH_2), 122.62–139.44 (m, arom.), 172.06 (s, *CO*).

3. Results and discussion

3.1. Spectroscopy

The ν(CO) band, which is sensitive to complexation, occurs at 1600 and 1610 cm^{-1} in the parent ylides Y^1 and Y^2, respectively [30,31]. Coordination of ylide through the carbon atom causes an increase in the ν(CO) band, whereas for O-coordination a lowering of the ν(CO) band is expected [32]. Thus the IR absorption bands for the complexes at higher frequencies indicate that C-coordination has occurred. The ν(P–C) band frequencies, which are also diagnostic of the coordination mode, occur at 848 and 887 cm^{-1} in the parent ylides Y^1 and Y^2, respectively, and are shifted to lower frequencies for the complexes, suggesting some removal of the electron density of the P–C bonds [33].

The presence of two chiral C centres (forming diastereoisomers) in **1b** (Scheme 1) is shown in the ^1H, ^{31}P and ^{13}C NMR spectra by two sets of signals with unequal populations for CH_2, CH, CO and PCH groups. The geometry of cis and trans may leads to the further peaks in the ^{31}P NMR spectra: 19.83, 20.80, 27.84 and 28.09 ppm for **1b** and 23.38 and 23.52 ppm at 25 °C for **1a** [34,35].

The two geometries for **1a** equilibrate rapidly at higher temperatures, leading to one signal for phosphorus centre (δ_P = 23.50 ppm at 55 °C) (Fig. 1).

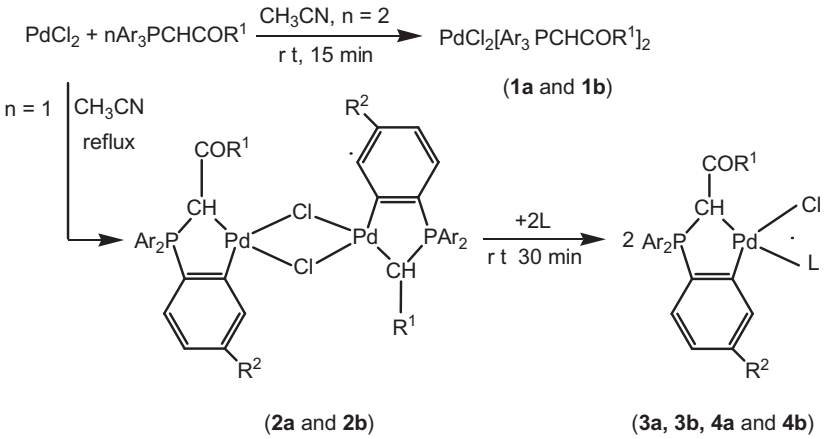

No	1a	2a	3a	4a	1b	2b	3b	4b
Ar	P(*p*-tolyl)$_3$	P(*p*-tolyl)$_3$	P(*p*-tolyl)$_3$	P(*p*-tolyl)$_3$	Ph	Ph	Ph	Ph
R^1	Me	Me	Me	Me	OCH_2Ph	OCH_2Ph	OCH_2Ph	OCH_2Ph
R^2	-	Me	Me	Me	-	H	H	H
L	-	-	PPh_3	P(*p*-tolyl)$_3$	-	-	PPh_3	P(*p*-tolyl)$_3$

Scheme 1.

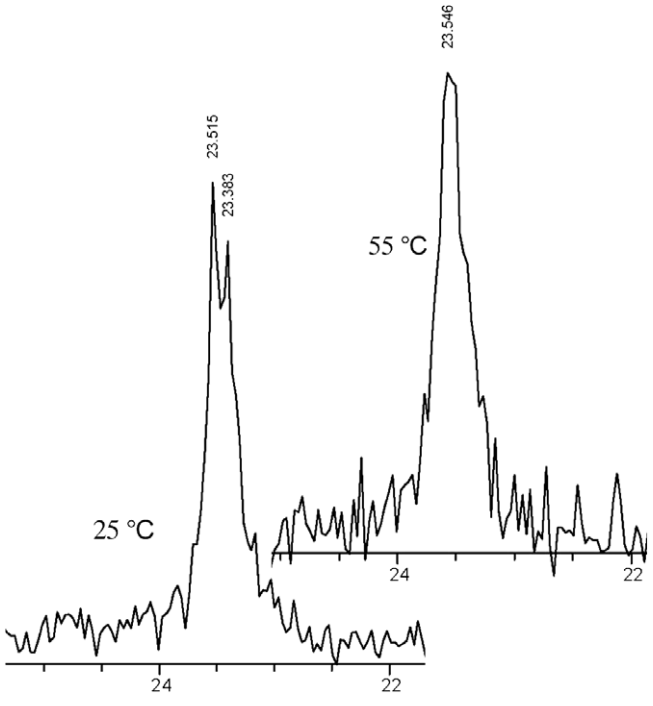

Fig. 1. Variable temperature ^{31}P NMR study on **1a**.

In the ^1H NMR spectra for **1a** and **1b**, the signals due to the methinic proton are broad (**1a**) or are a broad doublet (**1b**). This broadening is probably due to the presence of different geometries and the above mentioned diastereoisomers. A related insoluble complex, $[PdCl_2\{CH(PPh_3)CO_2Me\}_2]$, has been reported to be of a trans geometry on the basis of IR data [20]. An NMR study could not be performed on complexes **2a** and **2b** because they are very insoluble in the most common solvents. However their elemental analysis, IR spectra and the synthesis of **3a** and **4b** from complexes **2a** and **2b** adequately establish their identity, thus we propose for **2a** and **2b** the same structure as reported for the related complexes [17,20,22–26] (see Scheme 1). The bridge-splitting reaction of **2a** and **2b** with PPh_3 and P(*p*-tolyl)$_3$ is highly selective, affording exclusively the corresponding mononuclear compounds **3a, 4a**, **3b** and **4b**, respectively (Scheme 1). The ^1H and ^{31}P signals for the PCH group of complexes **3a**–**4b** are shifted downfield compared to that of the free ylide, as a consequence of the inductive effect of the metal centre. The ^1H NMR spectra of complexes **3a**–**4b** show one doublet of doublets signal for the CH group that must

Table 1
Crystal data and structure refinement for **4a**

Compound	4a
Empirical formula	$C_{45}H_{45}ClOP_2Pd$
Formula weight	805.62
Temperature (K)	120(2)
Wavelength (Å)	0.71073
Crystal system	triclinic
Space group	$P\bar{1}$
a (Å)	9.973(2)
b (Å)	13.211(3)
c (Å)	16.830(4)
α (°)	73.082(19)
β (°)	89.549(19)
γ (°)	68.566(18)
Volume (Å^3)	1962.6(8)
Z	2
D_{Calc} (Mg/m^3)	1.363
Absorption coefficient (mm^{-1})	0.656
F(000)	832
Crystal size (mm)	0.50 × 0.20 × 0.10
θ Range for data collection (°)	1.74–29.51
Reflections collected/unique (R_{int})	20212/10443 (0.0902)
Limiting indices	$-12 \leqslant h \leqslant 13$, $-18 \leqslant k \leqslant 18$, $-23 \leqslant l \leqslant 21$
Completeness to θ = 29.51° (%)	96.7
Absorption correction	numerical
Maximum and minimum transmission	0.930 and 0.850
Refinement method	full-matrix least-squares on F^2
Data/restraints/parameters	10443/0/450
Goodness-of-fit on F^2	1.088
Final *R* indices [$I > 2\sigma(I)$]	R_1 = 0.0905, wR_2 = 0.1877
R indices (all data)	R_1 = 0.0999, wR_2 = 0.1959
Extinction coefficient	0.019(3)
Largest difference in peak and hole (e Å^{-3})	1.723 and −1.918

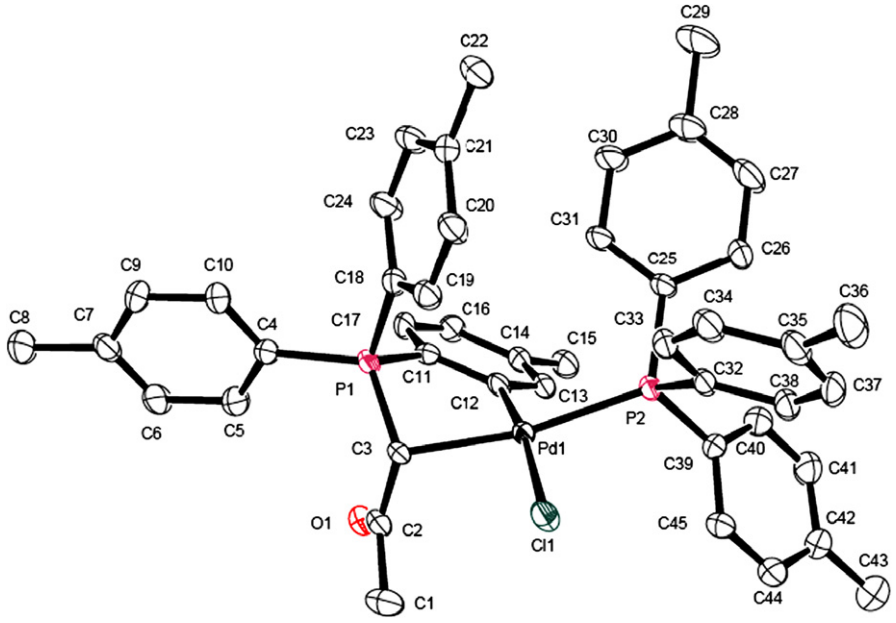

Fig. 2. ORTEP view of the X-ray crystal structure of $[Pd\{CH\{P(C_7H_6)(p\text{-tolyl})_2\}COCH_3\}Cl\{P(p\text{-tolyl})_3\}]$ (**4a**). Selected bond lengths (Å) and bond angles (°): Pd(1)–C(12), 2.021(5); Pd(1)–C(3), 2.166(5); Pd(1)–P(2), 2.2945(15); Pd(1)–Cl(1), 2.4241(14); C(2)–C(3), 1.478(8); C(2)–O(1), 1.219(8); C(11)–C(12), 1.415(7); C(11)–P(1), 1.782(6); C(3)–P(1), 1.780(5); C(12)–Pd(1)–C(3), 86.8(2); C(12)–Pd(1)–P(2), 93.06(14); C(3)–Pd(1)–P(2), 168.19(16); C(12)–Pd(1)–Cl(1), 170.58(14); C(3)–Pd(1)–Cl(1), 88.35(15); P(2)–Pd(1)–Cl(1), 93.33(5) (hydrogen atoms have been omitted for clarity).

arise from the simultaneously coupling with two phosphorus centres.

In ^{13}C NMR spectra, a higher shielding of the ylidic carbon atoms compared to those of the parent ylides is expected and we observed this for **3a**, **4a** and **1b**. Such a higher shielding was observed in $[PdCl(\eta^3\text{-}2\text{-}XC_3H_4)(C_6H_5)_3PCHCOR]$ (X = H, CH_3; R = CH_3, C_6H_5), and is due to the change in hybridization of the ylidic carbon atom on coordination [36]. Similar upfield shifts of 2–3 ppm with reference to the parent ylide were also observed in the case of $[(C_6H_5)_3PC_5H_4 \cdot HgI_2]_2$ [37] and in our synthesized complexes [30,38]. The downfield shift of the carbonyl C atom in **1a**, **3a**, **3b**, **4a** and **4b** compared to the same carbon atom in the parent ylides (190.38 ppm (Y^1) and 170.46 ppm (Y^2)), indicate a much lower shielding of the CO group in these complexes [30,38–40]. In this work, it is interesting that the expected upfield shift of the ylidic C atoms in **3b** and **4b** and downfield shift of the carbonyl C atom in **1b** are not in accordance with the expected process. This is probably due to the steric nature of Y^2, which is different from ketonic ylides.

3.2. X-ray crystallography

Table 1 provides the crystallographic results and refinement information for complex **4a**. The molecular structure and pertinent bond distances and angles are presented in Fig. 2.

Suitable crystals of **4a** were grown by the slow diffusion of diethyl ether into a chloroform solution. The Pd atom is located in a distorted square-planar environment, surrounded by one ylidic carbon (C3) and one metallated carbon (C12) that form a five-membered cycle, one chlorine (Cl1) and one phosphorus (P2) atom. The angles subtended by the ligands at the Pd(II) centre in **4a** vary from 86.8(2)° to 93.33(5)° and 168.19(16)° to 170.58(14)° indicating the distorted square-planar environment. The C(3)–Pd(1)–P(2) (168.19(16)°) and C(12)–Pd(1)–Cl(1) (170.58-(14)°) bond angles deviate a little from linearity. The Pd(1)–C(12) bond distance (2.021(5) Å) is statistically identical to those found in the orthopalladated complexes $[Pd\{\kappa^2\text{-}C,N\text{—}C_6H_4\text{-}1\text{-}[(3,5\text{-}Me_2\text{—}C_3N_2)\text{—}CH_2\text{—}(\eta^5\text{-}C_5H_4Fe(\eta^5\text{-}C_5H_5)]\}Cl(PPh_3)]$ (2.035(5) Å) [41] and $[Pd\{\kappa^2\text{-}C,O\text{—}C_6H_4\{C(O)Me\}\text{-}2\}Br\{P(o\text{-}To)_3\}]$ (2.021(2) Å) [42]. The distances Pd(1)–C(12) [2.021(5) Å] and Pd(1)–C(3) [2.166(5) Å] are different, probably reflecting the different trans effect of the phosphorus and chlorine atoms. The stabilized resonance structure for the parent ylide is destroyed by the complex formation, thus the C(2)–C(3) bond length (1.478(8) Å) is significantly longer than the corresponding distance found in the similar uncomplexed phosphoranes (1.407(8) Å [43] and 1.401(2) Å [44]). Likewise the C(3)–P(1) bond length in a similar ylide is 1.7194(17) Å [44], which shows that the corresponding bond in **4a** is considerably elongated to 1.780(5) Å.

4. Conclusion

The present study describes the synthesis and characterization of orthometallated Pd(II) complexes of phosphorus ylides. On the basis of the physico-chemical and spectroscopic data we propose that these ligands herein exhibit C-coordination to the metal centre, which is further confirmed by the X-ray crystal structure of complex **4a**. The structural study involved in this work demonstrates that phosphorus ylides can show transition metal induced activation of C–H bonds.

Acknowledgement

We are highly grateful to Mr. Zebarjadian for recording the NMR spectra.

Appendix A. Supplementary data

CCDC 684309 contains the supplementary crystallographic data for **4a**. These data can be obtained free of charge via http://www.ccdc.cam.ac.uk/conts/retrieving.html, or from the Cambridge Crystallographic Data Centre, 12 Union Road, Cambridge CB2 1EZ, UK; fax: (+44) 1223-336-033; or e-mail: deposit@ccdc.cam.ac.uk. Supplementary data associated with this article can be found, in the online version, at doi:10.1016/j.poly.2008.07.017.

References

[1] A.E. Shilov, G.B. Shul'pin, Chem. Rev. 97 (1997) 2879.
[2] F. Kakiuchi, N. Chatani, Adv. Synth. Catal. 345 (2003) 1077.
[3] R.B. Bedford, Chem. Commun. (2003) 1787.
[4] M.E. van der Boom, D. Milstein, Chem. Rev. 103 (2003) 1759.
[5] I. Omae, Coord. Chem. Rev. 248 (2004) 995.
[6] B. Schlummer, U. Scholz, Adv. Synth. Catal. 346 (2004) 1599.
[7] I.P. Beletskaya, A.V. Cheprakov, J. Organomet. Chem. 689 (2004) 4055.
[8] W.D. Jones, Inorg. Chem. 44 (2005) 4475.
[9] J. Dupont, C. Consorti, J. Spencer, Chem. Rev. 105 (2005) 2527.
[10] D. Kalyani, N.R. Deprez, L.V. Desai, M.S. Sanford, J. Am. Chem. Soc. 127 (2005) 7330.
[11] A. Zapf, M. Beller, Chem. Commun. (2005) 431.
[12] K. Godula, D. Sames, Science 312 (2006) 67.
[13] K.L. Hull, E.L. Lanni, M.S. Sanford, J. Am. Chem. Soc. 128 (2006) 14047.
[14] J. Vicente, J.A. Abad, M.J. Lopez–Saez, P.G. Jones, Organometallics 25 (2006) 1851.
[15] F. Lopez-Ortiz, Curr. Org. Synth. 3 (2006) 187.
[16] K. Onitsuka, M. Nishii, Y. Matsushima, S. Takahashi, Organometallics 23 (2004) 5630.
[17] E. Serrano, C. Valles, J.J. Carbo, A. Lledos, T. Soler, R. Navarro, E.P. Urriolabeitia, Organometallics 25 (2006) 4653.
[18] Y. Canac, S. Conejero, M. Soleilhavoup, B. Donnadieu, G. Bertrand, J. Am. Chem. Soc. 128 (2006) 459.
[19] A. Kawachi, T. Yoshioka, Y. Yamamoto, Organometallics 25 (2006) 2390.
[20] J. Vicente, M.T. Chicote, J. Femandez-Baeza, J. Organomet. Chem. 364 (1989) 407.
[21] D. Aguilar, M.A. Aragues, R. Bielsa, E. Serrano, R. Navarro, E.P. Urriolabeitia, Organometallics 26 (2007) 3541.
[22] J.C. Baldwin, W.C. Kaska, Inorg. Chem. 18 (1979) 686.
[23] M.L. Illingsworth, J.A. Teagle, J.L. Burmeister, W.C. Fultz, A.L. Rheingold, Organometallics 2 (1983) 1364.
[24] J.A. Teagle, J.L. Burmeister, Inorg. Chim. Acta 118 (1986) 65.
[25] J. Vicente, M.T. Chicote, M.C. Lagunas, P.G. Jones, E. Bembenek, Organometallics 13 (1994) 1243.
[26] D. Aguilar, M.A. Aragues, R. Bielsa, E. Serrano, T. Soler, R. Navarro, E.P. Urriolabeitia, J. Organomet. Chem. 693 (2008) 417.
[27] Stoe & Cie, X-AREA, Version 1.30: Program for the Acquisition and Analysis of Data, Stoe & Cie GmbH, Darmstadt, Germany, 2005.
[28] G.M. Sheldrick, SHELX97 Program for Crystal Structure Solution and Refinement, University of Göttingen, Germany, 1997.
[29] Stoe & Cie, X-STEP32, Version 1.07b: Crystallographic Package, Stoe & Cie GmbH, Darmstadt, Germany, 2000.
[30] S.J. Sabounchei, H. Nemattalab, S. Salehzadeh, S. Khani, M. Bayat, H.R. Khavasi, Polyhedron 27 (2008) 2015.
[31] S.J. Sabounchei, A.R. Dadrass, F. Akhlaghi, Z. Bolboli Nojini, H.R. Khavasi, Polyhedron 27 (2008) 1963.
[32] H. Koezuka, G. Matsubayashi, T. Tanaka, Inorg. Chem. 25 (1976) 417.
[33] W. Luttke, K. Wilhelm, Angew. Chem., Int. Ed. Engl. 4 (1965) 875.
[34] J. Vicente, M.T. Chicote, I. Saura-Llamas, J. Turpin, J. Fernandez-Baeza, J. Organomet. Chem. 333 (1987) 129.
[35] J. Vicente, M.T. Chicote, J.A. Cayuelas, J. Fernandez-Baeza, P.G. Jones, G.M. Sheldrick, P. Espinet, J. Chem. Soc., Dalton Trans. (1985) 1163.
[36] G. Facchin, R. Bertani, M. Calligaris, G. Nardin, M. Mari, J. Chem. Soc., Dalton Trans. (1987) 1381.
[37] N.L. Holy, N.C. Baenziger, R.M. Flynn, D.C. Swenson, J. Am. Chem. Soc. 98 (1976) 7823.
[38] S.J. Sabounchei, V. Jodaian, H.R. Khavasi, Polyhedron 26 (2007) 2845.
[39] S.J. Sabounchei, H. Nemattalab, S. Salehzadeh, M. Bayat, H.R. Khavasi, H. Adams, J. Organomet. Chem. 693 (2008) 1975.
[40] M. Kalyanasundari, K. Panchanatheswaran, W.T. Robinson, H. Wen, J. Organomet. Chem. 491 (1995) 103.
[41] A. González, C. López, X. Solans, M. Font-Bardía, E. Molins, J. Organomet. Chem. 693 (2008) 2119.
[42] J. Vicente, J.A. Abad, E. Martínez-Viviente, M.C. Ramírez de Arellano, Organometallics 19 (2000) 752.
[43] M. Kalyanasundari, K. Panchanatheswaran, V. Parthasarathi, W.T. Robinson, H. Wen, Acta Crystallogr. 50 (1994) 1738.
[44] S.J. Sabounchei, A. Dadrass, M. Jafarzadeh, H.R. Khavasi, Acta Crystallogr., Sect. E 63 (2007) 3160.

ligand adopts a μ_2-1,2-bridging coordination mode, which has been widely observed in other metal tetrazolate complexes. By contrast, the potassium, rubidium, and cesium Metetz complexes contain new coordination modes that entail bonding of two or more metal atoms to each nitrogen atom in the tetrazolate ligand. These new coordination modes lead to high solid state densities through extremely efficient packing. Achievement of high solid state densities in energetic materials is very important, since the detonation pressure and thus explosive performance of a compound is related to the square of the density [51].

2. Results and discussion

2.1. Preparation and characterization of sodium, potassium, rubidium, and cesium methyl tetrazolate complexes

Several group 1 Metetz complexes have been previously described, with varying levels of characterization. Na(Metetz) has been generated in solution by treatment of MetetzH with several different bases, and has been used as a nucleophilic tetrazolate transfer reagent [52,53]. The X-ray crystal structure of Na(Metetz)$(H_2O)_2$ was recently reported, although it was not described [38b]. K(Metetz) has been generated in solution by deprotonation of MetetzH and was used as an intermediate in the synthesis of functionalized tetrazoles [54,55]. Neither Rb(Metetz) nor Cs(Metetz) has been previously described. In the present work, MetetzH was treated with MOH or MOH · H_2O (M = Na, K, Rb, Cs) in water at room temperature, which afforded 92–97% isolated yields of Na(Metetz)$(H_2O)_2$ (**1**), K(Metetz) (**2**), Rb(Metetz) (**3**), and Cs(Metetz) (**4**) as colorless solids after workup (Eq. (1)). Complex **1** was isolated as the dihydrate, and the waters of hydration were not lost upon extended storage at room temperature. By contrast, **2**–**4** crystallized from concentrated aqueous solutions (**2**, **3**) or methanol/diethyl ether (**4**) as the anhydrous Metetz complexes. The crystal structures of **1**–**4** are described below. Several precautions were required during the synthetic procedures. To avoid formation of carbonates, reactions involving the metal hydroxides were conducted under argon in degassed, distilled water. A slight excess of MetetzH was employed in each synthesis, to assure complete consumption of the metal hydroxide starting materials. The excess MetetzH was subsequently removed by washing the crude reaction mixtures with tetrahydrofuran, since **1**–**4** are rigorously insoluble in this solvent, whereas MetetzH is very soluble. A small portion of each crude reaction product was also dissolved in water, and several drops of phenolphthalein solution were added. Formation of a light pink color indicated the presence of hydroxide ion, and thus incomplete reaction. Only products that afforded colorless solutions with the phenolphthalein test were employed further. Finally, although **2**–**4** crystallized as anhydrous materials, the crystals themselves were hygroscopic and formed gelatinous blobs upon standing in ambient atmosphere (0.25–2 h, depending on the humidity levels). Crystals of **2**–**4** were obtained upon slow evaporation of aqueous (**2**, **3**) or methanol/diethyl ether (**4**) solutions, but the crystals themselves were encased in greasy coatings that could not be removed without dissolving the crystals. In addition, only small amounts of crystals were obtained in each evaporation, with most of the product forming microcrystalline or syrupy materials. As a result, it was not possible to obtain analytical samples by crystallization. Infrared spectra of **2**–**4** obtained on the powders obtained after tetrahydrofuran washing and vacuum drying at ambient temperature for 18 h showed absorptions at ~3400 and ~1645 cm^{-1} that corresponded to vibrations from water molecules, indicating that these materials were hydrates. Carbon, hydrogen, and nitrogen microanalyses of these hydrated powders gave variable results, but generally suggested formulations of **2** · $(H_2O)_{0.5}$, **3** · $(H_2O)_{0.5}$, and **4** · $(H_2O)_{0.5}$. The waters of hydration could be removed by drying for 18 h at 111 °C/0.05 Torr in a drying pistol using refluxing toluene. Infrared spectra of **2**–**4** after this drying protocol did not show the absorptions at ~3400 and ~1645 cm^{-1}, demonstrating that these materials were anhydrous. The carbon, hydrogen, and nitrogen microanalysis values were consistent with analytically pure material for **2**. However, carbon, hydrogen, and nitrogen microanalysis values within 0.4% of the calculated values could not be obtained for **3** and **4**, despite three analyses for each compound. It has been previously established that the high nitrogen contents in tetrazoles can lead to difficulties in obtaining correct microanalyses [56].

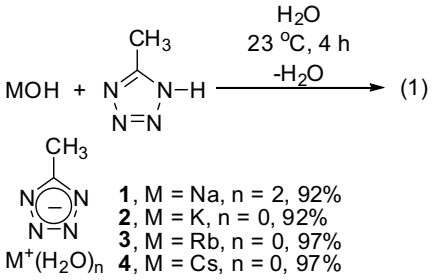

The ^1H NMR resonances for the methyl group hydrogen atoms in **1**–**4** appeared at δ 2.41 in methanol-d_4, while the $^{13}C\{^1H\}$ NMR spectra in the same solvent showed resonances between 159.14 and 159.17 ppm for the tetrazolate ring carbon atom and between 10.14 and 10.20 ppm for the methyl group carbon atom. These resonances suggest very similar solution structures that probably involve solvated, separated metal and methyl tetrazolate ions. The infrared spectrum of **1** showed absorptions due to the methyl tetrazolate ligand, as well as a strong, broad absorption at 3420 cm^{-1} and a sharp, medium intensity absorption at 1645 cm^{-1}. These latter absorptions correspond to the symmetric and asymmetric stretches of water and the bending of the water O–H bonds, respectively. The infrared spectra of dried samples of **2**–**4** revealed absorptions for the methyl tetrazolate ligand, and the water absorptions were absent.

Complexes **1** and **2** have melting points above 300 °C, while **3** and **4** melt at 254 and 257 °C, respectively. There was no evidence for detonation of **1**–**4** during the melting point experiments. Small samples of **1**–**4** (~5 mg) were placed on an iron anvil and were struck hard with a hammer. No detonations occurred during these procedures. Small samples (~10 mg) of **1**–**4** were placed on laboratory tissues in a large ceramic dish, and the tissues were lit with a match. No noise was heard upon burning **1**–**4**, and normal burning was observed (no deflagration). Passing sparks from a Tesla coil through ~5 mg samples of **1**–**4** on an iron anvil did not lead to detonation or even deflagration. These experiments suggest that **1**–**4** are not primary energetic materials, although they may still contain considerable energy. The thermal decomposition of **1**–**4** was further investigated by thermogravimetric analysis under a nitrogen atmosphere between 25 and 450 °C with a heating rate of 10 °C/min. The thermogravimetric analysis of **1** showed two events: loss of coordinated water with the onset at 92 °C (weight loss = 26.2% versus 25.4% expected for loss of two water molecules) and two step loss of dinitrogen with onsets at 352 and 395 °C (weight loss = 41.2% versus 39.4% expected for loss of 2 equiv. of dinitrogen). Complexes **2**–**4** showed single weight loss events with onsets at 350, 377, and 362 °C with total weight loss of 38.7%, 31.5%, and 21.9%, respectively. The weight losses for **2**–**4** are consistent with 85%, 95%, and 84%, respectively, of the mass losses expected for 2 equiv. of dinitrogen.

2.2. X-ray crystal structures of 1–4

Complexes **1**–**4** were subjected to X-ray crystal structure analyses to determine the bonding modes of the methyl tetrazolate ligands, the geometries around metal centers, and solid state densities. The X-ray crystal structure of **1** was reported recently [38b], but was not described in the publication. We describe the structure of **1** herein to allow comparison with **2**–**4**. Crystallographic data for **1**–**4** are summarized in Table 1, selected bond lengths and bond angles are listed in Tables 2–5, while perspective views are given in Figs. 1–4. In the structure discussion and throughout the paper, N_1–N_4 refer to the atom numbers within the tetrazolate ligand CN_4 core (Chart 1), whereas N(1) and N(2) refer specifically to the crystallographically unique nitrogen atoms within each structure.

The molecular structure of **1** is shown in Fig. 1. The structure consists of approximately octahedrally coordinated sodium ions that form infinite chains built up by two μ_2-aqua ligands and two μ_2-N_1,N_2-tetrazolate ligands between each sodium atom. The tetrazolate ligand nitrogen atoms are *trans* within the octahedron, and occupy the crystallographic mirror along with the sodium ion. The four oxygen atoms lie in an approximate plane containing the sodium ion. The sodium–nitrogen distances are 2.523(1) and 2.533(1) Å, while the nitrogen–sodium–nitrogen angle is 168.63(3)°. The nitrogen–sodium–oxygen angles range between 77.56° and 110.52°, which illustrate the distorted octahedral geometry. The sodium–oxygen distances are 2.422(1) and 2.435(1) Å, the *cis* oxygen–sodium–oxygen angles are between 84.74° and 93.36°, while the *trans* oxygen–sodium–oxygen angle is 166.40(2)°. The sodium–oxygen–sodium angle is 92.30(2)°. The linear chains containing the NaN_2O_4 octahedra form a larger structure that is cross-linked by O–H···N hydrogen bonds between the bridging aqua ligand hydrogen atoms and the uncoordinated N_3 and N_4 atoms of each Metetz ligand. These hydrogen bonds are characterized by oxygen-hydrogen distances of 0.843 and 0.847 Å, hydrogen–nitrogen distances of 2.078 and 2.132 Å, oxygen–nitrogen separations of 2.925 and 2.966 Å, and oxygen–hydrogen–nitrogen angles of 169.69° and 179.00°.

Complexes **2** and **3** are isostructural and have similar bonding interactions (Figs. 2 and 3). The metal ions in each complex are eight coordinate, and each has bonds to one η^2-N_1,N_2-tetrazolate ligand, one η^2-N_2,N_3-tetrazolate ligand, one η^2-N_3,N_4-tetrazolate ligand, one η^1-N_1-tetrazolate ligand, and one η^1-N_4-tetrazolate ligand. The η^2-N_1,N_2- and η^2-N_3,N_4-tetrazolate interactions are *syn* to each other within each Metetz ligand. Through these bonding motifs, each nitrogen atom in the Metetz ligand forms bonds to two potassium or rubidium ions. In **2**, the potassium–nitrogen distances range from 2.89 to 2.97 Å, while the rubidium–nitrogen distances in **3** are between 3.01 and 3.07 Å. There are no close contacts between the metal ions and the Metetz ligand core carbon atom in either **2** or **3**. In **2**, the nitrogen–potassium–nitrogen bite angle associated with the η^2-tetrazolate interactions are 26.00(5)° and 26.73(3)°. For **3**, the corresponding angles are 25.13(4)° and 25.65(2)°. The slightly smaller bite angles in **3** are consistent with the longer metal–nitrogen distances, compared to **2**.

Table 1
Crystal data and data collection parameters for **1**–**4**

	1	2	3	4
Empirical formula	$C_2H_7N_4NaO_2$	$C_2H_3KN_4$	$C_2H_3N_4Rb$	$C_2H_3CsN_4$
FW	142.11	122.18	168.55	215.99
Space group	*Pnma*	*Pnma*	*Pnma*	$P2_1/m$
a (Å)	6.9152(7)	7.2636(2)	7.5040(5)	4.3812(3)
b (Å)	6.9202(11)	6.2834(2)	6.4590(4)	6.9532(4)
c (Å)	12.1016(13)	10.0394(3)	10.1539(6)	8.8358(5)
β (°)				97.688(3)
V (Å^3)	579.12(10)	458.20(2)	492.14(5)	266.75(3)
Z	4	4	4	2
T (K)	100	100	100	100
λ (Å)	0.71073	0.71073	0.71073	0.71073
D_{calc} (g cm^{-3})	1.630	1.771	2.275	2.689
μ (mm^{-1})	0.198	1.007	9.918	6.810
R(*F*) (%)	3.03	2.61	1.79	1.34
$R_w(F)$ (%)	7.82	6.77	4.21	3.52

$R(F) = \sum||F_o| - |F_c||/\sum|F_o|$, $R_w(F)^2 = [\sum w(F_o^2 - F_c^2)^2/\sum w(F_o^2)^2]^{1/2}$ for $I > 2\sigma(I)$.

Table 2
Selected bond lengths (Å) and angles (°) for **1**

Na–O(1)	2.435(1)
Na–O(1)′	2.422(1)
Na–N(3)′	2.533(1)
Na–N(4)	2.523(1)
N(1)–N(2)	1.352(1)
N(2)–N(3)	1.316(1)
N(3)–N(4)	1.351(1)
N(1)–C(1)	1.337(1)
N(4)–C(1)	1.336(1)
O(1)–Na–O(1)′	93.36(2)
O(1)–Na–O(1)″	166.40(2)
O(1)–Na–O(1)‴	84.74(3)
O(1)–Na–N(4)	77.56(2)
O(1)′–Na–N(4)	88.87(2)
O(1)–Na–N(3)′	110.52(2)
O(1)′–Na–N(3)′	82.78(2)
N(4)–Na–N(3)′	168.63(3)
Na–N(4)–N(3)	124.81(6)
Na–O(1)–Na′	92.30(2)

Table 3
Selected interatomic distances (Å) and angles (°) for **2**

K–N(1)′	2.971(1)
K–N(2)	2.963(1)
K–N(2)′	2.886(1)
K–N(1)″	2.907(1)
N(1)–N(2)	1.356(2)
N(1)–N(1)′	1.308(2)
N(2)–C(1)	1.338(1)
K–K′	4.1863(4)
K–K″	4.5797(5)
N(1)′–K–N(2)′	26.73(3)

Table 4
Selected interatomic distances (Å) and angles (°) for **3**

Rb–N(1)	3.007(1)
Rb–N(1)′	3.074(1)
Rb–N(2)′	3.013(1)
Rb–N(2)″	3.057(1)
N(1)–N(2)	1.353(1)
N(1)–N(1)′	1.308(2)
N(2)–C(1)	1.339(1)
Rb–Rb′	4.3114(3)
N(1)–Rb–N(1)′	25.13(4)

Table 5
Selected interatomic distances (Å) and angles (°) for **4**

Cs–N(1)	3.337(1)
Cs–N(1)′	3.333(1)
Cs–N(2)	3.139(1)
Cs–N(2)′	3.207(1)
Cs–N(2)″	3.497(1)
N(1)–N(2)	1.357(1)
N(2)–N(2)′	1.314(2)
N(1)–C(1)	1.339(1)
Cs–Cs′	4.3662(2)
N(1)–Cs–N(2)	23.94(2)

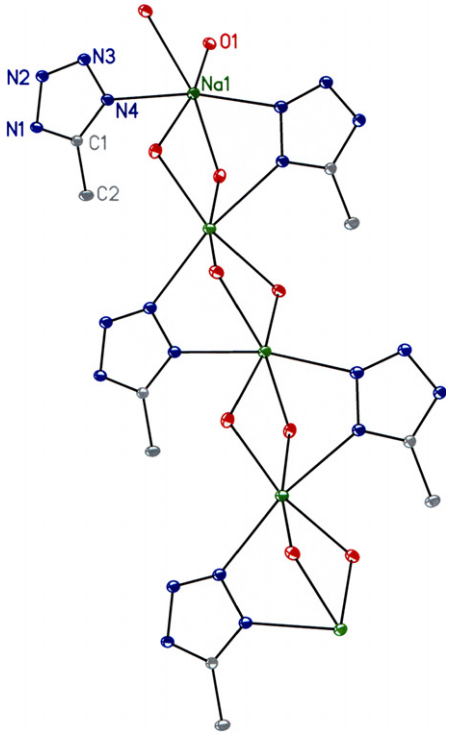

Fig. 1. Perspective view of **1** with thermal ellipsoids at the 50% probability level.

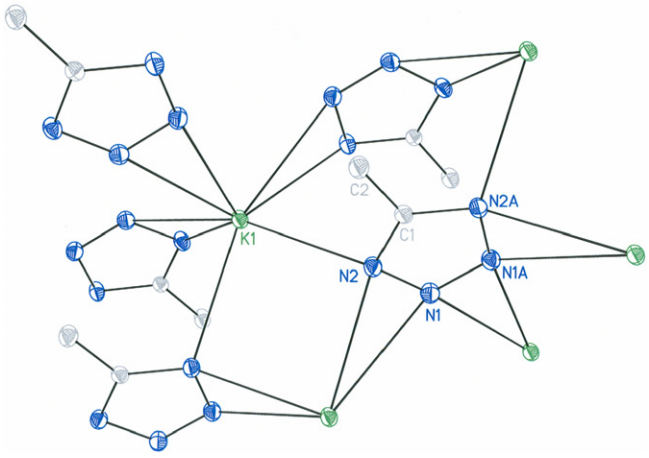

Fig. 2. Perspective view of **2** with thermal ellipsoids at the 50% probability level.

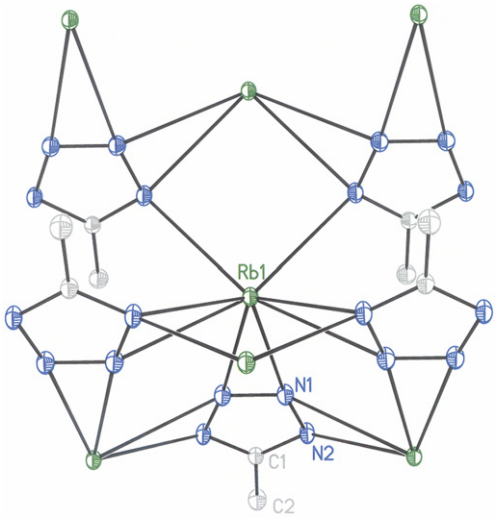

Fig. 3. Perspective view of **3** with thermal ellipsoids at the 50% probability level.

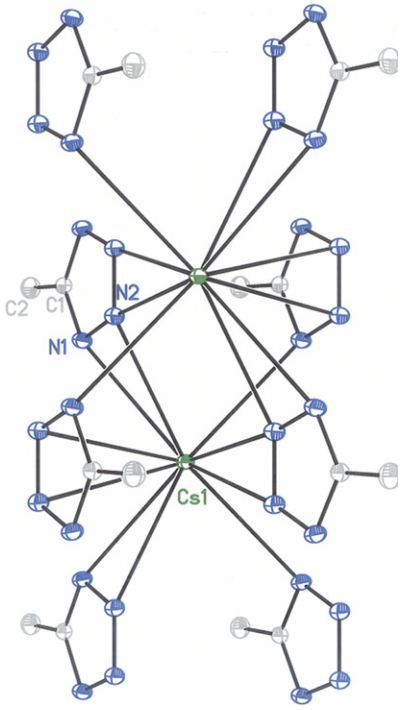

Fig. 4. Perspective view of **4** with thermal ellipsoids at the 50% probability level.

The cesium ions in **4** are 10-coordinate, and form bonds to one η^2-N_1,N_2-tetrazolate ligand, two η^2-N_2,N_3-tetrazolate ligands, one η^2-N_3,N_4-tetrazolate ligand, one η^1-N_1-tetrazolate ligand, and one η^1-N_4-tetrazolate ligand (Fig. 4). The cesium atoms lie slightly out of the CN_4 planes of the η^2-N_1,N_2- and η^2-N_3,N_4-tetrazolate ligands, but the CsN_2/CN_4 angles are small (21.3°). By contrast, the CsN_2/CN_4 angles associated with the two η^2-N_2,N_3-tetrazolate ligands are 95.6° and 0.9°. The cesium ion bonding vector makes an angle of 71.5° with the CN_4 planes of the η^1-N_1- and η^1-N_4-tetrazolate ligands. Through these cesium–nitrogen interactions, the two N(1) atoms of the Metetz ligands (adjacent to the core carbon atom) each form bonds with two cesium ions, whereas the two N(2) atoms (remote from the core carbon atom) each form bonds to three cesium ions. The cesium–nitrogen distances in **4** range between 3.14 and 3.50 Å. The η^2-1,2-N_1,N_2- and η^2-N_3,N_4-tetrazolate ligands have cesium–nitrogen distances of 3.337(1) Å to N(1) and 3.139(1) Å to N(2), and thus have a distorted η^2-interaction. The η^2-N_2,N_3-tetrazolate ligands are characterized by cesium–nitrogen distances of 3.207(1) Å for the in-plane interaction and 3.497(1) Å for the out-of-plane interaction. The latter interaction is the longest cesium–nitrogen bond in the complex, consistent with the presumably lower basicity of the out-of-plane π-orbitals, compared to the in-plane nitrogen-based lone pairs. The η^1-interactions have a cesium–nitrogen distance of 3.333(1) Å. The nitrogen–cesium–nitrogen bite angles associated with the η^2-tetrazolate interactions are 23.94(2)°, 23.65(4)°, and 21.66(4)°. These angles are smaller than those found in **2** and **3**, due to the longer cesium–nitrogen bond lengths in **4**. In addition, the latter bite angle in **4** (21.66(4)°) is associated with the out-of-plane η^2-N_2,N_3-tetrazolate interaction, and is smaller than the other two bite angles because of the longer cesium–nitrogen distances.

Chart 1. Numbering scheme for tetrazolate ligand core nitrogen atoms.

We have recently reported examples of intramolecular and intermolecular C-H···N hydrogen bonding between 18-crown-6 C–H bonds and the nitrogen atoms of tetrazolate ligands in group 1 and 2 complexes [48–50]. These interactions are important, since the metal–tetrazolate bonding interactions were distorted to facilitate the hydrogen bonding and because this weak hydrogen bonding possibly promotes higher densities through more efficient packing. The sum of the van der Waals radii for N and H is about 2.7–3.0 Å [57,58], so interactions in this range or shorter are diagnostic of C–H···N hydrogen bonding. The structure of **1** contains intermolecular C–H···N hydrogen bonding interactions with an H···N separation of 2.905 Å. Complexes **2** and **3** exhibit intermolecular C–H···N hydrogen bonding interactions with H···N separations of 2.551 and 2.693 Å, respectively. Complex **4** exhibits close H···N distances of 2.797, 2.896, and 2.901 Å.

2.3. Discussion

Chart 2 depicts the metal atom coordination modes to the Metetz ligands in **1**–**4**. Complex **1** contains N_1,N_2-μ_2-η^1:η^1-Metetz ligands, which is a common coordination mode for tetrazolate ligands. The same coordination mode has been observed in $[Cd[Cd(py)(H_2O)]_2(1,3\text{-BTB})_2]$ (1,3-BTB = 1,3-benzeneditetrazolate, py = pyridine) [16f]. One of the tetrazolate moieties within sodium *trans*-5,5′-ethylenetetrazolate [38d] and sodium 5,5′-azotetrazolate pentahydrate [38g] also exhibits the N_1,N_2-μ_2-η^1:η^1-coordination mode. The N_1,N_2-μ_2-η^1:η^1-coordination mode is also a common motif within more complex tetrazolate bridging ligand modes [1,16c,16e]. Complexes **2** and **3** contain the μ_8-η^1:η^1:η^2:η^2:η^2 coordination mode. A very similar coordination mode was observed in cesium cyanotetrazolate [38h], where η^1-cesium–nitrogen bonds occurred to N_1 and N_4 of the tetrazolate core, and η^2-interactions were observed to N_1–N_2, N_2–N_3, and N_3–N_4. The only difference between the coordination mode of the tetrazolate ligand cores in **2** and **3** and that in cesium cyanotetrazolate is that the η^2-interactions to N_1–N_2 and N_3–N_4 are *syn* within each tetrazolate ligand in the former two examples, but are anti in the last example. Interestingly, the tetrazolate moieties in rubidium 5,5′-azotetrazolate dihydrate exhibit a novel bridging coordination mode that entails η^1-coordination of N_1, two η^2-interactions to N_1 and N_2, and an η^2-interaction to N_2 and N_3 [38g]. This coordination pattern is very similar to that in **2** and **3**. However, N_3 and N_4 engage in hydrogen bonding to the water molecules, which interrupts coordination of the rubidium ion to all of the ligand core nitrogen atoms. Complex **4** contains the μ_{10}-η^1:η^1:η^2:η^2:η^2:η^2-Metetz ligand, which is a new coordination mode for a tetrazolate ligand. Interestingly, the Metetz ligand nitrogen atoms in **4** form bonds to 10 cesium ions, whereas the core nitrogen atoms in cesium cyanotetrazolate form bonds to only 8 cesium ions [38h]. This difference occurs because the cyano group nitrogen atom in cesium cyanotetrazolate bonds to three cesium ions, thereby reducing the overall number of cesium–nitrogen bonds to the cyanotetrazolate core nitrogen atoms. The X-ray crystal structure of cesium aminotetrazolate has also been reported [38d]. Each cesium ion is 9-coordinate, with eight cesium–nitrogen bonds to tetrazolate ring core nitrogen atoms and one cesium–nitrogen bond to the amino nitrogen atom. The core nitrogen atoms of the tetrazolate ligand are bonded to six cesium atoms, with two η^1-N_1, two η^1-N_4, and two η^2-N_2,N_3 interactions. Apparently, the coordination number at the cesium ion and the number of cesium atoms bonded to each tetrazolate core nitrogen atom are reduced in cesium aminotetrazolate, due to the formation of the cesium–nitrogen bond to the amino group as well as the N–H···N hydrogen bonding that is associated with the amino group hydrogen atoms. The X-ray crystal structure of the cesium salt of the dianion 5-cyanoiminotetrazoline has been described [38e]. In this structure, each CN_4 core nitrogen atom is bonded to three cesium ions with two η^1-N_1, two η^1-N_4, and two η^2-N_1,N_2, one η^2-N_2,N_3, and one η^2-N_3,N_4 interactions. However, the presence of two cesium ions per tetrazolate ring and the Lewis basic cyanoimino group makes the overall coordination spheres of the cesium ions very complex.

The X-ray crystal structure of Na(Htetz)(H_2O) has been determined [38i], and its coordination sphere consists of four nitrogen atoms from four tetrazolate ligands lying in an approximate plane and two *trans* oxygen atoms of the aqua ligands. Each tetrazolate ligand has four sodium–nitrogen bonds, and forms two η^1-N_1 and two η^1-N_4 interactions. The uncoordinated N_2 and N_3 atoms of each tetrazolate ligand are engaged in hydrogen bonding to the hydrogen atoms of the aqua ligands. Interestingly, the carbon-bound hydrogen atom has an intermolecular close contact of 2.782 Å to N_2 of an adjacent tetrazolate ion, which demonstrates that weak C–H···N hydrogen bonding is also present in the solid state. The thermal decomposition of Na(Htetz)(H_2O) was reported [59], and it exhibits water loss between 120 and 170 °C and loss of 1 equiv. of dinitrogen as a single event between 323 and 337 °C. For comparison, **1** underwent dehydration beginning at 92 °C, but lost 2 equiv. of dinitrogen in a two step process beginning at 352 °C. Complexes **2**–**4** lost 2 equiv. of dinitrogen in single step events at onset temperatures between 350 and 377 °C. Detonations of **1**–**4** were not observed in any of the thermogravimetric analysis experiments. By contrast, it was reported that thermogravimetric analyses with more than 10 mg of Na(Htetz)(H_2O) resulted in detonation [59]. It is likely that the Metetz complexes are less energetic than Na(Htetz)(H_2O), due to the lower nitrogen contents associated with the presence of the methyl groups in **1**–**4**.

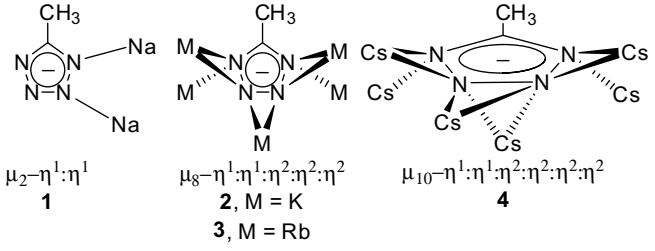

μ_2–η^1:η^1 **1**

μ_8–η^1:η^1:η^2:η^2:η^2 **2**, M = K; **3**, M = Rb

μ_{10}–η^1:η^1:η^2:η^2:η^2:η^2 **4**

Chart 2. Tetrazolate ligand coordination modes in 1–4.

3. Experimental

3.1. Caution

The compounds described herein have high nitrogen contents, and are potentially energetic. While **1**–**4** showed no evidence for detonation or shock sensitivity in our studies, safety precautions

such as a face shields, a leather apron and gloves, and hearing protection should be employed.

3.2. General considerations

The syntheses of **1**–**4** were conducted under an argon atmosphere using Schlenk line techniques, to avoid the formation of metal carbonates in the reaction solutions. Once isolated, **2**–**4** were handled under a dry argon atmosphere in a glove box to avoid the formation of hydrates. Methyl tetrazole, NaOH, KOH, $RbOH \cdot H_2O$, $CsOH \cdot H_2O$, and methanol were purchased from Aldrich Chemical Company and were used without further purification. ^1H and $^{13}C\{^1H\}$ NMR spectra were obtained at 300 and 75 MHz, respectively, in methanol-d_4. Infrared spectra were obtained as Nujol mulls on NaCl plates. Elemental analyses were performed by Midwest Microlab, Indianapolis, IN. Melting points were obtained on a Haake–Buchler HBI digital melting point apparatus and are uncorrected. Thermogravimetric analyses were conducted on a Perkin Elmer Pyris 1 TGA system between 25 and 450 °C, using nitrogen as the flow gas with a heating rate of 20 °C/min.

3.3. General procedure for the preparation of *1*–*4*

A 100-mL Schlenk flask was charged with the metal hydroxide, a stir bar, and degassed, distilled water (20 mL). To the stirred solution at ambient temperature, the methyl tetrazole (1.1 molar equiv.) was slowly added as a solution in 20 mL of degassed, distilled water. The resultant mixture was stirred for 4 h at ambient temperature. The volatile components were then removed under reduced pressure to afford colorless solids. The crude solids were washed with two 20 mL portions of tetrahydrofuran to remove the excess methyl tetrazole. A small sample of each complex was dissolved in dry, degassed water. To this solution was added a few drops of an aqueous phenolphthalein solution. A pink color at this stage indicated the presence of hydroxide ion, and thus an incomplete reaction. Only products that afforded colorless solutions upon addition of phenolphthalein were deemed successful. With **2**–**4**, the solids were dried for 18 h at 0.05 Torr in a drying pistol, using refluxing toluene (111 °C). Single crystals for the X-ray crystallographic analyses were obtained by slow evaporation of water at 23 °C for **1**–**3**, and by diffusion of diethyl ether into a methanol solution of **4** at 23 °C.

3.4. Sodium methyl tetrazolate dihydrate (*1*)

Prepared from sodium hydroxide (0.182 g, 4.55 mmol) and methyl tetrazole (0.421 g, 5.01 mmol) to afford **1** in 92% yield as a colorless solid: mp >300 °C; IR (Nujol, cm^{-1}) 3435 (vs), 1645 (s), 1302 (s), 1259 (m), 1169 (m), 1153 (m), 1125 (s), 1103 (s), 1068 (s), 1028 (s), 721 (s), 700 (s); ^1H NMR (CD_3OD, 23 °C, δ) 2.41 (s, 3H, CN_4CH_3); $^{13}C\{^1H\}$ NMR (CD_3OD, 23 °C, ppm) 159.14 (s, CN_4CH_3), 10.15 (s, CN_4CH_3).

Anal. Calc. for $C_2H_7N_4NaO_2$: C, 16.91; H, 4.97; N, 39.43. Found: C, 16.78; H, 5.15; N, 39.67%.

3.5. Potassium methyl tetrazolate (*2*)

Prepared from potassium hydroxide (0.216 g, 3.84 mmol) and methyl tetrazole (0.356 g, 4.23 mmol) to afford **2** in 92% yield as a colorless solid: mp >300 °C; IR (Nujol, cm^{-1}) 1305 (m), 1261 (m), 1200 (s), 1115 (s), 1108 (s), 1054 (s), 1018 (s), 799 (m), 716 (s), 696 (s); ^1H NMR (CD_3OD, 23 °C, δ) 2.41 (s, 3 H, CN_4CH_3); $^{13}C\{^1H\}$ NMR (CD_3OD, 23 °C, ppm) 159.16 (s, CN_4CH_3), 10.15 (s, CN_4CH_3).

Anal. Calc. for $C_2H_3N_4K$: C, 19.66; H, 2.48; N, 45.86. Found: C, 19.77; H, 2.57; N, 45.56%.

3.6. Rubidium methyl tetrazolate (*3*)

Prepared from rubidium hydroxide hydrate (0.394 g, 3.27 mmol) and methyl tetrazole (0.302 g, 3.60 mmol) to afford **3** in 97% yield as a colorless solid: mp 254–256 °C; IR (Nujol, cm^{-1}) 1306 (m), 1194 (s), 1117 (s), 1055 (s), 1019 (s), 997 (m), 716 (s), 694 (s); ^1H NMR (CD_3OD, 23 °C, δ) 2.41 (s, 3H, CN_4CH_3); $^{13}C\{^1H\}$ NMR (CD_3OD, 23 °C, ppm) 159.17 (s, CN_4CH_3), 10.14 (s, CN_4CH_3).

Anal. Calc. for $C_2H_3N_4Rb$: C, 14.25; H, 1.79; N, 33.24. Found: C, 13.61; H, 1.82; N, 32.64%.

3.7. Cesium methyl tetrazolate (*4*)

Prepared from cesium hydroxide hydrate (0.362 g, 2.16 mmol) and methyl tetrazole (0.199 g, 2.37 mmol) to afford **4** in 97% yield as a colorless solid: mp 257 °C; IR (Nujol, cm^{-1}) 1305 (m), 1261 (m), 1194 (s), 1114 (s), 1103 (m), 1049 (s), 1015 (s), 722 (s), 715 (s), 693 (s); ^1H NMR (CD_3OD, 23 °C, δ) 2.41 (s, 3H, CN_4CH_3); $^{13}C\{^1H\}$ NMR (CD_3OD, 23 °C, ppm) 159.17 (s, CN_4CH_3), 10.20 (s, CN_4CH_3).

Anal. Calc. for $C_2H_3CsN_4$: C, 11.12; H, 1.40; N, 25.94. Found: C, 10.49; H, 1.93; N, 25.52%.

3.8. X-ray crystallographic structure determinations of *1*–*4*

Diffraction data were measured on a Bruker *X8* APEX-II kappa geometry diffractometer with Mo radiation and a graphite monochromator. Frames were collected at 100 K as a series of sweeps with the detector set at 40 mm and 0.3° between each frame and were recorded for 5 or 10 s. APEX-II [60] and SHELX-97 [61] software were used in the collection and refinement of the models. Crystals of **1** grew as colorless plates. 15762 reflections were measured, yielding 1663 unique data. Hydrogen atom positions were placed in calculated and observed positions. The sodium, nitrogen, and carbon atoms all occupy crystallographic mirrors; the methyl hydrogen atoms are necessarily disordered through the mirror. The lattice contains a two-dimensional polymeric structure that is cross-linked by hydrogen bonds. Crystals of **2** were obtained as colorless rods. 6630 reflections were counted, which averaged to 1310 independent data. Hydrogen atoms were placed in observed positions. The atoms K(1), C(1), and C(2) occupy a crystallographic mirror plane. The structure consists of a three-dimensional polymer in which each nitrogen atom is bound to two potassium atoms, and every potassium atom is bound to 8 nitrogen atoms. Crystals of **3** were colorless plates. 10496 data were integrated, which averaged into 1256 independent data. The Rb(1), C(1), and C(2) atoms occupy the crystallographic mirror. Complex **3** is isostructural with **2**, although the unit cell is slightly larger in **3** due to the longer Rb–N distances compared to the K–N distances in **2**. Complex **4** crystallized as colorless rods. 5514 data were averaged into 1370 unique data. Hydrogen atoms were placed in calculated positions. The Cs, C(1), and C(2) atoms all occupy a crystallographic mirror. The structure consists of an extended three-dimensional ionic polymer.

Acknowledgement

We are grateful to the Office of Naval Research (Grant No. N00014-07-1-0105) for support of this work.

Appendix A. Supplementary data

CCDC 686698, 686699, 686700 and 686701 contain the supplementary crystallographic data for **1**–**4**. These data can be obtained free of charge via http://www.ccdc.cam.ac.uk/conts/retriev-

ing.html, or from the Cambridge Crystallographic Data Centre, 12 Union Road, Cambridge CB2 1EZ, UK; fax: (+44) 1223-336-033; or e-mail: deposit@ccdc.cam.ac.uk. Supplementary data associated with this article can be found, in the online version, at doi:10.1016/j.poly.2008.07.010.

References

[1] For a recent review of metal tetrazolate complexes, see: P.N. Gaponik, S.V. Voitekhovich, O.A. Ivashkevich, Russ. Chem. Rev. 75 (2006) 507.
[2] M. Friedrich, J.C. Gálvez-Ruiz, T.M. Klapötke, P. Mayer, B. Weber, J.J. Weigand, Inorg. Chem. 44 (2005) 8044.
[3] A. Hammerl, G. Holl, M. Kaiser, T.M. Klapötke, H. Piotrowski, Z. Anorg. Allg. Chem. 629 (2003) 2117.
[4] B.C. Tappan, C.D. Incarvito, A.L. Rheingold, T.B. Brill, Thermochim. Acta 384 (2002) 113.
[5] B.C. Tappan, M.H. Huynh, M.A. Hiskey, D.E. Chavez, E.P. Luther, J.T. Mang, S.F. Son, J. Am. Chem. Soc. 128 (2005) 6589.
[6] M.H.V. Huynh, M.A. Hiskey, T.J. Meyer, M. Wetzler, PNAS 103 (2006) 5409.
[7] B.C. Tappan, R.W. Beal, T.B. Brill, Thermochim. Acta 388 (2002) 227.
[8] F. Himo, Z.P. Demko, L. Noodleman, K.B. Sharpless, J. Am. Chem. Soc. 125 (2003) 9983.
[9] F. Himo, Z.P. Demko, L. Noodleman, K.B. Sharpless, J. Am. Chem. Soc. 124 (2002) 12210.
[10] P. Lin, W. Clegg, R.W. Harrington, R.A. Henderson, Dalton Trans. (2005) 2388.
[11] F.A. Mautner, C. Gspan, K. Gatterer, M.A.S. Goher, M.A.M. Abu-Youssef, E. Bucher, W. Sitte, Polyhedron 23 (2004) 1217.
[12] Z.-R. Qu, H. Zhao, X.-S. Wang, Y.-H. Li, Y.-M. Song, Y.-J. Liu, Q. Ye, R.-G. Xiong, B.F. Abrahams, Z.-L. Xue, X.-Z. You, Inorg. Chem. 42 (2003) 7710.
[13] C.-W. Chang, G.-H. Lee, Organometallics 22 (2003) 3107.
[14] A. Palazzi, S. Stagni, S. Bordoni, M. Monari, S. Selva, Organometallics 21 (2002) 3774.
[15] X. Xue, B.F. Abrahams, R.-G. Xiong, X.-Z. You, Aust. J. Chem. 55 (2002) 495.
[16] (a) S. Stagni, A. Palazzi, S. Zacchini, B. Ballarin, C. Bruno, M. Marcaccio, F. Paolucci, M. Monari, M. Carano, A.J. Bard, Inorg. Chem. 45 (2006) 695;
(b) X.-S. Wang, Y.-Z. Tang, X.-F. Huang, Z.-R. Qu, C.-M. Che, P.W.H. Chang, R.-G. Xiong, Inorg. Chem. 44 (2005) 5278;
(c) Q. Ye, Y.-H. Li, Y.-M. Song, X.-F. Huang, R.-G. Xiong, Z. Xue, Inorg. Chem. 44 (2005) 3618;
(d) T. Wu, B.-H. Yi, D. Li, Inorg. Chem. 44 (2005) 4130;
(e) C. Jiang, Z. Yu, S. Wang, C. Jiao, J. Li, Z. Wang, Y. Cui, Eur. J. Inorg. Chem. (2004) 3662;
(f) C. Jiang, Z. Yu, C. Jiao, S. Wang, J. Li, Z. Wang, Y. Cui, Eur. J. Inorg. Chem. (2004) 4669;
(g) J. Tao, Z.-J. Ma, R.-B. Huang, L.-S. Zheng, Inorg. Chem. 43 (2004) 6133;
(h) X. Xue, X.S. Wang, L.-Z. Wang, R.-G. Xiong, B.F. Abrahams, X.-Z. You, Z.-L. Xue, C.-M. Che, Inorg. Chem. 41 (2002) 6544.
[17] J. Vela, S. Vaddadi, S. Kingsley, C.J. Flaschenriem, R.J. Lachicotte, T.R. Cundari, P.L. Holland, Angew. Chem., Int. Ed. 45 (2006) 1607.
[18] J. Hitzbleck, G.B. Deacon, K. Ruhlandt-Senge, Angew. Chem., Int. Ed. 43 (2004) 5218.
[19] K.R. Gust, J.E. Knox, M.J. Heeg, H.B. Schlegel, C.H. Winter, Angew. Chem., Int. Ed. 41 (2002) 1591.
[20] D. Pfeiffer, M.J. Heeg, C.H. Winter, Angew. Chem., Int. Ed. 37 (1998) 2517.
[21] G.B. Deacon, E.E. Delbridge, C.M. Forsyth, P.C. Junk, B.W. Skelton, A.H. White, Aust. J. Chem. 52 (1999) 733.
[22] I.A. Guzei, A.G. Baboul, G.P.A. Yap, A.L. Rheingold, H.B. Schlegel, C.H. Winter, J. Am. Chem. Soc. 119 (1997) 3387.
[23] D. Röttger, G. Erker, M. Grehl, R. Frölich, Organometallics 13 (1994) 3897.
[24] J.E. Cosgriff, G.B. Deacon, B.M. Gatehouse, Aust. J. Chem. 46 (1993) 1881.
[25] C.W. Eigenbrot Jr., K.N. Raymond, Inorg. Chem. 21 (1982) 2653.
[26] S.M. Arachchige, M.J. Heeg, C.H. Winter, J. Organomet. Chem. 690 (2005) 4356.
[27] J.R. Perera, M.J. Heeg, H.B. Schlegel, C.H. Winter, J. Am. Chem. Soc. 121 (1999) 4536.
[28] J.C. Röder, F. Meyer, E. Kaifer, Angew. Chem., Int. Ed. 41 (2002) 2304.
[29] A. Steiner, G.T. Lawson, B. Walfort, D. Leusser, D. Stalke, J. Chem. Soc., Dalton Trans. (2001) 219.
[30] G.B. Deacon, E.E. Delbridge, C.M. Forsyth, B.W. Skelton, A.H. White, J. Chem. Soc., Dalton Trans. (2000) 745.
[31] F. Nief, Eur. J. Inorg. Chem. (2001) 891.
[32] J.E. Cosgriff, G.B. Deacon, Angew. Chem., Int. Ed. 37 (1998) 286.
[33] G. La Monica, G.A. Ardizzoia, Prog. Inorg. Chem. 46 (1997) 151.
[34] A.P. Sadimenko, S.S. Basson, Coord. Chem. Rev. 147 (1996) 247.
[35] S. Trofimenko, Prog. Inorg. Chem. 34 (1986) 115.
[36] S. Trofimenko, Chem. Rev. 72 (1972) 497.
[37] All X-ray crystallographic structure searches were carried out using version 5.29 of the Cambridge Crystallographic Database (November 2007).
[38] (a) A. Rodríguez-Diéguez, A. Salinas-Castillo, S. Galli, N. Masciocchi, J.M. Gutiérrez-Zorilla, P. Vitoria, E. Colacio, Dalton Trans. (2007) 1821;
(b) X.-M. Zhang, Y.-F. Zhao, H.-S. Wu, S.R. Batten, S.W. Ng, Dalton Trans. (2006) 3170;
(c) X.-F. Huang, Y.-M. Song, Q. Wu, Q. Ye, X.-B. Chen, R.-G. Xiong, X.-Z. You, Inorg. Chem. Commun. 8 (2005) 58;
(d) C.-Y. Geng, M.-C. Hu, S.-N. Li, Q.-G. Zhai, Y.-C. Jiang, Z.-H. Liu, Acta Chim. Sin. 21 (2005) 1974;
(e) T.M. Klapötke, C. Kuffer, P. Mayer, K. Polborn, A. Schulz, J.J. Weigand, Inorg. Chem. 44 (2005) 5949;
(f) G. Singh, R. Prajapati, R. Frohlich, J. Hazard. Mater. A118 (2005) 75;
(g) A. Hammerl, G. Holl, T.M. Klapötke, P. Mayer, H. Nöth, H. Piotrowski, M. Warchhold, Eur. J. Inorg. Chem. (2002) 834;
(h) H.P.H. Arp, A. Decken, J. Passmore, D.J. Wood, Inorg. Chem. 39 (2000) 1840;
(i) G.J. Palenik, Acta Crystallogr. 16 (1963) 596.
[39] V. Ernst, T.M. Klapötke, J. Stierstorfer, Z. Anorg. Allg. Chem. 633 (2007) 879.
[40] T.M. Klapötke, H. Radies, J. Stierstorfer, Z. Naturforsch. 62b (2007) 1343.
[41] X.-R. Hu, Y.-W. Wang, J.-M. Gu, Acta Crystallogr., Sect. E E61 (2005) m1686.
[42] L.A. Solovyov, A.M. Astachov, M.S. Molokeev, A.D. Vasiliev, Acta Crystallogr., Sect. B B61 (2005) 435.
[43] E.V. Tretyakov, S.V. Fokin, G.V. Romanenko, V.I. Ovcharenko, Polyhedron 22 (2003) 1965.
[44] D. Fernández, D. Vega, J.A. Ellena, G. Echeverría, Acta Crystallogr., Sect. C C58 (2002) m418.
[45] G.A. Stephenson, B.A. Diseroad, Int. J. Pharmaceut. 198 (2000) 167.
[46] Y. Nagao, T. Hirata, S. Goto, S. Sano, A. Kakehi, K. Iizuka, M. Shiro, J. Am. Chem. Soc. 120 (1998) 3104.
[47] J.P. Yevich, D.A. Temple Jr., R.R. Covington, D.A. Owens, R.J. Seidehamel, K.W. Dungan, J. Med. Chem. 25 (1982) 864.
[48] W. Zheng, M.J. Heeg, C.H. Winter, Angew. Chem., Int. Ed. 42 (2003) 2761.
[49] I. Kobrsi, W. Zheng, J.E. Knox, M.J. Heeg, H.B. Schlegel, C.H. Winter, Inorg. Chem. 45 (2006) 8700.
[50] I. Kobrsi, J.E. Knox, M.J. Heeg, H.B. Schlegel, C.H. Winter, Inorg. Chem. 44 (2005) 4894.
[51] L.E. Fried, M.R. Manaa, P.F. Pagoria, R.L. Simpson, Annu. Rev. Mater. Sci. 31 (2001) 291.
[52] H.J. Wadsworth, S.M. Jenkins, B.S. Orlek, F. Cassidy, M.S.G. Clark, F. Brown, G.J. Riley, D. Graves, J. Hawkins, C.B. Naylor, J. Med. Chem. 35 (1992) 1280.
[53] R.J. Spear, Aust. J. Chem. 37 (1984) 2453.
[54] A. Schmidpeter, G. Jochem, Z. Naturforsch. 48B (1993) 93.
[55] A.I. Podgurskii, S.G. Zlotin, M.M. Krayushkin, O.A. Luk'yanov, Izv. Akad. Nauk SSSR Ser. Khim. (1985) 236.
[56] M.M. Williams, W.S. McEwan, R.A. Henry, J. Phys. Chem. 61 (1957) 261.
[57] A. Bondi, J. Phys. Chem. 68 (1964) 441.
[58] N.L. Allinger, J.A. Hirsch, M.A. Miller, I.J. Tyminski, F.A. Van-Catledge, J. Am. Chem. Soc. 90 (1968) 1199.
[59] A.I. Lesnikovich, G.V. Printsev, O.A. Ivashkevich, P.N. Gaponik, V.A. Shandakov, Thermochim. Acta 184 (1991) 221.
[60] APEX II Collection and Processing Programs are Distributed by the Manufacturer, Bruker AXS Inc., Madison, WI, USA, 2005.
[61] G.M. Sheldrick, Acta Crystallogr., Sect. A 64 (2008) 112.

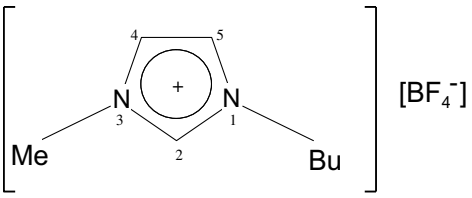

Chart 1. The ionic liquid used in this study.

ppm relative to tetramethylsilane (TMS) as external standard. The synthesized [BMIm][BF_4] has the following spectral characteristics: ^{1}H NMR ($CDCl_3$): 8.54 [s, 1H, H(2)]; 7.45 [s, 1H, H(4)]; 7.40 [s,1H, H(5)]; 4.07 [t, 2H, $^3J_{HH}$ = 6.6 Hz, H(6)]; 3.79 [s, 3H, H(10)]; 1.70 and 1.13 [2m, 4H, H(7) and H(8)]; 0.69 [t, 3H, $^3H_{HH}$ = 7.2 Hz, H(9)]. ^{13}C NMR ($CDCl_3$): 136.48 [C(2)]; 123.33 [C(4)]; 122.01 [C(5)]; 48.95 [C(6)]; 35.36 [C(10)]; 31.48 [C(7)]; 18.83 [C(8)]; 12.61 [C(9)].

Infrared spectra (IR) were recorded on ABB BOMEM model FTLA 2000-100 FTIR spectrometer using an Axiom Analytical DPR 207 immersion probe.

2.3. Water content analysis

The water content in the synthesized ILs was determined using a coulometric Karl–Fischer titration (Titrino 756 KF Metrohm) and duplicate measurements were performed with results agreeing to within 5%.

All aqueous solutions were prepared with deionized water that was purified using a LAB-UPW water purification system. The water employed has a conductivity value of less than 1.2 μS cm^{-1}.

2.4. Density measurements

All densities were determined by gravimetric analysis using a calibrated 10 mL volumetric pipette. Deionized water was employed as reference for calibration. All measurements were taken at 25.00 ± 0.01 °C using a thermostated water bath and repeated at least three times.

2.5. Viscosity measurements

The viscosities were determined using an Ubbelohde capillary viscosimeter. A 10 mL sample was used and the temperature was maintained at 25.00 ± 0.01 °C. The absolute viscosity (η) for each [BMIm][BF_4]/H_2O mixture was calculated using

$$\eta = \rho k t$$

where ρ is the density measured for each mixture, k is the constant of the viscosimeter and t is the mean flow time.

2.6. Surface tension measurements

The surface tension (γ) was measured by capillary ascension using

$$\Delta h \rho g = 2\gamma / r$$

where Δh is the capillary ascension, ρ is the density of the analyzed solution, g is the acceleration due to gravity and r is the radius of the capillary employed. The temperature was maintained constant at 25.00 ± 0.01 °C during the measurements.

2.7. Conductivity measurements

All the conductivity measurements were carried out with a Digimed DM-31 digital conductimeter equipped with a platinum electrodes cell calibrated at 25 °C by using aqueous KCl solution. The temperature of the sample was maintained at 25.00 ± 0.01 °C during the measurements.

3. Results and discussion

3.1. Water absorption by [BMIm][BF_4]

Atmospheric water is slowly absorbed by [BMIm][BF_4] as shown in Fig. 1 [room temperature and 80% air humidity]. It can be observed that the [BMIm][BF_4] absorbs water continuously and that the absorption rate decreases with time of exposure. After a 1 day exposure of [BMIm][BF_4] to an environment with 80% humidity, the water content attains only ca. 0.5 weight% and a composition of 4.0 weight% is obtained after 20-day exposure.

3.2. Physico-chemical properties

The physico-chemical properties studied in the present work (density, viscosity, excess molar volume, surface tension and conductivity) are summarized in Tables 1 and 2.

3.2.1. Density

Increasing the water content causes a decrease in solution density. Fig. 2a shows that the density depends linearly on the molar

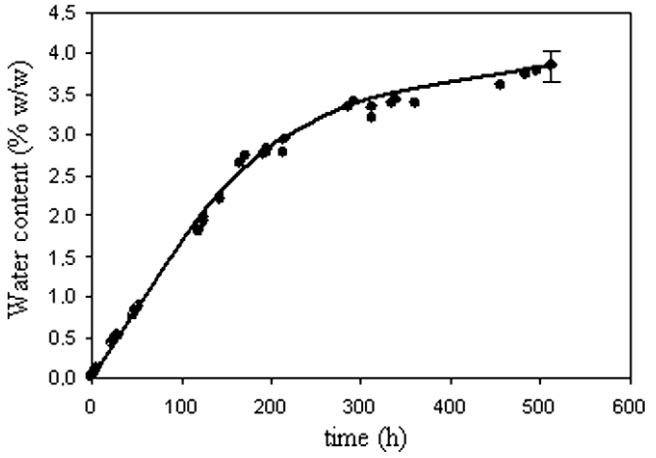

Fig. 1. Absorption of water by [BMIm][BF_4] from atmospheric air at 25 °C and 80% of humidity, with constant stirring as a function of the time exposure.

Table 1
The density, viscosity, excess molar volume and surface tension of aqueous solutions of [BMIm] [BF_4] at 25 °C and at different IL concentrations

IL concentration (C_{IL}/mol l^{-1})	IL Mole fraction (x_{IL})	Density (ρ/g cm^{-3})	Viscosity (η/cP)	Excess molar volume (V_{exc}/cm^3 mol^{-1})	Surface tension (γ/mN m^{-1})
5.367	1.0000	1.2131	106.820	0.000	36.43
5.130	0.9040	1.2101	86.020	0.137	36.82
5.099	0.6451	1.2011	40.110	0.199	
4.830	0.4626	1.1904	19.500	0.195	37.85
4.294	0.2767	1.1704	7.270	0.112	39.12
3.757	0.1825	1.1501	4.380	0.087	39.45
3.220	0.1255	1.1299	3.400	0.067	39.85
2.684	0.0873	1.1100	2.600	0.045	40.55
2.147	0.0600	1.0897	2.080	0.038	42.15
1.610	0.0394	1.0697	1.650	0.028	
1.073	0.0234	1.0501	1.350	0.012	47.67
0.537	0.0105	1.0298	1.120	0.008	56.03
0.054	0.0010	1.0119	0.992	0.002	
0.000	0.0000	1.0099	0.959	0.000	73.05

Table 2
The specific conductance at 25 °C of aqueous solutions of [BMIm] [BF_4] at different IL concentrations

IL concentration (C_{IL}/mol l^{-1})	IL Mole fraction (x_{IL})	Specific condutance (mS cm^{-1})
0.00000	0.0000	0.001113
0.00537	0.0001	0.587
0.01073	0.0002	0.987
0.02147	0.0004	1.345
0.03220	0.0006	1.627
0.04294	0.0008	2.00
0.05367	0.0010	2.40
0.08051	0.0015	3.70
0.10734	0.0019	4.70
0.21468	0.0040	8.70
0.32202	0.0061	12.10
0.42936	0.0082	15.90
0.53670	0.0105	19.40
0.64404	0.0129	23.00
0.75138	0.0153	26.80
0.85872	0.0179	29.80
0.96607	0.0206	33.00
1.07341	0.0234	36.20
1.34176	0.0309	39.60
1.61011	0.0394	42.40
2.14680	0.0600	46.30
2.68350	0.0873	48.30
3.22020	0.1255	47.70
3.75690	0.1825	45.50
4.29360	0.2767	38.90
4.83030	0.4626	28.90
5.09870	0.6451	18.32
5.31340	0.9045	9.56
5.36700	1.0000	5.86

concentration (d = 0.0376 C + 1.009), which can be useful to predict water concentrations in this class of ILs.

On the other hand, the dependence of the density with the mole fraction is not linear, as shown in Fig. 2b. Two regions are shown: a water-rich and a salt-rich region. When water is added to the IL in the salt-rich region, ($x_{[BMIm][BF_4]}$ = 1 to ca. 0.3), the density decreases slowly, but in the water-rich region, ($x_{[BMIm][BF_4]}$ = ca. 0.3 to 0) the density decreases rapidly with small additions until the value of pure water. Similar results have been described by Liu et al. [53] and Zhou et al. [54].

3.2.2. Viscosity

The viscosity of the IL solutions depends strongly on their concentration as shown in Figs. 3a and b. Table 1 shows that the viscosity for pure [BMIm][BF_4] (106.82 cP) is comparable to the density of a typical oil. The addition of water, whose viscosity is 0.959 cP, decreases solution viscosity as shown in Fig. 3. When the concentration is expressed as molarity (Fig. 3a) two regions can be observed, similarly to the previously described behavior of the density (Fig. 2b). Increasing the IL content of the mixture in the dilute region does not have much effect on increasing mixture viscosity. On the other hand, for the concentrated region, the viscosity increases rapidly with the IL concentration.

The viscosity of an IL solution can be correlated with the supramolecular structure of the liquid network. The experimental findings indicate that a small addition of water is enough to drastically change the intermolecular interactions and to affect the dependence between viscosity and concentration.

The curve viscosity versus concentration expressed in molar fraction, shown in Fig. 3b, can be fitted by an exponential function as

$$\eta = \eta_{IL}\exp(-x_{H_2O}/a)$$

where η is the viscosity of the system, η_{IL} is the viscosity of the pure IL, x_{H_2O} is the molar fraction of water and a is a constant with value of 0.212 for the [BMIm][BF_4]. This function enable the prediction of the viscosity at different water contents and also to determine water content through viscosity experiments.

The viscosity of the ILs has been described as decreasing with the addition of co-solvents proportionally to its dielectric constant [52,57,58]. Nevertheless, the viscosity of a mixture with a known IL concentration can be predicted, in general, by the exponential relationship, regardless of the co-solvent polarity [52].

3.2.3. Conductivity

Figs. 4a and b show the dependence of the specific conductivity of IL/water solutions on the concentration. The plots exhibit a maximum conductivity around 48 mS cm^{-1} at a concentration of 2.7 mol L^{-1} (Fig. 4a), corresponding to a 0.09 mole fraction (Fig. 4b).

Once again the system properties show a water-rich and a salt-rich region, shown by a maximum of the abovementioned specific conductivity. This maximum appears for a solution with an IL molarity ca. 2.7 mol L^{-1} or a mole fraction of 0.09. Fig. 4b shows that the conductivity increases rapidly in the water-rich region and decreases linearly in the salt-rich region, as IL concentration increases.

Thus, in the water-rich region, increasing conductivity may be attributed to the dissociation increase of the [BMIm][BF_4] ionic li-

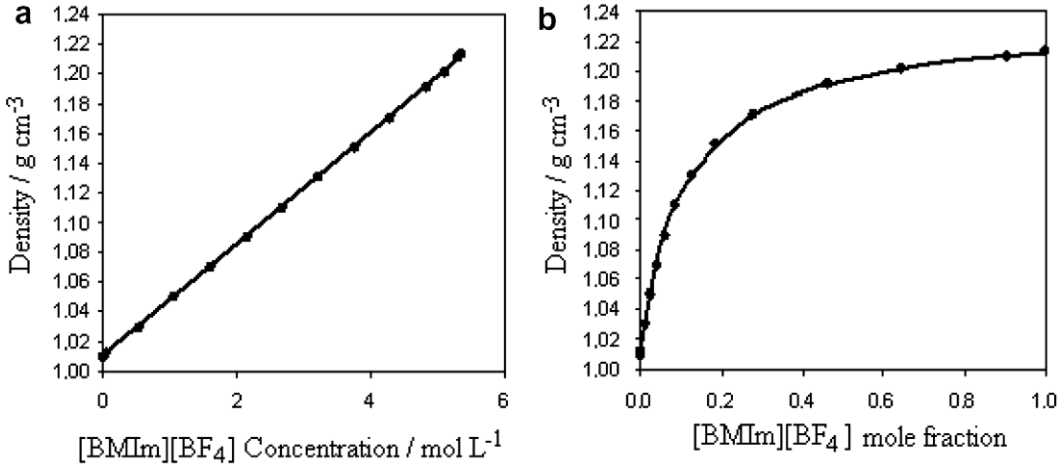

Fig. 2. Concentration dependence {molar concentration (a) and mole fraction (b)} of the density for aqueous [BMIm][BF_4] solutions.

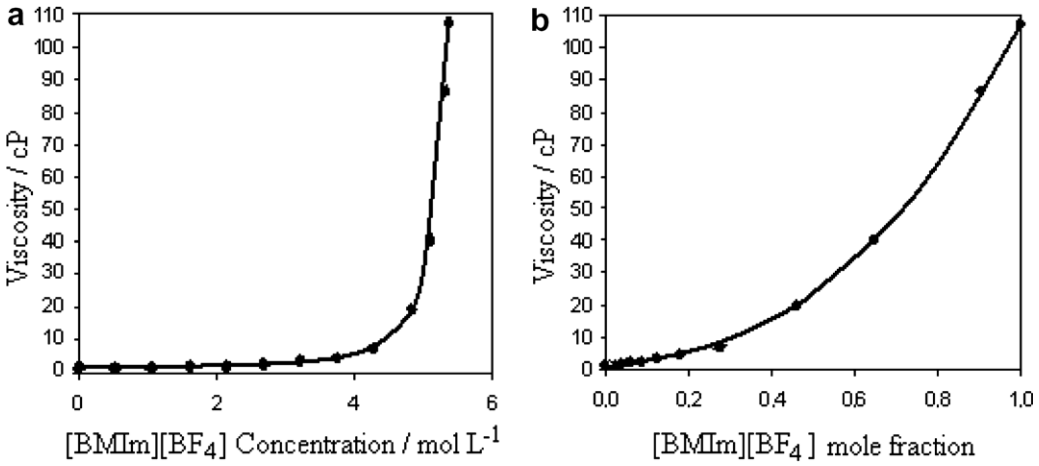

Fig. 3. Concentration dependence {molar concentration (a) and mole fraction (b)} of the viscosity for aqueous [BMIm][BF_4] solutions.

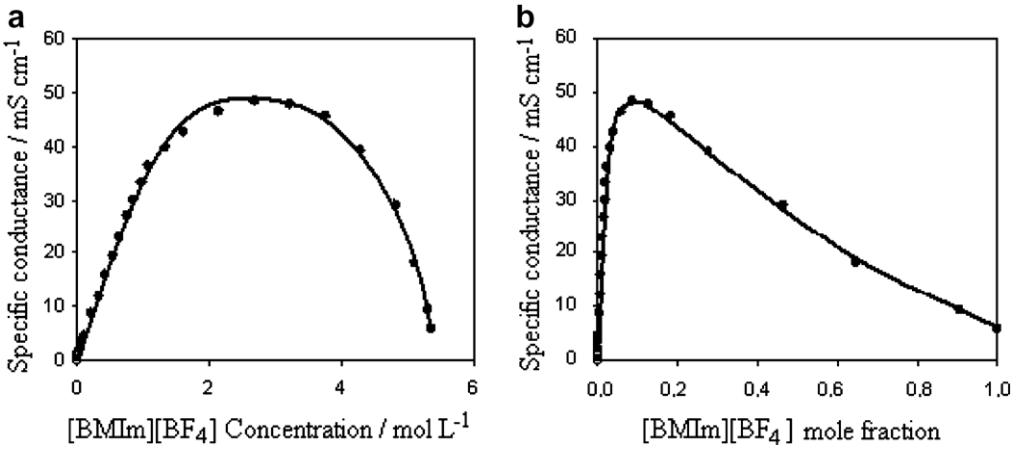

Fig. 4. Concentration dependence {molar concentration (a) and mole fraction (b)} of the specific conductance for aqueous [BMIm][BF_4] solutions.

quid. In this region, water acts as a solvent, interacting with the IL cations and anions. This interaction leads to the weakening and even breaking of the strong Coulombic forces involved in keeping ions dissociated. Therefore, in this region, solvated cations and anions are present and also water molecules that are not hydrogen bonded to the salt (the so-called "free water" [58]).

It is worthwhile pointing out that ILs may form contact ion-pairs and aggregates in solution, which cannot contribute to the ionic conduction as well as dissociated ions, responsible for conduction [59,60]. Moreover, ionic conductivity is proportional to the number of charge carrier ions and their mobility. Therefore it can be pointed out that the solvation effect of the water on the [BMIm][BF_4] has two important consequences. The first involves a reduction of the [BMIm][BF_4]$_{aq}$ structure size. In this respect, it was demonstrated that the structure of pure dialkylimidazolium ionic liquids can be considered as a highly ordered three-dimensional network of anions e cations, linked by hydrogen bonds [61–65]. The addition of water molecules to IL progressively reduces the electrostatic attractions between the ions, promoting its separation with a disruption of the hydrogen bond network leading to the formation of ionic aggregates, contact ions pairs and finally, in infinite dilution, solvated separated ion pairs. This process is expressed by the consequent increase of the ionic mobility of the ionic species. Moreover, the overall cohesive energy of the system is lowered and hence its viscosity is lowered too, as observed in Figs. 3a and b more specifically for the mixtures belonging to the water-rich region. The second immediate consequence of the dissociation of the ionic structure is the increasing number of charge carrier species responsible for electrical conduction of the system. In this way, both consequences are beneficial to increase the ionic conductivity, in agreement with experimental results obtained in this concentration region.

Another point to be considered is that the reduced cohesive energy is a likely cause of the volumetric expansion of the system from the pure IL, as will be demonstrated later.

In the salt-rich region, increasing concentration of [BMIm][BF_4] results in decreasing ionic specific conductivity. It is suggested that this is due to the exponential increase of the viscosity of the solutions in this region, as shown in Fig. 3b. Such behavior can be explained by Walden's rule [66], which is derived from the Stokes–Einstein equation, in which the diffusion coefficient of a fluid particle in a solution is inversely proportional to solution viscosity and from the Nernst–Einstein law, in which this diffusion coefficient is directly proportional to molar conductivity of the solution [67]. The resulting empirical rule is given by

$$\Lambda\eta = \text{constant}$$

which states that the product of molar conductivity (Λ) and viscosity (η) of hydrodynamic systems having moving conducting entities is a constant at a given temperature.

Thus, in the salt-rich region, the [BMIm][BF_4] solutions exhibit a decrease in the conductivity parallel to the increase in viscosity.

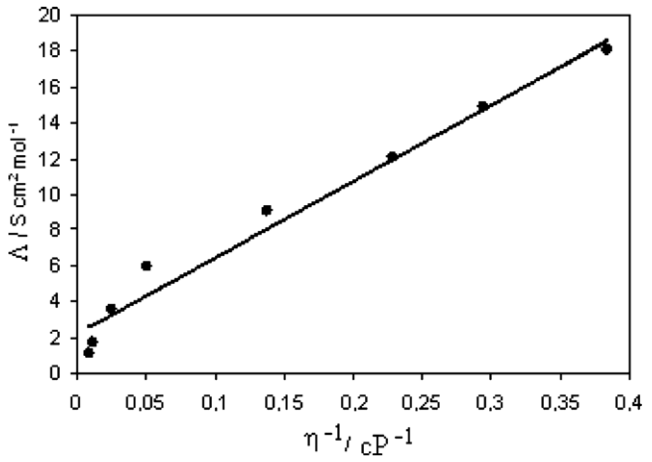

Fig. 5. Walden's plot: a plot of the molar conductivity (Λ) against the reciprocal of the viscosity (η^{-1}) for [BMIm][BF_4]. Data collected at 25 °C. — Linear plot corresponding to Walden's law.

Fig. 5 represents Walden's plot of the [BMIm][BF_4]/H_2O system for this region. The use of Walden's rule in the system studied evidence that, in the salt concentrated region, conductivity is related to the viscosity of the media i.e., in this region transport of the charge is controlled by the viscosity.

Another point that must be considered to explain the behavior observed in this region involves the reduction of the degree of dissociation of [BMIm][BF_4] because of the decreased water content, leading to a lower concentration of ionic mobile species in solution and hence decreasing the ionic conductivity. This result agrees with the general recognition that a lower degree of dissociation of a salt leads to lower conductivity due to the reduction of the charge carrier concentration.

In order to determine the limiting molar conductivity (Λ_o), the molar conductivity ($\Lambda = \kappa/C$) was plotted against the square root of the IL concentration and the Λ values in the low concentration domain were extrapolated to infinite dilution, as shown in Fig. 6. The extrapolated value found was 142.05 S cm^2 mol^{-1}. Similar results were found for other aqueous systems involving [DMIm]Br, [BMIm]Br and [EMIm]Cl [28,64].

The value of the limiting molar conductivity for solutions of [BMIm][BF_4] in water is in the same range as other classical salts like tetraalkylammonium salts [68], characteristic for 1:1 electrolytes. Thus, the solvation of [BMIm][BF_4] in water can be described by the equilibrium between the solvated contact ion pairs and the solvated unassociated ions, according to the following equation:

$$([BMIm^+ \cdots [BF_4]^-)_{H_2O} \leftrightarrow ([BMIm]^+)_{H_2O} + ([BF_4]^-)_{H_2O}$$

The specific conductivity behavior of the [BMIm][BF4]/H_2O system for low IL concentrations was studied in order to elucidate whether this IL can show association forming aggregates, i.e., micelles. A representative result is shown in Fig. 7.

It is apparent that the gradual increase of the IL concentration leads to two readily distinguishable linear dependencies. In the low concentration domain the increase of specific conductivity is due to the increasing number of $[BMIm]^+$ and $[BF_4]^-$ moieties. In this region the IL behaves like a strong electrolyte, suffering complete dissociation and behaving like a usual 1:1 electrolyte, as demonstrated by the use of Kohlrausch's law (Fig. 6). However, the abrupt change of the slope in the specific conductivity versus concentration plot indicates that micelles, start to form at the concentration corresponding to the break point, suggesting a structural resemblance of imidazolium IL to conventional cationic surfactants. The polar or hydrophilic group (the "head") is constituted by imidazolium cations, and the hydrophobic group (the "tail") is formed by nonpolar alkyl side chains. The tetrafluoroborate is the counter-ion, which has a fundamental role: when in adequate concentration, surrounding the positive charge of the aggregates, decreasing the repulsion of the head-groups. Micelles are not completely dissociated, i.e., only a small fraction remains free in solution, assuming the behavior of a weak electrolyte. The critical micellar concentration (cmc) determined is an intrinsic property and characteristic of each surface-active species.

The value obtained for the cmc for the [BMIm][BF_4]/H_2O system (around 1.0 mol L^{-1}) is considerably higher than those for typical cationic surfactants. This behavior is a consequence of the short, length of the alkyl substituents (methyl and butyl). It is well known [24–28] that, for single alkyl chain surfactants, the cmc value depends primarily on the number of carbon atom substituents incorporated in the IL structure. Above the critical micellar concentration (cmc) the increase of the specific conductivity has a smaller slope due to two reasons: (i) the association of a fraction of the counter-ion with the micellar surface results in an effective decrease in the number of ionic charge carriers and (ii) the micelles can contribute to the charge transport to a lesser extent than the free ions owing to their lower mobility. As the concentration of the surfactant ([BMIm][BF_4]) increases, the association between

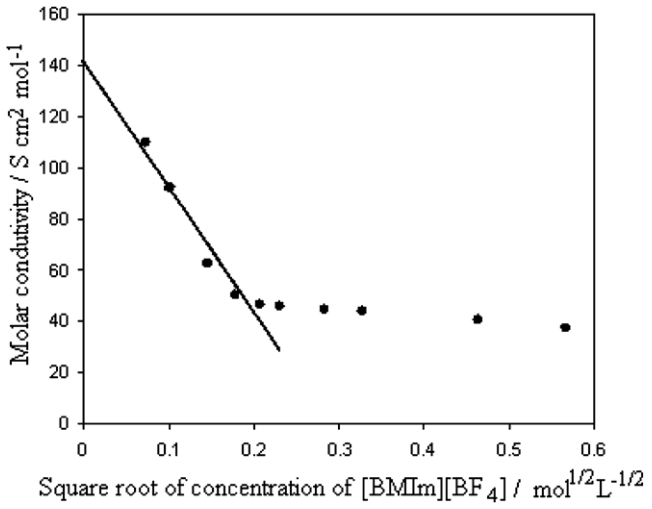

Fig. 6. Molar conductivity vs square root of concentration for aqueous [BMIm][BF_4] solutions. Data collected at 25 °C. — Linear plot corresponding to Kohlrausch's law.

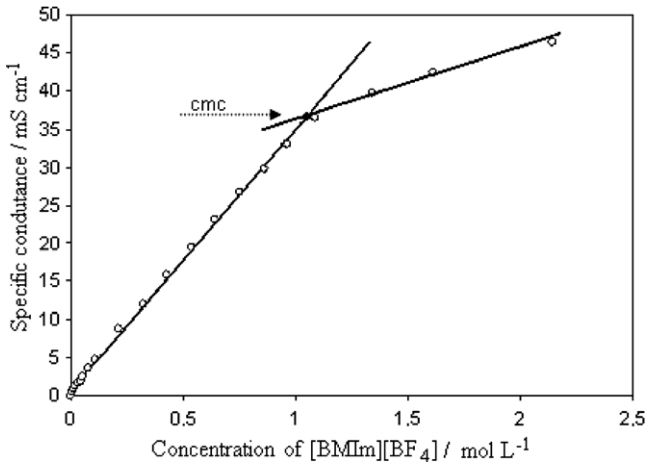

Fig. 7. Specific conductance vs concentration for aqueous [BMIm][BF_4] solutions.

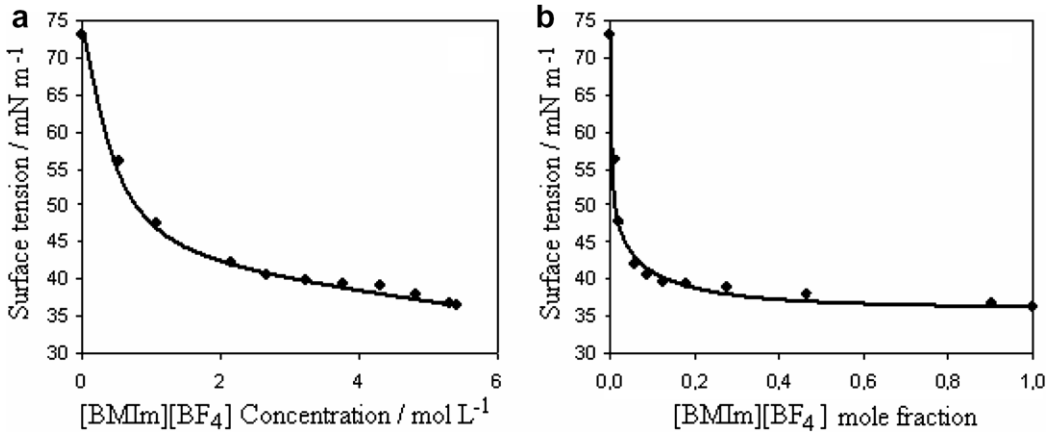

Fig. 8. Concentration dependence {molar concentration (a) and mole fraction (b)} of the surface tension for aqueous [BMIm][BF_4] solutions.

cations and anions is favored, thus resulting in a higher number of nonconducting aggregates of IL dispersed in water and a second interpenetrated phase is created within the first. The conductivity of the system, then, decreases until it reaches the low value of the pure IL, as previously explained.

3.2.4. Surface tension

As shown in Figs. 8a and b, the surface tension of the [BMIm][BF_4]/H_2O system reveals two distinct tendencies: it decreases rapidly in the water-rich region and becomes almost constant in the salt-rich region. This behavior is typical of surface active molecules showing that [BMIm][BF_4] acts as a surfactant in aqueous solution. The surface tension value obtained for pure [BMIm][BF_4] (36.43 mN m^{-1}) is somewhat higher than traditional organic solvents [69], whose values are in the 20–30 mN m^{-1} range and lower than water, which has a high surface tension, in the range of 72 mN m^{-1}, in accordance with Huddleston et al. [70].

An excess property of a solution is defined as the difference between the actual property of the mixture and that which would be obtained for an ideal solution at the same temperature, pressure and composition. So, the excess molar properties represent the deviation from ideal behavior of the mixtures and are very important for understanding the nature of the interactions and of the molecular aggregations existing in binary mixtures. The excess molar volumes (V_{exc}) were calculated from our measurements according to the following equation [71]:

$$V_{exc} = [x_1M_1 + x_2M_2/\rho] - [x_1M_1/\rho] - [x_2M_2/\rho_2]$$

where ρ is the viscosity of the mixtures, x_1 and x_2 are mole fractions, M_1 and M_2 are molar masses and ρ_1 and ρ_2 are densities of [BMIm][BF_4] and water, respectively. The plot of the excess molar volume in function of the [BMIm][BF_4] concentration is shown in Fig. 9.

From Fig. 9, it can be seen that the values of V_{exc} are positive throughout the range of composition, indicating a positive deviation from ideal behavior and suggesting that water reduces and even breaks the strong electrostatic attractions between cations and anions of the pure IL during the mixing process. This assumption was investigated using infrared spectroscopy for the [BMIm][BF_4]/H_2O system.

The IR spectra obtained for the [BMIm][BF_4] identified the characteristic C–H···F hydrogen bonding bands in the region of 3100–3200 cm^{-1} concerning the interactions of the H2, H4 and H5 of the imidazolium ring with the BF_4 anion [62,63]. The bands at 2800–3000 cm^{-1} are due to C–H stretches of methyl and butyl groups. It was observed that the bands at 3128 cm^{-1} and at 3166 cm^{-1}, ascribed to the C2 and C4, C5 hydrogen stretching,

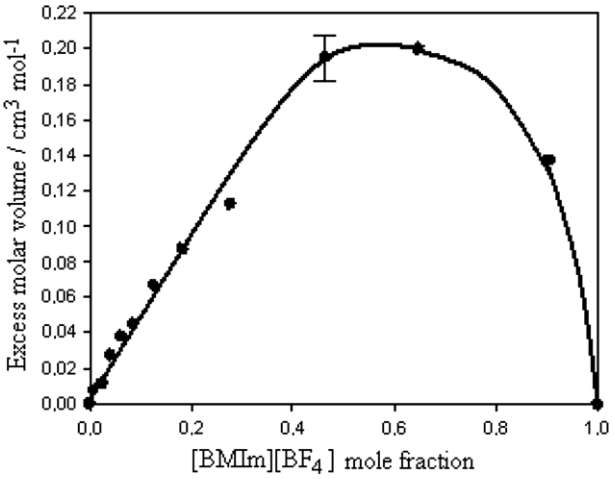

Fig. 9. Excess molar volume for [BMIm][BF_4]/H_2O mixtures at 25 °C vs mole fraction of [BMIm][BF_4].

respectively, both observed in the pure IL, are shifted as the water content increases, to 3142 cm^{-1} and 3198 cm^{-1}, respectively. This tendency suggests a weakening and even a breaking of the strong attraction forces involved between cations and anions. These results are in agreement with the conductivity measurements and excess molar volume values. The shift of the C–H stretching value can be observed until a concentration of 2.68 mol L^{-1}. For higher concentrations values, the bands pertaining to the water molecule completely overlapped the [BMIm][BF_4] bands.

4. Conclusions

The density, viscosity, and surface tension of the [BMIm][BF_4]/H_2O system depends on the molar fraction of the mixtures. It is clear that there are a water-rich and a salt-rich region in which the effect of water addition is drastically different. The presence of water strongly affects (i) the density and the surface tension of water-rich solutions and (ii) the viscosity of salt-rich solutions. Such behavior, characterized by an exponential dependence of the viscosity with the molar fraction, provides a practical method for the quantitative determination of the amount of water in the solution using simple measures of this physico-chemical property.

Specific conductivity of the IL solutions increases in the water-rich region and decreases in the salt-rich region, exhibiting a maximum at IL mole fraction ca. 0.09. Increasing specific conductivity

has been attributed to the weakness of the intermolecular interaction of the [BMIm][BF_4] structure provoked by adding water, increasing the dissociation and, consequently, increasing the ionic mobility of the ionic species. The decrease in the intermolecular interaction between the anionic and cationic species of [BMIm][BF_4] due to the addition of water has been shown by IR. The decrease of the specific conductivity in the salt-rich region has been explained taking into account the viscosity increase, which follows the empirical Walden's rule, and also considering the reduction of the dissociation degree of the IL.

Applying Kohlrausch's equation to specific conductivity for low IL concentration solutions (lower than 0.04 IL mol^{-1}) allows the determination of the [BMIm][BF_4] limiting molar conductivity. The observed value of 142.05 S cm^2 mol^{-1} is characteristic of a 1:1 electrolyte.

Conductivity and surface tension measurements, herein reported, shows that [BMIm][BF_4] IL displays cationic surfactant properties characteristic of micelles. The critical micellar concentration (cmc) of 1.07 mol L^{-1} determined through conductivity measurements indicates that [BMIm][BF_4] behaves like a weak electrolyte above this value.

Finally, the excess molar volume values of the water content IL solutions indicated a positive deviation from ideal behavior. These measures confirmed that added water in IL solution is responsible for a progressive weakness of the intermolecular interaction of IL molecules.

Thus, this study demonstrates that addition of water to [BMIm][BF_4] solutions affects density, viscosity, surface tension, specific conductivity and excess volume values which can be explained by change in the molecular organization of the solution. These results are helpful for a variety of different technological applications and in particular for electrochemical applications.

Acknowledgements

Financial support by PRONEX/FAPERGS, CNPq and the LAPPS – UFRGS for the water contents determination are gratefully acknowledged.

References

[1] H. Ohno, Electrochemical Aspect of the Ionic Liquids, first ed., John Wiley & Sons, New York, 2005.
[2] J.D. Holbrey, K.R. Seddon, J. Chem. Soc. (1999) 2133.
[3] T. Welton, Chem. Rev. 99 (1999) 2071.
[4] P.A.Z. Suarez, S. Einloft, J.E.L. Dullius, R.F. de Souza, J. Dupont, J. Chim. Phys. Phys. Chim. Biol. 95 (1998) 1626.
[5] J.E.L. Dullius, P.A.Z. Suarez, S. Einloft, R.F. de Souza, J. Dupont, J. Fischer, A. De Cian, Organometallics 17 (1998) 815.
[6] J.S. Wilkes, M.J. Zaworotko, J. Chem. Soc., Chem. Commun. (1992) 965.
[7] J.S. Wilkes, J.A. Lewisky, R.A. Wilson, C.L. Hussey, Inorg. Chem. 21 (1982) 1263.
[8] C. Chiappe, D. Pieraccini, P. Saullo, J. Org. Chem. 68 (2003) 6710.
[9] J. Dupont, R.F. de Souza, P.A.Z. Suarez, Chem. Rev. 102 (2002) 3667.
[10] P. Wasserscheid, W. Keim, Angew. Chem., Int. Ed. Engl. 39 (2000) 3772.
[11] M.J. Earle, K.R. Seddon, Pure Appl. Chem. 72 (2000) 1391.
[12] P.A.Z. Suarez, J.E.L. Dullius, S. Einloft, R.F. de Souza, J. Dupont, Polyhedron 15 (1996) 1217.
[13] C.M. Gordon, Appl. Catal. A 222 (2001) 101.
[14] H. Olivier, Y. Chauvin, Chem. Ind. 68 (1996) 249.
[15] Y. Chauvin, H. Olivier-Bourbigou, Chemtech 25 (1995) 26.
[16] L.C. Branco, J.G. Crespo, C.A.M. Afonso, Angew. Chem., Int. Ed. Engl. 41 (2002) 2771.
[17] A.G. Fadeev, M.M. Meagher, Chem. Commun. (2001) 295.
[18] J.G. Huddleston, H.D. Willaver, R.P. Swatloski, A.E. Visser, D. Rogers, Chem. Commun. (1998) 1765.
[19] S. Park, R. Kazlauskas, Curr. Opin. Biotechnol. 14 (2003) 432.
[20] P. Lozano, T. de Diego, D. Came, M. Vaultier, J.L. Iborra, Biotechnol. Prog. 19 (2003) 380.
[21] S.G. Cull, J.D. Holbrey, V. Vargas-Mora, K.R. Seddon, G.J. Lye, Biotechnol. Bioeng. 69 (2000) 227.
[22] R.A. Reich, P.A. Stewart, J. Bohaychick, J.A. Urbanski, Lub. Eng. 59 (2003) 16.
[23] C.F. Ye, W.M. Liu, Y.X. Chen, L.G. Yu, Chem. Commun. (2001) 2244.
[24] T. Inove, H. Ebina, B. Dong, L. Zheng, J. Colloid Interface Sci. 314 (2007) 236.
[25] O.A. El Seoud, P.A.R. Pires, T. Abdel-Moghny, E.L. Bastos, J. Colloid Interface Sci. 313 (2007) 296.
[26] R. Vanyúr, L. Biczók, Z. Miskolczy, Colloid Surf. A 299 (2007) 256.
[27] Q.Q. Baltazar, J. Chandawalla, K. Sawyer, J.L. Anderson, Colloid Surf. A 302 (2007) 150.
[28] J. Sirieix-Plénet, L. Gaillon, P. Letellier, Talanta 63 (2004) 979.
[29] A. Balducci, U. Bardi, S. Caporali, M. Mastragostino, F. Soavi, Electrochem. Commun. 6 (2004) 566.
[30] T. Sato, G. Masuda, K. Takagi, Electrochim. Acta 49 (2004) 3603.
[31] A. Lewandowski, A. Swiderska, Solid State Ionics 161 (2003) 243.
[32] M. Ue, M. Makeda, T. Takahashi, M. Takehara, Electrochem. Solid State Lett. 5 (2002) 119.
[33] B. Garcia, S. Lavallée, G. Perron, C. Michot, M. Armand, Electrochim. Acta 49 (2004) 4583.
[34] A. Webber, G.E. Blomgren, in: W.A. van Schalkwjik, B. Scrosati Kluver (Eds.), Advances in Lithium-Ion Batteries, Academic/Plenum Publishers, New York, 2002.
[35] M. Kosmulski, R.A. Osteryoung, M. Ciszkowska, J. Electrochem. Soc. 147 (2000) 1454.
[36] N. Papagerorgiou, Y. Athanassov, M. Armand, P. Bonhôte, H. Pettersson, A. Azam, M. Grätzel, J. Electrochem. Soc. 143 (1996) 3099.
[37] R.F. de Souza, J.C. Padilha, R.S. Gonçalves, J. Dupont, Electrochem. Commun. 5 (2003) 728.
[38] M. Grätzel, J. Photochem. Photobiol. A: Chem. 164 (2004) 3.
[39] P. Wang, S.M. Zakeeruddin, P. Comte, I. Exnar, M. Grätzel, J. Am. Chem. Soc. 125 (2003) 1166.
[40] A.P. Abbot, K.J. Mckenzie, Phys. Chem. Chem. Phys. 8 (2006) 4265.
[41] P.-Y. Chen, C.L. Hussey, Electrochim. Acta 52 (2006) 1857.
[42] Q.-X. Liu, S.Z. El Abedin, F. Endres, Surf. Coat Technol. 201 (2006) 1352.
[43] H. Ping, L. Hongtao, L. Zhiying, L. Jinghong, J. Electrochem. Soc. 152 (2005) 146.
[44] A.P. Abbot, G. Capper, D.L. Davies, R.K. Rasheed, J. Archet, C. Johns, Trans. Inst. Metal Finis. 82 (2004) 14.
[45] N. Koura, Y. Suzuki, F. Maatsumoto, Electrochemistry (Japan) 70 (2002) 203.
[46] A.P. Abbot, C.A. Eardley, N.R.S. Farley, G.A. Griffit, A. Pratt, J. Appl. Electrochem. 31 (2001) 1345.
[47] R.T. Carlin, J. Osteryoung, J. Electrochem. Soc. 136 (1989) 1409.
[48] F.H. Hurley, T.P. Wier, J. Electrochem. Soc. 98 (1951) 203.
[49] C. Comminges, R. Barhdadi, M. Laurent, M. Troupel, J. Chem. Eng. Data 51 (2006) 680.
[50] J. Wang, Y. Tian, Y. Zhao, K. Zhuo, Green Chem. 5 (2003) 618.
[51] T. Nishida, Y. Tashiro, Y. Masashi, J. Fluorine Chem. 120 (2003) 135.
[52] K.R. Seddon, A. Stark, M.-J. Torres, Pure Appl. Chem. 72 (2000) 2275.
[53] W. Liu, T. Zhao, Y. Zhang, H. Wang, M. Yu, J. Solution Chem. 35 (2006) 1337.
[54] Q. Zhou, L.-S. Wang, H.-P. Chen, J. Chem. Eng. Data 51 (2006) 905.
[55] L.P.N. Rebelo, V. Najdanovic-Visak, Z.P. Visak, M. Nunes, J. da Ponte, C.A. Szydlowski, J. Cerdeirina, L. Troncoso, J.M.S.S. Romani, H.J.R. Esperança, H.C. Guedes, H.C. de Sousa, Green Chem. 6 (2004) 369.
[56] J. Dupont, C.S. Consorti, P.A.Z. Suarez, R.F. de Souza, Org. Synth. 79 (2002) 236.
[57] R.L. Perry, K.M. Jones, W.D. Scott, Q. Liao, C.L. Hussey, J. Chem. Eng. Data 40 (1995) 615.
[58] M. Abraham, M.C. Abraham, Electrochim. Acta 31 (1986) 821.
[59] Y. Saito, K. Hirai, K. Matsumoto, R. Hagiwara, Y. Minamizaki, J. Phys. Chem. B 109 (2005) 2942.
[60] H. Shobukawa, H. Tokuda, S.-I. Tabata, M. Watanabe, Electrochim. Acta 50 (2004) 1.
[61] J.N.A. Canongia Lopes, A.A.H. Pádua, J. Phys. Chem. B 110 (2006) 3330.
[62] J. Dupont, J. Brazil Chem. Soc. 15 (2004) 341.
[63] P.A.Z. Suarez, S. Einloft, J.E.L. Dullius, R.F. de Souza, J. Dupont, J. Chim. Phys. 95 (1998) 1626.
[64] A.G. Avent, P.A. Chaloner, M.P. Day, K.R. Seddon, T. Welton, J. Chem. Soc., Dalton Trans. (1994) 3405.
[65] K.M. Dieter, C.J. Dymek, N.E. Heimer, J.W. Rovang, J.S. Wilkes, J. Am. Chem. Soc. 110 (1988) 2722.
[66] P. Walden, Z. Phys. Chem. 55 (1906) 207.
[67] J. O'M. Bockris, A.K.N. Reddy, Modern Electrochemistry, second ed., Plenum Press, New York and London, 1998.
[68] W.J. Geary, Coord. Chem. Rev. 7 (1971) 81.
[69] CRC Handbook of Chemistry and Physics, CRC Press, FL, 1992.
[70] J.G. Huddleston, A.E. Visser, M. Matthew Reichert, H.D. Willauer, G.A. Broker, R.D. Rogers, Green Chem. 3 (2001) 156.
[71] A. Hemtz, D. Klasen, K.L. Lehmann, J. Solution Chem. 31 (2002) 467.

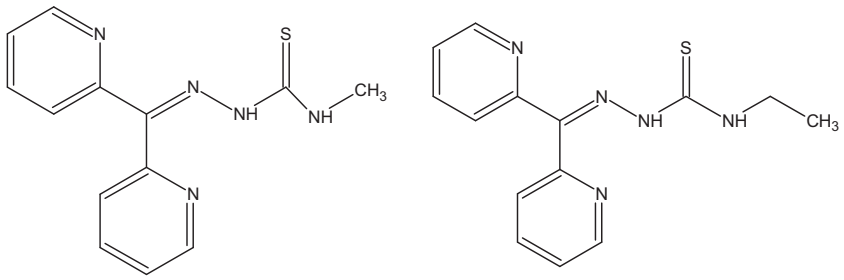

Scheme 1.

solution was heated at reflux for 3 hours and then kept at room temperature. The complex formed was filtered, washed thoroughly with ether and dried *in vacuo* over P_4O_{10}.

*2.3.3. Synthesis of [Mn(HDpyMeTsc)$_2$](ClO$_4$)$_2$ · H$_2$O (**3**)*

To a solution of HDpyMeTsc (0.271 g, 1 mmol) in hot ethanol was added $Mn(ClO_4)_2 \cdot 6H_2O$ (0.361 g, 1 mmol), and the resulting solution was heated at reflux for 3 hours and then kept at room temperature. The complex formed was filtered, washed thoroughly with ether and dried *in vacuo* over P_4O_{10}.

Single crystals of compound **1** suitable for X-ray diffraction were grown from a 1:1 (v/v) mixture of ethanol and methanol. Attempts were made to crystallize other complexes also, but unfortunately we could not isolate single crystals of suitable quality for single crystal XRD.

2.4. Physical measurements

Elemental analyses of the ligands and the complexes were done on a Vario EL III CHNS analyzer at SAIF, Kochi, India. The IR spectra were recorded on a Thermo Nicolet AVATAR 370 DTGS model FT-IR Spectrophotometer with KBr pellets at SAIF, Kochi. Electronic spectra in DMF solution were recorded on a Spectro UV–Vis Double Beam UVD-3500 spectrometer in the 200–900 nm range. The EPR spectra of the complexes were recorded on a Varian E-112 spectrometer using TCNE as the standard at the SAIF, IIT, Bombay, India. The molar conductance measurements of the complexes in dimethylformamide solutions (10^{-3} M) at room temperature were measured using a direct reading conductivity meter.

2.5. X-ray crystallography

Reddish brown crystals for the single crystal X-ray diffraction were grown by slow evaporation of the complex in ethanol/methanol (1:1) mixture. The crystallographic data and structure refinement parameters are given in Table 1. The data reduction and cell refinement were carried out using a CRYSALIS RED, Oxford Diffraction Ltd. at the National Single Crystal X-ray Diffraction facility, IIT, Bombay, India. The trial structure was solved using SHELXS-97 [16] and refinement was carried out by full-matrix least squares on F^2 (SHELXL-97) [16]. The molecular graphics employed were PLATON [17] and MERCURY [18].

Table 1
Crystal refinement parameters of [Mn(DpyMeTsc)$_2$]

Empirical formula	$C_{26}H_{24}Mn_1N_{10}S_2$
Formula weight (M)	595.63
Temperature (T) (K)	120(2)
Wavelength (Mo Kα) (Å)	0.71073
Crystal system	monoclinic
Space group	$P2_1/n$
Lattice constants	
a (Å)	10.6433(7)
b (Å)	15.1466(9)
c (Å)	17.2816(10)
α (°)	90.00
β (°)	92.179(6)
γ (°)	90.00
Volume V (Å^3)	2784.0(3)
Z	4
D_{calc} (ρ) (Mg m^{-3})	1.421
Absorption coefficient, μ (mm^{-1})	0.660
F(000)	1228
Crystal size (mm^3)	0.19 × 0.15 × 0.13
θ Range for data collection	2.94–25
Limiting indices	$-12 \leqslant h \leqslant 12$, $-18 \leqslant k \leqslant 18$, $-20 \leqslant l \leqslant 20$
Reflections collected	21 200
Unique reflections (R_{int})	4883 (0.1276)
Refinement method	full-matrix least-squares on F^2
Data/restraints/parameters	4883/0/362
Goodness-of-fit on F^2	1.026
Final R indices [$I > 2\sigma(I)$]	$R_1 = 0.0636$, $wR_2 = 0.0869$
R indices (all data)	$R_1 = 0.1463$, $wR_2 = 0.1142$
Largest difference peak and hole (e Å^{-3})	0.43 and −0.427

$R_1 = \sum||F_o| - |F_c||/\sum|F_o|$.
$wR_2 = [\sum w(F_o^2 - F_c^2)^2/\sum w(F_o^2)^2]^{1/2}$.

3. Results and discussion

All the four compounds are soluble in polar organic solvents like chloroform, DMF, DMSO, etc. In compounds **1** and **4**, the thiosemicarbazones deprotonate and chelate in the thiolate form, as proved by the IR spectral data. In **2** and **3**, the ligands are in the thione form. Elemental analyses and conductivity data are in agreement with the general empirical formula [Mn(DpyMeTsc)$_2$] for the complex part of compound **1** and [Mn(DpyETsc)$_2$] for compound **4**. Compounds **2** and **3** are [Mn(DpyMeTsc)Cl$_2$] and [Mn(DpyMeTsc)$_2$](ClO$_4$)$_2$, respectively. The colors, partial elemental analyses and molar conductivities of the metal complexes are shown in Table 2. The molar conductivity measurements in 10^{-3} M DMF solutions indicate that complexes **1**, **2**, and **4** are non-electrolytes and complex **3** is probably 1:2 electrolyte [19].

*3.1. Crystal structure of [Mn(DpyMeTsc)$_2$] (**1**)*

The molecular structure of the compound along with atom numbering scheme is given in Fig. 1. The compound crystallizes into a monoclinic lattice with $P2_1/n$ space group. The two molecules of monodeprotonated ligand, coordinate to manganese *via* pyridyl nitrogen, azomethine nitrogen and thiolato sulfur atoms to form four five membered chelate rings. The coordination of sulfur occurs through deprotonation after enolization, and was confirmed by the partial single and double bond nature of C1–S1 [1.728(5) Å] and N1–C1 [1.323(6) Å] bonds. There is a slight

Table 2
Colors, partial elemental analyses and molar conductivities of the complexes

Complex	Color	λ^{a}_{m}	Found (Calc.) (%)		
			C	H	N
$[Mn(DpyMeTsc)_2]$ (**1**)	Brown	8	52.18 (52.43)	4.17 (4.06)	23.06 (23.52)
$[Mn(HDpyMeTsc)Cl_2]$ (**2**)	Orange	48	39.92 (39.31)	3.46 (3.30)	17.92 (17.63)
$[Mn(HDpyMeTsc)_2](ClO_4)_2 \cdot H_2O$ (**3**)	Orange	182	38.34 (38.34)	3.16 (3.46)	17.32 (17.20)
$[Mn(DpyETsc)_2] \cdot 2H_2O$ (**4**)	Brown	12	50.38 (50.98)	4.31 (4.89)	21.15 (21.23)

[a] Molar conductivity of 10^{-3} M DMF solution, in ohm^{-1} cm^2 mol^{-1}.

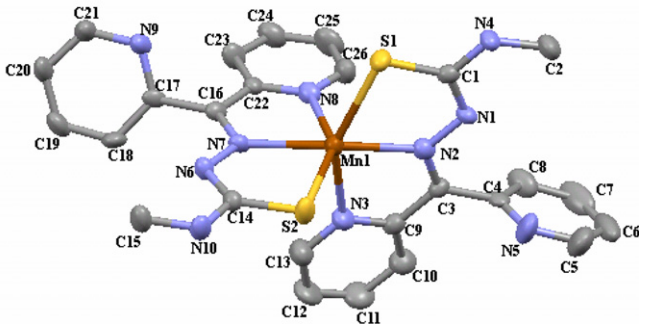

Fig. 1. The molecular structure of $[Mn(DpyMeTsc)_2]$ (**1**) along with the atom numbering scheme. The hydrogen atoms are omitted for clarity.

shortening of Mn–$N_{azomethine}$ bond distance compared to Mn–N_{py} distances; this may be attributed to the fact that the azomethine nitrogen is a stronger base compared with the pyridyl nitrogen. The ligands with their donor atoms are arranged around the manganese ion in a meridional fashion. In this compound, while S1, S2, N3 and N8 lie in the equatorial plane, N2 and N7 occupy the axial positions of the distorted octahedron. The MnN_2S_2 fragment is distorted from the mean plane by 0.013 Å. Each thiosemicarbazone fragment is subtending an angle of 147.38 and 148.41° at the Mn center, which is smaller than 180° that is expected for an ideal octahedron. The planes containing Mn, S1, N2, N3, N7 and Mn, S2, N2, N8, N7 are deviated from the mean plane by 0.179 and 0.166 Å (Mn), respectively. These factors suggest considerable distortion from an octahedral geometry around the Mn(II) center. The significant deviation from regular octahedron coordination geometry around the central metal is evident from the observed values of bond distances and angles as summarized in Table 3.

The molecules are connected in the crystal lattice through weak intermolecular hydrogen bonds; N4(H) of one molecule with S1 of another molecule [symmetry code: $2 - x$, $-y$, $1 - z$; with a H···S distance of 2.60(6) Å and angle 166(5)°] and vice-versa and N10(H) of same molecule with N(9) of another [symmetry code: $5/2 - x$, $1/2 + y$, $1/2 - z$; with a H···N distance of 2.28(6) Å and angle 169(5)°] leading to a three-dimensional network (Fig. 2). The network of electron delocalization brought about by the aromatic and metallo-aromatic [20] rings gives rise to diverse π–π and C–H···π interactions, invoking stable molecular arrangement in the unit cell. The interaction parameters are listed in Table 4.

Table 3
Selected bond lengths (Å) and bond angles (°) of $[Mn(DpyMeTsc)_2]$

Bond lengths (Å)		Bond angles (°)	
Mn(1)–N(2)	2.231(4)	N(2)–Mn(1)–N(7)	160.60(14)
Mn(1)–N(7)	2.249(4)	N(7)–Mn(1)–N(3)	94.95(14)
Mn(1)–N(3)	2.269(4)	N(2)–Mn(1)–N(3)	72.07(15)
Mn(1)–N(8)	2.254(4)	N(7)–Mn(1)–N(8)	72.23(14)
Mn(1)–S(1)	2.558(14)	N(2)–Mn(1)–N(8)	92.20(14)
Mn(1)–S(2)	2.495(15)	N(8)–Mn(1)–N(3)	86.55(14)
S(1)–C(1)	1.728(5)	N(7)–Mn(1)–S(1)	115.52(10)
N(2)–C(3)	1.298(5)	N(2)–Mn(1)–S(1)	75.45(11)
N(1)–N(2)	1.375(5)	N(3)–Mn(1)–S(1)	47.38(11)
N(1)–C(1)	1.323(6)	N(8)–Mn(1)–S(1)	1.73(10)
C(1)–N(4)	1.356(6)	N(7)–Mn(1)–S(2)	6.57(10)
N(6)–N(7)	1.375(5)	N(2)–Mn(1)–S(2)	17.10(10)
N(7)–C(16)	1.292(5)	N(3)–Mn(1)–S(2)	1.35(11)
C(14)–S(2)	1.738(5)	N(8)–Mn(1)–S(2)	48.41(11)
N(6)–C(14)	1.342(5)	S(2)–Mn(1)–S(1)	06.23(5)
N(10)–C(14)	1.335(6)		

3.2. Infrared and electronic spectra

To clarify the mode of bonding, the IR spectra of the free ligands and manganese(II) complexes were studied and assigned on the basis of a careful comparison of the latter with the free ligand. The tentative IR spectral assignments are listed in Table 5. The IR spectra of the ligands exhibit a medium band at *ca.* 3050 cm^{-1} assigned to ν(N–H) vibration, disappears in the spectra of complexes **1** and **4**, providing strong evidence for ligand coordination to the manganese(II) ion in the deprotonated thiolate form [12]. In complexes **2** and **3**, the ν(N–H) bands are shifted slightly but are indicative of the ligands in the thione form. The ν(C=N) bands of thiosemicarbazones are found to be shifted to lower frequencies in all the complexes indicating coordination *via* the azomethine nitrogen. The involvement of this nitrogen in bonding is also supported by a shift in ν(N–N) to higher frequencies. The appearance of new bands at *ca.* 1510 cm^{-1} in complexes **1** and **4** due to the newly formed ν(N=C) support the above observation. Coordination

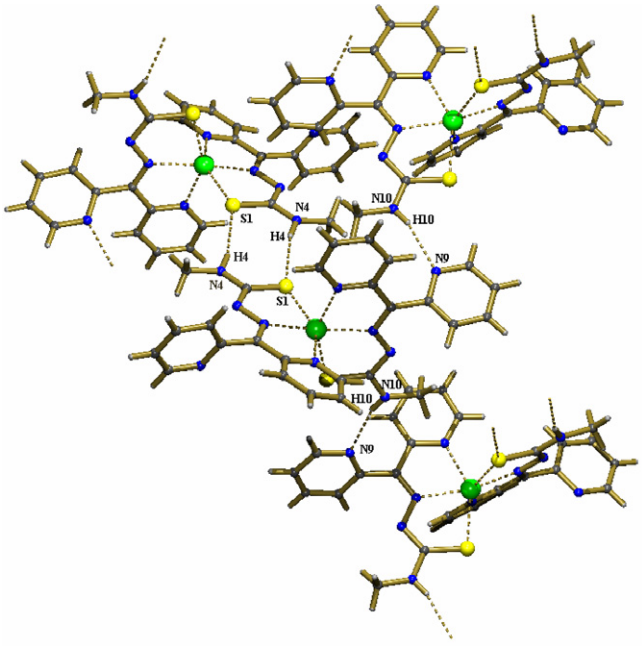

Fig. 2. Packing diagram of compound **1** showing H-bonding.

Table 4
H-bonding, π–π and C–H···π interaction parameters of the compound [Mn(DpyMeTsc)$_2$]

Donor···H···A (Å)	D–H	H···A	D···A	D–H···A
H-bonding				
N4(H)···S(1)	0.97	2.60	3.550	166
N10(H)···N(9)	0.83	2.28	3.100	169
π–π Interactions				
Cg(I)–Res(1)···Cg(J)	Cg–Cg (Å)	α (°)	β (°)	
Cg(2) [1] ⩾ Cg(6)[a]	4.023	20.76	23.74	
Cg(6) [1] ⩾ Cg(2)[b]	4.023	20.76	43.30	
Equivalent position codes				
a = 1 + *x*, *y*, *z*; b = −1 + *x*, *y*, *z*		Cg(2) = Mn(1), S(2),C(14), N(6), N(7); Cg(6) = N(5), C(4), C(5), C(6), C(7), C(8)		
C–H···π interaction				
X–H(I)···Cg(J)	H···Cg (Å)	XH···Cg (°)	X···Cg (°)	
C(19)–H(19) [1] ⩾ Cg(1)[a]	2.57	160	3.476	
Equivalent position code				
a = ½ + *x*, ½ − *y*, −1/2 + *z*		Cg(1) = Mn(1), S(1), C(1), N(1), N(2)		

D, donor; A, acceptor; Cg, centroid; α, dihedral angles between planes *I* and *J*; β, angle Cg(1)–Cg(J).

via the thiolate sulfur is indicated by the negative shift of the two bands assigned to ν(C=S) and δ(C=S) vibrations. The out-of-plane bending vibrations of the pyridine ring in uncomplexed ligands shift to higher frequencies on complexation, confirming the coordination of the ligands to the metal *via* the pyridine nitrogen [21].

The perchlorate complex shows a single broad band at 1098 cm^{-1} and a band at 637 cm^{-1}, indicating the presence of ionic perchlorate. The band at 1098 cm^{-1} is assignable to $\nu_3(ClO_4)$ and the unsplit band at 637 cm^{-1} is assignable to $\nu_4(ClO_4)$.

The ground state of the high spin octahedrally coordinated Mn^{2+} ion is $^6A_{1g}$. Since there are no other terms of sextet spin multiplicity, all the d-d transitions in high spin d^5 complexes are not only Laporte forbidden but also spin forbidden. The absorptions of the organic ligands tailing into the visible region obscure the very weak d–d absorption bands of the manganese(II) complexes. The broad band at *ca.* 24000 cm^{-1}, due to the $^4E_g \leftarrow {}^6A_{1g}$ transitions, is observed for all the complexes. The very weak bands at *ca.*18000 cm^{-1} are assigned to $^4T_{1g} \leftarrow {}^6A_{1g}$ transitions. The electronic spectral assignments are summarized in Table 6.

3.3. EPR spectra

The EPR spectra of Mn(II) may be described by the spin Hamiltonian

$$\hat{H} = g\beta HS + D[S_z^2 - S(S+1)/3] + E(S_x^2 - S_y^2)$$

where *H* is the magnetic field vector, *g* is the spectroscopic splitting factor, β is the Bohr magneton, *D* is the axial zero field splitting term, *E* is rhombic zero field splitting parameter and *S* is the electron spin vector [22]. If *D* and *E* are very small compared to *gβHS*, five EPR transitions are expected. The solid state EPR spectra of complexes **2** and **4** at 298 K are characterized by broad signals with *g* values of 2.031 and 2.097 respectively, broadening is due to dipolar interactions and random orientation of the Mn^{2+} ions [21]. Compound **3** is characterized by two *g* values at 2.073 and 5.241. The solid state EPR spectrum of complex **1** consists of five *g* values due to zero field splitting and Kramers degeneracy. The solution spectra in DMF at 77 K displayed a hyperfine sextet with *g* values 1.999 and 1.997, and *A* values 99 and 96 G, respectively for complexes **2** and **3** (Figs. 3 and 4). For complex **3,** a broad signal in the low field region is also observed with *g* value 4.642. The six hyperfine lines are due to the interaction of electron spin with the nuclear spin (^{55}Mn, *I* = 5/2). The frozen solution spectra of the complexes **1** and **4** in DMF, displayed two *g* values. The EPR spectral data of the complexes are summarized in Table 7.

The observed *g* values are very close to the free electron spin value, suggestive of the absence of spin orbit coupling in the ground state. The A_{iso} values are somewhat lower than pure ionic compounds, which reflects the covalent nature of the metal–ligand bond in the complexes. The mixing of the nuclear hyperfine levels with the zero field splitting factor produces low intensity

Table 6
Electronic spectral assignments of the ligands and the complexes

Compound	π → π*	n → π*	$^6A_{1g} \rightarrow {}^4T_{1g}$	$^6A_{1g} \rightarrow {}^4E_g$
HDpyMeTsc	34600	28980		
[Mn(DpyMeTsc)$_2$] (**1**)	35210	29070	18790	24030
[Mn(HDpyMeTsc)Cl$_2$] (**2**)	33890	28160	17360	23980
[Mn(HDpyMeTsc)$_2$](ClO$_4$)$_2$ · H$_2$O (**3**)	31250	29850	18110	24210
HDpyETsc	34560	28930		
[Mn(DpyETsc)$_2$] · 2H$_2$O (**4**)	34250	29190	18690	23980

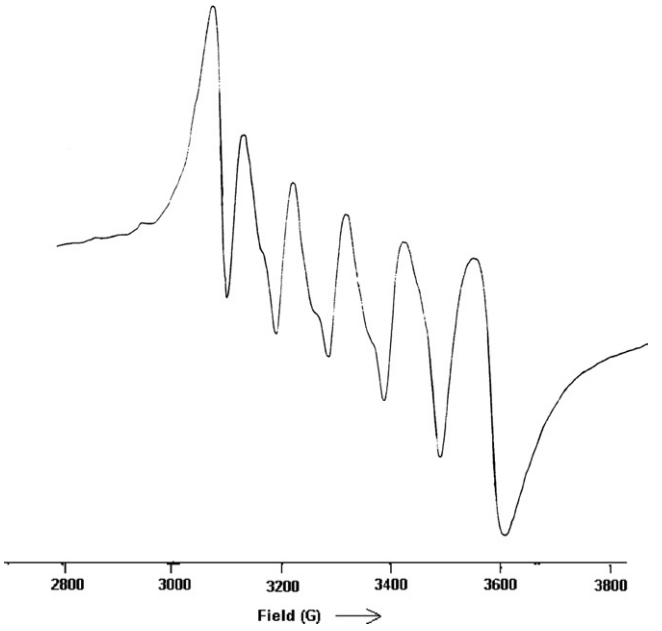

Fig. 3. EPR spectrum of [Mn(HDpyMeTsc)Cl$_2$] (**2**) in DMF at 77 K.

Table 5
Infrared spectra (cm^{-1}) of *N*(4)-substituted thiosemicarbazones and their manganese(II) complexes

Compound	ν(C=N)	ν(N–N)	ν/δ(C–S)	py(ip)	ν(^{1}N–H)	ν(^{4}N–H)	ν(Mn–N)
HDpyMeTsc	1588	1110	1431, 800	618	3050	3263	
[Mn(DpyMeTsc)$_2$] (**1**)	1560	1151	1329, 786	634		3332	444
[Mn(HDpyMeTsc)Cl$_2$] (**2**)	1533	1175	1328, 741	650	3065	3260	402
[Mn(HDpyMeTsc)$_2$](ClO$_4$)$_2$ · H$_2$O (**3**)	1555	1168	1332, 747	623	3083	3303	404
HDpyETsc	1585	1109	1431, 799	615	2979	3200	
[Mn(DpyETsc)$_2$] · 2H$_2$O (**4**)	1518	1147	1325, 742	635		3315	412

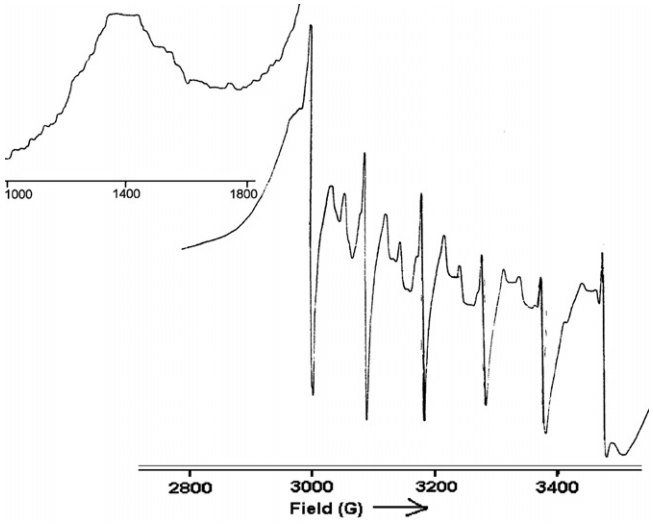

Fig. 4. EPR spectrum of $[Mn(HDpyMeTsc)_2](ClO_4)_2 \cdot H_2O$ (**3**) in DMF at 77 K. Spectrum in the lower field region is given in inset.

Table 7
EPR spectral data for the complexes

Compound	g Values	
	Polycrystalline at 298 K	DMF at 77 K
$[Mn(DpyMeTsc)_2]$ (**1**)	2.037, 2.882, 4.261, 5.700, 11.605	2.093, 4.133
$[Mn(HDpyMeTsc)Cl_2]$ (**2**)	2.031	1.999
$[Mn(HDpyMeTsc)_2](ClO_4)_2 \cdot H_2O$ (**3**)	2.073, 5.241	1.997, 4.642
$[Mn(DpyETsc)_2] \cdot 2H_2O$ (**4**)	2.097	2.054, 4.763

forbidden lines lying between each of the two main hyperfine lines in the frozen solution spectra of the complexes [13].

Acknowledgements

S. Renjusha thanks the CSIR, New Delhi, India for financial support in the form of a Fellowship. The authors are thankful to the National Single Crystal X-ray Diffraction Facility, IIT, Bombay, India for providing single crystal XRD results and Sophisticated Analytical Instruments Facility, Kochi, India for the elemental analyses.

Appendix A. Supplementary data

CCDC 672181 contains the supplementary crystallographic data for $Mn(DpyMeTsc)_2$. These data can be obtained free of charge via http://www.ccdc.cam.ac.uk/conts/retrieving.html, or from the Cambridge Crystallographic Data Centre, 12 Union Road, Cambridge CB2 1EZ, UK; fax: (+44) 1223-336-033; or e-mail: deposit@ccdc.cam.ac.uk.

References

[1] A. Sreekanth, S. Sivakumar, M.R.P. Kurup, J. Mol. Struct. 655 (2003) 47.
[2] E. Manoj, M.R.P. Kurup, Polyhedron 27 (2008) 275.
[3] E.J. Blanz, F.A. French, Cancer Res. 28 (1968) 2419.
[4] M.C. Miller, C.N. Stineman, J.R. Vance, D.X. West, I.M. Hall, Anticancer Res. 18 (1998) 4131.
[5] M.C. Miller, C.N. Stineman, J.R. Vance, D.X. West, I.M. Hall, Appl. Organomet. Chem. 13 (1999) 9.
[6] J.P. Scovill, D.L. Klayman, C. Lambros, G.E. Childs, W. Antholine, D.H. Petering, J. Med. Chem. 27 (1984) 87.
[7] A. Sreekanth, M. Joseph, H.-K. Fun, M.R.P. Kurup, Polyhedron 25 (2006) 1408.
[8] M. Maneiro, M.R. Bermejo, M. Fondo, A.M. Gonzalez, J. Sanmartin, J.C. Garcia-Monteagudo, R.G. Pritchard, A.M. Tyryshkin, Polyhedron 20 (2001) 711.
[9] D. Huang, X. Zhang, C. Chen, F. Chen, Q. Liu, D. Liao, L. Li, L. Sun, Inorg. Chim. Acta 353 (2003) 284.
[10] A. Usman, I.A. Razak, S. Chantrapromma, H.-K. Fun, A. Sreekanth, S. Sivakumar, M.R.P. Kurup, Acta Crystallogr., Sect. C 58 (2002) m461.
[11] M.B. Ferrari, G.G. Fava, C. Pelizzi, P. Tarasconi, G. Tori, J. Chem. Soc., Dalton Trans. (1987) 227.
[12] V. Philip, V. Suni, M.R.P. Kurup, M. Nethaji, Spectrochim. Acta, Part A 64 (2006) 171.
[13] P.F. Rapheal, E. Manoj, M.R.P. Kurup, Polyhedron 26 (2007) 5088.
[14] J.K. Swearingen, D.X. West, Trans. Met. Chem. 26 (2001) 252.
[15] D.R. Richardson, P.C. Sharpe, D.B. Lovejoy, D. Senaratne, D.S. Kalinowski, M. Islam, P.V. Bernhardt, J. Med. Chem. 49 (2006) 6510.
[16] G.M. Sheldrick, SHELXL-97 and SHELXS-97 Program for the Solution of Crystal Structures, University of Göttingen, Germany, 1997.
[17] A.L. Spek, J. Appl. Cryst. 36 (2003) 7.
[18] C.F. Macrae, P.R. Edgington, P. McCabe, E. Pidcock, G.P. Shields, R. Taylor, M. Towler, J. Van de Streek, J. Appl. Cryst. 39 (2006) 453.
[19] W.J. Geary, Coord. Chem. Rev. 7 (1971) 81.
[20] H. Masui, Coord. Chem. Rev. 219 (2001) 957.
[21] B.S. Garg, M.R.P. Kurup, S.K. Jain, Y.K. Bhoon, Trans. Met. Chem. 13 (1988) 92.
[22] D.J.E. Ingram, Spectroscopy at Radio and Microwave Frequencies, 2nd ed., Butterworth, London, 1967.

of the 4-nitrobenzoates of the alkaline-earths [24–28]. The triad of compounds $[Mg(H_2O)_6](4\text{-nba})_2 \cdot 2H_2O$, $[Mg(H_2O)_2(Im)_2(\eta^1\text{-}4\text{-nba})_2]$ (Im = imidazole) and $[Mg(H_2O)(N\text{-MeIm})_2(\eta^1\text{-}4\text{-nba})(\mu_2\text{-}\eta^1\text{:}\eta^1\text{-}4\text{-nba})]_2$ (*N*-MeIm = *N*-methylimidazole) demonstrate a rich and variable chemistry of 4-nitrobenzoates of Mg in terms of the binding modes of 4-nba anions as well as secondary H-bonding interactions. For calcium we reported on the structure and properties of a seven coordinated monomeric complex $[Ca(H_2O)_4(\eta^1\text{-}4\text{-nba})(\eta^2\text{-}4\text{-nba})]$ **1** [24], which exhibits both mono (η^1) and bidentate (η^2) coordination of 4-nba and $[Ca(H_2O)_3(Im)(\eta^1\text{-}4\text{-nba})_2] \cdot Im$ [25] which shows η^1 ligation of 4-nba and contains coordinated as well as free imidazole. In this paper, we present the details of the investigation of the thermal reaction of the seven coordinated Ca compound **1** in the presence of *N*-methylimidazole (*N*-MeIm) and imidazole (Im), resulting in the formation of the anhydrous mixed ligand complexes of composition $[Ca(L)(4\text{-nba})_2]$ (L = *N*-MeIm **2**; L = Im **3**).

2. Experimental

2.1. Materials and methods

All the chemicals used in this study were of reagent grade and were used as received. The starting materials and reaction products are air stable and hence were prepared under normal laboratory conditions. The complex $[Ca(H_2O)_4(\eta^1\text{-}4\text{-nba})(\eta^2\text{-}4\text{-nba})]$ **1** was prepared as described earlier [24]. Infrared (IR) spectra were recorded on a Shimadzu (IR Prestige-21) FT-IR spectrometer in the range 4000–400 cm^{-1}. The samples for the IR spectra were diluted with KBr in the solid state and the signals referenced to polystyrene bands. Electronic spectra were recorded using matched quartz cells on a Shimadzu (UV-2450) spectrophotometer. ^1H NMR spectra were recorded in DMSO-d_6 on a Bruker 400 MHz FT-NMR spectrometer. TG-DSC measurements were performed in Al_2O_3 crucibles on a STA-409PC simultaneous thermal analyzer from Netzsch in flowing air. A heating rate of 10 K min^{-1} was employed for all measurements. X-ray powder pattern were recorded on a Phillips PW-3710 diffractometer using Cu K_α radiation over 2θ range of 15–75° at a scan rate of 3° min^{-1}. The insoluble 4-nbaH obtained on acid treatment of the complexes was weighed as described earlier [15] and metal analysis was performed titrimetrically following a standard procedure. Isothermal weight loss studies were performed in an electric furnace fitted with a temperature controller.

2.2. Preparation of $[Ca(H_2O)(4\text{-nba})_2]$ **1a**

A powdered sample of **1** (0.444 g) was heated on a steam bath for ~30 min. The heat-treated sample was kept in a desiccator and allowed to cool to room temperature and weighed to obtain **1a**. The observed decrease in weight (12.15%) corresponds to the removal of three moles of water. The yield was quantitative. The compound is insoluble in MeOH, CH_3CN, etc.

Anal. Calc. for $C_{14}H_{10}CaN_2O_9$: Ca, 10.25; 4-nbaH, 85.68; CaO, 14.35. Found: Ca, 10.01; 4-nbaH, 84.8, CaO, 14.0%.

IR data: 3611–3100(br), 3113(s), 2849(w), 1944(w), 1813(w), 1612(s), 1558(s), 1524(m), 1493(sh), 1414(s), 1346(s), 1319(s), 1171(m), 1142(m), 1107(s), 1015(s), 980(s), 880(s), 839(s), 799(s), 725(s), 511(s) cm^{-1}.

DSC data (in °C): 260 (*exo*), 410 (*exo*), 447 (*exo*), 558 (*exo*).

2.3. Preparation of $[Ca(N\text{-MeIm})(4\text{-nba})_2]_n$ **2**

2.3.1. Method 1

N-Methylimidazole (0.082 g, 1 mmol) was added into a freshly prepared sample of **1a** and the reaction mixture was left in a desiccator for ~30 min. The reaction mixture was washed with ether and dried to obtain **2**. Alternatively **2** can also be prepared by directly heating a mixture of a finely powdered sample of **1** (0.45 g, 1 mmol) and *N*-MeIm (0.082 g, 1 mmol) in a steam bath for ~30 min. The hot reaction mixture was cooled and washed well with ether and dried in air. Yield: (quantitative).

Anal. Calc. for $C_{18}CaH_{14}N_4O_8$ (454.43) **2**: Ca, 8.8; 4-nbaH, 73.11; CaO, 12.34; C, 47.53; H, 3.0; N, 12.32. Found: Ca, 8.8; 4-nbaH, 73, CaO, 12.2; C, 47.6; H, 3.03; N, 11.81%.

IR data: 3121(s), 2967(s), 2855(w), 1614(s), 1584(s), 1520(m), 1402(s), 1375(s), 1344(s), 1321(s), 1279(s), 1230(m), 1107(s), 1014(s), 1082(m), 934(s), 878(s), 822(s), 800(s), 752(s), 727(s), 667(s), 621(s), 559(s), 509(s) cm^{-1}.

UV–Vis 274 nm (23 775 L mol^{-1} cm^{-1}).

^1H NMR (DMSO-d_6) δ (in ppm): 3.63 (s, 3H); 6.86 (s, 1H); 7.09 (s, 1H); 7.55 (s, 1H); 8.16 (m, 4H).

DSC data (in °C): 188 (*endo*), 412 (*exo*), 558 (*exo*).

2.3.2. Method 2

A powdered sample of **1** (1.78 g, 4 mmol) was heated with *N*-MeIm (1.4 ml, 17 mmol) on a steam bath for ~1 h to obtain a light yellow solid. To this hot mass distilled water (~8 ml) was added and the mixture reheated to obtain a pale yellow solution. The hot solution was quickly filtered and kept aside for crystallization. Fine colorless blocks of crystals suitable for X-ray study, which separated were washed with ether (5 ml) and dried in air. Yield: 60%. The use of reduced amounts of *N*-MeIm in the thermal reaction or excess water for recrystallisation results in the formation of the tetraaqua compound **1** in accordance with its hydration characteristics (*vide infra*). The infrared spectrum and the DSC thermogram of this product is identical with that of the product obtained in the thermal reaction.

2.4. Preparation of $[Ca(Im)(4\text{-nba})_2]$ **3**

Imidazole (0.068 g, 1 mmol) was added into a freshly prepared sample of **1a** and the reaction mixture was left in a desiccator for ~30 min. The reaction mixture was washed with ether and dried to obtain **3**. Alternatively **3** can also be prepared by directly heating a mixture of a finely powdered sample of **1** (0.45 g, 1 mmol) and Im (0.068 g, 1 mmol) in a steam bath for ~30 min. The hot reaction mixture was cooled and was washed well with ether and dried in air. Yield: (quantitative).

Anal. Calc. for $C_{17}CaH_{12}N_4O_8$ **3**: Ca, 9.08; 4-nbaH, 75.88; CaO, 12.73; C, 46.31; H, 2.72; N, 12.71. Found: Ca, 8.9; 4-nbaH, 74.28; CaO, 12.3; C, 45.95; H, 3.13; N, 10.94%.

IR data: 3381(s), 3223(s), 3061(w), 2941(w), 1604(w), 1570(s), 1516(s), 1490(m), 1402(s), 1348(s), 1321(s), 1261(s), 1171(m), 1142(m), 1107(s), 1066(s), 1014(s), 935(s), 918(s), 860(s), 825(s), 802(s), 752(s), 740(s), 723(s), 659(s), 617(s), 497(s), 511(s) cm^{-1}.

^1H NMR (DMSO-d_6) δ (in ppm): 7.00 (s, 2H); 7.63 (s, 1H); 8.13 (m, 4H).

DSC data (in °C): 198 (*endo*), 415 (*exo*), 547 (*exo*).

2.5. Rehydration studies

A powdered sample of **2** (200 mg) was suspended in water (~5 ml) and the reaction mixture left undisturbed overnight. The reaction mixture was filtered and the residue was washed with alcohol followed by ether and dried to obtain **1** in quantitative yields. The formation of **1** is evidenced by its characteristic IR spectrum and DSC thermogram. Alternatively **2** can be transformed to **1** by suspending an amount (200 mg) of **2** in water (5 ml) and heating the solution till dissolution of the solid. The hot solution is cooled to obtain **1** in quantitative yield. The equilibration of a powdered sample of **3** over water vapour, resulted in the

formation of the starting compound **1** in quantitative yield in about a day as evidenced by its characteristic IR spectrum and DSC thermogram.

2.6. X-ray crystallography

Intensity data for **2** were collected on a Bruker Smart Apex CCD diffractometer using graphite-monochromated Mo Kα radiation. The data integration and reduction were processed with SAINT software [29]. An empirical absorption correction was applied to the collected reflections with SADABS [30]. The structure was solved with direct methods using SHELXS-97 and refinement was done against F^2 using SHELXL-97 [31]. All non-hydrogen atoms were refined anisotropically. Aromatic hydrogens were introduced on calculated positions and included in the refinement riding on their respective parent atoms. The technical details of data acquisition and some selected refinement results for **2** are listed in Table 1.

3. Results and discussion

3.1. Synthesis and spectroscopy

Heating of a solid sample of the tetrahydrate **1** at 100 °C resulted in the loss of three moles of water leading to the formation of a monohydrate $[Ca(H_2O)(4\text{-nba})_2]$ **1a** (Scheme 1). The presence of water in **1a** is evidenced by the strong and broad absorption around 3500 cm^{-1} in its infrared spectrum assignable to O–H vibration. It is to be noted that the profile of the O–H signal of compound **1a** is quite different as compared to that of the tetrahydrate compound **1**. In addition the IR signals of the nitro and carboxylate functionalities, which occur between 1300 and 1650 cm^{-1} are broadened in **1a** as compared to the spectrum of **1** (Fig. 1). On exposure to moisture the monohydrate rapidly transforms into the seven coordinated starting material **1.** Interestingly, the reaction of *N*-MeIm or Im with the monohydrate **1a** results in the displacement of water by the N-donor ligands and the formation of anhydrous mixed ligand compounds **2** or **3** having molar composition of Ca:4-nba:*N*-MeIm(Im) 1:2:1 (Scheme 1). The use of excess *N*-MeIm or Im in the thermal reaction did not result in the formation of new products containing additional N-donor ligands. The anhydrous mixed ligand compounds **2** or **3** can also be synthesized in a single step by directly heating a mixture of powdered sample of **1** and *N*-MeIm in a 1:1 mole ratio. The presence of the N-donor ligands in compounds **2** and **3** can be readily confirmed by their NMR spectra which exhibit the characteristic signals of 4-nba, *N*-MeIm or Im. The formation of the anhydrous compounds **2** or **3** is evidenced by their IR spectra, which are devoid of the signals for O–H vibrations of water and is further confirmed by the appearance of additional bands due to the incorporation of the N-donor ligand in its mid IR spectrum (Fig. 1). Compounds **2** and **3** are relatively stable compared to the moisture sensitive monohydrate **1a**. However, both **2** and **3** can be transformed to **1** by suspending them in water overnight or alternatively by heating **2** or **3** in water (Scheme 1). Crystals of **2** suitable for structure determination were prepared by heating a mixture of **1** and excess *N*-MeIm at 100 °C followed by recrystallisation from minimum water. Similar attempts to prepare compound **3** in crystalline form suitable for

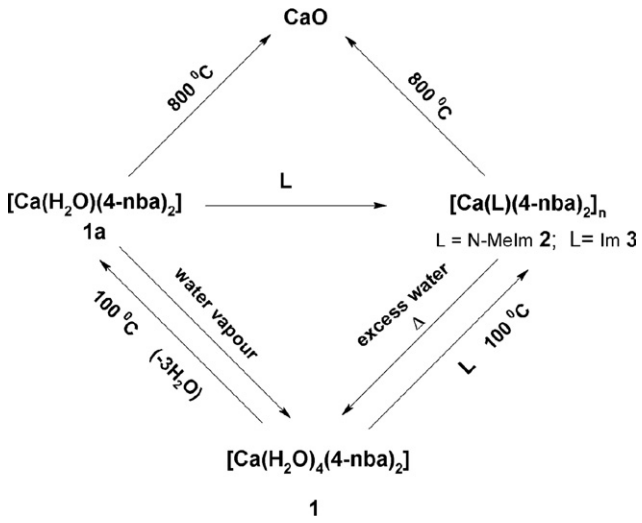

Scheme 1.

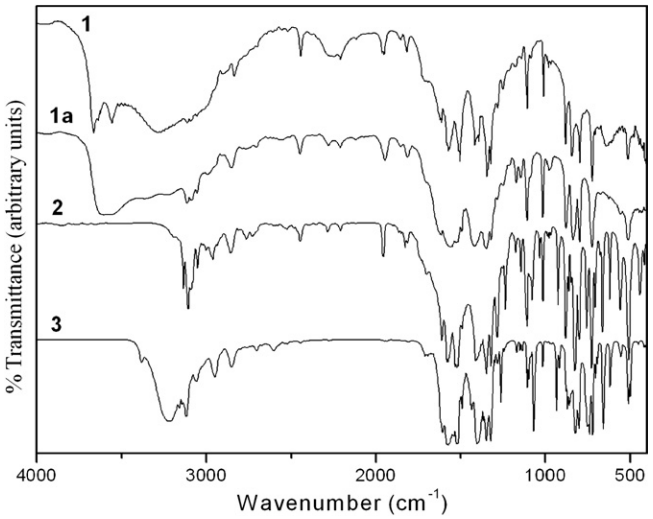

Fig. 1. IR spectra of compounds **1**, **1a**, **2** and **3**.

Table 1
Crystal data and structure refinement for $[Ca(N\text{-MeIm})(4\text{-nba})_2]_n$ **2**

Empirical formula	$C_{18}H_{14}CaN_4O_8$
Formula weight (g mol^{-1})	454.41
Temperature (K)	293(2)
Wavelength (Å)	0.71073
Crystal system	triclinic
Space group	$P\bar{1}$
Unit cell dimensions	
a (Å)	5.5313(5)
b (Å)	12.7904(12)
c (Å)	14.9226(15)
α (°)	113.08(1)
β (°)	95.72(1)
γ (°)	97.64(1)
Volume (Å^3)	950.11(16)
Z	2
D_{calc} (mg/m^3)	1.588
Absorption coefficient (mm^{-1})	0.388
$F(000)$	468
Crystal size (mm^3)	0.38 × 0.28 × 0.20
Theta range for data collection (°)	1.50–26.0
Index ranges	$-6 \leqslant h \leqslant 6$, $-15 \leqslant k \leqslant 15$, $-18 \leqslant l \leqslant 18$
Reflections collected	9475
Independent reflections (R_{int})	3696 (0.0205)
Completeness to theta = 26.0°	99.3%
Refinement method	full-matrix least-squares on F^2
Data/restraints/parameters	3696/0/285
Goodness-of-fit on F^2	1.057
Final R indices [$I > 2\sigma(I)$]	$R_1 = 0.0348$, $wR_2 = 0.0900$
R indices (all data)	$R_1 = 0.0392$, $wR_2 = 0.0929$
Largest difference in peak and hole (e Å^{-3})	0.338 and −0.235

X-ray structure determination by solution method always resulted in the formation of the known monomeric compound $[Ca(H_2O)_3(Im)(\eta^1\text{-4-nba})_2]\cdot Im$. The compounds **1a**, **2** and **3** were formulated based on the elemental analysis and the mass loss leading to the formation of CaO on pyrolysis in a Bunsen flame. All the compounds exhibit several signals in the mid IR region indicating the presence of the organic moieties. However, based only on the infrared data the exact nature of the binding of the 4-nba ligand cannot be confirmed. The UV–Vis spectra of all compounds exhibit an absorption in the UV region around 274 nm assignable to the charge transfer of the aromatic 4-nba ligand.

3.2. Crystal structure description of **2**

Compound **2** crystallises in the triclinic space group $P\bar{1}$ and all atoms are situated in general positions. The structure reveals that **2** is a polymer and can be formulated as *catena*-poly[[(*N*-methylimidazole)calcium(II)](μ_2-η^1:η^1-4-nitrobenzoato)(μ_3-η^2:η^1-4-nitrobenzoato)]. The structure of $[[Ca(N\text{-MeIm})](\mu_2\text{-}\eta^1\text{:}\eta^1\text{-4-nba})(\mu_3\text{-}\eta^2\text{:}\eta^1\text{-4-nba})]_n$ **2** consists of a central Ca(II) ion, a terminal *N*-MeIm ligand and two crystallographically independent 4-nba ligands. In the crystal structure, each Ca(II) is bonded to a nitrogen atom of *N*-MeIm and five oxygen atoms from five symmetry related 4-nba ligands resulting in a distorted $\{CaO_5N\}$ octahedron (Fig. 2). The geometric parameters of the 4-nba anions and *N*-MeIm are in the normal range and are comparable with literature values [24–27]. The Ca–O distances in **2** range from 2.2823(12) to 2.4507(11) Å (Table 2) and are in agreement with literature values [24,25]. The Ca–N bond is longer at 2.5088(14) Å. The *cis* O–Ca–O and O–Ca–N angles range from 73.71(4)° to 107.39(4)° while the trans O–Ca–O and O–Ca–N angles range from 163.97(4)° to 175.54(4)° indicating a distorted octahedron. It is interesting to note that both 4-nitrobenzoates in each formula unit are coordinated to the central Ca(II) in different bridging modes (Fig. 2). One of the two 4-nba anions in each formula unit functions as a bridging bidentate ligand (μ_2-η^1:η^1-4-nba) (Supplementary data, Fig. 1) and is linked to two symmetry related Ca(II) ions via O5 and O6 atoms resulting in the formation of an infinite chain extending along *a* axis with a Ca···Ca separation of 5.531(1) Å. The second independent ligand (μ_3-η^2:η^1-4-nba) is coordinated to three different Ca(II) ions with both the carboxylate oxygen atoms O1 and O2 linked to the same infinite chain formed earlier and one of the carboxylate oxygen atoms (O1) functioning as a monoatomic bridge between two symmetry related Ca(II) ions (Supplementary data, Figs. 2 and 3). This monoatomic bridge serves to link the two infinite chains with a shorter Ca···Ca separation of 3.8585(7) Å resulting in the formation of a one-dimensional ladder structure (Fig. 3).

It is to be noted that Ca(II) forms a polymeric compound with 4-nba in the presence of *N*-MeIm unlike Mg(II) which forms a centrosymmetric dimeric complex $[Mg(H_2O)(N\text{-MeIm})_2(\eta^1\text{-4-nba})(\mu_2\text{-}\eta^1\text{:}\eta^1\text{-4-nba})]_2$ [26]. The coordination polymer **2** and the previously reported monomeric compounds $[Ca(H_2O)_4(\eta^1\text{-4-nba})(\eta^2\text{-4-nba})]$ **1** [24] and $[Ca(H_2O)_3(Im)(\eta^1\text{-4-nba})_2]\cdot Im$ [25] constitute a triad of Ca(II) compounds having Ca:4-nba in a 1:2 mole ratio and showing different binding modes of the 4-nba ligand. In terms of secondary interactions **1** shows only O–H···O interactions while the monomeric imidazole compound is involved in three varieties of H-bond-

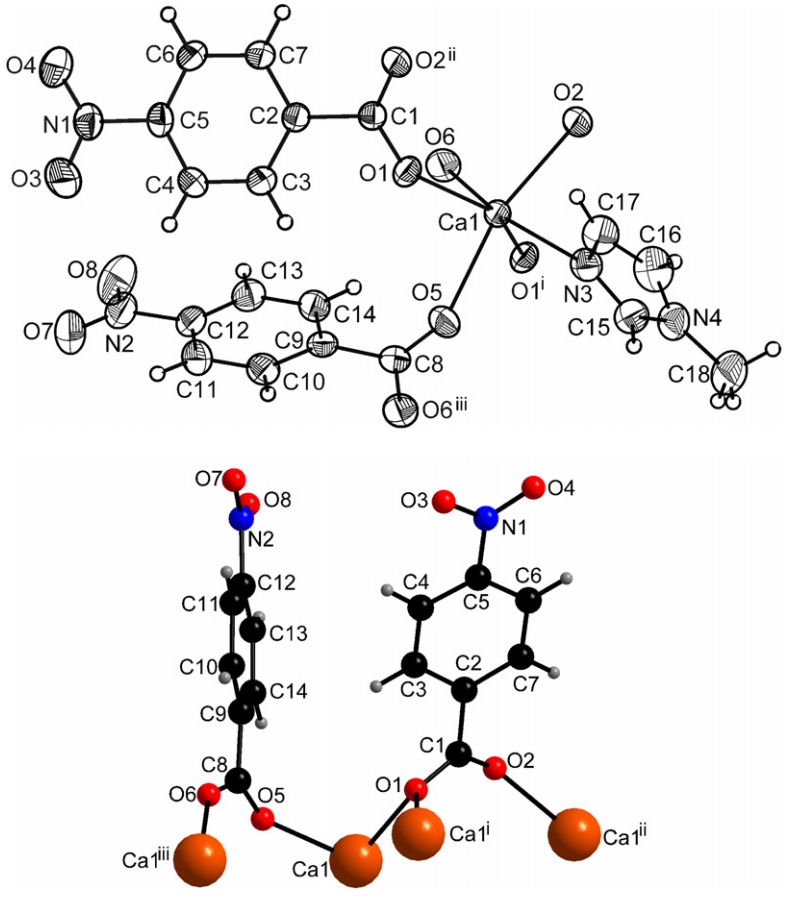

Fig. 2. The coordination sphere of Ca(II) in **2** showing the atom-labeling scheme. Displacement ellipsoids are drawn at the 50% probability level except for the H atoms, which are shown as circles of arbitrary radius (top). The μ_2-η^1:η^1 (O5,O6) and μ_3-η^2:η^1 (O1, O1, O2) bridging binding modes of the 4-nitrobenzoate ligands in **2** (bottom). Symmetry code: (i) $-x+1, -y+1, -z+1$; (ii) $-x+2, -y+1, -z+1$; (iii) $x-1, y, z$.

Table 2
Selected bond lengths (Å) and bond angles (°) for $[Ca(N\text{-MeIm})(4\text{-nba})_2]_n$ **2**

Ca(1)–N(3)	2.5088(14)	Ca(1)–O(5)	2.3074(12)
Ca(1)–O(1)	2.3710(11)	Ca(1)–O(6)	2.2823(12)
Ca(1)^{i}–O(1)	2.4507(11)	Ca(1)–Ca(1)^{iii}	5.531(1)
Ca(1)–O(2)	2.3292(11)	Ca(1)–Ca(1)^{i}	3.8585(7)
O(6)–Ca(1)–O(5)	96.22(5)	O(2)–Ca(1)–O(1)^{i}	93.23(4)
O(6)–Ca(1)–O(2)	92.78(4)	O(1)–Ca(1)–O(1)^{i}	73.71(4)
O(5)–Ca(1)–O(2)	165.10(4)	O(6)–Ca(1)–N(3)	88.01(5)
O(6)–Ca(1)–O(1)	90.60(4)	O(5)–Ca(1)–N(3)	84.47(5)
O(5)–Ca(1)–O(1)	91.47(4)	O(2)–Ca(1)–N(3)	84.00(4)
O(2)–Ca(1)–O(1)	100.31(4)	O(1)–Ca(1)–N(3)	175.54(4)
O(6)–Ca(1)–O(1)^{i}	163.97(4)	O(1)^{i} –Ca(1)–N(3)	107.39(4)
O(5)–Ca(1)–O(1)^{i}	81.25(4)		

Symmetry transformations used to generate equivalent atoms: (i) $-x+1, -y+1, -z+1$, (iii) $x-1, y, z$.

Table 3
Hydrogen-bonding geometry (Å, °) for $[Ca(N\text{-MeIm})(4\text{-nba})_2]_n$ **2**

D–H···A	*d*(D–H)	*d*(H···A)	*D*(D···A)	∠DHA
C13–H13···O8^{iv}	0.93	2.67	3.456(3)	143
C13–H13···O4^{v}	0.93	2.69	3.586(2)	161
C6–H6···O7^{vi}	0.93	2.63	3.519(2)	160
C4–H4···O3^{v}	0.93	2.62	3.495(2)	157
C18–H18B···O7^{vii}	0.93	2.44	3.378(3)	167

Symmetry codes: (iv) $-x+1, -y, -z$, (v) $-x, -y+1, -z$, (vi) $-x+1, y+1, -z$, (vii) $x+1, y, z+1$.

ing interactions namely O–H···O, N–H···O and O–H···N. The absence of coordinated water as well as methylation of the nitrogen atom in *N*-MeIm in **2** blocks the O–H···O, N–H···O and O–H···N interactions. An analysis of the structure of **2** reveals that the anhydrous compound is involved in only C–H···O interactions (Supplementary data, Fig. 4) with the oxygen atoms of the nitro groups functioning as H-acceptors and the methyl group of imidazole as well as H atoms on the aromatic ring functioning as H-donors. The geometric parameters of these hydrogen bonds are listed in Table 3.

3.3. Comparative study of Ca(II) coordination polymers

A survey of the reported structures of Ca(II) carboxylates reveals that formation of a polymeric chain due to the bridging nature of the carboxylate ligand is a characteristic structural feature of many Ca(II) carboxylates. Several polymeric Ca(II) carboxylates of varying dimensionalities (D) [17–23,32–52] have been reported in the literature many of which are 1-D polymers (Table 4). A comparative study of 30 different Ca(II) 1-D polymers reveals that the coordination number of Ca(II) in these compounds varies from 6 to 10, with eight coordination observed in many cases. Hexacoordination around Ca(II) is observed in compound **2** as well as $[Ca(Sa)_2(Phen)]_n$ and $[Ca(H_2O)_2(C_9H_8NO_4)_2]\cdot 2.5H_2O]_n$ (for abbreviations see Table 4). Of the several Ca(II) coordination polymers reported in the literature using substituted benzene carboxylic acids, compound **2** constitutes the first example of a Ca(II) coordination polymer derived from 4-nba ligand as the two other known Ca(II) compounds of 4-nba are monomeric in nature. A wide range of Ca···Ca distances between 3.612(1) and 9.816(1) Å are observed for the different Ca(II) 1-D polymeric compounds listed in the comparative table. The Ca···Ca separation of 3.8585(7) Å between the chains in the ladder compound is comparable with the Ca–Ca distance of around 4.0 Å observed in several coordination polymers listed in Table 4 while the Ca···Ca separation of 5.531(1) Å across the chains in **2** is relatively longer. A very long Ca···Ca distance of 9.816(1) Å is observed in the one-dimensional polymer $[[Ca(H_2O)_4(AlP)_2](H_2O)]_n$ containing the 5-aminoisophthalate dianion. Interestingly in the related 1-D Ca(II) polymer derived from isophthalic acid which exhibits a triple helix structure, Ca···Ca separations of 3.6402(3) and 3.8705(4) Å are reported. These observations indicate that the Ca···Ca distances across the polymeric chain in the coordination polymers are determined by a combination of several factors, which include the electronic and steric requirements of the central metal, the denticity, flexibility, bridging behavior, H-bonding characteristics of the carboxylate ligand, presence of ancillary ligands, etc.

3.4. Thermal studies

The temperature for the thermal synthesis of compounds **2** and **3** was chosen based on the thermal characteristics of compound **1**. A comparison of the thermal behavior of the tetrahydrate **1** and the monohydrate **1a** reveals that the DSC thermograms of **1a** is identical to that of compound **1** above 100 °C when the tetrahydrate **1** emits three moles of water forming the monohydrate (see Supple-

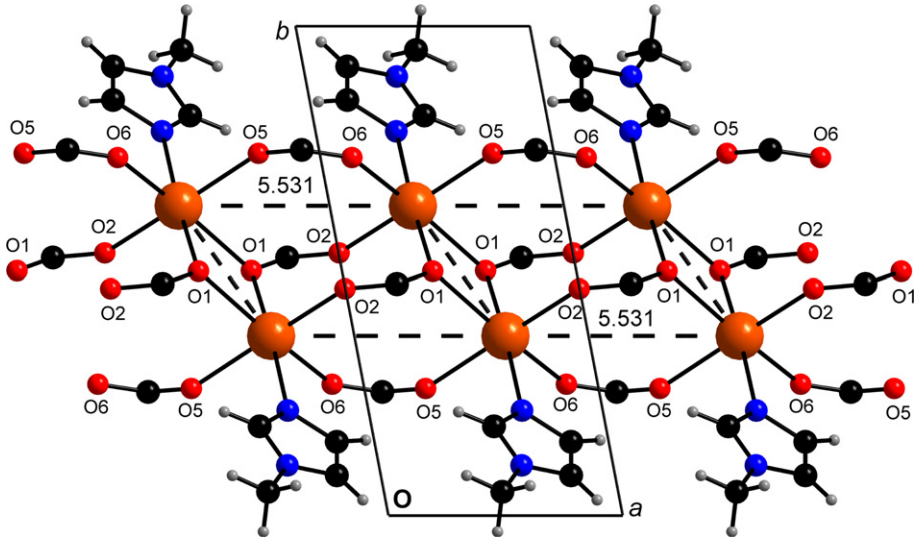

Fig. 3. A view of the bridging bidentate coordination (μ_2-η^1:η^1) of 4-nba through O5 and O6 leading to a one-dimensional polymeric Ca(II) chain extending along *a* with Ca···Ca separation of 5.531(1) Å. The monoatomic bridging mode of O1 in the second 4-nba ligand results in the linking of two infinite chains. In the chains each Ca(II) is bonded to five O atoms and one N atom. For clarity only the carboxylate groups are shown.

Table 4
Ca···Ca distances across the chain in reported one-dimensional (1-D) Ca(II) coordination polymers

Compound	C.N.	Ca···Ca distance (Å)	Reference
$[[Ca(H_2O)_3(4\text{-fba})](4\text{-fba})]_n$	8	3.612(1)	[32]
$[Ca(H_2O)_3(benz)_2]_n$	8	3.6146(4)	[33]
$[Ca(H_2O)_3(1,4\text{-bdc})]_n$	8	3.637(2)	[34]
$[[Ca(H_2O)_2(1,3\text{-bdc})]_{2.5} \cdot 4H_2O]_n$ *	8, 8, 9	3.6402(3), 3.8705(4)	[21]
$[[Ca_5(1,3\text{-bdc})_5(H_2O)_9] \cdot 8H_2O]_n$	8, 8, 9	3.659	[35]
$[[Ca(H_2O)]_2(L)(\mu\text{-}H_2O)]_n$	8	3.71	[36]
$[[Ca(NH_2\text{-}NH\text{-}CO_2)_2] \cdot H_2O]_n$	8	3.70, 3.87	[37]
$[Ca(gly)_2 \cdot H_2O]_n$	8	3.749	[22]
$[Ca(N\text{-MeIm})(4\text{-nba})_2]$	6	3.8585(7), 5.531(1)	This work
$[Ca(H_2O)(dnSa)]_n$	7	3.8665(8), 4.1067(5)	[38]
$[Ca(H_2O)_2(4\text{-aba})_2]_n$	8	3.9047(5)	[39]
$[Ca(H_2O)(DMF)(benz)_2]_n$	8	3.956	[40]
$[Ca_2(H_2O)_2(Oac)_3(NO_3)]_n$	8	3.9953(8)	[41]
$[Ca(H_2O)_2(3\text{-aba})_2]_n$	8	4.0034(5)	[42]
$[[Ca(H_2O)_4][Ca(L^1)(H_2O)_2]_2 \cdot 7H_2O]_n$	7	4.008(1)	[43]
$[Ca(leu)_2 \cdot 3H_2O]_n$	8	4.020	[22]
$[Ca(H_2O)_2(4\text{-CNbenz})_2]_n$	8	4.023(15)	[20]
$[Ca(H_2O)[(O_2C)_2C_6H_3CO_2H]]_n$ **	8	4.0290(7)	[23]
$[[Ca(H_2O)_2(Nic)_2] \cdot (H_2O)_3]_n$	7	4.055	[44]
$[Ca(H_2O)_2(C_8H_5O_3)_2]_n$	8	4.0651(3)	[45]
$[Ca(H_2O)_2(2\text{-OPA})_2]_n$	8	4.1022	[46]
$[Ca(H_2O)_3(2\text{-aba})_2]_n$	7	4.699(1)	[47]
$[[Ca(Hpdc)(H_2O)_4] \cdot H_2O]_n$	8	4.751(1)	[48]
$[Ca(Sa)_2(Phen)]_n$	6	4.831(1)	[49]
$[Ca(val)_2(H_2O)]_n$	7	6.073	[22]
$[[Ca(PY\text{-Threonato})_2(H_2O)_2](H_2O)_2]_n$	8	6.404	[50]
$[[Ca(H_2O)_4(Hpdc)] \cdot 2H_2O]_n$	7	6.867(2)	[48]
$[[Ca(H_2O)_2(C_9H_8NO_4)_2] \cdot 2.5H_2O]_n$	6	7.669	[51]
$[Ca(H_2O)_3(C_9H_{11}N_6O_5)_2]_n$	10	7.701	[52]
$[[Ca(H_2O)_4(AIP)_2](H_2O)]_n$	8	9.816(1)	[19]

Abbreviations used: C.N. = coordination number; * three unique Ca(II) ions. ** 2-D polymer.
4-fba = 4-fluorobenzoate; benz = benzoate; 1,4-bdc = 1,4-benzenedicarboxylate; 1,3-bdc = 1,3-benzenedicarboxylate; L = 4-(2-nitrophenyl)-3,6-dioxaoctane dioate; $(NH_2–NH–CO_2)$ = hydrazine carboxylate; gly = glycinate; dnSa = 3,5-dinitrosalicylato; 4-aba = 4-amino benzoate; DMF = *N*,*N*-dimethylformamide; OAc = acetate; 3-aba = 3-aminobenzoate; L^1 = 2,2′,2″-nitrilotribenzoate; leu = rac-leucinate; 4-CNbenz = 4-cyanobenzoate; $(O_2C)_2C_6H_3CO_2H$ = 1,2,4-benzenetricarboxylate; Nic = nicotinate; $C_8H_5O_3$ = 2-formylbenzoate; 2-OPA = 2-oxo-1,2-dihydropyridine-1-acetate; 2-aba = 2-aminobenzoate; Hpdc = 3,5-pyrazoledicarboxylate; Sa = salicylato; Phen = 1,10-phenanthroline; val = rac-valinate; PY = *N*-(6-amino-3,4-dihydro-3-methyl-5-nitroso-4-oxopyrimidin-2-yl); $C_9H_8NO_4$ = 2-(pyridinium-1-yl)butanedioate $C_9H_{11}N_6O_5$ = bis[*N*-(6-amino-3,4-dihydro-3-methyl-5-nitroso-4-oxopyrimidine-2-yl) glycylglycinate; AIP = 5-aminoisopthalate.

mentary data, Figs. 5 and 6). Both **1** and **1a** decompose at higher temperatures forming CaO as the final product as evidenced by the observed mass loss and also the featureless infrared spectra of the residues indicating the loss of organics. The DSC thermogram of **2** (Fig. 4) exhibits an endothermic peak at 188 °C, which can be

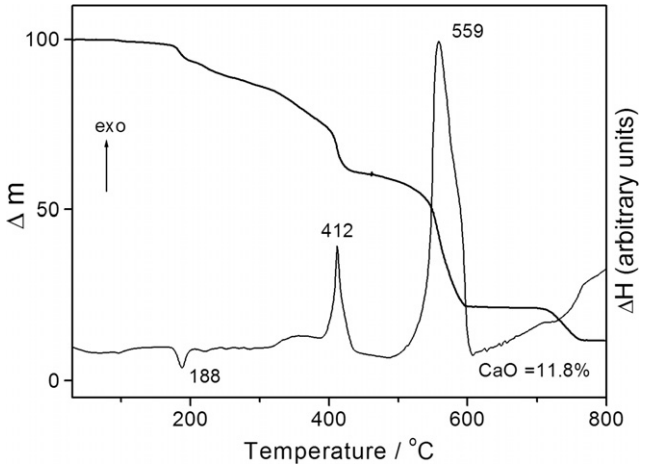

Fig. 4. TG-DSC thermogram of compound **2**.

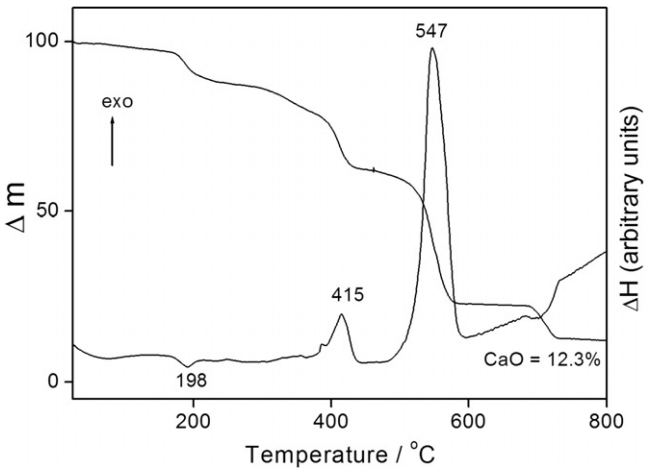

Fig. 5. TG-DSC thermogram of compound **3**.

attributed to the removal of *N*-methylimidazole and exothermic events above 400 °C assignable to the decomposition of the carboxylate ligand resulting in the formation of CaO. This assignment gains more credence as all the compounds **1**, **1a**, **2** and **3** exhibit the first exothermic event at around 410 °C. The removal of *N*-MeIm leads to further decomposition of **2** as evidenced by a steep drop in the TG curve of **2**. A scrutiny of **2** by isothermal weight loss studies at 185 °C, revealed a weight loss of 21.67% corresponding to the loss of one mole of *N*-MeIm, while further heating to 800 °C resulted in a total mass loss of 88% with 12% residue corresponding to the formation of CaO. However, our efforts to prepare the anhydrous compound $[Ca(4\text{-nba})_2]$ by heating **2** were not successful. The TG-DSC thermogram of **3** exhibits three thermal events at 198, 415 and 547 °C, respectively (Fig. 5). The endothermic signal at 198 °C can be assigned for the loss of the neutral Im ligand. This process appears to be complex and is not well resolved as evidenced by further drop in the TG curve. The exothermic signals at 415 and 547 °C can be attributed to the degradation of the carboxylate moieties leading to the decomposition of **3** to CaO with a residual mass of 12.3%, which is in good agreement with the calculated value. In the absence of associated mass spectral data of the emitted fragments the exact nature of the thermal decomposition taking place above 400 °C cannot be commented upon for both **2** and **3**. The formation of CaO as the final residue can be unambiguously confirmed by weight loss studies of compounds **2** and **3** in a temperature controlled furnace, as well as their characteristic X-ray powder pattern (see Supplementary data, Figs. 7 and 8). The diffractograms of the residues are in very good agreement with that of the reported CaO phase in the JCPDS file No. 37-1497.

4. Conclusions

In summary, we have shown that the zero dimensional mononuclear tetraaqua Ca(II) compound **1** can be transformed into the Ca(II) coordination polymer $[Ca(N\text{-MeIm})(4\text{-nba})_2]_n$ **2** by heating it in the presence of *N*-MeIm. The key step in this transformation is the formation of an intermediate monohydrate compound, which undergoes ligand substitution and incorporation of N-donor ligand into the coordination sphere of Ca(II). The use of imidazole instead of *N*-MeIm in the thermal reaction resulted in the formation of the anhydrous mixed ligand compound $[Ca(Im)(4\text{-nba})_2]_n$ **3**.

Acknowledgements

B.R.S. thanks Dr. Samar K. Das School of Chemistry, University of Hyderabad, for the X-ray intensity data of compound **2** and the

powder diffraction data of the residues. This work is supported by the Department of Science and Technology, New Delhi under Grant No. SR/S1/IC-41/2003.

Appendix A. Supplementary data

CCDC 658462 contains the supplementary crystallographic data for this paper. These data can be obtained free of charge via http://www.ccdc.cam.ac.uk/conts/retrieving.html, or from the Cambridge Crystallographic Data Centre, 12 Union Road, Cambridge CB2 1EZ, UK; fax: (+44) 1223-336-033; or e-mail: deposit@ccdc.cam.ac.uk. Additional figures related to the crystal structure of **2**, comparative DSC thermograms of compounds **1**, **1a**, **2** and **3**, X-ray powder pattern of the residue of compounds **2** and **3** are available. Supplementary data associated with this article can be found, in the online version, at doi:10.1016/j.poly.2008.07.020.

References

[1] C.N.R. Rao, S. Natarajan, R. Vaidhyanathan, Angew. Chem., Int. Ed. 43 (2004) 1466.
[2] M. Eddaoudi, D.B. Moler, H. Li, B. Chen, T M Reineke, M. O'Keeffe, O.M. Yaghi, Acc. Chem. Res. 34 (2001) 319.
[3] J. Kim, B. Chen, T.M. Reineke, H. Li, M. Eddaoudi, D.B. Mole, M. O'Keeffe, O.M. Yaghi, J. Am. Chem. Soc. 123 (2001) 8239.
[4] Y. Li, N. Hao, Y. Lu, E. Wang, Z. Kang, C. Hu, Inorg. Chem. 42 (2003) 3119.
[5] J.L.C. Rowsell, O.M. Yaghi, J. Am. Chem. Soc. 128 (2006) 1304.
[6] S. Surblé, F. Millange, C. Serre, T. Düren, M. Latroche, S. Bourrelly, P.L. Llewellyn, G. Férey, J. Am. Chem. Soc. 128 (2006) 14889.
[7] T.M. Reineke, M. Eddaoudi, M. O'Keeffe, O.M. Yaghi, Angew. Chem., Int. Ed. 38 (1999) 2590.
[8] M.J. Platers, R.A. Howie, A.J. Roberts, Chem. Commun. (1997) 893.
[9] M.J. Plater, A.J. Roberts, J. Marr, E.E. Lachowski, R.A. Howie, J. Chem. Soc., Dalton Trans. (1998) 797.
[10] H. Zhu, Z. Zhang, W. Sun, T. Okamura, N. Ueyama, Cryst. Growth Des. 5 (2005) 177.
[11] C.A. Williams, A.J. Blake, C. Wilson, P. Hubberstey, M. Schroder, Cryst. Growth Des. 8 (2008) 911.
[12] R.C. Mehrotra, R. Bohra, Metal Carboxylates, Academic Press, London, 1983.
[13] R.C. Mehrotra, A. Singh, Prog. Inorg. Chem. 46 (1997) 239.
[14] F.A. Cotton, G. Wilkinson, C.A. Murillo, M. Bochmann, Advanced Inorganic Chemistry, 6th ed., John Wiley & Sons, Inc., Chichester, 1999.
[15] B.R. Srinivasan, S. C Sawant, Thermochim. Acta 402 (2003) 45.
[16] B.R. Srinivasan, S.C. Sawant, S.K. Das, Indian J. Chem. 43A (2004) 1066.
[17] A. Grirrane, A. Pastor, E. Álvarez, R. Moyano, A. Galindo, Inorg. Chem. Commun. 10 (2007) 1125.
[18] Q. Shuai, S. Chen, S. Gao, Inorg. Chim. Acta 360 (2007) 1381.
[19] R. Murugavel, P. Kumar, M.G. Walawalkar, R. Mathialagan, Inorg. Chem. 46 (2007) 6828.
[20] R.-X. Yuan, R.-G. Xiong, Z.-F. Chen, X.-Z. You, S.-M. Peng, G.-H. Lee, Inorg. Chem. Commun. 4 (2001) 430.
[21] L.-C. Yu, Z.-F. Chen, H. Liang, C.-S. Zhou, Y. Li, J. Mol. Struct. 750 (2005) 35.
[22] S. Fox, I. Büsching, W. Barklage, H. Strasdeit, Inorg. Chem. 46 (2007) 818.
[23] C. Volkringer, T. Loiseau, G. Férey, J.E. Warren, D.S. Wragg, R.E. Morris, Solid State Sci. 9 (2007) 455.
[24] B.R. Srinivasan, J.V. Sawant, P. Raghavaiah, Indian J. Chem. 45A (2006) 2392.
[25] B.R. Srinivasan, J.V. Sawant, P. Raghavaiah, J. Chem. Sci. 119 (2007) 11.
[26] B.R. Srinivasan, J.V. Sawant, C. Näther, W. Bensch, J. Chem. Sci. 119 (2007) 243.
[27] B.R. Srinivasan, P. Raghavaiah, J.V. Sawant, Acta Crystallogr., Sect. E 63 (2007) m2251.
[28] B.R. Srinivasan, J.V. Sawant, S. C Sawant, P. Raghavaiah, J. Chem. Sci. 119 (2007) 593.
[29] Bruker SMART V5.630 and SAINT-PLUS V6.45, Bruker-Nonius Analytical X-ray Systems Inc., Madison, WI, USA, 2003.
[30] SADABS, Empirical Absorption Correction Program, Bruker AXS Inc., Madison, WI, USA, 1997.
[31] G.M. Sheldrick, Acta Crystallogr., Sect. A 64 (2008) 112.
[32] A. Karipides, C. Mc Kinney, K. Peiffer, Acta Crystallogr., Sect. C 44 (1988) 46.
[33] I. Senkovska, U. Thewalt, Acta Crystallogr., Sect. C 61 (2005) m448.
[34] R.H. Groeneman, J.L. Atwood, Cryst. Eng. 2 (1999) 241.
[35] S.H. Dale, M.R.J. Elsegood, Acta Crystallogr., Sect. C 59 (2003) m540.
[36] A. Bacchi, M. Carcelli, C. Pelizzi, G. Pelizzi, P. Pelagatti, D. Rogolino, M. Tegoni, C. Viappiani, Inorg. Chem. 42 (2003) 5871.
[37] A. Brainbanti, A.M.M. Lanfredi, M.A. Pellinghelli, A. Tiripicchio, Chem. Commun. (1970) 377.
[38] W.-D. Song, X.-X. Guo, C.-H. Zhang, Acta Crystallogr., Sect. E 63 (2007) m399.
[39] R. Murugavel, V.V. Karambelkar, G. Anantharaman, Indian J. Chem. 39A (2000) 843.
[40] S. Yano, M. Numata, M. Kato, S. Motoo, T. Nishimura, Acta Crystallogr., Sect. E 57 (2001) m488.
[41] B.G. Cooksey, L.T. Gibson, A.R. Kennedy, D. Littlejohn, L. Stewart, N.H. Tennent, Acta Crystallogr., Sect. C 55 (1999) m324.
[42] R. Murugavel, S. Banerjee, Inorg. Chem. Commun. 6 (2003) 810.
[43] S. Wörl, I.O. Fritsky, D. Hellwinkel, H. Pritzkow, R. Krämer, Eur. J. Inorg. Chem. (2005) 759.
[44] B.L. Cole, E.M. Holt, Inorg. Chim. Acta 108 (1985) 159.
[45] M. Odabaşoğlu, O. Büyükgüngör, Acta Crystallogr., Sect. E 63 (2007) m712.
[46] J.-G. Zhao, S. Gao, Z.-Y. Zhang, L.-H. Huo, H. Zhao, Acta Crystallogr., Sect. E 62 (2006) m278.
[47] R. Murugavel, V.V. Karambelkar, G. Anantharaman, M.G. Walawalkar, Inorg. Chem. 39 (2000) 1381.
[48] L. Pan, T. Frydel, M.B. Sander, X. Huang, J. Li, Inorg. Chem. 40 (2001) 1271.
[49] R. Murugavel, R. Korah, Inorg. Chem. 46 (2007) 11048.
[50] M.L.G. Salido, P.A. Mascaros, R.L. Garzon, M.D.G. Valero, J.N. Low, J.F. Gallagher, C. Glidewell, Acta Crystallogr., Sect. B 60 (2004) 46.
[51] D.K. Tian, S.L. Li, J.F. Hou, Acta Crystallogr., Sect. E 62 (2006) m130.
[52] J.N. Low, P. Arranz, J. Cobo, M.A. Fontecha, M.L. Godino, R. Lopez, D. Cannon, A. Quesada, C. Glidewell, Acta Crystallogr., Sect. C 57 (2001) 680.

25,26,27,28-tetrakis-(dimethylphosphinoylmethoxy)calix[4]arene, S) on the solvent extraction of five selected lanthanoid ions (La^{3+}, Nd^{3+}, Eu^{3+}, Ho^{3+} and Lu^{3+}) with 4,4,4-trifluoro-1-(2-thienyl)-1,3-butanedione (HL) in $CHCl_3$ and to determine the stoichiometry and the structure of solid complexes of Eu with the extractants by elemental analysis, IR, NMR and X-ray investigations.

2. Experimental

2.1. Reagents

The commercial product 4,4,4-trifluoro-1-(2-thienyl)-1,3-butanedione, (purity > 99%, Fluka) was used as received. IR(KBr): ν(C=O), 1655(s) cm^{-1}; ν(Ar), 1606(m), 1522(m) cm^{-1}; ν(C–H in –H_2C–C(O)–), 1409(m) cm^{-1}; γ(C–H in thienyl), 1521(m) cm^{-1}; $\nu(CF_3)$, 1312(m) cm^{-1}. ^{1}H NMR (250MHz, CD_3OD, 25 °C): δ = 7.209 (dd, J = 3.9, 5.0 Hz, 1H, 4-Ar), 7.894 (dd, J = 1.1, 5.0 Hz, 1H, 3-Ar), 7.908 (dd, J = 1.1, 3.9 Hz, 1H, 5-Ar); ^{19}F{^{1}H} NMR (235 MHz, CD_3OD, 25 °C): δ = −82.07 ppm.

The lower rim substituted calix[4]arene, S, was synthesized according to the method described in [21]. The structural formula of S is shown in Fig. 1. Its quality has been checked by ^{1}H NMR in $CDCl_3$ (250 MHz, 25 °C): δ = 1.074 (s, 36H, $(CH_3)_3C$), 1.532 (d, $^2J_{HP}$ = 12.9 Hz, 24H, $(CH_3)_2P{=}O$), 3.268 (d, $^2J_{HH}$ = 13.0 Hz, 4H, Ar–CH_2–Ar), 4.688 (d, $^2J_{HP}$ = 1.3 Hz, 8H, $CH_2P{=}O$), 4.836 (d, $^2J_{HH}$ = 13.0 Hz, 4H, Ar–CH_2–Ar), 6.800 (s, 8H, Ar–H) and in CD_3OD (250 MHz, 25 °C): δ = 1.001 (s, 36H, $(CH_3)_3C$), 1.527 (d, $^2J_{HP}$ = 13.1 Hz, 24H, $(CH_3)_2P{=}O$), 3.292 (d, $^2J_{HH}$ = 13.2 Hz, 4H, Ar–CH_2–Ar), 4.668 (d, $^2J_{HP}$ = 1.3 Hz, 8H, $CH_2P{=}O$), 4.780 (d, $^2J_{HH}$ = 13.2 Hz, 4H, Ar–CH_2–Ar), 6.891 (s, 8H, Ar–H).

Stock solutions of La(III), Nd(III), Eu(III), Ho(III) and Lu(III) were prepared by dissolving of appropriate amounts of their oxides (Fluka, puriss.) in concentrated hydrochloric acid and diluting to required volume. The diluent was $CHCl_3$ (Merck, p.a.). Arsenazo III (Fluka) was of analytical grade purity as were the other reagents used.

2.2. Apparatus

S-20 Spectrophotometer Boeco (Germany) was used for measuring absorbances and pH 211 HANNA digital pH meter was used for pH measurements in the solvent extraction studies.

The melting points (uncorrected) of the solid complexes were measured on a Boetzius microheating plate PHMK05 (Germany).

Infrared spectra (400–4000 cm^{-1}) were recorded on a FTIR Bruker IFS113v IR spectrometer in KBr pellets.

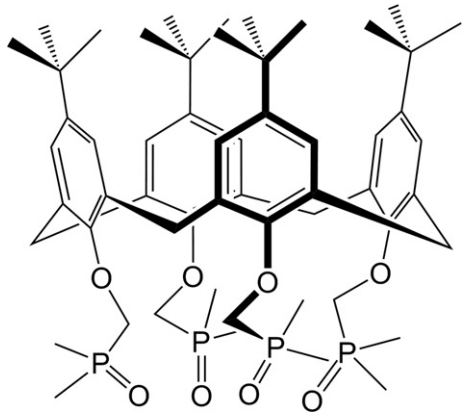

Fig. 1. Structural formula of 5,11,17,23-tetra-*tert*-butyl-25,26,27,28-tetrakis-(dimethylphosphinoylmethoxy)calix[4]arene.

The ^{1}H and ^{19}F NMR spectra were recorded on Bruker Avance DRX 250 MHz, while the ^{31}P NMR spectra were measured on Bruker Avance II+ 600 MHz high performance digital FT-NMR spectrometers. The ^{1}H NMR chemical shifts are given relative to TMS, the ^{19}F NMR chemical shifts are referenced to $CFCl_3$, while the ^{31}P NMR chemical shifts are calibrated relative to external 85% H_3PO_4.

X-ray data collection was carried out at 290 K on an Enraf-Nonius CAD-4 diffractometer with graphite monochromatized Mo Kα radiation (α = 0.71073 Å).

2.3. Solvent extraction procedure

The experiments were carried out using 10 cm^3 volumes of aqueous and organic phases. The samples were shaken mechanically for 45 min at room temperature which was sufficient to reach equilibrium. After the separation of the phases, the metal concentration in the aqueous phase was determined photometrically using Arsenazo III [22, p. 172]. The concentration of the metal ion in the organic phase was obtained by material balance. The acidity of the aqueous phase was measured by a pH-meter with an accuracy of 0.01 pH unit. The ionic strength was maintained at 0.1 mol dm^{-3} with (Na, H)Cl. The initial concentration of the metal ions was 2.5×10^{-4} mol dm^3 in all experiments.

The distribution coefficients of the lanthanoid ions were determined in three series of experiments, viz.:

- with fixed HL and S concentrations and varied pH;
- with fixed pH and S concentration and varied HL concentration;
- with fixed pH and HL concentration and varied S concentration.

2.4. Preparation of metal complexes

2.4.1. Complex of Eu(III) with 4,4,4-trifluoro-1-(2-thienyl)-1,3-butanedione (HL)

The solution of 148 mg (0.5 mmol) $EuCl_3 \cdot 2H_2O$ in 30 cm^3 absolute ethanol was added at room temperature to a transparent solution of 334 mg (1.5 mmol) 4,4,4-trifluoro-1-(2-thienyl)-1,3-butanedione in 2 cm^3 absolute ethanol and stirred for 5 h. The reaction mixture was light yellow transparent solution. It was concentrated under reduced pressure to 10 cm^3 and cooled. The crystal product was filtered, washed twice with absolute ethanol and dried in high vacuum over P_2O_5. It melts at 74–76 °C. Yield 320 mg (88.0%).

Anal. Calc. for $C_{16}H_8ClEuF_6O_4S_2 \cdot 3H_2O$ (M 683.81): C, 28.10; H, 2.06; S, 9.38. Found: C, 28.19; H, 2.28; S, 9.60%. IR(KBr): ν(C=O), 1605(vs) cm^{-1}; ν(Ar), 1605(vs), 1542–1510(s) cm^{-1}; ν(C–H in –H_2C–C(O)–), 1412(s) cm^{-1}; $\nu(-CF_3)$, 1029(m) cm^{-1}. ^{1}H NMR (250 MHz, CD_3OD, 25 °C): δ = 3.89 (bs, 1H, 3-Ar), 5.68 (bs, 1H, 4-Ar), 6.52 (bs, 1H, 5-Ar); ^{19}F{^{1}H} NMR (235 MHz, CD_3OD, 25 °C): δ = −83.69 ppm.

2.4.2. Complex of Eu(III) with 4,4,4-trifluoro-1-(2-thienyl)-1,3-butanedione (HL) and 5,11,17,23-tetra-tert-butyl-25,26,27,28-tetrakis-(dimethylphosphinoylmethoxy)calix[4]arene (S)

A colorless solution of 30 mg (0.1 mmol) $EuCl_3 \cdot 2H_2O$ in 2 cm^3 absolute ethanol was added at room temperature to a solution containing 101 mg (0.1 mmol) S and 67 mg (0.3 mmol) HL in 3 cm^3 absolute ethanol. The reaction mixture was limpid solution and after 40 min it became a white gel. After stirring for 5 h the product was isolated by centrifugation, washed three times with absolute ethanol and dried in high vacuum over P_2O_5. The solid product does not melt up to 370 °C. Yield 160 mg (96%).

Anal. Calc. for $C_{72}H_{92}ClEuF_6O_{12}P_4S_2 \cdot 2H_2O$ (M 1674.96): C, 51.63; H, 5.78; S, 3.83. Found: C, 51.73; H, 5.52; S, 4.07%. IR(KBr): ν(C=O), 1617(vs) cm^{-1}; ν(P=O), 1144 (vs) cm^{-1}; ν(P–C–H in H_3C–P), 1300(vs) cm^{-1}; ν(1,2,3,5-tetrasubst Ar), 1478(m), 940(s) cm^{-1}; ν(Ar), 1617–1600 cm^{-1} (overlap with ν(C=O)), 1502(s) cm^{-1}; ν(C–H in –H_2C–C(O)–), 1414(m) cm^{-1}; γ(C–H in thienyl), 1537(m) cm^{-1}; ν(ArC–H), 1186(s) cm^{-1}; ν(Ar–O–C), 1029(m) cm^{-1}; ν(C–H in *t*-Bu), 3075–2870(m) cm^{-1}; ν(CF_3), 1360(m) cm^{-1}. ^{1}H NMR (250 MHz, CD_3OD, 25 °C) δ = 1.010 (s, 36H, (CH_3)$_3$C), 1.387 (d, $^2J_{HP}$ = 13.3 Hz, 24H, (CH_3)$_2$P=O), 3.63 (bs, 8H, CH_2P=O), 3.80 (bs, 4H, Ar–CH_2–Ar), 5.20 (bs, 4H, Ar–CH_2–Ar), 5.48 (bs, 2H, 3-Ar), 6.17 (bs, 2H, 4-Ar), 6.894 (d, *J* = 4.6 Hz, 2H, 5-Ar), 6.978 (s, 8H, Ar–*H*); ^{19}F{^{1}H} NMR (235 MHz, CD_3OD, 25 °C): δ = −80.00 ppm.

2.5. X-ray crystallography of the complex of Eu(III) with 4,4,4-trifluoro-1-(2-thienyl)-1,3-butanedione (HL)

The crystals of the complex were prepared by slow crystallization from a diluted ethanol solution at room temperature with the possibility of partial evaporation of the solvent. A single crystal suitable for X-ray diffraction was used. The unit cell parameters were determined by least square refinement of 22 reflections, 18° < θ < 20°. The $\omega/2\theta$ technique was used for data collection using Nonius Diffractometer Control Software [23]. Lorentz and polarization corrections were applied to intensity data using the WINGX [24]. The structure was solved by direct methods using SHELXS-97 [25] and refined by full-matrix least-squares procedure on F^2 with SHELXL-97 [25]. The H atoms were placed in idealized positions ($CH_{aromartic}$ = 0.93 Å, CH_{methyl} = 0.96 Å, $CH_{methylen}$ = 0.97 Å) and were constrained to ride on their parent atoms, with $U_{iso}(H) = 1.2U_{eq}$.

3. Results and discussion

3.1. Synergistic solvent extraction of Ln(III) with mixtures of HL–S

The solvent extraction of the lanthanoid(III) ions with 4,4,4-trifluoro-1-(2-thienyl)-1,3-butanedione (HL) in $CHCl_3$ has been studied previously [2]. It has been found that the metal extraction can be represented by the following equation:

$$Ln^{3+}_{(aq)} + 3HL_{(o)} \rightleftharpoons [LnL_3]_{(o)} + 3H^+_{(aq)} \quad (1)$$

The synergistic solvent extraction of the lanthanoids was studied using a traditional method called "slope analysis". It is based on an examination of the variation of $D_{L,S}$ (the distribution coefficient due to the synergistic effect) as a function of the relevant experimental variables. As the lanthanoid extraction with the calix[4]arene alone is negligible under the experimental conditions of the present study, the values of the distribution coefficient *D* obtained experimentally are the sum of $D_{L,S}$ and D_L (D_L is the distribution coefficients due to the lanthanoid extraction with HL alone under the same experimental conditions). So, the values of $D_{L,S}$ were calculated as $D - D_L$. A log–log plots of $D_{L,S}$ versus one of the variables [H^+], [HL] and [S] keeping the other two constant, indicate the stoichiometry of the extractable complex. This leads to the derivation of a suitable equilibrium expression and then to the calculation of the equilibrium constant. If the concentration of the extractants is constant and the hydrolysis in the aqueous phase as well as the polymerization in the organic phase occur to a negligible extent only, then the plots will be straight lines and their slopes will give the number of the ligands in the adducts.

The experimental data for the extraction of the lanthanoid(III) ions with mixture of HL and S are given in Figs. 2–4. The plots of log$D_{L,S}$ versus pH and log[HL] are linear with slope close to three and the plots of log$D_{L,S}$ versus log[S] – with slope close to two.

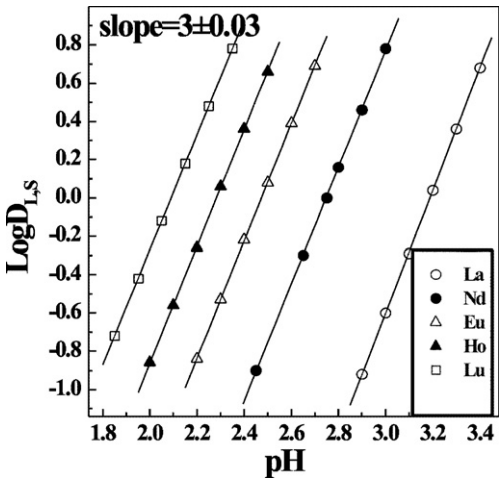

Fig. 2. Log$D_{L,S}$ vs. pH for the extraction of lanthanoid ions with mixtures of HL–S at [HL] = 6 × 10^{-2} mol dm^{-3} and [S] = 1 × 10^{-3} mol dm^{-3}.

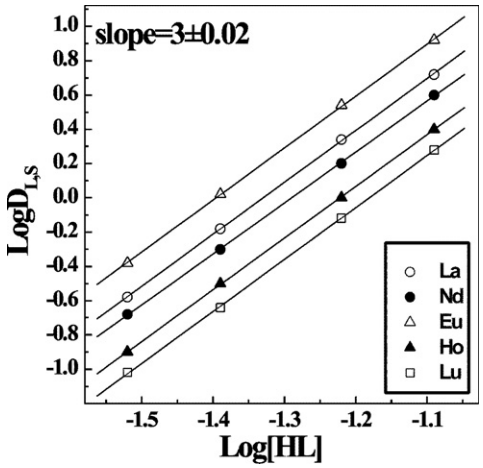

Fig. 3. Log$D_{L,S}$ vs. [HL] for the extraction of lanthanoid ions with mixtures of HL–S at [S] = 1 × 10^{-3} mol dm^{-3}; La, pH = 3.30; Nd, pH = 2.75; Eu, pH = 2.65; Ho, pH = 2.35; Lu, pH = 2.05.

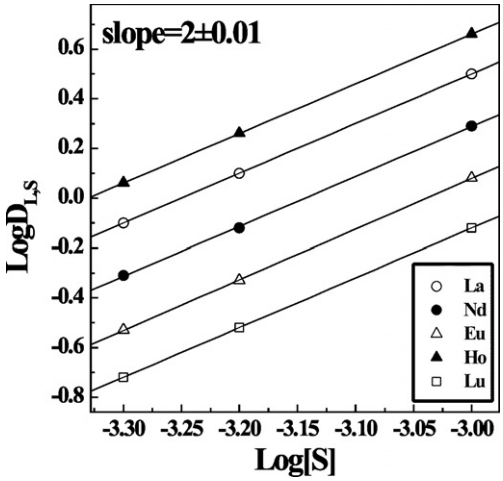

Fig. 4. Log$D_{L,S}$ vs. [S] for the extraction of lanthanoid ions with mixtures of HL–S at [HL] = 6 × 10^{-2} mol dm^{-3}; La, pH = 3.35; Nd, pH = 2.85; Eu, pH = 2.50; Ho, pH = 2.50; Lu, pH = 2.05.

Table 1
Values of the equilibrium constants K_L, $K_{L,S}$, $\beta_{L,S}$, synergistic coefficients ([HL] = 6×10^{-2} mol dm^{-3}, [S] = 1×10^{-3} mol dm^{-3}, pH = 2.50) and separation factors for the Ln(III) extraction with HL–S mixtures in $CHCl_3$

Ln^{3+}	log K_L[2]	log $K_{L,S}$	log $\beta_{L,S}$	S.C.	S.F.		
						HL	HL–S
La^{3+}	−11.06	−3.22	7.84	1.84	Nd/La	8.70	21.37
Nd^{3+}	−10.12	−1.89	8.23	2.23	Eu/Nd	27.54	6.60
Eu^{3+}	−8.68	−1.07	7.61	1.61	Ho/Eu	1.32	3.72
Ho^{3+}	−8.56	−0.50	8.06	2.06	Lu/Ho	2.57	3.80
Lu^{3+}	−8.15	0.08	8.23	2.23			

Note: The values of the equilibrium constants are calculated on the basis of the 38 experimental points, statistical confidence 95%, confidence interval ⩽±0.06.

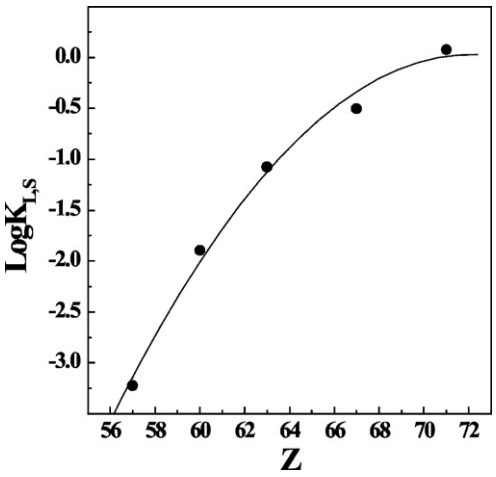

Fig. 5. Log $K_{L,S}$ vs. atomic number Z of La, Nd, Eu, Ho and Lu.

Therefore, in the presence of HL–S combination the lanthanoid extraction can be expressed by the following equation:

$$Ln^{3+}_{(aq)} + 3HL_{(o)} + 2S_{(o)} \rightleftharpoons [LnL_3S_2]_{(o)} + 3H^+_{(aq)} \quad (2)$$

where Ln^{3+} denotes a lanthanoid ion and the subscripts "aq" and "o" denote aqueous and organic phases, respectively.

Taking into account that the partition of HL [26] and S [21] toward the aqueous phase is very low, the overall equilibrium constant values $K_{L,S}$ can be determined by the equation

$$\log K_{L,S} = \log D_{L,S} - 3\log[HL] - 2\log[S] - 3pH \quad (3)$$

The formation of mixed complexes in the organic phase can be described by the following equation:

$$[LnL_3]_{(o)} + 2S_{(o)} \rightleftharpoons [LnL_3S_2]_{(o)} \quad (4)$$

The equilibrium constant $\beta_{L,S}$ for the organic phase synergistic reaction can be determined as

$$\log \beta_{L,S} = \log K_{L,S} - \log K_L \quad (5)$$

The values of the equilibrium constants $K_{L,S}$ and $\beta_{L,S}$ calculated from the experimental data are given in Table 1. The equilibrium constants are based on the assumption that the activity coefficients of the species do not change significantly under the experimental conditions i.e. they are concentration constants. The data presented in Table 1 show that the addition of the calix[4]arene to the system Ln(III)–HL leads to a very large increase of the values of $K_{L,S}$ in comparison with those of K_L (8 orders of magnitude approximately) as well as that the values of this constant increase from La(III) to Lu(III) as expected from their decreasing ionic radii. The values of log $K_{L,S}$ are smaller (up to 2 log units) than those obtained for the extraction of the same lanthanoids with mixtures 4-benzoyl-3-methyl-1-phenyl-5-pyrazolone (HP) and the same calix[4]arene [20]. This fact can be explained taking into account that HL is more weak acid than HP (pK_a = 6.2 [26], and pK_a = 3.95

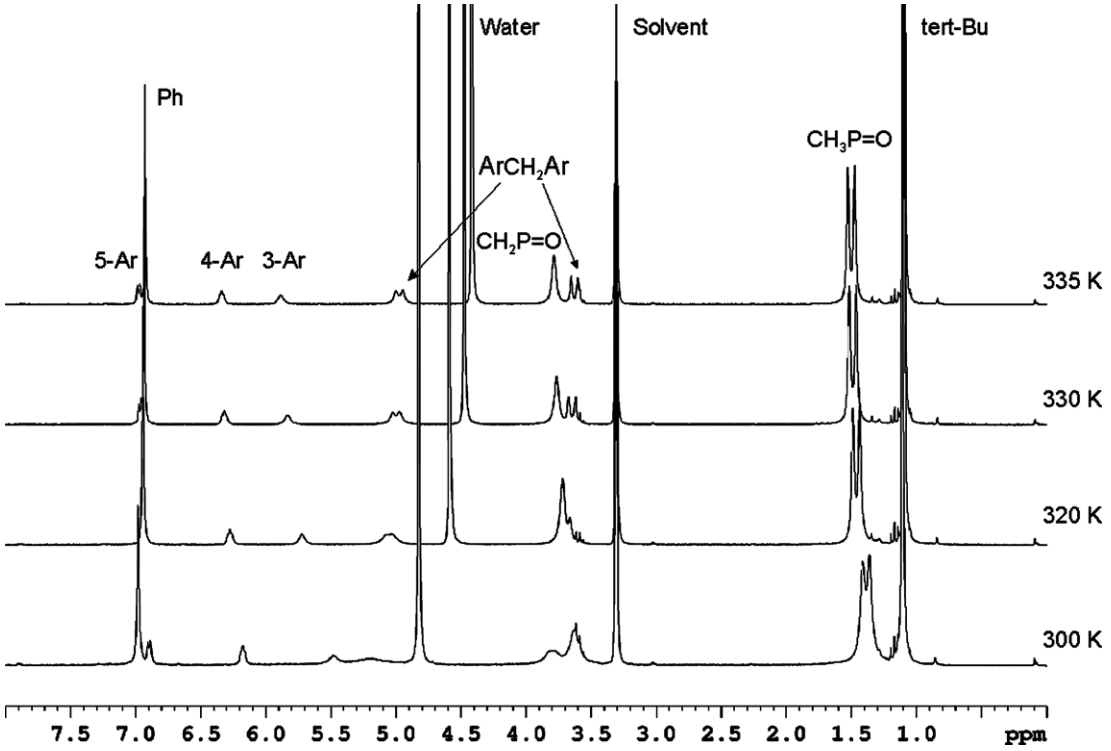

Fig. 6. The ^{1}H NMR spectra of the [EuL_2S]Cl complex in CD_3OD at 300, 320, 330 and 335 K. The assignment of signals in spectrum at 335 K is done by running 2D COSY spectrum at the same temperature.

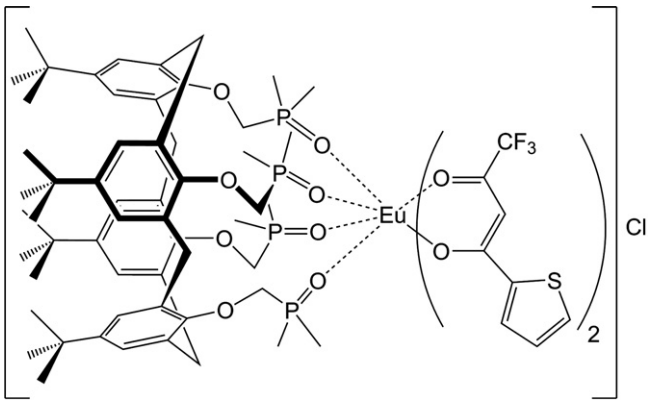

Fig. 7. Structure of the solid complex $[EuL_2S]Cl$ proposed on the basis of IR and NMR data.

[2], respectively). On the other hand, the lanthanoid(III) ions are more effectively extracted using the present mixture of extractants in comparison with the cases when 1-(2-pyridylazo)-naphthol [27], dibenzo-18-crown-6 or dibenzo-24-crown-8 [28], tri-(n-butyl)phosphate [2] or 2,2′-dipyridil [2] were used as synergistic agents in combination with HL. Similar value of the overall equilibrium constant ($\log K_{L,S} = 1.08$) has been obtained for Eu(III) extraction with mixtures of HL and tri(*n*-octyl)phosphine oxide in $CHCl_3$ and complexes of the same type, $[EuL_3S_2]$, has been found [2].

The variation of the equilibrium constant $K_{L,S}$ values versus the atomic number Z of the investigated lanthanoids is given in Fig. 5. It is seen that the values of $\log K_{L,S}$ do not increase monotonically with Z.

The synergistic enhancement produced by HL–S mixtures can be determined using the synergistic coefficients (S.C.). They were calculated according to [1] viz. $S.C. = \log(D_{1,2}/D_1 + D_2)$ where $D_{1,2}$ is the distribution coefficient of a metal obtained using mixture of the two extractants and D_1 and D_2 – the distribution coefficient values of the same metal using the extractants separately. The values of the synergistic coefficients are listed in Table 1. It is seen that the lanthanoids are extracted synergistically (S.C. > 0). So, the addition of S to the chelating extractant improves the extraction efficiency of the lanthanoid ions and produces rather large synergistic effects.

The separation of the lanthanoids using HL–S mixtures can be assessed by the separation factors (S.F.) calculated as a ratio of the distribution coefficients of two lanthanoids (the heavier and the lighter one). When the metal ions form complexes of the same type (as in the present case), the separation factors can be determined as a ratio of the equilibrium constants $K_{L,S}$. Their values are also given in Table 1. It is seen that the separation factors obtained for the extraction of the investigated lanthanoid ions with HL alone are smaller than those with HL–S combination with exception of the Eu/Nd pair. So, the synergistic mixture used in the present study combines (in the most cases) higher extraction efficiency with improved selectivity as compared with HL.

The comparison of the data for synergistic coefficients and separation factors found for the present synergistic system with those for 4-benzoyl-3-methyl-1-phenyl-5-pyrazolone and the same synergistic agent [20] shows that in the present case the synergistic enhancement is lower but the separation factors for the heavier lanthanoids are higher.

3.2. IR, ^1H, ^{19}F and ^{31}P NMR spectra and X-ray structure determination of the complexes

The elemental analysis, IR, NMR and X-ray studies of the isolated solid complexes give a possibility to make conclusions about the composition and the structure of the complexes.

In the IR spectrum of 4,4,4-trifluoro-1-(2-thienyl)-1,3-butanedione the characteristic band observed at 1655 cm^{-1} for enol group in β-diketones is shifted to 1605 cm^{-1} in the complex of HL with

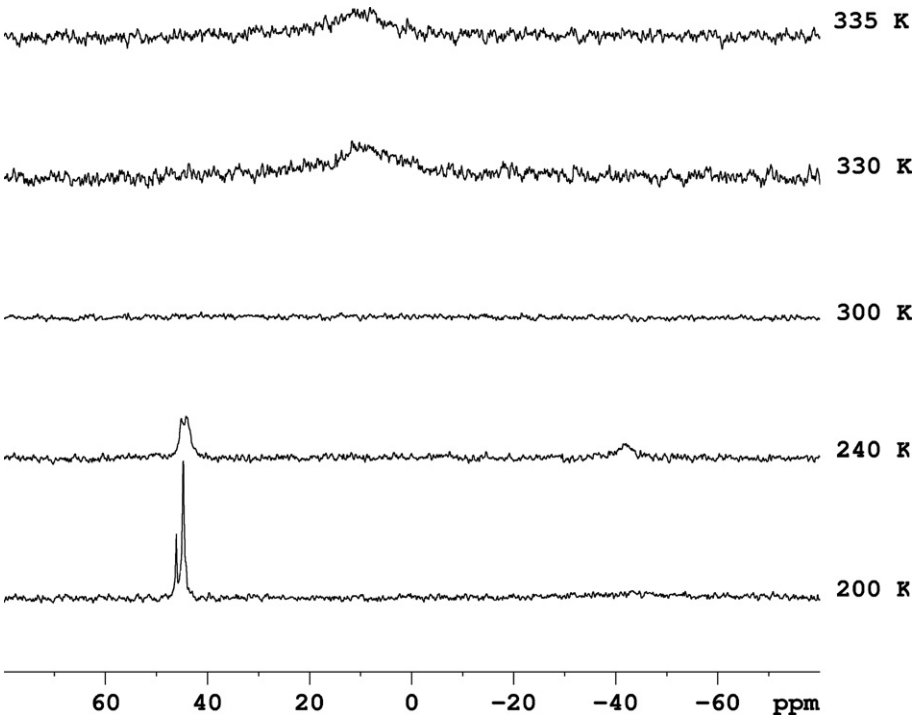

Fig. 8. The $^{31}P\{^1H\}$ NMR spectra of the $[EuL_2S]Cl$ complex in CD_3OD at 200, 240, 300, 330 and 335 K. The signals at about 45 ppm are assigned for noncoordinated P=O moieties, while the broad signal at about −40 ppm is assigned for coordinated P=O moieties. This assignment is based on the $^{31}P\{^1H\}$ NMR spectra of S (49.71 ppm) and EuS (6.13 ppm) at 300 K (Búnzli and Varbanov – unpublished results). The similar low chemical shifts of Eu(III) complexes with bisphosphonates (−50.6, −65.4 and −81 ppm) have been already reported by Platt et al. [29,30].

Eu(III) and at 1617 cm^{-1} in the complex of Eu(III), HL and calix[4]-arene. They are overlaped with the bands for aromatic rings.

The position of the bands typical for aromatic rings are around 1600 cm^{-1} and around 1500 cm^{-1} in the HL and its complexes with calix[4]arene and Eu(III).

The IR spectra show shift of the band for P=O group from 1160 cm^{-1} in the free calix[4]arene to 1144 cm^{-1} in the crystal complex of Eu with HL and S.

The expected ^1H NMR resonances of HL are significantly shifted to higher field upon coordination ($\Delta\delta$ is from −1.4 to −4.0 ppm in $[EuL_2]Cl$, while in $[EuL_2S]Cl$ it is from −1.0 to −2.4 ppm), while the signals of S are relatively less influenced ($\Delta\delta$ is less than 1.0 ppm). On the other hand, the signal of 3-Ar(HL) proton is the most shifted to higher field signal indicating proximity to the metal ion (Fig. 6).

There is no change in the symmetry of ligand S upon coordination and all resonances of S remain in the same form as for free S ligand, which indicates uniform interaction of all P=O with Ln(III) ion within the ^1H NMR time scale. The ^1H NMR spectra of Eu–HL–S complex at 300, 320, 330 and 335 K are presented in Fig. 6. At the highest temperature the signals are sufficiently resolved and on the basis of their integral intensity the ratio of the ligands in the synthesized complex was calculated as HL:S = 2:1. Therefore the composition of the complex can be represented by the formula $[EuL_2S]Cl$. The proposed structure of the complex is presented in Fig. 7.

The variable temperature $^{31}P\{^1H\}$ NMR measurements showed dynamic processes of exchanging phosphine oxides moieties. At 335 K intermediate exchange is observed, while at 240 K slow exchange between bounded and non bounded P=O groups is seen (Fig. 8). Most probably the all possible coordinations are realized at low temperature and the ratio between them is changed with the temperature (spectra at 200 K and 240 K). Although the existence of different S coordinations at low temperature, the structure given on Fig. 7 represents the picture at 335 K, which we state to be the most probable according to the coordination number of Eu.

The crystal structure of the complex of Eu(III) with HL is illustrated in Fig. 9. The X-ray data showed that the composition of this

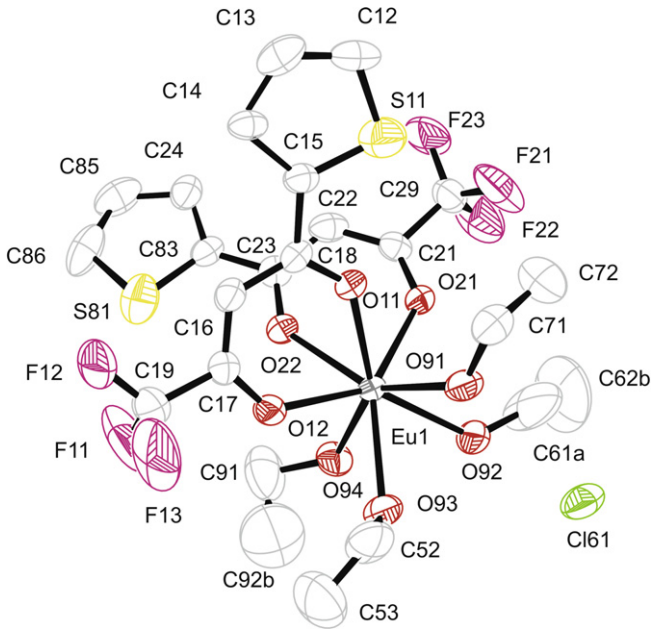

Fig. 9. View of the structure of the complex $[Eu(L)_2(C_2H_5OH)_4]Cl$ and the atom-numbering scheme showing 50% probability displacement ellipsoids. H atoms are omitted for clarity.

Table 2
Crystal data and structure solution methods and refinement results for $[EuL_2(C_2H_5OH)_4]Cl$

Empirical formula	$C_{24}H_{34}ClF_6O_8S_2Eu$
Formula weight	816.07
Temperature (K)	290(2)
Wavelength (Å)	0.71073
Crystal system	monoclinic
Space group	*C*2/*c*
Unit cell dimensions	
a (Å)	41.350(9)
b (Å)	11.152(2)
c (Å)	15.521(3)
α (°)	90
β (°)	111.33(3)
γ (°)	90
V (Å^3)	6666.9(7)
Z, D_{calc} (mg/m^3)	8, 1.626
Absorption coefficient (mm^{-1})	2.161
F(000)	3264
Crystal size (mm)	0.32 × 0.31 × 0.22
Crystal color/shape	yellow/prismatic
θ Range for data collection (°)	1.29–25.97
Index ranges	
Reflections collected/unique (R_{int})	12910/6546 (0.050)
Completeness (%)	100 (to 25.97)
Observed reflections [$I > 2\sigma(I)$]	4581
Refinement method	full-matrix least-squares procedure on F^2
Weight, *w*	$1/[\sigma^2(F_o^2) + (0.0720P)^2 + 0.7043P]$ where $P = (F_o^2 + 2F_c^2)/3$
Data/restrains/parameters	6546/0/385
Goodness of fit on F^2	1.068
Final *R* indices [$I > 2\sigma(I)$]	$R_1 = 0.0543$, $wR_2 = 0.1533$
R indices (all data)	$R_1 = 0.0873$, $wR_2 = 0.1725$
Extinction coefficient	none
Largest peak and hole (Å^{-3})	1.652 and −1.009

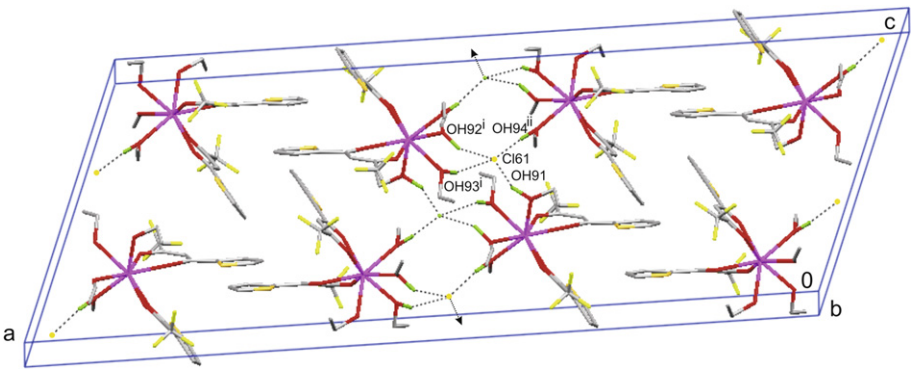

Fig. 10. A view of the molecular packing in $[Eu(L)_2(C_2H_5OH)_4]Cl$. Hydrogen bonds are represented by dotted lines. [Symmetry codes: (i) −1 − *x*, 1 − *y*, 1 − *z*; (ii) *x*, 1 − *y*, ½ + *z*].

complex is $[Eu(L)_2(C_2H_5OH)_4]Cl$. Basic crystallographic data for the complex, data collection and structural refinement are listed in Table 2. The complex shows a typical for Eu eight coordination sphere incorporating two bidentate 4,4,4-trifluoro-1-(2-thienyl)-1,3-butanedione ligands while ethanol molecules complete the distorted square antiprism geometry. The thiophene ring is nearly planar (r.m.s. deviation of 0.01(6) Å) and forms an angle of 8.45(7)° with the extended trifluoro-3-oxobutanal plane (r.m.s. deviation of 0.03(5) Å).

The three-dimensional crystal packing is stabilized trough $O_{ethanol}$–H···Cl interactions producing chains propagating along *c* axis (Fig. 10). The head-to-head interaction of the ethanol molecules is in the inner side of the chains while on the outer side the thiophene ring blocks the formation of strong non-covalent interactions.

4. Conclusion

Selected lanthanoid(III) ions (La, Nd, Eu, Ho, Lu) are synergistically extracted by HL–S combination as $[LnL_3S_2]$ species. The addition of the phosphorus-containing *p-tert*-butylcalix[4]arene (S) produces a large synergistic effect and, in the most cases, improves the selectivity among the lanthanoid ions in comparison with HL alone.

On the basis of elemental analysis, IR and NMR spectra the stoichiometry of the complexes in solid state is found and the structure is proposed. The crystallographic data for the complex of Eu with HL have shown that Eu(III) is eight coordinated and its composition can be represented with the formula $[Eu(L)_2(C_2H_5OH)_4]Cl$. The coordination polyhedron of the complex is distorted square antiprism.

5. Supplementary data

CCDC 670123 contains the supplementary crystallographic data for $[Eu(L)_2(C_2H_5OH)_4]Cl$. These data can be obtained free of charge via http://www.ccdc.cam.ac.uk/conts/retrieving.html, or from the Cambridge Crystallographic Data Centre, 12 Union Road, Cambridge CB2 1EZ, UK; fax: (+44) 1223-336-033; or e-mail: deposit@ccdc.cam.ac.uk.

Acknowledgements

The financial support from the Bulgarian National Science Foundation – Grant X-1408 (N. Vassilev) and Project'VU X 13/2007 (I. L. Dukov, M. Atanassova) as well as from the Swiss National Science Foundation – Project SCOPES 2000–2003: 7BUPJ062293.00/1 (S. Varbanov) is acknowledged with gratitude.

References

[1] J.N. Mathur, Solvent Extr. Ion Exch. 1 (1983) 349.
[2] J. Stary, H. Freiser, Equilibrium Constants of Liquid–Liquid Distribution Reactions. Part IV. Chelating extractants (IUPAC Chemical Data Series, No. 18), Pergamon Press, Oxford, 1978.
[3] K. Gschneidner, J. Bünzli, V. Pecharsky (Eds.), Handbook on the Physics and Chemistry of Rare Earths, vol. 35, Elsevier, Amsterdam, 2005, pp. 107–272 (Chapter 225).
[4] R. Ludwig, D. Lentz, T. Nguyen, Radiochim. Acta 88 (2000) 335.
[5] F. Arnaud-Neu, R. Arneck, V. Böhmer, S. Faunni, J. Gordon, M. Weill, W. Vogt, J. Chem. Soc., Perkin Trans. 2 (1996) 1855.
[6] F. Arnaud-Neu, J. Cremin, S. Harris, M. McKervey, M. Weill, P. Schwinte, A. Walker, J. Chem. Soc., Dalton Trans. (1997) 329.
[7] F. Arnaud-Neu, J. Browne, D. Byrne, D. Marrs, M. McKervey, P. O'Hagan, M. Weill, Chem. Eur. J. 5 (1999) 175.
[8] F. Arnaud-Neu, J. Barboso, V. Böhmer, F. Brisach, L. Delman, J. Dozol, O. Moyck, E. Paulis, M. Saadioni, A. Shivanyuk, Aust. J. Chem. 56 (2003) 1113.
[9] M. Baaden, M. Burgard, C. Boehme, G. Wipff, Phys. Chem. Chem. Phys. 3 (2001) 1317.
[10] O. Klumchuk, L. Atamas, S. Mirochnichenko, V. Kalchenko, I. Smirnov, V. Babain, A. Varnek, G. Wipff, J. Incl. Phenom. Macrocycl. Chem. 49 (2004) 47.
[11] M.R. Yaftian, M. Burgard, D. Matt, C.B. Dieleman, F. Rastegar, Solvent Extr. Ion Exch. 15 (1997) 975.
[12] R. Ludwig, Fres. J. Anal. Chem. 376 (2000) 103.
[13] W. Sliwa, J. Incl. Phenom. Macrocycl. Chem. 52 (2005) 13.
[14] W. Sliwa, Croat. Chim. Acta 75 (2002) 131.
[15] L. Kuznetsova, A. Mustafina, J. Podjavlev, E. Kazakova, A. Burilov, M. Pudovic, Russ. Coord. Chem. 24 (1998) 623.
[16] L. Kuznetsova, A. Mustafina, A. Ziganshina, E. Kazakova, A. Konovalov, J. Incl. Phenom. Macrocycl. Chem. 39 (2001) 65.
[17] L. Kuznetsova, G. Pribalova, A. Mustafina, I. Tananaev, B. Myasoedov, A. Konovalov, Russ. Radiochem. 46 (2004) 277.
[18] M. Kyrš, K. Svoboda, P. Lhotak, S. Alexova, J. Radioanal. Nucl. Chem. 254 (2002) 455.
[19] M. Kyrš, K. Svoboda, P. Lhotak, J. Radioanal. Nucl. Chem. 258 (2003) 497.
[20] M. Atanassova, V. Lachkova, N. Vassilev, S. Varbanov, I. Dukov, J. Incl. Phenom. Macrocycl. Chem. 58 (2007) 173.
[21] L. Saulnier, S. Varbanov, R. Scopelliti, M. Elhabriri, J. Bünzli, J. Chem. Soc., Dalton Trans. (1999) 3919.
[22] S.B. Savvin, Arsenazo III, Atomizdat, Moskva, 1966.
[23] Enraf-Nonius diffractometer control software, Release 5.1. Enraf-Nonius, Delft, The Netherlands, 1993.
[24] L.J. Farrugia, J. Appl. Crystallogr. 32 (1999) 837.
[25] G.M. Sheldrick, SHELXS-97. Program for the Solution of Crystal Structures, Universität of Göttingen, Germany, 1990.
[26] A. De, S. Khopkar, R. Chalmers, Solvent Extraction of Metals, Van Nostraud, Holland, 1970.
[27] M. Atanassova, I. Dukov, Sep. Purif. Technol. 49 (2006) 101.
[28] M. Atanassova, I. Dukov, Sep. Sci. Technol. 40 (2005) 1103.
[29] A.W.G. Platt, D. Simpson, J. Fawcett, D.R. Russell, Inorg. Chim. Acta 223 (1994) 43.
[30] A.M.J. Lees, J.M. Charnock, R.A. Kresinski, A.W.G. Platt, Inorg. Chim. Acta 312 (2001) 170.

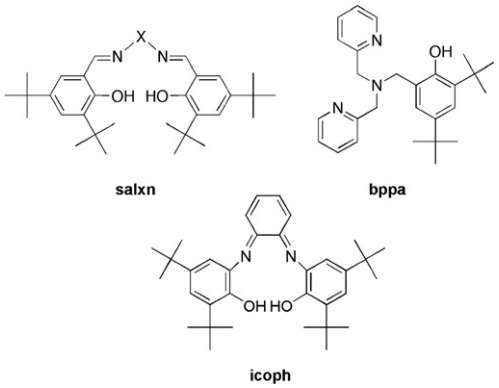

Chart 1. Ligand structures of bppa, icoph, and salxn, where X = $-CH_2CH_2-$ (salen), $-CH_2CH_2CH_2-$ (salpen), or $-CH_2CH_2CH_2CH_2-$ (salben).

aminium cations [20,21], which is significantly smaller than the apparent λ for the related tyrosine oxidation [19]. While the above suggests that the $PhO^{\cdot/-}$ ET reaction is subject to a smaller kinetic barrier than that of protonated phenols, it is unclear how this translates to the redox reactivity of metal-coordinated phenolates.

As the cofactors found in GalOx and CAO are proposed to form via oxidation of a copper–tyrosine precursor [27–32], our work was motivated by a desire to understand the ET reactivity of metal coordinated phenolates [33]. For these studies, the roughly square–planar complexes Cu(salxn) (H_2salxn, bis-salicylidinediamine) were synthesized to vary the planarity of the Cu(O_2N_2) center, as well as the more easily oxidized complexes Cu(bppa) (Hbppa, bis-pyridyl phenolamine) and Cu(icoph) (H_2icoph, bis-iminocatechol *o*-phenylenediamine) (Chart 1). Cu(salxn) complexes were observed to be efficient energy-transfer quenchers of $Ru(bpy)_3^{2+*}$, likely due to spectral overlap with a copper ligand-field state. In contrast, Cu(bppa) and Cu(icoph) quenched $Ru(bpy)_3^{2+*}$ by electron transfer, with observed reorganization energy $\lambda = 22$ kcal/mol. While this reactivity difference likely arises from the more favorable driving force for electron transfer in the case of Cu(bppa) and Cu(icoph), the large self-exchange reorganization energy calculated for the Cu-coordinated phenolate suggests that the CAO and GalOx cofactors may be poor $1e^-$ redox centers.

2. Materials and methods

Chemicals were obtained from commercial sources and used without further purification. For the electrochemical and time-resolved studies, CH_2Cl_2 and CH_3CN were dried over calcium hydride and distilled. ^1H NMR spectra were collected using a Bruker Avance 400 MHz NMR spectrometer. Electronic spectra were recorded using a Hewlett Packard 8453 UV–Vis spectrometer. Elemental analyses were performed at the University of Massachusetts Microanalysis Laboratory.

$Ru(bpy)_3(PF_6)_2$, $Ru(dMebpy)_3(PF_6)_2$, and $Ru(dOMebpy)_3(PF_6)_3$ were prepared according to literature procedures and recrystallized using CH_3CN/ether; $Ru(bpy)_3(PF_6)_3$ was prepared by oxidizing $Ru(bpy)_3^{2+}$ in 7 M H_2SO_4 using MnO_2. [34] The complexes Cu(bppa) [17] and Cu(icoph) [35] were produced and purified following literature methods. H_2salen, H_2salpen, H_2salben, and H_2saloph were synthesized through the condensation reaction of 3,5-di-*tert*-butyl-2-hydroxybenzaldehyde and the appropriate diamine. Copper(II) complexes were produced by adding $Cu(OAc)_2$ to the ligands in ethanol. The resulting compounds were recrystallized in CH_2Cl_2/ether and characterized using elemental analysis.

Cu(salen), Copper(II) *N,N′*-disalicylidene-1,2-ethylenediamine. Cu(salen) · $0.5H_2O$. *Anal.* Calc. for $C_{32}H_{47}N_2CuO_{2.5}$: C, 68.23; H, 8.41; N, 4.97. Found: C, 68.36; H, 8.21; N, 4.96%.

Cu(salpen), Copper(II) *N,N′*-disalicylidene-1,3-propylenediamine. Cu(salpen) · $0.5H_2O$. *Anal.* Calc. for $C_{33}H_{49}N_2CuO_{2.5}$: C, 68.66; H, 8.56; N, 4.85. Found: C, 68.84; H, 8.52; N, 4.80%.

Cu(salben), Copper(II) *N,N′*-disalicylidene-1,4-butylenediamine. Anal. Calc. for $C_{34}H_{50}N_2CuO_2$: C, 70.13; H, 8.65; N, 4.81. Found: C, 69.98; H, 8.67; N, 4.80%.

Electrochemical measurements were performed using a Bioanalytical Systems BAS CV-50 W potentiostat with a standard three electrode cell. Glassy carbon (working), Pt wire (auxiliary), and Ag/AgCl (reference) electrodes were used. 1 mM solutions of each complex were prepared using CH_3CN or CH_2Cl_2 with 0.1 M of tetra-*n*-butylammonium hexafluorophosphate (TBA) as the supporting electrolyte and ferrocene as an internal standard. Samples were sparged with Ar before collection.

Lifetime experiments were performed using a Photon Technology International PL-2300 nitrogen laser at 23 °C. The emission was filtered using a 695 nm filter and detected using a photomultiplier. Decay traces were acquired using a digital oscilloscope triggered by a photodiode. The $Ru(R_2bpy)_3^{2+}$ concentration was approximately 5 μM while the quencher solutions contained $Ru(R_2bpy)_3^{2+}$ with an additional 0.3–4 mM metal phenolate. Since Cu(bppa) is a positively charged species in solution, 0.1 M TBA was added to attenuate any electrostatic interactions for that sample.

The lifetime of $Ru(R_2bpy)_3^{2+}$ alone, τ_0, was determined for each individual experiment, then aliquots of the quencher solution were transferred via a Hamilton gas-tight syringe to the cuvette, and lifetime measurements taken after each sequential addition. The lifetime values were determined from the slope of semilog plots [36]. The quenching efficiency (K_{SV}) for each quencher was determined from Stern–Volmer plots of τ_0/τ vs. quencher concentration. The observed quenching rate constants (k_{obs}) were determined from the relationship $k_{obs} = K_{SV} \times \tau_0$ and corrected for the rate of diffusion (k_{diff}) to obtain the diffusion-corrected quenching rate constant, k_q according to the equation $1/k_{obs} = 1/k_{diff} + 1/k_q$.

X-band (9.764 GHz) EPR experiments were performed on a Bruker ESP-300 spectrometer, with a liquid nitrogen finger-dewar used to control the sample temperature to 77 K. The modulation amplitude was 10 gauss and the frequency 100 kHz. Spectra were collected using 20 mW power. 0.9 mM solutions of Cu(salophen) and Zn(salophen) were prepared separately in CH_2Cl_2, then combined with an equal volume of 0.9 mM $Ru(bpy)_3^{3+}$ in CH_3CN. The mixtures were immediately transferred to EPR tubes and frozen in liquid nitrogen manually. Simulations were run using XSophe [37,38].

3. Results and discussion

3.1. $Ru(bpy)_3^{3+}$ oxidizes Cu-phenolates

$Ru(R_2bpy)_3^{3+}$ oxidized metal-coordinated phenolates, as expected from literature reports of non-coordinated phenolate oxidation. [19–21,39] Cu(salophen) (0.9 mM, CH_2Cl_2) and Zn(salophen) (0.9 mM, CH_2Cl_2) were separately mixed with $Ru(bpy)_3^{3+}$ (0.9 mM, CH_3CN), then added to an EPR tube and quickly frozen in liquid nitrogen. Zn(salophen) exhibited no EPR signal, as expected for this S = 0 ground state (Fig. 1A); upon reaction with ~1 equiv. of $Ru(bpy)_3^{3+}$, a narrow isotropic signal at $g_{eff} \sim 2.01$ appeared (Fig. 1C). This narrow signal is assigned to the phenoxyl radical (S = ½) of Zn(salophen)$^+$. Similarly, Cu(salophen) exhibited an axial signal with fine structure, as expected for a an S = 1/2 Cu^{2+} (Fig. 1D). This spectrum was simulated with $g_\perp = 2.034$, $g_{||} = 2.196$, and Cu-hyperfine coupling of $A_\perp = 3.0$ mT, $A_{||} = 19.2$ mT (Fig. 1E). These electronic parameters are similar to those reported for other square–pyramidal Cu(II) complexes with a predominantly $d_{(x^2-y^2)}$ ground state [40,41]. Oxidation of Cu(salophen) by ~1 equiv. of $Ru(bpy)_3^{3+}$ attenuated this Cu^{2+} signal, while a broad

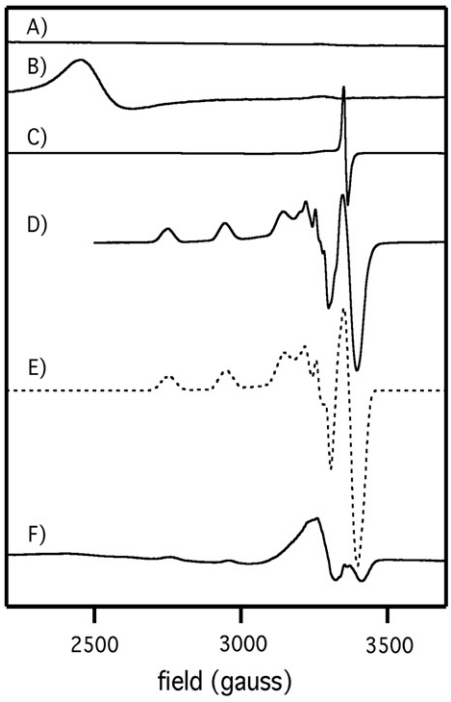

Fig. 1. 9.764 GHz EPR spectra at 77 K: (A) Zn(salophen); (B) $Ru(bpy)_3^{3+}$; (C) Zn(salophen) mixed with $Ru(bpy)_3^{3+}$ (×0.25); (D) Cu(salophen) (×0.75); (E) simulation for Cu(salophen) (×0.75, see text for details); (F) Cu(salophen) mixed with $Ru(R_2bpy)_3^{3+}$ (×2).

$g_{eff} \sim 2.1$ signal appeared, which we attribute to weak magnetic coupling between Cu^{2+} ($S = 1/2$) and a phenoxyl radical ($S = 1/2$) on $Cu(salophen)^+$.

The EPR spectra clearly indicated that $Ru(bpy)_3^{3+}$ oxidized the salophen ligand for both Cu(salophen) and Zn(salophen) to form the metal-coordinated phenoxyl radical. Cyclic voltammetry confirmed that such reactions were exothermic (Table 1). As we were interested in the electron-transfer reactivity of metal-phenolates, we attempted to measure the rate constants for metal-phenolate oxidation by stopped-flow methods. These experiments were unsuccessful, largely due to solvent incompatibilities. Rapid mixing of CH_2Cl_2 solutions of Cu-phenolate with CH_3CN solutions of $Ru(R_2bpy)_3^{3+}$ led to extensive turbidity, due to mixing, leading us to abandon this approach in favor of photo-induced experiments.

3.2. Quenching of $Ru(bpy)_3^{2+*}$ by Cu(salxn) through energy transfer

As $Ru(bpy)_3^{2+}$ is sufficiently soluble in CH_2Cl_2, and the photo-excited state has a long lifetime, transient fluorescence of Ru $(bpy)_3^{2+*}$ was monitored to determine the mechanism for quenching by Cu(salxn). The lowest-lying excited state, $Ru(bpy)_3^{2+*}$, is a charge-separated state conveniently represented as $[Ru(III)(bpy)_2(bpy^-)]^{2+}$ which may be deactivated either by oxidizing Cu(salxn) to form $Ru(bpy)_3^{1+}$, or else by energy transfer. As the electron transfer between $Ru(bpy)_3^{2+*}$ and Cu(salxn) would be exothermic, it was expected to form a phenoxyl radical as seen in the oxidation of Cu(salophen) by $Ru(bpy)_3^{3+}$ (Fig. 1)

$$Cu(II)(salxn) + Ru(bpy)_3^{2+*} \rightarrow Cu(II)(salxn)^{+\cdot} + Ru(bpy)_3^{1+} \quad (2)$$

The fluorescence lifetime of $Ru(bpy)_3^{2+*}$ was efficiently quenched by Cu(salxn), yielding concentration-dependent quenching data (Fig. 2). The normalized fluorescence quenching (τ_0/τ) was proportional to the Cu(salxn) concentration, as predicted by the Stern–Volmer equation (Eq. (3)) in which K_{SV} is the quenching efficiency. The linear Stern–Volmer plots indicate that a dynamic quenching mechanism is operative, in which a bimolecular collision between Cu(salxn) and $Ru(bpy)_3^{2+*}$ deactivates the excited state

$$\tau_0/\tau = 1 + K_{SV}[Cu(salxn)] \quad (3)$$

Table 2 lists the quenching data for Cu(salxn) complexes, indicating that the observed rate constants approach the rate of diffusion. Furthermore, the observed quenching rates for Cu(salxn) displayed no discernable dependence on driving force over the modest range of 4 kcal/mol spanned by this series, suggesting that Cu(salxn) quenched $Ru(bpy)_3^{2+*}$ either by diffusion-limited electron transfer, or by energy transfer. Treating k_{obs} with Marcus theory (Eq. (1)) indicated that the reorganization energy would need to be very small, $\lambda \sim 10$ kcal/mol, for diffusion limited kinetics. Thus, while thermodynamic arguments indicated that fluorescence quenching could occur by electron transfer, the rates were much faster than anticipated for quenching to occur by bimolecular electron transfer.

Energy transfer is the more likely mechanism for dynamic quenching of $Ru(bpy)_3^{2+*}$ by Cu(salxn), due to their spectral overlap. Förster and Dexter energy transfer are the two energy-transfer

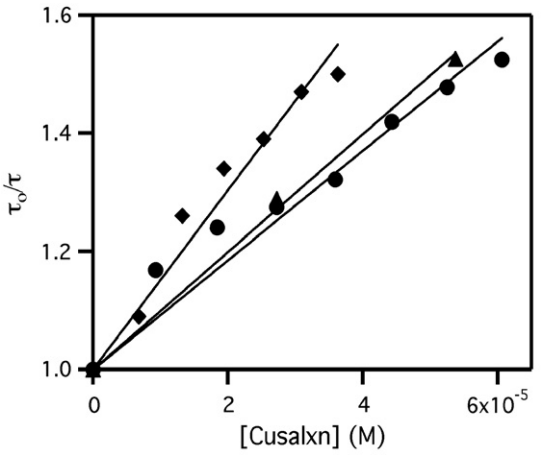

Fig. 2. Time-resolved Stern–Volmer data of $Ru(bpy)_3^{2+*}$ quenching by Cu(salen) (▲); Cu(salpen) (♦); Cu(salben) (●); see text for details.

Table 1
Midpoint reduction potentials measured by cyclic voltammetry

Complex	$E_{1/2}$[c] (mV)
$Ru(bpy)_3(PF_6)_2$[a]	896
$Ru(dmbpy)_3(PF_6)_2$[a]	737
$Ru(dobpy)_3(PF_6)_2$[a]	566
Cusalen[b]	454
Cusalpen[b]	463
Cusalben[b]	485
Cu(salophen)[b]	549
Zn(salophen)[b]	415
Cu(bppa)[a]	40
Cu(icoph)[b]	−60

[a] CH_3CN, 0.1 M TBA.
[b] CH_2Cl_2, 0.1 M TBA.
[c] vs. $Fc^{+/0}$.

Table 2
Time-resolved quenching of $Ru(R_2bpy)_3^{2+*}$ by Cu(salxn) in CH_2Cl_2

Quencher	Sensitizer	k_{obs} ($\times 10^{10}$ M^{-1} s^{-1})	ΔG° (kcal/mol)
Cusalen	$Ru(bpy)_3^{2+}$	1.7	−3.1
Cusalpen	$Ru(bpy)_3^{2+}$	0.8	−2.9
Cusalben	$Ru(bpy)_3^{2+}$	2.2	−2.4
Cusalen	$Ru(dmbpy)_3^{2+}$	1.7	0.8

Lifetimes in CH_2Cl_2 (μs): $Ru(bpy)_3^{2+}$ (0.6); $Ru(dmbpy)_3^{2+}$ (1.0).

mechanisms, with Förster energy transfer requiring spectral overlap between the emission of $Ru(bpy)_3^{2+*}$ and an absorption band of Cu(salxn) [42], The visible absorption spectra for Cu(salxn) was overlayed with the $Ru(bpy)_3^{2+*}$ emission spectrum (Fig. 3). A low energy electronic transition in the 570–670 nm range which is weakly allowed ($\varepsilon \sim 500\ M^{-1}\ cm^{-1}$) is observed for each Cu(salxn), which is appropriate for the ligand-field transition of Cu(II). As the overlap of this absorption with the $Ru(bpy)_3^{2+*}$ emission is considerable, it is likely that this would allow for quenching of $Ru(bpy)_3^{2+*}$ through energy transfer with Cu(salxn).

The excited-state lifetime of $Ru(bpy)_3^{2+}$ could have also changed due to complexation with Cu(salxn), as intermolecular aggregation would alter the local solvent environment. Such an effect was observed with phenols, which form a weak adduct with $Ru(bpy)_3^{2+}$ through face-to-face π–π stacking in weakly acidic aqueous solution; binding was enhanced for electron-withdrawing chlorophenols [43]. Complexation with phenol decreased the observed decay rates of $Ru(bpy)_3^{2+*}$, however, chlorophenols did not affect the excited-state properties of $Ru(bpy)_3^{2+*}$ [44]. We attempted to test for intermolecular complexation by observing the emission spectrum of $Ru(bpy)_3^{2+*}$ in the presence of increasing Cu(salxn) concentrations, and observed no changes in the peak emission wavelength. However, significant inner filter effects due to the absorption of Cu(salxn) would have precluded us from observing small wavelength shifts. As the bulky *tert*-butyl groups on the Cu(salxn) phenolic rings would strongly disfavor π–π stacking, we consider energy transfer as the more likely mechanism for $Ru(bpy)_3^{2+*}$ quenching by Cu(salxn).

3.3. Quenching of $Ru(bpy)_3^{2+*}$ by Cu(bppa), Cu(icoph) through electron transfer

As Cu(bppa) and Cu(icoph) are more easily reduced than Cu(salxn), their oxidations by $Ru(bpy)_3^{2+*}$ were calculated to be much more favorable (Table 3). The reactions of $Ru(bpy)_3^{2+*}$ by Cu(bppa) and Cu(icoph) were monitored by transient fluorescence quenching, with each yielding linear Stern–Volmer plots indicating a dynamic quenching reaction. The observed quenching rate constants for Cu(bppa) or Cu(icoph) ($k_{obs} \sim 10^9\ M^{-1}\ s^{-1}$) were noticeably slower than those observed for Cu(salxn), indicating that diffusion was not rate-limiting in these cases.

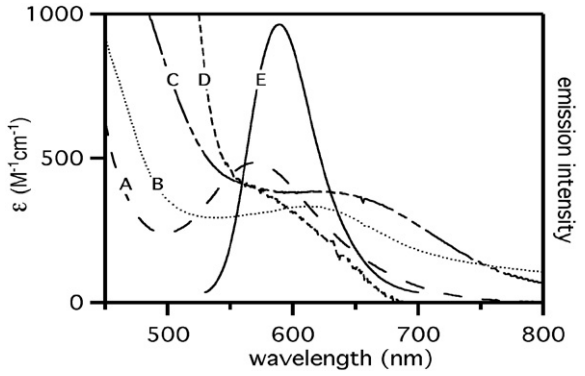

Fig. 3. Absorption spectrum of Cu(salxn) complexes: (A) Cusalen; (B) Cusalpen; (C) Cusalben; (D) Cusalophen; (E) Fluorescence of $Ru(bpy)_3^{2+}$.

Table 3
Time-resolved quenching of $Ru(R_2bpy)_3^{2+*}$ by Cu(bppa), Cu(icoph)

Quencher	Sensitizer	k_{obs} ($\times 10^9\ M^{-1}\ s^{-1}$)	k_q ($\times 10^9\ M^{-1}\ s^{-1}$)	ΔG° (kcal/mol)
Cu(icoph)	$Ru(bpy)_3^{2+}$	8.1	18	−14.9
Cu(bppa)	$Ru(bpy)_3^{2+}$	1.1	1.2	−12.6
Cu(icoph)	$Ru(dmbpy)_3^{2+}$	5.8	9.5	−11.1
Cu(bppa)	$Ru(dmbpy)_3^{2+}$	0.95	0.99	−8.8
Cu(bppa)	$Ru(dombpy)_3^{2+}$	1.9	2.1	−5.9

Lifetimes (μs): $Ru(bpy)_3^{2+}$ (0.6, CH_2Cl_2; 1.2; CH_3CN); $Ru(dmbpy)_3^{2+}$ (1.4, CH_2Cl_2; 1.6; CH_3CN); $Ru(dombpy)_3^{2+}$ (0.4; CH_3CN).

The observed rates (k_{obs}) were corrected for the rate of diffusion (k_{diff}) to obtain diffusion-corrected quenching rates (k_q), $k_q^{-1} = k_{obs}^{-1} - k_{diff}^{-1}$. The diffusion rate was estimated as $k_{diff} = 1.6 \times 10^{10}\ M^{-1}\ s^{-1}$ using the Smoluchowski equation (Eq. (4)), in which k_{diff} is a function of the solution viscosity ($\eta = 0.41$ cP for CH_2Cl_2, $\eta = 0.341$ cP for CH_3CN) [45], the radius of $Ru(bpy)_3^{2+}$ ($r_R = 7.1$ Å) [46], and the radius of Cu(bppa) and Cu(icoph) ($r_Q = 5.3$ Å) [47]

$$k_{diff} = \frac{2RT}{3\eta}\left\{2 + \frac{r_R}{r_Q} + \frac{r_Q}{r_R}\right\} \quad (4)$$

The diffusion corrected quenching rates (k_q) of $Ru(bpy)_3^{2+*}$ by Cu(bppa) or Cu(icoph) were correlated with driving force (Table 3), as predicted for an electron transfer quenching mechanism. Marcus theory predicts that intermolecular electron transfers will exhibit a parabolic $\ln k_q$ vs. ΔG° curve, cresting at $-\Delta G^\circ = \lambda$ [24]. Our quenching data (Fig. 4) was fitted to Eq. (1), yielding $\lambda = 20$ (±2) kcal/mol by fixing the collisional rate at $Z = 1.6 \times 10^{10}\ M^{-1}\ s^{-1}$. The good fit for the quenching data for Cu(bppa) and Cu(icoph) to the electron transfer model is in direct contrast to the driving force independent quenching data for Cu(salxn), suggesting that the more favorable driving force for Cu(bppa) and Cu(icoph) makes oxidation much faster than any energy-transfer quenching.

The reorganization energy for the Cu(bppa) and Cu(icoph) oxidations were very similar to those reported for comparable reactions. The oxidation of an appended tyrosine by $Ru(bpy)_3^{3+}$ apparently exhibited $\lambda = 46$ kcal/mol [19], however that reaction required the release of a proton to the bulk, leading to a significant additional kinetic barrier [19,25]. At elevated pH, when the tyrosine was deprotonated, the reorganization energy for oxidation by $Ru(bpy)_3^{3+}$ was 22 kcal/mol [19,25]. The oxidation of a substituted phenol with internal hydrogen-bonding by aminium radicals exhibited $\lambda = 34$ kcal/mol; while the proton was not released to bulk solvent, the proton-transfer within the internal hydrogen bond would likely impart some additional kinetic barrier [20,21]. The oxidization of substituted phenolates by photo-excited $Ru(NN)_3^{2+*}$ (NN indicates an aromatic diimine) in basic H_2O and H_2O/CH_3CN solution exhibited $\lambda = 25$ kcal/mol [22,23]. It is apparent that the reorganization energy for the $Ru(bpy)_3^{n+}$ oxidations of deprotonated phenolates by ET are all very similar, with values ranging from $\lambda = 20$–25 kcal/mol, and much smaller than those for phenol oxidation which require proton transfer in a PCET.

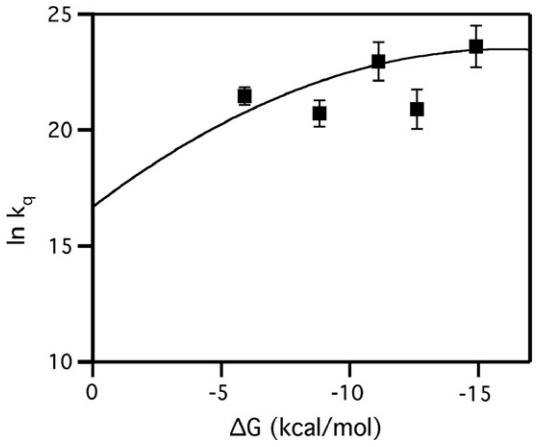

Fig. 4. Marcus plot for the reaction of Cu(bppa) and Cu(icoph) with $Ru(R_2bpy)_3^{2+*}$; see text for fitting details.

The Marcus cross-relation predicts that the reorganization energy for Cu(bppa) and Cu(icoph) oxidation by $Ru(bpy)_3^{2+*}$ should be the average of the self-exchange reorganization energies: $\lambda = \frac{1}{2}(\lambda_{Ru} + \lambda_{PhO})$ [24]. As the reorganization energy for the $Ru(bpy)_3^{2+*/1+}$ couple is dominantly due to outer-sphere reorganization [34], it is rather small. Marcus described the outer-sphere reorganization energy in terms of a dielectric continuum mode (Eq. (5)) [24,48], in which e is the charge of the electron, r_R is the radius of $Ru(bpy)_3^{2+*}$, and D_{op} and D_S are the optical and static dielectric constants of the solvent. Inserting tabulated values for the dielectric constants into Eq. (5) [45], we calculated that $\lambda_{Ru} = 9$ and 12 kcal/mol in CH_2Cl_2 and CH_3CN, respectively

$$\lambda_{Ru} \approx \lambda_o = e^2 \left[\frac{1}{2r_R}\right]\left[\frac{1}{D_{op}} + \frac{1}{D_s}\right] \quad (5)$$

These relationships allow us to estimate the self-exchange reorganization energy for $Cu(bppa)^{+/2+\cdot}$ and $Cu(icoph)^{0+/+\cdot}$ as $\lambda_{PhO.} \approx 30$ kcal/mol, assuming that both complexes have similar values for λ. This implies that, to the extent that these complexes are reasonable models for the Cu-associated tyrosine-derived cofactors found in CAO and GalOx, those proteins may undergo sluggish ET reactions. Typical biological redox proteins, such as those found in cytochromes *c* or azurin, exhibit $\lambda \sim 20$ kcal/mol [49], however the specific function of such proteins is to catalyze ET in energy-transformation pathways. As CAO and GalOx catalyze the $2e^-$ oxidation of small molecules, one-electron redox reactivity may suppressed to minimize inactivation pathways.

Acknowledgements

The authors thank Meaghan Germain for providing samples of Cu(bppa); and Professors S. Thayumanavan (fluorimeter), H. Stidham (PTI instrument), and the UMass-Amherst EPR facility (NSF CHE-0443180) for access to instrumentation. This research was supported by the ACS-PRF #40033-G4.

References

[1] J. Stubbe, W.A. van der Donk, Chem. Rev. 98 (1998) 705.
[2] V.L. Davidson, Biochemistry 46 (2007) 5283.
[3] J.P. Klinman, Bba-Proteins Proteom. 1647 (2003) 131.
[4] S.M. Janes, D. Mu, D. Wemmer, A.J. Smith, S. Kaur, D. Maltby, A.L. Burlingame, J.P. Klinman, Science 248 (1990) 981.
[5] N. Ito, S.E.V. Phillips, K.D.S. Yadav, P.F. Knowles, J. Mol. Biol. 238 (1994) 794.
[6] M.M. Whittaker, J.W. Whittaker, J. Biol. Chem. 263 (1988) 6074.
[7] M.S. Rogers, D.M. Dooley, Curr. Opin. Chem. Biol. 7 (2003) 189.
[8] N.M. Okeley, W.A. van der Donk, Chem. Biol. 7 (2000) R159.
[9] M. Rogers, S. Firbank, P. Knowles, M. McPherson, S. Phillips, D. Dooley, J. Inorg. Biochem. 86 (2001) 404.
[10] R.H. Moore, M.A. Spies, M.B. Culpepper, T. Murakawa, S. Hirota, T. Okajima, K. Tanizawa, M. Mure, J. Am. Chem. Soc. 129 (2007) 11524.
[11] J.L. DuBois, J.P. Klinman, Biochemistry 44 (2005) 11381.
[12] J.P. Klinman, Chem. Rev. 96 (1996) 2541.
[13] S. Itoh, M. Taki, S. Takayama, S. Nagatomo, T. Kitagawa, N. Sakurada, R. Arakawa, S. Fukuzumi, Angew. Chem., Int. Ed. 38 (1999) 2774.
[14] Y.D. Wang, J.L. DuBois, B. Hedman, K.O. Hodgson, T.D.P. Stack, Science 279 (1998) 537.
[15] P. Chaudhuri, M. Hess, J. Muller, K. Hildenbrand, E. Bill, T. Weyhermuller, K. Wieghardt, J. Am. Chem. Soc. 121 (1999) 9599.
[16] R.C. Pratt, T.D.P. Stack, Inorg. Chem. 44 (2005) 2367.
[17] A. Philibert, F. Thomas, C. Philouze, S. Hamman, E. Saint-Aman, J.L. Pierre, Chem. Eur. J. 9 (2003) 3803.
[18] M. Sjodin, S. Styring, B. Akermark, L.C. Sun, Philos. Trans. Roy. Soc. B 357 (2002) 1471.
[19] M. Sjodin, S. Styring, B. Akermark, L.C. Sun, L. Hammarstrom, J. Am. Chem. Soc. 122 (2000) 3932.
[20] I.J. Rhile, T.F. Markle, H. Nagao, A.G. DiPasquale, O.P. Lam, M.A. Lockwood, K. Rotter, J.M. Mayer, J. Am. Chem. Soc. 128 (2006) 6075.
[21] I.J. Rhile, J.M. Mayer, J. Am. Chem. Soc. 126 (2004) 12718.
[22] P. Thanasekaran, S. Rajagopal, C. Srinivasan, J. Chem. Soc., Faraday Trans. 94 (1998) 3339.
[23] K. Swarnalatha, E. Rajkumar, S. Rajagopal, R. Ramaraj, Y.L. Lu, K.L. Lu, P. Ramamurthy, J. Photochem. Photobiol. A171 (2005) 83.
[24] R.A. Marcus, N. Sutin, Biochim. Biophys. Acta 811 (1985) 265.
[25] C. Carra, N. Iordanova, S. Hammes-Schiffer, J. Am. Chem. Soc. 125 (2003) 10429.
[26] M. Sjodin, T. Irebo, J.E. Utas, J. Lind, G. Merenyi, B. Akermark, L. Hammarstrom, J. Am. Chem. Soc. 128 (2006) 13076.
[27] M. Mure, Acc. Chem. Res. 37 (2004) 31.
[28] J.L. DuBois, J.P. Klinman, Arch. Biochem. Biophys. 433 (2005) 255.
[29] C.E. Ruggiero, J.A. Smith, K. Tanizawa, D.M. Dooley, Biochemistry 36 (1997) 1953.
[30] M.C.J. Wilce, D.M. Dooley, H.C. Freeman, J.M. Guss, H. Matsunami, W.S. McIntire, C.E. Ruggiero, K. Tanizawa, H. Yamaguchi, Biochemistry 36 (1997) 16116.
[31] B. Schwartz, J.E. Dove, J.P. Klinman, Biochemistry 39 (2000) 3699.
[32] J.E. Dove, B. Schwartz, N.K. Williams, J.P. Klinman, Biochemistry 39 (2000) 3690.
[33] (a) Reviews of related modelling chemistry: B.A. Jazdzewski, W.B. Tolman, Coord. Chem. Rev. 200 (2000) 633;
(b) V. Mahadevan, R.J.M.K. Gebbink, T.D.P. Stack, Curr. Opin. Chem. Biol. 4 (2000) 228;
(c) P. Chaudhuri, K. Wieghardt, in: K.D. Karlin (Ed.), Progress in Inorganic Chemistry, vol. 50, John Wiley and Sons, New York, 2001, p. 151.
[34] M. Biner, H.B. Burgi, A. Ludi, C. Rohr, J. Am. Chem. Soc. 114 (1992) 5197.
[35] P. Chaudhuri, M. Hess, T. Weyhermuller, K. Wieghardt, Angew. Chem., Int. Ed. 38 (1999) 1095.
[36] C.T. Lin, W. Bottcher, M. Chou, C. Creutz, N. Sutin, J. Am. Chem. Soc. 98 (1976) 6536.
[37] G.R. Hanson, K.E. Gates, C.J. Noble, M. Griffin, A. Mitchell, S. Benson, J. Inorg. Biochem. 85 (2004) 903.
[38] M. Griffin, A. Muys, C. Noble, D. Wang, C. Eldershaw, K.E. Gates, K. Burrage, G.R. Hanson, Mol. Phys. Rep. 26 (1999) 60.
[39] T. Rajendran, P. Thanasekaran, S. Rajagopal, G.A. Gnanaraj, C. Srinivasan, P. Ramamurthy, B. Venkatachalapathy, B. Manimaran, K.L. Lu, Phys. Chem. Chem. Phys. 3 (2001) 2063.
[40] R.C. Pratt, L.M. Mirica, T.D.P. Stack, Inorg. Chem. 43 (2004) 8030.
[41] A. Sokolowski, H. Leutbecher, T. Weyhermuller, R. Schnepf, E. Both, E. Bill, P. Hildebrandt, K. Wieghardt, J. Biol. Inorg. Chem. 2 (1997) 444.
[42] A. Gilbert, J. Baggott, Essentials of Molecular Photochemistry, CRC Press, Inc., Boca Raton, FL, 1991.
[43] C. Li, M.Z. Hoffman, C. Pizzocaro, G. Maihot, M. Bolte, Inorg. Chem. 37 (1998) 3078.
[44] C. Li, M.Z. Hoffman, C. Pizzocaro, G. Mailhot, M. Bolte, J. Phys. Chem. A102 (1998) 7370.
[45] J.A. Riddick, W.B. Bunger, T.K. Sakano, Organic Solvents: Physical Properties and Methods of Purification, John Wiley and Sons, New York, 1986.
[46] N. Kitamura, H.B. Kim, S. Okano, S. Tazuke, J. Phys. Chem. 93 (1989) 5750.
[47] Spartan, Wavefunction, Irvine, CA, 2004.
[48] R.A. Marcus, J. Chem. Phys. 24 (1956) 966.
[49] H.B. Gray, J.R. Winkler, in: I. Bertini, H.B. Gray, E.I. Stiefel, J.S. Valentine (Eds.), Biological Inorganic Chemistry: Structure and Reactivity, University Science Books, Sausalito, CA, 2007, p. 261.

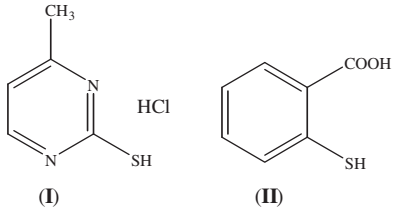

Scheme 1. Formulae of the ligands used; 2-mercapto-4-methyl-pyrimidine hydrochloride (I) and 2-mercapto-benzoic acid (II).

structures, it would be of interest to know the difference for obtaining either structure, if possible. The complexes {[Ph_3Sn(MPMT)]} (**1**) and {[Me_2Sn(MPMT)]$_2$} (**2**) were also prepared by Ma et al [16] by reacting 2-mercapto-4-methyl-pyrimidine hydrochloride with organtoin(IV) chlorides in benzene solution in the presence of EtONa. Crystals of complexes **1** and **2** were grown from ether and ether–dichloromethane solutions, respectively. All four complexes reported here were prepared again, with a slightly modified method, using a mixture of MeOH/H_2O of 1:2 in order to investigate the possible solvent effect in their preparation. Different solvents were also used for their crystallization (see below).

In addition, the inhibitory activity of these four organotin(IV) complexes [14,16] **1–4**, on the catalytic oxidation of linoleic acid to hydroperoxylinoleic acid by the enzyme lipoxygenase LOX is also reported. Such an inhibition may be the cause of the antitumor action of tin complexes [12,13] (Scheme 1).

Table 1
^{119}Sn Mössbauer spectroscopic data for complexes **1**, **3**, and **4**

Complex	Temperature (K)	IS (mm s^{-1})	ΔE_q (mm s^{-1})	Area (%)	IS (mm s^{-1})	ΔE_q (mm s^{-1})	Area (%)
1	80	1.28	1.48	75	1.40	2.53	25
3	80	1.39	3.23	50	1.52	3.32	50
4	80	1.27	2.95	50	1.32	3.26	50

2. Results and discussion

2.1. General aspects

The synthesis of complexes **1–4** were achieved with an alternative method to the one used previously for the synthesis of these complexes [14,16]. Instead of using EtONa, a methanolic/water (1:2) solution of the reactants and KOH were used. Crystallizations were achieved by slow evaporation of methanol/acetonitrile (1:1) solutions for **1** and **2**, and in the case of complexes **3** and **4** dichloromethane/methanol/toluene (3:1:1) solutions were used.

$$R_nSnCl_{4-n} + (4\text{-}n)\ HMPMT \xrightarrow{KOH} \{R_nSn(MPMT)_{4-n}\} + (4\text{-}n)\ KCl$$

n=3; R= Ph- (**1**) and n= 2; R= Me- (**2**);

$$2n\ R_2SnCl_2 + 2n\ H_2MBA \xrightarrow{KOH} \{[R_2Sn(MBA)]_2\}_n + 2n\ KCl$$

n= infinite; R= *n*-Bu- (**3**) and Me- (**4**)

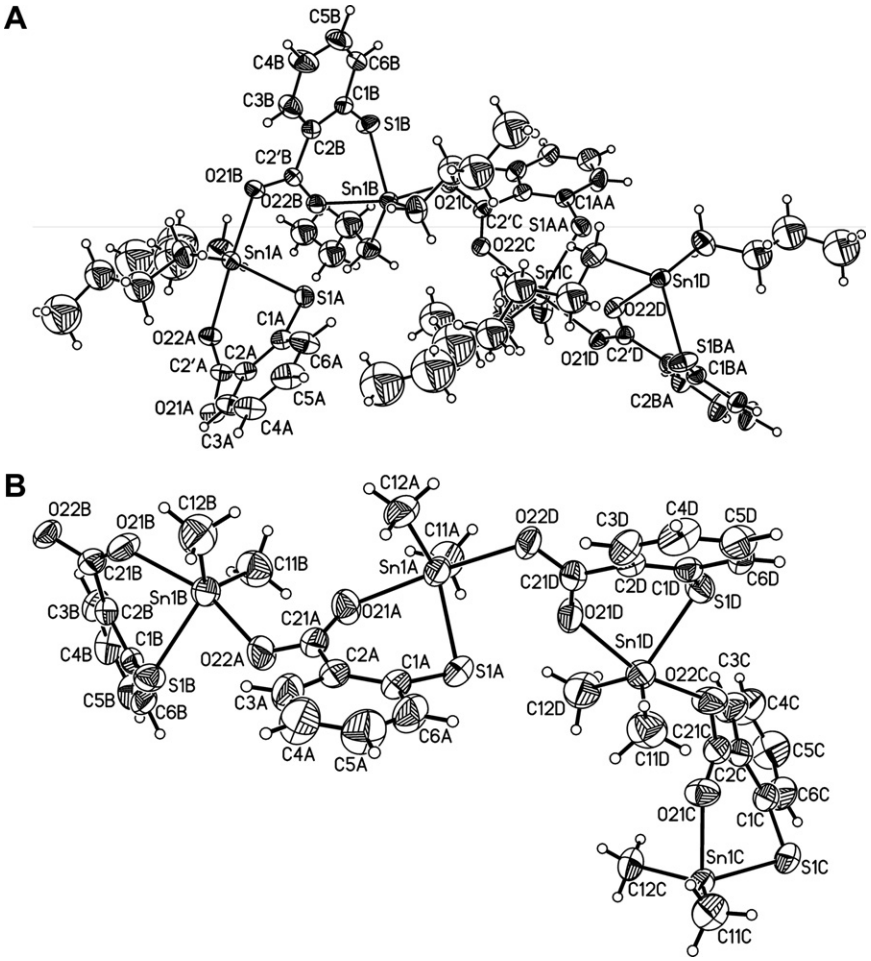

Fig. 1. ORTEP diagrams together with the atomic numbering schemes of the complexes {[(*n*-Bu)$_2$Sn(MBA)]$_2$}$_n$ (**3**) (**A**) and {[Me_2Sn(MBA)]$_2$}$_n$ **(4)** (**B**) measured at 293(2) K.

Both complexes **3** and **4** have a polymeric helical supramolecular structure. The structure of **3** was refined to $R = 6.1\%$, compared to the previous R value of 9.9%. The crystal structure of complex **2** has a monoclinic $P2_1$ space group in contrast to the structure already published with an orthorhombic $Cmc2_1$ space group [16]. The crystal structure of **1** was found to be identical with the previous one [16].

2.2. ^{119m}Sn Mössbauer spectroscopy

The solid state ^{119m}Sn Mossbauer spectroscopic data of complexes **1**, **3** and **4** are given in Table 1. The two symmetric Lorentzian doublets (50:50) observed for **3** and **4**, confirmed the presence of two tin atoms in different chemical environments in the dimers [8,10], which was also confirmed by the X-ray analysis (vide infra). The ΔE_q values of complexes **3** and **4** lie between 2.95 and 3.32 mm s^{-1} in both complexes, indicating distorted trigonal bipyramidal to octahedral geometries. The two symmetric Lorentzian doublets (75:25) observed for **1** indicate the presence of two structural isomers. The ΔE_q value of 1.48 mm s^{-1} corresponds to a complex with a tetrahedral arrangement (75%) while the ΔE_q value of 2.53 mm s^{-1} to a complex with a trigonal bipyramidal geometry around tin (25%) [2].

2.3. Crystal and molecular structure of complexes *1–4*

The structures of **3** and **4** (Fig. 1 and Table 2) consist of dimeric $\{[R_2Sn(MBA)]_2\}$ building blocks (R = Me– or *n*-Bu-group), infinitely repeated in space.

The polymeric structure of **4** consists of dimeric building blocks with a distorted trigonal bi-pyramidal arrangement around Sn(IV). The ligand undergoes double deprotonation upon coordination. In the case of the $[Me_2Sn(MBA)]_2$ dimer, selected distances are Sn1A–S1A 2.4050(11), Sn1A–O21A 2.235(3) and Sn1A–O22D 2.203(3) Å in the first moiety and Sn1B–S1B 2.4197(10), Sn1B–O21B 2.267(3) and Sn1B–O22A 2.174(3) Å for the second moiety (Fig. 1). The corresponding bond distances in the $[(n\text{-Bu})_2Sn(MBA)]_2$ dimer are Sn1A–S1A 2.4141(19), Sn1A–O22A 2.312(4) and Sn1A–O21B 2.191(5) Å for the first moiety and Sn1B–S1B 2.4155(18), Sn1B–O22B 2.1282(6) and Sn1B–O21C 2.216(4) Å for the second. These two units in both complexes are infinitely repeated to form the polymers **3** and **4**. The Sn–O and Sn–S bond distances found in **3** and **4** are similar with the corresponding bond distances measured in the complexes **5** and **6** [15].

Selected angles around the Sn1A atom of the first moiety of the dimer $[Me_2Sn(MBA)]_2$ are O21A–Sn1A–O22D 171.59(9)° and C11A–Sn1A–C12A 129.89(16)°, while those around the Sn1B atom of the second moiety are O21B–Sn1B–O22A 158.02(10)° and S1B–Sn1B–C12B 125.45(13)°. The corresponding angles around the Sn1A atom of $[(n\text{-Bu})_2Sn(MBA)]_2$ are O21B–Sn1A–O22A 177.22(17)° and C11A–Sn1A–C21A 130.35(3)° and those around Sn1B are O21C–Sn1B–O22B 164.35(16)° and C11B–Sn1B–C21B 129.93(3)°. According to Reedijk's criteria [17] the geometry around a metal center is octahedral when the parameter $\tau = (\beta - \alpha)/60$ equals zero and when τ is one it is trigonal bipyramidal. In the case of the $[Me_2Sn(MBA)]_2$ dimer, the τ values are 0.70 and 0.54 for Sn1A and Sn1B, respectively, while in the case of $[(n\text{-Bu})_2Sn(MBA)]_2$ the τ values are 0.78 and 0.57, thus justifying their description as distorted trigonal bipyramidal. The weak Sn···O contacts (Sn1A···O21D = 3.235 and Sn1B···O21A = 3.328 Å in **4** and Sn1A···O22B = 3.076 and Sn1B···O22C = 3.140 Å in **3**) confirm the distortions of the geometry (Fig. 1). The intra-molecular hydrogen bonding interactions observed, C3A[H3A]···O22A = 2.719(5) Å in **4** and C13C[H13C]···O22A = 3.471(4) Å in **3**, stabilize the structures in our case. π–π interactions were observed only in **4**, stabilizing the supramolecular assembly (3.647 Å), (Fig. 2). It is noteworthy that no X–H···O hydrogen bonding interactions were found in the case of complexes **5** and **6**, which have macrocyclic structures [15].

Table 2
Selected bond lengths (Å) and angles (deg) for the tri-organotin(IV) complexes **3** and **4** measured at room temperature (293(2)), e.s.d.'s in parentheses

Complex **3**		Complex **4**	
(a) Bond lengths		*(a) Bond lengths*	
Sn1A–S1A	2.4141(19)	Sn1A–S1A	2.4050(11)
Sn1A–O22A	2.312(4)	Sn1A–O21A	2.235(3)
Sn1A–C11A	2.1177(6)	Sn1A–C11A	2.114(4)
Sn1A–C21A	2.1175(6)	Sn1A–C12A	2.103(4)
Sn1A–O21B	2.191(5)	Sn1A–O22D[a]	2.203(3)
Sn1B–S1B	2.4155(18)	Sn1B–S1B	2.4197(10)
Sn1B–O21C[b]	2.216(4)	Sn1B–O21B	2.267(3)
Sn1B–O22B	2.260(4)	Sn1B–O22A	2.174(3)
Sn1B–C11B	2.1129(6)	Sn1B–C11B	2.111(5)
Sn1B–C21B	2.1282(6)	Sn1B–C12B	2.108(4)
S1A–C1A	1.790(7)	S1A–C1A	1.768(4)
S1B–C1B	1.773(7)	S1B–C1B	1.783(4)
(b) Angles		*(b) Angles*	
S1A–Sn1A–O22A	82.58(12)	S1A–Sn1A–O21A	84.03(7)
S1A–Sn1A–C11A	111.57(6)	S1A–Sn1A–C11A	115.39(12)
S1A–Sn1A–C21A	117.44(6)	S1A–Sn1A–C12A	114.31(12)
S1A–Sn1A–O21B	94.80(13)	S1A–Sn1A–O22D[a]	89.78(7)
O22A–Sn1A–C11A	93.33(11)	O21A–Sn1A–C11A	90.11(13)
O22A–Sn1A–C21A	85.61(11)	O21A–Sn1A–C12A	88.91(13)
O21B–Sn1A–O22A	177.2(2)	O21A–Sn1A–O22B[a]	171.59(9)
C11A–Sn1A–C21A	130.35(3)	C11A–Sn1A–C12A	129.89(16)
O21B–Sn1A–C11A	88.48(14)	O22B[a]–Sn1A–C11A	97.71(13)
O21B–Sn1A–C21A	94.83(13)	O22B[a]–Sn1A–C12A	88.45(13)
S1B–Sn1B–O21C[b]	83.68(13)	S1B–Sn1B–O21B	82.45(7)
S1B–Sn1B–O22B	82.12(12)	S1B–Sn1B–O22A	82.45(8)
S1B–Sn1B–C11B	112.09(6)	S1B–Sn1B–C11B	111.94(13)
S1B–Sn1B–C21B	117.15(6)	S1B–Sn1B–C12B	125.45(13)
O21A[b]–Sn1B–O22B	164.35(16)	O21B–Sn1B–O22A	158.02(10)
O21A[b]–Sn1B–C11B	99.81(12)	O21B–Sn1B–C11B	95.17(13)
O21Aii–Sn1B–C21B	94.04(12)	O21B–Sn1B–C12B	85.43(13)
O22B–Sn1B–C11B	91.61(11)	O22A–Sn1B–C11B	105.26(13)
O22B–Sn1B–C21B	86.65(11)	O22A–Sn1B–C12B	90.43(13)
C11B–Sn1B–C21B	129.93(3)	C11B–Sn1B–C12B	122.04(18)

Symmetry codes: [a]: $(-x + 3/2, y + 1/2, -z + 1/2)$, [b]: $(-x + 1/2, y + 1/2, -z + 1/2)$.

The torsional angles Sn–O···O′–Sn′ (namely Sn1B–O22A···O21A–Sn1A, Fig. 1) are −166.18° and 141.98° for **4** and −144.61° and 156.8° in the case of **3** (Sn1A–O22B···O22B–Sn1B). Thus, there is a difference of −24.2° in **4** and −12.2° in **3**, resulting in the formation of helical structures. In contrast, the six such torsional angles in the case of **6** are −151.38°, −164.40°, −160.90° followed by 151.38°, 164.40° and 160.90°, compensating the differences and resulting in the formation of hexanuclear macrocycles [15]. Similarly for **5**, the six torsional angles are 153.50°, −151.13°, 177.59° and −153.50°, 151.13°, −177.59°.

To study the influence of temperature and solvents in the preparation of complex **4** on its structure (helical polymeric or macrocyclic), XRPD spectra were recorded and compared (Fig. 3). The XRPD spectra of the product with the reaction carried out at 40 °C (Fig. 3A), 20 °C (Fig. 3B) and using EtOH as a recrystallization solvent (Fig. 3C) were extremely similar to the simulated spectrum (Fig. 3D) with the helical-polymer structure and were different from the simulated spectrum (Fig. 3E) of the macrocyclic product reported by Ma et al. [15].

The supramolecular assembly of compound **4** exhibits a helical pattern where in every two asymmetric units appreciable π–π stacking interactions between neighboring phenyl groups exist. The interplanar distance is 3.67 Å and the interplanar angle is 0°, implying completely parallel phenyl groups. The angle formed by the plane of the phenyl ring and the stack column axis is 19.89 °, characterizing this interaction as a parallel displaced non-covalent interaction [18]. It is likely that these π–π interactions play an important role in the stabilization of the molecular units. However

this is not the case in the butyl analog **3** where the interaction between the neighboring phenyl groups is considered as point-to-face C–H···π, with the distance between the centroid of the ring and the nearest carbon atom being 3.99 Å and the H···centroid distance being 3.37 Å. On the other hand, the weak intermolecular C–H···S hydrogen bonds together with stronger C–H···O ones, may also play an important role in the supramolecular arrangements.

2.4. DFT calculations

In an attempt to better understand the formation of two structurally different complexes of the formulae $\{[Me_2Sn(MBA)]_2\}_n$ (**4**) and $\{[Me_2Sn(MBA)]_6\ H_2O\}$ (**6**) we have also used computational DFT methods. Due to the requirement of lesser computational resources, only the methyl derivative has been examined here. Ignoring solid-state effects, symmetry plays a significant role to the computed outcome, since non-symmetric structures tend to converge to symmetric ones [19]. This fact led us to follow two different procedures: (i) to fully optimize all the geometrical parameters (ii) to impose symmetry constrains with the intention of improving the approximation of the solid state motif obtained from X-ray diffraction techniques. These constrains concern the dihedral angles of the six-membered rings formed by Sn, S, O, and two C atoms of each of the phenyl rings. As it is evident from the calculated data, although the standard LANL2DZ basis set is known to provide reliable results [20], the 3-21G** type basis set takes account of polarization functions on all atoms and consequently gives a more precise description of the tin-ligand interactions. The model with no constrains applied gave marginally better results than the one with the preset dihedral angles. The results showed that the energy difference between the two different structures, macrocycle [15] and helical [14], differ only slightly with ΔE = 1.65 Kcal/mol.

Fig. 4 shows the molecular diagrams of complexes **1** and **2**.

The crystal structure of complex **2** has now been refined in the monoclinic $P2_1$ space group, with no significant differences in the bond distances and angles from those found previously [16]. Thus

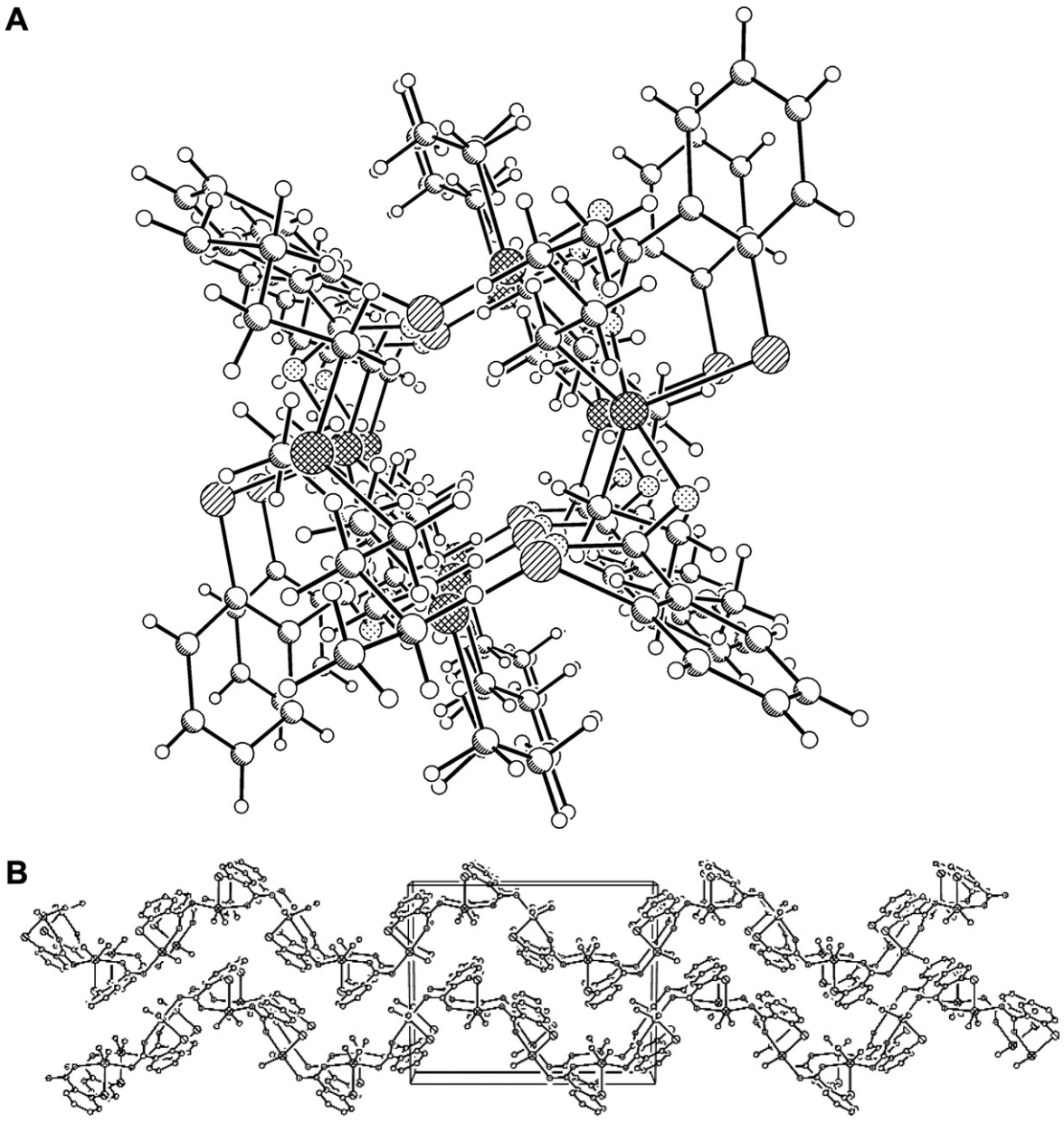

Fig. 2. The unit cell of the complexes **3** (**A**) and **4** (**B**). There are two independent helixes in the cell of **4**.

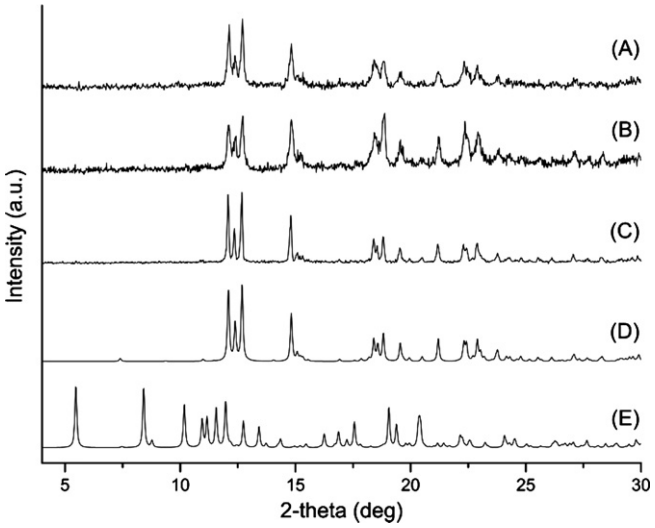

Fig. 3. XRPD diagrams of the reaction products (**A**) at 40 °C, (**B**) at 20 °C, (**C**) after recrystallization in EtOH and the simulated XRPD diagrams from the pattern of the single crystal X-ray diffraction of **4** (**D**) and **5** (**E**).

two sulfur and two nitrogen atoms from thiol ligands are coordinated to Sn(IV) forming a distorted octahedral arrangement around the metal center in case of **2**. This coordination mode through N, S donor atoms of the ligand is similar to that observed previously in $[Me_2Sn(PMT)_2]$ (HPMT = 2mercapto-pyrimidine) [21]. The presence of the methyl substituent, however, at the 5-position in the pyrimidine ring in the case of the 2-mercapto-5-methyl-pyrimidine ligand generates isomerism upon coordination to the tin atom. Thus in the case of **2** the ligand is coordinated through its adjacent and remote forms (Fig. 4B). The Sn–S bond distances are 2.490(3) and 2.496(2) Å, respectively in contrast to the 2.480(2) and 2.484(3) Å reported previously [16]. Table 3 summarizes the selected bond distances and angles found for complex **2** within this work in comparison to those previously reported [16]. The structure of **1** is found to be identical with that previously reported [16].

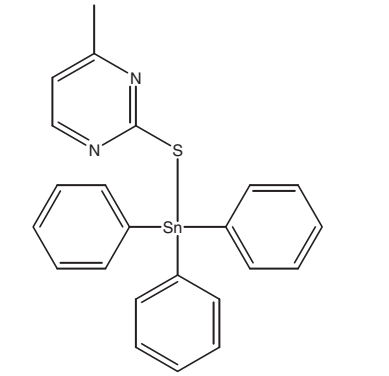

(**1**)

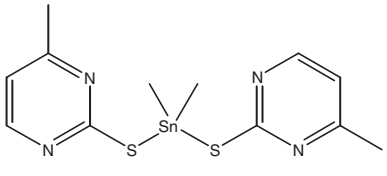

(**2**)

Fig. 4. Molecular diagrams of complexes **1** and **2**.

Table 3
Selected bond distances (Å) and angles (deg) found for complex **2** in this work in contrast to the previously reported values [16]

This work		Reported in Ref. [16]	
(a) Bond lengths		*(a) Bond lengths*	
Sn1–S12	2.490(3)	Sn(1)–S(1)	2.480(2)
Sn1–S22	2.496(2)	Sn(1)–S(2)	2.484(3)
Sn1–C1A	2.103(7)	Sn(1)–C(11)	2.102(5)
S12–C12	1.762(15)	S(1)–C(1)	1.773(9)
S22–C22	1.751(9)	S(2)–C(6)	1.782(15)
(b) Angles		*(b) Angles*	
S12–Sn1–S22	87.73(8)	S(1)–Sn(1)–S(2)	88.64(9)
S12–Sn1–C1A	108.31(16)	C(11)–Sn(1)–S(1)	107.95(12)
S22–Sn1–C1A	107.50(18)	C(11)–Sn(1)–S(2)	109.23(12)
C1A–Sn1–C1B	129.5(3)	C(11)#1–Sn(1)–C(11)	127.0(3)

#1 is the geometrical equivalent C atom of C(11), bonded to Sn (See Ref. [16]).

*2.5. Study of the peroxidation of linoleic acid by the enzyme of lipoxygenase (LOX) in the presence of complexes **1–4***

The influence of the complexes **1–4** on the oxidation of linoleic acid by the enzyme LOX were studied over a wide concentration range. The degree of LOX activity (**A**, %) in the presence of each complex was calculated according to the method described previously [5–11]. The IC_{50} values determined are 23 (**1**), 30 (**2**), 30 (**3**) and 30 (**4**) μM, respectively, while no such activity was shown for cisplatin [5–11]. These values lie at the higher range to those found for other similar Sn(IV) complexes. For example, the IC_{50} values found for the organotin compounds tested towards LOX, were 26 and 14 μM for $[(C_6H_5)_2SnCl(HMNA)]$ and $[(C_6H_5)_3Sn(MNA)\text{-}Sn(C_6H_5)_3$ (acetone)] (H_2MNA = 2-thiobarbituric acid), respectively [9], 19, 16 and 21 μM for $[(C_6H_5)_3Sn(MBZT)]$, $[(C_6H_5)_3Sn(MBZO)]$, and $[(C_6H_5)_3Sn(CMBZT)]$ (MBZT = 2-mercapto-benzothiazole, MBZO = 2-mercapto-benzoxazole and CMBZT = 5-chloro-2-mercapto-benzothiazole), respectively [6], 10, 13 and 14 μM for $[(C_6H_5)_2Sn(CMBZT)_2]$, $[(n\text{-}C_4H_9)_2Sn(CMBZT)_2]$, and $[(CH_3)_2Sn\text{-}(CMBZT)_2]$, respectively [6], 61.3, 26.2, 20.5 and 16.9 μM for $[(CH_3)_2Sn(PMT)_2]$, $[(n\text{-}C_4H_9)_2Sn(PMT)_2]$, $[(C_6H_5)_2Sn(PMT)_2]$, and $[(C_6H_5)_3Sn(PMT)]$ (PMT = 2mercapto-pyrimidine), respectively, [7] and 25 μM for $[(n\text{-}Bu)_3Sn(TBA)\cdot H_2O]$ (HTBA = 2-thiobarbituric acid) [5].

3. Conclusions

The antiproliferative activity of organotin(IV)-thioamide complexes were found to correspond to the regularity of inhibition of the lipoxygenase (LOX) activity [5–11]. This inhibition activity was also found to be independent of the geometry or the number and type of the aryl and alkyl substituents at the tin(IV) ion, but it is determined to a great extent by the ligand nature [5–11]. Therefore the IC_{50} values towards LOX activity found for complexes 1–4 (20–30 μM), which lie at the higher range of the corresponding ones for similar complexes, suggest mild or low antitumor activity [5–11].

On the other hand, slight modifications in the synthetic and crystallization conditions in the case of complexes **3** and **4** results in different conformations of the products, independent of the hydrogen bonding and π–π interactions [15]. The small ΔE = 1.65 Kcal/mol between the two conformations (helical or macrocycle) observed in the dialkyltin derivatives with 2-mercapto-benzoic acid may easily be overcome subject to slight solvent or temperature modifications, leading to macrocycles or polymers. Thus, there are inherent physicochemical reasons which lead to the particular packing characteristics of each structure. The self-assembly process of these type of complexes, seems to be fortuity dependent and not based on intermolecular C–H···S weak

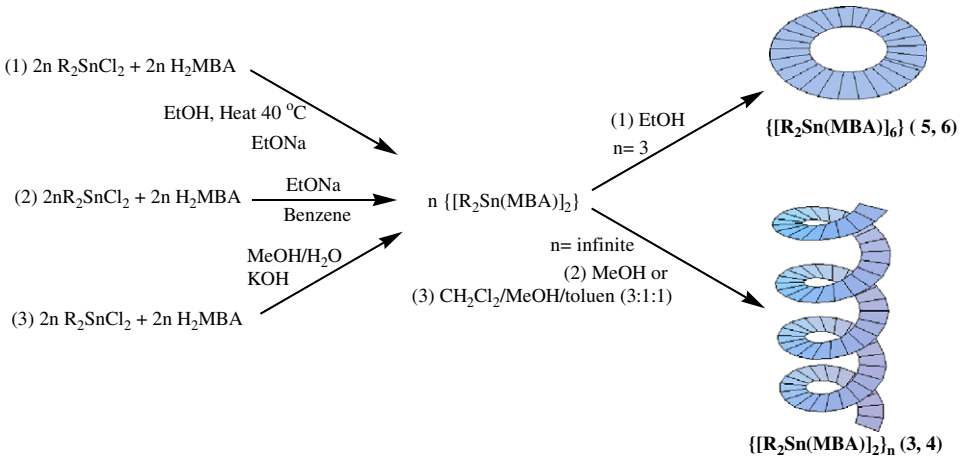

Fig. 5. Reaction conditions and structures obtained.

hydrogen bonds and π–π interactions. The results are summarized in Fig. 5.

4. Experimental

4.1. Materials and instruments

All solvents used were of reagent grade. 2-Mercapto-benzoic acid and the diorganotin dichlorides (Aldrich) were used with no further purification. Elemental analyses for C, H, N, and S were carried out with a Carlo Erba EA model 1108 elemental analyzer. The ^{119}Sn Mössbauer spectra were collected at various sample temperatures (85–150 K), with a constant acceleration spectrometer equipped with $CaSnO_3$ source kept RT. The calibration of the spectrometer was carried out with a ^{57}Co source and Fe absorber at room temperature. The line widths were very close to the natural width (0.28 mm/s). The content of the tin samples was calculated to be approximately 4 mg Sn in a 2 cm^2 area of sample holder. X-ray powder diffraction patterns, from powder derived from the crystals, were obtained using a Bruker AXS D8 Advance diffractometer in Bragg–Brentano geometry equipped with a Cu sealed-tube radiation source (λ = 1.54178 Å) and a secondary beam graphite monochromator.

4.2. Synthesis and crystallization of 1–4

A methanolic (3 cm^{-3}) solution of $(C_6H_5)_3SnCl$ (0.385 g, 1 mmol, (**1**)) and $(CH_3)_2SnCl_2$ (0.219 g, 1 mmol (**2**)) was added to a clear solution of 2-mercapto-4-methyl-pyrimidine (0.162 g, 1 mmol (**1**) and 0.326 g, 2 mmol (**2**)) in distilled water (8 cm^{-3}) which was treated with KOH 1 N (2 cm^{-3}, 2 mmol (**1**) and 4 cm^{-3}, 4 mmol (**2**)). A white precipitate formed immediately, which was filtered off after stirring for 3 h, washed with 5 ml of cold distilled water and dried *in vacuo* over silica gel. Complexes **3** and **4** were prepared by a similar method. A suspension of 2-mercapto-benzoic acid (0.308 g, 2 mmol) in distilled water (8 cm^{-3}) was treated with a solution of KOH 1 N (4 cm^{-3}, 4 mmol), giving a clear solution. A methanolic (3 cm^{-3}) solution of the diorganotin(IV) dichloride ($(n\text{-}C_4H_9)_2SnCl_2$ 0.304 g, 1 mmol, (**3**) and $(CH_3)_2SnCl_2$ 0.219 g, 1 mmol (**4**)) was subsequently added. A white precipitate formed immediately, which was filtered off after stirring for 3 h, washed with 5 ml of cold distilled water and dried *in vacuo* over silica gel. The yields of the preparations are 60% for **1**, **2,** and **4** and 50% for **3**. Crystals of complexes **1** and **2** suitable for X-ray analysis were formed by slow evaporation of methanol/acetonitrile (1:1) solutions while crystals of **1** and **2** suitable for X-ray analysis were formed by slow evaporation of dichloromethane/methanol/toluene (3:1:1) solutions.

4.3. Computational details

Using the crystallographic data reported above as a starting point, we performed geometry optimization at the gradient-corrected density functional theory (DFT) level by utilizing Becke's three-parameter fit of the exact exchange correlation potential [22] in combination with the gradient-corrected functional of Lee et al. [23], (B3LYP), within the GAUSSIAN 03 software package [24]. For this study, the all-electron, split-valence 3-21G** basis set and the LANL2DZ double-zeta effective core potential basis set were utilized. Attempts to use a mixed basis set (LANL2DZ/6-31G**) for increased accuracy were not successful as the optimization did not meet the convergence criterion. To characterize the nature of the stationary points, a harmonic vibrational calculation was carried out. No imaginary frequencies were computed.

4.4. X-ray structure determination

Data were collected by the ω scan technique in the range 2.6° < 2θ < 28.8° (**1**), 2.3° < 2θ < 29.0° (**2**), 2.8° < 2θ < 25.0° (**3**) and 2.6° < 2θ < 25.0° (**4**) on a KUMA KM4CCD four-circle diffractometer [25] with a CCD detector, using graphite-monochromated Mo Kα radiation (λ = 0.71073 Å) at room temperature. Cell parameters were determined by a least-squares fit [25]. All data were corrected for Lorentz-polarization effects and absorption [26].

The structure was solved with direct methods with SIR-92 [27] and refined by full-matrix least-squares procedures on F^2 with SHELXL97 [28]. In **4** all non-hydrogen atoms were refined anisotropically, hydrogen atoms were located at calculated positions and refined as a 'riding model' with isotropic thermal parameters fixed at 1.2 times (1.3 for methyl groups) the U_{eq}'s of the appropriate carrier atom. In **3** the *n*-butyl chains were disordered over two positions. Weak constraints for the molecular geometry were applied; the disordered atoms were refined isotropically, all other non-hydrogen atoms were refined anisotropically. Hydrogen atoms were treated as in **1**. Significant crystal data are given below:

Compound **1**: $C_{23}H_{20}N_2SSn$, orthorhombic, *Pbca*, a = 9.4530(19) Å, b = 15.525(3) Å, c = 28.170(6) Å, V = 4134.2(15) Å^3, Z = 8, T = 293(2) K, $\rho_{(calc)}$ = 1.527 g cm^{-3}, μ(Mo Kα) = 1.3 mm^{-1}, reflections collected: 17766, unique: 4984 (R_{int} = 0.019), 3969 observed data [$I > 2\sigma(I)$], final R: 0.0231, wR_2 [$I > 2\sigma(I)$] 0.0498, S = 1.04, min/max $\Delta\rho$: −0.73/1.01 e Å^{-3}.

Compound **2**: $C_{12}H_{16}N_4S_2Sn$, monoclinic, $P2_1$, $a = 7.5720(10)$ Å, $b = 17.704(2)$ Å, $c = 12.062(2)$ Å, $V = 1617.0(4)$ Å^3, $Z = 4$, $T = 293(2)$ K, $\rho_{(calc)} = 1.640$ g cm^{-3}, μ(Mo Kα) = 1.8 mm^{-1}, reflections collected: 2328, unique: 1191 ($R_{int} = 0.039$), 1029 observed data [$I > 2\sigma(I)$], final R: 0.0341, wR_2 [$I > 2\sigma(I)$] 0.0789, $S = 1.11$, min/max $\Delta\rho$: −1.09/0.99 e Å^{-3}.

Compound **3**: $C_{30}H_{44}O_4S_2Sn_2$, monoclinic, $P2_1/n$, $a = 10.9297(6)$ Å, $b = 14.8199(8)$ Å, $c = 22.3115(9)$ Å, $\beta = 97.739(4)°$, $V = 3581.0(3)$ Å^3, $Z = 4$, $T = 293(2)$ K, $\rho_{(calc)} = 1.429$ g cm^{-3}, μ(Mo Kα) = 1.5 mm^{-1}, reflections collected: 16256, unique: 6229 ($R_{int} = 0.036$), 4439 observed data [$I > 2\sigma(I)$], final R: 0.0612, wR_2 [$I > 2\sigma(I)$] 0.1950, $S = 1.08$, min/max $\Delta\rho$: −0.79/2.02 e Å^{-3}.

Compound **4**: $C_{18}H_{20}O_4S_2Sn_2$, monoclinic, $P2_1/n$, $a = 7.6430(10)$ Å, $b = 18.850(2)$ Å, $c = 15.7150(10)$ Å, $\beta = 100.870(10)°$, $V = 2223.4(4)$ Å^3, $Z = 4$, $T = 293(2)$ K, $\rho_{(calc)} = 1.798$ g cm^{-3}, μ(Mo Kα) = 2.5 mm^{-1}, reflections collected: 10044, unique: 3838 ($R_{int} = 0.032$), 2424 observed data [$I > 2\sigma(I)$], final R: 0.0263, wR_2 [$I > 2\sigma(I)$] 0.0419, $S = 0.84$, min/max $\Delta\rho$: −0.42/0.70 e Å^{-3}.

Acknowledgements

This research was co-funded by the European Union in the framework of the program 'Heraklitos' of the 'Operational Program for Education and Initial Vocational Training' of the 3rd Community Support Framework of the Hellenic Ministry of Education, funded by 25% from national sources and by 75% from the European Social Fund (ESF) and was carried out in partial fulfillment of the requirements for the Ph.D. thesis of Miss MNX within the graduate program in Bioinorganic Chemistry, coordinated by Prof. Nick Hadjiliadis.

Appendix A. Supplementary data

CCDC 691678, 691677, 674874 and 674067 contain the supplementary crystallographic data for **1, 2, 3, 4**, respectively. These data can be obtained free of charge via http://www.ccdc.cam.ac.uk/conts/retrieving.html, or from the Cambridge Crystallographic Data Centre, 12 Union Road, Cambridge CB2 1EZ, UK; fax: (+44) 1223 336 033; or e-mail: deposit@ccdc.cam.ac.uk. Supplementary data associated with this article can be found, in the online version, at doi:10.1016/j.poly.2008.07.030.

References

[1] A.G. Davis, Organotin Chemistry, VCH, Verlagsgesellschaft, Weinheim, Germany, 1997.
[2] P.J. Smith, Chemistry of Tin, Blackie Academic & Professional an imprint of Thomson Science, London, UK, 1998.
[3] M. Gielen, E.R.T. Tiekink, in: M. Gielen, E.R.T. Tiekink (Eds.), Tin compounds and their therapeutic potential, Metallotherapeutic Drugs and Metal-Based Diagnostic Agents: The Use of Metals in Medicine, John Wiley & Sons, Ltd., 2005, p. 421.
[4] S.K. Hadjikakou, N. Hadjiliadis, Coord. Chem. Rev. (2008), doi:10.1016/j.ccr.2007.12.026.
[5] V.I. Balas, S.K. Hadjikakou, N. Hadjiliadis, N. Kourkoumelis, M.E. Light, M. Hursthouse, A.K. Metsios, S. Karkabounas, Bioinorg. Chem. Appl. (2008) (Article ID 654137).
[6] M.N. Xanthopoulou, S.K. Hadjikakou, N. Hadjiliadis, E.R. Milaeva, J.A. Gracheva, V.-Y. Tyurin, N. Kourkoumelis, K.C. Christoforidis, A.K. Metsios, S. Karkabounas, K. Charalabopoulos, Eur. J. Med. Chem. 43 (2008) 327.
[7] M.N. Xanthopoulou, S.K. Hadjikakou, N. Hadjiliadis, N. Kourkoumelis, E.R. Milaeva, J.A. Gracheva, V.-Y. Tyurin, I.I. Verginadis, S. Karkabounas, M. Baril, I.S. Butler, Russ. Chem. Bull. 56 (2007) 767.
[8] M.N. Xanthopoulou, S.K. Hadjikakou, N. Hadjiliadis, M. Kubicki, S. Skoulika, T. Bakas, M. Baril, Ian S. Butler, Inorg. Chem. 46 (2007) 1187.
[9] Marianna N. Xanthopoulou, Sotiris K. Hadjikakou, Nick Hadjiliadis, Maciej Kubicki, Spyros Karkabounas, Konstantinos Charalabopoulos, Nikolaos Kourkoumelis, Thomas Bakas, J. Organomet. Chem. 691 (2006) 1780.
[10] M.N. Xanthopoulou, S.K. Hadjikakou, N. Hadjiliadis, M. Schurmann, K. Jurkschat, A. Michaelides, S. Skoulika, T. Bakas, J.J. Binolis, S. Karkabounas, K. Charalabopoulos, J. Inorg. Biochem. 96 (2003) 425.
[11] M.N. Xanthopoulou, S.K. Hadjikakou, N. Hadjiliadis, M. Schurmann, K. Jurkschat, J. Binolis, S. Karkabounas, K. Charalabopoulos, Bioinorg. Chem. Appl. 1 (2003) 227.
[12] B. Samuelsson, S.E. Dahlen, J. Lindgren, C.A. Rouzer, C.N. Serhan, Science 237 (1987) 1171.
[13] M.J. Knapp, J.P. Klinman, Biochemistry 42 (2003) 11466.
[14] H. Yin, H. Xu, K. Li, G. Li, J. Inorg. Organomet. Polym. Mater. 15 (2005) 319.
[15] C. Ma, Q. Zhang, R. Zhang, D. Wang, Chem. Eur. J. 12 (2006) 420.
[16] C. Ma, J. Zhang, G. Tian, R. Zhang, J. Organomet. Chem. 690 (2005) 519.
[17] A.W. Addison, T. Nageswara Rao, J. Reedijk, J. van Rijk, G.C. Verschoor, J. Chem. Soc., Dalton Trans. (1984) 1349.
[18] C. Janiak, J. Chem. Soc., Dalton Trans. (2000) 3885.
[19] M.A. Buntine, V.J. Hall, F.J. Kosovel, E.R.T. Tiekink, J. Phys. Chem. A 102 (1998) 2472.
[20] J.B. Foresman, A. Frisch, Exploring Chemistry with Electronic Structure Methods, 2nd ed., Gaussian, Inc., Pittsburgh, PA, 1996, p. 101.
[21] S.K. Hadjikakou, M.A. Demertzis, M. Kubicki, D. Kovala-Demertzi, Appl. Organometal. Chem. 14 (2000) 727.
[22] A.D. Becke, J. Chem. Phys. 98 (1993) 5648.
[23] C. Lee, W. Yang, R.G. Parr, Phys. Rev. B 37 (1988) 785.
[24] M.J. Frisch, G.W. Trucks, H.B. Schlegel, G.E. Scuseria, M.A. Robb, J.R. Cheeseman, J.A. Montgomery, Jr., T. Vreven, K.N. Kudin, J.C. Burant, J.M. Millam, S.S. Iyengar, J. Tomasi, V. Barone, B. Mennucci, M. Cossi, G. Scalmani, N. Rega, G.A. Petersson, H. Nakatsuji, M. Hada, M. Ehara, K. Toyota, R. Fukuda, J. Hasegawa, M. Ishida, T. Nakajima, Y. Honda, O. Kitao, H. Nakai, M. Klene, X. Li, J.E. Knox, H.P. Hratchian, J.B. Cross, V. Bakken, C. Adamo, J. Jaramillo, R. Gomperts, R.E. Stratmann, O. Yazyev, A.J. Austin, R. Cammi, C. Pomelli, J.W. Ochterski, P.Y. Ayala, K. Morokuma, G.A. Voth, P. Salvador, J.J. Dannenberg, V.G. Zakrzewski, S. Dapprich, A.D. Daniels, M.C. Strain, O. Farkas, D.K. Malick, A.D. Rabuck, K. Raghavachari, J.B. Foresman, J.V. Ortiz, Q. Cui, A.G. Baboul, S. Clifford, J. Cioslowski, B.B. Stefanov, G. Liu, A. Liashenko, P. Piskorz, I. Komaromi, R.L. Martin, D.J. Fox, T. Keith, M.A. Al-Laham, C.Y. Peng, A. Nanayakkara, M. Challacombe, P.M.W. .Gill, B. Johnson, W. Chen, M.W. Wong, C. Gonzalez, J.A. Pople, GAUSSIAN 03, Revision C.02, Gaussian, Inc., Wallingford CT, 2004.
[25] CrysAlisCCD (version 1.171.29.9), Oxford Diffraction, Wrocław, Poland, 2006.
[26] CrysAlisRED (version 1.171.29.9), Oxford Diffraction, Wrocław, Poland, 2006.
[27] A. Altomare, G. Cascarano, C. Giacovazzo, A. Gualardi, J. Appl. Crystallogr. 26 (1993) 343.
[28] G.M. Sheldrick, SHELX97, Program for the Solution and Refinement of Crystal Structures. University of Göttingen, Germany, 1997.

2.4. Physical measurements

Melting points were determined using an Electrothermal digital m.p. apparatus. Magnetic susceptibility was measured with a Sherwood Auto MSB at 298 K. All susceptibilities were corrected for the diamagnetic contribution using Pascal's constant. Carbon, hydrogen, nitrogen and sulfur analyses were carried out using a Leco CHNS-932 analyzer. The IR spectra were recorded in the range of 400–4000 cm^{-1} with KBr pellets on either a Perkin Elmer 1650X or 1750X infrared spectrophotometer. The molar conductance of a 10^{-3} M solution of each metal complex in DMSO was measured at 29 °C using a Jenway 4310 conductivity meter and a dip-type cell with platinized electrode. The UV–Vis spectra were recorded on a Shimadzu UV-2501 PC spectrophotometer (800–200 nm). ^1H NMR spectra were recorded on a NMR JNM ECA400 spectrometer. Metal determinations were carried out using a Perkin Elmer Plasma 1000 emission spectrometer.

2.5. X-ray structure determination

Crystals of SBNBODTC formed when an ethanol solution was allowed to slowly evaporate over a couple of weeks. A single crystal was selected and mounted on a glass fibre using perfluoropolyether oil and cooled rapidly to 150 K in a stream of cold N_2 using an Oxford Cryosystems CRYOSTREAM unit. Diffraction data were measured using an Enraf-Nonius Kappa CCD diffractometer (graphite-monochromated Mo Kα radiation, $\lambda = 0.71073$ Å). Intensity data were processed using the DENZO-SMN package [9]. The crystal was found to be triclinic with $a = 9.7080(2)$ Å, $b = 11.2247(3)$ Å, $c = 14.1051(4)$ Å and $\alpha = 85.6063(11)°$, $\beta = 75.8090(11)°$, $\gamma = 74.1825(12)°$. The structure was solved in the space group $P\{\bar{1}\}$ using the direct-methods program [10] to locate all non-hydrogen atoms. Subsequent full-matrix least-squares refinement on F^2 was carried out using CRYSTALS Program Suite [11]. Coordinates and anisotropic thermal parameters of all non-hydrogen atoms were refined. Hydrogen atoms were located through a difference Fourier map. Hydrogens on the N and C were refined positionally and isotropically. Further crystallographic and refinement details are shown in Table 5.

2.6. Bioactivity

Antimicrobial and cytotoxic activities were evaluated at the Animal Cell and Tissue Culture Laboratory, Department of Biotechnology, Universiti Putra Malaysia.

2.7. Target microorganisms

Eight pathogens were used to test the biological potential of the ligands and metal complexes. They were methicillin-resistant *Staphylococcus* (MRSA); *Pseudomonas aeruginosa* (60690); *Bacillus subtilis* mutant defective DNA repair (B28) *Saccharomyces typhimurium* (S-T), *Candida albicans* (C.A), *Aspergillus ochraceous* (398), *Saccharomyces cereviceae* (20341), *Candida lypolytica* (2075). The sources of microbes and culture maintenance were as previously described [12,13].

2.8. Qualitative antimicrobial assay

Antimicrobial activity of each compound was qualitatively determined by a modified disk diffusion method [12]. A lawn of microorganisms was prepared by pipetting and evenly spreading inoculum (10^{-4} cm^3, adjusted turbidometrically to 10^5–10^6 cfu cm^3 (cfu: colony forming units) on to agar set in Petri dishes, using nutrient agar (NA) for the bacteria and potato dextrose agar (PDA) for fungi. Whatman no. 1 filter paper disks of 6 mm diameter were impregnated with stock solution of the compound (100 mg cm^{-3}) and dried under sterile conditions. The dried disks were then placed on the previously inoculated agar surface. The plates were inverted and incubated for 24 h at 30 °C for bacteria and 37 °C for fungi. Antimicrobial activity is indicated by the presence of clear inhibition zones around the disks. Commercially available streptomycin was used as antibacterial control and nystatin as antifungal control.

2.9. Cytotoxic assay

HL-60 (human myeloid leukemia) cell line was obtained from the American Type Culture Collection, USA HL-60 was cultured in RPMI-1640 (Sigma) medium supplemented with 10% fetal calf serum, Cytotoxicity was determined using the microtitration of 3-(4, 5-dimethylthiazol-2-yl)-2,5-diphenyltetrazolium bromide (MTT) (Sigma, USA) following Mosmann's method [14]. Controls that contained only cells were included for each sample. Cytotoxicity was expressed as IC_{50}, i.e. the concentration that reduced the absorbance of treated cells by 50% with reference to the control (untreated cells). Doxorubicin and Tamoxifen were used as cytotoxic standards.

3. Results and discussion

3.1. Infrared and nuclear magnetic resonance spectra

The physical and analytical data for the SBNBODTC and its metal complexes are shown in Table 1. All analytical data obtained are in agreement with proposed structures. Important absorption bands in the IR spectra of these compounds are shown in Table 2.

S-Benzyl-β-*N*-(benzoyl) dithiocarbazate was formed from reaction of SBDTC with benzoyl chloride in the presence of potassium hydroxide. In solution, the thione tautomer of SBDTC is unstable and converted to the more stable thiolo forms by enethiolization [8]. Through the loss of a proton, SBDTC behaves as a uninegatively charged weak base due to resonance involving the nonbonding pair of electrons on the nitrogen atom thus the benzoyl group is directed to the α-nitrogen on SBDTC forming *S*-benzyl-β-*N*-(benzoyl) dithiocarbazate [15]. Steric hindrance due to the benzyl group in SBDTC also contributes to the formation of *S*-benzyl-β-*N*-(benzoyl) dithiocarbazate. Four tautomeric forms are possible for SBNBODTC (Fig. 1).

The spectrum of SBNBODTC shows sharp and strong υ(C=O) in addition to absorption bands in common with SBDTC. The υ_{asym}(N–H) and υ_{sym}(N–H) bands associated with the free amine group in SBDTC were replaced with a medium intensity band at 3062 cm^{-1} in the spectrum of SBNBODTC which is assigned to secondary υ(N–H). The absence of υ(S–H) and υ(O–H) from its IR spectrum, shows that SBNBODTC exists primarily as the thione tautomer (Fig. 1a) in the solid state (Table 2). The presence of the peak at 3.38 ppm attributed to the S–H proton and the absence of O–H in ^1H NMR spectrum confirmed that SBNBODTC exists as the thiol in DMSO-*d*6 solution. The signal at δ10.99 ppm is attributed to the N–H group on the aliphatic nitrogen atom, and resonance peaks associated with the aromatic groups are observed in the range δ 7.23–7.91 ppm. Combination of IR and NMR spectra verify that SBNBODTC exists in the thione form in solid state but undergoes enethiolization to form more stable thiolo tautomer in solution [8].

Both SBDTC and SBNBODTC display strong bands indicating the presence of C=S at 1048 cm^{-1} and 1052 cm^{-1}, respectively. However, this band is absent in the spectra of all the complexes indicating that ligation occurred through the thiolo sulfur. This is further supported by the splitting of υ(CSS) in these IR spectra. The υ(C=O) band exhibited a negative shift for all complexes clearly showing participation of carbonyl oxygen in the coordination to the metal

Table 1
Physical and analytical data of SBNBODTC and its complexes

Compound	Color	M.p. (°C)	Found (Calculated %)				Metal (%)	Yield (%)
			C	H	N	S		
$C_{16}H_{16}N_2OS_2$ (SBNBODTC)	white	143–144	60.43 (60.73)	5.62 (5.10)	8.35 (8.85)	20.99 (20.27)		75
$Cd(C_{16}H_{16}N_2OS_2)_2$	white	168–169	51.04 (51.43)	4.69 (4.59)	7.76 (7.50)	17.33 (17.16)	15.00 (15.04)	86
$Co(C_{16}H_{16}N_2OS_2)_2$	orange	216–217	55.51 (55.39)	4.94 (4.94)	8.53 (8.07)	18.36 (18.49)	8.42 (8.49)	84
$Cu(C_{16}H_{16}N_2OS_2)_2$	dark blue	240–241	53.28 (55.03)	4.98 (4.91)	8.32 (8.02)	19.89 (18.36)	9.17 (9.10)	86
$Ni(C_{16}H_{16}N_2OS_2)_2$	brown	249–250	54.83 (55.41)	4.38 (4.94)	7.93 (8.08)	18.49 (18.49)	8.47 (8.46)	84
$Pb(C_{16}H_{16}N_2OS_2)_2$	yellow	165–166	45.77 (45.64)	3.93 (4.07)	6.73 (6.65)	14.95 (15.23)	24.65 (24.61)	88

Table 2
Selected IR bands of SBDTC, SBNBODTC and its metal complexes

Compound	IR bands (cm^{-1})				
	υ(N–H)	υ(C=S)	υ(CSS)	υ(C=O)	υ(N–N)
SBDTC	3304, 3180	1048	950		1346
SBNBODTC (OS)	3062	1052	906	1638	1272
$Cd(OS)_2$	3060		966, 900	1608	1280
$Co(OS)_2$	3062		968, 902	1602	1306
$Cu(OS)_2$	3058		966, 850	1584	1292
$Ni(OS)_2$	3058		972, 930	1600	1294
$Pb(OS)_2$	3058		946, 908	1600	1294

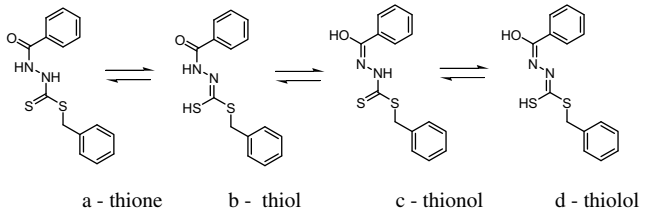

Fig. 1. Thione–thiol–thionol–thiolol tautomerism.

[16,17]. That there was no significant shift in either υ(N–N) or υ(N–H) corresponding to the *sec* NH group of SBNBODTC upon complexation shows that coordination did not occur through nitrogen.

3.2. Magnetic and conductivity data

The molar conductance data (Table 3) showed that all the metal complexes are essentially non-electrolytes in DMSO, indicating that they do not dissociate in solution. At room temperature, the cobalt, copper and nickel complexes are paramagnetic (Table 3). These paramagnetic Ni^{2+} and Co^{2+} complexes are expected to be tetrahedral while the Cu^{2+} complex should be square planar [18].

3.3. Electronic spectra

The spectrum of the SBNBODTC exhibits bands at ~281 and 260 nm attributed to $\pi \rightarrow \pi^*$ and $n \rightarrow \pi^*$ transitions respectively. These do not shift significantly upon complexation. $Cd(OS)_2$ showed absorption bands at 280–322 nm which may be attributed to intra-ligand transitions. $Co(OS)_2$ displayed absorption bands at 361 nm corresponding to the $^1T_{2g} \leftarrow {}^1A_{1g}$ d–d transition and at 281 nm, caused by intra ligand charge transfer, $n \rightarrow \pi^*$. $Cu(OS)_2$ exhibited absorption at 504 nm corresponding to the $^2E_{1g} \leftarrow {}^2B_{1g}$ transition [6]. The band at 276 nm is presumably due to charge transfer. This low spin complex thus has a square planar stereochemistry.

$Ni(OS)_2$ exhibits d–d transition bands at 729 and 537 nm attributable to $^3T_1(P) \leftarrow {}^3T_1(F)$, which may be observed as doublet due to the spin–orbital coupling compatible with the $Ni(OS)_2$ in an distorted tetrahedral environment [18]. The remaining bands at 387 and 280 nm were caused by charge transfer. The electronic spectra for $Pb(OS)_2$ exhibit charge transfer bands at 326 and 273 nm. (see Table 4).

3.4. X-ray crystal structure of S-benzyl-β-N-(benzoyl) dithiocarbazate(SBNBODTC)

A perspective view of SBNBODTC with its numbering scheme is shown in Fig. 2. A summary of crystal data and structure refinement parameters is given in Table 5. The relevant bond distances and bond angles are given in Table 6. The asymmetric unit consists of two independent *S*-benzyl-β-*N*-(benzoyl) dithiocarbazate molecules. Both asymmetric unit SBNBODTC crystallized as the thione in *cis–cis* conformation with the N–N bond adopting a *cis* geometry with respect to C=S, while the *S*-benzyl group adopts a *cis* geometry with respect to the thione sulfur atom across the C–S bond. Both molecules are related with a 179.21° rotation across [−1.0, −0.7, 0.6]. The asymmetric units deviates to each other in 25.76(5)°. The differences of the bond lengths of both independent molecules are below 3σ except for C2–N4 and S3–C2 (3.1σ and 3.2σ).

The C=S bond distances for SBNBODTC are shorter than that in SBDTC (1.678(3) Å) [19] but are comparable with Schiff bases derived from SBDTC [20,21]. These lengths are intermediate between the C–S and C=S bonds [22] showing there are conjugation effect along the –C–N–N–C(=S) bond. The C=O bond distances are comparable with previous literature as double bond character [22]. These two bonds are essential to confirm that SBNBODTC exist as thione tautomer.

The N4–N5 [1.384(2) Å] and N24–N25 [1.389(2) Å] are slightly longer than in Schiff bases of SBDTC, e.g. 1.3765(19) Å [20],

Table 3
UV–Vis, conductivity and magnetic susceptibility measurements data of SBNBODTC and its metal complexes

Compound	Λ ($\Omega\ cm^{-2}\ mol^{-1}$)	λ_{max}, nm (log ε, $cm^{-1}\ mol^{-1}\ L$)	μ_{eff} (B.M.)
SBNBODTC (OS)	0.1	281 (4.208), 260 (4.195)	
$Cd(OS)_2$	2.705	322 (3.942), 308 (3.921), 280.0 (4.217)	diamagnetic
$Co(OS)_2$	2.275	361 (3.607), 281 (4.140)	4.538
$Cu(OS)_2$	0.07	509 (3.207), 322 (4.330), 271 (4.374)	1.868
$Ni(OS)_2$	0.1	729 (2.068), 537 (2.068), 387 (3.868), 280 (3.993)	3.241
$Pb(OS)_2$	0.725	326 (4.266), 273 (4.391)	diamagnetic

Table 4
Cytotoxic activity of SBNBODTC ligand and its metal complexes

Compound	HL-60 (IC_{50}, μg cm^{-3})[a]
SBNBODTC (OS)	1.00
$Cd(OS)_2$	5.23
$Co(OS)_2$	5.62
$Cu(OS)_2$	2.15
$Ni(OS)_2$	3.62
$Pb(OS)_2$	1.54
Doxorubicin	0.1
Tamoxifen	36

[a] IC_{50} = inhibition concentration at 50%, i.e., the concentration to reduce growth of cancer cells by 50%. IC_{50} <5.0 μg cm^{-3} – strongly active; 5.0 ⩽ 10.0 μg cm^{-3} – moderately active; 10.0–25.0 μg cm^{-3} – weakly active; >25.0 μg cm^{-3} – not active.

Table 5
Crystal structure data for *S*-benzyl-β-*N*-(benzoyl)dithiocarbazate

Crystal structure	*S*-Benzyl-β-*N*-(benzoyl)dithiocarbazate
Chemical formula	$C_{15}H_{14}N_2O_1S_2$
Formula weight	M_r = 302.42
Crystal class, space group	triclinic, $P\{\bar{1}\}$
a (Å)	9.7080 (2)
b (Å)	11.2247 (3)
c (Å)	14.1051 (4)
α (°)	85.6063(11)
β (°)	75.8090(11)
γ (°)	74.1825(12)
Size (mm)	0.08 × 0.26 × 0.28
Colour, shape	colourless, plate
Volume (Å^3)	1433.62 (6)
Z	4
Temperature (K)	150
D_x (mg m^{-3})	1.401
μ (mm^{-1})	0.37
Data collection	
Diffractometer type	KAPPACCD
Absorption type	multi–scan
Scan type	OMEGA
Radiation type, wavelength	Mo Kα, 0.710730
Reflections measured	11369
Independent reflections	6505
R_{int}	0.034
θ_{max}	27.5
H_{min}, H_{max}	−12 12
K_{min}, K_{max}	−14 13
L_{min}, L_{max}	−18 18
Refinement on F^2	
$\Delta\rho_{min}$ (e Å^{-3})	−0.67
$\Delta\rho_{max}$ (e Å^{-3})	0.54
Reflections used	6505
Parameter refined	361
R-factor, weighted *R*-factor	0.077, 0.107

1.3747(13) Å [21], which may due to delocalization along –C–N–N–C– involving C6–O7 and C26–O27 double bonds (1.240(2) Å and 1.233(2) Å).

The intramolecular hydrogen bonds, N4–H41···O7 [2.903(4) Å] and N24–H241···O27 [2.816(4) Å] stabilize the *cis–cis* conformation (Fig. 3) by imposing angle strain, N25–C26–O27 [122.61 (18)°], N24–N25–C26 [120.18(17)°], N4–N5–C6 [118.98(16)°] and N5–C6–O7 [120.88(17)°]. The N5–H51···O27 and N25—H251···O7 contacts are intermolecular hydrogen bonds that connects the molecules in its 3D packing [Fig. 3].

3.5. Biological activity

3.5.1. Antimicrobial assay

Clear inhibition zones less than 15 mm indicated that the all compounds synthesized are inactive against the pathogens tested. SBNBODTC was moderately active against Methicillin resistant *Staphyloccus* (MRSA) (9 mm diameter inhibition zone). $Cu(OS)_2$ is moderately active towards both *Pseudomonas aeruginosa* (60690) and *Saccharomyces typhimurium* (S–T). This result contrasts with

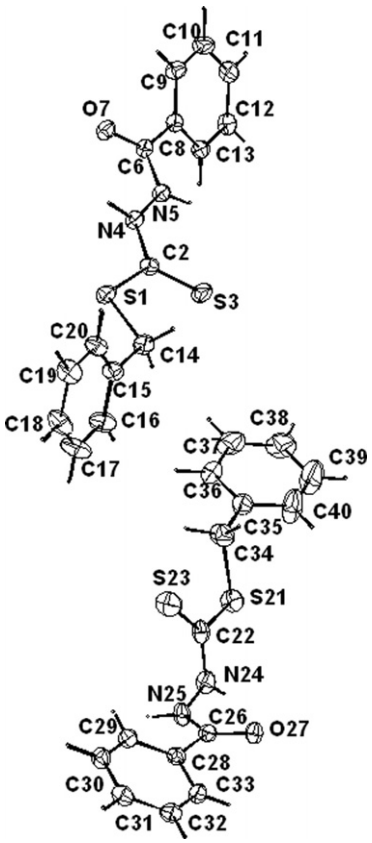

Fig. 2. Molecular structure and atomic numbering scheme of *S*-benzyl-β-N-(benzoyl)dithiocarbazate (OS).

Table 6
Selected bond lengths, bond angles and hydrogen bond geometry for *S*-benzyl-β-*N*-(benzoyl) dithiocarbazate

Selected bond lengths (Å)		Selected bond angles (°)	
S1–C2	1.762 (2)	C2–S1–C14	101.30 (10)
S1–C14	1.809 (2)	S1–C2–S3	125.27 (12)
C2–S3	1.655 (2)	S1–C2–N4	110.99 (15)
C2–N4	1.338 (3)	S3–C2–N4	123.74 (15)
N4–N5	1.384 (2)	C2–N4–N5	120.01 (17)
N5–C6	1.343 (3)	N4–N5–C6	118.98 (16)
C6–O7	1.240 (2)	N5–C6–O7	120.88 (17)
S21–C22	1.761 (2)	N5–C6–C8	115.47 (17)
S21–C34	1.814 (3)	O7–C6–C8	123.64 (18)
C22–S23	1.646 (2)	S1–C14–C15	108.75 (15)
C22–N24	1.352 (3)	C22–S21–C34	102.91 (11)
N24–N25	1.389 (2)	S21–C22–S23	125.32 (14)
N25–C26	1.349 (3)	S21–C22–N24	110.32 (15)
C26–O27	1.233 (2)	S23–C22–N24	124.33 (16)
		C22–N24–N25	120.09 (18)
		N24–N25–C26	120.18 (17)
		N25–C26–O27	122.61 (18)
		N25–C26–C28	115.85 (18)
		O27–C26–C28	121.53 (18)
		S21–C34–C35	108.08 (17)

Hydrogen bond geometry

D–H···A	D–H (Å)	H···A (Å)	D···A (Å)	D–H···A (°)
N5–H51···O27i	0.87	2.48	3.038 (4)	123
N4–H41···O7ii	0.89	2.08	2.903 (4)	154
N25–H251···O7iii	0.88	2.09	2.925 (4)	158
N24–H241···O27iv	0.88	1.95	2.816 (4)	171

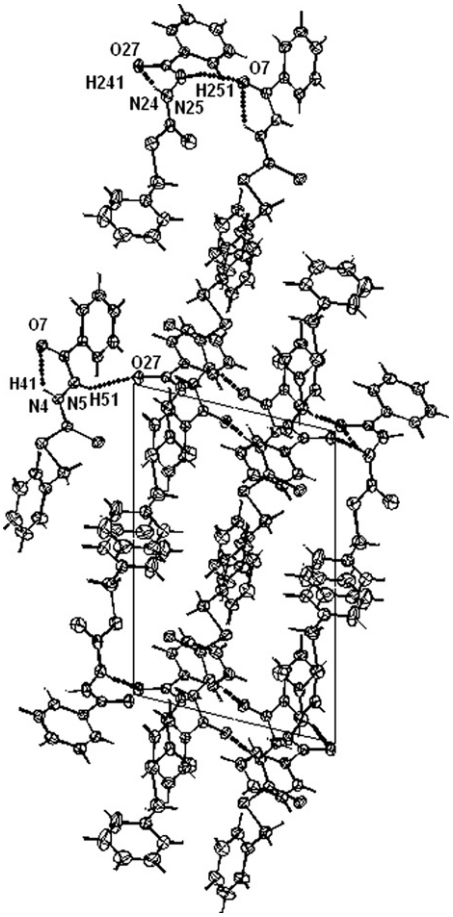

Fig. 3. Packing of the molecules along the *b*-axis with intramolecular and intermolecular hydrogen bonds represented as dotted lines.

the marked activity of SBDTC and its metal complexes against bacteria and fungi [6,7]. The addition of the benzoyl functionality has rendered it moderately active.

3.5.2. Cytotoxic activity

SBNBODTC, $Cu(OS)_2$, $Ni(OS)_2$ and $Pb(OS)_2$ displayed marked cytotoxicity ($IC_{50} < 5.0\ \mu g\ cm^{-3}$) against HL-60 (human myeloid leukemia). $Cd(OS)_2$ and $Co(OS)_2$ are moderately active against HL-60 with IC_{50} of 5.23 and 5.62, respectively. The rank order of potency as a function of chelated metal ion follows the order Co < Cd < Ni < Cu < Pb. That there was no enhancement in cytotoxicity upon complexation of SBNBODTC with metal ions was unexpected considering that such enhancement has often been observed for related complexes containing NS donor ligands.

Acknowledgements

The authors thank the Department of Chemistry and the Institute of Bioscience, Universiti Putra Malaysia, for the provision of laboratory facilities. We sincerely thank David J. Watkin, Oxford, for his helpful suggestions. We also thank the Ministry of Science, Technology and Innovation (MOSTI), Malaysia, for funding this research under the Intensification of Research in Priority Areas Scheme (IRPA Grant No. 09-02-04-0755-EA001). FHNF gratefully acknowledges MOSTI, for awarding her a National Science Fellowship.

Appendix A. Supplementary data

Crystallographic data for structural analysis have been deposited with the Cambridge Crystallographic Data Centre, CCDC no. 262560. Copies of this information may be obtained free of charge from The Director, CCDC, 12 Union Road, Cambridge, CB2 1EZ, UK (fax: +44 1223 336033; e-mail: deposit@ccdc.cam.ac.uk or http://www.ccdc.cam.ac.uk). Supplementary data associated with this article can be found, in the online version, at doi:10.1016/j.poly.2008.07.022.

References

[1] H. Zhou, D. Li, P. Wang, L. Cheng, Y. Gao, Y. Zhu, J. Wu, Y. Tian, Z. Tao, M. Jiang, H.K. Fun, J. Mol. Struct. 826 (2-3) (2007) 205.
[2] X. Wang, Z. Deng, B. Baokang Jin, Y. Tian, Xiangqin Lin, Bull. Chem. Soc. Jpn. 75 (2002) 1269.
[3] M.T.H. Tarafder, A.M. Ali, D.J. Wee, K. Azahari, S. Silong, K.A. Crouse, Transition Met. Chem. 25 (2000) 456.
[4] M.T.H. Tarafder, M.A. Ali, N. Saravanan, W.Y. Weng, S. Kumar, N. Umar-Tsafe, K.A. Crouse, Transition Met. Chem. 25 (2000) 295.
[5] M.A. Ali, A.H. Mirza, R.J. Butcher, M.T.H. Tarafder, M.A. Ali, Inorg. Chim. Acta 320 (2001) 1.
[6] M.T.H. Tarafder, A. Kasbollah, K.A. Crouse, A.M. Ali, B.M. Yamin, H.K. Fun, Polyhedron 20 (18) (2001) 2363.
[7] M.T.H. Tarafder, A. Asmadi, M.S.S. Talib, A.M. Ali, K.A. Crouse, Transition Met. Chem. 26 (2001) 170–174.
[8] M.A. Ali, M.T.H. Tarafder, J. Inorg. Nucl. Chem. 39 (1977) 1785.
[9] Z. Otwinowski, W. Minor, in: C.W. Carter Jr., R.M. Sweet (Eds.), Methods Enzymol. Macromolecular Cryst., Part A, vol. 276, Academic Press, New York, 1997, pp. 307–326.
[10] A. Altomare, G. Cascarano, C. Giacovazzo, A. Guagliardi, J. Appl. Cryst. 27 (1994) 435.
[11] P.W. Betteridge, J.R. Carruthers, R.I. Cooper, K. Prout, D.J. Watkin, J. Appl. Cryst. 36 (2003) 1487.
[12] A.W. Bauer, M.D.K. Kirby, J.C. Sherris, M. Turck, Am. J. Clin. Path. 45 (1966) 493.
[13] C.D. Hufford, A.M. Clark, Discovery and development in the new drugs for systematic opportunistic infections, in: Atta-ur-Rahman (Ed.), Studies in Natural Product Chemistry, vol. 2, Elsevier, Amsterdam, 1988, p. 421.
[14] T. Mosmann, J. Immunol. Meth. 65 (1–2) (1983) 55.
[15] T.W.G. Solomons, C.B. Fryhle, Organic Chemistry, Seventh ed., John Wiley and Sons Inc., 1988.
[16] M.A. Ali, H.J.H. Abu Bakar, A.H. Mirza, S.J. Smith, L.R. Gahan, P.V. Bernhardt, Polyhedron 27 (2008) 71.
[17] M.B. Ferrari, C. Pelizzi, G. Pelosi, M.C. Rodríguez-Argüelles, Polyhedron 21 (2002) 2593.
[18] A.A.A. Emara, B.A. El-Sayed, E.A.E. Ahmed, Spectrochim. Acta Part A 69 (2008) 757.
[19] S.S.S.R. Shanmuga, B.M. Yamin, Y.A. Yussof, M.T.H. Tarafder, H.K. Fun, K.A. Crouse, Acta Crystallogr., Sect. C 56 (2000) 1236.
[20] M.H.E. Chan, K.A. Crouse, M.T.H. Tarafder, B.M. Yamin, Acta Crystallogr., Sect. E. 59 (2003) o628.
[21] F.N.-F. How, D.J. Watkin, K.A. Crouse, M.I.M. Tahir, Acta Crystallogr., Sect. E, 63 (2007) o3023–o3024.
[22] F.H. Allen, O. Kennard, D.G. Watson, L. Brammer, A.G. Orpen, R. Taylor, J. Chem. Soc., Perkin Trans. 2 (1987) S1: 19.

The similar reaction of ferrocenoylacetone (2.485 g, 9 mmol) and *N*-(2-hydroxyethyl)-1,2-diaminoethane (0.959 g, 9 mmol) in 25 ml of THF for 24 h afforded 2.70 g (84%) of enaminone $H_3\mathbf{L}^2$ as a dark red solid. M.p. 113 °C. *Anal.* Calc. for $C_{18}H_{24}FeN_2O_2$: C, 60.69; H, 6.79; N, 7.86. Found: C, 60.60; H, 6.75; N, 7.84%. IR (KBr disk, cm^{-1}): ν(OH) and ν(secondary amine NH), 3334 (br, m), ν(enamine NH) 3098 (w), ν(C=O) and ν(C=C) 1596 (vs) and 1527 (s). UV (nm, in DMF): λ_{max} ($\varepsilon \times 10^4$, in $dm^3\ mol^{-1}\ cm^{-1}$) 271.00 (B-band) (0.45), 342.50 (K-band) (1.27), 452.50 (CT-band) (0.08). ^1H NMR ($CDCl_3$, ppm): δ 1.93 (s, 1H, NH), 2.01 (s, 1H, OH), 2.02 (s, 3H, CH_3), 2.80–2.85 (t, 2H), 2.90–2.92 (t, 2H), 3.40–3.43 (q, 2H), 3.66–3.68 (t, 2H, OCH_2), 4.15 (s, 5H, C_5H_5), 4.34 (s, 2H, (H^3, H^4) of C_5H_4 ring), 4.71 (s, 2H, (H^2, H^5) of C_5H_4 ring), 5.29 (s, 1H, CH), 11.10 (s, 1H, enamino NH).

2.2. Syntheses of mixed-ligand complexes **I** and **II**

A solution of $Cu(OAc)_2 \cdot H_2O$ (0.1997 g, 1 mmol) and $H\mathbf{L}^1$ (0.360 g, 1 mmol) in 20 ml of absolute ethanol was stirred for 6 h at room temperature. The mixture was filtered to afford the brown crude product. The resulting solid was recrystallized from dichloromethane and petroleum ether to give 0.395 g (82%) of **I** as brown crystals. M.p. 176.2–176.8 °C. *Anal.* Calc. for $C_{22}CuH_{22}FeN_2O_3$: C, 54.84; H, 4.60; N, 5.81. Found: C, 54.92; H, 4.72; N, 5.73%. IR (KBr disk, cm^{-1}): ν(C=O) 1601 (vs), ν(C=C) 1509 (vs). UV (nm, in DMF): λ_{max} ($\varepsilon \times 10^4$, in $dm^3\ mol^{-1}\ cm^{-1}$) 270.00 (B-band) (1.08), 354.80 (2.43) (K-band), 454.20 (0.46) (CT-band).

A solution of $Cu(OAc)_2 \cdot H_2O$ (0.057 g, 28 mmol) and $H_3\mathbf{L}^2$ (0.102 g, 0.28 mmol) in 20 ml of absolute ethanol was stirred for 10 h at room temperature. The solvent was removed under vacuum, and the residue was recrystallized from dichloromethane and petroleum ether (60–90 °C) to afford 0.122 g (91%) of **II** as black crystals. M.p. 101.5–101.9 °C. *Anal.* Calc. for $C_{20}CuH_{26}FeN_2O_4$: C, 50.27; H, 5.48; N, 5.86. Found: C, 50.55; H, 5.64; N, 5.65%. IR (KBr disk, cm^{-1}): ν(OH) and ν(secondary amine NH), 3243 (s), ν(C=O) 1582 (s), ν(C=C) 1507 (vs). UV (nm, in DMF): λ_{max} ($\varepsilon \times 10^4$, in $dm^3\ mol^{-1}\ cm^{-1}$) 290.00 (B-band) (6.19), 340.00 (2.06) (K-band), 450.00 (0.12) (CT-band).

2.3. Crystal structure determinations

X-ray data were collected on an Enraf-Nonius CAD4 diffractometer for $H\mathbf{L}^1$, **I** and **II** at 295 K using graphite-monochromated Mo Kα radiation (λ = 0.71073 Å). The structures were solved by direct methods and subsequently refined on F^2 by using full-matrix least-squares methods, all non-hydrogen atoms were anisotropically refined, and hydrogen atoms were located at calculated positions [12]. A summary of the data collection and structure refinement parameters of $H\mathbf{L}^1$, **I** and **II** is given in Table 1. Published plots of $H\mathbf{L}^1$, **I** and **II** are drawn using the PLATON software [13]. In complex **I**, the unsubstituted cyclopentadienyl ring is disordered over two positions.

Table 1
Summary of the data collection and structure refinement parameters of $H\mathbf{L}^1$, **I** and **II**

Compound	$H\mathbf{L}^1$	**I**	**II** · CH_2Cl_2
Formula	$C_{20}H_{20}FeN_2O$	$C_{22}H_{22}CuFeN_2O_3$	$C_{20}H_{26}CuFeN_2O_4 \cdot CH_2Cl_2$
Formula weight	360.23	481.82	562.75
Crystal size (mm)	0.21 × 0.17 × 0.12	0.4 × 0.1 × 0.1	0.2 × 0.1 × 0.1
Crystal system	monoclinic	monoclinic	triclinic
Space group	$P2_1/c$	$P2_1/n$	P-1
Unit cell dimensions			
a (Å)	7.7592 (16)	8.0230 (10)	10.0320 (10)
b (Å)	7.8092 (16)	23.599 (3)	11.009 (2)
c (Å)	27.491 (2)	10.899 (2)	11.403 (2)
α (°)			84.31 (3)
β (°)	90.591 (17)°	106.55 (3)°	73.95 (2)
γ (°)			79.722 (18)
V (Å^3)	1665.7 (5)	1978.1 (6)	1189.2 (4)
Z	4	4	2
D_{calc} (g cm^{-1})	1.436	1.618	1.572
F(000)	752	988	578
T (K)	295	295	295
μ (Mo Kα)(mm^{-1})	0.91	1.84	1.76
Scan mode	ω–2θ	ω–2θ	ω–2θ
θ Range (°)	1.48–25.97	1.73–26.97	1.86–25.97
Limiting indices			
	$0 \leqslant h \leqslant 9$, $\leqslant k \leqslant 9$, $-33 \leqslant l \leqslant 33$,	$-10 \leqslant h \leqslant 9$, $0 \leqslant k \leqslant 30$, $0 \leqslant l \leqslant 13$,	$0 \leqslant h \leqslant 12$, $-13 \leqslant k \leqslant 13$, $-13 \leqslant l \leqslant 14$
Absorption correction	PSI-scan	PSI-scan	PSI-scan
Reflections collected	3533	4297	4944
Independent reflections (R_{int})	3283 (0.047)	4297 (0.054)	4659 (0.017)
Number of parameters refined	217	287	276
Final R indices [$I > 2.0\sigma(I)$]	R, 0.044; wR, 0.123	R, 0.0713; wR, 0.1723	R, 0.0503; wR, 0.1281
R indices (all data)	R, 0.0606; wR, 0.1312	R, 0.1179; wR, 0.2106	R, 0.0666; wR, 0.1423
Goodness-of-fit	1.22	1.08	1.02
Maximum peak and hole (e Å^{-3})	0.29 and −0.73	0.75 and −0.94	0.88 and −1.40

3. Results and discussion

3.1. Syntheses of multidentate enaminones and mixed-ligand complexes

The reactions of ferrocenoylacetone with 2-(aminomethyl)pyridine and *N*-(2-hydroxyethyl)-1,2-diaminoethane afford the multidentate enaminones $H\mathbf{L}^1$ and $H_3\mathbf{L}^2$, as shown in Scheme 1. For $H\mathbf{L}^1$, its chromatography should be carried out with neutral Al_2O_3, because it decomposes on silica gel. For $H_3\mathbf{L}^2$, using THF as a solvent leads to a higher yield, because ethanol results in a complex mixture that is hard to separate. Reactions of copper acetate with $H\mathbf{L}^1$ and $H_3\mathbf{L}^2$ give the corresponding mixed-ligand complexes **I** and **II**, formulated as [Cu$\mathbf{L}^1$(OAc)] and [Cu($H_2\mathbf{L}^2$)(OAc)], respectively (Scheme 2). All the new compounds have been characterized by elemental analyses and IR, NMR and UV spectra. The structures of $H\mathbf{L}^1$, **I** and **II** have been unambiguously determined by single-crystal X-ray crystallography.

3.2. Crystal structures

3.2.1. Crystal structure of $H\mathbf{L}^1$

The molecular structure of $H\mathbf{L}^1$ is shown in Fig. 1. Selected geometric parameters for $H\mathbf{L}^1$ are listed in Table 2. $H\mathbf{L}^1$ crystallizes with Z = 4 in the space group $P2_1/c$. As noted in enaminones previously reported, the O=C–C=C–N moiety is planar and the bond lengths indicate electron delocalization [5,14]. The O=C–C=C–N plane is twisted with respect to the substituted cyclopentadienyl ring by 17.66(17)°. Moreover, the dihedral angle between the substituted cyclopentadienyl ring and the cyclopentadienyl ring is 2.4(2)°. Consistent with the large dihedral angle between the O=C–C=C–N plane and substituted cyclopentadienyl ring, the C10–C11 bond of 1.482(4) Å linking the O=C–C=C–N moiety and the substituted cyclopentadienyl ring is typical of a single bond (Csp^2–Csp^2), suggesting that the substituted cyclopentadienyl ring is not involved in the conjugation of the O=C–C=C–N moiety. As

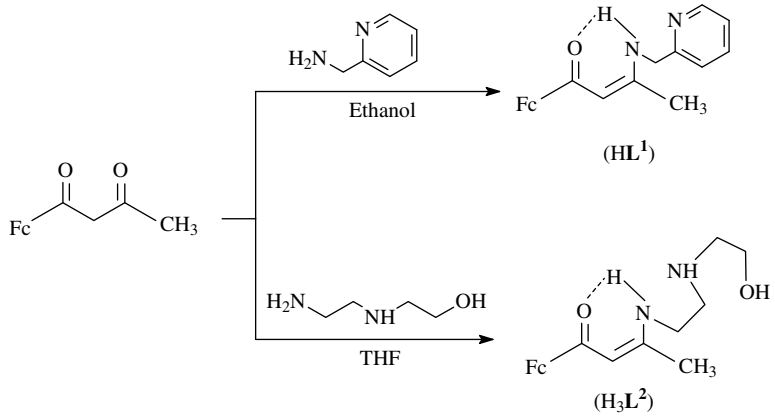

Scheme 1. Syntheses of multidentate enaminones.

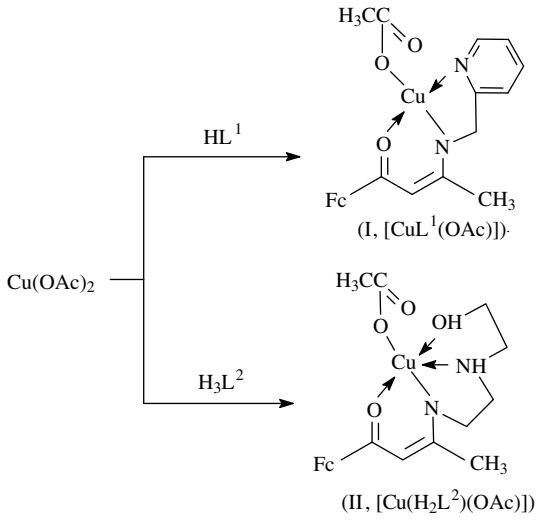

Scheme 2. Syntheses of mixed-ligand complexes

found in other enaminones, H**L**^{1} has a strong [N–H···O=C] intramolecular hydrogen bond. Furthermore, a [C–H···O=C] intermolecular hydrogen bond in which atom C19 in the molecule at (x, y, z) acts as a hydrogen-bond donor to the carbonyl atom O1 in the molecule at ($2 - x$, $2 - y$, $1 - z$) is also observed. By the intermolecular hydrogen bond, molecules of H**L**^{1} form centrosymmetric dimers.

3.2.2. Crystal structure of *I*

The molecular structure of complex **I** is shown in Fig. 2. Selected geometric parameters for complex **I** are listed in Table 3. Complex **I** crystallizes with $Z = 4$ in the space group $P2_1/n$. In **I**, H**L**^{1} acts as a tridentate monoanionic ligand after deprotonation of the enamine nitrogen atom, namely it is an N2O donor. The Cu1–O2 and Cu1–O3 distances are 1.930(5) and 2.823(5) Å, respectively. Since the Cu1–O3 distance is in excess of 2.8 Å, the O3 atom cannot be included in the first coordination sphere. Hence the acetate anion is monodentate. However, the distance of 2.823(5) Å indicates there is a short intramolecular contact between the Cu1 and O3 atoms [13]. The copper(II) ion is coplanar with four donor atoms O1, O2, N1 and N2; hence the coordination geometry of the copper(II) ion is square-planar. The Cu1–O1 bond length of 1.907(5) Å is close to the corresponding ones of copper complexes with enaminones previously reported, whereas the Cu1–N1 bond length of 1.918(5) Å is shorter than the reported values. Similar to a planar copper complex of Hacpa derived from acetylacetone and 2-aminomethylpyridine, the Cu–N(pyridyl) bond (Cu1–N2 = 2.001(5) Å) is longer than the Cu–N(enamine) bond [15,16].

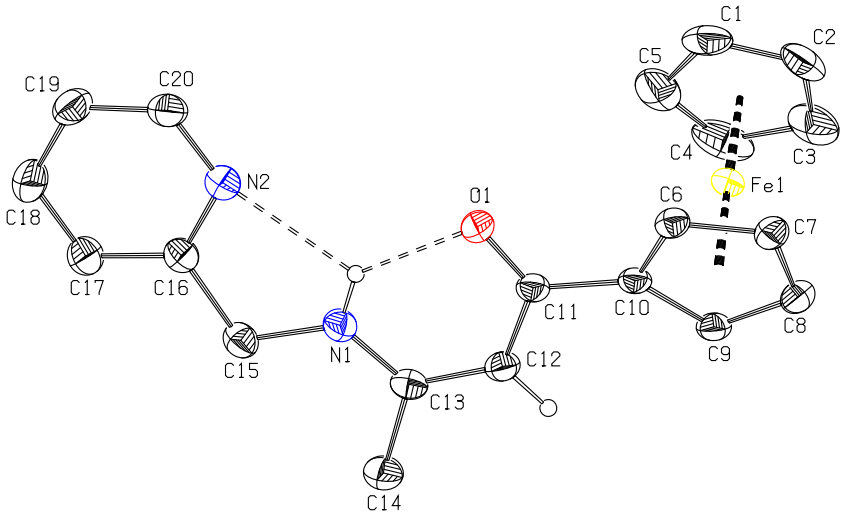

Fig. 1. ORTEP plot of H**L**^{1} showing the atom labelling, thermal ellipsoids are drawn as 30% probability ellipsoids. The intramolecular hydrogen bond is shown as a dashed line.

Table 2
Selected geometric parameters (Å, °) for H**L**[1]

O1–C11	1.252 (4)	C10–C11	1.483 (4)
N1–C13	1.325 (4)	C11–C12	1.427 (4)
N1–C15	1.440 (4)	C12–C13	1.382 (5)
N1···O1	2.692 (3)	C19···O1^{i}	3.284 (5)
O1–C11–C10	118.5 (3)	N1–C13–C12	121.9 (3)
O1–C11–C12	123.3 (3)	N1–C13–C14	118.1 (3)
C10–C11–C12	118.2 (3)	C13–N1–C15	125.4 (3)
C11–C12–C13	124.1 (3)	N1–H1N···O1	134
C12–C13–C14	120.0 (3)	C19–H19···O1^{i}	133

Symmetry code: (i) $2-x, 2-y, 1-z$.

Table 3
Selected geometric parameters (Å, °) for **I**

Cu1–O1	1.907 (5)	N1–C13	1.321 (8)
Cu1–O2	1.930 (5)	N1–C15	1.474 (8)
Cu1–O3	2.823 (5)	C10–C11	1.480 (9)
Cu1–N1	1.918 (5)	C11–C12	1.377 (9)
Cu1–N2	2.001 (5)	C12–C13	1.397 (9)
O1–C11	1.300 (7)	C14···O2^{i}	3.353 (9)
C17···O3^{ii}	3.176 (10)	C20···O2	3.048 (9)
O1–Cu1–O2	90.1 (2)	O1–C11–C12	125.1 (6)
O1–Cu1–N1	94.3 (2)	C10–C11–C12	119.9 (6)
O1–Cu1–N2	176.9 (2)	C11–C12–C13	126.6 (6)
O2–Cu1–N1	175.0 (2)	N1–C13–C12	122.5 (6)
O2–Cu1–N2	92.9 (2)	N1–C13–C14	121.3 (7)
N1–Cu1–N2	82.7 (2)	C12–C13–C14	116.3 (6)
O1–C11–C10	115.0 (6)	C14–H14A···O2^{i}	136
C17–H17···O3^{ii}	141	C20–H20···O2	114

Symmetry codes: (i) $-x, 1-y, 1-z$; (ii) $1-x, 1-y, 1-z$.

The bond lengths and angles of the O=C–C=C–N moiety in **I** are analogous with those of H**L**[1], the related bond lengths in the O=C–C=C–N moiety are indicative of electron delocalization [5–11,14]. As expected, the dihedral angle between the two cyclopentadienyl rings is 1.4(10)° and shows that they are parallel to each other. The dihedral angle between the O=C–C=C–N moiety and the substituted cyclopentadienyl ring is 17.3(5)°. The C(10)–C(11) bond length of 1.479(10) Å is a typical single bond, thus suggesting that the substituted cyclopentadienyl ring is not involved in the conjugation of the O=C–C=C–N moiety. In addition to the [C–H···O=C] intramolecular hydrogen bond involving atom C20 as a hydrogen-bond donor to atom O2 of an acetate anion, for **I**, atom C17 in the molecule at (x, y, z) acts as a hydrogen-bond donor to the carbonyl atom O3 of an acetate in the molecule at $(1-x, 1-y, 1-z)$, resulting in the formation of centrosymmetric dimers. These dimers, linked by a C–H···O=C hydrogen bond, viz. atom C14 in the molecule at (x, y, z) as a donor via atom H14A to atom O2 of an acetate anion at $(-x, 1-y, 1-z)$, form an infinite double-chain in the [100] direction.

3.2.3. Crystal structure of *II*

The molecular structure of complex **II** is shown in Fig. 3. Selected geometric parameters for complex **II** are listed in Table 4. Complex **II**, solvated by CH_2Cl_2, crystallizes with $Z = 2$ in the space group $P\bar{1}$. In **II**, H_3**L**[2] acts as a tetradentate monoanionic ligand upon deprotonation of the enamine nitrogen atom, namely an N2O2 donor. Similarly, the acetate anion in **II** is a monodentate ligand. The O2, O3 and N1 atoms lie on the equatorial plane and the O1 and N2 atoms occupy the axial sites. The O1–Cu1–N2 bond angle of 173.45(14)° shows that the five-coordinate copper(II) ion adopts a distorted trigonal bipyramidal configuration. In **II**, the Cu1–O1 and Cu1–N1 bonds of 1.919(3) and 1.942(3) Å are stronger than the Cu1–O2 and Cu1–N2 bonds of 2.377(3) and 2.020(3) Å. The Cu1–O3 bond length of 1.994(3) Å is longer than the Cu1–O2 bond of 1.930(4) Å in **I**. The bond lengths and angles of the O=C–C=C–N system in **II** are similar to the corresponding values of **I**. Just like **I**, the bond lengths in the O=C–C=C–N skeleton indicate electron delocalization [5–11,14]. As expected, the dihedral angle between the cyclopentadienyl rings is 1.9(4)° and this shows that they are parallel to each other. However, the small dihedral angle of 8.1(3)° between the O=C–C=C–N skeleton and the substituted cyclopentadienyl ring and the short C(10)–C(11) bond length of 1.468(6) Å suggest that the substituted cyclopentadienyl ring is to some extent engaged in the conjugation of the O=C–C=C–N skeleton.

For **II**, atom O2 in the molecule at (x, y, z) acts as a hydrogen-bond donor to the carbonyl atom O3 of an acetate in the molecule at $(1-x, 1-y, 2-z)$, thus leading to the formation of centrosymmetric dimers. These dimers, linked by an N–H···O=C hydrogen

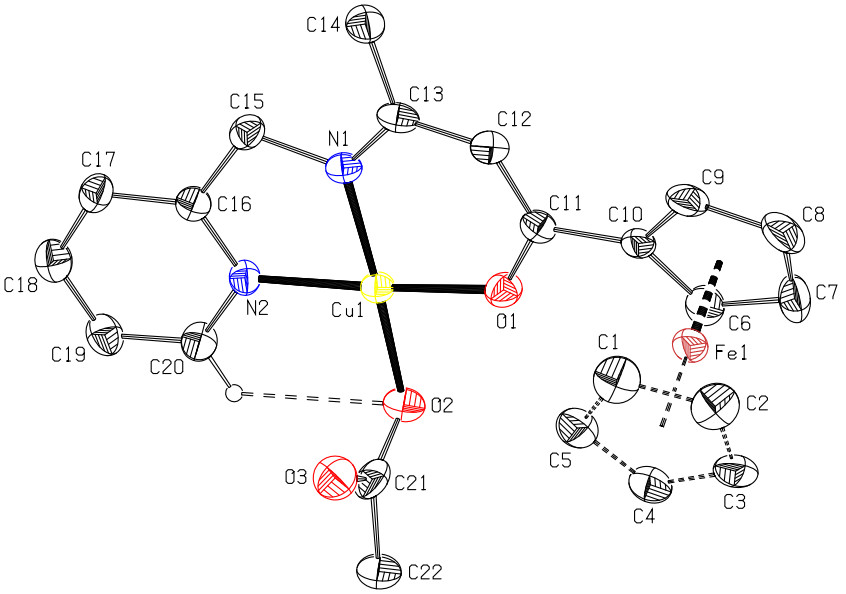

Fig. 2. ORTEP plot of **I** showing atom labelling, thermal ellipsoids are drawn as 30% probability ellipsoids.

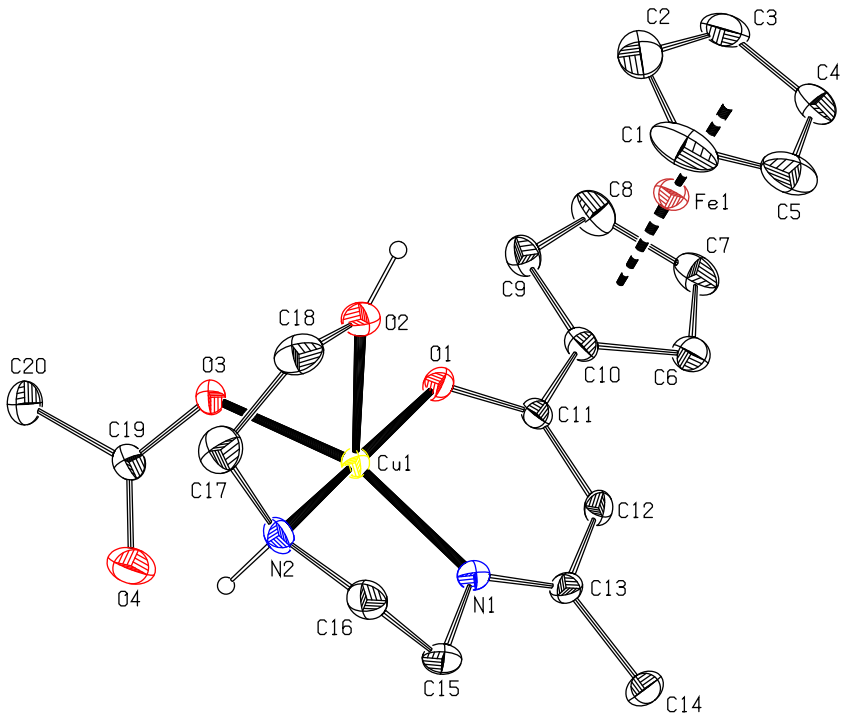

Fig. 3. ORTEP plot of **II** showing atom labelling, thermal ellipsoids are drawn as 30% probability ellipsoids.

Table 4
Selected geometric parameters (Å, °) for **II**

Cu1–O1	1.919 (3)	O4–C19	1.225 (6)
Cu1–O2	2.377 (3)	N1–C13	1.309 (5)
Cu1–O3	1.994 (3)	N1–C15	1.460 (5)
Cu1–N1	1.942 (3)	C10–C11	1.469 (6)
Cu1–N2	2.020 (3)	C11–C12	1.391 (6)
O1–C11	1.289 (5)	C12–C13	1.415 (6)
O3–C19	1.270 (5)	N2···O4	3.080 (6)
N2···O4^{i}	3.135 (6)	O2···O3^{ii}	2.683 (5)
O1–Cu1–N1	94.35 (13)	O3–Cu1–N2	93.44 (14)
O1–Cu1–O3	89.84 (12)	O1–Cu1–O2	98.33 (12)
N1–Cu1–O3	158.03 (14)	N1–Cu1–O2	110.92 (13)
O1–Cu1–N2	173.45 (14)	O3–Cu1–O2	89.71 (12)
N1–Cu1–N2	84.71 (15)	N2–Cu1–O2	76.04 (14)
N2–H2N···O4	123	N2–H2N···O4^{i}	140
O2–H2O···O3^{ii}	126		

Symmetry codes: (i) $-x, 1-y, 2-z$; (ii) $1-x, 1-y, 2-z$.

bond, viz. atom N2 in the molecule at (x, y, z) as a donor via atom H2N to atom O4 of an acetate anion at $(-x, 1-y, 2-z)$, generate an infinite double-chain in the [100] direction. In addition, an N–H···O=C intramolecular hydrogen bond is found. It is noted that a C–H···O intermolecular hydrogen bond [C21···O1 = 3.312(8) Å; C21–H21A···O1 = 172°] between CH_2Cl_2 and **II** in the same asymmetric unit is also observed.

3.3. ^1H NMR spectra

The spectrum of H**L**^{1} displays two singlets at δ 4.30 and 4.68 ppm, which are attributed to protons at the 3, 4- and 2, 5-positions of the substituted cyclopentadienyl ring. Another singlet signal at δ 4.10 ppm is assignable to the unsubstituted cyclopentadienyl ring protons. The CH_2 group exhibits one doublet at δ 4.57–4.58 ppm. The pyridyl group display two doublets at δ 5.51–5.52 and 7.26–7.28 ppm and two triplets at 7.13–7.15 and 7.61–7.64 ppm. The NH group appears at δ 11.30 ppm [5–11,14]. In addition, protons of the C(O)CH=CCH$_3$ moiety also show two singlets at δ 5.32 and 1.96 ppm, respectively. In the spectrum of H_3**L**^{2}, the methyl protons as one singlet appear at δ 2.02 ppm. Just like H**L**^{1}, the ferrocenyl group displays three singlets at δ 4.15, 4.34 and 4.71 ppm. The olefinic proton of the C(O)CHC moiety also shows a singlet at δ 5.29 ppm. Protons of the $NCH_2CH_2NCH_2CH_2O$ group appear as four triplets at δ 3.40–3.43, 2.80–2.85 (NCH_2CH_2N) and 2.90–2.92, 3.66–3.68 (NCH_2CH_2O) ppm. The secondary amine NH and OH groups exhibit two singlets at δ 1.93 and 2.01 ppm while the enamine NH group displays a signal at δ 11.10 ppm [5,7,9]. These singlets, generated from active hydrogens, disappear in the presence of D_2O.

3.4. IR spectra

In the IR spectra, complex **I** displays significant changes compared with H**L**^{1}. The band at 3086 cm^{-1} in the spectrum of H**L**^{1} due to ν(NH) does not appear in that of **I**, being indicative of deprotonated bonding of the enamine N atom. Furthermore, upon coordination, the strong bands assignable to stretching vibrations of the skeleton C=C and O=C groups, which are observed at 1539 and 1595 cm^{-1} in H**L**^{1}, respectively, are shifted to 1509 and 1601 cm^{-1} [5–10]. As usual, coordination of the enaminone O=C group leads to a red-shift of the O=C stretching vibration. Therefore, the blue-shift suggests that an acetate anion is involved in coordination. In other words, the band for the coordinated acetate anion obscures that of the coordinated O=C group of the enaminone. In fact, the IR spectrum of **I** displays only one O=C band. Although the IR spectrum does not afford unambiguous information on coordination of the pyridyl group and the acetate anion because of bands being overlapped, fortunately, the N2O bonding mode of H**L**^{1} and the monodentate bonding mode of the acetate anion are confirmed by the crystal structure of **I**, described above.

Compared with H_3**L**^{2}, the IR spectrum of complex **II** shows that a very broad band at 3334 cm^{-1} which is attributed to the ν(OH) and secondary amine ν(NH) is red-shift, suggesting that the hydroxy O and secondary amine N atoms participate in coordination. The

absence of the band at *ca.* 3098 cm^{-1}, which is due to the enaminone ν(NH), indicates that $H_3\mathbf{L}^2$ is coordinated to the copper(II) ion as the monoanionic ligand. Moreover, strong bands assignable to stretching vibrations of the skeleton C=C and O=C groups, which are observed at 1527 and 1596 cm^{-1} in $H_3\mathbf{L}^2$, are all red-shifted to 1507 and 1582 cm^{-1} in **II**, so revealing coordination of the enaminone O=C group. Although the IR spectrum does not give the clear information on coordination of the acetate anion because of bands being overlapped, fortunately, the N2O2 bonding mode of $H_3\mathbf{L}^2$ and the monodentate bonding mode of the acetate anion are confirmed by the crystal structure of **II**, described above.

3.5. UV spectra

In the UV spectra, the four compounds show three maxima at *ca.* 257.00–290.00, 340.00–354.80 and 424.20–454.20 nm which are attributed to the B-band, K-band and CT-band [5–9]. For each of complexes **I** and **II**, three absorption bands display red-shifts compared with the corresponding enaminones $H\mathbf{L}^1$ and $H_3\mathbf{L}^2$. Notably, the expected d–d absorption band of the copper(II) ion for each of **I** and **II**is not observed [5,15].

4. Conclusion

The reactions of ferrocenoylacetone with 2-(aminomethyl)pyridine and *N*-(2-hydroxyethyl)-1,2-diaminoethane afford the multidentate enaminones $H\mathbf{L}^1$ and $H_3\mathbf{L}^2$, respectively. Reactions of copper acetate with the two enaminones give the corresponding mixed-ligand complexes **I** and **II**, which are formulated as [Cu-$\mathbf{L}^1$(OAc)] and [Cu($H_2\mathbf{L}^2$)(OAc)], respectively. The structures of $H\mathbf{L}^1$, **I** and **II** have been determined by single-crystal X-ray crystallography. In complex **I**, the coordination geometry of the central metal is square planar in which the ligand acts as a monoanionic N2O donor via the carbonyl oxygen, deprotonated enamine nitrogen and pyridyl nitrogen atoms and the acetate anion is a unidentate donor. In complex **II**, the coordination geometry of the central metal is a distorted trigonal bipyramid in which the ligand is a monoanionic N2O2 donor via the carbonyl oxygen, deprotonated enamine nitrogen, secondary amine nitrogen and hydroxy oxygen atoms and the acetate anion is a monodentate donor.

Acknowledgements

The authors thank the National Nature Science Foundation of China (No. 20572091) and Nature Science Foundation of Jiangsu Province (No. 05KJB150151) for financial support of this work.

Appendix A. Supplementary data

CCDC 682991, 682992 and 682993 contain the supplementary crystallographic data for $H\mathbf{L}^1$, **I** and **II**. These data can be obtained free of charge via http://www.ccdc.cam.ac.uk/conts/retrieving.html, or from the Cambridge Crystallographic Data Centre, 12 Union Road, Cambridge CB2 1EZ, UK; fax: (+44) 1223-336-033; or e-mail: deposit@ccdc.cam.ac.uk. Supplementary data associated with this article can be found, in the online version, at doi:10.1016/j.poly.2008.04.057.

References

[1] A.A. Elassar, A.A. El-Khair, Tetrahedron 59 (2003) 8463.
[2] C. Kascheres, J. Braz. Chem. Soc. 14 (2003) 945.
[3] M. Pešková, P. Sÿimůnek, V. Bertolasi, V. Macháček, A. Lyčka, Organometallics 25 (2006) 2025.
[4] J. Kim, J.W. Hwang, Y. Kim, M.H. Lee, Y. Han, Y. Do, J. Organomet. Chem. 620 (2001) 1.
[5] Y.-C. Shi, H.-M. Yang, W.-B. Shen, C.-G. Yan, X.-Y. Hu, Polyhedron 23 (2004) 15.
[6] Y.-C. Shi, H.-M. Yang, H.-B. Song, C.-G. Yan, X.-Y. Hu, Polyhedron 23 (2004) 567.
[7] Y.-C. Shi, W.-B. Shen, H.-M. Yang, H.-B. Song, X.-Y. Hu, Polyhedron 23 (2003) 749.
[8] Y.-C. Shi, H.-M. Yang, H.-B. Song, Y.-H. Liu, Polyhedron 23 (2004) 1541.
[9] Y.-C. Shi, C.-X. Sui, H.-B. Song, P.-M. Jian, J. Coord. Chem. 58 (2005) 363.
[10] Y.-C. Shi, Acta Crystallogr., Sect. E 61 (2005) m873.
[11] Y.-C. Shi, S.-H. Zhang, H.-J. Cheng, W.-P. Sun, Acta Crystallogr., Sect. C 62 (2006) m407.
[12] G.M. Sheldrick, SHELXS97 and SHELXL97, University of Göttingen, Germany, 1997.
[13] A.L. Spek, J. Appl. Crystallogr. 36 (2003) 7.
[14] P. Gilli, V. Bertolasi, V. Ferretti, G. Gilli, J. Am. Chem. Soc. 122 (2000) 10405.
[15] H. Oshio, T. Kikuchi, T. Ito, Inorg. Chem. 35 (1996) 4938.
[16] H. Oshio, K. Toriumi, Y. Maeda, Y. Takashima, Inorg. Chem. 30 (1991) 4252.

neither soluble nor volatile, which limits their application as precursors. We were interested to develop soluble as well as volatile Cu/Zn metallo-organic SSPs for the preparation of nanostructured Cu/ZnO catalyst systems and other technological applications in powder or even thin film form.

Herein we report the synthesis and structure of a heterobimetallic precursor of copper and zinc, which is a potential SSP for the deposition of Cu–ZnO thin films.

2. Experimental

All manipulations were carried out under an atmosphere of dry argon using schlenk and glovebox techniques. Solvents were rigorously dried on sodium benzophenoate. 1,3-Bis(dimethylamino)-2-propanol (bdmapH) was purchased from Aldrich and used without further purification, while $[Cu(OCH_3)Cl]_4$ was prepared by literature procedure [24]. All other reagents were also purchased from Aldrich.

Elemental analysis was performed by the University of Manchester micro-analytical laboratory. Melting point was determined in a capillary tube using an electrothermal melting point apparatus, model MP.D Mitamura Riken Kogyo (Japan) and was uncorrected. FT-IR spectrum was recorded on a specie single reflectance ATR instrument (4000–400 cm^{-1}, resolution 4 cm^{-1}). TGA measurements were carried out by using a Seiko SSC/S200 thermal analyzer at a heating rate of 10 °C/min under N_2 flow. Mass spectrum was recorded on a Kratos concept IS instrument. PXRD studies were carried out by means of a Bruker AXS D8 diffractometer using monochromatic Cu Kα radiation. The morphology of films was determined by a FEG-SEM Philips XL30. Samples were carbon coated before observation and EDAX-DX_4 was used to calculate the composition (metallic ratio) of films. The thickness of films was measured with a Dektak 8 Stylus profilometer. The voltage–current characteristics of thin films were measured with Jandel Voltmeter, Model RM3, by the four-probe method.

2.1. Synthesis of $[Zn_2(OAc)_6(\mu\text{-}O)_2Cu_4(bdmap)_2Cl_2]$ (**1**)

0.32 g (2.2 mmol) of 1,3-bis(dimethylamino)-2-propanol (bdmapH) was added to a suspension of 0.50 g (4.4 mmol) $[Cu(OCH_3)Cl]_4$ and 0.72 g (3.3 mmol) $Zn(OAc)_2 \cdot 2H_2O$ in 25 ml toluene at room temperature. Reaction mixture was stirred for 3 h and filtered through cannula to remove the insoluble by-products. The blue solution was vacuum evaporated to dryness and the solid was redissolved in dichloromethane to recrystallize. Blue cubic crystals suitable for single crystal analysis were obtained. Yield 70%, m.p. 175 °C. *Anal.* Calc. for $C_{26}H_{46}Cl_2Cu_4N_4O_{16}Zn_2$: C, 27.72; H, 4.12; N, 4.97. Found: C, 27.14; H, 3.96; N, 4.53%. FT-IR (KBr, cm^{-1}): 2982w, 2927m, 2841w, 1612vs, 1442s, 1335m, 1204w, 1098m, 1021m, 993m, 890m, 860w, 826w, 672m, 663m, 616w, 534m, 507m, 456w. MALDI-MS (positive mode): *m*/*z* calc. (found) 896.5 (896) $[M-Cu_2Cl_2(O)_2]^+$, 783 $[M-Cu_2Cl_2(bdmap)]^+$, 719.7 (721) $[M-Cu_3Cl_2(bdmap)]^+$, 522.1 (523) $[M-Cu_4Cl_2(bdmap)(OAc)_2(O)]^+$, 479 (478) $[M-Cu_4Cl_2(bdmap)(OAc)_3]^+$, 388 (389) $[M-Cu_4Cl_2(bdmap)(OAc)_4(O)_2]^+$, 333.8 (333) $[M-Cu_4Cl_2(bdmap)_2(OAc)_3]^+$, 305 $[Zn(OAc)(bdmap)Cl]^+$, 285.6 (285) $[Zn(OAc)(bdmap)(O)]^+$. TGA: 160–189 °C (7.41 wt% loss), 189–226 °C (11.11 wt% loss), 226–340 °C (residue 37.2%).

2.2. X-ray crystallography

Single crystal X-ray data were collected on a Bruker Smart Apex CCD diffractometer using Mo radiation. Crystallographic and structure refinement data for complex (**1**): Empirical formula; $C_{26}H_{46}Cl_2Cu_4N_4O_{16}Zn_2$, F.wt. 1126.47, Temp. = 100(2) K, λ = 0.71073 Å, monoclinic, space group $P2(1)/n$, a = 12.076(2), b = 10.1958(18), c = 17.624(3) Å, α = 90°, β = 99.997(3)°, γ = 90°, V = 2137.1(6) $Å^3$, Z = 2, ρ_{calc} = 1.751 mg m^{-3}, μ = 3.250 mm^{-1}, 14468 reflections collected, 4369 unique (R_{int} = 0.1093), Refinement was by full-matrix least-squares on F^2; goodness-of-fit on F^2 was 1.021. Final R indices where $I > 2\sigma(I)$ are R_1 = 0.0611 and wR_2 = 0.1370. The R indices with all data are R_1 = 0.1114 and wR_2 = 0.1561. The largest difference peak and hole are 1.264 and 0.595 e $Å^{-3}$, respectively.

2.3. Deposition of thin films

Thin film deposition was performed via aerosol assisted chemical vapour deposition (AACVD) by dissolving 0.1 g of precursor in 13 ml THF + 2 ml dichloromethane in a two neck round bottomed flask. On one side, the flask was connected via tubing to a quartz reactor loaded with 2.5 × 1 cm glass substrates inside a carbolite tube furnace and a flow of argon gas was regulated using a platon flow gauge on the other. The flask was set in an ultrasonic humidifier equipped with a piezoelectric transducer, that generated droplets of the precursor solution, which were then transferred by the carrier gas into reactor chamber. Glass substrates were washed in concentrated nitric acid, subsequently washed with deionized water several times, and then oven dried. Deposition was done at four different temperatures i.e., 250, 325, 400 and 475 °C at a constant nitrogen flow rate of 130 ml/min on glass substrates for 2.5 h.

3. Results and discussion

3.1. Synthesis and characterization

Heterometallic hexanuclear complex (**1**), was prepared by mixing stoichiometric amounts of $Zn(OAc)_2 \cdot 2H_2O$, $[Cu(OCH_3)Cl]_4$ and 1,3-bis(dimethylamino)-2-propanol (bdmapH) in toluene for three hours as shown in chemical Eq. (1). The complex is readily soluble in common organic solvents such as toluene, dichloromethane and alcohols and is stable in air under normal conditions.

$$4[Cu(OCH_3)Cl]_4 + 3Zn(OAc)_2 \cdot 2H_2O + 2bdmapH \xrightarrow{Toluene} Zn_2(OAc)_6(\mu\text{-}O)_2Cu_4(bdmap)_2Cl_2 + ZnCl_2 + 4CH_3OH + 4H_2O \quad (1)$$

The composition of the complex (**1**) was ascertained by CHN analysis. IR absorption frequency of carboxylate appear at 1612 cm^{-1} for $\nu_{as}(CO_2)$ and 1442 cm^{-1} for $\nu_s(CO_2)$. The difference $\Delta = \nu_{as}(CO_2) - \nu_s(CO_2)$ suggests a dominant chelating or chelating-bridging behaviour for the acetate ligands [25,26].

MALDI mass spectrum of complex (**1**) did not show the molecular ion peak while molecular ion fragments of different *m*/*z* ratios indicating the formation of complex were found. The largest fragment was of *m*/*z* (896) $[M-Cu_2Cl_2(O)_2]^+$ and the base peak at *m*/*z* (783) corresponding to $[M-Cu_2Cl_2(bdmap)]^+$ were present.

3.2. Structural analysis

Selected interatomic distances and angles for (**1**) are listed in Table 2. The molecule of (**1**) (Fig. 1) possesses an inversion center and two asymmetric units, each having two copper and one zinc atoms, connected by μ_2-oxygen of bdmap and bridging acetate ligands. In this heterohexanuclear complex, six metal atoms are linked by four μ_2-acetate, two μ_3-acetate, two μ_3-O and two μ_2-bdmap groups in a cyclic fashion whereas the remaining two chloride atoms behave as termini without any contribution in connecting the metals. Considering only copper atoms, a twelve membered ring comprised of four copper atoms, two CO_2 units

Table 1
Deposition conditions and analysis of copper–zinc oxide composite films from (**1**)

Deposition temperature (°C)	Crystallite size (μm)	EDAX composition Cu/Zn (at%)	Film thickness (μm)	Resistivity (Ω cm)
250	0.2–0.5		0.49	
325	0.3–0.8	1:1.1	1.62	
400	0.4–0.8	1:1.2	4.59	2×10^{-5}
475	0.4–0.9		4.31	1.6×10^{-5}

Table 2
Selected bond distances (Å) and angles (°) for complex (**1**)

Bond distances (Å)			
Cu(1)–N(1)	2.044(4)	Cu(2)–O(1)	1.923(3)
Cu(1)–O(1)	1.933(3)	Cu(2)–O(2)	1.955(3)
Cu(1)–O(6)	2.421(3)	Cu(2)–O(5)	2.563(3)
Cu(1)–O(8)	1.946(3)	Zn(1)–Cl(1)	2.2536(13)
Cu(1)–O(5)	2.725(3)	Zn(1)–O(7)	1.933(3)
Cu(1)–O(3)	1.930(3)	Zn(1)–O(4)	1.961(3)
Cu(2)–N(2)	2.015(4)	Zn(1)–O(8)	2.039(2)
Cu(2)–Cl(1)	3.090(15)		
Bond angles (°)			
O(1)–Cu(1)–N(1)	84.01(14)	O(5)–Cu(2)–N(2)	106.93(12)
O(8)–Cu(1)–N(1)	176.03(13)	O(1)–Cu(2)–O(2)	175.07(12)
O(1)–Cu(1)–O(6)	94.94(12)	O(1)–Cu(2)–N(2)	84.88(14)
O(8)–Cu(1)–O(6)	88.32(11)	O(2)–Cu(2)–N(2)	90.56(14)
N(1)–Cu(1)–O(6)	92.77(14)	O(7)–Zn(1)–O(4)	112.73(13)
O(3)#–Cu(1)–O(1)	173.51(13)	O(7)–Zn(1)–O(8)	113.40(12)
O(5)–Cu(1)–O(6)	162.63(10)	O(4)–Zn(1)–O(8)	104.89(12)
O(5)–Cu(1)–N(1)	104.50(13)	O(7)–Zn(1)–Cl(1)	113.23(10)
O(5)–Cu(1)–O(8)	74.62(9)	O(4)–Zn(1)–Cl(1)	111.31(11)
O(5)–Cu(2)–O(8)	78.55(10)	O(8)–Zn(1)–Cl(1)	100.35(8)

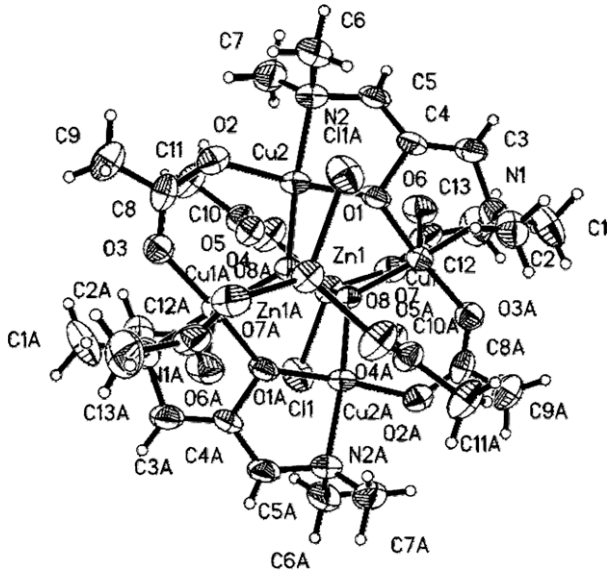

Fig. 1. ORTEP drawing showing the molecular structure of complex (**1**).

and two oxygen atoms is formed which is almost planar. The four copper atoms represent an approximate rectangular arrangement, Cu(1)–Cu(2) = 3.622 Å, Cu(2)–Cu(1)A = 3.282 Å, Cu(1)A–Cu(2)A = 3.622 Å, Cu(2)ACu(1) = 3.282 Å. Such type of arrangement and similar bonding pattern has been observed in the literature [27]. The bdmap ligand acts as a tridentate group and bridges two copper atoms through oxygen and two nitrogen atoms. The acetate ligands are bridging either two metals [Cu(1), Cu(2); Cu(1), Zn(1)] or three metal atoms, connecting Cu(1), Cu(2) of one asymmetric unit with Zn(1) of the other (Fig. 1).

The core unit of complex (1) (Fig. 2) indicates that the asymmetric unit consisting of three metal atoms, has three different geometric environments, with Cu(1) octahedral, Cu(2) square pyramidal and Zn(1) tetrahedral coordination spheres (Fig. 3). In each asymmetric unit, a triply bridged oxygen atom links three metal centers [Cu(1), Cu(2) and Zn(1)], in addition to two acetate ligands bridging two metal atoms [acetate group with C(8) bridges Cu(1), Cu(2), while that of C(12) links Cu(1), Zn(1)]. Oxygen atom O(5) of one acetate group [based on C(10)] again bridges Cu(1) and Cu(2).

The environment of the Cu(1) atom is tetragonally elongated octahedral with the ligation set CuO_5N, comprised of oxygen atoms [O(3), O(6)] of two doubly bridged acetate groups, a bridging oxygen [O(5)] of one triply bridged acetate ligand [based on C(10)], a triply bridged oxygen [O(8)], an oxygen [O(1)] and nitrogen atom [N(1)] of a chelating-bridging bdmap group. The Cu–O/N bond lengths in the basal planes range from 1.930(3) to 2.044(4) Å {normal values}, while the weaker apical bonds to oxygen atoms of acetate groups are 2.420(3) and 2.725(3) Å. The distorsion is further evident from the deviation of the O(5)–Cu(1)–O(6) angle (162.62°) from 180°, while the O(5)–Cu(1)–O(8) (74.62°) and O(5)–Cu(1)–N(1) (104.47°) angles from 90°. Distortion in octahedral geometry around $Cu^{II}(1)$, expected from the Jahn-Teller theorem [28], is due to the unequally occupied e_g (d_{z^2} and $d_{x^2-y^2}$) orbitals, the two axial acetate ligands based on O(5) and O(6) are repelled more strongly than the other four coordinating ligands. The overall geometry around Cu(2) is a square pyramidal, with a CuO_4N core, generated by a chelating-bridging bdmap ligand [O(1), N(2)], [the oxygen of which connects Cu(2) of one asymmetric unit to Cu(1) of the other], an oxygen atom of bridged acetate [O(2)], a triply bridged oxygen atom [O(8)], [connecting Cu(2) with Cu(1) and Zn(1)], and an oxygen atom of triply bridged acetate group [O(5)], [which links Cu(2) with Cu(1)]. Slight distortion in square pyramidal geometry is due to the doubly bridged oxygen [O(9)], being displaced towards O(8) and away from N(2), resulting in an O(5)–Cu(2)–N(2) angle being enlarged from the ideal 90 to 106.93° and O(5)–Cu(2)–O(8) being reduced to 78.54°. Again also the copper–oxygen bond distance of Cu(2) to apical oxygen atom [O(5)] is greater (2.563 Å) than the other Cu–O bond lengths, which are compatible to the sum of the ionic radii, 1.92 Å. Considering the chloride ion at 3.090(15) Å, the coordination environment of Cu(2)

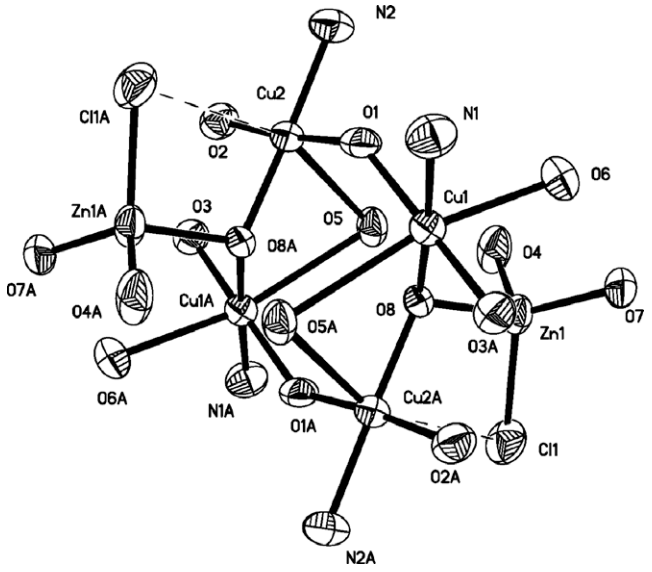

Fig. 2. The core unit of complex (**1**). Dashed lines show weak interactions. All carbon and hydrogen atoms are omitted for clarity (symmetry transformations used to generate equivalent atoms $-x+2$, $-y+2$, $-z+2$).

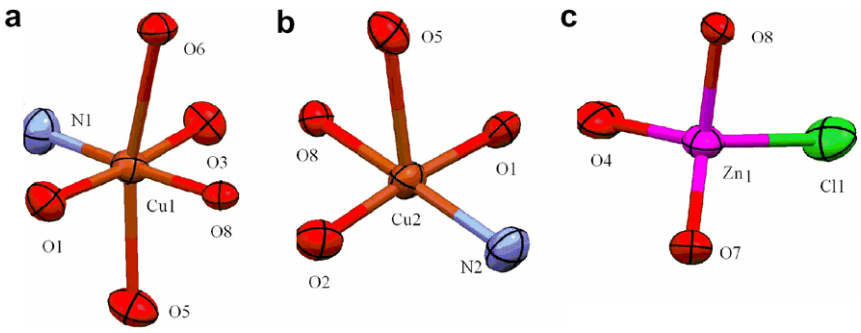

Fig. 3. Geometric spheres of (**1**), (a) distorted octahedral Cu(1), (b) square pyramidal Cu(2) and (c) tetrahedral Zn(1).

can also be described as tetragonally elongated octahedral with Cu–O/N bond distances in the basal plane ranging from 1.923(3) to 2.015(4) Å and weak apical bonds to oxygen and chloride atoms of 2.563(3) and 3.090(15) Å (Table 2). Zn(1) has a coordination number of four having a coordination environment almost tetrahedral, with ZnO_3Cl set of ligating atoms, composed of an oxygen of bridged acetate group [O(7)], an oxygen of triply bridged acetate ligand [O(4)], [that links Zn(1) with Cu(1) and Cu(2) of two asymmetric units], the μ_3-oxygen atom [O(8)], [which bridges three metal centers of asymmetric units] and a terminal chloride atom. The Zn–O bond distances around Zn(1), which range from 1.933(3) to 2.039(2) Å are in good agreement with the literature [29].

3.3. Thermal decomposition studies and characterization of thin films

TGA traces of complex (**1**) (Fig. 4) shows three step weight loss beginning at 160 °C and completed at 340 °C, leaving a residue of 37.2% of the initial weight, which is close to the expected composition of $Cu_4Zn_2O_2$ (37.01%). The residual mass also indicates the removal of most of the carboneous matter from the organic groups, leaving negligibly small carbon impurity in the composite and the complex (**1**) decomposes according to Eq. (2).

$$Zn_2(OAc)_6(\mu\text{-}O)_2Cu_4(bdmap)_2Cl_2 \xrightarrow{AACVD} 4Cu + 2ZnO + Volatiles \quad (2)$$

Deposition of the films was studied at four different temperatures i.e., 250, 325, 400 and 475 °C. The films deposited at 250 °C were amorphous, brown in colour with poor film coverage and adhesion to the substrate. The films deposited at 325 and 400 °C were crystalline, dark in colour and reflecting in nature. Diffractogram of the films (Fig. 5) obtained at 400 °C shows formation of cubic Cu and hexagonal ZnO phases which match very well with the JCPDS standard data 01-085-1326 and 01-079-0207, respectively. The PXRD of the films deposited at 475 °C (Fig. 6) shows high degree of crystallinity and appearance of new phase of Cu_2O at 2θ values of 42.4° and 61.4°.

Scanning electron microscopic images (Fig. 7) show that film deposition experiments performed at different temperatures result in different surface morphologies. In all the four cases, the particles are homogenously dispersed with well defined grain boundaries, especially at temperatures 325 and 400 °C. The image of films deposited at 250 °C shows less compact morphology having rela-

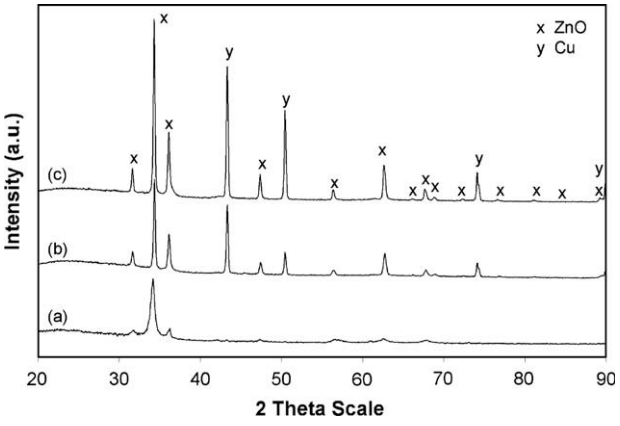

Fig. 5. Powder X-ray diffractograms of Cu–ZnO films obtained from precursor (**1**) at (a) 250 °C, (b) 325 °C and (c) 400 °C.

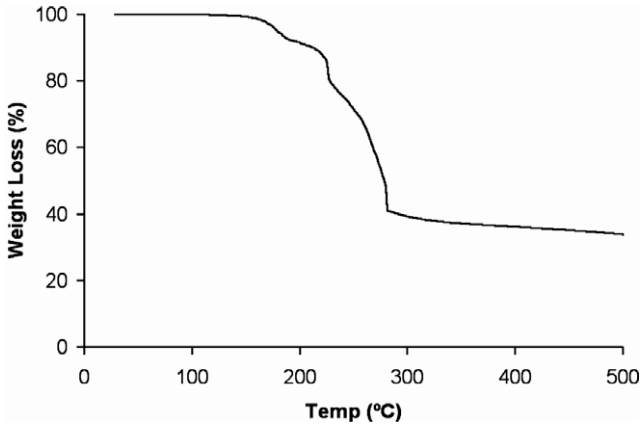

Fig. 4. Thermogram of the complex (**1**), showing loss in weight with rise in temperature.

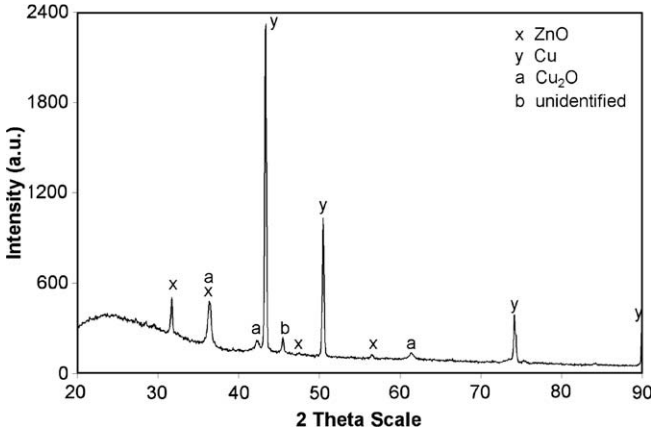

Fig. 6. Powder X-ray diffractograms of the films obtained from precursor (**1**) at 475 °C.

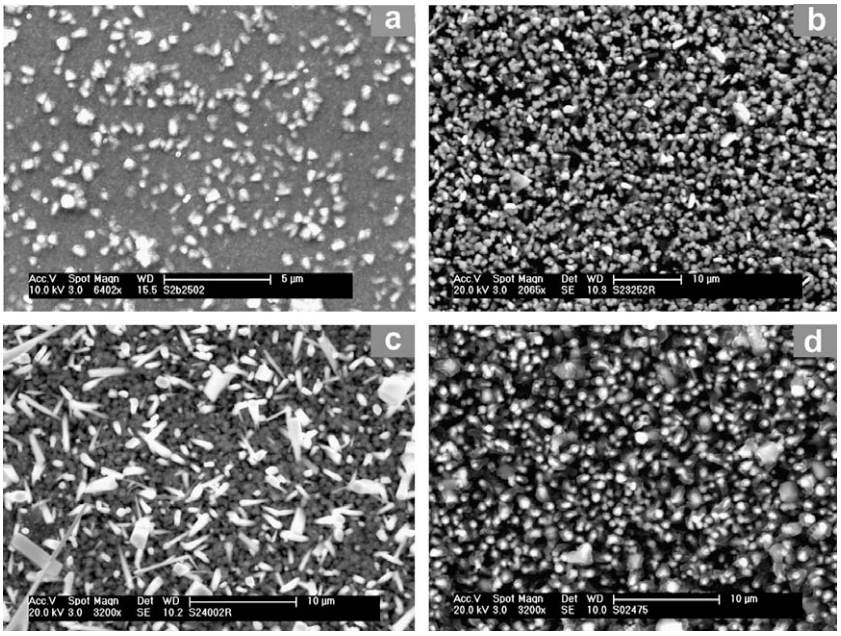

Fig. 7. SEM micrographs of films deposited from precursor (**1**) at (a) 250 °C, (b) 325 °C, (c) 400 °C and (d) 475 °C.

tively small individual rectangular crystallites ranging from 0.2 to 0.5 μm, while relatively large individual oval shaped grains, 0.4 to 0.9 μm, were obtained from the films deposited at 475 °C. At 325 and 400 °C, spherical with elongated strands like grains were obtained indicating dependence of grain shape and size on deposition temperature. The energy dispersive X-ray analysis (EDAX) was performed for the metallic Cu/Zn ratio in films deposited at 325 and 400 °C. The analysis indicates that the ratio of Cu/Zn is 1:1.1 and 1:1.2 for the films deposited at 325 and 400 °C, respectively. The deviation of Cu/Zn ratio from 2:1 indicates evaporation of copper with the rise in temperature from the surface of the film under CVD conditions [30].

The variation of the Cu–ZnO film's thickness as a function of deposition temperature is shown in Fig. 8. At 250 °C, the thickness of the film is monitored by surface decomposition reaction of the precursors. In the intermediate region i.e., 325–400 °C, the film growth rate is diffusion or mass transport limited, where all the reactants that reach the substrate essentially decompose. Finally, above 420 °C, the film thickness decreases with rise in temperature because of an increased desorption rate of the film components in addition to depletion of reactants by the reaction at the reactor walls. This observation is supported by EDAX analysis as stated earlier. The *V–I* curve (Fig. 9) is linear, indicating ohmic conduction.

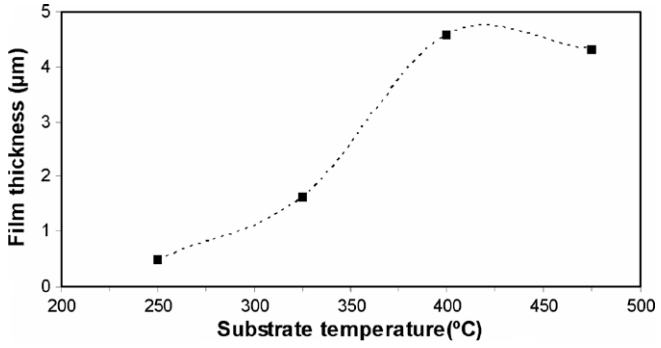

Fig. 8. Variation of Cu–ZnO thin film thickness as a function of substrate temperature with a dynamic nitrogen flow rate of 130 ml/min.

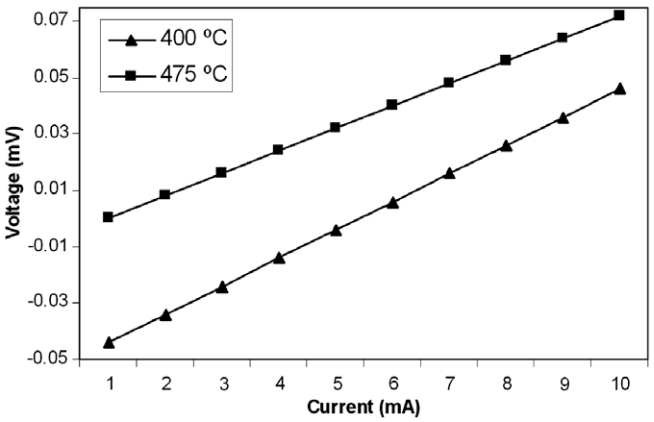

Fig. 9. *V–I* curves of Cu–ZnO films deposited at 400 and 475 °C.

The resistances determined from the slope of the curve are 10×10^{-3} and 8×10^{-3} Ω for the films deposited at 400 and 475 °C, respectively. The resistivity of the films at 400 and 475 °C were found to be 2×10^{-5} Ω cm and 1.6×10^{-5} Ω cm, respectively, using $\rho = 4.532(V/I) \times d$, where ρ is the resistivity in Ω cm, 4.532 is the instrument constant, V/I is the slope of curve in Ω and d is the film's thickness (Table 1), showing conducting nature of the films.

4. Conclusion

Heterobimetallic precursor $[Zn_2(OAc)_6(\mu\text{-}O)_2Cu_4(bdmap)_2Cl_2]$ (**1**) was prepared following a simple method by the reaction of $Cu(OCH_3)Cl$, $Zn(OAc)_2 \cdot 2H_2O$ and bdmapH in toluene at room temperature. Spectroscopic and single crystal X-ray analysis confirmed the identity of complex (**1**). The complex is stable for periods of several months at room temperature and is soluble in most organic solvents, which made it potentially useful precursor for the deposition of copper–zinc oxide thin films. The films deposited from (**1**) were characterized by PXRD, SEM, EDAX and thickness measurements. It was found that the morphology and the thickness of the films including the shape and size of the crystallites changed

with the change in the deposition temperature. The *V–I* measurements indicate that films are ohmic conductors.

Acknowledgements

M.S. and M.M. would like to thank "Higher Education Commission of Pakistan for financial support through the "Indigenous 5000 Ph.D Scholarship Scheme".

Appendix A. Supplementary data

CCDC 664476 contains the supplementary crystallographic data for **1**. These data can be obtained free of charge via http://www.ccdc.cam.ac.uk/conts/retrieving.html, or from the Cambridge Crystallographic Data Centre, 12 Union Road, Cambridge CB2 1EZ, UK; fax: (+44) 1223-336-033; or e-mail: deposit@ccdc.cam.ac.uk. Supplementary data associated with this article can be found, in the online version, at doi:10.1016/j.poly.2008.07.018.

References

[1] M.D. Ward, Chem. Soc. Rev. 24 (1995) 121.
[2] (a) O. Kahn, Molecular Magnetism, VCH, New York, 1993;
(b) O. Kahn, Adv. Inorg. Chem. 43 (1995) 179;
(c) D. Gatteschi, Adv. Mater. 6 (1994) 635.
[3] L.G. Hubert-Pfalzgraf, Polyhedron 13 (1994) 1181.
[4] M. Veith, S. Mathur, C. Mathur, Polyhedron 17 (1998) 1005.
[5] K.G. Caulton, L.G. Hubert-Pfalzgraf, Chem. Rev. 90 (1990) 3.
[6] (a) W.A. Herrmann, N.W. Huber, O. Runte, Angew. Chem. 107 (1995) 2371;
(b) W.A. Herrmann, N.W. Huber, O. Runte, Angew. Chem., Int. Ed. Engl. 34 (1995) 2187.
[7] M. Veith, Chem. Rev. 90 (1990) 3.
[8] C.D. Chandler, C. Roger, M.J. Hampden-Smith, Chem. Rev. 93 (1993) 1205.
[9] R. Amigo, J. Asenjo, E. Krotenko, F. Torres, J. Tejada, Chem. Mater. 12 (2000) 573.
[10] J.A. Rodriguez, J.C. Hanson, S. Chaturvedi, A. Maiti, J.L. Brito, J. Chem. Phys. 112 (2000) 935.
[11] D. Heinz, W.F. Hoelderich, S. Krill, W. Boeck, K. Huthmacher, J. Catal. 192 (2000) 1.
[12] (a) D. Kiessling, G. Went, K. Hagenau, R. Schoellner, Appl. Catal. 71 (1991) 69–78;
(b) H. Watanabe, Y. Koyasu, Appl. Catal. A 194 (2000) 479.
[13] S. Angelov, D. Mehandjiev, B. Piperov, V. Zarkov, A. Terlecki-Baricevic, D. Jovanovic, Z. Jovanovic, Appl. Catal. 16 (1985) 431.
[14] (a) K. Fujimoto, T. Oba, Appl. Catal. 13 (1985) 289;
(b) X. Xiaoding, E.B.M. Doesburg, J.J.F. Sholten, Catal. Today 2 (1987) 125;
(c) J.E. Baker, R. Burch, S.E. Golunski, Appl. Catal. 53 (1989) 279. and references therein.
[15] A. Sugier, E. Freund, US Patent 4122110, 1978.
[16] G. Fornasari, S. Gusi, F. Trifir, A. Vaccari, Ind. Eng. Chem. Res. 26 (1987) 1500. and references therein.
[17] W. Kaim, B. Schwederski, Bioinorganic Chemistry: Inorganic Elements in the Chemistry of Life, Wiley, Chichester, 1995.
[18] M. Hamid, A.A. Tahir, M. Mazhar, M. Zeller, A.D. Hunter, Inorg. Chem. 46 (2007) 4120.
[19] M. Veith, S. Faber, R. Hempelmann, S. Janssen, J. Prewo, H. Eckerlebe, J. Mater. Sci. 31 (1996) 2009.
[20] R. Becker, J. WeiB, M. Winter, K. Merz, R.A. Fischer, J. Organomet. Chem. 630 (2001) 253. and references therein.
[21] A. Cybulski, Catal. Rev. Sci. Eng. 36 (1994) 557.
[22] M.S. Spencer, Catal. Lett. 66 (2000) 255.
[23] T. Fujitani, J. Nakamura, Appl. Catal. A. Gen. 191 (2000) 111.
[24] M. Hamid, A.A. Tahir, M. Mazhar, M. Zeller, A.D. Hunter, Inorg. Chem. 45 (2006) 10457.
[25] G.B. Deacon, R.J. Phillips, Coord. Chem. Rev. 33 (1980) 227.
[26] B.H. Ye, X.Y. Li, I.D. Williams, X.M. Chen, Inorg. Chem. 41 (2002) 6426.
[27] S. Wang, S.J. Trepanier, J.C. Zheng, M.J. Wagner, Inorg. Chem. 31 (1992) 2118.
[28] J.D. Lee, Concise Inorganic Chemistry, 5th ed., Chapman Hall, London, 1996. 216.
[29] M. Hamid, A.A. Tahir, M. Mazhar, F. Ahmad, K.C. Molloy, G. Kociok-Kohn, Inorg. Chim. Acta 361 (2008) 188.
[30] Y. Hu, M. Afzaal, M.A. Malik, P. O' Brien, J. Cryst. Growth 297 (2006) 61.

but also for alkali-metal ions. These "ligand complexes" may act as a host molecule and include a guest metal ion by coordinating through cis-oxygen atoms such that new bi- or trinuclear metal complexes are produced [10]. Hence this adduct formation method may also be considered as host–guest chemistry. On this basis, Lindoy and Truter reported the X-ray structures of the sodium perchlorate adducts of [Ni(acacen)] [11] and [Cu(salen)] [12] [acacen = *N*,*N*′-ethylenebis(acetylacetoneiminate) and salen = *N*,*N*′-ethylenebis(salicylideneiminate)]. The structures of some other adducts of copper(II) chelates with alkali-metal salts have been reported since then [12–15]. From these results, it is observed that the structure of one sodium adduct of Cu-acacen [14], one potassium adduct each of Cu-acacen [14] and Cu-acactn [13] (acactn = *N*,*N*′-propylenebis(acetylacetoneiminate) are known with the acetylacetone derived Schiff bases. Interestingly, variable temperature magnetic properties of any such simple adducts have not been studied yet although it is well known that magnetic exchange between the paramagnetic centers can be mediated through the alkali-metal or other diamagnetic metal ions [16–20].

In this circumstances, we have systematically explored the formation of the 1:2 adduct of sodium perchlorate and square planar [CuL] complexes, where L stands for tetradentate di-Schiff-base ligands containing an acetylacetone moiety and one of the following diamines: 1,2-diaminoethane, 1,2-diaminopropane and 1,3-diaminopropane (Scheme 1). This effort has resulted in the formation of three new trinuclear Cu(II)–Na(I)–Cu(II) complexes, which have been characterized by X-ray single crystal structure analyses. The temperature-dependent magnetic properties of the complexes have been investigated.

2. Experimental

The diamines (1,2-diaminoethane, 1,2-diaminopropane and 1,3-diaminopropane) and triethylamine were dried over potassium hydroxide and distilled prior to use. Pentane-2,4-dione was dried over anhydrous sodium sulfate and distilled; the fraction boiling at 138–139 °C was collected. All the other chemicals were of reagent grade and used without further purification.

2.1. Preparation of the ligands H_2L^1, H_2L^2 and H_2L^3

The three di-Schiff-base ligands, H_2L^1, H_2L^2 and H_2L^3 were prepared by standard methods. Briefly, 10 mmol of pentane-2,4-dione (1.10 cm^3) were mixed with 5 mmol of the required amine [1,2-diaminoethane (0.31 cm^3), 1,2-diaminopropane (0.38 cm^3) and 1,3-diaminopropane (0.38 cm^3), respectively] in methanol (10 cm^3). The resulting solutions were refluxed for ca. 2 h, and allowed to cool. The Schiff-base ligands were not isolated and the yellow colored methanolic solutions were used directly for complex formation.

2.2. Synthesis of $[Cu(L^1)] \cdot H_2O$ (**A**), $[Cu(L^2)] \cdot H_2O$ (**B**) and $[CuL^3] \cdot H_2O$ (**C**)

A solution of $Cu(ClO_4)_2 \cdot 6H_2O$ (1.85 g, 5 mmol) in methanol (10 cm^3) was added to a solution of H_2L^1 (5 mmol), H_2L^2 (5 mmol) or H_2L^3 (5 mmol), separately, in methanol (10 cm^3) with constant stirring. Triethylamine (1.40 cm^3, 10 mmol) in methanol (5 cm^3) was added drop wise to each of these solutions with constant stir-

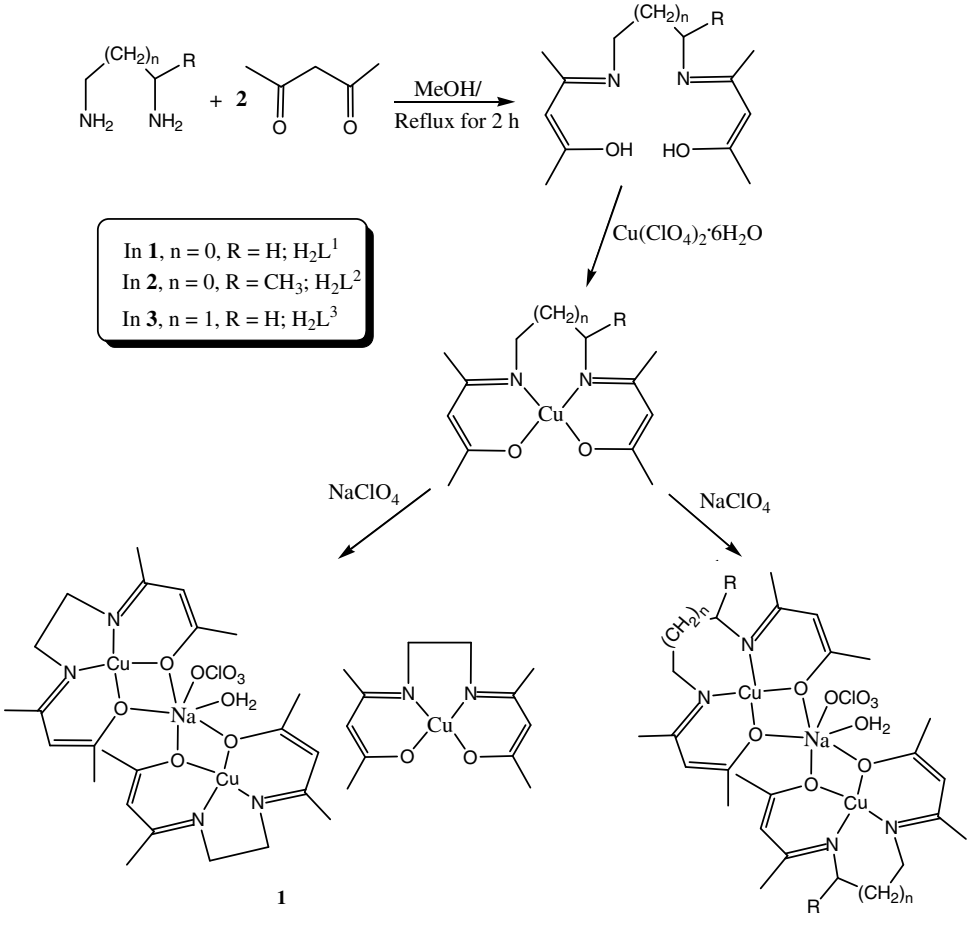

Scheme 1.

ring. The mixture was stirred for 1 h at room temperature and then filtered. The filtrate was left to stand overnight in air, when purple crystalline compound of **A** and **B** and green compound of **C** appeared at the bottom of the vessel on slow evaporation of the solvent.

Complex **A**: (yield: 1.06 g; 70%). *Anal.* Calc. for $C_{12}H_{20}CuN_2O_3$ (303.84) C, 47.33; H, 6.63; N, 9.22. Found: C, 47.32; H, 6.77; N, 9.19%. λ_{max}/nm (ε_{max}/dm^3 mol^{-1} cm^{-1}) (methanol), 540 (420); IR: ν(O–H), 3474 cm^{-1}, ν(C=N), 1593 cm^{-1}.

Complex **B**: (yield: 1.20 g; 75%). *Anal.* Calc. for $C_{13}H_{24}CuN_2O_3$ (319.89) C, 48.81; H, 7.56; N, 8.76. Found: C, 48.52; H, 7.87; N, 8.62%. λ_{max}/nm (ε_{max}/dm^3 mol^{-1} cm^{-1}) (methanol), 541 (405); IR: ν(O–H), 3470 cm^{-1}, ν(C=N), 1598 cm^{-1}.

Complex **C**: (yield: 1.04 g; 65%). *Anal.* Calc. for. $C_{13}H_{24}CuN_2O_3$ (319.89) C, 48.81; H, 7.56; N, 8.76. Found: C, 48.52; H, 7.87; N, 8.62%. λ_{max}/nm (ε_{max}/dm^3 mol^{-1} cm^{-1}) (methanol), 540 (298); IR: ν(O–H), 3485 cm^{-1}, ν(C=N), 1603 cm^{-1}.

2.3. Synthesis of $[(CuL^1)_2Na(ClO_4)(H_2O)]$ $[CuL^1]$ (**1**), $[(CuL^2)_2Na(ClO_4)(H_2O)]$ (**2**) and $[(CuL^3)_2Na(ClO_4)(H_2O)]$ (**3**)

To methanolic solutions (10 cm^3) of **A** (5 mmol, 1.43 g), **B** (5 mmol, 1.49 g) or **C** (5 mmol, 1.49 g), solution of $NaClO_4$ (2.5 mmol, 0.305 g) in methanol (10 cm^3) was added with constant stirring. The resultant purple solutions of **A** and **B** and dark green solution of **C**, on keeping overnight at room temperature yielded purple (both for **1** and **2**) and green (**3**) single crystals suitable for X-ray analysis.

Complex **1**: (yield: 1.24 g; 75%). *Anal.* Calc. for $C_{36}H_{56}ClCu_3N_6NaO_{11}$ (997.93) C, 43.33; H, 5.66; N, 8.42. Found: C, 43.12; H, 5.87; N, 8.19%. λ_{max}/nm (ε_{max}/dm^3 mol^{-1} cm^{-1}) (methanol), 541 (447); IR: ν(O–H), 3427 cm^{-1}, ν(C=N), 1598 cm^{-1}, $\nu(ClO_4^-)$, 1091 cm^{-1}.

Complex **2**: (yield: 1.29 g; 70%). *Anal.* Calc. for $C_{26}H_{44}ClCu_2N_4NaO_9$ (742.18) C, 42.08; H, 5.98; N, 7.55. Found: C, 42.12; H, 5.87; N, 7.32%. λ_{max}/nm (ε_{max}/dm^3 mol^{-1} cm^{-1}) (methanol), 540 (570); IR: ν(O–H), 3510 cm^{-1}, ν(C=N), 1603 cm^{-1}, $\nu(ClO_4^-)$, 1093 cm^{-1}.

Complex **3**: (yield: 1.21 g; 65%). *Anal.* Calc. for $C_{26}H_{44}ClCu_2N_4NaO_9$ (742.18) C, 42.08; H, 5.98; N, 7.55. Found: C, 42.32; H, 6.16; N, 7.24%. λ_{max}/nm (ε_{max}/dm^3 mol^{-1} cm^{-1}) (methanol), 593 (379); IR: ν(O–H), 3487 cm^{-1}, ν(C=N), 1584 cm^{-1}, $\nu(ClO_4^-)$, 1105 cm^{-1}.

2.4. Physical measurements

Elemental analyses (carbon, hydrogen and nitrogen) were performed using a Perkin–Elmer 240C elemental analyzer. IR spectra in KBr (4500–500 cm^{-1}) were recorded using a Perkin–Elmer RXI FT-IR spectrophotometer. Electronic spectra in methanol (1200–350 nm) were recorded in a Hitachi U-3501 spectrophotometer. Cyclic voltammetry was carried out using Sycopel model AEW2 1820 F/S instrument. The measurements were performed at 300 K using 0.2 M TEAP as supporting electrolyte and 10^{-3} M Cu(II) complexes deoxygenated by bubbling with nitrogen. The working, counter, and reference electrodes used were a platinum wire, a platinum coil, and an SCE. The magnetic measurements were carried out on polycrystalline samples using a Quantum Design SQUID MPMS-XL7 magnetometer in the temperature range of 1.9–300 K at an applied magnetic field of 1 or 0.05 T above and below 30 K, respectively, to avoid any saturation effects. The field-dependent magnetization was measured in the applied magnetic field range 0–5 T at 2 K. The diamagnetic corrections were evaluated from Pascal's constants. The X-band EPR spectra were recorded on powder samples with a Bruker E300 automatic spectrometer, varying the temperature between 4 and 300 K.

2.5. Crystallographic studies

Crystal data are given in Table 1. Intensity data were measured at 150 K using the Oxford Xcalibur CCD System using Mo Kα radiation. The crystals were positioned at 50 mm from the CCD. 321 frames were measured with a counting time of 3 s. Data analyses were carried out with the CRYSALIS program [21]. The structures were solved using direct methods with the SHELXS 97 program [22]. The non-hydrogen atoms were refined with anisotropic thermal parameters. The hydrogen atoms bonded to carbon were included in geometric positions and given thermal parameters equivalent to 1.2 times those of the atom to which they were attached. Hydrogen atoms on water molecules were not located. Absorption corrections were carried out using the ABSPACK program [23]. The structures were refined on F^2 using SHELXL 97 [22]. Selected bond lengths and bond angles are presented in Table 2.

3. Results and discussion

3.1. General characterization

All three Schiff-base ligands (H_2L^1–H_2L^3) and their Cu(II) complexes, were synthesized in the usual way. The three tetradentate Schiff-base ligands are very similar but the general formula of complex **1** is different from that of complexes **2** and **3**. In complex **1,** an additional $[CuL^1]$ unit is present along with the main trinuclear part. Interestingly, even on decreasing the $[CuL^1]$: $NaClO_4$ ratio to 1:1 during incorporation of sodium ion guest from methanol

Table 1
Crystal data and refinement details of complexes **1**–**3**

Complex	**1**	**2**	**3**
Formula	$C_{36}H_{58}ClCu_3N_6NaO_{12}$	$C_{26}H_{44}ClCu_2N_4NaO_9$	$C_{26}H_{44}ClCu_2N_4NaO_9$
M	1015.94	742.18	742.18
Space group	orthorhombic, *Fd2d*	triclinic, $P\bar{1}$	triclinic, $P\bar{1}$
Cell dimensions			
a (Å)	10.402(1)	10.789(1)	11.002(2)
b (Å)	23.835(2)	11.626(1)	11.813(2)
c (Å)	35.920(4)	14.967(2)	13.553(3)
α (°)	(90)	85.01(1)	86.09(2)
β (°)	(90)	70.37(1)	79.46(2)
γ (°)	(90)	66.74(1)	69.24(2)
V (Å^3)	8906.1(14)	1622.3(3)	1619.3(6)
Z, dm (g cm^{-3})	8, 1.515	2, 1.519	2, 1.522
Number of reflections measured	14959	11465	10800
Reflections/constraints/ parameters	6435/31/294	9097/0/398	8557/0/396
R_1, wR_2 ($I > 2\sigma(I)$)	0.0704, 0.1855	0.0623, 0.1534	0.0764, 0.1674
R_1,wR_2 (all data)	0.1025, 0.1904	0.1235, 0.1620	0.1065, 0.1793
Largest peak/hole (e Å^{-3})	1.687, −0.661	0.883, −0.966	0.940, −0.846

Table 2
Selected bond lengths (Å) and bond angles (°) for complexes **1**–**3**, respectively

Complex	**1**	**2**	**3**
	$x = 8$, $y = 2$	$x = 8$, $y = 2$	$x = 9$, $y = 3$
Cu(1)–O(11)	1.938(5)	1.906(3)	1.955(4)
Cu(1)–N(15)	1.910(7)	1.937(4)	1.979(4)
Cu(1)–N(1*x*)	1.943(6)	1.925(3)	1.970(5)
Cu(1)–O(2*y*)	1.908(5)	1.926(3)	1.940(4)
Cu(2)–O(31)	1.897(5)	1.920(3)	1.947(4)
Cu(2)–N(35)	1.989(7)	1.945(4)	1.988(4)
Cu(2)–N(3*x*)		1.923(4)	1.981(4)
Cu(2)–O(4*y*)		1.910(3)	1.948(4)
Na(1)–O(11)	2.439(7)	2.462(3)	2.425(4)
Na(1)–O(2*y*)	2.348(6)	2.487(3)	2.359(4)
Na(1)–O(31)		2.359(3)	2.403(4)
Na(1)–O(4*y*)		2.390(3)	2.419(4)
Na(1)–O(94)	2.372(11)	2.505(6)	2.517(5)
Na(1)–O(100)		2.347(4)	2.450(5)
O(11)–Cu(1)–N(15)	92.8(3)	94.3(2)	90.2(2)
O(11)–Cu(1)–N(1*x*)	174.7(3)	178.0(1)	172.0(2)
O(11)–Cu(1)–O(2*y*)	86.6(3)	85.7(1)	81.8(2)
N(15)–Cu(1)–N(1*x*)	86.8(3)	86.0(1)	96.4(2)
N(15)–Cu(1)–O(2*y*)	177.2(3)	179.3(1)	168.7(2)
N(1*x*)–Cu(1)–O(2*y*)	94.1(3)	94.0(1)	92.3(2)
O(31)–Cu(2)–N(35)	94.4(2)	93.6(2)	91.6(2)
O(31)–Cu(2)–N(3*x*)*	177.4(2)	178.6(2)	169.1(2)
O(31)–Cu(2)–O(4*y*)*	85.2(4)	86.7(1)	81.7(2)
N(35)–Cu(2)–N(3*x*)*	86.0(4)	85.9(2)	97.6(2)
N(35)–Cu(2)–O(4*y*)		179.6(2)	172.4(2)
N(38)–Cu(2)–O(42)		93.7(2)	89.4(2)

* The numbering system in **1** is different for these starred atoms due to the imposed symmetry around Cu(2) in [CuL1].

solution, the stoichiometric ratio of host: guest remains the same in complex **1**. Thus the numbers of guest molecules, which are incorporated in the hosts, seem to be determined by the requirement of the crystal lattice.

Besides elemental analysis all three complexes were initially characterized by IR spectra. The 'ligand complexes' [CuL] are neutral complexes and do not have any anion, whereas all three compounds, **1**, **2** and **3**, contain perchlorate as counter anion. Therefore, the appearance of characteristic intense peak for perchlorate (ν_3) in the IR spectra of **1**, **2** and **3** at 1091, 1093 and 1105 cm^{-1}, respectively, clearly indicate the formation of the adducts. The rest of the spectral pattern and band positions of respective adducts and the 'ligand complexes' are very similar. In all three complexes, a strong and broad band, centering at 3427, 3510 and 3487 cm^{-1} for **1**, **2** and **3**, respectively, is due to the presence of water molecule as is also found in the corresponding 'ligand complexes'. The other characteristic bands e.g. azomethine ν(C=N) appear at 1598, 1603 and 1584 cm^{-1} for **1**, **2** and **3**, respectively.

The electronic spectra of the complexes were recorded in methanol solution. A single absorption band at 541, 540 and 591 nm in the visible region and 293, 305 and 307 nm in the UV region are observed for **1**, **2** and **3**, respectively. In the visible region the bands indicate typical d–d transition in the square-planar environment around Cu(II) and the bands in UV region are due to charge transfer transitions. Electronic spectra are also measured for the starting "ligand complexes", **A**, **B** and **C** (**A** = [CuL^1], **B** = [CuL^2] and **C** = [CuL^3]). The positions and intensities of the bands in both UV and Vis regions for **A**, **B** and **C** are almost the same as that of complexes **1**, **2** and **3**, respectively.

The cyclic voltammograms of three sets of complexes, the "ligand complexes" and their corresponding sodium perchlorate adducts (A and **1**, B and **2** and C and **3**) are recorded in methanol (Pt electrode) under nitrogen at the potential range +1.0 to −1.0 V. All the complexes display an irreversible reductive response attributed to the Cu(II)/Cu(I) couple at −0.75 V (Ep_c) and −0.72 V (Ep_c) versus SCE for A and **1**, respectively, −0.78 V (Ep_c) and −0.76 V (Ep_c) versus SCE for B and **2**, respectively, and −0.72 V (Ep_c) and −0.78 V (Ep_c) versus SCE for C and **3**, respectively, during the cathodic potential scan. The appearance of nearly identical UV spectra and electrochemical responses of the adducts and their corresponding mononuclear 'ligand complexes' indicates that the trinuclear adducts probably dissociate in solution.

3.2. Description of structures of complexes *1*–*3*

The structures of complexes **1**–**3** have been solved by single crystal XRD and crystal data for the three compounds are given in Table 1. The trinuclear structures in the three complexes are similar and have a general formula $[(CuL)_2Na(ClO_4)(H_2O)]$ as shown in Fig. 1 (for complex **1**), Fig. 2 (for complex **2**) and *Fig.* S1 (for complex **3**), together with the atom-numbering scheme. The selected bond lengths and angles are summarized in Table 2. In all the three complexes, two neutral [CuL] units (where L represents the deprotonated, tetradentate, di-Schiff-base ligand) are bonded to a sodium cation Na(1) forming the trinuclear entity. The copper atoms are four coordinate with a square planar environment being bonded to two oxygen atoms and two nitrogen atoms of the Schiff-base ligand. The bond lengths in the trinuclear unit of **1** and **2** are very similar with average Cu–O 1.923(21) and 1.916(9) Å and average Cu–N 1.926(23) and 1.932(11) Å in **1** and **2**, respectively. In **3**, however, the ligand contains one more carbon atom in a central position giving rise to a six-membered chelate ring. As a consequence, the bond lengths are significantly greater with average Cu–O 1.947(6) Å and Cu–N 1.980(7) Å. In the previously reported [CuL^1] and [CuL^3] chelates [13,24] the average Cu–O distances (1.920 and 1.932 Å, respectively) are slightly lower than in **1** and **3**, indicating that upon adduct formation Cu–O bond lengths increase. The average O–Cu–N trans angles in the trinuclear units are 176.0(18)°, 178.9(7)°, 170.5(19)° for **1**, **2** and **3**, respectively, indicating that there is slight tetrahedral distortion from the ideal square planar geometry particularly in the later structure. The tetrahedral distortion is also apparent since one pair of diagonal donor atoms clearly lies below the plane while the other pair is above the plane with the metal ion in the mean plane. The dihedral angles between the two N–Cu–O planes in the trinuclear units are 5.79°, 1.28° and 8.99° for complexes **1**, **2** and **3**, respectively, considering 0° for a perfectly square-planar arrangement, and 90° for a perfect tetrahedral arrangement. The r.m.s. deviations of the five fitted atoms in the Cu–N_2O_2 plane are 0.10, 0.08 Å in **3** compared to 0.06 Å in **1** and 0.02, 0.01 Å in **2.** The increase in ring size in **3** compared to **1** and **2** results in higher tetrahedral distortion.

In **1**, the sodium cation has a six-coordinate distorted octahedral environment: four oxygen atoms from the two different "ligand complexes" are bonded to Na(1) ion and two terminal oxygen atoms complete its coordination sphere. The sodium ion is positioned on a twofold axis and it is assumed that the two terminal sites are occupied by a water molecule and a perchlorate anion both of which had 50% occupancy. O(94) was refined with 100% occupancy describing both the water molecule and a perchlorate oxygen atom in equivalent positions but the remainder of the perchlorate was refined with 50% occupancy.[1] On the other side, the perchlorate anion and water molecule can be observed separately occupying adjacent sites in the sodium coordination sphere for

[1] A referee has suggested that the structure should be refined in triclinic space group *P*1 to check on the disorder. In this space group there are two $[(CuL^1)_2Na(ClO_4)(H_2O)]$ dimers and two [CuL^1] monomers. However the disorder between perchlorate and water molecules persisted and no ordered dimers could be found which confirms that the structure solution in orthorhombic *Fd2d* is the optimum for this structure.

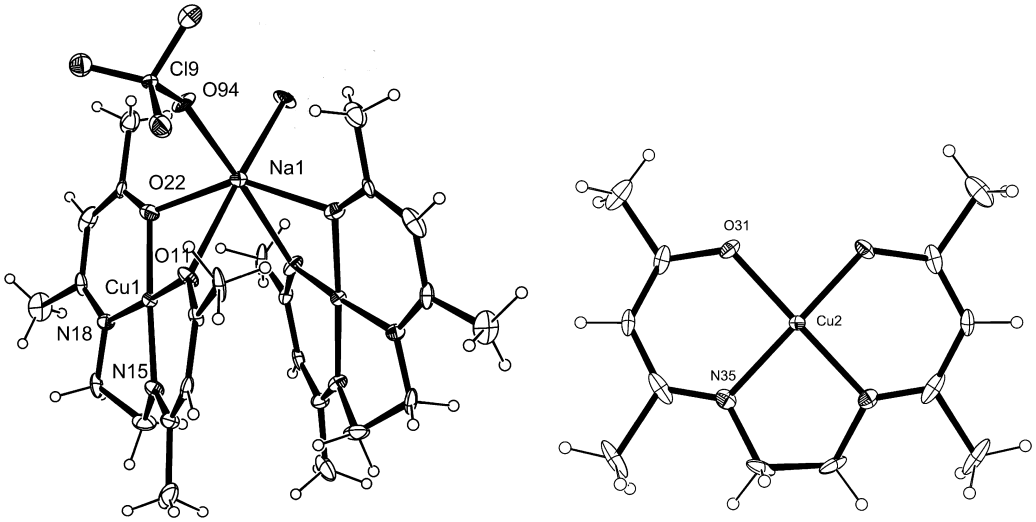

Fig. 1. Ortep-3 view of complex **1** with atom-numbering scheme (50% thermal ellipsoids).

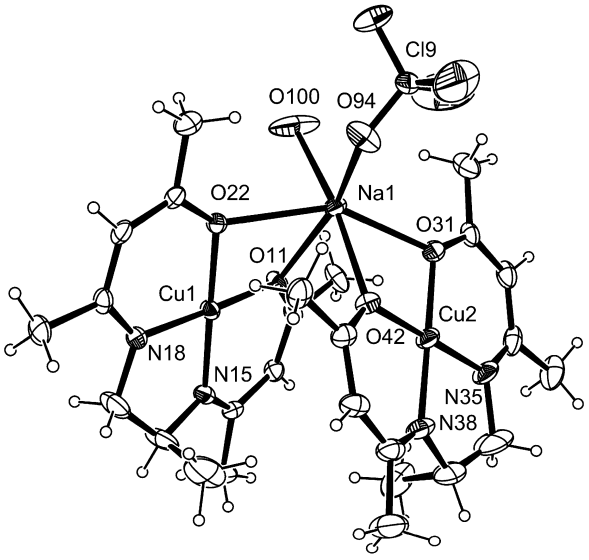

Fig. 2. Ortep-3 view of complex **2** with atom-numbering scheme (50% thermal ellipsoids).

complexes **2** and **3**. The four oxygen atoms of the Schiff-base ligands coordinate in facial manner to the central Na(1) resulting in a bent structure. The small bite of [CuL] on coordinating to Na(1) (66.9(2)°* for the trinuclear unit of **1**, 63.5(1)°, 67.3(1)° for **2** and 64.4(1)°, 63.8(1)° for **3**) is the main cause of distortion from the ideal octahedron of Na(1). In all the three complexes, the six-membered chelate rings incorporating the acetylacetone fragments are essentially planar with no atoms deviating more than 0.09 Å in **1** and **2** and 0.15 Å in **3** from their respective mean planes. In the trinuclear units of **1** and **2**, the five-membered rings comprising the diamine fragment adopt an envelope conformation, while the six-membered ring in **3** adopts a boat conformation.

In **1**, in addition to the trimer, there is a discrete [CuL^1] molecule which has crystallographic *C*2 symmetry (Fig. 1). The Cu(2) atom is four coordinate with a square planar environment being bonded to two oxygen atoms and two nitrogen atoms of the Schiff-base ligand. The *trans* angle is 177.4(2)° indicating that there is a slight tetrahedral distortion from the ideal square planar geometry. The dihedral angles between the two N(35)–Cu(2)–O(31) planes in the monomeric unit of complex **1** are 3.48°. The bond lengths in the discrete monomer [CuL^1] in **1** are somewhat different, with Cu(2)–O(31) 1.897(5) Å and Cu(2)–N(35) 1.989(7) Å, to that of trinuclear unit of **1** where average distances are 1.923(21) for Cu–O and 1.926(23) Å for Cu–N. Hence, the increase of Cu–O bond distances upon Na perchlorate adduct formation is confirmed, although there does seem to be a concomitant decrease in Cu–N distance.

In compound **1**, the trinuclear [$(CuL^1)_2Na(ClO_4)(H_2O)$] and the mononuclear [CuL^1] units are connected through H-bonding interactions (*Fig.* S2; Supplementary data) involving the water molecule O200 and the oxygen atoms O31 and O94. In compound **2**, the water molecule O100 and the oxygen atom O91 being involved in hydrogen bonding, forms dimeric entity as shown in *Fig.* S3.

3.3. Magnetic properties

The magnetic behavior for compounds **1**–**3** has been studied. The variable temperature susceptibilities for complexes **1**, **2** and **3** were measured over the range 2–300 K.

3.3.1. Complex *1*

Complex **1** shows a structure composed of alternated [Cu_2Na] and Cu(II) mononuclear discrete units. Accordingly, both of them have been considered in the magnetic study. The magnetic behavior of **1** is shown in Fig. 3 as the $\chi_M T$ *versus T* plot, χ_M being the molar susceptibility per three Cu(II) ions and *T* the temperature. At room temperature, the $\chi_M T$ value is 1.20 $cm^3\ mol^{-1}$ K which is slightly higher than the spin-only value, 1.13 $cm^3\ mol^{-1}$ K, expected for three Cu(II) ions with $S = 1/2$ and assuming a $g = 2$, suggesting higher values of *g* as is usual for Cu(II) ions. As the temperature is lowered, the $\chi_M T$ value is kept approximately constant until 40 K. Below that temperature the $\chi_M T$ *versus T* curve abruptly decreases until a final value of $\chi_M T = 1.02$ $cm^3\ mol^{-1}$ K is reached at 2 K. The low-temperature magnetic behavior confirms the presence of a weak antiferromagnetic exchange that could have its origin on either intra or intermolecular interactions. On the one hand, intramolecular exchange would undoubtedly take place through the different O–Na–O′ bridges present on the [Cu_2Na] unit, each oxygen atom corresponding to one different "ligand complex" of the unit. Such bridges are the only covalently bonded pathways by which unpaired electrons of the two Cu(II) atoms of the molecular unit could interact. The Cu···Cu intramolec-

ular distances are 4.134(2), 4.524(2), 3.966(1) Å, respectively, in the three structures.

Some examples have been previously published in the literature in which magnetic exchange coupling has been observed between paramagnetic species through diamagnetic metallic ions [16–20]. On the other hand, a detailed structural analysis of the intermolecular hydrogen bonds between one [Cu_2Na] and one discrete Cu(II) unit in complex **1** confirms that the possible intermolecular magnetic exchange pathway between Cu(II) ions would only be possible through the Na^+ ion, and would definitely contain two more atoms and therefore longer Cu(II)–Cu(II) distances compared to the intramolecular pathway.

Hence, it seems reasonable to assume that intermolecular interactions will be significantly weaker than intramolecular ones and so, only the intramolecular Cu(II)–Cu(II) coupling-type will be considered in our study. In order to quantify the magnitude of the intramolecular exchange interaction between Na^+ bridged-Cu(II) ions (J_{12}), an isotropic Heisenberg–Dirac–van Vleck Hamiltonian formalism for a dinuclear molecule plus a mononuclear discrete unit was used in the analysis [Eq. (1)]

$$\widehat{H}| = g_1\beta HS_1 + g_2\beta HS_2 + J_{12}S_1S_2 + g_3\beta HS_3 \quad (1)$$

where H is the value of the magnetic field and g_i, β and S_i have their usual meanings. Since intermolecular interactions in complex **1** are believed to be even weaker than intramolecular ones, no terms concerning this long-distance coupling have been introduced in the equation. Experimental data for **1**, corrected from diamagnetic contributions and TIP (180×10^{-6} cm^3 mol^{-1}/Cu atom) were analyzed by Eq. (1) on $\chi_M T$. In the fit procedure, $g_1 = g_2 \neq g_3$ was considered since the two Cu(II) ions in the [Cu_2Na] unit are structurally equivalent and different with respect to the Cu(II) ion located at the mononuclear entity. The g_3 value was fixed at 2.07 based on the value extracted from the epr spectrum at room temperature (see text below) which is considered as an average value of the parallel and perpendicular components of the anisotropic **g** tensor. The best fit parameters obtained are: $g_1 = g_2 = 2.07(0)$, $J = -1.09(1)$ cm^{-1} and $R = 2 \times 10^{-5}$ where R is the agreement factor defined as $R = \sum[(\chi_M T)_{calc} - (\chi_M T)_{obs}]^2 / \sum(\chi_M T)^2_{obs}$. These results confirm the weak antiferromagnetic exchange interaction between Cu(II) ions. The curve derived from the fit is plotted in Fig. 3 along with the experimental data. The value of the molar magnetization at 2 K and 5 T for complex **1** tends to 3 Nβ and it almost reaches saturation as seen in Fig. 4. Such low-temperature value of the magnetization confirms the weakness of the magnetic coupling in accordance with the temperature-dependent magnetic behavior.

3.3.2. Complexes *2* and *3*

The magnetic behavior of complexes **2** and **3** is shown in Fig. 3 as the $\chi_M T$ *versus* T *plot, being* χ_M the molar susceptibility per two Cu(II) ions and T the temperature. At room temperature, for both complexes, the $\chi_M T$ value is 0.80 cm^3 mol^{-1} K which is slightly higher than the spin-only value, 0.75 cm^3 mol^{-1} K, expected for two Cu(II) ions with $S = 1/2$ and assuming $g = 2$, suggesting higher values of g as usual for Cu(II) ions. As the temperature is lowered, the $\chi_M T$ value is kept approximately constant until 40 K. Below that temperature the $\chi_M T$ *versus* T curves abruptly decrease until a final value of $\chi_M T = 0.71$ and 0.68 cm^3 mol^{-1} K is reached at 2 K for complex **2** and **3**, respectively. The low-temperature magnetic behavior indicates the presence of a weak antiferromagnetic ex-

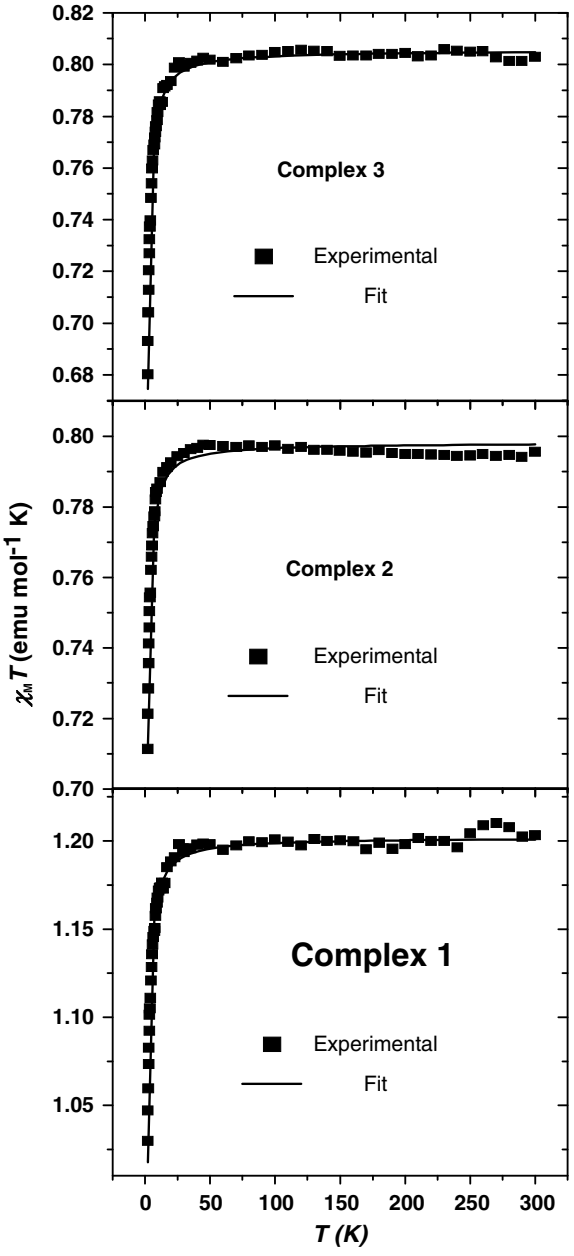

Fig. 3. Temperature dependence of the susceptibilities in the form of $\chi_M T$ vs T for complexes **1** (bottom), **2** (middle) and **3** (top). The solid lines are the fittings in the range between 300 to 1.9 K.

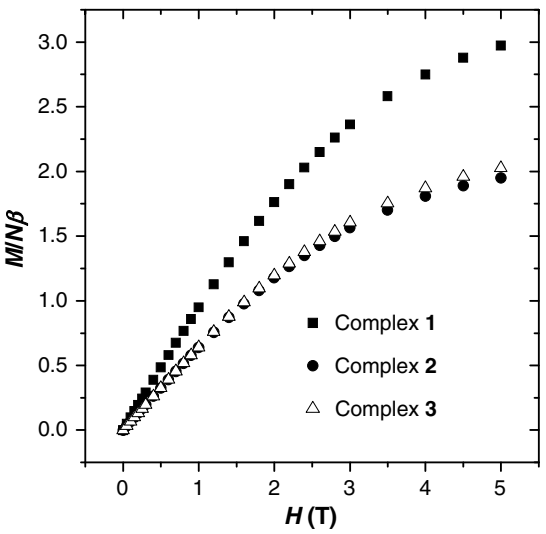

Fig. 4. Field dependence of the magnetization for complexes **1** (■), **2** (●) and **3** (△).

change. For the same reasons that stated for complex **1**, magnetic exchange mediated by intermolecular interactions will be much weaker than the intramolecular exchange coupling and hence they will not be considered in the magnetic analysis.

Complexes **2** and **3** are structurally similar and both show only [Cu_2Na] units in the crystal lattice with just one type of Cu(II) ion per structure. The different O–Na–O′ bridges present on each [Cu_2Na] unit, involving one Na^+ ion and four oxygen atoms of two different "ligand complexes", are responsible for the magnetic exchange coupling between Cu(II) ions. Taking in consideration all this information, an isotropic Heisenberg–Dirac–van Vleck Hamiltonian formalism for a dinuclear molecule was used in the fit of the experimental temperature-dependent $\chi_M T$ data [Eq.(2)],

$$\widehat{H} = g_1 \beta H S_1 + g_2 \beta H S_2 + J_{12} S_1 S_2 \quad (2)$$

where g_1 was considered equal to g_2 due to the symmetry equivalence of the two Cu(II) ions in the dimer. Experimental data for complexes **2** and **3**, corrected from diamagnetic contributions and TIP (120×10^{-6} cm^3 mol^{-1}/Cu atom) were analyzed by Eq. (2). The best fit parameters obtained are: $g_1 = g_2 = 2.06(0)$, $J = -0.55(1)$ cm^{-1} and $R = 0.5 \times 10^{-5}$ for complex **2** and $g_1 = g_2 = 2.07(0)$, $J = -0.80(1)$ cm^{-1} and $R = 0.4 \times 10^{-5}$ for complex **3** where R is the agreement factor defined as $R = \sum[(\chi_M T)_{calc} - (\chi_M T)_{obs}]^2 / \sum(\chi_M T)^2_{obs}$. These results confirm the weak antiferromagnetic exchange interaction between Cu(II) ions. The curves derived from the fits are plotted in Fig. 3 along with the experimental data. The value of the molar magnetization at 2 K and 5 T for complex **2** and **3** tends to 2 Nβ in both cases and they almost reach saturation as seen in Fig. 4. Such low-temperature values of the magnetization confirm that even at 2 K the unpaired electrons still populate the $S = 1$ excited state due to the weakness of the magnetic coupling. These data are in accordance with the fit of the temperature-dependent magnetic behavior of both complexes from which a very low value of the magnetic exchange constant was obtained.

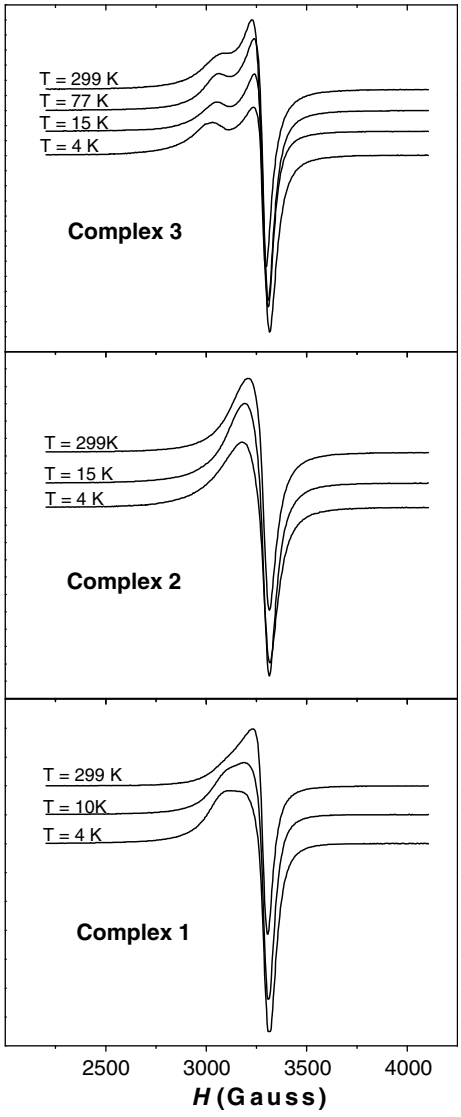

Fig. 5. Temperature-dependent EPR spectra for complexes **1** (bottom), **2** (middle) and **3** (top).

3.4. EPR spectra

The X-band epr spectra for complexes **1**–**3** were recorded on powder samples varying the temperature between 4 and 295 K (Fig. 5). The bands observed in the EPR spectra of the complexes have been analyzed as those corresponding to the transitions between $m_s = -1/2$ and $m_s = 1/2$ of non-interacting Cu(II) ions due to the extremely weak magnetic coupling that takes place in the dimeric unit. The profile of the spectra seems to be in agreement with the structural characterization of the complexes.

3.4.1. Complex *1*

At room temperature, complex **1** shows a broad absorption peak centered at $g_{eff} = 2.07$. With the temperature decrease, the same peak is observed but the slower relaxation dynamics of the complex allow to differentiate two different transitions with maxima at $g_{eff} = 2.13$ and 2.17, respectively. Due to their similar intensities the transitions can not be assigned to the $g_{\|}$ and $g_{\perp}$ components of the same **g**-tensor. The structure of complex **1** unambiguously shows the presence of two non-equivalent Cu(II) ions in the structure, both of them with a square planar environment. We attribute the observed peaks to the $g_{\perp}$ components of the two different Cu(II) ions. The peaks of the parallel transitions of both ions are probably overlapped with their perpendicular counterparts and only wide bands are observed even at low temperature. This fact does not allow to resolve the axial anisotropy of the metallic ions in the complex under these conditions.

3.4.2. Complexes *2* and *3*

The EPR spectra for complexes **2** and **3** show almost no evolution with temperature, confirming that only one transition coming from non-coupled metallic ions is observed. However, while for complex **2** only one broad absorption peak is observed, for complex **3** two different peaks are solved. Complexes **2** and **3** show just one type of Cu(II) ion in the crystal. In both cases Cu(II) ions are four coordinated with a square planar environment. Hence we expect to observe two different EPR transitions in each complex due to the axial anisotropy of the paramagnetic ions. Only in the spectra of complex **3** both $g_{\|}$ and $g_{\perp}$ components of the **g**-tensor can be observed while, for complex **2**, the low intensity parallel transition ($g_{\|}$) peak seems to be overlapped by the more intense perpendicular component ($g_{\perp}$). The reason for the more evidenced anisotropy of complex **3** could have a structural origin. Actually, the organic ligand L^3 used in the synthesis of complex **3** differs in length, from that used for complex **2**, containing one more carbon atom. This seems to have two main consequences in the bond lengths of the coordination sphere of the Cu(II) ions: (i) complex **3** shows much longer bond lengths with respect to complex **2** and ii) while in complex **2** Cu–O and Cu–N bond lengths show values in the same range (1.90–1.94 Å), in complex **3** their values belong to different ranges, such being 1.94–1.95 and 1.97–1.99 Å, respectively. These

structural differences could accentuate the magnetic anisotropy of the central ion.

3.5. Discussion

Several examples are available in the literature in which magnetic exchange between paramagnetic species takes place through bridges that contain diamagnetic metallic ions. The antiferromagnetic coupling has been reported between two Cu(II) ions with bridges containing a Zn(II) ion [16], a diamagnetic Ni(II) or Pd(II) ion [17], and a Na(I) ion [18]. On the other hand, ferromagnetic coupling has been also observed between two Cu(II) ions with bridges containing either a Zn(II) [19] or a CrO_4^{2-} moiety [20]. The values of the magnetic exchange constants (J) are generally very low, $-5 < J < 5\ cm^{-1}$, in agreement with what we observe in our [Cu_2Na] adducts. The ferromagnetic character of the coupling in the previously mentioned compounds has been usually rationalized in terms of strict orthogonality of the two magnetic orbitals that cancels their own overlapping [19,20]. The symmetry of the bridging ligand and the magnetic orbitals is responsible for that and probably the d-orbitals of the diamagnetic ion of the bridging ligand are somehow involved in the superexchange pathway. When either the symmetry of the bridging moiety or alternatively steric and electronic characteristics of the complex favor the overlapping of the magnetic orbitals, losing the previous orthogonality, the coupling between the two Cu(II) ions becomes clearly antiferromagnetic [16,17]. Neither in the case of complexes **1**–**3**, the $d_{x^2-y^2}$ magnetic orbitals of the paramagnetic ions show strict orthogonality nor hence an antiferromagnetic superexchange is expected and further confirmed by the corresponding magnetic analysis. However, due to the bent structure of the adducts (see Section 3.2), the magnetic orbitals of the two Cu(II) ions in the [Cu_2Na] units are tilted one from the other in contrast with the planar geometry of the molecule observed by Journaux et al. [16] and Chaudhuri et al. [17] for other molecular systems, and hence their overlapping could be substantially diminished leading to a very weak coupling.

The [Cu_2Na] units in complexes **1**–**3** are magnetically diluted in the crystal due to the absence of significant intermolecular interactions. This characteristic allows clearly identifying and studying the magnetic coupling through diamagnetic metallic ions without the interference of other long-distance couplings that could compete in strength with such particular kind of intramolecular interaction.

4. Conclusion

In the present study, it has been shown that sodium ion can be incorporated by the building block like [Cu(II)L] unit, simply on crystallization from methanol solution containing dissolved sodium perchlorate to result in trinuclear Cu_2Na adducts. Spectral and electrochemical analyses of both ligand complexes and sodium adducts indicate that the later exists in the solid state but breaks in solution. The temperature-dependent magnetic susceptibility measurements indicate that, in complexes **1–3** the two terminal paramagnetic Cu(II) centers are weakly antiferromagnetically coupled through Na(I) ion.

Acknowledgments

This work was supported by CSIR, Government of India [Junior Research Fellowship to P.M., Sanction No. 09/028 (0663)/2006-EMR-I] and by the Spanish Government (Grant CTQ2006-03949). We thank Núria Clos, Unitat de Mesures Magnètiques, Serveis Científics i Tècnics, Universitat de Barcelona, for the magnetic measurements. We also thank EPSRC and the University of Reading for funds for the Xcalibur system.

Appendix A. Supplementary data

CCDC 685933, 685934 and 685935 contain the supplementary crystallographic data for **1**, **2** and **3**. These data can be obtained free of charge via http://www.ccdc.cam.ac.uk/conts/retrieving.html, or from the Cambridge Crystallographic Data Centre, 12 Union Road, Cambridge CB2 1EZ, UK; fax: (+44) 1223-336-033; or e-mail: deposit@ccdc.cam.ac.uk. The ORTEP diagram for complex **3** and dimeric unit of **1**. Supplementary data associated with this article can be found, in the online version, at doi:10.1016/j.poly.2008.07.025.

References

[1] (a) J.M. Lehn, Supramolecular Chemistry Concepts and Perspectives, VCH, Weinheim, 1995;
(b) D.S. Lawrence, T. Jiang, M. Levett, Chem. Rev. 95 (1995) 2229;
(c) A.P. de Silva, H.Q.N. Gunaratne, T. Gunnlaugsson, A.J.M. Huxley, C.P. McCoy, J.T. Rademacher, T.E. Rice, Chem. Rev. 97 (1997) 1515;
(d) M. Fujita, Chem. Soc. Rev. 27 (1998) 417;
(e) D.L. Caulder, K.N. Raymond, Acc. Chem. Res. 32 (1999) 975;
(f) P.J. Stang, B. Olenyuk, Acc. Chem. Res. 30 (1997) 502;
(g) M.M. Conn, J. Rebek, Chem. Rev. 97 (1997) 1647;
(h) C.J. Jones, Chem. Soc. Rev. 27 (1998) 289;
(i) S. Leininger, B. Olenyuk, P.J. Stang, Chem. Rev. 100 (2000) 853.
[2] (a) V. Balzani, A. Juris, M. Venturi, S. Campagna, S. Serroni, Chem. Rev. 96 (1996) 759;
(b) V. Balzani, S. Campagna, G. Denti, A. Juris, S. Serroni, M. Venturi, Acc. Chem. Res. 31 (1998) 26;
(c) R.V. Slone, K.D. Benkstein, S. Belanger, J.T. Hupp, I.A. Guzei, A.L. Rheingold, Coord. Chem. Rev. 171 (1998) 221;
(d) T. Kusukawa, M. Fujita, J. Am. Chem. Soc. 124 (2002) 13576;
(e) M. Vitale, P.C. Ford, Coord. Chem. Rev. 219–221 (2001) 3;
(f) I. Pal, F. Basuli, T.C.W. Mak, S. Bhattacharya, Angew. Chem., Int. Ed. 40 (2001) 2923;
(g) X. Sun, D.W. Johnson, D.L. Caulder, K.N. Raymond, E.H. Wong, J. Am. Chem. Soc. 123 (2001) 2752.
[3] (a) U. Bossek, T. Weyhermuller, K. Weighardt, B. Nuber, J. Weiss, J. Am. Chem. Soc. 112 (1990) 6387;
(b) Y. Naruta, M. Sasayama, T. Sasaki, Angew. Chem., Int. Ed. Engl. 33 (1994) 1839.
[4] (a) M.D. Vargas, J.N. Nicholls, Adv. Inorg. Chem. Radiochem. 30 (1986) 123;
(b) A. Simon, Angew. Chem. 100 (1988) 163.
[5] (a) S.M. Owen, Polyhedron 7 (1988) 253;
(b) D.M.P. Mingos, Nat. Phys. Sci. (London) 236 (1972) 99;
(c) K. Wade, Adv. Inorg. Chem. Radiochem. 18 (1976).
[6] D.M.P. Mingos, M.J. Watson, Adv. Inorg. Chem. 39 (1992) 327.
[7] (a) R.A. Reynolds III, D. Coucouvanis, J. Am. Chem. Soc. 120 (1988) 209;
(b) M. Murrie, S. Parsons, R.E.P. Winpenny, J. Chem. Soc., Dalton Trans. (1998) 1423;
(c) E.K. Brechin, A. Graham, S.G. Harris, S. Parsons, R.E.P. Winpenny, J. Chem. Soc., Dalton Trans. (1997) 3405.
[8] (a) A. Muller, F. Peters, M.J. Pope, D. Gatteschi, Chem. Rev. 98 (1998) 239;
(b) Y. Zhang, P.J. Zapf, L.M. Meyer, R.C. Haushalter, J. Zubieta, Inorg. Chem. 36 (1997) 2159;
(c) L. Suber, M. Bonamico, V. Fares, Inorg. Chem. 36 (1997) 2030.
[9] (a) Y.-M. Jeon, J. Kim, D. Whang, K. Kim, J. Am. Chem. Soc. 118 (1996) 9790;
(b) H. Piotrowski, K. Polborn, G. Hilt, K. Severin, J. Am. Chem. Soc. 123 (2001) 2699;
(c) Li.-Y. Wang, S. Igarashi, Y. Yukawa, Y. Hoshino, O. Roubeau, G. Aromí, R.E.P. Winpenny, Dalton Trans. (2003) 2318.
[10] E. Sinn, C.M. Harris, Coord. Chem. Rev. 4 (1969) 391.
[11] L.G. Armstrong, L.F. Lindoy, P.A. Tasker, J. Chem. Soc., Dalton Trans. (1977) 1771.
[12] H. Milburn, M.R. Truter, B.L. Vickery, J. Chem. Soc., Dalton Trans. (1974) 841.
[13] Y.P. Cai, C.Y. Su, A.W. Xu, B.S. Kang, Y.X. Tong, H.Q. Liu, S. Jie, Polyhedron 20 (2001) 657.
[14] L. Shen, G. Sheng, J. Qiu, Y. Zhang, J. Coordin. Chem. 56 (2003) 603.
[15] F. Corazza, C. Floriani, M. Zehnderb, J. Chem. Soc., Chem. Commun. (1986) 1270.
[16] Y. Journaux, J. Sletten, O. Kahn, Inorg. Chem. 25 (1986) 439.
[17] P. Chaudhuri, M. Winter, B.P.C. Della Vedova, E. Bill, A. Trautwein, S. Gehring, P. Fleischhauer, B. Nuber, J. Weiss, Inorg. Chem. 30 (1991) 2148.
[18] P.K. Nanda, G. Aromí, D. Ray, Inorg. Chem. 45 (2006) 3143.
[19] R. Ruiz, M. Julve, J. Faus, F. Lloret, M.C. Muñoz, Y. Journaux, C. Bois, Inorg. Chem. 36 (1997) 3434.
[20] H. Oshio, T. Kikuchi, T. Ito, Inorg. Chem. 35 (1996) 4938.
[21] Crysalis, Oxford Diffraction Ltd, Version 1, 2005.
[22] SHELXS 97 and SHELXL 97, G.M. Sheldrick, Programs for Crystal Structure Calculations, University of Gottingen, 1997.
[23] ABSPACK, Oxford Diffraction Ltd, 2005.

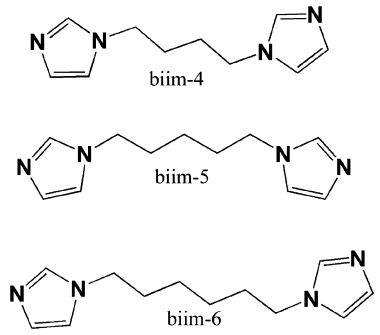

Scheme 1. Structures of bis(imidazole) ligands in this work.

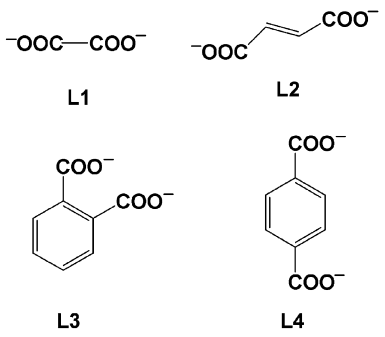

Scheme 2. Structures of the carboxylate anions in this work.

ring. After biim-6 (0.436 g, 2 mmol) in 1 mL ethanol was added, a blue precipitate was obtained. A minimum amount of ammonia (14 M) was added to give a blue solution. Suitable crystals were obtained after standing at room temperature for several days. The crystals were collected in a 75% yield based on Cu^{2+}. Elemental *Anal.* Calc. for $C_{14}H_{20}CuN_4O_5$: C, 43.35; H, 5.20; N, 14.44. Found: C, 43.42; H, 5.27; N, 14.57%. IR (KBr, cm^{-1}): 3741 (w), 3110 (s), 2858 (w), 1613 (s), 1560 (vs), 1516 (vs), 1358 (m), 1229 (m), 1109 (s), 829 (w), 784 (m), 663 (s), 659 (s), 487 (w).

*2.1.2. Synthesis of [ZnL1(biim-6)] · H_2O (**2**)*

After a mixture of $ZnCO_3$ (0.125 g, 1 mmol), oxalic acid dihydrate (0.126 g, 1 mmol) in water was stirring for 10 min at room temperature, biim-6 (0.436 g, 2 mmol) in 1 mL ethanol was added to the solution with stirring and still precipitate was obtained. A minimum amount of ammonia (14 M) was added to give a colorless solution. Suitable colorless crystals were obtained from the filtrate after standing at room temperature in a 45% yield based on $ZnCO_3$. Elemental *Anal.* Calc. for $C_{14}H_{20}ZnN_4O_5$: C, 43.15; H, 5.26; N, 14.37. Found: C, 43.27; H, 5.31; N, 14.48%. IR (KBr, cm^{-1}): 3741 (s), 3108 (w), 2933 (w), 1652 (vs), 1611 (s), 1454 (s), 1364 (m), 1313 (m), 1229 (w), 828 (s), 790 (s), 492 (m).

*2.1.3. Synthesis of [MnL1(biim-6)] · H_2O (**3**)*

A mixture of $MnCO_3$ (0.115 g, 1 mmol), oxalic acid dihydrate (0.126 g, 1 mmol) in water (8 mL), and biim-6 (0.436 g, 2 mmol) in ethanol (1 mL) was sealed in a Teflon-lined stainless steel autoclave and heated at 140 °C for 4 days, and then it was cooled to room temperature at 10 °C h^{-1}. Colorless crystals were obtained in a 56% yield based on $MnCO_3$. Elemental *Anal.* Calc. for $C_{14}H_{20}MnN_4O_5$: C, 44.33; H, 5.32; N, 14.77. Found: C, 44.44; H, 5.39; N, 14.70%. IR (KBr, cm^{-1}): 3550 (w), 3413 (m), 3112 (m), 2932 (w), 2858 (w), 1668 (vs), 1615 (vs), 1516 (vs), 1362 (s), 1230 (m), 1227 (m), 1110 (s), 827 (m), 734 (w), 662 (s), 627 (m), 489 (m).

*2.1.4. Synthesis of [MnL1(biim-4)] (**4**)*

A mixture of $MnCO_3$ (0.115 g, 1 mmol), oxalic acid dihydrate (0.126 g, 1 mmol) in water (8 mL), and biim-4 (0.380 g, 1 mmol) in ethanol (1 mL) was sealed in a Teflon-lined stainless steel autoclave and heated at 140 °C for 4 days prior to being cool to room temperature at 10 °C h^{-1}. Colorless crystals were obtained in a 69% yield based on $MnCO_3$. Elemental *Anal.* Calc. for $C_{12}H_{14}MnN_4O_4$: C, 43.26; H, 4.24; N, 16.81. Found: C, 43.14; H, 4.27; N, 16.75%. IR (KBr, cm^{-1}): 3742 (s), 3116 (w), 2928 (w), 1679 (vs), 1652 (vs), 1618 (m), 1515 (vs), 1389 (m), 1229 (w), 1111 (w), 789 (w), 667 (s), 475 (m).

*2.1.5. Synthesis of [Co_2(L2)$_2$(biim-5)$_3$ · 6H_2O] · 8H_2O (**5**)*

A mixture of $CoCO_3$ (0.119 g, 1 mmol), fumaric acid (0.116 g, 1 mmol) in water was stirring for 10 min at room temperature. Then biim-5 (0.408 g, 2 mmol) was added to the mixture with stirring for 1 h and pink solution was obtained. Pink crystals were obtained from the filtrate after standing at room temperature for several days in a 75% yield based on $CoCO_3$. Elemental *Anal.* Calc. for $C_{41}H_{80}Co_2N_{12}O_{22}$: C, 40.66; H, 6.66; N, 13.88. Found: C, 40.74; H, 6.70; N, 13.95%. IR (KBr, cm^{-1}): 3670 (w), 3136 (m), 2945 (w), 2858 (w), 1568 (vs), 1455 (m), 1240 (vs), 1108 (vs), 991 (m), 843 (s), 763 (s), 663 (vs).

*2.1.6. Synthesis of [ZnL3(biim-6)] (**6**)*

A mixture of $ZnCO_3$ (0.125 g, 1 mmol), phthalic anhydride (0.148 g, 1 mmol) in water (8 mL), and biim-6 (0.437 g, 2 mmol) in ethanol (1 mL) was sealed in a Teflon-lined stainless steel autoclave and heated at 180 °C for 4 days, and then it was cooled to room temperature at 10 °C h^{-1}. Colorless crystals were obtained in a 60% yield based on $ZnCO_3$. Elemental *Anal.* Calc. for $C_{20}H_{22}ZnN_4O_4$: C, 53.65; H, 4.95; N, 12.51. Found: C, 53.77; H, 4.97; N, 12.65%. IR (KBr, cm^{-1}): 3123 (w), 3090 (w), 2865 (w), 1619 (vs), 1560 (vs), 1524 (s), 1475 (m), 1377 (vs), 1249 (m), 1144 (m), 950 (m), 768 (s), 655 (vs), 454 (w).

*2.1.7. Synthesis of [ZnL3(biim-5)] (**7**)*

A mixture of $ZnCO_3$ (0.125 g, 1 mmol), phthalic anhydride (0.148 g, 1 mmol) in water (8 mL), and biim-5 (0.408 g, 2 mmol) in ethanol (1 mL) was sealed in a Teflon-lined stainless steel autoclave and heated at 170 °C for 4 days, and then it was cooled to room temperature at 10 °C h^{-1}. Colorless crystals were obtained in a 66% yield based on $ZnCO_3$. Elemental *Anal.* Calc. for $C_{19}H_{20}ZnN_4O_4$: C, 52.61; H, 4.65; N, 12.92. Found: C, 52.77; H, 4.61; N, 12.81%. IR (KBr, cm^{-1}): 3421 (m), 3111 (m), 2938 (w), 1617 (vs), 1565 (vs), 1516 (s), 1457 (s), 1365 (vs), 1246 (m), 1147 (m), 953 (m), 833 (m), 756 (m), 659 (m), 478 (w).

*2.1.8. Synthesis of [CdL3(biim-5) · 1.5H_2O] · 0.5H_2O (**8**)*

A mixture of $Cd(OH)_2$ (0.146 g, 1 mmol), phthalic anhydride (0.148 g, 1 mmol) in water (8 mL), and biim-5 (0.408 g, 2 mmol) in ethanol (1 mL) was sealed in a Teflon-lined stainless steel autoclave and heated at 170 °C for 4 days, and then it was cooled to room temperature at 10 °C h^{-1}. Colorless crystals were obtained in a 56% yield based on $Cd(OH)_2$. Elemental *Anal.* Calc. for $C_{19}H_{24}CdN_4O_6$: C, 44.16; H, 4.68; N, 10.84. Found: C, 44.27; H, 4.60; N, 10.95%. IR (KBr, cm^{-1}): 3742 (w), 3118 (w), 2933 (w), 2862 (w), 1646 (m), 1560 (vs), 1516 (s), 1481 (m), 1397 (vs), 1235 (m), 1112 (m), 937 (m), 841 (m), 751 (s), 652 (vs), 438 (s).

*2.1.9. Synthesis of [CdL4(biim-6) · 2H_2O] (**9**)*

A mixture of $Cd(OH)_2$ (0.146 g, 1 mmol), *p*-phthalic acid (0.166 g, 1 mmol) in water (8 mL), and biim-6 (0.436 g, 2 mmol) in ethanol (1 mL) was sealed in a Teflon-lined stainless steel autoclave and heated at 180 °C for 4 days, and then it was cooled to room temperature at 10 °C h^{-1}. Colorless crystals were obtained

in a 67% yield based on $Cd(OH)_2$. Elemental *Anal.* Calc. for $C_{20}H_{26}CdN_4O_6$: C, 45.25; H, 4.94; N, 10.55. Found: C, 45.17; H, 4.86; N, 10.42%. IR (KBr, cm^{-1}): 3743 (w), 3414 (vs), 2935 (w), 2862 (w), 1643 (s), 1616 (s), 1560 (vs), 1515 (s), 1465 (s), 1383 (vs), 1235 (w), 1116 (m), 745 (m), 651 (m), 452 (m).

2.2. X-ray crystallography

Single-crystal X-ray diffraction data for compounds **1, 2** and **4** were recorded on a Bruker Apex CCD diffractometer with graphite-monochromated Mo Kα radiation (λ = 0.71073 Å) at 293 K. Crystallographic data for compounds **3** and **5–9** were collected on a Rigaku RAXIS-RAPID single-crystal diffractometer with Mo Kα radiation (λ = 0.71073 Å) at 293 K. Absorption corrections were applied using multi-scan technique. All the structures were solved by Direct Method of SHELXS-97 [25] and refined by full-matrix least-squares techniques using the SHELXL-97 program [26] within WINGX [27]. Non-hydrogen atoms were refined with anisotropic temperature parameters. The hydrogen atoms attached to carbons were generated geometrically; the aqua hydrogen atoms were located from difference Fourier maps and refined with isotropic displacement parameters. Analytical expressions of neutral-atom scattering factors were employed, and anomalous dispersion corrections were incorporated [28]. The disordered C atoms in compounds **4** and **5** and disordered O atoms in compound **8** were refined using C or O atoms split over two sites, with a total occupancy of 1. The water H atoms in compounds **1–3** and **8** could not be positioned reliably and were omitted from the final model. The bond distance restraints were used in the refinement for the water molecules in compound **5**.

Detailed crystallographic data and structure refinement parameters for **1–9** are summarized in Table 1. Selected bond distances and angles for compounds **1–9** are listed in Table S1 (see the Supplementary data).

3. Results and discussion

3.1. Descriptions of crystal structures

3.1.1. Structure of $[CuL1(biim\text{-}6)] \cdot H_2O$ (**1**)

Compounds **1–3** are isostructural and crystallize in the monoclinic *C2/c* space groups; therefore the structure descriptions of compounds **2** and **3** will be neglected.

As shown in Fig. 1a, each Cu(II) atom lies on an inversion center and six-coordinated by four O atoms from two oxalate anions (Cu–O 2.006(1)–2.321(1) Å) and two N atoms from biim-6 ligands (Cu–N 2.011(2) Å). Due to the Jahn–Teller effect, the Cu–O distance of axial site is much longer than those in the equatorial plane. Each oxalate anion coordinates to two Cu atoms to form a 1D chain with a Cu···Cu distance of 5.58 Å. The neutral ligand biim-6 connects two Cu atoms and a 2D network is obtained (Fig. 1b).

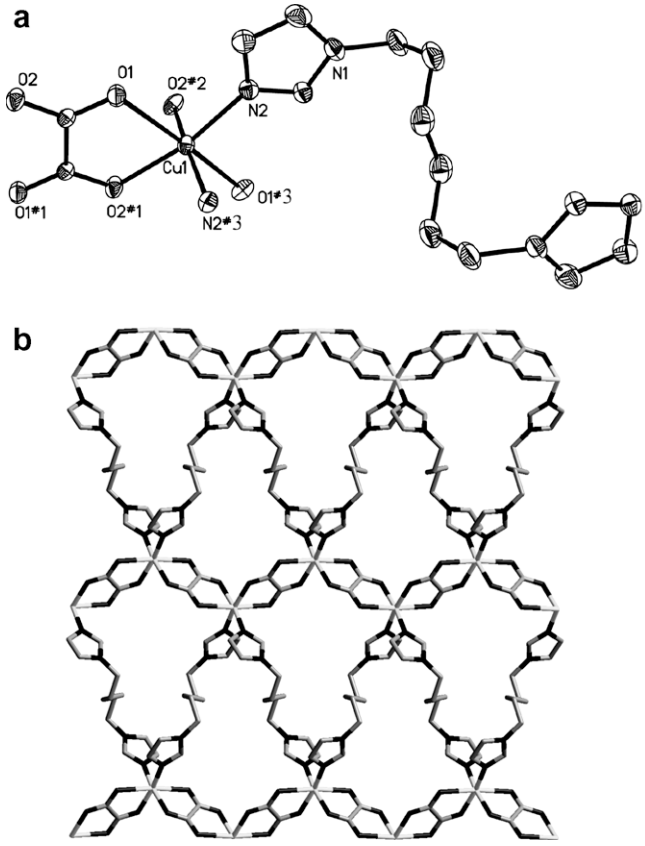

Fig. 1. (a) Coordination environment of the copper cation in **1**. (b) View of a single layer of **1**.

3.1.2. Structure of [MnL1(biim-4)] (**4**)

As illustrated in Fig. 2a, each central Mn(II) atom in **4** is coordinated by four O atoms (Mn–O 2.199(3)–2.211(3) Å) of two oxalate anions and two N atoms (Mn–N 2.198(4)–2.231(4) Å) from biim-4

Table 1
Crystal data and structure refinements for compounds **1–9**

	1	**2**	**3**	**4**	**5**	**6**	**7**	**8**	**9**
Formula	$C_{14}H_{20}CuN_4O_5$	$C_{14}H_{20}N_4O_5Zn$	$C_{14}H_{20}MnN_4O_5$	$C_{12}H_{14}MnN_4O_4$	$C_{41}H_{80}Co_2N_{12}O_{22}$	$C_{20}H_{22}ZnN_4O_4$	$C_{19}H_{20}ZnN_4O_4$	$C_{19}H_{24}CdN_4O_6$	$C_{20}H_{26}CdN_4O_6$
Molecular weight	387.88	389.71	379.28	333.21	1211.03	447.79	433.76	516.82	530.85
Crystal system	monoclinic	monoclinic	monoclinic	triclinic	triclinic	triclinic	orthorhombic	monoclinic	triclinic
Space group	*C2/c*	*C2/c*	*C2/c*	$P\bar{1}$	$P\bar{1}$	$P\bar{1}$	*Pbca*	*C2/c*	$P\bar{1}$
a (Å)	12.721(9)	12.758(7)	12.640(3)	8.056(2)	9.021(3)	9.677(4)	10.340(2)	16.591(7)	5.669(2)
b (Å)	13.578(8)	13.876(8)	14.330(3)	9.889(3)	13.004(5)	9.968(5)	13.539(3)	16.472(4)	8.868(6)
c (Å)	9.624(9)	9.437(7)	9.680(2)	9.989(2)	25.752(7)	11.716(6)	27.813(7)	14.641(6)	10.497(8)
α (°)	90	90.	90	103.585(4)	82.51(1)	78.69(2)	90	90	76.781(3)
β (°)	99.761(1)	99.557(2)	98.400(9)	97.253(6)	86.76(1)	74.02(3)	90	92.564(2)	86.480(4)
γ (°)	90	90	90	107.040(4)	71.12(1)	68.61(4)	90	90	84.391(3)
V (Å^3)	1638(2)	1648(2)	1734.5(7)	723.1(3)	2834(2)	1005.8(9)	3894(1)	3997(3)	510.9(6)
Z	4	4	4	2	2	2	8	8	1
Goodness-of-fit	1.127	1.036	1.176	1.031	1.061	1.050	1.046	1.006	1.085
$R_1[I > 2\sigma(I)]$	0.0309	0.0450	0.1016	0.0630	0.0461	0.0330	0.0345	0.0568	0.0399
wR_2 [all data]	0.0895	0.1323	0.1994	0.1709	0.1276	0.0764	0.0811	0.1291	0.0780

$R_1 = \sum||F_o| - |F_c||/\sum|F_o|$, $wR_2 = |\sum w(|F_o|^2 - |F_c|^2)|/\sum|w(F_o^2)^2|^{1/2}$.

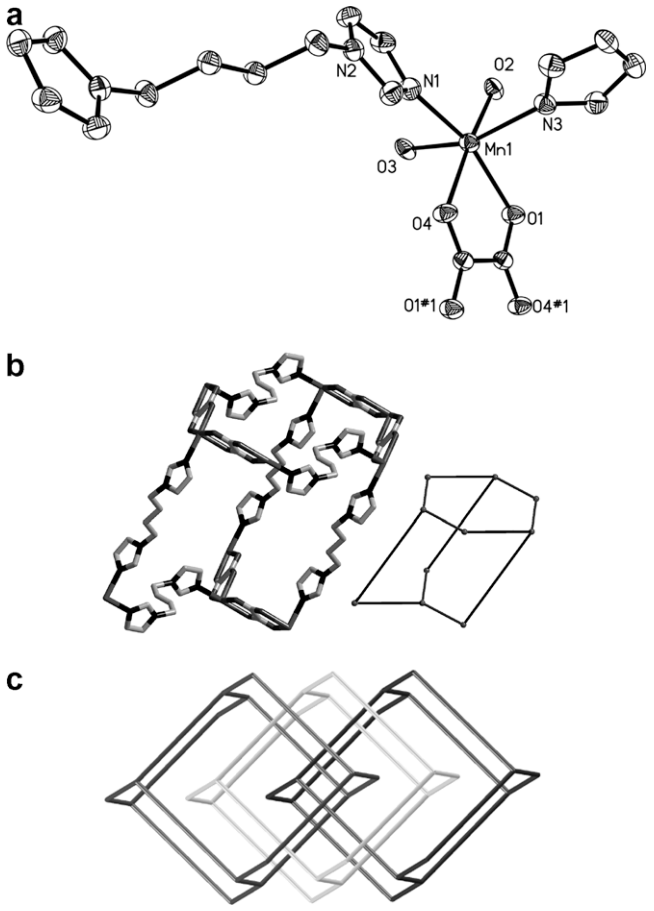

Fig. 2. (a) Coordination environment of the manganese cation in **4**. (b) Single adamantanoid cage. (c) Three interpenetrating diamondoid cages.

ligands to furnish a disordered octahedron geometry. Two crystallographically biim-4 ligands adopt "*S*" shaped and "zigzag" shaped conformations, respectively. The topology of the whole structure can be described as a typically diamondoid framework (Fig. 2b). As can be seen, the diamondoid cage are elongated significantly in one direction, and exhibit maximum dimensions (corresponding to the longest intracage Mn···Mn distances) of 21.37 Å × 20.18 Å × 18.90 Å. Because of the spacious nature of the single network, it allows two identical diamondoid networks to interpenetrate it in a normal mode giving rise to a threefold interpenetrating structure (Fig. 2c). According to topology classification, compound **4** belongs to Class Ia (all the independent nets are related by a single vector and the whole interpenetrating arrays are generated by translating a single net 2 times) [29], with the translating vector of [1 0 0] (8.06 Å).

3.1.3. Structure of $[Co_2(L2)_2(biim\text{-}5)_3 \cdot 6H_2O] \cdot 8H_2O$ (**5**)

As shown in Fig. 3a, there are three kinds of crystallographically unique Co centers in the structure of **5**. Co1 is coordinated by two N atoms (Co–N 2.111(2)–2.112(2) Å) from two neutral ligands and four water molecules (Co–O 2.095(2)–2.153(2) Å), showing a slightly disordered octahedral geometry. Co2 lies at an inversion center and is six-coordinated by four N atoms (Co–N 2.128(2)–2.137(2) Å) from biim-5 ligands and two water molecules (Co–O 2.154(2) Å). Co3 has the same coordination environment to that of Co2. The fumariate anions act as counterions. There exist two kinds of chains. For Co1, each biim-5 ligand connects two Co1 atoms to a 1D polymeric chain (Fig. 3b). For Co2 and Co3, the Co(II) atoms are joined by biim-5 ligands to form a double-stranded

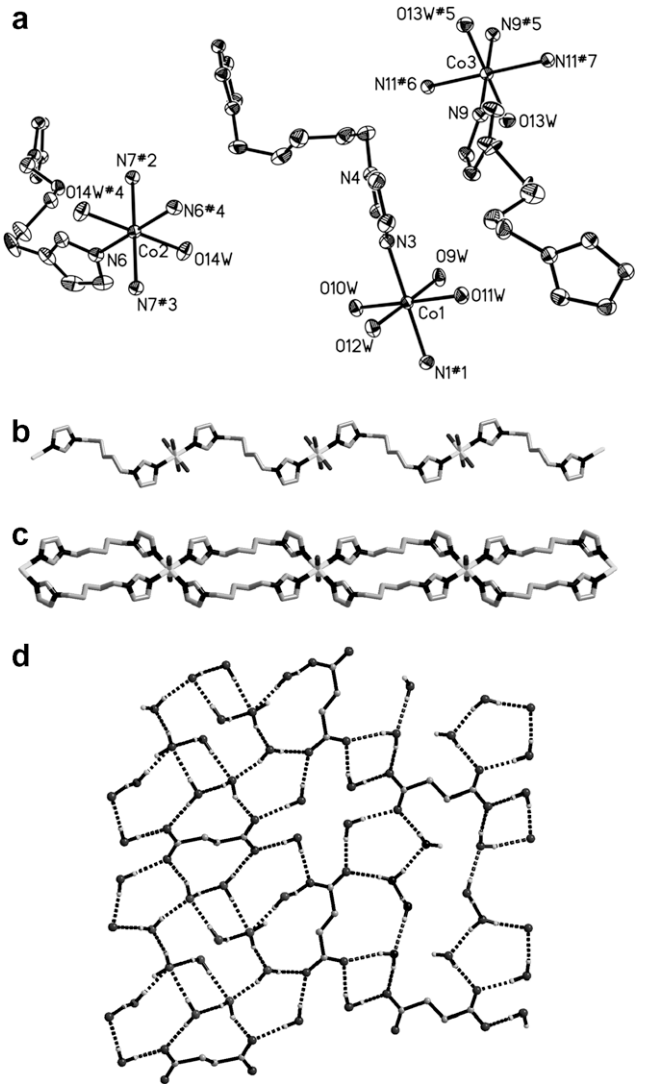

Fig. 3. (a) Coordination environment of the cobalt cations in **5**. (b) View of single chain composed of Co1 and biim-5 ligands. (c) View of double-stranded chain composed of Co2, Co3 and biim-5 ligands. (d) The hydrogen-bonded layer of L2 and water molecules.

chain (Fig. 3c). These two kinds of chains are connected by hydrogen bonds to construct a 3D supramolecular structure (Fig. S1a). As shown in Fig. 3d, the hydrogen bonds lead the water molecules and L2 anions to a 2D supramolecular network. In addition, a notable feature of **6** is the presence of two types of water clusters, namely $(H_2O)_{12}$ and $(H_2O)_8$. Within the $(H_2O)_{12}$ cluster, four water molecules (O8W, $O8W^{\#13}$, $O13W^{\#5}$ and $O13W^{\#12}$, symmetry code: $^{\#5}-x+1, -y+1, -z$; $^{\#12}1+x, y, z$; $^{\#13}2-x, 1-y, -z$) act as hydrogen bonds donors and others act as both donors and acceptors (Fig. S1b). In this water cluster, $O1W^{\#2}$, O2W, $O6W^{\#5}$, $O13W^{\#5}$ and $O1W^{\#3}$, $O2W^{\#13}$, $O6W^{\#12}$, $O13W^{\#12}$ (symmetry code: $^{\#2}-x, -y+2, -z$; $^{\#3}1+x, -1+y, z$) form two types 4-membered $(H_2O)_4$ rings, respectively and these rings are connected by $O7W^{\#2}$ and $O7W^{\#3}$ to form a much lager $(H_2O)_{10}$ ring. The $(H_2O)_{10}$ ring are joined by O8W and $O8W^{\#13}$ to form a $(H_2O)_{12}$ cluster. Moreover, the oxygen atoms O2, O3, O19 and O9 from L2 anions are involved in hydrogen bonds with water molecules, which helped to stabilize the $(H_2O)_{12}$ cluster. In $(H_2O)_{12}$ cluster, the average hydrogen bond is 2.78 Å, while these distances in regular ice, liquid water, and water vapor are 2.74, 2.85, and 2.98 Å, respectively [30]. In $(H_2O)_8$ cluster, four crystallographically unique lattice water molecules ($O3W^{\#8}$, O4W and $O5W^{\#9}$ act as both hydrogen-bond donors

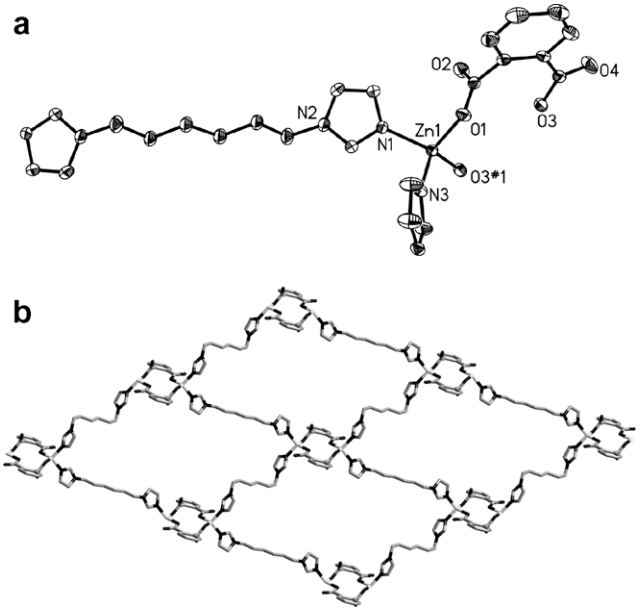

Fig. 4. (a) Coordination environment of the zinc cation in **6**. (b) View of a single layer.

and acceptors, while O14W$^{\#4}$ only acts as a hydrogen-bond donor) and their symmetry-related molecules link to each other to form a $(H_2O)_8$ cluster through hydrogen bonds (Fig. S1c). Furthermore, the oxygen atoms O1, O6$^{\#14}$, O21 and O22$^{\#8}$ from L2 anions (symmetry code: $^{\#14}2-x, 1-y, 1-z$) are involved in hydrogen bonds with water molecules to stabilize the $(H_2O)_8$ cluster.

3.1.4. Structure of [ZnL3(biim-6)] (*6*)

In compound **6**, L3 was introduced to replace L1 ligand of compound **2**. As illustrated in Fig. 4a, each Zn(II) atom is four-coordinated by two O atoms (Zn–O 1.951(2)–1.957(2) Å) from two L3 anions and two N atoms (Zn–N 2.003(2)–2.035(2) Å) from biim-6 ligands to furnish a distorted tetrahedron geometry. The phthalate anions adopt bis(monodentate) coordination mode to connect two central Zn(II) atoms. Every two L3 anions coordinate with the same two Zn(II) atoms and form a dimer. Biim-6 ligands display two kinds of conformations, which link the dimers to a 2D layer network (Fig. 4b).

3.1.5. Structure of [ZnL3(biim-5)] (*7*)

As shown in Fig. 5a, every Zn(II) atom in **7** is four-coordinated by two O atoms from two L3 anions and two N atoms from two biim-5 ligands. The L3 anion adopts bis(monodentate) coordination mode and connects two Zn(II) atoms. As bridged ligand, each biim-5 connects two Zn(II) atoms to form a dimer (Fig. 5b). These dimers are connected by L3 anions to a 2D network with (6,3) topology (Fig. 5c).

3.1.6. Structure of [CdL3(biim-5) · 1.5H_2O] · 0.5H_2O (*8*)

In compound **8**, cadmium ion was introduced to replace zinc ion in compound **7**. As illustrated in Fig. 6a, each Cd(II) atom is eight-coordinated by four O atoms (Cd–O 2.359(5)–2.626(7) Å) [31,32] from two L3 anions, two N atoms (Cd–N 2.264(5)–2.278(5) Å) from two biim-5 ligands and two water molecules (Cd–O 2.487(6)–2.56(2) Å). Two L3 anions connect to the same two Cd(II) atoms in the chelating modes to form a dimer (Fig. 6b). These dimers are joined by biim-5 ligands to a 2D layer network (Fig. 6b).

3.1.7. Structure of [CdL4(biim-6) · 2H_2O] (*9*)

As illustrated in Fig. 7a, each Cd(II) atom in **9** lies on an inversion center and is six-coordinated by two O atoms from two L4 anions, two N atoms from two biim-6 ligands and two water molecules. Each L4 adopts bis(monodentate) coordination mode and connects with two Cd(II) atoms to a 1D chain. These chains are joined by biim-6 ligands to propagate a 2D layer network (Fig. 7b). In addition, hydrogen bonds between L4 and water molecules exist in **9**. These hydrogen bonds link L4 anions and water molecules resulting a 1D infinite chain. These chains stabilize the structure and connect the adjacent layers to form a 3D supramolecular structure (Fig. 7c).

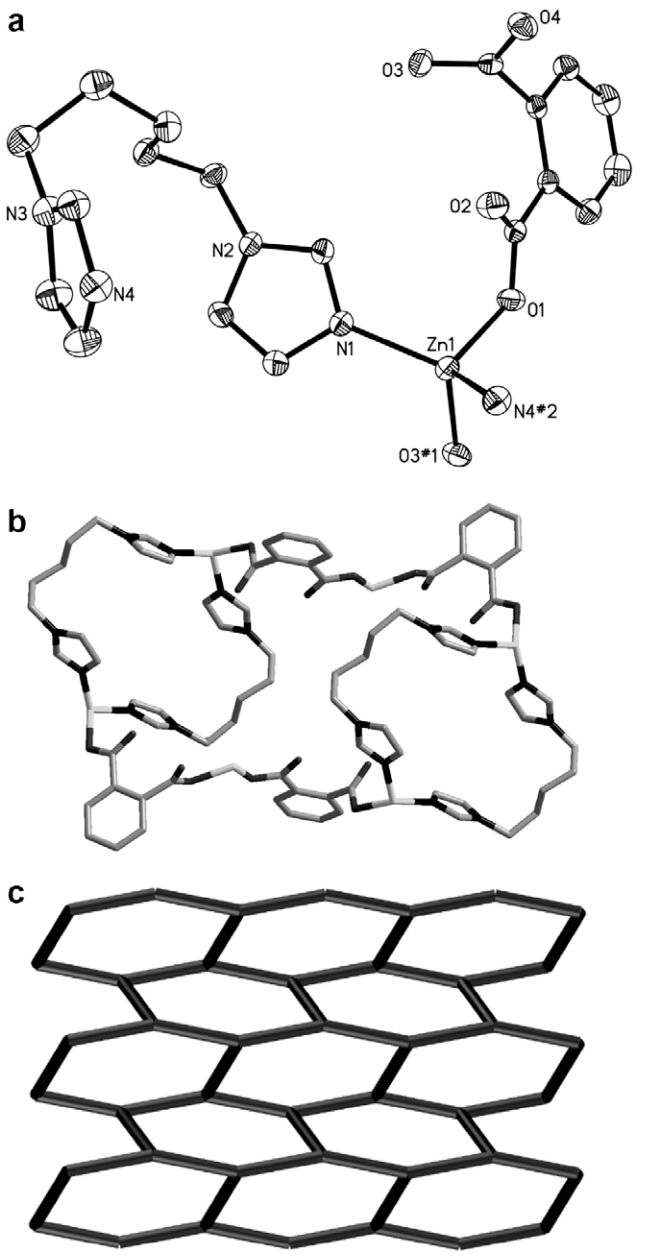

Fig. 5. (a) Coordination environment of the zinc cation in **7**. (b) View of the large ring of (6, 3) network. (c) View of a layer of (6, 3) topology.

3.2. Discussion

3.2.1. Effect of carboxylate anions

As expected, carboxylate anion plays an important role in determining the final structures. All of the L1 anions in **1**-**4** adopt bis(chelating) coordination modes, and M(II) centers are bridged

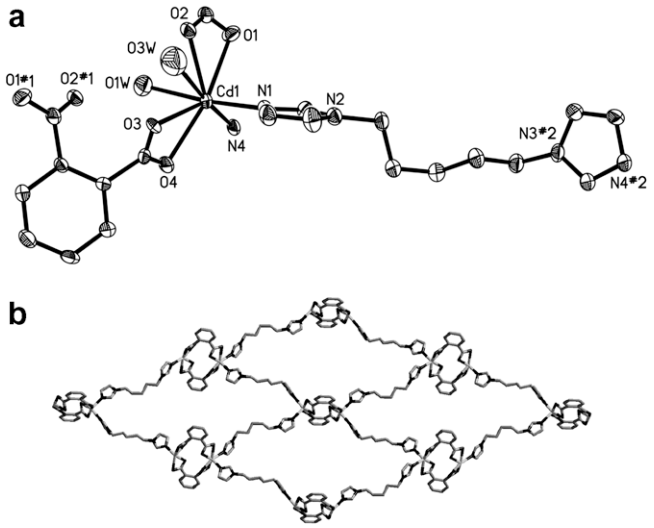

Fig. 6. (a) Coordination environment of the cadmium cation in **8**. (b) View of a single layer of compound **8**.

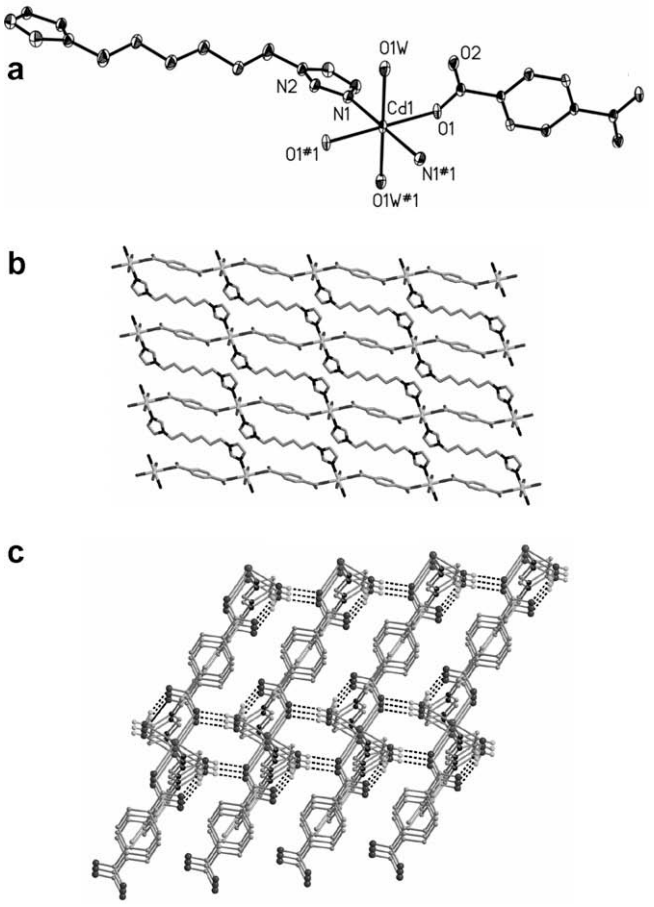

Fig. 7. (a) Coordination environment of the cadmium cation in **9**. (b) View of a single layer. (c) View of the 3D supramolecular structure formed by hydrogen bonds.

by L1 anions to form 1D chain skeletons. L2 anions in **5** act as counterions. Although the L2 anions in **5** are not coordinated with Co(II) ions, they joined by hydrogen bonds with water molecules, which also modulate the whole structure of **5**. L3 anions in **6** and **7** adopt bis(monodentate) coordination modes; and L3 anion in **8** adopts bis(chelating) coordination mode. The M(II) centers in **6** and **8** are linked by L3 anions to dimers, respectively, and the M(II) centers in **7** are linked by L3 anions to a chain. L4 anion in **9** adopts bis(monodentate) mode, and the L4 anions link M(II) center to form a chain.

3.2.2. Effect of bis(imidazole) ligands

In the structures of biim-6, biim-5 and biim-4, the imidazole groups are bridged by different spacers: 1,6-hexyl, 1,5-pentyl and 1,4-butyl. By comparing of the structures of compounds **1**–**9**, it was found that the flexibilities of the bis(imidazole) methylene groups have a great influence to the frameworks, because adjustments in the framework occur to accommodate the bend of the molecules. In compounds **1**–**3**, **6** and **9**, the neutral ligands are biim-6. The methylene groups of **1**–**3** display "*S*" conformations, with the distance between neighboring M(II) centers linked by biim-6 ligands being 11.77–12.34 Å. The methylene groups of **6** and **9** display zigzag conformations, with the distance between neighboring M(II) centers linked by biim-6 ligands being 14.19–16.49 Å. In compounds **5**, **7** and **8**, the neutral ligands are biim-5, and the methylene groups display "*S*" and "3" formed conformations, the distance between neighboring M(II) centers linked by biim-5 ligands are 8.39–15.12 Å. In compounds **4**, the neutral ligand is biim-4, and the methylene groups display "*S*" and zigzag conformations, with the distance between neighboring Mn(II) centers linked by the biim-4 ligands being 13.74 and 14.06 Å.

Comparing compounds **6** with **7**, it can be seen that the neutral ligands biim-6 of **6** display two kinds of conformations. The $[Zn(L3)_2Zn]$ dimers are linked by biim-6 to a 2D network (Fig. 4b). In **7**, biim-5 adopt only one kind of conformation to connect the central Zn(II) atoms to $[Zn(biim\text{-}5)_2Zn]$ dimers (Fig. 5b). By comparing **3** with **4**, the changes are more noticeable. Compound **3** has a 2D layer network, while compound **4** displays a 3D network with diamondoid topology.

3.3. Thermal analysis

In order to characterize the compounds more fully in terms of thermal stability, some of their thermal behaviors were studied by TGA (Fig. S2). The experiments were performed on samples consisting of numerous single crystals of **3**, **5** and **8**–**9** under N_2 atmosphere with a heating rate of 10 °C/min.

For compound **3**, the weight loss corresponding to the release of water molecules are observed from room temperature to 135 °C (obsd 3.9%, calcd 4.75%). The anhydrous compound begins to decompose at 253 °C. For compound **5**, the weight loss corresponding to the release of water molecules are observed from room temperature to 105 °C (obsd 19.1%, calcd 20.83%). The anhydrous compound begins to decompose at 253 °C. For compound **8**, the weight loss corresponding to the release of water molecules are observed from room temperature to 175 °C (obsd 4.7%, calcd 3.57%). The anhydrous compound begins to decompose at 240 °C. For compound **9**, the weight loss corresponding to the release of water molecules are observed from 120 to 236 °C (a weight loss of 5.1% is smaller than the calculated value 6.78% probably resulting from a slow losing of the guest molecules in the air at room temperature). The anhydrous compound begins to decompose at 305 °C.

3.4. Luminescent properties

The luminescence spectra of neutral ligands biim-5 and biim-6 were examined in an ethanol solution, because the solid samples cannot be isolated at room temperature (Table 2, Fig. S3). The solid state luminescence spectra of free carboxylate ligands, compounds

Table 2
The wavelengths of the emission maximums and excitation (nm)

Compound	2	6	7	8	9
λ_{em}	403	427	406	441	429
λ_{ex}	348	315	346	366	352
Ligand	Biim-5	Biim-6	Phthalic anhydride		H_2L4
λ_{em}	400	363, 379	389		390
λ_{ex}	342	343	352		347

2 and **6–9** were examined at room temperature (Table 2, Figs. S4 and S5).

Biim-5 shows an emission at 400 nm; and biim-6 shows a maximum at 379 nm and a shoulder at 363 nm. The peaks of the ligands biim-5 and biim-6 are probably due to $\pi^* \rightarrow \pi$ transitions [33].

The emissions of free ligands of phthalic anhydride (389, λ_{ex} = 352 nm) and H_2L4 (390 nm, λ_{ex} = 347 nm) [34] can also exhibit fluorescence at room temperature. The emission bands of the dicarboxylate ligands can be assigned to the $\pi^* \rightarrow n$ transitions [35]. The Zn(II) compounds (**2**, **6** and **7**) exhibit emissions at about 403 nm for **2**, at 427 nm for **6**, and at 406 nm for **7**. The emission peaks for these compounds may be attributed to the ligand-to-metal charge-transfer (LMCT) transitions [36,37]. The luminescent spectra of Cd(II) compounds **8** (441 nm) and **9** (429 nm) may also be assigned as LMCT [37].

3.5. Magnetic properties

The temperature-dependent magnetic susceptibility data of compounds **1**, **3** and **4** have been measured from polycrystalline samples at an applied magnetic field of 1000 Oe in the temperature range of 2–300 K (Fig. 8). Although compounds **1** and **3** are two-dimensional, and **4** is three-dimensional, from a magnetic point of view, the systems can be considered as one-dimensional owing to the long M···M distances (11.77 Å for **1**, 12.34 Å for **3** and 12.46 Å for **4**) along the bis(imidazole) ligands, for which we can assume a negligible magnetic exchange through the biim-6 and biim-4 ligands [38].

For **1**, the $\chi_m T$ value at 300 K is 0.451 $cm^3\ mol^{-1}$ K (1.900 μ_B), which is as expected (1.732 μ_B, considering g = 2.00) for a magnetically isolated spin doublet. Upon cooling, $\chi_m T$ gradually increase, reaching a value of 0.551 $cm^3\ mol^{-1}$ K at 2 K. This feature is indicative of the occurrence of an overall weak ferromagnetic coupling between the Cu(II) ions [39–43]. The magnetic susceptibility in the range of 300–100 K obeys the Curie–Weiss law with the Curie constant, C = 0.451 $cm^3\ mol^{-1}$ K, and the Weiss constant, Θ = 0.329 K.

For **3**, the $\chi_m T$ value at 300 K is 5.077 $cm^3\ mol^{-1}$ K (6.372 μ_B), which is slightly higher than the spin-only value (5.916 μ_B, considering g = 2.00) expected for a high-spin d^5 Mn(II) ion. Upon cooling, the values of $\chi_m T$ keep smoothly decreasing in 300–34 K range, and then exhibit a maximum value of 2.899 $cm^3\ mol^{-1}$ K at 32 K before goes down quickly to a minimum value of 0.186 $cm^3\ mol^{-1}$ K at 2 K. This behavior is indicative of antiferromagnetic coupling between the Mn(II) centers through the oxalate-bridging ligands. The inflexion at 32 K may be due to a small canting of the sub-lattice or a small amount of impurity [34]. The magnetic susceptibility above 34 K can be well fit to Curie–Weiss law with C = 5.66 $cm^3\ mol^{-1}$ K, Θ = –35.62 K. The negative Θ value further confirms the presence of antiferromagnetic interaction in **3**.

The magnetic behavior of compounds **3** and **4** is quite similar. For **4**, the $\chi_m T$ value at 300 K is 4.841 $cm^3\ mol^{-1}$ K (6.223 μ_B). Upon cooling, the values of $\chi_m T$ keep smoothly decreasing in 300–34 K range, and then go down quickly to a minimum value of 0.183 $cm^3\ mol^{-1}$ K at 2 K, indicating an overall antiferromagnetic coupling in compound **4**. There also exists an inflexion at 32 K [44]. The magnetic susceptibility above 34 K can be well fit to Curie–Weiss law with C = 5.38 $cm^3\ mol^{-1}$ K, Θ = –35.06 K.

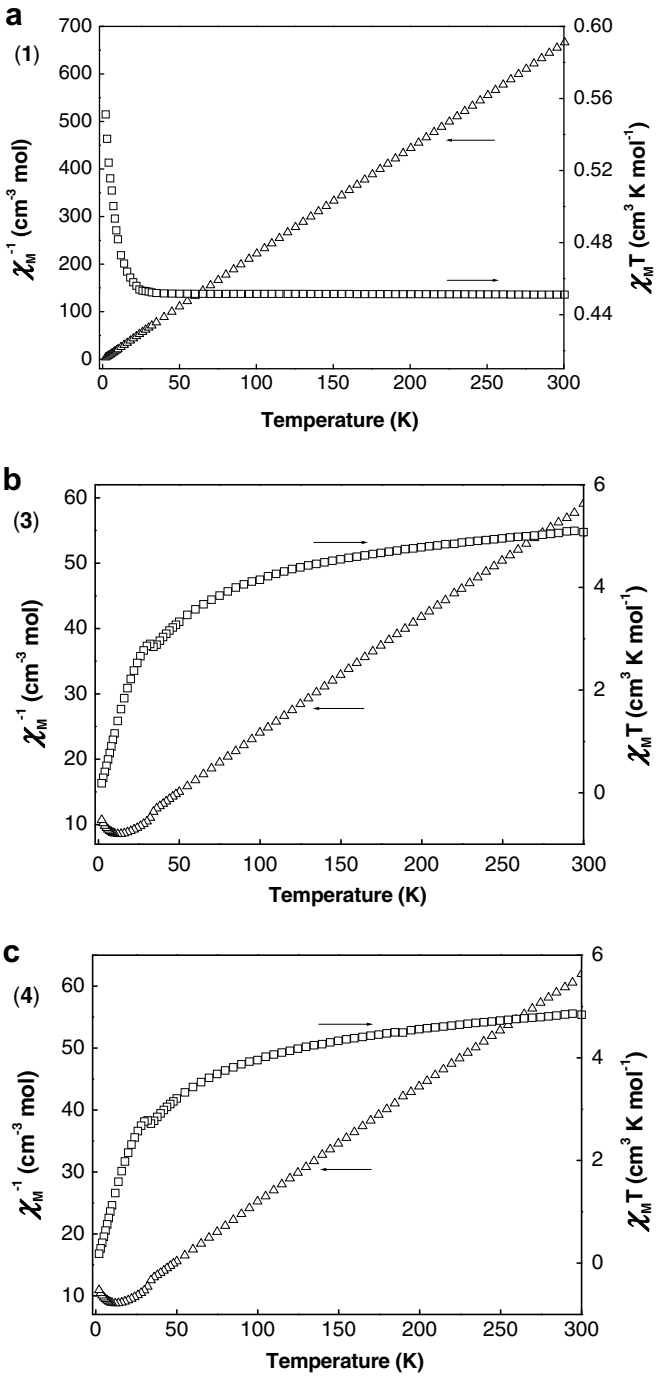

Fig. 8. Plots of the temperature dependence of $\chi_m T$ (squares) and χ_m^{-1} (triangles) for compounds **1**, **3** and **4**.

Acknowledgments

We thank the Program for New Century Excellent Talents in Chinese University (NCET-05-0320), Program for Changjiang Scholars and Innovative Research Teams in Chinese University and the Analysis and Testing Foundation of Northeast Normal University for support.

Appendix A. Supplementary data

CCDC 671105–671113 contain the supplementary crystallographic data for **1**–**9**. These data can be obtained free of charge via http://www.ccdc.cam.ac.uk/conts/retrieving.html, or from the Cambridge Crystallographic Data Centre, 12 Union Road, Cambridge CB2 1EZ, UK; fax: (+44) 1223-336-033; or e-mail: deposit@ccdc.cam.ac.uk. Supplementary data associated with this article can be found, in the online version, at doi:10.1016/j.poly.2008.07.026.

References

[1] S. Kitagawa, R. Kitaura, S.I. Noro, Angew. Chem., Int. Ed. 43 (2004) 2334.
[2] O.R. Evans, W. Lin, Acc. Chem. Res. 35 (2002) 511.
[3] X.H. Bu, M.L. Tong, H.C. Chang, S. Kitagawa, S.R. Batten, Angew. Chem., Int. Ed. 43 (2004) 192.
[4] M. Munakata, L.P. Wu, T. Kuroda-Sowa, M. Maekawa, K. Moriwaki, S. Kitagawa, Inorg. Chem. 36 (1997) 5416.
[5] Y. Suenaga, S.G. Yan, L.P. Wu, I. Ion, T. Kuroda-Sowa, M. Maekawa, M. Munakata, J. Chem. Soc., Dalton Trans. 23 (1998) 1121.
[6] K.A. Hirsch, S.R. Wilson, J.S. Moore, Inorg. Chem. 36 (1997) 2960.
[7] L. Carlucci, G. Ciani, P. Macchi, D.M. Proserpio, A. Sironi, Chem. Commun. (1997) 631.
[8] B.-H. Ye, M.-L. Tong, X.-M. Chen, Coord. Chem. Rev. 249 (2005) 545.
[9] J. Yang, Q. Yue, H.M. Yuan, J.S. Chen, S.N. Wang, Inorg. Chem. 45 (2006) 2857.
[10] C.N.R. Rao, S. Natarajan, R. Vaidhyanathan, Angew. Chem., Int. Ed. 43 (2004) 1466.
[11] G. Férey, C. MellotDraznieks, C. Serre, F. Millange, Acc. Chem. Res. 38 (2005) 217.
[12] X.-L. Wang, C. Qin, E.-B. Wang, Z.-M. Su, Chem. Eur. J. 12 (2006) 2680.
[13] B.F. Hoskins, R. Robson, D.A. Slizys, J. Am. Chem. Soc. 119 (1997) 2952.
[14] E.-Q. Gao, Y.-X. Xu, C.-H. Yan, CrystEngComm. 6 (2004) 298.
[15] J. Fan, C. Slebodnick, R. Angel, B.E. Hanson, Inorg. Chem. 44 (2005) 552.
[16] L. Zhang, X.-Q. Lü, C.-L. Chen, H.-Y. Tan, H.-X. Zhang, B.-S. Kang, Cryst. Growth Des. 5 (2005) 283.
[17] X. Li, R. Cao, W. Bi, Y. Wang, Y. Wang, X. Li, Z. Guo, Cryst. Growth Des. 5 (2005) 1651.
[18] G.-H. Cui, J.-R. Li, J.-L. Tian, X.-H. Bu, S.R. Batten, Cryst. Growth Des. 5 (2005) 1775.
[19] J.-F. Ma, J. Yang, G.-L. Zheng, L. Li, J.-F. Liu, Inorg. Chem. 42 (2003) 7531.
[20] J.-F. Ma, J. Yang, G.-L. Zheng, L. Li, Y.-M. Zhang, F.-F. Li, J.-F. Liu, Polyhedron. 23 (2004) 553.
[21] J. Yang, J.-F. Ma, Y.-Y. Liu, J.-C. Ma, H.-Q. Jia, N.-H. Hu, Eur. J. Inorg. Chem. (2006) 1208.
[22] J. Yang, J.-F. Ma, Y.-Y. Liu, S.-L. Li, G.-L. Zheng, Eur. J. Inorg. Chem. (2005) 2174.
[23] Y.-H. So, Macromolecules 25 (1992) 516.
[24] Y. Wang, X.-F. Wang, T.-A. Okanura, B. Xu, W.-Y. Sun, N. Ueyama, Chinese J. Inorg. Chem. 22 (2006) 1487.
[25] G.M. Sheldrick, SHELXS-97 Programs for X-ray Crystal Structure Solution, University of Göttingen, Göttingen, Germany, 1997.
[26] G.M. Sheldrick, SHELXL-97, Programs for X-ray Crystal Structure Refinement, University of Göttingen, Göttingen, Germany, 1997.
[27] L.J. Farrugia, WINGX, A Windows Program For Crystal Structure Analysis, University of Glasgow, Glasgow, UK, 1988.
[28] T. Comer, International Tables for X-ray Crystallography, vol. C, Kluwer Academic Publisher, Dordercht, The Netherlands, 1992.
[29] V.A. Blatov, L. Carlucci, G. Ciani, D.M. Proserpio, CrystEngComm. 6 (2004) 377.
[30] R. Ludwig, Angew. Chem., Int., Ed. 40 (2001) 1808.
[31] J. Zhang, Z.-J. Li, Y. Kang, J.-K. Cheng, Y.-G. Yao, Inorg. Chem. 43 (2004) 8085.
[32] W. Clegg, J.T. Cressey, A. Mcamley, B.P. Straughan, Acta Crystallogr., Sect. C 51 (1995) 234.
[33] Z. Guo, R. Cao, X. Li, D. Yuan, W. Bi, X. Zhu, Y. Li, Eur. J. Inorg. Chem. (2007) 742.
[34] W. Chen, J.-Y. Wang, C. Chen, H.-M. Yuan, J.-S. Chen, S.-N. Wang, Inorg. Chem. 42 (2003) 944.
[35] Y.-S. Song, B. Yan, Z.-X. Chen, J. Solid State Chem. 179 (2006) 4037.
[36] J. Tao, M.L. Tong, J.X. Shi, X.M. Chen, S.W. Ng, Chem. Commun. (2000) 2043.
[37] M. Li, J. Xiang, L. Yuan, S. Wu, S. Chen, J. Sun, Cryst. Growth Des. 6 (2006) 2036.
[38] O. Kahn, Molecular Magnetism, VCH, Weinheim, Germany, 1993. references therein.
[39] P. Day, Science 261 (1993) 431.
[40] S. Decurtins, H.W. Schmalle, P. Schneuwly, R. Schneuwly, L.M. Zheng, J. Ensling, A. Hauser, Inorg. Chem. 34 (1995) 5501.
[41] E. Coronado, J.R. Galán-Mascarós, C. Martí-Gastaldo, Inorg. Chem. 45 (2006) 1882.
[42] E. Coronado, P. Day, Chem. Rev. 104 (2004) 5419.
[43] U. García-Couceiro, O. Castillo, A. Luque, J.P. García-Terán, G. Beobide, P. Román, Cryst. Growth Des. 6 (2006) 1839.
[44] M.B. Salah, S. Vilminot, T. Mhiri, M. Kurmoo, Eur. J. Inorg. Chem. (2004) 2272.

of the metal ions. Schrauzer and Windgassen [10] found that inorganic metal complexes might exhibit conducting properties, which are nowadays the subject of an active research area both in the field of solid state physics and inorganic chemistry; especially in nano-chemistry [11]. Conducting and semiconducting compounds have attracted considerable focus because of their useful function in molecular electronics and vital biological life processes [12]. Such semiconducting metal complexes stand on the threshold of a bright and exciting future. One of the most important aspects of the studies of electronic characteristics of such compounds is the relationship to their chemical structures, which is yet to be explored in detail. It is also considered that different applications might be found for supramolecular inorganic semiconductors, which do not necessarily parallel to the present uses for organic and discrete inorganic semiconducting materials. Much attention has also been paid to the optical properties of such compounds because of their application in material chemistry, particularly in optoelectronics. There are very rare reports on Schiff base [13] complexes that have such properties. Their preparation is still extremely challenging.

Keeping in view the aspects stated above, which open up new vistas for synthesizing unique metal complexes of both fundamental and technological importance, our aim is to prepare new Schiff base metal complexes and to tune their properties. We report here the synthesis and characterization of a new hexadentate N_4O_2 donor symmetrical Schiff base ligand having two carboxylic acid groups and its metal complexes, paying special attention to their X-ray crystal structures, electrical conductivity and optical properties. In all the three complexes prepared, both carboxylic acid groups remain non-coordinated to the metal ions, but surely exert their influence on the formation of mono- and bifurcated hydrogen bondings, which help to build up the supramolecular architecture and its persuasion in conductivity. This is in contrast to similar disalicylidene type complexes [14] that have no carboxylic acid moiety.

Density functional theory (DFT) calculations have also been carried out to optimize the structures and comparisons have been made with the experimental geometries. Moreover, the theoretical outcome of the DFT approach gives insight into the electronic structure and spectral properties of the complexes.

2. Experimental

2.1. Materials and general methods

Triethylenetetramine was purchased from Aldrich and used as such. 3-Formylsalicylic acid was synthesized according to Duff and Bills [15]. Spectrograde solvents were used for physical measurements. All the other reagents and solvents were purchased from commercial sources, purified and dried by standard procedures [16].

2.2. Physical measurements

The elemental analyses were carried out on Elementar Vario EL III, Carlo Erba 1108 elemental analyzers at the Sophisticated Analytical Instrument Facility (SAIF), Central Drug Research Institute, Lucknow. The electronic spectra (in DMSO and other media as indicated in the text) were recorded on a Shimadzu UV-2401PC spectrophotometer and infrared spectra (KBr) on a Perkin–Elmer L120-000A spectrophotometer. The ESR spectrum was measured in an ESR spectrometer at SAIF, IIT Madras. The molar conductance (10^{-3} M in DMSO) was measured using an Elico conductivity bridge and the magnetic data were measured on a Guoy Balance.

The samples for electrical conductivity measurements were prepared from the complexes in the form of tablets; their thickness was 0.1 cm at a pressure of approximately 1×10^8 Pa. These tablets were placed between two copper electrodes with silver paste and contacts were tested to be ohmic. The electrical conductivities of the prepared complexes were measured with a Keithley 6514 system electrometer, by applying a dc voltage using a Keithely 230 programmable voltage source. The conductivities were calculated by using the general equation $\sigma = (I/V_c)(d/a)$, where (I) is the current in amperes, V_c the potential drop across the sample of cross-sectional area (a) and thickness (d). Optical absorption spectra (in the solid state) were taken using a Perkin–Elmer Lambda 2S Double Beam spectrophotometer.

2.3. Computational details

The calculations were carried out using the Amsterdam density functional (ADF) program package [17]. Triple-ζ STO (Slater-type orbital) basis sets with one additional polarization function were used throughout. [Ar3d], [Ne] and [He] core definitions were used for Cd, Ni/Mn and C/N/O, respectively. Hence the valence set on the metals includes the $(n-1)$s and $(n-1)$p shells. The density functional chosen for the calculations was BP (Becke's gradient correction for exchange [18] plus Perdew's gradient correction for correlation [19]), which has been shown to yield satisfactory numerical results in previous computations. Electron excitation energies related to the electronic absorption spectra were calculated using the time-dependent density functional response theory (TDDFT) [20] as implemented in the ADF program. The recent implementation of TDDFT in the updated ADF program allows calculations of excitation energies for open-shell systems. Calculations of open-shell systems were spin-unrestricted. The spin multiplicities (2S + 1) for the Ni-, Cd- and Mn-complexes are 3, 1 and 6, respectively.

2.4. Preparation of the ligand. 1,8-N-Bis(3-carboxy)disalicylidene-3,6-diazaoctane1,8-diamine, (H_4fsatrien)

3-Formylsalicylic acid (3-fsa) (1.66 g, 10 mmol) was dissolved in methanol (25 ml), to which triethylenetetramine (trien) (0.73 g, 5 mmol) taken in methanol (20 ml) was added dropwise with stirring. Immediately, a yellow solution was obtained. Glacial acetic acid (3–4 drops) were then added to it with stirring to facilitate completion of the condensation reaction; stirring was continued for 6 h at −10 °C until the separation of a yellow powdery compound at room temperature. It was filtered off, washed with methanol and ether, and dried in vacuo over fused $CaCl_2$. Yield 25%. *Anal.* Calc. for $C_{22}H_{26}N_4O_6$ (H_4fsatrien): C, 59.72; H, 5.92; N, 12.66. Found: C, 59.63; H, 5.89; N, 12.71%. IR (KBr, cm^{-1}): 3412, 3290 (ν_{OH}, ν_{NH}), 1657 ($\nu_{C=N}$). UV–Vis (DMSO, λ_{max}, nm (ε, $L\,M^{-1}\,cm^{-1}$)): 265, 360, 495 (1128), 895 (23). ^{1}H NMR (DMSO-d_6, 300 MHz, ppm, 298 K): δ 12.28 (2H, s, COO*H*), 10.8(2H, s, O*H*), 8.94 (2H, s, C*H*=N), 7.91 (2H, d, Ar-*H*), 7.33 (2H, d, Ar-*H*), 6.67 (2H, t, Ar-*H*), 6.2 (2H, br, N*H*), 3.00–3.83 (8H, m, C*H*2), 2.50–2.79 (4H, m, C*H*2). ^{13}C NMR (DMSO-d_6, 300 MHz, ppm, 298 K): δ 172 (*C*OOH), 161.5 (*C*=N), 167.1, 139.1, 136.6, 130.3, 116.93, 114.09 (Ar-*C*), 51.2, 50.2, 49.15 (*C*H2).

Due to the poor yield of the ligand, we used the *in situ* reaction procedure for the synthesis of the metal complexes.

2.5. Syntheses of the metal complexes. [M(H_2fsatrien)] (M = Ni (**1**), Cd (**2**) and Mn (**3**))

A solution of the ligand H_4fsatrien was prepared by the method described above, by reacting 3-formylsalicylic acid (1.66 g, 10 mmol) and trien (0.73 g, 5 mmol) in methanol (45 ml). The metal(II) acetate (5 mmol), dissolved in minimum volume of methanol (15 ml), was then added dropwise to the Schiff base solution with stirring, and the mixture was kept under reflux for 1 h.

Precipitation occurred for all of the above complexes during the refluxing, and the precipitates were collected by filtration under the hot conditions. The precipitates were washed thoroughly with methanol and diethyl ether, and dried in vacuum over fused $CaCl_2$. The concentration, cooling and slow evaporation of the mother liquor produced crystalline compounds, suitable for single X-ray crystal study, for the nickel(II) and cadmium(II) complexes. The X-ray quality crystal of the manganese(II) complex was obtained by slow evaporation of a solution of the complex in methanol–dichloromethane–acetonitrile. Yield 70–85%. *Anal.* Calc. for $C_{22}H_{24}N_4O_6Ni$ (**1**): C, 52.94; H, 4.85; N, 11.22. Found: C, 52.89; H, 4.93; N, 11.16%. IR (KBr, cm^{-1}): 3425, 3266 (ν_{OH}, ν_{NH}), 1644 ($\nu_{C=N}$). UV–Vis (DMSO, λ_{max}, nm (ε, L M^{-1} cm^{-1})): 385 (261), 585 (9.1), 850 (20.4), 990 (15.9); (Nujol, λ_{max}, nm): 350, 400 (sh), 540 (sh), 594 (sh), 822 (sh), 940, 1025. Molar conductivity (DMSO): Λ_M = 14.1 Ω^{-1} mol^{-1} cm^2. Magnetism (solid state, room temperature): μ_{eff} = 3.05 BM. Colour: snuff.

Anal. Calc. for $C_{22}H_{24}N_4O_6Cd$ (**2**): C, 47.79; H, 4.37; N, 10.13. Found: C, 47.83; H, 4.41; N, 10.19%. IR (KBr, cm^{-1}): 3420, 3275 (ν_{OH}, ν_{NH}), 1637 ($\nu_{C=N}$). UV–Vis (DMSO, λ_{max}, nm (ε, L M^{-1} cm^{-1})): 267, 353. Molar conductivity (DMSO): Λ_M = 15.3 Ω^{-1} mol^{-1} cm^2. Magnetism (solid state, room temperature): Diamagnetic. ^1H NMR (DMSO-d_6, 300 MHz, ppm, 298 K): δ 8.49 (2H, s, C*H*=N), 7.15 (2H, d, Ar-*H*), 6.81 (2H, d, Ar-*H*), 6.62 (2H, t, Ar-*H*), 6.08 (2H, br, NH), 3.02–3.44 (8H, m, C*H*2), 2.41–2.70 (4H, m, C*H*2). ^{13}C NMR (DMSO-d_6, 300 MHz, ppm, 298 K): δ 176 (*C*OOH), 169.2 (*C*=N), 168.6, 140.1, 133.3, 126.5, 119, 112.2 (Ar-*C*), 55.3, 49.1, 46 (*C*H2). Colour: off white.

Anal. Calc. for $C_{22}H_{24}N_4O_6Mn$ (**3**): C, 53.34; H, 4.88; N, 11.31. Found: C, 53.29; H, 4.92; N, 11.35%. IR (KBr, cm^{-1}): 3451, 3264 (ν_{OH}, ν_{NH}), 1640 ($\nu_{C=N}$). UV–Vis (DMSO, λ_{max}, nm (ε, L M^{-1} cm^{-1})): 241 (10889), 262.5 (28752), 348.5 (18894), 867 (87), 874.5 (85); (DMF, λ_{max}, nm (ε, L M^{-1} cm^{-1})): 400 (21300) (br), 405 (9873) (sh). Molar conductivity (DMSO): Λ_M = 16.2 Ω^{-1} mol^{-1} cm^2. Magnetism (solid state, room temperature): μ_{eff} = 5.81 BM. ESR (at RT polycrystalline state): g_{av} = 2.0. Colour: shining yellow.

Table 1
Crystal data and structure refinement parameters for **1**, **2** and **3**

	1	2	3
Empirical formula	$C_{22}H_{24}NiN_4O_6$	$C_{22}H_{24}CdN_4O_6$	$C_{22}H_{24}MnN_4O_6$
Formula weight	499.16	552.85	495.39
Crystal size (mm)	0.28 × 0.17 × 0.06	0.32 × 0.29 × 0.21	0.40 × 0.30 × 0.20
Crystal system	orthorhombic	monoclinic	orthorhombic
Space group	*P*2(1)2(1)2(1)	*P*2(1)/*c*	*Pbca*
Temperature (K)	120(2)	120(2)	120(2)
a (Å)	8.7826(14)	12.686(2)	16.055(2)
b (Å)	15.209(3)	14.723(3)	15.2764(19)
c (Å)	15.545(3)	11.620(2)	17.230(2)
α (°)	90	90	90
β (°)	90	91.279(2)	90
γ (°)	90	90	90
Cell volume (Å^3)	2076.4(6)	2169.7(7)	4226.0(9)
F(000)	1040	1120	2056
Z	4	4	8
D_{calc} (Mg m^{-3})	1.597	1.692	1.557
μ (mm^{-1})	0.985	1.055	0.674
θ Range for data collection (°)	1.87–28.29	1.61–28.18	2.19–28.26
T_{max}, T_{min}	0.9433, 0.7701	0.8089, 0.7289	0.8770, 0.7742
Goodness-of-fit on F^2	1.038	1.030	1.039
Final *R* indices [$I > 2\sigma(I)$]	R_1 = 0.0412, wR_2 = 0.0977	R_1 = 0.0262, wR_2 = 0.0685	R_1 = 0.0347, wR_2 = 0.0963
R indices (all data)	R_1 = 0.0493, wR_2 = 0.1022	R_1 = 0.0284, wR_2 = 0.0699	R_1 = 0.0358, wR_2 = 0.0974
Largest difference in peak and hole (e Å^{-3})	0.783 and −0.380	1.039 and −0.298	0.419 and −0.251

2.6. Crystallographic data collection and structure determination

The crystal data and refinement details are summarized in Table 1. In each case, a single crystal was mounted using Paratone(g) oil onto a glass fiber and cooled to the data collection temperature. Data were collected on a Brüker-AXS APEX CCD diffractometer with monochromatized Mo Kα radiation (λ = 0.71073 Å). Unit cell parameters were obtained from 60 data frames, 0.3° ω, from three different sections of the Ewald sphere. The systematic absences in the diffraction data and the unit cell parameters were uniquely consistent with the reported space groups. An inspection of the packing diagram of complex (**1**) displays no overlooked symmetry and the cell analysis routines in PLATON suggested no other unit cell or space group [21]. The data-set was treated with SADABS absorption corrections based on redundant multiscan data [22]. The structures were refined by full matrix least squares, based on F^2. Refinement of the absolute structure parameter in complex (**1**) yielded the Flack parameter 0.497(16), suggesting a twinned data set. All non-hydrogen atoms were refined with anisotropic displacement parameters. Hydrogen atoms on the hydroxyl groups, H(1) and H(2), were located from the electron density difference map and refined with a riding model. All other hydrogen atoms were treated as idealized contributions. Structure factors were contained in the SHELXTL 6.12 program library [23].

3. Results and discussion

The new dibasic hexadentate ligand 1,8-*N*-bis(3-carboxy)disalicylalidene-3,6-diazaoctane-1,8-diamine, H_4fsatrien, was prepared by the condensation reaction of 3-formylsalicylic acid with triethylenetetramine (2:1 molar ratio) in methanol, as described later and shown in Scheme 1. The *in situ* reaction of the ligand components and $Ni(CH_3COO)_2 \cdot 4H_2O$, $Cd(CH_3COO)_2 \cdot 2H_2O$ and $Mn(CH_3COO)_2 \cdot 2H_2O$ in methanol (Scheme 1) yielded the complexes (**1**)–(**3**) in good yield and purity. The ligand and all the complexes gave correct the elemental analyses and were further characterized by IR, UV–Vis, NMR, ESR, molar conductivity, magnetic measurements and X-ray crystallography.

3.1. Crystal and DFT-optimized structures

All the three complexes (**1**)–(**3**) were derived from the same polydentate ligand utilizing N_4O_2 donor sites. Complexes (**1**) and (**2**) crystallize in different crystallographic systems, orthorhombic (space group *P*2(1)2(1)2(1)) and monoclinic (space group *P*2(1)/*c*), respectively, while complex (**3**) crystallizes in the same crystal system as (**1**), with the space group *Pbca*. The crystallographic and refinement data are summarized in Table 1. Selected bond lengths and angles, from both the experiment and the DFT optimization, are given in Table 2. All cartesian coordinates are provided in the Supporting information (S1 and S2).

In general, there is good agreement between the calculated and X-ray crystal structural parameters, especially for the Ni-complex, where the largest deviation is 0.1 Å for the bond lengths and 5° for the bond angles. Relatively large discrepancies with the X-ray crystal measurements are found for the Mn-complex, where the largest deviation is 0.19 Å for the bond lengths and 8° for the bond angles. While the optimized Mn–N(2) and Mn–N(3) bond lengths are somewhat larger than the experimental ones, the Mn–N(1) and Mn–N(4) bond lengths optimized are notably (up to 0.2 Å) smaller than those in the crystal structure. Nevertheless, both experiment and theoretical calculations show an octahedral environment for the central metal ions. In the case of the Cd-complex, the calculated structural parameters compared in most cases favorably with the experimental ones.

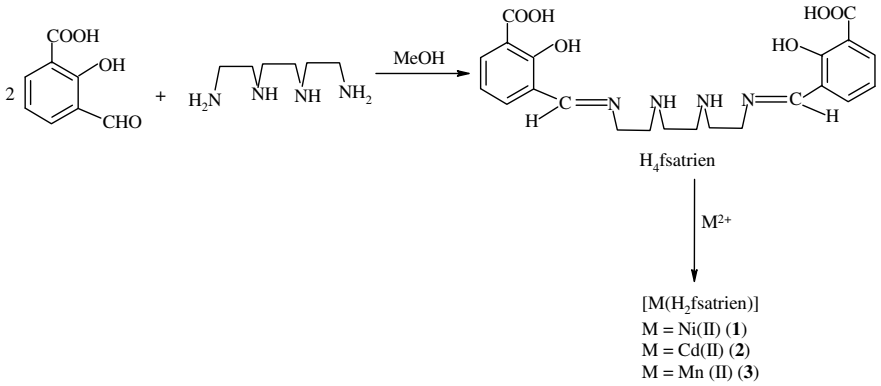

Scheme 1.

The molecular structures of these complexes consist of pseudo-octahedrally coordinated metal ions with a hexadentate ligand. The ORTEP drawings of these molecular structures are depicted in Fig. 1 (**1**), Fig. 2 (**2**) and Fig. 3 (**3**). The metal ions are surrounded by two oxygen atoms in *cis* positions, two imino nitrogen atoms and two amine nitrogen atoms to complete the distorted octahedron. This arrangement is consistent with that of Ni(sal)$_2$trien · 3H$_2$O [24].

Table 2
Selected bond lengths (Å) and bond angles (°) for **1**, **2** and **3**

Bonds (in Å)/angles (°)	Experimental	Theoretical
*Ni-complex (**1**)*		
Ni–N(2)	2.110(3)	2.159
Ni–N(3)	2.145(3)	2.249
Ni–N(4)	2.041(3)	2.016
Ni–N(1)	2.034(3)	2.001
Ni–O(4)	2.039(2)	2.049
Ni–O(1)	2.053(2)	2.039
O(4)···O(6)[a]	2.445(3) (1.663)	2.511 (1.538)
O(1)···O(2)[a]	2.456(3) (1.675)	2.513 (1.537)
N(4)–Ni–N(1)	172.3	175.0
N(3)–Ni–O(4)	167.4	162.3
N(2)–Ni–O(1)	165.7	164.5
O(6)–H(6)···O(4)	153.9	157.7
O(2)–H(2)···O(1)	153.8	157.5
*Cd-complex (**2**)*		
Cd–N(2)	2.3544(16)	2.500
Cd–N(3)	2.3566(16)	2.512
Cd–N(4)	2.3041(17)	2.312
Cd–N(1)	2.3060(16)	2.311
Cd–O(1)	2.3070(14)	2.319
Cd–O(4)	2.3024(13)	2.313
O(2)···O(1)[a]	2.430(2) (1.477)	2.506 (1.516)
O(5)···O(4)[a]	2.455(2) (1.673)	2.513 (1.524)
N(4)–Cd–N(1)	155.7	164.3
N(2)–Cd–O(1)	143.7	139.1
N(3)–Cd–O(4)	144.6	140.1
O(2)–H(2)···O(1)	159.2	159.6
O(5)–H(5A)···O(4)	154.0	159.5
*Mn-complex (**3**)*		
Mn–N(2)	2.3116(13)	2.394
Mn–N(3)	2.3047(13)	2.378
Mn–N(4)	2.2334(13)	2.044
Mn–N(1)	2.2387(13)	2.056
Mn–O(4)	2.1267(11)	2.006
Mn–O(3)	2.1130(11)	2.000
O(4)···O(5)[a]	2.462(2) (1.633)	2.555 (1.596)
O(3)···O(7)[a]	2.468(2) (1.577)	2.557 (1.601)
N(4)–Mn–N(1)	174.7	174.3
N(3)–Mn–O(4)	155.4	154.1
N(2)–Mn–O(3)	151.7	152.5
O(2)–H(1)···O(3)	159.0	150.8
O(54)–H(2)···O(4)	159.1	157.4

[a] O···H bond distance is in parentheses.

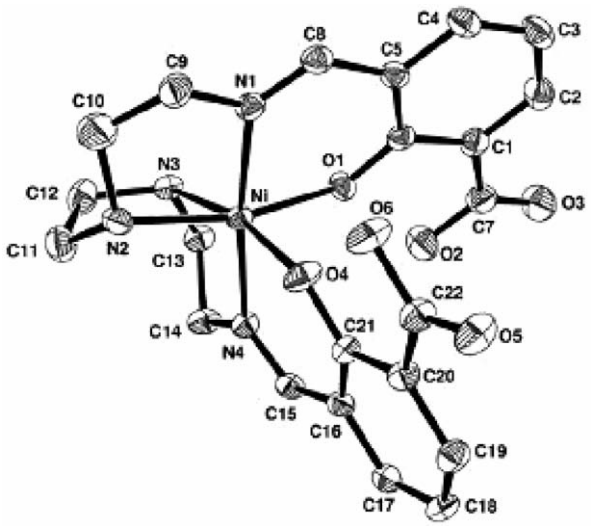

Fig. 1. ORTEP view of the Ni-complex with ellipsoids drawn at the 50% probability level.

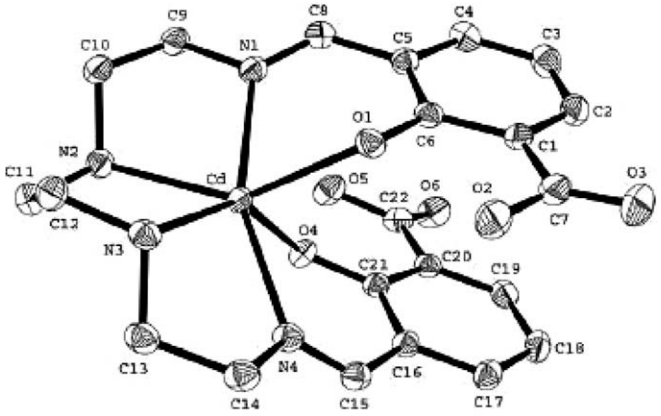

Fig. 2. ORTEP view of the Cd-complex with ellipsoids drawn at the 50% probability level.

The two imino nitrogen atoms [*d*(Mn–N) = 2.2387(13) and 2.2334(13) Å; *d*(Cd–N) = 2.3041(17) and 2.3060(16) Å; *d*(Ni–N) = 2.034(3) and 2.041(3) Å] are coordinated to the metal ions more strongly than the other two amine nitrogen atoms [*d*(Mn–N) = 2.3047(13) and 2.3116(13) Å; *d*(Cd–N) = 2.3544(16) and 2.3566(16) Å; *d*(Ni–N) = 2.110(3) and 2.145(3) Å]. This unequiva-

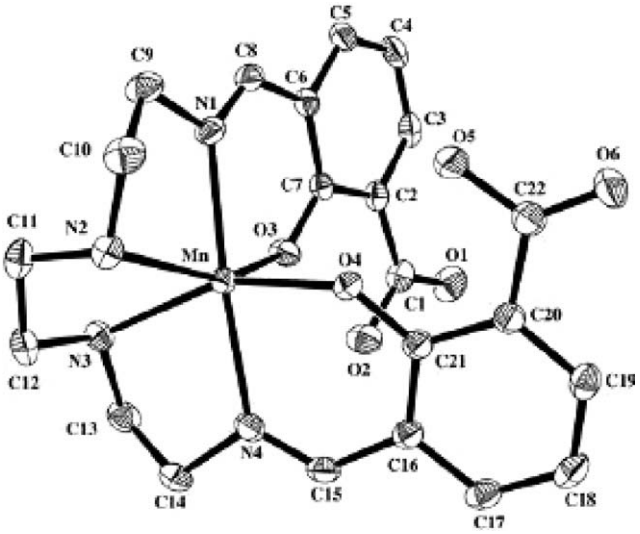

Fig. 3. ORTEP view of the Mn-complex with ellipsoids drawn at the 50% probability level.

lency in coordination of the metal-nitrogen bonds can be explained by the fact that imino nitrogens are better donors than amine nitrogens; the latter are somewhat influenced by the stereo-chemical arrangement of the trien and carboxylic acid groups. The axial bond angles of N_1–M–N_4 vary from 155.7(6)° to 175.0° and agree well with distorted octahedral structures. In most cases the metal–oxygen bond distances [2.039(2) and 2.053(2) Å for **1**; 2.3024(13) and 2.3070(14) Å for **2**; 2.1130(11) and 2.1267(11) Å for **3**] are shown to be shorter than the metal–nitrogen distances as a consequence of the negative charge borne by the phenolic oxygen atoms. The steric effect of the carboxyl group on the aromatic ring compels the *o*-phenolato plane to bend away from the central atom, which is helped by the presence of the highly flexible trien group [24]. The binding of the N_4O_2 hexadentate ligand by the metal ions results in the formation of three five-membered and two six-membered chelate rings, fused together creating large geometrical constraints. These steric strains, caused mainly by the formation of five-membered chelate rings, give rise to larger distortions from the octahedral angles, as reflected by numerous bond angles smaller or larger than 90°.

In the complex [Ni(H_2fsatrien)] (**1**), the adjacent mononuclear units are locked by face-to-face π–π interactions (distance between the centroids of the interacting rings, 3.968 Å; dihedral angle, 11.65°) exerted by terminal phenyl moieties and by hydrogen bonding interactions (Table 3). The molecules are arranged in an offset manner to maximize such interactions and generate a 1-D chain along the *c*-direction (Fig. 4). The adjacent zigzag chains are interwoven through C–H···π interactions with a ∠C–H···π angle of 161° and a C···π distance of 3.548 Å (Table 3), and are responsible for the formation of the 2-D supramolecular architecture in the *bc*-plane (Fig. 5).

The solid-state structure of [Mn(H_2fsatrien)] (**3**) is very similar to that of complex (**1**), but the π–π and C–H···π weak interactions in the former are stronger. Here the adjacent discrete molecular units are arranged into a 1-D chain along the *b*-direction (Fig. 6) *via* strong face-to-face π–π stacking interactions between the phenyl groups of the ligand with a centroid–centroid distance of 3.626 Å and dihedral angle of 6.50°. Furthermore, the adjacent zigzag 1-D chains are linked together to generate a supramolecular 2-D sheet in the *bc*-plane (Fig. 7) through C–H···π interactions, having a ∠C–H···π angle of 162° and a C···π distance of 3.428 Å (Table 4). The disposition of the adjacent sheets is shown in Fig. 8.

Table 3
Weak force interactions (Å, °) for the Ni-complex

D–H···A	D–H	H···A	D···A	∠D–H···A
Hydrogen bonding interactions				
O2–H2···O1	0.84	1.67	2.456(3)	154.00
O6–H6···O4[a]	0.84	166	2.445(3)	154.00
N2–H2B···O3	0.93	2.24	3.154(4)	167.00

C–H→π(*j*)	H···R (Å)	∠C–H···R (°)	C···R (Å)
C–H···π interactions			
C10–H10A→R(1)[(ii)]	2.60	161	3.548

π(*i*)→π(*j*)	Dihedral angle (*i*,*j*) (°)	Distance between the barycenters(Å)
π–π interactions (face-to-face)		
R(1)→R(2)[(i)]	11.65	3.968

Symmetry code: (a) 1/2 − *x*, −*y*, −1/2 + *z*; (i) = ½ − *x*, −*y*, ½ + *z*; (ii) −x, ½ + *y*, ½ − z. R(*i*)/R(*j*) denotes the centroids of the *i*th/*j*th ring; R(1)→C1–C2–C3–C4–C5–C6. R(2)→C16–C17–C18–C19–C20–C21.

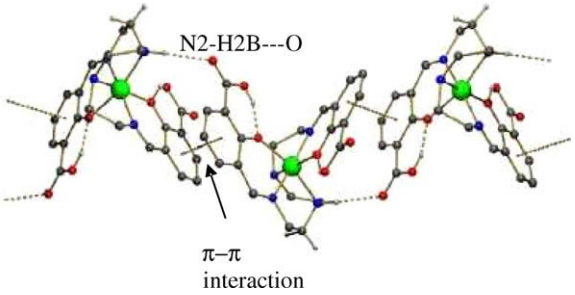

Fig. 4. The 1-D coordination structure of the Ni-complex.

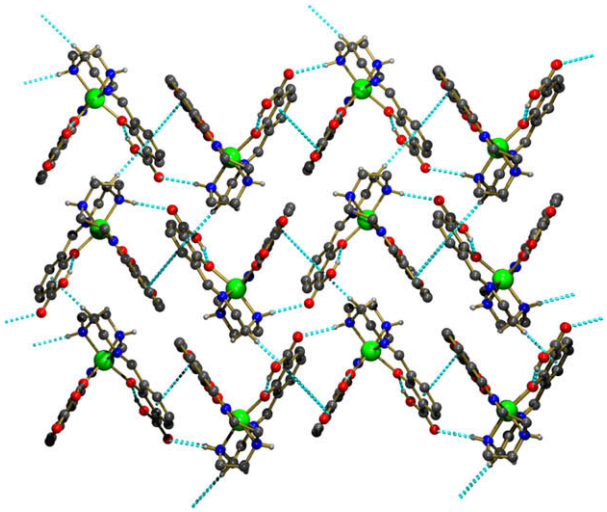

Fig. 5. The 2-D coordination structure of the Ni-complex showing intramolecular C–H···π and π–π interactions.

Unlike the complexes of Mn(II) and Ni(II), the supramolecular structure of the Cd(II) complex exhibits a 3-D architecture. Two terminal phenyl rings of the two closest mononuclear complexes of (**2**) are linked through face-to-face π interactions (distance between the barycentres of the interacting rings, 3.912 Å; dihedral angle, 10.05°) and through C–H···π interactions (∠C– H···π angle, 158° and C···π distance, 3.604 Å), and are responsible for the formation of the 1-D chain along the *a*-direction (Fig. 9). The 1-D chains pack alongside one another, and the 1-D columns are held

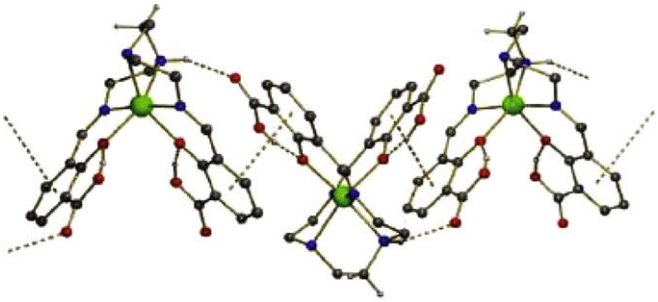

Fig. 6. The 1-D coordination structure of the Mn-complex.

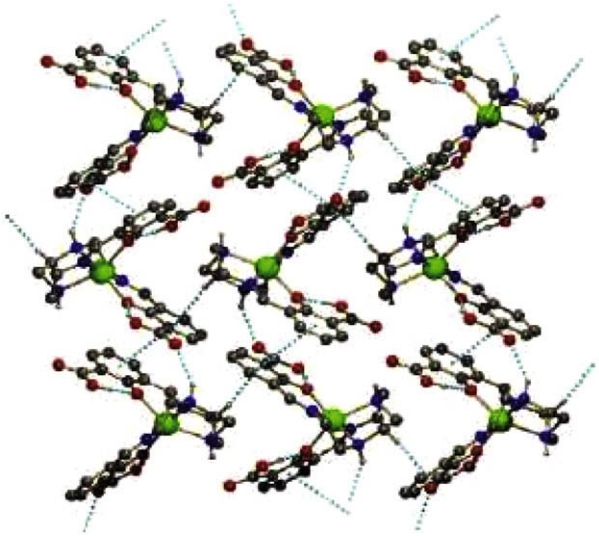

Fig. 7. The 2-D coordination structure of the Mn-complex showing intramolecular C–H···π and π–π interactions.

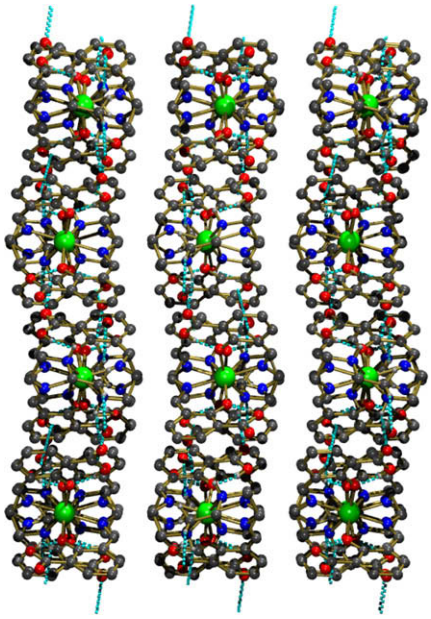

Fig. 8. Perspective view of the adjacent sheets in the Mn-complex.

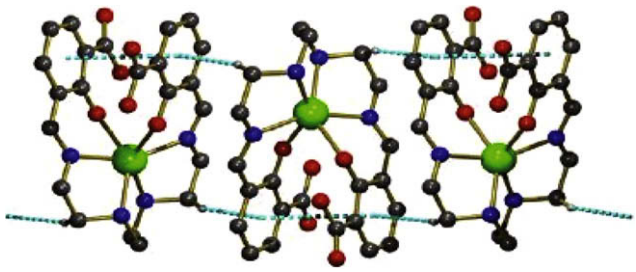

Fig. 9. The 1-D coordination structure of the Cd-complex.

Table 4
Weak force interactions (Å, °) for the Mn-complex

D–H···A	D–H	H···A	D···A	∠D–H···A
Hydrogen bonding interactions (Å, °)				
O2–H1···O3	0.93	1.58	2.468(2)	159.00
O5–H2···O4	0.87	1.63	2.462(2)	159.00
N3–H3B···O6[a]	0.93	2.25	3.031(2)	141.00

C–H→π(*j*)	H···R (Å)	∠C–H···R (°)	C···R (Å)
C–H···π interactions			
C12–H12B→R(2)[(ii)]	2.47	162	3.428

π(*i*)→π(*j*)	Dihedral angle (*i*,*j*) (°)	Distance between the barycenters (Å)
π–π interactions (face-to-face)		
R(1)→R(2)[(i)]	6.50	3.626

Symmetry code: (a) $-x, -1/2+y, 1/2-z$; (i) $-x, -½+y, ½-z$; (ii) $x, ½-y, ½+z$.
R(*i*)/R(*j*) denotes the centroids of the *i*th/*j*th ring; R(1)→C2–C3–C4–C5–C6–C7.
R(2)→C16–C17–C18–C19–C20–C21.

Table 5
Weak force interactions (Å, °) for the Cd-complex

D–H···A	D–H	H···A	D···A	∠D–H···A
Hydrogen bonding interactions (Å, °)				
O2–H2···O1	0.99	1.48	2.430(2)	159.00
N2–H2B···O5[a]	0.93	2.58	3.273(2)	132.00
N2–H2B···O6[a]	0.93	2.06	2.938(2)	157.00
N3–H3A···O2[b]	0.93	2.39	3.030(2)	126.00
N3–H3A···O3[b]	0.93	2.23	3.106(2)	156.00
O5–H5A···O4	0.84	1.67	2.455(2)	154.00

C–H→π(*j*)	H···π(Å)	∠C–H···π (°)	C···π (Å)
C–H···π interactions			
C10–H10A→R(1)[(i)]	2.67	158	3.604
C13–H13A→R(2)[(ii)]	2.72	158	3.656

π(*i*)→π(*j*)	Dihedral angle (*i*,*j*) (°)	Distance between the barycenters (Å)
π–π interactions (face-to-face)		
R(1)→R(2)	10.05	3.912

Symmetry code: (a) $x, 3/2-y, -1/2+z$; (b) $x, 5/2-y, -1/2+z$; (i) $2-x, 2-y, 1-z$; (ii) $1-x, 2-y, 1-z$.
R(*i*)/R(*j*) denotes the centroids of the *i*th/*j*th ring; R(1)→C1–C2–C3–C4–C5–C6; R(2)→C16–C17–C18–C19–C20–C21.

together through O–H···O and N–H···O hydrogen bonding interactions (Table 5) to form a grid-like structure when viewed along the *a*-direction (Fig. 10), which also involves bifurcated H-bonding [25]. In this structure the sheets are arranged parallel to the *ab*-plane to generate a 3-D supramolecular architecture (Fig. 11), where another C–H...π interaction (∠C–H···π angle, 158° and C···π distance, 3.656 Å) (Table 5) is mainly responsible for the formation of the solid-state structure.

3.2. Electronic structures

The valence molecular orbital (MO) energy level diagrams of the ligands and their M^{II}-complexes (M = Ni, Cd, Mn) are illustrated in

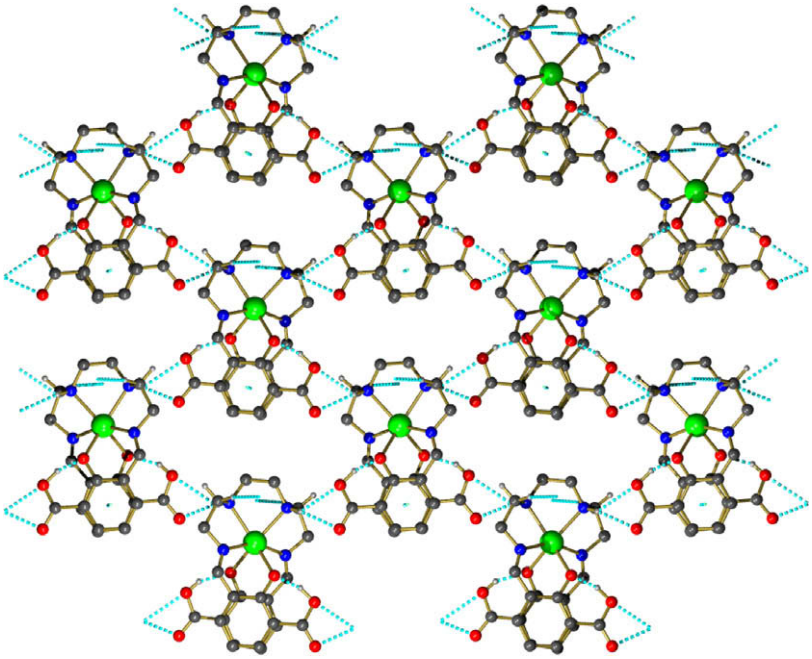

Fig. 10. The perspective view of the 2-D structure of the Cd-complex with bifurcated H-bonding.

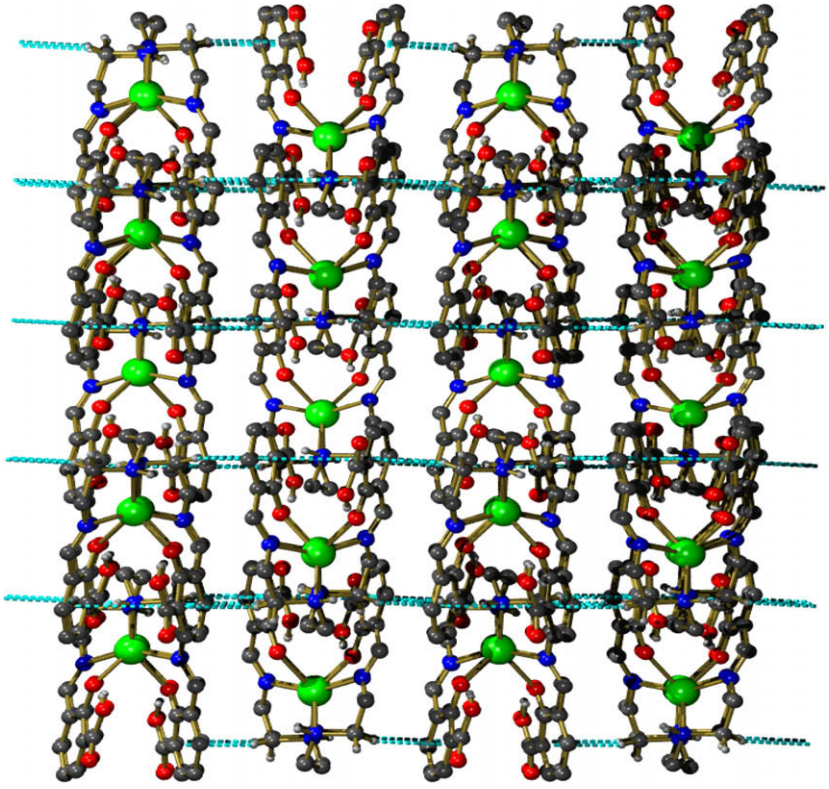

Fig. 11. A 3-D supramolecular assembly of the Cd-complex.

Fig. 12, from which we can see the change of the electronic structure on going from the ligand to the M^{II}–ligand complex. According to the calculations, the neutral ligand (H_2fsatrien) itself has an open-shell. This result is expected by examining the orbital energy level diagram of H_2fsatrien, where the HOMO (highest occupied molecular orbital) and second HOMO (i.e. HOMO − 1) are close to each other and therefore two unpaired electrons will enter the two orbitals, respectively. To confirm the open-shell ground state for the ligand, other density functionals (such as PW91, mPW, BLYP, PBE) were also tested and they gave the same results. We may note that the orbital energy level diagrams of H_2fsatrien are slightly different for different [M(H_2fsatrien)]. This is because

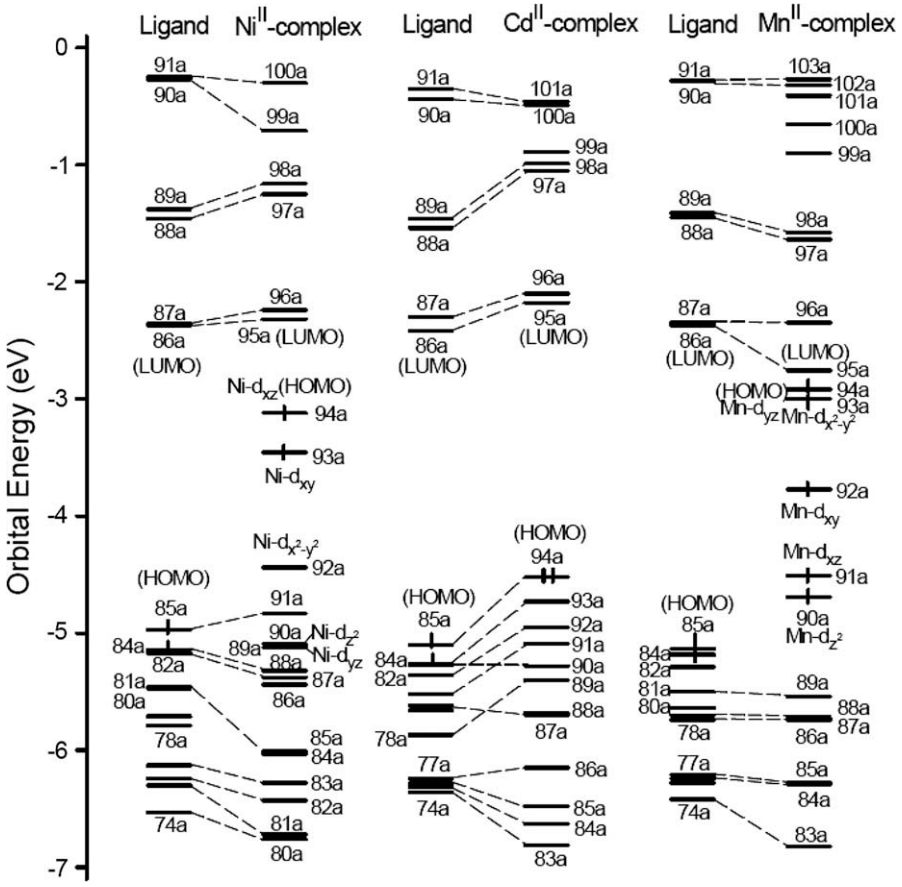

Fig. 12. Valence molecular orbital energy level diagrams of the ligands and their M^{II}-complexes (M = Ni, Cd, Mn)).

when we calculated the orbital energies of H_2fsatrien, the structure of H_2fsatrien in the respective [M(H_2fsatrien)] was adopted and this structure is somewhat different for different M. This also reflects slight perturbations of the ligand energy states by the different metals. The Ni- and Mn-complexes are open-shell as well, where some unpaired electrons are on the metal d-orbitals. Upon complexation, the singly occupied orbitals of the ligand become doubly occupied by obtaining electrons from the metal ns-orbitals. The Cd-complex has a closed-shell ground state because the Cd d-orbitals are fully occupied.

With M = Ni or Mn, the HOMO and LUMO (lowest unoccupied molecular orbital) are associated with the metal and ligand components, respectively. A very large splitting is found between the metal d-derived orbitals. The Mn-complex is calculated to be high-spin (2S + 1 = 6); that is, it has five unpaired electrons on the metal–d orbitals, in agreement with the magnetic susceptibility measurements. The low-spin state (2S + 1 = 2) is about 0.3 eV higher in energy than the high-spin state according to our calculations. The energies of the Mn–d orbitals are higher than those of the Ni–d ones so that the energy gap between the HOMO and LUMO is small in the Mn-complex. In the case of M = Cd, the d-orbitals are especially low in energy, so they do not appear in the valence set of the orbitals.

3.3. Electronic spectrum and TDDFT calculations

The UV–Vis (in DMSO) spectra were recorded both for the ligand and its metal complexes. The measured UV–Vis spectral data for the Ni(II), Cd(II) and Mn(II) complexes are presented in Table 6. To have a better insight into the electronic spectra, TDDFT calculations were performed for the allowed transitions from the ground state to the excited states. The theoretical results, obtained for both the crystal and optimized structures, are provided in the same table to compare the experimental data. The characters of the absorption bands are indicated by the contributions listed in the

Table 6
UV–Vis data for the complexes

Complex	Experimental		Calculated		
	λ_{max}[a]	E_{max}[b]	E[c]	f[d]	Contribution[e] (%)
Ni-complex	385	3.22	3.35 (3.28)	0.0125	41 (85a→93a); 16 (87a→95a)
	585	2.12	2.18 (2.15)	0.0015	90 (91a→93a)
	850	1.46			
	990	1.25			
Cd-complex	260	4.77	4.66 (4.71)	0.0075	49 (87a→97a); 37 (88a→97a)
	352	3.52	3.53 (3.51)	0.0023	50 (94a→97a); 34 (94a→98a)
	427(sh)	2.9	2.90 (2.92)	0.0574	37 (93a→95a); 33 (93a→96a)
Mn-complex	400	3.1	3.12 (3.02)	0.0009	67 (89a→96a); 13 (85a→90a)
	405 (sh)	3.06	3.03 (3.00)	0.0084	53 (90a→96a); 12 (86a→95a)
	867	1.43	1.45 (1.07)	0.0039	95 (94a→96a)
	874	1.42	1.36 (0.79)	0.0274	99 (94a→95a)

[a] Absorption maxima in nm.
[b] Experimental energy in eV.
[c] TDDFT energy in eV; the values in parentheses are the results calculated for the optimized structure.
[d] Oscillator strength.
[e] See Fig. 12 for the orbitals.

last column of the table. More calculated excitation energies (E^{exc}) for other, various (allowed) transitions are given in the Supporting information (S3–S5). Also, the calculated E^{exc} values for the complexes agree quite well with the experimental data.

The present TDDFT method is not able to calculate optical spectra of bulk materials. From Figs. 4–11, we see that the molecular units in all the crystal structures are rather discrete and are assembled through different weak force interactions. Therefore, the UV–Vis spectra (in the solution state) of the bulk materials can largely be represented by the spectra of the discrete molecules; although the optical spectra (in the solid state) show some features of band structure (see Section 3.6).

3.4. Magnetic moments, ESR and molar conductance values

The magnetic susceptibilities of the three complexes under investigation were measured in the solid state at room temperature. The complexes [Ni(H_2fsatrien)] (**1**) and [Mn(H_2fsatrien)] (**3**) are paramagnetic, while the complex [Cd(H_2fsatrien)] (**2**) is diamagnetic. Magnetic moments of octahedral nickel(II) complexes are usually found in the range 2.9–3.3 BM [26]. The observed magnetic moment of 3.10 BM for the nickel(II) complex, [Ni(H_2fsatrien)] (**1**) falls in the range for octahedral nickel(II) [27]. This eliminates the possibility of attaining other geometries by nickel(II) in the complex. The manganese(II) complex exhibits a magnetic mo-

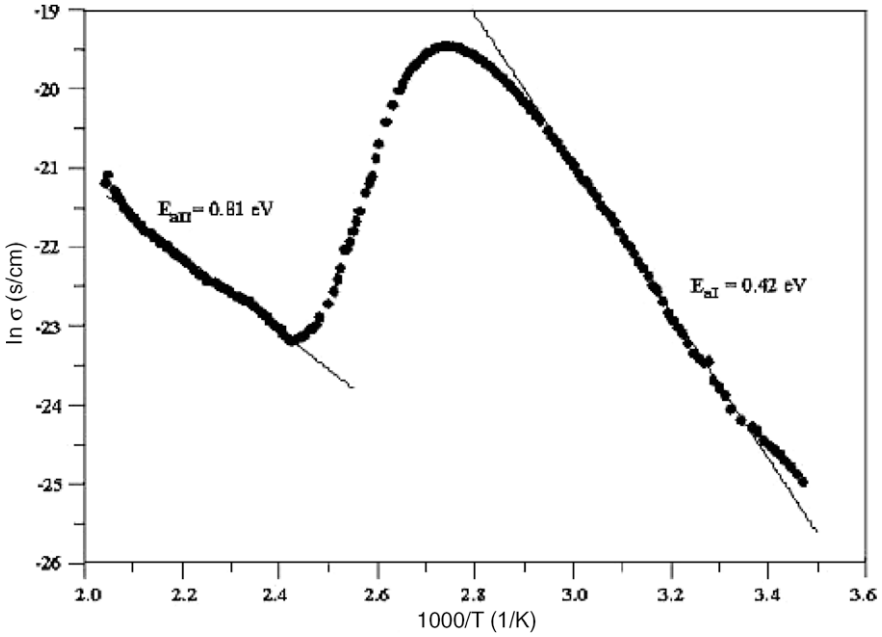

Fig. 13. Temperature dependence of the electrical conductivity of complex (**1**).

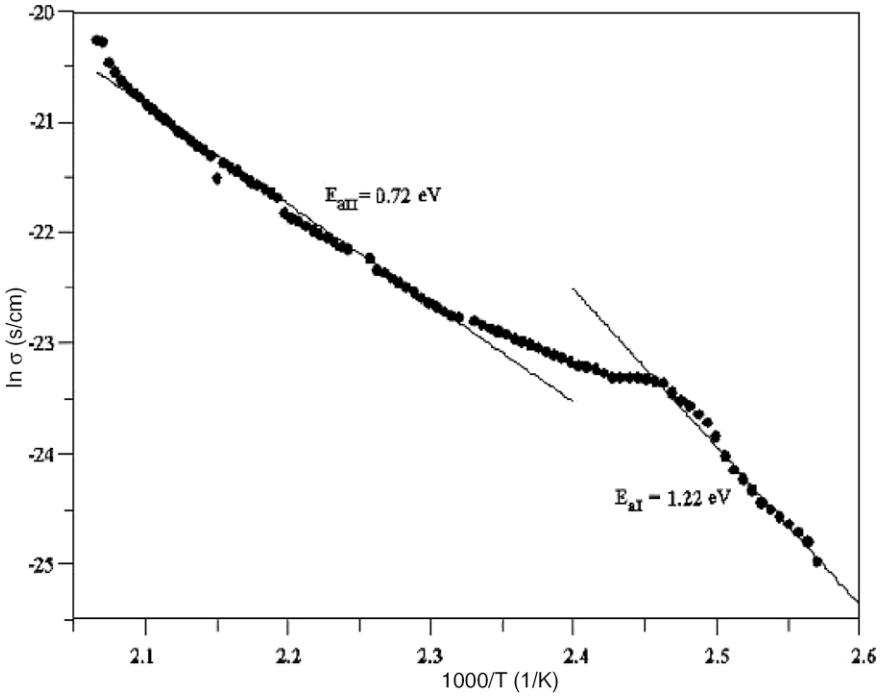

Fig. 14. Temperature dependence of the electrical conductivity of complex (**3**).

ment of 5.82 BM at room temperature and is indicative of a high-spin manganese(II) centre. The complex also exhibits a strong but broad ESR signal centered at $g = 2$, consistent with manganese(II) [28].

The molar conductance values of the complexes (**1**) to (**3**) in DMSO solution are found in the range $\Lambda_M = 15.3–16.4$ Ω^{-1} cm^2 mol^{-1}, indicating the non-electrolytic nature of the complexes in the DMSO solution [29].

3.5. Electrical conductivity

The electrical conductivity variations with temperature for the complexes (**1**) and (**3**) (shaped as a pellet) were measured and the $\ln\sigma - 1000/T$ graphs are given in Figs. 13 and 14. It can be observed that complex (**1**) shows three distinct regions, depending on the temperature (Fig. 13). At low temperatures (290–360 K) (large $1/T$) extrinsic behaviour dominates [22,30]. It can be seen from the figures that the conductivity is virtually temperature-independent at the beginning of the extrinsic region, where the increase in the number of electrons donated from the donor levels in its effect on the conductivity and is balanced by the decrease in the mean free path, being fully ionized, i.e., completely emptied. The conductivity starts dropping as a result of phonon scattering in the temperature range 360–410 K, until the onset of intrinsic conduction (at a temperature of 410 K), when the conductivity increases again with temperature [31]. Intrinsic conductivity occurs at high temperatures (410–480 K), as shown in the intrinsic region for the complex (**1**). The extrinsic and intrinsic regions have a positive temperature coefficient of electrical conductivity.

In spite of showing insulating properties at low temperatures, complex (**3**) showed conduction properties at about 390 K (Fig. 14). Complex (**3**) has a positive temperature coefficient between 390–405 K and 410–480 K. The conductivity is constant in the region between 405 and 410 K. We can say that the behaviour is similar to the behaviour in the exhausting region.

The increasing of conduction with temperature is semiconductor behaviour. The Arrhenius equation for the extrinsic region of n-type semiconductors is

$$\sigma = \sigma_0 \exp(-E_a/kT) \quad (1)$$

where σ_0 is the pre-exponential factor, E_a is the activation energy and k is the Boltzmann's constant. By using this equation, the activation energy can be calculated [22,26]. The slope in the extrinsic region for an n-type semiconductor is given by $(E_g - E_d)/k$ and $E_g/2k$ in the intrinsic region [22]. The calculated activation energies for complex (**1**) were found to be low (0.42 eV) in the lower temperature range (290–360 K), but considerably higher (0.81 eV) in the high-temperature range (410–480 K). The activation energies of complex (**3**) in the extrinsic region (390–405 K) and the intrinsic region (410–480 K) are 1.22 eV and 0.72 eV, respectively. Thus the conductivity of the compound shows the typical Arrhenius-type dependence on temperature. Such an n-type electrical semiconductivity mechanism of the present Schiff base complexes may be explained in terms of transfer of electrons in two possible ways. Firstly [32] the conduction process may be assumed to start with the delocalization of the π-electrons and then the excitation of electrons from the HOMO to the LUMO of π-MOs, which actually switch over the metal complexes to the semiconducting state. In a second [33] way, the electrons hop from one localized metal site to the next, i.e. in this case the holes have little effect on the mobility of negative charges. When the electron lands on a new site, it causes the surroundings to adjust their localization and the electron is trapped temporarily in the potential well and it resides until activated to migrate to another nearby site. Thus the electrons are supposed to tunnel from one molecular unit to the comparable unfilled level of the adjacent molecular unit. In this case the tunneling of electrons is observed through the intermolecular potential barrier to occupy the corresponding orbital in the adjacent unit *via* π–π stacking, C–H···π interactions and extensive H-bonding.

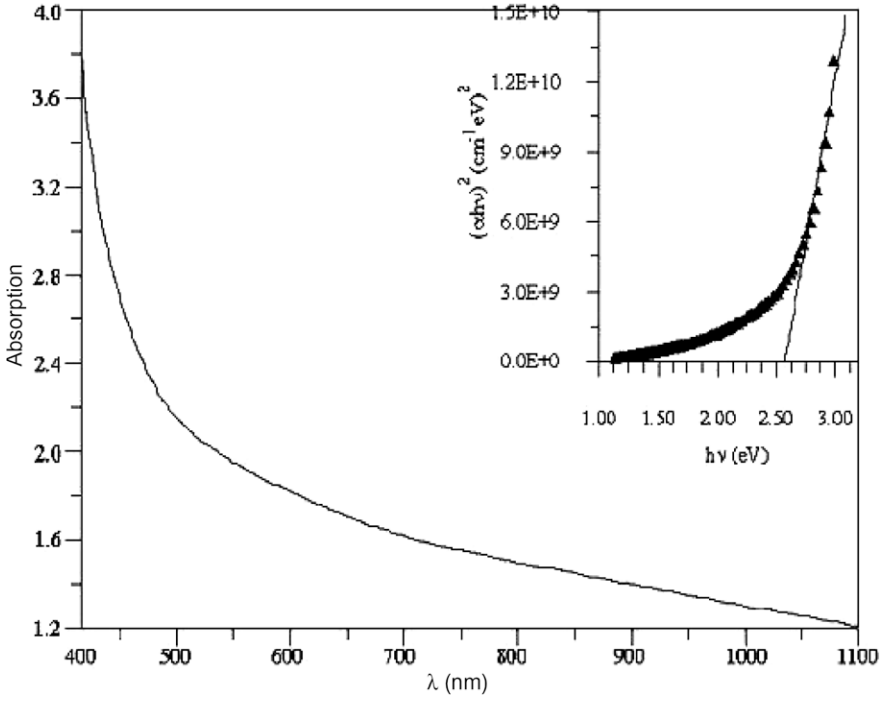

Fig. 15. The optical absorption spectra for complex (**1**).

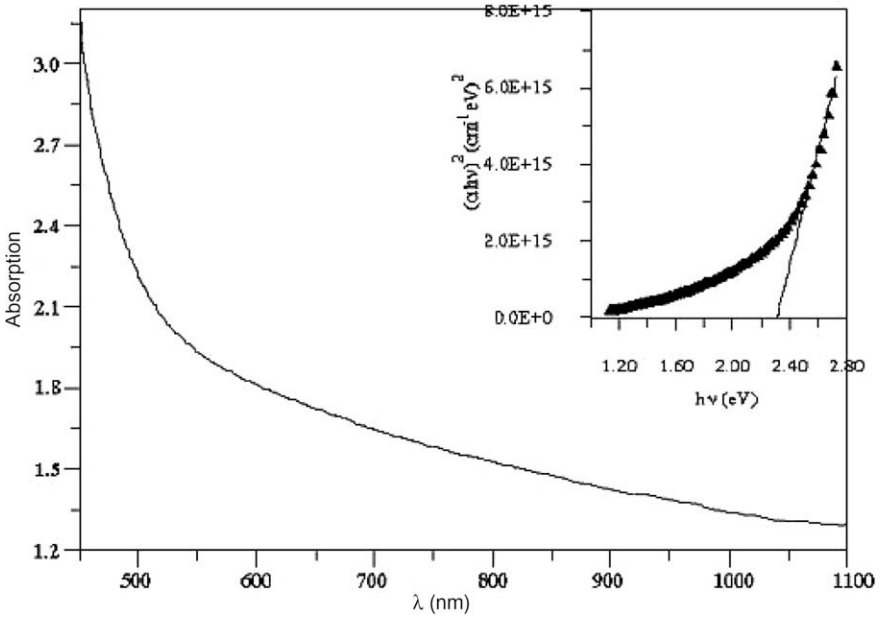

Fig. 16. The optical absorption spectra for complex (**3**).

3.6. Optical properties

To obtain the energy-band gaps and the nature of the optical transition involved in the complexes, the optical spectra were recorded at room temperature and the fundamental absorption edge is analyzed within the framework of the theory of Mott and Davis [30]. The optical band gaps of the samples were determined by applying the relation [31,34],

$$\alpha h\nu = A(h\nu - E_g)^n \quad (2)$$

where α is the linear absorption coefficient, $h\nu$ is the photon energy, E_g is the energy gap between the top of the valence band and bottom of the conduction band at the same value of wave number and n depends on the kind of optical transitions. Specifically, n is 1/2, 3/2, 2 and 3 for transitions which are directly allowed, directly forbidden, indirectly allowed and indirectly forbidden, respectively. A is a constant involving the properties of the bands.

The energy gap for allowed direct (E_{gd}) and indirect (E_{gi}) transitions can be determined by relating

$$\alpha h\nu = A_a(h\nu - E_{gd})^{1/2} \quad (3)$$

and

$$\alpha h\nu = A_i(h\nu - E_{gi})^2 \quad (4)$$

where A_a and A_i are the characteristic parameters for the respective transitions, independent of ν. From Eqs. (3) and (4), E_g can be determined from the extrapolation to zero of the linear parts of the $(\alpha h\nu)^2 = f(h\nu)$ and $(\alpha h\nu)^{1/2} = f(h\nu)$ curves.

The optical absorption spectra, i.e. the plots of $(\alpha h\nu)^2$ versus $h\nu$, are given in Figs. 15 and 16 for complexes (**1**) and (**3**) and analysis of the absorption data was carried out to determine the predominant optical transition. A satisfactory fit was obtained for $(\alpha h\nu)^2$ as a function of $h\nu$, showing the existence of a direct gap. The extrapolation of the graphs to $(\alpha h\nu)^2 = 0$ yields the optical band gap E_{gd}. The values of the optical band gap E_{gd} were determined from Figs. 15 and 16 by least squares fitting of the data. In this study, the optical band gaps, E_{gd}, of complexes (**1**) and (**3**) were found to be 2.57 and 2.30 eV, respectively.

4. Conclusions

The synthesis, characterization and crystal structures of three complexes [M(H_2fsatrien)] (M = Ni (**1**), Cd (**2**) and Mn (**3**)) with a new symmetrical hexadentate Schiff base (N_4O_2 donor) as a ligand have been described. Both the X-ray crystal structure determinations and theoretical calculations demonstrate that the complexes are all pseudo-octahedral with some variations in their configurations. Some intermolecular weak forces, such as π–π stacking, C–H···π interactions, unusual H-bonding interactions also play important roles by linking the discrete subunits and low-dimensional entities into high-dimensional (1-D, 2-D, 3-D) supramolecular coordination networks. The electrical semiconducting character of the metal complexes has been nicely correlated with these structural patterns. On the other hand, optical studies indicate that complexes (**1**) and (**3**) have direct band gaps. DFT/TDDFT calculations agree well with the experimentally observed structures and absorption spectra of the molecules.

Acknowledgments

One of the authors (K.D.) is thankful to the UGC, New Delhi for awarding Emeritus Fellowship and Financial grants to carry out this work. We are grateful to the Sophisticated Analytical Instrument Facility, Central Drug Research Institute, Lucknow and IIT Madras for elemental analyses and some spectroscopic measurements and IICB, Kolkata for NMR analysis. We are also grateful to the reviewers for their valuable comments.

Appendix A. Supplementary data

CCDC 677239, 677240 and 677238 contain the supplementary crystallographic data for complexes **1**, **2** and **3**. These data can be obtained free of charge via http://www.ccdc.cam.ac.uk/conts/retrieving.html, or from the Cambridge Crystallographic Data Centre, 12 Union Road, Cambridge CB2 1EZ, UK; fax: (+44) 1223-336-033; or e-mail: deposit@ccdc.cam.ac.uk. Supplementary data associated with this article can be found, in the online version, at doi:10.1016/j.poly.2008.07.034.

References

[1] (a) E.C. Constable, in: J.-M. Lehn, L. Atwood, J.E.D. Davis, D.D. MacNicol, F. Vögtle (Eds.), Comprehensive Supramolecular Chemistry, Pergamon, Oxford, UK, 1996;
(b) J.-M. Lehn, Supramolecular Chemistry – Concepts and Perspectives, VCH, Weinheim, Germany, 1995;
(c) P. Cucos, M. Pascu, R. Sessoli, N. Avarvari, F. Ppointillart, M. Andruh, Inorg. Chem. 45 (2006) 7035;
(d) M. Andruh, Chem. Commun. (2007) 2565.

[2] (a) O.M. Yaghi, H. Li, T.L. Groy, J. Am. Chem. Soc. 118 (1996) 9096;
(b) N.L. Rosi, J. Kim, M. Eddaoudi, B. Chen, M. O'Keeffe, O.M. Yaghi, J. Am. Chem. Soc. 127 (2005) 1504;
(c) M. Fujita, D. Oguro, M. Miyzawa, H. Oka, K. Yamaguchi, K. Ogura, Nature 378 (1995) 469;
(d) K.N. Power, T.L. Hennigar, M.J. Zaworotko, Chem. Commun. (1998) 595;
(e) N.W. Ockwig, O. Delgado-Friedrichs, M. O'Keeffe, O.M. Yaghi, Acc. Chem. Res. 38 (2005) 176.

[3] (a) G.R. Desiraju, Acc. Chem. Res. 29 (1996) 441;
(b) T.N. Gruu Rao, Coord. Chem. Rev. 183 (1999) 81;
(c) S.S. Kuduva, D.C. Craig, A. Nangia, G.R. Desiraju, J. Am. Chem. Soc. 121 (1999) 1936;
(d) E.S. Alekseyeva, A.S. Batsanov, L.A. Boyd, M.A. Fox, T.G. Hibbert, J.A.K. Howard, J.A.H. MacBride, A. Mackinnon, K. Wade, J. Chem. Soc., Dalton Trans. (2003) 475.

[4] (a) I. Unamuno, J.M. Gutiérrez-Zorrilla, A. Luque, P. Román, L. Lezama, R. Calvo, T. Rojo, Inorg. Chem. 37 (1998) 6452;
(b) S. Biswas, S. Sarkar, I.M. Steele, S. Sarkar, G. Mostafa, B.B. Bhaumik, K. Dey, Polyhedron 26 (2007) 5061;
(c) A.N. Khlobystov, A.J. Blake, N.R. Champness, D.A. Lemenovski, A.G. Majouga, N.V. Zyk, M. Schröder, Coord. Chem. Rev. 222 (2001) 155;
(d) M.C. Tse, K.K. Cheung, M.C.W. Chan, C.M. Che, Chem. Commun. (1998) 2295.

[5] (a) M. Ruben, J. Rojo, F.J. Romero-Salguero, L.H. Uppadine, J.-M. Lehn, Angew. Chem., Int. Ed. 43 (2004) 3644;
(b) S.G. Telfer, R. Kuroda, Coord. Chem. Rev. 242 (2003) 33;
(c) M. Albrecht, I. Janser, S. Meyer, P. Weis, R. Fröhlich, Chem. Commun. (2003) 2854;
(d) S. Leininger, B. Olenyuk, P.J. Stang, Chem. Rev. 100 (2000) 853;
(e) B. Moulton, M.J. Zaworotko, Chem. Rev. 101 (2001) 1629;
(f) L.C. Tabares, J.A.R. Navarro, J.M. Salas, J. Am. Chem. Soc. 123 (2001) 383.

[6] (a) A.J. Blake, N.R. Champness, P. Hubberstey, W.S. Li, M.A. Withersby, M. Schröder, Coord. Chem. Rev. 183 (1999) 117;
(b) J.-P. Sauvage (Ed.), Transition metals in Supramolecular Chemistry; Perspectives in Supramolecular Chemistry, vol. 5, Wiley, London, 1999;
(c) H.-H. Lin, S. Mohanta, C.-J. Lee, H.-H. Wei, Inorg. Chem. 42 (2003) 1584;
(d) G.R. Desiraju (Ed.), The Crystal as a Supramolecular Entity Perspectives in Supramolecular Chemistry, vol. 2, Wiley, London, 1996;
(e) D. Braga, L. Maini, Chem. Commun. (2004) 976;
(f) R. Koner, M. Nayak, G. Ferguson, J.N. Low, C. Glidewell, P. Misra, S. Mohanta, Cryst. Eng. Commun. 7 (2005) 129.

[7] (a) X.H. Bu, M.L. Tong, H.C. Chang, S. Kitagawa, S.R. Batten, Angew. Chem., Int. Ed. 43 (2003) 192;
(b) Y. Wan, L. Zhang, L. Jin, S. Gao, S. Lu, Inorg. Chem. 42 (2003) 4985;
(c) Z.M. Sun, J.G. Mao, Y.Q. Sun, H.Y. Zeng, A. Clearfield, Inorg. Chem. 43 (2004) 336;
(d) S.L. Zheng, J.P. Zhang, X.M. Chen, Z.L. Huang, Z.Y. Lin, W.T. Wong, Chem. Eur. J. 9 (2003) 3888.

[8] L. Salmon, A. Bousseksou, B. Donnadieu, J.-P. Tuchagues, Inorg. Chem. 44 (2005) 1763.

[9] (a) J.S. Miller, Angew. Chem., Int. Ed. 42 (2003) 27;
(b) O. Kahn, J. Kröber, C. Jay, Adv. Mater. 4 (1992) 718;
(c) S. Hayami, Z.-Z. Gu, H. Yoshiki, A. Fujishima, O. Sato, J. Am. Chem. Soc. 123 (2001) 11644;
(d) Y. Sunatsuki, Y. Ikuta, N. Matsumoto, H. Ohta, M. Kojima, S. Iijima, S. Hayami, Y. Maeda, S. Kaizaki, F. Dahan, J.-P. Tuchagues, Angew. Chem., Int. Ed. 42 (2003) 1614.

[10] G.N. Schrauzer, R.J. Windgassen, J. Am. Chem. Soc. 89 (1967) 143.

[11] R. Seoudi, A.A. Shabaka, M.M. Elokr, A. Sobhi, Mater. Lett. 61 (2007) 3451.

[12] Y. Okamoto, W. Brenner, Organic Semiconductors, Reinhold Publishing Corporation, Chapman and Hall, Ltd., London, 1964.

[13] S. Sarkar, Y. Aydogdu, F. Dagdelen, B.B. Bhaumik, K. Dey, Mater. Chem. Phys. 88 (2004) 357.

[14] Y. Yamamoto, S. Tsukuda, Bull. Chem. Soc. Jpn. 58 (1985) 1509.

[15] J.C. Duff, E.J. Bills, J. Chem. Soc. (1932) 1987.

[16] D. Perrin, W.L.F. Armarigo, D.R. Perrin, Purification of Laboratory Chemicals, 2nd ed., Pergamon, Oxford, England, 1980.

[17] (a) E.J. Baerends, D.E. Ellis, P. Ros, Chem. Phys. 2 (1973) 41;
(b) G. te Velde, F.M. Bickelhaupt, E.J. Baerends, C. Fonseca-Guerra, S.J.A. van Gisbergen, J.G. Snijders, T. Ziegler, J. Comput. Chem. 22 (2001) 931;
(c) C. Fonseca-Guerra, J.G. Snijders, E.J. Baerends, G. te Velde, Theor. Chem. Acc. 99 (1998) 391;
(d) ADF2006.01; SCM: Theoretical Chemistry, Vrije Universiteit, Amsterdam, The Netherlands. <http://www.scm.com>.

[18] A.D. Becke, Phys. Rev. A 38 (1988) 3098.

[19] J.P. Perdew, Phys. Rev. B 33 (1986) 8822.

[20] S.J.A. van Gisbergen, J.G. Snijders, E.J. Baerends, Comput. Phys. Commun. 118 (1999) 119.

[21] A.L. Spek, Acta Crystallogr., Sect. A 46 (1990) C34.

[22] J.F. Shackelford, Materials Science for Engineers, 6th ed., Pearson Prentice Hall, 2005.

[23] G. Sheldrick, Brüker-AXS, 2001.

[24] N. Chantarasiri, V. Ruangpornvisuti, N. Muangsin, H. Detsen, T. Mananunsap, C. Batiya, N. Chaichit, J. Mol. Struct. 701 (2004) 93.

[25] (a) A. Castiñeiras, D. Choquesillo-Lazarte, J.M. González-Pérez, R. Carballo, J. Niclós-Gutiérrez, Z. Anorg. Allg. Chem. 623 (2006) 845;
(b) X. Ren, J. Xie, Y. Chen, R.K. Kremer, J. Mol. Struct. 660 (2003) 139.

[26] L. Sacconi, R.L. Carlin (Eds.), Transition Metal Chemistry, vol. 4, Marcel Dekker, New York, 1968.

[27] K. Dey, R. Bhowmick, S. Sarkar, S. Biswas, D. Koner, Synth. React. Inorg. Met.-Org. Nano Met. Chem. 35 (2005) 285.

[28] R.S. Drago, Physical Methods in Inorganic Chemistry, 2nd ed., van Nostrand Reinhold Company, New York, 1965.

[29] W.J. Geary, J. Coord. Chem. 7 (1971) 81.

[30] N.F. Mott, E.A. Davis, Electronic Processes in Non-crystalline Materials, Clarendon Press, Oxford, 1971.

[31] F. Gutmann, Organic Semiconductors, John Wiley and Sons Inc., New York, London, Sydney, 1967.

[32] (a) G.B. El-Hefnawey, M.M. Ayad, A.E. El-Trass, Thermochim. Acta 198 (1992) 345 and references cited therein;
(b) K.Y. El-Baradie, M. Gaber, M.M. Abou-Sekkina, Thermochim. Acta 246 (1994) 175. and references cited therein.

[33] (a) F. Yakuphanoglu, S. Sarman, Y. Aydogdu, Z. Ilter, M. Coskun, J. Appl. Polym. Sci. 87 (2003) 741;
(b) Y. Aydogdu, F. Yakuphanoglu, A. Aydogdu, M. Sekerci, C. Alkan, Balkan Phys. Lett. 7 (1999) 294.

[34] J.I. Pankove, Optical Processes in Semiconductors, Prentice Hall Inc., New Jersey, 1971.

12-diphenyl-1,4,8,11-tetraazacyclo-tetradeca-7,12-diene) with oxamido bridge has been successfully synthesized. Based on this precursor, two trinuclear complexes $[Cu(VOL)_2(H_2O)_2](ClO_4)_2 \cdot 1.5H_2O$ (**2**) and $[Mn(VOL)_2(CH_3OH)_2](ClO_4)_2 \cdot 5CH_3OH$ (**3**) have been prepared and structurally characterized. Their spectroscopic properties and magnetic properties have also been investigated.

2. Experimental

2.1. General

All reagents were of analytical grade and were used as received from commercial sources without further purification. The complex H_2L' (H_2L' = 2,2′-(oxalyldiimino)bis(benzophenone)) was prepared as described elsewhere [27]. Elemental analyses were performed on a Perkin–Elmer 240 element analyzer. FT-IR spectra were recorded using KBr discs on a Bruker Tensor 27 spectrophotometer in the 4000–600 cm^{-1} region. Electronic spectra were measured on a JASCO V-570 spectrophotometer using DMF as the solvent. Magnetic susceptibility data were collected over the temperature range 2–300 K on a Quantum Design MPMS-7 SQUID magnetometer.

2.2. Synthesis of the complexes

2.2.1. Synthesis of VOL (*1*)

The precursor complex ligand VOL (**1**) was prepared by a solvent-thermal reaction. The reaction mixture of $VOSO_4 \cdot H_2O$ (0.178 g, 1 mmol), H_2L' (0.448 g, 1 mmol), ethylenediamine (1.2 mL, 2 mmol) and methanol (15 mL) was sealed in a 25 mL Teflon-lined stainless steel autoclave vessel at 140 °C under autogenous pressure for 72 h. After slow cooling, the resulting major phase of dark red crystals was filtered, washed with distilled water, methanol and dried in air at ambient temperature. Yield: 0.339 g (63%). Elemental *Anal.* Calc. for $C_{30}H_{22}N_4O_3V$: C, 67.04; H, 4.13; N, 10.42. Found: C, 67.1; H, 4.07; N, 10.4%. FT-IR (KBr, cm^{-1}): 3417 (m) 1671 (s), 1587 (s), 1547 (m), 1472 (w), 1442 (m), 1357 (m), 1326 (m), 1301 (w), 992 (s), 948 (s), 751 (m), 702 (m).

2.2.2. Synthesis of $[Cu(VOL)_2(H_2O)_2](ClO_4)_2 \cdot 1.5H_2O$ (*2*)

A methanol solution of $Cu(ClO_4)_2 \cdot 6H_2O$ (0.038 g, 0.1 mmol) was added dropwise to a methanol solution (25 mL) of VOL (0.11 g, 0.2 mmol). The mixture was refluxed with stirring for 5 h, and the resulting red solution was cooled and filtered. Light red single crystals suitable for X-ray analysis were obtained by slow evaporation of the filtrate in the open air at room temperature two weeks later. The sample is stable in air and soluble in most common organic solvents. Yield: 0.12 g (85%). Elemental *Anal.* Calc. for $C_{60}H_{51}Cl_2CuN_8O_{17.5}V_2$: C, 51.42; H, 3.64; N, 8.0. Found: C, 51.35; H, 3.51; N, 8.05%. FT-IR (KBr, cm^{-1}): 3422 (m), 1601 (s), 1588 (s), 1476 (w), 1443 (m), 1322 (m), 1105 (s), 994 (s), 951 (s), 756 (m), 704 (m), 625 (m).

2.2.3. Synthesis of $[Mn(VOL)_2(CH_3OH)_2](ClO_4)_2 \cdot 5CH_3OH$ (*3*)

Complex **3** was obtained as pale red crystals by using the analogous procedure used to prepare complex **2** except that $Cu(ClO_4)_2 \cdot 6H_2O$ was substituted with $Mn(ClO_4)_2 \cdot 6H_2O$. However, the red microcrystalline product is not air-stable and quickly turns to into an amorphous phase, due to the loss of CH_3OH molecules, when it is removed from the mother liquid, so the compound should be stored under low temperature and crystallographic data were also collected under a liquid nitrogen atmosphere. Yield: 0.125 g (80%). Elemental *Anal.* Calc. for $C_{67}H_{72}Cl_2MnN_8O_{21}V_2$: C, 51.76; H, 4.63; N, 7.21. Found: C, 51.66; H, 4.55; N, 7.24%. FT-IR (KBr, cm^{-1}): 3418 (m), 1600 (s), 1586 (s), 1477 (w), 1445 (m), 1326 (m), 1109 (s), 1009 (s), 953 (s), 755 (m), 705 (m), 625 (m).

2.3. Crystal structure determination and refinement

Crystals of **1**–**3** suitable for single-crystal X-ray diffraction were mounted on a BRUKER SMART 1000 diffractometer with graphite-monochromatized Mo Kα radiation (λ = 0.71073 Å), using the ω scan technique at 294(2) K for **1** and **2** and 113(2) K for **3**. Empirical absorption corrections were applied using the SADABS program. The structures were solved by direct methods and refined by the full-matrix least-squares on F^2 with anisotropic thermal parameters for all non-hydrogen atoms [28]. All hydrogen atoms were added in idealized positions and refined isotropically. For **2**, the phenyl ring of the macrocyclic ligand experiences a serious disorder over two positions and the site occupancy factors of the disordered atoms were initially refined and later fixed at 0.5/0.5. Moreover, three oxygen atoms of the ClO_4^- anion were also disordered in two positions with a 0.4/0.6 site occupancy distribution, these effects probably give rise to the relatively higher final *R* index. For **3**, the oxygen atoms of the ClO_4^- anion and one of the CH_3OH molecules were also found to be disordered. 944 parameters and 72 restraints have been used in the final least-squares refinement. Further details of the structure analyses are summarized in Table 1.

Table 1
Crystal data and structure refinement for complexes **1**–**3**

Complexes	**1**	**2**	**3**
Empirical formula	$C_{30}H_{22}N_4O_3V$	$C_{60}H_{51}Cl_2CuN_8O_{17.50}V_2$	$C_{67}H_{72}Cl_2MnN_8O_{21}V_2$
Formula mass	537.46	1400.41	1553.05
Crystal system	triclinic	triclinic	triclinic
Space group	$P\bar{1}$	$P\bar{1}$	$P\bar{1}$
a (Å)	10.946(3)	9.820(9)	10.805(2)
b (Å)	11.250(3)	12.128(11)	17.787(3)
c (Å)	11.311(3)	14.577(13)	18.572(3)
α (°)	70.229(4)	88.405(17)	93.148(3)
β (°)	86.132(4)	80.052(16)	101.772(3)
γ (°)	74.297(4)	76.619(15)	100.227(2)
V (Å^3)	1261.3(5)	1663(3)	3423.3(11)
Z	2	1	2
D_{calc} (g cm^{-3})	1.415	1.398	1.507
μ (mm^{-1})	0.434	0.744	0.609
size (mm)	0.28 × 0.20 × 0.16	0.20 × 0.18 × 0.12	0.20 × 0.20 × 0.20
Range of indices	$-13 \leqslant h \leqslant 13$ $-14 \leqslant k \leqslant 6$ $-14 \leqslant l \leqslant 13$	$-11 \leqslant h \leqslant 11$ $-14 \leqslant k \leqslant 14$ $-17 \leqslant l \leqslant 11$	$-14 \leqslant h \leqslant 14$ $-23 \leqslant k \leqslant 22$ $-15 \leqslant l \leqslant 24$
T (K)	294(2)	294(2)	113(2)
λ (Å)	0.71073	0.71073	0.71070
Reflections collected	7161	8292	30474
Unique reflections (R_{int})	5072 (0.0246)	5794 (0.0588)	16008 (0.0372)
Goodness-of-fit on F^2	1.022	1.005	1.089
R_1 wR_2 ($I > 2\theta$)[a]	R_1 = 0.0509, wR_2 = 0.1152	R_1 = 0.0830, wR_2 = 0.2121	R_1 = 0.0702, wR_2 = 0.1688
R_1 wR_2 (all data)[b]	R_1 = 0.0859, wR_2 = 0.1352	R_1 = 0.1871, wR_2 = 0.2912	R_1 = 0.0962, wR_2 = 0.1895
Largest difference in peak and hole (e Å^{-3})	0.957 and −0.829	0.830 and −0.513	0.795 and −0.636

[a] $R_1 = \sum|F_o| - |F_c|/\sum|F_o|$.
[b] $wR_2 = [\sum_w(F_o^2 - F_c^2)2/\sum_w(F_o^2)^2]^{1/2}$.

3. Result and discussion

3.1. Synthesis and spectroscopy

The synthesis route for the precursor mononuclear complex **1** comprises the solvent-thermal in situ reaction of ethylenediamine, H_2L' and a VO(IV) source, which is different from the traditional reflux routes for other CuL and NiL complexes [29]. This route not only tends to afford large single crystals suitable for X-ray crystallography, due to slow crystallization, directly but also prevents the oxidation of V^{IV} to V^{V} in a sealed and pressurized environment. The synthesis of trinuclear complexes are both performed in a basic methanol solution of VOL under refluxing conditions. Some experimental parameters, including the reactant molar ratio, are varied, but the resulting products remain the same. Finally, a VO/Cu (or Mn) ratio of 2:1 was used. Although the two trinuclear complexes are made in a similar way and have similar structures, complex **2** is more stable in air than complex **3**.

The IR spectra of complexes **2** and **3** show the characteristic bands of the bridging oxamide moiety around 1600 cm^{-1} ($\nu_{C=O}$), which are significantly lower than that for the mononuclear entity (1670 cm^{-1}), suggesting a strong coordination of the oxamido carbonyl oxygens. In addition, the particular absorptions at ca. 1105 cm^{-1} are consistent with the presence of perchlorate ions. For complexes **1–3**, the stretching vibrations of vanadyl V=O are indicated by strong bands at around 951 and 993 cm^{-1}, and the ν(C=N) mode of the macrocyclic complexes are seen at 1587 cm^{-1}. Absorptions at 3418 cm^{-1} may be assigned to O–H stretching in H_2O or CH_3OH.

The electronic absorption spectra of the two trinuclear complexes in DMF at ca. 278 and 355 nm are dominated by intense bands due to intraligand π–π^* transitions and the charge-transfer transitions of the VO^{2+} chromophore. In the visible region, they both exhibit broad weak bands centered at ca. 495 and 605 nm, which are most likely due to $^2B_2 \rightarrow {}^2A_1$ and $^2B_2 \rightarrow {}^2B_1$ d–d electron transitions of VO^{2+} with an idealized C_{4V} symmetry [30]. The spin-allowed transition $^2B_{1g} \rightarrow {}^2E_g$ and $^2B_{1g} \rightarrow {}^2B_{2g}$ for the octahedral Cu(II) ion of complex **2** is probably obscured by this absorption [31]. For complex **3**, the coordination environment of Mn(II) is distorted octahedral. Thus, according to ligand-field theory and assuming O_h symmetry, the ground-state of Mn(II) is $^6A_{1g.}$ Because d–d transitions of Mn(II) ($^6A_{1g} \rightarrow {}^4T_{1g}$ (G), $^4T_{2g}$ (G), $^4A_{1g}\ldots$) are spin-forbidden, no characteristic band of Mn(II) is found in the electronic spectrum [32].

3.2. Description of the crystal structures

3.2.1. Mononuclear complex VOL (*1*)

The asymmetric unit of the mononuclear complex **1** is shown in Fig. 1. Selected bond lengths and angles are presented in Table 2. The central vanadium atom is in a square pyramidal environment: two nitrogen atoms (N1 and N2) from the deprotonated oxamide and another two (N3 and N4) from ethylenediamine form the basal plane, and the apical position is occupied by the terminal oxo ligand (O3). The deviations of the four N atoms from their least-squares plane are −0.022(8) (N1), +0.022(8) (N2), −0.021(8) (N3) and +0.021(8) (N4) Å, and the central vanadium(IV) atom is 0.667(4) Å out of the plane. Of the four V–N bonds, the bonds to the deprotonated oxamide nitrogens, N1 [1.977(2) Å] and N2 [1.993(2) Å], are somewhat shorter than V–N3 [2.063(2) Å] and V–N4 [2.066(2) Å]. This is in agreement with the fact that the deprotonated oxamide nitrogen is a very strong σ-donor. The short V=O bond length (1.590(2) Å) indicates considerable π-bond character, as in other monomeric V(IV) complexes with similar coordination geometries [30c,33]. The C=O distances of the oxamido bridge are 1.212(4) Å for C1–O1 and 1.219(4) Å for C2–O2, analogous to the situation of other oxamido bridges [29a].

3.2.2. $[Cu(VOL)_2(H_2O)_2](ClO_4)_2 \cdot 1.5H_2O$ (*2*)

The single-crystal X-ray analysis reveals that complex **2** consists of a trinuclear cation $[Cu(VOL)_2(H_2O)_2]^{2+}$, with ClO_4^- counter anions and 1.5 molecules of lattice water. The perspective view of the cation is given in Fig. 2 (the ClO_4^- and H_2O and hydrogen atoms have been omitted for clarity). Selected bond distances and angles are given in Table 3. The trinuclear unit is centrosymmetric, in which V1 and V1A also adopt a square pyramidal geometry and reside in the N4 cavity of macrocyclic complex ligand, with the four donor atoms deviating from their mean plane by −0.053(6) (N1), 0.053(0) (N2), −0.051(3) (N3) and 0.051(9) (N4) Å, and the vanadium atom is −0.6385 Å out of the plane. There are some differences in the V–N bond lengths when compared to the mononuclear complex **1**: both V–N1 and V–N2 have distances of 2.012(5) Å, which is somewhat longer than that of **1**, while V–N3 [2.057(5) Å] and V–N4 [2.054(6) Å] are shorter than the corresponding bond lengths as a result of the interaction of the copper ion and the oxygen atoms of the oxamido bridge. On the other hand, the V=O (terminal) distance (1.588(5) Å) compares well with that observed in the mononuclear complex. The central Cu(II) is located on a centrosymmetric center and is set in a distorted octahedral coordination sphere. The equatorial plane is defined by the four donor oxygen atoms from the oxamido macrocyclic ligand with bond lengths of Cu1–O1 2.105(5) Å and Cu1–O2 1.992(4) Å. The other oxygen atoms of the two coordinated water molecules are positioned in the remaining axial sites above and below the

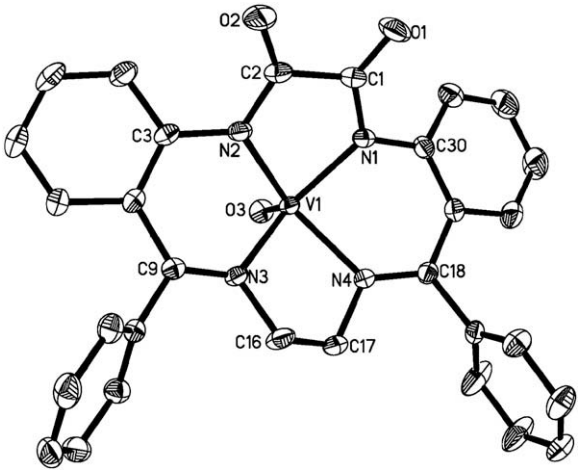

Fig. 1. ORTEP plot of compound **1** at the 30% probability level.

Table 2
Selected bond lengths (Å) and angles (°) for complex **1**

V(1)–N(1)	1.977(2)	V(1)–N(2)	1.993(2)
V(1)–N(3)	2.063(2)	V(1)–N(4)	2.066(2)
V(1)–O(3)	1.590(2)	O(1)–C(1)	1.212(4)
O(2)–C(2)	1.219(4)	N(1)–C(1)	1.361(4)
N(2)–C(2)	1.356(4)		
O(3)–V(1)–N(1)	111.8(1)	O(3)–V(1)–N(2)	111.0(1)
O(3)–V(1)–N(3)	108.2(1)	O(3)–V(1)–N(4)	106.1(1)
N(1)–V(1)–N(2)	81.3(1)	N(1)–V(1)–N(3)	140.1(1)
N(1)–V(1)–N(4)	86.2(1)	N(2)–V(1)–N(3)	85.8(1)
N(2)–V(1)–N(4)	142.9(1)	N(3)–V(1)–N(4)	81.8(1)
C(1)–N(1)–V(1)	117.0(2)	C(2)–N(2)–V(1)	116.2(2)
O(1)–C(1)–N(1)	127.9(3)	O(2)–C(2)–N(2)	127.9(3)

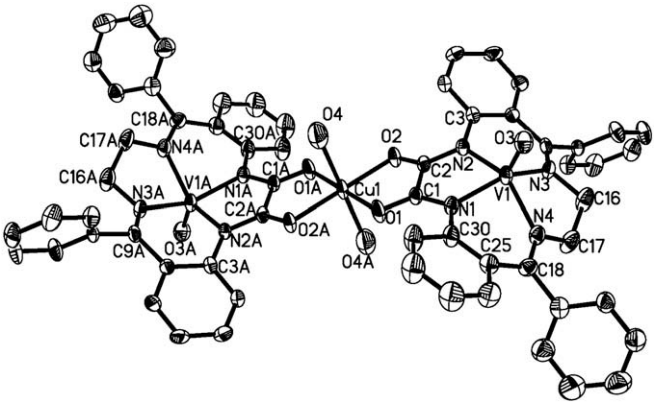

Fig. 2. ORTEP plot of $[Cu(VOL)_2(H_2O)_2]^{2+}$ at the 30% probability level.

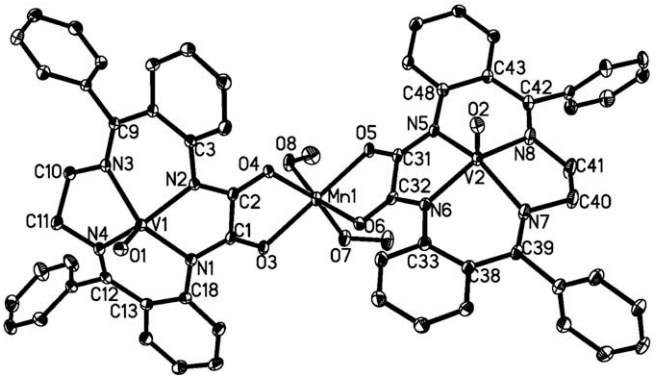

Fig. 3. ORTEP plot of $[Mn(VOL)_2(CH_3OH)_2]^{2+}$ at the 30% probability level.

Table 3
Selected bond lengths (Å) and angles (°) for complex **2**

V(1)–N(1)	2.012(5)	V(1)–N(2)	2.012(5)
V(1)–N(3)	2.057(5)	V(1)–N(4)	2.054(6)
V(1)–O(3)	1.588(5)	O(1)–C(1)	1.247(7)
O(2)–C(2)	1.240(7)	N(1)–C(1)	1.331(8)
N(2)–C(2)	1.336(7)	Cu(1)–O(1)	2.105(5)
Cu(1)–O(2)	1.992(4)	Cu(1)–O(4)	2.125(7)
O(3)–V(1)–N(1)	108.1(2)	O(3)–V(1)–N(2)	111.7(2)
O(3)–V(1)–N(3)	105.4(3)	O(3)–V(1)–N(4)	108.1(3)
N(1)–V(1)–N(2)	81.2(2)	N(1)V(1)–N(3)	146.5(2)
N(1)–V(1)–N(4)	86.4(2)	N(2)–V(1)–N(3)	87.6(2)
N(2)–V(1)–N(4)	140.2(2)	N(3)–V(1)–N(4)	82.2(2)
C(1)–N(1)–V(1)	115.3(4)	C(2)–N(2)–V(1)	114.9(4)
O(1)–C(1)–N(1)	129.8(6)	O(2)–C(2)–N(2)	128.9(6)
O(2)–Cu(1)–O(1)	81.1(2)	O(2)–Cu(1)–O(4)	88.1(2)
O(1)–Cu(1)–O(4)	93.0(2)		

Symmetry codes: $-x+2$, $-y+1$, $-z+1$.

copper ion at Cu1–O4 distances of 2.125(7) Å. The Cu···V separation across the oxamido bridge is 5.393 Å.

3.2.3. $[Mn(VOL)_2(CH_3OH)_2](ClO_4)_2 \cdot 5CH_3OH$ (**3**)

The crystal structure of complex **3** is built up of the heterotrinuclear cation $[Mn(VOL)_2(CH_3OH)_2]^{2+}$, two perchlorate ions and five uncoordinated methanol molecules. The main skeleton unit (Fig. 3) is asymmetric, which is appreciably different from the X-ray structure of complex **2** discussed above. The two VOL fragments are nearly perpendicular to each other with a dihedral angle of 87.91\. The central manganese also possesses a distorted octahedral geometry, surrounded by six oxygen atoms, four from the oxamido macrocyclic ligand and the other two from the coordinated methanol molecules. All the Mn–O bond lengths are different from each other, and are in the range 2.136(3) to 2.203(3) Å (detailed bond lengths and angles are available in Table 4). In the two VOL fragments, the vanadium atoms V1 and V2 are crystallographically distinct, though they both have square pyramidal geometries. However, N1–N4 substantially deviate from their mean plane by 0.104(8), −0.104(4), 0.101(3) and −0.100(6) Å, respectively, and the V1 atom is −0.669(6) out of the plane, while N5–N8 are nearly in the same plane with the largest deviations of 0.014(1) and −0.014(1) Å for N5 and N6, respectively, whilst the V2 atom is 0.564(9) Å above the mean plane. The V1···Mn1 separation (5.552 Å) is also slightly longer than that of V2···Mn1 (5.526 Å). The V=O (terminal) distance are very similar and they are both longer than the relative bond observed in the mononuclear complex **1**. In the $C_2O_2N_2$ bridge plane, the average C–O and C–N bond lengths in **3** are 1.248 and 1.333 Å, respectively, while the corresponding distances for the mononuclear precursor are 1.215 and 1.359 Å, respectively. The increase in the C–O and the decrease in the C–N distance in the trinuclear complex reflect the delocalization of the electron density from the N-atoms towards the O-atoms upon the coordination of the O-atoms to the Mn(II) ion [34].

3.3. Magnetic properties

Variable temperature (2–300 K) magnetic susceptibility measurements were collected for polycrystalline samples of complexes **2** and **3** in an applied magnetic field of 2 kOe. Diamagnetic corrections were made with Pascal's constants for all the constituent atoms [35]. As a predigesting approach to simulate the experimental magnetic behavior, the single *g* factor was treated as the sum of the contributions of the central atom, Cu(II) or Mn(II), and its neighbouring VO(IV) ions from the macrocyclic oxamido ligands.

The plot of χ_M and μ_{eff} versus *T* for compound **2** is shown in Fig. 4. At room temperature, the effective magnetic moment μ_{eff} is 3.11 μ_B, which is a little higher than the spin-only value (3.00 μ_B) expected for an isolated $V^{IV}_2Cu^{II}$ paramagnetic system. As the temperature decreases, the μ_{eff} value increases continuously over the whole range. These features are typical of a ferromagnetic exchange propagated between the VO(IV) and Cu(II) ions.

Table 4
Selected bond lengths (Å) and angles (°) for complex **3**

V(1)–N(1)	2.017(3)	V(1)–N(2)	2.000(3)
V(1)–N(3)	2.072(3)	V(1)–N(4)	2.057(3)
V(1)–O(1)	1.598(3)	V(2)–O(2)	1.597(3)
V(2)–N(5)	2.004(3)	V(2)–N(6)	1.998(3)
V(2)–N(7)	2.062(3)	V(2)–N(8)	2.045(3)
O(3)–C(1)	1.246(4)	O(4)–C(2)	1.251(4)
O(5)–C(31)	1.245(4)	O(6)–C(32)	1.249(4)
Mn(1)–O(3)	2.186(2)	Mn(1)–O(4)	2.203(3)
Mn(1)–O(5)	2.187(2)	Mn(1)–O(6)	2.171(2)
Mn(1)–O(7)	2.136(3)	Mn(1)–O(8)	2.155(3)
O(1)–V(1)–N(1)	114.6(1)	O(1)–V(1)–N(2)	108.2(1)
O(1)–V(1)–N(3)	109.8(1)	O(1)–V(1)–N(4)	104.3(1)
N(1)–V(1)–N(2)	81.4(1)	N(1)–V(1)–N(3)	135.6(1)
N(2)–V(1)–N(3)	86.0(1)	N(2)–V(1)–N(4)	147.5(1)
N(3)–V(1)–N(4)	81.7(1)	O(2)–V(2)–N(5)	106.6(1)
O(2)–V(2)–N(6)	106.1(1)	O(2)–V(2)–N(7)	104.9(1)
O(2)–V(2)–N(8)	107.1(1)	N(5)–V(2)–N(7)	148.5(1)
N(5)–V(2)–N(8)	87.9(1)	N(6)–V(2)–N(7)	88.0(1)
N(6)–V(2)–N(8)	146.7(1)	N(8)–V(2)–N(7)	82.9(1)
O(3)–Mn(1)–O(4)	75.2(9)	O(5)–Mn(1)–O(4)	100.0(9)
O(3)–Mn(1)–O(5)	173.0(1)	O(6)–Mn(1)–O(5)	75.6(9)
O(6)–Mn(1)–O(4)	89.6(1)	O(6)–Mn(1)–O(3)	99.2(1)
O(7)–Mn(1)–O(3)	87.2(1)	O(8)–Mn(1)–O(5)	89.1(1)
O(7)–Mn(1)–O(4)	162.3(1)	O(7)–Mn(1)–O(5)	97.7(1)
O(7)–Mn(1)–O(6)	94.8(1)	O(7)–Mn(1)–O(8)	87.1(1)

A magnetic analysis has been made using the magnetic susceptibility expression (1) based on the isotropic Heisenberg model. A molecular field approximation has also been introduced to take into account the small intermolecular interactions between the trinuclear entities using Eq. (2).

$$\hat{H} = -2J(\hat{S}_{V1}\hat{S}_{Cu} + \hat{S}_{V2}\hat{S}_{Cu})$$

$$\chi = \frac{Ng^2\beta^2}{4KT}\left[\frac{5+\exp(-3J/KT)}{1+\exp(-3J/KT)}\right] + N_\alpha \quad (1)$$

$$\chi_M = \frac{\chi}{1-(2zj'/Ng^2\beta^2)\chi} \quad (2)$$

where J is the exchange interaction parameter between the VO(IV) and Cu(II) ions, N_α is the temperature-independent paramagnetic term, and is set as 120×10^{-6} m^3 mol^{-1}, zJ' stands for the intermolecular interactions and the other symbols have their usual meanings. On this basis, the least squares fitting of the experimental data led to $J = 9.09$ cm^{-1}, $g = 2.00$ and $zJ' = 5.0 \times 10^{-3}$ cm^{-1}. The agreement factor defined as $R = \sum((\chi_M T)_{obs} - (\chi_M T)_{calc})^2 / \sum(\chi_M T)^2_{obs}$ is equal to 3.59×10^{-4}.

The magnetic behavior of complex **2** can be rationalized by the orthogonality of the magnetic orbitals. As already noted from the crystal structure of **2**, the symmetries of the metallic sites and the bridge in the Cu–VO region are very close to *Cs*. The magnetic orbital on the Cu(II) center, $d_{x^2-y^2}$ is roughly parallel to the copper-donor directions in the basal plane and is engaged in σ overlap with the bridging oxamido oxygens, and transforms as an α′ irreducible representation of the *Cs* group. On the other hand, the magnetic orbital on VO(IV), d_{xy}, which approximately bisects the equatorial donor-vanadium-donor angles, is delocalized toward the oxamido nitrogens by a π-type overlap and transforms as a α″ irreducible representation of the *Cs* group. Thus, for the magnetic orbitals (Φ_{Cu}, Φ_{VO}) being symmetry-related orthogonal, there is essentially zero overlap ($\langle\Phi_{Cu}|\Phi_{VO}\rangle \approx 0$), and no chemical bonding. This implies that in the expression for the singlet–triplet energy gap, $2J = J_{AF} + J_F$, the negative antiferromagnetic contribution J_{AF} is insignificant [36]. So the coupling is purely ferromagnetic.

The magnetic behavior of complex **3** is shown in Fig. 5. The effective magnetic moment μ_{eff} at 300 K (6.03 μ_B) is slightly lower than the spin-only value (6.40 μ_B) for the non-interaction of two vanadium(IV)-oxo and one manganese(II) ion. With the decreasing temperature, μ_{eff} decreases smoothly over the entire temperature region, and reaches a minimum value of 5.37 μ_B at 2 K. These behaviors are indicative of an overall weak antiferromagnetic coupling. The experimental data are fitted by using Eq. (3) derived from the spin-exchange Hamiltonian.

$$\hat{H} = -2J(\hat{S}_{V1}\hat{S}_{Mn} + \hat{S}_{V2}\hat{S}_{Mn})$$

$$\chi_M = \frac{Ng^2\beta^2}{4K(T-\theta)}\left[\frac{35+10\exp(-7J/KT)+35\exp(-2J/KT)+84\exp(5J/KT)}{3+2\exp(-7J/KT)+3\exp(-2J/KT)+4\exp(5J/KT)}\right] \quad (3)$$

The symbols in the expression have the same meaning as in expression (1) and θ is the correction term for the intermolecular interactions. For a satisfactory fit, the following parameters: $J = -0.27$ cm^{-1}, $g = 1.97$, $\theta = -0.03$ K are used with the agreement factor $R = 4.76 \times 10^{-4}$.

It is not difficult to rationalize the occurrence of weak antiferromagnetic coupling between the Mn(II) ion and VO(IV) ions. In a trinuclear system, with many electrons on metal centers, the exchange coupling parameter J is given by Eq. (4) [37].

$$J = \frac{1}{n_A n_B}\sum\nolimits_{\mu,\nu} J_{\mu,\nu} = \frac{1}{n_A n_B}[J_{AF} + J_F] \quad (4)$$

Where n_A and n_B are the number of unpaired electrons associated with the transition metal ions A and B, respectively. $J_{\mu,\nu}$ is the exchange between two singly occupied orbitals of symmetry μ and ν. When two orbitals have the same symmetry, they overlap and an antiferromagnetic contribution (J_{AF}, negative) arises. On the other hand, when two orbitals have different symmetries, the orthogonality leads to a ferromagnetic contribution (J_F, positive), the resulting sign of J is determined by a competition between them.

In the case of **3**, the Mn(II) site has five d_{xy}, d_{yz}, d_{xz}, $d_{x^2-y^2}$, d_{z^2} magnetic orbitals, and the VO(IV) site has only one d_{xy} orbital. By simple symmetry considerations, the J_{xy-xy} pathway involves an interaction between two magnetic orbitals of the same symmetry which contributes antiferromagnetically (J_{AF}) to the exchange, and it is expected to give the most important contribution in absolute value, while the other four routes (J_{xy-yz}, J_{xy-xz}, $J_{xy-x^2-y^2}$, J_{xy-z^2}) involve two orthogonal orbitals which lead to a ferromagnetic contribution (J_F). Consequently, the weak interaction will be overwhelmed by the opposite effects. The existence of the net antiferromagnetic interaction in **3** is indicative that the J_{xy-xy} pathway dominates the overall interaction.

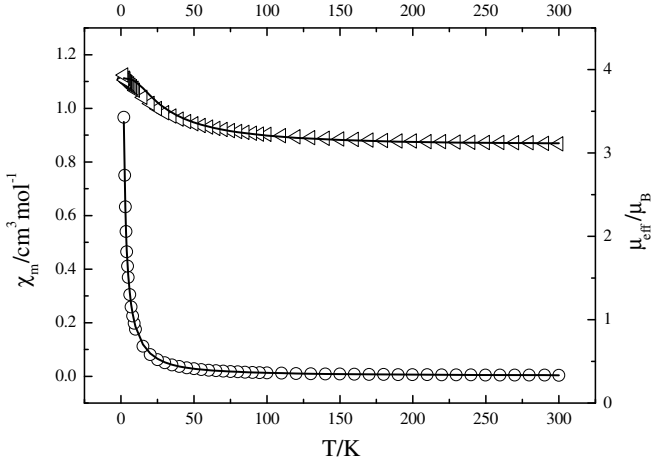

Fig. 4. Plots of χ_M vs. T (open circles) and μ_{eff} vs. T (open triangles) for **2**. The solid line shows the fitting values.

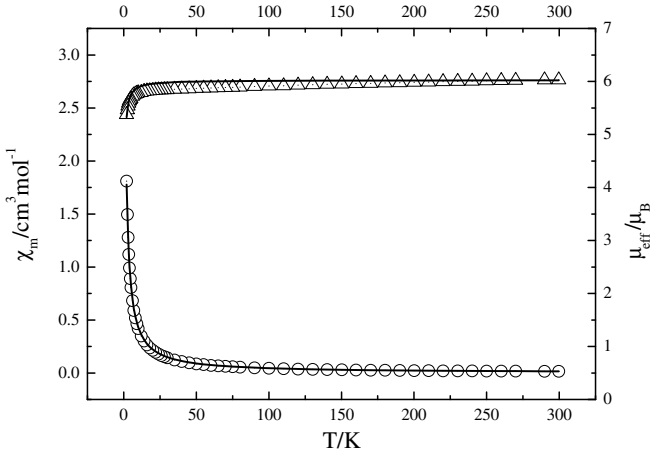

Fig. 5. Plots of χ_M vs. T (open circles) and μ_{eff} vs. T (open triangles) for **3**. The solid line shows the fitting values.

4. Conclusion

In summary, a new vanadium-oxo macrocyclic ligand with an oxamido bridge has been solvent-thermally synthesized, and based on the precursor ligand, two trinuclear complexes have been constructed and structurally as well as magnetically characterized. Both compounds **2** and **3** tend to adopt a trinuclear configuration as a result of the larger bulk of the rigid co-ligand VOL and the geometry around the central Cu(II) and Mn(II) ions is a distorted octahedron. Compound **2** exhibits ferromagnetic behavior, which is in accord with other Cu(II)–VO(IV) systems [36,38], while compound **3** shows a very weak antiferromagnetic coupling. The temperature dependence of the magnetic susceptibility for the complexes were analyzed by means of the Heisenberg Hamiltonian $\hat{H} = -2J\hat{S}_1\hat{S}_2$, leading to $J = 9.09\ \mathrm{cm}^{-1}$, $zJ' = 5.0 \times 10^{-3}\ \mathrm{cm}^{-1}$ for complex **2** and $J = -0.27\ \mathrm{cm}^{-1}$, $\theta = -0.03$ K for complex **3**. The present study reports, for the first time, a substitute VO(IV) ion for copper or nickel acting as the template metal ion of the macrocyclic ligand. It is clear from the above discussion that in this system the magnetic interactions may be tunable by changing the metal ions in the complex ligand or the central ions, and further investigations on this and similar systems are in progress in our laboratory.

Acknowledgements

The work was supported by the National Natural Science Foundation of China (Nos. 20571046 and 20601014) and the Natural Science Foundation of Tianjin (No. 013603711).

Appendix A. Supplementary data

CCDC 633452–633454 contains the supplementary crystallographic data for this paper. These data can be obtained free of charge via http://www.ccdc.cam.ac.uk/conts/retrieving.html, or from the Cambridge Crystallographic Data Centre, 12 Union Road, Cambridge CB2 1EZ, UK; fax: (+44) 1223-336-033; or e-mail: deposit@ccdc.cam.ac.uk. Supplementary data associated with this article can be found, in the online version, at doi:10.1016/j.poly.2008.07.032.

References

[1] O. Kahn, Struct. Bond. 68 (1987) 89.
[2] O. Kahn, Adv. Inorg. Chem. 43 (1996) 179.
[3] G.A. Melson (Ed.), Coordination Chemistry of Macrocyclic Compounds, Plenum, New York, 1979.
[4] E. Colacio, M. Ghazi, R. Kivekas, J.M. Moreno, Inorg. Chem. 39 (2000) 2882.
[5] E.Q. Gao, G.M. Yang, D.Z. Liao, Z.H. Jiang, S.P. Yan, G.L. Wang, J. Chem. Res. (1999) 278.
[6] G.M. Yang, J. Shi, S.P. Yan, D.Z. Liao, Z.H. Jiang, Q.L. Wang, Polyhedron 17 (1998) 1587.
[7] O. Kahn, Y. Pei, M. Verdaguer, J.P. Renard, J. Sletten, J. Am. Chem. Soc. 110 (1988) 782.
[8] P.A. Vigato, S. Tamburini, D.E. Fenton, Coord. Chem. Rev. 106 (1990) 25.
[9] (a) S. Mohanta, K.K. Nanda, R. Werner, W. Haase, A.K. Mukherjee, S.K. Dutta, K. Nag, Inorg. Chem. 36 (1997) 4656;
(b) K.K. Nanda, A. Addison, W.N. Paterson, E. Sinn, L.K. Thompson, U. Sakaguchi, Inorg. Chem. 37 (1998) 1028.
[10] D. Christodoulou, M.G. Kanatzidis, D. Coucouvanis, Inorg. Chem. 29 (1990) 191.
[11] (a) S.B. Wang, G.M. Yang, D.Z. Liao, L.C. Li, Inorg. Chem. 43 (2004) 852;
(b) L. Zhang, S.B. Wang, G.M. Yang, J.K. Tang, D.Z. Liao, Z.H. Jiang, P. Cheng, Inorg. Chem. 42 (2003) 1462;
(c) S.B. Wang, G.M. Yang, R.F. Li, Y.F. Wang, D.Z. Liao, Eur. J. Inorg. Chem. (2004) 4907.
[12] D. Gatteschi, A. Caneschi, R. Sessoli, A. Cornia, Chem. Soc. Rev. 25 (1996) 101.
[13] (a) S.J. Gruber, C.M. Harris, E. Sinn, J. Inorg. Nucl. Chem. 30 (1986) 1805;
(b) N.B. Brien, T.O. Maier, I.C. Paul, R.S. Drago, J. Am. Chem. Soc. 95 (1973) 6640;
(c) H. Ojima, K. Nonoyama, Coord. Chem. Rev. 92 (1988) 85;
(d) A. Escuer, R. Vicente, J. Ribas, R. Costa, X. Solans, Inorg. Chem. 31 (1992) 2627.
[14] (a) A. Bencini, M.D. Vaira, A.C. Fabretti, D. Gatteschi, C. Zanchini, Inorg. Chem. 23 (1984) 1620;
(b) H. Okawa, Y. Kawahara, M. Mikuriya, S. Kida, Bull. Chem. Soc. Jpn. 53 (1980) 549;
(c) M. Verdaguer, O. Kahn, M. Julve, A. Gleizes, Nouv. J. Chim. 9 (1985) 325.
[15] C.T. Chen, K.S. Suslick, Coord. Chem. Rev. 128 (1993) 293.
[16] D. Dhristodoulou, M.G. Kanatzidis, D. Coucouvanis, Inorg. Chem. 29 (1990) 191.
[17] M. Schindler, F.C. Hawthorne, W.H. Baur, Chem. Mater. 12 (2000) 1248.
[18] I. Pasha, A. Choudhury, C.N.R. Rao, Inorg. Chem. 42 (2003) 409.
[19] Z.M. Dai, Z. Shi, G.H. Li, X.B. Chen, X.Y. Lu, Y.H. Xu, S.H. Feng, J. Solid State Chem. 172 (2003) 205.
[20] Z.M. Dai, X.B. Chen, Z. Shi, D. Zhang, G.H. Li, S.H. Feng, Inorg. Chem. 42 (2003) 908.
[21] Z. Shi, D. Zhang, S. Feng, G.H. Li, Z.M. Dai, W.S. Fu, X.B. Chen, J. Hua, J. Chem. Soc., Dalton Trans. (2002) 1873.
[22] Z.M. Dai, Z. Shi, G.H. Li, D. Zhang, W.S. Fu, H.Y. Jin, W. Xu, S.H. Feng, Inorg. Chem. 42 (2003) 7396.
[23] (a) S. Aschwanden, H.W. Schmalle, A. Reller, H.R. Oswald, Mater. Res. Bull. 28 (1993) 45;
(b) J.R.D. DeBord, Y. Zhang, R.C. Haushalter, J. Zubieta, C.J. O'Connor, J. Solid State Chem. 122 (1996) 251;
(c) Y. Zhang, J.R.D. DeBord, C.J. O'Connor, R.C. Haushalter, A. Clearfield, J. Zubieta, Angew. Chem., Int. Ed. Engl. 35 (1996) 989;
(d) L.M. Zheng, J.S. Zhao, K.H. Li, L.Y. Zhang, Y. Liu, X.Q. Xin, J. Chem. Soc., Dalton Trans. (1999) 939.
[24] (a) Y. Zhang, P.J. Zapf, L.M. Meyer, R.C. Haushalter, J. Zubieta, Inorg. Chem. 36 (1997) 2159;
(b) R.L. LaDuca Jr, C. Brodkin, R. Finn, J. Zubieta, Inorg. Chem. Commun. 3 (2000) 248;
(c) R.L. LaDuca Jr, R. Finn, J. Zubieta, Chem. Commun. (1999) 1669;
(d) P.J. Hagrman, C. Bridges, J.E. Greedan, J. Zubieta, J. Chem. Soc., Dalton Trans. (1999) 2901;
(e) L.M. Zheng, X.Q. Wang, Y.S. Wang, A.J. Jacobson, J. Mater. Chem. 11 (2001) 1100.
[25] S. Ushak, E. Spodine, E. Le Fur, D. Venegas-Yazigi, J.Y. Pivan, W. Schnelle, R. Kniep, Inorg. Chem. 45 (2006) 5393.
[26] (a) E.Q. Gao, W.M. Bu, G.M. Yang, D.Z. Liao, Z.H. Jiang, S.P. Yan, G.L. Wang, J. Chem. Soc., Dalton Trans. (2000) 1431;
(b) E.Q. Gao, G.M. Yang, J.K. Tang, D.Z. Liao, Z.H. Jiang, S.P. Yan, Polyhedron 18 (1999) 3643;
(c) J.K. Tang, L.Y. Wang, L. Zhang, E.Q. Gao, D.Z. Liao, Z.H. Jiang, S.P. Yan, P. Cheng, J. Chem. Soc., Dalton Trans. (2002) 1607;
(d) J.K. Tang, Q.L. Wang, E.Q. Gao, J.J. Chen, D.Z. Liao, Z.H. Jiang, S.P. Yan, P. Cheng, Helv. Chim. Acta 85 (2002) 175;
(e) E.Q. Gao, D.Z. Liao, Z.H. Jiang, S.P. Yan, Polyhedron 20 (2001) 923;
(f) S.B. Wang, R.F. Li, G.M. Yang, D.Z. Liao, Z.H. Jiang, S.P. Yan, Inorg. Chem. Acta 358 (2005) 2595;
(g) S.B. Wang, G.M. Yang, R.F. Li, L.C. Li, D.Z. Liao, Inorg. Chem. Commun. 7 (2004) 1082;
(h) Y.Q. Sun, G.M. Yang, D.Z. Liao, Z.H. Jiang, S.P. Yan, Inorg. Chem. Commun. 6 (2003) 799;
(i) Y.Q. Sun, M. Liang, W. Dong, G.M. Yang, D.Z. Liao, Z.H. Jiang, S.P. Yan, P. Cheng, Eur. J. Inorg. Chem. (2004) 1514;
(j) M. Yu, R.F. Li, G.F. Xu, Q.L. Wang, Y. Song, G.M. Yang, D.Z. Liao, Inorg. Chem. Commun. 9 (2006) 1015.
[27] R.H. Zhang, Q.L. Wang, Y.F. Wang, G.M. Yang, Z.Q. Liu, B. Ding, G.F. Xu, J. Coord. Chem. 58 (2005) 857.
[28] G.M. Sheldrick, SHELXS-97 and SHELXL-97, Software for Crystal Structure Analysis, Siemens Analytical X-ray Instruments Ins, Wisconsin, Madison, USA, 1997.
[29] (a) St.C. David, Inorg. Nucl. Chem. 12 (1976) 657;
(b) Y.H. Zhang, Q.L. Wang, G.M. Yang, Trans. Met. Chem. 31 (2006) 856.
[30] (a) S. Bhattacharyya, S. Mukhopadhyay, S. Samanta, T.J.R. Weakley, M. Chaudhury, Inorg. Chem. 41 (2002) 2433;
(b) K.D. Soulti, A. Troganis, A. Papaioannou, T.A. Kabanos, A.D. Keramidas, Y.G. Deligiannakis, C.P. Raptopoulou, A. Terzis, Inorg. Chem. 37 (1998) 6785;
(c) M. Ebel, D. Rehder, Inorg. Chem. 45 (2006) 7083.
[31] H. Elliott, B.J. Hathaway, R.C. Slade, Inorg. Chem. 5 (1966) 669.
[32] D.Z. Liao, J. Shi, Z.H. Jiang, S.P. Yan, P. Cheng, G.L. Wang, Polyhedron 11 (1992) 2621.
[33] M. Mahroof-Tahir, A.D. Keramidas, R.B. Goldfarb, O.P. Anderson, M.M. Miller, D.C. Crans, Inorg. Chem. 36 (1997) 1657.
[34] E.Q. Gao, J.K. Tang, D.Z. Liao, Z.H. Jiang, S.P. Yan, G.L. Wang, Helv. Chim. Acta 84 (2001) 908.
[35] P.W. Selwood, Magnetochemistry, Interscience, New York, 1956. 78.
[36] O. Kahn, J. Galy, Y. Journaux, J. Jaud, I. Morgenstern-Badarau, J. Am. Chem. Soc. 104 (1982) 2165.
[37] O. Kahn, Molecular Magnetism, VCH, New York, 1993.
[38] (a) Y.T. Li, C.W. Yan, Z.Y. Wu, C.Y. Zhu, J. Magn. Magn. Mater. 292 (2005) 418;
(b) S. Mohanta, K.K. Nanda, L.K. Thompson, U. Flo1rke, K. Nag, Inorg. Chem. 37 (1998) 1465;
(c) T. Glaser, H. Theil, I. Liratzis, T. Weyhermuller, E. Bill, Inorg. Chem. 45 (2006) 4889;
(d) A. Bencini, C. Benelli, A. Dei, D. Gatteschi, Inorg. Chem. 24 (1985) 695.

tetraphenylporphyrin, T(*p*-ClP)P = tetra(4-chlorophenyl)porphyrin, T(*p*-MeP)P = tetra(4-methylphenyl)porphyrin, T(*m*-ClP)P = tetra(3-chlorophenyl)porphyrin, T(*m*-MeP)P = tetra(3-methylphenyl)porphyrin). The Ce^{IV}(porphyrin)$_2$ complexes were prepared by the method described by Buchler et al. [41]. The crude products were chromatographed on alumina by using *n*-hexane/toluene as eluent. The purification of the complexes was confirmed via UV–Vis and nuclear magnetic resonance spectroscopy. UV–Vis absorption spectra were obtained with a 1 cm quart cell using a Hewlett-Packard 8450 A diode array spectrophotometer. NMR experiments were performed on a 300 MHz Bruker instrument. Infrared spectra of the samples in KBr pellets were recorded on a Nicolet 550 spectrometer. The spectral slit width was 1 cm^{-1}.

3. Results

The infrared spectra of Ce(OEP)$_2$ and Ce(OEP)(TPP) are shown in Fig. 1. It is interesting to note that the features of the IR spectrum of the porphyrin dimer, Ce(OEP)$_2$, are closely related to those of the metalloporphyrin monomers [30–32,34]. To the best of our knowledge, the similarity of the IR spectra of the OEP monomer and dimer systems has not been fully discussed yet. In order to facilitate a comparison of the IR spectra, tentative assignments of the IR signals were carried out on the basis of the similar features of the IR spectra between the porphyrin dimers and metalloporphyrin monomers. However, it should be noted that the mode labelling is formally inappropriate for the porphyrin dimers as their symmetry is at most D_{4d} [14].

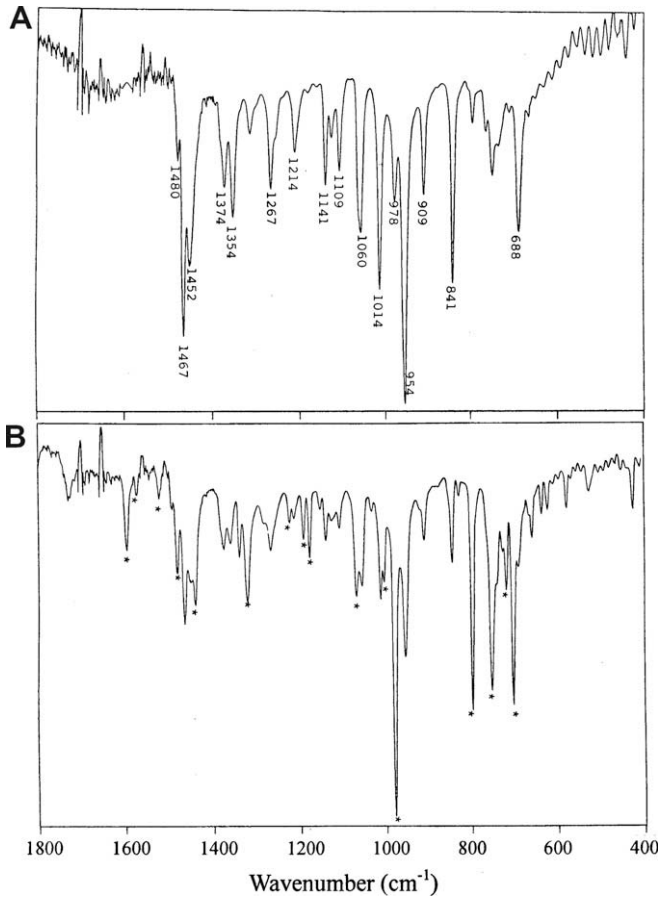

Fig. 1. IR spectra of (A) Ce(OEP)$_2$ and (B) Ce(OEP)(TPP) in KBr pellets. The IR signals from the TPP moiety are labelled with an asterisk.

The infrared spectrum of Ce(OEP)$_2$ displays three bands in the region between 1500 and 1450 cm^{-1}. Since they are similar to those of the metalloporphyrin monomers, the band observed at 1480 cm^{-1} is readily assigned to the core vibration, and the bands at 1467 and 1452 cm^{-1} are assigned to alkyl group vibrations. The region between 1400 and 1100 cm^{-1} contains several medium-intensity bands. Except for the band at 1354 cm^{-1}, its corresponding band in the metalloporphyrin monomers is too weak to be assigned, all the other signals can be readily assigned to their corresponding bands in the monomers. Additionally, an intensity change is also observed in this region especially for those of the skeletal modes at 1267, 1214 and 1141 cm^{-1}. After normalization, the relative intensities of these bands are shrunk to about one half of those of the corresponding bands in the metalloporphyrin monomers. The remaining absorptions in the region from 1100 to 600 cm^{-1} contain several strong bands. Except for the medium-strong bands at 841 and 688 cm^{-1}, the intensities of the other core vibrations at 978 and 909 cm^{-1} are much weaker than those of the alkyl group vibrations at 1060, 1014 and 954 cm^{-1}. Collectively, the overall feature of the IR spectrum Ce(OEP)$_2$ is highly correlated to that of the metalloporphyrin monomer. The major differences between these two systems are confined to the frequency shifts and the subtle changes in the relative intensities between the core vibrations and the group vibrations. It is worthwhile to note that the intensities of these two types of vibrations in the metalloporphyrin monomers are about the same generally, whereas in the Ce(OEP)$_2$ system, the intensities of the typical core vibrations, observed at 1267, 1214, 1141 and 978 cm^{-1}, are much weaker than those of the group vibrations at 1467, 1014 and 954 cm^{-1}.

In order to make the data comparison consistent, we have re-taken the IR spectrum of Ce(TPP)$_2$. As we have seen in the OEP system, most of the prominent IR bands in Ce(TPP)$_2$ can still find their corresponding signals in M(TPP) [33,38] (where M = Cu, and Zn). As shown in Fig. 2, the medium-intensity band observed at 1599 cm^{-1} in Ce(TPP)$_2$ can be easily assigned to the phenyl mode. The position and the relative intensity of this characteristic band are about the same in both monomer and dimer systems. It is interesting to note that this particular mode of the phenyl group is almost inert to the π–π interactions whereas the frequencies of the ethyl modes in the OEP dimers are all downshifted from their corresponding monomer signals. The following bands at 1575, 1525, 1483 and 1441 cm^{-1} are essentially unshifted from those of Zn(TPP). The location of the band at 1327 cm^{-1} corresponds to the electron-density-sensitive ν_4(Cα–N) mode of the

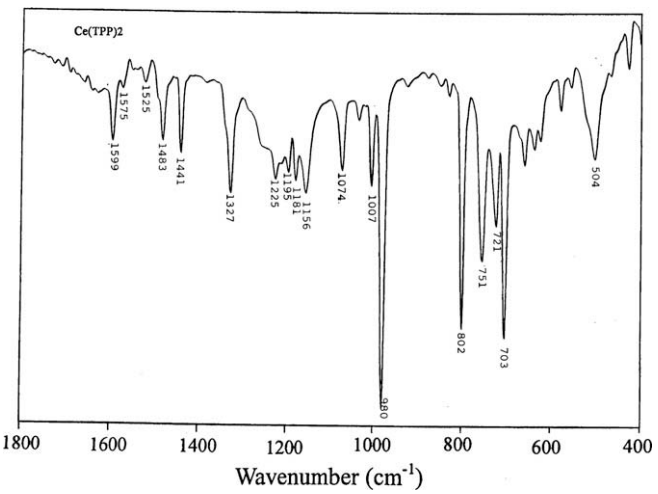

Fig. 2. IR spectrum of Ce(TPP)$_2$ in a KBr pellet.

metalloporphyrins [38]. This band, as well as the other two bands at 1599 cm^{-1} and 1007 cm^{-1}, has also been shown to have phenyl mode contributions, but only the band at 1327 cm^{-1} is downshifted by 12 cm^{-1} from the counterparts of Zn(TPP). There are four relatively weak signals observed around 1200 cm^{-1}. Except for the band at 1195 cm^{-1}, being downshifted, the remaining three bands at 1225, 1181 and 1156 cm^{-1} are all upshifted by 5–11 cm^{-1} from their corresponding signals of Zn(TPP). The medium-intensity band at 1074 cm^{-1} was assigned as a pyrrole-hydrogen bending mode [33] and was observed to be upshifted by 5 cm^{-1}. There are several strong and medium-strong bands that appear in the low frequency region. The band at 980 cm^{-1} is observed to be downshifted by 12 cm^{-1} whereas the bands at 802 and 721 cm^{-1} are upshifted by 7 and 5 cm^{-1}, respectively. The remaining two bands at 751 and 703 cm^{-1} are essentially unchanged from the monomer to dimer systems. Collectively, the π–π interactions do not cause all the IR frequencies of $Ce(TPP)_2$ to downshift from their corresponding monomer signals. These observations are in contrast to the monotonic change of the band frequencies in OEP systems. In addition, the relative intensity of the IR signals of $Ce(TPP)_2$ are essentially the same as those of Zn(TPP).

The methyl and chloro substituents represent typical electron donor and acceptor groups, respectively. Any change of the electronic configuration or geometrical conformation will in turn perturb the π–π interactions. Consequently, systematic studies of the IR spectra of the dimer complexes with suitable substituents should be able to reveal the perturbations of the inductive as well as the steric effects on the π–π interactions of the macrocycles.

The IR spectra of four different derivatives of $Ce(TPP)_2$ are shown in Figs. 3 and 4. In general, the features of these spectra are different to that of $Ce(TPP)_2$ with regard to the relative intensity and the number of signals. In order to explore the origin of these differences, we have also synthesized and compared the IR spectrum (not shown here) of Cu[T(*m*-clP)P] with those of the Ce[T(*m*-clP)P]$_2$ dimer. The results indicate that most of the prominent IR bands in Ce[T(*m*-clP)P]$_2$ can still find the corresponding signals in Cu[T(*m*-clP)P]. The typical bands at 1326 and 985 cm^{-1} are downshifted by 18 and 20 cm^{-1}, respectively, whereas the bands at 804, 782, 745, 724 and 697 cm^{-1} are all upshifted by 2–9 cm^{-1}. All these results indicate that both the nature and the position of the substituent groups perturb the IR spectra of the TPP monomer and dimer systems to a different extent. These substituent effects complicate the comparisons of the IR spectra of $Ce(TPP)_2$ with its dimer derivatives. However, the prominent signals at around 1327, 980, 802 and 724 cm^{-1} are relatively unaffected by the substituent groups.

Regarding heterodimers, the IR spectrum of Ce(OEP)(TPP) (as shown in Fig. 1) displays more complex features than those of either $Ce(OEP)_2$ or $Ce(TPP)_2$. A detailed analysis indicated that this spectrum can be de-convoluted to a simple combination of the IR spectra of $Ce(OEP)_2$ and $Ce(TPP)_2$. This result is similar to those obtained from a resonance Raman study on this complex [40]. Clearly, the effect of the symmetry decreasing does not play a major role in the heterodimers either. The similar properties of the linear combination of the IR spectra were also observed in other heterodimer derivatives (as shown in Figs. 5 and 6). Although most of the frequencies of the prominent signals are essentially unaffected on going from the homoleptic dimers to heteroleptic dimer, minor changes are still observed in both components. For example, the band at 845 cm^{-1} originating from the OEP moiety is upshifted by 4 cm^{-1} from its corresponding signal of $Ce(OEP)_2$. For those signals originating from the TPP moiety, the band at 1323 cm^{-1} is downshifted by 4 cm^{-1}, whereas the bands at 1069 and 798 cm^{-1} are downshifted by 5 and 4 cm^{-1}, respectively from their corresponding signals of $Ce(TPP)_2$.

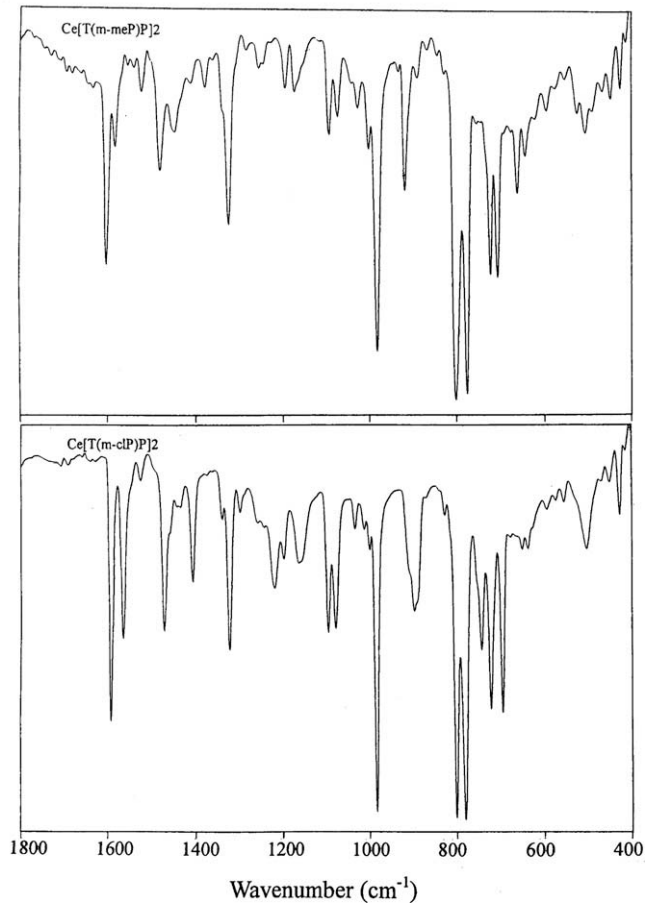

Fig. 3. IR spectra of Ce[T(*m*-MeP)P]$_2$ and Ce[T(*m*-ClP)P]$_2$ in KBr pellets.

Figs. 7 and 8 display the high frequency region of the IR spectra of $Ce(OEP)_2$, Ce(OEP)(TPP) and the heterodimer derivatives Ce(OEP)(TPP*) (where TPP* represents the derivatives of TPP). Coincidentally, they all display four signals at 2963, 2930, 2868 and 2850 cm^{-1}. These signals have previously been assigned to the vibrations of the ethyl group on the OEP macrocycle [30]. Similar to the other ethyl vibrations in the low frequency region, the frequencies of these bands are observed to be downshifted by about 4 cm^{-1} from their corresponding monomer signals. The distinction of these complexes can be characterized by the relative intensities of these four signals. Basically, the relative intensities of these four bands decline from 2963 to 2850 cm^{-1} in $Ce(OEP)_2$. However, in Ce[OEP][TPP], the relative intensities of the bands at 2963 and 2930 cm^{-1}, as well as the other two bands at 2868 and 2850 cm^{-1}, are inversed relative to those of the bands in $Ce(OEP)_2$. The relative intensities of these bands are also sensitive to the substituent groups on the TPP moiety. The IR spectra of the *para*-substituted heteroleptic dimers, Ce[OEP][T(*p*-ClP)P] and Ce[OEP][T(*p*-MeP)P], have similar contours to those of Ce[OEP][TPP] in this high frequency region, except for a minor difference between the signals at 2868 and 2850 cm^{-1}. However, both the *meta*-substituted heteroleptic dimers, Ce[OEP][T(*m*-MeP)P] and Ce[OEP][T(*m*-ClP)P], exhibit different IR figures to that of Ce[OEP][TPP]. The relative intensities of these four bands in Ce[OEP][T(*m*-MeP)P] are essentially similar to those in $Ce(OEP)_2$. Whereas in the case of Ce[OEP][T(*m*-ClP)P], the relative intensities of the bands at 2868 and 2850 cm^{-1} are similar to those in $Ce(OEP)_2$, the other two bands at 2963 and 2930 cm^{-1} display as the intermediate between $Ce(OEP)_2$ and Ce[OEP][TPP].

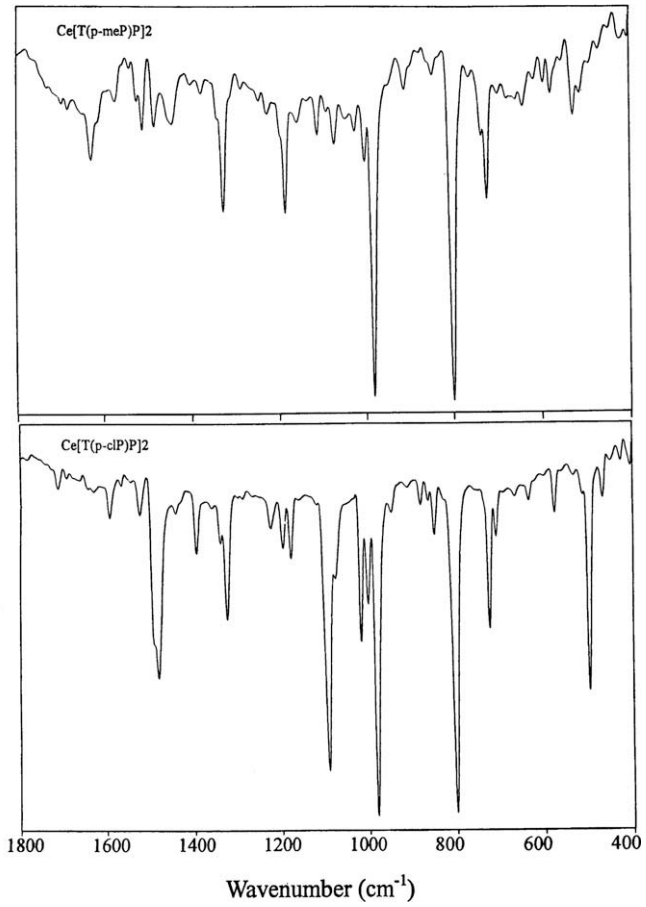

Fig. 4. IR spectra of Ce[T(*p*-MeP)P]$_2$ and Ce[T(*p*-ClP)P]$_2$ in KBr pellets.

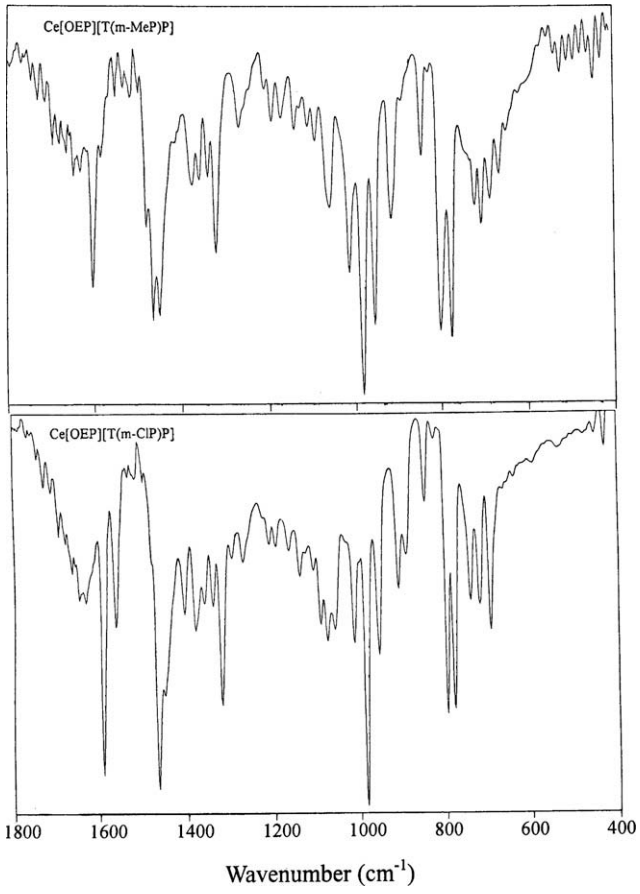

Fig. 5. IR spectra of Ce[OEP][T(*m*-MeP)P] and Ce[OEP][T(*m*-ClP)P] in KBr pellets.

4. Discussion

Although the IR spectrum is characterized by the geometry of the whole molecule, it turns out that certain groups of atoms give rise to bands at or near the same frequency regardless of the structure of the rest of the molecule. The intrinsic properties of these characteristic bands usually provide key information about the subtle change of the geometric and the electronic structure of the molecule. As has been shown in some typical metalloporphyrin monomers, the prominent IR spectra can be divided into two classes: the core vibrations, which are sensitive to the central metal ions, and the group vibrations, which are nearly unaffected by the central metal ions [31]. Since a change of the central metal ions also causes a structural change, the persistence of these characteristic group vibrations indicate that these bands are essentially inert to the structure perturbation of the macrocycle. Due to the similar features of the IR spectra between the porphyrin dimers and monomers, the dimer molecules can be treated as simple derivatives of metalloporphyrin monomers. Each macrocycle is acting as a special substituent group to each other. Following the same categorization of the IR signals in the monomer systems, we should be able to correlate the frequency and the relative intensity changes of the IR signals in the dimer systems to the effects of the induced π–π interactions between these two macrocycles.

In the case of Ce(OEP)$_2$, the IR bands of the core vibrations at 1480, 1267, 1214, 1141, 978, 909, 841, 749 and 688 cm^{-1} are observed to be downshifted by 5–21 cm^{-1} whereas the bands of the group vibrations at 1467, 1452, 1374, 1316, 1109, 1060, 1014 and 954 cm^{-1} are observed to be downshifted by 1–10 cm^{-1} from the corresponding signals of Ni(OEP). Since the group vibrations are nearly unaffected by the central metal ions in the metalloporphyrin monomers, the frequency shifts of these group vibrations observed in the Ce(OEP)$_2$ complex are then totally attributed to the effects of the π–π interaction between the macrocycles. In contrast to the relative simple effects of the π–π interaction on the group vibrations, the extent of the π–π interaction on the core vibrations is much harder to be resolved quantitatively, since the frequencies of the core vibrations are sensitive to the ionic radii of the central metal ions as well as the molecule conformations. These results imply that the dimerization of the macrocycles could lead to the adjustment of the mode composition and contributions of the core vibrations through the conformational change of the macrocycles. Unlike the other core vibrations, the strong band near 846 cm^{-1}, which has been assigned to a C_m–H out-of-plane bending vibration, is observed to be insensitive to the types of the central metal ions [30]. Any change of this particular mode reflects the extent of the π–π interactions on the core vibrations. The 5 cm^{-1} downshift of this band in the Ce(OEP)$_2$ dimer is consistent with the trend of the frequency changes in other group vibrations. The general trend of the frequency downshifts indicates that the π–π interaction causes bond weakness for the entire molecule.

In addition to the frequency changes caused by the π–π interactions, the change in the relative intensities of the core vibrations and the group vibrations is attributed to the symmetry change from the monomer to the dimer systems. Since the descending symmetry of the molecular structure could cause a significant signal split as well as intensity change, the minor change of the relative intensities of the core vibrations and the group vibrations accompanying the non-splitting of the signals implies that the π–π interactions rather than the symmetry change dominate the physical properties of the Ce(OEP)$_2$ complex.

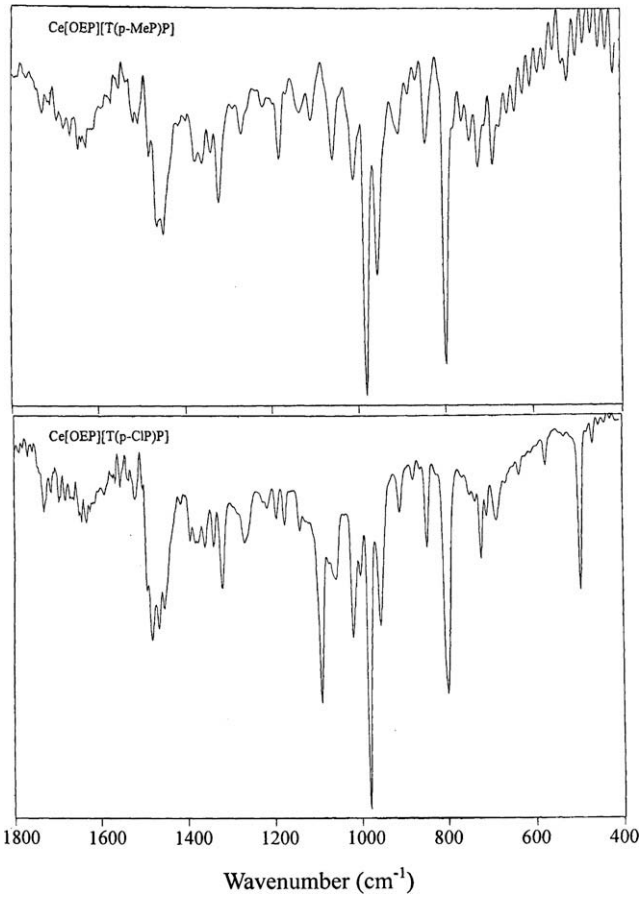

Fig. 6. IR spectra of Ce[OEP][T(*p*-MeP)P] and Ce[OEP][T(*p*-ClP)P] in KBr pellets.

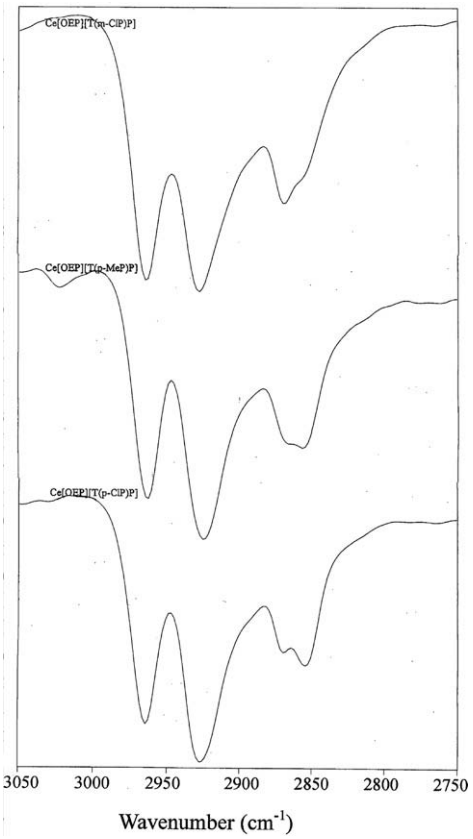

Fig. 8. The high frequency region of the IR spectra of Ce[OEP][T(*m*-ClP)P], Ce[OEP][T(*p*-MeP)P] and Ce[OEP][T(*p*-ClP)P] in KBr pellets.

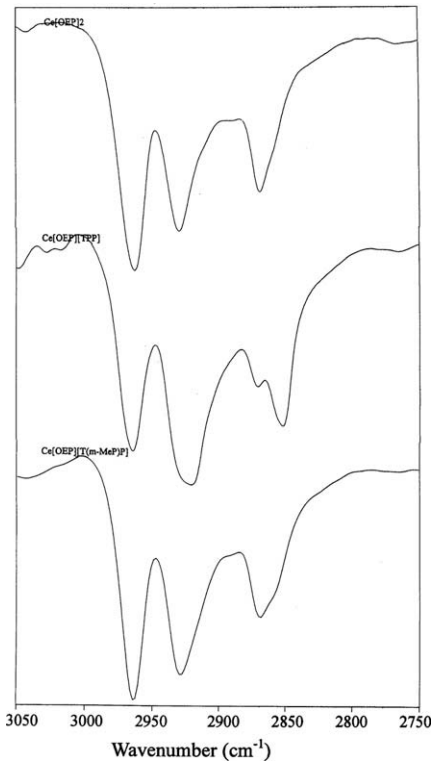

Fig. 7. The high frequency region of the IR spectra of $Ce[OEP]_2$, Ce[OEP][TPP] and Ce[OEP][T(*m*-MeP)P] in KBr pellets.

Significant effects of the π–π interactions are also observed in the IR spectra of the TPP system. The intimate correlation properties between the TPP monomer and dimer systems indicate again that the symmetry change caused by the dimerization does not induce a severe change on the vibrational modes of the porphyrin macrocycles. However, differences between the TPP and OEP systems are observed. In contrast to the regular change of the frequencies in the OEP systems, the π–π interactions in the TPP systems do not cause all the dimer vibrations to be downshifted from their corresponding monomer signals. Since the *meso*-substitution can affect the mode composition and contributions in the TPP system [36], the interactions of the vibrational modes might have been further perturbed in the TPP dimer. Consequently, the irregular alternations of the IR frequencies in the TPP dimer systems are attributed to the readjustment of the mode composition and contributions accompanying the π–π interactions between the macrocycles.

Symmetry insensitive properties also exist in the IR spectra of the heteroleptic dimer system. As we mentioned before, the IR spectrum of Ce(OEP)(TPP) is the simple composition of the IR spectra of $Ce(OEP)_2$ and $Ce(TPP)_2$ instead of the OEP and TPP monomers. These results indicate that the vibrational modes of each macrocycle are not mixed with each other, and the IR signals of each component are mainly affected by the π–π interactions of these two macrocycles. The substituent groups on the macrocycles exhibit very little perturbations on the vibrational modes of the opposite components. These deductions are further supported by the similar trends of the prominent IR signals of the OEP component in other heteroleptic $Ce(OEP)(TPP^*)$ complexes. Since the peripheral substituent groups were attached on the phenyl group rather than the tetrapyrrole macrocycle, the inductive effects of

these groups on the π–π interactions of the porphyrin dimers are believed to be weak. The frequency changes of the bands at 1323, 1069 and 798 cm^{-1}, originating from the TPP moiety, as well as the C_m–H out-of-plane bending vibration [31,34] at 845 cm^{-1}, originating from the OEP moiety, are then attributed to the mutual steric effects of the macrocycles.

In the region 2800–3000 cm^{-1}, $Ce(OEP)_2$ and its derivatives $Ce(OEP)(TPP^*)$ all display the same set of ethyl vibrations at 2963, 2930, 2868 and 2850 cm^{-1}. These results indicate again that the OEP moiety experiences the same magnitude of π–π interactions, no matter what the opposite component is – the OEP or TPP system. The similar contours of the IR spectra of Ce[OEP][T(*p*-ClP)P], Ce[OEP][T(*p*-MeP)P] and Ce[OEP][TPP] imply that both the inductive and the steric effects of the *para*-substituted groups are too small to be detected. However, for those of the *meta*-substituted heteroleptic dimers, significant changes of the band intensities are observed. These results indicate that the steric effects of the *meta*-substituted groups are not strong enough to cause changes of the frequencies by perturbing the electronic structure of the macrocycle π-electrons, the local perturbations on the molecular structure do affect the IR signals through the subtle changes of the band intensities. Referring to the crystallography study of porphyrin dimers, it has been shown that the porphyrin macrocycles are not perfectly flattened [11]. Both of the porphyrin rings are domed and the cerium metal ion protrudes from the porphyrinato plane. The whole molecule is arranged into five layers. The metal ion sits in the center of the molecule, the next pair of layers are formed by 4 nitrogens of each macrocycle, and the outer layers are formed by carbons of each macrocycle. It was also pointed out that the OEP ring is more deformed than the TPP ring [3]. The different deformations in the saucer-like geometries are believed to be responsible for the intensity changes of these four bands in $Ce(OEP)_2$ and Ce[OEP][TPP]. Since the substituent groups on the *para*-positions are not big enough to display effective steric effects, the IR spectra of these four bands in Ce[OEP][T(*p*-ClP)P], Ce[OEP][T(*p*-MeP)P] and Ce[OEP][TPP] are then similar to each others. However, the *meta*-substituted derivatives exhibit a different extent of steric effects on the porphyrin dimers. These effects lead to the perturbations of the porphyrin rings. Intrinsically, the methyl group has a larger steric effect than the chloride group. The essentially similar IR features of these four bands in Ce[OEP][T(*m*-MeP)P] and $Ce(OEP)_2$ imply that the deformations of the porphyrin rings are also similar in these two complexes. Finally, the intermediate IR features of these four bands in Ce[OEP][T(*m*-ClP)P] relative to those of $Ce(OEP)_2$ and Ce[OEP][TPP] are consistent with the weaker deformations of the porphyrin rings caused by the smaller chloride groups. Collectively, these four bands could be used as characteristic bands to monitor the deformations of the porphyrin rings.

5. Conclusions

The similar features of the IR spectra between porphyrin dimers and monomers indicate that the vibrational properties of the dimer molecules can be systematically compared to those of the metalloporphyrin monomers. The symmetry changes induced by the dimerization of the porphyrin rings only lead to a minor perturbation of the vibrational modes of the macrocycles. For the $Ce(OEP)_2$ complex, the frequency downshifts of the group vibrations, which are nearly unaffected by the central metal ions in the metalloporphyrin monomers, indicate that the π–π interactions of the porphyrin rings result in a weakness of the bonds in the dimer molecule. Additionally, the similar IR spectra of the OEP moiety in these different porphyrin dimers reveal that the effects the π–π interactions depend only on the π electrons of the macrocyclic rings instead of the electron configurations of the whole molecule. Finally, the systematic alterations of the IR intensities in the region of 2800–3000 cm^{-1} suggest that these group vibrational modes of the OEP moiety can be used as characteristic bands to monitor the subtle deformations of the porphyrin rings caused by the steric hindrance of the substituents in the dimer complexes.

Acknowledgment

Financial support from the National Kaohsiung Normal University is gratefully acknowledged.

References

[1] J.W. Buchler, K. Elsasser, M. Kihn-Botulinski, B. Scharbert, Angew. Chem., Int. Ed. Engl. 25 (1986) 286.
[2] J.W. Buchler, B. Scharbert, J. Am. Chem. Soc. 110 (1988) 4272.
[3] J.W. Buchler, A. De Cian, J. Fischer, P. Hammerschmitt, J. Loffler, B. Scharbert, R. Weiss, Chem. Ber. 122 (1989) 2219.
[4] O. Bilsel, J. Rodriguez, D. Holten, G.S. Girolami, S.N. Milam, K.S. Suslick, J. Am. Chem. Soc. 112 (1990) 4075.
[5] G.S. Girolami, C.L. Hein, K.S. Suslick, Angew. Chem., Int. Ed. Engl. 35 (1996) 1223.
[6] J. Deisenhofer, H. Michel, Angew. Chem. 101 (1989) 872.
[7] J. Deisenhofer, H. Michel, Angew. Chem., Int. Ed. Engl. 28 (1989) 829.
[8] J. Diesenhofer, H. Michel, Science 245 (1989) 1463.
[9] B.M. Hoffman, J.A. Ibers, Acc. Chem. Res. 16 (1983) 15.
[10] J. Martinsen, L. Stanton, R.L. Greene, J. Tanaka, B.M. Hoffman, J.A. Ibers, J. Am. Chem. Soc. 107 (1985) 6915.
[11] J.W. Buchler, A. DeCian, J. Fischer, M. Kihn-Botulinski, H. Paulus, R. Weiss, J. Am. Chem. Soc. 108 (1986) 3652.
[12] P. Turek, P. Petit, J.-J. Andre, J. Simon, R. Even, B. Boudjema, G. Guillaud, M. Maitrot, J. Am. Chem. Soc. 109 (1987) 5119.
[13] X. Yan, D. Holten, J. Phys. Chem. 92 (1988) 409.
[14] R.J. Donohoe, J.K. Duchowski, D.F. Bocian, J. Am. Chem. Soc. 110 (1988) 6119.
[15] J.W. Buchler, A. DeCian, J. Fischer, M. Kihn-Botulinski, R. Weiss, Inorg. Chem. 27 (1988) 339.
[16] J.K. Duchowski, D.F. Bocian, J. Am. Chem. Soc. 112 (1990) 3312.
[17] G.S. Girolami, S.M. Milam, K.S. Suslick, Inorg. Chem. 26 (1987) 343.
[18] J.-H. Perng, J.K. Duchowski, D.F. Bocian, J. Phys. Chem. 94 (1990) 6684.
[19] J.-H. Perng, J.K. Duchowski, D.F. Bocian, J. Phys. Chem. 95 (1991) 1319.
[20] E.M. Davoras, G.A. Spyroulias, E. Mikros, A.G. Coutsolelos, Inorg. Chem. 33 (1994) 3430.
[21] D. Chabach, M. Tahiri, A. DeCian, J. Fischer, R. Weiss, M. El Maloul Bibout, J. Am. Chem. Soc. 117 (1995) 8548.
[22] G.A. Spyroulias, A.G. Coutsolelos, Inorg. Chem. 35 (1996) 1382.
[23] G.A. Spyroulias, A.G. Coutsolelos, D. de Montauzon, R. Poiblane, J. Coord. Chem. 39 (1996) 89.
[24] J.L. Sessler, A.E. Vivian, D. Seidel, A.K. Burrell, M. Hoehner, T.D. Mody, A. Gebauer, S.J. Weghorn, V. Lynch, Coord. Chem. Rev. 216–217 (2001) 411.
[25] J.P. Collman, J.L. Kendall, J.L. Chen, K.A. Collins, J.-C. Marchon, Inorg. Chem. 39 (2000) 1661.
[26] N. Pan, Y. Bian, T. Fukuda, M. Yokoyama, R. Li, S. Neya, J. Jiang, N. Kobayashi, Inorg. Chem. 43 (2004) 8242.
[27] T. Takami, T. Ye, D.P. Arnold, K.-I. Sugiura, R. Wang, J. Jiang, P.S. Weiss, J. Phys. Chem. C 111 (2007) 2077.
[28] F.-L. Lu, Polyhedron 26 (2007) 3939.
[29] R.L. Keiter, J. Chem. Educ. 60 (1983) 625.
[30] H. Ogoshi, N. Masai, Z. Yoshida, J. Takemoto, K. Nakamoto, Bull. Chem. Soc. Jpn. 44 (1971) 49.
[31] K. Kincaid, M.W. Urban, T. Watanabe, K. Nakamoto, J. Phys. Chem. 87 (1983) 3096.
[32] K. Xu, J.G. Rankin, T.D. Lash, Vib. Spectrosc. 18 (1998) 175.
[33] L.A. Andersson, T.M. Loehr, C. Sotiriou, W. Wu, C.K. Chang, J. Am. Chem. Soc. 108 (1986) 2908.
[34] K. Itoh, K. Nakahasi, H. Toeda, J. Phys. Chem. 92 (1988) 1464.
[35] R.S. Czernuszewicz, K.A. Macor, X.-Y. Li, J.R. Kincaid, T.G. Spiro, J. Am. Chem. Soc. 111 (1989) 3860.
[36] X.-Y. Li, R.S. Czernuszewicz, J.R. Kincaid, O. Su, T.G. Spiro, J. Phys. Chem. 94 (1990) 31.
[37] X.-Y. Li, R.S. Czernuszewicz, J.R. Kincaid, P. Stein, T.G. Spiro, J. Phys. Chem. 94 (1990) 47.
[38] L.A. Andersson, T.M. Loehr, R.G. Thompson, S.H. Strauss, Inorg. Chem. 29 (1990) 2142.
[39] J.-H. Perng, D.F. Bocian, J. Phys. Chem. 96 (1992) 4804.
[40] J.K. Duchowski, D.F. Bocian, Inorg. Chem. 29 (1990) 4158.
[41] J.W. Buchler, H.-G. Kapellmann, M. Knoff, K.-L. Lay, S.Z. Pfeifer, Naturforsch. B. Anorg. Chem. Org. Chem. 38B (1983) 1339.

In this work, the synthesis of new octa alkylthio and triethyleneoxysulfonyl substituted oxotitanium phthalocyanines (**1a** and **2a**) is described. The mesogenic properties of these new materials are studied by differential scanning calorimetry and optical microscopy. The electrical dark conductivities (σ_d) and photoconductivities (σ_{ph}) of deposited films of the oxotitanium Pcs on interdigitated electrodes were investigated. Also the photoconductivity mechanism and formation of Pc^+ which is positive charge carrier under the light irradiation of the phthalocyanine molecules are demonstrated using the theoretical calculations.

The first goal is to explore the effect of oxygen concentration on the dark and photoconductivity of differently substituted oxotitanium(IV) phthalocyanines under the same conditions, from the conductivity measurements. The second is to demonstrate the photoconductivity mechanism and formation of Pc^+ which is positive charge carrier under the light irradiation of phthalocyanine molecule, using the theoretical calculations.

To the best of our knowledge, it is the first time to report the theoretical investigation of oxygen doped photoconductivity of substituted oxotitanium phthalocyanine molecules. The theoretical data about oxygen effect on the photoconductivity of oxotitanium phthalocyanine molecules in question are not exist in the literature, although semi-empirical and density functional theory (DFT) calculations of oxotitanium phthalocyanine concerning the electronic spectra have been reported [16–20]. For this purposes, we have carried out semi-empirical calculations to elucidate the oxygen doped photoconductivity mechanism of substituted oxotitanium phthalocyanine molecules.

2. Experimental

2.1. Materials and equipment

1,2-Di(13,17-dioxa nonacosane-15-sulfanyl)phthalonitrile **(1)** [9] and 4,5-bis(4,7,10-trioxaundecan-1-sulfonyl)phthalonitrile **(2)** [10] were synthesized according to the reported procedures. All other reagents and solvents were reagent-grade quality, obtained from commercial suppliers and were dried as described in Perrin and Armarego [21] before use. Elemental analyses were obtained from Thermo Finnigan Flash 1112. Infrared spectra in KBr pellets were recorded on a Bio-Rad FTS 175C FT-IR spectrophotometer. Optical spectra in UV–Vis region were recorded with a Shimadzu 2001 UV PC spectrophotometer using 1 cm pathlength cuvette at room temperature. The mass spectra were recorded on a LCQ-ion trap (Thermofinnigan, San Jose, CA,USA), equipped with an ES (Electrospray) source. ^1H and ^{13}C NMR spectra were recorded in $CDCl_3$ solutions on a Varian 500 MHz spectrometer. Thermogravimetric analyses were carried out on Mettler Toledo Star^e Thermal Analysis System at a rate of 10 °C min^{-1} in a nitrogen flow (50 ml min^{-1}). The phase transition behavior of these compounds was observed by means of polarizing microscope (Leitz Wetzler Orthoplan-pol.) equipped with the hot stage (Linkam TMS 93) and temperature-controller (Linkam LNP). Transition temperatures were determined with the scan rate of 5 °C min^{-1} using a Mettler Toledo Star^e Thermal Analysis System/DSC 822^e. Differential scanning calorimeter system was calibrated with indium from 3 to 4 mg samples under nitrogen atmosphere.

2.2. Synthesis

2.2.1. 2,3;9,10;16,17;23,24-Octakis (13,17-dioxa nonacosane-15-sulfanyl)phthalocyaninato titanium(IV) oxides (**1a**)

Under argon atmosphere, 1,2-Di(13,17-dioxa nonacosane-15-sulfanyl)phthalonitrile (**1**) (0.800 g, 0.788 mmol), urea (30 mg, 0.30 mmol) and three drops of DBU was heated in 3 ml of 1-pentanol to 120 °C, then 100 mg (0.29 mmol) titanium(IV) butoxide was added. The mixture was refluxed for 6 h. After cooling to room temperature, the crude product was poured into MeOH and precipitated. The oxotitanium phthalocyanine was purified with column chromatography [silica gel, eluent CH_2Cl_2/*n*-hexane, 1:1 (v/v)]. Yield: 85 mg (11%). *Anal.* Calc. for $C_{248}H_{448}N_8TiO_{17}S_8$ (4115): C, 72.00; H, 11.35; N, 2.71. Found: C, 72.10; H, 10.95; N, 2.63%. IR (KBr) ν_{max} (cm^{-1}) 3040, 2950–2855 (CH_2, CH_3), 1600 (C_{ar}=N), 1460, 1370, 1330, 1120, 1105, 964 (Ti=O). MS (ES-MS), *m*/*z* (%): 2058 $[M]^{2+}$. ^1H NMR (500 MHz, $CDCl_3$): δ 1.10 (t, 48H, CH_3), 1.8 (m, 32H, CH_2), 3.25 (m, 64H, CH_2), 3.52–3.80 (m, 256H, CH_2), 3.90 (d, 32H, CH_2O), 4.05 (m, 8H, CH), 9.12 (s, 8H, CH_{ar}). ^{13}C NMR (500 MHz, $CDCl_3$): δ 13.56 (CH_3), 22.00 (CH_2), 26.50 (CH_2), 29.58–32.05 (CH_2), 32.16 (CH_2), 40.00 (CH_2), 59.50 (CH), 69.10–72.90 (CH_2), 122.05 ($C_{ar}H$), 134.12 (C_{ar}), 141.60 (C_{ar}–S), 151.10 (C_{ar} C=N).

2.2.2. 2,3;9,10;16,17;23,24-Octakis (4,7,10-trioxaundecan-1-sulfonyl)phthalocyaninato titanium(IV) oxides (**2a**)

A round-bottomed flask fitted with a condenser was degassed and flame-dried under dry argon. The flask was charged under argon with 4,5-bis(4,7,10-trioxaundecan-1-sulfonyl) (**2**) (0.75 g, 1.55 mmol), 4 ml of 1-pentanol, urea (40 mg, 0.66 mmol) and four drops of DBU (1,8-diazabicyclo[5.4.0.]undec-7-ene) and the reaction mixture were heated to 120 °C. At that temperature, 174 mg (0.51 mmol) titanium(IV) butoxide was added. The mixture was refluxed for 6 h. After cooling the mixture and the crude brownish green product was precipitated by addition of hexane and then the product was purified with column chromatography [silica gel, eluent CH_2Cl_2/MeOH, 15:1 (v/v)]. Yield: 95 mg (12%). *Anal.* Calc. for $C_{88}H_{128}N_8O_{25}S_8Ti$ (2001): C, 52.78; H, 6.44; N, 5.60. Found: C, 52.90; H, 6.48; N, 5.30%. IR (KBr): ν_{max} (cm^{-1}) 2925–2858 (CH_2, CH_3), 1592 (C_{ar}=N), 1530, 1352 (C–N), 1290, 1250, 1200, 1120 (C–O–C), 1140–1070, 949 (Ti=O). MS (ES-MS), *m*/*z* (%): 2002 (100) $[M+H]^+$, 1824 (25) $[M-6(OCH_3)]$. ^1H NMR (500 MHz, $CDCl_3$): δ 3.43 (s, 24H, CH_3), 3.53 (t, 16H, CH_2), 3.65 (t, 16H, SCH_2), 3.73 (t, 16H, CH_2), 3.76 (t, 16H, CH_2), 3.85 (t, 16H, CH_2), 4.11 (t, 16H, CH_2), 9.12 (s, 8H, CH_{ar}). ^{13}C NMR (500 MHz, $CDCl_3$): δ 34.35 (SCH_2), 57.45 (CH_3), 69.50 (CH_2), 70.18 (CH_2), 70.30 (CH_2), 70.50 (CH_2), 71.80 (CH_2), 122.05 ($C_{ar}H$), 138.12 (C_{ar}), 139.60 (C_{ar}–S), 158.10 (C_{ar} C=N).

2.3. Dark conductivity and photoconductivity measurements

The conductivity measurements were carried out on the Pc thin films deposited on a photolithographically patterned microelectrode array on a glass substrate. This array consisted of 10 interdigital pairs of gold fingers, evaporated in a Leybold Univex 450 coater system equipped with an Inficon Deposition Monitor (XTM/2), with a thickness of 120 nm, 100 μm wide and spaced 100 μm from the next finger, called interdigital electrodes (IDE). The overlapping length of the IDEs was 5 mm. The coating solutions containing oxotitanium(IV) phthalocyanines (**1a** and **2a)** were prepared as 5 mg of Pc per 2 ml chloroform which were deposited on the interdigital electrodes with the jet-spray method in a glove box in nitrogen atmosphere at room temperature. Compounds **1a** and **2a** form liquid crystals layers at room temperature. After coating the samples slowly adopt a mesophase without annealing and form homogenous layers. Generally, liquid crystals are so flexible that they can be spread uniformly on a plate and between two electrodes.

Dark current and photocurrent measurements of **1a** and **2a** under different conditions (such as in vacuum, atmosphere, 0–35% oxygen in nitrogen) at room temperature (the room is air conditioned and hold at temperature of 20 °C and relative humidity 35% RH) were carried out in a stainless steel chamber with electrical feedthrough, a quartz optic window for photoconductivity investigations and valves for adjusting partial pressure of oxygen. The *I*–*V*

characteristics were recorded with a sweep rate of 50 mV/s starting from 0 V to +1 V, from +1 V to −1 V and from −1 V to 0 V as a cycle with a Keithley 6517A Electrometer/High Resistance Meter.

The conductivity can be calculated from the *I–V* curves using the equation

$$\sigma = \frac{1}{V}\frac{d}{(2n-1)l\cdot h} \quad (1)$$

where d is spacing between fingers, n is the number of fingers, h is thickness of fingers and l is the overlapping length of the fingers [22].

For photoconductivity measurements the samples in the measurement chamber were irradiated by a 100 W halogen tungsten lamp through a monochromator. The light coming through the monochromator was focused onto the sample making sure that the region between the two electrodes is fully illuminated. Light intensities for different wavelengths were measured by a Lumacare Fiber Optic Probe. The photoconductivity data were calculated from photocurrent measurements and normalized dividing by normalized intensities. The photocurrent of the samples biased at +1.0 V were obtained by directing monochromatic light from a halogen lamp onto the sample under different conditions (in vacuum, atmosphere, 0–35% oxygen in nitrogen) at room temperature. During the measurement, the data were recorded to a computer using a home made program. For oxygen measurements, the desired oxygen concentration in nitrogen flowed through the measurement chamber until the oxygen diffusion reaches a steady state (ca. 1 h) [20].

2.4. Computational method

In the present study, the structures of the oxotitanium compounds **1a** and **2a** were subjected to geometry optimization using PM3 type semi-empirical quantum chemical method. All calculations were carried out at Hartree–Fock level with no configuration interaction [21]. The geometry optimizations were achieved using the steepest descent technique followed by the Polak Ribiere algorithm which is one of the conjugate gradient method until the root mean square (RMS) gradient was permanently staying less than 0.01 [22] .

Using the optimized structures, UV–Vis spectra have been calculated using ZINDO/S method [23–27]. ZINDO/S singly excited configuration interaction (CI) calculations involving 10 of each the uppermost occupied and the lower most unoccupied molecular orbital with the overlap weighting factors 1.267 and 0.585 for s–s and p–p types, respectively [28].

3. Results and discussion

3.1. Synthesis and characterization

The alkylthia substituted phthalocyaninatotitanium(IV) oxides (**1a** and **2a**) are obtained from the dinitrilles **1** [9] and **2** [10], urea and titanium(IV) butoxide in 1-pentanol, under the conditions given in Scheme 1.

The ^{1}H and ^{13}C NMR spectra of the phthalocyanine compounds **1a** and **2a** in $CDCl_3$ confirmed the proposed structure. The ^{1}H NMR spectra of **1a** and **2a** have broad absorptions relative to those of the phthalonitrile derivatives. It is likely that broadness is due to both chemical exchange caused by aggregation–disaggregation equilibrium. The phthalocyanines were found to be pure by ^{1}H NMR spectroscopy with all the substituents and ring protons observed in their respective regions. In the IR spectra the disappearance of the dinitrile stretches at ca. 2230 cm^{-1} and the presence of Ti=O stretching at ca. 960 cm^{-1} confirmed the formation of MPc.

In the electronic spectrum of the phthalocyanine derivatives (**1a** and **2a**) show intense Q absorption bands about 730 nm (Table 1). The effect of the central metal ion appears as a shift of these intense Q bands to higher wavelengths in comparison with their nickel and metal free derivatives [9,10].

3.2. The mesogenic properties of the oxotitanium complexes (*1a* and *2a*)

The phase transition temperatures were determined by differential scanning calorimetry (DSC). The DSC measurements were performed on the virgin materials with scanning rate of 10 °C min^{-1}. The DSC-measurements of **2a** show no significant sharp peaks representing melting or any other phase transition from −30 °C to 200 °C. Ni derivatives of **2a** were shown similar behavior in the DSC measurement [10]. This investigation indicates that compound **2a** exhibits a thermotropic liquid crystalline phase in the measured temperature range. The heating cycle was interrupted before reaching any clearing point to avoid decomposition However, the thermogram of compound **1a** recorded with increasing temperature showed clearly two endothermic peaks. We assume that the first peaks are related to the transitions from the crystal phases to discotic mesophases, and the second ones to the transitions from discotic mesophases to isotropic liquid phases. Phase transition temperatures and the corresponding enthalpy changes of the Pc complexes (**1a** and **2a**) are summarized in Table 2.

Also, the phase transition temperatures of the complexes (**1a** and **2a**) have been surveyed by polarization microscopy. Fig. 1 shows the photomicrograph of the mesophase of **2a** at 120 °C. For this typical fan-shaped texture often observed for Col_h, these mesophases could be thus confirmed as the Col_h phases [9–11,29].

A decrease in the melting point and an increase in the clearing temperatures was observed for the coordination of Ti^{4+} for **1a** in comparison with their Ni(II) and free derivatives [9]. It could be seen that coordination of Ti^{4+} to the phthalocyanine core extend the temperature range between mesophase and isotropic phase.

3.3. Dark conductivity

The dark conductivities of the compounds under different conditions (in vacuum, atmosphere, 0–35% oxygen in nitrogen were calculated from *I–V* curves using Eq. (1). The devices measured were operating in the ohmic region of the *I–V* characteristics in vacuum and in nitrogen ambient. With increasing oxygen concentration, space charge limited behavior and hysteretic effect were observed. This effect may be caused by ion migration and/or polarization in sample after oxygen exposure. As a typical example, the *I–V* characteristics of **1a** in the various ambient are shown in Fig. 2. Hysteresis widths are 0.03 V, 0.03 V, 0.05 V, 0.17 V, 0.26 V, 0.28 V and 0.39 V for vacuum, nitrogen, 5% oxygen, 15% oxygen, atmosphere, 25% oxygen and 35% oxygen ambient, respectively. The dark conductivities of samples are calculated using a linear fit of the *I–V* curves as σ_d = 8.68E−12 S/cm for **1a** and σ_d = 6.56E−11 S/cm for **2a** in vacuum and σ_d = 1.51E−11 S/cm for **1a** and σ_d = 2.95E−10 S/cm for **2a** in 35% oxygen in nitrogen. The dark current increases with increasing oxygen concentration slowly for both compounds (Fig. 6). The increase of dark conductivity with oxygen concentration is reversible; if we remove the oxygen in the ambient the dark current goes the vacuum level.

3.4. Photoconductivity

Figs. 3 and 4 show the photoconductivity curves of **1a** and **2a** versus wavelength for the different measurement conditions, respectively. Compounds **1a** and **2a** demonstrate a pronounced

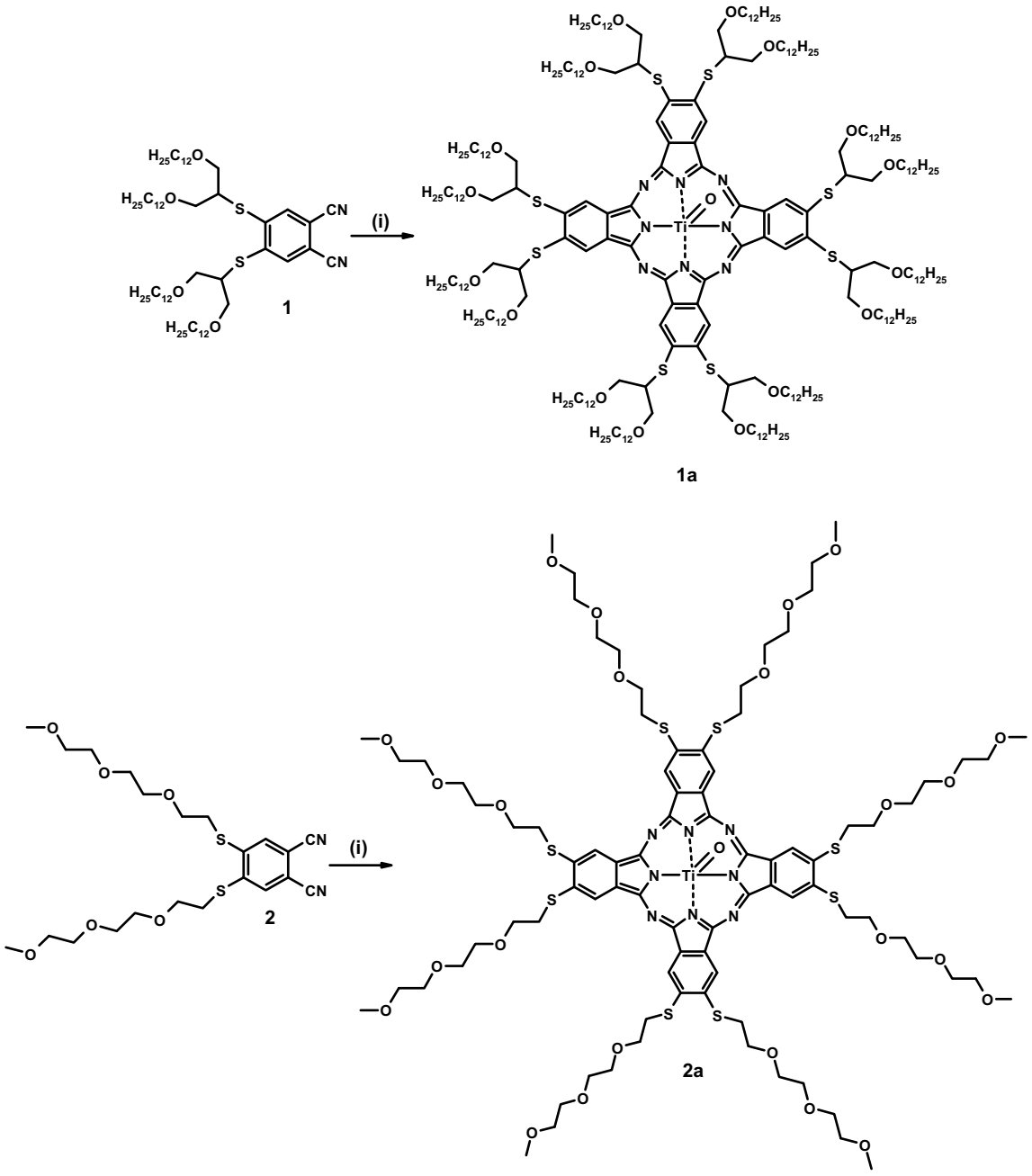

Scheme 1. Synthetic route of compound **1a** and **2a** (i) 1-pentanol, urea, $Ti(OBu)_4$, DBU, reflux, 6h.

Table 1
Electronic spectrum of the phthalocyanines in chloroform

Compound	λ_{max} (nm) ($\varepsilon/10^4$ dm^3 mol^{-1} cm^{-1})	
	Soret band region	Q band region
1a	430 (7.7), 347 (16.0)	727 (28.0), 657 (7.13)
2a	451 (3.6), 337 (8.6)	733 (24.0), 659 (4.84)

Table 2
Phase transition temperatures (°C) and in parentheses – enthalpy changes ΔH (in kJ/mol) by DSC (heating and cooling rates are 10 °C min^{-1}) for compound **1a** and **2a**

Compound	Heating $C \rightarrow Col_h \rightarrow I$		Cooling $I \rightarrow Col_h \rightarrow C$	
1a	−2.70 (20.45)	22.12 (105.65)	−8.29(27.19)	16.87 (117.51)
2a	Not observed	Not observed	Not observed	Not observed

C: solid phase, Col_h: hexagonal discotic columnar mesophase, I: isotropic phase.

photoconductivity response under visible light illumination. The photoconductivities of both compounds **1a** and **2a** calculated as $\sigma_{Ph} = 1.33 \times 10^{-11}$ S/cm and $\sigma_{Ph} = 9.1 \times 10^{-11}$ S/cm in vacuum and $\sigma_{Ph} = 7.24 \times 10^{-11}$ S/cm at 35% oxygen in nitrogen media at 680 nm and $\sigma_{Ph} = 1.09 \times 10^{-9}$ S/cm at 35% oxygen in nitrogen media at 740 nm using Eq. (1), respectively. In the ambient with 35% oxygen in nitrogen, the photoconductivity values of the compounds are greater than the dark conductivity values with a factor of 4 for **1a** and with a factor of 10 for **2a**. Compared each other σ_{Ph} of **2a** is greater 2–3 times than σ_{Ph} of **1a**. The oxygen induced increase of σ_{Ph} is also completely reversible; the current goes the value of photocurrent in vacuum.

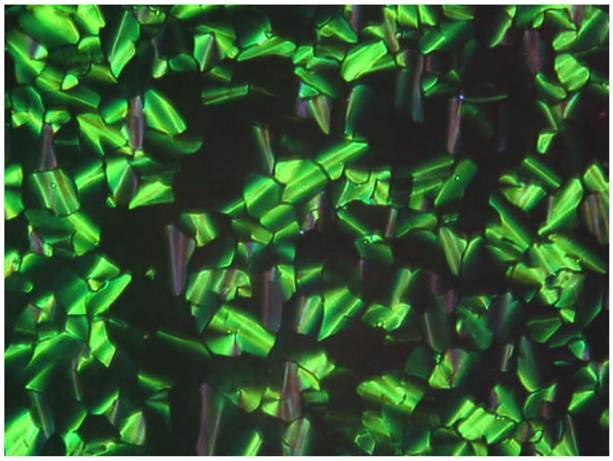

Fig. 1. Optical texture of **2a** observed at 120 °C (Magnification ×16).

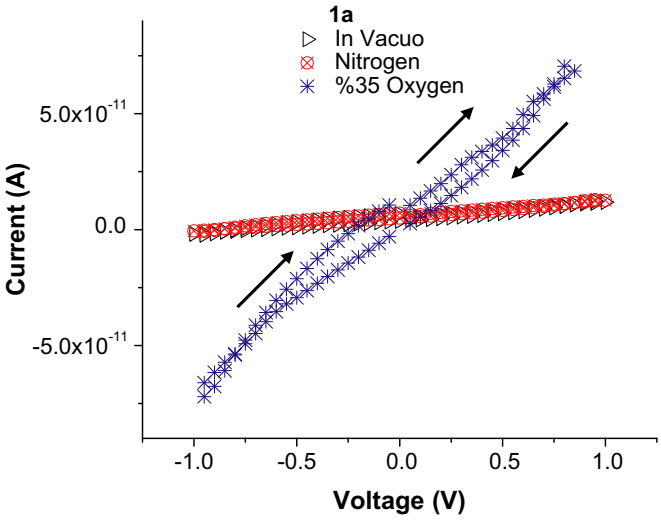

Fig. 2. *I–V* characteristics of **1a** in the various ambient.

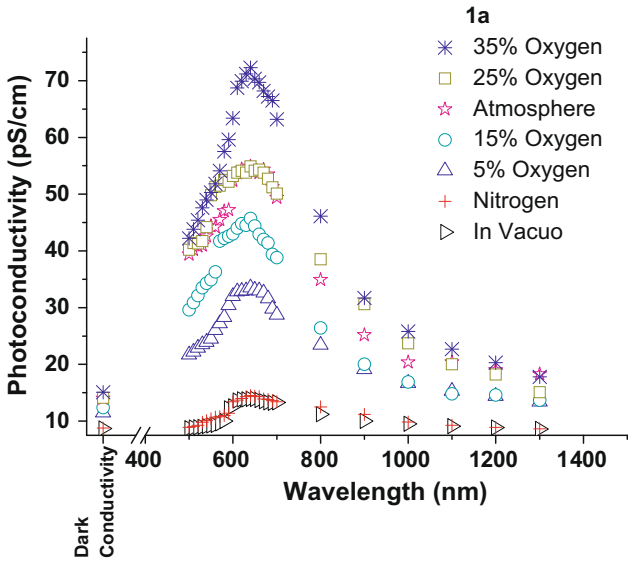

Fig. 3. Photoconductivity curves of **1a** function of wavelength.

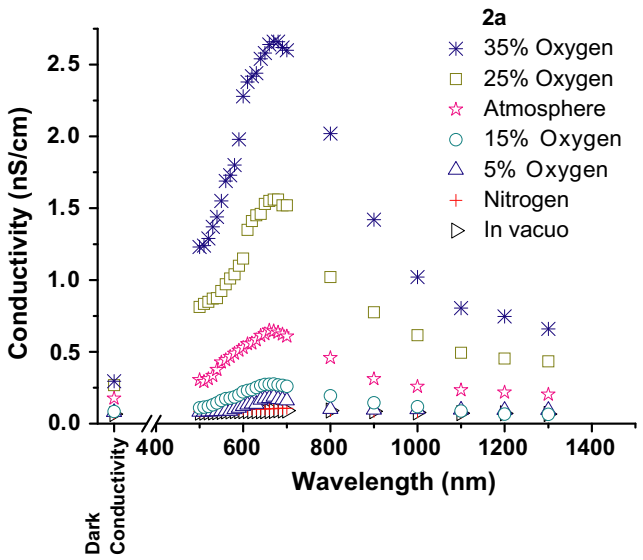

Fig. 4. Photoconductivity curves of **2a** function of wavelength.

Fig. 5 presents optical absorption spectra for the solution of TiOPc derivatives in dichloromethane and as-deposited films on quartz substrates. TiOPc derivatives in dichloromethane show Q bands as intense peaks at 727 and 733 nm with shoulders around 633, 659 and 699 nm for the derivatives **1a** and **2a**, respectively. The Q band in the films became broadened and the maxima were blue shifted to 705 and 689 nm for compounds **1a** and **2a**, respectively. The spectra of thin films are broader and they are shifted to longer wavelengths. The spectra of **1a** and **2a** suggest that they would be sensitive to visible sources. Because of low molecular weight, phthalocyanines are in the visible region of light absorbing semiconductors; photoconducting behavior is observed under irradiation [7]. Corresponding peaks observed in both UV–Vis and photoconductivity spectra of the TiOPc film in the range of 300–800 nm confirm that photoconductivity is generated via the excitation of TiOPc molecules.

Fig. 6 shows dark conductivity and photoconductivity curves of **1a** (a) and **2a** (b) exposed to different oxygen concentration at ambient atmosphere. The dark conductivities undergo a nearly 2-fold increase for **1a** and 4-fold increase for **2a** with increasing oxygen content whereas the values of photoconductivity undergo a nearly 5-fold increase for **1a** and 20-fold increase for **2a** with increasing oxygen content. The increase in σ_{Ph} is clearly correlated to the oxygen concentration. Compound **2a** offers rather intense photoconductivity as probe for the interaction with oxygen. When compared to the influence of substitution with alkoxy and polyoxo group upon the electrical properties of the Pc derivatives **1a** and **2a** the photoconductivity of **2a** substituted with polyoxo was higher than that of the alkoxy derivatives. The high photoconductivity of **2a** is thought to be caused by electronegative effects of oxygen atoms in the substitute group on phthalocyanine ring.

3.5. Computational works

PM3 Hamiltonian optimized structures of TiOPc molecules used in ZINDO/S calculations can regenerate excellent results. Excited-state energies of two TiOPc molecules have been calculated using ZINDO/S method as summarized in Table 3. Compound **2a** has the longest wavelength transition at 738 nm which corresponds to $\pi \rightarrow \pi^*$ transition (HOMO → LUMO). The introduction of polyoxo chains in **2a** can lead to extent the conjugation of Pc core. The strong electronegativity of oxygen atoms in polyoxo chains are

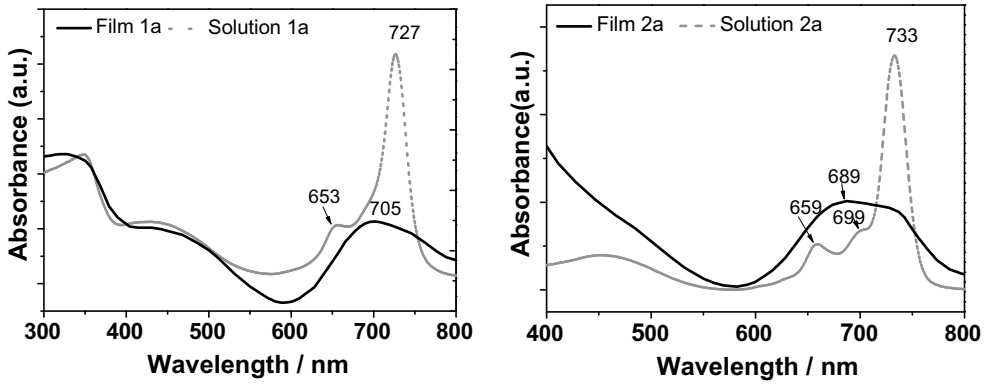

Fig. 5. Absorption spectra of **1a** and **2a** in dichloromethane and the films.

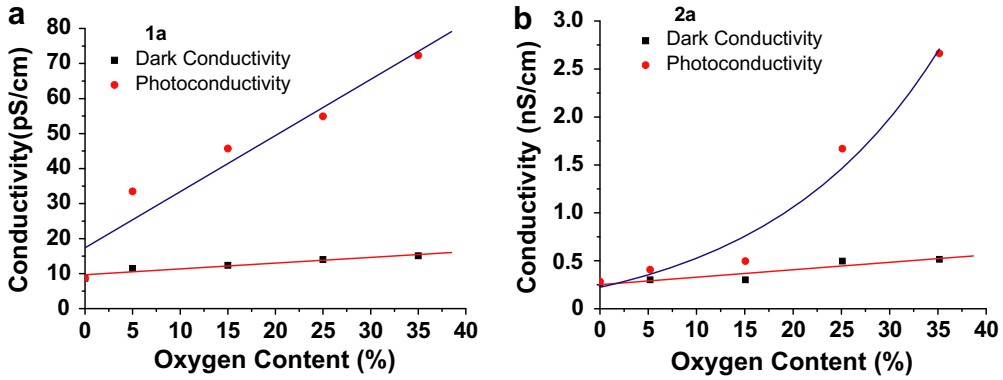

Fig. 6. Dark conductivity and photoconductivity curves of **1a** (a) and **2a** (b) exposed to different oxygen concentration at ambient atmosphere.

responsible from that effect. The extension of the conjugation can also cause the interfrontier molecular orbital energy gap (HOMO–LUMO energy difference) to narrow as compared to **1a** which is equivalent to a bathochromic shift in **2a** (Table 4). The HOMO–LUMO gap differences between **1a** and **2a** is about 3.41 kJ/mol (0.0354 eV). The charges on Ti and O (bonded to Ti) atoms are an evident to the extension of the conjugation. The dipole moments at the ground and first excited states were calculated using PM3 method (Table 5). The large dipole moment difference between the ground and first excited state results in increase in photoconductivity [30].

Another reason to higher photoconductivity of **2a** can be attributed to the larger difference dipole moment, $\Delta\mu$, value of compound **2a**. The quantum chemical calculations have been carried out to shed light on the oxygen induced increase of photoconductivity in substituted TiOPc's, **1a** and **2a** (Table 6). The predominant mechanism for charge-carrier formation is based on an oxygen-induced charge separation enhanced by illumination. Holes are charge carriers whilst electrons are trapped on a phthalocyanine oxygen complex. The positive charge carrier Pc^+ display very different behavior as seen Table 6. The oxygen-induced increase of photoconductivity in TiOPc's is due to the enhanced formation of charge carriers, Pc^+, by TiOPc–oxygen exciplexes, $(Pc^{\delta+}O_2^{\delta-})^*$, which are formed by the trapping of singlet excitons, Pc^*, at weakly bound charge-transfer adducts between TiOPc and oxygen (PcO_2) [31] (see Eq. (2)).

$$Pc, O_2 \xrightarrow{h\nu} Pc^*, O_2 \rightarrow \underset{(\text{hole})}{Pc^{\delta+}} \cdot O_2^{\delta-} \quad (2)$$

The effect of oxygen doping on the photoconductivity of differently substituted TiOPc compounds can clearly be seen in this study. The molecule, such as **1a**, is substituted with bulky group

Table 3
ZINDO/S calculated electronic excitation spectrum of **1a** and **2a** for major singlet transitions: optical Q absorption band (HOMO → LUMO)

	λ (nm) Q band	f (osc. strength)	Experimental λ (nm)
1a	726	0.8845	726
2a	738	0.8840	733

Table 4
Calculated properties using PM3 semi-empirical method

	1a	2a
Energy HOMO (eV)	−7.75241	−7.83013
Energy LUMO (eV)	−2.73201	−2.84529
HOMO–LUMO Gap (eV)	−5.0204	−4.98498
Charge on Ti atom	0.2603	0.3933
Charge on O atom[a]	−0.6389	−0.4845

[a] Oxygen atom bonded to titanium.

Table 5
The dipole moments at the ground state, first excited state and the differences between these states of two compounds

Compound	μ_{ground} (D)	$\mu_{excited}$ (D)	$\Delta\mu(=\mu_{excited}-\mu_{ground})$ (D)
1a	8.466	6.970	−1.496
2a	7.001	4.253	−2.748

The total energy of two compounds at the first excited state and the ground state.

Table 6
ZINDO/s calculated orbital energies of neutral and positively charged **1a** and **2a** at their ground states

Orbital energy	**1a** (TiOPc, neutral)	**1a** ($TiOPc^+$, positively charged)	**2a** (TiOPc, neutral)	**2a** ($TiOPc^+$, positively charged)
HOMO (eV)	−5.3302	−6.1739	−5.4200	−6.3333
LUMO (eV)	−1.6004	−3.8759	−1.7051	−4.0299
HOMO–LUMO gap (eV)	−3.2798	−2.2980	−3.7149	−2.3034
(kcal mol^{-1})	−86.0125	−52.9932	−85.6676	−53.1180

or contains highly branching substituent may not allow the hopping electron between the two TiOPc molecules. More bulky structure (**1a**) has larger distances between the TiOPc molecules comparing to structure which is much less branching (**2a**). It increases the activation barrier of electron hopping which is strongly distance dependent parameter and can be elucidated on the basis of Marcus theory [32]. Furthermore, it weakens intermolecular π-π interactions resulting in to reduced propensity of crystallization and increased distance between the conjugated phthalocyanine cores. As a result, charge and energy transfer are rigorously diminished. Oxygen diffusion should be taken into account when the oxygen doping photoconductivity is elaborately discussed. Oxygen diffusion into the TiOPc molecules can also be severely effected by highly branched structures due to possible longer diffusion channel in those structures [33].

3.6. Comparision of conductivity measurements and computational results

We explored the effect of oxygen concentration on the dark and photoconductivity of differently substituted oxotitanium(IV) phthalocyanines under the same conditions. The present experimental results have shown that the electrical dark conductivities and photoconductivities of oxotitanium(IV) phthalocyanine derivatives increase with increasing oxygen concentrations. Theoretical calculation's results agree well with the observed results. Electrical dark and photoconductivities of vapor deposited films of unsubstituted oxotitanium phthalocyanine were investigated as a function of oxygen of variable pressure by Lüer et al. [23]. The dark conductivity value was obtained as 1×10^{-13} S/cm for unsubstituted TiOPc. Dark conductivity values of **1a** and **2a** obtained by us are nearly 100 times higher than obtained by Lüer at al. Fig. 7 shows calculated orbital energies of unsubstituted TiOPc [34] and neutral and positively charged **1a** and **2a** at their ground states. The HOMO–LUMO energy differences are −3.853 eV, −3.2798 eV and −3.7149 eV for unsubstituted TiOPc, **1a** (neutral) and **2a** (neutral), respectively. The narrower HOMO–LUMO gap of **1a** and **2a** stem from oxygen atoms in polyoxo chains. It results in higher dark conductivity. In the another work, alkyl substituted TiOPc films were studied by following the increase of electric photoconductivity of the films under fine vacuum during oxygen sorption and the photoconductivity was obtained as 4.27×10^{-11} S/cm by Lüer et al. [35]. We obtained photoconductivity curves of **1a** and **2a** exposed to different oxygen concentrations in nitrogen at atmospheric pressure. Photoconductivity values of **2a** were calculated as $\sigma_{Ph} = 9.1 \times 10^{-11}$ S/cm in vacuum and $\sigma_{Ph} = 1.09 \times 10^{-9}$ S/cm at 35% oxygen in nitrogen. Photoconductivity values obtained by us are slightly higher than the values obtained by Lüer.

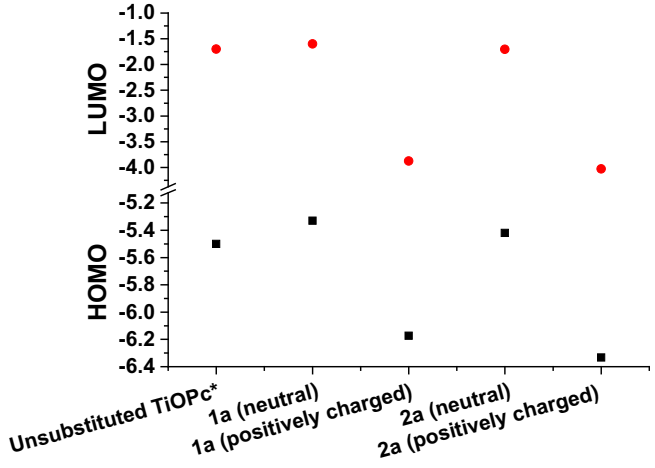

Fig. 7. Calculated orbital energies of TiOPc derivatives (* from [34]).

4. Conclusion

In the present work, the synthesis of the alkylthia and triethyleneoxysulfonyl substituted oxotitanium(IV) phthalocyanines was described. The oxotitanium(IV) phthalocyanine derivatives exhibit a hexagonal columnar (Col_h) structure. The electrical dark conductivities and photoconductivities of oxotitanium(IV) phthalocyanine derivatives were investigated as a function of the atmosphere containing different oxygen concentrations. The interaction of oxygen results from a reversible interaction with Pc, which is photo assisted. This interaction enhances rates of exciton dissociation, enhances photoconductivity. These comparative findings have been rationalized by computational methods. Electronic spectra, dipole moment, HOMO, LUMO energies and atomic charges of two susbstituted oxotitanium(IV) phthalocyanine molecules have been studied for clarification of the oxygen effect on the photoconductivity using PM3 and ZINDO/S methods. In general, our results are in good agreement with the spectroscopic experimental data and conductivity measurements. Our theoretical study of excited states and electronic spectra of substituted oxotitanium(IV) phthalocyanine molecules has shown that the electronic absorption spectra and HOMO–LUMO gap, dipole moments of the corresponding neutral and positively charged molecules clearly describe the distinctions between the oxygen-doped photoconductivity and dark conductivity. The effects of different substitution on photoconductivity of oxotitanium(IV) phthalocyanine molecules can be demonstrated by theoretical calculations as good as in experimental data. When compared to alkyl chain (**1a**) and polyoxo ethylene chain (**2a**) substitution, increasing of the number of oxygen atoms in substitute group increases the photoconductivity.

Acknowledgements

This work was supported by Research Fund of Gebze Institute of Technology (Project No.: 2006-A-07) and the authors wish to thank Colette Lebrun (CEA-Grenoble) for the mass spectra.

References

[1] P.M. Borsenberger, D.S. Weiss, Organic Photoreceptors for Imaging Systems, Marcel Dekker, New York, 1993.
[2] X.Q. Zhou, L.W. Li, H.Z. Chen, M. Wang, Mater. Chem. Phys. 58 (1999) 249.
[3] K.Y. Law, Chem. Rev. 93 (1993) 449.

[4] C.W. Tang, Appl. Phys. Lett. 48 (1986) 183.
[5] S. Zhou, W. Qui, W. Hu, Y. Liu, F. Bai, D. Zhu, Thin Solid Films 375 (2000) 263.
[6] Y. Arslanoğlu, A.M. Sevinç, E. Hamuryudan, A. Gül, Dyes Pigments 68 (2006) 129.
[7] J. Simon, J.J. Andre, Molecular Semiconductors, Springer Verlag, Berlin, 1985.
[8] J. Simon, P. Bassoul, in: C.C. Leznoff, A.B.P. Lever (Eds.), Phthalocyanines: Properties and Applications, vol. 2, VCH, New York, 1993 (Chapter 5).
[9] A.G. Gürek, V. Ahsen, F. Heineman, P. Zugenmaier, Mol. Cryst. Liq. Cryst. 338 (2000) 75.
[10] S. Dabak, V. Ahsen, F. Heinemann, P. Zugenmaier, Mol. Cryst. Liq. Cryst. 348 (2000) 11.
[11] A.G. Gürek, M. Durmuş, V. Ahsen, New J. Chem. 28 (2004) 693.
[12] T.V. Basova, A.G. Gürek, V. Ahsen, Mater. Sci. Eng. C 22 (2002) 99.
[13] V. Ahsen, M. Özdemir, Z.Z. Öztürk, A. Gül, Ö. Bekaroğlu, J. Chem. Res. (S) 2 (1995) 348.
[14] T.V. Basova, B.A. Kolesov, A.G. Gürek, V. Ahsen, Thin Solid Films 385 (2001) 246.
[15] T.V. Basova, C. Taşaltın, A.G. Gürek, M.A. Ebeoğlu, Z.Z. Öztürk, V. Ahsen, Sensors Actuat. B96 (2003) 70.
[16] J. Mizuguchi, G. Rihs, H.R. Karfunkel, J. Phys. Chem. 99 (1995) 16217.
[17] Y. Sakurai, H. Shiozaki, M. Yokoyama, J. Mol. Struct. Theochem. 766 (2006) 41.
[18] F. Henari, A. Davey, W. Blau, P. Haisch, M. Hanack, J. Porphyrins Phthalocyanines 3 (1999) 331.
[19] W.-D. Cheng, D.-S. Wu, H. Zhang, J.-T. Chen, Phys. Rev. B 64 (2001) 125109/1.
[20] K. Nakai, K. Ishii, N. Kobayashi, H. Yonehara, C. Pac, J. Phys. Chem. B 107 (2003) 9749.
[21] D.D. Perrin, W.L. Armarego, Purification of Laboratory Chemical, Pergamon Press, Oxford, 1980.
[22] W. Snow, W.R. Barger, Phthalocyanine films in chemical sensors, in: C.C. Leznoff, A.B.P. Lever (Eds.), Phthalocyanines. Properties and Applications, VCH, New York, 1989.
[23] L. Lüer, H.-J. Egelhaaf, D. Oelkrug, Opt. Mater. 9 (1998) 454.
[24] M.S.J. Dewar, E.G. Zoebish, E.F. Healey, J.J.P. Stewart, J. Am. Chem. Soc. 107 (1985) 3902.
[25] A.R. Leach, Molecular Modelling, Longman, Essex, 1997.
[26] E. Ridley, M.C. Zerner, Theor. Chim. Acta 42 (1976) 223.
[27] A.D. Bacon, M.C. Zerner, Theor. Chim. Acta 53 (1979) 21.
[28] J. Del Bene, H.H. Jaffe, J. Chem. Phys. 48 (1968) 1807.
[29] F. Yüksel, D. Atilla, V. Ahsen, Polyhedron 26 (2007) 4551.
[30] D.S. Chemla, J. Zyss, Nonlinear Optical Properties of Organic Molecules and Crystals, Acedemic Press, Orlando, 1987.
[31] C.C. Leznoff, A.B.P. Lever (Eds.), Phthalocyanines: Properties and Applications, vols. 1–4, VCH Publishers Inc., New York, 1996.
[32] R. Marcus, Ann. Rev. Phys. Chem. 15 (1964) 155.
[33] E. Magori, G. Reinhardt, M. Fleischer, R. Mayer, H. Meixner, Sensors Actuat. B: Chem. 95 (2003) 162.
[34] L. Lüer, Ph.D. Thesis, Über den Einfluss des Sauerstoffs auf die elektrische Leitfähigkeit und Photostabilität von dünnen Filmen π-konjugierter Verbindungen, Fakultät für Chemie und Pharmazie, Eberhard-Karls-Universität Tübingen, 2001.
[35] L. Lüer, H.-J. Egelhaaf, D. Oelkrug, G. Winter, M. Hanack, A. Weber, H. Bertagnolli, Synth. Metals 138 (2003) 305.

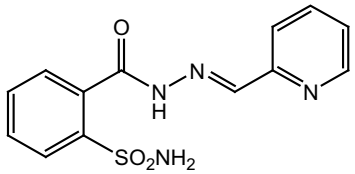

(HL)

Scheme 1.

and *p*-toluensulfonic acid (*ca.* 20 mg) as catalyst. The mixture was stirred and heated under reflux using a Dean–Stark trap. The resulting solid was separated by filtration, washed with methanol and ether and dried under vacuum. M.p. 142 °C. Calc. for $C_{13}H_{12}N_4O_3S$ (mol. wt. 304.32): C, 51.3; H 4.0; N 18.4; S 10.5. Found: C 51.2; H, 4.0; N 18.4; S 10.4%. IR (cm^{-1}): 3204(m), 1668(s), 1545(s), 1588(s), 1567(s), 1474(s), 1435(s), 1317(s), 1153(s). EI-MS (*m*/*z*): 304 (39.0%) [HL], 183 (33.6%) [O=C–$C_6H_6 \cdot SO_2NH_2$, 120 (100%) [py–C=N–NH]. ^1H NMR (DMSO-d_6, ppm): δ 12.33 [s, 1H, NH(I)]; 12.11 [s, 1H, OH(II)]; 8.61 [d, 1H(α), H(αpy(I)], 8.49 [d, 1H, H(αpy(II)]; 8.30 [s, 1H, CH=N(I)], 8.06 [s, 1H, CH=N(II)]; 8.01–7.30 [m, 8H, aromatic]; 7.23 [s, 2H, SO_2NH_2(II)]; 7.15 [s, 2H, SO_2NH_2(I)]. ^{13}C NMR (DMSO-d_6, ppm): δ 170 and 164 (C–O), 152.6 and 152.3 [C=N], 149.3 and 149.1 [C(2)-py], 148.4 [C(6-py)]; signals at δ = 143.8–119.8 ppm were assigned to the phenyl or pyridine group.

2.3. Synthesis of the complexes

All of the complexes were prepared by an electrochemical procedure [11]. The cell consisted of a metal anode suspended from a platinum wire and the cathode was also a platinum wire. The ligand was dissolved in acetonitrile and a small amount of tetraethylammonium perchlorate was added to the solution as a supporting electrolyte (*Caution*: perchlorate compounds are potentially explosive and should be handled in small quantities and with great care). Applied voltages of 10–15 V allowed sufficient current flow for smooth dissolution of the metal. During electrolysis, nitrogen was bubbled through the solution to provide an inert atmosphere and also to stir the reaction mixture. Under these conditions, the electrochemical cell can be summarized as

$$M_{(+)}/CH_3CN + HL/Pt_{(-)}; M = Co, Ni, Cu, Zn, Cd.$$

2.3.1. $[CoL_2]$

Electrochemical oxidation of a cobalt anode in a solution of HL (0.202 g, 0.661 mmol) and Et_4NClO_4 (*ca.* 20 mg) in acetonitrile (40 mL) at 12 V and 10 mA for 1.75 h caused 18.8 mg of cobalt to be dissolved; E_f = 0.49 mol F^{-1}. During the electrolysis hydrogen was evolved at the cathode and at the end of the reaction a brown crystalline solid appeared at the bottom of the vessel. The solid was filtered off, washed with acetonitrile and ether, dried under vacuum and characterized as $[CoL_2]$. *Anal.* Calc. for $C_{26}H_{22}N_8O_6S_2Co$ (mol. wt. 665.56): C, 46.9; H, 3.3; N, 16.8; S, 9.6. Found: C, 46.6; H, 3.6; N, 16.6; S, 9.6%. IR (cm^{-1}): 1606(s), 1570(s), 1560(s), 1491(s), 1458(s), 1430(s), 1343(s), 1163(s). FAB MS: *m*/*z*: 666.0 (79.0%) (CoL_2). Crystals of $[CoL_2]$ (**1**) suitable for X-ray analysis were obtained by crystallization of the initial product from 1:1 isopropanol/dichloromethane.

2.3.2. $[NiL_2] \cdot 2.5(CH_3CN)$

Following a similar procedure to that described above, starting from a nickel anode, HL (0.200 g, 0.660 mmol) and Et_4NClO_4 (*ca.* 25 mg) in acetonitrile (40 mL), at 15 V and 10 mA for 1.75 h, 18.0 mg of nickel were dissolved from the anode, E_f = 0.48 mol F^{-1}. At the end of the electrolysis the resulting solution was filtered to remove insoluble impurities and concentrated to give a brown crystalline solid. The solid was filtered off, washed with acetonitrile and ether, dried under vacuum and characterized as $[NiL_2] \cdot 2.5(CH_3CN)$. *Anal.* Calc. for $C_{31}H_{24.5}N_{10.5}O_6S_4Ni$ (mol. wt. 767.95): C, 48.9; H, 3.9; N, 19.1; S, 8.3. Found: C, 48.4; H, 3.8; N, 19.2; S, 8.2%. IR (cm^{-1}): 1562(s), 1608(s), 1493(s), 1460(s), 1433(s), 1346(s), 1163(s). FAB MS: *m*/*z*: 665.0 (6.12%) (NiL_2). Crystals of $[NiL_2] \cdot 2.5(CH_3CN)$ **(2)** suitable for X-ray analysis were obtained from the mother liquor.

2.3.3. $[CuL_2]$

Electrolysis of a solution of the ligand (0.207 g, 0.67 mmol) and a small amount of Et_4NClO_4 in acetonitrile (40 mL) at 10 V, 10 mA for 1.75 h dissolved 41.7 mg of Cu, E_f = 1.0 mol F^{-1}. The solution changed from colourless to green and at the end of the electrolysis the green solid was filtered off, washed with acetonitrile and ether, dried under vacuum and characterized as $[CuL_2]$. *Anal.* Calc. for $C_{26}H_{22}N_8O_6S_2Cu$ (mol. wt. 670.18): C, 46.7; H, 3.3; N, 16.8; S, 9.6. Found: C, 46.0; H, 3.5; N, 16.2; S, 9.2%. IR (cm^{-1}): 1606(s), 1571(s), 1565(s), 1491(m), 1459(s), 1433(s), 1343(s), 1161(s). FAB MS: *m*/*z*: 670.0 (11.87%) (CuL_2). Crystals of $[CuL_2] \cdot 2(CH_2Cl_2)$ **(3)** suitable for X-ray studies were obtained by crystallization of the initial product from 1:1 hexane/dichloromethane.

2.3.4. $[ZnL_2]$

HL (0.201 g, 0.66 mmol), acetonitrile (50 mL), Et_4NClO_4 (*ca.* 20 mg), 15 V, 10 mA, 1.75 h, 22.0 mg of Zn dissolved, E_f = 0.51 mol F^{-1}. At the end of the reaction the crystalline solid was filtered off, washed with acetonitrile and ether, dried under vacuum and characterized as $[ZnL_2]$. *Anal.* Calc. for $C_{26}H_{22}N_8O_6S_2Zn$ (mol. wt. 672.01): C, 46.5; H, 3.3; N, 16.7; S, 9.5. Found: C, 46.9; H, 3.4; N, 16.9; S, 9.5%. IR (cm^{-1}): 1598(s), 1565(s), 1498(s), 1462(s), 1434(s), 1345(s), 1163(s). ^1H NMR (DMSO-d_6, ppm): δ 8.80 [s, 1H, CH=N]; 8.14 [d, 1H, H(α-Npy]; 8.05–7.46 [m, 8H, aromatic], 7.51 [s, 2H, SO_2NH_2]. FAB MS: *m*/*z*: 670.9 (11.45%) (ZnL_2). Crystals of $[ZnL_2]$ **(4)** suitable for X-ray studies were obtained by crystallization of the initial product from 1:1 methanol/dichloromethane.

2.3.5. $[CdL_2] \cdot CH_3CN$

HL (0.201 g, 0.66 mmol), acetonitrile (50 mL), Et_4NClO_4 (*ca.* 25 mg), 12 V, 10 mA, 1.75 h, 38.6 mg of cadmium dissolved, E_f = 0.52 mol F^{-1}. At the end of the reaction the solution was filtered and concentrated in air to give crystals of $[CdL_2] \cdot CH_3CN$. *Anal.* Calc. for $C_{28}H_{25}N_9O_6S_2Cd$ (mol. wt. 760.09): C, 44.2; H, 3.3; N, 16.6; S, 8.4. Found: C, 44.2; H, 3.0; N, 16.7; S, 8.8%. IR (cm^{-1}): 1594(s), 1563(s), 1497(s), 1461(s), 1437(s), 1344(s), 1161(s). ^1H NMR (DMSO-d_6, ppm): δ 8.67 [s, 1H, $^3J(^{113}Cd–^1H)$ = 42.4 Hz, CH=N]; 8.32 [d, 1H, H(α-Npy]; 7.98–7.44 [m, 8H, aromatic], 7.63 [s, 2H, SO_2NH_2]. FAB MS: *m*/*z*: 720.0 (2.42%) (CdL_2). Crystals of $[CdL_2] \cdot CH_3CN$ **(5)** suitable for X-ray analysis were obtained from the mother liquor.

2.4. X-ray crystallographic studies

Intensity data sets for all compounds were collected using a Siemens Smart-CCD-1000 Bruker diffractometer (Mo Kα radiation, λ = 0.71073 Å) equipped with a graphite monochromator. Crystals of **1**, **3** and **5** were measured at 293 K while **2** and **4** were measured at 120 K. Compounds **2** and **4** are isostructural and the unit cell parameters are practically identical. The asymmetric unit of **2** contains two complex molecules and five acetonitrile molecules of crystallization. The asymmetric unit of **4** also contains two complex molecules and five acetonitrile molecules, although in this case the poor quality of the diffraction data did not allow the posi-

tions of these molecules to be resolved clearly. As a result, in this case the solvent was removed from the structure using the SQUEEZE program [12] implemented in PLATON [13]. In an analogous way, the crystal structure of the cobalt complex **1** has two complex molecules per asymmetric unit and disordered solvent molecules in the voids in the crystal lattice, although once again the poor quality of the diffraction data made refinement of these solvent units impossible and these were removed from the structure using the aforementioned program. In any case, analysis of the holes in the structure seems to indicate that the network contains 1.5 molecules of isopropanol, half a molecule of dichloromethane and one molecule of water per asymmetric unit. Each of the two complex molecules in the asymmetric unit in the crystal structures of compounds **1**, **2** and **4** have very similar structural parameters to each other.

The ω scan technique was employed to measure intensities in all crystals. Decomposition of the crystals did not occur during data collection. The intensities of all data sets were corrected for Lorentz and polarization effects. Absorption effects in all compounds were corrected using the program SADABS [14]. The crystal structures of all compounds were solved by direct methods. Crystallographic programs used for structure solution and refinement were those of SHELX97 [15]. Scattering factors were those provided with the SHELX program system. Missing atoms were located in the difference Fourier map and included in subsequent refinement cycles. The structures were refined by full-matrix least-squares refinement on F^2. Hydrogen atoms were placed geometrically and refined using a riding model with U_{iso} constrained at 1.2 (for non-methyl groups) and 1.5 (for methyl groups) times U_{eq} of the carrier C atom. For all structures non-hydrogen atoms were anisotropically refined. In the last cycles of refinement of all structures a weighting scheme was used, with weights calculated using the following formula $w = 1/[\sigma^2(F_o^2) + (aP)^2 + bP]$, where $P = (F_o^2 + 2F_c^2)/3$.

Pertinent details of the data collections and structure refinements are collected in Table 1. Further details regarding the data collections, structure solutions and refinements are included in the Supplementary data. ORTEP3 drawings [16] with the numbering schemes used are shown in Figs. 1–5.

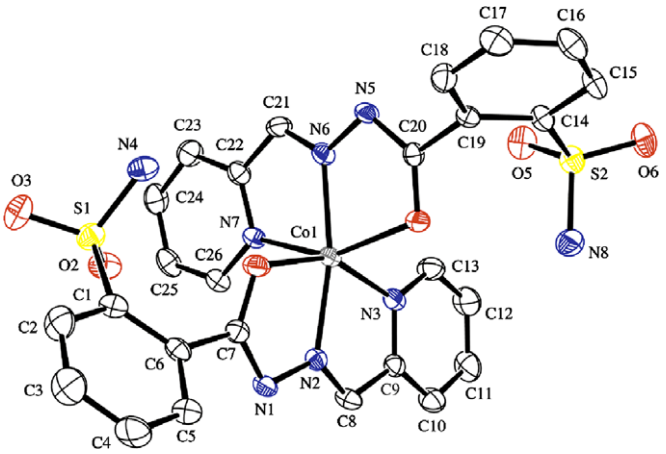

Fig. 1. Molecular structure of $[CoL_2]$ (**1**).

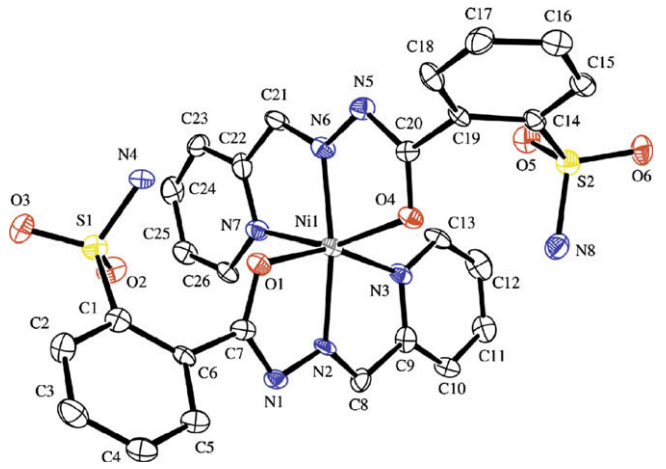

Fig. 2. Molecular structure of $[NiL_2] \cdot 2.5(CH_3CN)$ (**2**).

Table 1
Summary of crystal data for the compounds **1**–**5**

	1	**2**	**3**	**4**	**5**
Empirical formula	$C_{52}H_{44}N_{16}O_{12}S_4Co_2$	$C_{62}H_{59}N_{21}O_{12}S_4Ni_2$	$C_{28}H_{26}Cl_4N_8O_6S_2Cu$	$C_{52}H_{44}N_{16}O_{12}S_4Zn_2$	$C_{28}H_{25}N_9O_6S_2Cd$
M	1331.13	1535.96	840.03	1344.01	760.09
Crystal size (mm)	0.21 × 0.19 × 0.06	0.36 × 0.20 × 0.05	0.20 × 0.20 × 0.15	0.44 × 0.27 × 0.10	0.38 × 0.23 × 0.09
Temperature (K)	293(2)	120(2)	293(2)	120(2)	293(2)
Wavelength (Å)	0.71073	0.71073	0.71073	0.71073	0.71073
Crystal symmetry	monoclinic	monoclinic	triclinic	monoclinic	monoclinic
Space group	*I*2/*a*	*C*2/*c*	$P\bar{1}$	*C*2/*c*	*P*2(1)/*c*
a (Å)	32.5241(18)	42.615(5)	11.3371(16)	42.944(6)	9.1161(15)
b (Å)	11.7204(6)	11.5931(14)	12.8251(18)	11.7143(17)	26.186(4)
c (Å)	38.218(2)	32.441(4)	13.4900(19)	32.245(5)	13.577(2)
α (°)	90.00	90.00	85.205(2)	90.00	90.00
β (°)	105.7830(10)	120.553(3)	75.243(2)	121.073(2)	91.252(3)
γ (°)	90.00	90.00	71.791(2)	90.00	90.00
V (Å3)	14019.3(13)	13802(3)	1801.7(4)	13893(4)	3240.3(9)
Z	8	8	2	8	4
μ (mm^{-1})	0.655	0.743	1.071	0.874	0.858
Collected reflections	62746	70140	20641	79462	32349
Independent reflections (R_{int})	10070 (0.0940)	11835 (0.3619)	7354 (0.0422)	11789 (0.1466)	4639 (0.1730)
Data/restraints/parameters	62746/8/799	11835/16/940	7354/4/495	11879/8/800	4639/48/428
Goodness-of-fit	1.018	1.033	1.020	0.993	1.025
$R_1(F)$,[a]/$[I > 2\sigma(I)]$	0.0447	0.0770	0.0533	0.0575	0.0791
$wR_2(F^2)$,[b]/$[I > 2\sigma(I)]$	0.1107	0.1699	0.1284	0.1382	0.1867

[a] $R_1 = \sum[|F_o| - |F_c|/\sum|F_o|]$.
[b] $wR_2 = [\sum(F_o^2 - F^2c)/\sum(F_o^2)]^{1/2}$.

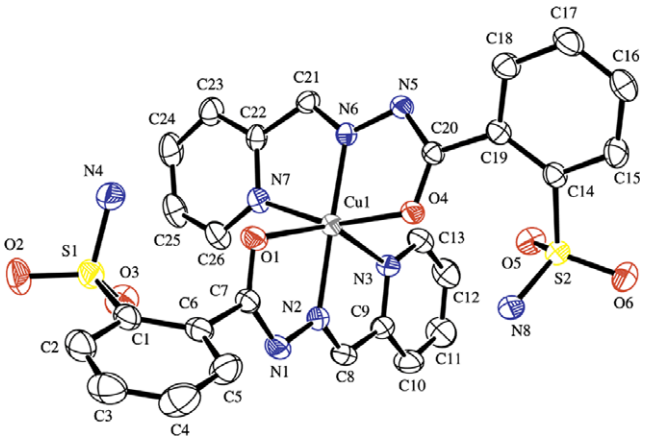

Fig. 3. Molecular structure of $[CuL_2]$ $2(CH_2Cl_2)$ (**3**).

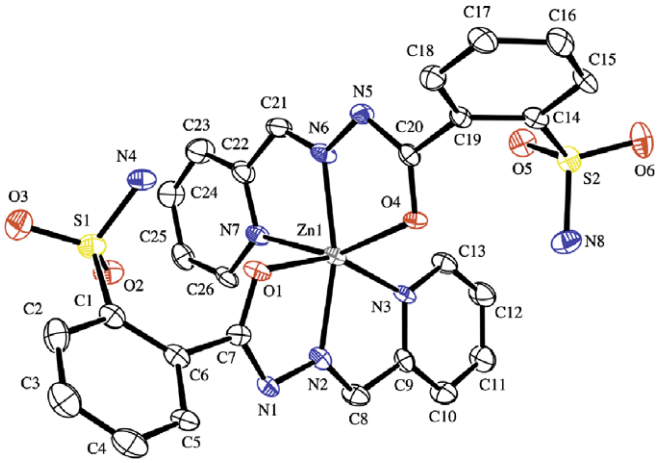

Fig. 4. Molecular structure of $[ZnL_2]$ (**4**).

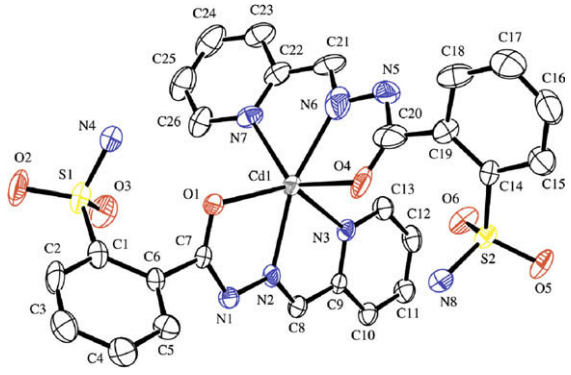

Fig. 5. Molecular structure of $[CdL_2]$ CH_3CN (**5**).

3. Results and discussion

3.1. Synthesis

Metal complexes were easily prepared in good yield by oxidation of the metal anode in a cell containing a solution of the ligand (HL) in acetonitrile and a small amount of tetraethylammonium perchlorate as an electrolytic carrier. The compounds were obtained as crystalline solids at the bottom of the cell.

The *electrochemical efficiency*, E_f, defined as the number of moles of metal dissolved per Faraday of charge, was close to 0.5 mol F^{-1} for the Co, Ni, Zn and Cd complexes. These values, along with the evolution of hydrogen at the cathode, are compatible with the following mechanism:

$$\text{Cathode}: 2HL + 2e^- \rightarrow 2L^- + H_2$$

$$\text{Anode}: M \rightarrow M^{2+} + 2e^-$$

$$\text{Solution}: M^{2+} + 2L^- \rightarrow [ML_2]$$

M = Co, Ni, Zn, Cd

In the synthesis of the copper complex the electrochemical efficiency was close to 1.0 mol F^{-1}. This is compatible with an anodic oxidation to Cu(I) and deprotonation of the ligand at the cathode:

$$\text{Cathode}: HL + e^- \rightarrow L^- + 1/2H_2$$

$$\text{Anode}: Cu + L^- \rightarrow [CuL] + e^-$$

followed by oxidation to Cu(II) in solution:

$$[CuL] + HL \rightarrow [CuL_2] + 1/2H_2$$

Similar behaviour has already been observed in other copper systems in which low oxidation state species are the initial products [17].

The complexes are stable to air and moderately soluble in common organic solvents. They were characterized by microanalysis, IR spectroscopy, mass spectrometry and X-ray diffraction. The zinc and cadmium complexes were also studied in solution by ^1H NMR spectroscopy and the cobalt, nickel and copper complexes were analysed by UV–Vis spectroscopy.

3.2. Description of the structures

All metal compounds were studied by X-ray diffraction. The crystal parameters and experimental details for data collection are given in Table 1. Bond distances and angles for all these compounds are provided as Supplementary data. Figs. 1–5 show the molecular structure of the complexes along with the numbering schemes employed. In order to make direct comparison easier, the numbering schemes are the same for each compound. Given the great similarities between the complexes they will be discussed together in a comparative manner. A selection of bond distances and angles, with the estimated standard deviations, are given in Tables 2–6.

Table 2
Selected bond distances and angles for $[CoL_2]$ (**1**)

Molecule 1		Molecule 2	
Co(1)–O(1)	2.091(3)	Co(2)–O(7)	2.087(3)
Co(1)–O(4)	2.129(3)	Co(2)–O(10)	2.115(3)
Co(1)–N(2)	2.024(3)	Co(2)–N(10)	2.024(3)
Co(1)–N(3)	2.138(3)	Co(2)–N(11)	2.107(4)
Co(1)–N(6)	2.017(3)	Co(2)–N(14)	2.021(3)
Co(1)–N(7)	2.143(3)	Co(2)–N(15)	2.147(4)
O(1)–Co(1)–O(4)	97.74(11)	O(7)–Co(2)–O(10)	94.44(12)
O(1)–Co(1)–N(2)	75.27(12)	N(14)–Co(2)–N(10)	167.19(15)
O(1)–Co(1)–N(3)	151.62(13)	O(7)–Co(2)–N(10)	74.86(12)
O(1)–Co(1)–N(6)	92.84(12)	O(7)–Co(2)–N(11)	150.65(14)
O(1)–Co(1)–N(7)	93.04(12)	O(7)–Co(2)–N(14)	93.88(12)
O(4)–Co(1)–N(2)	110.68(12)	O(7)–Co(2)–N(15)	96.11(13)
O(4)–Co(1)–N(3)	91.43(12)	O(10)–Co(2)–N(10)	111.79(13)
O(4)–Co(1)–N(6)	74.90(12)	O(10)–Co(2)–N(11)	90.66(14)
O(4)–Co(1)–N(7)	149.76(12)	O(10)–Co(2)–N(14)	74.59(13)
N(2)–Co(1)–N(6)	167.28(14)	O(10)–Co(2)–N(15)	149.62(13)
N(2)–Co(1)–N(7)	99.36(13)	N(10)–Co(2)–N(11)	76.40(15)
N(2)–Co(1)–N(3)	76.35(14)	N(10)–Co(2)–N(15)	98.45(14)
N(3)–Co(1)–N(6)	115.51(14)	N(11)–Co(2)–N(14)	115.30(15)
N(3)–Co(1)–N(7)	92.32(13)	N(11)–Co(2)–N(15)	93.88(15)
N(6)–Co(1)–N(7)	76.42(13)	N(14)–Co(2)–N(15)	76.34(14)

Table 3
Selected bond distances and angles for $[NiL_2] \cdot 2.5(CH_3CN)$ **(2)**

Molecule 1		Molecule 2	
Ni(1)–O(1)	2.076(7)	Ni(2)–O(7)	2.094(7)
Ni(1)–O(4)	2.116(7)	Ni(2)–O(10)	2.075(7)
Ni(1)–N(2)	1.978(8)	Ni(2)–N(10)	1.971(9)
Ni(1)–N(3)	2.095(9)	Ni(2)–N(11)	2.055(9)
Ni(1)–N(6)	1.968(9)	Ni(2)–N(14)	1.966(9)
Ni(1)–N(7)	2.084(9)	Ni(2)–N(15)	2.088(9)
O(1)–Ni(1)–O(4)	93.3(3)	O(7)–Ni(2)–O(10)	92.2(3)
O(1)–Ni(1)–N(2)	77.6(3)	O(7)–Ni(2)–N(10)	76.6(3)
O(1)–Ni(1)–N(3)	156.0(3)	O(7)–Ni(2)–N(11)	154.9(3)
O(1)–Ni(1)–N(6)	93.2(3)	O(7)–Ni(2)–N(14)	106.8(3)
O(1)–Ni(1)–N(7)	91.0(3)	O(7)–Ni(2)–N(15)	92.2(3)
O(4)–Ni(1)–N(2)	107.4(3)	O(10)–Ni(2)–N(10)	95.4(3)
O(4)–Ni(1)–N(3)	91.2(3)	O(10)–Ni(2)–N(11)	92.8(3)
O(4)–Ni(1)–N(6)	76.4(3)	O(10)–Ni(2)–N(14)	76.7(3)
O(4)–Ni(1)–N(7)	154.9(3)	O(10)–Ni(2)–N(15)	155.0(3)
N(2)–Ni(1)–N(6)	170.1(4)	N(10)–Ni(2)–N(11)	78.4(4)
N(2)–Ni(1)–N(7)	97.7(4)	N(10)–Ni(2)–N(14)	171.4(4)
N(2)–Ni(1)–N(3)	78.6(4)	N(10)–Ni(2)–N(15)	109.6(4)
N(3)–Ni(1)–N(6)	110.8(4)	N(11)–Ni(2)–N(14)	98.3(4)
N(3)–Ni(1)–N(7)	94.8(3)	N(11)–Ni(2)–N(15)	93.6(3)
N(6)–Ni(1)–N(7)	78.7(4)	N(14)–Ni(2)–N(15)	78.4(4)

Table 4
Selected bond distances and angles for $[CuL_2] \cdot 2(CH_2Cl_2)$ **(3)**

Cu(1)–O(1)	2.322(3)	Cu(1)–N(3)	2.309(4)
Cu(1)–O(4)	2.052(3)	Cu(1)–N(6)	1.926(3)
Cu(1)–N(2)	1.972(3)	Cu(1)–N(7)	2.082(4)
O(1)–Cu(1)–O(4)	96.47(12)	O(4)–Cu(1)–N(7)	157.77(13)
O(1)–Cu(1)–N(2)	74.16(12)	N(2)–Cu(1)–N(3)	76.54(13)
O(1)–Cu(1)–N(3)	150.22(11)	N(2)–Cu(1)–N(6)	178.52(15)
O(1)–Cu(1)–N(6)	105.86(12)	N(2)–Cu(1)–N(7)	101.57(14)
O(1)–Cu(1)–N(7)	88.41(13)	N(3)–Cu(1)–N(6)	103.57(13)
O(4)–Cu(1)–N(2)	100.63(13)	N(3)–Cu(1)–N(7)	92.34(14)
O(4)–Cu(1)–N(3)	93.98(12)	N(6)–Cu(1)–N(7)	79.91(14)
O(4)–Cu(1)–N(6)	77.89(12)		

Table 5
Selected bond distances and angles for $[ZnL_2]$ (**4**)

Molecule 1		Molecule 2	
Zn(1)–O(1)	2.150(3)	Zn(2)–O(7)	2.133(4)
Zn(1)–O(4)	2.149(3)	Zn(2)–O(10)	2.145(4)
Zn(1)–N(2)	2.054(4)	Zn(2)–N(10)	2.054(4)
Zn(1)–N(3)	2.156(4)	Zn(2)–N(11)	2.194(5)
Zn(1)–N(6)	2.056(4)	Zn(2)–N(14)	2.054(4)
Zn(1)–N(7)	2.201(4)	Zn(2)–N(15)	2.145(5)
O(1)–Zn(1)–O(4)	94.39(12)	O(7)–Zn(2)–O(10)	92.67(14)
O(1)–Zn(1)–N(2)	74.10(14)	O(7)–Zn(2)–N(10)	74.32(15)
O(1)–Zn(1)–N(3)	150.87(14)	O(7)–Zn(2)–N(11)	149.82(15)
O(1)–Zn(1)–N(6)	91.50(15)	O(7)–Zn(2)–N(14)	112.51(15)
O(1)–Zn(1)–N(7)	91.72(14)	O(7)–Zn(2)–N(15)	92.95(17)
O(4)–Zn(1)–N(2)	111.67(14)	O(10)–Zn(2)–N(10)	94.86(15)
O(4)–Zn(1)–N(3)	93.45(14)	O(10)–Zn(2)–N(11)	93.95(16)
O(4)–Zn(1)–N(6)	74.42(14)	O(10)–Zn(2)–N(14)	73.86(15)
O(4)–Zn(1)–N(7)	149.68(13)	O(10)–Zn(2)–N(15)	149.75(16)
N(2)–Zn(1)–N(3)	76.93(15)	N(10)–Zn(2)–N(11)	75.79(17)
N(2)–Zn(1)–N(6)	164.51(16)	N(10)–Zn(2)–N(14)	166.71(18)
N(2)–Zn(1)–N(7)	98.57(15)	N(10)–Zn(2)–N(15)	115.27(18)
N(3)–Zn(1)–N(6)	117.63(16)	N(11)Zn(2)–N(14)	97.61(17)
N(3)–Zn(1)–N(7)	95.51(15)	N(11)–Zn(2)–N(15)	95.97(19)
N(6)–Zn(1)–N(7)	75.75(15)	N(14)–Zn(2)–N(15)	76.54(18)

The structures of compounds consist of monomer units with the metal atoms bonded to two monoanionic tridentate ligands that are coordinated to the metal through two nitrogen atoms and the oxygen atoms. In all cases the environment around the metal is distorted octahedral. Coordination of the ligand to the metal gives rise to the formation of two five-membered rings with O–M–N chelate angles in the range 68.5(5)–77.89(12)° and N–M–N chelate angles in the range 65.6(6)–79.91(14)°, in both cases these values are low and outside the theoretical value expected for a regular geometry. These angles are the main cause of distortion from a regular octahedral geometry. The disposition of the two ligands in each of the complexes is such that the meridional isomer is obtained, probably due to the rigidity of the tridentate ligands. In this way each complex has two *trans* O–M–N bond angles in the range 131.7(5)–157.77(13)°, where donor atoms from the same ligand are involved, and a *trans* N–M–N bond angle in the range 163.6(5)–178.52(15)°, which involves donor atoms from two different ligands. All of the values are significantly different to the theoretical value of 180° expected for a regular geometry.

Table 6
Selected bond distances and angles for $[CdL_2] \cdot CH_3CN$ **(5)**

Cd(1)–O(1)	2.321(9)	Cd(1)–N(3)	2.410(11)
Cd(1)–O(4)	2.358(10)	Cd(1)–N(6)	2.285(18)
Cd(1)–N(2)	2.252(11)	Cd(1)–N(7)	2.360(12)
N(2)–Cd(1)–N(6)	163.6(5)	N(6)–Cd(1)–N(7)	65.6(6)
O(1)–Cd(1)–N(2)	69.0(4)	O(1)–Cd(1)–N(7)	95.1(4)
O(1)–Cd(1)–N(6)	123.2(5)	O(4)–Cd(1)–N(7)	131.7(5)
O(4)–Cd(1)–N(2)	100.5(4)	N(2)–Cd(1)–N(3)	70.4(4)
O(4)–Cd(1)–N(6)	68.5(5)	N(3)–Cd(1)–N(6)	98.1(5)
O(1)–Cd(1)–O(4)	97.3(4)	O(1)–Cd(1)–N(3)	138.7(4)
N(2)–Cd(1)–N(7)	127.4(5)	O(4)–Cd(1)–N(3)	96.8(4)

Three different types of bond distance can be found in the complexes and these correspond to the three types of donor atom that exist in the ligand (Table 7). With the exception of the cadmium complex, the similar covalent radii for the different metals mean that these bond distances in the different complexes are very similar, regardless of the metal in question. It is worth pointing out the existence of two bond distances in the copper complex, Cu(1)–O(1) 2.322(3) Å and Cu(1)–N(3) 2.309(4) Å (Table 4), clearly longer than the other four, in the range 1.926(3)–2.082(4) Å, as the result of the tetragonal distortion experienced by the complex due to the Jahn–Teller effect, which is typical copper(II) complex with an octahedral environment.

In general, all of the bond distances between metals and the donor atoms in question can be considered normal and are similar to those found in other compounds that contain similar monoanionic tridentate hydrazine ligands (HL′) with the metal in an octahedral environment. For example, $[NiL'_2]$ complexes with these types of ligand have Ni–O, Ni–N(iminic) and Ni–N(pyridinic) bond distances in the ranges 2.134–2.086 Å, 1.992–1.974 Å and 2.132–2.078 Å, respectively [18], and these are very similar to those in complex **2**. Analogous zinc complexes $[ZnL'_2]$ with this type of ligand show values for these three distances in the ranges 2.138–1.947 Å, 2.077–2.038 Å and 2.268–2.044 Å, respectively [19,18d], which are also very close to those found in the complex reported here. In copper complexes $[CuL'_2]$, the existence of two significantly longer bond lengths is a characteristic feature of these complexes [20]. Structural data for cobalt and cadmium complexes with this stoichiometry are not available in the literature, but values are

Table 7
Summary of selected bond lengths (Å) for the complexes (average values)

	[1]	[2]	[3]	[4]	[5]
M–O	2.105(3)	2.090(7)	2.187(3)	2.144(8)	2.340(9)
M–N(imine)	2.022(3)	1.971(9)	1.949(3)	2.055(8)	2.269(11)
M–N(pyridine)	2.134(4)	2.081(9)	2.196(4)	2.174(5)	2.385(12)
C=N(imine)	1.276(5)	1.278(12)	1.277(6)	1.282(6)	1.286(16)
C–N(amide)	1.320(5)	1.338(13)	1.320(6)	1.333(7)	1.329(16)
N–N	1.380(4)	1.395(12)	1.388(5)	1.380(6)	1.375(15)
C–O	1.276(5)	1.294(12)	1.272(5)	1.275(6)	1.271(16)

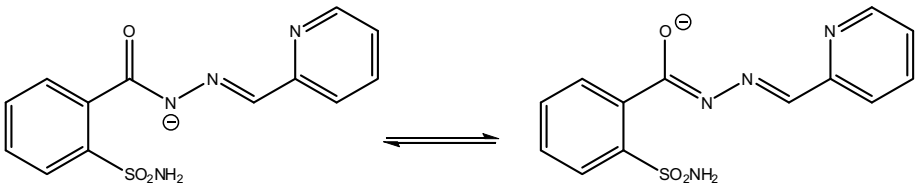

(I) (II)

Scheme 2.

available for the corresponding distances in pentacoordinated complexes with the general formulae [CoL″] [21] and [CdL″] [22], in which L″ represents a pentadentate dianionic Schiff base derived from 2,6-diacetylpyridine. In all of these cases the values reported for these distances are very similar to those found in the complexes described here.

As far as the structural parameters of the ligand are concerned, it is worth highlighting the variation observed in some of the bond distances in comparison to those found in the free ligand. Although the crystal structure of the free ligand HL is not available, structural data for related ligands (HL′) are known [23]. In these compounds the C–O bond lengths are in the range 1.230–1.219 Å and the C–N(amide) bond lengths are in the range 1.373–1.347 Å. Comparison of these values with those found in the complexes reported here shows that the corresponding C–O distances, in the range 1.292(12)–1.258(15) Å, are in all cases slightly longer whereas the C–N(amide) distances, in the range 1.351(13)–1.317(6) Å, are always shorter. These data are consistent with the increased conjugation experienced by the ligand in its deprotonated form.

3.3. Spectroscopy studies

In the IR spectra of the complexes the ν(N–H) (at 3204 cm^{-1}) and ν(C=O) (at 1668 cm^{-1}) stretching vibrations corresponding to the free ligand are not observed. This fact, along with the presence of a medium intensity band at *ca.* 1260 cm^{-1} assignable to ν(C–O), indicates that the hydrogen atoms of the amide group are lost during the electrochemical synthesis and the deprotonated ligand is predominantly in the enolate resonance form (II) in the complexes (Scheme 2).

The IR spectra of the complexes also show a sharp band in the range 1560–1570 cm^{-1}, attributed to ν(C=N), which is shifted to higher frequency on going from the free ligand (at 1545 cm^{-1}) to the complexes. This is indicative of the coordination of the imine nitrogen to the metal [24] and is consistent with by X-ray diffraction results. Bands at 1161–1164 cm^{-1} and 1343–1346 cm^{-1} can be assigned, respectively, to the symmetric and asymmetric $\nu(SO_2)$ vibrations and these are slightly shifted with respect to those in the free ligand.

The ^1H and ^{13}C NMR spectra of the free ligand (Section 2) indicate that, in solution, this compound exists in an equilibrium between two forms, with the amide as the predominant one. The ^1H spectra of the complexes confirm the loss of the amide proton in the synthetic procedure and that the anionic ligand is in the enolate form in the complexes. The signal for the imine proton in the zinc and cadmium complexes appears at 8.80 and 8.67 ppm, respectively, and these are shifted downfield with respect to the corresponding signal in the free ligand, indicating that the metal–nitrogen bond is retained in solution. In the case of the cadmium complex this signal shows satellite peaks due to the coupling of the proton to ^{113}Cd, with a ^3J(113Cd–1H) value of 42.4 Hz. Finally, the doublet assigned to H(6) of the pyridine ring (8.14 and 8.32 ppm, respectively, for the two complexes) is shifted to lower field in the complexes consistent with coordination through the pyridine nitrogen.

The compounds were also characterized by mass spectrometry using the FAB (m/z) technique with *m*-nitrobenzyl alcohol as matrix. In all cases the mass spectra show the peaks associated with [ML_2] species (see Section 2) and they have the appropriate isotopic distribution. Peaks corresponding to fragments of the parent ion are not observed.

The diffuse spectrum in the near IR–visible region of the cobalt complex shows the presence of three bands at ν_1 = 8810 cm^{-1} $^4T_{2g}(P) \leftarrow {}^4T_{1g}(F)$, ν_2 = 12 050 cm^{-1} $^4A_{2g} \leftarrow {}^4T_{1g}(P)$ and ν_3 = 20 400 cm^{-1} $^4T_{1g}(P) \leftarrow {}^4T_{1g}(F)$, and these are characteristic of a six-coordinate high spin Co(II) complex in a distorted octahedral geometry [25]. The spectrum of the nickel complex shows three bands in the near IR–visible region at ν_1 = 9025 cm^{-1} $^3T_{2g} \leftarrow {}^3A_{2g}$, ν_2 = 11 550 cm^{-1} $^3T_{1g}(F) \leftarrow {}^3A_{2g}$ and ν_3 = 21 460 cm^{-1} $^3T_{1g}(P) \leftarrow {}^3A_{2g}$. These frequencies are well within the range expected for octahedral Ni(II) complexes. Finally, the spectrum of the copper complex shows two bands at 13 400 cm^{-1} $^2E_g \leftarrow {}^2B_{1g}$ and 7590 cm^{-1} $^2B_{2g} \leftarrow {}^2B_{1g}$ and these are characteristic of hexacoordinated copper complexes with a tetragonal distortion.

4. Conclusions

The work described in this paper involved the synthesis and structural characterization of a series of cobalt, nickel, copper, zinc and cadmium complexes with a Schiff base ligands derived from hydrazone. The complexes were prepared using an electrochemical procedure that involved anodic oxidation of the metal and deprotonation of the ligand at the cathode. All of the complexes were studied by spectroscopic techniques and their structures in solid state were determined by X-ray diffraction. In all cases the metal is in an octahedral environment with the three donor atoms of each ligand in a meridional position.

Acknowledgements

This work was supported by the Ministerio de Ciencia y Tecnologia (Spain) (Grant CTQ2006-05298) and by the Xunta de Galicia (Spain) (Grant PGIDIT07PXIB-203038PR).

Appendix A. Supplementary data

CCDC 684345, 684346, 684347, 684348 and 684349 contain the supplementary crystallographic data for this paper. These data can be obtained free of charge via http://www.ccdc.cam.ac.uk/conts/retrieving.html, or from the Cambridge Crystallographic Data Centre, 12 Union Road, Cambridge CB2 1EZ, UK; fax: (+44) 1223-336-033; or e-mail: deposit@ccdc.cam.ac.uk. Supplementary data associated with this article can be found, in the online version, at doi:10.1016/j.poly.2008.08.011.

References

[1] (a) R.H. Holm, in: G.L. Eirchorn (Ed.), Inorganic Biochemistry, vol. 2, Elsevier, Amsterdam, 1974, p. 1137;
(b) S. Yamada, Coord. Chem. Rev. 1 (1966) 126;
(c) L. Sacconi, Coord. Chem. Rev. 1 (1966) 112.

[2] (a) T. Katsuki, Coord. Chem. Rev. 140 (1995) 189;
(b) Y.N. Ito, T. Katsuki, Bull. Chem. Soc. Jpn. 72 (1999) 603;
(c) P.K. Pospisil, D.H. Carsten, E.N. Jacobsen, Chem. Eur. J. 2 (1996) 974;
(d) T. Katsuki, J. Mol. Catal. 113 (1996) 87.

[3] N. Noshimo, Coord. Chem. Rev. 113 (1998) 87.

[4] L. Canali, D.C. Sherrintong, Chem. Soc. Rev. 28 (1999) 85.

[5] (a) T. Sogo, J. Romero, A. Sousa, A. de Blas, M.L. Durán, E.E. Castellano, Z. Naturforsch. B 43 (1988) 611;
(b) N.M. Atherton, D.E. Fenton, G.J. Hewson, C.H. McLean, R. Bastida, J. Romero, A. Sousa, E.E. Castellano, J. Chem. Soc., Dalton Trans. (1988) 1059;
(c) M.L. Durán, J.A. García-Vázquez, A. Macias, J. Romero, A. Sousa, E.B. Rivero, Z. Anorg. Allg. Chem. 573 (1989) 215;
(d) E. Labisbal, A. de Blas, J.A. García-Vazquez, J. Romero, M.L. Durán, A. Sousa, N.A. Bailey, D.E. Fenton, P.B. Leeson, R.V. Parish, Polyhedron 11 (1992) 227;
(e) E. Labisbal, J.A. García-Vazquez, J. Romero, A. Sousa, A. Castiñeiras, C. Maichle-Mössmer, U. Russo, Inorg. Chim. Acta 223 (1994) 87.

[6] (a) J.A. Castro, J. Romero, J.A. García-Vázquez, A. Castiñeiras, M.L. Durán, A. Sousa, Z. Anorg. Allg. Chem. 615 (1992) 155;
(b) J.A. Castro, J. Romero, J.A. García-Vázquez, M.L. Durán, A. Sousa, E.E. Castellano, J. Zukerman-Schpector, Polyhedron 11 (1992) 235;
(c) J.A. Castro, J.E. Vilasánchez, J. Romero, J.A. García-Vázquez, M.L. Durán, A. Sousa, E.E. Castellano, J. Zukerman-Schpector, Z. Anorg. Allg. Chem. 612 (1992) 83;
(d) J.A. Castro, J. Romero, J.A. García-Vázquez, A. Sousa, E.E. Castellano, J. Zukerman-Schpector, Polyhedron 12 (1993) 31;
(e) J.A. Castro, J. Romero, J.A. García-Vázquez, A. Macias, A. Sousa, U. Englert, Polyhedron 12 (1993) 1391;
(f) J.A. Castro, J. Romero, J.A. García-Vázquez, A. Sousa, A. Castiñeiras, J. Chem. Crystallogr. 24 (1994) 7;
(g) J. Castro, J. Romero, J.A. García-Vázquez, M.L. Durán, A. Castiñeiras, A. Sousa, D.E. Fenton, J. Chem. Soc., Dalton Trans. (1990) 3255.

[7] (a) E.S. Raper, Coord. Chem. Rev. 165 (1997) 475;
(b) J.A. García-Vázquez, J. Romero, A. Sousa, Coord. Chem. Rev. 193 (1999) 475;
(c) J.A. García-Vázquez, J. Romero, A. Sousa-Pedrares, M.S. Louro, A. Sousa, J. Zubieta, J. Chem. Soc., Dalton Trans. (2000) 559.

[8] L. Antolini, L.P. Battaglia, A. Bonamartini, G. Marcotrigliano, L. Menablue, G.C. Pellacani, J. Am. Chem. Soc. 107 (1985) 1369.

[9] (a) M.L. Durán, J.A. García-Vázquez, C. Gómez, A. Sousa-Pedrares, J. Romero, A. Sousa, Eur. J. Inorg. Chem. (2002) 2348;
(b) J. Sánchez-Piso, A. García-Vázquez, M.L. Durán, A. Sousa-Pedrares, J. Romero, E. Labisbal, O.R. Nacimento, Inorg. Chim. Acta 28 (2002) 111;
(c) I. Beloso, J. Castro, J.A. García-Vázquez, P. Pérez-Lourido, J. Romero, A. Sousa, Inorg. Chem. 44 (2005) 336.

[10] C.W. Whitehead, J.J. Traverso, J. Org. Chem. 25 (1960) 413.

[11] (a) D.G. Tuck, Pure Appl. Chem. 51 (1979) 2005;
(b) M.C. Chakravorti, G.V.B. Subrahmanyam, Coord. Chem. Rev. 135 (1994) 65;
(c) A.M. Vecchio-Sadus, J. Appl. Electrochem. 23 (1993) 401.

[12] P. Sluis, A.L. Spek, Acta Crystallogr., Sect. A 46 (1990) 194.

[13] (a) A.L. Spek, Acta Crystallogr., Sect. A 46 (1990) C34;
(b) A.L. Spek, PLATON, A Multipurpose Crystallographic Tool, Utrecht University, Utrecht, The Netherlands, 1998.

[14] G.M. Sheldrick, SADABS, Program for Absorption Correction of Area Detector Data, University of Göttingen, Germany, 1996.

[15] G.M. Sheldrick, SHELX97 [Includes SHELXS97, SHELXL97, CIFTAB] – Programs for Crystal Structure Analysis (Release 97-2). Institüt für Anorganische Chemie der Universität, Tammanstrasse 4, D-3400 Göttingen, Germany, 1998.

[16] J.L. Farrugia, J. Appl. Crystallogr. 30 (1997) 565.

[17] R. Kumar, H.E. Mabruk y, D.G. Tuck, J. Chem. Soc., Dalton Trans. 1045 (1988).

[18] (a) G.V. Karunakar, N.R. Sangeetha, V. Susila, S. Pal, J. Coord. Chem. 50 (2000) 51;
(b) P. Domiano, A. Musatti, M. Nardelli, C. Pelizzi, J. Chem. Soc., Dalton Trans. (1975) 295;
(c) S. Seth, C. Chakraborty, Acta Crystallogr., Sect. C 40 (1984) 1530;
(d) C.M. Armstrong, P.V. Bernhardt, P. Chin, D.R. Richardson, Eur. J. Inorg. Chem. (2003) 1145.

[19] (a) P. Domiano, C. Pelizzi, G. Predieri, C. Vignali, G. Palla, Polyhedron 3 (1984) 281;
(b) H. Sur, S. Roychowdhuri, S. Seth, Acta Crystallogr., Sect. C 49 (1993) 870.

[20] (a) J. Pushparaju, N.R. Sangeetha, S. Pal, Transition Met. Chem. 25 (2000) 529;
(b) Xiu-Tang Zhang, Xiao-Ping Zhan, Ding-Ming Wu, Wen-Bin Yang, Can-Zhong Lu, Jiegou Huaxue, J. Struct. Chem. 21 (2002) 280;
(c) P. Domiano, A. Musatti, M. Nardelli, C. Pelizzi, G. Predieri, J. Chem. Soc., Dalton Trans. (1979) 1266.

[21] (a) T.J. Giordano, G.J. Palenik, R.C. Palenik, D.A. Sullivan, Inorg. Chem. 18 (1979) 2445;
(b) K.A. Abboud, R.C. Palenik, G.J. Palenik, Acta Crystallogr., Sect. C 52 (1996) 2994;
(c) S.W. Gaines, G.J. Palenik, R.C. Palenik, Cryst. Struct. Commun. 10 (1981) 673;
(d) M.R. Bermejo, M. Fondo, A.M. González, O.L. Hoyos, A. Sousa, C.A. McAuliffe, W. Hussain, R. Pritchard, V.M. Novotorsev, J. Chem. Soc., Dalton Trans. (1999) 2211.

[22] M. Fondo, A. Sousa, M.R. Bermejo, A. García-Deibe, A. Sousa-Pedrares, O.L. Hoyos, M. Helliwell, Eur. J. Inorg. Chem. (2002) 703.

[23] (a) D.R. Richardson, E. Becker, P.V. Bernhardt, Acta Crystallogr., Sect. C 55 (1999) 2102;
(b) M. Bakir, O. Green, Acta Crystallogr., Sect. C 58 (2002) 263;
(c) N.R. Sangeetha, S. Pal, Polyhedron 19 (2000) 2713;
(d) P. Domiano, A. Musatti, C. Pelizzi, G. Predieri, Cryst. Struct. Commun. 3 (1974) 531;
(e) K.A. Abboud, C.G. Ortiz, R.C. Palenik, G.J. Palenik, Acta Crystallogr., Sect. C 53 (1997) 1322.

[24] S.G. Teoh, G.Y. Yeap, C.C. Loah, L.-W. Foong, S.-B. Teo, H.-K. Fun, Polyhedron 16 (1997) 2213 and references cited therein.

[25] A.B.P. Lever, Inorganic Electronic Spectroscopy, 2nd ed., Elsevier, Amsterdam, 1984.

antibacterial, antiviral, cytotoxic, antifungal and anti-inflammatory properties [26]. The guanidinium counterions also favour the stabilization of the crystal network by extensive hydrogen bonding. No complexes of any of the peroxo metal compounds with quinaldic acid have been synthesized or structurally characterized.

Therefore, we report on the synthesis, the spectroscopic data and the X-ray structure of $(gu)_2[Nb(O_2)_3(quin\text{-}2\text{-}c)]\cdot H_2O$ with the distinctive feature of having the metal atom in a five-membered N-/O-chelation ring and the Nb–N(quin) bond significantly long. In addition the present work introduces the first DFT study for the triperoxo complex containing the quinaldate ligand in order to explain the spectroscopic, bonding and reactivity properties of the complex. A comparison of the NMR, electronic, vibrational and thermogravimetric data of the triperoxo and tetraperoxo complexes is expected to reveal the relationship of their properties.

2. Experimental

2.1. Materials and methods

Potassium niobate, quinoline-2-carboxylate acid and guanidinium carbonate obtained from Aldrich were used without further purification. Hydrogen peroxide (35%) obtained from Merck was used as received and de-ionized and distilled water was used throughout this study. Deuterated solvents for use in the NMR, D_2O and DMSO-d_6 were purchased from Merck. Elemental analyses were performed using a Perkin–Elmer 240B elemental analyzer. IR spectra were recorded using a KBr pellet on a Perkin–Elmer 880 IR spectrophotometer. High-frequency Raman spectra were recorded with a Perkin–Elmer GX Fourier transform spectrometer with a diode pumped Nd:YAG laser at 1064 nm as the excitation source. The UV–Vis absorption spectra in the range 900–200 nm were recorded using a Cary 3E spectrophotometer. ^1H and ^{13}C NMR spectra were recorded on a Varian UNITY plus operating at 300 MHz spectrometer using TSP (2,2,3,3-tetradeutero-3-trimethylsilylpropionic acid) or the solvent peak as an internal reference. Thermogravimetric (TG) and differential thermal analysis (DTA) were carried out on a Mettler Toledo S R apparatus in N_2 atmosphere (temperature range: 40–1000 °C; heating rate: 10 °C/min).

2.2. Preparation of $(gu)_3[Nb(O_2)_4]$ (**2**)

The starting reactant was synthesized according the following procedure that differs from the reported one [27]. A solution of potassium niobate (0.9 g, 5 mmol) in 35% H_2O_2 (20 mL) was treated with $(gu)_2CO_3$ (1.36 g, 7.5 mmol) in 40 mL distilled water. The cloudy solution is agitated for a few hours. Then the solid is filtered off in order to avoid the presence of any niobium oxide. Addition of acetone in the filtered solution yields a white precipitate, which was filtered off, washed with acetone and air dried. Yield: 80%. *Anal.* Calc. for $C_3H_{18}NbN_9O_8$: C, 8.98; H, 4.52; N, 31.43. Found: C, 9.09; H, 4.44; N, 31.81%.

2.3. Preparation of $(gu)_2[Nb(O_2)_3(quin\text{-}2\text{-}c)]\cdot H_2O$ (**1**)

Quinoline-2-carboxylate acid (0.108 g, 0.625 mmol) was dissolved in water (2.5 mL) and added to a solution of the tetraperoxo niobate (0.25 g, 0.625 mmol) in 35% H_2O_2 (2.5 mL) while stirring. The pH value of the solution was recorded as approximately 4.5. Yellow crystals were obtained upon storage at 4 °C, filtered off and dried in the air. Yield: 70%. The X-ray diffraction analysis was carried out on the crystals and they correspond to the above stoichiometry. *Anal.* Calc. for $C_{12}H_{20}NbN_7O_9$: C, 28.36; H, 4.16; N, 19.29. Found: C, 28.66; H, 4.17; N, 19.32%.

2.4. X-ray diffraction

Diffraction measurements were made on a Crystal Logic dual goniometer diffractometer using graphite monochromated Cu Kα radiation (λ = 1.54187 Å) at a temperature of 220(2) K. Unit cell dimensions were determined by the angular settings of reflections in the range $6.88° < 2\theta < 72.52°$. Lorentz, polarization corrections were applied using Crystal Logic software. The structure was solved by direct methods using SHELX-86 and refined in full-matrix least-squares procedure on F^2 with SHELX-97 [28]. All non-hydrogen atoms in the structure were refined anisotropically. All hydrogen atoms were located by difference maps and were refined isotropically. Structure presentations were prepared by ORTEP for Windows and the calculation of the dihedral angles was calculated with MERCURY [29].

3. Computational details

Ground-state electronic structure calculations of the niobium complex (**1**) have been performed using density functional theory (DFT) [30] methods employing the GAUSSIAN 98 [31] and 03 [32] software packages. The functional used throughout this study was the B3LYP, consisting of a hybrid exchange functional as defined by Becke's three-parameter equation [33] and the Lee–Yang–Parr correlation functional [34]. The ground state geometry was obtained in the gas phase by full geometry optimization, starting from structural data and the optimum structure located as stationary point on the potential energy surface was verified by the absence of imaginary frequencies. The final wavefunction was found free from internal instabilities.

The basis set used throughout this study is the full double-ζ LANL2DZ basis functions together with the corresponding effective core potential for niobium [35]. Percentage compositions of molecular orbitals from the contributing molecular fragments were calculated and analyzed using the AOMIX and AOMIX-S programs [36].

The first 36 singlet excited states of the closed shell complexes were calculated within the TDDFT formalism [37–41]. The percentage of different transitions contributing to a state and the simulations of calculated UV–Vis spectra, when needed, were calculated with the aid of SWIZARD [42].

The graphics presented in the report have been prepared with the aid of MOLEKEL [43] and CHEMCRAFT [44].

4. Results and discussion

4.1. Crystal structure

The complex (**1**) crystallizes in the triclinic space group P1. Details concerning crystal data and refinement are given in Table 1. The structural unit consists of two anions (**1a** and **1b**), four guanidinium cations and of three molecules of water and is stabilized by identical hydrogen-bonding patterns involving several ring motifs. The hydrogen-bonding parameters for the complex are listed in Table 2. The structure and numbering scheme of the atoms of the complex anion are presented in Fig. 1 and the selected atomic distances and bond angles are collected in Table 3. The formation of hydrogen bonds to peroxo oxygen atoms and nitrogen atoms from the guanidinium ion has the major role in controlling the crystal packing (Fig. 2).

The niobium atom is surrounded by seven oxygen atoms belonging to three n^2-peroxo groups and a carboxylato group and a nitrogen atom from the deprotonated quinaldate ligand. The quinaldate ligand allows the formation of the five-membered chelation ring, while the picolinate ligand of the corresponding triperoxo niobate complex gave a six-membered ring coordinated

Table 1
Crystal data and structure refinement for $(gu)_2[Nb(O_2)_3(quin\text{-}2\text{-}c)] \cdot 1.5H_2O$ complex

Empirical formula	$C_{12}H_{21}N_7NbO_{9.50}$
Formula weight	508.27
Crystal size (mm)	0.20 × 0.30 × 0.80
Temperature (K)	220(2)
Wavelength (Å)	1.54187
Crystal system	triclinic
Space group	*P*1
Unit cell dimensions	
a (Å)	10.1903(2)
b (Å)	10.7214(2)
c (Å)	19.1635(4)
α (°)	97.2640(10)
β (°)	102.0790(10)
γ (°)	103.7930(10)
V (Å^3)	1953.73(7)
Z	4
D_{calc} (mg/m^3)	1.728
F(000)	1036
Absorption coefficient (mm^{-1})	5.629
θ Range for data collection (°)	6.88–72.52
Index range	$-12 \leqslant h \leqslant 12$; $-13 \leqslant k \leqslant 7$; $-18 \leqslant l \leqslant 23$
Reflections collected/unique	18594/6934
Reflections observed	6564
Independent reflections (R_{int})	0.0415
Goodness-of-fit (on F^2)	1.077
R	0.0344
Rw	0.090

Table 2
Distances and bending angles for hydrogen bonds in structure of complex **1**

D–H···A	D–H	H···A	D···A	∠D–H···A	
O–H donors of water molecules					
OW1–HW1A·· O2	0.78(4)	1.98(4)	2.762(5)	177(5)	2_676
OW1–HW1B···O7	0.78(6)	2.43(6)	3.158(4)	157(5)	
OW1–HW1B···O8	0.78(6)	2.01(6)	2.761(4)	164(6)	
OW2–HW2A···O13	0.94(6)	2.00(6)	2.904(3)	159(6)	2_566
OW3–HW3B···O15	0.75(5)	2.48(5)	3.197(4)	162(6)	
N–H donors from guanidinium ions					
N21–H21A···O11	0.91(4)	1.99(4)	2.898(4)	173(4)	1_554
N21–H21B···O15	0.73(4)	2.51(4)	3.121(4)	143(4)	2_556
N21–H21B···O16	0.73(4)	2.37(4)	3.041(4)	153(4)	2_556
N22–H22A···O14	0.82(4)	2.07(4)	2.889(4)	179(5)	2_556
N22–H22B···O1	0.80(4)	2.46(4)	3.193(4)	155(3)	2_666
N23–H23A···O12	0.78(4)	2.26(4)	3.014(4)	165(4)	1_554
N23–H23B···O5	0.88(4)	2.08(4)	2.942(4)	167(4)	2_666
N24–H24A···O1	0.77(4)	2.34(4)	3.091(5)	164(4)	2_666
N24–H24A···O2	0.77(4)	2.46(4)	3.091(5)	140(4)	2_666
N24–H24B···OW1	0.84(4)	2.26(4)	2.986(5)	145(4)	2_566
N25–H25A···O5	0.76(4)	2.22(4)	2.965(4)	166(4)	2_666
N25–H25B ···O7	0.83(4)	2.08(4)	2.897(5)	167(4)	
N26–H26A···O8	0.74(4)	2.11(4)	2.843(4)	171(5)	
N26–H26B···OW1	0.92(4)	2.00(4)	2.817(5)	149(3)	2_566
N27–H27A···O3	0.85(4)	2.16(4)	3.002(4)	171(3)	1_545
N27–H27A···O4	0.85(4)	2.56(4)	3.244(3)	138(3)	1_545
N27–H27B···O18	0.86(4)	2.16(4)	2.992(3)	162(4)	
N28–H28A···O4	0.99(4)	1.88(4)	2.842(4)	164(4)	1_545
N29–H29A···O17	0.80(4)	2.22(4)	2.995(4)	164(4)	
N29–H29A···O18	0.80(4)	2.49(4)	3.108(4)	135(3)	
N30–H30A···	0.76(4)	2.14(4)	2.872(4)	161(4)	
N31–H31A···O18	0.85(4)	2.21(4)	3.052(4)	170(4)	
N31–H31B···O6	0.78(4)	2.19(4)	2.946(4)	165(4)	
N32–H32A···O3	0.89(5)	2.27(5)	3.048(4)	146(4)	
N32–H32A···O4	0.89(5)	2.03(5)	2.907(4)	169(4)	
C–H donors from quinoline ring					
C3–H3···O2	0.83(5)	2.58(5)	2.846(5)	100(3)	
C9–H9···O3	0.85(4)	2.53(4)	2.985(4)	115(3)	
C9–H9···O8	0.85(4)	2.46(4)	3.132(4)	137(3)	
C13–H13···O12	0.88(4)	2.57(4)	2.854(4)	100(3)	
C19–H19···O14	0.92(4)	2.29(4)	3.114(4)	148(3)	

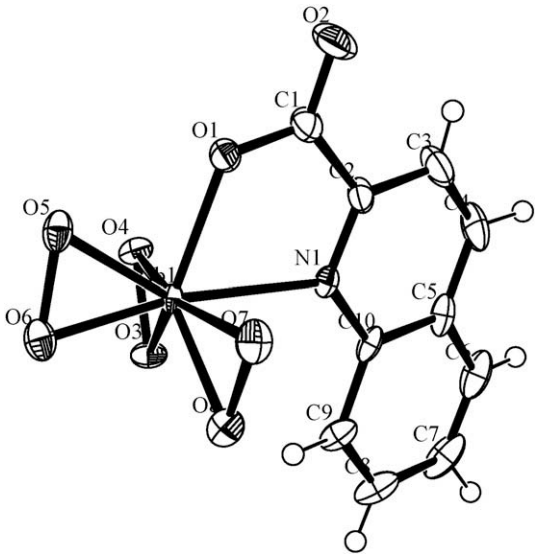

Fig. 1. Structure and atom numbering of $[Nb(O_2)_3(quin\text{-}2\text{-}c)]^{2-}$. Thermal ellipsoids are drawn at the 50% probability level.

Table 3
Comparison of calculated selected bond lengths (Å) and angles (°) with the experimental values from X-ray analysis for the two structures present in the unit cell, **1a** and **1b**, respectively

Structural index	$Nb(O_2)_3L$		
	1a	**1b**	Calc.
Nb–O3(O14)	1.980	1.999	2.065
Nb–O4(O13)	2.000	1.995	2.036
Nb–O5(O15)	1.983	1.963	2.015
Nb–O6(O16)	1.961	1.978	2.024
Nb–O7(O17)	1.978	1.983	2.036
Nb–O8(O18)	1.998	1.983	2.065
O3–O4	1.506	1.504	1.543
O5–O6	1.485	1.468	1.553
O7–O8	1.502	1.496	1.543
Nb–O1	2.113	2.123	2.220
Nb–N1	2.414	2.412	2.547
O1–C1	1.290	1.286	1.302
N1–C2	1.314	1.331	1.338
C1–C2	1.496	1.491	1.525
C1–O2	1.210	1.232	1.275
O6–Nb–O5	44.2	43.7	45.2
O8–Nb–O7	44.4	44.3	44.2
O4–Nb–O3	44.5	44.2	44.2
O1–Nb–N1	70.8	70.1	68.3
O8–Nb–N1	84.6	79.6	80.6
O6–Nb–O3	92.7	89.7	90.4

via the oxidized nitrogen atom of the heteroligand [19]. The environment of the metal atom in both complexes is identical. The coordination polyhedron around the niobium atom is a dodecahedron. The two bidentate peroxide groups are in *cis* configuration and the third one is in *trans* position to the quinaldate ligand. The coordination distances fall in the range, which is typical of heteroleptic peroxo complexes of niobium(V) [19,27,45,46]. If one assumes that the peroxo ligand occupies one vertex of the polyhedron, then the coordination polyhedron of niobium may be described as a strongly distorted pseudotrigonal bipyramid with the N,O (quin) atoms in the equatorial positions and the peroxo ligands, O (3, 4) and O (7, 8) in the axial positions. The dihedral angle between the pseudoequatorial and pseudoaxial planes of the pseudotrigonal bipyramid (O5, O6, O1, N1/O3, O4, O7, O8) equals 89.1° and 87.5° in each anionic entity of the structure, respectively.

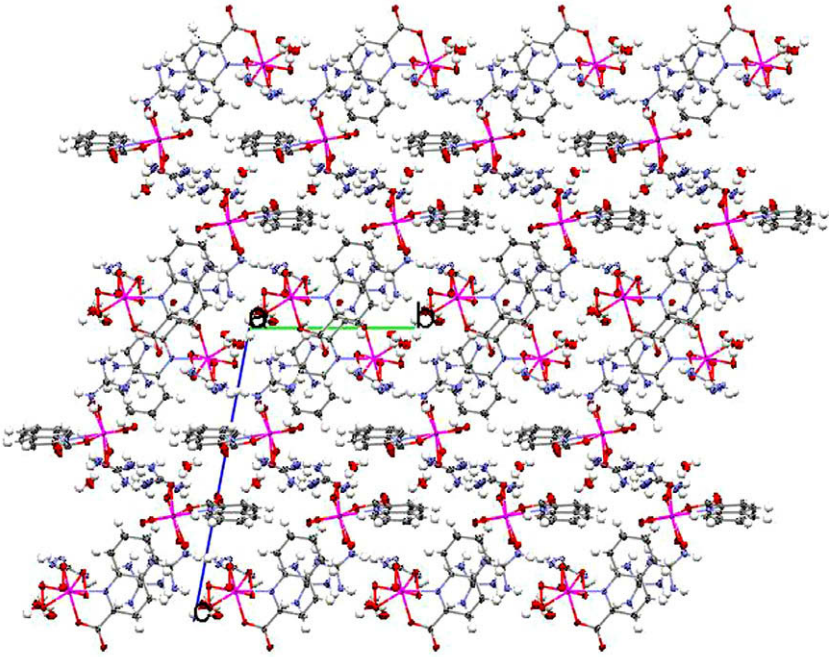

Fig. 2. A packing diagram of the title peroxo complex viewed down the α axis.

The angles between the corresponding planes in the peroxo niobate analogue with picolinate N-oxide reach 89.8° and 89.9° for each anionic entity, respectively [19].

It is interesting to point out that the quinoline ring and the five-membered ring formed via the N,O coordination with niobium atom are almost in the same plane due to the small folding of the coordination ring. This is shown by the following angles of the planes: Nb1, O1, N1/O1, C1, C2, N1 equals to 3.33° and Nb2, O11, N11/O11, C11, C12, N11 equals to 13.34° in each entity of the quinaldate peroxo complex, which has not been referenced before for the complexes of this class. It should be noted that the folding of the ring of the peroxo analogue with the picolinate N-oxide ligand is maximized as the angle between the planes containing Nb1, O7, O9/O7, O9, C2, C8, N1 equals to 24.88° and Nb2, O27, O29/O27, C28, C22, N21, O29 equals to 20.35° (Fig. 3). This difference can be attributable to the hydrogen-bonding between the guanidinium counterion and the carboxylate group. The value of the dihedral angle between the plane of COOH group and quinoline rings in the neutral molecule of the free quinoline-2-carboxylic acid equals 23.7° [47]. The main difference between the quinaldate peroxo complex (**1**) and the picolinato N-oxide one is that the metal atom in the complex **1** is in a five-membered chelate ring and coordinates directly to the nitrogen atom of the heteroligand which implies in that case the oxidation of the quinaldate ligand is not favoured. The folding angle observed in the case of the picO complex may also be enhanced by the coordination through the oxygen atoms, which provides a six-membered chelation ring.

It is worth noting that the coordination bond lengths between the quinoline N atom and the metal ion and between the carboxylate oxygen atom and the metal ion differs from the corresponding bond lengths in other metal quinaldate complexes [20–23,25,48,49]. The Nb–O(carboxylate) distance is 2.113(2) Å and 2.123(2) and the Nb–N bond distance reach 2.414(2) and 2.412(2) Å which are longer than that found for Ga^{III}, Fe^{II}, Co^{II}, Ni^{II} and Re^{V} quinaldate complexes and slightly shorter than that found for the quinaldate complex with Sn^{IV}, indicating a weaker coordination of the quinaldate ligand to the niobium atom due to the strong Nb-peroxo σ-bonding. The Nb–O(peroxo) bond lengths

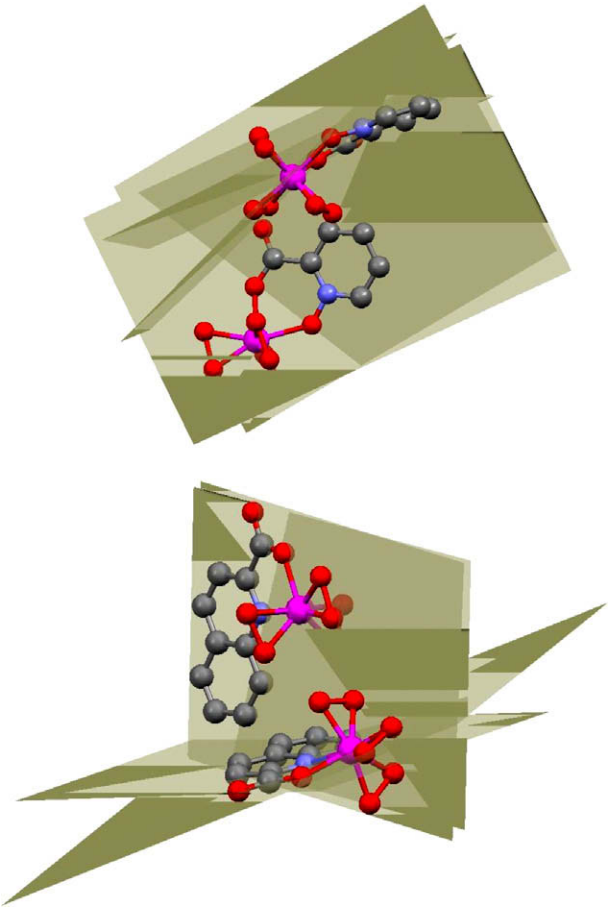

Fig. 3. The folding for the crystal structure reported in the literature [19] (up) and for the crystal structure of $[Nb(O_2)_3(quin\text{-}2\text{-}c)]^{2-}$ (down). The counterions and the water molecules are omitted for clarity.

range from 1.961 to 2.000 Å and the (O–O) distances range from 1.468 to 1.506 Å which are in good correlation with the corresponding ones in other triperoxo niobate complexes [50]. On the axial plane, the bonds $O–O_{ax}$ are longer than the bond $O–O_{eq}$ on the equatorial plane, as a result of the slightly higher contribution of the O_{eq} in HOMO (vide infra). Three water molecules are cocrystallized in the structure and all of the species are hydrogen bonded with the guanidinium cations, the oxygen atom of the ligand and between themselves.

4.2. Ground state structure

In order to study more thoroughly the electronic properties of **1**, we have used a standard DFT approach to optimize its ground state geometry and hence extract its frontier orbitals. In Table 3, calculated bond lengths and angles are depicted along with the experimental data as received from its crystal structure (vide supra).

From a comparison of the data of Table 3, we observe that all the calculated bonds are systematically overestimated. As this is anticipated [51] we can judge that the agreement between the theoretical and experimental data is satisfactory. We should also note that the ground state geometries were obtained in the gas phase by full geometry optimization, as free from intermolecular hydrogen bonds.

Table 4
Contribution of different fragments to complexes' valence orbitals

MO	E_{eV}	Nb	O_2 eq[a]	O_2 ax[b]	L
Unoccupied					
104	6.48	64.2	10.9	24.0	0.9
103	6.42	40.5	2.6	6.8	50.1
102	5.35	0.4	0.0	0.6	98.9
101	4.37	0.0	0.0	0.4	99.5
100	**3.51**	**0.0**	**0.2**	**3.2**	**96.6**
Occupied					
99	**1.74**	**0.6**	**49.4**	**47.2**	**2.8**
98	1.50	2.6	9.1	86.6	1.6
97	1.38	2.2	40.5	55.2	2.0
96	0.28	10.2	29.0	53.0	7.8
95	0.03	14.5	4.7	63.8	16.9
94	−0.31	10.9	20.8	30.0	38.2
93	−0.61	6.0	7.1	10.8	76.1
92	−0.95	3.9	2.1	17.4	76.6
91	−1.24	0.0	1.4	4.0	94.5

HOMO and LUMO orbitals are shown in bold.
[a] Oxygen atoms that lie opposite the quinoline-carboxylate ligand
[b] Oxygen atoms that lie in the axial positions of the pseudo-octahedral arrangement.

4.3. Molecular orbitals

The orbital energies, the contributions of the different fragments and the contour plots of the frontier orbitals are depicted in Table 4 and Fig. 4.

As we can notice, the three highest occupied orbitals are localized on the three peroxo units and are strongly π-antibonding in character with respect to the O–O bonds. HOMO − 6 to HOMO − 9 contain metal d_z^2 sigma and d_{yz} π-bonding contributions to the carboxylate moiety and the peroxo ligands. On the contrary, HOMO − 3 to HOMO − 5 are strongly Nb-peroxo σ-bonding, while smaller bonding and antibonding contributions from Nb quinoline-carboxylate ligand are also present.

LUMO, LUMO + 1 and LUMO + 2 are formed mainly by p_z bonding and antibonding contributions of the ring atoms of the quinoline-carboxylate ligand. LUMO + 3/+5 are formed by metal's d_{xy}/oxygen p_π antibonding contributions, while the LUMO + 4 is a peroxo sigma antibonding orbital.

Special attention should be drawn on the HOMO − 3 and HOMO − 5 orbitals. Both of them are indicative of the electron transfer from the main ligand to the $Nb(O_2)_3$ moiety. Our analysis according to the Frenking's decomposition analysis [36,51,52] showed that the former contains a contribution of 3.4% from the LUFO + 1 of $Nb(O_2)_3$, while the latter contains a contribution of 3.2% from the LUFO of the same fragment. The aforementioned scheme is supported by the total 10.6% of contributions of occupied

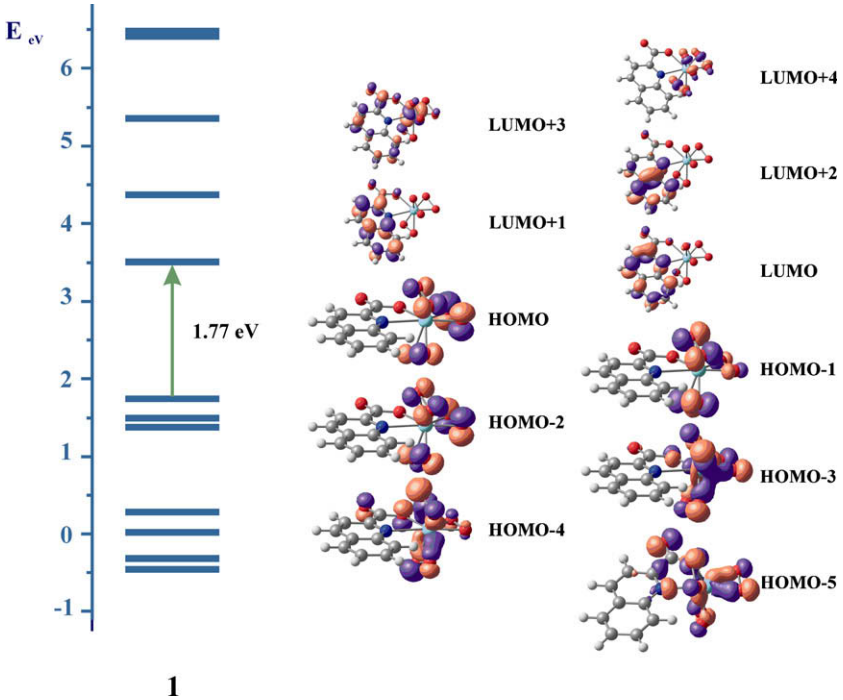

Fig. 4. Energy level diagram and graphic representation of frontier orbitals of **1**, given through isodensity surfaces of 0.05 a.u.

ligand orbitals to compound's unoccupied molecular orbitals. Thus, the net charge transfer from the quinoline-2-carboxylate to the Nb-peroxo core is calculated to be 0.19 electrons.

Besides, an unoccupied orbital with a predominant d(σ^*) character was not found among the spectroscopically important orbitals. Thus, low lying LF states, contradictory to the arguments of the traditional ligand field theory, are not expected.

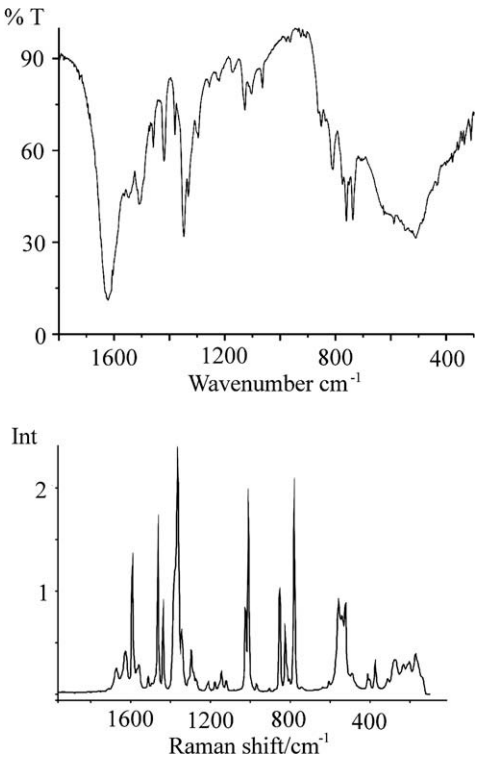

Fig. 5. IR and Raman spectra of the triperoxo complex.

Table 5
Infrared (theoretical and experimental) and Raman data (in cm^{-1}) for complexes **1** and **2**

Assign.			**1**	**2**
ν(O–O)	IR	Exp.	853, 836, 809	846, 814
		Calc.	881 (41), 865 (39), 861 (38)[b]	886, 861[a]
	Raman		852, 824, 804	850
ν_s(Nb–O_2)	IR	Exp.		552
		Calc.	560 (30), 517 (25), 497 (23)[b]	483[a]
	Raman		523	525
ν_{as}(Nb–O_2)	IR	Exp.	511	594
		Calc.	539 (28), 449 (22)[b]	502[a]
	Raman		539	535
ν_{as}(COO)	IR	Exp.	1622	
		Calc.	1606 (62)[b]	
	Raman		1624	
ν_s(COO)	IR	Exp.	1348	
		Calc.	1332 (55)	
	Raman		1362	

[a] Theoretical results reported in the literature [45] and used in this work for comparison.

[b] Theoretical results obtained in the present work and fundamental vibration in parenthesis.

4.4. Infrared and Raman data

The IR and Raman spectra of the triperoxo niobate complex displayed a sufficiently well resolved spectral pattern (Fig. 5). The theoretical results reported in the literature for the tetraperoxo complex and obtained in the present work for the complex **1** and some representative vibrational modes of the coordinated heteroligand are summarized in Table 5.

In the IR spectrum of the tetraperoxo niobate complex the prominent band at 814 cm^{-1} assigned to the O–O stretching vibration and another two broad bands with the same intensity appearing at 594 and 552 cm^{-1} attributable to ν_{as}(Nb–O_2) and ν_s(Nb–O_2) modes, respectively, gave the indication of the presence side-on bound peroxo ligands in the complex. In the Raman spectrum the stretching vibration of the peroxo group is observed at 850 cm^{-1}, which is active due to the symmetric vibration. As far as the metal–peroxo stretching Nb–O_2 vibrations are concerned two bands are observed at 535 and 525 cm^{-1}. These results are consistent with the results obtained by Bayot et al. for the same

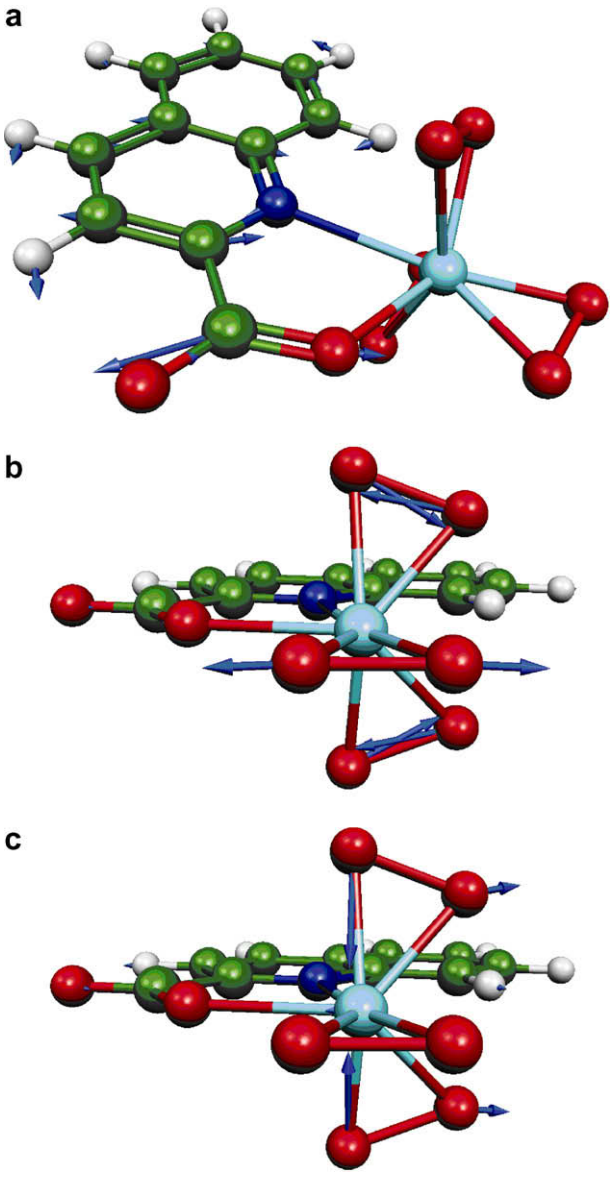

Fig. 6. Graphic representations of the compound's normal modes observed at 1622 cm^{-1} (a), 853 cm^{-1} (b) and 511 cm^{-1} (c).

tetraperoxo compound [27,45]. The additional bands occurring in the IR spectrum in the range 1390–1700 cm^{-1} are due to the bending vibration of the NH_2 and CN_3 groups presented in the guanidinium ion [53].

In the case of the triperoxo complex, the theoretical results confirmed the empirical rule which states that the presence of three ν(O–O) bands in the IR spectrum indicates the formation of the triperoxo complex. There are three calculated frequencies corresponding to the O–O vibration modes are 881, 865 and 861 cm^{-1} which are in agreement with the experimental spectra. In the Raman spectrum of the complex **1** the vibration modes which involve the O–O stretching are observed at 852, 824 and 804 cm^{-1}. The triperoxo complex also shows two characteristic Nb–peroxo modes calculated around 560 cm^{-1} in the IR spectrum as confirmed by the experimental observations as well as the Raman spectrum provides the corresponding vibrations at 539 and 523 cm^{-1}. Moreover, the triperoxo complex displays two bands calculated at 1606 cm^{-1} and 1332 cm^{-1} for the asymmetric and symmetric modes of the carboxylate moiety complexed to niobium, respectively. The coordination of the niobium atom by the carboxylato groups in the monodentate mode is evidenced by the broadening of this ν_{as}(COO) band, by the value of $\nu_{as} - \nu_s = 274$ cm^{-1} [54] and by its shift from a value of ca. 1694 cm^{-1} in the free carboxylic acid to ca. 1622 cm^{-1} in the complex. In any case the calculation fits well with the experimental results and some of the aforementioned modes are depicted in Fig. 6.

4.5. Thermal analyses

Thermogravimetric (TG) and differential thermal analysis (DTA) data of the peroxo niobate complexes provide crucial information regarding composition of the compounds and their thermal stability. They indicated that the existence of the heteroligand in the coordination sphere of the niobium atom gives different thermal

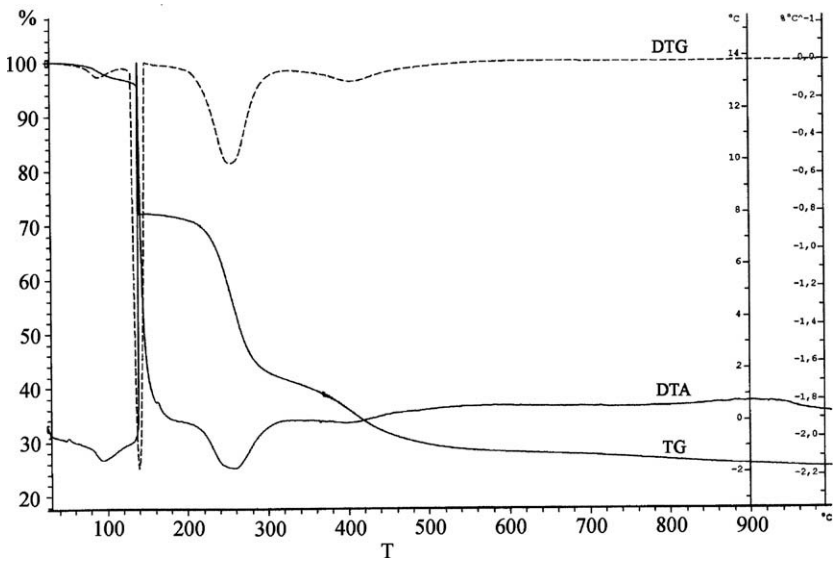

Fig. 7. TG, DTG and DTA of the triperoxo compound $(gu)_2[Nb(O_2)_3(quin\text{-}2\text{-}c)] \cdot H_2O$ in air (10 °C/min).

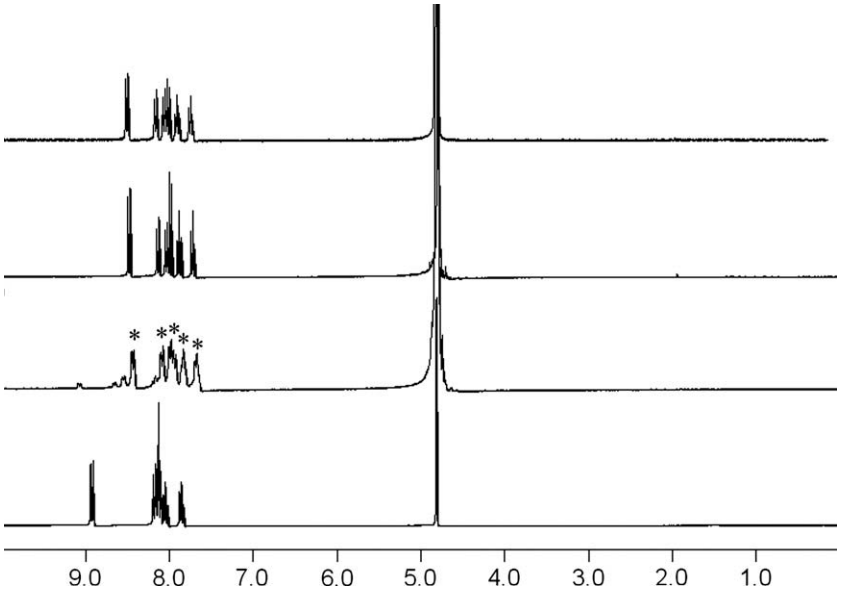

Fig. 8. ^1H NMR spectra of the quinaldate ligand, the triperoxo $(gu)_2[Nb(O_2)_3(quin\text{-}2\text{-}c)] \cdot H_2O$ 5 min and 90 min after dissolution and the quinaldate salt with the guanidinium ion in D_2O solution (from bottom to top). The peaks marked with an asterisk are from the quinaldate salt.

stability. The thermogram of the peroxo compound **1** is illustrated in Fig. 7. The first stage of decomposition occurs at 51–119 °C is believed to be associated with the liberation of the outer sphere H_2O molecule with a weight loss of 3.1% which is in agreement with the calculated value (3.5%). Another decomposition stage follows in the temperature region 123–157 °C. It has been shown that the guanidinium ion's decomposition starts at these temperatures [55]. This process seems to be exothermic and quite violent with considerable dispersion of the residue and a drastic weight loss of 24.5%. This value corresponds to the loss of the two guanidinium counterions (calc. value 23.6%). The decomposition gases released during the thermal degradation of the guanidinium moiety have been reported in the literature [55]. The next two steps of decomposition (temperature region 182–328 °C and 331–544 °C) continued with an experimental loss 43% are characterized by rather complex degradation mechanism of the peroxo groups and the quinaldic acid. The calculated loss of the coordinated peroxo groups and the quinoline moiety from the quinaldic acid is 44.3% [56]. According to the literature the loss of the peroxo groups in the tetraperoxo niobate complex occurs at lower temperature (187 °C) suggesting that the quinaldate ligand stabilize the peroxo complex [3].

The final decomposition temperature appears at 544 °C where the complex undergoes a complete degradation into Nb_2O_5. The weight of the residue was recorded to be 29.4% and the content per niobium is 19.1% which is in agreement with the theoretically calculated value of 18.3%.

4.6. NMR spectroscopy

The peroxo complexes of niobium were investigated with ^1H NMR spectroscopy in D_2O and DMSO solutions. Despite the difficulties in the measurements due to the rapid degradation in water of the complexes, the NMR analyses revealed information on their relative stability in aqueous solution and their relative catalytic activity in DMSO solution. The NMR spectra of all the solution of the complexes measured immediately on adding the complexes in water and DMSO. From the NMR solution spectra it is evident that no information is provided regarding the nature of the original solid compounds **1** and **2**. The relative stability and catalytic activity have been studied by obtaining spectra at different time for over a period of 48 h.

Fig. 8 illustrates the ^1H NMR spectrum of the triperoxo complex 5 min after the dissolution in D_2O showing broad signals around $\delta = 7.7$ and $\delta = 9.2$ ppm. The peaks of low intensity appear at lower fields compared to the free ligand suggesting that the decomposition of the complex has occurred. Several additional major peaks are observed at higher fields compared to the free ligand indicating the formation of a different 'compound' of the ligand. In order to confirm the main peaks observed in the spectrum, we prepared the quinaldate salt with the guanidinium counterion. Mixing equimolar amounts of the quinaldic acid and guanidinium carbonate in ethanol:water 1:1 results a white solid characterized by elemental analysis and IR spectroscopy (our work with all the experimental results and the crystal structure of this compound will be published elsewhere). The ^1H NMR spectrum of the salt in D_2O is identical with that of the triperoxo complex after dissolution in D_2O (Fig. 8, top). Remarkable at the spectrum is the decrease in the chemical shifts for the salt in comparison to the appropriate chemical shifts in the spectrum of the free ligand. A similar influence on the value of the chemical shifts of protons is mentioned for the alkali metal picolinates versus picolinic acid [57]. The assignment of the peaks that correspond to the protons of the free quinaldic acid is based on the ^1H–^1H COSY spectrum (Fig. 9). The corresponding proton shifts from the free ligand show that H_4 (0.5 ppm upfield)

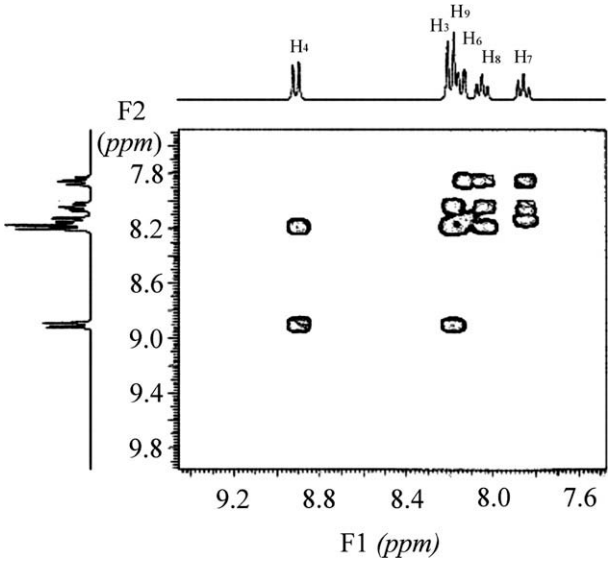

Fig. 9. COSY-NMR spectrum of quinaldic acid in D_2O.

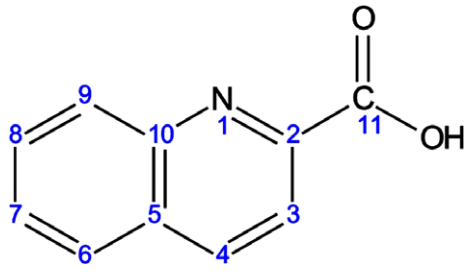

Scheme 1. Quinoline-2-carboxylate acid with atom numbering.

is more affected followed by the separation of H_3 and H_9 signals (Scheme 1).

The ^1H NMR spectrum of the triperoxo complex in DMSO (Fig. 10) 5 min after the dissolution displays a set of peaks with low intensity occurring in the region of the aromatic protons and assigned to the coordinated quinaldate ligand. The protons of the

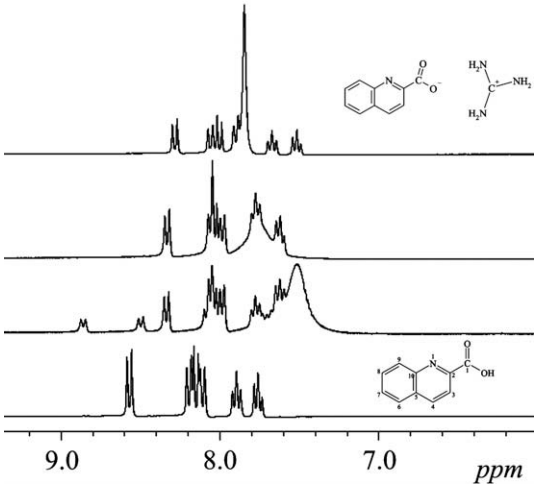

Fig. 10. ^1H NMR spectra of the quinaldate ligand and the triperoxo $(gu)_2[Nb(O_2)_3(quin\text{-}2\text{-}c)] \cdot H_2O$ (5 min and 90 min after dissolution) and the quinaldate salt in DMSO solution (from bottom to top).

ligand are shifted downfield in comparison to those of the free ligand, which results from the asymmetrical charge distribution in the valence orbital of the metal. The resulting paramagnetic moment deshields the ligand's protons. It is reported that in the tin quinaldate complex the protons are shifted slightly to the low field compared with the free ligand while a reverse tendency was reported for the aluminum and gallium complexes with the quinaldic acid [25,49]. The spectrum also displays additional more intense peaks attributed to the resulting liberated ligand salt with the guanidinium counterion. After 48 h of the dissolution the peaks attributed to the coordinated ligand disappear, the characteristic set of peaks due to the ligand salt remains and a peak at 3.012 ppm appears due to the protons of the dimethylsulfone. The latter peak is indicative of the oxidation of DMSO.

Fig. 11 illustrates the ^{1}H NMR spectra of the tetraperoxo and triperoxo complexes in the region of the dimethylsulfoxide protons in order to reveal the difference in the rate of the oxidation reaction catalyzed by the complexes mentioned. Oxidation of DMSO with a variety of oxidants has been studied [58] but no examples of peroxo metal complexes have been described as catalysts in the mentioned oxidation reaction. As it is observed in the spectrum of the tetraperoxo complex, the peak at 3.012 ppm is much more intense compared to this in the spectrum of the triperoxo complex indicating that the triperoxo complex in this period had lower catalytic activity on the oxidation in DMSO in comparison with the tetraperoxo complex. The reaction of dimethylsulfoxide with hydrogen peroxide was compared to that of the more reactive tetraperoxo complex. The oxidation of DMSO with hydrogen peroxide yields dimethylsulfone which is the main product [59] at low conversion and dimethylether as by-product. The increase in the intensity of the peak at 3.012 ppm is significant in the case of the tetraperoxo complex which means that the reaction is much faster than that of the reaction with hydrogen peroxide. A proposed mechanism of the oxygen transfer reaction in the oxidation of DMSO is represented in Scheme 2.

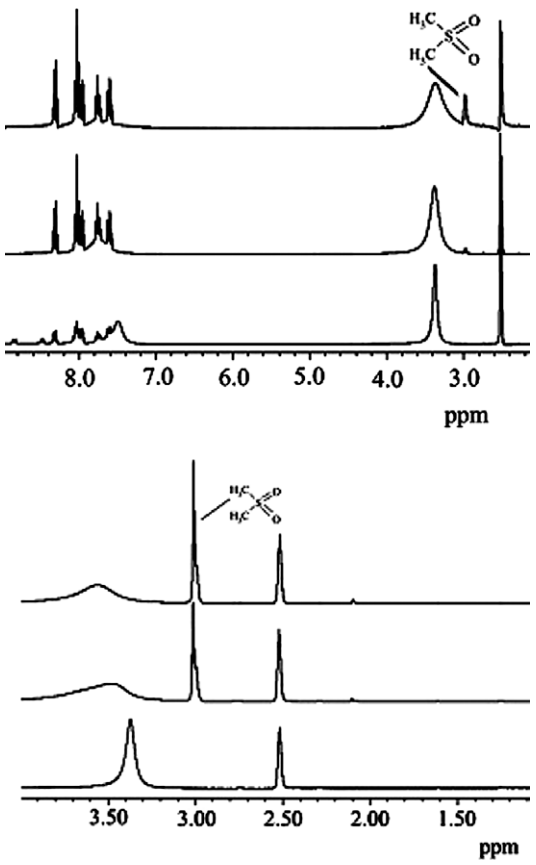

Fig. 11. ^{1}H NMR spectra of the triperoxo (up) and the tetraperoxo (down) complexes in DMSO solution

4.7. Absorption spectroscopy

The peroxo-niobate complexes **1** and **2** are soluble but not very stable in water. An amorphous precipitate forms after 1 h in both solutions and using IR spectroscopy the precipitate is identified as peroxoniobium hydrate (ESI). At low pH a condensation reaction probably occur to form polymeric niobium complexes. However, the freshly prepared aqueous solutions of **1** and **2** have the UV absorption peaks attributed to the peroxo metal charge transfer. The UV–Vis spectra of the peroxo niobate complexes are shown in Fig. 12. A UV absorption band around 280 nm is observed for the tetraperoxo complex and two bands around 280 and 330 nm for the triperoxo complex. According to the literature the complexes with peroxo:Nb mole ratios 1:1 show the characteristic absorption band in the range 255–260 nm while these with 2:1 and 3:1 mole ratios in the range 330–380 nm [9]. Therefore, the peroxo-complex containing the quinaldic ligand seems to be more stable than the homoleptic one since the latter loses easily the peroxide groups coordinated to the metal.

In order to investigate the lowest lying singlet states of **1**, TDDFT calculations have been performed. The most important calculated states along with their vertical excitation energies and oscillator strengths are gathered in Table 6. The lowest in energy

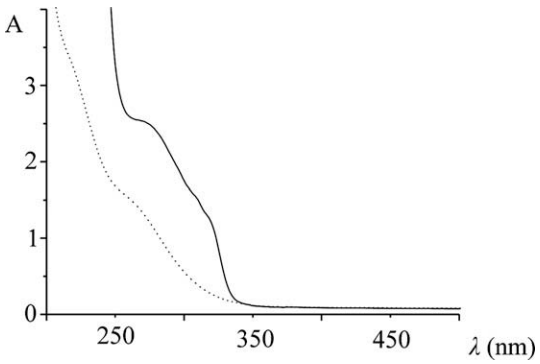

Fig. 12. UV–Vis spectrum of the triperoxo (solid line) and tetraperoxo (dot line) complexes in aqueous solutions.

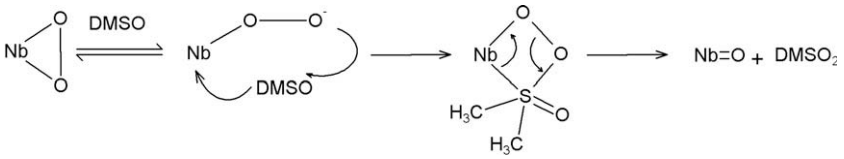

Scheme 2. The proposed mechanism of oxygen transfer reactions in the oxidation of dimethylsulfoxide by the peroxo niobate complexes.

Table 6
TDDFT calculated energies and compositions of the eight lowest lying singlet electronic transitions of **2** owning $f > 0.0070$

State	Composition[a]	ΔE[b]	f[c]	Character
2	HOMO → LUMO, *90%*	1.27	0.0250	π^*(peroxo) → quin (LLCT)
4	HOMO − 2 → LUMO, *93%*	1.59	0.0133	π^*(peroxo) → quin (LLCT)
5	HOMO → LUMO + 1, *94%*	2.07	0.0119	π^*(peroxo) → quin/carb (LLCT)
7	HOMO − 2 → LUMO + 1, *96%*	2.44	0.0076	π^*(peroxo) → quin/carb (LLCT)
10	HOMO → LUMO + 2, *92%* HOMO − 2 → LUMO + 2, *6%*	3.03	0.0083	π^*(peroxo) → quin/carb (LLCT)
22	HOMO − 7 → LUMO, *89%*	3.84	0.0097	carb/π^*(axperoxo) → quin ($\pi \rightarrow \pi^*$)
29	HOMO − 8 → LUMO, *65%* HOMO − 12 → LUMO, *9%* HOMO − 8 → LUMO + 1, *7%* HOMO − 8 → LUMO, *5%*	4.30	0.0405	quin → quin ($\pi \rightarrow \pi^*$) quin→quin/carb ($\pi \rightarrow \pi^*$)
33	HOMO − 1 → LUMO + 6, *35%* HOMO − 10 → LUMO, *25%* HOMO − 1 → LUMO + 8, *10%* HOMO − 8 → LUMO, *7%* HOMO − 8 → LUMO + 1, *7%*	4.43	0.0198	π^*(peroxo) → Nb (LMCT) π^*(peroxo) → quin (LLCT) π (peroxo) → Nb (LMCT) quin → quin ($\pi \rightarrow \pi^*$) quin → quin/carb ($\pi \rightarrow \pi^*$)

[a] Compositions of electronic transitions are expressed in terms of contributing excitations between ground-state Kohn–Sham molecular orbitals.
[b] Transition energy from the ground state in eV.
[c] Oscillator strength.

electronic transition can be ascribed as a HOMO–LUMO transition. As it can be seen from Fig. 4, the HOMO and LUMO orbitals are delocalized amongst the peroxo and quinoline-carboxylate ligand so a LLCT (ligand-to-ligand charge transfer) description can be used. The aforementioned band is not observed in the experimental spectrum due to the decomposition of the complex in water as we have indicated with the NMR experiments and have been discussed before. The experimental spectrum of the complex **1** exhibits the absorption band at 280 nm assigned to the transition of π^* orbital of the peroxo unit into the d ($\pi^* \rightarrow$ d LMCT) and the band at 330 nm resulting mainly from the $\pi_{quin} \rightarrow \pi^*_{quin}$ transition of the ligand. The intraligand transitions of the free quinaldate acid are assigned to the absorption bands below 320 nm (S2).

5. Conclusions

The synthesis, characterization and crystallographic analysis of a novel complex $(gu)_2[Nb(O_2)_3(quin\text{-}2\text{-}c)] \cdot H_2O$ are presented. The crystal data shows that the niobium atom displays eightfold coordination with the quinaldate ligand bound in a bidentate mode via the nitrogen atom and the carboxylato group. The structure is characterized by the presence of the unusual five-membered N-/O-chelation ring and is stabilized by the extended hydrogen bonds. First DFT calculations performed on this triperoxo niobate complex provide an insight on the nature of the chemical bonds in the peroxide group with Nb and new information on spectral properties. The triperoxo complex is also investigated for the relative stability and catalytic reactivity in comparison with the tetraperoxo niobate complex.

Acknowledgments

The present work was supported by the Special Research Account of Athens University (E.L.K.E. 70/4/6495). We are grateful to As. Prof. A. Moutsatsou (Chemical Engineering Department, National Technical University of Athens) for collecting the thermogravimetric data.

Appendix A. Supplementary data

CCDC 680571 contains the supplementary crystallographic data for this paper. These data can be obtained free of charge from The Cambridge Crystallographic Data Centre via www.ccdc.cam.ac.uk/data_request/cif. Supplementary data associated with this article can be found, in the online version, at doi:10.1016/j.poly.2008.08.006.

References

[1] D. Bayot, M. Devillers, Coord. Chem. Rev. 250 (2006) 2610.
[2] M.H. Dickman, M.T. Pope, Chem. Rev. 94 (1994) 569.
[3] L.C. Passoni, M.R.H. Siddiqui, A. Steiner, I.V. Kozhevnikov, J. Mol. Catal. A: Chem. 153 (2000) 103.
[4] J.H. Enemark, J.J.A. Cooney, J.J. Wang, R.H. Holm, Chem. Rev. 104 (2004) 1175.
[5] D.C. Crans, J.J. Smee, E. Gaidamauskas, L.Q. Yang, Chem. Rev. 104 (2004) 849.
[6] E.C. Niederhoffer, J.H. Timmons, A.E. Martell, Chem. Rev. 84 (1984) 137.
[7] J. Li, G. Elberg, D. Gefel, Y. Shechter, Biochemistry 34 (1995) 6218.
[8] Y. Shechter, I. Goldwaser, M. Mironchik, M. Fridkin, D. Gefel, Coord. Chem. Rev. 237 (2003) 3.
[9] Y. Narendar, G.L. Messing, Chem. Mater. 9 (1997) 580.
[10] J.C. Zhao, C.C. Chen, W.H. Ma, Top. Catal. 35 (2005) 269.
[11] A.G.S. Prado, E.A. Faria, J.R. Souzade, J.D. Torres, J. Mol. Catal. A-Chem. 237 (2005) 115.
[12] Z. Zou, H. Arakawa, J. Photochem. Photobiol. A: Chem. 158 (2003) 145.
[13] A. Maniatakou, S. Parsons, A. Karaliota, J. Photochem. Photobiol. A: Chem. 192 (2007) 29.
[14] G. Mathern, R. Weiss, R. Rohmer, Chem. Commun. (1970) 153.
[15] G. Mathern, R. Weiss, Acta Crystallogr., Sect. B 27 (1971) 1582.
[16] C. Djordjevic, N. Vuletic, Inorg. Chem. 7 (1968) 1864.
[17] V. de Oliveira, R.A.D. San Gil, E.R. Lachter, Polyhedron 20 (2001) 2647.
[18] M.T.H. Tarafder, Orient. J. Chem. 15 (1999) 207.
[19] D. Bayot, M. Degand, B. Tinant, M. Devillers, Inorg. Chim. Acta 359 (2006) 1390.
[20] D. Dobrzyńska, M. Duczmal, L.B. Jerzykiewicz, J. Warchulska, K. Drabent, Eur. J. Inorg. Chem. (2004) 110.
[21] D. Dobrzyńska, L.B. Jerzykiewicz, M. Duczmal, Polyhedron 24 (2005) 407.
[22] B. Machura, J. Kusz, Polyhedron 27 (2008) 87.
[23] B. Machura, R. Kruszynski, Polyhedron 26 (2007) 3686.
[24] P. Zhou, D. O'Hagan, U. Mocek, Z. Zeng, L.D. Yuen, T. Frenzel, C.J. Unkefer, J.M. Beale, H.G. Floss, J. Am. Chem. Soc. 111 (1989) 7274.
[25] W. Li, M.M. Olmstead, D. Miggins, R.H. Fish, Inorg. Chem. 35 (1996) 51.
[26] E.D. Raczyńska, M.K. Cyrański, M. Gutowski, J. Rak, J.F. Gal, P.C. Maria, M. Darowska, K. Duczmal, J. Phys. Org. Chem. 16 (2003) 91.
[27] D. Bayot, B. Tinant, M. Devillers, Catal. Today 78 (2003) 439.
[28] (a) G.M. Sheldrick, SHELXS-86, Structure Solving Program, University of Gőttingen, Germany, 1986;
(b) G.M. Sheldrick, SHELXL-97, Program for the Refinement of Crystal Structures from Diffraction Data, University of Gőttingen, Germany, 1997.
[29] (a) J. Farrugia, J. Appl. Crystallogr. 30 (1997) 565;
(b) MERCURY, Version 1.4, <http://www.ccdc.cam.ac.uk>.
[30] R.G. Parr, W. Yang, Density Functional Theory of Atoms and Molecules, Oxford University Press, Oxford, 1989.
[31] M.J. Frisch, G.W. Trucks, H.B. Schlegel, G.E. Scuseria, M.A. Robb, J.R. Cheeseman, V.G. Zakrzewski, J.A. Montgomery, Jr., R.E. Stratmann, J.C. Burant, S. Dapprich, J.M. Millam, A.D. Daniels, K. N. Kudin, M.C. Strain, O. Farkas, J. Tomasi, V. Barone, M. Cossi, R. Cammi, B. Mennucci, C. Pomelli, C. Adamo, S. Clifford, J.

Ochterski, G.A. Petersson, P.Y. Ayala, Q. Cui, K. Morokuma, D.K. Malick, A.D. Rabuck, K. Raghavachari, J.B. Foresman, J. Cioslowski, J.V. Ortiz, A.G. Baboul, B.B. Stefanov, G. Liu, A. Liashenko, P. Piskorz, I. Komaromi, R. Gomperts, R.L. Martin, D.J. Fox, T. Keith, M.A. Al-Laham, C.Y. Peng, A. Nanayakkara, M. Challacombe, P.M.W. Gill, B. Johnson, W. Chen, M.W. Wong, J.L. Andres, C. Gonzalez, M. Head-Gordon, E.S. Replogle, J.A. Pople, GAUSSIAN 98, Revision A.9, Gaussian, Inc., Pittsburgh, PA, 1998.

[32] M.J. Frisch, G.W. Trucks, H.B. Schlegel, G.E. Scuseria, M.A. Robb, J.R. Cheeseman, J.A. Montgomery, Jr., T. Vreven, K. N. Kudin, J.C. Burant, J.M. Millam, S.S. Iyengar, J. Tomasi, V. Barone, B. Mennucci, M. Cossi, G. Scalmani, N. Rega, G.A. Petersson, H. Nakatsuji, M. Hada, M. Ehara, K. Toyota, R. Fukuda, J. Hasegawa, M. Ishida, T. Nakajima, Y. Honda, O. Kitao, H. Nakai, M. Klene, X. Li, J.E. Knox, H.P. Hratchian, J.B. Cross, C. Adamo, J. Jaramillo, R. Gomperts, R.E. Stratmann, O. Yazyev, A.J. Austin, R. Cammi, C. Pomelli, J.W. Ochterski, P.Y. Ayala, K. Morokuma, G.A. Voth, P. Salvador, J.J. Dannenberg, V.G. Zakrzewski, S. Dapprich, A.D. Daniels, M.C. Strain, O. Farkas, D.K. Malick, A.D. Rabuck, K. Raghavachari, J.B. Foresman, J.V. Ortiz, Q. Cui, A.G. Baboul, S. Clifford, J. Cioslowski, B.B. Stefanov, G. Liu, A. Liashenko, P. Piskorz, I. Komaromi, R.L. Martin, D.J. Fox, T. Keith, M.A. Al-Laham, C.Y. Peng, A. Nanayakkara, M. Challacombe, P.M.W. Gill, B. Johnson, W. Chen, M.W. Wong, C. Gonzalez, J.A. Pople, GAUSSIAN 03, Revision B.1, Gaussian, Inc., Pittsburgh PA, 2003.

[33] A.D. Becke, J. Chem. Phys. 98 (1993) 5648.

[34] C. Lee, W. Yang, R.G. Parr, Phys. Rev. B 37 (1988) 785.

[35] (a) T.H. Dunning Jr., P.J. Hay, in: H.F. Schaefer III (Ed.), Modern Theoretical Chemistry, vol. 3, Plenum Press, New York, 1976;
(b) P.J. Hay, W.R. Wadt, J. Chem. Phys. 82 (1985) 270.

[36] [a] S.I. Gorelsky, AOMIX program, revision 6.36 and AOMIX-CDA program, revision 2.18, <http://www.sg-chem.net/>.;
(b) S.I. Gorelsky, A.B.P. Lever, J. Organomet. Chem. 635 (2001) 187.

[37] R. Stratmann, G. Scuseria, M. Frisch, J. Chem. Phys. 109 (1998) 8218.

[38] J.P. Perdew, K. Burke, M. Ernzerhof, Phys. Rev. Lett. 78 (1997) 1396.

[39] A.D. McLean, G.S. Chandler, J. Chem. Phys. 72 (1980) 5639.

[40] R. Krishnan, J.S. Binkley, R. Seeyer, J.A. Pople, J. Chem. Phys. 72 (1980) 650.

[41] D. Andrae, U. Haeussermann, M. Dolg, H. Stoll, H. Preuss, Theor. Chim. Acta 77 (1990) 123.

[42] S.I. Gorelsky, SWIZARD program, revision 4.4, <http://www.sg-chem.net/>.

[43] P. Flükiger, H.P. Lüthi, S. Portman, J. Weber, MOLEKEL, Version 4.3, Swiss Center for Scientific Computing, Manno, Switzerland, 2000–2002.

[44] CHEMCRAFT, Version 1.5, <http://www.chemcraftprog.com>.

[45] D. Bayot, M. Devillers, D. Peeters, Eur. J. Inorg. Chem. (2005) 4118.

[46] G. Mathern, R. Weiss, Acta Crystallogr., Sect. B 27 (1971) 1572.

[47] D. Dobrzyńska, L.B. Jerzykiewicz, J. Chem. Crystallogr. 34 (2004) 51.

[48] N. Okabe, Y. Muranishi, Cryst. Struct. Commun. Acta Cryst. 59 (2003) 228.

[49] H.D. Yin, Q.B. Wang, S.C. Xue, J. Organomet. Chem. 690 (2005) 3111.

[50] V.S. Sergienko, Crystallogr. Rep. 49 (2004) 907.

[51] (a) C. Makedonas, C.A. Mitsopoulou, F.J. Lahoz, Inorg. Chem. 42 (2003) 8853;
(b) C. Makedonas, C.A. Mitsopoulou, Spectrochim. Acta A 64 (2006) 918;
(c) C. Makedonas, C.A. Mitsopoulou, Inorg. Chim. Acta 360 (2007) 3997.

[52] (a) S. Dapprich, G. Frenking, J. Chem. Phys. 99 (1995) 9352;
(b) G. Frenking, N. Fröhlich, Chem. Rev. 100 (2000) 717;
(c) C. Makedonas, I. Veroni, C.A. Mitsopoulou, Eur. J. Inorg. Chem. 1 (2007) 120.

[53] M. Drozd, J. Mol. Struct.: THEOCHEM 756 (2005) 173.

[54] G.B. Deacon, R.J. Phillips, Coord. Chem. Rev. 33 (1980) 227.

[55] J. Neutz, O. Grosshardt, S. Schaufele, H. Schuppler, W. Schweikert, Propellants, Explosives, Pyrotechnics 28 (2003) 181.

[56] A.S.M. Goher, A.K. Hafez, T.C.W. Mak, Polyhedron 20 (2001) 2583.

[57] G. Świderski, M. Kalinowska, S. Wojtulewski, W. Lewandowski, Spectrochim. Acta A 64 (2006) 24.

[58] D.C. Bilehal, R.M. Kulkarni, S.T. Nandibewoor, React. Kinet. Catal. Lett. 73 (2001) 349.

[59] B. Ballesteros, N.R. Jensen, J. Hjorth, J. Atmos. Chem. 43 (2002) 135.

2.3. Preparation of [Zn(pchlorben)$_2$(py)$_2$] (**3**)

Complex **3** was prepared by using 4-chlorobenzoic acid (pchlorbenH) in similar way to that of (**1**), but was crystallised from a mixed solvent comprising of DMSO and pyridine. Yield: 46% (based on Zn). Elemental *Anal.* Calc. for $C_{24}H_{18}Cl_2N_2O_4Zn$: C, 53.87; H, 3.37. Found C, 53.90; H, 3.38%. FT-IR (KBr, cm^{-1}): 3223 (br s), 1925 (w), 1649 (m), 1611 (s), 1593 (s), 1550 (s), 1508 (m), 1383 (s), 1291 (w), 1172 (s), 1139 (w), 1115 (w), 868 (s), 849 (s), 791 (s), 763 (s), 633 (s); ^{1}H NMR (DMSO-d_6, 400 MHz): 8.62 (2H, br s), 7.93 (2H, d, J = 8.4 Hz), 7.83 (1H, t, J = 7.6 Hz), 7.46 (4H, m).

2.4. Preparation of [Zn$_2$(μ^2-mtol)$_4$(py)$_2$] (**4**)

3-Methylbenzoic acid (0.272 g, 2 mmol) and zinc sulfate heptahydrate (0.287 g, 1 mmol) and sodium hydroxide (0.08 g, 2 mmol) were finely ground in a mortar and heated at 100 °C for 20 min. The mixture was cooled to room temperature and methanol (10 ml) was added to it and the heterogeneous mixture was transferred to a round bottom flask. To this solution pyridine (0.079 g, 1 mmol) was added and stirred at room temperature for 5 min. Colorless crystals were obtained after 5 days and dried in air. Yield: 48% (based on Zn). Elemental *Anal.* Calc. for $C_{42}H_{38}N_2O_8Zn_2$: C, 60.76; H, 4.58. Found: C, 60.79; H, 5.01%. FT-IR (KBr, cm^{-1}): 3431 (br s), 3064 (w), 3030 (w), 2912 (w), 1823 (w), 1644 (s), 1602 (s), 1583 (s), 1403 (br s), 1214 (m), 1082 (m), 1069 (m), 1046 (m), 788 (s), 755 (s), 747 (s), 693 (m), 674 (w), 642 (w), 493 (m), 458 (m). ^{1}H NMR (DMSO-d_6, 400 MHz): 8.84 (2H, br s), 8.07 (1H, t, J = 6.8 Hz), 7.95 (2H, s), 7.92 (2H, t, J = 4 Hz), 7.67 (2H, t, J = 6.8 Hz), 7.46 (4H, d, J = 5.2 Hz), 2.50 (12H, s).

2.5. Preparation of [Zn$_5$(μ^2-mtol)$_6$(mtol)$_2$(μ^3-OH)$_2$(py)$_2$] (**5**)

3-Methylbenzoic acid (0.272 g, 2 mmol), zinc sulfate heptahydrate (0.287 g, 1 mmol) and sodium hydroxide (0.08 g, 2 mmol) were finely ground in a mortar and heated at 100 °C for 15 min. The solid mixture was cooled to room temperature, transferred into a round bottom flask and dimethylsulfoxide: water (4:1) was added to it. The heterogeneous mixture was stirred at room temp for 5 min followed by addition of pyridine (0.079 g, 1 mmol). The colourless liquid was filtered and was left undisturbed. Colourless crystals were collected after 15 days and dried in air. Yield: 34% (based on Zn). Elemental *Anal.* Calc. for $C_{74}H_{68}N_2O_{18}Zn_5$: C, 55.49; H, 4.25. Found C, 55.52; H, 4.28%. FT-IR (KBr, cm^{-1}): 3432 (br s), 2919 (m), 1623 (s), 1601 (s), 1578 (s), 1531 (s), 1428 (s), 1404 (s), 1289 (w), 1229 (w), 1088 (m), 787 (s), 764 (s), 673 (m), 589 (m), 492 (s). ^{1}H NMR (DMSO-d_6, 400 MHz): 7.76 (4H, s), 7.73 (5H, m), 7.30 (6H, m) 2.38 (12H, s).

2.6. Preparation of [Zn$_2$(μ^2-otol)$_4$(py)$_2$] (**6**)

2-Methylbenzoic acid (0.272 g, 2 mmol), zinc sulfate heptahydrate (0.287 g, 1 mmol) and sodium hydroxide (0.08 g, 2 mmol) were finely ground in a mortar and heated at 100 °C for 20 min. The mixture was transferred to a round bottom flask and methanol (10 ml) was added, followed by pyridine (0.079 g, 1 mmol). The resultant mixture was stirred at room temperature for half an hour and then was filtered. The colourless filtrate was left undisturbed. Colourless crystals were obtained after 8 days and dried in air. Yield: 41% (based on Zn). Elemental *Anal.* Calc. for $C_{42}H_{38}N_2O_8Zn_2$: C, 60.76; H, 4.58. Found C, 60.81; H, 5.01%. FT-IR (KBr, cm^{-1}): 3420 (br s), 3064 (w), 3021 (w), 2929 (w), 1634 (s), 1609 (s), 1568 (s), 1435 (s), 1403 (br s), 1219 (m), 1157 (m), 1103 (m), 1071(m), 1048 (m), 852 (m), 741 (s), 700 (s), 665 (s), 550 (m). ^{1}H NMR (DMSO-d_6, 400 MHz): 8.62 (2 H, br s), 7.87 (1H, t, J = 6.8 Hz), 7.75 (2H, d, J = 7.2 Hz), 7.47 (2H, t, J = 6.8 Hz), 7.27 (2H, t, J = 8.0 Hz), 7.18 (4H, d, J = 7.6 Hz), 2.50 (12H, s).

2.7. Preparation of [Zn$_4$(μ^2-otol)$_6$(μ^4-O)(DMSO)$_2$] (**7**)

2-Methylbenzoic acid (0.272 g, 2 mmol), zinc sulfate heptahydrate (0.287 g, 1 mmol) and sodium hydroxide (0.08 g, 2 mmol) were finely ground in a mortar and heated at 100 °C for 15 min. The heated mixture was cooled to room temperature, transferred

Table 1
Crystal data and refinement parameters for compound **1–7**

	1	**2**	**3**	**4**	**5**	**6**	**7**
Formulae	$C_{16}H_{18}O_6Zn$	$C_{18}H_{22}N_2O_{11}S_2Zn$	$C_{24}H_{18}Cl_2N_2O_4Zn$	$C_{42}H_{38}N_2O_8Zn_2$	$C_{74}H_{68}N_2O_{18}Zn_5$	$C_{42}H_{38}N_2O_8Zn_2$	$C_{52}H_{54}O_{15}S_2Zn_4$
Molecular weight	371.67	571.87	534.67	829.48	1600.2	829.48	1244.6
Crystal system	monoclinic	triclinic	monoclinic	tetragonal	monoclinic	monoclinic	orthorhombic
Space group	*C*2/*c*	*P*$\bar{1}$	*C*2/*c*	*I*-42*d*	*C*2/*c*	*P*2$_1$/*c*	*Pca*2(1)
a (Å)	26.8543(12)	6.0159(5)	28.3367(4)	12.4107(2)	15.9469(8)	10.7319(10)	23.7229(8)
b (Å)	5.0620(2)	7.7149(5)	6.23450(10)	12.4107(2)	22.1141(8)	10.9111(10)	11.3117(4)
c (Å)	12.0699(6)	26.7675(17)	15.4315(3)	24.7015(5)	21.6548(13)	18.7835(15)	41.1802(14)
α (°)	90	84.584(5)	90	90	90	90	90
β (°)	106.837(5)	84.464(4)	119.9150(10)	90	107.563(4)	114.387(5)	90
γ (°)	90	70.371(3)	90	90	90	90	90
V (Å^3)	1570.40(12)	1162.13(14)	2362.98(7)	3804.66(12)	7280.6(6)	2003.2(3)	11050.6(7)
Z	4	2	4	4	4	2	8
Density (Mg m^{-3})	1.572	1.634	1.503	1.448	1.46	1.375	1.496
Absorption coefficient (mm^{-1})	1.592	1.298	1.299	1.317	1.693	1.251	1.855
Absroption correction	none	none	none	none	none	none	none
F(000)	768	588	1088	1712	3280	856	5104
Total number of reflections	9890	14736	17074	23239	39072	26347	125528
Reflections, $I > 2\sigma(I)$	1937	5405	4156	2361	8910	4860	26306
Maximum 2θ (°)	28.28	28.2	28.3	28.29	28.46	28.23	28.3
Ranges	$-35 \leqslant h \leqslant 35$ $-6 \leqslant k \leqslant 6$ $-15 \leqslant l \leqslant 16$	$-7 \leqslant h \leqslant 7$ $-9 \leqslant k \leqslant 10$ $-35 \leqslant l \leqslant 35$	$-37 \leqslant h \leqslant 37$ $-8 \leqslant k \leqslant 8$ $-20 \leqslant l \leqslant 20$	$-16 \leqslant h \leqslant 16$ $-16 \leqslant k \leqslant 15$ $-32 \leqslant l \leqslant 32$	$-21 \leqslant h \leqslant 19$ $-28 \leqslant k \leqslant 29$ $-15 \leqslant l \leqslant 28$	$-14 \leqslant h \leqslant 14$ $-14 \leqslant k \leqslant 14$ $-24 \leqslant l \leqslant 21$	$-31 \leqslant h \leqslant 31$ $-15 \leqslant k \leqslant 12$ $-54 \leqslant l \leqslant 52$
Complete to 2θ (%)	99.2	94.8	98.5	99.7	96.8	98.0	99.7
Data/restraints/parameters	1937/0/106	5405/0/316	2901/0/150	2361/0/124	8910/529/455	4860/0/246	26306/902/1335
Goof (F^2)	1.086	1.030	1.035	1.038	1.136	1.062	0.975
R indices [$I > 2\sigma(I)$]	0.0356	0.0500	0.0375	0.0248	0.0813	0.0272	0.0422
R indices (all data)	0.0495	0.0628	0.0558	0.0365	0.2085	0.0356	0.1005

into a round bottom flask and dimethylsulfoxide: water (4:1) was added to it. The heterogeneous mixture was stirred at room temperature. The reaction mixture was filtered, the solid precipitate was discarded and the colourless filtrate was left undisturbed. Block type colourless crystals were obtained after 10 days and dried in air. Yield: 24% (based on Zn). Elemental *Anal.* Calc. for $C_{52}H_{54}O_{15}S_2Zn_4$: C, 50.14; H, 4.34. Found C, 50.19; H, 4.38%. FT-IR (KBr, cm^{-1}): 3422 (br s), 2968 (m), 2929 (m), 1611 (s), 1591 (s), 1566 (s), 1437 (s), 1399 (s), 1286 (w), 1196 (w), 1160 (m), 1103 (m), 1004 (s), 953 (w), 785 (m), 749 (s), 666 (m), 535 (w). ^1H NMR (DMSO-d_6, 400 MHz): 7.75 (6H, d, J = 9.2 Hz), 7.27 (6H, t, J = 7.2 Hz), 7.18 (10H, d, J = 7.2 Hz), 7.15 (2H, s), 2.52 (40H, m).

3. Structure determination

The X-ray data were collected at 296 K with Mo Kα radiation (λ = 0.71073 Å) using a Bruker Nonius SMART CCD diffractometer equipped with a graphite monochromator. SMART software was used for data collection and also for indexing the reflections and determining the unit cell parameters; the collected data were integrated using SAINT software. The structures were solved by direct methods and refined by full-matrix least-squares calculations using SHELXTL software. All the non-H atoms were refined in the anisotropic approximation against F^2 of all reflections. The H-atoms, except those attached to N and O, were placed at their calculated positions and refined in the isotropic approximation; those attached to the heteroatoms (N, O) were located in the difference Fourier maps, and refined with isotropic displacement coefficients. The crystal data for the complexes are listed in Table 1.

4. Results and discussion

A series of combined solid and solution phase reactions of the sodium salt of substituted benzoic acids with zinc sulfate heptahydrate, followed by dissolution of the reactant in methanol or dimethylsulfoxide in the presence or absence of pyridine were carried out (Scheme 1). A variety of complexes, as listed in Scheme 1, was obtained and each of the complexes was characterized by X-ray crystallography. This combined phase reaction methodology is in accordance with our earlier observation on the variation of product formation as compared to solution chemistry [5]. From the para-substituted benzoic acids, 4-methylbenzoic acid, 4-nitrobenzoic acid and 4-chlorobenzoic acid, on reaction with zinc sulfate and pyridine we could prepare mononuclear zinc complexes. However, the compositions and coordination geometries of the products were different in each case and depend on the solvent

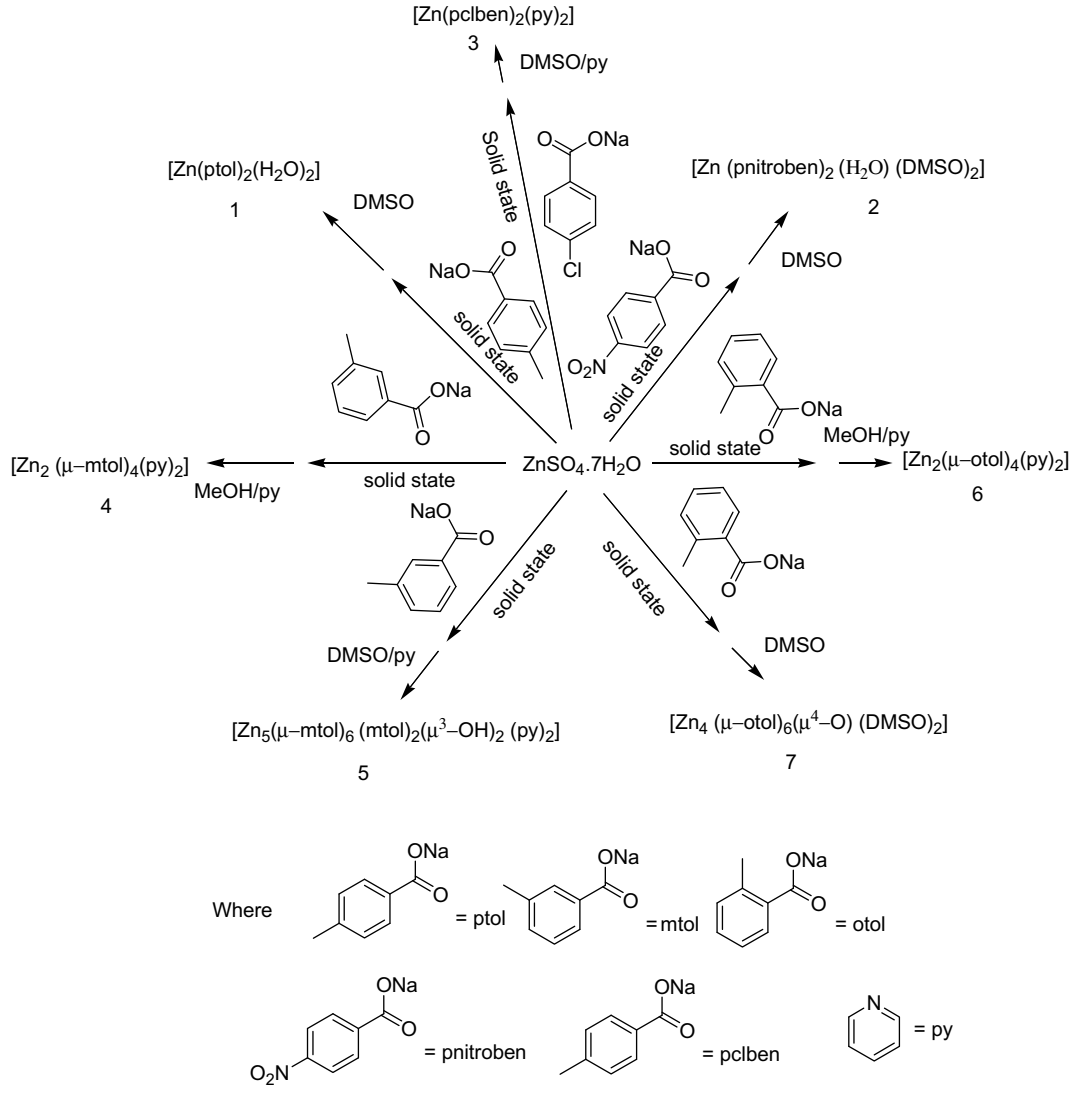

Scheme 1.

of crystallization. For example, complex **1** has the composition $[Zn(ptol)_2(H_2O)_2]$, having two water ligands, complex **2** has dimethylsulfoxide ligands with the composition $[Zn(pnitroben)_2(H_2O)(DMSO)_2]$ and **3** has pyridine ligands [5a] with the composition $[Zn(pchlorben)_2(py)_2]$. These complexes were characterized by various spectroscopic techniques and also by X-ray crystallography. The structures of the three complexes are shown in Fig. 1. Complex **2** has a penta-coordinated structure close to a square pyramidal geometry with two DMSO and two carboxylate groups opposite to each other in the basal plane, and with a water molecule occupying an axial position. The complex shows sharp IR signals at 3368 cm^{-1} for the aqua ligand and 1010 cm^{-1} for DMSO. The monodentate carboxylate stretching appears at 1617 cm^{-1} and 1578 cm^{-1} (sym) and the anti-symmetric stretching appears at 1345 cm^{-1}. The monodentate nature of the carboxylate group is reflected in the Zn–O distances in the crystal structure; the distances between the two carbonyl oxygen atoms that are not participating in the metal ligand bond and zinc, namely Zn1–O6 and Zn–O1, are 3.166 Å and 2.584, whereas the other metal ligand bond distances, Zn–O2, Zn1–O5, Zn1–O9,

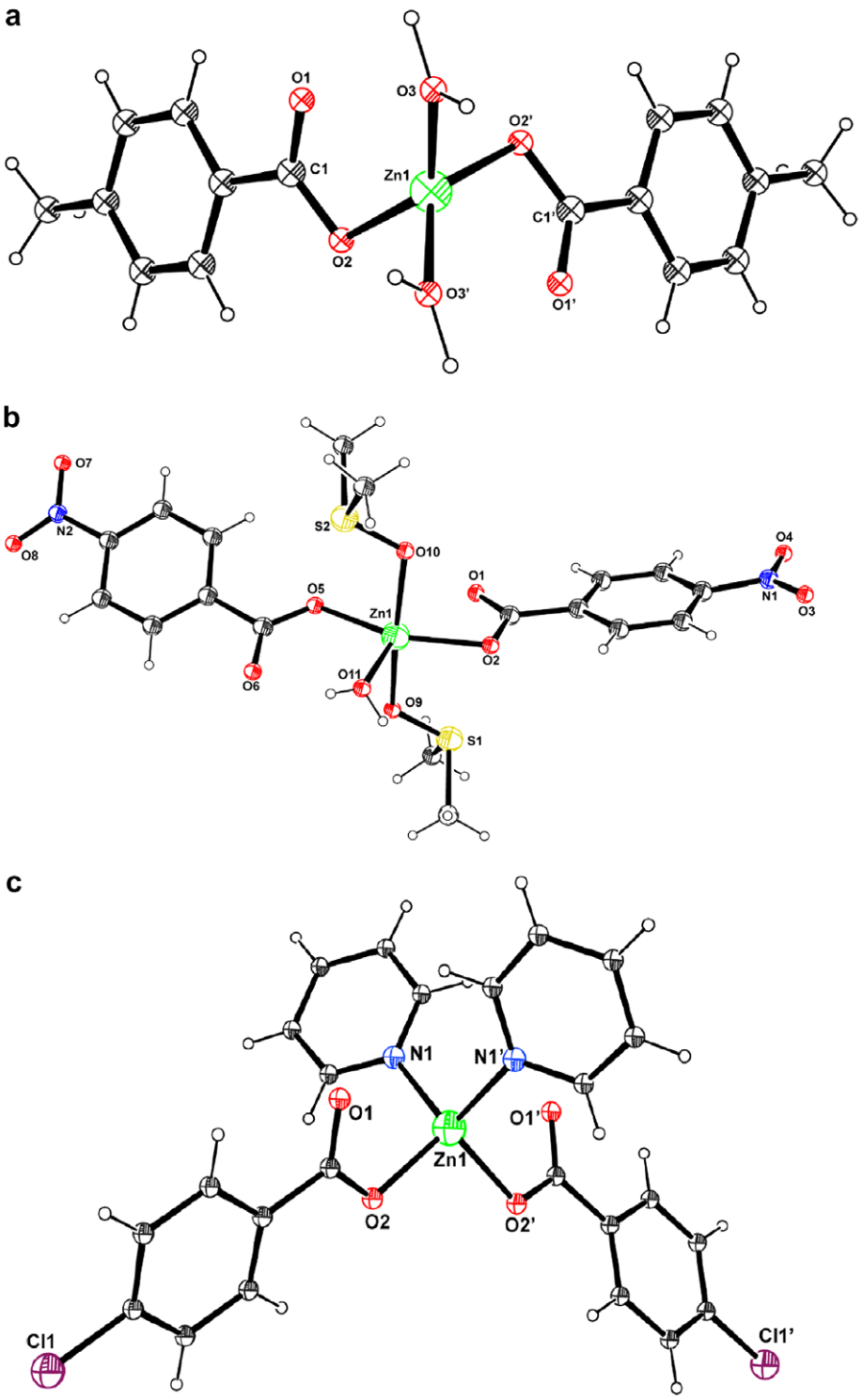

Fig. 1. The solid state structures of (a) $[Zn(ptol)_2(H_2O)_2]$ (**1**), (b) $[Zn\ (pnitroben)_2(H_2O)\ (DMSO)_2]$ (**2**) and (c) $[Zn(pchlorben)_2(py)_2]$ (**3**).

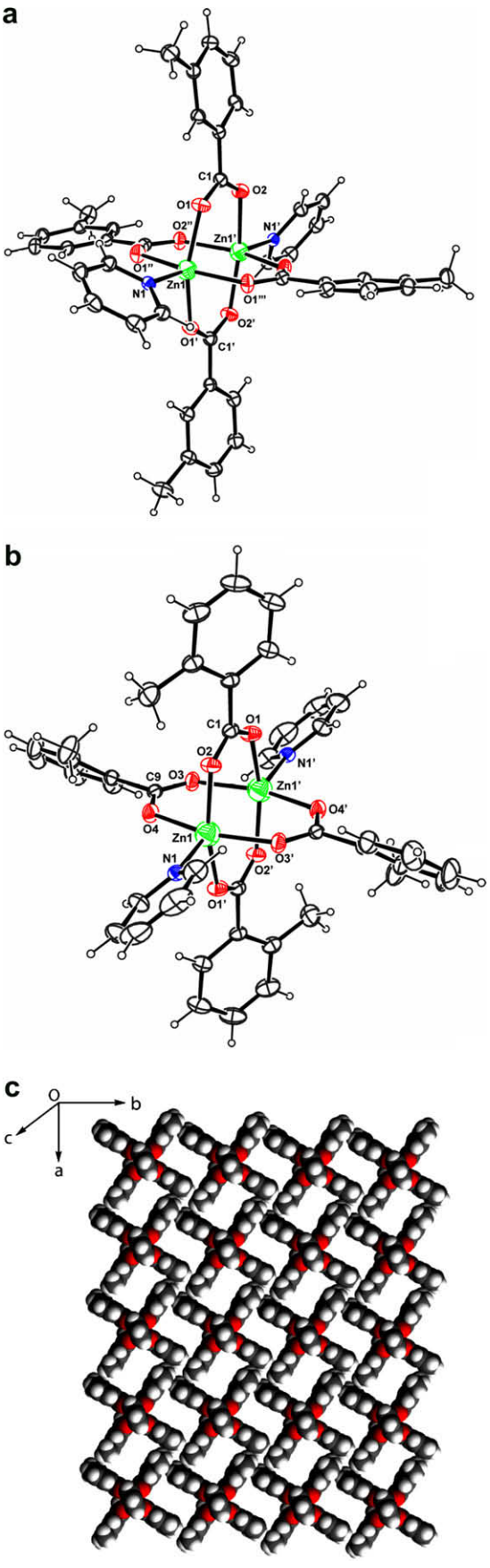

Fig. 2. The solid state structure of (a) $[Zn_2(\mu\text{-mtol})_4(py)_2]$ (**4**), (b) $[Zn_2(\mu\text{-otol})_4(py)_2]$ (**6**) and (c) the packing pattern in (**4**).

Zn1–O10 and Zn1–O11, are 2.045, 2.011, 2.120, 2.109 and 2.004 Å, respectively. The lone pairs of electrons on the two sulfur atoms of the dimethylsulfoxide ligands in the complex project in opposite directions and it becomes one of the factors for the five coordination geometry around the zinc centre. However, there are other very weak interactions such as C–H···O and S···N(pi) interactions [9] that also contribute to this geometry. These lone pairs in this complex also push the two carbonyl oxygens of the carboxylate away from each other and thereby making space for a water ligand to approach the metal center. In the case of complexes **1** and **3** such effects are not present; complex **1** can be considered to have a distorted square planar structure with two symmetric halves, having two types of Zn–O bonds (Zn1–O2, 2.009 Å and Zn1–O3, 1.990 Å). Complex **1** has an IR absorption at 3430 cm^{-1} and has two closely spaced carboxylate stretching frequencies at 1621 and 1608 cm^{-1}. Whereas complex **3** has the coordination number four with a distorted tetrahedral geometry in which the two carboxylate groups are monodentate. The molecule has a mirror plane and the Zn1–N1 and Zn1–O2 bond distances are 2.043 and 1.961 Å, respectively. The distance of separation between Zn1 and O1 is 2.787 Å, suggesting no bond formation between them and making the carboxylate group bind in a monodentate fashion. Mononuclear complexes of 2,6-dichlorobenzoate and 2,6-difluorobenzoate are characterized in the literature and have six and five coordination geometries, respectively [3a]. However our reactions are done under thermodynamically favorable conditions and the product composition varies from substituent, as observed in earlier studies. In our earlier study we have shown that the number of ancillary ligands in a carboxylate complex is decided by the substituent attached to the aromatic ring [6].

The reaction of zinc(II) sulfate heptahydrate with sodium salts of 3-methylbenzoic acid or 2-methylbenzoic acids in a methanolic solution containing pyridine gave dinuclear zinc complexes having a paddlewheel type structure with two pyridine ligands at axial positions (Fig. 2a and 2b). The metal ligand bond distances and angles are listed in Tables 2 and 3. In each case there are four carboxylate ligands bridging the two zinc centers. On a careful look at the geometry of the complexes it is observed that in the case of complex **4** the orientation of the two planes of the pyridine rings are perpendicular to each other, whereas in the case of **6** the two rings

Table 2
Selected internuclear distances (in Å) and angles (in °) in **4**

Bond distances		Bond angles	
Zn(1)–O(1)	2.0346(19)	O(1)–Zn(1)–O(1′)	152.25(10)
Zn(1)–N(1)	2.0361(19)	O(1)–Zn(1)–N(1)	103.87(5)
Zn(1)–O(2)	2.0557(19)	O(1)–Zn(1)–O(2)	88.32(8)
Zn(1)–Zn(1′)	2.9799(5)	N(1)–Zn(1)–O(2)	97.45(5)
C(1)–O(1)	1.250(3)	O(1)–Zn(1)–O(2′)	88.12(7)
C(1)–O(2)	1.255(3)	O(2)–Zn(1)–O(2′)	165.10(10)

Table 3
Selected internuclear distances (in Å) and angles (in °) in **6**

Bond distances		Bond angles	
Zn(1)–O(1)	2.0340 (12)	N1–Zn1–O3	101.81(5)
Zn(1)–O(2)	2.0544 (12)	O1–Zn1–O3	89.23(6)
Zn(1)–O(3)	2.0340 (12)	N1–Zn1–O4	98.27(5)
Zn(1)–O(4)	2.0465 (12)	O1–Zn1–O4	88.97(6)
Zn(1)–N(1)	2.0287 (13)	O3–Zn1–O4	159.72(5)
Zn(1)–Zn(1′)	2.9341 (4)	N1–Zn1–O2	96.92(6)
C(1)–O(1)	1.247(2)	O1–Zn1–O2	159.88(5)
C(1)–O(2)	1.251(2)	O3–Zn1–O2	87.41(6)
C(9)–O(3)	1.246(2)	O4–Zn1–O2	87.36(6)
C(9)–O(4)	1.252(2)		

lies in one plane. The orientation of the rings is attributed to the steric effect of the methyl groups on the crystal packing. The packing pattern of **4** is shown in Fig. 2c, which has a grid-like structure. Dinuclear paddlewheel structure benzoate complexes have been reported [7], but these have not been studied in detail. It has also been observed that non-symmetric carboxylato bridged complexes of zinc can be prepared with pyridine as an ancillary ligand [3a]. We have also recently shown that binuclear or co-crystals of bi and trinclear zinc benzoate complexes can be prepared by varying the reaction conditions [4].

The reaction of zinc sulfate with sodium salts of 3-methylbenzoic acid and 2-methylbenzoic acid in dimethylsulfoxide gave the tetranuclear and pentanuclear zinc complexes **5** and **7,** respectively. From the observation of the formation of two paddle wheel type structures in the case of **4** and **6**, it is clear that methanol has no role in the formation of these dinuclear structures, whereas DMSO, being a more coordinating solvent, leads to an expansion of the nuclearity. The IR spectrum of the dinuclear complex **4**, prepared in methanol solution, shows clear distinctions as compared to the tetranuclear complex **6**, as shown in Fig. 3. Distinctions between the dinuclear complex **5** and the pentanuclear complex **7** are also observed, again shown in Fig. 3. In the case of **5** all the carboxylate groups are bridging, whereas in complex **7** there are bridging as well as monodentate carboxylate ligands. The monodentate carboxylate of **5** shows an IR absorption at 1623 cm^{-1}, whereas for the bridging carboxylate absorptions of the complex, ν_a are at 1601 cm^{-1} and 1578 cm^{-1} and ν_{sCOO} stretchings appear at 1428 cm^{-1} and 1404 cm^{-1}. Complex **4** has ν_a at 1602 cm^{-1} and 1583 cm^{-1} along with a ν_{sCOO} stretching at 1403 cm^{-1}. It has an absorption at 1644 cm^{-1} due to a C=C absorption of the pyridine ring. In a similar manner, complex **6** has a C=C absorption from pyridine at 1634 cm^{-1}, ν_{aCOO-} at 1602 cm^{-1} and 1583 cm^{-1} and ν_{sCOO} stretching at 1403 cm^{-1}. However, complex **7** has all bridging carboxylate ligands and IR absorptions at 1611, 1591 (ν_{sCOO}) and 1399 cm^{-1} (ν_{aCOO}) are observed. The S=O stretching of coordinated DMSO appears at 1004 cm^{-1}.

Complex **7** is a tetranuclear complex having one oxy-ligand shared by four zinc centers. The oxy anion acts as a central point in a tetrahedral geometry formed by four zinc ions and one oxide anion. Among the four zinc centers, three zinc centers are equivalent, are anchored by three carboxylate bridges and are attached to the central oxygen, whilst the other zinc center is bridged by three carboxylate, one oxy ligand and two dimethylsulfoxide ligands. Complex **5** has two symmetry non-equivalent molecules per unit cell. This is a rare example of a polynuclear complex having symmetry non- equivalent molecules in the unit cell. The bond distances and bond angles of zinc with the different ligands, as illustrated in Fig. 4c and d, are listed in Tables 4 and 5. Both the complexes have a combination of six and four coordination geometry around zinc. Complex **7** is symmetric and has a mirror plane that bisects two halves containing the two tetrahedral units anchored by a six coordinated zinc. The complex has two hydroxyl ligands bridging Zn1, Zn2 and Zn3 centers, in which the OH are intramolecularly hydrogen bonded with two free carbonyl groups of the monodentate carboxylate hydrogen. The donor acceptor bond distances in this intramolecular hydrogen bonding O9–

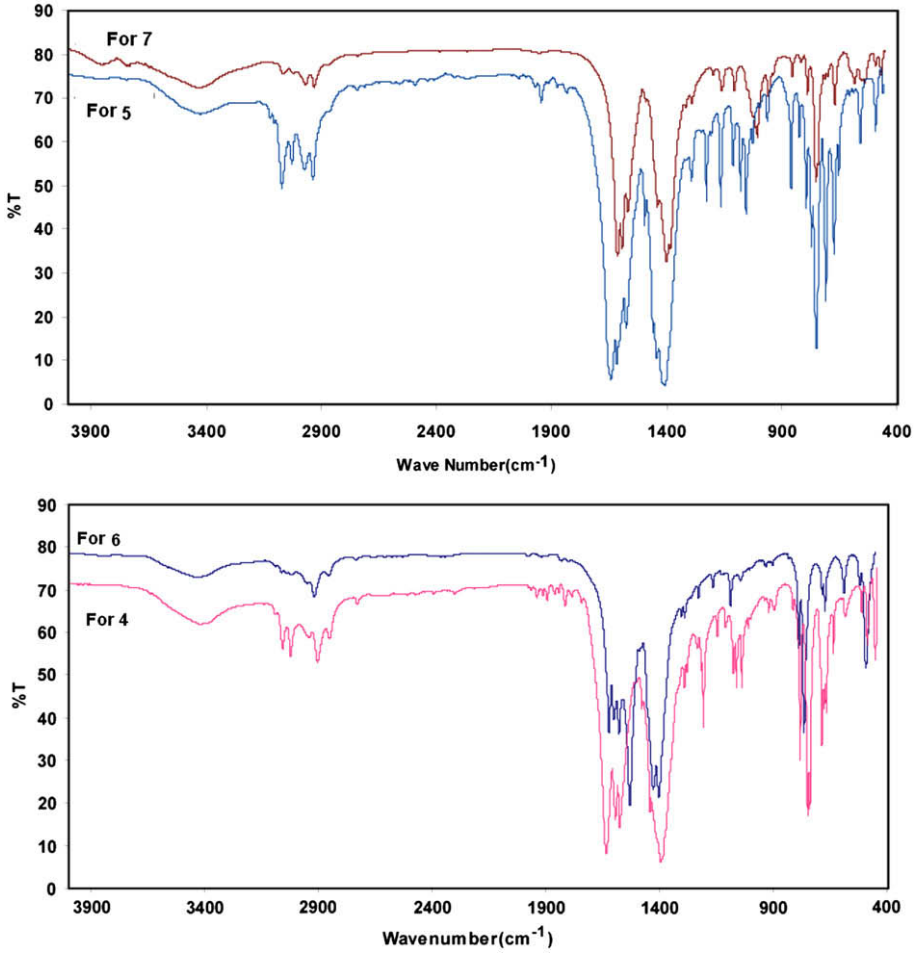

Fig. 3. The solid state IR spectra (KBr) of complexes **4–7.**

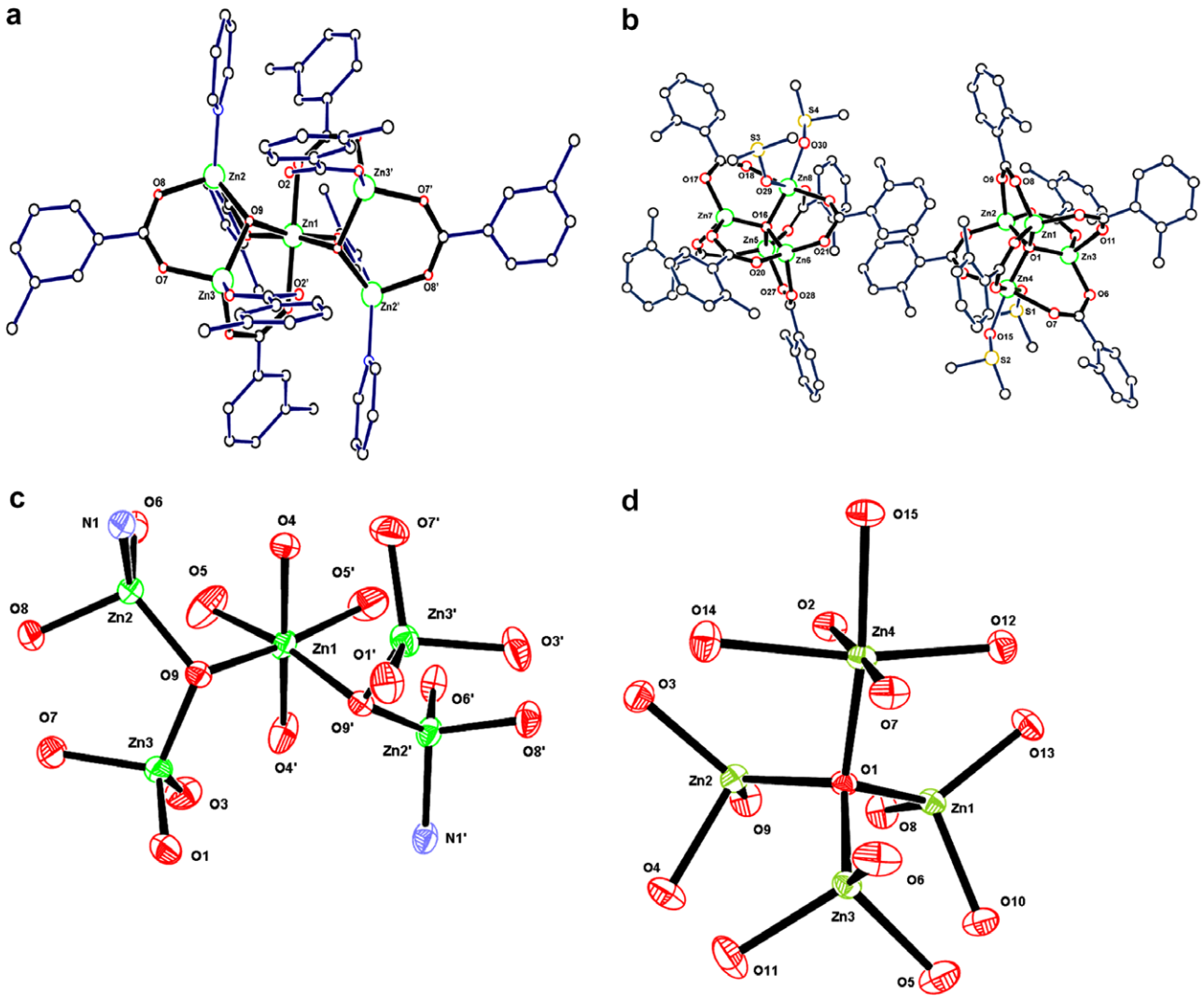

Fig. 4. The crystal structures of (a) $[Zn_5(\mu^2\text{-mtol})_6(\text{mtol})_2(\mu^3\text{-OH})_2(\text{py})_2]$ (**5**) (b) $[Zn_4(\mu^2\text{-otol})_6(\mu^4\text{-O})(\text{DMSO})_2]$ (**7**) (the hydrogen atoms are omitted for clarity). The ligand environments around (c) **5** and (d) **7.**

Table 4
Selected internuclear distances (in Å) and angles (in °) in **5**

Bond distances			Bond angles
Zn(1)–O(4)	2.061(5)	O(4)–Zn(1)–O(4′)	175.2(3)
Zn(1)–O(5)	2.080(5)	O(4)–Zn(1)–O(5)	85.9(2)
Zn(1)–O(9)	2.096(4)	O(4′)–Zn(1)–O(5)	91.0(3)
Zn(2)–N(1)	2.016(6)	O(5)–Zn(1)–O(5′)	96.8(4)
Zn(2)–O(6)	1.938(5)	O(4)–Zn(1)–O(9)	98.7(2)
Zn(2)–O(9)	1.954(4)	O(4′)–Zn(1)–O(9)	84.64(18)
Zn(2)–O(8)	1.974(5)	O(5)–Zn(1)–O(9)	86.8(2)
Zn(2)–O(1)	1.920(5)	O(5′)–Zn(1)–O(9)	169.9(2)
Zn(3)–O(3)	1.936(6)	O(9)–Zn(1)–O(9′)	91.2(2)
Zn(3)–O(9)	1.956(4)	O(6)–Zn(2)–O(9)	122.9(2)
Zn(3)–O(7)	1.978(5)	O(6)–Zn(2)–O(8)	103.3(2)
C(1)–O(1)	1.285(10)	O(9)–Zn(2)–O(8)	105.59(18)
C(1)–O(2)	1.216(10)	O(6)–Zn(2)–N(1)	108.7(2)
C(9)–O(3)	1.264(14)	O(8)–Zn(2)–N(1)	111.3(2)
C(9)–O(4)	1.259(14)	O(21)–Zn(2)–N(1)	102.8(2)
C(17)–O(5)	1.276(13)	O(1)–Zn(3)–O(3)	117.3(2)
C(17)–O(6)	1.221(13)	O(1)–Zn(3)–O(9)	112.0(2)
C(25)–O(7)	1.232(10)	O(3)–Zn(3)–O(9)	114.8(2)
C(25)–O(8)	1.249(10)	O(1)–Zn(3)–O(7)	104.3(2)
		O(3)–Zn(3)–O(7)	101.2(3)
		O(9)–Zn(3)–O(7)	105.02(19)

H9···O2 are d_{D-H} 0.77 Å, $d_{D-A,intra}$ 2.73 Å; ⟨D–H···A 170.93°. On the six coordinated zinc center the two bulky groups occupy *cis* positions, which also comply with the strong intramolecular hydrogen bonding. The presence of two uncoordinated carbonyl oxygens at this position could be responsible for further abstraction of protons from the hydroxyl groups. Complex **5**, however, has a central oxy ligand which coordinates to four independent zinc centers to complete three tetrahedral and an octahedral geometry. Complex **5** is similar to the tetranuclear symmetric zinc core reported by Straughan et al. [8], but with the difference that one of the zinc centers gets coordinated to solvent making the complex less symmetric. Additionally such a change of coordination environment by a ligand with the retention of four uniformly coordinated geometries in tetranuclear zinc clusters is known in the literature [3a]. The presence of hexa and tetra coordinated zinc makes our clusters structurally unique. Thus, our clusters possess a new motif containing four coordinated zinc centers along with six coordinated zinc centers. Recently a tetranuclear oxo-cluster of zinc has been reported and it was observed that molecular oxygen is responsible for the formation of such clusters from organo-zinc reactions [2d]. In organo-zinc complexes there is a Zn–C bond, leaving scope for reactions with molecular oxygen, whilst in our reactions the oxo or hydroxo species are generated from water molecules in the sol-

Table 5
Selected internuclear distances (in Å) and angles (in °) in **7**

	Bond distances		Bond angles
Zn(1)–O(1)	1.909(3)	O(1)–Zn(1)–O(13)	118.10(15)
Zn(1)–O(8)	1.956(4)	O(1)–Zn(1)–O(10)	112.00(16)
Zn(1)–O(10)	1.944(4)	O(13)–Zn(1)–O(10)	107.05(19)
Zn(1)–O(13)	1.930(4)	O(1)–Zn(1)–O(8)	111.60(15)
Zn(2)–O(1)	1.924(3)	O(13)–Zn(1)–O(8)	104.38(18)
Zn(2)–O(3)	1.912(4)	O(10)–Zn(1)–O(8)	102.3(2)
Zn(2)–O(4)	1.966(4)	O(3)–Zn(2)–O(1)	120.01(14)
Zn(2)–O(9)	1.983(4)	O(3)–Zn(2)–O(4)	106.50(17)
Zn(3)–O(1)	1.935(3)	O(1)–Zn(2)–O(4)	112.91(15)
Zn(3)–O(5)	1.958(4)	O(3)–Zn(2)–O(9)	106.89(17)
Zn(3)–O(6)	1.928(4)	O(1)–Zn(2)–O(9)	110.36(15)
Zn(3)–O(11)	2.046(4)	O(4)–Zn(2)–O(9)	97.73(17)
Zn(4)–O(1)	2.007(3)	O(6)–Zn(3)–O(1)	121.81(14)
Zn(4)–O(2)	2.104(4)	O(6)–Zn(3)–O(5)	112.24(17)
Zn(4)–O(7)	2.257(4)	O(1)–Zn(3)–O(5)	117.11(16)
Zn(4)–O(12)	2.104(3)	O(6)–Zn(3)–O(11)	97.16(16)
Zn(4)–O(14)	2.195(3)	O(1)–Zn(3)–O(11)	105.70(15)
Zn(4)–O(15)	2.077(3)	O(5)–Zn(3)–O(11)	96.53(17)
Zn(5)–O(16)	1.912(3)	O(1)–Zn(4)–O(15)	170.65(14)
Zn(5)–O(24)	1.936(4)	O(1)–Zn(4)–O(2)	96.22(14)
Zn(5)–O(25)	1.946(4)	O(15)–Zn(4)–O(2)	87.90(14)
Zn(5)–O(27)	1.968(4)	O(1)–Zn(4)–O(12)	99.72(13)
Zn(6)–O(16)	1.919(3)	O(15)–Zn(4)–O(12)	88.36(13)
Zn(6)–O(20)	1.949(4)	O(2)–Zn(4)–O(12)	93.54(15)
Zn(6)–O(21)	1.912(4)	O(1)–Zn(4)–O(14)	79.68(12)
Zn(6)–O(28)	1.982(4)	O(15)–Zn(4)–O(14)	92.02(13)
Zn(7)–O(16)	1.936(3)	O(2)–Zn(4)–O(14)	89.15(14)
Zn(7)–O(17)	1.946(4)	O(12)–Zn(4)–O(14)	177.29(15)
Zn(7)–O(19)	1.979(4)	O(1)– Zn(4)–O(7)	92.12(14)
Zn(7)–O(26)	2.036(4)	O(15)–Zn(4)–O(7)	83.06(14)
Zn(8)–O(16)	2.004(3)	O(2)–Zn(4)–O(7)	170.02(15)
Zn(8)–O(18)	2.224(4)	O(12)–Zn(4)–O(7)	90.45(14)
Zn(8)–O(22)	2.096(4)	O(14)–Zn(4)–O(7)	86.94(14)
Zn(8)–O(23)	2.082(4)	O(16)–Zn(5)–O(24)	117.06(15)
Zn(8)–O(29)	2.216(4)	O(16)–Zn(5)–O(25)	112.12(16)
Zn(8)–O(30)	2.068(3)	O(24)–Zn(5)–O(25)	107.84(18)
C(1)–O(2)	1.252(6)	O(16)–Zn(5)–O(27)	111.51(16)
C(1)–O(3)	1.270(6)	O(24)–Zn(5)–O(27)	104.48(18)
C(9)–O(4)	1.258(6)	O(25)–Zn(5)–O(27)	102.60(19)
C(9)–O(5)	1.269(6)	O(21)–Zn(6)–O(16)	121.73(14)
C(17)–O(6)	1.268(6)	O(21)–Zn(6)–O(20)	105.38(18)
C(17)–O(7)	1.237(6)	O(16)–Zn(6)–O(20)	110.93(16)
C(25)–O(12)	1.239(6)	O(21)–Zn(6)–O(28)	106.45(17)
C(25)–O(13)	1.257(6)	O(16)–Zn(6)–O(28)	110.71(15)
C(41)–O(10)	1.248(6)	O(20)–Zn(6)–O(28)	99.16(17)
C(41)–O(11)	1.226(6)	O(16)–Zn(7)–O(17)	123.03(15)
C(53)–O(17)	1.283(7)	O(16)–Zn(7)–O(19)	115.12(15)
C(53)–O(18)	1.243(7)	O(17)–Zn(7)–O(19)	112.66(18)
C(61)–O(19)	1.245(7)	O(16)–Zn(7)–O(26)	104.59(15)
C(61)–O(20)	1.240(7)	O(17)–Zn(7)–O(26)	98.54(17)
C(69)–O(21)	1.276(6)	O(19)–Zn(7)–O(26)	96.94(16)
C(69)–O(22)	1.238(6)	O(16)–Zn(8)–O(30)	167.77(14)
C(85)–O(25)	1.244(6)	O(16)–Zn(8)–O(23)	100.61(13)
C(85)–O(26)	1.234(6)	O(30)–Zn(8)–O(23)	90.80(14)
C(93)–O(27)	1.236(6)	O(16)–Zn(8)–O(22)	96.77(14)
C(93)–O(28)	1.246(6)	O(30)–Zn(8)–O(22)	86.66(15)
		O(23)–Zn(8)–O(22)	94.31(16)
		O(16)–Zn(8)–O(29)	80.32(13)
		O(30)–Zn(8)–O(29)	88.00(14)
		O(23)–Zn(8)–O(29)	175.93(15)
		O(22)–Zn(8)–O(29)	89.51(15)
		O(16)–Zn(8)–O(18)	90.48(15)
		O(30)–Zn(8)–O(18)	85.28(15)
		O(23)–Zn(8)–O(18)	89.01(16)
		O(22)–Zn(8)–O(18)	171.32(16)
		O(29)–Zn(8)–O(18)	87.01(15)

vent and hydrated salts, as these reactions proceed under nitrogen atmosphere and the use of dry solvents led to poor yields of the clusters. DMSO, being an aprotic coordinating solvent, allows the deprotonation of water in basic medium whereas in methanol the labile hydrogen is in a large excess; this thus facilitates the formation of neutral dinuclear species. The formation of the mononuclear aqua complex in the case of **1** suggests that not only the reaction conditions but also the substituent controls the formation of different zinc complexes.

5. Supplementary data

Crystallographic details of the compounds in the form of CIF files are available and they have the CCDC numbers 668242, 668243, 676945–676948 and 612955. These data can be obtained free of charge via http://www.ccdc.cam.ac.uk/conts/retrieving.html or from the Cambridge Crystallographic Data Centre, 12 Union Road, Cambridge CB2 1EZ, UK; fax: (+44) 1223-336-033; or e-mail: deposit@ccdc.cam.ac.uk.

Acknowledgement

The authors thank the Department of Science and Technology, New Delhi, India, for financial assistance.

References

[1] (a) B.-H. Ye, X.-Y. Li, I.D. Williams, X.-M. Chen, Inorg. Chem. 41 (2002) 6426;
(b) B. Singh, J.R. Long, F. Fabrizi de Biani, D. Gatteschi, P. Stavropoulos, J. Am. Chem. Soc. 119 (1997) 7030.
[2] (a) Y. Wei, H. Hou, L. Li, Y. Fan, Y. Zhu, Cryst. Growth Des. 5 (2005) 1405;
(b) M. Alexioun, E. Katsoulakou, C. Dendrinou-Samara, C.P. Raptopoulou, V. Psycharis, E. Manessi-Zoupa, S.P. Perlepes, D.P. Kessissoglou, Eur. J. Inorg. Chem. (2005) 1964;
(c) A. Exleben, J. Hermann, J. Chem. Soc., Dalton Trans. (2000) 569;
(d) J. Lewiński, W. Bury, M. Dutkiewicz, M. Maurin, I. Justyniak, J. Lipkowski, Angew. Chem., Int. Ed. 47 (2008) 573;
(e) C.S. McCowan, T.L. Groy, M.T. Caudle, Inorg. Chem. 41 (2002) 1120.
[3] (a) D.J. Darensbourg, J.R. Wildeson, J.C. Yarbrough, Inorg. Chem. 41 (2002) 973;
(b) T. Tsuruta, Y. Kawakami, Tetrahedron 29 (1973) 1179;
(c) K. Soga, E. Imai, I. Hattori, Polym. J. (Japan) 13 (1981) 407;
(d) M. Super, E. Berluche, C. Costello, E. Beckman, Macromolecules 30 (1997) 368;
(e) D.J. Darensbourg, M.S. Zimmer, Macromolecules 32 (1999) 2137.
[4] A. Karmakar, R.J. Sarma, J.B. Baruah, Inorg. Chem. Commun. 9 (2006) 1169.
[5] (a) A. Karmakar, R.J. Sarma, J.B. Baruah, Eur. J. Inorg. Chem. (2007) 643;
(b) A. Karmakar, R.J. Sarma, J.B. Baruah, Eur. J. Inorg. Chem. (2006) 4673.
[6] N. Barooah, A. Karmakar, R.J. Sarma, J.B. Baruah, Inorg. Chem. Commun. 9 (2006) 1251.
[7] T. Ohmura, W. Mori, T. Takei, T. Ikeda, A. Maeda, Mater. Sci. – Poland 23 (2005) 729.
[8] W. Clegg, D. Harbron, C. Holman, P. Hunt, I. Little, B. Straughan, Inorg. Chim. Acta 186 (1991) 51.
[9] J. Lewinski, W. Bury, T. Kopec, E. Tratkiewicz, I. Justyniak, J. Lipkowski, Eur. J. Inorg. Chem. (2005) 3414.

system. In this work, we present the synthesis, characterization and photophysical studies of monometallic and bimetallic complexes of rhenium(I) and osmium(II) complexes.

2. Experimental

2.1. Materials

$Re_2(CO)_{10}$ (Alfa), $(NH_4)_2OsCl_6$ (Aldrich), 2,2′-bipyridine (Merck), 4,4′-bipyridine (Fluka), $AgCF_3SO_3$ (Alfa) and NH_4PF_6(Alfa) were used as received. All solvents used for the synthesis were of reagent grade and for spectral measurements spectral grade solvents were used.

2.2. Physical Measurements

UV–Vis spectra were recorded on an Analtikjena Specord S100 spectrophotometer and emission spectra were measured in a JASCO FP6300 spectrofluorimeter. All the samples used for emission were purged with dry nitrogen gas for about 20 min. The emission quantum yield was calculated using $[Ru(bpy)_3]^{2+}$ as a standard, which has a quantum yield of 0.062 in degassed CH_3CN. IR spectra were measured using a JASCO FT-IR spectrophotometer. The samples were recorded in the form of KBr pellets. ^1H NMR spectra were recorded on a Bruker 300 MHz NMR spectrometer using $(CD_3)_2SO$ as the solvent. All the mass spectra were recorded using a Quattro LC triple-quadrupole mass spectrometer (Micromass, Manchester, UK) interfaced to an (Electro Spray ionization) ESI source; data acquisition was done under the control of MASSLYNX software (version 3.2). The ESI capillary voltage was maintained between 4.0 and 4.2 kV and the cone voltage kept at 25 V. Nitrogen was used as the desolvation and nebulization gas. The source and desolvation temperatures were 100 °C.

2.3. Electrochemistry

The redox potentials of the complexes were determined by cyclic voltammetric and differential pulse voltammetric techniques using an EG & G Princeton Applied Research Potentiostat/Galvanostat Model 273 A. Measurements were performed by purging the solution in acetonitrile (spectroscopic grade) by dry nitrogen gas for 30 min. The supporting electrolyte was 0.1 M TBAP, Pt was the working electrode, and the Ag/AgCl was the reference electrode.

2.4. Lifetime and transient measurements

The excited state lifetime measurements for all the complexes were made, after degassing the solutions with argon for 30 min, using the time correlated single photon counting (TCSPC) technique and the details are given in previous reports [49]. Transient absorption measurements were made with the laser flash photolysis technique as described elsewhere [49a].

2.5. Synthesis

The complexes $Re^I(CO)_5Br$ [50], $(bpy)(CO)_3ReBr$ [51], $[(bpy)(CO)_3Re(4,4'\text{-bpy})](PF_6)$ [52], $[\{(bpy)(CO)_3Re\}_2(4,4'\text{-bpy})](PF_6)_2$ [52], $[Cl(bpy)_2Os(4,4'\text{-bpy})](PF_6)$ [53] and $[Cl(bpy)_2Os(4,4'\text{-bpy})Os(bpy)_2Cl](PF_6)_2$ [53] were synthesized according to literature procedures.

2.6. $[(CO)_3(bpy)Re(4,4'\text{-bpy})Os(bpy)_2Cl](PF_6)_2$

$Re(CO)_3(bpy)Br$ (0.05 g, 0.099 mmol) and $AgCF_3SO_3$ (0.025 g, 0.099 mmol) were dissolved in MeOH (20 mL) and reluxed for 1 h under a nitrogen blanket. A white precipitate of AgBr was formed. The solution was cooled and filtered to remove the AgBr. To the filtrate was added $[Os(bpy)_2Cl(4,4'\text{-bpy})](PF_6)$ (0.041 g, 0.049 mmol) and the resulting mixture was refluxed for 8 h under an inert atmosphere. After completion of the reaction, the solvent was evaporated under reduced pressure and the residue was dried. The product was separated by column chromatography using alumina as the solid support and a mixture of CH_3CN/toluene as the eluent. A yellow band of unreacted rhenium(I) eluted first, and then increasing the composition of CH_3CN leads to the elution of unreacted $[Os(bpy)_2Cl(4,4'\text{-bpy})](PF_6)$. Finally a brownish band of the product $[(CO)_3(bpy)Re(4,4'\text{-bpy})Os(bpy)_2Cl](PF_6)_2$ got eluted. Yield 64%, ^1H NMR (CD_3COCD_3, δ in ppm): 9.4 (d, 6H), 8.7 (d, 4H), 8.6 (d, 6H), 8.4 (t), 8.0 (t, 6H), 7.7 (m, 6H). ES-MS: m/z = 1265 ($M-PF_6$). IR and electronic spectral data and redox potentials are given in Tables 1 and 2.

3. Results and Discussion

3.1. Preparation

The schematic structures of the complexes that are the focus of the present investigation are illustrated in Chart 1. The rhenium(I) complexes [52], **I**, **II** and osmium(II) complexes [53] **III**, **IV** were prepared by reported procedures. The rhenium(I)–osmium(II) heterobimetallic complex **V** was prepared by the complex as metal/complex as ligand approach [54]. The heterobinuclear complex was synthesized by reacting the monometallic osmium complex carrying the bridging ligand 4,4′-bipyridine with the rhenium precursor complex $[(CO)_3(bpy)Re(CH_3CN)](CF_3SO_3)$. These complexes were characterized by NMR, ESIMS, FT-IR, cyclic voltammetry, UV–Vis and luminescence spectroscopy.

3.2. Infra red spectra

The IR spectral data of the monometallic and bimetallic complexes are gathered in Table 1. The infra red spectra of the rhenium(I) complexes are characterized by intense carbonyl stretching frequencies, ν(CO). Three ν(CO) stretching frequencies are in general observed between 1900 cm^{-1} and 2040 cm^{-1}, corresponding to the facial orientation. The highest energy CO stretching band appears as a very sharp band around 2030 cm^{-1} and the other two bands are relatively broad and overlap considerably. When we compare the ν(CO) stretching frequencies of rhenium complexes **I** and **II** with the heterobimetallic complex **V**, little change is observed. This indicates that the interaction between the Re(I) unit and Os(II) unit is weak.

3.3. ESIMS

The monometallic and bimetallic complexes are characterized by the ESIMS spectral technique. The m/z values for complexes **I**, **III** and **V** are 582, 693 and 1264, respectively, corresponding to the loss of a PF_6^- ion. Other peaks are assigned to the loss of 4,4′-bipyridine and CO moieties. The ESIMS spectra of complexes **III** and **V** are shown in Figs. S1 and S2.

3.4. Electrochemistry

The electrochemical behavior of the monometallic and bimetallic complexes is studied in acetonitrile solution, and the relevant redox potentials are listed in Table 1. For the rhenium(I) complexes the oxidation occurs at 1.73 V. The oxidation/reduction potentials are not observed for the Re(I) complexes at a scan rate higher than 50 mV s^{-1}. In the cathodic region of the cyclic voltammogram, the

Table 1
IR spectral and electrochemical data of the monometallic and bimetallic complexes **I–V**

Complex	$E_{1/2}$ (V) $Os^{3+/2+}$	E_p (V) $Re^{2+/+}$	$E_{1/2}$ (V)			ν (CO) cm^{-1}
			$Re^{+/0}$	$bpy^{0/-}$	4,4′-$bpy^{0/-}$	
I		1.75	−1.27	−1.09	−0.96	2034, 1936, 1920
II		1.72	−1.26	−1.10	−0.89	2032, 1940, 1919
III	0.30			−1.50		
IV	0.31			−1.49		
V	0.35	1.71	−1.10	−1.50	−0.84	2028, 1936, 1918

Table 2
Absorption and photophysical data of complexes **I–V** in CH_3CN at room temperature

Complex	λ_{max} ($\varepsilon/10^4$ M^{-1} cm^{-1}) nm	$\lambda_{em,max}$ nm	τ (ns)	Φ_{em}	k_r 10^4	k_{nr} 10^6
I	306 (1.5), 348 (0.5)	580	240	0.090	1.50	36.0
II	268 (4.8), 306 (3.9), 350 (1.23)	580	270	0.029	7.80	35.0
III	294 (5.9), 408 (1.7), 511 (1.5)	690	56	0.0065	11.6	17.7
IV	296 (10.5), 408 (3.1), 512 (2.9)	690	56	0.0034	6.10	17.7
V	295 (7.4), 346 (2.0), 425 (1.8), 510 (1.7)	690	80	0.0021	2.60	12.5

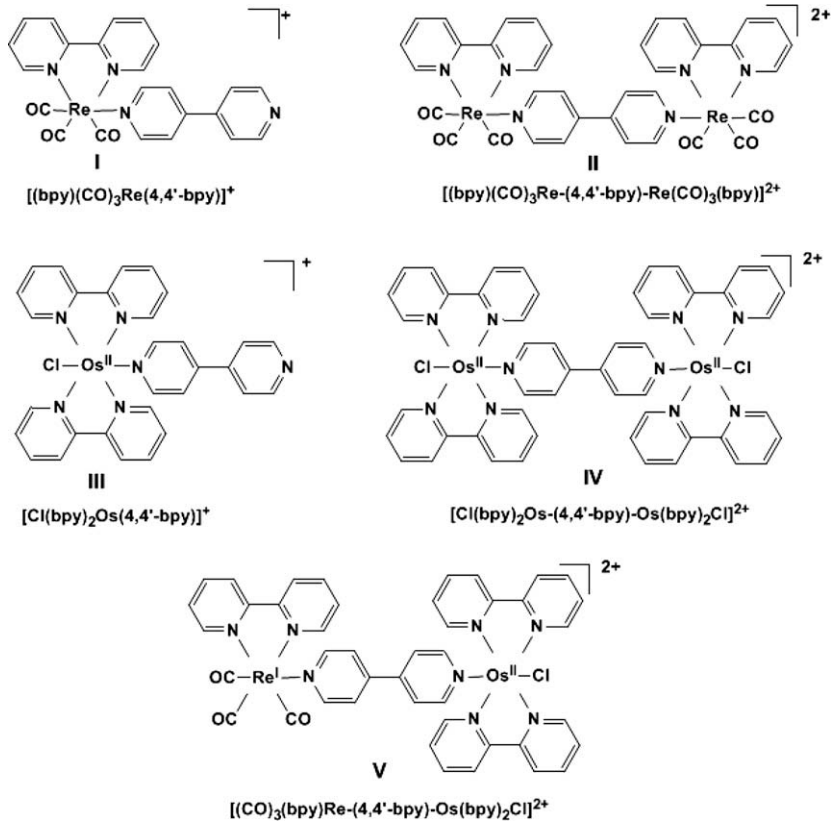

Chart 1. Structure of the complexes.

reduction at a less negative potential can be assigned to that of the bridging ligand. An irreversible wave at −1.20 V can be assigned to the $Re^{I/0}$ reduction. The osmium complexes **III** and **IV** show reversible waves with $E_{1/2}$ values of 0.30 and 0.31 V, respectively, with the anodic and cathodic peak separation (ΔE_p) of 72 mV. The cyclic voltammogram of complex **III** is shown in Fig. 1. In the case of homobimetallic complexes the oxidation potential of the two metal centers is hardly distinguishable. In the cathodic region reduction of the ligands occurs, and the first reduction occurs at a considerably lower potential (−0.84 V), which can be assigned to the reduction of bridging ligand, and the other two reductions at large negative potentials can be assigned to the reduction of the 2,2′-bipyridine ligands.

In the case of the rhenium(I)–osmium(II) heterobimetallic complex **V**, the $E_{1/2}$ value of the $Os^{II/III}$ couple is slightly shifted to a more positive region, which indicates the attachment of the electron withdrawing Re(I) unit to the osmium(II) unit (Fig. 1). The osmium unit shows a nice reversible wave having an $E_{1/2}$ value of 0.35 V. The rhenium(I) oxidation occurs at 1.71 V. In the negative part of the cyclic voltammogram, the bridging ligand reduction

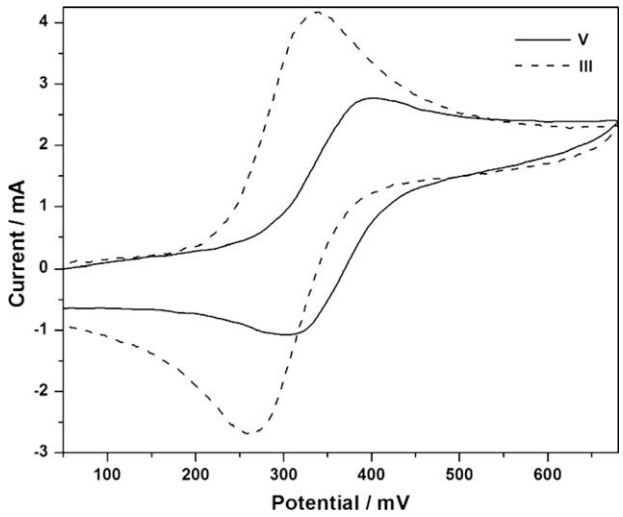

Fig. 1. Cyclic voltammogram of **III** (---) and **V** (—) recorded in CH_3CN at RT with 0.1 M TBAP.

gets merged with the rhenium(I) reduction, which occurs at −1.10 V. As seen in complex **I**, the 2,2′-bipyridine ligand reductions occur at higher negative potentials.

3.5. Absorption spectra

The absorption spectra for all the complexes are recorded in CH_3CN at room temperature and the data are summarized in Table 2. The absorption spectrum of **II** is shown in Fig. 2. For the rhenium(I) monometallic **I** and homobimetallic **II** complexes, the peak in the high energy region is assigned to a ligand centered $\pi \rightarrow \pi^*$ transition and a ^{1}MLCT transition is observed in the region 340–350 nm. For the osmium(II) complexes **III** and **IV**, the intense peak observed in the UV region can be assigned to a ligand centered $\pi \rightarrow \pi^*$ transition occurring in the bipyridine ligand. The bands seen in the visible region between 400 and 560 nm are assigned to spin-allowed ^{1}MLCT transitions and relatively less intense bands seen at wavelengths longer than 560 nm are attributed to a spin-forbidden ^{3}MLCT transition (Fig. 2). Since osmium is a heavy metal, enhanced spin–orbit coupling occurs, which leads to the spin-forbidden ^{3}MLCT transition occurring in the longer wavelength region. In the case of the Re–Os heterobimetallic complex **V**, a peak at *ca.* 348 nm is seen due to the Re(d π) $\rightarrow \pi^*$ MLCT transition and bands in the region 400–550 nm correspond to a Os(d π) $\rightarrow \pi^*$ ^{1}MLCT transition. A relatively less intense peak seen at *ca.* 656 nm is assigned to a ^{3}MLCT transition, arising out of the direct transition from the ground state to the triplet state, owing to spin–orbit coupling seen in osmium complexes. On comparing the absorption spectrum of the Re–Os heterobimetallic complex **V** with that of the rhenium(I) and osmium(II) homobimetallic complexes **II** and **IV**, the bands seen are similar to the latter complexes, except the band around 420 nm is shifted (Fig. 2). This indicates that in the heterobimetallic complex **V** there is only less interaction between the two metal centers.

3.6. Emission

The emission spectra of all the complexes were recorded in CH_3CN at room temperature. The rhenium(I) monometallic complex **I** and bimetallic complex **II** show an emission at *ca.* 580 nm and the emission occurs from a low lying ^{3}MLCT state upon excitation at 348 nm (Fig. 3). When the osmium(II) complexes **III** and **IV** are excited at the wavelength corresponding to the ^{1}MLCT absorption, they display an emission maximum at 690 nm from the ^{3}MLCT state. The Re–Os heterobimetallic complex **V** also shows emission at *ca.* 690 nm, indicating emission from the ^{3}MLCT state of osmium (Fig. 3). When complex **V** is excited at 290 nm, where the ligand centered absorption is predominant, it still shows an emission at 690 nm (Fig. 4). This indicates that irrespective of the excitation wavelength, complex **V** displays an emission at 690 nm from the osmium unit. Since in complex **V**, the lowest energy level may be the ^{3}MLCT state of osmium(II), the emission takes place from osmium. The quenching of emission from the rhenium(I) chromophore at 580 nm on excitation at 290 and 348 nm indicates that an energy transfer process takes place from the rhenium(I) chromophore to osmium(II). The uncorrected excitation spectrum of **V** is shown in Fig. 5, which closely matches the absorption spectrum. This indicates that no photochemical reaction takes place upon irradiation.

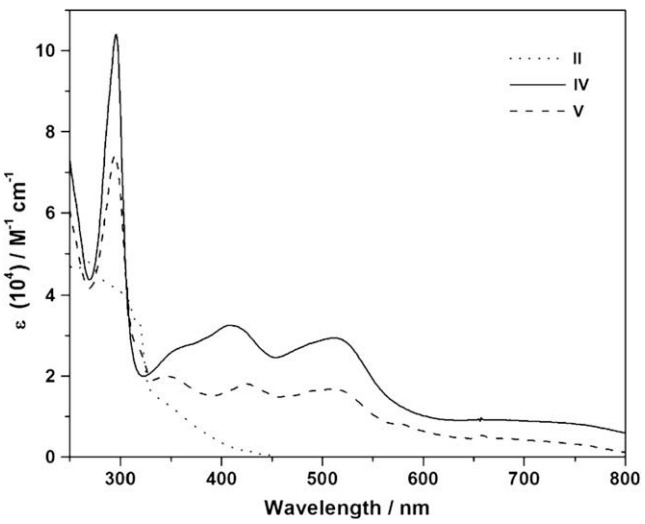

Fig. 2. Absorption spectra of complexes **II** (···), **IV**(—) and **V**(---) in CH_3CN at room temperature.

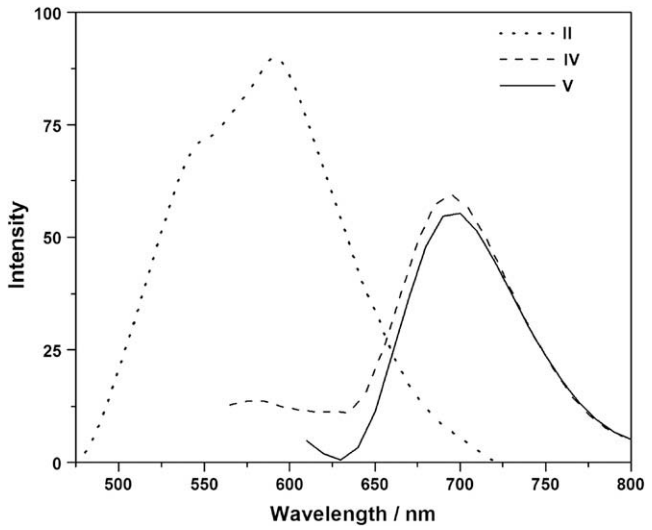

Fig. 3. Emission spectra of complexes **II** (···), **IV**(---) and **V**(—) in CH_3CN at room temperature.

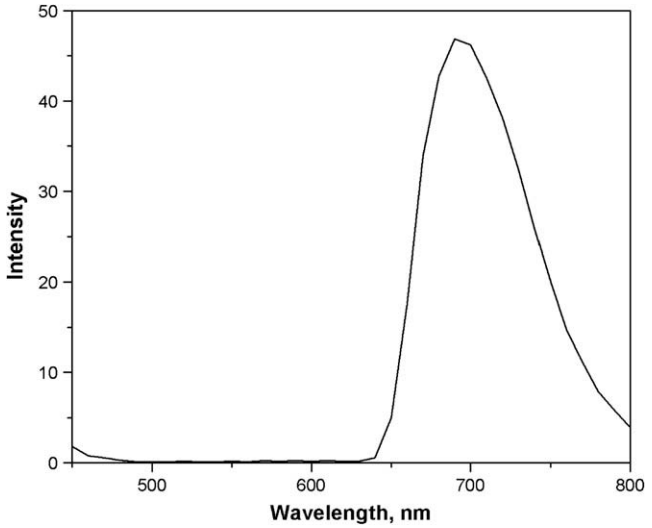

Fig. 4. Emission spectrum of complex **V** in CH_3CN at room temperature, (λ_{ex} = 290 nm).

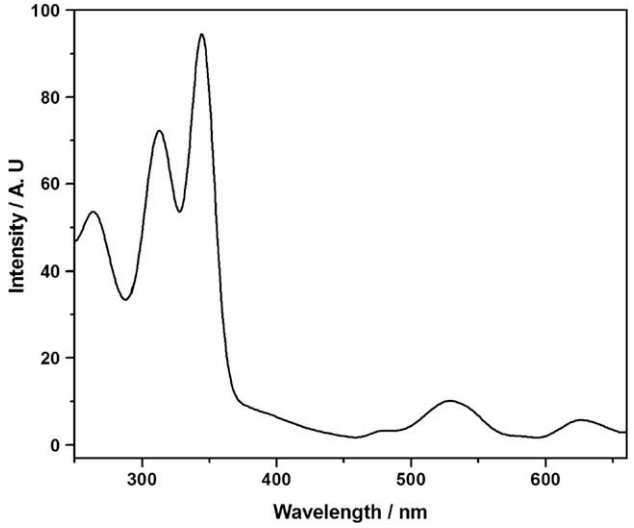

Fig. 5. Excitation spectrum (uncorrected) of **V**.

3.7. Excited state lifetime

The excited state lifetime of all the complexes were recorded in acetonitrile at 298 K and the results are given in Table 2. The excited state lifetime data show that the lifetimes of the rhenium(I) complexes are higher than the osmium(II) complexes. This is because in the osmium(II) complexes, the energy difference between the ground and excited ^{3}MLCT state is less. According to the energy gap law, the non-radiative rate increases exponentially with a decreasing energy gap between the ground state and excited state. So this leads to enhanced non-radiative decay and a decreased lifetime for the osmium(II) complexes. The rhenium(I) complexes **I** and **II** have excited state lifetimes of 240 and 270 ns, respectively. The excited state lifetimes observed here are in accordance with the reported values [52]. The osmium(II) complexes **III** and **IV** have excited state lifetimes of 56 ns each. The lifetimes of the osmium(II) complexes **III** and **IV** are comparable to that of $[Os(bpy)_3]^{2+}$, which has an excited state lifetime of 49 ns in CH_3CN [55]. The rhenium(I)–osmium(II) heterobimetallic complex **V** has an excited state lifetime of 80 ns. The lifetime data indicates that the Re–Os heterobimetallic complex behaves more like the osmium(II) complex.

When we look into the luminescence quantum yield values of the complexes (Table 2), the values are very much higher for the rhenium(I) complexes **I** and **II**. The rhenium(I)–osmium(II) heterobimetallic complex also has a quantum yield similar to that of the osmium(II) complexes. From the excited state lifetime (τ) and quantum yield (Φ_{em}), the radiative and non-radiative rate constants can be calculated using Eqs. (1) and (2):

$$k_r = \Phi_{em}/\tau \quad (1)$$

$$k_{nr} = 1/\tau - k_r \quad (2)$$

The radiative (k_r) and non-radiative (k_{nr}) rate constants for all the complexes are given in Table 2.

The experimental energy transfer rate constant can be calculated using the following equation:

$$k_{et} = (1/\tau) - (1/\tau^0) \quad (3)$$

where τ^0 and τ are the phosphorescence lifetime of **I** and quenched lifetime of the Re(I) component in **V**, respectively. The energy transfer rate constant is found to be 8.7×10^7 s^{-1}.

3.8. Transient spectra

The transient spectra of the complexes were recorded in acetonitrile at room temperature. The transient spectra of the rhenium(I) complexes **I** and **II** show a broad absorption from the near UV to mid-visible region, with higher intensity in the region 370–390 nm (Fig. 6). This corresponds to the formation of the Re^{II}(bpy$^{\cdot}$) excited state [52a]. The bleach, with a maximum occurring at 580 nm, corresponds to the emission of light from the ^{3}MLCT state. The transient spectrum of the osmium(II) complex **III** is shown in Fig. 7. A bleach is observed in the region 450–550 nm with the maximum occurring at 510 nm. This corresponds to the loss of the ground state MLCT absorption of osmium(II). When we compare the transient spectrum of the rhenium(I)–osmium(II) heterobimetallic complex **V** (Fig. 8) with the osmium(II) monometallic complex **III** (Fig. 7), a similar ground state bleach in the region 480–560 nm is observed for the heterobimetallic complex **V**. On the contrary, a broad absorption is seen in this region in the transient spectra of the rhenium(I) complexes **I** and **II** (Figs. 6 and 8). These spectral features indicate the occurrence of an energy

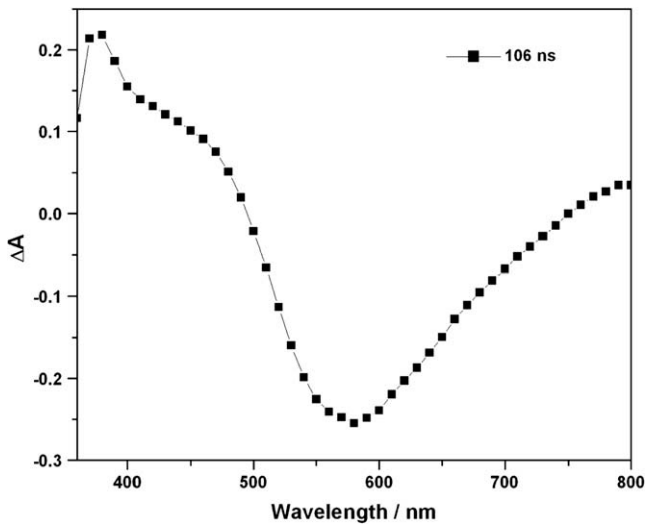

Fig. 6. Transient absorption spectrum of **I** recorded in argon degassed CH_3CN upon excitation at 355 nm at RT. Recorded at 106 ns after excitation.

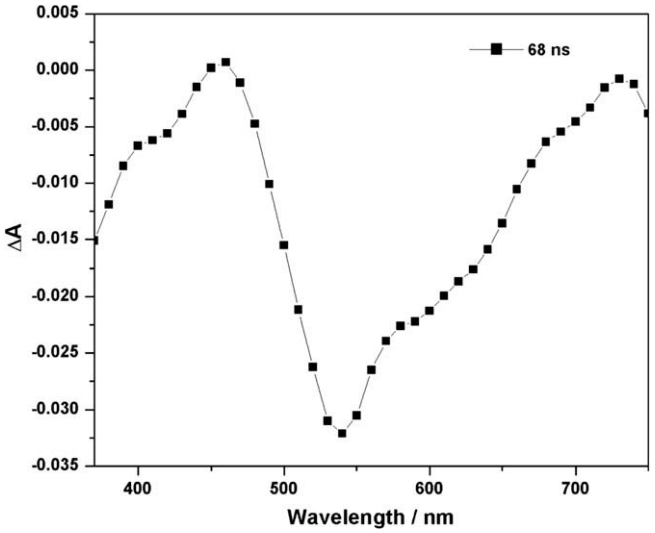

Fig. 7. Transient absorption spectrum of **III** recorded in argon degassed CH_3CN upon excitation at 355 nm at RT. Recorded at 68 ns after excitation.

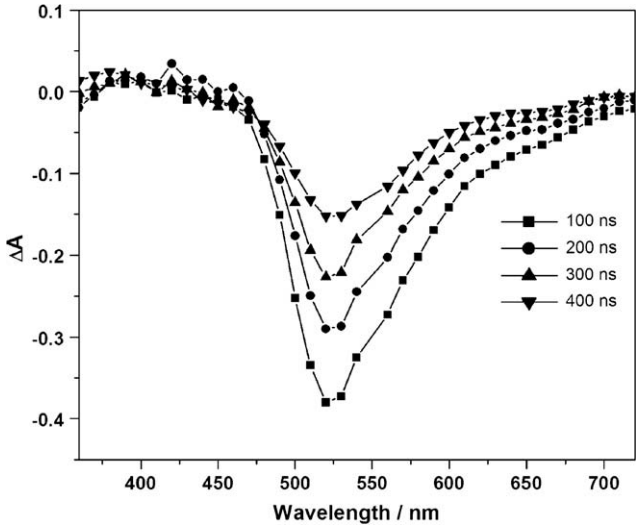

Fig. 9. Transient absorption spectra of **V** recorded at various time intervals in CH_3CN at room temperature.

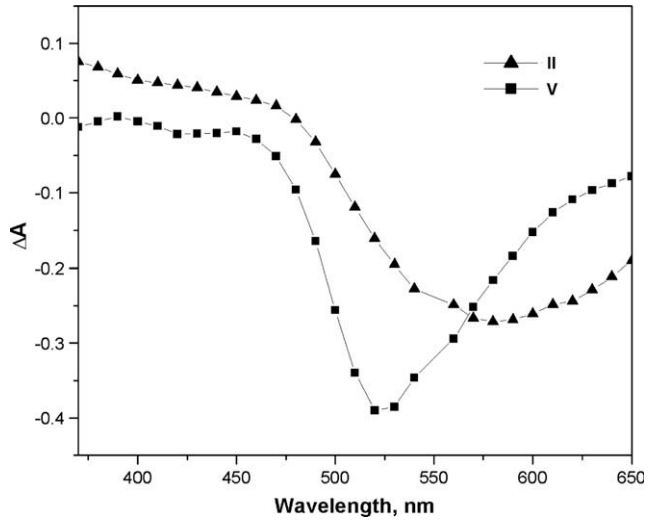

Fig. 8. Transient absorption spectra of **II** (-▲-) and **V** (-■-) recorded in argon degassed CH_3CN upon excitation at 355 nm at RT.

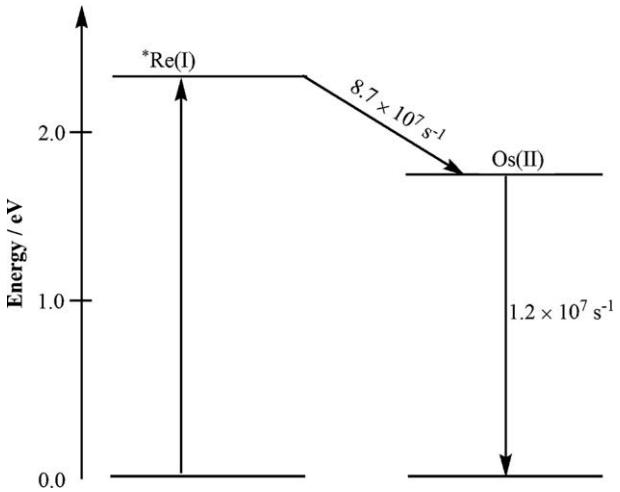

Fig. 10. Energy level diagram depicting the energy transfer from *Re(I) to Os(II) in **V**.

transfer process from the ^{3}MLCT state of *Re(I) to that of the osmium(II) chromophore in **V**. The transient absorption spectra of **V** recorded at various time intervals is shown in Fig. 9. Iha et al. [47b] have studied a series of bimetallic Re(I)–Os(II) complexes, $[(CO)_3(phen)ReLOs(trpy)(bpy)]^{3+}$ (phen = 1,10-phenanthroline, trpy = 2,2′:6′,2″-terpyridine and L = 4,4′-bipyridine (4,4′-bpy), *trans*-1,2-bis(4-pyridyl)ethylene (*t*-bpe) or 1,2-bis(4-pyridyl)ethane (bpa)) and found that an intramolecular energy transfer takes place from *Re(I) to Os(II) with an energy transfer rate constant $k_{en} > 4 \times 10^7\ s^{-1}$. Thus the value of k_{en} calculated in this work is close to the value reported by Iha et al. Also in Ru–Os heterobimetallic complexes, the bleach seen in the transient spectra is due to the decay of the ground state MLCT of osmium(II) because of energy transfer from *Ru(II) [23d,56]. Even in the case of Re(I)–Ru(II) heterobimetallic complexes, an intramolecular energy transfer occurs from *Re(I) to Ru(II) [57] and it is in the range $1.7 \times 10^8\ s^{-1}$–$1.2 \times 10^9\ s^{-1}$ for the complexes studied by Furue et al. [58] Based on the spectral features, a possible energy level diagram depicting the energy transfer process is shown in Fig. 10.

4. Conclusions

A series of monometallic and bimetallic complexes of rhenium(I) and osmium(II) **I**–**V** have been synthesized and characterized by various spectral techniques. The electrochemical and photophysical properties of all the complexes have been studied. From the emission and transient spectral studies it is found that an intramolecular energy transfer occurs from *Re(I) to Os(II). The energy transfer rate constant is found to be $8.7 \times 10^7\ s^{-1}$. The occurrence of energy transfer from Re(I) to Os(II) implies that this heterobinuclear complex has the potential to act as a light harvesting antenna.

Acknowledgements

M.V. and S.R. thank the Department of Science and Technology (DST), New Delhi, India for sanctioning a Project (No. SR/S1/IC-30/2002 dated 08-05-2003 and 15-07-2003) to carry out this research work.

References

[1] (a) H. Ringsdorf, B. Schlarb, J. Venzmer, Angew. Chem., Int. Ed. Engl. 27 (1988) 113;
(b) J.-M. Lehn, Angew. Chem., Int. Ed. Engl. 27 (1988) 89.
[2] W.R. Browne, N.M. O'Boyle, J. Mc Garvey, J.G. Vos, Chem. Soc. Rev. 34 (2005) 641.
[3] (a) H. Hofmeier, U.S. Schubert, Chem. Soc. Rev. 33 (2004) 373;
(b) F. Würthner, C. You, C.R. Saha-Möller, Chem. Soc. Rev. 33 (2004) 133.
[4] M. Beley, S. Chodorowski, J.-P. Collin, J.-P. Sauvage, L. Flamigni, F. Barigelletti, Inorg. Chem. 33 (1994) 2543.
[5] K.J. Brewer, L.M. Vogler, Inorg. Chem. 35 (1996) 818.
[6] C. Chiorboli, S. Fracasso, M. Ravaglia, F. Scandola, S. Campagna, K.L. Wouters, R. Konduri, F.M. MacDonnell, Inorg. Chem. 44 (2005) 8368.
[7] S. Serroni, S. Campagna, R.S. Nascone, G.S. Hanan, G.J.E. Davidson, J.-M. Lehn, Chem. Eur. J. 5 (1999) 3523.
[8] A. Juris, L. Prodi, A. Harriman, R. Ziessel, M. Hissler, A. El-ghayoury, F. Wu, E.C. Riesgo, R.P. Thummel, Inorg. Chem. 39 (2000) 3590.
[9] F. Weldon, L. Hammarström, E. Mukhtar, R. Hage, E. Gunneweg, J.G. Haasnoot, J. Reedijk, W.R. Browne, A.L. Guckian, J.G. Vos, Inorg. Chem. 43 (2004) 4471.
[10] (a) M.I.J. Polson, F. Loiseau, S. Campagna, G.S. Hanan, Chem. Commun. (2006) 1301;
(b) M. Venturi, F. Marchioni, V. Balzani, D.M. Opris, O. Henze, A.D. Schluter, Eur. J. Org. Chem. (2003) 4227.
[11] (a) B. O'Regan, M. Grätzel, Nature 353 (1991) 737;
(b) M. Grätzel, Comments Inorg. Chem. 12 (1991) 93;
(c) A. Hagfeldt, M. Grätzel, Chem. Rev. 95 (1995) 49;
(d) J.N. Demas, E.W. Harris, C.M. Flynn Jr., D. Diemente, J. Am. Chem. Soc. 97 (1975) 3838.
[12] H. Zabri, F. Odobel, S. Altobello, S. Caramori, C.A. Bignozzi, J. Photochem. Photobiol. A 166 (2004) 99.
[13] P.G. Hoertz, T.E. Mallouk, Inorg. Chem. 44 (2005) 6828.
[14] C.G. Garcia, J.F. de Lima, N.Y.M. Iha, Coord. Chem. Rev. 196 (2000) 219.
[15] (a) N. Sabbatini, M. Guardigli, J.-M. Lehn, Coord. Chem. Rev. 123 (1993) 201;
(b) C. Devadoss, P. Bharathi, J.S. Moore, J. Am. Chem. Soc. 118 (1996) 9635;
(c) L.M. Dupray, M. Devenney, D.R. Striplin, T.J. Meyer, J. Am. Chem. Soc. 119 (1997) 10243.
[16] (a) P.G. Van Patten, A.P. Shreve, J.S. Lindsey, R.J. Donohoe, J. Phys. Chem. B 102 (1998) 4209;
(b) V. Balzani, S. Campagna, G. Denti, A. Juris, S. Serroni, M. Venturi, Acc. Chem. Res. 31 (1998) 26.
[17] G.T. Higgins, B.V. Bergeron, G.M. Hasselmann, F. Farzad, T.J. Meyer, J. Phys. Chem. B 110 (2006) 2598.
[18] (a) F. Farzad, D.W. Thompson, C.A. Kelly, G.J. Meyer, J. Am. Chem. Soc. 121 (1999) 5577;
(b) S.A. Trammell, T.J. Meyer, J. Phys. Chem. B 103 (1999) 104;
(c) S.A. Trammell, J. Yang, M. Sykora, C.N. Fleming, F. Odobel, T.J. Meyer, J. Phys. Chem. B 105 (2001) 8895.
[19] (a) K. Westermark, H. Rensmo, A.C. Lees, J.G. Vos, H. Slegbahn, J. Phys. Chem. B 106 (2002) 10108;
(b) P.G. Hoertz, A. Staniszewski, A. Marton, G.T. Higgins, C.D. Incavito, A.L. Rheingold, G.J. Meyer, J. Am. Chem. Soc. 128 (2006) 8234;
(c) T.W. Hamann, F. Gstrein, B.S. Brunschwig, N.S. Lewis, J. Am. Chem. Soc. 127 (2005) 13949.
[20] (a) F. Odobel, D. Massiot, B.S. Harrison, K.S. Schanze, Langmuir 19 (2003) 30;
(b) A.C. Lees, C.J. Kleverlaan, C.A. Bignozzi, J.G. Vos, Inorg. Chem. 40 (2001) 5343.
[21] (a) E.C. Constable, R.W. Handel, C.E. Housecroft, A.F. Morales, L. Flamigni, F. Barigelletti, J. Chem. Soc., Dalton Trans. (2003) 1220;
(b) T. Akasaka, J. Otsuki, K. Araki, Chem.-Eur. J. 8 (2002) 130;
(c) S.J.A. Pope, C.R. Rice, M.D. Ward, A.F. Morales, G. Accorsi, N. Armaroli, F. Barigelletti, J. Chem. Soc., Dalton Trans. (2001) 2228.
[22] T. Akasaka, H. Inoue, M. Kuwabara, T. Mutai, J. Otsuki, K. Araki, J. Chem. Soc., Dalton Trans. (2003) 815.
[23] (a) B. Maubert, N.D. McClenaghan, M.T. Indelli, S. Campagna, J. Phys. Chem. A 107 (2003) 447;
(b) A. Börje, O. Köthe, A. Juris, J. Chem. Soc., Dalton Trans. (2002) 843;
(c) C.N. Fleming, L.M. Dupray, J.M. Papanikolas, T.J. Meyer, J. Phys. Chem. A 106 (2002) 2328;
(d) H.B. Baudin, J. Davidson, S. Serroni, A. Juris, V. Balzani, S. Campagna, L. Hammarström, J. Phys. Chem. A 106 (2002) 4312.
[24] (a) C.N. Fleming, K.A. Maxwell, J.M. Desimone, T.J. Meyer, J.M. Papanikolas, J. Am. Chem. Soc. 123 (2001) 10336;
(b) M. Sommovigo, G. Denti, S. Serroni, S. Campagna, C. Mingazzini, C. Mariotti, A. Juris, Inorg. Chem. 40 (2001) 3318;
(c) F. Scandola, M.T. Indelli, C. Chiorboli, C.A. Bignozzi, Top. Curr. Chem. 158 (1990) 73.
[25] T.J. Meyer, Acc. Chem. Res. 22 (1989) 163.
[26] (a) S. Ott, M. Borgström, L. Hammarström, O. Johansson, J. Chem. Soc., Dalton Trans. (2006) 434;
(b) S. Encinas, L. Flamigni, F. Barigelletti, E.C. Constable, C.E. Housecroft, E.R. Schofield, E. Figgemeier, D. Fenske, M. Neuburger, J.G. Vos, M. Zehnder, Chem. Eur. J. (2002) 137.
[27] (a) R.J. Forster, E. Figgemeier, P. Loughman, A. Lees, J. Hjelm, J.G. Vos, Langmuir 16 (2006) 7871;
(b) D.M. D'Alessandro, P.H. Dinolfo, M.S. Davies, J.T. Hupp, F.R. Keene, Inorg. Chem. 45 (2006) 3261;
(c) A.C. Benniston, A. Harriman, P. Li, C.A. Sams, J. Am. Chem. Soc. 127 (2005) 2553;
(d) I. Ciofini, P.P. Lainé, F. Bedioui, C. Adamo, J. Am. Chem. Soc. 126 (2004) 10763.
[28] S. Chardon–Noblat, A. Deronzier, F. Hartl, J. van Slageren, T. Mahabiersing, Eur. J. Inorg. Chem. (2001) 613.
[29] (a) Y. Nakabayashi, A. Omayu, S. Yagi, K. Nakamura, J. Motonaka, Anal. Sci. 17 (2001) 945;
(b) C. Xue, F.-T. Luo, J. Chen, H. Liu, Anal. Chim. Acta 569 (2006) 27;
(c) C. Zhang, T. Haruyama, E. Kobatake, M. Aizawa, Anal. Chim. Acta 408 (2000) 225;
(d) M.V. del Pozo, A.F. Pariente, E. Lorenzo, Anal. Chem. 77 (2005) 2550;
(e) W. Xu, K.A. Kneas, J.N. Demas, B.A. DeGraff, Anal. Chem. 68 (1996) 2605;
(f) M.C. Jung, N. Munro, G. Shi, A.C. Michael, S.G. Wener, Anal. Chem. 78 (2006) 1761.
[30] M.K. Itokazu, A.S. Polo, N.Y. Murakami Iha, J. Photochem. Photobiol. A: Chem. 160 (2003) 27.
[31] (a) B. Carlson, G.D. Phelan, W. Kaminsky, L. Dalton, X. Jiang, S. Liu, A. K.-Y. Jen, J. Am. Chem. Soc. 124 (2002) 14162;
(b) P. Chou, Y. Chi, Eur. J. Inorg. Chem. (2006) 3319;
(c) T. Albrecht, A. Guckian, J. Ulstrup, J.G. Vos, Nano Lett. 5 (2005) 1451;
(d) R.C. Evans, P. Douglas, C.J. Winscam, Coord. Chem. Rev. 250 (2006) 2093.
[32] (a) B. Li, M. Li, Z. Hong, W. Li, T. Yu, H. Wei, Appl. Phys. Lett. 85 (2004) 4786;
(b) H.L. Wong, L.S.M. Lam, K.W. Cheng, K.Y.K. Man, W.K. Chan, C.Y. Kwong, A.B. Djurisic, Appl. Phys. Lett. 84 (2004) 2557.
[33] (a) V. Balzani, A. Juris, M. Venturi, S. Campagna, S. Serroni, Chem. Rev. 96 (1996) 759;
(b) A. Juris, V. Balzani, F. Barigelletti, S. Campagna, P. Belser, A. von Zelewsky, Coord. Chem. Rev. 84 (1988) 85.
[34] (a) D.J. Stufkens, Comments Inorg. Chem. 13 (1992) 359;
(b) V. Wing-WahYam, C.-C. Ko, N. Zhu, J. Am. Chem. Soc. 126 (2004) 12734;
(c) L. Zhao, H. Odaka, H. Ono, S. Kajimoto, K. Hatanaka, J. Hobley, H. Fukumura, Photochem. Photobiol. Sci. 4 (2005) 113.
[35] (a) K. Kalyanasundaram, Photochemistry of Polypyridine and Porphyrin Complexes, Academic Press, London, 1992;
(b) M.T. Indelli, F. Scandola, J.-P. Collin, J.-P. Sauvage, A. Sour, Inorg. Chem. 35 (1996) 303;;
(c) K. Kalyanasundaram, M. Grätzel, M.K. Nazeeruddin, J. Phys. Chem. 96 (1992) 5865.
[36] (a) F. Vogtle, M. Frank, M. Nieger, A. von Zelewsky, V. Balzani, F. Barigelletti, L. De Cola, L. Flamigni, Angew. Chem., Int. Ed. Engl. 32 (1993) 1643;
(b) A. Harriman, R. Ziessel, Chem. Commun. (1996) 1707;
(c) V. Grosshenny, A. Harriman, R. Ziessel, Angew. Chem., Int. Ed. Engl. 34 (1995) 1100;
(e) A. Harriman, A. Khatyr, R. Ziessel, J. Chem. Soc., Dalton Trans. (2003) 2061.
[37] (a) L. De Cola, S. Welter, K. Brunner, J.W. Hofstraat, Nature 421 (2003) 54;
(b) D. Xu, J.Z. Zhang, B. Hong, J. Phys. Chem. A 105 (2001) 7979;
(c) P.F.H. Schwab, M.D. Levin, J. Michl, Chem. Rev. 99 (1999) 1863.
[38] (a) S.S. Isied, A. Vassilian, J.F. Wishart, C. Creutz, H.A. Schwartz, N. Sutin, J. Am. Chem. Soc. 110 (1988) 635;
(b) S. Welter, N. Salluce, P. Belser, M. Groeneveld, L. De Cola, Coord. Chem. Rev. 249 (2005) 1360;
(c) A. Beyeler, P. Belser, Coord. Chem. Rev. 230 (2002) 29.
[39] (a) A.G. Hyslop, M. Orphanide, V. Javed, E.G. Megehee, Inorg. Chim. Acta 355 (2003) 272;
(b) Z. Murtaza, P. Herman, J.R. Lakowicz, Biophys. Chem. 80 (1990) 143.
[40] D.M. Roundhill, Photochemistry and Photophysics of Metal Complexes, Plenum Press, New York, 1994.
[41] (a) E.M. Kober, B.P. Sullivan, W.J. Dressick, J.V. Caspar, T.J. Meyer, J. Am. Chem. Soc. 102 (1980) 7383;
(b) S. Li, Y. Cheng, Y. Yeh, C. Hsu, P. Chou, S. Peng, Y. Tung, P. Wu, Y. Chi, F. Wu, C. Shu, Chem. Eur. J. 11 (2005) 6347;
(c) K. Kalyanasundaram, M.K. Nazeeruddin, Chem. Phys. Lett. 158 (1989) 45;
(d) M.M. Richter, K.J. Brewer, Inorg. Chim. Acta 180 (1991) 125.
[42] (a) J.P. Sauvage, J.P. Collin, J.C. Chambron, S. Guillerez, C. Coudret, V. Balzani, F. Barigelletti, L. Decola, L. Flamigni, Chem. Rev. 94 (1994) 993;
(b) P.A. Anderson, F.R. Keene, T.J. Meyer, J.A. Moss, G.F. Strouse, J.A. Treadway, J. Chem. Soc., Dalton Trans. (2002) 3820.
[43] P. Laine, F. Bedioui, P. Ochsenbein, V. Marvaud, M. Bonin, E. Amouyal, J. Am. Chem. Soc. 124 (2002) 1364.
[44] (a) D.M. Adams, L. Brus, C.E.D. Chidsey, S. Creager, C. Creutz, C.R. Kagan, P.V. Kamat, M. Lieberman, S. Lindsay, R.A. Marcus, R.M. Metzger, M.E. Michel-Beyerle, J.R. Miller, M.D. Newton, D.R. Rolison, O. Sankey, K.S. Schanze, J. Yardley, X.Y. Zhu, J. Phys. Chem. B 107 (2003) 6668;
(b) S. Vaduvescu, P.G. Potvin, Eur. J. Inorg. Chem. (2004) 1763.
[45] (a) M.H.V. Huynh, D.M. Dattelbaum, T.J. Meyer, Coord. Chem. Rev. 249 (2005) 457;
(b) F. Puntoriero, S. Serroni, M. Galletta, A. Juris, A. Licciardello, C. Chiorboli, S. Campagna, F. Scandola, ChemPhysChem. 6 (2005) 129.
[46] P.J. Low, J. Chem. Soc., Dalton Trans. (2005) 2821.
[47] (a) S. Goeb, A. De Nicola, R. Ziessel, C. Sabatini, A. Barbieri, F. Barigelletti, Inorg. Chem. 45 (2006) 1173;
(b) R. Argazzi, E. Bertolasi, C. Chiorboli, C.A. Bignozzi, M.K. Itokazu, N.Y. Murakami Iha, Inorg. Chem. 40 (2001) 6885.

[48] (a) M. Casanova, E. Zangrando, F. Munini, E. Iengo, E. Alessio, J. Chem. Soc., Dalton Trans. (2006) 5033;
(b) J.L. Smithback, J.B. Helms, E. Schutte, S.M. Woessner, B.P. Sullivan, Inorg. Chem. 45 (2006) 2163;
(c) L. Cuesta, M.A. Huertos, D. Morales, J. Pérez, L. Riera, V. Riera, D. Miguel, A. Menéndez-Velázquez, S. García-Granda, Inorg. Chem. 46 (2007) 2836.
[49] (a) P. Thanasekaran, T. Rajendran, S. Rajagopal, C. Srinivasan, R. Ramaraj, P. Ramamurthy, B. Venkatachalapathy, J. Phys. Chem. A 101 (1997) 8195;
(b) T. Rajendran, S. Rajagopal, C. Srinivasan, P. Ramamurthy, J. Chem. Soc., Faraday Trans. 93 (1997) 3155.
[50] E. Abel, G. Wilkinson, J. Chem. Soc. (1959) 1501.
[51] L.A. Worl, R. Duessing, P. Chen, L.D. Ciana, T.J. Meyer, J. Chem. Soc., Dalton Trans. (1991) 849.
[52] (a) G. Tapolsky, R. Duesing, T.J. Meyer, Inorg. Chem. 29 (1990) 2285;
(b) R. Lin, Y. Fu, C.P. Brock, T.F. Guarr, Inorg. Chem. 31 (1992) 4346.
[53] K.D. Demadis, G.A. Neyhart, E.M. Kober, P.S. White, T.J. Meyer, Inorg. Chem. 38 (1999) 5948.
[54] S. Serroni, S. Campagna, F. Puntoriero, C. Di Pietro, N.D. McClenaghan, F. Loiseau, Chem. Soc. Rev. 30 (2001) 367.
[55] E.M. Kober, J.V. Caspar, R.S. Lumpkin, T.J. Meyer, J. Phys. Chem. 90 (1986) 3722.
[56] A. El-ghayoury, A. Harriman, R. Ziessel, J. Phys. Chem. A 104 (2000) 7906.
[57] (a) T. Lazarides, A. Barbieri, C. Sabatini, F. Barigelletti, H. Adams, M.D. Ward, Inorg. Chim. Acta 360 (2007) 814;
(b) S. Van Wallendael, D. Paul Rillema, Coord. Chem. Rev. 111 (1991) 297.
[58] M. Furue, M. Naiki, Y. Kanematsu, T. Kushida, M. Kamachi, Coord. Chem. Rev. 111 (1991) 221.

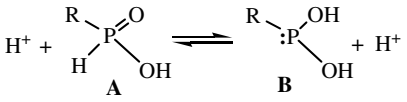

'inactive' form 'active' form (I)

The species in the alkaline solutions are $RHPO_2^-$ (**A**) and $R:P(O)_2^{2-}$ (**B**). The conductivity data of sodium salt of phosphinic acid supports the species HPO_2^{2-} [18], which is intermediate in the base catalysed exchange of hydrogen on phosphinic anion [19] besides being the reactive entity in the oxidations by $Fe(CN)_6^{3-}$ [9], $[Ag(OH)_4]^-$ [20] and Ru(VII) [21] in alkaline solution.

2. Experimental

2.1. Material

The solution of hexacyanoferrate(III) (Fluka, Puriss), prepared from an accurately weighed sample, is stored in the dark. The purity of the sample is ensured by measuring its absorptivity coefficient, 990, that compares well with the value 1000 $dm^3\ mol^{-1}\ cm^{-1}$ at 420 nm [22,23]. The ε value is independent of pH [23] and ionic strength [24]. Subsequent solutions are standardised using ε_{420} = 1000 $dm^3\ mol^{-1}\ cm^{-1}$.

The 50% phosphinic acid solution (Fisher) is iodometrically analysed for H_2PO_3 and H_3PO_3 [25]. The sample had 9.21 and 0.1 mol dm^{-3} of H_2PO_3 and H_3PO_3, respectively. The $C_6H_5H_2PO_2$ sample (Fluka, Technical) is twice recrystallised from hot water. The m.p. of the recrystallised sample is 70–71 °C (lit. 71 °C [26]). The suitably prepared aqueous solutions of RH_2PO_2 are neutralised with a known solution of sodium hydroxide (Sarabhai-M, GR) and are standardised by cerimetry at room temperature [27]. Although the atmospheric oxidation of the $RHPO_2^-$ solutions is not detected over a week yet fresh solutions are prepared every 2–3 days.

The OsO_4 solution is prepared by the dissolution of a known weight of the sample (Johnson Matthey) in 0.1 mol dm^{-3} NaOH solution and stored in a refrigerator from which suitable dilutions are made and standardised by iodometry [9] and spectrophotometrically (ε_{316} = 500 $dm^3\ mol^{-1}\ cm^{-1}$) [28].

Sodium perchlorate solution is prepared by the neutralisation of a known weight of sodium carbonate (BDH, AnalaR) with a known perchloric acid (E. Merck, GR) solution and standardised as described [20]. Solutions of sodium chloride (Sarabhai-M, GR) and potassium chloride (Sarabhai-M, GR) are prepared by direct weighing of the respective samples.

The water is first distilled under mild alkaline conditions using a pinch of potassium permanganate. The first distillate is once again distilled and the second distillate is used through out for the preparation of the solutions. These solutions, if needed, are purged with nitrogen gas before use.

2.2. Rate measurements

The rates are measured at constant ionic strength (μ = 1 mol dm^{-3}, $NaClO_4$), ($[RHPO_2^-] \gg [Fe(CN)_6^{3-}]$), by measuring the disappearance of $Fe(CN)_6^{3-}$ at 420 nm using a Spectrochem Mk (II) colorimeter [29]. The linear plots of $(A_t - A_\infty)$ against time for more than three half-lives of the reaction rules out the biphasic nature of the reaction where A_t and A_∞ are the optical density at a given time and infinite time, respectively. Any contribution to the measured optical density from OsO_4 is negligible because of its very low concentration in the reaction mixture. A_∞ is measured few hours after completion of the reaction. The pseudo zero-order rate constant k_o is calculated by dividing the slope of the plots of $(A_t - A_\infty)$ against time by ε (=1000 $dm^3\ mol^{-1}\ cm^{-1}$). The Beers–Lambert law holds good over the concentrations used. The reproducibility of the pseudo zero-order rate constant k_o is with in ± 5%.

The EXCEL program is used to draw the plots and to obtain the least-square values of the slopes and intercepts. The program ACTE by H. Strahlow is used to calculate the activation parameters. The thermodynamic parameters are calculated with a computer program EQLBPARA written in basic in our laboratory.

2.3. Stoichiometry

The stoichiometry of the reaction is studied from several reaction mixtures with $Fe(CN)_6^{3-}$ in excess over the substrate. The disappearance of $Fe(CN)_6^{3-}$ is measured at 420 nm till the optical density has a constant value using a Hewlett Packard 8452A UV–Vis diode spectrophotometer with a bandwidth of 2 nm and integration time of 0.1 s. The calculated concentration of reacted $Fe(CN)_6^{3-}$ in each mixture indicated that $\Delta[Fe(CN)_6^{3-}]/\Delta[RHP(O)O^-] = 2 \pm 0.05$, which is consistent with the stoichiometry equation (1) and the stoichiometry reported previously [5,9].

$$2Fe(CN)_6^{3-} + RHPO_2^- + 2OH^- \xrightarrow{OsO_4} 2Fe(CN)_6^{4-} + RHPO_3^- + H_2O \quad (1)$$

2.4. Test for free radicals

The nitrogen purged solutions of $Fe(CN)_6^{3-}$ and $RHPO_2^-$ having appropriate concentrations of OsO_4 are taken separately and 2 ml of distilled acrylonitrile is added to each solution. The solutions do not show cloudiness over several minutes. These solutions are then mixed to initiate the reaction and no cloudiness or precipitate is observed over several minutes confirming that free radicals are not generated in the reaction.

3. Results

The zero-order dependence in hexacyanoferrate(III) ion is confirmed by proportionate increase in the $t_{1/2}$ and almost constant value of k_o over a 10-fold variation in the initial $Fe(CN)_6^{3-}$ (Table 1).

The k_o values measured over a 10-fold variation in the initial $[H_2PO_2^-]$ and $[C_6H_5HPO_2^-]$, at different $[OH^-]$ and temperatures, Tables 2 and 3, respectively, indicate that for the same concentrations the rate of $C_6H_5HPO_2^-$ oxidation is slower than that of $H_2PO_2^-$. The results provided linear plots of k_o^{-1} against $[RHPO_2^-]^{-1}$, Fig. 1, with intercepts on the rate ordinate indicating the formation of the intermediate osmium(VIII)–$RHPO_2^-$ complex. The formation of a similar complex is reported in the oxidation of $H_2PO_2^-$ ion [5] but the oxidation of $H_2PO_3^-$ ion does not report the formation of a similar complex [11]. The intercept and slope values of the plots in Fig. 1, Table 4, indicate that these decrease with the increase in the initial $[OH^-]$.

The k_o values increased proportionately with the increase in $[OsO_4]$ (Table 5). The linear plot of k_o against $[OsO_4]$, Fig. 2, almost passes through the origin confirming first-order dependence in OsO_4 and that the reaction between $Fe(CN)_6^{3-}$ and $RHPO_2^-$ is negligibly slow.

The increasing $[OH^-]$, Table 6, increases the k_o and the correlation between k_o and $[OH^-]$ is discussed in the mechanism section. A similar increase in the rate with OH^- is reported in the oxidation of phosphite ion [11] though the nature of dependence is different.

The effect of added NaCl and KCl, Table 7, indicated that the rates are almost the same in the presence of Na^+ and K^+ ions indicating the absence of specific cation effects in the reaction. The plot of k_o against [alkali metal ions] are linear with intercept on the rate ordinate.

Table 1
Dependence of k_o (mol dm^{-3} s^{-1}) on the initial $[Fe(CN)_6^{3-}]$ $10^6[OsO_4] = 1.25$, $[OH^-] = 0.1$, $[RHPO_2^-] = 0.01$ and $\mu = 1.0$ mol dm^{-3}

$10^4[Fe(CN)_6^{3-}]$ (mol dm^{-3})		1.0	3.0	4.5	6.4	8.0	10.0
$10^7 k_o$ (30 °C)	R = C_6H_5	0.873	0.878	0.882	0.888	0.878	0.892
$10^7 k_o$ (35 °C)	R = H	1.36	1.41	1.39	1.44	1.35	1.37

Table 2
Dependence of k_o (mol dm^{-3} s^{-1}) on $[H_2PO_2^-]$ at different $[OH^-]$ and temperatures

$[H_2PO_2^-]$ (mol dm^{-3})		$10^7 k_o$ (mol dm^{-3} s^{-1})				
Temperature (°C)	$[OH^-]$ (mol dm^{-3})	0.005	0.01	0.02	0.03	0.05
30	0.1	0.558	0.966	1.66	2.04	2.83
35		0.770	1.36	2.24	2.82	3.60
40		1.05	1.73	2.81	3.55	4.21
45		1.38	2.35	3.62	4.42	5.37
30	0.2	0.709	1.21	2.15	2.69	3.72
35		1.01	1.79	2.93	3.70	4.69
40		1.34	2.35	3.78	4.59	5.68
45		1.83	3.10	4.77	5.81	7.04
30	0.5	1.07	1.94	3.21	4.06	5.78
35		1.75	3.09	5.00	6.32	8.00
40		2.30	4.05	6.37	7.40	9.80
45		3.09	5.25	8.10	9.86	11.9
30	0.7	1.37	2.43	4.11	5.15	6.99
35		2.22	3.91	6.29	7.91	10.1
40		3.01	5.15	8.00	10.2	12.6
45		3.82	6.53	10.1	12.4	15.1
30	1.0	1.80	3.58	5.01	6.77	10.3
35		2.97	5.25	8.51	10.7	13.6
40		3.97	6.84	10.6	13.3	16.5
45		5.26	8.92	13.7	16.6	20.1

$10^4[Fe(CN)_6^{3-}] = 4.0$, $10^6[OSO_4] = 1.25$ and $\mu = 1.0$ mol dm^{-3}.

Table 3
Dependence of k_o (mol dm^{-3} s^{-1}) on $[C_6H_5HPO_2^-]$ at different $[OH^-]$ and temperatures

$[C_6H_5HPO_2^-]$ (mol dm^{-3})		$10^7 k_o$ (mol dm^{-3} s^{-1})				
Temperature (°C)	$[OH^-]$ (mol dm^{-3})	0.005	0.01	0.02	0.03	0.05
30	0.1	0.531	0.873	1.29	1.54	1.82
35		0.607	1.00	1.45	1.72	2.05
40		0.748	1.22	1.78	2.09	2.47
45		0.983	1.59	2.30	2.69	3.13
30	0.2	0.625	1.03	1.51	1.79	2.10
35		0.876	1.42	2.16	2.50	2.96
40		1.04	1.68	2.45	2.86	3.33
45		1.19	1.93	2.76	3.27	3.77
30	0.5	0.869	1.43	2.07	2.50	2.89
35		1.10	1.79	2.66	3.15	3.70
40		1.31	2.11	3.03	3.61	4.16
45		1.79	2.90	4.08	4.86	5.56
30	0.7	1.01	1.57	2.51	2.87	3.49
35		1.38	2.29	3.26	3.95	4.58
40		1.77	2.86	4.19	4.89	5.64
45		2.18	3.54	4.98	5.92	6.64
30	1.0	1.16	1.96	2.87	3.40	4.03
35		1.59	2.78	3.81	4.49	5.32
40		2.00	3.22	4.74	5.45	6.42
45		2.78	4.46	6.44	7.46	8.67

$10^4[Fe(CN)_6^{3-}] = 4.0$, $10^6[OSO_4] = 1.25$ and $\mu = 1.0$ mol dm^{-3}.

4. Mechanism and discussion

It would be instructive to consider the mechanisms of the OsO_4-catalysed [5] and uncatalysed [9] oxidation of $H_2PO_2^-$ with alkaline hexacyanoferrate (III) ion.

$$H_2PO_2^- + OsO_4(OH)^- \underset{k_{-4}}{\overset{k_4}{\rightleftharpoons}} [complex]^{2-} \quad (i)$$

$$complex^{2-} + OH^- \overset{k'}{\rightarrow} HP^+O_2^- + OsO_3(OH)_3^{3-} \quad (ii)$$

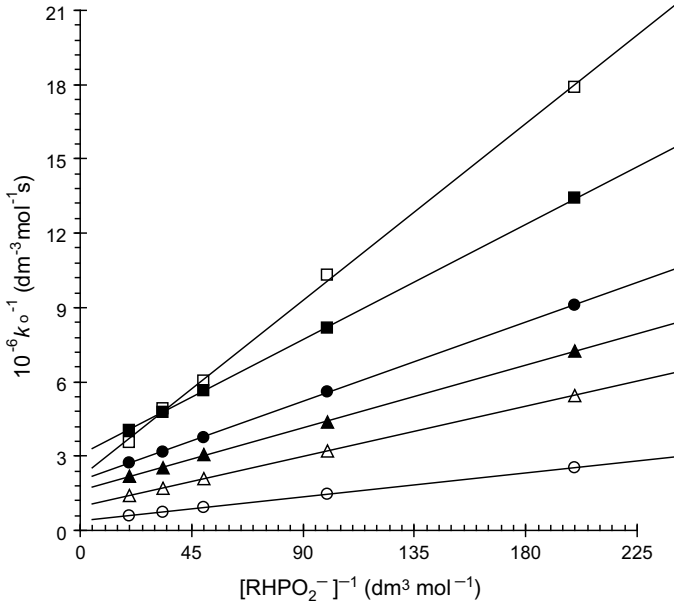

Fig. 1. Some of the linear plots of k_o^{-1} against $[RHPO_2^-]^{-1}$ with intercepts on the rate ordinate are consistent with Eq. (21). For R = H: (□) 30 °C and $[OH^-] = 0.1$; (○) 40 °C and $[OH^-] = 1.0$; (△) 45 °C and $[OH^-] = 0.2$ and for R = C_6H_5: (●) 35 °C and $[OH^-] = 0.5$; (▲) 35 °C and $[OH^-] = 0.7$ and (■) 40 °C and $[OH^-] = 0.1$ mol dm^{-3}. $10^4[Fe(CN)_6^{3-}] = 4.0$, $[OsO_4] = 1.25$ and $\mu = 1$ mol dm^{-3}.

Table 4
The values of intercepts and slopes from plots such as in Fig. 1 at different temperatures and $[OH^-]$

$[OH^-]$ (mol dm^{-3})	10^{-6} (intercept, dm^3 mol^{-1} s)				
Substrate	0.1	0.2	0.5	0.7	1.0
$H_2PO_2^-$					
30 °C	2.13	1.60	0.988	0.822	0.580
35 °C	1.65	1.26	0.758	0.610	0.442
40 °C	1.57	1.10	0.676	0.530	0.401
45 °C	1.26	0.974	0.567	0.447	0.341
$C_6H_5HPO_2^-$					
30 °C	4.03	3.50	2.55	2.15	1.78
35 °C	3.64	2.48	1.99	1.61	1.37
40 °C	3.03	2.26	1.82	1.32	1.18
45 °C	2.41	2.01	1.37	1.13	0.879
	10^{-4} (slope, s)				
$H_2PO_2^-$					
30 °C	7.94	6.28	4.18	3.25	2.45
35 °C	5.68	4.32	2.48	1.95	1.46
40 °C	4.01	3.17	1.83	1.40	1.06
45 °C	2.99	2.24	1.34	1.08	0.780
$C_6H_5HPO_2^-$					
30 °C	7.38	6.24	4.47	3.93	3.40
35 °C	6.42	4.47	3.56	2.81	2.42
40 °C	5.18	3.67	2.91	2.16	1.91
45 °C	3.89	3.19	2.10	1.72	1.36

$$2Fe(CN)_6^{3-} + OsO_3(OH)_3^{3-} \overset{fast}{\rightarrow} 2Fe(CN)_6^{4-} + HOsO_5^- + H_2O \quad (iii)$$

$$HP^+O_2^- + H_2O \overset{fast}{\rightarrow} H_2PO_3^- + H^+ \quad (iv)$$

$$\frac{-d[Fe(CN)_6^{3-}]}{dt} = \frac{2k_4k'[OH^-][H_2PO_2^-][OsO_4^-]}{k_{-4} + k'[OH^-]} \quad (v)$$

Table 5
Dependence of k_o (mol dm^{-3} s^{-1}) on the initial [OsO_4]

10^6[OsO_4] (mol dm^{-3})	10^7k_o				
Substrate	1.25	2.50	5.0	10.0	12.5
$H_2PO_2^-$, 35 °C	1.36	2.75	5.15	10.6	13.3
$C_6H_5HPO_2^-$, 30 °C	0.873	1.76	3.57	7.25	8.80

$10^4[Fe(CN)_6^{3-}] = 8.0$, [$OH^-$] = 0.1, [$RHPO_2^-$] = 0.01 and μ = 1.0 mol dm^{-3}.

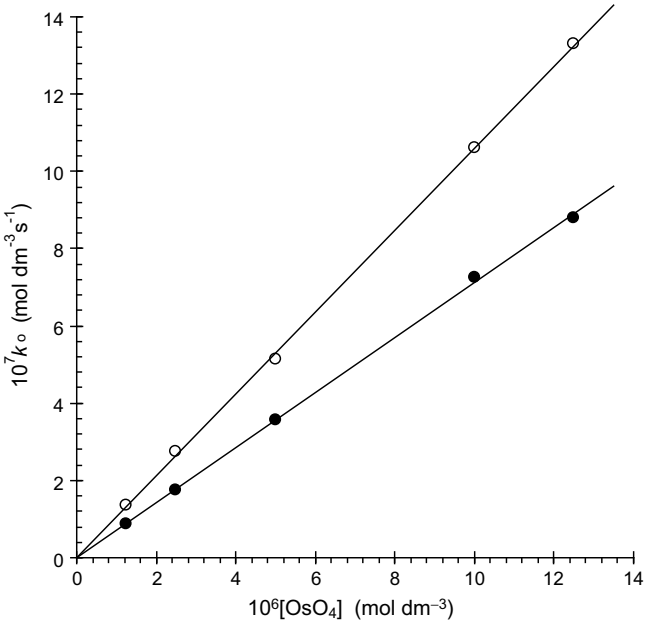

Fig. 2. The dependence of k_o on the initial [OsO_4] for the oxidation of $C_6H_5HPO_2^-$ at 30 °C (●) and for $H_2PO_2^-$ at 35 °C (○). $10^4[Fe(CN)_6^{3-}] = 8.0$, [$OH^-$] = 0.1, [$RHPO_2^-$] = 0.01 and μ = 1 mol dm^{-3}.

Table 6
Dependence of k_o (mol dm^{-3} s^{-1}) on the initial [OH^-]

[OH^-] (mol dm^{-3})	10^7k_o					
Substrate	0.1	0.2	0.4	0.5	0.7	1.0
$H_2PO_2^-$, 35 °C	1.36	1.77	2.37	2.94	3.74	5.10
$C_6H_5HPO_2^-$, 30 °C	0.873	1.03	1.21	1.43	1.57	1.96

$10^4[Fe(CN)_6^{3-}] = 8.0$, 10^6[OsO_4] = 1.25, [$RHPO_2^-$ = 0.01] and μ = 1.0 mol dm^{-3}.

Table 7
Dependence of k_o (mol dm^{-3} s^{-1}) on the initial ionic strength varied with MCl

[MCl] (mol dm^{-3})	10^7k_o				
Substrate	0.1	0.2	0.5	0.7	1.0
$H_2PO_2^-$, 35 °C					
M = Na	0.596	0.705	0.927	1.13	1.48
M = K	0.592	0.692	0.916	1.10	1.44
$C_6H_5HPO_2^-$, 30 °C					
M = Na	0.382	0.442	0.596	0.744	0.888
M = K	0.372	0.451	0.606	0.732	0.881

$10^4[Fe(CN)_6^{3-}] = 4.0$, 10^6[OsO_4] = 1.25, [OH^-] = 0.1, [$RHPO_2^-$] = 0.01.

and for the uncatalysed reaction,

$$H_2PO_2^- + OH^- \rightleftharpoons H_3PO_3^{2-} \quad (a)$$

$$H_3PO_3^{2-} + Fe(CN)_6^{3-} \xrightarrow{k''} H_3PO_3^- + Fe(CN)_6^{4-} \quad (b)$$

$$H_3PO_3^- + Fe(CN)_6^{3-} \xrightarrow{fast} H_3PO_3 + Fe(CN)_6^{4-} \quad (c)$$

The empirical rate equation (2) based on the present results is different from the rate equation (v) [5] in respect of dependence on OH^- and $H_2PO_2^-$ ions. The present results indicate an additional path which is independent of OH^- ion. It is therefore imperative that the reaction has a different mechanism.

$$\frac{-d[Fe(CN)_6^{3-}]}{dt} = k_o = \frac{(a + b[OH^-])[RHPO_2^-][OsO_4]_o}{m + n[RHPO_2^-]} \quad (2)$$

Eq. (2) is similar to the rate equation in the oxidation of $H_2PO_2^-$ by square-planar $Ag(OH)_4^-$ ion [20]. However, $m \gg n[H_2PO_2]$ in the $Ag(OH)_4^-$ oxidation is not observed in the present reaction. The reason for the difference is attributable to the relative stability of the complex $H_2PO_2^-$ forms with $Ag(OH)_4^-$ and $OsO_4(OH)^-$/$OsO_4(OH)_2^{2-}$ ions. The osmium species form a stable complex whereas a transition complex is formed by $Ag(OH)_4^-$ ion.

In view of the zero-order dependence in $Fe(CN)_6^{3-}$ ion, an interaction between OH^- and $Fe(CN)_6^{3-}$ is unlikely and is not reported in the literature. It is for this reason that the OH^- dependence in the oxidation of $H_2PO_2^-$ is explained by invoking the equilibrium (a) [9]. A similar equilibrium is also considered in the mechanism of $H_2PO_2^-$ ion oxidation with $Ag(OH)_4^-$ ion [20]. It might be noted that OH^- ion does not react either with $Fe(CN)_6^{3-}$ or $Ag(OH)_4^-$ ions.

However, the equilibrium (a) is not considered in the present reaction for the reason that the equilibrium amount of HPO_2^{2-} is small under basic conditions used and that the (composite) second pK of H_3PO_2 is above 14. On the other hand OsO_4 forms various species with OH^- ions, which are in equilibrium with each other.

In the aqueous solution of OsO_4 the species OsO_4 and H_2OsO_5 are in equilibrium which is shifted more towards OsO_4. The apparent primary ionization constant K_{a1} (1×10^{-12} mol dm^{-3}, μ = 1 mol dm^{-3}, 25 °C) of OsO_4 in weakly KOH solution and the second ionization constant K_{a2} (3×10^{-15} mol dm^{-3}) in the more strong KOH solution are determined spectrophotometrically [30] and are defined by Eqs. (3) and (4), respectively, where $[OsO_4]_o$ is the analytical concentration.

$$K_{a1} = \frac{[H^+][OsO_4OH^-]}{[OsO_4]_o[H_2O]} \quad (3)$$

$$K_{a2} = \frac{[H^+][OsO_4(OH)_2^-]}{[OsO_4(OH)^-][H_2O]} \quad (4)$$

trans-$[OsO_4(OH)_2]^{2-}$ is formed in NaOH and KOH [31,32] in two steps as shown in Eqs. (5) and (6) whereas $[OsO_4OH]^-$, $[O_4Os(\mu\text{-}OH)OsO_4]^-$ and *trans*-$[OsO_4(OH)_2]^{2-}$ ions are formed with RbOH and CsOH [33]. The equilibrium constants K_1 and K_2, estimated from the known K_{a1} and K_{a2} [30] using the relation $K_n = K_{an}/K_w$, have the values 5.55×10^{13} and 16.6 dm^3 mol^{-1}, respectively [32], the later is in fair agreement with the value 24 ± 4 dm^3 mol^{-1} estimated spectrophotometrically [11]. However, K_1 = 302 dm^3 mol^{-1} is reported in another estimate [34], and the use of it indicated that about 95% of OsO_4 existed as $[OsO_4(OH)]^-$. Hence, it is assumed that equilibrium (5) is almost shifted to the right so that OsO_4 is entirely present as $[OsO_4OH]^-$ even in very dilute alkali solution.

trans-$[OsO_4(OH)_2]^{2-}$ is obviously more likely to be the additional reactive species in addition to $[OsO_4(OH)]^-$ in view of the acceleration of the rate with OH^- and the equilibrium (6). The most likely mechanism of the reaction in view of the kinetics results is presented in Scheme 1. The formation of the $OsO_4(OH)RHPO_2^{2-}$ complex is consistent with the observed Michaelis-Menten kinetics [35] with respect to $RHPO_2^-$ ion. However, the formation of a similar complex by $OsO_4(OH)_2^{2-}$ and $RHPO_2^-$ ions is considered unlikely because of the relatively strong repulsion between these ions which react through a bimolecular collision.

The $Fe(CN)_6^{3-}$ ions may form $MFe(CN)_6^{2-}$ with M^+ ions (M = Li, Na, K, Rb). The specific catalytic effect of M^+ ion has been observed

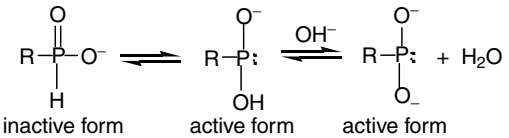

(II)

$$OsO_4 + OH^- \underset{}{\overset{K_1}{\rightleftharpoons}} OsO_4OH^- \quad (5)$$

$$OsO_4(OH)^- + OH^- \underset{}{\overset{K_2}{\rightleftharpoons}} OsO_4(OH)_2^{2-} \quad (6)$$

$$OsO_4(OH)^- + RHPO_2^- \underset{}{\overset{\beta}{\rightleftharpoons}} OsO_4(OH)RHPO_2^{2-} \quad (7)$$

$$OsO_4(OH)RHPO_2^{2-} \xrightarrow{k} OsO_3(H_2O) + RP(O)O_2^{2-} \quad (8)$$

$$OsO_4(OH)_2^{2-} + RHPO_2^- \xrightarrow{k_2} RPO_3^{2-} + OsO_3(H_2O)(OH)^- \quad (9)$$

$$OsO_3(H_2O) + 2Fe(CN)_6^{3-} + 2OH^- \xrightarrow{fast} OsO_4(H_2O)_2 + 2Fe(CN)_6^{4-} \quad (10)$$

$$OsO_3(H_2O)(OH)^- + 2Fe(CN)_6^{3-} + OH^- \xrightarrow{fast} OsO_4(H_2O)_2 + 2Fe(CN)_6^{4-} \quad (11)$$

Scheme 1.

in the $Fe(CN)_6^{3-}$ oxidation of SO_3^{2-} [36], L-ascorbic acid [37], and substituted anilines [38]. $NaClO_4$ and KCl increased the rate in the alkaline $Fe(CN)_6^{3-}$ oxidation of $H_2PO_2^-$ but spectrophotometric measurements did not substantiate the ion pair formation even in presence of high [NaC1O$_4$] or [KCl] [9].

The zero order dependence in $Fe(CN)_6^{3-}$ ion precludes ion pair formation between $Fe(CN)_6^{3-}$ and M^+ ions. However, the ion pairs Na^+—$OsO_4(OH)^-$/Na^+—$OsO_4(OH)_2^{2-}$ can be speculated which are not reported even in the concentrated alkali solutions. M^+ ions are therefore unlikely to act as a bridge between $OsO_4(OH)^-$/$OsO_4(OH)_2^{2-}$ ions and $RHPO_2^-$ ions. The electrostatic repulsion between the negative species is, probably, reduced by the strong hydration of the negatively charged ions. Thus the solvent H_2O molecule is the likely bridge between the two anionic species.

Therefore, the rate acceleration by Na^+ and K^+ ions is attributed to the change in the ionic strength of the medium and the assertion is supported by the application of the Davies' equation (12) [39] since the plot of $\log k_o$ against $(\sqrt{\mu}/1+\sqrt{\mu}-0.01\mu)$ is linear with slopes 1.93 in $C_6H_5HPO_2^-$ and 1.98 in $H_2PO_2^-$. The slope values are consistent with the reaction between $OsO_4(OH)_2^{2-}$ and $RHPO_2^-$ ions.

$$\log k_o = \log k + z_a z_b \left(\frac{\sqrt{\mu}}{1+\sqrt{\mu}} - 0.01\mu\right) \quad (12)$$

The apparent rates of the reaction between $OsO_4(OH)_2^{2-}$ and $RHPO_2^-$ ions is more than four times the rate between OsO_4OH^- and $H_2PO_2^-$ ions and more than three times the rate between OsO_4OH^- and $C_6H_5HPO_2^-$ ions. Hence the major contribution to the effect of the ionic strength is from the reaction (9).

The rate equation derived from the reactions in Scheme 1 is given by Eq. (13).

$$\frac{-d[Fe(CN)_6^{3-}]}{dt} = (k\beta + k_2K_2[OH^-])[OsO_4OH^-][RHPO_2^-] \quad (13)$$

The mass balance of the osmium species considered in Eqs. (6) and (7) is given by Eq. (14).

$$[OsO_4OH^-] = \frac{[OsO_4]_o}{1 + K_2[OH^-] + \beta[RHPO_2^-]} \quad (14)$$

The relation expressed in Eq. (15) can be established in view of the reaction (10) or (11).

$$\frac{d[OsO_4]}{dt} = \frac{d[Fe(CN)_6^{3-}]}{2dt} \quad (15)$$

The substitution of the value of $[OsO_4OH^-]$ from Eq. (14) into Eq. (13) and the application of the relation expressed in Eq. (15), changes Eq. (13) to (24), which modifies to Eq. (25) on the assumption that $(1+\beta[RHP(O)O^-]) \gg K_2[OH^-]$ because K_2 is likely to have less value than the estimated values[1] in the present context because the concentrations of OsO_4OH^- and $OsO_4(OH)_2^{2-}$ are being constantly depleted by the reaction with $RHPO_2^-$ ion.

$$\frac{-d[Fe(CN)_6^{3-}]}{dt} = k_o = \frac{2(k\beta + k_2K_2[OH^-])[OsO_4]_o[RHPO_2^-]}{1 + K_2[OH^-] + \beta[RHPO_2^-]} \quad (16)$$

$$k_o = \frac{2(k\beta + k_2K_2[OH^-])[OsO_4]_o[RHPO_2^-]}{1 + \beta[RHPO_2^-]} \quad (17)$$

Eq. (25) is consistent with the linear plot of k_o against $[OsO_4]$, Fig. 2, that passes through the origin and the linear plots of k_o against $[OH^-]$, Fig. 3, with intercepts on the rate ordinate. The inverted Eq. (25) is given in Eq. (18).

$$\frac{1}{k_o} = \frac{1}{2(k\beta + k_2K_2[OH^-])[OsO_4]_o[RHPO_2^-]} + \frac{\beta}{2(k\beta + k_2K_2[OH^-])[OsO_4]_o} \quad (18)$$

Eq. (18) is consistent with the double reciprocal plots such as shown in Fig. 1. The estimated intercept and slope values of such plots, Table 4, are used to estimate the values of β (=intercept/slope) given in Table 8. It is noted that the β value is independent of the initial $[OH^-]$, which is in agreement with the Eq. (18) which further suggests that the correlation of the slope and intercept values, Table 4, with the $[OH^-]$ are given by Eqs. (19) and (20).

$$\text{Slope}^{-1} = 2(k\beta + k_2K_2[OH^-])[OsO_4]_o \quad (19)$$

$$\text{Intercept}^{-1} = 2(k + k_2K_2\beta^{-1}[OH^-])[OsO_4]_o \quad (20)$$

[1] Calculated values of K_2 from the data in [17] are 27, 30, 36 and 42.5 dm^3 mol^{-1} at 30, 35, 40 and 45 °C, respectively.

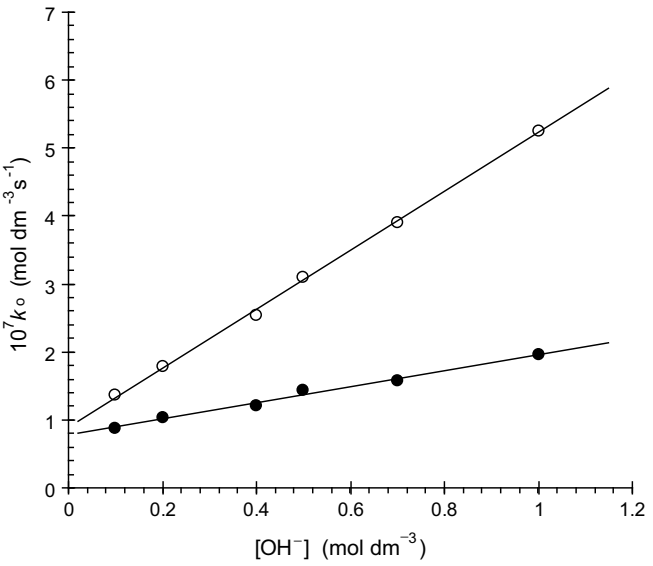

Fig. 3. Some representative plots of the dependence of k_o on the initial [OH$^-$] for the oxidation of $C_6H_5HPO_2^-$ at 30 °C (●) and (○) for $H_2PO_2^-$ at 35 °C. 10^4[Fe(CN)$_6^{3-}$] = 8.0, 10^6[OsO$_4$] = 1.25, [$RHPO_2^-$] = 0.01 and μ = 1 mol dm^{-3}.

The values of β, k and k_2K_2, Table 9, are calculated from the slope and intercept values of the plots in Figs. 4 and 5. The k and k_2K_2 values, calculated from the two plots, are in fair agreement and thus the proposed mechanism is supported. Although the K_2 values (footnote 2) are known yet the k_2 values are not separated from the estimated k_2K_2 values because the equilibria 6 and 7, from which the K_2 values were estimated, are disturbed by the depletion of the concentrations of the species OsO_4OH^- and $OsO_4(OH)_2^{2-}$ because of their reaction with the $RHPO_2^-$ ions as shown in reactions (8)–(10). Thus, K_2 is unlikely to retain the reported values during the course of the redox reaction. The Arrhenius plots for k, k_2K_2 and β are shown in Fig. 6.

The higher β value in the oxidation of $C_6H_5HPO_2^-$ is ascribed to the presence of nucleophilic C_6H_5 group which stabilises the Os(VIII)–$C_6H_5HPO_2^-$ complex. This is consistent with the significantly lower ΔH° and ΔS° values for $C_6H_5HPO_2^-$ than those for $H_2PO_2^-$ ion. It is further noted that the ΔG° value for $H_2PO_2^-$ and $C_6H_5HPO_2^-$ is almost identical indicating the compensatory effect of ΔH° and ΔS°. The plot of ΔH° against ΔS° to establish the isokinetic effect is not attempted because there are only two points.

The k and k_2K_2 values in $H_2PO_2^-$ are about two times the values in $C_6H_5HPO_2^-$ because the chances of C–H fission in $C_6H_5HPO_2^-$ are statistically reduced by half of those possible in $H_2PO_2^-$ ion. Another reason for the low values of k_2K_2 in $C_6H_5HPO_2^-$ is the steric effect of the bulky phenyl group. The $\Delta H_k^\ddagger$, $\Delta S_k^\ddagger$ and $\Delta G_k^\ddagger$ values for $H_2PO_2^-$ and $C_6H_5HPO_2^-$ are almost similar and so are the values of $\Delta H_{k_2K_2}^\ddagger$, $\Delta S_{k_2K_2}^\ddagger$ and $\Delta G_{k_2K_2}^\ddagger$ supporting the common mechanism. The negative entropies in both the cases are supportive of the bond making in the formation of the intermediate or the transition state. However, the $\Delta S_k^\ddagger$ corresponding to the intermediate $OsO_4(OH)RHPO_2^{2-}$ complex is significantly more negative than $\Delta S_{k_2K_2}^\ddagger$ which corresponds to the transition state is consistent with the expectation for the intermediate is more tightly held than the transition state. And another reason is that the large number of water molecules form the hydration sphere around the intermediate because of the increased charge on it so that the degree of freedom of water molecules is greatly curtailed.

Table 8
The values of β, which are independent of [OH$^-$], at different temperatures and related thermodynamic parameters

[OH$^-$] (mol dm^{-3})	β (dm^3 mol^{-1})					
Temperature (°C)	0.1	0.2	0.5	0.7	1.0	Mean value
30, $H_2PO_2^-$	26.8	25.5	23.6	25.3	23.7	25 ± 1.3
35	29.0	29.2	30.6	31.3	30.3	30 ± 1
40	39.1	34.7	36.9	37.8	37.8	37.3 ± 1.6
45	42.1	43.5	42.3	41.4	43.7	42.6 ± 1
$\Delta H^\circ = 29 \pm 1$ kJ mol^{-1}, $\Delta S^\circ = 122 \pm 5$ J K^{-1} mol^{-1}, $\Delta G^\circ = -8 \pm 1$ kJ mol^{-1}						
30, $C_6H_5HPO_2^-$	54.6	56.1	57.0	54.7	52.3	55 ± 1.8
35	56.7	55.5	55.9	57.3	56.6	56.4 ± 0.7
40	58.2	61.6	62.5	61.1	61.8	61 ± 1.7
45	63.6	65.4	65.2	65.6	63.2	64.6 ± 1.1
$\Delta H^\circ = 8 \pm 1$ kJ mol^{-1}, $\Delta S^\circ = 62 \pm 3$ J K^{-1} mol^{-1}, $\Delta G^\circ = -10 \pm 1$ kJ mol^{-1}						

Table 9
The temperature dependence of the rate constant k (s^{-1}) and k_2K_2 (dm^3 mol^{-1} s^{-1}), calculated from the intercept and slope of the plots shown in Figs. 5 and 6, and the related values of $\Delta H^\ddagger$, $\Delta G^\ddagger$ (kJ mol^{-1}) and $-\Delta S^\ddagger$ (J K^{-1} mol^{-1})

Substrates	$H_2PO_2^-$				$C_6H_5HPO_2^-$			
	From plots in Fig. 5		From plots in Fig. 6		From plots in Fig. 5		From plots in Fig. 6	
Temperature (°C)	k	k_2K_2	k	k_2K_2	k	k_2K_2	k	k_2K_2
30	0.149	0.459	0.134	0.500	0.091	0.262	0.086	0.257
35	0.158	0.753	0.167	0.724	0.106	0.365	0.107	0.359
40	0.176	0.864	0.187	0.841	0.117	0.402	0.119	0.390
45	0.203	0.969	0.224	0.954	0.128	0.500	0.133	0.486
$\Delta H^\ddagger$	14 ± 2	36 ± 10	24 ± 2	31 ± 6	16 ± 1	30 ± 5	20 ± 3	30 ± 5
$-\Delta S^\ddagger$	198 ± 7	116 ± 32	166 ± 7	131 ± 20	197 ± 5	139 ± 15	182 ± 9	142 ± 16
$\Delta G^\ddagger$	73 ± 3	70 ± 12	73 ± 2	70 ± 7	75 ± 2	71 ± 8	74 ± 4	71 ± 5

$H_2PO_2^-$		$C_6H_5HPO_2^-$	
Mean $\Delta H_k^\ddagger = 19 \pm 6$	Mean $\Delta H_{k_2K_2}^\ddagger = 33 \pm 8$	Mean $\Delta H_k^\ddagger = 18 \pm 3$	Mean $\Delta H_{k_2K_2}^\ddagger = 30 \pm 4$
Mean $-\Delta S_k^\ddagger = 182 \pm 18$	Mean $-\Delta S_{k_2K_2}^\ddagger$ 121 ± 23	Mean $-\Delta S_k^\ddagger = 188 \pm 11$	Mean $-\Delta S_{k_2K_2}^\ddagger = 140 \pm 14$
Mean $\Delta G_k^\ddagger = 73 \pm 2$	Mean $\Delta G_{k_2K_2}^\ddagger = 70 \pm 9$	Mean $\Delta G_k^\ddagger = 74 \pm 3$	Mean $\Delta G_{k_2K_2}^\ddagger = 71 \pm 6$

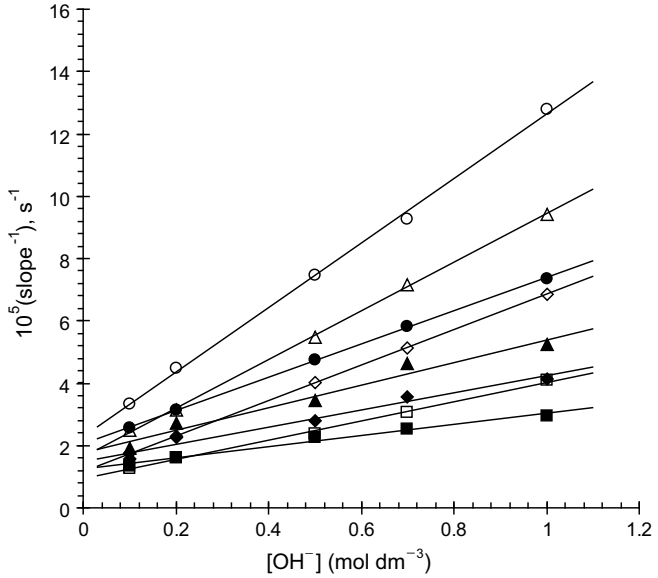

Fig. 4. The linear plots of slope^{-1} against [OH$^-$] with intercepts are consistent with Eq. (22) at temperatures 30 °C (□), 35 °C (◇), 40 °C (△) and 45 °C (○) for $H_2PO_2^-$, and for $C_6H_5HPO_2^-$ at 30 °C (■), 35 °C (♦), 40 °C (▲) and 45 °C (●). The slope values are from the plots such as shown in Fig. 1.

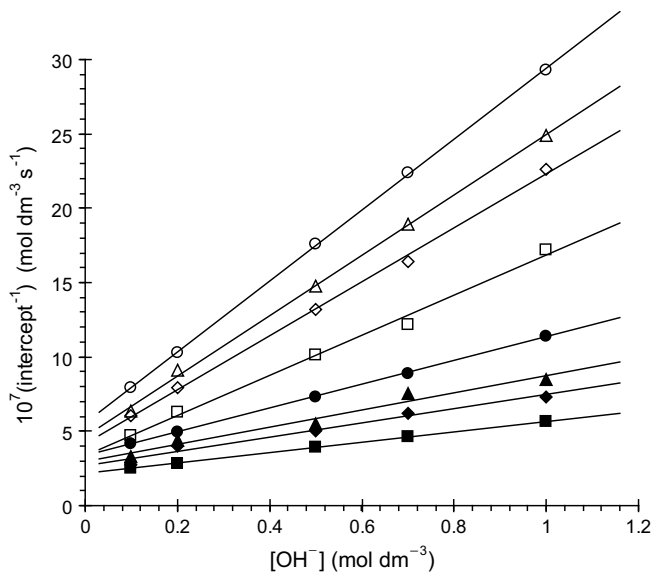

Fig. 5. The linear plots of intercept^{-1} against [OH$^-$] with intercepts are consistent with Eq. (23) at temperatures 30 °C (□), 35 °C (◇), 40 °C (△) and 45 °C (○) for $H_2PO_2^-$, and for $C_6H_5HPO_2^-$ at 30 °C (■), 35 °C (♦), 40 °C (▲) and 45 °C (●). The intercept values are from the plots such as shown in Fig. 1.

The considerably higher value of $\Delta H^{\ddagger}_{k_2K_2}$ than $\Delta H^{\ddagger}_{k}$ is obvious considering that a bimolecular reaction between $OsO_4(OH)_2^{2-}$ and $RHPO_2^-$ ions will have a high value of activation enthalpy than the activation enthalpy corresponding to the decomposition of the complex.

The structure of the complex $[OsO_4RP(O)O]^{2-}$ and the nature of electron transfer with in the complex and the bimolecular reaction between $[OsO_4(OH)_2]^{2-}$ and $RHP(O)O^-$ is shown in Eqs. Eqs. (21)–(23).

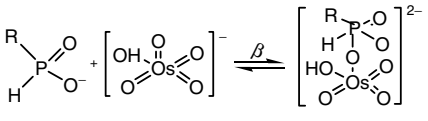

(21)

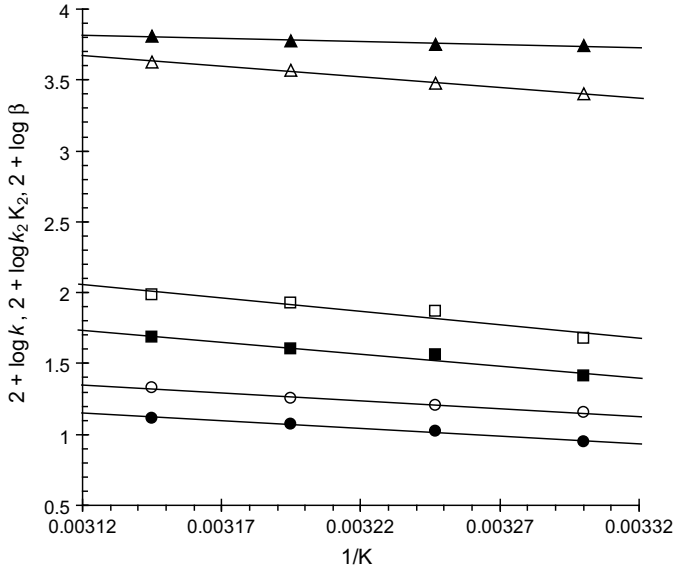

Fig. 6. The plots of log$k$ (□), logk_1 (○) and logβ (△) for $H_2PO_2^-$ and, that of log$k$ (■), logk_1 (●) and logβ (▲) for $C_6H_5HPO_2^-$ against 1/K.

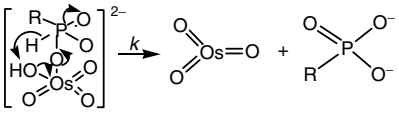

(22)

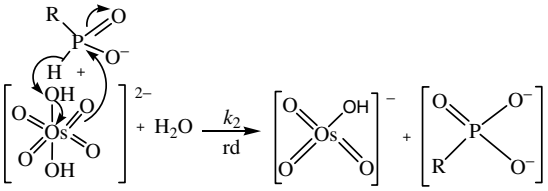

(23)

It is interesting to note that the Arrhenius energy of activation (83 kJ mol^{-1}, [19]) for the formation of the active tautomer from the inactive tautomer of $H_2PO_2^-$ ion is higher than those corresponding to the rate constants k and k_2K_2 for the rate determining steps considered in the mechanism. It is therefore considered appropriate to assume that the inactive tautomer is the reactant species and the active tautomer does not participate in the mechanism. Since the behaviour of $C_6H_5PO_2^-$ ion is similar to that of $H_2PO_2^-$ ion, therefore a similar conclusion can be made in respect of the reactive tautomeric form of $C_6H_5PO_2^-$ ion.

5. Conclusion

In conclusion it is surmised that the zero order in $Fe(CN)_6^{3-}$ preclude the ion pair formation between $Fe(CN)_6^{3-}$ and the alkali metal M^+ ions. Since the size of M^+ does not affect the rate, the M^+ ions are considered to contribute to the observed ionic strength. The major part of the slope of the Davies' plot, ~2, is probably contributed by the reaction between $OsO_4(OH)_2^{2-}$ and $H_2PO_2^-$ ($z_az_b = 2$) and the minor part by the reaction between OsO_4OH^- and $H_2PO_2^-$ ions ($z_az_b = 1$). it may be the resultant value of the two rate determining steps. The two osmium(VIII) species, which are in equilibrium with each other in the alkali solution, differ from each other by one hydroxyl ion and both of these are reactive. Thus the component of the rate independent of OH^- is ascribed to the reaction of $RHPO_2^-$ with the OsO_4OH^- ion. The reaction between $OsO_4(OH)_2^{2-}$ and $RHPO_2^-$ ions is probably through a bimolecular collision. The Michaelis-Menten plot is ascribed to the formation of the intermediate complex $OsO_4(OH)RHPO_2^{2-}$ by $OsO_4(OH)^-$

and $RHPO_2^-$ ions. This conclusion is based on the comparison of the rate limiting constants involving OsO_4OH^- and $OsO_4(OH)_2^{2-}$ ions. Therefore, the reaction does not have a resemblance with the mechanism of the oxidation of phosphinic acid by tetrahydroxoargentate(III) ion in which the OH^- ion attacks the transition state [20].

Acknowledgements

Thanks are due to the CSIR and DST Grant No. 2/17/83-STP-III for the financial support of the work. Thanks are also due to Kriti Mehrotra, my grand daughter, at Cornell University, in helping with certain references.

References

[1] J.M. Leal, B. Garcia, P.L. Domingo, Coord. Chem. Rev. 173 (1998) 79.
[2] B.S. Thyagarajan, Chem. Rev. 58 (1958) 439.
[3] M.C. Agrawal, S.K. Upadhyay, J. Sci. Indus. Res. 42 (1983) 508.
[4] F. Solymosi, Naturwissenschaften 44 (1957) 374.
[5] K.K. Sengupta, S. Basu, Indian J. Chem. 15A (1977) 108.
[6] Y. Zhong, P.K. Lim, J. Am. Chem. Soc. 111 (1989) 8398. and 8404.
[7] V.K. Jindal, M.C. Agrawal, S.P. Mushran, J. Chem. Soc. (A) (1970) 2060.
[8] V.K. Jindal, M.C. Agrawal, S.P. Mushran, Z. Naturforsch. 25B (1970) 100.
[9] D. Mohan, V.K. Chhabra, Y.K. Gupta, J. Chem. Soc., Dalton Trans. (1975) 1737.
[10] R.K. Panda, G. Neogi, D. Ramaswamy, Bull. Chem. Soc. Jpn. 55 (1982) 587.
[11] D. Mohan, Y.K. Gupta, J. Chem. Soc., Dalton Trans. (1977) 1085.
[12] K.K. Sengupta, J.K. Chakladar, B.B. Pal, D.C. Mukherji, J. Chem. Soc., Perkin Trans. II (1973) 926.
[13] Raj N. Mehrotra, Can J. Chem. 63 (1985) 663.
[14] A. Fratiello, E.W. Anderson, J. Am. Chem. Soc. 85 (1963) 519.
[15] W.A. Jenkins, D.M. Yost, J. Inorg. Nucl. Chem. 11 (1959) 297.
[16] J.R. Van Wazer, Phosphorous and its Compounds, vol. 1, Interscience, New York, 1958.
[17] A.W. Frank, J. Org. Chem. 26 (1961) 850.
[18] W.V. Bhagwat, N.R. Dhar, J. Indian Chem. Soc. 6 (1929) 781.
[19] G.C. Roper, T.E. Hass, H.P. Gilman, Inorg. Chem. 9 (1970) 1049.
[20] Raj N. Mehrotra, Louis J. Kirschenbaum, Inorg. Chem. 28 (1989) 4327.
[21] S.J. Paton, C.H. Brubaker Jr., Inorg. Chem. 12 (1973) 1402.
[22] F. Aziz, G.A. Mirza, Talanta 11 (1964) 889.
[23] G.J. Brigardt, W.A. Waters, I.R. Wilson, J. Chem. Soc. (1973) 1582.
[24] B.M. Chadwick, A.G. Sharpe, in: H.J. Emelius, A.G. Sharpe (Eds.), Advances Inorganic Chemistry Radiochemistry, vol. 8, Academic Press, New York, NY, 1966, p. 83.
[25] R.T. Jones, E.H. Swift, Anal. Chem. 25 (1953) 1272.
[26] V.M. Plets, Zh. Obsheh. Khim. 6 (1936) 1198.
[27] D.N. Bernhart, Anal. Chem. 26 (1954) 1798.
[28] R.K. Panda, G. Neogi, D. Ramaswamy, Bull. Chem. Soc. Jpn. 55 (1982) 587.
[29] Vimal Soni, R.S. Sindal, Raj N. Mehrotra, Polyhedron 24 (2005) 1167.
[30] R.D. Sauerbrum, E.B. Sandell, J. Am. Chem. Soc. 75 (1953) 4170.
[31] F.A. Cotton, G. Wilkinson, Advanced Inorganic Chemistry, 5th ed., John Wiley, New York, 1988.
[32] Raj N. Mehrotra, R.C. Kapoor, S.K. Vajpai, J. Chem. Soc., Dalton Trans. (1984) 999.
[33] W. Levason, J. Chem. Soc., Dalton Trans. (1985) 199.
[34] J.G. Leipoldt, C.R. Dennis, A.J. Van Wyk, L.D.C. Bok, Inorg. Chim. Acta 34 (1979) 237.
[35] L. Michaelis, M.L. Menten, Biochem. Z. 49 (1913) 333.
[36] D.V.S. Jain, F.S. Nandel, J. Chem. Soc., Dalton Trans. (1977) 949.
[37] J.M. Leal, P.L. Domingo, B. García, S. Ibeas, J. Chem. Soc., Faraday Trans. (1993) 3571.
[38] J.M. Leal, P.L. Domingo, B. García, S. Ibeas, New J. Chem. 18 (1994) 1233.
[39] C.W. Davies, Ion Association, Butterworths, London, 1962.

2.1.2. Preparation of the ligands

The ligands SMDTC and SBDTC have been synthesized according to the known methods of Audrieth et al. [23] and Ali and Tarafdar [24], respectively. Briefly, 11.4 g of (0.2 mol) KOH in 70 ml of absolute ethanol with 10 g (0.2 mol) of hydrazine hydrate was kept in an ice bath (temperature below 5 °C) and chilled CS_2 (0.2 mol, 15.2 g) was added dropwise over a period of 1 h with constant stirring (caution! CS_2 should not be added at a faster rate). A yellow mass was obtained after the complete addition of CS_2 and the reaction mixture was stirred for another half an hour. The yellow mass was separated and dissolved in cold 40% aqueous ethanol (60 ml). The mixture was again kept in an ice bath and CH_3I (0.2 mol, 20.8 g) for SMDTC or benzyl chloride (0.2 mol, 25.2 g) for SBDTC was added dropwise such that the temperature of the solution was maintained between 0 and 5 °C. After the complete addition of CH_3I or $PhCH_2Cl$, a white product formed which was filtered off and finally washed with water. Recrystallisation from CH_2Cl_2 gave the pure white crystalline ligand. The yield is 65–70% in each case. ^{1}H NMR of SMDTC (ppm, DMSO-d_6): δ 10.79 (1H, s, N*H*, thiol form), 5.06 (2H, s, NH_2), 3.48 (3H, s, SCH_3), 2.70 (1H, s, N*H* thione form). ^{1}H NMR of SBDTC (ppm, DMSO-d_6): δ 10.86 (1H, s, N*H*), 7.42–7.20 (5H, m, C_6H_5), 4.38 (2H, s, CH_2, thione form), 4.37 (2H, s, CH_2, thiol form).

2.1.3. General method of preparation of the complexes

To 1 mmol (0.331 g) of cadmium nitrate tetrahydrate dissolved in ethanol (10 ml) (ACS grade, ≥99.5%) was added the appropriate *S*-alkyl/aryl dithiocarbazate (2 mmol) in the same solvent (20 ml). The resulting solution was heated at 60 °C while being stirred for 20 min, whereupon a white flocculent precipitate formed. The solid thus obtained was filtered off and washed with hot aqueous ethanol and dried over silica gel. The crude products were recrystallized from water. During recrystallization good quality colorless single crystals of **1** were obtained for X-ray data collection. Yield: 55–60% in each case. For **1**: m.p. (decomposition) 120–122 °C, $\Lambda_m = 180\ \Omega^{-1}\ cm^{-2}\ mole^{-1}$, *Anal.* Calc. for $C_6H_{18}N_8S_6O_6Cd$: C, 11.95; H, 2.98; N, 18.59; S, 31.87. Found: C, 11.78; H, 2.93; N, 18.81; S, 31.79%. ^{1}H NMR (ppm, DMSO-d_6): δ 10.93 [1H, br s, N*H*], 3.73 [1H, m, CN*H*]. For **2**: m.p. (decomposition): 152–154 °C, $\Lambda_m = 175\ \Omega^{-1}\ cm^{-2}\ mole^{-1}$, *Anal.* Calc. for $C_{16}H_{20}N_6S_4O_6Cd$: C, 30.36; H, 3.16; N, 13.28; S, 20.24. Found: C, 30.45; H, 3.17; N, 13.15; S, 20.38%. ^{1}H NMR (ppm, DMSO-d_6): δ 10.97 [1H, br s, N*H*], 7.35 [5H, m, C_6H_5], 4.46 [2H, s, CH_2].

2.2. Characterization

2.2.1. Instrumentations

Elemental analyses were carried out with a FISONS EA-1108 CHN analyzer. The molar conductances of 10^{-3} (M) solutions of the metal complexes in DMSO were measure at 30 °C using a Thermo Orion model 550A conductivity meter and a dip-type cell with a platinised electrode. IR spectra (4000–500 cm^{-1}) were recorded on a Bruker EQUINOX 55 FT-IR spectrophotometer with samples prepared in KBr pellets. The electronic spectra of the complexes were recorded with a Varian Cary 5000 spectrophotometer. The TG analyses were recorded in a TGA Q500 V6.7 Build 203 TG instrument at a heating rate of 10 °C/min under nitrogen. The ^{1}H NMR spectra were recorded on a Bruker AMX-500 FTNMR spectrophotometer at room temperature using DMSO-d_6 as the solvent.

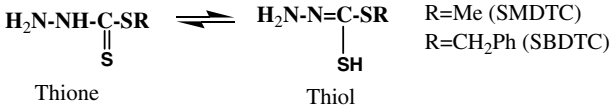

Scheme 1. Thione–thiol tautomerism of the ligands.

2.2.2. Crystal structure determination by X-ray Crystallography

The epoxy-coated crystal was mounted on a Bruker SMART APEX II X-ray diffractometer equipped with graphite-monochromated Mo Kα radiation (λ = 0.71073 Å) and a CCD area detector. The intensity data were collected in the phi and omega scan mode, operating at 50 kV, 30 mA at 296 K [25]. The data reduction was performed using the SAINT and SADABS programs [26].

All calculations in the structural solution and refinement were performed using the Bruker SHELXTL program [27]. The structure was solved by the heavy atom method and refined by full-matrix least-squares methods. All the non-hydrogen atoms were refined anisotropically; the hydrogen atoms were geometrically positioned and fixed with isotropic thermal parameters. The final difference of electron density maps contained no significant features.

3. Results and discussion

The ligand molecules have a proton adjacent to the thiocarbonyl group and consequently can exhibit thione–thiol tautormerism (Scheme 1). The IR spectra do not display any ν_{S-H} band at *ca.* 2600 cm^{-1}, but exhibit ν_{NH} bands in the range 3100–3200 cm^{-1}, indicating that the ligands remain in the thio-keto tautomer in the solid state. The ^{1}H NMR spectra of the ligands in DMSO-d_6 show that the ligands exist in solution with a second isomer. A sharp singlet, which integrates as one hydrogen at δ = *ca.* 10.80 ppm, is assigned by the reduced intensity of the α-NH of the ligand molecule. Another singlet at δ = 5.06 ppm in the spectrum of SMDTC corresponds to NH_2 protons but the corresponding signal does not appear in the spectrum of SBDTC. Furthermore the existence of the thiol form is indicated by the presence of two overlapping signals for CH_2 at 4.37 and 4.38 ppm in the ^{1}H NMR spectrum of SBDTC [28].

3.1. Characterization of the complexes

Solid state isolation and the satisfactory results of elemental analysis, conductance values and spectral studies including thermogravimetric analysis revealed that the reported cadmium(II) complexes derived from SMDTC and SBDTC were of good purity. The complexes are stable at room temperature and may stored in a desiccator over silica gel for a long time without any sign of decomposition and they are soluble in polar coordinating solvents like water, pyridine, DMF and DMSO. The molar conductivity

Table 1
Characteristic IR data of the ligands and their cadmium(II) complexes

Compound	ν_{NH/NH_2}	ν_{C-N}	$\nu_{C=S}$	ν_{N-N-C}	Mixed ν_{C-N} and ν_{N-N}
SMDTC	3178	1495	941	1360	1615
$[Cd(SMDTC)_3]\cdot 2NO_3$ (**1**)	3154	1523	954	1382	1626s
SBDTC	3177	1468	950	1344	1608
$[Cd(SBDTC)_2]\cdot 2NO_3$ (**2**)	3159	1496	963	1383	1601

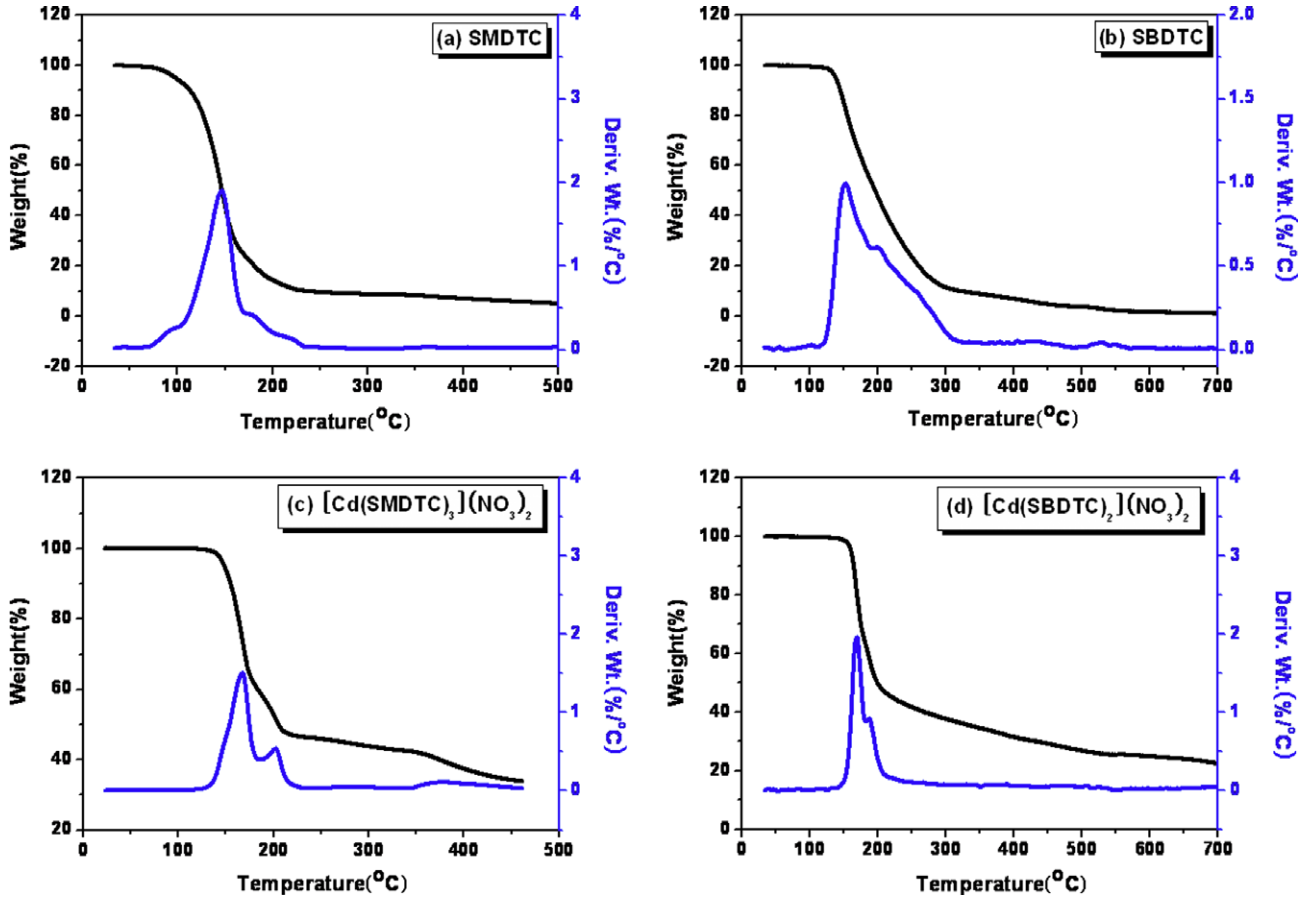

Fig. 1. TGA and DrTGA of the ligands and their cadmium(II) complexes.

values of the complexes in DMSO are quite close to those expected for 1:2 electrolytes and also confirm that the ligands coordinate to the cadmium atom in their neutral thione forms.

Infrared spectral studies (4000–500 cm^{-1}) for the uncomplexed ligands show two significant broad bands in the range 3300–3175 cm^{-1} which are attributed to the asymmetric and symmetric stretching modes of the NH_2 group and the absence of a band in the region 2600–2500 cm^{-1} indicates the absence of a free –SH group, at least in the solid state of the ligands [2]. The bands in the range 1468–1495 cm^{-1} and 1608–1615 cm^{-1} in the free ligand have been assigned to ν_{C-N} and mixed vibration ν_{C-N} and ν_{N-N}, respectively whereas the band in the region 1345–1360 cm^{-1} is due to the ν_{C-N-N} vibration. The other band in the range 950–941 cm^{-1} is ascribed to the C=S stretching vibration of the free ligands [10,22]. A comparative study of the IR spectral data of the reported complexes with those of the uncomplexed ligand (Table 1) provide meaningful information regarding the bonding sites of the ligand molecule. The strong IR band appearing in the range 3300–3175 cm^{-1} in the free ligand spectra has been found to shift to the lower frequency region in the spectra of the complexes, due to probable involvement of the nitrogen of the NH_2 group in bonding. The positive shift of the ν_{C-N} frequencies in the range 1468–1495 cm^{-1} (in the free ligands spectra) to 1496–1523 cm^{-1} on complexation with a cadmium ion indicates involvement of the nitrogen atom in bonding, indicating shorter C–N bond lengths. The vibration bands in the range 954–963 cm^{-1}, due to the C=S stretching vibration, shift to the high energy side by *ca.*15 cm^{-1} in comparison with the free ligands pointing to the participation

Table 2
Characteristic TGA data of the ligands and their cadmium(II) complexes

Complex	Loss in weight % found (calcd)	Assignment	Temperature range (°C)
SMDTC	70.17(72.13)	Loss of CH_3SH and H_2NNH_2 Loss of sulfur	80–160
	26.22(24.92)		160–240
$[Cd(SMDTC)_3] \cdot 2NO_3$ (**1**)	39.64(40.50)	Loss of two ligand	120–182
	13.71(14.94)	Loss unit $H_2NHNCSCH_3$	182–224
	12.91(12.61)	Loss of N_2O_3	230–400
	33.74(34.59)	Residue CdS and "2S"	400–461
SBDTC	46.07(45.95)	Loss of $PhCH_2$- unit	110–191
	52.16(54.05)	Loss of remaining part	191–700
$[Cd(SBDTC)_2] \cdot 2NO_3$ (**2**)	36.35(38.92)	Loss of two unit $PhCH_2S$	137–182
	21.96(19.60)	Loss of two NO_3 group	183–256
	18.76(18.65)	Loss of $SCNHNH_2$ and $CNHNH_2$ simultaneously	256–700
	22.33(22.83)	Residue CdS	>700

Table 3
Crystal data and structure refinement details for $[Cd(SMDTC)_3] \cdot 2NO_3$ (**1**)

Chemical formula	$C_6H_{18}N_8O_6S_6Cd$
Formula weight	603.04
Temperature (K)	296(2)
Wavelength (Å)	0.71073
Crystal system	monoclinic
Space group	$P21/n$
Unit cell dimensions	
a (Å)	14.9513(2)
b (Å)	7.9769(1)
c (Å)	19.4887(3)
α (°)	90
β (°)	111.418(1)
γ (°)	90
V (Å^3)	2163.80(5)
Z	4
D_{calc} (g cm^{-3})	1.851
μ(Mo Kα) (mm^{-1})	1.628
F(000)	1208
Crystal size (mm)	0.39 × 0.30 × 0.15
θ range for data collection (°)	1.48–28.38
Index range	$-19 \le h \le 14$, $-10 \le k \le 10$, $-26 \le l \le 26$
Reflections measured	22434
Independent reflections	5373 (R_{int} = 0.0218)
Completeness to θ = 28.38° (%)	99.1
Absorption correction	multi-scan
Maximum and minimum transmission	0.7923, 0.5694
Refinement method	full-matrix least-squares on F^2
Data/restraints/parameters	5373/0/244
Goodness of fit on F^2	1.009
Final R indices [$I > 2\sigma(I)$]	0.0283, 0.0625
R indices (all data)	0.0421, 0.0685
Largest difference in peak and hole (e Å^{-3})	0.528, −0.555

of the sulfur atom of the C=S group as a possible coordination site [29,30].

The complexes were prepared using a metal:ligand molar ratio of 1:2. For complex **2** the elemental analysis is consistent with the proposition having a 1:2 molar ratio, whereas the elemental analysis result of complex **1** indicates that the complex has a metal–ligand ratio of 1:3. The reaction was repeated using a 1:3 metal:ligand ratio and the product had the same decomposition temperature and IR spectrum as that prepared using a 1:2 stoichiometry, this is also further substantiated by the crystal structure analysis of **1**. The electronic spectra of the ligands exhibit two distinct absorption bands with very high intensity above 25000 cm^{-1} because of the presence of the chromophore. The UV–Vis spectra of the complexes are similar in this region. The presence of very high intensity bands in the ligands results in the overlapping of the ligand bands and the charge-transfer bands electronic spectra, and are therefore not useful in deducing the structure of the complexes. However the spectra of most of the reported four coordinated complexes have tetrahedral structures [31,32], so the structure of complex **2** is also expected to be tetrahedral.

The ^{1}H NMR spectra of the cadmium(II) complexes, when compared to that of the free ligands, show slightly downfield shifts of the positions of the NH_2 protons, NH proton and SCH_2 protons (with different chemical environments), ascribed to the fact that the coordination of the ligands to the cadmium(II) center through the β-nitrogen and thione sulfur reduces the electron density at these atoms to different extents. The appearance of a peak at a δ value of *ca.* 10.95 ppm in the spectra of the complexes for an exchangeable proton of the ligands indicates that the coordination occurs with the thione form, which is also in accordance with the findings of the IR spectra. The presence of all the characteristic peaks slightly downfield in the spectra of the complexes with respect to their ligand spectra, along with the solvent peaks, which appears nearly at the same position both in the spectra of the ligands and complexes, indicates that the ligand molecules still remain coordinated with the cadmium ion in the presence of the strongly coordinating DMSO solvent. The ^{1}H NMR spectra thus provide support for the bonding characteristic of the primary ligand in forming complexes with cadmium(II) ion as a neutral 'NS' donor [28].

The thermogravimetric analyses (TGA) are conducted to evaluate the physical behavior of the complexes. The TGA and DrTGA curves of the ligands and complexes are presented in Fig. 1 and the results are tabulated in Table 2. From the TGA/DrTGA curve of SMDTC, it can be concluded that the decomposition of the ligand is initiated at 80 °C and loses almost 90.26% by 240 °C. The 4.88% residue may be due to some trace amount of elemental sulfur or

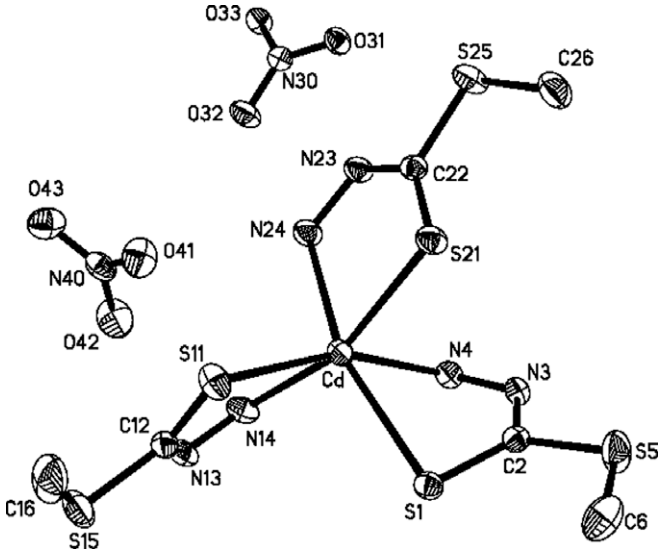

Fig. 2. ORTEP drawing of $[Cd(SMDTC)_3] \cdot 2NO_3$ (**1**) with the atomic numbering. Thermal ellipsoids are drawn at the 25% probability level.

Table 4
Selected bond lengths (Å) and angles (°) for $[Cd(SMDTC)_3] \cdot 2NO_3$ (**1**)

Cd–S(1)	2.7234(7)	Cd–N(4)	2.386(2)
Cd–S(11)	2.6090(7)	Cd–N(14)	2.379(2)
Cd–S(21)	2.6428(6)	Cd–N(24)	2.368(2)
S(1)–C(2)	1.676(2)	C(2)–N(3)	1.321(3)
N(3)–N(4)	1.403(3)	C(2)–S(5)	1.736(2)
S(5)–C(6)	1.772(4)	S(11)–C(12)	1.663(3)
C(12)–N(13)	1.323(3)	N(13)–N(14)	1.408(3)
C(12)–S(15)	1.748(3)	S(15)–C(16)	1.789(4)
S(21)–C(22)	1.664(2)	C(22)–N(23)	1.323(3)
N(23)–N(24)	1.410(3)	C(22)–S(25)	1.744(2)
S(25)–C(26)	1.792(3)	N(30)–O(31)	1.250(2)
N(30)–O(32)	1.239(2)	N(30)–O(33)	1.255(2)
N(40)–O(41)	1.231(3)	N(40)–O(42)	1.225(3)
N(40)–O(43)	1.247(3)		
S(1)–Cd–N(4)	70.58(5)	S(1)–Cd–S(11)	92.10(2)
S(1)–Cd–N(14)	103.93(6)	S(1)–Cd–S(21)	94.42(2)
S(1)–Cd–N(24)	162.28(6)	N(4)–Cd–S(11)	160.41(5)
N(4)–Cd–N(14)	99.30(7)	N(4)–Cd–S(21)	87.50(5)
N(4)–Cd–N(24)	94.18(8)	S(11)–Cd–N(14)	75.45(6)
S(11)–Cd–S(21)	103.37(2)	S(11)–Cd–N(24)	104.24(6)
N(14)–Cd–S(21)	161.63(6)	N(14)–Cd–N(24)	87.04(7)
S(21)–Cd–N(24)	75.40(5)	Cd–S(1)–C(2)	91.06(9)
Cd–N(4)–N(3)	107.7(1)	Cd–S(11)–C(12)	98.1(1)
Cd–N(14)–N(13)	113.5(2)	Cd–S(21)–C(22)	97.72(8)
Cd–N(24)–N(23)	115.1(1)	S(1)–C(2)–N(3)	123.1(2)
C(2)–N(3)–N(4)	120.9(2)	S(1)–C(2)–S(5)	125.3(2)
C(2)–S(5)–C(6)	103.8(2)	N(3)–C(2)–S(5)	111.6(2)
S(11)–C(12)–N(13)	126.0(2)	C(12)–N(13)–N(14)	122.3(2)
S(11)–C(12)–S(15)	122.7(2)	C(12)–S(15)–C(16)	103.1(2)
N(13)–C(12)–S(15)	111.3(2)	S(21)–C(22)–N(23)	126.4(2)
C(22)–N(23)–N(24)	122.5(2)	S(21)–C(22)–S(25)	123.2(2)
C(22)–S(25)–C(26)	103.1(1)	N(23)–C(22)–S(25)	110.4(2)
O(31)–N(30)–O(32)	119.8(2)	O(31)–N(30)–O(33)	120.0(2)
O(32)–N(30)–O(33)	120.2(2)	O(41)–N(40)–O(42)	118.8(3)
O(41)–N(40)–O(43)	120.5(3)	O(42)–N(40)–O(43)	120.7(3)

impurities. SBDTC shows two significant mass losses in the temperature ranges 110–191 °C (46.07%) and 191–700 °C (52.16%) due to loss of the benzyl unit and the other residual part of the ligand, respectively. The TGA curve of complex **1** (Fig. 1c) shows three weight losses in the temperature ranges 120–182, 182–224 and 230–461 °C. The first mass loss can be attributed to the loss of two moles of SMDTC ligand, while the second represents loss of the $H_2NHNCSCH_3$ unit from the remaining ligand and N_2O_3 from nitrate groups is lost in the third stage. CdS formation starts from this stage and is complete at 461 °C. The TGA curve of complex **2** shows three stages (Fig. 1d). The first with a loss of 36.35% of the total weight of the complex is due to the loss of two units of $PhCH_2S$ at 137–182 °C. The second stage corresponds to the loss of 21.96% weight and is assigned to the loss of two NO_3 groups at 183–256 °C. The last stage can be assigned to the loss of 18.76% at 256–700 °C due to decomposition of the complex into CdS residue, which is very close to the 22.33% of the total weight of the complex. TGA analysis shows that the complexes are relatively volatile with respective to the other reported complexes derived from Schiff bases of *S*-alkyl dithiocarbazates [6,33] and thus these complexes will be very susceptible to give CdS nanoparticles in solvothermal processes.

3.2. Crystal structure of $[Cd(SMDTC)_3] \cdot 2NO_3$ (**1**)

The crystallographic data and detailed information on the structure solution and refinement for $[Cd(SMDTC)_3] \cdot 2NO_3$ (**1**) are listed in Table 3. The molecular structure with the atomic numbering is shown in Fig. 2. The molecular structure of complex **1** consists of a cadmium cation chelated by neutral SMDTC molecules and free nitrate anions in a 1:2 ratio. The cadmium(II) cation and nitrate anions are mainly constructed through ionic bonds. The central cadmium(II) atom is six-coordinated by three SMTDC ligands and

Table 5
Hydrogen bonds for $[Cd(SMDTC)_3] \cdot 2NO_3$ (**1**)

D–H···A	H···A (Å)	D···A (Å)	D–H···A (°)
N(3)–H(3a)···O(33)$^{\#1}$	2.13	2.872(2)	144.5
N(4)–H(4a)···O(43)$^{\#2}$	2.20	3.082(3)	167.7
N(4)–H(4a)···O(41)$^{\#2}$	2.43	3.137(3)	135.6
N(4)–H(4a)···N(40) $^{\#2}$	2.63	3.502(3)	163.3
N(4)–H(4b)···O(31) $^{\#1}$	2.25	3.005(3)	141.6
N(13)–H(13a)···O(33)$^{\#3}$	2.07	2.916(3)	169.6
N(13)–H(13a)···O(32)$^{\#3}$	2.64	3.130(3)	117.3
N(14)–H(14a)···O(42)	2.35	3.161(4)	149.6
N(14)–H(14a)···O(43)$^{\#3}$	2.52	3.207(3)	133.5
N(14)–H(14a)···O(41)	2.56	3.185(4)	127.1
N(14)–H(14b)···O(32)$^{\#3}$	2.38	2.976(3)	123.8
N(23)–H(23a)···O(31)	2.08	2.942(3)	175.2
N(23)–H(23a)···O(32)	2.54	3.090(3)	122.6
N(23)–H(23a)···N(30)	2.67	3.440(3)	149.9
N(24)–H(24a)···O(43)$^{\#3}$	2.20	3.034(3)	153.9
N(24)–H(24b)···O(41)	2.17	2.921(3)	140.9

Symmetry transformations used to generate equivalent atoms: #1; $-x+1$, $-y+1$, $-z$, #2; x, $y+1$, z, #3; $-x+3/2$, $y+1/2$, $-z+1/2$.

forms three five-membered chelate rings with N and S donor atoms of each ligand molecule. The coordination environment around the cadmium(II) atom is octahedral. The N donor groups of the SMDTC ligand are directed towards a nitrate anion while the S donor groups are directed to the opposite faces of a nitrate anion. This conformation of ligands is very significance for the crystal packing structure and hydrogen bond networks. Selected bond lengths and angles for complex **1** are listed in Table 4. The bond lengths of Cd–N and Cd–S are within the range 2.368(2)–2.386(2) and 2.6090(7)–2.7234(7) Å, respectively, and are slightly longer than that of the previously reported structure [1]. The bond angles of N–Cd–N and S–Cd–S are in the range 87.04(7)–103.37(2)° while the bond angles of N–Cd–S are in the range 70.58(5)–75.45(6)° and 160.41(5)–162.28(6)°. The bond lengths and angles of the *S*-methyldithiocarbazate ligand and nitrate anion are within the normal ranges and are very similar to those of previously reported structures [1,34].

The crystal-packing diagram (see the Supplementary data) of this complex reveals a discrete structure and the conformation of each complex is arranged parallel to the *ac*-plane. The crystal structure consists of parallel layers of cations and anions. The SMDTC molecules in the cations are arranged with their N donor groups directed towards the anionic layer in an alternating fashion and form hydrogen bonds with the O atoms of the anion. There are inter-molecular weak hydrogen bonds between the N–H moieties of the SMDTC ligands and the O atoms of the nitrate ions. As listed in Table 5, the hydrogen bonds of N_{SMDTC}–H···$O_{nitrate}$ vary greatly in their lengths and linearity and are in the range H···$O_{nitrate}$ 2.07–2.64 Å, N_{SMDTC}···$O_{nitrate}$ 2.872(2)-3.207(3) Å, N_{SMDTC}–H···$O_{nitrate}$ 117.3–175.2°. The hydrogen bond lengths and angles of N(4)–H(4a)···O(43) (2.20 Å, 167.7°), N(13)–H(13a)···O(33) (2.07 Å, 169.6°), N(23)–H(23a)···O(31) (2.08 Å, 175.2°) and N(24)–H(24a)···O(43) (2.20 Å, 153.9°) are shorter and more linear than other hydrogen bonds. The N–H···O hydrogen bonds are linked together into two-dimensional hydrogen bond layers. These hydrogen-bonding interactions lead to a self-assembled molecular conformation and contribute to the stabilization of the crystal structure.

Attempts to grow crystals of complex **2** suitable for X-ray diffraction have been unsuccessful. Further work on the crystallization of complex **2** is in progress.

4. Conclusion

SMDTC and SBDTC behave as neutral bidentate ligands with a cadmium(II) center, as envisaged by the spectroscopic studies.

The IR spectra of the free ligands indicate that in the solid state the ligand remains in the thione form, where the existence of both tautomeric forms may be expected in solution. On the basis of the available physicochemical data and TG analysis, along with a representative crystal structure determination, it can be reasonably concluded that the ligand, SMDTC, coordinates through the nitrogen atom of the NH_2 group and the sulfur atom of the thiocarbonyl group in its neutral thione form in an approximately octahedral environment in complex **1**, whereas complex **2** is expected to be a tetrahedral complex with same set of donor atoms with a larger phenyl substituent of SBDTC in its neutral thione form. The presence of the phenyl group makes the ligand SBDTC bulkier than SMDTC and consequently only two SBDTC ligands are expected to be sufficient to meet the coordination saturation of the central cadmium atom in $[Cd(SBDTC)_2] \cdot 2NO_3$. The TG analysis of the complexes also reveals that both complexes are volatile above 100 °C and finally give a CdS residue, thus these complexes may be used as single source molecular precursors for CdS nanoparticle syntheses at moderately low temperatures. A primary investigation to synthesis CdS nanoparticles using these complexes gave positive results and further work on this is in progress. To the best of our knowledge, these cadmium(II) complexes of *S*-alkyl/aryl dithiocarbazates have been reported for the first time along with the determination of the crystal structure of one of the reported compounds.

Acknowledgements

This research was supported both by the Korea Foundation for International Cooperation of Science and Technology through the Global Research Lab. (GRL) Program funded by the Ministry of Education, Science and Technology, by a grant from the Fundamental R&D Program for Core Technology of Materials funded by the Ministry of Knowledge Economy, and the Republic of Korea.

Appendix A. Supplementary data

CCDC 690742 contains the supplementary crystallographic data for this paper. These data can be obtained free of charge from The Cambridge Crystallographic Data Centre via www.ccdc.cam.ac.uk/data_request/cif. Supplementary data associated with this article can be found, in the online version, at doi:10.1016/j.poly.2008.07.039.

References

[1] K.B. Chew, M.T.H. Tarafder, K.A. Crouse, A.M. Ali, B.M. Yamin, H.K. Fun, Polyhedron 23 (2004) 1385.
[2] M.T.H. Tarafder, A. Asmadi, S.M.S. Talib, A.M. Ali, K.A. Crouse, Trans. Met. Chem. 26 (2001) 170.
[3] M.E. Hossain, M.N. Alam, J. Begum, M.A. Ali, M. Nazimuddin, F.E. Smith, R.C. Hynes, Inorg. Chim. Acta 249 (1996) 207.
[4] K.A. Crouse, K.B. Chew, M.T.H. Tarafder, A. Kasbollah, A.M. Ali, B.M. Yamin, H.K. Fun, Polyhedron 23 (2004) 161.
[5] M.R. Maurya, S. Khurana, S. Shailendra, A. Azam, W. Zhang, D. Rehder, Eur. J. Inorg. Chem. (2003) 1966.
[6] N. Bharti, M.R. Maurya, F. Naqvi, A. Bhattacharya, S. Bhattacharya, A. Azam, Eur. J. Med. Chem. 35 (2000) 481.
[7] Y.P. Tian, M.L. Zhang, Z.J. Hu, H.M. Hu, J.Y. Wu, X.J. Zhang, S.Y. Zhang, X.T. Tao, M.H. Jiang, H.P. Chen, S. Chantapromma, H.K. Fun, Trans. Met. Chem. 30 (2005) 778.
[8] H. Zhou, D. Li, P. Wang, L. Cheng, Y. Gao, Y. Zhu, J. Wu, Y. Tian, X. Tao, M. Jiang, H.K. Fun, J. Mol. Struct. 826 (2007) 205.
[9] X.H. Zhu, X.F. Chen, Y. Zhang, X.Z. You, W.L. Tan, W. Ji, Chem. Lett. (1999) 1211.
[10] L.H. van Poppel, T.L. Groy, M. Tyler Caudle, Inorg. Chem. 43 (2004) 3180.
[11] D. Fan, M. Afzaal, M.A. Mallik, C.Q. Nguyen, P. O'Brien, P. Thomas, Coord. Chem. Rev. 251 (2007) 1878.
[12] N. Revaprasadu, M.A. Malik, P. O'Brien, G. Wakefield, Chem. Commun. (1999) 1573.
[13] P.S. Nair, N. Revaprasadu, T. Radhakrishnan, G.A. Kolawole, J. Mater. Chem. 11 (2001) 1555.
[14] T. Trindade, P. O'Brien, Adv. Mater. 8 (1996) 161.
[15] M. Green, P. O'Brien, Chem. Commun. (1999) 2235.
[16] B. Ludolph, M.A. Malik, Chem. Commun. (1998) 1849.
[17] T. Trindade, P. O'Brien, J. Mater. Chem. 6 (1996) 343.
[18] N. Pradhan, S. Efrima, J. Am. Chem. Soc. 125 (2003) 2050.
[19] Y. Sun, S. Lee, N. Kang, J. Cheon, J. Am. Chem. Soc. 123 (2001) 5150.
[20] G. Kedarnath, V.K. Jain, S. Ghoshal, G.K. Dey, C.A. Ellis, E.R.T. Tiekink, Eur. J. Inorg. Chem. (2007) 1566.
[21] D.X. West, S.B. Padhye, P.B. Sonawane, Struct. Bond (Berl.) 76 (1991) 1.
[22] M.A. Ali, A.H. Mirza, M.H.S.A. Hamid, P.V. Bernhardt, O. Atchade, X. Song, G. Eng, L. May, Polyhedron 27 (2008) 977.
[23] L.F. Audrieth, E.S. Scott, P.S. Kippur, J. Org. Chem. 19 (1954) 733.
[24] M.A. Ali, M.T.H. Tarafdar, J. Inorg. Nucl. Chem. 39 (1977) 1785.
[25] Bruker, SMART (Version 5.625) Data Collection Program, Bruker AXS Inc., Madison, Wisconsin, USA, 2001.
[26] Bruker, SAINT (Version 6.28a) and SADABS (Version 2.03) Data Reduction and Absorption Correction Program, Bruker AXS Inc., Madison, Wisconsin, USA, 2001.
[27] G M. Sheldrick, SHELXTL (Version 6.12) Structure Analysis Program, Bruker AXS Inc., Madison, Wisconsin, USA, 2001.
[28] K. Tampouris, S. Coco, A. Yannopoulos, S. Koinis, Polyhedron 26 (2007) 4269.
[29] W. Han, M. Gao, Cryst. Growth Des. 8 (2008) 1023.
[30] X. Chen, Z. wang, X. Wang, J. Wan, J. Liu, Y. Qian, Inorg. Chem. 44 (2005) 951.
[31] M. Chan, K. Crouse, M.I.M. Tahir, R. Rosli, N.U. Tsafe, A.R. Cowley, Polyhedron 27 (2008) 1141.
[32] M.T.H. Tarafder, A. Kasbollah, K.A. Crouse, A.M. Ali, B.M. Yamin, H.K. Fun, Polyhedron 20 (2001) 2363.
[33] A.A.M. Aly, Trans. Met. Chem. 16 (1991) 249.
[34] M.A. Ali, A.H. Mirza, M. Nazimuddin, H. Rahaman, R.J. Butcher, Trans. Met. Chem. 27 (2002) 268.

2.2. Syntheses of $[La_2(PDP)_3(H_2O)_2]$ (**1**) and $[Eu_2(PDP)_3(H_2O)_2]$ (**2**)

A mixture of $La(NO_3)_3 \cdot 6H_2O$ (0.117 g, 0.27 mmol) and H_2PDP (0.060 g, 0.27 mmol) was placed in a Teflon-lined Parr bomb containing 5 mL of deionized water. The bomb was sealed, heated at 170 °C for 3 days, and allowed to cool to room temperature. Yellow crystals of **1** were isolated by decanting the supernatant; washed with deionized water, *N*,*N*-dimethylformamide (DMF), and ethanol; and air-dried to give 0.0195 g of product (44%). Main IR absorption bands (cm^{-1}): 1541 (s), 1410 (s), 1337 (m), 1318 (m), 1291 (m), 1237 (m), 875 (m), 845 (m), 826 (m).

Compound **2** was prepared analogously in 72% yield using $Eu(NO_3)_3 \cdot 6H_2O$. Main IR absorption bands (cm^{-1}): 1545 (s), 1425 (s), 1340 (m), 1320 (m), 1292 (m), 1234 (m), 877 (m), 847 (m), 823 (m).

2.3. X-ray crystallography

Several crystals of each compound were indexed on a Bruker SMART CCD diffractometer using 40 frames with an exposure time of 20 s per frame. One crystal of each compound with good reflection quality was chosen for data collection. The exposure time was 20 s for each frame. The reflections were collected in the hemisphere of the reciprocal lattice of the triclinic cell to ensure enough redundancy. An empirical absorption correction using the program SADABS [16] was applied to all observed reflections. The structure was solved with direct methods using the SHELXTL program [16,17]. Full matrix least-squares refinement on F^2 was carried out using the SHELXTL program [16]. The unit cell information and refinement details are summarized in Table 1.

3. Results and discussion

Compounds **1** and **2** have been synthesized from the hydrothermal reactions of lanthanide(III) nitrates with H_2PDP. They occur as crystalline solids that are insoluble in water or common organic solvents such as acetone and ethanol. The IR spectra of **1** and **2** are similar, both showing intense absorption bands around 1541 and 1410 cm^{-1} that are diagnostic of metal-coordinated carboxylate groups [18]. The absence of the strong carboxyl absorption band at 1703 cm^{-1} indicates complete deprotonation of H_2PDP.

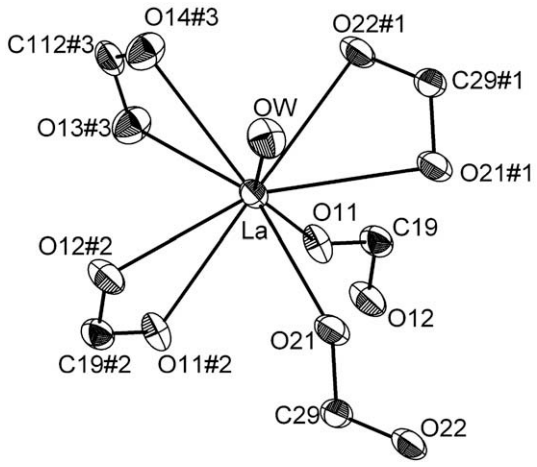

Fig. 1. An ORTEP diagram showing the lanthanum coordination environment in **1**. Thermal ellipsoids are at 30% probability. Symmetry labels #1–#3 are specified in Table 2.

Compounds **1** and **2** are isostructural, as shown by single-crystal X-ray diffraction analysis, and the structure of **1** is described here representatively. There exist one crystallographically independent La(III) ion and one and a half PDP moieties in the asymmetric unit. The La(III) ion is, apparently due to its large size, coordinated by nine oxygen atoms, eight of them from five carboxylate groups of different PDP units and one from a water molecule (Fig. 1). This coordination geometry can be regarded as a distorted tricapped trigonal prism, with O14#3, O22#1, OW, O11, O21, and O11#2 filling the vertices and O12#2, O13#3, and O21#1 capping the rectangular faces. We have previously observed a similar coordination environment for the nine-coordinate La(III) ion in $[La_2(PDA)_3(H_2O)] \cdot 2H_2O$ [12]. The La–O (carboxylate) bond distances in **1** range from 2.485(9) to 2.665(9) Å, and that of the La–O (aqua) bond is 2.534(9) Å, all of which are consistent with those observed for $[La_2(PDA)_3(H_2O)] \cdot 2H_2O$ [12]. Selected bond distances and angles are presented in Table 2.

In the network structure of **1**, each La(III) ion is interconnected through two COO groups with two other La(III) ions, forming an

Table 1
Crystal data and structure refinement for compounds **1** and **2**

	1	**2**
Empirical formula	$La_2C_{36}H_{40}O_{14}$	$Eu_2C_{36}H_{40}O_{14}$
Formula weight	974.52	1000.60
Crystal system	triclinic	triclinic
Space group	$P\bar{1}$	$P\bar{1}$
a (Å)	6.5262(15)	6.2642(5)
b (Å)	11.608(3)	11.61790(10)
c (Å)	12.552(3)	12.8199(2)
α (°)	70.908(4)	70.418(12)
β(°)	83.942(5)	84.950(15)
γ (°)	81.274(4)	81.833(15)
V (Å^3)	886.6(4)	869.30(7)
Z	1	1
T (K)	293(2)	293(2)
D_{calcd} (g/cm^3)	1.825	1.911
λ (Mo Kα) (Å)	0.71073	0.71073
μ (mm^{-1})	2.447	3.646
Data/restraints/parameters	2989/0/254	3921/0/235
Final R indices $[I > 2\sigma(I)]$		
R_1	0.0870	0.0356
wR_2	0.1573	0.0726
R indices (all data)		
R_1	0.1025	0.0419
wR_2	0.1634	0.0761

* $R_1 = \sum||F_o| - |F_c||/\sum|F_o|$; $wR_2 = [\sum[w(F_o^2 - F_c^2)^2]/\sum[w(F_o^2)^2]]^{1/2}$.

Table 2
Bond lengths [Å] and angles [°] for compound **1**

La–O(11)	2.485(9)	La–O(13)#3	2.567(9)
La–O(21)	2.506(9)	La–O(14)#3	2.582(10)
La–OW	2.534(9)	La–O(11)#2	2.634(9)
La–O(22)#1	2.556(9)	La–O(21)#1	2.665(9)
La–O(12)#2	2.560(9)		
O(11)–La–O(21)	90.3(3)	O(11)–La–O(11)#2	68.0(3)
O(21)–La–O(11)#2	80.3(3)	O(13)#3–La–O(14)#3	50.3(3)
OW–La–O(11)#2	130.8(3)	O(12)#2–La–O(14)#3	80.5(3)
O(22)#1–La–O(11)#2	146.4(3)	O(22)#1–La–O(14)#3	74.8(3)
O(12)#2–La–O(11)#2	49.7(3)	OW–La–O(14)#3	71.6(3)
O(13)#3–La–O(11)#2	71.2(3)	O(21)–La–O(14)#3	146.2(3)
O(14)#3–La–O(11)#2	108.8(3)	O(11)–La–O(14)#3	123.5(3)
O(11)–La–O(21)#1	81.8(3)	O(12)#2–La–O(13)#3	80.0(3)
O(21)–La–O(21)#1	66.2(3)	O(22)#1–La–O(13)#3	88.9(3)
OW–La–O(21)#1	72.5(3)	OW–La–O(13)#3	121.3(3)
O(22)#1–La–O(21)#1	49.7(3)	O(21)–La–O(13)#3	151.6(3)
O(12)#2–La–O(21)#1	143.2(3)	O(11)–La–O(13)#3	79.0(3)
O(13)#3–La–O(21)#1	136.4(3)	O(22)#1–La–O(12)#2	154.6(3)
O(14)#3–La–O(21)#1	116.2(3)	OW–La–O(12)#2	83.7(3)
O(11)#2–La–O(21)#1	134.5(3)	O(21)–La–O(12)#2	81.9(3)
O(11)–La–OW	154.3(3)	O(11)–La–O(12)#2	117.6(3)
O(21)–La–OW	8.0(3)	OW–La–O(22)#1	82.7(3)
O(11)–La–O(22)#1	82.0(3)	O(21)–La–O(22)#1	115.9(3)

Symmetry transformations used to generate equivalent atoms: #1, $-x-1$, $-y+1$, $-z+2$; #2, $-x$, $-y+1$, $-z+2$; #3, $x+1$, $y-1$, z.

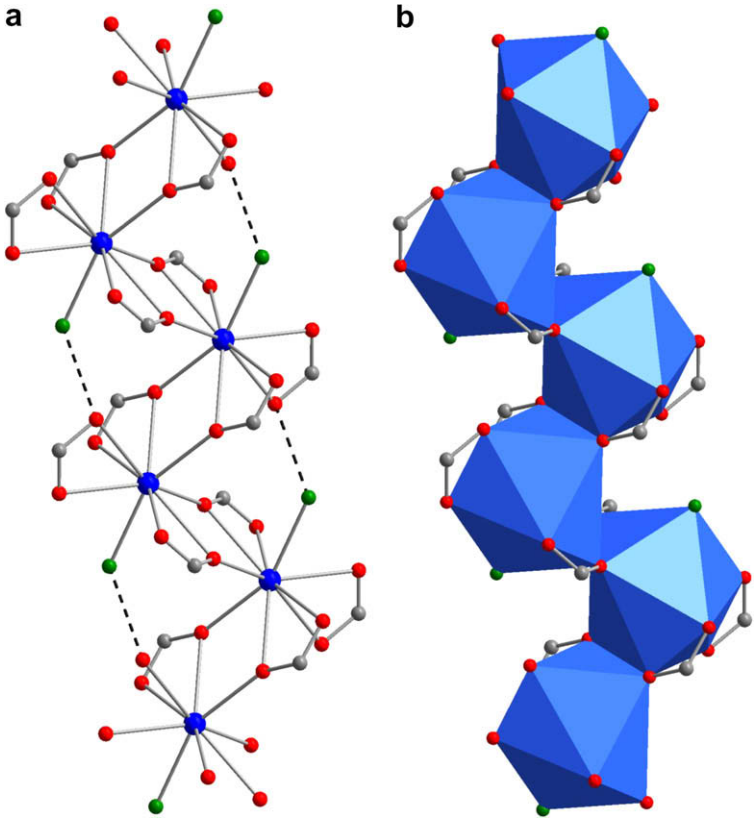

Fig. 2. (a) A ball-and-stick representation of the 1D La(H_2O)–OOC chain showing the interconnections between lanthanum ions, as well as the OW–O (carboxylate) hydrogen bonds (dashed lines). (b) A representation highlighting lanthanum coordination polyhedra. Color scheme: La, blue; O, red; C, dark gray. (For interpretation of the references to colour in this figure legend, the reader is referred to the web version of this article.)

infinite La(H_2O)–OOC zigzag chain that extends along the crystallographic *a* axis (Fig. 2a). The La(III) ions act as nodes in the chain, and the two symmetry-equivalent COO moieties bridge two adjacent La(III) ions in tridentate bonding mode, affording two La–O–C–O–La strands. Although no hydrogen atoms were located for the coordinated water molecule, the OW–O (carboxylate) distances suggest that there is one class of hydrogen bonding interaction for O13···OW at 2.755(9) Å, as indicated by the dashed lines in Fig. 2a. A better view of the 1D zigzag chain is provided by a representation that highlights lanthanum coordination polyhedra (Fig. 2b). These infinite 1D chains constitute supramolecular SBUs that are cross-linked via $-CH_2CH_2C_6H_4CH_2CH_2-$ tethers of the PDP anions,

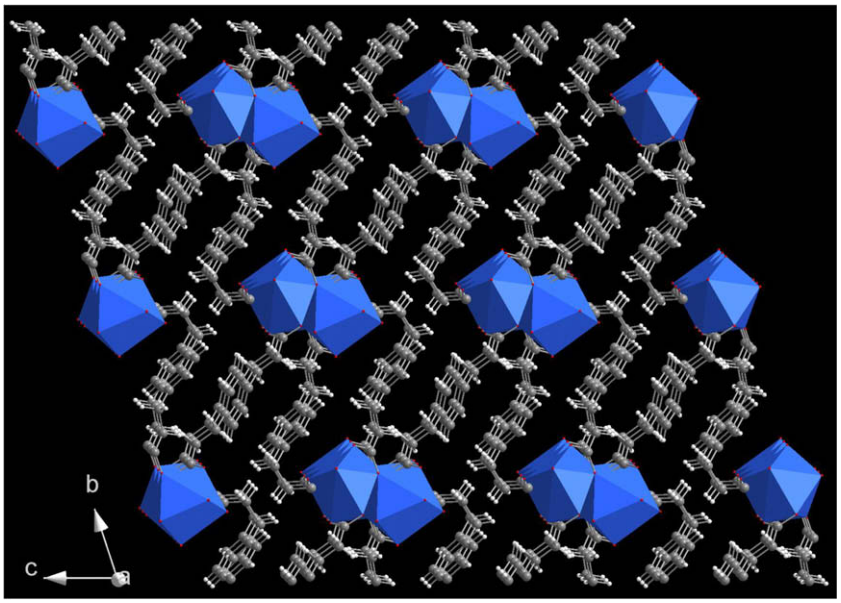

Fig. 3. The 3D network structure of [$La_2(PDP)_3(H_2O)_2$] viewed along the *a* axis. Color scheme: La coordination polyhedron, blue; C, gray; H, white. (For interpretation of the references to colour in this figure legend, the reader is referred to the web version of this article.)

affording a 3D coordination polymer (Fig. 3). A space-filling model analysis of the network structure of **1** indicates that the void in the structure is not large enough to include guest water molecules. This explains why compound **1**, $[La_2(PDP)_3(H_2O)_2]$, contains only coordinated water and no guest water. Compared with $[Ln_2(PDA)_3(H_2O)] \cdot 2H_2O$ [12], compound **1** has a more condensed structure. Apparently, the more flexible $-CH_2CH_2C_6H_4CH_2CH_2-$ tether renders the atoms closer to one another, leaving little empty space in the channels.

In conclusion, we have synthesized $[Ln_2(PDP)_3(H_2O)_2]$ (Ln = La, Eu), two novel isostructural lanthanide–carboxylate coordination polymers. The 3D network structure of $[Ln_2(PDP)_3(H_2O)_2]$ consists of infinite 1D $La(H_2O)$–OOC chains that are cross-linked by organic spacer groups. These structures lend support to the notion of infinite supramolecular SBUs. We have also offered an insight into the condensedness of the structure of $[Ln_2(PDP)_3(H_2O)_2]$. Currently, we are investigating other ditopic carboxylates, hoping to correlate their structures with the frameworks of the resulting lanthanide–carboxylate coordination polymers.

Supplementary data

CCDC 658050 and 658051 contain the supplementary crystallographic data for **1** and **2**. These data can be obtained free of charge via http://www.ccdc.cam.ac.uk/conts/retrieving.html, or from the Cambridge Crystallographic Data Centre, 12 Union Road, Cambridge CB2 1EZ, UK; fax: (+44) 1223-336-033; or e-mail: deposit@ccdc.cam.ac.uk.

Acknowledgements

The authors gratefully acknowledge support for this work from the donors of The Petroleum Research Fund, administrated by the ACS; the National Science Foundation (Grant DMR-0094872); Research Corporation; and Beijing Institute of Petrochemical Technology.

References

[1] (a) S. Kitagawa, S.-i. Noro, T. Nakamura, Chem. Commun. (2006) 701;
(b) A.K. Cheetham, C.N.R. Rao, R.K. Feller, Chem. Commun. (2006) 4780;
(c) R.J. Hill, D.-L. Long, N.R. Champness, P. Hubberstey, M. Schröder, Acc. Chem. Res. 38 (2005) 335;
(d) S. Kitagawa, R. Kitaura, S.-i. Noro, Angew. Chem., Int. Ed. 43 (2004) 2334;
(e) C. Janiak, Dalton Trans. (2003) 2781;
(f) O.M. Yaghi, M. O'Keeffe, N.W. Ockwig, H.K. Chae, M. Eddaoudi, J. Kim, Nature 423 (2003) 705;
(g) O.R. Evans, W. Lin, Acc. Chem. Res. 35 (2002) 511;
(h) B. Moulton, M.J. Zaworotko, Chem. Rev. 101 (2001) 1629.
[2] S. Muniappan, S. Lipstman, S. George, I. Goldberg, Inorg. Chem. 46 (2007) 5544.
[3] S. Neogi, P.K. Bharadwaj, Polyhedron 25 (2006) 1491.
[4] X.-J. Zheng, T.-T. Zheng, L.-P. Jin, J. Mol. Struct. 740 (2005) 31.
[5] A. Thirumurugan, S. Natarajan, Eur. J. Inorg. Chem. (2004) 762.
[6] Y. Wan, L. Jin, K. Wang, L. Zhang, X. Zheng, S. Lu, New J. Chem. 26 (2002) 1590.
[7] L. Pan, N. Zheng, Y. Wu, S. Han, R. Yang, X. Huang, J. Li, Inorg. Chem. 40 (2001) 828.
[8] T.M. Reineke, M. Eddaoudi, M. O'Keeffe, O.M. Yaghi, Angew. Chem., Int. Ed. 38 (1999) 2590.
[9] T.M. Reineke, M. Eddaoudi, M. Fehr, D. Kelley, O.M. Yaghi, J. Am. Chem. Soc. 121 (1999) 1651.
[10] V. Kiritsis, A. Michaelides, S. Skoulika, S. Golhen, L. Ouahab, Inorg. Chem. 37 (1998) 3407.
[11] L. Pan, E.B. Woodlock, X. Wang, Inorg. Chem. 39 (2000) 4174.
[12] L. Pan, K.M. Adams, H.E. Hernandez, X. Wang, C. Zheng, Y. Hattori, K. Kaneko, J. Am. Chem. Soc. 125 (2003) 3062.
[13] N.L. Rosi, J. Kim, M. Eddaoudi, B. Chen, M. O'Keeffe, O.M. Yaghi, J. Am. Chem. Soc. 127 (2005) 1504.
[14] Y. Kim, M. Suh, D.-Y. Jung, Inorg. Chem. 43 (2004) 245.
[15] S.K. Ghosh, P.K. Bharadwaj, Inorg. Chem. 43 (2004) 2293.
[16] G.M. Sheldrick, SHELXTL. Version 5; Siemens Analytical Instruments Inc.: Madison, Wisconsin, 1994.
[17] A. Altomare, G. Cascarano, C. Giacovazzo, A. Guagliardi, M.C. Burla, G. Polidori, M. Camalli, J. Appl. Crystallogr. 27 (1994) 435.
[18] K. Nakamoto, Infrared and Raman Spectra of Inorganic and Coordination Compounds, fifth ed., Wiley & Sons, New York, 1997.

used in tumor therapeutics [25]. Cobalt(III) nitrogen mustard complex has also been shown to be potential hypoxia-activated prodrug [26,27]. Some of the cobalt(II) complexes, such as $[Co(tfa)_2(happ)]$, are known to function as specific probe for DNA bulges due to its ability to cleave DNA specifically [28].

Our research group currently focuses on metallo-intercalators of various metals incorporating terpyridine ligands [29–31]. Terpyridine ligands are known for intercalation and due to the presence of conjugated aromatic core, exhibit several interesting luminescence properties. Like the excited state of the ruthenium(II) complex, excited state of cobalt(II) and cobalt(III) complexes too can bring about cleavage of macromolecules like protein and DNA. Schiff base ligand in the presence of cobaltous chloride has been shown to induce site-specific photocleavage of protein [32]. However, cobalt(II) and cobalt(III) complexes have not been exploited for photodynamic therapy. We have shown that some of the cobalt complexes with tridentate ligands like bzimpy and ptpy are good candidates for photoactivated DNA strand cleavage [33,34]. Towards achieving our goal of developing cobalt complexes of tridentate ligands, which may find therapeutic applications due to their oxidative cleavage or photocleavage of DNA, we report here the syntheses, characterization, DNA binding and cleavage studies of two new cobalt complexes, namely $[Co(Itpy)]^{2+}$ **1** and $[Co(Itpy)]^{3+}$ **2** derived from tridentate imidazole terpyridine ligand (Scheme 1).

A host of physical methods like absorption, fluorescence, cyclic voltammetry and viscosity measurements have been used to probe the interactions of the cobalt complexes with CT-DNA.

2. Experimental

2.1. Materials

Chemicals such as 2-acetyl pyridine and imidazole-2-carboxaldehyde used for ligand synthesis were purchased from Aldrich Chemicals and used as received. All other chemicals used in this study like ammonium acetate, potassium permanganate, sodium perchlorate and solvents like acetonitrile, dimethyl sulfoxide, diethyl ether, methanol, perchloric acid and hydrochloric acid, purchased from Rankem, were of analytical grade and used as received without further purification. The ligand imidazole terpyridine (Itpy) was prepared using published procedures [35]. Calf thymus DNA was purchased from SRL (India). Agarose (molecular biology grade) and Ethidium bromide were procured from Sigma chemicals. Buffers were prepared using deionised and sonicated triple distilled water. Tris (hydroxymethyl) aminomethane–HCl (Tris–HCl) buffer (pH, 7.2) was used for all DNA binding and cleavage studies. Concentrated stock solutions of CT-DNA (7 mM) were prepared in Tris buffer. A solution of CT-DNA in the buffer gave the UV absorbance ratio of ~1.8–1.9:1, at 260 and 280 nm indicating that the DNA was sufficiently free of protein [36]. DNA concentration, more precisely nucleotide phosphate (NP) concentration, was determined by UV absorbance at 260 nm. The extinction coefficient was taken to be 6600 mol^{-1} cm^{-1} [37]. Stock solutions of DNA were stored at 4 °C and used within 4 days.

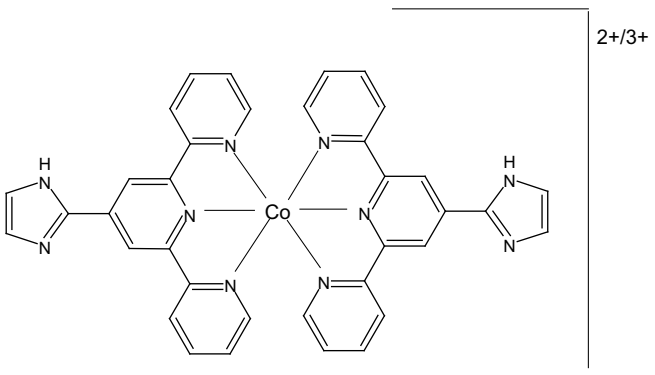

Scheme 1. Complex **1** is dipositive and **2** is tripositive complex.

2.2. Physical measurements

UV–Vis spectra of the complexes and absorption titration studies were conducted using Perkin–Elmer Lambda 35 double beam spectrophotometer at 25 °C. Elemental Analyses were done using Heraeus CHN–O– Rapid Analyser. The infrared spectra of the complexes were recorded on Perkin–Elmer FT-IR spectrometer. Positive ion electrospray ionization mass spectra of the complexes were obtained by using Thermo Finnigan LCQ 6000 advantage max ion trap mass spectrometer. The emission spectra were recorded in varian spectrofluorimeter. Cyclic Voltammetric experiments were performed on CH instrument (USA) model CH-620 B, electrochemical analyzer. The three electrode configuration, a glassy carbon as working electrode, saturated calomel electrode as reference electrode and platinum electrode as auxillary electrode was used. Deoxygenated, anhydrous acetonitrile solutions containing tetrabutyl ammonium perchlorate (TBAP) as supporting electrolyte were used for the electrochemical measurements. All measurements were carried out in 10 mM Tris buffer, 50 mM NaCl (pH 7.2). ^1H NMR was recorded in DMSO-d_6 solvent using JEOL-500 MHz spectrometer. Chemical shifts (δ) are given in ppm.

Caution! Perchlorate salts are potentially explosives and should be handled only in small quantities with care.

2.3. Synthesis of bis(imidazole-terpyridine) cobalt(II) perchlorate, $[Co(Itpy)_2](ClO_4)_2$, (**1**)

The ligand imidazole terpyridine (Itpy) was prepared by slight modification of the reported procedure and the authenticity confirmed from ESI-MS, m/z = 300 [Itpy+H^+]. The cobalt(II) complex **1** was prepared directly by the addition of cobaltous chloride and the ligand imidazole terpyridine (Itpy) in 1:2 mole ratio, using methanol as reaction medium. The ligand Itpy (0.60 g, 2 mmol) in methanolic solution was added to the boiling methanolic solution of cobaltous chloride (0.23 g, 1 mmol). The solution immediately turned dark red. An aqueous solution of sodium perchlorate was added. Upon slow cooling, the dark red precipitate settled down. The crude precipitate was recrystallised from acetonitrile/methanol mixture (1:1 v/v) and the recrystallised product was filtered, washed with diethyl ether and then dried under vacuum. Yield: 85%. Elemental *Anal.* Calc. for $[Co(C_{18}H_{13}N_5)_2](ClO_4)_2$: C, 50.5; H, 3.04; N, 16.37; Co, 6.90. Found: C, 50.43; H, 3.7; N, 16.81; Co, 6.80%. ESI-MS m/z, 328.8, $[Co(Itpy)_2]^{2+}$. IR (KBr phase, cm^{-1}): 3461 br, 1629 m, 1473 w, 1114 m, 629 w (s, strong; w, weak; m, medium; br, broad). Single crystals of the complex were grown by ether diffusion method and the dark red crystals obtained were used for XRD studies.

2.4. Synthesis of bis(imidazole-terpyridine) cobalt(III) perchlorate, $[Co(Itpy)_2](ClO_4)_3$, (**2**)

Complex **2** was prepared from complex **1**. Cobalt(II) complex **1** prepared above was dissolved in methanol and few drops of dilute perchloric acid was added. To this solution 2.5 ml of hydrogen peroxide (30% w/v) was added and slightly warmed. Slowly, the colour of the solution turned deep yellow indicating the oxidation of cobalt(II) to cobalt(III). On standing, the solution yielded a yellow microcrystalline solid of the complex which was filtered, washed

with diethyl ether and then dried under vacuum. Yield: 80%. Elemental *Anal.* Calc. for $[Co(C_{18}H_{13}N_5)_2](ClO_4)_3$: C, 45.28; H, 2.73; N, 14.68; Co, 6.18. Found: C, 45.98; H, 3.1; N, 14.23; Co, 6.45%. ESI-MS *m/z*, 219.3, $[Co(Itpy)_2]^{3+}$. IR (KBr phase, cm^{-1}): 3401 m, 1610 m, 1482 m, 1420 w, 1087 br, 788 w, 629 m (s, strong; w, weak; m, medium; br, broad). ^1H NMR (DMSO-d_6) δ 9.67 (s, 2H); δ 8.8 (d, 2H); δ 8.35 (t, 2H); δ 7.48 (t, 2H); δ 7.63 (d, 2H); δ 7.8 (s, 2H); δ 4.7 (s, 1H) (s, singlet; d,doublet; t,triplet). The yellow solid was dissolved in a mixture of acetonitrile–water (1:1 v/v) in the presence of two drops of 0.5 N perchloric acid and kept for slow evaporation. After a few days, complex **2** crystallized as yellow needles, which were found suitable for single crystal X-ray analysis.

2.5. X-ray crystallographic data collection and refinement of the structures

Both dark red crystal of complex **1** and yellow coloured single crystal of complex **2** were coated with perfluoropolyether, picked up with a nylon fibre and mounted in the nitrogen cold stream (100 K) of a Bruker-Nonius KappaCCD diffractometer equipped with a Mo-target rotating-anode X-ray source and a graphite monochromator (Mo Kα, λ = 0.71073 Å). Final cell constants were obtained from a least squares fit of all integrated reflections. The Siemens SHELXTL [38] software package was used for solution and artwork of the structure, SHELXL97 [39] was used for the refinement. The structure was readily solved by Patterson method and subsequent difference Fourier techniques. All the non-hydrogen atoms were refined using anisotropic thermal parameter. Hydrogen atoms attached to carbon atoms were placed at calculated positions and refined as riding atoms with isotropic displacement parameters. The structural diagram was drawn using ORTEP-3 for Windows [40]. Crystallographic data for both complexes **1** and **2** are given in Table 1. For complex **2**, the perchlorate anion containing Cl(60) was found to be disordered and was split on two positions. The occupation factor refined to about 0.5 for both sets. In order to obtain a reasonable model, Cl–O and O–O distances were refined to be equal within errors and equal thermal displacement parameters were refined for corresponding atoms of the split model using SADI and EADP restraints of SHELXL.

Table 1
Crystallographic data for complexes **1** $[Co(Itpy)_2]Cl_2 \cdot 7H_2O$ and **2** $[Co(ItpyH)_2](ClO_4)_5 \cdot 5H_2O$

Parameters	1	2
Chemical formula	$C_{36}H_{40}Cl_2CoN_{10}O_7$	$C_{36}H_{38}C_{l5}CoN_{10}O_{25}$
Fw	854.61	1246.94
Crystal system, space group	monoclinic, *C*2/*c*, No. 15	monoclinic, *P*2(1)/*c*
a (Å)	28.8001(9)	16.9334(7)
b (Å)	14.6385(5)	14.4492(6)
c (Å)	21.7264(8)	19.5607(9)
α (°)	90	90
β (°)	123.250(3)	92.253(4)
γ (°)	90	90
V (Å)	7660.1(5)	4782.3(4)
Z	8	4
T (K)	100(2)	100(4)
ρ_{calc} (g cm^{-3})	1.482	1.732
Reflections collected/$2\theta_{max}$	72468/52.98	49600/46.5
Unique reflections	7897	6781
Number of parameters/restraints	536/15	751/35
μ (cm^{-1})/λ (Å)	6.50/0.71073	7.40/0.71073
R_1[a]/goodness of fit[b]	0.0626/1.045	0.0665/1.038
wR_2[c] ($I > 2\sigma(I)$)	0.1825	0.1288
Residual density (e $Å^{-3}$)	+1.480/−1.276	+0.717/−0.560

[a] Observation criterion: $I > 2\sigma(I)$. $R_1 = \sum||F_o| - |F_c||/\sum|F_o|$.
[b] Goodness-of-fit = $[\sum[w(F_o^2 - F_c^2)^2]/(n-p)]^{1/2}$.
[c] $wR_2 = [\sum[w(F_o^2 - F_c^2)^2]/\sum[w(F_o^2)^2]]^{1/2}$ where $w = 1/\sigma^2(F_o^2)+(aP)^2 + bP$, $P = (F_o^2 + 2F_c^2)/3$.

2.6. DNA binding and cleavage experiments

Concentrated stock solutions of metal complexes were prepared by dissolving the complex in acetonitrile and diluted suitably with 10 mM Tris buffer (1:10 as acetonitrile:buffer) to required concentrations for all the experiments. Absorption spectral titration experiments were carried out with both the complexes by maintaining a constant concentration of the complex (20 μM) and varying the CT-DNA concentration (20–500 μM). Equal concentrations of DNA in the sample and reference cells were maintained in order to eliminate the absorbance of DNA itself. The intrinsic binding constant was estimated using the following equation [41]:

$$[DNA]/(\varepsilon_a - \varepsilon_f) = [DNA]/(\varepsilon_b - \varepsilon_f) + 1/K_b(\varepsilon_b - \varepsilon_f),$$

where ε_a, ε_f and ε_b correspond to A_{obsd}/[Co], the extinction coefficient for the free cobalt complex, and the extinction coefficient for the cobalt complex in the fully bound form, respectively. A plot of [DNA]/($\varepsilon_a - \varepsilon_f$) versus [DNA], gives K_b, the intrinsic binding constant as the ratio of the slope to the intercept. For emission spectral titration measurements, Tris buffer was used as a blank to make preliminary adjustments. DNA was pretreated with ethidium bromide in the ratio [DNA]/[EB] = 2.5 for 30 min at room temperature. The excitation wavelength was fixed at 500 nm and the emission intensity was measured at 603 nm. The effect on emission intensity was measured by varying the concentration of complexes from 0 to 50 μM.

For viscosity measurements, the Ubberhold viscometer (3 mL capacity) was thermostated in water-bath maintained at 28 °C. The flow time for each sample was measured three times using digital stopwatch and an average flow time was calculated. The rate of flow of the buffer (10 mM Tris), DNA (100 μM) and DNA with the cobalt complexes at various concentrations were measured. The relative specific viscosity was calculated using the equation $\eta = (t - t_o)/t_o$, where t_o is the flow time for the buffer and t is the observed flow time for DNA in the absence and presence of the complex. Data are presented as $(\eta/\eta_o)^{1/3}$ versus $1/R$ (R = [complex]/[DNA]) where η is the viscosity of DNA in the presence of complex and η_o is the viscosity of DNA alone [42,43].

The cleavage of DNA was monitored using agarose gel electrophoresis. The experiments were performed using supercoiled pBR322 DNA. The DNA (0.5 μg) in Tris buffer, was treated with 100 μM and 140 μM of complex **2** and varying amounts of ascorbic acid and hydrogen peroxide. The samples were incubated at 28 °C for 1 h. The reactions were quenched using the loading buffer (0.25% bromophenol blue, EDTA and 40% sucrose). The reaction samples were then loaded on 0.8% agarose gel containing ethidium bromide and were run at 60 V for 2 h in Tris (boric acid) ethylenediaminetetraacetic acid (TBE) buffer, pH 7.2. The bands were viewed by placing the gel on UV illuminator and were photographed using gel documentation system.

3. Results and discussion

3.1. Synthesis and characterization of the complexes

Complex **1** was prepared by the direct addition of cobaltous chloride and the ligand in 1:2 molar ratio using methanol as reaction medium. Complex **2** was prepared by the oxidation of complex **1** using hydrogen peroxide. Both the complexes were obtained in good yield and showed well defined m/z = $[Co(Itpy)_2]^{2+/3+}$, peaks in acetonitrile as obtained from ESI mass spectrometry. Complexes **1** and **2** were isolated as perchlorate salts as evident from the presence of band at 1114–1089 cm^{-1} in the IR spectrum. Fig. 1 shows the electronic spectra of complexes **1** (1) and **2** (2) in the spectral range of 200–400 nm. The spectra

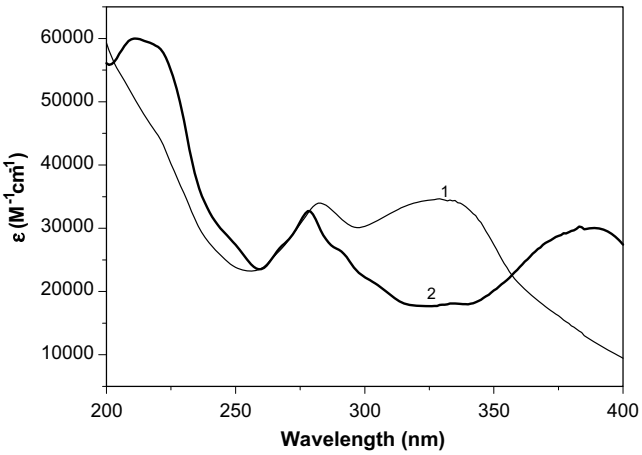

Fig. 1. Electronic absorption spectra (1) of complex **1** and (2) **2** in acetonitrile in the spectral range of 200–400 nm.

for ligand and both the complexes were taken in acetonitrile. The free ligand shows bands at 250, 283, 316 nm. These bands are due to the aromatic nature of the imidazole terpyridine ligand. Complex **1** shows bands at 284 and 330 nm. Complex **2** on the other hand shows absorption bands at 267, 279, 292 and 387 nm. These bands are due to the ligand centered transitions. Complex **2** showed NMR spectrum due to low spin, diamagnetic nature of the cobalt(III) complex. Cyclic voltammogram of complexes **1** and **2** show reversible redox wave in acetonitrile due to the Co(II)/Co(III) couple with cathodic (E_{pc}) and anodic peak potential (E_{pa}) 0.102 and 0.168 V, respectively, versus SCE. The peak separation (ΔE_p) was found to be 66mv at the scan rate of 0.1 V s^{-1} which is expected for a one electron reversible redox process.

3.2. Description of the structures

Complexes **1** and **2** were characterized structurally by X-ray crystallography. In both the complexes, cobalt ion is coordinated to two tridentate ligand to form CoN_6 octahedral complex. The perspective view of complex **1** is shown in Fig. 2. The structure shows that the cobalt(II) forms distorted octahedron with two Itpy ligands. Complex **1** crystallized with the molecular formula $[Co(L)_2](Cl)_2 \cdot 7H_2O$ and space group *C*2/*c*. Single crystal analysis of cobalt(III) complex **2** revealed that the compound crystallized with the molecular formula $[Co(LH)_2](ClO_4)_5 \cdot 5H_2O$ and space group *P*2(1)/*c*. The ORTEP diagram of complex **2** is shown in Fig. 3. The free nitrogen atom of the imidazole ring in the ligand is protonated in complex **2** (since single crystals were obtained in

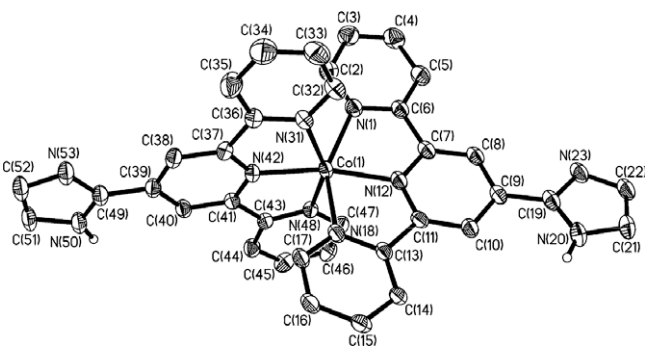

Fig. 2. ORTEP view of complex **1** and hydrogen atoms are being omitted for clarity.

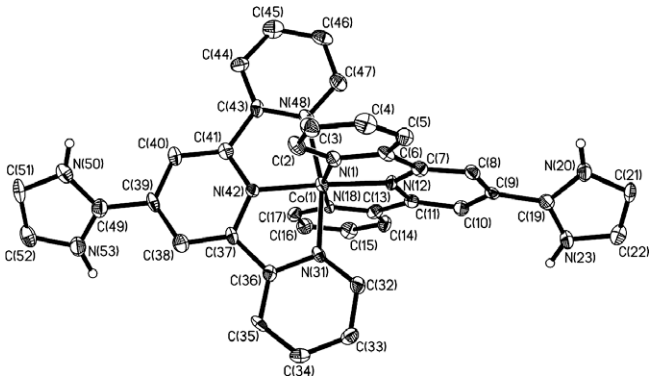

Fig. 3. ORTEP drawing of complex **2.** Hydrogen atoms are omitted for clarity.

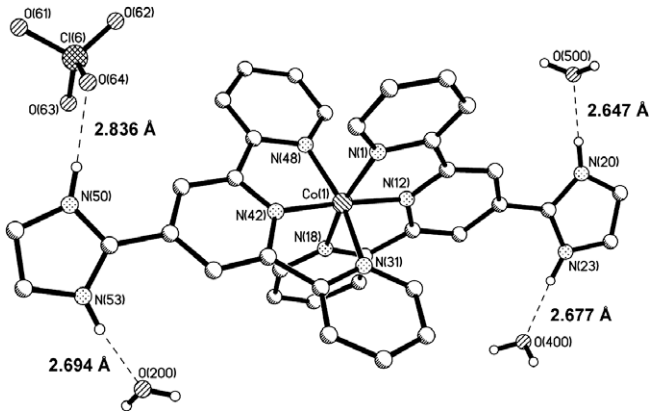

Fig. 3a. Represents ORTEP diagram of complex **2** with hydrogen bonding.

the presence of dilute perchloric acid), thereby leading to an overall increase in the positive charge of the complex. So, complex **2** contains five perchlorate counter anions in their crystal structure. The crystal structure of cobalt(III) imidazole terpyridine complex shows five water molecules, three of which are hydrogen bonded to three –NH moieties and their bond lengths vary from 2.647 Å to 2.697 Å. One of the –NH is seen hydrogen bonded to one perchlorate anion with a bond length of 2.836 Å (Fig. 3a). The crystal structure of complex **1** shows that the free imidazole nitrogen atom is not protonated and crystallizes as dication with two chloride counter ions. It is evident from the ORTEP diagrams, that both the complexes form distorted octahedron with meridional configuration and belong to monoclinic crystal system. Important bond lengths and bond angles for complexes **1** and **2** are given in Tables 2 and 3, respectively. Co(1)–N(1) and Co(1)–N(48) bond lengths in complex **1** were almost equidistant when compared to other Co–N bonds. The N–Co–N (76–169°) bond angles deviate largely from 180°. For complex **2**, Co–N bond lengths are similar to those reported for low spin cobalt(III) complexes and their bond lengths are much smaller than the cobalt(II) complex. The nitrogen atom of central pyridine ring of the two tridentate ligands is found to be closer to the central metal ion, than the other two terminal nitrogen atoms of each ligand by 0.08 Å. Interestingly, one of the remaining four Co–N bonds, namely Co(1)–N(1), has an unusually smaller bond length of 1.927 Å as against 1.942, 1.948 and 1.950 Å for Co(1)–N(18), Co(1)–N(31) and Co(1)–N(48) bonds, respectively. The N(42)–Co(1)–N(12) bond angle is found to be 176.7° while the remaining bond angles show deviations and vary from 82° to 165°.

Table 2
Important bond distances and bond angles of complex **1** $[Co(Itpy)_2]Cl_2 \cdot 7H_2O$

Bond distances (Å)			
Co(1)–N(42)	2.0353(17)	C(19)–N(20)	1.342(4)
Co(1)–N(12)	2.0444(18)	C(19)–N(23)	1.344(3)
Co(1)–N(31)	2.133(2)	N(20)–C(21)	1.370(3)
Co(1)–N(1)	2.150(2)	C(22)–N(23)	1.367(3)
Co(1)–N(48)	2.152(2)	N(31)–C(32)	1.340(3)
Co(1)–N(18)	2.170(2)	N(31)–C(36)	1.355(3)
N(1)–C(2)	1.338(4)	C(37)–N(42)	1.340(3)
N(1)–C(6)	1.347(3)	C(41)–N(42)	1.342(3)
C(7)–N(12)	1.346(3)	C(43)–N(48)	1.360(3)
C(11)–N(12)	1.346(3)	C(47)–N(48)	1.342(3)
C(11)–C(13)	1.487(3)	C(49)–N(53)	1.334(3)
C(13)–N(18)	1.351(3)	C(49)–N(50)	1.353(3)
C(17)–N(18)	1.336(3)	N(50)–C(51)	1.378(3)
Bond angles (°)			
N(42)–Co(1)–N(12)	168.75(9)	N(18)–C(13)–C(11)	114.6(2)
N(42)–Co(1)–N(31)	76.33(8)	N(18)–C(17)–C(16)	123.3(2)
N(12)–Co(1)–N(31)	110.96(8)	C(17)–N(18)–C(13)	118.1(2)
N(42)–Co(1)–N(1)	113.87(8)	C(17)–N(18)–Co(1)	126.95(17)
N(12)–Co(1)–N(1)	75.56(8)	C(13)–N(18)–Co(1)	114.92(15)
N(31)–Co(1)–N(1)	88.78(8)	N(20)–C(19)–N(23)	111.9(2)
N(42)–Co(1)–N(48)	76.33(8)	N(20)–C(19)–C(9)	123.8(2)
N(12)–Co(1)–N(48)	97.18(8)	N(23)–C(19)–C(9)	124.3(2)
N(31)–Co(1)–N(48)	51.72(7)	C(32)–N(31)–Co(1)	126.45(17)
N(1)–Co(1)–N(48)	95.71(8)	C(36)–N(31)–Co(1)	115.60(17)
N(42)–Co(1)–N(18)	95.52(8)	N(31)–C(36)–C(37)	114.0(2)
N(12)–Co(1)–N(18)	76.12(8)	N(42)–C(37)–C(36)	113.96(19)
N(31)–Co(1)–N(18)	91.56(8)	N(42)–C(41)–C(40)	121.4(2)
N(1)–Co(1)–N(18)	149.76(7)	C(37)–N(42)–C(41)	120.50(18)
N(48)–Co(1)–N(18)	98.12(8)	C(37)–N(42)–Co(1)	119.45(16)
C(2)–N(1)–C(6)	118.7(2)	C(41)–N(42)–Co(1)	119.61(15)
C(2)–N(1)–Co(1)	125.64(15)	N(48)–C(43)–C(44)	122.0(2)
C(6)–N(1)–Co(1)	115.69(17)	N(48)–C(43)–C(41)	114.3(2)
N(12)–C(11)–C(10)	121.7(2)	N(48)–C(47)–C(46)	122.9(2)
C(7)–N(12)–C(11)	119.65(19)	C(47)–N(48)–C(43)	118.2(2)
C(7)–N(12)–Co(1)	120.46(17)	C(47)–N(48)–Co(1)	126.85(15)
C(11)–N(12)–Co(1)	119.88(14)	C(43)–N(48)–Co(1)	114.83(15)
N(18)–C(13)–C(14)	122.2(2)	N(53)–C(49)–N(50)	111.2(2)
N(18)–C(13)–C(11)	114.6(2)	N(53)–C(49)–C(39)	124.3(2)

Table 3
Important bond distances and bond angles of complex **2** $[Co(ItpyH)_2](ClO_4)_5 \cdot 5H_2O$

Bond distances (Å)			
Co(1)–N(42)	1.855(5)	C(19)–N(20)	1.331(8)
Co(1)–N(12)	1.865(5)	N(20)–C(21)	1.373(7)
Co(1)–N(1)	1.927(5)	N(31)–C(32)	1.339(7)
Co(1)–N(18)	1.942(5)	N(31)–C(36)	1.378(7)
Co(1)–N(31)	1.948(5)	C(37)–N(42)	1.344(7)
Co(1)–N(48)	1.950(5)	C(41)–N(42)	1.344(7)
N(1)–C(2)	1.331(8)	C(43)–N(48)	1.370(7)
N(1)–C(6)	1.385(7)	C(47)–N(48)	1.333(8)
C(7)–N(12)	1.345(7)	C(49)–N(53)	1.317(8)
C(11)–N(12)	1.350(7)	C(49)–N(50)	1.329(8)
C(13)–N(18)	1.377(7)	N(50)–C(51)	1.368(8)
C(17)–N(18)	1.332(8)	C(51)–C(52)	1.337(9)
C(19)–N(23)	1.328(8)	C(52)–N(53)	1.377(8)
Bond angles (°)			
N(42)–Co(1)–N(12)	176.7(2)	C(17)–N(18)–C(13)	118.3(5)
N(42)–Co(1)–N(1)	99.2(2)	C(17)–N(18)–Co(1)	127.8(4)
N(12)–Co(1)–N(1)	82.6(2)	C(13)–N(18)–Co(1)	113.8(4)
N(42)–Co(1)–N(18)	95.3(2)	N(23)–C(19)–N(20)	108.6(5)
N(12)–Co(1)–N(18)	82.9(2)	C(19)–N(20)–C(21)	108.9(5)
N(1)–Co(1)–N(18)	165.5(2)	C(22)–C(21)–N(20)	106.8(5)
N(42)–Co(1)–N(31)	82.7(2)	C(21)–C(22)–N(23)	107.3(6)
N(12)–Co(1)–N(31)	94.5(2)	C(19)–N(23)–C(22)	108.4(5)
N(1)–Co(1)–N(31)	90.7(2)	C(32)–N(31)–C(36)	118.7(5)
N(18)–Co(1)–N(31)	91.50(19)	C(32)–N(31)–Co(1)	127.8(4)
N(42)–Co(1)–N(48)	82.5(2)	C(36)–N(31)–Co(1)	113.4(4)
N(12)–Co(1)–N(48)	100.2(2)	N(42)–C(37)–C(36)	112.4(5)
N(1)–Co(1)–N(48)	90.4(2)	C(38)–C(39)–C(49)	119.8(6)
N(18)–Co(1)–N(48)	91.1(2)	C(41)–N(42)–Co(1)	118.3(4)
N(31)–Co(1)–N(48)	165.2(2)	C(37)–N(42)–Co(1)	118.0(4)
C(2)–N(1)–C(6)	118.0(5)	C(44)–C(43)–N(48)	122.2(6)
C(2)–N(1)–Co(1)	127.3(4)	N(48)–C(43)–C(41)	112.9(5)
C(6)–N(1)–Co(1)	114.6(4)	C(47)–N(48)–C(43)	118.9(5)
C(7)–N(12)–Co(1)	118.8(4)	C(47)–N(48)–Co(1)	127.3(4)
C(11)–N(12)–Co(1)	117.9(4)	C(43)–N(48)–Co(1)	113.7(4)
C(14)–C(13)–N(18)	121.8(5)	N(53)–C(49)–N(50)	107.5(6)
C(14)–C(13)–C(11)	125.3(5)	N(53)–C(49)–C(39)	127.9(6)
N(18)–C(17)–C(16)	122.2(6)	N(50)–C(49)–C(39)	124.5(6)

4. DNA binding experiments

4.1. Electronic absorption spectra

Interaction of metal complexes with DNA can be monitored by absorption spectral titration [44]. In general, metal complex binding to DNA through intercalation, results in hypochromism and red shift (bathochromism), due to the strong stacking interaction between aromatic chromophore of the complex and the base pairs of DNA. The intercalative binding strength is determined by the extent of hypochromism exhibited by the complex. The absorption spectra of complex **2** in the absence and presence of calf thymus DNA is shown in Fig. 4. The cobalt(III) complex exhibits intense absorption bands in the UV–Vis region which is attributed to intraligand π–π^* transition of the coordinated groups. The absorption spectra of both complexes **1** and **2** showed hypochromism upon addition of CT-DNA which is suggestive of an intercalative mode of binding for both the complexes. This is due to the imidazole terpyridine ligand which possesses greater planar area and extended system, thereby leading to deeper penetration and stronger binding within the DNA base pairs.

In order to compare the DNA binding strengths of complexes **1** and **2** quantitatively, the intrinsic binding constant, K_b for both the complexes were obtained by monitoring the changes in the intraligand band. K_b for both the complexes were determined from the plot of $[DNA]/(\varepsilon_a - \varepsilon_f)$ versus [DNA] and found to be $(5.07 \pm 0.12) \times 10^3\ M^{-1}$ and $(7.46 \pm 0.16) \times 10^3\ M^{-1}$ for complexes **1** and **2**, respectively. The intrinsic binding constant values for both the complexes were found to be much smaller than that reported for the classical intercalators and our previous work on pytpy [45,34]. This is probably due to the absence of planarity of the imidazole ring with the terpyridine unit. From the crystal structure, it is seen that the imidazole moiety is twisted by about 33° away from the plane of the adjacent pyridine ring of the terpyri-

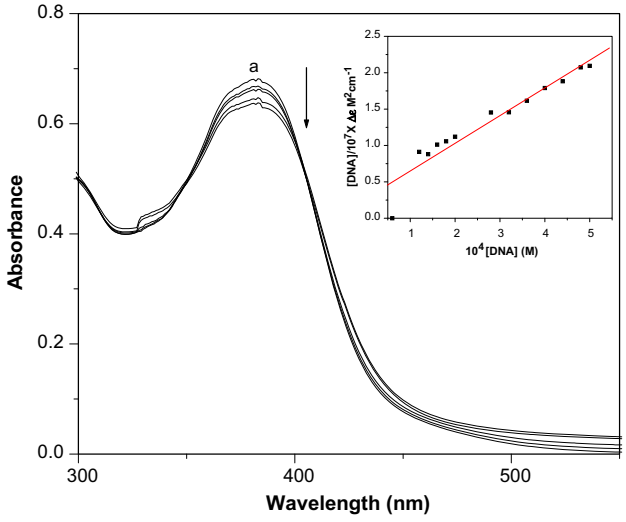

Fig. 4. Absorption spectra of complex **2** in the absence (a) and in the presence of increasing amounts of DNA. [Co] = 20 μM; [DNA] = 0–500 μM. The arrow shows the spectral changes on increasing DNA concentration. Inset: plot of $[DNA]/(\varepsilon_a - \varepsilon_f)$ vs. [DNA].

dine ligand. This deviation from planarity affects the magnitude of binding of these complexes although the mode of binding remains unaffected.

4.2. Competitive binding studies

Excitation of complexes **1** and **2**, either in aqueous solution or in the presence of CT-DNA did not result in any fluorescence emission at the room temperature. Competitive ethidium bromide binding studies were undertaken to gain support for the extent of binding of the metal complexes with DNA. The extent of quenching of emission of EB bound to DNA by competitive displacement is a measure of strength of intercalation between the second molecule and DNA [46]. EB emits intense fluorescence in the presence of DNA, due to its strong intercalation between the adjacent DNA base pairs. Increasing the concentration of both complexes **1** and **2** with respect to DNA pretreated with EB, causes an appreciable quenching in the emission intensity, indicating the displacement of EB fluorophore by these complexes. The fluorescence quenching curve of EB bound to DNA by complex **2** is shown in Fig. 5. The quenching behavior is then analyzed by Stern–Volmer equation [47], $I_0/I = 1+K_{sv}r$, where I_0 and I are fluorescence intensities in the absence and presence of the complex. K_{sv} is the linear Stern–Volmer quenching constant and r is the ratio of the total concentration of the complex to that of DNA. From the plot of I_0/I versus [complex]/[DNA], K_{sv} is given by the ratio of slope to the intercept. The K_{sv} value calculated for complex **2** is 4.25 which is in good agreement with the reported intercalators such as $[Co(phen)_2(pdta)]^{3+}$ and $[Co(phen)_2(pdtp)]^{3+}$ [48]. These results further confirm that both the complexes show an intercalative binding mode to CT-DNA.

4.3. Viscosity measurements

Though photophysical experiments, give necessary information about the binding modes of the metal complexes with DNA, they do not provide conclusive evidences for the exact mode of binding. Hydrodynamic measurements such as viscosity which is sensitive to length changes are regarded as the least ambiguous and the most critical tests of binding modes in solution [49]. It is considered as the convincing test for intercalative mode of binding. Viscosity of DNA is increased in the case of classical intercalators due to increase in the length of the DNA helix, as base pairs are separated to accommodate the intercalator. In contrast, decrease in DNA viscosity is noted in the partial or non-classical intercalator, because it may bend (or kink) DNA helix, thereby decreasing its effective length and therefore the viscosity. The effect of cobalt complexes **1** and **2** on the viscosity of rod-like DNA are shown in Fig. 6. Upon addition of complexes **1** and **2** (10–160 μM), the viscosity of rod-like calf thymus DNA increases steadily till the ratio of the complex to DNA reaches 0.8, which confirms that both the complexes bind to DNA through intercalation. This result parallels the observation found in the absorption spectral and emission studies. The more pronounced changes in relative viscosity of DNA observed in the case of complex **2** as compared to **1** is indicative of the fact that this complex is relatively better intercalator than complex **1**. This is also reflected in the DNA binding constant of the two complexes.

4.4. Differential pulse voltammetry

Binding of metal complexes to DNA is better understood by monitoring the DNA-induced changes in the electrochemical properties of small molecules. Both cyclic voltammetry (CV) and differential pulse voltammetry (DPV) techniques were employed to study metallointercalation. Both these techniques differ on their time scales τ. Under the same experimental conditions, the τ for CV is 250 ms and DPV is 17 ms. Therefore, the reversibility of heterogeneous electron transfer kinetics will be different for these two techniques [50]. Quantitative information about the interaction of metal complexes with DNA can be obtained from DPV. Fig. 7 shows DPV curve of 0.25 mM complex **2** in the absence and presence of 0.5 mM DNA. It is noted from the figure that there is a shift in the potential of cobalt(III) complex on the addition of CT-DNA. The observed shift in the potential is possibly because of the fact that the metal complex bound to the large macromolecule diffuses slowly to the electrode compared to the free metal complex [51]. Bard and co-workers have shown that the electrochemical potential of small molecules shift positively when it is intercalated into the base pairs of DNA and negatively when it is bound to DNA by electrostatically [52]. In the present case, the observed positive shift implies that the complex could bind to DNA by intercalation.

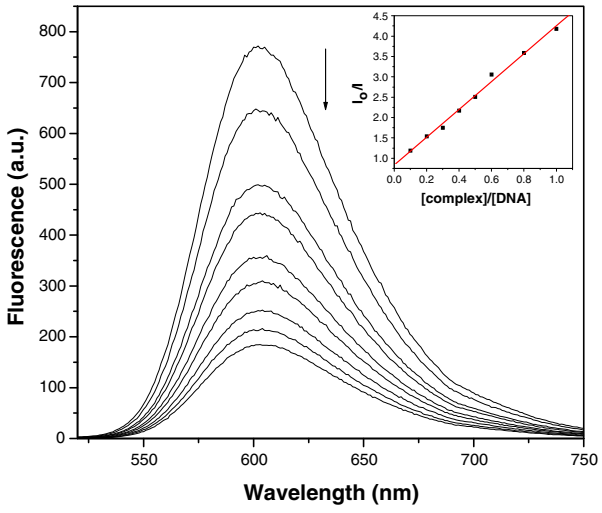

Fig. 5. Emission spectra of EB bound to DNA in the presence of complex **2** ([DNA]/[EB] = 2.5, [Co] = 0–50 μM, λ_{ex} = 500 nm. The arrow shows the intensity changes upon increasing the complex concentration. Inset: Fluorescence quenching curve of EB-DNA by complex **2**.

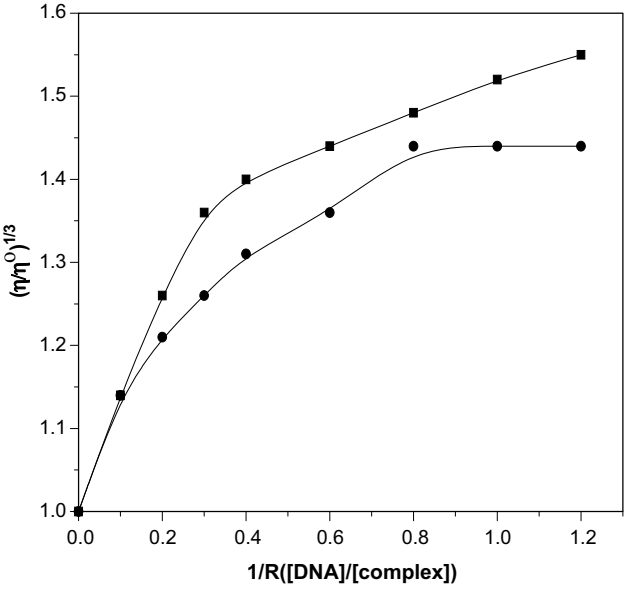

Fig. 6. Effect of increasing amounts of cobalt complexes **1** (●) and **2** (■) on the relative viscosity of CT-DNA at 28.0(±0.1) °C.

Differential pulse voltammetry can be used to calculate the corresponding equilibrium constant for one electron redox process, provided both the oxidized and reduced forms are associated with a third species (DNA) in the solution using the following equation [52]:

$$E_b^0 - E_f^0 = 0.059 \log(K_{II}/K_{III})$$

where E_b^0 and E_f^0 are the formal potentials of Co(III)/Co(II) couple in the bound and free forms, respectively. K_{II} and K_{III} are the binding constants for the binding of the oxidized and reduced forms to DNA. The addition of 0.5 mM CT-DNA to complex **2** results in a potential shift of 8 mV and the ratio of the binding constant (K_{II}/K_{III}) was calculated to be 0.73. This indicates the stronger DNA binding aptitude of the cobalt(III) complex as compared to cobalt(II) due to its higher nuclear charge.

4.5. Cleavage of plasmid PBR 322 DNA

In order to explore the metallonuclease activity of the newly synthesized cobalt(III) complexes, agarose gel electrophoresis experiments were carried out with plasmid pBR322 DNA. The DNA cleaving ability of complex **2** was analyzed by monitoring the conversion of supercoiled DNA (Form I) to nicked circular (Form II) and linear (Form III) forms and the gel electrophoretogram is given in Fig. 8. Complexes **1** and **2** does not bring about any hydrolytic or photocleavage of DNA. In order to explore the possibility of oxidative cleavage of DNA by the synthesised complexes, plasmid DNA was treated with complex **2** in the presence of hydrogen peroxide. No significant cleavage of DNA was observed even under high concentrations of peroxide (Lanes 1–3). However, on treatment of DNA with the complex in the presence of both hydrogen peroxide and ascorbic acid, significant cleavage was observed (Lanes 4–6). On varying the concentration of ascorbic acid and hydrogen peroxide, it is seen that the cleavage efficiency of complex **2** remarkably increases with increase in the concentration of ascorbic acid (200–600 μM). It was found that the cleavage remained almost unaffected beyond a certain minimum concentration of hydrogen peroxide (500 μM). Complex **1** (100 μM) on the other hand brought about DNA cleavage in the presence of hydrogen peroxide alone as seen from Lane 7.

The mechanism of cleavage in the present case involves the well-known Fenton type chemistry. The cobalt(III) complex bound to DNA through outer sphere gets reduced to cobalt(II) complex by ascorbic acid, which in turn reacts with hydrogen peroxide to generate the highly reactive hydroxyl radicals. The freely diffusible hydroxyl radical brings about the cleavage of DNA. This mechanism is supported by the fact that complex **1,** which is a Co(II) complex

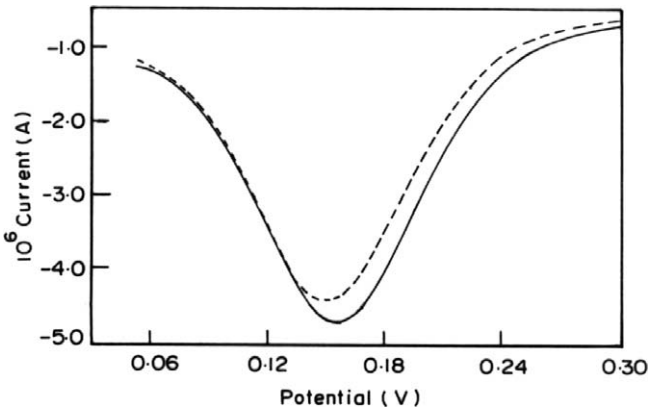

Fig. 7. DPV curves of 0.25 mM of complex **2** in the absence (—) and presence (- - -) of 0.5 mM of CT-DNA in 10 mM Tris buffer pH 7.2.

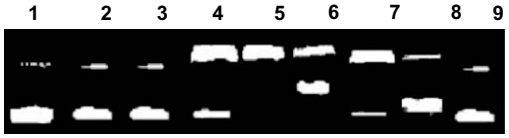

Fig. 8. Cleavage of pBR 322 DNA by cobalt complex **2** in the presence of hydrogen peroxide and ascorbic acid and complex **1** in the presence of hydrogen peroxide. [DNA] = 200 ng was incubated with complex **2** for 75 min in Tris buffer pH 7.2. Lane 1, DNA control; Lane 2, DNA + 100 μM of complex **2**; Lane 3, DNA + 100 μM of **2** + H_2O_2; Lane 4, DNA + 100 μM of **2** + 200 μM of ascorbic acid + 500 μM of H_2O_2; Lane 5, DNA + 100 μM of **2** + 400 μM of ascorbic acid + 500 μM of H_2O_2; Lane 6, DNA + 100 μM of **2** + 600 μM of ascorbic acid + 500 μM of H_2O_2; Lane 7, DNA + 100 μM of **1** + 500 μM of H_2O_2; Lane 8, DNA + 100 μM of **2** + 600 μM of ascorbic acid + 500 μM of H_2O_2 + 0.05 M of DMSO; Lane 9, DNA + 100 μM of **1** + 500 μM of H_2O_2 + 0.05 M of DMSO.

brings about DNA cleavage even in the absence of ascorbic acid as a co-reagent. Further, addition of hydroxyl radical scavenger DMSO, results in the inhibition of cleavage activity, as shown in Lanes 8 and 9, indicating that the hydroxyl radical is responsible for the nuclease activity exhibited by the complexes. Our previous reports on a similar cobalt(III) ptpy complex shows that the complex brings about photocleavage of DNA [34]. In the present case, however photocleavage was clearly ruled out. Normally, photocleavage mechanism in cobalt(III) complexes involves electron transfer from the excited state of the metal leading to guanine base oxidation [53]. The excited state properties of the metal ion are greatly influenced by the ligands coordinated to it [54]. In the present case, it is possible that, the presence of imidazole ring in the ligand lowers the excited state redox potential of the metal and thereby, makes guanine base oxidation impossible. Further studies on excited state properties of these complexes are underway.

5. Conclusion

Cobalt(II) and cobalt(III) complexes of tridentate ligand, imidazole terpyridine, were synthesized and characterized spectroscopically. Both the complexes were structurally characterized by X-ray crystallography and belong to monoclinic crystal system. The imidazole ring of the terpyridine ligand of complex **2** was protonated and hydrogen bonded to either water or perchlorate anion as evident from its crystal structure. The DNA binding capabilities of both complexes **1** and **2** were studied by spectroscopic, hydrodynamic and electrochemical techniques. The complexes exhibit intercalative mode of binding and the binding constant values from absorption spectral studies were found to be $(5.07 \pm 0.12) \times 10^3$ and $(7.46 \pm 0.16) \times 10^3\ M^{-1}$ for complexes **1** and **2**, respectively. The stronger DNA binding aptitude of cobalt(III) complex as compared to that of cobalt(II) complex was due to its higher nuclear charge. Further, viscosity and electrochemical studies offer further support for the intercalative mode of binding of these complexes. The cobalt(III) imidazole terpyridine complex exhibits efficient nuclease activity in the presence of ascorbic acid and hydrogen peroxide, whereas the corresponding cobalt (II) complex brings about DNA cleavage in the presence of hydrogen peroxide as a co-reagent.

Acknowledgements

R.I. thanks DST, India, for a pre-doctoral fellowship under "New Initiatives in Bioinorganic Chemistry".

Appendix A. Supplementary data

CCDC 684149 and 628606 contain the supplementary crystallographic data for complex **1** and **2**. These data can be obtained free

of charge via http://www.ccdc.cam.ac.uk/conts/retrieving.html, or from the Cambridge Crystallographic Data Centre (CCDC), 12 Union Road, Cambridge CB2, IEZ, UK; fax: (+44) 1223-336-033; or e-mail: deposit@ccdc.cam.ac.uk. Supplementary data associated with this article can be found, in the online version, at doi:10.1016/j.poly.2008.08.003.

References

[1] K.E. Erkkila, D.T. Odom, J.K. Barton, Chem. Rev. 99 (1999) 2777 and references cited therein.
[2] P.K. Bhattacharya, J.K. Barton, J. Am. Chem. Soc. 123 (2001) 8649.
[3] S. Delaney, J. Yoo, E.D.A. Stemp, J.K. Barton, PNAS 101 (2004) 10511.
[4] R.E. Hemin, J.A. Yao, J.K. Barton, Inorg. Chem. 38 (1999) 174.
[5] M. Demeunynck, C. Bailly, W.D. Wilson (Eds.), DNA and RNA Binders: From Small Molecules to Drugs, Wiley-VCH, Weinheim, 2003.
[6] J.K. Barton, A.J. Danishefsky, J.P. Goldberg, J. Am. Chem. Soc. 106 (1984) 2172.
[7] J.M. Kelly, M.J. Murphy, D.J. McConell, C. OhUigin, Nucleic Acids Res. 13 (1989) 167.
[8] R. Hartmann, A. Robert, V. Duarte, B.K. Keppler, B. Meunier, J. Biol. Inorg. Chem. 2 (1997) 143.
[9] S.R. Rajski, R.M. Williams, Chem. Rev. 98 (1998) 2723.
[10] M.V. Keek, S.J. Lippard, J. Am. Chem. Soc. 114 (1992) 3386.
[11] Q.L. Zhang, J.G. Liu, H. Xu, H. Li, J.Z. Liu, H. Zhou, L.H. Qu, L.-N. Ji, Polyhedron 20 (2001) 3049.
[12] C.H. Ng, H.K.A. Ong, C.W. Kong, K.W. Tan, R.N.Z.R.A. Rahman, B.M. Yamin, S.W. Ng, Polyhedron 25 (2006) 3118.
[13] L.-N. Ji, X.–H. Zou, J.G. Liu, Coord. Chem. Rev. 216–217 (2001) 513.
[14] G.A. Eichhorn, Y.A. Shin, J. Am. Chem. Soc. 90 (1968) 7323.
[15] S.J. Lippard, in: I. Bertini, H.B. Gray, S.J. Lippard, J.S. Valentine (Eds.), Bioinorganic Chemistry, University Science Books, Mill Valley, CA, 1994, p. 505.
[16] M. Gielen, E.R.T. Tiekink (Eds.), Metallotherapeutic Drugs and Metal-Based Diagnostic Agents: The Use of Metals in Medicine, John Wiley & Sons, London, 2005.
[17] L.-F. Tan, H. Chao, K.-C. Zhen, J.-J. Fei, F. Wang, Y.-F. Zhou, L.-N. Ji, Polyhedron 26 (2007) 5458.
[18] A.K.D. Mesmaeker, J.-P. Lecomte, J.M. Kelly, Top. Curr. Chem. 177 (1996) 25.
[19] C. Turro, J.K. Barton, J. Am. Chem. Soc. 90 (1968) 7323.
[20] A. Sitlani, E.C. Long, A.M. Pyle, J.K. Barton, J. Am. Chem. Soc. 114 (1992) 2303.
[21] C. Turro, D.B. Hall, W. Chen, H. Zuilhof, J.K. Barton, N.J. Turro, J. Phys. Chem. A 102 (1998) 5708.
[22] J. Widom, R.L. Baldwin, J. Mol. Biol. 144 (1980) 431.
[23] J. Widom, R.L. Baldwin, Biopolymers 22 (1983) 1595.
[24] J.W. Kieltyka, C.S. Chow, J. Am. Soc. Mass Spectrom. 17 (2006) 1376.
[25] R. Gust, I. Ott, D. Posselt, K. Sommer, J. Med. Chem. 47 (2004) 5837.
[26] D.C. Ware, P.J. Brothers, G.R. Clark, W.A. Denny, B.D. Palmer, W.R. Wilson, J. Chem. Soc., Dalton Trans. (2000) 925.
[27] L.C. Perrin, W.R. Wilson, W.A. Denny, W.D. McFadyen, Anticancer Drug Des. 14 (1999) 231.
[28] C.C. Cheng, Y.N. Kuo, K.S. Chuang, C.F. Luo, W.J. Wang, Angew. Chem., Int. Ed. Engl. 38 (1999) 1255.
[29] V. Uma, M. Kanthimathi, T. Weyhermuller, B.U. Nair, J. Inorg. Biochem. 99 (2005) 2299.
[30] V. Uma, M. Elango, B.U. Nair, Eur. J. Inorg. Chem. 2007 (2007) 3484.
[31] V.G. Vaidyanathan, B.U. Nair, Eur. J. Inorg. Chem. 9 (2004) 1840.
[32] H.Y. Shrivastava, M. Kanthimathi, B.U. Nair, Biochim. Biophys. Res. Commun. 265 (1999) 311.
[33] V.G. Vaidyanathan, B.U. Nair, J. Inorg. Biochem. 94 (2003) 121.
[34] R. Indumathy, S. Radhika, M. Kanthimathi, T. Weyhermuller, B.U. Nair, J. Inorg. Biochem. 101 (2006) 434.
[35] G.W.V. cave, C.L. Raston, J. Chem. Soc., Perkin Trans. 1 (2001) 3258.
[36] J. Murmur, J. Mol. Biol. 3 (1961) 208.
[37] M.F. Reichmann, S.A. Rice, C.A. Thomas, P. Doty, J. Am. Chem. Soc. 76 (1954) 3047.
[38] SHELXTL V. 5, Siemens Analytical X-ray Instruments, Inc., Madison, Wisconsin, USA, 1994.
[39] G.M. Sheldrick, SHELXL97, University of Göttingen, 1997.
[40] L.J. Farrugia, J. Appl. Crystallogr. 30 (1997) 565.
[41] A.M. Pyle, J.P. Rehmann, R. Meshoyrer, C.V. Kumar, N.J. Turro, J.K. Barton, J. Am. Chem. Soc. 111 (1989) 3051.
[42] B. Chaires, N. Dattaguota, D.M. Crothers, Biochemistry 21 (1982) 3933.
[43] G. Cohen, H. Eisenberg, Biopolymers 8 (1969) 45.
[44] T.M. Kelly, A.B. Tossi, D.J. McConnell, T.C. Strekas, Nucleic Acids Res. 13 (1985) 6017.
[45] S. Arounagiri, B.G. Maiya, Inorg. Chem. 35 (1996) 4267.
[46] B.C. Baguley, M. Lebert, Biochemistry 23 (1984) 937.
[47] J.R. Lakowicz, G. Webber, Biochemistry 12 (1973) 4161.
[48] X.-L. Wang, H. Chao, H. Li, X.-L. Hong, Y.-J. Liu, L.-F. Tan, L.N. Ji, J. Inorg. Biochem. 98 (2004) 1143.
[49] G. Yang, J.Z. Wu, L. Wang, L.-N. Ji, X. Tian, J. Inorg. Biochem. 66 (1997) 141.
[50] A.J. Bard, l.R. Faulkner, in: Electrochemical Methods: Fundamentals and Applications, 2nd ed., John Wiley, New York, 2001.
[51] J. Sun, D.K.Y. Soliman, J. Inorg. Biochem. 40 (1990) 271.
[52] M.T. Carter, M. Rodriguez, A.J. Bard, J. Am. Chem. Soc. 111 (1989) 8901.
[53] A. Kirsch-De Mesmaeker, G. Orellana, J.K. Barton, N.J. Turro, Photochem. Photobiol. 52 (1990) 461.
[54] S.D. Cummings, R. Eisenberg, J. Am. Chem. Soc. 118 (1996) 1949.

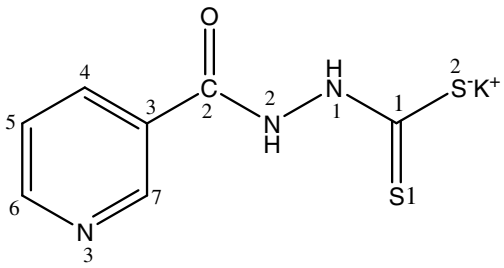

Fig. 1. [*N*′-(Pyridine-3-carbonyl)-hydrazine]-carbodithioate [$K^+(H_2L)^-$].

prepared potassium[*N*′-(pyridine-3-carbonyl)-hydrazine]-carbodithioate [$K^+(H_2L)^-$] (2 g, 8 mmol) in methanol (15 ml) and the reaction mixture was stirred continuously for 2 h at room temperature. On evaporation of the solvent and acidification of the product with dilute CH_3COOH (20% v/v), a yellow precipitate was obtained. This was suction filtered, washed with water, dried in vacuo and crystallized from hot methanol.

*2.3.1.1. Compound (**1a**).* Yellow single crystals of **(1a)** suitable for X-ray analyses were obtained by slow evaporation of its methanolic solution over a period of 10 days. Yield (68%); mp 172 °C. *Anal.* Calc. for $C_9H_{11}N_3OS_2$: C, 44.79; H, 4.59; N, 17.41; S, 26.67. Found: (241.33): C, 44.85; H, 4.55; N, 17.46; S, 26.62%. IR data (ν cm^{-1}, KBr): ν(NH) 3241 m; ν(C=O) 1672s; [β(NH)+ν(CN)] (Thioamide I) 1450s; [β(CN)+ν(NH)] (Thioamide II) 1348s; ν(N-N) 905m; ν(C=S) 1119; pyridine ring 649; (CH_3) 2979; (CH_2) 2930.

^{1}H NMR (DMSO-d_6; δ ppm): 11.57, 11.30 (m, 2H, –NH), 2.51 (m, 2H, >CH_2), 1.30 (m, 3H, –CH_3), 9.04, 8.81, 7.61, 8.24 (4H, pyridine ring). ^{13}C NMR (DMSO-d_6, δ ppm): 127.52 (C1), 152.96 (C2), 148.36 (C3), 123.87 (C4), 135.31 (C5), 163.92 (>C6=O), 203.11 (>C7=S), 27.88 (>C8H_2), 13.75 (–C9H_3). The structure was confirmed by XRD (Fig. 1a).

2.3.2. Synthesis of 1b (Method B)

The compound (**1b**) was synthesized by the reaction of CS_2 (1.5 ml, 22 mmol) with a methanol solution (20 ml) of nicotinic acid hydrazide (3 g, 22 mmol) in the presence of triethylamine (1.5 ml). Ethyl iodide (1.8 ml, 22 mmol) was added drop wise to the above clear solution and stirred continuously for 2 h at room temperature. On evaporation of the excess solvent and acidification of the residual mass with dilute CH_3COOH (20% v/v) a yellow precipitate was obtained which was suction filtered, washed with water, dried and crystallized from hot methanol.

*2.3.2.1. Compound (**1b**).* Dark yellow single crystals of **(1b)** suitable for X-ray analyses were obtained by slow evaporation of its methanolic solution over a period of 25 days. Yield 75%; mp 170 °C. *Anal.* Calc. for $C_9H_{11}N_3OS_2$: C, 44.79; H, 4.59; N, 17.41; S, 26.67. Found: (241.33): C, 44.64; H, 4.54; N, 17.39; S, 26.72%. IR (ν cm^{-1}, KBr): ν(NH) 3223m; ν(>C=O) 1646s; [β(NH)+ν(CN)] (Thioamide I)1429s; [β(CN)+ν(NH)] (Thioamide II) 1350s; ν(N-N) 901m; ν(>C=S) 1115m; pyridine ring 661; (CH_3) 2963; (CH_2) 2917. ^{1}H NMR (DMSO-d_6; δ ppm): 11.58, 11.31 (m, 2H, –NH), 2.50 (m, 2H, >CH_2), 1.31(m, 3H, –CH_3), 9.04, 8.79, 7.59, 8.24 (4H, pyridine ring).

^{13}C NMR (DMSO-d_6, δ ppm): 127.61 (C1), 152.98 (C2), 148.41 (C3), 123.94 (C4), 135.39 (C5), 164.02(>C6=O), 203.19(>C7=S), 27.97(>C8H_2), 13.81 (—C9H_3). The structure was confirmed by XRD. (Fig. 1b)

2.3.3. Preparation of complex (2)

A solution of H_2pchc (**1a**) (0.482 g, 2 mmol) in MeOH (10 ml) was added to a MeOH solution (10 ml) of $Mn(OAc)_2{\cdot}4H_2O$ (0.249 g, 1 mmol). This mixture was magnetically stirred for 3 h at room temperature. The resulting precipitate was filtered off, washed thoroughly with EtOH and air dried. This was suspended in MeOH to which *o*-phen (0.200 g, 1 mmol) was added and magnetically stirred for 2 h at room temperature. The clear yellow solution was filtered off and kept for crystallization.

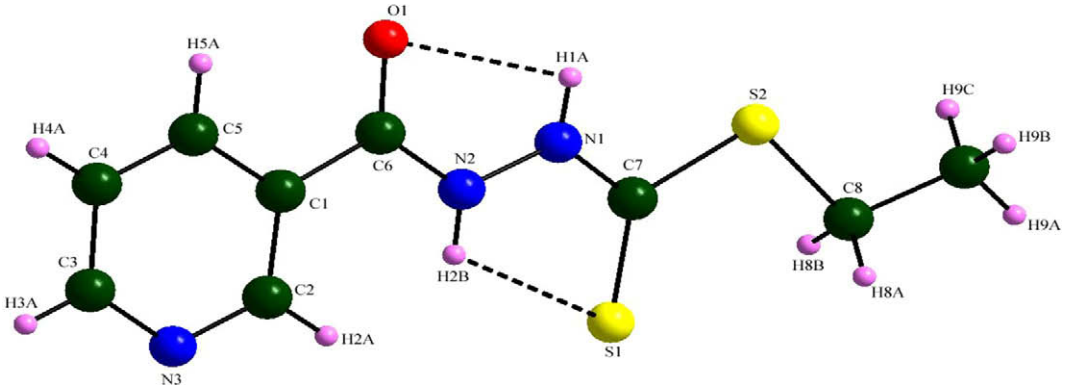

Fig. 1a. Crystal structure of H_2pchc (**1a**), showing the atom numbering scheme and intramolecular hydrogen bonding.

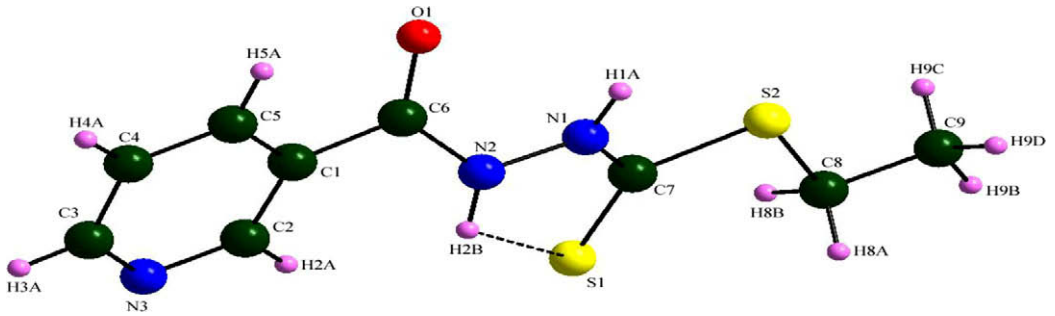

Fig. 1b. Crystal structure of H_2pchc (**1b**), showing the atom numbering scheme and intramolecular hydrogen bonding.

*2.3.3.1. Complex (**2**).* Light yellow single crystals of **(2)** suitable for X-ray analyses were obtained by slow evaporation of the above methanolic solution over a period of 7 days. Yield 58%; mp 176 °C, μ_{eff} = 6.10 BM. *Anal.* Calc. for $C_{30}H_{28}MnN_8O_2S_4$: C, 50.34; H, 3.94; N, 15.65; S, 17.92; Mn, 7.68. Found: (715.78): C, 50.34; H, 3.96; N, 15.62; S, 17.90; Mn, 7.72%. IR(ν cm^{-1}, KBr): ν(NH) 3224 m; ν(>C=O) 1646s; Thioamide(I) ν[β(NH)+ν(CN)] 1473s; Thioamide(II) [β(CN)+ν(NH)] 1353s; ν(N–N) 972m; ν(>C=S) 1117; (pyridine ring) 663; (CH_3) 2962; (CH_2) 2919. The structure was further confirmed by XRD (Fig. 4).

3. Analyses and physical measurements

Carbon, hydrogen, nitrogen and sulfur contents were estimated on a CHN Model CE-440 Analyser and on an Elementar Vario EL III Carlo Erbo 1108. By following standard procedure, the complex was analyzed for its metal content, after decomposition with a mixture of conc. HNO_3 and HCl, followed by conc. H_2SO_4 [18]. Magnetic susceptibility measurement was performed at room temperature on a Cahn Faraday balance using Hg[Co(NCS)$_4$] as the calibrant and electronic spectra were recorded on an UV-1700 Pharmaspec spectrophotometer. IR spectra were recorded in the 4000–400 cm^{-1} region as KBr pellets on a Varian Excalibur 3100 FT-IR spectrophotometer. ^{1}H and ^{13}C NMR spectra were recorded in DMSO-d_6 on a JEOL AL300 FT NMR spectrometer using TMS as an internal reference.

4. Crystal Structure determination

Single crystal X-ray diffraction measurements of **1a, 1b** and **2** were carried out with a Bruker SMART CCD area detector diffractometer equipped with a graphite crystal monochromator situated in the incident beam for data collection at 293(2) K and 173(2) K. Data collections were performed with Mo Kα radiation (λ = 0.71073 Å) by the phi and omega scan mode and the radiation source was a fine focus sealed tube. The structure was solved by direct methods (SHELX-97) and refined against all data by full-matrix least-squares on F^2 using anisotropic displacement parameters for all non-hydrogen atoms. All hydrogen atoms were included in the refinement at geometrically ideal positions and refined with a riding model [19,20]. MERCURY and DIAMOND packages were used for molecular graphics [21,22]. Crystal structure diagrams were generated by use of the ORTEP-3 for windows program [23].

5. Results and discussion

With an aim to obtaining N′-acylhydrazine carbodithioic acid ester ligand, H_2pchc was synthesized by the reaction of freshly prepared K$^+$[(H$_2$L)$^-$] and C_2H_5I in equivalent molar ratio in methanolic solution. Owing to the presence of amide and thioamide functional groups, it can exhibit keto–enol and thione–thiol forms [3]. The high polarizability, relatively weak C=S bond and the greater ability of sulfur with respect to oxygen to accommodate a negative charge makes NH–C=S more acidic [24]. But the IR (KBr) and ^{1}H NMR (DMSO-d_6) spectra are devoid of any peak to be attributed to SH for thiol form indicating that H_2pchc exists in thione form in solid (also by XRD) as well as in solution. Due to the more acidic character of NHC=S, this proton undergoes deprotonation during complexation. After deprotonation of NH(C=S), the extensive delocalization of π electron in (Hpchc)$^-$ on NHC=O moiety may be responsible for the retention of this proton. H_2pchc loses a proton directly from the HNC=S group to compensate the positive charge of the metal ion. The ligand H_2pchc reacts with $Mn(OAc)_2 \cdot 4H_2O$ to give a yellow solid product. The resulting solid was suspended in MeOH and reacted with *o*-phen which resulted in a clear solution of complex **2**. Complex **2** has been obtained as single crystals and analyzed, which shows that the carbonyl-oxygen and NH(C=S) nitrogen (after loss of proton) participate in bonding. The ligand and the complex are air-stable and can be kept in desiccators over a prolonged period without sign of decomposition.

5.1. IR spectra

The ligand H_2pchc **(1a and 1b)** contain the thioamide group (NHCS), which should give rise to characteristic bands namely, thioamide I, thioamide II and thioamide IV having contributions from [β(NH)+ν(CN)], [β(CN)+ν(NH)], ν(C=S) modes of vibrations, respectively. The IR spectra of H_2pchc (**1a** and **1b)** show only one band at 3241, 3223 cm^{-1}, respectively for –NH groups. The others bands at 1672–1646, 1450–1429, 1348–1350, 905–901, 1119–1115 cm^{-1} correspond to ν(>C=O), [β(NH)+ν(CN)] (thioamide I), [β(CN)+ν(NH)] (thioamide II), ν(N-N) and ν(>C=S), respectively. The pyridine ring, –CH_2 and –CH_3 bands occur at 649–661, 2930–2917, 2979–2963 cm^{-1}, respectively.

Comparison of the main vibrational bands of H_2pchc (**1a**) is used to establish its ligating behavior in its complex **2**. The bands at 3224 and 1646 cm^{-1} in **2** are assigned to ν(NH) and ν(C=O), respectively. A negative shift of 26 cm^{-1} in ν(C=O) indicates the involvement of carbonyl oxygen in bonding. The bonding through the sulfur of C=S is not indicated because ν(C=S) remains unchanged in the complex **2** in comparison to the free ligand H_2pchc **(1a)**. The involvement of the hydrazinic nitrogen in bonding is supported by a positive shift of 67 cm^{-1} in ν(N–N). The ν(NH) peak in complex **2** shows a negative shift as compared to the ligand **1a** due to disappearance of hydrogen bonding N–H···O during complexation. The pyridine ring vibrations at 649 cm^{-1} in the complex remains unchanged, as compared to the ligand H_2pchc (**1a)** indicating that the ring nitrogen is not involved in bonding.

5.2. ^{1}H and ^{13}C NMR spectra

The ^{1}H NMR spectra of H_2pchc (**1a** and **1b**) show peaks due to –NH, –CH_2, –CH_3 and multiplets for pyridine ring in aromatic region. The ^{1}H NMR spectra of H_2pchc (**1a** and **1b**) exhibit two signals at δ 11.57–11.58 and 11.30–11.31 ppm for the amide and thioamide protons, respectively. The protons due to the pyridine ring appear as multiplets between δ 7.61–9.04 ppm for **1a** and 7.59–9.03 ppm for **1b**. In solution downfield chemical shifts for hydrazinic protons as compared to K$^+$(H$_2$L)$^-$ (δ_H = 11.57 [NH(CS)], 11.30 [(NH(CO)] ppm for (**1a**) and (δ_H = 11.58 [NH(CS)], 11.31 [(NH(CO)] ppm for (**1b**) indicate the involvement of N–H group in intramolecular hydrogen bonding N2–H2···S1 and N1–H1···O1 in **1a** and N2–H2···S1 in **1b**, respectively (Figs. 1a and 1b). The ^{13}C NMR spectra exhibit signals due to >(C=S), >(C=O), –CH_2, –CH_3 and pyridine ring carbons as expected for the structures shown in Figs. 1a and 1b. The ^{13}C NMR spectra of both **1a** and **1b** show 9 signals for nine carbon atoms, of which the signals at δ 203.11–203.19 and 163.92–164.02 ppm are due to the >C=S and >C=O, carbons, respectively. The signals for >CH_2 and >CH_3 carbons are observed at 27.88–27.97 and 13.75–13.81 ppm, respectively. The pyridine ring carbons appear at C1:127.52–127.61, C2:152.96–152.98, C3:148.36–148.41, C4:123.87–123.94 and C5:135.31–135.39 ppm.

6. Electronic spectra and magnetic moment

The electronic spectra of **1a** and **1b** in MeOH show two bands at 288 and 214 nm which can be assigned to the $\pi \rightarrow \pi^*$ transition in the ligand. The magnetic moment of 6.10 B.M. for [Mn(Hpchc)$_2$(*o*-phen)] suggests a high spin Mn(II) with five unpaired electrons. The electronic spectrum of the complex shows d–d bands at 631,

548, 454 and 431 nm which are assigned to the $^6A_{1g} \rightarrow {}^4T_{1g}(G)$, $^6A_{1g} \rightarrow {}^4T_{2g}(G)$ and $^6A_{1g} \rightarrow {}^4E_g(G)$ and $^4A_{1g}(G)$ transitions, respectively for six coordinated high spin Mn(II) centre possessing distorted octahedral geometry [25].

7. Crystal structure description

7.1. Crystal structure of H_2pchc (**1a**)

The crystal structure of **1a** and **1b** are shown in Figs. 1a and 1b, respectively, with atomic numbering scheme. Crystallographic data and structural refinement details are given in Table 1 for compounds **1a** and **1b**. The hydrogen bonding parameters and intermolecular interactions are listed in Table 3. The main bond distances, bond angles and torsional angles of both ligands (**1a** and **1b**) are listed in Table 2. In the compound **1a,** the crystal packing is dominated by weaker C(4)–H(4A)···O(1) (2.561 Å) and stronger hydrogen bonding N(1)–H(1)···N(3) (1.963 Å). Views of the molecular packing in **1a** are shown in Fig. 2. Due to the presence of the intermolecular hydrogen bonding N–H···N and weak interaction C(8)–(S2)···N(3) (3.343 Å), the two adjacent molecules of the ligand are orthogonally arranged with respect to each other. The adjacent orthogonal arrangement of the molecules gives a twisted molecular conformation leading to a ladder type of arrangement where each step of the ladder happens due to the presence of hydrogen bonding between pyridine ring nitrogen and hydrazinic hydrogen (Fig. 2b). A similar arrangement has been reported by Gulyani et al. [26] and Suresh et al. [27]. This crystal is twined. i.e., forms a regular aggregates consisting of crystals of the same species joined together in some definite mutual orientation [28]. The pyridine ring carbon C3 shows a weak interaction with the O1 and hydrazinic hydrogen of N3. In the crystal lattice, the molecules are connected via intermolecular N–H···N hydrogen bond and form a twisted chain along *a*-axis (Fig. 2c). The distances and angle are: N(1)–H(1) = 0.860 Å, H(1)···N(1) = 1.963 Å, ∠N(1)–H(1)···N(3) = 171.44°. One hydrogen of methylene group [C(sp^3)-H(s)] of one molecule shows weak van der Waals interaction with a methylene hydrogen of another molecule (view along *b*-axis) with H···H distance of 2.363 Å. The H···H interaction between the **1a** molecules moves the chain in upward direction along *b*-axis. The packing of **1a** in the crystal lattice is stabilized by hydrogen bonding which is responsible for producing β-sheet pattern (Fig. 2a). The C–H···O hydrogen bond [d(H···A) = 2.5614 Å with an angle of ∠C–H···O = 132.71°] is formed between the hydrogen atom of sp^2 carbon of pyridine ring at position 4 and the amide oxygen. The sheet further grows in *b* direction by C4–H4A···O(1)═C(6). The values found for, H···A, ∠C–H···O is close to the bond distance and

Table 1
Crystallographic data and structure refinements for **1a**, **1b** and **2**

Compounds	1a	1b	2
Chemical formula	$C_9H_{11}N_3OS_2$	$C_9H_{11}N_3OS_2$	$C_{30}H_{28}MnN_8O_2S_4$
Formula weight	241.33	241.33	715.78
T (K)	293(2)	173(2)	173(2)
λ (Mo Kα) (Å)	0.71073	0.71073	0.71073
Crystal system	monoclinic	triclinic	monoclinic
Space group	*C*2/*c*	P1	*C*2/*c*
a (Å)	37.202(8)	4.8809	17.9507(15)
b (Å)	4.100(1)	7.0553	11.2218(9)
c (Å)	14.267(2)	8.463	16.8359(14)
α (°)	90	78.927(4)	90
β (°)	99.16(1)	76.140(4)	106.082(1)
γ (°)	90	77.063(3)	90
V (Å^3)	2148.3	272.80(12)	3258.7(5)
Z	8	1	4
M (mm^{-1})	0.471	0.464	0.704
$\rho_{calc.}$ (Mg/cm^3)	1.492	1.469	1.459
F (000)	1008	126	1476
Crystal size (mm^3)	0.38 × 0.33 × 045	0.51 × 0.28 × 0.08	0.39 × 0.35 × 0.20
θ Range for data collected (°)	1.11 to 29.70	2.51 to 29.80	2.33 to30.52
Index ranges	$-51 \leqslant h \leqslant 50$ $0 \leqslant k \leqslant 5$ $0 \leqslant l \leqslant 19$	$-6 \leqslant h \leqslant 6$ $-9 \leqslant k \leqslant 9$ $-11 \leqslant l \leqslant 11$	$-25 \leqslant h \leqslant 25$ $-15 \leqslant k \leqslant 15$ $-23 \leqslant l \leqslant 23$
Number of reflections collected	3343	2968	17990
Number of indent reflections (R_{int})	3387 [R_{int} = 0.0000]	2411 [R_{int} = 0.0179	4723 [R_{int} = 0.0227]
Number of data/ restraints/ parameters	3387/0/138	2411/3/144	4723/0/205
Goodness-of-fit on F^2	1.225	1.070	1.033
R_1,[a] wR_2[b] ($I > 2\ (I)$)	0.0671, 0.2069	0.0320, 0.0845	0.0405, 0.0969
R_1,[a] wR_2[b] (all data)	0.0689, 0.2087	0.0324, 0.0848	0.0496, 0.1023
Largest differences in peak/hole, e Å^{-3}	0.727 and −0.584	0.499 and −0.400	1.065 and −0.624

[a] $R_1 = \Sigma||F_o| - |F_c||/\Sigma|F_o|$.
[b] $R_2 = [\Sigma w(|F_o^2| - |F_c^2|)^2/\Sigma w|F_o^2|^2]^{1/2}$.

Table 2
Selected bond lengths (Å) and angles (°) for **1a** and **1b**

	1a	1b
Bond lengths		
S(2)–C(7), S(2)–C(8)	1.765(4), 1.818(4)	1.7660(18), 1.805(2)
S(1)–C(7)	1.663(4)	1.6580(19)
O(1)–C(6)	1.220(5)	1.229(2)
N(1)–C(7)	1.332(5)	1.338(2)
N(1)–N(2)	1.383(4)	1.386(2)
N(2)–C(6)	1.338(5)	1.340(2)
C(1)–C(6)	1.493(5)	1.497(2)
C(8)–C(9)	1.512(6)	1.524(3)
Bond angles		
C(7)–S(2)–C(8)	102.7(2)	102.96(10)
C(7)–N(1)–N(2)	119.3(3)	119.39(16)
C(6)–N(2)–N(1)	120.2(3)	120.09(15)
C(2)–C(1)–C(6)	124.5(4)	122.04(17)
C(5)–C(1)–C(6)	117.4(3)	118.86(16)
O(1)–C(6)–N(2)	122.5(4)	122.90(16)
O(1)–C(6)–C(1)	121.5(4)	121.36(16)
N(2)–C(6)–C(1)	115.9(3)	115.73(15)
N(1)–C(7)–S(1)	123.5(3)	124.23(13)
N(1)–C(7)–S(2)	111.0(3)	110.71(13)
S(1)–C(7)–S(2)	125.5(3)	125.06(11)
C(9)–C(8)–S(2)	107.8(3)	108.31(16)
Torsion angles		
C(7)–N(1)–N(2)–C(6)	−174.2(4)	−145.54(18)
N(1)–N(2)–C(6)–O(1)	1.8(6)	−2.6(3)
N(1)–N(2)–C(6)–C(1)	−179.2(3)	178.76(16)
C(2)–C(1)–C(6)–O(1)	178.0(4)	150.49(18)
C(5)–C(1)–C(6)–O(1)	−0.3(6)	−26.2(2)
C(2)–C(1)–C(6)–N(2)	−1.1(6)	−30.8(2)
C(5)–C(1)–C(6)–N(2)	−179.4(3)	152.50(17)
N(2)–N(1)–C(7)–S(1)	4.9(5)	1.8(2)
N(2)–N(1)–C(7)–S(2)	−174.7(3)	−177.50(12)
C(8)–S(2)–C(7)–S(1)	−4.4(3)	−7.24(14)

Table 3
Summary of intermolecular interactions and hydrogen bonds for **1a** (Å and °)

D–H···A	*d*(D–H)	*d*(H···A)	*d*(D···A)	∠(DHA)
N(1)–H(1A)···N(3)#1	0.86	1.96	2.816(5)	171.5
C(4)–H(4A)···O(1)	0.93	2.56	3.264	137.71
N(1)–H(1A)···O(1)	0.86	2.45	2.695	97.20
N(2)–H(2B)···S(1)	0.86	2.56	2.94	107.44
N(1)–H(1A)···C(3)	0.86	3.330	4.186	175.93
C(6)–O(1)···C(3)	1.24	3.127	4.087	135.46

Symmetry transformations used to generate equivalent atoms: #1 $x, -y-1, z-1/2$.

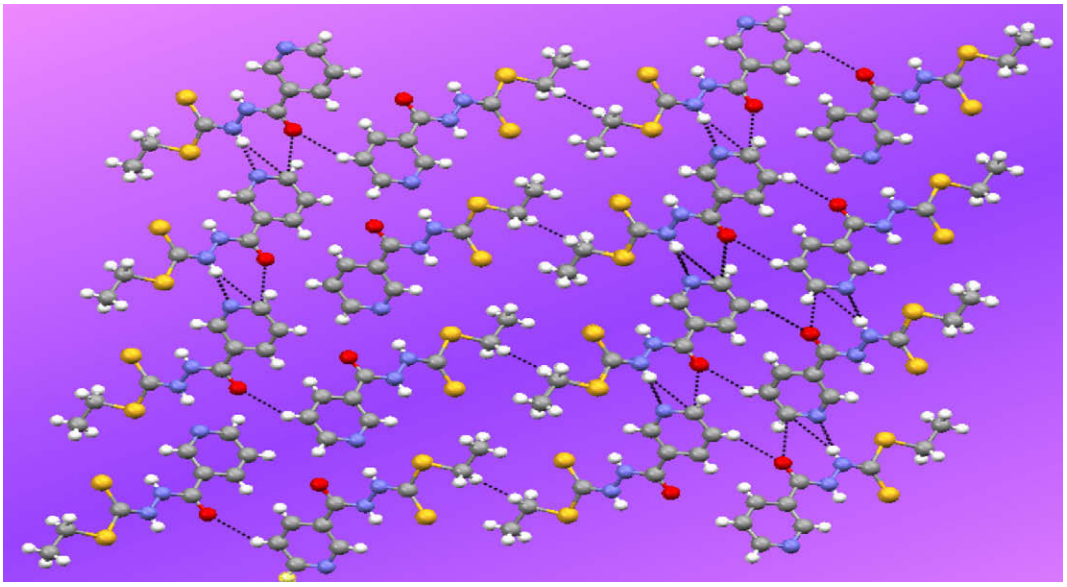

Fig. 2a. View of the crystal packing in H_2pchc (**1a**) along the *b* direction resulting in 1D chain.

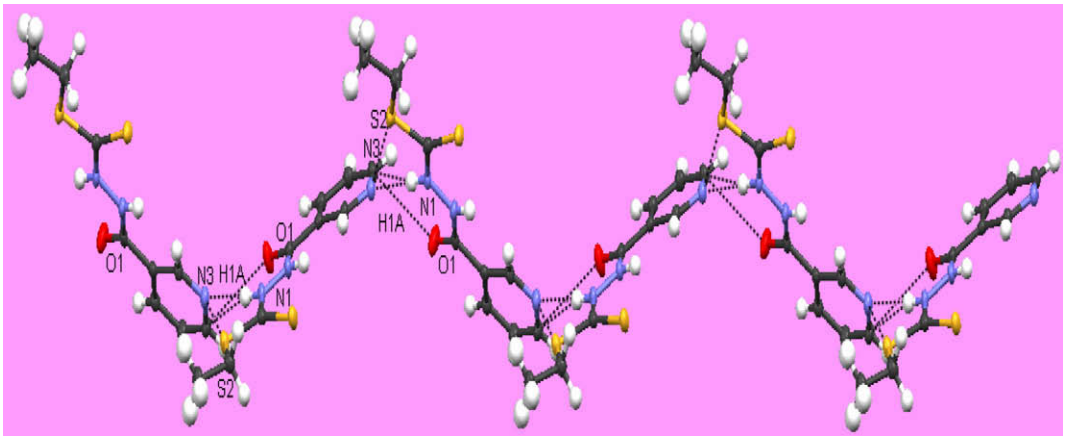

Fig. 2b. The orientation of pyridine rings forming N1–H1A···N3 intermolecular hydrogen bonding and C8–S2···N short contact, along *a*-axis.

bond angle reported by Suresh et al [25]. These weak interactions link the layers into 3D network. There is no π···π interactions operating in the structure of **1a.**

7.2. Crystal structure of H_2pchc (**1b**)

The hydrogen bonding parameters and intermolecular interactions are listed in Table 4. In the crystal structure of **1b**, the intermolecular N(1)–H(1A)···N(3) and N(2)–H(2B)···O(1) hydrogen bonding are present with the distances of 2.020 Å and 2.105 Å, respectively. However, **1b** lacks the N–H···O intramolecular hydrogen bonding which is present in **1a.** The structure is in turn stabilized by intramolecular N–H···S hydrogen bonding as also reported by Srinivasan and Chacko [29].

The intermolecular N–H···N and N–H···O hydrogen bonding give layers of the molecules stacked upon each other, along *a*-axis (Fig. 3a). This stacking results in face to face interaction between pyridine ring with centroid–centroid (Cp–Cp)* separation of 4.881 Å (Fig. 3b). However distance of centroid separation indicates that there is no co-facial interaction between successive pyridine rings. The molecules are linked together to form chain along *a*-axis via linear H···H weak interaction. One hydrogen atom of methyl group (Csp^3) shows van der Waals interaction with the hydrogen atom of pyridine ring at position 3 (Fig. 3c). There is edge to face interaction between the centroid of a pyridine ring (Cp) and methylene hydrogen atom (H8B) with a distance of 2.939 Å (C8–H8B···Cp, Cp = centroid of pyridine ring) and an angle ⩾C–H···Cp of 147.53°. The molecules of **1a** and **1b** also show extensive electron delocalization on the amide and thioamide due to intermediate bond distances found for –C(O)NHNHC(S)S– moiety [13]. Both **1a** and **1b** are stabilized by the presence of weak interactions, intermolecular and intramolecular hydrogen bonding.

7.3. Comparison of **1a** and **1b**

The ligands **1a** and **1b** crystallized in different crystal systems, monoclinic and triclinic, respectively, and show different molecular packing. The basic difference between **1a** and **1b** is that **1a** crystallized as twinned crystal in a regular orthogonal arrangement of molecules [28]. The bond lengths and bond angles in **1a** and **1b** are almost similar but the torsional angles of both are completely different [[N(1)–N(2)–C(6)–C(1) = −179.2(3), C(5)–C(1)–C(6)–O(1) = −0.3(6), C(2)–C(1)–C(6)–N(2) = −1.1(6) for **1a** and N(1)–N(2)–C(6)–C(1) = 178.76(16), C(2)–C(1)–C(6)–O(1) = 150.49(18), C(5)–C(1)–C

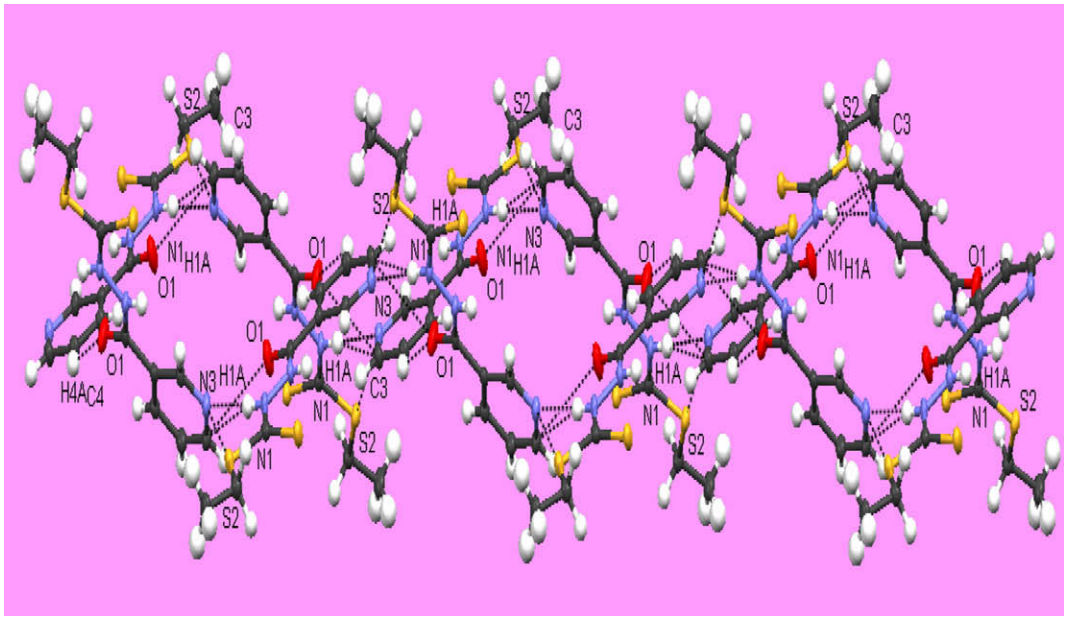

Fig. 2c. Crystal packing of H_2pchc (**1a**), along *a*-axis showing molecules stacked with each other to form helix like structure.

Table 4
Summary of intermolecular interactions and hydrogen bonds for **1b** (Å and °)

D–H···A	*d*(D–H)	*d*(H···A)	*d*(D···A)	∠(DHA)
N(1)–H(1A)···N(3)#1	0.88	2.02	2.900(2)	176.7
N(2)–H(2B)···O(1)#2	0.88	2.10	2.906(2)	151.0
N(2)–H(2B)···S(1)	0.88	2.713	2.956	97.23
C(3)–H(3A)···O(1)	0.95	2.485	3.0109	123.26
C(2)–H(2A)···S(2)	0.95	2.887	3.551	127.95
C(6)–O(1)···C(3)	1.24	3.109	3.930	123.92

Symmetry transformations used to generate equivalent atoms: #1 $x-1, y+1, z$ #2 $x+1, y, z$.

(6)–O(1) = −26.2(2), C(2)–C(1)–C(6)–N(2) = −30.8(2) for **1b**]. The ligand **1a** shows two types of intramolecular hydrogen bonding (NH···S and NH···O) while **1b** has only NH···S hydrogen bonding. Compound **1a** contains only one type of inter molecular hydrogen bonding N–H···$N_{(py)}$ while **1b** forms two types of hydrogen bonding i.e. N–H···$O_{(carbonyl)}$ and N–H···$N_{(py)}$.

7.4. Crystal structure of complex (*2*)

Fig. 4 shows an ORTEP diagram of the Mn(II) complex together with the atom numbering scheme. The structural refinement data related to complex **2** are listed in Table 1 and the selected bond distances, bond angles and torsion angles are listed in Table 5. The hydrogen bonding and weak interactions are listed in Table 6.

The metal center in complex **2** is coordinated in an N4O2 core by two uninegative bidentate ligands using hydrazine nitrogen (N1, after loss of proton) and carbonyl oxygen. The N2H2 nitrogen does not take part in bonding because of the presence of hydrogen bonding between N2–H2B···S1 atoms, both in the ligand and the complex. Various distances found within the chelate rings are intermediate between single and double bond lengths and also shorter or longer than the corresponding bond lengths in H_2pchc (**1a**). The average bond lengths in complex **2** are: O1–C6 = 1.247(19)(L), N2–C6 = 1.331(2)(S), N1–N2 = 1.392(18)(L), N1–C7 = 1.322(2)(S) Å (L = longer, S = shorter) which suggest considerable

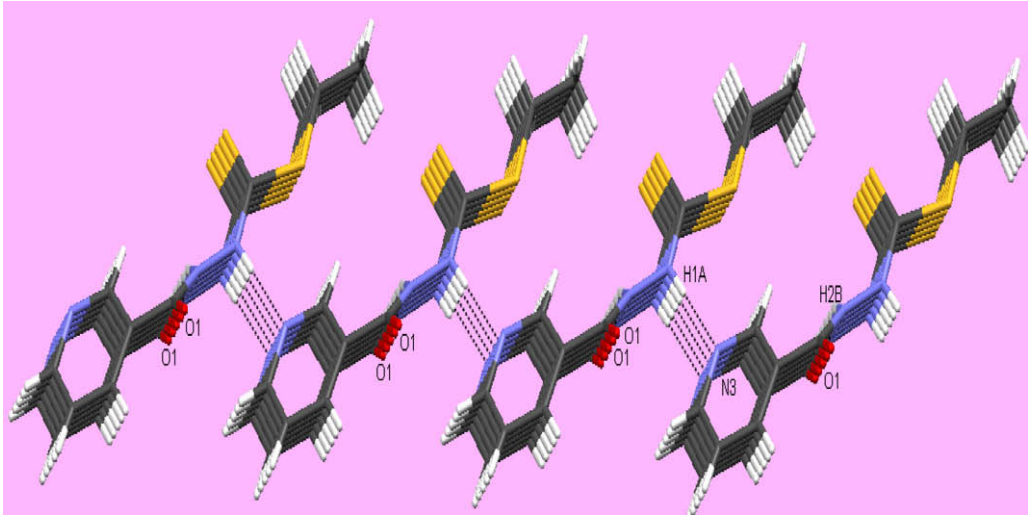

Fig. 3a. Crystal packing of H_2pchc (**1b**), along *a*-axis showing molecules stacked and superimposed on each other.

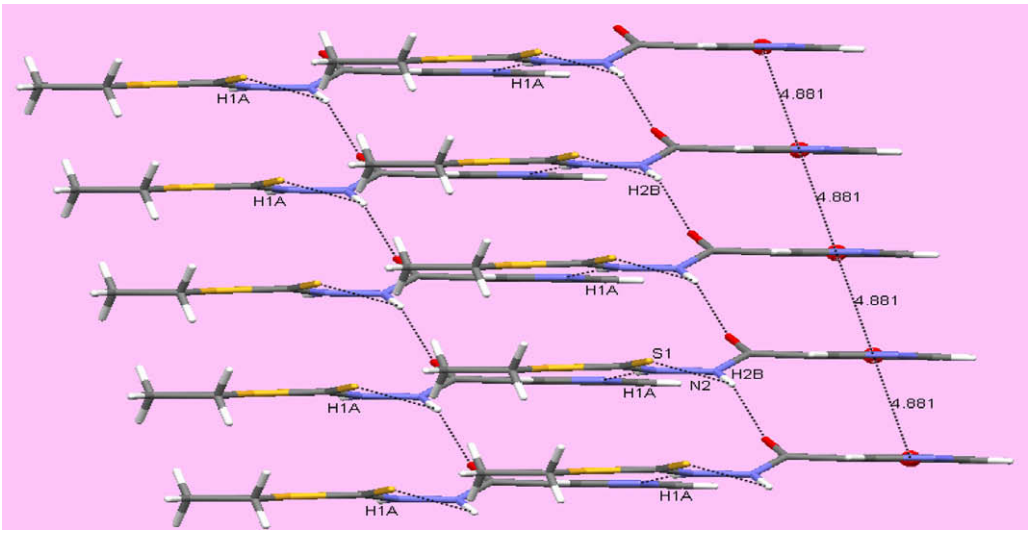

Fig. 3b. Molecular packing indicating centroid–centriod (Cp–Cp)* separation between pyridine ring.

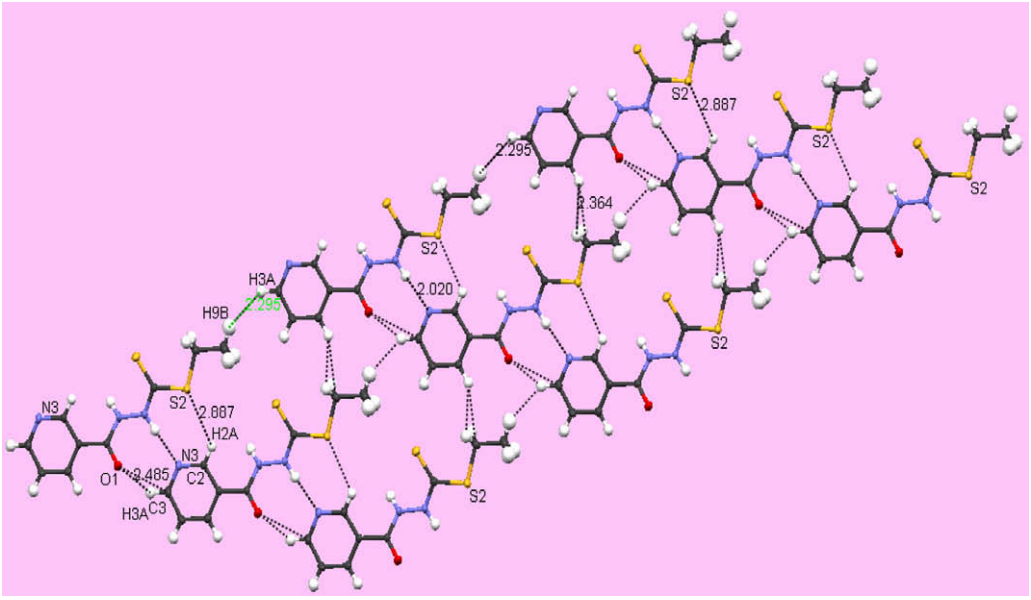

Fig. 3c. Crystal packing of H_2pchc (**1b**), reinforced by weak interactions along *a*-axis.

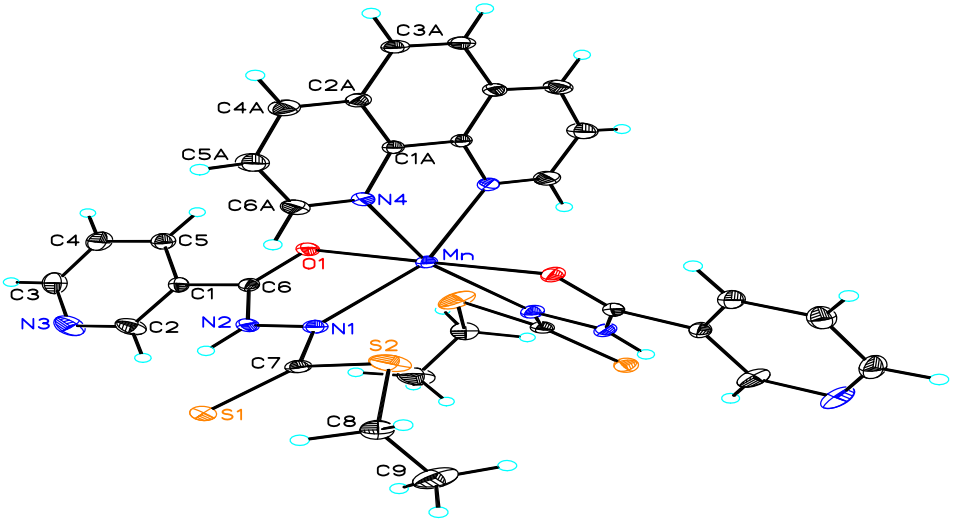

Fig. 4. ORTEP diagram of [Mn(Hpchc)$_2$(*o*-phen)] showing atomic numbering scheme with ellipsoid of 30% probability.

Table 5
Selected bond lengths (Å), bond angles (°) and torsional angles (°) for complex **2**

Bond lengths (Å)			
Mn–O(1)#1	2.1832(12)	S(1)–C(7)	1.6943(17)
Mn–O(1)	2.1833(12)	S(2)–C(7)	1.7727(17)
Mn–N(1)#1	2.2487(14)	S(2)–C(8)	1.785(2)
Mn–N(1)	2.2488(14)	O(1)–C(6)	1.2472(19)
Mn–N(4)#1	2.2585(14)	N(1)–C(7)	1.322(2)
Mn–N(4)	2.2586(14)	N(1)–N(2)	1.3916(18)
N(2)–C(6)	1.331(2)		
C(8)–C(9)	1.480(3)		
Bond angles (°)			
O(1)#1–Mn–O(1)	179.35(6)	O(1)#1–Mn–N(1)#1	73.82(5)
C(1A)–N(4)–Mn	115.18(11)	O(1)–Mn–N(1)	73.82(5)
O(1)–Mn–N(1)#1	106.62(5)	N(1)#1–Mn–N(4)#1	96.67(5)
O(1)#1–Mn–N(1)	106.62(5)	N(1)–Mn–N(4)	96.67(5)
O(1)–Mn–N(4)#1	88.77(5)	O(1)–Mn–N(4)	90.71(5)
O(1)#1–Mn–N(4)	88.77(5)	O(1)#1–Mn–N(4)#1	90.72(5)
N(1)#1–Mn–N(4)	160.30(5)	C(6)–O(1)–Mn	114.93(10)
N(1)–Mn–N(4)#1	160.30(5)	C(7)–N(1)–Mn	137.79(11)
N(4)#1–Mn–N(4)	73.94(7)	N(2)–N(1)–Mn	108.89(10)
N(1)#1–Mn–N(1)	97.11(8)	C(6A)–N(4)–Mn	126.54(12)
C(7)–S(2)–C(8)	105.45(9)	C(6)–N(2)–N(1)	118.63(13)
C(9)–C(8)–S(2)	115.04(18)	C(7)–N(1)–N(2)	113.32(13)
C(2)–C(1)–C(6)	123.34(17)	O(1)–C(6)–N(2)	121.89(14)
C(5)–C(1)–C(6)	118.86(15)	O(1)–C(6)–C(1)	120.92(15)
N(2)–C(6)–C(1)	117.19(14)	N(1)–C(7)–S(2)	109.40(12)
N(1)–C(7)–S(1)	126.29(13)	S(1)–C(7)–S(2)	124.25(10)
Torsional angles (°)			
O(1)#1–Mn–	−144.66(12)	N(1)#1–Mn–	81.69(12)
O(1)–C(6) Mn–N(1)–N(2)–C(6)	−11.18(17)	O(1)–C(6) N(1)–Mn–O(1)–C(6)	−11.05(12)
N(4)#1–Mn–O(1)–C(6)	178.29(12)	O(1)#1–Mn–N(1)–C(7)	9.08(19)
N(4)–Mn–O(1)–C(6)	−107.79(12)	O(1)–Mn–N(1)–C(7)	−170.43(19)
N(4)#1–Mn–N(1)–C(7)	−141.67(17)	O(1)#1–Mn–N(1)N(2)	−169.44(10)
N(4)–Mn–N(1)–C(7)	−81.63(18)	O(1)–Mn–N(1)–N(2)	11.05(10)
N(1)#1–Mn–N(1)–C(7)	84.26(17)	N(4)–Mn–N(1)–N(2)	99.86(11)
N(1)#1–Mn–N(1)–N(2)	−94.26(11)	C(7)–N(1)–N(2)–C(6)	169.90(15)
N(4)#1–Mn–N(1)–N(2)	39.8(2)		

Table 6
Summary of intermolecular interactions and hydrogen bonds for **2** (Å and °)

D–H···A	d(D–H)	*d*(H···A)	*d*(D···A)	∠(DHA)
N(2)–H(2B)···S(1)	0.88	2.45	2.8769(15)	110.3
C(3A)–H(3AA)···S(1)	0.95	2.995	3.846	149.74
C(9)–H(9A)···S(2)	0.98	2.935	3.724	138.24
C(5A)–H(5AA)···Cg (py)	0.95	2.927	3.748	145.46
C(3)–H(3A)···Cg (ph)	0.95	2.707	3.615	160.17

Symmetry transformations used to generate equivalent atoms: #1 $-x, y, -z + 1/2$.

delocalization of charge [30]. The metal ligand bond lengths in **2** are found to be shorter than typical single bond which may be due to the π – donating or π – back bonding interactions between the metal and the ligand. Thus, the charge is transferred from the metal and the ligand into an orbital that is bonding with respect to the metal-ligand bond. Masui suggested that if an active electron delocalization within a metal–*N*-heterocyclic chelate ring is present it would exhibit some degree of metalloaromaticity [31]. The transition metal complexes in which bonding of the ligand takes place through carbonyl oxygen and nitrogen and also bonded with *N*-heterocyclic bases such as *o*-phen, 2,2′-bpy are prone to exhibit metalloaromaticity [32–34]. The above criteria of metalloaromaticity are fulfilled in complex **2**. The most noteworthy structural feature of complex **2** is that two *ortho*-H atoms from *o*-phen ring point towards the centre of the corresponding $MnOCN_2$ chelate rings [35]. This delocalized charge in the chelate ring forms an unusual intramolecular C–H···π interaction with ortho hydrogen of the adjacent phenyl ring of *o*-phen [31,32] (Fig. 5). The H···Cg, C···Cg and H···chelate ring plane distances are 3.375, 3.613 and 2.858 Å and C–H···Cg angle is 96.84° (below the optimal value of 180°) for the strongest C–H···π interactions, which may be due to the steric constraints in the molecule. Both chelate rings around Mn(II) formed by the $(Hpchc)^-$ are almost orthogonal to each other forming a dihedral angle of 86.44°. In the complex the chelate rings and the pyridine rings lie nearly in the same plane forming a dihedral angle of 20.75°. The pyridine rings thus make an extended coplanar system with both chelate rings forming a bite angle of 73.82° and with coligand, the bite angle is 73.94°. However, it has been observed that both the ligands coordinated to Mn(II) are antioriented with respect to each other, to minimize the steric hindrance by similar groups. The O(1)#1–Mn–O(1) angle involving the carbonyl oxygen of the two ligands is 179.35(6)°, showing less distortion from an octahedral geometry in complex **2**. The bond distances Mn–O, Mn–N and Mn–N_{phen} are 2.183, 2.249 Å and 2.259 Å which are comparable to the bond lengths reported for $[Mn_3(O_2CCH_3)_6(N–N)_2]$ (where N–N = *o*-phen) [36] and $[Mn_2(phen)(Hdcbi)]_n$ (Hdcbi = 4,5-dicarboxyimidazole) [37]. Due to deprotonation of hydrazinic hydrogen, the intermolecular hydrogen bonding present between the N(3) pyridine nitrogen and H1A–N1 of hydrazinic hydrogen in **1a** disappears in **2**. The intramolecular hydrogen bonding C=O···H1A–N1 is also absent due to involvement of carbonyl oxygen in coordination with Mn(II).

7.5. Crystal packing

There is notable intermolecular hydrogen bonding C3–H3AA···S1 (*o*-phen ring) in the complex **2** which gives stacking due to which the molecules are exactly superimposed on each other (Fig. S1). The shortest centroid to centroid separation found between parallel pyridine rings is 5.813(2) Å which rules out the possibility of face to face (π···π) interaction between pyridine rings in the crystal structure of **2** (Fig. 6). The C–H···π (edge to

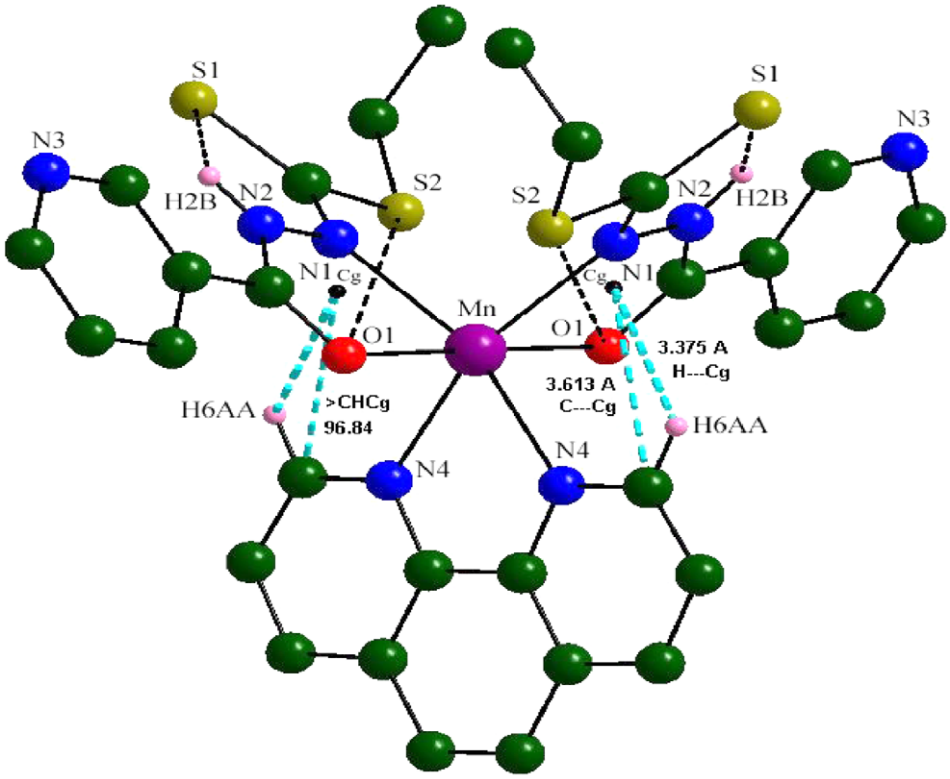

Fig. 5. Crystal structure of [Mn(Hpchc)$_2$(*o*-phen)], showing unusual intramolecular C–H···π interaction with Mn(II) chelate ring and intramolecular hydrogen bonding. For clarity other hydrogen atoms are omitted.

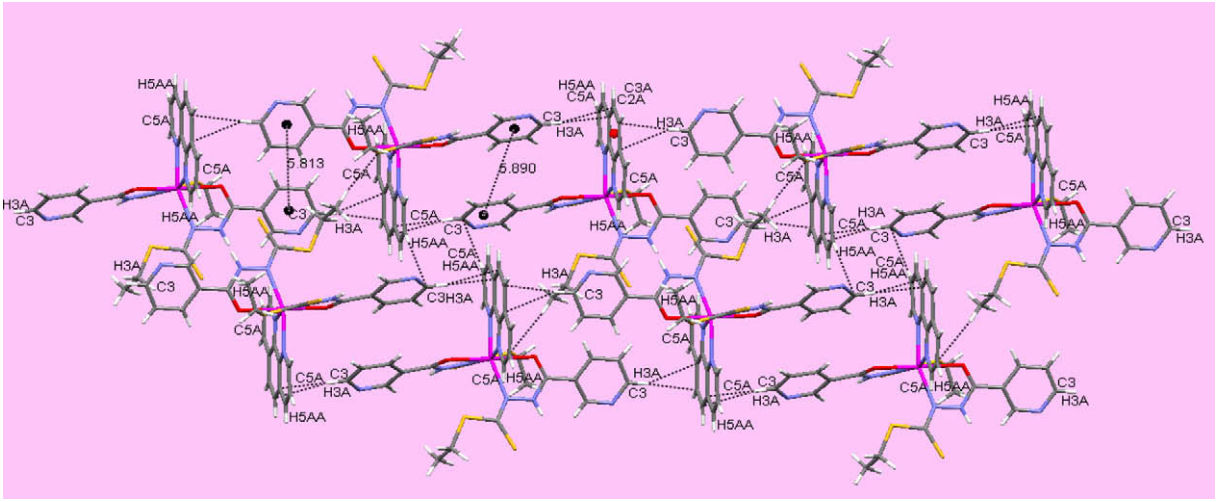

Fig. 6. Crystal packing of complex 2, showing centroid–centroid (Cp–Cp)* separation and edge to face interactions.

face) contacts follows a network of interconnected pattern giving rise to three dimensional supramolecular arrangement (Fig. 6, Fig. S2). The strong N(1)–H(1)···S(1) interaction serves as structure directing factor. The geometric parameters describing the intermolecular interactions in **2** are collected in Table 6. The extended supramolecular system is obtained due to the presence of three types of weak interactions C(3)–H(3A)···C(2A) (*o*-phen) = 2.839 Å, C(3)–H(3A)···C3A (*o*-phen) = 2.724 Å and C(5)–H(5AA)···C(3)(pyridine ring) = 2.927 Å. The crystal structure is in turn stabilized by intramolecular and intermolecular hydrogen bonding. The additional stabilization in the complex is due to intramolecular C–H···π interaction (Fig. 5).

8. Conclusion

Two different forms of a new *N′*-(pyridine-3-carbonyl) hydrazinecarbodithioic acid ethyl ester (**1a** and **1b**) and the Mn(II) complex (2) of **1a** have been synthesized. The crystals of **1a** are twined and show ladder like regular arrangement. The molecular packing of **1b** and **2** show layering and stacking upon each other. The

complex **2** shows an unusual intramolecular C–H···π (chelate ring) interaction which gives structural support for metalloaromaticity.

Acknowledgement

One of the authors (M. Singh) is thankful to CSIR, New Delhi, India for the award of SRF in a Project supported by Grant No. 01(2152)07/EMR-II.

Appendix A. Supplementary data

CCDC 650160, 650161 and 650162 contain the supplementary crystallographic data for **1a**, **1b** and **2**. These data can be obtained free of charge via http://www.ccdc.cam.ac.uk/conts/retrieving.html, or from the Cambridge Crystallographic Data Centre, 12 Union Road, Cambridge CB2 1EZ, UK; fax: (+44) 1223 336 033; or e-mail: deposit@ccdc.cam.ac.uk. Supplementary data associated with this article can be found, in the online version, at doi:10.1016/j.poly.2008.08.007.

References

[1] (a) M.A. Ali, A.H. Mirza, T.B.S.A. Ravoof, P.V. Bernhardt, Polyhedron 23 (2004) 2031;
(b) M.A. Ali, A.H. Mirza, L.K. Wei, A.L. Tan, P.V. Bernhardt, Polyhedron 23 (2004) 2037;
(c) M.A. Ali, A.H. Mirza, C.W. Voo, A.L. Tan, P.V. Bernhardt, Polyhedron 22 (2003) 3433;
(d) M.A. Ali, A.H. Mirza, M. Nazimuddin, R. Ahmed, L.R. Gahan, P.V. Bernhardt, Polyhedron 22 (2003) 1471;
(e) M.A. Ali, A.H. Mirza, S.T.W. Keng, R.J. Butcher, Transition Met. Chem. 28 (2003) 241.
[2] (a) M.A. Ali, A.H. Mirza, R.J. Butcher, M.T.H. Tarafder, T.B. Keat, A.M. Ali, J. Inorg. Biochem. 92 (2002) 141;
(b) M.A. Ali, A.H. Mirza, M. Nazimuddin, P.K. Dhar, R.J. Butcher, Transition Met. Chem. 27 (2002) 27;
(c) M.A. Ali, A.H. Mirza, R.J. Butcher, M.T.H. Tarafder, A.M. Ali, Inorg. Chim. Acta 320 (2001) 1.1.
[3] K.A. Crouse, K.-T. Chew, M.T.H. Tarafder, A. Kasbollah, A.M. Ali, B.M. Yamin, H.-K. Fun, Polyhedron 23 (2004) 161.
[4] K.A. Crouse, K.-T. Chew, B.M. Yamin, S.-W. Nq, M.T.H. Tarafder, Acta Crystallogr., Sect. E 59 (2003) 148.
[5] (a) Y.-C. Shi, H.-M. Yang, H.-B. Song, C.-G. Yan, X.-Y. Hu, Polyhedron 23 (2004) 567;
(b) W. Wang, F.-L. Zeng, X. Wang, M.-y. Tan, Polyhedron 15 (1996) 1699.
[6] (a) M. Das, S.E. Livingstone, Inorg. Chim. Acta 19 (1976) 5;
(b) A. Marchi, L. Uccelli, L. Marvelli, R. Rossi, M. Giganti, V. Bertolasi, V. Ferretti, J. Chem. Soc., Dalton Trans. (1996) 3105;
(c) A.I. El-Said, Transition Met. Chem. 28 (2003) 749.
[7] M.A. Ali, A.H. Mirza, M.H.S.A. Hamid, P.V. Bernhardt, Polyhedron 23 (2004) 2405.
[8] N.R. Pramanik, S. Ghosh T.K.R. Chaudhuri, S. Ray, R.J. Butcher, S.S. Mandal, Polyhedron 23 (2004) 1595.
[9] M.A. Ali, A.H. Mirza, M. Nazimuddin, R. Ahmed, L.R. Gahan, P.V. Bernhardt, Polyhedron 22 (2003) 1471.
[10] M.A. Ali, A.H. Mirza, A.L. Tan, L.K. Wei, P.V. Bernhardt, Polyhedron 23 (2004) 2037.
[11] S. Gou, X. You, Z. Zhou, K. Yu, Polyhedron 10 (1991) 1363.
[12] (a) C. Klofutar, S. Paljk, F. Krasovec, P. Suhae, Kem. Ind. 24 (1975) 361;
(b) C. Klofutar, S. Paljk, F. Krasovec, P. Suhae, Chem. Abstr. 84 (1976) 84739;
(c) R.A. Sanchez-Delgado, K. Lazardi, L. Rincon, J.A. Urbina, J. Med. Chem. 36 (1993) 2041.
[13] (a) N.K. Singh, M. Singh, R.J. Butcher, Acta Crystallogr., Sect. E 63 (2007) o4679;
(b) M. Singh, A.K. Srivastava, N.K. Singh, R.J. Butcher, A. Shrivastav, R.K. Sharma, Acta Crystallogr., Sect. E 64 (2008) o339.
[14] A. Shrivastav, N.K. Singh, P. Tripathi, T. George, J.R. Dimmock, R.K. Sharma, Biochimie 88 (2006) 1209–1216.
[15] A. Shrivastav, P. Tripathi, N.K. Singh, A.K. Shrivastava, R.K. Sharma, Eur. J. Med. Chem. 43 (2008) 577.
[16] T. Curtius, J. Prakt. Chem. 50 (1894) 278.
[17] M. Singh, R.J. Butcher, N.K. Singh, Polyhedron (2008), doi:10.1016/j.poly.2008.06.038.
[18] A.I. Vogel, A Text Book of Quantitative Inorganic Analysis, third ed., ELBS, 380 Longman, London, 1969.
[19] G.M. Sheldrick, Acta Crystallogr., Sect. A 46 (1990) 467.
[20] G.M. Sheldrick, SHELXL-97, Program for Crystal Structure Refinement, University of Göttingen, Germany, 1997.
[21] I.J. Bruno, J.C. Cole, P.R. Edgington, M. Kessler, C.F. Macrae, P. McCabe, J. Pearson, R. Taylor, Acta Crystallogr., Sect. B 58 (2002) 389.
[22] K. Brandenburg, H. Putz, DIAMOND, Version 3.0, University of Bonn, Germany, 2004.
[23] L.J. Farrugia, J. Appl. Cryst. 30 (1997) 565.
[24] S. Padhye, G.B. Kauffman, Coord. Chem. Rev. 65 (1985) 127.
[25] A.B.P. Lever, Inorganic Electronic Spectroscopy, Elsevier, Amsterdam, 1984.
[26] A. Gulyani, R.S. Gopalan, G.U. Kulkarni, S. Bhattacharya, J. Mol. Struct. 616 (2002) 103.
[27] B. Venkataramanan, M.-A. Saifudin, V. Jagadese, V. Suresh, Cryst. Eng. Commun. 6 (2004) 284.
[28] C. Giacovazzo, Fundamentals in Crystallography, I.U.Cr.& O.U.P., Oxford, UK, 1992.
[29] R. Srinivasan, K.K. Chacko, Conformation of Biopolymers, vol. 2, Academic Press, New York, 1967.
[30] J.R. Dilworth, J. Hyde, P. Lyford, P. Vella, K. Venkatasubramaman, J.A. Zubieta, Inorg. Chem. 18 (1979) 268.
[31] (a) M. Calvin, K. Wilso, J. Am. Chem. Soc. 67 (1945) 2003;
(b) H. Masui, Coord. Chem. Rev. 219 (2001) 957.
[32] (a) G.A. Bogdanovic, A.S. De Bire, S.D. Zaric, Eur. J. Inorg. Chem. (2002) 1599;
(b) Z.D. Tomic, V.M. Leovac, S.V. Pokorni, D. Zobel, S.D. Zaric, Eur. J. Inorg. Chem. (2003) 1222;;
(c) S.D. Zaric, Eur. J. Inorg. Chem. (2003) 2197.
[33] (a) A. Bogdanovic, V. Medakovic, M.K. Milicic, S.D. Zaric, Int. J. Mol. Sci. (2004) 174;
(b) V.B. Medakovic, M.K. Milicic, G.A. Bogdanovic, S.D. Zaric, J. Inorg. Biochem. 98 (2004) 1867;
(c) A. Castin-eiras, A.G. Sicilia-Zafra, J.M. González-Pèrez, D. Choquesillo-Lazarte, J. Niclós-Gutièrrez, Inorg. Chem. 41 (2002) 6956.
[34] (a) E. Craven, C. Zhang, C. Janiak, G. Rheinwald, H. Lang, Z. Anorg. Allg. Chem. 629 (2003) 2282;
(b) H.H. Monfared, Z. Kalantari, M.A. Kamyabi, C. Janiak, Z. Anorg. Allg. Chem. 633 (2007) 1945.
[35] M. Trivedi, D.S. Pandey, Q. Xu, Inorg. Chim. Acta 360 (2007) 2492.
[36] S.G. Baca, Y. Sevryugina, R. Clerac, I. Malaestean, N. Gerbeleu, M.A. Petrukhina, Inorg. Chem. Commun. 8 (2005) 474.
[37] X. Zhang, D. Huang, F. Chen, C. Chen, Q. Liu, Inorg. Chem. Commun. 8 (2004) 662.

and after slow evaporation yellow crystals separated out, which were collected, washed with ether and dried over P_4O_{10} *in vacuo*.

Zn(HL)Br_2 (**1**): Yield ~0.35 g; found (calc): C, 40.16 (40.76); H, 2.79 (2.78); N, 12.91 (13.25); IR data (cm^{-1}): 3239, 1597, 1661, 1147, 407.

Zn(HL)Cl_2 (**2**): Yield ~0.28 g; found (calc): C, 47.66 (47.72); H, 3.33 (3.41); N, 15.44 (15.57); IR data (cm^{-1}): 3369, 1597, 1667, 1153, 404.

ZnL(OAc) (**3**): Yield ~0.32 g; found (calc): C, 54.25 (53.73); H, 4.33 (4.30); N, 15.82 (15.71); IR data (cm^{-1}): 1597, 1521, 1156, 414, 516.

2.3.2. Synthesis of $ZnLN_3$ (**4**)

A solution of the ligand HL (0.317 g, 1 mmol) in methanol was treated with a methanolic solution of $Zn(OAc)_2 \cdot 2H_2O$ (0.219 g,1 mmol). The solution was heated under reflux and sodium azide (0.130 g, 2 mmol) was added in portions to the solution and further refluxed for 4 h. The resulting solution was allowed to stand at room temperature and upon slow evaporation gave yellow crystals. The crystals that separated out were collected, washed with ether and dried over P_4O_{10} *in vacuo*. Yield ~0.25 g; found (calc): C, 54.25 (53.73); H, 3.33 (3.27); N, 26.44 (26.56); IR data (cm^{-1}): 1595, 1518, 1148, 404, 502.

2.3.3. Synthesis of ZnL_2 (**5**)

A solution of the ligand HL (0.317 g, 1 mmol) in 20 ml of methanol was treated with a methanolic solution of $Zn(OAc)_2 \cdot 2H_2O$ (0.109 g, 0.5 mmol). The solution was heated under reflux for 2 h. The resulting solution was allowed to stand at room temperature and after slow evaporation yellow crystals were separated out, which were collected, washed with ether and dried over P_4O_{10} *in vacuo*. Yield ~0.20 g; found (calc): C, 61.53 (61.94); H, 3.96 (4.04); N, 20.01 (20.07); IR data (cm^{-1}): 1597, 1515, 1223, 420, 518.

2.3.4. Synthesis of $ZnL_2 \cdot H_2O$ (**6**)

A solution of the ligand HL (0.317 g, 1 mmol) in methanol was treated with a methanolic solution of $Zn(OAc)_2 \cdot 2H_2O$ (0.219 g, 1 mmol). The solution was heated under reflux and sodium azide (0.065 g, 1 mmol) was added in portions to the solution and further refluxed for 4 h. The resulting solution was allowed to stand at room temperature and upon slow evaporation gave yellow crystals. The crystals that separated out were collected, washed with ether and dried over P_4O_{10} *in vacuo*. Yield ~0.16 g; found (calc): C, 59.87 (60.38); H, 4.01 (4.22); N, 19.25 (19.56); IR data (cm^{-1}): 1597, 1515, 1229, 416, 520.

2.4. X-ray crystallography

Single crystals of compound **1** suitable for X- ray diffraction were obtained by slow evaporation of its solution in a 1:1:1 mixture of CH_3OH, $CHCl_3$ and CH_2Cl_2. Single crystals of compound **5** were obtained by slow evaporation of its solution in a 1:1 mixture of CH_3OH and CH_3CN, and of compound **6** by slow evaporation of its solution in a 1:1:1:1 mixture of DMF, $CHCl_3$, CH_3CN and CH_3OH. X-ray diffraction measurements were carried out on a CRYSALIS CCD diffractometer with graphite-monochromated Mo Kα (λ = 0.71073 Å) radiation. The program CRYSALIS RED was used for data reduction and cell refinement [8]. The structure was solved by direct methods using SHELXS [9] and refined by full-matrix least-squares refinement on F^2 using SHELXL [10]. The N–H hydrogen atoms were located from difference Fourier maps and refined isotropically. The remainder of the H-atoms were included in calculated positions and refined as riding atoms using default SHELXL parameters. Compound **6** is non-centrosymmetric and its Flack *x* parameter is 0.001(12). As this value is near 0, with small standard uncertainty, the absolute structure given by the structure refinement is likely correct [11]. The structures of the compounds were

Table 1
Crystal data and structure refinement parameters for [Zn(HL)Br_2] (**1**), [ZnL_2] (**5**) and [ZnL_2] · 0.3H_2O (**6**)

	1	**5**	**6**
Empirical formula	$C_{18}H_{15}Br_2N_5OZn$	$C_{36}H_{28}N_{10}O_2Zn$	$C_{36}H_{28}N_{10}O_2Zn \cdot 0.3H_2O$
Formula weight	542.54	698.05	702.85
Temperature, K	120(2)	120(2)	120(2)
Wavelength, Å	0.71073	0.71073	0.71073
Crystal system	monoclinic	monoclinic	orthorhombic
Space group	$P2_1/n$	$P2_1/n$	$P2_12_12_1$
Unit cell dimensions			
a (Å)	7.3466(3)	11.0982(2)	8.5993(4)
b (Å)	14.5893(4)	16.6320(3)	17.0904(6)
c (Å)	18.5267(5)	17.8826(4)	22.3002(11)
α (°)	90	90	90
β (°)	98.315(3)	98.690(2)	90
γ (°)	90	90	90
V (Å^3)	1964.85(11)	3262.97(11)	3277.4(3)
Z	4	4	4
D_{calc} (Mg/m^3)	1.834	1.421	1.424
Absorption coefficient (mm^{-1})	5.335	0.803	0.801
F(000)	1064	1440	1450
Crystal size (mm^3)	0.32 × 0.28 × 0.26	0.26 × 0.21 × 0.19	0.18 × 0.11 × 0.08
θ range for data collection (°)	3.01–25.00	2.99–25.00	2.99–25.00
Index ranges	$-8 \leqslant h \leqslant 8$, $-17 \leqslant k \leqslant 17$, $-21 \leqslant l \leqslant 22$	$-13 \leqslant h \leqslant 12$, $-19 \leqslant k \leqslant 18$, $-21 \leqslant l \leqslant 21$	$-10 \leqslant h \leqslant 10$, $-20 \leqslant k \leqslant 20$, $-26 \leqslant l \leqslant 26$
Reflections collected	16909	30049	31407
Independent reflections	3445 [*R*(int) = 0.0341]	5729 [*R*(int) = 0.0358]	5772 [*R*(int) = 0.1000]
Refinement method	full-matrix least-squares on F^2	full-matrix least-squares on F^2	full-matrix least-squares on F^2
Data/restraints/parameters	3445/0/252	5729/0/450	5772/0/454
Goodness-of-fit on F^2	1.058	1.073	1.010
Final *R* indices [$I > 2\sigma(I)$]	R_1 = 0.0273, wR_2 = 0.0532	R_1 = 0.0306, wR_2 = 0.0638	R_1 = 0.0500, wR_2 = 0.0661
R indices (all data)	R_1 = 0.0507, wR_2 = 0.0632	R_1 = 0.0444, wR_2 = 0.0711	R_1 = 0.0741, wR_2 = 0.0734
Largest difference in peak and hole (e A^{-3})	0.362 and −0.262	0.272 and −0.290	0.608 and −0.415

$R_1 = \sum||F_o| - |F_c||/\sum|F_o|$.
$wR_2 = [\sum w(F_o^2 - F_c^2)^2/\sum w(F_o^2)^2]^{1/2}$.

plotted using the program ORTEP [12]. The crystallographic data along with the structural refinements are given in Table 1.

3. Results and discussion

3.1. Synthesis of complexes

Di-2-pyridyl ketone N^4-phenyl-3-semicarbazone (HL) reacts with zinc(II) halides in a 1:1 molar ratio to form **1** and **2**, complexes of the type $Zn(HL)X_2$ where X = Br and Cl. Complexes **3** and **4** were consistent with the general formula ZnLY where Y = OAc and N_3 and for complexes **5** and **6**, the composition ZnL_2 was obtained. For the preparation of complexes **3** and **5**, $Zn(OAc)_2 \cdot 2H_2O$ and HL were taken in 1:1 and 1:2 ratios, respectively, and for complexes **4** and **6**, $Zn(OAc)_2 \cdot 2H_2O$, HL and NaN_3 were taken in 1:1:2 and 1:1:1 ratios, respectively. In complex **6**, however, the azide added was not coordinated and $ZnL_2 \cdot H_2O$ was obtained accidentally, though the yield was much lower. Although the molecular formulae of **5** and **6** are same, the crystallographic parameters are different.

3.2. Description of the crystal structures of $Zn(HL)Br_2$ (**1**), ZnL_2 (**5**) and $ZnL_2 \cdot 0.3H_2O$ (**6**)

The molecular structure of complex **1**, along with the atom numbering scheme, is presented in Fig. 2. The compound crystallizes in the monoclinic crystal system with the space group $P2_1/n$. In this compound, the Zn atom is coordinated by an azomethine nitrogen (N2), pyridyl nitrogen (N1), ketoxy oxygen (O1) and two bromide ions (Br1 and Br2). The bond distances to Zn are in the order $Zn–N_{(azo)} < Zn–N_{(py)} < Zn–O_{(ketoxy)} < Zn–Br1 < Zn–Br2$. The bond lengths, $Zn–N_{(py)}$, 2.154(3) Å and $Zn–N_{(azo)}$, 2.130(3) Å are very similar compared to other Zn complexes of thiosemicarbazones [13–15]. The Zn–Br bond distances are 2.3561(5) and 2.4026(6) Å, but there is a difference of 0.0465 Å between the Zn–Br bonds of $[Zn(HL)Br_2]$. The basal plane could involve either Br1 or Br2 with the semicarbazone moiety, but because Zn–Br1 is marginally shorter and it can be designated as the apical position. The Zn atom is displaced by a distance of 0.8335 Å above the basal plane and elongated towards Br1. Selected bond lengths and bond angles are given in Table 2.

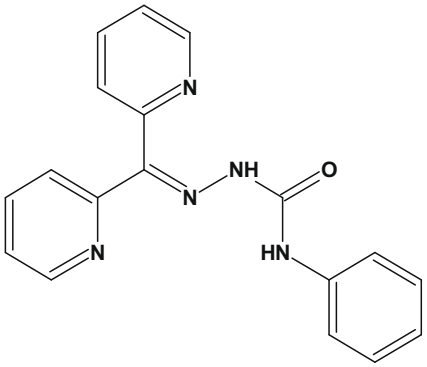

Fig. 1. Structure of HL.

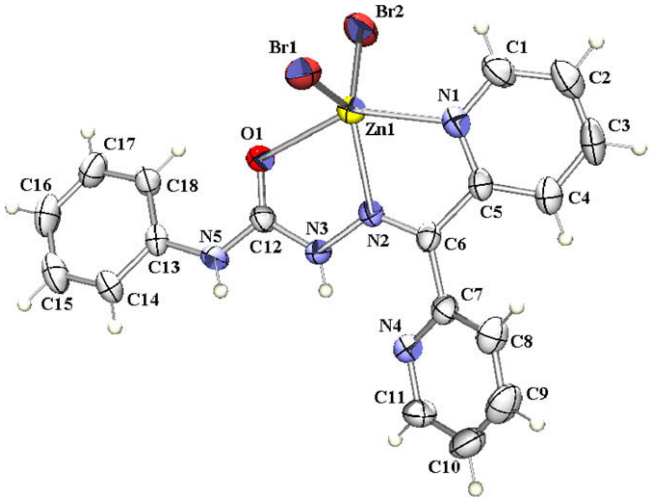

Fig. 2. Molecular structure of $Zn(HL)Br_2$.

According to Addison et al., for five coordinated complexes, the angular structural parameter (τ) is used to propose an index of trigonality. The value of τ is defined by an equation represented by $\tau = (\beta - \alpha)/60$, where β is the greatest basal angle and α is the second greatest angle; τ is 0 for rectangular pyramidal forms and 1 for trigonal bipyramidal forms [16,17]. However, in the case of five-coordinate systems, the structures vary from near regular trigonal bipyramidal (RTB) to near square based pyramidal (SBP). The τ value for the compound **1** of 0.27 indicates that the coordination geometry around Zn(II) is best described as a distorted square based pyramidal geometry [18].

The deviations from the least-square plane through the O1, N1, N2 and Br2 atoms comprising the square plane are 0.3697, 0.5336, −0.6794 and −0.0054 Å, respectively, and the Zn1 atom is deviated by 0.8335 Å in the direction of the Br1 atom. Ring puckering analysis and least square plane calculations show that the rings Cg(1) comprising of atoms Zn1, O1, C12, N3 and N2 and Cg(2) comprising of atoms Zn1, N1, C5, C6 and N2 adopt a twisted conformation [Cg(1) on N2–Zn1 and Cg(2) on C5–C6] [19]. In the crystal packing four molecules are present and two of them are complementary to each other (Fig. 3). In the unit cell π–π, C–H···π and hydrogen

Table 2
Selected bond lengths (Å) and bond angles (°) for $[Zn(HL)Br_2]$ (**1**), $[ZnL_2]$ (**5**) and $[ZnL_2] \cdot 0.3H_2O$ (**6**)

1	5	6
Bond lengths		
Zn1–N2 2.130(3)	Zn1–N7 2.0716(17)	Zn1–N2 2.073(3)
Zn1–N1 2.154(3)	Zn1–N2 2.0851(17)	Zn1–N7 2.077(3)
Zn1–O1 2.243(2)	Zn1–O1 2.0950(14)	Zn1–O1 2.097(3)
Zn1–Br1 2.3561(5)	Zn1–O2 2.1234(13)	Zn1–O2 2.099(3)
Zn1–Br2 2.4026(6)	Zn1–N1 2.1499(17)	Zn1–N1 2.155(3)
O1–C12 1.233(3)	Zn1–N6 2.2047(16)	Zn1–N6 2.221(3)
N1–C1 1.328(4)	O1–C12 1.257(2)	O1–C12 1.252(4)
N1–C5 1.345(4)	O2–C30 1.257(2)	O2–C30 1.256(4)
N2–C6 1.287(4)	N5–C12 1.363(3)	N1–C1 1.339(4)
N2–N3 1.355(4)	N5–C13 1.403(3)	N1–C5 1.352(5)
N3–C12 1.369(4)	N3–N2 1.352(2)	N2–C6 1.296(5)
		N2–N3 1.347(4)
Bond angles		
N2–Zn1–N1 73.88(10)	N7–Zn1–N2 165.27(6)	
N2–Zn1–O1 72.60(9)	N7–Zn1–O1 109.11(6)	N2–Zn1–N7 167.20(14)
N1–Zn1–O1 146.06(9)	N2–Zn1–O1 76.14(6)	N2–Zn1–O1 76.08(11)
N2–Zn1–Br1 129.81(8)	N7–Zn1–O2 76.17(6)	N7–Zn1–O1 109.42(11)
N1–Zn1–Br1 99.40(7)	N2–Zn1–O2 118.01(6)	N2–Zn1–O2 115.77(12)
O1–Zn1–Br1 97.86(6)	O1–Zn1–O2 91.14(5)	N7–Zn1–O2 76.30(12)
N2–Zn1–Br2 114.29(8)	N7–Zn1–N1 99.93(6)	O1–Zn1–O2 90.11(10)
N1–Zn1–Br2 101.82(8)	N2–Zn1–N1 75.49(6)	N2–Zn1–N1 75.84(12)
O1–Zn1–Br2 96.60(6)	O1–Zn1–N1 150.95(6)	N7–Zn1–N1 99.40(12)
Br1–Zn1–Br2 115.75(2)	O2–Zn1–N1 96.65(6)	O1–Zn1–N1 151.17(11)
C12–O1–Zn1 114.11(19)	N7–Zn1–N6 74.92(6)	O2–Zn1–N1 96.25(11)
	N2–Zn1–N6 90.96(6)	N2–Zn1–N6 92.80(13)
	O1–Zn1–N6 96.57(6)	N7–Zn1–N6 75.15(13)
	O2–Zn1–N6 151.03(6)	O1–Zn1–N6 98.13(11)
	N1–Zn1–N6 90.05(6)	O2–Zn1–N6 151.42(11)
	C12–O1–Zn1 111.16(13)	N1–Zn1–N6 89.61(11)
		C12–O1–Zn1 110.7(3)

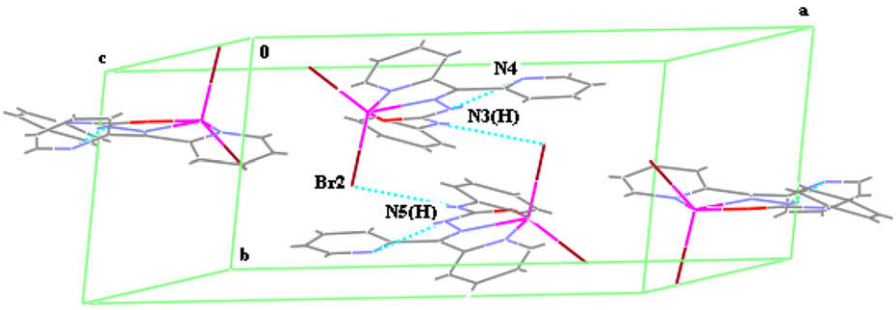

Fig. 3. Partial unit cell packing diagram for compound **1** with intra- and intermolecular hydrogen bonding interactions shown as dotted lines.

bonding interactions were observed. The π–π interaction is perceived at 4.0873 Å for Cg(1)–Cg(1)[a] [Cg(1) = Zn1–O1–C12–N3–N2; *a* = 1 − *x*, 1 − *y*, 1 − *z*]. Only one C–H···π interaction is shown in the unit cell and that is between C(8)–H(8)···Cg(5)[b] [Cg(5) = C(13)–C(14)–(15)–C(16)–C(17)–C(18); d_{H-Cg} = 2.95 Å; *b* = 1 − *x*, 1 − *y*, 1 − *z*]. One intra- and one intermolecular hydrogen bonding interaction were observed, *ie*, N3(H) and N4 of the same molecule and N5(H) of one molecule with Br2 of the other molecule [N(3)–H(3 N)···N(4), D–H = 0.80(3) Å, H···A = 2.04(3) Å, D···A = 2.669(4) Å, D–H···A = 135(3)°; N(5)–(H5N)···Br(2)[c], D–H = 0.70(3) Å, H···A = 2.68(3) Å, D···A = 3.374(3) Å, D–H···A = 170(3)°, *c* = 1 − *x*, 1 − *y*, 1 − *z*].

Figs. 4 and 5 show the molecular structures of compounds **5** and **6** along with the atom numbering schemes. Compound **5** crystallizes in the monoclinic crystal system with the space group $P2_1/n$, while compound **6** in the orthorhombic crystal system with the space group $P2_12_12_1$. In both the compounds [ZnL_2], the Zn atom is six coordinate in which both ligands are coordinated in their deprotonated enolate forms *via* the pyridine nitrogen, azomethine nitrogen and enolate oxygen atoms. The ligands with their donor atoms are arranged around the zinc ion in a meridional fashion and both compounds are polymorphic. In compound **5**, atoms O1, O2, N1 and N6 lie in the equatorial plane, and N2 and N7 occupy the axial positions, while in compound **6**, atoms O1, O2, N1 and N6 lie in the equatorial plane, and N2 and N7 occupy the axial positions of the distorted octahedron. In both compounds **5** and **6**, the atoms Zn1, O1, O2, N1, N6 do not deviate significantly from the least square plane [0.0034 Å for **5** and 0.0015 Å for **6**]. Each of the semicarbazone fragments {(O1 and N1, O2 and N6 for **5**); (O1 and N1, O2 and N6 for **6**)} are coordinated to the Zn centre with an angle of 150.95(6)°, 151.03(6)° and 151.17(11)°, 151.42(11)°, respectively, for **5** and **6**, having a large distortion from an ideal octahedron (180°). The planes containing Zn1, O1, N1, N2, N7 (plane 1) and Zn1, O2, N2, N6, N7 (plane 2) are deviated from the central metal atom (Zn1) by 0.0837 and 0.0248 Å, respectively, in compound **5**, similarly in compound **6**, the planes containing Zn1, O2, N7, N6, N2 (plane 3) and Zn1, O1, N2, N1, N7 (plane 4) are deviated from the central metal atom (Zn1) by 0.0314 and 0.0610 Å, respectively. The dihedral angle formed by the planes 1 and 2 is 85.81(0.04)° for compound **5** and by the planes 3 and 4 in compound **6** is 85.69 (0.08)°, consistent with a nearly 90° octahedral angle. Selected bond lengths and bond angles are given in Table 2.

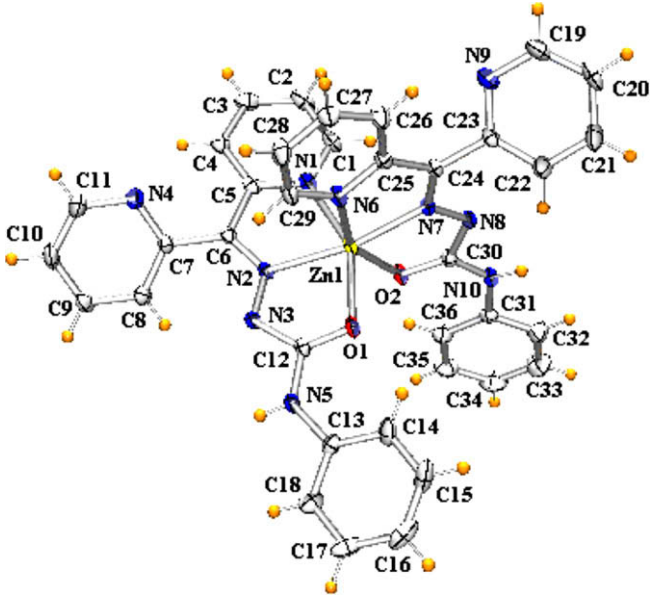

Fig. 4. Molecular structure of ZnL_2.

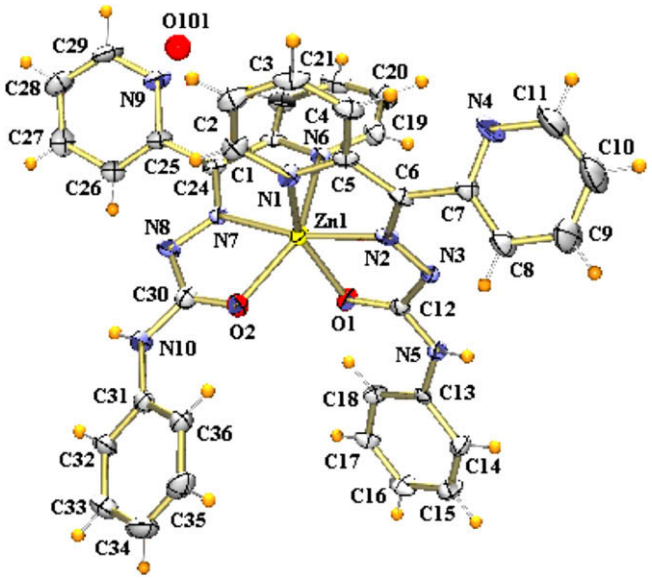

Fig. 5. Molecular structure of $ZnL_2 \cdot 0.3H_2O$.

In compound **5**, when viewed along *a* axis, the molecules are arranged in an opposite manner and are interconnected through N5(H) and N3 of the same molecule with N8 and N10(H) of the nearby molecule, respectively (Fig. 6) [D–H···A, N(5)–H(5)···N(8)[d]; D–H = 0.84(3) Å; H···A = 2.13(3) Å; D···A = 2.961(2) Å; D–H···A = 170.(2)°; Symmetry code, *d* = 1/2 − *x*, 1/2 + *y*, 3/2 − *z*; D–H···A, N(10)–H(10)···N(3)[e]; D–H = 0.83(2) Å; H···A = 2.21(2) Å; D···A = 3.023(2) Å; D–H···A = 170.(2)°; Symmetry code, *e* = 1/2 − *x*, −1/2 + *y*, 3/2 − *z*]. Intramolecular hydrogen bonding interactions were also observed i.e., C4(H) with N4 and C8(H) with N3 and C14(H) with O1 [D–H···A, C(4)–H(4)···N(4); D–H = 0.93 Å; H···A = 2.42 Å; D···A = 2.984(3) Å; D–H···A = 119°;

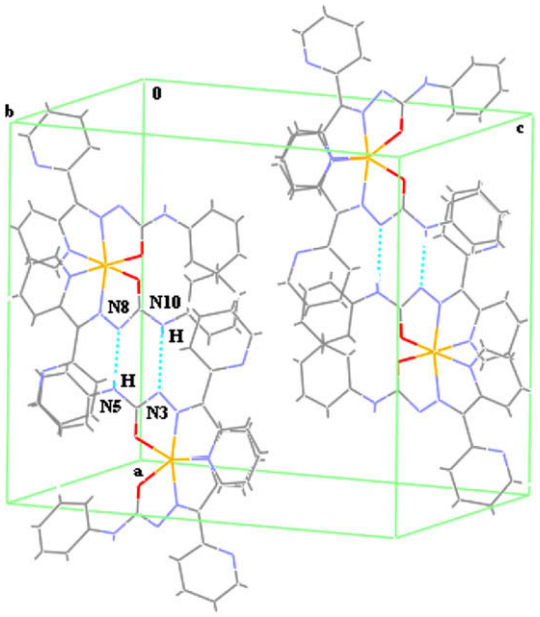

Fig. 6. Partial unit cell packing diagram for compound **5** with intermolecular hydrogen bonding interactions shown as dotted lines.

D–H···A, C(8)–H(8)··N(3)i; D–H = 0.93 Å; H···A = 2.56 Å; D···A = 2.940(3) Å; D–H···A = 105°; D–H···A, C(14)–H(14)···O(1); D–H = 0.93 Å; H···A = 2.32 Å; D···A = 2.901(3) Å; D–H···A = 120°]. In compound **6**, two intermolecular hydrogen bonding interactions are observed i.e., N5(H) and N8 and with N10(H) and N3, which are arranged in an opposite manner (Fig. 7) [D–H···A, N(5)–H(5)···N(8)[f]; D–H = 0.84(3) Å; H···A = 2.15(3) Å; D···A = 2.992(5) Å; D–H···A = 179(5)°; Symmetry code, f = 1 − *x*, 1/2 + *y*, 1/2 − *z*; D–H···A, N(10)–H(10)···N(3)[g]; D–H = 0.84(3) Å; H···A = 2.18(3) Å; D···A = 3.018(5) Å; D–H···A = 176(3)°; Symmetry code, *g* = 1 − *x*, −1/2 + *y*, 1/2 l− *z*]. Intramolecular hydrogen bonding interactions were also observed i.e., C4(H) with N4 and C14(H) with O1 and C22(H) with N9 [D–H···A, C(4)–H(4)···N(4); D–H = 0.95 Å; H···A = 2.45 Å; D···A = 3.041(6) Å; D–H···A = 120°;

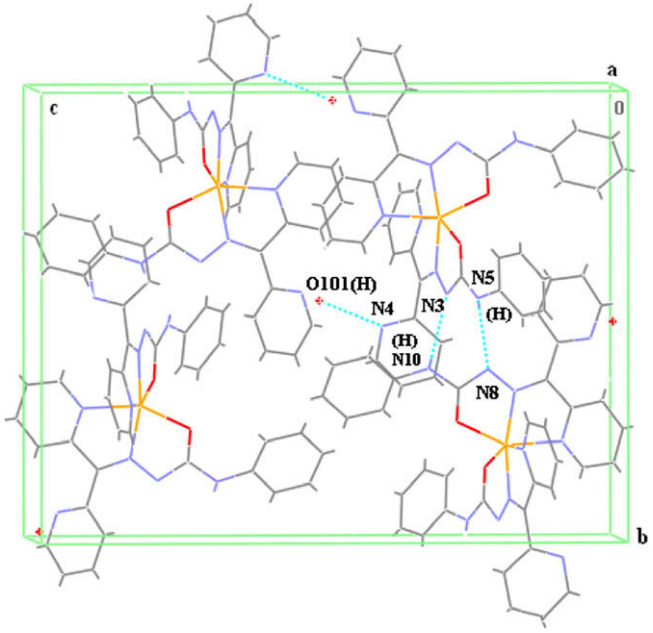

Fig. 7. Intermolecular hydrogen bonding interactions of compound **6**.

Table 3
Interaction parameters of the compounds $[Zn(HL)Br_2]$ (**1**), $[Zn(L)_2]$ (**5**) and $[Zn(L)_2] \cdot 0.3H_2O$ (**6**)

Cg(I)–Res(1)···Cg(J)	Cg–Cg(Å)	α °	β °
π···π Interactions			
Cg(1) [1] → Cg(1)[a]	4.0874	0.02	31.75
Equivalent position codes: [a] = 1 − *x*, 1 − *y*, 1 − *z*			
Cg(1) = Zn(1), O(1), C(12), N(3), N(2)			
XH(I)···Cg(J)	H···Cg (Å)	X–H···Cg (°)	X···Cg (Å)
CH···π interactions			
C(8)–H(8)[1] → Cg(5)[b]	2.95	118	3.447(4)
Equivalent position codes: [b] = 1 − *x*, 1 − *y*, 1 − *z*			
Cg(1) = C(13), C(14), C(15), C(16), C(17), C(18)			
D–H···A	D–H	H···A	D···A	D–H···A
H bonding				
$[Zn(HL)Br_2]$ (**1**)				
N(3)–H(3N)···N(4)	0.80(3)	2.04(3)	2.669(4)	135(3)
N(5)–H(5N)···Br(2)[c]	0.70(3)	2.68(3)	3.374(3)	170(3)
$[Zn(L)_2]$ (**5**)				
N(5)–H(5N)···N(8)[d]	0.84(3)	2.13(3)	2.961(2)	170(2)
N(10)–H(10N)···N(3)[e]	0.83(2)	2.21(2)	3.023(2)	170(2)
C(4)–H(4)···N(4)	0.93	2.42	2.984(3)	119
C(8)–H(8)···N(3)	0.93	2.56	2.940(3)	105
C(14)–H(14)···O(1)	0.93	2.32	2.901(3)	120
$[Zn(L)_2]0.3H_2O$ (**6**)				
N(5)–H(5N)···N(8)[f]	0.84(3)	2.15(3)	2.992(5)	179(5)
N(10)–H(10N)···N(3)[g]	0.84(3)	2.18(3)	3.018(5)	176(3)
C(4)–H(4)···N(4)	0.95	2.45	3.041(6)	120
C(14)–H(14)···O(1)	0.95	2.36	2.921(5)	118
C(22)–H(22)···N(9)	0.95	2.61	3.026(5)	107

Equivalent position codes: [c] = 1 − *x*, 1 − *y*, 1 − *z*.
[d] = 1/2 − *x*, 1/2 + *y*, 3/2 − *z*; [e] = 1/2 − *x*, −1/2 + *y*, 3/2 − *z*; [f] = 1 − *x*, 1/2 + *y*, 1/2 − *z*; [g] = 1 − *x*, −1/2 + *y*, 1/2 − *z*.
(D = donor, A = acceptor, Cg = centroid, α = dihedral angles between planes I and *J*, β = angle Cg(1)–Cg(J).

D–H···A, C(14)–H(14)···O(1); D–H = 0.95 Å; H···A = 2.36 Å; D···A = 2.921(5) Å; D–H···A = 118°; D–H···A, C(22)–H(22)···N(9); D–H = 0.95 Å; H···A = 2.61 Å; D···A = 3.026(5) Å; D–H···A = 107°] (Table 3).

3.3. Infrared and electronic spectral studies

The infrared spectral data of the zinc(II) complexes are given in Table 4. The ν_a(NH) vibrations of the imino group are observed at *ca.* 3369 cm^{-1} in the IR spectrum of HL. The lack of an N–H stretching vibration in the spectra of the complexes ZnL(OAc) and $ZnLN_3$ endorses the ligand coordination to zinc(II) ion in the deprotonated enolate form. However in the complexes $Zn(HL)Br_2$ and $Zn(HL)Cl_2$ the presence of bands at 3239 and 3369 cm^{-1}, corresponding to ν(NH) vibrations, indicates that the semicarbazone is coordinated in the neutral form. A strong band at 1591 cm^{-1} in the IR spectrum of HL corresponds to the ν(N3–C6) stretching, which suffers a positive shift on complexation. Coordination of the azomethine nitrogen atom is also consistent with the presence of a band in the 404–420 cm^{-1} region, assignable to ν(Zn–N) for these complexes

Table 4
IR spectral assignments for the ligand and the zinc(II) complexes

Compound	ν(NH)	ν(C=N)	ν(CO)	ν(N=C)	ν(N–N)	ν(Zn–N)	ν(Zn–O)
HL	3369	1591	1718		1129		
$Zn(HL)Br_2$ (**1**)	3239	1597	1661		1147	407	
$Zn(HL)Cl_2$(**2**)	3369	1597	1667		1153	404	
ZnL(OAc) (**3**)		1597		1521	1156	414	516
$ZnLN_3$(**4**)		1595		1518	1148	404	502
ZnL_2(**5**)		1597		1515	1223	420	518
$ZnL_2 \cdot H_2O$ (**6**)		1597		1515	1229	416	520

Table 5
Electronic spectral assignments for the ligand and the zinc(II) complexes

compound	π–π^*	n–π^*	MLCT
HL	40000	30770	
$Zn(HL)Br_2$ (**1**)	37630	31840	24220
$Zn(HL)Cl_2$ (**2**)	37460	31450	24280
ZnL(OAc) (**3**)	37410	31350	24280
$ZnLN_3$ (**4**)	37200	32250	24210
ZnL_2 (**5**)	37280	32230	24230
$ZnL_2 \cdot H_2O$ (**6**)	37270	32240	24210

[20–22]. A band at 1718 cm^{-1} in the ligand has significant contribution from the C=O stretching vibration and it is shifted to 1667 cm^{-1} in $Zn(HL)Cl_2$ and 1661 cm^{-1} in $Zn(HL)Br_2$ confirming the keto form of HL in these complexes. In complexes **3**–**6**, the bands at 502–520 cm^{-1} are assignable to ν(Zn–O), consistent with oxygen coordination. The spectra of the complexes exhibit a systematic shift in the position of the ν(N–N) bands in the region 1129–1229 cm^{-1}. A medium band around 601 cm^{-1}, indicating an out-of-plane pyridyl ring vibration in the uncomplexed ligand, shifts to higher frequencies on complexation which confirms the coordination of the ligand to the metal via the pyridine nitrogen [23–26]. Compound $ZnLN_3$ exhibits strong bands at 2076 and 1302 cm^{-1} corresponding to the asymmetric and symmetric stretching of the coordinating azido group. For the complex ZnL(OAc) the asymmetric and symmetric stretching vibrations of the acetate group appear at 1562 and 1433 cm^{-1} respectively. The presence of a band at 3440 cm^{-1} for $ZnL_2 \cdot H_2O$ indicates the presence of the H_2O molecule.

The electronic spectral data of the zinc(II) complexes are given in Table 5. The ligand HL has an absorption at 40000 cm^{-1} due to the intra-ligand π–π^* transitions of the pyridyl ring and imine function of the semicarbazone moiety. Another band at 30770 cm^{-1} for HL corresponding to a n–π^* transition of the amide function, which undergoes a small blue shift on complexation, indicating coordination via the pyridyl nitrogen with a reduction in intensity [27]. The shift of the π–π^* bands to the longer wavelength region is the result of the C=O bond being weakened and the conjugated system being enhanced after the formation of the complexes. The metal–ligand CT bands are found around 24200 cm^{-1}.

Acknowledgement

M.R.P. Kurup is thankful to the Council of Scientific and Industrial Research (CSIR), New Delhi, India for the financial assistance. The authors are thankful to the National Single Crystal X-ray diffraction Facility, IIT, Bombay, India for providing single crystal XRD results.

Appendix A. Supplementary data

CCDC 648484, 648485 and 648486 contain the supplementary crystallographic data for **1**, **5** and **6**. These data can be obtained free of charge via http://www.ccdc.cam.ac.uk/conts/retrieving.html, or from the Cambridge Crystallographic Data Centre, 12 Union Road, Cambridge CB2 1EZ, UK; fax: (+44) 1223-336-033; or e-mail: deposit@ccdc.cam.ac.uk. Supplementary data associated with this article can be found, in the online version, at doi:10.1016/j.poly.2008.08.014.

References

[1] J.S. Casas, M.S. Garcia-Tasende, J. Sordo, Coord. Chem. Rev. 209 (2000) 197.
[2] Q. Li, H. Tang, Y. Li, M. Wang, L. Wang, C. Xia, J. Inorg. Biochem. 78 (2000) 167.
[3] T. Matsukura, H. Tanaka, Biochemistry 65 (2000) 817.
[4] T.A. Reena, E.B. Seena, M.R.P. Kurup, Polyhedron 27 (2008) 1825.
[5] H. Cerecetto, M. González, Curr. Topics Med. Chem. 2 (2002) 1185.
[6] H. Cerecetto, R. Di Maio, G. Ibarruri, G. Seoane, A. Denicola, C. Quijano, G. Pelluffo, M. Paulino, Farmaco 53 (1998) 89.
[7] V. Martinez, H. Cerecetto, Bioorg. Med. Chem. 9 (2001) 1025.
[8] CRYSALIS CCD and CRYSALIS RED Versions 1.171.29.2 (CRYSALIS171. NET), Oxford Diffraction Ltd, Abingdon, Oxfordshire, England, 2006.
[9] G.M. Sheldrick, Acta Crystallogr., Sect. A 46 (1990) 467.
[10] G.M. Sheldrick, SHELXL97 and SHELXS97, University of Göttingen, Germany, 1997.
[11] H.D. Flack, G. Bernardinelli, J. Appl. Crystallogr. 33 (2000) 1143.
[12] L.J. Farrugia, J. Appl. Crystallogr. 30 (1997) 565.
[13] K.A. Ketcham, J.K. Swearingen, A. Castineiras, I. Garcia, E. Bermejo, D.X. West, Polyhedron 20 (2001) 3265.
[14] E. Bermejo, A. Castineiras, I. Garcia-Santos, D.X. West, Z. Anorg. Allg. Chem. 630 (2004) 1097.
[15] I. Garcia, E. Bermejo, A.K. El Sawaf, A. Castineiras, D.X. West, Polyhedron 21 (2002) 729.
[16] A.W. Addison, T.N. Rao, J. Reedijk, J. Van Rijn, G.C. Verschoor, J. Chem. Soc., Dalton Trans. (1984) 1349.
[17] G. Murphy, C.O. Sullivan, B. Murphy, B. Hathaway, Inorg. Chem. 37 (1998) 240.
[18] M. Vaidyanathan, R. Balamurugan, U. Sivagnanam, M. Palaniandavar, J. Chem. Soc., Dalton Trans. (2001) 3498.
[19] D. Cremer, J.A. Pople, J. Am. Chem. Soc. 97 (1975) 1354.
[20] K. Nakamoto, Infrared and Raman Spectra of Inorganic and Coordination compounds, fifth ed., Wiley, New York, 1997.
[21] D.F. Xiang, C.Y. Duan, X.S. Tan, Q.W. Hang, W.X. Tang, J. Chem. Soc., Dalton Trans. (1998) 1201.
[22] M.J.M. Campbell, Coord. Chem. Rev. 17 (1975) 279.
[23] E. Bayer, C.G. Witte, J. Coord. Chem. 7 (1997) 13.
[24] D.F. Little, C.J. Long, Inorg. Chem. 7 (1968) 3401.
[25] M. Canadas, E. Lopez-Torres, A. Martinez-Arias, M.A. Mendiola, M.T. Sevilla, Polyhedron 19 (2000) 2059.
[26] R.A. Bailey, S.L. Kozak, T.W. Michelsen, W.N. Mills, Coord. Chem. Rev. 6 (1971) 407.
[27] V. Philip, V. Suni, M.R.P. Kurup, M. Nethaji, Polyhedron 24 (2005) 1133.

2. Experimental

2.1. Materials and physical measurements

All the chemicals were of analytical grade and were used as received without further purification. The precursor complex, [bis(salicylaldiminato)manganese(II)], was prepared according to the procedure described previously [21]. XRD patterns were recorded by a Rigaku D-max C III, X-ray diffractometer using Ni-filtered Cu Kα radiation. Elemental analyses were obtained from a Carlo ERBA Model EA 1108 analyzer. Scanning electron microscopy (SEM) images were obtained on a Philips XL-30ESEM equipped with an energy dispersive X-ray spectroscopy. Transmission electron microscopy (TEM) images were obtained on a Hitachi H-800 transmission electron microscope with an accelerating voltage of 200 kV. The surface of the manganese compound was characterized by X-ray photoelectron spectroscopy (XPS). An ESCA-3000 electron spectrometer with non-monochromatic Mg Kα radiation was used to excite the photoelectrons. The metallic impurities were identified using an inductively coupled plasma-optical emission spectrometer (ICP-OES) Model Perkin–Elmer PLASMA-1000. FT-IR spectra were recorded on a Shimadzu Varian 4300 spectrophotometer in KBr pellets.

2.2. Preparation of Mn_3O_4 nanoparticles

The fabrication method of Mn_3O_4 nanoparticles was identical to that reported earlier [22], which was based on a thermal decomposition process of [bis(salicylaldiminato)manganese(II)], $[Mn(Sal)_2]$, without the presence of a catalyst. The current synthetic procedure is a modified version of the method developed by Hyeon and coworkers for the synthesis of nanocrystals for metals that employs the thermal decomposition of transition metal complexes [23]. Unless otherwise noted, all reactions were carried out in a dry-argon atmosphere. The overall synthetic procedure is shown in Scheme 1. In this synthesis Mn_3O_4 nanoparticles were prepared by the thermal decomposition of a $[Mn(sal)_2]$-oleyl amine complex. First, the $[Mn(sal)_2]$-oleyl amine complex was prepared by the reaction of 0.6 g of $[Mn(sal)_2]$ and 2 ml of oleyl amine. The mixed solution was placed in a 50 ml three-neck distillation flask and heated up to 100 °C for 90 min. During all the experimental processes, the flask was flushed with high-purity Ar gas to avoid oxidation. The resulting metal-complex solution was injected into 5 g of triphenylphosphine at 210 °C. The color of the solution changed from orange to black, indicating that colloidal nanoparticles were generated. The black solution was aged at 210 °C for 45 min, and was then cooled to room temperature. The nanoparticles were precipitated by adding excess ethanol to the solution. The precipitated nanoparticles were retrieved by centrifugation. The yield of the overall synthesis was 60% based on the amount of $[Mn(sal)_2]$. The final products were dispersed into *n*-hexane or toluene (Scheme 1).

3. Results and discussion

The presence of triphenylphosphine led the particles to be well dispersed with no agglomeration; while much larger particles flocculating together were synthesized in the absence of triphenylphosphine (TPP) [24]. Triphenylphosphine is a high-boiling point surfactant with a patulous long chain structure providing greater steric hindrance. So, this agent might slow the addition rate of materials to the nanoparticles during their growth, resulting in much smaller nanoparticles. Furthermore, the surfactants in the solution coordinated onto the metal of the nanoparticles, providing a dynamic organic structure that stabilizes the nanoparticles in solution. The addition of TPP into the mixture of oleyl amine and complex as an additional surfactant reduced the particle size much further and resulted in very uniform size distribution (Scheme 1). Oleyl amine is known as a ligand that binds tightly to the metal nanoparticle surface. The combined effects of TPP and oleyl amine were much more profound than those of the individual components.

Fig. 1 shows the XRD of Mn_3O_4 nanoparticles using thermal decomposition. The powders showed a crystalline pattern and the observed d-lines matched the reported values for the tetragonal Mn_3O_4 phase (JCPDS; 1–1127). The calculated lattice parameters, by a least square fit, are $a = 5.752$ Å and $c = 9.421$ Å. The additional lines that are not indexed may arise from intermediate phases that are formed during the reaction. The surface area of these powders was found to be 130 m^2/g. The crystallite size measurements were also carried out using the Scherrer equation, $D = k\lambda/\beta\cos\theta$, where D is the crystallite size, k is a constant (=0.9 assuming that the particles are spherical), λ is the wavelength of the X-ray radiation, β is the line width (obtained after correction for the instrumental broadening) and θ is the angle of diffraction. The average particle size obtained from the XRD data is 25 nm.

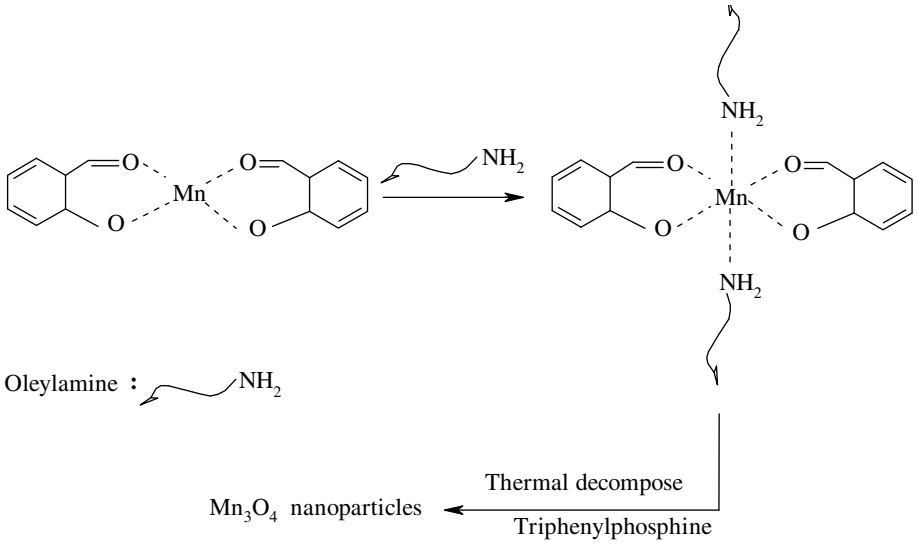

Scheme 1. Synthesis of Mn_3O_4 nanoparticles by the thermal decomposition of Mn-oleyl amine complexes.

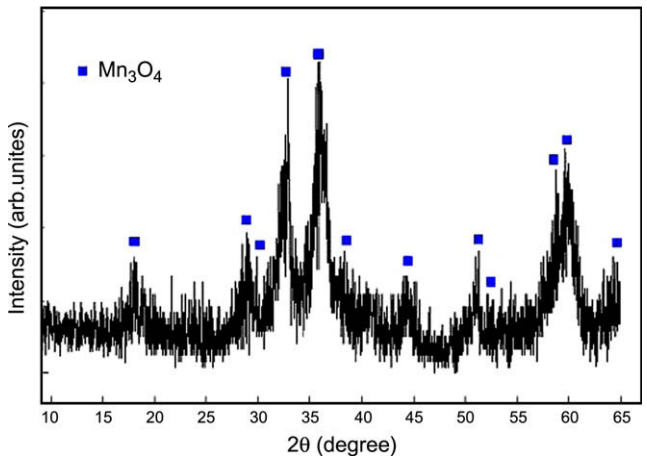

Fig. 1. X-ray diffraction (XRD) pattern of the as-synthesized Mn_3O_4 nanoparticles.

No diffraction peaks for metallic Mn were seen in Fig. 1. The absence of the Mn phase in our sample was ascribed to the high reactivity of Mn at high temperatures, resulting in complete oxidation of Mn in air.

Fig. 2 depicts the SEM pictures of sample Mn_3O_4 nanoparticles. From the micrograph, it was observed that the nanoparticles were agglomerated but were almost uniform in size. The particle morphology observed was either spherical or cubic like with uneven shapes.

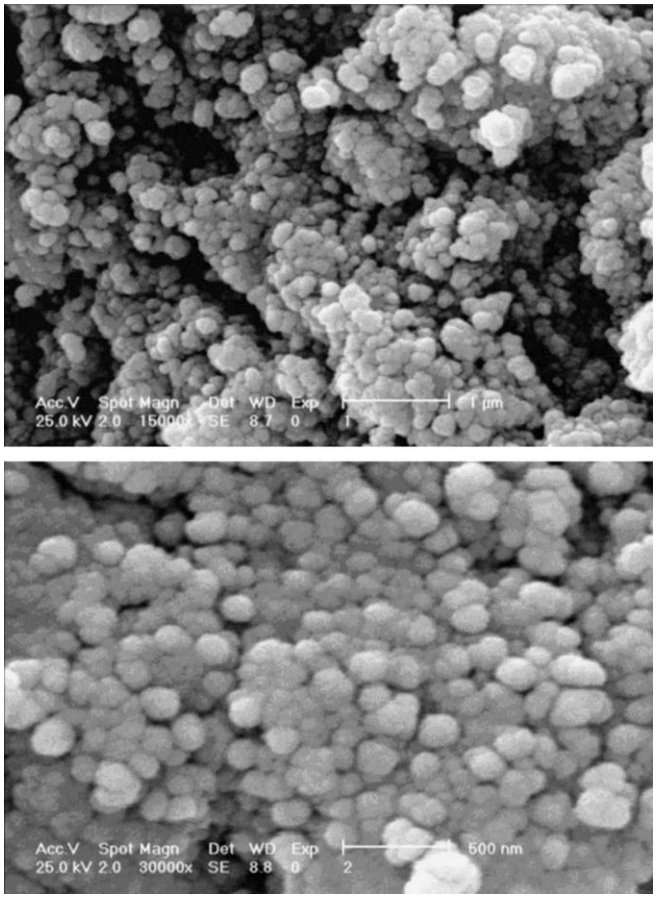

Fig. 2. SEM images of Mn_3O_4 nanoparticles.

As-synthesized samples were subjected to ICP-OES analysis for the identification of the metallic impurity level, wherein it was observed that impurities such as Na, Ca and Cu were at a considerably low level (<0.01%). It implies that better quality Mn_3O_4 can be obtained by thermal decomposition.

The morphology, size distribution and microstructure of the products were further studied by TEM. Fig. 3 shows a representative TEM image of the sample at low magnification. It is interesting to note that most of the particles appear to have a spherical morphology. Statistical analysis of the diameter distribution of the nanoparticles indicates that the mean diameter is about 20–30 nm.

Fig. 4 shows the FT–IR spectra of the obtained Mn_3O_4 powders by thermal decomposition of $[Mn(sal)_2]$. It can be seen from Fig. 4 that there are no characteristic IR absorption bands of salicyclaldehyde, oleyl amine and triphenylphosphine, indicating that the Mn_3O_4 product was free of solvent. The FT-IR spectra of the product demonstrated a notable resemblance to those of Mn_3O_4 in the previous studies [25–27]. In the region from 650 to 400 cm^{-1}, three absorption peaks were observed at 642, 521 and 423 cm^{-1} due to Mn–O vibrations.

The surface of the Mn_3O_4 nanoparticles was characterized by X-ray photoelectron spectroscopy (Fig. 5). A hemispherical sector analyzer with a multi-channel detector was used to detect the ejected electrons energy wise. All the measurements were carried out with reference to the C 1s binding energy (285 eV) as an internal standard. All the spectra were recorded in an optimized high vacuum, 10^{-9} Torr. The details about the electron spectrometer were given in an earlier publication [28]. The XPS spectra of Mn $2p_{3/2}$, Mn $2p_{1/2}$ Mn 3s and O 1s energy levels were recorded. The Mn 2p peak is broad due to multiple splitting. The binding energy value of Mn $2p_{3/2}$ is 641.7 eV. The spin–orbit splitting is the difference between BE values of Mn $2p_{3/2}$ and Mn $2p_{1/2}$ levels. The observed spin–orbit splitting is 11.6 eV, the same as manganese oxides [29]. There is no change in the spin–orbit splitting as compared with the various manganese oxides. The BE value of Mn $2p_{3/2}$ (641.7 eV) and spin–orbit splitting (11.6 eV) are well matching with the reported values of manganese oxide. The BE of the 3s level is 86.1 eV and the multiple splitting is 5.2 eV. The magnitude of the splitting is proportional to the number of unpaired electrons in the d-orbital. The observed BE values and the splitting of the 3s levels exactly match with the reported values of the Mn_3O_4 compound [30]. The O 1s spectra is broad and shows a symmetry towards higher BE sides. It is resolved into two components. The BE values are 529.7 and 532.5 eV for the first and the second peak, respectively. The first peak is assigned to the lattice oxygen of manganese

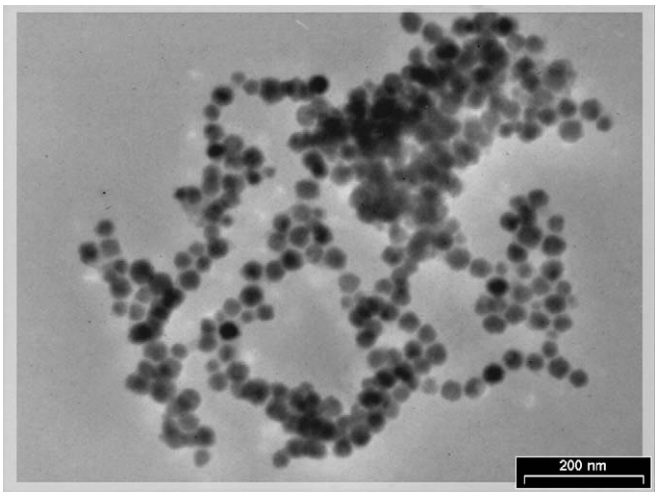

Fig. 3. TEM images of Mn_3O_4 nanoparticles.

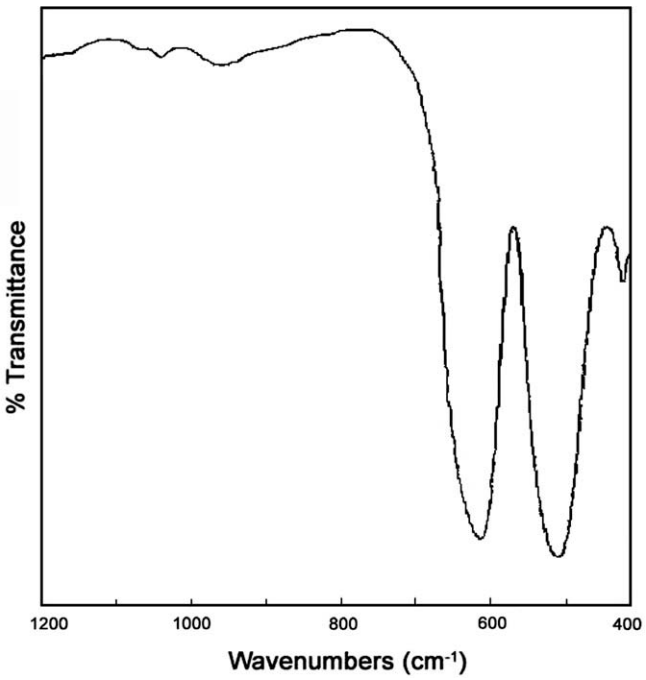

Fig. 4. FT-IR spectra of Mn_3O_4 nanoparticles.

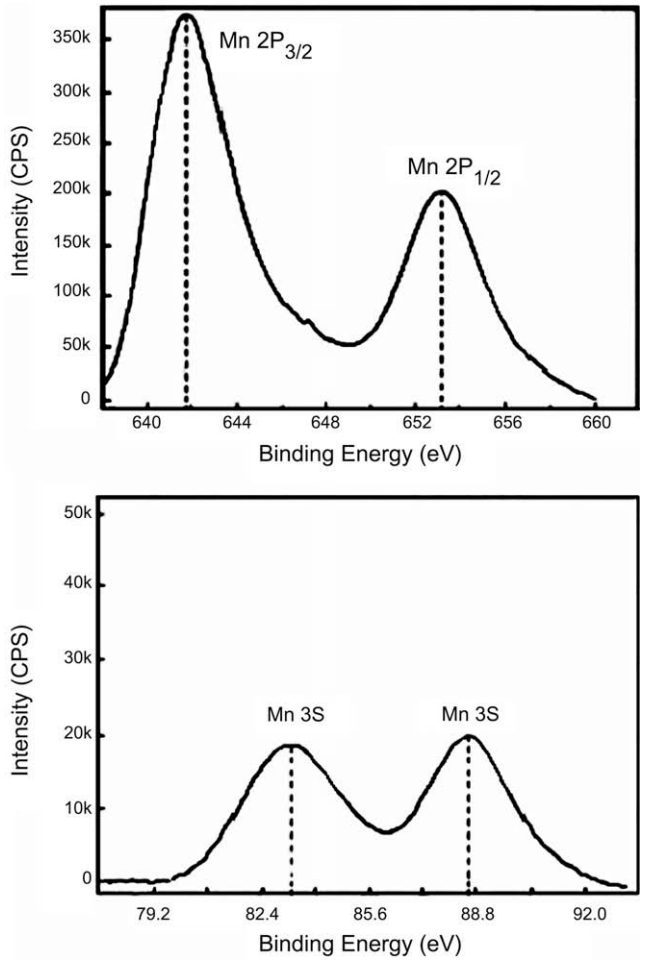

Fig. 5. XPS spectra of Mn_3O_4 prepared by thermal decomposition of $[Mn(Sal)_2]$.

oxide and second can be assigned to either carbonate species or OH species present on the surface. In the present case, it is due to hydroxyl species of the surface.

Recently, amine compounds have been used due to their moderate reducibility [31–34]. At certain pressures, 1,2-diaminoethane mainly performs the role of an electron transfer agent, displaying moderate intensity reductive characteristics [30,31]. In view of this, in our case we feel that the formation of Mn_3O_4 by thermal decomposition at high temperature in oleyl amine may also be a form of typical mild reduction process. In the present case, after coordination of oleyl amine to the manganese precursor solution there may be formation of MnO(OH). These amines are also acting as the solvent. Being a polarizing solvent, oleyl amine can greatly enhance the solubility, diffusion and reactivity of the reactant species. Especially, when oleyl amine is coordinated with manganese, the short distance between the manganese and nitrogen or oxygen atom in the compound is favorable for electron transfer from N or O to manganese [31–34], resulting in the formation of Mn_3O_4. The synthesis of phase pure Mn_3O_4 using the hydrothermal method has rarely been reported in the literature. However, good quality Mn_3O_4 formation by thermal decomposition is attributed to the instant reaction due to localized superheating. In the hydrothermal method, the formation of Mn_3O_4 takes a very long time (24 h). MnO(OH) is always present as one of the phases in the Mn_3O_4 prepared by the hydrothermal method. Surprisingly, MnO(OH) is not present in the Mn_3O_4 prepared by the thermal decomposition method.

In addition Mn_3O_4 nanoparticles have been prepared under different conditions. By controlling the quality of the nanoparticles, Mn_3O_4 with various sizes and morphologies can be formed. For example, mixing and heating 0.6 g $[Mn(sal)_2]$ and 2 ml of oleyl amine led to 10–15 nm Mn_3O_4 nanoparticles, but the obtained nanoparticles were irregular and not monodispersed. To prepare monodispersed Mn_3O_4 nanoparticles, the same procedure was executed with a temperature of 100 °C for 90 min. The resulting metal-complex solution was injected into 5 g of triphenylphosphine at 210 °C. Uniform-shaped Mn_3O_4 nanoparticles with an average size of 20–30 nm were obtained. In this experimental TPP was used as a stabilizing agent.

4. Conclusion

Pure phase Mn_3O_4 nanoparticle powder was synthesized successfully by the thermal decomposition method from [bis(salicylidiminato)manganese(II)] in the presence of oleyl amine and triphenylphosphine. The particles were mostly tetragonal Mn_3O_4 phase and had a size in the range 20–30 nm. The BE values of the Mn $2p_{3/2}$ (641.7 eV) and spin–orbit splitting (11.6 eV) is well matching with the reported value of the manganese oxide. Significantly, the metallic impurities were below 0.01%, and so high quality products were prepared.

Acknowledgement

Authors are grateful to the council of the University of Kashan for providing financial support to undertake this work.

References

[1] A.R. Armstrong, P.G. Bruce, Nature 381 (1996) 499.
[2] Y.F. Shen, R.P. Zerger, R.N. Deguzman, S.I. Suib, L. Mccurdy, D.I. Potter, C.I. Oyoung, Science 260 (1993) 511.
[3] A.H. De Vries, L. Hozoi, R. Broer, Phys. Rev. B 66 (2002) 035108.
[4] Y. Yamashita, K. Mukai, J. Yoshinobu, M. Lippmaa, T. Kinoshita, M. Kawasaki, Surf. Sci. 514 (2002) 54.
[5] V.V. Pankov, Ceram. Int. 14 (1988) 87.
[6] I. Ursu, R. Alexandrescu, I.N. Mihailescu, J. Phys. B 19 (1986) L825.
[7] P. Gibot, L. Laffont, J. Solid State Chem. 180 (2007) 695.

[8] M. Anilkumar, V. Ravi, Mater. Res. Bull. 40 (2005) 605.
[9] M. Yoshimura, MRS Bull. 25 (2000) 17.
[10] X. Hong, G. Zhang, Y. Zhu, H. Yang, Mater. Res. Bull. 38 (2003) 1695.
[11] K.J. Rao, P.D. Ramesh, Bull. Mater. Sci. 18 (1995) 447.
[12] D. Chen, K. Tang, G. Shen, J. Sheng, Z. Fang, X. Liu, H. Zheng, Y. Qian, Mater. Chem. Phys. 82 (2003) 206.
[13] N.R. Jana, Y. Chen, X. Peng, Chem. Mater. 16 (2004) 3931.
[14] X. Sun, Y.W. Zhang, R. Si, C.H. Yan, Small 11 (2005) 1081.
[15] S. Sun, H. Zeng, D.B. Robinson, S. Raoux, P.M. Rice, S.X. Wang, G. Li, J. Am. Chem. Soc. 26 (2004) 273.
[16] N.V. Loginova, A.A. Chernyavskaya, M.S. Parfenova, N.P. Osipovich, G.I. Polozov, Yu.A. Fedutik, T.V. Koval'chuk, G.P. Shevchenko, Polyhedron 25 (2006) 1723.
[17] P.S. Nair, T. Radhakrishnan, N. Revaprasadu, G.A. Kolawole, P. O'Brien, Polyhedron 22 (2003) 3129.
[18] J. Cusack, M.G.B. Drew, T.R. Spalding, Polyhedron 23 (2004) 2315.
[19] I. Gilbert, A. Milla'n, F. Palacio, A. Falqui, E. Snoeck, V. Serin, Polyhedron 22 (2003) 2457.
[20] W.S. Seo, H.H. Jo, K. Lee, B. Kim, S.J. Oh, J.T. Par, Angew. Chem., Int. Ed. 43 (2004) 1115.
[21] M. Salavati-Niasari, M. Shaterian, M.R. Ganjali, P. Norouzi, J. Mol. Catal. A: Chem. 261 (2007) 147.
[22] M. Salavati-Niasari, F. Davar, M. Mazaheri, M. Shaterian, J. Magn. Magn. Mater. 320 (2008) 575.
[23] T. Hyeon, S.S. Lee, J. Park, Y. Chung, H.B. Na, J. Am. Chem. Soc. 123 (2001) 12798.
[24] J. Park, E. Kang, C.J. Bae, J.-G. Park, H.-J. Noh, J.-Y. Kim, J.-H. Park, H.M. Park, T. Hyeon, J. Phys. Chem. B 108 (2004) 13594.
[25] B. Gillot, M. El Guendouzi, M. Laarj, Mater. Chem. Phys. 70 (2001) 54.
[26] F.A. AL Sagheer, M.A. Hasan, L. Pasupulety, J. Mater. Sci. Lett. 18 (1999) 209.
[27] M. Ishii, M. Nakahira, Solid State Commun. 11 (1972) 209.
[28] A.D. Gole, C. Dash, A.B. Mandale, M. Rao, M. Sastri, Anal. Chem. 72 (2000) 4301.
[29] J.S. Foord, R.B. Jackman, G.C. Allen, Philos. Magn. A 49 (1984) 657.
[30] S. Ardizzon, C.L. Bianchi, D. Tirelli, Colloids Surf., A 134 (1998) 305.
[31] Y.C. Zhang, T. Qiao, X.Y. Hu, J. Solid State Chem. 177 (2004) 4093.
[32] J. Xiao, Y. Xie, Y. Xiong, J. Mater. Chem. 11 (2001) 1417.
[33] Y. Gao, H. Niu, C. Zeng, Chem. Phys. Lett. 367 (2003) 141.
[34] B. Mayers, Y.N. Xia, Adv. Mater. 14 (2002) 279.

$[Et_3NH]_4[V_{10}O_{26}(OH)_2]$ (**1**) ($V_{10}C_{24}H_{66}N_4O_{28}$): C, 21.07; H, 4.86; N, 4.09. Found: C, 20.92; H, 4.73; N, 3.97%.

2.4. Synthesis of $[Me_2HN(CH_2)_2NHMe_2]_3[V_{10}O_{28}] \cdot 4H_2O$ (**2**)

Compound **2** was synthesized from aqueous medium in 47% yield by following a very similar procedure as described for **1** using *N*,*N*,*N*′,*N*′-tetramethylethylenediamine (3.3 mmol) instead of triethylamine. *Anal.* Calc. for $[Me_2HN(CH_2)_2NHMe_2]_3[V_{10}O_{28}] \cdot 4H_2O$ (**2**) ($V_{10}C_{18}H_{62}N_6O_{32}$): C, 15.62; H, 4.51; N, 6.07. Found: C, 15.45; H, 4.42; N, 5.89%.

2.5. X-ray crystallography

X-ray quality single crystals of **1** and **2** were collected directly from the products obtained during synthesis. Unit cell parameters and the intensity data were obtained on a Bruker-Nonius SMART APEX CCD single crystal diffractometer, equipped with a graphite monochromator and a Mo Kα fine-focus sealed tube (λ = 0.71073 Å). Data were collected at 298 K with a scan width of 0.3° in ω and an exposure time of 10 s/frame. The SMART and the SAINT-PLUS packages [22] were used for data acquisition and extraction, respectively. In each case, the SADABS program [23] was used for absorption correction. The SHELX-97 programs [24] available in the WINGX package [25] were used for structure solution by direct method and refinement on F^2 by full-matrix least-squares procedures. All non-hydrogen atoms were refined anisotropically. In the case of **1**, the hydrogen atoms of the ammonium N–H groups and the hydrogen atoms of the dihydrogendecavanadate were located on a difference map and refined isotropically. In the case of **2**, the hydrogen atoms of the ammonium groups and the water molecules were also located on a difference map. The N–H hydrogens were refined with $U_{iso}(H) = 1.2U_{eq}(N)$ and the water hydrogen atoms were refined with geometric restraints and $U_{iso}(H) = 1.5U_{eq}(O)$. All other hydrogen atoms in both structures were included at idealized positions by using a riding model. The ORTEX6a [26] and PLATON [27] packages were used for molecular graphics. Selected crystallographic data are listed in Table 1.

Table 1
Crystallographic data for $[Et_3NH]_4[V_{10}O_{26}(OH)_2]$ (**1**) and $[Me_2HN(CH_2)_2NHMe_2]_3[V_{10}O_{28}] \cdot 4H_2O$ (**2**)

	1	**2**
Empirical formula	$V_{10}C_{24}H_{66}N_4O_{28}$	$V_{10}C_{18}H_{62}N_6O_{32}$
Formula weight	1368.21	1384.14
Crystal size (mm)	0.43 × 0.22 × 0.07	0.26 × 0.21 × 0.14
Crystal system	monoclinic	monoclinic
Space group	$P2_1/n$	$C2/m$
a (Å)	13.345(2)	12.1180(9)
b (Å)	21.569(4)	17.4770(13)
c (Å)	17.096(3)	11.9955(9)
β (°)	100.985(3)	113.634(1)
V (Å^3)	4831.0(14)	2327.4(3)
Z	4	2
ρ_{calc} (g/cm^3)	1.881	1.975
μ (mm^{-1})	1.930	2.011
F(000)	2768	1396
Reflections collected	54891	12093
Unique reflections	11585	2358
Observed reflections ($I \geqslant 2\sigma(I)$)	9632	2058
Data/restraints/parameters	11585/0/631	2358/5/180
Goodness-of-fit on F^2	1.083	1.044
R_1, wR_2 ($I \geqslant 2\sigma(I)$)	0.0515, 0.1194	0.0372, 0.1066
R_1, wR_2 (all data)	0.0635, 0.1256	0.0427, 0.1106
Largest peak and hole (e/Å^3)	0.965 and −0.631	0.937 and −0.720

3. Results and discussion

3.1. Synthesis and characterization

Both **1** and **2** have been prepared by treating an aqueous suspension of V_2O_5 with the corresponding amine under boiling condition. The elemental analysis data are consistent with the empirical formula obtained from the X-ray structures. Each of the two compounds is diamagnetic and EPR silent in the solid state indicating the +5 oxidation state of all the vanadium centres.

The infrared spectral features of both compounds are very similar to that reported for polyvanadates [10–14,16,17,19]. The spectra of **1** and **2** display the terminal V=O stretching bands within 1000–930 cm^{-1}. The asymmetric and symmetric vibrations of the bridging V–O–V fragments appear in the ranges 850–730 and 600–450 cm^{-1}, respectively. Compound **1** shows several weak bands within 3370–2485 cm^{-1}. These are possibly due to the O–H, N–H and C–H stretches. Two moderately strong bands are observed at 3486 and 3044 cm^{-1} in the spectrum of **2**. The former is most likely associated with the water of crystallization and the latter is attributed to the N–H stretching.

^{51}V NMR spectra were recorded using aqueous solutions of **1** and **2**. The spectra of both compounds are very similar and typical of decavanadate containing species. Three resonances observed at −426, −507 and −525 ppm for **1** and at −424, −501 and −516 ppm for **2** are within the range reported previously [10,12].

3.2. Thermal studies

Thermogravimetric measurements with both compounds have been performed in the temperature range 50–800 °C with a scan rate of 10°/min in the presence of a nitrogen flow. The profiles of the thermal decomposition curves obtained for **1** and **2** are comparable with that reported for decavanadates containing organic cations [11,14,19]. The anhydrous compound **1** is stable up to 160 °C. After this temperature the decomposition starts in two successive steps due to the loss of the organic cations. In the relatively sharp first step up to 200 °C the weight loss is about 12%. A further 18% weight loss occurs in the following step which continues up to 310 °C. Above this temperature up to 800 °C there is a small progressive weight loss without any clear peak. The hydrated compound **2** shows the loss of water (obsd. 5.6%, calcd. 5.2%) in the temperature range 60–115 °C. After the water loss there is a stable form up to 160 °C. The loss of the organic cations occurs in two steps. In the sharp first step between 160 and 175 °C the weight loss is about 7%. In the broad second step between 175 and 380 °C the weight loss is about 19%. As observed for **1**, there is a small but progressive weight loss without any peak in the temperature range 380–800 °C.

3.3. Description of structures

Compound **1** crystallizes in the space group $P2_1/n$. The asymmetric unit contains four triethylammonium cations and the dihydrogendecavanadate anion $[V_{10}O_{26}(OH)_2]^{4-}$. The crystal structure of **1** synthesized by a different procedure has been reported earlier in the space group $P2_1/c$ [18]. Compound **2** crystallizes in the space group $C2/m$. The asymmetric unit contains half of one disordered diammonium cation, one fourth of a second diammonium cation, one fourth of the decavanadate anion $[V_{10}O_{28}]^{6-}$ and two water molecules each having half occupancy. The methylene groups of the disordered diammonium are found in four places. The intracation bond parameters are unexceptional for both **1** and **2**. The structures of $[V_{10}O_{26}(OH)_2]^{4-}$ and $[V_{10}O_{28}]^{6-}$ are shown in Fig. 1. Two hydrogen atoms of $[V_{10}O_{26}(OH)_2]^{4-}$ are bonded to a μ_2-oxo

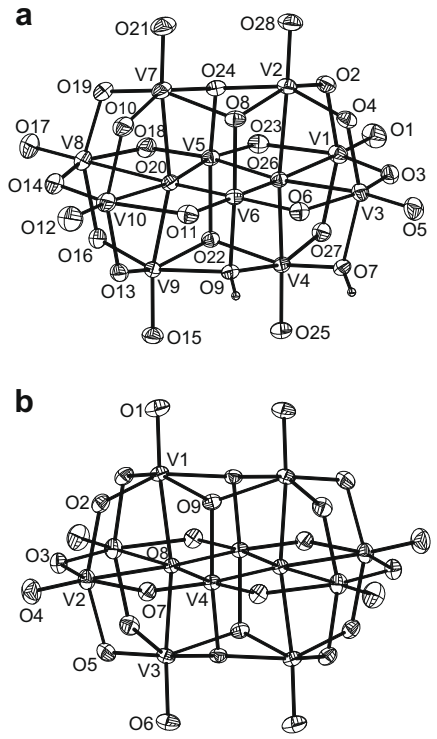

Fig. 1. The structures of (a) $[V_{10}O_{26}(OH)_2]^{4-}$ and (b) $[V_{10}O_{28}]^{6-}$ with the atom-labeling schemes. All non-hydrogen atoms are represented by their 40% probability thermal ellipsoids.

atom (O7) and a μ_3-oxo atom (O9). All the metal centres in both decavanadates are in distorted O_6 octahedra. The bond parameters associated with the metal centres in both compounds are comparable with that reported for structurally characterized decavanadates [10–21]. The *cis* and *trans* O–V–O bond angles are in the ranges 72.53(10)–107.78(12)° and 150.88(10)–177.26(11)°, respectively. All the V–O bond lengths for **1** and **2** are listed in Tables 2 and 3, respectively. Eight terminal V=O bond lengths are within 1.598(2)–1.622(2) Å. Each metal centre of these terminal V=O groups has a very long V–O bond length (2.217(2)–2.427(2) Å) involving the hexacoordinated O-atoms (O20 and O26 for **1** and O8 for **2**). Other V–O bond lengths for these eight metal centres are in the range 1.731(2)–2.129(2) Å. Remaining two central metal centres (V5 and V6 for **1** and V4 for **2**) without terminal oxo group have two short (1.667(2)–1.700(2) Å), two medium (1.865(2)–2.049(2) Å) and two long (2.050(2)–2.160(2) Å) V–O bond lengths.

Table 2
Selected bond lengths (Å) for $[Et_3NH]_4[V_{10}O_{26}(OH)_2]$ (**1**)

V(1)–O(1)	1.603(2)	V(6)–O(6)	1.700(2)
V(1)–O(2)	1.863(2)	V(6)–O(8)	1.865(2)
V(1)–O(3)	1.798(2)	V(6)–O(9)	2.049(2)
V(1)–O(23)	2.041(2)	V(6)–O(11)	1.667(2)
V(1)–O(26)	2.298(2)	V(6)–O(20)	2.050(2)
V(1)–O(27)	1.940(2)	V(6)–O(26)	2.160(2)
V(2)–O(2)	1.819(2)	V(7)–O(8)	2.036(2)
V(2)–O(4)	1.878(2)	V(7)–O(10)	1.823(2)
V(2)–O(8)	1.989(2)	V(7)–O(19)	1.814(3)
V(2)–O(24)	1.944(2)	V(7)–O(20)	2.313(2)
V(2)–O(26)	2.320(2)	V(7)–O(21)	1.602(2)
V(2)–O(28)	1.603(2)	V(7)–O(24)	2.000(2)
V(3)–O(3)	1.849(2)	V(8)–O(14)	1.825(3)
V(3)–O(4)	1.817(2)	V(8)–O(16)	1.943(2)
V(3)–O(5)	1.598(2)	V(8)–O(17)	1.602(3)
V(3)–O(6)	2.000(2)	V(8)–O(18)	2.021(3)
V(3)–O(7)	1.983(2)	V(8)–O(19)	1.836(3)
V(3)–O(26)	2.272(2)	V(8)–O(20)	2.427(2)
V(4)–O(7)	1.941(2)	V(9)–O(9)	2.108(2)
V(4)–O(9)	2.129(2)	V(9)–O(13)	1.826(2)
V(4)–O(22)	1.886(2)	V(9)–O(15)	1.622(2)
V(4)–O(25)	1.615(2)	V(9)–O(16)	1.738(2)
V(4)–O(26)	2.217(2)	V(9)–O(20)	2.218(2)
V(4)–O(27)	1.731(2)	V(9)–O(22)	2.007(2)
V(5)–O(18)	1.683(2)	V(10)–O(10)	1.874(2)
V(5)–O(20)	2.113(2)	V(10)–O(11)	2.111(3)
V(5)–O(22)	1.954(2)	V(10)–O(12)	1.602(3)
V(5)–O(23)	1.685(2)	V(10)–O(13)	1.861(2)
V(5)–O(24)	1.912(2)	V(10)–O(14)	1.816(3)
V(5)–O(26)	2.131(2)	V(10)–O(20)	2.325(2)

Table 3
Selected bond lengths (Å) for $[Me_2HN(CH_2)_2NHMe_2]_3[V_{10}O_{28}] \cdot 4H_2O$ (**2**)

V(1)–O(1)	1.601(3)	V(3)–O(5)[a]	1.811(2)
V(1)–O(2)	1.826(2)	V(3)–O(9)[b]	2.023(2)
V(1)–O(2)[a]	1.826(2)	V(3)–O(9)[c]	2.023(2)
V(1)–O(9)[a]	2.006(2)	V(3)–O(8)	2.223(3)
V(1)–O(9)	2.006(2)	V(4)–O(7)	1.698(2)
V(1)–O(8)	2.261(3)	V(4)–O(7)[c]	1.698(2)
V(2)–O(4)	1.599(2)	V(4)–O(9)	1.9178(19)
V(2)–O(3)	1.8432(16)	V(4)–O(9)[c]	1.9178(19)
V(2)–O(2)	1.870(2)	V(4)–O(8)[b]	2.0987(17)
V(2)–O(5)	1.873(2)	V(4)–O(8)	2.0987(17)
V(2)–O(7)	2.034(2)	O(3)–V(2)[a]	1.8432(16)
V(2)–O(8)	2.325(2)	O(8)–V(4)[b]	2.0987(17)
V(3)–O(6)	1.616(3)	O(8)–V(2)[a]	2.325(2)
V(3)–O(5)	1.811(2)	O(9)–V(3)[b]	2.023(2)

Symmetry transformations used to generate equivalent atoms:
[a] $x, -y, z$.
[b] $-x, -y, -z+1$.
[c] $-x, y, -z+1$.

3.4. Hydrogen bonding and self-assembly

Both **1** and **2** contain several classical hydrogen bond donor and acceptor centres. We have investigated the self-assembly patterns of both **1** and **2** via intermolecular hydrogen bonding. Dihydrogendecavanadates are known to form hydrogen bonded dimeric aggregates in the crystal lattice [16–18]. Compound **1** also forms discrete dimeric units (Fig. 2). The $[V_{10}O_{26}(OH)_2]^{4-}$ anion dimerises via two pairs of complementary O–H···O hydrogen bonds involving the two hydroxy groups (O7–H and O9–H) and two terminal V=O group O-atoms (O15 and O25). The O7···O15 and the O9···O25 distances are

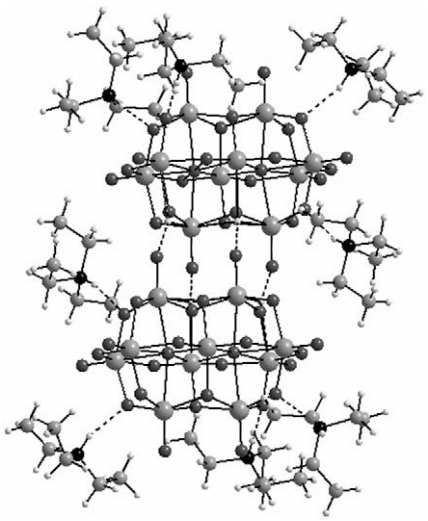

Fig. 2. The dimeric aggregate of $[Et_3NH]_4[V_{10}O_{26}(OH)_2]$ (**1**).

2.734(3) and 2.708(3) Å, respectively. The O7–H···O15 and the O9–H···O25 angles are 167(4)° and 166(4)°, respectively. The triethylammonium moieties are connected to the corresponding anions through N–H···O hydrogen bonds. Four μ_2-oxo atoms (O2, O4, O10 and O13) of the dihydrogendecavanadate act as donors in these N–H···O hydrogen bonds. The N···O distances and the N–H···O angles are in the ranges 2.713(4)–2.833(4) Å and 160(4)–176(5)°, respectively. Due to the presence of the diammonium cations and water of crystallization the self-assembly of **2** is more intricate in comparison to that of **1**. The disordered diammonium cations, water molecules and the $[V_{10}O_{28}]^{6-}$ anion form a two-dimensional sheet structure via N–H···O and O–H···O hydrogen bonds (Fig. 3a). In the N–H···O hydrogen bonds, μ_2-oxo atom (O3) of the decavanadate unit is involved. The N2···O3 distance and the N2–H···O3 angle are 2.634(5) Å and 178(6)°, respectively. The μ_2-oxo atom O2 and the terminal V=O group O-atom O6 of $[V_{10}O_{28}]^{6-}$ are involved in the O–H···O hydrogen bonds with the water molecules. The O10···O2 and the O11···O6 distances are 2.850(3) and 2.853(4) Å, respectively. The O10–H···O2 and O11–H···O6 angles are 147(2) and 166(5)°, respectively. The third diammonium cation connects the parallel sheets through N–H···O hydrogen bonds and a three-dimensional network of **2** is formed (Fig. 3b). The acceptor in this N–H···O hydrogen bond is the μ_3-oxo atom O9 of the anion. The N1···O9 distance and the N1–H···O9 angle are 3.010(4) Å and 161(5)°, respectively.

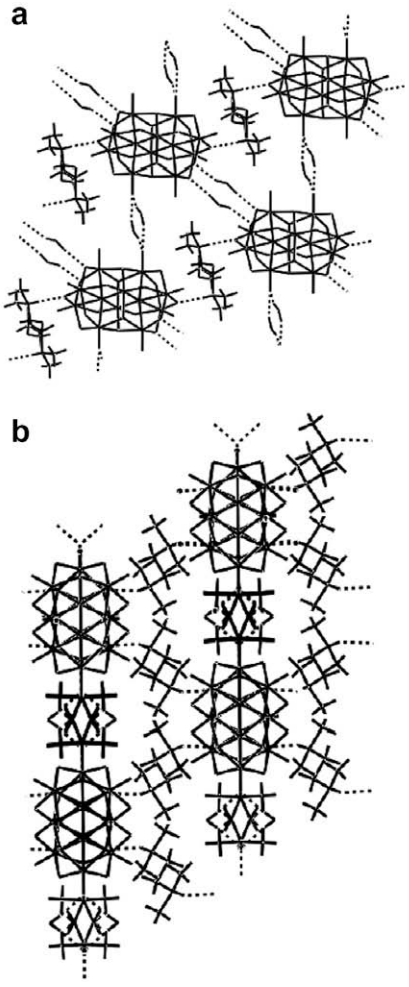

Fig. 3. Packing of $[Me_2HN(CH_2)_2NHMe_2]_3[V_{10}O_{28}] \cdot 4H_2O$ (**2**): (a) two-dimensional ordering of the two diammonium cations, the anion and the water molecules and (b) bridging of the parallel two-dimensional sheets by the remaining diammonium cation to form a three-dimensional network.

4. Conclusion

In conclusion, triethylammonium and *N*,*N*,*N*′,*N*′-tetramethylethylenediammonium decavanadates have been synthesized and characterized by elemental analysis, magnetic, thermal, IR and NMR measurements. The X-ray structures of both compounds have been determined. The $[V_{10}O_{26}(OH)_2]^{4-}$ is isolated with $[Et_3NH]^+$ in anhydrous form, while the $[Me_2HN(CH_2)_2NHMe_2]^{2+}$ salt of $[V_{10}O_{28}]^{6-}$ is obtained in tetrahydrated form. The self-assembly patterns via intermolecular hydrogen bonding have been scrutinized. The structure of $[Et_3NH]_4[V_{10}O_{26}(OH)_2]$ reveals that the four cations are simply connected to the anion via N–H···O hydrogen bonds but due to complementary interanionic O–H···O hydrogen bonds the compound forms discrete dimeric aggregates. On the other hand, the diammonium cations and the water molecules help to form a complex three-dimensional network of $[Me_2HN(CH_2)_2NHMe_2]_3[V_{10}O_{28}] \cdot 4H_2O$ through N–H···O and O–H···O hydrogen bonds.

5. Supplementary data

CCDC 678220 and 678221 contain the supplementary crystallographic data for **1** and **2**, respectively. These data can be obtained free of charge via http://www.ccdc.cam.ac.uk/conts/retrieving.html, or from the Cambridge Crystallographic Data Centre, 12 Union Road, Cambridge CB2 1EZ, UK; fax: (+44) 1223-336-033; or e-mail: deposit@ccdc.ac.uk.

Acknowledgments

This work was supported in part by the Department of Science and Technology (DST) (Grant No. SR/S1/IC-10/2007). Ms. A. Sarkar thanks the Council of Scientific and Industrial Research for a fellowship. X-ray structures were determined at the National Single Crystal Diffractometer Facility, School of Chemistry, University of Hyderabad (established by DST). We thank the University Grants Commission for the facilities provided under the UPE and CAS programs.

References

[1] C.L. Hill (Ed.), Polyoxometalates, Chem. Rev. 98 (1998) 1.
[2] M.T. Pope, A. Müller (Eds.), Polyoxometalate Chemistry: From Topology Via Self-Assembly to Applications, Kluwer Academic, Dordrecht, 2000.
[3] E. Coronado, P. Day, Chem. Rev. 104 (2004) 5419.
[4] E. Coronado, C. Giménez-Saiz, C.J. Gómez-García, Coord. Chem. Rev. 249 (2005) 1776.
[5] D.-L. Long, E. Burkholder, L. Cronin, Chem. Soc. Rev. 36 (2007) 105.
[6] C.L. Hill (Ed.), Polyoxometalates in Catalysis, J. Mol. Catal. A: Chem. 262 (2007) 1.
[7] A. Proust, R. Thouvenot, P. Gouzerh, Chem. Commun. (2008), doi:10.1039/b715502f.
[8] L. Petterson, I. Andersson, B. Hedman, Chem. Scripta 25 (1985) 309.
[9] D.C. Crans, Comments Inorg. Chem. 16 (1994) 1.
[10] V.W. Day, W.G. Klemperer, D.J. Maltbie, J. Am. Chem. Soc. 109 (1987) 2991.
[11] J.M. Arrieta, Polyhedron 11 (1992) 3045.
[12] D.C. Crans, M. Mahroof-Tahir, O.P. Anderson, M.M. Miller, Inorg. Chem. 33 (1994) 5586.
[13] P. Román, A. Aranzabe, A. Luque, J.M. Gutiérrez-Zorrilla, M. Martínez-Ripoll, J. Chem. Soc., Dalton Trans. 20 (1995) 2225.
[14] A.S.J. Wery, J.M. Gutiérrez-Zorrilla, A. Luque, P. Roman, M. Martínez-Ripoll, Polyhedron 15 (1996) 4555.
[15] M. Farahbakhsh, P. Kögerler, H. Schmidt, D. Rehder, Inorg. Chem. Commun. 1 (1998) 111.
[16] S. Nakamura, T. Ozeki, J. Chem. Soc., Dalton Trans. (2001) 472.
[17] J.L. Ferreira da Silva, M.F. Minas da Piedade, M.T. Duarte, Inorg. Chim. Acta 356 (2003) 222.
[18] I. Correia, F. Avecilla, S. Marcão, J.C. Pessoa, Inorg. Chim. Acta 357 (2004) 4476.
[19] Y. Gong, C. Hu, H. Li, W. Tang, K. Huang, W. Hou, J. Mol. Struct. 784 (2006) 228.
[20] S. Pacigová, E. Rakovský, M. Sivák, Z. Žák, Acta Crystallogr., Sect. C 63 (2007) m419.
[21] C.-Y. Zhu, Y.-T. Li, Z.-Y. Wu, N.-Y. Xiao, Acta Crystallogr., Sect. E 63 (2007) m547.

[22] SMART V5.630 and SAINT-PLUS V6.45, Bruker-Nonius Analytical X-ray Systems Inc., Madison, WI, 2003.
[23] G.M. Sheldrick, SADABS Empirical Absorption Correction Program, University of Göttingen, Göttingen, Germany, 1997.
[24] G.M. Sheldrick, SHELX-97 Structure Determination Software, University of Göttingen, Göttingen, Germany, 1997.
[25] L.J. Farrugia, J. Appl. Crystallogr. 32 (1999) 837.
[26] P. McArdle, J. Appl. Crystallogr. 28 (1995) 65.
[27] A.L. Spek, PLATON A Multipurpose Crystallographic Tool, Utrecht University, Utrecht, The Netherlands, 2002.

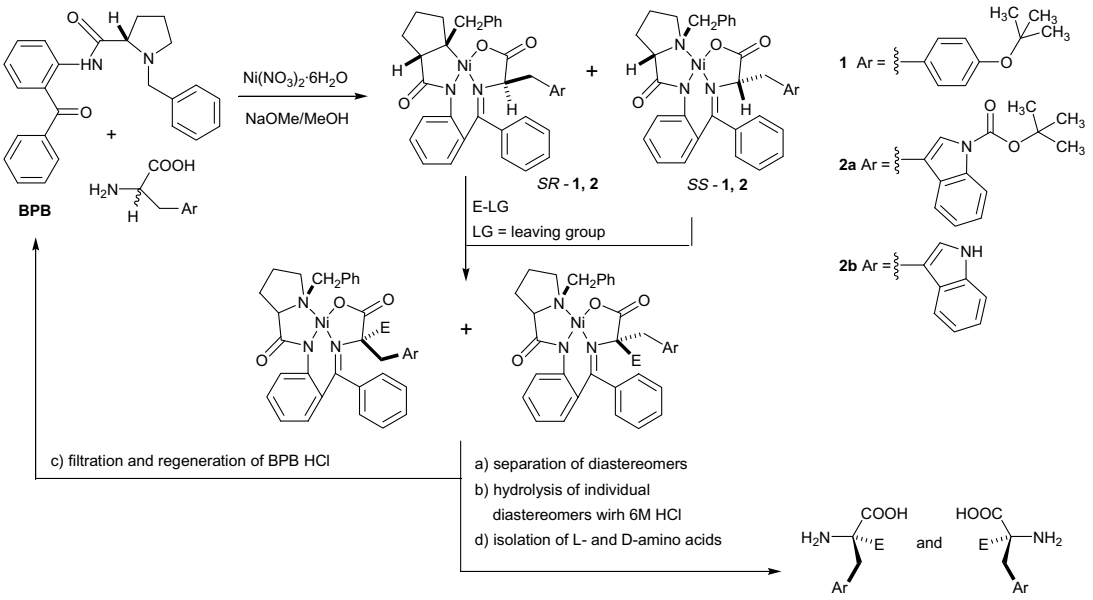

Scheme 1.

complexes was assessed using a model complex derived from tyrosine protected by a methyl group in the side chain.

2. Results and discussion

Ratios of starting compounds for the preparation of complexes were chosen from a previous optimisation protocol of the ratio of starting compounds for the preparation of the glycine-derived complex [5]. Twenty percent excess of nickel nitrate(II) to BPB was predicted to be optimal for both maximisation of the yield of complexes and minimisation of the amount of nickel in waste water. Five and fifty percent excess were also tested (Table 1). Unlike glycine used in the previous work, both side-chain protected amino acids are relatively expensive. Thus, the previously applied two-fold excess of amino acid was considered to be uneconomical. Ten, twenty and forty percent excess of amino acid to BPB were tested (Table 1). Experiments demonstrated that in this particular case the Boc-protective group of the indole residue nitrogen is unstable during chromatographic purification on silica gel. A significant amount of the complex derived from the protected tryptophan lost the protective group during quick preparative TLC purification of an analytical sample. Clean deprotection was observed in all the four preparative syntheses followed by time-consuming purification of the product by column chromatography on silica gel. No observations of low stability of indole nitrogen Boc-protected derivatives of tryptophan [9] were found in the literature. Deprotection was confirmed by NMR, MS/MS and X-ray data. In order to demonstrate the necessity of including the protective group for the preparation of quaternary α-amino acids via C-methylation of carbanion generated from tertiary precursor [7b], a sample of deprotected complex was methylated with an excess of CH_3I/KOH in 1,3-dimethylimidazolidin-2-one (DMI). This resulted in pure N-methylated product without any traces of the C-methylated product as confirmed by both MS^n and X-ray data (Scheme 2, Figs. 1C, D, 2 and 3).

Table 1
Yields of complexes (both *SS* and *SR* diastereomers) depending on the ratios of the starting compounds used

$Ni(NO_3)_2 \cdot 6H_2O$ excess	Amino acid excess	BPB	Yield of complex **1** (sum of diastereomers)	Yield of complex **2b** (sum of diastereomers)
1.05	1.1	1	57	55
1.2	1.2	1	79	61
1.2	1.4	1	83	86
1.5	1.4	1	87	79

Development of an alternative purification method was successful, but the methylation of the *N*-Boc protected complex with an excess of CH_3I/KOH in DMI resulted in complete deprotection followed by complete N-methylation [10]. Similar *N*-Si(*i*-Pr)$_3$ protected tryptophan complex is stable during chromatographic purification on silica gel, but its methylation with an excess of CH_3I/KOH in DMI also resulted in almost complete deprotection followed by predominant N-methylation and less than 1% of C-methylation (Scheme 3). *tert*-Butyl protection of the phenolic group of tyrosine is perfectly compatible with the reaction conditions used and with column chromatography on silica gel (Fig. 1A, B).

Typical ions in the first-order positive-ion ESI mass spectra are protonated molecules and adducts with alkali metal ions, such as $[M+Na]^+$ and $[M+K]^+$ (Fig. 1A). The presence of these ions was used for the determination of molecular weights of all analysed compounds (see Section 3 for more details). Based on the determination of the molecular weights, the presence or the absence of a protective group or another substituent on the aromatic nitrogen (for tryptophan) or oxygen atom (for tyrosine side-chains) can be recognised [10]. Furthermore, the presence of a protective group can be confirmed using tandem mass spectrometry by the typical neutral losses associated with a particular group. In the case of complex 1, the typical neutral losses are $\Delta m/z$ 56 (butene) and 106 (see Fig. 1B). For deprotected complex 2b, the characteristic neutral loss is $\Delta m/z$ 129 (see Fig. 1C). However, the difference neutral loss $\Delta m/z$ 145 is observed in the spectra of N-methylated complex 3 (see Fig. 1D).

Both complexes *SS*-**2b** and *SS*-**3** crystallize with solvent molecules in the crystalline lattice. The crystals loose some solvent molecules during drying in air at ambient temperature. For such crystallosolvates, X-ray crystallography of shock-frozen single crystals is an informative method of structure characterisation.

2.1. SS-2b

There are 2 crystallographically different complexes co-crystallized with 3 benzene molecules in the asymmetric unit. Both complexes suffer from disorder at C2 atoms and one of them even has

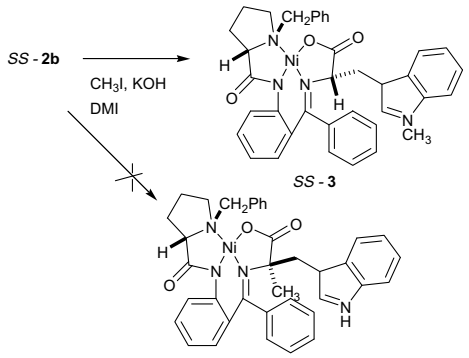

Scheme 2.

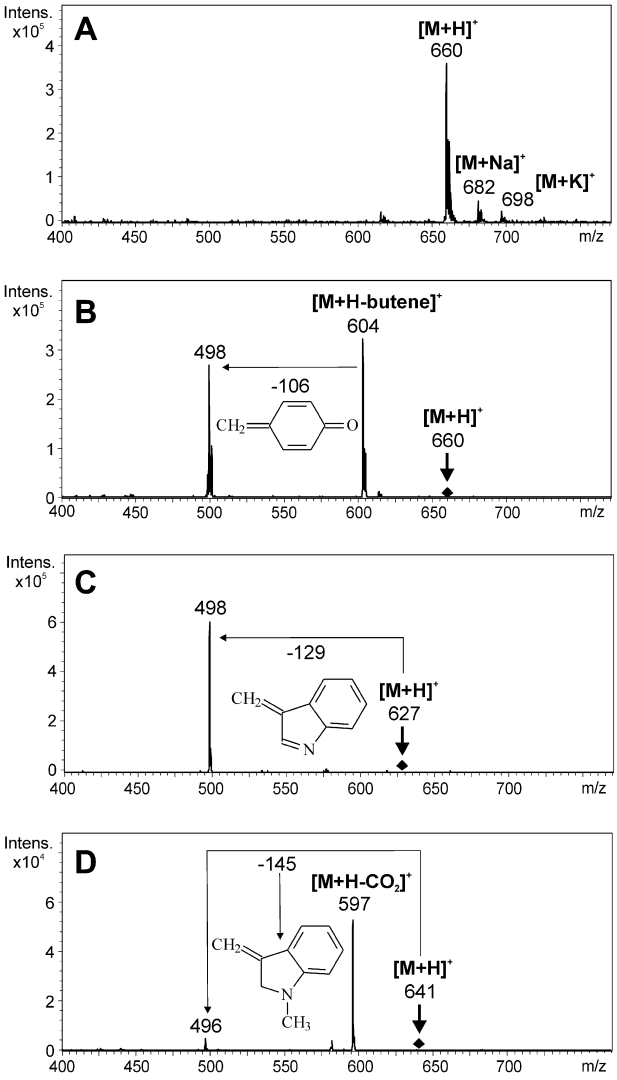

Fig. 1. Positive-ion electrospray ionization mass spectra: (A) First-order spectrum of **1**, (B) MS/MS spectrum of ion *m*/*z* 660 $[M+H]^+$ for **1**, (C) MS/MS spectrum of ion *m*/*z* 627 $[M+H]^+$ for **2b**, (D) MS/MS spectrum of ion *m*/*z* 641 $[M+H]^+$ for **3**.

the disorder of the phenyl group, see Figs. 2 and 5 (in Supplementary material). There are hydrogen bonds in the structure producing an helical arrangement of the complexes, see Figs. 6 and 7 (in Supplementary material). Packing in the unit cell along the monoclinic *b*-axis is shown in Fig. 8 (in Supplementary material).

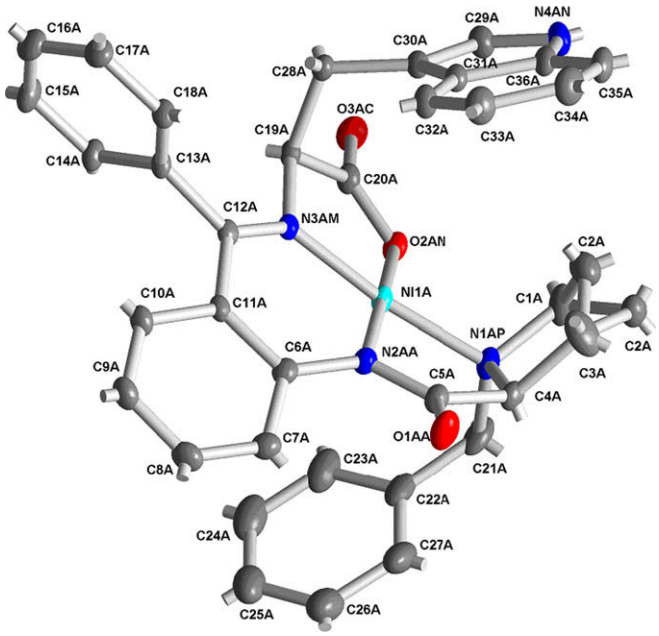

Fig. 2. The numbering scheme for *SS*-**2b**, the first complex, with atomic displacement ellipsoids at 30% probability level. Note disorder of C2A. Hydrogens are omitted for clarity.

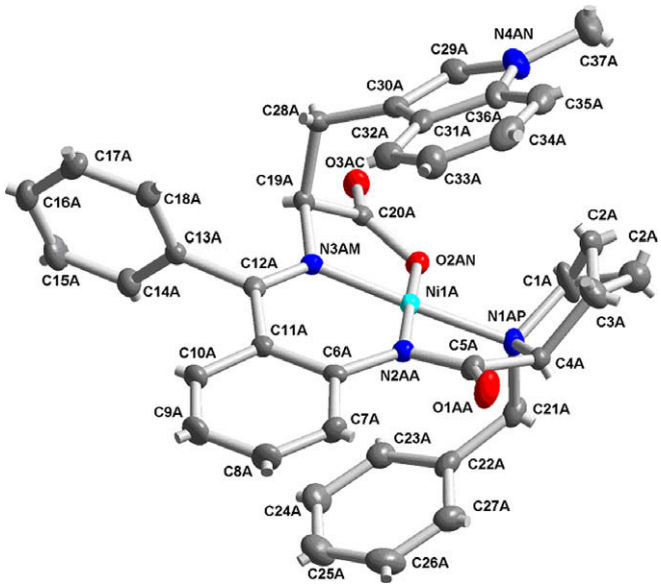

Fig. 3. The numbering scheme for *SS*-**3**, the first complex, with atomic displacement ellipsoids at 30% probability level. Note disorder of C2A. Hydrogens are omitted for clarity.

2.2. *SS*-**3**

There are 2 crystallographically different complexes co-crystallized with 2 benzene and 2 water molecules in the asymmetric unit. Again, both complexes suffer from disorder at C2 atoms see Figs. 3 and 9 (in Supplementary material). There are hydrogen bonds in the structure producing an helical arrangement of the complexes, see Figs. 10 and 11 (in Supplementary material). Packing in the unit cell along the orthorhombic *a*-axis is shown in Fig. 12 (in Supplementary material).

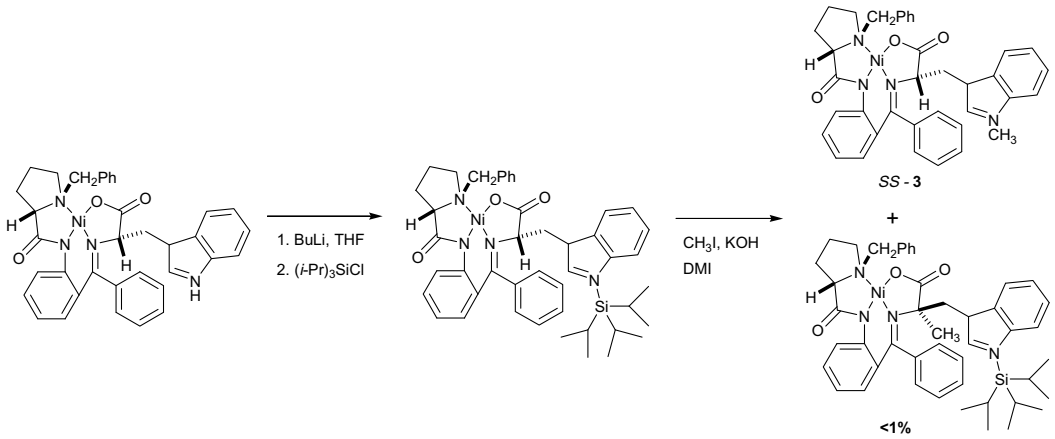

Scheme 3.

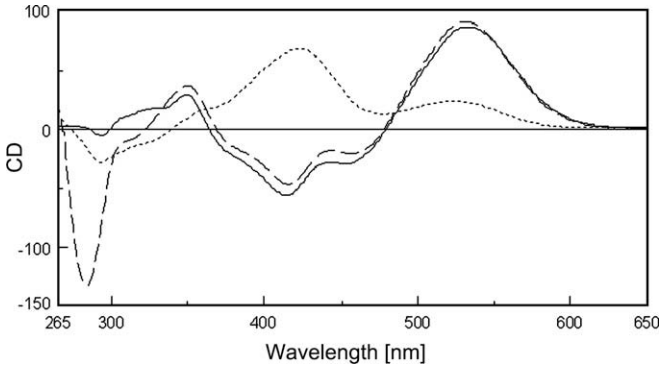

Fig. 4. CD spectra of *SS*-**4** (—), the first fraction, *SS*-**5** (— — —) and the second fraction *SR*-**5** (. . . . . .).

For both structures, the absolute structures were unambiguously determined. All nickel complexes show square-planar coordination geometry with small pyramidal distortions.

Five and ten percent excess of nickel nitrate and amino acid, respectively, led to poor yields of both complexes (Table 1). This result corresponds with the low yield of glycine-derived complex obtained with five percent excess of nickel nitrate [5]. As expected, twenty percent excess of nickel nitrate led to the high yield of both complexes. With such an excess of nickel salt, a higher excess of amino acid gave a slightly higher excess of complex **1** derived from tyrosine, and led to significantly higher yield of the complex derived from tryptophan (**2a** → **2b**) (Table 1). Lower yield of this complex, in the case when fifty percent excess of nickel nitrate was used, is consistent with the previously observed relationship between an excess of nickel nitrate used and yields of the complexes derived from glycine. Diastereomeric excess of (*SS*)-diastereomers in all cases was >95%. Minor (*SR*)-diastereomers were collected and partially characterised. Due to retroracemisation of the amino acid chiral centre in basic conditions, in further alkylation reaction mixtures of both diastereomers could be used without separation [8].

Due to poor preparative TLC separation of diastereomeric products of α-methylation of complex *SS*-**1**, its analogue complex *SS*-**4** (carrying methyl protective group of the side chain instead of *tert*-Bu) was used to assess the stereochemistry of products of α-methylation of such complexes (Scheme 4). These diastereomeric products of methylation *SS*-**5** and *SR*-**5** are separable by preparative TLC on silicagel while for the separation of many other similar diastereomers expensive preparative HPLC is necessary.

Stereochemistry of the diastereomers of 5 was assessed by circular dichroism (CD) and ^{13}C NMR spectroscopy:

- Two intense peaks were observed in the ^{13}C NMR spectrum of the reaction mixture after alkylation of *SS*-**4** with $^{13}CH_3I$/KOH in DMI (Scheme 4): minor at δ 29.3 ppm and major at δ 28.5 ppm. According to the integral intensities of peaks in ^{13}C NMR spectra, the diastereomeric excess of methylation was 6.9%;
- Two fractions were obtained after the preparative TLC separation of the reaction mixture. The first fraction giving a main ^{13}C NMR peak at δ 29.3 ppm was associated with the minor diastereomer. The second fraction where the main peak was at δ 28.5 ppm, was associated with the major diastereomer;
- CD spectra of starting *SS*-**4** and both diastereomers of **5** were recorded. Cotton effects in the spectra of both *SS*-**4** and the first TLC fraction (minor diastereomer) of **5** were similar in two areas (650–480 nm and 480–360 nm). Cotton effect in the spectrum of the second TLC fraction (major diastereomer) of **5** in the range 480–360 nm had an opposite sign (Fig. 4). Based on these CD data, the *SS* configuration was assigned to the first fraction (minor diastereomer) and the *SR* configuration was assigned to the second fraction (major diastereomer). This assignment is consistent with the proposed predominance of *Si*-alkylation leading to the major formation of *SR*-**5** (Scheme 4)[8].

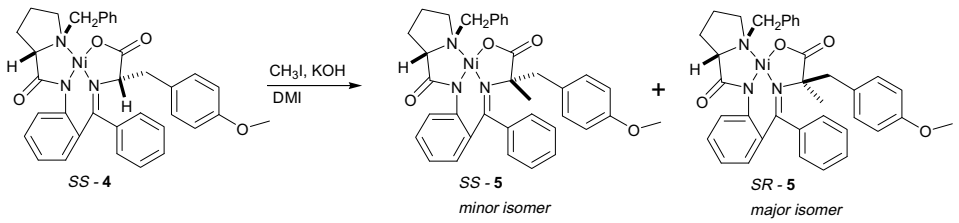

Scheme 4.

3. Experimental

The ^1H and ^{13}C NMR spectra were obtained in $CDCl_3$ solutions using a Bruker AMX-360 or Bruker 500 spectrometer equipped with a multinuclear 5 mm tunable probe. ^1H NMR chemical shifts δ are expressed in parts per million (ppm) downfield from tetramethylsilane as an internal standard. Coupling constants J are given in Hz. ^{13}C NMR chemical shifts are given with respect to the solvent signal (δ = 77 ppm). Data are given in the following order: δ value (number of protons, multiplicity (s, singlet; d, doublet; dd doublet of doublet; m, multiplet; t, triplet; br s, broad singlet).

Positive-ion electrospray ionization (ESI) mass spectra were measured on an Esquire 3000 ion trap analyzer (Bruker Daltonics, Bremen, Germany) in the range m/z 50–1000. The samples were dissolved in 100% acetonitrile and analyzed by direct infusion at the flow rate 5 μl/min. The selected precursor ions were further analyzed by MS/MS analyses under the following conditions: the isolation width m/z = 8, the collision amplitude (in the range 0.8–1.0 V depending on the precursor ion stability), the ion source temperature (300 °C), the tuning parameter compound stability (100%), the flow rate and the pressure of nitrogen (4 l/min and 10 psi), respectively. The elemental composition of the complexes *SS*-**1** and *SS*-**2b** was confirmed on an orthogonal hybrid quadrupole time-of-flight (QTOF) mass spectrometer fitted with electrospray ionization source (Bruker Daltonics). The instrument was externally calibrated using ESI tunning mix before the measurement. The samples were dissolved in acetonitrile and analyzed by direct infusion at the flow rate of 3 μl/min. Interface parameters were set as follows: capillary voltage −4.5 kV, drying temperature 200 °C, the flow rate and pressure of nitrogen were 4 l/min and 0.4 bar, respectively. For the recording of exact masses, QTOF data were acquired by the summation of 50 000 scans with 10 rolling averages. The typical ions observed in the first-order positive-ion mass spectra were $[M+H]^+$, $[M+Na]^+$ and $[M+K]^+$, and the elemental composition was confirmed by the comparison of experimental and theoretical values for all studied compounds. Table 2 shows mass accuracies for monoisotopic masses, mean mass accuracies correspond to the mean value for all isotopic peaks, and the sigma is a combined value for the standard deviation of masses and intensities for all peaks.

The elemental composition of the complexes *SS*-**5** and *SR*-**5** was confirmed on a sector mass spectrometer fitted with electron-impact ionization source (VG Analytical) by a commercial analytical laboratory.

Diffraction data were collected using a Siemens SMART CCD diffractometer with Mo Kα radiation (λ = 0.71073 Å, graphite monochromator). The crystals were cooled to 173(2) K by a flow of nitrogen gas using the LT-2A device. A full sphere of reciprocal space was scanned by 0.3 steps in ω with a crystal-to-detector distance of 3.97 cm. Preliminary orientation matrices were obtained from the first frames using SMART program. The collected frames were integrated using the preliminary orientation matrices which were updated every 100 frames. Final cell parameters were obtained by refinement of the positions of reflections with $I > 10\sigma(I)$ after the integration of all the frames using SAINT software [11]. The data were empirically corrected for absorption and other effects using the SADABS program [12]. The structures were solved by direct methods and refined by full-matrix least-squares analysis on all $|F^2|$ data using SHELXTL software [13]. The crystallographic and refinement data are summarized in Tables 3 and 4. The hydrogen bonding geometrical parameters are summarized in Tables 5 and 6 (in Supplementary material). Selected bond lengths, selected bond angles and their estimated standard deviations are listed in Tables 7 and 8 (in Supplementary material). The molecular graphics (Figs. 2,3,5–12) were prepared using the program DIAMOND [14]. Circular dichroism spectra were recorded using a Jasco J-715 spectropolarimeter.

Table 2
Mass accuracies and sigma values used

		$[M+H]^+$	$[M+Na]^+$	$[M+K]^+$
Complex *SS*-**1**	Mass accuracy (ppm)	1.0	0.3	0.7
$C_{38}H_{39}N_3O_4Ni$	Mean mass accuracy (ppm)	−1.4	−0.3	0.6
	Sigma	0.015	0.005	0.025
Complex *SS*-**2b**	Mass accuracy (ppm)	1.5	0.6	0.0
$C_{36}H_{32}N_4O_3Ni$	Mean mass accuracy (ppm)	−0.7	0.548	0.0
	Sigma	0.025	0.013	0.024

3.1. General procedure for the synthesis of complexes

2.47 M MeONa/MeOH (7.9 ml, 19.5 mmol) was added to a stirred suspension of BPB (500 mg, 1.3 mmol) and the corresponding amount of nickel nitrate and protected amino acid (Table 1) in dry MeOH (4 ml) under argon at 50 °C. The volume of the reaction mixture was then adjusted to 20 ml with dry MeOH. After stirring at 55 °C for 30 min, the mixture was poured into 0.7% aqueous citric acid (300 ml), stirred and the resulting precipitate was filtered off, washed with water on a filter and dried on air. The dry precipitate was purified by column chromatography using silica gel (Merck 40/63) and eluted with chloroform.[1] The first red fractions containing minor (*SR*)-diastereomers and the second red fractions containing major (*SS*)-diastereomers were collected. Yields of complex formation are given in Table 1. Complexes *SS*-**2b** and *SS*-**3** were purified by preparative TLC followed by crystallisation from a (wet) acetone-benzene mixture which gave a crystallosolvate. Resulting red single crystals are unstable in air at ambient temperature; they loose benzene (and water in the case of *SS*-**3**) and decompose within tens of minutes.

3.1.1. (SR)-Diastereomer of complex **2b**

δ_H (360.13 MHz, $CDCl_3$; Me_4Si) 1.36 (2H, m), 1.84 (1H, m), 2.21 (1H, m), 2.30 (1H, m), 3.07 (5H, m), 3.64 (1H, m), 4.30 (1H, t), 6.76 (1H, m), 6.84 (1H, m), 7.05 (1H, m), 7.10 (3H, m), 7.15 (1H, m), 7.20 (1H, m), 7.31 (4H, m), 7.38 (2H, d), 7.49 (2H, m), 7.55 (2H, m), 8.39 (1H, br s, NH), 8.52 (1H, d). δ_C (90.57 MHz, $CDCl_3$) 23.57 CH_2, 30.92 CH_2, 31.11 CH_2, 54.91 CH_2, 58.66 CH_2, 68.30 CH, 72.25 CH, 110.35 C_q, 111.17 CH, 120.11 CH, 120.44 CH, 120.67 CH, 122.50 CH, 123.76 CH, 124.81 CH, 126.08 C_q, 127.19 CH, 128.16 CH, 128.55 2 × CH, 128.67 CH, 128.72 C_q, 128.81 CH, 129.27 CH, 129.69 CH, 131.76 C_q, 131.90 2 × CH, 132.59 CH, 133.76 CH, 134.83 C_q, 136.57 C_q, 143.23 C_q, 170.96 C_q, 179.22 C_q, 181.88 C_q.

3.1.2. (SS)-Diastereomer of complex **2b**

δ_H (360.13 MHz, $CDCl_3$; Me_4Si) 1.42 (1H, m), 1.79 (2H, m), 1.89 (1H, m), 2.11 (1H, m), 2.80 (1H, m), 3.07 (1H, dd, A part of AMX system), 3.21 (1H, dd, M part of AMX system), 3.36 (1H, dd, X part of AMX system), 3.40 (1H, d, A part of AB system of CH_2Ar, $^2J_{AB}$ 12.6), 4.21 (1H, d, B part of AB system of CH_2Ar, $^2J_{AB}$ 12.6), 4.35 (1H, t), 6.74 (2H, m), 6.92 (2H, m), 7.01 (1H, t), 7.19 (3H, m), 7.36 (6H, m), 7.56 (2H, m), 8.01 (2H, d), 8.30 (1H, d), 8.93 (1H, br s, NH). δ_C (90.57 MHz, $CDCl_3$) 22.58 CH_2, 30.22 CH_2, 30.52 CH_2, 56.91 CH_2, 63.12 CH_2, 70.27 CH, 71.55 CH, 109.41 C_q, 111.25 CH, 119.50 CH, 119.78 CH, 120.48 CH, 122.10 CH, 123.35 CH, 124.42 CH, 126.12 C_q, 127.17 CH, 127.90 CH, 128.26 Cq, 128.63 2 × CH, 128.65 CH, 128.70 CH, 128.95 CH, 129.58 CH, 131.42 2 × CH, 132.20 CH, 133.16 C_q, 133.45 CH, 134.03 C_q, 136.50 C_q, 142.68 C_q, 170.73 C_q,

[1] As chloroform is known to be a human carcinogen, for preparative applications a gradient elution using $CH_2Cl_2 \rightarrow CH_2Cl_2$: Me_2CO = 7:1 or toluene → toluene: Me_2CO = 2:1 is strongly recommended.

Table 3
Crystal data and structure refinement for *SS*-**2b**

Empirical formula	$C_{45}H_{41}N_4NiO_3$
Formula weight	744.53
Temperature (K)	173(2)
Wavelength (Å)	0.71073
Crystal system	monoclinic
Space group	$P2_1$
Unit cell dimensions	
a (Å)	15.5711(5)
b (Å)	9.6236(3)
c (Å)	25.6788(9)
α (°)	90
β (°)	106.729(1)
γ (°)	90
V (Å^3)	3685.1(2)
Z	4
D_{calc} (Mg/m^3)	1.342
Absorption coefficient (mm^{-1})	0.574
F(000)	1564
Crystal size (mm^3)	0.91 × 0.62 × 0.36
Theta range for data collection (°)	2.27–30.56
Index ranges	$-22 \leqslant h \leqslant 22$
	$-13 \leqslant k \leqslant 13$
	$-36 \leqslant l \leqslant 36$
Reflections collected	62093
Independent reflections	22451
	[R(int) = 0.0445]
Completeness to theta = 30.56°	99.7 %
Absorption correction	multi-scan
Maximum and minimum transmission	0.8200 and 0.6231
Refinement method	full-matrix least-squares on F^2
Data/restraints/parameters	22451/685/1030
Goodness-of-fit on F^2	1.055
Final R indices [I > 2sigma(I)]	R_1 = 0.0570
	wR_2 = 0.1428
R indices (all data)	R_1 = 0.0718
	wR_2 = 0.1519
Absolute structure parameter	0.019(9)
Largest difference in peak and hole (e Å^{-3})	1.392 and −0.445

Table 4
Crystal data and structure refinement for *SS*-**3**

Empirical formula	$C_{43}H_{42}N_4NiO_4$
Formula weight	737.52
Temperature	173(2) K
Wavelength	0.71073 Å
Space group	$P2_12_12_1$
Unit cell dimensions	
a (Å)	13.9338(2)
b (Å)	14.6081(2)
c (Å)	36.1605(5)
α (°)	90
β (°)	90
γ (°)	90
V (Å^3)	7360.34(18)
Z	8
D_{calc} (Mg/m^3)	1.331
Absorption coefficient (mm^{-1})	0.576
F(000)	3104
Crystal size (mm^3)	0.44 × 0.26 × 0.19
Theta range for data collection	2.10–25.00°
Index ranges	$-16 \leqslant h \leqslant 16$
	$-17 \leqslant k \leqslant 17$
	$-43 \leqslant l \leqslant 43$
Reflections collected	77400
Independent reflections	12942
	[R(int) = 0.0583]
Completeness to theta = 25.00°	99.8%
Absorption correction	multi-scan
Maximum and minimum transmission	0.8984 and 0.7857
Refinement method	Full-matrix least-squares on F^2
Data/restraints/parameters	12942/6/972
Goodness-of-fit on F^2	1.026
Final R indices [I > 2sigma(I)]	R_1 = 0.0518
	wR_2 = 0.1268
R indices (all data)	R_1 = 0.0593
	wR_2 = 0.1320
Absolute structure parameter	0.025(13)
Largest difference peak and hole (e Å^{-3})	1.141 and −0.378

179.47 C_q, 180.08 C_q. Positive-ion mass spectra: m/z 665 $[M+K]^+$, m/z 649 $[M+Na]^+$, m/z 627 ($[M+H]^+$, 100%), m/z 498 $[M+H-129]^+$. MS/MS of m/z 627: m/z 498 $[M+H-129]^+$. For the single crystal structure, see Fig. 2.

3.1.3. (SS)-Diastereomer of complex **3**

Positive-ion mass spectra: m/z 679 $[M+K]^+$, m/z 663 ($[M+Na]^+$, 100%), m/z 641 $[M+H]^+$. MS/MS of m/z 641: m/z 597 $[M+H-CO2]^+$, m/z 496 $[M+H-145]^+$. For the single crystal structure, see Fig. 3.

3.1.4. (SR)-Diastereomer of complex **1**

δ_H (360.13 MHz, $CDCl_3$; Me_4Si) 1.34 (9H, s), 1.80 (1H, m), 1.99 (1H, m), 2.38 (1H, m), 2.49 (1H, m), 2.60 (1H, m), 2.89 (1H, dd, A part of AMX system), 3.13 (2H, m, M part of AMX system and one of proline protons), 3.32 (1H, dd, X part of AMX system), 3.45 (1H, d, A part of AB system of CH_2Ar, $^2J_{AB}$ 12.7), 4.22 (1H, t), 4.28 (1H, d, B part of AB system of CH_2Ar, d, 1H, $^2J_{AB}$ 12.7), 6.65 (2H, m), 6.70 (1H, m), 6.97 (2H, m), 7.03 (2H, m), 7.16 (2H, m), 7.26 (1H, m), 7.31 (2H, t), 7.38 (1H, m), 7.51 (2H, m), 8.03 (2H, d), 8.23 (1H, d). δ_D (90.57 MHz, $CDCl_3$) 23.23 CH_2, 28.84 3 × CH_3, 30.80 CH_2, 39.54 CH_2, 57.32 CH_2, 63.22 CH_2, 70.39 CH, 71.66 CH, 78.28 C_q, 120.55 CH, 123.34 CH, 123.93 2 × CH, 126.12 C_q, 127.16 CH, 127.84 CH, 128.74 2 × CH, 128.76 CH, 128.80 CH, 128.95 CH, 129.64 CH, 130.10 C_q, 130.95 2 × CH, 131.49 2 × CH, 132.28 CH, 133.25 C_q, 133.49 CH, 134.09 C_q, 142.77 C_q, 155.21 C_q, 171.00 C_q, 178.62 C_q, 180.44 C_q.

3.1.5. (SS)-Diastereomer of complex **1**

δ_H (360.13 MHz, $CDCl_3$; Me_4Si) 1.28 (1H, m), 1.33 (9H, s), 1.53 (1H, m), 1.94 (1H, m), 2.14 (1H, m), 2.68 (1H, m), 2.85 (1H, dd, A part of AMX system), 2.98 (1H, dd, M part of AMX system), 3.48 (1H, d, A part of AB system of CH_2Ar $^2J_{AB}$ 13.8), 3.54 (1H, dd, X part of AMX system), 3.74 (1H, d, B part of AB system of CH_2Ar $^2J_{AB}$ 13.8Hz), 4.05 (1H, m), 4.20 (1H, t), 6.77 (2H, m), 6.96 (1H, d), 7.07 (2H, m), 7.17 (2H, m), 7.30 (1H, m), 7.38 (3H, m), 7.51 (6H, m), 8.43 (1H, d). δ_C (90.57 MHz, $CDCl_3$) 23.60 CH_2, 28.81 3 × CH_3, 31.19 CH_2, 39.41 CH_2, 56.50 CH_2, 60.59 CH_2, 69.14 CH, 71.72 CH, 78.44 C_q, 120.81 CH, 123.80 CH, 124.12 2 × CH, 126.36 C_q, 127.19 CH, 127.89 CH, 128.68 2 × CH, 128.78 CH, 128.81 CH, 129.23 CH, 129.79 CH, 130.39 C_q, 131.54 2 × CH, 132.08 2 × CH, 132.51 C_q, 132.58 CH, 133.73 CH, 134.16 C_q, 143.08 C_q, 155.29 C_q, 171.01 C_q, 178.42 C_q, 181.74 C_q. Positive-ion mass spectra: m/z 698 $[M+K]^+$, m/z 682 $[M+Na]^+$, m/z 660 ($[M+H]^+$, 100%). MS/MS of m/z 660: m/z 604 $[M+H-butene]^+$, m/z 498 $[M+H-butene-106]^+$.

(*SS*)-diastereomer of complex **4** was prepared according to the published procedure [15].

3.1.6. α-(^{13}C)Methylation of SS-4

Under an atmosphere of Ar at 20 °C to a solution of *SS*-**4** (62 mg, 0.1 mmol) in DMI (3 ml), excess of KOH and $^{13}CH_3I$ (63 μl, 1 mmol) was added and the reaction mixture was stirred for 30 min. The reaction mixture was poured into 10% aqueous citric acid (50 ml), stirred and the resulting red oil was filtered off. The filter was dried and extracted with chloroform. The extract was evaporated in vacuo. The diastereomeric excess was calculated based on the ratio of the integral intensities of the $^{13}CH_3$-signals in the ^{13}C NMR spectra of the mixtures of the diastereomers. *SS*-**5** and *SR*-**5** were separated by preparative TLC using silica gel (Merck 60H) eluted with CH_2Cl_2. Yield of *SS*-**5** and *SR*-**5** varies (40–70%) depending on the dryness of KOH used for the synthesis.

*3.1.7. (SS)-Diastereomer of complex **5***

The first fraction, red solidified oil, *SS*-**5**. The obtained complex was then purified by chromatography on Sephadex LH-20 with toluene: MeOH = 2:1. δ_H (500.13 MHz, $CDCl_3$; Me_4Si) 8.10 (1H, d), 7.99 (2H, m), 7.47 (1H, m), 7.37 (1H, m), 7.30 (5H, m) 7.25 (1H, s), 7.20 (1H, m), 7.10 (2H, m), 6.98 (3H, m), 6.59 (2H, s), 4.29 (1H, d, A part of AB system of CH_2Ar, $^2J_{AB}$ 12.6 Hz) and 3.54 (1H, d, B part of AB system of CH_2Ar, $^2J_{AB}$ 12.6 Hz), 3.81 (3H, s), 3.27 (1H, m), 3.10 (2H, m), 2.34 (1H, m), 2.24 (2H, m), 2.10 (1H, m), 1.91 (1H, m), 1.70 (1H, m), 1.13 (3H, $^{13}CH_3$, d, ^1J(H, C) = 130 Hz). δ_C (125.77 MHz, $CDCl_3$) 29.32 ($^{13}CH_3$). Calculated mass for $C_{35}{}^{13}CH_{35}N_3O_4Ni$ $[M]^+$ = 632.2015. High resolution EI-MS found $[M]^+$ = 632.2015.

*3.1.8. (SR)-Diastereomer of complex **5***

The second fraction, red crystals, *SR*-**5**. The obtained complex was then purified by chromatography on Sephadex LH-20 with toluene: MeOH = 2:1. Mp 274–276 °C (from acetone). δ_H (500.13 MHz, $CDCl_3$; Me_4Si) 7.86 (1H, d), 7.75 (2H, m), 7.51 (1H, m), 7.41 (2H, m), 7.33 (2H, m), 7.25–7.01 (6H, m), 6.94 (2H, m), 6.70 (1H, m), 6.62 (1H, t), 4.13 (1H, d, A part of AB system of CH_2Ph, $^2J_{AB}$ 14.3 Hz) and 3.39 (1H, d, B part of AB system of CH_2Ph, $^2J_{AB}$ 14.3 Hz), 3.72 (3H, s), 3.32 (1H, m), 3.06 (1H, m), 2.99 (1H, d, A part of AB system of CH_2Ar, $^2J_{AB}$ 14.7 Hz) and 2.86 (1H, d, B part of AB system of CH_2Ar, $^2J_{AB}$ 14.7 Hz), 2.32 (1H, m), 2.13 (2H, m), 1.91 (1H, m), 1.42 (3H, $^{13}CH_3$, d, ^1J(H, C) = 130 Hz).). δ_C (125.77 MHz, $CDCl_3$) 28.58 ($^{13}CH_3$). Calculated mass for $C_{35}{}^{13}CH_{35}N_3O_4Ni$ $[M]^+$ = 632.2015. High resolution EI-MS found $[M]^+$ = 632.2018.

NMR data are consistent with published data for similar complexes derived from α-methylphenylalanine or α-methyltyrosine-(OBn) [8a]. Half-minute intervals between pulses were applied for the recording of integral intensities of signals in ^{13}C NMR spectra.

4. Conclusions

A preparative procedure for the synthesis of a practically important chiral synthon of side-chain protected tyrosine was developed and optimised for the maximum reduction of nickel salts waste. While preparing a similar side-chain protected tryptophan synthon, unexpected low stability of Boc-protective group of tryptophan aromatic nitrogen was found during purification on silica gel. Stereochemistry of diastereomers of α-methylated complexes was disclosed using model compounds.

Acknowledgements

The authors thank Mr. Joe Bird and Dr. Katrin Probst for language corrections and acknowledge the support of Project Grants MSM0021627501 and MSM0021627502 sponsored by the Ministry of Education, Youth and Sports of the Czech Republic.

Appendix A. Supplementary data

Supplementary data associated with this article can be found, in the online version, at doi:10.1016/j.poly.2008.08.009.

References

[1] H.C. Dunathan, Adv. Enyzmol. Relat. Areas Mol. Biol. (1971) 79.
[2] (a) Y.N. Belokon, Izv. Acad. Nauk, Ser. Khim. (1992) 1106;
(b) Y.N. Belokon, Bull. Russ. Acad. Sci., Div. Chem. Sci. 41 (1992) 868 (Engl. Trans.) and references cited therein;
(c) Y.N. Belokon, Pure Appl. Chem. 64 (1992) 191;
(d) V.A. Soloshonok, D.V. Avilov, V.P. Kukhar, V.I. Tararov, T.F. Saveleva, T.D. Churkina, N.S. Ikonnikov, K.A. Kochetkov, S.A. Orlova, A.P. Pisarevsky, Y.T. Struchkov, N.I. Raevsky, Y.N. Belokon, Tetrahedron: Asymmetry 6 (1995) 1741;
(e) B.B. De, N.R. Thomas, Tetrahedron: Asymmetry 8 (1997) 2687;
(f) Y.N. Belokon, V.I. Tararov, V.I. Maleev, T.F. Saveleva, M.G. Ryzhov, Tetrahedron: Asymmetry 9 (1998) 4249;
(g) S. Collet, P. Bauchat, D. Danion-Bougot, R. Danion, Tetrahedron: Asymmetry 9 (1998) 2121;
(h) V.A. Soloshonok, C.Z. Cai, V.J. Hruby, Tetrahedron 55 (1999) 12045;
(i) X. Tang, V.A. Soloshonok, V.J. Hruby, Tetrahedron: Asymmetry 11 (2000) 2917;
(j) C. Cai, V.A. Soloshonok, V.J. Hruby, J. Org. Chem. 66 (2001) 1339;
(k) Y.N. Belokon, K.A. Kochetkov, N.S. Ikonnikov, T.V. Strelkova, S.R. Harutyunyan, A.S. Saghiyan, Tetrahedron: Asymmetry 12 (2001) 481;
(l) A. Debache, S. Collet, P. Bauchat, D. Danion, L. Euzenat, A. Hercouet, B. Carboni, Tetrahedron: Asymmetry 12 (2001) 761;
(m) A. Popkov, A. Gee, M. Nádvorník, A. Lyčka, Transition Met. Chem. 27 (2002) 884;
(n) O.V. Larionov, T.F. Saveleva, K.A. Kochetkov, N.S. Ikonnokov, S.I. Kozhushkov, D.S. Yufit, J.A.K. Howard, V.N. Khrustalev, Y.N. Belokon, A. de Meijere, Eur. J. Org. Chem. (2003) 869;
(o) Y.N. Belokon, K.A. Kochetkov, D.A. Borkin, Mendeleev Commun. (2003) 132;
(p) H. Ueki, T.K. Ellis, C.H. Martin, T.U. Boettiger, S.B. Bolene, V.A. Soloshonok, J. Org. Chem. 68 (2003) 7104;
(q) A.S. Saghiyan, A.V. Geolchanyan, S.G. Petrosyan, T.V. Ghochikyan, V.S. Haroutunyan, A.A. Avetisyan, Y.N. Belokon, K. Fischer, Tetrahedron: Asymmetry 15 (2004) 705;
(r) X.Y. Gu, J.A. Ndungu, W. Qiu, J.F. Ying, M.D. Carducci, H. Wooden, V.J. Hruby, Tetrahedron 60 (2004) 8233;
(s) S. Vadon-Legoff, S. Dijols, D. Mansky, J.-L. Boucher, Org. Process Res. Develop. 9 (2005) 677;
(t) V.A. Soloshonok, C. Cai, T. Yamada, H. Ueki, Y. Ohfune, V.J. Hruby, J. Am. Chem. Soc. 127 (2005) 15296;
(u) J.C. Pessoa, I. Correia, A. Galvão, A. Gameiro, V. Felix, E. Fiuza, J. Chem. Soc., Dalton Trans. (2005) 2312;
(v) A. Popkov, I. Císařová, J. Sopková, J. Jirman, A. Lyčka, K.A. Kochetkov, Collect. Czech. Chem. Commun. 70 (2005) 1397;
(w) A.S. Saghiyan, H.H. Hambardzumyan, L.L. Manasyan, A.A. Petrosyan, V.I. Maleev, A.S. Peregudov, Synth. Commun. 35 (2005) 449;
(x) A.S. Saghiyan, S.A. Dadayan, S.G. Petrosyan, L.L. Manasyan, A.V. Geolchanyan, S.M. Djamgaryan, S.A. Andreasyan, V.I. Maleev, V.N. Khrustalev, Tetrahedron: Asymmetry 17 (2006) 455;
(y) T. Kitamoto, S. Marubayashi, T. Yamazaki, Tetrahedron 64 (2008) 1888;
(z) Application of the complexes for preparation of helically chiral precursors of nanostructures:V.A. Soloshonok, H. Ueki, J. Am. Chem. Soc. 129 (2007) 2426.
[3] Y.N. Belokon, DSc. Thesis, A. N. Nesmeyanov Institute of Organoelement Compounds, Acad. Sci. USSR, 1979.
[4] V.I. Tararov, R. Kadyrov, C. Fischer, A. Börner, Synlett (2004) 1961.
[5] M. Nádvorník, A. Popkov, Green Chem. 4 (2002) 78.
[6] R.N. Krasikova, O.F. Kuznetsova, O.S. Fedorova, V.I. Maleev, T.F. Saveleva, Y.N. Belokon, Bioorg. Med. Chem. 16 (2008) 4994.
[7] (a) A. Popkov, M. Nádvorník, P. Kružberská, A. Lyčka, M. Eisenhut, N.M. Gillings, J. Labelled Compd. Radiopharm. 46 (2003) S227;
(b) A. Popkov, M. Nádvorník, P. Kružberská, A. Lyčka, S. Lehel, N.M. Gillings, J. Labelled Compd. Radiopharm. 50 (2007) 370;
(c) Y. Sakai, C. Dobson, M. Diksic, M. Aubé, E. Hamel, Neurology 70 (2008) 431;
(d) M.S. Judenhofer, H.F. Wehrl, D.F. Newport, C. Catana, S.B. Siegel, M. Becker, A. Thielscher, M. Kneilling, M.P. Lichy, M. Eichner, K. Klingel, G. Reischl, S. Widmaier, M. Röcken, R.E. Nutt, H.-J. Machulla, K. Uludag, S.R. Cherry, C.D. Claussen, B.J. Pichler, Nature Med. 14 (2008) 459;
(e) For a review of tomographic methods see:B.J. Pichler, J. Nucl. Med. 49 (2008) S5.
[8] (a) Y.N. Belokon, V.I. Bakhmutov, N.I. Chernoglazova, K.A. Kochetkov, S.V. Vitt, N.S. Garbalinskaya, V.M. Belikov, J. Chem. Soc., Perkin Trans. 1 (1988) 305;
(b) For reviews of methods of asymmetric preparation of α-methyl amino acids, see:C. Cativiela, M.D. Días-de-Villegas, Tetrahedron: Asymmetry 9 (1998) 3517;
(c) C. Cativiela, M.D. Días-de-Villegas, Tetrahedron: Asymmetry 11 (2000) 645;
(d) H. Vogt, S. Bräse, Org. Biomol. Chem. 5 (2007) 406;
(e) C. Najera, J.M. Sansano, Chem. Rev. 107 (2007) 4584;
(f) C. Cativiela, D. Días-de-Villegas, Tetrahedron: Asymmetry 18 (2007) 569.
[9] H. Franzen, L. Grehn, U.J. Ragnarsson, J. Chem. Soc., Chem. Commun. (1984) 1699.
[10] R. Jirásko, M. Holčapek, L. Kolářová, M. Nádvorník, A. Popkov, J. Mass Spectrom. 43 (2008) 1274.
[11] Bruker AXS Inc., SMART and SAINT, Area Detector Control and Integration Software, Madison, WI, USA, 2003.
[12] G.M. Sheldrick, SADABS, Program for Empirical Absorption Correction for Area Detectors, Version 2.10, University of Göttingen, Germany, 2003.
[13] Bruker, SHELXTL, Solution and Refinement Package, Version 6.12, Bruker AXS Inc., Madison, Wisconsin, USA, 2001.
[14] K. Brandenburg, DIAMOND, Crystal and Molecular Structure Vizualization, Version 3.1d, Crystal Impact GbR, Bonn, Germany, 2006.
[15] P. Řehulka, A. Popkov, M. Nádvorník, J. Planeta, K. Mazanec, J. Chmelík, J. Mass Spectrom. 41 (2006) 448.

of ligands, as well as other factors, is still important and necessary to be studied.

In order to prepare functional supramolecular complexes with intriguing structures and potential applications especially in catalysis and to systematically investigate the substituent effect of an organic ligand on the structure of zinc-carboxylate containing coordination polymers, in this work, we have reacted Zn-benzoate with pyrazine (pyz) and its derivatives, 2,3-dimethylpyrazine (2,3-Me_2pyz), 2,5-dimethylpyrazine (2,5-Me_2pyz), 2,6-dimethylpyrazine (2,6-Me_2pyz), and quinoxaline, and report herein five new Zn(II)-benzoate coordination architectures, **1** ($Zn_2(O_2CPh)_4$(quinoxaline)$_2$), **2** ($Zn_3(O_2CPh)_6$(2,3-Me_2pyz)$_2$), **3** ($Zn_5(\mu_3\text{-}OH)_2(O_2CPh)_8$(2,6-$Me_2$pyz)$_2$), **4** (1-D, $[Zn_2(O_2CPh)_4(2,5\text{-}Me_2pyz)]_n$), **5** (2-D, $[Zn(O_2CPh)(\mu_2\text{-}O_2CPh)(\mu_2\text{-}pyz)_{0.5}]_n$). Assembly of zinc(II)-benzoate with different types of pyrazine shows different structures, from dinuclear, trinuclear and pentanuclear complexes to one-dimensional and two-dimensional coordination polymers. Moreover, compounds **1**–**5** catalyzed efficiently the transesterification of a variety of esters.

2. Experimental

2.1. Materials

Acetone, methanol, ethanol, propanol, 2-propanol, *para*-substituted phenyl acetate, *para*-substituted phenyl benzoate, methylacetate, methylbenzoate, quinoxaline, 2,3-dimethylpyrazine, 2,6-dimethylpyrazine, 2,5-dimethylpyrazine, pyrazine, ammonium benzoate, and zinc nitrate were purchased from Aldrich and were used as received. 4-Fluorophenyl acetate and 4-nitrophenyl benzoate were obtained from Lancaster.

2.2. Instrumentation

Elemental analysis for carbon, nitrogen, and hydrogen was carried out by using an EA1108 (Carlo Erba Instrument, Italy) in the Organic Chemistry Research Center of Sogang University, Korea. IR spectra were measured on a BIO RAD FTS 135 spectrometer as KBr pellets. Product analysis for the transesterification reaction was performed on either a Hewlett–Packard 5890 II Plus gas chromatograph interfaced with Hewlett–Packard Model 5989B mass spectrometer or a Donam Systems 6200 gas chromatograph equipped with a FID detector using 30-m capillary column (Hewlett–Packard, HP-1, HP-5, and Ultra 2).

2.3. Synthesis of dinuclear zinc-benzoate with quinoxaline ligand ($Zn_2(O_2CPh)_4$(quinoxaline)$_2$) (**1**)

Thirty-eight milligrams (0.125 mmol) of $Zn(NO_3)_2 \cdot 6H_2O$ and 36.0 mg (0.25 mmol) of $C_6H_5COONH_4$ were dissolved in 4 mL water and carefully layered by 4 mL methanol solution of quinoxaline ligand (29.0 μL, 0.25 mmol). The yield was 55.0 mg (50.5%) for compound **1**. Suitable crystals of compound **1** for X-ray analysis were obtained in a month. *Anal.* Calc. for $C_{44}H_{32}N_4O_8Zn_2$ (875.48), **1**: C, 60.36; H, 3.69; N, 6.40. Found: C, 60.01; H, 3.62; N, 6.70%. IR (KBr): $\nu(cm^{-1})$ = 3434(br), 3068(w), 2369(m), 1641(s), 1574(w), 1505(w), 1402(s), 1068(w), 1039(w), 967(w), 866(w), 840(w), 764(m), 717(s), 680(m), 464(m).

2.4. Synthesis of trinuclear zinc-benzoate with 2,3-dimethylpyrazine ligand ($Zn_3(O_2CPh)_6$(2,3-Me_2pyz)$_2$) (**2**)

Thirty-eight milligrams (0.125 mmol) of $Zn(NO_3)_2 \cdot 6H_2O$ and 36.0 mg (0.25 mmol) of $C_6H_5COONH_4$ were dissolved in 4 mL water and carefully layered by 4 mL acetone solution of 2,3-dimethylpyrazine ligand (27.0 μL, 0.25 mmol). The yield was 60.0 mg (42.2%) for compound **2**. Slow evaporation of the diffused mixture provided suitable crystals of **2** for X-ray crystallography in a month. *Anal.* Calc. for $C_{54}H_{46}N_4O_{12}Zn_3$ (1139.06), **2**: C, 56.94; H, 4.08; N, 4.92. Found: C, 56.54; H, 4.10; N, 4.73%. IR (KBr): $\nu(cm^{-1})$ = 3061(s), 3030(w), 1973(w), 1919(w), 1829(w), 1638(br s), 1572(br s), 1421(br s), 1258(w), 1178(s), 1071(s), 1024(s), 978(m), 942(m), 884(w), 862(s), 841(s), 819(m), 723(s), 680(s), 596(w), 466(s), 438(m).

2.5. Synthesis of pentanuclear zinc-benzoate with 2,6-dimethylpyrazine ligand ($Zn_5(\mu_3\text{-}OH)_2(O_2CPh)_8$(2,6-$Me_2$pyz)$_2$) (**3**)

Thirty-eight milligrams (0.125 mmol) of $Zn(NO_3)_2 \cdot 6H_2O$ and 36.0 mg (0.25 mmol) of $C_6H_5COONH_4$ were dissolved in 4 mL methanol and carefully layered by 4 mL acetone solution of 2,6-dimethylpyrazine ligand (28.0 mg, 0.25 mmol). The yield was 32.0 mg (16.6%) for compound **3**. Slow evaporation of the diffused mixture provided suitable crystals of **3** for X-ray crystallography in a month. *Anal.* Calc. for $C_{68}H_{58}N_4O_{18}Zn_5$ (1546.03), **3**: C, 52.82; H, 3.79; N, 3.62. Found: C, 52.55; H, 4.00; N, 3.88%. IR (KBr): $\nu(cm^{-1})$ = 3440(br), 3066(m), 1603(s), 1565(s), 1416(br s), 1309(w), 1259(w), 1174(m), 1070(m), 1025(m), 942(w), 842(m), 719(s), 685(s), 576(w), 472(s).

2.6. Synthesis of one-dimensional polymeric compound containing zinc-benzoate with 2,5-dimethylpyrazine ligand (1-D, $[Zn_2(O_2CPh)_4(2,5\text{-}Me_2pyz)]_n$) (**4**)

Thirty-eight milligrams (0.125 mmol) of $Zn(NO_3)_2 \cdot 6H_2O$ and 36.0 mg (0.25 mmol) of $C_6H_5COONH_4$ were dissolved in 4 mL methanol and carefully layered by 4 mL acetone solution of 2,5-dimethylpyrazine ligand (27.0 μL, 0.25 mmol). The yield was 75.0 mg (72.8%) for compound **4**. Slow evaporation of the diffused mixture provided suitable crystals of **4** for X-ray crystallography in a month. *Anal.* Calc. for $C_{40}H_{36}N_4O_8Zn_2$ (831.47), **4**: C, 57.78; H, 4.37; N, 6.74. Found: C, 58.02; H, 4.11; N, 6.35%. IR (KBr): $\nu(cm^{-1})$ = 3741(w), 3431(br w), 3064(w), 2360(w), 1637(s), 1573(w), 1499(w), 1406(s), 1171(w), 1082(w), 1049(w), 1027(w), 840(w), 727(s), 715(s), 680(m), 464(w), 429(w).

2.7. Synthesis of two-dimensional polymeric compound containing zinc-benzoate with simple pyrazine ligand (2-D, $[Zn(O_2CPh)(\mu_2\text{-}O_2CPh)(\mu_2\text{-}pyz)_{0.5}]_n$) (**5**)

Thirty-eight milligrams (0.125 mmol) of $Zn(NO_3)_2 \cdot 6H_2O$ and 36.0 mg (0.25 mmol) of $C_6H_5COONH_4$ were dissolved in 4 mL water and carefully layered by 4 mL methanol solution of pyrazine ligand (20.0 mg, 0.25 mmol). The yield was 43.0 mg (24.7%) for compound **5**. Slow evaporation of the diffused mixture provided suitable crystals of **5** for X-ray crystallography in a month. *Anal.* Calc. for $C_{64}H_{48}N_4O_{16}Zn_4$ (1390.54), **5**: C, 55.28; H, 3.49; N, 4.03. Found: C, 54.96; H, 3.40; N, 3.98%. IR (KBr): $\nu(cm^{-1})$ = 3127(w), 3070(w), 1598(s), 1555(s), 1428(s), 1398(m), 1157(w), 1121(m), 1067(s), 1024(w), 859(w), 828(m), 715(s), 688(s), 558(w), 461(s), 424(m).

2.8. Catalytic activity of compounds **1**–**5**

Catalytic homogeneous reaction conditions: Ester (0.05 mmol) was dissolved in an appropriate solvent (1 mL), methanol or propanol, and the catalyst (1.0 mg, 1.14×10^{-3} mmol for **1**, 1.0 mg, 0.88×10^{-3} mmol for **2**, 1.0 mg, 0.65×10^{-3} mmol for **3**, 1.0 mg, 1.20×10^{-3} mmol for **4**, and 1.0 mg, 0.72×10^{-3} mmol for **5**, respectively) was added and shaken in an incubator at 50 °C (450 rpm). Reaction conversion was monitored by GC/Mass analy-

sis of 20 μL aliquots withdrawn periodically from the reaction mixture. All reactions were run at least three times and the average conversion yields are presented. We had the same results under N_2 instead of air, suggesting that air does not effect the transesterification reaction.

2.9. X-ray crystallography

The X-ray diffraction data for all five compounds were collected on a Bruker SMART APX diffractometer equipped with a monochromator in the Mo Kα (λ = 0.71073 Å) incident beam. Each crystal was mounted on a glass fiber. The CCD data were integrated and scaled using the Bruker-SAINT software package, and the structure was solved and refined using SHEXTL V6.12 [24]. All hydrogen atoms were placed in the calculated positions. The crystallographic data for compounds **1**–**5** are listed in Table 1.

3. Results and discussion

3.1. Synthesis and spectral characterization

To investigate the effect of structure and substituent of organic ligands on the structure of their metal complexes, four pyrazine derivative ligands, quinoxaline, 2,3-dimethylpyrazine, 2,6-dimethylpyrazine, 2,5-dimethylpyrazine and simple pyrazine, were used to react with Zn(II)-benzoate. The coordination complexes **1**–**5** were prepared cleanly as single phase crystalline products and shows dinuclear **1**, trinuclear **2**, pentanuclear complexes **3**, one-**4** and two-dimensional **5** polymeric compounds, respectively. All five compounds are shown in Scheme 1. The infrared spectra of **1**–**5** were fully consistent with their formulations [25]. Sharp medium intensity bands in the range of ~1300 cm^{-1} to ~700 cm^{-1} were ascribed to stretching modes of the pyrazine ring moiety. Asymmetric and symmetric C=O stretching modes of the ligated benzoate moieties were evidenced by very strong, slightly broadened bands at ~1600 cm^{-1} and ~1400 cm^{-1}. The absence of any bands in the area of ~1710 cm^{-1} indicates full deprotonation of all carboxylate groups in **1**–**5**.

3.2. Dinuclear zinc-benzoate with quinoxaline ligand ($Zn_2(O_2CPh)_4(quinoxaline)_2$) (**1**)

Asymmetric unit contains half of whole molecule, and there is an inversion center in the middle of Zn–Zn bond. Symmetric operation ($-x+2$, $-y+1$, $-z+1$) produces a paddle-wheel type dinuclear zinc-benzoate complex **1** (Fig. 1). The paddle-wheel type dinuclear complex is constructed by four bridging benzoate groups and two terminal quinoxaline ligands. Thus each Zn atom is NO4 donor penta-coordinated to form square pyramidal geometry. The similar paddle-wheel type of structures from zinc-benzoate or zinc-acetate have been reported in literature [19,26]. Zn–O bond distances range from 2.0191(15) to 2.0537(17) Å, Zn–N bond distance is 2.0792(18) Å which is typical in Zn(II) complexes, and Zn–Zn distance is 2.9900(7) Å (Table 2).

3.3. Trinuclear zinc-benzoate with 2,3-dimethylpyrazine ligand ($Zn_3(O_2CPh)_6(2,3\text{-}Me_2pyz)_2$) (**2**)

Asymmetric unit contains half of whole molecule, and there is a crystallographic inversion center on the central Zn atom. Symmetric operation ($-x+2$, $-y+2$, $-z+1$) produces a trinuclear zinc-benzoate complex **2** constructed by six bridging benzoate ligands and two axial 2,3-dimethylpyrazine ligands (Fig. 2) which is similar to the previously described trinuclear zinc-benzoate with axial pyridine ligands [19b]. Out of three Zn centers the central Zn is all O-donor hexa-coordinated from six benzoate groups to form a distorted octahedral geometry. The other two Zn centers are symmetric to each other, and each has a terminal 2,3-dimethylpyrazine ligand and four oxygen atoms from benzoate ligands. Thus each Zn2 center has NO4 coordination environment with a distorted trigonal bipyramid geometry. The coordination modes of benzoate ligands show two kinds of bridging modes [15]: one mode is a typical bridging mode, and the other is the unusual coordination mode that chelates to one Zn2 atom and, at the same time, bridges the other Zn1 atom as shown in Fig. 2. This unusual coordination mode of carboxylate group provides a big distortion around Zn2. In the typical bridging carboxylate coordination mode, Zn1–$O_{bridging}$ distances are 2.0362(15) and 2.0894(16) Å, and Zn2–$O_{bridging}$

Table 1
Crystallogrphic data for compounds **1**, **2**, **3**, **4**, and **5**

	1	**2**	**3**	**4**	**5**
Empirical formula	$C_{44}H_{32}N_4O_8Zn_2$	$C_{54}H_{46}N_4O_{12}Zn_3$	$C_{68}H_{58}N_4O_{18}Zn_5$	$C_{40}H_{36}N_4O_8Zn_2$	$C_{64}H_{48}N_4O_{16}Zn_4$
Formula weight	875.48	1139.06	1546.03	831.47	1390.54
Temperature (K)	293(2)	170(2)	170(2)	170(2)	170(2)
Wavelength (Å)	0.71073	0.71073	0.71073	0.71073	0.71073
Space group	$P\bar{1}$	$P\bar{1}$	$P2/c$	$P\bar{1}$	$P2_1/c$
a (Å)	10.146(3)	10.7629(13)	11.644(12)	9.868(3)	14.197(3)
b (Å)	10.338(3)	11.3112(13)	11.639(13)	10.012(3)	6.2166(12)
c (Å)	10.444(3)	11.7684(14)	23.67(3)	11.865(3)	16.306(3)
α (°)	65.677(4)	61.846(2)	90.000	65.386(4)	90.000
β (°)	72.974(4)	78.843(2)	95.231(19)	89.490(5)	95.557(3)
γ (°)	81.781(4)	80.246(2)	90.000	63.081(4)	90.000
Volume ($Å^3$)	954.2(4)	1234.3(3)	3194(6)	926.6(4)	1432.4(5)
Z	1	1	2	1	1
D_{calc} (Mg/m^3)	1.524	1.532	1.607	1.490	1.612
Absorption coefficient (mm^{-1})	1.319	1.515	1.927	1.353	1.732
Crystal size (mm)	0.20 × 0.08 × 0.08	0.05 × 0.05 × 0.05	0.10 × 0.05 × 0.05	0.25 × 0.10 × 0.03	0.25 × 0.10 × 0.08
Reflections collected	5351	6947	17173	5202	7587
Independent reflections (R_{int})	3659 (0.0162)	4737 (0.0163)	6264 (0.0512)	3539 (0.0282)	2818 (0.0289)
Data/restraints/parameters	3659/0/262	4737/0/333	6264/0/435	3539/0/246	2818/0/199
Goodness-of-fit on F^2	1.099	1.037	1.056	0.946	1.059
Final R indices [$I > 2\sigma(I)$]	R_1 = 0.0315, wR_2 = 0.0827	R_1 = 0.0306, wR_2 = 0.0784	R_1 = 0.0391, wR_2 = 0.1007	R_1 = 0.0439, wR_2 = 0.0921	R_1 = 0.0327, wR_2 = 0.0815
R indices (all data)	R_1 = 0.0378, wR_2 = 0.0848	R_1 = 0.0392, wR_2 = 0.0811	R_1 = 0.0584, wR_2 = 0.1117	R_1 = 0.0631, wR_2 = 0.0966	R_1 = 0.0421, wR_2 = 0.0841
Largest difference in peak and hole (e $Å^{-3}$)	0.226 and −0.371	0.317 and −0.513	0.550 and −0.418	0.598 and −0.300	0.487 and −0.260

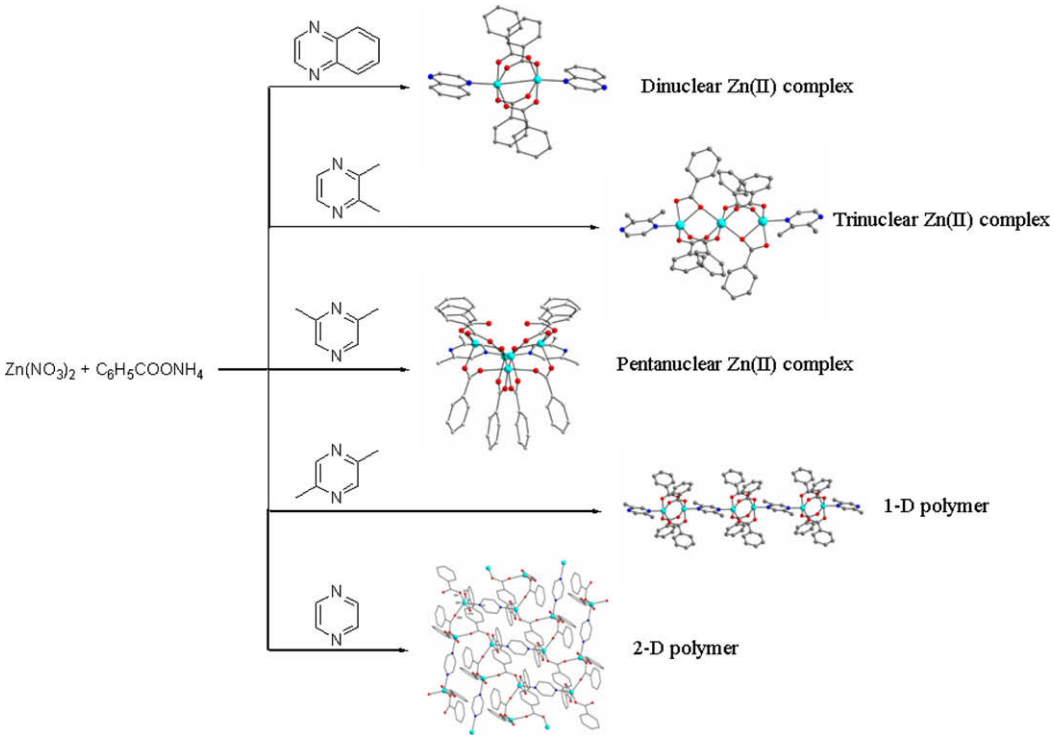

Scheme 1.

distances are 1.9532(16) and 1.9453(16) Å. In the unusual coordination mode, Zn1–$O_{bridging}$ distance is 2.1744(16) Å which is a little longer than typical one, and Zn2–$O_{chelating}$ distances are 2.1804(17) and 2.1798(18) Å. Zn–N bond distance is 2.075(2) Å which is typical in Zn complexes. The Zn–Zn distance is 3.362(4) Å which is much longer than that of dinuclear one (Table 2).

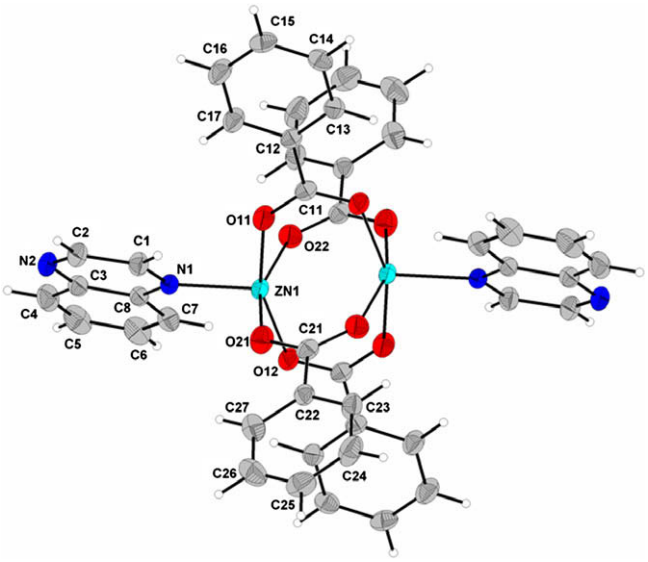

Fig. 1. Structure of dinuclear Zn complex **1**. Displacement ellipsoids are shown at the 30% probability level.

3.4. Pentanuclear zinc-benzoate with 2,6-dimethylpyrazine ligand ($Zn_5(\mu_3\text{-}OH)_2(O_2CPh)_8(2,6\text{-}Me_2pyz)_2$) (**3**)

Asymmetric unit contains half of whole molecule, and there is a C_2 axis through the middle Zn atom. Symmetric operation ($-x+1$, y, $-z+1/2$) produces a pentanuclear zinc-benzoate complex **3** constructed by six bridging benzoate ligands, two μ_3-hydoxyl ligands, two terminal 2,6-dimethylpyrazine ligands, and two terminal monodentate dangling benzoate ligands (Fig. 3). The central Zn1 ion is all O-donor hexa-coordinated from four benzoate ligands and two hydroxyl ligands to form a distorted octahedral geometry, and another two Zn2 ions are all O-donor tetra-coordinated from two bridging benzoate ligands, a dangling (monodentate)-benzoate ligand and a hydroxyl ligand to form a distorted tetrahedral geometry, and another two Zn3 ions are NO3-donor tetra-coordinated from two bridging benzoate ligands, a hydroxyl ligand and a 2,6-dimethylpyrazine ligand to form a distorted tetrahedral geometry. Importantly, this Zn-containing pentanuclear complex is unprecedented, to our best knowledge. The coordination modes of benzoate ligands are two types, bridging and monodentate (dangling) modes as shown in Fig. 3. A hydroxyl ligand bridges three Zn atoms. Zn–$O_{benzoate}$ bond distances range from 1.933(3) to

Table 2
Selected bond distances for compounds **1**, **2**, **3**, **4**, and **5**

	1	2	3	4	5
Zn–O (Å)	2.0191(15)–2.0537(17)	1.9454(16)–2.1804(17)	Zn–O(benzoate) 1.933(3)– 2.083(3) Zn–O(hydroxyl) 1.941(3)–2.111(3)	2.017(2)–2.063(2)	Zn–O(bridging benzoate) 1.9627(17), 1.9924(17) Zn–O(chelating benzoate) 2.0068(18), 2.3407(18)
Zn–N (Å)	2.0792(18)	2.075(2)	2.013(3)	2.083(2)	2.085(2)
Zn–Zn (Å)	2.9900(7)	3.362(4)	3.143(2)–3.397(4)	2.9525(10)	N/A

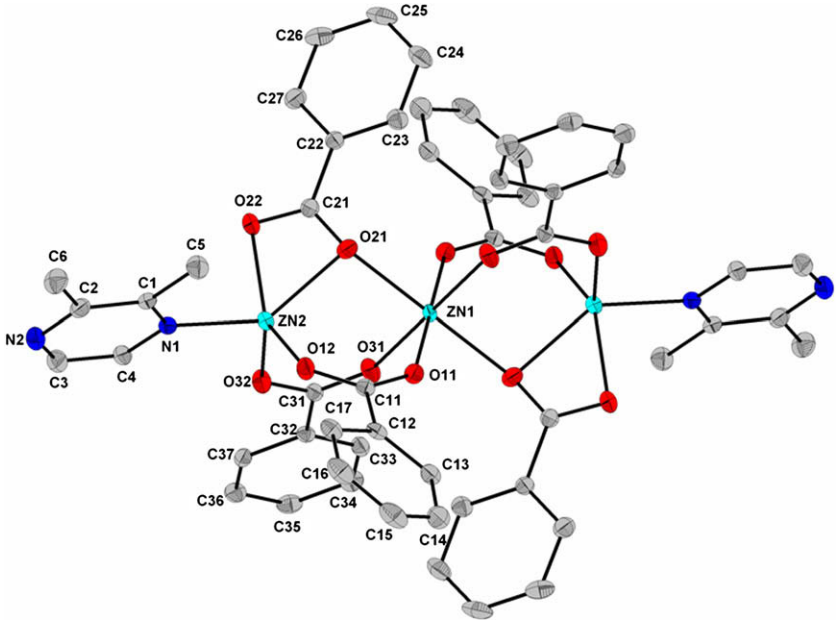

Fig. 2. Structure of trinuclear Zn complex **2**. Displacement ellipsoids are shown at the 30% probability level.

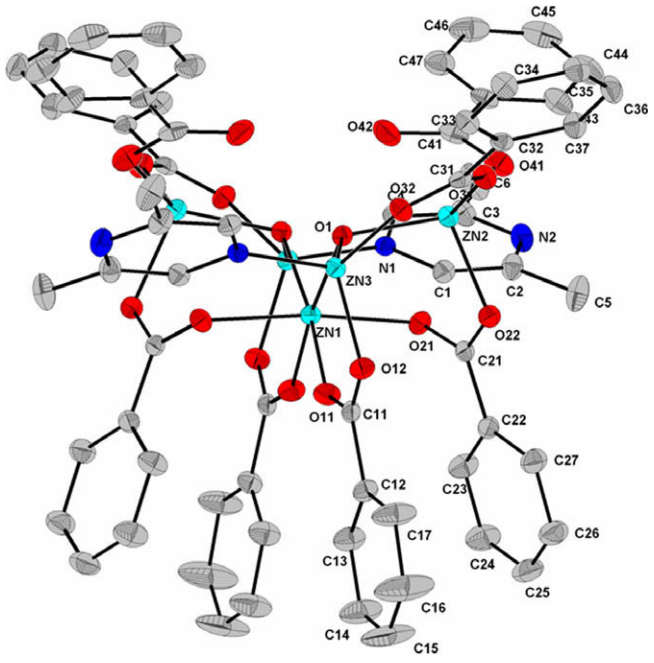

Fig. 3. Structure of pentanuclear Zn complex **3**. Displacement ellipsoids are shown at the 30% probability level. All hydrogen atoms were omitted for clarity.

2.083(3) Å, Zn–$O_{hydroxyl}$ bond distances range from 1.941(3) to 2.111(3) Å, and Zn–N bond distance is 2.013(3) Å which is typical in Zn complexes. The Zn1–Zn2, Zn1–Zn3, and Zn2–Zn3 distances are 3.295(21), 3.397(4), 3.143(2) Å, respectively (Table 2).

3.5. One-dimensional polymeric compound containing zinc-benzoate with 2,5-dimethylpyrazine ligand (1-D, $[Zn_2(O_2CPh)_4(2,5\text{-}Me_2pyz)]_n$) (**4**)

The crystal structure of **4** is shown in Fig. 4. The paddle-wheel type units are bridged by 2,5-dimethylpyrazine to form a one-dimensional polymeric compound. The paddle-wheel type units are similar to those of compound **1**. Zn–O bond distances range from 2.017(2) to 2.063(2) Å, which are almost close to those in **1**, and Zn–N bond distance is 2.083(2) Å which is typical in Zn(II) complexes. Zn–Zn distance is 2.9525(10) Å (Table 2), that is shorter than that of the discrete dinuclear complex **1**. The Zn′–Zn–N bond angle (175.25(1)°) shows a nearly linear chain structure. Interestingly, this compound shows an one-dimensional structure unlike **1**, **2**, and **3**. The coordination mode of benzoate shows only bridging type as shown in Fig. 4. In case of similar one-dimensional compound $[Zn_2(bpy)(OAc)_4]_n$, acetate bridged dinuclear Zn_2 unit is not a paddle-wheel type, and each Zn(II) ion has different coordination geometry: Zn1 has an octahedral geometry and Zn2 has a trigonal bipyramid geometry [27].

3.6. Two-dimensional polymeric compound containing zinc-benzoate with simple pyrazine ligand (2-D, $[Zn(O_2CPh)(\mu_2\text{-}O_2CPh)(\mu_2\text{-}pyz)_{0.5}]_n$) (**5**)

Asymmetric unit contains a Zn atom, two benzoate ligands, and half pyrazine, and symmetry operations $(-x+2, -y+3, -z+2)$, $(-x+2, y+1/2, -z+3/2)$, and $(-x+2, y-1/2, -z+3/2)$ produce a two-dimensional polymeric compound (Fig. 5). Mononuclear $Zn(O_2CPh)$ units are bridged by bridging benzoate and pyrazine ligands to form a two-dimensional sheet. Thus, the Zn atom has NO4-donor penta-coordinated environment. The coordination modes of benzoate ligands show two types, bridging and chelating modes as shown in Fig. 5. Zn–$O_{bridging}$ bond distances are 1.9627(17) and 1.9924(17) Å, and Zn–$O_{chelating}$ bond distances are 2.0068(18) and 2.3407(18) Å. Zn–N bond distance is 2.085(2) Å which is typical in Zn complexes (Table 2). Pyrazine does not have any substituents on its own ring, indicating no steric effect. Therefore, pyrazine may produce 2-D structure. However, in case of using acetate ligands instead of benzoate ligands, an unusual heptanuclear complex $Zn_7(\mu_4\text{-}O)_2(OAc)_{10}(pyz)_2$ has been made by reaction of $Zn(OAc)_2 \cdot 2H_2O$ with pyrazine (pyz) in refluxing ethanol [21]. The structure of the heptanuclear complex revealed a central Zn core in which two pseudo-tetrahedral Zn_4 units are joined at a common vertex, and two pyrazine molecules are bound as terminal ligands. Furthermore, $Cu_2(O_2CPh)_4$-pyz system showed a linear one-dimensional [28]. The structure of $Cu_2(O_2CPh)_4$-pyz showed the linear geometry with the chain skeleton bridged by pyrazine in axial direction of the paddle-wheel type Cu_2 core which is similar to our one-dimensional compound **4** containing

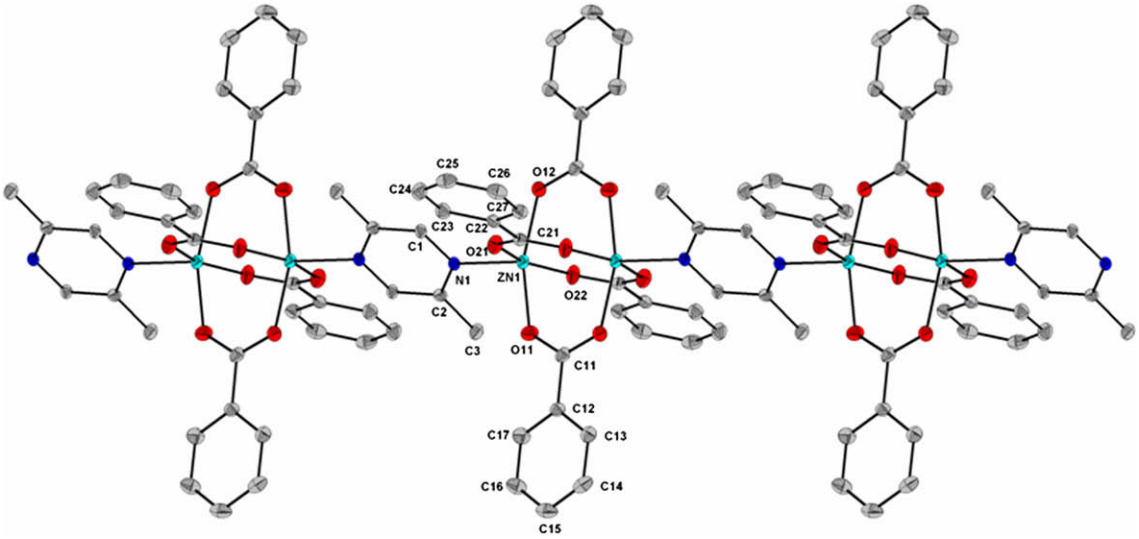

Fig. 4. Structure of one-dimensional Zn complex **4** containing paddle-type dinuclear Zn units. Displacement ellipsoids are shown at the 30% probability level. All hydrogen atoms were omitted for clarity.

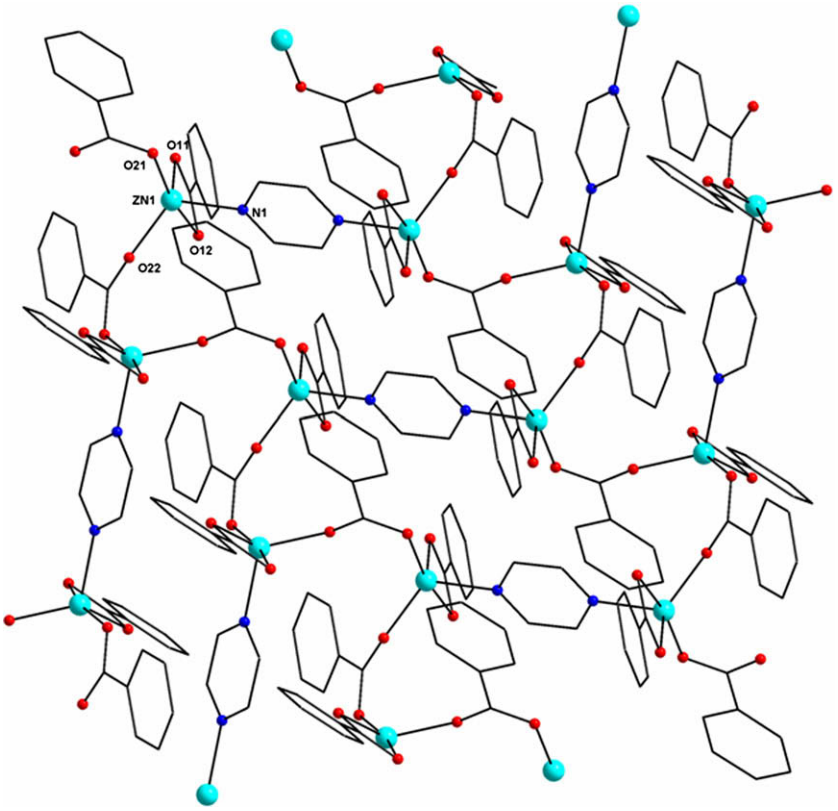

Fig. 5. Structure of two-dimensional Zn complex **5** containing $Zn(O_2CC_6H_5)$ units. All hydrogen atoms were omitted for clarity.

2,5-dimethylpyrazine. These different results might be because of (1) using different metal ions (Cu(II) versus Zn(II)), (2) using different ligands (acetate versus benzoate) and (3) using different reaction conditions from our self-assembly system.

3.7. Influence of the substituents of the organic ligand on the structure of the coordination compounds

To investigate how the change of the substituents of the bridging pyrazine ligand influences on construction of Zn-benzoate complexes, substituted pyrazine ligands (2,3-dimethylpyrazine, 2,6-dimethylpyrazine, 2,5-dimethylpyrazine, and quinoxaline) as well as simple pyrazine have been employed. Simple pyrazine and 2,5-dimethlpyrazine are used as bridging ligands to form two-dimensional and one-dimensional polymeric compounds, respectively. The other quinoxaline and two dimethyl-substituted pyrazine ligands are used only as terminal ligands to form dinuclear, trinuclear, and pentanuclear complexes. The structures of complexes **1**–**5** clearly show that the change of the substituents on the pyrazine ring are critical in the construction of molecular architecture of Zn-benzoate complexes. The coordination modes of benzoate ligand are also different according to the change of the

substituents of pyrazine. Complexes **1** and **4** have only a bridging coordination mode, and **2** shows two different coordination modes, unusual chelating and bridging. **3** and **5** have two different coordination modes (bridging and monodentate (dangling) modes for **3** and bridging and chelating modes for **5**). These results suggest that selection of appropriate substituted groups would be an ideal way to construct novel metal-pyz coordination polymers.

3.8. Catalytic transesterification reactions by the compounds *1–5*

Transesterifications are important transformations in organic synthesis in industrial as well as in academic laboratories [29]. Although there are many catalysts available for transesterification, they require harsh reaction conditions such as high reaction temperatures and acidic conditions [30]. Such drawback experienced with these catalysts derives us to develop new catalysts that operate under milder conditions. Therefore, as part of our efforts to design transesterification catalysts based on metal ions that are not redox active, we have recently reported that Zn-containing coordination polymers could carry out the catalytic transesterification of a range of esters with methanol at room temperature under the mild conditions [31]. While these catalyst systems constitute a promising class of catalysts that appears to be an efficient, mild, and easily recyclable method for the alcoholysis of esters, there is still more demand to develop new type of catalysts that show a high efficiency. Based on the previous results, therefore, compounds **1–5** have been also employed as a homogeneous catalyst for transesterification reaction in methanol. The ester, *p*-nitrophenyl acetate, was initially used as a substrate (Eq. (1)).

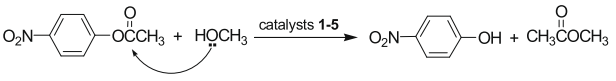

(1)

We observed that compounds **1–5** catalyzed the reaction of methanol with phenyl acetate, with quantitative conversion to methyl acetate in 0.04–0.5 day (1–12 h; see the entry 1 of Table 3) at 50 °C under the homogeneous neutral conditions. Among them, pentanuclear complex **3** shows the most efficient reactivity. Importantly, this result is best among the catalytic systems reported previously in Zn-containing coordination and polymeric compounds, to our best knowledge [31,32]. Once having established that **1–5** represent excellent catalysts for the transesterification reaction of *p*-nitrophenyl acetate with methanol, we have investigated the transesterification of various *p*-substituted phenyl acetates and benzoates. The substrates with the electron-withdrawing substituents have undergone faster transesterification (entries 1 and 5), while those with the electron-donating ones have shown slow reaction (entries 4 and 8). In addition, *p*-nitrophenyl acetate and *p*-nitrophenyl benzoate, known to be problematic substrates for the transesterification reaction due to undesirable side reactions such as isomerization or polymerization [33], were also converted quantitatively to the corresponding products.

Transesterification of esters with alcohol cannot, sometimes, achieve high conversions since the reaction is reversible. To solve this problem, therefore, enol esters are usually used as acylating agents, since the resultant enolate is converted to an aldehyde or ketone that is unable to participate in the reverse reaction [34]. In this work, vinyl acetate was used as an acylating agent and, expectedly, converted efficiently to the product methyl acetate within 0.06–0.5 day by **1–5** (entry 9), suggesting that this catalytic system can be useful for preparing various esters by transesterification.

Moreover, this promising result led us to test the transesterification with more challenging nucleophiles such as ethanol, 2-propanol, and propanol, in the presence of the most efficient catalyst **3**. Phenyl acetate reacted very slowly with either ethanol (70 days) or 2-propanol (75 days), respectively, whereas propanol drove the reaction to completion within 4 days (the sixth column in Table 3). Various esters were also examined with propanol as a nucleophile in the presence of **3**. The substrates with the electron-withdrawing substituents have undergone faster conversion to the corresponding products (entries 1 and 5 of the sixth column), while those with the electron-donating ones have shown slow transesterification reaction (entries 4 and 8 of the sixth column).

Table 3
Transesterification of esters by methanol and propanol in the presence of compounds **1**, **2**, **3**, **4**, and **5** at 50 °C[a]

Entry	Substrate	**1** (time/days)[b]	**2** (time/days)[b]	**3** (time/days)[b]		**4** (time/days)[b]	**5** (time/days)[b]
		MeOH[c]	MeOH[c]	MeOH[c]	PrOH[d]	MeOH[c]	MeOH[c]
1	4-Nitrophenyl acetate	0.21	0.5	0.04	1	0.25	0.13
2	4-Fluorophenyl acetate	4	1.5	1	4	3	2
3	Phenyl acetate	2	1.5	0.37	4	2	2
4	4-Methylphenyl acetate	9	4	1	8	6	6
5	4-Nitrophenyl benzoate[e]	3	0.5	0.21	13	3	3
6	4-Chlorophenyl benzoate	3	2	1	11	3	4
7	Phenyl benzoate	7	4	0.83	26	7	7
8	4-Methylphenyl benzoate	6	3	1	25	6	6
9	Vinyl acetate	0.46	0.5	0.06	3	0.35	0.42

[a] All esters were completely converted to the corresponding products, methyl acetate and methyl benzoate. Reaction conditions: esters; 0.05 mmol, catalyst; 1.14×10^{-3} mmol for **1**, 0.88×10^{-3} mmol for **2**, 0.65×10^{-3} mmol for **3**, 1.20×10^{-3} mmol for **4**, 0.72×10^{-3} mmol for **5**, solvent; methanol or propanol (1 mL). See Section 2 for the detailed reaction conditions.
[b] Time necessary for the complete conversion of substrate to product.
[c] Transesterification of esters was carried out in methanol (MeOH).
[d] Transesterification of esters was carried out in propanol (PrOH).
[e] The solvent was a mixture of MeOH/CH_2Cl_2 or PrOH/CH_2Cl_2 (1/1) because of low solubility of substrate in MeOH or PrOH.

Protection of a primary alcohol in the presence of a secondary alcohol is useful in natural product synthesis [34,35]. Therefore, selectivity of primary over secondary alcohol protection has been tested with the catalyst **3**. In a mixture of propanol and 2-propanol in the presence of **3** and phenyl acetate, only the propanol reacted, providing propyl acetate in 99.7% yield while the secondary acetate formed in <0.3% yield. This reaction clearly demonstrates the potential utility of our catalyst in selecting for primary alcohols.

Though we do not know, at this moment, about the exact reactive species and the reaction mechanism for the transesterification reaction by the catalysts, it has been proposed that the mechanism of metal ion catalyzed transesterification probably involves electrophilic activation of the carbon center of the carbonyl moiety by binding of the metal to the carbonyl oxygen [16]. Therefore, Lewis acidity of the metal center may be important in catalytic transesterification. Based on this idea, a possible transesterification mechanism in this catalyst system can be proposed. The substrate phenyl acetate substitutes a labile ligand, maybe benzoate, to give the adduct –Zn–O=$CR_1(OR_2)$R. Then, the nucleophile methanol would attack the carbon atom of carbonyl moiety of the adduct to produce the product methyl acetate. Detailed mechanistic studies are currently under investigation.

4. Conclusions

To investigate the influence of the substituent change of ligands on the crystal structure, five new coordination polymers constructed by self-assembly of the pyrazine and its derivatives and

zinc(II)-benzoate have been structurally characterized. Simple pyrazine and 2,5-dimethlpyrazine are used as bridging ligands to form two-dimensional and one-dimensional polymeric compounds, respectively. The other quinoxaline and two dimethyl-substituted pyrazine ligands are used only as terminal ligands to form dinuclear, trinuclear, and pentanuclear complexes. The structural differences between such complexes reveal that the change of the substituents of the ligands has a great influence on the complex structures. This approach may be useful for synthesizing other complexes with high-dimensional structures. We have also shown that the compounds **1**–**5** catalyzed efficiently the transesterification of a variety of esters. Among them, pentanuclear complex **3** shows the most efficient reactivity. In addition, the scope of the application of **3** as a transesterification catalyst has been expanded to now include ethanol and propanol. Moreover, selectivity test of primary over secondary alcohol protection in the presence of **3** and phenyl acetate has provided, exclusively, the primary acetate propyl acetate, demonstrating the potential utility of our catalyst in selecting for primary alcohols. Furthermore, this observation is very significant since it encourages us to construct new polymeric compounds that might be efficiently used as heterogeneous catalysts friendly to the environment.

Acknowledgements

Financial support from Environmental Technology Educational Innovation Program (2006) of the Ministry of Environment, the Korea Research Foundation (2006-312-C00569 and 2007-314-C00159), The SEOUL R & BD Program, and the SRC program of the Korea Science and Engineering Foundation (KOSEF) through the Center for Intelligent Nano-Bio Materials at Ewha Womans University (Grant R11-2005-008-00000-0) is gratefully acknowledged.

Appendix A. Supplementary data

CCDC 661363, 661364, 661365, 661366 and 661367 contain the supplementary crystallographic data for **1**, **2**, **3**, **4** and **5**. These data can be obtained free of charge via http://www.ccdc.cam.ac.uk/conts/retrieving.html, or from the Cambridge Crystallographic Data Centre, 12 Union Road, Cambridge CB2 1EZ, UK; fax: (+44) 1223-336-033; or e-mail: deposit@ccdc.cam.ac.uk. X-ray powder diffraction patterns on the bulk samples for **1**–**5** are also available. Supplementary data associated with this article can be found, in the online version, at doi:10.1016/j.poly.2008.08.010.

References

[1] (a) S.R. Batten, R. Robson, Angew. Chem., Int. Ed. 37 (1998) 1460;
(b) D.B. Moler, H. Li, B. Chen, T.M. Reineke, M. O'Keeffe, O.M. Yaghi, Acc. Chem. Res. 34 (2001) 319;
(c) B. Moulton, M.J. Zaworotko, Chem. Rev. 101 (2001) 1629;
(d) K. Kim, Chem. Soc. Rev. 31 (2002) 96;
(e) O.R. Evans, W. Lin, Acc. Chem. Res. 35 (2002) 511;
(f) C. Janiak, Dalton Trans. (2003) 2781.
[2] (a) P.J. Hagrman, D. Hagrman, J. Zubieta, Angew. Chem., Int. Ed. 38 (1999) 2638;
(b) S. Noro, R. Kitaura, M. Komdo, S. Kitagawa, T. Ishii, H. Matsuzaka, M. Yamashita, J. Am. Chem. Soc. 124 (2002) 2568. and references cited therein;
(c) S.L. James, Chem. Soc. Rev. 32 (2003) 276.
[3] (a) K.S. Min, M.P. Suh, J. Am. Chem. Soc. 122 (2000) 6834;
(b) J. Fan, L. Gan, H. Kawaguchi, W.-Y. Sun, K.-B. Yu, W.-X. Tang, Chem. Eur. J. 9 (2003) 3965.
[4] (a) A.J. Fletcher, E.J. Cussen, D. Bradshaw, M.J. Rosseinsky, K.M. Thomas, J. Am. Chem. Soc. 126 (2004) 9750;
(b) D.N. Dybtsev, H. Chun, K. Kim, Angew. Chem., Int. Ed. 43 (2004) 5033;
(c) E.-Y. Choi, K. Park, C.-M. Yang, H. Kim, J.-H. Son, S.W. Lee, Y.H. Lee, D. Min, Y.-U. Kwan, Chem. Eur. J. 10 (2004) 5535;
(d) J.L.C. Rowsell, O.M. Yaghi, Angew. Chem., Int. Ed. 44 (2005) 4670;
(e) B. Kesanli, Y. Cui, M.R. Smith, E.W. Bittner, B.C. Bockrath, W. Lin, Angew. Chem., Int. Ed. 44 (2005) 72;
(f) H. Chun, D.N. Dybtsev, H. Kim, K. Kim, Chem. Eur. J. 11 (2005) 3521.
[5] G.A. Mines, B.-C. Tzeng, K.J. Stevenson, J. Li, J.T. Hupp, Angew. Chem., Int. Ed. 41 (2002) 154.
[6] (a) S.-K. Yoo, J.Y. Ryu, J.Y. Lee, C. Kim, S.-J. Kim, Y. Kim, Dalton Trans. (2003) 1454;
(b) S. Takizawa, H. Somei, D. Jayaprakash, H. Sasai, Angew. Chem., Int. Ed. 42 (2003) 5711;
(c) S.J. Hong, J.Y. Ryu, J.Y. Lee, C. Kim, S.-J. Kim, Y. Kim, Dalton Trans. (2004) 2697;
(d) S. Kitagawa, R. Kitaura, S.-I. Noro, Angew. Chem., Int. Ed. 43 (2004) 2334;
(e) S.J. Hong, J.S. Seo, J.Y. Ryu, J.H. Lee, C. Kim, S.-J. Kim, Y. Kim, A.J. Lough, J. Mol. Struct. 751 (2005) 22;
(f) C.-D. Wu, A. Hu, L. Zhang, W. Lin, J. Am. Chem. Soc. 127 (2005) 8940;
(g) X. Wang, X. Wang, H. Guo, Z. Wang, K. Ding, Chem. Eur. J. 11 (2005) 4078;
(h) H. Han, S. Zhang, H. Hou, Y. Fan, Y. Zhu, Eur. J. Inorg. Chem. (2006) 1594;
(i) D.N. Dybtsev, A.L. Nuzhdin, H. Chun, K.P. Bryliakov, E.P. Talsi, V.P. Fedin, K. Kim, Angew. Chem., Int. Ed. 45 (2006) 916;
(j) S. Hasegawa, S. Horike, R. Matsuda, S. Furukawa, K. Mochizuki, Y. Kinoshita, S. Kitagawa, J. Am. Chem. Soc. 129 (2007) 2607.
[7] (a) M.C. Hong, Y.J. Zhao, W.P. Su, R. Cao, M. Fujita, Z.Y. Zhou, A.S.C. Chan, J. Am. Chem. Soc. 122 (2000) 4819;
(b) J.F. Ma, J.F. Liu, X. Yan, H.Q. Jia, Y.H. Lin, J. Chem. Soc., Dalton Trans. (2000) 2403.
[8] (a) D.M. Shin, I.S. Lee, Y.-A. Lee, Y.K. Chung, Inorg. Chem. 42 (2003) 2977;
(b) C. Richardson, P.J. Steel, D.M. D'Alessandro, P.C. Junk, F.R. Keene, J. Chem. Soc., Dalton Trans. (2002) 2775;
(c) K. Biradha, M. Fujita, J. Chem. Soc., Dalton Trans. (2000) 3805.
[9] (a) O.-S. Jung, S.H. Park, K.M. Kim, H.G. Jang, Inorg. Chem. 37 (1998) 5781;
(b) M.A. Withersby, A.J. Blake, N.R. Champness, P.A. Cooke, P. Hubberstey, W.-S. Li, M. Schröder, Inorg. Chem. 38 (1999) 2259.
[10] (a) W.-X. Chen, S.-T. Wu, L.-S. Long, R.-B. Huang, L.-S. Zheng, Cryst. Growth Des. 7 (2007) 1171;
(b) R.-Q. Fang, X.-M. Zhang, Inorg. Chem. 45 (2006) 4801;
(c) Y.B. Go, X. Wang, E.V. Anokhina, A.J. Jacobson, Inorg. Chem. 44 (2005) 8265.
[11] (a) Y.-B. Dong, Y.-Y. Jiang, J. Li, J.-P. Ma, F.-L. Liu, B. Tang, R.-Q. Huang, S.R. Batten, J. Am. Chem. Soc. 129 (2007) 4520;
(b) C.-M. Liu, S. Gao, D.-Q. Zhang, D.-B. Zhu, Cryst. Growth Des. 7 (2007) 1312.
[12] (a) L. Carlucci, G. Ciani, D.M. Proserpio, S. Rizzato, Chem. Eur. J. 5 (1999) 237;
(b) H.-P. Wu, C. Janiak, G. Rheinwald, H. Lang, J. Chem. Soc., Dalton Trans. (1999) 183.
[13] (a) A.J. Blake, N.R. Brooks, N.R. Champness, P.A. Cooke, A.M. Deveson, D. Fenske, P. Hubberstey, M. Schroder, J. Chem. Soc., Dalton Trans. (1999) 2103;
(b) R.W. Saalfrank, I. Bernt, M.M. Chowdhry, F. Hampel, G.B.M. Vaughan, Chem. Eur. J. 7 (2001) 2765.
[14] (a) V.R. Pedireddi, S. Varughese, Inorg. Chem. 43 (2004) 450;
(b) M.T. Ng, T.C. Deivaraj, W.T. Klooster, G.J. McIntyre, J.J. Vittal, Chem. Eur. J. 10 (2004) 5853;
(c) M.-L. Tong, H.-J. Chen, X.-M. Chen, Inorg. Chem. 39 (2000) 2235;
(d) Y.-S. Zhang, G.D. Enright, S.R. Breeze, S. Wang, New J. Chem. 23 (1999) 625;
(e) R. Wang, F. Jiang, Y. Zhou, L. Han, M. Hong, Inorg. Chim. Acta 358 (2005) 545;
(f) L.-G. Zhu, S. Kitagawa, H. Miyasaka, H.-C. Chang, Inorg. Chim. Acta 355 (2003) 121;
(g) N.L. Toh, M. Nagarathinam, J.J. Vittal, Angew. Chem., Int. Ed. 44 (2005) 2237;
(h) B. Conerney, P. Jensen, P.E. Kruger, B. Moubaraki, K.S. Murray, CrystEngComm 5 (2003) 454;
(i) R. Carballo, B. Covelo, M.S.E. Fallah, J. Ribas, E.M. Vazquez-Lopez, Cryst. Growth Des. 7 (2007) 1069;
(j) A.M. Goforth, K. Gerth, M.D. Smith, S. Shotwell, U.H.F. Bunz, H.-C. zur Loye, Solid State Sci. 7 (2005) 1083;
(k) M.V. Marinho, M.I. Yoshida, K.J. Guedes, K. Krambrock, A.J. Bortoluzzi, M. Horner, F.C. Machado, W.M. Teles, Inorg. Chem. 43 (2004) 1539;
(l) B.-H. Ye, X.-M. Chen, F. Xue, L.-N. Ji, T.C.W. Mak, Inorg. Chim. Acta 299 (2000) 1.
[15] (a) M. Casarin, C. Corvaja, C.D. Nicola, D. Falcomer, L. Franco, M. Monari, L. Pandolfo, C. Pettinari, F. Piccinelli, Inorg. Chem. 44 (2005) 6265;
(b) B.-H. Ye, M.-L. Tong, X.-M. Chen, Coord. Chem. Rev. 249 (2005) 545;
(c) F. Li, T. Li, X. Li, X. Li, Y. Wang, R. Cao, Cryst. Growth Des. 6 (2006) 1458.
[16] (a) F.E. Jacobsen, J.A. Lewis, S.M. Cohen, J. Am. Chem. Soc. 128 (2006) 3156;
(b) J. Weston, Chem. Rev. 105 (2005) 2151;
(c) G. Parkin, Chem. Rev. 104 (2004) 699;
(d) W.D. Horrocks Jr., J.N. Ishley, R.R. Whittle, Inorg. Chem. 21 (1982) 3265;
(e) W.D. Horrocks Jr., J.N. Ishley, R.R. Whittle, Inorg. Chem. 21 (1982) 3270.
[17] (a) A.-L. Cheng, N. Liu, Y.-F. Yue, Y.-W. Jiang, E.-Q. Gao, C.-H. Yan, M.-Y. He, Chem. Commun. (2007) 407;
(b) D. Sun, D.J. Collins, Y. Ke, J.-L. Zuo, H.-C. Zhou, Chem. Eur. J. 12 (2006) 3768;
(c) B. Chen, S. Ma, F. Zapata, E.B. Lobkovsky, J. Yang, Inorg. Chem. 45 (2006) 5718;
(d) D. Sun, Y. Ke, T.M. Mattox, S. Parkin, H.-C. Zhou, Inorg. Chem. 45 (2006) 7566.
[18] (a) M.A. Malik, M. Motevalli, P. O'Brien, Inorg. Chem. 34 (1995) 6223;
(b) X.-M. Chen, Z.-T. Xu, T.C.W. Mak, Polyhedron 13 (1994) 3329;
(c) T.C.W. Mak, W.-H. Yip, G. Smith, E.J. O'Reilly, C.H.L. Kennard, Inorg. Chim. Acta 84 (1984) 57.
[19] (a) T. Ohmura, W. Mori, T. Ikeda, A. Maeda, Sci.-Poland 23 (2005) 729;
(b) A. Karmaker, R.J. Sarma, J.B. Baruah, Inorg. Chem. Commun. 9 (2006) 1169;

(c) W. Clegg, I.R. Little, B.P. Straughan, J. Chem. Soc., Dalton Trans. (1986) 1283;
(d) P. Chaudhuri, C. Stockheim, K. Wieghardt, W. Deck, R. Gregorzik, H. Vahrenkamp, B. Nuber, J. Weiss, Inorg. Chem. 31 (1992) 1451;
(e) S. Uhlenbrock, B. Krebs, Angew. Chem., Int. Ed. 31 (1992) 1647.
[20] W. Clegg, D.R. Harbron, C.D. Homan, P.A. Hunt, I.R. Little, B.P. Straughan, Inorg. Chim. Acta 186 (1991) 51.
[21] A. Waheed, R.A. Jones, J. McCarty, X. Yang, J. Chem. Soc. Dalton Trans. (2004) 3840.
[22] (a) D.S. Sun, Y. Ke, T.M. Mattox, S. Parkin, H.-C. Zhou, Inorg. Chem. 45 (2006) 7566;
(b) Z. Shi, G. Li, L. Wang, L. Gao, X. Chen, J. Hua, S. Feng, Cryst. Growth Des. 4 (2004) 25.
[23] (a) X.-C. Huang, J.-P. Zhang, Y.-Y. Lin, X.-M. Chen, Chem. Commun. (2005) 2232;
(b) Y.-P. Ren, X.J. Kong, X.-Y. Hu, M. Sun, L.-S. Long, R.-B. Huang, L.-S. Zheng, Inorg. Chem. 45 (2006) 4016;
(c) N.L. Rosi, J. Kim, M. Eddaoudi, B. Chen, M. O'Keeffe, O.M. Yaghi, J. Am. Chem. Soc. 127 (2005) 1504;
(d) Q.-G. Zhai, X.-Y. Wu, S.-M. Chen, C.-Z. Lu, W.-B. Yang, Cryst. Growth Des. 6 (2006) 2126;
(e) C. Nather, J. Greve, I. Je, C. Wickleder, Solid State Sci. 5 (2003) 1167;
(f) D.J. Chesnut, D. Plewak, J. Zubieta, J. Chem. Soc., Dalton Trans. (2001) 2567.
[24] Bruker, SHELXTL/PC. Version 6.12 for Windows XP, Bruker AXS Inc., Madison, Wisconsin, USA, 2001.
[25] (a) K. Nakamoto, Infrared and Raman Spectra of Inorganic and Coordination Compounds, John Wiley & Sons, New York, 1986;
(b) J. Tao, M.-L. Tong, X.-M. Chen, J. Chem. Soc., Dalton Trans. (2000) 3669;
(c) W. Chen, J.-Y. Wang, C. Chen, Q. Yue, H.-M. Yuan, J.-S. Chen, S.-N. Wang, Inorg. Chem. 42 (2003) 944.
[26] B. Singh, J.R. Long, F.F. de Biani, D. Gattesch, P. Stavropoulos, J. Am. Chem. Soc. 119 (1997) 7030.
[27] T.-W. Lee, P.-K. Lau, W.-T. Wong, Polyhedron 23 (2004) 999.
[28] (a) S. Takamizawa, E. Nakata, H. Yokoyama, Inorg. Chem. Commun. 6 (2003) 763;
(b) R. Nukada, W. Mori, S. Takamizawa, M. Mikuriya, M. Handa, H. Naono, Chem. Lett. (1999) 367;
(c) S. Takamizawa, T. Hiroki, E. Nakata, K. Mochizuki, W. Mori, Chem. Lett. (2002) 1208.
[29] (a) M.-H. Lin, T.V. RajanBabu, Org. Lett. 2 (2000) 997;
(b) G.A. Grasa, R.M. Kissling, S.P. Nolan, Org. Lett. 4 (2002) 3583;
(c) G.A. Grasa, T. Guveli, R. Singh, S.P. Nolan, J. Org. Chem. 68 (2003) 2812.
[30] (a) R.L.E. Furlan, E.G. Mata, O.A. Mascaretti, Tetrahedron Lett. 39 (1998) 2257;
(b) C.E. Rehberg, C.H. Fisher, J. Org. Chem. 12 (1947) 226.
[31] (a) J.Y. Lee, S.J. Hong, C. Kim, S.-J. Kim, Y. Kim, Inorg. Chem. Commun. 8 (2005) 692;
(b) Y.M. Lee, S.J. Hong, H.J. Kim, S.H. Lee, H. Kwak, C. Kim, S.-J. Kim, Y. Kim, Inrog. Chem. Commun. 10 (2007) 287.
[32] (a) J.S. Seo, D. Whang, H. Lee, S.I. Jun, J. Oh, Y.J. Jeon, K. Kim, Nature 404 (2000) 982;
(b) J.Y. Ryu, J.H. Han, J.Y. Lee, S.J. Hong, S.H. Choi, C. Kim, S.-J. Kim, Y. Kim, Inorg. Chim. Acta 358 (2005) 3659;
(c) Y. Kim, S.-J. Kim, S.H. Choi, J.H. Han, S.H. Nam, J.H. Lee, H.J. Kim, C. Kim, D.W. Kim, H.G. Jang, Inorg. Chim. Acta 359 (2006) 2534.
[33] V.K. Aggarwal, A. Mereu, Chem. Commun. (1999) 2311.
[34] (a) G.W. Nyce, J.A. Lamboy, E.F. Connor, R.M. Waymouth, J.L. Hedrick, Org. Lett. 4 (2002) 3587;
(b) D. Tashiro, Y. Kawasaki, S. Sakaguchi, Y. Ishii, J. Org. Chem. 62 (1997) 8141;
(c) Y. Ishii, M. Takeno, Y. Kawasaki, Y. Muromachi, Y. Nishiyama, S. Sakaguchi, J. Org. Chem. 61 (1996) 3088.
[35] A. Orita, A. Mitsutome, J. Otera, J. Org. Chem. 63 (1998) 2420.

and H_2O (10 mL) was heated to 150 °C for 50 h in a 23 mL Teflon-lined stainless-steel autoclave and then it was cooled to room temperature at 10 °C h^{-1} to obtain colorless plate-like single crystals of **1** (yield: 52% based on Eu). *Anal.* Calc. for $Ag_2EuC_{24}H_{26}N_4O_{17}Cl$: C, 27.57; H, 2.51; N, 5.36. Found: C, 27.53; H, 2.53; N, 5.38%. IR frequencies (KBr, cm^{-1}): 3431, 1612, 1560, 1411, 1203, 1099, 840, 756, 692, 538, 420.

2.2.2. $[Ag_2Gd(nic)_4(H_2O)_4 \cdot (ClO_4) \cdot H_2O]$ (**2**)

An identical procedure as for **1** was used to prepare **2** except that Eu_2O_3 was replaced by Gd_2O_3. Colorless plate-like single crystals of (**2**) were obtained (yield: 57% based on Gd) *Anal. Calc.* for $Ag_2GdC_{24}H_{26}N_4O_{17}Cl$: C, 27.43; H, 2.49; N, 5.33. Found: C, 27.40; H, 2.50; N, 5.35%. IR frequencies (KBr, cm^{-1}): 3437, 1614, 1560, 1411, 1203, 1097, 840, 756, 696, 534, 420.

2.2.3. $[AgTb(nic)_2(ox)_{0.5}(H_2O)_2 \cdot (ClO_4) \cdot H_2O]$ (**3**)

A mixture of nicotinic acid (0.123 g; 1 mmol), $Na_2C_2O_4$ (0.0335 g; 0.25 mmol); $AgNO_3$ (0.100 g; 0.59 mmol), Tb_4O_7 (0.100 g, 0.284 mmol), $HClO_4$ (0.385 mmol) and H_2O (10 mL) was heated to 150 °C for 50 h in a 23 mL Teflon-lined stainless-steel autoclave. Colorless plate-like single crystals (**3**) were obtained (yield: 48% based on Tb) on cooling the solution to room temperature at 10 °C h^{-1}. *Anal. Calc.* for $AgTbC_{13}H_{12}N_2O_{12}Cl$: C, 22.61; H, 1.75; N, 4.06. Found: C, 22.62; H, 1.73; N, 4.07%. IR frequencies (KBr, cm^{-1}): 3423, 1612, 1568, 1421, 1201, 1072, 864, 756, 692, 623, 551, 424.

2.2.4. $[AgYb(nic)_2(ox)_{0.5}(H_2O)_2 \cdot (ClO_4) \cdot H_2O]$ (**4**)

An identical procedure as for **3** was used to prepare **4** except that Tb_4O_7 was replaced by Yb_2O_3. Colorless plate-like single crystals (**4**) were obtained (yield: 41% based on Yb) *Anal. Calc.* for $AgYbC_{13}H_{12}N_2O_{12}Cl$: C, 22.16; H, 1.72; N, 3.98. Found: C, 22.12; H, 1.75; N, 3.94%. IR frequencies (KBr, cm^{-1}): 3423, 1612, 1568, 1421, 1201, 1064, 864, 759, 696, 623, 557, 418.

2.3. Crystal structure determination

Single-crystal X-ray diffraction data collections of **1–4** were performed on a Bruker Apex II CCD diffractometer operating at 50 kV and 30 mA using Mo Kα radiation (λ = 0.71073 Å). Data collection and reduction were performed using the APEX II software [9]. Multi-scan absorption corrections were applied for all data sets using the algorithms implemented in APEX II [9]. All four structures were solved by direct methods and refined by full-matrix least squares on F^2 using the SHELXTL program package [9]. All non-hydrogen atoms were refined with anisotropic displacement parameters. Hydrogen atoms attached to carbon were placed in geometrically idealized positions and refined using a riding model. Hydrogen atoms on water molecules were located from difference Fourier maps and were also refined using a riding model. Crystallographic data for **1–4** are listed in Table 1 and selected bond lengths and angles for all compounds are given in Table 2. Hydrogen bonding parameters for **1** and **3** are given in Table 3.

3. Results and discussion

3.1. Synthesis and characterization

We initially tried to isolate single crystals of the target compounds by the reactions of lanthanide salts with a mixture of $AgNO_3$, nicotinic acid and/or oxalate salt using conventional solution methods; however, only white precipitates were obtained. Hydrothermal synthesis has been proven to be a powerful method for the construction of organic–inorganic hybrid compounds [10]. By introducing hydrothermal techniques, we obtained a small quantity of microlite unsuitable for single-crystal X-ray diffraction when lanthanide salts were used as the lanthanide source. In our previous work, lanthanide oxides and perchloric acid have been proven to play an important role in the formation of unusual Ln–M coordination polymers [11]. Therefore, we tried lanthanide oxides as the lanthanide source and perchloric acid to synthesize new Ln–M coordination frameworks under hydrothermal conditions.

3.1.1. Structures of $[Ag_2Ln(nic)_4(H_2O)_4 \cdot (ClO_4) \cdot H_2O]$ (Ln = Eu **1**; Gd **2**)

Single-crystal X-ray diffraction studies revealed that compounds **1** and **2** are isostructural, and only the structure of **1** is representatively described here in detail. It exhibits novel 2D wave-like heterometallic coordination frameworks constructed from 1D zigzag chains and perchlorate anions, and crystallizes in the orthorhombic space group *Cmca*. The asymmetric unit of **1** exhibits half a europium ion, one silver ion, half a perchlorate anion, two crystallographically unique nicotinate ligands, and two coordinated and half a non-coordinated water molecule (Fig. 1). Each Eu(III) center lies on an inversion center and is bonded to four oxygen atoms from monodentate nicotinate ligands, and to four

Table 1
Crystal data details of the structure determination for complexes **1–4**

Complex	1	2	3	4
Formula	$Ag_2EuC_{24}H_{26}N_4O_{17}Cl$	$Ag_2GdC_{24}H_{26}N_4O_{17}Cl$	$AgTbC_{13}H_{12}N_2O_{12}Cl$	$AgYbC_{13}H_{12}N_2O_{12}Cl$
Formula weight	1045.64	1050.93	690.49	704.61
Wavelength (Å)	0.71073	0.71073	0.71073	0.71073
Crystal system	orthorhombic	orthorhombic	monoclinic	monoclinic
Space group	*Cmca*	*Cmca*	$P2_1/c$	$P2_1/c$
a (Å)	35.2066(12)	35.2066(12)	14.8129(4)	14.6528(4)
b (Å)	12.3551(3)	12.3551(3)	12.7377(3)	12.6997(5)
c (Å)	15.0970(4)	15.0970(4)	9.8903(2)	9.8257(4)
β (°)	90	90	93.269(2)	92.838(2)
V (Å^3)	6566.9(3)	6566.9(3)	1863.09(8)	1826.18(11)
Z	8	8	4	4
D_{calc} (g/cm^3)	2.115	2.126	2.462	2.563
μ (mm^{-1})	3.231	3.341	5.029	6.379
F(000)	4064	4072	1316	1336
Parameters	236	236	296	271
Goodness-of-fit (F^2)	0.997	1.133	1.157	1.043
R_1 [$I > 2\sigma(I)$][a]	0.0644	0.0457	0.0409	0.0383
wR_2 (all data)[b]	0.1752	0.1369	0.1037	0.0838

[a] $R_1 = \sum||F_o| - |F_c||/\sum|F_o|$.
[B] $wR_2 = \{\sum[w(F_o^2 - F_c^2)^2]/\sum(F_o^2)^2\}^{1/2}$.

Table 2
Selected bond distances (Å) and angles (°) for complexes **1**–**4**

Complex ***1***			
Ag(1)–N(1)$^{\#1}$	2.176(10)	Ag(1)–N(2)	2.187(9)
Ag(1)–Ag(1)$^{\#2}$	3.333(2)	Eu(1)–O(1)$^{\#3}$	2.468(7)
Eu(1)–O(3)	2.328(7)	Eu(1)–O(1*w*)	2.431(7)
Eu(1)–O(2*w*)	2.385(7)		
N(1)$^{\#1}$–Ag(1)–N(2)	173.7(4)	N(1)$^{\#1}$–Ag(1)–Ag(1)$^{\#2}$	70.7(3)
N(2)–Ag(1)–Ag(1)$^{\#2}$	114.7(3)	O(1)$^{\#3}$–Eu(1)–O(1)	129.5(4)
O(3)–Eu(1)–O(1)	75.6(3)	O(3)–Eu(1)–O(1)$^{\#3}$	139.4(3)
O(3)–Eu(1)–O(2*w*)	146.6(3)	O(3)$^{\#3}$–Eu(1)–O(2*w*)	90.0(3)
O(3)$^{\#3}$–Eu(1)–O(2*w*)	69.6(3)	O(1*w*)–Eu(1)–O(1)	70.7(2)
O(1*w*)–Eu(1)–O(1)$^{\#3}$	133.1(3)	O(1*w*)–Eu(1)–O(1*w*)$^{\#3}$	131.1(3)
O(2*w*)–Eu(1)–O(2*w*)$^{\#3}$	91.3(4)	O(2*w*)$^{\#3}$–Eu(1)–O(1)$^{\#3}$	73.2(3)
O(2*w*)$^{\#3}$–Eu(1)–O(1*w*)	142.8(3)		
Complex ***2***			
Ag(1)–N(1)$^{\#1}$	2.180(7)	Ag(1)–N(2)	2.184(7)
Ag(1)–Ag(1)$^{\#2}$	3.3404(15)	Gd(1)–O(1)	2.462(5)
Gd(1)–O(3)	2.321(5)	Gd(1)–O(1*w*)	2.426(5)
Gd(1)–O(2*w*)$^{\#3}$	2.381(5)		
N(1)$^{\#1}$–Ag(1)–N(2)	174.0(3)	N(1)$^{\#1}$–Ag(1)–Ag(1)$^{\#2}$	70.52(19)
N(2)–Ag(1)–Ag(1)$^{\#2}$	114.76(19)	O(1)–Gd(1)–O(1)$^{\#3}$	129.8(3)
O(3)–Gd(1)–O(1)	75.59(18)	O(3)–Gd(1)–O(1)$^{\#3}$	139.37(18)
O(3)–Gd(1)–O(3)$^{\#3}$	106.1(3)	O(3)–Gd(1)–O(1*w*)	81.45(19)
O(3)–Gd(1)–O(2*w*)	146.80(19)	O(3)–Gd(1)–O(2*w*)$^{\#3}$	90.12(19)
O(3)$^{\#3}$–Gd(1)–O(1*w*)	69.50(18)	O(1*w*)–Gd(1)–O(1)	70.74(18)
O(2*w*)–Gd(1)–O(1)	73.40(18)	O(2*w*)–Gd(1)–O(1)$^{\#3}$	72.12(19)
O(2*w*)$^{\#3}$–Gd(1)–O(1*w*)	142.85(19)	O(2*w*)$^{\#3}$–Gd(1)–O(2*w*)	91.40(3)
Complex ***3***			
Ag(1)–N(1)	2.144(7)	Ag(1)–N(2)	2.157(7)
Tb(1)–O(1)	2.352(6)	Tb(1)–O(2)$^{\#2}$	2.320(6)
Tb(1)–O(3)$^{\#1}$	2.302(6)	Tb(1)–O(4)$^{\#3}$	2.345(5)
Tb(1)–O(9)	2.432(5)	Tb(1)–O(10)$^{\#4}$	2.424(6)
Tb(1)–O(1*w*)	2.407(6)	Tb(1)–O(2*w*)	2.463(7)
N(1)–Ag(1)–N(2)	174.4(3)	O(1)–Tb(1)–O(1*w*)	75.8(2)
O(1)–Tb(1)–O(9)	139.9(2)	O(2)$^{\#2}$–Tb(1)–O(9)	73.3(2)
O(2)$^{\#2}$–Tb(1)–O(4)$^{\#3}$	105.9(2)	O(2)$^{\#2}$–Tb(1)–O(1*w*)	141.7(3)
O(2)$^{\#2}$–Tb(1)–O(2*w*)	71.0(2)	O(3)$^{\#1}$–Tb(1)–O(10)$^{\#4}$	71.2(2)
O(4)$^{\#3}$–Tb(1)–O(1)	146.5(2)	O(3)$^{\#1}$–Tb(1)–O(2*w*)	143.8(2)
O(10)$^{\#4}$–Tb(1)–O(9)	66.95(19)	O(4)$^{\#3}$–Tb(1)–O(9)	73.6(2)
O(1*w*)–Tb(1)–O(9)	139.0(2)	O(4)$^{\#3}$–Tb(1)–O(1*w*)	75.2(2)
O(1*w*)–Tb(1)–O(2*w*)	71.6(2)	O(10)$^{\#4}$–Tb(1)–O(2*w*)	138.1(2)
Complex ***4***			
Ag(1)–N(1)	2.150(6)	Ag(1)–N(2)	2.157(6)
Yb(1)–O(1)	2.291(5)	Yb(1)–O(2)$^{\#2}$	2.254(5)
Yb(1)–O(3)$^{\#1}$	2.238(5)	Yb(1)–O(4)$^{\#3}$	2.274(5)
Yb(1)–O(5)	2.382(5)	Yb(1)–O(6)$^{\#4}$	2.374(5)
Yb(1)–O(1*w*)	2.359(6)	Yb(1)–O(2 *w*)	2.403(5)
N(1)–Ag(1)–N(2)	174.9(3)	O(1)–Yb(1)–O(5)	140.49(1)
O(1)–Yb(1)–O(6)$^{\#4}$	74.15(18)	O(2)$^{\#2}$–Yb(1)–O(5)	72.98(18)
O(1)–Yb(1)–O(2 *w*)	75.01(17)	O(2)$^{\#2}$–Yb(1)–O(1)	142.2(2)
O(4)$^{\#3}$–Yb(1)–O(1)	146.3(2)	O(3)$^{\#1}$–Yb(1)–O(1)	100.62(1)
O(6)$^{\#4}$–Yb(1)–O(5)	68.29(17)	O(3)$^{\#1}$–Yb(1)–O(6)$^{\#4}$	71.46(19)
O(1*w*)–Yb(1)–O(5)	137.94(18)	O(3)$^{\#1}$–Yb(1)–O(2)	143.0(2)
O(1*w*)–Yb(1)–O(2*w*)	70.5(2)	O(4)$^{\#3}$–Yb(1)–O(5)	73.03(18)

Symmetry code for **1**–**2**: (#1) *x*, −*y* + 1/2, *z* + 1/2; (#2) *x*, −*y*, −*z* + 1; (#3) −*x* + 1/2, *y* + 0, −*z* + 1/2; (#4) *x*, −*y* + 1/2, *z* − 1/2; (#5) −*x*+1, *y*, *z*.
Symmetry code for **3**–**4**: (#1) *x* + 1, −*y* + 1/2, *z* + 1/2; (#2) *x*, −*y* + 1/2, *z* − 1/2; (#3) *x* + 1, *y*, *z*; (#4) −*x* + 2, −*y* + 1, −*z* + 2; (#5) *x*, −*y* + 1/2, *z* + 1/2; (#6) *x* − 1, −*y* + 1/2, *z* − 1/2; (#7) *x*−1, *y*, *z*.

Table 3
Hydrogen bond parameters of **1** and **3**

D–H···A	*d*(D–H), Å	*d*(H···A), Å	*d*(D···A), Å	∠(DHA), °
Complex ***1***				
O(1)–H(1*w*)···O(2)$^{\#1}$	0.83	2.18	2.785(12)	130
O(1)–H(2*w*)···O(2)$^{\#5}$	0.82	1.98	2.784(12)	168
O(2)–H(3*w*)···O(3)$^{\#4}$	0.82	1.82	2.636(11)	171
O(2)–H(4*w*)···O(2)$^{\#3}$	0.82	1.89	2.670(11)	159
O(3)–H(5*w*)···O(2*w*)$^{\#2}$	0.85	2.29	2.926(11)	131
Complex ***3***				
O(1*w*)–H(1*w*)···O(2)	0.83	2.51	3.032(9)	122
O(1*w*)–H(1*w*)···O(5)$^{\#6}$	0.83	2.08	2.881(8)	162′
O(2*w*)–H(3*w*)···O(6)$^{\#7}$	0.82	2.00	2.808(8)	167
O(2*w*)–H(4*w*)···O(8)	0.83	2.01	2.788(12)	156

Symmetry code: (#1) 1/2 − *x*, 1/2 + *y*, *z*; (#2) *x*, 3/2 − *y*, 1/2 + *z*; (#3) 1/2 − *x*, *y*, 1/2 − *z* ; (#4) *x*, 1 − *y*, 1 − *z*; (#5) −*x*, *y*, *z*; (#6) *x*, 1/2 − *y*, 1/2 + *z*; (#7) 2 − *x*, −1/2 + *y*, 3/2 − *z* .

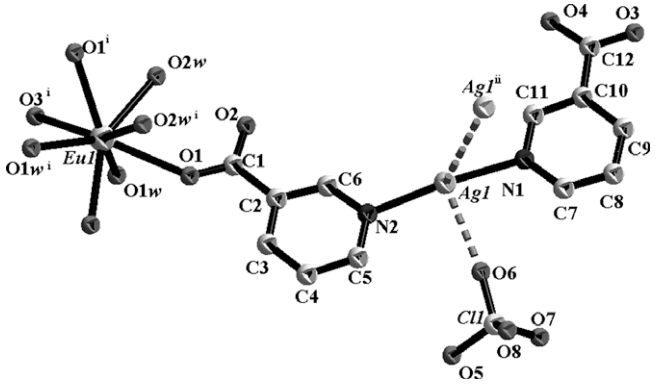

Fig. 1. Perspective view of the asymmetric unit of **1** (the disorder of the perchlorate anion is omitted for clarity).

water oxygen atoms. The 8-fold coordination polyhedron of the europium center can be described as a slightly distorted square antiprism. The Eu–O bond lengths and O–Eu–O bond angles are all within the range of those observed for other eight-coordinate Eu(III) complexes with oxygen donor ligands [12] and range from 2.328(7) to 2.468(7) Å and 69.6(3)° to 146.6(3)°, respectively. The Ag(I) ion is coordinated in a linear fashion by each of the two pyridyl nitrogen atoms of the nicotinate ligands. This coordination is augmented by a weaker interaction with one oxygen atom from the ClO_4^- anion, and the silver cations also exhibit argentophilic interactions with an Ag···Ag bond length of 3.333(2) Å, which is smaller than the sum of the van der Waals radii for two silver atoms (3.44 Å) [13]. The two Ag–N distances are 2.176(10) and 2.187(9) Å and the N–Ag–N angle is 173.7(4)°; the pyridyl rings of the nicotinate ligands coordinating to this Ag ion are almost coplanar and have a dihedral angle of only 1.74(3)°. The two unique nicotinate ligands in compound **1** exhibit only one type of coordination mode as shown in Chart 1a. The nitrogen atom connects to one Ag center and the carboxylate group bonds to one Eu center via monodentate coordination.

In the polymeric structure of **1**, the cationic $Ag(nic)_2^+$ units interconnect europium centers to form an infinite zigzag chain (Fig. 2a). These chains are further extended into a 2D layer in the *a*-axis direction through bridging perchlorate ions by the weak Ag–O interactions (Fig. 2b). It should be noted that the layer is

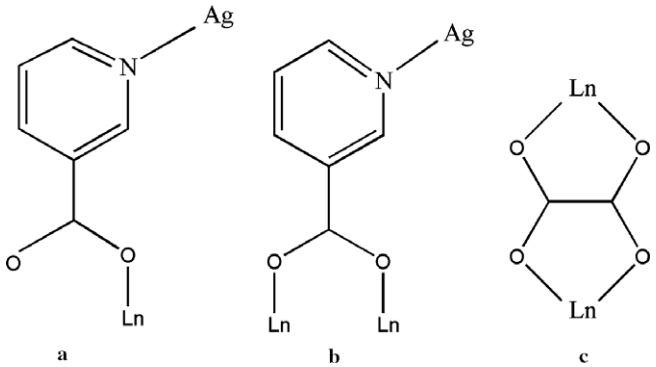

Chart 1. Coordination modes of nicotinate and oxalate ligands in compounds **1**–**4**.

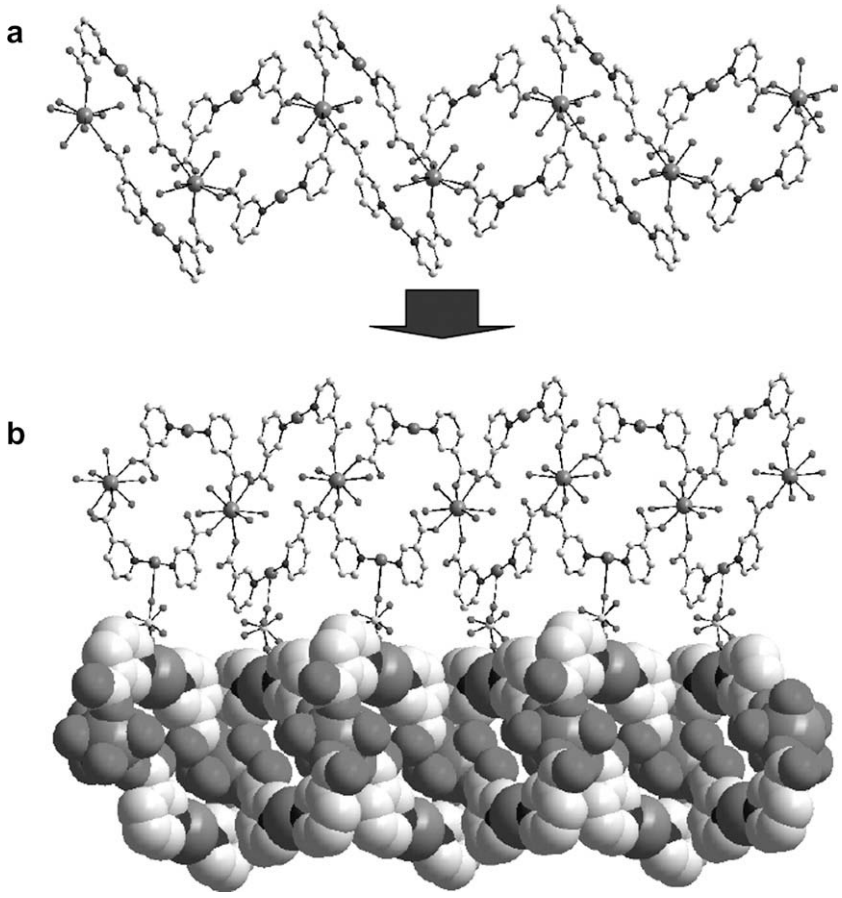

Fig. 2. View of a zigzag chain of **1** (a), view of 2D wave-like layer assembled by weak Ag–O contacts (b).

not smooth but is wave-like. The water molecules act as both H-bond donors and acceptors (Table 3), and play an important part in the structural packing, thus linking neighboring layers to form a three-dimensional network structure. Moreover, the above-mentioned Ag···Ag bonds and π···π stacking interactions enhance the structure's stability. The adjacent pyridyl rings within these connecting layer have centroid to centroid distances of 3.661(2) Å, and the offset value between them is less than 1.5 Å, indicating a normal π···π stacking interaction [14].

*3.1.2. Structures of $[AgLn(nic)_2(ox)_{0.5}(H_2O)_2 \cdot (ClO_4) \cdot H_2O]$ (Ln = Tb **3**; Yb **4**)*

Single-crystal X-ray diffraction studies revealed that compounds **3** and **4** are also novel 3D heterometallic coordination framework constructed from the linkage of lanthanide–oxalate layers and cationic $[Ag(nic)_2]^+$ units, crystallizing in the monoclinic space group $P2_1/c$. Because **3** and **4** are also isostructural, only the structure of **3** is described here in detail. In the asymmetric unit of **3**, there are one Tb(III) ion, one Ag(I) ion, half an oxalate ligand, one ClO_4^- anion, two crystallographically unique nic ligands and two coordinated water molecules (Fig. 3). The Tb(III) ion is surrounded by eight oxygen atoms and exhibits a slightly distorted square antiprismatic coordination geometry: four oxygen atoms from four bis(monodentate) bridging nicotinate ligands, two oxygen atoms from one oxalate ligand and two oxygen atoms from two water molecules. The Tb–O bond lengths range from 2.302(6) to 2.463(7) Å, all of which are within the range of those observed for other eight-coordinate Tb(III)-carboxylate complexes [15]. The O–Tb–O bond angles fall in the range 67.0(2)–146.5(2)°. The Ag(I) ion is coordinated in a linear fashion by each of the two pyridyl nitrogen atoms of the nic ligands. The Ag–N distances are 2.144(7) and 2.157(7) Å and the N–Ag–N angle is 174.4(4)°. The dihedral angle between the pyridyl rings of the nicotinate ligands coordinated to the Ag ion is 16.3(4)°. In compound **3**, the two nicotinate ligands adopt a bridging coordination mode different from that in **1** and **2**, as depicted in Chart 1b. The nitrogen atom coordinates to one Ag center and the carboxylate group connects two Tb centers through a bis-monodentate coordination. The oxalate ligand bonds to two Tb centers through a bridging and chelating coordination (Chart 1c).

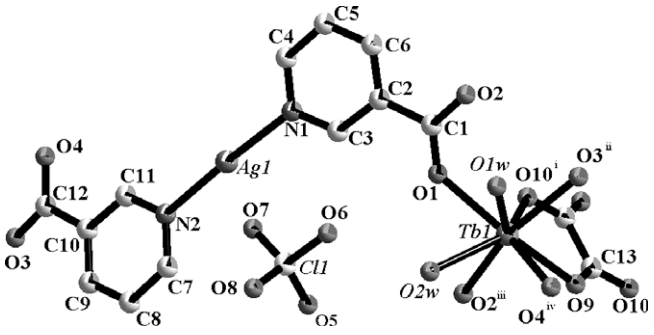

Fig. 3. Perspective view of the asymmetric unit of **3**.

In the polymeric structure of **3**, the carboxylate groups of the nicotinate ligands link the oxalate-connected dimeric terbium subunits to form a smooth layered network perpendicular to the *a*-axis (Fig. 4a). These layers are in turn connected through the pyridyl coordinated silver ions to form a three-dimensional network

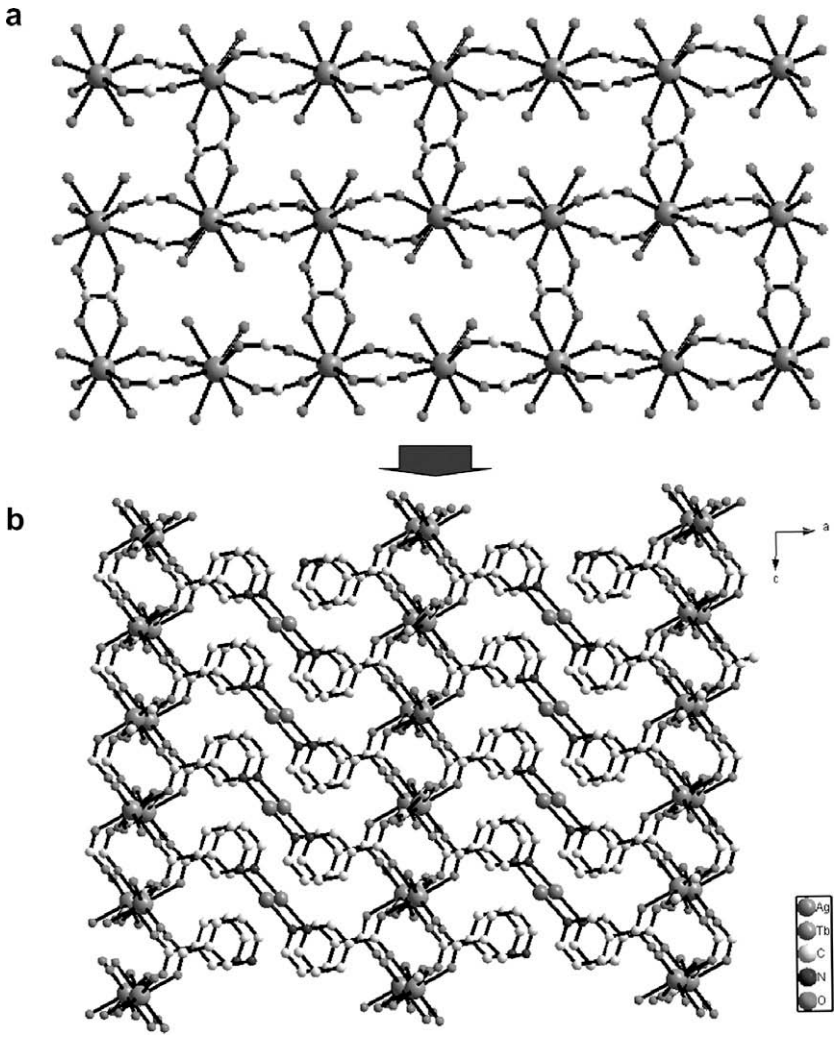

Fig. 4. View of lanthanide–oxalate layer of **3** (a), view of 3D network of **3** constructed by lanthanide–oxalate layers and $Ag(nic)_2$ units (b).

(Fig. 4b). Hydrogen bonds (Table 3) between the coordinated water molecules and the carboxylate groups of the nicotinate ligands also stabilize the structure. The shortest Ag···Ag distance is 3.602(2) Å, which is larger than the sum of the van der Waals radii for two silver atoms (3.44 Å) [13]. This complex thus shows no significant Ag···Ag interactions. The charge balancing perchlorate ions are well separated from both the Tb and Ag ions with separations between adjacent Ag and O atoms being between 2.723 and 2.748 Å.

3.2. IR spectroscopy

The IR spectra of compounds **1–4** shows the characteristic bands of the asymmetric stretching vibrations of carboxylate groups in the range 1560–1614 cm^{-1}, those for symmetric stretching vibrations are at 1411 cm^{-1}. The broad band at around 3430 cm^{-1} is assigned to the vibration of the water molecules in these compounds. Another broad band in the region 1099–1064 cm^{-1} can be ascribed to the ClO_4^- stretching vibrations [16].

3.3. Luminescent properties

Owing to the excellent luminescent properties of Eu(III) and Tb(III) ions, the room temperature photoluminescence in the solid state of nicotinate as well as of **1** and **3** were investigated. The emission peak of the nicotinate ligand is observed at about 378 nm (λ_{ex} = 329 nm) with a relatively intense broad band (Fig. S1).

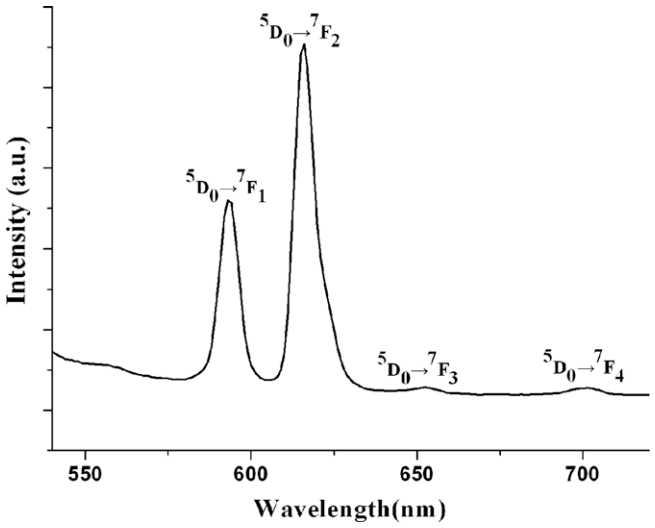

Fig. 5. Solid-state emission spectrum of **1** at room temperature.

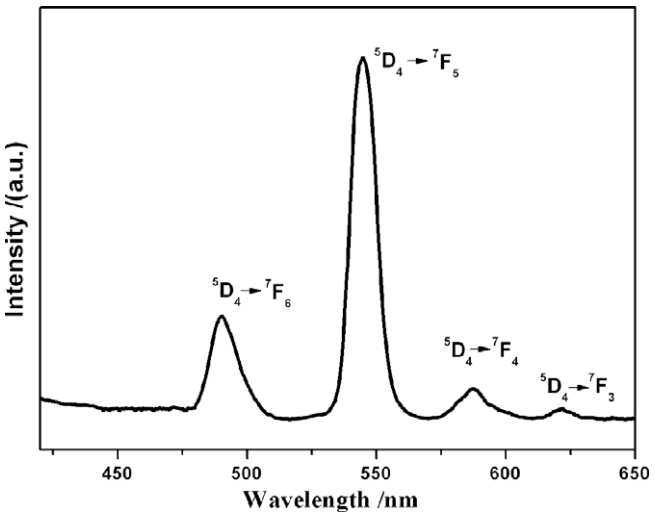

Fig. 6. Solid-state emission spectrum of **3** at room temperature.

As shown in Fig. 5, the emission spectrum of **1** at room temperature upon excitation at 394 nm displays intense red luminescence and exhibits the characteristic transitions of $^5D_0 \rightarrow {}^7F_n$ (n = 1–4) of Eu(III) ions at 593, 615, 652 and 701 nm, respectively, which indicate a moderately efficient of ligand-to-metal (europium) energy transfer (LMCT) [17,7b]. The band at 615 nm can be attributed to an electric-dipolar $^5D_0 \rightarrow {}^7F_2$ transition, the band at 593 nm can be assigned to $^5D_0 \rightarrow {}^7F_1$ and the band at 701 nm to a $^5D_0 \rightarrow {}^7F_4$ transition. The $^5D_0 \rightarrow {}^7F_1$ emission peak at 593 nm is a magnetic dipole transition and its intensity should vary with the crystal field strength acting on the Eu(III) ion. The strongest $^5D_0 \rightarrow {}^7F_2$ transition is an electric dipole transition and the intensity of this transition increases as the site symmetry of the Eu(III) ions decreases. The intensity of the $^5D_0 \rightarrow {}^7F_2$ transition is stronger than that of the $^5D_0 \rightarrow {}^7F_1$ transition, the intensity ratio $I(^5D_0 \rightarrow {}^7F_2)/I(^5D_0 \rightarrow {}^7F_1)$ is ca. 1.7, which indicates that the Eu(III) ions have a low symmetric coordination environment [18]. The luminescent spectrum of **3** is shown in Fig. 6. The bands at 489, 545, 588 and 623 nm can be attributed to the $^5D_4 \rightarrow {}^7F_6$, $^5D_4 \rightarrow {}^7F_5$, $^5D_4 \rightarrow {}^7F_4$ and $^5D_4 \rightarrow {}^7F_3$ transitions, respectively [19]. The peak at 545 nm is the strongest. The quantum yield of luminescence of **1** and **3**, determined as described by Bünzli and coworkers [20], are 3.2% and 7.6%, respectively. As powders, the complexes feature long luminescence lifetimes of 2.01(2) ms for **1** and 2.50(1) ms for **3** [21]. Thus, **1** and **3** may be candidates for use in luminescent materials.

4. Conclusion

In conclusion, we have successfully synthesized four new 4d–4f coordination frameworks based on oxalate and nicotinate ligands. They all represent unusual structural examples of heterometallic coordination frameworks by spontaneous assembly of N-/O-donor ligands. This successful synthetic idea can be used to prepare other novel high-dimensional lanthanide–transition metal heterometallic coordination polymers materials with particular functions.

Acknowledgements

We kindly acknowledge the financial support from the South China Normal University.

Appendix A. Supplementary data

CCDC 684003, 684004, 684005, 684006 contain the supplementary crystallographic data for **1**–**4**. These data can be obtained free of charge via http://www.ccdc.cam.ac.uk/conts/retrieving.html, or from the Cambridge Crystallographic Data Centre, 12 Union Road, Cambridge CB2 1EZ, UK; fax: (+44) 1223-336-033; or e-mail: deposit@ccdc.cam.ac.uk. Supplementary data associated with this article can be found, in the online version, at doi:10.1016/j.poly.2008.07.035.

References

[1] (a) F. Mori, T. Nyui, T. Ishida, T. Nogami, K.Y. Choi, H. Nojin, J. Am. Chem. Soc. 128 (2006) 1440;
(b) F.C. Liu, Y.F. Zeng, J. Jiao, J.R. Li, X.H. Bu, J. Ribas, S.R. Batten, Inorg. Chem. 45 (2006) 6129;
(c) Y. O Yang, W. Zhang, N. Xu, G.F. Xu, D.Z. Liao, K. Yoshimura, S.P. Yan, P. Cheng, Inorg. Chem. 46 (2007) 8454;
(d) A.C. Rizzi, R. Calvo, R. Baggio, M.T. Garland, O. Pena, M. Perec, Inorg. Chem. 41 (2002) 5609.
[2] (a) G. Ballester, E. Coronado, C. Giménez-Saiz, F. Romero, Angew. Chem. 113 (2001) 814;
(b) Y. Pei, P. Bergerat, O. Kahn, J. Am. Chem. Soc. 116 (1994) 3866;
(c) E. Coronado, J.R. Galán-Mascarós, C.J. Gómez-García, J. Ensling, P. Gütlich, Chem. Eur. J. 6 (2000) 552;
(d) S. Singh, S.K. Dhar, P. Manfrinetti, A. Palenzona, J. Magn. Magn. Mater. 250 (2002) 190.
[3] (a) M.C. Yin, X.F. Lei, M. Li, L.J. Yuan, J.T. Sun, J. Phys. Chem. Solids 67 (2006) 1372;
(b) C. Edder, C. Piguet, J.C.G. Bünzli, G. Hopfgartner, Chem. Eur. J. 7 (2001) 3014;
(c) S.J.A. Pope, B.J. Coe, S. Faulkner, E.V. Bichenkova, X. Yu, K. Douglas, J. Am. Chem. Soc. 126 (2004) 9490.
[4] O. Margeat, P.G. Lacroix, J.P. Costes, B. Donnadieu, C. Lepetit, K. Nakatani, Inorg. Chem. 43 (2004) 4743.
[5] (a) B. Zhao, P. Cheng, X.Y. Chen, C. Cheng, W. Shi, D.Z. Liao, S.P. Yan, Z.H. Jiang, J. Am. Chem. Soc. 126 (2004) 3012;
(b) H. Deng, S.G. Shore, J. Am. Chem. Soc. 113 (1991) 8538;
(c) Y.P. Ren, L.S. Long, B.W. Mao, Y.Z. Yuan, R.B. Huang, L.S. Zheng, Angew. Chem., Int. Ed. 42 (2003) 532.
[6] (a) C.E. Plecnik, S. Liu, S.G. Shore, Acc. Chem. Res. 36 (2003) 499;
(b) C.L. Cahill, D.T. de Lill, M. Frisch, CrystEngComm. 9 (2007) 15;
(c) Y.F. Zhou, M.C. Hong, X.T. Wu, Chem. Commun. (2006) 135.
[7] (a) R.G. Pearson, J. Am. Chen. Soc. 85 (1963) 3533;
(b) X.J. Gu, D.F. Xue, Inorg. Chem. 45 (2006) 9257;
(c) S.C. Manna, S. Konar, E. Zangrando, J. Ribas, N.R. Chaudhuri, Polyhedron 26 (2007) 2507;
(d) S. Ueki, A. Okazawa, T. Ishida, T. Nogami, H. Nojiri, Polyhedron 26 (2007) 1970.
[8] (a) W. Su, R. Cao, M.C. Hong, J. Chen, J. Liu, Chem. Commun. (1998) 1389;
(b) Y.P. Ren, L.S. Long, B.W. Mao, Y.Z. Yuan, R.B. Huang, L.S. Zheng, Angew. Chem., Int. Ed. 42 (2003) 532;
(c) H. Maas, A. Currao, G. Calzaferri, Angew. Chem., Int. Ed. 41 (2002) 2495;
(d) H.Z. Kou, B.C. Zhou, S. Gao, R.J. Wang, Angew. Chem. 115 (2003) 3410.
[9] (a) Bruker, APEX II software, Version 6.12, Bruker AXS Inc., Madison, WI, USA, 2004;
(b) G.M. Sheldrick, SHELXL-97, Program for X-ray Crystal Structure Refinement, University of Göttingen, Göttingen, Germany, 1997.
[10] (a) Y.B. Dong, M.D. Smith, H.C. zurLoye, Angew. Chem. 112 (2000) 4438;
(b) J.W. Cheng, J. Zhang, S.T. Zheng, M.B. Zhang, G.Y. Yang, Angew. Chem., Int. Ed. 45 (2006) 73;
(c) J.Y. Lu, Coord. Chem. Rev. 246 (2003) 327.
[11] Y.C. Qiu, H.G. Liu, Y.H. Li, H. Deng, R.H. Zeng, G.Y. Zhou, M. Zeller, Inorg. Chem. Commun. 10 (2007) 1399.
[12] (a) F.A. Cotton, L.M. Daniels, P.L. Huang, Inorg. Chem. Commun. 4 (2001) 319;
(b) C. Turta, D. Prodius, V. Mereacre, S. Shova, M. Gdaniec, Y.A. Simonov V. Kuncser, G. Filoti, A. Caneschi, L. Sorace, Inorg. Chem. Commun. 7 (2004) 576.
[13] (a) A. Bondi, J. Phys. Chem. 68 (1964) 441;
(b) B. Zhao, X.Y. Chen, W.Z. Wang, P. Cheng, B. Ding, D.Z. Liao, S.P. Yan, Z.H. Jiang, Inorg. Chem. Commun. 8 (2005) 178.
[14] E.C. Lee, D. Kim, P. Jurecka, P. Tarakeshwar, P. Hobza, K.S. Kim, J. Phys. Chem. A 111 (2007) 3446.
[15] (a) X.D. Guo, G.S. Zhu, Z.Y. Li, Y. Chen, X.T. Li, S.L. Qiu, Inorg. Chem. 45 (2006) 4065;
(b) T. Akitsu, Y. Einaga, Polyhedron 25 (2006) 2655.
[16] (a) A. Majumder, G.M. Rosair, A. Mallick, N. Chattopadhyay, S. Mitra, Polyhedron 25 (2006) 1753;
(b) H. Keypour, S. Salehzadeh, R.G. Pritchard, R.V. Parish, Polyhedron 19 (2000) 1633.

[17] (a) T. Yamada, S. Shinoda, H. Sugimoto, J. Uenishi, H. Tsukube, Inorg. Chem. 42 (2003) 7932;
(b) S. Petoud, S.M. Cohen, J.C.G. Bünzli, K.N. Raymond, J. Am. Chem. Soc. 125 (2003) 13324.
[18] (a) G.R. Choppin, D.R. Peterman, Coord. Chem. Rev. 174 (1998) 283;
(b) B. Zhao, X.Y. Chen, P. Cheng, D.Z. Liao, S.P. Yan, Z.H. Jiang, J. Am. Chem. Soc. 126 (2004) 15394.
[19] (a) Z.Y. Li, G.S. Zhu, X.D. Guo, X.J. Zhao, Z. Jin, S.L. Qiu, Inorg. Chem. 46 (2007) 5174;
(b) X.P. Yang, R.A. Jones, J. Am. Chem. Soc. 127 (2005) 7686;
(c) D.A. Chengelis, A.M. Yingling, P.D. Badger, C.M. Shade, S. Petoud, J. Am. Chem. Soc. 127 (2005) 16752;
(d) H. Xin, Y. Ebina, R. Ma, K. Takada, T. Sasaki, J. Phys. Chem. B 110 (2006) 9863.
[20] S. Petoud, J.-C.G. Bünzli, K.J. Schenk, C. Piguet, Inorg. Chem. 36 (1997) 1345.
[21] C. Marchal, Y. Filinchuk, D. Imbert, J.-C G. Bü1nzli, M. Mazzanti, Inorg. Chem. 45 (2007) 4262.

antitumor properties (such as cytostasan [16]). With regard to the aim to achieve reduced cytotoxicity and increasing the bioavailability of the benzimidazole-platinum complexes different modifications of this heterocycle have been reported [17,18]. Here we report on the synthesis, crystal structure, UV–Vis, IR, Raman, EPR and NMR spectroscopic properties of new Cd(II) and Cu(II) complexes with chelating ligand. Their coordination chromophores and shape of polyhedra have also been compared.

2. Experimental

2.1. Physical measurements and instrumentation

Elemental analyses were run on a Model 240 Perkin–Elmer CHN Analyzer. Infrared spectra (Perkin–Elmer 180 spectrophotometer; 4000–400 cm^{-1}) were recorded in KBr and FIR spectra (400–30 cm^{-1}) in Nujol with specimens applied as suspension of the complexes in Nujol onto a polyethylene window. Raman spectra were performed at room temperature with a Bio-Rad spectrometer, resolution 4 cm^{-1}. The incident radiation (λ = 1064 nm) was provided by a Neodymium laser YAG (Spectra-Physics). The electronic spectra (Cary 5 UV–Vis–NIR spectrophotometer; 5000–30 000 cm^{-1}) were recorded in Nujol mulls. The visible-range absorption spectra of Cu(II) complexes in aqueous solution were recorded on a Specord M-500 (Carl Zeiss, Jena) spectrophotometer.

Magnetic measurements were carried out on a magnetic susceptibility balance (Sherwood Scientific) at room temperature by Guoy's method using $Hg[Co(NCS)_4]$ as the calibrant.

Electron paramagnetic resonance (EPR) spectra were performed on a Bruker ESP 300 E spectrometer at the X-band frequency (about 9.45 GHz) and equipped with the Bruker NMR gaussmeter ER 035 M and the Hewlett–Pacard microwave frequency counter HP 5350B [19]. The spectra were analyzed by a computer simulation program written by dr Andrew Ozarowski, National High Magnetic Field Laboratory, Florida University, as well as applying BRUKER program WIN EPR SimFonia version 1.25.

^1H and ^{13}C NMR spectra were run on Mercury-400BB spectrometer. ^1H NMR spectra were recorded at 400.09 MHz. Chemical shifts were referenced to the residual proton signals of CD_3OD (3.30 ppm). ^{13}C NMR were run at 100.60 Hz (standard methanol $^{13}CD_3OD$, 50.28 ppm). $Cd(NO_3)_2 \cdot 4H_2O$ and $Cu(NO_3)_2 \cdot 3H_2O$ were purchased from Merck Chemical Company and 2-hydroxymethylbenzimidazole (Aldrich 97%) were used as received.

2.2. Synthesis

2.2.1. Preparation of $[CdL_2(NO_3)_2]$ (1)

2-CH_2OHBIm (L; 0.5 mmol) dissolved in 25 ml of pure EtOH was stirred with $Cd(NO_3)_2 \cdot 4H_2O$ dissolved in 25 ml of redistilled water. The molar ratio *M*/*L* was 1:2. The solution was left to crystallize at room temperature. After six weeks, colourless crystals, suitable for X-ray, were obtained. The precipitate was separated by filtration and washed with isopropanol, before drying under vacuum. The product was collected in 75% yield.

Anal. Calc. for $C_{16}H_{16}N_6O_8Cd$: C, 36.34; H, 3.03; N, 15.77. Found: C, 36.34; H, 2.95; N, 15.73%. ^1H NMR: (400.09 MHz, 295 K, CD_3OD) δ: 4.85 (1H, O*H*), 4.90 (s, 2H, CH_2), C–$H_{\text{benzimidazole ring}}$: 7.28 H(5), 7.31 H(6), 7.62 H(7), 7.64 H(4); ^{13}C NMR: (100.60 MHz, 295 K, CD_3OD) δ: 58.39 (CH_2OH), 138.87 (*C*=N), $C_{\text{benzimidazole ring}}$: 116.67 C(4,7), 125.47 C(5,6), 157.17 C(8,9);

IR (KBr, Nujol): ν (cm^{-1}) 3206 (vb), 1775 (m), 1735 (m), 1628 (s), 1596 (s), 1555 (s), 1457 (vs), 1412 (vs), 1385 (vs), 1334 (vs), 1278 (vs), 1080 (vs), 1032 (vs), 750 (vs), 644 (m), 486 (s), 426 (s), 398 (m), 278 (s), 198 (vb), 152 (vb), 121 (vb);

2.2.2. Preparation of $[CuL_2(NO_3)](NO_3)(H_2O)$ (2) and mer-$[CuL_3](NO_3)_2(H_2O)$(*i*-PrOH) (**4**)

The coordination compounds **2** and **4** were prepared according to the following general procedure: 1 mmol (0.2416 g) of the $Cu(NO_3)_2 \cdot 3H_2O$ and 2 mmol (0.2964 g) of the ligand were each dissolved in ca. 10 mL of ethanol/water (2:1) solution. Under vigorous stirring the ligand solution was then added slowly to the Cu(II)-salt solution. After the addition was complete, the coloured solution was stirred for 1 h and filtered off to remove any undissolved material. Usually, after a few days green crystals of $[CuL_2(NO_3)](NO_3)(H_2O)$ **2** were separated as the first fraction. These were isolated by filtration and dried under high vacuum.

Anal. Calc. for $C_{16}H_{18}N_6O_9Cu$: C, 38.29; H, 3.62; N, 16.75. Found: C, 38.41; H, 3.50; N, 16.42%. IR (KBr,): ν (cm^{-1}) 3369 (vb), 3229 (vb), 3210 (vb), 1627 (m), 1593 (s), 1549 (s), 1476(s), 1459 (s), 1436 (vb), 1383 (vs), 1317 (vs), 1283 (vs), 1066 (vs), 1038 (vs), 763 (s), 750 (vs), 430 (vs), 397 (s), 330 (vs), 309 (vs), 290 (vs), 241 (m), 211 (s), 175 (s), 142 (vb); Raman: ν (cm^{-1}) 3203 (m), 3076 (vs), 2946 (vs), 2875 (s), 1625 (s), 1549 (vs), 1447 (s), 1344 (m), 1282 (vs), 1241 (m), 1096 (vs), 1048 (vs), 811 (s), 706 (s), 576 (s), 532 (m), 420 (s), 320 (s), 293 (s), 220 (s), 184 (vs).

After ca. one week turquoise blue crystals of $[CuL_3](NO_3)_2(H_2O)$ were separated from the remaining solution (second fraction). The complex was filtered off and re-crystallized from isopropanol (note: the solvent participates in the structure of the compounds: $[CuL_3](NO_3)_2(H_2O)$(*i*-PrOH) **4**) and dried under high vacuum.

Anal. Calc. for $C_{27}H_{34}N_8O_{11}Cu$: C, 45.66; H, 4.83; N, 15.78. Found: C, 45.86; H, 4.60; N, 15.77%. IR (KBr,): ν (cm^{-1}) 3490 (vb), 3216 (vb), 2915 (vb), 2843 (vs), 1624 (m), 1593 (s), 1455 (s), 1436 (vb), 1378 (vs), 1343 (vs), 1072 (vs), 1038 (vs), 743 (s), 487 (m), 437 (m), 432 (m), 385 (s), 333(s), 329 (s), 300 (s), 286 (m), 247 (m), 208 (m), 167 (vb), 142 (vb). Raman: ν (cm^{-1}) 3077 (s), 2915 (vs), 2881 (vs), 2849 (vs), 1598 (vs), 1542 (s), 1458 (s), 1280 (vs), 1240 (m), 1096 (m), 1046 (vs), 1008 (s), 706 (s), 639 (s), 540 (s), 501 (s), 430 (s), 350 (m), 307 (m), 276 (s), 193 (s).

2.2.3. Preparation of $[CdL_3](NO_3)_2$ L(EtOH)$_{0.25}$ (**3**)

The ligand (0.5 mmol) dissolved in 20 mL of pure EtOH was added to cadmium salts ($Cd(NO_3)_2 \cdot 4H_2O$, 2 mmol) dissolved in redistilled water (20 mL). The molar ratio *M*/*L* was 1:4. The mixture was stirred for about 2 h and left to crystallize at lower temperature (2–5 °C). After four weeks, colourless crystals suitable for X-ray were obtained. The product was collected by filtration and washed with the same solvent as used in the first complex of cadmium. The crystals were dried in vacuum box. The precipitate was collected in 70% yield.

Anal. Calc. for $C_{32.5}H_{33.5}N_{10}O_{10.5}Cd$: C, 46.43; H, 4.03; N, 16.66. Found: C, 46.17; H, 3.74; N, 16.73%. ^1H NMR: (400.09 MHz, 295 K, CD_3OD) δ_{complex}: 4.90 (1H, O*H*), 4.95 (s, 2H, CH_2), C–$H_{\text{benzimidazole ring}}$: 7.23 H(5), 7.25 H(6), 7.56 H(7), 7.58 H(4); δ_{EtOH}: 1.17 (s, 3H, CH_3), 3.61 (s, 2H, CH_2), 3.13 (1H, O*H*); ^{13}C NMR: (100.60 MHz, 295 K, CD_3OD) δ: 58.70 (CH_2OH), 139.31 (*C*=N), $C_{\text{benzimidazole ring}}$: 116.50 C(4,7), 125.21 C(5,6), 157.32 C(8,9); δ_{EtOH}: 58.70 (CH_2), 19.21 (CH_3); IR (KBr, Nujol): ν (cm^{-1}) 3198 (vb), 1625 (s), 1597 (s), 1545 (s), 1457(vs), 1385 (vs), 1334 (vs), 1279 (vs), 1073 (vs), 1035 (vs), 914 (s), 825 (s), 750 (vs), 734 (vs), 648 (m), 483 (s), 428 (s), 387 (vs), 319 (vb), 277(s), 252 (m), 190 (vb), 118 (vb).

2.3. Crystal structure determination

Diffraction intensity data for single crystal of the Cd(II) and Cu(II) complexes were collected at room temperature on a KappaCCD (Nonius) diffractometer with graphite-monochromated MoK_α radiation (λ = 0.71073 Å). Corrections for Lorentz, polarization and absorption effects [20,21] were applied. The structures

Table 1
Crystal data and structure refinement for **1, 2, 3** and **4**

Empirical formula	**1**	**2**	**3**	**4**
Formula weight	532.75	501.90	840.59	710.16
Temperature (K)	293(2)	293(2)	293(2)	293(2)
Wavelength (Å)	0.71073	0.71073	0.71073	0.71073
Crystal system, space group	tetragonal, $P4_32_12$	triclinic, $P\bar{1}$	monoclinic, $C2/c$	triclinic, $P\bar{1}$
Unit cell dimensions				
a (Å)	8.2891(2)	8.5639(2)	24.3190(2)	9.6793(2)
b (Å)	8.2891(2)	9.5933(3)	25.4282(2)	13.2706(3)
c (Å)	29.0428(6)	13.5311(3)	15.1217(1)	13.2941(2)
α (°)	90	80.141(2)	90	90.744(1)
β (°)	90	79.195(2)	127.261(1)	108.259(1)
γ (°)	90	66.475(1)	90	102.522(1)
Volume (Å^3)	1995.51(8)	995.45(4)	7442.4(1)	1577.03(5)
Z, Calculated density (Mg/m^3)	4, 1.773	2, 1.674	8, 1.500	2, 1.496
Absorption coefficient (mm^{-1})	1.153	1.162	0.656	0.764
F(000)	1064	514	3428	738
Crystal size (mm)	0.37 × 0.35 × 0.32	0.32 × 0.17 × 0.05	0.30 × 0.20 × 0.10	0.15 × 0.12 × 0.10
Theta range for data collection (°)	3.55–27.50	3.44–30.04	2.36–27.44	3.16–27.47
Limiting indices	$-12 \leqslant h \leqslant 12$, $-8 \leqslant k \leqslant 8$, $-29 \leqslant l \leqslant 43$	$-10 \leqslant h \leqslant 12$, $-12 \leqslant k \leqslant 13$, $-16 \leqslant l \leqslant 19$	$0 \leqslant h \leqslant 31$, $-32 \leqslant k \leqslant 32$, $-19 \leqslant l \leqslant 15$	$-12 \leqslant h \leqslant 12$, $-16 \leqslant k \leqslant 17$, $-16 \leqslant l \leqslant 17$
Reflections collected/unique/observed [$I > 2$sigma(I)]	4209/2221 [$R_{int} = 0.022$]	9137/5754 [$R_{int} = 0.0255$]	16477/8389 [$R_{int} = 0.0121$]	12405/7175 [$R_{int} = 0.0192$]
Completeness to 2θ (%)	$2\theta = 27.50$ 98	$2\theta = 30.04$ 98.7	$2\theta = 27.44$ 98.8	$2\theta = 27.47$ 99.2
Absorption correction	Semi-empirical from equivalents	Semi-empirical from equivalents	Semi-empirical from equivalents	Semi-empirical from equivalents
Maximum and minimum transmission	0.6950 and 0.6615	0.9442 and 0.7074	0.9373 and 0.8275	0.9275 and 0.8940
Refinement method	Full-matrix least-squares on F^2	Full-matrix least-squares on F^2	Full-matrix least-squares on F^2	Full-matrix least-squares on F^2
Data/restraints/parameters	2221/1/141	5754/4/313	8389/3/494	7175/34/430
Goodness-of-fit on F^2	1.090	1.047	1.124	1.069
Final R indices [$I > 2$sigma(I)]	$R_1 = 0.0234$, $wR_2 = 0.0514$	$R_1 = 0.0421$, $wR_2 = 0.0982$	$R_1 = 0.0397$, $wR_2 = 0.1037$	$R_1 = 0.0407$, $wR_2 = 0.1094$
R indices (all data)	$R_1 = 0.0258$, $wR_2 = 0.0523$	$R_1 = 0.0593$, $wR_2 = 0.1074$	$R_1 = 0.0506$, $wR_2 = 0.1180$	$R_1 = 0.0468$, $wR_2 = 0.1147$
Largest differences in peak and hole (e Å^3)	0.196 and −0.178	0.333 and −0.463	0.887 and −0.755	0.654 and −0.498

were solved by direct methods using the program package SIR-92 [22] and refined using a full-matrix least square procedure on F^2 using SHELXL-97 [23]. Anisotropic displacement parameters for all non-hydrogen atoms and isotropic temperature factors for hydrogen atoms were introduced. Further details of the structures analysis are given in Table 1 and in the Supplementary data.

3. Results and discussion

3.1. Crystal structure

3.1.1. The molecular structure of $[CdL_2(NO_3)_2]$ (**1**)

The cadmium complex crystallizes in the tetragonal system (space group $P4_32_12$) (Fig. 1.).

Two molecules of 2-CH_2OHBIm **(L)** and two nitrate ions are bounded directly to the metal ion, as bidentate ligands, to give a CdN_2O_6 chromophore. Thus, the Cd atom is eight-coordinated with two pyridinic N-atoms of the benzimidazole rings [N(3) and N(3a)] and six oxygen atoms, two of hydroxymethyl groups O(10) and O(10a), and four of the nitrate ions [O(21), O(23), O(21a), O(23a)]. Cadmium-nitrogen bond distances of 2.268(2) Å are relatively short and cadmium-oxygen distances of 2.377(2)–2.827(2) Å are, in general, in agreement with those found in the literature [25–31]. Selected geometrical data for **1** are given in Table 2. The most interesting feature of the cadmium complex is the shape of coordination polyhedron which can be described as a transition form between the dodecahedron and the tetragonal antiprism. It consists of an equatorial plane [O(23), O(21), O(23a), O(21a)] – typical for the antiprism, and a part of the dodecahedron, in which the oxygen atoms occupy the vertices with the five neighbours and the nitrogen atoms are in the vertices with four neighbours (compare Fig. 1).

The crystal packing is stabilized by the moderate intermolecular hydrogen bonds of N–H···O and O–H···O types (Table 6). Additionally, weak interactions of C–H···π type exist between C(5)-H and C(10)-H and π electron systems of the neighbouring benzimidazole rings (Fig. 2.).

3.1.2. The molecular structure of $[CuL_2(NO_3)](NO_3)(H_2O)$ (**2**)

The copper ion is five-coordinated with ligation of N, O-donor atoms of two 2-CH_2OHBIm residues and one oxygen atom of the nitrate ion (Fig. 3). Cu(II) polyhedron could be described as a distorted tetragonal pyramid with a structural index parameter (τ) value of 0.105 (the trigonality index τ is calculated using the equation $\tau = (\beta - \alpha)/60$ [32]; for perfect square pyramidal and trigonal bipyramidal geometries the values of τ are zero and unity, respectively). The form of distortion in the $[CuL_2(NO_3)]^+$ cation involves not only bond-length but also apparent bond-angles distortion (Table 3). In the case of coordination cation, both N(imidazole)- and O(hydroxymethyl)-donors of each of two 2-CH_2OHBIm ligands are involved in a five-membered chelate rings, from which one is rather symmetric with Cu–N(23) = 1.9525(2) Å and Cu–O(2) = 2.0385(2) Å, and the second – clearly asymmetric (Cu–N(3) = 1.9467(2) Å; Cu–O(1) = 2.2812(2) Å). The basal plane of the distorted pyramid is formed by N(3), N(23), O(2) and O(41) and the apex of the pyramid is occupied by the oxygen atom, O(1), of the hydroxymethyl group. Selected bond distances and valence angles are listed in Table 3.

The H_2O molecule and NO_3^- ion present in the complex molecule are engaged in very strong hydrogen bonding interactions. There are two kinds of hydrogen bonds between N–H imidazole molecules and nitrate oxygen atoms: typical N–H···O bonds. The water molecule participates in hydrogen bonding to the oxygen atom of the hydroxymethyl group of the ligand, to oxygen atom of NO_3^- ion and to oxygen atoms of coordinated and non-coordinated nitrate group. The details of the hydrogen bond geometry are given in Table 6.

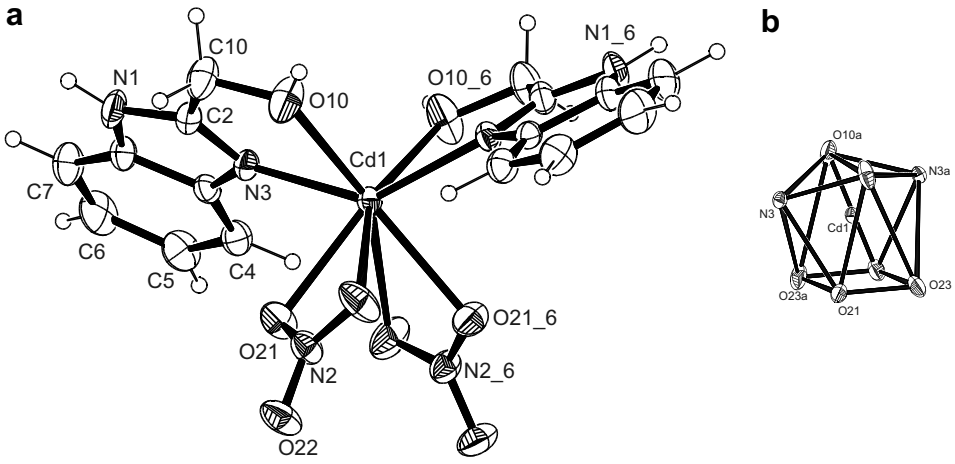

Fig. 1. Molecular structure with the atom numbering scheme (a) and coordination polyhedron (b) of **1**. Atomic displacement ellipsoids are shown at the 30% probability level (ORTEP-32 [24]).

Table 2
Bond lengths (Å) and valence angles (°) for **1**

Bond lengths (Å)			
Cd(1)–N(3)	2.268(2)	Cd(1)–O(21)	2.398(2)
Cd(1)–O(10)	2.377(2)	Cd(1)–O(23)	2.827(2)
Valence angles (°)			
N(3)–Cd(1)–O(10)	70.15(9)	N(3)a–Cd(1)–O(21)	133.90(7)
N(3)a–Cd(1)–N(3)	140.17(1)	N(3)–Cd(1)–O(21)	80.40(7)
N(3)–Cd(1)–O(10)a	85.98(7)	O(10)a–Cd(1)–O(21)	150.87(8)
N(3)a–Cd(1)–O(10)	85.98(7)	O(10)–Cd(1)–O(21)	92.85(9)
O(10)a–Cd(1)–O(10)	106.67(1)	N(3)–Cd(1)–O(21)a	133.90(7)
O(10)–Cd(1)–O(21)a	150.87(8)	O(21)–Cd(1)–O(21)a	78.75(1)

3.1.3. The molecular structure of $[CdL_3](NO_3)_2L(EtOH)_{0.25}$ (**3**)

The molecular structure of cadmium(II) complex **3**, which crystallizes in the monoclinic space group *C*2/c, is shown in Fig. 4.

The central ion is surrounded by three molecules of 2-CH_2OH-BIm, which act as bidentate ligands. 2-CH_2OHBIm is bound to the metal through the pyridine-like nitrogen atoms of the benzimidazole ring and oxygen atoms of the hydroxymethyl groups. Structural data indicated that coordination geometry around the Cd(II) ion can be considered as distorted pseudo-octahedron (chromophore type CdN_3O_3). The equatorial plane is formed by N(3), N(23), N(33) and O(3) atoms with Cd-N bond lengths ranging from 2.207(2) to 2.247(2) Å and Cd–O = 2.497(2) Å. Two coordination axial sites are occupied by O(1) and O(2) oxygen atoms of $-CH_2OH$ groups with Cd–O distances of 2.427(3) and 2.450(2) Å. Selected bond distances and valence angles are given in Table 4. The most interesting features of the crystal packing is existence of channels running along [1 0 1] direction, filled with the free ligand and ethanol molecules (Fig. 5).

The channels comprise 26.5% of the unit cell volume (6.625% per each of four symmetry-related voids). Complex molecules are held together by hydrogen bonds of the O–H···O and N–H···O types, the geometry of which is given in Table 6.

3.1.4. The molecular structure of mer-$[CuL_3](NO_3)_2(H_2O)$(*i*-PrOH) (**4**)

The crystal of *mer*-$[CuL_3] \cdot (NO_3)_2 \cdot H_2O \cdot i$PzOH consist of CuL_3^{2+} cation, nitrate anions, and water and propan-2-ol molecules as co-crystallizing solvents. The copper atom has a distorted tetragonal bipyramid coordination geometry with the equatorial plane formed by three nitrogen atoms, N(23), N(3), N(33), from the imid-

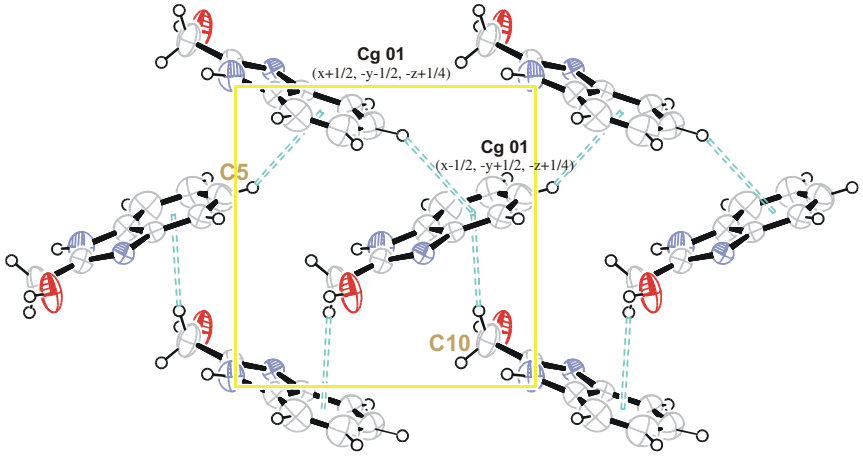

Fig. 2. Weak hydrogen bond of C–H···π type (category II and III in the classification of Malone at al [42]) in the complex **1**. Cg 01denotes the gravity centre of the C(5)-C(9) benzene ring

D-H···A	D-H (Å)	H···A (Å)	D···A (Å)	∠ D-H···A (°)
C(5)-H(5)···Cg 01$_{(x+1/2, -y-1/2, -z+1/4)}$	0.93	3.095	3.880	143.2
C(10)-H(10b)···Cg 01$_{(x-1/2, -y+1/2, -z+1/4)}$	0.97	2.780	3.706	159.0

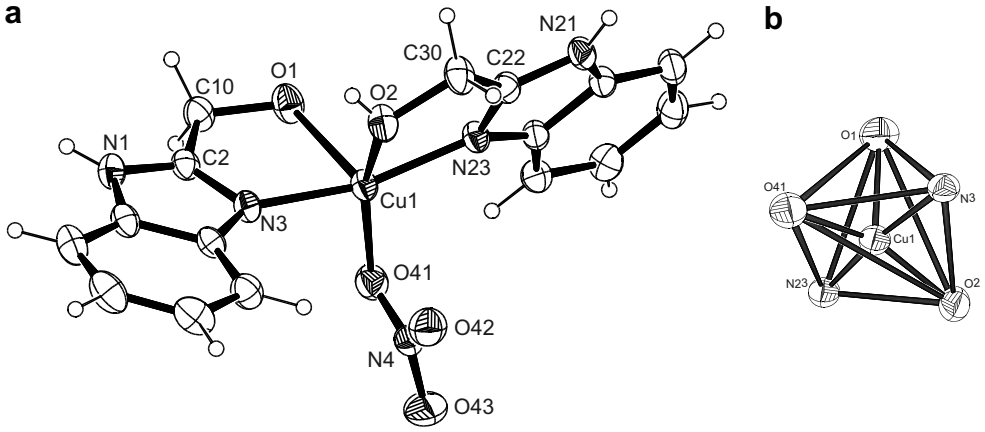

Fig. 3. Molecular structure with the atom numbering scheme (a) and coordination polyhedron (b) of **2**. Details as for Fig. 1.

Table 3
Selected bond lengths (Å) and valence angles (°) for **2**

Bond lengths (Å)				
Cu(1)–N(3)	1.9467(2)	Cu(1)–O(2)	2.0385(2)	
Cu(1)–N(23)	1.9525(2)	Cu(1)–O(1)	2.2812(2)	
Cu(1)–O(41)	2.0340(2)			
Bond angles (°)				
N(3)–Cu(1)–N(23)	166.10(7)		O(41)–Cu(1)–O(2)	157.27(8)
N(3)–Cu(1)–O(41)	96.40(7)		N(3)–Cu(1)–O(1)	77.17(7)
N(23)–Cu(1)–O(41)	96.78(7)		N(23)–Cu(1)–O(1)	98.00(7)
N(3)–Cu(1)–O(2)	88.75(7)		O(41)–Cu(1)–O(1)	91.84(7)
N(23)–Cu(1)–O(2)	80.76(7)		O(2)–Cu(1)–O(1)	110.89(7)

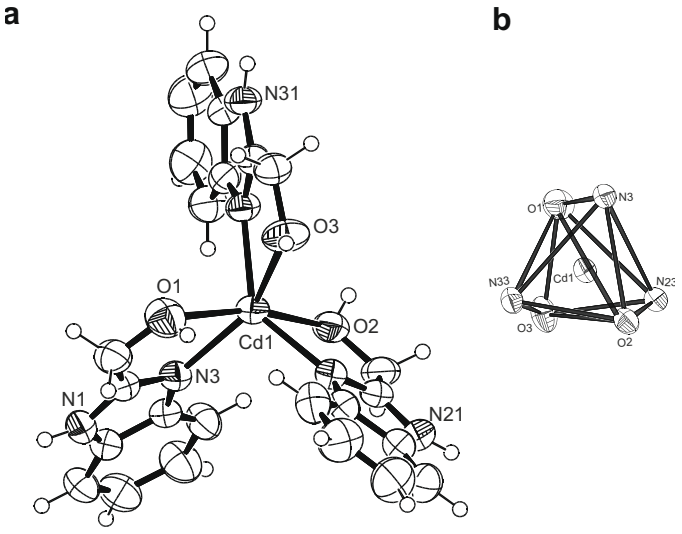

Fig. 4. Molecular structure with the atom numbering scheme (a) and coordination polyhedron (b) of **3**. Details as for Fig. 1.

azole rings of 1-CH_2OHBIm molecules and one oxygen atom O(1), of the hydroxymethyl group of the ligand. Therefore, the structure of the complex (Fig. 6) is assigned as *mer*-$[CuL_3] \cdot (NO_3)_2 \cdot H_2O \cdot$ *i*P-zOH isomer.

The Cu–N distances vary from 1.967(2) to 1.987(2) Å, while Cu–O distance is a little bit longer, 2.057(2) Å (Table 5). The axial positions are occupied by the oxygen atoms of the hydroxymethyl groups of two remaining 2-CH_2OHBIm molecules. The Cu–O apex distances, 2.370(2) and 2.465(2) Å, are longer due to the Jahn–Teller effect. The three ligands act as bidentate, forming a five-membered chelate rings with central ion, however, two of them are asymmetric because of the longer *z*-axis distances. The crystal structure of the complex is stabilized by complicated network of typical and bifurcated hydrogen bonds with the geometric details given in Table 6.

Table 4
Bond lengths (Å) and valence angles (°) for **3**

Bond lengths (Å)			
Cd(1)–N(33)	2.207(2)	Cd(1)–O(1)	2.427(3)
Cd(1)–N(23)	2.226(2)	Cd(1)–O(2)	2.450(2)
Cd(1)–N(3)	2.247(2)	Cd(1)–O(3)	2.497(2)
Valence angles (°)			
N(33)–Cd(1)–N(23)	136.92(9)	N(33)–Cd(1)–N(3)	115.10(9)
N(23)–Cd(1)–N(3)	105.73(8)	N(3)–Cd(1)–O(2)	96.61(8)
N(33)–Cd(1)–O(1)	101.55(9)	O(1)–Cd(1)–O(2)	165.62(8)
N(23)–Cd(1)–O(1)	104.31(1)	N(33)–Cd(1)–O(3)	69.11(8)
N(33)–Cd(1)–O(2)	90.02(8)	N(23)–Cd(1)–O(3)	85.00(8)
N(23)–Cd(1)–O(2)	71.65(9)	N(3)–Cd(1)–O(3)	145.89(9)
O(1)–Cd(1)–O(3)	75.15(9)	O(2)–Cd(1)–O(3)	117.47(9)
N(3)–Cd(1)–O(1)	70.84(8)		

3.2. UV–Vis, EPR spectra and magnetic studies

The UV/Visible spectra of copper(II) complexes suggest that water solution structure of the **2** and **4** complexes are very similar. Within the visible region of **2** and **4** of the Cu(II)-complexes manifest absorption with the λ_{max} of 330 ($\varepsilon = 614\ M^{-1}\ cm^{-1}$) and 726 nm ($\varepsilon = 59\ M^{-1}\ cm^{-1}$) and 330 ($\varepsilon = 760\ M^{-1}\ cm^{-1}$) and 715 nm ($\varepsilon = 61\ M^{-1}\ cm^{-1}$), respectively. This suggests that the Cu centre of **2** can accommodate the H_2O molecule as a sixth ligand and both complexes exist as six coordinated species. In each case, the higher energy transition is assigned to a ligand-based π-π^* transition [33–35] the lower energy of the feature is assigned to d-d transition of hexacoordinated Cu(II) complexes with distorted octahedral geometry. The UV–Vis spectra of **2** in the solid state differ from those found in the solution. The reflectance spectra exhibit a very broad intense absorption between 550 and 900 nm. By means of the Gaussian distribution the following peaks position are established: 625, 875 nm which are typical of pentacoordinated Cu(II) complexes [33] with distorted square pyramidal geometry ($d_{xz},d_{yz}) \leftarrow d_{x^2-y^2}$ and $d_{z^2} \leftarrow d_{x^2-y^2}$, respectively). In addition, the electronic spectra of all the Cu(II) complexes feature a characteristic absorption in the 200–400 nm range. The position of individual bands for **2** and **4** obtained from Gaussian analysis were 228, 263, 321 and 248, 313, 387 nm, respectively which are typical of π–π^* transition of benzimidazole moiety. Furthermore, both of

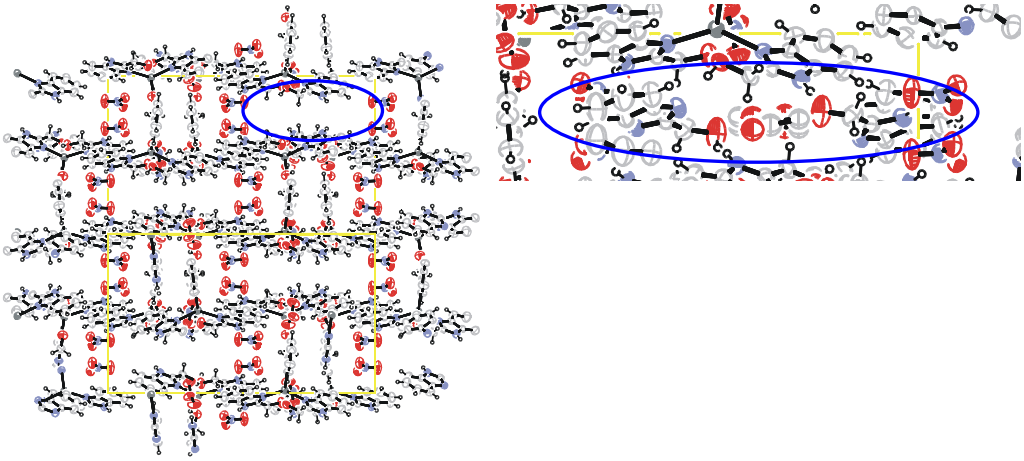

Fig. 5. Crystal packing of $[CdL_3](NO_3)_2L(EtOH)_{0.25}$ with channels viewed along [1 0 1] empty and filled with the free ligand and ethanol molecules.

Table 5
Bond lengths (Å) valence angles (°) for **4**

Bond lengths (Å)			
Cu(1)–N(3)	1.967(2)	Cu(1)–O(1)	2.057(2)
Cu(1)–N(23)	1.982(2)	Cu(1)–O(2)	2.370(2)
Cu(1)–N(33)	1.987(2)	Cu(1)–O(3)	2.465(2)
Valence angles (°)			
N(3)–Cu(1)–N(23)	161.03(7)	N(33)–Cu(1)–O(1)	164.53(7)
N(3)–Cu(1)–N(33)	99.84(7)	N(3)–Cu(1)–O(2)	88.50(7)
N(23)–Cu(1)–N(33)	94.92(7)	N(23)–Cu(1)–O(2)	76.54(7)
N(3)–Cu(1)–O(1)	80.09(7)	N(33)–Cu(1)–O(2)	103.05(7)
N(23)–Cu(1)–O(1)	88.84(6)	O(1)–Cu(1)–O(2)	92.42(6)

Table 6
Hydrogen bonds for **1, 2, 3** and **4** (Å and °)

	D–H···A	D–H (Å)	H···A (Å)	D···A (Å)	∠DHA (°)
1	N(1)–H(1)···O(21)$_{x-1/2,-y+1/2,-z+1/4}$	0.86	2.08	2.918(3)	165
	O(10)–H(10)···O(22)$_{y-1,x,-z}$	0.82	1.91	2.709(3)	165
2	O(2)–H(2O)···O(3)	0.81(1)	1.76(1)	2.550(3)	167(3)
	O(1)–H(1O)···O(23)$_{x,y+1,z}$	0.81(1)	2.14(2)	2.856(3)	147(3)
	O(1)–H(1O)···O(22)$_{x,y+1,z}$	0.81(1)	2.35(2)	3.096(3)	153(3)
	N(1)–H(1N)···O(21)$_{-x,-y,-z}$	0.84(3)	2.12(3)	2.941(3)	164(3)
	N(21)–H(21N)···O(22)$_{-x,-y,\ -z+1}$	0.84(3)	2.08(3)	2.898(3)	165(3)
	O(3)–H(31)···O(43)$_{x-1,y,z}$	0.81(1)	2.13(1)	2.935(4)	175(4)
	O(3)–H(32)···O(22)	0.81(1)	2.15(2)	2.932(4)	161(4)
3	N(1)–H(1)···O(21)$_{-x+3/2,-y+1/2,-z+3/2}$	0.86	2.02	2.850(3)	163
	N(1)–H(1)···O(23)$_{-x+3/2,y+1/2,-z+3/2}$	0.86	2.44	3.156(4)	141
	O(1)–H(1O)···O(41)	0.82	2.03	2.824(4)	162
	N(21)–H(21)···O(4)$_{-x+3/2,y+1/2,-z+3/2}$	0.86	2.01	2.830(4)	160
	O(2)–H(2O)···N(43)$_{x,-y,z-1/2}$	0.82	1.86	2.675(3)	175
	N(31)–H(31)···O(41)$_{-x+1,-y,-z+1}$	0.86	2.10	2.937(3)	165
	N(31)–H(31)···O(43)$_{-x+1,-y,-z+1}$	0.86	2.44	3.125(4)	138
	O(3)–H(3O)···O(22)$_{x-1/2,-y+1/2,z-1/2}$	0.82	1.97	2.758(4)	162
	N(41)–H(41)···O(42)	0.86	2.13	2.956(4)	160
	O(4)–H(4A)···O(22)$_{-x+3/2,y-1/2,-z+3/2}$	0.82	2.16	2.977(6)	171
4	N(1)–H(N1)···O(22)$_{-x+1,-y,-z+2}$	0.86	2.17	2.967(3)	154
	N(1)–H(N1)···O(23)$_{-x+1,-y,-z+2}$	0.86	2.41	3.034(3)	130
	O(1)–H(O1)···O(21)	0.82	1.94	2.736(3)	162
	O(1)–H(O1)···O(23)	0.82	2.41	3.088(3)	141
	N(21)–H(N21)···O(21)$_{-x+1,-y+1,-z+2}$	0.86	2.06	2.842(3)	152
	O(2)–H(O2)···O(4)$_{x+1,y,z,}$	0.82	1.86	2.673(3)	169
	N(31)–H(N31)···O(41)$_{x,y,z-1}$	0.86	2.15	2.955(3)	157
	N(31)–H(N31)···O(42)$_{x,y,z-1}$	0.86	2.48	3.177(4)	139
	O(3)–H(O3)···O(5)$_{-x,-y,-z+2}$	0.82	1.91	2.730(3)	173
	O(4)–H(41O)···O(22)	0.81(1)	2.30(3)	2.913(3)	133(4)
	O(4)–H(42O)···O(43)	0.82(1)	2.10(1)	2.902(4)	169(4)
	O(5)–H(5O)···O(43)	0.82	2.28	3.068(4)	160

the complexes show bands at 399 (**2**) and 387 nm (**4**) which are assigned to LMCT transition from the benzimidazole to the Cu(II) metal centre [33,36,37].

3.3. EPR spectra and magnetic studies

3.3.1. $[CuL_2(NO_3)](NO_3)(H_2O)$ (**2**), mer-$[CuL_3](NO_3)_2(H_2O)(i\text{-}PrOH)$ (**4**)

The powder EPR spectrum of **2** exhibits rhombic character of *g* parameters ($g_z = 2.32$, $g_x = 2.11$, $g_y = 2.04$) in agreement with the apparent distortion of the square-pyramidal geometry of the complex [38] towards trigonal pyramid. On other hand, the EPR spectrum of **4** corresponds to the axial g parameters typical for tetragonal Cu(II) complexes ($g_{II} = 2.255$, $g\perp$ and $A_{II} = 190 \times 10^{-4}\ cm^{-1}$) [39] and shows the copper hyperfine splitting of parallel orientation, a very rare case for solid state Cu(II) complexes (Fig. 7).

This effect is usually observed for Cu(II) centres at relatively long distance and was previously observed by us for the Cu(II) complex coordinated by four 1-benzyl-2-hydroxymethylimidazoles, with a Cu-Cu distance of 9.6 Å [39]. This parameter is in the 8.56–8.98 Å range (except for Cu1–Cu1$_{(-x+1,\ -y,\ -z+1)}$ = 6.83 Å) in **2** and in the 8.96–9.36 Å range in **4**. The EPR parameters of **4** in the solid state are strongly suggestive of O(1)N(3)N(23)N(33) coordination in Cu(II) plane realized by three ligands, in agreement with the crystal structure data. It is noteworthy that the EPR parameters for **4** in methanol solution show a significant increase of g_{II} and decrease of A_{II} ($g_{II} = 2.303$, $g_\perp = 2.062$ and $A_{II} = 155 \times 10^{-4}\ cm^{-1}$, $A_\perp 14 \times 10^{-4}\ cm^{-1}$) as compared to the solid state spectrum. The frozen solution spectrum exhibits seven lines nitrogen hyperfine splitting ($A(^{14}N) = 13 \times 10^{-4}\ cm^{-1}$) in the region of Cu(II) perpendicular orientation (Fig. 8), strongly indicating that three nitrogen donors are still involved in Cu(II) coordination. In view of the spectral parameters the fourth position in Cu(II) plane is most likely substituted by the solvent. The EPR spectrum of the compound **2** in methanol solution exhibits slight rhombic distortion according to $g_z = 2.325$, $g_x = 2.058$, $g_z = 2.073$ and $A_z = 142 \times 10^{-4}\ cm^{-1}$, $A_x = A_y = 14 \times 10^{-4}\ cm^{-1}$ and five line splitting of the perpendicular orientation line due to hyperfine interactions with two nitrogen nuclei $A(^{14}N) = 13 \times 10^{-4}\ cm^{-1}$ (Fig. 8). It supports (X-ray data) that two nitrogen donors are coordinated in the Cu(II) plane. A relatively greater g_{II} and smaller A_{II} as compared to those observed for complexes with two *bis* chelating ON ligands implies [39] mono-

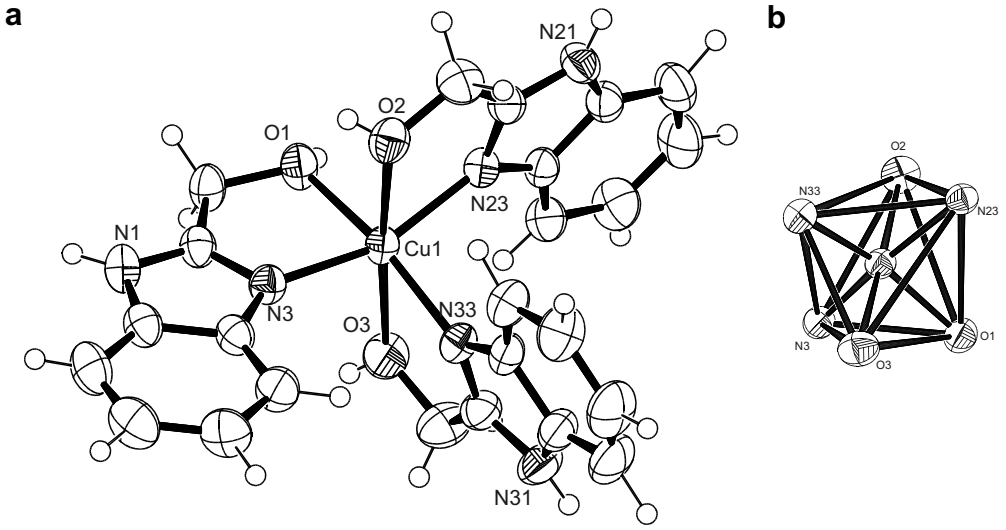

Fig. 6. Molecular structure with the atom numbering scheme (a) and coordination polyhedron (b) of **4**. Details as for Fig. 1.

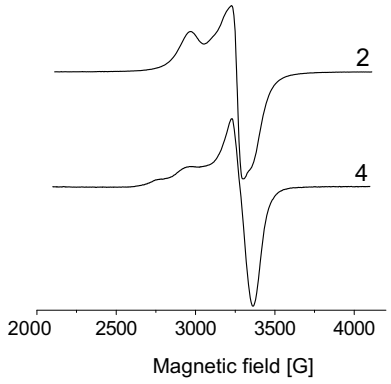

Fig. 7. The EPR spectra of the powdered compounds **2** and **4** at 77 K.

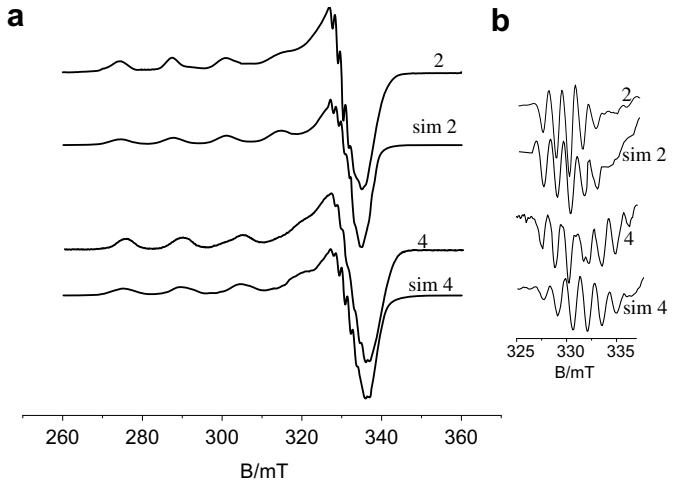

Fig. 8. (a) The EPR spectra of the compounds **2** and **4** in frozen (77 K) methanol solutions together with the spectra simulated using Bruker program, WIN EPR SimFonia version 1.25 with the parameters presented in the text; (b) the fragments of the experimental and simulated spectra after differentiation of dA/dB signals.

dentate binding of the ligands; the remaining coordination positions are occupied by solvent molecules.

The magnetic susceptibility was measured for powder samples of the complexes **2** and **4** at room temperature. The calculated magnetic moment values for copper(II) complexes are 1.82 MB and 1.93 MB, respectively, which are very close to that of the spin only value (1.73 MB) expected for complexes having one Cu(II) ion with single unpaired electron sited in an essentially $d_{x^2-y^2}$ orbital.

3.4. IR(R) spectra

Selected vibration bands of the free ligand and their Cu(II), Cd(II) complexes, which are useful for determining the ligand's mode of coordination, are given in Table 7. In the IR spectra the $\nu_{(O\text{-}H)}$ bands of 2-hydroxymethylbenzimidazole complexes are shifted by 27–58 cm^{-1} to lower wavenumbers and the intense heteroatomic ring vibrations (C=N) are shifted by 17–21 cm^{-1} to higher wavenumbers in comparison to the absorption of the free ligand. Such shifts in the mentioned bands upon coordination are consistent with bidentate coordination of the ligand through the hydroxymethyl oxygen and pyridine-like nitrogen atom of 2-hydroxymethylbenzimidazole. In addition, the electron accepting capabilities of the central ion can be estimated by comparing the O–H and C=N stretching vibration bonds of the ligand. For this reason Table 7 shows a comparison of IR stretching vibrations between the free ligand and **1**, **2**, **3** and **4** compounds. The Δ values calculated from IR data indicate that Cd(II) ions are evidently better acceptors compared to Cu(II). Furthermore, the IR spectra have presented evidence for the different coordination mode of the NO_3^- ions (in agreement with X-ray data). The frequency difference of the vibrations $\Delta\nu = 40$ ($\Delta\nu = 1774–1735$ cm^{-1}) [40,41] indicate the bidentate coordination of nitrate in the **1**. Two kinds of bands 1432 and 1383 cm^{-1} in **2** confirm the existence of monocoordinated and non-coordinated NO_3^- ion, respectively. For other **3** and **4** compounds the absorption bands at 1385 and 1378 cm^{-1} reveal that the charge of the cationic complex is balanced by two non-coordinated nitrate anions. Moreover, in the far-IR spectra new bands, not detected in the spectrum of 2-hydroxymethylbenzimidazole, are observed, which arise from ν(M–O) and ν(M–N) stretches, respectively (Table 7).

3.5. NMR spectra

The NMR spectra confirmed X-ray data of the chelating mode of coordination of 2-hydroxymethylbenzimidazole. Metal coordina-

Table 7
Selected IR (*R*) spectral data for **1, 2, 3** and **4** (cm^{-1})

Assignment	Ligand	**1**	**2**	**3**	**4**
$\nu(OH)_{H_2O}$			3369		3490
ν (O–H)	3256b	3206 ($\Delta = -50$)	3229 ($\Delta = -27$)	3198vb ($\Delta = -58$)	3216 ($\Delta = -40$)
ν benzene ring	1620(*1625*)	1628	1627 (*1625*)	1628	1624 (*1622*)
δ (C=C, C=N)	1588, 1487, 1438 (*1591, 1489, 1454*)	1596, 1457 ($\Delta = 19$)	1596, 1459 ($\Delta = 21$) (*1598, 1447*)	1597, 1457 ($\Delta = 19$)	1593, 1455 ($\Delta = 17$) (*1598, 1458*)
ν (NO_3)		1412, 1775,1735,$\Delta = 40$	1432, 1383	1385	1378
δ (C–O)	1055, 1036 (*1061, 1034*)	1080, 1032	1066, 1038 (*1096, 1048*)	1073, 1035	1072, 1038 (*1096, 1046*)
ν M–O		278s	330(*338*)	277s	333, 329 (*320*)
ν M–N		198vb	290(*293*)	190vb	286(*290*)

Table 8
^1H and ^{13}C NMR data for the **1** and **3**

	(1H, O*H*)	(s, 2H, CH_2)	H(5)	H(6)	H(7)	H(4)
Ligand	4.82	4.83	7.17	7.19	7.50	7.53
1 $\Delta\delta$	4.85 (+0.03)	4.90 (+0.07)	7.28 (+0.11)	7.31 (+0.12)	7.62 (+0.12)	7.64 (+0.11)
3 $\Delta\delta$	4.90(+0.08)	4.95 (+0.12)	7.23 (+0.06)	7.25 (+0.06)	7.56 (+0.06)	7.58 (+0.05)
Ligand			C(4,7)	C(5,6)		C(8,9)
1 $\Delta\delta$			116.67 (+0.20)	125.47 (+1.23)		157.17 (+0.16)
3 $\Delta\delta$			116.50 (+0.03)	125.21 (+0.97)		157.32 (+0.31)

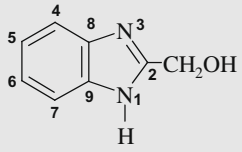

tion of the oxygen atom should lead to deshielding the H and C of the –CH_2OH group of the ligand (Table 8). Such a dieshielding is actually observed with $\Delta\delta$ values of 1.09–1.4 ppm for the ^{13}C resonances while the ^1H resonances (0.03–0.08 ppm) are so close to those of the free alcohol that they cannot be discussed. Likewise the ^{13}C NMR spectra confirm coordination of pyridine-like nitrogen atom of 2-CH_2OHBIm with Cd(II) ion of **1** and **3** (chemical shifts for (*C*=N) are 0.28 and 0.84 ppm, respectively (Table 8). Moreover, the data from Table 8 indicate that the ^{13}C NMR method can be a powerful tool to study weak C–H···π type interactions which were extracted from X-ray data of **1** (see Fig. 2.)

4. Conclusions

The new complexes of Cd(II) (**1**,**3**) and Cu(II) (**2**,**4**) with 2-hydroxymethylbenzimidazole have been prepared and their crystal structures solved using single-crystal X-ray diffraction data. It is noteworthy that the NMR, IR, R and X-ray studies have confirmed a bidentate fashion of coordination of the 2-CH_2OHBIm to the Cd(II) as well to the Cu(II) ions. This results in the formulation of a five-membered chelate ring in which both the N(imidazole) and O(hydroxymethyl) donors of the ligand are involved. Formation of the chelates is not accompanied by loss of a proton from the hydroxyalkyl substituent. The X-ray data extracted from a comparison of Cu(II) ($[CuL_3](NO_3)_2(H_2O)(i\text{-}PrOH)$) **4** and Cd(II) ($[CdL_3](NO_3)_2L(EtOH)_{0.25}$) **3** model complexes with N, O-donor ligand show that both metals may form complexes which exhibit identical structures (distorted octahedral) forming chromophores of the MN_3O_3 type. The most interesting feature of the crystal packing of **3** is the existence of channels running along the [101] direction, filled with the free ligand and ethanol molecules. The channels comprise 26.5% of the unit cell volume (6.625% for each of the four symmetry-related voids). Complex molecules are held together by hydrogen bonds of the O–H···O and N–H···O type. On the other hand, when the central ions are associated with two molecules of 2-CH_2OHBIm, the metals exhibit different structures because of the different role of NO_3^- ions which are employed as additional ligands. Copper complex **2** is five-coordinated with a tetragonal pyramid as coordination polyhedron (CuN_2O_3) however, cadmium forms an eight-coordinated (CdN_2O_6) complex **1**. The interesting feature of the eight-coordinated cadmium complex is the shape of the coordination polyhedron which can be described as a transition form between the dodecahedron and the tetragonal antiprism. The IR data (ν_{O-H} and $\nu_{C=N}$ stretching vibration bonds) indicated that Cd(II) is considerably better acceptor (Lewis acid) than Cu(II) ion for the N, O-donor ligand. But the lower acceptor strength of Cu(II) does not result in longer Cu–N and Cu–O bonds. The similarities and differences revealed in the coordination behaviour of Cu(II) and Cd(II) towards the N, O-donor ligand should be treated as a test of the possibility that copper(II) ions might be displaced by cadmium(II), for example, in intracellular sites. The effective substitution may result in increased ionic copper concentration but is also expected to be one of the possible pathways for heavy-metal intoxication of the redox process in biological systems.

Appendix A. Supplementary data

CCDC 645635, 645636, 645637 and 645638 contains the supplementary crystallographic data for **1**, **2**, **3** and **4**. These data can be obtained free of charge via http://www.ccdc.cam.ac.uk/conts/retrieving.html, or from the Cambridge Crystallographic Data Centre, 12 Union Road, Cambridge CB2 1EZ, UK; fax: (+44) 1223-336-033; or e-mail: deposit@ccdc.cam.ac.ukSupplementary data associated with this article can be found, in the online version, at doi:10.1016/j.poly.2008.07.038.

References

[1] G. Multhaup, A. Schlisksupp, L. Hesse, D. Beher, T. Ruppert, C.L. Masters, K. Beyreuther, Science 271 (1996) 1406.
[2] G. Multhaup, T. Ruppert, A. Schlisksupp, L. Hesse, E. Bill, R. Pipkorn, C.L. Masters, K. Beyreuther, Biochemistry 37 (1998) 7224.
[3] D.R. Brown, H. Kozłowski, J. Chem. Soc., Dalton Trans. (2004) 1907.
[4] M. Waisberg, P. Joseph, B. Hale, D. Beyersmann, Toxicology 192 (2003) 95.
[5] P. O'Brien, H.J. Salacinski, Arch. Toxicol. 72 (1998) 690.

[6] M.J. Sánchez-Moreno, A. Fernández-Botello, R.B. Gómez-Coca, R. Griesser, J. Ochocki, A. Kotynski, J. Niclós-Gutiérrez, V. Moreno, H. Siegel, Inorg. Chem. 43 (2004) 1311.
[7] M.J. Sánchez-Moreno, R.B. Gómez-Coca, A. Fernández-Botello, J. Ochocki, A. Kotynski, R. Griesser, H. Siegel, Org. Biomol. Chem. 1 (2003) 1819.
[8] L.E. Kapinos, B. Song, H. Siegel, Chem. Eur. J. 5 (1999) 1794.
[9] L.E. Kapinos, A. Holý, J. Günter, H. Siegel, Inorg. Chem. 40 (2001) 2500.
[10] F. Seela, T. Wenzel, Helv. Chim. Acta 78 (1995) 833.
[11] K.M. Guckian, J.C. Morales, E.T. Kool, J. Org. Chem. 63 (1998) 9652.
[12] J.W. Ellingboe, W. Spinelli, M.W. Winkley, Y.T. Nguyen, R.W. Parsons, I.F. Moubarak, J.M. Kitzen, D. Von Engen, J.F. Bagli, J. Med. Chem. 39 (1992) 705.
[13] Y. He, J. Yang, B. Wu, L. Risen, E.E. Swayze, Bioorg. Med. Chem. Lett. 14 (2004) 1217.
[14] S. Saluja, R. Zou, J.C. Drach, L.B. Townsend, J. Med. Chem. 39 (1996) 881.
[15] H. Sigel, Chem. Soc. Rev. 3 (2004) 191.
[16] P.N. Preston, Chem. Rev. 74 (1974) 279.
[17] F. Gümüş, F. Izgü, Ö. Algül, FABADJ. Pharm. Sci. 21 (1996) 7.
[18] F. Gümüş, Ö. Algül, J. Inorg. Biochem. 68 (1997) 71.
[19] U. Sakaguchi, Y. Arata, S. Fujiwara, J. Magn. Reson. 9 (1973) 118.
[20] B. V. Nonius, Nonius COLLECT, Delft, The Netherlands 1997-2000.
[21] Z. Otwinowski, W. Minor, Methods Enzymol. 276 (1997) 307.
[22] A. Altomare, G. Cascarano, C. Giacovazzo, C. Guagliardi, M.C. Burla, G. Palidori, M. Camalli, J. Appl. Cryst. 27 (1994) 435.
[23] G.M. Scheldrick, SHELXL-97: Program for Crystal Structure Refinement, University of Göttingen, Germany, 1997.
[24] L. Faruggia, J. Appl. Cryst. 32 (1999) 837.
[25] F. Hueso-Ureña, S.B. Jiménez-Pulido, M.N. Moreno-Carretero, M. Quirós-Olozábal, J.M. Salas-Peregrín, Inorg. Chim. Acta 277 (1998) 103.
[26] M.A. Romero, M.N. Moreno, J. Ruiz, M.P. Sánchez, F. Nieto, Inorg. Chem. 25 (1986) 1498.
[27] E.R. Acuña-Cueva, R. Faure, N.A. Illán-Cabeza, S.B. Jiménez-Pulido, M.N. Moreno-Carretero, M. Quirós-Olozábal, Inorg. Chim. Acta 342 (2003) 209.
[28] A.A. Naiini, V. Young, J.G. Verkade, Polyhedron 14 (1995) 393.
[29] J.M. Grevy, F. Tellez, S. Bernés, H. Nöth, R. Contreras, N. Barba-Behrens, Inorg. Chim. Acta 339 (2002) 532.
[30] N. Niklas, F. Hampel, G. Liehr, A. Zahl, R. Alsfasser, Chem. Eur. J. 7 (2001) 5135.
[31] B. Barszcz, S. Hodorowicz, A. Jabłońska-Wawrzycka, K. Stadnicka, Polyhedron 24 (2005) 627.
[32] A.W. Addison, T.N. Rao, J. Reedijk, J. van Rijn, G.C. Verschoor, J. Chem. Soc., Dalton. Trans. (1984) 1349.
[33] A.B.P. Lever, Inorganic Electronic Spectroscopy, 2nd ed., Elsevier, Amsterdam, 1984.
[34] T.G. Fawcett, E.E. Bernarducci, K. Krogh-Jespersen, H.J. Schugar, J. Am. Chem. Soc. 102 (1980) 2598.
[35] A.K. Nairn, S.J. Archibald, R. Bhalla, B.C. Gilbert, E.J. MacLean, S.J. Tead, P.H. Walton, J. Chem. Soc., Dalton Trans. (2006) 172.
[36] D. Zurita, C. Scheer, J.-L. Pierre, E. Saint-Aman, J. Chem. Soc., Dalton Trans 12 (1996) 4331.
[37] Y. Wang, T.D.P. Stack, J. Am. Chem. Soc. 118 (1996) 13097.
[38] B. Kurzak, A. Kamecka, K. Bogusz, J. Jezierska, Polyhedron 26 (2007) 4345. and reference therein.
[39] B. Barszcz, T. Glowiak, J. Jezierska, Polyhedron 18 (1999) 3713.
[40] K. Nakamoto, Infrared and Raman Spectra of Inorganic and Coordination Compounds, 4th ed., Wiley, New York, 1986.
[41] A.B.P. Lever, Inorganic Electronic Spectroscopy, 2nd ed., Elsevier, Amsterdam, 1984.
[42] J.F. Malone, M.C. Murray, M.H. Charlton, R. Docherty, J. Lavery, J. Chem Soc., Faraday Trans. 93 (1997) 3429.

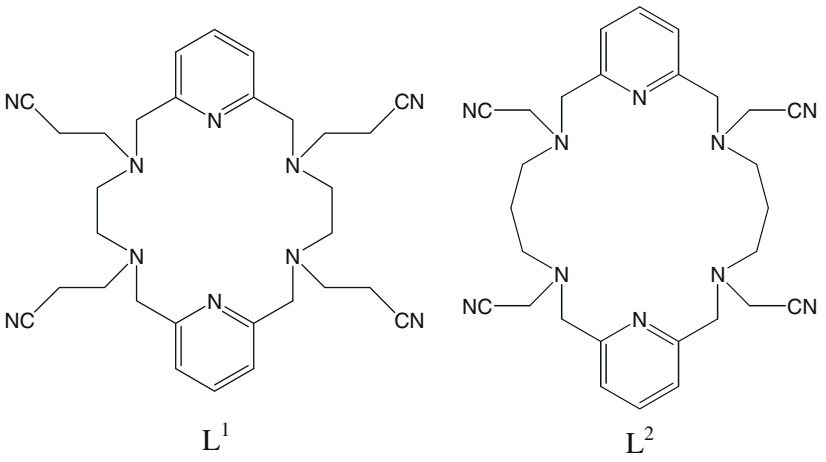

Scheme 1.

2.2.1. $[CdL^1](NO_3)_2$

Anal. Calc. for $CdC_{30}H_{38}N_{12}O_6$ (MW: 775.12): C, 46.5; H, 4.9, N, 21.7. Found: C, 46.3, H, 5.1, N, 21.5%. Yield: 57%. IR (KBr, cm^{-1}): 1604, 1582, 1466 [ν(C=C) and $\nu(C{=}N)_{py}$], 2251, 2426 [ν(C≡N)], 1384 [$\nu(NO_3^-)$]. MS (LSI, *m/z*): $[CdL^1(NO_3)]^+$ 714. $\Lambda_M/\Omega^{-1}cm^2\ mol^{-1}$ (in CH_3CN): 265 (2:1). Colour: white.

2.2.2. $[CdL^1](ClO_4)_2 \cdot CH_3CN$

Anal. Calc. for $CdC_{32}H_{41}Cl_2N_{11}O_8$ (MW: 891.06): C, 43.1; H, 4.6, N, 17.3. Found: C, 43.1, H, 4.7, N, 17.2%. Yield: 62%. IR (KBr, cm^{-1}): 1604, 1583, 1463 [ν(C=C) and $\nu(C{=}N)_{py}$], 2248, 2425 [ν(C≡N)], 1114, 626 [$\nu(ClO_4^-)$]. MS (LSI, *m/z*): $[CdL^1(ClO_4)]^+$ 751. $\Lambda_M/\Omega^{-1}cm^2\ mol^{-1}$ (in CH_3CN): 242 (2:1). Colour: white.

2.2.3. $[CdL^2](NO_3)_2$

Anal. Calc. for $CdC_{28}H_{34}N_{12}O_6$ (MW: 747.06): C, 45.0; H, 4.6, N, 22.5. Found: C, 45.2, H, 4.4, N, 22.6%. Yield: 52%. IR (KBr, cm^{-1}): 1604, 1582, 1466 [ν(C=C) and $\nu(C{=}N)_{py}$], 2251 [ν(C≡N)], 1384 [$\nu(NO_3^-)$]. MS (LSI, *m/z*): $[CdL^2]^{2+}$ 624. $\Lambda_M/\Omega^{-1}cm^2\ mol^{-1}$ (in CH_3CN): 260 (2:1). Colour: white.

2.2.4. $[CdL^2](ClO_4)_2 \cdot H_2O$

Anal. Calc. for $CdC_{28}H_{36}Cl_2N_{10}O_9$ (MW: 839.97): C, 40.0; H, 4.3, N, 16.7. Found: C, 39.8, H, 4.5, N, 16.7%. Yield: 65%. IR (KBr, cm^{-1}): 1612, 1583, 1475, 1459 [ν(C=C) and $\nu(C{=}N)_{py}$], 2248 [ν(C≡N)], 1100, 626 [$\nu(ClO_4^-)$]. MS (LSI, *m/z*): $[CdL^2(ClO_4)]^+$ 723. $\Lambda_M/\Omega^{-1}cm^2\ mol^{-1}$ (in CH_3CN): 233 (2:1). Colour: white.

Table 1
Crystal data and structure refinement for $[CdL^1](NO_3)_2$, $[CdL^1](ClO_4)_2 \cdot CH_3CN$, and $[CdL^2](ClO_4)_2 \cdot H_2O$

	$[CdL^1](NO_3)_2$	$[CdL^1](ClO_4)_2 \cdot CH_3CN$	$[CdL^2](ClO_4)_2 \cdot H_2O$
Empirical formula	$C_{60}H_{76}N_{24}O_{12}Cd_2$	$C_{32}H_{41}N_{11}O_8Cl_2Cd$	$C_{28}H_{36}CdCl_2N_{10}O_9$
Formula weight	1550.25	891.06	839.97
Temperature (K)	293(2)	293(2)	293(2)
Wavelength (Å)	0.71073	0.71073	0.71073
Crystal system, space group	triclinic, $P\bar{1}$	triclinic, $P\bar{1}$	monoclinic, *C2/c*
Unit cell dimensions			
a (Å)	10.9488(7)(10)	10.290(2)	13.314(9)
b (Å)	15.4054	10.822(2)	15.964(11)
c (Å)	19.8693(13)	17.251(3)	17.079(11)
α (°)	90.0450(10)	84.914(3)	
β (°)	93.9350(10)	85.626(3)	102.767(14)
γ (°)	90.0220(10)	77.022(3)	
Volume ($Å^3$)	3343.5(4)	1861.4(6)	3540(4)
Z, D_{calc} (g/cm^3)	2, 1.540	2, 1.590	4, 1.573
Absorption coefficient (mm^{-1})	0.715	0.796	0.832
Crystal size (mm^3)	0.35 × 0.33 × 0.20	0.23 × 0.20 × 0.07	0.23 × 0.13 × 0.11
θ Range for data collection (°)	1.67–28.05	1.19–28.38	2.02–28.17
Index ranges	$-14 \le h \le 8$, $-18 \le k \le 19$, $-25 \le l \le 22$	$-13 \le h \le 13$, $-13 \le k \le 14$, $0 \le l \le 22$	$-17 \le h \le 17$, $-20 \le k \le 19$, $-22 \le l \le 11$
Reflections collected	19821	23263	8204
Independent reflections (R_{int})	13935 (0.0267)	8851 (0.0341)	3581 (0.1248)
Completeness to θ	85.9% (28.05)	94.8% (28.38)	82.4% (28.17)
Absorption correction	SADABS	SADABS	SADABS
Maximum and minimum transmission	0.8702 and 0.7879	0.9464 and 0.8382	0.9140 and 0.8316
Refinement method	full-matrix least-squares on F^2	full-matrix least-squares on F^2	full-matrix least-squares on F^2
Data/restraints/parameters	13935/0/883	8851/0/488	3581/0/233
Goodness-of-fit on F^2	0.911	1.038	0.859
Final *R* indices [$I > 2\sigma(I)$]	$R_1 = 0.0379$, $wR_2 = 0.0835$	$R_1 = 0.0401$, $wR_2 = 0.0910$	$R_1 = 0.0754$, $wR_2 = 0.1622$
R indices (all data)	$R_1 = 0.0569$, $wR_2 = 0.0888$	$R_1 = 0.0674$, $wR_2 = 0.1062$	$R_1 = 0.1716$, $wR_2 = 0.1921$
Largest differences in peak and hole ($e\ Å^{-3}$)	1.051 and −1.178	0.537 and −0.800	0.908 and −1.954

2.3. Physical measurements

Elemental analyses were performed in a Carlo-Erba EA microanalyser. Infra-red spectra were recorded as KBr discs on a Bruker IFS-66 V spectrophotometer. LSI mass spectra were recorded using a Kratos-MS-50T spectrometer connected to a DS90 data system using 3-nitrobenzyl alcohol as the matrix. Conductivity measurements were carried out in 10^{-3} mol dm^{-3} acetonitrile solutions at 20 °C using a WTW LF3 conductivimeter. ^{1}H and ^{13}C, COSY, DEPT, and HMQC NMR spectra were recorded on a Varian 400 MHz, and CD_3CN was used as solvent.

2.4. Crystal structure determination

By slow recrystallisation from acetonitrile, crystals of $[CdL^1](NO_3)_2$, $[CdL^1](ClO_4)_2 \cdot CH_3CN$ and $[CdL^2](ClO_4)_2 \cdot H_2O$ suitable for X-ray diffraction were obtained. The details of the X-ray crystal data, and the structure solution and refinement for all them are given in Table 1. Measurements were made on a Nonius CAD4 for L and on a Bruker SMART CCD 1000 area diffractometer for the metal complexes. All data were corrected for Lorentz and polarization effects. Empirical absorption corrections were also applied for all the crystal structures obtained [19]. Complex scattering factors were taken from the program package SHELXTL [20]. The structures were solved by direct methods which revealed the position of all non-hydrogen atoms. All the structures were refined on F^2 by a full-matrix least-squares procedure using anisotropic displacement parameters for all non hydrogen atoms. The hydrogen atoms were located in their calculated positions and refined using a riding model. Molecular graphics were generated using ORTEP-3 [21].

3. Results and discussion

3.1. Crystal structure of $[CdL^1](NO_3)_2$ and $[CdL^1](ClO_4)_2 \cdot CH_3CN$

Colourless prisms of $[CdL^1](NO_3)_2$ and $[CdL^1](ClO_4)_2 \cdot CH_3CN$ were obtained by slow recrystallization of the obtained compounds in acetonitrile. The asymmetric unit of $[CdL^1](NO_3)_2$ is comprised by two $[CdL^1]^{2+}$ cations and four well resolved nitrate ions, while in $[CdL^1](ClO_4)_2 \cdot CH_3CN$ the asymmetric unit shows the presence of the $[CdL^1]^{2+}$ cation, two independent perchlorate counterions and an interstitial acetonitrile molecule. Only the ORTEP diagram of one $[CdL^1]^{2+}$ cation of $[CdL^1](NO_3)_2$, is shown in Fig. 1 together with selected bond lengths and angles. Fig. 2 shows the ORTEP diagram of the $[CdL^1]^{2+}$ cation of $[CdL^1](ClO_4)_2 \cdot CH_3CN$. Both $[CdL^1]^{2+}$ cations in $[CdL^1](NO_3)_2$ are similar, and only present small bond lengths and angles deviations between them. Also, these cations are similar to that present in $[CdL^1](ClO_4)_2 \cdot CH_3CN$.

In all cases, the $[CdL^1]^{2+}$ cation contains the Cd(II) ion sited in the middle of the macrocyclic cavity in a distorted octahedral geometry arising from coordination by the six donor nitrogen atoms of the macrocyclic backbone.

The six Cd–N bond lengths are in the range 2.237–2.440 Å, affording an average Cd–N bond distance of 2.356 Å. The distances found are shorter than other found in previously reported Cd(II) complexes with the metal ion in octahedral environments with similar N donor ligands [22,23]. The shortest bond distances correspond to the pyridinic nitrogen atoms according with bond distances found in similar complexes.

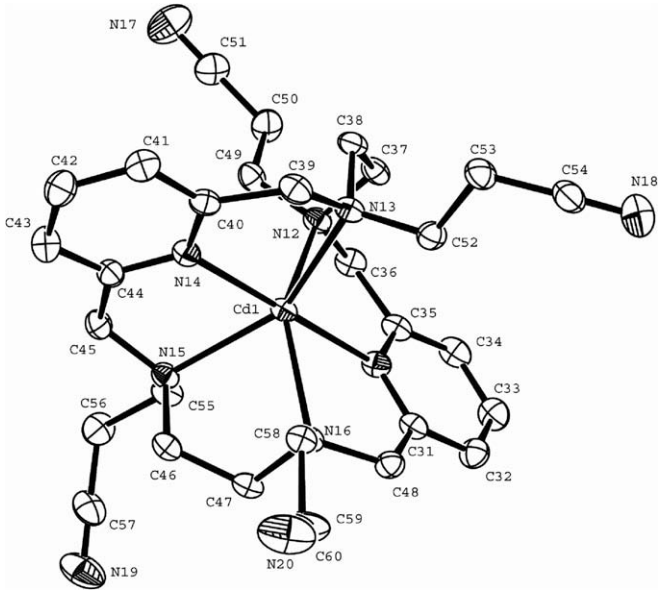

Fig. 1. ORTEP drawing of the molecular structure of one of the $[CdL^1]^+$ cations in $[CdL^1](NO_3)_2$ with displacement ellipsoids drawn at 50% probability level with selected bond lengths (Å) and angles (°). Hydrogen atoms are omitted for clarity. N(1)–Cd(2) 2.250(2), N(2)–Cd(2) 2.397(2), N(3)–Cd(2) 2.422(2), N(4)–Cd(2) 2.237(2), N(5)–Cd(2) 2.411(2), N(6)–Cd(2) 2.406(2), N(11)–Cd(1) 2.254(2), N(12)–Cd(1) 2.393(2), N(13)–Cd(1) 2.414(2), N(14)–Cd(1) 2.240(2), N(15)–Cd(1) 2.419(2), N(16)–Cd(1) 2.405(2), N(14)–Cd(1)–N(11) 179.88(10), N(14)–Cd(1)–N(12) 106.33(8), N(11)–Cd(1)–N(12) 73.77(9), N(14)–Cd(1)–N(16) 107.37(8), N(11)–Cd(1)–N(16) 72.53(8), N(12)–Cd(1)–N(16) 146.28(8), N(14)–Cd(1)–N(13) 74.01(8), N(11)–Cd(1)–N(13) 106.08(9), N(12)–Cd(1)–N(13) 79.86(8), N(16)–Cd(1)–N(13) 108.41(8), N(14)–Cd(1)–N(15) 73.46(8), N(11)–Cd(1)–N(15) 106.45(9), N(12)–Cd(1)–N(15) 111.02(9), N(16)–Cd(1)–N(15) 79.99(8), N(13)–Cd(1)–N(15) 147.43(8), N(4)–Cd(2)–N(1) 179.89(10), N(4)–Cd(2)–N(2) 106.37(8), N(1)–Cd(2)–N(2) 73.65(9), N(4)–Cd(2)–N(6) 107.32(8), N(1)–Cd(2)–N(6) 72.66(8), N(2)–Cd(2)–N(6) 146.28(8), N(4)–Cd(2)–N(5) 73.95(8), N(1)–Cd(2)–N(5) 106.16(9), N(2)–Cd(2)–N(5) 79.73(8), N(6)–Cd(2)–N(5) 108.39(8), N(4)–Cd(2)–N(3) 73.52(9), N(1)–Cd(2)–N(3) 106.36(9), N(2)–Cd(2)–N(3) 111.01(8), N(6)–Cd(2)–N(3) 80.14(8), N(5)–Cd(2)–N(3) 147.44(8).

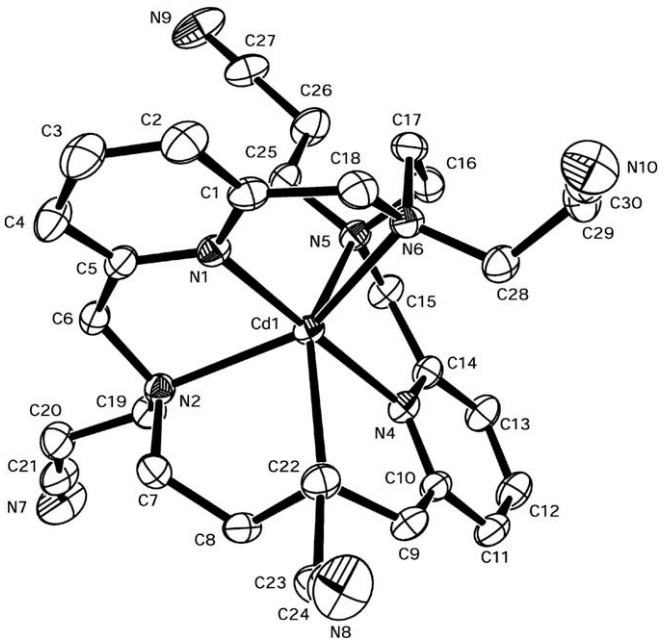

Fig. 2. ORTEP drawing of the molecular structure of the $[CdL^1]^+$ cation in $[CdL^1](ClO_4)_2 \cdot CH_3CN$ drawn as for Fig. 1 with selected bond lengths (Å) and angles (°). N(1)–Cd(1) 2.237(3); N(2)–Cd(1) 2.419(3); N(3)–Cd(1) 2.440(3); N(4)–Cd(1) 2.231(3); N(5)–Cd(1) 2.394(3); N(6)–Cd(1) 2.443(3); N(4)–Cd(1)–N(1) 174.89(10); N(4)–Cd(1)–N(5) 74.26(10); N(1)–Cd(1)–N(5) 108.96(9); N(4)–Cd(1)–N(2) 108.82(10); N(1)–Cd(1)–N(2) 73.87(9); N(5)–Cd(1)–N(2) 112.91(9); N(4)–Cd(1)–N(3) 73.11(10); N(1)–Cd(1)–N(3) 103.49(10); N(5)–Cd(1)–N(3) 147.34(9); N(2)–Cd(1)–N(3) 79.38(9); N(4)–Cd(1)–N(6) 104.39(10); N(1)–Cd(1)–N(6) 72.70(10); N(5)–Cd(1)–N(6) 80.05(9); N(2)–Cd(1)–N(6) 146.51(9); N(3)–Cd(1)–N(6) 106.74(9).

The ligand adopts a typical 'twist-wrap' conformation with the two pyridine rings oriented at 86.73 (0.10)° and 86.55 (0.10)° for each one of the cationic complexes of $[CdL^1](NO_3)_2$ and 87.43 (0.11)° for $[CdL^1](ClO_4)_2 \cdot CH_3CN$.

The angle between the pyridinic nitrogen atoms and the metal ion, N(4)–Cd(2)–N(1) 179.89(10) and N(14)–Cd(1)–N(11) 179.88(10) for $[CdL^1](NO_3)_2$ and N(4)–Cd(1)–N(1) 174.89(10) for $[CdL^1](ClO_4)_2 \cdot CH_3CN$, shows that the macrocycle is slightly folded in the perchlorate complex.

The nitrile groups are not interacting with the metal ion due to their linear nature as has been found in previously related crystal structures [14–17].

The nitrate and perchlorate ions were refined with no disorder giving bond distances and angles typical for these ions.

Inter- or intramolecular π,π-stacking interactions between the pyridine rings are not observed, however, as has been previously described in other reported nitrate complexes with this type of nitrile derivates ligands [14–17], interactions between nitrate anions, nitrile groups and pyridine rings from the macrocycle have been observed in the crystal structure of $[CdL^1](NO_3)_2$ (Fig. 3a). One nitrate ion is situated between a pyridine ring and a pendant nitrile group interacting with the π-systems of these groups.

If we consider the distance between the centroid of the pyridine and the N atom of the nitrate group as analogous to the centroid–centroid distance, this distance (d_{C-N}) is 3.4 Å. Table 2 contains some atom–atom distances between this nitrate ion and the pyridine ring and nitrile group of one pendant-arm, suggesting an interaction between the nitrate ion and the π-shell of the nitrile pendant group.

In the case of $[CdL^1](ClO_4)_2 \cdot CH_3CN$ the acetonitrile molecule is occupying the position of the nitrate ion in the previously described compound and it is this solvent molecule which interacts with the π-shell of the pyridine ring and the nitrile pendant group (Fig. 3b). Table 2 shows also atom–atom distances for $[CdL^1](ClO_4)_2 \cdot CH_3CN$.

3.2. Crystal structure of $[CdL^2](ClO_4)_2 \cdot H_2O$

By recrystallization of the Cd(II) perchlorate complex with L^2 in acetonitrile, crystals suitable for X-ray diffraction were obtained. The details of the X-ray crystal structure and refinement of $[CdL^2](ClO_4)_2 \cdot H_2O$ are given in Table 1. The molecular structure of the $[CdL^2]^+$ cation with selected bond lengths and angles are given in Fig. 4.

The complex is mononuclear and contains the Cd(II) ion endomacrocyclically coordinated in a distorted N6 octahedral geometry by coordination of the six donor nitrogen atoms from the macrocyclic framework. The cyanomethyl pendant arms remain not coordinated as happened with the complexes described for L^1.

Table 2
Intermolecular atom–atom distances (Å) shorter than 3.5 Å for $[CdL^1](NO_3)_2$ and $[CdL^1](ClO_4)_2 \cdot CH_3CN$

$[CdL^1](NO_3)_2$	$[CdL^1](ClO_4)_2 \cdot CH_3CN$
O1N–C60 3.385 Å	N1S–C1 3.432 Å
O2N–C40 3.153 Å	N1S–C2 3.309 Å
O3N–C42 3.363 Å	N1S–N8 3.443 Å
O2N–N20 3.453 Å	N1S–C24 3.449 Å
O2N–C60 3.368 Å	C1S–C2 3.304 Å
	C1S–C3 3.348 Å

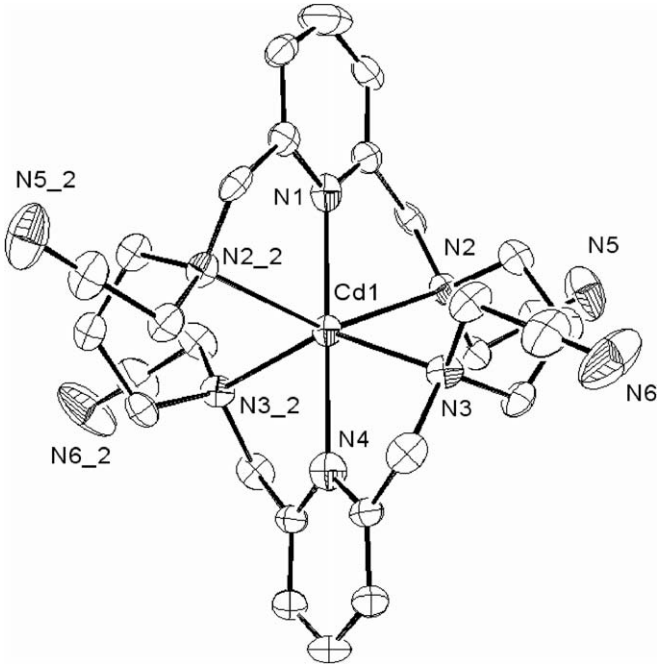

Fig. 4. ORTEP drawing of the molecular structure of the $[CdL^2]^+$ cation in $[CdL^2](ClO_4)_2 \cdot H_2O$ drawn as for Fig. 1 with selected bond lengths (Å) and angles (°). N(1)–Cd(1) 2.185(11); N(2)–Cd(1) 2.503(7); N(3)–Cd(1) 2.520(7); N(4)–Cd(1) 2.207(11); N(1)–Cd(1)–N(4) 180.000(2); N(1)–Cd(1)–N(2) 71.25(17); N(4)–Cd(1)–N(2) 108.75(17); N(2)–Cd(1)–N(2)#1 142.5(3); N(1)–Cd(1)–N(3) 108.51(16); N(4)–Cd(1)–N(3) 71.49(16); N(2)–Cd(1)–N(3) 85.7(2); N(2)–Cd(1)–N(3)#1 106.2(2); N(3)–Cd(1)–N(3)#1 143.0(3).

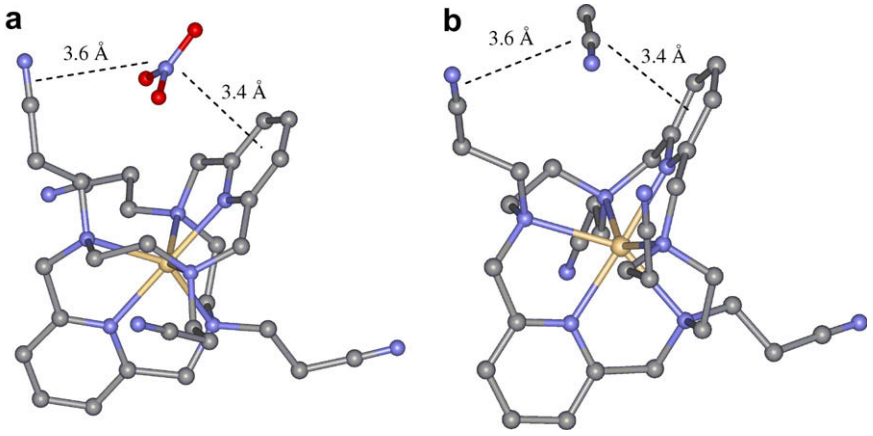

Fig. 3. Triple π-stacking interaction between (a) the pyridine ring, the nitrile group and the nitrate ion in $[CdL^1](NO_3)_2$, and (b) the pyridine ring, the nitrile group and the acetonitrile molecule in $[CdL^1](ClO_4)_2 \cdot CH_3CN$.

The structure shows also a 'twist-wrap' typical conformation where the macrocycle adopts a helical shape with the two pyridine rings oriented at 65.34° relative to each other. The angle between the pyridinic nitrogen atoms and the metal ion [N(1)–Cd(1)–N(4), 180.000(2)], shows that the macrocycle is not folded.

The pyridine groups provides again the shortest bond distance to the Cd(II) atom [Cd(1)–N(1) 2.185(11) and Cd(1)–N(4) 2.207(11) Å], while the bond lengths of the tertiary amine groups [N(2)–Cd(1) 2.503(7) and N(3)–Cd(1) 2.520(7)] are similar than those found in similar complexes that have been reported previously [22,23]. The perchlorate ions are not coordinated to the metal; they were refined with no disorder, giving bond distances and angles typical for these ions.

Inter- or intramolecular π,π-stacking interactions between the pyridine rings are not observed.

3.3. Spectroscopic studies

The IR spectra of the complexes (KBr discs) show in all cases that the ν(C=N) vibration band of the pyridine groups are shifted to higher wavenumber than in the free ligands suggesting coordination to the metal atom [24]. The IR spectra of the Cd(II) complexes of L^1 show two bands at *ca.* 2250 and 2425 cm^{-1}, assigned to the ν(C≡N) band that can be related with the interaction of the nitrile pendant groups with different π systems present in the structures (pyridine rings, nitrate ions or acetonitrile molecules), accordingly with the crystal structures found for these complexes [15,17]. However, in the case of the Cd(II) complexes of L^2, the spectra show only one band at *ca.* 2250 cm^{-1}, similar than in the free ligand.

The IR spectra of the perchlorate complexes feature absorptions attributable to ionic perchlorate at 1100 and 626 cm^{-1}, indicating that these groups are not coordinated to the metal centers in any case [25,26]. The IR spectra of the nitrate complexes present the band at 1384 cm^{-1} associated with the ionic nitrate groups [27].

The LSI mass spectra of the complexes confirm in all cases the mononuclear nature of the complexes.

Molar conductivity data, measured at room temperature using acetonitrile as solvent, showed the presence of ionic counterions, since they are in the range reported in that solvent for 2:1 electrolytes [28]. This is in agreeing with the results obtained from the IR and X-ray studies.

The ^{1}H NMR spectra of the complexes were recorded in CD_3CN. The spectra are in general more complicated than expected showing that fast interconversion of isomer in solution does not occur. All the spectra show in general that the signals are shifted downfield compared with the free ligands.

The ^{1}H NMR spectra of $[CdL^1](NO_3)_2$ and $[CdL^1](ClO_4)_2 \cdot CH_3CN$ are similar. They show that pyridyl protons appear at δ 8.3 and 7.8 ppm as a triplet and a doublet, respectively. However, the aliphatic signals appear as different multiplets: the adjacent to pyridine protons appear at δ 4.4–4.2 ppm while the remaining aliphatic protons collapse in a multiplet at δ 3.3–2.3 ppm.

The ^{1}H NMR spectra of $[CdL^2](ClO_4)_2 \cdot H_2O$ and $[CdL^2](NO_3)_2$ are also similar. In this case, the pyridyl protons appear again as a triplet and a doublet at δ 8.3 and 7.8 ppm, respectively, the adjacent to pyridine and the pendant arms proton signals collapse in a multiplet between δ 3.9 and 4.4 ppm, and the remaining aliphatic protons appears as a multiplet at δ 2.5–3.0 ppm.

4. Conclusion

In summary, we described the synthesis of different nitrate and perchlorate cadmium(II) complexes with two cyano pendant arm azamacrocyclic ligands (L^1 and L^2). The structure of the complexes $[CdL^1](NO_3)_2$, $[CdL^1](ClO_4)_2 \cdot CH_3CN$ and $[CdL^2](ClO_4)_2 \cdot H_2O$ have been determined by X-ray analysis, showing that they are mononuclear complexes with the metal atom endomacrocyclicly coordinated in all cases to the six nitrogen donor atoms from the macrocyclic framework being the pendant groups not coordinated. In all cases, the geometry around the Cd(II) ion can be described as N6 distorted octahedral. Also, different interactions between nitrate ions, nitrile groups and pyridine rings from the macrocycle were found in the $[CdL^1](NO_3)_2$ and $[CdL^1](ClO_4)_2 \cdot CH_3CN$ structures.

Acknowledgments

We thank the Xunta de Galicia (PGIDT07PXIB209039PR) for financial support. Intensity measurements were performed at the Unidade de Raios X. RIAIDT. University of Santiago de Compostela, SPAIN.

Appendix A. Supplementary data

CCDC 694572, 694573, and 694574 contain the supplementary crystallographic data for $[CdL^1](NO_3)_2$, $[CdL^1](ClO_4)_2 \cdot CH_3CN$, and $[CdL^2](ClO_4)_2 \cdot H_2O$. These data can be obtained free of charge via http://www.ccdc.cam.ac.uk/conts/retrieving.html, or from the Cambridge Crystallographic Data Centre, 12 Union Road, Cambridge CB2 1EZ, UK; fax: (+44) 1223-336-033; or e-mail: deposit@ccdc.cam.ac.uk.

References

[1] A. Bianchi, M. Micheloni, P. Paoletti, Coord. Chem. Rev. 110 (1991) 17, and references cited therein.
[2] G.A. Nelson (Ed.), Coordination Chemistry of Macrocyclic Compounds, Plenum Press, New York, 1979.
[3] M. Mitewa, P.R. Bontchev, Coord. Chem. Rev. 135/136 (1994) 129.
[4] R.M. Izatt, J.S. Bradshaw, S.A. Nielsen, J.D. Lamb, J.J. Christensen, D. Sen, Chem. Rev. 85 (1985) 271.
[5] K.E. Krakowiak, J.S. Bradshaw, D.J. Zamecka-Krakowiak, Chem. Rev. 89 (1989) 929.
[6] P. Guerriero, S. Tamburini, P.A. Vigato, Coord. Chem. Rev. 139 (1995) 17 and references cited therein.
[7] T. Koike, M. Inoue, E. Kimura, J. Am. Chem. Soc. 118 (1996) 3091.
[8] C. Bazzicalupi, A. Bencini, A. Bianchi, M. Cecchi, B. Escuder, V. Fusi, E. Gracia-España, C. Giorgi, S.V. Luis, C. Maccagni, V. Marcelino, P. Paoletti, P. Valtancoli, J. Am. Chem. Soc. 121 (1999) 6807.
[9] K.A. Arnold, L. Echegoyen, F.R. Fronczek, R.D. Gandour, V.J. Gatto, B.D. White, G.W. Gokel, J. Am. Chem. Soc. 109 (1987) 3716.
[10] G.L. Rothermel, L. Miao, A.L. Hill, S.C. Jackels, Inorg. Chem. 31 (1992) 4854.
[11] E.V. Rybak-Akinova, A.Y. Nazarenko, S.S. Silchenco, Inorg. Chem. 38 (1999) 2974.
[12] M. Botta, Eur. J. Inorg. Chem. (2000) 399.
[13] K.P. Wainwright, Adv. Inorg. Chem. 52 (2001) 293.
[14] S. Gonzalez, L. Valencia, R. Bastida, D.E. Fenton, A. Macías, A. Rodríguez, J. Chem. Soc., Dalton Trans. (2002) 3551.
[15] L. Valencia, R. Bastida, Madel C. Fernandez-Fernandez, A. Macías, M. Vicente, Inorg. Chim. Acta 358 (2005) 2618.
[16] Mªdel C. Fernandez-Fernandez, R. Bastida, A. Macías, P. Pérez-Lourido, L. Valencia, Inorg. Chem. 45 (2006) 2266.
[17] Mªdel C. Fernandez-Fernandez, R. Bastida, A. Macías, P. Pérez-Lourido, L. Valencia, Polyhedron 26 (2007) 5317.
[18] G.L. Rothermel, L. Miao Jr., A.L. Hill, S.C. Jackels, Inorg. Chem. 31 (1992) 4854.
[19] G.M. Sheldrick, SADABS Program for Empirical Absorption Correction of Area Detector Data, University of Gottingen, Germany, 1996.
[20] SHELXTL version, An integrated system for solving and refining crystal structures from diffraction data (Revision 5.1), Bruker AXS LTD.
[21] L.J. Farrugia, J. Appl. Crystallogr. 30 (1997) 565.
[22] Madel C. Fernandez-Fernandez, R. Bastida, A. Macías, P. Pérez-Lourido, L. Valencia, Polyhedron 25 (2006) 783.
[23] R. Bastida, D.E. Fenton, M. López-Deber, A. Macías, L. Valencia, M. Vicente, Inorg. Chim. Acta 355 (2003) 292.
[24] N.S. Gill, R.H. Nuttall, D.E. Scaife, D.W. Sharp, J. Inorg. Nucl. Chem. 18 (1961) 79.
[25] M.R. Rosenthal, J. Chem. Educ. 50 (1973) 331.
[26] A.J. Hathaway, A.E. Underhill, J. Chem. Soc., Dalton Trans. (1961) 3091.
[27] P. Gueriero, U. Casellato, S. Tamburini, P.A. Vigato, R. Graziani, Inorg. Chim. Acta 129 (1987) 127.
[28] W.J. Geary, Coord. Chem. Rev. 7 (1971) 81.

purification. Copper oxalate precursor was synthesized according to this procedure: the $Cu(OOCCH_3)_2 \cdot H_2O$ (2 mmol) was dissolved into 10 mL of distilled water to form a homogeneous solution. A stoichiometric amount of potassium oxalate dissolved in an equal volume of distilled water was dropwise added into the above solution under magnetic stirring. The solution was stirred for about 15 min and a blue precipitate was centrifuged and washed with ethanol several times. The product was dried at 50 °C. The copper oxalate, $Cu(O_4C_2)$, was characterized by elemental analyses, powder X-ray diffraction (XRD) and thermo gravimetric analysis (TGA) [31,34]. *Anal.* Calc. for $[Cu(O_4C_2)]$: C, 15.84; Cu, 41.93. Found: C, 15.75; Cu, 41.84%.

2.2. Characterization

XRD patterns were recorded by a Rigaku D-max C III, X-ray diffractometer using Ni-filtered Cu Kα radiation. Elemental analyses were obtained from Carlo ERBA Model EA 1108 analyzer. Scanning electron microscopy (SEM) images were obtained on Philips XL-30ESEM equipped with an energy dispersive X-ray spectroscopy. Transmission electron microscopy (TEM) images were obtained on a Philips EM208 transmission electron microscope with an accelerating voltage of 200 kV. Fourier transform infrared (FT-IR) spectra were recorded on Shimadzu Varian 4300 spectrophotometer in KBr pellets. Thermogravimetric-differential thermal analysis (TG-DTA) were carried out using a thermal gravimetric analysis instrument (Shimadzu TGA-50H) with a flow rate of 20.0 mL min^{-1} and a heating rate of 10 °C min^{-1}. The electronic spectra of the complexes were taken on a Shimadzu UV–Vis scanning spectrometer (Model 2101 PC).

2.3. Synthesis of Cu nanoparticles

The current synthetic procedure is a modified version of the method developed by Hyeon and others for the synthesis of metal nanoparticles which employs the thermal decomposition of transition metal complexes [32,33,35]. The synthetic pathway is shown in Scheme 1. In this synthesis Cu nanoparticles were prepared by the thermal decomposition of copper oxalate, $[Cu(O_4C_2)]$–oleylamine complex as precursor. First, the $[Cu(O_4C_2)]$–oleylamine complex was prepared by reaction 0.6 g of $Cu(O_4C_2)$ and 5 mL of oleylamine. The mixed solution was placed in a 50 mL three-neck distillation flask and heated up to 140 °C for 60 min under an argon atmosphere. The resulting metal-complex solution was injected into 5 g of triphenylphosphine (TPP) at 240 °C. As the thermal decomposition proceeded, the azury solution turned to red, indicating the formation of metallic copper. The reddish solution was aged at 240 °C for 45 min, and was then cooled to room temperature. The reddish nanoparticles were precipitated by adding excess ethanol to the solution. The final product was washed with ethanol several times to remove excessive surfactant. This product could easily be re-dispersed in nonpolar organic solvents, such as hexane or toluene (Scheme 1).

3. Results and discussion

The TGA curve of the as-prepared precursor is shown in Fig. 1. There is only one weight loss step in the temperature range 250–310 °C. The weight loss at 250–315 °C may be ascribed to the decomposition of the oxalate. The weight loss is about 43.23%, which is close to the theoretical value.

X-ray powder diffraction (XRD) patterns of Cu nanoparticles at room temperature shows in Fig. 2. The XRD pattern is consistent with the spectrum of copper, and no peak attributable to possible impurities is observed. The peak positions are consistent with metallic copper. All possible peaks of copper are observed, which indicates the polycrystalline nature of the product. Bragg's reflections for Cu nanoparticles are observed in XRD pattern at 2θ value of 43.6°, 50.7° and 74.45° representing [111], [200] and [220] planes of fcc structure of copper with the space group of *Fm3m*

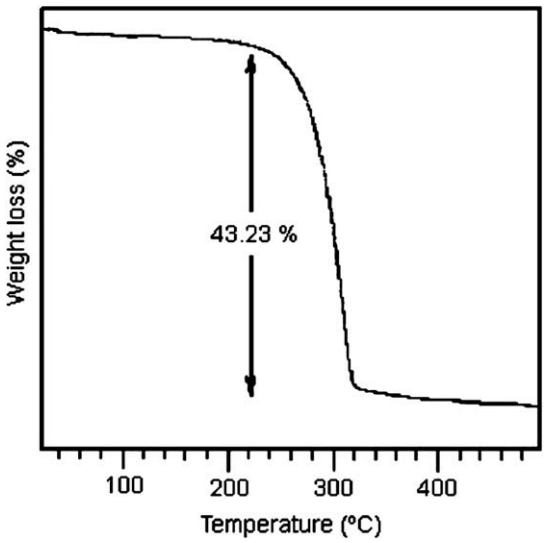

Fig. 1. TGA of the copper oxalate precursor, $Cu(O_4C_2)$.

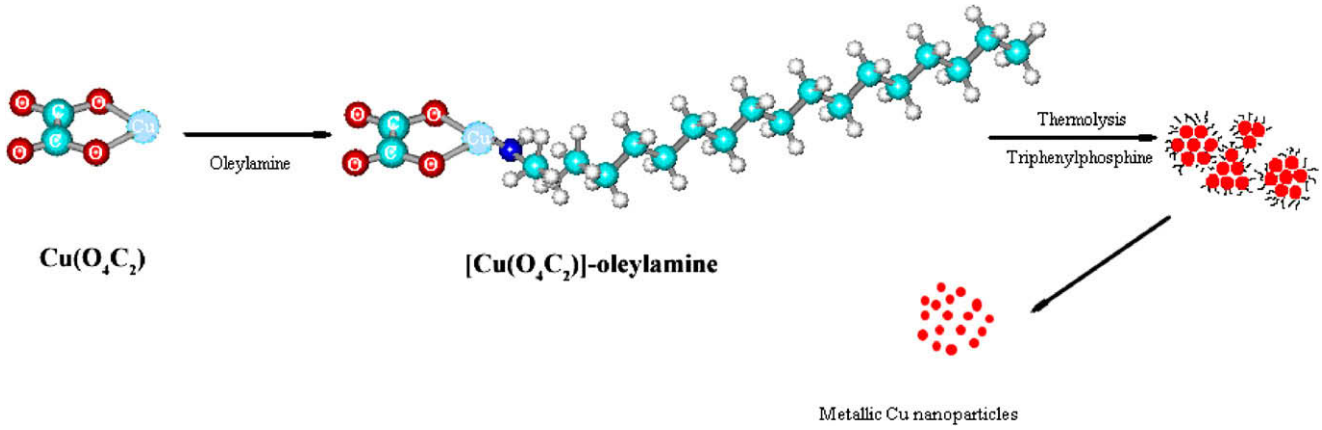

Scheme 1. Schematic depiction of the selective formation of Cu nanoparticles.

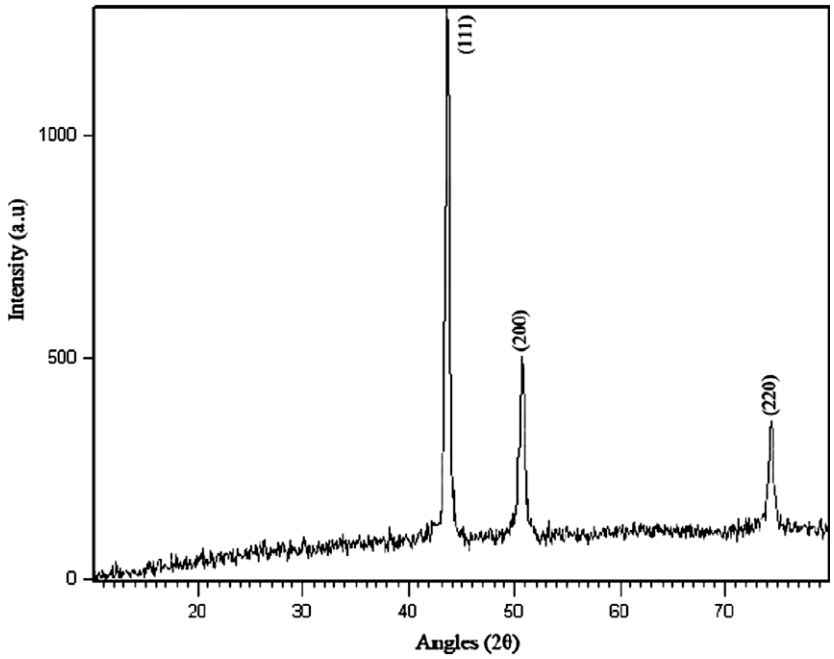

Fig. 2. XRD pattern of the copper nanoparticles.

(JCPDS No. 4–0836). The size of the crystallites was estimated from Debye–Scherrer equation is about 40 nm.

FT-IR spectroscopy is a useful tool to understand the functional group of any organic molecule. The infrared spectra of free TPP, oleylamine and copper nanoparticles coated with oleylamine and TPP are shown in Fig. 3. By comparing the infrared spectra of the nanoparticles with free surfactants in Fig. 3 we can see that the organic molecules have indeed become a part of the nanoparticles. As shown in Fig. 3a and b, peaks corresponding to P–ph stretching at 1710 cm^{-1}, rocking and bending mode of the methylene group $\omega(CH_2)$ at 1270 cm^{-1}, bending mode of the phenyl group $\gamma(=CH)$ at 742 cm^{-1} and υ (benzene ring) at 697 cm^{-1} can be seen clearly. The only difference among these characteristic peaks is either the peak intensity or a slight shift in the peak position. For example, the peak position of the longitudinal modes of oleylamine and TPP shifts to lower wavenumbers after TPP and oleylamine are adsorbed on the surface of the copper nanoparticles. The FT-IR of the copper nanoparticles shows the intense adsorption peaks at 2920 and 2850 cm^{-1} attributed to the alkyl chains of oleylamine. The bands attributed to the antisymmetric and symmetric vibration modes of –N–H are observed at 3437 and 3232 cm^{-1}, respectively (Fig. 3c). Due to the coordination of the unpaired electron couple of the nitrogen atom, the vibration bands are observed in lower values than those expected for the free amine group, i.e., 3500 and 3300 cm^{-1}, respectively. This indicates that oleylamine is bound on the surface through the unpaired electron couple of the amine group [36]. From these results, a chemical bond can be formed between N and Cu atoms and a coordinate bond between P and Cu atoms on the surface of the nanoparticles. Thus, the phenyl stretching mode ν(P–ph) at 1430 cm^{-1} is still visible in Fig. 3c. So the oleylamine and TPP serves as the capping ligand that controls growth. Triphenylphosphine (TPP) was widely used in the synthesis of phosphine-stabilized cobalt or other metal nanoparticles

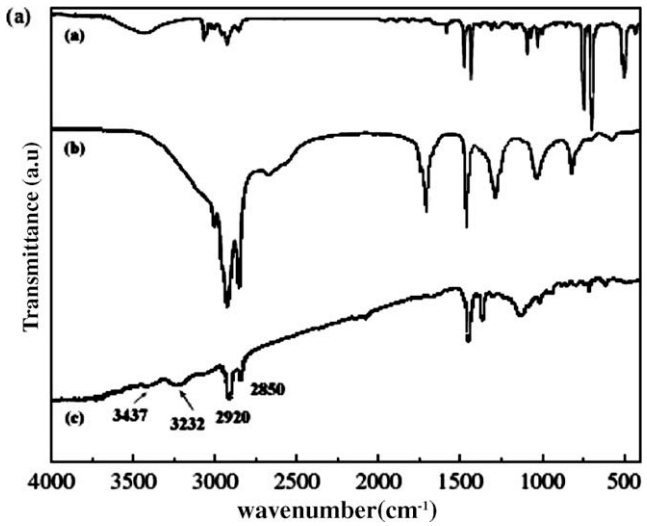

Fig. 3. FT-IR spectra of (a) free TPP absorption, (b) free oleylamine and (c) Cu nanoparticles coated by oleylamine and TPP.

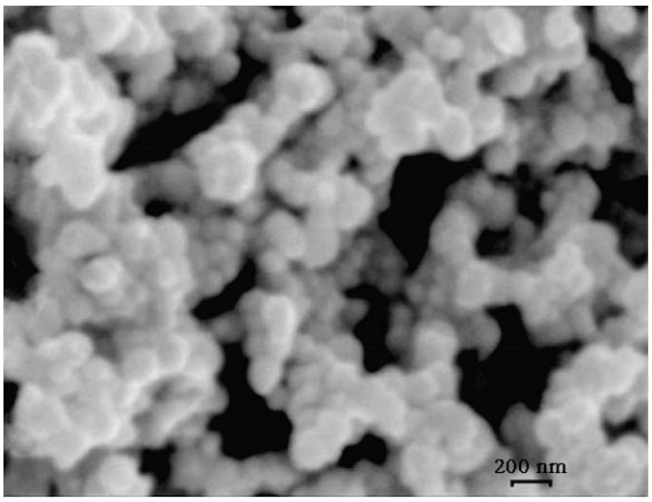

Fig. 4. SEM image of Cu nanoparticles.

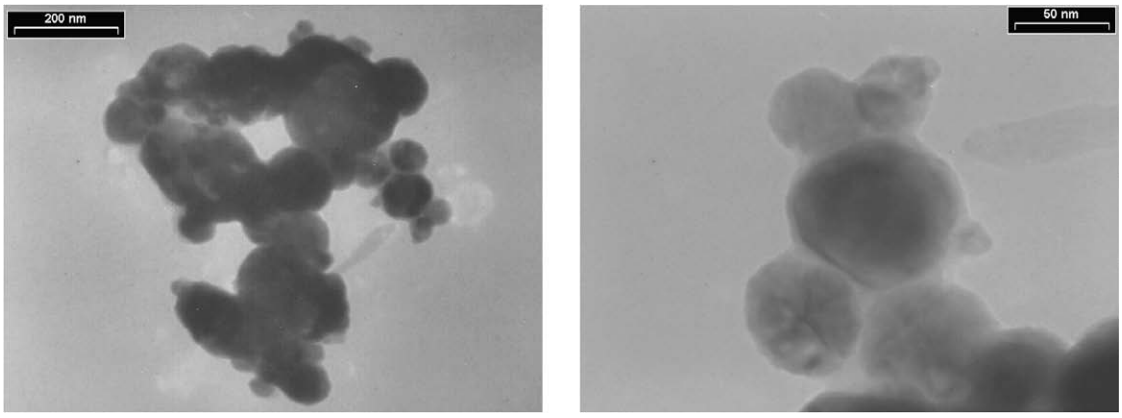

Fig. 5. TEM images of Cu nanoparticles.

[37]. The phenyl groups in TPP can provide greater steric hindrance than straight-chained alkyl groups such as tributyl and trioctyl to control the size of nonmagnetic metal nanoparticles and to stabilize efficiently the magnetic nanoparticles.

The morphology of the Cu nanoparticles is examined by SEM (Fig. 4). From the micrograph, it was observed that the nanoparticles were agglomerated. The TEM image (Fig. 5) shows the presence of dense agglomerates. The particles have an irregular shape, and their distribution, likewise, is not uniform (30–80 nm).

The growth mechanism could be well understood on the basis of the following reactions and the crystal habits of Cu. In the presence of oleylamine as solvent [$Cu(O_4C_2)$]–oleylamine were synthesized. After addition of TPP to these solutions at high temperature the complexes were decomposed. TPP is a high-boiling point surfactant with a patulous long-chain structure providing great steric hindrance. The addition of TPP into the mixture of oleylamine and complex as an additional surfactant reduced the particle size much further and resulted in nanoparticles with very thin arrays. Oleylamine is known as a ligand that binds tightly to the metal nanoparticles surface. The combined effects of TPP and oleylamine were much more profound than those of individual contributions. On the other hand these complexes transform to Cu under an argon atmosphere. When the triphenylphopsphine (TPP) was used as the complexing agent, the spherical nanoparticles capped by this surfactant were obtained. The growth of the Cu nanoparticles can be explained on the basis of the schematic view presented in Scheme 1. The Cu nanoparticles agglomerated together to form a spherical structure. In this synthetic rout oleylamine acts not only as the reaction solution but also as the stabilizer, which prevents the nanoparticles from oxidizing. Recently, copper oxalate was used as precursor for synthesizing CuO. In that method copper oxalate was calcined at 400 °C for 4 h [31] or 350 °C for 10 h [34] without any capping agent and argon atmosphere. So, metal oxide nanoparticles obtained. But here with use of capping agent, metallic nanoparticles obtained. We believe that capping agents used here help to the formation of metal rather than metal oxide.

Nanosized particles exhibit unique optical properties with an exponential-decay Mie scattering profile with decreasing photon energy. Some transition metal nanoparticles show a distinct surface-plasmon resonance (SPR). The SPR is very sensitive to metal size, dielectric constant of metal and embedding medium (here is oleylamine) [20,29]. For instance, Cu nanoparticles typically exhibit SPR at around 600 nm [38]. However, for the fresh Cu nanoparticles synthesized here show an absorption peak at around 572 nm (Fig. 6). This peak can be assigned to the absorption of nanoparticles of copper [38]. A modest blue shift (about 28 nm) of the absorption edge relative to that of the bulk copper powder is

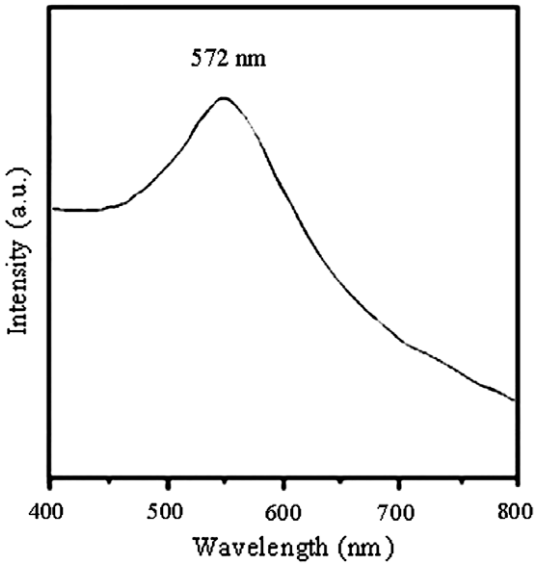

Fig. 6. UV–Vis absorption of the Cu nanoparticles.

observed. This observation alludes to the size effect to the Cu nanoparticles. The synthesized particles were stable for ~6 days. This kind of stabilization of Cu nanoparticles was due to the capping of particles by oleylamine in thermal treatment. The arrangement of capping agent, oleylamine surrounding the nanoparticles is size dependent. After a few days, slow oxidation of copper particles sets in with the disappearance of absorption peaks [39] and finally the as-synthesized product becomes black. This indicated that the sample was oxidized.

4. Conclusion

In summary, Cu nanoparticles with diameters from 30 to 80 nm have been successfully synthesized via thermal decomposition of [$Cu(O_4C_2)$]-oleylamine complex. This method employed an inexpensive, reproducible process for the large-scale synthesis of copper nanoparticles.

Acknowledgment

Authors are grateful to council of University of Kashan for providing financial support to undertake this work.

References

[1] A. Roucoux, J. Schulz, H. Patin, Chem. Rev. 102 (2000) 3757.
[2] L.K. Yeung, R.M. Crooks, Nano Lett. 1 (2001) 14.
[3] K.R. Gopidas, J.K. Whitesell, M.A. Fox, Nano Lett. 3 (2003) 1757.
[4] S. Gan, L. Liang, D. Baer, M. Sievers, G. Herman, C. Peden, J. Phys. Chem. B 105 (2001) 2412.
[5] N. Toshima, Y. Wang, Langmuir 10 (1994) 4574.
[6] C. Yong, B.C. Zhang, C.S. Seet, A. See, L. Chan, J. Sudijono, S.L. Liew, C.-H. Tung, H.C. Zeng, J. Phys. Chem. B 106 (2002) 12366.
[7] Y. Takedaa, O.A. Plaksin, K. Kono, N. Kishimoto, Surf. Coat. Technol. 196 (2005) 30.
[8] M. Tada, R. Bal, S. Namba, Y. Iwasawa, Appl. Catal., A 307 (2006) 78.
[9] A.K. Verma, R. Kumar, P. Chaudhary, A. Saxena, R. Shankar, S. Mozumdar, R. Chandra, Tetrahedron Lett. 46 (2005) 5229.
[10] S. Panigrahi, S. Kundu, S.K. Ghosh, S. Nath, S. Praharaj, S. Basu, T. Pal, Polyhedron 25 (2006) 1263.
[11] Z.P. Liu, Y. Yang, J.B. Liang, Z.K. Hu, S. Li, S. Peng, Y.T. Qian, J. Phys. Chem. B 107 (2003) 12658.
[12] E.K. Athanassiou, R.N. Grass, W.J. Stark, Nanotechnology 17 (2006) 1668.
[13] E.R. Savinova, E.N. Savinov, V.N. Parmon, J. Mol. Catal. 48 (1988) 231.
[14] T. Miao, L. Wang, Tetrahedron Lett. 48 (2007) 95.
[15] M. Kidwai, N.K. Mishra, V. Bansal, A. Kumar, S. Mozumdar, Tetrahedron Lett. 48 (2007) 8883.
[16] X. Liu, B. Geng, Q. Dua, J. Ma, X. Liu, Mater. Sci. Eng., A 448 (2007) 7.
[17] Y.H. Kim, D.K. Lee, B.G. Jo, J.H. Jeong, Y.S. Kang, Colloids Surf. A: Physicochem. Eng. Aspects 284–285 (2006) 364.
[18] A.G. Nasibulin, P.P. Ahonen, O. Richard, E.I. Kauppinen, I.S. Altman, J. Nanoparticle Res. 3 (2001) 385.
[19] L. Daroczi, M.T. Beck, D.L. Beke, M. Kis-Varga, L. Harasztosi, N. Takacs, Mater. Sci. Forum. 319 (1998) 269.
[20] S. Chen, J.M. Sommers, J. Phys. Chem. B 105 (2001) 8816.
[21] H. Zhu1, C. Zhang, Y. Yin, Nanotechnology 16 (2005) 3079.
[22] S.S. Joshi, S.F. Patil, V. Iyer, S. Mahumuni, Nanostruct. Mater. 10 (1998) 1135.
[23] M.P. Pileni, B.W. Ninham, T. Gulik-Krzywicki, J. Tanori, I. Lisiecki, A. Filankembo, Adv. Mater. 11 (1999) 1358.
[24] K.J. Ziegler, R.C. Doty, K.P. Johnston, B.A. Korgel, J. Am. Chem. Soc. 123 (2001) 7797.
[25] R.G. Song, M. Yamaguchi, O. Nishimura, M. Suzuki, Appl. Surf. Sci. 253 (2007) 3093.
[26] B.K. Park, S. Jeong, D. Kim, J. Moon, S. Lim, J.S. Kim, J. Colloid Interf. Sci. 311 (2007) 417.
[27] T. Xin-ling, R. Ling, S. Ling-na, I. Wei-guo, C. Min-hua, H. Chang-wen, Chem. Res. Chin. U 22 (2006) 547.
[28] X.F. Zhang, X.L. Dong1, H. Huang, D.K. Wang, B. Lv, J.P. Lei, Nanotechnology 18 (2007) 275701.
[29] N.A. Dash, C.P. Raj, A. Gedanken, Chem. Mater. 10 (1998) 1446.
[30] K. Simeonidis, S. Mourdikoudis, M. Moulla, I. Tsiaoussis, C.M. Boubeta, M. Angelakeris, C.D. Samara, O. Kalogirou, J. Magn. Magn. Mater. 316 (2007) e1.
[31] X. Zhang, D. Zhang, X. Ni, H. Zheng, Solid-State Electron. 52 (2008) 245.
[32] M. Salavati-Niasari, F. Davar, M. Mazaheri, Mater. Lett. 62 (2008) 1890.
[33] M. Salavati-Niasari, F. Davar, M. Mazaheri, M. Shaterian, J. Magn. Magn. Mater. 320 (2008) 575.
[34] Z. Jia, L. Yue, Y. Zheng, Z. Xu, Mater. Res. Bull. 43 (2008) 2434.
[35] H.M. Park, E. Kang, S.U. Son, H.M. Park, M.K. Lee, J. Kim, K.W. Kim, H. Noh, J. Park, C.J. Bae, J. Park, T. Hyeon, Adv. Mater. 17 (2005) 429.
[36] B.A. Korgel, S. Fullam, S. Connolly, D. Fitzmaurics, J. Phys. Chem. B 102 (1998) 8379.
[37] H.T. Yang, Y.K. Su, C.M. Shen, T.Z. Yang, H.J. Gao, Surf. Interf. Anal. 36 (2004) 155.
[38] J.A. Creighton, D.G. Eadon, J. Chem. Soc., Faraday Trans. 87 (1991) 3881.
[39] Z. Liu, Y. Bando, Chem. Phys. Lett. 378 (2003) 85.

graphical user interface. Least square refinements were performed by the full-matrix method with SHELXL [29]. The hydrogen atom positions were geometrically fixed.

2.2. Preparation of chiral p-tert-butyl-calix[4]arene bisphosphites (L^1 and L^2)

Triethylamine (2.33 g, 23×10^3 mol) was added to a stirred suspension of *p-tert*-butyl-calix[4]arene (3.11 g, 4.8×10^3 mol) in 60 cm^3 THF, and the reaction mixture was stirred at room temperature for 15 min. The solution was cooled in an ice bath and (1*S*,2*R*,5*R*)-(+)-*iso*-menthyl phosphorodichloridite (2.47 g, 9.6×10^3 mol) was slowly added through a dropping funnel at 0 °C. The reaction mixture was allowed to attain ambient temperature and stirred for 4 h. During this time, a white precipitate was formed. The ^{31}P NMR spectrum of the reaction mixture showed the formation of the expected product. The precipitate was filtered off and the filtrate was evaporated under reduced pressure to obtain a yellowish-white foamy solid. The mixture was subjected to column chromatographic separation over silica gel using petrol/EtOAc (200:1 v/v) as the eluant. The initial fraction contained *p-tert*-butyl-calix[4]arene *iso*-menthyl bisphosphite ($\mathbf{L}^1$). Yield: 1.36 g (28%); m.p. = 136–142 °C; $[\alpha]_D^{25} = 77.7$ (*c* 1.0, $CHCl_3$); *Anal.* Calc. for $C_{64}H_{90}O_6P_2$ (mol. wt.: 1017.5): C, 75.5; H, 8.9. Found: C, 75.9; H, 8.4%; ^1H NMR $\delta = 0.72$ (d, 6H, $J = 2.8$ Hz), 0.84 (d, 6H, $J = 4.2$ Hz), 0.94 (d, 6H, $J = 3.8$ Hz), 1.01 (s, 18H, Bu^t), 1.08–1.58 (m, 18H, *iso*-menthyl group + 18H, Bu^t), 3.25 (d, 2H, Hb_2, $J = 5.2$ Hz), 3.28 (d, 2H, Hb_1, $J = 6.0$ Hz), 4.55 (br s, 2H-methyne protons of the *iso*-menthyl group), 4.56 (d, 2H, Ha_2, $J = 13.2$ Hz), 4.81 (d, 2H, Ha_1, $J = 14.4$ Hz), 6.74 (s), 6.82 (s) (8H, aromatic protons of the calixarene); ^{13}C NMR (100 MHz, $CDCl_3$) $\delta = 15.54$, 22.26, 22.88, 24.91, 27.02, 31.27, 31.29, 31.32, 31.36, 31.38, 31.64, 31.68, 31.82, [33.83 and 34.08 (bridged methylene carbons)], 34.32, 38.54, 44.61, 48.66 (aliphatic carbons), 76.42 (*iso*-menthyl carbon), 124.13, 124.24, 125.81, 126.06, 131.87, 133.52 (aromatic carbons) 145.11, 146.23, 147.59, 148.84 (aromatic carbons directly attached to the oxygen atoms).

p-tert-Butyl-calix[4]arene menthyl bisphosphite ($\mathbf{L}^2$) was synthesized as described above for ligand ($\mathbf{L}^1$): Yield: 1.41 g (29%); m.p. = 132–138 °C; $[\alpha]_D^{25} = 93.7$ (*c* 1.0, $CHCl_3$); *Anal.* Calc. for $C_{64}H_{90}O_6P_2$: (mol. wt.: 1017.5): C, 75.5; H, 8.9. Found: C, 75.8; H, 8.2%; ^1H NMR $\delta = 0.60$ (d, 6H, $J = 3.0$ Hz), 0.63 (d, 6H, $J = 3.2$ Hz), 0.88 (d, 6H, $J = 3.8$ Hz), 0.91 (s, 18H, Bu^t), 1.09–1.62 (m, 18H, menthyl group + 18H, Bu^t), 3.22 (d, 2H, Hb_2, $J = 4.6$ Hz), 3.26 (d, 2H, Hb_1, $J = 8.4$ Hz), 4.06 (br s, 2H-methyne protons of the menthyl group), 4.56 (d, 2H, Ha_2, $J = 13.2$ Hz), 4.74 (d, 2H, Ha_1, $J = 14.4$ Hz), 6.59 (s), 6.86 (s) (8H, aromatic protons of calixarene); ^{13}C NMR (100 MHz, $CDCl_3$) $\delta = 15.43$, 22.14, 22.82, 24.88, 26.98, 31.18, 31.26, 31.26, 31.30, 31.37, 31.60, 31.64, 31.75, [33.77 and 34.03 (bridged methylene carbons)], 34.24 38.49, 44.45, 48.55 (aliphatic carbons), 76.09 (menthyl carbon), 123.83, 124.17, 125.73, 125.96, 131.83, 133.45 (aromatic carbons), 145.03, 146.32, 147.56, 148.78 (aromatic carbons directly attached to the oxygen atoms).

2.3. Preparation of achiral p-tert-butyl-calix[4]arene bisphosphite (L^3)

The title compound ($\mathbf{L}^3$) was prepared as described above for ligand ($\mathbf{L}^1$) by the reaction of *p-tert*-butyl-calix[4]arene (3.11 g, 4.8×10^3 mol) with 2.98 g (9.6×10^3 mol) of $ROPCl_2$ (R = C_6H_4-Bu^t-4) in toluene in the presence of triethylamine for 8 h. Yield: 1.83 g (38%); m.p. = 166–172 °C; *Anal.* Calc. for $C_{64}H_{78}O_6P_2$ (mol. wt.: 1004.4): C, 76.5; H, 7.8. Found C, 77.1; H, 7.4%; ^1H NMR (400 MHz,$CDCl_3$) $\delta = 1.12$ (s, 36H, Bu^t), 1.27 (s, 18H, Bu^t), 3.34 (d, 2H, Hb_2, $J = 8.4$ Hz), 3.44 (d, 2H, Hb_1, $J = 12.6$ Hz), 4.64 (d, 2H, Ha_2, $J = 14.4$ Hz), 4.88 (d, 2H, Ha_1, $J = 14.8$ Hz), 6.80 (s), 6.90 (s), (8H, aromatic protons of calixarene), 7.17 (d, 4H, $J = 7.4$ Hz, aromatic protons), 7.24 (d, 4H, $J = 7.8$ Hz, aromatic protons); ^{13}C NMR (100 MHz, $CDCl_3$) $\delta = 31.43$, 31.89, 33.55, [33.77 and 34.18 (bridged methylene carbons)], 34.76, 38.56, 38.72 (aliphatic carbons), 120.44, 124.68, 126.23, 126.54, 131.60, 132.22, 144.36, 146.57, 148.06 (aromatic carbons).

2.4. Preparation of chiral p-tert-butyl-calix[4]arene iso-menthyl bisphosphite–$PdCl_2$ complex (**1**) and menthyl bisphosphite–$PdCl_2$ complex (**4**)

Chiral *p-tert*-butyl-calix[4]arene *iso*-menthyl bisphosphite ($\mathbf{L}^1$) (107 mg, 10.5×10^5 mol) was treated with [$PdCl_2$(COD)] (30 mg, 10.5×10^5 mol) or $PdCl_2(PhCN)_2$ (40 mg, 10.5×10^5 mol) in THF (20 ml) and the reaction mixture was stirred for 1 h. The solvent was evaporated and the residue was washed several times with petrol to obtain complex (**1**) as a light yellow powder. The product was crystallized from THF:petrol (1:3) to obtain pale yellow crystals. Yield: 120 mg (96%); m.p. = 289–294 °C; *Anal.* Calc. for $C_{64}H_{90}O_6P_2PdCl_2$ (mol. wt.: 1194.6): C, 64.3; H, 7.5. Found C, 64.8; H, 7.8%; ^1H NMR $\delta = 0.80$ (d, 6H, $J = 3.4$ Hz), 0.85 (d, 6H, $J = 3.8$ Hz), 0.94 (d, 6H, $J = 3.6$ Hz), 1.06–1.69 (m, 18H, *iso*-menthyl group + 18H, Bu^t +18H, Bu^t), 3.44 (d, 2H, Hb_2, $J = 6.4$ Hz), 3.48 (d, 2H, Hb_1, $J = 7.6$ Hz), 4.56 (d, 2H, Ha_2, $J = 16.4$ Hz), 4.60 (d, 2H, Ha_1, $J = 13.6$ Hz), 5.77 (br s, 2H-methyne protons of the *iso*-menthyl group), 6.90 (s), 6.96 (s) (8H, aromatic protons of calixarene); ^{13}C NMR (100 MHz, $CDCl_3$) $\delta = 18.66$, 19.99, 20.35, 21.53, 26.44, 28.26, 31.24, 31.28, 32.18, [34.06 and 34.18 bridged methylene carbons], 34.22, 37.18, 38.36, 47.29 (aliphatic carbons); 85.69 (*iso*-menthyl carbon), 125.48, 125.69, 126.65, 126.79, 129.38, 129.76, 132.49, 132.88 (aromatic carbons), 147.14, 147.24 148.22, 148.31 (aromatic carbons directly attached to the oxygen atom).

The palladium dichloride complex (**4**) of chiral *p-tert*-butyl-calix[4]arene menthyl bisphosphite ($\mathbf{L}^2$) was prepared as described above for complex (**1**): pale yellow crystals, yield: 118 mg (94%); m.p. = 284–292 °C; *Anal.* Calc. for $C_{64}H_{90}O_6P_2PdCl_2$ (mol. wt.: 1194.6): C, 64.3; H, 7.5. Found C, 64.7; H, 7.8%; ^1H NMR $\delta = 0.80$ (d, 6H, $J = 2.6$ Hz), 0.86 (d, 6H, $J = 3.4$ Hz), 0.94 (d, 6H, $J = 3.8$ Hz), 1.03 (s, 18H, Bu^t), 1.06–1.72 (m, 18H, menthyl group + 18H, Bu^t), 3.42 (d, 2H, Hb_2, $J = 6.2$ Hz), 3.49 (d, 2H, Hb_1, $J = 7.4$ Hz), 4.54 (d, 2H, Ha_2, $J = 12.2$ Hz), 4.66 (d, 2H, Ha_1, $J = 12.4$ Hz), 5.74 (bs, 2H-methyne protons of the menthyl group), 6.73 (s), 6.83 (s), (8H, aromatic protons of calixarene); ^{13}C NMR (100 MHz, $CDCl_3$) $\delta = 18.61$, 19.97, 20.30, 21.52, 26.41, 28.20, 31.19, 31.26, 32.09 [33.94 and 34.15 (bridged methylene carbons)], 34.21, 37.16, 38.33, 47.27 (aliphatic carbons), 85.68 (menthyl carbon), 125.47, 125.67, 126.63, 126.76, 129.36, 129.74, 132.47, 132.86 (aromatic carbons), 147.11, 147.28, 148.21, 148.29 (aromatic carbons directly attached to the oxygen atoms).

2.5. Preparation of chiral p-tert-butyl-calix[4]arene iso-menthyl bisphosphite–$PtCl_2$ complex (**2**) and menthyl bisphosphite–$PtCl_2$ complex (**5**)

The platinum dichloride complex (**2**) was prepared by the reaction of chiral *p-tert*-butyl-calix[4]arene *iso*-menthyl bisphosphite ($\mathbf{L}^1$) (107 mg, 10.5×10^5 mol) with [$PtCl_2$(COD)] (39 mg, 10.5×10^5 mol) in 20 ml of toluene and the reaction mixture was stirred for 1 h. The solvent was evaporated and the residue was washed several times with petrol to obtain complex (**2**). The product was crystallized from chloroform:petrol (1:3) to obtain colorless crystals: Yield 113 mg (84%); m.p. = 291–298 °C; *Anal.* Calc. for $C_{64}H_{90}O_6P_2PtCl_2$ (mol. wt.: 1283.5): C, 59.9; H, 7.1; Found C, 60.2; H, 6.9%; ^1H NMR $\delta = 0.79$ (d, 6H, $J = 2.8$ Hz), 0.84 (d, 6H, $J = 3.6$ Hz), 0.92 (d, 6H, $J = 3.2$ Hz), 1.04–1.67 (m, 18H, *iso*-menthyl group + 18H, Bu^t + 18H, Bu^t), 3.42 (d, 2H, Hb_2, $J = 6.2$ Hz), 3.46 (d,

2H, Hb_1, J = 7.4 Hz), 4.54 (d, 2H, Ha_2, J = 16.0 Hz), 4.59 (d, 2H, Ha_1, J = 13.4 Hz), 5.76 (br s, 2H-methyne protons of the *iso*-menthyl group), 6.90 (s), 6.95 (s) (8H, aromatic protons of calixarene); ^{13}C NMR (100 MHz, $CDCl_3$) δ = 18.66, 19.99, 20.35, 21.53, 26.44, 28.26, 31.24, 31.28, 32.18, [34.06 and 34.18, bridged methylene carbons] 34.22, 37.18, 38.36, 47.29 (aliphatic carbons), 85.69 (*iso*-menthyl carbon), 125.48, 125.69, 126.65, 126.79, 129.38, 129.76, 132.49, 132.88 (aromatic carbons), 147.14, 147.29, 148.22, 148.31 (aromatic carbons directly attached to the oxygen atoms).

The menthyl bisphosphite-platinum dichloride complex (**5**) was synthesized as described above for complex (**2**). Yield: 115 mg (85%); m.p. = 287–294 °C; *Anal.* Calc. for $C_{64}H_{78}O_6P_2PtCl_2$: (mol. wt.: 1283.5): C, 59.9; H, 7.1; Found C, 60.4; H 7.4%; ^{1}H NMR δ = 0.79 (d, 6H, J = 3.4 Hz), 0.87 (d, 6H, J = 3.8 Hz), 0.96 (d, 6H, J = 3.6 Hz), 1.06–1.54 (m, 18H, menthyl group + 18H, Bu^t + 18H, Bu^t), 3.24 (d, 2H, Hb_2, J = 3.9 Hz), 3.29 (d, 2H, Hb_1, J = 4.8 Hz), 4.12 (br s, 2H-methyne protons of the menthyl group), 4.56 (d, 2H, Ha_2, J = 14.2 Hz), 4.81 (d, 2H, Ha_1, J = 14.4 Hz), 6.73 (s), 6.83 (s) (8H, aromatic protons of calixarene); ^{13}C NMR (100 MHz, $CDCl_3$) δ = 16.45, 21.11, 21.95, 22.54, 30.89, 30.93, 31.13, 31.62, 32.20 [33.85 and 33.93, bridged methylene carbons), 34.49, 37.23, 47.22, 48.62 (aliphatic carbons), 87.22 (menthyl carbon), 125.14, 125.68, 127.30, 127.80, 130.77, 131.38, 135.32 (aromatic carbons), 146.84, 146.91, 147.50, 148.77 (aromatic carbons directly attached to the oxygen atom).

2.6. Preparation of chiral p-tert-butyl-calix[4]arene iso-menthyl bisphosphite PdMeCl complex (3) and menthyl bisphosphite PdMeCl complex (6)

Chiral *p-tert*-butyl-calix[4]arene *iso*-menthyl bisphosphite (**L**^{1}) (107 mg, 10.5×10^5 mol) was treated with PdMeCl(COD) (28 mg, 10.5×10^5 mol) in 20 ml of toluene. The reaction mixture was stirred for 30 min. The solvent was evaporated and the residue was washed several times with petrol to obtain complex (**3**) as a colorless powder. Yield: 110 mg (82%); m.p. = 279–284 °C; *Anal.* Calc. for $C_{65}H_{93}O_6P_2PdCl$ (mol. wt.: 1174.4): C, 66.4; H, 7.9; Found C, 66.9; H 8.2%; ^{1}H NMR δ = 0.68 (d, 3H, J = 2.4 Hz), 0.72 (d, 3H, J = 2.6 Hz), 0.76 (dd, 3H, Pd–Me), 0.81 (d, 3H, J = 3.8 Hz) 0.84 (d, 3H, J = 3.2 Hz) 0.86 (d, 3H, J = 2.6 Hz), 0.92 (d, 3H, J = 4.2 Hz), 1.04–1.60 (m, 18H, *iso*-menthyl group + 18H, Bu^t + 18H, Bu^t), 3.38 (d, 2H, Hb_2, $Hb_{2'}$, J = 14.2 Hz), 3.44 (d, 2H, Hb_1, $Hb_{1'}$, J = 9.4 Hz), 4.57 (d, 2H, Ha_2, $Ha_{2'}$, J = 12.6 Hz), 4.70 (d, 2H, Ha_1, $Ha_{1'}$, J = 14.0 Hz), 4.98 (br s, H-methyne protons of the *iso*-menthyl group, *cis* to the methyl group), 6.04 (br s, H-methyne protons of the *iso*-menthyl group, *trans* to the methyl group), 6.80 (s), 6.86 (s), 6.88 (s), 7.19 (s) (aromatic protons of calixarene); ^{13}C NMR (100 MHz, $CDCl_3$) δ = 16.62, 16.74, 21.15, 21.42, 21.95, 22.17, 22.51, 22.82, 25.69, 26.23, 30.90, 30.99, 31.04, 31.25, 31.42, 31.60, 31.66, 31.84, 32.05, 33.80 (Pd–Me), 34.10, 34.11, 34.35, 37.49, 37.96, 42.87, 43.97, 48.64, 48.87 (aliphatic carbons), 82.15, 82.48 (*iso*-menthyl carbons), 124.63, 124.76, 124.97, 125.18, 125.58, 125.88, 126.66, 127.15, 127.71, 128.62, 128.94, 131.23, 131.68, 134.51, 135.11, 146.49, 146.68, 146.88, 147.11, 147.13, 147.51, 147.84 (aromatic carbons).

Complex (**6**) was synthesized by the same procedure as that described above for complex (**3**). Yield: 106 mg (79%); m.p. = 278–281 °C; *Anal.* Calc. for $C_{65}H_{93}O_6P_2PdCl$ (mol. wt.: 1174.4): C, 66.4; H, 7.9; Found C, 66.8; H 7.5%; ^{1}H NMR δ = 0.79 (d, 3H, J = 2.4 Hz), 0.80 (d, 3H, J = 3.2 Hz), 0.83 (d, 3H, J = 3.6 Hz), 0.84 (d, 3H, J = 2.8 Hz), 0.86 (d, 3H, J = 3.2 Hz), 0.87 (d, 3H, J = 3.4 Hz), 0.89 (dd, 3H, Pd–Me), 0.90 (s, 9H, Bu^t), 0.92 (s, 9H, Bu^t), 1.06–1.54 (m, 18H, menthyl group + 18H, Bu^t), 3.34 (d, 2H, Hb_2, $Hb_{2'}$, J = 8.2 Hz), 3.40 (d, 2H, Hb_1, $Hb_{1'}$, J = 12.0 Hz), 4.32 (br s, H-methyne protons of the menthyl group, *cis* to the methyl group), 4.57 (d, 2H, Ha_2, $Ha_{2'}$, J = 16.2 Hz), 4.60 (d, 2H, Ha_1, $Ha_{1'}$, J = 18.2 Hz), 5.75 (br s, H-methyne protons of the menthyl group, *trans* to the methyl group), 6.63 (s), 6.65 (s), 7.03 (s), 7.22 (s) (8H, aromatic protons of calixarene); ^{13}C NMR (100 MHz, $CDCl_3$) δ = 16.59, 16.68, 21.12, 21.40, 21.93, 22.16, 22.50, 22.80, 25.67, 26.20, 30.89, 30.98, 31.03, 31.23, 31.43, 31.58, 31.65, 31.82, 32.03, 33.84 (Pd–Me), 34.09, 34.09, 34.33, 37.48, 37.95, 42.85, 43.78, 48.63, 48.85 (aliphatic carbons), 82.14, 82.46 (menthyl carbons), 124.64, 124.75, 124.95, 125.18, 125.56, 125.87, 126.62, 127.12, 127.70, 128.59, 128.92, 131.21, 131.67, 134.50, 135.10, 146.47, 146.67, 146.86, 147.02, 147.14, 147.49, 147.81 (aromatic carbons).

2.7. Preparation of achiral p-tert-butyl-calix[4]arene bisphosphite–$PdCl_2$ complex (7) and $PtCl_2$ Complex (8)

The $PdCl_2$ complex (**7**) was prepared by the reaction of achiral *p-tert*-butyl-calix[4]arene bisphosphite (**L**^{3}) (105 mg, 10.5×10^5 mol) with [$PdCl_2$(COD)] (30 mg, 10.5×10^5) or $PdCl_2(PhCN)_2$ (40 mg, 10.5×10^5) in 20 ml of toluene and the reaction mixture was stirred for 2 h. The reaction mixture was worked up as described above for the synthesis of complex (**1**). The product was crystallized from dichloromethane:petrol (1:3) and few drops of acetone to obtain yellow crystals. Yield: 108 mg (87%); m.p. = 295–298 °C; *Anal.* Calc. for $C_{64}H_{78}O_6P_2PdCl_2(CH_3COCH_3)$ (mol. wt.: 1240.6): C, 64.9; H, 6.8; Found C, 65.3; H 7.2%; ^{1}H NMR δ = 1.08 (s, 36H, Bu^t), 1.21 (s, 18H, Bu^t), 3.45 (d, 2H, Hb_2, J = 3.2 Hz), 3.49 (d, 2H, Hb_1, J = 5.2 Hz), 4.57 (d, 2H, Ha_2, J = 15.2 Hz), 4.69 (d, 2H, Ha_1, J = 13.6 Hz), 6.82 (s), 6.90 (s) (8 H, aromatic protons of calixarene), 7.14 (d, J = 8.4 Hz), 7.18 (d, J = 7.8 Hz) (8H, aromatic protons); ^{13}C NMR (100 MHz, $CDCl_3$) δ = 31.13, 31.36, 34.18, 37.11 (aliphatic carbons), 118.27, 125.86, 126.25, 129.01, 132.45, 146.96, 147.59, 148.36, 148.71 (aromatic carbons).

The analogous $PtCl_2$ complex (**8**) was prepared by the reaction of ligand (**L**^{3}) (105 mg, 10.5×10^5 mol) with [$PtCl_2$(COD)] (39 mg, 10.5×10^5 mol) in 20 ml of toluene and the reaction mixture was stirred for 2 h. The reaction mixture was worked up as described above for the synthesis of complex (**2**). The product was crystallized from chloroform:petrol (1:3) to obtain colorless crystals. Yield: 112 mg (84%); m.p. = 292–295 °C; *Anal.* Calc. for $C_{64}H_{78}O_6P_2PtCl_2(CHCl_3, H_2O)$ (mol. wt.: 1408.6): C, 55.4; H, 5.8; Found C, 56.1; H, 5.3%; ^{1}H NMR δ = 1.07 (s, 36H, Bu^t), 1.22 (s, 18H, Bu^t), 3.44 (d, 2H, Hb_2, J = 3.4 Hz), 3.51 (d, 2H, Hb_1, J = 5.4 Hz), 4.62 (d, 2H, Ha_2, J = 15.4 Hz), 4.75 (d, 2H, Ha_1, J = 14.2 Hz), 6.82 (s), 6.90 (s) (8H, aromatic protons of calixarene), 7.16 (d, J = 8.2 Hz), 7.19 (d, J = 8.4 Hz) (8H, aromatic protons); ^{13}C NMR (100 MHz, $CDCl_3$) δ = 31.14, 31.37, 34.15, 37.09 (aliphatic carbons), 117.98, 125.80, 126.06, 126.70, 128.96, 132.48, 146.86, 147.25, 148.48, 148.81 (aromatic carbons).

3. Results and discussion

3.1. Synthesis of calix[4]arene bisphosphites and their NMR spectra

Chiral *p-tert*-butyl-calix[4]arene *iso*-menthyl bisphosphite (**L**^{1}) and menthyl bisphosphite (**L**^{2}) have been synthesized in moderate yields (~30%) by the reaction of *p-tert*-butyl-calix[4]arene with (1S,2*R*,5*R*)-(+)-*iso*-menthyl or (1*R*,2*S*,5*R*)-(−)-menthyl phosphorodichloridites, respectively, in the presence of Et_3N. Similarly, the achiral *p-tert*-butyl-calix[4]arene bisphosphite (**L**^{3}) has been isolated from the reaction of *p-tert*-butyl-calix[4]arene with *p-tert*-butyl-phenyl-phosphorodichloridite (Scheme 1). Bisphosphites of the type **L**^{1}–**L**^{3}, in which a single phosphorus atom is bonded to two phenolic oxygen atoms of the calixarene framework, were first reported by Paceillo et al. [14] and Mahalakshmi et al. [19a,30].

The ^{31}P NMR chemical shift values for ligands (**L**^{1}–**L**^{3}) and their palladium and platinum complexes (**1**–**8**) are listed in Table 1. The

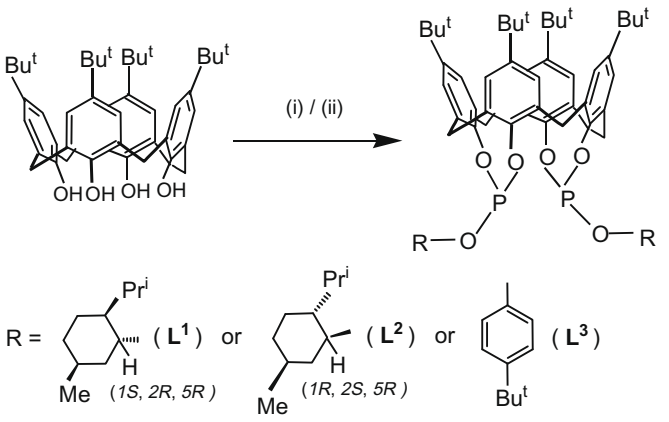

Scheme 1. (i) $ROPCl_2$, THF, Et_3N, 25 °C, 4 h ($\mathbf{L}^1$ or $\mathbf{L}^2$); (ii) $ROPCl_2$, toluene, Et_3N, 25 °C, 8 h ($\mathbf{L}^3$).

^{31}P NMR spectra of ligands ($\mathbf{L}^1$), ($\mathbf{L}^2$) and ($\mathbf{L}^3$) display singlets indicating the magnetic equivalence of the two phosphorus centres. The ^1H NMR spectra show two AB patterns for the methylene protons as would be anticipated for a cone conformation of the calix[4]arene framework [1a,19a] (see Section 3.3). The ^1H NMR spectrum of ligand ($\mathbf{L}^1$) shows a broad singlet at 4.55 ppm for the proton attached to the *iso*-menthyl carbon atom carrying the oxygen atom. This signal merges with the resonances arising from the methylene protons which exist outside the phosphite cage and away from the calixarene cavity. However, the ^1H NMR spectrum of ligand ($\mathbf{L}^2$) shows a broad singlet at 4.06 ppm for the proton attached to the menthyl carbon bearing the oxygen atom. This resonance is flanked by the resonances arising from the two sets of methylene protons which point towards and away from the calix[4]arene cavity. It is also noteworthy that two distinct signals are observed for the *tert*-butyl (CMe_3) protons of the calix[4]arene framework in both ($\mathbf{L}^1$) and ($\mathbf{L}^2$) because of the presence of the chiral *iso*-menthyl or menthyl group.

3.2. Palladium and platinum complexes of chiral and achiral p-tert-butyl-calix[4]arene bisphosphite ligands

The reaction of bisphosphite ligands ($\mathbf{L}^1$), ($\mathbf{L}^2$) and ($\mathbf{L}^3$) with one molar equivalent of $PdCl_2(COD)$ or $PdCl_2(PhCN)_2$ in THF or toluene gives, respectively, the complexes [$PdCl_2(\mathbf{L}^1)$] (**1**), $PdCl_2(\mathbf{L}^2)$ (**4**) and $PdCl_2(\mathbf{L}^3)$ (**7**) which are isolated as pale yellow solids. The analogous Pt complexes [$PtCl_2(\mathbf{L}^1)$] (**2**), [$PtCl_2(\mathbf{L}^2)$] (**5**) and [$PtCl_2(\mathbf{L}^3)$] (**8**) are prepared by the reaction of $PtCl_2(COD)$ with the ligands ($\mathbf{L}^1$), ($\mathbf{L}^2$) and ($\mathbf{L}^3$), respectively. The methyl palladium complexes [PdMeCl($\mathbf{L}^1$)] (**3**) and [PdMeCl($\mathbf{L}^2$)] (**6**) are obtained by the reaction of [PdMeCl(COD)] with the chiral bisphosphite ligands ($\mathbf{L}^1$) and ($\mathbf{L}^2$), respectively. These reactions are shown in Scheme 2.

The ^{31}P NMR chemical shifts for the palladium and platinum dichloride complexes (**1**), (**4**), (**7**) and (**8**) lie very much upfield to those of the free ligands (see Table 1). The ^1H NMR spectra of the complexes display four doublets for the methylene protons of the calix[4]arene framework. The *cis* stereochemistry around the palladium metal centre can be inferred from the far IR spectra which show two ν(Pd–Cl) bands for each of the complexes. The ^{31}P NMR spectra of the platinum complexes (**2**), (**5**) and (**8**) show large $^1J_{Pt-P}$ couplings (see Table 1), confirming the *cis* stereochemistry [18a,31]. The structures of the $PdCl_2$ complexes (**1**), (**4**) and (**7**) and the $PtCl_2$ complex (**8**) have been confirmed by single crystal X-ray diffraction analysis. The exclusive formation of *cis*-chelate complexes and the absence of oligomeric products (as shown by the ^{31}P NMR spectra of the reaction mixtures) is presumably due to the strong "*cis*-preference" exhibited by phosphite ligands in their palladium and platinum complexes, as pointed out by Pringle and coworkers [31].

The ^{31}P NMR spectra of the PdMeCl complexes (**3**) and (**6**) show an AB pattern because of the chemical non-equivalence of the two phosphorus nuclei. The ^{31}P chemical shifts lie in a region, which is in between those for the free ligands and the dichloride complexes (see Table 1). The $^2J_{P-P}$ coupling constants are 113.2 and 106.4 Hz, respectively, for the two complexes. The proton-coupled ^{31}P NMR spectrum of complex (**6**) shows a doublet of quartets for the downfield phosphorus resonance (centered at 113.5 ppm) because of further splitting by coupling with the protons of the methyl group attached to palladium. Hence the downfield resonance can be assigned to the phosphorus which is *trans* to the methyl group. The ^1H NMR spectra of these complexes (**3**) and (**6**) show two broad singlets {6.04 and 4.98 ppm for complex (**3**); 5.75 and 4.32 ppm for complex (**6**)} for the two different methyne protons of the *iso*-menthyl/menthyl carbon atoms directly attached to the oxygen atoms. Although the eight methylene protons of the calix[4]arene framework in the complexes (**3**) and (**6**) are magnetically non-equivalent, only four doublets are observed at room temperature.

3.3. X-ray crystallographic studies

The solid-state structures of complexes (**1**), (**4**), (**7**) and (**8**) have been determined by single crystal X-ray diffraction analysis. Details pertinent to data collection, structure solution and refinement are summarized in Table 2. Selected bond lengths and angles are given in Tables 3 and 4. The data are comparable to those observed for calix[4]arene bisphosphite–$PdCl_2$ complexes reported by Matt and coworkers [17]. There is a slight deviation from a square planar geometry around the metal in all these complexes, presumably because of the involvement of chlorine atom(s) in hydrogen bonding (see below).

The ORTEP plots of the molecular structures of the palladium dichloride complexes (**1**) and (**4**) are presented in Figs. 1 and 2, respectively. The crystal packing diagrams are shown in Fig. S1 (see Supplementary information). When viewed down the *c*-axis, one can clearly see a hexagonal shaped self-assembly of molecules of complexes (**1**) or (**4**) resulting in a hydrophobic channel surrounded by alkyl groups of the *iso*-menthyl and menthyl unit,

Table 1
The ^{31}P {^1H} NMR data for ligands ($\mathbf{L}^1$–$\mathbf{L}^3$) and their palladium and platinum complexes (**1**)–(**8**)[a]

Ligand	δ	Pd complex	δ	$\Delta\delta$	Pt complex[c]	δ	$\Delta\delta$
L^1	126.7	$PdCl_2(L^1)$	80.1	46.6	$PtCl_2(L^1)$	54.3	72.4
		PdMeCl(L^1)[b]	117.4(d), 114.2 (d)				
L^2	125.2	$PdCl_2(L^2)$	78.6	46.6	$PtCl_2(L^2)$	51.9	73.3
		PdMeCl(L^2)[b]	113.5(d), 107.9(d)				
L^3	115.7	$PdCl_2(L^3)$	77.9	37.8	$PtCl_2(L^3)$	53.9	61.8

[a] Recorded in $CDCl_3$ at 25 °C and at 161.9 MHz, δ in ppm, $\Delta\delta = (\delta_{ligand} - \delta_{complex})$ in ppm.
[b] $^2J_{P-P}$ = 113.2, 106.4 Hz for complexes (**3**), (**6**), respectively.
[c] $^1J_{Pt-P}$ = 6056, 6045, 5345 Hz for complexes (**2**), (**5**) and (**8**), respectively.

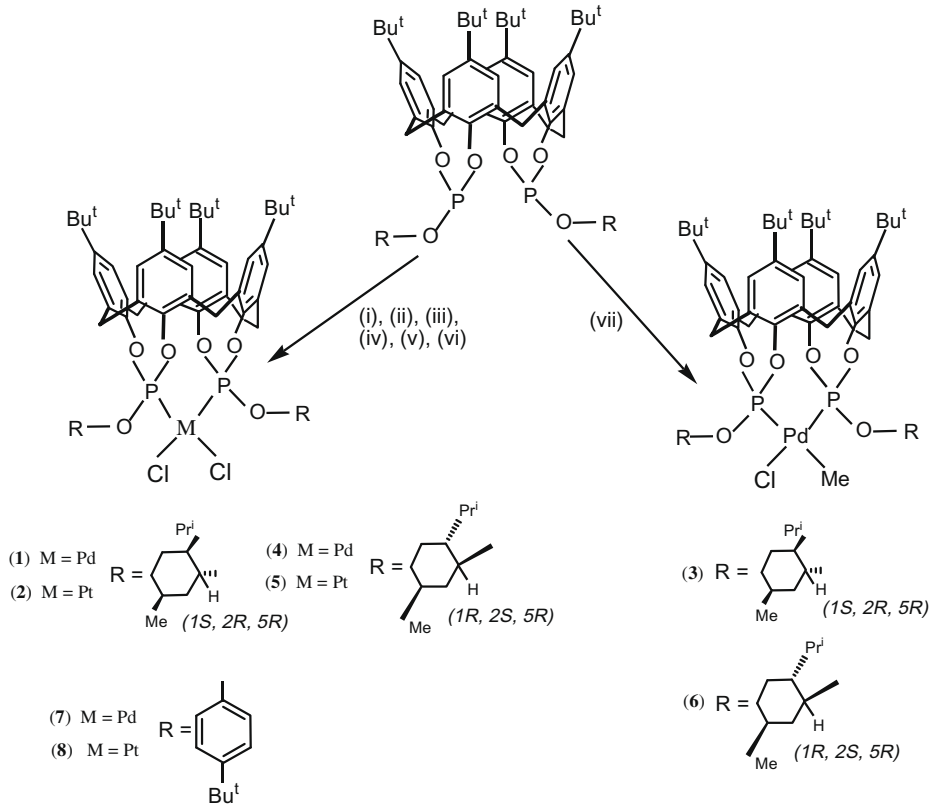

Scheme 2. (i) $PdCl_2$ (COD) or $PdCl_2$ $(PhCN)_2$, THF, 25 °C, 1 h; (ii) $PtCl_2$ (COD), toluene, 25 °C, 1 h; (iii) $PdCl_2$ (COD) or $PdCl_2$ $(PhCN)_2$, THF, 25 °C, 1 h; (iv) $PtCl_2$ (COD), toluene, 25 °C, 1 h; (v) $PdCl_2$ (COD) or $PdCl_2$ $(PhCN)_2$, toluene, 25 °C, 2 h; (vi) $PtCl_2$ (COD), toluene, 25 °C, 2 h; (vii) PdMeCl (COD), toluene, 25 °C, 30 min.

Table 2
Crystal data for complexes (**1**), (**4**), (**7**) and (**8**)

Empirical formula	$C_{64}H_{90}Cl_2O_6P_2Pd$ (**1**)	$C_{64}H_{90}Cl_2O_6P_2Pd$ (**4**)	$C_{67}H_{84}Cl_2O_7P_2Pd$ (**7**)	$C_{65}H_{81}Cl_5O_7P_2Pt$ (**8**)
Formula weight	1194.60	1194.60	1240.58	1408.58
Temperature (K)	293(2)	293(2)	293(2)	293(2)
Wavelength (Å)	0.71073	0.71073	0.71073	0.71073
Crystal system	hexagonal	hexagonal	monoclinic	monoclinic
Space group	$P6_122$	$P6_122$	$C2/c$	$C2/c$
Unit cell dimensions				
a (Å)	19.469(3)	19.4130(14)	37.656(10)	37.936(3)
b (Å)	19.469(3)	19.4130(14)	16.379(4)	16.3639(1)
c (Å)	33.857(9)	33.917(5)	23.670(9)	24.0908(2)
α (°)	90	90	90	90
β (°)	90	90	110.547(5)	111.998(1)
γ (°)	120	120	90	90
Volume (Å^3)	11114(4)	11070(2)	13670(6)	13866(2)
Z	6	6	8	8
$D_{calc.}$ (Mg/m^3)	1.07	1.075	1.206	1.369
Absorption coefficient (mm^{-1})	0.406	0.408	0.444	2.310
$F(000)$	3792	3792	5216	5760
Crystal size (mm)	0.59 × 0.28 × 0.21	0.48 × 0.38 × 0.32	0.52 × 0.46 × 0.26	0.34 × 0.28 × 0.22
Theta range for data collection (°)	1.21–26.03	1.21–26.37	1.84–25.00	1.16–25.00
Index ranges	$-24 \leqslant h \leqslant 21$, $-24 \leqslant k \leqslant 24$, $-41 \leqslant l \leqslant 40$	$-24 \leqslant h \leqslant 24$, $-24 \leqslant k \leqslant 24$, $-42 \leqslant l \leqslant 42$	$-44 \leqslant h \leqslant 44$, $-19 \leqslant k \leqslant 18$, $-28 \leqslant l \leqslant 28$	$-45 \leqslant h \leqslant 45$, $-19 \leqslant k \leqslant 19$, $-28 \leqslant l \leqslant 28$
Reflections collected	86587	87563	48476	66157
Independent reflections (R_{int})	7307(0.0998)	7558(0.1606)	12035(0.0759)	12239(0.0861)
Completeness to θ (%)	99.9	99.9	99.9	100.0
Absorption correction	empirical	empirical	empirical	empirical
Maximum and minimum transmission	0.9196 and 0.7956	0.8806 and 0.8283	0.8925 and 0.8007	0.6303 and 0.5070
Refinement method	full-matrix-least-squares on F^2	full-matrix-least-squares on F^2	full-matrix-least-squares on F^2	full-matrix-least-squares on F^2
Data/restraints/parameters	5416/1/348	7558/1/348	12035/0/732	12239/0/738
Goodness-of-fit	0.787	1.005	0.949	1.016
Final R indices [$I > 2\sigma(I)$]	$R_1 = 0.0604$, $wR_2 = 0.1802$	$R_1 = 0.1428$, $wR_2 = 0.3114$	$R_1 = 0.0869$, $wR_2 = 0.2134$	$R_1 = 0.0629$, $wR_2 = 0.1523$
R indices (all data)	$R_1 = 0.0825$, $wR_2 = 0.2060$	$R_1 = 0.1761$, $wR_2 = 0.3357$	$R_1 = 0.1029$, $wR_2 = 0.2242$	$R_1 = 0.0883$, $wR_2 = 0.1650$
Largest difference in peak and hole (e Å^{-3})	0.825 and −0.299	1.386 and −0.542	1.045 and −1.382	2.626 and −1.729
Absolute structure parameter	−0.04(5)	0.05(10)		

Table 3
Selected structural parameters for the $PdCl_2$ complexes (**1**) and (**4**) (distances in Å, angles in °)

Bond distance	(**1**)	(**4**)	Bond angle	(**1**)	(**4**)
P(1)–Pd(1)	2.227(1)	2.215(3)	P(1)–Pd(1)–P(1′)	91.39(6)	91.93(2)
Cl(1)–Pd(1)	2.333(2)	2.338(4)	P(1)–Pd(1)–Cl(1)	92.21(6)	90.77(1)
P(1)–O(1)	1.556(4)	1.557(9)	P(1)–Pd(1)–Cl(1′)	161.69(5)	163.27(1)
P(1)–O(2)	1.595(3)	1.585(8)	Cl(1′)–Pd(1)–Cl(1)	90.0(1)	91.4(3)
P(1)–O(3)	1.585(3)	1.598(8)	O(3)–P(1)–O(2)	103.8(2)	104.3(4)
			O(3)–P(1)–Pd(1)	118.1(1)	117.9(3)
			O(1)–P(1)–Pd(1)	115.0(1)	116.7(3)
			O(2)–P(1)–Pd(1)	109.8(1)	110.1(3)
			O(3)–P(1)–O(1)	102.65(2)	100.4(4)
			O(1)–P(1)–O(2)	106.3(2)	106.1(5)

Table 4
Selected structural parameters for the complexes (**7**) and (**8**) (distances in Å, angles in °)

Bond distance	(**7**) [M = Pd]	(**8**) [M = Pt]	Bond angle	(**7**) [M = Pd]	(**8**) [M = Pt]
P(1)–M(1)	2.224(2)	2.196(2)	P(2)–M(1)–P(1)	91.37(6)	91.58(7)
P(2)–M(1)	2.213(2)	2.197(2)	P(2)–M(1)–Cl(2)	89.54(6)	89.02(7)
Cl(1)–M(1)	2.348(2)	2.328(2)	P(1)–M(1)–Cl(1)	88.75(6)	91.69(7)
Cl(2)–M(1)	2.328(2)	2.352(2)	Cl(2)–M(1)–Cl(1)	91.92(6)	88.76(7)
P(1)–O(1)	1.584(4)	1.587(6)	O(3)–P(1)–O(1)	101.9(2)	99.0(3)
P(1)–O(2)	1.584(4)	1.592(5)	O(3)–P(1)–O(2)	106.0(2)	107.4(3)
P(1)–O(3)	1.593(5)	1.585(6)	O(1)–P(1)–O(2)	105.3(2)	103.7(3)
P(2)–O(4)	1.587(5)	1.590(5)	O(3)–P(1)–M(1)	114.66(2)	117.5(2)
P(2)–O(5)	1.599(5)	1.579(5)	O(1)–P(1)–M(1)	116.23(2)	118.2(2)
P(2)–O(6)	1.588(5)	1.581(6)	O(2)–P(1)–M(1)	111.56(2)	109.5(2)
			O(6)–P(2)–O(5)	106.3(3)	106.4(3)
			O(6)–P(2)–O(4)	98.9(3)	101.6(3)
			O(5)–P(2)–O(4)	104.7(2)	105.0(3)
			O(6)–P(2)–M(1)	117.59(2)	114.9(2)
			O(5)–P(2)–M(1)	109.45(2)	112.3(2)
			O(4)–P(2)–M(1)	118.46(2)	115.5(2)

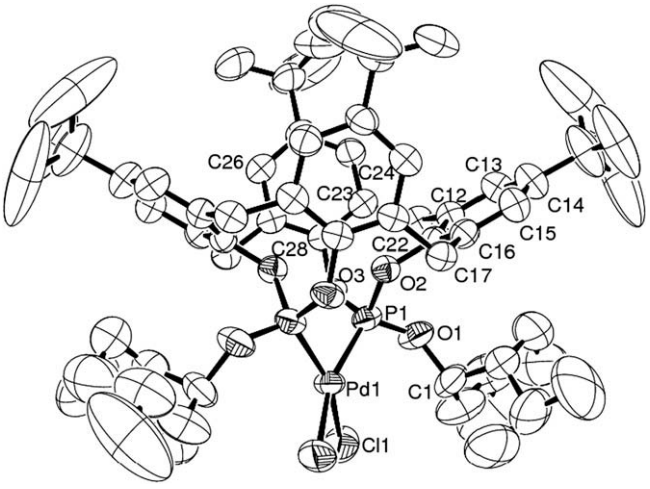

Fig. 1. ORTEP plot of calix[4]arene *iso*-menthyl bisphosphite–palladium dichloride complex (**1**). Only selected atoms are labelled and hydrogen atoms are omitted for clarity.

respectively. A significant difference in the hydrophobic channels of these two complexes is that in complex (**1**), the alkyl groups of the *iso*-menthyl unit surround the channel without any gaps but in complex (**4**), the alkyl groups of the menthyl unit surround the channel with discrete gaps. This difference may be due to the orientation of the *iso*-menthyl and menthyl subunits in the two complexes.

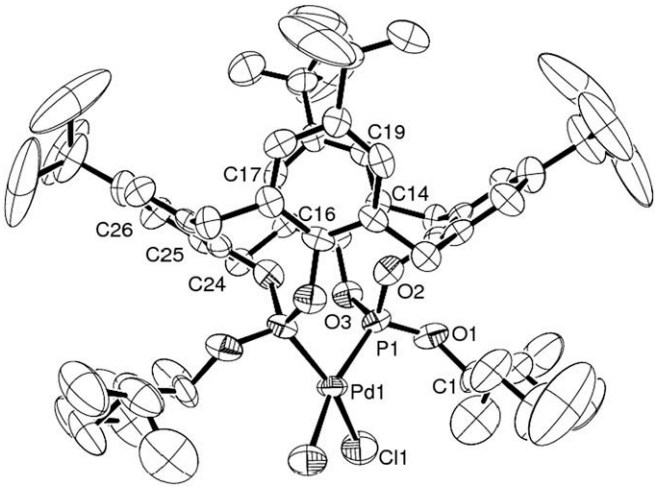

Fig. 2. ORTEP plot of calix[4]arene menthyl bisphosphite–palladium dichloride complex (**4**). Only selected atoms are labelled and hydrogen atoms are omitted for clarity.

The near perfect hexagonal shaped packing of molecules of complexes (**1**) and (**4**) in their crystal lattices arises because of hydrogen bonding interactions as shown in Fig. S2 (see Supplementary information) and Fig. 3, respectively. The crystal lattice of complex (**1**) features a bifurcated hydrogen bond involving Cl(1) and the *ortho*-aryl protons of the calix[4]arene back bone [Cl(1)–aryl proton H(24) distance = 2.936 Å, Cl(1)–aryl proton H(13) distance = 2.954 Å]. We also observed an intramolecular hydrogen bond between an oxygen and a methylene proton [O(1)···H(22B) methylene proton distance = 2.343 Å] (Fig. S2). In the structure of complex **4**, there is an intermolecular hydrogen bond between the chlorine atom and an *ortho*-proton of the calix[4]arene back bone [Cl(1)···H(1) aromatic proton distance = 2.576 Å]. In addition, two intramolecular hydrogen bonds, one between Cl(1) and a methyne proton (H19) of the menthyl unit and another between O(1) and the methylene proton H(13B) of the

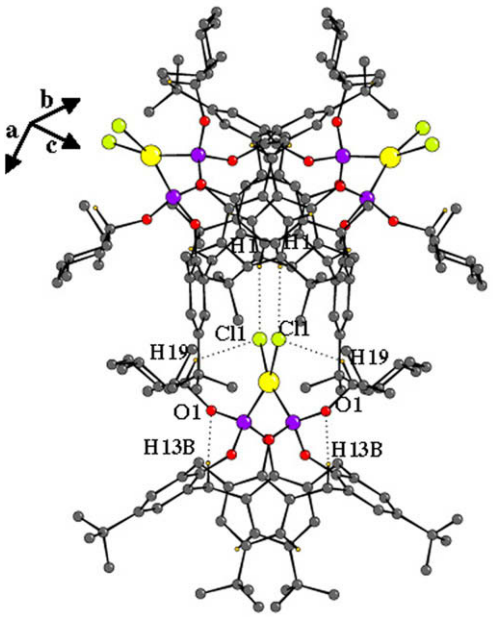

Fig. 3. A view of a crystal segment of palladium dichloride complex (**4**) showing the bifurcated intermolecular and intramolecular hydrogen bonding interactions.

calix[4]arene framework [Cl(1)···H(19) menthyl proton distance = 2.833 Å, O(1)···H(13B) distance = 2.322 Å] are observed (Fig. 3).

The $PdCl_2$ and $PtCl_2$ complexes (**7**) and (**8**) crystallize in the monoclinic C2/c space group and are isostructural. The ORTEP plots of the molecular structures of complexes (**7**) and (**8**) are shown in Figs. 4 and 5, respectively. The structural features are similar to those of the chiral *p*-*tert*-butyl-calix[4]arene *iso*-menthyl and menthyl palladium dichloride complexes (**1**) and (**4**) described above.

The packing of molecules of complex (**7**) in the crystal lattice shows a layer-like arrangement along the *b*-axis; the orientations of the two adjacent molecules are different from each other. Each molecule is surrounded by two other molecules connected by intermolecular hydrogen bonds formed between the chlorine atom and a methylene proton [Cl(1)···H(2A) distance = 2.867 Å], and also between the oxygen atom and alkyl proton of the *tert*-butyl group [O(3)···H(51A) distance = 2.694 Å]. There is also an intramolecular hydrogen bond formed between the oxygen atom and a methylene proton [O(6)···H(14B) distance = 2.311 Å] (see Fig. 6). In the crystal lattice of complex (**8**), each discrete molecule is surrounded by two other molecules and one solvent molecule. The observed intra- and intermolecular hydrogen bonds are shown in Fig. S3 (see Supplementary information). The relevant data are given in Table 5.

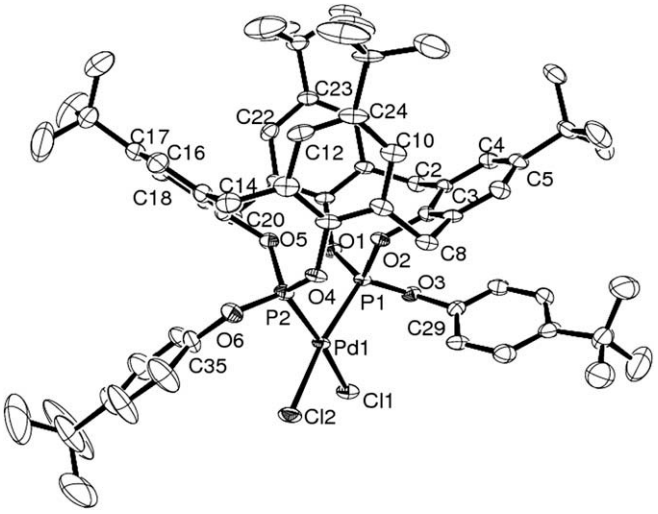

Fig. 4. ORTEP plot of calix[4]arene 4-*tert*-butyl-phenyl bisphosphite-palladium dichloride complex (**7**). Selected atoms are labelled and hydrogen atoms and solvent molecules are omitted for clarity.

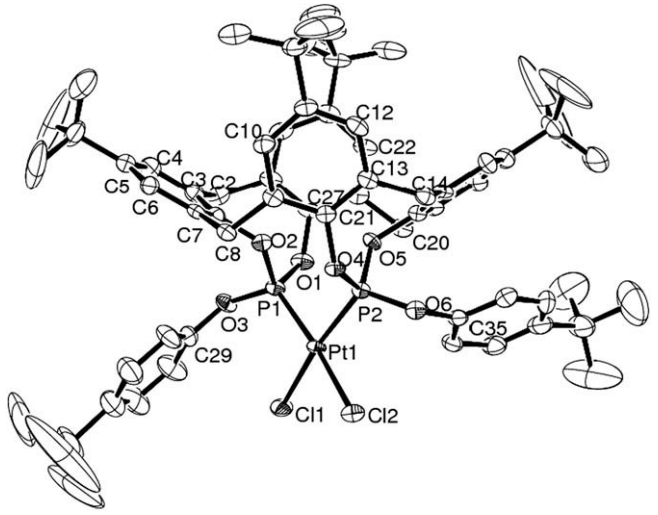

Fig. 5. ORTEP plot of calix[4]arene 4-*tert*-butyl-phenyl bisphosphite–platinum dichloride complex (**8**). Selected atoms are labelled and hydrogen atoms and solvent molecules are omitted for clarity.

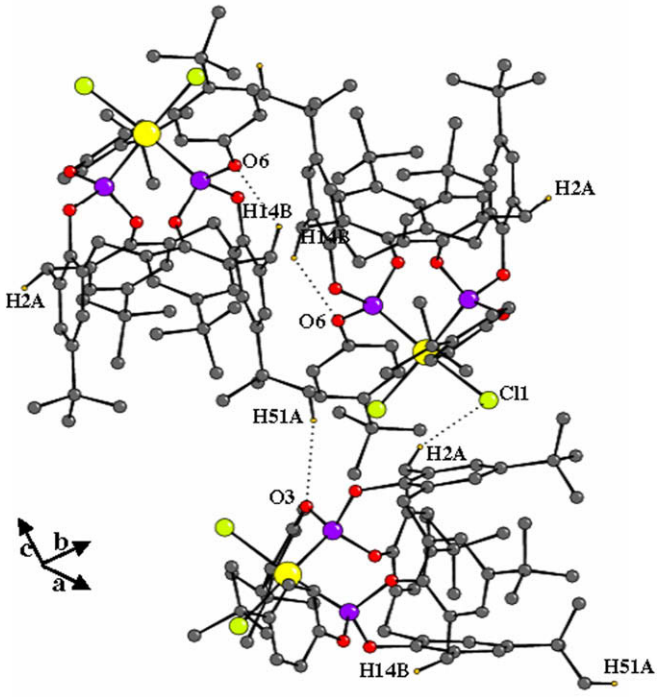

Fig. 6. A view of a crystal segment of palladium dichloride complex (**7**) showing the intra and intermolecular hydrogen bonding interactions.

The calix[4]arene framework in all these compounds (**1**), (**4**), (**7**) and (**8**) adopts a cone conformation. The conformation of the calix[4]arene backbone can be discussed in terms of either torsion angles or dihedral angles. The dihedral angles of the calix[4]arene aryl rings (A = A′ and B = B′) with the plane X of the four methylene carbon atoms{C17, C22, C17′ and C22′ for the complex (**1**) and C13, C24, C13′ and C24′ for complex (**4**)} are listed in Table S-1 (see Supplementary information). These data show that there is a distortion of the cone conformation in the two complexes. The torsion angles involving the bridging methylene carbon atoms and aryl ring carbon atoms for the complexes (**1**) and (**4**) are listed in Table S-2 (see Supplementary information). The sequence of signs for the two torsion angles ϕ and χ is found to be +−, +−, +−, +− and confirms the cone conformation for both the complexes. A comparison of the observed torsion angles ϕ and χ for the two palladium complexes (**1**) and (**4**) with those expected for an ideal cone conformation [90° and 90°, respectively] shows that there is a larger deviation for two aryl rings (larger torsion angles) and a smaller deviation for the other two aryl rings (smaller torsion angles). The two aryl rings with larger torsion angles are parallel with respect to each other; the other two aryl rings with smaller torsion angles are tilted from the mean plane X of the methylene carbon atoms. This type of conformation is known as a "flattened cone conformation" [32]. Similar results are observed for the palladium and platinum dichloride complexes, (**7**) and (**8**). The relevant dihedral angles and torsion angles are listed in Tables S-3 and S-4, respectively (see Supplementary information). These values indicate that the cone conformation is more flattened in complexes (**1**), (**4**), (**7**) and (**8**) than in the free calix[4]arene bisphosphites [19a,33].

Table 5
Hydrogen bonding parameters for complexes (**1**), (**4**), (**7**) and (**8**)

D–H···A	r(H···A) (Å)	r(D···A) (Å)	Angle (D–H···A) (°)
*A: Hydrogen bonding (C–H···Cl and C–H···O) parameters for [$PdCl_2$(L^1)] (**1**)*			
C(22)–H(22B) ···O(1)	2.343[0]	3.069[0]	131.0[0]
C(13)–H(13) ···Cl(1)	2.954[i]	3.695[i]	137.6[i]
C(24)–H(24) ···Cl(1)	2.936[i]	3.838[i]	163.8[i]
Symmetry codes: [0] *x*, *y*, *z*; [i] *y* + 1, +*x*, −*z* + 1/3 + 1.			
*B: Hydrogen bonding (C–H…Cl and C–H…O) parameters for [$PdCl_2$(L^2)] (**4**)*			
C(1)–H(1)···Cl(1)	2.576[0]	3.222[0]	133.0[0]
C(13)–H(13B)···O(1)	2.322[0]	3.051[0]	132.2[0]
C(19)–H(19)···Cl(1)	2.833[i]	3.748[i]	167.9[i]
Symmetry codes: [0] *x*, *y*, *z*; [i] *y* + 1, +*x*, −*z* + 1/3.			
*C: Intra and intermolecular hydrogen bonding (C–H···Cl and C–H···O) parameters for complex (**7**)*			
C(2)···H(2A)···Cl(1)	2.867 [i]	3.795[i]	160.6[i]
C(51)···H(51A)···O(3)	2.694[ii]	3.619[ii]	162.1[ii]
C(14)···H(14B)···O(6)	2.311[0]	3.043[0]	131.6[0]
Symmetry codes: [0] *x*, *y*, *z*; [i] *x* + 1/2, +*y* − 1/2, *z* + 1/2 + 1; [ii] *x*, *y*, +*z* − 1/2.			
*D: Intra and intermolecular hydrogen bonding (C–H···Cl and C–H···O) parameters for complex (**8**)*			
C(2)···H(2A)···O(3)	2.299[0]	3.034[0]	131.9[0]
C(14)···H(14B)···O(6)	2.353[0]	3.078[0]	131.1[0]
C(42)···H(42B)···O(1)	2.881[iii]	3.804[iii]	161.6[iii]
C(14)···H(14A)···Cl(2)	2.810[i]	3.754[i]	164.6[i]
C(40)···H(40)···Cl(1)	2.888[i]	3.756[i]	155.9[i]
C(43)···H(43C)···O(6)	2.823[ii]	3.749[ii]	162.6[ii]
C(43)···H(43C)···O(4)	2.958[ii]	3.698[ii]	134.8[ii]
C(52)···H(52B)···Cl(4)	2.967[0]	3.771[0]	142.1[0]
Symmetry codes: [0] *x*, *y*, *z*; [i] −*x* + 1/2, *y* + 1/2, *z* + 1/2, [ii] *x*, *y* + 1, +*z* − 1/2; [iii] −*x* + 1/2, *y* + 1/2, *z*.			

4. Conclusions

We have described the synthesis of new chiral and achiral bisphosphites anchored to a *p-tert*-butyl-calix[4]arene framework. These bisphosphites behave as chelating ligands in palladium(II) and platinum(II) complexes. These complexes provide examples of the presence of non-covalent interactions such as intermolecular C–H···Cl and C–H···O hydrogen bonds which lead to novel structural motifs in the solid state. These rigid chiral and achiral bisphosphites with hydrophobic cavities may have significant applications in homogeneous catalysis.

Acknowledgements

We thank the Department of Science and Technology, New Delhi, India for financial support and also for data collection using the CCD X-ray facility at IISc, Bangalore set up under the IRHPA program. S.S.K. thanks the Indian National Science Academy, New Delhi for a Senior Scientist position.

Appendix A. Supplementary data

CCDC 692825, 692826, 692827 and 692828 contain the supplementary crystallographic data for **8**, **7**, **1** and **4**. These data can be obtained free of charge via http://www.ccdc.cam.ac.uk/conts/retriving.html, or from the Cambridge Crystallographic Data Centre, 12 Union Road, Cambridge CB2 1EZ, UK; fax (+44) 1223-336-033; e-mail: deposit@ccdc.cam.ac.uk. Supplementary data associated with this article can be found, in the online version, at doi:10.1016/j.poly.2008.08.008.

References

[1] (a) C.D. Gutsche, Calixarenes Revisited, The Royal Society of Chemistry, Cambridge, 1998;
(b) L. Mandolini, R. Ungaro, Calixarenes in Action, Imperial College Press, London, 2000.
[2] V. Bohmer, Angew. Chem., Int. Ed. 34 (1995) 713.
[3] S. Shinkai, Tetrahedron 49 (1993) 8933.
[4] (a) P. Buhlmann, E. Pretsch, E. Bakker, Chem. Rev. 98 (1998) 1593;
(b) B.R. Cameron, S.J. Loeb, Chem. Commun. (1996) 2003;
(c) Y. Kubo, S. Maruyama, N. Ohhara, M. Nakamura, S. Tokita, J. Chem. Soc., Chem. Commun. (1995) 727.
[5] (a) L. Baldini, A. Casnati, F. Sansone, R. Ungaro, Chem. Soc. Rev. 36 (2007) 254;
(b) S.J. Delgarno, P.K. Thallapallly, L.J. Barbour, J.L. Atwood, Chem. Soc. Rev. 36 (2007) 236.
[6] G.R. Desiraju, Acc. Chem. Res. 35 (2002) 565.
[7] (a) G.R. Desiraju, Angew. Chem., Int. Ed. 34 (1995) 2311;
(b) G.R. Desiraju, Angew. Chem., Int. Ed. 46 (2007) 8342.
[8] C.B. Akeroy, T.A. Evans, K.R. Saddon, I. Palinko, New. J. Chem. (1999) 145.
[9] P.K. Thallapally, A. Nangia, Cryst. Eng. Commun. 27 (2001) 1.
[10] C.B. Dieleman, C. Loeber, D. Matt, A. De Cian, J. Fischer, J. Chem. Soc., Dalton Trans. (1995) 3097.
[11] (a) C. Wieser, D. Matt, L. Toupet, H. Bourgeois, J.P. Kintzinger, J. Chem. Soc., Dalton Trans. (1996) 4041;
(b) C.B. Dieleman, D. Matt, P.G. Jones, J. Organomet. Chem. (1997) 461.
[12] (a) C. Wieser, C.B. Dieleman, D. Matt, Coord. Chem. Rev. 165 (1997) 93;
(b) C. Jeunesse, D. Armspach, D. Matt, Chem. Commun. (2005) 5603.
[13] (a) C. Loeber, D. Matt, A. De Cian, J. Fischer, J. Organomet. Chem. 475 (1994) 297;
(b) C.B. Dieleman, D. Matt, I. Neda, R. Schmutzler, H. Thoennessen, P.G. Jones, A. Harriman, J. Chem. Soc., Dalton Trans. (1998) 2115.
[14] R. Paciello, L. Siggel, M. Roper, Angew Chem., Int. Ed. 38 (1999) 1920.
[15] W. Xu, R.J. Puddephatt, L.M. Muir, K.W. Muir, C.S. Frampton, J. Inclusion Phenom. 19 (1994) 277.
[16] M. Stolmar, C. Floriani, A. Chiesi-Villa, C. Rizzoli, Inorg. Chem. 36 (1997) 1694.
[17] S. Steyer, C. Jeunesse, J. Harrowfield, D. Matt, J. Chem. Soc., Dalton Trans. (2005) 1301.
[18] (a) C.J. Cobley, D.D. Ellis, A.G. Orpen, P.G. Pringle, J. Chem. Soc., Dalton Trans. (2000) 1101;
(b) C.J. Cobley, D.D. Ellis, A.G. Orpen, P.G. Pringle, J. Chem. Soc., Dalton Trans. (2000) 1109.
[19] (a) L. Mahalakshmi, M. Nethaji, S.S. Krishnamurthy, Curr. Sci. 83 (2002) 870;
(b) A. Sarkar, M. Nethaji, S.S. Krishnamurthy, Polyhedron 26 (2007) 3904.
[20] J.-M. Brunel, G. Buono, J. Org. Chem. 58 (1993) 7313.
[21] D. Drew, J.R. Doyle, Inorg. Synth. 13 (1972) 52.
[22] J.R. Doyle, P.E. Slade, H.B. Jonassen, Inorg. Synth. 6 (1960) 218.
[23] F.T. Ladipo, G.K. Anderson, Organometallics 13 (1994) 303.
[24] D. Drew, J.R. Doyle, Inorg. Synth. 13 (1972) 48.
[25] Bruker SMART, V. 6.028, Bruker AXS Inc., Madison Wisconsin, USA, 1998.
[26] Bruker SAINT, V. 6.02, Bruker AXS Inc., Madison Wisconsin, USA, 1998.
[27] G.M. Sheldrick, SADABS, University of Göttingen, Germany, 1997.

[28] G.M. Sheldrick, SHELXS-97, Program for Crystal Structure Solution, University of Göttingen, Göttingen, Germany, 1997.
[29] G.M. Sheldrick, SHELXL-97, Program for Refinement of Structure, University of Göttingen, Göttingen, Germany, 1997.
[30] L. Mahalakshmi, Synthesis, structure and coordination chemistry of phosphorus functionalized calixarenes, Ph.D. Thesis, Indian Institute of Science, Bangalore, 1999.
[31] A. Crispini, K.N. Harrison, A.G. Orpen, P.G. Pringle, J.R. Wheatcroft, J. Chem. Soc., Dalton Trans. (1996) 1069.
[32] F. Ugozzoli, G.D. Andreetti, J. Inclusion Phenom. 13 (1992) 337.
[33] P. Maji, Phosphite ligands based on the calix[4]arene scaffold and their palladium, platinum and rhodium complexes, Ph.D. Thesis, Indian Institute of Science, Bangalore, 2005.

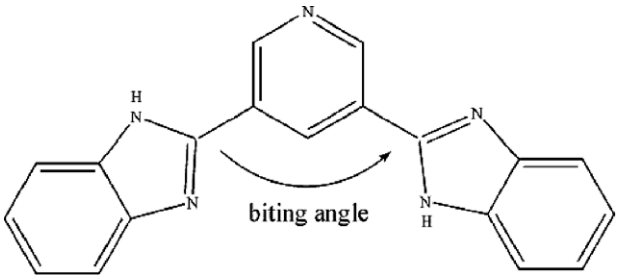

Scheme 1. Schematic view of pyridine-3,5-bis(benzimidazole-2-yl).

2. Experimental

2.1. Materials and analyses

All reagents and solvents were used directly as supplied commercially without further purification, except that the ligand (pbb) was prepared. Elemental analyses (C, H, and N) were determined with a Perkin–Elmer model 240 °C automatic instrument. Infrared spectra on KBr pellets were performed in a BRUKER EQUINOX–55 spectrometer in the range of 4000–400 cm^{-1}. ^1H NMR spectra were recorded using an INOVA–400 MHZ (Varian, America). Mass spectra were obtained with a JEOL HX–110 HF double focusing spectrometer operating in the positive ion detection mode. A Micro DSC III Thermal Activity Monitor (Setaram, France) was used to determine the power-time curves of *Escherichia coli* growth.

2.2. Syntheses

The formation of **1**, **2**, **3,** and **4** with the experimental conditions are shown in Scheme 2. Their syntheses are given in the sequel.

2.2.1. Preparation of the ligand

The ligand (pbb) was prepared from o-phenylenediamine and 3,5-pyridinedicarboxylic acid monohydrate by a modified literature method [11]. The product was a pale-yellow powder in 60% yield, mp > 280 °C. *Anal.* Calc. for $C_{19}H_{13}N_5$: C, 73.29; H, 4.21; N, 22.49. Found: C, 73.28; H, 4.18; N, 22.50%. IR (cm^{-1}, KBr): 3386 (s), 3185 (s), 2930 (s), 1602 (w), 1514 (w), 1437 (m), 1322 (w), 1279 (m), 1224 (w), 1118 (w), 1016 (w), 959 (w), 898 (w), 734 (s), 699 (m). MS (FAB): *m/z* (%) = 312.3 (pbb). ^1H NMR (ppm, DMSO): δ = 9.319 (s, 1H, 1-H), 9.426 (s,2H,2-H), 13.347 (s, 2H, 3-H), 7.682 (dd, 4H, 4-H), 7.281 (m, 4H, 5-H).

2.2.2. $[pbb(Hpbb)_2]SO_4 \cdot 7H_2O$ (**1**)

A mixture of pbb (31 mg, 0.1 mmol), $ZnSO_4 \cdot 7H_2O$ (29 mg, 0.1 mmol) and 10 mL H_2O was sealed in a 25 mL Telfon-lined stainless steel container, which was heated to 140 °C for 72 h. After cooling to room temperature at a rate of 2 °C per hour, well-shaped yellow block crystals of **1**, suitable for X-ray diffraction, were obtained. The final pH value of the mixture was about 5. Notably, **1** was obtained under the emergence of $ZnSO_4$. It has been confirmed that the existence of $ZnSO_4$ is required in this process, although the mechanism is not clear. *Anal.* Calc. for $C_{57}H_{57}N_{15}O_{12}S$ (1176.24): C, 58.20; H, 4.88; N, 17.86. Found: C, 58.20; H, 4.89; N, 17.88%. IR (cm^{-1}, KBr): 3745 (m), 3381 (s), 1596 (m), 1490 (w), 1429 (s), 1342 (m), 1312 (m), 1275 (m), 1254 (m), 1137 (w), 1015 (w), 955 (w), 896 (w), 857 (w), 742 (s), 616 (m).

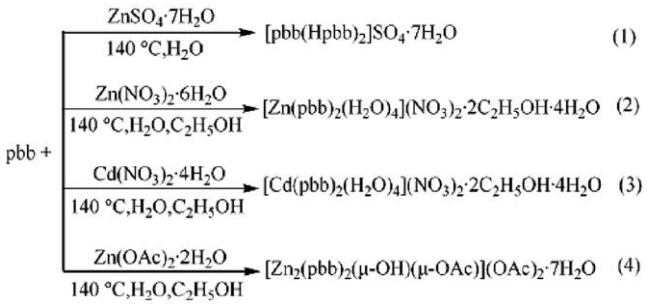

Scheme 2. The formation of **1**–**4** together with the experimental conditions.

2.2.3. $[Zn(pbb)_2(H_2O)_4](NO_3)_2 \cdot 2C_2H_5OH \cdot 4H_2O$ (**2**)

A mixture of pbb (31 mg, 0.1 mmol), $Zn(NO_3)_2 \cdot 6H_2O$ (30 mg, 0.1 mmol) and 10 mL water–ethanol (1:1) was sealed in a 25 mL Telfon-lined stainless steel container, which was heated to 140 °C for 72 h. Slow cooling of the reaction mixture to room temperature gave light-yellow block crystals in ca. 60% yield. *Anal.* Calc. for $C_{42}H_{54}N_{12}O_{16}Zn$ (1048.34): C, 48.12; H, 5.19; N, 16.03. Found: C, 48.11; H, 5.14; N, 16.02%. IR (cm^{-1}, KBr): 3443 (s), 1764 (w), 1628 (m), 1481 (m), 1385 (s), 1224 (m), 1025 (w), 904 (w), 826 (w), 743 (m), 693 (w).

2.2.4. $[Cd(pbb)_2(H_2O)_4](NO_3)_2 \cdot 2C_2H_5OH \cdot 4H_2O$ (**3**)

The preparation of **3** was similar to that of **2** except that $Cd(NO_3)_2 \cdot 4H_2O$ (0.1 mmol) was used instead of $Zn(NO_3)_2 \cdot 6H_2O$. Pale-yellow block crystals were obtained in ca. 66% yield. *Anal.* Calc. for $C_{42}H_{54}N_{12}O_{16}Cd$ (1095.37): C, 46.05; H, 4.97; N, 15.34. Found: C, 46.04; H, 4.96; N, 15.36%. IR (cm^{-1}, KBr): 3467 (s), 1763 (w), 1623 (m), 1478 (m), 1423 (m), 1383 (s), 1225 (w), 1123 (w), 1045 (w), 961 (w), 901 (w), 826 (w), 735 (m), 690 (m).

2.2.5. $[Zn_2(pbb)_2(\mu\text{-}OH)(\mu\text{-}OAc)](OAc)_2 \cdot 7H_2O$ (**4**)

The preparation of **4** was similar to that of **2** except that $Zn(OAc)_2 \cdot 2H_2O$ (0.1 mmol) was used instead of $Zn(NO_3)_2 \cdot 6H_2O$. Pale-yellow block crystals were obtained in ca. 48% yield. *Anal.* Calc. for $C_{44}H_{50}N_{10}O_{14}Zn_2$ (1073.68): C, 49.22; H, 4.69; N, 13.04. Found: C, 49.24; H, 4.69; N, 13.10%. IR (cm^{-1}, KBr): 3121 (s), 1591 (s), 1482 (m), 1430 (m), 1332 (m), 1277 (m), 1227 (w), 1184 (w), 1132 (w), 1051 (w), 1021 (w), 960 (w), 932 (w), 903 (w), 847 (w), 744 (s), 699 (s), 614 (w).

2.3. X-ray crystallography

Diffraction experiments for **1**, **2**, **3,** and **4** were carried out with Mo Kα radiation using a BRUKER SMART APEX CCD diffractometer at 293 (2) or 296 (2) K. The structures were solved by direct methods and refined with the full-matrix least-squares technique on F^2 using the SHELXS–97 and SHELXL–97 [12] programs. All non-hydrogen atoms were refined anisotropically. A summary of the crystallographic data and structure refinement is shown in Table 1, selected bond lengths and angles of the complexes are listed in Table 2, and possible hydrogen bond geometries are given in Table 3.

2.4. Biological activity tests

Bacteria (*E. coli*, *Staphylococcus aureus,* and *Bacillus subtilis)* and mould (*Glomerella cingulata*, *Alternaria solani,* and *Monilinia fructicola)* strains were provided by the College of Life Sciences at Northwest University (China). The antimicrobial activities of pbb and its complexes were examined by the bacteriostatic ring test method. The antibacterial activity was measured as the diameter of the inhibitory zones in the soft agar layer stained after 24 h incubation at 37 °C, while inhibition again mould after 72 h at 28 °C. An inhibitory zone with a diameter less than 6 mm corresponds to lack of activity (6 mm is the diameter of the spot). Control experiments with solvents show that the solvents have no activity. Selected duplicates were run to ensure reproducibility.

Table 1
Crystal data and structure refinements for complexes **1**–**4**

Complexes	**1**	**2**	**3**	**4**
Empirical formula	$C_{57}H_{57}N_{15}O_{12}S$	$C_{42}H_{54}N_{12}O_{16}Zn$	$C_{42}H_{54}N_{12}O_{16}Cd$	$C_{44}H_{50}N_{10}O_{14}Zn_2$
Formula mass	1176.24	1048.34	1095.37	1073.68
Temperature (K)	293(2)	296(2)	296(2)	296(2)
Crystal system	triclinic	triclinic	triclinic	monoclinic
Space group	$P\bar{1}$	$P\bar{1}$	$P\bar{1}$	$C2/c$
a (Å)	12.495(3)	7.690(3)	7.888(2)	16.7513(14)
b (Å)	15.367(3)	11.015(4)	11.214(3)	13.5444(12)
c (Å)	15.976(3)	15.332(6)	15.004(4)	20.7377(19)
α (°)	73.050(3)	70.791(7)	70.349(5)	90
β (°)	72.760(3)	89.738(7)	88.439(5)	95.5710(10)
γ (°)	82.380(3)	75.442(7)	74.617(5)	90
V (Å^3)	2798.9(10)	1182.87(7)	1202.3(5)	4682.9(7)
Z	2	1	1	4
D_{calc} (g cm^{-3})	1.396	1.472	1.513	1.523
μ (mm^{-1})	0.136	0.603	0.537	1.103
F[000]	1232	548	566	2224
θ (°)	2.47–25.50	1.41–25.10	2.00–25.09	1.94–25.10
Data/restraints/parameters	10346/0/766	4136/0/356	4175/12/356	4166/0/319
Goodness-of-fit on F^2	0.992	0.861	0.870	1.058
Final R[a] indices [$I > 2\sigma(I)$]	$R_1 = 0.0735$	$R_1 = 0.0666$	$R_1 = 0.0566$	$R_1 = 0.0495$
	$wR_2 = 0.1680$	$wR_2 = 0.1494$	$wR_2 = 0.1332$	$wR_2 = 0.1139$
R indices (all data)	$R_1 = 0.1524$	$R_1 = 0.1547$	$R_1 = 0.1021$	$R_1 = 0.0875$
	$wR_2 = 0.2134$	$wR_2 = 0.1814$	$wR_2 = 0.1590$	$wR_2 = 0.1349$

[a] $R_1 = \sum(|F_0| - |F_C|)/\sum|F_0|$; $wR_2 = [\sum w(|F_0^2| - |F_C^2|)^2/\sum w(|F_0^2|)^2]^{1/2}$.

Table 2
Selected bond lengths (Å) and angles (°) for complexes **1**–**4**

Complex **1**			
N(1)–C(7)	1.327(5)	N(2)–C(7)	1.349(5)
N(4)–C(13)	1.334(5)	N(5)–C(13)	1.361(5)
N(6)–C(26)	1.368(5)	N(7)–C(26)	1.306(5)
N(9)–C(32)	1.331(5)	N(10)–C(32)	1.353(5)
N(11)–C(45)	1.359(5)	N(12)–C(45)	1.323(5)
N(14)–C(51)	1.349(5)	N(15)–C(51)	1.346(5)
N(1)–C(7)–C(8)	126.9(3)	N(5)–C(13)–C(11)	125.3(3)
N(6)–C(26)–C(27)	124.5(4)	N(9)–C(32)–C(29)	125.7(4)
N(11)–C(45)–C(46)	124.0(3)	N(14)–C(51)–C(49)	125.2(3)
Complex **2**			
Zn(1)–O(1)	2.112(5)	Zn(1)–O(2)	2.098(4)
Zn(1)–N(1)	2.158(5)	O(2)–Zn(1)–O(1)	86.8(2)
O(1)–Zn(1)–N(1)	89.5(2)	O(2)–Zn(1)–N(1)	86.9(2)
Complex **3**			
Cd(1)–O(1)	2.30(1)	Cd(1)–O(2)	2.30(1)
Cd(1)–N(3)	2.32(1)	O(2)–Cd(1)–O(1)	84.0(5)
O(2)–Cd(1)–N(3)	94.2(5)	O(1)–Cd(1)–N(3)	90.8(4)
Complex **4**			
Zn(1)–O(1)	1.970(3)	Zn(1)–O(2)	1.916(2)
Zn(1)–O(3)	1.956(3)	Zn(1)–N(1)	2.063(3)
O(2)–Zn(1)–O(3)	127.7(2)	O(2)–Zn(1)–O(1)	108.3(2)
O(3)–Zn(1)–O(1)	110.7(2)	O(2)–Zn(1)–N(1)	101.8(1)
O(3)–Zn(1)–N(1)	100.1(2)	O(1)–Zn(1)–N(1)	105.0(2)

Microcalorimetry is an important tool for measuring metabolic activities of cells and biological tissues [13]. Here, the power-time curves for growth of *E.* coli at 37 °C were determined in the presence of pbb and its complexes by using a microcalorimetric method. In the exponential growth phase of *E. coli*, the thermal power given out by the microbe and time are related with the following equation [14]:

$$\ln P_t = \ln P_o + kt$$

where P_t and P_0 are the thermal power at time t and t_0, respectively, k is the growth rate constant. Using the experimental data, P_t and t obtained from the thermal power-time curves under various concentrations of the samples, the corresponding growth rate constant k can be calculated from linear regression analysis. Under the same cultivation conditions, the experimental results (the thermal power-time curves) display high repeats.

Table 3
Hydrogen-bonding geometries for complexes **1**–**4**

D–H···A	D–H (Å)	H···A (Å)	D···A (Å)	D–H···A (°)
Complex **1**				
O(1)–H(1W)···O(3)	0.84	1.92	2.762(6)	177.5
O(3)–H(6W)···O(2)	0.85	2.23	3.079(7)	179.4
O(4)–H(7W)···O(3)	0.83	1.84	2.594(6)	150.5
O(5)–H(9W)···O(4)	0.85	2.44	2.899(7)	114.4
O(5)–H(10W)···O(12)#2	0.85	1.83	2.651(4)	161.7
O(6)–H(11W)···O(9)	0.85	2.02	2.866(5)	179.3
O(8)–H(15W)···O(4)#2	0.83	1.97	2.747(5)	154.0
N(9)–H(9D)···O(6)	0.86	1.79	2.625(5)	162.2
N(5)–H(5D)···O(12)#2	0.86	1.92	2.759(4)	165.9
N(1)–H(1D)···O(5)	0.86	1.80	2.625(4)	159.2
N(14)–H(14D)···O(11)	0.86	1.91	2.728(4)	157.3
Complex **2**				
O(1)–H(1WB)···O(8)#1	0.832	1.871	2.691	167.85
O(2)–H(2WA)···O(7)	0.827	1.905	2.720	168.24
O(2)–H(2WB)···O7#2	0.828	2.054	2.790	147.84
O(7)–H(7WB)···O(8)	0.835	2.044	2.792	148.69
N(2)–H(2A)···O(3)	0.860	2.152	2.999	168.29
Complex **3**				
O(1)–H(1A)···O(8)#1	0.832	1.889	2.681	158.76
O(7)–H(7B)···O(8)#2	0.837	1.963	2.793	170.84
N(4)–H(4A)···O(3)	0.860	1.981	2.825	166.63
N2-H2A···O(5)#3	0.860	2.190	3.039	169.27
Complex **4**				
O(7)–H(7B)···O(3)	0.81	2.06	2.862(4)	169.0
O(7)–H(7C)···O(5)#4	0.82	1.96	2.751(3)	161.6
O(6)–H(6B)···O(7)	0.85	2.03	2.870(5)	169.0
O(6)–H(6C)···O(8)	0.85	1.87	2.689(5)	161.5
O(8)–H(8B)···O(2)#4	0.82	1.99	2.790(5)	164.3

For **1**: #2 $-x+1$, $-y+1$, $-z+1$. For **2**: #1 $-x+1$, $-y+1$, $-z+1$; #2 $-x$, $-y+1$, $-z+1$. For **3**: #1 $x, y, z-1$; #2 $-x+1$, $-y+1$, $-z+1$; #3 $-x+1$, $-y+1$, $-z$. For **4**: #4 $x-1/2$, $y-1/2$, z.

3. Results and discussion

The pale-yellow powder pbb is obtained in good yield. In order to confirm the identity of the product, the MS and ^{1}H NMR spectra of pbb were measured, and the spectra are given in Fig. S1.

3.1. Description of structures

3.1.1. Crystal Structure of **1**

The single-crystal X-ray structural analysis of complex **1** reveals a H_2SO_4 solvate of pbb, in which three pbb molecules, eight water molecules and one SO_4^{2-} ion are observed. As shown in Fig. 1a, two of the three pbb molecules are protonated, and intramolecular dihedral angels between the benzimidazolic rings are 9.04, 12.31, and 3.92 °. The bite angles of the three rings are 125.97, 133.69, and 124.56 °, respectively. The above data suggest that the middle pbb molecule may be potentially affected by the other two via π–π stacking interactions. Notably, there are O–H···O hydrogen bonds and weak O···O interactions in the unit of **1**, forming 1D chains in which three six-membered rings and one four-membered ring units are alternately arranged (Fig. S2).

The most striking feature of these chains is that the six-membered rings formed by free water molecules adopt a chair conformation (Fig. 1b), of which four oxygen atoms are located in the same geometry plane (O···O···O angles: 71.372° and 108.628°) and the remaining two oxygen atoms are symmetrically arranged on the bilateral sides of the plane (the dihedral angel between the plane O1A, O2, O3 and the plane O1A, O2, O1 is 49.39°). Here, the hexameric water cluster is unlike the previously published hexamer clusters [1b,15]. In the inter-$(H_2O)_6$ rings, water–water connections have an average O···O distance of 2.853 Å, which is very close to the corresponding value observed in liquid water (2.85 Å) [16] and longer than corresponding value of 2.759 Å in hexagonal ice (I_h) [17]. The emergence of a chair conformation, to some extent, may have a significant effect on the construction of a stable supramolecular network. Further, each $(H_2O)_6$ subunit and two $(H_2O)_3$ subunits are associated to form a centrosymmetric $(H_2O)_{12}$ cluster by hydrogen-bonds. Two dangling trimeric water molecules at the periphery are situated alternately right and left of the $(H_2O)_6$ subunit, so as to associate with the SO_4^{2-} ion. A closer view of the $(H_2O)_{12}$ cluster illustrates that each water monomer, except for O8, acts as both a hydrogen-bonding donor and acceptor. In the supramolecular $(H_2O)_{12}$ morphology, the O···O distances range from 2.592 to 3.079 Å, resulting in an average O···O distance of 2.800 Å, which is very close to those observed in liquid water (2.80 Å) [18] and comparable to the corresponding value in the ice phase (2.77–2.84 Å) [19]. However, the O···O···O angles vary widely (ca. 71.439–131.023°) with an average of 102.447°, considerably deviating from the preferred ideal tetrahedral geometry of water. Compared with other water morphologies reported recently [20], our observation of $(H_2O)_{12}$ clusters in such a water framework may be due to its different interactions with surrounding water molecules and the SO_4^{2-} ions. The present association mode of the $(H_2O)_{12}$ cluster, comprising of a chair conformation $(H_2O)_6$ ring core and the additional two dangling trimeric water clusters, in **1** is rather unusual.

Moreover, 1D supramolecular chains are linked with pbb molecules through N···O hydrogen-bonding to give rise to 2D layers (Fig. S3). The adjacent layers are connected further to afford a 3D supramolecular structure, in which face-to-face π–π stacking interactions between the aromatic rings (centroid-to-centroid distances: 3.531, 3.598, 3.616, and 3.658 Å) are dominant.

3.1.2. Crystal structures of ***2*** and ***3***

Complexes **2** and **3** are isomorphous, and thus only the structure of **2** is described here in detail. Complex **2** crystallizes in the triclinic space group $P\bar{1}$ and is composed of a mononuclear unit. The coordination geometry around each Zn^{II} atom can be attributed to a slightly distorted octahedron with four water molecules in the equatorial sites and two nitrogen atoms from pyridine rings of two pbb molecules in the axial positions (Fig. 2a). The Zn–N (2.158 Å) and Zn–O (2.112 and 2.098 Å) bond lengths are in the normal range and are similar to those of mononuclear Zn^{II} complexes reported in literature [21]. The biting angle of pbb in **2** is 123.27°, and the intramolecular dihedral angel between the benzimidazole groups is 4.87°, which are different from the corresponding values in **1**. As expected, hydrogen-bonding and π–π stacking interactions are also present, arranging and stabilizing of the

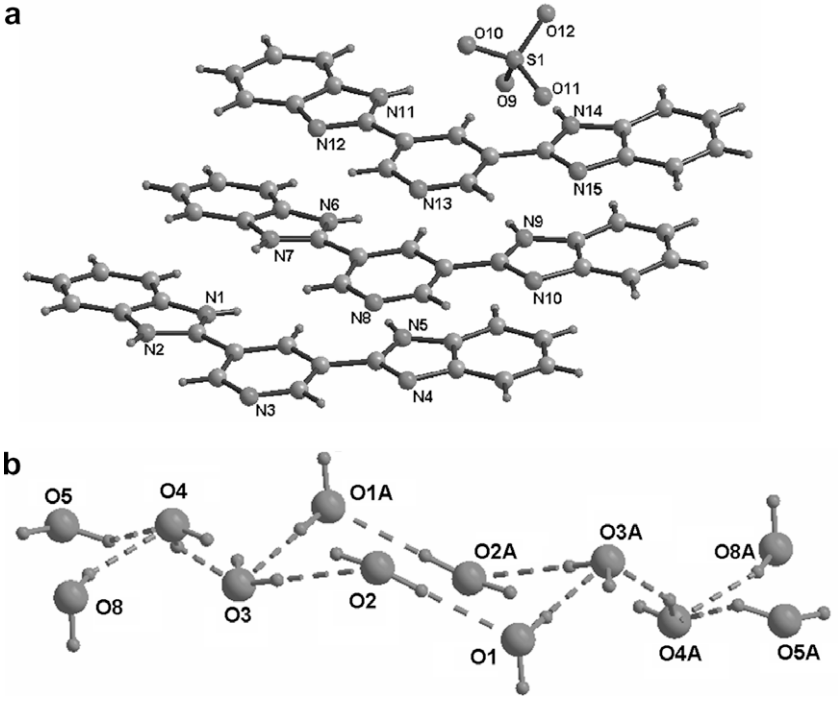

Fig. 1. (a) Molecular structure of **1** (the water molecule is omitted for clarity); (b) Perspective view of the discrete $(H_2O)_{12}$ cluster containing a chair conformation. Dash lines show the hydrogen bonding between water molecules.

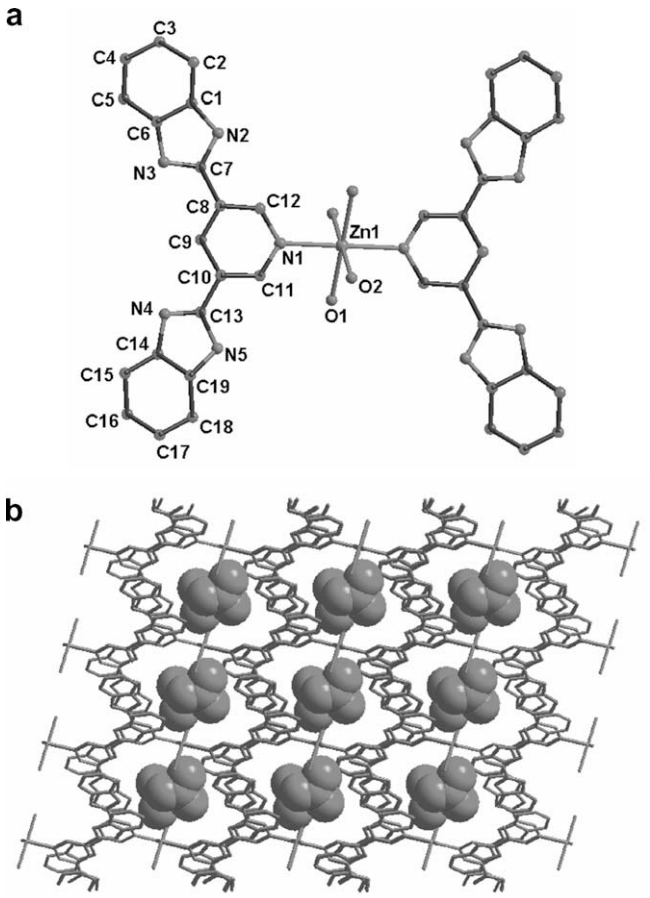

Fig. 2. (a) View of the coordination environment of Zn(II) in **2**; (b) 3D network of **2** containing 1D open channels encapsulating NO_3^- ions.

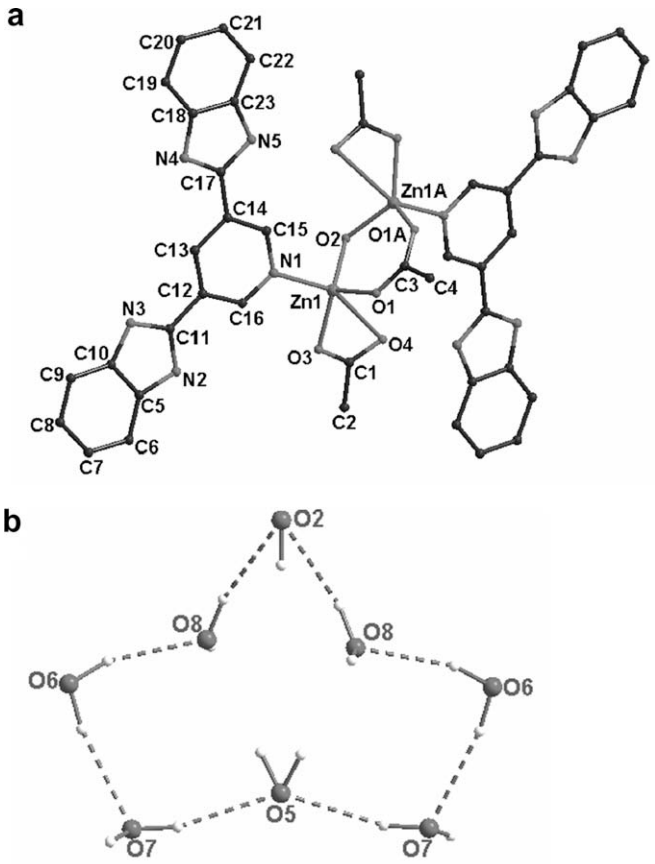

Fig. 3. (a) Coordination environment of Zn(II) in **4**; (b) Perspective view of the crown-like ring formed by hydrogen bonding.

supramolecular framework of **2**. There exist intense O–H···O interactions between the coordinated water and the free water, forming 1D chair chains (Fig. S4). The range of the O···O distances is approximately from 2.690 to 2.791 Å. It is interesting that four oxygen atoms (O2, O2A, O7, and O7A) are arranged in one plane, whilst O8 and O8A are symmetrically arranged on both sides of the plane. That is, similar to **1**, a chair conformation is built by these six oxygen atoms in **2**. The dihedral angel between the plane O1A, O2, O3 and the plane O1A, O2, O1 is 52.43°. Further, the 1D chair chains are connected into a 2D layered structure via weak N···O interactions (2.748 and 2.786 Å) and strong π–π stacking interactions between the two imidazole rings (minimum centroid-to-centroid distance: 3.512 Å) (Fig. S5). Adjacent 2D layers are further linked by hydrogen bonds (N2–H2···O3 2.999 Å) to give a 3D structure with 1D open channels encapsulating NO_3^- ions (Fig. 2b).

3.1.3. Crystal structure of *4*

Unlike **2** and **3**, the basic structure of **4** consists of a binuclear unit (Fig. 3a). The Zn^{II} center in **4** is four-coordinate with a distorted tetrahedral geometry, and is coordinated by one nitrogen atom in the pyridine ring of pbb and one oxygen atom in an acetate group. Zn1 and Zn1A are linked by one μ_2-OH (O2) and one μ_2-OAc (O1, O1A) with a Zn1···Zn1A distance of 3.215 Å. The bite angle of pbb in **4** is 123.55° and this is similar to that found in **2**. However, the intramolecular dihedral angels between the benzimidazole groups in **4** are 2.60°, which is very different to those of **1** and **2**. The bond distances of Zn–N and Zn–O in **4** are shorter than those in **2**, which may be as a result of the different coordination environment of Zn^{II}. Similar to **2**, there also exist rich hydrogen-bonding and strong π–π stacking interactions in **4**. A 1D chain (Fig. S6) is obtained due to hydrogen bonding interactions (O7–H7···O3 2.862, O7–H7···O5 2.751 Å) between three lattice water molecules and the oxygen atoms of the acetate groups. Interestingly, free water and the bridge oxygen (O2) are associated by hydrogen bonding to form a crown-like ring, as shown in Fig. 3b. In the eight-membered ring, the O···O distances fall in the range 2.696–2.868 Å, with an average of 2.768 Å, which is very close to the corresponding value of 2.759 Å in ice I_h [17], but is shorter than those observed in containing-water rings [16a,22]. This might be attributed to its different modes of connectivity with the surrounding water molecules. Furthermore, these rings link adjacent 1D chains to give rise to a 2D layered supramolecular structure (Fig. S7). Strong face-to-face π–π stacking interactions (minimum centroid-to-centroid distance 3.517 Å) contribute to the stabilization of the 3D supramolecular network of **4**. Additional hydrogen bonds involve the coordinated/uncoordinated carboxylate oxygen atoms, uncoordinated nitrogen atoms and free water molecules.

3.2. Biological results and discussion

3.2.1. Inhibitory zone test method

The antimicrobial activities of pbb and its complexes (**2**, **3**, and **4**) against bacteria (*E. coli*, *S. aureus*, and *B. subtilis*) and mould (*G. cingulata*, *M. fructicola*, *A. solani*) were examined by the inhibitory zone test method. The selected results obtained by this method are shown in Fig. 4. In this model, it could turn out that the samples have some antibacterial activity against the selected strains, the diameter of the inhibitory zone ranges from 7 to 25 mm. Inhibition

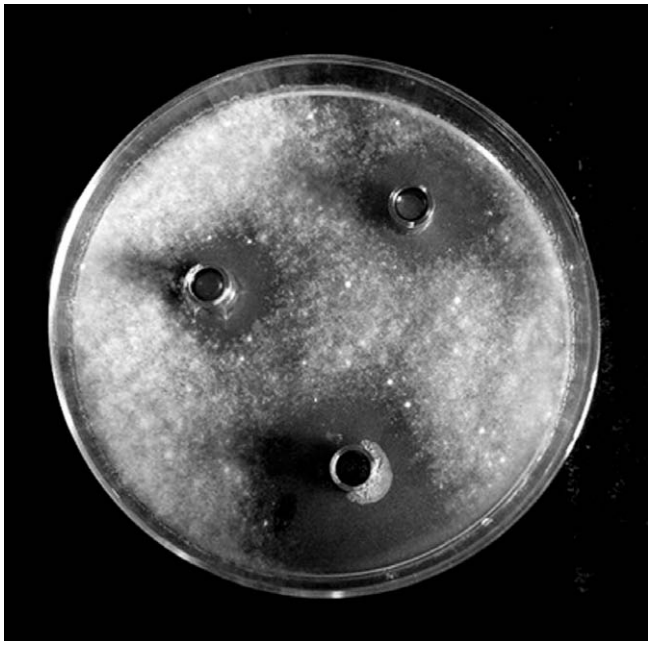

Fig. 4. Effect of concentrations of **2** on the growth of *Alternaria solani*: top left—2.5 μg mL^{-1}; top right—5 μg mL^{-1}; bottom—7.5 μg mL^{-1}.

again mould was observed clearly, whilst when the moulds were replaced by bacteria, there was a general decrease in activity. The ability of the samples to inhibit growth of the tested strains is listed in Table 4. From the viewpoint of the test, four samples exhibit only poor activity against *E. coli* and *S. aureus*, but an inhibition ring with a diameter of 7–8 mm against *B. subtilis* was found. Comparatively, it seems that the germproof ability of the samples against mould is superior to that against bacteria. However, different strains result in a different antibacterial effect of the samples. The average inhibitive ring diameters are, respectively, 21 mm (*G. cingulata*), 13 mm (*M. fructicola*) and 24 mm (*A. solani*). In addition, the antibacterial activity of pbb and its complexes against the same strain give distinctness. The ligand pbb presents optimal antibacterial activity versus *G. cingulata* and *A. solani* whereas **2–4** have good antibacterial activity against *M.* fructicola and are slightly active against *B. subtilis*.

These results indicate that pbb and its complexes possess selective antimicrobial properties for the tested objects. That is, they maybe possess higher antimicrobial activities against mould than bacteria. Consequently, pbb and its complexes are expected to have higher special bio-activity through further survey.

3.2.2. Microcalorimetric method

On the other hand, the antimicrobial activities of pbb and **2–4** were also investigated by the microcalorimetric method. Take *E. coli* as an example. Their partly thermal power-time (p–t) curves at 37 °C are shown in Fig. 5. All the curves are similar in shape,

Table 4
Biological results[a]

Sample	pbb	2	3	4
Escherichia coli	–	–	–	–
Bacillus subtilis	+	+	+	+
Staphylococcus aureus	–	–	–	–
Glomerella Cingulata	++	+	+	+
Alternaria Solani	++	+	+	+
Monilinia fructicola	+	++	++	++

[a] –, weak or no inhibition; +, inhibition; ++, strong inhibition.

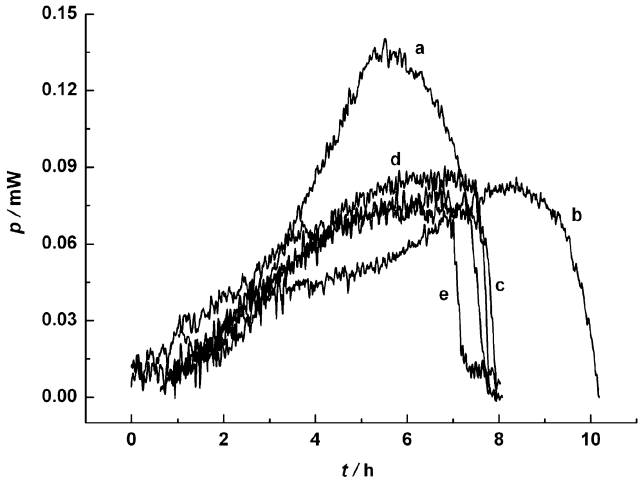

Fig. 5. Power–time curves of *E. coli* at 37 °C under different conditions in: (a) blank; (b) pbb, c = 2 μg mL^{-1}; (c) **2**, c = 2 μg mL^{-1}; (d) **3**, c = 5 μg mL^{-1}; (e) **4**, c = 3 μg mL^{-1}.

which testifies the good reappearance using this method. However, the thermal powers in the growth phase for *E. coli* are reduced evidently in the presence of pbb or its complexes. This result shows that the samples (pbb, **2**, **3**, and **4**) can inhibit the growth of *E. coli*.

According to the p–t curves, the corresponding growth rate constant k can be calculated from linear regression analysis. The k versus c curves of pbb and **2–4** were obtained, as illustrated in Fig. 6. The k value is ca. 0.83 h^{-1} when the concentration of the samples is 0 μg mL^{-1}. It can be seen that the k values clearly decrease due to the addition of the samples. The results can be described that pbb and its complexes exhibit good activities against *E. coli*. In the concentration range 2–100 μg mL^{-1}, the k values increase, then decrease. Therefore it may be predicted that the concentration of the samples is important to the antibacterial action [23]. What is more, one concentration peak value c_p can be observed in every k–c curve. It is clear that the c_p values of **2–4** are less than that of pbb. It could be deduced that, under the same conditions, the antibacterial actions of the complexes against *E. coli* are superior to that of the ligand. That means the presence of metal ions has improved the antibacterial activity of ligand. Accordingly, we believe that this work may contribute basic information to the further

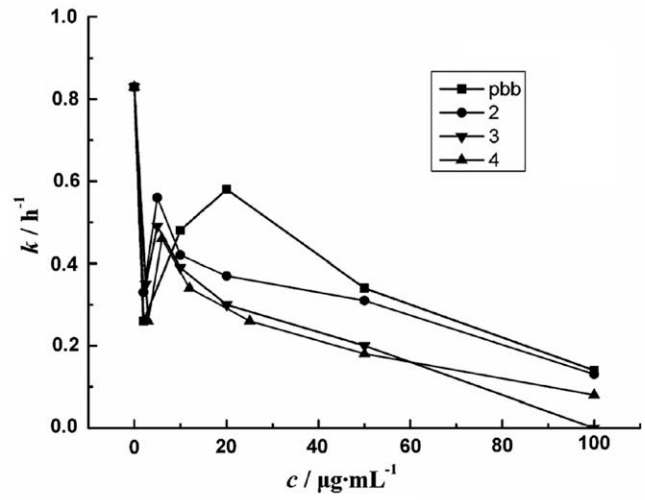

Fig. 6. The k–c curves of *E. coli* at 37 °C with different concentrations of pbb, **2**, **3**, and **4**.

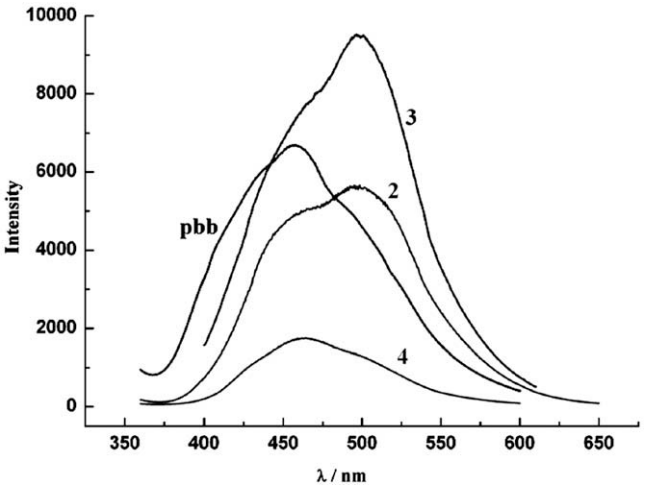

Fig. 7. Solid-state fluorescence emission spectra of pbb, **2**, **3**, and **4** at room temperature.

application of pbb and its complexes in the field of biological chemistry.

3.3. Fluorescent properties

The solid-state fluorescent properties of pbb and complexes **2–4** were investigated at room temperature (Fig. 7). Free pbb exhibits an intense emission peak at 458 nm upon excitation at 320 nm. The emission should be assigned to the intraligand π–π^* transitions. Excitation at 300 nm leads to a fluorescent emission band at about 465 nm for **4**. The emission spectra of **2** and **3** show a main peak at 498 nm (λ_{ex} = 305 nm) and 497 nm (λ_{ex} = 340 nm), respectively. It can be seen that complexes **2–4** clearly exhibit a red-shift with respect to free pbb. We tentatively assign it to a ligand-to-metal charge transfer (LMCT) [1g]. The differences of the peak positions may be considered to be a result of the dissimilar coordination of the metal centers because the emission behavior is closely associated to the metal ions and ligands around them [1d]. These complexes may be good candidates for stable fluorescent materials.

4. Conclusion and perspectives

In this paper, we have successfully synthesized a new ligand, pbb, and four of its complexes with different architectures and properties. It is worth mentioning that a rarely known discrete $(H_2O)_{12}$ cluster, with a chair conformation, and a crown-like eight-membered ring have been observed in **1**–**4**. These results indicate that these complexes enrich the supramolecular chemistry of organic aromatic derivatives. Our studies also show that hydrogen-bonding, π–π stacking interactions and weak interaction between atoms play a crucial role in connecting the low-dimensional units into high-dimensional supramolecular structures. Importantly, the strong fluorescent properties and the selective bioactivity of pbb and **2**–**4** make them excellent candidates for potential photoactive materials and bio-inhibitors. Further studies will focus on the construction of new metal-organic coordination polymers from pbb, and their bioactivities.

Acknowledgement

This work was supported by the National Natural Science Foundation of China (Grant No. 20771090), TRAPOYT and the Specialized Research Fund for the Doctoral Program of Higher Education (No. 20050697005).

Appendix A. Supplementary data

CCDC 690764, 690765, 691177 and 690766 contain the supplementary crystallographic data for **1**, **2**, **3,** and **4**. These data can be obtained free of charge via http://www.ccdc.cam.ac.uk/conts/retrieving.html, or from the Cambridge Crystallographic Data Centre, 12 Union Road, Cambridge CB2 1EZ, UK; fax: (+44) 1223-336-033; or e-mail: deposit@ccdc.cam.ac.uk. Supplementary data associated with this article can be found, in the online version, at doi:10.1016/j.poly.2008.08.018.

References

[1] (a) R.L. Sang, L. Xu, Inorg. Chem. 44 (2005) 3731;
(b) Y.P. Wu, C.J. Wang, Y.Y. Wang, P. Liu, W.P. Wu, Q.Z. Shi, S.M. Peng, Polyhedron 25 (2006) 3533;
(c) K.T. Holman, A.M. Pivovar, J.A. Swift, M.D. Ward, Acc. Chem. Res. 34 (2001) 107;
(d) X.L. Wang, Y.F. Bi, G.C. Liu, H.Y. Lin, T.L. Hu, X.H. Bu, CrystEngCommun 10 (2008) 349;
(e) Y.T. Wang, G.M. Tang, W.Y. Ma, W.Z. Wan, Polyhedron 26 (2007) 782;
(f) M. Du, Z.H. Zhang, X.J. Zhao, H. Cai, Cryst. Growth Des. 6 (2006) 114;
(g) G.B. Che, C.B. Liu, B. Liu, Q.W. Wang, Z.L. Xu, CrysEngCommun 10 (2008) 84;
(h) X.P. Zhou, W.X. Ni, S.Z. Zhan, J. Ni, D. Li, Y.G. Yin, Inorg. Chem. 46 (2007) 2345.
[2] (a) M.P. Hogerheide, J. Boersma, G.V. Koten, Coord. Chem. Rev. 155 (1996) 87;
(b) D. Imbert, M. Cantuel, J.-C.G. Bünzli, G. Bemardinelli, C. Piguet, J. Am. Chem. Soc. 125 (2003) 15698;
(c) N.M. Shavaleev, L.P. Moorcraft, S.J.A. Pope, Z.R. Bell, S. Faulkner, M.D. Ward, Chem. Commun. (2003) 1134;
(d) S.I. Klink, H. Keizer, F.C.J.M. van Veggel, Angew. Chem., Int. Ed. 39 (2000) 4319.
[3] (a) M. Albrecht, M. Lutz, A.L. Spek, G. van Koten, Nature 406 (2000) 970;
(b) C.D. Wu, A. Hu, L. Zhang, W. Lin, J. Am. Chem. Soc. 127 (2005) 8940;
(c) D.N. Dybtsev, H. Chun, S.H. Yoon, D. Kim, K. Kim, J. Am. Chem. Soc. 126 (2004) 1308;
(d) K. Uemura, S. Kitagawa, M. Knodo, K. Fukui, R. Kitaura, H.C. Chang, T. Mizutani, Chem. Eur. J. 8 (2002) 3587;
(e) M.H. Zeng, X.L. Feng, X.M. Chen, J. Chem. Soc., Dalton Trans. (2004) 2217;
(f) O.M. Yaghi, H. Li, J. Am. Chem. Soc. 118 (1996) 295.
[4] (a) B.J. Holliday, C.A. Mirkin, Angew. Chem., Int. Ed. 40 (2001) 2022;
(b) J.W. Steed, J.L. Atwood, Supramolecular Chemistry, Wiley, Chichester, UK, 2000.
[5] (a) B. Zhao, H.L. Gao, X.Y. Chen, P. Cheng, W. Shi, D.Z. Liao, S.P. Yan, Z.H. Jiang, Chem. Eur. J. 12 (2006) 149;
(b) C.S. Liu, X.S. Shi, J.R. Li, J.J. Wang, X.H. Bu, Cryst. Growth Des. 6 (2006) 656;
(c) Q. Yue, J. Yang, G.H. Li, G.D. Li, W. Xu, J.S. Chen, S.N. Wang, Inorg. Chem. 44 (2005) 5241;
(d) B.Q. Ma, D.S. Zhang, S. Gao, T.Z. Jin, C.H. Yan, Angew. Chem., Int. Ed. 39 (2000) 3644;
(e) R.Q. Zou, H. Sakurai, Q. Xu, Angew. Chem., Int. Ed. 45 (2006) 2542;
(f) P. Li, H.M. Liu, X.G. Lei, X.Y. Huang, D.H. Olson, N.J. Turro, J. Li, Angew. Chem., Int. Ed. 42 (2003) 542;
(g) J.S. Seo, D. Whang, H. Lee, S.I. Jun, J. Oh, Y. Jeon, K. Kim, Nature 404 (2000) 982.
[6] W.R. Roderick, C.W. Nordeen, A.M. Von Esch, R.N. Appell, J. Med. Chem. 15 (1972) 655.
[7] (a) K.S. Yeung, N.A. Meanwell, Z. Qiu, D. Hernandez, S. Zhang, F. McPhee, S. Weinheimer, J.M. Clark, J.W. Janc, Bioorg. Med. Chem. Lett. 11 (2001) 2355;
(b) S.G. Liu, J.L. Zuo, Y.Z. Li, X.Z. You, J. Mol. Struct. 705 (2004) 153;
(c) V. Gayathri, E.G. Leelamani, N.M.N. Gowda, G.K.N. Reddy, Polyhedron 18 (1999) 2351;
(d) L. Tong, Chem. Rev. 102 (2002) 4609;
(e) F.G. Lootiens, P. Regenfuss, A. Zechel, L. Dumortier, R.M. Clegg, Biochemistry 29 (1990) 9029.
[8] (a) J.D. Geratz, R.R. Tidwell, R.J. Lombardy, J.H. Schwab, S.K. Anderle, K.B. Pryzwansly, Am. J. Pathol. 139 (1991) 921;
(b) M.J. Tebbe, W.A. Spitzer, F. Victor, J. Med. Chem. 40 (1997) 3937.
[9] M. Du, C.P. Li, X.J. Zhao, Q. Yu, CrystEngCommun 9 (2007) 1011.
[10] (a) R. Fu, S. Xiang, S. Hu, L. Wang, Y. Li, X. Huang, X. Wu, Chem. Commun. (2005) 5292;
(b) M. Munakata, L.P. Wu, G.L. Ning, T. Kuroda-Sowa, M. Maekawa, Y. Suenaga, N. Maeno, J. Am. Chem. Soc. 121 (1999) 4968;
(c) M. Munakata, L.P. Wu, T. Kuroda-Sowa, M. Maekawa, Y. Suenaga, K. Sugimoto, Inorg. Chem. 36 (1997) 4903.
[11] A.W. Addison, P.J. Burke, J. Heterocycl. Chem. 18 (1981) 803.
[12] (a) G.M. Sheldrick, SHELXS 97, Program for Crystal Structure Solution, University of Göttingen, Germany, 1997;

(b) G.M. Sheldrick, SHELXL 97, Program for Crystal Structure Refinement, University of Göttingen, Germany, 1997.
[13] A.J. Fontana, L.D. Hansen, R.W. Breidenbach, R.S. Criddle, Thermochim. Acta 172 (1990) 105.
[14] (a) C.L. Xie, H.K. Tang, Z.H. Song, S.S. Qu, Thermochim. Acta 123 (1988) 33;
(b) H.K. Tang, C.L. Xie, Z.H. Song, S.S. Qu, Y.T. Liao, H.S. Liu, Acta Phys. Chim. Sin. 3 (1987) 113.
[15] (a) U. Mukhopadhyay, I. Bernal, Cryst. Growth Des. 5 (2005) 1687;
(b) R.J. Doedens, E. Yphannes, M.I. Khan, Chem. Commun. (2002) 62;
(c) B.H. Ye, B.B. Ding, Y.Q. Weng, X.M. Chen, Inorg. Chem. 43 (2004) 6866.
[16] (a) R.J. Speedy, J.D. Madura, W.L. Jorgensen, J. Phys. Chem. 91 (1987) 909;
(b) A.H. Narten, W.E. Thiessen, L. Blum, Science 217 (1982) 1033.
[17] D. Eisenberg, W. Kauzmann, The Structure and Properties of Water, Oxford University Press, Oxford, 1969.
[18] L.F. Ma, Y.Y. Wang, L.Y. Wang, J.Q. Liu, Y.P. Wu, J.G. Wang, Q.Z. Shi, S.M. Peng, Eur. J. Inorg. Chem. (2008) 693.
[19] (a) G.A. Jeffrey, An Introduction to Hydrogen Bonding 1, Oxford University Press, Oxford, 1997;
(b) Y.G. Huang, Y.Q. Gong, F.L. Jiang, D.Q. Yuan, M.Y. Wu, Q. Gao, W. Wei, M.C. Hong, Cryst. Growth Des. 7 (2007) 1385.
[20] (a) H. Wang, J.Q. Liu, Y.N. Zhang, Y.Y. Wang, G.L. Wen, C.Y. Guo, Q.Z. Shi, Inorg. Chem. Commun. 11 (2008) 129;
(b) I. Ravikumar, P.S. Lakshminarayanan, E. Suresh, P. Ghosh, Cryst. Growth Des. 6 (2006) 2630;
(c) S. Neogi, G. Savitha, P.K. Bharadwaj, Inorg. Chem. 43 (2004) 3771;
(d) Pallepohu Raghavaiah, Sabbani Supriya, Samar K. Das, Chem. Commum. (2006) 2762.
[21] B. Liu, X.C. Zhang, Y.H. Chen, Inorg. Chem. Commun. 10 (2007) 498.
[22] (a) A.H. Narten, W.E. Thiessen, L. Blum, Science 217 (1982) 1033;
(b) L.F. Ma, L.Y. Wang, X.K. Huo, Y.Y. Wang, Y.T. Fan, J.G. Wang, S.H. Chen, Cryst. Growth Des. 8 (2008) 620.
[23] H.L. Zhang, X.F. Yu, X.X. Li, X.R. Pan, Thermochim. Acta 416 (2004) 71.

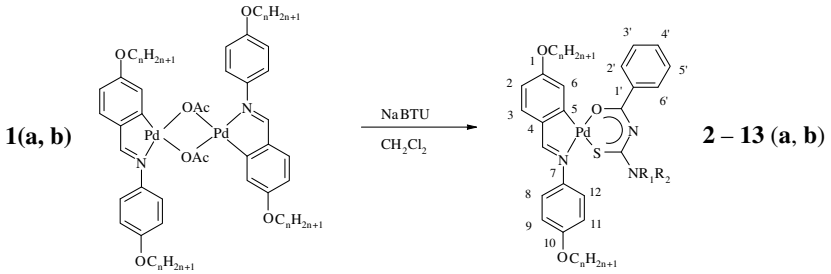

n = 1, **a**

n = 6, **b**

$R_1 = R_2 =$	*n*-Et	**2**	$R_1 = H, R_2 =$	Ph	**7**
	n-Pr	**3**		*p*-Me-Ph	**8**
	n-Bu	**4**		*m*-Me-Ph	**9**
	n-Hex	**5**		*p*-F-Ph	**10**
	n-Oct	**6**		*p*-Cl-Ph	**11**
				p-Br-Ph	**12**
				p-MeO-Ph	**13**

Scheme 1. Synthesis of the new complexes and the *N*-benzoyl thiourea derivatives used in this study.

The new mononuclear complexes were obtained in moderate to good yields as yellow microcrystalline solid products, which are stable under atmospheric conditions. Their structures were confirmed by elemental analysis, IR spectroscopy as well as ^{1}H and ^{13}C NMR spectroscopy and X-ray diffraction.

The coordination of the *N*-benzoyl thiourea derivatives in the deprotonated form was confirmed by the disappearance of the ν_{NH} frequency in the IR spectra of the Pd(II) complexes, which suggests the absence of the NH hydrogen located between the carbonyl and the thiocarbonyl groups of the benzoyl thioureic moiety, information that is further supported by ^{1}H NMR spectroscopy. The formation of the *ortho*-metallated mononuclear complexes can be confirmed readily by ^{1}H NMR spectroscopy where a pattern specific to 1,3,4-substitution of an aromatic ring can be seen as two doublets (H-2, H-3, $^3J_{H2,H3} = 8.4$ Hz) and a doublet of doublets (H-6, $^4J_{H2,H6} = 2.4$ Hz).

Also, the ^{1}H NMR spectra indicate the presence of only one isomer in solution (one set of signals) for all the prepared complexes, though it is possible for the complexes to exist as a mixture of two isomers with the sulfur atom of the *N*-benzoyl thiourea ligand in a *trans* or *cis* position to the nitrogen atom of the imine group of the Schiff base ligand. This information is supported by X-ray diffraction studies that showed only one isomer in the solid state for the complexes isolated as single crystals.

The ^{13}C NMR spectra show all the expected signals. The shift of the signals ($\Delta\delta \sim 13$ ppm) due to the imine and C-5 carbon atoms are consistent with the existence of a Pd–N and a Pd–C-5 bond. This deshielding effect caused by Pd bonding ($\Delta\delta = 4$–9 ppm) is also visible for the *ortho* positions with respect with the metallated position (C-4, C-6). In the case of the benzoyl moiety of the *N*-benzoyl thiourea derivative, coordination to the metal center leads to a deshielding of C-1′ ($\Delta\delta = 5$ ppm) and *para* C-4′ ($\Delta\delta = 2$ ppm), as compared with the free ligand. The signals corresponding to C=O and C=S undergo relatively large downfield and upfield chemical shifts of $\Delta\delta = 7$ and 6 ppm, respectively. This behaviour is similar to that observed for simple Pd(II) complexes with other *N*,*N*-dialkyl-*N*′-aroyl or acyl thiourea derivatives [13].

It is interesting to note that for the complexes **2–6a** the signals corresponding to the alkyl groups from the $N(Alk)_2$ moiety are not magnetically equivalent, both in the ^{1}H and ^{13}C NMR spectra. This is due to a hindered rotation about the C–$N(Alk)_2$ bond, which in turn can be explained through the conjugation between the amine and the Pd containing ring.

2.2. Structures

Single crystals of **2a**, **10a** and **13a** suitable for analysis by X-ray diffraction were obtained from a mixture of dichloromethane and ethanol (ca. 1/1 v/v) at −25 °C. Complex **13a** crystallised with two independent molecules in the structural unit. The crystallographic data are collected in Table 1, while selected bond lengths and angles for all three complexes are presented in Table 2.

The molecular structure of **2a** is shown in Fig. 1. The palladium atom is surrounded by one sulfur atom and one oxygen atom of the *N*-benzoyl thiourea ligand, one aromatic carbon atom (metallated phenyl ring) and one nitrogen atom (imine group) in an approximatively square-planar arrangement, with the sulfur atom located *cis* to the nitrogen atom of the imine group. The corresponding chelate ring around the Pd centre is essentially planar with a maximum deviation from the mean plane of 0.040 Å. However, while the metallated phenyl ring is almost coplanar with respect to the mean plane, the unmetallated ring of the imine ligand is twisted by 37.7° with respect to the core plane. The phenyl ring of the benzoyl group from the *N*,*N*-diethyl-*N*′-benzoyl thiourea ligand is also twisted by 32.9° with respect to the mean plane.

The Pd–Pd distance between two neighbouring molecules is 8.2 Å, precluding any Pd–Pd interactions. The Pd–C and Pd–N bond lengths are comparable with the values reported for similar *ortho*-palladated complexes with Schiff bases, while the Pd–O and Pd–S bond lengths are very well situated between the two values found for the simple *cis* complex of Pd(II) with *N*,*N*-diethyl-*N*′-benzoyl thiourea, which are 2.10 and 1.99 Å for the Pd–O bonds and 2.215 and 2.31 Å for the Pd–S bonds [14].

Complex **10a** (Fig. 2) crystallised with the same square-planar arrangement around the palladium atom; indeed the bond lengths and angles for the central core are all very similar to those found in

Table 1
Crystallographic data for **2a**, **10a** and **13a**

Compound	**2a**	**10a**	**13a**
Empirical formula	$C_{27}H_{29}N_3O_3PdS$	$C_{29}H_{24}FN_3O_3PdS$	$C_{30}H_{27}N_3O_4PdS$
Formula weight ($g\,mol^{-1}$)	581.99	619.97	632.01
Temperature (K)	110(2)	110(2)	110(2)
Wavelength (Å)	0.71073	0.71073	0.71073
Crystal system	triclinic	monoclinic	monoclinic
Space group	$P\bar{1}$	$P2(1)/n$	$P2(1)/c$
Unit cell dimensions			
a (Å)	7.6707(8)	19.813(17)	17.8784(13)
b (Å)	11.6553(12)	6.436(6)	9.3708(7)
c (Å)	15.4545(16)	20.501(17)	32.105(2)
α (°)	111.219(2)	90	90
β (°)	97.100(2)	90.18(2)	99.993(2)
γ (°)	97.386(2)	90	90
Volume ($Å^3$)	1255.5(2)	2614(4)	5297.1(6)
Z	2	4	8
D_{calc} ($Mg\,m^{-3}$)	1.539	1.575	1.585
Absorption coefficient (mm^{-1})	0.857	0.834	0.822
$F(000)$	596	1256	2576
Crystal	yellow	yellow	yellow
Crystal size (mm)	0.22 × 0.14 × 0.13	0.28 × 0.09 × 0.04	0.30 × 0.24 × 0.16
θ Range for data collection (°)	1.44–28.30	1.43–28.34	1.16–30.02
Index ranges	$-10 \leqslant h \leqslant 10$, $-15 \leqslant k \leqslant 15$, $-20 \leqslant l \leqslant 20$	$-26 \leqslant h \leqslant 15$, $-8 \leqslant k \leqslant 8$, $-27 \leqslant l \leqslant 26$	$-24 \leqslant h \leqslant 24$, $-13 \leqslant k \leqslant 13$, $-44 \leqslant l \leqslant 45$
Reflections collected	12837	16695	58726
Independent reflections (R_{int})	6170 (0.0204)	6420 (0.0599)	15249 (0.0429)
Completeness to $\theta = 27.48°$ (%)	99.8	98.3	98.5
Absorption correction	semi-empirical from equivalents	semi-empirical from equivalents	semi-empirical from equivalents
Maximum and minimum transmission	0.890 and 0.814	0.970 and 0.724	0.877 and 0.762
Refinement method	full-matrix least-squares on F^2	full-matrix least-squares on F^2	full-matrix least-squares on F^2
Data/restraints/parameters	6170/0/320	6420/0/386	15249/0/717
Goodness-of-fit on F^2	1.045	0.930	1.111
Final R indices $[F^2 > 2\sigma(F^2)]$	$R_1 = 0.0253$, $wR_2 = 0.0619$	$R_1 = 0.0387$, $wR_2 = 0.0750$	$R_1 = 0.0374$, $wR_2 = 0.0870$
R indices (all data)	$R_1 = 0.0283$, $wR_2 = 0.0632$	$R_1 = 0.0648$, $wR_2 = 0.0828$	$R_1 = 0.0487$, $wR_2 = 0.0962$
Largest difference in peak and hole ($e\,Å^{-3}$)	0.592 and −0.681	0.700 and −0.530	1.605 and −0.774

Table 2
Selected bond lengths (Å) and angles (°)

	2a	**10a**	**13a**	
			Molecule A	Molecule B
Pd–C	1.9856(17)	1.984(3)	1.988(2)	1.977(2)
Pd–N	2.1003(14)	2.055(3)	2.1113(18)	2.1015(19)
Pd–S	2.2382(5)	2.2394(16)	2.2457(6)	2.2382(6)
Pd–O	2.0847(12)	2.063(2)	2.0877(15)	2.0759(16)
N–C(Ph)	1.325(2)	1.342(4)	1.330(3)	1.335(3)
N–C(S)	1.342(2)	1.321(4)	1.342(3)	1.343(3)
N–C(O)	1.339(2)	1.344(4)	1.341(3)	1.347(3)
C–O	1.265(2)	1.260(3)	1.260(3)	1.257(3)
C–S	1.7345(18)	1.745(3)	1.723(2)	1.723(2)
C(O)–C(Ph)	1.503(2)	1.487(4)	1.504(3)	1.499(3)
C–N (imine)	1.295(2)	1.306(3)	1.300(3)	1.301(3)
C–Pd–N	81.35(7)	81.17(11)	81.17(3)	81.41(9)
N–Pd–O	95.63(1)	92.61(8)	96.74(7)	96.24(7)
O–Pd–S	92.38(4)	92.28(6)	92.78(4)	91.87(5)
S–Pd–C	90.67(5)	93.84(9)	89.58(6)	90.32(7)

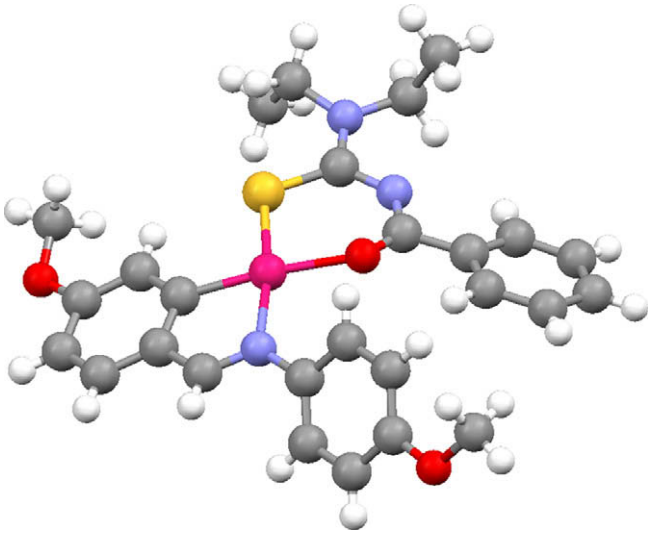

Fig. 1. The molecular structure of **2a**.

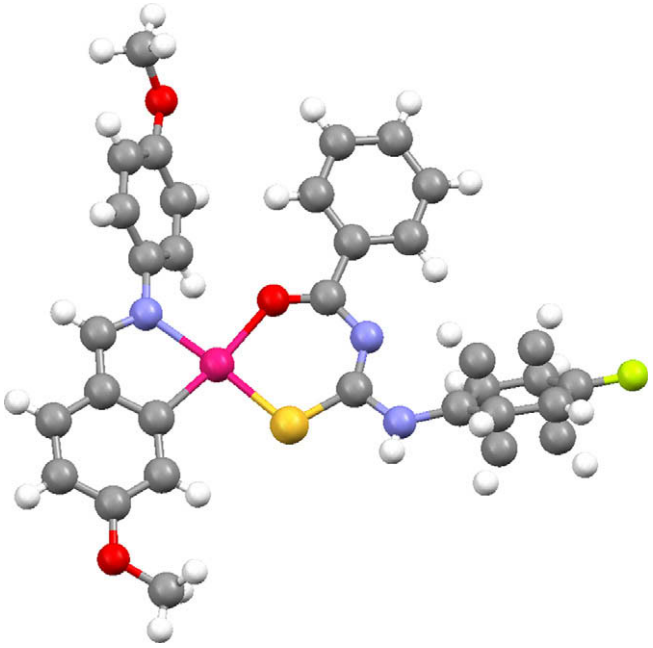

Fig. 2. The molecular structure of **10a**.

2a. The same orientation with respect to the core plane was found for the unmetallated ring of the imine ligand, which is twisted by 54.2°, a larger value when compared to **2a**. The phenyl ring of the benzoyl group from the *N*-benzoyl thiourea ligand is also twisted in respect to the core plane by 14.2°, a smaller value compare to that found for **2a**. An interesting feature of this complex is the two possible configurations adopted by the *p*-F-phenyl ring of the *N*-benzoyl thiourea ligand, with a twist of 73.6°, each with 50% probability as revealed by the site occupancy factors. In both cases there is a twist of this ring by 49.4° and 57.2° with respect to the core plane. Another factor that contributes to the crystal packing of **10a** are intermolecular –C–H···F–C– interactions, found between the fluorine atom of the *N*-benzoyl thiourea ligand and the methoxy group of the metallated ring of the imine ligand. The measured H···F distance is 2.50 Å, which is smaller than the sum of the van der Waals' radii of fluorine and hydrogen of 2.67 Å (the van der Waals' radius of fluorine is 1.47 Å)[15].

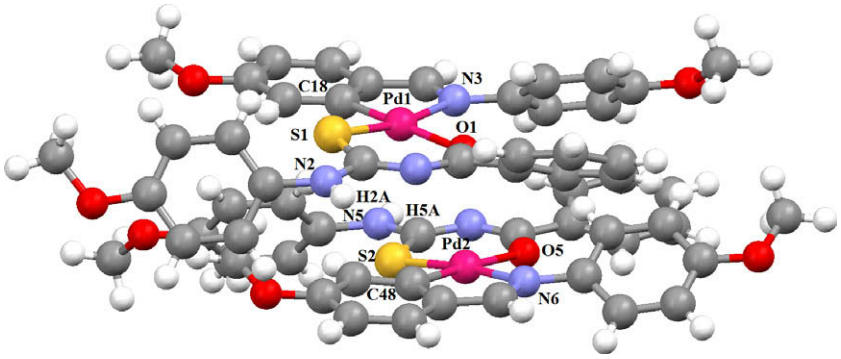

Fig. 3. The molecular structure of **13a**.

Complex **13a** crystallises in the monoclinic crystal system, group *P2*(1)/*c*, as a dimer (Fig. 3). The crystal structure of this compound shows Pd(II) in a square-planar environment bound to the imine ligand in an *ortho*-metallated fashion and chelated to the *N*-benzoyl thiourea derivative with the same coordinated atoms (one aromatic C atom (metallated ring), one N atom (imine group), one O atom (carbonyl group) and one S atom (thiocarbonyl group)) as found for **2a** and **10a**. The two five- and six-membered chelate rings are almost co-planar with the metallated ring of the imine ligand while the unmetallated ring is twisted in respect to the core plane by 34.9° for one molecule, and by 36.3° for the second.

For this compound the maximum deviation from the mean plane is 0.063 and 0.047 Å for Pd_1 and Pd_2, respectively. In this case, the complexes are arranged so that one sits over another with a short Pd–Pd distance of 3.92 Å. This distance is greater than twice the van der Waals' radius of Pd. Additionally, within the dimer the Pd···Pd vector deviates from orthogonality to the coordination plane (25° angle with the plane normal) and so the relative disposition of the complexes is not felt to be due to any intermolecular metal–metal interaction. The C–O and C–S bond lengths of the *N*-benzoyl thiourea ligand in **13a** are longer than those found in the free ligand (1.231 and 1.659 Å, respectively) while the N–C(S) and N–C(O) bond lengths are shorter in **13a** than in the free ligand (1.392 and 1.376 Å, respectively) as a consequence of the coordination of the ligand to the palladium centre in the deprotonated form which leads to the partial double-bond character of the C–N bonds [16]. An important factor that contributes to the crystal packing of **13a** is intermolecular N–H···S hydrogen bonds, found between the S atom of the thiocarbonyl group and the hydrogen atom of the amino –NHR group from the *N*-benzoyl thiourea ligand.[1] This type of interaction is usually found in the uncomplexed *N*-benzoyl thiourea ligands and is typically shorter than the interactions found for **13a** [17,18].

2.3. Thermal behaviour

The palladium complexes, bearing alkoxy groups with six carbon atoms chains (**2**–**13b**), were investigated for their potential liquid crystal properties by hot stage polarising optical microscopy and differential scanning calorimetry (DSC). DSC data were recorded only for those compounds showing mesomorphic behaviour. The thermal data are summarised in Table 3. Mesophases were assigned by their optical texture and two examples are shown in Fig. 4.

[1] Hydrogen bonds for **13a**: N(5)–H(5A)···S(2)#1, 3.772(2) Å and N(2)–H(2A)···S(1)#2, 3.6967(19) Å. Symmetry transformations used to generate equivalent atoms: (1) $-x+1, y-1/2, -z+1/2$; (2) $-x, y+1/2, -z+1/2$.

Table 3
Thermal data for the palladium(II) complexes

Compound	Transition	T (°C)	ΔH (kJ mol^{-1})
2b	Cr–I (N–I)[b]	110 (61)	23.8 (0.3[d])
3b	Cr–I (I–N) (N–Cr)	104 (64[a])	30.8 (20.4[c])
5b	Cr–Cr′ Cr′–I (I–N) (N–Cr)	102 108 (78[a])	18.2 21.5 (29.8[c])
6b	Cr–Cr′ Cr′–I (I–N) (N–Cr)	53 95 (58[a])	3.4 29.9 (22.2[c])

[a] These values represent the temperatures taken from microscopy.
[b] In this case $T_{(N-I)}$ is quoted as the sample was cooled from isotropic to nematic and then re-heated back to the isotropic phase.
[c] The two transitions could not be separated and the values represent the combined enthalpies.
[d] Compound **2b** was the only compound for which it was possible to extract the enthalpy parameter associated with the isotropic to nematic phase transition. The nematic phase of **2b** is stable up to room temperature for several hours after which a slow crystallization process occurs.

This family of complexes offers a broad and systematic picture of the possibility to use *N*-benzoyl thiourea derivatives in designing liquid crystalline materials as well as the effects of changing the substituents on this type of ligand on the mesogenic behaviour. The nature of the *N*-benzoyl thiourea derivative, more specific the R_1 and R_2 substituents, has a major influence on the mesogenic properties of these complexes (Table 3), though it is very clear that their mesogenic behaviour is driven by the *ortho*-metallated imine fragment. Thus, complexes **7**–**13b** show no mesomorphic properties and this behaviour could be assigned to the more flexible structures adopted by the *N*-benzoyl thiourea derivatives bearing aromatic fragments, in particular due to the aromatic groups linked to the nitrogen atom, which imposes a less favourable molecular shape in connection with the intermolecular hydrogen bonds N–H···S that can be formed between the S atom of the thiocarbonyl group and the hydrogen atom of the amino –NHR group. This type of intermolecular interaction (hydrogen bonding between the NH_2 and the carboxyl groups within the amino acids groups) within the crystal lattice was supposed to be responsible for increasing the melting points of the liquid crystals based on *ortho*-metallated Pd imine complexes with amino acids [5b]. On the other hand, the Pd(II) complexes with *N*,*N*-dialkyl-*N*′-benzoyl thiourea derivatives (**2**–**6b**) show a monotropic nematic phase on cooling, except for **4b** ($R_1 = R_2 = Bu$) for which no mesophase was seen either on heating or cooling. This behaviour could be dis-

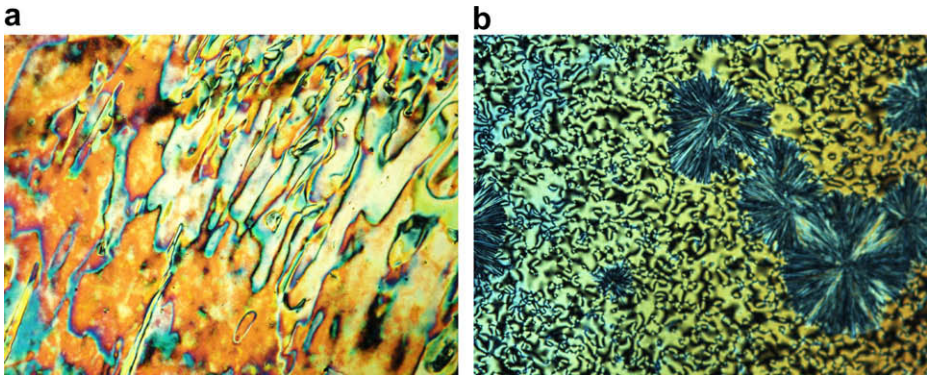

Fig. 4. Polarised optical micrograph of the nematic phase of **2b** at 60 °C (a) and of **6b** at 58 °C (b). In the later case the transition to the nematic phase occurs just before the crystallisation process.

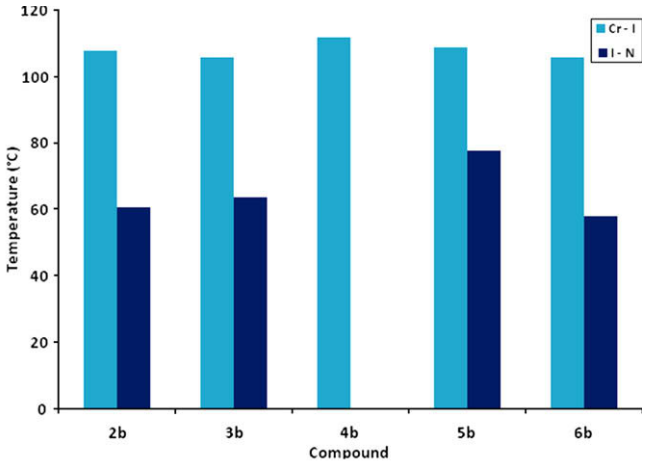

Fig. 5. Thermotropic behaviour of Pd(II) complexes **2–6b.**

cussed in terms of molecular anisotropy of these complexes, e.g. the length-to-breadth ratio [19]. As the terminal alkoxy chains of the imine are not changed, increasing the length of the alkyl chain of the *N*-benzoyl thiourea derivative leads to an increase of the breadth of the molecule with immediate consequences on the mesogenic behaviour. One can assume that the maximum breadth of the molecule is reached for $R_1 = R_2 =$ butyl, when the mesogenic behaviour is being totally suppressed.

Fig. 5 shows the influence of the chain length on the mesogenic properties of Pd(II) complexes with *N*,*N*-dialkyl-*N*′-benzoyl thiourea derivatives. Though the melting points and the temperature of the transition from isotropic to nematic phase do not follow the same trend, there is a clear tendency of increase of T_{I-N} with the increasing chain length up to hexyl groups, followed by a significant drop, 20 °C, on going from hexyl to octyl groups. The same effect of decreasing the transition temperatures with increasing the alkyl chain length from ethyl to octyl has been seen for *ortho*-metallated imine Pd(II) complexes with dialkyldithiocarbamates as chelating ligands [7].

It is very clear that compared with the other types of co-ligands, such as β-diketones or β-aminoenonates, the use of *N*-benzoyl thiourea derivatives as co-ligands destabilise the mesogenic behaviour to such an extent that only monotropic behaviour is seen, with the transitions to the nematic mesophase occurring at approximately 30–50 °C below the clearing point. While changing β-diketones to β-aminoenonate co-ligands leads to more accessible nematic phase but over slightly narrower temperature [3a], the effect of introducing the *N*-benzoyl thiourea derivatives is to further decrease the melting points and the mesophase range together with a change of transition type.

3. Conclusions

A series of organometallic palladium(II) complexes bearing imine ligands and different types of *N*-benzoyl thiourea derivatives as co-ligands were prepared and investigated for their liquid crystal properties. The structures of three of the complexes have been solved by X-ray diffraction.

The first liquid crystals based on metal complexes containing the *N*-benzoyl thiourea moiety are reported here and their mesogenic properties are compared to those of palladium complexes with other types of co-ligands. The use of *N*-benzoyl thiourea derivatives as co-ligands in company of the *ortho*-palladated imine fragment destabilise the mesogenic behaviour of these complexes. Thus, in the case of complexes bearing *N*,*N*-dialkyl-*N*′-benzoyl thiourea derivatives only monotropic behaviour is seen, with the transitions to nematic mesophase occurring approximately 30–50 °C below the clearing point, while in the case where *N*-aryl-*N*′-benzoyl thiourea derivatives were employed, the mesomorphic behaviour was totally suppressed.

These results suggest the possibility of using these simple *N*-benzoyl thiourea derivatives in designing liquid crystals together with the *ortho*-metallated imine fragment but, probably, the mesogenic behaviour of such compounds can be considerably improved by changing the type of imine ligand employed.

4. Experimental

Dichloromethane was distilled from phosphorus pentaoxide, while acetone was distilled from calcium chloride; other chemicals were used as supplied. Proton and carbon NMR spectra were recorded on a Varian Gemini 300 BB spectrometer operating at 300 MHz, using $CDCl_3$ as solvent. ^1H chemical shifts were referenced to the solvent peak position, δ 7.26 ppm. Analysis by DSC was carried out using a Perkin–Elmer DSC7 instrument using a 10 °C/min heating rate. Mesomorphism was studied by hot stage polarising microscopy using a Nikon 50i Pol microscope equipped with a Linkam THMS600 hot stage and a TMS94 temperature controller. Mesophases were assigned by their optical texture [20].

Diffraction data were collected at 110 K on a Bruker Smart Apex diffractometer with Mo Kα radiation (λ = 0.71073 Å) using a SMART CCD camera. Diffractometer control, data collection and initial unit cell determination was performed using "SMART" (v5.625 Bruker-AXS). Frame integration and unit-cell refinement was carried out with the "SAINT+" (v6.22, Bruker AXS) sofware. Absorption correc-

tions were applied by SADABS (v2.03, Sheldrick). Structures were solved by "direct methods" using SHELXS-97 [21] and refined by full-matrix least squares using SHELXL-97 [21]. All non-hydrogen atoms were refined anisotropically. Hydrogen atoms (except for NH hydrogens) were placed using a "riding model" and were included in the refinement at calculated positions. NH hydrogens were found by a difference map after all other atoms were found.

The synthesis of the μ-acetato bridged Pd(II) complexes (**1a**,**b**) was carried out as described elsewhere [22]. The *N*-benzoyl thiourea derivatives used in this work were prepared according to the methods published in literature [8].

4.1. Preparation of the sodium salts of N-benzoyl thiourea derivatives

The sodium salts of *N*-benzoyl thiourea derivatives were prepared by reacting the corresponding *N*-benzoyl thiourea with sodium ethoxide (1:1 molar ratio) in petroleum ether for 2 h under reflux. A white or off-white precipitate developed for all *N*-benzoyl thiourea derivatives, which was filtered off and washed with petroleum ether several times. The sodium salts were used in the next step without further purification. Their formation was checked by IR spectroscopy. Their IR spectra confirmed the loss of the proton by the disappearance of ν_{NH} (~3300 cm^{-1}) and $\nu_{C=O}$ (~1670 cm^{-1}) frequencies (compare to the IR spectra of the free ligands) together with a shift of ν_{C-N} frequency towards lower wavenumbers.

4.2. Synthesis of **2a**

The solid sodium salt of *N*,*N*-diethyl-*N*'-benzoyl thiourea (0.0715 g, 0.27 mmol) was added to a solution of the binuclear palladium complex (0.075 g, 0.09 mmol) in CH_2Cl_2 (15 cm^3) and the mixture was stirred at room temperature for 24 h. Evaporation of the solvent gave a yellow solid, which was purified by chromatography on silica using CH_2Cl_2 as the eluant to give a yellow solid. This was recrystallised from a mixture of CH_2Cl_2/C_2H_5OH (1/1) at −25 °C.

4.2.1. Compound **2a**

Yield: 52%, m.p. 144 °C. *Anal.* Calc. for $C_{27}H_{29}N_3O_3PdS$: C, 55.7; H, 4.6; N, 7.2. Found: C, 55.3; H, 4.1; N, 7.5%.

^{1}H NMR (300 MHz, $CDCl_3$): 8.13 (s, 1H), 7.73 (m, 2H), 7.41–7.18 (m, 6H), 7.03 (d, ^4J = 2.4 Hz, 1H), 6.97 (AA′BB′ system, ^3J = 8.8 Hz, 2H), 6.60 (dd, ^3J = 8.4 Hz, ^4J = 2.4 Hz, 1H), 3.99 (q, ^3J = 7.1 Hz, 2H), 3.88–3.82 (m, 8H), 1.40 (t, ^3J = 7.1 Hz, 3H), 1.25 (t, ^3J = 7.1 Hz, 3H). ^{13}C NMR (75 MHz, $CDCl_3$): 172.7 (C–S), 170.9 (CH=N), 170.2 (C-O), 160.3, 158.6, 158.2, 141.6, 140.4, 138.2 (C-1, C-4, C-5, C-7, C-10, C-1′), 130.7 (C-4′), 130.2 (C-3), 129.4 (C-3′, C-5′), 127.3 (C-2′, C-6′), 124.4 (C-8, C-12), 118.9 (C-6), 113.9 (C-9, C-11), 109.2 (C-2). IR (cm^{-1}): 1582($\nu_{C=N}$); 1496(δ_{NH}); 1418(ν_{CN+CS}).

4.3. Synthesis of **2b** and **3–13a**,*b*

Compounds **2b** and **3–13a,b** were prepared in the same manner as **2a** by using the binuclear palladium complex/sodium salt of *N*-benzoyl thiourea in a molar ratio of 1:3.

4.3.1. Compound **2b**

Yield: 50%, m.p. 108 °C. *Anal.* Calc. for $C_{37}H_{49}N_3O_3PdS$: C, 61.5; H, 6.8; N, 5.8. Found: C, 61.3; H, 6.4; N, 5.3%.

^{1}H NMR (300 MHz, $CDCl_3$): 8.04 (s, 1H), 7.66 (m, 2H), 7.32–7.11 (m, 6H), 6.93 (d, ^4J = 2.4 Hz, 1H), 6.89 (AA′BB′ system, ^3J = 8.9 Hz, 2H), 6.51 (dd, ^3J = 8.4 Hz, ^4J = 2.5 Hz, 1H), 3.94 (m, 6H), 3.78 (q, ^3J = 7.0 Hz, 2H), 1.80–1.22 (m, 19H), 1.18 (t, ^3J = 7.0 Hz, 3H), 0.84 (m, 6H). ^{13}C NMR (75 MHz, $CDCl_3$): 172.9 (C–S), 170.9 (CH=N), 170.2 (C–O), 160.3, 158.2, 141.5, 140.2, 138.4 (C-1, C-4, C-5, C-7, C-10, C-1′), 130.7 (C-4′), 130.3 (C-3), 129.4 (C-3′, C-5′), 127.4 (C-2′, C-6′), 124.3 (C-8, C-12), 119.1 (C-6), 114.5 (C-9, C-11), 109.9 (C-2). IR (cm^{-1}): 1585($\nu_{C=N}$); 1525(δ_{NH}); 1418(ν_{CN+CS}).

4.3.2. Compound **3a**

Yield: 55%, m.p. 161 °C. *Anal.* Calc. for $C_{29}H_{33}N_3O_3PdS$: C, 57.1; H, 5.4; N, 6.9. Found: C, 56.9; H, 5.9; N, 6.5%.

^{1}H NMR (300 MHz, $CDCl_3$): 8.14 (s, 1H), 7.74–7.70 (m, 2H), 7.42–7.18 (m, 6H), 7.02 (d, ^4J = 2.3 Hz, 1H), 6.97 (AA′BB′ system, ^3J = 8.9 Hz, 2H), 6.59 (dd, ^3J = 8.3 Hz, ^4J = 2.4 Hz, 1H), 3.90–3.71 (m, 10H), 1.95–1.67 (m, 4H), 1.03 (t, ^3J = 7.3 Hz, 3H), 0.92 (t, ^3J = 7.4 Hz, 3H). ^{13}C NMR (75 MHz, $CDCl_3$): 173.0 (C–S), 170.9 (CH=N), 170.2 (C–O), 160.3, 158.6, 158.4, 141.1, 140.3, 138.3 (C-1, C-4, C-5, C-7, C-10, C-1′), 130.6 (C-4′), 130.1 (C-3), 129.4 (C-3′, C-5′), 127.3 (C-2′, C-6′), 124.3 (C-8, C-12), 117.8 (C-6), 113.9 (C-9, C-11), 110.0 (C-2). IR (cm^{-1}): 1582($\nu_{C=N}$); 1507(δ_{NH}); 1418 (ν_{CN+CS}).

4.3.3. Compound **3b**

Yield: 51%, m.p. 106 °C. *Anal.* Calc. for $C_{39}H_{55}N_3O_3PdS$: C, 62.3; H, 7.3; N, 5.6. Found: C, 62.0; H, 7.7; N, 5.3%.

^{1}H NMR (300 MHz, $CDCl_3$): 8.11 (s, 1H), 7.73 (m, 2H), 7.40–7.19 (m, 6H), 7.01 (d, ^4J = 2.4 Hz, 1H), 6.96 (AA′BB′ system, ^3J = 8.9 Hz, 2H), 6.59 (dd, ^3J = 8.4 Hz, ^4J = 2.5 Hz, 1H), 4.03 (m, 4H), 3.90–3.74 (m, 4H), 1.95–1.31 (m, 20H), 1.04 (t, ^3J = 7.4 Hz, 3H), 0.93 (m, 9H). ^{13}C NMR (75 MHz, $CDCl_3$): 172.9 (C-S), 170.9 (CH=N), 170.2 (C–O), 160.1, 158.6, 158.3, 141.7, 140.3, 138.5 (C-1, C-4, C-5, C-7, C-10, C-1′), 130.7 (C-4′), 130.2 (C-3), 129.4 (C-3′, C-5′), 127.4 (C-2′, C-6′), 124.5 (C-8, C-12), 118.6 (C-6), 114.6 (C-9, C-11), 110.7 (C-2). IR (cm^{-1}): 1582($\nu_{C=N}$); 1540(δ_{NH}); 1420(ν_{CN+CS}).

4.3.4. Compound **4a**

Yield: 60%, m.p. 140 °C. *Anal.* Calc. for $C_{31}H_{37}N_3O_3PdS$: C, 58.4; H, 5.8; N, 6.6. Found: C, 57.9; H, 5.9; N, 6.2%.

^{1}H NMR (300 MHz, $CDCl_3$): 8.13 (s, 1H), 7.72 (m, 2H), 7.41–7.17 (m, 6H), 7.02 (d, ^4J = 2.4 Hz, 1H), 6.97 (AA′BB′ system, ^3J = 8.9 Hz, 2H), 6.59 (dd, ^3J = 8.4 Hz, ^4J = 2.5 Hz, 1H), 3.99 (q, ^3J = 7.1 Hz, 2H), 3.94–3.77 (m, 10H), 1.88–1.28 (m, 8H), 1.02 (t, ^3J = 7.3 Hz, 3H), 0.91 (t, ^3J = 7.3 Hz, 3H). ^{13}C NMR (75 MHz, $CDCl_3$): 173.0 (C–S), 168.7 (CH=N), 171.0 (C–O), 160.4, 158.7, 158.5, 141.7, 140.3, 138.3 (C-1, C-4, C-5, C-7, C-10, C-1′), 130.7 (C-3), 130.2 (C-4′), 129.5 (C-3′, C-5′), 127.4 (C-2′, C-6′), 124.4 (C-8, C-12), 118.9 (C-6), 113.9 (C-9, C-11), 110 (C-2). IR (cm^{-1}): 1581($\nu_{C=N}$); 1511(δ_{NH}); 1418(ν_{CN+CS}).

4.3.5. Compound **4b**

Yield: 43%, m.p. 112 °C. *Anal.* Calc. for $C_{41}H_{57}N_3O_3PdS$: C, 63.3; H, 7.3; N, 5.4. Found: C, 62.9; H, 7.0; N, 5.0%.

^{1}H NMR (300 MHz, $CDCl_3$): 8.11 (s, 1H), 7.75 (m, 2H), 7.40–7.19 (m, 6H), 7.02 (d, ^4J = 2.4 Hz, 1H), 6.97 (AA′BB′ system, ^3J = 8.8 Hz, 2H), 6.59 (dd, ^3J = 8.4 Hz, ^4J = 2.4 Hz, 1H), 4.06–3.75 (m, 8H), 1.92–1.29 (m, 24H), 1.04 (t, ^3J = 7.3 Hz, 3H), 0.91 (m, 9H). ^{13}C NMR (75 MHz, $CDCl_3$): 173.0 (C–S), 170.9 (CH=N), 170.2 (C–O), 160.3, 158.6, 158.4, 141.1, 140.3, 138.3 (C-1, C-4, C-5, C-7, C-10, C-1′), 130.8 (C-3), 130.3 (C-4′), 129.7 (C-3′, C-5′), 127.5 (C-2′, C-6′), 124.5 (C-8, C-12), 118.3 (C-6), 114.6 (C-9, C-11), 110.9 (C-2). IR (cm^{-1}): 1582($\nu_{C=N}$); 1540, 1516(δ_{NH}); 1420(ν_{CN+CS}).

4.3.6. Compound **5a**

Yield: 69%, m.p. 138 °C. *Anal.* Calc. for $C_{35}H_{47}N_3O_3PdS$: C, 60.6; H, 6.5; N, 6.1. Found: C, 60.2; H, 6.1; N, 6.2%.

^{1}H NMR (300 MHz, $CDCl_3$): 8.13 (s, 1H), 7.73 (m, 2H), 7.42–7.18 (m, 6H), 7.03 (d, ^4J = 2.5 Hz, 1H), 6.98 (AA′BB′ system, ^3J = 8.9 Hz, 2H), 6.60 (dd, ^3J = 8.3 Hz, ^4J = 2.4 Hz, 1H), 3.92–3.75 (m, 10H),

1.87–1.23 (m, 16H), 0.94–0.82 (m, 6H). IR (cm^{-1}): 1583($\nu_{C=N}$); 1522(δ_{NH}); 1421(ν_{CN+CS}).

4.3.7. Compound ***5b***

Yield: 59%, m.p. 109 °C. *Anal.* Calc. for $C_{45}H_{65}N_3O_3PdS$: C, 64.8; H, 7.8; N, 5.0. Found: C, 64.3; H, 7.4; N, 4.8%.

^1H NMR (300 MHz, $CDCl_3$): 8.10 (s, 1H), 7.76 (m, 2H), 7.40–7.19 (m, 6H), 7.02 (d, ^4J = 2.5 Hz, 1H), 6.97 (AA′BB′ system, ^3J = 8.9 Hz, 2H), 6.58 (dd, ^3J = 8.2 Hz, ^4J = 2.3 Hz, 1H), 4.05–3.77 (m, 8H), 1.96–1.27 (m, 32H), 0.95–0.83 (m, 12H). ^{13}C NMR (75 MHz, $CDCl_3$): 173.3 (C–S), 171.0 (CH=N), 170.2 (C–O), 160.1, 158.5, 158.3, 141.7, 140.3, 138.5 (C-1, C-4, C-5, C-7, C-10, C-1′), 130.8 (C-3), 130.4 (C-4′), 129.6 (C-3′, C-5′), 127.5 (C-2′, C-6′), 124.5 (C-8, C-12), 118.6 (C-6), 114.6 (C-9, C-11), 110.6 (C-2). IR (cm^{-1}): 1582($\nu_{C=N}$); 1518(δ_{NH}); 1419(ν_{CN+CS}).

4.3.8. Compound ***6b***

Yield: 51%, m.p. 106 °C. *Anal.* Calc. for $C_{49}H_{73}N_3O_3PdS$: C, 66.0; H, 8.4; N, 4.7. Found: C, 65.6; H, 8.7; N, 4.4%.

^1H NMR (300 MHz, $CDCl_3$): 8.06 (s, 1H), 7.70 (m, 2H), 7.35–7.13 (m, 6H), 6.96 (d, ^4J = 2.4 Hz, 1H), 6.91 (AA′BB′ system, ^3J = 8.9 Hz, 2H), 6.54 (dd, ^3J = 8.4 Hz, ^4J = 2.3 Hz, 1H), 3.98 (q, ^3J = 6.6 Hz, 4H), 3.87–3.71 (m, 4H), 1.84–1.16 (m, 38H), 0.91–0.78 (m, 12H).

4.3.9. Compound ***7a***

Yield: 60%, m.p. 145 °C. *Anal.* Calc. for $C_{29}H_{25}N_3O_3PdS$: C, 57.9; H, 4.2; N, 7.0. Found: C, 57.3; H, 4.6; N, 6.6%.

^1H NMR (300 MHz, $CDCl_3$): 8.13 (s, 1H), 7.72 (m, 2H), 7.58 (m, 2H), 7.42–7.20 (m, 9H), 6.99 (AA′BB′ system, ^3J = 8.9 Hz, 2H), 6.90 (d, ^3J = 2.3 Hz, 1H), 6.61 (dd, ^3J = 8.4 Hz, ^4J = 2.5 Hz, 1H), 3.88 (s, 3H), 3.86 (s, 3H). IR (cm^{-1}): 3295(ν_{NH}); 1585($\nu_{C=N}$); 1526, 1501(δ_{NH}); 1428(ν_{CN+CS}).

4.3.10. Compound ***7b***

Yield: 47%, m.p. 115 °C. *Anal.* Calc. for $C_{39}H_{45}N_3O_3PdS$: C, 63.1; H, 6.0; N, 5.7. Found: C, 63.0; H, 6.5; N, 5.3%.

^1H NMR (300 MHz, $CDCl_3$): 8.10 (s, 1H), 7.75 (broad d, 2H), 7.58 (m, 2H), 7.43–7.18 (m, 9H), 6.97 (AA′BB′ system, ^3J = 8.8 Hz, 2H), 6.89 (broad s, 1H), 6.60 (m, 1H), 4.02 (t, ^3J = 6.6 Hz, 4H), 1.94–1.25 (m, 16H), 0.94 (m, 6H). IR (cm^{-1}): 3128(ν_{NH}); 1585($\nu_{C=N}$); 1540, 1502(δ_{NH}); 1422(ν_{CN+CS}).

4.3.11. Compound ***8a***

Yield: 47%, m.p. 218 °C. *Anal.* Calc. for $C_{30}H_{27}N_3O_3PdS$: C, 58.5; H, 4.4; N, 6.8. Found: C, 58.1; H, 4.8; N, 6.4%.

^1H NMR (300 MHz, $CDCl_3$): 8.13 (s, 1H), 7.72 (d broad, 2H), 7.47–7.16 (m, 10H), 6.98 (AA′BB′ system, ^3J = 8.9 Hz, 2H), 6.90 (s broad, 1H), 6.60 (dd, ^3J = 8.2 Hz, ^4J = 2.4 Hz, 1H), 3.88 (s, 3H), 3.84 (s, 3H), 2.35 (s, 3H). IR (cm^{-1}): 3363(ν_{NH}); 1583($\nu_{C=N}$); 1520(δ_{NH}); 1419(ν_{CN+CS}).

4.3.12. Compound ***8b***

Yield: 45%, m.p. 156 °C. *Anal.* Calc. for $C_{40}H_{47}N_3O_3PdS$: C, 63.5; H, 6.2; N, 5.6. Found: C, 63.8; H, 6.0; N, 5.2%.

^1H NMR (300 MHz, $CDCl_3$): 8.11 (s, 1H), 7.75 (broad d, 2H), 7.48–7.17 (m, 10H), 6.98 (AA′BB′ system, ^3J = 8.9 Hz, 2H), 6.90 (d broad, 1H), 6.60 (dd, ^3J = 8.3 Hz, ^4J = 2.4 Hz, 1H), 4.03 (t, ^3J = 6.6 Hz, 4H), 2.36 (s, 3H), 1.90–1.34 (m, 16H), 0.93 (m, 6H). IR (cm^{-1}): 3321(ν_{NH}); 1584($\nu_{C=N}$); 1510(δ_{NH}); 1425(ν_{CN+CS}).

4.3.13. Compound ***9a***

Yield: 81%, m.p. 153 °C. *Anal.* Calc. for $C_{30}H_{27}N_3O_3PdS$: C, 58.5; H, 4.4; N, 6.8. Found: C, 58.2; H, 4.8; N, 6.7%.

^1H NMR (300 MHz, $CDCl_3$): 8.12 (s, 1H), 7.74 (m, 2H), 7.41–7.20 (m, 10H), 6.99 (AA′BB′ system, ^3J = 8.9 Hz, 2H), 6.90 (d, ^4J = 2.4 Hz, 1H), 6.61 (dd, ^3J = 8.4 Hz, ^4J = 2.4 Hz, 1H), 3.88 (s, 3H), 3.86 (s, 3H), 2.36 (s, 3H). IR (cm^{-1}): 3298(ν_{NH}); 1584($\nu_{C=N}$); 1501(δ_{NH}); 1399(ν_{CN+CS}).

4.3.14. Compound ***9b***

Yield: 45%, m.p. 179 °C. *Anal.* Calc. for $C_{40}H_{47}N_3O_3PdS$: C, 63.5; H, 6.2; N, 5.6. Found: C, 63.9; H, 6.0; N, 5.3%.

^1H NMR (300 MHz, $CDCl_3$): 8.14 (s, 1H), 7.85 (broad d, 2H), 7.53–7.02 (m, 12H), 6.98 (d broad, 1H), 6.65 (dd, ^3J = 8.4 Hz, ^4J = 2.3 Hz, 1H), 4.08 (t, ^3J = 6.5 Hz, 4H), 2.43 (s, 3H), 1.95–1.40 (m, 16H), 1.01 (m, 6H). IR (cm^{-1}): 3126(ν_{NH}); 1584($\nu_{C=N}$); 1508(δ_{NH}); 1451(ν_{CN+CS}).

4.3.15. Compound ***10a***

Yield: 52%, m.p. 171 °C. *Anal.* Calc. for $C_{29}H_{24}FN_3O_3PdS$: C, 56.2; H, 3.9; N, 6.8. Found: C, 55.9; H, 3.5; N, 6.4%.

^1H NMR (300 MHz, $CDCl_3$): 8.12 (s, 1H), 7.79 (broad d, 2H), 7.53–7.19 (m, 8H), 7.06 (AA′MXX system, ^3J = 8.3 Hz, 2H), 6.98 (AA′BB′ system, ^3J = 8.9 Hz, 2H), 6.87 (broad s, 1H), 6.61 (dd, ^3J = 8.3 Hz, ^4J = 2.4 Hz, 1H), 3.88 (s, 3H), 3.84 (s, 3H), 2.36 (s, 3H). IR (cm^{-1}): 3267(ν_{NH}); 1583($\nu_{C=N}$); 1536, 1503(δ_{NH}); 1405(ν_{CN+CS}).

4.3.16. Compound ***10b***

Yield: 41%, m.p. 171 °C. *Anal.* Calc. for $C_{39}H_{44}FN_3O_3PdS$: C, 60.3; H, 5.7; N, 5.4. Found: C, 59.8; H, 5.4; N, 5.0%.

^1H NMR (300 MHz, $CDCl_3$): 8.03 (s, 1H), 7.62 (broad d, 2H), 7.43 (AA′MXX system, ^3J = 8.3 Hz, $^4J_{HF}$ = 4.9 Hz, 2H), 7.35–7.12 (m, 6H), 6.99 (AA′MXX system, ^3J = 8.4 Hz, 2H), 6.89 (AA′BB′ system, ^3J = 9.0 Hz, 2H), 6.78 (broad s, 1H), 6.52 (dd, ^3J = 8.3 Hz, ^4J = 2.4 Hz, 1H), 3.94 (t, ^3J = 6.6 Hz, 4H), 1.91–1.24 (m, 16H), 0.84 (m, 6H). IR (cm^{-1}): 3111(ν_{NH}); 1583($\nu_{C=N}$); 1544, 1507(δ_{NH}); 1400(ν_{CN+CS}).

4.3.17. Compound ***11a***

Yield: 61%, m.p. 199 °C. *Anal.* Calc. for $C_{29}H_{24}ClN_3O_3PdS$: C, 54.7; H, 3.8; N, 6.6. Found: C, 54.3; H, 3.9; N, 6.2%.

^1H NMR (300 MHz, $CDCl_3$): 8.13 (s, 1H), 7.69 (d broad, 2H), 7.52 (AA′BB′ system, ^3J = 8.8 Hz, 2H), 7.45–7.21 (m, 8H), 6.98 (AA′BB′ system, ^3J = 8.9 Hz, 2H), 6.87 (d, ^4J = 2.3 Hz, 1H), 6.61 (dd, ^3J = 8.3 Hz, ^4J = 2.4 Hz, 1H), 3.88 (s, 3H), 3.85 (s, 3H). IR (cm^{-1}): 3209(ν_{NH}); 1582($\nu_{C=N}$); 1527(δ_{NH}); 1415(ν_{CN+CS}).

4.3.18. Compound ***11b***

Yield: 43%, m.p. 199 °C. *Anal.* Calc. for $C_{39}H_{44}ClN_3O_3PdS$: C, 60.3; H, 5.7; N, 5.4. Found: C, 60.0; H, 5.8; N, 5.0%.

^1H NMR (300 MHz, $CDCl_3$): 8.10 (s, 1H), 7.71 (broad d, 2H), 7.52 (AA′BB′ system, ^3J = 8.9 Hz, 2H), 7.44–7.21 (m, 8H), 6.97 (AA′BB′ system, ^3J = 8.9 Hz, 2H), 6.87 (d, ^4J = 2.4 Hz, 1H), 6.60 (dd, ^3J = 8.3 Hz, ^4J = 2.4 Hz, 1H), 4.02 (t, ^3J = 6.6 Hz, 4H), 1.89–1.32 (m, 16H), 0.93 (m, 6H). IR (cm^{-1}): 3209(ν_{NH}); 1584($\nu_{C=N}$); 1525(δ_{NH}); 1424(ν_{CN+CS}).

4.3.19. Compound ***12a***

Yield: 66%, m.p. 201 °C. *Anal.* Calc. for $C_{29}H_{24}BrN_3O_3PdS$: C, 51.1; H, 3.5; N, 6.2. Found: C, 50.9; H, 3.9; N, 6.9%.

^1H NMR (300 MHz, $CDCl_3$): 8.13 (s, 1H), 7.69 (m, 2H), 7.47–7.21 (m, 10H), 6.99 (AA′BB′ system, ^3J = 8.7 Hz, 2H), 6.87 (d, ^4J = 2.4 Hz, 1H), 6.61 (dd, ^3J = 8.2 Hz, ^4J = 2.4 Hz, 1H), 3.88 (s, 3H), 3.85 (s, 3H). IR (cm^{-1}): 3298(ν_{NH}); 1584($\nu_{C=N}$); 1501(δ_{NH}); 1399(ν_{CN+CS}).

4.3.20. Compound ***12b***

Yield: 33%, m.p. 191 °C. *Anal.* Calc. for $C_{39}H_{44}BrN_3O_3PdS$: C, 57.0; H, 5.4; N, 5.1. Found: C, 56.8; H, 5.0; N, 4.9%.

^1H NMR (300 MHz, $CDCl_3$): 8.02 (s, 1H), 7.64 (m, 2H), 7.36–7.14 (m, 10H), 6.90 (AA′BB′ system, ^3J = 8.8 Hz, 2H), 6.79 (d, ^4J = 2.4 Hz,

1H), 6.52 (dd, ^3J = 8.4 Hz, ^4J = 2.4 Hz, 1H), 3.94 (t, ^3J = 6.6 Hz, 4H), 1.80–1.24 (m, 16H), 0.86 (m, 6H). IR (cm^{-1}): 3210(ν_{NH}); 1584($\nu_{C=N}$); 1510(δ_{NH}); 1423(ν_{CN+CS}).

*4.3.21. Compound **13a***

Yield: 56%, m.p. 162 °C. *Anal.* Calc. for $C_{30}H_{27}N_3O_4PdS$: C, 57.0; H, 4.3; N, 6.7. Found: C, 56.9; H, 4.6; N, 6.3%.

^1H NMR (300 MHz, $CDCl_3$): 8.11 (s, 1H), 7.67 (m, 2H), 7.57–7.19 (m, 10H), 6.99–6.87 (m, 3H), 6.59 (dd, ^3J = 8.2 Hz, ^4J = 2.4 Hz, 1H), 3.86 (s, 3H), 3.81 (s, 3H). IR (cm^{-1}): 3298(ν_{NH}); 1584($\nu_{C=N}$); 1501(δ_{NH}); 1399(ν_{CN+CS}).

*4.3.22. Compound **13b***

Yield: 51%, m.p. 165 °C. *Anal.* Calc. for $C_{40}H_{47}N_3O_4PdS$: C, 62.4; H, 6.2; N, 5.5. Found: C, 61.9; H, 6.0; N, 5.2%.

^1H NMR (300 MHz, $CDCl_3$): 8.10 (s, 1H), 7.72 (br, 2H), 7.49–7.20 (m, 10H), 6.97 (AA′BB′ system, ^3J = 8.8 Hz, 2H), 6.92 (d, ^4J = 2.4 Hz, 1H), 6.52 (dd, ^3J = 8.4 Hz, ^4J = 2.4 Hz, 1H), 4.01 (t, ^3J = 6.6 Hz, 2H), 3.82 (t, ^3J = 6.6 Hz, 2H), 1.90–1.32 (m, 16H), 0.91 (m, 6H). IR (cm^{-1}): 3220(ν_{NH}); 1585($\nu_{C=N}$); 1509(δ_{NH}); 1420(ν_{CN+CS}).

Acknowledgements

The authors wish to thank MEdC (Romanian Ministry of Education and Research, Project CEEX ET-31 and Project PNII ID_954) and NATO for funding this study and to Prof. Duncan W. Bruce (University of York, UK) for his support.

Appendix A. Supplementary data

CCDC 684867, 684868 and 684869 contain the supplementary crystallographic data for **2a**, **10a** and **13a**. These data can be obtained free of charge via http://www.ccdc.cam.ac.uk/conts/retrieving.html, or from the Cambridge Crystallographic Data Centre, 12 Union Road, Cambridge CB2 1EZ, UK; fax: (+44) 1223-336-033; or e-mail: deposit@ccdc.cam.ac.uk. Supplementary data associated with this article can be found, in the online version, at doi:10.1016/j.poly.2008.08.023.

References

[1] B. Donnio, D. Guillon, R. Deschenaux, D.W. Bruce, in: J.A. McCleverty, T.J. Meyer (Eds.), Comprehensive Coordination Chemistry II, vol. 7, Elsevier, Oxford, 2003, p. 357 (Chapter 7.9).
[2] B. Donnio, D. Guillon, R. Deschenaux, D.W. Bruce, in: R.H. Crabtree, D.M.P. Mingos (Eds.), Comprehensive Organometallic Chemistry III, vol. 12, Elsevier, Oxford, UK, 2006, p. 195 (Chapter 12.05).
[3] (a) J. Buey, P. Espinet, J. Organomet. Chem. 507 (1996) 137;
(b) M.J. Baena, P. Espinet, M.B. Ros, J.L. Serrano, Angew. Chem., Int. Ed. Engl. 30 (1991) 711;
(c) L. Omnès, B.A. Timimi, T. Gelbrich, M.B. Hursthouse, G.R. Luckhurst, D.W. Bruce, Chem. Commun. (2001) 2248;
(d) G.W.V. Cave, D.P. Lydon, J.P. Rourke, J. Organomet. Chem. 555 (1998) 81;
(e) V. Cîrcu, T.J.K. Gibbs, L. Omnès, P.N. Horton, M.B. Hursthouse, D.W. Bruce, J. Mater. Chem. 16 (2006) 4316.
[4] J. Buey, P. Espinet, H.S. Kitzerow, J. Strauss, Chem. Commun. (1999) 441.
[5] (a) D.J. Huang, N.Y. Xiong, J. Yang, S.M. Wang, G.N. Li, L.F. Zhang, Mol. Cryst. Liq. Cryst. 231 (1993) 191;
(b) D.J. Saccomando, C. Black, G.W.V. Cave, D.P. Lydon, J.P. Rourke, J. Organomet. Chem. 601 (2000) 305.
[6] D.P. Lydon, G.W.V. Cave, J.P. Rourke, J. Mater. Chem. 7 (1997) 403.
[7] L. Diez, P. Espinet, J.A. Miguel, J. Chem. Soc., Dalton Trans. (2001) 1189.
[8] I.B. Douglass, F.B. Dains, J. Am. Chem. Soc. 56 (1934) 719.
[9] (a) L. Beyer, E. Hoyer, J. Liebscher, H. Hartmann, Z. Chem. 21 (1981) 81;
(b) P. Muhl, K. Gloe, F. Dietze, E. Hoyer, L. Beyer, Z. Chem. 26 (1986) 81;
(c) K.R. Koch, Coord. Chem. Rev. 216–217 (2001) 473.
[10] T. Seshadri, H.-J. Haupt, J. Mater. Chem. 8 (1998) 1345.
[11] T. Seshadri, H.-J. Haupt, U. Flörke, G. Henkel, Liq. Cryst. 34 (2007) 33.
[12] A. Deleanu, M. Ilis, T. Rosu, V. Cîrcu, Rev. Chim. (Bucharest) 57 (2006) 1216.
[13] A.N. Mautjana, J.D.S. Miller, A. Gie, S.A. Bourne, K.R. Koch, J. Chem. Soc., Dalton Trans. (2003) 1952.
[14] G. Fitzl, L. Beyer, J. Sieler, R. Richter, J. Kaiser, E. Hoyer, Z. Anorg. Allg. Chem. 433 (1977) 237.
[15] A. Bondi, J. Phys. Chem. 68 (1964) 441.
[16] Y. Cao, B. Zhao, Y.-Q. Zhang, D.-C. Zhang, Acta Crystallogr., Sect. C 52 (1996) 1772.
[17] S. Shanmuga Sundara Raj, K. Puviarasan, D. Velmurugan, G. Jayanthi, H.-K. Fun, Acta Crystallogr., Sect. C 55 (1999) 1318.
[18] P. Wagner, S. Niemczyk-Baltro, M. Kubicki, Acta Crystallogr., Sect. C 59 (2003) o83.
[19] P.J. Collings, M. Hird, Introduction to Liquid Crystals Chemistry and Physics, Taylor & Francis, London and New York, 2004.
[20] I. Dierking, Textures of Liquid Crystals, Wiley-VCH Verlag, Weinheim, 2003.
[21] G.M. Sheldrick, SHELXS-97, Program for Refinement of Crystal Structures, University of Göttingen, Germany, 1997.
[22] L. Omnès, V. Cîrcu, P.T. Hutchins, S.J. Coles, P.N. Horton, M.B. Hursthouse, D.W. Bruce, Liq. Cryst. 32 (2005) 1437.

by the full-matrix least-squares method on all F^2 data using the program SHELXL-97 [5]. Geometrical analysis was performed using SHELXL-97. The structures were drawn by ORTEP-3 for Windows. The single crystal suite WINGX was used as an integrated system for all crystallographic programs and software for preparing the material for publication [6]. Crystal data and conditions of data collection and refinement are reported in Table 1.

2.3. Preparation of the complexes

2.3.1. Cu(meclof)$_2$H$_2$O

To an aqueous solution of copper(II) sulfate (5 mmol), an aqueous solution of meclofenamate and an equimolar quantity of sodium hydroxide (10 mmol) were added, and the reaction mixture was refluxed for 30 min. The blue green precipitate that formed was filtered off and dried at ambient temperature.

Elemental *Anal.* Calc. for $C_{28}H_{22}N_2O_5Cl_4Cu$: C, 50.06; H, 3.30; N, 4.17; Cu, 9.46. Found: C, 49.84; H, 3.32; N, 4.68; Cu, 9.48%. UV–Vis spectrum: 675 nm (band I) and 375 nm (band II).

Cu(meclof)$_2$L$_2$ (L = 2-pyridylcarbinol (2-pyca), 3-pyridylcarbinol (3-pyca), nicotinamide (na) and *N*,*N*-diethylnicotinamide (dena)).

A solution of L (10 mmol) in methanol (20 ml) was added to a solution of Cu(meclof)$_2$H$_2$O (5 mmol) in methanol (50 ml). The resulting solution was heated and left to stand at ambient temperature. The blue precipitate that formed was collected by filtration, washed with cold methanol and finally dried at ambient temperature (the yield of the complexes was ~70%).

Elemental *Anal.* Cu(meclof)$_2$(2-pyca)$_2$: Calc. for $C_{40}H_{34}N_4O_6Cl_4$-Cu(%): C, 55.09; H, 3.93; N, 6.42; Cu, 7.29. Found: C, 54.32; H, 4.11; N, 6.67; Cu, 7.31%. UV–Vis spectrum: 615 nm (band I) and 330 nm (band II).

Cu(meclof)$_2$(3-pyca)$_2$: Calc. for $C_{40}H_{34}N_4O_6Cl_4Cu$: C, 55.09; H, 3.93; N, 6.42; Cu, 7.29. Found: C, 54.76; H, 4.03; N, 6.65; Cu, 7.35%. UV–Vis spectrum: 615 nm (band I) and 330 nm (band II).

Table 1
Crystal data and structure refinement for the complex Cu(meclof)$_2$(2-pyca)$_2$

Internal index	mk16
Compound	[Cu$_2$(meclof)$_2$(2-pyca)$_2$]
Empirical formula	$C_{40}H_{34}O_6N_4Cl_4Cu$
Formula weight	872.05
Wavelength (Å)	0.71073
Crystal system, space group	monoclinic, C2/c
Unit cell dimensions	
a (Å)	10.723(1)
b (Å)	15.333(1)
c (Å)	18.721(2)
α (°)	90
β (°)	108.434(6)
γ (°)	90
Volume (Å^3)	3978.2(8)
Z, D_{calc} (Mg m^{-3})	4, 1.456
Absorption coefficient (mm^{-1}), F(000)	1.100, 1452
Crystal size (mm)	0.126 × 0.26 × 0.52
θ Range for data collection (°)	2.48–25.23
Limiting indices	$-1 \leqslant h \leqslant 40$, $-1 \leqslant k \leqslant 11$, $-24 \leqslant l \leqslant 22$
Reflections collected/unique (R_{int})	4238/3479 (0.0481)
Completeness to θ = 25.23 (%)	96.8
Absorption correction	psi-scan
Refinement method	full-matrix least-squares on F^2
Data/restraints/parameters	5720/84/236
Goodness-of-fit on F^2	0.903
Final R indices [$I > 2\sigma(I)$]	R_1 = 0.0706, wR_2 = 0.1465
R indices (all data)	R = 0.1723, wR_2 = 0.1780
Largest difference in peak and hole (e Å^{-3})	0.624 and −0.282
CCDC	685931

Cu(meclof)$_2$(na)$_2$: Calc. for $C_{40}H_{32}N_6O_6Cl_4Cu$: C, 53.50; H, 3.59; N, 9.36; Cu, 7.08. Found: C, 51.59; H, 4.07; N, 9.45; Cu, 7.14%. UV–Vis spectrum: 640 nm (band I) and 330 nm (band II).

Cu(meclof)$_2$(dena)$_2$(H$_2$O)$_2$: Calc. for $C_{48}H_{52}N_6O_8Cl_4Cu$: C, 55.10; H, 5.01; N, 8.03; Cu, 6.07. Found: C, 53.95; H, 5.17; N, 8.19; Cu, 6.08%. UV–Vis spectrum: 605 nm (band I) and 325 nm (band II).

3. Results and discussion

An ORTEP plot of Cu(meclof)$_2$(2-pyca)$_2$ is shown in Fig. 1, and selected bond distances and angles are given in Table 2. In the structure of the complex, the Cu(II) atom is six-coordinated and the coordination polyhedron can be described as a tetragonally distorted octahedron. Two equatorial positions are occupied by two oxygen atoms [Cu1–O1 1.968(3) Å] from the carboxyl groups of two meclofenamate anions, which are coordinated to the central atom in an unidentate manner. Two heterobidentate (O, N) 2-pyridylcarbinol ligands, which span the equatorial plane [Cu1–N1 2.021(5) Å] and the axial positions [Cu1–O3 2.387(4) Å], complete the distorted tetragonal bipyramidal arrangement. The value of the angle which is part of the five-membered metallocycles (N1$_{(eq)}$–Cu1–O3$_{(ax)}$) of 76.8(2)°) is about 7.87° smaller than those of (O1$_{(eq)}$–Cu1–O3$_{(ax)}$) 84.67(14)°. However, the (N1$_{(eq)}$–Cu1–O3$_{(ax)}$) angle from the cis-angles is the most open, with a value of 103.2(2)°. All the trans L–Cu–L angles are linear (180.0°).

The structural chemistry for over 600 coordinated monomeric copper(II) compounds has been reviewed by us [7]. From the three principal forms of distortion of the octahedron, all of which occur in the chemistry of Cu(II) to varying degrees, the tetragonal distor-

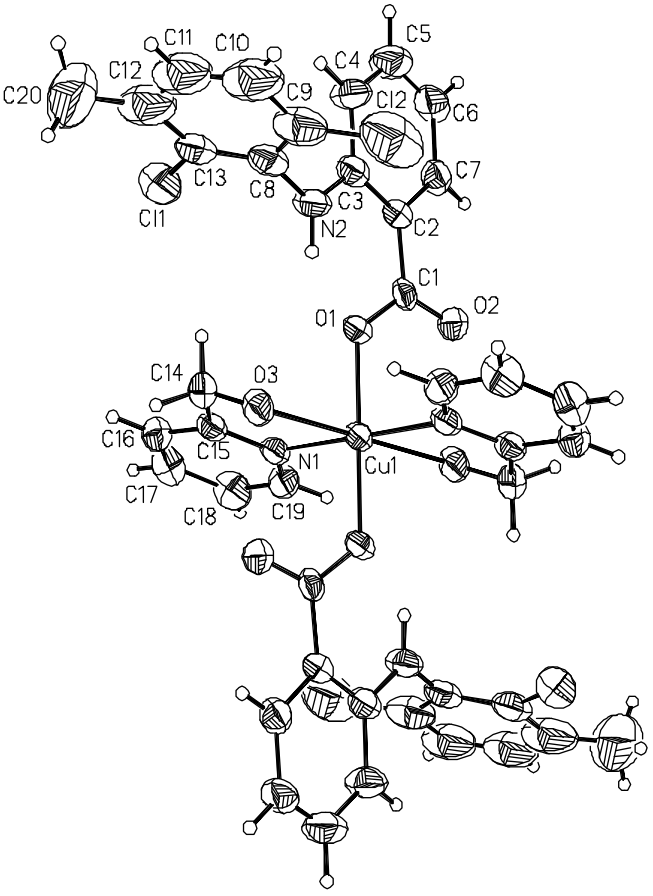

Fig. 1. ORTEP-plot of Cu(meclof)$_2$(2-pyca)$_2$. Thermal ellipsoids are drawn at the 30% probability level.

Table 2
Selected distances (Å) and angles (°) for complex the Cu(meclof)$_2$(2-pyca)$_2$

Cu1–O1	1.973(3)	O1–Cu1–O3	84.89(2)
Cu1–N1	2.018(5)	O1–Cu1–N1	89.62()
Cu1–O3	2.386(4)	N1–Cu1–O3	76.89(2)
O1–C1	1.278(6)	Cu1–O3–C14	103.7(4)
O2–C1	1.245(7)	O3–C14–C15	115.7(6)
C1–C2	1.467(8)	C14–C15–N1	117.4(6)
O3–C14	1.438(7)	C15–N1–Cu1	120.1(4)
N1–C15	1.329(7)	Cu1–O1–C1	127.2(4)
		O1–C1–O2	123.9(5)

tion most commonly involves an elongation of one C_4 axis. There are some examples of the general formula $CuX_2(2\text{-pyca})_2$ (X = mefanamate, clofibriate, salicylate, 2-bromopropionate and meclofenamate) and selected data of these complexes are given in Table 3. The value of the T ($T = R_S/R_L$) parameter for $CuX_2(2\text{-pyca})_2$, indicating the degree of the tetragonal distortion about the Cu(II) centers, decreases in the order: X = salicylate 0.850 > meclofenamate 0.835 > clofibriate 0.832 > 2-bromopropionate 0.829 > mefanamate 0.819.

The IR spectrum of Cu(meclof)$_2$H$_2$O shows two absorption bands at 3308 and 3248 cm^{-1}. These bands correspond to the antisymmetric and symmetric OH stretch and confirm the presence of water in the complex. Moreover, the IR spectrum exhibits characteristic bands at approximately 850 and 550 cm^{-1} assigned to the rocking and wagging mode of the coordinated water molecule [12]. Each complex showed carboxylate stretching frequencies, $V_{as}(COO^-)$ and $V_s(COO^-)$, which are in the expected region (Table 4). The broad bands at about 1610 cm^{-1} (assigned to the asymmetric stretch $V_{as}(COO^-)$) are overlapped with the stretching vibration of C=N of the pyridine ring. The difference between the asymmetric and symmetric stretching vibration ($\Delta\nu = V_{as}(COO^-) - V_s(COO^-)$) (Table 4), which gives information on the carboxylate bonding mode, especially for Cu(meclof)$_2 \cdot$ H$_2$O, could not be determined accurately. However, splitting of the bands assigned to $V_s(COO^-)$ indicates that the meclofenamate anion as a ligand in Cu(meclof)$_2 \cdot$ H$_2$O is coordinated as a bidentate bridging carboxyl group (see electronic and EPR spectra). The difference $\Delta\nu = 245$ cm^{-1} for Cu(meclof)$_2 \cdot$ (2-pyca)$_2$ is typical for a unidentately bonded carboxylic group of meclofenamate (see the crystal structure). The smaller Δ values from 164 to 188 cm^{-1} for the complexes Cu(meclof)$_2 \cdot$ L$_2$ (L = 3-pyca, na, dena) indicate that the meclofenamate anions are coordinated as asymmetrically bidentate chelating carboxylic groups.

The electronic spectrum of Cu(meclof)$_2 \cdot$ H$_2$O shows a broad absorption band (band I) in the visible region at 675 nm, which could be assigned to the $d_{xz,yz} \rightarrow d_{x^2y^2}$ transition [13]. Moreover, the spectrum displays a shoulder at 375 nm (band II). Band II has been assigned to a charge transfer LMCT absorption [14] and is believed to be indicative of a dimeric structure [15]. The electronic spectra of all the remaining Cu(meclof)$_2 \cdot$ L$_2$ complexes exhibit a broad asymmetrical ligand field band with a maximum in the range 605–610 nm (Table 5). For complexes Cu(meclof)$_2 \cdot$ L$_2$ (L = 3-pyca, na and dena) there is also a charge transfer band at about 330 nm.

Table 4
IR-data (cm^{-1})

L	Carboxylic groups		$\Delta\nu$
	$V_{as}(COO^-)$	$V_s(COO^-)$	
dena	1624, 1613	1457, 1426	~177
3-pyca	1612	1448	164
2-pyca	1609	1364	245
na	1615	1427	188

Table 5
Electronic spectra (nm)

L	Band I	Band II
dena	605	325
3-pyca	615	
2-pyca	615	330
na	640	330

The EPR spectrum of a powdered sample of Cu(meclof)$_2 \cdot$ H$_2$O was made at room temperature. The spectrum exhibit feature typical of those for dimeric carboxylate copper(II) complexes [16], absorption at low and high field ($H_{Z1} \sim 300$ G and $H_{Z2} \sim 6000$ G, respectively) and line $H_{\perp 2} \sim$ about 4700 G. Absorption at about 3200 G ($g = 2100$) confirms monomeric impurities in measured powered sample of ~2.6%. The EPR spectrum was interpreted by using the effective spin Hamiltonian [17] for a randomly oriented triplet state, $S = 1$:

$$H = g\beta H\acute{S} + D\acute{S}_z^2 + E(\acute{S}_x^2 - \acute{S}_y^2) - 2/3 \cdot D$$

where D and E are the axial and rhombic zero-field splitting parameters, and x, y, z are the principal axes of a coordinated system fixed with respect to the Cu–Cu bond. The obtained parameters are $g_\perp = 2.090$, $g_{||} = 2.397$, $g_{av} = 2.192$, $|D| = 0.331$ cm^{-1} and $E = 0.003$ cm^{-1}.

The EPR spectra of all the remainding complexes exhibit a monomeric type of signal and have either axial (complexes Cu(meclof)$_2 \cdot$ L$_2$, L = 2-pyca, 3-pyca and na) or rhombic symmetry (Cu(meclof)$_2$dena$_2$) with $g_\perp < g_{||}$. This indicates that the unpaired electron is located mostly on the $d_{x^2-y^2}$ orbital of the copper(II) atom. The values of the g factors are summarized in Table 6. Complexes Cu(meclof)$_2 \cdot$ L$_2$ (L = 3-pyca and dena) also exhibit well-resolved parallel hyperfine splitting with $A_{||}$ values of 166 and 157 G, respectively.

On the basis of the spectral data observed, a dimeric structure for Cu(meclof)$_2 \cdot$ H$_2$O can be proposed, in which two copper(II) atoms are held together by four bidentate meclofenamate anions in a *syn–syn* arrangement. Each Cu(II) atom is penta-coordinated with four oxygen atoms of four different meclofenamate anions assuming the basal positions in a tetragonal pyramidal arrangement and molecule water occupying an apical position.

For Cu(meclof)$_2 \cdot$ L$_2$ (L = 3-pyca, na and dena) we proposed, on the basis of the spectroscopic data observed, a monomeric structure with a tetragonal bipyramidal geometry around the Cu(II) atom. We propose that meclofenamate use both carboxylate

Table 3
Selected lengths (Å) and angles (°) for the $CuX_2(2\text{-pyca})_2$ complexes

	Mefanamate [8]	Clofibriate [9]	Salicylate [10]	2-Bromopropionate [11]	Meclofenamate, this work
Cu–O$_{eq}$	1.966(2)	1.997(2)	1.981(1)	2.003(2)	1.968(3)
Cu–N$_{eq}$	1.990(3)	1.978(2)	1.981(1)	1.984(2)	2.021(5)
Cu–O$_{ax}$	2.415(3)	2.388(2)	2.331(2)	2.404(2)	2.387(4)
N$_{eq}$–Cu–O$_{ax}$	75.82(1)	76.83(7)	77.62(7)	76.97(7)	76.79(2)
N$_{eq}$–Cu–O$_{ax}$	96.26(9)	94.19(6)	95.13(5)	96.15(7)	90.38(3)

Table 6
EPR-data

L	$g_{\perp}$		$g_{\parallel}$	g_{av}
	g_1	g_2		
dena	2.029	2.066	2.303	3.133
3-pyca	2.066		2.178	2.137
2-pyca	2.068		2.290	2.142
na	2.080		2.301	2.154

oxygens for binding to the metal atom in an asymmetrical manner. Each of the L ligands (=3-pyca, na and dena) coordinated unidentately via the ring nitrogen atom and complete the tetragonal bipyramid. The mean *g*-values of the complexes (Table 6) slightly decrease in the order: 2.154 (L = na) > 2.142 (2-pyca) > 2.137 (3-pyca) > 2.133 (dena), which seems to be associated with a lowering of the symmetry of coordination geometry in the given order.

Acknowledgements

We thank the Scientific Grant Agency of the Ministry of Education of Slovak Republic and the Slovak Academy of Sciences for financial support (1/0353/08 and 1/4454/07).

Appendix A. Supplementary data

CCDC 685931 contains supplementary crystallographic data for $Cu(meclof)_2(2\text{-pyca})_2$. These data can be obtained free of charge via http://www.ccdc.cam.ac.uk/conts/retrieving.html, or from the Cambridge Crystallographic Data Centre, 12 Union Road, Cambridge CB2 1EZ, UK; fax: (+44) 1223-336-033; or e-mail: deposit@ccdc.cam.ac.uk. Supplementary data associated with this article can be found, in the online version, at doi:10.1016/j.poly.2008.08.017.

References

[1] R.J. Sorenson, in: HiSigel (Ed.), Metal ions in Biological Systems, vol. 14, Marcel Decker, New York, 1982.
[2] Siemens, XEMP.Version 4.2, Siemens Analytical X-ray Instruments Inc., Madison, Wisconsin, USA, 1990.
[3] Siemens, Siemens Analytical X-ray Instruments Inc., Madison, Wisconsin, USA, 1994.
[4] G.M. Sheldrick, Acta Crystallogr., Sect. A 46 (1990) 467.
[5] G.M. Sheldrick, SHELXL97, University of Göttingen, Germany, 1997.
[6] L.J. Farrugia, J. Appl. Crystallogr. 30 (1997) 565.
[7] M. Melník, M. Kabešová, Ľ. Macášková, C.E. Holloway, J. Coord. Chem. 45 (1998) 31.
[8] M. Koman, M. Melník, J. Moncoľ, Š. Lörinc, T. Glowiak, in: M. Melník, A. Sirota (Eds.), Progress in Coordination and Bioinorganic Chemistry, Slovak Technical University Press, Bratislava, 2003. p. 121.
[9] J. Moncoľ, B. Kaliňaková, J. Švorec, M. Kleinová, M. Koman, D. Hudecová, M. Melník, M. Mazúr, M. Valko, Inorg. Chim. Acta 357 (2004) 3211.
[10] N.N. Hoang, F. Valach, M. Dunaj-Jurčo, M. Melník, Acta Crystallogr., Sect. C 48 (1992) 443.
[11] J. Moncoľ, M. Múdra, P. Lönnecke, M. Koman, M. Melník, J. Coord. Chem. 57 (2004) 1056.
[12] K. Nakamoto, Infrared and Raman spectra Inorganic and Coordination Compounds, Part B, 5th ed., Wiley, New York, 1997. p. 23.
[13] M. Kato, Y. Muto, Coord. Chem. Rev. 92 (1988) 45.
[14] Y. Caterick, P. Thornton, Adv. Inorg. Chem. Radiochem. 20 (1977) 291.
[15] M. Melník, I. Potočňák, Ľ. Macášková, D. Miklóš, Polyhedron 15 (1996) 2159.
[16] M. Melník, Coord. Chem. Rev. 36 (1981) 1.
[17] A. Abragan, B. Bleaney, Electron Paramagnetic Resonance of Transition Ions, Clarendon Press, Oxford, 1971.

2.3. Computational method

The geometry of the resulting complexes $[Mn(L_{22pyfp})Cl]^+$ and $[Cd(L_{22pyfp})NO_3]^+$ in the gas phase were fully optimized at both the Hartree–Fock and DFT (B3LYP) [18] levels of theory using the GAUSSIAN 98 set of program (Figs. 1 and 2) [19]. The atomic coordinates of the complexes in their crystal structures were used for ab initio calculations. Both complexes were optimized using the standard LanL2MB [20] for all atoms, or 3-21G* and/or 6-31G* basis sets [21,22] for ligand atoms, and LanL2DZ for the metal ions [23]. The optimized structures of the ligands of both complexes were used for molecular orbital analysis and time-dependent DFT (TD-DFT) calculations at the B3LYP/LanL2MB level of theory. Calculations were performed on a Pentium-PC computer with a 4400 MHz processor.

2.4. Synthesis

2.4.1. Synthesis of $[Cd(L_{22pyfp})NO_3](ClO_4)\cdot H_2O$ (**1**)

This complex was prepared by the template condensation method [5]. L_{22py}.3HCl (0.1 g, 0.33 mmol) and NaOH (0.039 g, 0.99 mmol) were mixed and heated under reflux for 30 min in EtOH (15 ml). The NaCl which formed upon cooling was filtered off. The filtrate was added to 2-pyridinecarboxaldehyde (0.07 g, 0.66 mmol) in dry EtOH (40 ml) and the solution was stirred. $Cd(NO_3)_2\cdot 4H_2O$ (0.1 g, 0.33 mmol) dissolved in MeOH (5 ml) was subsequently added. The mixture was stirred at 50–60 °C for 24 h, then $NaClO_4$ (0.92 g, 0.66 mmol) was added. The solution was filtered and the filtrate was reduced to ca. 10 cm^3. A crystalline compound was obtained by slow diffusion of Et_2O vapor into this solution. Yield of the complex $[Cd(L_{22pyfp})NO_3](ClO_4)\cdot H_2O$ (**1**), 0.15 g, 75%. *Anal.* Calc. for ($C_{22}H_{26}CdClN_7O_8$): C, 39.77; H, 3.92; N, 14.75. Found: C, 39.21; H, 3.65; N, 14.17%. IR (KBr, cm^{-1}): 1667 (νC=N schiff base), 1591 (νC=N pyridine), 1568 (νC=C), 1081. ^{1}H NMR (DMSO, ppm, 300 MHz, py = pyridine): δ 2.76 (m, 2H, 1-Hα), 3.12 (m, 2H, 1-H$_\beta$), 3.95 (4H, t, 2-H), 4.24 (s, 2H, CH_2-Py), 7.37 (t, 1H), 7.57 (d, 1H), 7.84 (t, 2H) 7.96 (t, 1H), 8.01 (d, 2H), 8.26 (m, 5H) 8.82 (s, 2H, with two satellite peaks in the ratio 1:6:1 relative to the main signal $^3J(^{111/113}Cd\text{-}^1H) = 44.53$ Hz). ^{1}H COSY (DMSO, 300 MHz) δ: 2.76/312 (1-Hα/1-H$_\beta$), 2.76/3.95 (1-Hα/2-Hα), 2.76/3.95 (1-Hα/2-H$_\beta$), 312/3.95 (1-H$_\beta$/2-H$_\alpha$), 312/3.95 (1-H$_\beta$/2-H$_\beta$), ^{13}C NMR (DMSO, ppm, 300 MHz): δ 53.83 (C-1), 54.69 (C-2), 57.66 (C-3), 124.53 (C-8), 125.50 (C-6), 129.28 (C-9 and C-5), 140.17 (C-7), 141.06 (C-13), 147.43 (C-11), 149.39 (C-12), 150.04 (C-10), 156.95 (C-14), 162.47 (C-4).

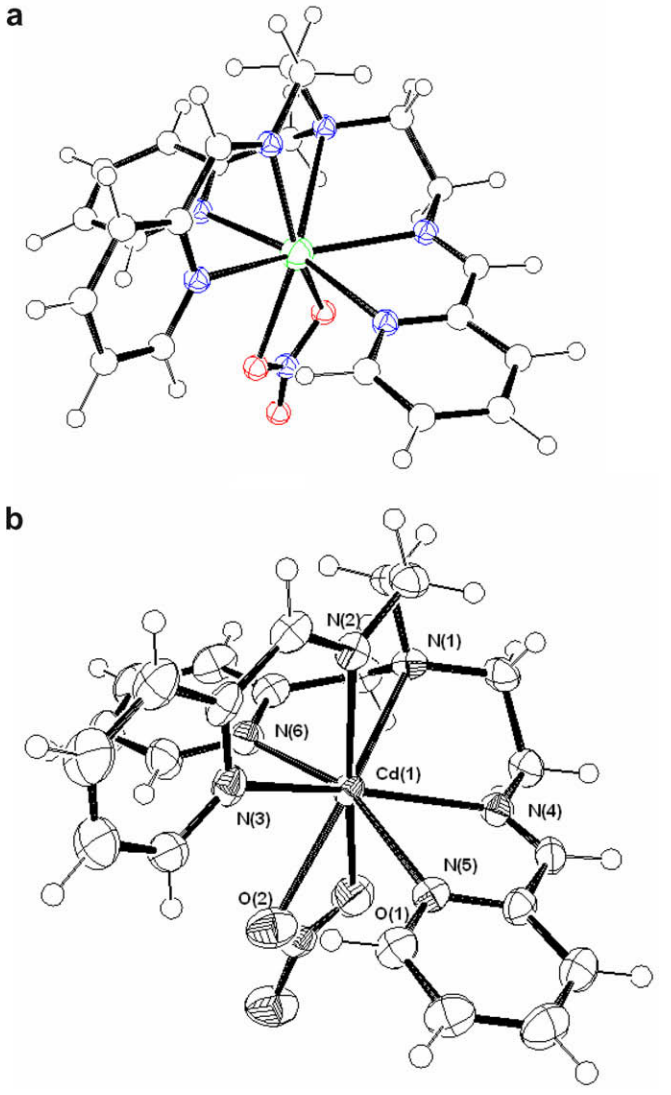

Fig. 1. DFT optimized (a) and crystal structure (b) of compound **1**. The perchlorate anion and solvated H_2O are omitted for clarity.

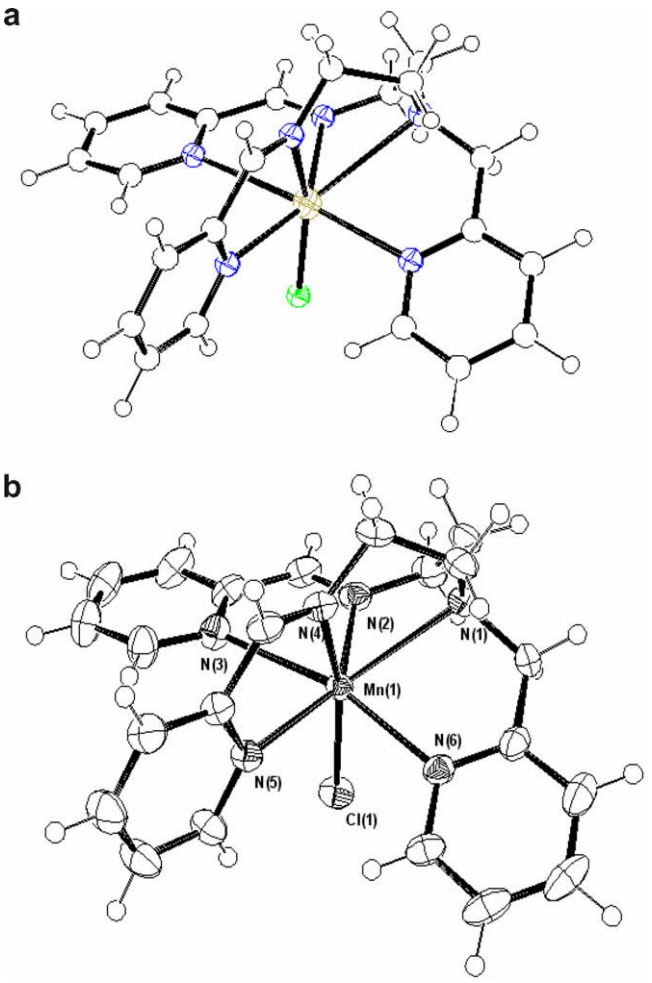

Fig. 2. RHF optimized (a) and crystal structure (b) of compound **2**. The perchlorate anion and solvated MeOH are omitted for clarity.

2.4.2. Synthesis of $[Mn(L_{22pyfp})Cl](ClO_4)\cdot MeOH$ (**2**)

Compound **2** was prepared in an analogous method to **1**. $L_{22py}\cdot 3HCl$ (0.1 g, 0.33 mmol) and NaOH (0.039 g, 0.99 mmol)

were mixed and heated under reflux for 30 min in EtOH (15 ml). The resulting solution was worked up as previously stated, however $MnCl_2{\cdot}6H_2O$ (0.65 g, 0.33 mmol) was added in place of $Cd(NO_3)_2 \cdot 4H_2O$. Yield of the complex $[Mn(L_{22pyfp})Cl](ClO_4) \cdot MeOH$ (**2**), (0.08 g, 40%). *Anal.* Calc. for ($C_{23}H_{28}Cl_2MnN_6O_5$): C, 46.47; H, 4.71; N, 14.13. Found: C, 46.15; H, 4.31; N, 13.86%. IR (KBr, cm^{-1}): 1660 (νC=N Schiff base), 1596 (νC=N pyridine), 1569 (νC=C), 1094.

3. Results and discussion

3.1. Synthesis and characterization

Both complexes **1** and **2** were readily synthesized by the templated condensation of the neutralized L_{22py} tripodal ligand [5] with 2-pyridinecarboxaldehyde in the presence of either Mn(II) or Cd(II) metal ions, respectively. These compounds are quite stable in air and can be stored in a desiccator for long periods of time without decomposition. The resulting compounds were characterized by, IR, elemental analysis and X-ray diffraction, and by ^1H NMR in the case of Cd(II). Condensation of all the primary amino group is confirmed by the lack of N–H stretching bands in the IR reign (3150–3450 cm^{-1}) and the presence of strong C=N (Schiff base) stretching bands at 1668 and 1660 cm^{-1} for **1** and **2**, respectively. The band observed at 1387 cm^{-1}, for complex **1**, can be assigned to the bidentate nitrate group. A broad intense band at ca. 1100 cm^{-1} due to ClO_4^- shows no splitting, indicating the absence of coordination of ClO_4^- for both complexes. The NMR studies of **1** are completely consistent with its formulation. The electronic spectra of both complexes in acetonitrile (10^{-4} M) show two intense bands in the UV region, at 200–300 nm as expected for imino-substituted pyridines [24].

3.2. X-ray crystal structure analysis

Suitable crystals of **1** and **2** were obtained by slow diffusion of diethyl ether vapor into a methanol-ethanol solution of the corresponding complexes. ORTEP diagrams of the molecular structures of **1** and **2** are shown in Figs. 1 and 2, respectively, with the atomic numbering. Selected bond lengths and bond angles are listed in Tables 2 and 3. The Cd–N and Mn–N bond lengths are within the normal range. The crystal structure of **1** consists of a cadmium metal center coordinated to six nitrogen and two oxygen donor atoms from the nitrate counter ion and the crystal structure of **2** consist of a manganese metal center coordinated to six nitrogen atoms and a chloride ion. Eight-coordinate systems are found to adopt a cube, a square antiprism or a triangulated dodecahedron (TD) arrangement [25]. On the basis of the observed angles, (N–Cd–N, N–Cd–O and O–Cd–O), complex **1** adopts a slightly distorted TD geometry [26] with N(2) as the lone capping atom, whereas O(1) and O(2) are the shared capping atoms (see Fig. 3). The two Cd–O distances [2.643(3) and 2.436(3) Å] in the cadmium complex differ substantially, one being short and the other long. The Cd–O distance for the bidentate nitrate group (*av*. 2.539 Å) is comparable with the calculated mean value [2.482(144) Å] observed in 28 eight-coordinate Cd(II) complexes obtained from the Cambridge Structural Database [27], navigated using CONQUEST [28], thus both oxygen atoms are coordinated to the central cadmium ion. The Cd–N distances are in the normal range [from 2.344(3) to 2.659(2) Å)]. The bond distance between the atom Cd(1) and the tertiary nitrogen atom N(1) of complex **1** is 2.659(2) Å, which is much longer that the nor-

Table 1
Crystal data and structure refinement for compounds **1** and **2**

Empirical formula	$C_{22}H_{26}CdClN_7O_s$	$C_{23}H_{2S}Cl_2MnN_6O_5$
Formula weight	664.35	594.35
Temperature (K)	150(2)	150(2)
Wavelength (A)	0.71073	0.71073
Crystal system	orthorhombic	monoclinic
Space group	*Pna*2(l)	*P*2(1)/*c*
Unit cell dimensions		
a (Å)	17.9766(8)	15.316(2)
b (Å)	19.8297(9)	7.6486(11)
c (Å)	7.6340(4)	22.991(4)
α (°)	90	90
β (°)	90	103.935(8)
γ (°)	90	90
$V(A^3)$	2721.3(2)	2614.0(7)
Z	4	4
D_{calc} (Mg/m^3)	1.622	1.510
Absorption coefficient (mm^{-1})	0.959	0.756
F(000)	1344	1228
Crystal size (mm)	0.28 × 0.16 × 0.09	0.18 × 0.08 × 0.06
θ Range for data collection (°)	1.53–29.32	1.37–27.50
Index ranges	$-24 \le h \le 24$, $-27 \le k \le 27$, $-10 \le l \le 10$	$-19 \le h \le 19$,$-9 \le k \le 9$, $-29 \le l \le 29$
Reflections collected	79535	37230
Independent reflections	7396	5945
R_{int}	0.0358	0.0403
Completeness to $\theta = 29.32°$ (%)	99.4	99.3
Absorption correction	semi-empirical from equivalents	semi-empirical from equivalents
Maximum and minimum transmission	0.9187 and 0.7750	0.9561 and 0.8760
Refinement method	full-matrix least-squares on F^2	full-matrix least-squares on F^2
Data/restraints/parameters	7396/4/351	5945/48/352
Goodness-of-fit on F^2	1.125	1.036
Final *R* indices	$R_1 = 0.0293$	$R_1 = 0.0479$
$[I > 2\sigma(I)]$	$wR_2 = 0.0784$	$wR_2 = 0.1208$
R indices (all data)	$R_1 = 0.0325$, $wR_2 = 0.0802$	$R_1 = 0.0668$, $wR_2 = 0.1339$
Absolute structure parameter	0.00(2)	
Largest difference in peak and hole (e $Å^{-3}$)	0.785 and −0.806	0.803 and −0.836

Table 2
Selected experimental and calculated bond lengths (Å) and bond angles (°) for complex **1**

	X-ray	LanL2MB		Computational level[a]			
				3-21G*		6-31G*	
				(LanL2DZ for Cd)		(LanL2DZ for Cd)	
Bond lengths							
Cd(1)–N(4)	2.344(3)	**2.377**	2.302	**2.241**	2.278	**2.441**	2.371
Cd(1)–N(2)	2.348(3)	**2.391**	2.346	**2.256**	2.300	**2.466**	2.358
Cd(1)–N(6)	2.371(2)	**2.461**	2.260	**2.306**	2.357	**2.493**	2.461
Cd(1)–O(2)	2.436(3)	**2.323**	2.257	**2.390**	2.377	**2.334**	2.315
Cd(1)–N(3)	2.498(3)	**2.478**	2.482	**2.663**	2.541	**2.561**	2.564
Cd(1)–N(5)	2.541(3)	**2.611**	2.617	**2.483**	2.625	**2.624**	2.649
Cd(1)–O(1)	2.643(3)	**2.388**	2.356	**2.454**	2.418	**2.413**	2.437
Cd(1)–N(1)	2.659(2)	**2.610**	2.620	**2.754**	2.646	**2.715**	2.694
Bond angles							
N(4)–Cd(1)–N(2)	101.84(9)	**97.89**	98.28	**113.81**	100.43	**98.37**	98.64
N(4)–Cd(1)–N(6)	123.47(9)	**131.00**	130.36	**117.87**	128.66	**125.90**	125.60
N(2)–Cd(1)–N(6)	92.92(9)	**87.54**	87.58	**98.48**	87.97	**87.21**	87.46
N(4)–Cd(1)–O(2)	108.81(10)	**109.48**	107.54	**136.53**	113.80	**115.50**	114.86
O(2)–Cd(1)–N(2)	145.67(10)	**144.56**	146.18	**101.38**	142.99	**143.23**	143.46
N(6)–Cd(1)–O(2)	83.02(9)	**91.01**	91.83	**79.09**	81.68	**84.29**	84.67
N(4)–Cd(1)–N(3)	146.45(9)	**142.76**	142.80	**139.19**	143.87	**143.06**	143.03
N(2)–Cd(1)–N(3)	68.35(9)	**67.89**	68.06	**56.02**	66.55	**66.14**	65.93
N(6)–Cd(1)–N(3)	89.69(9)	**84.18**	84.95	**102.93**	85.89	**88.14**	88.56
O(2)–Cd(1)–N(3)	77.52(10)	**76.73**	78.19	**48.98**	77.26	**77.87**	78.23
N(4)–Cd(1)–N(5)	67.50(9)	**66.29**	66.22	**69.41**	65.52	**65.39**	64.86
N(2)–Cd(1)–N(5)	100.24(8)	**90.71**	90.27	**99.55**	94.51	**95.77**	94.86
N(6)–Cd(1)–N(5)	160.82(9)	**162.69**	163.41	**155.12**	164.93	**167.87**	168.87
O(2)–Cd(1)–N(5)	78.24(9)	**80.49**	80.87	**80.65**	87.48	**86.32**	87.02
N(3)–Cd(1)–N(5)	82.37(8)	**79.22**	78.92	**73.71**	81.51	**82.37**	82.49
N(4)–Cd(1)–O(1)	73.80(9)	**75.54**	75.71	**85.23**	75.32	**75.48**	75.85
N(2)–Cd(1)–O(1)	159.85(9)	**152.96**	152.52	**157.08**	153.59	**156.14**	158.31
N(6)–Cd(1)–O(1)	74.38(9)	**78.13**	77.02	**82.29**	75.64	**78.53**	79.36
O(2)–Cd(1)–O(1)	49.78(9)	**59.49**	58.26	**56.08**	55.68	**54.66**	52.73
N(3)–Cd(1)–O(1)	125.86(9)	**131.93**	131.64	**101.33**	131.07	**131.46**	130.12
N(5)–Cd(1)–O(1)	96.19(9)	**109.61**	110.73	**74.45**	106.72	**102.17**	101.38
N(4)–Cd(1)–N(1)	67.87(9)	**68.67**	68.60	**70.14**	68.65	**66.95**	67.07
N(2)–Cd(1)–N(1)	69.06(8)	**69.21**	69.21	**77.32**	68.97	**67.29**	67.42
N(6)–Cd(1)–N(1)	67.54(9)	**68.14**	67.84	**67.29**	67.69	**66.15**	65.98
O(2)–Cd(1)–N(1)	137.24(8)	**141.52**	140.65	**145.57**	135.90	**138.04**	138.14
N(3)–Cd(1)–N(1)	129.96(9)	**129.26**	129.65	**130.98**	128.44	**127.23**	127.19
N(5)–Cd(1)–N(1)	130.34(8)	**126.98**	126.41	**133.76**	126.99	**125.81**	124.91
O(1)–Cd(1)–N(1)	91.39(9)	**84.12**	83.81	**123.05**	85.52	**89.34**	91.37

[a] The parameters obtained at the HF level are given as plain text, those for the B3LYP level are in bold.

mal bond distance. This phenomenon is probably attributed to the steric requirements of the tripodal ligand. The Cd–N_{imine} bond lengths are shorter than the Cd–$N_{pyridine}$ bond lengths due to the fact that the imine nitrogens are involved in two chelate rings. The X-ray crystallography of **2** reveals a seven-coordinate Mn atom best described as a distorted pentagonal bipyramid, with five nitrogen atoms lying in an approximately pentagonal ring (forming a distorted equatorial plane). The axial positions are occupied by one of the two imine nitrogen atoms and the chloride ion with an axial *trans* angle N(4)–Mn–Cl(1) = 164.47(7)°. The longest bond is found between Mn and N(3) [2.562(3) Å] and the shortest bond is between Mn and N(4) [2.242(2) Å]. All of the three equatorial five-membered chelate bond angles subtended by the ligand at the manganese atom are close to the ideal value of the pentagonal bipyramidal geometry (72°), [N(1)–Mn–N(2) = 69.75(9)°, N(2)–Mn–N(3) = 67.76(9) and N(1)–Mn–N(6) = 68.36(8)°]. The Mn–N_{imine} bond lengths, similar to those in **1**, are shorter than the Mn–$N_{pyridine}$ bond lengths.

3.3. NMR spectra

The NMR spectra of the cadmium complex confirm the formation of a fully condensed Schiff base complex. The ^{13}C NMR and DEPT 135° of this complex shows three distinct methylene carbons in the aliphatic region. It is interesting that the ^{1}H NMR spectrum (Fig. 4) of this complex shows two kinds of protons for the methylene group adjacent to the tertiary nitrogen atom. The COSY spectrum confirms the geminal coupling between the latter protons, indicating that the protons are diastereotopic in the rigid five-membered rings. We have reported similar observations for all methylene groups involved in the six-membered rings of seven-coordinate tripodal cadmium complexes [8,10]. It is clear from the COSY spectrum that both diastereotopic protons of C(1) (Scheme 1a) display coupling to protons of C(2) in addition to the above observations the ^{1}H NMR spectrum of the cadmium complex synthesized here, which shows that the signal corresponding to the imine proton displays two satellite peaks (^{3}J = 44.4 Hz) with intensities in the ratio 1:6:1 (Fig. 4) due to coupling with the neighboring $^{111/113}$Cd nucleus (^{111}Cd, 12.81; ^{113}Cd, 12.22%). The very similar magnetogyric ratio of ^{113}Cd and ^{111}Cd, −5.93303 and −5.6720 × 10^{-7} rad/Ts, respectively, lead to satellite overlap at the collection frequency. It should be noted that there are several reports of $^{111/113}$Cd–^{1}H heteronuclear coupling, [29–33] and we very recently published clear illustrations of such satellites very similar to that shown in Fig. 4 [5,10,11]. The coupling constant observed here is in the range expected for tripodal Schiff base cadmium complexes [5,10,11]. Obviously the observation of such coupling suggests that the Cd–N_{im} bond remains intact in

Table 3
Selected experimental and calculated bond lengths (Å) and bond angles (°) for complex **2**

	X-ray	LanL2MI		Computational level[a]		
				3-21G*		6-31G*
				(LanL2DZ for Mn)		(LanL2DZ for Mn)
Bond lengths						
Mn(1)–N(4)	2.242(2)	**2.213**	2.302	**2.241**	2.278	2.371
Mn(1)–N(2)	2.261(2)	**2.216**	2.346	**2.256**	2.300	2.358
Mn(1)–N(5)	2.332(2)	**2.295**	2.260	**2.306**	2.357	2.461
Mn(1)–N(6)	2.346(2)	**2.326**	2.281	**2.388**	2.439	2.454
Mn(1)–Cl(1)	2.489(8)	**2.480**	2.418	**2.401**	2.472	2.446
Mn(1)–N(1)	2.555(2)	**2.481**	2.609	**2.468**	2.538	2.827
Mn(1)–N(3)	2.562(3)	**2.481**	2.353	**2.689**	2.644	2.627
Bond angles						
N(4)–Mn(1)–N(2)	103.48(9)	**106.02**	103.42	**104.74**	105.07	100.42
N(4)–Mn(1)–N(5)	71.26(8)	**72.77**	73.12	**72.73**	70.90	68.35
N(2)–Mn(1)–N(5)	145.34(9)	**143.72**	149.56	**141.44**	144.52	148.32
N(4)–Mn(1)–N(6)	93.81(8)	**91.92**	93.51	**87.72**	86.84	89.89
N(2)–Mn(1)–N(6)	125.92(9)	**130.46**	124.83	**134.51**	130.96	118.72
N(5)–Mn(1)–N(6)	88.73(8)	**85.48**	85.58	**84.05**	84.48	91.52
N(4)–Mn(1)–Cl(1)	164.47(7)	**165.22**	167.68	**168.13**	166.20	160.58
N(2)–Mn(1)–Cl(1)	90.00(7)	**86.83**	87.15	**86.83**	88.39	96.85
N(5)–Mn(1)–Cl(1)	93.27(6)	**92.69**	94.50	**97.28**	96.44	92.25
N(6)–Mn(1)–Cl(1)	84.20(6)	**84.73**	85.49	**85.90**	86.47	89.56
N(4)–Mn(1)–N(1)	71.19(9)	**72.89**	70.86	**73.50**	72.08	66.46
N(2)–Mn(1)–N(1)	69.75(9)	**71.72**	68.12	**72.41**	70.74	65.57
N(5)–Mn(1)–N(1)	134.02(8)	**136.75**	133.81	**137.06**	134.71	127.97
N(6)–Mn(1)–N(1)	68.36(8)	**70.35**	68.97	**69.66**	68.29	64.30
Cl(1)–Mn(1)–N(1)	121.65(6)	**118.92**	119.87	**113.36**	116.26	129.88
N(4)–Mn(1)–N(3)	87.84(9)	**90.39**	86.10	**90.48**	91.43	90.76
N(2)–Mn(1)–N(3)	67.76(9)	**68.32**	70.28	**66.42**	66.50	66.47
N(5)–Mn(1)–N(3)	77.72(8)	**75.39**	79.29	**75.04**	78.24	83.67
N(6)–Mn(1)–N(3)	165.05(8)	**159.10**	164.30	**158.51**	162.21	174.52
Cl(1)–Mn(1)–N(3)	90.22(6)	**87.78**	91.52	**91.79**	91.26	88.01
N(1)–Mn(1)–N(3)	125.93(8)	**129.92**	125.18	**130.06**	127.81	120.85

[a] The parameters obtained at the HF level are given as plain text, those for the B3LYP level are in bold.

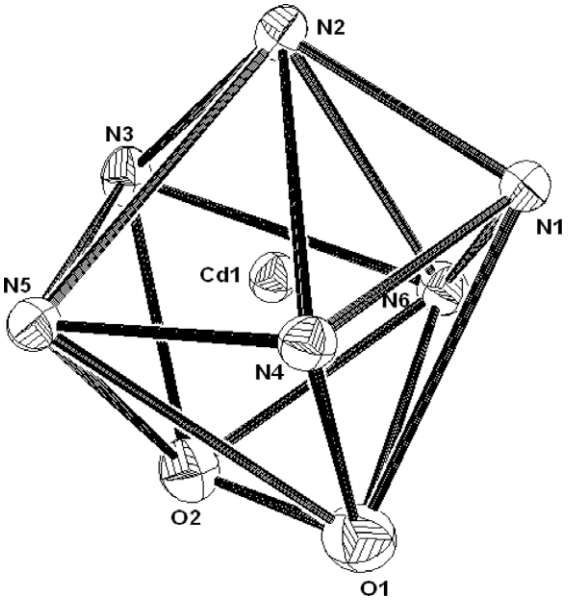

Fig. 3. View of the dodecahedron coordination polyhedron for **1**.

solution. It should be noted that the value of the $^{111/113}$Cd–^{1}H heteronuclear coupling in coordinated Schiff base compounds can be considerably dependent on the value of the torsion angle of the H–C=N–Cd bond. The mean value for the latter torsion angle in compound **1** is 173.76° and is very close to calculated values (172–178°) for seven-coordinate tripodal Schiff base cadmium complexes [5,10,11]. Thus this is a clear reason for the fact that the coupling constant observed here is in the range expected for the latter tripodal Schiff base cadmium complexes.

3.4. Ab initio and DFT studies

The geometry of both complexes was fully optimized at both the Hartree–Fock (HF) and density functional B3LYP levels of theory. As can be seen, the degree of agreement between the theoretical and experimental data depends on both the method and the basis sets. The results show that the gas-phase structures of both complexes are similar to their solid state structures. It should be note that we could not optimize the Mn complex at the DFT level of theory using the 6-31G* basis set in a reasonable time. We also carried out a LanL2MB basis set for the calculation of the highest occupied molecular orbital (HOMO) and the lowest-unoccupied molecular orbital (LUMO) and the energy gap of complexes **1** and **2**. The calculated energies for the HOMO and LUMO of these compounds are given in Table 4. The HOMO and LUMO for compounds **1** and **2** are illustrated in Fig. 5. As can be seen, in the Cd(II) complex the HOMO is a bonding π orbital that is essentially distributed on the metal atom and the coordinated nitrate ion and the LUMO is an anti-bonding π orbital that is distributed on one of the pyridine Schiff base rings. In the Mn (II) complex the HOMO is a bonding σ orbital that is essentially distributed on the metal and chloride ions and the LUMO is an anti-bonding π orbital that, similar to the Cd(II) complex, is distributed on one of the pyridine Schiff base rings. The results of the TD-DFT calculations at the B3LYP/lanl2mb level of theory for compounds **1** and **2** and the corresponding free Schiff

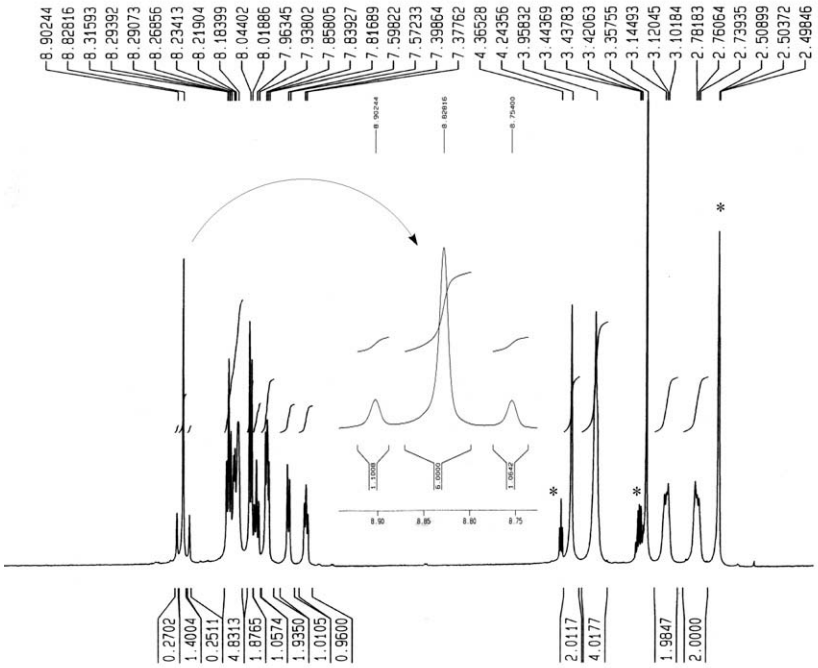

Fig. 4. The ^{1}H NMR spectrum of the complex $[Cd(L_{22pyfp})NO_3](ClO_4)$ and the observed satellites for the CH=N hydrogen resonances. The signals marked with an asterisk are related to MeOH and solvent impurities.

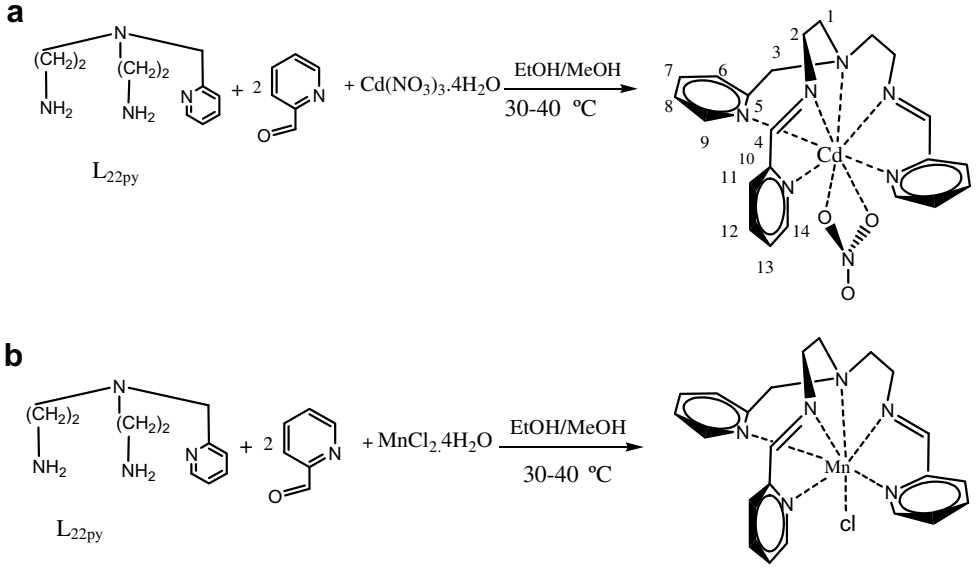

Scheme 1. The syntheses of the cadmium (**a**) and manganese (**b**) complexes and the NMR numbering of the Cd(II) complex (**a**).

Table 4
Frontier molecular orbital of compounds **1** and **2** (Hartree) and the energy EAN (eV) obtained from DFT calculations

	Energy	
	1	**2**
HOMO	−0.11714	−0.12819
LUMO	−0.18843	−0.24610
Gap (eV)	1.9399	3.2085

base tripodal ligand (optimized at the same level of theory) are given in Table 5. It is clear that the results of the latter calculations for complexes **1** and **2** agree with the relative size of the HOMO-LUMO energy gap in these complexes. On the other hand, the result does not agree with the observed spectra for the latter complexes. Note that both complexes do not have any spin-allowed electronic transitions. Thus the experimental spectra must be related to intra-ligand (LL) transitions. Fortunately there is a good agreement between the results of the TD-DFT calculations on the ligand itself with the experimental data.

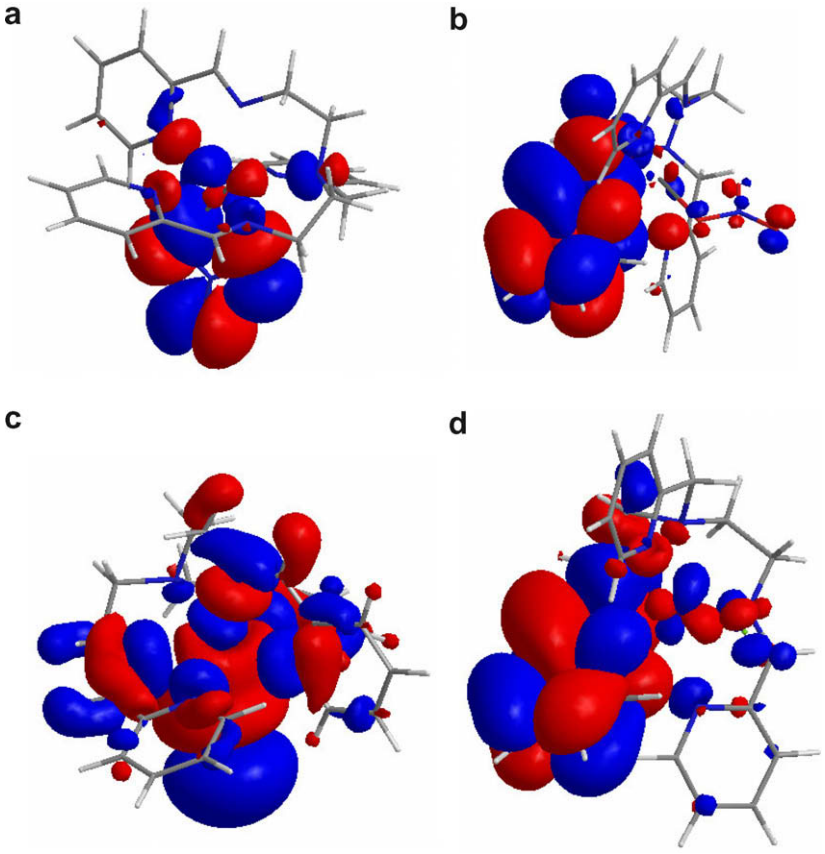

Fig. 5. Calculated HOMO (a, c) and LUMO (b, d) for compounds **1** (up) and **2** (down).

Table 5
Calculated excitation energy for compounds **1** and **2** and the free tripodal Schiff base ligand (L_{22pyfp})

1		**2**		L_{22pyfp}	
λ (nm)	E (eV)	λ (nm)	E (eV)	λ (nm)	E (eV)
888.08	1.3961	525.72	2.3584	322.59	3.8433
750.78	1.6514	493.20	2.5139	319.23	3.8838
686.84	1.8051	479.16	2.5876	293.21	4.2284

Appendix A. Supplementary data

CCDC 689988 and 689989 contain the supplementary crystallographic data for **1** and **2**. These data can be obtained free of charge via http://www.ccdc.cam.ac.uk/conts/retrieving.html, or from the Cambridge Crystallographic Data Centre, 12 Union Road, Cambridge CB2 1EZ, UK; fax: (+44) 1223-336-033; or e-mail: deposit@ccdc.cam.ac.uk.

References

[1] A.D. Granvoskii, A.L. Nivorozhkin, V.I. Minkin, Coord. Chem. Rev. 126 (1993) 1.
[2] V. Alexander, Chem. Rev. 95 (1995) 273.
[3] M.A.V. Ribeiro Da Silva, M.D.M.C. Ribeiro Da Silva, M.J.S. Monte, J.M. Goncalves, E.M.R. Fernandes, J. Chem. Soc., Dalton Trans. (1997) 1257.
[4] R. Atkins, G. Brewer, E. Kokot, G.M. Mockler, E. Sinn, Inorg. Chem. 24 (1985) 127.
[5] S. Salehzadeh, R. Golbedaghi, J. Chem. Res. (S) (2007) 94.
[6] H. Keypour, S. Salehzadeh, R.G. Pitchard, R.V. Parish, Inorg. Chem. 39 (2000) 5787.
[7] H. Keypour, S. Salehzadeh, Transition Met. Chem. 25 (2000) 204.
[8] H. Keypour, S. Salehzadeh, R.G. Pitchard, R.V. Parish, Polyhedron 19 (2000) 633.
[9] S. Salehzadeh, S.M. Nouri, H. Keypour, M. Bagherzadeh, Polyhedron 24 (2005) 478.
[10] S. Salehzadeh, S.A. Javarsineh, H. Keypour, J. Mol. Struct. 785 (2006) 54.
[11] S. Salehzadeh, H. Keypour, Asian J. Chem. 18 (2006) 1387.
[12] H. Keypour, M. Dehdari, S. Salehzadeh, K.P. Wainwright, Transition Met. Chem. 28 (2003) 425.
[13] S. Salehzadeh, M. Bayat, Chem. Phys. Lett. 427 (2006) 455.
[14] S. Salehzadeh, M. Bayat, M. Hashemi, J. Phys. Chem. A 111 (2007) 8188.
[15] SMART, SAINT, and SADABS Packages, Version 5.1, Bruker AXS, Madison, W I, 1997–1999.
[16] G.M. Sheldrick, SHELXS-97, Program for Automatic Solution of Crystal Structures, University of Göttingen, Germany, 1997.
[17] G.M. Sheldrick, SHELX-97, Program for Crystal Structure Refinement, University of Göttingen, Germany, 1997.
[18] A.D. Becke, J. Chem. Phys. 98 (1993) 5648.
[19] M.J. Frisch, G.W. Trucks, H.B. Schlegel, G.E. Scuseria, M.A. Robb, J.R. Cheeseman, V.G. Zakrazewski, J.A. Montgomery, Jr. R.E. Startmann, J.C. Burant, S. Dapprich, J.M. Millam, A.D. Daniels, K.N. Kudin, M.C. Strain, O. Farkas, J. Tomasi, V. Barone, M. Cossi, R. Cammi, B. Mennucci, C. Adamo, S. Clifford, J. Ochterski, G.A. Petersson, P.Y. Ayala, Q. Cui, K. Morokuma, D.K. Malik, A.D. Rabuck, K. Raghavachar, J.B. Foresman, J. Cioslowski, J.V. Ortiz, B.B. Stefanov, G. Liu, A. Liashenko, P. Piskorz, I. Komaromi, R. Gomperts, R.L. Martin, D.J. Fox, T. Keith, M.A. Al-Laham, C.Y. Peng, A. Nanyakkara, C. Gonzalez, M. Challacombe, P.M.W. Gill, B. Johnson, W. Chen, M.W. Wong, J.L. Andres, M. Head-Gordon, E.S. Replogle, J.A. Pople, GAUSSIAN 98, Revision A.6, Gaussian Inc. Pittsburg, PA, USA.
[20] P.J. Hay, W.R. Wadt, J. Chem. Phys. 82 (1985) 270.
[21] K.D. Dobbs, W.J. Hehre, J. Comput. Chem. 8 (1987) 880.
[22] P.C. Hariharan, J.A. Pople, Theor. Chim. Acta 28 (1973) 213.
[23] P.J. Hay, W.R. Wadts, J. Chem. Phys. 82 (1985) 299.
[24] H. Keypour, S. Salehzadeh, R.G. Pritchard, R.V. Parish, Transition Met. Chem. 23 (1998) 605.
[25] J.R. Gispert, Quimica de coordination, Omega, Barcelona, 2000.
[26] F.J.B. García, F.L. Giles, M.A.M. Rogado, E.V. Zahínos, Polyhedron 25 (2006) 43.
[27] I.J. Bruno, J.C. Cole, P.R. Edington, M. Kessler, C.F. Macrae, P. Mccabe, J. Pearson, R. Taylor, Acta Crystallogr., Sect. B 58 (2002) 389.
[28] F.H. Allen, Acta Crystallogr., Sect. B 58 (2002) 380.
[29] (a) J.S. Casas, M.V. Castano, M.S. Garcia-Tasende, I. Martinez-Santamarta, J. Sordo, E.E. Castellano, J. Zuckerman-Schpector, J. Chem. Res. (S) (1992) 324;

(b) J.S. Casas, M.V. Castano, M.S. Garcia- Tasende, I. Martinez-Santamarta, J. Sordo, E.E. Castellano, J. Zuckerman-Schpector, J. Chem. Res. (M) (1992) 2626.
[30] O. Zerbe, D.L. Pountney, W.V. Philipsborn, M. Vasak, J. Am. Chem. Soc. 116 (1994) 77.
[31] D.C. Bebout, S.W. Stokes, R.J. Butcher, Inorg. Chem. 38 (1999) 26.
[32] L. Valencia, H. Adams, R. Bastida, D.E. Fenton, A. Macias, Inorg. Chem. Acta 317 (2001) 45.
[33] X. Liang, J.A. Parkinson, S. Parsons, M. Weishaupl, P.J. Sadler, Inorg. Chem. 41 (2002) 4539.

We intended to employ the ethynyl group in the construction of supramolecular compounds such as **A**,[1] which are built by the ethynyl group cooperating with the extended hypervalent bonds of Z_4 4c–6e (Z = S [25j,26] and Se [25b,e,26]). As a first step to study such compounds, the factors that control the structures of 1-(arylethynylselanyl)naphthalenes [**1**: 1-(*p*-$YC_6H_4C{\equiv}CSe)C_{10}H_7$, 1-(ArC-CSe)Nap] have been investigated very recently, together with the structures [27]. One factor is called the ethynyl effect. The ethynyl group operates to determine the fine structures of **1**, which are completely different from those in 1-(arylselanyl)naphthalenes [**I**: 1-(*p*-$YC_6H_4Se)C_{10}H_7$] [28b]. The effect of G substituted at the 8-position of **1** also operates to control the fine structures. 8-G-1-(*p*-$YC_6H_4C{\equiv}CSe)C_{10}H_6$ [**2** (G = Cl) and **3** (G = Br): Y = H (**a**), OMe (**b**), Me (**c**), F (**d**), Cl (**e**), CN (**f**) and NO_2 (**g**)] have been prepared and the NMR spectra were measured, in addition to **1** (G = H). The fine structures were determined by X-ray crystallographic analysis exemplified by **2b**, **2e** and **2g**, to clarify the factor which controls the fine structures. The factor is called the G-dependence in **2**.

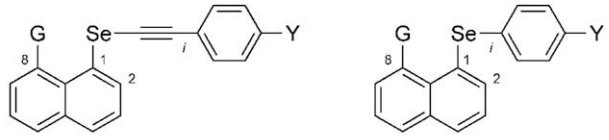

1 (G = H), **2** (G = Cl), **3** (G = Br) **I** (G = H)

	a	b	c	d	e	f	g
Y =	H	OMe	Me	F	Cl	CN	NO_2

The structures of the naphthalene system are well explained by three types, defined as **A**, **B** and **C**, where the Se–C_{sp} bond is perpendicular to the naphthyl plane in **A**, it is placed on the plane in **B** and **C** is intermediate between **A** and **B** [25c,d,f–i,28b]. The **A**, **B** and **C** notations are employed to specify the structures around the Se–C_{Nap} bonds in **1**–**3**. The planar (**pl**), perpendicular (**pd**) and non-planar and non-perpendicular (**np**) notations are also used to specify the structures around the linear Se–C_{sp}–C_{sp}–C_{Ar} alignment in **1**–**3**. Scheme 1 illustrates plausible structures of **1**–**3**. Combined notations such as (**A**: **pl**) and (**B**: **pd**) are employed for the structures.

We often worry about the structures of compounds in solution when investigations are carried out in solution and the compounds have plural dominant conformers. NMR spectroscopy plays an important role in determining the structures in solutions through the careful examination of the chemical shift values. The structures of **2** and **3** in solution are examined based on the NMR data, employing standard values of ^{1}H and ^{77}Se NMR parameters which are useful to determine structures in solutions, as proposed recently.

Here, we report the fine structure of **2**, determined by X-ray crystallographic analysis, together with the factors that controls the fine structure. Quantum chemical (QC) calculations are employed to understand the origin of the factors, which reveals that the G-dependence arises from the non-bonded $n_p(G)\cdots\sigma^*(Se–C_{sp})$ 3c–4e interaction or the $G\cdots Se–C_{sp}–C_{sp}–C_{sp2}$ 5c–6e type interaction. The behaviors of **2** and **3**, together with **1**, in solution are also examined to estimate the efficiency of the factors based on NMR parameters.

[1] **A** with *n* = 0 and 1 were prepared and the structure of **A** (*n* = 0) was determined by X-ray analysis. The results will be reported elsewhere.

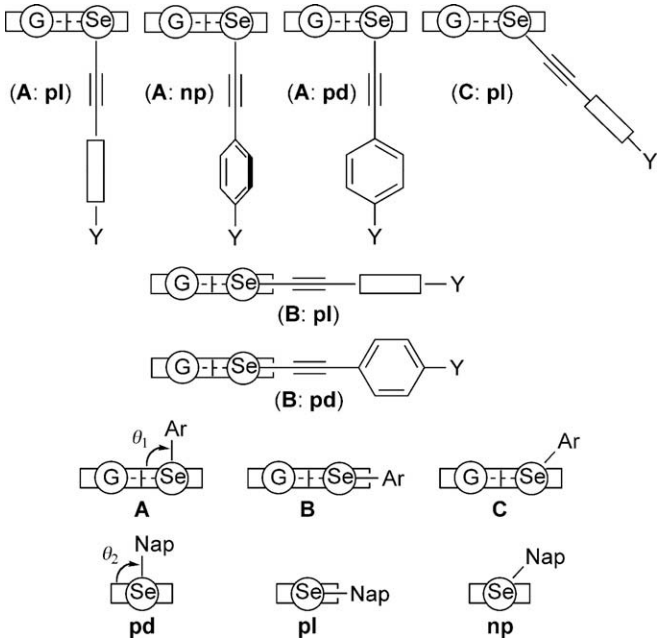

Scheme 1. Plausible structures of **1**–**3** together with the **A**, **B** and **C** notations.

2. Experimental

2.1. General experimental considerations

Manipulations were performed under an argon atmosphere with standard vacuum-line techniques. Glassware was dried at 130 °C overnight. Solvents and reagents were purified by standard procedures as necessary. Melting points were determined on a Yanaco MP-S3 melting point apparatus and are uncorrected. NMR spectra were recorded at room temperature on a JEOL AL-300 spectrometer (^{1}H, 300 MHz; ^{13}C, 75 MHz; ^{77}Se, 57 MHz) and on a JEOL Lambda-400 spectrometer (^{1}H, 400 MHz; ^{13}C, 100 MHz; ^{77}Se, 76 MHz). The ^{1}H, ^{13}C and ^{77}Se NMR spectra were recorded in $CDCl_3$ solution. Chemical shifts are given in ppm relative to Me_4Si for the ^{1}H and ^{13}C NMR spectra, and relative to the reference compound Me_2Se for the ^{77}Se NMR spectra. Column chromatography was performed using silica gel (Fujishilysia PSQ-100B) and basic alumina (E. Merck).

2.2. Preparation of the 8-G-1-(arylethynylselanyl)naphthalenes

2.2.1. 8-Chloro-1-(phenylethynylselanyl)naphthalene (*2a*)

Under an argon atmosphere, ethynylbenzene (0.13 g, 1.25 mmol) was dissolved in anhydrous THF (10 mL), and LDA (diisopropylamine (0.13 g, 1.31 mmol) and *n*-BuLi (0.8 mL, 1.31 mmol, 1.62 M)) were added to the solution at 0 °C. After the mixture was stirred for 1 h at 0 °C, 8-chloro-1-naphthylselanyl bromide in anhydrous THF (10 mL) was added to the above solution at 0 °C. The reaction mixture was stirred for 2 h at 0 °C, and allowed to warm up to room temperature. Then, acetone (5 mL) was added, evaporated and the mixture dried in vacuo. The crude product was purified by column chromatography (flash column, SiO_2, acidic alumina, hexane). **2a** was isolated in 65% yield as colorless prisms, m.p. 59.5–60.5 °C; $C_{18}H_{11}ClSe$ requires C, 63.27; H, 3.24. Found: C, 63.18; H, 3.12%; δ_H (300 MHz; $CDCl_3$; Me_4Si) 7.30–7.40 (m, 4H), 7.43 (t, *J* 7.9 Hz, 1H), 7.52–7.63 (m, 3H), 7.73 (dd, *J* 0.8, 8.3 Hz, 1H), 7.76 (dd, *J* 1.2, 8.4 Hz, 1H), 8.38 (dd, *J* 1.1, 7.6 Hz, 1H); δ_C (75 MHz; $CDCl_3$; Me_4Si) 73.1, 105.3, 123.2, 125.9, 127.0, 127.6, 127.9, 128.4, 128.6, 128.7, 128.7, 129.5, 129.5, 130.6, 131.9, 137.0; δ_{Se} (57 MHz; $CDCl_3$; Me_2Se) 327.9.

*2.2.2. 8-Chloro-1-(p-anisylethynylselanyl)naphthalene (**2b**)*

A similar method to that described for the preparation of **2a** was used. Compound **2b** was isolated in 82% yield as colorless prisms, m.p. 157.5–158.5 °C; $C_{19}H_{13}ClOSe$ requires C, 61.39; H, 3.53. Found: C, 61.35; H, 3.54%; δ_H (300 MHz; $CDCl_3$; Me_4Si) 3.84 (s, 3H), 6.89 (d, *J* 9.0 Hz, 2H), 7.35 (t, *J* 7.9 Hz, 1H), 7.41 (t, *J* 7.9 Hz, 1H), 7.52 (d, *J* 9.0 Hz, 2H), 7.54 (dd, *J* 1.3, 7.4 Hz, 1H), 7.71 (dd, *J* 0.9, 8.2 Hz, 1H), 7.76 (dd, *J* 1.1, 8.2 Hz, 1H), 8.37 (dd, *J* 1.2, 7.7 Hz, 1H); δ_C (75 MHz; $CDCl_3$; Me_4Si) 55.4, 71.2, 105.4, 114.0, 115.3, 125.9, 127.0, 127.8, 128.0, 128.6, 128.7, 129.4, 129.8, 130.7, 133.8, 137.0, 160.1; δ_{Se}(57 MHz; $CDCl_3$; Me_2Se) 327.1.

*2.2.3. 8-Chloro-1-(p-tolylethynylselanyl)naphthalene (**2c**)*

A similar method to that described for the preparation of **2a** was used. Compound **2c** was isolated in 70% yield as light yellow prisms, m.p. 103.5–104.5 °C; $C_{19}H_{13}ClSe$ requires C, 64.15; H, 3.68. Found: C, 63.89; H, 3.64%; δ_H (400 MHz; $CDCl_3$; Me_4Si) 2.38 (s, 3H), 7.18 (d, *J* 8.2 Hz, 2H), 7.35 (t, *J* 7.8 Hz, 1H), 7.42 (t, *J* 7.8 Hz, 1H), 7.47 (d, *J* 7.8 Hz, 2H), 7.54 (dd, *J* 0.9 and 7.8 Hz, 1H), 7.72 (dd, *J* 0.9 and 7.8 Hz, 1H), 7.76 (dd, *J* 0.9 and 8.2 Hz, 1H), 8.37 (dd, *J* 0.9 and 7.8 Hz, 1H); δ_C (100 MHz; $CDCl_3$; Me_4Si) 21.6, 72.1, 105.5, 120.1, 125.9, 127.0, 127.8, 127.9, 128.6, 128.7, 129.2, 129.4, 129.8, 130.7, 131.9, 137.0, 139.1; δ_{Se} (76 MHz; $CDCl_3$; Me_2Se) 329.2.

*2.2.4. 8-Chloro-1-(p-fluorophenylethynylselanyl)naphthalene (**2d**)*

A similar method to that described for the preparation of **2a** was used. Compound **2d** was isolated in 64% yield as colorless prisms, m.p. 116.5–117.5 °C; $C_{18}H_{10}ClFSe$ requires C, 60.11; H, 2.80. Found: C, 59.88; H, 3.01%; δ_H (300 MHz; $CDCl_3$; Me_4Si) 7.06 (t, *J* 8.7 Hz, 2H), 7.36 (t, *J* 7.9 Hz, 1H), 7.42 (t, *J* 7.9 Hz, 1H), 7.51–7.59 (m, 3H), 7.73 (dd, *J* 1.1, 8.5 Hz, 1H), 7.77 (dd, *J* 1.2, 8.2 Hz, 1H), 8.34 (dd, *J* 1.1, 7.6 Hz, 1H); δ_C (75 MHz; $CDCl_3$; Me_4Si) 68.9 ($^5J_{C,F}$ 1.9 Hz), 101.6, 115.7 ($^2J_{C,F}$ 22.4 Hz), 119.3 ($^4J_{C,F}$ 3.7 Hz), 125.5, 126.3, 126.5, 126.9, 127.2, 128.4, 128.8, 129.1, 132.2, 133.8 ($^3J_{C,F}$ 8.7 Hz), 134.1, 162.7 ($^1J_{C,F}$ 250.0 Hz); δ_{Se} (57 MHz; $CDCl_3$; Me_2Se) 327.7.

*2.2.5. 8-Chloro-1-(p-chlorophenylethynylselanyl)naphthalene (**2e**)*

Under an argon atmosphere, *p*-chloroethynylbenzene (0.17 g, 1.25 mmol) was dissolved in anhydrous THF (10 mL), and LDA (diisopropylamine (0.13 g, 1.31 mmol) and *n*-BuLi (0.8 mL, 1.31 mmol, 1.62 M)) were added to the solution at −78 °C. After the mixture was stirred for 1 h at 0 °C, 8-chloro-1-naphthylselanylbromide in anhydrous THF (10 mL) was added to the above solution at −78 °C. The reaction mixture was stirred for 2 h at −78 °C, and allowed to warm up to 0 °C. Then, acetone (5 mL) was added, evaporated, and the mixture dried in vacuo. The crude product was purified by column chromatography (flash column, SiO_2, acidic alumina, hexane). Compound **2e** was isolated in 40% yield as colorless prisms, m.p. 142.5–143.5 °C; $C_{18}H_{10}Cl_2Se$ requires C, 57.48; H, 2.68. Found: C, 57.46; H, 2.84%; δ_H (300 MHz; $CDCl_3$; Me_4Si) 7.34 (d, *J* 7.3 Hz, 2H), 7.36 (t, *J* 7.8 Hz, 1H), 7.43 (t, *J* 7.9 Hz, 1H), 7.49 (d, *J* 8.7 Hz, 2H), 7.55 (dd, *J* 1.0, 7.5 Hz, 1H), 7.73 (dd, *J* 1.0, 8.2 Hz, 1H), 7.77 (dd, *J* 1.0, 8.2 Hz, 1H), 8.33 (dd, *J* 1.1, 7.7 Hz, 1H); δ_C (75 MHz; $CDCl_3$; Me_4Si) 74.5, 104.1, 121.7, 126.0, 126.9, 127.3, 128.0, 128.7, 128.7, 128.8, 129.4, 129.7, 130.6, 133.1, 134.8, 137.0; δ_{Se} (57 MHz; $CDCl_3$; Me_2Se) 329.0.

*2.2.6. 8-Chloro-1-(p-cyanophenylethynylselanyl)naphthalene (**2f**) [33]*

α-(*p*-Cyanophenylcarbonyl)-α-(8-chloronaphthylselanyl)phosphorane (**4**) (0.40 g, 0.62 mmol) was heated under vacuum (0.1 mmHg) at 230 °C for 5 min. The crude product was purified by column chromatography (flash column, SiO_2, hexane:benzene = 9:1). Compound **2f** was isolated in 27% yield as colorless prisms, m.p. 164.5–165.0 °C; $C_{19}H_{10}ClNSe$ requires C, 62.23; H, 2.75; N, 3.82. Found: C, 62.01; H, 2.74; N, 3.98%; δ_H (300 MHz; $CDCl_3$; Me_4Si) 7.38 (t, *J* 7.8 Hz, 1H), 7.45 (t, *J* 7.9 Hz, 1H), 7.57 (dd, *J* 1.3, 7.4 Hz, 1H), 7.59–7.67 (m, 4H), 7.76 (dd, *J* 0.9, 6.4 Hz, 1H), 7.79 (dd, *J* 1.1, 6.4 Hz, 1H), 8.30 (dd, *J* 1.1, 7.7 Hz, 1H); δ_C (75 MHz; $CDCl_3$; Me_4Si) 79.4, 103.7, 111.6, 118.5, 126.1, 126.7, 126.9, 127.9, 128.3, 128.8, 129.5, 129.7, 130.5, 131.9, 131.9, 132.1, 137.0; δ_{Se} (57 MHz; $CDCl_3$; Me_2Se) 332.7.

*2.2.7. α-(p-Cyanophenylcarbonyl)-α-(8-chloronaphthylselanyl)phosphorane (**4**) [33]*

Under an argon atmosphere, (*p*-cyanophenylcarbonylmethylidene)triphenylphosphorane [34] (1.20 g, 2.96 mmol) was dissolved in benzene (26 mL), and added to a benzene solution (6 mL) of 1-naphthylselanylbromide at the room temperature, and stirred for 2 h at room temperature. A white suspension was formed, and the solid was filtered out from the reaction mixture. The filtrate was evaporated and dried in vacuo. The crude product was purified by column chromatography (flash column, SiO_2, CH_2Cl_2). Compound **4** was isolated in 21% yield as yellow prisms, m.p. 228.0–229.5 °C; $C_{37}H_{25}ClNOPSe$ requires C, 68.90; H, 3.91; N, 2.17. Found: C, 68.58; H, 3.94; N, 2.19%; δ_H (300 MHz; $CDCl_3$; Me_4Si) 7.19–7.39 (m, 9H), 7.39–7.48 (m, 3H), 7.48–7.68 (m, 10H), 7.80 (d, *J* 8.4 Hz, 2H), 8.31 (dd, *J* 1.1, 7.5 Hz, 1H); δ_C (75 MHz; $CDCl_3$; Me_4Si) 57.2 ($^1J_{C,P}$ 88.2 Hz), 112.1, 119.1, 125.5, 126.0 ($^1J_{C,P}$ 101.6 Hz), 125.9, 126.5 ($^3J_{C,P}$ 10.5 Hz), 127.6, 128.1 ($^4J_{C,P}$ 1.9 Hz), 128.3, 128.4 ($^3J_{C,P}$ 12.5 Hz), 130.4, 131.3, 131.7, 132.0, 132.0 ($^4J_{C,P}$ 1.9 Hz), 133.6 ($^2J_{C,P}$ 9.6 Hz), 136.6, 137.4 ($^4J_{C,P}$ 1.9 Hz), 146.3 ($^3J_{C,P}$ 12.5 Hz), 190.5 ($^2J_{C,P}$ 10.5 Hz); δ_{Se} (57 MHz; $CDCl_3$; Me_2Se) 406.8 ($J_{Se,P}$ 6.0 Hz).

*2.2.8. 8-Chloro-1-(p-nitorophenylethynylselanyl)naphthalene (**2g**) [33]*

α-(*p*-Nitrophenylcarbonyl)-α-(8-chloronaphthylselanyl)phosphorane (**5**) (0.30 g, 0.79 mmol) was heated under vacuum (0.1 mmHg) at 250 °C for 5 min. The crude product was purified by column chromatography (flash column, SiO_2, hexane:benzene = 4:1). Compound **2g** was isolated in 7% yield as yellow prisms, m.p. 173.0–174.0 °C; $C_{18}H_{10}ClNO_2Se$ requires C, 55.91; H, 2.61; N, 3.62. Found: C, 55.59; H, 2.62; N, 3.69%; δ_H (300 MHz; $CDCl_3$; Me_4Si) 7.39 (t, *J* 7.8 Hz, 1H), 7.46 (t, *J* 7.8 Hz, 1H), 7.57 (dd, *J* 1.2, 7.5 Hz, 1H), 7.66 (d, *J* 9.0 Hz, 2H), 7.77 (dd, *J* 1.0, 8.2 Hz, 1H), 7.79 (dd, *J* 1.0, 8.2 Hz, 1H), 8.23 (d, *J* 9.0 Hz, 2H), 8.31 (dd, *J* 1.1, 7.7 Hz, 1H); δ_C (75 MHz; $CDCl_3$; Me_4Si) 80.7, 103.6, 123.7, 126.1, 126.6, 126.9, 128.4, 128.8, 128.8, 129.6, 129.7, 129.9, 130.4, 132.0, 137.0, 147.0; δ_{Se} (57 MHz; $CDCl_3$; Me_2Se) 334.2.

*2.2.9. α-(p-Nitrophenylcarbonyl)-α-(8-chloronaphthylselanyl)-phosphorane (**5**) [33]*

A similar method to that described for the preparation of **4** was used. Compound **5** was isolated in 33% yield as yellow prisms, m.p. 138.0–139.0 °C; $C_{36}H_{25}ClNO_3PSe \cdot 2H_2O$ requires C, 61.68; H, 4.17; N, 2.00. Found: C, 61.49; H, 3.90; N, 2.01%; δ_H (300 MHz; $CDCl_3$; Me_4Si) 7.21–7.29 (m, 5H), 7.30–7.39 (m, 6H), 7.42–7.49 (m, 2H), 7.53–7.68 (m, 7H), 7.82 (d, *J* 8.9 Hz, 2H), 8.07 (d, *J* 9.0 Hz, 2 H), 8.31 (dd, *J* 1.1, 7.5 Hz, 1H); δ_C (75 MHz; $CDCl_3$; Me_4Si) 57.7 ($^1J_{C,P}$ 88.3 Hz), 122.7, 125.2, 125.5, 125.9, 126.4, 126.6, 127.6, 128.1 ($^4J_{C,P}$ 1.3 Hz), 128.4 ($^3J_{C,P}$ 12.5 Hz), 128.5 ($^3J_{C,P}$ 11.8 Hz), 129.4 ($^1J_{C,P}$ 100.9 Hz), 131.6, 132.1 ($^4J_{C,P}$ 3.1 Hz), 133.7 ($^2J_{C,P}$ 9.3 Hz), 136.6, 137.2 ($^4J_{C,P}$ 2.5 Hz), 147.8, 148.3 ($^3J_{C,P}$ = 11.8 Hz), 190.4 ($^2J_{C,P}$ 11.2 Hz); δ_{Se} (57 MHz; $CDCl_3$; Me_2Se) 406.4 ($J_{Se,P}$ 6.0 Hz).

*2.2.10. 8-Bromo-1-(phenylethynylselanyl)naphthalene (**3a**)*

A similar method to that described for the preparation of **2a** was used. Compound **3a** was isolated in 65% yield as colorless prisms,

m.p. 90.5–91.5 °C; $C_{18}H_{11}BrSe$ requires C, 55.99; H, 2.87. Found: C, 55.93; H, 2.86%; δ_H (300 MHz; $CDCl_3$; Me_4Si) 7.28 (t, *J* 7.8 Hz, 1H), 7.33–7.38 (m, 3H), 7.41 (t, *J* 7.8 Hz, 1H), 7.53–7.59 (m, 2H), 7.74 (dd, *J* 1.1, 8.1 Hz, 1H), 7.77–7.84 (m, 2H), 8.44 (dd, *J* 1.1, 7.7 Hz, 1H); δ_C (75 MHz; $CDCl_3$; Me_4Si) 73.7, 104.7, 119.5 123.2, 126.3, 126.9, 128.3, 128.4, 128.4, 128.7, 129.4, 130.3, 131.3, 131.9, 132.9, 137.3; δ_{Se} (57 MHz; $CDCl_3$; Me_2Se) 323.7.

2.2.11. 8-Bromo-1-(p-anisylethynylselanyl)naphthalene (**3b**)

A similar method to that described for the preparation of **2a** was used. Compound **3b** was isolated in 33% yield as colorless prisms, m.p. 161.5–162.5 °C; $C_{19}H_{13}BrOSe$ requires C, 54.83; H, 3.15. Found: C, 54.69; H, 3.33%; δ_H (300 MHz; $CDCl_3$; Me_4Si) 3.84 (s, 3 H), 6.89 (d, *J* 8.9 Hz, 2H), 7.27 (t, *J* 7.8 Hz, 1H), 7.40 (t, *J* 7.9 Hz, 1H), 7.51 (d, *J* 8.9 Hz, 2H), 7.72 (dd, *J* 1.1, 8.1 Hz, 1H), 7.77–7.83 (m, 2H), 8.43 (dd, *J* 1.1, 7.7 Hz, 1H); δ_C (75 MHz; $CDCl_3$; Me_4Si) 55.4, 71.8, 104.7, 114.0, 115.3, 119.6, 126.3, 126.9, 128.2, 128.7, 129.4, 130.2, 131.3, 132.9, 133.7, 137.2, 160.1; δ_{Se} (57 MHz; $CDCl_3$; Me_2Se) 323.2.

2.2.12. 8-Bromo-1-(p-tolylethynylselanyl)naphthalene (**3c**)

A similar method to that described for the preparation of **2a** was used. Compound **3c** was isolated in 70% yield as light yellow prisms, m.p. 115.0–116.0 °C; $C_{19}H_{13}BrSe$ requires C, 57.03; H, 3.27. Found: C, 57.05; H, 3.52%; δ_H (400 MHz; $CDCl_3$; Me_4Si) 2.38 (s, 3H), 7.17 (d, *J* 7.8 Hz, 2H), 7.27 (t, *J* 7.8 Hz, 1H), 7.41 (t, *J* 7.8 Hz, 1H), 7.46 (d, *J* 8.2 Hz, 2H), 7.73 (dd, *J* 0.9, 8.2 Hz, 1H), 7.77–7.83 (m, 2H), 8.44 (dd, *J* 1.4, 7.3 Hz, 1H); δ_C (100 MHz; $CDCl_3$; Me_4Si) 21.6, 72.7, 104.9, 119.6, 120.1, 126.3, 126.9, 128.3, 128.5, 129.2, 129.4, 130.2, 131.3, 131.9, 132.9, 137.2, 139.0; δ_{Se} (76 MHz; $CDCl_3$; Me_2Se) 325.2.

2.2.13. 8-Bromo-1-(p-fluorophenylethynylselanyl)naphthalene (**3d**)

A similar method to that described for the preparation of **2a** was used. Compound **3d** was isolated in 48% yield as colorless prisms, m.p. 105.0–106.0 °C; $C_{18}H_{10}BrFSe$ requires C, 53.50; H, 2.49. Found: C, 53.31; H, 2.64%; δ_H (300 MHz; $CDCl_3$; Me_4Si) 7.05(t, *J* 8.8 Hz, 2H), 7.27 (t, *J* 7.8 Hz, 1H), 7.41 (t, *J* 7.8 Hz, 1H), 7.49–7.59 (m, 2 H), 7.73 (dd, *J* 0.9, 8.2 Hz, 1H), 7.77–7.84 (m, 2H), 8.40 (dd, *J* 1.1, 7.7 Hz, 1H); δ_C (75 MHz; $CDCl_3$; Me_4Si) 73.5 ($^5J_{C,F}$ 1.9 Hz), 103.5, 115.7 ($^2J_{C,F}$ 22.4 Hz), 119.3 ($^4J_{C,F}$ 3.7 Hz), 119.5, 126.3, 126.9, 128.2, 128.4, 129.4, 130.2, 131.3, 133.0, 134.0 ($^3J_{C,F}$ 8.1 Hz), 137.3, 162.8 ($^1J_{C,F}$ = 250.0 Hz); δ_{Se} (57 MHz; $CDCl_3$; Me_2Se) 323.71.

2.2.14. 8-Bromo-1-(p-chlorophenylethynylselanyl)naphthalene (**3e**)

A similar method to that described for the preparation of **2e** was used. Compound **3e** was isolated in 15% yield as colorless prisms, m.p. 147.0–148.0 °C; $C_{18}H_{10}BrClSe$ requires C, 51.40; H, 2.40. Found: C, 51.36; H, 2.33%; δ_H (300 MHz; $CDCl_3$; Me_4Si) 7.28 (t, *J* 7.8 Hz, 1H), 7.33 (d, *J* 8.8 Hz, 2H), 7.41 (t, *J* 7.8 Hz, 1H), 7.48 (d, *J* 8.8 Hz, 2H), 7.75 (dd, *J* 1.0, 8.1 Hz, 1H), 7.78–7.83 (m, 2H), 8.39 (dd, *J* 1.1, 7.6 Hz, 1H); δ_C (75 MHz; $CDCl_3$; Me_4Si) 75.0, 103.4, 119.5, 121.7, 126.4, 126.9, 128.1, 128.5, 128.8, 129.4, 130.3, 131.3, 133.0, 133.1, 134.8, 137.3; δ_{Se} (57 MHz; $CDCl_3$; Me_2Se) 324.8.

While the 8-chloro derivatives **2f** and **2g** were obtained by the Wittig reaction via triphenylphosphine ylides, similarly to the case of **1f** and **1g** [27,33], the 8-bromo derivatives **3f** and **3g** were not obtained due to facile C_8–Br bond cleavage.

2.3. X-ray structure determination

Single crystals of **2b**, **2e** and **2g** were obtained by slow evaporation of dichloromethane–hexane at room temperature. X-ray diffraction data were collected on a Rigaku/MSC Mercury CCD diffractometer equipped with a graphite-monochromated Mo Kα radiation source (λ = 0.71070 Å) at 103(2) K. The structures were solved by direct methods (SHELXS-97 [35], SIR97 [36] and SIR-2004 [37], respectively) [38] and refined by the full-matrix least squares method on F^2 for all reflections (SHELXL-97) [39].

2.4. Quantum chemical calculations

Quantum chemical (QC) calculations were performed on **1a**–**3a** and their related species. The 6-311+G(d,p) basis set of the GAUSSIAN 03 program [40] was employed for geometry optimizations at the density functional theory (DFT) level of the Becke three-parameter hybrid functionals combined with the Lee–Yang–Parr correlation functional (B3LYP) [41].[2,3] QC calculations were also performed at the Møller–Plesset second order energy correlation (MP2) level [42–44], employing the 6-311+G(d) basis set for Se, Cl and Br and the 4-31G(d) basis set for C and H of the GAUSSIAN 03 program [40].[2,3] The natural bond orbital analysis (NBO) [45–47] and atoms-in-molecules (AIM) analysis [48,49] were also carried out to evaluate the magnitudes of the $n_p(G)\cdots\sigma^*(Se–C_{sp})$ interactions (G-dependence).

3. Results and discussion

3.1. Structures of *2* in crystals

Single crystals were obtained for **2a**–**g**, via slow evaporation of dichloromethane–hexane solutions. X-ray crystallographic analysis was carried out for suitable crystals of **2b**, **2e** and **2g**. Figs. 1–3 show the structures of **2b**, **2e** and **2g**, respectively. The crystallographic data are collected in Table 1. Table 2 collects the selected interatomic distances, angles and torsional angles necessary for the discussion. Scheme 2 shows the structural changes from **1** to **2**, which is called G-dependence.

As shown in Figs. 1–3 and Table 2, the structures are (**B**: **pd**) for **2b** and **2e** and (**B**: **pl**) for **2g**. The results exhibit that the structure of **1b** (**A**: **pl**) changes dramatically to **2b** (**B**: **pd**) by substitution of H with Cl at the 8-position in **2**. We call the effect the G-dependence in **2**. The effect fixes the structure of **2** to **B**. While a variety of structures, such as (**A**: **pl**), (**B**: **pd**) or (**B**: **pl**), are observed in **1**, the observed structure is only **B** in **2**. The observation is quite different from that in **1**. The Y-dependence in **2** must be very similar to that in **1**.

The G-dependence in **2** (**B**: **pd**) should arise from the energy lowering effect of the $n_p(Cl)\cdots\sigma^*(Se–C_{sp})$ 3c–4e interaction, together with the $n_p(Cl)$–π(Nap)–$n_p(Se)$–π(C≡C) interaction of the through bond type. Scheme 3 illustrates the plausible interactions in **2** (**B**: **pd**) and **2** (**B**: **pl**). Y at the *p*-position in **2** (**B**: **pd**) seems not to stabilize the electrons in $n_p(Se)$ due to the orthogonal orientations between $n_p(Y)$ and $n_p(Se)$. The G-dependence must also operate in **3**, which fixes the structures of **3** to be (**B**: **pd**) or (**B**: **pl**) more strongly, since the energy lowering effect of the $n_p(Br)\cdots\sigma^*(Se–C)$ 3c–4e interaction is expected to be larger than the case of G = Cl.

How does the G-dependence stabilize (**B**: **pd**) and (**B**: **pl**)? Factors that control the fine structures of **2** and **3**, together with **1**, are examined based on the QC calculations.

[2] Our procedure for the optimization is explained and exemplified by **2a**: Three structures of types **A**, **B** and **C** are plausible around the Se–C_{Nap} bond in **2a**, with three conformers of **pl**, **pd** and **np** around the linear Se–C≡C–C_{Ar} alignment for each. Consequently, nine structures are expected to exist for **1a** in all. The nine structures are pre-optimized with the B3LYP/3-21G* method. Some structures will fuse to others. Then a few conformers are identified, which are optimized with the B3LYP/6-311+G(d,p) method. The optimized structures with the B3LYP/6-311+G(d,p) method are further optimized at the MP2 level employing suitable basis sets. The results are shown in Table 3, although higher energy species could exist.

[3] The optimized structures are available in the Supplementary data.

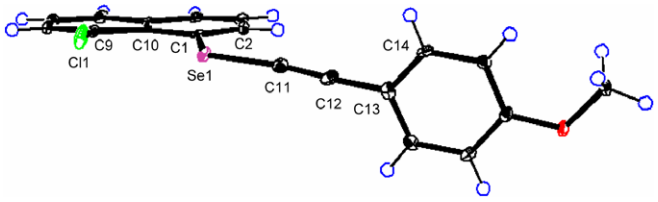

Fig. 1. Structure of **2b** (thermal ellipsoids are shown at the 50% probability level).

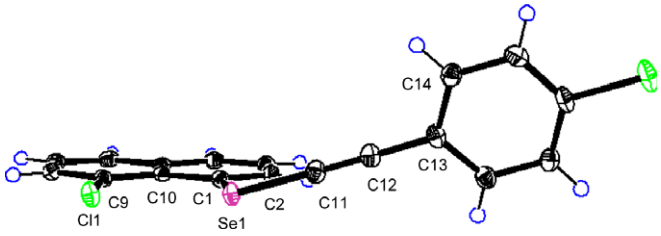

Fig. 2. Structure of **2e** (thermal ellipsoids are shown at the 50% probability level).

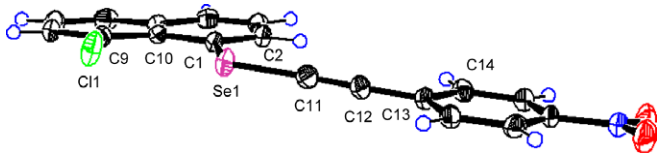

Fig. 3. Structure of **2g** (thermal ellipsoids are shown at the 50% probability level).

3.2. QC calculations

3.2.1. QC calculations on *1a–3a*

QC calculations were performed on (**A**: **pl**), (**B**: **pd**) and (**B**: **pl**) of **1a–3a**[2,3,4] with the B3LYP/6-311+G(d,p) method [41] of the GAUSSIAN 03 program [40]. QC calculations were also performed at the MP2 level [42–44] by employing the 6-311+G(d) basis set for Se, Cl and Br, and the 4-31G(d) basis set for C and H of the GAUSSIAN 03 program [40]. The results are collected in Table 3.

The relative stability of (**A**: **pl**) is predicted to be almost equal to that of (**B**: **pd**) and (**B**: **pl**) at the B3LYP level or the former is more stable than the latter at the MP2 level in **1a**. However, (**A**: **pl**) becomes much less stable relative to (**B**: **pd**) and (**B**: **pl**) in **2a** and **3a**. The $n_p(G)\cdots\sigma^*(Se–C_{sp})$ 3c–4e interaction in (**B**: **pd**) and (**B**: **pl**) must play an important role to lower the energy of the structures. The energy differences between (**B**: **pd**) and (**B**: **pl**) are very small in **2** and **3**, and therefore, the two conformers would be in equilibrium in solution.

How does the $n_p(G)\cdots\sigma^*(Se–C_{sp})$ 3c–4e interaction operate to stabilize (**B**: **pd**) and (**B**: **pl**) in **2** and **3**? Natural bond orbital analysis (NBO) and atoms-in-molecules analysis (AIM) were carried out on the models of **2** and **3**, as well as **2a** and **3a**.

[4] The (**B**: **pd**) and (**B**: **pl**) structures are optimized assuming C_s symmetry. Then they are calculated assuming C_1 symmetry, starting from those very close to the optimized C_s structures. The optimized structures of C_1 symmetry are very close to those of the C_s symmetry for **1a** (**B**: **pd**), **2a** (**B**: **pd**) and **3a** (**B**: **pd**): The frequency analysis of **1a** (**B**: **pd**) showed that it is the global minimum. The calculations are converged to (**B**: **pd**) for **1a–3a**, when started from the structures of C_1 symmetry very close to the optimized (**B**: **pl**) structures of C_s symmetry for **1a–3a**, respectively: The frequency analysis of **1a** (**B**: **pd**) showed that it is a transition state. Table 4 shows the results of the calculations for (**B**: **pd**) and (**B**: **pl**), although **2b** and **2e** are observed as C_1. See also footnote 2 and the Supplementary data (Table S2) of Ref. [27].

Table 1
Crystallographic data for **2b**, **2e** and **2g**

	2b	**2e**	**2g**
Empirical formula	$C_{19}H_{13}ClOSe$	$C_{18}H_{10}Cl_2Se$	$C_{18}H_{10}ClNO_2Se$
Formula weight	371.70	376.12	386.68
Temperature (K)	103(2)	103(2)	103(2)
Crystal system	triclinic	triclinic	triclinic
Space group	$P\bar{1}$	$P\bar{1}$	$P\bar{1}$
Unit cell dimensions			
a (Å)	8.034(3)	7.4652(3)	6.9934(2)
b (Å)	9.861(3)	8.3832(3)	7.9240(2)
c (Å)	10.483(3)	12.5213(3)	14.1861(4)
α (°)	96.743(5)	86.0500(12)	78.2838(13)
β (°)	95.2551(18)	73.0138(16)	89.1488(17)
γ (°)	111.216(4)	79.351(2)	80.290(2)
Volume (Å^3)	760.8(4)	736.43(4)	758.57(4)
Z	2	2	2
D_{calc} (g cm^{-3})	1.623	1.696	1.693
$F(000)$	372	372	384
Crystal size (mm)	0.45 × 0.30 × 0.20	0.30 × 0.15 × 0.10	0.12 × 0.10 × 0.05
μ (cm^{-1})	2.641	2.900	2.659
Reflections collected	4494	6478	5409
Reflections unique	2520	2696	2764
Reflections observed [$I > 2\sigma(I)$]	2205	2576	2393
Parameters	200	230	208
Final R indices R_1	0.0538,	0.0241,	0.0266,
[$I > 2\sigma(I)$] wR_2	0.1384	0.0573	0.0646
R indices (all data) R_1	0.0558,	0.0252,	0.0337,
wR_2	0.1392	0.0577	0.0670
Goodness-of-fit on F^2	1.249	1.202	1.028

Table 2
Selected interatomic distances, angles and torsional angles around the Se atom, observed in **2b**, **2e** and **2g**

	2b	**2e**	**2g**
r(Se1,Cl1) (Å)	2.9495(16)	2.9753(17)	2.9454(15)
r(Se1,C1) (Å)	1.946(4)	1.9458(18)	1.945(2)
r(Se1,C11) (Å)	1.831(5)	1.8383(19)	1.829(2)
r(Cl1,C9) (Å)	1.749(4)	1.7443(18)	1.744(2)
∠Cl1Se1C11 (°)	179.18(15)	165.51(17)	175.70(15)
∠Se1C11C12 (°)	167.2(4)	173.07(17)	170.6(2)
∠C1Se1C11 (°)	99.7(2)	98.47(8)	99.32(10)
∠C2C1Se1 (°)	118.0(3)	117.64(14)	117.70(17)
∠C10C1Se1 (°)	121.7(3)	122.39(13)	122.21(16)
∠C10C1Se1C11 (°)	170.5(3)	−164.16(15)	171.80(19)
∠C1Se1C13C14 (°)	104.41(6)	102.59(8)	3.68(7)
Structure	(**B**: **pd**)	(**B**: **pd**)	(**B**: **pl**)

3.2.2. NBO and AIM analyses of the G-dependence

NBO [45–47] and AIM [48,49] analyses were performed on 8-G-1-(HC≡CSe)Nap (**6** (**B**): G = Cl and Br), 8-G-1-(H_2C=CHSe)Nap (**7** (**B**): G = Cl and Br) and 8-G-1-(CH_3CH_2Se)Nap (**8** (**B**): G = Cl and Br), together with **2a** (**B**: **pd**) and **3a** (**B**: **pd**). The B3LYP/6-311+(d,p) method [41] was employed at the B3LYP level and the 6-311+G(d) basis set for Se, Cl and Br and the 4-31G(d) basis set for C and H are at the MP2 level [42–44]. The structures were optimized to be C_s symmetry for **6** (**B**) and **8** (**B**). **7** (**B**) was optimized by placing the S–C_{sp2} bond in the naphthyl plane.

$$E(2) = \Delta E_{ij} = q_i F(i,j)^2/(\varepsilon_j - \varepsilon_i) \quad (1)$$

The CT interactions can be evaluated as the second order perturbation of the Fock matrix in NBO, which is defined by Eq. (1). For each donor NBO (i) and acceptor NBO (j), the stabilization energy $E(2)$ associated with delocalization is estimated as in Eq. (1), where q_i is the donor orbital occupancy, ε_j and ε_i are diagonal ele-

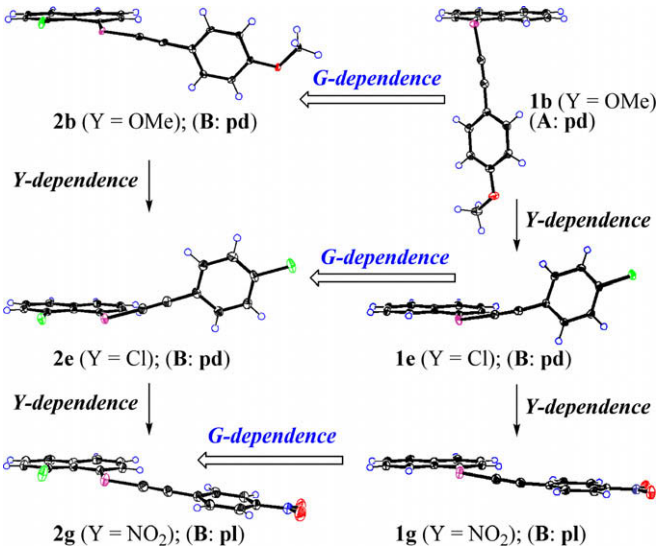

Scheme 2. The G-dependence in **2**: The Y-dependence in **2** must be very similar to that in **1**.

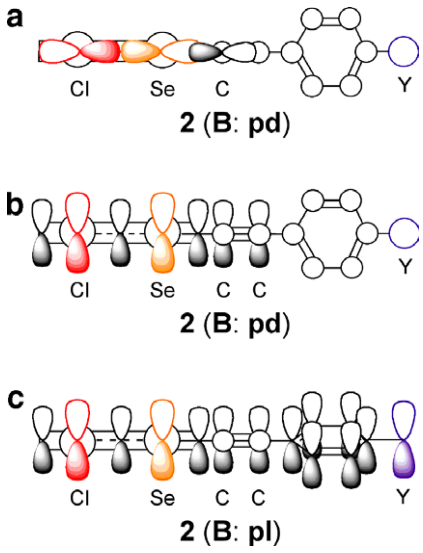

Scheme 3. Orbital interactions: (a) $n_p(Cl)\cdots\sigma^*(Se–C_{sp})$ 3c–4e interaction in **2** (**B**: **pd**), (b) $n_p(Cl)–\pi(Nap)–n_p(Se)–\pi(C{\equiv}C)$ interaction in **2** (**B**: **pd**) and (c) $n_p(Cl)–\pi(Nap)–n_p(Se)–\pi(C{\equiv}C)–\pi(C_6H_4)–n_p(Y)$ interaction in **2** (**B**: **pl**).

ments (orbital energies) and $F(i,j)$ is the off-diagonal NBO Fock matrix element. The results of NBO analysis at the B3PLY level are very similar to those at the MP2 level. The results of the MP2 calculations are collected in Table 4.[5]

The magnitudes of the $n_p(G)\cdots\sigma^*(Se–C)$ interactions are larger than those of the corresponding $n_s(G)\cdots\sigma^*(Se–C)$ interactions and the latter seem not to affect the conclusions. Those of the $n_p(Br)\cdots\sigma^*(Se–C)$ interactions are predicted to be larger than those of the corresponding $n_p(Cl)\cdots\sigma^*(Se–C)$ interactions. The magnitudes of the $n_p(G)\cdots\sigma^*(Se–C)$ interactions of **6** (**B**)–**8** (**B**), shown in Table 4, are summarized as shown in Relation (2). The order shown in Relation (2) show that the contributions stabilize the system through the $n(G)\cdots\sigma^*(Se–C)$ interactions. The optimized non-bonded G···Se distances become longer in the inverse order shown in Relation (2). The results show that the magnitudes of the energy

[5] Those at the B3LYP level are shown in the Supplementary data (Table S1).

Table 3
Results of QC calculations on (**A**: **pl**), (**B**: **pd**) and (**B**: **pl**) of **1a**–**3a**

Compound Symmetry	(**A**: **pl**) C_1	(**B**: **pd**) C_s[a]	(**B**: **pd**) C_1	(**B**: **pl**) C_s[b]
B3LYP[c]				
Compound ***1a***				
E (au)[d]	−3094.8055	−3094.8061		−3094.8057
ΔE (kJ mol^{-1})	1.6	0.0[e]		1.1
r(Se···H$_8$) (Å)	2.8122	2.6657		2.6609
$\angle C_9C_1Se_1C_{sp}$ (°)	70.6	180.0		180.0
$\angle C_1SeC_iC_o$ (°)[f]	162.9	91.0		180.0
Compound ***2a***				
E (au)[d]	−3554.4111	−3554.4178	−3554.4177	−3554.4174
ΔE (kJ mol^{-1})	17.6	0.0[e]	< 0.3	1.1
r(Se···Cl) (Å)	3.2638	3.0220	3.0225	3.0191
$\angle C_9C_1Se_1C_{sp}$ (°)	72.0	180.0	−179.98	180.0
$\angle C_1SeC_iC_o$ (°)[f]	168.1	91.7	91.56	180.0
Compound ***3a***				
E (au)[d]	−5668.3285	−5668.3349	−5668.3349	−5668.3345
ΔE (kJ mol^{-1})	16.8	0.0[e]	0.0	1.1
r(Se···Br) (Å)	3.3668	3.1251	3.1272	3.1252
$\angle C_9C_1Se_1C_{sp}$ (°)	70.0	180.0	−179.81	180.0
$\angle C_1SeC_iC_o$ (°)[f]	178.3	92.0	−92.48	180.0
MP2[g]				
Compound ***1a***				
E (au)[d]	−3089.2287	−3089.2268		−3089.2263
ΔE (kJ mol^{-1})	−5.0	0.0[e]		1.3
r(Se···H$_8$) (Å)	2.8204	2.6782		2.6740
$\angle C_9C_1Se_1C_{sp}$ (°)	61.1	180.0		180.0
$\angle C_1SeC_iC_o$ (°)[f]	144.1	90.4		180.0
Compound ***2a***				
E (au)[d]	−3548.2794	−3548.2826		−3548.2819
ΔE (kJ mol^{-1})	8.4	0.0[e]		1.8
r(Se···Cl) (Å)	3.2552	3.0116		3.0102
$\angle C_9C_1Se_1C_{sp}$ (°)	58.8	180.0		180.0
$\angle C_1SeC_iC_o$ (°)[f]	109.0[h]	90.8		180.0
Compound ***3***[a]				
E (au)[d]	−5661.2811	−5661.2833		−5661.2826
ΔE (kJ mol^{-1})	5.8	0.0[e]		1.8
r(Se···Br) (Å)	3.3730	3.1159		3.1150
$\angle C_9C_1Se_1C_{sp}$ (°)	50.0	180.0		180.0
$\angle C_1SeC_iC_o$ (°)[f]	147.1	90.9		180.0

[a] Global minimum for **1a**[i] and substantially equal to the optimized structures of the C_1 symmetry for **2a** and **3a**.
[b] Transition state for **1a**[i] and converged to (**B**: **pd**) when started from the C_1 symmetry for **2a** and **3a**.
[c] With the 6-311+G(d,p) basis sets.
[d] On the energy potential surface.
[e] Taken as the standard.
[f] $\angle C_1SeC_{ipso}C_{ortho}$.
[g] With the 6-311+G(d) basis set for Se, Cl and Br, and the 4-31G(d) basis sets for C and H.
[h] Optimized to be the (**A**: **pd**) structure.
[i] Supplementary data (Table S2) of Ref. [27].

lowering effect by the $n(G)\cdots\sigma^*(Se–C)$ interactions are closely related to the optimized non-bonded G···Se distances.

$$Se–C_{sp3} \leqslant Se–C_{sp2} < Se–C_{CCAr}\ (\mathbf{2a}(\mathbf{B}\text{: }\mathbf{pd})\text{ and }\mathbf{3a}\ (\mathbf{B}\text{: }\mathbf{pd})) < Se–C_{sp} \quad (2)$$

The results of AIM analysis at the B3PLY level are very close to those at the MP2 level. Table 5 shows the results of the MP2 calculations on the optimized structures of **6** (**B**)–**8** (**B**), **2a** (**B**: **pd**) and **3a** (**B**: **pd**) at the bond critical points (BCPs) for the non-bonded $n(G)\cdots\sigma^*(Se–C)$ (G = Br and Cl) interactions.

The total electron energy density at the BCP ($H_b(r_c)$) is recognized to be a better parameter to discuss weak interactions, as well as the electron density at BCP ($\rho_b(r_c)$) and the Laplacian ($\nabla^2\rho_b(r_c)$). The interactions are ionic and covalent in nature when the values of $H_b(r_c)$ and $\nabla^2\rho_b(r_c)$ are positive and negative, respectively. The nature of the interactions must be close to that of hydrogen bonds

Table 4
NBO analysis for the non-bonded n(G)···σ*(Se–C) interactions in 8-G-1-(RSe)$C_{10}H_6$ (**6** (**B**)–**8** (**B**)), together with **2a** (**B**: **pd**) and **3a** (**B**: **pd**) at the MP2 level.[a]

Compound Donor NBO (*i*)[b]	G = Cl *r*(Se,Cl) (Å)	*E*(2) (kcal mol^{-1})	G = Br *r*(Se, Br) (Å)	*E*(2) (kcal mol^{-1})
*8-G-1-(HC≡CSe)Nap (**6** (**B**))*				
n_s(G)	3.0064	1.42	3.1114	1.31
n_p(G)	3.0064	8.69	3.1114	10.12
*8-G-1-(H_2C=CHSe)Nap (**7** (**B**))*				
n_s(G)	3.0431	1.24	3.1469	1.13
n_p(G)	3.0431	6.88	3.1469	8.08
*8-G-1-(CH_3CH_2Se)Nap (**8** (**B**))*				
n_s(G)	3.0480	1.18	3.1522	1.06
n_p(G)	3.0480	6.71	3.1522	7.83
2a **(B: pd)/*3a* (B: pd)**				
n_s(G)	3.0116	1.40	3.1159	1.29
n_p(G)	3.0116	8.48	3.1159	9.90

[a] With the 6-311+G(d) basis sets for Se, Cl and Br, and the 4-31G(d) basis sets for C and H.
[b] Acceptor NBO (*j*) being σ*(Se–C).

Table 5
AIM Analysis for the non-bonded n(G)···σ*(Se–C) interactions in **6** (**B**)–**8** (**B**), together with **2a** (**B**: **pd**) and **3a** (**B**: **pd**) at the MP2 level[a]

Compound	G	$\rho_b(r_c)$ (ea$_o^3$)	$\nabla^2\rho_b(r_c)$ (ea$_o^5$)	$H_b(r_c)$ (au)	$H_b(r_c)$ (kJ mol^{-1})
6 (**B**)	Cl	0.0184	0.0660	0.00183	4.8
6 (**B**)	Br	0.0186	0.0585	0.00119	3.1
7 (**B**)	Br	0.0177	0.0564	0.00126	3.3
8 (**B**)	Br	0.0178	0.0563	0.00123	3.2
2a (**B**: **pd**)	Cl	0.0182	0.0656	0.00183	4.8
3a (**B**: **pd**)	Br	0.0184	0.0582	0.00120	3.2

[a] With the 6-311+G(d) basis sets for Se, Cl and Br and the 4-31G(d) basis sets for C and H.

(or the CT interactions in molecular complexes), since the values are all positive with small magnitudes. The $H_b(r_c)$ values for the n(Br)···σ*(Se–C) interactions are smaller than those for the n(Cl)···σ*(Se–C) interactions, which shows that the former are substantially stronger than the latter. The n(Br)···σ*(Se–C_{sp}) interaction seems slightly stronger than other n(Br)···σ*(Se–C) interactions, judging from the $H_b(r_c)$ values.

Fig. 4 draws the results of AIM analysis of **3a** (**B**: **pd**). Fig. 4a shows the BCPs, ring critical points (RCPs) and bond paths of **3a** (**B**: **pd**). Fig. 4b shows contour map of $\rho_b(r_c)$ for **3a** (**B**: **pd**), together with BCPs, RCPs and bond paths. The BCP between Br and Se clearly shows the n(Br)···σ*(Se–C_{sp}) interaction in **3a** (**B**: **pd**). While a bond path is detected between H_2 and C_{sp}, the interaction must be very small.

The nature of the G-dependence of the n(G)···σ*(Se–C) interactions as factors to control the fine structures of **2** and **3** is well clarified by the NBO and AIM analyses. The next extension is to examine the structures in solution.

3.3. Behavior of *1–3* in solution based on NMR spectroscopy

^{1}H and ^{77}Se NMR spectra of **1**–**3** are measured in chloroform-*d* solution (0.050 M) at 297 K.[6] Table 6 collects the $\delta(H_2)$, $\delta(H_8)$ and δ(Se) values for **1**–**3**. The values change depending on Y, although not by much. How are the values correlated with the structures in solution? The δ(H) and δ(Se) values of 9-(arylselanyl)anthracenes [9-(*p*-YC_6H_4Se)$C_{14}H_9$: **9**] and 1-(arylselanyl)anthraquinones [9-(*p*-YC_6H_4Se)$C_{14}H_7O_2$: **10**] are demonstrated to serve as standards to determine the structures of (**A**: **pl**) and (**B**: **pd**) in solution, respectively [50,51]. Scheme 4 illustrates the structures of **9** (**A**: **pl**) and **10** (**B**: **pd**). The values for **9** and **10** are also given in Table 6.

The $\delta(H_2)$ values of **1**–**3** are plotted versus $\delta(H_1)$ of **9** (δ (H_1: **9**)) and $\delta(H_2$: **10**). Fig. 5 shows the plots. The correlations are collected in Table 7 (entries 1–6). The $\delta(H_2)$ values appear more downfield in the order $\delta(H_2$: **1**) ≪ $\delta(H_2$: **2**) < $\delta(H_2$: **3**) (Table 6 and Fig. 5). The results are in accordance with the expectation that each H_2 in **2** and **3**

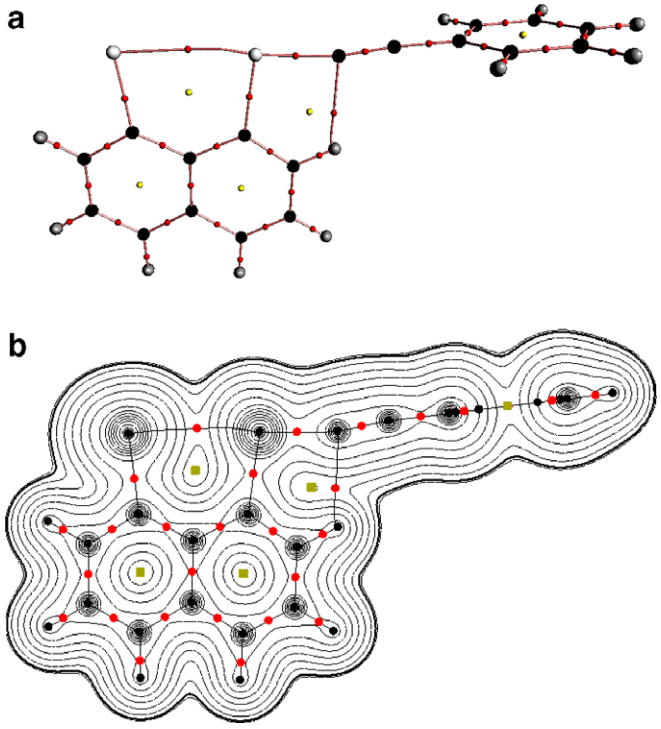

Fig. 4. AIM analysis of **3a** (**B**: **pd**): (a) BCPs (●), RCPs (●) and bond paths and (b) BCPs (●), RCPs (■) and bond paths on the contour map of $\rho_b(r_c)$.

Table 6
^{1}H and ^{77}Se NMR chemical shifts in **1**–**3**, together with those in **9** and **10**[a,b]

Y	OMe **b**	Me **c**	H **a**	F **d**	Cl **e**	CN **f**	NO_2 **g**
*Compound **1***							
$\delta(H_2)$	7.779	7.787	7.798	7.803	7.809	7.845	7.857
$\delta(H_8)$	8.010	8.019	8.033	8.038	8.045	8.087	8.102
δ(Se)	240.9	241.4	241.4	240.5	241.3	243.9	244.9
*Compound **2***							
$\delta(H_2)$	8.368	8.371	8.377	8.338	8.326	8.298	8.309
δ(Se)	327.1	329.2	327.9	327.7	329.0	332.7	334.2
*Compound **3***							
$\delta(H_2)$	8.432	8.430	8.440	8.399	8.389		
δ(Se)	323.1	325.2	323.7	323.7	324.8		
*Compound **9***							
$\delta(H_1)$	8.929	8.889	8.884	8.856	8.809	8.698	8.666
δ(Se)	236.8	242.4	249.0	245.4	247.5	275.2	279.3
*Compound **10***							
$\delta(H_2)$	7.260	7.261	7.237	7.199	7.220	7.181	7.185
$\delta(H_8)$	8.374	8.365	8.352	8.357	8.363	8.363	8.370
δ(Se)	497.3	503.4	512.3	502.2	505.3	504.1	509.8

[a] In $CDCl_3$.
[b] From TMS for δ(H) and from Me_2Se for δ(Se).

[6] The concentration dependence of δ(H) is carefully examined for **1**–**3**. No dependence on the concentrations was detected in the measurements, which shows that the contribution from dimers is negligible in **1**–**3**, although dimers are detected for **1a**–**c** in the crystalline state. For the concentration dependence see also Ref. [49].

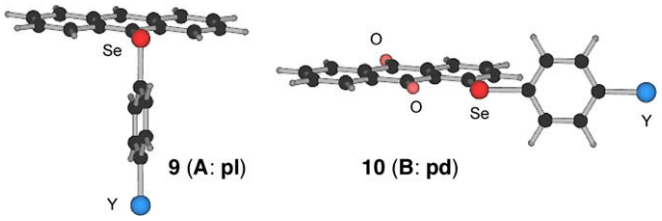

Scheme 4. Illustration of the **9** (**A**: **pl**) and **10** (**B**: **pd**) structures.

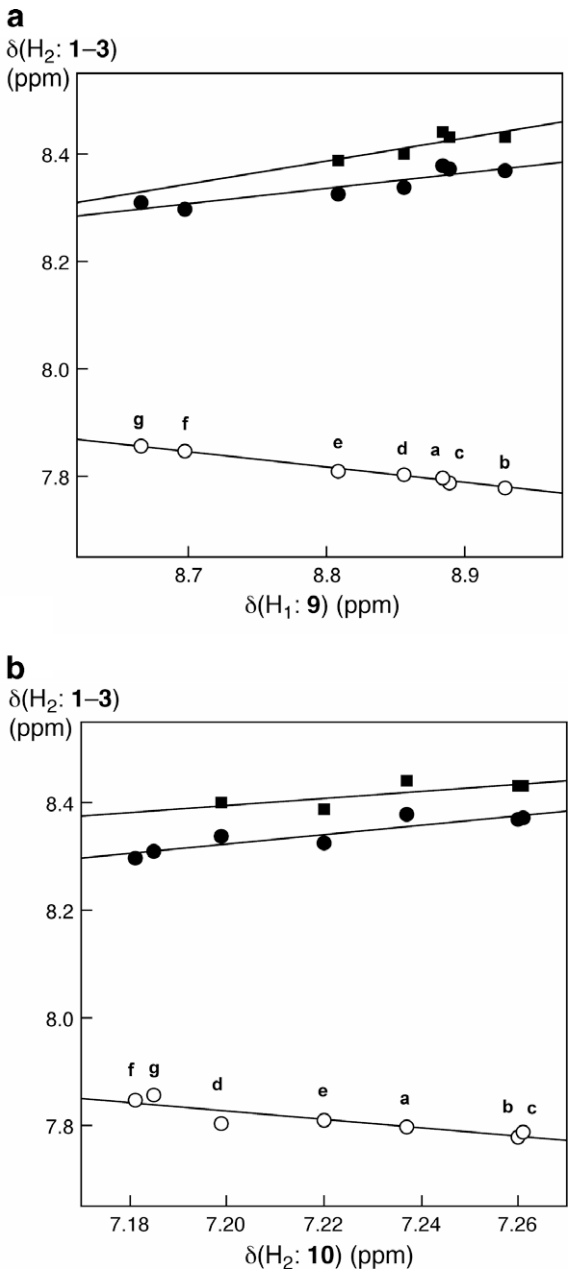

Fig. 5. Plots of $\delta(H_2$: **1**–**3**$)$ vs. $\delta(H_1$: **9**$)$ (a) and $\delta(H_2$: **10**$)$ (b): ○ stands for **1**, ● for **2** and ■ for **3**.

is more deshielded due to the location above the C≡C bond. Namely, the structures of **2** and **3** must be **B** in solution. The anisotropic effect of the C≡C bond in **3** seems to be stronger than that in **2**. The results imply the substantive contributions of (**A**: **pd**) and (**B**: **pl**) to **1** in solution.

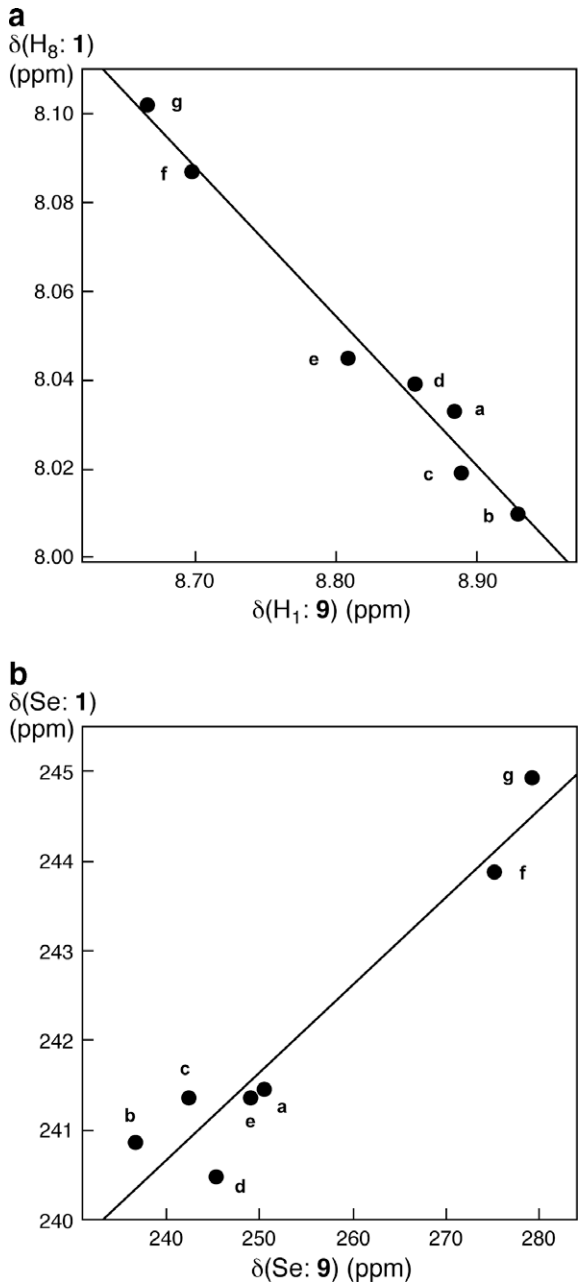

Fig. 6. Plots of $\delta(H_8$: **1**$)$ vs. $\delta(H_1$: **9**$)$ (a) and δ(Se: **1**) vs. δ(Se: **9**) (b).

$\delta(H_8$: **1**$)$ and δ(Se: **1**) are plotted versus $\delta(H_1$: **9**$)$ and δ(Se: **9**), respectively. Fig. 6 shows the results. The correlations are shown in Table 7 (entries 7 and 8, respectively). The correlation in Fig. 6a is good (entry 7), which means that the structures of **1** are closely related to those of **9** (**A**: **pl**). Namely, (**A**: **pl**) contributes predominantly to the structures of **1**, although the correlation constant is a negative value of −0.34. The negative value is a reflection of the inverse anisotropic effect between the phenyl π system and the ethynyl group. It is concluded that the structures of **1** in solution are substantially (**A**: **pl**) with some contributions of (**B**: **pd**) and/or (**B**: **pl**) through an equilibrium. The correlation of the plots of δ(Se: **1**) versus δ(Se: **9**) also supports the conclusion (entry 8).

The preferential contribution of **B** is predicted for **2** and **3** based on the $\delta(H_2)$ values. However, the plots of $\delta(H_2$: **2**$)$ versus $\delta(H_2$: **10**$)$ (entry 5) and those of δ(Se: **2**) versus δ(Se: **10**) (entry 9) do not give good correlations. The plots of δ(Se: **2**) versus δ(Se: **9**) give rather a

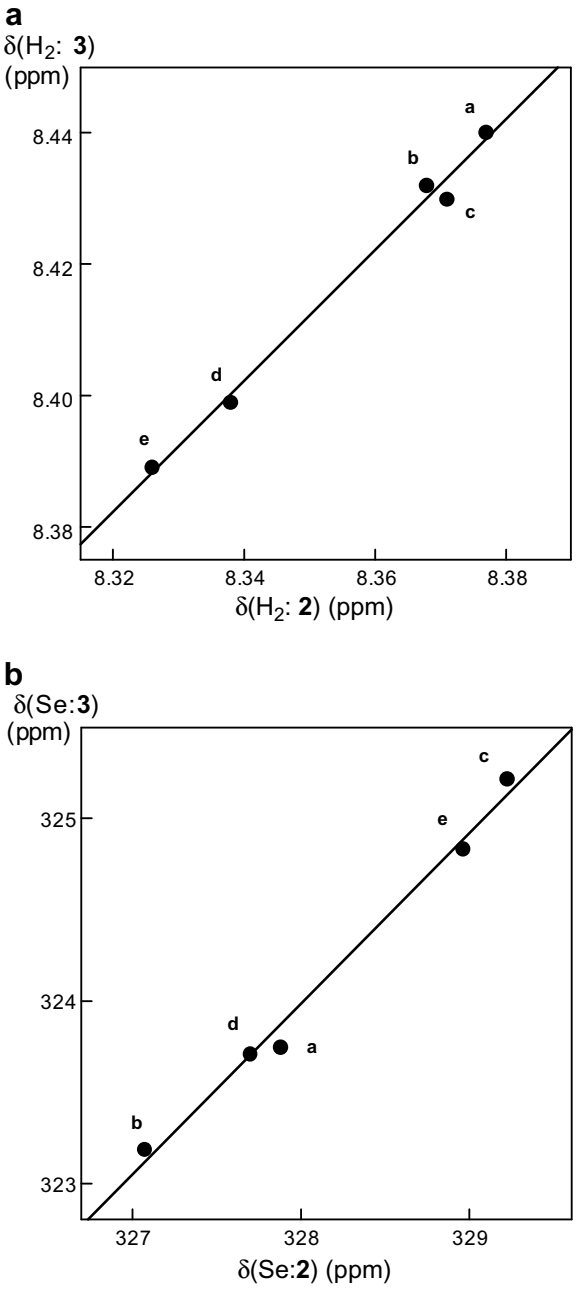

Fig. 7. Plots of $\delta(H_2$: **3**) vs. $\delta(H_2$: **2**) (a) and δ(Se: **3**) vs. δ(Se: **2**) (b).

Table 7
Correlations of δ(H) and δ(Se) in solution for **1**–**3**, **9** and **10**[a]

Entry	*y*	*x*	*a*	*b*	*r*
1	$\delta(H_2$: **1**)	$\delta(H_1$: **9**)	−0.290	10.37	0.992
2	$\delta(H_2$: **2**)	$\delta(H_1$: **9**)	0.289	5.79	0.917
3	$\delta(H_2$: **3**)	$\delta(H_1$: **9**)	0.430	4.60	0.845
4	$\delta(H_2$: **1**)	$\delta(H_2$: **10**)	−0.784	13.47	0.895
5	$\delta(H_2$: **2**)	$\delta(H_2$: **10**)	0.856	2.16	0.906
6	$\delta(H_2$: **3**)	$\delta(H_2$: **10**)	0.646	3.74	0.763
7	$\delta(H_8$: **1**)	$\delta(H_1$: **9**)	−0.337	11.02	0.990
8	δ(Se: **1**)	δ(Se: **9**)	0.098	217.2	0.961
9	δ(Se: **2**)	δ(Se: **10**)	0.261	197.0	0.786
10	δ(Se: **2**)	δ(Se: **9**)	0.157	289.8	0.957
11	$\delta(H_2$: **3**)	$\delta(H_2$: **2**)	0.994	0.11	0.996
12	δ(Se: **3**)	δ(Se: **2**)	0.939	16.1	0.995

[a] Analyzed according to $y = ax + b$ (r: correlation coefficient).

good correlation (entry 10). The discrepancy must come mainly from the equilibrium between (**B**: **pd**) and (**B**: **pl**). The consideration is supported by the QC calculations displayed in Table 3. Compilation of these results led us to the conclusion that the structures of **2** are predominantly **B**, which are in equilibrium between (**B**: **pd**) and (**B**: **pl**). The equilibrium with **A** could exist but the contribution must be small for most of Y.

What are the structures of **3** in solution? Fig. 7 shows the plots of $\delta(H_2$: **3**) versus $\delta(H_2$: **2**) and δ(Se: **3**) versus δ(Se: **2**). The correlations are excellent as shown in Table 7 (entries 11 and 12, respectively). The results show that effects and behavior of G = Br in **3** on the structures are very similarly to the case of G = Cl in **2** in solution.

4. Conclusions

The ethynyl π and π^* orbitals play an important role in the appearance of specific properties, but the ethynyl σ and σ^* orbitals must also be of interest for the functionalities of the materials. 8-G-1-(*p*-$YC_6H_4C{\equiv}CSe)C_{10}H_6$ [**2** (G = Cl) and **3** (G = Cl): Y = H (**a**), OMe (**b**), Me (**c**), F (**d**), Cl (**e**), CN (**f**) and NO_2 (**g**)] have been prepared and the chemical shifts measured. Structures have been determined by X-ray crystallographic analysis for **2b**, **2e** and **2g**. The structures are all **B** around the Se–C_{Nap} bonds, in our definition. The structures around the linear Se–C_{sp}–C_{sp}–C_{Ar} alignment are **pd** for Y = OMe and Cl and **pl** for Y = NO_2. The **1b** (**A**: **pl**) structure with Y = OMe changes dramatically to **2b** (**B**: **pd**) with G = Cl at the 8-position in **2**. The effect is called G-dependence. The G-dependence must arise from the energy lowering effect of the $n_p(Cl)\cdots\sigma^*$(Se–C_{sp}) 3c–4e interaction. The $n_p(Cl)$–π(Nap)–n_p(Se)–π(CC) interaction may also contribute to the stabilization of the structure. The **B** structures must be greatly stabilized by the $n_p(Cl)\cdots\sigma^*$(Se–C_{sp}) 3c–4e interaction (G-dependence) even if the structures of **2** and **3** are not changed from those of **1**. The G-dependence can be analyzed as the G···Se–C_{sp}–C_{sp}–C_{sp2} 5c–6e type interaction. The structures of **2** and **3** were also examined in solution based on NMR parameters for (**A**: **pl**) of 1-(arylselanly)anthracene (**9**) and (**B**: **pd**) of 1-(arylselanly)anthracene (**10**). The results show that **2** and **3** behave very similarly in solution and the structures of **2** and **3** are predominantly **B** in solution, with some equilibrium between (**B**: **pd**) and (**B**: **pl**). The observed results and the origin of the G-dependence in **2** and 3 are well rationalized by QC calculations containing NBO and AIM analyses.

Acknowledgments

This work was partially supported by a Grant-in-Aid for Scientific Research (Nos. 16550038, 19550041 and 20550042) from the Ministry of Education, Culture, Sports, Science, and Technology, Japan.

Appendix A. Supplementary data

CCDC 687206, 687207 and 687208 contain the supplementary crystallographic data for **2b**, **2e** and **2g**. These data can be obtained free of charge via http://www.ccdc.cam.ac.uk/conts/retrieving.html, or from the Cambridge Crystallographic Data Centre, 12 Union Road, Cambridge CB2 1EZ, UK; fax: (+44) 1223-336-033; or e-mail: deposit@ccdc.cam.ac.uk. Supplementary data associated with this article can be found, in the online version, at doi:10.1016/j.poly.2008.08.026.

References

[1] P.J. Stang, F. Diederich, Modern Acetylenic Chemistry, Wiley-VCH, Weiheim, 1995.

[2] F. Diederich, P.J. Stang, R.R. Tykwinski, Acetylene Chemistry: Chemistry, Biology and Material Science, Wiley-VCH, Weinheim, 2005.
[3] A.J. Zucchero, J.N. Wilson, U.H.F. Bunz, J. Am. Chem. Soc. 128 (2006) 11872.
[4] E.L. Spitler, L.D. Shirtcliff, M.M. Haley, J. Org. Chem. 72 (2007) 86–96.
[5] H. Hinrichs, A.J. Boydston, P.G. Jones, K. Hess, R. Herges, M.M. Haley, Chem. Eur. J. 12 (2006) 7103.
[6] J.A. Marsden, M.M. Haley, J. Org. Chem. 70 (2005) 10213.
[7] Y. Jiang, D. Perahia, Y. Wang, U.H.F. Bunz, Macromolecules 39 (2006) 4941.
[8] K. Tahara, S. Furukawa, H. Uji-i, T. Uchino, T. Ichikawa, J. Zhang, W. Mamdouh, M. Sonoda, F.C. De Schryver, S. De Feyter, Y. Tobe, J. Am. Chem. Soc. 128 (2006) 16613.
[9] A. Nomoto, M. Sonoda, Y. Yamaguchi, T. Ichikawa, K. Hirose, Y. Tobe, J. Org. Chem. 71 (2006) 401.
[10] E.E. Nesterov, Z. Zhu, T.M. Swager, J. Am. Chem. Soc. 127 (2005) 10083.
[11] A. Orita, T. Nakano, D.L. An, K. Tanikawa, K. Wakamatsu, J. Otera, J. Am. Chem. Soc. 126 (2004) 10389.
[12] A. Orita, D.L. An, T. Nakano, J. Yaruva, N. Ma, J. Otera, Chem. Eur. J. 8 (2002) 2005.
[13] D.B. Werz, R. Gleiter, J. Org. Chem. 68 (2003) 9400.
[14] S. Husebye, E.A. Meyers, R.A. Zingaro, A.L. Braga, J.V. Comasseto, N. Petragnani, Acta Crystallogr., Sect. C 42 (1986) 1789.
[15] P.C. Bell, W. Skranc, X. Formosa, J. O'Leary, J.D. Wallis, J. Chem. Soc., Perkin Trans. 2 (2002) 878.
[16] S. Scheiner, Molecular Interactions. From Van der Waals to Strongly Bound Complexes, Wiley, New York, 1997.
[17] K.D. Asmus, Acc. Chem. Res. 12 (1979) 436.
[18] W.K. Musker, Acc. Chem. Res. 13 (1980) 200.
[19] A. Kucsman, I. Kapovits, Non-bonded Sulfur–Oxygen Interaction, in: F. Bernardi, I.G. Csizmadia, A. Mangini (Eds.), Organic Sulfur Chemistry: Theoretical and Experimental Advances, Elsevier, Amsterdam, 1985.
[20] R.S. Glass, S.W. Andruski, J.L. Broeker, Rev. Heteroatom Chem. 1 (1988) 31.
[21] R.S. Glass, S.W. Andruski, J.L. Broeker, H. Firouzabadi, L.K. Steffen, G.S. Wilson, J. Am. Chem. Soc. 111 (1989) 4036.
[22] R.S. Glass, L. Adamowicz, J.L. Broeker, J. Am. Chem. Soc. 113 (1991) 1065.
[23] N. Furukawa, Bull. Chem. Soc. Jpn. 70 (1997) 2571.
[24] N. Furukawa, K. Kobayashi, S. Sato, J. Organomet. Chem. 611 (2000) 116.
[25] (a) W. Nakanishi, Chem. Lett. (1993) 2121;
(b) W. Nakanishi, S. Hayashi, S. Toyota, Chem. Commun. (1996) 371;
(c) W. Nakanishi, S. Hayashi, H. Yamaguchi, Chem. Lett. (1996) 947;
(d) W. Nakanishi, S. Hayashi, A. Sakaue, G. Ono, Y. Kawada, J. Am. Chem. Soc. 120 (1998) 3635;
(e) W. Nakanishi, S. Hayashi, S. Toyota, J. Org. Chem. 63 (1998) 8790;
(f) S. Hayashi, W. Nakanishi, J. Org. Chem. 64 (1999) 6688;
(g) W. Nakanishi, S. Hayashi, T. Uehara, J. Phys. Chem. A 103 (1999) 9906;
(h) W. Nakanishi, S. Hayashi, J. Org. Chem. 67 (2002) 38;
(i) S. Hayashi, H. Wada, T. Ueno, W. Nakanishi, J. Org. Chem. 71 (2006) 5574;
(j) W. Nakanishi, S. Hayashi, T. Arai, Chem. Commun. (2002) 2416;
(k) W. Nakanishi, S. Hayashi, N. Itoh, Chem. Commun. (2003) 124;
(l) W. Nakanishi, S. Hayashi, N. Itoh, J. Org. Chem. 69 (2004) 1676;
(m) W. Nakanishi, T. Nakamoto, S. Hayashi, T. Sasamori, N. Tokitoh, Chem. Eur. J. 13 (2007) 255;
(n) W. Nakanishi, S. Hayashi, S. Yamaguchi, K. Tamao, Chem. Commun. (2004) 140.
[26] W. Nakanishi, Hypervalent Chalcogen Compounds, in: F.A. Devillanova (Ed.), Handbook of Chalcogen Chemistry: New Perspectives in Sulfur, Selenium and Tellurium, Royal Society of Chemistry, London, 2006 (Chapter 10.3).
[27] K. Yamane, S. Hayashi, W. Nakanishi, T. Sasamori, N. Tokitoh, Polyhedron 27 (2008) 2478.
[28] (a) W. Nakanishi, S. Hayashi, H. Kihara, J. Org. Chem. 64 (1999) 2630;
(b) W. Nakanishi, S. Hayashi, T. Uehara, Eur. J. Org. Chem. (2001) 3933.
[29] M. Iwaoka, S. Tomoda, J. Am. Chem. Soc. 116 (1994) 4463.
[30] M. Iwaoka, S. Tomoda, J. Am. Chem. Soc. 118 (1996) 8077.
[31] H. Komatsu, M. Iwaoka, S. Tomoda, Chem. Commun. (1999) 205.
[32] K.-y. Akiba, Chemistry of Hypervalent Compounds, Wiley-VCH, New York, 1999.
[33] A.L. Braga, J.V. Comasseto, N. Petragnani, Synthesis (1984) 240.
[34] The starting α-acylphosphoranes were prepared according to procedures previously described T. Thiemann, K. Umeno, J. Wang, Y. Tabuchi, K. Arima, M. Watanabe, Y. Tanaka, H. Gorohmaru, S. Mataka, J. Chem. Soc., Perkin Trans. 1 (2002) 2090.
[35] G.M. Sheldrick, SHELXL-97 Program for the Refinement of Crystal Structures, University of Göttingen, Germany, 1997.
[36] A. Altomare, M.C. Burla, M. Camalli, G.L. Cascarano, C. Giacovazzo, A. Guagliardi, A.G.G. Moliterni, G. Polidori, R. Spagna, J. Appl. Crystallogr. 32 (1999) 115.
[37] M.C. Burla, R. Caliandro, M. Camalli, B. Carrozzini, G.L. Cascarano, L.D. Caro, C. Giacovazzo, G. Polidori, R. Spagna, J. Appl. Crystallogr. 38 (2005) 381.
[38] For the absorption correction: multi-scan, Jacobson, RA (1998). REQAB. Version 1.1. Molecular Structure Corporation, R.H. Blessing, Acta Crystallogr. AS1 (1995) 33–38.
[39] C.F. Matta, R.J. Boyd, An Introduction to the Quantum Theory of Atoms in Molecules, in: C.F. Matta, R.J. Boyd (Eds.), The Quantum Theory of Atoms in Molecules: From Solid State to DNA and Drug Design, Wiley-VCH, Weinheim, 2007 (Chapter 1).
[40] M.J. Frisch, G.W. Trucks, H.B. Schlegel, G.E. Scuseria, M.A. Robb, J.R. Cheeseman, J.A. Montgomery Jr., T. Vreven, K.N. Kudin, J.C. Burant, J.M. Millam, S.S. Iyengar, J. Tomasi, V. Barone, B. Mennucci, M. Cossi, G. Scalmani, N. Rega, G.A. Petersson, H. Nakatsuji, M. Hada, M. Ehara, K. Toyota, R. Fukuda, J. Hasegawa, M. Ishida, T. Nakajima, Y. Honda, O. Kitao, H. Nakai, M. Klene, X. Li, J.E. Knox, H.P. Hratchian, J.B. Cross, V. Bakken, C. Adamo, J. Jaramillo, R. Gomperts, R.E. Stratmann, O. Yazyev, A.J. Austin, R. Cammi, C. Pomelli, J.W. Ochterski, P.Y. Ayala, K. Morokuma, G.A. Voth, P. Salvador, J.J. Dannenberg, V.G. Zakrzewski, S. Dapprich, A.D. Daniels, M.C. Strain, O. Farkas, D.K. Malick, A.D. Rabuck, K. Raghavachari, J.B. Foresman, J.V. Ortiz, Q. Cui, A.G. Baboul, S. Clifford, J. Cioslowski, B.B. Stefanov, G. Liu, A. Liashenko, P. Piskorz, I. Komaromi, R.L. Martin, D.J. Fox, T. Keith, M.A. Al-Laham, C.Y. Peng, A. Nanayakkara, M. Challacombe, P.M. W. Gill, B. Johnson, W. Chen, M.W. Wong, C. Gonzalez, J.A. Pople, GAUSSIAN 03 (Revision D.02), Gaussian, Inc., Wallingford, CT, 2004.
[41] (a) A.D. Becke, Phys. Rev. A 38 (1988) 3098;
(b) A.D. Becke, J. Chem. Phys. 98 (1993) 5648;
(c) C. Lee, W. Yang, R.G. Parr, Phys. Rev. B 37 (1988) 785;
(d) B. Miehlich, A. Savin, H. Stoll, H. Preuss, Chem. Phys. Lett. 157 (1989) 200.
[42] C. Møller, M.S. Plesset, Phys. Rev. 46 (1934) 618.
[43] J. Gauss, J. Chem. Phys. 99 (1993) 3629.
[44] J. Gauss, Ber. Bunsenges, Phys. Chem. 99 (1995) 1001.
[45] A.E. Reed, R.B. Weinstock, F. Weinhold, J. Chem. Phys. 83 (1985) 735.
[46] J.E. Carpenter, F. Weinhold, J. Mol. Struct. (THEOCHEM) 169 (1988) 41.
[47] E.D. Glendening, A.E. Reed, J.E. Carpenter, F. Weinhold, NBO Ver. 3.1.
[48] R.F.W. Bader, Atoms in Molecules. A Quantum Theory, Oxford University Press, Oxford, 1990.
[49] (a) R.F.W. Bader, T.S. Slee, D. Cremer, E. Kraka, J. Am. Chem. Soc. 105 (1983) 5061;
(b) R.F.W. Bader, Chem. Res. 91 (1991) 893;
(c) R.F.W. Bader, J. Phys. Chem. A 102 (1998) 7314;
(d) F.W. Biegler-König, R.F.W. Bader, T.H. Tang, J. Comput. Chem. 3 (1982) 317;
(e) R.F.W. Bader, Acc. Chem. Res. 18 (1985) 9;
(f) T.H. Tang, R.F.W. Bader, P. MacDougall, Inorg. Chem. 24 (1985) 2047;
(g) F. Biegler-König, J. Schönbohm, D. Bayles, J. Comput. Chem. 22 (2001) 545;
(h) F. Biegler-König, J. Schönbohm, J. Comput. Chem. 23 (2002) 1489.
[50] W. Nakanishi, S. Hayashi, D. Shimizu, M. Hada, Chem. Eur. J. 12 (2006) 3829.
[51] S. Hayashi, K. Yamane, W. Nakanishi, J. Org. Chem. 72 (2007) 7587.

ent cytotoxic effects. Although differences between oxaliplatin and cisplatin in DNA binding, adduct formation, strand breaks, and apoptosis have been reported, the mechanisms behind the more potent cytotoxic activity of oxaliplatin compared with cisplatin against colon cancer cells have not yet been completely elucidated.

On the theoretical front, the interaction of cisplatin with water has been studied by various authors [19–35]. However, to our knowledge, no such studies have been reported for the third generation platinum drug, oxaliplatin (eloxatin). In view of the biological importance of this compound, we have carried out a systematic study of the structural properties of oxaliplatin and its various conformational forms. After comparing the relative energies of various conformers, we identified the most stable one. To check the accuracy of the methods used, the results of our density functional (DF) calculations were also compared with the experimental results, wherever possible. In addition, the experimental FT-IR spectrum was determined for the more potent isomer and compared with the theoretically predicted values.

2. Methods

2.1. Computational details

First-principles density functional (DF) calculations were performed on the various conformers of oxaliplatin using the DMol^3 code [36–39] available from Accelrys Inc. in the MATERIALS STUDIO 3.2 package. Our calculations employed numerical basis sets of double-ζ quality plus polarization functions (DNP) to describe the valence orbitals. This is the numerical equivalent of the Gaussian 6-31G** basis set. The core electrons were treated using DFT semilocal pseudopotentials (DSSP) [40]. These core potentials include some degree of relativistic effects and are thus very useful approximations for heavier elements, and, furthermore, the calculation is less computationally expensive since the core electrons are dropped. Details of the calculations are described elsewhere [41].

Geometry optimizations, without restrictions, were performed using delocalized internal coordinates. The exchange-correlation contribution to the total electronic energy was treated in a spin-polarized generalized-gradient corrected (GGA) form with the Perdew-Wang-91 correlation (PW91). Density functional calculations at the GGA level are expected to give good prediction for the bond lengths and bonding energies. We chose PW91 for our study because the Perdew-Wang density functional is superior to other DFT methods for the simultaneous prediction of both molecular geometries and vibrational frequencies of platinum(II) complexes [42]. The vibrational frequencies were calculated and these were used to calculate the zero-point corrections to the energies and to confirm that the structures are minima on the potential energy surface, i.e. all the vibrational frequencies are real. Free valences and bond orders were calculated using Mayer's procedure [43].

2.2. Experimental details

Oxaliplatin was purchased from the Sigma Chemical Company and used as such without further purification. The FT-IR spectrum (4000–400 cm^{-1}) was recorded on a Perkin Elmer FT-IR Spectrometer Spectrum 2000. High quality KBr was used as the dispersal medium.

3. Results and discussion

3.1. Conformers of DACH

The spectator ligand DACH plays an important role in determining the higher biological activity of oxaliplatin compared to cisplatin. Besides imparting lipophilic character to the complex, DACH is expected to display a wide range of possible conformers because of the presence of the cyclohexane ring. Investigations on this type of chiral complexes showed that the *trans* isomer *trans-l (trans-(−)-1R,2R)* is more efficacious than the corresponding *trans-d (trans-(+)-1S,2S)* and the *cis*-isomer (1*R*,2*S*) [17]. Thus, the activity might be explained by speculating on the stereochemical structures of the complexes.

The cyclohexane ring of DACH can have various conformations, such as chair, boat or twist boat. The chair form, expected to be the most stable one, is the obvious choice for the study, but the twist boat form has also been reported to exist [44], and is higher in energy than the other possible conformers in which the cyclohexane moiety is in the chair form.

The ligand DACH has two amino groups attached to two adjacent carbons. Each amino group may be attached at either the axial or equatorial position. The chair form of DACH may exist in three conformers:

(i). *cis*-Cyclohexyl-1,2-diamine [cis-(1*R*,2*S*)], in which one amine group is axial (a) and the other is equatorial (e).
(ii). *trans-d*-Cyclohexyl-1,2-diamine [*trans-d* (1*S*,2*S*)], in which both the amine groups are in equatorial position, and
(iii). *trans-l*-Cyclohexyl-1,2-diamine [*trans-l* (1*R*,2*R*)], in which both the amine groups are in equatorial position.

The (ii) and (iii) forms are optical isomers of each other.

In addition to these three isomers, we have also incorporated another form, in which the cyclohexane ring is in a twist boat conformation, in our studies.

3.2. Relative energies

In oxaliplatin, platinum is bound on one side to the two amine nitrogens of the large 1,2-diaminocyclohexane (DACH) ligand and to the other side by two oxalate oxygens in a chelating fashion (see Fig. 1). Taking the various conformers of the cyclohexane ring in turn, the energies of the complexes were determined, and the relative energies are listed in Table 1.

As expected, the diaxial conformation of DACH is not preferred in the complex (relative energy = 36.9 kcal/mol), and the equilibria between the diaxial and diequatorial conformations for the *trans* isomers favor the latter. This is due to the increased steric hindrance of axial locations. The relative energy of 6.6 kcal/mol obtained for the twist boat form proves theoretically the possibility of existence of the complex with DACH in the twist boat form at higher temperatures. No such complex has been experimentally reported as yet.

Both the *trans* forms are most stable. However, a close inspection of the relative energy values for *trans-(S,S), trans-(R,R)* and *cis-(R,S)* isomers reveals that they all co-exist at room temperature, as the energy difference between them is significantly less than 5 kcal/mol. Of these, *trans-d* (*S*,*S*) and *trans-l* (*R*,*R*) deserve special mention as they are optical isomers and the energy difference

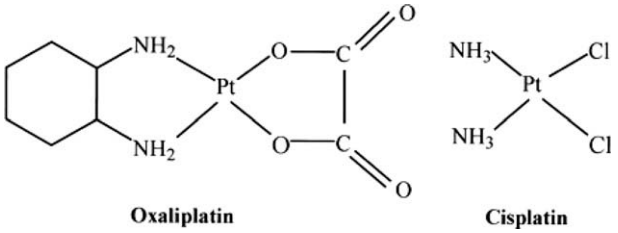

Fig. 1. Chemical structures of oxaliplatin and cisplatin.

Table 1
DFT relative energies (kcal/mol) of the various isomers of oxaliplatin

DACH conformation	Relative energy
trans ee (*S*,*S*)	0.0[a]
trans ee (*R*,*R*)	0.3
cis ae (*R*,*S*)	1.1
Twist boat form	6.6

[a] ZPVE corrected energy: −576828.2 kcal/mol.

between them is negligibly small. On the basis of these calculations, we expect both isomers to have almost an equal population at room temperature.

Our expectations are borne out by the experimental results. In an effort to solve the structure of the active species of oxaliplatin, an X-ray structural investigation was carried out on oxaliplatin [45]. The complex was prepared by reacting the enantiomerically pure isomer *trans-l* (*trans*-(−)-1*R*,2*R*-diaminocyclohexane (DACH)) and the platinum salt $K_2[PtCl_4]$ in H_2O. They found that the oxaliplatin which was isolated does not consist only of the desired isomer, but a mixture of both the *trans-l* and *trans-d* isomers. No retention of optical isomerism was observed despite the fact that the enantiomerically pure DACH ligand was utilized, although it had been earlier reported [46] that only the absolute configuration of the *trans-l*-DACH ligand exists in the platinum complex.

The Pt complexes of the three isomers [*cis-(R,S)*, *trans-l* (*R*,*R*) and *trans-d* (*S*,*S*)] interact differently with DNA. It has been shown that the *trans-l* (*R*,*R*) isomer of oxaliplatin is the most effective against cisplatin-sensitive and cisplatin-resistant cancer cell lines [17].

Proteins that discriminate between cisplatin–DNA adducts and oxaliplatin-DNA adducts are thought to be responsible for the differences in tumor range, toxicity, and mutagenicity of these two important chemotherapeutic agents. However, the structural basis for differential protein recognition of these adducts has not been determined and could be important for the design of more effective platinum anti-cancer agents. Recently, a lot of work has been devoted to understanding the differences between cisplatin and oxaliplatin binding to DNA [47–50]. Several significant conformational differences were observed between the cisplatin–GG adduct and the oxaliplatin–GG adduct [49,50]. It has also been demonstrated [51,52] that the chirality at the carrier ligand of oxaliplatin can affect its biological effects.

Thus, the stereochemistry of the carrier amine ligands of cisplatin analogues can modulate their anti-cancer and mutagenic properties. The significance of this finding is also reinforced by the fact that, in general, interstrand cross-links formed by various compounds of biological significance result in greater cytotoxicity than is expected for monofunctional adducts or other intrastrand DNA lesions [53]. Therefore, the unique properties of the interstrand cross-links of oxaliplatin are at least partly responsible for this drug's unique antitumor effects.

3.3. Optimized geometries

Geometry optimizations were performed on all possible conformers. The isomers differ in the orientations related to the cyclohexane ring of the DACH ligand. As far as the coordination sphere is concerned, all the isomers exist in the square planar geometry. This is expected, as Pt(II) compounds show stability in this form only [54]. The oxalate group is not only planar in itself but also in plane with the coordination sphere. All the optimized structures are shown in Fig. 2.

The calculated bond lengths and bond angles for the *trans-l* (*trans*-(−)-1*R*,2*R*) isomer are listed in Table 2 along with the corresponding experimental data [46] obtained from single crystal X-ray analysis of oxaliplatin. The numbering scheme used in these optimized structures is displayed below (Scheme 1):

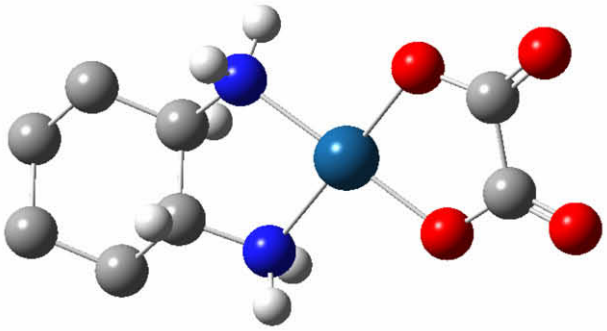

[Pt(1,2-*trans*-*R*,*R*-diaminocyclohexane)(O-O-oxalato)]

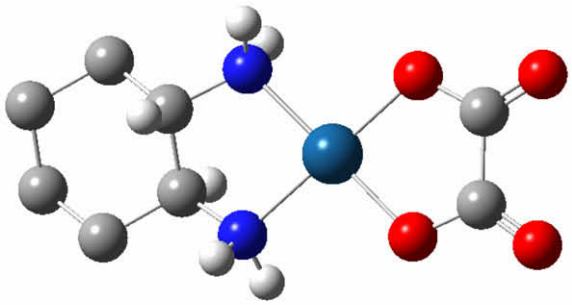

[Pt(1,2-*trans*-*S*,*S*-diaminocyclohexane)(O-O-oxalato)]

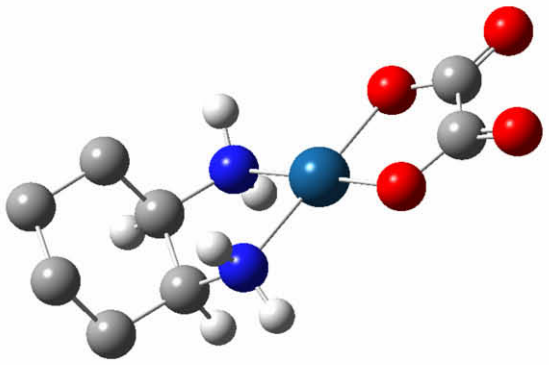

[Pt(1,2-*cis*-*R*,*S*-diaminocyclohexane)(O-O-oxalato)]

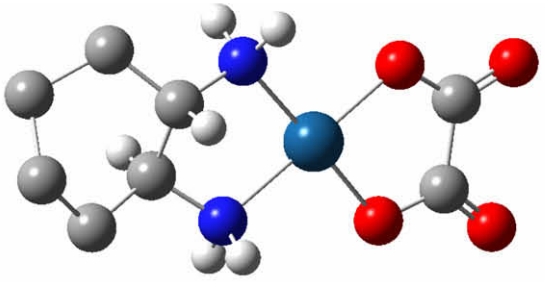

Twist boat form of oxaliplatin

Fig. 2. Structures of four oxaliplatin isomers. Colour code: H-white, C-grey, N-blue, O-red, and Pt-Prussian blue. (For interpretation of the references to colour in this figure legend, the reader is referred to the web version of this article.)

Table 2
Optimized geometry of the *trans-R,R* form (bond lengths in Ångstroms; bond angles in degrees)

Parameters[a]	Calculated	Experimental[b]	Parameters[a]	Calculated	Experimental[b]
N_1–Pt	2.10	2.06	N_2PtN_1	82.4	83.8
N_2–Pt	2.11	2.04	C_7O_1Pt	112.6	112.0
O_1–Pt	2.01	2.01	C_8O_2Pt	112.7	141.0
O_2–Pt	2.01	2.04	$C_8C_7O_1$	115.4	122.0
N_1–C_1	1.49	1.54	$O_3C_7O_1$	122.5	124.0
N_2–C_2	1.49	1.54	$O_3C_7C_8$	122.2	114.0
O_1–C_7	1.34	1.21	$C_7C_8O_2$	122.1	110.0
O_2–C_8	1.34	1.32	$O_4C_8O_2$	122.7	124.0
C_7–C_8	1.56	1.56	$O_4C_8C_7$	122.1	125.0
C_7–O_3	1.22	1.29	C_1N_1Pt	108.6	107.0
C_8–O_4	1.22	1.19	C_2N_2Pt	109.3	106.0
C_1–C_2	1.54	1.49	$C_2C_1N_1$	108.1	107.0
C_1–C_6	1.53	1.57	$C_6C_1N_1$	113.9	105.0
C_2–C_3	1.53	1.51	$C_6C_1C_2$	111.4	111.0
C_6–C_5	1.53	1.61	$C_1C_2N_2$	108.2	103.0
C_3–C_4	1.53	1.50	$C_3C_2N_2$	113.7	113.0
C_5–C_4	1.53	1.53	$C_3C_2C_1$	111.4	111.0
O_2PtO_1	84.2	82.5	$C_5C_6C_1$	111.0	106.0
N_1PtO_1	96.8	96.0	$C_4C_3C_2$	111.1	111.0
N_2PtO_1	179.1	175.6	$C_4C_5C_6$	111.3	112.0
N_1PtO_2	178.2	169.7	$C_5C_4C_3$	111.3	111.0
N_2PtO_2	96.6	98.6			

[a] See Scheme 1 for numbering.
[b] From Ref. [46].

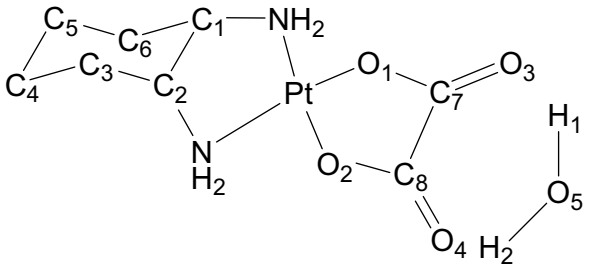

Scheme 1. Structure and numbering scheme of $[Pt(C_2O_4)(DACH)] \cdot H_2O$.

Although the computed gas phase free structure cannot be compared with the X-ray structure for the solid state, in the absence of any other available data we compared the structural parameters of the *trans-(R,R)* form with the X-ray crystallographic data. It is found that the DFT results are in good agreement with experiment (Table 2).

The optimized geometries of all the investigated isomers are compared in Table 3. Our earlier hypothesis that the difference between the isomers is limited to the DACH ligand area only has been proved by a comparison of the geometric parameters of the isomers (Table 3). All the isomers have very close values as far as the oxalate ligand parameters are concerned, since the calculated O_1–Pt, O_2–Pt, C_7–C_8, O_1–C_7 and O_2–C_8 bond lengths have very little difference among all the isomers. In a similar fashion, all the C–C bond lengths, except C_1–C_2, which is slightly higher for the *cis* isomer, have quite similar values.

The two amino groups are bound to platinum in a way to form a distorted square planar geometry of the coordinate sphere, and the Pt–N bond lengths are ~2.1 Å in all the complexes. Except in the *trans*-(+)-*S,S* isomer, there is considerable difference in the N_1-Pt and N_2-Pt bond lengths, but the O_1–Pt and O_2–Pt bond lengths are similar. The ∠NPtO bond angles are much larger than the ∠NPtN and ∠OPtO bond angles.

Hence we conclude that all the chair forms have almost equal thermal stability, and are much more stable than the twist boat conformer. Of the three stable chair forms, the *trans-(R,R)* conformer has been found to be the most potent [17]. Thus we consider only the two *trans*-forms for further studies.

3.4. Charge population analysis

Table 4 presents the calculated Hirshfeld [55,56] and Mulliken partial atomic charges on the various atoms in the free ligands, DACH and oxalate anion, and the two *trans* complexes of Pt(II). The Hirshfeld charges are considered to give a better description of the charge distribution than the Mulliken charges, which show a large dependence on the basis set.

The charge of the metal ion in the free state is +2.0. It is seen that the positive charge of the metal ion decreases in the complex to +0.18, which indicates that transfer of electrons from the ligands to the metal ion has occurred and the coordination bonds have formed. To see how the charge transfer occurs, we compared the values of partial atomic charges on the free ligand with that of the Pt(II) complex (oxaliplatin), in which the charge transfer takes place.

Although there is no change in the charge density on the carbon atoms of DACH on complexation, a decrease of 0.13 *e* in the charge density on each of the two nitrogens indicates that transfer of electron density to the metal ion occurs through these coordinated atoms.

The observation from the Mulliken charges is quite the opposite, i.e. an appreciable increase (~0.1) in the negative charge on each of the C_3, C_4, C_5 and C_6 carbon atoms of DACH, and practically no change on the nitrogen atoms.

A decrease (~0.3) in negative charge on each of the oxygens of oxalate shows that a considerable amount of charge is transferred from these four oxygens to the metal ion. Simultaneously, an increase of about ~0.1 in the positive charges of C_7 and C_8 is also noted. These observations indicate contribution of the whole of the ligand in the charge transfer from the oxalate ion to the metal ion.

A noteworthy point is the similarity in the charge distributions of all the isomers, signifying that electronic differences are not the reason for the differences in their reactivity.

According to Pearson's HSAB concept, Pt^{2+} is a soft acid and O^{2-} is a soft base, while NH_3 is a hard base. This indicates that there

Table 3
Optimized geometry of different conformers (bond lengths in Ångstroms; bond angles in degrees)

Parameter[a]	*trans*-(−)-*R*,*R*	*trans*-(+)-*S*,*S*	*cis*-*R*,*S*	*cis*-*R*,*S* · H_2O		Twist boat
				Calculated	Experimental[b]	
N_1–Pt	2.103	2.100	2.097	2.094	2.011	2.097
N_2–Pt	2.109	2.101	2.100	2.092	2.028	2.100
O_1–Pt	2.009	2.007	2.009	2.012	2.021	2.010
O_2–Pt	2.008	2.009	2.009	2.012	2.033	2.011
N_1–C_1	1.493	1.493	1.497	1.498	1.500	1.495
N_2–C_2	1.493	1.494	1.497	1.500	1.506	1.495
O_1–C_7	1.336	1.336	1.335	1.329	1.302	1.334
O_2–C_8	1.335	1.335	1.335	1.329	1.282	1.335
C_7–C_8	1.555	1.556	1.557	1.555	1.563	1.557
C_7–O_3	1.217	1.217	1.218	1.221	1.206	1.218
C_8–O_4	1.218	1.218	1.217	1.221	1.228	1.217
C_1–C_2	1.535	1.537	1.542	1.540	1.530	1.534
N_2PtN_1	82.4	82.6	82.5	82.6	83.8	82.3
O_2PtO_1	84.2	84.2	84.2	84.2	82.8	84.1
N_1PtO_1	96.8	96.3	96.6	96.6	95.5	96.1
N_2PtO_2	96.6	96.9	96.7	96.6	98.0	97.5
N_1PtO_2	178.2	179.4	179.1	179.0	177.4	179.6
N_2PtO_1	179.1	178.5	178.7	179.1	178.9	178.3
O_3–H_1				2.149		
O_4–H_2				2.140		

[a] See Scheme 1 for the numbering of atoms.
[b] From Ref. [57].

Table 4
The calculated Hirshfeld partial charges (Mulliken charges are in parentheses) of the optimized complexes and the ligands (DACH and oxalate ion)

Atom*	Free DACH	Free oxalate	*trans*- (*R*,*R*)	*trans*- (*S*,*S*)	*cis*-(*R*,*S*)	*cis*- (*R*,*S*) · H_2O
C_1	0.03 (0.09)		0.03 (0.05)	0.03 (0.05)	0.03 (0.03)	0.03 (0.03)
C_2	0.03 (0.09)		0.03 (0.05)	0.03 (0.05)	0.03 (0.04)	0.03 (0.04)
C_3	−0.06 (−0.07)		−0.06 (−0.17)	−0.06 (−0.17)	−0.06 (−0.17)	−0.06 (−0.17)
C_4	−0.05 (−0.06)		−0.05 (−0.17)	−0.05 (−0.17)	−0.05 (−0.18)	−0.05 (−0.18)
C_5	−0.05 (−0.06)		−0.05 (−0.17)	−0.05 (−0.17)	−0.05 (−0.17)	−0.05 (−0.17)
C_6	−0.06 (−0.07)		−0.06 (−0.17)	−0.06 (−0.17)	−0.06 (−0.18)	−0.06 (−0.18)
N_1	−0.22 (−0.39)		−0.09 (−0.38)	−0.09 (−0.38)	−0.09 (−0.37)	−0.09 (−0.37)
N_2	−0.22 (−0.39)		−0.09 (−0.38)	−0.09 (−0.38)	−0.09 (−0.39)	−0.09 (−0.39)
C_7		0.05 (0.36)	0.13 (0.45)	0.13 (0.45)	0.13 (0.45)	0.14 (0.46)
C_8		0.05 (0.36)	0.13 (0.45)	0.13 (0.45)	0.13 (0.45)	0.14 (0.46)
O_1		−0.53 (−0.68)	−0.25 (−0.51)	−0.25 (−0.51)	−0.25 (−0.51)	−0.25 (−0.51)
O_2		−0.53 (−0.68)	−0.25 (−0.51)	−0.25 (−0.51)	−0.25 (−0.51)	−0.25 (−0.51)
O_3		−0.53 (−0.68)	−0.27 (−0.39)	−0.27 (−0.39)	−0.27 (−0.39)	−0.24 (−0.41)
O_4		−0.53 (−0.68)	−0.27 (−0.39)	−0.27 (−0.39)	−0.27 (−0.39)	−0.24 (−0.42)
Pt			0.18 (0.22)	0.18 (0.22)	0.18 (0.22)	0.20 (0.23)
H_1						0.11 (0.28)
H_2						0.10 (0.28)
O_5						−0.35 (−0.58)

* See Scheme 1 for the numbering of atoms.

should be stronger interaction between Pt^{2+} and O^{2-} than between Pt^{2+} and the NH_2 groups of DACH. Our calculations are in accord with this principle, as there is a transfer of only 0.6 *e* from DACH to Pt while 1.2 *e* is transferred by oxalate. This shows that a total charge of ~1.8 *e* is transferred to Pt(II) during the complexation, and the net charge on Pt(II) reduces to ~0.2 *e*. The electronic configuration of platinum in the complex is: [core] $5s^2 6s^{0.92} 5p^{5.99} 6p^{0.35} 5d^{8.53}$. This shows that, out of the total charge density donated by the ligands to Pt^{2+}, approximately one electron goes to the 6s orbital, and approximately one-half to 5d, and the rest of the electron density is gained by the 6p orbital.

3.5. Bond order analysis

We calculated the Mayer bond orders for all the bonds of the complex and the results are produced in Table 5.

Table 5 shows that there is practically no difference in the bonding pattern of the two complexes. The N–Pt and O–Pt bond orders are around 0.6 and 0.7, respectively, which indicates covalent character in the bonds. Reduction in the bond order of O_1–C_7 and O_2–C_8 from 1.6 to 1.15 shows that charge has been carried away from these bonds. The C_7–O_3 and C_8–O_4 bonds regain their double bond character which was lost in the free oxalate ion due to resonance. However, there is a slight increase in the C_7–C_8 bond order of the oxalate group. The N–C and C–C bond orders of the DACH ligand decrease due to electron density transfer from these bonds.

We also examined the ligand orbitals in free DACH, oxalate ion and complex. Fig. 3a gives a plot of the highest occupied molecular orbital (HOMO) of DACH. This orbital has an energy of −4.71 eV. It is clear that the HOMO is centered on the nitrogens, which being thus electron rich, can donate charge density to the vacant metal ion orbital.

Fig. 3b gives the plot of the HOMO of the oxalate ion. In oxalate, as expected, the HOMO comprises the four oxygen atoms equally. The energy of this orbital is 6.26 eV.

Fig. 3c shows the plot of the HOMO of oxaliplatin. It can be seen from the plot of the HOMO of the complex that not only are the oxalate ligand orbitals retained, but the metal *d* orbitals also

Table 5
Calculated Mayer bond orders for DACH, oxalate ion and the isomers of oxaliplatin

Bond*	Free DACH	Free oxalate	*trans*- (*R*,*R*)	*trans*- (*S*,*S*)	*cis*- (*R*,*S*)	*cis*- (*R*,*S*) · H_2O
N_1–Pt			0.61	0.61	0.62	0.63
N_2–Pt			0.61	0.61	0.62	0.63
O_1–Pt			0.70	0.69	0.69	0.68
O_2–Pt			0.70	0.70	0.69	0.68
N_1–C_1	1.01		0.89	0.89	0.91	0.90
N_2–C_2	1.01		0.89	0.89	0.88	0.88
C_1–C_2	0.97		0.95	0.95	0.96	0.96
O_1–C_7		1.61	1.15	1.15	1.15	1.18
O_2–C_8		1.61	1.15	1.15	1.15	1.17
C_7–O_3		1.61	1.90	1.90	1.90	1.85
C_8–O_4		1.61	1.90	1.90	1.90	1.85
C_7–C_8		0.90	0.93	0.93	0.93	0.93
O_3···H_1						0.04
O_4···H_2						0.04

* See Scheme 1 for the numbering of atoms.

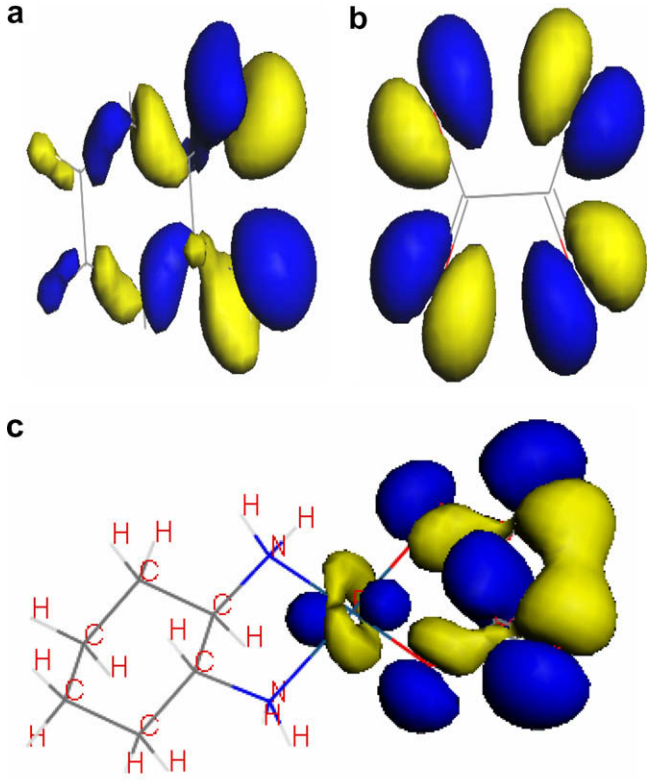

Fig. 3. Plot of HOMOs of (a) 1,2-diaminocyclohexane (DACH), (b) oxalate, (c) Pt(II) complex (oxaliplatin).

become part of the HOMO for the square planar Pt(II) complex, showing an interaction between oxalate and Pt(II) orbitals. The energy of the HOMO of the Pt(II) complex is −4.68 eV. It is interesting to note that the HOMO of the other ligand (DACH) is not a part of the HOMO of the complex. This can be explained quite conveniently by comparing the energies of the HOMOs of the two ligands. Oxalate ion, being negatively charged, has a high energy HOMO, which can contribute electron density to Pt^{2+}, forming the complex whose HOMO lies above the HOMO of DACH.

3.6. Vibrational analysis

The FT-IR spectrum of oxaliplatin was recorded in the range 400–4000 cm^{-1}. The detailed list of calculated frequencies and the corresponding intensities, as well as the experimental FT-IR and the corresponding computed infrared absorption spectrum are given as Supplementary data. The spectra have a very complicated pattern, as each band corresponds to mixed vibrations.

3.6.1. Pt–Ligand Vibrations

The platinum–ligand vibrations are expected to occur in a very low frequency range (below 600 cm^{-1}). In the process of assigning the frequencies obtained from the theoretical IR spectra, we found that the band at 551 cm^{-1} corresponds to the symmetric stretching vibration, ν_s(Pt–N). Calculations have also revealed that the frequency of the asymmetric Pt–N stretching vibration ν_a(Pt–N), which is at 559 cm^{-1}, is very close to ν_s(Pt–N). It is clear that both the symmetric and asymmetric Pt–N stretching vibrations in oxaliplatin contribute to a strong band observed in the experimental FT-IR spectrum at 573 cm^{-1}. The frequency of Pt–N stretching in oxaliplatin is higher in comparison to that in carboplatin and cisplatin. In the FT-Raman spectrum of cisplatin, the strongest band observed at 522 cm^{-1} and weaker band at 506 cm^{-1} were assigned to the symmetric and asymmetric Pt–N stretching vibrations [57], respectively. However in the FT-IR spectrum of carboplatin, the strong band at 545 cm^{-1} and a weak band at 548 cm^{-1} were assigned to the symmetric and asymmetric Pt–N stretching vibrations [58].

The theoretical results consistently indicate that the strong band at 780 cm^{-1} should be assigned to the asymmetric Pt–O stretching and the band at 854 cm^{-1} to the symmetric Pt–O stretching, coupled with the symmetric stretching of the C–C bond of the oxalate group. Similarly the very strong band at 808 cm^{-1} in the experimental FT-IR spectrum is assigned to the symmetric Pt–O stretching. The medium intensity band at 306 cm^{-1} in the calculated theoretical spectra is assigned to O–Pt–O bending. The band in the range of 50–173 cm^{-1} in the theoretically predicted IR spectrum is assigned to the N–Pt–O bending. Similarly the band at 195 cm^{-1} is assigned to the N–Pt–N bending. Comparison of the experimental and theoretical spectra has revealed that both the positions and intensities of the bands are well predicted by the PW-91 method.

3.6.2. Oxalate group vibrations

In the calculated theoretical spectrum, the very weak band at 339 cm^{-1} is assigned to the O–C=O in-plane bending. A strong band at 433 cm^{-1} is assigned to the O–C=O out-of-plane bending. The strong band at 1142 cm^{-1} in the calculated theoretical spectrum is assigned to the asymmetric C–O stretching. However, very strong bands at 1282 cm^{-1} and 1284 cm^{-1} are assigned to the Pt–O symmetric stretching, coupled with the C–C stretching. The band for C–O stretching in the experimental FT-IR occurs at 1226 cm^{-1}.

In the region 1550–1700 cm^{-1}, the ν(C=O) stretching vibrations and the NH_2 degenerate deformations, $\delta_d(NH_2)$ are expected to occur. In the FT-IR spectrum of oxaliplatin, two closely lying strong bands at 1662 and 1700 cm^{-1} are undoubtedly due to the C=O stretching vibrations; however, in the theoretical spectrum the bands at 1723 and 1741 cm^{-1} are assigned to the C=O stretching vibrations.

3.6.3. DACH group vibrations

The diaminocyclohexane ring vibrations are further discussed in two subsections:

3.6.3.1. Cyclohexane ring vibrations. In the calculated FT-IR spectrum of oxaliplatin, the strong band at 1039 cm^{-1} is assigned to the C–N stretching vibrations; similarly, in the theoretical spectrum the very strong band at 1012 cm^{-1} is assigned to the C–N stretching. In the theoretically calculated spectrum the bands at 1026–1062 cm^{-1} are assigned to the characteristic ν(C–C) stretching of the cyclohexane ring, similarly the strong band at 1106 cm^{-1} corresponds to the symmetric stretching of the C–C bond of the two carbons attached to nitrogens.

The scissoring vibrations of the methylene group in oxaliplatin are assigned to the bands observed at 1444 and 1456 cm^{-1} in the calculated theoretical spectrum. Similar results are recorded for the theoretical spectrum of carboplatin in which the scissoring vibrations of methylene group were observed at 1436 and 1463 cm^{-1} [58]. The band in the range of 2954–3058 cm^{-1} is assigned to the C–H stretching vibration in the calculated theoretical spectrum; similar bands at 2928 and 3085 cm^{-1} appear in the experimental FT-IR spectrum.

3.6.3.2. Amino group vibrations. The strong band at 3085, 3158 and 3212 cm^{-1} in the experimental FT-IR spectrum and the bands in the range of 3364–3460 cm^{-1} in the calculated theoretical spectrum are assigned to the N–H stretching vibrations of the amino groups of oxaliplatin.

The degenerate deformation vibration of ammonia gives a strong band at 1610 cm^{-1} in the FT-IR spectrum; similarly, we get two strong bands at 1609 and 1620 cm^{-1} which correspond to wagging of NH_2. The symmetric deformation vibrations of NH_2 are coupled with the degenerate deformation mode (twisting and wagging vibrations) of the methylene group and generate the medium intensity bands at 1444 and 1456 cm^{-1} in the calculated theoretical spectrum. However, in the experimental FT-IR spectrum, these vibrations give a very strong band at 1377 cm^{-1}. No peak corresponding to NH_2 rocking vibrations is found in the FT-IR spectrum since, as shown by theoretical calculations, NH_2 rocking vibrations give rise to the bands at 659 and 697 cm^{-1} of negligible intensity.

3.7. Oxaliplatin monohydrate

Al-Allaf et al. [59] synthesized crystals of oxaliplatin for X-ray determination. It was found that, although the complex was prepared starting from the enantiomerically pure isomer *trans-l* (1*R*,2*R*) as confirmed by X-ray analysis [45], it does not consist of the desired (1*R*,2*R*) isomer, but rather the (1*R*,2*S*) isomer. This encouraged them to prepare the platinum complex of the *cis* isomer of the DACH ligand in order to study its behavior from the X-ray point of view and to compare the results with those of the isomeric complex [Pt(C_2O_4){(1*R*,2*R*)-DACH}] reported previously [46]. It was seen that the [Pt(C_2O_4)(*cis*-DACH)] complex crystallizes with one molecule of water as [Pt(C_2O_4)(*cis*-DACH)] · H_2O in well-shaped colorless crystals.

The water molecule is reported to be placed at the oxalate end, in plane with the oxalate group and oriented to have two H-bonds with the two non-bound oxygens of the oxalate ligand [59]. We therefore restricted our studies to this position of the water molecule. The hydrated molecule thus has following structure:

3.7.1. Optimized geometries

The optimized geometry of *cis*-(*R*,*S*) was taken as calculated earlier. The water molecule is placed in such a way that the two hydrogen of the water molecule are in close contact with the two carbonyl oxygens of the oxalate ring, as has been previously reported [59], and geometry optimization was performed on the resulting structure. The numbering scheme and the optimized structure of [Pt(C_2O_4)(*cis*-DACH)] · H_2O are shown in Figs. 2 and 4.

The calculated bond lengths and bond angles for the [Pt(C_2O_4)(*cis*-DACH)] · H_2O isomer are listed in Table 3, together with the corresponding experimental data obtained from single crystal X-ray analysis of [Pt(C_2O_4)(*cis*-DACH)] · H_2O [59] to check the accuracy of our calculation.

It is found that the DFT results are in good agreement with the experimental data within the error range, considering that the former are obtained for the gas phase and the latter are for the solid state.

To gauge the effect of hydrogen bonding on the geometry and stabilization of the complex we compared the geometric parameters of the hydrated complex with the anhydrous complex. It is found that there is no major change in the geometric parameters of DACH in the hydrated and anhydrous [Pt(C_2O_4)(*cis*-DACH)] forms of the complex.

A slight change is noted in the geometric parameters of the coordination sphere. In the hydrated form, the equatorial N–Pt bond is shorter by 0.003 Å, while for the axial N–Pt bond this change is 0.008 Å. The O–Pt bond gets elongated by 0.003 Å. No change is noted in the equatorial N_1–C_1 bond, but the equatorial N_2–C_2 bond increases by 0.003 Å.

The effect on the bond lengths of the oxalate ring in the hydrated form is found to be larger, as expected. The O_1–C_7 and O_2–C_8 bond lengths decrease by 0.006 Å, while an increase in bond length by 0.004 Å is noted in case of the C_7–O_3 and C_8–O_4 bonds. The distance of 2.1 Å between the carbonyl oxygen of the oxalate group and the hydrogens of water, indicates hydrogen bonding between the two, as this is much smaller than the sum of the van der Waals radii of oxygen and hydrogen (2.72 Å).

3.7.2. Charge population analysis

Table 4 represents the calculated Hirshfeld partial atomic charges in [Pt(C_2O_4)(*cis*-DACH)] · H_2O and anhydrous [Pt(C_2O_4)(*cis*-DACH)]. No significant change is noted in the charge densities on the atoms of the DACH ring in the anhydrous and hydrated *cis* complex. A decrease of 0.03 in the negative charge on O_3 and O_4 is noted, showing the decrease in electron density at these two oxygens on hydration, as these two oxygens are directly involved in hydrogen bonding.

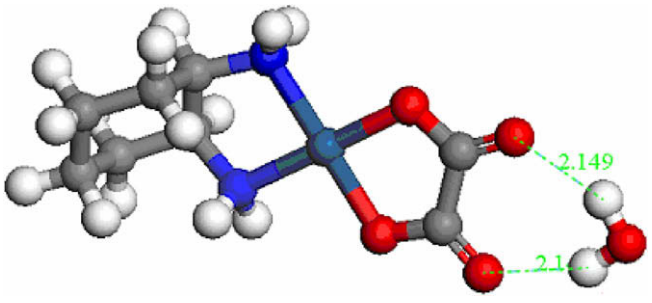

Fig. 4. Optimized structure for Pt(C_2O_4)(*cis*-DACH)] · H_2O.

3.7.3. Bond order analysis

We calculated the Mayer bond order for the bonds in [Pt(C_2O_4)(*cis*-DACH)] · H_2O, and the results are compared with those in the anhydrous [Pt(C_2O_4)(*cis*-DACH)] complex to find out the structural difference caused by the hydrogen bonding on the metal ligand binding. Table 5 shows the calculated bond orders for [Pt(C_2O_4)(*cis*-DACH)] · H_2O and the anhydrous complex.

Compared to the anhydrous complex, the Pt–N bond strengthens slightly, while the Pt–O bond becomes slightly weaker. Thus, coordination with a water molecule increases the capacity of oxalate as a leaving group. No significant change is noted in the bond orders of the bonds involved in the DACH ring for the hydrated and anhydrous forms.

The O_1–C_7 and O_2–C_8 bond orders increase by about 0.02. A major change is noted in case of the C_7–O_3 and C_8–O_4 bonds. The bond orders here decrease by about 0.05, which indicates the weakening of these bonds as a result of the transfer of electrons away from them, due to hydrogen bonding with water.

The O_3···H_1 and O_4···H_2 bond orders are expected to be zero, but a value of 0.04 is calculated, which indicates that hydrogen bonds have formed.

4. Conclusions

We have performed density functional calculations at the GGA-PW91 level in order to gain an understanding into the structure of the third generation anti-cancer drug, oxaliplatin. We have paid particular emphasis on the conformation of the DACH ligand and have found that the *trans* forms of the ligand are more stable than the *cis* form. However, of the two equally stable enantiomers, the *trans-l* (1*R*,2*R*) one is found to be more potent biologically. Since very minor differences are observed in the electronic structures of the two enantiomers, their difference in activity may be attributed to the chiral recognition of the ligand by DNA. The calculated vibrational frequencies are in good agreement with our experimental FT-IR spectrum. It has been observed that the *trans-d* (1*S*,2*S*) and the *cis*-(1*R*,2*S*) isomers are less active than the *trans-l* (1*R*,2*R*) isomer, but have similar activities. Calculations were also performed on the *cis* isomer and its monohydrate, experimental data on whose geometry is known. Comparison between the theoretically predicted geometries and the experimental ones yielded good correspondence, validating our methodology, although these calculations pertain to the gas phase, and the experimental data are for the solid state, in which crystal-field effects may affect the relative energies of the conformers and the geometries. In the biological environment, hydrogen bonding with the solvent is also expected to affect the relative energies of the conformers, but the good correspondence between our calculations and experimental data suggest that crystal packing and hydrogen bonding effects are negligible.

Acknowledgements

The authors thank University of Delhi's "Scheme to Strengthen R&D Doctoral Research Programme by Providing Funds to University Faculty". One of the authors (PG) also thanks the Council of Scientific and Industrial Research, New Delhi, for a Senior Research Fellowship.

References

[1] B. Rosenberg, L. Van Camp, T. Krigas, Nature 205 (1965) 698.
[2] B. Rosenberg, Platinum complexes for the treatment of cancer: Why the search goes on, in: B. Lippert (Ed.), Cisplatin Chemistry and Biochemistry of a Leading Anticancer Drug, Wiley-VCH, New York, 1999, p. 1.
[3] R.B. Weiss, M.C. Christian, Drugs 46 (1993) 360.
[4] D.S. Alberts, J.K. Noel, Anticancer Drugs 6 (1965) 369.
[5] M.P. Goren, R.K. Wright, M.E. Horowitz, Cancer Chemother. Pharmacol. 18 (1986) 69.
[6] F.P.T. Hamers, W.H. Gispen, J.P. Neijt, Eur. J. Cancer 27 (1991) 372.
[7] M.J. Cleare, J.D. Hoeschele, Bioinorg. Chem. 2 (1973) 187.
[8] T.A. Connors, M.J. Cleare, K.R. Harrap, Cancer Treat. Rep. 63 (1979) 1499.
[9] A.S. Abu-Surrah, Mini-Rev. Med. Chem. 7 (2007) 203.
[10] E. Raymond, S.G. Chaney, A. Taama, E. Cvitkovic, Ann. Oncol. 9 (1998) 1053.
[11] E. Raymond, S. Faivre, J. Woynarowski, S.G. Chaney, Semin. Oncol. 25 (1998) 4.
[12] P. Soulié, A. Bensma, C. Garrino, P. Chollet, E. Brain, M. Fereres, C. Jasmin, M. Musset, J.L. Misset, E. Cvitkovic, Eur. J. Cancer 33 (1997) 1400.
[13] P. Soulié, E. Raymond, S. Brienza, E. Cvitkovic, Bull. Cancer 84 (1997) 665.
[14] E. Cvitkovic, Cancer Treat. Rev. 24 (1998) 265.
[15] E. Cvitkovic, Brit J. Cancer 77 (1998) 8.
[16] J.F. Llory, P. Soulié, E. Cvitkovic, J.L. Misset, J. Natl. Cancer Inst. 86 (1994) 1098.
[17] Y. Kidani, K. Inagaki, M. Iigo, A. Hoshi, K. Kuretani, J. Med. Chem. 21 (1978) 1315.
[18] A. Ghezzi, M. Aceto, C. Cassino, E. Gabano, D. Osella, J. Inorg. Biochem. 98 (2004) 73.
[19] P. Carloni, M. Sprik, W. Andreoni, J. Phys. Chem. B 104 (2000) 823.
[20] J. Raber, C. Zhu, L.A. Eriksson, Mol. Phys. 102 (2004) 2537.
[21] J.V. Burda, M. Zeizinger, J. Leszczynski, J. Comput. Chem. 26 (2005) 907.
[22] J.K-C. Lau, D.V. Deubel, J. Chem. Theory Comput. 2 (2006) 103.
[23] T. Song, P. Hu, J. Chem. Phys. 125 (9) (2006). DOI:10.1063/1.233642, art. no. 091101.
[24] J.F. Lopes, V.S.d.A. Menezes, H.A. Duarte, W.R. Rocha, W.B. De Almeida, H.F. Dos Santos, J. Phys. Chem. B 110 (2006) 12047.
[25] A. Springer, C. Bürgel, V. Böhrsch, R. Mitrić, V. Bonaccčić-Koutecký, M.W. Linscheid, ChemPhysChem. 7 (2006) 1779.
[26] A. Robertazzi, J.A. Platts, Chem. Eur. J. 12 (2006) 5747.
[27] K. Spiegel, A. Magistrato, Org. Biomol. Chem. 4 (2006) 2507.
[28] J.V. Burda, J. Leszczynski, Inorg. Chem. 42 (2003) 7162.
[29] J.V. Burda, M. Zeizinger, J. Leszczynski, J. Chem. Phys. 120 (2004) 1253.
[30] J. Raber, C. Zhu, L.A. Eriksson, J. Phys. Chem. B 109 (2005) 11006.
[31] A. Robertazzi, J.A. Platts, Inorg. Chem. 44 (2005) 267.
[32] K. Spiegel, U. Rothlisberger, P. Carloni, J. Phys. Chem. B 108 (2004) 2699.
[33] M. Zeizinger, J.V. Burda, J. Leszczynski, J. Phys. Chem. Chem. Phys. 6 (2004) 3585.
[34] R. Wysokiński, K. Hernik, R. Szostak, D. Michalska, Chem. Phys. 333 (2007) 37.
[35] R. Wysokiński, J. Kuduk-Jaworska, D. Michalska, J. Mol. Struct.: THEOCHEM 758 (2006) 169.
[36] B. Delley, J. Chem. Phys. 92 (1990) 508.
[37] B. Delley, J. Chem. Phys. 94 (1991) 7245.
[38] B. Delley, J. Phys. Chem. 100 (1996) 6107.
[39] B. Delley, J. Chem. Phys. 113 (2000) 7756.
[40] B. Delley, Phys. Rev. B 66 (2002) 155125/1.
[41] R. Kakkar, R. Grover, P. Gahlot, Polyhedron 25 (2006) 759.
[42] R. Wysokiński, D. Michalska, J. Comput. Chem. 22 (2001) 901.
[43] I. Mayer, Int. J. Quantum Chem. 29 (1986) 477.
[44] E.L. Eliel, S.H. Wilen, L.N. Stereochemistry of Organic Compounds, Wiley, New York, 1994.
[45] A.S. Abu-Surrah, T.A.K. Al-Allaf, M. Klinga, M. Ahlgren, Polyhedron 22 (2003) 1529.
[46] M.A. Bruck, R. Bau, M. Noji, K. Inagaki, Y. Kidani, Inorg. Chem. Acta 92 (1984) 279.
[47] B. Spingler, D.A. Whittington, S.J. Lippard, Inorg. Chem. 40 (2001) 5596.
[48] P.M. Takahara, A.C. Rosenzweig, C.A. Frederick, S.J. Lippard, Nature 377 (1995) 649.
[49] Y. Wu, D. Bhattacharyya, C.L. King, I. Baskerville-Abraham, S.H. Huh, G. Boysen, J.A. Swenberg, B. Temple, S.L. Campbell, S.G. Chaney, Biochemistry 46 (2007) 6477.
[50] Y. Wu, P. Pradhan, J. Havener, G. Boysen, J.A. Swenberg, S.L. Campbell, S.G. Chaney, J. Mol. Biol. 341 (2004) 1251.
[51] J. Malina, O. Novakova, M. Vojtiskova, G. Natile, V. Brabec, Biophys J. 93 (2007) 3950.
[52] J. Kasparkova, M. Vojtiskova, G. Natile, V. Brabec, Chem. Eur. J. 14 (2007) 1330.
[53] R. Corradini, S. Sforza, T. Tedeschi, R. Marchelli, Chirality 19 (2007) 269.
[54] E. Tornaghi, W. Andreoni, P. Carloni, J. Hutter, M. Parinello, Chem. Phys. Lett. 246 (1995) 469.
[55] F.L. Hirshfeld, Theor. Chim. Acta 44 (1977) 129.
[56] K.B. Wiberg, P.R. Rablen, J. Comp. Chem. 14 (1993) 1504.
[57] D. Michalska, R. Wysokinski, Chem. Phys. Lett. 403 (2005) 211.
[58] R. Wysokinski, K. Kuduk-Jaworska, D. Michalska, J. Mol. Struct.: THEOCHEM 758 (2006) 169.
[59] T.A.K. Al-Allaf, L.J. Rashan, D. Steinborn, K. Merzweiler, C. Wagner, Transition Metal Chem. 28 (2003) 717.

to the identity of the $Mn^{III}/H_2salox/RCO_2^-$ (R = Ph) reaction system, i.e. the synthesis, structural and physical properties studies of the hexanuclear complexes $[Mn^{III}_6(\mu_3\text{-}O)_2(O_2CPh)_2(salox)_6(L_1)_2(L_2)_2] \cdot x MeCN \cdot y MeOH \cdot z H_2O \cdot w Me_2CO$ (L_1 = py, $L_2 = H_2O$, $x = 6$, $y = 0$, $z = 0$, $w = 0$ (**1**); $L_1 = Me_2CO$, $L_2 = H_2O$, $x = 0$, $y = 0$, $z = 0$, $w = 2$ (**2**); $L_1 = L_2$ = MeOH, $x = 0$, $y = 1$, $z = 0.5$, $w = 0$ (**3**)) and the 1D complexes $[Mn^{III}_3Na(\mu_3\text{-}O)(O_2CPh)_2(salox)_3(S)]_n \cdot nS$ (S = MeCN (**4**); S = Me_2CO (**5**)).

2. Experimental

2.1. General and spectroscopic measurements

All manipulations were performed under aerobic conditions using materials as received (Aldrich Co). All chemicals and solvents were of reagent grade. $[Mn^{III}_2Mn^{II}(\mu_3\text{-}O)(O_2CPh)_6(py)_2(H_2O)]$ [15] and $(NBu^n_4)[Mn^{III}_4O_2(O_2CPh)_9(H_2O)]$ [16] were synthesized as previously described. Elemental analysis for carbon, hydrogen, and nitrogen was performed on a Perkin Elmer 2400/II automatic analyzer. Infrared spectra were recorded as KBr pellets in the range 4000–400 cm^{-1} on a Bruker Equinox 55/S FT-IR spectrophotometer. Variable-temperature magnetic susceptibility measurements were carried out on polycrystalline samples of **1** and **5** using a Quantum Design MPMS SQUID susceptometer. DC data were collected in the 2–300 K temperature range under magnetic fields of 0.1, 0.5, 1, 2.5 and 5 T for **1** and under a field of 0.5 T for **5**. AC data for **1** were collected between 2 and 7.5 K, with an oscillating field of 1 G amplitude oscillating at frequencies of 0.1, 1, 10, 33, 99.9, 332, 997, 1400 Hz. Diamagnetic corrections for the complexes were estimated from Pascal's constants. The magnetic susceptibility of **5** has been computed by exact calculation of the energy levels associated with the spin Hamiltonian through diagonalization of the full matrix with a general program for axial symmetry [17]. Least-squares fittings were accomplished with an adapted version of the function-minimization program MINUIT [18]. The error factor R is defined as $R = \sum \frac{(x_{exp} - x_{calc})^2}{N x^2_{exp}}$, where N is the number of experimental points. ^1H pulsed NMR experiments on polycrystalline sample of **1** were performed at 2.4 T using a coherent spectrometer operating at 2.4 T (100 MHz for ^1H NMR). An Oxford 1200 CF continuous flow cryostat was employed for measurements in the range 5–300 K. The T_1 spin-lattice relaxation time was obtained using the standard saturation technique [19].

2.2. Compound preparations

2.2.1. $[Mn^{III}_6(\mu_3\text{-}O)_2(O_2CPh)_2(salox)_6(py)_2(H_2O)_2] \cdot 6MeCN$ (**1** · 6MeCN)

2.2.1.1. Method A. Solid H_2salox (0.014 g, 0.10 mmol) was added to a red brown solution of $[Mn_3(\mu_3\text{-}O)(O_2CPh)_6(py)_2(H_2O)]$ (0.108 g, 0.10 mmol) in MeCN (30 mL) and the resulting brown solution was refluxed for 1 h. Small portions of an orange-brown precipitate were filtered off, and the brown filtrate was left for slow evaporation. After 5 days, a mixture of green-brown prismatic crystals of **1** and orange cubic crystals were formed. The latter identified as the mixed-valence hexanuclear complex $[Mn^{II}_4Mn^{III}_2(\mu_4\text{-}O)_2(O_2CPh)_{10}(py)_2(H_2O)(MeCN)] \cdot 2MeCN$ by unit cell determination [20].

2.2.1.2. Method B. Solid H_2salox (0.069 g, 0.50 mmol) was added to a red brown solution of $[Mn_3(\mu_3\text{-}O)(O_2CPh)_6(py)_2(H_2O)]$ (0.184 g, 0.17 mmol) in MeCN (50 mL) and the resulting brown solution was refluxed for 1 h. The brown solution was left for slow evaporation and after 20 days green-brown prismatic crystals of **1** were formed, which were filtered off, washed with cold MeCN and dried *in vacuo* (yield: 0.093 g, 67% based on the metal). The resulting powder was analyzed as solvent free. $C_{66}H_{54}Mn_6N_8O_{20}$ requires: C, 49.27; H, 3.38; N, 6.96. Found: C, 49.02; H, 3.36; N, 6.93%. FT-IR (KBr pellets, cm^{-1}): 3450(br), 3054(w), 3013(w), 2927(w), 1598(vs), 1529(vs), 1472(m), 1440(vs), 1394(vs), 1358(w), 1324(m), 1283(vs), 1200(m), 1154(m), 1126(m), 1068(w), 1043(s), 1027(vs), 1009(m), 961(w), 918(s), 851(w), 826(m), 754(s), 721(s), 678(vs), 652(m), 625(w), 530(w), 472(m).

2.2.2. $[Mn^{III}_6(\mu_3\text{-}O)_2(O_2CPh)_2(salox)_6(Me_2CO)_2(H_2O)_2] \cdot 2Me_2CO$ (**2** · $2Me_2CO$)

2.2.2.1. Method A. Solid H_2salox (0.034 g, 0.25 mmol) was added to a refluxed red brown solution of $[Mn_3(\mu_3\text{-}O)(O_2CPh)_6(py)_2(H_2O)]$ (0.092 g, 0.085 mmol) in Me_2CO (30 mL) and the resulting brown solution was further refluxed for 15 min. Vapor diffusion of Et_2O to the brown reaction mixture afforded X-ray quality brown needle-like crystals of **2**, which were filtered off, and dried *in vacuo* (yield: 0.040 g, 60% based on the metal). The resulting powder was analyzed as solvent free. $C_{62}H_{56}Mn_6N_6O_{22}$ requires: C, 47.53; H, 3.60; N, 5.36. Found: C, 47.29; H, 3.57; N, 5.33%. FT-IR (KBr pellets, cm^{-1}): 3410(br), 3056(w), 3015(w), 1701(m), 1634(sh), 1597(vs), 1536(vs), 1472(s), 1440(vs), 1396(vs), 1327(m), 1282(vs), 1202(s), 1152(m), 1125(m), 1044(vs), 1028(vs), 956(w), 917(vs), 856(w), 825(m), 755(s), 722(s), 676(vs), 648(s), 550(w), 531(m), 465(s).

2.2.2.2. Method B. Solid H_2salox (0.034 g, 0.25 mmol) and solid NaOMe (0.027 g, 0.50 mmol) were added to a refluxed red brown solution of $[Mn_3(\mu_3\text{-}O)(O_2CPh)_6(py)_2(H_2O)]$ (0.092 g, 0.085 mmol) in Me_2CO (30 mL) and the resulting brown solution was further refluxed for 20 min. Small portions of a white precipitate (probably insoluble NaOMe) were filtered off, and the brown filtrate was layered with Et_2O/*n*-hex to afford brown crystals, which were filtered off and dried *in vacuo* (yield: 0.043 g, 65% based on the metal). The brown crystals were identified as compound **2** · $2Me_2CO$ by unit cell determination (a = 32.948(1), b = 32.948(1), c = 14.381(1) Å, V = 15611.6(2) $Å^3$, see Table 1).

2.2.3. $[Mn^{III}_6(\mu_3\text{-}O)_2(O_2CPh)_2(salox)_6(MeOH)_4] \cdot MeOH \cdot 0.5H_2O$ (**3** · $MeOH \cdot 0.5H_2O$)

Solid H_2salox (0.034 g, 0.25 mmol) and solid MeONa (0.027 g, 0.50 mmol) were added to a red brown solution of $[Mn_3(\mu_3\text{-}O)(O_2CPh)_6(py)_2(H_2O)]$ (0.092 g, 0.085 mmol) in MeOH (30 mL) and the resulting green-brown solution was refluxed for half hour, upon which time the solution turned to brown. Small portions of a dark brown precipitate were filtered off, and the brown filtrate was left for slow evaporation. After a period of one month, brown prismatic crystals of **3** were formed, which were filtered off, washed with cold MeOH and dried *in vacuo* (yield: 0.039 g, 60% based on the metal). The resulting powder was analyzed as solvent free. $C_{60}H_{56}Mn_6N_6O_{22}$ requires: C, 46.71; H, 3.66; N, 5.45. Found: C, 46.47; H, 3.63; N, 5.42%. FT-IR (KBr pellets, cm^{-1}): 3420(br), 3052(w), 3011(w), 2926(w), 1597(vs), 1527(vs), 1471(m), 1440(vs), 1393(vs), 1358(w), 1322(m), 1282(vs), 1200(m), 1154(m), 1126(m), 1067(w), 1042(s), 1027(vs), 1009(m), 960(w), 918(s), 851(w), 826(m), 755(s), 722(s), 679(vs), 652(m), 625(w), 531(w), 474(m).

2.2.4. $[Mn^{III}_3Na(\mu_3\text{-}O)(O_2CPh)_2(salox)_3(MeCN)]_n \cdot nMeCN$ (**4** · $nMeCN$)

2.2.4.1. Method A. Solid H_2salox (0.034 g, 0.25 mmol) and solid NaOMe (0.027 g, 0.50 mmol) were added to a refluxed red-brown solution of $[Mn_3(\mu_3\text{-}O)(O_2CPh)_6(py)_2(H_2O)]$ (0.092 g, 0.085 mmol) in MeCN (30 mL), and the resulting brown solution was further refluxed for half hour. Small portions of a white precipitate (probably insoluble NaOMe) were filtered off, and the brown filtrate was left undisturbed in closed vials. After one week X-ray quality brown needle-like crystals were formed, which were filtered off and dried *in vacuo* (yield: 0.053 g, 70% based on the metal). The resulting

Table 1
Crystallographic data for complexes **1** · 6MeCN, **2** · $2Me_2CO$, **3** · MeOH · $0.5H_2O$, **4** · *n*MeCN and **5** · nMe_2CO

	1 · 6MeCN	**2** · $2Me_2CO$	**3** · MeOH · $0.5H_2O$	**4** · *n*MeCN	**5** · nMe_2CO
Formula	$C_{78}H_{72}Mn_6N_{14}O_{20}$	$C_{68}H_{68}Mn_6N_6O_{24}$	$C_{61}H_{61}Mn_6N_6O_{23.5}$	$C_{39}H_{31}Mn_3N_5NaO_{11}$	$C_{41}H_{37}Mn_3N_3NaO_{13}$
Fw	1855.14	1682.92	1583.80	933.50	967.56
Space group	$P\bar{1}$	$I4_1/a$	$P\bar{1}$	$P2_1/c$	$P2_1/c$
T (°C)	25	25	−170	25	25
λ (Å)	Mo Kα (0.71073 Å)	Cu Kα (1.54187 Å)	Mo Kα (0.71069 Å)	Cu Kα (1.54187 Å)	Mo Kα (0.71069 Å)
a (Å)	12.588(7)	32.8892(6)	12.797(1)	14.5372(3)	15.2662(9)
b (Å)	12.841(7)	32.8892(6)	14.146(2)	17.6493(3)	17.8828(10)
c (Å)	13.438(7)	14.3012(3)	19.830(2)	16.1490(3)	16.1926(10)
α (°)	77.16(2)		86.310(3)		
β (°)	77.89(2)		69.983(3)	108.2725(7)	93.456(2)
γ (°)	87.81(2)		81.465(3)		
V Å^3	2070.6(2)	15469.6(5)	3335.2(7)	3934.5(1)	4412.6(5)
Z	1	8	2	4	4
ρ_{calc} (g cm^{-3})	1.488	1.445	1.577	1.576	1.456
μ (mm^{-1})	0.965 (Mo Kα)	8.382 (Cu Kα)	1.184 (Mo Kα)	8.405 (Cu Kα)	0.920 (Mo Kα)
R_1[a]	0.0660[b]	0.0475[c]	0.0773[d]	0.0524[e]	0.0972[f]
wR_2[a]	0.1769[b]	0.1236[c]	0.1938[d]	0.0969[e]	0.2270[f]

[a] $w = 1/[\sigma^2(F_o^2)+(aP)^2 + bP]$ and $P = (\max(F_o^2,0) + 2F_c^2)/3$; $R_1 = \sum(|F_o| - |F_c|)/\sum(|F_o|)$ and $wR_2 = \{\sum[w(F_o^2 - F_c^2)^2]/\sum[w(F_o^2)^2]\}^{1/2}$.
[b] For 5740 reflections with $I > 2\sigma(I)$.
[c] For 4251 reflections with $I > 2\sigma(I)$.
[d] For 6754 reflections with $I > 2\sigma(I)$.
[e] For 5301 reflections with $I > 2\sigma(I)$.
[f] For 3739 reflections with $I > 2\sigma(I)$.

powder was analyzed as solvent free. $C_{37}H_{28}Mn_3N_4NaO_{11}$ requires: C, 49.80; H, 3.16; N, 6.28. Found: C, 49.55; H, 3.14; N, 6.24%. FT-IR (KBr pellets, cm^{-1}): 3428(br), 3056(w), 3012(w), 2927(w), 1654(s), 1596(vs), 1534(vs), 1473(s), 1440(vs), 1394(vs), 1367(s), 1322(m), 1277(vs), 1203(s), 1152(m), 1121(m), 1105(w), 1067(w), 1040(sh), 1022(vs), 957(w), 916(vs), 853(w), 825(m), 758(s), 720(s), 707(s), 672(vs), 653(sh), 551(w), 531(m), 478(m), 462(s).

2.2.4.2. Method B. Solid H_2salox (0.014 g, 0.10 mmol) and solid $NaClO_4 \cdot H_2O$ (0.028 g, 0.20 mmol) were added to a red-brown solution of $(NBu^n_4)[Mn_4O_2(O_2CPh)_9(H_2O)]$ (0.040 g, 0.025 mmol) in MeCN (30 mL). The resulting brown solution was refluxed for 45 min. Layer of Et_2O to the brown reaction mixture afforded X-ray quality brown crystals which were filtered off and dried *in vacuo* (yield: 0.014 g, 63% based on the metal). The brown crystals were identified as compound **4** · *n*MeCN by unit cell determination (a = 14.554(2), b = 17.670(3), c = 16.168(3) Å, β = 108.258(6)°, V = 3948.6(2) Å^3, see Table 1).

*2.2.5. $[Mn^{III}_3Na(\mu_3\text{-}O)(O_2CPh)_2(salox)_3(Me_2CO)]_n \cdot nMe_2CO$ (**5** · nMe_2CO)*

Solid H_2salox (0.014 g, 0.10 mmol) and solid $NaClO_4 \cdot H_2O$ (0.028 g, 0.20 mmol) were added to a red-brown solution of $(NBu^n_4)[Mn_4O_2(O_2CPh)_9(H_2O)]$ (0.040 g, 0.025 mmol) in Me_2CO (30 mL). The resulting brown solution was refluxed for 45 min. Layering or vapor diffusion of Et_2O or Et_2O/*n*-hex to the brown reaction mixture afforded X-ray quality brown crystals which were filtered off and dried *in vacuo* (yield: 0.024 g, 74% based on the metal). The resulting powder was analyzed as solvent free. $C_{41}H_{37}Mn_3N_3NaO_{13}$ requires: C, 50.90; H, 3.86; N, 4.34. Found: C, 50.64; H, 3.84; N, 4.31. FT-IR (KBr pellets, cm^{-1}): 3422(br), 3057(w), 3011(w), 2930(w), 1705(m), 1652(s), 1595(vs), 1537(vs), 1472(s), 1440(vs), 1395(vs), 1365(s), 1323(m), 1278(vs), 1204(s), 1154(m), 1123(m), 1106(w), 1069(w), 1040(sh), 1024(vs), 959(w), 917(vs), 854(w), 826(m), 759(s), 721(s), 706(s), 673(vs), 653(sh), 550(w), 531(m), 478(m), 462(s).

2.3. Single-crystal X-ray crystallography

A green-brown prismatic crystal of **1** (0.18 × 0.36 × 0.70 mm) was mounted in capillary. Diffraction measurements were made on a Crystal Logic Dual Goniometer diffractometer using graphite-monochromated Mo Kα radiation. Unit cell dimensions were determined and refined by using the angular settings of 25 automatically centred reflections in the range 11° < 2θ < 23°. Three standard reflections monitored every 97 reflections showed less than 3% intensity fluctuation and no decay. Lorentz, polarization corrections were applied using Crystal Logic software. Brown crystals of **2** (0.08 × 0.12 × 0.60 mm), **4** (0.08 × 0.25 × 0.25 mm), and **5** (0.08 × 0.55 × 0.65 mm) were mounted in capillaries with drops of mother liquor. A brown crystal of **3** (0.09 × 0.09 × 0.19 mm) was taken directly from the mother liquor and immediately cooled to −170 °C. Diffraction measurements for **2–5** were made on a Rigaku R-AXIS SPIDER Image Plate diffractometer using graphite monochromated Mo Kα (**3**, **5**) and Cu Kα radiation (**2**, **4**). Data collection (ω-scans) and processing (cell refinement, data reduction and empirical absorption correction) were performed using the CRYSTALCLEAR program package [21]. Important crystal data and parameters for data collection are reported in Table 1. The structures were solved by direct methods using SHELXS-97 [22] and refined by full matrix least-squares techniques on F^2 with SHELXL-97 [23]. Further experimental crystallographic details for **1**: $2\theta_{max}$ = 50°; reflections collected/unique/used, 7648/7276 [R_{int} = 0.0217]/7276; 611 parameters refined; $(\Delta/\sigma)_{max}$ = 0.004; $(\Delta\rho)_{max}/(\Delta\rho)_{min}$ = 1.192/−01.409 e/Å^3; R/R_w (for all data), 0.0830/0.1955. Hydrogen atoms were located by difference maps and were refined isotropically, except those of the coordinated pyridine and the solvate molecules which were introduced at calculated positions as riding on bonded atoms. All non-H atoms were refined anisotropically. The crystals of **2** were very thin needles. Repeating efforts to increase their size proved unsuccessful. Data were collected to $2\theta_{max}$ = 144° but only those to $2\theta_{max}$ = 125° were used for the refinement, since in greater θ values more than 50% of the collected data were unobserved. Further experimental crystallographic details for **2**: $2\theta_{max}$ = 125°; reflections collected/unique/used, 31770/5864 [R_{int} = 0.0491]/5864; 557 parameters refined; $(\Delta/\sigma)_{max}$ = 0.008; $(\Delta\rho)_{max}/(\Delta\rho)_{min}$ = 0.564/−0.341 e/Å^3; R/R_w (for all data), 0.0758/0.1423. Hydrogen atoms were located by difference maps and were refined isotropically, except those of the methyl groups which were introduced at calculated positions as riding on bonded atoms. All non-H atoms were refined anisotropically. The crystals of **3** were very small in size. Repeating efforts to increase their size proved unsuc-

cessful. Data were collected to $2\theta_{max} = 55°$ but only those to $2\theta_{max} = 46.5°$ were used for the refinement, since in greater θ values more than 50% of the collected data were unobserved. Further experimental crystallographic details for **3**: reflections collected/unique/used, 19418/9471 [$R_{int} = 0.0684$]/9471; 884 parameters refined; $(\Delta/\sigma)_{max} = 0.007$; $(\Delta\rho)_{max}/(\Delta\rho)_{min} = 0.847/-0.673$ e/Å^3; R/R_w (for all data), 0.1034/0.2107. Hydrogen atoms were introduced at calculated positions as riding on bonded atoms; no H-atoms for the water solvate molecule were included in the refinement. All non-H atoms were refined anisotropically. The solvate water molecule was refined anisotropically with occupation factor fixed to 0.50. Further experimental crystallographic details for **4**: $2\theta_{max} = 144.1°$; reflections collected/unique/used, 27919/7418 [$R_{int} = 0.0662$]/7418; 634 parameters refined; $(\Delta/\sigma)_{max} = 0.005$; $(\Delta\rho)_{max}/(\Delta\rho)_{min} = 0.418/-0.705$ e/Å^3; R/R_w (for all data), 0.0814/0.1110. Hydrogen atoms were located by difference maps and were refined isotropically, except those of the methyl groups which were introduced at calculated positions as riding on bonded atoms. All non-H atoms were refined anisotropically. The crystals of **5** showed poor diffraction ability (despite their sufficient size) and signs of twinning. Data were collected to $2\theta_{max} = 54°$ but only those to $2\theta_{max} = 45°$ were used for the refinement, since in greater θ values more than 50% of the collected data were unobserved. The twinning problem was handled by omitting reflections showing large F^2_o compared to the expected F^2_c values because an exact twin law could not be found. As it was proved after the solution of the structure, compound **5** is analogous to **4** thus we felt that the complete structural characterization would not add further significant information to our work. Therefore, we have not attempted to improve the quality of the crystals. Further experimental crystallographic details for **5**: $2\theta_{max} = 45°$; reflections collected/unique/used, 40444/5493 [$R_{int} = 0.1240$]/5493; 554 parameters refined; $(\Delta/\sigma)_{max} = 0.017$; $(\Delta\rho)_{max}/(\Delta\rho)_{min} = 2.162/-0.608$ e/Å^3; R/R_w (for all data), 0.1204/0.2448. Hydrogen atoms were introduced at calculated positions as riding on bonded atoms. All non-H atoms were refined anisotropically.

3. Results and discussion

3.1. Syntheses

Previous investigation of the use of H_2salox in manganese carboxylate chemistry by Perlepes and his co-workers has led to the hexanuclear compounds $[Mn^{III}_6(\mu_3\text{-}O)_2(O_2CR)_2(salox)_6(EtOH)_4]$ (R = Me, Ph) [14] isolated from the 1:1 $Mn(O_2CR)_2 \cdot 2H_2O/H_2$salox molar ratio reaction in EtOH. Both complexes exhibit single-molecule magnetism (SMM) behaviour [24], and have been isolated under identical reaction conditions suggesting that the nature of the carboxylate ligand does not affect the identity of the products. Recently Brechin and co-workers have expanded this family of clusters by changing the carboxylate groups and/or by introducing steric bulk at the oximate carbon atom [25]; these modifications led to dramatic improvement of the SMM properties [25b,c]. In order to further investigate the parameter space of this reaction system, we have decided to modify other key factors and in particular: (i) the Mn/H_2salox stoichiometry, (ii) the reaction media, (iii) the source of the manganese ions, (iv) the addition of base and/or counterions, and (v) the crystallization method, in order to study their influence on the metal ions' topology, oxidation state and nuclearity. Thus, reaction of one equivalent of $[Mn^{III}_2Mn^{II}(\mu_3\text{-}O)(O_2CPh)_6(py)_2(H_2O)]$ with one equivalent of H_2salox in MeCN and slow evaporation of the reaction mixture afforded green-brown prismatic crystals of $[Mn^{III}_6(\mu_3\text{-}O)_2(O_2CPh)_2(salox)_6(py)_2(H_2O)_2]$ (**1**) and orange cubic crystals of the known mixed-valence hexanuclear complex $[Mn^{II}_4Mn^{III}_2(\mu_4\text{-}O)_2(O_2CPh)_{10}(py)_2(H_2O)(MeCN)]$ [20] in mixture. With the identity of **1** established by X-ray crystallography the stoichiometric Mn:H_2salox reaction has been performed which afforded pure **1** for further physical measurements (Scheme 1). Further investigation of

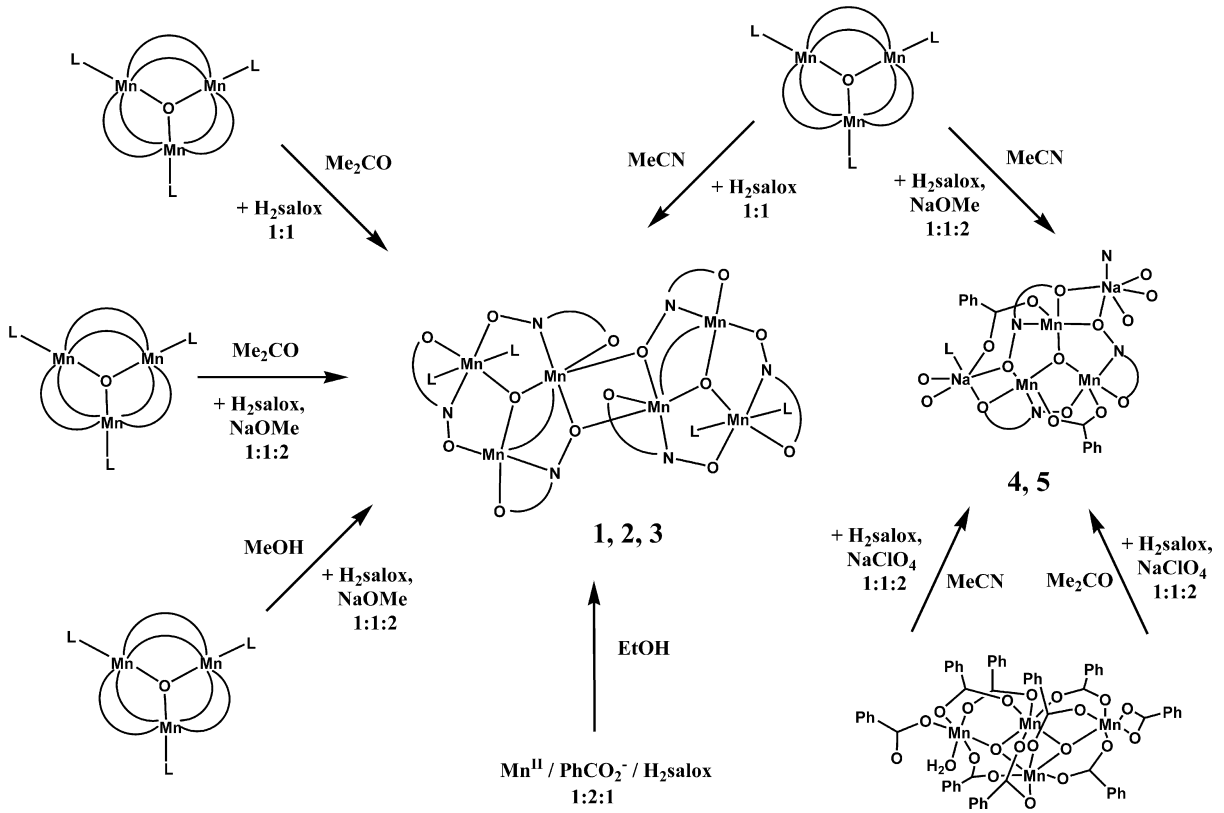

Scheme 1. The synthetic routes employed for the preparation of **1**–**5** (see text for details).

the reaction media, by reaction of one equivalent of $[Mn^{III}_2Mn^{II}(\mu_3\text{-}O)(O_2CPh)_6(py)_2(H_2O)]$ with three equivalents of H_2salox in Me_2CO afforded compound $[Mn^{III}_6O_2(O_2CPh)_2(salox)_6(Me_2CO)_2(H_2O)_2]$ (**2**) either by slow evaporation or layering of Et_2O or vapour diffusion of Et_2O or Et_2O/*n*-hexane (Scheme 1).

Compounds **1** and **2** are quite similar to the previously reported hexanuclear complexes $[Mn_6(\mu_3\text{-}O)_2(O_2CR)_2(salox)_6(EtOH)_4]$ (R = Me, Ph), suggesting that these species are spontaneously formed, perhaps due to their thermal and/or thermodynamic stability, and/or their insolubility in the reaction solvent. Thus, changes in the source of the manganese ions and the reaction media have not affected the identity of the product isolated, whereas the change of the reactants stoichiometry (excess of manganese ions in the case of **1**) most likely promotes the simultaneous isolation of the known mixed-valence compound $[Mn^{II}_4Mn^{III}_2(\mu_4\text{-}O)_2(O_2CPh)_{10}(py)_2(H_2O)(MeCN)]$. Of course the presence of other more soluble species in the reaction mixture cannot be excluded.

In order to examine the influence of the base and/or counterions we have employed reactions analogous to those leading to **1** and **2** in the presence of NaOMe and/or $NaClO_4.H_2O$. Thus, reaction of one equivalent of $[Mn^{III}_2Mn^{II}(\mu_3\text{-}O)(O_2CPh)_6(py)_2(H_2O)]$ with three equivalents of H_2salox in the presence of six equivalents of NaOMe in MeOH yielded compound $[Mn^{III}_6O_2(O_2CPh)_2(salox)_6(MeOH)_4]$ (**3**), which is completely analogous to **1** and **2**. On the other hand, the analogous reaction in MeCN yielded only the 1D complex $[Mn^{III}_3Na(\mu_3\text{-}O)(O_2CPh)_2(salox)_3(MeCN)]_n$ (**4**) whose structure is completely different than **1**–**3**, whereas the same reaction mixture in Me_2CO afforded only **2** as confirmed by X-ray crystallography (Scheme 1). Finally the reaction of one equivalent of $(NBu^n_4)[Mn^{III}_4O_2(O_2CPh)_9(H_2O)]$ with four equivalents of H_2salox in the presence of eight equivalents of $NaClO_4 \cdot H_2O$ in MeCN also afforded compound **4**, whereas the analogous reaction in Me_2CO afforded the 1D complex $[Mn^{III}_3Na(\mu_3\text{-}O)(O_2CPh)_2(salox)_3(Me_2CO)]_n$ (**5**) which is analogous to **4** (Scheme 1).

In conclusion, the reaction media, the use of oligonuclear manganese complexes as starting materials and the crystallization methods have not affected the identity of the hexanuclear complexes **1**–**3**, whereas analogous modifications on the salicylaldoximato iron(III) carboxylate chemistry revealed that the reaction media is determinative for the identity of the product. Trinuclear $[Fe_3(\mu_3\text{-}O)(O_2CPh)_5(salox)(L_1)(L_2)]$ ($L_1 = L_2$ = MeOH, L_1 = EtOH and $L_2 = H_2O$ depending on the reaction solvent) [10] or hexanuclear $[Fe_6(\mu_3\text{-}O)_2(O_2CPh)_{10}(salox)_2(L)_2]$ ($L = H_2O$, $MeCONH_2$) [8a] complexes have been isolated from alcoholic or MeCN solutions, respectively; the former being transformed to the latter by simple recrystallization from MeCN solutions. Compounds **1**–**3** and $[Fe_6(\mu_3\text{-}O)_2(O_2CPh)_{10}(salox)_2(L)_2]$ contain the same $[M^{III}_6(\mu_3\text{-}O)_2(\mu_2\text{-}OR)_2]^{12+}$ core, although the rest of the ligation pattern is different. On the other hand, the presence of sodium ions in the reaction mixtures in MeCN and Me_2CO, either as NaOMe or $NaClO_4 \cdot H_2O$, revealed dramatic changes to the identity of the products isolated yielding the 1D complexes **4** and **5**.

3.2. Description of structures

Compound **1** crystallizes in the triclinic space group $P\bar{1}$ with one molecule per unit cell. The molecular structure of **1** is given in Fig. 1 and selected bond distances and angles are listed in Table 2. The structure contains the $[Mn_6(\mu_3\text{-}O)_2(\mu_2\text{-}OR)_2]^{12+}$ core, whose topology consists of six manganese(III) ions arranged as two centrosymmetrically related off-set stacked $[Mn_3(\mu_3\text{-}O)]^{7+}$ subunits bridged by two oximato oxygen atoms (O(12) and O(12′)). In each $[Mn_3(\mu_3\text{-}O)]^{7+}$ subunit, there are two Mn···Mn pairs [Mn(1)/Mn(3) and Mn(1)/Mn2)] bridged by a μ_2 oxide and a μ_2-κ*O*:κ*O*′:κ*N* salox^{2-} ligand, while the third pair [Mn(2)/Mn(3)] is further bridged by a μ_2 benzoato ligand. The coordination

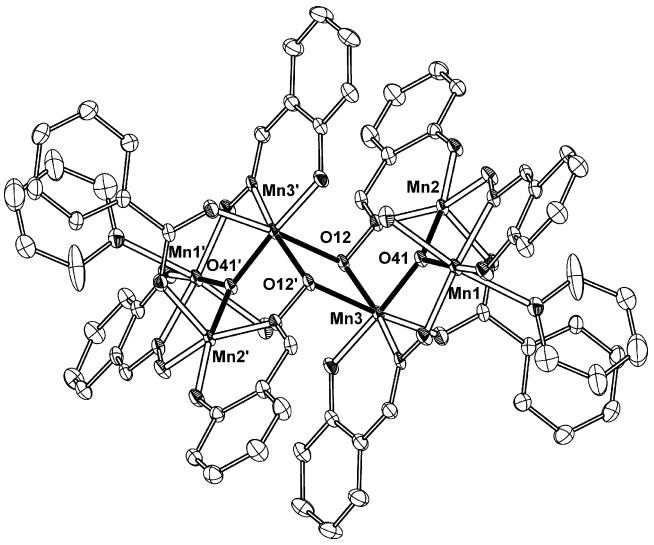

Fig. 1. Partially labelled ORTEP plot of **1** with ellipsoids drawn at the 30% probability level. For clarity hydrogen atoms have been omitted. Primed atoms are generated by symmetry (′ = −*x*, 2 − *y*, 1 − *z*).

geometry around Mn(1) is distorted octahedral where the equatorial positions are occupied by one salox^{2-} ligand (through $O_{phenolic}$ and $N_{oximato}$ atoms), the $O_{oximato}$ atom of a second salox^{2-} ligand and the oxide group, while the Jahn–Teller axis of the octahedron is completed by a pyridine and a coordinated water molecule. The coordination geometry around Mn(2) is square pyramidal comprised by one salox^{2-} ligand (through $O_{phenolic}$ and $N_{oximato}$ atoms), the $O_{oximato}$ atom of a second salox^{2-} ligand and the oxide group occupying the equatorial plane, while the apical position is occupied by an oxygen atom of the μ_2 benzoato ligand. Finally, the coordination geometry about Mn(3) is distorted octahedral comprised by one salox^{2-} ligand (through $O_{phenolic}$ and $N_{oximato}$ atoms), the oxide group and the $O_{oximato}$ atom of a second salox^{2-} directed in the equatorial plane of the octahedron, while the Jahn–Teller positions are completed by a benzoato oxygen and an $O_{oximato}$ atom of a third salox^{2-} ligand. Thus, in each $[Mn_3(\mu_3\text{-}O)]$ subunit two of the salox^{2-} ligands adopt the common μ_2-κ*O*:κ*O*′:κ*N* coordination mode, while the third one presents the rare μ_3-κ^2*O*:κ*O*′:κ*N* coordination mode (Scheme 2), that has been also observed in $[Mn_6(\mu_3\text{-}O)_2(O_2CR)_2(salox)_6(R'OH)_4]$ [14,25a], $[Fe_6(\mu_3\text{-}O)_2(O_2CPh)_{10}(salox)_2(H_2O)_2]$ [8a], and in $[M^{III}_6(\mu_3\text{-}O)_2(salox)_6(\mu_2\text{-}O_2CR)_2(OH_2)_2\ (RCN)_2]$ (M = V^{III}, Cr^{III}, Mn^{III}, Fe^{III}, $RCO_2^- = Ph_3CCO_2^-$, $Me_3CCO_2^-$, $Ph_2C(OH)CO_2^-$, $PhCO_2^-$, $C_2H_5CO_2^-$) [26], but also in trinuclear and tetranuclear complexes [27].

The three Mn^{III} ions in each $[Mn_3(\mu_3\text{-}O)]^{7+}$ subunit form an almost isosceles triangle (see Table 2). The Mn(2)···Mn(3) separation (3.158(2) Å) is shorter than the other two in the triangular subunit (3.248(5), 3.273(5) Å) due to the presence of the extra benzoate bridge. The Mn···Mn distance in the central $[Mn_2(\mu_2\text{-}O)_2]$ core is 3.335(5). The central μ_3-O^{2-} ion in each $[Mn_3(\mu_3\text{-}O)]$ subunit is displaced at 0.17 Å out of the $[Mn_3]$ mean plane, an observation that has been also seen in the analogous compound $[Mn_6(\mu_3\text{-}O)_2(O_2CR)_2(salox)_6(R'OH)_4]$ [14,25a] as well as in the trinuclear complexes $[Mn_3(\mu_3\text{-}O)(O_2CR)_3(mpko)_3](ClO_4)$ (R = Me, Et, Ph; mpkoH = methyl-2-pyridyl ketone oxime, 0.30 Å) [28]. The Mn–O_{oxo} bond distances are in the range 1.863–1.881 Å. The Mn–$O_{phenoxo}$ and the Mn–$N_{oximato}$ bond lengths are ~1.86 and ~2.0 Å, respectively. The Mn–$O_{oximato}$ chelating bond distances are ~1.94 Å while the corresponding bridging bond distances are significantly longer (2.420 Å). All the salox^{2-} ligands are planar and make an angle of 5.1°, 13.3° and 28.7° (for the salox^{2-} ligands defined by O(1), O(11), and O(21), respectively) with the $[Mn_3]$ mean

Table 2
Selected bond distances (Å) and angles (°) for complex **1** · 6MeCN

Distances					
Mn(1)–O(1)	1.859(3)	Mn(2)–O(11)	1.864(3)	Mn(3)–O(21)	1.866(3)
Mn(1)–O(41)	1.882(3)	Mn(2)–O(41)	1.862(3)	Mn(3)–O(41)	1.868(3)
Mn(1)–O(22)	1.922(3)	Mn(2)–O(2)	1.900(3)	Mn(3)–O(12)	1.942(3)
Mn(1)–N(1)	1.998(4)	Mn(2)–N(11)	2.011(4)	Mn(3)–N(21)	1.998(4)
Mn(1)–O(w)	2.310(4)	Mn(2)–O(31)	2.123(4)	Mn(3)–O(32)	2.137(4)
Mn(1)–N(41)	2.391(4)	Mn(1)···Mn(2)	3.273(5)	Mn(3)–O(12′)	2.419(3)
Mn(1)···Mn(3)	3.248(5)	Mn(2)···Mn(3)	3.158(2)	Mn(3)···Mn(3′)	3.335(5)
Angles					
O(1)–Mn(1)–O(41)	174.5(2)	O(11)–Mn(2)–O(41)	169.4(2)	O(21)–Mn(3)–O(41)	175.6(2)
O(1)–Mn(1)–O(22)	88.8(2)	O(11)–Mn(2)–O(2)	87.2(1)	O(21)–Mn(3)–O(12)	88.4(1)
O(41)–Mn(1)–O(22)	92.3(1)	O(41)–Mn(2)–O(2)	91.0(2)	O(41)–Mn(3)–O(12)	89.8(1)
O(1)–Mn(1)–N(1)	91.9(2)	O(11)–Mn(2)–N(11)	89.0(2)	O(21)–Mn(3)–N(21)	90.9(2)
O(41)–Mn(1)–N(1)	87.6(1)	O(41)–Mn(2)–N(11)	89.4(1)	O(41)–Mn(3)–N(21)	89.9(1)
O(22)–Mn(1)–N(1)	174.8(2)	O(2)–Mn(2)–N(11)	161.4(2)	O(12)–Mn(3)–N(21)	165.9(2)
O(1)–Mn(1)–Ow	88.2(2)	O(11)–Mn(2)–O(31)	98.1(2)	O(21)–Mn(3)–O(32)	94.1(2)
O(41)–Mn(1)–Ow	86.3(1)	O(41)–Mn(2)–O(31)	92.5(1)	O(41)–Mn(3)–O(32)	90.1(1)
O(22)–Mn(1)–Ow	97.8(2)	O(2)–Mn(2)–O(31)	104.2(2)	O(12)–Mn(3)–O(32)	96.6(2)
N(1)–Mn(1)–Ow	87.5(2)	N(11)–Mn(2)–O(31)	94.3(2)	N(21)–Mn(3)–O(32)	97.5(2)
O(1)–Mn(1)–N(41)	89.3(2)	Mn(1)–O(41)–Mn(2)	121.9(2)	O(21)–Mn(3)–O(12′)	88.9(1)
O(41)–Mn(1)–N(41)	96.1(1)	Mn(1)–O(41)–Mn(3)	120.1(2)	O(41)–Mn(3)–O(12′)	86.8(1)
O(22)–Mn(1)–N(41)	90.9(2)	Mn(2)–O(41)–Mn(3)	115.7(2)	O(12)–Mn(3)–O(12′)	80.8(1)
N(1)–Mn(1)–N(41)	83.9(2)	Mn(3)–O(12)–Mn3′)	99.2(1)	O(32)–Mn(3)–O(12′)	176.0(1)
Ow–Mn(1)–N(41)	170.9(2)			N(21)–Mn(3)–O(12′)	85.1(1)

Symmetry transformations used to generate equivalent atoms: ′ = −*x*, 2 − *y*, 1 − *z*.

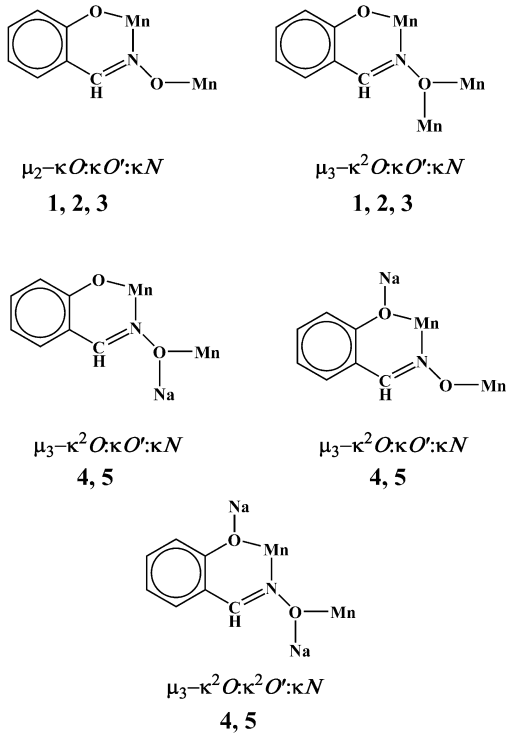

Scheme 2. The coordination modes of salox^{2-} ligands in the structures of **1**–**5** (see text for details).

plane. The benzoate ligands are coordinated through the common *syn*,*syn* μ$_2$-κ*O*:κ*O*′ mode. The Mn–O$_{carboxylate}$ bond distances are ~2.13 Å. There is a moderate twisting of the Mn–O–N–Mn moieties within each Mn$_3$ subunit; this is evidenced by the Mn–N–O–Mn torsion angles which are 5.9°, 22.3° and 19.8° for the Mn(1)/Mn(2), Mn(2)/Mn(3) and Mn(3)/Mn(1) pairs (and their symmetry-equivalents), respectively.

Compound **2** crystallizes in the tetragonal space group $I4_1/a$, with eight molecules per unit cell, and compound **3** crystallizes in the triclinic space group $P\bar{1}$ with two half molecules in the asymmetric unit. The molecular structures of **2** and **3** (Figs. 2 and 3, respectively) are completely analogous to **1** and they will not be discussed further. Selected bond distances and angles are given as Supplementary material (Tables S1 and S2, respectively); a comparison of their structural characteristics with those of **1** is given in Table 4.

Compound **4** crystallizes in the monoclinic space group $P2_1/c$ with one molecule per asymmetric unit. The molecular structure of **4** consists of anionic trinuclear oxo-centered units, [Mn$^{III}_3$(μ$_3$-O)(O$_2$CPh)$_2$(salox)$_3$]$^-$, sodium cations and MeCN molecules. An ORTEP plot of the structure of **4** is given in Fig. 4, selected bond distances and angles are listed in Table 3. The trinuclear anion contains a central [Mn$_3$(μ$_3$-O)]$^{7+}$ core, in which two Mn···Mn pairs [Mn(1)/Mn(2) and Mn(2)/Mn(3)] are bridged by a μ$_2$ oxide and a μ$_2$-κ*O*:κ*O*′:κ*N* salox^{2-} ligand, while the third pair [Mn(1)/Mn(3)] is further bridged by a μ$_2$ benzoato ligand. The coordination geometry

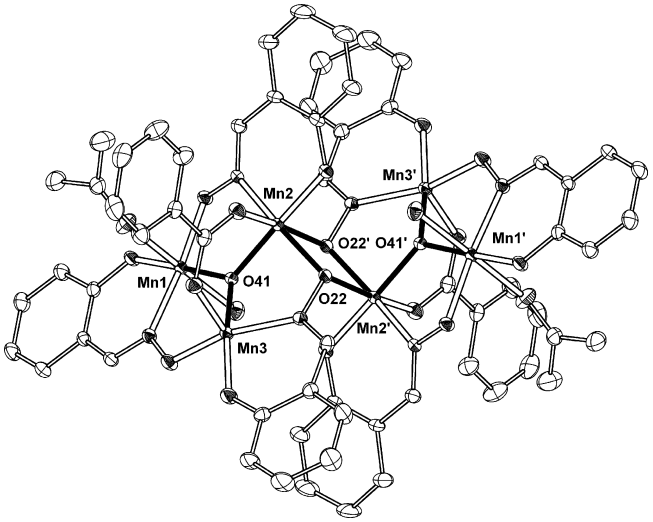

Fig. 2. Partially labelled ORTEP plot of **2** with ellipsoids drawn at the 30% probability level. For clarity hydrogen atoms have been omitted. Primed atoms are generated by symmetry (′ = 1 − *x*, 1 − *y*, −*z*).

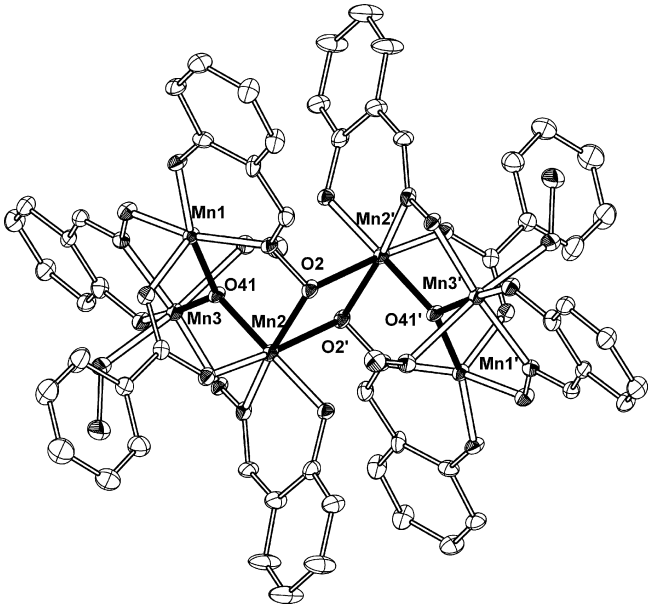

Fig. 3. Partially labelled ORTEP plot of one of the crystallographically independent hexanuclear molecules in the structure of **3** with ellipsoids drawn at the 30% probability level. For clarity hydrogen atoms have been omitted. Primed atoms are generated by symmetry (′ = 1 − *x*, −*y*, −*z*).

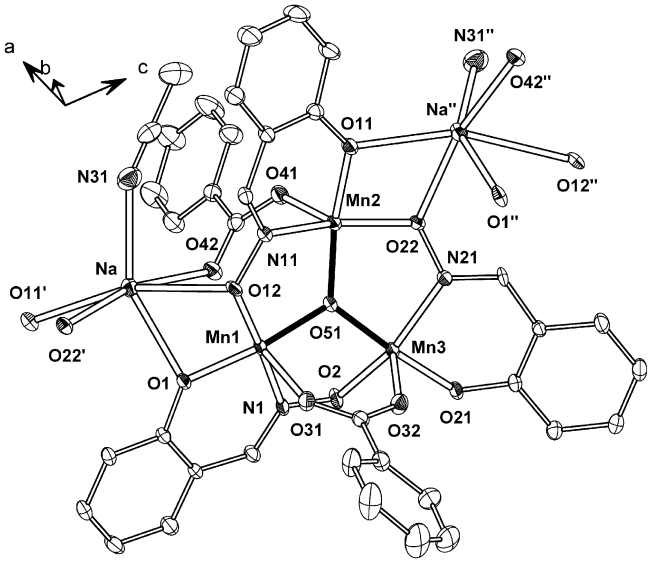

Fig. 4. Partially labelled ORTEP plot of a small fragment of the chains of **4** with ellipsoids drawn at the 30% probability level. For clarity hydrogen atoms have been omitted. Symmetry transformations used to generate equivalent atoms: ′ = *x*, 0.5 − *y*, −0.5 + *z*; ″ = *x*, 0.5 − *y*, 0.5 + *z*.

around each Mn^{III} ion is square pyramidal where the basal positions are occupied by one $salox^{2-}$ ligand (through $O_{phenolic}$ and $N_{oximato}$ atoms), the $O_{oximato}$ atom of a second $salox^{2-}$ ligand and the oxide group, and the apical position is occupied by a carboxylato oxygen atom [O(31), O(41) and O(32) for Mn(1), Mn(2) and Mn(3), respectively].

The three Mn^{III} ions in the $[Mn_3(\mu_3\text{-}O)]^{7+}$ subunit form a scalene triangle with edges 3.138(1)–3.305(1) Å (Table 3). The central $\mu_3\text{-}O^{2-}$ ion lies in the plane defined by the three Mn^{III} ions, as in the case of the 'basic carboxylates' of the general formula $[M^{III}_3(\mu_3\text{-}O)(O_2CR)_6(L)_3]^+$ (M = Mn, Fe, Cr; L = neutral monodentate ligands) [29], suggesting that the replacement of the carboxylato and monodentate ligands by the tridentate $salox^{2-}$ ligand has not affected the structural characteristics of the planar $[Mn_3(\mu_3\text{-}O)]^{7+}$ core. The Mn–O_{oxo} bond distances are in the range 1.845–1.867 Å. The average Mn–$O_{phenoxo}$, Mn–$O_{oximato}$ and Mn–$N_{oximato}$ bond lengths are 1.863, 1.914 and 2.008 Å, respectively.

All the $salox^{2-}$ ligands are planar and make an angle of 18.6°, 16.8° and 25.8° (for the $salox^{2-}$ ligands defined by O(1), O(11), and O(21), respectively) with the $[Mn_3]$ mean plane. The three $salox^{2-}$ ligands adopt different coordination modes, bridging pairs of Mn^{III} ions of the anionic complex with the sodium cations. Two of the $salox^{2-}$ ligands (defined by O(1) and O(21)) adopt the $\mu_3\text{-}\kappa^2O{:}\kappa O'{:}\kappa N$ coordination mode bridging Mn(3)/Mn(1) and Mn(3)/Mn(2) pairs to Na through the μ_2 phenoxo oxygen O(1) and through the μ_2 oximato oxygen O(22), respectively. The third $salox^{2-}$ ligand (defined by O(11)) adopts the $\mu_4\text{-}\kappa^2O{:}\kappa^2O'{:}\kappa N$ coordination mode bridging Mn(1)/Mn(2) pair to two adjacent Na atoms through the μ_2 phenoxo oxygen O(11) and through the μ_2 oximato oxygen O(12). The coordinational flexibility of the $salox^{2-}$ ligands is reflected in the Mn–N–O–Mn torsion angles in the Mn_3 subunit, suggesting a moderate twisting of the Mn–O–N–Mn moieties in the case of $\mu_3\text{-}\kappa^2O{:}\kappa O'{:}\kappa N$ ligands (22.1° and 16.7° for the Mn(1)/Mn(3) and Mn(3)/Mn(2) pairs, respectively), whereas the same moiety is planar (0.8° for the Mn(2)/Mn(1) pair) in the case of the $\mu_4\text{-}\kappa^2O{:}\kappa^2O'{:}\kappa N$ ligand.

The two benzoato ligands also adopt different coordination modes. One of them bridges Mn(1) and Mn(3) in the trinuclear anion through the common *syn,syn* $\mu_2\text{-}\kappa O{:}\kappa O'$ coordination mode, whereas the second one bridges the trinuclear anion to the sodium cation through the *syn,anti* $\mu_2\text{-}\kappa O{:}\kappa O'$ coordination mode. The Mn–$O_{carboxylate}$ bond distances range from 2.045 to 2.170 Å. The coordination geometry around the Na^+ ions is distorted octahedral comprised of two phenoxo and two oximato oxygen atoms belonging to four $salox^{2-}$ ligands, one carboxylato oxygen atom and one MeCN molecule. Each Na^+ ion is triply and doubly bridged to its adjacent trinuclear anions forming 1D polymeric arrays which extend parallel to the crystallographic *c*-axis. The Na–O bond interatomic distances range from 2.406 to 2.673 Å.

Compound **5** crystallizes in the monoclinic space group $P2_1/c$ with one molecule per asymmetric unit, and is completely analogous to **4**; the only difference being the solvate molecule coordinated to the Na^+ ions. An ORTEP plot of a small fragment of the chains of **5** is given in Fig. 5, selected bond distances and angles are given as Supplementary material (Table S3), and a comparison of its structural characteristics with those of **4** is given in Table 4.

Compounds **1**–**5** join a small family of structurally characterized Mn complexes with the mono-($Hsalox^-$) and/or the dianion ($salox^{2-}$) of salicylaldoxime as ligand. Other members are the "butterfly" complex $[Mn^{III}_4O_2(salox)_2L_3L'_2](ClO_4)$ [30], where L is the diphenylglycolate(−1) ligand and L′ is 1,4,7-trimethyl-1,4,7-triazacyclononane, and the structurally similar $[Mn^{III}_6O_2(O_2CR)_2(salox)_6(R'OH)_4]$ (R = H, Me, Ph; R′ = Me, Et) mentioned above [14,25a]. Compounds **1**–**3** are also members of a small family of Mn^{III}_6 complexes whose cores are based on two linked trinuclear $[Mn^{III}_3(\mu_3\text{-}O)]^{7+}$ subunits [14,25,31]. Compounds **4** and **5** represent the first trinuclear oxo-centered Mn^{III} anionic complexes with $salox^{2-}$. Recently, a neutral trinuclear oxo-centered Mn^{III} complex has been reported which contains Me-$salox^{2-}$, compound $[Mn_3O(O_2CMe)(Me\text{-}salox)_3(py)_4]$ [32].

3.3. Magnetic susceptibility studies

3.3.1. DC susceptibility

The $\chi_M T$ product of **1** (Fig. 6) at 300 K (1 T) is 15.62 $cm^3\ mol^{-1}$ K, lower than the theoretically expected value for six non-interacting $S = 2$ spins (18.01 $cm^3\ mol^{-1}$ K, $g = 2$), indicating the interplay of antiferromagnetic interactions. Upon cooling, this progressively decreases to a minimum of

Table 3
Selected bond distances (Å) and angles (°) for complex **4** · *n*MeCN

Distances					
Mn(1)–O(1)	1.865(3)	Mn(2)–O(51)	1.845(2)	Mn(3)–O(21)	1.856(3)
Mn(1)–O(51)	1.867(2)	Mn(2)–O(11)	1.869(3)	Mn(3)–O(51)	1.865(2)
Mn(1)–O(12)	1.915(3)	Mn(2)–O(22)	1.920(2)	Mn(3)–O(2)	1.906(3)
Mn(1)–N(1)	1.992(3)	Mn(2)–N(11)	2.028(3)	Mn(3)–N(21)	2.003(3)
Mn(1)–O(31)	2.170(3)	Mn(2)–O(41)	2.045(3)	Mn(3)–O(32)	2.085(3)
Na–O(22′)	2.406(3)	Na–N(31)	2.419(5)	Na–O(42)	2.490(3)
Na–O(1)	2.414(3)	Na–O(11′)	2.451(3)	Na–O(12)	2.673(3)
Mn(1)···Mn(2)	3.206(1)	Mn(1)···Mn(3)	3.138(1)	Mn(2)···Mn(3)	3.305(1)
Mn(1)···Na	3.187(2)	Mn(2)···Na″	3.443(2)		
Angles					
O(1)–Mn(1)–O(51)	169.4(1)	O(51)–Mn(2)–O(11)	167.5(1)	O(21)–Mn(3)–O(51)	174.8(1)
O(1)–Mn(1)–O(12)	86.9(1)	O(51)–Mn(2)–O(22)	89.2(1)	O(21)–Mn(3)–O(2)	90.7(1)
O(51)–Mn(1)–O(12)	92.7(1)	O(11)–Mn(2)–O(22)	85.7(1)	O(51)–Mn(3)–O(2)	90.9(1)
O(1)–Mn(1)–N(1)	90.8(1)	O(51)–Mn(2)–N(11)	89.2(1)	O(21)–Mn(3)–N(21)	90.7(1)
O(51)–Mn(1)–N(1)	89.0(1)	O(11)–Mn(2)–N(11)	90.7(1)	O(51)–Mn(3)–N(21)	85.8(1)
O(12)–Mn(1)–N(1)	176.2(1)	O(22)–Mn(2)–N(11)	155.2(1)	O(2)–Mn(3)–N(21)	155.1(1)
O(1)–Mn(1)–O(31)	98.6(1)	O(51)–Mn(2)–O(41)	95.9(1)	O(21)–Mn(3)–O(32)	91.3(1)
O(51)–Mn(1)–O(31)	92.1(1)	O(11)–Mn(2)–O(41)	96.7(1)	O(51)–Mn(3)–O(32)	93.4(1)
O(12)–Mn(1)–O(31)	93.4(1)	O(22)–Mn(2)–O(41)	111.0()	O(2)–Mn(3)–O(32)	98.1(1)
N(1)–Mn(1)–O(31)	89.9(1)	N(11)–Mn(2)–O(41)	93.9(1)	N(21)–Mn(3)–O(32)	106.8(1)
O(22′)–Na–O(1)	86.3(1)	N(31)–Na–O(11′)	108.9(1)	O(22′)–Na–O(12)	99.2(1)
O(22′)–Na–N(31)	108.0(1)	O(22′)–Na–O(42)	165.2(1)	O(1)–Na–O(12)	61.2(1)
O(1)–Na–N(31)	149.0(1)	O(1)–Na–O(42)	79.1(1)	N(31)–Na–O(12)	88.8(1)
O(22′)–Na–O(11′)	64.1(1)	N(31)–Na–O(42)	83.8(1)	O(11′)–Na–O(12)	158.3(1)
O(1)–Na–O(11′)	102.1(1)	O(11′)–Na–O(42)	121.5(1)	O(42)–Na–O(12)	71.4(1)
Mn(2)–O(51)–Mn(3)	125.9(1)	Mn(2)–O(51)–Mn(1)	119.5(1)	Mn(3)–O(51)–Mn(1)	114.5(1)
Mn(1)–O(12)–Na	86.3(1)	Mn(1)–O(1)–Na	95.4(1)	Mn(2)–O(11)–Na″	104.9(1)
Mn(2)–O(22)–Na″	104.9(1)				

Symmetry transformations used to generate equivalent atoms: ′ = *x*, 0.5 − *y*, −0.5 + *z*; ″ = *x*, 0.5 − *y*, 0.5 + *z*.

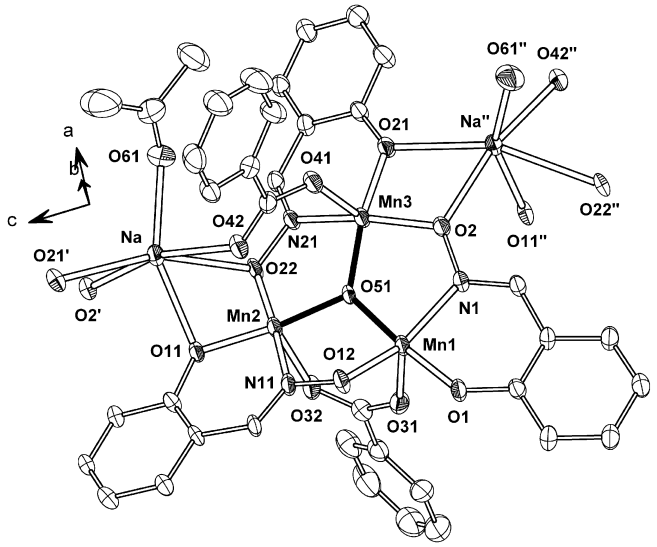

Fig. 5. Partially labelled ORTEP plot of a small fragment of the chains of **5** with ellipsoids drawn at the 30% probability level. For clarity hydrogen atoms have been omitted. Symmetry transformations used to generate equivalent atoms: ′ = *x*, 0.5 − *y*, 0.5 + *z*; ″ = *x*, 0.5 − *y*, −0.5 + *z*.

7.63 $cm^3\ mol^{-1}\ K$ at 30 K, and then increases to a maximum of 9.22 $cm^3\ mol^{-1}\ K$ at 10 K, before falling to 4.71 $cm^3\ mol^{-1}\ K$ at 2 K. This overall behaviour shows the interplay of both ferro- and antiferromagnetic interactions. The drop below 10 K is associated with zero-field splitting effects of the Mn^{III} ions. The maximum around 10 K is field-dependent, being suppressed and shifted to higher temperatures with increase of the applied magnetic field. This is attributed to the additional Zeeman splitting of the ground multiplet.

The overall behavior is very similar to that encountered in complexes $[Mn_6(\mu_3\text{-}O)_2(O_2CR)_2(salox)_6(EtOH)_4]$ (R = Me, Ph) [8], which is in accord with the structural similarities of the complexes. *M* versus HT^{-1} plots (Fig. 6) confirm that in **1** an $S = 4$ ground state is also stabilized. Fits of the low-temperature data, and assuming a well-isolated ground state, yield values of $|D| \sim 0.5\ cm^{-1}$ and $g = 2.00$ for the ground state. The magnitude of *D* for the ground state of complex **1**, is lower than the values previously reported ($|D| = 1.22$ [14] and 1.39 cm^{-1} [25a]) for the respective Mn_6 complexes with $S = 4$ ground states. Although these fits qualitatively confirm the ground state as an $S = 4$ one, they fail to accurately reproduce the data, probably due to the existence of low-lying excited states. This is to be expected, given the relatively weak exchange couplings between Mn^{III} ions, which lead to a closely

Table 4
Structural characteristics of compounds **1**–**5**

	Mn···Mn in $[Mn_3O]$ core (Å)	Mn···Mn in $[Mn_2O_2]$ core (Å)	Displacement of O^{2-}/$[Mn_3]$ plane (Å)	Mn–N–O–Mn torsion angle (average) (°)
1	3.159(2)–3.274(5)	3.335(5)	0.17	6.1, 19.7, 22.5 (16.1)
2	3.163(2)–3.268(2)	3.314(2)	0.17	1.1, 21.6, 24.5 (15.7)
3[a]	3.150(1)–3.278(2)	3.287(2)	0.18	6.6, 22.7, 32.9 (20.7)
	3.164(2)–3.262(2)	3.304(2)	0.20	13.1, 13.3, 29.8 (18.7)
4	3.138(1)–3.305(1)		0.00	0.8, 16.7, 22.1 (13.2)
5	3.142(2)–3.301(2)		0.00	2.5, 14.0, 22.6 (13.0)

[a] For the two crystallographically independent molecules in the asymmetric unit.

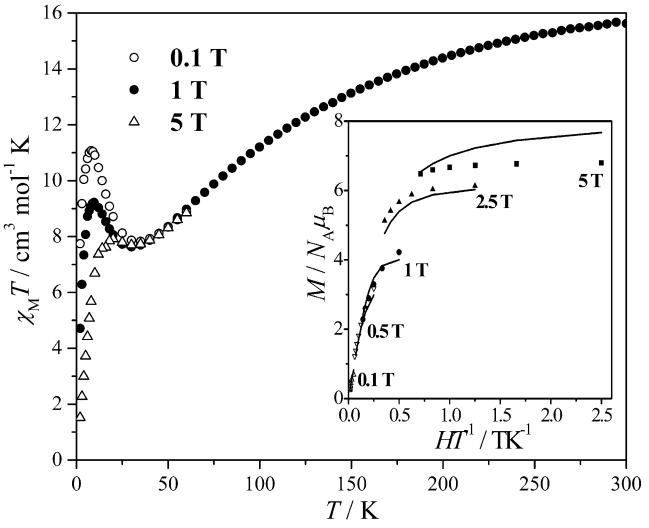

Fig. 6. $\chi_M T$ vs. T data for **1** under various magnetic fields. The M vs. HT^{-1} dependence along with a fit assuming an isolated $S = 4$ ground state are shown in the inset.

spaced energy spectrum. Thus, the values of the above fits should not be considered as quantitatively accurate.

The $S = 4$ ground state is in accord [25] with the moderate twisting of the Mn–N–O–Mn moieties within each Mn_3 subunit, the average torsion angle being $\alpha_v = 16°$. Brechin and co-workers recently showed [25b,c] that when this twisting in this family of Mn_6^{III} SMMs becomes severe (as a consequence of the use of bulky substituents on the oximate carbon), e.g. $\alpha_v = 36.5°$ or 39.1°, the resulting ground state is $S = 12$ and record U_{eff} values up to 86.4 K can be achieved.

The $\chi_M T$ product of **5** (Fig. 7) at 300 K (0.5 T) is 6.64 cm^3 mol^{-1} K, lower than the theoretically expected value for three non-interacting $S = 2$ spins (9.00 cm^3 mol^{-1} K, $g = 2$), indicating the interplay of antiferromagnetic interactions. Upon cooling, this rapidly decreases, attaining a value of 0.51 cm^3 mol^{-1} K at 2 K.

In order to interpret the experimental data, an isosceles model of three interacting $S = 2$ spins was assumed, based on the repeating unit of the complex. Due to its polymeric structure, intra-unit interactions are expected, while significant single-ion zero-field splitting parameters D, are also common for Mn^{III} complexes. The former was accounted for by a mean-field correction term zj, while the latter by an axial zfs parameter D, common for all spins ($D = D_1 = D_2 = D_3$). Initial fitting attempts over 2–300 K yielded very poor results. It was then decided that the intramolecular interactions might be too complex to be successfully accounted for by a mean-field term, while the single-ion zfs parameters might be substantially different for the three sites. In addition, it was also acknowledged that since both parameters zj and D are mainly manifested in the low temperature range, inclusion of both in our model might lead to overparametrization of our problem. Thus, a simpler model was used, considering only the intra-unit exchange couplings, while the data over the 300–100 K range were fitted. The corresponding Hamiltonian is given in Eq. (1):

$$\hat{H} = -2[J_1(\hat{\mathbf{S}}_1\hat{\mathbf{S}}_2 + \hat{\mathbf{S}}_1\hat{\mathbf{S}}_3) + J_1\hat{\mathbf{S}}_2\hat{\mathbf{S}}_3] \quad (1)$$

Best-fit parameters for this model were $J_1 \sim J_2 = -11.8$ cm^{-1}, $g = 2.01$ with $R = 4.1 \times 10^{-5}$, corresponding to a $S = 2$ ground state.

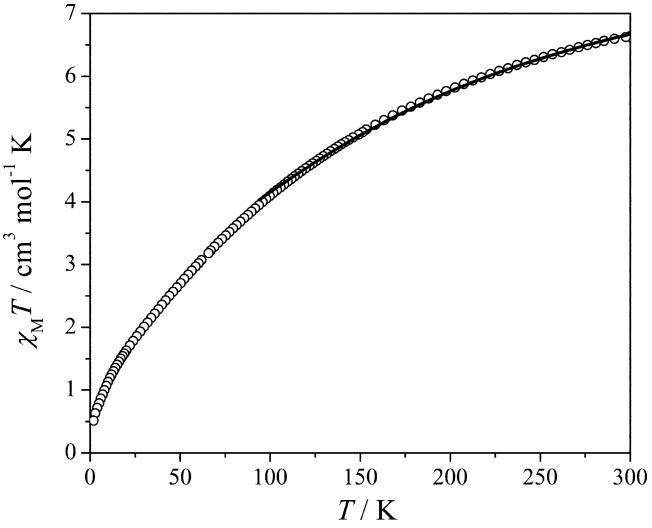

Fig. 7. $\chi_M T$ vs. T data for **5** and best fit according to the model described in the text.

3.3.2. AC susceptibility

Given the pronounced similarities of **1** with $[Mn_6(\mu_3\text{-}O)_2(O_2CR)_2(salox)_6(EtOH)_4]$ (R = Me, Ph), we decided to test whether it also behaves as an SMM. Thus, in order to probe its relaxation properties, AC susceptibility experiments were carried out at low temperatures (Fig. 8). These showed characteristic out-of-phase signals attributed to slow magnetic relaxation phenomena. The signals show clear maxima between 2.13 K (10 Hz) and 3.50 K (1400 Hz). For lower frequencies the maxima occur below 1.9 K, which is the lower limit of our instrument. Fits of these data to an Arrhenius law, $\tau = \tau_0 \cdot e^{U_{eff}/k_BT}$, yielded parameters

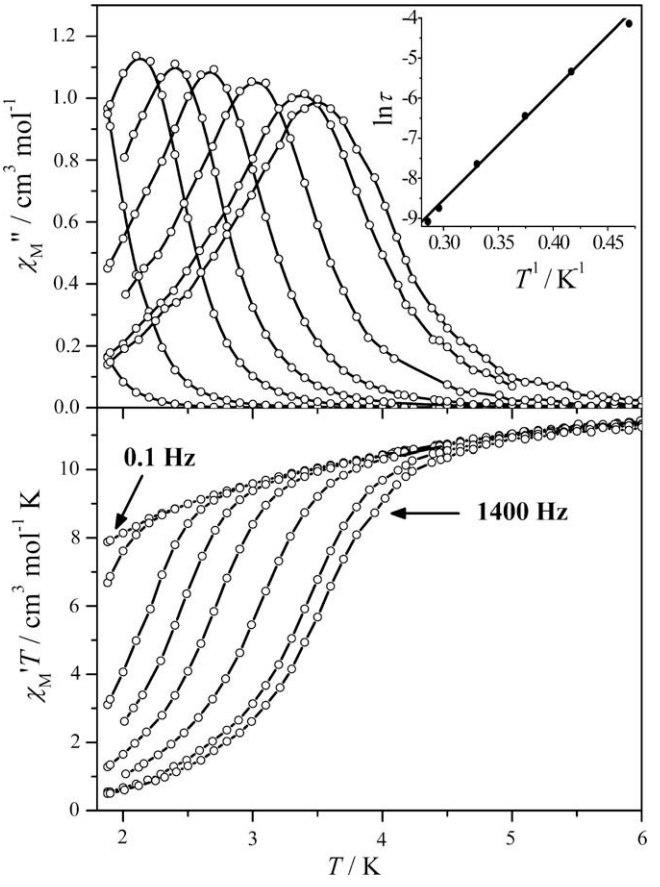

Fig. 8. χ'_M (top) and $\chi''_M T$ vs. T data for **1** between 1.9 and 6 K for oscillating magnetic fields of 0.1, 1, 10, 33, 100, 333, 1000 and 1400 Hz. A fit of the out-of-phase data to an Arrhenius law is shown in the inset.

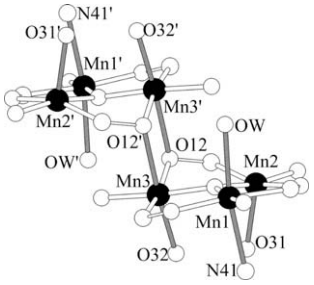

Fig. 9. Simplified view of **1**, showing the coordination spheres of the Mn^{III} ions. The Jahn–Teller elongated bonds (shown in gray) are roughly parallel to each other.

$\tau_0 = 5.5 \times 10^{-8}$ s and $U_{eff} = 27.4$ K = 19.0 cm^{-1}. For an $S = 4$ ground state and considering that $\Delta E = S^2|D| > U_{eff}$, it turns that the lowest limit for $|D|$ is 1.2 cm^{-1}, or in other words $D < -1.2$ cm^{-1}. These results are in close agreement with the results obtained for $[Mn_6(\mu_3\text{-}O)_2(O_2CR)_2(salox)_6(R'OH)_4]$ (R = H, Me, Ph; R′ = Me, Et) [14,25a].

The relatively high value of D predicted by the relaxation experiments deserves some comment. Generally speaking, the anisotropy of the ground state is related to the single-ion anisotropies of the coupled spins. The projection of each single-ion anisotropy on the molecular anisotropy axis (i.e. the z-axis) contributes to the total anisotropy. High-spin ($S = 2$) Mn^{III} ions, are highly anisotropic ions, with their easy axes coinciding with their Jahn–Teller axes. In the case of **1** we observe that the Jahn–Teller elongation axes are roughly parallel (Fig. 9). This should have an important effect on the total D value. We should note that for a D value of -1.2 cm^{-1}, a cluster like Mn_{12} ($S = 10$) should present a spin-reversal energy barrier of ca. 120 cm^{-1}. This relatively high D value should be responsible for the fact that clear out-of-phase signals are observed despite the relatively low spin ($S = 4$) of the ground state.

3.4. Solid state NMR studies

Nuclear magnetic resonance is a powerful tool in order to probe the internal fields that are present in paramagnetic and magnetic solids. In particular the nuclear T_1 spin-lattice relaxation is sensitive to the electron spin dynamics of the system since the nuclei under investigation probe the fluctuating local magnetic fields induced at the nuclear sites through the hyperfine interaction.

The ^1H T_1 spin-lattice relaxation time of complex **1** was measured at an applied magnetic field $H = 2.4$ T, between room and liquid-helium temperatures. The nuclear relaxation rate $1/T_1$ as a function of temperature is shown in Fig. 10.

At high temperatures $1/T_1$ is nearly temperature independent while below 70 K the rate increases exponentially with an appearance of a peak at around 15 K. This behaviour has been frequently encountered in previous ^1H NMR studies of molecular clusters, rings and single-molecule magnets and it is observed when the temperature is of the order of the magnetic exchange constant J/k_B between the magnetic ions [33].

In these molecular clusters, due to finite size of the spin system, the low-lying energy states are well separated among themselves and at low temperatures, the spin dynamics is governed by magnetic excitations between the ground state and the next excited state separated by an energy difference Δ. This energy difference Δ is largely determined by the exchange interaction J/k_B and the peak of the nuclear relaxation rate $1/T_1$ occurs when the temperature is of the order of the energy gap. Thus the appearance of the NMR peak provide us with a direct estimate of the energy difference between the ground state and the first excited state and can be compared with results of magnetic measurements.

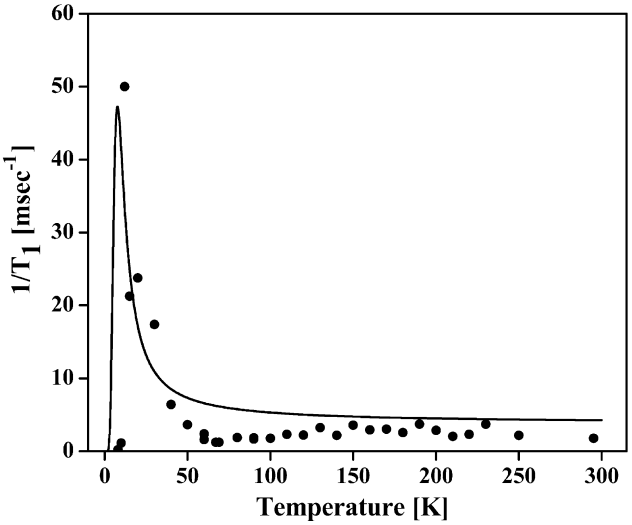

Fig. 10. ^1H NMR $1/T_1$ spin-lattice relaxation rate of complex **1** as a function of temperature (solid line represents the fitted data according to Eq. (2)).

For the analysis of the NMR data, we adopt a simple model, originally proposed by Hardeman et al. [34] based on a two level scheme for the fluctuations of the orientation of the magnetic moment.

In this model the NMR relaxation is caused by the local field fluctuations originating from the magnetic excitations from the ground state to the excited state, separated by the energy difference Δ. Assuming that the Mn spin system remains in the ground state for an average time τ_0 and in the excited state for a lifetime τ_1, during which an effective transverse local field $h_\perp$ appears at the nuclear site, the relaxation rate is expressed as [34]

$$\frac{1}{T_1} = (\gamma_N h_\perp)^2 \frac{\tau_1 \tau_0}{(\tau_1 + \tau_0)^2} \frac{\tau}{(\omega_N \tau)^2 + 1} \tag{2}$$

where

$$\frac{1}{\tau} = \frac{1}{\tau_0} + \frac{1}{\tau_1},$$

γ_N is the proton gyromagnetic ratio and ω_N is the Larmor angular frequency.

This model has been frequently employed for the nuclear magnetic relaxation in paramagnets [29d,33a,35].

Considering an activation-type process for the excitation, we set

$$\frac{1}{\tau_0} = B_0 \exp\left(-\frac{\Delta}{k_B T}\right) \tag{3}$$

where Δ represents the energy-level spacing between the ground state and the first excited state. For the lifetime τ_1 we consider a temperature independent term:

$$1/\tau_1 = C_1 \tag{4}$$

Setting $\nu_N = 100$ MHz ($H = 4.7$ T), and using Eqs. (3) and (4), the experimental NMR points are fitted to Eq. (2), shown as solid line in Fig. 10. The fitted parameters are $\Delta/k_B = 20$ K for the energy gap and $B_0 = 5\times10^9$ s^{-1} and $C = 5\times10^8$ s^{-1}, which are slow fluctuations of the order of the Larmor frequency. We observe that the line describes the overall experimental features rather well.

Therefore the NMR analysis of the low-frequency dynamics of the Mn electron spin system clearly demonstrates the existence of a sizeable energy gap between the ground state and the first excited multiple. Also we have given a measure of the magnitude

of the local-field fluctuations present in the electronic spin system.

4. Conclusions

Three hexanuclear compounds presenting the $[Mn_6(\mu_3\text{-}O)_2(\mu_2\text{-}OR)_2]^{12+}$ core, complexes $[Mn^{III}_6(\mu_3\text{-}O)_2(O_2CPh)_2(salox)_6(L_1)_2(L_2)_2]$ (L_1 = py, L_2 = H_2O (**1**); L_1 = Me_2CO, L_2 = H_2O (**2**); L_1 = L_2 = MeOH (**3**)) have been prepared. The influence of the reactants stoichiometry, the reaction media, the use of oligonuclear manganese clusters as starting materials and crystallization, on the isolation of the congener compounds **1**–**3** is negligible. On the other hand, the presence of Na^+ ions (either as NaOMe or $NaClO_4 \cdot H_2O$) in the corresponding MeCN and Me_2CO solutions, dramatically influenced the identity of the products, yielding the 1D complexes $[Mn^{III}_3Na(\mu_3\text{-}O)(O_2CPh)_2(salox)_3(S)]_n$ (S = MeCN (**4**), Me_2CO (**5**)). The magnetic properties of the representative compounds **1** (hexanuclear) and **5** (polymeric) have been studied. The magnetic susceptibility measurements from polycrystalline samples of **1** revealed the interplay of both ferro- and antiferromagnetic interactions stabilizing an $S = 4$ ground state as confirmed by M versus HT^{-1} plots. The AC susceptibility measurements at 1.9–6 K showed characteristic out-of-phase signals due to slow magnetic relaxation phenomena. Fits of the AC data to the Arrhenius law, yielded parameters $\tau_0 = 5.5 \times 10^{-8}$ s and $U_{eff} = 27.4$ K = 19.0 cm^{-1}. The magnetic behavior of **1** is analogous to the SMM behavior displayed by the prototype complexes of this series, compounds $[Mn_6(\mu_3\text{-}O)_2(O_2CR)_2(salox)_6(R'OH)_4]$ (R = Me, Ph; R′ = Et). Investigation of the electron spin dynamics of **1** carried out by solid state ^1H NMR measurements, clearly revealed an energy gap of $\Delta/k_B = 20$ K between the ground and the first excited state. Magnetic susceptibility measurements from polycrystalline samples of **5** revealed the presence of antiferromagnetic interactions in the $[Mn^{III}_3]$ unit. The data were fitted in the 100–300 K range by considering only intra-unit exchange couplings and yielded $J = -11.8$ cm^{-1}, corresponding to an $S = 2$ ground state.

Appendix A. Supplementary data

CCDC 694623, 694624, 694625, 694626 and 694627 contain the supplementary crystallographic data for **1** · 6MeCN, **2** · $2Me_2CO$, **3** · MeOH · $0.5H_2O$, **4** · *n*MeCN and **5** · nMe_2CO. These data can be obtained free of charge via http://www.ccdc.cam.ac.uk/conts/retrieving.html, or from the Cambridge Crystallographic Data Centre, 12 Union Road, Cambridge CB2 1EZ, UK; fax: (+44) 1223-336-033; or e-mail: deposit@ccdc.cam.ac.uk. Tables of selected bond distances and angles for **2** · $2Me_2CO$, **3** · MeOH · $0.5H_2O$ and **5** · nMe_2CO are also available. Supplementary data associated with this article can be found, in the online version, at doi:10.1016/j.poly.2008.08.021.

References

[1] (a) For some recent examples on manganese iron complexes see: P. Baran, R. Boča, I. Chakraborty, J. Giapintzakis, R. Herchel, Q. Huang, J.E. McGrady, R.G. Raptis, Y. Sanakis, A. Simopoulos, Inorg. Chem. 47 (2008) 645;
(b) J. Ballmann, S. Dechert, E. Bill, U. Ryde, F. Meyer, Inorg. Chem. 47 (2008) 1586;
(c) A. Mishra, W. Wernsdorfer, K.A. Abboud, G. Christou, Chem. Commun. (2005) 54;
(d) A. Mishra, Y. Pushkar, J. Yano, V.K. Yachandra, W. Wernsdorfer, K.A. Abboud, G. Christou, Inorg. Chem. 47 (2008) 1940;
(e) R. Tagore, R.H. Crabtree, G.W. Brudvig, Inorg. Chem. 47 (2008) 1815.

[2] (a) For some recent examples see: A. Mishra, A.J. Tasiopoulos, W. Wernsdorfer, E.E. Moushi, B. Moulton, M.J. Zaworotko, K.A. Abboud, G. Christou, Inorg. Chem. 47 (2008) 4832;
(b) V. Chandrasekhar, B. Murugesa Pandian, R. Boomishankar, A. Steiner, J.J. Vittal, A. Houri, R. Clérac, Inorg. Chem. 47 (2008) 4918;
(c) D. Li, R. Clé rac, O. Roubeau, E. Harté, C. Mathonière, R. Le Bris, S.M. Holmes, J. Am. Chem. Soc. 130 (2008) 252;
(d) X. Yang, R.A. Jones, W.-K. Wong, Dalton Trans. (2008) 1676;
(e) I.S. Lee, Y.K. Chung, Inorg. Chem. Commun. 10 (2007) 593.

[3] R.E.P. Winpenny, J. Chem. Soc., Dalton Trans. (2002) 1.

[4] (a) As the most characteristic example of this approach we mention the replacement of the bridging carboxylato ligands in the $[Mn_{12}]$ family of complexes. See for example: P. Artus, C. Boskovic, J. Yoo, W.E. Streib, L.-C. Brunel, D.N. Hendrickson, G. Christou, Inorg. Chem. 40 (2001) 4199;
(b) N.E. Chakov, W. Wernsdorfer, K.A. Abboud, D.N. Hendrickson, G. Christou, J. Chem. Soc., Dalton Trans. (2003) 2243;
(c) J.M. Lim, Y. Do, J. Kim, Eur. J. Inorg. Chem. (2006) 711;
(d) E. Coronado, A. Forment-Aliaga, A. Gaita-Ariño, C. Giménez-Saiz, F.M. Romero, W. Wernsdorfer, Angew. Chem., Int. Ed. 43 (2004) 6152.

[5] (a) See for example: V. Marvaud, C. Decroix, A. Scuiller, C. Guyard-Duhayon, J. Vaissermann, F. Gonnet, M. Verdaguer, Chem. Eur. J. 9 (2003) 1677;
(b) Z.-G. Gu, W. Liu, Q.-F. Yang, X.-H. Zhou, J.-L. Zuo, X.-Z. You, Inorg. Chem. 46 (2007) 3236;
(c) A.J. Tasiopoulos, A. Vinslava, W. Wernsdorfer, A. Abboud, G. Christou, Angew. Chem., Int. Ed. 43 (2004) 2117;
(d) M. Soler, E. Rumberger, K. Folting, D.N. Hendrickson, G. Christou, Polyhedron 20 (2001) 1365;
(e) M. Soler, W. Wernsdorfer, K. Folting, M. Pink, G. Christou, J. Am. Chem. Soc. 126 (2004) 2156;
(f) X. Ottenwaelder, J. Cano, Y. Journaux, E. Rivière, C. Brennan, M. Nierlich, R. Ruiz-García, Angew. Chem., Int. Ed. 43 (2004) 850.

[6] (a) See for example: J.-P. Costes, F. Dahan, W. Wernsdorfer, Inorg. Chem. 45 (2006) 5;
(b) J.-P. Costes, F. Nicodème, Chem. Eur. J. 8 (2002) 3442;
(c) J.-P. Costes, F. Dahan, F. Nicodème, Inorg. Chem. 42 (2003) 6556;
(d) L.K. Thompson, T.L. Kelly, L.N. Dawe, H. Grove, M.T. Lemaire, J.A.K. Howard, E.C. Spencer, C.J. Matthews, S.T. Onions, Inorg. Chem. 43 (2004) 7605;
(e) S.K. Dey, L.K. Thompson, L.N. Dawe, Chem. Commun. (2006) 4967;
(f) L.N. Dawe, L.K. Thompson, Angew. Chem., Int. Ed. 46 (2007) 7440.

[7] (a) See for example: C.P. Raptopoulou, V. Tangoulis, E. Devlin, Angew. Chem., Int. Ed. 41 (2002) 2386;
(b) A.K. Boudalis, C.P. Raptopoulou, B. Abarca, R. Ballesteros, M. Chadlaoui, J.-P. Tuchagues, A. Terzis, Angew. Chem., Int. Ed. 45 (2006) 432;
(c) C.P. Raptopoulou, V. Tangoulis, V. Psycharis, Inorg. Chem. 39 (2000) 4452.

[8] (a) See for example: C.P. Raptopoulou, A.K. Boudalis, Y. Sanakis, V. Psycharis, J.M. Clemente-Juan, M. Fardis, G. Diamantopoulos, G. Papavassiliou, Inorg. Chem. 45 (2006) 2317;
(b) A.K. Boudalis, B. Donnadieu, V. Nastopoulos, J.M. Clemente-Juan, A. Mari, Y. Sanakis, J.-P. Tuchagues, S.P. Perlepes, Angew. Chem., Int. Ed. 43 (2004) 2266;
(c) A.K. Boudalis, Y. Sanakis, J.M. Clemente-Juan, B. Donnadieu, V. Nastopoulos, A. Mari, Y. Coppel, J.-P. Tuchagues, S.P. Perlepes, Chem. Eur. J. 14 (2008) 2514.

[9] For a comprehensive review of our work see A.K. Boudalis, Y. Sanakis, C.P. Raptopoulou, V. Psycharis, A. Terzis, Polyhedron 25 (2006) 1391 and references 7–10 cited therein.

[10] C.P. Raptopoulou, A.K. Boudalis, Y. Sanakis, V. Psycharis, Polyhedron 24 (2005) 711.

[11] (a) A.K. Boudalis, V. Nastopoulos, A. Terzis, C.P. Raptopoulou, S.P. Perlepes, Z. Naturforsch. 56b (2001) 122;
(b) C. Gkioni, A.K. Boudalis, Y. Sanakis, L. Leondiadis, V. Psycharis, C.P. Raptopoulou, Polyhedron 27 (2008) 2315.

[12] Th.C. Stamatatos, A.K. Boudalis, Y. Sanakis, C.P. Raptopoulou, Inorg. Chem. 45 (2006) 7372.

[13] C.P. Raptopoulou, V. Psycharis, Inorg. Chem. Commun. 11 (2008) 1194.

[14] C.J. Milios, C.P. Raptopoulou, A. Terzis, F. Lloret, R. Vicente, S.P. Perlepes, A. Escuer, Angew. Chem., Int. Ed. 43 (2004) 210.

[15] J.B. Vincent, H.-R. Chang, K. Folting, J.C. Huffman, G. Christou, D.N. Hendrickson, J. Am. Chem. Soc. 109 (1987) 5703.

[16] M.W. Wemple, H.-L. Tsai, S. Wang, J.P. Claude, W.E. Streib, J.C. Huffman, D.N. Hendrickson, G. Christou, Inorg. Chem. 35 (1996) 6437.

[17] J.-M. Clemente-Juan, C. Mackiewicz, M. Verelst, F. Dahan, A. Bousseksou, Y. Sanakis, J.-P. Tuchagues, Inorg. Chem. 41 (2002) 1478.

[18] F. James, M. Roos, Comput. Phys. Commun. 10 (1975) 343.

[19] E. Fukushima, S.B.W. Roeder, Experimental Pulse NMR, Addison Wesley, Reading, MA, 1981.

[20] S. Parsons, M. Murie, R. Winpenny, P. Wood, Private Communication to the CCDC, Code XAJVEK.

[21] Rigaku/MSC CRYSTALCLEAR, Rigaku/MSC Inc., The Woodlands, Texas, USA, 2005.

[22] G.M. Sheldrick, SHELXS-97: Structure Solving Program, University of Göttingen, Germany, 1997.

[23] G.M. Sheldrick, SHELXL-97: Crystal Structure Refinement, University of Göttingen, Germany, 1997.

[24] (a) For reviews see: G. Aromi, E.K. Brechin, Struct. Bond. 122 (2006) 1;
(b) D. Gatteschi, R. Sessoli, Angew. Chem., Int. Ed. 42 (2003) 268;
(c) G. Christou, D. Gatteschi, D.N. Hendrickson, R. Sessoli, MRS Bull. 25 (2000) 66.

[25] (a) C.J. Milios, A. Vinslava, A.G. Whittaker, S. Parsons, W. Wernsdorfer, G. Christou, S.P. Perlepes, E.K. Brechin, Inorg. Chem. 45 (2006) 5272;
(b) C.J. Milios, A. Vinslava, P.A. Wood, S. Parsons, W. Wernsdorfer, G. Christou, S.P. Perlepes, E.K. Brechin, J. Am. Chem. Soc. 129 (2007) 8;
(c) C.J. Milios, A. Vinslava, W. Wernsdorfer, S. Moggach, S. Parsons, S.P. Perlepes, G. Christou, E.K. Brechin, J. Am. Chem. Soc. 129 (2007) 2754;

(d) C.J. Milios, A. Vinslava, W. Wernsdorfer, A. Prescimone, P.A. Wood, S. Parsons, S.P. Perlepes, G. Christou, E.K. Brechin, J. Am. Chem. Soc. 129 (2007) 6547;
(e) C.J. Milios, R. Inglis, A. Vinslava, R. Bagai, W. Wernsdorfer, S. Parsons, S.P. Perlepes, G. Christou, E.K. Brechin, J. Am. Chem. Soc. 129 (2007) 12505.
[26] P. Chaudhuri, Coord. Chem. Rev. 243 (2003) 143.
[27] (a) J.M. Thorpe, R.L. Beddoes, D. Collison, C.D. Garner, M. Helliwell, J.M. Holmes, P.A. Tasker, Angew. Chem., Int. Ed. 38 (1999) 1119;
(b) P. Chaudhuri, M. Hess, E. Rentschler, T. Weyhermüller, U. Flörke, New J. Chem. (1998) 553;
(c) V. Zerbib, F. Robert, P. Gouzerh, J. Chem. Soc., Chem. Commun. (1994) 2179.
[28] (a) Th.C. Stamatatos, D. Foguet-Albiol, C.C. Stoumpos, C.P. Raptopoulou, A. Terzis, W. Wernsdorfer, S.P. Perlepers, G. Christou, J. Am. Chem. Soc. 127 (2005) 15380;
(b) Th.C. Stamatatos, D. Foguet-Albiol, S.-C. Lee, C.C. Stoumpos, C.P. Raptopoulou, A. Terzis, W. Wernsdorfer, S.O. Hill, S.P. Perlepers, G. Christou, J. Am. Chem. Soc. 129 (2007) 9484.
[29] (a) R. Wu, M. Poyraz, F.E. Sowrey, C.E. Anson, S. Wocadlo, A.K. Powell, U.A. Jayasooriya, R.D. Cannon, T. Nakamoto, M. Katada, H. Sano, Inorg. Chem. 37 (1998) 1913;
(b) J. An, Z.-D. Chen, J. Bian, X.-L. Jin, S.-X. Wang, G.-X. Xu, Inorg. Chim. Acta 287 (1999) 82;
(c) J. Li, S. Yang, F. Zhang, Z. Tang, S. Ma, Q. Shi, Q. Wu, Z. Huang, Inorg. Chim. Acta 294 (1999) 109;
(d) A. Vlachos, V. Psycharis, C.P. Raptopoulou, N. Lalioti, Y. Sanakis, G. Diamantopoulos, M. Fardis, M. Karayanni, G. Papavassiliou, A. Terzis, Inorg. Chim. Acta 357 (2004) 3162;
(e) V. Psycharis, C.P. Raptopoulou, A.K. Boudalis, Y. Sanakis, M. Fardis, G. Diamantopoulos, G. Papavassiliou, Eur. J. Inorg. Chem. (2006) 3710.
[30] P. Chaudhuri, E. Rentschler, F. Birkelbach, C. Krebs, E. Bill, T. Weyhermüller, U. Flörke, Eur. J. Inorg. Chem. (2003) 541.
[31] (a) N.E. Chakov, L.N. Zakharov, A.L. Rheingold, K.A. Abboud, G. Christou, Inorg. Chem. 44 (2005) 4555;
(b) X. Xia, M. Verelst, J.-C. Daran, J.-P. Tuchagues, J. Chem. Soc., Chem. Commun. (1995) 2155.
[32] C.J. Milios, P.A. Wood, S. Parsons, D. Foguet-Albiol, C. Lampropoulos, G. Christou, S.P. Perlepes, E.K. Brechin, Inorg. Chim. Acta 360 (2007) 3932.
[33] (a) M. Fardis, G. Diamantopoulos, M. Karayianni, G. Papavassiliou, V. Tangoulis, A. Konsta, Phys. Rev. B 65 (2001) 014412;
(b) D. Procissi, B.J. Suh, A. Lascialfari, F. Borsa, A. Caneschi, A. Cornia, J. Appl. Phys. 91 (2002) 7173;
(c) M. Belesi, A. Lascialfari, D. Procissi, Z.H. Jang, F. Borsa, Phys. Rev. B 72 (2005) 014440.
[34] G.E.G. Hardeman, N.J. Poulis, W.v.D. Lugt, Physica (Utrecht) 22 (1956) 48.
[35] (a) T. Kohmoto, T. Goto, S. Maegawa, N. Fujiwara, Y. Fukuda, M. Kunitomo, M. Mekata, Phys. Rev. B 49 (1994) 6028;
(b) T. Goto, T. Koshiba, T. Kubo, K. Agawa, Phys. Rev. B 67 (2003) 104408.

2. Results and discussion

$PPhpy_2$ and Ppy_3 react with tricarbonyl complexes of rhenium(I) or technetium(I) under coordination of two pyridyl rings. Complexes of the composition $[M(CO)_3X(PPhpy_2\text{-}N,N')]$ were obtained in moderate yields from reactions of $(NEt_4)_2[M(CO)_3X_3]$ (M = Tc, X = Cl; M = Re; X = Br) with 1 equiv. of $PPhpy_2$ in acetonitrile at room temperature Eq. (1). The respective yields can be increased by concentration of the mother liquors, the purity of the resulting second crops of products, however, is lower and the separation from oily side-products causes is difficult.

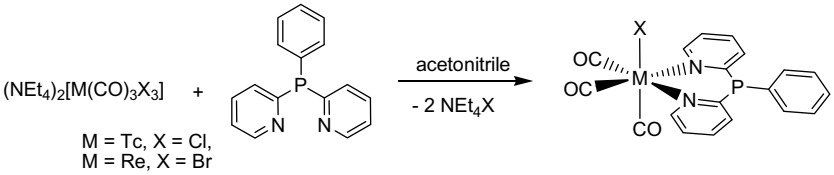

(1)

$[Re(CO)_3Br(PPhpy_2\text{-}N,N')]$ crystallizes from a xylene solution in form of yellow blocks, while $[Tc(CO)_3Cl(PPhpy_2\text{-}N,N')]$ was isolated as colorless needles from the mother liquor. The air and moisture stable compounds are readily soluble in organic solvents. Strong bands in the infrared spectrum of the rhenium complex at 2021 and 1909 cm^{-1} and in that of the technetium compound at 2033 and 1925 cm^{-1} can be assigned to the $\nu_{(C\equiv O)}$ stretches and confirm the retention of the *fac*-$[M(CO)_3]^+$ cores. The ^{99}Tc NMR spectrum of the technetium compound shows a signal at −990.06 ppm. This corresponds to a to high-field shift of about 120 ppm with regard to the resonance of the precursor, which appears at −868.16 ppm. The finding is in good agreement with the positions of the ^{99}Tc NMR signals of the tricarbonyl complexes *mer*-$[Tc(CO)_3Br(py)_2]$ (−946 ppm) and *fac*-$[Tc(CO)_3Br(bipy)]$ (−1078 ppm) [13]. The $^{31}P\{^1H\}$ NMR spectra of $[Re(CO)_3Br(PPhpy_2\text{-}N,N')]$ and $[Tc(CO)_3Cl(PPhpy_2\text{-}N,N')]$ show signals at 1.04 ppm and −2.24 ppm, respectively. They belong to non-coordinated phosphorus atoms, while signals of coordinated phosphines typically appear at lower field in such complexes [5d]. Moreover, the detection of H^6 signals in the ^1H NMR spectra at 9.52 ppm for the rhenium complex and at 9.36 ppm for the technetium analog confirm the coordination of two pyridyl rings. The signals of ^6H protons, adjacent to nitrogen in the pyridyl group, generally appear downfield from the other protons in the phenyl region. For non-coordinated pyridylphosphines, such signals appear as multiplets [14] in the range of 8.60–8.75 ppm ($CDCl_3$) [7b,14,15]. The coordination of the nitrogen atom, however, displaces the signal positions to 9–10 ppm [5d,7b,16].

$[Tc(CO)_3Cl(PPhpy_2\text{-}N,N')]$ as well as $[Re(CO)_3Br(PPhpy_2\text{-}N,N')]$ have been also characterized by X-ray structure analysis. Their structures are isotypic and the coordination environments of the metal atoms are slightly distorted octahedra with the carbonyl ligands in facial configuration. $PPhpy_2$ coordinates with the two nitrogen atoms forming six-membered chelate rings. Chlorine or bromine atoms occupy the remaining coordination sites. Fig. 1 shows an ellipsoid representation of the technetium complex. The structure of the rhenium analog is virtually identical and the same atomic labeling scheme has been applied. Therefore, it is not shown separately. Selected bond lengths and angles of both compounds are compared in Table 1. Main distortions from an ideal octahedron are mainly due to the restricting bite angle of the chelating ligand. The mean values of the M-N, M-C and M-X bond lengths are fully in agreement with the values of structurally related compounds [9,17].

The reaction of $(NEt_4)_2[Tc(CO)_3Cl_3]$ with 1 equiv. of Ppy_3 in THF at room temperature affords $[Tc(CO)_3Cl(Ppy_3\text{-}N,N')]$. The complex crystallizes directly from the mother liquor as colorless needles. The air and moisture stable complex is moderately soluble in THF, acetonitrile or CH_2Cl_2. Strong carbonyl bands at 2032, 1948 and 1882 cm^{-1} are observed in the IR spectrum of the compound.

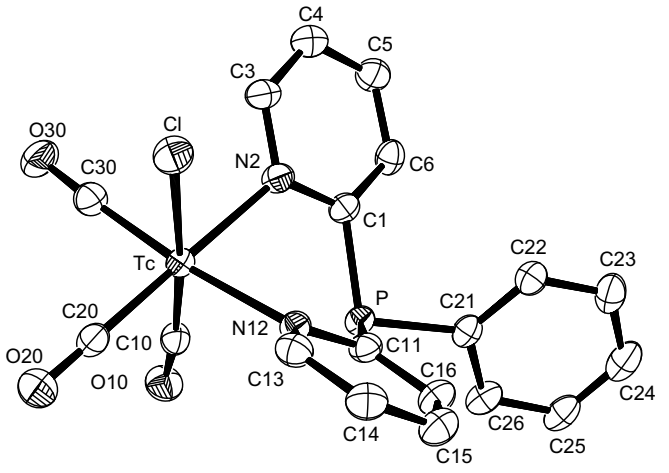

Fig. 1. Ellipsoid representation [26] of $[Tc(CO)_3Cl(PPhpy_2\text{-}N,N')]$. Thermal ellipsoids represent 50% probability. H atoms have been omitted for clarity.

Table 1
Selected bond lengths (Å) and angles (°) in the $[M(CO)_3X(PPhpy_2\text{-}N,N')]$ complexes (M = Tc, Re; X = Cl, Br)

	$[Re(CO)_3Br(PPhpy_2\text{-}N,N')]$	$[Tc(CO)_3Cl(PPhpy_2\text{-}N,N')]$
M–C10	1.90(1)	1.904(4)
M–C20	1.91(1)	1.909(4)
M–C30	1.91(1)	1.906(4)
M–N2	2.205(8)	2.218(3)
M–N12	2.223(9)	2.202(3)
M–Br/Cl	2.635(1)	2.499(1)
C30–M–C20	89.1(5)	89.1(2)
C30–M–N2	95.4(4)	91.8(1)
C20–M–N12	91.6(4)	95.4(1)
N2–M–N12	83.9(3)	83.7(1)
C10–M–X	175.6(4)	175.0(1)

The atomic labeling scheme of the technetium complex in Fig. 1 has also been applied for the rhenium compound.

The latter two values refer to a broad, splitted $\nu_{(C\equiv O)}$ band. The ^{99}Tc NMR signal is observed at −988.42 ppm, which is almost perfectly the value, which was observed for [Tc(CO)$_3$Cl(PPhpy$_2$-*N*,*N*′)] and strongly suggests a bidentate *N*,*N*′ coordination mode also for Ppy$_3$ in the technetium complex under study. The ^{1}H NMR signals of the H^6 protons appear at 9.36 and 8.99 ppm with a 2:1 ratio and, thus, support this suggestion. [Tc(CO)$_3$Cl(Ppy$_3$-*N*,*N*′)] crystallizes as a racemic twin in the orthorhombic space group Pna2$_1$ with two molecules per asymmetric unit. The Flack parameter has a value of 0.56(5). All attempts to refine the structure in the corresponding centrosymmetric space group *Pnma* were not successful. A slightly distorted octahedron with facial configuration of the carbonyl ligands represents the coordination environment of the technetium atom as is shown in Fig. 2. Ppy$_3$ coordinates solely via two nitrogen atoms and the sixth coordination position is occupied by a chloro ligand. Thus, the structure is isotypic with the [M(CO)$_3$X(PPhpy$_2$-*N*,*N*′)] (M = Tc, Re; X = Cl, Br) complexes discussed above and in agreement with the bonding mode, which was proposed for analogous rhenium complex on the basis of spectroscopic data [12]. There are only marginal differences in the bond lengths and angles (Table 2). The position of the nitrogen atom of the non-coordinated pyridyl ring was derived on the basis of the thermal parameters.

In all our reactions of (NEt$_4$)$_2$[M(CO)$_3$X$_3$] complexes with PPhpy$_2$ and Ppy$_3$, we never observed the coordination of the phosphine (i) as monodentate phosphorus donor as previously observed in (NEt$_4$)[Re(CO)$_3$Br$_2$(PPh$_2$py-P)] [9], (ii) as P,N chelate, or (iii) in a tripodal *N*,*N*′,*N*″ arrangement. The first two facts can be explained by the preferred formation of the more stable six-membered chelate rings and the well-known high tendency of [M(CO)$_3$]$^+$ centers to bind to aromatic amines, which has been demonstrated previously and finds application in the labeling of histidine-rich protein sites [18,19]. A simple explanation for our observation, that the formation of species of the composition [M(CO)$_3$(Ppy$_3$-*N*,*N*′,*N*″)]$^+$ (M = Re, Tc) is less favored, however, cannot be given in the light that a number of transition metal complexes with N$_3$-tripodal Ppy$_3$ ligands are reported, and also the isotypic molybdenum(0) complex [Mo(CO)$_3$(Ppy$_3$-*N*,*N*′,*N*″)] has been isolated and characterized by X-ray crystallography [7]. In the case of the corresponding technetium and rhenium complexes, obviously charge compensation by the coordination of an anionic ligand is preferred. This assumption is supported by the results of our attempt to support tripodal coordination by the removal of all halide ligands from the metal atom.

In order to avoid the co-coordination of halide, we added 3 equiv. of the AgNO$_3$ to a solution of (NEt$_4$)$_2$[Re(CO)$_3$Br$_3$] in water/THF or water/MeOH mixtures. After removal of the precipitated AgBr, the remaining solution, which mainly contains the [Re(CO)$_3$(OH$_2$)$_3$]$^+$ cation, was brought to dryness. The resulting oil was redissolved in THF and 1 equiv. PPy$_3$ was added. The mixture was stirred for 1 h at room temperature Eq. (2). Colorless crystals of [Re(CO)$_3$(NO$_3$)(Ppy$_3$-*N*,*N*′)] deposited from the yellow mother liquor upon standing for 2 days. The compound is only sparingly soluble in water or organic solvents. Its IR spectrum shows two strong carbonyl bands at 2029 and 1913 cm^{-1}. The N–O frequency of the coordinated NO$_3^-$ ligand appears at 1281 cm^{-1} and is in agreement with values of the similar nitrato complexes (NEt$_4$)[ReBr$_2$(CO)$_2$(NO$_3$)NO] and (NMe$_4$)[Re(CO)$_2$(NO$_3$)$_3$NO] [20].

A single-crystal diffraction study on [Re(CO)$_3$(NO$_3$)(Ppy$_3$-*N*,*N*′)] confirms the coordination of a nitrato ligand and the role of Ppy$_3$ as an *N*,*N*′ chelating ligand. An ellipsoid representation of the neutral complex is shown in Fig. 3. Selected bond lengths and angles are summarized in Table 3. The position of the nitrogen atom in

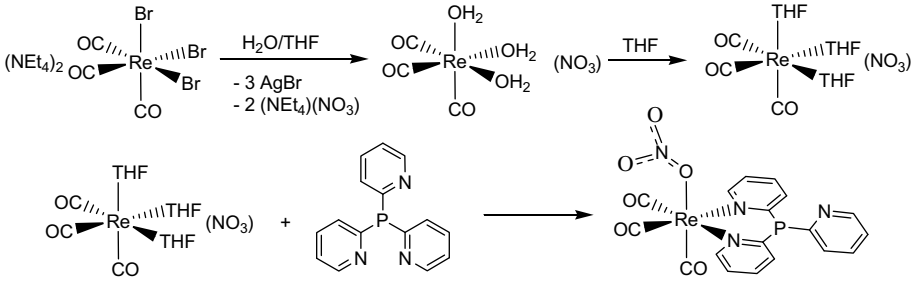

(2)

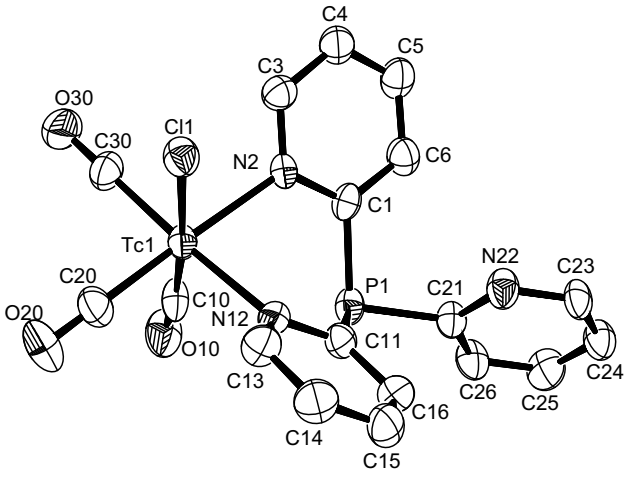

Fig. 2. Ellipsoid representation [26] of [Tc(CO)$_3$Cl(Ppy$_3$-*N*,*N*′)]. Thermal ellipsoids represent 50% probability. H atoms have been omitted for clarity.

Table 2
Selected bond lengths (Å) and angles (°) in [Tc(CO)$_3$Cl(Ppy$_3$-*N*,*N*′)] (values for two independent species)

Molecule 1		Molecule 2	
Tc1–C10	1.886(8)	Tc2–C40	1.922(9)
Tc1–C20	1.915(7)	Tc2–C50	1.904(7)
Tc1–C30	1.933(6)	Tc2–C60	1.916(8)
Tc1–N2	2.215(5)	Tc2–N32	2.196(6)
Tc1–N12	2.204(5)	Tc2–N42	2.198(6)
Tc1–Cl1	2.484(2)	Tc2–Cl2	2.482(2)
C30–Tc1–C20	88.6(3)	C60–Tc2–C50	89.6(4)
C30–Tc1–N2	94.8(2)	C60–Tc2–N32	94.8(3)
C20–Tc1–N12	92.1(3)	C50–Tc2–N42	91.2(3)
N2–Tc1–N12	84.1(2)	N32–Tc2–N42	84.4(2)
C10–Tc1–Cl1	175.7(2)	C40–Tc2–Cl2	174.9(3)

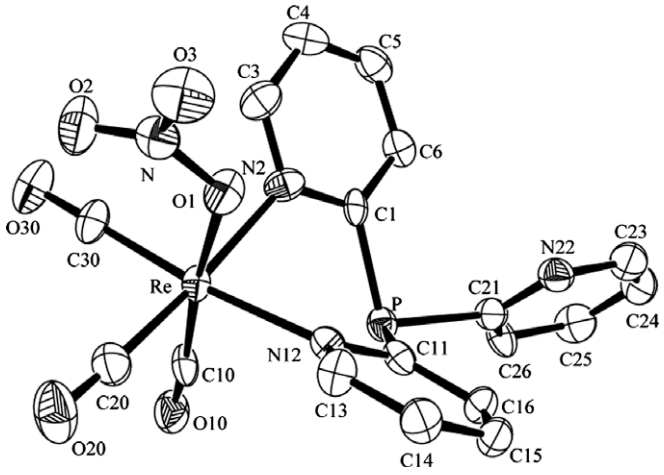

Fig. 3. Ellipsoid representation [26] of $[Re(CO)_3(NO_3)(Ppy_3\text{-}N,N')]$. Thermal ellipsoids represent 50% probability. H atoms have been omitted for clarity.

Table 3
Selected bond lengths (Å) and angles (°) in $[Re(CO)_3(NO_3)(Ppy_3\text{-}N,N')]$

Re–C10	1.92(1)	Re–C20	1.92(1)
Re–C30	1.92(1)	Re–N2	2.199(9)
Re–N12	2.202(8)	Re–O1	2.175(7)
O1–N	1.30(1)	N–O2	1.21(1)
N–O2	1.228(12)		
C10–Re–C20	87.3(5)	C10–Re–C30	88.3(4)
C10–Re–N2	99.7(4)	C10–Re–N12	95.2(4)
C10–Re–O1	173.3(4)	C20–Re–C30	88.5(5)
C20–Re–N2	172.9(5)	C20–Re–N12	96.4(4)
C20–Re–O1	92.5(4)	C30–Re–N2	90.1(4)
C30–Re–N12	174.1(4)	C30–Re–O1	98.4(4)
N2–Re–N12	84.6(3)	N2–Re–O1	80.8(3)
N12–Re–O1	78.2(3)	O1–N–O2	120.9(9)
O1–N–O3	115.3(9)	O2–N–O3	123.8(9)
Re–O1–N	124.6(6)		

the non-coordinated pyridyl ring was derived from a comparison of the thermal parameters of the corresponding atoms. Some distortions from an ideal octahedron are due to the small bite angle of the Ppy_3 and steric effects caused by the nitrato ligand, which is bent away from the two pyridine rings. The Re–O1 bond length of 2.175(7) Å is relatively long, but is in agreement with values found in analogous complexes and the weakness of such bonds [20,21]. This weakness is supported by a mass spectrometric study on the complex, which shows in addition to the molecular ion a peak at $m/z = 552$, which can be assigned to a deprotonation product of $[Re(CO)_3(OH_2)(Ppy_3)]$.

Concluding it must stated, that $PPhpy_2$ and Ppy_3 in all the isolated products coordinate to $\{M(CO)_3\}^+$ fragments (M = Re, Tc) exclusively as *N*,*N*′ bidentate ligands under formation of six-membered chelate rings. The unoccupied P or P,N donor positions recommend such compounds for the synthesis of bimetallic compounds.

3. Experimental

$(NEt_4)_2[Tc(CO)_3Cl_3]$ [22] and $(NEt_4)_2[Re(CO)_3Br_3]$ [23] were prepared by literature procedures. $PPhPy_2$ and PPy_3 were synthesized by a modification of a procedure previously reported by Kurtev et al. [5e]. ^{99}Tc is a weak β^--emitter. All manipulations with this isotope were performed in a laboratory approved for the handling of low-level radioactive materials. Normal glassware provides adequate protection against the low-energy beta emission of the technetium compounds. Secondary X-rays (bremsstrahlung) play an important role only when larger amounts of ^{99}Tc are used. IR spectra were measured as KBr pellets on a Shimadzu FTIR-spectrometer 8300. FAB^+ mass spectra were recorded with a TSQ (Finnigan) instrument using a nitrobenzyl alcohol matrix. Elemental analysis of carbon, hydrogen and nitrogen were determined using a Heraeus (vario EL) elemental analyzer. ^1H, ^{13}C, $^{31}P\{^1H\}$ and ^{99}Tc NMR spectra were taken with a JEOL 400 MHz multinuclear spectrometer.

3.1. $PPhpy_2$ and Ppy_3

n-Butyllithium (50 ml of a 1.6 m solution in *n*-hexane) was cooled to −70 °C under an atmosphere of dry argon. 2-Bromopyridine (7.7 ml, 80 mmol) in 50 ml of dry diethylether was added dropwise with stirring. The resulting red-brown solution was diluted with additional 20 ml of diethylether and stirred for 4 h. $PPhCl_2$ (40 mmol) or PCl_3 (27 mmol) were added dropwise in 10 ml diethylether, and an extra amount of 40 ml diethylether was added when the addition of the phosphine was completed. The resulting turpid, orange-brown suspension was vigorously stirred for 2 h at −70 °C and slowly warmed to room temperature. The mixture was extracted with 100 ml of degassed 2 m sulfuric acid. The pH was adjusted to 8–9 by the addition of concentrated NaOH. The resulting yellow solid was filtered off, washed with water and petrol ether, and recrystallized from acetone/petrol ether. Yield about 50%.

$PPhpy_2$: *Anal.* Calc. for $C_{16}H_{13}N_2P$: N, 10.61; C, 72.70; H, 4.96. Found: N, 10.54; C, 72.53; H, 4.63%. IR (ν_{max}, cm^{-1}): 3036 (m), 2985 (w), 2916 (w), 1562 (vs), 1477 (w), 1442 (s), 1416 (s), 1273 (w), 1142 (w), 1092 (m), 1038 (w), 984 (m), 768 (s), 694 (s), 617 (w), 478 (s), 440 (m). $^{31}P\{^1H\}$ NMR (δ, $CDCl_3$): −2.05 ppm. ^1H NMR (δ, $CDCl_3$): 8.71 (m, $2H^6$-py); 7.60–7.17 (m, 11H, rest of aromatic protons) ppm.

Ppy_3: Anal. Calc. for $C_{15}H_{12}N_3P$: N, 15.85; C, 67.90; H, 4.56%. Found: N, 15.64; C, 67,78; H, 4.58%. IR (ν_{max}, cm^{-1}): 3035 (m), 2978 (w), 1566 (vs), 1450 (s), 1416 (s), 1276 (m), 1215 (w), 1050 (m), 1045 (m), 984 (m), 771 (s), 740 (m), 617 (w), 501 (s), 432 (m). $^{31}P\{^1H\}$ NMR (δ, $CDCl_3$): −0.17 ppm. ^1H NMR (δ, $CDCl_3$): 8.70 (m, $3H^6$-py); 7.63-7.19 (m, 9H, rest of aromatic protons) ppm.

3.2. $[Tc(CO)_3Cl(PPhpy_2\text{-}N,N')]$

$(NEt_4)_2[Tc(CO)_3Cl_3]$ (54.6 mg, 0.1 mmol) and $PPhpy_2$ (26.4 mg, 0.1 mmol) were dissolved each in 1.5 ml acetonitrile and the phosphine solution was added dropwise to the technetium compound. The solution was stirred for 2 h at room temperature. Colorless crystals of $[Tc(CO)_3Cl(PPhpy\text{-}N,N')]$ deposited from the light brown solution upon standing overnight. The crystals were filtered off and washed with methanol. Yield: 14 mg (30%). IR (ν_{max}, cm^{-1}): 2033 (vs, CO), 1925 (vs, br, CO). ^{99}Tc NMR (δ, $CDCl_3$): −990.06 ppm. ^1H NMR (δ, $CDCl_3$): 9.36 (*m*, 2H, H^6- pyridine); 7.77–7.05 (*m*, 11H, rest of the aromatic protons) ppm. $^{31}P\{^1H\}$ NMR (δ, $CDCl_3$): −2.24 ppm.

3.3. $[Tc(CO)_3Cl(Ppy_3\text{-}N,N')]$

$(NEt_4)_2[Tc(CO)_3Cl_3]$ (54.6 mg, 0.1 mmol) and Ppy_3 (26.5 mg, 0.1 mmol) were dissolved each in 1.5 ml THF, and the phosphine was added dropwise to the technetium complex. The solution was stirred for 2 h at room temperature. Colorless crystals of $[Tc(CO)_3Cl(Ppy_3\text{-}N,N')]$ deposited from the light brown solution upon standing overnight. The crystals were filtered off and washed with methanol. Yield: 20 mg (40%). IR (ν_{max}, cm^{-1}): 2033 (vs, CO), 1948 (vs, br, CO), 1882 (vs, br, CO). ^{99}Tc NMR (δ, $CDCl_3$): −988.42 ppm. ^1H NMR (δ, $CDCl_3$): 9.36 (*m*, 2H, H^6 coordinated py); 8.99 (*m*, 1H, H^6 non-coordinated py); 8.15–6.91 (*m*, 9H, rest of the aromatic protons) ppm.

Table 4
X-ray structure data collection and refinement parameters

	$[Re(CO)_3Br(PPhpy_2\text{-}N,N')]$	$[Tc(CO)_3Cl(PPhpy_2\text{-}N,N')]$	$[Tc(CO)_3Cl(Ppy_3\text{-}N,N')]$	$[Re(CO)_3(NO_3)(Ppy_3\text{-}N,N')]$
Formula	$C_{19}H_{13}BrN_2O_3PRe$	$C_{19}H_{13}ClN_2O_3PTc$	$C_{18}H_{12}ClN_3O_3PTc$	$C_{18}H_{12}N_4O_6PRe$
MW	614.39	481.73	482.73	597.49
Crystal system	monoclinic	triclinic	orthorhombic	triclinic
a (Å)	14.363(3)	9.547(1)	22.395(2)	8.818(1)
b (Å)	12.596(4)	9.645(1)	10.649(1)	10.992(1)
c (Å)	20.798(4)	10.687(1)	16.022(1)	11.614(1)
α (°)	90	102.53(1)	90	110.79(1)
β (°)	90.25(2)	100.88(1)	90	91.19(1)
γ (°)	90	98.62(1)	90	109.88(1)
V (Å^3)	3763.0(15)	924.5(2)	3820.9(5)	976.8(2)
Space group	$C2/c$	$P\bar{1}$	$Pna2_1$ [a]	$P\bar{1}$
Z	8	2	8	2
D_{calc} (g cm^{-3})	2.169	1.731	1.678	2.032
μ (mm^{-1})	8.690	1.035	1.001	6.347
Number of reflections	4573	7656	17115	8155
Number of independent	4082	3848	9084	4121
Number of parameters	244	244	488	271
R_1/wR_2	0.0513/0.1013	0.0302/0.0658	0.0478/0.1152	0.0498/0.0967
Goodness-of-fit	1.045	0.825	0.932	1.000
Device/T (°K)	CAD4/293(2)	IPDS, STOE/200(2)	IPDS, STOE/200(2)	IPDS, STOE / 200(2)

[a] Racemic twin, Flack parameter 0.56(5). All attempts to calculate the structure in a centrosymmetric space group were not successful.

3.4. $[Re(CO)_3Br(PPhpy_2\text{-}N,N')]$

$(NEt_4)_2[Re(CO)_3Br_3]$ (76.8 mg, 0.1 mmol) and $PPhpy_2$ (26.4 mg, 0.1 mmol) were dissolved each in 1.5 ml acetonitrile, and the phosphine was added dropwise to the rhenium complex. The solution was stirred for 1 h at room temperature. The color changed slowly to yellow. Finally, 1 ml of xylene was added and NEt_4Br precipitated. The solution was filtered and the solvent was removed in vacuum. The obtained oil was crystallized from xylene to give yellow blocks. Yield: 25 mg (40%). *Anal.* Calc. for $C_{19}H_{13}N_2O_3PBrRe$: N, 4.56; C, 37.14; H, 2.13. Found: N, 4.35; C, 36.59; H, 2.32%. IR (ν_{max}, cm^{-1}): 2021 (vs, CO), 1909 (vs, CO). $^{31}P\{^1H\}$ NMR (δ, $CDCl_3$): 1.04 ppm. ^1H NMR (δ, $CDCl_3$): 9.54 (m, $2H^6$-Py); 7.77–7.05 (m, 11H, rest of aromatic protons) ppm. FAB$^+$ MS: m/z 614 ($[Re(CO)_3Br(PPhpy_2)]^+$); 535.0 ($[Re(CO)_3(PPhpy_2)]^+$); 451.0 ($[Re(PPhpy_2)]^+$).

3.5. $[Re(CO)_3(NO_3)(Ppy_3\text{-}N,N')]$

$(NEt_4)_2[Re(CO)_3Br_3]$ (76.8 mg, 0.1 mmol) was dissolved in 10 ml THF and ca. 1 ml H_2O. $AgNO_3$ (51.0 mg, 0.3 mmol) was added. The mixture was stirred for 2 h at room temperature. AgBr was filtered off and the mother liquor was brought to dryness under vacuum. The resulting oil was redissolved in 1.5 ml THF and Ppy_3 (26.5 mg, 0.1 mmol) was added in 1.5 ml THF. The solution was stirred for 1 h at room temperature. A colorless solid of $[Re(CO)_3(NO_3)(Ppy_3\text{-}N,N')]$ deposited from the light yellow solution upon standing for 2 d. Single crystals were grown from MeOH. Yield: 25.4 mg (42.5%). *Anal.* Calc. for $C_{18}H_{12}N_4O_6PRe$: N, 9.37; C, 36.12; H, 2.02. Found: N, 9.13; C, 36.51; H, 1.95%. IR (ν_{max}, cm^{-1}): 2029 (vs, CO), 1913 (vs, CO), 1281 (m, NO_3). NMR spectra of sufficient quality could not be obtained due to the low solubility of the compound. FAB$^+$ MS: m/z 552 ($[Re(CO)_3O(Ppy_3)]^+$); 536 ($[Re(CO)_3(Ppy_3)]^+$).

3.6. X-ray structure determinations

The intensities for the X-ray determinations were collected on CAD4 (Enraf-Nonius) or STOE IPDS automated single crystal diffractometers with Mo Kα radiation. The structures were solved by direct methods using SIR 92 [24], SHELXS-86 [25] or SHELXS-97 [25]. Subsequent Fourier-difference map analyses yielded the position of the non-hydrogen atoms. Refinement was performed using SHELXL-97 [25]. Hydrogen atom positions were calculated for idealized positions and treated with the 'riding model' option of SHELXL. Crystal data and more details of the data collections and refinements are contained in Table 4.

Supplementary data

CCDC 698149, 698150, 698151 and 698152 contain the supplementary crystallographic data for $[Tc(CO)_3Cl(PPhpy_2\text{-}N,N')]$, $[Re(CO)_3Br(PPhpy_2\text{-}N,N')]$, $[Tc(CO)_3Cl(Ppy_3\text{-}N,N')]$ and $[Re(CO)_3(NO_3)(Ppy_3\text{-}N,N')]$. These data can be obtained free of charge via http://www.ccdc.cam.ac.uk/conts/retrieving.html, or from the Cambridge Crystallographic Data Centre, 12 Union Road, Cambridge CB2 1EZ, UK; fax: (+44) 1223-336-033; or e-mail: deposit@ccdc.cam.ac.uk.

Acknowledgements

We gratefully acknowledge financial support from CONACYT (Mexico) and DAAD (Germany).

References

[1] R. Alberto, in: J.A. McCleverty, T.J. Meyer (Eds.), Technetium, Comprehensive Coordination Chemistry II, Elsevier, Amsterdam, 2004, pp. 126–276.
[2] U. Abram, in: J.A. McCleverty, T.J. Meyer (Eds.), Rhenium, Comprehensive Coordination Chemistry II, Elsevier, Amsterdam, 2004, pp. 271–402.
[3] (a) G.R. Newkome, Chem. Rev. 93 (1993) 2067;
(b) Z.-Z. Zhang, H. Cheng, Coord. Chem. Rev. 147 (1996) 1. and literature cited therein;
(c) P. Espinet, K. Soulantica, Coord. Chem. Rev. 193–195 (1999) 499. and literature cited therein.
[4] T. Zhang, C. Chen, Y. Qin, X. Meng, Inorg. Chem. Commun. 9 (2006) 72.
[5] (a) M.G. Ehrlich, F.R. Fronczek, S.F. Watkins, G.R. Newkome, D.C. Hager, Acta Cryst. C40 (1984) 78;
(b) K. Wajda-Hermanowicz, F.P. Pruchnik, Transition Met. Chem. 13 (1988) 22;
(c) G. Zhang, J. Zhao, G. Raudaschl-Sieber, E. Herdtweck, F.E. Kühn, Polyhedron 21 (2002) 1737;
(d) P. Espinet, P. Gómez-Elipe, F. Villafañe, J. Organomet. Chem. 450 (1993) 145;
(e) K. Kurtev, D. Ribola, A.J. Richard, D.J. Cole-Halmiton, G. Wilkinson, J. Chem. Soc., Dalton Trans. (1980) 55;
(f) A.J. Deeming, M.B. Smith, J. Chem. Soc., Chem. Commun. (1993) 844;
(g) Y. Xie, C.-L. Lee, Y. Yang, S.J. Retting, B.R. James, Can. J. Chem. 70 (1992) 751;
(h) C.J.L. Lock, M.A. Turner, Acta Cryst. C43 (1987) 2096.
[6] (a) T. Zhang, Y. Qin, D. Wu, C. Wang, C. Liu, J. Coord. Chem. 58 (2005) 1485;
(b) J.A. Casares, P. Espinet, J.M. Martín-Alvarez, V. Santos, Inorg. Chem. 43 (2004) 189;

(c) J.A. Casares, P. Espinet, J.M. Martín-Alvarez, V. Santos, Inorg. Chem. 45 (2006) 6628.
[7] (a) R.K. Boggess, D.A. Zakto, J. Coord. Chem. 4 (1975) 217;
(b) J.A. Casares, P. Espinet, R. Hernando, G. Iturbe, F. Villafañe, Inorg. Chem. 36 (1997) 44;
(c) C.-Y. Kuo, Y.-S. Fuh, J.-Y. Shiue, S.J. Yu, G.-H. Lee, S.-M. Peng, J. Organomet. Chem. 588 (1999) 260. and literature cited therein.
[8] (a) T.J. Barder, S.M. Tetrick, R.A. Walton, F.A. Cotton, G.L. Powell, J. Am. Chem. Soc. 105 (1983) 4090;
(b) T.J. Barder, F.A. Cotton, G.L. Powell, S.M. Tetrick, R.A. Walton, J. Am. Chem. Soc. 106 (1984) 1323;
(c) A.R. Cutler, P.E. Fanwick, R.A. Walton, Inorg. Chem. 26 (1987) 3811;
(d) H.G. Ang, W.L. Kwik, P.T. Lau, Polyhedron 9 (1990) 1479;
(e) P.W. Schrier, D.R. Derringer, P.E. Fanwick, R.A. Walton, Inorg. Chem. 29 (1990) 1290.
[9] U. Abram, R. Alberto, J.R. Dilworth, Y. Zheng, K. Ortner, Polyhedron 18 (1999) 2995.
[10] T. Nicholson, M. Hirsch-Kuchma, A. Shellenbarger-Jones, A. Davison, A.G. Jones, Inorg. Chim. Acta 267 (1998) 319.
[11] (a) B. Machura, R. Kruszynski, Polyhedron 25 (2006) 1985;
(b) B. Machura, R. Kruszynski, J. Mol. Struct. 837 (2007) 92.
[12] P.A. Anderson, F.R. Keene, E. Horn, E.R.T. Tiekink, Appl. Organomet. Chem. 4 (1990) 523.
[13] B. Lorenz, M. Findeisen, B. Olk, K. Schmidt, Z. Anorg. Allg. Chem. 566 (1988) 160.
[14] G.E. Griffin, W.A. Thomas, J. Chem. Soc. B (1970) 477.
[15] H. Schmidbaur, Y. Inoguchi, Z. Naturforsch. B: Anorg. Chem. Org. Chem. 35 (1980) 1329.
[16] K. Wadja-Hermanowicz, F.P. Pruchnik, Transition Met. Chem. 13 (1988) 101.
[17] (a) Y.-D. Chen, L.-Y. Zhang, Z.-N. Chen, Acta Cryst. E61 (2005) m121;
(b) L.A. García-Escudero, D. Miguel, J.A. Turiel, J. Organomet. Chem. 691 (2006) 3434;
(c) M.M. Saw, P. Kurz, N. Agorastos, T.S.A. Hor, F.X. Sundram, Y.K. Yan, R. Alberto, Inorg. Chim. Acta 359 (2006) 4087;
(d) S. Das, B.K. Panda, Polyhedron 25 (2006) 2289.
[18] (a) R. Alberto, R. Schibli, R. Waibel, U. Abram, A.P. Schubiger, Coord. Chem. Rev. 190–192 (1999) 901;
(b) M. Casanova, E. Zangrando, F. Munini, E. Iengo, E. Alessio, Dalton Trans. (2006) 5033.
[19] R. Waibel, R. Alberto, J. Wiluda, R. Finnern, R. Schibli, A. Stichelberger, A. Egli, U. Abram, J.-P. Mach, A. Plückthun, P.A. Schubiger, Nat. Biotechnol. 17 (1999) 897.
[20] (a) R. Schibli, N. Marti, P. Maurer, B. Spingler, M.-L. Lehaire, V. Gramlich, C.L. Barnes, Inorg. Chem. 44 (2005) 683;
(b) P. Kurz, D. Rattat, D. Angst, H. Schmalle, B. Spingler, R. Alberto, H. Berke, W. Beck, Dalton Trans. (2005) 804.
[21] (a) D. Rattat, A. Verbruggen, H. Schmalle, H. Berke, R. Alberto, Tetrahedron Lett. 45 (2004) 4089;
(b) M.Q. Dequeant, P.M. Bradley, G.-L. Xu, D.A. Lutterman, C. Turro, T. Ren, Inorg. Chem. 43 (2004) 7887.
[22] R. Alberto, R. Schibli, A. Egli, P.A. Schubiger, W.A. Herrmann, G. Artus, U. Abram, T.A. Kaden, J. Organomet. Chem. 493 (1995) 119.
[23] (a) D. Vitali, F. Calderazzo, Gazz. Chim. Ital. 102 (1972) 587;
(b) M. Hinrichs, F.R. Hofbauer, P. Klüfers, M. Suhanji, Inorg. Chem. 45 (2006) 6688.
[24] A. Altomare, G. Cascarano, C. Giacovazzo, A. Guagliardi, J. Appl. Crystallogr. 26 (1993) 343.
[25] (a) G.M. Sheldrick, Acta Cryst. A46 (1990) 467;
(b) G.M. Sheldrick, SHELX97 – A Programme Package for the Solution and Refinement of Crystal Structures, University of Göttingen, Germany, 1997.
[26] L.J. Farrugia, J. Appl. Crystallogr. 30 (1997) 565.

2. Experimental

2.1. General consideration

All starting materials were obtained commercially from Aldrich. IR spectra were recorded on a JASCO FTIR-410 spectrometer using KBr pellets. UV/Vis spectra were recorded on a Perkin–Elmer Lambda25 UV/Vis spectrophotometer. Thermogravimetric analysis was performed on a Mettler Toledo Star system from room temperature to 700 °C with a heating rate of 10 °C/min. Elemental analysis was carried out using a Perkin–Elmer 1400 C analyzer. Magnetic susceptibility measurements were performed on a George Associate Faraday Force Magnetometer.

2.2. Preparation of $[Co(tmb)_2(4,4'\text{-bpy})_2(H_2O)_2](Htmb)_2$ (**1**)

A mixture of cobalt acetate tetrahydrate (0.0311 g, 0.125 mmol), Htmb (0.041 g, 0.250 mmol), 4,4′-bpy (0.039 g, 0.250 mmol) and water (2.5 mL) was stirred for 30 min, sealed in a 23 mL polyfluoroethylene-lined stainless steel bomb, and kept at 100 °C under autogenous pressure for 72 h. After cooling at a ramp of 10 °C/h to room temperature, pink colored crystals of 1 were collected by filtration, washed with deionized water followed by diethyl ether, and then dried (0.0858 g, 65% yield).

For **1**: *Anal.* Calc. for $C_{60}H_{66}N_4O_{10}Co$: C, 67.85; H, 6.26; N, 5.28. Found: C, 68.25; H, 6.02; N, 5.60%.

2.3. Preparation of $\{[Ni(tmb)_2(\mu\text{-}4,4'\text{-bpy})_2(H_2O)_2]\ (4,4'\text{-bpy})\}_n$ (**2**)

A mixture of nickel acetate tetrahydrate (0.0311 g, 0.125 mmol), Htmb (0.041 g, 0.250 mmol), 4,4′-bpy (0.039 g, 0.250 mmol) and water (2.5 mL) was stirred for 30 min, sealed in a 23 mL polyfluoroethylene-lined stainless steel bomb, and kept at 75 °C under autogenous pressure for 72 h. After cooling at a ramp of 10 °C/h to room temperature, green colored crystals of **2** were collected by filtration, washed with de-ionized water followed by diethyl ether, and then dried (0.0641 g, 70% yield).

For **2**: *Anal.* Calc. for $C_{40}H_{42}N_4O_6Ni$: C, 65.50; H, 5.77; N, 7.64. Found: C, 66.23; H, 5.49; N, 7.51%.

2.4. X-ray data collection and structure refinement of **1** and **2**

X-ray single-crystal diffraction data for compound **1** was collected on a CAD-4 diffractometer equipped with graphite monochromated Mo Kα radiation at 293 K. The data was collected by the $\omega/2\theta$ scan mode. The standard direct method was used to position the heavy atoms. The remaining non-H atoms were located from the subsequent difference Fourier synthesis. All non-H atoms were refined anisotropically. All H atoms were calculated in ideal positions and were riding on their respective carbon atoms (Biso = 1.2 Beq and 1.5 Beq). The structure was refined in a full matrix least-squares calculation on F^2. Programs used to solve and refine the structure: SHELXS97 and SHELXL97 [15]. Molecular graphics: ORTEP-3 for windows [16].

X-ray single-crystal diffraction data for compound **2** was collected on a Bruker Apex II CCD diffractometer at 293(2) K. A semi-empirical absorption correction was applied using SADABS [17] and the SAINT program [18] was utilized for integration of the diffraction profiles. The structure was solved by direct methods using the SHELXS program of the SHELXTL package [19] and refined with SHELXL. The final refinement was implemented by full-matrix least-squares methods on F^2 with anisotropic thermal parameters for all the non-H atoms. In general, H atoms attached to the ligands were placed geometrically and allowed to ride during the subsequent refinement. The crystal data for both complexes are presented in Table 1, and selected bond distances and angles are in Tables 2 and 3.

3. Results and discussion

3.1. Structural description of $[Co(tmb)_2(4,4'\text{-bpy})_2(H_2O)_2](Htmb)_2$

Compound **1** crystallizes in the monoclinic space group $P2_1/n$. The cobalt center locates on the inversion center and coordinates to two nitrogen atoms from two 4,4′-bipyridyl, two oxygen atoms from two 2,4,6-trimethylbenzoate groups, and two oxygen atoms from a pair of water molecules to form an octahedral geometry. In this complex, there exist two unique 2,4,6-trimethylbenzoic acid moieties (see Fig. 1), one in anionic form to constitute the $[Co(tmb)_2(4,4'\text{-bpy})_2(H_2O)_2]$ monomer via coordination with car-

Table 1
Crystal data and structure refinement for **1** and **2**

Complex	**1**	**2**
Empirical formula	$C_{60}H_{66}N_4O_{10}Co$	$C_{40}H_{42}N_4O_6Ni$
Formula weight	1062.1	733.49
Temperature (K)	293(2)	294(2)
Wavelength (Å)	0.71073	0.71073
Crystal system	monoclinic	orthorhombic
Space group	*P*121/*n*1	*Ccca*
Unit cell dimensions		
a (Å)	10.4363(8)	12.992(2)
b (Å)	13.0223(9)	26.101(4)
c (Å)	20.6962(12)	22.618(4)
V (Å^3)	2812.0(3)	7670(2)
Z	2	8
D_{calc} (mg m^{-3})	1.254	1.270
Absorption coefficient (mm^{-1})	0.366	0.556
F(000)	1122	3088
Crystal size (mm)	0.38 × 0.28 × 0.23	0.40 × 0.32 × 0.20
θ Range for data collection (°)	1.85–28.31	1.56–27.85
Limiting indices	$-13 \leqslant h \leqslant 13$ $-17 \leqslant k \leqslant 17$ $-27 \leqslant l \leqslant 26$	$-17 \leqslant h \leqslant 16$ $-33 \leqslant k \leqslant 32$ $-21 \leqslant l \leqslant 29$
Reflections collected/unique	30218/6982	22765/4564
R_{int}	0.0474	0.0336
Completeness to θ (%)	100.0	100.0
Absorption correction	none	none
Refinement method	full-matrix least-squares on F^2	
Data/restraints/parameters	6982/0/357	4564/0/236
Goodness-of-fit on F^2	1.017	1.025
R_1 and wR_2 [$I > 2\sigma(I)$]	0.0479, 0.1148	0.0354, 0.0878
R_1 and wR_2 (all data)	0.0828, 0.1340	0.0629, 0.1016
Largest difference in peak and hole (e Å^3)	0.541 and −0.350	0.278 and −0.326

Table 2
Selected bond lengths (Å) and angles (°) for **1**

Co–O(1)#1	2.0749(16)	C(10)–N(11)	1.318(4)
Co–O(1)	2.0749(16)	C(20)–O(21)	1.248(3)
Co–O(21)#1	2.1338(14)	C(20)–O(22)	1.261(3)
Co–O(21)	2.1338(14)	C(32)–O(34)	1.194(3)
Co–N(2)#1	2.1787(16)	C(32)–O(33)	1.306(3)
Co–N(2)	2.1787(16)	O(33)–H(33)	0.9300(4)
O(1)#1–Co–O(1)	180.00(11)	O(21)–Co–N(2)	88.19(6)
O(1)#1–Co–O(21)	93.25(6)	O(21)#1–Co–N(2)	91.81(6)
O(1)–Co–O(21)	86.75(6)	O(1)#1–Co–N(2)#1	90.66(6)
O(1)#1–Co–O(21)#1	86.75(6)	O(1)–Co–N(2)#1	89.34(6)
O(1)–Co–O(21)#1	93.25(6)	O(21)–Co–N(2)#1	91.81(6)
O(21)–Co–O(21)#1	180.00(11)	O(21)#1–Co–N(2)#1	88.19(6)
O(1)#1–Co–N(2)	89.34(6)	N(2)–Co–N(2)#1	180.00(12)
O(34)–C(32)–O(33)	122.3(3)	O(1)–Co–N(2)	90.66(6)
O(21)–C(20)–O(22)	123.6(2)		

Symmetry transformation used to generate equivalent atoms: #1 $-x+1, -y, -z$.

Table 3
Selected bond lengths (Å) and angles (°) for **2**

Ni(1)–O(1)	2.0419(14)	Ni(1)–N(2)#2	2.105(2)
Ni(1)–O(1)#1	2.0419(14)	O(1)–C(7)	1.259(2)
Ni(1)–O(3)	2.0835(13)	O(2)–C(7)	1.248(2)
Ni(1)–O(3)#1	2.0835(13)	N(2)–Ni(1)#3	2.105(2)
Ni(1)–N(1)	2.1041(18)		
O(1)–Ni(1)–O(1)#1	177.04(7)	O(1)#1–Ni(1)–N(1)	88.52(3)
O(1)–Ni(1)–O(3)	90.39(5)	O(3)–Ni(1)–N(1)	88.77(3)
O(1)#1–Ni(1)–O(3)	89.54(5)	O(3)#1–Ni(1)–N(1)	88.77(3)
O(1)–Ni(1)–O(3)#1	89.54(5)	O(1)–Ni(1)–N(2)#2	91.48(3)
O(1)#1–Ni(1)–O(3)#1	90.39(5)	O(1)#1–Ni(1)–N(2)#2	91.48(3)
O(3)–Ni(1)–O(3)#1	177.55(7)	O(3)–Ni(1)–N(2)#2	91.23(3)
O(1)–Ni(1)–N(1)	88.52(3)	O(2)–C(7)–O(1)	125.32(18)

Symmetry transformations used to generate equivalent atoms: #1 $-x+1/2, -y, z$; #2 $x, -y, z-1/2$; #3 $x, -y, z+1/2$.

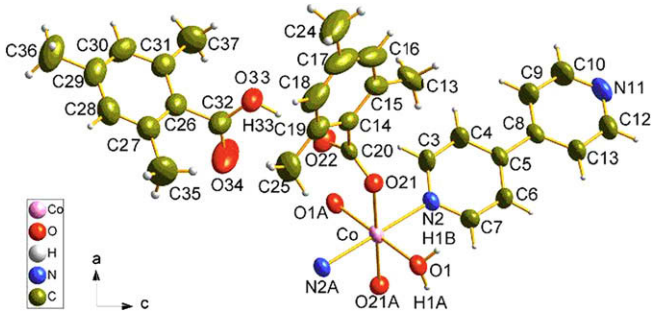

Fig. 1. A portion view of **1** with atom labeling of the asymmetry unit and metal coordination sphere. Symmetry code (A) $-x+1, -y, -z$.

boxylate and the other in the free acid form that is involved in hydrogen bonding linkage.

The bond lengths involving 4,4′-bipyridyl and 2,4,6-trimethyl benzoate ligands, Co(1)–N(2) [2.1787(16) Å], Co(1)–O(1) [2.0749(16) Å] and Co(1)–O(21) [2.1338(14) Å], are comparable to those found in similar cobalt complexes [20]. The *cis*-O–Co–O/N angles are in the range of 86.75(6)–91.81(6)° and the O–C–O angle is 123.6(2)°.

Due to the trans-disposition of the aqua molecules and both types of organic ligands at each metal center, a square grid layer network is propagated along the crystallographic bc plane with the adjacent Co–Co distance of 13.022 Å via intermolecular O–H···N interactions, as shown in Fig. 2 [21]. The bridging role of 4,4′-bipyridyl ligand via both coordination and H-bonded contacts leads to the formation of a (4,4) sheet, in which the ligated 2,4,6-trimethyl benzoate moieties lie along the shorter diagonals within each subunit and the unligated 2,4,6-trimethyl benzoic acid molecules recline the length of the longer diagonal by virtue of hydrogen bonds (Scheme 1).

In detail, the water ligands form strong intermolecular hydrogen bonds to the uncoordinating carboxylate oxygen atoms with $d_{O1-H1A\cdots O22\ (-x+1,\ -y,\ -z)} = 2.660(2)$ Å and ∠ = 158(3)°, and also to the uncoordinating N atoms of 4,4′-bipyridyl, with $d_{O1-H1B\cdots N11\ (-x+3/2,\ y+1/2,\ -z+1/2)} = 2.767(3)$ Å and ∠ = 179(4)°. In addition, there exist strong hydrogen bonds between the 2,4,6-trimethyl benzoic acid guests and the unligated O atoms of the 2,4,6-trimethyl benzoate ligands with $d_{O33-H33\cdots O22} = 2.586(3)$ Å and ∠ = 175(4)°.

Also, there are C–H···O interactions present in the structure [$d_{C36-H36B\cdots O21\ (x+1/2,\ -y+1/2,\ z-1/2)} = 3.594(4)$ Å and ∠ = 163.86(2)°], [$d_{C10-H10\cdots O34\ (x+1/2,\ -y-1/2,\ z+1/2)} = 3.333(4)$ Å and ∠ = 154.77(20)°], [$d_{C7-H7\cdots O34(-x+1,\ -y,\ -z)} = 3.630(4)$ Å and ∠ = 152.04(15)°], and [$d_{C3-H3\cdots O22} = 3.721(3)$ Å and ∠ = 143.81(16)°], which play a significant role in stabilizing the overall 3D structure (see Fig. 3). The parameters of hydrogen bonds are given in Table 4.

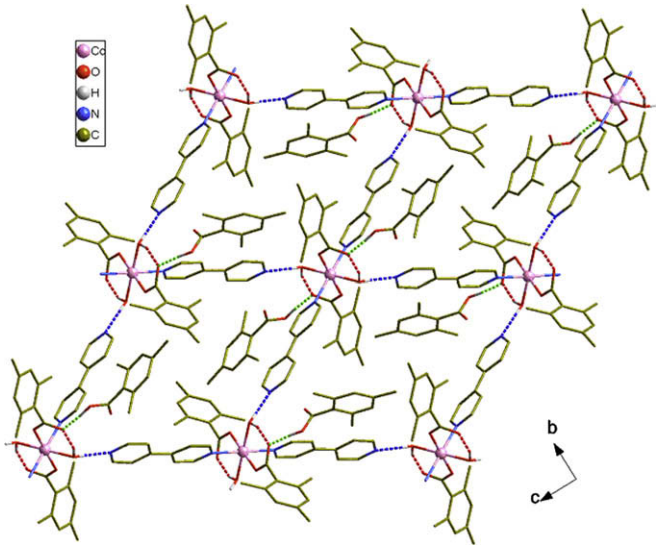

Fig. 2. A perspective view of the 2D H-bonding layer in **1** along the [100] direction. (H-bonds are shown in red, blue, and green broken lines). (For interpretation of the references to colour in this figure legend, the reader is referred to the web version of this article.)

From the least square plane calculations, the phenyl rings of two 2,4,6-trimethylbenzoate anions and the two 4,4′-bipyridyl ligands are located in the parallel planes and separated by the distances of 1.914 and 0.264 Å, respectively.

The dihedral angle between the 4,4′-bipyridyl ring and a phenyl ring of 2,4,6-trimethyl benzoate anion is 63.79° for the planes containing (C14, C15, C16, C17, C18, and C19) and (N2, C3-C10, N11, C12, and C13), and the dihedral angle between the phenyl rings of coordinated and uncoordinated acids is 63.20° for the planes containing (C14, C15, C16, C17, C18, and C19) and (C26, C27, C28, C29, C30, and C31) [22].

The group of atoms (N2, C3-C10, N11, C12, and C13) in the 4,4′-bipyridyl unit deviate significantly from planarity. Among all, C4 has the highest deviation of 0.0877 Å. The group of atoms (C14–C20 and C23–C25) of the trimethyl benzoate moiety also deviate significantly from planarity and C24 has the highest deviation of 0.1668 Å.

The group of atoms (C20, O21, and O22) in the carboxylate moiety are coplanar but, almost perpendicular (dihedral angle 88.84°) to its phenyl ring (C14–C19). The group of atoms (C26–C32 and C35–C37) deviates significantly from planarity, and C32 has the higher deviation of 0.0182 Å. From the puckering parameters (φ_2, θ_2, and Q) [23,24] the conformation for ring 1 (C14–C19) is boat conformation $^{1,4}B$, for ring 2 (C26–C31) is twist conformation $^{4}T_2$, for ring 3 (N2 and C3–C7) is twist conformation $^{3}T_1$, and for ring 4 (C8–C9, N11, C12, and C13) is sofa conformation $^{3}S_4$.

3.2. Structural description of *{[Ni(tmb)$_2$(μ-4,4′-bpy)(H$_2$O)$_2$](4,4′-bpy)}$_n$*

Compound **2** crystallizes in the orthorhombic space group *Ccca*. It is a 1:1:2 complex with Ni ion, 2,4,6-trimethylbenzoic acid (Htmb), and 4,4′-bipyridyl. The Ni atom lies on a diad axis and has a *trans*-N_2O_4 octahedral coordination through bonds to two 4,4′-bpy N atoms, two equivalent water O atoms and two equivalent carboxylate-O atoms. In the asymmetric unit, both COOH group of Htmb and 4,4′-bpy interact with Ni(II). Thus, each Ni(II) is connected to two 4,4′-bpy molecules that lie at the axial positions and two Htmb to complete the six coordination sites with the aid of two water molecules (Fig. 4). As a result, in this case, infinite linear polymeric chains of –Ni–bpy–Ni–bpy– are formed

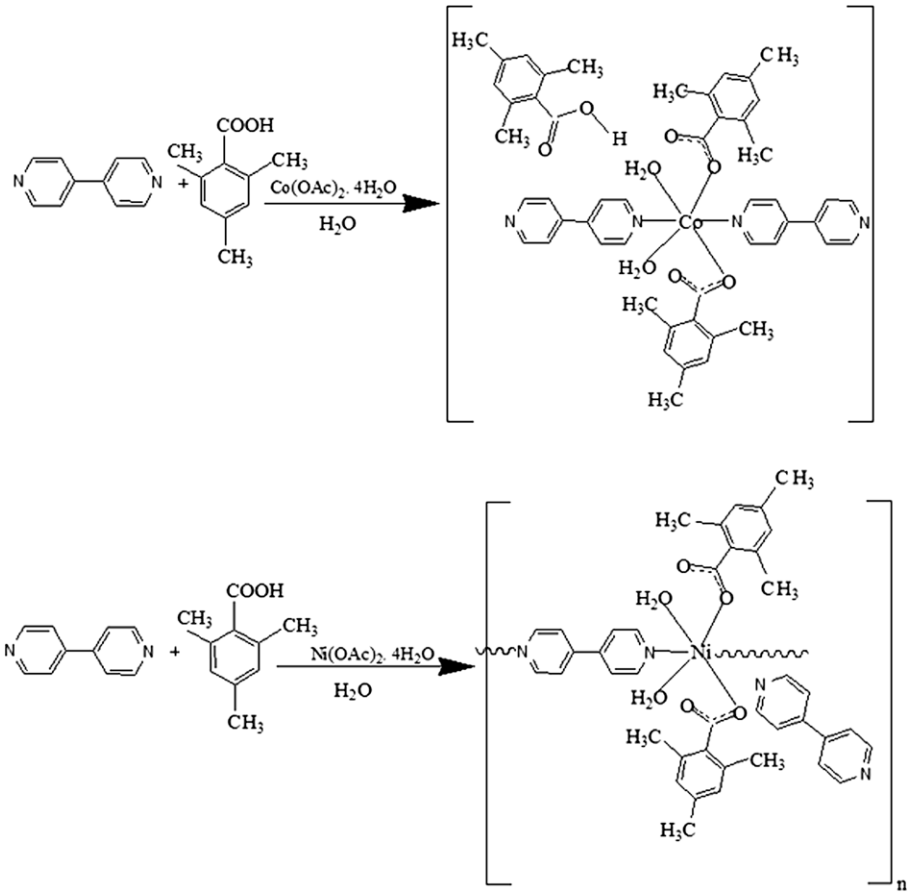

Scheme 1.

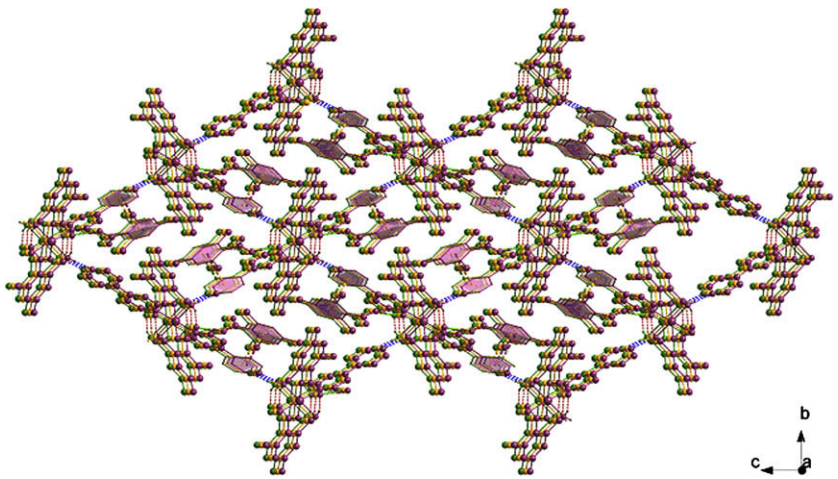

Fig. 3. 3D packing diagram of **1**, in which the interlayer aromatic interactions are indicated by pink. (For interpretation of the references to colour in this figure legend, the reader is referred to the web version of this article.)

running parallel to the *c*-axis by repeated operations of *c*-glide (see Fig. 5), with the 4,4′-bpy connectors joining the adjacent Ni^{II} octahedrons using their typical bridging role. In each chain, the basal plane of carboxylate and water O atoms is stabilized by O3–H···O2 hydrogen bonding from water to the uncoordinated carboxylate O.

These polymeric chains are further held together by O3–H···N(bpy)N···H–O3 bridges. In short, there is much symmetry including glide planes and 2-fold rotation axes in all three directions, 2-fold screw axes in two directions, inversion centers, and lattice centering in this structure.

In the structure of 2, two unique 4,4′-bipyridyl molecules are found, one of which coordinates to the nickel center via its nitrogen atoms, whereas the other is involved only in hydrogen bonded linkage. Both types of 4,4′-bipyridyl units are nonplanar, having torsional twists about their central linking bonds of ca. 16.3° and 43.1°, respectively. Notably, the non-coordinated 4,4′-bipyridyl guest is positioned over a crystallographic inversion center, and

Table 4
Hydrogen bonds exhibited by **1** and **2**

D–H	d(D–H)	d(H···A)	∠D–H···A	d(D···A)	A [symmetry]
Complex 1					
O33–H33	0.93(4)	1.66(4)	175(4)	2.586(3)	O22 [*x*,*y*,*z*]
O1–H1B	0.78(4)	1.98(4)	179(4)	2.767(2)	N11 [$-x+3/2$, $y+1/2$, $-z+1/2$]
O1– H1A	0.86(3)	1.84(4)	158(3)	2.660(2)	O22 [$-x+1$, $-y$, $-z$]
Complex 2					
O3–H3A	0.85	1.964	167.30(1)	2.799	N3 [$x-1/2$, y, $-z+1$]
O3–H3B	0.85	1.82	164.76(1)	2.65	O2 [$-x+1/2$, $-y$, $+z$]
C5–H5	0.93	2.514	178.34(1)	3.444	O2 [$-x+1$, $-y$, $-z+1$]
C21–H21	0.93	2.299	163.25(1)	3.201	O1 [$x+1/2$, y, $-z+1$]

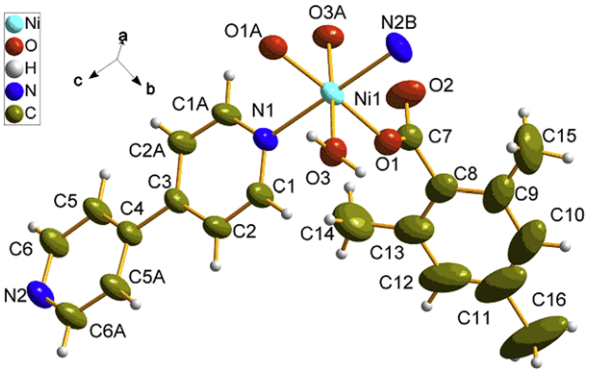

Fig. 4. A molecular diagram showing the coordination geometry of Ni^{II} in **2**. Symmetry codes (A) $-x+1/2$, $-y$, z; (B) $-x+1/2$, y, $z-1/2$.

therefore, there is a statistical reversal of the N–N axis throughout the structure, which however does not change the crosslinking hydrogen bonding role of it.

The least square plane calculations show that the dihedral angle between the phenyl rings of two 2,4,6-trimethylbenzoate anions is 8.32° for the planes containing (C8, C9, C10, C11, C12, and C13) and (C8a, C9a, C10a, C11a, C12a, and C13a), and the dihedral angle between the two 4,4′-bipyridyl units is 73.51° for the planes containing (N1, C1–C6, N2, and C1′–C6′) and (N1a, C1a–C6a, N2a, and C1a′–C6a′), and the dihedral angle between the 4,4′-bipyridyl ring and a phenyl ring of 2,4,6-trimethyl benzoate anion is 48.41° for the planes containing (C8, C9, C10, C11, C12 and C13) and (N1, C1–C6, N2 and C1′–C6′).

The bond lengths involving 4,4′-bipyridyl and 2,4,6-trimethyl benzoate ligands are Ni–O(carboxyl) [2.042(1) Å], Ni–O(water) [2.0084(1) Å], and Ni–N [2.104(1) and 2.105(2) Å], being virtually similar to the mean database values for these bonds [2.061, 2.087, and 2.103 Å, respectively]. The O–Ni–O angles are in the range of 89.54(5)–177.55(7)° with the average value of 118.99° and the O–C–O angle is 125.32(18)°.

Each coordinated water molecule provides one H atom to the coordinating carboxylate O atom and the other to the N atom of uncoordinated 4,4′-bpy [$d_{O3-H3A\cdots N3\ (x-1/2,y,-z+1)}$ = 2.799(0) Å and ∠ = 167.30(1)°] and [$d_{O3-H3B\cdots O2\ (-x+1/2,\ -y,\ z)}$ = 2.650(0) Å and ∠ = 164.76(1)°]. The strong hydrogen bonds are apparently responsible for the supramolecular assembly of the 1D coordination chains to generate 3D networks. In fact, considering these H-bonds, each metal center behaves as a planar four-connected node to constitute 3D $CdSO_4$ topological frameworks [25], which are interestingly of 2-fold interpenetration in the crystalline lattice (see Figs. 6–8). Intermolecular C–H···O interactions [$d_{C5-H5\cdots O2\ (-x+1,-y,-z+1)}$ = 3.444 Å and ∠ = 178.34(1)°] and [$d_{C21-H21\cdots O1\ (x+1/2,\ y,\ -z+1)}$ = 3.201 Å and ∠ = 163.25(1)°] are also found, which play a significant role in stabilizing this structure. The vibrational frequencies [26] of **1** and **2** are given in Table 5.

3.3. Magnetic properties

Temperature-dependent magnetic susceptibility measurements for complexes **1** and **2** were performed on polycrystalline samples. The effective magnetic moments of **1** and **2** are 5.68 and 3.42 μ_B, being close to the expected values (5.2 and 3.9 μ_B) for the isolated high-spin Co(II) and Ni(II) ($S = 5/2$). A χ_M versus T plot for **1** over the temperature range of 23.7–291.8 K (Fig. 9), in which χ_M is the corrected magnetic susceptibility per Co(II) unit, could be fitted according to the Curie–Weiss law $\chi_M = C/(T-\theta)$, giving a Curie constant C = 4.03 $cm^3\ mol^{-1}$ K, and a Weiss constant $\theta = -22.51$ K. The negative value of θ indicates weak antiferromagnetic interactions between Co(II), since the adjacent Co(II) ions are separated with distance of 13.022 Å as revealed by X-ray crystal structure. The χ_M value of 1.2×10^{-2} $cm^3\ mol^{-1}$ at room temperature increases as the temperature decreases, attaining 9.8×10^{-2} $cm^3\ mol^{-1}$ at 23.7 K. A χ_M versus T plot for **2** over the temperature range of 8.4–296.7 K (Fig. 10), in which χ_M is the corrected magnetic susceptibility per Ni(II) unit, could be fitted according to the Curie–Weiss law $\chi_M = C/(T-\theta)$, giving a Curie constant C = 1.46 $cm^3\ mol^{-1}$ K, and a Weiss constant $\theta = -34.92$ K. Similarly, the negative value of θ indicates antiferromagnetic interactions between Ni(II), since the adjacent Ni(II) ions are separated by 4,4′-bpy ligands with distance of 11.3 Å. The χ_M value of 4.91×10^{-3} $cm^3\ mol^{-1}$ at room temperature increases as the temperature decreases, attaining 6.8×10^{-2} $cm^3\ mol^{-1}$ at 8.4 K.

3.4. Thermal properties

Thermal analysis (TGA) of complexes **1** and **2** were performed between room temperature and 700 °C under the nitrogen atmo-

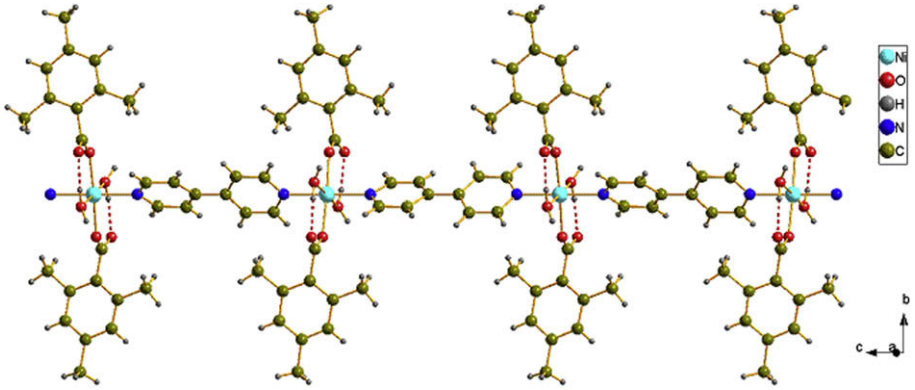

Fig. 5. The polymeric single chain in **2**.

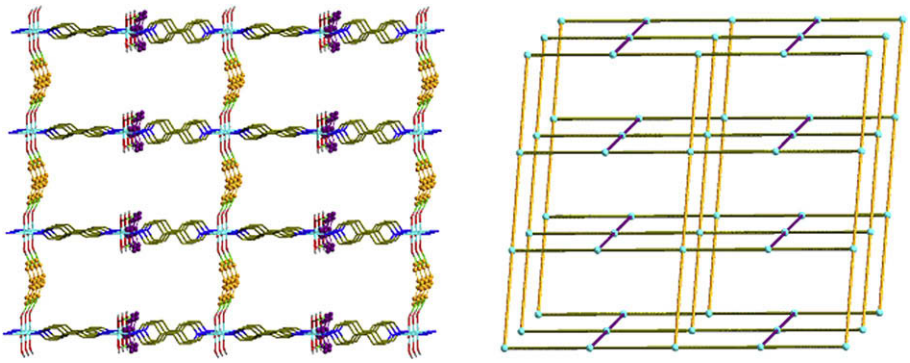

Fig. 6. A single 3D network in **2** (left). A schematic representation of the cds ($CdSO_4$) topology (right). The 4,4′-bipy molecules involving in H-bonds are shown in violet and orange, respectively, and the 2,4,6-trimethyl benzencarboxylic acid ligands are omitted for clarity. (For interpretation of the references to colour in this figure legend, the reader is referred to the web version of this article.)

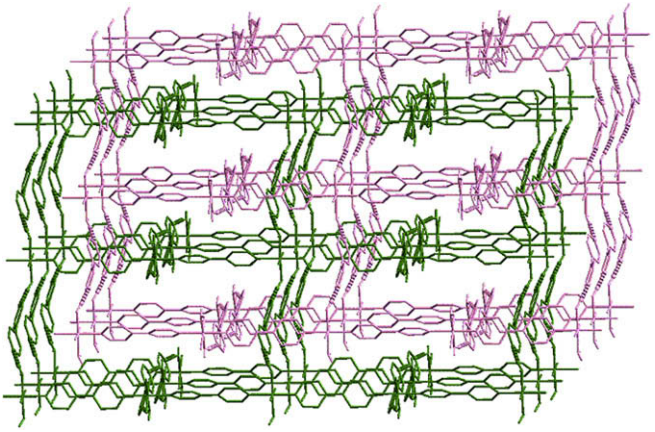

Fig. 7. 2-Fold interpenetrating structure of **2**. The two cds arrays are shown in green and rose, respectively. (For interpretation of the references to colour in this figure legend, the reader is referred to the web version of this article.)

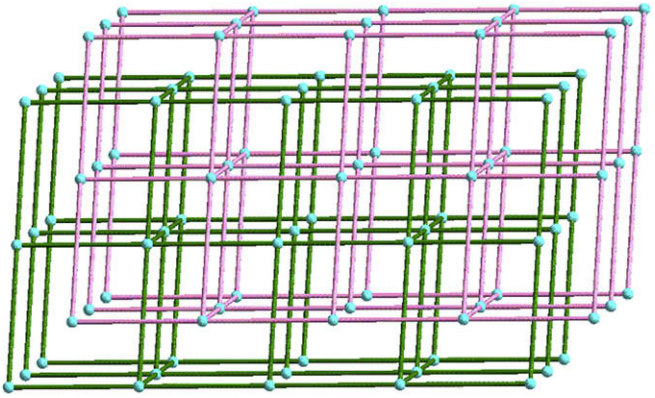

Fig. 8. A schematic view of two interpenetrating networks.

sphere. The TGA results indicate that **1** undergoes a weight loss of 3.7% (Calc. 3.3%) in the temperature range of 85–106 °C, corresponding to the removal of two coordinated water molecules. The second stage has the weight loss of 52.2% (Calc. 51.5%) in the temperature range of 146–274 °C, corresponding to removal of two 4,4′-bpy moieties and an unligated Htmb. The third stage occurs with the gradual decomposition of the remaining species, leading to the formation of cobalt oxide. The saturation temperature above which there is no obvious weight loss occurs at ~425 °C.

The TGA results indicate that complex **2** loses 5.1% (Calc. 4.9%) of its mass in the temperature range of 92–108 °C, corresponding

Table 5
Infrared spectral data of **1** and **2**

Frequency range (cm^{-1})		Mode of vibration
Compound **1**	Compound **2**	
3388	3415	O–H_{str} (water)
	3133	inter molecular H-bonding
3059	3061	aromatic C–H_{str}
2919 and 2857	2929 and 2863	aliphatic C–H_{str}
1604 and 1544	1609 and 1531	COO^- asymmetric and COO^- symmetric stretching [26]
1439–1004	1450–946	C=C and C–N stretching vibrations
764 and 806	754 and 846	C–H out of plane bending
Below 600	below 600	M–N and M–O stretching vibrations

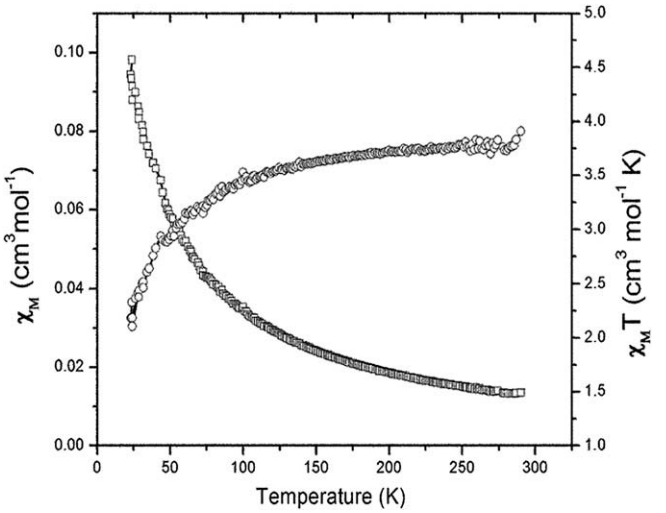

Fig. 9. χ_M and $\chi_M T$ vs. T plots for complex **1**. The solid lines represent the best fit of the experimental data.

to the loss of coordinated water molecules. The second stage involves the loss of 85.7% (Calc. 87.0%) of its mass in the temperature range of 290–395 °C, corresponding to the loss of two 4,4′-bpy and two tmb components. The third stage occurs with the gradual decomposition of the remaining species, leading to the formation of nickel oxide. The saturation temperature above which there is no obvious weight loss occurs at ~530 °C.

3.5. Electronic absorption spectra

In the electronic spectrum for complex **1**, the ligand 4,4′-bipyridyl exhibits a low energy band at 320 nm region, which is gener-

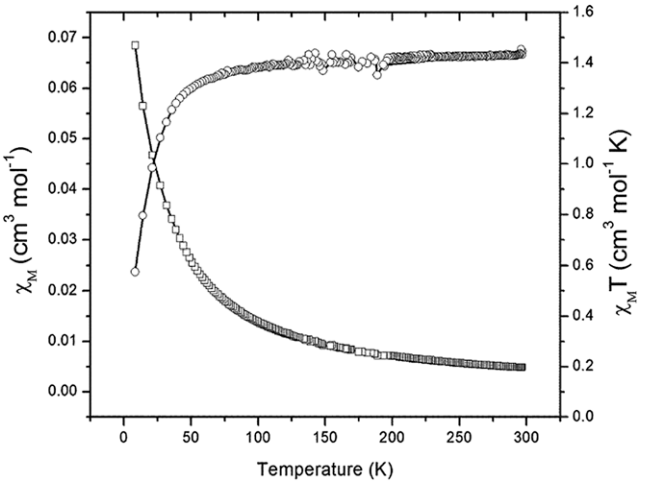

Fig. 10. χ_M and $\chi_M T$ vs. T plots for complex **2**. The solid lines represent the best fit of the experimental data.

ally assigned to π–π^* transition of the benzenoid and/or (C=N) chromophore of the ligand. As a rule, the longer wavelength bands in the spectra of metal complexes may be considered as evidence for the complex formation. The absorption band at 535 nm due to the $^4T_{1g} \rightarrow {}^4T_{1g}$ (P) transition, suggests a high-spin octahedral sphere. However, the presence of an additional absorption band as a shoulder in the 680 nm region, assigned to the $^4T_{1g} \rightarrow {}^4A_{2g}$ transition, suggests a distorted-octahedral configuration due to the Jahn–Teller effect.

The electronic spectrum of the Ni(II) complex **2** shows two absorption bands at 390 and 700 nm due to the MLCT transitions, as generally observed for octahedral Ni(II) complexes.

3.6. Antibacterial and antifungal activity

The *in vitro* biological screening effects of both complexes were tested against the bacteria: *Escherichia coli, Staphylococcus aureus, Pseudomonas aeruginosa,* and *Bacillus subtilis* by the well-diffusion method [27] using agar nutrient as the medium. The antifungal activities were also evaluated by the well-diffusion method against the fungi viz., *Aspergillus niger, Aspergillus flavus* and *Rhizoctonia bataicola* cultured on potato dextrose agar as medium. The compounds were tested at a concentration of 50 μg/0.01 mL in aqueous solution. In a typical procedure [28], a well was made on the agar medium inoculated with microorganisms. The well was filled with the test solution using a micropipette and the plate was incubated for 24 h for bacteria and 72 h for fungi at 35 °C. During this period, the test solution diffused and the growth of the inoculated microorganisms was affected. The inhibition zone was developed, at which the concentration was noted. The percentage inhibition was calculated as $100(C - T)/C$, where C is the average diameter of bacteria or fungal growth on the control plate (water) and T is the average diameter of bacteria or fungal growth on the test plate.

The susceptibility zones were measured in diameter (mm) and the results are shown in Tables 6 and 7. The susceptibility zones measured are the clear zones around the discs killing the bacteria. The complexes individually exhibit varying degrees of inhibitory effect on the growth of the tested bacterial species. On complexation, the polarity of the metal ion will be reduced to a greater extent due to the overlap of the ligand orbital and partial sharing of the positive charge of the metal ion with the donor groups. Further, it increases the delocalization of π-electrons over the whole ligand and enhances the penetration of complexes into lipid membranes and blocking of the metal binding sites in the enzymes of microorganisms. The complexes may also disturb the respiration process of the cell and thus block the synthesis of proteins, which restricts further growth of the organism [29].

Table 6
Antibacterial activity of the complexes **1** and **2**

Complex	Bacterial species				
	a	b	c	d	e
$[Co(tmb)_2(4,4'\text{-bpy})_2](Htmb)_2$	+++	++	++	+++	+++
$[Ni(tmb)_2(\mu\text{-}4,4'\text{-bpy})(H_2O)_2]_n(4,4'\text{-bpy})$	+++	++	++	+++	+++

a: *Escherichia coli*, b: *Staphylococcus aureus*, c: *Pseudomonas aeruginosa*, d: *Bacillus subtilis*; e: *Klebsiella pneumoniae*. Inhibition zone diameter mm (% inhibition): +, 6–10 (27–45%); ++, 10–14 (45–64%); +++, 14–18 (64–82%); ++++, 18–22 (82–100%). Percent inhibition values were relative to inhibition zone (22 mm) of standard antibacterials (sulfadiazine, sulfathiazole), considered as 100% inhibition, tested under the same conditions as the new compounds reported here.

Table 7
Antifungal activity of the complexes **1** and **2**

Complex	Fungal species		
	a	b	c
$[Co(tmb)_2(bpy)_2](Htmb)_2$	+++	++	++
$[Ni(tmb)_2(\mu\text{-}4,4'\text{-bpy})(H_2O)_2]_n(4,4'\text{-bpy})$	+++	++	++

a: *Aspergillus niger*, b: *Aspergillus flavus*, c: *Rhizoctonia bataicola*. Inhibition zone diameter mm (% inhibition): +, 6–10 (27–45%); ++, 10–14 (45–64%); +++, 14–18 (64–82%); ++++, 18–20 (82–100%), (–) = no inhibition zone. Percent inhibition values were relative to inhibition zone (20 mm) of standard antifungal (Bavistin), considered as 100% inhibition, tested under the same conditions as the new compounds reported here.

4. Conclusion

In summary, two new supramolecular complexes of Co^{II} and Ni^{II} using 2,4,6-trimethyl benzoic acid and 4,4′-bipyridyl as ligands have been synthesized by hydrothermal reaction and characterized by X-ray crystallography, IR, UV/Vis spectra, elemental analysis and magnetic susceptibility measurements. Both complexes display interesting 3D hydrogen-bonded assemblies from the fundamental discrete or 1D coordination arrays. Weak intermolecular antiferromagnetic interactions are found in **1** and **2**, which also show good antibacterial and antifungal activity.

Acknowledgement

The authors (MI and RR) acknowledge CSIR, New Delhi for providing financial support through Senior Research Fellowship. The authors greatly acknowledge Dr. H.N. Vasan, Principal Research Scientist, SSCU, Indian Institute of Science, Bangalore-12 for his constant encouragement and moral support. M.D. also acknowledges the financial support from Tianjin Normal University.

Appendix A. Supplementary data

CCDC 680843 and 680844 contain the supplementary crystallographic data for this paper. These data can be obtained free of charge via http://www.ccdc.cam.ac.uk/conts/retrieving.html, or from the Cambridge Crystallographic Data Centre, 12 Union Road, Cambridge CB2 1EZ, UK; fax: (+44) 1223-336-033; or e-mail: deposit@ccdc.cam.ac.uk. Supplementary data associated with this article can be found, in the online version, at doi:10.1016/j.poly.2008.09.003.

References

[1] S. Kitagawa, R. Kitaura, S. Noro, Angew. Chem., Int. Ed. 43 (2004) 2334.
[2] F. Mori, T. Nyui, T. Ishida, T. Nogami, K. Ychoi, H. Nojiri, J. Am. Chem. Soc. 128 (2006) 1440.
[3] B. Zhao, X.Y. Chen, P. Cheng, D.Z. Liao, S.P. Yan, Z.H. Jiang, J. Am. Chem. Soc. 126 (2004) 15394.
[4] A. Cingolani, S. Galli, N. Masciocchi, L. Pandolfo, C. Pettinari, A. Siroin, J. Am. Chem. Soc. 127 (2005) 6144.
[5] (a) C.M. Liu, D.Q. Zhang, J.L. Luo, N.L. Wang, H.M. Hu, D.B. Zhu, Eur. J. Inorg. Chem. (2003) 3618;
(b) M. Kondo, T. Okubo, A. Asami, S. Noro, T. Yoshitomi, S. Kitagawa, T. Ishii, H. Matsuzaka, K. Seki, Angew. Chem., Int. Ed. 38 (1999) 140;
(c) L. Mao, S.J. Rettig, R.C. Thompson, J. Trotter, S.-H. Xia, Can. J. Chem. 74 (1996) 2413;
(d) S.K. Ghosh, P.K. Bharadwaj, Inorg. Chem. 43 (2004) 6887;
(e) S.K. Ghosh, P.K. Bharadwaj, Eur. J. Inorg. Chem. (2005) 4880;
(f) Y. Liang, R. Cao, W.P. Zhu, M.C. Hong, W.J. Zhang, Angew. Chem., Int. Ed. 39 (2000) 3304;
(g) Y. Liang, M.C. Hong, W.P. Zhu, R. Cao, W.J. Zhang, Inorg. Chem. 40 (2001) 4574.
[6] M.J. Zaworotko, Chem. Commun. (2001) 1.
[7] S.R. Batten, R. Robson, Angew. Chem., Int. Ed. 37 (1998) 1460.
[8] M.L. Tong, H.K. Lee, X.M. Chen, R.B. Huang, T.C.W. Mak, J. Chem. Soc., Dalton Trans. (1999) 3657.
[9] M. Andruh, H.W. Roesky, M. Noltemeyer, H.G. Schmidt, Z. Naturforsch., Teil. B B49 (1994) 31.
[10] K. Biradha, M. Fujita, Chem. Commun. (2001) 15.
[11] Q. Wang, X. Wu, W. Zhang, T. Sheng, P. Lin, J. Li, Inorg. Chem. 38 (1999) 2223.
[12] K. Biradha, M. Sarkar, L. Rajput, Chem. Commun. (2006) 4169.
[13] B.F. Hoskins, P.J. Oliver, G. Winter, Inorg. Chim. Acta 86 (1984) L21.
[14] C.L. Ma, J.K. Li, R.F. Zhang, D.Q. Wang, Inorg. Chim. Acta 359 (2006) 2407.
[15] G.M. Sheldrick, SHELXL97 and SHELXS97, University of Göttingen, Germany, 1997.
[16] L.J. Farrugia, J. Appl. Crystallogr. 30 (1997) 565.
[17] SADABS, Empirical Absorption Correction Program, University of Göttingen, Göttingen, Germany, 1997.
[18] G.M. Sheldrick, SAINT, 5.1 ed., Siemens Industrial Automation Inc., Madison, WI, 1995.
[19] G.M. Sheldrick, SHELXTL Reference Manual: Version 5.1; Bruker AXS: Madison, WI, 1997.
[20] Y. Sun, Z. Wang, H. Zhang, Y. Cao, S. Zhang, Y. Chen, C. Huang, X. Yu, Inorg. Chim. Acta 360 (2007) 2565.
[21] Y.-H. Liu, Y.-L. Lu, H.-L. Tsai, J.-C. Wang, K.-L. Lu, J. Solid State Chem. 158 (2001) 315.
[22] F. Jin, J. Li, H. Zhou, J. Wu, J. Yang, Y. Tian, M. Jiang, J. Mol. Struct. 829 (2007) 202.
[23] J.C.A. Boeyens, J. Cryst. Mol. Struct. 8 (1978) 317.
[24] D. Cremer, J.A. Pople, J. Am. Chem. Soc. 97 (1975) 1354.
[25] D.M.L. Goodgame, D.A. Grachvogel, A.J.P. White, D.J. Williams, Inorg. Chem. 40 (2001) 6180.
[26] K. Nakamoto, Infrared and Raman Spectra of Inorganic and Coordination Compounds, Fourth ed., Wiley, New York, 1986.
[27] C. Perez, M. Pauli, P. Bazerque, Acat Biol. Et. Med. Exp. 15 (1990) 113.
[28] M.J. Pelczar, E.C.S. Chan, N.R. Krieg, Microbiology, fifth ed., Blackwell, Science, New York, 1998.
[29] N. Dharmaraj, P. Viswanathamurthi, K. Natarajan, Transition Met. Chem. 26 (2001) 105.

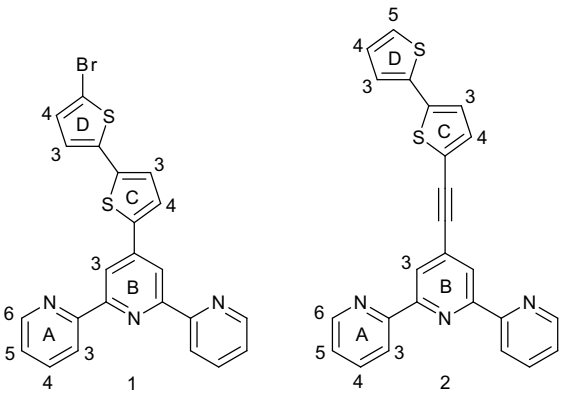

Scheme 1. Structures of ligands **1** and **2**, and numbering scheme used for the NMR spectroscopic assignments.

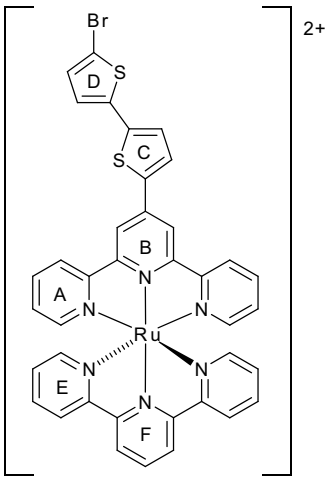

Scheme 2. Ring labelling for the NMR spectroscopic assignments in $[Ru(tpy)(1)]^{2+}$. The same scheme is used in $[Ru(tpy)(2)]^{2+}$.

2.3. 4′-(5-Bromo-2,2′-bithien-5′-yl)-2,2′:6′,2″-terpyridine (*1*)

4′-(2,2′-Bithien-5′-yl)-2,2′:6′,2″-terpyridine [39] (0.31 g, 0.81 mmol) was dissolved in a mixture of glacial acetic acid (5 cm^3) and *N*-bromosuccinimide (0.17 g, 0.97 mmol) and stirred at room temperature overnight in the absence of light. The reaction mixture was neutralised with aqueous $NaHCO_3$ and the solution was extracted into CH_2Cl_2 (3 × 25 cm^3). The CH_2Cl_2 extracts were dried over Na_2SO_4 and the solvent was removed. Compound **1** was isolated as a yellow solid (0.26 g, 0.55 mmol, 68%). m.p. = 185.6 °C. ^{1}H NMR (500 MHz, $CDCl_3$) δ/ppm 8.72 (ddd, *J* 4.8, 1.8, 0.9 Hz, 2H, H^{A6}), 8.64 (s, 2H, H^{3B}), 8.63 (dt, *J* 7.5, 1.0 Hz, 2H, H^{A3}), 7.86 (dt, *J* 7.7, 1.8 Hz, 2H, H^{A4}), 7.68 (d, *J* 3.9 Hz, 1H, H^{C4}), 7.35 (ddd, *J* 7.5, 4.8, 1.2 Hz, 2H, H^{A5}), 7.15 (d, *J* 3.9 Hz, 1H, H^{C3}), 7.00 (s, 2H, H^{D3+D4}). ^{13}C NMR (125 MHz, $CDCl_3$) δ/ppm 156.2 (C^{B2}), 156.0 (C^{A2}), 149.3 (C^{A6}), 143.0 (C^{B4}), 140.9 (C^{C5}), 138.7 (C^{D2}), 138.2 (C^{C2}), 137.2 (C^{A4}), 131.0 (C^{D4}), 126.9 (C^{C4}), 125.1 (C^{C3}), 124.5 (C^{D3}), 124.2 (C^{A5}), 121.6 (C^{A3}), 116.9 (C^{B3}), 111.9 (C^{C5}). EI MS *m/z* 476 $[M]^+$. $C_{23}H_{14}BrN_3S_2 \cdot 1.5H_2O$ requires C, 54.87; H, 3.40; N, 8.35. Found: C, 54.26; H, 2.83; N, 8.25%.

2.4. $[Ru(tpy)(\mathbf{1})][PF_6]_2$

$[Ru(tpy)Cl_3]$ (0.12 g, 0.27 mmol) was added to a stirring solution of compound **1** (0.13 g, 0.25 mmol) in EtOH (20 cm^3) with a few drops of *N*-ethylmorpholine. The mixture was stirred at room temperature for 15 min, and then heated at reflux for 5 h in the absence of light. The mixture was cooled to room temperature, and was added to aqueous NH_4PF_6 and the solution diluted with water (100 cm^3). The resulting precipitate was collected and dissolved in MeCN and purified by column chromatography (SiO_2, MeCN:H_2O:aqueous KNO_3 9:0.9:0.1). The second (red) band was collected, excess aqueous NH_4PF_6 was added and solvent was removed. The solid was dissolved in acetonitrile, and the product precipitated by addition to water. Recrystallization from MeCN/Et_2O gave $[Ru(tpy)(1)][PF_6]_2$ as a red solid (40 mg, 0.036 mmol, 13%). ^{1}H NMR (500 MHz, CD_3CN) δ/ppm 8.88 (s, 2H, H^{B3}), 8.75 (d, *J* 8.2 Hz, 2H, H^{F3}), 8.64 (d, *J* 8.1 Hz, 2H, H^{A3}), 8.49 (d, *J* 8.0 Hz, 2H, H^{E3}), 8.41 (t, *J* 8.2 Hz, 1H, H^{F4}), 8.11 (d, *J* 3.9 Hz, 1H, H^{C4}), 7.95 (dt, *J* 7.8, 1.3 Hz, 2H, H^{A4}), 7.92 (dt, *J* 7.9, 1.4 Hz, 2H, H^{E4}), 7.51 (d, *J* 3.9 Hz, 1H, H^{C3}), 7.43 (d, *J* 5.5 Hz, 2H, H^{A6}), 7.34 (d, *J* 5.6 Hz, 2H, H^{E6}), 7.29 (d, *J* 3.9 Hz, 1H, $H^{D3/D4}$), 7.22 (d, *J* 3.9 Hz, 1H, $H^{D3/D4}$), 7.17 (m, 4H, H^{A5+E5}). $^{13}C\{^1H\}$ NMR (125 MHz, CD_3CN) δ/ppm 159.1 ($C^{A2/E2}$), 158.9 ($C^{A2/E2}$), 156.5 ($C^{B2/F2}$), 156.4 ($C^{B2/F2}$), 153.6 ($C^{A6/E6}$), 153.5 ($C^{A6/E6}$), 141.7 (C^{B4}), 140.6 ($C^{C2/D2}$), 139.8 (C^{C5}), 139.2 ($C^{A4/E4}$), 139.1 ($C^{A4/E4}$), 138.8 ($C^{C2/D2}$), 136.9 (C^{F4}), 132.9 (C^{D4}), 130.4 (C^{C4}), 128.6 ($C^{A5/E5}$), 128.5 ($C^{A5/E5}$), 127.2 (C^{C3}), 126.8 (C^{D3}), 125.7 ($C^{A3/E3}$), 125.5 ($C^{A3/E3}$), 124.8 (C^{F3}), 120.3 (C^{B3}), 113.2 (C^{D5}). ESI MS *m/z* 957 $[M-PF_6]^+$, 405 $[M-2PF_6]^{2+}$. $C_{38}H_{25}Br_1F_{12}N_6P_2Ru_1S_2 \cdot H_2O$ requires C, 40.80; H, 2.43; N, 7.51. Found: C, 41.10; H, 2.77; N, 7.18%.

2.5. $[Ru(\mathbf{1})_2][PF_6]_2$

$RuCl_3 \cdot 3H_2O$ (31 mg, 0.12 mmol), **1** (110 mg, 0.23 mmol) and $AgNO_3$ (0.06 g, 0.35 mmol) were added to DMF (15 cm^3). The solution was stirred at room temperature for 15 min, after which time it was heated at reflux for 8 h in the absence of light. The reaction mixture was filtered to remove AgCl, and then saturated aqueous NH_4PF_6 (excess) was added to the filtrate to precipitate the product which was purified by column chromatography (SiO_2, MeCN:aqueous KNO_3, 15:1). The main red fraction was collected and saturated aqueous NH_4PF_6 was added to effect nitrate/hexafluorophosphate exchange. Solvent was removed, the solid residue dissolved in MeCN, and the product precipitated by addition of water. $[Ru(1)_2][PF_6]_2$ was recrystallized from MeCN/Et_2O and was isolated as an orange-red solid (80 mg, 0.060 mmol, 52%). ^{1}H NMR (400 MHz, CD_3CN) δ/ppm 8.89 (s, 4H, H^{B3}), 8.64 (d, *J* 8.0 Hz, 4H, H^{A3}), 8.11 (d, *J* 4.0 Hz, 2H, H^{C4}), 7.95 (dt, *J* 7.9, 1.5 Hz, 4H, H^{A4}), 7.51 (d, *J* 3.9 Hz, 2H, H^{C3}), 7.43 (d, *J* 4.8 Hz, 4H, H^{A6}), 7.29 (d, *J* 3.9 Hz, 2H, $H^{D3/D4}$), 7.23 (d, *J* 3.9 Hz, 2H, $H^{D3/D4}$), 7.18 (m, 4H, H^{A5}). ESI MS *m/z* 1198 $[M-PF_6]^+$.

2.6. Ligand *2*

4′-Ethynyl-2,2′:6′,2″-terpyridine (100 mg, 0.388 mmol), 5-bromo-2,2′-bithiophene (100 mg, 0.408 mmol), $[Pd(PPh_3)_2Cl_2]$ (14 mg, 0.020 mmol) and CuI (4 mg, 0.021 mmol) were dissolved in Et_3N (8 cm^3). The solution was heated under reflux for 48 h. The solvent was then evaporated under reduced pressure. The crude material was dissolved in hexane (200 cm^3). After filtration, solvent from the filtrate was removed under reduced pressure. The crude product was purified by several, sequential column chromatographic separations (see text) (Al_2O_3, hexane:ethyl acetate 1:1), and the third band was collected. Compound **2** was isolated as a yellow solid (45 mg, 0.11 mmol, 28%). M.p. = 152.4 °C. ^{1}H NMR (500 MHz, CD_3CN) δ/ppm 8.70 (d, *J* 4.6 Hz, 2H, H^{A6}), 8.60 (d, *J* 7.9 Hz, 2H, H^{A3}), 8.53 (s, 2H, H^{B3}), 7.85 (dt, *J* 7.8, 1.7 Hz, 2H, H^{A4}), 7.33 (dd, *J* 7.2, 4.8, 0.7 Hz, 2H, H^{A5}), 7.25 (dd, *J* 5.0, 1.0 Hz, 1H, H^{D3}), 7.24 (d, *J* 3.9 Hz, 1H, H^{C4}), 7.21 (d, *J* 3.7 Hz, 1H, H^{D5}), 7.08 (d, *J* 3.8 Hz, 1H, H^{C3}), 7.02 (dd, *J* 3.8, 5.0 Hz, 1H, H^{D4}). $^{13}C\{^1H\}$ NMR (125 MHz, CD_3CN) δ/ppm 155.8 ($C^{A2/B2}$), 155.7 ($C^{A2/}$

^{E2}), 149.4 (C^{A6}), 140.5 ($C^{D2/C5}$), 137.1 (C^{A4}), 136.7 (C^{C2}), 134.3 (C^{C4}), 133.3 (C^{B4}), 128.2 (C^{D4}), 125.5 ($C^{D3/D5}$), 124.3 ($C^{D3/D5}$), 124.1 (C^{A5}), 123.9 (C^{C3}), 122.5 (C^{B3}), 121.4 (C^{A3}), 121.1 ($C^{D2/C5}$), 92.6 ($C^{tpyC\equiv C}$), 87.4 ($C^{tpyC\equiv C}$). EI MS *m/z* 421.1 $[M]^+$. $C_{25}H_{15}N_3S_2 \cdot 1.5H_2O$ requires C, 66.94; H, 4.04; N, 9.37. Found: C, 67.35; H, 3.87; N, 8.68%.

2.7. [Ru(**2**)(tpy)][PF_6]$_2$

Ligand 2 (40 mg, 0.095 mmol) and [Ru(tpy)Cl_3] (41 mg, 0.094 mmol) were dissolved in EtOH (40 cm^3). A few drops of *N*-ethylmorpholine were added. The reaction mixture was heated under reflux for 48 h, then filtered through Celite, and washed through with EtOH. The filtrate was concentrated under reduced pressure and aqueous NH_4PF_6 was added to precipitate the product. The crude product was filtered through Celite, washed with Et_2O and dissolved in MeCN. It was purified by column chromatography (SiO_2, MeCN:H_2O:saturated aqueous KNO_3 7:2:2). The third band (orange-red) was collected, and was concentrated under reduced pressure. Aqueous NH_4PF_6 was added to precipitate the product, which was collected on Celite and was washed with Et_2O and dissolved in MeCN. Removal of solvent gave [Ru(2)(tpy)][PF_6]$_2$ as a dark red powder (23 mg, 0.030 mmol, 32%). ^{1}H NMR (500 MHz, CD_3CN) δ/ppm 8.84 (s, 2H, H^{B3}), 8.76 (d, *J* 8.2 Hz, 2H, H^{F3}), 8.49 (overlapping d, *J* 8.1 Hz, 4H, H^{A3+E3}), 8.43 (t, *J* 8.2 Hz, 1H, H^{F4}), 7.95 (dt, *J* 8.0, 1.3 Hz, 2H, H^{A4}), 7.91 (dt, *J* 8.0, 1.3 Hz, 2H, H^{E4}), 7.56 (d, *J* 3.8 Hz, 1H, H^{C4}), 7.51 (d, *J* 3.9 Hz, 1H, H^{D5}), 7.48 (dd, *J* 5.0, 0.9 Hz, 1H, H^{D3}), 7.44 (dd, *J* 3.6, 0.9 Hz, 1H, H^{D3}), 7.39 (d, *J* 5.5 Hz, 2H, H^{A6}), 7.36 (m, 3H, H^{E6+C3}), 7.18 (m, 4H, H^{A5+E5}), 7.15 (t, *J* 4.3 Hz, 1H, H^{D4}), ^{13}C{^{1}H} NMR (125 MHz, CD_3CN) δ/ppm 159.0 (C^{B2}), 158.6 (C^{E2}), 156.4 (C^{F2}), 156.2 (C^{A2}), 153.6 ($C^{A6/E6}$), 153.55 ($C^{A6/E6}$), 142.7 (C^{C5}), 139.3 ($C^{A4/E4}$), 139.2 ($C^{A4/E4}$), 137.2 (C^{F4}), 137.0 (C^{C4}), 136.7 (C^{D2}), 130.6 (C^{B4}), 129.6 (C^{D4}), 128.7 ($C^{A5/E5}$), 128.5 ($C^{A5/E5}$), 127.8 (C^{D5}), 126.6 (C^{D3}), 125.7 ($C^{A3/E3}$), 125.6 ($C^{A3/E3}$), 125.5 (C^{B3}), 124.8 (C^{F3}), 120.3 (C^{C2}), 92.2 ($C^{tpyC\equiv C}$), 91.0 ($C^{tpyC\equiv C}$). FAB MS *m/z* 900 $[M-PF_6]^+$, 755 $[M-2PF_6]^+$. $C_{40}H_{26}F_{12}N_6P_2RuS_2 \cdot 2H_2O$ requires C, 44.41; H, 2.80; N, 7.77. Found: C, 43.96; H, 2.87; N, 7.79%.

2.8. Crystal structure determination

Data were collected on a Bruker Nonius Kappa CCD instrument; data reduction, solution and refinement used the programs COLLECT [40], SIR92 [41], DENZO/SCALEPACK [42] and CRYSTALS [43]. Structures have been analysed using Mercury v. 1.4.2 [44].

2.9. 4′-(5-Bromo-2,2′-bithien-5′-yl)-2,2′:6′,2″-terpyridine (**1**)

$C_{23}H_{14}BrN_3S_2$, M = 476.42, colourless blocks, monoclinic, space group $P2_1/a$, a = 8.3099(1), b = 11.5704(1), c = 20.5872(3) Å, β = 99.9846(7)°, U = 1949.46(4) Å^3, Z = 4, D_{calc} = 1.623 Mg m^{-3}, μ(Mo K_α) = 2.338 mm^{-1}, T = 173 K, 5691 reflections collected. Refinement of 3901 reflections (262 parameters) with $I > 3\sigma(I)$ converged at final R_1 = 0.0257 (R_1 all data = 0.0394), wR_2 = 0.0294 (wR_2 all data = 0.0396), Goodness-of-fit = 1.072.

3. Results and discussion

We approached the assembly of a conjugated system connecting tpy, thienyl and alkynyl domains by two strategies: by starting with 4′-(2,2′-bithien-5′-yl)-2,2′:6′,2″-terpyridine [39], or by using 4′-ethynyl-2,2′:6′,2″-terpyridine [36] as the precursor. Bromination of 4′-(2,2′-bithien-5′-yl)-2,2′:6′,2″-terpyridine by NBS in acetic acid in the absence of light produced ligand **1** (Scheme 1) in 68% yield after workup. This reaction proved to be sensitive to the scale, and optimum yields of **1** were obtained under the conditions described in Section 2. The electron impact mass spectrum of **1** exhibited a parent ion at *m/z* 476 with the characteristic isotope pattern of a monobromo-derivative. The ^{1}H NMR spectrum was assigned using COSY and NOESY techniques, the doublet for thiophene proton H^{C4} (see Scheme 1) being assigned on the basis of a NOESY cross peak to the signal for tpy proton H^{B3}. The signals for thiophene protons H^{D3} and H^{D4} are coincident and give rise to a singlet at δ 7.00 ppm. The ^{13}C NMR spectrum was fully assigned using HMQC and HMBC experiments; the bromo-attached carbon atom C^{D5} appears at lowest frequency at δ 111.9 ppm. X-ray quality crystals of 1 were grown by slow diffusion of hexane into a chloroform solution of the compound. Fig. 1 shows the molecular structure of **1** and gives selected bond parameters. The ligand deviates somewhat from planarity, although not sufficiently that conjugation along the tpy-bithiophene backbone will be significantly perturbed (angles between the least squares planes of the rings containing atoms N1 and N2, N2 and N3, N2 and S1, and S1 and S2 are 17.65(8)°, 18.9(1)°, 12.52(8)° and 14.14(8)°). Molecules assemble in the crystal lattice so that there are segregated domains of bithiophene units and of tpy units (Fig. 2). Within the former, the closest S···S atom contacts are S2···S2i of 3.6447(6) Å (symmetry code i = $-x$, $1-y$, $1-z$) which is less than the sum of the van der Waals radii (3.70 Å).

Ligand **1** was incorporated into the homoleptic complex [Ru(**1**)$_2$]$^{2+}$ and heteroleptic complex [Ru(tpy)(**1**)]$^{2+}$ by treament of $RuCl_3 \cdot 3H_2O$ with two equivalents of **1** in the presence of $AgNO_3$, and by the reaction of [Ru(tpy)Cl_3] with **1** in the presence of *N*-ethylmorpholine, respectively. Both complexes were isolated as the hexafluorophosphate salts, although it was difficult to obtain pure samples of the homoleptic complex. The highest mass peak in the electrospray mass spectrum of [Ru(1)$_2$][PF_6]$_2$ appeared at *m/z* 1198 and exhibited the correct isotope pattern for the ion $[M-PF_6]^+$. For [Ru(tpy)(**1**)][PF_6]$_2$, the electrospray mass spectrum showed peaks both for $[M-PF_6]^+$ (*m/z* = 957) and $[M-2PF_6]^{2+}$ (*m/z* = 405), again with the correct isotopic distrubtions. The appearance of the ^{1}H NMR spectrum of [Ru(**1**)$_2$][PF_6]$_2$ confirmed the presence of a single ligand environment. The significant shift in the signal for proton H^{A6} from δ 8.72 ppm in free **1** to δ 7.43 ppm in [Ru(**1**)$_2$][PF_6]$_2$ is consistent with coordination of the tpy domain to the ruthenium(II) centre. Coordination also has the effect of separating the signals for thiophene protons H^{D3} and H^{D4} which appear as doublets (*J* 3.9 Hz) at δ 7.23 and 7.29 Hz, compared to δ 7.00 ppm in the uncoordinated ligand. The ^{1}H NMR spectrum of

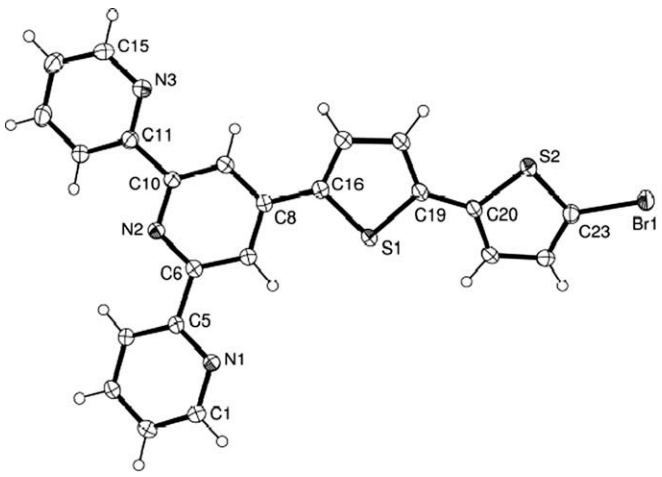

Fig. 1. The structure of ligand **1** with thermal ellipsoids plotted at 40% probability level. Selected bond distances and angles: C8–C16 = 1.465(2), Br1–C23 = 1.875(2), S1–C16 = 1.731(2) , S1–C19 = 1.726(2), S2–C20 = 1.730(2), S2–C23 = 1.720(2) Å; C16–S1–C19 = 92.22(8), C20–S2–C23 = 91.12(8), C8–C16–S1 = 120.6(1), S1–C19–C20 = 119.9(1), C19–C20–S2 = 120.6(1), Br1–C23–S2 = 120.9(1)°.

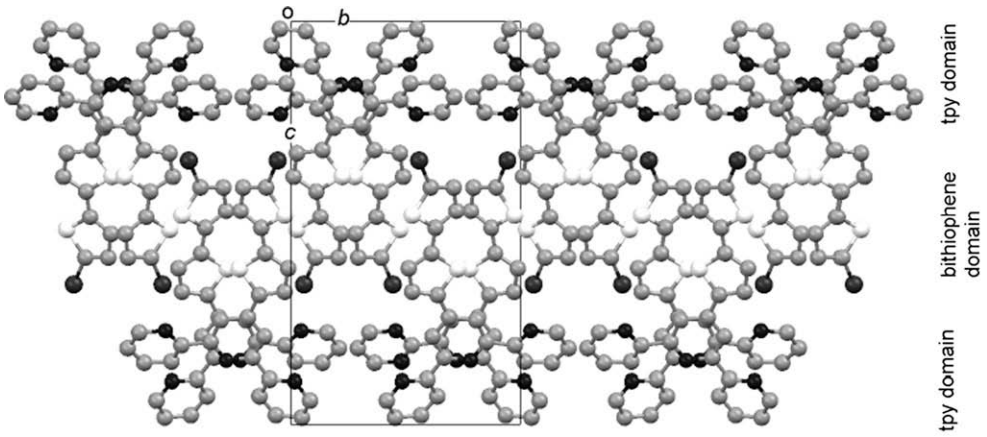

Fig. 2. Packing of molecules of **1** in the solid state, viewed down the crystallographic *a*-axis and showing separated bithiophene and tpy domains.

$[Ru(tpy)(\mathbf{1})][PF_6]_2$ was assigned by use of 2D-NMR spectroscopic techniques and by comparison with the spectra for $[Ru(\mathbf{1})_2][PF_6]_2$ and $[Ru(tpy)_2][PF_6]_2$ [45]. The spectrum of the heteroleptic complex is essentially a superimposition of the spectra of the two homoleptic complexes. Residual impurities in the sample of $[Ru(\mathbf{1})_2][PF_6]_2$ precluded us from obtaining a satisfactory elemental analysis, and the ^{13}C NMR spectrum was not well resolved. The ^{13}C NMR spectrum of $[Ru(tpy)(\mathbf{1})][PF_6]_2$ was assigned by use of HMQC and HMBC experiments, and as for the free ligand **1**, the lowest frequency signal (δ 113.2 ppm) was assigned to carbon atom C^{D5}. Attempts to carry out Suzuki coupling reactions between $[Ru(tpy)(\mathbf{1})]^{2+}$ and HC≡C(TIPS) did not yield the desired product within reasonable reaction times (for example, >2 h in a Biotage Initiator 8 microwave reactor at 120 °C). Hence, this strategy towards ruthenium(II)-centred building blocks terminated with conjugated bithienyl-alkynyl units was abandoned in favour of a second approach which yielded more promising results.

Our second strategy (Scheme 3) involved the attachment of a pendant bithiophene unit to directly coupled alkyne and tpy units. The reaction of 4′-ethynyl-2,2′:6′,2″-terpyridine with 5-bromo-2,2′-bithiophene under Sonogashira conditions [46,47] resulted in the formation of ligand **2**. Initial purification of the ligand using a single pass through a chromatography column (see Section 2) gave a product, the EI mass spectrum of which showed a base peak at *m/z* 421 corresponding to $[M]^+$ for **2**. However, in addition, a peak at *m/z* 501 exhibiting an isotope pattern consistent with a monobromo-derivative was also observed. This was assigned to compound **3** (Scheme 4). We had observed that the synthesis of 5-bromo-2,2′-bithiophene also produced 5,5′-dibromo-2,2′-bithiophene [38] as an impurity which was difficult to separate, and its presence was presumably responsible for the formation of **3**. In the ^1H NMR spectrum ($CDCl_3$ solution) of the mixture of **2** and **3**, most signals for the two derivatives overlapped. However, the presence of **3** was most easily seen by the appearance to two singlets for H^{B3}, δ 8.53 ppm for **2**, and δ 8.52 ppm for **3**, and by doublets ($J \approx 7.8$ Hz) for H^{A3} centred at δ 8.60 pm for **2** and δ 8.59 pm for **3**. The thienyl protons for **3** give rise to four doublets (δ 7.21, 7.00, 6.97 and 6.94 ppm, each with $J \approx 3.8$ Hz). Ligand **2** was eventually purified by sequential column chromatography. The ^1H and ^{13}C NMR spectra of **2** were assigned by a combination of COSY, NOESY, HMQC and HMBC techniques. In thiophene ring C, proton H^{C3} was distinguished from H^{C4} by the appearance of a cross peak in the NOESY spectrum between H^{C3} and H^{D3}. A cross peak in the HMBC

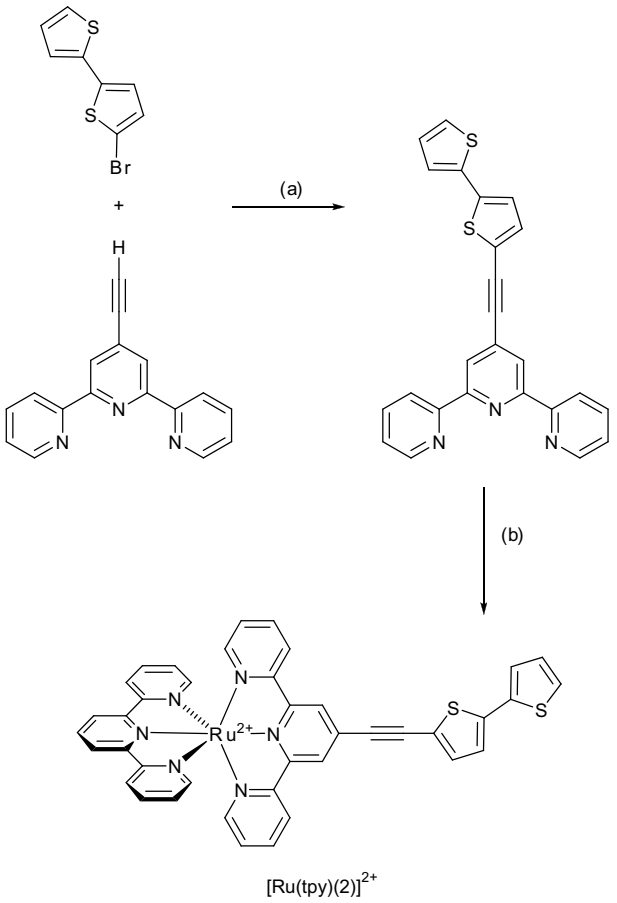

Scheme 3. Strategy for the formation of a ruthenium(II) centred building block containing conjugated tpy, bithienyl and alkynyl substituents: (a) $[Pd(PPh_3)_2Cl_2]$, CuI in Et_3N, reflux; (b) $[Ru(tpy)Cl_3]$, *N*-ethylmorpholine in EtOH.

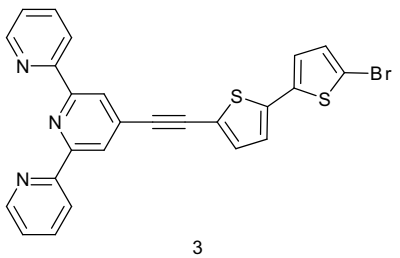

3

Scheme 4. Structure of **3**; proton labelling is as for **2**.

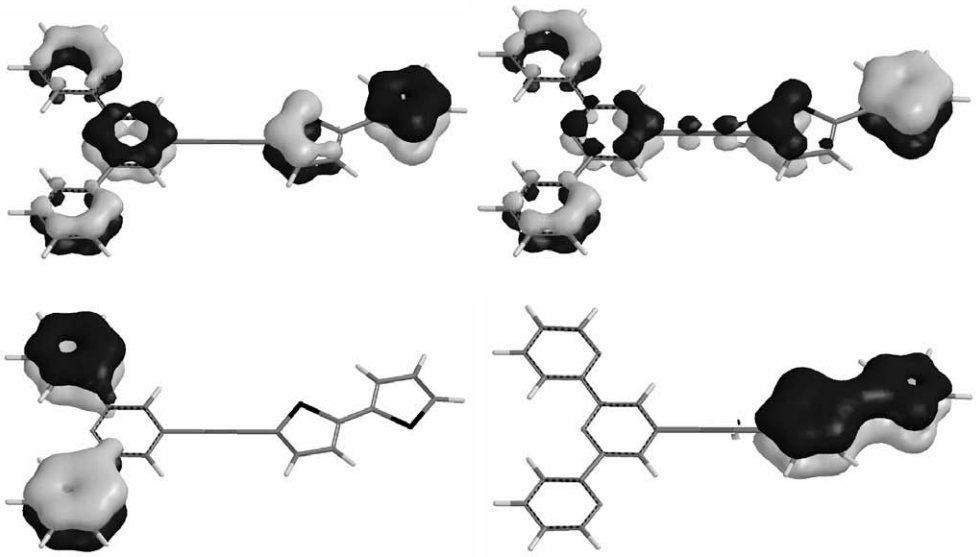

Fig. 3. Representations of the four lowest-lying, occupied π-MOs of ligand **2**.

spectrum to proton H^{B3} allowed the two alkyne carbon signals in the ^{13}C NMR spectrum to be distinguished ($C^{tpyC\equiv C}$at δ 92.6 ppm, and $C^{tpyC\equiv C}$ at δ 87.4 ppm).

In order to gain insight into the degree of conjugation across the tpy, alkynyl and thienyl units, we have run approximate molecular orbital calculations on ligand **2** at the HF 6-31G* level, the structure having been first optimised at the PM3 level [48]. The energy minimised structure indicates that all the heterocyclic rings lie approximately in plane. Fig. 3 illustrates the composition of the lowest-lying π-molecular orbitals, and the appearance of π-character delocalized across the tpy–C≡C–thiophene domains in one of the MOs is consistent with there being electronic communication along the molecule through the π-bonding electrons.

The heteroleptic complex $[Ru(tpy)(\mathbf{2})]^{2+}$ was prepared by treatment of $[Ru(tpy)Cl_3]$ with one equivalent of ligand **2** in the presence of *N*-ethylmorpholine as the reducing agent. The complex was isolated as the hexafluorophosphate salt, and the FAB mass spectrum exhibited peak envelopes at *m/z* 900 and 755, with isotope distributions that matched those predicted for $[M-PF_6]^+$ and $[M-2PF_6]^+$, respectively. The ^1H NMR spectrum of a CD_3CN solution of $[Ru(tpy)(\mathbf{2})][PF_6]_2$ confirmed the presence of two tpy environments. In addition to the use of 2D-techniques, one set of signals could be assigned to the unsubstituted tpy by comparison with spectra of $[Ru(tpy)_2][PF_6]_2$ [45] and $[Ru(tpy)(\mathbf{1})][PF_6]_2$. For ligand **2**, coordination to ruthenium(II) leads to the expected shift to lower frequency for the signal for H^{A6} (from δ 8.70 ppm in **2** in $CDCl_3$, to δ 7.39 ppm for $[Ru(tpy)(\mathbf{2})][PF_6]_2$ in CD_3CN). Sets of thiophene protons belonging to rings C and D were assigned through a COSY experiment, and protons H^{C3} and H^{D3} were distinguished by a cross peak in the NOESY spectrum. Each of the five thiophene proton signals shifts to higher frequency upon coordination of ligand **2**, and largest change being for the signal for H^{C4} ($\Delta\delta$ = +0.32 ppm). The ^{13}C NMR spectrum of the complex was fully assigned using HMQC and HMBC spectra; the signals for the alkyne carbon atoms (δ 92.2 and 91.0 ppm) were only slightly shifted from those of the free ligand (δ 92.6 and 87.4 ppm). Attempts to grow good quality crystals of the complex for X-ray diffraction analysis were unsuccessful.

4. Conclusions

In this exploratory investigation, we have demonstrated that a ligand incorporating π-conjugated tpy, alkynyl and bithienyl units is most conveniently assembled through the reaction of 4′-ethynyl-2,2′:6′,2″-terpyridine with 5-bromo-2,2′-bithiophene under Sonogashira conditions. Use of 5,5′-dibromo-2,2′-bithiophene leads to a bromo-functionalized analogue (**3**) of the first ligand (**2**). Protection–deprotection strategies need to be tailored to the individual alkyne derivatives. A representative ruthenium(II) complex, $[Ru(tpy)(\mathbf{2})][PF_6]_2$, has been prepared and characterized. In subsequent work, we plan to investigate the bromination of this and related complexes, and the synthesis of complexes incorporating ligand **3** in order to produce building blocks suitable for the assembly of larger systems using reactions of coordinated ligands rather than conventional linear ligand synthesis.

Supplementary data

CCDC 693514 contains the supplementary crystallographic data for ligand **2**. These data can be obtained free of charge via http://www.ccdc.cam.ac.uk/conts/retrieving.html, or from the Cambridge Crystallographic Data Centre, 12 Union Road, Cambridge CB2 1EZ, UK; fax: (+44) 1223-336-033; or e-mail: deposit@ccdc.cam.ac.uk.

Acknowledgements

We thank the Swiss National Science Foundation, the Swiss National Center of Competence in Research in Nanoscale Science, the Swiss Energy Ministry (Project NEFIOS) and the University of Basel for support. Thanks are due to Dr. David Scanu for providing the precursor for the synthesis of 4′-ethynyl-2,2′:6′,2″-terpyridine, Pirmin Rösel for recording ESI-MS, and Ana Hernandez Redondo for recording 500 MHz NMR spectra.

References

[1] S. Ott, M. Borgstrom, M. Kritikos, R. Lomoth, J. Bergquist, B. Akermark, L. Hammarstrom, L. Sun Licheng, Inorg. Chem. 43 (2004) 4683.
[2] L. Cheng, G.E. Pacey, J.A. Cox, Anal. Chem. 73 (2001) 5607.
[3] L. Cheng, J.A. Cox, Chem. Mater. 14 (2002) 6.
[4] M. Grätzel, Inorg. Chem. 44 (2005) 6841.
[5] Md.K. Nazeeruddin, M. Grätzel, in: J.A. McCleverty, T.J. Meyer (Eds.), Comprehensive Coordination Chemistry II, vol. 9, Elsevier, Oxford, 2004, p. 719.
[6] U.S. Schubert, H. Hofmeier, G.R. Newkome, Modern Terpyridine Chemistry, Wiley-VCH, Weinheim, 2006.
[7] E.C. Constable, Coord. Chem. Rev. 52 (2008) 842.
[8] E.C. Constable, Chem. Soc. Rev. 36 (2007) 246.
[9] H. Hofmeier, U.S. Schubert, Chem. Soc. Rev. 33 (2004) 373.

[10] M. Beley, D. Delabouglise, G. Houppy, J. Husson, J.-P. Petit, Inorg. Chim. Acta 358 (2005) 3075.
[11] E.C. Constable, S.J. Dunne, D.G.F. Rees, C.X. Schmitt, Chem. Commun. (1996) 1169.
[12] E.C. Constable, R. Handel, C.E. Housecroft, M. Neuburger, E.R. Schofield, M. Zehnder, Polyhedron 23 (2004) 135.
[13] E.C. Constable, R.W. Handel, C.E. Housecroft, A.F. Morales, L. Flamigni, F. Barigelletti, J. Chem. Soc., Dalton Trans. (2003) 1220.
[14] S. Etienne, M. Beley, Inorg. Chem. Commun. 9 (2006) 68.
[15] E. Figgemeier, V. Aranyos, E.C. Constable, R.W. Handel, C.E. Housecroft, C. Risinger, A. Hagfeldt, E. Mukhtar, Inorg. Chem. Commun. 7 (2004) 117.
[16] C. Houamer-Rassin, F. Chaignon, C. She, D. Stockwell, E. Blart, P. Buvat, T. Lian, F. Odobel, J. Photochem. Photobiol. A 192 (2007) 56.
[17] S. Krompiec, M. Krompiec, H. Ignasiak, M. Łapkowski, S. Baj, D. Grabarczyk, Catal. Commun. 8 (2007) 1457.
[18] A. Juris, V. Balzani, F. Barigelletti, S. Campagna, P. Belser, A. von Zelewsky, Coord. Chem. Rev. 84 (1988) 85.
[19] A. Harriman, R. Ziessel, Chem. Commun. (1996) 1707.
[20] V. Grosshenny, A. Harriman, R. Ziessel, Angew. Chem., Int. Ed. 34 (1995) 1100.
[21] A.C. Benniston, V. Grosshenny, A. Harriman, R. Ziessel, Dalton Trans. (2004) 1227.
[22] E.C. Constable, C.E. Housecroft, E.R. Schofield, S. Encinas, N. Armaroli, F. Barigelletti, L. Flamigni, E. Figgemeier, J.G. Vos, Chem. Commun. (1999) 869.
[23] J. Hjelm, E.C. Constable, E. Figgemeier, A. Hagfeldt, R. Handel, C.E. Housecroft, E. Mukhtar, E. Schofield, Chem. Commun. (2002) 284.
[24] S. Encinas, L. Flamigni, F. Barigelletti, E.C. Constable, C.E. Housecroft, E. Schofield, E. Figgemeier, D. Fenske, M. Neuburger, J.G. Vos, M. Zehnder, Chem. Eur. J. 8 (2002) 137.
[25] J. Hjelm, R.W. Handel, A. Hagfeldt, E.C. Constable, C.E. Housecroft, R.J. Forster, Electrochem. Commun. 6 (2004) 193.
[26] J. Hjelm, R.W. Handel, A. Hagfeldt, E.C. Constable, C.E. Housecroft, R.J. Forster, Inorg. Chem. 44 (2005) 1073.
[27] A. Winter, D.A.M. Egbe, U.S. Schubert, Org. Lett. 9 (2007) 2345.
[28] A. Barbieri, B. Ventura, F. Barigelletti, A. De Nicola, M. Quesada, R. Ziessel, Inorg. Chem. 43 (2004) 7359.
[29] A.C. Benniston, A. Harriman, D.J. Lawrie, S.A. Rostron, Tetrahedron Lett. 45 (2004) 2503.
[30] A.C. Benniston, A. Harriman, D.J. Lawrie, A. Mayeux, Phys. Chem. Chem. Phys. 6 (2004) 51.
[31] A. De Nicola, C. Ringenbach, R. Ziessel, Tetrahedron Lett. 44 (2003) 183.
[32] C. Ringenbach, A. De Nicola, R. Ziessel, J. Org. Chem. 68 (2003) 4708.
[33] M. Büschel, M. Helldobler, J. Daub, Chem. Commun. (2002) 1338.
[34] A. Harriman, A. Mayeux, A. De Nicola, R. Ziessel, Phys. Chem. Chem. Phys. 4 (2002) 2229.
[35] B.P. Sullivan, M.J. Calvert, T.J. Meyer, Inorg. Chem. 19 (1980) 1404.
[36] Y. Pan, M. Lu, Z. Peng, J.S. Melinger, Org. Biomol. Chem. 1 (2003) 4465.
[37] R. Wu, J.S. Schumm, D.L. Pearson, J.M. Tour, J. Org. Chem. 61 (1996) 6906.
[38] P.A. Chaloner, S.R. Gunatunga, P.B. Hitchcock, J. Chem. Soc., Perkin Trans. 2 (1997) 1597.
[39] J. Hjelm, R.W. Handel, A. Hagfeldt, E.C. Constable, C.E. Housecroft, R.J. Forster, J. Phys. Chem. B 107 (2003) 10431.
[40] COLLECT Software, Nonius BV, 1997–2001.
[41] A. Altomare, G. Cascarano, G. Giacovazzo, A. Guagliardi, M.C. Burla, G. Polidori, M. Camalli, J. Appl. Crystallogr. 27 (1994) 435.
[42] Z. Otwinowski, W. Minor, in: C.W. Carter, R.M. Sweet (Eds.), Methods in Enzymology, vol. 276, Academic Press, New York, 1997, p. 307.
[43] P.W. Betteridge, J.R. Carruthers, R.I. Cooper, K. Prout, D.J. Watkin, J. Appl. Crystallogr. 36 (2003) 1487.
[44] I.J. Bruno, J.C. Cole, P.R. Edgington, M.K. Kessler, C.F. Macrae, P. McCabe, J. Pearson, R. Taylor, Acta Crystallogr., Sect. B 58 (2002) 389.
[45] E.C. Constable, A.M.W. Cargill Thompson, D.A. Tocher, M.A.M. Daniels, New J. Chem. 16 (1992) 855.
[46] K. Sonogashira, Y. Tohda, N. Hagihara, Tetrahedron Lett. 16 (1975) 4467.
[47] K. Sonogashira, J. Organomet. Chem. 653 (2002) 46.
[48] SPARTAN '04, © 1991-2004 by Wave function Inc., Irvine, CA.

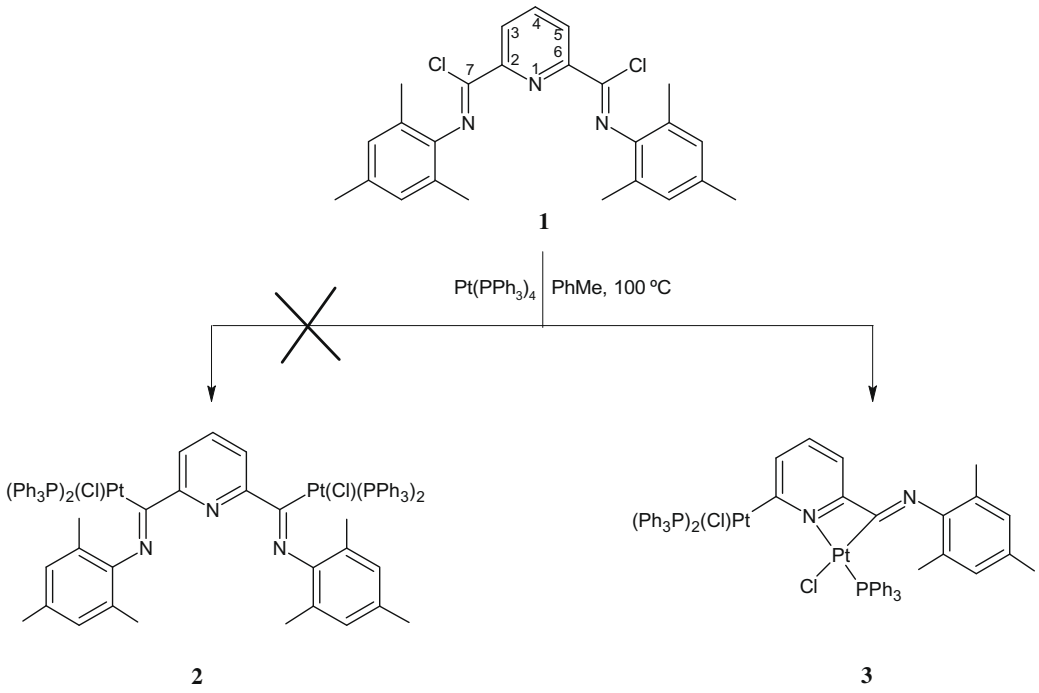

Fig. 1. Reaction of imidoyl chlorides with low valent transition metal complexes.

2.2. Synthesis of the title complex and analytical characterization

2.2.1. Synthesis of ***3***

A mixture of *N*,*N*′-bis(2,4,6-trimethylphenyl)pyridine-2,6-carboxyimidoyl dichloride (88 mg, 0.2 mmol) and [$Pt(PPh_3)_4$] (500 mg, 0.4 mmol) in toluene (20 mL) was stirred under argon for 2 h at 100 °C. After cooling, the solvent was removed *in vacuo* and the waxy residue was suspended in pentane and stirred for 1 h at ambient temperature to form a fine powder. The pentane was discarded and the residue was extracted with pentane to remove the remaining PPh_3. The crude product was then recrystallized from CH_2Cl_2 to precipitate impurities. After filtration, crystallization of the product was induced by slowly diffusing pentane into the CH_2Cl_2 solution to afford the complex as a light brown crystals.

Yield: 0.210 g (63%). *Anal.* Calc. for $C_{69}H_{59}Cl_2N_2P_3Pt_2$: C, 56.37; H, 4.04; N, 1.91. Found: C, 57.06; H, 3.57; N, 2.38%. ^{1}H NMR (δ in ppm, 400 MHz, *J* in Hz, $CDCl_3$): 1.58 (s, 6H, *o*-CH_3-Mes), 2.14 (s, 3H, *p*-CH_3-Mes), 6.6 (s, 2H, *CH*-Mes), 7.43 (m, 18H, *oH*-P*Ph*$_3$), 7.73 (m, *pH*-P*Ph*$_3$, 9H), 7.82 (m, *H*-Py and *mH*-P*Ph*$_3$, 21H) ^{13}C NMR (δ in ppm, 101 MHz, $CDCl_3$): 14.21, 18.74, 127.79, 127.85, 128.37, 128.42, 128.49, 128.54, 129.19, 129.83, 130.73, 131.17, 132.04, 134.12, 134.18, 134.23, 134.75, 134.81, 134.86.

Table 1
Crystal data and details of the structure refinement for the title complex.

Empirical formula	$C_{69}H_{59}N_2P_3Cl_2Pt_2$
Formula weight	1470.17
Crystal system, space group	triclinic, $P\bar{1}$
Unit cell dimensions	
a (Å)	11.9074(5)
b (Å)	12.1059(5)
c (Å)	25.7888(10)
α (°)	96.294(3)
β (°)	93.269(3)
γ (°)	117.350(3)
V (Å^3)	3257.6(3)
Z, D_{calc} (g/cm^3)	2, 1.499
μ (Mo Kα) (mm^{-1})	4.485
F(000)	1444
Crystal size (mm^3)	0.60 × 0.36 × 0.18
Absorption correction	integration
θ Range for data collection (°)	1.60–26.15
Reflections collected/unique (R_{int})	58735/12790 (0.045)
Data/restrain/parameters	10093/0/703
Final *R* indices [$I > 2\sigma(I)$]	$R = 0.0310/R_w = 0.0762$
R indices (all data)	$R = 0.0423/R_w = 0.0791$
Goodness-of-fit (GoF) on F^2	0.993
Highest peak/deepest hole (e Å^{-3})	2.210/−1.231

2.3. Crystal structure determination

Light brown single crystals suitable for data collection were mounted on a glass fibre and the diffraction intensity data were collected at room temperature on a STOE IPDS 2 diffractometer using graphite-monochromatized Mo Kα radiation (λ = 0.71073 Å). A summary of crystallographic data and details of the structure refinement are listed in Table 1. The cell parameters were determined by using X-AREA software [13] on the setting angles of 58735 reflections [1.60° < θ < 26.15°]. Absorption correction was achieved by the integration method via X-RED software [13]. A total of 58735 reflections were collected for $h_{min} = -14$, $h_{max} = 14$, $k_{min} = -14$, $k_{max} = 14$, $l_{min} = -31$, $l_{max} = 31$. The crystal structure was solved by SHELXS-97 [14]. The refinement (on F^2) was carried out by full-matrix least square techniques using the SHELXL-97 program [15]. All non-hydrogen atoms were refined anisotropically. All hydrogen atoms were treated as riding atoms, with C–H distances of 0.93 Å for aromatic H atoms and 0.96 Å for methyl H atoms.

Examination of the structure of the title compound with PLATON [16] showed that there was a solvent-accessible void (380 Å^3) in the region around (1/2, 1/2, 1). The reflection (*hkl*) data were modified using the SQUEEZE option of PLATON. Although the empty space seemed large enough to accommodate small solvent molecules, the spaces are too constricted to hold any molecule larger than water. Since no water was present during the synthesis or recrys-

tallization, and since little electron density in the area of the void was found, we conclude that the voids are empty.

3. Results and discussion

Pyridine-2,6-dicarboxyimidoyl dichloride (**1**) is an interesting diimidoyl chloride that has been reported recently. Keeping the above mentioned facts in mind and in continuation of our study with aminocarbene complexes [17], we treated **1** with tetrakis(triphenylphosphine)platinum(0) in toluene at 100 °C for 2 h with the hope of obtaining **2**. The easy cleavage of the C_2–C_7 bond implies that this bond is probably the weakest bond in **1**. However, ^{1}H NMR solution studies on the crystalline light brown solid revealed the presence of a pyridine skeleton with one mesityl substituent. In order to determine the atom connectivity we performed a crystallographic study which confirmed unequivocally the structure depicted as **3**. The mechanistic details of the cleavage reaction are not fully understood.

In summary, pyridine-2,6-dicarboxyimidoyl dichloride (**1**) experiences complex transformations when reacted with $[Pt(PPh_3)_4]$. The mechanistic aspect of this process remains to be elucidated.

An ORTEP3 [18] view of the title complex is shown in Fig. 2. The title compound crystallizes in the triclinic space group $P\bar{1}$.

The asymmetric unit contains one neutral binuclear complex. The coordination environments of the Pt centres are different. The coordination geometry around Pt1 atom is distorted square-planar, formed by the C and N atoms of the platinalactam ring, Cl atom and P atom from the triphenylphosphine group. The N1–Pt1–C1 angle is acute, with a value of 66.68(15)°, but is comparable to those found in similar metallalactam complexes [19–21]. The Cl1–Pt1–P1 angle is more obtuse [97.17(4)°] to accommodate the steric bulk of the PPh_3 ligand. The maximum deviation of the coordination plane formed by the Pt1/Cl1/C1/N1/P1 atoms is −0.050 Å for Pt1. The Pt2 atom has the expected square-planar geometry, involving one Cl atom, the coordinating C atom of the pyridine ring and two P atoms from the triphenylphosphine groups, with no atom deviating by more than 0.077 Å [for Pt2] from the coordination plane defined by Pt2/Cl2/P2/P3/C2. The coordination planes are almost perpendicular to each other [88.12(5)°].

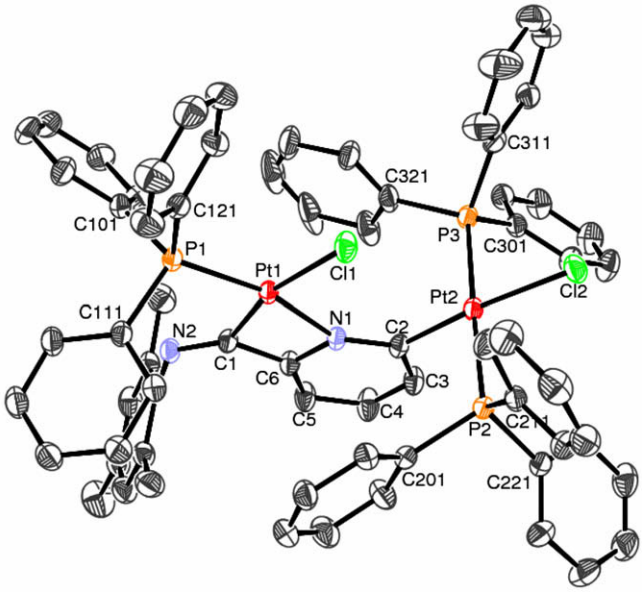

Fig. 2. An ORTEP3 view of the title compound. Displacement ellipsoids are shown at the 20% probability level and hydrogen atoms have been omitted for clarity.

Table 2
Selected geometrical parameters (Å, °) for the title complex.

Pt1–Cl1	2.374(1)	Pt2–Cl2	2.381(1)
Pt1–C1	1.984(5)	Pt2–C2	1.992(5)
Pt1–N1	2.105(3)	N2–C1	1.278(5)
N1–C6	1.367(6)	C1–C6	1.486(6)
N2–C7	1.423(6)	N1–C2	1.324(5)
N1–Pt1–Cl1	98.86(10)	C2–Pt2–P3	89.77(13)
P1–Pt1–Cl1	97.17(4)	C2–Pt2–P2	90.58(13)
N1–Pt1–P1	163.58(10)	P3–Pt2–Cl2	90.10(5)
C1–Pt1–Cl1	165.16(12)	P2–Pt2–Cl2	89.20(4)
C6–C1–Pt1	95.3(3)	P3–Pt2–P2	177.25(4)
C6–N1–Pt1	94.0(2)	C2–Pt2–Cl2	172.62(12)
N2–C1–Pt1	134.0(3)	N1–C2–Pt2	125.0(3)
C2–N1–Pt1	143.0(3)	C3–C2–Pt2	118.3(3)
C1–N2–C7	122.3(4)		

The Pt–P and Pt–N coordination distances are in the expected range and are in accordance with other reported Pt structures [19,22–24]. Selected interatomic distances, bond and torsion angles for the title complex are listed in Table 2.

The mesityl ring is rotated with respect to the platinalactam ring (Pt1/N1/C1/C6) plane by 89.5(3)°. The Pt2-P2 and Pt2-P3 bonds [2.298(1) and 2.297(1) Å] are significantly longer than the Pt1–P1 bond *trans* to the platinalactam N atom [2.216(1) Å]. This difference appears to be a result of a stronger *trans* influence of the P atom.

In the crystal structure, the molecules of the title compound are linked by C–H···N weak hydrogen bonds into centrosymmetric dimmers, as shown in Fig. 3. The C113 atom in the molecule at (x,y,z) acts as a weak hydrogen-bond donor, via atom H113, to the N2 atom at $(1-x,1-y,1-z)$, thus forming a dimer characterized by an $R_2^2(16)$ motif [25] with an inversion centre at (1/2,1/2,1/2) with

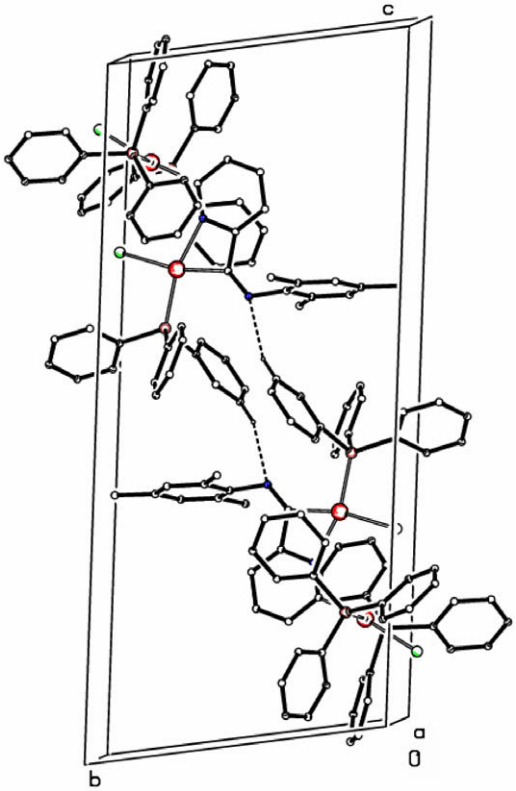

Fig. 3. Part of the crystal structure of the title compound showing the centrosymmetric dimer containing the $R_2^2(16)$ ring. For the sake of clarity, all H atoms except H113 have been omitted.

dimensions H113···N2^a = 2.62 Å, C113···N2^a = 3.505(7) Å and ∠C113–H113···N2^a = 160° (a: $1-x, 1-y, 1-z$).

4. Supplementary data

CCDC 666496 contains the supplementary crystallographic data for this paper. These data can be obtained free of charge via http://www.ccdc.cam.ac.uk/conts/retrieving.html, or from the Cambridge Crystallographic Data Centre, 12 Union Road, Cambridge CB2 1EZ, UK; fax: (+44) 1223-336-033; or e-mail: deposit@ccdc.cam.ac.uk.

Acknowledgements

The authors acknowledge the Faculty of Arts and Sciences, Ondokuz Mayıs University, Turkey, for the use of the Stoe IPDS-II diffractometer (purchased under Grant No. F279 of the University Research Fund) and Dokuz Eylül University Research Funds (Project No.: 04.KB.FEN.100).

References

[1] A. Togni, L.M. Venanzi, Angew. Chem., Int. Ed. Engl. 33 (1994) 497.
[2] S. Yamada, Coord. Chem. Rev. 190 (1999) 537.
[3] F. Fache, E. Schulz, M.L. Tommasino, M. Lemaire, Chem. Rev. 100 (2000) 2159.
[4] B. Clercq, F. Verpoort, Adv. Synth. Catal. 344 (2002) 639.
[5] H. Hofmeier, U.S. Schubert, Chem. Soc. Rev. 33 (2004) 373.
[6] G. Desimoni, G. Faita, P. Quadrelli, Chem. Rev. 103 (2003) 3119.
[7] (a) O. Dayan, B. Çetinkaya, J. Mol. Catal. A-Chem. 271 (2007) 134;
(b) T. Seçkin, S. Köytepe, E. Çetinkaya, J. Polym. Res. 11 (2004) 119.
[8] M.F. Lappert, A.J. Oliver, J. Chem. Soc., Chem. Commun. (1972) 274.
[9] P.M. Treichel, J.J. Benedict, R.W. Hess, J.P. Stenson, J. Chem. Soc., Chem. Commun. (1970) 1627.
[10] D.F. Christian, G.R. Clark, W.R. Roper, J.M. Waters, K.R. Whittle, J. Chem. Soc., Chem. Commun. (1972) 458.
[11] L. Malatesta, C. Cariello, J. Chem. Soc. (1958) 2323.
[12] T.M. Smit, A.K. Tomov, V.C. Gibson, A.J.P. White, D.J. Williams, Inorg. Chem. 43 (2004) 6511.
[13] Stoe & Cie, X-AREA (Version 1.18) and X-RED32 (Version 1.04), Darmstadt, Germany, 2002.
[14] G.M. Sheldrick, SHELXS-97 Program for the solution of Crystal Structures, University of Goettingen, Germany, 1997.
[15] G.M. Sheldrick, SHELXL-97 Program for the refinement of Crystal Structures, University of Goettingen, Germany, 1997.
[16] A.L. Spek, J. Appl. Crystallogr. 36 (2003) 7.
[17] M.E. Günay, M. Aygün, A. Kartal, B. Çetinkaya, E. Kendi, Cryst. Res. Technol. 41 (2006) 615.
[18] L.J. Farrugia, J. Appl. Crystallogr. 32 (1999) 837.
[19] W. Henderson, A.G. Oliver, C.E.F. Rickard, Inorg. Chim. Acta 310 (2000) 242.
[20] W. Henderson, B.K. Nicholson, A.G. Oliver, J. Organomet. Chem. 620 (2001) 182.
[21] W. Henderson, A.G. Oliver, C.E.F. Rickard, L.J. Baker, Inorg. Chim. Acta 292 (1999) 260.
[22] M.D. Meijer, A.W. Kleij, M. Lutz, A.L. Spek, G. van Koten, J. Organomet. Chem. 640 (2001) 166.
[23] W. Henderson, A.G. Oliver, B.K. Nicholson, Inorg. Chim. Acta 298 (2000) 84.
[24] E. Dubler, H.W. Schmalle, F. Arod, A. Schneider, Acta Crystallogr., Sect. C 58 (2002) m111.
[25] J. Bernstein, R.E. Davis, L. Shimoni, N.-L. Chang, Angew. Chem., Int. Ed. Engl. 34 (1995) 1555.

These two dipyridyl ligands can coordinate to the metal centers through their pyridyl nitrogen atoms and interact with each other through hydrogen bonds involving the amide groups, which are important for molecular recognition and constructing supramolecular arrays. The syntheses, structures, thermal and luminescent properties of the coordination polymer complexes $[Cu(\mathbf{L1})_2X_2]_\infty$ (X = Cl, **1** and X = Br, **2**), $\{[Cu(\mathbf{L1})_2(DMF)](NO_3)_2\}_\infty$, **3**, $\{[Ag_2(\mathbf{L1})_2](SO_4)\}_\infty$, **4** and $\{[Cu(\mathbf{L2})(DMSO)_2(NO_3)](NO_3)\}_\infty$, **5**, form the subject of this report.

2. Experimental

2.1. General procedures

All manipulations were carried out under dry, oxygen-free nitrogen by using Schlenk techniques, unless otherwise noted. Solvents were dried and deoxygenated by refluxing over the appropriate reagents before use. Diethyl ether was purified by distillation from sodium/benzophenone, methanol from Mg/I_2. The UV–Vis spectra were recorded on a Shimadzu UV-2450 spectrophotometer. ^1H NMR spectra in DMSO-d_6 were measured on a Bruker Avance 300 MHz spectrometer. IR spectra (KBr disk) were obtained from a Jasco FT/IR-460 plus spectrometer. Elemental analyses were obtained from a PE 2400 series II CHNS/O analyzer or a HERAEUS VaruoEL analyzer.

2.2. Materials

The reagents $CuBr_2$ and $Cu(NO_3)_2 \cdot 3H_2O$ were purchased from Strem Chemical Co. *N*,*N*-Dimethylformamidine (DMF), dimethyl sulfoxide (DMSO), 4,4′-diaminodiphenylmethane, triphenyl phosphite, and pyridine were purchased from Aldrich Chemical Co. $CuCl_2 \cdot H_2O$, Ag_2SO_4, nicotinic acid and isonicotinic acid were purchased from Merck Co. All the reagents were used as received.

2.3. Preparation of *N*,*N*′-(methylenedi-p-phenylene)bis(pyridine-4-carboxamide) (*L1*)

Isonicotinic acid (2.46 g, 20.00 mmol) was placed in a flask containing 20 mL of pyridine, followed by addition of 4,4′-diaminodiphenylmethane (1.98 g, 10.00 mmol) and triphenyl phosphite (6.83 g, 22.00 mmol) in 30 mL of pyridine. This mixture was refluxed for 6 h. After cooling to room temperature, the residue was added to deionized water (800 mL) with stirring. The light yellow solid was collected by filtration, washed with deionized water and then dried under vacuum. Yield: 3.37 g (83%). *Anal.* Calc. for $C_{25}H_{20}N_4O_2$ (MW = 408.46): C, 73.51; H, 4.94; N, 13.72. Found: C, 73.11; H, 5.18; N, 13.75%. IR (cm^{-1}): 3359(w), 3039(br), 1654(s), 1594(m), 1523(s), 1486(w), 1405(s), 1322(s), 1259(w), 1205(m), 1162(m), 1014(m), 944(br), 825(m), 759(w), 678(w). ^1H NMR (ppm): 10.44 (s, N*H*, 2H), 8.75 (d, aromatic, 4H), 7.82 (d, aromatic, 4H), 7.66 (d, aromatic, 4H), 7.20 (d, aromatic, 4H), 3.88 (s, CH_2, 2H).

2.4. Preparation of *N*,*N*′-(methylenedi-p-phenylene)bis(pyridine-3-carboxamide) (*L2*)

Prepared as described for **L1** except nicotinic acid (2.46 g, 20.00 mmol) was used. Yield: 3.45 g (84%). *Anal.* Calc. for $C_{25}H_{20}N_4O_2$ (MW = 408.46): C, 73.51; H, 4.94; N, 13.72. Found: C, 73.22; H, 4.97; N, 13.81%. IR (cm^{-1}): 3345(w), 3041(br), 1662(s), 1596(m), 1529(s), 1409(s), 1317(s), 1261(w), 1195(m), 1110(m), 1024(m), 823(s), 771(w), 700(w), 647(w). ^1H NMR (ppm): 10.38 (s, N*H*, 2H), 9.06 (d, aromatic, 2H), 8.72 (d, aromatic, 2H), 8.25 (t, aromatic, 2H), 7.66 (d, aromatic, 4H), 7.54 (t, aromatic, 2H), 7.20 (d, aromatic, 4H), 3.34 (s, CH_2, 2H).

2.5. Preparation of $[Cu(\mathbf{L1})_2Cl_2]_\infty$, *1*

To a solution of **L1** (0.80 g, 2.00 mmol) in 20 mL of DMF was added a solution of $CuCl_2 \cdot H_2O$ (0.17 g, 1.00 mmol) in 30 mL of water. The mixture was then stirred at room temperature for 20 h to give a light blue solution with some blue precipitate. The solid was filtered, washed with diethyl ether and then dried under vacuum. Yield: 0.29 g (30% based on Cu). *Anal.* Calc. for $C_{50}H_{40}Cl_2CuN_8O_4$ (MW = 951.34), C, 63.12; H, 4.24; N, 11.78. Found: C, 63.05; H, 4.01; N, 12.08%. IR (cm^{-1}): 3197(br), 3152(br), 1677(m), 1652(s), 1600(s), 1523(br), 1497(s), 1413(s), 1321(s), 1268(w), 1106(m), 1062(s), 1024(m), 904(w), 850(s), 808(w), 765(m), 684(s). Blue crystals suitable for X-ray diffraction were grown by layering H_2O solution of $CuCl_2 \cdot H_2O$ with **L1** in DMF for several weeks.

2.6. Preparation of $[Cu(\mathbf{L1})_2Br_2]_\infty$, *2*

Prepared as described for **1** except $CuBr_2$ (0.22 g, 1.00 mmol) was used. Yield: 0.35 g (34% based on Cu). *Anal.* Calc. for $C_{50}H_{40}Br_2CuN_8O_4$ (MW = 1040.26), C, 57.73; H, 3.88; N, 10.77. Found: C, 57.94; H, 4.07; N, 10.68%. IR (cm^{-1}): 3152(br), 1671(m), 1654(s), 1602(s), 1536(br), 1503(s), 1413(s), 1322(s), 1267(w), 1105(m), 1062(s), 1025(m), 906(w), 854(s), 767(m), 684(s). Crystals suitable for X-ray diffraction were grown by layering H_2O solution of $CuBr_2$ with **L1** in DMF for several weeks.

2.7. Preparation of $\{[Cu(\mathbf{L1})_2(DMF)](NO_3)_2\}_\infty$, *3*

Prepared as described for **1** except $Cu(NO_3)_2 \cdot 3H_2O$ (0.24 g, 1.00 mmol) was used. Yield: 0.42 g (39% based on Cu). *Anal.* Calc. for $C_{53}H_{47}CuN_{11}O_{11}$ (MW = 1077.56), C, 59.08; H, 4.40; N, 14.30. Found: C, 58.97; H, 4.07; N, 14.27. IR (cm^{-1}): 3188(br), 3152(br), 1654(m), 1604(s), 1542(br), 1503(s), 1411(s), 1384(s), 1324(m), 1265(w), 1114(m), 1058(s), 1018(m), 948(w), 825(s), 767(m), 684(s). Crystals suitable for X-ray diffraction were grown by layering H_2O solution of $Cu(NO_3)_2 \cdot 3H_2O$ with **L1** in DMF for several weeks.

2.8. Preparation of $\{[Ag_2(\mathbf{L1})_2](SO_4)\}_\infty$, *4*

Prepared as described for **1** except Ag_2SO_4 (0.31 g, 1.00 mmol) was used. Yield: 0.47 g (42% based on Ag). *Anal.* Calc. for $C_{50}H_{40}Ag_2N_8O_8S$ (MW = 1128.70), C, 53.21; H, 3.57; N, 9.93. Found: C, 53.14; H, 3.87; N, 9.63. IR (cm^{-1}): 3426(w), 3148(br), 1656(s), 1600(s), 1536(br), 1497(s), 1328(s), 1249(w), 1213(m), 1122(m), 931(s), 823(s), 759(m), 678(s), 613(w). Crystals suitable for X-ray diffraction were grown by layering H_2O solution of Ag_2SO_4 with **L1** in DMF for several weeks.

2.9. Preparation of $\{[Cu(\mathbf{L2})(DMSO)_2(NO_3)](NO_3)\}_\infty$, *5*

To a solution of **L2** (0.80 g, 2.00 mmol) in 20 mL of DMSO was added a solution of $Cu(NO_3)_2 \cdot 3H_2O$ (0.48 g, 2.00 mmol) in 30 mL of methanol. The mixture was then stirred at room temperature for 12 h, resulting in a blue solution with some blue precipitate. The solid was filtered off and layered with diethyl ether to give blue plate crystals. The crystal was collected, washed with diethyl ether and then dried under vacuum. Yield: 0.48 g (32% based on Cu). *Anal.* Calc. for $C_{29}H_{32}CuN_6O_{10}S_2$ (MW = 752.27), C, 46.30; H, 4.29; N, 11.17. Found: C, 45.97; H, 4.39; N, 11.04%. IR (cm^{-1}): 3372(w), 3152(br), 2395(w), 1913(w), 1762(s), 1656(s), 1604(s), 1532(m), 1485(s), 1383(s), 1324(s), 1199(w), 1117(m), 1059(m), 1019(s), 950(s), 921(m), 899(s), 860(w), 824(m), 777(m), 733(s), 654(w), 512(m), 446(s), 418(m).

3. X-ray crystallography

The diffraction data for complexes **1, 2** and **4** were collected on a Bruker AXS P4 diffractometer while those of **3** and **5** were collected on a Bruker AXS SMART-1000 diffractometer and a Bruker-Nonius APEXII CCD diffractometer at 22 °C, respectively, which were equipped with a graphite-monochromated Mo Kα (λ_α = 71073 Å) radiation. Data reduction was carried by standard methods with use of well-established computational procedures [9]. A blue crystal of **1** was mounted on the top of a glass fiber with epoxy cement. The hemisphere data collection method was used to scan the data points at $4.26° < \theta < 50.00°$. The structure factors were obtained after Lorentz and polarization correction. The positions of some of the heavier atoms, including the copper atom, were located by the direct methods. The remaining atoms were found in a series of alternating difference Fourier maps and least-square refinements [10].

For the structures of complexes **1–5,** all the hydrogen atoms were added by using the HADD program in SHELXTL 5.10 [10]. Disordered solvent molecules, presumably to be DMF and/or water molecules, were present in complexes **1–5**, and PLATON/SQUEEZE tool was applied [11]. Large solvent void volumes were observed for these structures. The relative percentages per unit cell are 40.5% for **1** (2662.1 out of 6579.6 Å^3), 45.4% for **2** (3085.5 out of 6800.0 Å^3), 21.7% for **3** (672.2 out of 3092.9 Å^3), 27.2% for **4** (805.2 out of 2960.7 Å^3) and 3.9% for **5** (134.5 out of 3430.5 Å^3), respectively. Where relevant, data cited in are given without disordered solvent contribution. The bonded DMSO molecule of **5** is disordered such that for each sulfur and methyl carbon atom, two positions each with occupancy of 0.5 were located. The crystallographic procedures for **2–5** were similar to those for **1**. Basic information pertaining to crystal parameters and structure refinement is summarized in Table 1. Selected bond distances and angles for complexes **1–5** are listed in Table S1 as Supplementary data.

4. Results and discussion

4.1. Syntheses and spectroscopic studies

The angular dipyridyl ligands *N,N′*-(methylenedi-*p*-phenylene)bis(pyridine-4-carboxamide), **L1**, and *N,N′*-(methylenedi-*p*-phenylene)bis(pyridine-3-carboxamide), **L2**, were prepared by the reactions of isonicotinic acid and nicotinic acid, respectively, with 4,4′-diaminodiphenylmethane and triphenyl phosphite in refluxing pyridine. The reactions of **L1** with $CuCl_2 \cdot H_2O$, $CuBr_2$, $Cu(NO_3)_2 \cdot 3H_2O$, and Ag_2SO_4 in DMF/H_2O afforded the complexes $[Cu(\mathbf{L1})_2X_2]_\infty$ (X = Cl, **1** and X = Br, **2**) and $\{[Cu(DMF)(\mathbf{L1})_2](NO_3)_2\}_\infty$, **3**, and $\{[Ag_2(\mathbf{L1})_2](SO_4)\}_\infty$, **4**. Complex $\{[Cu(\mathbf{L2})(DMSO)_2(NO_3)](NO_3)\}_\infty$, **5**, was prepared by reaction of $Cu(NO_3)_2 \cdot 3H_2O$ with **L2** in methanol/DMSO at room temperature. Complexes **1–5** are very stable in air at ambient temperature and almost insoluble in common solvents such as water, ethanol, methanol, THF, acetonitrile, chloroform and acetone. Table 2 lists the emission data for **L1**, **L2** and complexes **1–5**. There is no significant energy shift observed upon coordination of the ligands to the metal atoms and hence the emission bands may be tentatively assigned as intraligand (IL) $\pi \rightarrow \pi^*$ transitions.

Table 1
Crystal data for complexes **1–5**

Compound	1	2	3	4	5
Formula	$C_{50}H_{40}Cl_2CuN_8O_4$	$C_{50}H_{40}Br_2CuN_8O_4$	$C_{53}H_{47}CuN_{11}O_{11}$	$C_{50}H_{40}Ag_2N_8O_8S$	$C_{27}H_{32}CuN_6O_{10}S_2$
fw	951.34	1040.26	1077.56	1128.70	752.27
Crystal system	monoclinic	monoclinic	triclinic	triclinic	orthorhombic
Space group	*C*2/*c*	*C*2/*c*	$P\bar{1}$	$P\bar{1}$	*Pbcm*
a (Å)	25.987(3)	26.737(4)	13.0788(10)	8.9863(13)	8.8020(3)
b (Å)	19.128(3)	19.056(4)	16.1648(12)	17.0138(15)	22.7059(7)
c (Å)	15.500(2)	15.746(3)	16.8279(12)	20.087(3)	17.1647(6)
α (°)	90	90	105.6630(10)	100.407(12)	90
β (°)	121.353(9)	122.044(13)	94.3490(10)	101.125(14)	90
γ (°)	90	90	112.7670(10)	90.537(10)	90
V (Å^3)	6579.6(15)	6800(2)	3092.9(4)	2960.7(7)	3430.5(2)
Z	4	4	2	4	4
D_{calc} (g/cm^3)	0.0960	1.016	1.157	1.266	1.474
F(000)	1964	2108	1118	1140	1576
Crystal size (mm^3)	0.5 × 0.6 × 0.7	0.1 × 0.2 × 0.6	0.4 × 0.3 × 0.2	0.4 × 0.4 × 0.4	0.20 × 0.35 × 0.50
μ(Mo Kα) (mm^{-1})	0.451	1.533	0.413	0.748	0.823
Range(2θ) for data collection (°)	$4.26 \leqslant 2\theta \leqslant 50.00$	$3.60 \leqslant 2\theta \leqslant 50.00$	$3.44 \leqslant 2\theta \leqslant 52.16$	$3.50 \leqslant 2\theta \leqslant 50.00$	$3.58 \leqslant 2\theta \leqslant 58.32$
Temperature (°C)	22	22	22	22	22
Limiting indices	$-1 \leqslant h \leqslant 30$, $-1 \leqslant k \leqslant 22$, $-18 \leqslant l \leqslant 16$	$-1 \leqslant h \leqslant 31$, $-22 \leqslant k \leqslant 1$, $-18 \leqslant l \leqslant 16$	$-16 \leqslant h \leqslant 15$, $-19 \leqslant k \leqslant 15$, $-20 \leqslant l \leqslant 20$	$-1 \leqslant h \leqslant 10$, $-19 \leqslant k \leqslant 19$, $-23 \leqslant l \leqslant 23$	$-12 \leqslant h \leqslant 5$, $-30 \leqslant k \leqslant 27$ $-22 \leqslant l \leqslant 23$
Reflections collected	6550	6715	17641	12412	19838
Independent reflections (R_{int})	5748 (0.0258)	5910 (0.0647)	12012 (0.0215)	10296 (0.0243)	4735 (0.0705)
Refinement method	full-matrix least-squares on F^2	full-matrix least-squares on F^2	full-matrix least-squares on F^2	full-matrix least-squares on F^2	full-matrix least-squares on F^2
Data/restraints/parameters	5748/0/294	5910/0/294	12012/0/685	10296/0/623	4735/5/256
Quality-of-fit indicator[c]	1.036	0.942	1.056	1.032	1.058
Final *R* indices [$I > 2\sigma(I)$][a,b]	R_1 = 0.0661, wR_2 = 0.1474	R_1 = 0.0756, wR_2 = 0.1991	R_1 = 0.0576, wR_2 = 0.1628	R_1 = 0.0519, wR_2 = 0.1005	R_1 = 0.0761, wR_2 = 0.1626
R indices (all data)	R_1 = 0.0940, wR_2 = 0.1564	R_1 = 0.1332, wR_2 = 0.2180	R_1 = 0.0799, wR_2 = 0.1730	R_1 = 0.0686, wR_2 = 0.1061	R_1 = 0.1430, wR_2 = 0.1778
Largest difference in peak and hole (e/Å^3)	0.264 and 0.729	0.952 and 0.929	1.031 and −0.498	0.906 and −1.232	1.117 and −1.016

[a] $R_1 = \sum||F_o| - |F_c||/\sum|F_o|$.
[b] $wR_2 = [\sum w(F_o^2 - F_c^2)^2/\sum w(F_o^2)^2]^{1/2}$. $w = 1/[\sigma^2(F_o^2) + (ap)^2 + (bp)]$, $p = [\max(F_o^2 \text{ or } 0) + 2(F_c^2)]/3$. a = 0.0100, b = 40.1720, **1**; a = 0.1241, b = 0.0000, **2**; a = 0.1078, b = 0.0000, **3**. a = 0.0000, b = 9.1247, **4**; a = 0.0000, b = 10.1717, **5**.
[c] Quality-of-fit = $[\sum w(|F_o^2| - |F_c^2|)^2/(N_{observed} - N_{parameters})]^{1/2}$.

Table 2
The emission and excitation wave-lengths (nm) of **L1**, **L2** and compounds **1–5** in the solid state at room temperature

Compound	Emission in solid state	
	λ_{em}	λ_{ex}
L1	403	247
L2	400	245
1	399	246
2	396	245
3	401	245
4	395	245
5	400	247

4.2. Structures of *1* and *2*

The structures of $[Cu(\mathbf{L1})_2Cl_2]_\infty$, **1** and $[Cu(\mathbf{L1})_2Br_2]_\infty$, **2**, were solved in the space group *C*2/*c*. Fig. 1a shows a representative asymmetric unit for complexes **1** and **2**, which contains a half copper(II) atom, one complete **L1** ligand and one coordinated halide atom. Fig. 1b depicts the molecular structures for complexes **1** and **2**, showing the arrangements about the Cu(II) metal centers and Fig. 1c presents a space-filling model showing the rhombohedral molecular squares for **1** and **2**. The coordination environment of the copper(II) atoms are elongated tetragonal bipyramidal and the tetragonal planes are built up by four pyridyl nitrogen atoms [Cu–N = 2.036(3) and 2.036(4) Å for **1**; 2.022(5) and 2.042(5) Å for **2**]. The *cis* N–Cu–N bond angles show some deviations from perpendicularity [N–Cu–N = 88.0(2), 90.31(13) and 91.40(19)° for **1**; 87.7(3), 90.3(2) and 91.7(3)° for **2**]. The adjacent Cu atoms are linked to each other through the pyridyl nitrogen atoms to form double-stranded chains involving 44-membered rings with a dimension of 16.95 × 19.13 Å^2 for **1** and 17.03 × 19.06 Å^2 for **2**, respectively. The cavity sizes were defined by measuring the Cu–Cu distances and the distances between two methylene carbon atoms. The halogen atoms, occupying the axial positions of the square planes, interacts with the Cu metal atoms through weak Cu–X [Cu–Cl = 2.840(3) Å and Cl–Cu–Cl = 175.36(4)° for **1**; Cu–Br = 2.998(4) Å and Br–Cu–Br = 176.71(3)° for **2**] interactions. Hathaway and Hodgson have investigated the dependence of *T* ($T = R_S/R_L$, tetragonality) on the parameters R_S and R_L for some copper complexes, where R_S is the average value of the four interatomic distances in the equatorial plane and R_L is the average value of central atom–donar atom distance at the fifth and sixth

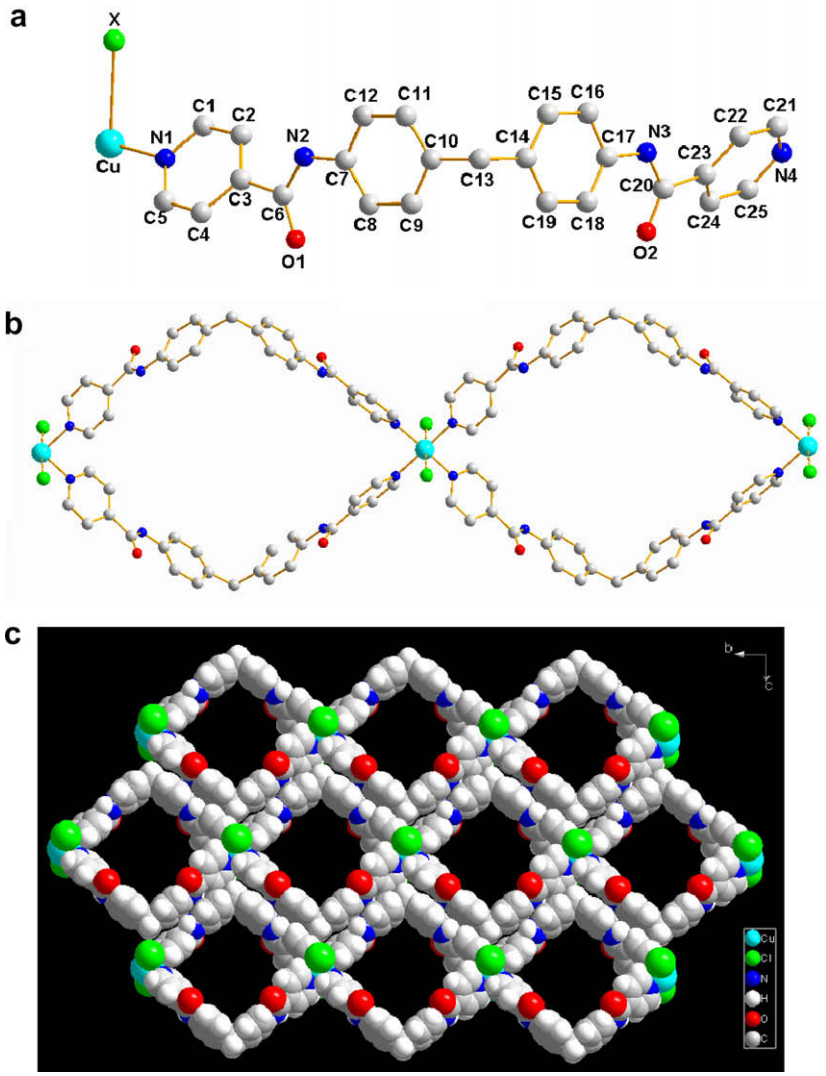

Fig. 1. (a) A representative molecular structure showing the asymmetric unit of complexes **1** (X = Cl) and **2** (X = Br). (b) A representative molecular structure showing the coordination environments of **1** (X = Cl) and **2** (X = Br). Hydrogen atoms are omitted for clarity. (c) The space-filling model showing the rhombohedral molecular squares for **1** and **2**, looking down the *a*-axis.

coordination sites for coordination number 4 + 2 (tetragonally distorted octahedron) [12]. The values of the *T* parameter show the degree of tetragonal distortion about the copper(II) centers. The calculated *T* values for **1** and **2** are 0.715 and 0.678, respectively, which indicate that the bromo complex **2** distorted more from octahedron.

4.3. Structure of **3**

The structure of $\{[Cu(\mathbf{L1})_2(DMF)](NO_3)_2\}_\infty$, **3** was solved in the space group $P\bar{1}$. Fig. 2a shows a representative asymmetric unit for complex **3**, which contains one copper(II) atom, two complete **L1** ligands, one bonded DMF ligand and two uncoordinated nitrate anions. The copper metal center adopts a slightly distorted square pyramidal coordination geometry with the bond angles only deviates slightly from 90° or 180°. The Cu atom is bonded to four pyridyl nitrogen atoms [Cu–N = 2.014(2)–2.042(2) Å] from four different **L1** ligands in the basal plane. The Cu atom is also bonded to one DMF ligand [Cu–O(5) = 2.277(2) Å] in the axial position to complete the distorted square pyramidal coordination geometry. The *cis* N–Cu–N bond angles show significant deviation from perpendicularity [N–Cu–N = 87.35(9), 90.27(9), 90.41(9) and 91.04(9)°]. The Cu atoms are linked to each other through the pyridyl nitrogen atoms to form 1-D double-stranded polymeric chains involving 44-membered rings with a dimension of 16.66×19.94 Å^2, Fig. 2b. The space-filling model is shown in Fig. 2c.

4.4. Structure of **4**

The structure of $\{[Ag(\mathbf{L1})_2](SO_4)\}_\infty$, **4**, was solved in the space group $P\bar{1}$. Fig. 3a shows the asymmetric unit of **4**, which contains two silver(I) atoms, two complete **L1** ligands and an uncoordinated sulfate anion. Fig. 3b shows its infinite one-dimensional chains. Both the silver(I) metal centers, Ag(1) and Ag(2), adopt the bent coordination geometry [N(1)–Ag(1)–N(8) = 161.45(16) and N(4)–Ag(2)–N(5A) = 161.75 (17)°]. The Ag(I) atoms are bonded to two pyridyl nitrogen atoms [Ag(1)–N(1) = 2.173(4) Å, Ag(1)–N(8) = 2.173(4) Å, Ag(2)–N(4) = 2.150(4) Å and Ag(2)–N(5A) = 2.142(4) Å] from two different **L1** ligands. The uncoordinated sulfate ions

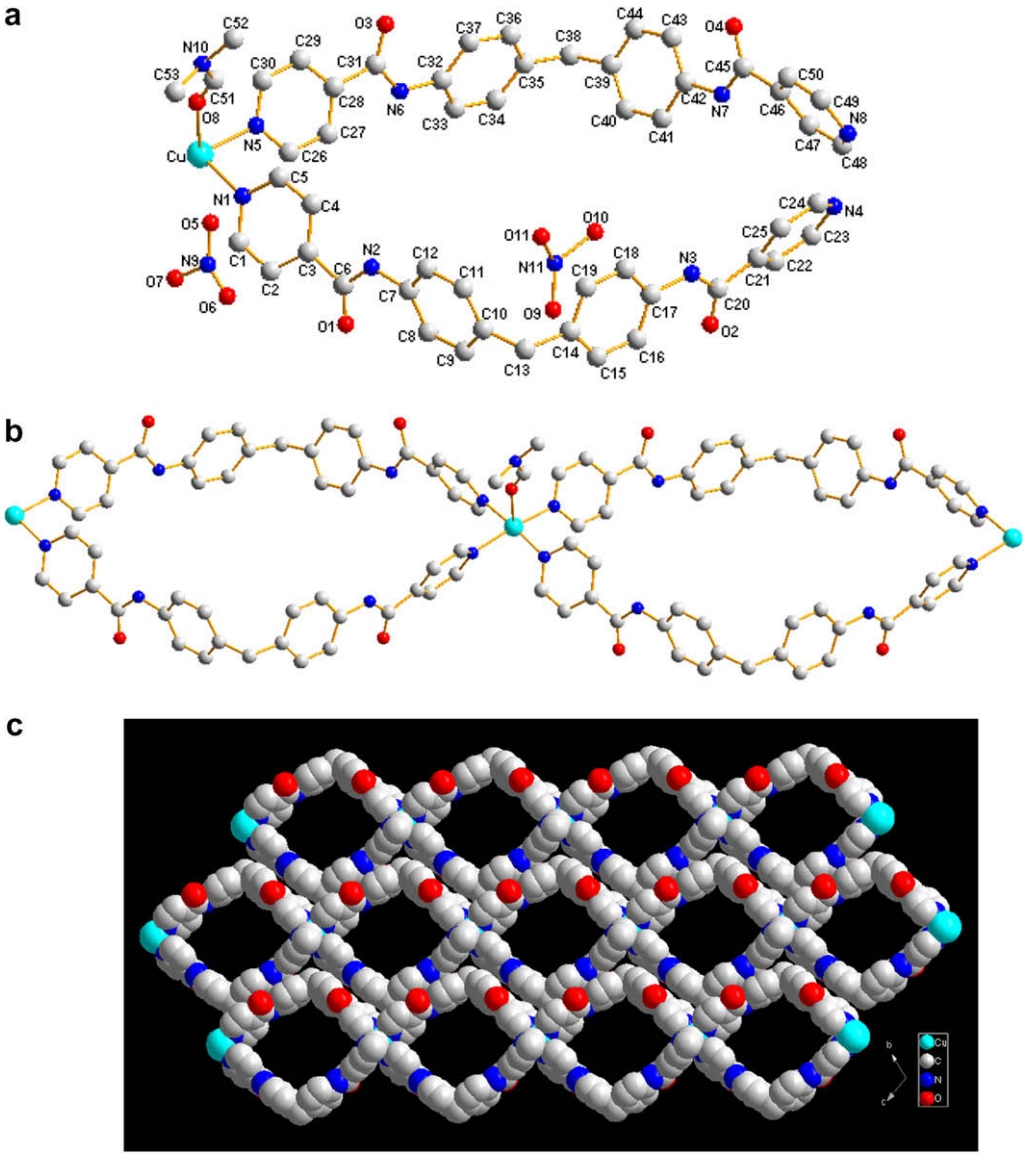

Fig. 2. (a) A molecular structure showing the asymmetric unit of complex **3**. (b) A molecular structure showing the coordination environment of **3**. Hydrogen atoms are omitted for clarity. (c) The space-filling model showing the rhombohedral molecular squares for **3**, looking down the *a*-axis.

interact with the Ag(I) centers in the zigzag chains through the Ag–O interactions [Ag(1)–O(5) = 2.658(4), Ag(1)–O(7) = 2.668(4), Ag(2)–O(6) = 2.757(5) and Ag(2)–O(8) = 2.724(4) Å] forming the 1-D ladder like chain structure, as shown in Fig. 3c. Fig. 3d shows a space-filling model. The Ag–O distances are significantly shorter than their van der Waals contact of 3.24 Å (van der Waals radius for Ag = 1.72 and O = 1.52 Å). It is noted that the typical range of Ag–O bonds is 2.3–2.6 Å [13]. The Ag–Ag distances in the zigzag polymeric chains separated by the bridging **L1** are 19.487(3) and 20.496(4) , while the distance between the zigzag chains separated by the bridging SO_4^{2-} anion is 6.535(2) . No significant hydrogen bond was observed.

4.5. Structure of *5*

The complex $\{[Cu(\mathbf{L2})(DMSO)_2(NO_3)](NO_3)\}_\infty$, **5**, was solved in the space group *Pbcm* and each asymmetric unit contains one copper(II) atom, one **L2** ligand, two DMSO molecules and two NO_3^- anions. Fig. 4a shows the coordination geometry about the Cu metal center. The copper metal center adopts slightly distorted square pyramidal coordination geometry with the bond angles only deviates slightly from 90 or 180°. The Cu atom is bonded to two *trans* pyridyl nitrogen atoms [Cu–N(1) = 2.018(4) Å] and two *trans* oxygen atoms, which are one of the monodentate nitrate groups [Cu–O(4) = 2.029(9) Å] and one of the DMSO ligands [Cu–O(3) = 1.810(5) Å] in the basal plane. The Cu atom is also bonded to one DMSO ligand [Cu–O(2) = 2.260(6) Å] in the axial position to complete the distorted square pyramidal coordination geometry. Along the *c*-axis, adjacent Cu atoms are bridging through the pyridyl nitrogen atoms of **L2** ligands to form a 1-D sinusoidal chain, as shown in Fig. 4b, where the sinusoidal waves propagate along the axis formed by linking the methylene carbon atoms. The Cu–Cu distance in the polymeric chain separated by the bridging **L2** ligand is 18.529(2).

4.6. Conformations of the ligands

The structures of **1–5** provide an opportunity to investigate the conformation of **L1** and **L2** ligands. Based on the relative orientation of the C=O (or N–H) groups, each conformation can adopt a *cis* or *trans* arrangement as shown in Fig. 5. Thus, the ligand **L1** can possibly show two different conformations in the solid state. In addition to the *cis* and *trans* conformations, the *syn* and *anti* designations, which indicate the relative positions of the pyridyl nitrogen atoms can also be applied to the **L2** ligands. Thus, the ligand **L2** can possibly show four different conformations in the solid state as shown in Fig. 5. Based on this descriptor, the conformations of the ligand **L1** in complexes **1, 2** and **3** are assigned as *cis* while that in complex **4** is *trans*, and the ligand **L2** in complex **5** is *trans-anti*.

4.7. Structural comparisons

Complexes **1**–**5** make interesting comparisons with the metal complexes of *N*,*N*′-bis(4-pyridylcarbonyl)-4,4′-diaminodiphenyl ether (**L**′) [14]. Table S2 inSupplementary data lists some important parameters of the rhomboidal area formed by two metal atoms and two methylene carbon atoms of **L1** ligands or two oxygen atoms of **L**′ ligands, where the X denotes the central carbon and oxygen atoms of **L1** and **L**′, respectively. The area of the rhomboidal area was calculated by using the long diagonal length (d_{M-M}) and the

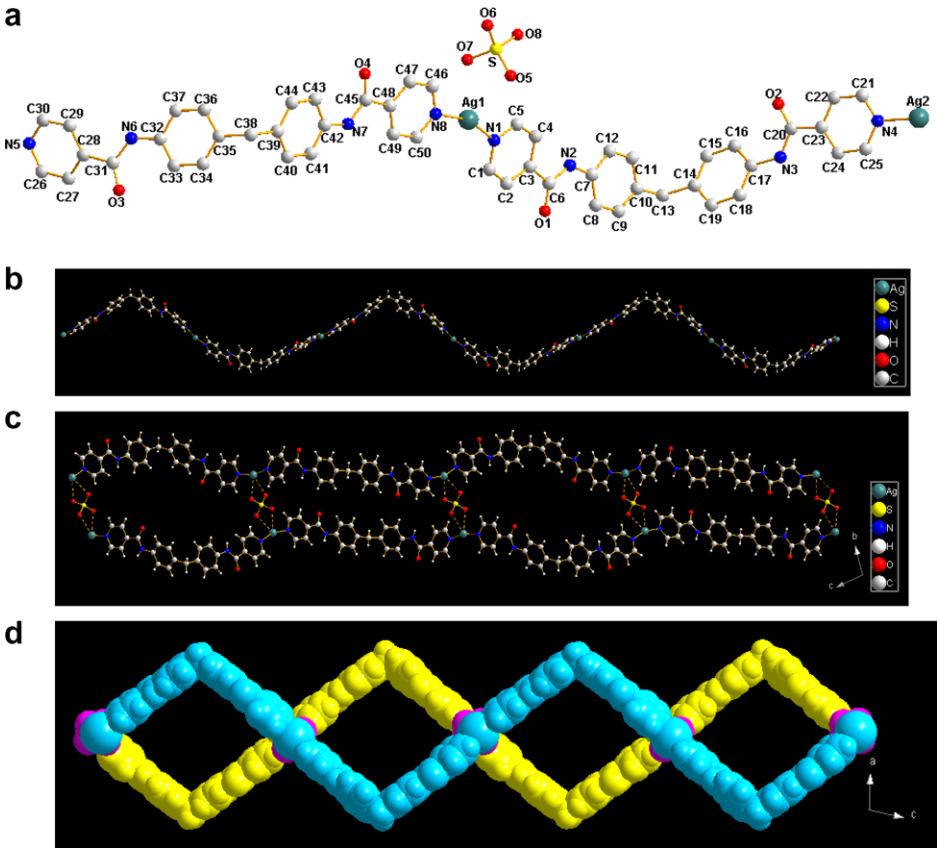

Fig. 3. (a) A molecular structure showing the asymmetric unit of complexes **4**. (b) A molecular structure showing the coordination environment of **4**. (c) The 1-D chains are linked by the SO_4^{2-} anions through Ag–O interactions to form 1-D ladder-like chain like structure. (d) The space-filling model showing the rhombohedral molecular squares for **4**, looking down the *a*-axis.

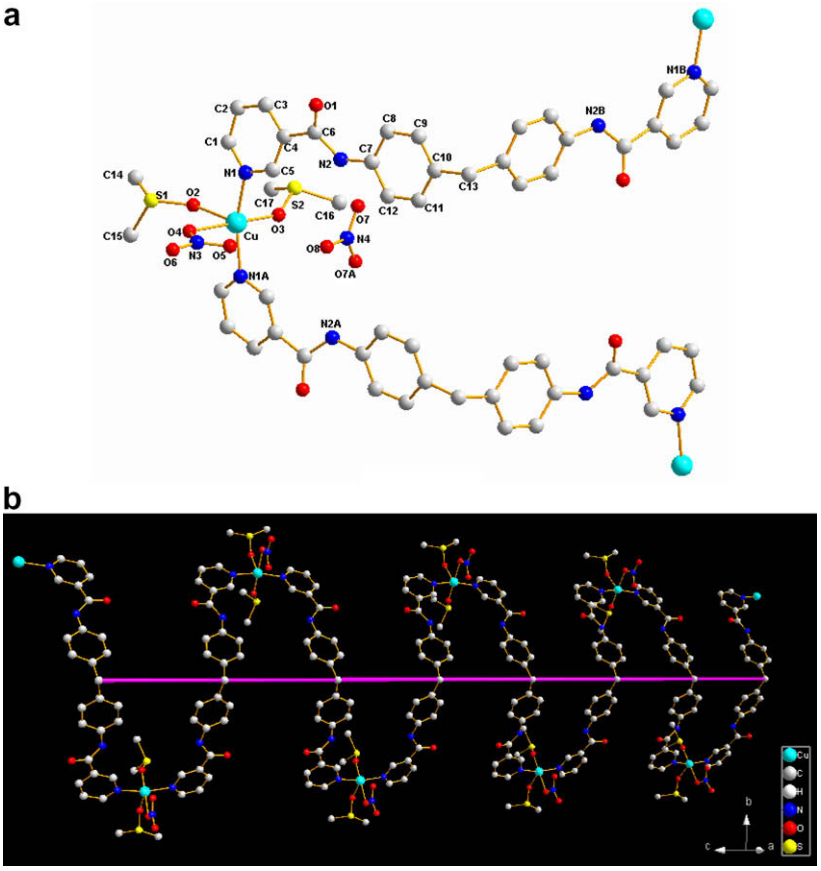

Fig. 4. (a) A molecular structure showing the geometry about the Cu center of complex. (b) A view of the 1-D sinusoidal polymeric chains of **5**.

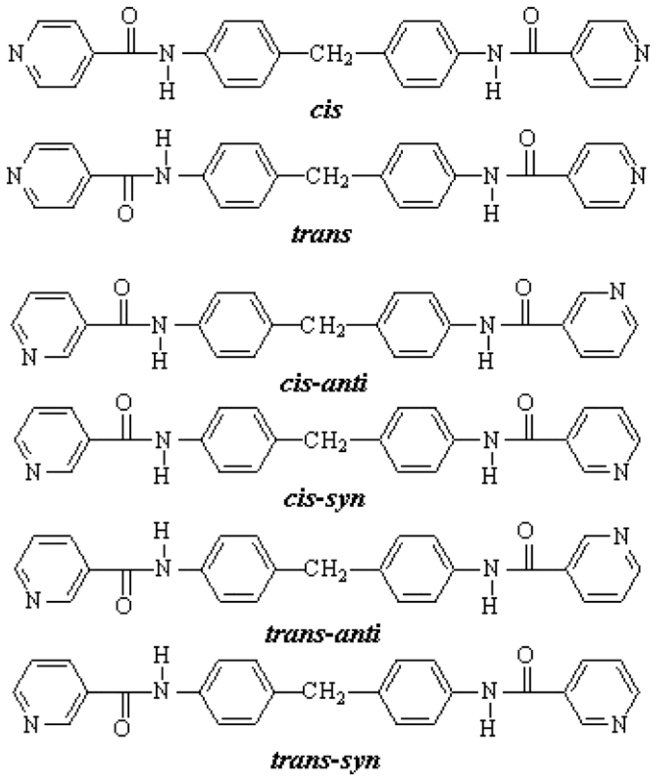

Fig. 5. Possible conformations for **L1** and **L2** ligands.

short diagonal length (d_{X-X}). The result shows that complexes **1**–**3** have the larger sizes than those of the complexes prepared from the **L′** ligands, which may be ascribed to the smaller C–X–C and larger N–Cu–N angles in complexes **1**–**3**.

4.8. Thermal properties

Thermal gravimetric analyses (TGA) were carried out to examine the thermal stability of **1**–**5**. The samples were heated up in air at 1 atm pressure with the heating rate of 10 °C min^{-1}. A weight loss of 42.8% and 39.3% occurred in the temperature range 245–425 °C for **1** and 250–420 °C for **2**, respectively, due to the removal of the first **L1** ligand per formula unit (calcd. 42.9% and 39.1%). Another weight loss occurred in the temperature range 425–590 °C for **1** and 420–587 °C for **2**, corresponding to the removal of the second **L1** ligand and decomposition of the structure. Finally, the residual product weights of 8.7% for **1** and 8.1% for **2** were found in the temperature range 590–700 and 587–700 °C, corresponding to the formation of CuO (calcd. 8.4% and 7.6%), respectively. TGA for **3** showed the loss of two NO_3^- anions and DMF groups in the range 120–232 °C (calcd. 18.4%, obs. 18.1%), followed by the loss of two **L1** ligands above 232–584 °C. The residual product weight of 7.6% was finally found in the temperature range 584–700 °C, corresponding to the formation of CuO (calcd. 7.4%). For complexes **1**–**3**, the results show that the nature of the anions has no significant effect on the decomposition of the double-stranded chains.

The TGA curve shows that **4** is stable up to 300 °C. A total weight loss of 8.7% occurred in the temperature range 300–330 °C, presumably due to the removal of the SO_4^{2-} anions per

formula unit (calcd. 8.5%). A weight loss of 71.9% occurred in the temperature range 330–550 °C, corresponding to the removal of **L1** ligands (calcd. 72.4%) and decomposition of the chain structure. TGA for **5** showed the first loss took place between 123 and 185 °C and was associated with the loss of the coordinated NO_3^- anions and DMSO molecules (calcd. 18.6%, obs. 18.8%). The second loss took place between 185 and 250 °C, corresponding to the loss of the bounded NO_3^- anions and another DMSO groups. A loss occurred in the temperature range 250–485 °C, corresponding to the removal of the **L2** ligands and decomposition of the chains. The residual product weight of 11.0% was found in the temperature range 485–700 °C, corresponding to the formation of CuO (calcd. 10.5%). The TGA results show that complexes **1–5**, which contain the ligands with multi-phenyl and pyridyl groups, are thermal stable and the **L1** or **L2** ligands decomposed at temperatures above 230 °C.

5. Conclusion

In this study, the coordination chemistry of two new angular dipyridyl ligands *N,N′*-(methylenedi-*p*-phenylene)bis(pyridine-4-carboxamide), **L1**, and *N,N′*-(methylenedi-*p*-phenylene)bis(pyridine-3-carboxamide), **L2**, with Cu(II) and Ag(I) salts was investigated. Complexes **1–3** show 1-D double-stranded polymeric chains involving M_2L_2 rhombic molecular squares with the dimensions of 16.95×19.13 for **1**, 17.03×19.06 for **2** and 16.66×19.94 Å^2 for **3**, which are larger than those of the complexes containing the *N,N′*-bis(4-pyridylcarbonyl)-4,4′-diaminodiphenyl ether (**L′**) ligand. Complex **4** forms infinite 1-D zigzag polymeric chains, which are interlinked through a series of Ag–O interactions to form wavy 1-D ladder like chains, while complex **5** shows 1-D bent sinusoidal chains. Table S3 in Supplementary data summarizes some important parameters of these complexes.

The conformations of the **L1** and **L2** ligands are susceptible to the change in the structural type. The **L1** ligands in complexes **1, 2** and **3** adopt the *cis* conformation to present 1-D double-stranded polymeric chains with rhombic molecular squares and those in **4** adopts the adopts *trans* conformation to show 1-D zigzag polymeric chains, while the **L2** ligands in complex **5** adopt the *trans-anti* conformation to give the 1-D sinusoidal chains. Although the **L1** ligands in complexes **1–3** adopt the same *cis* conformation, significant differences in the dihedral angles between the rings were observed, presumably due to the supramolecular interactions. Thus, the *cis* conformation is necessary for coordination polymers containing the angular dipyridyl ligand bearing amide spacer to form structures with rhombic molecular squares, while the *trans* conformation produces the open 1-D chains. Obviously, the **L1** and **L2** ligands are sufficiently flexible to adjust to the stereochemical requirements for the formation of the complexes **1–5**, which adopt the conformation that maximizes the intra- and intermolecular forces.

Acknowledgments

We are grateful to the National Science Council of the Republic of China for support. This research was also supported by the project of the specific research fields in Chung Yuan Christian University, Taiwan, R.O.C. under grant CYCU-97-CR-CH.

Appendix A. Supplementary data

CCDC 684912, 684913, 684914, 684915 and 684916 contain the supplementary crystallographic data for this paper. These data can be obtained free of charge via http://www.ccdc.cam.ac.uk/conts/retrieving.html, or from the Cambridge Crystallographic Data Centre, 12 Union Road, Cambridge CB2 1EZ, UK; fax: (+44) 1223-336-033; or e-mail: deposit@ccdc.cam.ac.uk. Supplementary data associated with this article can be found, in the online version, at doi:10.1016/j.poly.2008.09.008.

References

[1] E.R.T. Tiekink, J.J. Vittal, Frontiers in Crystal Engineering, John Wiley & Sons, Ltd, England, 2006.
[2] (a) R. Robson, B.E. Abrahams, S.R. Batten, R.W. Gable, B.F. Hoskins, J. Lieu, Supramolecular Architecture, ACS Publications, Washington, DC, 1992;
(b) S.R. Batten, R. Robson, Angew. Chem., Int. Ed. 37 (1998) 1460;
(c) O.M. Yaghi, H. Li, C. Davis, D. Richardson, T.L. Groy, Acc. Chem. Res. 31 (1998) 474;
(d) H. Gudbjartson, K. Biradha, K.M. Poirier, M.J. Zaworotko, J. Am. Chem. Soc. 121 (1999) 2599;
(e) C.B. Aakeröy, K.R. Seddon, Chem. Soc. Rev. (1993) 397;
(f) M. Fujita, K. Ogura, Coord. Chem. Rev. 148 (1996) 249;
(g) S.-I. Noro, R. Kitauta, M. Kondo, S. Kitagawa, T. Ishii, H. Matauzaka, M. Yamashita, J. Am. Chem. Soc. 124 (2002) 2568;
(h) S. Kitagawa, M. Kondo, Bull. Chem. Soc. Jpn. 71 (1998) 1739.
[3] (a) R.P. Sijbesma, E.W. Meijer, Curr. Opin. Colloid Interface Sci. 4 (1999) 24;
(b) S.C. Zimmerman, P.S. Corbin, Struct. Bond. 96 (2000) 63;
(c) D.C. Sherrington, K.A. Taskinen, Chem. Soc. Rev. 30 (2001) 83;
(d) D.S. Lawrence, T. Jiang, M. Levett, Chem. Rev. 95 (1995) 2229.
[4] (a) S. Muthu, J.H.K. Yip, J.J. Vittal, J. Chem. Soc., Dalton Trans. (2002) 4561;
(b) Z. Qin, M. Jennings, R.J. Puddephatt, Inorg. Chem. 40 (2001) 6220;
(c) Y. Kajikawa, N. Azuma, K. Tajima, Inorg. Chim. Acta 283 (1998) 61.
[5] (a) T. Hennigar, D.C. MacQuarrie, P. Loiser, R.D. Rogers, M.J. Zaworotko, Angew. Chem., Int. Ed. Engl. 36 (1997) 972;
(b) L. Carlucci, G. Ciani, D.M. Proserpio, S. Rizzato, Chem. Commun. (2000) 1319;
(c) Z. Qin, M.C. Jennings, R.J. Puddephatt, Chem. Eur. J. 8 (2002) 735;
(d) L. Applegarth, A.E. Goeta, J.W. Steed, Chem. Commun. (2005) 2405;
(e) J. Wang, B. Djukic, J. Cao, A. Alberola, F.S. Razavi, M. Pilkington, Inorg. Chem. 46 (2007) 8560.
[6] (a) M.B. Zaman, M.D. Smith, H.-C.z. Loye, Chem. Commun. (2001) 2256;
(b) M. Du, X.-H. Bu, Y.-M. Guo, H. Liu, S.R. Batten, J. Ribas, T.C.W. Mak, Inorg. Chem. 41 (2002) 4904;
(c) M.-L. Tong, Y.-M. Wu, J. Ru, X.-M. Chen, H.-C. Chang, S. Kitagawa, Inorg. Chem. 41 (2002) 4846;
(d) Z.-Y. Fu, X.-T. Wu, J.-C. Dai, S.-M. Hu, W.-X. Du, New J. Chem. 26 (2002) 978;
(e) M.J. Plater, M.R.St.J. Foreman, T. Gelbrich, M.B. Hursthouse, J. Chem. Soc., Dalton Trans. (2000) 1995.
[7] (a) M.J. Plater, M.R.St.J. Foreman, T. Gelbrich, S.J. Coles, M.B. Hursthouse, J. Chem. Soc., Dalton Trans. (2000) 3065;
(b) M. Fujita, Y.J. Kwon, M. Miyazawa, K. Ogure, J. Chem. Soc., Chem. Commun. (1994) 1977;
(c) M. Fujita, Y.J. Kwon, O. Sasaki, K. Yamaguchi, K. Ogura, J. Am. Chem. Soc. 117 (1995) 7287;
(d) X.-C. Su, S.-R. Zhu, H.-K. Lin, X.-B. Leng, Y.-T. Chen, J. Chem. Soc., Dalton Trans. (2001) 3163;
(e) M.O. Awaleh, A. Badia, F. Brisse, Cryst. Growth Des. 5 (2005) 1897;
(f) M. Du, C.-P. Li, X.-J. Zhao, Cryst. Growth Des. 6 (2006) 335.
[8] (a) Y.-F. Hsu, J.-D. Chen, Eur. J. Inorg. Chem. (2004) 1488;
(b) H.-L. Hu, C.-W. Yeh, J.-D. Chen, Eur. J. Inorg. Chem. (2004) 4696;
(c) H.-C. Chen, H.-L. Hu, Z.-K. Chan, C.-W. Yeh, H.-W. Jia, C.-P. Wu, J.-D. Chen, J.-C. Wang, Cryst. Growth Des. 7 (2007) 698;
(d) L.-M. Chiang, C.-W. Yeh, Z.-K. Chan, K.-M. Wang, Y.-C. Chou, J.-D. Chen, J.-C. Wang, J.Y. Lai, Cryst. Growth Des. 8 (2008) 470;
(e) Y.-F. Hsu, C.-H. Lin, J.-D. Chen, J.-C. Wang, Cryst. Growth Des. 8 (2008) 1094.
[9] SMART/SAINT/ASTRO, Release 4.03, Siemens Energy & Automation, Inc., Madison, Wisconsin, USA, 1995.
[10] SHELXTL 5.10. Bruker Analytical X-ray Instruments Inc., Karlsruhe, Germany, 1997.
[11] A.L. Spek, J. Appl. Crystallogr. 36 (2003) 7.
[12] B.J. Hathaway, P.G. Hodgson, J. Inorg. Nucl. Chem. 35 (1973) 4071.
[13] S. Muthu, J.H.K. Yip, J.J. Vittal, J. Chem. Soc., Dalton Trans. (2002) 4561.
[14] (a) Y.W. Shin, T.H. Kim, K.Y. Lee, K.-M. Park, S.W. Han, S.S. Lee, J.S. Kim, J. Kim, Bull. Korean Chem. Soc. 26 (2005) 473;
(b) Y.W. Shin, T.H. Kim, J. Seo, S.S. Lee, J. Kim, Bull. Korean Chem. Soc. 27 (2006) 1915;
(c) Y.W. Shin, T.H. Kim, K.Y. Lee, K.-M. Park, S.S. Lee, J. Kim, Inorg. Chem. Commun. 7 (2004) 374;
(d) Y.-X. Li, Y.-H. Li, X.-R. Zeng, R.-G. Xiong, X.-Z. You, H.-K. Fun, Inorg. Chem. Commun. 6 (2003) 1144.

tetrakis cyclopentadienyl tin(IV) intermediate is produced, which undergoes additional transmetallation to isolate the desired organotin dichloride [19]. The reaction scheme can be viewed in Scheme 1.

Within this paper we present the synthesis, preliminary cytotoxicity and antibacterial studies of a series of three organotin dichloride derivatives, modelled on Titanocene **Y**.

2. Experimental

2.1. General conditions

Manipulations of air and moisture sensitive compounds were performed under an inert atmosphere of nitrogen or argon using standard Schlenk techniques. Tin tetrachloride ($SnCl_4$ 1.0 M solution in heptane) and Super Hydride ($LiBEt_3H$, 1.0 M solution in THF) were obtained commercially from Sigma–Aldrich. All solvents were dried and distilled according to standard methods. ^1H and ^{13}C NMR spectra were measured on a Varian 500 MHz spectrometer with C_6D_6 as solvent and TMS as internal standard. ^{119}Sn NMR spectra were measured on a Varian 500 MHz spectrometer with C_6D_6 as solvent and t-But_2SnCl_2 as internal standard. IR spectra were recorded on a Perkin Elmer Paragon 1000 FT-IR Spectrometer employing NaCl discs. UV/Vis spectra were recorded on a Unicam UV4 Spectrometer. Electron spray mass spectrometry (MS) was performed on a quadrupole tandem mass spectrometer (Quattro Micro, Micromass/Water's Corp., USA), using solutions made up in 50% dichloromethane and 50% methanol. MS spectra were obtained in the ES- (electron spray negative ionisation) mode for compounds **4a** and **4b**. Compound **4c** was obtained in ES+ (electron spray positive) mode. X-ray diffraction data for compound **5** was collected using a Bruker SMART APEX CCD area detector diffractometer. A full sphere of reciprocal space was scanned by phi–omega scans. Pseudo-empirical absorption correction based on redundant reflections was performed by the program SADABS [20]. The structures were solved by direct methods using SHELXS-97 [21] and refined by full matrix least-squares on F^2 for all data using SHELXL-97 [21]. In **5**, hydrogen atoms were added at calculated positions and refined using a riding model. Their isotropic temperature factors were fixed to 1.2 times (1.5 times for methyl groups) the equivalent isotropic displacement parameters of its parent atom. Anisotropic thermal displacement parameters were used for all non-hydrogen atoms. The chloroform molecule could not be located in the unit cell. Platon SQUEEZE [22] was used to compensate for the spread electron density. The solvent is included in the overall formula, $F(000)$, absorption coefficient and density. Further details about the data collection are listed in Table 2, as well as reliability factors. Suitable crystals of **5** were formed from the slow evaporation of a saturated trichloromethane solution.

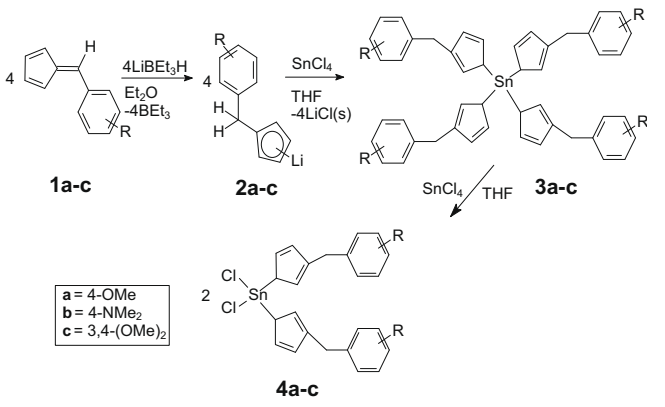

Scheme 1. General reaction scheme for the synthesis of benzyl-substituted organotin dichloride derivatives.

2.2. Synthesis

6-(*p*-Methoxyphenyl) fulvene **1a**, 6-(*p*-*N*,*N*-dimethylaminophenyl) fulvene **1b** and 6-(3,4-dimethoxyphenyl) fulvene **1c** were synthesised according to already published procedures [23–24].

2.2.1. Synthesis of bis-[(p-methoxybenzyl)cyclopentadienyl] tin(IV) dichloride, $[\eta^1$-C_5H_4–CH_2–C_6H_4–O–$CH_3]_2SnCl_2$ (**4a**)

15.0 ml (15.0 mmol) of 1 M solution of Super Hydride ($LiBEt_3H$) in THF was concentrated by removal of the solvent by heating it to 60 °C under reduced pressure of 10^{-2} mbar for forty minutes and then to 90 °C for 20 min in a Schlenk flask. The concentrated Super Hydride was dissolved in 30 ml of dry diethyl ether to give a cloudy white suspension. 2.40 g (13.0 mmol) of the red solid **1a** was added to a Schlenk flask and was dissolved in 90 ml dry diethyl ether to give a red solution. The red fulvene solution was transferred to the Super Hydride solution *via cannula*. The solution was left to stir for 8 h to give a white precipitate of the lithium cyclopentadienide intermediate and the solution had changed colour from orange/red to colourless with a white precipitate formed. The precipitate was filtered on to a frit and was washed with 20 ml of diethyl ether. The white precipitate was dried briefly under reduced pressure and was transferred to a Schlenk flask under nitrogen. 2.06 g (10.7 mmol, 82.2% yield) of the lithiated cyclopentadienide intermediate **2a** was obtained. 2.68 ml (2.68 mmol) of a 1 M solution of tin tetrachloride in heptane was dissolved in 30 ml of dry toluene in a Schlenk flask. The lithium cyclopentadienide intermediate was dissolved in 60 ml of dry toluene to give a colourless solution. The solution of tin tetrachloride was added to the lithium cyclopentadienide intermediate solution slowly at 0 °C *via cannula* to give a yellow solution. The tin solution was allowed to stir for 16 h at room temperature followed by the removal of the solvent under reduced pressure which yielded a yellow solid, tetrakis-[η^1-*(p-methoxybenzyl)cyclopentadienyl] tin(IV)* intermediate **3a**. The yellow solid was dissolved in 30 ml of dry toluene and 2.68 ml (2.68 mmol) of a 1 M solution of tin tetrachloride in heptane was added slowly at 0 °C. The solution was stirred at room temperature for 2 h after which it was allowed to settle, followed by filtration in an inert atmosphere of nitrogen using a frit. The resulting clear yellow solution was reduced under vacuum to yield the title compound as a light yellow, waxy and air sensitive solid (0.960 g, 1.71 mmol, 31.9% yield) **4a**.

^1H NMR (δ ppm C_6D_6, 500 MHz): 3.28 [s, 6H, C_6H_4–OCH_3], 3.61 [s, 4H, C_5H_4–CH_2], 5.15 [s, 4H, C_5H_4–CH_2], 6.05 [s, 4H, C_5H_4–CH_2], 6.75 [d, 4H, J 7.82 Hz, C_6H_4–OCH_3], 7.04 [d, 4H, *J* 7.82 Hz, C_6H_4–OCH_3].

^{13}C NMR (δ ppm C_6D_6, 125 MHz, proton decoupled): 35.5 [C_5H_4–CH_2], 54.4 [C_6H_4–OCH_3], 97.1, 114.0, 123.3, 129.8, 132.3, 145.8, 158.4.

^{119}Sn NMR (δ ppm C_6D_6, 186 MHz, proton decoupled): −36.5.

MS (m/z, QMS-MS/MS): 559 $[M-H]^-$.

IR absorptions (NaCl, cm^{-1}): 2996, 2905, 2833, 1610, 1575, 1511, 1463, 1431, 1300, 1247, 1176, 1036, 919, 803.

UV–Vis (toluene, nm): λ 216 (ε 56000), λ 239 (ε 53000), λ 266 (ε 49000), λ 274 (ε 39000), λ 299 (ε 13000), λ 321 (ε 7800), λ 337 (ε 2000), λ 425 (ε 5900), λ_{max} 555 (ε 600).

2.2.2. Synthesis of bis-[(p-N,N-dimethylaminobenzyl)cyclopentadienyl] tin(IV) dichloride, $[\eta^1$-C_5H_4–CH_2–C_6H_4–N–$(CH_3)_2]_2SnCl_2$ (**4b**)

15.0 ml (15.0 mmol) of 1 M solution of Super Hydride ($LiBEt_3H$) in THF was concentrated by removal of the solvent by heating it to 60 °C under reduced pressure of 10^{-2} mbar for forty minutes and then to 90 °C for 20 min in a Schlenk flask. The concentrated Super

Hydride was dissolved in 30 ml of dry diethyl ether to give a cloudy white suspension. 2.38 g (12.1 mmol) of the red solid **1b** was added to a Schlenk flask and was dissolved in 90 ml dry diethyl ether to give a red solution. The red fulvene solution was transferred to the Super Hydride solution *via cannula*. The solution was left to stir for 8 h to give a white precipitate of the lithium cyclopentadienide intermediate and the solution had changed colour from orange/red to faint yellow. The precipitate was filtered on to a frit and was washed with 20 ml of diethyl ether. The white precipitate was dried briefly under reduced pressure and was transferred to a Schlenk flask under nitrogen. 1.94 g (9.45 mmol, 78.2% yield) of the lithiated cyclopentadienide intermediate **2b** was obtained. 2.36 ml (2.36 mmol) of a 1 M solution of tin tetrachloride in heptane was dissolved in 30 ml of dry toluene in a Schlenk flask. The lithium cyclopentadienide intermediate was dissolved in 60 ml of dry toluene to give a colourless solution. The solution of tin tetrachloride was added to the lithium cyclopentadienide intermediate solution slowly at 0 °C *via cannula* to give a yellow solution with a white precipitate. The tin solution was allowed to stir for 16 h at room temperature followed by the removal of the solvent under reduced pressure which yielded a dark yellow solid, tetrakis-[η^1-*(p-dimethylaminobenzyl)cyclopentadienyl] tin(IV)* intermediate **3b**. The dark yellow solid was dissolved in 30 ml of dry toluene and 2.36 ml (2.36 mmol) of a 1 M solution of tin tetrachloride in heptane was added slowly at 0 °C. The solution was stirred at room temperature for 2 h after which it was allowed to settle, followed by filtration in an inert atmosphere of nitrogen using a frit. The resulting clear yellow solution was reduced under vacuum to yield the title compound as a yellow, waxy and air sensitive solid (1.21 g 2.06 mmol, 43.7% yield) **4b**.

^{1}H NMR (δ ppm C_6D_6, 500 MHz): 2.23 [s, 12H, C_6H_4–N(CH_3)$_2$], 3.36 [s, 2H, C_5H_4–CH_2], 3.43 [s, 2H, C_5H_4–CH_2], 4.93 [s, 2H, C_5H_4–CH_2], 4.98 [s, 2H, C_5H_4–CH_2], 5.72 [s, 2H, C_5H_4–CH_2], 5.86 [s, 2H, C_5H_4–CH_2], 6.32 [d, 4H, J 8.31 Hz, C_6H_4–N(CH_3)$_2$], 6.82 [d, 4H, *J* 8.31 Hz, C_6H_4–N(CH_3)$_2$].

^{13}C NMR (δ ppm C_6D_6, 125 MHz, proton decoupled): 35.4 [C_5H_4–CH_2], 40.2 [C_6H_4–N-(CH_3)$_2$], 97.0, 100.3, 113.0, 121.6, 123.4, 129.5, 146.3, 148.1, 149.3.

^{119}Sn NMR (δ ppm C_6D_6, 186 MHz, proton decoupled): −26.8

MS (*m*/*z*, QMS-MS/MS): 585 $[M-H]^-$.

IR absorptions (near, NaCl windows, cm^{-1}): 3007, 2888, 2798, 1614, 1567, 1518, 1478, 1444, 1347, 1224, 1162, 1131, 947, 805.

UV–Vis (toluene, nm): λ 218 (ε 42 000), λ 227 (ε 36 000), λ 236 (ε 43 000), λ 246 (ε 41 000), λ 263 (ε 48 000), λ 299 (ε 20 000), λ 322 (ε 8400), λ 426 (ε 4500), λ 555 (weak).

*2.2.3. Synthesis of bis-[(3,4-dimethoxybenzyl)cyclopentadienyl] tin(IV) dichloride, [η^1-C_5H_4–CH_2–C_6H_3–$(OCH_3)_2$]$_2$$SnCl_2$ (**4c**)*

16.0 ml (16.0 mmol) of 1 molar solution of Super Hydride (Li-BEt_3H) in THF was concentrated by removal of the solvent by heating it to 60 °C under reduced pressure of 10^{-2} mbar for 40 min and then to 90 °C for 20 min in a Schlenk flask. The concentrated Super Hydride was dissolved in 30 ml of dry diethyl ether to give a cloudy white suspension. 2.40 g (11.2 mmol) of the red solid **1c** was added to a Schlenk flask and was dissolved in 90 ml dry diethyl ether to give a red solution. The red fulvene solution was transferred to the Super Hydride solution *via cannula*. The solution was left to stir for 8 h to give a white precipitate of the lithium cyclopentadienide intermediate and the solution had changed colour from orange/red to faint yellow with a white precipitate formed. The precipitate was filtered on to a frit and was washed with 20 ml of diethyl ether. The white precipitate was dried briefly under reduced pressure and was transferred to a Schlenk flask under nitrogen. 2.16 g (9.72 mmol, 86.8% yield) of the lithiated cyclopentadienide intermediate **2c** was obtained. 2.43 ml (2.43 mmol) of a 1 molar solution of tin tetrachloride in heptane was dissolved in 30 ml of dry toluene in a Schlenk flask. The lithium cyclopentadienide intermediate was dissolved in 60 ml of dry toluene to give a colourless solution. The solution of tin tetrachloride was added to the lithium cyclopentadienide intermediate solution slowly at 0 °C *via cannula* to give a yellow solution. The tin solution was allowed to stir for 16 h at room temperature followed by the removal of the solvent under reduced pressure which yielded a dark brown solid, tetrakis-[η^1-(*p-N,N*-dimethylaminobenzyl)cyclopentadienyl] *tin(IV)* intermediate **3c**. The dark yellow solid was dissolved in 30 ml of dry toluene and 2.43 ml (2.43 mmol) of a 1 M solution of tin tetrachloride in heptane was added slowly at 0 °C. The solution was stirred at room temperature for 2 h after which it was allowed to settle, followed by filtration in an inert atmosphere of nitrogen using a frit. The resulting clear brown solution was reduced under vacuum to yield the title compound as a brown, waxy and air sensitive solid (0.740 g 1.20 mmol, 24.6% yield) **4c**.

^{1}H NMR (δ ppm C_6D_6, 500 MHz): 3.14 [s, 6H, C_6H_3-(OCH_3)$_2$], 3.18 [s, 6H, C_6H_3–(OCH_3)$_2$], 3.46 [s, 4H, C_5H_4–CH_2], 4.77 [s, 4H, C_5H_4–CH_2], 5.95 [s, 4H, C_5H_4–CH_2], 6.37 [d, 2H, J 8.31 Hz, C_6H_3–(OCH_3)$_2$], 6.48 [s, 2H, C_6H_3–(OCH_3)$_2$], 6.52 [d, 2H, J 8.31 Hz, C_6H_3–(OCH_3)$_2$].

^{13}C NMR (δ ppm C_6D_6, 125 MHz, proton decoupled): 35.1 [C_5H_4–CH_2], 54.2 [C_6H_3–(OCH_3)$_2$], 99.2, 111.7, 112.1, 120.0, 120.9, 131.7, 146.3, 149.2.

^{119}Sn NMR (δ ppm C_6D_6, 186 MHz, proton decoupled): −48.9.

MS (*m*/*z*, QMS-MS/MS): 621 $[M+H]^+$.

IR absorptions (neat, NaCl windows, cm^{-1}): 2998, 2934, 2833, 1609, 1590, 1510, 1463, 1417, 1235, 1139, 1028, 804, 733.

UV–Vis (toluene, nm): λ 213 (ε 63 000), λ 230 (ε 53 000), λ 240 (ε 55 000), λ 248 (ε 56 000), λ 266 (ε 58 000), λ 300 (ε 8600), λ 321 (ε 5600), λ 426 (ε 4300), λ_{max} 555 (ε 400) (see Fig. 1).

2.3. Antibacterial Studies

Two different strains of the Gram-positive bacteria *Staphylococcus aureus* (SA) were used; a clinical isolate of Methicillin-resistant SA (MRSA identified as isolate CC), and the commercially available Methicillin-sensitive SA (MSSA ATCC 6538). For comparison, a Gram-negative bacterium was also tested (*Escherichia coli,* lab strain BL21).

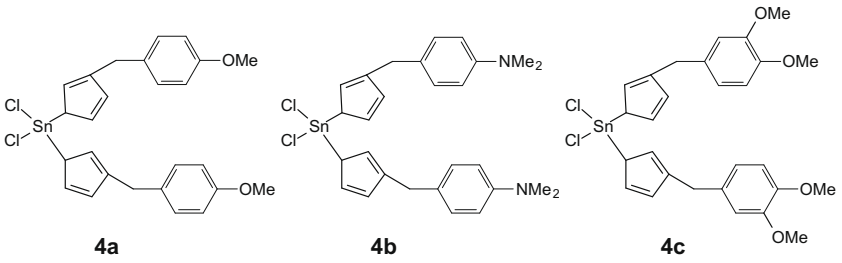

Fig. 1. Structures of η^1 organotin dichlorides **4a–c**.

Table 1
Zone of clearance for compounds **4a–c** in mm

Bacteria	DMSO	**4a** (mm)	**4b** (mm)	**4c** (mm)
Gram-positive				
MRSA	N/A	5	10	14
MSSA	N/A	8	8	14
Gram–negative				
E. coli	N/A	5	6	5

To assess the biological activity of compounds **4a–c**, the Kirby–Bauer disk-diffusion method was applied [25]. All bacteria were individually cultured from a single colony in sterile LB medium [26] overnight at 37 °C (orbital shaker incubator). All the work carried out was performed under sterile conditions.

For each strain, 50 μl of culture were spread evenly on agar-LB medium. Four 5 mm diameter paper discs were placed evenly separated on each plate. 50 mg of each sample (**4a** 0.089 M, **4b** 0.085 M and **4c** 0.081 M) were dissolved in 1 ml of DMSO to prepare the drug formulation. 5 μl of **4a–c** solution (250 μg) were placed on the paper discs and 5 μl of DMSO was placed on the fourth circle of filter paper as a control. The plates were covered and placed in an incubator at 30 °C for 24 h. The plates were then removed and the zone of clearance (defined as the diameter of inhibited bacterial growth around the filter paper) for each sample was measured in mm (see Table 1).

2.4. Cytotoxicity studies

Preliminary *in vitro* cell tests were performed on the cell line LLC-PK (long-lasting cells–pig kidney) in order to compare the cytotoxicity of the compounds presented in this paper. This cell line was chosen based on their regular and long-lasting growth behaviour, which is similar to the one shown in kidney carcinoma cells. It was obtained from the ATCC (American Tissue Cell Culture Collection) and maintained in Dulbecco's Modified Eagle Medium containing 10% (v/v) FCS (foetal calf serum), 1% (v/v) penicillin streptomycin and 1% (v/v) L-glutamine. Cells were seeded in 96-well plates containing 200 μl microtitre wells at a density of 5000-cells/200 μl of medium and were incubated at 37 °C for 24 h to allow for exponential growth. Then the compounds used for the testing were dissolved in the minimal amount of DMSO (dimethylsulfoxide) possible and diluted with medium to obtain stock solutions of 5×10^{-4} M in concentration and less than 0.7% of DMSO. The cells were then treated with varying concentrations of the compounds and incubated for 48 h at 37 °C. Then, the solutions were removed from the wells and the cells were washed with PBS (phosphate buffer solution) and fresh medium was added to the wells. Following a recovery period of 24 h incubation at 37 °C, individual wells were treated with a 200 μl of a solution of MTT (3-(4,5-dimethylthiazol-2-yl)-2,5-diphenyltetrazolium bromide) [27] in medium. The solution consisted of 30 mg of MTT in 30 ml of medium. The cells were incubated for 3 h at 37 °C. The medium was then removed and the purple formazan crystals were dissolved in 200 μl DMSO per well. A Wallac Victor (Multilabel HTS Counter) Plate Reader was used to measure absorbance at 540 nm. Cell viability was expressed as a percentage of the absorbance recorded for control wells. The values used for the dose response curves represent the values obtained from four consistent MTT-based assays for each compound tested.

Table 2
Crystal data and structure refinement for **5**

Identification code	**5**
Empirical formula	$C_{47}H_{43}N_4O_2Cl_9Sn_2$
Molecular formula	$(C_{23}H_{21}N_2OCl_3Sn)_2xCHCl_3$
Formula weight	1252.28
Temperature (K)	100(2)
Wavelength (Å)	0.71073
Crystal system	monoclinic
Space group	$P2_1/n$ (#14)
Unit cell dimensions	
a (Å)	14.7176(11)
b (Å)	8.2667(6)
c (Å)	20.4595(16)
α (°)	90
β (°)	96.649(2)
γ (°)	90
V (Å^3)	2472.5(3)
Z	2
D_{calc} (Mg/m^3)	1.682
Absorption coefficient (mm^{-1})	1.540
$F(000)$	1244
Crystal size (mm^3)	0.40 × 0.05 × 0.03
θ range for data collection (°)	1.62–26.43
Index ranges	$-18 \le h \le 18$, $-10 \le k \le 10$, $-25 \le l \le 25$
Reflections collected	21282
Independent reflections	5081 [R(int) = 0.0426]
Completeness to θ = 26.43°	99.8%
Absorption correction	semi-empirical from equivalents
Maximum and minimum transmission	0.9553 and 0.7701
Refinement method	full-matrix least-squares on F^2
Data/restraints/parameters	5081/0/272
Goodness-of-fit on F^2	1.041
Final R indices [I > 2sigma(I)]	R_1 = 0.0347, wR_2 = 0.0777
R indices (all data)	R_1 = 0.0434, wR_2 = 0.0805
Largest difference in peak and hole (e Å^{-3})	0.907 and −0.536

3. Discussion

3.1. Synthesis

The lithium intermediates used in the synthesis of derivatives **4a–c** were synthesised by the hydridolithiation reaction of aryl-fulvenes with Super Hydride ($LiBEt_3H$). This form of nucleophilic addition to the exocyclic double bond of the fulvene is highly selective due to the increased polarity as a result of the inductive effect of the corresponding phenyl ring. There is no nucleophilic attack seen at the diene element of the aryl-fulvenes. The lithiated cyclopentadienide intermediate was isolated with good yields of 79–87%.

Four equivalents of the lithiated cyclopentadienide intermediate were then transmetallated with one equivalent of tin tetrachloride to form a tetrakis cyclopentadienyl tin(IV) intermediate and lithium chloride as a by-product. This tetrakis cyclopentadienyl tin(IV) intermediate was isolated but not characterised due to extreme air sensitivity. This was then further reacted with 1 equiv. of tin tetrachloride to yield the organotin dichlorides **4a**, **4b**, and **4c** in yields of 25–44%. Elemental analysis was not possible due to the level of air and moisture sensitivity of the compounds.

Derivatives **4a**, **4b**, and **4c** are soluble in organic non-chlorinated solvents, but decompose rapidly in chlorinated solvents such as dichloromethane. The synthesis of organotin dichlorides is dependent upon the solvent. The expected dichloride species were formed only when toluene or benzene was used as the solvent.

A notable feature of the organotin species **4a**, **4b**, and **4c** is the η^1-bonded Cp ligand in these molecules. This results in an interesting ^{1}H NMR spectrum, which appears to suggest a η^5-bonding due to the symmetry of two singlet peaks for the cyclopentadienyl hydrogens, approximately 1 ppm apart. This can be rationalised by fast sigma tropic shift in solution.

3.2. Structural discussion

Despite the effort to crystallise the organotin derivatives **4a-c**, no crystal structures were obtained. 2,2-Bipyridine was success-

fully used as a bidentate nitrogen base in an attempt to crystallise a six co-ordinated tin complex for the organotin dichloride species. This produced single crystals of the bipyridine adduct of η^1-(*p*-methoxybenzyl)cyclopentadienyl tin(IV) trichloride (**5**), where one of the Cp ligands is replaced with a Cl atom, which can be viewed in Fig. 2. This shows that the tin(IV) cyclopentadienyl chlorides undergo more than one exchange reaction: The above mentioned sigma tropic shift and a ligand exchange in a Schlenk-type equilibrium. The structure is monoclinic and contains $CHCl_3$ solvent molecules in the crystal (see Table 3).

The bond lengths for Sn–Cl(1) 2.420 Å, Sn–Cl(2) 2.442 Å, and Sn–Cl(3) 2.414 Å of the six co-ordinated Sn species are slightly longer when compared with other tin(IV) complexes [28], due to the increased electron density surrounding the central Sn atom. Also, the bond length of the Sn–C(3) 2.222 Å is comparable with other organotin complexes such as Me_2SnCl_2 where the Sn–C bond

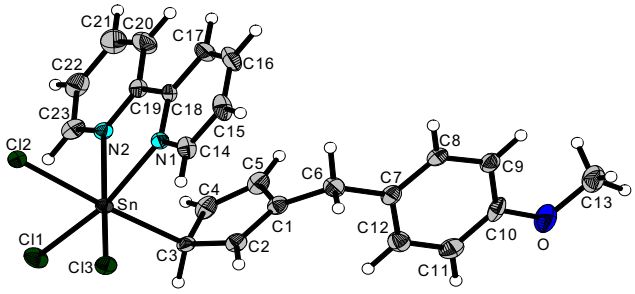

Fig. 2. X-ray diffraction structure of **5**; thermal ellipsoids are drawn on the 50% probability level.

Table 3
Selected bond lengths and angles from the crystal structure of **5**

Identification code	**5**
Bond	*Bond length* (Å)
Sn–C(3)	2.222
Sn–N(1)	2.231
Sn–N(2)	2.278
Sn–Cl(3)	2.414
Sn–Cl(1)	2.420
Sn–Cl(2)	2.442
C(1)–C(2)	1.349
C(1)–C(5)	1.453
C(1)–C(6)	1.494
C(2)–C(3)	1.482
C(3)–C(4)	1.460
C(4)–C(5)	1.346
C(6)–C(7)	1.521
N(1)–C(14)	1.347
N(1)–C(18)	1.355
C(19)–N(2)	1.337
C(19)–C(18)	1.482
C(23)–N(2)	1.342
Bond angles	
C(3)–Sn–N(1)	91.73
C(3)–Sn–N(2)	95.38
N(1)–Sn–N(2)	72.51
C(3)–Sn–Cl(3)	93.98
N(1)–Sn–Cl(3)	93.59
N(2)–Sn–Cl(3)	163.44
C(3)–Sn–Cl(1)	92.82
N(1)–Sn–Cl(1)	165.49
N(2)–Sn–Cl(1)	93.34
Cl(3)–Sn–Cl(1)	99.83
C(3)–Sn–Cl(2)	176.83
N(1)–Sn–Cl(2)	85.48
N(2)–Sn–Cl(2)	82.34
Cl(3)–Sn–Cl(2)	87.72
Cl(1)–Sn–Cl(2)	89.53

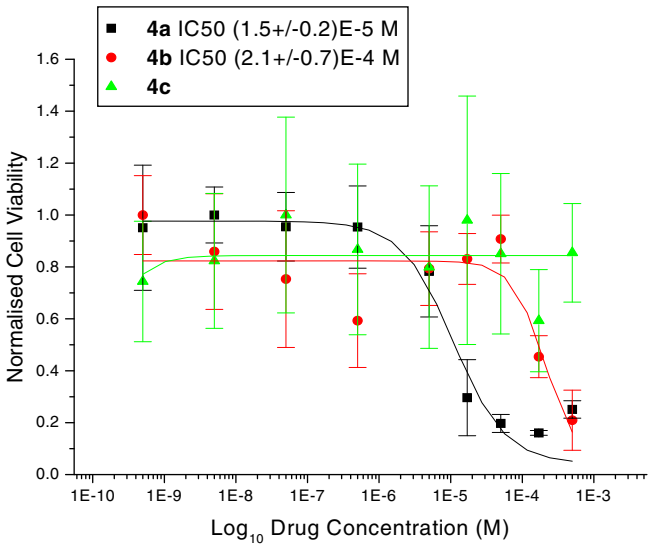

Fig. 3. Cytotoxicity curves from typical MTT assays showing the effect of compounds **4a–c** on the viability of LLC-PK cells.

lengths are in the region of 2.210 Å [29]. This structure also demonstrates the η^1-bonded conformation for the Sn–C bond, which is believed to be present in complexes **4a–c**. The two double bonds present in the cp ring are evident due to the shortening of the carbon-carbon bond lengths, C(1)–C(2) 1.349 Å and C(4)–C(5) 1.346 Å. The longer single CC bonds within the Cp ring were; C(2)–C(3) 1.482 Å, C(3)–C(4) 1.460 Å, and C(1)–C(5) 1.453 Å. The structure displays a distorted octahedral conformation, with the N(1)–Sn–N(2) angle of 72.51° being compressed due to the co-ordinated bipyridine ligand.

3.3. Biological evaluation

Almost no antibacterial effect was observed for complexes **4a–c** against the Gram-negative bacteria *E. coli* using the Kirby–Bauer disk diffusion method. Against the Gram-positive bacteria MRSA and MSSA however, a low to medium effect was observed with the compounds **4b** and **4c** having the greatest effect over 24 h. The solvent used to prepare the stock solutions (DMSO) played no role in growth inhibition. These results are in keeping with other organotin(IV) results found in the literature.

3.4. Cytotoxicity studies

As seen in Fig. 3, compounds **4a** and **4b** showed IC50 values 15 and 210 μM respectively. Complex **4c** displayed no antitumor activity. All three compounds suffered from very poor solubility along with decomposition due to certain air sensitivity of the compounds, which resulted in relatively large error margins for compounds **4b** and **4c**. Compound **4a** showed surprisingly good results of 15 μM with reduced error margins when compared with the titanium equivalent, Titanocene **Y**, which yielded an IC50 value of 21 μM. This result emphasises the importance of the *p*-methoxy phenyl moiety that is present in both **4a** and Titanocene **Y**. However the IC50 value for **4a** did not reach the level set by cisplatin with an IC50 value of 3.3 μM.

4. Conclusion and outlook

The hydridolithiation of 6-aryl substituted fulvenes followed by transmetallation has been found to be a very effective and reproducible way to medium to highly cytotoxic benzyl-substituted

organotin complexes. Although preliminary anti-bacterial results were lower than expected, **4a** yielded a promising anti-tumour IC50 value of 15 μM. While the possibility of **4a** becoming a viable anti-cancer drug are low due to high air sensitivity of **4a** and general toxicity of organotin compounds, these results are encouraging enough to warrant further work in this area.

Supplementary data

CCDC 699232 contains the supplementary crystallographic data for **5**. These data can be obtained free of charge via http://www.ccdc.cam.ac.uk/conts/retrieving.html, or from the Cambridge Crystallographic Data Centre, 12 Union Road, Cambridge CB2 1EZ, UK; fax: (+44) 1223-336-033; or e-mail: deposit@ccdc.cam.ac.uk.

Acknowledgements

The authors thank the Higher Education Authority (HEA), the Centre for Synthesis and Chemical Biology (CSCB), University College Dublin (UCD), COST D39 and the Central European Society for Anticancer Drug Research (CESAR) for funding.

References

[1] T. Schilling, B.K. Keppler, M.E. Heim, G. Niebch, H. Dietzfelbinger, J. Rastetter, A.R. Hanauske, Invest. New Drugs 13 (1996) 327.
[2] E. Melendez, Crit. Rev. Oncol./Hematol. 42 (2002) 309.
[3] F. Caruso, M. Rossi, Metal Ions Biol. Syst. 42 (2004) 353.
[4] G. Lummen, H. Sperling, H. Luboldt, T. Otto, H. Rubben, Cancer Chemoth. Pharmacol. 42 (1998) 415.
[5] N. Kröger, U.R. Kleeberg, K. Mross, L. Edler, G. Saß, D. Hossfeld, Onkologie 23 (2000) 60.
[6] O.R. Allen, L. Croll, A.L. Gott, R.J. Knox, P.C. McGowan, Organometallics 23 (2004) 288.
[7] K. Strohfeldt, M. Tacke, Chem. Soc. Rev. 37 (2008) 1174.
[8] N.J. Sweeney, O. Mendoza, H. Müller-Bunz, C. Pampillón, F.-J.K. Rehmann, K. Strohfeldt, M. Tacke, J. Organomet. Chem. 690 (2005) 4537.
[9] P. Quevauviller, R. Ritsema, R. Morabit, W.M.R. Dirkx, Appl. Organomet. Chem. 8 (1994) 541.
[10] M. Jain, S. Nehra, P.C. Trivedi, R.V. Singh, Metal Based Drugs 9 (2002) 53.
[11] M. Jain, S. Gaur, V.P. Singh, R.V. Singh, Appl. Organomet. Chem. 18 (2004) 73.
[12] M. Jain, S. Gaur, S.C. Diwedi, S.C. Joshi, R.V. Singh, A. Bansal, Phosphorus, Sulfur, Silicon 179 (2004) 1517.
[13] S. Belwal, S.C. Joshi, R.V. Singh, Main Group Met. Chem. 20 (1997) 301.
[14] S.A. Sadeek, M.S. Refat, H.A. Hashem, J. Coord. Chem. 59 (2006) 759.
[15] A. Chaudhary, R.V. Singh, Phosphorus, Sulfur, Silicon 178 (2003) 603.
[16] J. Crowe, Appl. Organomet. Chem. 1 (1987) 143.
[17] K. Shahid, S. Ali, S. Shahzadi, A. Badshah, K.M. Khan, G.M. Maharvi, Synth. React. Inorg. Met.-Org. Chem. 33 (2003) 1221.
[18] P. Álvarez-Boo, J.S. Casas, M.D. Couce, R. Farto, V. Fernández-Moreira, E. Freijanes, J. Sordo, E. Vázquez-López, J. Organomet. Chem. 691 (2006) 45.
[19] D.L. Tomaja, J.J. Zuckerman, Synth. React. Inorg. Metal-Org. Chem. 6 (1976) 323.
[20] G.M. Sheldrick, SADABS Version 2.03, University of Göttingen, Germany, 2002.
[21] G.M. Sheldrick, SHELXS-97 and SHELXL-97, University of Göttingen, Germany, 1997.
[22] A.L. Spek, J. Appl. Crystallogr. 36 (2003) 7.
[23] N.J. Sweeney, O. Mendoza, H. Müller-Bunz, C. Pampillón, F.-J.K. Rehmann, K. Strohfeldt, M. Tacke, J. Organomet. Chem. 690 (2005) 4537.
[24] F.-J.K. Rehmann, A.J. Rous, O. Mendoza, N.J. Sweeney, K. Strohfeldt, W.M. Gallagher, M. Tacke, Polyhedron 24 (2005) 1250.
[25] A. Bondi, H.E. Spaulding, E.D. Smith, C.C. Dietz, Am. J. Med. Sci. 213 (1947) 221.
[26] S.E. Luria, Bacteriol Rev. 11 (1947) 1.
[27] T. Mosmann, J. Immunol. Methods 65 (1983) 55.
[28] S. Alshehri, J. Burgess, J. Fawcett, S.A. Parsons, D.R. Russel, Polyhedron 19 (2000) 399.
[29] H. Schumann, B.C. Wassermann, M. Frackowiak, B. Omotowa, S. Schutte, J. Velder, S.H. Mühle, W. Krause, J. Organomet. Chem. 609 (2000) 189.

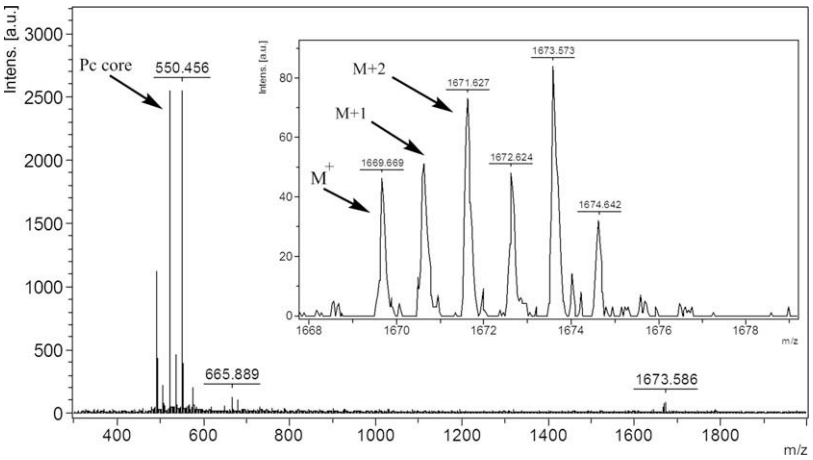

Fig. 1. The positive ion and linear mode MALDI-TOF-MS spectrum of **3** (1669 Da), obtained in 7-hydroxycoumarin (umbelliferone) MALDI matrix, using a nitrogen laser, accumulating 50 laser shots. Inset spectrum shows the expanded molecular mass region of the complex.

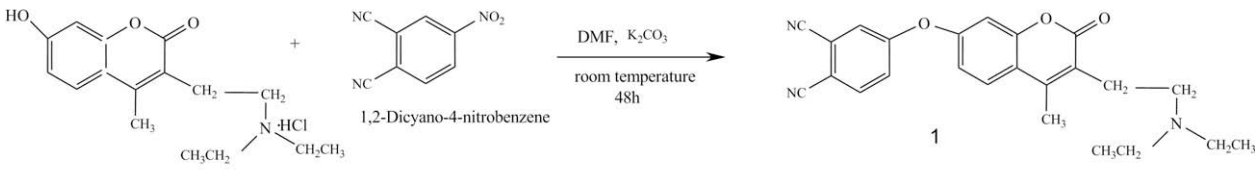

3-[(2-Diethylamino)ethyl]-7-hydroxy-4-methylcoumarin hydrochloride

3-[(2-Diethylamino)ethyl]-7-[(3,4-dicyanophenoxy)]-4-methylcoumarin

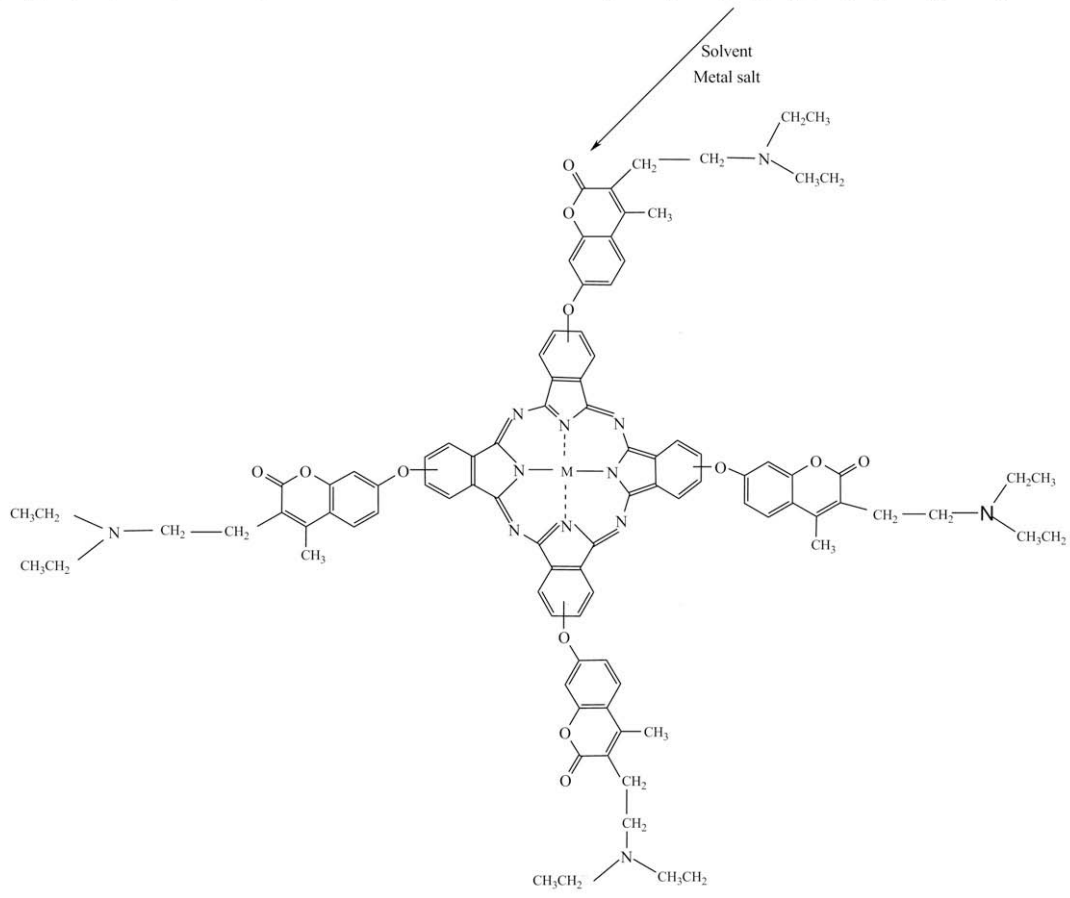

Scheme 1. Synthesis of the starting compounds, metal-free and metallo phthalocyanines.

Inova 500 MHz NMR spectrophotometer using TMS as an internal reference at the Bogazici University Laboratory. Elemental analysis was performed by the Instrumental Analysis Laboratory of TUBITAK Ankara Test and Analysis Laboratory. Mass spectra were performed on a Bruker Daltonic Autoflex MALDI-TOF spectrometer at Marmara University.

1,2-Dicyano-4-nitrobenzene was synthesized according to a reported procedure [16] and 3-[(2-diethylamino)ethyl]-7-hydroxy-4-methylcoumarin hydrochloride was purchased from the Aldrich Chemical Company.

2.1. Synthesis of 3-[(2-diethylamino)ethyl]-7-[(3,4-dicyanophenoxy)]-4-methylcoumarin (*1*)

3-[(2-Diethylamino)ethyl]-7-hydroxy-4-methylcoumarin hydrochloride (0.500 g, 1.60 mmol) and 1,2-dicyano-4-nitrobenzene (0.270 g, 1.60 mmol) were added successively with stirring to dry DMF (10 ml). After stirring for 15 min, finely ground anhydrous K_2CO_3 (0.330 g, 2.40 mmol) was added portionwise over 2 h and the mixture was stirred vigorously at room temperature for a further 48 h. Then the reaction mixture was poured into water (100 ml) and the precipitate that formed was filtered off, and washed with water until neutral. The yellow product (**1**) was obtained in the pure form. The compound is soluble in ethanol, methanol, tetrahydrofuran, chloroform, dichloromethane, dimethylformamide and dimethylsulfoxide.

Compound **1**: Yield: 0.500 g (86%); m.p.: 280–285 °C. IR (KBr) γ_{max} (cm^{-1}): 3074 (aryl CH), 2804–2957 (alkyl CH), 2229 (C≡N), 1704 (C=O lactone), 1589 and 1489 (C=C), 1245 (Ar–O–Ar). ^1H NMR ($CHCl_3$) δ_H (ppm): 7.75 (d, 1H, Ar–H), 7.66 (d, 1H, Ar–H), 7.33 (d, 1H, Ar–H), 7.31 (dd, 1H, Ar–H), 7.01 (d, 1H, Ar–H), 6.97 (dd, 1H, Ar–H), 3.41 (t, 2H, $ArCH_2CH_2$), 2.82 (q, 4H, NCH_2), 2.06 (t, 2H, $ArCH_2$), 2.45 (s, 3H, CH_3), 1.09 (t, 6H, CH_2CH_3). ^{13}C NMR (DMSO) δ_C (ppm): 161.1 (C=O), 153.7 (CH_3–C=C–CH_2), 118.1 (CH_3–C=C–CH_2), 115.3 (CN), 114.8 (CN), 160.7, 155.5, 146.0, 135.8, 126.9, 125.0, 122.4, 122.3, 118.9, 116.2, 110.2, 108.6, 51.0, 47.1, 47.1, 25.2, 15.3 ($ArCH_3$), 12.2, 12.2 ppm. UV–Vis ($CHCl_3$) λ_{max} (log ε) (nm): 320 (4.85). *Anal. Calc.* for $C_{24}H_{23}N_3O_3$: C, 71.82; H, 5.73; N, 10.47. Found: C, 70.64; H, 5.02; N, 10.41%. MS (MALDI-TOF) *m/z*: 401 $[M]^+$, 402 $[M+1]^+$.

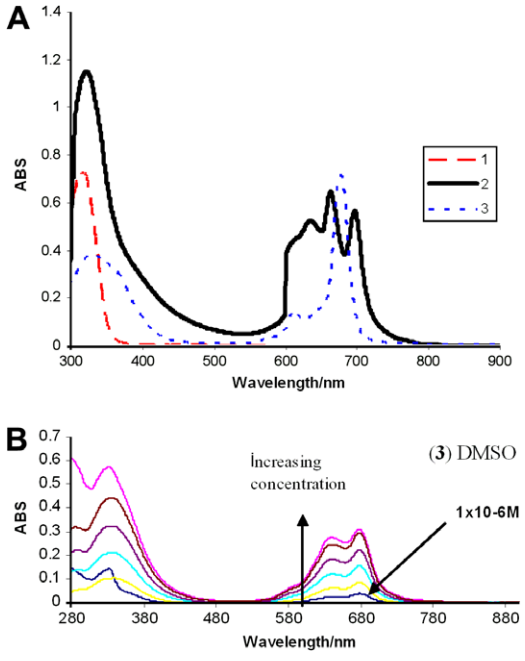

Fig. 2. UV–Vis spectra of **1** in $CHCl_3$ (1×10^{-5} M), **2** in CH_3COOH (1×10^{-5} M), **3** in DMF (1×10^{-5} M) (A), and the effect of increasing concentration on the UV–Vis spectra of 1×10^{-6} mol dm^{-3} **3** in DMSO (B).

2.2. Synthesis of the metal-free and zinc phthalocyanines (*2* and *3*)

2.2.1. Synthesis of 2,9,16,23-tetrakis[7-oxo-(3-[(2-diethylamino)ethyl)]-4-methylcoumarin] phthalocyanine (*2*)

3-[(2-Diethylamino)ethyl]-7-[(3,4-dicyanophenoxy)]-4-methylcoumarin (**1**) (0.050 g, 0.12 mmol) was heated with 2 ml dry 2-*N*,*N*-dimethylaminoethanol in a sealed tube. The mixture was held at 145 °C for 48 h. After cooling to room temperature, the reaction mixture was treated with dilute HCl, then filtered off and washed with water until the filtrate became neutral. The green product was purified by washing with tetrahydrofuran, chloroform, dichloromethane, acetonitrile, acetone, ethylacetate and ether, and the dried. The compound is soluble in acetic acid, dimethylformamide (slightly) and dimethylsulfoxide (slightly).

Compound **2**: Yield: 0.020 g (57%); m.p.: >300 °C. IR γ_{max} (cm^{-1}): 3269 (N–H), 3058 (aryl CH), 2850–2970 (alkyl CH), 1701 (C=O lactone), 1604 (C=C), 1242 (Ar–O–Ar). ^1H NMR (DMSO) δ_H (ppm): 7.0–8.04 (m, 24H, Ar–H), 2.88 (m, 32H, CH_2), 2.45 (s, 12H, CH_3), 1.12 (s, 24H, CH_2CH_3), −2.85 (s, 2H, NH). UV–Vis (CH_3COOH) λ_{max} (log ε) (nm): 707 (3.69), 674 (3.85), 325 (4.95). *Anal. Calc.* for $C_{96}H_{94}N_{12}O_{12}$: C, 71.73; H, 5.85; N, 10.46. Found: C, 70.68; H, 5.22; N, 10.20%. MS (MALDI-TOF) *m/z*: 1606 $[M]^+$, 1607 $[M+1]^+$.

2.2.2. Synthesis of 2,9,16,23-tetrakis[7-oxo-(3-[(2-diethylamino)ethyl)]-4- methylcoumarin] phthalocyaninatozinc (*3*)

A mixture of compound **1** (0.050 g, 0.12 mmol) and $Zn(CH_3COO)_2 \cdot 2H_2O$ (0.007 g, 0.03 mmol) were heated at 160 °C with 2 ml dry 2-*N*,*N*-dimethylaminoethanol in a sealed tube, and stirred for 24 h. After cooling to room temperature, the reaction mixture was treated with ethyl acetate, and the precipitate that formed was filtered off and washed with water to remove unreacted $Zn(CH_3COO)_2 \cdot 2H_2O$. The green product was purified by washing with tetrahydrofuran, chloroform, dichloromethane, acetonitrile, acetone, ethylacetate, ether and then dried. The compound is soluble in dimethylformamide and dimethylsulfoxide.

Compound **3**: Yield: 0.040 g (77%); m.p.: >300 °C. IR γ_{max} (cm^{-1}): 3051 (aryl CH), 2916–2947 (alkyl CH), 1701 (C=O lactone), 1604, 1465 (C=C), 1238 (Ar–O–Ar). UV–Vis (DMF) λ_{max} (log ε) (nm): 679 (4.08), 617 (4.38), 337 (4.56). *Anal. Calc.* for $C_{96}H_{92}N_{12}O_{12}Zn$: C, 69.02; H, 5.51; N, 10.06. Found: C, 68.16; H, 5.59; N, 9.84%. MS (MALDI-TOF) *m/z*: 1669 $[M]^+$, 1670 $[M+1]^+$ (Fig. 1).

2.3. Synthesis of 2,9,16,23-tetrakis[7-oxo-(3-[(2-diethylaminomethyliodide)ethyl)]-4-methylcoumarin] phthalocyaninatozinc (*4*)

To a solution of 2,9,16,23-tetrakis[7-oxo-(3-[(2-diethylamino)-ethyl)]-methylcoumarin]-phthalocyaninatozinc (0.020 g, 0.012 mmol) **(3)** in dry DMSO (10 ml) was added CH_3I (0.017 g, 0.12 mmol). The mixture was stirred vigorously at room temperature for 48 h. Then the reaction mixture was poured into ethylacetate (20 ml) and the precipitate formed was filtered off. The green product was purified by washing with ethylacetate, ethanol, methanol, acetone and tetrahydrofuran. The compound is soluble in DMF, DMSO and water. Yield: 0.015 g (56%); m.p.: >300 °C. IR γ_{max} (cm^{-1}): 3054 (aryl CH), 2920–2964 (alkyl CH), 1704 (C=O lactone), 1603, 1459 (C=C), 1234 (Ar–O–Ar). UV–Vis (DMF) λ_{max} (log ε) (nm): 680 (5.38), 617 (4.64), 330 (5.15). *Anal. Calc.* for $C_{100}H_{104}N_{12}O_{12}ZnI_4$: C, 53.64; H, 4.64; N 7.51. Found: C, 50.26; H, 5.01; N, 6.64%. MS (MALDI-TOF) *m/z*: 2237 $[M]^+$ (Fig. 3).

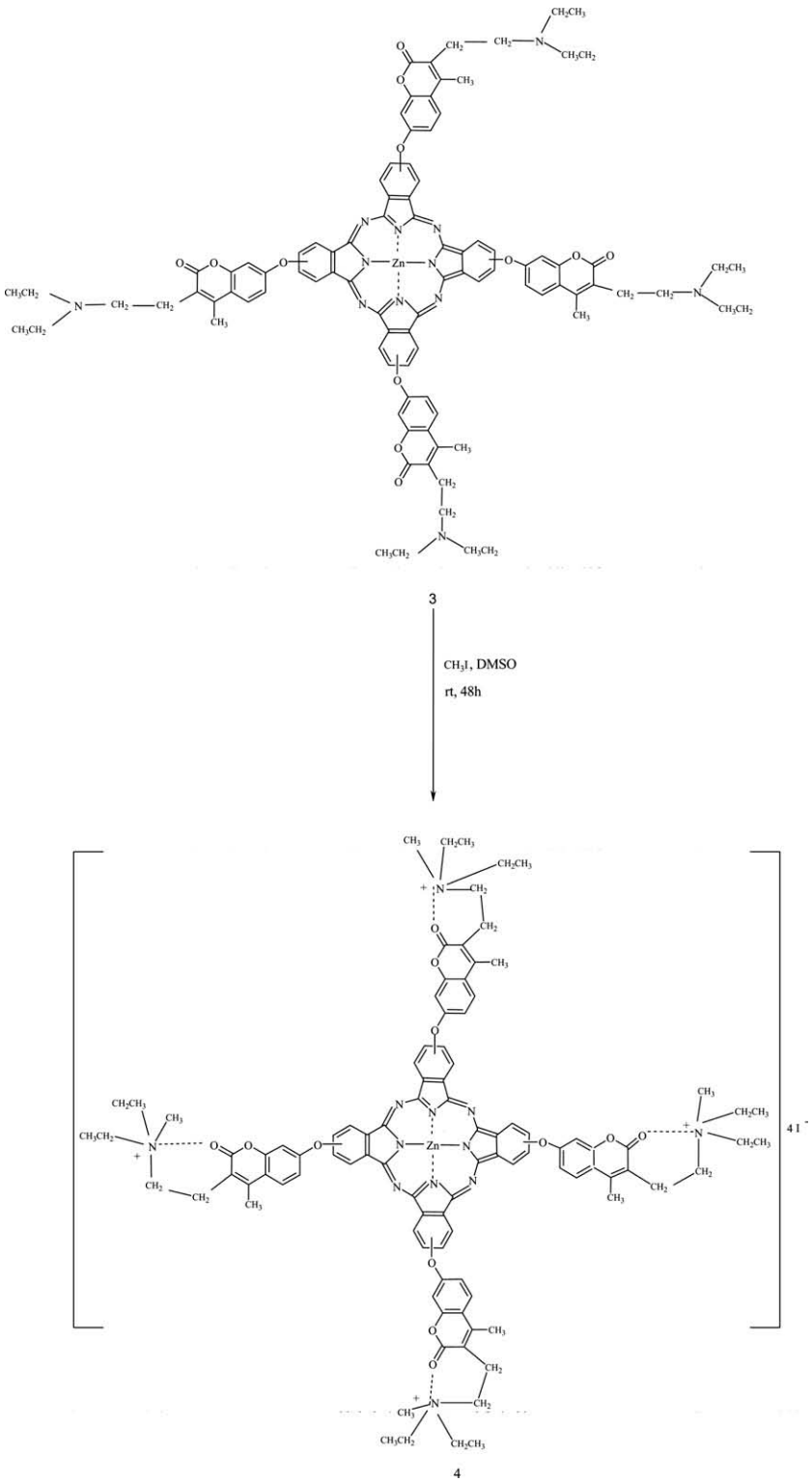

Scheme 2. Synthesis of the phthalocyanine bearing quaternizable coumarin (**4**).

3. Result and discussion

The novel 3-[(2-diethylamino)ethyl]-7-[(3,4-dicyanophenoxy)]-4-methylcoumarin (**1**) was prepared by a base catalyzed nucleophilic aromatic nitro displacement of 1,2-dicyano-4-nitrobenzene with 3-[(2-diethylamino)ethyl]-7-hydroxy-4-methylcoumarin hydrochloride. The reaction was carried out in a single step synthesis by using K_2CO_3 as the nitro-displacing base at room temperature in dimethylformamide under a N_2 atmosphere, and the yield was 86%. Cyclotetramerization of the phthalonitrile derivative (**1**) to the metal-free Pc (**2**) was accomplished in 2-*N*,*N*-dimethylaminoethanol (DMAE) at 145 °C in sealed tube. The Zn Pc (**3**) was obtained from the dicyano derivative (**1**) and the $Zn(CH_3COO)_2 \cdot 2H_2O$ salt in the anhydrous solvent DMAE

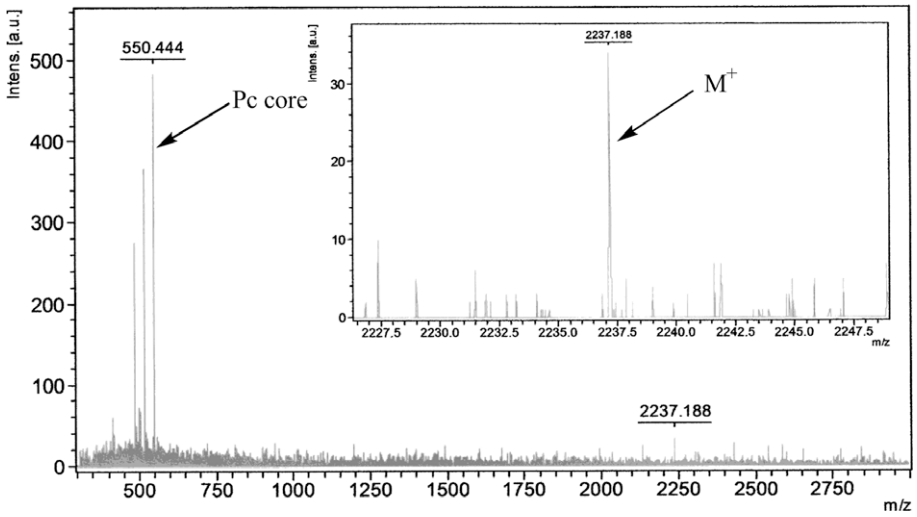

Fig. 3. The positive ion and linear mode MALDI-TOF-MS spectrum of **4** (2237 Da), obtained in 7-hydroxycoumarin (umbelliferone) MALDI matrix, using a nitrogen laser, accumulating 50 laser shots. Inset spectrum shows the expanded molecular mass region of the complex.

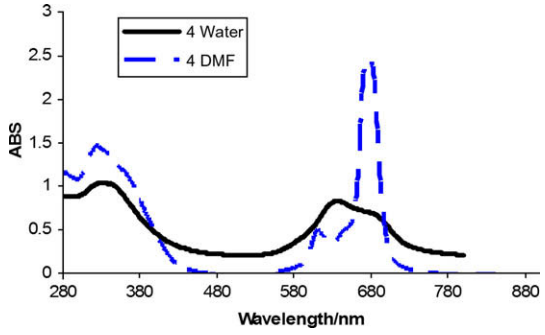

Fig. 4. UV–Vis spectra of **4** in water and DMF (1×10^{-5} M).

(Scheme 1). The tetraoxycoumarin substituted Pc products (**2**,**3**), purified by washing with tetrahydrofuran, acetone, acetonitrile, ethylacetate and ether, are soluble in DMF and DMSO. Characterization of the products involved a combination of methods including elemental analysis, ^{1}H and ^{13}C NMR, UV–Vis and MALDI-TOF spectroscopy.

Spectral data of the newly synthesized compounds are consistent with the proposed structures. The IR spectrum clearly indicates the formation of compound **1**, with the appearance of new absorption bands at 2229 cm^{-1} (C≡N) and 1245 cm^{-1} (Ar–O–Ar). After conversion of the dinitrile derivative (**1**) into the Pcs (**2**,**3**), the sharp peak for the C≡N vibration around 2229 cm^{-1} disappeared. The IR spectra of the metal-free Pc **2** and the zinc complex (**3**) are very similar, with the exception of **2** showing a NH stretching band

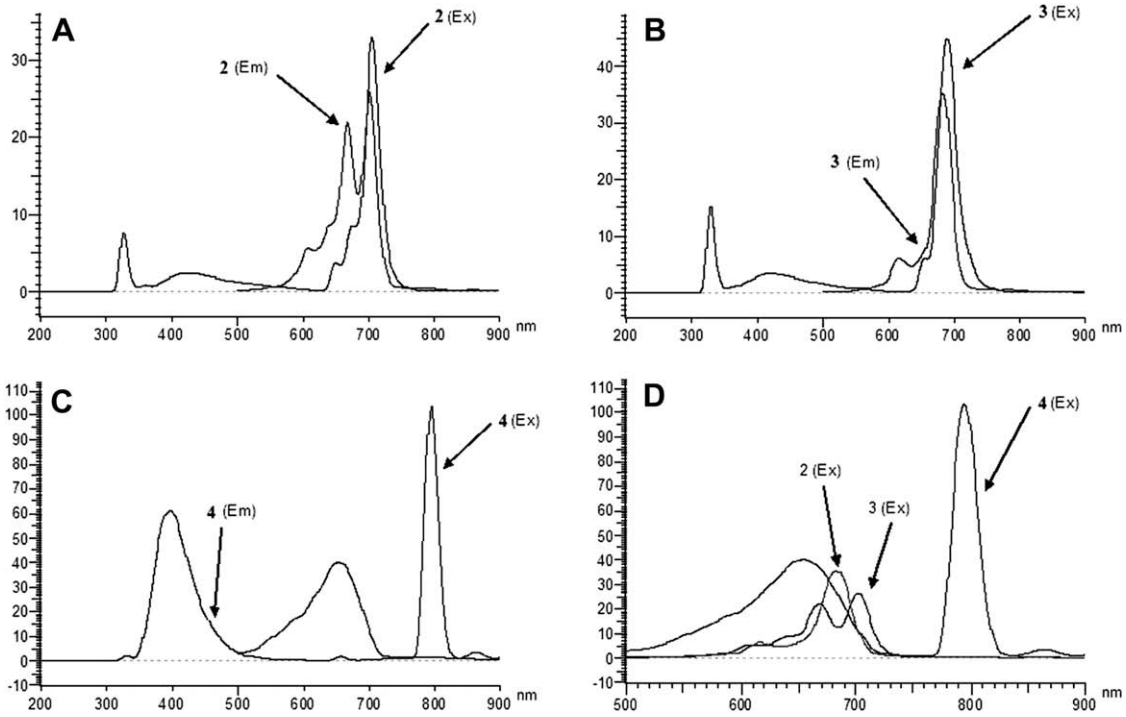

Fig. 5. Excitation and emission spectra of compound **2** (A), compound **3** (B) in DMF, compound **4** (C) in water and all the complexes overlapped (6×10^{-6} M).

due to the inner core. These bands were absent from the spectra of the complexes. The NH group of the metal-free Pc (**2**) in the inner core gave a weak absorption peak at 3269 cm^{-1}. The C=O and C=C bands for the Pcs in the IR spectra were broader and shorter than those of **1** because of H-type aggregation of the coumarin moiety.

The ^1H NMR spectrum of **1** was almost identical except for small shifts; The ^1H NMR spectrum exhibited aromatic protons at 7.75, 7.66, 7.33, 7.31, 7.01 and 6.97 ppm and methyl protons at 2.45 ppm. The ^{13}C NMR data are accord with the expected structure. The ^{13}C NMR spectrum of compound **1** indicate nitrile carbons at 115.3 and at 114.8 ppm, and the carbonyl carbon of the lactone ring appears at 161.1 ppm for **1**.

The ^1H NMR spectrum of Pc **2** was as expected . A common feature of this spectrum is the broad absorptions caused by the aggregation of the Pc. The NH protons of the metal-free Pc (**2**) were also identified in the ^1H NMR spectrum with a broad peak at $\delta = -2.85$ ppm, and the signals disappeared after the addition of D_2O.

A closed investigation of the mass spectra of the Pcs confirmed the proposed structures. In the mass spectra of the compounds, the [M^+] peaks were identified easily, as is shown as an example in Fig. 1 for **3**. The MALDI-TOF-MS spectra provided definitive characterization of the structures of all complexes. The linear mode positive ion MALDI mass spectra could be obtained in 7-hydroxycoumarin (umbelliferone) MALDI matrix. The protonated molecular ion peaks of the complexes were observed at 401 Da for **1**, 1606 Da for **2**, 1669 Da for **3** and 2237 Da for **4**. These mass values overlapped with the theoretical calculated mass values for the molecular ions of all the complexes.

The coumarins show maximum absorption with a single band at 310 nm. The UV–Vis spectrum of **1** in $CHCl_3$ showed a band at 320 nm (Fig. 2). Pcs **2** and **3** show typical electronic spectra with two strong absorption regions, a typical spectrum of the metal-free Pc (**2**) in acetic acid showed a doublet in the Q band region at 707 and 674 nm, and a B band region at 325 nm; while the ZnPc (**3**) each gave an intense Q band at 679 and 617 nm and a B band region at 337 nm. The UV–Vis spectrum of **3** in DMSO is remarkably different from that in DMF. The spectra of **3** in DMF and DMSO are shown in Fig. 2A and B. As shown in Fig. 2B for **3**, the appearance of a new band around 643 nm, at the blue side of the main Q band absorption, in DMSO suggests clearly the presence of aggregated species. Aggregation is usually depicted as a coplanar association and is strongly dependent on the concentration and nature of the solvent. Fig. 2B indicates the effect of increasing concentration on the UV–Vis spectra of 1×10^{-6} mol dm^{-3} **3** in DMSO, as an example. At the beginning (for 1×10^{-6} mol dm^{-3} **3**), the intensities of the two bands are approximately equal to each other. As the concentration of **3** is increased, the band with the lower wavelength becomes more intense than the other band.

2,9,16,23-Tetrakis[7-oxo-(3-[(2-diethylaminomethyliodide) ethyl)]-4-methylcoumarin]-phthalocyaninatozinc (**4**), bearing quaternizable coumarin, was synthesized from 2,9,16,23-tetrakis[7-oxo-(3-[(2-diethylamino)ethyl)]-methylcoumarin]-phthalocyaninatozinc (**3**) by methylation with CH_3I. The product (**4**) shows good solubility in solvents such as DMF, DMSO and water (Scheme 2). The mass spectra of **4** confirmed the proposed structure, with the molecular ion being easily identified at 2237 [M^+] (Fig. 3).

A typical UV-spectrum of 2,9,16,23-tetrakis[7-oxo-(3-[(2-diethylaminomethyliodide)ethyl)]-4-methylcoumarin]-phthalocyaninatozinc (**4**) in DMF showed a Q band at 680 nm and a B band at 330 nm (Fig. 4). The shoulder of **4** registered at 617 nm. The UV–Vis spectrum of **4** in water is different from that in DMF. Typical spectra of **4** in DMF and water are shown in Fig. 4. The appearance of a new band around 639 nm at the blue side of the main Q band absorption in water suggests clearly the presence of aggregated species.

Fig. 5 shows the fluorescence emission and excitation spectra for complexes **2**, **3** and **4** in DMF (for **2** and **3**) and in water (**4**). Fluorescence emission peaks were observed at: 709 nm for **2**, 700 nm for **3** and 693 nm for **4**. The excitation spectra were similar to the absorption spectra and both were mirror images of the fluorescent spectra in DMF for complexes **2** and **3**, and in water for **4**. For complex **4** in water, an excitation peak was indicated, which shifted to a more longer wavelength than the emission peak (red shifted), because of α,β-electron delocalization over the carbonyl oxygen of the lactone ring up to the nitrogen cation (Scheme 2).

Acknowledgements

We are thankful to the Scientific and Research Council of Turkey (TUBITAK) (107T347) and the Research Found of Marmara University, Commission of Scientific Research Project FEN-C-YLP-030408-0081.

References

[1] (a) V.B. Fiedler, J.J. Scholtholt, Pharm. Col. Exp. Ther. 217 (1981) 306;
(b) D. Opherk, G. Schuler, W. Waas, R. Dietz, W. Kubler, Eur. Heart J. 11 (1990) 342.
[2] (a) F.H. Moser, A.L. Thomas, in: A.L. Thomas (Ed.), The Phthalocyanines Properties, vol. 1, CRC, Boca Raton, Florida, 1983, p. 79;
(b) N.B. Mc Keown, in: B. Dunn, J.W. Goodby, A.R. West (Eds.), Phthalocyanine Material Synthesis Structure and Function, vol. 5, Cambridge University Press, Cambridege, 1998, p. 101.
[3] (a) D. Wöhrle, G. Meyer, Kontakte (1985) 338;
(b) D. Wöhrle, Kontakte 1 (1986) 24.
[4] (a) R.D.H. Murray, J. Mendez, S.A. Brown, The Natural Coumarins Occurrence Chemistry and Biochemistry, Wiley & Sons, New York, 1982;
(b) A. Banrji, B. Mallick, A. Chatterjee, H. Budzikiewicz, M. Breuer, Tetrahedron Lett. 29 (1988) 1557;
(c) R. O'Kennedy, R.D. Thornes, Coumarins Biology Applications and MADE of Action, Wiley & Sons, Chichester, 1997.
[5] P. Tiew, J.R. Ioset, U. Kokpal, W. Chavasir, K. Hostettmam, Phytother. Res. 17 (2003) 190.
[6] L.K. Jurd, K. Mihara, Phytochemistry 10 (1971) 2965.
[7] S.M. Seshadri, K. Horita, R.G. Micetich, S. Nishibe, M. Daneshtalab, Bioorg. Med. Chem. 7 (1999) 1933.
[8] M. Mazze, R. Dondero, E. Sottotattari, E. Melloni, R. Minafra, Eur. J. Med. Chem. 36 (2001) 851.
[9] V.R.R. Kasinadhuni, G. Rajashekbar, R. Rajogopalan, V.M. Sharma, C.V. Krishna, P. Sairam, G.S. Prasad, S. Sadhukhan, G.G. Rao, Fitoterapia 70 (1999) 93.
[10] (a) N. Mala, J. Ruchi, E. George, S. Xueqing, K. Ashok, J. Organomet. Chem. 690 (2005) 134;
(b) N. Mala, J. Ruchi, E. George, S. Xueqing, K. Ashok, Spectrochim. Acta Part A 61 (2005) 3155.
[11] (a) D. Yu, M. Suzuki, L. Xie, S.L. Morris-Natschke, K.H. Lee, Med. Res. Rev. 23 (2003) 322;
(b) R.D.H. Murray, J. Mendez, S.A. Brown, The Natural Coumarins, Wiley, Chichester, UK, 1982.
[12] P.T. Kaye, M.A. Musa, A.T. Nichinda, X.W. Nocanda, Communication 34 (2004) 2575.
[13] M. Hanack, H. Heckmann, R. Polley, in: E. Schaumann (Ed.), Methods of Organic Chemistry (Houben Wcyl), George Thieme, Stuttgant, 1998, p. 717.
[14] (a) H.R.P. Karaoğlu, A. Gül, M.B.K. Kocak, Dyes Pigments 76 (2008) 231;
(b) H.A. Dincer, A. Koca, A. Gül, M.B. Koçak, Dyes Pigments 75 (2008) 825;
(c) Z.A. Bayır, Dyes Pigments 6 (2005) 235.
[15] (a) A.A. Esenpınar, M. Bulut, Dyes Pigments 76 (2008) 249;
(b) M. Çamur, M. Bulut, Dyes Pigments 77 (2008) 165.
[16] J.G. Young, W. Onyebuagu, J. Org. Chem. 55 (1990) 2155.
[17] D. Wrobel, A. Boguta, J. Photochem. Photobiol. A: Chem. 150 (2002) 67.
[18] (a) M.N. Yarasır, M. Kandaz, A. Koca, B. Salih, Polyhedron 26 (2007) 1139;
(b) M. Çamur, A.R. Özkaya, M. Bulut, Polyhedron 26 (2007) 2638;
(c) N. Sheng, R. Li, C. Choi, W. Su, D.K.P. Cui, X. Ng, K. Yoshida, N. Kobayashi, J. Jiang, Inorg. Chem. 45 (2006) 3794.

2. Results and discussion

2.1. Preparation of complexes

Copper(II) complexes **1** and **3** were obtained by a reaction of copper(II) sulfate with 6-methylpicolinic or 6-bromopicolinic acid, respectively, in mildly alkaline aqueous solution. Both **1** and **3** can be prepared as well in highly acidic solutions (pH = 1) without the addition of the base, but with smaller yields and rates of formation due to the lower concentration of anionic form of ligands in the acidic solutions. The same thing was observed during the synthesis of copper(II) complex with 3-methylpicolinic acid, $[Cu(3\text{-}Mepic)_2] \cdot 2H_2O$ [31]. Thus, the pH value of the reaction solution does not influence on the type of the complexes formed, but it affects their formation rates, leading to the slower crystallization and, eventually, to smaller yields in the case of lower pH values. Slow evaporation of the pyridine solution of **1** leads to the formation of **2** by replacing the coordinated water molecule in **1** with the coordinated pyridine molecule.

All isolated complexes **1**–**3** are air-stable, blue crystalline substances, less soluble in water and alcohols, but well soluble in solvents with pronounced donor properties (such as DMF, DMSO, pyridine and 4-picoline).

2.2. Structural description of *1*

ORTEP-3 view of the molecular structure of **1** is depicted in Fig. 1a and its crystal structure in Fig. 2a. The selected molecular

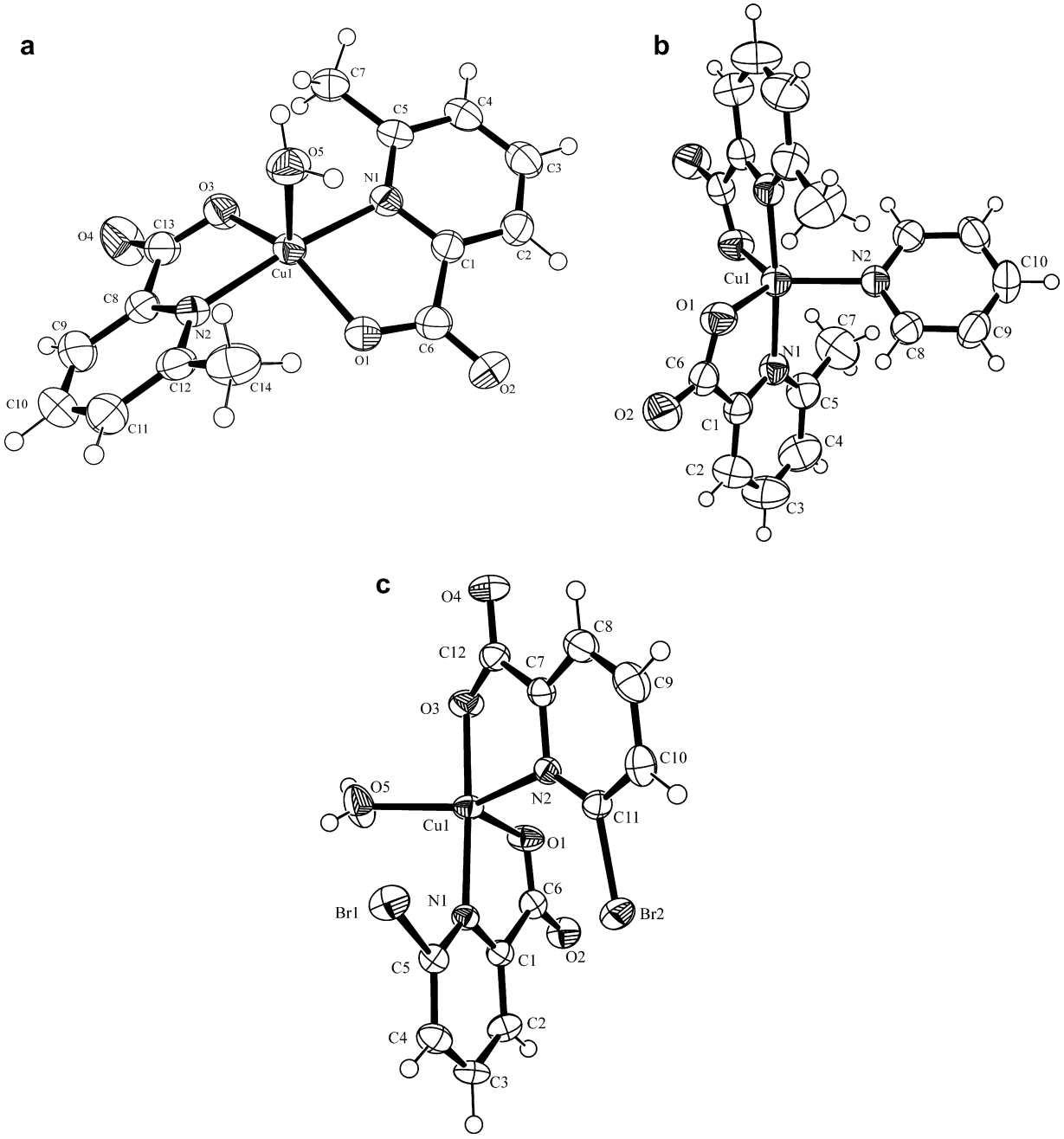

Fig. 1. ORTEP-3 drawing of (a) $[Cu(6\text{-}Mepic)_2(H_2O)]$ (**1**), (b) $[Cu(6\text{-}Mepic)_2(py)]$ (**2**) and (c) $[Cu(6\text{-}Brpic)_2(H_2O)]$ (**3**) with the atomic numbering scheme of the asymmetric unit. The thermal ellipsoids are drawn at the 50% probability level at 296 K.

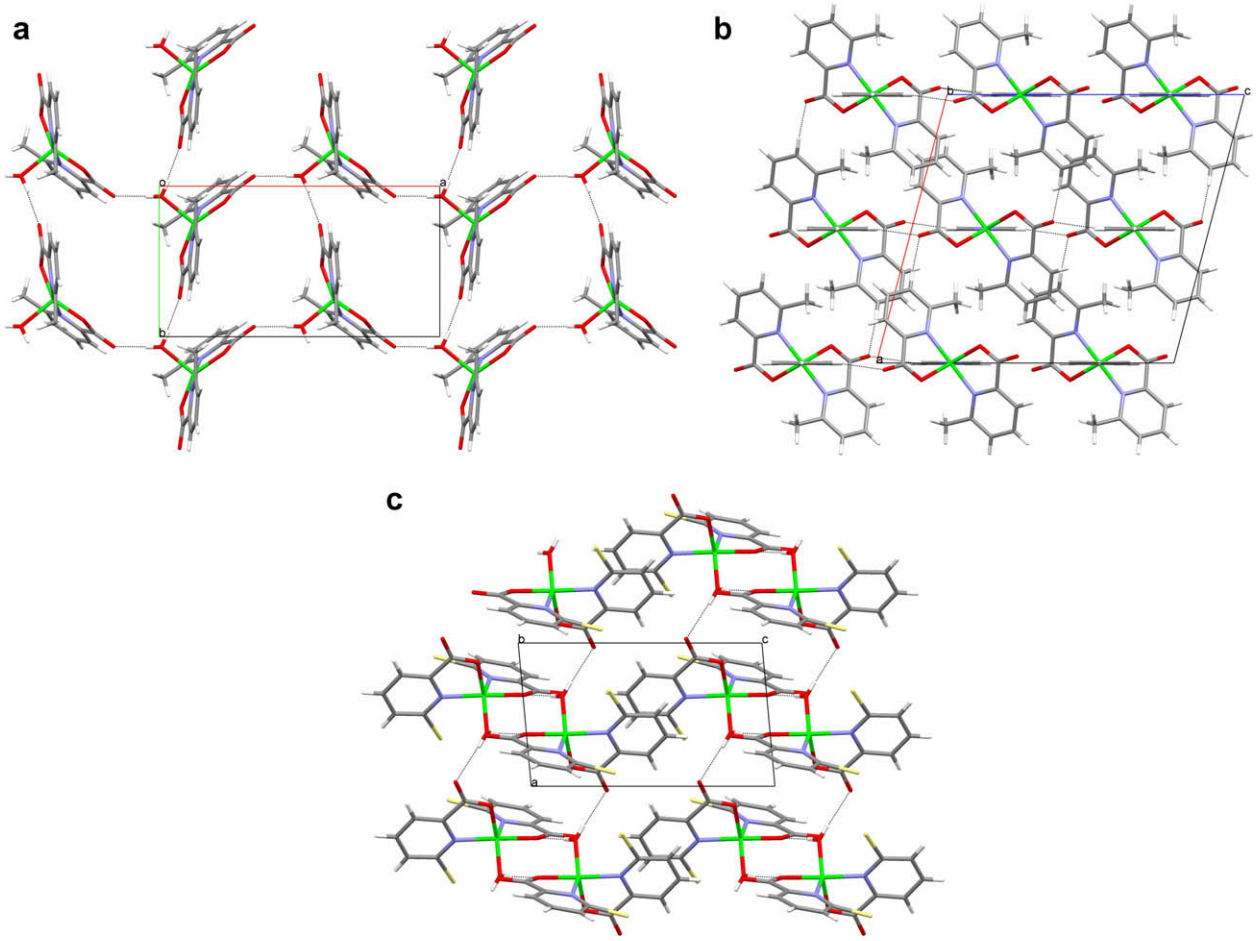

Fig. 2. (a) A view of the crystal packing of $[Cu(6\text{-Mepic})_2(H_2O)]$ (**1**) in *ab* plane, showing molecules linked into a two-dimensional network by hydrogen bonds of the O–H···O type, represented by dotted lines. (b) A view of the crystal packing of $[Cu(6\text{-Mepic})_2(py)]$ (**2**) in *ac* plane, showing a part of the three-dimensional structure. Intermolecular hydrogen bonds of C–H···O type are represented by dotted lines. (c) A view of the crystal packing of $[Cu(6\text{-Brpic})_2(H_2O)]$ (**3**) in *ac* plane, showing centrosymmetric dimers linked into chains in a [100] direction by hydrogen bonds of the O–H···O type (represented by dotted lines). Chains are mutually assembled in a [001] direction by π···π stacking interaction between pyridine rings defined by atoms N1/C1/C2/C3/C4/C5.

geometry parameters are listed in Table 1 and hydrogen bond geometry in Table 2.

The copper(II) ion in **1** is coordinated by two 6-methylpicolinato ligands which are both bound in a bidentate *N*,*O*-chelated mode, forming a five-membered chelate ring, and by one water molecule (Fig. 1a). The geometry around this pentacoordinated copper(II) ion can be best described as an intermediate between a square pyramid and a trigonal bipyramid since $\tau = 0.45[\tau = (\alpha - \beta)/60°$ (α and β are the largest angles), 0 for the ideal square pyramid, 1 for the ideal trigonal bipyramid] [32].

The dihedral angle between the least squares calculated planes through the atoms of pyridine ring (N1/C1/C2/C3/C4/C5) and the corresponding five-membered chelate ring (Cu1/N1/C1/C6/O1) is 2.0(1)°, while the analogous angle (between planes defined by atoms N2/C8/C9/C10/C11/C12 and Cu1/N2/C8/C13/O3) is 7.7(1)°.

The crystal packing of **1** is controlled by two intermolecular hydrogen bonds of the O–H···O type, while an additional weak intramolecular hydrogen bond of the C–H···O type [33–35] is also present (Fig. 2a and Table 2). Molecules of **1** are linked by the intermolecular O–H···O hydrogen bonds into a two-dimensional network in *ab* plane (Fig. 2a). These networks are mutually assembled in a [001] direction only by the π···π stacking interaction [36] between the pyridine rings defined by atoms N2/C8/C9/C10/C11/C12 (centroid–centroid distance 3.652(1) Å, dihedral angle 0°, slippage 0.959 Å, slip angle 15.2°, symmetry code $-x$, $1-y$, $-z$), forming a three-dimensional supramolecular architecture.

There is one more π···π stacking interaction [36] between the pyridine rings defined by atoms N1/C1/C2/C3/C4/C5 (centroid–centroid distance 3.625(1) Å, dihedral angle 0°, slippage 1.094 Å, slip angle 17.6°, symmetry code $1/2-x$, $1/2-y$, $1/2-z$) and an intermolecular interaction between five-membered chelate ring defined by atoms Cu1/N1/C1/C6/O1 and pyridine ring (N1/C1/C2/C3/C4/C5) (centroid–centroid distance 3.683(1) Å, dihedral angle 2.0(1)°, slip angle 20.3°, symmetry code $1/2-x$, $1/2-y$, $1/2-z$).

2.3. Structural description of **2**

ORTEP-3 view of the molecular structure of **2** is depicted in Fig. 1b and its crystal structure in Fig. 2b. The selected molecular geometry parameters are listed in Table 1 and hydrogen bond geometry in Table 2.

Copper(II) ion in **2** is situated on a twofold symmetry axis and its coordination environment can be described as a distorted trigonal bipyramid since $\tau = 0.87$. The equatorial plane of the pyramid is defined by two carboxylato O atoms from two 6-methylpicolinato ligands and one pyridine N atom from coordinated pyridine molecule. The axial positions are occupied by two pyridine N atoms from two 6-methylpicolinato ligands which are both bound to

Table 1
Selected bond distances (Å) and angles (°) for [Cu(6-Mepic)$_2$(H$_2$O)] (**1**), [Cu(6-Mepic)$_2$(py)] (**2**) and [Cu(6-Brpic)$_2$(H$_2$O)] (**3**)

1		**2**		**3**	
Bond distances					
Cu1–N1	2.022(2)	Cu1–N1	2.005(1)	Cu1–N1	1.986(2)
Cu1–N2	2.016(2)	Cu1–N2	2.085(2)	Cu1–N2	2.142(2)
Cu1–O1	1.960(2)	Cu1–O1	2.009(1)	Cu1–O1	2.070(2)
Cu1–O3	1.955(2)			Cu1–O3	1.910(2)
Cu1–O5	2.221(2)			Cu1–O5	2.013(2)
Bond angles					
O3–Cu1–O1	145.9(1)	N1–Cu1–O1	82.3(1)	O3–Cu1–N1	176.7(1)
O3–Cu1–N2	81.9(1)	N1–Cu1–O1^{i}	94.6(1)	O3–Cu1–O5	86.5(1)
O1–Cu1–N2	93.5(1)	N1–Cu1–N2	93.0(1)	N1–Cu1–O5	90.7(1)
O3–Cu1–N1	98.1(1)	O1–Cu1–N2	120.8(1)	O3–Cu1–O1	98.1(1)
O1–Cu1–N1	82.3(1)	N1–Cu1–N1^{i}	174.0(1)	N1–Cu1–O1	81.4(1)
N2–Cu1–N1	172.6(1)	O1^{i}–Cu1–O1	118.4(1)	O5–Cu1–O1	111.2(1)
O3–Cu1–O5	110.7(1)			O3–Cu1–N2	81.2(1)
O1–Cu1–O5	103.4(1)			N1–Cu1–N2	102.1(1)
N2–Cu1–O5	95.3(1)			O5–Cu1–N2	139.6(1)
N1–Cu1–O5	91.7(1)			O1–Cu1–N2	108.6(1)

Symmetry code (i) $-x, y, 1/2 - z$.

Table 2
Hydrogen bond geometry (Å, °) for [Cu(6-Mepic)$_2$(H$_2$O)] (**1**), [Cu(6-Mepic)$_2$(py)] (**2**) and [Cu(6-Brpic)$_2$(H$_2$O)] (**3**)

D–H···A	D–H	H···A	D···A	∠DHA	Symmetry code
(***1***)					
O5–H15O···O2	0.85(3)	1.94(3)	2.783(3)	176(3)	$x - 1/2, -y, z$
O5–H25O···O4	0.85(3)	1.91(3)	2.751(2)	170(3)	$x, y - 1, z$
C14–H14A···O1	0.96	2.26	3.082(3)	143.0	
(***2***)					
C4–H4···O2	0.93	2.52	3.425(3)	166.0	$x + 1/2, y + 1/2, z$
C8–H8···O2	0.93	2.31	3.200(2)	159.0	$-x, -y, 1 - z$
C9–H9···O2	0.93	2.59	3.435(2)	151.0	$x, y + 1, z$
(***3***)					
O5–H15O···O2	0.73(3)	2.02(3)	2.748(3)	172(3)	$x - 1, y, z$
O5–H25O···O3	0.79(4)	1.98(3)	2.764(3)	177(4)	$1 - x, 1 - y, -z$
C2–H2A···O2	0.93	2.43	3.213(3)	142.0	$2 - x, 1 - y, 1 - z$
C3–H3···O4	0.93	2.49	3.251(3)	139.0	$x, y, z + 1$
C10–H10···O2	0.93	2.38	3.304(3)	170.0	$x, y - 1, z$

the copper(II) ion in a bidentate *N*,*O*-chelated mode forming a five-membered chelate ring (Fig. 1b).

The dihedral angle between the least squares calculated planes through the atoms of pyridine ring (N1/C1/C2/C3/C4/C5) and the corresponding five-membered chelate ring (Cu1/N1/C1/C6/O1) is 4.4(1)°.

There are three weak intermolecular hydrogen bonds of the C–H···O type [33–35] in the crystal packing of **2** (Fig 2b and Table 2) which assemble molecules of **2** into a three-dimensional supramolecular architecture.

2.4. Structural description of *3*

ORTEP-3 view of the molecular structure of **3** is depicted in Fig. 1c and its crystal structure in Fig. 2c. The selected molecular geometry parameters are listed in Table 1 and hydrogen bond geometry in Table 2.

The copper(II) ion in **3** is coordinated by two 6-bromopicolinato ligands which are both bound in a bidentate *N*,*O*-chelated mode, forming a five-membered chelate ring, and by one water molecule (Fig. 1c). The coordination environment around this pentacoordinated copper(II) ion can be described as an intermediate between a trigonal bipyramid and a square pyramid since $\tau = 0.62$.

The dihedral angle between the least squares calculated planes through the atoms of pyridine ring (N1/C1/C2/C3/C4/C5) and the corresponding five-membered chelate ring (Cu1/N1/C1/C6/O1) is 0.9(1)°, while the analogous angle (between planes defined by atoms N2/C7/C8/C9/C10/C11 and Cu1/N2/C7/C12/O3) is 7.8(1)°.

The crystal packing of **3** is dominated by two intermolecular hydrogen bonds of the O–H···O type, while three weak intermolecular hydrogen bonds of C–H···O type [33–35] are also present (Fig. 2c and Table 2). Molecules of **3** are linked into centrosymmetric dimers by two O5–H25O···O3 hydrogen bonds. These dimers are further connected into an infinite chain in [100] direction by O5–H15O···O2 hydrogen bond. The chains are mutually assembled in [010] direction only by weak interactions such as C10–H10···O2 hydrogen bond and π···π stacking interaction [36] between pyridine rings defined by atoms N2/C7/C8/C9/C10/C11 (centroid–centroid distance 3.677(2) Å, dihedral angle 0°, slippage 1.431 Å, slip angle 22.9°, symmetry code $2 - x, -y, -z$), forming a layer in *ab* plane (Fig. 2c). The layers are assembled together in a [001] direction by weak C2–H2A···O2 and C3–H3···O4 hydrogen bonds and by π···π stacking interaction [36] between pyridine rings defined by atoms N1/C1/C2/C3/C4/C5 (centroid–centroid distance 3.678(2) Å, dihedral angle 0°, slippage 1.281 Å, slip angle 20.4°, symmetry code $1 - x, 1 - y, 1 - z$), forming a three-dimensional supramolecular architecture.

2.5. Vibrational spectroscopy

Infrared spectroscopy data for **1**, **2** and **3** confirm the coordination of 6-methylpicolinato ligand to copper(II) ion in **1** and **2** and the coordination of 6-bromopicolinato ligand to copper(II) ion in **3** *via* the carboxylate group. Tentative assignments for the origin of the bands in the spectra are based on those found in the literature for cobalt complex with 6-methylpicolinic acid [25] and for complexes of 3-hydroxypicolinic acid [13,37], especially the ones with copper(II) [14]. In the spectra of **1**, **2** and **3**, the band associated to the asymmetric stretching vibrational mode, $\nu_{asym}(-COO^-)$, appears at 1651 cm^{-1} (**1**), 1641 cm^{-1} (**2**) and 1631 and 1683 cm^{-1} (**3**), together with the $\nu_{sym}(-COO^-)$ band at 1365 cm^{-1} (**1**), 1355 cm^{-1} (**2**) and 1335 and 1371 cm^{-1} (**3**). The measured value of $\Delta(\nu_{asym}(-COO^-) - \nu_{sym}(-COO^-))$ amounts 286 cm^{-1} for both **1** and **2**, and 304 cm^{-1} (average Δ value) for **3**, indicating the presence of carboxylato group coordinated to copper(II) ion in the unidentate mode [14,38,39], which is in agreement with the crystal structures of **1**, **2** and **3**. The typical stretching ν(C–N) vibrational mode of substituted pyridines appears for the uncoordinated 6-methylpicolinato ligand at 1612 cm^{-1} and shows shifts (9 cm^{-1} for **1** and 10 cm^{-1} for **2**) to lower wave numbers. These shifts are in a good agreement with *N*,*O*-chelation (involving the endocyclic nitrogen atom of 6-methylpicolinato ligand) proposed for both **1** and **2**. The broad absorption band at 3407 cm^{-1} (**1**) and 3217 cm^{-1} (**3**) indicates hydrogen bonds involving coordinated water molecule present in **1** and **3** [39].

2.6. EPR spectroscopy

The EPR spectrum of **1** shows one copper(II) spin $S = ½$ signal. The signal is weakly resolved and may be related to an elongated axial symmetry of the coordination sphere ($g_{\perp(x,y)} = 2.09$, $g_{\parallel(z)} = 2.21$, Fig. 3). This is in agreement with a distorted square-pyramidal environment around copper(II) (which is very close to the intermediate between trigonal bipyramid and square pyramid) in **1**, suggesting the $\{d_{x^2-y^2}\}^1$ ground state.

The spectrum of **2** reveals one almost isotropic symmetry signal with $g_{av} = 2.16$. This agrees with the same range of lengths for all five coordination bonds to the central copper(II) ion (Cu–O,N 2.005(1)–2.085(2) Å). The determination of the complex ground state is thus not clearcut.

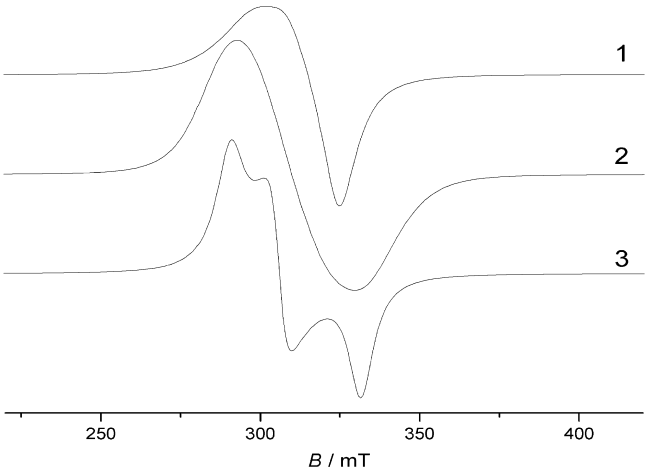

Fig. 3. The EPR spectra of $[Cu(6\text{-}Mepic)_2(H_2O)]$ (**1**), $[Cu(6\text{-}Mepic)_2(py)]$ (**2**) and $[Cu(6\text{-}Brpic)_2(H_2O)]$ (**3**), showing three different types of copper(II) $S = ½$ symmetry signals (**1** – elongated axial, **2** – isotropic, **3** – rhombic).

The spectrum of **3** shows three distinctive signals of the rhombic symmetry with $g_1 = 2.01$, $g_2 = 2.18$ and $g_3 = 2.29$ (Fig. 3). Due to the $g_1 \ll g_2 < g_3$ and $g_1 \sim g_e$, the possibility of the $\{d_{z^2}\}^1$ ground state may be assumed for this complex [40]. The distorted axially compressed trigonal-bipyramidal coordination sphere (which is very close to the intermediate between trigonal bipyramid and square pyramid) in **3** is also in favour of the $\{d_{z^2}\}^1$ ground state, instead of the $\{d_{x^2-y^2}\}^1$, more commonly observed for copper(II) $S = ½$.

2.7. Thermal analysis (TGA/DTA)

Compound **1** is thermally stable up to 150 °C. One water molecule was released in a step with an endothermic peak at 193.5 °C (observed weight loss 5.1%, calculated 5.1%). The thermal decomposition of **1** continues through step with an endothermic peak at 270.3 °C, corresponding to the release of both 6-methylpicolinato ligands (61.3%). The observed residue (33.6%) at 600 °C corresponds to CuO.

Compound **2** is thermally stable up to 130 °C. One pyridine molecule was evolved in a step with an endothermic peak at 155.3 °C (observed weight loss 18.8%, calculated 19.1%). The thermal decomposition of **2** finishes with a step with an endothermic peak at 279.1 °C, corresponding to the release of both 6-methylpicolinato ligands (53.5%). The observed residue (27.7%) at 600 °C corresponds to CuO.

Compound **3** is thermally stable up to 190 °C. One water molecule (observed weight loss 5.0%, calculated 3.7%) and one 6-bromopicolinato ligand (observed weight loss 41.2%, calculated 41.6%) were evolved in a cumulative step with an endothermic peak at 226.2 °C. The further step of the decomposition (22.2%) occurs in the wide temperature range of 310–600 °C and results with the complete decomposition of **3**. The observed residue (31.6%) at 600 °C corresponds to CuO.

2.8. Magnetic measurements

The susceptibility measurements for the complexes **1** and **2** reveal constant $\chi_M \cdot T$ values of 0.42 cm^3 K/mol in the temperature range of 2–300 K suggesting paramagnetic behaviour of both complexes. Differently for **3**, a significant decrease of $\chi_M \cdot T$ appears below 100 K, revealing an antiferromagnetic interaction. The structure of **3** shows a mononuclear molecule, as found also for **1** and **2**. Therefore, the magnetic interaction takes place *via* an alternative path, either through hydrogen bonding (Table 2) or π···π stacking interaction. The hydrogen bonds are connecting the mononuclear units into chains (O5–H15O···O2), as well as into binuclear units (O5–H25O···O3), while π···π stacking into binuclear units (*via* two N1 rings or two N2 rings). To estimate the magnitude of the antiferromagnetic coupling, the magnetic susceptibility data were fitted to the Bleaney-Bowers equation (Eq. (1)) for two interacting copper(II) ions with the Hamiltonian in the form $H = -2J\ S_1 \cdot S_2$ [41]. The least-squares fitting of the data with Eq. (1) leads to $2J = -7.2\ cm^{-1}$, $g = 2.19$, $\rho = 0.035$ (residual paramagnetic contribution) and the theoretical curve using the above parameters is shown as a solid line in Fig. 4. On the other hand, the fitting with the Bonner-Fisher model [41] for 1D chain showed significantly less successful fit with the experimental data. Therefore, the origin for the antiferromagnetic interaction is suggested to be an intradinuclear (e.g. $[Cu(6\text{-}Brpic)_2(H_2O)]_2$) and not within the chain (e.g. $[Cu(6\text{-}Brpic)_2(H_2O)]_n$). Due to the mononuclear coordination moieties in **3**, with no coordination bridges between the Cu(II) species, the alternative or pseudobinuclear units may be suggested. One option for the intradinuclear bridging is by two H-bonds (Cu–O3···H25O–O5–Cu′ and vice versa), but that path may not be appropriate due to the water O5 atom in the equatorial

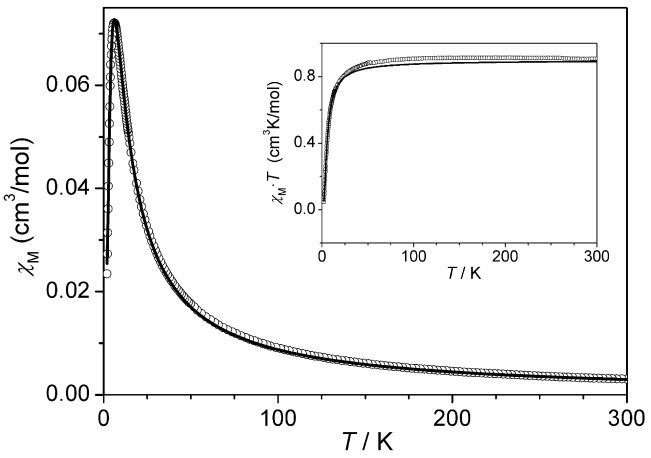

Fig. 4. χ_M and $\chi_M T$ (inset) vs. T experimental (○) and fitted (solid line) curves for $[Cu(6\text{-}Brpic)_2(H_2O)]$ (**3**). Parameters for the Bleaney-Bowers equation of the binuclear moiety are: $2J = -7.2\ cm^{-1}$, $g = 2.19$, $\rho = 0.035$.

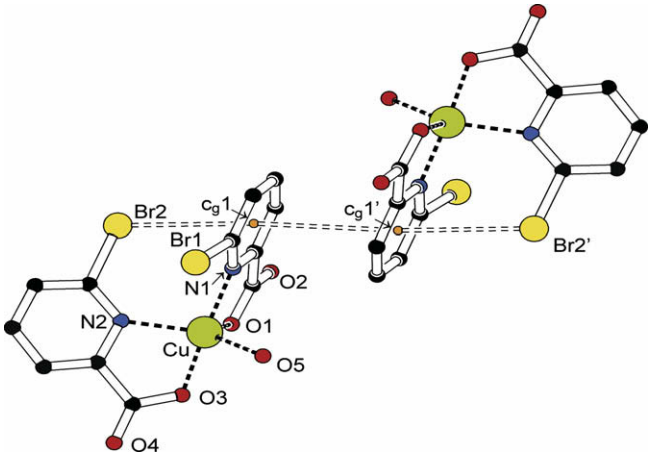

Fig. 5. An almost linear Br···c_g···c_g'···Br′ connection of the bromine atoms and the centroids of the N1 ring atoms into a pseudobinuclear units as found in the structure of $[Cu(6\text{-}Brpic)_2(H_2O)]$ (**3**). Hydrogen atoms are omitted for clarity.

Cu coordination plane (non-magnetic Cu orbital in that direction for the compressed axial geometry), although the oxygen O3 is axially coordinated to copper (magnetic Cu orbital in that direction for the compressed axial geometry). The structure is additionally stabilized by a π···π stacking *via* the ligand pyridine rings, where each ring is stacked by the same type of ring from the adjacent molecule. The N1 pyridine ring is coordinated axially to the copper(II) coordination sphere (the magnetic d_{z^2} orbital), while the N2 ring coordinated equatorially (the non-magnetic $d_{x^2-y^2}$ orbital). Therefore, the N1 rings path (Cu–N1(py)···N1′(py)–Cu′) seems to be the most suitable candidate to maintain the antiferromagnetic interaction in **3**. Interestingly, on almost the same line as both adjacent N1 ring centroids (c_g) are, also two Br atoms from the N2 ligands of the same mononuclear units are present at relatively short distance Br···c_g of 3.478(1) Å, showing a line Br···c_g···c_g'···Br′ within a symmetrical binuclear unit (Fig. 5). This may well be related to the anion (atom)···π interactions, a topic investigated intensively in the last years [42–44].

Table 3
Crystal data and details of the structure determination for [Cu(6-Mepic)$_2$(H$_2$O)] (**1**), [Cu(6-Mepic)$_2$(py)] (**2**) and [Cu(6-Brpic)$_2$(H$_2$O)] (**3**)

Compound	**1**	**2**	**3**
Formula	$C_{14}H_{14}CuN_2O_5$	$C_{19}H_{17}CuN_3O_4$	$C_{12}H_8Br_2CuN_2O_5$
M_r	353.81	414.91	483.56
Colour and habit	blue, prism	blue, prism	blue, plate
Crystal system, space group	monoclinic, *I*2/*a*	monoclinic, *C*2/*c*	triclinic, $P\bar{1}$
Crystal dimensions (mm^3)	0.25 × 0.15 × 0.14	0.21 × 0.20 × 0.19	0.43 × 0.14 × 0.08
Unit cell parameters			
a (Å)	14.6320(3)	14.1463(3)	6.9237(2)
b (Å)	7.8311(2)	8.8583(2)	9.1011(4)
c (Å)	24.4343(5)	15.1514(4)	11.4405(4)
α (°)	90	90	86.963(3)
β (°)	94.0180(18)	104.727(2)	84.259(3)
γ (°)	90	90	77.010(3)
V (Å^3)	2792.91(11)	1836.28(8)	698.59(5)
Radiation, Mo Kα (Å)		0.71073	
Z	8	4	2
D_{calc} (g cm^{-3})	1.683	1.501	2.299
μ (mm^{-1})	1.590	1.219	7.308
θ Range for data collection (°)	3.95–30.00	4.17–29.99	3.98–30.00
h,*k*,*l* range	−20:20; −11:10, −34:34	−19:19; −12:12, −21:21	−9:9; −12:12, −16:16
Number of measured reflections	31145	23008	20552
Number of independent reflections (R_{int})	4055 (0.0500)	2661 (0.0412)	4052 (0.0406)
Number of observed reflections, $I \geqslant 2\sigma(I)$	1955	1478	2597
Number of refined parameters	209	125	207
R[a], wR[b] [$I \geqslant 2\sigma(I)$]	0.0321, 0.0711	0.0291, 0.0665	0.0284, 0.0572
R, wR [all data]	0.0746, 0.0806	0.0573, 0.0725	0.0529, 0.0646
g_1, g_2 in w[c]	0.0431, 0	0.0403, 0	0.0344, 0
Goodness-of-fit on F^2, S[d]	0.821	0.854	0.906
Maximum, minimum electron density (e Å^{-3})	0.560, −0.279	0.215, −0.293	0.702, −0.571
Maximum Δ/σ	<0.001	<0.001	0.001
Absorption correction type	multi-scan	multi-scan	multi-scan
Range of transmission factors minimum, maximum	0.760, 0.810	0.770, 0.790	0.310, 0.560

[a] $R = \sum||F_o| - |F_c||/\sum|F_o|$.
[b] w$R = [\sum(F_o^2 - F_c^2)^2/\sum w(F_o^2)^2]^{1/2}$.
[c] $w = 1/[\sigma^2(F_o^2) + [(g_1P)^2 + g_2P]]$ where $P = (F_o^2 + 2F_c^2)/3$.
[d] $S = \sum[w(F_o^2 - F_c^2)^2/(N_{obs} - N_{param})]^{1/2}$.

$$\chi_M = \frac{2Ng^2\beta^2}{kT(3 + e^{-2J/kT})}(1 - \rho) + \frac{Ng^2\beta^2}{2kT}\rho \quad (1)$$

In the last section, the magnetic interaction within the binuclear units in **3** is discussed due to the presumed $\{d_{z^2}\}^1$ ground state, as at least at first glance could most easily be explained from the structural and the EPR data. Nevertheless, the intermediate geometry between trigonal bipyramid and square pyramid (e.g. $\tau = 0.62$) may clearly suggest a strong d-orbital mixing, so the unpaired electron density is probably in multiple d-orbitals. Therefore, the other *d*-orbitals may as well play an important role in the predominantly binuclear magnetic interaction found for **3**. If that would be the case, another intrabinuclear path should be decisive for the antiferromagnetism in **3**, either N2(py)···N2′(py) or O5–H25O···O3 double H-bond bridges. To verify these pathways, some theoretical calculations would be necessary.

3. Conclusion

We have prepared and fully characterized three copper(II) complexes, namely aquabis(6-methylpyridine-2-carboxylato-*N*,*O*)copper(II), [Cu(6-Mepic)$_2$(H$_2$O)] (**1**), bis(6-methylpyridine-2-carboxylato-*N*,*O*)(pyridine)copper(II), [Cu(6-Mepic)$_2$(py)] (**2**) and aquabis(6-bromopyridine-2-carboxylato-*N*,*O*)copper(II), [Cu(6-Brpic)$_2$(H$_2$O)] (**3**) which were characterized by elemental analysis, IR and EPR spectroscopy and by thermal methods (TGA/DTA), while their crystal structures were determined by X-ray single-crystal diffractometry method. The magnetic susceptibility of powdered polycrystalline samples of **1**–**3** were measured in order to obtain more information about their magnetic behaviour.

Synthesis of **1** and **3** were done in mildly alkaline solution, although **1** and **3** can be prepared in acidic solution as well, but with smaller yields. The X-ray structural analysis revealed the intermediate between square-pyramidal and trigonal-bipyramidal coordination around copper(II) ion in both **1** and **3**. It is evident that substituent in the ligands' pyridine ring (electron-donating methyl group in 6-methylpicolinic acid or electron-withdrawing bromine atom in 6-bromopicolinic acid) has influence on the crystal packing patterns of **1** and **3**. Molecules of **1** are assembled by intermolecular O–H···O hydrogen bonds into 2D network. These networks interact through π···π stacking in the third dimension. Molecules of **3** are linked into centrosymmetric dimers which are connected into infinite chains, both by intermolecular O–H···O hydrogen bonds. These chains are linked into 3D structure by π···π stacking. Complex **2** was prepared by a recrystallization of **1** from pyridine. Substitution of water molecule by pyridine molecule affects both coordination polyhedron and crystal packing pattern, leading to a trigonal-bipyramidal geometry of **2** in contrast to **1**. 3D supramolecular structure of **2** is supported only by weak interactions such as intermolecular hydrogen bonds of C–H···O type.

The methyl group or bromine atom, as a substituent in the ligands' pyridine ring, mostly affect the type of the coordination polyhedron around copper(II), leading to the pentacoordinated copper(II) ion in **1**, **2** and **3**. This is quite different from the copper(II) complexes with picolinic [45], 3-hydroxypicolinic [8] and 6-hydroxypicolinic acid [12] reported in the literature. The coordination environments in these complexes are usually square-planar or octahedral and square-pyramidal only in copper(II) complex with 3-methylpicolinic acid [31]. However, the Cu–N and Cu–O

bond distances in **1**, **2** and **3** are in agreement with the values reported in the literature for the abovementioned complexes [8,12,31,45].

EPR spectra show three different types of copper(II) $S = ½$ symmetry signals. Most probably they could be assigned to the elongated axial in **1**, the isotropic in **2** and the rhombic in **3**. The ground state is suggested to be $\{d_{x^2-y^2}\}^1$ for **1** and $\{d_{z^2}\}^1$ for **3**, while we were unable to determine it for **2**.

The measurements of magnetic susceptibility revealed paramagnetic behaviour of both **1** and **2**, as it was expected. On the other hand, **3** exhibits an antiferromagnetic interaction. This interaction is ascribed to the formation of pseudobinuclear units by $\pi\cdots\pi$ stacking between pyridine rings.

4. Experimental

4.1. Materials and physical measurements

All chemicals for the syntheses were used as received without further purification. Copper(II) sulfate pentahydrate was purchased from Merck, while 6-methylpicolinic and 6-bromopicolinic acids were purchased from Aldrich.

CHN analyses were performed on Perkin–Elmer 2400 Series II CHNS analyzer in the Analytical Services Laboratories of the Ruđer Bošković Institute, Zagreb, Croatia.

The IR spectra were obtained from KBr pellets in the range 4000–450 cm^{-1} with a Perkin–Elmer Spectrum RXI FTIR-spectrometer.

TGA/DTA measurements were performed at a heating rate of 5 °C/min for **1** and **3** and 10 °C/min for **2** in the temperature range of 25–600 °C, under nitrogen flow of 10 mL/min on instrument Mettler-Toledo TGA/SDTA 851[e]. Approximately 10 mg of sample were placed in standard aluminium crucible (40 μL).

X-band powder EPR spectra were recorded at room temperature on a Bruker ESP-300 electron spin resonance spectrometer. The g values were calculated by the equation $E = h\nu = g\beta_e B$.

The magnetic susceptibility data of powdered polycrystalline samples were measured with a Quantum Design SQUID MPMS-XL-5 magnetometer, equipped with a 5 T magnet. The molar magnetic susceptibility χ_M was investigated in the temperature interval between 300 and 2 K in a magnetic field strength $H = 1000$ Oe. The data were corrected for the experimentally determined contribution of the sample holder. Corrections for the diamagnetic response of the compounds, due to closed atomic shells as estimated from the Pascal's constants, were applied [41].

4.2. Synthesis of aquabis(6-methylpyridine-2-carboxylato-N,O)copper(II), [Cu(6-Mepic)$_2$(H_2O)] (**1**)

A solution of 6-methylpicolinic acid (0.40 g, 2.92 mmol) in water (15 mL) was added to a solution of copper(II) sulfate pentahydrate (0.36 g, 1.44 mmol) in water (5 mL). The pH value of the resulting deep blue solution was adjusted to 8 by adding a few drops of concentrated ammonia solution. The blue product was formed immediately and it was left to stand at room temperature until the next day to complete precipitation. The product was then filtered off, washed with water and dried in a desiccator over $CaCl_2$. Yield: 0.44 g (86.3%). *Anal.* Calc. for $C_{14}H_{14}CuN_2O_5$ (353.81): C, 47.52; H, 4.00; N, 7.92. Found: C, 47.27; H, 4.17; N, 8.57%. IR data (KBr pellet, cm^{-1}): 3407m, 1651s, 1603s, 1573m, 1468m, 1407m, 1365s, 1260m, 803m, 767s.

The crystals suitable for X-ray crystal structure analysis were obtained by slow evaporation of the mother liquor solution, remained after filtration of the product described above, at room temperature.

4.3. Synthesis of bis(6-methylpyridine-2-carboxylato-N,O)(pyridine)copper(II), [Cu(6-Mepic)$_2$(py)] (**2**)

A solution of **1** (0.20 g, 0.57 mmol) in pyridine (7 mL) was left to stand at room temperature for five days to give a blue product, which was filtered off and dried *in vacuo*. Yield: 0.14 g (59.7%). *Anal.* Calc. for $C_{19}H_{17}CuN_3O_4$ (414.91): C, 54.99; H, 4.14; N, 10.13. Found: C, 54.95; H, 4.29; N, 11.20%. IR data (KBr pellet, cm^{-1}): 1641s, 1602s, 1572m, 1448m, 1355s, 1255m, 795m, 769m, 712m.

The crystals suitable for X-ray crystal structure analysis were obtained by recrystallization from pyridine.

4.4. Synthesis of aquabis(6-bromopyridine-2-carboxylato-N,O)copper(II), [Cu(6-Brpic)$_2$(H_2O)] (**3**)

A solution of 6-bromopicolinic acid (0.20 g, 0.99 mmol) in water (15 mL) was added to a solution of copper(II) sulfate pentahydrate (0.12 g, 0.48 mmol) in water (5 mL). The pH value of the resulting light blue solution was adjusted to 7 by adding a few drops of concentrated ammonia solution. The blue product was formed slowly and it was left to stand at room temperature until the next day to complete precipitation. The product was then filtered off, washed with water and dried in a desiccator over $CaCl_2$. Yield: 0.18 g (78.3%). *Anal.* Calc. for $C_{12}H_8Br_2CuN_2O_5$ (483.56): C, 29.80; H, 1.67; N, 5.79. Found: C, 29.54; H, 1.70; N, 6.20%. IR data (KBr pellet, cm^{-1}): 3217m, 3078m, 1683s, 1653m, 1631s, 1588s, 1552s, 1437s, 1408m, 1371s, 1335s, 1247m, 1177m, 1161s, 1140m, 1124m, 1078m, 1004m, 784s, 775m, 750m, 668m.

The crystals suitable for X-ray crystal structure analysis were obtained by slow evaporation of the mother liquor solution, remained after filtration of the product described above, at room temperature.

4.5. X-ray single-crystal structure determination

Suitable single crystals of **1**, **2** and **3** were selected and mounted in air onto thin glass fibres. The data collection was carried out on Oxford Diffraction Xcalibur four-circle kappa geometry single-crystal diffractometer with Xcalibur Sapphire 3 CCD detector by applying the CRYSALIS Software system, Version 171.32.4 at room temperature (296 K) [46]. Data reduction has been applied by the same programme [46]. Eleven runs containing 1277 data collection frames for **1**, 11 runs containing 1425 data collection frames for **2** and 13 runs containing 1603 data collection frames for **3** were collected at the crystal–detector distance of 60 mm with the exposure time of 20, 20 and 15 s for **1**, **2** and **3**, respectively, and with ω scan type for all structures.

The X-ray diffraction data have been corrected for Lorentz-polarization factor and scaled for absorption effects by multi-scan. The structures were solved by direct methods. Refinement procedure by full-matrix least squares methods based on F^2 values against all reflections has been performed including anisotropic displacement parameters for all non-H atoms.

The positions of hydrogen atoms belonging to the carbon atoms Csp^2 and methyl Csp^3 atoms were geometrically optimized applying the riding model [Csp^2–H, Csp^3(methyl)–H, 0.93 Å and 0.96 Å, respectively; $U_{iso}(H) = 1.2U_{eq}(C)$ for Csp^2 and $1.5U_{eq}(C)$ for Csp^3(methyl)]. H atoms belonging to water molecules in **1** and **3** were found in difference Fourier maps and restrained with the average O–H value of 0.82(5) Å using SHELXL-97 DFIX instruction.

Calculations were performed with SHELXS-97 [47], SHELXL-97 [47] and PLATON [48]. The molecular graphics were done with ORTEP-3 [49] and MERCURY (Version 1.4.2) [50].

Crystal data and details of the structure determination for **1**, **2** and **3** are given in Table 3.

Acknowledgements

This work was supported by the Ministry of Science, Education and Sports of the Republic of Croatia (Grant No. 119–1193079–1332) and MVZT P1–0175–103, Republic of Slovenia. We thank Dr. M. Šentjurc, EPR Centre, Jožef Stefan Institute, Ljubljana, Slovenia.

Appendix A. Supplementary data

CCDC 688516, 688517 and 688518 contain the supplementary crystallographic data for this paper. These data can be obtained free of charge via http://www.ccdc.cam.ac.uk/conts/retrieving.html, or from the Cambridge Crystallographic Data Centre, 12 Union Road, Cambridge CB2 1EZ, UK; fax: (+44) 1223-336-033; or e-mail: deposit@ccdc.cam.ac.uk. Structure factor table is available from the authors. Supplementary data associated with this article can be found, in the online version, at doi:10.1016/j.poly.2008.09.011.

References

[1] B. Moulton, M.J. Zaworotko, Chem. Rev. 101 (2001) 1629.
[2] A.Y. Robin, K.M. Fromm, Coord. Chem. Rev. 250 (2006) 2127.
[3] J.J. Vittal, Coord. Chem. Rev. 251 (2007) 1781.
[4] R. Horikoshi, T. Mochida, Coord. Chem. Rev. 250 (2006) 2595.
[5] N.R. Champness, Dalton Trans. (2006) 877.
[6] V.B. Di Marco, A. Tapparo, G.G. Bombi, Ann. Chim. 91 (2001) 595.
[7] P.C.R. Soares-Santos, H.I.S. Nogueira, V. Félix, M.G.B. Drew, R.A. Sá Ferreira, L.D. Carlos, T. Trindade, Chem. Mater. 15 (2003) 100.
[8] C. Sun, X. Zheng, L. Jin, J. Mol. Struct. 646 (2003) 201.
[9] C. Sun, X. Zheng, L. Jin, Z. Anorg. Allg. Chem. 630 (2004) 1342.
[10] G.-Q. Bian, T. Kuroda-Sowa, H. Konaka, M. Maekawa, M. Munakata, Acta Crystallogr., Sect. C 60 (2004) m338.
[11] V.B. Di Marco, A. Tapparo, A. Dolmella, G.G. Bombi, Inorg. Chim. Acta 357 (2004) 135.
[12] A. Şengül, O. Büyükgüngör, Acta Crystallogr., Sect. C 61 (2005) m119.
[13] P.I. Girginova, F.A.A. Paz, H.I.S. Nogueira, N.J.O. Silva, V.S. Amaral, J. Klinowski, T. Trindade, Polyhedron 24 (2005) 563.
[14] P.I. Girginova, F.A.A. Paz, H.I.S. Nogueira, N.J.O. Silva, V.S. Amaral, J. Klinowski, T. Trindade, J. Mol. Struct. 737 (2005) 221.
[15] M. Nakai, F. Sekiguchi, M. Obata, C. Ohtsuki, Y. Adachi, H. Sakurai, C. Orvig, D. Rehder, S. Yano, J. Inorg. Biochem. 99 (2005) 1275.
[16] X.-L. Zhang, S.W. Ng, Acta Crystallogr., Sect. E 61 (2004) m1140.
[17] B. Żurowska, J. Mroziński, K. Ślepokura, Polyhedron 26 (2007) 3379.
[18] B.-M. Kukovec, Z. Popović, G. Pavlović, M. Rajić Linarić, J. Mol. Struct. 882 (2008) 47.
[19] Z. Popović, B.-M. Kukovec, K. Molčanov, G. Pavlović, M. Rajić Linarić, First European Chemistry Congress, Abstract Book, Budapest, Hungary, 2006, p. 368.
[20] B.-M. Kukovec, Z. Popović, G. Pavlović, Fifteenth Slovenian-Croatian Crystallographic Meeting, Book of Abstracts, Jezersko, Slovenia, 2006, p. 57.
[21] J.L. Hoare, K.J. Cavell, R. Hecker, B.W. Skelton, A.H. White, J. Chem. Soc., Dalton Trans. (1996) 2197.
[22] À. Leiva, W. Clegg, L. Cucurull-Sánchez, P. González-Duarte, J. Pons, J. Chem. Cystallogr. 29 (1999) 1097.
[23] C.B. Aakeröy, A.M. Beatty, K.R. Lorimer, J. Chem. Soc., Dalton Trans. (2000) 3869.
[24] Y. Yoshikawa, E. Ueda, K. Kawabe, H. Miyake, T. Takino, H. Sakurai, Y. Kojima, J. Biol. Inorg. Chem. 7 (2002) 68.
[25] R. March, W. Clegg, R.A. Coxall, L. Cucurull- Sánchez, L. Lezama, T. Rojo, P. González-Duarte, Inorg. Chim. Acta 353 (2003) 129.
[26] B.-M. Kukovec, P.D. Vaz, Z. Popović, M.J. Calhorda, K. Furić, G. Pavlović, M. Rajić Linarić, Cryst. Growth Des. 8 (2008) 3465.
[27] J. Pons, R. March, J. Rius, J. Ros, Inorg. Chim. Acta 357 (2004) 3789.
[28] G.-H. Xu, J.-F. Ma, Y.-Y. Liu, S.-L. Li, Acta Crystallogr., Sect. C 62 (2006) m581.
[29] B.-M. Kukovec, Z. Popović, G. Pavlović, Acta Crystallogr., Sect. C 63 (2007) m615.
[30] B.-M. Kukovec, Z. Popović, G. Pavlović, Acta Crystallogr., Sect. C 63 (2007) m389.
[31] B.-M. Kukovec, Z. Popović, G. Pavlović, J. Coord. Chem. 61 (2008) 3092.
[32] A.W. Addison, T. Nageswara Rao, J. Reedijk, J. van Rijn, G.C. Verschoor, J. Chem. Soc., Dalton Trans. (1984) 1349.
[33] G.R. Desiraju, T. Steiner, The Weak Hydrogen Bond in Structural Chemistry and Biology, IUCr Monographs on Crystallography, Oxford University Press, Oxford, 2001.
[34] G.R. Desiraju, Acc. Chem. Res. 35 (2002) 565.
[35] G.A. Jeffrey, An Introduction to Hydrogen Bonding, Topics in Physical Chemistry, Oxford University Press, Oxford, 1997.
[36] C. Janiak, J. Chem. Soc., Dalton Trans. (2000) 3885.
[37] S.M.O. Quintal, H.I.S. Nogueira, V. Félix, M.G.B. Drew, New J. Chem. 24 (2000) 511.
[38] G.B. Deacon, R.J. Phillips, Coord. Chem. Rev. 33 (1980) 227.
[39] K. Nakamoto, Infrared and Raman Spectra of Inorganic and Coordination Compounds, 4th ed., Wiley-Interscience, New York, 1986.
[40] M.A. Halcrow, J. Chem. Soc., Dalton Trans. (2003) 4375.
[41] O. Kahn, Molecular Magnetism, VCH, New York, 1993.
[42] B.L. Schottel, H.T. Chifotides, K.R. Dunbar, Chem. Soc. Rev. 37 (2008) 68.
[43] T.J. Mooibroek, C.A. Black, P. Gamez, J. Reedijk, Cryst. Growth Des. 8 (2008) 1082.
[44] P. Gamez, T.J. Mooibroek, S.J. Teat, J. Reedijk, Acc. Chem. Res. 40 (2007) 435.
[45] C.-X. Zhang, Y.-Y. Zhang, J. Sheng, J. Coord. Chem. 58 (2005) 189.
[46] Oxford Diffraction, CRYSALIS CCD and CRYSALIS RED. Versions 171.32.4, Oxford Diffraction Ltd., Abingdon, Oxfordshire, England, 2007.
[47] G.M. Sheldrick, Acta Crystallogr., Sect. A 64 (2008) 112.
[48] A.L. Spek, J. Appl. Crystallogr. 36 (2003) 7.
[49] L.J. Farrugia, J. Appl. Crystallogr. 30 (1997) 565.
[50] C.F. Macrae, P.R. Edgington, P. McCabe, E. Pidcock, G.P. Shields, R. Taylor, M. Towler, J. van de Streek, J. Appl. Crystallogr. 39 (2006) 453.

grade. The epoxides and used solvents were purified by standard procedures.

2.2. Apparatus

IR spectra were recorded as KBr pellets on a Perkin–Elmer 781 spectrophotometer and on an Impact 400 Nicolet FTIR spectrophotometer. ^{1}H NMR spectra were recorded with a 400 MHz spectrometer in dimethylsulfoxide (DMSO) using tetramethylsilane (TMS) as an internal reference. The melting points were determined by a Yanagimoto micro melting point apparatus. The purity determination of the substrates and reaction monitoring were accomplished by thin layer chromatography (TLC) on silica gel polygram SILG/UV 254 plates. The chromatography was carried out on Silica Gel 60 (70–230 mesh).

2.3. General procedure

2.3.1. General procedure for the preparation of the Schiff base ligands

To a mixture of salicylaldehyde (0.4 g, 3.27 mmol) in MeOH was added the diamine (1.65 mmol) with stirring in one portion. The stirring was continued to completion the reaction. The progress of the reaction was monitored by thin layer chromatography (TLC). After the completion of the reaction, a colored substance was obtained. The solid product was filtered off and washed with cold MeOH. The crude product was purified by recrystallization from ethanol and the pure Schiff base was obtained in high yield after leaving for the appropriate time. The Schiff base products were identified by physical and spectroscopic data and by a comparison with authentic samples prepared in accordance to the literature procedures [20].

2.3.2. General procedure for the preparation of the Schiff base complexes of metal(II)

To a solution of the Schiff base ligand (1 mmol) in MeOH (10 ml) was added $M(O_2CCH_3)_2$ (1 mmol) dropwise under reflux conditions. The reaction mixture was stirred to completion the reaction. The progress of the reaction was monitored by TLC. After the completion of complex formation, a colored substance was obtained. The solid product was filtered off and washed with MeOH. The crude product was purified by recrystallization from methanol and the pure Schiff base complex was obtained. The complex products were identified by comparison with authentic samples prepared in accordance to the literature procedures [20].

2.3.3. General procedure for the preparation of the catalysts

Alumina was activated by treatment at 500 °C for 8 h. Then 2 g of activated alumina was added to 0.02 mmols of each of the complexes and the obtained mixture was stirred for 0.5 h. The catalysts were analyzed by dissolving a known amount of catalyst in concentrated hydrochloric acid, then using an atomic absorption spectrophotometer.

2.3.4. General procedure for conversion of epoxides to β-halohydrins

A mixture of 1.0 g catalyst **2a**, 25 ml CH_2Cl_2 as solvent and 10 mmol substituted epoxide was stirred in a 50 ml round-bottom flask equipped with a condenser and a dropping funnel at room temperature. Then a solution of 10 mmol halogen (Br_2 or I_2) in 5 ml dichloromethane was added dropwise over 20 min to the above-mentioned mixture. The progress of the reaction was monitored by gas chromatography (GC) and TLC. After the complete disappearance of the starting material, the reaction mixture was filtered and the obtained solution was washed with 10% aqueous $Na_2S_2O_3$ (2×10 ml) and water (2×10 ml). The aqueous layer was further extracted with CH_2Cl_2 (2×10 ml). The combined organic layer was dried over $MgSO_4$. The solvent was evaporated, and the pure halo alcohol was obtained. The halo alcohol products were identified by a comparison with authentic samples prepared accordance to the literature procedures [20,23–29].

2-Iodo-1-phenylethanol. IR (neat): 748 (m), 915 (m), 1032 (s), 1121 (w), 1243 (s), 1365 (m), 1492 (m), 1602 (s), 2885 (m), 2930 (s), 3061 (m), 3398 (br s) cm^{-1}.

^{1}H NMR: δ 2.02 (s, 1H), 3.76 (d, 2H, J = 5.5 Hz), 4.78 (t, 1H, J = 5.0 Hz), 7.17–7.35 (m, 5H).

^{13}C NMR: δ 54.96, 66.90, 128.22, 129.10, 129.21, 138.17.

1-Iodo-3-phenoxy-2-propanol. IR (neat): 650 (w), 678 (w), 760 (m), 823 (m), 1038 (s), 1113 (w), 1240 (s), 1375 (m), 1494 (s), 1588 (s), 2877 (m), 2927 (s), 3050 (m), 3418 (br s) cm^{-1}.

^{1}H NMR: δ 3.1 (s, 1H), 3.48 (d, 2H, J = 5.0 Hz), 4.06 (tt, 1H, J_1 = 7.0, J_2 = 5.0 Hz), 4.13 (d, 2H, J = 5.6 Hz), 6.78–6.90 (m, 3H), 7.36 (m, 2H).

^{13}C NMR: δ 67.18, 69.67, 70.01, 114.98, 116.87, 121.79, 129.89, 132.86.

1-Iodo-2-octanol. IR (neat): 725 (m), 1015 (br s), 1105 (m), 1130 (m), 1185 (s), 1385 (s), 1425 (s), 1465 (s), 1475 (s), 2870 (vs), 2940 (vs), 3400 (br s) cm^{-1}.

^{1}H NMR: δ 0.89 (t, 3H, J = 7.0 Hz), 1.26–1.58 (m, 10H), 2.24 (s, 1H), 3.24–3.55 (m, 3H).

^{13}C NMR: δ 14.09, 16.45, 22.62, 25.56, 29.12, 31.70, 36.89, 70.91.

2-Iodocyclohexanol. IR (neat): 690 (s), 790 (w), 870 (m), 948 (s), 1038 (w), 1082 (br s), 1123 (m), 1189 (s), 1372 (m), 1462 (s), 2882 (s), 2960 (br s), 3425 (br s) cm^{-1}.

^{1}H NMR: δ *1.26–1.44* (m, 3H), 1.75–1.95 (m, 3H), 2.15–2.3 (m, 1H), 2.3–2.35 (m, 1H), 2.72 (s, 1H), 3.58–3.62 (m, 1H), 3.9–4.0 (m, 1H).

^{13}C NMR: δ 24.51, 26.56, 32.75, 35.40, 59.84, 71, 59.

2-Bromo-1-phenylethanol. IR (neat): 689 (m), 766 (m), 823 (m), 1036 (s), 1115 (w), 1233 (s), 1375 (m), 1494 (m), 1600 (s), 2875 (m), 2935 (s), 3064 (m), 3405 (br s) cm^{-1}.

^{1}H NMR: δ 1.98 (s, 1H), 4.01 (m, 2H), 4.98 (t, 1H, J = 5.0 Hz), 7.19–7.39 (m, 5H).

^{13}C NMR: δ 57.39, 67.97, 128.32, 129.30, 129.37, 138.98.

1-Bromo-3-phenoxy-2-propanol. IR (neat): 641 (w), 688 (m), 756 (m), 823 (m), 1038 (s), 1112 (w), 1239 (s), 1375 (m), 1494 (s), 1588 (s), 2878 (m), 2925 (s), 3059 (m), 3415 (br s) cm^{-1}.

^{1}H NMR: δ 2.75 (s, 1H), 3.61 (d, 2H, J = 5.3 Hz), 4.03 (tt, 1H, J_1 = 7.1 Hz, J_2 = 5.0 Hz), 4.11 (d, 2H, J = 7.0 Hz), 6.78 (d, 1H, J = 5 Hz), 6.94 (d, 2H, J = 8.0 Hz), 7.35 (m, 2H).

^{13}C NMR: δ 69.58, 69.77, 69.93, 115.01, 116.82, 121.86, 129.99, 132.79.

1-Bromo-2-octanol. IR (neat): 720 (m), 830 (m), 1050 (s), 1075 (s), 1125 (m), 1225 (m), 1265 (m), 1385 (m), 1425 (m), 1470 (s), 2860 (vs), 2935 (vs), 2970 (vs) 3380 (br s) cm^{-1}.

^{1}H NMR: δ 0.89 (t, 3H, J = 6.5 Hz), 1.25–1.63 (m, 8H), 1.86 (q, 2H, J = 7.1 Hz), 2.22 (s, 1H), 3.42 (d, 2H, J = 7.1 Hz), 3.75–3.84 (m, 1H).

^{13}C NMR: δ 14.01, 22.52, 25.58, 29.14, 31.68, 35.05, 40.73, 71.02.

2-Bromocyclohexanol. IR (neat): 690 (s), 793 (w), 865 (m), 960 (s), 1038 (m), 1075 (br s), 1123 (m), 1189 (s), 1372 (m), 1460 (s), 2882 (s), 2960 (br s), 3425 (br s) cm^{-1}.

^{1}H NMR: δ 1.26–1.42 (m, 3H), 1.78–1.98 (m, 3H), 2.18–2.32 (m, 1H), 2.32–2.38 (m, 1H), 2.68 (s, 1H), 3.58–3.64 (m, 1H), 3.82–3.92 (m, 1H).

^{13}C NMR: δ 24.48, 27.02, 33.95, 36.59, 62.13, 75.66.

3. Results and discussion

Schiff base complexes of metal (II) have been recognized as being among the most promising catalysts for various reactions. These complexes show wide applicability and are now used as catalysts for a variety of enantioselective reactions, such as oxidation [30,31], aziridination [32], cyclopropanation [33], the Diels–Alder reaction [34,35], the addition of TMSCN to aldehydes [36,37], the Sterecker reaction [38], and the conversion of 1,2-epoxyethanes to 2-haloethanols with molecular halogen [20]. Metal(II)-salen complexes can be readily synthesized from metal(II) salts and salen ligands, which are prepared by simply mixing 1 mol of various diamines and 2 mol of salicylaldehyde.

Indeed the whole area of supported transition metal complex catalysts is rapidly expanding again as the advantages which arise from ease of handling, recovery, separation and recycling, coupled with the potential for automation which has become recognized by more and more rank-and-file industrial and academic synthetic chemists [39,40]. Nowadays, on the basis to immobilize the transition metal complex catalysts, key targets are highly active and selective asymmetric catalysts. Heterogeneous analogues [41] of these homogeneous catalysts would not only simplify their use and facilitate product separation and isolation, but would also offer considerable economic benefits if recycling and their reuse were possible.

The preparation of catalysts readily occurred via the immobilized complexes on activated alumina (alumina was activated at 500 °C for 8 h before use) [21] and were estimated by dissolving a known amount of the catalyst in concentrated HCl (Scheme 1). From this solution, transition metal contents were estimated on an atomic absorption spectrometer (AAS) [21]. The concentration of the metal ions was 0.01 mmol/gr.

In this study, the reaction of styrene oxide with iodine and bromine in the presence of some alumina-supported Mn(II) Schiff base-complexes as the catalyst were carried out (Scheme 2).

A mixture of 1.0 g catalyst, 25 ml solvent and 10 mmol styrene oxide was stirred in a 50 ml round-bottom flask equipped with a condenser and a dropping funnel at room temperature. Then 10 mmol of halogen (solution in 5 ml dichloromethane) was added dropwise. The resulting mixture was stirred at 25 °C and was checked by GC and TLC analysis up to the end of the reaction. After filtration and washing with solvent, workup of the filtrate with thiosulfate and concentration of the solution, was obtained the

Table 1
Reaction of styrene oxide with elemental iodine and bromine in the presence of various Al_2O_3–SB complexes as catalysts in CH_2Cl_2 at 25 °C

Entry	Catalyst	Iodination		Bromination	
		Time (h)	Yield (%)[a]	Time (h)	Yield (%) [a]
1	**2a**	0.4	95	0.25	>95
2	**2b**	0.4	92	0.3	95
3	**2c**	0.5	92	0.3	92
4	**2d**	1.5	73	0.9	78
5	**2e**	2.2	70	1.1	75
6	**2f**	2.7	68	1.2	75
7[b]	None	Several days	0	1	30[c]

[a] GC yield, based on epoxide.
[b] In the presence of excess of halogen.
[c] Only one isomer, 2-bromo-2-phenyl-ethanol was formed.

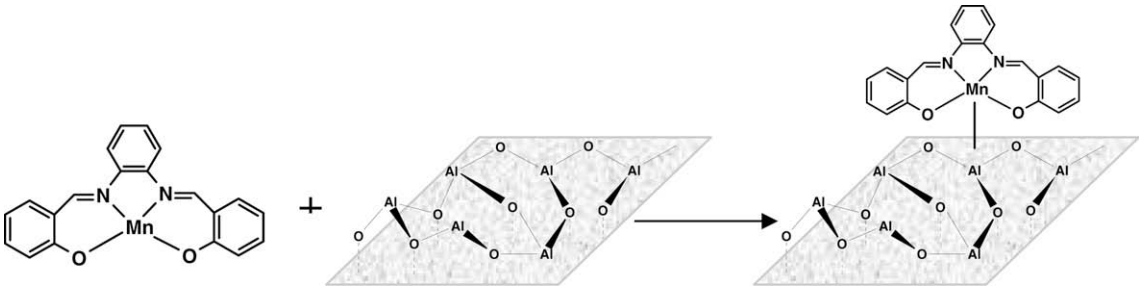

Scheme 1. Preparation of the catalysts via immobilizing the complexes on the activated alumina.

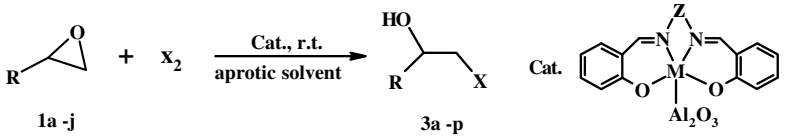

R of epoxides		R of products x=I	R of products x=Br
Ph	a	a	i
$PhOCH_2$	b	b	j
p-Cl-$PhOCH_2$	c	c	k
p-Me-$PhOCH_2$	d	d	l
t-Bu-OCH_2	e	e	m
3-Buten	f	f	n
CH_3	g	g	o
Cyclohexane	h	h	p

M	Z	
Mn(II)		a
	$-(CH_2)_2-$	b
	$-(CH_2)_8-$	c
Co(II)		d
Ni(II)		e
Cu(II)		f

Scheme 2. The reaction of styrene oxide with iodine and bromine in the presence of alumina-supported Mn(II) Schiff base-complexes as a catalyst.

Table 2
Reaction of various epoxides with elemental iodine and bromine in the presence of catalyst **2a**

Entry	Epoxide **1a–h**	Conditions	Time (h)	Yield[a] (%)	Product(s) **3a–p**	Ref.
1		I_2, **2a**, r.t., CH_2Cl_2	0.4	92		
2	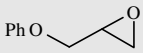	I_2, **2a**, r.t., CH_2Cl_2	3.9	83	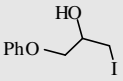	
3	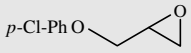	I_2, **2a**, r.t., CH_2Cl_2	4.3	87	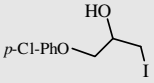	
4	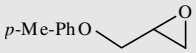	I_2, **2a**, r.t., CH_2Cl_2	4.5	85	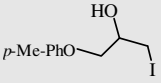	
5		I_2, **2a**, r.t., CH_2Cl_2	6.5	73		
6	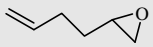	I_2, **2a**, r.t., CH_2Cl_2	4.6	68	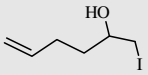	
7	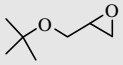	I_2, **2a**, r.t., CH_2Cl_2	5.8	74	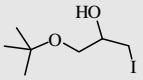	
8		I_2, **2a**, r.t., CH_2Cl_2	3.5	72		
9	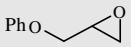	I_2, r.t., CH_2Cl_2	Several days	0		[32,17]
10	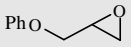	I_2, r.t., acetone		94 (53:47)	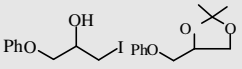	[32,17]
11	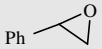	I_2, r.t., acetone	2	83		[32]
12	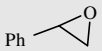	[*n*-Bu_4N]Br/$Mg(NO_3)_2$, $CHCl_3$	5	78 (5:1)	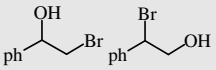	[35]
13	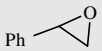	$(Me_2N)_2BBr/CH_2Cl_2$, N_2 atm.	12	75 (1:4.5)	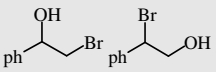	[36]
14	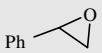	HI, CH_2Cl_2	0.25	99	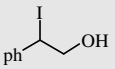	[34]
15	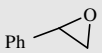	HBr, CH_2Cl_2	0.25	99	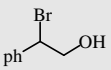	[20]
16	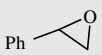	LiI, AcOH, THF, r.t.	1.3	87 (1:2)	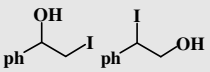	[20]
17	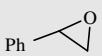	Br_2, **2a**, r.t., CH_2Cl_2	0.3	91		
18	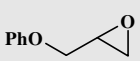	Br_2, **2a**, r.t., CH_2Cl_2	0.9	90	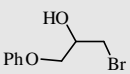	

Table 2 (*continued*)

Entry	Epoxide **1a–h**	Conditions	Time (h)	Yield[a] (%)	Product(s) **3a–p**	Ref.
19	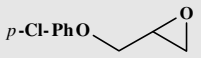	Br_2, **2a**, r.t., CH_2Cl_2	1.2	88	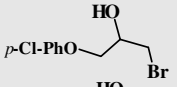	
20	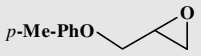	Br_2, **2a**, r.t., CH_2Cl_2	1.3	89	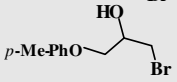	
21		Br_2, **2a**, r.t., CH_2Cl_2	2.3	85		
22	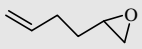	Br_2, **2a**, r.t., CH_2Cl_2	2	76	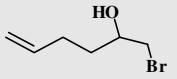	
23	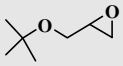	Br_2, **2a**, r.t., CH_2Cl_2	1.6	78	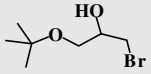	
24		Br_2, **2a**, r.t., CH_2Cl_2	1.2	75	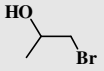	

[a] Isolated product yields based on epoxide.

neat products (**3a–p**). The results of the reaction of 1,2-epoxy-3-phenylpropane with elemental iodine and bromine in the presence of the above-mentioned catalysts are summarized in Table 1.

In each case, cleavage of the epoxide ring occurs. The reaction product was 2-halo-1-phenylethanol, and the yields were determined by GC and TLC analysis. The catalysts were easily recovered and could be reused several times.

In comparison, the cleavage behavior of styrene oxide with elemental iodine and bromine in the absence of catalyst is given in Table 1, entry 7. Iodination of styrene oxide did not occur with excess elemental iodine in the absence of a catalyst even under refluxing conditions and an extension of the reaction time to several days [42]. In addition, the yield and regioselectivity of the bromination reaction were very low in the absence of catalyst. As shown in Table 1, the yields of both iodination and bromination with this new methodology are quite fair. The catalysts **2a**, **2b** and **2c** are the most effective ones in these reactions.

It seems that immobilizing of the complexes obtained from the Schiff base ligand obtained from ortho phenylene diamine on an alumina surface is stronger and more suitable than the other ones; as a result the utilized catalyst has a better effect in the reaction. As it is shown in the results, the yield of the products of β-halohydrin in the reactions with these Schiff base ligands is more significant.

Moreover, the effect of various first-row transition metals(II) in supported Schiff base complexes as catalysts on the reaction rate and the yield of bromination and iodination reactions are featured in Table 1 (entries 4–6). As can be seen by using the supported Mn(II)-salen complex as a catalyst, the iodo alcohol and bromo alcohol were formed in high yields and the reaction rate was much faster than other metal complexes. These results are comparable with the results of the usage of Schiff base complexes as catalysts presented previously [20].

To ascertain the scope and limitation of the ring-opening reactions promoted by the above mentioned supported complexes, the reactions on various epoxides were carried out (Scheme 2). The results of the reactions with some representative epoxides in the presence of complex **2a** as the catalyst are indicated in Table 2.

However, other factors can exert a controlling influence such as; (1) steric hindrance of the epoxides (for example, compare in Table 2, entry 7 with entry 8); (2) the nature of the solvent; (3) the rate of admixing the reagents; and (4) the order in which the reagents are combined. Each one can have a pronounced effect on the observed ratio of β-halohydrins isomers and the overall yield.

The order and rate in which the reagents are combined were found to exert a subtle influence on the yield and regioselectivity in both bromohydrin and iodohydrin formation. For example, if bromine is added to the epoxide before the catalyst is added, two bromohydrin isomers are produced, but if the epoxide is added to the catalyst and then bromine is added dropwise over a period of time, only one isomer is formed. Furthermore, it appears that fast addition of bromine can reduce the regioselectivity too.

The results of the ring opening of styrene oxide in the presence of catalyst **2a** in various solvents are summarized in Table 3. The iodination and bromination reactions can cleanly proceed in dichloro-methane, while those performed in THF, DMSO, chloroform, diethylether and acetonitrile lead to a lower yield of the β-halohydrins.

As shown in Table 2 (entry 5), where only the *trans* isomers were detected, the reactions are completely *anti*-stereoselective. A contra-Markovnikov-type [3,43] regioselectivity is generally observed in these reactions. In many cases, this type of regioselectivity appears to be the opposite of that observed in the ring opening of the same epoxides with aqueous hydrohalogenic acid, under classic conditions [44] (entries 14 and 15). However, this new method appears to be highly competitive with the other methods reported in the literature. The reaction occurs under neutral and

Table 3
Halogenative reaction of styrene oxide in the presence of catalyst **2a** in various solvents at 25 °C

Entry	Solvent	Iodination		Bromination	
		Time (h)	Yield[a] (%)	Time (h)	Yield[a] (%)
1	CH_2Cl_2	0.4	95	0.25	>95
2	$CHCl_3$	0.4	95	0.3	95
3	CH_3CN	0.8	82	0.5	90
4	DMSO	1.1	80	0.5	82
5	THF	1.4	77	0.7	75
6	Diethylether	1.8	75	0.9	78

[a] GC yield.

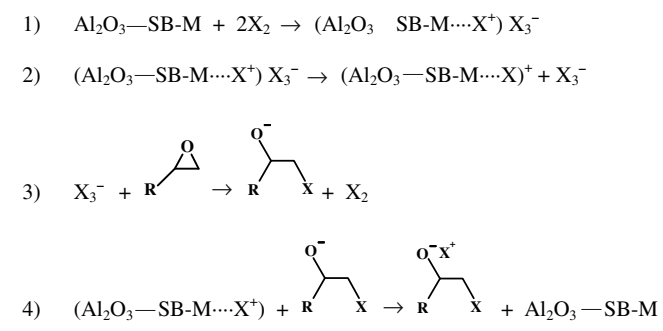

Scheme 3. The mechanism of halogenative cleavage of epoxides with the Al_2O_3–SB-M catalyst.

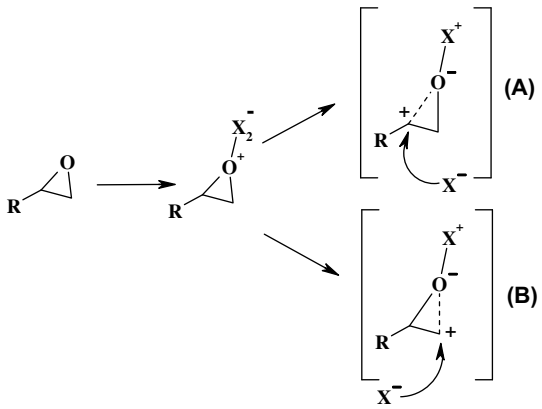

Scheme 4. The cleavage of epoxides in the absence of a catalyst.

mild conditions on the acid sensitive substrates and vicinal halohydrins were obtained in high yields and with high regioselectivity.

The regiochemical mode of epoxide cleavage by elemental iodine or bromine in the presence of alumina supported Schiff base complexes as a catalyst can be viewed as occurring via nucleophilic attack by a halide ion on the less sterically hindered epoxide carbon. This mechanism closely resembles the S_N2 model for aliphatic nucleophilic displacement. On the basis of accomplished research on the complexation of Schiff base metals [20] and other works reported on different ligands [42,45–48] with elemental halogen, the mechanism of halogenative cleavage of epoxides with this new catalyst follows the given mechanism for the same reaction with Schiff base complexes as catalysts [20] and is done in the following four steps (Scheme 3):

The first step (Eq. (1), Scheme 3) involves the formation of a 1:2 or 1:1 molecular complex between the catalyst and elemental halogen, in which the halogen ion (X_3^-) exists as a contact ion pair [49]. In the second step (Equation 2) this complex is further decomposed to release the X_3^- ion into the solution. Therefore, in this way, molecular iodine or bromine is converted to a nucleophilic halogen species in the presence of Al_2O_3–SB-M and, in the third step (Eqs. (3) and (4)), this ion participates in the ring opening reaction of the epoxides, and the catalyst is reproduced and is used in the first step again. These steps occur continuously until all of the epoxides and halogen are consumed, and after filtrations, the catalyst can be recovered easily.

On the other hand, when the catalyst is not present, cleavage of epoxides can occur via two limiting mechanistic pathway, either electrophilic attack by molecular halogen, behaving as a Lewis acid, giving the more stable carbonium ion-like transition state **A** (Scheme 4), or via nucleophilic attack by the halide ion on the epoxide or epoxide-halogen complex, giving the more stable transition state **B**. Most Lewis acidic compounds, such as titanium halides, foster electrophilic opening of the epoxide ring to yield transition state **A**. When weaker Lewis acids are employed, namely bromine or iodine, nucleophilic attack, by the halide ions generated, should be fostered and transition state **B** may be expected to be lower in energy. In this case, the cleavage leads to a mixture of secondary and primary alcohol products [3].

In addition, the advantages such as high regio- and stereoselectivity of the reactions, stability, commercially availability, inexpensive catalysts, high yield and ease of workup make this method a useful addition to the present methodologies in organic synthesis. All the products are known compounds and yields refer to GC yields.

4. Conclusions

In conclusion, this new method for the preparation of vicinal haloalcohols have some advantages such as high regioselectivity, high yields of products, short reaction times relative to other procedures, and simplicity of workup. This reaction occurs under neutral and mild conditions on acid sensitive substrates and appears to be highly competitive with the other methods reported in the literature.

Acknowledgement

We are grateful to The University of Kashan Research Council for the partial support of this work.

References

[1] P.A. Bartlett, J.D. Morrison, Asymmetric Synthesis, vol. 3, Academic Press, New York, 1984. p. 411.
[2] G. Righi, C. Bonini, Synthesis (1994) 225.
[3] G.X. Zheng, J.J. Eisch, Z.R. Lui, X. Ma, J. Org. Chem. 57 (1992) 5140.
[4] S.C. Maynard, Y. Ueda, Tetrahedron Lett. 29 (1998) 5197.
[5] T.M. Tarasow, J.P. Konopelski, M.A. Boehler, J. Org. Chem. 54 (1989) 4966.
[6] G.H. Coleman, H.F. Gohnstone, Org. Synth. Coll. I (1944) 158.
[7] H.B. Donahoe, C.A. Vanderwerf, Org. Synth. Coll. IV (1963) 157.
[8] C.A. Vanderwerf, C.A. Stewart, J. Am. Chem. Soc. 76 (1954) 1259.
[9] P.A. Tardella, M.A. Loreto, L. Pellacani, Synth. Commun. 11 (1981) 287.
[10] W.J. Rae, J.N. Coxon, M.P. Hartshorn, Tetrahedron 26 (1970) 1091.
[11] H.R. Kricheldorf, G. Morber, W. Regel, Synthesis (1981) 383.
[12] M.R. Detty, M.D. Seidler, Tetrahedron Lett. 23 (1982) 2543.
[13] R. Caputo, C. Ferreri, S. Noviello, G. Palumbo, Synthesis (1986) 499.
[14] N.N. Joshi, M. Srebnic, H.C. Brown, J. Am. Chem. Soc. 110 (1988) 6246.
[15] T.W. Bell, J.A. Ciiaccio, Tetrahedron Lett. 27 (1986) 827.
[16] P. Bovicelli, E. Mincion, G. Ortaggi, Tetrahedron Lett. 32 (1991) 3719.
[17] J.A. Ciaccio, E. Heller, A. Talbot, Synlett (1991) 248.
[18] Z.X. Guo, A.H. Haines, R.J.K. Taylor, Synlett (1993) 607.
[19] H. Kotsuki, T. Shimanouchi, Tetrahedron Lett. 37 (1996) 1845.
[20] H. Sharghi, H. Naeimi, Bull. Chem. Soc. Jpn. 72 (1999) 1525.
[21] M. Salavati-Niasari, S.H. Banitaba, J. Mol. Catal. A 201 (2003) 43.
[22] M. Salavati-Niasari, F. Farzaneh, M. Ghandi, J. Mol. Catal. A 186 (2002) 101.
[23] R.C. Anderson, J.S. Bajwa, Tetrahedron Lett. 32 (1991) 3021.
[24] P. Salehi, N. Iranpoor, F. Kazemi, Synth. Commun. 27 (1997) 1247.
[25] Y. Ishii, H. Masuda, K. Takase, M. Nishio, A. Hasegawa, Y. Nishiyama, J. Org. Chem. 59 (1994) 5550.
[26] R. Rosenthal, C.O. Guss, J. Am. Chem. Soc. 77 (1955) 2549.
[27] K. Bauer, P. Pfeiffer, Chem. Ber. 80 (1947) 7.
[28] R. Filler, S.M. Naqvi, J.P. Horwits, J. Am. Chem. Soc. 79 (1957) 6283.
[29] W. Yuanliu, Z. Ailian, Y. Huaxue, 13 (1993) 616.
[30] T. Katsuki, J. Mol. Catal. A 113 (1996) 87.
[31] E.N. Jacobsen, in: Catalytic Asymmetric Synthesis, I. Ojima (Ed.), VCH Publishers Inc., New York, 1993, p. 159.
[32] T. Katsuki, K. Hori, H. Sugihara, N. Ito, Tetrahedron Lett. 40 (1999) 5207.
[33] T. Katsuki, T. Fukuda, Tetrahedron 53 (1997) 7201.
[34] T. Katsuki, Y. Yamashita, Synlett (1995) 829.
[35] E.N. Jacobsen, J. Branalt, S.E. Schaus, J. Org. Chem. 63 (1998) 403.
[36] M. Tasinazzo, Y. Belokon, M. Felego, J. Chem. Soc., Perkin Trans. 1 (1997) 1293.

[37] L. Yashkina, Y. Belokon, N. Ikonnikov, Tetrahedron: Asymmetry 7 (1996) 851.
[38] E.N. Jacobsen, M.S. Sigma, J. Am. Chem. Soc. 120 (1998) 5315.
[39] D.C. Sherrington, Polymer-Supported Synthesis, in: J.H. Clark (Ed.), Chemistry of Waste Minimization, Blackie, London, 1995, p. 141.
[40] S.J. Shuttlewoth, S.M. Allin, P.K. Sharma, Synthesis (1997) 1218.
[41] P. Hodge, Polymer-Supported Asymmetric Organic Synthesis, in: R. Epton (Ed.), Solid Phase Synthesis, SPCC (UK) Ltd, Birmingham, 1990, p. 173.
[42] E. Turos, M.I. Konaklieva, M.L. Dahi, Tetrahedron Lett. 33 (1992) 7093.
[43] P.B.D. DE la Mare, R. Bolton, Electrophilic Addition to Unsaturated Systems, Elsevier Scientific, Amsterdam, 1996.
[44] F. Macchia, M. Chini, P. Crotti, C. Gardelli, Tetrahedron 48 (1992) 3805.
[45] Y.S. Cho, Y.G. Suh, B.A. Koo, J.A. Ko, Chem. Lett. (1993) 1907.
[46] J.A. Ciaccio, T.W. Bell, Tetrahedron Lett. 27 (1986) 827.
[47] A. Semnani, M. Shamsipur, J. Chem. Soc., Dalton Trans. (1999) 2215.
[48] H. Sharghi, A.R. Massah, M. Abedi, Talanta 49 (1999) 531.
[49] T.I. Petrenko, Y.A. Serguchev, Teor. Eksp. Khim. 13 (1977) 705.

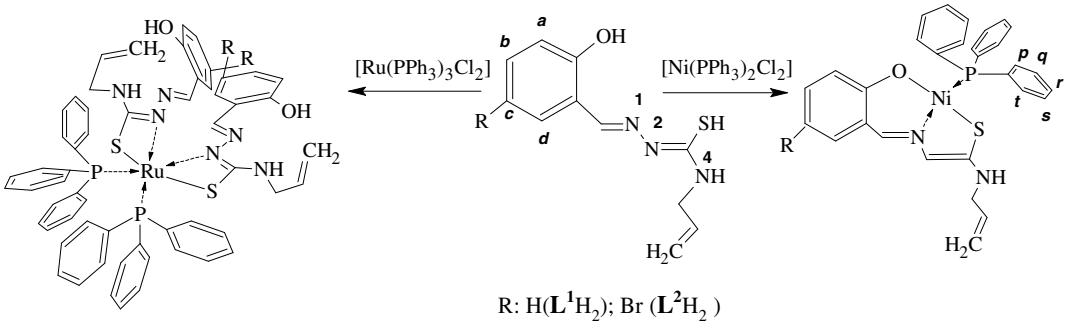

Fig. 1. The formation of the [Ni(L)(PPh$_3$)] and [Ru(HL)$_2$(PPh$_3$)$_2$] complexes.

complexes were recorded in 10^{-4} M $CHCl_3$ solution with an ATI-Unicam spectrometer in the 800–200 nm range. The ^{1}H and ^{31}P NMR spectra were recorded on a Bruker Avance-500 model spectrometer using DMSO-d_6 as solvent, relative to $SiMe_4$ and H_3PO_4, respectively. Magnetic measurements were carried out at room temperature with a Sherwood Scientific MK I apparatus by using $CuSO_4.5H_2O$ as the calibrant. The molar conductivities of the compounds were measured in 10^{-3} M DMSO solution at 25 ± 1 °C using a digital WPA CMD 750 conductivity meter.

The APCI MS analyses were carried out in the positive ion mode using a Thermo Finnigan LCQ Advantage MAX LC/MS/MS. The mobile phase consisted of MeOH. A hypersil Betabasic-8 (5 μ, 100 mm × 4.6 mm) column was used at a flowrate of 0.5 ml/min at 25 °C. APCI-MS inlet conditions in the positive ion mode: heated capillary temp. 200 °C; vaporizer temp. 450 °C.

2.2. Synthesis of the ligands and complexes

2.2.1. Ligands

The ligands, $\mathbf{L^1}H_2$ and $\mathbf{L^2}H_2$, were prepared by the literature method [34]. The colours, m.p. (°C), yields (%), R_f value (hexane–EtAc, 2:1), elemental analysis, UV–Vis. (λ_{max} (ε), nm (dm^3 cm^{-1} mol^{-1})), IR (cm^{-1}) and ^{1}H NMR (ppm, J in Hz) data of the ligands are as follows:

$\mathbf{L^1}H_2$: Cream, 155-157; 82; 0.50. *Anal.* Calc. for $C_{11}H_{13}N_3OS$ (235.3 g): C, 56.15; H, 5.57; N, 17.86; S, 13.63. Found: C, 56.19; H, 5.57; N, 17.95; S, 13.61%. UV–Vis: 217 (36520), 243 (8650), 295 (shoulder), 306 (11930), 335 (12630), 345 (shoulder), 631 (90). IR: ν(N^{4}H) 3430, ν(OH) 3407, ν(N^{2}H) 3153, ν(C=CH$_2$) 3000, δ (N^{4}H) 1623, δ (N^{2}H) 1623, ν(C=N^1) 1607, ν(–CS–NH) 1538, 1292, ν(–C=S) 1223. ^{1}H NMR: 11.42 (s, 1H, O*H*), 9.86 (s, 1H, N^2*H*), 8.56 (t, J = 5.85, 1H, N^4*H*), 8.37 (s, 1H, C*H*=N), 7.92 (dd, J = 1.46, J = 7.80, 1H, *d*), 7.20 (td, J = 1.46, J = 8.78, 1H, *b*), 6.86 (d, J = 7.32, 1H, *a*), 6.82 (t, J = 7.81, 1H, *c*), 5.90 (m, 1 H, –C*H*=), 5.14 (dq, J = 1.95, J = 1.46, J = 17.57, 1H, =CH_{2a}), 5.08 (dq, J = 1.46, J = 1.46, J = 10.24, 1H, =CH$_{2b}$), 4.20 (t, J = 5.86, 2H, N–CH_2–).

$\mathbf{L^2}H_2$: Light yellow; 179–180; 69; 0.45. *Anal.* Calc. for $C_{11}H_{12}N_3OSBr$ (314.2 g): C, 42.05; H, 3.85; N,13.37; S, 10.21. Found: C, 42.09; H, 3.81; N, 13.28; S, 10.25%. UV–Vis: 218 (8450), 248 (10446), 306 (shoulder), 315 (14040), 346 (14986), 354 (shoulder), 460 (110). IR: ν(N^4 H) 3438, ν(OH) 3384, ν(N^{2}H) 3153, δ (N^{4}H) 1646, δ (N^{2}H) 1623, ν(C=N^1) 1607, ν(C=CH$_2$) 3092, 3000, ν(–CS–NH) 1538, ν(C=S) 1230. ^{1}H NMR: 11.21 (s, 1H, O*H*), 10.30 (s, 1H, N^{2}H), 8.51 (t, 1H, N^{4}H), 8.07 (s, 1H, C*H*=N), 7.89 (d, J = 2.24, 1H, *d*), 7.11 (dd, J = 2.49, J = 8.71, 1H, *b*), 6.60 (d, J = 8.72, 1H, *a*), 5.65 (m, 1H, –C*H*=), 4.89 (d, J = 1.52, J = 17.88, 1H, =CH_{2a}), 4.86 (dd, J = 1.28, J = 10.69, 1H, =CH$_{2b}$), 3.96 (d, J = 5.03, 2H, N–CH_2–).

2.2.2. Complexes

2.2.2.1. Synthesis of [NiL^1(PPh$_3$)] (I). A solution of 2-hydroxy-benzaldehyde-4-allyl-thiosemicarbazone ($\mathbf{L^1}H_2$) (50 mg, 1 mmol) in dichloromethane (10 ml) was added dropwise to a solution of [Ni(PPh$_3$)$_2$Cl$_2$] (139 mg, 1 mmol) in 10 ml of absolute ethanol under a nitrogen atmosphere. The solution was stirred for 5 h at room temperature. The resulting dark red precipitate was collected by filtration, and dried over anhydrous $CaCl_2$.

The complex [Ni($\mathbf{L^2}$)(PPh$_3$)] was prepared in a similar manner. The colours, m.p. (°C), yields (%), R_f ($CHCl_3$), μ_{eff} value (BM), molar conductivity (ohm^{-1} cm^2 mol^{-1}), elemental analysis, electronic, IR (cm^{-1}) and NMR (ppm, J in Hz, *p–t* are the symbols for the PPh$_3$ protons) data of the nickel complexes are as follows:

*[Ni(L^1)(PPh$_3$)](**I**):* Red; 198-199; 85; 0.52; 0.12; 8.2. *Anal.* Calc. for $C_{29}H_{26}N_3OPSNi$ (554.27 g): C, 62.84; H, 4.73; N, 7.58; S, 5.79; Ni, 10.59. Found: C, 62.79; H, 4.79; N, 7.43; S, 5.99; Ni, 10.68%. UV–Vis (nm, dm^3 cm^{-1} mol^{-1}): 246 (76320), 299 (shoulder), 366 (12420), 412 (7110), 819 (80), 962 (30). IR: ν(N^{4}H) 3430, ν(C=CH$_2$) 3075, 3048, ν(–CH$_2$–) 2964, 2921, 2852, δ (N^4 H) 1639, ν(C=N^1) 1601, 1562, ν(–CS–NH) 1539, ν(PPh$_3$) 1435, 1096, 1027, 996, 754, 692, ν(–C–S) 1208. ^{1}H NMR: 8.40 (d, J = 8.29, 1H, C*H*=N), 7.79 (dd, J = 8.3, J = 9.27, 6H, *p, t*), 7.62 (d, J = 6.35, 3H, *r*), 7.58 (d, J = 6.83; 6H, *q, s*), 7.44 (d, J = 7.32, 1H, *d*), 7.20 (br s, 1H, N^{4}H), 7.09 (t, J = 7.81, 1H, *b*), 6.33 (d, J = 8.29, 1H, *a*), 5.87 (m, 1H, –C*H*=), 5.17 (dd, J = 1.46, J = 17.12, 1H, =CH_{2a}), 5.08 (d–d, J = 1.95, J = 10.24, 1H, =CH$_{2b}$), 3.81 (s, broad, 2H, N–CH_2–); ^{31}P NMR: 18.54. *m/z* (+c APCI-MS, % relative abundance): [M$^+$] 554.27 (100.00), [M+H$^+$] 555.5 (49.58), [M+2H$^+$] 556.2 (40.21), [M−H$^+$] 553.8 (31.19), [M−2H$^+$] 552.3 (20.18), [PPh$_3$OH]$^{2+}$ 279.2 (18.24), [PPh$_3$OH$_2$]$^{2+}$ 280.4 (10.24), [Ni$\mathbf{L^1}$] 291.8 (7.13), [Ni$\mathbf{L^1}$(PPh$_3$)$_2$] 816.5 (11.10), [Ni($\mathbf{L^1}$)$_2$(PPh$_3$)$_2$] 1050.6 (9.06).

*[Ni(L^2)(PPh$_3$)] (**II**):* Red; 215–216; 84; 0.59; 0.19; 5.9. *Anal.* Calc. for $C_{29}H_{25}N_3OPSNiBr$ (633,17 g): C, 55.01; H, 3.98; N,6.64; S, 5.06; Ni, 9.27. Found: C, 55.06; H, 3.94; N, 6.67; S, 5.09; Ni, 9.30. UV–Vis (nm, dm^3 cm^{-1} mol^{-1}): 251 (33458), 270 (shoulder), 303 (shoulder), 372 (11072), 418 (6300) 762 (90), 963 (30). IR: ν(N^{4}H) 3415, ν(C=CH$_2$) 3061, 3015, ν(–CH$_2$–) 2915, 2861, δ (N^4 H) 1638, ν(C=N^1) 1600, ν(–CS–NH) 1538, ν(PPh$_3$) 1438, 1100, 1030, 1000, 753, 700, ν(–C–S) 1192. ^{1}H NMR: 8.36 (d, J = 7.94, 1H, C*H*=N), 7.70 (d, J = 7.78, 6H, *p, t*), 7.56 (3H, *r*), 7.52 (t, J = 7.32, J = 7.81, 6H, *q, s*), 7.62 (d, J = 7.94, 1H, *d*), 7.31 (br s, 1H, N^{4}H), 7.11 (d, J = 8.39, 1H, *b*), 6.19 (d, J = 8.38, 1H, *a*), 5.80 (m, 1H, –C*H*=), 5.11 (d, J = 17.12, 1H, =CH_{2a}), 5.03 (d, J = 10.31, 1H, =CH$_{2b}$), 3.75 (s, 2H, N–CH_2–); ^{31}P NMR: 20.53. *m/z* (+c APCI-MS, % relative abundance): [M$^+$] 633.2 (100.00), [M+H$^+$] 634.3 (34.17), [M+2H$^+$] 635.3 (29.9), [M−H$^+$] 632.3 (27.09), [M−2H$^+$] 631.3 (21.30), [PPh$_3$OH]$^{2+}$ 279.3 (11.85), [PPh$_3$OH$_2$]$^{2+}$ 280.3 (15.69), [Ni$\mathbf{L^2}$] 370.8 (6.7), [Ni$\mathbf{L^2}$(PPh$_3$)$_2$] 895.4 (9.35), [Ni($\mathbf{L^2}$)$_2$(PPh$_3$)$_2$] 1209.5 (6.06).

2.2.2.2. Synthesis of [Ru(L^{1}H)$_2$(PPh$_3$)$_2$](III). Triethylamine was used to pluck the acidic –SH proton in the synthesis of the Ru complexes because the ruthenium complexes were not obtained according to the syntheses procedure of the nickel complexes. To the solution of

the salicylaldehyde-4-allyl-thiosemicarbazone ligand (100 mg; 1 mmol) in absolute ethanol (15 ml) was added triethylamine (0.15 ml), and the mixture was stirred for 1 h under a nitrogen atmosphere at room temperature. The mixture was combined with a suspension of $[Ru(PPh_3)_3Cl_2]$ (408 mg, 1 mmol) in 10 ml of dichloromethane and refluxed for 5 hours. After several days, yellow plates were isolated and dried over anhydrous $CaCl_2$.

The complex $[Ru(\mathbf{L^2}H)_2(PPh_3)_2]$ (**IV**) was synthesized by means of the same procedure. The colours, m.p. (°C), yields (%), R_f (pet-ether:$CHCl_3$, 1:1), μ_{eff} value (BM), molar conductivity ($ohm^{-1}\,cm^2\,mol^{-1}$), elemental analysis electronic, IR (cm^{-1}) and NMR (ppm, *J* in Hz) data of the **III** and **IV** are as follows:

$[Ru(L^1H)_2(PPh_3)_2]$ (**III**)*:* Yellow; 174–175; 71; 0.38; 0.22; 9.9. *Anal.* Calc. for $C_{58}H_{54}N_6O_2P_2S_2Ru$ (1094.24 g): C, 63.66; H, 4.97; N, 7.68; S, 5.86. Found: C, 63.59; H, 4.92; N, 7.65; S, 5.88%. UV–Vis (nm, $dm^3\,cm^{-1}\,mol^{-1}$): 242 (65260), 322 (shoulder), 330 (shoulder), 346 (13870), 382 (12750), 762 (90), 960 (20). IR: *ν*(OH) 3469, *ν*(N^4H) 3438, *ν*(C=CH_2) 3084, 3053, *ν*(–CH_2–) 2923, 2861, *δ* (N^4 H) 1638, 1623, *ν*(C=N^1) 1600, *ν*(–CS–NH) 1546, *ν*(PPh_3) 1438, 1092, 1038, 1000, 753, 700, *ν*(C–S) 1238. ^{1}H NMR: 10.05 (s, 2H, O*H*), 8.98 (s, 2H, C*H*=N), 7.27 (dd, *J* = 8.3, *J* = 7.82, 12H, *p, t*), 7.25 (t, *J* = 7.32, 6H, *r*), 7.08 (t, *J* = 7.32, 12H, *q,s*), 7.23 (s, 2H, *d*), 7.03 (dd, *J* = 5.86, *J* = 6.34, 2H, N^4H), 7.20 (ddd, *J* = 1.47, *J* = 7.81, 2H, *b*), 6.89 (ddd, *J* = 0.97, *J* = 7.32, 2H, *c*), 6.83 (d, *J* = 7.81, 2H, *a*), 5.60 (m, 2H, –C*H*=), 4.94 (dq, *J* = 1.46, *J* = 12.20, *J* = 17.07, 2H, =CH_{2a}), 4.80 (dq, *J* = 1.47, *J* = 5.37, *J* = 10.25, 2H, =$CH2_b$), 3.68 (m, 2H, N–CH_{2a}–), 3.62 (m, 2H, N-CH_{2b}-). ^{31}P NMR: 23.13, −75,28. *m/z* (+c APCI-MS,% relative abundance): [M^+] 1094.2 (100.00), [M+H^+] 1095.5 (34.17), [M+2H^+] 1096.6 (41.13), [M−H^+] 1093.2 (23.81), [M−2H^+] 1092.1 (25.14), $[PPh_3OH]^{2+}$ 279.3 (21.34), $[PPh_3OH_2]^{2+}$ 280.3 (11.42), $[Ru\mathbf{L^1}(PPh_3)]$ 596.9 (9.07), $[Ru\mathbf{L^1}(PPh_3)_2]$ 859.2 (12.12), $[Ru(\mathbf{L^1})_2(PPh_3)]$ 831.9 (11.05), $[Ru(\mathbf{L^1})_3(PPh_3)]$ 1591.5 (8.75), $[Ru(\mathbf{L^1})_2(PPh_3)_3O]$ 1372.5 (8.45), $[Ru(\mathbf{L^1})_3(PPh_3)OH]$ 1373.8 (11.05).

$[Ru(L^2H)_2(PPh_3)_2]$ (**IV**)*:* Yellow; 198–199; 58; 0.59; 0.18; 10.9. *Anal.* Calc. for $C_{58}H_{52}N_6O_2P_2S_2RuBr_2$ (1252.03 g): C, 55.64; H, 4.19; N,6.71; S, 5.12. Found: C, 55.67; H, 4.17; N, 6.68; S, 5.08%. UV–Vis (nm, $dm^3\,cm^{-1}\,mol^{-1}$): 247 (13460), 324 (shoulder), 355 (5620), 393 (4840), 832 (90), 967 (50). IR: *ν*(OH) 3469, *ν*(N^4 H) 3423, *ν*(C=CH_2) 3076, 3023, 2992, *ν*(–CH_2–) 2915, 2876, *δ* (N^4H) 1638, 1623, *ν*(C=N^1) 1600, *ν*(CS–NH) 1546, *ν*(PPh_3) 1438, 1092, 1030, 1000, 753, 700, *ν*(C–S) 1238. ^{1}H NMR: 10.04 (s, 2H, O*H*), 8.84 (s, 2H, C*H*=N), 7.19 (m, 18H, *p, t, r*), 7.00 (t, 12H, *J* = 6.72, *q, s*), 7.45 (s, 2H, *d*), 7.8 (broad, 2H, N^4H), 7.02 (d, *J* = 6.72, 2H, *b*), 6.75 (d, *J* = 7.95, 2H, *a*), 5.58 (m, 2H, –C*H*=), 4.88 (d, *J* = 17.00, 2H, =CH_{2a}), 4.76 (d, *J* = 9.93, 2H, =CH_{2b}), 3.60 (d, *J* = 14.93, 4H, N–CH_2–). ^{31}P NMR: 24.02, −76.86. *m/z* (+c APCI-MS,% relative abundance): [M^+] 1252.2 (100.00), [M+H^+] 1253.2 (81.36), [M+2H^+] 1254.1 (48.05), [M−H^+] 1251.2 (29.13), [M−2H^+] 1250.0 (36.71), $[PPh_3OH]^{2+}$ 279.3 (15.16), $[PPh_3OH_2]^{2+}$ 280.4 (8.49), $[Ru\mathbf{L^2}(PPh_3)]$ 675.7 (11.57), $[Ru\mathbf{L^2}(PPh_3)_2]$ 937.3 (15.94), $[Ru(\mathbf{L^2})_2(PPh_3)]$ 989.7 (11.05), $[Ru(\mathbf{L^2})_3(PPh_3)]$ 1828.3 (10.84), $[Ru(\mathbf{L^2})_2(PPh_3)_3O]$ 1530.0 (11.54), $[Ru(\mathbf{L^2})_3(PPh_3)OH]$ 1531.2 (10.25).

2.3. X-ray crystallography

2.3.1. $[NiL^2(PPh_3)]$ (II)

A red prism crystal of $C_{29}H_{25}BrN_3NiOPS$ of dimensions 0.60 × 0.40 × 0.20 mm was mounted on a glass fiber. All measurements were made on a Rigaku RAXIS RAPID imaging plate area detector with graphite monochromated Mo Kα radiation. The absorption correction was applied using the multi-scan technique [35]. The structure was solved by direct methods [36] and the molecular structure is shown in Fig. 2. The non-hydrogen atoms were refined anisotropically. H atoms were positioned geometrically and treated using a riding model, fixing the bond lengths at

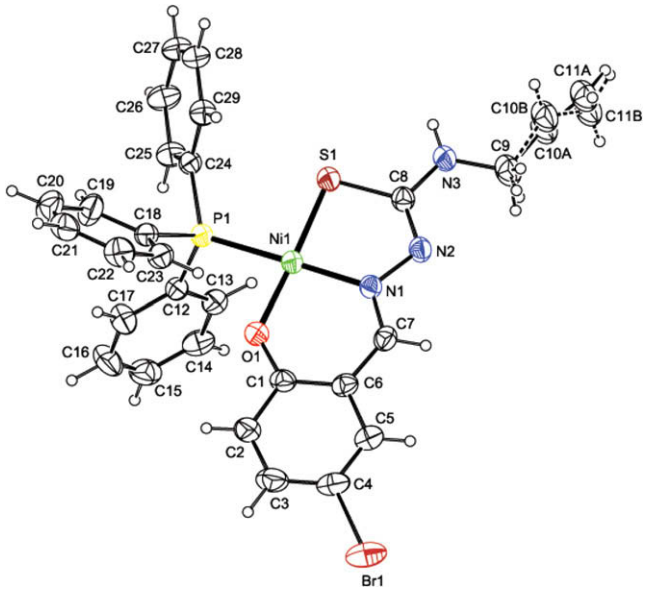

Fig. 2. Molecular structure of $[Ni(L^2)(PPh_3)]$, showing 30% probability displacement ellipsoids and the atom numbering scheme. The H atoms have been omitted for clarity.

0.97 Å for atom C9, 0.93 Å for the phenyl rings and atoms C7, C10 and C11, and 0.86 Å for the NH group. The displacement parameters of the H atoms were constrained as $U_{iso}(H) = 1.2U_{eq}$ of the parent atom. In the molecule, the (C10–C11) group shows positional disorder and the refined site-occupancy factors of the disordered parts, viz. C10A–C11A and C10B–C11B, are 70(1) and 30(1)%, respectively. The disordered atoms were refined using the following restraints: SIMU, DELU and SADI [37].

2.3.2. $[Ru(L^1H)_2(PPh_3)_2]$(III)

A brown prism crystal of $C_{58}H_{54}N_6O_2P_2RuS_2$ of dimensions 0.72 × 0.52 × 0.28 mm was mounted on a glass fiber. All measurements were made on a STOE IPDS 2 imaging plate area detector with graphite monochromated Mo Kα radiation. The absorption correction was applied using X-RED32 [39]. The structure was solved by direct methods [36] and refined by full-matrix least-squares refinement [37]. H atoms bounded to C atoms were positioned geometrically and treated using a riding model, fixing the bond lengths at distances in the range 0.93–0.97 Å, and with $U_{iso}(H) = 1.2U_{eq}(C)$. The H atoms bound to the N and O atoms were found from a Fourier map and refined freely.

3. Results and discussion

3.1. Some physical properties of the compounds

The thiosemicarbazone ligands are in the form of powder crystals, and they are soluble in methanol, ethanol and chlorinated hydrocarbons. The reactions of the ligands with $[NiCl_2(PPh_3)_2]$ and $[RuCl_2(PPh_3)_3]$ in a 1:1 molar ratio in ethanol-dichloromethane mixture yielded the 1:1 and 1:2 complexes of the formula $[Ni(L)(PPh_3)]$ and $[Ru(LH)_2(PPh_3)_2]$, respectively. The complexes (I–IV) form as very fine crystal materials, and they are very soluble in common organic solvents. The relative low molar conductances of **I**–**IV** between 5.9 and 10.9 $ohm^{-1}\,cm^2\,mol^{-1}$ indicate non-ionic structures. All the complexes are stabile in air, and the magnetic susceptibility values (0.12–0.22 BM) evince a square planar environment of the d^8 nickel ion and a low-spin structure (d^6) of the ruthenium ion in the 2+ oxidation state.

3.2. Spectral data

UV–Vis spectra of the ligands and complexes showed the expected $\pi \rightarrow \pi^*$ bands at 217–251 nm. The bands in the range 270–355 nm may be assignable to $n \rightarrow p^*$ transitions of the azomethine and thioamide region of the thiosemicarbazone moiety [39]. The spectra of the nickel complexes show broad bands in the visible region that are probably due to the expected MLCT transitions. The absorptions at 336 (for I) and 372 (for II) nm may be attributed to S → nickel(II) charge-transfer transitions, Although these bands did not separate, the triple band appearance of absorptions in the visible region indicate that **I** and **II** consist of a square planar geometry around the nickel(II) ion [40]. For the ruthenium complexes, the $(4d\pi) \rightarrow \pi^*$(thioamide) transitions appear at 382 and 393 nm, respectively for **III** and **IV**. The bands at 960 (for III) and 967 (for IV) nm can be designated as d–d transition bands of a spin-paired d^6 species with a distorted octahedral structure [41].

The chelation of the thiosemicarbazone ligands can be easily monitored by means of IR and ^{1}H NMR spectra. In the infrared spectra of the ligands, the bands of the NH and OH groups were clearly visible in the regions 3500–3150 and 1640–1550 cm^{-1}. After the complexation, ν(OH) and one of the N^2H and N^4H bands, probably N^2H, disappear in the IR spectra of the nickel complexes (**I** and **II**), while only the vibrations of N^2H were removed from the spectra of the ruthenium complexes **III** and **IV**. The $\nu(C{=}N^1)$ bands of **I**–**IV** were recorded with a shift of approx. 8 cm^{-1} to lower frequencies compared to the free ligands.

The NMR signals of the ligand protons showed the expected chemical shift values [38–40]. After chelation of the nickel(II) ion, the proton signals of OH and N^2H were absent in the spectra of **I** and **II**. Because $\mathbf{L^1}$ and $\mathbf{L^2}$ act as bidentate ligands through the N^2 and S atoms towards ruthenium(II), the signals of the phenolic proton can be still observed at *ca.* 10 ppm in the spectra of **III** and **IV**. In all the complex spectra, the chemical shifts of the N^4H protons were recorded at a higher field compared to the free ligands, but the CH=N protons were to a lower field region.

In the ^{31}P NMR spectra of the nickel and ruthenium complexes, the bands which were observed in the range 18.54–24.02 ppm are attributed to the P atom in the basal plane, while the bands at −75.28 ppm (**III**), −76.86 ppm (**IV**) in the spectra of the ruthenium complexes are assigned to an apical P atom.

The analytical and spectral results indicate that the nickel complexes give 1:1 complexes with an ONS coordination mode, and the

Table 1
Crystallographic data for $[Ni(L^2)(PPh_3)]$ and $[Ru(L^1H)_2(PPh_3)_2]$

	$[Ni(\mathbf{L^2})(PPh_3)]$	$[Ru(\mathbf{L^1}H)_2(PPh_3)_2]$
Empirical formula	$C_{29}H_{25}BrN_3NiOPS$	$C_{58}H_{54}N_6O_2P_2RuS_2$
Formula weight	633.17	1094.23
Temperature (K)	293.1	293.1
Wavelength (Å)	0.71073	0.71069
Crystal system	monoclinic	triclinic
Space group	$P2_1/c$	$P\bar{1}$
Unit cell		
a (Å)	13.5835(5)	11.6232(7)
b (Å)	11.5596(3)	11.8379(6)
c (Å)	18.5590(7)	19.6654(11)
α (°)	90	96.917(4)
β (°)	105.658(2)	97.740(5)
γ (°)	90	98.725(4)
V (Å^3)	2805.99(16)	2622.6(3)
Z	4	2
D_{calc} (g/cm^3)	1.499	1.386
λ (Mo Kα) (cm^{-1})	22.78	4.89
F(000)	1288	1132
h, k, l Range	$-16 \leqslant h \leqslant 16$	$-14 \leqslant h \leqslant 14$
	$-12 \leqslant k \leqslant 13$	$-15 \leqslant k \leqslant 15$
	$-22 \leqslant l \leqslant 22$	$-22 \leqslant l \leqslant 25$
Reflections collected	51753	25964
Unique reflections	4908	11409
R_{int}	0.0493	0.0672
Data/restraints/parameters	4870/58/353	4870/0/676
R [$I > 2\sigma(I)$]	0.0762	0.0416
R_w [$I > 2\sigma(I)$]	0.1215	0.1062
Goodness-of-fit on Indicator	1.456	0.97
Structure determination	SHELXS-97	
Refinement	Full matrix	

Table 2
Bond lengths and selected bond and torsion angles for $[Ni(L^2)(PPh_3)]$

Bond lengths (Å)		Coordinate bond angles (°)		Torsion angle (°)	
Ni1–O1	1.857(4)	O1–Ni1–N1	95.53(17)	P1–Ni1–S1–C8	172.67
Ni1–N1	1.878(4)	O1–Ni1–S1	77.23(12)	N1–Ni1–S1–C8	−2.51
Ni1–S1	2.1260(15)	N1–Ni1–S1	87.23(13)	C7–N1–Ni1–S1	−178.03
Ni1–P1	2.1923(15)	O1–Ni1–P1	85.20(12)	S1–Ni1–P1–C12	−120.98
		N1–Ni1–P1	175.13(13)	S1–Ni1–P1–C18	119.65
		S1–Ni1–P1	92.03(6)	S1–Ni1–P1–C24	−1.73
		C8–S1–Ni1	96.09(18)	O1–Ni1–P1–C12	59.08
		C12–P1–Ni1	106.88(17)	O1–Ni1–P1–C18	−60.29
		C24–P1–Ni1	119.50(17)	O1–Ni1–P1–C24	178.33
		C18–P1–Ni1	115.54(18)	P1–Ni1–O1–C1	−177.57

Table 3
Hydrogen bond parameters (Å and °) in $[Ni(L^2)(PPh_3)]$

D–H···A	d(D–H)	d(H···A)	d(D···A)	<(DHA)
C23–H23···O1	0.93	2.51	3.144(7)	125.8
C11B–H11C···Br1	0.93	2.63	3.554(19)	172.4

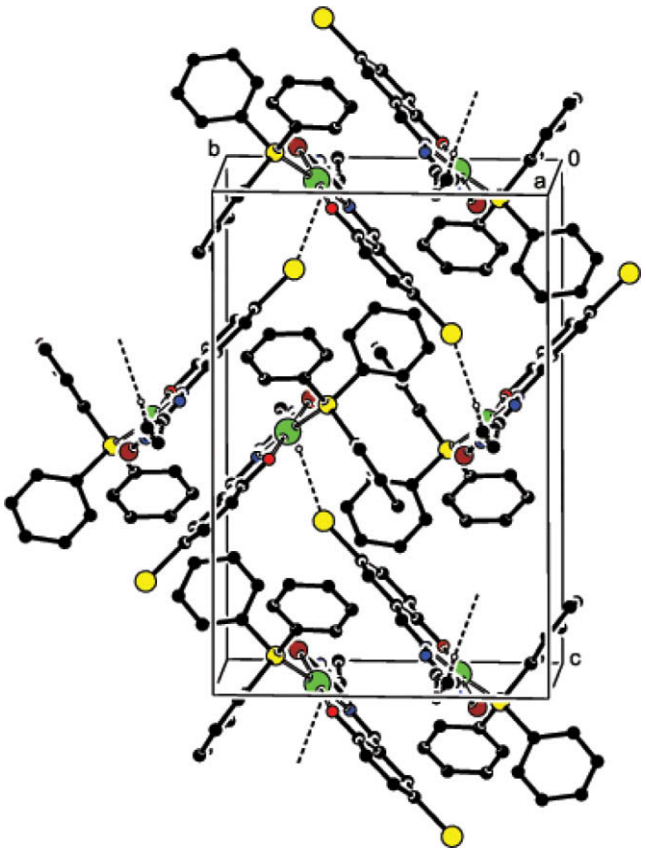

Fig. 3. Part of the crystal structure of $[Ni(L^2)(PPh_3)]$, showing the formation of a C(13) chain along [0 1 0]. For the sake of clarity, only H atoms involved in hydrogen bonding have been included.

Table 4
Bond lengths and selected bond and torsion angles for $[Ru(L^1H)_2(PPh_3)_2]$

Bond lengths (Å)		Coordinate bond angles (°)		Torsion angle (°)	
Ru1–S1	2.4372(6)	S1–Ru1–P1	88.25(2)	Ru1–S1–C77–N3	177.8(3)
Ru1–S2	2.4229(6)	S1–Ru1–P2	105.76(2)	Ru1–S2–C97–N6	179.8(3)
Ru1–P1	2.3231(7)	S1–Ru1–N2	65.72(6)	Ru1–S2–C97–N5	−1.1(2)
Ru1–P2	2.3176(7)	S1–Ru1–N5	98.86(5)	Ru1–P1–C10–C15	−76.7(2)
Ru1–N2	2.147(2)	S2–Ru1–P1	104.58(2)	Ru1–P1–C20–C25	160.4(3)
Ru1–N5	2.166(2)	S2–Ru1–P2	88.96(2)	Ru1–P1–C10–C11	99.1(2)
		S2–Ru1–N2	97.08(6)	Ru1–P1–C30–C35	−46.4(3)
		S2–Ru1–N5	65.82(5)	Ru1–P1–C30–C31	132.2(3)
		P1–Ru1–P2	98.71(3)	Ru1–P1–C20–C21	−18.4(3)
		P1–Ru1–N2	90.50(6)	Ru1–P2–C60–C61	93.3(2)
		P1–Ru1–N5	167.68(6)	Ru1–P2–C40–C41	−47.9(2)
		P2–Ru1–N2	167.40(6)	Ru1–P2–C50–C55	−11.6(2)
		P2–Ru1–N5	89.09(6)	Ru1–P2–C60–C65	−81.5(2)
		N2–Ru1–N5	83.37(8)	Ru1–P2–C50–C51	166.7(2)
		Ru1–S1–C77	81.55(9)	Ru1–P2–C40–C45	130.0(2)
		Ru1–S2–C97	81.94(8)	C76–N1–N2–Ru1	−22.8(4)
		Ru1–P1–C10	111.98(8)	Ru1–N2–C77–N3	−177.4(2)
		Ru1–P1–C20	120.68(9)	Ru1–N2–C77–S1	3.03(19)
		Ru1–P1–C30	119.02(11)	Ru1–N5–C97–S2	1.2(2)
		Ru1–P2–C40	117.83(8)	Ru1–N5–C97–N6	−179.7(3)
		Ru1–P2–C50	121.58(8)		
		Ru1–P2–C60	112.56(8)		

ruthenium complexes form 1:2 complexes through a bidentate function of the ligands (NS mode). As supplementary spectral data, it can be mentioned that the ^{31}P NMR values of **I–IV** justify the compositions, and also the M^+ and $M+H^+$ peaks in the mass spectra for **III** and **IV**.

Table 5
Hydrogen bond parameters (Å and °) in $[Ru(L^1H)_2(PPh_3)_2]$

D–H···A	d(D–H)	d(H···A)	d(D···A)	<(DHA)
O1–HO1···N1	0.86(5)	1.89(5)	2.656(4)	147(4)
O2–HO2···N4	0.72(5)	2.03(5)	2.667(4)	148(4)
C21–H21···S2	0.9300	2.4400	3.312(4)	155.00
C41–H41···S2	0.9300	2.7900	3.624(4)	150.00
C55–H55···S1	0.9300	2.4900	3.374(3)	160.00
C76–H76···S2	0.9300	2.6400	3.387(3)	138.00
C96–H96···S1	0.9300	2.6000	3.470(3)	155.00

Single crystals of **I–IV** were grown by crystallization from ethanol by ether diffusion. Crystallographic analyses of **II** and **III** were carried out and are reported here.

3.3. X-ray structure determination

3.3.1. Crystal structure of $[NiL^2(PPh_3)]$ (II)

Additional information for the structure determinations are given in Table 1. Selected bond distances, angles and torsion angles are listed in Table 2.

In the $[Ni(\mathbf{L^2})(PPh_3)]$ complex (Fig. 2), the structure of the molecule adopts a square planar geometry with O1–Ni1–S1 and N1–Ni1–P1 bond angles of 177.23(12) and 175.13(13)°, respectively (Table 2). The Ni atom almost lies in the basal plane containing the P, N, S and O donor atoms. The geometric parameters are comparable to those observed in other similar complexes [42].

In the Ni complex, the molecular conformation is stabilized by C–H···O and C–H···Br intramolecular hydrogen bonding interactions (Table 3). The crystal packing interactions and the hydrogen bonds of the title complex are shown in Fig. 3.

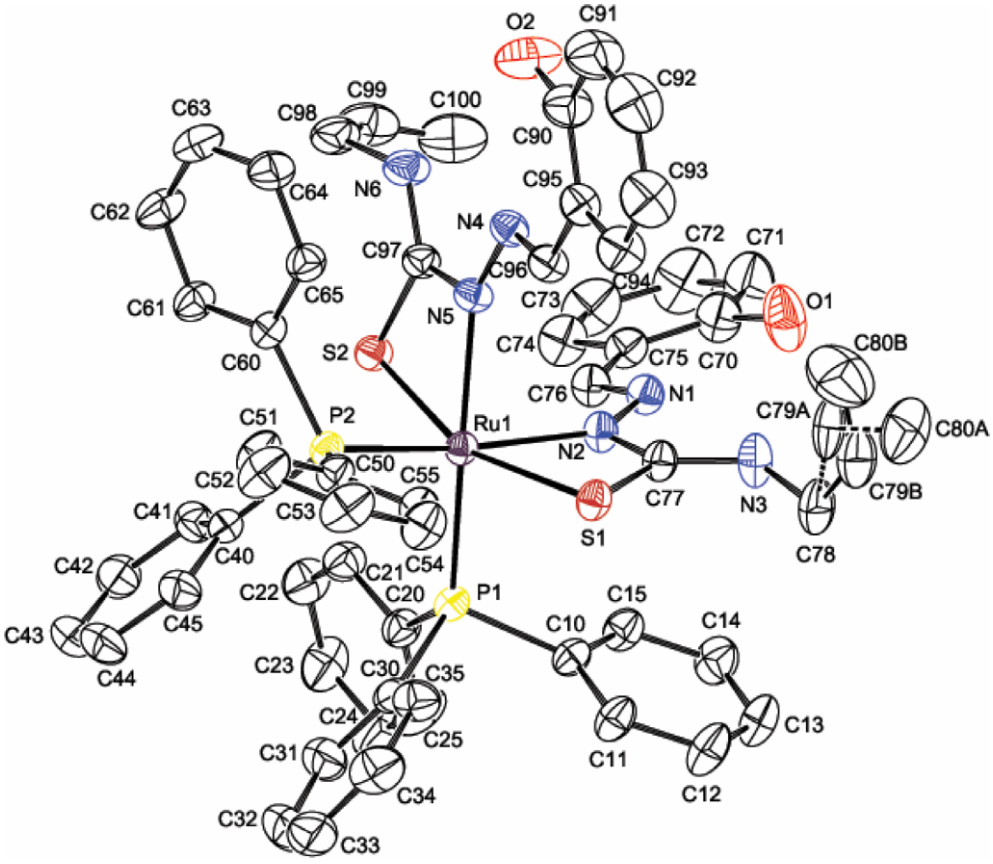

Fig. 4. Molecular structure of $[Ru(L^1H)_2(PPh_3)_2]$, showing 30% probability displacement ellipsoids and the atom numbering scheme. The H atoms have been omitted for clarity.

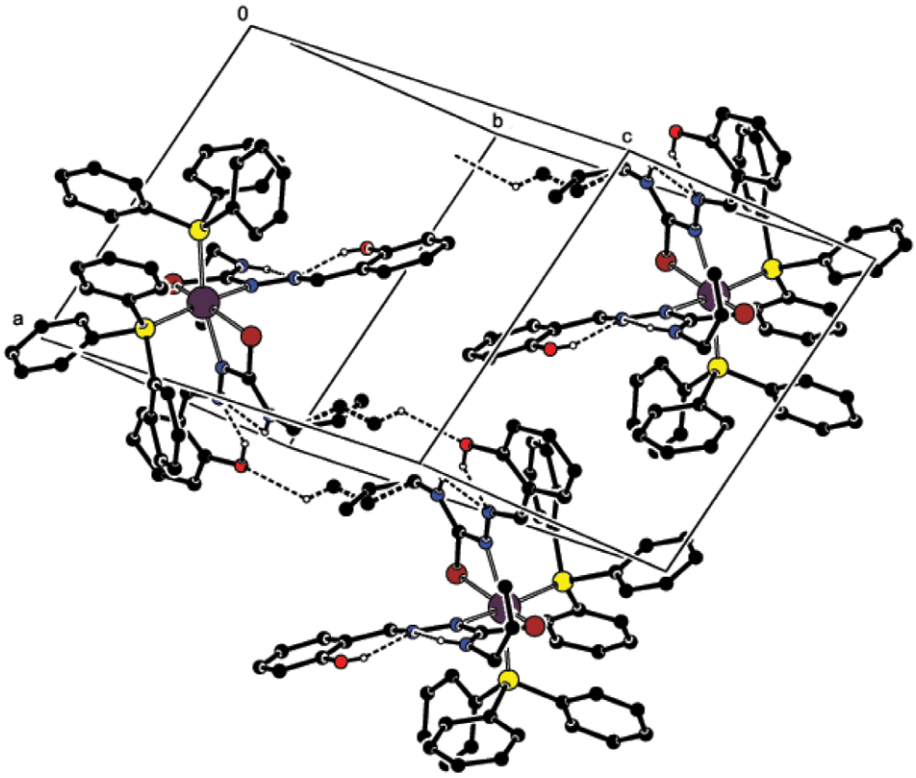

Fig. 5. A view the packing and hydrogen bonding of $[Ru(L^1H)_2(PPh_3)_2]$. H atoms not involved in hydrogen bonding have been omitted for clarity.

3.3.2. Crystal structure of $[Ru(L^1H)_2(PPh_3)_2]$(III)

In the molecule, the (C79–C80) group shows positional disorder and the refined site-occupancy factors of the disordered parts, viz. C79A–C80A and C79B–C80B, are 45(1)% and 55(1)%, respectively. Additional information on the structure determination is given in Table 1. Selected bond distances, angles and torsion angles are listed in Table 4.

In the $[Ru(\mathbf{L^1}H)_2(PPh_3)_2]$ complex (Fig. 4), the Ru atom is coordinated by two N atoms, two S atoms and two P atoms in a distorted octahedral geometry. The Ru–N distances are in the range 2.147 (2)–2.166 (2) Å, Ru–S distances 2.4229 (6)–2.4372 (6) Å and Ru–P distances 2.3176 (7)–2.3231 (7) Å. These distances are comparable to those found in other similar complexes [43–51]. Within the ligands, other geometric parameters all lie within the expected ranges.

In the Ru complex, the molecular conformation with the four-membered chelate ring formed by the ligand [52] and the distorted octahedral coordination geometry of the Ru atom are stabilized by C–H···S and O–H···N type-intramolecular hydrogen bonding interactions (Table 5). The crystal packing interactions and the hydrogen bonds of the title complex are shown in Fig. 5.

4. Conclusion

The interaction of $[NiCl_2(PPh_3)_2]$ with the dianionic ligands, $\mathbf{L^1}$ and $\mathbf{L^2}$, yielded the expected ON^1S chelates, **I** and **II** (Fig. 2). However, $[RuCl_2(PPh_3)_3]$ gave the 1:2 complexes (**III** and **IV**) through the N^2S donor set in the monoanionic forms of the ligands, even when a 1:1 mole ratio of the reactants was used (Figs. 4 and 5). Taking into consideration our data together previous studies [25–31] it is obvious that the substituents on the aryl and amide region of the tridendate thiosemicarbazones do not effect their chelating preferences. As for the reason of these interesting results, it can be said that ruthenium(II) prefers the higher symmetry of the octahedral geometry than of the bipyramidal geometry.

Acknowledgments

This work was supported by the Research Fund of Istanbul University. Project number, 233/29042004 and 516/050506. The authors acknowledge the Faculty of Arts and Sciences, Ondokuz Mayıs University, Turkey, for the use of the Stoe IPDS 2 diffractometer (purchased under grant F.279 of the University Research Fund).

Appendix A. Supplementary data

CCDC 674770 and 674769 contain the supplementary crystallographic data for [Ni(L2)(PPh3)] and [Ru(L1 H)2(PPh3)2]. These data can be obtained free of charge via http://www.ccdc.cam.ac.uk/conts/retrieving.html, or from the Cambridge Crystallographic Data Centre (CCDC), 12 Union Road, Cambridge CB2, IEZ, UK; fax: (+44) 1223-336-033; or e-mail: deposit@ccdc.cam.ac.uk.

References

[1] G. Simmons, L.B. Hobson, A. Resnick, R. de Nicola, R.H. Bennett, G. Rake, Trans Annu. Meet. Natl. Tuberc. Assoc. 46 (1950) 124.
[2] F. Gıaldı, R. Poncı, Farmaco 6 (3) (1951) 332.
[3] P. Mantegazza, R. Tommasını, Farmaco 6 (2) (1951) 264.
[4] A. Kolocouris, K. Dimas, C. Pannecouque, et al., Bioorg. Med. Chem. Lett. 12 (5) (2002) 723.
[5] A. De Logu, M. Saddi, V. Onnis, C. Sanna, C. Congiu, R. Borgna, M. Teresa Cocco, Int. J. Antimicrob. Ag. 26 (1) (2005) 28.
[6] M.R. Maurya, S.K. Shailendra, A. Azam, W. Zhang, D. Rehder, Eur. J. Inorg. Chem. 24 (2003) 43.
[7] E.W. Ainscough, A.M. Brodie, W.A. Denny, G.J. Finlay, J.D. Ranford, J. Inorg. Biochem. 70 (3–4) (1998) 175.
[8] L.S. Chin, S.F. Murray, D.H. Harter, J. Biomed. Sci. 6 (1999) 213.
[9] D.K. Sau, R.J. Butcher, S. Chaudhuri, N. Saha, Mol. Cell. Biochem. 253 (1–2) (2003) 21.
[10] T. Bal, B. Atasever, Z. Solakoğlu, S. Erdem-Kuruca, B. Ülküseven, Eur. J. Med. Chem. 42 (2) (2007) 161.
[11] T. Varadinova, D. Kovala-Demertzi, M. Rupelieva, M. Demertzis, P. Genova, Acta Virol. 45 (2) (2001) 87.

[12] V. Mishra, S.N. Pandeya, C. Pannecouque, M. Witvrouw, E. De Clercq, Arch. Pharm. 335 (5) (2002) 183.
[13] H. Beraldo, D. Gambino, Mini Rev. Med. Chem. 4 (2004) 159.
[14] A. Karam, R. Tenia, M. Martínez, F. López-Linares, et al., J. Mol. Catal. A: Chem. 265 (1–2) (2007) 127.
[15] M.R. Buchmeiser, K. Wurst, J. Am. Chem. Soc. 121 (1999) 11101.
[16] M. Cai, J. Sha, Catal. Commun. 8 (11) (2007) 1691.
[17] T.E. Barder, J. Am. Chem. Soc. 128 (2006) 898.
[18] H. Weissman, L.J.W. Shimon, D. Milstein, Organometallics 23 (16) (2004) 3931.
[19] G.B.W.L. Ligthart, R.H. Meijer, M.P. Hulshof, Tetrahedron Lett. 44 (2003) 1507.
[20] S.D. Robinson, M.F. Uttley, J. Chem. Soc., Dalton Trans. (1973) 1912.
[21] A. Dijksman, A.M. Gonzalez, A.M.I. Payeras, I.W.C.E. Arends, R.A. Sheldon, J. Am. Chem. Soc. 123 (2001) 6826.
[22] V. Mahalingam, R. Karvembu, V. Chinnusamy, K. Natarajan, Spectrochim. Acta, A 64 (2006) 886.
[23] S. Grguric-Sipka, C.R. Kowol, S.-M. Valiahdi, R. Eichinger, M.A. Jakupec, A. Roller, S. Shova, V.B. Arion, B.K. Kepler, Eur. J. Inorg. Chem. (2007) 2870.
[24] S. Rathinasamy, S.S. Karki, S. Bhattacharya, L. Manikandan, S.G. Prabakaran, M. Gupta, et al., J. Enzym. Inhib. Med. Chem. 21 (2006) 501.
[25] F. Basuli, M. Ruf, C.G. Pierpont, S. Bhattacharya, Inorg. Chem. 37 (1998) 6113.
[26] F. Basuli, S.M. Peng, S. Bhattacharya, Inorg. Chem. 36 (1997) 5645.
[27] T.S. Lobana, G. Bawa, R.J. Butcher, B.J. Liaw, C.W. Liu, Polyhedron 25 (15) (2006) 2897.
[28] D. Mishra, S. Naskar, M.G.B. Drew, S.K. Chattopadhyay, Polyhedron 24 (2005) 1861.
[29] D. Mishra, S. Naskar, M.G.B. Drew, S.K. Chattopadhyay, Inorg. Chim. Acta 359 (2006) 585.
[30] P. Sengupta, R. Dinda, S. Ghosh, Transition Met. Chem. 27 (2002) 665.
[31] K.P. Balasubramanian, R. Karvembu, R. Prabhakaran, V. Chinnusamy, K. Natarajan, Spectrochim. Acta, A 68 (1) (2007) 50.
[32] R. Prabhakaran, R. Karvembu, T. Hashimoto, K. Shimizu, K. Natarajan, Inorg. Chim. Acta 358 (2005) 2093.
[33] L.E. Nikolaeva, T.N. Tarkhova, N.V.G.I. Belov, Kristallografiya 19 (1974) 746.
[34] C. Yamazaki, Can. J. Chem. 53 (1975) 614.
[35] T. Higashi, Program for Absorption Correction. Rigaku Corporation, Tokyo, Japan, 1995.
[36] G.M. Sheldrick, SHELXS-97, Program for Crystal Structure Solution, University of Göttingen, Germany, 1997.
[37] G.M. Sheldrick, SHELXL-97, Program for Crystal Structure Refinement, University of Göttingen, Germany, 1997.
[38] Stoe & Cie, X-RED32, Stoe & Cie, Darmstadt, Germany, (2002).
[39] L.M. Fostiak, I. Garcia, J.K. Swearingen, E. Bermejo, A. Castineiras, D.X. West, Polyhedron 22 (2003) 83.
[40] H. Beraldo, L.P. Boyd, D.X. West, Transition Met. Chem. 23 (1998) 67.
[41] D.X. West, P.M. Ahweiler, G. Ertem, J.P. Scovill, et al., Transition Met. Chem. 10 (1985) 264.
[42] Tülay Bal-Demirci, Polyhedron 27 (2008) 440.
[43] V. Mahalingam, N. Chitrapriya, F.R. Fronczek, K. Natarajan, Polyhedron 27 (2008) 1917.
[44] L. Otero, P. Nobilia, D. Gambino, H. Cerecetto, M. González, J.A. Ellena, O.E. Piro, Inorg. Chim. Acta 344 (2003) 85.
[45] R. Cini, G. Tamasi, S. Defazio, M. Corsini, P. Zanello, L. Messori, G. Marcon, F. Piccioli, R. Orioli, Inorg. Chem. 42 (2003) 8038.
[46] P. Braunstein, C. Graiff, F. Naud, A. Pfaltz, T. Tiripicchio, Inorg. Chem. 39 (2000) 4468.
[47] S.A. Serron, C.M. Haar, S.P. Nolan, Organometallics 16 (1997) 5120.
[48] R.C. van der Drift, E. Bouwman, E. Drent, H. Kooijman, A.L. Spek, A.B. van Oort, W.P. Mul, Organometallics 21 (2002) 3401.
[49] N. Chitrapriya, V. Mahalingam, M. Zeller, K. Natarajan, Polyhedron 27 (2008) 1573.
[50] A. García-Fernández, J. Díez, Ã. Manteca, J. Sánchez, M.P. Gamasa, E. Lastra, Polyhedron 27 (2008) 1214.
[51] A.H. Murray, Z. Yue, A.I. Wallbank, T.S. Cameron, R. Vadavi, B.J. MacLean, M.A.S. Aquino, Polyhedron 27 (2008) 1270.
[52] D. Mishra, S. Naskar, M.G.B. Drew, S.K. Chattopadhyay, Polyhedron 24 (2005) 1861.

research opportunities and potential applications is chemical functionalization.

Functionalization of carbon nanotubes is an effective way to enhance the physical properties and improve the solubility. However, the aromatic character of nanotubes restricts the possible addition reactions. The functionalization of carbon nanotubes may extend the range of their potential applications. The electric properties of CNTs can be modified using chemical functionalization and the contact resistance between the interconnected tubes can be reduced by chemically binding functional groups. Suitable functionalization enables the linking of individual carbon nanotubes to form complex networks for nanoscale electronic circuits [17]. The functionalization solubilizes the nanotubes in a variety of solvents [18,19], allows chemical manipulations and improves the dispersion in composite applications. In nanocomposites, the functional groups attached to the walls of CNTs can form strong chemical bonds with the surrounding polymer matrix, increasing the binding force between the nanotube and the polymer [20,21].

Some of the functionalization approaches previously reported have involved the formation of covalent bonds [22–25], while others have employed non-covalent interactions [26–29]. Both non-covalent and covalent modifications of the surface have been developed to improve solubility. Non-covalent chemistry includes surfactant modification [30–32], polymer wrapping [33] and polymer absorption [34] in which the polymers were produced by an in situ ring-opening metathesis polymerization or emulsion polymerization. The initial attempts for covalent functionalization took advantage of the higher reactivity of carbon atoms at the ends of the nanotubes to carry out the series of reaction steps leading to the covalent attachment.

In this paper, we report the synthesis and characterization of manganese(II) complex of the Schiff-base ligand; *N*,*N*-bis(4-hydroxysalicylidene)-ethylene-1,2-diamine, $H_2[(OH)_2$-salen]; and this complex was covalently attached on MWNTs (Scheme 1), [Mn($(OH)_2$-salen)]@MWNTs, and used in the oxidation of cyclohexene with TBHP. As far as we know, our report constitutes the first example of MWNTs as a support for a manganese(II) salen complex in heterogeneous catalysis.

2. Experimental

2.1. Materials

All the solvents were purchased from Merck (pro analysi) and were distilled and dried using molecular sieves (Linde 4 Å). Manganese(ll) acetate, 4-hydroxysalicyclaldehyde and *tert*-butylhydroperoxide (solution 80% in di-*tert*-butylperoxide) were obtained from Merck Co. Cyclohexene was distilled under nitrogen and stored over molecular sieves (4 Å). Cyclohexanone was used as an internal standard for the quantitative analysis of the product using gas chromatography. Reference samples of 2-cyclohexene-1-ol and 2-cyclohexene-1-one (Aldrich) were distilled and stored in a refrigerator.

2.2. Physical measurements

^{1}H NMR (400 MHz) spectra were measured in DMSO solutions and referenced to the solvent signals. XRD patterns were recorded by a Rigaku D-max C III, X-ray diffractometer using Ni-filtered Cu Kα radiation. Transmission electron microscopy (TEM) images were obtained on a Hitachi H-800 transmission electron microscope with an accelerating voltage of 200 kV. FT-IR spectra were recorded on a Shimadzu Varian 4300 spectrophotometer in KBr pellets. The electronic spectra of the neat complexes were taken on a Shimadzu UV–Vis scanning spectrometer (Model 2101 PC). The stability of the complex covalently attached to the MWNTs was checked after the reaction by UV–Vis and possible leaching of the complex was investigated by UV–Vis in the reaction solution after filtration of the heterogeneous catalyst. The amounts of manganese complex grafted in the MWNTs matrix were determined by the elemental analysis and by subtracting the amount of manganese complex left in the solutions after the synthesis of the

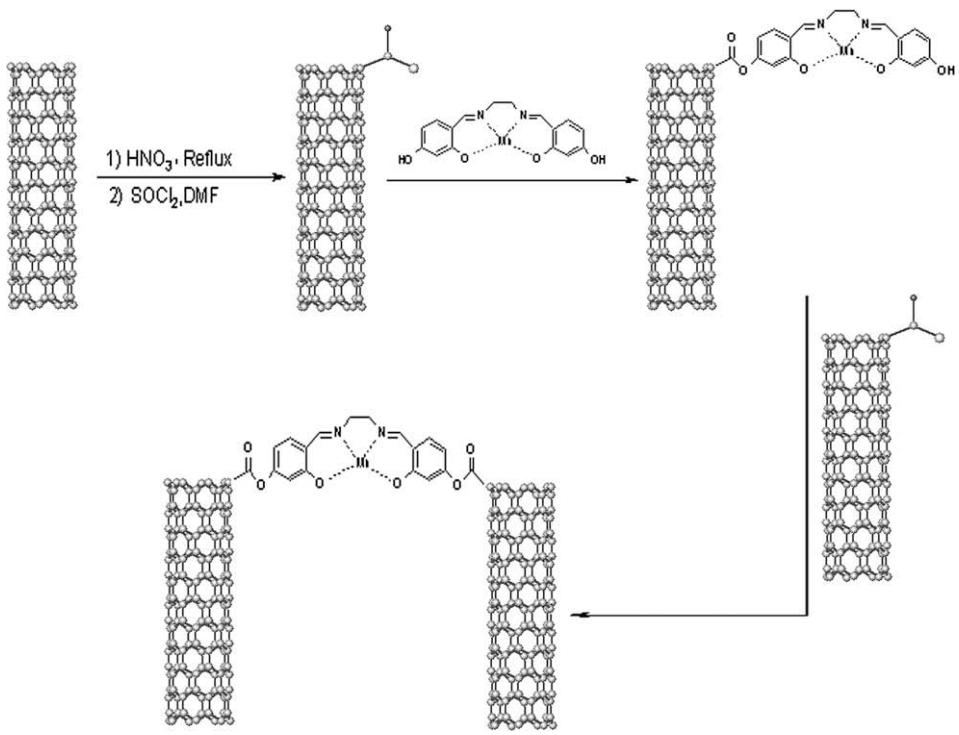

Scheme 1.

catalysts, as determined by UV–Vis spectroscopy, from the amount taken for the synthesis. Atomic absorption spectra (AAS) were recorded on a Perkin–Elmer 4100–1319 spectrophotometer using a flame approach, after acid (HF) dissolution of known amounts of the nanotubes. Diffuse reflectance spectra (DRS) were registered on a Shimadzu UV/3101 PC spectrophotometer in the range 1500–200 nm, using MgO as a reference. The elemental analysis (carbon, hydrogen and nitrogen) of the materials was obtained from a Carlo ERBA Model EA 1108 analyzer. XPS (small area X-ray photoelectron spectroscopy) data were recorded with the PHI-5702 Multi-Technique System, Power Source by Mg Kα line and Ag $3d_{5/2}$ FWHM $\leqslant$ 0.48 eV. Thermogravimetric-differential thermal analysis (TG-DTA) were carried out using a thermal gravimetric analysis instrument (Shimadzu TGA-50H) with a flow rate of 20.0 mL min^{-1} and a heating rate of 10 °C min^{-1}. The products were analyzed by GC–MS, using a Philips Pu 4400 Chromatography (1.5 m, 3% OV-17 Column), Varian 3400 Chromatography (25 m, DB- 5 Column) coupled with a QP Finnegan MAT INCOF 50, 70 eV.

2.3. Preparation of N,N-bis(4-hydroxysalicylidene)ethylene-1,2-diamine; $H_2[(OH)_2$-salen]

A stoichiometric amount of 4-hydroxysalicylaldehyde (0.02 mol, 2.76 g) in dissolved methanol (25 ml) was added drop by drop to a 1,2-diaminoethane solution (0.01 mol, 0.60 g) in 25 ml methanol. The contents were refluxed for 4 h and a bright yellow precipitate of the symmetrical Schiff-base ligand, $H_2[(OH)_2$-salen], was obtained. The yellow precipitate was separated by filtration, washed and dried in vacuum. It was then recrystallized from methanol to yield $H_2[(OH)_2$-salen]. Yield 97% (3.26 g); orange solid; mp > 230 °C; IR (KBr, cm^{-1}) $\nu_{C=N}$ 1640. *Anal.* Calc. for the Schiff-base ligand: C, 63.99; H, 5.37; N, 9.33; C/N, 6.86. Found: C, 63.80; H, 5.20; N, 9.46; C/N, 6.74%. ^{1}H NMR (DMSO-d_6, ppm) δ 3.76 (s, 4H), 6.14 (d, 2H), 6.24 (dd, 2H), 7.15 (d, 2H), 8.35 (s, 2H), 12.6 (s, 4H).

2.4. Preparation of $[Mn((OH)_2$-salen)]

The Schiff-base ligand (3.30 g, 0.011 mol) was dissolved in 100 ml of refluxing ethanol and a stream of nitrogen was purged through the solution for 4 h to eliminate any oxygen. A solution containing 2.7 g (0.011 mol) of manganese(II) acetate tetrahydrate in water was added dropwise to the deoxygenated ligand solution. The resulting mixture was agitated and refluxed under nitrogen with 5 ml of ethanol followed by 5 ml of water. The mixture was then cooled and filtered under reduced pressure. The collected solid was washed with diethyl ether and dried in air to give yellow crystalline $[Mn((OH)_2$-salen)], which was purified by recrystallization from chloroform (Yield: 51%). *Anal.* Calc. for $[Mn((OH)_2$-salen)]: C, 54.40; H, 3.99; N, 7.93; C/N, 6.86; Mn, 15.55; Mn/N, 1.96. Found: C, 54.27; H, 3.82; N, 8.08; C/N, 6.72; Mn, 15.32; Mn/N, 1.90%; IR (KBr, cm^{-1}) $\nu_{C=N}$ 1633.

2.5. Multi-wall carbon nanotubes (MWNTs) preparation and purification

The multi-wall carbon nanotubes (MWNTs) used in this study were prepared by chemical vapor deposition (provided by Jiang Youg Trade Co. (China)) with diameters ranging from 20 nm to 40 nm, lengths varying from 1 mm to 10 mm and a purity of 85%. The raw product was first immersed in an aqueous solution of HF to remove SiO_2, then filtered, washed with distilled water, and refluxed in diluted HNO_3 for 4 h to remove the metals and amorphous carbon. The resulting solid was then thoroughly washed with deionized water and THF, and dried in vacuum. TEM analysis showed that the carbon nanotubes exhibited a multi-wall structure and their diameters were about 20–40 nm.

2.6. Chlorination of MWNTs

The purified MWNTs (100 mg) previously dried under vacuum were suspended in a solution of $SOCl_2$ (25 ml) and DMF (1 ml). The suspension was stirred at 65 °C for 24 h. The solid was then separated by filtration and washed with anhydrous THF and dried in vacuum.

2.7. Anchoring the manganese(II) salen complex to the MWNTs; $[Mn((OH)_2$-salen)]@MWNTs

The MWNs were added (50 mg) to a solution of $[Mn((OH)_2$-salen)] (100 mg) in degassed $CHCl_3$ (8 ml), and the suspension was stirred for 20 h under N_2 atmosphere at 70 °C. The solid was then separated by filtration and exhaustively washed with THF and CH_2Cl_2, and dried in a vacuum. The loading of the $[Mn((OH)_2$-salen)] complex in the MWNTs, determined by elemental (N) analysis, was 0.4 mg. The Mn content for the manganese(II) complexes on MWNTs was below the detection limit of quantitative absorption spectroscopy.

Anal. Calc. for $[Mn((OH)_2$-salen)]@MWNTs: Mn/N, 1.78%; IR (KBr, cm^{-1}) $\nu_{C=N}$ 1604. Elemental and spectroscopic analysis of $[Mn((OH)_2$-salen)] and $[Mn((OH)_2$-salen)]@MWNTs confirmed the molecular composition of ligand.

2.8. Oxidation of cyclohexene

The catalytic oxidation of cyclohexene was carried out using both the catalysts. In a typical reaction, an aqueous solution of TBHP (2.28 g, 20 mmol), cyclohexene (0.82 g, 10 mmol) and catalyst (9.2×10^{-5} mol) were mixed in 20 ml of CH_3CN and the reaction mixture was heated at 80 °C with continuous stirring in an oil bath. The progress of the reaction was monitored as mentioned above and the identity of the various products confirmed by GC–MS. The concentration of the products was determined using cyclohexanone as an internal standard.

3. Results and discussion

Synthesis of the manganese(II) complex involved heating and stirring of stoichiometric amounts of $H_2[(OH)_2$-salen] and manganese(II) acetate in methanol. The desired complex crystallized upon cooling and was recrystallized from chloroform. Elemental analysis indicates that the complex is a monomeric species formed by coordination of 1 mol of Mn(II) and 1 mol of $[(OH)_2$-salen]. The metal chelates in this study are insoluble in water but soluble in most organic solvents. Electrical conductivity measurements of the manganese(II) complex gave Λ_M values of 11 Ω^{-1} cm^{-1} mol^{-1} and confirmed that it is a non-electrolyte. The manganese content of the MWNTs catalysts were estimated by dissolving known amounts of the heterogeneous catalyst in concentrated HNO_3 and from these solutions, transition metal contents were estimated by atomic absorption spectrometry. The chemical composition confirmed the purity and stoichiometry of the neat and MWNTs-grafted complex. The chemical analysis of the samples revealed the presence of organic matter with a Mn/N ratio roughly similar to that of the neat complex. The loading of the complex was 82 μ mol g^{-1}. The chemical composition confirmed the purity and stoichiometry of the neat and multi-wall carbon nanotube complex.

MWNTs-Schiff-base complexes have enhanced chemical stability in most common solvents and enhanced thermal stability. The

homogeneous suspension of the MWNTs-Schiff-base complexes in methanol without any surfactant can be formed by stirring and remains very stable for at least 2 months at room temperature (no breakdown was detected even after high-speed centrifugation or high temperature treatment), while pristine MWNTs are easy to breakdown after high-speed centrifugation or high temperature treatment. The enhanced chemical and thermal stability of the MWNTs-Schiff-base complexes might result from the covalent interaction between the MWNTs and the Schiff-base complex. Because the Schiff-base complexes are covalently bonded to the MWNTs, the strong and super-stable covalent bond interactions between the Schiff-base complexes and MWNTs are responsible for the thermal stability of the MWNTs-Schiff-base complexes material.

Comparison of the spectra of this catalyst with the ligand provides evidence for the coordinating mode of the ligand in the catalyst. The ligand exhibits a broad band in the 2450–2750 cm^{-1} range due to extensive hydrogen bonding between the phenolic hydrogen and nitrogen of the azomethine group. Absence of this band in the spectra of the covalently anchored complex indicates the destruction of the hydrogen bond followed by the coordination of the phenolic oxygen after deprotonation. The sharp band appearing at 1640 cm^{-1} due to ν(C=N) (azomethine), shifts to a lower wavenumber, and appears at 1633 cm^{-1}. This indicates the involvement of the azomethine nitrogen in coordination. The presence of multiple bands in the 2850–2935 cm^{-1} region in the ligand and its complexes with slight shifts suggests the presence of the CH_2 group of ethylene in the ligand as well as its complexes. The neat complex [Mn($(OH)_2$-salen)] exhibits a sharp band at 1633 cm^{-1} due to the ν(C=N) stretch, while on the covalently anchored manganese(II) complex the location of the bands due to the ν(C=N) structure shifts to a lower wavenumber and appears at 1604 cm^{-1}. The intensity of the peaks on the covalently anchored complex is weak, due to their low concentration on the MWNTs, though the spectra of the covalently anchored as well as the neat complex show essentially similar bands. Meanwhile, the disappearance of the band at 3400 cm^{-1} due to ν(OH) may be due to the covalent anchoring of the [Mn($(OH)_2$-salen)] complex on the modified MWNTs.

The most informative spectroscopic data to support the covalent anchoring of the [Mn($(OH)_2$-salen)] complex on the modified MWNTs were obtained from a comparison of the set of IR data corresponding to the purified MWNTs, HOOC@MWNTs, ClCO@MWNTs and [Mn($(OH)_2$-salen)]@MWNTs (Fig. 1). The sharp peak at A (1519 cm^{-1}) in the IR spectrum (a in Fig. 1) is from the stretch mode of the aromatic carbon–carbon bond in raw MWNTs. After the reaction of the shortened MWNTs with $SOCl_2$, the IR spectrum (Fig. 1) showed well defined bands at about 1724, 1221 and 615 cm^{-1} which are clearly related to the formation of the –COCl group on the ends and side-wall of the MWNTs. The near-IR region of the purified MWNTs is preserved upon functionalization in ClCO@MWNTs and [Mn($(OH)_2$-salen)]@MWNTs, thus showing that the multi-walled structure of the nanotubes has been preserved unaltered during the treatment (Fig. 1).

In addition, a control experiment in which a mechanical mixture of MWNTs and 100 μmol g^{-1} of commercial [bis(salicylidene)ethylene-1,2-diiminemanganese(II)], [Mn(salen)], (no covalent linkage between the complex and MWNTs) was submitted for an extraction procedure with $CHCl_3$ and this revealed that essentially all the complex can be recovered by our workup procedure.

The X-ray diffraction patterns of MWNTs containing the manganese(II) complex are similar to the MWNTs alone. This indicates that the crystallinity and morphology of the MWNTs are preserved during the grafting. Fig. 2 shows the XRD pattern of the MWNTs, which is similar to that of highly oriented pyrolytic graphite (HOPG). The (002) peak emerges at around 26°, corresponding to an inter-planar spacing of 0.342 nm, which is little greater than that of HOPG of about 0.336 nm. Fig. 2 shows the XRD patterns of MWNTs with the modification grafted method. It can be seen that the XRD patterns are similar to the raw MWNTs. Modified MWNTs still have the same cylinder wall structure as raw MWNTs and the inter-planar spacing of all samples remains the same.

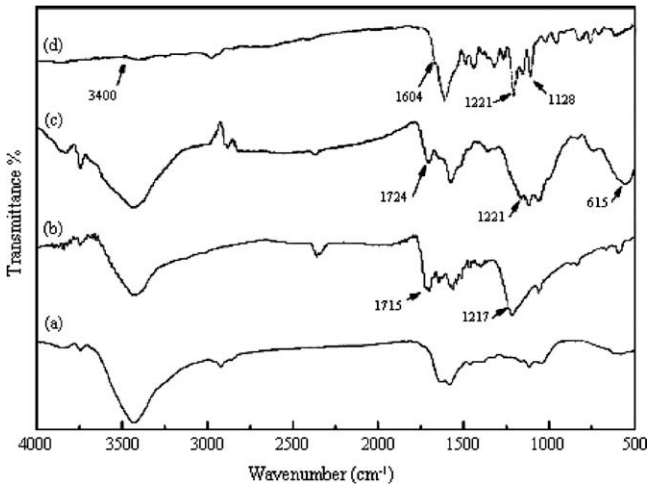

Fig. 1. FT-IR spectra of (a) raw MWNTs, (b) HOOC@MWNTs, (c) ClCO@MWNTs, (d) [Mn($(OH)_2$-salen)]@MWNTs.

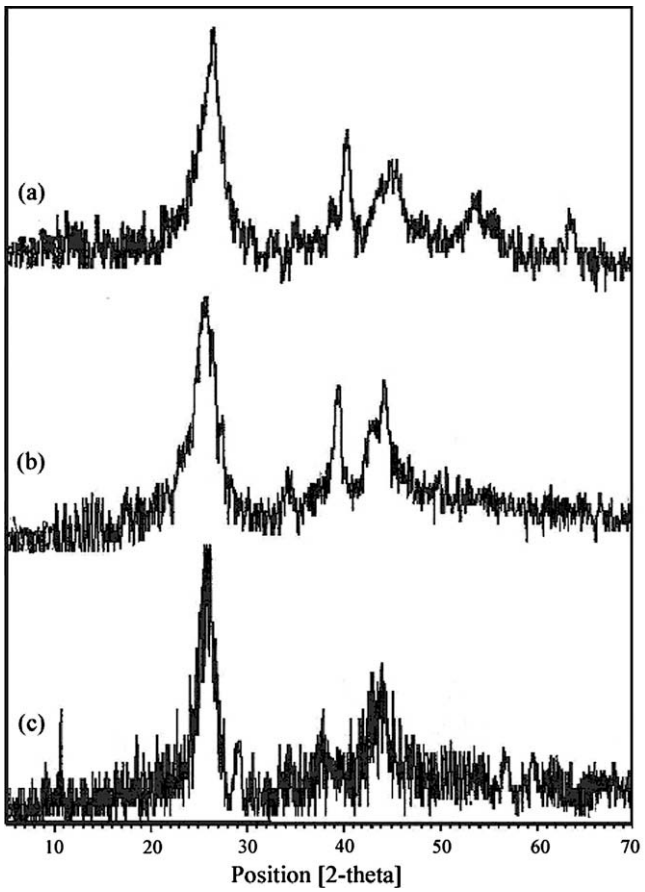

Fig. 2. XRD pattern for (a) MWNTs, (b) HOOC@MWNTs, (c) [Mn($(OH)_2$-salen)]@MWNTs.

Fig. 3 shows a TEM image of the MWNTs with high quality, uniform diameter and a high length/diameter ratio, which shows that the diameter is about 20–40 nm. From Fig. 3 it is found that each MWNTs before modification is mainly a long and folded pipe. The MWNTs-Schiff-base complexes exhibit a stretched or folded feature with the Schiff-base complex (black dots) mainly congregating in the convex surfaces of the MWNTs (Fig. 3). These images of the sample also confirm the junction formations through the Schiff-base complex. As expected most of the junctions occur at the tips of the MWNTs, as hydroxyl (OH) groups of the Schiff-base complex react with the carboxylic (COOH) groups at the open end of the MWNTs. Scheme 1 illustrates the synthetic step and the structure of the resulting [Mn((OH)$_2$-salen)] complex anchored to the MWNTs. According to Fig. 3 in which bundles of MWNTs rather than isolated tubes are seen, drawn in Scheme 1, multi-wall nanotubes represent a simplification of the functionalization process.

The electronic spectral data of the ligand and the complex are also given in the experimental section. The electronic spectral profiles of [Mn((OH)$_2$-salen)] and [Mn((OH)$_2$-salen)]@MWNTs are reproduced in Fig. 4. The electronic spectrum of the ligand H$_2$[(OH)$_2$-salen] exhibits three bands at 335, 265 and 208 nm and these are assigned due to $n \rightarrow \pi^*$, $\pi \rightarrow \pi^*$ and $\phi \rightarrow \phi^*$ transitions, respectively. All these bands shift to the higher wavelength side, indicating the restructuring of the ligand after coordination to the metal ion. The appearance of a weak band due to a ligand to metal transition underneath the $n \rightarrow \pi^*$ transition make this a band broad. No band could be located in the higher wavelength region due to the expected d–d transition in the covalently anchored complex. The neat complex exhibits at least one broad band at 340 nm for [Mn((OH)$_2$-salen)]. The magnetic measurement obtained at room temperature for the manganese complex in the powder state is 5.92 BM, *i.e.* close to the spin only value expected for high spin manganese(II) in a tetrahedral environment [35–37].

Further evidence for the modification of MWNTs comes from the XPS spectrum of the [Mn((OH)$_2$-salen)]-functionalized MWNTs, that reveals the surface chemical state as shown in Fig. 5a. The peaks at 294.8, 397.8 and 531.1 eV are attributed to C, N and O, respectively, [38]. By calculating the content of the elements on the surface of MWNTs by area for each element, we can show that the weight content of N is about 2%, indicating the presence of Schiff-base groups. It was found that O 1s can be fitted to three line shapes with binding energies at 532.7, 531.2 and 529.9 eV, which are assigned to –CO–, –C–O–C– and –C–O–Mn(II), respectively (Fig. 5b). The structure of the complexes could be confirmed as shown in Scheme 1. The XPS spectra relating to the core levels of Mn 2p are shown in Fig. 5c. The peaks at 640.0 and 651.4 eV are attributed to Mn 2p3/2 and Mn 2p1/2, respectively. These data confirm the loading of the [Mn((OH)$_2$-salen)] complex in the MWNTs.

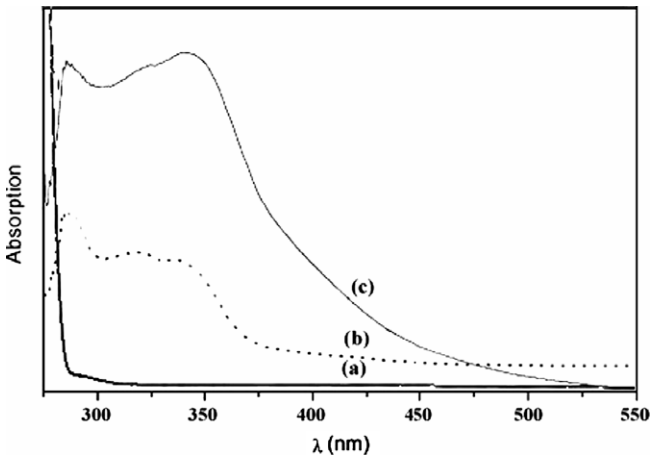

Fig. 4. UV–Vis spectra of the (a) raw MWNTs (b) [Mn((OH)$_2$-salen)]@MWNTs (c) Schiff-base complex.

TGA demonstrates that the composites of [Mn((OH)$_2$-salen)]@MWNTs have been prepared (Fig. 6). The mass loss in temperature range below 250 °C reflects the deprotonation of COOH, the loss of the acid group of HOOC@MWNTs and humidity. Also the mass loss in this temperature is related to the loss of COCl of the MWNTs. On the other hand, Fig. 6 is the TGA curve for the as-prepared MWNTs-Schiff-base complexes, [Mn((OH)$_2$-salen)]@MWNTs, presenting several weight losses in the temperature range 125–400 °C. According to Fig. 6, decomposition [Mn((OH)$_2$-salen)] starts above 250 °C. The significant weight loss of between 250 and 320 °C is due to the surface grown salen groups. Another weight loss below 200 °C corresponds to the loss of humidity. No further weight loss can be observed over 480 °C.

The complex [Mn((OH)$_2$-salen)]@MWNTs catalyzes the oxidation of cyclohexene by TBHP efficiently to give 2-cyclohexene-1-one, 2-cyclohexene-1-ol and 1-(*tert*-butylperoxy)-2-cyclohexene (Table 1). The reaction conditions have also been optimized for the maximum oxidation of cyclohexene by varying different parameters.

Three different TBHP:cyclohexene molar ratios, viz. 1:1, 2:1 and 3:1, were considered while keeping a fixed amount of cyclohexene (0.82 g, 10 mmol) and catalyst (9.2×10^{-5} mol) in 20 ml of CH_3CN, and the reaction was carried out at 75 °C. The percentage conversions noted at various times are presented in Fig. 7. A maximum of 52.1% conversion was noted for the TBHP to cyclohexene ratio of 1:1 after 2 h of reaction time. This conversion reached 63.4% at a TBHP to cyclohexene molar ratio of 2:1. On increasing the TBHP to cyclohexene ratio further to 3:1 results in only a 40.6%

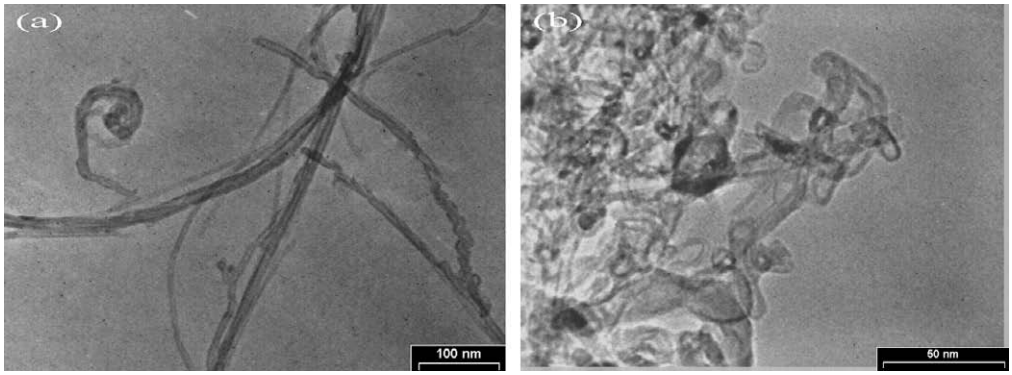

Fig. 3. Images TEM of (A) pristine MWNTs, B) MWNTs functionalized by Schiff-base complex.

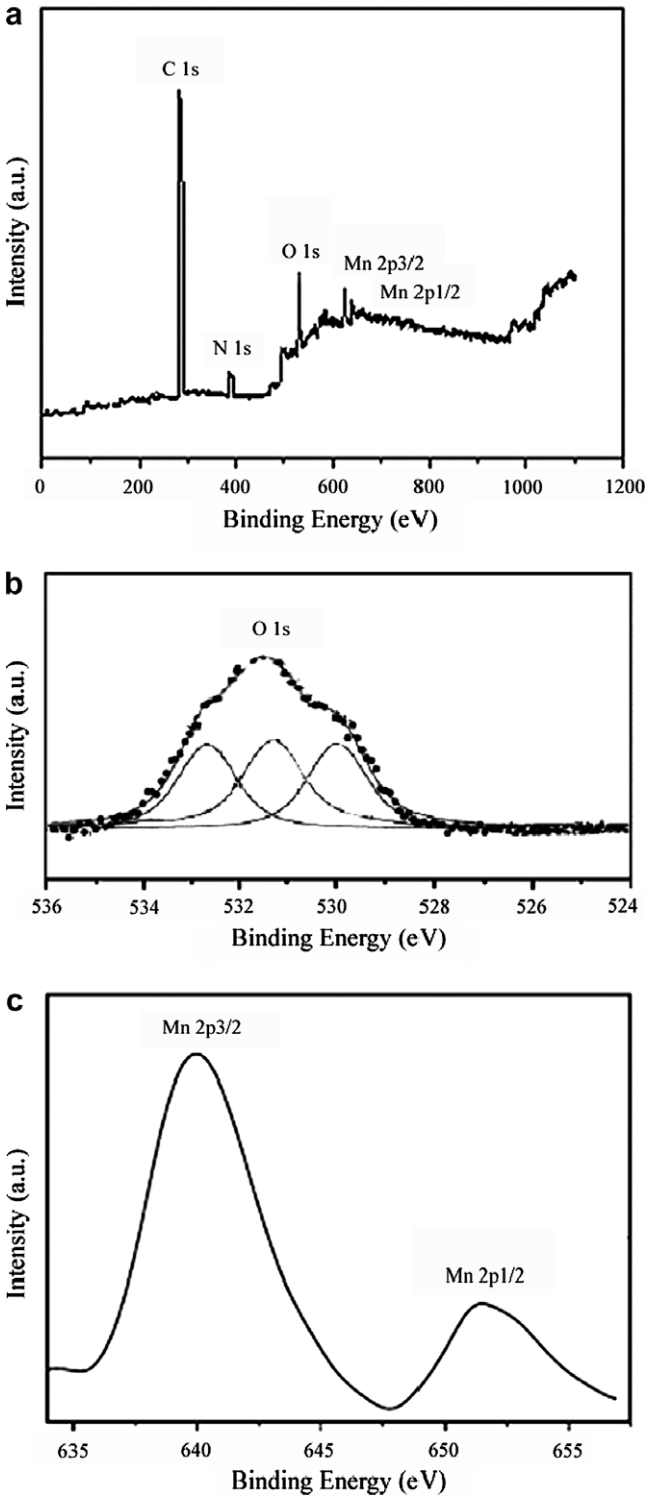

Fig. 5. Wide XPS spectra (a) of [Mn((OH)$_2$-salen)] functionalized MWNTs, (b) curve fitting of the O1s and (c) Mn 2p spectrum.

conversion of cyclohexene. This is possibly due to the presence of excess water, as has been noted earlier. Thus, a large amount of oxidant is not an essential condition to maximize the oxidation.

The effect of the amount of catalyst on the oxidation of cyclohexene is shown in Fig. 8. Three different amounts of catalyst, viz. 3.9×10^{-5} mol, 6.6×10^{-5} mol and 9.2×10^{-5} mol, were considered while keeping other conditions as above. It is clear from the plot that 9.2×10^{-5} mol catalyst amount is the best one to obtain the highest cyclohexene conversion. Temperature also has an influence on the oxidation of cyclohexene. As shown in Fig. 9, amongst the three temperatures of 55, 65 and 75 °C, the maximum conversion of cyclohexene was obtained at 75 °C. Thus, the optimized conditions for the oxidation of 10 mmol of cyclohexene were fixed as follow: 9.2×10^{-5} mol catalyst, 20 mmol TBHP, 20 ml CH_3CN and 75 °C reaction temperature. Under these reaction conditions the catalyst [Mn((OH)$_2$-salen)]@MWNTs gave 82.1%

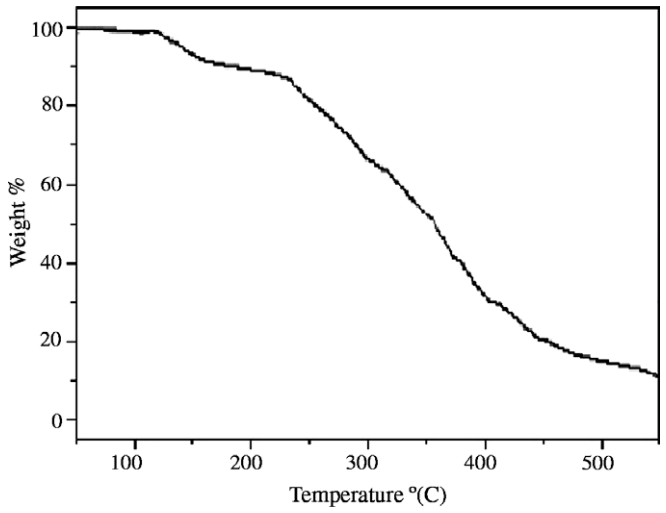

Fig. 6. TGA curve of [Mn((OH)$_2$-salen)]@MWNTs.

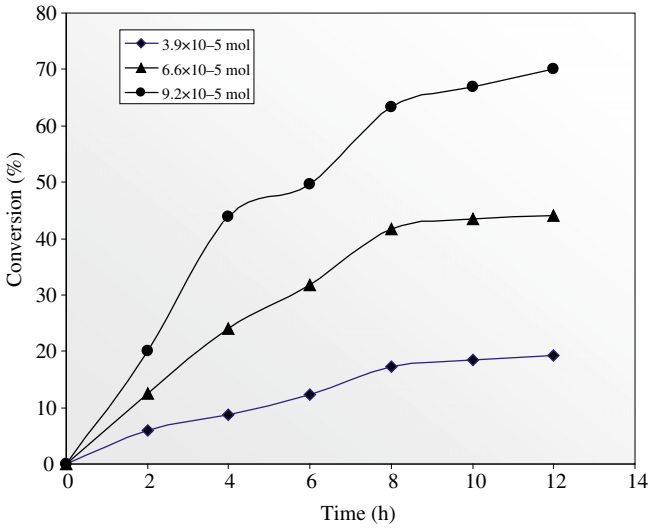

Fig. 8. Effect of the amount of catalyst on the oxidation of cyclohexene (reaction conditions: 20 mmol TBHP, 20 ml CH_3CN, 10 mmol of cyclohexene, temperature 75 °C, catalyst [Mn((OH)$_2$-salen)]@MWNTs).

conversion of cyclohexene with major reaction products of 2-cyclohexene-1-one, 2-cyclohexene-1-ol and 1-(*tert*-butylperoxy)-2-cyclohexene, as shown in Table 1. About 8 h was required to

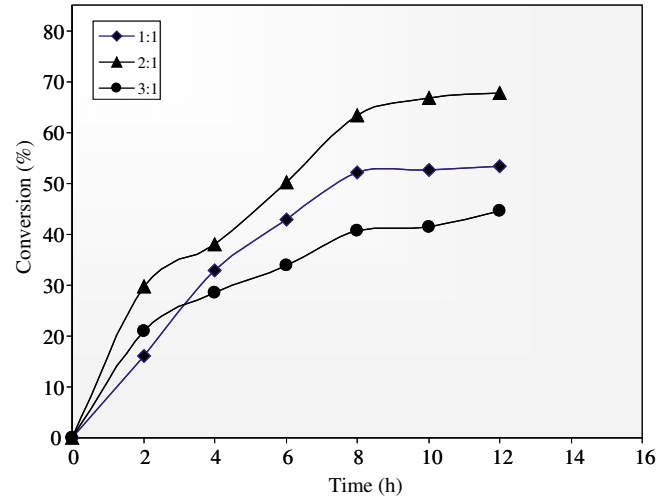

Fig. 7. Effect of TBHP concentration on the oxidation of cyclohexene (reaction conditions: 9.2×10^{-5} mol catalyst, 20 ml CH_3CN, temperature 75 °C, catalyst [Mn((OH)$_2$-salen)]@MWNTs).

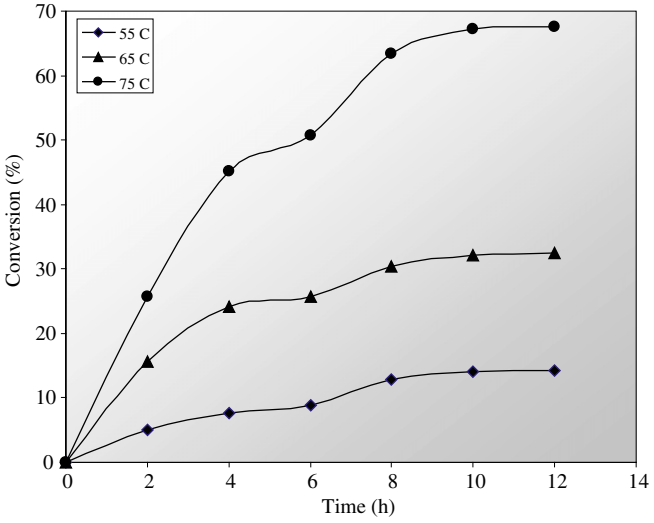

Fig. 9. Effect of temperature on the oxidation of cyclohexene (reaction conditions: 9.2×10^{-5} mol catalyst, 20 mmol TBHP, 20 ml CH_3CN, 10 mmol of cyclohexene, catalyst [Mn((OH)$_2$-salen)]@MWNTs).

Table 1
Effect of catalyst on the oxidation of cyclohexene and product selectivity[a]

Catalyst	Conversion (%)	Selectivity (%)		
		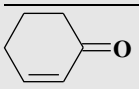	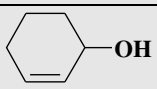	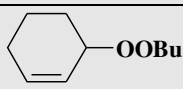
[Mn((OH)$_2$-salen)]	40.6	53.6	22.4	24.0
MWNTs	3.7	51.6	28.6	19.8
[Mn((OH)$_2$-salen)]@MWNTs	82.1	73.2	18.1	8.7
[Mn((OH)$_2$-salen)]@MWNTs[b]	79.7	72.5	19.3	8.2
[Mn((OH)$_2$-salen)]@MWNTs[c]	79.1	72.0	20.4	7.6
[Mn((OH)$_2$-salen)]@MWNTs[d]	79.0	71.1	21.7	7.2

[a] Reaction condition: 9.2×10^{-5} mol catalyst, 20 mmol TBHP, 20 ml CH_3CN, 10 mmol of cyclohexene, temperature 75 °C.
[b] First reuse.
[c] Second reuse.
[d] Third reuse.

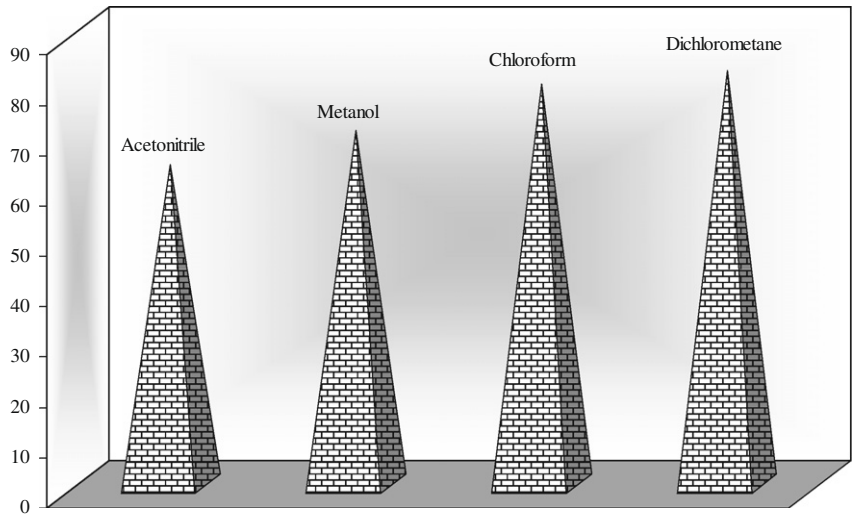

Fig. 10. Effect of solvent on the oxidation of cyclohexene (reaction conditions: 9.2×10^{-5} mol catalyst, 20 mmol TBHP, 20 ml solvent, 10 mmol of cyclohexene, catalyst [Mn($(OH)_2$-salen)]@MWNTs).

achieve equilibrium in these reactions. Amongst the various products formed, the selectivity of 2-cyclohexene-1-one was found to be highest while the selectivities of the other two products were much less. As a result 2-cyclohexene-1-one is the major product.

The solid was used as a heterogeneous catalyst for the oxidation of cyclohexene (Table 1). One of the major advantages of anchoring the [Mn($(OH)_2$-salen)] complex on the MWNTs as a support is the ease in which the catalyst can be suspended in the solvent due to the bundled agglomerates of MWNTs that aggregate slowly. Upon initial stirring of the suspension, the black solid remains suspended without setting down for long period of time.

The reusability of [Mn($(OH)_2$-salen)]@MWNTs was confirmed by performing a series of consecutive experiments in which the used catalyst was filtered, washed with fresh solvent, and re-employed without any further treatment in another run. The results shown in Table 1 clearly prove that no loss of activity occurs, giving a minimum productivity of 300 mol of product per mole of complex. Results of elemental (N) analysis exhibit that leaching of the Mn complex along with catalytic reaction does not occur.

The effect of various solvents for the oxidation of cyclohexene with the [Mn($(OH)_2$-salen)]@MWNTs catalyst was also studied (Fig. 10). The oxidation reactions were carried out in protic and aprotic solvents. The results are given in Fig. 10. In all the oxidation reactions, 2-cyclohexene-1-one was formed as the major product. When the reaction was carried out in a coordinating solvent like CH_3CN the conversion decreased by a factor of ~1.29 (Fig. 10). This might be attributed to the donor number of acetonitrile (14.1) and, therefore, to its higher ability to occupy the vacant spaces around the metal center and prevent the approach of oxidant molecules. In dichloromethane and chloroform the yields of 2-cyclohexene-1-o1 and 2-cyclohexene-1-one were higher and a lower yield of the peroxy species was obtained as compared to the other solvents. The efficiency of the catalysts for oxidation of cyclohexene in different solvents decreases in the order: dichloromethane > chloroform > methanol > acetonitrile.

The results clearly suggest that [Mn($(OH)_2$-salen)]@MWNTs efficiently catalyses the conversion of cyclohexene to 2-cyclohexene-1-one with 73.2% selectivity and a conversion of 82.1% in dichloromethane. The greater activity of the $(OH)_2$-salen system has clearly arisen from the existence of an electron donating ligand which facilitates the electron transfer rate, a process that has previously been observed by us in other oxidation reactions [39–44].

The trend observed in Table 1 can be explained by the donor ability of the ligand available in the complex catalysts. As Wang and co-workers have pointed out recently, the key point in the conversion of cyclohexene to the products is the reduction of ($(OH)_2$-salen)-Mn^{3+} to ($(OH)_2$-salen)-Mn^{2+}. This reduction to ($(OH)_2$-salen)-Mn^{2+} is facilitated by ligands available around the metal cation [45]. The formation of the allylic oxidation products 2-cyclohexene-1-one and 2-clohexene-1-ol shows the preferential attack of the activated C–H bond over the C=C bond. The formation of 1-(*tert*-butylperoxy)-2-cyclohexene shows the presence of radical reactions [46]. That TBHP as an oxidant promotes the allylic oxidation pathway and epoxidation is minimized, especially in presence of MWNTs with divalent and trivalent transition metal ions and complexes, has been observed by us and others [44–52].

4. Conclusion

MWNTs covalently bonded by a manganese(II) Schiff-base complex were successfully obtained via the method of chemical modification. The "neat" and MWNTs covalently anchored manganese(II) Schiff-base complex exhibit efficient catalytic activity in the oxidation of cyclohexene using TBHP. The reaction conditions have been optimized considering different parameters to get a maximum conversion of this substrate. A maximum of 82.1% conversion with three different oxidation products of cyclohexene has been obtained with [Mn($(OH)_2$-salen)]@MWNTs. The selectivity of these products follows the order: 2-cyclohexene-1-one (73.2%) > 2-cyclohexene-1-ol (18.1%) > 1-(*tret*-butylperoxy)-2-cyclohexene (8.7%). This complex is stable and does not leach during the catalytic reaction, as has been confirmed by testing the filtrate for the corresponding metal ion, thus suggest their heterogeneous nature. The high conversion of the complex makes this system a suitable catalyst for this catalytic oxidation. The extension of the method to different olefins is currently under investigation in our laboratory.

Acknowledgment

Authors are grateful to the Council of the University of Kashan for providing financial support to undertake this work.

References

[1] H. Arakawa, M. Aresta, J.N. Armor, M.A. Barteau, E.J. Beckman, A.T. Bell, J.E. Bercaw, C. Creutz, E. Dinjus, D.A. Dixon, K. Domen, D.L. Dubois, J. Eckert, E. Fujita, D.H. Gibson, W.A. Goddard, D.W. Goodman, J. Keller, G.J. Kubas, H.H. Kung, J.E. Lyons, L.E. Manzer, T.J. Marks, K. Morokuma, K.M. Nicholas, R. Periana, L. Que, J.R. Nielson, W.M.H. Sachtler, L.D. Schmidt, A. Sen, G.A. Somorjai, P.C. Stair, B.R. Stults, Chem. Rev. 101 (2001) 953.
[2] T. Katsuki, Coord. Chem. Rev. 140 (1995) 189.
[3] S. Iijima, Nature 354 (1991) 56.
[4] (a) M.M. Treacy, T.W. Ebbesen, J.M. Gibson, Nature 381 (1996) 678; (b) E.W. Wong, P.E. Sheehan, C.M. Lieber, Science 277 (1997) 1971.
[5] M.R. Falvo, G.J. Clary, R.M. Taylor II, V. Chi, F.P. Brooks Jr., S. Washburn, R. Superfine, Nature 389 (1997) 582.
[6] W.A. de Heer, A. Chatelain, D. Ugarte, Science 270 (1995) 1179.
[7] H. Dai, E.W. Wong, C.M. Lieber, Science 272 (1996) 523.
[8] T.W. Ebbesen, H.J. Lezec, H. Hiura, J.W. Bennett, H.F. Ghaemi, T. Thio, Nature 382 (1996) 54.
[9] J.W. Wildöer, L.C. Venema, A.G. Rinzler, R.E. Smalley, C. Dekker, Nature 391 (1998) 59.
[10] Z. Wang, Q. Wu, F.-Y. Zhang, Y.-Y. Cui, Mat. Lett. 61 (2007) 1955.
[11] Y.B. Li, B.Q. Wei, J. Liang, Q. Yu, D.H. Wu, Carbon 37 (1999) 493.
[12] Y.A. Kim, T. Hayashi, Y. Fukai, M. Endo, T. Yanahisawa, M.S. Dresselhaus, Chem. Phys. Lett. 355 (2002) 279.
[13] K.B. Shelimov, R.O. Esenaliev, A.G. Rinzler, C.B. Huffman, R.E. Smalley, Chem. Phys. Lett. 282 (1998) 429.
[14] J. Hilding, E.A. Grulke, Z.G. Zhang, F.J. Lockwood, Dispersion Sci. Technol. 24 (2003) 1.
[15] J.E. Riggs, D.B. Walker, D.L. Carroll, Y.P. Sun, J. Phys. Chem. B 104 (2000) 7071.
[16] O. Matarredona, H. Rhoads, Z. Li, J. Harwell, L. Balzano, D. Resasco, J. Phys. Chem. B 107 (2003) 13357.
[17] P.W. Chiu, G.S. Duesberg, U. Dettlaff-Weglikowska, S. Roth, Appl. Phys. Lett. 80 (2002) 3811.
[18] J. Chen, M.A. Hamon, H. Hu, Y. Chen, A.M. Rao, P.C. Eklund, R.C. Haddon, Science 282 (1998) 95.
[19] E.T. Mickelson, I.W. Chiang, J.L. Zimmerman, P.J. Boul, J. Lozano, J. Liu, R.E. Smalley, R.H. Hauge, J.L. Margrave, J. Phys. Chem. B 103 (1999) 4318.
[20] K.T. Lau, D. Hui, Carbon 40 (2002) 1605.
[21] A. Garg, S.B. Sinnott, Chem. Phys. Lett. 295 (1998) 273.
[22] J.L. Bahr, J. Yang, D.M. Kosynkin, M.J. Bronikowski, R.E. Smalley, J.M. Tour, J. Am. Chem. Soc. 123 (2001) 6536.
[23] F. Pompeo, D. Reasaco, Nano Lett. 2 (2002) 369.
[24] C.A. Dyke, J.M. Tour, Nano Lett. 3 (2003) 1215.
[25] M.S. Strano, C.A. Dyke, M.L. Usrey, P.W. Barone, M.J. Allen, H. Shan, C. Kittrell, R.H. Hauge, J.M. Tour, R.E. Smalley, Science 301 (2003) 1519.
[26] J. Chen, A.M. Rao, S. Lyuksyutov, M.E. Itkis, M.A. Hamon, H. Hu, R.W. Cohn, P.C. Eklund, D.T. Colbert, R.E. Smalley, R.C. Haddon, J. Phys. Chem. B 105 (2001) 2525.
[27] M.C. O'Connell, P. Boul, L.M. Ericson, C. Huffman, Y. Wang, E. Haroz, C. Kuper, J. Tour, K.D. Ausman, R.E. Smalley, Chem. Phys. Lett. 342 (2001) 265.
[28] D. Chattopadhyay, S. Lastella, S. Kim, F. Papadimitrikapoulos, J. Am. Chem. Soc. 124 (2002) 728.
[29] D. Chattopadhyay, I. Galeska, F. Papadimitrikapoulos, J. Am. Chem. Soc. 125 (2003) 3370.
[30] M.J. O'Connell, S.M. Bachilo, C.B. Huffman, V.C. Moore, M.S. Strano, E.H. Haroz, K.L. Rialon, P.J. Boul, W.H. Noon, C. Kittrell, J.P. Ma, R.H. Hauge, R.B. Weisman, R.E. Smalley, Science 297 (2002) 593.
[31] M.F. Islam, E. Rojas, D.M. Bergey, A.T. Johnson, A.G. Yodh, Nano Lett. 3 (2003) 269.
[32] Y.J. Kang, T.A. Taton, J. Am. Chem. Soc. 125 (2003) 5650.
[33] A. Star, J.F. Stoddart, Macromolecules 35 (2002) 7516.
[34] A. Star, J.F. Stoddart, D. Steuerman, M. Diehl, A. Boukai, E.W. Wong, X. Yang, S.W. Chung, H. Choi, J.R. Heath, Angew. Chem., Int. Ed. 40 (2001) 1721.
[35] C.J. Ballhausen, H.B. Gray, Molecular Orbital Theory, Benjamin, New York, 1965.
[36] M. Salavati-Niasari, Micropor. Mesopor Mater. 95 (2006) 248.
[37] A.B.P. Lever, Crystal field spectra, first ed., Inorganic Electronic Spectroscopy, Elsevier, Amsterdam, 1968. pp. 249–360.
[38] J. Cui, W.P. Wang, Y.Z. You, C. Liu, P. Wang, Polymer 45 (2004) 8717.
[39] M. Salavati-Niasari, Chem. Lett. 34 (2005) 244.
[40] M. Salavati-Niasari, Chem. Lett. 34 (2005) 1444.
[41] M. Salavati-Niasari, Micropor. Mesopor. Mater. 92 (2006) 173.
[42] M. Salavati-Niasari, H. Banitaba, J. Mol. Catal. A: Chem. 201 (2003) 43.
[43] M. Salavati-Niasari, J. Hasanalian, H. Najafian, J. Mol. Catal. A: Chem. 209 (2004) 204.
[44] M. Salavati-Niasari, H. Najafian, J. Chem. Res. 9 (2003) 586.
[45] M. Wang, C.J. Hao, Y.P. Wang, S.B. Li, J. Mol. Catal. 147 (1999) 173.
[46] D. Koola, J.K. Kochi, J. Org. Chem. (1987) 4545.
[47] A.H. Gemeay, M.A. Salem, I.A. Salem, Colloid Surface 117 (1996) 245.
[48] W. Nam, R. Ho, J.S. Valentine, J. Am. Chem. Soc. 113 (1991) 7052.
[49] M. Salavati-Niasari, J. Mol. Catal. A: Chem. 217 (2004) 87.
[50] V. Bagchi, D. Bandyopadhyay, Polyhedron 27 (2008) 1387.
[51] S.G. Baca, M.T. Reetz, R. Goddard, I.G. Filippova, Y.A. Simonov, M. Gdaniec, N. Gerbeleu, Polyhedron 25 (2006) 1215.
[52] M. Salavati-Niasari, M. Bazarganipour, J. Mol. Catal. A: Chem. 278 (2007) 173.

These are some examples of the importance of PCr and Cu(II) which explain why it is important to know how these two species interact to form a Cu–PCr complex.

At physiological pH, PCr is present as the anion PCr^{2-} and this species can coordinate to metal cations [3] (Fig. 1). The PCr molecule has three possible donor atoms: one oxygen atom of the phosphate group, the nitrogen atom of the guanidine group and the oxygen atom of the carboxylate group. Thus, there is the possibility of PCr acting as a tridentate ligand.

In previous studies performed by us in solution we could see that PCr acts as a bidentate ligand, the guanidine group being one of the donor atoms. However, it was not possible to conclude whether the second donor atom was the oxygen atom of the phosphate or of the carboxylate group [1,2]. For this reason we decided to synthesize a complex of Cu–PCr in solid state in order to understand better the coordination site therein. The present work reports the synthesis and characterization of a solid binary Cu–PCr compound, and the results suggest that PCr in solid state is acting as a tridentate ligand.

2. Experimental

2.1. Materials

Na_2PCr was purchased from Sigma–Aldrich and was used as received. $CuSO_4 \cdot 5H_2O$ (Merck) was used to prepare $Cu(OH)_2$ (synthesized according to reported method [16]). All other chemicals were reagent-grade and were used without further purification.

Table 1
TGA data for the CuPCr complex

Compound	Step	ΔT (°C)	Mass loss% Exp. (calc.)	Probable species
CuPCr	1	20–120	5.1 (5.8)	OH
	2	120–311	11.8 (11.3)	$CH_3 + H_2O$
	3	311–899	23.9 (23.4)	$CO–CH_2–N–C$
	4	Residue	59.0 (58.3)	PO_2 + CuONHC

Table 2
DFT:B3LYP/6-311G bond length and inter-bond angles in the [Cu(PCr)(H_2O)] complex

i,j atoms	Bond lengths (Å)	*i,j,k* atoms	Inter-bond angles (°)	*i,j,k* atoms	Inter-bond angles (°)
1,4	1.960	4,1,8	89.087	6,8,21	111.818
1,8	1.967	4,1,12	153.106	9,7,15	117.787
1,12	1.912	4,1,13	93.634	7,9,10	114.316
1,13	1.958	1,4,2	124.666	7,9,16	107.572
2,4	1.631	8,1,12	98.267	7,9,17	108.868
2,14	1.569	8,1,13	173.015	7,15,23	114.414
3,18	0.973	1,8,6	97.751	7,15,24	113.330
5,6	1.375	1,8,21	112.902	7,15,25	108.895
5,22	1.008	12,1,13	82.152	10,9,16	108.288
6,7	1.352	1,12,10	132.413	10,9,17	107.740
6,8	1.348	1,13,19	108.851	9,10,11	118.469
7,9	1.479	1,13,20	126.254	9,10,12	117.488
7,15	1.470	4,2,14	122.039	16,9,17	110.028
8,21	1.020	4,2,3	105.774	11,10,12	124.028
9,10	1.548	4,2,5	104.082	19,13,20	116.342
9,16	1.088	14,2,3	114.915	23,15,24	109.267
9,17	1.086	14,2,5	109.382	23,15,25	108.583
10,11	1.243	18,3,2	115.946	24,15,25	108.280
10,12	1.327	6,5,22	123.438	3,2,5	97.366
13,19	0.971	5,6,7	121.530		
13,20	0.964	5,6,8	119.422		
15,23	1.092	6,5,2	117.671		
15,24	1.088	22,5,2	118.220		
15,25	1.088	7,6,8	118.284		
2,3	1.732	6,7,9	118.750		
2,5	1.803	6,7,15	123.009		

2.2. Synthesis

Binary Cu–PCr compound was synthesized by suspending $Cu(OH)_2$ and PCr in 4 mL of distilled water using the stoichiometric ratio 1:1. The initially blue suspension obtained was stirred for 6 h at 30 °C and then the solvent was slowly filtered. After solvent filtration the suspension was mixed again for 4 h at 15 °C. The blue powder was precipitated by reducing the solution temperature to −10 °C and using H_2SO_4 as a desiccant agent. The blue powder was dried at 47 °C for 4 h. After compound purification with water and a 5:1 water/ether mixture, the solid was kept in a vessel containing $CaCl_2$.

2.3. Elemental analysis and melting point

Carbon, hydrogen and nitrogen determinations were performed in an elemental analyzer EA 1110 from CE Instruments. The copper content was determined by atomic absorption spectrometry in a Varian AA5 Instrument. The measurements were taken using a wavelength of 324.7 nm and a slit of 0.1 nm. Melting Points were obtained with a MQAPF-302 apparatus.

Yield: 47%; M.p. 210 °C (decomposition). Elemental *Anal.* Calc. for $C_4H_{10}N_3PO_6Cu$: C, 16.52; H, 3.44; N, 14.45; Cu, 21.85. Found: C, 17.12; H, 3.31; N, 15.03; Cu, 21.23%.

2.4. Thermogravimetric analysis

Thermogravimetric analyses were performed with a Perkin–Elmer TGA 7. The temperature range used was from 20 to 900 °C, with a scanning rate of 10.0 °C min^{-1} in a nitrogen atmosphere.

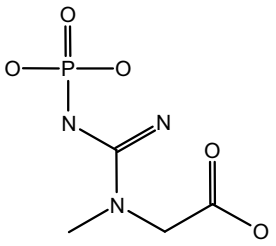

Fig. 1. Structure of phosphocreatine.

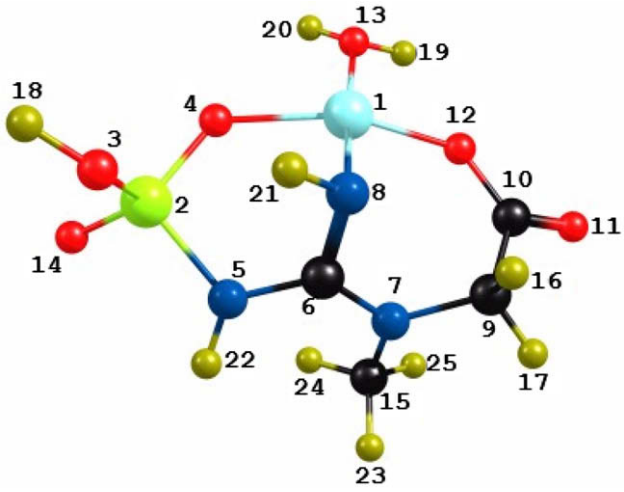

Fig. 2. DFT:B3LYP/6-311G calculated structure of the [Cu(PCr)(H_2O)] complex showing the atom numbering.

2.5. Spectroscopic measurements

The infrared spectra were carried out using a model FT-IR 2000 Perkin–Elmer spectrophotometer. Samples were prepared as KBr pellets for the range of 4000–370 cm^{-1} and polyethylene ones for the range of 710–30 cm^{-1}. Electron paramagnetic resonance (EPR) spectra were obtained at room temperature (300 K) on a Bruker ESP300E apparatus with modulation frequency of 100 kHz

Table 3
Experimental FT-IR spectrum and calculated DFT: B3LYP/6-311G vibrational wave numbers for the [Cu(PCr)(H_2O)] complex (units in cm^{-1})

DFT: B3LYP/6-311G calculated	DFT scaled values × 0.9613	FT-IR wn. (% T)	2nd derivative	Approximate assignment
3869	3719			ν_{as}(OH)(H_2O)
3714	3570	3630		ν(OH)phosph.
3673	3531	3591	3594	ν_s(OH)(H_2O)
3625	3485	3568	3568	ν(NH)
3463	3329	3404	3429	ν(NH)
3144	3022			$\nu(CH)_{as}CH_2$
3129	3008			$\nu(CH)_{as}CH_3$
3099	2979	2958	2963	ν(CH)CH_3
3076	2957	2922	2922	$\nu(CH)_sCH_2$
3025	2908	2852	2854	$\nu(CH)_sCH_3$
1656	1592	1720	1718	ν(C=O)
1620	1557	1704		δ(C=NH) + δ(NCN)
1592	1530	1658	1656	δ(HOH)H_2O
1550	1490	1620	1613	δ(HCH)CH_3
1541	1481	1561	1551	$\delta(HCH)_3$
1494	1436	1544		$\delta(HCH)_3$
1486	1428	1512	1511	$\delta(CH)_2$
1454	1398	1478		ν(C=N)
1390	1326	1461	1462	δ(HNH)
1376	1323	1428	1399	δ(HCH)CH_2 + δ(HNC)
1354	1302	1401		δ(HNC)
1280	1230	1349	1349	ν(C–O) + δ(HNC) + ν(CC)
1270	1221	1262	1248	δ(HNC) + ν(C–O) + ν(CC)
1224	1176			ν(C–N) + ρ(CH)CH_3
1160	1115			δ(HCH)
1146	1102		1134	δ(HCH)
1067	1026	1114	1102	ν(P=O) + δ(HOP)
1049	1008	1046	1048	ρ(CH)CH_3
1015	976		1024	δ(HOP)
980	942	993	993	$\rho(CH)_2$
964	927			ρ(NH)
904	869	897	899	δ(OC=O) + ν(Cu–O)
845	812	850	853	ν(P–O)
835	803			ν(P–O) + ν(CN)
777	747			δ(NCN) + ν(CCO)
726	698	740	736	ρ(NH) out of plane
717	689			ν(CN) + ρ(OH)H_2O
681	655	692	687	ρ (OH)H_2O
665	639	671	673	δ(HOP)
606	582	622	621	δ(NCN)
597	574		592	ρ(OH)H_2O + δ(HCH)wagg + ν_s(CuO)
564	542	562	564	ρ(NH) out of plane
548	527			δ(HOH)wagg
528	507			ν_{as}(CuO) + δ(HOH)wagg + $\rho(CH_2)$
491	472			ν(CuO) + ν(CuN)
480	461		474	ν(CuO) + ν(CuN)
440	423	458	456	$\rho(CH_2)$ + ν(CuO)
408	392		397	ν(CuO) + δ(OPN) + ν(CuN)
404	388	404		δ(CuOC) + δ(OPO)
386	371			δ(POCu) + δ(NCuO) + δ(PNC)
374	359			ρ(OH)H_2O
364	350		357	Angle ring distortion
358	344			$\rho(CH_3)$ out of plane
347	333	325	324	δ(OPO) + ρ(OH)H_2O
311	299	301	298	ν(CuO) + angle ring distortion
266	256	282	279	ρ(OH)phosp
244	234	236	240	δ(POCu) + torsion CH_3
228	219	220	213	ρ(OH)phosp + torsion CH_3
203	195	208		Angle ring distortion
179	172	192	195	Angle ring distortion
159	153	168		ρ(OH)phosp
150	144	158	158	Torsion
123	118	119		Torsion
111	107			Torsion
91	87			Torsion
85	82	82		Torsion
79	76			Torsion
65	62	67		Torsion
40	38	53		Torsion

operating at 9.5 GHz (X-band); solid samples for EPR analyses were firmly accommodated in quartz tubes; aqueous solutions spectra were obtained at room temperature (300 K) in a quartz flat cell. The EPR parameter values were obtained by treating and simulating the experimental spectra using the Windows software programs WIN-EPR and SIMFONIA, and the WEAK PITCH BRUKER sample pattern.

3. Results and discussion

3.1. General

The presence of three donor groups in phosphocreatine and, thus, the possibility of different types of coordination is a source of controversy, particularly in solution studies [2,3]. To obtain insight about the coordination properties of the system involving PCr and copper(II) ion, one solid complex was synthesized. The composition of the compound was confirmed by elemental analysis and is in agreement with a [Cu(PCr)(H_2O)] species and a molar ratio of 1:1. The coordination mode was determined based on the EPR, IR and thermogravimetric analyses and confirmed by theoretical calculations.

3.2. TG analysis

The decomposition CuPCr complex was observed by TG analysis. Thermal analysis results are in agreement with the assignments of the coordination sites.

Dry Na_2PCr salt decomposes in three steps with the inflexion points at 114 °C, 195 °C, and 308 °C. Above 900 °C there is a residue corresponding to 40.7% (calc. 40%) of the total mass. It is probably associated with the phosphate moiety, which is present in the residue of the complex as described below.

CuPCr undergoes a four-stage decomposition process. Calculations based on mass loss confirmed the stoichiometry of one PCr ligand and one H_2O molecule *per* metal. Between 20 and 120 °C a small part of the phosphate unit is probably lost. The experimental mass loss of 5.1% is in agreement with a mass of 5.8% calculated for the hydroxide molecule from phosphate. The next step occurs between 120 and 311 °C and the experimental mass loss is in agreement with a mass loss of a CH_3 species from phosphocreatine and a water molecule. This temperature is in agreement with a loss of a coordinated water molecule. The TG curve of the CuPCr interpretation is difficult to determine. The suggested species proposed for step 3 and the residue are shown in Table 1. Above 900 °C the curve attains a plateau with the formation of a stable residue corresponding to 59.1% of the total mass (calc. at 59.5%).

3.3. Electron paramagnetic resonance

The EPR parameters found for the CuPCr compound are: $g_{||}$ 2.3150; $A_{||}$ 170 $cm^{-1} \times 10^4$; $g_{\perp}$ 2.0860; $A_{\perp}$ 25 $cm^{-1} \times 10^4$. We can see that the perpendicular parameters, A and g, are in accordance with those found for copper(II) complexes with approximately axial symmetry [17]. The EPR parallel parameter values for the CuPCr complex $A_{||}$ $g_{||}$ are between those for Cu(II) bounded to four oxygen atoms and four nitrogen atoms [18,19], which is consistent with the hypothesis of complexation through three oxygen atoms and one nitrogen atom (two oxygen atoms of the PCr ligand, one oxygen atom of a molecule of water, and one nitrogen atom from PCr).

3.4. Optimization of the geometrical parameters

Ab initio optimization of the geometrical parameters, and hence a structural analysis of copper and phosphocreatine, [Cu(PCr)(H_2O)], was carried out employing DFT levels with B3LYP/6-311G basis set. The calculated stabilization energy was E(RB=HF-LYP) = −2755.91 a.u. The calculated bond lengths for the Cu–O bond were 1.958, 1.960 and 1.912 Å for the Cu–OH_2, Cu–O(carboxylate) and Cu–O(phosphate) bonds, respectively. For the phosphate group we found the following values: P–O 1.631 Å; P–O(H) 1.732 Å; P═O 1.569 Å. The calculated value for the Cu–N bond was 1.967 Å. Selected bond lengths and bond angles are given in Table 2. The full [Cu(PCr)(H_2O)] complex structure is shown in Fig. 2.

3.5. Vibrational assignments

The infrared spectra of the complex are shown in Fig. 3. Vibrational assignments were carried out with the aid of density functional theory (DFT) [20–22] calculations with B3LYP/6-311G basis set. To discuss the vibrational assignments, we took the functional density (DFT) calculated wave numbers corrected by a scale factor of 0.9613. For an accurate description of the normal modes in the metal–ligand spectral range, instead of the potential energy distribution (PED) we used the normalized percentage of deviation of the geometrical parameters (PDPG) [23] from the equilibrium position. This way we were able to obtain the percentage of participation of the bond stretching and bending internal vibrational coordinates in the normal modes.

3.5.1. N–H stretching

There are two NH groups in phosphocreatine. We observed two infrared bands at 3568 and at 3404 cm^{-1}, and calculated at 3483 and at 3329 cm^{-1}. These bands were assigned to the NH stretching.

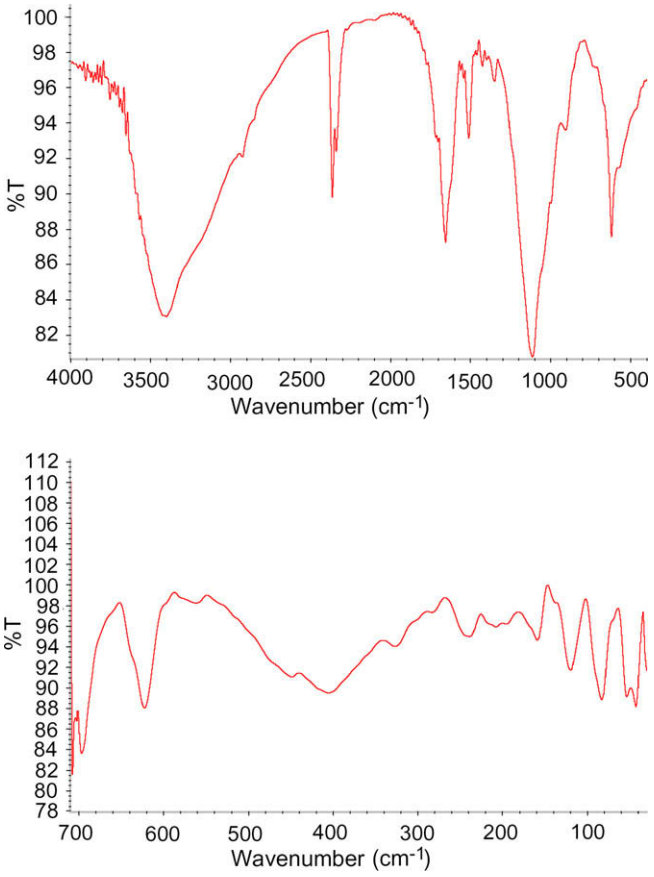

Fig. 3. FT-IR spectra of complex [Cu(PCr)(H_2O)] in the region of 4000–370 cm^{-1} and in the region of 700–30 cm^{-1}.

3.5.2. O–H stretching

One water molecule coordinates the Cu(II)–phosphocreatine complex, creating two O–H stretchings. In the phosphate group after deprotonation one P–O–H group remains, displaying one O–H stretching. In the infrared spectrum we observed a very broad band in the region of the O–H absorptions from which we can assign the peaks at 3630 and at 3591 cm^{-1} as the bands pertaining to the phosphate group and to the water molecule, the latter being the O–H symmetrical stretching. The DFT scaled calculated values were: 3719, 3570 and 3530 cm^{-1}, for O–H (H_2O), O–H (phosphate) and O–H (H_2O), respectively.

3.5.3. C–H stretching

We expected to observe five infrared bands pertaining to the phosphocreatine ligand in the [Cu(PCr)(H_2O)] complex. The calculated DFT values were: 3022, 3007, 2979, 2957 and 2907 cm^{-1}. These wave numbers can be correlated with the experimental ones found at 2958, 2922 and 2852 cm^{-1}. There were two very weak bands observed at 3270 and 3176 cm^{-1} which were assigned preferentially as combination bands.

3.5.4. C=O and C=N stretching

Recently we informed the synthesis, structural and vibrational analysis of the guanidinoaceticserinenickel (II) complex [Ni(GAA)-(Ser)] [24], in which the DFT calculation showed that the C=N stretching is at a higher energy position than the C=O stretching, and the experimental data were in good agreement. In the case of [Cu(PCr)(H_2O)], the $(NH)_2C{=}NH$ group binds to the Cu atom through the –C=NH group, and the C=N bond becomes weak and shifts the C=N stretching wave number to a lower region. As discussed by Bellamy [25], the position of the C=N absorption in conjugated cyclic systems is not very clear, and the C=N absorptions have been assigned as being within the range of 1660–1480 cm^{-1}. We observed the C=N stretching at 1478 cm^{-1}, according to the calculated value at 1454 cm^{-1}. The C=O stretching was assigned at 1720 cm^{-1}. The calculated value was 1657 cm^{-1}.

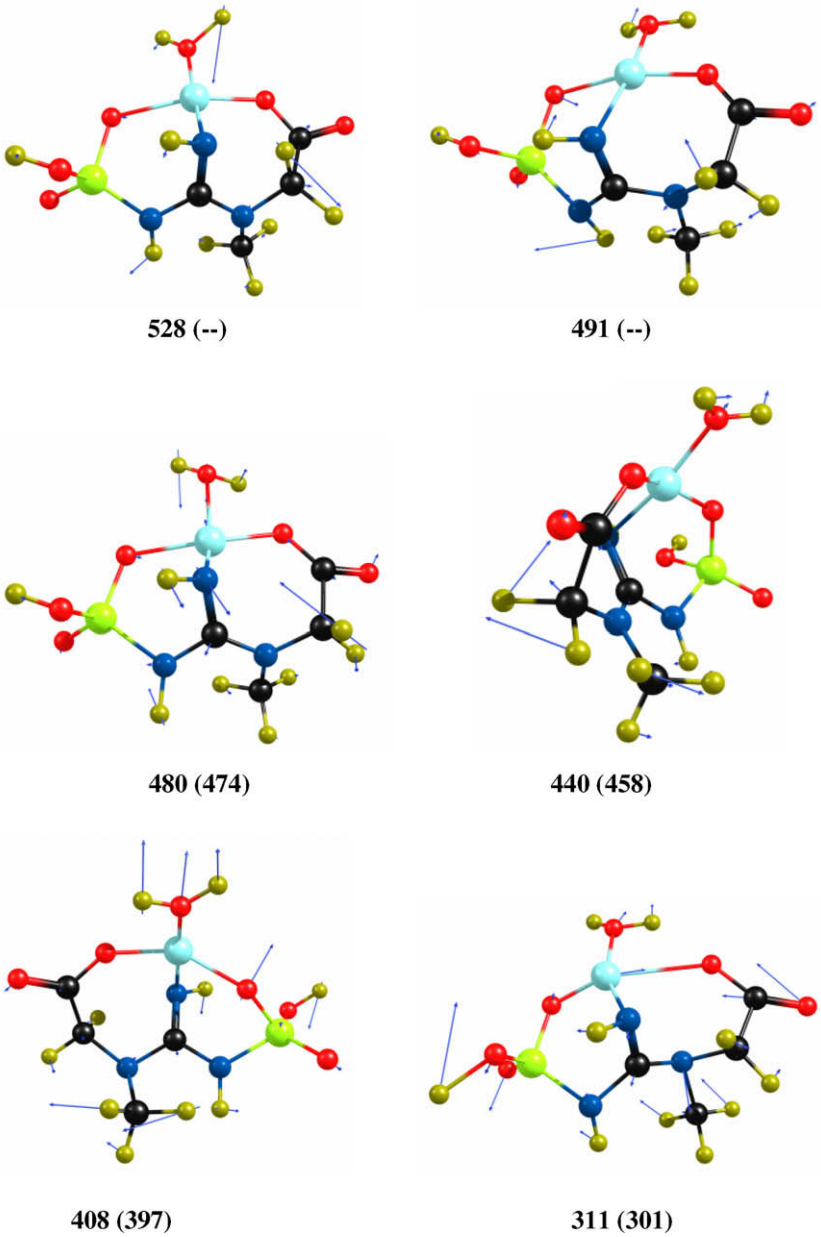

Fig. 4. Distorted geometries of some normal modes.

3.5.5. P=O and P–O stretching

The assignments for the phosphorous compounds present some difficulties due to structural effects caused by the surrounding atoms. The DFT calculated spectra indicate the following assignments for the P=O and P–O stretching: 1114 cm^{-1} (1067 cm^{-1} calculated), 850 cm^{-1} (845 cm^{-1} calculated) and (835 cm^{-1} calculated) for the ν(P=O), ν_s(P–O) and ν_{as}(P–O) vibrational modes, respectively. The experimental bands found at 1114 cm^{-1} agree well with earlier assignments for phosphorous compounds.

3.5.6. CNH and HCH bending vibrations

In general terms, the CNH and HCH bending vibrations are considered as characteristic wave numbers. As usual we can differentiate scissoring, wagging, twisting and rocking vibrations within the $-CH_2$ group. The two CNH structural fragments in the complex can form two δ(CNH)/or δ(CuNH) and δ(CNH)/or δ(PNH) bendings. In total we have expected to assign 13 bendings including the rocking vibrational modes. The DFT calculated spectra indicate the following assignments: the observed band at 1704 cm^{-1} (calculated value at 1620 cm^{-1}) can be assigned to the coupled mode as δ(C=NH) + δ(NCN). The infrared bands found at 1620 cm^{-1} (calculated at 1550 cm^{-1}), 1561 cm^{-1} (1541 cm^{-1} calculated) and 1544 cm^{-1} (1494 cm^{-1} calculated) were assigned to the δ(HCH) of the CH_3 group. The bands observed at 1512 cm^{-1} (1486 cm^{-1} calculated), 1428 cm^{-1} (1376 cm^{-1} calculated), 1173 cm^{-1} (1160 cm^{-1} calculated) and 1134 cm^{-1} (1146 cm^{-1} calculated) were assigned to the δ(HCH) of the CH_2 group. For the rocking vibrations of the $-CH_3$ and $-CH_2$ groups we found the following results: 1046 cm^{-1} (1049 cm^{-1} calculated) and 993 cm^{-1} (980 cm^{-1} calculated), respectively. The observed band at 740 cm^{-1} (727 cm^{-1} calculated) was assigned to one of the ρ(NH) vibrational modes. Descriptions of the assignments of these modes are given in Table 3.

3.5.7. CN, CO, and CC stretching vibrations

The C–O stretchings were assigned at 1342 cm^{-1} (1280 cm^{-1} calculated) and at 1252 cm^{-1} (1270 cm^{-1} calculated), both vibrations coupled with ν(CC). The band found by means of the second derivative at 1205 cm^{-1} (1225 cm^{-1} calculated) can be assigned as the coupled mode ν(CN) + ρ(CH)CH_3. The other bands that could be assigned to the C–N stretching present higher coupling degrees; they are 835 cm^{-1} calculated and 717 cm^{-1} calculated.

3.5.8. Skeletal framework vibrations

A clear identification of the metal–ligand vibrations is not straightforward due to the greater mixture of the different internal coordinates which form part of the description of the normal mode. With the purpose of better understanding this energy region and of achieving a better assignment of the low energy vibrational bands, we have studied the distorted geometry of some vibrational modes whose description is not clear under visual inspection. Our goal was to obtain a better description of the coupling degree between the different internal coordinates which compose the normal mode. Analysis of the low energy yielded the following approximate assignments in which the Cu–O and Cu–N stretching spread out in several vibrational modes with different participation degree: the calculated band at 528 cm^{-1} (no observed band) can be assigned as the coupled mode ν(Cu–O) + δ(HOH)wagging + $\rho(CH_2)$; the calculated band at 492 cm^{-1} (no observed band) corresponds to the coupled mode ν(Cu–O) + ν(Cu–N) with distortions of the order of 12% and 8%, respectively; the observed band at 474 cm^{-1} (second derivative) may be assigned as ν(Cu–N) + ν(Cu–O) with distortions of the order of 14% and 13%, respectively. The band found at 458 cm^{-1} may be assigned as $\rho(CH_2)$ + ν(Cu–O). The second derivative band found at 397 cm^{-1} corresponds approximately to the mode ν(Cu–O) + δ(OPN) + ν(Cu–N). The observed band at 301 cm^{-1} may be assigned to the mode ν(Cu–O) + angle ring distortion. The remaining assignments are given in Table 3. Fig. 4 shows the distorted geometry of some of the normal modes which were discussed above. The images were captured using the free CHEMKRAFT program [26].

4. Conclusions

The data reported here show that the reactions lead to a compound with a 1:1 metal/ligand ratio.

Solution studies involving PCr and copper(II) ions show that PCr acts as a bidentate ligand where one center of metallation is the nitrogen atom of the guanidine group, but are not conclusive about the second donor atom from PCr, as to whether it is the oxygen atom of the phosphate or the oxygen atom of the carboxylate groups from PCr [2,3]. The experimental and calculated data obtained for CuPCr has led us to propose that in solid state PCr acts as a tridentate ligand and coordinates to the metal ion through two oxygen atoms, one from the phosphate and one from the carboxylate group, as well as one nitrogen atom from the guanidine group. The fourth position is occupied by a water molecule. These results show that PCr has different behaviors in solution and in solid state. Calculations made from thermogravimetric curves suggest that the last remaining bond is that of Cu–phosphate. Phosphate is present in the residue of the thermal decomposition, and the coordination seems to increase its thermal stability.

Infrared spectral analysis combined with the quantum mechanical DFT:B3LYP/6-311G was useful to determine the geometrical structure of the [Cu(PCr)(H_2O)] complex, and to determine the description of the coupling degree of the Cu–O and Cu–N stretching internal coordinates and the associated framework bending coordinates in the composition of the normal modes belonging to the low energy region.

Mechanisms of many processes involving phosphocreatine and metal ions have not been explained yet. Thus, knowledge about the coordination modes of this system can be useful for a better understanding of its behavior in living organisms.

Acknowledgement

The authors thank CNPq (Conselho Nacional de Pesquisa e Desenvolvimento), Brazil, for their financial support.

References

[1] D.C.N. Lopes, Doctorate Dissertation, Department of Chemistry, PUC-Rio, 2001.
[2] A.M. Silva, A.L.R. Mercê, A.S. Mangrich, C.A.T. Soto, J. Felcman, Polyhedron 25 (2006) 1319.
[3] F. Cecconi, C. Frassineti, P. Gans, S. Lotti, S. Midollini, A. Sabatini, A.C. Vacca, Polyhedron 21 (2002) 1481.
[4] G.W. Allen, P. Haake, J. Am. Chem. Soc. 98 (1976) 16.
[5] M.L. Semnovski, V.I. Shumakov, V.G. Sharov, G.M. Mogilewsky, A.V. Asmolovsky, L.A. Makhotine, V.A. Saks, J. Thorac. Cardia. Surg. 94 (1987) 762.
[6] G. Prabhakar, L. Vana-Davis, D. Murray, P. Lakhani, G. Murray, J. Am. Coll. Surg. 197 (5) (2003) 786.
[7] J.T. Saari, Can. J. Physiol. Pharmacol. 78 (10) (2000) 845.
[8] K.B. Wallace, Pharmacol. Toxicol. 93 (2003) 105.
[9] G. Minotti, P. Menna, E. Salvatorelli, G. Cairo, L. Gianni, Pharmacol. Rev. 56 (2004) 185.
[10] S.D. Williams, L.H. Eichhorn, Adv. Internal Med. 27 (1982) 531.
[11] G.S.H. Mayor, Life Sci. 32 (1983) 685.
[12] G. Ara, T. Kusumoto, T.T. Korbut, F. Cullere-Luengo, B.A. Teicher, Cancer 54 (1994) 1497.
[13] A. De-Vizcaya-Ruyz, A. Rivero-Mueller, L. Ruiz-Ramirez, G.E. Lass, L.R. Kelland, R.M. Orr, M. Dobrota, Toxicol. In Vitro 14 (2000) 1.
[14] I. Gracia-Mora, L. Ruiz-Ramirez, C. Gómez-Ruiz, M. Tinoco-Méndez, A. Márquez-Quiñones, L. Romero-De Lira, A. Marin-Hernández, L. Macias-Rosales, M.E. Bravo-Gómez, Met-Based Drugs 8 (2001) 19.
[15] L. Hernández-Esquivel, A. Marín-Hernández, N. Pavón, K. Carvajal, R. Moreno-Sánchez, Toxicol. Appl. Pharmacol. 212 (2006) 79.

[16] George Brauer (Ed.), Handbook of Preparative Inorganic Chemistry, Academic Press, 1965.
[17] N.A. Rey, K.C. Santos, M.A.B.C. Menezes, A.S. Mangrich, E.C.P. Maia, J. Braz. Chem. Soc. 17 (3) (2006) 497.
[18] L. Lomozick, A. Gasowska, L. Bolewski, J. Inorg. Biochem. 63 (1996) 191.
[19] I. Somasundaram, M. Palaniandavar, J. Inorg. Biochem. 53 (1994) 95.
[20] R.G. Parr, W. Yang, Density-Functional Theory of Atoms and Molecules, Oxford University Press, Oxford, 1989.
[21] A.D. Becke, J. Chem. Phys. 98 (1993) 1372.
[22] M.J. Frisch, G.W. Trucks, H.B. Schlegel, G.E. Scuseria, M. A. Robb, J.R. Cheeseman, V.G. Zakrzewski Jr., J.A. Montgomery, R. E. Stratmann, J.C. Burant, S. Dapprich, J.M. Millam, A.D. Daniels, K.N. Kudin, M.C. Strain, O. Farkas, J. Tomasi, V. Barone, N.M. Cossi, R. Cammi, B. Mennucci, C. Pomelli, C. Adamo, S. Clifford, J. Ochterski, G.A. Peterson, P.Y. Ayala, Q. Cui, K. Morokuma, D.K. Malick, A.D. Rabuck, K. Raghavachari, J.B. Foresman, J. Cioslowski, J.V. Ortiz, A.G. Baboul, B.B. Stepanov, G. Liu, A. Liashenko, P. Piskorz, I. Komaromi, R. Gomperts, R.L. Martin, D.J. Fox, T. Keith, M.A. Al-Laham, C.Y. Peng, A. Nanayakkara, C. González, M. Challacombe, P.M.W. Gill, B. Johnson, W. Chen, M.W. Wong, J.L. Andresw, C. González, M. Head-Gordon, E.S. Repogle, J.A. Pople, GAUSSIAN 98, Revision A. 7, Gaussian Inc., Pittsburgh, PA, 1998.
[23] C.A. Téllez, S.E. Hollauer, M.A. Mondragon, V.M. Castaño, Spectrochim. Acta, Part A 57 (2001) 993.
[24] J.M. Ramos, O. Versiane, J. Felcman, C.A. Téllez, Spectrochim. Acta, Part A 67 (2007) 1037.
[25] L.J. Bellamy, The Infrared Spectra of Complex Molecules, Methuen & Co. Ltd., London, 1968.
[26] CHEMKRAFT. <http://www.chemkraftprog.com/order.htlm>.

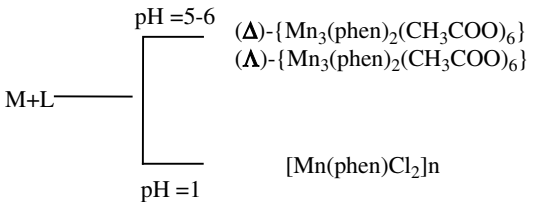

Scheme 1.

about 48% based on Mn). *Anal.* Calc. for **1**: C, 49.27; H, 3.90; N, 6.37. Found: C, 49.34; H, 3.94; N, 6.42%. IR (KBr): 1587 s, 1515 m, 1425 s, 1342 m, 1222 w, 1140 w, 1102 w, 1047 w, 1016 m, 942 w, 849 s, 776 w, 728 s, 657 m, 617w.

2.2.2. Synthesis of $[Mn(phen)Cl_2]_n$ (**2**)

The crystals of complex **2** were obtained in a similar method to complex **1**, just adjusting the pH to about **1** with hydrochloric acid. Yellow prism single crystals suitable for X-ray diffraction were obtained after three weeks (yield: about 32% based on Mn). *Anal.* Calc. for **1**: C, 47.09; H, 2.64; N, 9.15. Found: C, 47.15; H, 2.71; N, 9.22%. IR (KBr): 1621 m, 1586 m, 1515 m, 1423 s, 1349 w, 1284 w, 1224 w, 1144 m, 1104 m, 1046 w, 985 w, 950 w, 862 s, 748 m, 728 s, 638 w.

2.3. Crystallographic data collection and structure determination

A single-crystal X-ray diffraction study of complexes **1**–**2** was performed on a Bruker SMART diffractometer equipped with a CCD area detector with a graphite monochromator situated in the incident beam for data collection. The determination of unit cell parameters and data collections were performed with Mo Kα radiation ($\lambda = 0.71073$ Å) by the ω scan mode in the range $1.56 \leqslant \theta \leqslant 31.96$ (for **1**), and $2.33 \leqslant \theta \leqslant 35.59$ (for **2**) at 293(2) K. All data were corrected by the semi-empirical method using the SADABS program. The program SAINT [9] was used for integration of the diffraction profiles.

Both structures were solved by direct methods using the SHELXS program of the SHELXTL-97 package and refined with SHELXL [10]. The metal atom centers were located from the E-maps and other non-hydrogen atoms were located in successive difference Fourier syntheses. The final refinements were performed by full matrix least-squares methods with anisotropic thermal parameters for non-hydrogen atoms on F^2. All the hydrogen atoms were first found in difference electron density maps, and then placed in the calculated sites and included in the final refinement in the riding model approximation with displacement parameters derived from the parent atoms to which they were bonded. Further crystallographic data and experimental details for the structural analyses of both complexes are summarized in Table 1, and selected bond lengths and angles with their estimated standard deviations for complexes **1** and **2** are in Tables 2 and 3, respectively.

3. Results and discussion

3.1. Description of the crystal structures of complexes *1* and *2*

3.1.1. (Δ, Λ)-$\{Mn_3(phen)_2(CH_3COO)_6\}$ (**1**)

Structural analysis revealed that **1** is a kind of neutral trinuclear cluster. In each trinuclear cluster there are two crystallographically distinct Mn atoms, and the three Mn^{II} atoms are in a linear form linked by six acetate groups with Mn···Mn distances of 3.266 Å, and with two 1,10-phenanthroline ligands as terminal ligands (Fig. 1a). All of the three Mn^{II} atoms have a distorted octahedral geometry and two adjacent manganese octahedra share a triangular face. The middle Mn^{II} atom of the linear trinuclear cluster is coordinated by six oxygen atoms (Mn–O = 2.123(6) – 2.163(5) Å) belonging to three crystallographically distinct acetate carboxylate groups, while each of the two terminal Mn^{II} atoms is coordinated by four oxygen atoms (Mn–O = 2.171(5) – 2.406(13) Å) belonging to three different acetate carboxylate groups and two nitrogen atoms (Mn–N = 2.256(4) – 2.282(4) Å) of one chelate 1,10-phenanthroline. Interestingly, the acetate carboxylate group O3–C13–O4 chelates the terminal Mn(2) atom to form an O(3)–Mn(2)–O(4) angle of 50.7(3)°, and the O(3) atom acts as a bridge to link Mn(1) and Mn(2) with a Mn(1)–O(3)–Mn(2) angle of 95.9(4)° and distances Mn(1)–O(3) = 2.117(11)° and Mn(2)–O(3) = 2.441(12)°.

The structural analysis revealed that the two terminal chelating 1,10-phenanthroline molecules of one neutral trinuclear cluster

Table 1
Crystallographic data and structure refinement summary for complexes **1** and **2**

	1	**2**
Formula	$C_{36}H_{34}Mn_3N_4O_{12}$	$C_{12}H_8Cl_2MnN_2$
Mr	879.49	306.04
Temperature (K)	290(2)	290(2)
Wavelength (Å)	0.71073	0.71073
Crystal system	monoclinic	monoclinic
Space group	*C*2/*c*	*C*2/*c*
a (Å)	11.410(7)	17.269(5)
b (Å)	12.423(9)	10.455(3)
c (Å)	26.407(2)	7.052(3)
β (°)	98.677(4)	112.033(2)
V (Å^3)	3700.3(4)	1180.14(7)
Z	4	4
D_{calc} (g cm^{-3})	1.579	1.723
Crystal size (mm)	0.24 × 0.22 × 0.20	0.22 × 0.20 × 0.18
Theta range (°)	1.56–31.96	2.33–35.59
Reflections collected/unique	18533/6006	6269/2373
R_{int}	0.0275	0.0160
Completeness to theta	99.0% (25.00°)	99.9% (25.49°)
Data/restraints/parameters	3217/0/252	1107/0/79
Refinement method	full-matrix least-squares on F^2	full-matrix least-squares on F^2
Goodness-of-fit on F^2	1.002	1.055
Final R_1 and wR_2 indices	$R_1 = 0.0806$, $wR_2 = 0.1885$	$R_1 = 0.0216$, $wR_2 = 0.1023$
R_1 and wR_2 indices (all data)	$R_1 = 0.0913$, $wR_2 = 0.1937$	$R_1 = 0.0225$, $wR_2 = 0.1040$
Minimum and maximum peaks (e Å^{-3})	0.921 and −0.803	0.247 and −0.232

Table 2
Selected bond lengths (Å) and angles (°) for complex **1**

Mn(1)–O(1)	2.126(8)	Mn(2)–O(2)	2.184(6)	O2–C15	1.233(11)
Mn(1)–O(3)	2.117(11)	Mn(2)–O(3)	2.441(12)	O3–C13	1.239(12)
Mn(1)–O(5)	2.159(6)	Mn(2)–O(4)	2.338(8)	O4–C13	1.200(9)
Mn(2)–N(1)	2.251(5)	Mn(2)–O(6)	2.171(5)	O5–C17	1.247(10)
Mn(2)–N(2)	2.283(5)	O1–C15	1.248(11)	O6–C17	1.246(9)
O(1)–Mn(1)–O(3)	87.4(4)	O(2)–Mn(2)–O(3)	97.6(3)	O(4)–Mn(2)–O(6)	168.2(2)
O(1)–Mn(1)–O(5)	87.2(3)	O(2)–Mn(2)–O(4)	89.5(2)	O(4)–Mn(2)–N(1)	89.3(2)
O(1)–Mn(1)–O(1)#1	89.1(3)	O(2)–Mn(2)–O(6)	95.3(2)	O(4)–Mn(2)–N(2)	88.9(2)
O(1)–Mn(1)–O(3)#1	94.9(4)	O(2)–Mn(2)–N(1)	92.2(2)	O(6)–Mn(2)–N(1)	101.4(2)
O(1)–Mn(1)–O(5)#1	176.2(3)	O(2)–Mn(2)–N(2)	165.5(2)	O(6)–Mn(2)–N(2)	89.1(2)
O(3)–Mn(1)–O(5)	84.3(3)	O(3)–Mn(2)–O(4)	50.7(3)	N(1)–Mn(2)–N(2)	73.33(19)
O(3)–Mn(1)–O(3)#1	176.8(3)	O(3)–Mn(2)–O(6)	117.8(3)	O(1)–C(15)–O(2)	124.6(8)
O(3)–Mn(1)–O(5)#1	93.6(3)	O(3)–Mn(2)–N(1)	138.3(3)	O(3)–C(13)–O(4)	114.1(9)
O(5)–Mn(1)–O(5)#1	96.6(2)	O(3)–Mn(2)–N(2)	92.6(3)	O(5)–C(17)–O(6)	122.9(7)
Mn(1)–O(3)–Mn(2)	95.9(4)				

Symmetry transformations used to generate equivalent atoms: #1 $-x+1, y, -z+1/2$.

Table 3
Selected bond lengths (Å) and angles (°) for complex **2**

Mn(1)–Cl(1)	2.4809(3)	Mn(1)–Cl(1)#3	2.6630(3)
Mn(1)–Cl(1)#1	2.4809(3)	Mn(1)–N(1)	2.2608(10)
Mn(1)–Cl(1)#2	2.6630(3)	Mn(1)–N(1)#1	2.2608(10)
Cl(1)–Mn(1)–Cl(1)#1	102.293(17)	N(1)#1–Mn(1)–N(1)	73.41(6)
Cl(1)#1–Mn(1)–Cl(1)#2	84.136(10)	N(1)#1–Mn(1)–Cl(1)	93.13(3)
Cl(1)#1–Mn(1)–Cl(1)#3	98.176(11)	N(1)–Mn(1)–Cl(1)	162.03(3)
Cl(1)#2–Mn(1)–Cl(1)#3	176.342(14)	N(1)#1–Mn(1)–Cl(1)#2	84.60(3)
Mn(1)–Cl(1)–Mn(1)#3	95.866(10)	N(1)–Mn(1)–Cl(1)#2	92.46(3)

Symmetry transformations used to generate equivalent atoms: #1 $-x, y, -z+1/2$; #2 $x, -y, z+1/2$; #3 $-x, -y, -z$.

are not in a plane, but have a torsion angle of 36.44(6)°, which means **1** exists as two kinds of chiral neutral trinuclear enantiomers. The absolute configurations of these are as shown in Fig. 1b. Compound **1a** adopts a Δ configuration, while **1b** adopts a Λ configuration.

Detailed structural analysis revealed that the distance between the two planes of two adjacent 1,10-phenanthroline molecules in two neighboring trinuclear clusters is about 3.480(8) Å, within the range of π···π packing interactions (3.3–3.7 Å). It is the π···π packing interactions that link these clusters to result in the crystal of **1** as depicted in Fig. 1c.

3.1.2. $[Mn(phen)Cl_2]_n$ (**2**)

X-ray single crystal structure determination reveals that complex **2** is a coordination polymer based on neutral one-dimensional infinite coordination chains. In each asymmetric unit of **2**, one Mn^{II} center coordinates to two N donors (Mn–N = 2.2608(10) Å) of 1,10-phenanthroline and four chlorine atoms (Mn–Cl = 2.4809(3)-2.6630(3) Å), forming a distorted octahedral geometry as shown in Fig. 2a.

Detailed structural analysis revealed that the neutral one-dimensional infinite chain of **2** is assembled by Δ-configuration and Λ-configuration Mn^{II} units, alternately. In each Mn^{II} unit, one Mn^{II} coordinates to (i) two N donors of a 1,10-phenanthroline ligand, forming a Mn1–N1–C1–C2–N2–Mn1 five-member ring and (ii) four chlorine atoms which are bridge coordinated with another two neighboring units, forming two Mn1–Cl1–Mn2–Cl2–Mn1 four-member rings. As a result, two kinds of configuration of Mn^{II} units are formed, one in a Δ configuration and the other in a Λ configuration [11], as shown in Fig. 2b. Then they assemble alternately to form the one-dimensional chains of **2** (Fig. 2c).

Analysis of the crystal packing of **2** indicates that the distance between two planes of two adjacent 1,10-phenanthroline molecules of two neighboring chains is about 3.251(6) Å, which indicates strong π···π packing interactions. The inter-chains π···π packing interactions link these one-dimensional infinite coordination chains to result in the coordination polymer of **2** as depicted in Fig. 2d.

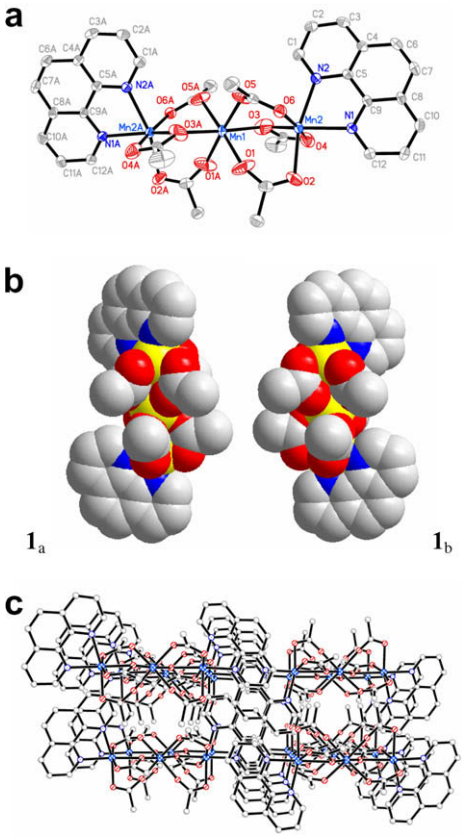

Fig. 1. (a) Perspective view of **1**, showing the linear trinuclear cluster, hydrogen atoms are omitted for clarity; (b) perspective view of the Δ configuration and Λ configuration of compound **1a** (left) and **1b** (right), respectively; (c) crystal packing diagram of **1** along the *c* axis, showing the π···π packing interactions between two adjacent trinuclear clusters.

3.2. Magnetic properties

The variations of the molar magnetic susceptibilities χ_M were investigated for compounds **1** and **2** in the temperature range 2–300 K at a field of 1000 Oe. The study of the temperature

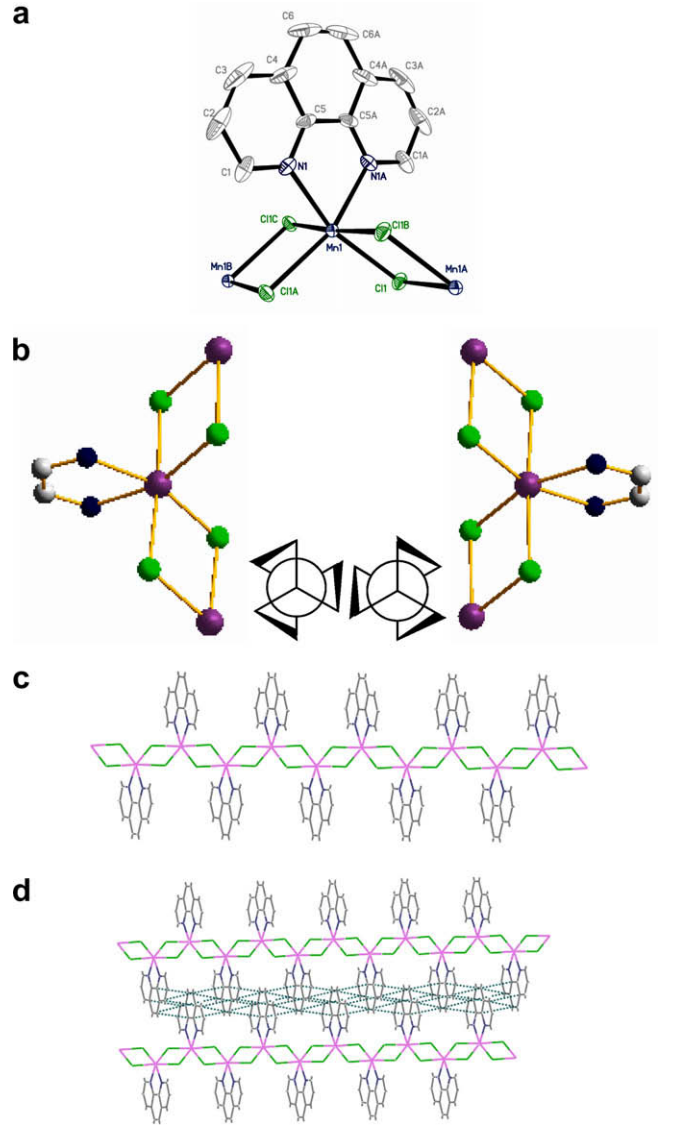

Fig. 2. (a) Perspective view of an asymmetric unit of **2**, hydrogen atoms are omitted for clarity; (b) perspective view of the Δ configuration (left) and Λ configuration (right) of Mn^{II} units of **2**; (c) the neutral hetero-assembled one-dimensional infinite coordination chains of **2**, (d) crystal packing diagram of **2**, showing the π···π packing interactions between two adjacent 1-D infinite coordination chains of **2**.

dependent magnetic susceptibilities revealed that **1** shows an antiferromagnetic coupling between the Mn^{II} ions while **2** displays a ferromagnetic interaction within the chain.

The χ_M^{-1} and $\chi_M T$ *versus* T plots of **1** are displayed in Fig. 3a. The inverse susceptibility plot as a function of temperature is linear (above 80 K), following the Curie–Weiss law $\chi_M = C/(T-\theta)$ for Mn^{II} centers with the Curie constant $C = 14.72\ cm^3\ K\ mol^{-1}$ and Weiss temperature $\theta = -24.6$ K. Below this temperature, a departure from the line may be caused by antiferromagnetic interactions. The $\chi_M T$ versus T plot exhibits a value of 13.63 cm^3 K mol^{-1} at 300 K, which is slightly above the expected value $\chi_M T = 13.12\ cm^3\ K\ mol^{-1}$ for three uncoupled Mn^{II} ions with $S = 5/2$ and $g = 2$ each [12]. It continuously decreases on cooling to a value of 1.167 $cm^3\ mol^{-1}$ K at 2 K. Such magnetic behavior is typical for antiferromagnetic coupling between Mn^{II} ions [13].

Taking into account the structure of the isolated and linear Mn(II) trimer units in **1** and assuming that the exchange coupling within the cluster is isotropic and that there is no interaction

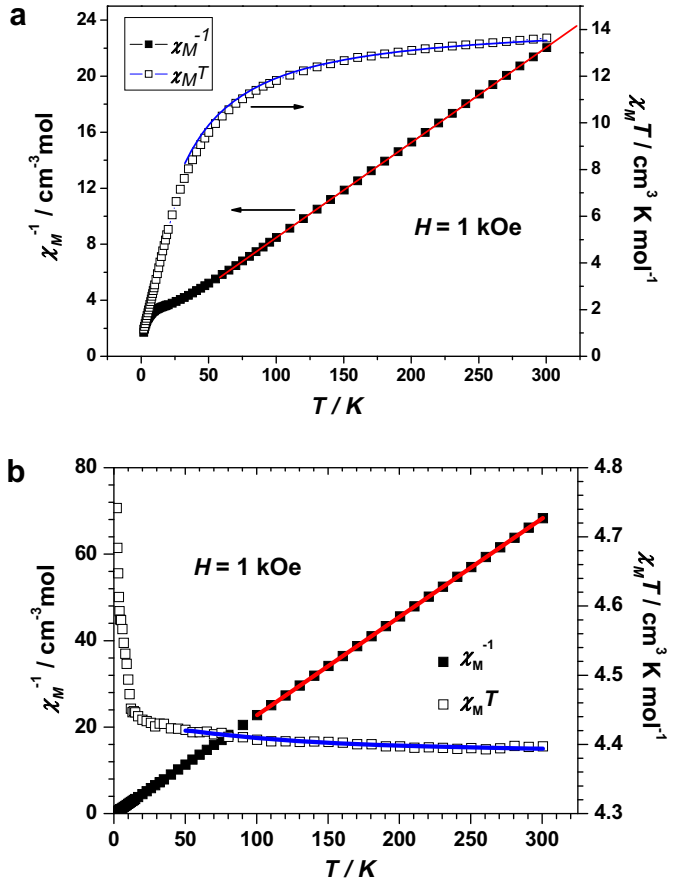

Fig. 3. The χ_M^{-1} and $\chi_M T$ vs. T plots, (a) for **1** and (b) for **2** at $H = 1000$ Oe. The red solid lines represent the best fit for the Curie–Weiss Law and the blue ones are the fitting lines with the models mentioned in the text.

between the two terminal Mn(II) ions, the Heisenberg Hamiltonian for the trimer system can be written as

$$H = -J(S_1S_2 + S_2S_3)$$

where J is the exchange coupling constant (negative for antiferromagnetic and positive for ferromagnetic interactions) and S_1, S_2, $S_3 = 5/2$ for the three Mn(II). By application of Van Vleck's equation, [14] a theoretical expression for the molar susceptibility may be derived as follows:

$$\chi_M = \frac{Ng^2\beta^2}{3kT}\left(\frac{3F_1}{4F_2}\right)$$

where $F_1 = 680\ e^{27.5x} + 455(e^{20x} + e^{25x}) + 286(e^{13.5x} + e^{18.5x} + e^{22.5x}) + 165(e^{8x} + e^{13x} + e^{17x} + e^{20x}) + 84(e^{3.5x} + e^{8.5x} + e^{12.5x} + e^{15.5x} + e^{17.5x}) + 35(e^{15x} + e^{5x} + e^{9x} + e^{12x} + e^{14x}) + 10(e^{2.5x} + e^{6.5x} + e^{9.5x} + e^{11.5x}) + (e^{5x} + e^{8x}) + 35,$

$F_2 = 8\ e^{27.5x} + 7(e^{20x} + e^{25x}) + 6(e^{13.5x} + e^{18.5x} + e^{22.5x}) + 5(e^{8x} + e^{13x} + e^{17x} + e^{20x}) + 4(e^{3.5x} + e^{8.5x} + e^{12.5x} + e^{15.5x} + e^{17.5x}) + 3(e^{15x} + e^{5x} + e^{9x} + e^{12x} + e^{14x}) + 2(e^{2.5x} + e^{6.5x} + e^{9.5x} + e^{11.5x}) + (e^{5x} + e^{8x}) + 3$

$$x = J/(kT)$$

The best fitting for the data from 32 to 300 K gives $J = -6.60\ cm^{-1}$ and $g = 2.10$. The negative J value indicates antiferromagnetic coupling between the Mn^{II} ions, which is consistent with similar compounds [14].

The magnetic properties of **2** are shown in Fig. 3b. The molar susceptibility also follows the Curie–Weiss law in the range 100–

300 K, with a value of the Curie constant $C = 4.39\ cm^3\ K\ mol^{-1}$ and Weiss temperature $\theta = +0.43$ K, as shown in Fig. 3b. At 300 K, the $\chi_M T$ value of **2** is $4.40\ cm^3\ K\ mol^{-1}$ per Mn^{II}, which is slightly above the expected value for $S = 5/2$ of a spin-only ground state for per couple of uncorrelated Mn^{II} centers ($4.35\ cm^3\ K\ mol^{-1}$). Then it continuously increased to a maximum of $4.74\ cm^3\ K\ mol^{-1}$ when the temperature was cooled to 2 K. This behavior of the $\chi_M T$ curve shows that **2** is a one-dimensional ferromagnetic coupled chain [15].

The value of the exchange interaction of **2** has been estimated according to the Fisher model of the isotropic Heisenberg antiferromagnet for a $S = 1/2$ system and later modified by Wagner and Friedberg [16] for the Mn(II) system of $S = 5/2$. The molar susceptibility of the Fisher chain can be expressed as

$$\chi = \frac{NS(S+1)}{3kT} g^2 \beta^2 \frac{1-u(K)}{1+u(K)}$$

where $u(K)$ is $1/K - \coth(K)$, $K = 2JS(S+1)/kT$, $g = 2$ and $S = 5/2$. The best fitting to the data from 50 to 300 K gives $J = +0.02\ cm^{-1}$, $g = 2.00$. The small positive J value shows a slightly ferromagnetic interaction within the Mn^{II} chain.

4. Conclusions

By the strategy of pH-directed assembly, we have synthesized two polynuclear manganese(II) complexes. In the pH range 5–6, chiral linear trinuclear manganese molecules were obtained, while on adjusting the pH to about 1 with hydrochloric acid, one-dimensional infinite manganese chains were gained. Further studies on the preparation of polynuclear manganese functional complexes are under way in our laboratory.

Supplementary data

CCDC 603481 and 603482 contain the supplementary crystallographic data for this paper. These data can be obtained free of charge via http://www.ccdc.cam.ac.uk/conts/retrieving.html, or from the Cambridge Crystallographic Data Centre, 12 Union Road, Cambridge CB2 1EZ, UK; fax: (+44) 1223-336-033; or e-mail: deposit@ccdc.cam.ac.uk.

Acknowledgements

We gratefully acknowledge the financial support of Beijing Natural Science Foundation (No. 2052007).

References

[1] (a) G.B. Conyers, G. Wu, M.J. Bessman, A.S. Mildvan, Biochemistry 39 (2000) 2347;
(b) S.V. Antonyuk, V.R. Melikadamyan, A.N. Popov, V.S. Lamzin, P.D. Hempstead, P.M. Harrison, P.J. Artymyuk, V.V. Barynin, Crystallogr. Rep. 45 (2000) 105;
(c) M.C. Bewley, P.D. Jeffrey, M.L. Patchett, Z.F. Kanyo, E.N. Baker, Struct. Fold. Des. 7 (1999) 435;
(d) M.C.J. Wilce, C.S. Bond, N.E. Dixon, H.C. Freeman, J.M. Guss, P.E. Lilley, J.A. Wilce, Proc. Nat. Acad. Sci. USA 95 (1998) 3472.
[2] (a) O. Kahn (Ed.), Molecular Magnetism a Supramolecular Function, Kluwer, Dordrecht, Netherlands, 1996;
(b) O. Kahn, Molecular Magnetism, VCH, Weinheim, Germany, 1993.
[3] (a) E.J. Schelter, F. Karadas, C. Avendano, A.V. Prosvirin, W. Wernsdorfer, K.R. Dunbar, J. Am. Chem. Soc. 129 (2007) 8139;
(b) S. Piligkos, G. Rajaraman, M. Soler, N. Kirchner, J.V. Slageren, R. Bircher, S. Parsons, H.-U. Güdel, J. Kortus, W. Wernsdorfer, G. Christou, E.K. Brechin, J. Am. Chem. Soc. 127 (2005) 5572;
(c) D. Gatteschi, R. Sessoli, Angew. Chem., Int. Ed. 42 (2003) 268;
(d) M. Soler, W. Wernsdorfer, K.A. Abboud, J.C. Huffman, E.R. Davidson, D.N. Hendrickson, G. Christou, J. Am. Chem. Soc. 125 (2003) 3576.
[4] (a) R. Sessoli, H.-L. Ysai, A.R. Schake, S. Wang, J.B. Vincent, K. Folting, D. Gatteschi, G. Christou, D.N. Hendrickson, J. Am. Chem. Soc. 115 (1993) 1804;
(b) R. Sessoli, D. Gatteschi, A. Caneschi, M.A. Novak, Nature 356 (1993) 141;
(c) G. Christou, D. Gatteschi, D.N. Hendrickson, R. Sessoli, MRS Bull. 25 (2000) 66.
[5] H. Gudbjartson, K. Biradha, K.M. Poirier, M.J. Zaworotko, J. Am. Chem. Soc. 121 (1999) 2599.
[6] (a) H.P. Wu, C. Janiak, G. Rheinwald, H. Lang, J. Chem. Soc., Dalton Trans. (1999) 183;
(b) M.A. Withersby, A.J. Blake, N.R. Champness, P.A. Cooke, P. Hubberstey, W.S. Li, M. Schröder, Inorg. Chem. 38 (1999) 2259.
[7] N. Niklas, F. Hampel, R. Alsfasser, Chem. Commun. (2003) 1586.
[8] J. Kim, J.M. Lim, Y. Do, Eur. J. Inorg. Chem. (2003) 2563.
[9] Bruker AXS, SAINT Software Reference Manual, Madison, WI, 1998.
[10] G.M. Sheldrick, SHELXTL NT Version 5.1. Program for Solution and Refinement of Crystal Structures, University of Göttingen, Germany, 1997.
[11] F.A. Cotton, G. Wilkinson, C.A. Murillo, M. Bochmann, Advanced Inorganic Chemistry, John Wiley & Sons, New York, 1999, p. 32.
[12] C.J. Milios, T.C. Stamatatos, P. Kyritsis, A. Terzis, C.P. Raptopoulou, R. Vicente, A. Escuer, S.P. Perlepes, Eur. J. Inorg. Chem. (2004) 2885.
[13] (a) P. Yin, S. Gao, Z.-M. Wang, C.-H. Yan, L.-M. Zheng, X.-Q. Xin, Inorg. Chem. 44 (2005) 2761;
(b) S.C. Manna, S. Konar, E. Zangrando, K. Okamoto, J. Ribas, N.R. Chaudhuri, Eur. J. Inorg. Chem. (2005) 4646;
(c) X.-M. Lu, P.-Z. Li, X.-T. Wang, S. Gao, X.-J. Wang, S. Wang, Y.-H. Deng, L. Zhou, Y.-J. Zhang, Polyhedron (2008) 2402.
[14] K.-F. Hsu, S.-L. Wang, Inorg. Chem. 39 (2000) 1773.
[15] (a) K. Inoue, K. Kikuchi, M. Ohba, H. Ōkawa, Angew. Chem., Int. Ed. 42 (2003) 4810;
(b) H.-R. Wen, C.-F. Wang, Y.-Z. Li, J.-L. Zuo, Y. Song, X.-Z. You, Inorg. Chem. 45 (2006) 7032;
(c) S.C. Manna, S. Konar, E. Zangrando, K. Okamoto, J. Ribas, N.R. Chaudhuri, Eur. J. Inorg. Chem. (2005) 4646.
[16] (a) G.R. Wagner, S.A. Friedberg, Phys. Lett. 9 (1964) 11;
(b) T. Somchai, P.A.F. Francesca, R.A. David, V.K. Konstantin, R. Neil, J. Am. Chem. Soc. 128 (2006) 9205.

2. Experimental

2.1. Chemicals and starting materials

All the solvents were purified by conventional procedures and distilled prior to use. Commercially available chemicals (Aldrich) were used as supplied without further purification.

2.2. Synthesis of the ligand dmpt

The ligand (*R*,*R*)-(+)-di-*N*,*N*′-methylpyridino-tartramide (dmpt) (Fig. 1) was prepared as previously described and was characterized by IR, ^1H–^{13}C NMR and elemental analysis [19].

2.3. Synthesis of the complexes

2.3.1. Synthesis of $Na[Cu_2(dmptH_{-3})(CO_3)] \cdot 8H_2O$ (**1**)

A solution of $Cu(ClO_4)_2 \cdot 6H_2O$ (0.74 g, 2 mmol) in 15 mL of ethanol was added dropwise to a solution of dmpt (0.33 g, 1 mmol) dissolved in 20 mL of absolute ethanol. Then, solid Na_2CO_3 (0.21 g, 2 mmol) was added in small portions and the mixture was stirred for 20 min and filtered. Slow evaporation of the solution at room temperature yielded blue crystals suitable for X-ray diffraction analysis. Yield: 0.45 g (67%). *Anal.* Calc. for $C_{17}H_{31}Cu_2N_4NaO_{15}$: C, 29.96; H, 4.54; N, 8.22; Cu, 18.6. Found: C, 30.11; H, 4.40; N, 8.24; Cu, 19%. IR (KBr) (cm^{-1}): 3424 (s, ν_{O-H}), 1614 (vs, $\nu_{C=O}$), 1585 (s, $\nu_{pyridine\ ring}$), 1420, (s, νCO_2), 1560 and 1319 (s, ν_{C-N} and δ_{N-H}). UV–Vis λ_{max} (nm) (ε, $mol^{-1}\,dm^3\,cm^{-1}$): (solid state) 640, broad; (H_2O) 640 (310); (DMF) 610 (280).

2.3.2. Synthesis of $[Ni_2(dmptH_{-2})_2] \cdot 2H_2O$ (**2**)

$Ni(OH)_2$ was freshly obtained by adding 2 equiv. of NaOH to an aqueous solution of nickel chloride. $Ni(OH)_2$ (0.09 g, 1 mmol) was added to a solution of dmpt (0.33 g, 1 mmol) in 10 mL of a mixture of CH_3OH and H_2O (v/v = 1/1), and stirred for 2 h. The blue-purple precipitate obtained was filtered, washed with ethanol and dried in vacuum. Yield: 0.3 g (75%). *Anal.* Calc. for $C_{32}H_{36}N_8Ni_2O_{10}$: C, 47.4; H, 4.4; N, 13.8; Ni, 14.5. Found: C, 47.7; H, 4.5; N, 14.1; Ni, 14.1%. IR (KBr) (cm^{-1}): 3386 (s, ν_{O-H}), 1608 (vs, $\nu_{C=O}$), 1563 and 1480 (s, $\nu_{pyridine\ ring}$), 1565 and 1399 (s, ν_{C-N} and δ_{N-H}). UV–Vis λ_{max} (nm) (ε, $mol^{-1}\,dm^3\,cm^{-1}$): (solid state) 365, 568, 987 (broad); (CH_3OH) 280 (68), 575 (9), 975 (33).

$[Ni_2(dmptH_{-2})_2] \cdot 9.75H_2O$ (**2**), was obtained as monocrystals by mixing a solution of $Ni(ClO_4)_2 \cdot 6H_2O$ (0.37 g, 1 mmol) in 10 mL of ethanol and a solution of dmpt (0.33 g, 1 mmol) in 20 mL of ethanol. Then, potassium *tert*-butoxide (0.224 g, 2 mmol) dissolved in 5 mL of ethanol was added and the mixture was stirred for 2 h and filtered. The resulting purple solution concentrated at room temperature gave blue-purple crystals suitable for X-ray diffraction analysis.

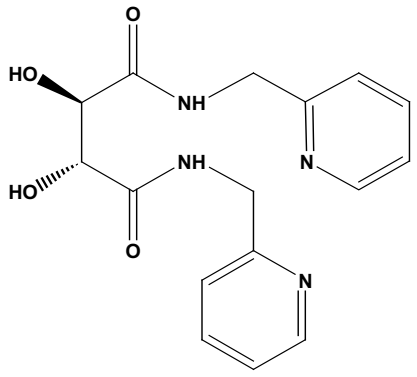

Fig. 1. Schematic structure of the ligand dmpt (neutral form).

2.3.3. Synthesis of $[Co_2(dmptH_{-3})(\mu\text{-}OH)] \cdot NaClO_4 \cdot 5H_2O$ (**3**)

To avoid cobalt oxidation the synthesis was monitored in a glovebox under N_2 atmosphere. A solution of $Co(ClO_4)_2 \cdot 6H_2O$ (0.37 g, 1 mmol) in 10 mL of ethanol was added dropwise to a solution of dmpt (0.165 g, 0.5 mmol) in 20 mL of ethanol. Then, sodium hydroxide (0.08 g, 2 mmol) dissolved in 5 mL of water was added. The mixture was heated at 60 °C, and stirred for 1 h. The red powder which precipitated was then filtered, washed with ethanol and dried in vacuum; yield 0.16 g (50%). *Anal.* Calc. for $C_{16}H_{24}Co_2N_4O_{13}NaCl$: C, 28.4; H, 3.8; N, 8.3; Co, 17.4; Na, 3.4. Found: C, 28.8; H, 3.9; N, 8.6; Co, 17.8, Na 3.3%. IR (KBr) (cm^{-1}): 3422 (s, ν_{O-H}), 2899 (vs, ν_{CH}), 1586 (vs, $\nu_{C=O}$), 1560 (s, ν_{C-N} and δ_{N-H}), 1085 (s, ν_{ClO_4}). UV–Vis λ_{max} (nm) (ε, $mol^{-1}\,dm^3\,cm^{-1}$): (CH_3OH) 503 (75), 560 (52), 582 (46).

2.4. Physical measurements

Elemental analyses (C, H and N) were carried out on a Perkin–Elmer 2400 C, H, N element analyzer in our university. The metal analysis was performed on an ICP AES Liberty Series II Varian apparatus.

ESI-MS experiments were monitored on a hybrid tandem quadrupole/time-of-flight (Q-TOF) instrument, equipped with a pneumatically assisted electrospray (Z-spray) ion source (Micromass, Manchester, UK) operated in the positive mode. The electrospray potential was set to 3 kV in the positive ion mode and the extraction cone voltage was usually varied between 30 and 90 V in order to obtain optimized mass spectra.

Magnetic measurements were performed at the Institut de Physique et Chimie des Matériaux de Strasbourg (UMR CNRS-ULP 7504) using a Quantum Design MPMS-XL SQUID magnetometer. The susceptibility measurement was performed in the 300–1.8 K temperature range with an applied magnetic field of 0.5 T. Magnetization measurements at different fields at a given temperature confirm the absence of ferromagnetic impurities. Data were corrected for the sample holder and diamagnetism was estimated from Pascal constants.

The UV–Vis spectra in solution were recorded on a Perkin–Elmer Lambda 6 spectrophotometer. In the solid state, the visible spectra were obtained on a Beckman 5240 spectrophotometer by depositing the compound on a Schleicher and Schul ash-free filter paper. The paper was used as the reference. IR spectra were obtained in KBr pellets with a Nicolet Avatar 320. Thermogravimetric analysis (TGA) studies were carried out in the 25–300 °C range using a 2950 TA-Analyser. Electrochemical measurements were performed at room temperature in DMF using an Autolab PGSTAT12 potentiostat equipped with a three-electrode assembly comprising a glassy carbon-working electrode, a Pt counter electrode and a Ag/AgCl reference electrode. The ferrocenium(1+)/ferrocene couple was used as an internal standard. All potentials were reported relative to the Ag/AgCl reference electrode. The $E_{½}$ value of the ferrocenium/ferrocene (Fc^+/Fc) system under the experimental conditions was 630 mV in DMF and ΔEp for Fc^+/Fc was 110 mV. Tetrabutylammonium hexafluorophosphate (10^{-1} mol L^{-1}) was used as the supporting electrolyte. The sample concentration was 10^{-3} mol L^{-1} and the solution was de-aerated with Argon gas for at least 20 min before measurement.

2.5. Crystal structure determination

The intensity data were collected in the phi scan mode at 293 K for compound **1** and at 100 K for compound **2** on a Bruker-Nonius

Kappa-CCD diffractometer, equipped with a graphite monochromator, using Mo Kα radiation (λ = 0.71073 Å). The structures were solved by direct methods using the SIR92 software package [20] and refined by full matrix least-squares on F^2 using SHELXL97 [21]. The intensities were corrected for Lorentz and polarization effects. In both crystal structure determinations, non-hydrogen atoms were located in the difference Fourier syntheses and were refined with anisotropic thermal parameters. Not all hydrogen atoms were observed in the difference Fourier syntheses, in particular those belonging to the alcohol groups and to 12 disordered water molecules in **2**. Observed hydrogen atoms were placed at calculated positions using a riding model, except those of water molecules which were either refined (**1**) or restrained to the mean Ow–H distances (0.97 Å) and H–Ow–H angles (~107°) observed from neutron diffraction data (**2**). In both crystal structure determinations, a global isotropic thermal parameter was refined for the H-atoms. Within each dimer of the asymmetric unit of **2**, one pyridylmethyl group of each ligand was found to be disordered. When compared to each other, the groups exhibited a very similar disorder, and the moieties show statistically equivalent site occupation factors (0.61(2)/0.39(2) and 0.63(2)/0.37(2)). In fact, the dimers of **2** are related by twofold axes pseudo-symmetry elements, which could eventually lead to the orthorhombic $C\,222_1$ space group. However, close inspection of the systematic absences clearly indicates the good choice of the monoclinic $P2_1$ space group, the pseudo-symmetry elements being non-crystallographic mainly due to the co-crystallized water molecules (many of them are disordered).

Crystal data and refinement details for $Na[Cu_2(dmptH_{-3})(CO_3)]\cdot 8H_2O$ (**1**) and $[Ni_2(dmptH_{-2})_2]\cdot 9.75H_2O$ (**2**) are shown in Table 1. Additional experimental information, including atomic positional parameters, is supplied in CIF format as described in the Supplementary data.

2.6. XAS data collection and analysis

The XANES (X-ray Absorption Near Edge Structure) and EXAFS (Extended X-ray Absorption Fine Structure) spectra were collected at the ELETTRA Synchrotrone (Trieste, Italy) on the Beamline 11.1 of the storage ring operating at 2/2.4 GeV with an optimal storage beam current of around 300/130 mA. The measurements were carried out at the cobalt *K*-edge (≈7709 eV) and the incident beam was mono-chromatized with a Si(1 1 1) double crystal. The energy was calibrated by measuring the absorption edge of a cobalt metallic foil (fixed at 7709 eV). The detectors were low-pressure (≈0.2 atm) air-filled ionization chambers and the measurements were performed at room temperature in the transmission mode. The XANES spectra were the sum of three recordings in the range 7660–7780 eV, and the EXAFS spectra were the sum of three recordings in the range 7660–8660 eV (including the cobalt *K*-edge (≈7709 eV)). The spectra were recorded using sampling steps of 0.2 eV (XANES) and 2 eV (EXAFS), and an integration time of 2.0 s per point was used in both cases. The spectrum of the 0.5 μm metallic foil was recorded just before the unknown XANES spectra to check the energy calibration. Spectra were measured on well-powdered samples mixed with boron nitride, to give a sample thickness of *ca.* 1 mm, placed in aluminium sample holders and held in place by Kapton tape.

The EXAFS data analysis was performed using the "EXAFS pour le Mac" and EXAFS98 programs [22,23]. The $\chi(k)$ functions were extracted from the data with a linear pre-edge background and a polynomial atomic-absorption background, and normalized using the Lengeler–Eisenberger method [24]. The extraction procedure was conducted as previously described [25]. In this work, all Fourier transforms were calculated and presented without phase correction. The major peak below 2 $Å^{-1}$ in the Fourier transformed curve was isolated and back-Fourier transformed. An *R* range of ≈0.80–2.15 $Å^{-1}$ was used for the first peak. This back-Fourier transformed peak was fit in *k* space. Structural parameters (R_i, distances between neighbours, N_i, number of neighbours and σ_i, Debye-Waller factor) were extracted with fits to the standard EXAFS formula, realized in the framework of a single scattering. The estimated errors for distances and coordination numbers are ±0.02 Å and ±20%, respectively. The backscattering phase, $\Phi_i(k,R_i)$, and amplitude, $A_i(k,R_i)$, functions were obtained using the ab initio FEFF 7 code [26]. The validity of the theoretical functions was ascertained using a reference compound of known crystallographic structure: Co^{III}[1,12-bis(2-pyridyl)-5,8-dioxa-2,11-diazadodecane] [27] for the Co–O and Co–N waves. Moreover, the FEFF 7 code was used to check if the multiple scattering of our reference compounds of known crystallographic structure was negligible in the 0–3 Å range. No constraints were placed on the fitting parameters of the first neighbour O shells, but the Debye-Waller factor (σ^2) of the oxygen atom from water molecules was fixed at 0.01 $Å^2$ to reduce the number of free parameters in the fitting procedure.

Table 1
Crystal data and details of the refinement of the crystal structures of $Na[Cu_2(dmptH_{-3})(CO_3)]\cdot 8H_2O$ (**1**) and $[Ni_2(dmptH_{-2})_2]\cdot 9.75H_2O$ (**2**).

	1	**2**
Formula	$C_{17}H_{31}Cu_2N_4NaO_{15}$	$C_{32}H_{51.5}N_8Ni_2O_{17.75}$
M	681.39	949.73
Crystal system	orthorhombic	monoclinic
Crystal size (mm^3)	0.16 × 0.14 × 0.04	0.30 × 0.20 × 0.20
Space group	$P\,2_12_12_1$	$P\,2_1$
a (Å)	6.7561(1)	12.6485(3)
b (Å)	14.4773(3)	29.1767(7)
c (Å)	26.6954(5)	13.0691(3)
α (°)	90	90
β (°)	90	121.099(1)
γ (°)	90	90
V ($Å^3$)	2611.08(8)	4129.85(17)
T (K)	293	100
Z	4	2
μ(Mo Kα) (mm^{-1})	1.723	0.995
Reflections measured	7106	35 600
Number of independent reflections [R_{int}]	5977 [0.04]	18 552 [0.05]
F(0 0 0)	1332	1990
Goodness-of-fit on F^2	1.114	1.224
Final *R* indices	R_1 = 0.036	R_1 = 0.0625
[$I > 2\sigma(I)$]	wR_2 = 0.051	wR_2 = 0.1609
R indices (all data)	R_1 = 0.046	R_1 = 0.0738
	wR_2 = 0.082	wR_2 = 0.1776

3. Results and discussion

3.1. Synthesis

The new complexes with deprotonated forms of the ligand, $Na[Cu_2(dmptH_{-3})(CO_3)]\cdot 8H_2O$ (**1**), $[Ni_2(dmptH_{-2})_2]\cdot 2H_2O$ and $[Ni_2(dmptH_{-2})_2]\cdot 9.75H_2O$ (**2**) and $[Co_2(dmptH_{-3})(\mu\text{-}OH)]\cdot NaClO_4\cdot 5H_2O$ (**3**) were synthesized in a mixture of water and ethanol under basic conditions (pH ≈ 8). NaOH, Na_2CO_3, $KtBuO^-$ and/or $Ni(OH)_2$ were used as bases to deprotonate the NH amido- and the OH alcohol groups of the ligand. When NaOH is used in the preparation of the copper complex (**1**), the absorption of atmospheric CO_2 during the recrystallization leads to the formation of a carbonato bridged complex.

3.2. Thermal decomposition

For the Cu(II), Ni(II) and Co(II) complexes, TGA experiments were monitored under a nitrogen atmosphere in the temperature

range 20–250 °C. For complexes (**2**) and (**3**), the analytical data show a weight loss, which occurs in one step in the temperature range 50–100 °C, corresponding to the loss of coordinated and uncoordinated water molecules. This weight loss corresponds to 13.6% in the case of complex (**3**), in agreement with the empirical formula $[Co_2(dmptH_{-3})(\mu\text{-}OH)] \cdot NaClO_4 \cdot 5H_2O$ (theoretical weight loss 13.7%). For the $[Ni_2(dmptH_{-2})_2] \cdot 2H_2O$ complex, the weight loss is equal to 4.6% (theoretical weight loss 4.4%), and is equal to 18.4% for the $[Ni_2(dmptH_{-2})_2] \cdot 9.75H_2O$ complex (**2**) (theoretical weight loss 18.5%). For complex (**1**), the thermal curve shows that the decomposition occurs in three steps, which correspond to the release of 3 (42 °C), 2 (47 °C) and 3 (120 °C) water molecules, giving a total weight loss of 20.9%, in accordance with the empirical formula $Na[Cu_2(dmptH_{-3})(CO_3)] \cdot 8H_2O$ (theoretical weight loss 21.1%).

3.3. X-ray diffraction studies

3.3.1. $Na[Cu_2(dmptH_{-3})(CO_3)] \cdot 8H_2O$ (**1**)

Complex (**1**) crystallizes as a water solvate in the space group $P2_12_12_1$ with four formula units present in the unit cell. The molecular structure consists of a dinuclear $[Cu_2(dmptH_{-3})(CO_3)]^-$ anion with one sodium cation and eight water molecules of crystallization. In the crystal lattice, the sodium cation is coordinated by six water molecules in an octahedral fashion with Na···OH_2 distances in the range 2.3–2.5 Å. Moreover, these octahedra are aligned into chains with μ-OH_2 bridges from the equatorial water ligand and OH···O hydrogen bonds from the axial water ligands. Selected bond lengths and angles are listed in Table 2. A Platon [28] drawing of the $[Cu_2(dmptH_{-3})(CO_3)]^-$ anion together with the labelling-scheme is shown in Fig. 2.

The dinuclear core is composed of two copper(II) ions bridged by one deprotonated endogenous alcohol group of the ligand and also by the carbonate anion. The Cu···Cu separation in the compound is 3.379 Å. Both copper(II) ions are tetracoordinated with an identical set of N_2O_2 donors atoms in a distorted square planar geometry. However, the coordination of the deprotonated alcohol O(2) has led to the existence of asymmetry in the compound: there are two five-membered chelate rings formed around Cu(1) with *cis* angles of 82.5° and 84.3°, whereas Cu(2) possesses one five-membered chelate ring and one six-membered chelate ring with *cis* angles of 82.9° and 95.6°, respectively. This implies a lengthening of the N_{amido}–Cu(2) bond of 0.041 Å compared to the N_{amido}–Cu(1) bond and a shortening of the $O_{carbonate}$–Cu(2) bond of 0.011 Å compared to the $O_{carbonate}$–Cu(1). The bond lengths involving the pyridylmethylamido nitrogen atoms are entirely consistent with those in other Cu(II) amido complexes [29,30]. The *trans* angles

Table 2
Selected bond lengths (Å) and angles (°) for $Na[Cu_2(dmptH_{-3})(CO_3)] \cdot 8H_2O$.

Bond lengths			
Cu(1)–N(1)	2.002(2)	Cu(2)–N(4)	2.004(2)
Cu(1)–N(2)	1.884(2)	Cu(2)–N(3)	1.925(2)
Cu(1)–O(2)	1.919(2)	Cu(2)–O(2)	1.908(2)
Cu(1)–O(6)	1.887(2)	Cu(2)–O(5)	1.914(2)
O(5)–C(17)	1.284(4)	O(2)–C(8)	1.418(3)
O(6)–C(17)	1.283(4)	O(3)–C(9)	1.420(4)
O(7)–C(17)	1.281(4)	Cu(1)–Cu(2)	3.379(1)
Bond angles			
N(1)–Cu(1)–N(2)	82.5(1)	N(3)–Cu(2)–N(4)	82.9(1)
N(1)–Cu(1)–O(2)	166.7(1)	N(4)–Cu(2)–O(2)	162.5(1)
N(1)–Cu(1)–O(6)	93.8(1)	N(4)–Cu(2)–O(5)	90.4(1)
N(2)–Cu(1)–O(2)	84.3(1)	N(3)–Cu(2)–O(2)	95.6(1)
N(2)–Cu(1)–O(6)	175.8(1)	N(3)–Cu(2)–O(5)	163.1(1)
O(2)–Cu(1)–O(6)	99.3(1)	O(2)–Cu(2)–O(5)	95.4(1)
Cu(1)–O(2)–Cu(2)	124.4(1)	O(5)–C(17)–O(6)	122.5(3)
C(8)–O(2)–Cu(1)	113.5(2)	C(8)–O(2)–Cu(2)	119.7(2)

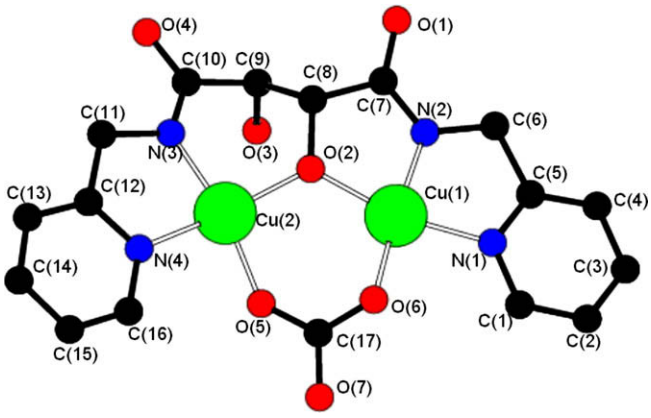

Fig. 2. Platon drawing of the anion $[Cu_2(dmptH_{-3})(CO_3)]^-$ and the atom labelling-scheme. Hydrogen atoms are omitted for clarity.

in Cu(2) of 162.5° and 163.1°, smaller than their analogues of 166.7° and 175.8° in Cu(1), reflect the larger distortion around Cu(2).

3.3.2. $[Ni_2(dmptH_{-2})_2] \cdot 9.75H_2O$ (**2**)

Complex **2** crystallizes in the monoclinic system (space group $P2_1$) with four dimeric complexes and 39 co-crystallized water molecules per unit cell. Selected bond lengths and angles are summarized in Table 3, and a Platon drawing of the molecular structure of the dimer $[Ni_2(dmptH_{-2})_2]$ is shown in Fig. 3.

The molecular structure of each dimer is symmetric, with each half unit consisting of the first pyridylmethylamido group and the undeprotonated alcohol oxygen donor of the ligand coordinated to one nickel centre, with the same set of donor atoms of the same ligand being coordinated to the second nickel centre. In each dimer complex one pyridylmethyl group is disordered. It should be noted that, in spite of the hydrogen atoms of the alcohol groups not being found in the structure determination, the range and average of the C–$O_{alcohol}$ and $O_{alcohol}$–Ni^{2+} bond distances observed in **2** (1.429 < C–$O_{alcohol}$ < 1.445 Å, average 1.437 Å and 2.151 < $O_{alcohol}$–Ni^{2+} < 2.259 Å, average 2.165 Å) are significantly closer to those observed in Ni(II) complexes with undeprotonated alcohol groups, as found in the Cambridge Structural Database (corresponding to 25 hits, 1.399 < C–OH < 1.478 Å, average 1.444 Å; 1.901 < $O_{alcohol}$–Ni^{2+} < 2.182 Å, average 2.097 Å, respectively). In the same database, there was no hit corresponding to a nickel complex in which the ligand is coordinated through the deprotonated alcohol group, but 13 hits show a deprotonated alcohol group of the ligand in which the oxygen atom behaves as a bridge between two metallic ions, as observed in complex **1** (see above). In these metal ions (M^{2+} = Cu^{2+}, Zn^{2+}, Fe^{2+}), the C–$O^-_{alcohol}$ and M–$O^-_{alcohol}$ bond distances are: 1.363 < C–O^- < 1.453 Å, average 1.397 Å; 1.908 < O^-–M^{2+} < 2.021 Å, average 1.946 Å.

The intramolecular Ni···Ni separations within each dimer of the asymmetric unit are 5.268 and 5.269 Å. The geometry around the nickel atoms in both dimers is essentially identical and they are therefore discussed together, giving average values for the four coordinations. Both coordination geometries are distorted octahedral, with an N_4O_2 donor set of atoms coming from four nitrogen atoms from the two pyridylmethylamido moieties in the equatorial plane and two oxygen donor atoms from undeprotonated alcohol groups in the axial positions. Around each nickel centre, the two pyridyl nitrogen atoms and two alcohol oxygen atoms are each mutually trans. The average Ni–$N_{pyridyl}$ bond length of 2.086 Å is comparable to those observed in other six coordinate nickel(II) complexes with a pyridylcarboxamido moiety [31–34]. The average Ni–N_{amido} bond length of 1.977 Å, shorter than Ni–$N_{pyridyl}$, is

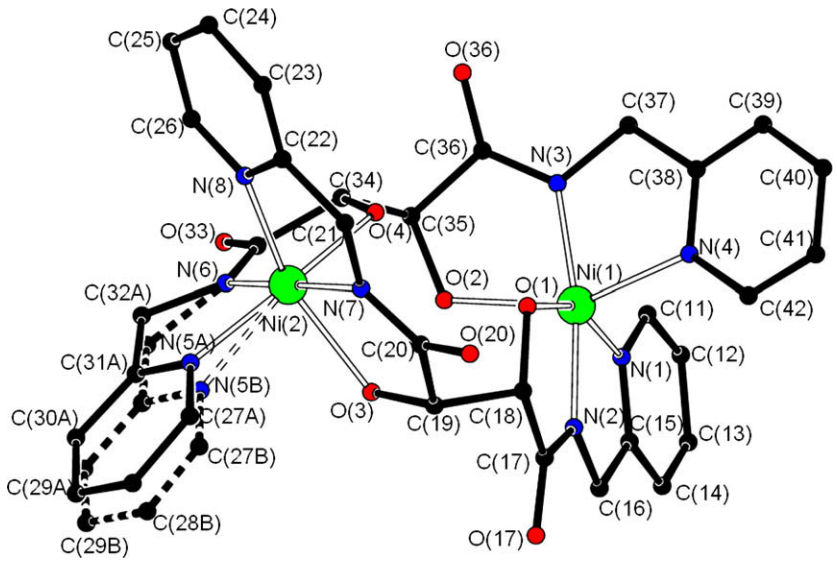

Fig. 3. Platon drawing of the dimer $[Ni_2(dmptH_{-2})_2]$ and the atom labelling-scheme. Water molecules and hydrogen atoms are omitted for clarity.

Table 3
Selected bond lengths (Å) and angles (°) for $[Ni_2(dmptH_{-2})_2] \cdot 9.75H_2O$ (**2**). The Ni–N bonds distance and N–Ni–N, or N–Ni–O bonds angles showing two values correspond to the disordered nitrogen atoms.

Bond lengths			
Ni(1)–N(1)	2.077(5)	Ni(2)–N(5)	2.000(9)/2.216(17)
Ni(1)–N(2)	1.975(5)	Ni(2)–N(6)	1.969(5)
Ni(1)–N(3)	1.986(5)	Ni(2)–N(7)	1.975(5)
Ni(1)–N(4)	2.086(5)	Ni(2)–N(8)	2.049(6)
Ni(1)–O(1)	2.259(4)	Ni(2)–O(1)	2.174(4)
Ni(1)–O(2)	2.166(4)	Ni(2)–O(2)	2.151(4)
Bond angles			
N(1)–Ni(1)–N(2)	80.5(2)	N(5A)–Ni(2)–N(6)	78.7(3)/85.1(5)
N(1)–Ni(1)–N(3)	104.0(2)	N(5A)–Ni(2)–N(7)	105.1(3)/97.9(5)
N(1)–Ni(1)–N(4)	99.1(2)	N(5A)–Ni(2)–N(8)	99.3(3)/107.8(5)
N(1)–Ni(1)–O(1)	156.66(19)	N(5A)–Ni(2)–O(3)	91.8(3)/81.2(5)
N(1)–Ni(1)–O(2)	95.25(17)	N(5A)–Ni(2)–O(4)	157.5(3)/157.9(4)
N(2)–Ni(1)–N(3)	170.5(2)	N(6)–Ni(2)–N(7)	174.2(2)
N(2)–Ni(1)–N(4)	107.7(2)	N(6)–Ni(2)–N(8)	101.9(2)
N(2)–Ni(1)–O(1)	76.20(16)	N(6)–Ni(2)–O(3)	97.8(2)
N(2)–Ni(1)–O(2)	95.48(18)	N(6)–Ni(2)–O(4)	79.70(19)
N(3)–Ni(1)–N(4)	80.2(2)	N(7)–Ni(2)–N(8)	81.9(2)
N(3)–Ni(1)–O(1)	99.20(18)	N(7)–Ni(2)–O(3)	77.92(19)
N(3)–Ni(1)–O(2)	75.81(18)	N(7)–Ni(2)–O(4)	96.02(18)
N(4)–Ni(1)–O(1)	87.64(16)	N(8)–Ni(2)–O(3)	158.94(17)
N(4)–Ni(1)–O(2)	154.44(19)	N(8)–Ni(2)–O(4)	91.01(19)
O(1)–Ni(1)–O(2)	87.47(14)	O(4)–Ni(2)–O(3)	85.11(15)

consistent with the stronger donor ability of the deprotonated amido nitrogen atoms. This amido bond length is well within the range of Ni–N_{amido} distances noted in similar complexes [31–35]. The average trans bond angles $N_{pyridyl}$–Ni–$O_{alcohol}$ and N_{amido}–Ni–N_{amido} (157.1° and 172.5°, respectively) deviate from the ideal octahedral trans angle of 180°. The range of the four five-membered chelate ring bond angles subtended by the ligands at the nickel atoms 75.8-81.2° (average, 78.5°) differ from 90°, indicating a large distortion around each nickel centre.

3.4. XAS investigations of $[Co_2(dmptH_{-3})(\mu\text{-}OH)] \cdot NaClO_4 \cdot 5H_2O$

XANES spectra were used to probe the oxidation state of the cobalt. There are a number of characteristic features in the XANES spectra of cobalt(II) and cobalt(III) complexes. Many cobalt compounds display a weak pre-edge feature at ~7709 eV that can be assigned to the 1s → 3d transition. Most cobalt(III) spectra show two main peaks, the absorption edge peak at ~7727 eV and a neighbouring peak at around ~7736 eV. Both peaks can be assigned to the 1s → 4p transitions [36]. In contrast, the XANES spectra of cobalt(II) complexes show a single main absorption peak at ~7723 eV. This is in accordance with several studies which have shown that the main absorption peak is shifted to lower values with a decreased effective charge of the nucleus [36,37]. Finally, the post-edge minima of the XANES spectra for cobalt(III) complexes are observed in the range 7757–7762 eV, whereas those of most cobalt(II) complexes occur in the range 7749–7750 eV. This post-edge minimum is a consequence of multiple-scattering phenomena which depend upon inter-atomic distances and angles [38–40].

Fig. 4 shows the Co *K*-edge XANES spectra of the $Co^{II}Cl_2$ reference compound and $[Co_2(dmptH_{-3})(\mu\text{-}OH)] \cdot NaClO_4 \cdot 5H_2O$ in the solid state and in solution. The three spectra exhibit a weak pre-edge feature at 7709 eV, which corresponds to a 1s → 3d transition. The relatively weak intensity of this pre-edge is consistent with an octahedral symmetry. Indeed, for this point group, a weak pre-edge feature is observed, despite being theoretically forbidden by the centre of symmetry. This is because the point group represents a static model derived by time-averaging the asymmetric vibrations within the molecule, whereas XAS reacts to the individual, and constantly changing, structures of the local environment as intramolecular vibrations which momentarily eliminate the

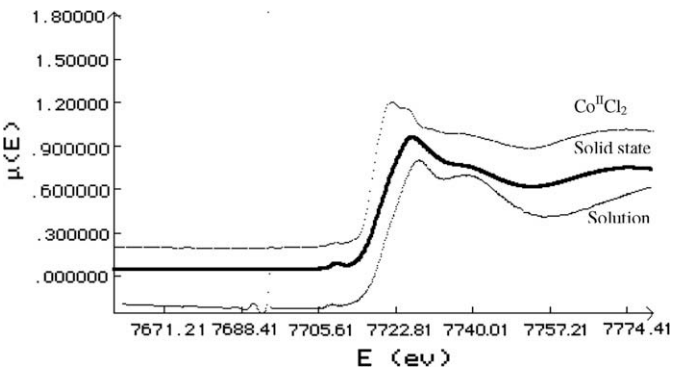

Fig. 4. Normalized XANES spectra of the $Co^{II}Cl_2$ reference compound and of $[Co_2(dmptH_{-3})(\mu\text{-}OH)] \cdot NaClO_4 \cdot 5H_2O$ in solid state and in solution.

centre of symmetry [41]. The absorption edge (1s → 4p transition) of the solid complex is at 7725.4 eV, whereas in solution the absorption edge is shifted to a higher value (7728.1 eV). The former value is in accordance with a +II oxidation state of the cobalt cation, which is oxidized in solution to cobalt(III). The presence of cobalt(II) is in agreement with the magnetic measurements. This oxidation state is also supported by the fact that the post-edge minimum in the XANES spectra differs between the solid state and solution. As a solid, cobalt(II) has its post-edge minimum at 7752.8 eV, while the complex in solution has its minimum at 7756.0 eV. Nevertheless, this difference may also be due to a strong effect of the coordination environment, which limits its usefulness in the determination of an oxidation state in complex systems [36]. However, this shift in the post-edge minimum combined with the one absorption edge confirms the +II oxidation state of the solid cobalt complex.

The experimental and least-squares fitting of the first shell filtered EXAFS spectra of the $[Co_2(dmptH_{-3})(\mu\text{-}OH)] \cdot NaClO_4 \cdot 5H_2O$ complex in solid state are shown in Fig. 5 with their corresponding Fourier transforms. A single shell fitting was performed to obtain the local structural parameters because the different atomic contributions to EXAFS oscillations do not interfere with one another, so each contribution to the EXAFS oscillation could be well resolved. The first shell was fitted with two Co–N/O contributions with a distance of 2.03 ± 0.02 Å and four Co–O/N contributions with a distance of 2.01 ± 0.02 Å. Even if the oxygen and nitrogen atoms have very similar phase and similar amplitude functions, the nature of the ligand allows us to propose a CoN_2O_4 chromophore: the two nitrogen atoms coming from pyridyl and amidic groups and the two bridged oxygen atoms from a deprotonated alcohol group and an hydroxyl group; the hexacoordination is achieved by two water molecules as depicted in Fig. 6. These results are in agreement with those obtained by UV–Vis spectroscopy and magnetism measurements, which underline a slightly distorted octahedral geometry around the cobalt(II) metallic cation.

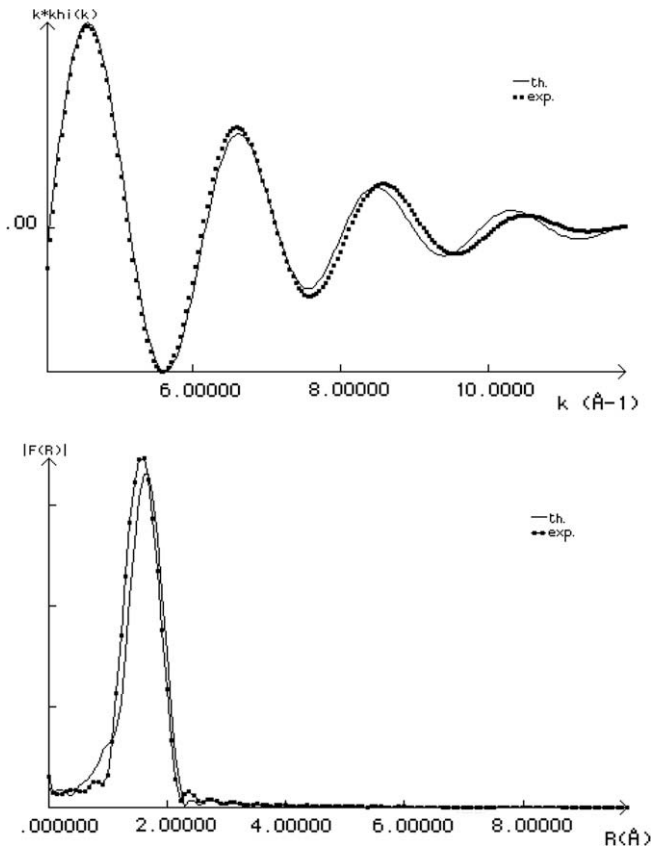

Fig. 5. First shell filtered Co *K*-edge EXAFS spectra (top) and the corresponding Fourier transforms (bottom) of the $[Co_2(dmptH_{-3})(\mu\text{-}OH)] \cdot NaClO_4 \cdot 5H_2O$ complex.

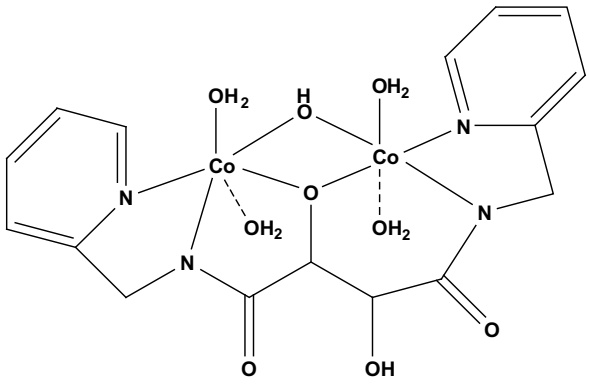

Fig. 6. Proposed structure for the complex $[Co_2(dmptH_{-3})(\mu\text{-}OH)]$.

Unfortunately, no significant peak on the Fourier transform at higher *R* values (>2.15 Å) could be interpreted. Indeed, fitting attempts which were performed at higher values on the very weak peaks lead to insignificant contributions. This is in accordance with a metal–metal distance higher than the one found for the copper complex (3.379 Å).

4. Spectral studies

4.1. IR spectroscopy

All the complexes exhibit broad bands around 3400 and 3500 cm^{-1}, which is caused by the OH vibration of coordinated and uncoordinated water molecules. The binding metal–ligand is indicated by a shift of the ν(CO) vibration from 1673 cm^{-1} in the free ligand to 1614, 1608 and 1586 cm^{-1} in the complexes (**1**), (**2**) and (**3**), respectively. The dinuclear copper complex (**1**), which is bridged by a carbonate ion, showed a strong $\nu(CO_2)$ band around 1420 cm^{-1} [42]. The presence of an uncoordinated perchlorate anion in complex (**3**) is inferred from the bands around 1085 and 630 cm^{-1} [42].

4.2. UV–Vis spectroscopy

4.2.1. Nickel complex

The UV–Vis spectra of the nickel complex in methanol and in DMF show three bands corresponding to the predicted $^3A_{2g} \rightarrow {}^3T_{2g}$ (950–800 nm), $^3A_{2g} \rightarrow {}^3T_{1g}(F)$ (560–500 nm) and $^3A_{2g} \rightarrow {}^3T_{1g}(P)$ (300–400 nm) transitions for a d^8 metallic cation held in an octahedral symmetry [43,44]. The overall pattern of the spectra for the solid state and solution are closely similar, which confirms that the complex structure is retained in the solution state. Moreover, ESI-MS analysis (in the positive mode) of the complex dissolved in CH_3OH solution is in agreement with the retention in solution of the dinuclear structure. The ESI-MS spectrum shows a major peak at *m*/*z* equal to 773.2 (*m*/*z* of the first peak of the isotopic clump), which corresponds to the formula $[Ni_2(dmptH_{-2})_2+H]^+$.

4.2.2. Copper complex

The electronic absorption spectra in water and in DMF exhibit a broad absorption band in the visible region with a maximum at 640 (ε = 310 mol^{-1} dm^3 cm^{-1}) and 610 nm (ε = 280 mol^{-1} dm^3 cm^{-1}), respectively. The symmetrical shape of the absorption band is typical of tetragonally distorted Cu(II) in a square

pyramidal geometry [34,45–47]. The small blue shift of the absorption maximum observed in DMF compared to the one in water is in accordance with the coordination of an additional solvent molecule to the copper centre compared to the coordination observed in the solid state. The electronic spectrum of the copper complex in the solid state exhibits two main transitions. The moderately intense peak close to 375 nm is probably due to a metal–ligand charge transfer, whereas the very broad band at λ_{max} equal to 640 nm is due to a d–d transition, which confirms the square planar geometry in the solid state.

4.2.3. Cobalt complex

The electronic absorption spectrum of $[Co_2(dmptH_{-3})(\mu\text{-}OH)] \cdot NaClO_4 \cdot 5H_2O$ dissolved in CH3OH is typical of a high spin Co(II) complex. The spectrum exhibits a broad band in the 450-650 nm region, which can be deconvoluted into three contributions: 503 ($\varepsilon = 75\ mol^{-1}\ dm^3\ cm^{-1}$), 560 ($\varepsilon = 52\ mol^{-1}\ dm^3\ cm^{-1}$) and 582 nm ($\varepsilon = 46\ mol^{-1}\ dm^3\ cm^{-1}$), which correspond respectively to the following forbidden transitions $4T_{1g}(F) \rightarrow 4B_{1g}(F)$, $4T_{1g}(F) \rightarrow 4E_g(P)$ and $4T_{1g}(F) \rightarrow 4A_{2g}(P)$ in D_4h symmetry [42,48].

5. EPR and magnetic susceptibility studies

The copper complexes are EPR-silent in the solid state and in a H_2O–CH_3OH solution at 150 K, suggesting an anti-ferromagnetic coupling between the copper ions. Such behaviour is confirmed by the temperature dependence of the molar magnetic susceptibility χ_M and of the product $\chi_M T$, depicted in Fig. 7a. The value of $\chi_M T$ at 300 K is 0.336 $cm^3\ K\ mol^{-1}$, well below the spin-only value for two Cu(II) ions (0.75 $cm^3\ K\ mol^{-1}$, considering $g = 2$). Upon cooling, χ_M and $\chi_M T$ decrease steadily, indicating a strong antiferromagnetic coupling between the Cu(II) ions. Below 10 K, a "Curie tail" appears in the χ_M versus T curve, which is attributed to the presence of a small quantity of a paramagnetic impurity. The experimental data were reproduced correctly using the following spin Hamiltonian where all parameters have their usual meaning [49] and where the spin operator $\mathbf{S}$ is defined as $\mathbf{S} = \mathbf{S_{Cu1}} + \mathbf{S_{Cu2}}$:

$$\mathscr{H} = -J\mathbf{S_{Cu1}}\mathbf{S_{Cu2}} + g\beta H\mathbf{S}$$

To satisfactorily reproduce the data, we had to consider a certain amount ρ of paramagnetic impurity, which was assumed to be a mononuclear copper(II) species ($\mathbf{S_{impur}} = ½$). The best-fit parameters are $J = -329.3(1)\ cm^{-1}$, $g = 1.92(1)$ and ρ = 0.18% with an excellent agreement factor $R = 3.2 \times 10^{-5}$ which is defined as: $R = \frac{\sum(\chi_{exp} - \chi_{calc})^2}{\sum \chi^2_{exp}}$.

These medium anti-ferromagnetic couplings should be correlated to a significant overlap between the two magnetic orbitals of the two copper(II) ions in the complexes through the oxo bridge. The coordination sphere around the two copper ions is square pyramidal and the unpaired electron of copper(II) occupies the $d(x^2–y^2)$ orbital, which points along the Cu–O bond. Short Cu–O bonds and large Cu–O–Cu angles in square-planar dinuclear copper complexes result in a strong overlap of the $d(x^2–y^2)$ orbitals and thus produce strong to very strong anti-ferromagnetic coupling. In the literature, much research has been undertaken to describe the relationship between the Cu–O–Cu angle and the magnetic interaction [50–55]. It has been clearly established [53] that large Cu–O–Cu angles (>110°) have a strongly anti-ferromagnetic contribution. The J value ($-329\ cm^{-1}$) follows the magneto-structural correlation between the Cu–O–Cu angle reported by Van Albada and co-workers [53]. The ferromagnetic interaction via the $Cu(\mu CO_3)Cu$ bridge observed in compounds in which the carbonate is monodentately bound to two copper ions by two oxygen atoms and the third oxygen, being uncoordinated [56–58], can be considered as negligible in our compound, taking into account the high J value.

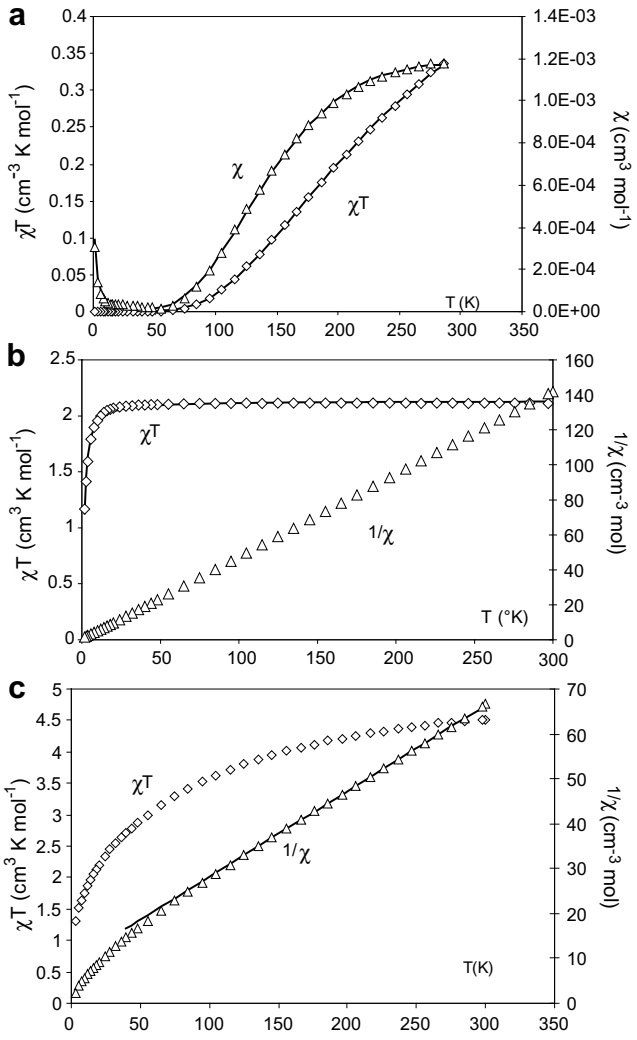

Fig. 7. Plots of $\chi_M T$ (◇) and χ_M (or $1/\chi_M$) (△) versus T for the copper (a), nickel (b) and cobalt (c) complexes. The solid lines are the fit of the data.

The magnetic behaviour of the nickel dimer is presented Fig. 7b. From room temperature to around 50 K, the χT product is almost constant (2.11 $cm^3\ K\ mol^{-1}$), indicating two almost non-coupled octahedral Ni(II) ions, with a g value of 2.05 [42,44,59–61]. The decrease of χT below 50 K (2.10 $cm^3\ K\ mol^{-1}$ at 50 K down to 1.17 $cm^3\ K\ mol^{-1}$ at 1.8 K) may be attributed to a zero-field splitting of the Ni(II) ions and/or to a very weak intramolecular antiferromagnetic coupling, in agreement with the long intramolecular Ni–Ni distance. Fitting the curve by considering zero-field splitting of Ni(II) ions and/or intramolecular anti-ferromagnetic coupling leads nearly to the same value of the agreement factor, which does not permit the two possibilities from being distinguished.

The plots of χ^{-1} and χT versus temperature for the Co(II) dinuclear complex are shown in Fig. 7c. The μ_{eff} value of this complex at 300 K, is 6.05 MB ($\chi_M T = 4.57\ cm^3\ K\ mol^{-1}$), which is consistent with the literature reports for high spin d^7 Co(II) [62–64]. The value of χT decreases regularly upon cooling from 4.57 $cm^3\ K\ mol^{-1}$ at room temperature to 1.26 $cm^3\ K\ mol^{-1}$ at 1.8 K. This decrease may be due to a spin-orbit coupling and/or to anti-ferromagnetic interactions. Above 50 K, the χ^{-1} versus T plot obeys the Curie-Weiss law, and the fitting provides a Curie constant C of 2.62 $cm^3\ K\ mol^{-1}$/Co and a Weiss temperature θ of −47.5 K. The

absence of crystallographic structure, as well as the existence of a spin–orbit coupling, prevented us from performing an accurate determination of the *g* and *J* parameters for this complex.

6. Electrochemistry

The range of potential recording is limited to −2.2 V to 0.9 V versus Fc^+/Fc taking into account the intrinsic redox processes of the ligand. The ligand voltammogram underlines an oxidation peak at 0.18 V versus Fc^+/Fc.

The cyclic voltammograms recorded in the negative potential range for the Ni(II) and Cu(II) complexes do not show any significant reduction process.

The cyclic voltammogram of the $Na[Cu_2(dmptH_{-3})CO_3]$ complex is shown in Fig. 8a. The cyclic voltammetry experiments underline two irreversible oxidation waves at 0.25 V (peak a) and 0.50 V (peak b) versus Fc/Fc^+. These two peaks corresponds to the successive oxidation of the two copper(II) centres into Cu(III), following two consecutive mono-electronic oxidation processes. Peak c corresponds to the ligand oxidation. The irreversible nature of the oxidation process suggests that the hypothetical Cu(III) species are highly reactive and might lead to ligand degradation. Within the functional groups present, the bridging alkoxide functions are most susceptible to be oxidized, which can produce aldehyde and carboxylic acid derivatives or C–C coupled products [65]. The dinuclear $[Ni_2(dmptH_{-2})_2]$ complex has two similar environments around the nickel atoms (see Section 3.3) and, consequently, these atoms present the same electrochemical behaviours. The cyclic voltammogram (Fig. 8b) in the positive potential range shows one single step of electron transfer processes at an $E_{1/2}$ value of 0.15 V versus (Fc^+/Fc). It corresponds to the simultaneous oxidation of the two Ni(II) centres, which indicates that the distance between the two metallic centres is sufficiently important so that the oxidation of one Ni(II) is not affected by the oxidation of the other centre. The second peak corresponds to the ligand oxidation. Cyclic voltammograms recorded between 0 and 1 V at three scan rates show that the oxidation process corresponding to the formation of the Ni(III)–Ni(III) complex is quasi reversible, taking into account the following criteria: (i) the $E_{1/2}$ values are independent of the scan rate, (ii) ΔEp increases with increasing scan rate and is always greater than 60 mV and (iii) the peak currents i_{pc} and i_{pa} are not equal [66].

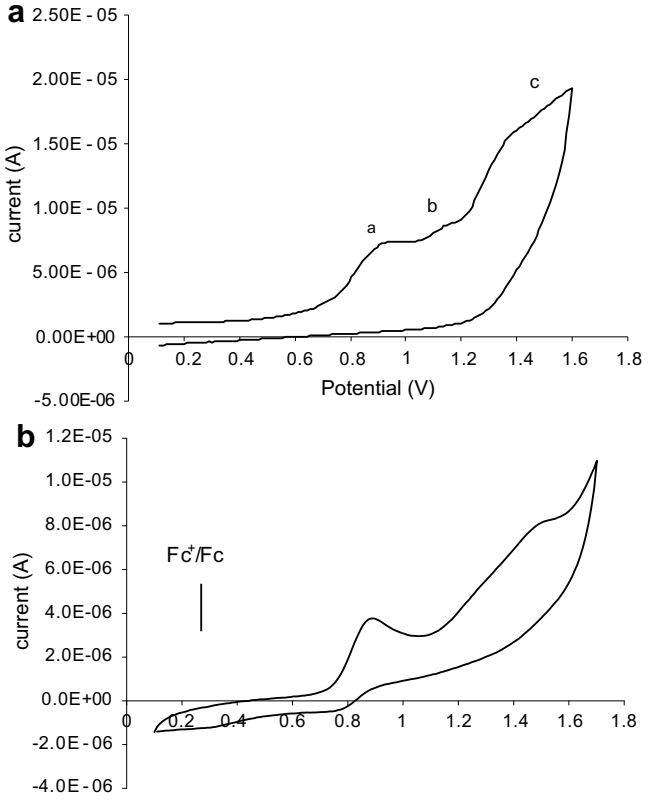

Fig. 8. Oxidation peaks for the copper (a) and nickel (b) complexes. Data were recorded in a 0.1 mol L^{-1} solution of Bu_4NPF_6 in DMF using Fc^+/Fc as a reference.

Under our experimental conditions, the cyclic voltammogram of the Co(II) dinuclear complex does not show any redox processes. This seems to indicate that the oxidation in solution of Co(II) into Co(III), which was revealed by the XANES experiments, is probably a process which requires the contribution of atmospheric oxygen.

7. Conclusion

We have described the synthesis and structure of new Cu(II), Ni(II) and Co(II) dinuclear complexes formed with a tartramide ligand. These complexes were characterized by X-ray diffraction study or XAS experiments, UV–Vis spectroscopy and cyclic voltammetry. The magnetic properties were also investigated using EPR spectroscopy and variable temperature magnetic measurements. In the dinuclear copper complex, the two metallic centres are in a square planar geometry and are linked together by alkoxo (Cu···O···Cu) and carbonato bridges. The short Cu···Cu distance and the large Cu–O–Cu angle favor strong antiferromagnetic interactions between the two copper centres. The octahedral geometry around the Ni(II) ions enhances the formation of the dimer species $[Ni_2(dmptH_{-2})_2]$ in which the metallic centres are coordinated by the nitrogen atoms of the pyridyl groups and the deprotonated amide functions, as well as the hydroxyl groups of the ligands. In this structure, the metal centres are weakly coupled. The cobalt(II) complex was obtained as a powder and the structural investigation was monitored by XAS, which leads us to consider an octahedral coordination around the metal centres. The study of the variable temperature magnetic behaviour of the complex shows that the two metallic cobalt(II) cations are also weakly coupled.

Acknowledgements

The authors are grateful to Dr S. Belin (Synchrotron Soleil) and Dr L. Olivi (Staff Beamline) for their help in XAS data recording. Assistance of Dr E. Wenger, Pr. P. Leconte and Pr. E. Espinosa for X-ray diffraction, and Dr F. Massicot, R. Plantier-Royon and C. Portella for ligand synthesis is greatly appreciated. We also thank Dr D. Harakat for ESI-MS spectra recording and helpful discussions.

The XAS experiments were financially supported by the European Community Research Infrastructure Action under the PF6 "Structuring the European Research Area" Program (RII3-CT-2004-506008).

We thank the Conseil Général de la Marne for a grant to N. Tounsi and for its financial support.

Appendix A. Supplementary data

CCDC 652895 and 652896 contain supplementary crystallographic data for $Na[Cu_2(dmptH_{-3})(CO_3)] \cdot 8H_2O$ and $[Ni_2(dmptH_{-2})_2] \cdot 9.75H_2O$. These data can be obtained free of charge via http://www.ccdc.cam.ac.uk/conts/retrieving.html, or from the Cambridge Crystallographic Data Centre, 12 Union Road, Cambridge CB2 1EZ, UK; fax: (+44) 1223-336-033; or e-mail: deposit@ccdc.cam.ac.uk Supplementary data associated with this article can be found, in the online version, at doi:10.1016/j.poly.2008.09.020.

References

[1] C.J. Cairns, D.H. Busch, Coord. Chem. Rev. 69 (1986) 1.
[2] A.J. Atkins, D. Black, A.J. Black, A. Marin-Bacerra, S. Parsons, L. Ruiz-Ramirez, M. Schroder, Chem. Commun. (1996) 457.
[3] O. Kahn, Struct. Bond. 68 (1987) 89.
[4] P. Guerriero, S. Tamburini, P.A. Vigato, Coord. Chem. Rev. 139 (1995) 17.
[5] J. Reims, B. Krebs, J. Chem. Soc., Dalton Trans. (1997) 3793.
[6] R. Wegner, M. Gottschaldt, H. Gorls, E. Jager, D. Klemm, Chem. Eur. J. 7 (2001) 2143.
[7] S. Striegler, M. Dittel, J. Am. Chem. Soc. 125 (2003) 11518.
[8] D.J. Berger, J.R. Telford, Inorg. Chim. Acta 341 (2002) 132.
[9] H. Carlsson, M. Hauka, A. Bousseksou, J.M. Latour, E. Nordlander, Inorg. Chem. 43 (2004) 8252.
[10] D.A. Brown, W. Errington, W.K. Glass, W. Haase, T.J. Kemp, H. Nimir, S.M. Ostrovsky, R. Werner, Inorg. Chem. 40 (2001) 5962.
[11] M.H. Sazinsky, M. Merkx, E. Cadieux, S. Tang, S.J. Lippard, Biochemistry 43 (2004) 16263.
[12] H. Chao, L.-N. Ji, in: M. Gielen, E.R.T. Tiekink (Eds.), Metallotherapeutic, Drugs and Metal-Based Diagnostic Agents, Wiley, Chichester, 2005 (Chapter 11).
[13] S.M. Ostrovsky, R. Werner, D.A. Brown, W. Haase, Chem. Phys. Lett. 353 (2002) 290.
[14] N.Dj. Lazarov, V. Spasojevic, V. Kusigerski, V.M. Matić, M. Milić, J. Magn. Magn. Mater. 272 (2004) 065.
[15] D.A. Brown, W.K. Glass, N.J. Fitzpatrick, T.J. Kemp, W. Errington, G.J. Clarkson, W. Haase, F. Karsten, A.H. Mahdy, Inorg. Chim. Acta 357 (2004) 1411.
[16] N. Tounsi, L. Dupont, E. Guillon, M. Aplincourt, Inorg. Chim. Acta 360 (2007) 2598.
[17] N. Tounsi, L. Dupont, A. Mohamadou, M. Aplincourt, R. Plantier-Royon, F. Massicot, C. Portella, l'Actualité Chimique 293 (2006) 12.
[18] R. Plantier-Royon, F. Massicot, A.V.R.L. Sudha, C. Portella, L. Dupont, A. Mohamadou, M. Aplincourt, C.R. Chimie 7 (2004) 119.
[19] F. Massicot, R. Plantier-Royon, D. Saleur, A.V.R.L. Sudha, C. Portella, Synthesis 16 (2001) 2441.
[20] A. Altomare, M.C. Burla, M. Camalli, G.L. Cascarano, C. Giacovazzo, A. Guagliardi, A.G.G. Moliterni, G. Polidori, G. Spagna, J. Appl. Crystallogr. 32 (1999) 115.
[21] G.M. Sheldrick, SHELXS97 and SHELXL97, University of Göttingen, Germany, 1997.
[22] A. Michalowicz, Logiciels pour la Chimie, 102, Société Française de Chimie, Paris, 1991.
[23] A. Michalowicz, J. Chem. Phys. 7 (1997) 235.
[24] B. Lengeler, P. Eisenberger, Phys. Rev. B21 (1980) 4507.
[25] E. Guillon, P. Merdy, M. Aplincourt, Chem. Eur. J. 9 (2003) 4479.
[26] S.I. Zabinsky, J.J. Rehr, A. Ankudinov, R.C. Albers, M.J. Eller, Phys. Rev. B 52 (1995) 2995.
[27] A. Mohamadou, C. Jubert, J.P. Barbier, Inorg. Chim. Acta 359 (2006) 273.
[28] A.L. Spek, J. Appl. Crystallogr. 36 (2003) 7.
[29] A.K. Patra, M. Ray, R. Mukherjee, Polyhedron 19 (2000) 1423.
[30] D. Marcos, R. Martinez-Manez, J.V. Folgado, A. Bertran-Porter, D. Bertran-Porter, A. Fuertes, Inorg. Chim. Acta 159 (1989) 11.
[31] C. Jubert, A. Mohamadou, C. Gérard, S. Brandes, A. Tabard, J.P. Barbier, J. Chem. Soc., Dalton Trans. (2002) 2260.
[32] L.A. Tyler, M.M. Olmstead, P.K. Mascharak, Inorg. Chim. Acta 321 (2001) 135.
[33] S. Chatel, M. Rat, S. Dijols, P. Leduc, J.P. Tuchagues, D. Mansuy, I. Artaud, J. Inorg. Biochem. 80 (2000) 239.
[34] M.M. Chavez, P.K. Olmstead, P.K. Mascharak, Inorg. Chem. 36 (1997) 6323.
[35] E.J. Billo, Inorg. Nucl. Chem. Lett. 10 (1974) 613.
[36] P.D. Bonnitcha, M.D. Hall, C.K. Underwood, G.J. Foran, M. Zhang, P.J. Beale, T.W. Hambley, J. Inorg. Biochem. 100 (2006) 963.
[37] P.K. Awasthi, K. Srivastava, J. Prasad, J. Phys. C 2 (1988) 5025.
[38] J.M. Chen, J.K. Simons, K.H. Tan, R.A. Rosenberg, Phys. Rev. B 48 (1993) 10047.
[39] A. Bianconi, A. Di Cicco, N.V. Pavel, M. Benfatto, A. Marcelli, C.R. Natoli, P. Pianetta, J. Woicik, Phys. Rev. B 36 (1987) 6426.
[40] J. Garcia, M. Benfatto, C.R. Natoli, A. Bianconi, I. Davoli, A. Marcelli, Solid State Commun. 58 (1986) 595.
[41] A. Moen, D.G. Nicholson, M. Ronning, G.M. Lamble, J.F. Lee, H. Emerich, J. Chem. Soc., Dalton Trans. 93 (1997) 4071.
[42] K. Shannaga Barathi, A.K. Rahiman, K. Rajesh, S. Sreedaran, P.G. Aravidan, D. Velmurugan, V. Narayanan, Polyhedron 35 (2006) 2859.
[43] M.F. Cabral, B. Murphy, J. Nelson, Inorg. Chim. Acta 90 (1984) 169.
[44] T.C. Higgs, C.J. Carrano, Inorg. Chem. 36 (1997) 298.
[45] R.L. Belford, M. Calvin, G. Belford, J. Chem. Phys. 26 (1957) 1165.
[46] K. Bertoncello, G.D. Fallon, J.H. Hodgin, K.S. Murray, Inorg. Chem. 27 (1988) 4750.
[47] D. Reinen, C. Friedel, Inorg. Chem. 23 (1984) 791.
[48] A.B.P. Lever, in: Inorganic Electronic Spectroscopy, Elsevier, Amsterdam, 1984. pp. 376–572.
[49] O. Kahn, Molecular Magnetism, Wiley, VCH, New-York, 1993.
[50] C.J. Boxwell, R. Bhalla, L. Cronin, S.S. Turner, P.H. Walton, J. Chem. Soc., Dalton Trans. (1998) 2449.
[51] K.S. Burger, P. Chaudhuri, K. Wieghardt, J. Chem. Soc., Dalton Trans. (1996) 247.
[52] S. Alvarez, A.A. Palacio, G. Aullon, Coord. Chem. Rev. 185-186 (1999) 431.
[53] G.A. Van Albada, I. Mutikainen, U. Turpainen, J. Reedijk, Polyhedron 25 (2006) 81.
[54] V.H. Crawford, H.W. Richardson, J.R. Wasson, D.J. Hogdson, W.E. Hatfield, Inorg. Chem. 15 (1976) 2107.
[55] W.E. Hatfield, in: R.D. Willett, D. Gatteschi, O. Kahn (Eds.), Magneto-Structural Correlations in Exchange Coupled Systems. NATO ASI Series, Reidel, Dordrecht, 1985.
[56] S. Youngme, C. Pakawatchai, W. Somjitsripunya, K. Chinnakali, H.K. Fun, Inorg. Chim. Acta 303 (2000) 181.
[57] A.K. Gregson, N.T. Moxon, Inorg. Chem. 21 (1982) 3464.
[58] A.L. Van den Brenk, K.A. Byriel, D.P. Fairlie, L.R. Gahan, G.R. Hanson, C.J. Hawkins, A. Jones, C.H.L. Kennard, B. Moubaraki, K.S. Murray, Inorg. Chem. 33 (1994) 3549.
[59] S.S. Massoud, F.A. Mautner, R. Vincente, B.M. Rodrigue, Inorg. Chim. Acta 359 (2006) 3321.
[60] A. Horn Jr., L. Fim, A.J. Bortoluzzi, B. Szpoganisz, M.S. Silva, M.A. Novak, M. Benassi Neto, L.S. Eberlin, R.R. Catharino, M.N. Eberlin, C. Fernandes, J. Mol. Struct. 797 (2006) 154.
[61] M.P. Suh, B.Y. Shim, T.S. Yoon, Inorg. Chem. 33 (1994) 5509.
[62] R.L. Carlin, Magnetochemistry, Springer, Berlin, Heidelberg, 1986.
[63] K.L. Zhang, Z. Zhang, H. Zhang, Y. Zhu, X.Z. You, J. Mol. Struct. 693 (2004) 193.
[64] I.A. Koval, M. Huisman, A.F. Stassen, P. Gamez, M. Lutz, A.L. Spek, D. Pursche, B. Krebs, J. Reedjik, Inorg. Chim. Acta 357 (2004) 294.
[65] T. Jocher, W. Pape, W. Seidel, P. Gamez, J. Reedijk, F. Eckerhardt Hahn, Eur. J. Inorg. Chem. (2005) 4914.
[66] N. Sengottuvelan, J. Manonmani, M. Kandaswamy, Polyhedron 21 (2002) 2767.

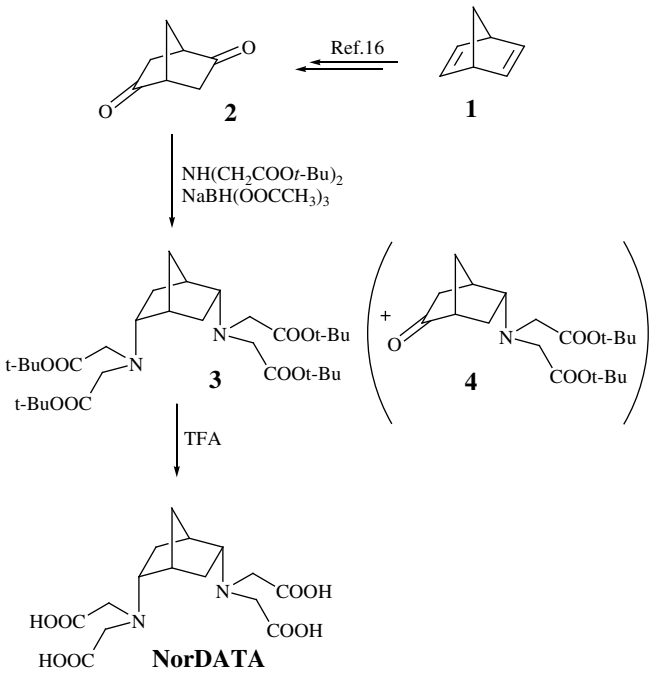

Scheme 1. Synthesis of **NorDATA**.

nitrogen atoms sticking out from a rigid bicyclic structure seemed promising for stable coordination of metal ions. Thus we decided to synthesize the aminocarboxylate ligand we christened **NorDATA** (Scheme 1) that is derived from the above diamine by adding four carboxymethyl arms to it, and subsequently to evaluate its potential as chelating agent.

Norbornadiene **1** was converted to 2,5-norbornanedione **2** by double addition of formic acid and subsequent Jones oxidation, according to a published procedure [16]. A direct reductive amination was then performed with di-*t*-butyl iminodiacetate and sodium triacetoxyborohydride [17], yielding tetraester **3**. A minor amount of a byproduct arising from a single reductive amination was also isolated. NMR analysis of **3** confirmed the *endo,endo* configuration of the amino groups. Removal of *t*-butyl ester groups in neat trifluoroacetic acid completed this short and efficient synthesis of **NorDATA**. The ligand was then characterized and studied for its complexing properties.

Table 1
Protonation constants of the ligands **NorDATA**, BDTA, DCTA and EDTA

Ionic strength	NorDATA 0.1 M KCl		BDTA[18] 0.1 M KNO_3		CDTA[19] 0.1 M KNO_3		EDTA[20a] 0.1 M KCl	
	$\log \beta$	$\log K_i^H$	$\log \beta$	$\log K_i^H$	$\log \beta$	$\log K_i^H$	$\log \beta$	$\log K_i^H$
$\log \beta_{011}$	10.54 (0.01)	10.54	10.45	10.45	12.3	12.3	10.18	10.18
$\log \beta_{021}$	18.17 (0.01)	7.63	19.43	8.98	18.42	6.12	16.33	6.15
$\log \beta_{031}$	20.80 (0.02)	2.63	22.11	2.68	22.01	3.59	19.03	2.7
$\log \beta_{041}$	22.71 (0.02)	1.91	24.11	2.0	24.43	2.42	21.11	2.08

2.2. Determination of complexing properties

In order to characterize the complexation properties of the ligand **NorDATA**, its protonation constants were first determined. The protonation constants ($\log \beta_i$) of **NorDATA** determined by pH-potentiometry are listed in Table 1 (standard deviations are shown in parentheses) and compared to those of archetypal EDTA (1,2-ethylenediamine-*N*,*N*,*N*′,*N*′-tetraacetic acid), monocyclic CDTA (1,2-cyclohexanediamine-*N*,*N*,*N*′,*N*′-tetraacetic acid) and structurally related BDTA (1,4-butanediamine-*N*,*N*,*N*′,*N*′-tetraacetic acid), the latter sharing with **NorDATA** the number of carbon atoms lying between the coordinating nitrogen atoms.

On the basis of previously reported information, the protonation scheme of the BDTA, DCTA and EDTA is well defined [19,21]. We assume that the protonation sites and sequence of **NorDATA** are similar because all these ligands have similar structures and donor groups array. For all of them, starting from basic pH values, the first and second protonation take place at the nitrogen atoms of the ligand backbone. The third and fourth protonations involve two carboxylate groups. For **NorDATA**, all protonation constants are comparable to those of the flexible "parent" BDTA, but the second protonation constant of **NorDATA** $\log K_2^H = 7.63$ is appreciably lower than the corresponding one in parent BDTA $\log K_2^H = 8.98$, in which protonations occur practically independently. This difference may be ascribed to the larger electrostatic repulsion between the close protonated amino groups that reduces the basicity of the second one. This lower basicity and the rigid structure of the molecule result in slightly different complexation properties for **NorDATA** as compared to BDTA. The stability constants obtained by pH-potentiometric titration for some divalent metal and lanthanide ions are presented in Table 2 and Table 3, where the corresponding data for BDTA, DCTA and EDTA are also reported.

By comparing the stability constants of complexes formed by aminopolycarboxylate ligands with the same donor atoms we could shed some light on the complexation behavior of **NorDATA**. The inspection of data presented in Table 2 indicates that $\log \beta_{101}$ values of **NorDATA** complexes formed with metal ions of lower size (Mg^{2+}, Cu^{2+}, Zn^{2+}) do not differ much from those of EDTA complexes. This suggests that the distance between the two nitrogen atoms in the rigid **NorDATA** allows the coordination of the iminodiacetate ("imda") groups in the complexes. The $\log \beta_{101}$ values of the **NorDATA** complexes of Cu^{2+} and Zn^{2+} are somewhat higher than those of BDTA, which shows that in the "preorganized" **Nor-**

Table 2
Cumulative stability and protonation constants of **NorDATA**, BDTA, DCTA and EDTA complexes

Ionic strength	NorDATA 0.1 M KCl			BDTA[21] 0.5 M $NaClO_4$			CDTA[23] 1.0 M KCl	EDTA[20a] 0.1 M KCl
	$\log \beta_{101}$	$\log \beta_{111}$	$\log \beta_{121}$	$\log \beta_{101}$	$\log \beta_{111}$	$\log \beta_{121}$	$\log \beta_{101}$	$\log \beta_{101}$
Mg^{2+}	7.13 (0.02)	14.13 (0.05)	20.98 (0.03)	6.23[22]	14.16[22]		10.32[20b]	8.69
Ca^{2+}	7.44 (0.02)	14.14 (0.05)	20.65 (0.03)	5.66	14.31	21.76	12.5[20b]	10.61
Cu^{2+}	17.73 (0.01)	20.67 (0.01)		17.33[22]	21.52[22]		21.92[20b]	18.78
Zn^{2+}	16.08 (0.04)	18.75 (0.06)		14.89[22]	17.99[22]		18.6[20b]	16.44
La^{3+}	9.47 (0.02)	15.88 (0.04)	22.03 (0.01)	9.04	16.74		16.3	15.46
Ce^{3+}	9.52 (0.03)	15.75 (0.03)	21.82 (0.02)				16.97	15.94
Nd^{3+}	9.62 (0.01)	15.7 (0.03)	21.7 (0.08)				17.73	16.56
Gd^{3+}	10.23 (0.01)	16.15 (0.02)	21.63 (0.01)	9.94	16.6	21.96	18.97	17.35
Er^{3+}	10.43 (0.01)	15.93 (0.03)	20.65 (0.01)	10.94	17.14	22.12	20.63	18.83
Lu^{3+}	10.51 (0.02)	16.07 (0.03)	20.69 (0.02)	11.4	17.34	22.1	21.52	19.80

Table 3
Stepwise protonation constants of **NorDATA** and BDTA complexes

	NorDATA		BDTA	
	$\log K^{H}_{MNorDATA}$	$\log K^{H}_{MHNorDATA}$	$\log K^{H}_{MBDTA}$	$\log K^{H}_{MHBDTA}$
Mg^{2+}	7.00	6.85	7.93	
Ca^{2+}	6.70	6.51	8.65	7.45
Cu^{2+}	2.94		4.19	
Zn^{2+}	2.67		3.10	
La^{3+}	6.41	6.15	7.70	
Ce^{3+}	6.23	6.07		
Nd^{3+}	6.08	6.00		
Gd^{3+}	5.92	5.48	6.66	5.36
Er^{3+}	5.50	4.72	6.2	4.98
Lu^{3+}	5.56	4.62	5.94	4.76

DATA ligand the imda groups lies in a more favorable position. In the Cu^{2+} and Zn^{2+} **NorDATA** complexes the coordination of the two nitrogen atoms with the formation of a seven-membered ring leads to a chelate effect, as their $\log \beta_{101}$ values (Table 2) are higher than the $\log \beta_{102}$ values of the Cu(imda)$_2$ ($\log \beta_{102}$ = 16.68) [22] and Zn(imda)$_2$ ($\log \beta_{102}$ = 12.6) [22] complexes. However the stability constants of both Ln(**NorDATA**) and Ln(BDTA) complexes are low and significantly lower than the $\log\beta_{102}$ values of Ln(imda)$_2$ complexes (e.g., for Lu(imda)$_2$ $\log \beta_{102}$ = 13.73) [22], indicating the absence of a chelate effect. As it was found by Hancock and Martell, the hard metal ions of larger size, like Ln^{3+}, prefer to form the five-membered chelate rings in their complexes, while metal ions of lower size are able to form larger-size chelate rings [24].

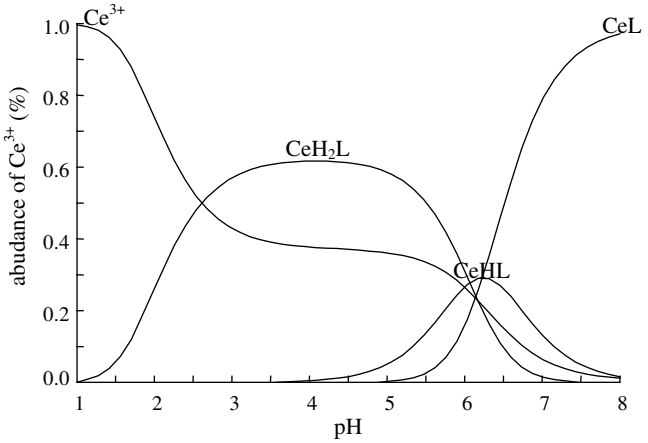

Fig. 1. Distribution diagram of the Ce^{3+}-**NorDATA** system ([Ce^{3+}] = [L] = 0.001 M).

In the protonated complexes formed with Cu^{2+}, as well as in Zn(**NorDATA**), protonation probably occurs at a carboxylate group of the ligand, because $\log K^{H}_{MNorDATA}$ values are relatively low (Table 3). However, the protonation constants of complexes formed with Mg^{2+}, Ca^{2+} and Ln^{3+} ions are large, suggesting that the nitrogen atoms of the coordinated ligand are protonated. The large $\log K^{H}_{MNorDATA}$ and $\log K^{H}_{MHNorDATA}$ values show that the interactions of Mg^{2+}, Ca^{2+} and Ln^{3+} ions with the nitrogen donor atoms are very weak.

The stability constants of Ln(**NorDATA**) complexes are relatively small; in fact the **NorDATA** ligand cannot prevent hydrolysis of Ln^{3+} ions at pH > 8.0. The stability constants of Ln(**NorDATA**) complexes increase from La^{3+} to Gd^{3+}, then remain practically constant for the heavier lanthanides. The stability constants of lanthanides complexes often increase with increasing atomic number because of the lanthanide contraction. For example, $\log \beta_{101}$ values of Ln(BDTA) complexes increase by 2.4 $\log \beta$ units from La^{3+} to Lu^{3+}. However, for Ln(**NorDATA**) complexes the increase in $\log \beta_{101}$ values is much lower, probably because of the more rigid structure of the **NorDATA** ligand.

The distribution diagram and UV-spectra of the Ce^{3+}-**NorDATA** system are reported in Figs. 1 and 2, respectively.

The UV-spectrum of the Ce^{3+}-**NorDATA** system was examined in order to ascertain the existence of each species. UV spectra show significant changes in the position of the absorption maxima as a result of complexation. In the pH range 1.8–4.5 a new absorption band appears at about 270 nm, which is related to the coordination of the carboxylates to the Ce^{3+}-ion and the formation of Ce(H_2**NorDATA**), a species in which N atoms are protonated. Above pH 4.5 the deprotonation and coordination of the N-atoms occur practically simultaneously, resulting in significant changes in absorption spectra. In general, the position of Ce^{3+} absorption bands depends on the number of the coordinated donor atoms [25]. For Ce(H_2**NorDATA**) the deprotonation and coordination of the N-atoms increase the number of the coordinated donor atoms and modify the coordination sphere of the Ce^{3+} ion, which is indicated by the 20 nm red shift in the maximum of the absorption bands. The absorption spectrum of Ce(**NorDATA**) at pH 6.7 is very similar to that of Ce(EDTA) [25]. This is not surprising, since in both complexes two N-atoms and four carboxylates are coordinated to the Ce^{3+} ion.

3. Experimental

3.1. General

All chemicals were purchased from Sigma-Aldrich or from Alfa-Aesar and were used without purification unless otherwise stated. NMR spectra were recorded on a JEOL ECP 300 (operating at

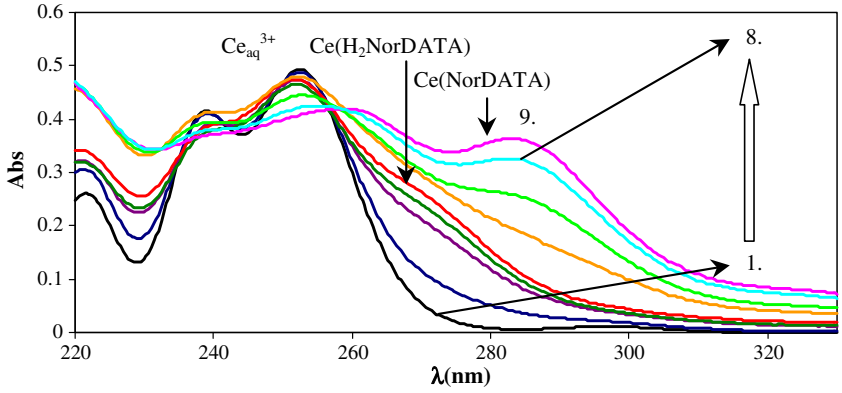

Fig. 2. Absorption spectra of the Ce^{3+}-NorDATA system. ([Ce^{3+}] = [NorDATA] = 7 × 10^{-4} M; (1) Ce^{3+}_{aq}; (2) pH 1.82; (3) pH 2.52; (4) pH 3.05; (5) pH 4.00; (6) pH 5.92; (7) pH 6.21; (8) pH 6.44; (9) pH 6.62, 25 °C, 0.1 M KCl).

7.05 T). ESI mass spectra were recorded on ThermoFinnigan LCQ-Deca XP-Plus and melting points (uncorrected) with a Stuart Scientific SMP3 apparatus.

3.2. Synthesis

3.2.1. ***NorDATA***, *tetra-t-butyl ester (**3**)*

In a 50-mL round-bottomed flask 2,5-norbornanedione[16] (**2**, 1.00 g, 8.06 mmol) and di-*t*-butyl iminodiacetate (3.96 g, 16.1 mmol) were dissolved in 1,2-dichloroethane (20 mL) at room temperature and under a dinitrogen atmosphere. Sodium triacetoxyborohydride (3.42 g, 16.1 mmol) was added in a single portion and the mixture stirred at room temperature. After 15 h a second portion of di-*t*-butyl iminodiacetate (0.79 g, 3.2 mmol) was added and stirring was maintained for another 70 h. The reaction mixture was poured in water and extracted with dichloromethane (3×20 mL). The combined extract were dried over Na_2SO_4, filtered and evaporated *in vacuo*. The viscous oily residue was subjected to column chromatography on silica gel (petroleum ether/ethyl acetate 9:1 as eluant), yielding pure **3** (3.140 g, 67% yield) and some compound **4** (0.69 g, 24%).

Compound **3**: white waxy solid. M.p. 66.9–67.8 °C. Mass spectrum (ESI) 583.1 (MH^+). *Anal.* Calc. for $C_{31}H_{54}N_2O_8$: 582.1. ^1H NMR ($CDCl_3$): 3.48 (d, 4H, J = 17.0 Hz), 3.37 (d, 4H, J = 17.0 Hz), 3.27 (m, 2H), 2.12 (m, 2H), 1.62 (m, 2H), 1.48–1.34 (m, 4H), 1.46 (s, 36H). ^{13}C NMR ($CDCl_3$): 171.1 (C), 80.6 (C), 64.2 (CH), 54.9 (CH_2), 40.4 (CH), 36.8 (CH_2), 28.2 (CH_3), 25.4 (CH_2).

Compound **4**: light yellow oil. Mass spectrum (ESI) 354.2 (MH^+). *Anal.* Calc. for $C_{19}H_{31}NO_5$: 353.2. ^1H NMR ($CDCl_3$): 3.63 (dt, 1H, J_1 = 9.6 Hz, J_2 = 4.1 Hz), 3.45 (d, 2H, J = 17.0 Hz), 3.36 (d, 2H, J = 17.0 Hz), 2.63 (m, 1H), 2.50 (m, 1H), 2.47 (d, 1H, J = 8.8 Hz), 1.99 (m, 1H), 1.89 (dd, 1H, J_1 = 17.8 Hz, J_2 = 4.4 Hz), 1.72 (m, 2H), 1.42 (s, 18H), 1.27 (m, 1H). ^{13}C NMR ($CDCl_3$): 216.6 (C), 170.5 (C), 81.2 (C), 61.0 (CH), 54.1 (CH_2), 50.3 (CH), 38.5 (CH), 37.5 (CH_2), 36.3 (CH_2), 30.3 (CH_2), 28.2 (CH_3).

3.2.2. NorDATA

Tetraester **3** (1.45 g, 2.49 mmol) was dissolved in trifluoroacetic acid (10 mL) and stirred at room temperature for 24 h. Volatiles were removed by vacuum evaporation, trifluoroacetic acid (10 mL) was added to the residue and the mixture stirred at room temperature for another 24 h. After evaporation, the oily crude product was redissolved in methanol (3 mL) and excess diethyl ether was added dropwise. **NorDATA** precipitated and was isolated by centrifugation, washed with diethyl ether and dried *in vacuo* to constant weight (0.65 g, 74%).

Amorphous off-white solid. M.p. 175.9-177.0 °C (dec.). Mass spectrum (ESI) 359.1 (MH^+), 381.1 (MNa^+). *Anal.* Calc. for $C_{15}H_{22}N_2O_8$: 358.1. ^1H NMR ($CDCl_3$): 4.21 (s, 8H), 3.98 (m, 2H), 2.72 (m, 2H), 2.15 (m, 2H), 1.95 (dd, 2H, J_1 = 14.7 Hz, J_2 = 5.6 Hz), 1.71 (s, 2H). ^{13}C NMR ($CDCl_3$): 169.2 (C), 69.4 (CH), 56.7 (CH_2), 38.3 (CH), 36.6 (CH_2), 23.7 (CH_2).

3.3. Equilibrium measurements

The chemicals used for the experiments were of the highest analytical grade. The $LnCl_3$ solutions were prepared from $LnCl_3 \cdot xH_2O$ (x = 5–7) (Aldrich; 99.9%). The concentration of $MgCl_2$, $CaCl_2$, $ZnCl_2$, $CuCl_2$ and $LnCl_3$ solutions were determined by complexometric titration with standardized Na_2H_2EDTA and xylenol orange ($ZnCl_2$, $LnCl_3$), murexide ($CuCl_2$), *Patton & Reeder* ($CaCl_2$) and eriochrome black T ($MgCl_2$) as indicators. The concentration of **NorDATA** was determined by pH-potentiometric titration either in the presence or the absence of a large (40-fold) excess of $CaCl_2$.

For the calculation of $[H^+]$ from the measured pH values, the method proposed by Irving et al. was used [26]. A 0.01 M HCl solution (0.1 M KCl) was titrated with a standardized KOH solution. The differences between measured and calculated pH values were used to obtain the H^+ concentration from the pH values, measured in the titration experiments. The ionic product of water was found to be 13.85 under these conditions. For pH measurements and titration, a Crison micro pH *2002* pH-meter, a Crison micro BU2030 autoburette and a Metrohm-6.0233.100 combined electrode were used. Equilibrium measurements were carried out at constant ionic strength (0.1 M KCl) on 10 mL sample at 25 ± 0.2 °C. The solutions were stirred while N_2 was being bubbled through. Titrations were performed in the pH range 1.7-11.7. For the calibration of the pH meter, buffer standard solutions, color-coded "pink" (pH 4.010) (Fluka) and "yellow" (pH 7.000) (Fluka) were used.

The protonation constants of **NorDATA** and the stability constants of the complexes it formed with Mg^{2+}, Ca^{2+}, Cu^{2+}, Zn^{2+} and Ln^{3+} ions were determined by pH-potentiometric titration. The equilibrium constants of ligands and complexes are defined by the following equations, where M, H and L are the metal ion, proton and ligand, respectively (i = 1, 2, ...).

$$pM^{n+} + qH^+ + rL \rightleftharpoons M_pH_qL_r$$

$$\beta_{pqr} = \frac{[M_pH_qL_r]}{[M^{n+}]^p[H^+]^q[L]^r}$$

$$H_{i-1}L + H^+ \rightleftharpoons H_iL$$

$$K_i^H = \frac{[H_iL]}{[H_{i-1}][H^+]}$$

$$MH_{i-1}L + H^+ \rightleftharpoons MH_iL$$

$$K^H_{MH_{i-1}L} = \frac{[MH_iL]}{[MH_{i-1}L][H^+]}$$

The protonation constants of **NorDATA** ($\log\beta$) were calculated from titration data (152 data points) obtained by the titration of 0.002 M solution samples. The metal/ligand concentration ratio was 1:1; for Cu^{2+} and Zn^{2+} complexes, titrations were also carried out at metal/ligand ratio of 2:1 in order to examine the possible formation of dinuclear complexes in the Zn^{2+}-**NorDATA** and Cu^{2+}-**NorDATA** systems (ligand concentration was 0.002 M). pH-potentiometric titration data obtained for the equilibrium study of metal ion – **NorDATA** systems could be described by the formation of ML, MHL and MH_2L species. The protonation and stability constants of Zn(**NorDATA**) and Cu(**NorDATA**) complexes were calculated separately from the titration curves obtained at 1:1 and 2:1 metal/ligand concentration ratios by using the model considering only the formation of the ML and MHL species. In both cases values of the protonation and stability constants of the ML complexes were identical, implying that dinuclear complexes were not involved. To calculate the stability and protonation constants of complexes formed in metal ion – **NorDATA** systems about 160 data points were normally used. Protonation and stability constants ($\log\beta$) were calculated with the PSEQUAD program [27].

The formation of Ce(**NorDATA**)$^-$ complex was studied at 25 °C in a thermostated cell holder with a Cary 1E spectrophotometer. The complexation equilibria were followed in the UV range 340–220 nm (the UV absorption band of Ce^{3+} resulting from the 4f–5d transition is very sensitive to complex formation). The concentration of **NorDATA** and $CeCl_3$ were 7×10^{-4} M in the presence of 0.1 M KCl.

4. Conclusion

In this paper we report the four-step synthesis of the novel polyaminopolycarboxylic ligand **NorDATA**, as well as its complexation behavior towards selected metal ions as assessed by potentiometry and UV–Vis spectrophotometry.

NorDATA complexes generally show higher stabilities than those formed by the acyclic congener BDTA, except for the smaller lanthanides. The stability constant of the Zn^{2+} chelate is close to that of the prototypal EDTA congener, while it is significantly smaller in the lanthanide series and in comparison with the monocyclic CDTA.

The result of using the rigid bicyclic skeleton with conformationally locked nitrogen atoms is manifest in the log K_2^H value and is probably responsible for the stability of alkaline earth and transition metal ion complexes. The lower affinity of lanthanides for **NorDATA** can possibly be ascribed to the less than optimal size match of the ligand cavity with the Ln^{3+} ion.

References

[1] (a) H.-U. Jäger, W. Schul, Münchner Beiträge zur Abwasser-, Fisch- und Flußbiologie 54 (2001) 207.;
(b) C.K. Schmidt, M. Fleig, F. Sacher, H.-J. Brauch, Environ. Pollut. 131 (2004) 107. and references cited therein;
(c) T. Knepper, Trends Anal. Chem. 22 (2003) 708.

[2] B. Nowack, Environ. Sci. Technol. 36 (2002) 4009.

[3] S. Aime, C. Cavallotti, E. Gianolio, G.B. Giovenzana, G. Palmisano, M. Sisti, Tetrahedron Lett. 43 (2002) 8387.

[4] S. Aime, C. Cavallotti, G. Cravotto, G.B. Giovenzana, G. Palmisano, Tetrahedron Lett. 45 (2004) 5901.

[5] G.B. Giovenzana, G. Palmisano, E. Del Grosso, L. Giovannelli, A. Penoni, T. Pilati, Org. Biomol. Chem. 3 (2005) 1489.

[6] M. Sisti, M. Botta, R. Artali, G. Palmisano, C. Cavallotti, G.B. Giovenzana, Org. Biomol. Chem. 5 (2007) 2441.

[7] G.B. Giovenzana, L. Tei, L. Piscopo, Z. Baranyai, S. Aime, M. Botta, Org. Biomol. Chem. 6 (2008) 2361.

[8] S. Aime, L. Calabi, C. Cavallotti, E. Gianolio, G.B. Giovenzana, P. Losi, A. Maiocchi, G. Palmisano, M. Sisti, Inorg. Chem. 43 (2004) 7588.

[9] R.A. Peralta, A. Neves, A.J. Bortoluzzi, A. Casellato, A. dos Anjos, A. Greatti, F.R. Xavier, B. Szpoganicz, Inorg. Chem. 44 (2005) 7690.

[10] J. Romba, D. Kuppert, B. Morgenstern, C. Neis, S. Steinhauser, T. Weyhermüller, K. Hegetschweiler, Eur. J. Inorg. Chem. (2006) 314.

[11] N.A. Rey, A. Neves, A.J. Bortoluzzi, C.T. Pich, H. Terenzi, Inorg. Chem. 46 (2007) 348.

[12] S. Ge, S. Bambirra, A. Meetsma, B. Hessen, Chem. Commun. (2006) 3320.

[13] S. Aime, G. Bombieri, C. Cavallotti, G.B. Giovenzana, D. Imperio, N. Marchini, Inorg. Chim. Acta 361 (2008) 1534.

[14] A. Berkessel, D. Menche, C.A. Sklorz, M. Schröder, I. Paterson, Angew. Chem., Int. Ed. 42 (2003) 1032.

[15] A. Berkessel, M. Schröder, C.A. Sklorz, S. Tabanella, N. Vogl, J. Lex, J.M. Neudörfl, J. Org. Chem. 69 (2004) 3050.

[16] R.T. Hawkins, R.S. Hsu, S.G. Wood, J. Org. Chem. 43 (1978) 4648.

[17] (a) A.F. Abdel-Magid, K.G. Carson, B.D. Harris, C.A. Maryanoff, R.D. Shah, J. Org. Chem. 61 (1996) 3849;
(b) A.F. Abdel-Magid, S.J. Mehrmann, Org. Process Res. Dev. 10 (2006) 971.

[18] M.L.S. Goncalves, A.M.A. Mota, J.J.R. Frausto Da Silva, Talanta 31 (1984) 531.

[19] J. Felcman, J.J.R. Frausto Da Silva, Talanta 30 (1983) 565.

[20] (a) A.E. Martell, R.M. Smith, Critical Stability Constants, vol. 4, Plenum Press, New York, 1974. 25 °C, 0.1 M KCl;
(b) A.E. Martell, R.M. Smith, Critical Stability Constants, vol. 4, Plenum Press, New York, 1974. 25° C, 0.1 M KNO_3.

[21] G. Choppin, J. Brock, Inorg. Chim. Acta 109 (1985) 99.

[22] G. Anderegg, Helv. Chim. Acta 47 (1964) 1801. 20 C, 0.1 M KNO_3.

[23] J. Charlier, E. Merciny, J. Fuger, Anal. Chim. Acta 192 (1987) 95.

[24] R.D. Hancock, A.E. Martell, Chem. Rev. 89 (1989) 1875.

[25] E. Brücher, L. Zékány, J. Inorg. Nucl. Chem. 43 (1981) 351.

[26] H.M. Irving, M.G. Miles, L. Pettit, Anal. Chim. Acta 38 (1967) 475.

[27] L. Zékány, I. Nagypál, in: D.J. Legett (Ed.), Computational Method for Determination of Formation Constants, Plenum, New York, 1985. p. 291.

2. Experimental

2.1. Materials and physical measurements

Purchased chemicals and solvents were used as received. Elemental analysis of **1** was performed on a VARIO EL (Heraeus) CHNS analyzer. The IR spectrum was recorded on a Perkin–Elmer Spectrum 2000 FT-IR spectrometer by using the KBr pellet technique in the scan range 4000–400 cm^{-1}, the UV–Vis–NIR spectrum on a Perkin–Elmer Lambda 900 spectrophotometer, in acetonitrile solution, in the range 250.0–1200.0 nm ($c = 5.571 \times 10^{-5}$ mol/L), and the EPR spectrum on a Bruker Elexsys E500 CW EPR spectrometer in frozen solution (acetone/chloroform 1:1) at 110 K, MW-power: 0.615 mW, frequency: 9.4374 GHz. The magnetic measurement was carried out at 298 K using a Quantum Design SQUID-based MPMSXL-5-type magnetometer at the University of Wroclaw (Poland). ^{1}H, ^{13}C and ^{195}Pt NMR spectra were attempted for **1** in $CDCl_3$ at room temperature using a 600 MHz Varian Unity spectrometer, but to no avail, since the sample is paramagnetic.

2.2. Synthesis of *1*

Benzene-1,2-dithiol (1.5 g, ≈10 mmol, Fluka 97%) in 95% ethanol (20 mL) was mixed together with a solution of $[NBu_4]Cl$ (2.7 g, ≈10 mmol, Fluka 99% +) in water (10 mL). The green-yellow solution was stirred at room temperature and treated with K_2PtCl_4 (1.1 g, ≈5 mmol, Degussa p.a.) dissolved in water (10 mL). The color of the reaction mixture rapidly turned deep green, and a thick green solid finally formed. After stirring for 1.5 h, the solid was separated by filtration, washed twice with water (3 mL), and dried in air between filter papers. The combined filtrates were evaporated to near complete dryness to produce an additional crop that was washed and dried likewise. The total yield of 0.7 g (97.49%) of crude material was recrystallized from saturated solutions in $CHCl_3$ or CH_3CN to afford large dark green crystals. M.p.: 184.3–184.5 °C. *Anal.* Calc. for $C_{28}H_{44}NPtS_4$ (MW 717.97): C, 46.84; H, 6.18; N, 1.95; S, 17.86. Found: C, 46.85; H, 6.32; N, 2.10; S, 17.80%. IR (KBr pellet, cm^{-1}) 3429.2 m; 3033.6 w; 2958.0 vs; 2870.7 s; 2508.8 vw; 1530.5 w; 1481.9 s; 1459.4 m; 1416.2 w; 1378.9 m; 1294.9 s; 1234 m; 1152.9 w; 1106.5 vw; 1073.4 s; 880.0 w; 750.1 vs; 665.3 w; 472.5 w; 439.1 w. UV–Vis–NIR: $\lambda_{max}1 = 270.2$ nm ($\varepsilon = 28\,715\ M^{-1}\ cm^{-1}$), $\lambda_{max}2 = 340.8$ nm ($\varepsilon = 2820\ M^{-1}\ cm^{-1}$), $\lambda_{max}3 = 365.0$ nm ($\varepsilon = 2326\ M^{-1}\ cm^{-1}$), $\lambda_{max}4 = 454.9$ nm ($\varepsilon = 444\ M^{-1}\ cm^{-1}$), $\lambda_{max}5 = 635.2$ nm ($\varepsilon = 1844\ M^{-1}\ cm^{-1}$), $\lambda_{max}6 = 707.3$ nm ($\varepsilon = 4058\ M^{-1}\ cm^{-1}$), and $\lambda_{max}7 = 867.1$ nm ($\varepsilon = 23\,345\ M^{-1}\ cm^{-1}$).

2.3. X-ray crystallography

Suitable single crystals of **1** were produced by slow evaporation of a saturated solution in $CHCl_3$ at room temperature. A dark green prismatic crystal of dimensions $0.2 \times 0.06 \times 0.06$ mm was used and data collection was carried out on a Siemens SMART [10a] CCD diffractometer using graphite-monochromated Mo Kα radiation ($\lambda = 0.71073$ Å). Data reduction with SAINT [10b], ω-scan rotation mode, structure solved by direct methods (SHELXS) [10c] and refined with SHELXL [10d], non-hydrogen atoms refined anisotropically, H atoms calculated on idealized positions and refined isotropically, empirical absorption correction with SADABS [10d], refinement by full-matrix least-squares on F^2. Crystal data and structure refinement parameters for **1** are given in Table 1, selected bond lengths and bond angles in Table 2.

Table 1
Crystal data and structure refinement for **1**

Empirical formula	$C_{28}H_{44}NPtS_4$
Formula weight	717.97
Temperature (K)	208(2)
Wavelength (Å)	0.71073
Crystal system	orthorhombic
Space group	$Pna2_1$
a (Å)	16.518(3)
b (Å)	19.790(3)
c (Å)	18.674(3)
Volume (Å^3)	6104.3(2)
Z	8
D_{calc} (Mg/m^3)	1.562
Absorption coefficient (mm^{-1})	4.888
$F(000)$	2888
Crystal size (mm)	$0.20 \times 0.06 \times 0.06$
θ Range for data collection (°)	1.50–31.66
Index ranges	$-18 \leqslant h \leqslant 23$, $-28 \leqslant k \leqslant 18$, $-26 \leqslant l \leqslant 23$
Reflections collected	50894
Independent reflections (R_{int})	17560 (0.0790)
Completeness to $\theta = 31.66°$	94.2%
Absorption correction	SADABS
Maximum and minimum transmission	0.7580 and 0.4414
Refinement method	full-matrix least-squares on F^2
Data/restraints/parameters	17560/1/621
Goodness-of-fit on F^2	0.960
Final R indices [$I > 2\sigma(I)$]	$R_1 = 0.0496$, $wR_2 = 0.0661$
R indices (all data)	$R_1 = 0.1084$, $wR_2 = 0.0793$
Absolute structure parameter	−0.002(5)
Largest difference in peak and hole (e Å^{-3})	1.720 and −0.834

Table 2
Selected bond lengths (Å) and bond angles (°) within the $[Pt1S_4]$ and $[Pt2S_4]$ cores of the crystallographically independent anions $[Pt1(bdt)_2]^-$ and $[Pt2(bdt)_2]^-$ in **1**

$[Pt1(bdt)_2]^-$		$[Pt2(bdt)_2]^-$	
Pt1–S2	2.260(2)	Pt2–S7	2.258(2)
Pt1–S1	2.262(2)	Pt2–S8	2.262(2)
Pt1–S4	2.267(2)	Pt2–S6	2.266(2)
Pt1–S3	2.268(2)	Pt2–S5	2.273(2)
S2–Pt1–S1	89.14(7)	S7–Pt2–S8	89.02(7)
S2–Pt1–S4	90.33(7)	S7–Pt2–S6	177.06(7)
S1–Pt1–S4	179.40(9)	S8–Pt2–S6	90.46(7)
S2–Pt1–S3	176.80(8)	S7–Pt2–S5	91.19(7)
S1–Pt1–S3	91.24(7)	S8–Pt2–S5	179.51(8)
S4–Pt1–S3	89.28(7)	S6–Pt2–S5	89.35(7)

3. Results and discussion

3.1. Formulation of *1*

In accord with the conclusions of Sellmann et al. [2a], we assume that the benzene-1,2-dithiol (H_2bdt) system behaves like a normal dithiolate, bdt^{2-}, and we logically suspect compound **1** to result from the straightforward reaction of Eq. (1), whereby Pt(II) is oxidized to Pt(III), presumably by air, similar to the oxidation of Ni(II) to Ni(III) [3f]:

$$K_2[PtCl_4] + [NBu_4]Cl + 2H_2bdt + 1/2O_2 \rightarrow [NBu_4][Pt(bdt)_2]\ (\mathbf{1}) + 2KCl + 3HCl + 1/2H_2O \quad (1)$$

3.2. Vibrational and electronic absorption spectra of *1*

3.2.1. The IR spectrum

The IR spectrum of **1** exhibits typical absorption peaks at $\nu = 3033.6\ cm^{-1}$ (w, Ar-H), at 2870.7–2958.0 cm^{-1} (s, m, C–H) [4],

at 1378–1482 cm^{-1} (w, m) characteristic of the alkane C–H bending mode, and a very strong peak at 750.1 cm^{-1} attributable to the Ar-H out-of-plane absorption. Most interestingly, previous IR studies [9a] have revealed that the presence of one or two π radical anions in bis(benzene-1,2-dithiolato)metal complexes considerably enhances the intensity of the ν(CS) stretching mode at 1100–1115 cm^{-1}. The IR spectrum of **1**, however, exhibits only a very weak peak at 1106 cm^{-1}, thus suggesting that the bdt^{2-} ligands in this case behave like normal dithiolates. This observation, as a matter of fact, is in line with the X-ray structural and EPR spectroscopic results discussed below; moreover, it nicely corroborates the virtual absence of the ν(CS) stretching band noticed earlier in the IR spectrum of the structurally closely related, but diamagnetic Cu(III) (d^8) complex anion, $[Cu^{III}(L^{Bu})_2]^-$, where $(L^{Bu})^{2-}$ = 3,5-di-*tert*-butylbenzene-1,2-dithiolate [9a].

3.2.2. The electronic spectrum

The UV–Vis–NIR spectrum of **1** exhibits seven absorption bands ($\lambda_{max}1$–$\lambda_{max}7$) mentioned above. Obviously bands $\lambda_{max}1$ to $\lambda_{max}3$ result from π–π* and n–π* electronic transitions within the bdt^{2-} ligands; band $\lambda_{max}4$ may be attributed to ligand-to-metal charge transfer (LMCT), bands $\lambda_{max}5$ and $\lambda_{max}6$ to d–d transitions, and band $\lambda_{max}7$ to ligand-to-ligand charge transfer (LLCT), or else, to intervalent charge transfer (IVCT) [9a].

3.3. The magnetic behavior of *1*

It is necessary to take a closer look at the magnetic behavior of compound **1** for the purpose of reliable comparisons with previous results obtained on closely related materials. Alves et al. [4] have pointed out that the number of Pt(III) complexes studied sofar by EPR spectroscopy is small. One such complex is the anion $[Pt(dcbdt)_2]^-$ contained in the salt $[NBu_4][Pt(dcbdt)_2]$ [4], which may be considered as derived from the parent anion $[Pt(bdt)_2]^-$ contained in the present salt, $[NBu_4][Pt(bdt)_2]$ (**1**). The close relationship between these complex ions is quite obvious, indeed. In the solid, however, the former ions are dimerized, hampering, therefore, any straightforward assessment of the fundamental question surrounding spin density at and oxidation state of the central platinum. The latter ions in **1**, by contrast, are well isolated in the solid state (*vide infra*). Thus, compound **1** now appears to provide the most suitable template system for reliable magnetic studies that may enable unequivocal assignment of the effective oxidation state of the central Pt atom as well as the paramagnetic spin density surrounding this atom.

The experimental EPR spectrum of **1** and a simulation with the resulting parameters is displayed in Fig. 1. The spectrum was simulated with the Bruker SIMFONIA Program [11] individually for $I = 0$ and $I = ½$ and combined in the ratio of the natural abundance (66.2:33.8). It is, moreover, strikingly similar to the rhombic spectra reported previously for the closely related Pt(III) complexes, $[NEt_4][Pt(C_2H_2S_2)_2]$ [1a] and $[NBu_4][Pt(dcbdt)_2]$ [4]. The spectrum can be described as arising from a doublet state ($S = 1/2$), showing rhombic anisotropy with the experimental parameters $g_1 = 1.797 \pm 0.002$, $g_2 = 2.052 \pm 0.002$, $g_3 = 2.220 \pm 0.002$ confirmed by the simulated spectrum (Fig. 1). An attribution of the tensor parameters to the *x*, *y*, z directions and a comparison to the crystallographic orientation from a frozen solution spectrum without detailed calculations (and/or single crystal studies) is nearly impossible, and it is not the aim of this research project anyway (see Ref. [9] for more details on related systems). The central intense line of each signal is attributed to the platinum isotopes with $I = 0$ (sum of 66.2% natural abundance), and the satellites (not resolved for the low field signal) correspond to the ^{195}Pt isotope ($I = 1/2$, 33.8% natural abundance). The experimental anisotropic hyperfine structure tensor parameters for **1** are $A_1 < 15 \times 10^{-4}$ cm^{-1} (not resolved), $A_2 = 63 \pm 1 \times 10^{-4}$ cm^{-1}, $A_3 = 34 \pm 1 \times 10^{-4}$ cm^{-1}. The spectrum of the liquid solution at room temperature (295 K) consists of a single unresolved broad signal (~400 G) with a *g*-value of approximately 2.03. These parameters are in good correlation with those of other Pt(III) dithiolato complexes reported previously [1a,12]. The magnitude of the hyperfine structure parameter indicates a significant contribution of the metal center to the singly occupied molecular orbital (SOMO) of the unpaired electron. Hence, the observed paramagnetism of **1** (first revealed by the failure to record a ^1H, ^{13}C and ^{195}Pt NMR spectrum) is assumed to be confined mainly to the PtS_4 core, without any remarkable contribution of the ligand backbone. Indeed, the room temperature magnetic susceptibility measurement yields an effective moment $\mu_{eff} = 1.80$ BM (Bohr magneton) compatible with a d^7 SOMO [4].

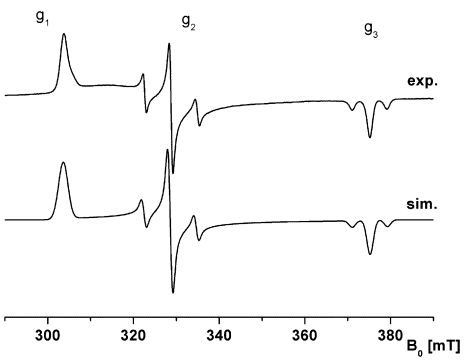

Fig. 1. Experimental (exp.) and simulated (sim.) X-band EPR spectrum of **1**, recorded at 110 K in acetone/$CHCl_3$ (1:1). The spectrum clearly displays rhombic symmetry and hyperfine structures of the transitions at g_2 and g_3, due to ^{195}Pt ($I = 1/2$, natural abundance 33.8%).

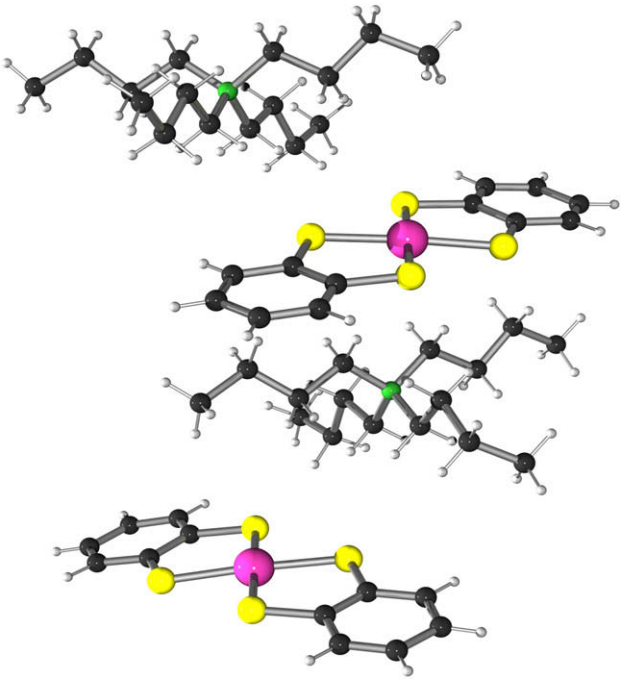

Fig. 2. Ball-and-stick picture of the crystallographically independent anions, $[Pt(bdt)_2]^-$, and cations $[NBu_4]^+$, in **1** (Pt = red, S = yellow). (For interpretation of the references to color in this figure legend, the reader is referred to the web version of this article.)

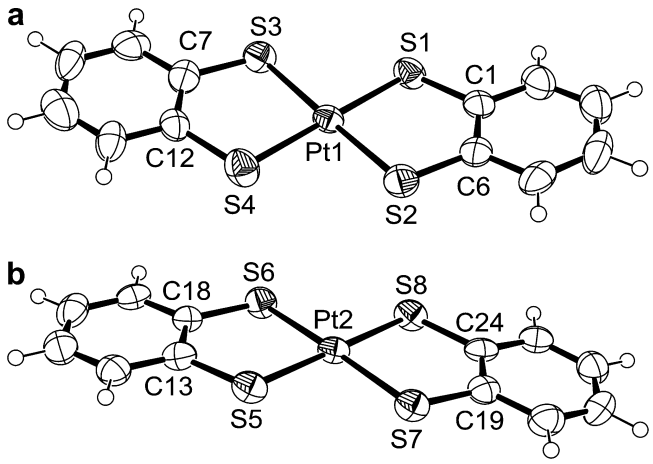

Fig. 3. ORTEP drawing [13] of the crystallographically independent complex anions, $[Pt1(bdt)_2]^-$ (a) and $[Pt2(bdt)_2]^-$ (b), in solid **1**, showing atoms labeling and numbering, and displacement ellipsoids at 50% probability. Note that these anions are rotated by an angle of nearly 90° relative to each other.

3.4. The crystal structure of *1*

Compound **1** represents the first well-resolved crystal structure of a complex based on benzene-1,2-dithiolato ligands coordinated to a Pt(III) central atom in a square-planar geometry. Compound **1** is isostructural to its Ni(III) counterpart, $[NBu_4][Ni(bdt)_2]$ [3a], crystallizing in the orthorhombic space group $Pna2_1$. The unit cell of **1** contains eight asymmetric units with two crystallographically independent $[Pt(bdt)_2]^-$ anions and two $[NBu_4]^+$ cations (Fig. 2). The ORTEP drawing [13] of the anions is displayed in Fig. 3. The spatial orientation of these anions is nearly a 90° rotation relative to each other, which would lead to the right angle stacking structure reported previously for the $Pt(bqd)_2$ system [7c] – bqd^- is benzene-1,2-dione dioximate(1−) – if they were allowed to pile up on top of one another. The [Pt1S1S2S3S4] and [Pt2S5S6S7S8] motifs occupy two distinct crystallographic positions, and the $[PtS_4]$ cores define quasi-perfect squares with Pt1 and Pt2, respectively, at the symmetry centers. Indeed, the Pt–S distances average 2.264 Å, and the angles within these cores are close to the values of 90° and 180° for a perfect S_4 square (Table 2). It should be noted that this particular structural feature differs quite noticeably from what was observed previously in a closely related Ni(III) salt, namely $[IB_zP_y][Ni(bdt)_2]$ (IB_zP_y = 1-(4-iodobenzyl)pyridinium) [3d], in which the corresponding bond angles depart markedly from square geometry. Within the benzene rings of **1**, C–C-bond lengths compare quite satisfactorily with classical aromatic values, with an average of 1.388 Å. The aliphatic C–C-bond lengths within the *n*-butyl groups of the cations average 1.513 Å, as expected.

The relative ordering of the complex anions within the unit cell of **1** is shown in Fig. 4. These anions are slightly bent and positioned in a fishbone manner parallel to the *a* axis. The Pt atoms are well separated from each other (Pt···Pt = 9.148 Å), so that there are no detectable contacts between them. Note that the $[NBu_4]^+$ countercations, omitted here for clarity, are embedded in this anionic framework. The packing of the bulk structure is insured by the mutual electrostatic attraction and the neat space filling of the cations and the anions.

4. Conclusion

We have prepared and characterized unambiguously compound **1** as the first well-resolved crystal structure of a complex based on benzene-1,2-dithiolate(2−) ligands coordinated to a central Pt(III) atom in a discrete square-planar PtS_4 geometry. It is obvious that the straightforward oxidation process (presumably by the oxygen of the air) of the starting Pt(II) to the final Pt(III) central atom in compound **1** is quite reminiscent of the well-documented oxidations of a whole range of central metal atoms such as Co(II), Fe(II), Ni(II), Pd(II), Pt(II), Cu(II), Au(II) [4]. The assignment of the Pt(III) oxidation state (d^7) in compound **1** is nicely confirmed by the value of μ_{eff} = 1.80 BM derived from the room temperature magnetic susceptibility measurement, quite in line with the effective moments of 1.90 and 1.74 BM obtained previously [12] for the related systems $[NBu_4][M(dmi\text{-}t)_2]$ (M = Ni^{III}, Pd^{III}, Pt^{III}; dmi-t = isotrithionedithiolate(2−)). Thus, as another seldom report on a well-characterized Pt(III) complex, this paper may be considered a significant empirical contribution that is expected to help shed more light on the sensitive theoretical discussion of effective oxidation states and magnetic spin density distributions within this important category of bis(dithiolene) or bis(dithiolato) transition metal complexes. It is noteworthy, finally, that the empirical conclusions arrived at in this work grossly parallel the detailed theoretical and experimental results reported recently by Grosshans et al. [14] and Cauchy et al. [15] on closely related materials such as the

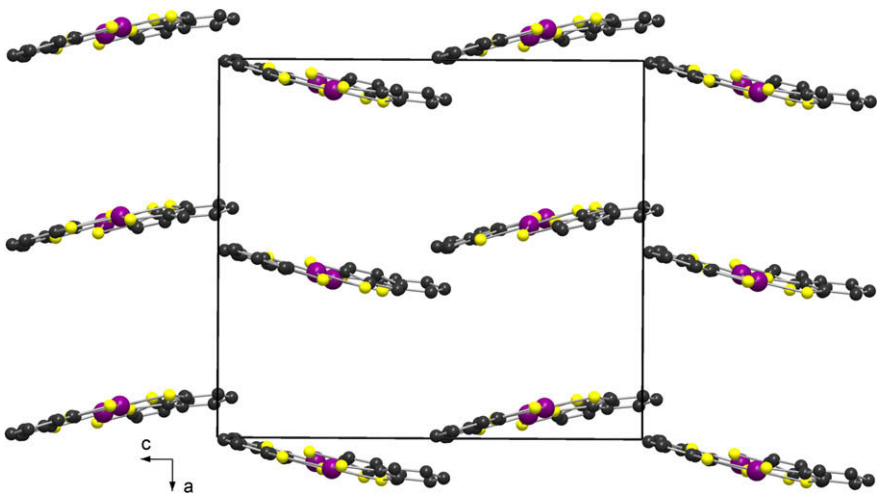

Fig. 4. Projection down the *b* axis of the unit cell of **1**, highlighting the relative ordering of the anionic complexes, $[Pt(bdt)_2]^-$. The counter cations, $[TBA]^+$ (left out for clarity) are actually embedded between these anions.

CpNi(bdt) neutral complexes. These workers have reliably demonstrated, indeed, that there is excellent agreement between DFT calculations and EPR measurements of spin density distributions within this class of complexes, with the SOMO at stake overwhelmingly confined to the inner sphere around the central metal site, and only faintly delocalized over the external benzene ring moieties.

5. Supplementary data

CCDC 682039 contains the supplementary crystallographic data for this paper. These data can be obtained free of charge via http://www.ccdc.cam.ac.uk/conts/retrieving.html, or from the Cambridge Crystallographic Data Centre, 12 Union Road, Cambridge CB2 1EZ, UK; fax: (+44) 1223-336-033; or e-mail: deposit@ccdc.cam.ac.uk.

Acknowledgments

The authors thank Prof. Jerzy Mrozinski (Univ. Wroclaw) for the susceptibility measurement, and one reviewer for drawing their attention to the important Refs. [14] and [15]; MMB is grateful to Deutscher Akademischer Austausch-Dienst, (DAAD), Bad-Godesberg (Germany) for a grant-in-research-stay at the University of Heidelberg.

References

[1] (a) E. Möller, R. Kirmse, Inorg. Chim. Acta 257 (1997) 273 and references cited therein;
(b) H.-J. Krüger, G. Peng, R.H. Holm, Inorg. Chem. 30 (1991) 734.
[2] (a) D. Sellmann, H. Binder, D. Häussinger, F.W. Heinemann, J. Sutter, Inorg. Chim. Acta 300–302 (2000) 829 and Ref. [4c] cited therein;
(b) E. Uhlig, Pure Appl. Chem. 60 (1988) 1235.
[3] (a) N. Robertson, S. Parsons, K. Awaga, W. Fujita, CrystEngCommun 2 (2000) 121 and Ref. [14] cited therein;
(b) R. Williams, E. Billig, J.H. Waters, H.B. Gray, J. Am. Chem. Soc. 88 (1966) 43;
(c) M.J. Baker-Hawkes, E. Billig, H.B. Gray, J. Am. Chem. Soc. 88 (1966) 4870;
(d) G.-X. Liu, P.-F. Wang, Y.-C. Chen, X.-M. Ren, Acta Crystallogr., Sect. E 62 (2006) m1746;
(e) C. Mahadevan, M. Seshasayee, P. Kuppusamy, P.T. Manoharan, J. Crystallogr. Spectrosc. Res. 15 (1985) 305;
(f) J. Ochoki, Ph. Chaudhuri, W.L. Driessen, R.A.G. De Graaf, F.B. Hulsbergen, J. Reedijk, Inorg. Chim. Acta 167 (1990) 15.
[4] H. Alves, D. Simão, I.C. Santos, V. Gama, R.T. Henriques, H. Novais, M. Almeida, Eur. J. Inorg. Chem. (2004) 1318.
[5] (a) Z.H. Kafafi, J.R. Lindle, S.R. Flom, R.G.S. Pong, C.S. Weisbecker, R.C. Claussen, F.J. Bartoli, Nonlinear Opt. III SPIE 1626 (1992) 440;
(b) J.R. Lindle, C.S. Weisbecker, F.J. Bartoli, R.G.S. Pong, Z.H. Kafafi, Mater. Res. Soc. Symp. Proc. 247 (1992) 277.
[6] D. Sellmann, S. Funfgelder, F. Knoch, M. Moll, Z. Naturforsch., Teil B 46 (1991) 1601.
[7] (a) M.M. Bélombé, Ph.D. Thesis, University of Heidelberg, Germany, 1974.;
(b) J.W. Brill, M.M. Bélombé, M. Novotny, J. Chem. Phys. 68 (1978) 585;
(c) M.M. Bélombé, J. Solid State Chem. 27 (1979) 389.
[8] (a) M.M. Bélombé, J. Phys. (Paris) Colloq. 44 (1983) C3-717;
(b) M.M. Bélombé, Synth. Met. 18 (1987) 605.
[9] (a) K. Ray, T. Weyhermüller, F. Neese, K. Wieghardt, Inorg. Chem. 44 (2005) 5345 and references cited therein;
(b) R. Kirmse, E. Möller, Chr. Seitz, J. Reinhold, Z. Anorg. Allg. Chem. 623 (1997) 159.
[10] (a) SMART: Area-Detector Software Package, Siemens Industrial automation, Inc., Madison, WI, 1993;
(b) SAINT: Area-Detector Integration Software. Version 6.01, Siemens Industrial Automation, Inc., Madison, WI, 1999;
(c) SHELX97 [Includes SHELXS97, SHELXL97] G.M. Sheldrick, SHELX97: Program for Crystal Structure Analysis (Release 97-2), University of Göttingen, Germany, 1997;
(d) G.M. Sheldrick, SADABS: Program for Scaling and Correction of Area-Detector Data, Göttingen, 1997.
[11] R.T. Weber: WIN-EPR-SIMFONIA, EPR Division, BRUKER Instruments Inc., Version 1.2, 1995.
[12] R. Kirmse, J. Stach, W. Dietzch, G. Steimecke, E. Hoyer, Inorg. Chem. 19 (1980) 2679.
[13] ORTEP3 for Windows: L.J. Farrugia, J. Appl. Crystallogr. 30 (1997) 565.
[14] P. Grosshans, P. Adkine, H. Sidorenkova, M. Nomura, M. Fourmigué, M. Geoffroy, J. Phys. Chem. A 112 (2008) 4067 and references cited therein.
[15] T. Cauchy, E. Ruiz, O. Jeannin, M. Nomura, M. Fourmigué, Chem. Eur. J. 13 (2007) 8858.

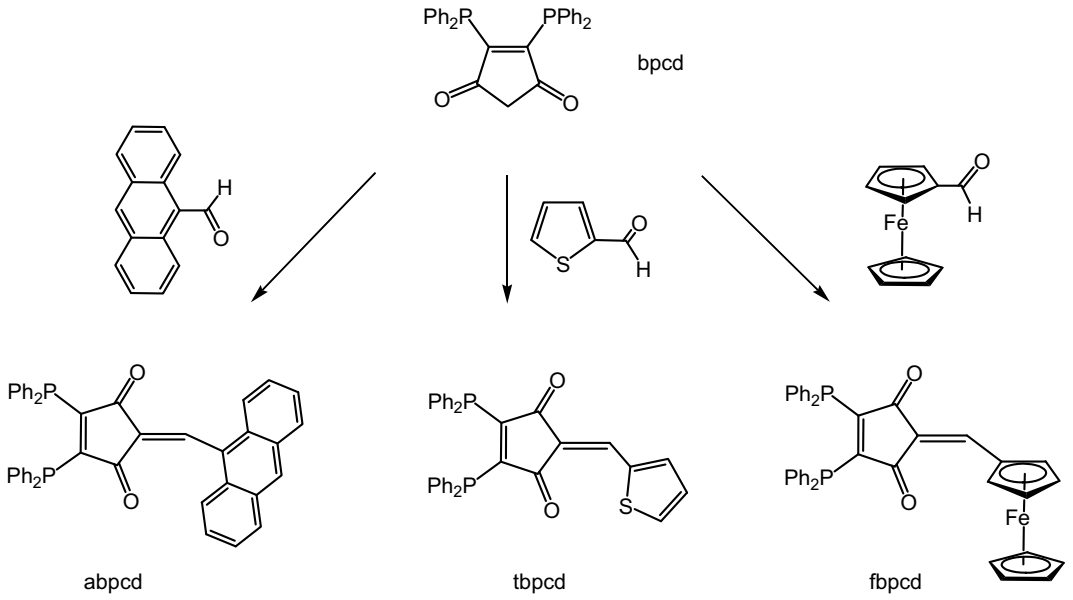

Scheme 1.

Given the dearth of Pt(diphosphine)(S–S) compounds that possess an energetically accessible phosphine-based LUMO, we have prepared and investigated the redox properties of Pt(fbpcd)(mnt) through the use of cyclic voltammetry and molecular orbital calculations at the extended Hückel level. The electrochemical and MO results are discussed with respect to related dithiolate-substituted platinum compounds.

2. Experimental

2.1. General

The $PtCl_2$(cod) starting material was prepared from $H_2PtCl_6 \cdot xH_2O$ and 1,5-cyclooctadiene (cod) according to the known procedure [12], and the fbpcd ligand synthesized via the condensation reaction of bpcd and ferrocenecarboxaldehyde [13]. The disodium maleonitriledithiolate (Na_2mnt) was prepared according the published literature procedure [14]. The chemicals cod and ferrocenecarboxaldehyde were purchased from Aldrich Chemical Co. All reaction and NMR solvents were distilled from an appropriate drying agent under argon using Schlenk techniques and stored under argon in storage vessels equipped with high-vacuum Teflon stopcocks [15].

All IR spectra were recorded on a Nicolet 20 SXB FT-IR spectrometer in amalgamated 0.1 mm NaCl cells, while the absorption spectra were recorded on a HP 8425A diode array spectrometer using 1.0 cm quartz UV–Vis cells that were equipped with a high-vacuum Teflon stopcock to facilitate handling on the vacuum line. The ^{1}H spectra were recorded at 200 MHz on a Varian Gemini-200 spectrometer, and the ^{31}P NMR spectra were collected in the proton-decoupled mode on a Varian 300-VXR spectrometer at 121 MHz, with the reported chemical shifts referenced to external H_3PO_4 (85%), taken to have $\delta = 0$. The ESI mass spectrum for **2** was recorded at the UNT mass spectrometry facility in the positive ion mode using a matrix composed of MeCN and 1% trifluoroacetic acid (UNT), while the mass spectral data for **3** were recorded at the University of the Pacific mass spectrometry facility in the negative ion mode.

2.2. Synthesis of the $PtCl_2$(fbpcd) (**2**)

To a small Schlenk flask under argon was added 0.10 g (0.27 mmol) of $PtCl_2$(cod) and 0.17 g (0.27 mmol) of the diphosphine ligand fbpcd, followed by 20 mL of CH_2Cl_2 via syringe. The reaction mixture was stirred at room temperature for ca. 0.5 h, and then solvent was removed under vacuum and the residue washed with 2×10 mL portions of hexane to remove the liberated cod ligand. The crude product was recrystallized from a 1:1 mixture of CH_2Cl_2/hexane to afford 0.22 g (90% yield) of **2**. IR (CH_2Cl_2): ν(CO) 1718 (w, sym dione), 1676 (vs, antisym dione) cm^{-1}. UV–Vis (CH_2Cl_2): λ_{max} 356 (ε = 12 149), 584 (ε = 2192). ^{1}H NMR ($CDCl_3$): δ 4.22 (s, 5H, Cp), 4.93 (s, br, 2H, Cp), 5.21 (s, br, 2H, Cp), 7.25–8.30 (m, 21H, aryls and alkenyl). ^{31}P NMR ($CDCl_3$): δ 26.51 (s, J_{Pt-P} = 1838 Hz), 27.44 (s, J_{Pt-P} = 1838 Hz). ESI-MS (m/z): 949.27 [**2** + Na]$^+$.

2.3. Synthesis of Pt(mnt)(fbpcd)

To 0.10 g (0.11 mmol) of $PtCl_2$(fbpcd) in a Schlenk tube was added 30 mL of acetone, after which 20 mg (0.11 mmol) of Na_2mnt was added in one portion. The solution was stirred for 3 h and then examined by TLC analysis, which revealed the desired product as a blue spot at R_f = 0.40 using CH_2Cl_2 as the eluent. The solvent was removed under vacuum and the crude product was purified by flash-column chromatography over silica gel. The isolated product was recrystallized from CH_2Cl_2 and hexane to afford compound **3** in 83% yield (90 mg). IR (CH_2Cl_2): ν(CN and CO) 2209 (m, nitrile), 1718 (w, sym dione), 1679 (s, antisym dione) cm^{-1}. UV–Vis (CH_2Cl_2): λ_{max} 360 (ε = 12 288), 582 (ε = 2750). ^{1}H NMR ($CDCl_3$): δ 4.20 (s, 5H, Cp), 4.93 (s, b, 2H, Cp), 5.20 (b, 2H, Cp), 7.45–7.95 (m, 21H, aryls and alkenyl). ^{31}P NMR ($CDCl_3$): δ 30.26 (s, J_{Pt-P} = 1420 Hz), 31.08 (s, J_{Pt-P} = 1420 Hz). ESI-MS (m/z): 874.04 [**3**-CpFe]$^-$.

2.4. X-ray diffraction data for clusters **2** and **3**

Tables 1 and 2 contain the X-ray data and processing parameters and selected bond distances and angles, respectively, for compounds **2** and **3**. Single crystals of **2** and **3** suitable for X-ray diffraction analysis were grown at 5 °C from CH_2Cl_2 solutions containing each compound that had been layered with hexane. The X-ray data for **2** · CH_2Cl_2 and **3** · CH_2Cl_2 were collected on an APEX II CCD-based diffractometer at 100 K. The frames were integrated with the available APEX2 [16] software package using a narrow-frame algorithm, and the structures were solved and refined using the SHELXTL program package [17]. The molecular structures were checked using PLATON [18], and all nonhydrogen atoms were refined

Table 1
X-ray crystallographic data and processing parameters for compounds **2** · CH_2Cl_2 and **3** · CH_2Cl_2

CCDC entry number	683128	683129
Crystal system	triclinic	monoclinic
Space group	$P\bar{1}$	$P2_1/n$
a (Å)	10.112(1)	10.1301(5)
b (Å)	14.481(2)	29.531(2)
c (Å)	14.585(2)	14.5702(8)
α (°)	100.194(2)	
β (°)	101.582(2)	106.700(1)
γ (°)	107.055(2)	
V (Å^3)	1935.7(4)	4174.9(4)
Molecular formula	$C_{40}H_{30}Cl_2FeO_2P_2Pt \cdot CH_2Cl_2$	$C_{44}H_{30}FeN_2O_2P_2PtS_2 \cdot CH_2Cl_2$
Fw	1011.35	1080.63
Formula units per cell (Z)	2	4
D_{calc} (Mg/m^3)	1.735	1.719
λ (Mo Kα) (Å)	0.71073	0.71073
μ (mm^{-1})	4.379	4.041
Absorption correction	numerical	analytical
Absorption correction factor	0.7791/0.3968	0.7936/0.4197
Total reflections	21 544	49 948
Independent reflections	7512	8733
Data/restraints/parameters	7512/0/460	8733/0/514
R_1[a] ($I \geqslant 2\sigma(I)$]	0.0286	0.0211
wR_2[b]	0.0698	0.0453
Goodness-of-fit on F^2	1.063	1.035
$\Delta\rho$(max), $\Delta\rho$(min) (e/Å^3)	2.807, −0.764	0.892, −0.450

[a] $R_1 = \sum||F_o| - |F_c||/\sum|F_o|$.
[b] $R_2 = \{\sum[w(F_o^2 - F_c^2)^2]/\sum[w(F_o^2)^2]\}^{1/2}$.

Table 2
Selected bond distances (Å) and angles (°) in compounds **2** · CH_2Cl_2 and **3** · CH_2Cl_2

Compound **2** · CH_2Cl_2			
Bond distances			
Pt(1)–P(1)	2.217(1)	Pt(1)–P(2)	2.218(1)
Pt(1)–Cl(1)	2.352(1)	Pt(1)–Cl(2)	2.342(1)
C(1)–C(2)	1.331(6)	C(1)–C(5)	1.518(6)
C(2)–C(3)	1.526(5)	C(3)–C(4)	1.478(6)
C(4)–C(6)	1.365(6)	C(4)–C(5)	1.468(6)
C(6)–C(7)	1.427(6)	C(7)–C(11)	1.436(7)
Cp(centroid)-Fe[a]	1.640(2)	Cp′(centroid)-Fe[a]	1.659(2)
Bond angles			
P(1)–Pt(1)–P(2)	89.42(4)	P(1)–Pt(1)–Cl(2)	89.94(4)
P(2)–Pt(1)–Cl(2)	176.51(4)	P(1)–Pt(1)–Cl(1)	173.88(4)
P(2)–Pt(1)–Cl(1)	88.64(4)	Cl(2)–Pt(1)–Cl(1)	92.34(4)
C(1)–P(1)–Pt(1)	105.7(1)	C(2)–P(2)–Pt(1)	105.5(1)
C(2)–C(1)–P(1)	119.0(3)	C(1)–C(2)–P(2)	119.9(3)
C(4)–C(6)–C(7)			
Compound **3** · CH_2Cl_2			
Bond distances			
Pt(1)–P(1)	2.2589(6)	Pt(1)–P(2)	2.2572(7)
Pt(1)–S(2)	2.3027(6)	Pt(1)–S(1)	2.3047(6)
S(1)–C(1)	1.737(3)	S(2)–C(3)	1.736(3)
N(1)–C(2)	1.145(3)	N(2)–C(4)	1.152(3)
C(1)–C(3)	1.365(4)	C(1)–C(2)	1.433(4)
C(3)–C(4)	1.426(4)	C(29)–C(30)	1.339(3)
C(29)–C(33)	1.516(3)	C(30)–C(31)	1.514(3)
C(31)–C(32)	1.482(3)	C(32)–C(34)	1.356(3)
C(32)–C(33)	1.470(3)	C(34)–C(35)	1.437(3)
Cp(centroid)-Fe[b]	1.641(1)	Cp′(centroid)-Fe[b]	1.655(1)
Bond angles			
P(2)–Pt(1)–P(1)	88.46(2)	P(2)–Pt(1)–S(2)	178.71(2)
P(1)–Pt(1)–S(2)	90.51(2)	P(2)–Pt(1)–S(1)	90.69(2)
P(1)–Pt(1)–S(1)	174.08(2)	S(2)–Pt(1)–S(1)	90.26(2)
C(1)–S(1)–Pt(1)	101.47(9)	C(3)–S(2)–Pt(1)	101.46(9)
C(2)–C(1)–S(1)	116.4(2)	C(4)–C(3)–S(2)	117.2(2)
N(1)–C(2)–C(1)	178.4(3)	N(2)–C(4)–C(3)	178.9(3)
C(32)–C(34)–C(35)	131.9(2)		

[a] **2** · CH_2Cl_2: Cp centroid defined by the atoms C(7)–C(11) and Cp′ centroid defined by the atoms C(12)–C(16).
[b] **3** · CH_2Cl_2: Cp centroid defined by the atoms C(35)–C(39) and Cp′ centroid defined by the atoms C(40)–C(44).

anisotropically. All hydrogen atoms were assigned calculated positions and allowed to ride on the attached carbon atom. The refinement for **2** · CH_2Cl_2 converged at $R_1 = 0.0286$ and $wR_2 = 0.0698$ for 7512 independent reflection with $I > 2\sigma(I)$, with **3** · CH_2Cl_2 yielding convergence values of $R_1 = 0.0211$ and $wR_2 = 0.0453$ for 8733 independent reflection with $I > 2\sigma(I)$.

2.5. Electrochemical studies

All cyclic voltammograms were recorded on a PAR Model 273 potentiostat/galvanostat, equipped with positive feedback circuitry to compensate for *i*R drop. The homemade three-electrode cell that was employed allowed the cyclic voltammograms to be recorded under oxygen- and moisture-free conditions. A platinum disk (area = 0.0079 cm^2) was utilized as the working and auxiliary electrode, and the reference electrode utilized a silver wire as a quasi-reference electrode, with the reported potential data standardized against the formal potential of the $Cp^*_2Fe/Cp^*_2Fe^+$ (internally added) redox couple, taken to have $E_{1/2} = -0.20$ V [19].

2.6. Extended Hückel MO calculations

The extended Hückel calculations reported here were carried out using the original program developed by Hoffmann [20], as modified by Mealli and Proserpio [21]. The weighted H_{ij}'s contained in the program were used in the calculations, and the input *Z*-matrices for **2** and **3** were constructed from the available X-ray data. The *Z*-matrix for the free ligand fbpcd was constructed from the appropriate bpcd and ferrocene fragments.

3. Results and discussion

3.1. Synthesis and spectroscopic characterization of compounds *2* and *3*

Treatment of $PtCl_2$(cod) at room temperature in CH_2Cl_2 with an equimolar amount of the diphosphine ligand 2-(ferrocenylidene)-4,5-bis(diphenylphosphino)-4-cyclopenten-1,3-dione (fbpcd) furnishes the expected product of cod displacement, namely $PtCl_2$(fbpcd). The structure of **2** is depicted in Scheme 2. Compound **2** was isolated in greater than 90% yield after recrystallization and was characterized initially by traditional spectroscopic methods and mass spectrometry. The IR spectrum reveals the presence of two vibrationally coupled carbonyl bands associated with the dione ring at 1718 (w) and 1676 (vs) cm^{-1}, whose frequencies are in good agreement with the data reported by us for the isomeric $Os_3(CO)_{10}$(fbpcd) clusters containing chelating and bridging fbpcd ligands [10]. The electronic absorption spectrum of **2** recorded in CH_2Cl_2 exhibits a moderately intense near UV–Vis absorbance at 356 nm in excellent agreement with the optical data reported by Eisenberg and coworkers for sundry Pt(mnt)(diphosphine) complexes [4b], with the weak visible band at 584 nm ascribed to a d–d transition localized on the pendant ferrocene moiety [22]. The four sets of ^{1}H NMR resonances at δ 4.22 (s, 5H, Cp), 4.93 (s, br, 2H, Cp), 5.21 (s, br, 2H, Cp), 7.25–8.30 (m, 21H, aryls and alkenyl) and the two inequivalent ^{31}P singlets at δ 26.51 and 27.44 are in accord with the formulated structure. The ESI mass spectrum of $PtCl_2$(fbpcd) displayed a prominent *m*/*z* peak at 949.27 consistent with the sodiated species $[\mathbf{2} + Na]^+$. The solid-state structure of **2**, as the CH_2Cl_2 solvate, confirms the presence of a four-coordinate, square-planar platinum center possessing two ancillary chlorine groups and a chelating fbpcd ligand. Fig. 1 shows the thermal ellipsoid plot of **2**. The Pt–P and Pt–Cl bonds display a mean distance of 2.218 Å and 2.347 Å, respectively, and agree with those bond distances in the related platinum(II) compounds $PtCl_2$[1,2-bis(diphenylphosphino)ethane], $PtCl_2$[(*Z*)-1,2-bis(diphenylphosphino)ethene], and derivatives based on diphosphine ligands having an ethano backbone [23]. The remaining bond distances and angles are unremarkable and require no comment.

The reaction of **2** with disodium maleonitriledithiolate (Na_2mnt) in acetone at room temperature afforded the corresponding mnt-substituted complex Pt(mnt)(fbpcd) (**3**) in good yield after flash-column chromatographic separation and recrystallization.

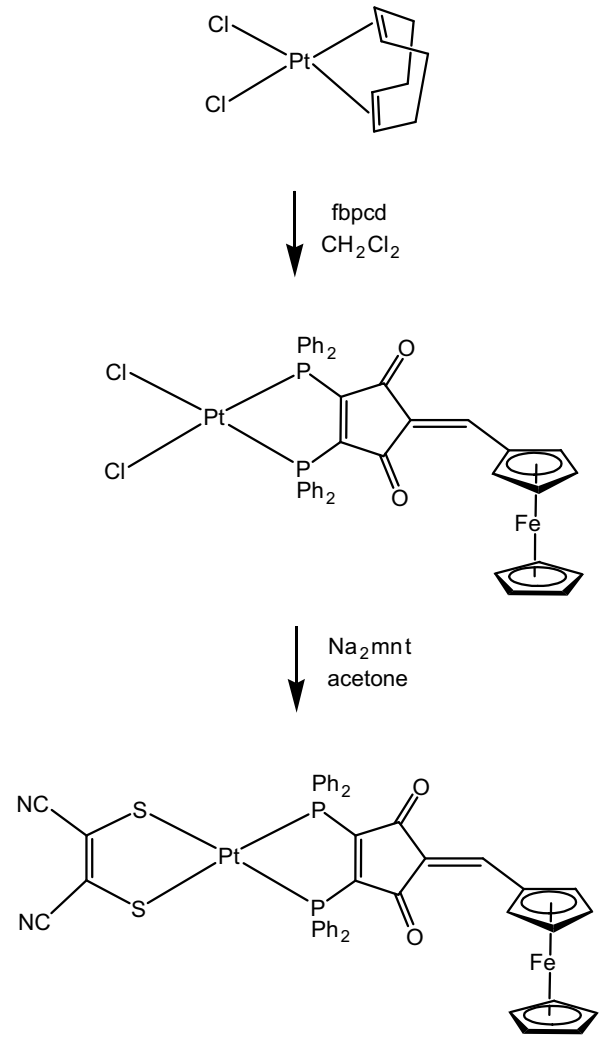

Scheme 2.

The new dithiolate complex was isolated as a navy blue colored solid that is stable under argon in the solid state but solutions containing **3** that have been exposed to oxygen are less stable, with decomposition observed after several hours. **3** was fully characterized by IR, UV–Vis, and NMR spectroscopies, and by ESI mass spectrometry and X-ray diffraction analysis. The IR spectrum of **3** recorded in CH_2Cl_2 revealed a moderately intense ν(CN) stretch at 2209 cm^{-1} for the two nitrile groups and a pair of ν(CO) bands at 1718 and 1679 cm^{-1} for the kinematically coupled dione groups in the fbpcd residue [24]. The UV–Vis and ^{1}H NMR spectral data for **3** parallel those data found in the dichloride precursor **2**. The ^{31}P NMR spectrum of **3** exhibits two singlets at δ 30.26 and 31.08, both of which display a pair of satellites from geminal coupling with a ^{195}Pt center. Interesting, the $^1J_{P-Pt}$ coupling of 1420 Hz recorded in **3** is 418 Hz smaller than that found in **2**, and strongly supports the existence of longer Pt–P bond distances in compound **3** compared to **2**. This empirical trend was initially discovered by Pidcock and coworkers in a series of four- and six-coordinated phosphine-substituted platinum compounds and was corroborated by the X-ray diffraction structures of compounds **2** and **3** [25]. Finally, **3** was examined by ESI mass spectrometry in the negative ion mode, where a peak at *m*/*e* 874.04 corresponding to [**3**-CpFe]$^-$ was found. Attempts to observe the molecular ion derived from **3** were unsuccessful as a result of the facile loss of the "CpFe" fragment, a phenomenon with ample literature precedent [26]. The X-ray structure of **3**, as the CH_2Cl_2 solvate, that is shown in Fig. 1 con-

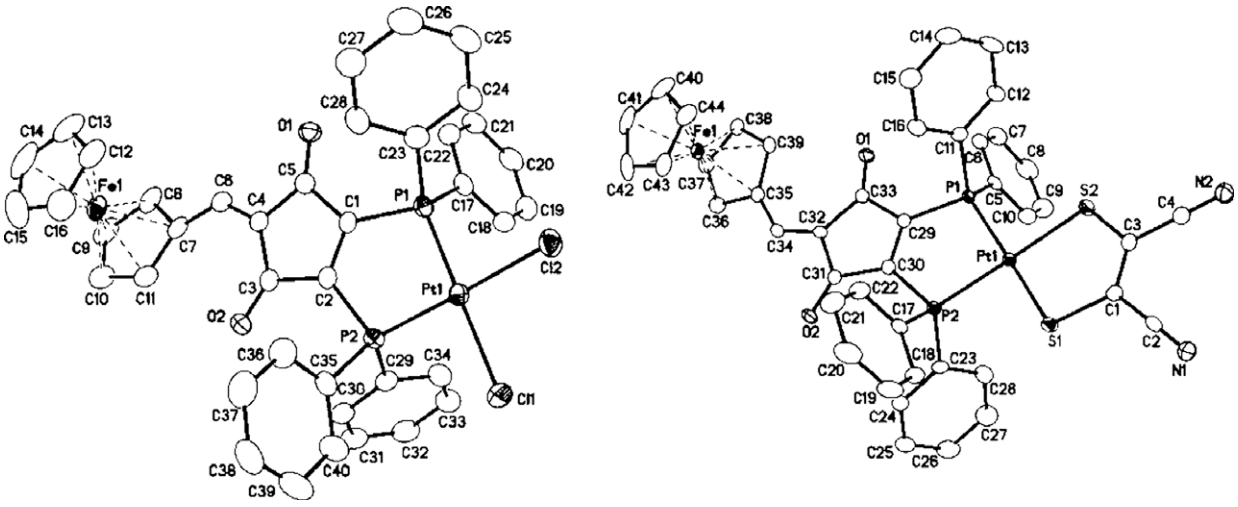

Fig. 1. Thermal ellipsoid plot of **2** · CH_2Cl_2 (left) and **3** · CH_2Cl_2 (right) showing the thermal ellipsoids at the 50% probability level. The CH_2Cl_2 solvent molecule in each plot has been omitted for clarity.

firms the formal replacement of the chlorine ligands by the mnt group. The two Pt–P bond lengths of 2.2589(6) Å [Pt(1)–P(1)] and 2.2572(7) Å [Pt(1)–P(2)] exhibit an average distance of 2.2581 Å and account for the aforementioned trend in the $^1J_{P-Pt}$ coupling constants in **2** and **3**. The mnt and fbpcd moieties in **3** exhibit bond distances and angles consistent with related derivatives containing these ligands.

3.2. Cyclic voltammetric and MO data on the ligand fbpcd and compounds *2* and *3*

Given the rich redox history of the organometallic compounds containing ferrocene, mnt, and bpcd ligands, we next investigated the cyclic voltammetric behavior of the fbpcd ligand and compounds **2** and **3**. The CV data were recorded at platinum electrodes in CH_2Cl_2 at room temperature using 0.2 M TBAP as the supporting electrolyte. The CV of the free ligand fbpcd when scanned at a rate of 250 mV/s over the potential range of −1.0 V to 1.5 V revealed two reversible, diffusion-controlled processes at $E_{1/2}$ = 0.63 and −1.08 V for the $0/1^+$ and $0/1^-$ redox couples [27]. The assignments for these redox couples are straightforward and ascribed to an oxidation and reduction of the ferrocene appendage [i.e., Fe(II) to Fe(III)] and dione moiety (i.e., e^- occupation of the ψ_4-based π^* MO) moiety, respectively, in good agreement with the reported redox potentials of related ferrocene derivatives and the parent ligand bpcd [7,10,28]. The assignments for the redox data were also corroborated by extended Hückel MO calculations, which yielded the expected ferrocene-based HOMO at −11.80 eV and a π^* LUMO at −10.40 eV at the dione platform of the fbpcd ligand.

Examination of **2** by CV in a manner identical to that of the free fbpcd ligand revealed the presence of two well-defined redox waves at $E_{1/2}$ = 0.62 and −0.63 V, as depicted in Fig. 2. While the oxidation potential of the ferrocene portion of the molecule remains unchanged relative to the free fbpcd ligand, an anodic shift of 0.45 V in the $0/1^-$ redox couple is observed upon coordination of the fbpcd ligand to the Pt(II) center. The electrochemical assignments in **2** were verified by carrying out extended Hückel MO calculations. The orbital composition and approximate energy of the HOMO and LUMO levels in **2**, which are shown below, are in keeping with the nature of the ancillary fbpcd ligand. The HOMO occurs at −11.82 eV and resembles the universally seen a_{1g} metal-based orbital for ferrocene and its derivatives [22a,29]. The LUMO in **2** occurs at −10.35 eV and traces its parentage to ψ_4 of the π system associated with the dione moiety [30]. The relatively low energy

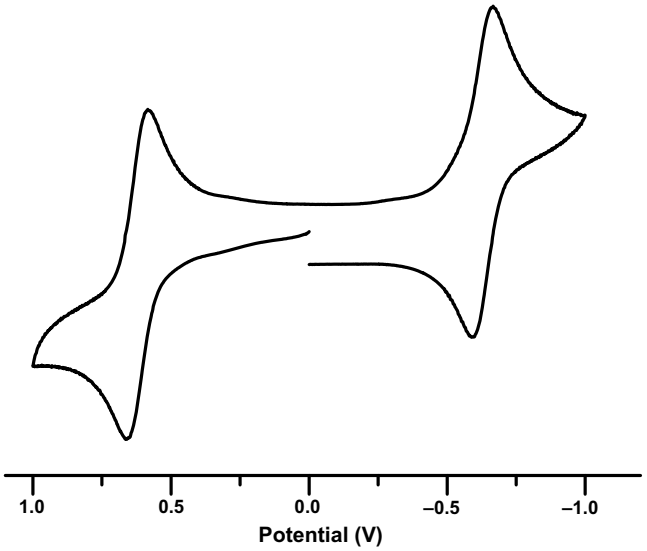

Fig. 2. Anodic scan cyclic voltammogram of **2** (ca. 10^{-3} M) in CH_2Cl_2 containing 0.2 M TBAP at 0.25 V/s at 298 K.

of this π^* orbital makes it a superb electron reservoir vis-á-vis common diphosphine ligands such as dppe and (*Z*)-$Ph_2PCH{=}CHPPh_2$ that do not possess an electrochemically accessible π^* counterpart.

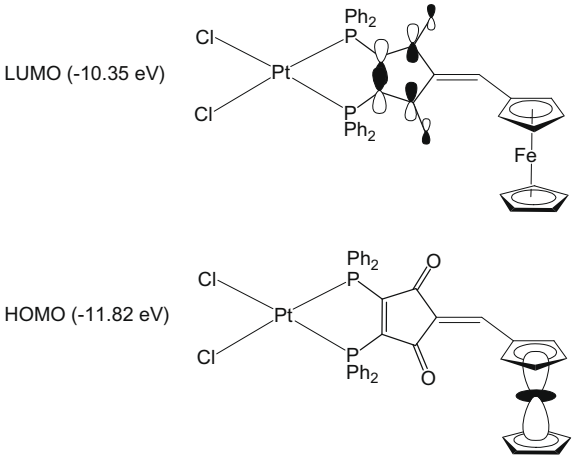

The CV of **3** exhibited three redox waves when examined over the potential range of −1.0 V to 1.5 V at a scan rate of 250 mV/s, with the one-electron reduction wave at $E_{1/2} = -0.57$ V unambiguously assigned to an electron accession at the dione residue. Unlike the straightforward assignment of the oxidation in compound **2** that had single, well-defined oxidation center, the diffusion-controlled waves at $E_{1/2} = 0.65$ (fully reversible) and 1.27 (quasi-reversible) V in **3** could not be made with certainty because dithiolate ligands in other four-coordinate Pt(II) compounds have also been reported to undergo oxidation in the same vicinity as the $E_{1/2}$ value displayed by **3**. The reported oxidation values for Pt(N–N)(S–S) and Pt(P–P)(S–S) compounds (where N–N = bpy and phen derivatives; S–S = mnt, dmit, ecda, tdt; P–P = $2PR_3$, diphosphine) vary considerably, ranging from ca. 0.30 V to 1.0 V depending on the donor/acceptor properties of the dithiolate ligand. For example, the platinum compounds Pt(dppe)(dmit) and Pt(bpy)(tdt) reveal a $0/1^+$ redox response at ca. 0.5 V that mirrors the oxidation potential recorded for **3** [3f,4a]. Oxidation of the HOMO in this latter genre of compounds is controlled exclusively by dπ–pπ interactions between the ancillary dithiolate ligand and platinum metal [3c].

The nature and orbital energies of the important HOMO and LUMO levels in **3** were established by MO analysis, as illustrated below. The LUMO in **3** is concentrated on the dione moiety and is unremarkable in comparison to the energy level and orbital composition of the LUMO found in free fbpcd ligand and compound **2**. The HOMO is best viewed as arising from an out-of-phase union of the $2b_1$ and d_{zy} orbitals of the $[mnt]^{2-}$ and $[Pt(fbpcd)]^{2+}$ fragments, respectively [31]. This particular interaction accounts nicely for observed pπ–dπ bond that is exhibited by the HOMO in compound **3** and that has been similarly found by Eisenberg in the compounds Pt(mnt)(bpy), $Pt(SPh)_2$(bpy), and other Pt(II) derivatives [3c]. In fact, the filled-filled or $4e^-$ interaction in play between these π-based fragments allows one, in theory, to control or tune the energy level associated with the HOMO in this family of compounds [32]. Our calculations on **3** reveal a HOMO energy of −11.45 eV that is in excellent agreement with those HOMO energies reported for Pt(mnt)(bpy) and $Pt(SPh)_2$(bpy) [3c]. Accordingly, the observed $0/1^+$ redox process at $E_{1/2} = 0.65$ in **3** is assigned to the oxidation of the mnt π^*-based orbital. Finally, the Hückel calculations demonstrate that the subjacent highest occupied molecular orbital (SHOMO) at −11.81 eV corresponds to the anticipated ferrocence-based a_{1g} molecular orbital, whose oxidation potential has been shifted to more positive potential relative to compound **2** that is dithiolate free.

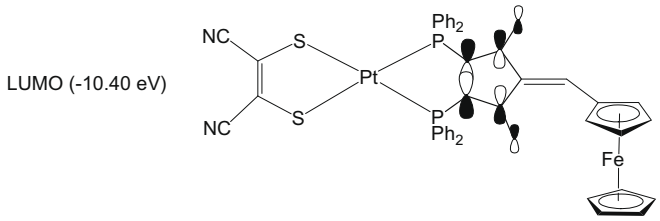

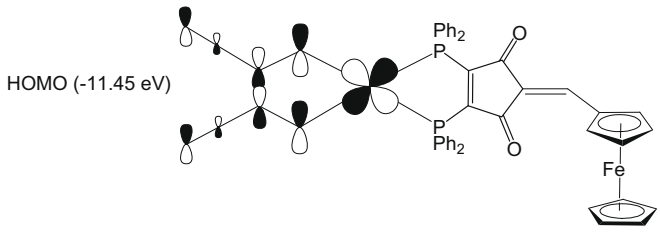

4. Conclusions

The synthesis and spectroscopic properties of the new platinum compounds $PtCl_2$(fbpcd) (**2**) and Pt(mnt)(fbpcd) (**3**) have been presented and discussed. The solid-state structures and the redox properties of $PtCl_2$(fbpcd) (**2**) and Pt(mnt)(fbpcd) (**3**) have been established through a combination of electrochemical and computational methods. Future studies will focus on the photophysical investigation of these and related compounds, and the luminescent properties will be reported in due course.

Acknowledgments

Financial support from the Robert A. Welch Foundation (B-1093-MGR) is much appreciated, and Prof. Guido F. Verbeck and graduate student Ms. Nicole Ledbetter (UNT) and Prof. Andreas H. Franz (University of the Pacific) are thanked for recording the mass spectra of compounds **2** and **3**, respectively.

Appendix A. Supplementary data

CCDC 683128 and 683129 contain the supplementary crystallographic data for $\mathbf{2} \cdot CH_2Cl_2$ and $\mathbf{3} \cdot CH_2Cl_2$. These data can be obtained free of charge via http://www.ccdc.cam.ac.uk/conts/retrieving.html, or from the Cambridge Crystallographic Data Centre, 12 Union Road, Cambridge CB2 1EZ, UK; fax: (+44) 1223-336-033; or e-mail: deposit@ccdc.cam.ac.uk. Cyclic voltammogram of **3** recorded in CH_2Cl_2 and 0.2 M TABP. Supplementary data associated with this article can be found, in the online version, at doi:10.1016/j.poly.2008.09.005.

References

[1] (a) C.N. Pettijohn, E.B. Jochnowitz, B. Chuong, J.K. Nagle, A. Vogler, Coord. Chem. Rev. 171 (1998) 85;
(b) C.J. Adams, N. Fey, J.A. Weinstein, Inorg. Chem. 45 (2006) 6105;
(c) M. Kato, Bull. Chem. Soc. Jpn. 80 (2007) 287;
(d) G.D. Batema, K.T.L. van de Westelaken, J. Guerra, M. Lutz, A.L. Spek, C.A. van Walree, C. de Mello Donegá, A. Meijerink, G.P.M. van Klink, G. Van Koten, Eur. J. Inorg. Chem. (2007) 1422;
(e) P. Du, J. Schneider, P. Jarosz, J. Zhang, W.W. Brennessel, R. Eisenberg, J. Phys. Chem. B 111 (2007) 6887;
(f) B.W. Smucker, J.M. Hudson, M.A. Omary, K.R. Dunbar, Inorg. Chem. 42 (2003) 4714.
[2] (a) F. Puntoriero, S. Campagna, M.L. Di Pietro, A. Giannetto, M. Cusumano, Photochem. Photobiol. Sci. 6 (2007) 357;
(b) M. Cusumano, M.L. Di Pietro, A. Giannetto, Inorg. Chem. 46 (2006) 230.
[3] (a) J.A. Zuleta, C.A. Chesta, R. Eisenberg, J. Am. Chem. Soc. 111 (1989) 8916;
(b) J.A. Zuleta, M.S. Burberry, R. Eisenberg, Coord. Chem. Rev. 97 (1990) 47;
(c) J.A. Zuleta, J.M. Bevilacqua, D.M. Proserpio, P.D. Harvey, R. Eisenberg, Inorg. Chem. 31 (1992) 2396;
(d) J.M. Bevilacqua, R. Eisenberg, Inorg. Chem. 33 (1994) 1886. 2913;
(e) S.D. Cummings, R. Eisenberg, Inorg. Chem. 34 (1995) 3396;
(f) S.D. Cummings, R. Eisenberg, J. Am. Chem. Soc. 118 (1996) 1949;
(g) W.B. Connick, D. Geiger, R. Eisenberg, Inorg. Chem. 38 (1999) 3264;
(h) J. Zhang, P. Du, J. Schneider, P. Jarosz, R. Eisenberg, J. Am. Chem. Soc. 129 (2007) 7726.
[4] (a) For reports on the synthesis, structural characterization, and photophysical properties of Pt(diphosphine)(S–S) compounds, see: R. Vicente, J. Ribas, X. Solans, M. Font-Altaba, A. Mari, P. De Loth, P. Cassoux, Inorg. Chim. Acta 132 (1987) 229;
(b) J.M. Bevilacqua, J.A. Zuleta, R. Eisenberg, Inorg. Chem. 33 (1994) 258;
(c) S. Takemoto, S. Kuwata, Y. Nishibayashi, M. Hidai, Inorg. Chem. 37 (1998) 6428;
(d) K.G. Landis, A.D. Hunter, T.R. Wagner, L.S. Curtin, F.L. Filler, S.A. Jansen-Varnum, Inorg. Chim. Acta 282 (1998) 155;
(e) D.-Y. Noh, E.-M. Seo, H.-J. Lee, H.-Y. Jang, M.-G. Choi, Y.H. Kim, J. Hong, Polyhedron 20 (2001) 1939;
(f) M. Nihei, M. Kurihara, J. Mizutani, H. Nishihara, J. Am. Chem. Soc. 125 (2003) 2964.
[5] R. Saha, M.A. Qaium, D. Debnath, M. Younus, N. Chawdhury, N. Sultana, G. Kociok-Köhn, L.-L. Ooi, P.R. Raithby, M. Kijima, Dalton Trans. (2005) 2760.
[6] (a) For bpcd ligand reactivity studies, see: H. Shen, S.G. Bott, M.G. Richmond, Organometallics 14 (1995) 4625;
(b) S.G. Bott, H. Shen, R.A. Senter, M.G. Richmond, Organometallics 22 (2003) 1953;

(c) W.H. Watson, G. Wu, M.G. Richmond, Organometallics 25 (2006) 930;
(d) W.H. Watson, S.G. Bodige, K. Ejsmont, J. Liu, M.G. Richmond, J. Organomet. Chem. 691 (2006) 3609;
(e) W.H. Watson, B. Poola, M.G. Richmond, J. Organomet. Chem. 691 (2006) 5579.
[7] (a) H.J. Becher, D. Fenske, M. Heymann, Z. Anorg. Allg. Chem. 475 (1981) 27;
(b) R. Meyer, D.M. Schut, K.J. Keana, D.R. Tyler, Inorg. Chim. Acta 240 (1995) 405;
(c) N.W. Duffy, R.R. Nelson, M.G. Richmond, A.L. Rieger, P.H. Rieger, B.H. Robinson, D.R. Tyler, J.C. Wang, K. Yang, Inorg. Chem. 37 (1998) 4849.
[8] For a report on Knoevenagel condensation reactions using 4,5-dichloro-4-cyclopenten-1,3-dione, the immediate precursor in the synthesis of the diphosphine ligand bpcd, see: R. Alfred, Z. Hellmut, Chem. Ber. 94 (1961) 1800.
[9] W.H. Watson, B. Poola, M.G. Richmond, J. Chem. Crystallogr. 36 (2006) 715.
[10] W.H. Watson, D. Wiedenfeld, A. Pingali, B. Poola, M.G. Richmond, Polyhedron 26 (2007) 3577.
[11] W.H. Watson, B. Poola, M.G. Richmond, Polyhedron 26 (2007) 3585.
[12] D. Drew, J.R. Doyle, Inorg. Synth. 28 (1990) 346.
[13] W.H. Watson, B. Poola, M.G. Richmond, Polyhedron 26 (2007) 3585.
[14] A. Davison, R.H. Holm, Inorg. Synth. 10 (1967) 8.
[15] D.F. Shriver, The Manipulation of Air-Sensitive Compounds, McGraw-Hill, New York, 1969.
[16] APEX2 Version 2.14, Bruker AXS, Inc. Copyright 2007, Madison, WI.
[17] SHELXTL Version 6.14, Bruker AXS, Inc. Copyright 2003, Madison, WI.
[18] A.L. Spek, PLATON – A Multipurpose Crystallographic Tool, Utrecht University, Utrecht, The Netherlands, 2006.
[19] M.F. Ryan, D.E. Richardson, D.L. Lichtenberger, N.E. Gruhn, Organometallics 13 (1994) 1190.
[20] (a) R. Hoffmann, W.H. Lipscomb, J. Chem. Phys. 36 (1962) 2179;
(b) R. Hoffmann, J. Chem. Phys. 39 (1963) 1397.
[21] C. Mealli, D.M. Proserpio, J. Chem. Ed. 67 (1990) 399.
[22] (a) Y.S. Sohn, D.N. Hendrickson, H.B. Gray, J. Am. Chem. Soc. 93 (1971) 3603;
(b) G.L. Geoffroy, M.S. Wrighton, Organometallic Photochemistry, Academic Press, New York, 1979.
[23] (a) W. Oberhauser, C. Bachmann, P. Brüggeller, Inorg. Chim. Acta 238 (1995) 35;
(b) W. Oberhauser, C. Bachmann, T. Stampfl, R. Haid, C. Langes, A. Rieder, P. Brüggeller, Inorg. Chim. Acta 274 (1998) 143;
(c) L.M. Engelhardt, J.M. Patrick, C.L. Raston, P. Twiss, A.H. White, Aust. J. Chem. 37 (1984) 2193;
(d) M.H. Johansson, T. Malmstrom, O.F. Wendt, Inorg. Chim. Acta 316 (2001) 149;
(e) J. Powell, M.J. Horvath, A. Lough, J. Chem. Soc., Dalton Trans. (1996) 1679.
[24] The observation of only one nitrile stretch for the two nitrile groups in compound **3**, as opposed to a set of vibrationally coupled symmetric and antisymmetric ν(CN) bands, is expected if the oscillator strength of the higher energy ν(CN) symmetric stretch is weak. See: N.B. Coltrup, L.H. Daly, S.E. Wiberley, Introduction to Infrared and Raman Spectroscopy, Academic Press, New York, 1990.
[25] G.G. Mather, A. Pidcock, G.J.N. Rapsey, J. Chem. Soc., Dalton Trans. (1973) 2095.
[26] (a) S. Barfuss, K.-H. Emrich, W. Hirschwald, P.A. Dowben, N.M. Boag, J. Organomet. Chem. 391 (1990) 209;
(b) E. Bullita, S. Tamburini, P.A. Vigato, M. Carbini, S. Catinella, P. Traldi, Rapid Commun. Mass Spectrom. 10 (1996) 490.
[27] (a) Electrochemical reversibility and electron stoichiometry were determined via the ususal methods, see: A.J. Bard, L.R. Faulkner, Electrochemical Methods, Wiley, New York, 1980;
(b) P.H. Rieger, Electrochemistry, Chapman and Hall, New York, 1994.
[28] (a) G. Gritzner, J. Kuta, Pure Appl. Chem. 56 (1984) 461;
(b) I. Ratera, C. Sporer, D. Ruiz-Molina, N. Ventosa, J. Baggerman, A.M. Brouwer, C. Rovira, J. Veciana, J. Am. Chem. Soc. 129 (2007) 6117;
(c) S.M. Batterjee, M.I. Marzouk, M.E. Aazab, M.A. El-Hashash, Appl. Organomet. Chem. 17 (2003) 291.
[29] (a) J.W. Lauher, R. Hoffmann, J. Am. Chem. Soc. 98 (1976) 1729;
(b) P. Zanello, G. Opromolla, F.F. de Biani, A. Ceccanti, G. Giorgi, Inorg. Chim. Acta 225 (1997) 47;
(c) M. Lein, J. Frunzke, A. Timoshkin, G. Frenking, Chem. Eur. J. 7 (2001) 4155.
[30] T.A. Albright, J.K. Burdett, M.H. Whangbo, Orbital Interactions in Chemistry, Wiley-Interscience, New York, 1985.
[31] (a) For some references dealing with the frontier orbitals of these fragments, see: T.A. Albright, R. Hoffmann, J.C. Thibeault, D.L. Thorn, J. Am. Chem. Soc. 101 (1979) 3801;
(b) T.A. Albright, R. Hoffmann, Y.-C. Tse, T. O'Ottavio, J. Am. Chem. Soc. 101 (1979) 3812;
(c) R. Hoffmann, Angew. Chem., Int. Ed. Engl. 21 (1982) 711;
(d) T.A. Albright, Acc. Chem. Res. 15 (1982) 149;
(e) S. Alvarez, R. Vicente, R. Hoffmann, J. Am. Chem. Soc. 107 (1985) 6253.
[32] K.G. Caulton, New J. Chem. 18 (1994) 25.

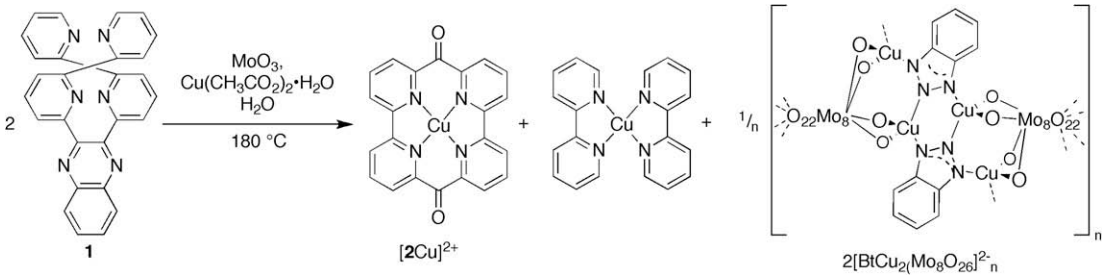

Scheme 1.

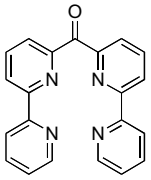

3

dication contains two planar 2-acyl-6,2′-bipyridyl (Bpy) fragments that are interrelated by the inversion center passing through the Cu center (Fig. 1). The constituent atoms of each plane are separated from its congener by 0.588–0.689 Å. In this conformation, the diameter of the macrocyclic cavity, as measured between pairs of opposing N atoms, is 3.95–4.00 Å. All bond lengths in **2**Cu^{2+} are within expected values, except for one of the two C–C lengths that are associated with the carbonyl groups (1.69(2) Å) and exhibit some disorder at the carbon sites [27,28].

The structure of **2**Cu^{2+} invites comparison to the Cu(II) complexes of **3**. This would be erroneous, since the latter do not simultaneously maintain molecular planarity and sp^2 hybridization of the carbonyl group. Arguably, this is a result of bond angle strain induced by the geometry about the carbonyl group, and would be relieved by a highly twisted global molecular geometry [29,30]. Alternatively, carbonyl hydration permits coplanarity of the heteroaromatic groups, but disrupts interannular conjugation. In contrast, **2**Cu^{2+} is largely coplanar and does not occur as a hydrate – in the crystal lattice *and* in spite of the reaction conditions. The observed widening of the angle around C=O, and of the opposite bite angle, would provide a means of strain relief.

To understand its anticipated electronic structure, we calculated the molecular orbitals and geometry of **2**Cu^{2+} using scalar relativistic ZORA DFT methods on ADF2005.01 [31]. Either full or D_{2h}-constrained optimization, followed by vibrational analysis, converged to a D_{2h} structure that was energetically preferred by 33.8 kcal mol^{-1} over C_i and C_{2h} symmetries. The resulting Cu–N distance, 1.989 Å, closely resembles commonly accepted values for d^9 square planar Cu(II) porphyrins and Bpy complexes [27,28], with ∠N4—Cu1—N5 being 96.4° (bite angle) and ∠C7—C17—C16 narrowing to 125.3°.

The HOMO is energetically disfavored by 1.02 eV, relative to the remaining filled orbitals, but stabilized by 1.29 eV relative to the B_{1u} symmetrical orbital that corresponds to the closest empty level with the same spin. We take this latter value to approximate the anticipated band gap in **2**Cu^{2+}. The corresponding LUMO is ligand centered and has overall anti-bonding character. See Figs. S2 and S3 in Supplementary data for diagrams of initial and final orbitals, plus energy levels.

In the lattice, **2**Cu^{2+} has closest through-space contacts to two symmetry-related Bt equivalents, which are parallel to, and within typical stacking distances from, inversion symmetry-related 2-acyl-6,2′-bipyridyl fragments (average separation of closest C_5H_3N to Bt mean plane: 3.425 Å; see Fig. 2). The Bt fragments occur in head-to-tail π-stacked pairs (average separation to plane: 3.522 Å) and dimerize by bridging of two symmetry-related Cu atoms to give N_4Cu_2-rings. Bt units that are related by either π-stacking or a dicopper bridge are associated with different **2**Cu^{2+} equivalents. Stacked and coordinating Bt pairs thus translate between the **2**Cu^{2+} equivalents.

The Cu atoms of the N_4Cu_2 rings and an additional Cu outside of the ring bond with tetrahedral ligand field to oxygen of Mo_8O_{24}. The Cu–N bond lengths, 1.898–1.960 Å, and the Cu–O distances, in the 1.916–2.263 Å range, are ~0.1–0.2 Å greater than in known Bt–Cu(II) complexes with oxygen-donor ligands (*loco cite* [32]) but do not allow distinguishing the Cu oxidation state.

Summarizing, we have uncovered a highly unusual synthesis of a electron-deficient, oligopyridyl-type macrocycle forming a planar Cu(II) complex. Future studies will focus on its mechanism of for-

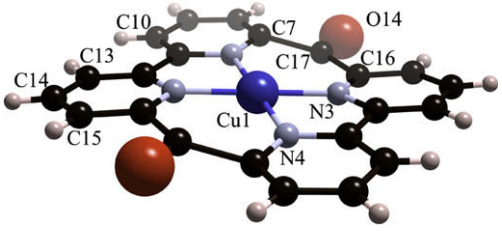

Fig. 1. Structure of **2**Cu^{2+} in the crystal. Selected bond angles: ∠C7–C17–C16: 130°; ∠N4–Cu1–N5: 97.9° (bite angle).

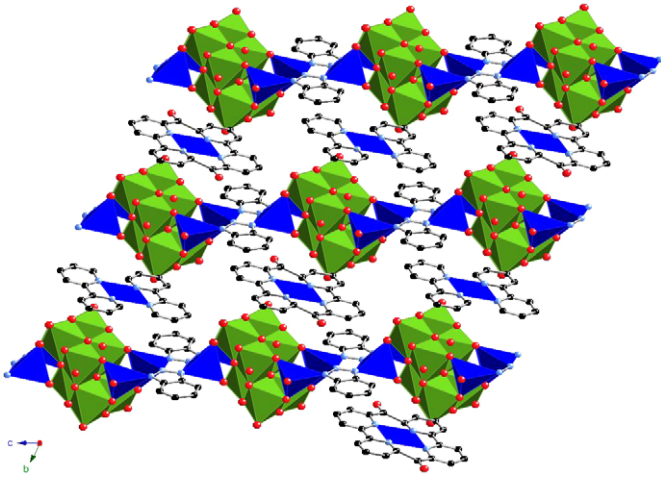

Fig. 2. Crystal lattice of [**2**Cu][bpy2Cu][$BtCu_2Mo_8O_{26}$]$_2$, emphasizing stacking of **2**Cu^{2+} and Bt; ligand fields: Cu: blue, Mo: green. (For interpretation of the references to colour in this figure legend, the reader is referred to the web version of this article.)

mation, optimization and generalization, plus confirmation and prediction of its spectroscopic and electronic properties.

Appendix A. Supplementary data

CCDC 690429 contains the supplementary crystallographic data for this paper. These data can be obtained free of charge via http://www.ccdc.cam.ac.uk/conts/retrieving.html, or from the Cambridge Crystallographic Data Centre, 12 Union Road, Cambridge CB2 1EZ, UK; fax: (+44) 1223-336-033; or e-mail: deposit@ccdc.cam.ac.uk. Supplementary data associated with this article (crystallographic CIF file, depiction of asymmetric unit, computational details and Kohn-Sham MO diagrams) can be found, in the online version, at doi:10.1016/j.poly.2008.09.007.

References

[1] F.R. Heirtzler, M. Neuburger, M. Zehnder, E.C. Constable, Liebigs Ann.-Recl. (1997) 297.
[2] W. Ouellette, V. Golub, C.J. O'Connor, J. Zubieta, Dalton Trans. (2005) 291.
[3] E. Burkholder, J. Zubieta, Inorg. Chim. Acta 357 (2004) 1229.
[4] P.J. Hagrman, D. Hagrman, J. Zubieta, Angew. Chem., Int. Ed. 38 (1999) 2639.
[5] D.R. Xiao, Y. Hou, E.B. Wang, J. Lu, Y.G. Li, L. Xu, C.W. Hu, Inorg. Chem. Commun. 7 (2004) 437.
[6] X.M. Zhang, Coord. Chem. Rev. 249 (2005) 1201.
[7] C.M. Liu, H.Y. Gao, D.Q. Zhang, D.B. Zhu, Lett. Org. Chem. 2 (2005) 712.
[8] S. Hu, J.C. Chen, M.L. Tong, B. Wang, Y.X. Yan, S.R. Batten, Angew. Chem., Int. Ed. 44 (2005) 5471.
[9] X.M. Zhang, M.L. Tong, X.M. Chen, Angew. Chem., Int. Ed. 41 (2002) 1029.
[10] J. Tao, Y. Zhang, M.L. Tong, X.M. Chen, T. Yuen, C.L. Lin, X.Y. Huang, J. Li, Chem. Commun. (2002) 1342.
[11] Q.H. Zhao, X.F. Wang, Y.Q. Liu, R.B. Fang, Chem. Lett. 33 (2004) 138.
[12] N.F. Zheng, X.H. Bu, P.Y. Feng, J. Am. Chem. Soc. 124 (2002) 9688.
[13] C.M. Liu, S. Gao, H.Z. Kou, Chem. Commun. (2001) 1670.
[14] S.L. Zheng, J.P. Zhang, W.T. Wong, X.M. Chen, J. Am. Chem. Soc. 125 (2003) 6882.
[15] Q. Ye, Y.-H. Li, Y.-M. Song, X.-F. Huang, R.-G. Xiong, Z. Xue, Inorg. Chem. 44 (2005) 3618.
[16] S. Ogawa, R. Narushima, Y. Arai, J. Am. Chem. Soc. 106 (1984) 5760.
[17] S. Ogawa, T. Uchida, T. Uchiya, T. Hirano, M. Saburi, Y. Uchida, J. Chem. Soc., Perkin Trans. 1 (1990) 1649.
[18] M. Hirai, K. Shinozuka, S. Ogawa, H. Sawai, Chem. Lett. (1996) 1113.
[19] C.C. Cheng, Y.N. Kuo, K.S. Chuang, C.F. Luo, W.J. Wang, Angew. Chem., Int. Ed. 38 (1999) 1255.
[20] W.J. Wang, K.S. Chuang, C.F. Luo, H.Y. Liu, Tetrahedron Lett. 41 (2000) 8565.
[21] A.J. Gallant, J.K.H. Hui, F.E. Zahariev, Y.A. Wang, M.J. MacLachlan, J. Org. Chem. 70 (2005) 7936.
[22] J.R. Nitschke, T.D. Tilley, Angew. Chem., Int. Ed. 40 (2001) 2142.
[23] R. Ibrahim, S. Tsuchiya, S. Ogawa, J. Am. Chem. Soc. 122 (2000) 12174.
[24] J. Costamagna, J. Canales, J. Vargas, G. Ferraudi, Pure Appl. Chem. 67 (1995) 1045.
[25] *Anal.* Calcd for $C_{33}H_{20}Cu_5Mo_8N_{10}O_{27}$: C, 19.1; H, 1.0; N, 6.8. Found: C, 19.7; H, 1.3; N, 6.6%.
[26] Crystal data for [**2**Cu][bpy$_2$Cu]{[{Cu$_2$(benzotriazolate)Mo$_8$O$_{26}$]}$_2$: triclinic space group, $P\bar{1}$, FW = 2073.86, a = 9.9538(7) Å, b = 11.4051(8) Å, c = 12.5150(9) Å, α = 64.535(10)°, β = 74.892(10)°, γ = 89.805(10)°, V = 1228.7(2) A^3, Z = 1, D_{calc} = 2.803 g cm^{-3}, μ(Mo Kα) = 4.180 mm^{-1}, R_1 = 0.0508, wR_2 = 0.0843.
[27] J. March, Advanced Organic Chemistry, 4th ed., John Wiley and Sons, New York, 1992.
[28] A.G. Orpen, L. Brammer, F.H. Allen, O. Kennard, D.G. Watson, R. Taylor, J. Chem. Soc., Dalton Trans. (1989) S1.
[29] A.C. Deveson, S.L. Heath, C.J. Harding, A.K. Powell, J. Chem. Soc., Dalton Trans. (1996) 3173.
[30] X.-D. Chen, T.C.W. Mak, Inorg. Chim. Acta 358 (2005) 1107.
[31] G. te Velde, F.M. Bickelhaupt, E.J. Baerends, C.F. Guerra, S.J.A. Van Gisbergen, J.G. Snijders, T. Ziegler, J. Comput. Chem. 22 (2001) 931.
[32] C. Richardson, P.J. Steel, Dalton Trans. (2003) 992.

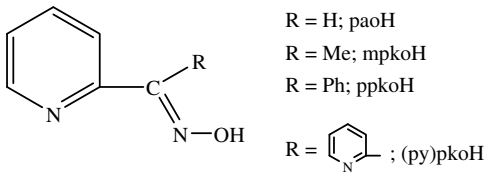

Fig. 1. General structural formula and abbreviations of the 2-pyridyl oximes that are used in our laboratories, including methyl 2-pyridyl ketone oxime (mpkoH) employed in this work.

[9–11]. As an extension to this work, we have now asked if other products might result from the $Mn/R'CO_2^-$/mpkoH reaction system. Four years ago, we described in detail the synthesis and structural, spectroscopic and magnetochemical characterization of the remarkable cluster $[Mn^{II}_4Mn^{III}_4O_2(OH)_2(O_2CPh)_{10}(ppko)_4]$ (**1**) and showed that it has a $S = 0$ ground state [7]. We have wondered if the $mpko^-$ analogue of **1** could be prepared and have thus pursued its synthesis. There are two reasons to prepare such a complex: (i) to determine if it would be isostructural with **1** and be isolated at the same oxidation level, and (ii) if it is isostructural, to assess any influence of the Me versus Ph difference on magnetochemical properties. We herein report the successful development of synthetic procedures to prepare the $mpko^-$ analogue of **1** and describe its characterization.

2. Experimental

2.1. General and physical measurements

All manipulations were performed under aerobic conditions using materials (reagent grade) and solvents as received. $Mn(O_2CPh)_2 \cdot 2H_2O$ [15a], $NBu^n_4MnO_4$ [15b], $(NBu^n_4)[Mn^{III}_4O_2(O_2CPh)_9(H_2O)]$ [15a] and $[Mn_3O(O_2CPh)_6(py)_2(H_2O)]$ [16] were synthesized according to published methods. Elemental analyses (C, H, N) were performed by the in-house facilities of the University of Florida Chemistry Department. IR spectra (4000–400 cm^{-1}) were recorded on Perkin–Elmer 16 PC and Nicolet Nexus 670 FTIR spectrometers with samples prepared as KBr pellets. Variable-temperature dc and ac magnetic susceptibility data were collected at the University of Florida using a Quantum Design MPMS-XL SQUID susceptometer equipped with a 7 T magnet. The sample was embedded in eicosane to prevent torquing. Diamagnetic corrections were applied to the observed paramagnetic susceptibilities using Pascal's constants.

2.2. Compound preparation

2.2.1. $[Mn(O_2CPh)_2(mpkoH)_2]$ (**2**)

Solid mpkoH (0.082 g, 0.60 mmol) was added to a pale pink solution of $Mn(O_2CPh)_2 \cdot 2H_2O$ (0.100 g, 0.30 mmol) in CH_2Cl_2 (30 mL). The solid soon dissolved to give a yellow solution. The solution was stirred for 30 min and layered with Et_2O/*n*-hexane (1:1 v/v, 60 mL). After 1 d, X-ray quality, yellow prismatic crystals of the product were collected by filtration, washed with Et_2O (2×2 mL), and dried in air. Yield: 85%. *Anal.* Calc. for $C_{28}H_{26}MnN_4O_6$: C, 59.05; H, 4.61; N, 9.84. Found: C, 58.97; H, 4.32; N, 9.72%. IR (KBr, cm^{-1}): ~3488mb, 3065w, 1599s, 1543s, 1478m, 1437m, 1404s, 1327m, 1255w, 1170w, 1137w, 1098w, 1047s, 1024m, 964w, 834w, 786s, 720s, 684m, 674s, 636w, 563w, 452m, 406w.

2.2.2. $[Mn_8O_2(OH)_2(O_2CPh)_{10}(mpko)_4]$ (**3**)

2.2.2.1. Method A. To a deep red solution of $(NBu^n_4)[Mn^{III}_4O_2(O_2CPh)_9(H_2O)]$ (0.160 g, 0.10 mmol) in CH_2Cl_2 (30 mL) was added solid mpkoH (0.054 g, 0.40 mmol). The resulting dark brown solution was stirred for 30 min, during which time no further colour change occurred. The solution was filtered and the filtrate layered with Et_2O/*n*-hexane (1:1 v/v, 60 mL). After 2 d, dark red prismatic crystals of $\mathbf{3} \cdot 1.8CH_2Cl_2 \cdot 1.8Et_2O$ were collected by filtration, washed with cold Et_2O (2×2 mL), and dried in air. Yield: 60%. The air-dried sample analyzed as $\mathbf{3} \cdot 2H_2O$. *Anal.* Calc. for $C_{98}H_{84}Mn_8N_8O_{30}$: C, 51.32; H, 3.70; N, 4.88. Found: C, 51.51; H, 3.84; N, 4.83%. IR (KBr, cm^{-1}): 3435mb, 3063w, 2921w, 1597s, 1553s, 1491w, 1484w, 1447m, 1404s, 1317w, 1273w, 1175w, 1151w, 1098w, 1068m, 1046m, 1025m, 934w, 820w, 778m, 718s, 689w, 676m, 639w, 604m, 537w, 457w.

2.2.2.2. Method B. Treatment of a stirred, dark brown solution of $[Mn_3O(O_2CPh)_6(py)_2(H_2O)]$ (0.108 g, 0.10 mmol) in CH_2Cl_2 (30 mL) with solid mpkoH (0.027 g, 0.20 mmol) gave a solution of essentially the same colour. This was stirred for 30 min and layered with Et_2O (60 mL). Slow mixing gave dark red prismatic crystals which were collected by filtration, washed with Et_2O (2×3 mL) and dried in air. Yield: 40%. The IR spectrum of the product was identical with that of the authentic material prepared by Method A.

2.2.2.3. Method C. Treatment of a stirred, pale pink solution of $Mn(O_2CPh)_2 \cdot 2H_2O$ (0.100 g, 0.30 mmol) in MeOH/MeCN (15 mL, 1:2 v/v) with solid $NBu^n_4MnO_4$ (0.040 g, 0.12 mmol) resulted in a dark brown solution. Solid mpkoH (0.040 g, 0.29 mmol) was slowly added to the solution, and it soon dissolved to give a somewhat darker solution that was stirred for a further 20 min. The solvents were then evaporated under reduced pressure. The dark brown residue was dissolved in CH_2Cl_2 (30 mL), filtered and the essentially black filtrate layered with Et_2O (60 mL). Slow mixing gave dark red crystals of the product after 4 d, which were collected by filtration, washed with cold CH_2Cl_2 (2×2 mL) and Et_2O (5 mL), and dried in air. Yield: ~35%. The IR spectrum of the product was identical with the spectra of the material from Methods A and B. The purity of the sample prepared from this method was also confirmed by microanalytical data.

2.3. Single-crystal X-ray crystallography

The crystallographic data and structure refinement details for the two complexes are summarized in Table 1. A selected crystal of **2** ($0.07 \times 0.35 \times 0.66$ mm) was mounted in air. Diffraction measurements were made on a Crystal Logic Dual Goniometer diffractometer using graphite-monochromated Mo radiation. Unit cell dimensions were determined and refined by using the angular settings of 25 automatically centered reflections in the range $11° < 2\theta < 23°$. Intensity data were recorded using a θ–2θ scan to a maximum 2θ value of 50°. Three standard reflections monitored every 97 reflections showed less than 3% variation and no decay. Lorentz, polarization corrections were applied using CRYSTAL LOGIC software. The structure was solved by direct methods using SHELXS-97 [17a] and refined on F^2 by full-matrix least squares techniques with SHELXL-97 [17b]. All H atoms were located by Fourier difference maps and refined isotropically. All non-H atoms were refined anisotropically.

A selected crystal of $\mathbf{3} \cdot 1.8CH_2Cl_2 \cdot 1.8Et_2O$ ($0.28 \times 0.30 \times 0.55$ mm), prepared by Method A, was taken from the mother liquor, mounted, and immediately cooled to 103(2) K. Data were collected on a Rigaku R-AXIS SPIDER Image Plate diffractometer using graphite-monochromated Mo radiation. Data collection (ω-scans) to a maximum 2θ value of 51° and processing (cell refinement, data reduction and empirical absorption correction) were performed using the CRYSTALCLEAR program package [17c]. The structure was solved by direct methods using SHELXS-97 [17a] and

Table 1
Crystallographic data for complexes **2** and **3** · $1.8CH_2Cl_2$ · $1.8Et_2O$

Parameter	**2**	**3** · $1.8CH_2Cl_2$ · $1.8Et_2O$
Formula	$C_{28}H_{26}MnN_4O_6$	$C_{107}H_{101.60}Mn_8N_8O_{29.80}Cl_{3.60}$
Formula weight	569.47	2543.50
Crystal system	triclinic	monoclinic
Space group	$P\bar{1}$	$C2/c$
a (Å)	11.013(4)	31.320(4)
b (Å)	11.608(5)	15.565(2)
c (Å)	11.265(5)	24.495(3)
α (°)	97.50(1)	90
β (°)	95.34(1)	109.49(1)
γ (°)	98.19(1)	90
V (Å^3)	1404.1(10)	11257(3)
Z	2	4
ρ_{calc} (g cm^{-3})	1.347	1.501
Radiation, λ (Å)	Mo Kα, 0.71073	Mo Kα, 0.71069
Temperature (K)	298	103
μ (mm^{-1})	0.517	1.031
Data collected/unique (R_{int})	5270/4954 (0.0137)	40 112/10 405 (0.0613)
Data with $I > 2\sigma(I)$	4221	8314
R_1 ($I > 2\sigma(I)$)[a]	0.0390	0.0831
wR_2 ($I > 2\sigma(I)$)[b]	0.1024	0.1973

[a] $R_1 = \sum(|F_o| - |F_c|)/\sum(|F_o|)$.
[b] $wR_2 = \{\sum[w(F_o^2 - F_c^2)^2]/\sum[w(F_o^2)^2]\}^{1/2}$.

refined by full-matrix least squares techniques on F^2 with SHELXL-97 [17b]. All H atoms were introduced at calculated positions and refined as riding on their bound atoms. All non-H atoms were refined anisotropically. Two of the benzoates as well as the solvate molecules were found disordered and refined in two orientations with occupancies adding up to 100%.

3. Results and discussion

3.1. Syntheses and IR spectroscopy

The preparation of pure **2** in excellent yield was achieved by the reaction of $Mn(O_2CPh)_2 \cdot 2H_2O$ with two equivalents of mpkoH in CH_2Cl_2, see Eq. (1):

$$Mn(O_2CPh)_2 \cdot 2H_2O + 2mpkoH \xrightarrow{CH_2Cl_2} [Mn(O_2CPh)_2(mpkoH)_2] + 2H_2O \quad (1)$$

Three procedures to $Mn^{II}_4Mn^{III}_4$ complex **3** were developed. The first (and best) involves the conversion of $[Mn^{III}_4O_2(O_2CPh)_9(H_2O)]^-$ into a higher nuclearity product. The anion, which contains only $PhCO_2^-$ and H_2O ligands [15a], is a very useful starting material for the synthesis of higher nuclearity clusters [15a,18]. Thus, treatment of the $NBu^n_4{}^+$ salt of $[Mn^{III}_4O_2(O_2CPh)_9(H_2O)]^-$ with an excess of mpkoH in CH_2Cl_2 led to pure crystalline **3** in good yields (~60%) upon layering of the reaction solution with precipitation solvents. The formation of **3** is summarized in Eq. (2). The $4Mn^{II}$, $4Mn^{III}$ description of **3** requires the reduction of four Mn^{III} ions to have occurred. The source of the reducing agent is probably an

$$2[Mn^{III}_4O_2(O_2CPh)_9(H_2O)]^- + 4mpkoH \xrightarrow{+4e^-} [Mn^{II}_4Mn^{III}_4O_2(OH)_2(O_2CPh)_{10}(mpko)_4] + 2PhCO_2H + 6PhCO_2^- + 2H_2O \quad (2)$$

impurity of the solvent or excess ligand groups, facilitated by the strongly oxidizing nature of Mn^{III} [15a]. An alternative means for the generation of the Mn^{II} ions in **3** might be disproportionation of Mn^{III}, in which case Mn^{IV}-containing species would be present in the coloured filtrate [15a]. We have not attempted to identify the exact origin of the Mn^{II} ions in the product, nor would it be a simple investigation.

The second procedure to **3** gave a lower yield and involved the reaction of $[Mn^{II}Mn^{III}_2O(O_2CPh)_6(py)_2(H_2O)]$ [16] with two equivalents of mpkoH in CH_2Cl_2. Many synthetic procedures to make polynuclear manganese carboxylate clusters rely on the reactions of triangular $[Mn_3O(O_2CR)_6L_xL'_y]^{0/+}$ species ($x + y = 3$) with a potentially chelating/bridging ligand [5b,11]. The formation of **3** by this method can be summarized in Eq. (3). As stated above, it is not uncommon to find Mn^{III} – a strong oxidizing agent – being reduced by ligand groups, solvent impurities, etc.:

$$8[Mn^{II}Mn^{III}_2O(O_2CPh)_6(py)_2(H_2O)] + 12mpkoH + 4H^+ \xrightarrow{+4e^-} 3[Mn^{II}_4Mn^{III}_4O_2(OH)_2(O_2CPh)_{10}(mpko)_4] + 18PhCO_2H + 16py + 4H_2O \quad (3)$$

Once the identity of **3** had been established, we also sought its synthesis from simpler starting materials, and we found that it can be prepared by the comproportionation between $Mn(O_2CPh)_2.2H_2O$ and $NBu^n_4MnO_4$ [15b] in a 2.5:1 ratio in the presence of mpkoH in MeOH/MeCN. Such comproportionation reactions between Mn^{II} and Mn^{VII} sources in the presence of appropriate ligand groups have found extensive prior use to produce clusters of several nuclearities at various Mn oxidation levels [11,15a,19]. The ratio employed in this work gives, on paper, an average Mn oxidation state in solution of $Mn^{+3.4}$, higher than that ($Mn^{+2.5}$) observed in solid **3**, but the MeOH can act as reducing agent. The yield was only ~35%, and it is possible there are other products in the coloured filtrates. We also explored higher Mn^{II}:Mn^{VII} ratios, but this led to **3** contaminated with $[Mn^{II}_4Mn^{III}_2O_2(O_2CPh)_{10}(MeCN)_4]$ [20] containing no bound $mpko^-$ groups.

Note that the $Mn(O_2CPh)_2 \cdot 2H_2O/MnO_4^-$/mpkoH and $[Mn_3O(O_2CPh)_6(py)_2(H_2O)]$/mpkoH reaction systems in EtOH or MeOH/MeCN/CH_2Cl_2 in the presence of appropriate counterions (e.g. ClO_4^-) have led to salts of the $[Mn_3O(O_2CPh)_3(mpko)_3]^+$ cation, which were amongst the first examples of SMMs with a triangular structure [9,11]. Thus, it is likely, as with many other reactions in higher oxidation state Mn chemistry, that the reaction solution contains a complicated mixture of several species in equilibrium, with factors such as relative solubilities, absence/presence of counterions, lattice energies, crystallization kinetics and others determining the identity of the isolated product [19].

The presence of neutral oxime groups in **2** is manifested by a broad IR band of medium intensity at 3488 cm^{-1}, assigned to $\nu(OH)_{oxime}$ [6,21]. The IR spectrum of **3** exhibits a medium band at 3435 cm^{-1} assignable [22] to $\nu(OH)_{OH^-}$. The broadness and relatively low wavenumber of these bands are both indicative of hydrogen-bonding. A medium-intensity band at 604 cm^{-1} is present in the spectrum of **3**; this band, which is absent from the spectrum of **2**, is tentatively assigned to a vibration involving a Mn^{III}–O^{2-} stretch [23]. The $\nu(CO_2)$ bands are difficult to assign in the spectra of **2** and **3** due to the appearance of overlapping carboxylate, phenyl, 2-pyridyl and oxime/oximate stretching vibrations in the 1600–1400 cm^{-1} region [24] and thus the application of the spectroscopic criterion of Deacon and Phillips [25] is very difficult.

3.2. Description of structures

The molecular structures of complexes **2** and **3** are depicted in Figs. 2 and 3, respectively. Selected interatomic distances and angles are listed in Tables 2 and 3.

Complex **2** crystallizes in the triclinic space group $P\bar{1}$. Its structure consists of well-separated $[Mn(O_2CPh)_2(mpkoH)_2]$ molecules. The Mn^{II} center is coordinated by two monodentate $PhCO_2^-$ groups and two *N*,*N*′-chelating (η^2) mpkoH ligands. The mpkoH donor atoms are the nitrogen atoms of the neutral oxime and the 2-pyridyl groups. The six-coordinate molecule is the *cis–cis–trans* isomer

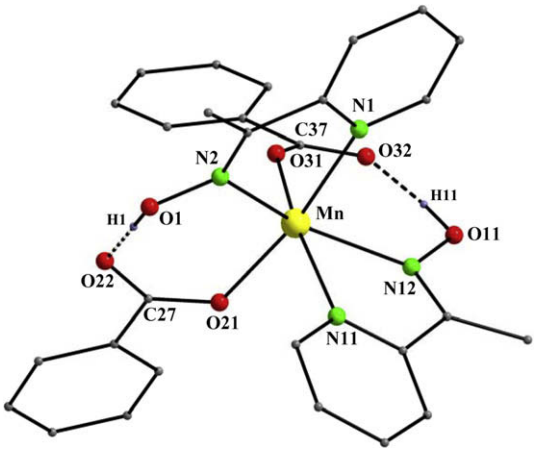

Fig. 2. Partially labelled plot of complex **2**. The dashed lines are H-bonds. Colour scheme: Mn^{II}, yellow; O, red; N, green; C, gray; H, purple. (For interpretation of the references to colour in this figure legend, the reader is referred to the web version of this article.)

with respect to the disposition of the benzoate oxygen, pyridyl nitrogen and oxime nitrogen atoms, respectively. The *cis* arrangement of the oxime groups seems unfavorable, probably due to the steric hindrance arising from the Me groups upon oxime coordination. The molecule has no imposed symmetry, although it closely approximates C_2 symmetry, with the pseudo C_2 axis bisecting the O(21)–Mn–O(31) angle. The main distortion from octahedral geometry is due to the small bite angles of the mpkoH chelates (70.2°, 70.6°). There are very strong intramolecular H-bonds between unbound oxime –OH groups and the unbound benzoate O atoms (O(22), O(32)). The dimensions are: O(1)···O(21) 2.542(4) Å, HO(1)···O(22) 1.650(4) Å, O(1)–HO(1)···O(22) 178.9(1)° and O(11)···O(32) 2.535 Å, HO(11)···O(32) 1.672(5) Å, O(11)–HO(11)···O(32) 170.5(1)°. Complex **2** joins a very small family of $[Mn^{II}(O_2CR')_2(L–L)_2]$ complexes (L–L = neutral 2-pyridyl oximes) with an analogous *cis–cis–trans* arrangement of the donor atoms [6–8].

Table 2
Selected bond lengths (Å) and angles (°) for complex **2**

Mn–O(21)	2.104(2)	Mn–N(12)	2.282(2)
Mn–O(31)	2.083(2)	C(27)–O(21)	1.259(3)
Mn–N(1)	2.302(2)	C(27)–O(22)	1.241(4)
Mn–N(2)	2.273(2)	C(37)–O(31)	1.244(3)
Mn–N(11)	2.287(2)	C(37)–O(32)	1.232(3)
O(21)–Mn–O(31)	88.4(1)	O(31)–Mn–N(12)	95.9(1)
O(21)–Mn–N(1)	169.1(1)	N(1)–Mn–N(2)	70.2(1)
O(21)–Mn–N(2)	99.1(1)	N(1)–Mn–N(11)	92.9(1)
O(21)–Mn–N(11)	88.5(1)	N(1)–Mn–N(12)	87.8(1)
O(21)–Mn–N(12)	102.8(1)	N(2)–Mn–N(11)	89.3(1)
O(31)–Mn–N(1)	92.9(1)	N(2)–Mn–N(12)	149.6(1)
O(31)–Mn–N(2)	105.7(1)	N(11)–Mn–N(12)	70.6(1)
O(31)–Mn–N(11)	165.0(1)		

Complex $\mathbf{3}\cdot 1.8CH_2Cl_2\cdot 1.8Et_2O$ crystallizes in the monoclinic space group *C*2/*c*. Its structure consists of the $[Mn_8O_2(O\text{-}H)_2(O_2CPh)_{10}(mpko)_4]$ molecule and solvate CH_2Cl_2 and Et_2O molecules; the latter will not be further discussed. The molecule lies on a crystallographic twofold axis. The eight Mn ions are held together by two μ_4-O^{2-} (O(71), O(71′)) and two μ_3-OH^- (O(72), O(72′)) groups to give a $[Mn_8(\mu_4\text{-}O)_2(\mu_3\text{-}OH)_2]^{14+}$ core (Fig. 4). Bond-valence sum (BVS) calculations [26] give values of 1.8 and 1.2 for O(71) and O(72), respectively, supporting their assignments as oxo and hydroxo oxygen atoms (Table 4). Peripheral ligation is provided by two monodentate (η^1) $PhCO_2^-$ (those containing the ligating atoms O(51) and O(51′)), four *syn,syn*-η^1:η^1:μ $PhCO_2^-$ (those containing O(41)/O(42), O(61)/O(62) and their symmetry-related partners), four η^1:η^2:μ_3 $PhCO_2^-$ groups (those containing O(21)/O(22), O(31)/O(32′) and their symmetry-related partners)

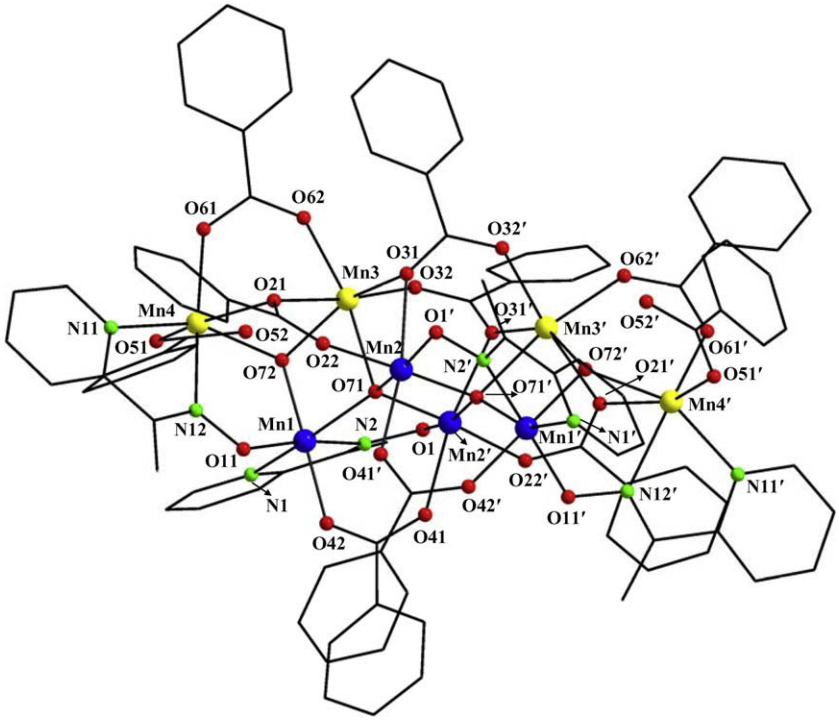

Fig. 3. Partially labelled plot of the Mn_8 molecule of complex **3**. Primed and unprimed atoms are related by the crystallographic two-fold axis. O(71) and O(71′) are the oxide ions, and O(72) and O(72′) are the hydroxide O atoms. Colour scheme: Mn^{II}, yellow; Mn^{III}, blue; O, red; N, green; C, gray. (For interpretation of the references to colour in this figure legend, the reader is referred to the web version of this article.)

Table 3
Selected interatomic distances (Å) and angles (°) for complex **3** · $1.8CH_2Cl_2$ · $1.8Et_2O$

Mn(1)···Mn(2)	3.870(6)	Mn(2)–O(31)	2.304(5)
Mn(1)···Mn(3)	3.290(2)	Mn(2)–O(41′)	2.173(5)
Mn(1)···Mn(4)	3.531(6)	Mn(2)–O(71)	1.908(4)
Mn(2)···Mn(3)	3.189(1)	Mn(2)–O(71′)	1.870(3)
Mn(2)···Mn(4)	5.346(2)	Mn(3)–O(21)	2.238(4)
Mn(3)···Mn(4)	3.365(1)	Mn(3)–O(31)	2.158(4)
Mn(2)···Mn(2′)	2.804(2)	Mn(3)–O(32)	2.133(4)
Mn(4)···Mn(4′)	10.910(5)	Mn(3)–O(62)	2.131(5)
Mn(1)–O(11)	1.891(4)	Mn(3)–O(71)	2.272(4)
Mn(1)–O(42)	1.954(4)	Mn(3)–O(72)	2.164(4)
Mn(1)–O(71)	2.180(4)	Mn(4)–O(21)	2.450(4)
Mn(1)–O(72)	1.942(4)	Mn(4)–O(51)	2.130(4)
Mn(1)–N(1)	2.273(5)	Mn(4)–O(61)	2.098(5)
Mn(1)–N(2)	2.039(5)	Mn(4)–O(72)	2.163(4)
Mn(2)–O(1′)	1.947(4)	Mn(4)–N(11)	2.237(5)
Mn(2)–O(22)	1.978(4)	Mn(4)–N(12)	2.238(6)
O(11)–Mn(1)–N(2)	170.8(2)	O(72)–Mn(4)–N(11)	153.2(2)
O(42)–Mn(1)–O(72)	177.7(2)	Mn(1)–O(71)–Mn(2)	142.3(2)
O(71)–Mn(1)–N(1)	157.2(2)	Mn(1)–O(71)–Mn(2′)	107.8(2)
O(1′)–Mn(2)–O(71)	167.5(2)	Mn(1)–O(71)–Mn(3)	95.3(2)
O(22)–Mn(2)–O(71′)	175.5(2)	Mn(2)–O(71)–Mn(2′)	95.8(2)
O(31)–Mn(2)–O(41′)	169.5(1)	Mn(2)–O(71)–Mn(3)	99.1(2)
O(21)–Mn(3)–O(32)	173.6(2)	Mn(2′)–O(71)–Mn(3)	118.0(2)
O(31)–Mn(3)–O(72)	150.6(2)	Mn(1)–O(72)–Mn(3)	106.4(2)
O(62)–Mn(3)–O(71)	168.8(2)	Mn(1)–O(72)–Mn(4)	118.5(2)
O(21)–Mn(4)–O(51)	161.2(2)	Mn(3)–O(72)–Mn(4)	102.1(2)
O(61)–Mn(4)–N(12)	156.3(2)		

[a] Primed atoms are related to the unprimed ones by the symmetry operation $-x, y, -z + 1/2$.

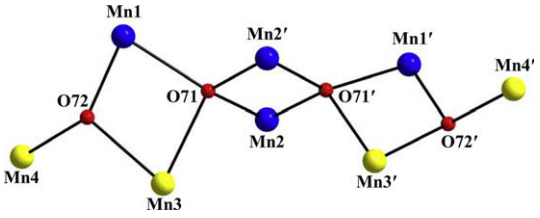

Fig. 4. The $[Mn_8(\mu_4\text{-}O)_2(\mu_3\text{-}OH)_2]^{14+}$ core of complex **3**; O(71) and O(71′) are the oxide ions, and O(72) and O(72′) are the OH^- ions. Colour scheme: Mn^{II}, yellow; Mn^{III}, blue; O, red. (For interpretation of the references to colour in this figure legend, the reader is referred to the web version of this article.)

Table 4
Bond valence sum (BVS) calculations[a,b] for the Mn and selected O atoms in complex **3**

Atom	Mn^{II}	Mn^{III}	Mn^{IV}
Mn(1)	3.17	*2.95*	3.02
Mn(2)	3.17	*2.90*	3.05
Mn(3)	*1.96*	1.79	1.88
Mn(4)	*1.98*	1.85	1.88
	BVS	Assignment	
O(71)	1.79	O^{2-}	
O(72)	1.17	OH^-	

[a] The italic value is the one closest to the charge for which it was calculated. The oxidation state of a particular Mn center can be taken as the nearest whole number to the italic value.

[b] An O BVS in the ~1.8–2.0, ~1.0–1.2 and ~0.2–0.4 ranges is indicative of zero, single, and double protonation, respectively.

and four $\eta^1{:}\eta^1{:}\eta^1{:}\mu$ $mpko^-$ ligands. Each $mpko^-$ ligand chelates one metal ion through its nitrogen atoms forming a five-membered ring and bridges this metal ion with a second one through the terminally ligated, deprotonated oximate O atom (O(1), O(1′), O(11), O(11′)). If we consider the monoatomic carboxylate bridges and the bridging diatomic oximate groups as part of the core, then the latter becomes $[Mn_8(\mu_4\text{-}O)_2(\mu_3\text{-}OH)_2(\mu\text{-}OR'')_4(\mu\text{-}ONR''')_4]^{6+}$;

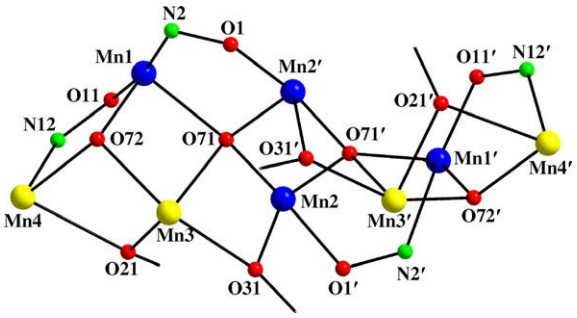

Fig. 5. The core of **3** emphasizing the oxime bridging modes. For the chemical nature of most atoms, see the caption of Fig. 4. O(21), O(31), O(21′) and O(31′) are the monoatomically bridging benzoate O atoms. N(2), O(1), N(12), and O(11) are the $mpko^-$ oximate groups. Colour scheme as in Fig. 3.

this view is emphasized in Fig. 5. The Mn_8 topology of **3** is shown in Fig. 6.

Mn(1) and Mn(4) are bound to an O_4N_2 set of donor atoms, while Mn(2) and Mn(3) to an O_6 set. Charge considerations require a $4Mn^{II}$, $4Mn^{III}$ mixed-valence description, and Mn(1) and Mn(2) are assigned as Mn^{III} on the basis of (i) their shorter average Mn-O bond lengths (2.015 Å) compared with those for Mn(3) and Mn(4) (average 2.194 Å, with no individual value shorter than 2.10 Å); (ii) a Jahn–Teller (JT) axial elongation at Mn(1) and Mn(2) (the JT elongation axes are O(71)–Mn(1)–N(1) and O(31)–Mn(2)–O(41′)), as expected for high-spin d^4 ions in near-octahedral geometry; and (iii) BVS calculations [26] (Table 4). Thus, the hydroxide group bridges one Mn^{III} and two Mn^{II} atoms, while the oxide group bridges one Mn^{II} and three Mn^{III} atoms.

The μ-O atom O(21) does not bridge the two Mn^{II} ions symmetrically, with Mn(3)–O(21) (2.238(4) Å) noticeably shorter than Mn(4)–O(21) (2.450(4) Å). The Mn(3,4)–O(72) bond distances (average (2.164(4) Å) are longer than the Mn(1)–O(72) distance (1.942(4) Å), consistent with a higher oxidation state for Mn1. It should also be noted that the O^{2-} groups (O(71), O(71′)) bridge the three Mn^{III} atoms in an asymmetric fashion. Thus, Mn(2,2′)–O(71) distances average 1.889(4) Å, whereas the Mn(1)–O(1) bond length is noticeably longer (2.180(4) Å). This is the result of O(71) lying on the JT elongation axis of Mn(1); Mn^{III}–O^{2-} distances at ~2.2 Å are extremely rare [27]. The Mn···Mn distances (Table 3) depend on the number and nature of the bridges between two given metal centers and on the oxidation state of each Mn atom. The central Mn(2)···Mn(2′) distance is the shortest (2.804(2) Å) and is typical for $\{Mn_2^{III,III}(\mu_4\text{-}O)_2\}^{2+}$ subunits in Mn^{III}-containing clusters [20,28]. The uncoordinated O atoms of the monodentate $PhCO_2^-$ ligands (O(52) and O(52′)) are H-bonded to the OH^- ligands, with the O(52)···O(72) distance being 2.777(2) Å.

The core of **3** can be described in various ways: (i) as two $\{Mn_2^{II}Mn_2^{III}(\mu_3\text{-}O)(\mu_3\text{-}OH)\}^{7+}$ subunits (atoms Mn(1)–Mn(4) and their symmetry equivalents) becoming linked through their μ_3-O

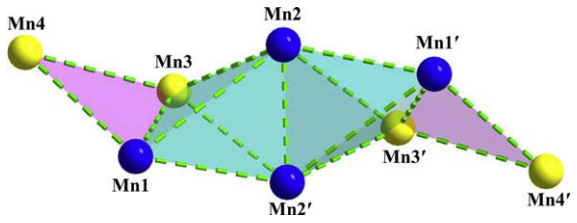

Fig. 6. The Mn_8 skeleton of **3** emphasizing the 'edge-sharing tetrahedra', 'butterfly-like' and various triangular subunits. Colour scheme: Mn^{II}, yellow; Mn^{III}, blue. (For interpretation of the references to colour in this figure legend, the reader is referred to the web version of this article.)

$^{2-}$ converting to μ_4 and thus providing the two 'inter-fragment' Mn(2)–O(71′) and Mn(2′)–O(71) bonds. The four metal ions in each subunit are nearly coplanar with the Mn(1)–Mn(2)–Mn(3)–Mn(4) torsion angle being 7.18°. The $\{Mn^{II}_2Mn^{III}_2(\mu_3\text{-}O)(\mu_3\text{-}OH)\}^{7+}$ subunit has not been seen before in a discrete Mn_4 cluster or as a recognizable sub-fragment of a higher nuclearity cluster; (ii) as a central $\{Mn^{II}_2Mn^{III}_4(\mu_4\text{-}O)\}^{12+}$ subunit (the oxidized version of the familiar $[Mn^{II}_4Mn^{III}_2(\mu_4\text{-}O)_2]^{10+}$ core [29]) with an additional Mn^{II} atom at each end linked through the μ_3-OH^- ion. The central $\{Mn^{II}_2Mn^{III}_4(\mu_4\text{-}O)_2\}^{12+}$ subunit consists of six Mn ions arranged as two edge-sharing tetrahedra, each with a central μ_4-O^{2-}. The Mn–μ_4-O^{2-}–Mn angles range from 95.3° to 142.3°, deviating significantly from the 109.5° ideal values of a tetrahedron. The central $\{Mn^{II}_2Mn^{III}_4(\mu_4\text{-}O)_2\}^{12+}$ subunit can also be considered as two $\{Mn_3O\}^{6+}$ triangular units (Mn(1,2,3) and Mn(1′,2′,3′) or, alternatively, Mn(1,2′,3) and Mn(1′,2,3′)) joined together by each of their μ_3-O^{2-} ions (O71 and O71′) becoming μ_4 by ligating to the Mn^{III} center of the adjacent unit. Note that this central $\{Mn_6O_2\}^{12+}$ subunit of **3** is similar to the recently reported Mn_6 cation $[Mn^{II}_2Mn^{III}_4O_2(OMe)_2(dapdo)_2(dapdoH)_4]^{2+}$ (dapdoH$_2$ = 2,6-diacetylpyridine dioxime) [5b]; and (iii) as a central $\{Mn^{III}_4(\mu_3\text{-}O)_2\}^{8+}$ butterfly-like [15a,30] subunit (atoms Mn(1), Mn(2), Mn(2′), Mn(1′), O(71), O(71′)) to which are attached two $\{Mn^{II,II}_2(\mu\text{-}OH)\}^{3+}$ subunits via the interfragment bonds Mn(1)–O(72), Mn(3)–O(71) and their symmetry equivalents; as a result, each OH^- group becomes μ_3, forming a bond with a 'wing-tip' Mn^{III} atom (Mn(1), Mn(1′)), and each O^{2-} group is converted to μ_4 forming a bond with one of the Mn^{II} atoms (Mn(3), Mn(3′)).

Complex **3** joins only a small family of Mn clusters of nuclearity eight, which currently comprise the metal oxidation levels Mn^{II}_8 [31], $Mn^{II}_6Mn^{III}_2$ [32], $Mn^{II}_4Mn^{III}_4$ [7,33], $Mn^{II}_2Mn^{III}_6$ [5b,15a,34], Mn^{III}_8 [35] and $Mn^{III}_2Mn^{IV}_6$ [36], and thus it becomes the fourth member of the $Mn^{II}_4Mn^{III}_4$ subfamily.

3.3. Magnetochemistry

Variable-temperature dc magnetic susceptibility data in a 0.1 T field and in the 5.0–300 K range were collected on a powdered microcrystalline sample of **3** restrained in eicosane to prevent torquing. The obtained data are plotted as χ_MT versus T in Fig. 7. The χ_MT value at 300 K is 29.34 cm^3 K mol^{-1}. This value is slightly less than that expected for a cluster comprising four Mn^{II} and four Mn^{III} non-interacting ions (29.50 cm^3 K mol^{-1} with g = 2). The χ_MT product gradually decreases with decreasing temperature to 15.12 cm^3 K mol^{-1} at 50 K before dropping to 2.99 cm^3 K mol^{-1} at

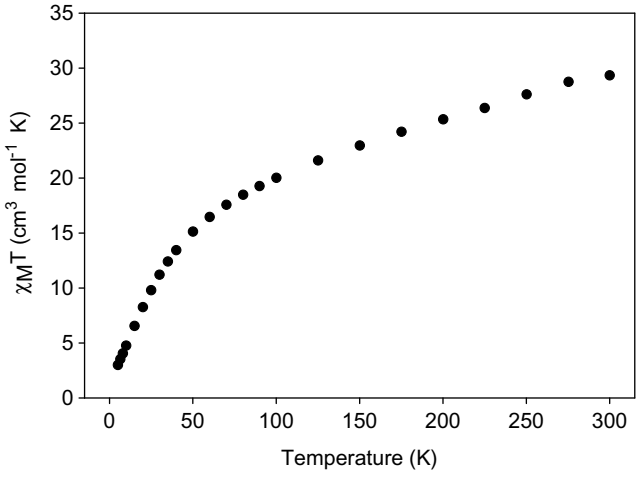

Fig. 7. Plot of χ_MT vs. T for cluster **3**.

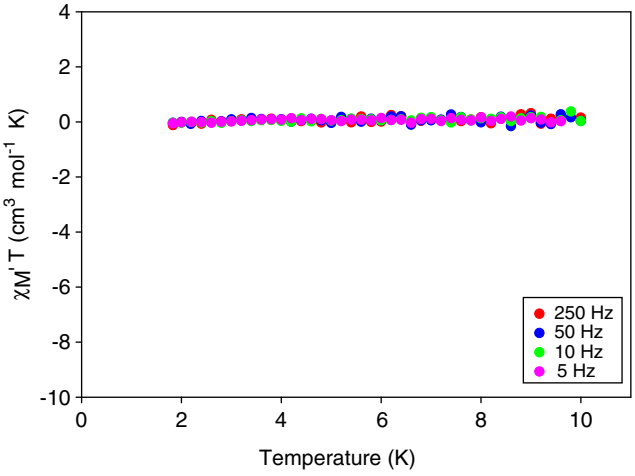

Fig. 8. Plot of the in-phase ac susceptibility signals as a χ'_MT vs. T plot for complex **3** in a 3.5 G field oscillating at the indicated frequencies.

5.0 K. The χ_MT versus T data appear to be heading for 0 cm^3 K mol^{-1} at 0 K. This behaviour is indicative of dominant antiferromagentic interactions between the metal centers with the low temperature value suggesting a small ground state spin of S = 0 or 1. To determine which one it is, and to avoid complications from an applied dc field, we employed the ac susceptibility technique [37] with a zero dc field and a 3.5 G ac field (Fig. 8). The χ'_MT signal below 10 K is zero, confirming an S = 0 ground state [29], and the essentially constant value in this temperature range indicates little population of excited states.

Similarly low or S = 0 ground states have been reported for the other $Mn^{II}_4Mn^{III}_4$ clusters in the literature [33], and we have provided elsewhere a detailed rationalization of the S = 0 ground state for the structurally similar cluster **1** [7] on the basis of the well-established magnetic behaviour of the central, butterfly-like $\{Mn^{III}_4(\mu_3\text{-}O)_2\}^{8+}$ subcore [30,38].

4. Conclusions

The present work extends the body of results that emphasize the ability of mpkoH to form interesting structural types in Mn carboxylate chemistry. In addition to the $[Mn^{III}_3O(O_2CR')_3(mpko)_3]^+$ cationic SMMs reported previously [9–11], the Mn/$PhCO_2^-$/mpkoH reaction system has provided access to the octanuclear $Mn^{II}_4Mn^{III}_4$ cluster **3** and the mononuclear Mn^{II} compound **2**. Complex **3** is a new addition to the Mn_8 family of clusters. Although this compound has been found to possess a S = 0 spin ground state, the potentially μ_3 mode of mpko$^-$ (which has not been realized in the present study) [13] would undoubtedly give Mn_x/RCO_2^-/mpko$^-$ products structurally different from **3** and which may have high-spin ground states. The bridging mode(s) of mpko$^-$ also suggests possibilities for other Mn_x non-carboxylate clusters to exist, e.g. clusters containing the strongly coordinating inorganic anions N_3^-, NCO^- and SO_4^{2-}.

As far as the specific goals of this work mentioned in the Introduction are concerned, it has been demonstrated that the attainment and stability of clusters containing the $[Mn^{II}_4Mn^{III}_4(\mu_4\text{-}O)_2(\mu_3\text{-}OH)_2]^{14+}$ core are not limited to the use of ppko$^-$ (Fig. 1), nor are they in some way a consequence of any specific property of this ligand, other than its chelating/bridging nature. The employment of mpko$^-$ leads to a product with the same formulation, superimposable cores and almost identical magnetic behaviour. In many ways, this was surprising given how often similarly small changes to a reaction, such as changing the carboxylate or solvent, can lead to a completely different product. There are examples in nickel chemistry

where mpkoH and ppkoH give different products in otherwise similar reactions [24,39]. The presence or absence of counteranions such as ClO_4^- does make a difference, however; its absence from the present reactions precludes formation of the trinuclear $[Mn_3O]^{7+}$-containing, mixed $R'CO_2^-/mpko^-$ complexes, another thermodynamically favorable arrangement and potential product of $Mn/R'CO_2^-/mpko^-$ components.

Acknowledgements

This work was supported by EPEAEK II (Program PYTHAGORAS I, Grant b.365.037 to S.P.P) and NSF (CHE-0414555 to G.C.).

Appendix A. Supplementary data

CCDC 693825 and 693826 contain supplementary crystallographic data for **2** and **3** · $1.8CH_2Cl_2$ · $1.8Et_2O$. These data can be obtained free of charge via http://www.ccdc.cam.ac.uk/conts/retrieving.html, or from the Cambridge Crystallographic Data Centre, 12 Union Road, Cambridge CB2 1EZ, UK; fax: (+44) 1223-336-033; or e-mail: deposit@ccdc.cam.ac.uk. Supplementary data associated with this article can be found, in the online version, at doi:10.1016/j.poly.2008.09.010.

References

[1] (a) K.N. Ferreira, T.M. Iverson, K. Maghlaoui, J. Barber, S. Iwata, Science 303 (2004) 1831;
(b) A recent comprehensive review:J. Barber, J.W. Murray, Coord. Chem. Rev. 252 (2008) 416.
[2] (a) A recent review: C.S. Mullins, V.L. Pecoraro, Coord. Chem. Rev. 252 (2008) 416;
(b) A. Mishra, W. Wernsdorfer, K.A. Abboud, G. Christou, Chem. Commun. (2005) 54;
(c) I.J. Hewitt, J.K. Tang, N.T. Maddhu, R. Clérac, G. Buth, C.F. Anson, A.K. Powell, Chem. Commun. (2006) 2650.
[3] (a) For reviews see: G. Christou, D. Gatteschi, D.N. Hendrickson, R. Sessoli, MR Bull. 25 (2000) 66;
(b) D. Gatteschi, R. Sessoli, Angew. Chem., Int. Ed. 42 (2003) 268;
(c) R. Birchner, G. Chaboussant, C. Dobe, H. Güdel, S.T. Ochsenbein, A. Sieber, O. Waldman, Adv. Funct. Mater. 16 (2006) 209;
(d) G. Aromi, E.K. Brechin, Struct. Bond. 122 (2006) 1.
[4] (a) Th.C. Stamatatos, G. Christou, Philos. Trans. Roy. Soc. (A) 366 (2008) 113;
(b) C.J. Milios, A. Vinslava, W. Wernsdorfer, S. Moggach, S. Parsons, S.P. Perlepes, G. Christou, E.K. Brechin, J. Am. Chem. Soc. 129 (2007) 2754.
[5] (a) G. Christou, Polyhedron 24 (2005) 2065;
(b) Th.C. Stamatatos, B.S. Luisi, B. Moulton, G. Christou, Inorg. Chem. 47 (2008) 1134. and references cited therein.
[6] C.J. Milios, E. Keffalloniti, C.P. Raptopoulou, A. Terzis, A. Escuer, R. Vicente, S.P. Perlepes, Polyhedron 23 (2004) 83.
[7] C.J. Milios, Th.C. Stamatatos, P. Kyritsis, A. Terzis, C.P. Raptopoulou, R. Vicente, A. Escuer, S.P. Perlepes, Eur. J. Inorg. Chem. (2004) 2885.
[8] C.J. Milios, P. Kyritsis, C.P. Raptopoulou, A. Terzis, R. Vicente, A. Escuer, S.P. Perlepes, Dalton Trans. (2005) 501.
[9] Th.C. Stamatatos, D. Foguet-Albiol, C.C. Stoumpos, C.P. Raptopoulou, A. Terzis, W. Wernsdorfer, S.P. Perlepes, G. Christou, Polyhedron 26 (2007) 2165.
[10] S.-C. Lee, Th.C. Stamatatos, D. Foguet-Albiol, S. Hill, S.P. Perlepes, G. Christou, Polyhedron 26 (2007) 2255.
[11] Th.C. Stamatatos, D. Foguet-Albiol, S.-C. Lee, C.C. Stoumpos, C.P. Raptopoulou, A. Terzis, W. Wernsdorfer, S.O. Hill, S.P. Perlepes, G. Christou, J. Am. Chem. Soc. 129 (2007) 9484.
[12] (a) For reviews see: V.Yu. Kukushkin, A.J.L. Pombeiro, Coord. Chem. Rev. 181 (1999) 147;
(b) A.G. Smith, P.A. Tasker, D.J. White, Coord. Chem. Rev. 241 (2003) 61;
(c) P. Chaudhuri, Coord. Chem. Rev. 243 (2003) 143.
[13] C.J. Milios, Th.C. Stamatatos, S.P. Perlepes, Polyhedron 25 (2006) 134 (Polyhedron Report).
[14] H. Miyasaka, R. Clérac, K. Mizushima, K. Sugiura, M. Yamashita, W. Wernsdorfer, C. Coulon, Inorg. Chem. 42 (2003) 8203.
[15] (a) M.W. Wemple, H.-L. Tsai, S. Wang, J.P. Claude, W.E. Streib, J.C. Huffman, D.N. Hendrickson, G. Christou, Inorg. Chem. 35 (1996) 6437;
(b) J.B. Vincent, K. Folting, J.C. Huffman, G. Christou, Inorg. Chem. 25 (1986) 996.
[16] J.B. Vincent, H.-R. Chang, K. Folting, J.C. Huffman, G. Christou, D.N. Hendrickson, J. Am. Chem. Soc. 109 (1987) 5703.
[17] (a) G.M. Sheldrick, SHELXS-97, Program for Crystal Structure Solution, University of Göttingén, Germany, 1997;
(b) G.M. Sheldrick, SHELXS-97, Program for the Refinement of Crystal Structures from Diffraction Data, University of Göttingén, Germany, 1997;
(c) Rigaku/MSC, CRYSTALCLEAR, The Woodlands, Texas, USA, 2008.
[18] (a) H.-L. Tsai, S. Wang, K. Folting, W.E. Streib, D.N. Hendrickson, G. Christou, J. Am. Chem. Soc. 117 (1995) 2503;
(b) R.C. Squire, S.M.J. Aubin, K. Folting, W.E. Streib, G. Christou, D.N. Hendrickson, Inorg. Chem. 34 (1995) 6463.
[19] N.C. Harden, M.A. Bolcar, W. Wernsdorfer, K.A. Abboud, W.E. Streib, G. Christou, Inorg. Chem. 42 (2003) 7067.
[20] M.A. Halcrow, W.E. Streib, K. Folting, G. Christou, Acta crystallogr. C 51 (1995) 1263.
[21] K.W. Nordquest, D.W. Phelps, W.F. Little, D.J. Hodgson, J. Am. Chem. Soc. 98 (1976) 1104.
[22] I. Chadjistamatis, A. Terzis, C.P. Raptopoulou, S.P. Perlepes, Inorg. Chem. Commun. 6 (2003) 1365.
[23] R.D. Cannon, R.P. White, Prog. Inorg. Chem. 36 (1988) 195.
[24] C. Papatriantafyllopoulou, C.G. Efthymiou, C.P. Raptopoulou, A. Terzis, E. Manessi-Zoupa, S.P. Perlepes, Spectrochim. Acta, Part A 70 (2008) 718.
[25] G.B. Deacon, R.J. Phillips, Coord. Chem. Rev. 33 (1980) 227.
[26] (a) I.D. Brown, D. Altermatt, Acta Crystallogr., Sect. B 41 (1985) 244;
(b) W. Liu, H.H. Thorp, Inorg. Chem. 32 (1993) 4102.
[27] H.J. Eppley, S.M.J. Aubin, W.E. Streib, J.C. Bollinger, D.N. Hendrickson, G. Christou, Inorg. Chem. 36 (1997) 109.
[28] A.G. Blackman, J.C. Huffman, E.B. Lobkovsky, G. Christou, Polyhedron 11 (1992) 251.
[29] Th.C. Stamatatos, D. Foguet-Albiol, S.P. Perlepes, C.P. Raptopoulou, A. Terzis, C.S. Patrickios, G. Christou, A.J. Tasiopoulos, Polyhedron 25 (2006) 1737. and references cited therein.
[30] J.B. Vincent, C. Christmas, H.-R. Chang, Q. Li, P.D.W. Boyd, J.C. Huffman, D.N. Hendrickson, G. Christou, J. Am. Chem. Soc. 111 (1989) 2086.
[31] (a) For example see: R.W. Saalfrank, N. Löw, B. Demleitner, D. Stalke, M. Teichert, Chem. Eur. J. 4 (1998) 1305;
(b) R.W. Saalfrank, N. Löw, S. Trummer, G.M. Sheldrick, M. Teichert, D. Stalke, Eur. J. Inorg. Chem. (1998) 559.
[32] (a) Th.C. Stamatatos, K.A. Abboud, G. Christou, J. Mol. Struct., in press. Available from:<http://dx.doi.org/10.1016/j.molstruc.2008.04.031>;
(b) C. Boskovic, W. Wernsdorfer, K. Folting, J.C. Huffman, D.N. Hendrickson, G. Christou, Inorg. Chem. 41 (2002) 5107;
(c) C. Boskovic, J.C. Huffman, G. Christou, Chem. Commun. (2002) 2502.
[33] (a) C.J. Milios, F.P.A. Fabbiani, S. Parsons, M. Murugesu, G. Christou, E.K. Brechin, Dalton Trans. (2006) 351;
(b) M. Murugesu, W. Wernsdorfer, K.A. Abboud, G. Christou, Angew. Chem., Int. Ed. 44 (2005) 892;
(c) M. Manoli, C.J. Milios, A. Mishra, G. Christou, E.K. Brechin, Polyhedron 26 (2007) 1923.
[34] (a) R. Bagai, K.A. Abboud, G. Christou, Inorg. Chem. 47 (2008) 621;
(b) E.K. Brechin, G. Christou, M. Soler, M. Helliwell, S.J. Teat, Dalton Trans. (2003) 513;
(c) C.J. Milios, R. Inglis, A. Vinslava, A. Prescimone, S. Parsons, S.P. Perlepes, G. Christou, E.K. Brechin, Chem. Commun. (2007) 2738.
[35] (a) For example see: S. Tanase, G. Aromi, E. Bouwman, H. Kooijman, A.L. Spek, J. Reedijk, Chem. Commun. (2003) 3147;
(b) E.K. Brechin, M. Soler, G. Christou, M. Helliwell, S.J. Teat, W. Wernsdorfer, Chem. Commun. (2003) 1276;
(c) V.A. Grillo, M.J. Knapp, J.C. Bollinger, D.N. Hendrickson, G. Christou, Angew. Chem., Int. Ed. 35 (1996) 1818;
(d) H.-L. Tsai, W. Wang, K. Folting, W.E. Streib, D.N. Hendrickson, G. Christou, J. Am. Chem. Soc. 117 (1995) 2503;
(e) S. Wang, H.-L. Tsai, K. Folting, J.D. Martin, D.N. Hendrickson, G. Christou, J. Chem. Soc., Chem. Commun. (1997) 671;
(f) E. Libby, K. Folting, C.J. Huffman, G. Christou, Inorg. Chem. 32 (1993) 2549;
(g) L.F. Jones, E.K. Brechin, D. Collison, J. Raftery, S.J. Teat, Inorg. Chem. 42 (2003) 6971.
[36] A.J. Tasiopoulos, K.A. Abboud, G. Christou, Chem. Commun. (2003) 580.
[37] E.C. Sañudo, V.A. Grillo, M.J. Knapp, J.C. Bollinger, J.C. Huffman, D.N. Hendrickson, G. Christou, Inorg. Chem. 41 (2002) 2441. and references cited therein.
[38] (a) E. Libby, J.K. McCusker, E.A. Schmitt, K. Folting, D.N. Hendrickson, G. Christou, Inorg. Chem. 30 (1991) 3486;
(b) S. Wang, K. Folting, W.E. Streib, E.A. Schmitt, J.K. McCusker, D.N. Hendrickson, G. Christou, Angew. Chem., Int. Ed. 30 (1991) 305;
(c) G. Aromi, S. Bhaduri, P. Artus, J.C. Huffman, D.N. Hendrickson, G. Christou, Polyhedron 21 (2002) 1799;
(d) C. Cañada-Vilalta, J.C. Huffman, G. Christou, Polyhedron 20 (2001) 1785.
[39] C. Papatriantafyllopoulou, C.P. Raptopoulou, A. Terzis, J.F. Janssens, S.P. Perlepes, E. Manessi-Zoupa, Z. Naturforsch. 62b (2007) 1123.

CCD diffractometer using graphite monochromated Mo Kα (λ = 0.7107 Å) radiation and the intensities were measured using the ω scan method. Preliminary lattice parameters and orientation matrices were obtained from four sets of frames. Unit cell dimensions were determined from the setting angles of 6903 reflections in the range 2.17° < θ < 25.79°. Integration and scaling of intensity data was accomplished using the SAINT program [20]. The structure was solved by direct methods using SHELXS97 [21] and refinement was carried out by full-matrix least-squares techniques using SHELXL97 [21]. Anisotropic displacement parameters were included for all non-hydrogen atoms. The side chain atoms were disordered and refined with site-occupation factors of 0.563(7) and 0.437(7). The geometries of the disordered atoms were refined with distance restraints. The displacement parameters of the disordered atoms were restrained with SIMU and DELU commands.

2.4. Synthesis and analyses

N,N′-Di-4-(4′-pentyloxybenzoate)salicylidene diaminoethane, **3** (Scheme 1), was synthesized from the precursor materials **1** and **2**, as reported earlier [15,16]. The [ML^5] (M = Mn, Co, Ni, Cu and Zn) complexes were prepared by refluxing solutions of the Schiff-base H_2L^5 and the corresponding metal acetate in a 1:1 molar ratio in dichloromethane/ethanol medium for ~2 h at 80 °C. The reaction mixture was left overnight in the flask, closed with a guard tube. The solid complex that separated out in each case was filtered under suction and washed repeatedly with cold ethanol and dried over fused $CaCl_2$ in a desiccator.

2.4.1. Synthesis of *N,N′*-di-4-(4′-pentyloxybenzoate)salicylidene diaminoethane, H_2L^5

N,N′-Di-4-(4′-pentyloxybenzoate)salicylidene diaminoethane, H_2L^5, was prepared by mixing together absolute ethanolic solutions of 4-pentyloxy-(4′-formyl-3′-hydroxy)benzoate (16.42 g, 50 mmol, in 100 mL) and 1,2-diaminoethane (1.9 mL, 25 mmol in 10 mL) and magnetically stirring for ~1 h in the presence of a few drops of acetic acid and leaving the resultant solution overnight in the reaction flask at room temperature. The micro-crystalline product was suction-filtered, thoroughly washed with cold ethanol, recrystallized from a solution of absolute ethanol/chloroform (v/v, 1/1) and dried at room temperature; yield: 12.76 g (75%) as a yellow solid; mp 230 °C. Calc. for $C_{40}H_{44}N_2O_8$ (680.31): C, 70.57; H, 6.51; N, 4.11. Found: C, 70.53; H, 6.53; N, 4.13%.

2.4.2. Synthesis of the Mn^{II} complex

Yield: 0.50 g (68%) as a brown coloured solid; mp 200 °C (decomposes). Calc. for $C_{40}H_{42}MnN_2O_8$ (733.71): C, 65.48; H, 5.77; N, 3.82; Mn, 7.49. Found: C, 65.50; H, 5.74; N, 3.80; Mn, 7.52%.

2.4.3. Co^{II} complex

Yield: 0.52 g (70%) as an olive green solid; mp 210 °C (decomposes). Calc. for $C_{40}H_{42}CoN_2O_8$ (737.70): C, 65.12; H, 5.74; N, 3.80; Co, 7.99. Found: C, 65.15; H, 5.72; N, 3.81; Co, 8.01%.

2.4.4. Ni^{II} complex

Yield: 0.58 g (79%) as a dark orange solid; mp 255 °C. Calc. for $C_{40}H_{42}N_2O_8Ni$ (737.46): C, 65.15; H, 5.74; N, 3.80; Ni, 7.96. Found: C, 65.27; H, 5.80; N, 3.85; Ni, 8.01%.

2.4.5. Cu^{II} complex

Yield 0.52 g (70%) as a violet solid; mp 260 °C. Calc. for $C_{40}H_{42}N_2O_8Cu$ (742.32): C, 64.72; H, 5.70; N, 3.77; Cu, 8.56. Found: C, 64.77; H, 5.72; N, 3.80; Cu, 8.53%.

2.4.6. Zn^{II} complex

Yield 0.48 g (65%) as a white solid; mp 140 °C. Calc. for $C_{40}H_{42}N_2O_8Zn$ (744.16): C, 64.56; H, 5.69; N, 3.76; Zn, 8.79. Found: C, 64.57; H, 5.71; N, 3.77; Zn, 8.78%.

3. Results and discussion

3.1. Physical properties and spectral investigation

The Schiff-base ligand H_2L^5 as well as the metal complexes are soluble in chloroform, dichloromethane, DMF and DMSO, but are

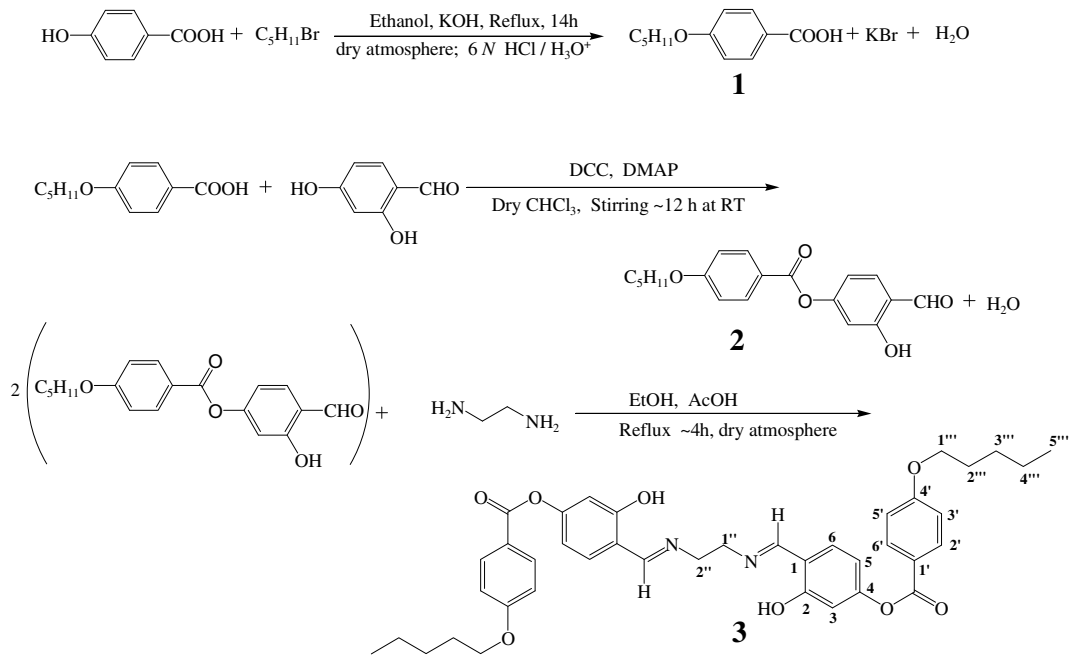

Scheme 1. Synthetic steps involved in the synthesis of **1** (*p*-pentyloxybenzoic acid), **2** (4-pentyloxy-(4′-formyl-3′-hydroxy)benzoate) and **3** (*N,N′*-di-4-(4′-pentyloxy benzoate)salicylidene diaminoethane, H_2L^5.

insoluble in water, methanol, ethanol and acetonitrile. The structure and purity of the parent ligand and the complexes were checked and confirmed by elemental analyses, IR, ^{1}H and ^{13}C NMR and FAB mass spectra. The mass spectral features of H_2L^5 were characterized by the base peak (m/e = 191 corresponding to the fragment $C_5H_{11}O$–Ph–CO^+), and the molecular ion peak (m/e = 681) with ~72% intensity, and those of ML^5 (M = Mn^{II}, Co^{II}, Ni^{II} and Cu^{II}) by the base peak (m/e = 121 corresponding to the fragment, HO–Ph–CO^+) and the molecular ion peak (m/e = 734, 737, 737 and 742, respectively) with ~92–98% intensity. Further, additional peaks (corresponding to the formation of dimeric units) were observed in the FAB mass spectra of the Mn^{II}, Co^{II} and Ni^{II} complexes; based on the decomposition behaviour of the former two complexes, they may be presumed to be polymeric, which upon bond rupture under the experimental conditions might give rise to dimeric units. A comparison of the ^{1}H and ^{13}C{^{1}H} NMR spectral data of the ligand with those of the diamagnetic Ni^{II} and Zn^{II} complexes shows the absence of the phenolic-OH signal (13.537 ppm) and a significant shift (8.358 to 7.195 and 8.458 ppm, respectively) in the peak position for –N=C*H* in the spectra of the metal complexes, which implies bonding through the phenolate anion and azomethine nitrogen atom [22] of the ligand. Similar shifts observed in the ^{13}C{^{1}H} NMR spectra were of considerable magnitude in the case of the carbon atoms directly attached to the bonding atoms. Thus, the NMR spectral data imply a tetra-dentate bonding of $(L^5)^{2-}$ through the two >C=N groups and two phenolate oxygen atoms. In the IR spectrum of H_2L^5 the broad absorptions centred at 3443 cm^{-1} may be assigned to the ν(O–H)$_{phenolic}$ vibration, and further the strong bands occurring at 1740 and 1255 cm^{-1} may be assigned [23] to ν(>C=O) and ν(C–O) modes of the aromatic ester; the band occurring at 1628 cm^{-1} may be due to the ν(C=N) absorption of the azomethine moiety. These bands are shifted to lower frequencies in the complexes, indicating that the nitrogen atom of the azomethine group is coordinated to the metal ion [24]. Coordination through one of the nitrogen atoms of the ligand is also implied by the appearance of a new band (468–472 cm^{-1}) in the complexes, assignable to ν(M–N) [25,26]. Coordination through the phenolate oxygen to the metal ion is implied by the shifts of the ν(C–O) band in the complexes [27] and by the appearance of new bands, assignable to ν(M–O), in the 440–448 cm^{-1} region in the spectra of the complexes.

Table 2
Crystal structure data and structure refinement parameters

Details	Ligand, H_2L^5 [*jpl5*]	$[NiL^5]_2$ [*jpni1*]	$[CuL^5]$ [*ac27*]
Formula	$C_{40}H_{44}N_2O_8$	$C_{40}H_{42}N_2O_9Ni$	$C_{40}H_{43}N_2O_9Cu$
FW	680.77	737.47	759.30
Crystal system	Orthorhombic	Monoclinic	Monoclinic
Space group	$Pna2_1$	$P2_1/c$	$P2_1/c$
a (Å)	20.573(4)	17.8641(19)	17.7902(12)
b (Å)	5.868(1)	18.6864(19)	18.7711(13)
c (Å)	29.867(7)	11.4267(12)	11.4585(8)
β (°)	90	104.004(2)	104.355(1)
V (Å^3)	3605.8(13)	3701.0(7)	3707.0(4)
Z	4	4	4
ρ_{calc} (g/cm^3)	1.254	1.324	1.361
μ(Mo Kα) (mm^{-1})	0.087	0.579	0.647
R [$I > 2\sigma(I)$]	0.0637	0.0588	0.0449
R_w	0.1468	0.0924	0.0547
Goodness-of-fit	1.027	1.053	1.061
F(000)	1448	1552	1592
2θ Range (°)	1.98–25.00	1.17–25.00	1.18–25.00
Range of h, k, l	−24, 23	−21, 21	−21, 21
	−6, 6	−21, 22	−22, 22
	−35, 35	−13, 13	−13, 13
Total number of reflections	24264	26479	35252
Unique reflections	3228	6517	6537
Number of parameters	461	524	524
$wR2$_all	0.1680	0.1673	0.1419
$wR2$_obs	0.1296	0.1472	0.1299
$\Delta\rho_{max}$, $\Delta\rho_{min}$ (e Å^{-3})	0.296, −0.248	0.604, −0.485	0.723, −0.466

The room temperature magnetic moments and electronic spectral data of the present complexes are included in Table 1 while the spectra of the complexes of Co^{II}, Ni^{II} and Cu^{II} are shown in Fig. 1. The overall geometry assigned to the metal ion is based not only on the μ_{eff} values and the nature of the electronic spectra, but also

Table 1
Magnetic and electronic spectral data[a] of the complexes of H_2L5

Complex	Colour	μ_{eff} (B.M)	d–d transitions (nm)	Transition		Assignment
				Ground state(s)	Excited state(s)	
$[MnL^5]_n$	Brown	5.85	317, 260	$^6A_{1g}$	$^4A_{2g}$(F); ^4E_g(D)	Octahedral with M–M bonding
$[CoL^5]_n$	Olive green	3.52	974, 895, 860	^2E_g	$^2A_1$	Octahedral with M–M bonding (l.s.)
$[NiL^5]_2$	Dark orange	Diamag	530, 406	$^1A_1$	^1E; $^1A_2$	Square-pyramidal (M–M bonding[b] of 3.337 Å)
$[CuL^5]$	Violet	2.74	562	*xz*, *yz*	x^2–y^2	Sq. planar (M–M distance[b] of 3.457 Å)

[a] Spectra recorded in chloroform solutions.
[b] Vide single crystal structure data.

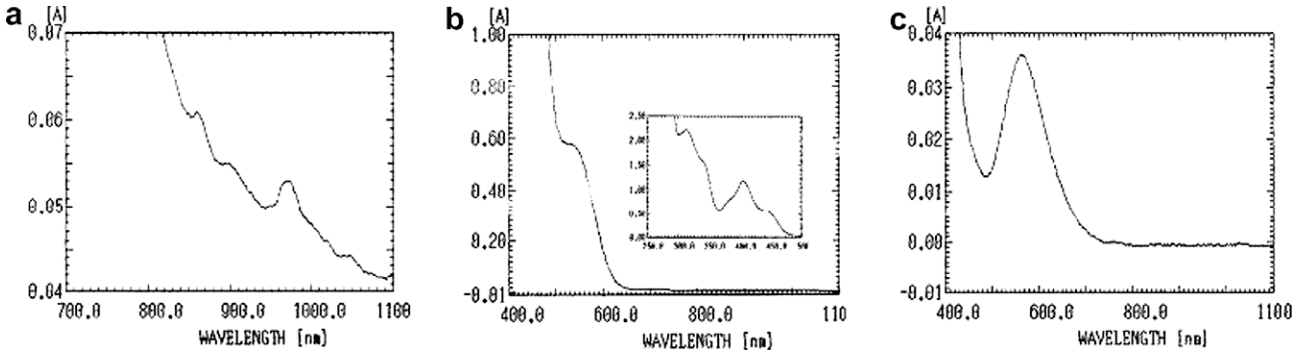

Fig. 1. Absorption spectra of: (**a**) $[CoL^5]$, (**b**) $[NiL^5]_2$ and (**c**) $[CuL^5]$.

on the denticity of the ligand (*vide* IR and NMR) and the number of such ligands coordinated to the metal ion (vide elemental analyses). Although the μ_{eff} values imply ferromagnetic type interactions in the Mn^{II}, Co^{II} and Cu^{II} complexes, no concrete conclusion to this effect could be drawn in the absence of variable temperature magnetic moment data. The $[MnL^5]_n$ complex gives rise to extremely weak bands in the electronic spectrum, presumably with an octahedral environment (square-planar units polymerically

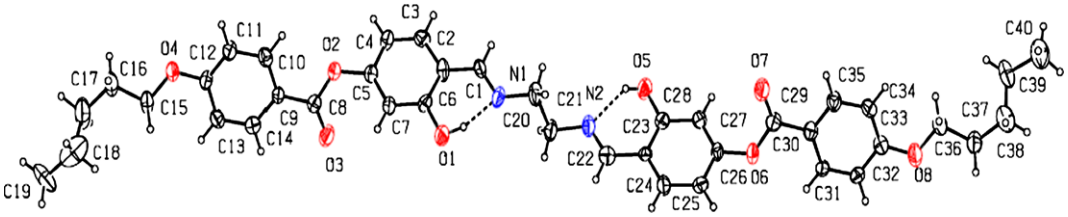

Fig. 2. The asymmetric unit of H_2L^5, with the atom numbering scheme. Displacement ellipsoids are drawn at the 30% probability level. H atoms are shown as small spheres of arbitrary radii. Hydrogen bonds are shown as dashed lines.

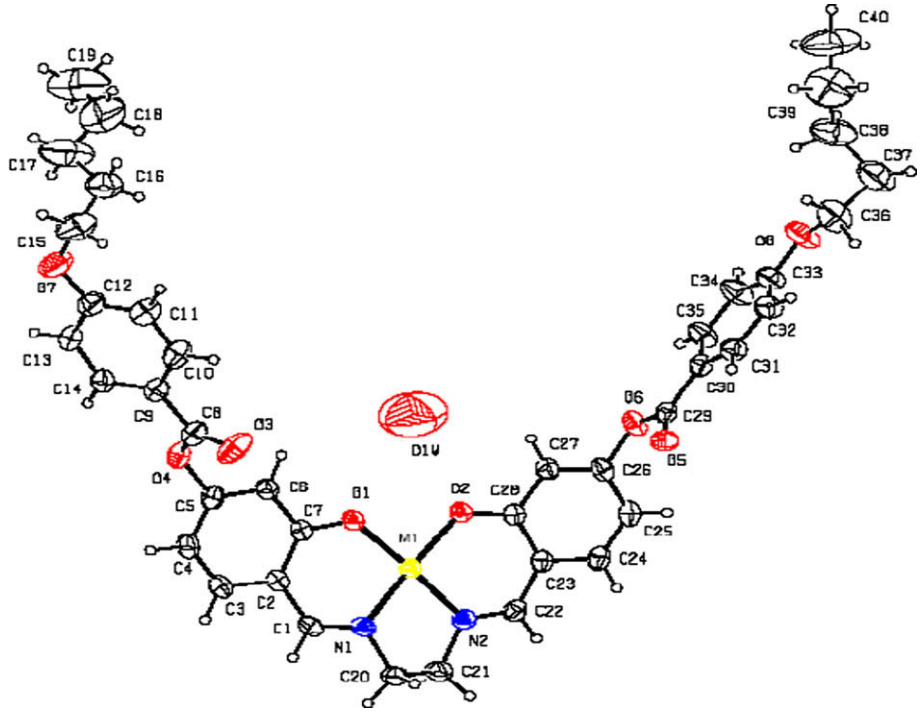

Fig. 3. The asymmetric unit of the isomorphous complexes $[ML^5]$ [M = Ni or Cu] with the atom numbering scheme. Displacement ellipsoids are drawn at the 30% probability level. The disordered atoms of the minor component (C161 and C361/C371/C381/C391/C401) have been omitted for clarity.

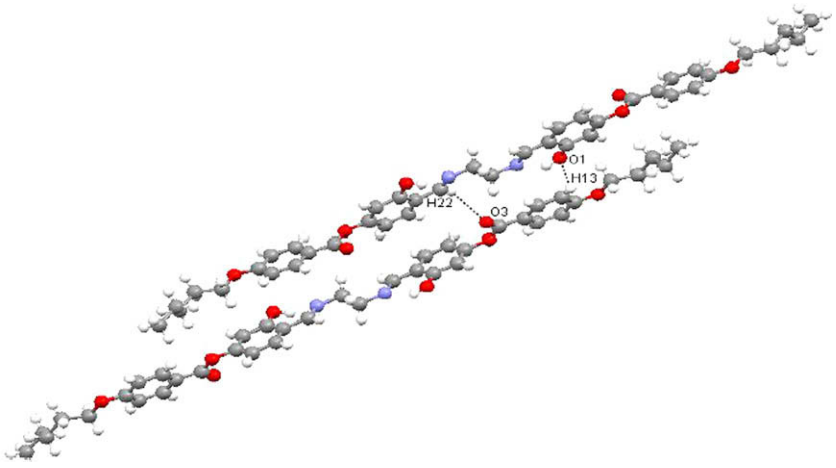

Fig. 4. A view of H_2L^5 molecules in the crystal lattice showing [C–H···O] intermolecular interactions along the *b* axis.

connected with M–M bonding) for the metal ion. The spectrum of the $[CoL^5]_n$ complex shows bands at 860, 895 and 974 nm which may be assigned to the transition(s) from the ^2E_g ground state to the $^2A_1$ excited state in an octahedral (low-spin) environment around the metal ion [28]. The electronic spectrum of the $[NiL^5]_2$ complex shows two absorptions at 406 and 530 nm which may be assigned to the ^1E and $^1A_2$ excited states from the $^1A_1$ ground state in a low-spin square-pyramidal environment of the diamagnetic metal ion [28]. The spectrum of $[CuL^5]$ shows a single band at 562 nm, assignable to the transition from the *xz, yz* ground state to the x^2–y^2 excited state in a square-planar environment [28].

3.2. Crystal structure and molecular association

The crystal data and structure refinement details for H_2L^5, $[NiL^5]_2$ and $[CuL^5]$ are given in Table 2. The molecular structure and atomic labelling scheme of the ligand and its nickel and copper complexes are as shown in Figs. 2 and 3, respectively, while their packing diagrams are shown in Figs. 5, 6 and 8.

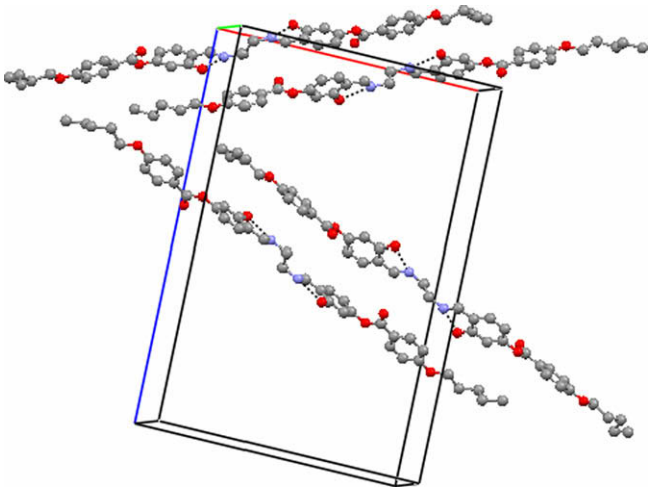

Fig. 5. Packing diagram of H_2L^5 showing intra molecular interactions along the *c* axis.

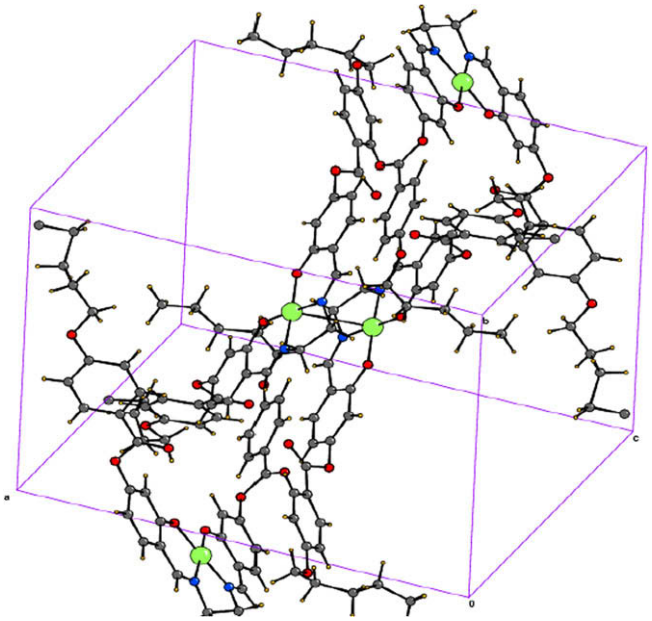

Fig. 6. Packing of molecules in the unit cell of $[NiL^5]_2$.

The Schiff-base crystallizes in the non-centrosymmetric space group $Pna2_1$ with $Z = 4$. The conformation of the ligand (Fig. 2) presents several interesting features: the molecule prefers to be as an extended linear conformation with all *trans* central linkages; the angle between the two six-membered rings adjacent to the central linkage is 0.39° (nearly planar); however, the angle between the adjacent rings in each flank is 52.50° (avg.); the extended arms of the aliphatic chains show large thermal vibrations compared to the central atoms, typical of any such molecule. Table 3 provides the details of the short intramolecular contacts while Fig. 4 represents a section of the intermolecular space, highlighting the C–H···O–H bond regions.

Both the isomorphic nickel and copper complexes $[NiL^5]_2$ and $[CuL^5]$ crystallize in the centrosymmetric space group $P2_1/c$ with

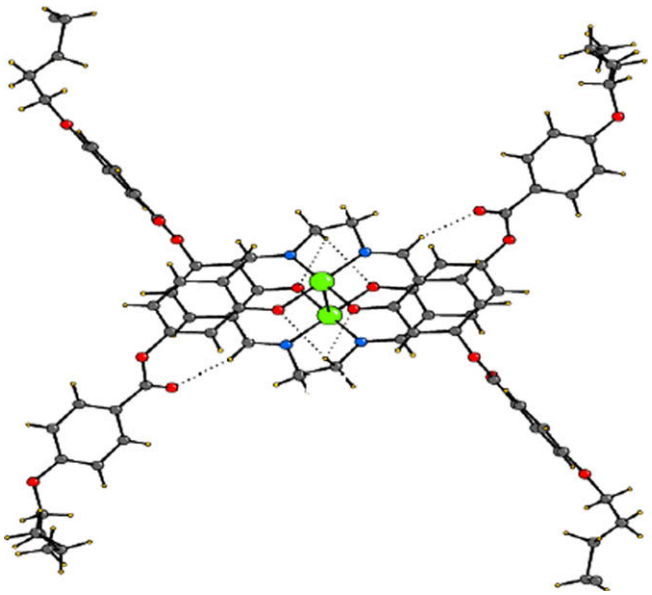

Fig. 7. A view of the $[NiL^5]_2$ molecule in the crystal lattice showing [C–H···O] inter molecular interactions.

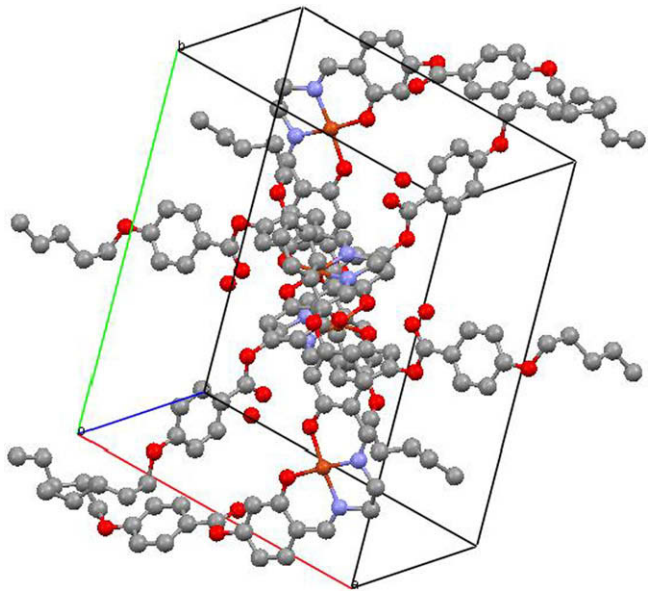

Fig. 8. Packing of molecules in the unit cell of $[CuL^5]$ along the *b* axis.

Table 3
Intramolecular hydrogen bonding data of H_2L^5

D–H···A	D–H (Å)	H···A (Å)	D···A (Å)	D–H···A (°)	Symmetry
O1–H1O...N1	0.87(7)	1.81(7)	2.582(10)	147(7)	*x,y,z*
O5–H5O...N2	0.86(9)	1.88(10)	2.576(10)	137(9)	*x,y,z*

Table 4
Selected bond lengths (Å) and bond angles (°) of the isomorphous $[NiL^5]_2$ and $[CuL^5]$[a] complexes

M1–O1	1.850(3) [1.8988(18)]	M1–N1	1.860(3) [1.933(2)]
M1–O2	1.848(3) [1.8956(17)]	M1–N2	1.846(4) [1.939(2)]
O1–M1–O2	84.9(1) [88.95(8)]	O1–M1–N2	178.0(2) [175.17(9)]
O1–M1–N1	94.6(2) [93.23(8)]	O2–M1–N2	94.7(1) [93.73(8)]
O2–M1–N1	177.2(2) [175.19(9)]	N2–M1–N1	85.9(2) [84.40(9)]

[a] The data for [CuL5] are given in square brackets.

Table 5
Transition temperatures and enthalpy changes of H_2L^5 and of the $[NiL^5]_2$ and $[CuL^5]$ complexes

Compound	Transition[a]	T[b] (°C)	δH[b] (kJ mol^{-1})
H_2L^5	Cr–N	174.81	35.06
	N–I	229.30	10.81
	I–N	216.04	1.69
$[NiL^5]_2$	Cr–Cr	144.72	8.79
	Cr–N	245.09	19.52
	N–I[c] (dec.)	255.00	
$[CuL^5]$	Cr–Cr	136.21	10.07
	Cr–N	224.94	20.25
	N–I[c]	260.50	
	N–Cr	199.84	5.39

[a] Cr: Crystal, N: Nematic, I: Isotropic liquid.
[b] Data as obtained from the first DSC cycle.

$Z = 4$ and the ORTEP diagram is shown in Fig. 3. It appears that the ligand takes up an entirely different conformation, effectively generating a "V" shaped molecular unit. The coordination around Ni^{II} is believed to be a distorted square-pyramidal environment, generating a tricyclic moiety, while that around Cu^{II} is considered to be square-planar with a *cis*-conformation, which may be invoked on the basis of the four adjacent bond angles around the metal ion which are close to 90° (84.40(9), 88.95(8), 93.23(8), 93.73(8)) and the angles between the diagonal atoms of the square plane are close to 180° (175.19(9), 175.17(9)).

Table 4 describes the conformational features of the isomorphous Ni^{II} and Cu^{II} complexes. The angle between the two six-membered rings nearest to Ni is 2.92° while such an angle on the outside flanks is 73.81°. As expected, the thermal ellipsoids are once again large on the terminal chain atoms on either side. It is noteworthy that the conformations of the two flanks are different from each other, with one of the flanks displaying an intramolecular C–H···O interaction (C10–H10···O3). Also, the angle between the adjacent six-membered rings in one flank is 88.04° while in the other it is 56.82°. The angle between the planes containing the C24, O2, Ni1 and N2 atoms and C5, O1, Ni1 and N1 atoms is 2.74°. The Ni atom is penta-coordinated with a Ni–Ni metal bond of 3.336 Å; the distortion of the square base from planarity is quite negligible since the angles between the diagonal atoms of the square base are close to 180° (N2NiO1: 177.83 and N1NiO2: 177.17) in both the planes of the dimeric unit. Fig. 7 shows the packing features of $[NiL^5]_2$ along with the intermolecular interactions.

The mesogenic nature of the ligand (H_2L^5) as well as the $[NiL^5]_2$ and $[CuL^5]$ complexes has been studied by two methods, using polarized optical microscopy and differential scanning calorimetry (DSC); the introduction of the metal ion into the metal-coordination sphere, as expected, resulted in the elevation of the transition temperature, melting and clearing points. The assignment of the mesophase (*nematic*) in each case is on the basis of the optical textures (Fig. 9a–c) and the DSC thermograms (Fig. 10a–c). The details of the transition temperatures, enthalpy changes and the mesophases of H_2L^5, $[NiL^5]$ and $[CuL^5]$ are given in Table 5. However, no such mesogenic property was observed with the complexes of Mn^{II}, Co^{II} and Zn^{II}.

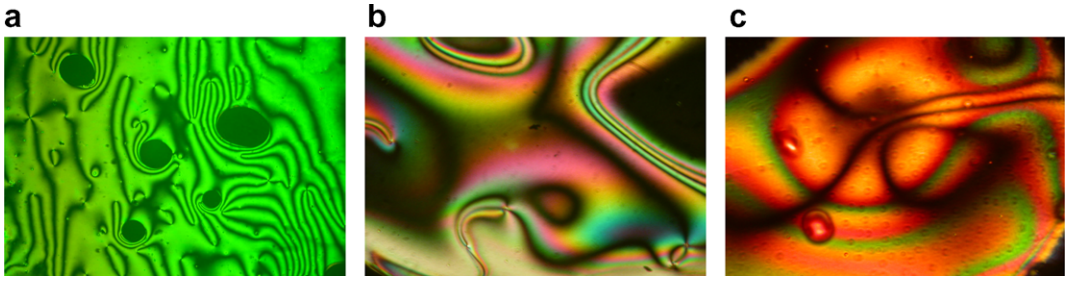

Fig. 9. Optical textures of: (a) H_2L^5 at 210 °C (b) $[NiL^5]_2$ at 252 °C and (c) $[CuL^5]$ at 245 °C.

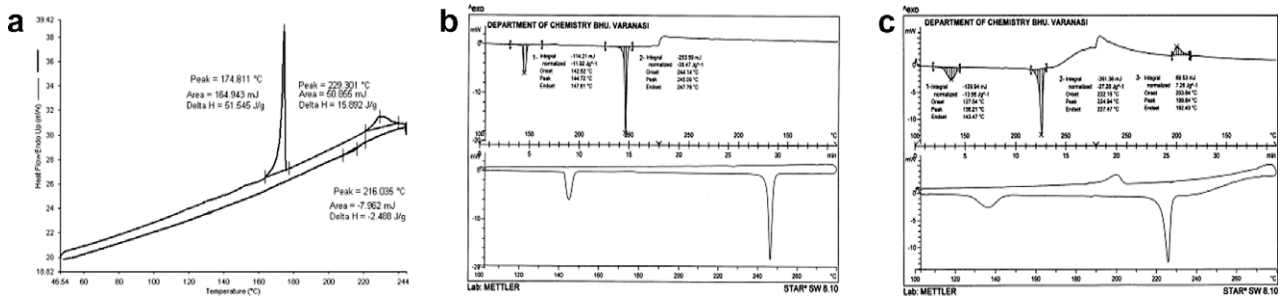

Fig. 10. DSC thermograms of: (**a**) H_2L^5 (**b**) $[NiL^5]_2$ and (**c**) $[CuL^5]$.

4. Conclusion

The mesogenic (*nematic)* Schiff-base *N,N′*-di-(4′-pentyloxybenzoate)salicylidene diaminoethane (H_2L^5) coordinates to Mn^{II}, Co^{II}, Ni^{II}, Cu^{II} and Zn^{II} to yield the isomorphous mesogenic (*nematic*) Ni^{II}, Cu^{II} complexes and the non-mesogenic Mn^{II}, Co^{II}, Zn^{II} complexes. The Schiff-base crystallizes in the non-centrosymmetric space group $Pna2_1$ with $Z = 4$ and the nickel and copper complexes, $[NiL^5]_2$ and $[CuL^5]$, in the centrosymmetric space group $P2_1/c$, with $Z = 4$. The coordination geometry around Ni^{II} is low-spin distorted square-pyramidal (*cis*-NiN_2O_2) while that of the Cu^{II} complex is square-planar with a *cis*-CuN_2O_2 configuration.

Acknowledgements

We wish to acknowledge the recording of FAB mass spectra and elemental analyses at the Central Drug Research Institute, Lucknow, India. One of the authors, T.R. Rao, gratefully acknowledges the financial grant received from the Council of Scientific & Industrial Research, New Delhi [vide Grant No. 01(1834)/03/EMR-II], the University Grants Commission, New Delhi [vide grant No. F.12-26/2003 (SR)] and the Department of Science and Technology, New Delhi [vide Grant No. SR/S1/IC-26/2004].

Appendix A. Supplementary data

CDC 660036, 660037 and 685718 contain the supplementary crystallographic data for this paper. These data can be obtained free of charge via http://www.ccdc.cam.ac.uk/conts/retrieving.html, or from the Cambridge Crystallographic Data Centre, 12 Union Road, Cambridge CB2 1EZ, UK; fax: (+44) 1223-336-033; or e-mail: deposit@ccdc.cam.ac.uk. Supplementary data associated with this article can be found, in the online version, at doi:10.1016/j.poly.2008.09.013.

References

[1] B. Donnio, D.W. Bruce, in: D.M.P. Mingos (Ed.), Structure and Bonding, Liquid Crystals II. Metallomesogens, Springer, 1999, p. 95.
[2] B. Donnio, D. Guillon, R. Deschenaux, D.W. Bruce, in: J.A. McCleverty, T.J. Meyer (Eds.), Metallomesogens in Comprehensive Coordination Chemistry, vol. 6, Elsevier, Oxford, 2003.
[3] A-M. Giroud-Godquin, P.M. Maitlis, Angew. Chem., Int. Ed. Engl. 30 (1991) 375.
[4] M.H. Chisholm, Acc. Chem. Res. 33 (2000) 53.
[5] P. Kirsch, M. Bremer, Angew. Chem., Int. Ed. Engl. 39 (2000) 4216.
[6] I. Aiello, M. Ghedini, M. La Deda, D. Pucci, O. Francescangeli, Eur. J. Inorg. Chem. (1999) 1367.
[7] J.L. Serrano, Metallomesogens: Synthesis, Properties and Applications, VCH, Weinheim, 1996.
[8] B. Donnio, D. Guillon, R. Deschenaux, D.W. Bruce, in: J.A. McCleverty, J.J. Meyer, M. Fujita, A. Powell (Eds.), Comprehensive Coordination Chemistry II, vol. 7, Elsevier, Oxford, 2003. p. 353.
[9] D.W. Bruce, R. Deschenaux, B. Donnio, D. Guillon, in: R.H. Crabtree, D.M.P. Mingos (Eds.), Comprehensive Organometallic Chemistry II, vol. 12, Elsevier, Oxford, UK, 2006, p. 195. Chapter 12.05.
[10] B. Donnio, D. Guillon, R. Deschenaux, D.W. Bruce, in: J.A. McCleverty, T.J. Meyer (Eds.), Comprehensive Coordination Chemistry, vol. 7, Elsevier, Oxford, UK, 2003, p. 357. Chapter 7.9.
[11] (a) A. Serrette, P.J. Carroll, T.M. Swager, J. Am. Chem. Soc. 114 (1992) 1887;
(b) A.M. Giroud-Godquin, P.M. Maitlis, Angew. Chem., Int. Ed. Engl. 30 (1991) 375.
[12] N. Hoshino, Coord. Chem. Rev. 174 (1998) 77.
[13] R. Paschke, D. Balkow, E. Sinn, Inorg. Chem. 41 (2002) 1949.
[14] (a) Y. Abe, K. Nakabayashi, N. Matsukawa, M. Iida, T. Tanase, M. Sugibayashia, K. Ohta, Inorg. Chem. Commun. 7 (2004) 580;
(b) Y. Abe, K. Nakabayashi, N. Matsukawa, H. Takashima, M. Iida, T. Tanase, M. Sugibayashi, H. Mukai, K. Ohta, Inorg. Chim. Acta 359 (2006) 3934;
(c) Y. Abe, N. Nakazima, T. Tanase, S. Katano, H. Mukai, K. Ohta, Mol. Cryst. Liq. Cryst. 466 (2007) 129;
(d) Y. Abe, A. Iyoda, K. Seto, A. Moriguchi, T. Tanase, H. Yokoyama, Eur. J. Inorg. Chem. 13 (2008) 2148.
[15] A.K. Singh, S. Kumari, K. Ravi Kumar, B. Sridhar, T.R. Rao, Polyhedron 27 (2008) 181.
[16] A.K. Singh, S. Kumari, K. Ravi Kumar, B. Sridhar, T.R. Rao, Polyhedron 27 (2008) 1937.
[17] N.V.S. Rao, M.K. Paul, T.R. Rao, A. Prasad, Liq. Cryst. 29 (2002) 1243.
[18] T.R. Rao, A. Prasad, Synth. React. Inorg. Met-Org. Nano-Metal Chem. 35 (2005) 299.
[19] A. Weisberger, F.S. Praskver, Organic Solvents, International Publishers Inc., New York, 1956. p. 1263.
[20] SMART and SAINT. Software Reference manuals. Versions 6.28a and 5.625, Bruker Analytical X-ray Systems Inc., Madison, Wisconsin, USA, 2001.
[21] G.M. Sheldrick, SHELXS97 and SHELXL97, Programs for crystal structure solution and refinement, University of Gottingen, Germany, 1997.
[22] K. Binnemans, K. Lodewyckx, R. van Deun, Y.G. Galyametdinov, D. Hinz, G. Meyer, Liq. Cryst. 28 (2001) 279.
[23] R.M. Silverstein, F.X. Webster, Spectroscopic Identification of Organic Compounds, 6th ed., John-Wiley & Sons. Inc., New York, 2002. pp. 82.
[24] A. Braibanti, F. Dallavalle, M.A. Pellinghelli, Inorg. Chem. 7 (1968) 1430.
[25] S.K. Agrawal, D.R. Tuflani, R. Gupta, S.K. Hajela, Inorg. Chim. Acta 129 (1987) 257.
[26] N. Saha, S. Sinha, Ind. J. Chem. 29 (1990) 292.
[27] K. Nakamoto, Infrared and Raman Spectra of Inorganic and Coordination Compounds, Wiley, New York, 1978.
[28] A.B.P. Lever, Inorganic Electronic Spectroscopy, Elsevier, Amsterdam, 1984. p. 490, 524, 571.

Polyhedron 27 (2008) 3717

Contents lists available at ScienceDirect

Polyhedron

journal homepage: www.elsevier.com/locate/poly

Erratum

Erratum to "Template synthesis and characterization of host (nanopores of zeolite-Y)/guest (Co(II)–tetraoxodithiatetraaza macrocyclic complexes) nanocomposite materials" [Polyhedron 27 (2008) 15]

Masoud Salavati-Niasari *

Institute of Nano Science and Nano Technology, University of Kashan, Kashan, P.O. Box 87317-51167, Islamic Republic of Iran
Department of Chemistry, Faculty of Science, University of Kashan, Kashan, P.O. Box 87317-51167, Islamic Republic of Iran

The journal regrets that the following error has occurred.
The scheme on page 3210 is incorrect. The correct scheme can be found below.

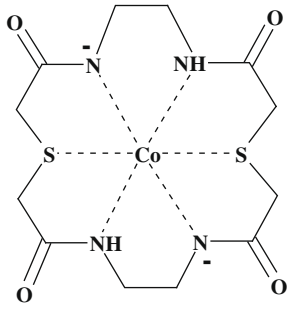

(I)

The journal apologizes for the error.

DOI of original article: 10.1016/j.poly.2008.07.008
* Address: Department of Chemistry, Faculty of Science, University of Kashan, Kashan, P.O. Box 87317-51167, Islamic Republic of Iran. Tel.: +98 361 555 333; fax: +98 361 552 930.
E-mail address: salavati@kashanu.ac.ir

0277-5387/$ - see front matter © 2008 Elsevier Ltd. All rights reserved.
doi:10.1016/j.poly.2008.10.003

POLYHEDRON

The International Journal for Inorganic and Organometallic Chemistry

Executive Editors

The Americas
G. Christou
Department of Chemistry, University of Florida,
Gainesville, FL 32611-7200, USA
E-mail: christou@chem.ufl.edu

Rest of the world
C.E. Housecroft
Department of Chemistry, University of Basel,
Spitalstrasse 51, CH-4056 Basel, Switzerland
E-mail: poly-chemie@unibas.ch

Associate Regional Editor for China
T.C.W. Mak
Department of Chemistry, University Science Centre,
The Chinese University of Hong Kong,
Shatin NT, Hong Kong, People's Republic of China
E-mail: tcwmak@cuhk.edu.hk

Polyhedron Reports
Editor
G. Christou *(Gainesville, FL, USA)*

Symposia-in-print
Editor
G. Parkin *(New York, NY, USA)*

Editorial Board
A.G. Blackman *(Dunedin, New Zealand)*
D.C. Bradley *(London, UK)*
A. Brodie *(Palmerston North, New Zealand)*
A. Castiñeiras *(Santiago de Compostela, Spain)*
X.-M. Chen *(Guangzhou, PR China)*
M.H. Chisholm *(Columbus, OH, USA)*
E.C. Constable *(Basel, Switzerland)*
L. Cronin *(Glasgow, UK)*
W.J. Evans *(Irvine, CA, USA)*
L.H. Gade *(Heidelberg, Germany)*
G. Girolami *(Urbana, IL, USA)*
J.-F. Halet *(Rennes, France)*
L. Hubert-Pfalzgraf *(Villeurbanne, France)*
C. Janiak *(Freiburg, Germany)*
C. Kepert *(NSW, Australia)*
P. Kruger *(Canterbury, New Zealand)*
I. Manners *(Bristol, UK)*
S. Perlepes *(Patras, Greece)*
P.P. Power *(Davis, CA, USA)*
T.B. Rauchfuss *(Urbana, IL, USA)*
J. Reedijk *(Leiden, The Netherlands)*
A.L. Rheingold *(Newark, DE, USA)*
M. Rosales Hoz *(Mexico, D.F., Mexico)*
P. Steel *(Christchurch, New Zealand)*
L.K. Thompson *(St John's, NF, Canada)*
M. Yamashita *(Sendai, Japan)*

Aims and Scope

Polyhedron will publish original, fundamental, experimental and theoretical work of the highest quality in all the major areas of inorganic chemistry. These include synthetic chemistry, coordination chemistry, organometallic chemistry, bioinorganic chemistry, and solid-state and materials chemistry. Papers should be complete pieces of work, and the inclusion of results from spectroscopic and/or physical techniques is encouraged. Papers merely reporting the preparation and X-ray structural characterization of only a single compound will not be considered appropriate unless the compound and its structure are particularly interesting.

Similarly, papers concerned solely with stability constants determined by potentiometric titration data unsupported by other e.g. spectroscopic techniques will not be acceptable nor will solvent extraction data unless supported by other data of interest to inorganic chemists. Unnecessary fragmentation of work is not acceptable.

In addition Polyhedron publishes specially commissioned review articles (Polyhedron Reports) and collections of original research papers (Polyhedron Symposia-in-Print) of appropriate timeliness.

Publication Information: Polyhedron (ISSN 0277-5387). For 2008, volume 27 is scheduled for publication. Subscription prices are available upon request from the Publisher or from the Regional Sales Office nearest you or from this journal's website (http://www.elsevier.com/locate/poly). Further information is available on this journal and other Elsevier products through Elsevier's website (http://www.elsevier.com). Subscriptions are accepted on a prepaid basis only and are entered on a calendar year basis. Issues are sent by standard mail (surface within Europe, air delivery outside Europe). Priority rates are available upon request. Claims for missing issues should be made within six months of the date of dispatch.

Orders, Claims and Journal Enquiries

(no manuscript enquiries)
Please contact the Regional Sales Office nearest you:

St. Louis
Elsevier, Customer Service Department, 11830 Westline Industrial Drive, St. Louis, MO 63146, USA; Tel.: (877) 8397126 [toll free within the USA]; (+1) (314) 4537076 [outside the USA]; Fax: (+1) (314) 5235153; E-mail: JournalCustomerService-usa@elsevier.com

Amsterdam
Elsevier, Customer Service Department, P.O. Box 211, 1000 AE Amsterdam, The Netherlands; Tel.: (+31) 20-485-3757; Fax: (+31) 20-485-3432; E-mail: JournalsCustomerServiceEMEA@elsevier.com

Tokyo
Elsevier K.K., Customer Service Department, 4F Higashi-Azabu, 1-Chome Bldg, 1-9-15 Higashi-Azabu, Minato-ku, Tokyo 106-0044, Japan; Tel.: (+81) 3-5561-5037; Fax: (+81) 3-5561-5047; E-mail: JournalsCustomerServiceJapan@elsevier.com

Singapore
Elsevier, Customer Service Department, 3 Killiney Road, #08-01 Winsland House 1, Singapore 239519, Tel.: (+65) 6349-0222; Fax: (+65) 6733-1510; E-mail: JournalsCustomerServiceAPAC@elsevier.com

USA mailing notice: *Polyhedron* (ISSN 0277-5387) is published triweekly by Elsevier B.V. (Radarweg 29, 1043 NX Amsterdam, the Netherlands). Periodical postage paid at Rahway NJ and additional mailing offices.
USA POSTMASTER: Send change of address to *Polyhedron*, Elsevier, Customer Service Department, 11830 Westline Industrial Drive, St. Louis, MO 63146, USA.
AIRFREIGHT AND MAILING in the USA by Mercury International Limited, 365 Blair Road, Avenel, NJ 07001.

Advertising Information
Advertising orders and enquiries can be sent to: **USA, Canada and South America:** Mr Tino DeCarlo, The Advertising Department, Elsevier Inc., 360 Park Avenue South, New York, NY 10010-1710, USA; tel.: (+1) (212) 633 3815; fax: (+1) (212) 633 3820; e-mail: t.decarlo@elsevier.com. **Europe and ROW:** Miss Katrina Barton, Commercial Sales, Elsevier, 84 Theobald's Road, London, WCIX 8RR, UK; phone: (+44) (0) 20 7611 4117; fax: (+44) (0) 20 7611 4463; e-mail: commercialsales@elsevier.com

Funding body agreements and policies
Elsevier has established agreements and developed policies to allow authors who publish in Elsevier journals to comply with potential manuscript archiving requirements as specified as conditions of their grant awards. To learn more about existing agreements and policies please visit http://www.elsevier.com/fundingbodies

POLYHEDRON

The International Journal for Inorganic and Organometallic Chemistry

Executive Editors

The Americas
G. Christou
Department of Chemistry, University of Florida,
Gainesville, FL 32611-7200, USA
E-mail: christou@chem.ufl.edu

Rest of the world
C.E. Housecroft
Department of Chemistry, University of Basel,
Spitalstrasse 51, CH-4056 Basel, Switzerland
E-mail: poly-chemie@unibas.ch

Associate Regional Editor for China
T.C.W. Mak
Department of Chemistry, University Science Centre,
The Chinese University of Hong Kong,
Shatin NT, Hong Kong, People's Republic of China
E-mail: tcwmak@cuhk.edu.hk

Polyhedron Reports
Editor
G. Christou *(Gainesville, FL, USA)*

Symposia-in-print
Editor
G. Parkin *(New York, NY, USA)*

Editorial Board
A.G. Blackman *(Dunedin, New Zealand)*
D.C. Bradley *(London, UK)*
A. Brodie *(Palmerston North, New Zealand)*
A. Castiñeiras *(Santiago de Compostela, Spain)*
X.-M. Chen *(Guangzhou, PR China)*
M.H. Chisholm *(Columbus, OH, USA)*
E.C. Constable *(Basel, Switzerland)*
L. Cronin *(Glasgow, UK)*
W.J. Evans *(Irvine, CA, USA)*
L.H. Gade *(Heidelberg, Germany)*
G. Girolami *(Urbana, IL, USA)*
J.-F. Halet *(Rennes, France)*
L. Hubert-Pfalzgraf *(Villeurbanne, France)*
C. Janiak *(Freiburg, Germany)*
C. Kepert *(NSW, Australia)*
P. Kruger *(Canterbury, New Zealand)*
I. Manners *(Bristol, UK)*
S. Perlepes *(Patras, Greece)*
P.P. Power *(Davis, CA, USA)*
T.B. Rauchfuss *(Urbana, IL, USA)*
J. Reedijk *(Leiden, The Netherlands)*
A.L. Rheingold *(Newark, DE, USA)*
M. Rosales Hoz *(Mexico, D.F., Mexico)*
P. Steel *(Christchurch, New Zealand)*
L.K. Thompson *(St John's, NF, Canada)*
M. Yamashita *(Sendai, Japan)*

Aims and Scope

Polyhedron will publish original, fundamental, experimental and theoretical work of the highest quality in all the major areas of inorganic chemistry. These include synthetic chemistry, coordination chemistry, organometallic chemistry, bioinorganic chemistry, and solid-state and materials chemistry. Papers should be complete pieces of work, and the inclusion of results from spectroscopic and/or physical techniques is encouraged. Papers merely reporting the preparation and X-ray structural characterization of only a single compound will not be considered appropriate unless the compound and its structure are particularly interesting.

Similarly, papers concerned solely with stability constants determined by potentiometric titration data unsupported by other e.g. spectroscopic techniques will not be acceptable nor will solvent extraction data unless supported by other data of interest to inorganic chemists. Unnecessary fragmentation of work is not acceptable.

In addition Polyhedron publishes specially commissioned review articles (Polyhedron Reports) and collections of original research papers (Polyhedron Symposia-in-Print) of appropriate timeliness.

Publication Information: Polyhedron (ISSN 0277-5387). For 2008, volume 27 is scheduled for publication. Subscription prices are available upon request from the Publisher or from the Regional Sales Office nearest you or from this journal's website (http://www.elsevier.com/locate/poly). Further information is available on this journal and other Elsevier products through Elsevier's website (http://www.elsevier.com). Subscriptions are accepted on a prepaid basis only and are entered on a calendar year basis. Issues are sent by standard mail (surface within Europe, air delivery outside Europe). Priority rates are available upon request. Claims for missing issues should be made within six months of the date of dispatch.

Orders, Claims and Journal Enquiries

(no manuscript enquiries)
Please contact the Regional Sales Office nearest you:

St. Louis
Elsevier, Customer Service Department, 11830 Westline Industrial Drive, St. Louis, MO 63146, USA; Tel.: (877) 8397126 [toll free within the USA]; (+1) (314) 4537076 [outside the USA]; Fax: (+1) (314) 5235153; E-mail: JournalCustomerService-usa@elsevier.com

Amsterdam
Elsevier, Customer Service Department, P.O. Box 211, 1000 AE Amsterdam, The Netherlands; Tel.: (+31) 20-485-3757; Fax: (+31) 20-485-3432; E-mail: JournalsCustomerServiceEMEA@elsevier.com

Tokyo
Elsevier K.K., Customer Service Department, 4F Higashi-Azabu, 1-Chome Bldg, 1-9-15 Higashi-Azabu, Minato-ku, Tokyo 106-0044, Japan; Tel.: (+81) 3-5561-5037; Fax: (+81) 3-5561-5047; E-mail: JournalsCustomerServiceJapan@elsevier.com

Singapore
Elsevier, Customer Service Department, 3 Killiney Road, #08-01 Winsland House 1, Singapore 239519, Tel.: (+65) 6349-0222; Fax: (+65) 6733-1510; E-mail: JournalsCustomerServiceAPAC@elsevier.com

USA mailing notice: *Polyhedron* (ISSN 0277-5387) is published triweekly by Elsevier B.V. (Radarweg 29, 1043 NX Amsterdam, the Netherlands). Periodical postage paid at Rahway NJ and additional mailing offices.
USA POSTMASTER: Send change of address to *Polyhedron*, Elsevier, Customer Service Department, 11830 Westline Industrial Drive, St. Louis, MO 63146, USA.
AIRFREIGHT AND MAILING in the USA by Mercury International Limited, 365 Blair Road, Avenel, NJ 07001.

Advertising Information
Advertising orders and enquiries can be sent to: **USA, Canada and South America:** Mr Tino DeCarlo, The Advertising Department, Elsevier Inc., 360 Park Avenue South, New York, NY 10010-1710, USA; tel.: (+1) (212) 633 3815; fax: (+1) (212) 633 3820; e-mail: t.decarlo@elsevier.com. **Europe and ROW:** Miss Katrina Barton, Commercial Sales, Elsevier, 84 Theobald's Road, London, WCIX 8RR, UK; phone: (+44) (0) 20 7611 4117; fax: (+44) (0) 20 7611 4463; e-mail: commercialsales@elsevier.com

Funding body agreements and policies
Elsevier has established agreements and developed policies to allow authors who publish in Elsevier journals to comply with potential manuscript archiving requirements as specified as conditions of their grant awards. To learn more about existing agreements and policies please visit http://www.elsevier.com/fundingbodies

POLYHEDRON

The International Journal for Inorganic and Organometallic Chemistry

Executive Editors

The Americas
G. Christou
Department of Chemistry, University of Florida,
Gainesville, FL 32611-7200, USA
E-mail: christou@chem.ufl.edu

Rest of the world
C.E. Housecroft
Department of Chemistry, University of Basel,
Spitalstrasse 51, CH-4056 Basel, Switzerland
E-mail: poly-chemie@unibas.ch

Associate Regional Editor for China
T.C.W. Mak
Department of Chemistry, University Science Centre,
The Chinese University of Hong Kong,
Shatin NT, Hong Kong, People's Republic of China
E-mail: tcwmak@cuhk.edu.hk

Polyhedron Reports
Editor
G. Christou *(Gainesville, FL, USA)*

Symposia-in-print
Editor
G. Parkin *(New York, NY, USA)*

Editorial Board

A.G. Blackman *(Dunedin, New Zealand)*
D.C. Bradley *(London, UK)*
A. Brodie *(Palmerston North, New Zealand)*
A. Castiñeiras *(Santiago de Compostela, Spain)*
X.-M. Chen *(Guangzhou, PR China)*
M.H. Chisholm *(Columbus, OH, USA)*
E.C. Constable *(Basel, Switzerland)*
L. Cronin *(Glasgow, UK)*
W.J. Evans *(Irvine, CA, USA)*
L.H. Gade *(Heidelberg, Germany)*
G. Girolami *(Urbana, IL, USA)*
J.-F. Halet *(Rennes, France)*
L. Hubert-Pfalzgraf *(Villeurbanne, France)*
C. Janiak *(Freiburg, Germany)*
C. Kepert *(NSW, Australia)*
P. Kruger *(Canterbury, New Zealand)*
I. Manners *(Bristol, UK)*
S. Perlepes *(Patras, Greece)*
P.P. Power *(Davis, CA, USA)*
T.B. Rauchfuss *(Urbana, IL, USA)*
J. Reedijk *(Leiden, The Netherlands)*
A.L. Rheingold *(Newark, DE, USA)*
M. Rosales Hoz *(Mexico, D.F., Mexico)*
P. Steel *(Christchurch, New Zealand)*
L.K. Thompson *(St John's, NF, Canada)*
M. Yamashita *(Sendai, Japan)*

Aims and Scope

Polyhedron will publish original, fundamental, experimental and theoretical work of the highest quality in all the major areas of inorganic chemistry. These include synthetic chemistry, coordination chemistry, organometallic chemistry, bioinorganic chemistry, and solid-state and materials chemistry. Papers should be complete pieces of work, and the inclusion of results from spectroscopic and/or physical techniques is encouraged. Papers merely reporting the preparation and X-ray structural characterization of only a single compound will not be considered appropriate unless the compound and its structure are particularly interesting.

Similarly, papers concerned solely with stability constants determined by potentiometric titration data unsupported by other e.g. spectroscopic techniques will not be acceptable nor will solvent extraction data unless supported by other data of interest to inorganic chemists. Unnecessary fragmentation of work is not acceptable.

In addition Polyhedron publishes specially commissioned review articles (Polyhedron Reports) and collections of original research papers (Polyhedron Symposia-in-Print) of appropriate timeliness.

Publication Information: Polyhedron (ISSN 0277-5387). For 2008, volume 27 is scheduled for publication. Subscription prices are available upon request from the Publisher or from the Regional Sales Office nearest you or from this journal's website (http://www.elsevier.com/locate/poly). Further information is available on this journal and other Elsevier products through Elsevier's website (http://www.elsevier.com). Subscriptions are accepted on a prepaid basis only and are entered on a calendar year basis. Issues are sent by standard mail (surface within Europe, air delivery outside Europe). Priority rates are available upon request. Claims for missing issues should be made within six months of the date of dispatch.

Orders, Claims and Journal Enquiries

(no manuscript enquiries)
Please contact the Customer Support Department at the Regional Sales Office nearest you:

Orlando
Elsevier
Customer Service Department
6277 Sea Harbor Drive
Orlando, FL 32887-4800
USA
Tel.: (877) 8397126
[toll free within the USA];
(+1) (407) 5636022
[outside the USA];
Fax: (+1) (407) 3631354
E-mail: JournalCustomerService-usa@elsevier.com

Amsterdam
Elsevier
Customer Service Department
P.O. Box 211
1000 AE Amsterdam
The Netherlands
Tel.: (+31) 20-485-3757
Fax: (+31) 20-485-3432
E-mail: nlinfo-f@elsevier.com

Tokyo
Elsevier K.K.
Customer Service Department
4F Higashi-Azabu, 1-Chome Bldg
1-9-15 Higashi-Azabu
Minato-ku, Tokyo 106-0044
Japan
Tel.: (+81) 3-5561-5037
Fax: (+81) 3-5561-5047
E-mail: jp.info@elsevier.com

Singapore
Elsevier
Customer Service Department
3 Killiney Road
#08-01 Winsland House 1
Singapore 239519
Tel.: (+65) 6349-0222
Fax: (+65) 6733-1510
E-mail: asiainfo@elsevier.com

USA mailing notice: *Polyhedron* (ISSN 0277-5387) is published triweekly by Elsevier Ltd. (P.O. Box 211, 1000 AE Amsterdam, The Netherlands). Annual subscription price in the USA US$ 8198.00 (valid in North, Central and South America), including air speed delivery. Periodical postage rate is paid at Rahway, NJ.
USA POSTMASTER: Send change of address to *Polyhedron*, Elsevier, 6277 Sea Harbor Drive, Orlando, FL 32887-4800.
AIRFREIGHT AND MAILING in the USA by Mercury International Limited, 365 Blair Road, Avenel, NJ 07001.

Advertising Information

Advertising orders and enquiries can be sent to: **South America:** Mr Tino DeCarlo, The Advertising Department, Elsevier Inc., 360 Park Avenue South, New York, NY 10010-1710, USA; tel.: (+1) (212) 633 3815; fax: (+1) (212) 633 3820; e-mail: t.decarlo@elsevier.com. **Europe, USA, Canada and ROW:** Miss Katrina Barton, Commercial Sales, Elsevier, 84 Theobald's Road, London, WCIX 8RR, UK; phone: (+44) (0) 20 7611 4117; fax: (+44) (0) 20 7611 4463; e-mail: commercialsales@elsevier.com

Funding body agreements and policies

Elsevier has established agreements and developed policies to allow authors who publish in Elsevier journals to comply with potential manuscript archiving requirements as specified as conditions of their grant awards. To learn more about existing agreements and policies please visit http://www.elsevier.com/fundingbodies

POLYHEDRON

The International Journal for Inorganic and Organometallic Chemistry

Executive Editors

The Americas
G. Christou
Department of Chemistry, University of Florida,
Gainesville, FL 32611-7200, USA
E-mail: christou@chem.ufl.edu

Rest of the world
C.E. Housecroft
Department of Chemistry, University of Basel,
Spitalstrasse 51, CH-4056 Basel, Switzerland
E-mail: poly-chemie@unibas.ch

Associate Regional Editor for China
T.C.W. Mak
Department of Chemistry, University Science Centre,
The Chinese University of Hong Kong,
Shatin NT, Hong Kong, People's Republic of China
E-mail: tcwmak@cuhk.edu.hk

Polyhedron Reports
Editor
G. Christou *(Gainesville, FL, USA)*

Symposia-in-print
Editor
G. Parkin *(New York, NY, USA)*

Editorial Board

A.G. Blackman *(Dunedin, New Zealand)*
D.C. Bradley *(London, UK)*
A. Brodie *(Palmerston North, New Zealand)*
A. Castiñeiras *(Santiago de Compostela, Spain)*
X.-M. Chen *(Guangzhou, PR China)*
M.H. Chisholm *(Columbus, OH, USA)*
E.C. Constable *(Basel, Switzerland)*
L. Cronin *(Glasgow, UK)*
W.J. Evans *(Irvine, CA, USA)*
L.H. Gade *(Heidelberg, Germany)*
G. Girolami *(Urbana, IL, USA)*
J.-F. Halet *(Rennes, France)*
L. Hubert-Pfalzgraf *(Villeurbanne, France)*
C. Janiak *(Freiburg, Germany)*
C. Kepert *(NSW, Australia)*
P. Kruger *(Canterbury, New Zealand)*
I. Manners *(Bristol, UK)*
S. Perlepes *(Patras, Greece)*
P.P. Power *(Davis, CA, USA)*
T.B. Rauchfuss *(Urbana, IL, USA)*
J. Reedijk *(Leiden, The Netherlands)*
A.L. Rheingold *(Newark, DE, USA)*
M. Rosales Hoz *(Mexico, D.F., Mexico)*
P. Steel *(Christchurch, New Zealand)*
L.K. Thompson *(St John's, NF, Canada)*
M. Yamashita *(Sendai, Japan)*

Aims and Scope

Polyhedron will publish original, fundamental, experimental and theoretical work of the highest quality in all the major areas of inorganic chemistry. These include synthetic chemistry, coordination chemistry, organometallic chemistry, bioinorganic chemistry, and solid-state and materials chemistry. Papers should be complete pieces of work, and the inclusion of results from spectroscopic and/or physical techniques is encouraged. Papers merely reporting the preparation and X-ray structural characterization of only a single compound will not be considered appropriate unless the compound and its structure are particularly interesting.

Similarly, papers concerned solely with stability constants determined by potentiometric titration data unsupported by other e.g. spectroscopic techniques will not be acceptable nor will solvent extraction data unless supported by other data of interest to inorganic chemists. Unnecessary fragmentation of work is not acceptable.

In addition Polyhedron publishes specially commissioned review articles (Polyhedron Reports) and collections of original research papers (Polyhedron Symposia-in-Print) of appropriate timeliness.

Publication Information: Polyhedron (ISSN 0277-5387). For 2008, volume 27 is scheduled for publication. Subscription prices are available upon request from the Publisher or from the Regional Sales Office nearest you or from this journal's website (http://www.elsevier.com/locate/poly). Further information is available on this journal and other Elsevier products through Elsevier's website (http://www.elsevier.com). Subscriptions are accepted on a prepaid basis only and are entered on a calendar year basis. Issues are sent by standard mail (surface within Europe, air delivery outside Europe). Priority rates are available upon request. Claims for missing issues should be made within six months of the date of dispatch.

Orders, Claims and Journal Enquiries

(no manuscript enquiries)
Please contact the Customer Support Department at the Regional Sales Office nearest you:

Orlando
Elsevier
Customer Service Department
6277 Sea Harbor Drive
Orlando, FL 32887-4800
USA
Tel.: (877) 8397126
[toll free within the USA];
(+1) (407) 5636022
[outside the USA];
Fax: (+1) (407) 3631354
E-mail: JournalCustomerService-usa@elsevier.com

Amsterdam
Elsevier
Customer Service Department
P.O. Box 211
1000 AE Amsterdam
The Netherlands
Tel.: (+31) 20-485-3757
Fax: (+31) 20-485-3432
E-mail: nlinfo-f@elsevier.com

Tokyo
Elsevier K.K.
Customer Service Department
4F Higashi-Azabu, 1-Chome Bldg
1-9-15 Higashi-Azabu
Minato-ku, Tokyo 106-0044
Japan
Tel.: (+81) 3-5561-5037
Fax: (+81) 3-5561-5047
E-mail: jp.info@elsevier.com

Singapore
Elsevier
Customer Service Department
3 Killiney Road
#08-01 Winsland House 1
Singapore 239519
Tel.: (+65) 6349-0222
Fax: (+65) 6733-1510
E-mail: asiainfo@elsevier.com

USA mailing notice: *Polyhedron* (ISSN 0277-5387) is published triweekly by Elsevier Ltd. (P.O. Box 211, 1000 AE Amsterdam, The Netherlands). Annual subscription price in the USA US$ 8198.00 (valid in North, Central and South America), including air speed delivery. Periodical postage rate is paid at Rahway, NJ.
USA POSTMASTER: Send change of address to *Polyhedron*, Elsevier, 6277 Sea Harbor Drive, Orlando, FL 32887-4800.
AIRFREIGHT AND MAILING in the USA by Mercury International Limited, 365 Blair Road, Avenel, NJ 07001.

Advertising Information

Advertising orders and enquiries can be sent to: **South America:** Mr Tino DeCarlo, The Advertising Department, Elsevier Inc., 360 Park Avenue South, New York, NY 10010-1710, USA; tel.: (+1) (212) 633 3815; fax: (+1) (212) 633 3820; e-mail: t.decarlo@elsevier.com. **Europe, USA, Canada and ROW:** Miss Katrina Barton, Commercial Sales, Elsevier, 84 Theobald's Road, London, WCIX 8RR, UK; phone: (+44) (0) 20 7611 4117; fax: (+44) (0) 20 7611 4463; e-mail: commercialsales@elsevier.com

Funding body agreements and policies

Elsevier has established agreements and developed policies to allow authors who publish in Elsevier journals to comply with potential manuscript archiving requirements as specified as conditions of their grant awards. To learn more about existing agreements and policies please visit http://www.elsevier.com/fundingbodies

POLYHEDRON

The International Journal for Inorganic and Organometallic Chemistry

Executive Editors

The Americas
G. Christou
Department of Chemistry, University of Florida,
Gainesville, FL 32611-7200, USA
E-mail: christou@chem.ufl.edu

Rest of the world
C.E. Housecroft
Department of Chemistry, University of Basel,
Spitalstrasse 51, CH-4056 Basel, Switzerland
E-mail: poly-chemie@unibas.ch

Associate Regional Editor for China
T.C.W. Mak
Department of Chemistry, University Science Centre,
The Chinese University of Hong Kong,
Shatin NT, Hong Kong, People's Republic of China
E-mail: tcwmak@cuhk.edu.hk

Polyhedron Reports
Editor
G. Christou *(Gainesville, FL, USA)*

Symposia-in-print
Editor
G. Parkin *(New York, NY, USA)*

Editorial Board

A.G. Blackman *(Dunedin, New Zealand)*
D.C. Bradley *(London, UK)*
A. Brodie *(Palmerston North, New Zealand)*
A. Castiñeiras *(Santiago de Compostela, Spain)*
X.-M. Chen *(Guangzhou, PR China)*
M.H. Chisholm *(Columbus, OH, USA)*
E.C. Constable *(Basel, Switzerland)*
L. Cronin *(Glasgow, UK)*
W.J. Evans *(Irvine, CA, USA)*
L.H. Gade *(Heidelberg, Germany)*
G. Girolami *(Urbana, IL, USA)*
J.-F. Halet *(Rennes, France)*
L. Hubert-Pfalzgraf *(Villeurbanne, France)*
C. Janiak *(Freiburg, Germany)*
C. Kepert *(NSW, Australia)*
P. Kruger *(Canterbury, New Zealand)*
I. Manners *(Bristol, UK)*
S. Perlepes *(Patras, Greece)*
P.P. Power *(Davis, CA, USA)*
T.B. Rauchfuss *(Urbana, IL, USA)*
J. Reedijk *(Leiden, The Netherlands)*
A.L. Rheingold *(Newark, DE, USA)*
M. Rosales Hoz *(Mexico, D.F., Mexico)*
P. Steel *(Christchurch, New Zealand)*
L.K. Thompson *(St John's, NF, Canada)*
M. Yamashita *(Sendai, Japan)*

Aims and Scope

Polyhedron will publish original, fundamental, experimental and theoretical work of the highest quality in all the major areas of inorganic chemistry. These include synthetic chemistry, coordination chemistry, organometallic chemistry, bioinorganic chemistry, and solid-state and materials chemistry. Papers should be complete pieces of work, and the inclusion of results from spectroscopic and/or physical techniques is encouraged. Papers merely reporting the preparation and X-ray structural characterization of only a single compound will not be considered appropriate unless the compound and its structure are particularly interesting.

Similarly, papers concerned solely with stability constants determined by potentiometric titration data unsupported by other e.g. spectroscopic techniques will not be acceptable nor will solvent extraction data unless supported by other data of interest to inorganic chemists. Unnecessary fragmentation of work is not acceptable.

In addition Polyhedron publishes specially commissioned review articles (Polyhedron Reports) and collections of original research papers (Polyhedron Symposia-in-Print) of appropriate timeliness.

Publication Information: Polyhedron (ISSN 0277-5387). For 2008, volume 27 is scheduled for publication. Subscription prices are available upon request from the Publisher or from the Regional Sales Office nearest you or from this journal's website (http://www.elsevier.com/locate/poly). Further information is available on this journal and other Elsevier products through Elsevier's website (http://www.elsevier.com). Subscriptions are accepted on a prepaid basis only and are entered on a calendar year basis. Issues are sent by standard mail (surface within Europe, air delivery outside Europe). Priority rates are available upon request. Claims for missing issues should be made within six months of the date of dispatch.

Orders, Claims and Journal Enquiries

(no manuscript enquiries)

Please contact the Customer Support Department at the Regional Sales Office nearest you:

Orlando
Elsevier
Customer Service Department
6277 Sea Harbor Drive
Orlando, FL 32887-4800
USA
Tel.: (877) 8397126
[toll free within the USA];
(+1) (407) 5636022
[outside the USA];
Fax: (+1) (407) 3631354
E-mail: JournalCustomerService-usa@elsevier.com

Amsterdam
Elsevier
Customer Service Department
P.O. Box 211
1000 AE Amsterdam
The Netherlands
Tel.: (+31) 20-485-3757
Fax: (+31) 20-485-3432
E-mail: nlinfo-f@elsevier.com

Tokyo
Elsevier K.K.
Customer Service Department
4F Higashi-Azabu, 1-Chome Bldg
1-9-15 Higashi-Azabu
Minato-ku, Tokyo 106-0044
Japan
Tel.: (+81) 3-5561-5037
Fax: (+81) 3-5561-5047
E-mail: jp.info@elsevier.com

Singapore
Elsevier
Customer Service Department
3 Killiney Road
#08-01 Winsland House 1
Singapore 239519
Tel.: (+65) 6349-0222
Fax: (+65) 6733-1510
E-mail: asiainfo@elsevier.com

USA mailing notice: *Polyhedron* (ISSN 0277-5387) is published triweekly by Elsevier Ltd. (P.O. Box 211, 1000 AE Amsterdam, The Netherlands). Annual subscription price in the USA US$ 8198.00 (valid in North, Central and South America), including air speed delivery. Periodical postage rate is paid at Rahway, NJ.

USA POSTMASTER: Send change of address to *Polyhedron*, Elsevier, 6277 Sea Harbor Drive, Orlando, FL 32887-4800.

AIRFREIGHT AND MAILING in the USA by Mercury International Limited, 365 Blair Road, Avenel, NJ 07001.

Advertising Information

Advertising orders and enquiries can be sent to: **South America:** Mr Tino DeCarlo, The Advertising Department, Elsevier Inc., 360 Park Avenue South, New York, NY 10010-1710, USA; tel.: (+1) (212) 633 3815; fax: (+1) (212) 633 3820; e-mail: t.decarlo@elsevier.com. **Europe, USA, Canada and ROW:** Miss Katrina Barton, Commercial Sales, Elsevier, 84 Theobald's Road, London, WCIX 8RR, UK; phone: (+44) (0) 20 7611 4117; fax: (+44) (0) 20 7611 4463; e-mail: commercialsales@elsevier.com

Funding body agreements and policies

Elsevier has established agreements and developed policies to allow authors who publish in Elsevier journals to comply with potential manuscript archiving requirements as specified as conditions of their grant awards. To learn more about existing agreements and policies please visit http://www.elsevier.com/fundingbodies

POLYHEDRON

The International Journal for Inorganic and Organometallic Chemistry

Executive Editors

The Americas
G. Christou
Department of Chemistry, University of Florida,
Gainesville, FL 32611-7200, USA
E-mail: christou@chem.ufl.edu

Rest of the world
C.E. Housecroft
Department of Chemistry, University of Basel,
Spitalstrasse 51, CH-4056 Basel, Switzerland
E-mail: poly-chemie@unibas.ch

Associate Regional Editor for China
T.C.W. Mak
Department of Chemistry, University Science Centre,
The Chinese University of Hong Kong,
Shatin NT, Hong Kong, People's Republic of China
E-mail: tcwmak@cuhk.edu.hk

Polyhedron Reports
Editor
G. Christou *(Gainesville, FL, USA)*

Symposia-in-print
Editor
G. Parkin *(New York, NY, USA)*

Editorial Board

A.G. Blackman *(Dunedin, New Zealand)*
D.C. Bradley *(London, UK)*
A. Brodie *(Palmerston North, New Zealand)*
A. Castiñeiras *(Santiago de Compostela, Spain)*
X.-M. Chen *(Guangzhou, PR China)*
M.H. Chisholm *(Columbus, OH, USA)*
E.C. Constable *(Basel, Switzerland)*
L. Cronin *(Glasgow, UK)*
W.J. Evans *(Irvine, CA, USA)*
L.H. Gade *(Heidelberg, Germany)*
G. Girolami *(Urbana, IL, USA)*
J.-F. Halet *(Rennes, France)*
L. Hubert-Pfalzgraf *(Villeurbanne, France)*
C. Janiak *(Freiburg, Germany)*
C. Kepert *(NSW, Australia)*
P. Kruger *(Canterbury, New Zealand)*
I. Manners *(Bristol, UK)*
S. Perlepes *(Patras, Greece)*
P.P. Power *(Davis, CA, USA)*
T.B. Rauchfuss *(Urbana, IL, USA)*
J. Reedijk *(Leiden, The Netherlands)*
A.L. Rheingold *(Newark, DE, USA)*
M. Rosales Hoz *(Mexico, D.F., Mexico)*
P. Steel *(Christchurch, New Zealand)*
L.K. Thompson *(St John's, NF, Canada)*
M. Yamashita *(Sendai, Japan)*

Aims and Scope

Polyhedron will publish original, fundamental, experimental and theoretical work of the highest quality in all the major areas of inorganic chemistry. These include synthetic chemistry, coordination chemistry, organometallic chemistry, bioinorganic chemistry, and solid-state and materials chemistry. Papers should be complete pieces of work, and the inclusion of results from spectroscopic and/or physical techniques is encouraged. Papers merely reporting the preparation and X-ray structural characterization of only a single compound will not be considered appropriate unless the compound and its structure are particularly interesting.

Similarly, papers concerned solely with stability constants determined by potentiometric titration data unsupported by other e.g. spectroscopic techniques will not be acceptable nor will solvent extraction data unless supported by other data of interest to inorganic chemists. Unnecessary fragmentation of work is not acceptable.

In addition Polyhedron publishes specially commissioned review articles (Polyhedron Reports) and collections of original research papers (Polyhedron Symposia-in-Print) of appropriate timeliness.

Publication Information: Polyhedron (ISSN 0277-5387). For 2008, volume 27 is scheduled for publication. Subscription prices are available upon request from the Publisher or from the Regional Sales Office nearest you or from this journal's website (http://www.elsevier.com/locate/poly). Further information is available on this journal and other Elsevier products through Elsevier's website (http://www.elsevier.com). Subscriptions are accepted on a prepaid basis only and are entered on a calendar year basis. Issues are sent by standard mail (surface within Europe, air delivery outside Europe). Priority rates are available upon request. Claims for missing issues should be made within six months of the date of dispatch.

Orders, Claims and Journal Enquiries

(no manuscript enquiries)
Please contact the Customer Support Department at the Regional Sales Office nearest you:

Orlando
Elsevier
Customer Service Department
6277 Sea Harbor Drive
Orlando, FL 32887-4800
USA
Tel.: (877) 8397126
[toll free within the USA];
(+1) (407) 5636022
[outside the USA];
Fax: (+1) (407) 3631354
E-mail: JournalCustomerService-usa@elsevier.com

Amsterdam
Elsevier
Customer Service Department
P.O. Box 211
1000 AE Amsterdam
The Netherlands
Tel.: (+31) 20-485-3757
Fax: (+31) 20-485-3432
E-mail: nlinfo-f@elsevier.com

Tokyo
Elsevier K.K.
Customer Service Department
4F Higashi-Azabu, 1-Chome Bldg
1-9-15 Higashi-Azabu
Minato-ku, Tokyo 106-0044
Japan
Tel.: (+81) 3-5561-5037
Fax: (+81) 3-5561-5047
E-mail: jp.info@elsevier.com

Singapore
Elsevier
Customer Service Department
3 Killiney Road
#08-01 Winsland House 1
Singapore 239519
Tel.: (+65) 6349-0222
Fax: (+65) 6733-1510
E-mail: asiainfo@elsevier.com

USA mailing notice: *Polyhedron* (ISSN 0277-5387) is published triweekly by Elsevier Ltd. (P.O. Box 211, 1000 AE Amsterdam, The Netherlands). Annual subscription price in the USA US$ 8198.00 (valid in North, Central and South America), including air speed delivery. Periodical postage rate is paid at Rahway, NJ.
USA POSTMASTER: Send change of address to *Polyhedron*, Elsevier, 6277 Sea Harbor Drive, Orlando, FL 32887-4800.
AIRFREIGHT AND MAILING in the USA by Mercury International Limited, 365 Blair Road, Avenel, NJ 07001.

Advertising Information

Advertising orders and enquiries can be sent to: **South America:** Mr Tino DeCarlo, The Advertising Department, Elsevier Inc., 360 Park Avenue South, New York, NY 10010-1710, USA; tel.: (+1) (212) 633 3815; fax: (+1) (212) 633 3820; e-mail: t.decarlo@elsevier.com. **Europe, USA, Canada and ROW:** Miss Katrina Barton, Commercial Sales, Elsevier, 84 Theobald's Road, London, WCIX 8RR, UK; phone: (+44) (0) 20 7611 4117; fax: (+44) (0) 20 7611 4463; e-mail: commercialsales@elsevier.com

Funding body agreements and policies

Elsevier has established agreements and developed policies to allow authors who publish in Elsevier journals to comply with potential manuscript archiving requirements as specified as conditions of their grant awards. To learn more about existing agreements and policies please visit http://www.elsevier.com/fundingbodies

POLYHEDRON

The International Journal for Inorganic and Organometallic Chemistry

Executive Editors

The Americas
G. Christou
Department of Chemistry, University of Florida,
Gainesville, FL 32611-7200, USA
E-mail: christou@chem.ufl.edu

Rest of the world
C.E. Housecroft
Department of Chemistry, University of Basel,
Spitalstrasse 51, CH-4056 Basel, Switzerland
E-mail: poly-chemie@unibas.ch

Associate Regional Editor for China
T.C.W. Mak
Department of Chemistry, University Science Centre,
The Chinese University of Hong Kong,
Shatin NT, Hong Kong, People's Republic of China
E-mail: tcwmak@cuhk.edu.hk

Polyhedron Reports
Editor
G. Christou *(Gainesville, FL, USA)*

Symposia-in-print
Editor
G. Parkin *(New York, NY, USA)*

Editorial Board

A.G. Blackman *(Dunedin, New Zealand)*
D.C. Bradley *(London, UK)*
A. Brodie *(Palmerston North, New Zealand)*
A. Castiñeiras *(Santiago de Compostela, Spain)*
X.-M. Chen *(Guangzhou, PR China)*
M.H. Chisholm *(Columbus, OH, USA)*
E.C. Constable *(Basel, Switzerland)*
L. Cronin *(Glasgow, UK)*
W.J. Evans *(Irvine, CA, USA)*
L.H. Gade *(Heidelberg, Germany)*
G. Girolami *(Urbana, IL, USA)*
J.-F. Halet *(Rennes, France)*
L. Hubert-Pfalzgraf *(Villeurbanne, France)*
C. Janiak *(Freiburg, Germany)*
C. Kepert *(NSW, Australia)*
P. Kruger *(Canterbury, New Zealand)*
I. Manners *(Bristol, UK)*
S. Perlepes *(Patras, Greece)*
P.P. Power *(Davis, CA, USA)*
T.B. Rauchfuss *(Urbana, IL, USA)*
J. Reedijk *(Leiden, The Netherlands)*
A.L. Rheingold *(Newark, DE, USA)*
M. Rosales Hoz *(Mexico, D.F., Mexico)*
P. Steel *(Christchurch, New Zealand)*
L.K. Thompson *(St John's, NF, Canada)*
M. Yamashita *(Sendai, Japan)*

Aims and Scope

Polyhedron will publish original, fundamental, experimental and theoretical work of the highest quality in all the major areas of inorganic chemistry. These include synthetic chemistry, coordination chemistry, organometallic chemistry, bioinorganic chemistry, and solid-state and materials chemistry. Papers should be complete pieces of work, and the inclusion of results from spectroscopic and/or physical techniques is encouraged. Papers merely reporting the preparation and X-ray structural characterization of only a single compound will not be considered appropriate unless the compound and its structure are particularly interesting.

Similarly, papers concerned solely with stability constants determined by potentiometric titration data unsupported by other e.g. spectroscopic techniques will not be acceptable nor will solvent extraction data unless supported by other data of interest to inorganic chemists. Unnecessary fragmentation of work is not acceptable.

In addition Polyhedron publishes specially commissioned review articles (Polyhedron Reports) and collections of original research papers (Polyhedron Symposia-in-Print) of appropriate timeliness.

Publication Information: Polyhedron (ISSN 0277-5387). For 2008, volume 27 is scheduled for publication. Subscription prices are available upon request from the Publisher or from the Regional Sales Office nearest you or from this journal's website (http://www.elsevier.com/locate/poly). Further information is available on this journal and other Elsevier products through Elsevier's website (http://www.elsevier.com). Subscriptions are accepted on a prepaid basis only and are entered on a calendar year basis. Issues are sent by standard mail (surface within Europe, air delivery outside Europe). Priority rates are available upon request. Claims for missing issues should be made within six months of the date of dispatch.

Orders, Claims and Journal Enquiries

(no manuscript enquiries)
Please contact the Customer Support Department at the Regional Sales Office nearest you:

Orlando
Elsevier
Customer Service Department
6277 Sea Harbor Drive
Orlando, FL 32887-4800
USA
Tel.: (877) 8397126
[toll free within the USA];
(+1) (407) 5636022
[outside the USA];
Fax: (+1) (407) 3631354
E-mail: JournalCustomerService-usa@elsevier.com

Amsterdam
Elsevier
Customer Service Department
P.O. Box 211
1000 AE Amsterdam
The Netherlands
Tel.: (+31) 20-485-3757
Fax: (+31) 20-485-3432
E-mail: nlinfo-f@elsevier.com

Tokyo
Elsevier K.K.
Customer Service Department
4F Higashi-Azabu, 1-Chome Bldg
1-9-15 Higashi-Azabu
Minato-ku, Tokyo 106-0044
Japan
Tel.: (+81) 3-5561-5037
Fax: (+81) 3-5561-5047
E-mail: jp.info@elsevier.com

Singapore
Elsevier
Customer Service Department
3 Killiney Road
#08-01 Winsland House 1
Singapore 239519
Tel.: (+65) 6349-0222
Fax: (+65) 6733-1510
E-mail: asiainfo@elsevier.com

USA mailing notice: *Polyhedron* (ISSN 0277-5387) is published triweekly by Elsevier Ltd. (P.O. Box 211, 1000 AE Amsterdam, The Netherlands). Annual subscription price in the USA US$ 8198.00 (valid in North, Central and South America), including air speed delivery. Periodical postage rate is paid at Rahway, NJ.
USA POSTMASTER: Send change of address to *Polyhedron*, Elsevier, 6277 Sea Harbor Drive, Orlando, FL 32887-4800.
AIRFREIGHT AND MAILING in the USA by Mercury International Limited, 365 Blair Road, Avenel, NJ 07001.

Advertising Information

Advertising orders and enquiries can be sent to: **South America:** Mr Tino DeCarlo, The Advertising Department, Elsevier Inc., 360 Park Avenue South, New York, NY 10010-1710, USA; tel.: (+1) (212) 633 3815; fax: (+1) (212) 633 3820; e-mail: t.decarlo@elsevier.com. **Europe, USA, Canada and ROW:** Miss Katrina Barton, Commercial Sales, Elsevier, 84 Theobald's Road, London, WCIX 8RR, UK; phone: (+44) (0) 20 7611 4117; fax: (+44) (0) 20 7611 4463; e-mail: commercialsales@elsevier.com

Funding body agreements and policies

Elsevier has established agreements and developed policies to allow authors who publish in Elsevier journals to comply with potential manuscript archiving requirements as specified as conditions of their grant awards. To learn more about existing agreements and policies please visit http://www.elsevier.com/fundingbodies

POLYHEDRON

The International Journal for Inorganic and Organometallic Chemistry

Executive Editors

The Americas
G. Christou
Department of Chemistry, University of Florida,
Gainesville, FL 32611-7200, USA
E-mail: christou@chem.ufl.edu

Rest of the world
C.E. Housecroft
Department of Chemistry, University of Basel,
Spitalstrasse 51, CH-4056 Basel, Switzerland
E-mail: poly-chemie@unibas.ch

Associate Regional Editor for China
T.C.W. Mak
Department of Chemistry, University Science Centre,
The Chinese University of Hong Kong,
Shatin NT, Hong Kong, People's Republic of China
E-mail: tcwmak@cuhk.edu.hk

Polyhedron Reports
Editor
G. Christou *(Gainesville, FL, USA)*

Symposia-in-print
Editor
G. Parkin *(New York, NY, USA)*

Editorial Board
A.G. Blackman *(Dunedin, New Zealand)*
D.C. Bradley *(London, UK)*
A. Brodie *(Palmerston North, New Zealand)*
A. Castiñeiras *(Santiago de Compostela, Spain)*
X.-M. Chen *(Guangzhou, PR China)*
M.H. Chisholm *(Columbus, OH, USA)*
E.C. Constable *(Basel, Switzerland)*
L. Cronin *(Glasgow, UK)*
W.J. Evans *(Irvine, CA, USA)*
L.H. Gade *(Heidelberg, Germany)*
G. Girolami *(Urbana, IL, USA)*
J.-F. Halet *(Rennes, France)*
L. Hubert-Pfalzgraf *(Villeurbanne, France)*
C. Janiak *(Freiburg, Germany)*
C. Kepert *(NSW, Australia)*
P. Kruger *(Canterbury, New Zealand)*
I. Manners *(Bristol, UK)*
S. Perlepes *(Patras, Greece)*
P.P. Power *(Davis, CA, USA)*
T.B. Rauchfuss *(Urbana, IL, USA)*
J. Reedijk *(Leiden, The Netherlands)*
A.L. Rheingold *(Newark, DE, USA)*
M. Rosales Hoz *(Mexico, D.F., Mexico)*
P. Steel *(Christchurch, New Zealand)*
L.K. Thompson *(St John's, NF, Canada)*
M. Yamashita *(Sendai, Japan)*

Aims and Scope

Polyhedron will publish original, fundamental, experimental and theoretical work of the highest quality in all the major areas of inorganic chemistry. These include synthetic chemistry, coordination chemistry, organometallic chemistry, bioinorganic chemistry, and solid-state and materials chemistry. Papers should be complete pieces of work, and the inclusion of results from spectroscopic and/or physical techniques is encouraged. Papers merely reporting the preparation and X-ray structural characterization of only a single compound will not be considered appropriate unless the compound and its structure are particularly interesting.

Similarly, papers concerned solely with stability constants determined by potentiometric titration data unsupported by other e.g. spectroscopic techniques will not be acceptable nor will solvent extraction data unless supported by other data of interest to inorganic chemists. Unnecessary fragmentation of work is not acceptable.

In addition Polyhedron publishes specially commissioned review articles (Polyhedron Reports) and collections of original research papers (Polyhedron Symposia-in-Print) of appropriate timeliness.

Publication Information: Polyhedron (ISSN 0277-5387). For 2008, volume 27 is scheduled for publication. Subscription prices are available upon request from the Publisher or from the Regional Sales Office nearest you or from this journal's website (http://www.elsevier.com/locate/poly). Further information is available on this journal and other Elsevier products through Elsevier's website (http://www.elsevier.com). Subscriptions are accepted on a prepaid basis only and are entered on a calendar year basis. Issues are sent by standard mail (surface within Europe, air delivery outside Europe). Priority rates are available upon request. Claims for missing issues should be made within six months of the date of dispatch.

Orders, Claims and Journal Enquiries

(no manuscript enquiries)

Please contact the Customer Support Department at the Regional Sales Office nearest you:

Orlando
Elsevier
Customer Service Department
6277 Sea Harbor Drive
Orlando, FL 32887-4800
USA
Tel.: (877) 8397126
[toll free within the USA];
(+1) (407) 5636022
[outside the USA];
Fax: (+1) (407) 3631354
E-mail: JournalCustomerService-usa@elsevier.com

Amsterdam
Elsevier
Customer Service Department
P.O. Box 211
1000 AE Amsterdam
The Netherlands
Tel.: (+31) 20-485-3757
Fax: (+31) 20-485-3432
E-mail: nlinfo-f@elsevier.com

Tokyo
Elsevier K.K.
Customer Service Department
4F Higashi-Azabu, 1-Chome Bldg
1-9-15 Higashi-Azabu
Minato-ku, Tokyo 106-0044
Japan
Tel.: (+81) 3-5561-5037
Fax: (+81) 3-5561-5047
E-mail: jp.info@elsevier.com

Singapore
Elsevier
Customer Service Department
3 Killiney Road
#08-01 Winsland House 1
Singapore 239519
Tel.: (+65) 6349-0222
Fax: (+65) 6733-1510
E-mail: asiainfo@elsevier.com

USA mailing notice: *Polyhedron* (ISSN 0277-5387) is published triweekly by Elsevier Ltd. (P.O. Box 211, 1000 AE Amsterdam, The Netherlands). Annual subscription price in the USA US$ 8198.00 (valid in North, Central and South America), including air speed delivery. Periodical postage rate is paid at Rahway, NJ.
USA POSTMASTER: Send change of address to *Polyhedron*, Elsevier, 6277 Sea Harbor Drive, Orlando, FL 32887-4800.
AIRFREIGHT AND MAILING in the USA by Mercury International Limited, 365 Blair Road, Avenel, NJ 07001.

Advertising Information

Advertising orders and enquiries can be sent to: **South America:** Mr Tino DeCarlo, The Advertising Department, Elsevier Inc., 360 Park Avenue South, New York, NY 10010-1710, USA; tel.: (+1) (212) 633 3815; fax: (+1) (212) 633 3820; e-mail: t.decarlo@elsevier.com. **Europe, USA, Canada and ROW:** Miss Katrina Barton, Commercial Sales, Elsevier, 84 Theobald's Road, London, WCIX 8RR, UK; phone: (+44) (0) 20 7611 4117; fax: (+44) (0) 20 7611 4463; e-mail: commercialsales@elsevier.com

Funding body agreements and policies

Elsevier has established agreements and developed policies to allow authors who publish in Elsevier journals to comply with potential manuscript archiving requirements as specified as conditions of their grant awards. To learn more about existing agreements and policies please visit http://www.elsevier.com/fundingbodies

POLYHEDRON

The International Journal for Inorganic and Organometallic Chemistry

Executive Editors

The Americas
G. Christou
Department of Chemistry, University of Florida,
Gainesville, FL 32611-7200, USA
E-mail: christou@chem.ufl.edu

Rest of the world
C.E. Housecroft
Department of Chemistry, University of Basel,
Spitalstrasse 51, CH-4056 Basel, Switzerland
E-mail: poly-chemie@unibas.ch

Associate Regional Editor for China
T.C.W. Mak
Department of Chemistry, University Science Centre,
The Chinese University of Hong Kong,
Shatin NT, Hong Kong, People's Republic of China
E-mail: tcwmak@cuhk.edu.hk

Polyhedron Reports
Editor
G. Christou *(Gainesville, FL, USA)*

Symposia-in-print
Editor
G. Parkin *(New York, NY, USA)*

Editorial Board

A.G. Blackman *(Dunedin, New Zealand)*
D.C. Bradley *(London, UK)*
A. Brodie *(Palmerston North, New Zealand)*
A. Castiñeiras *(Santiago de Compostela, Spain)*
X.-M. Chen *(Guangzhou, PR China)*
M.H. Chisholm *(Columbus, OH, USA)*
E.C. Constable *(Basel, Switzerland)*
L. Cronin *(Glasgow, UK)*
W.J. Evans *(Irvine, CA, USA)*
L.H. Gade *(Heidelberg, Germany)*
G. Girolami *(Urbana, IL, USA)*
J.-F. Halet *(Rennes, France)*
L. Hubert-Pfalzgraf *(Villeurbanne, France)*
C. Janiak *(Freiburg, Germany)*
C. Kepert *(NSW, Australia)*
P. Kruger *(Canterbury, New Zealand)*
I. Manners *(Bristol, UK)*
S. Perlepes *(Patras, Greece)*
P.P. Power *(Davis, CA, USA)*
T.B. Rauchfuss *(Urbana, IL, USA)*
J. Reedijk *(Leiden, The Netherlands)*
A.L. Rheingold *(Newark, DE, USA)*
M. Rosales Hoz *(Mexico, D.F., Mexico)*
P. Steel *(Christchurch, New Zealand)*
L.K. Thompson *(St John's, NF, Canada)*
M. Yamashita *(Sendai, Japan)*

Aims and Scope

Polyhedron will publish original, fundamental, experimental and theoretical work of the highest quality in all the major areas of inorganic chemistry. These include synthetic chemistry, coordination chemistry, organometallic chemistry, bioinorganic chemistry, and solid-state and materials chemistry. Papers should be complete pieces of work, and the inclusion of results from spectroscopic and/or physical techniques is encouraged. Papers merely reporting the preparation and X-ray structural characterization of only a single compound will not be considered appropriate unless the compound and its structure are particularly interesting.

Similarly, papers concerned solely with stability constants determined by potentiometric titration data unsupported by other e.g. spectroscopic techniques will not be acceptable nor will solvent extraction data unless supported by other data of interest to inorganic chemists. Unnecessary fragmentation of work is not acceptable.

In addition Polyhedron publishes specially commissioned review articles (Polyhedron Reports) and collections of original research papers (Polyhedron Symposia-in-Print) of appropriate timeliness.

Publication Information: Polyhedron (ISSN 0277-5387). For 2008, volume 27 is scheduled for publication. Subscription prices are available upon request from the Publisher or from the Regional Sales Office nearest you or from this journal's website (http://www.elsevier.com/locate/poly). Further information is available on this journal and other Elsevier products through Elsevier's website (http://www.elsevier.com). Subscriptions are accepted on a prepaid basis only and are entered on a calendar year basis. Issues are sent by standard mail (surface within Europe, air delivery outside Europe). Priority rates are available upon request. Claims for missing issues should be made within six months of the date of dispatch.

Orders, Claims and Journal Enquiries

(no manuscript enquiries)
Please contact the Customer Support Department at the Regional Sales Office nearest you:

Orlando
Elsevier
Customer Service Department
6277 Sea Harbor Drive
Orlando, FL 32887-4800
USA
Tel.: (877) 8397126
[toll free within the USA];
(+1) (407) 5636022
[outside the USA];
Fax: (+1) (407) 3631354
E-mail: JournalCustomerService-usa@elsevier.com

Amsterdam
Elsevier
Customer Service Department
P.O. Box 211
1000 AE Amsterdam
The Netherlands
Tel.: (+31) 20-485-3757
Fax: (+31) 20-485-3432
E-mail: nlinfo-f@elsevier.com

Tokyo
Elsevier K.K.
Customer Service Department
4F Higashi-Azabu, 1-Chome Bldg
1-9-15 Higashi-Azabu
Minato-ku, Tokyo 106-0044
Japan
Tel.: (+81) 3-5561-5037
Fax: (+81) 3-5561-5047
E-mail: jp.info@elsevier.com

Singapore
Elsevier
Customer Service Department
3 Killiney Road
#08-01 Winsland House 1
Singapore 239519
Tel.: (+65) 6349-0222
Fax: (+65) 6733-1510
E-mail: asiainfo@elsevier.com

USA mailing notice: *Polyhedron* (ISSN 0277-5387) is published triweekly by Elsevier Ltd. (P.O. Box 211, 1000 AE Amsterdam, The Netherlands). Annual subscription price in the USA US$ 8198.00 (valid in North, Central and South America), including air speed delivery. Periodical postage rate is paid at Rahway, NJ.
USA POSTMASTER: Send change of address to *Polyhedron*, Elsevier, 6277 Sea Harbor Drive, Orlando, FL 32887-4800.
AIRFREIGHT AND MAILING in the USA by Mercury International Limited, 365 Blair Road, Avenel, NJ 07001.

Advertising Information

Advertising orders and enquiries can be sent to: **South America:** Mr Tino DeCarlo, The Advertising Department, Elsevier Inc., 360 Park Avenue South, New York, NY 10010-1710, USA; tel.: (+1) (212) 633 3815; fax: (+1) (212) 633 3820; e-mail: t.decarlo@elsevier.com. **Europe, USA, Canada and ROW:** Miss Katrina Barton, Commercial Sales, Elsevier, 84 Theobald's Road, London, WCIX 8RR, UK; phone: (+44) (0) 20 7611 4117; fax: (+44) (0) 20 7611 4463; e-mail: commercialsales@elsevier.com

Funding body agreements and policies

Elsevier has established agreements and developed policies to allow authors who publish in Elsevier journals to comply with potential manuscript archiving requirements as specified as conditions of their grant awards. To learn more about existing agreements and policies please visit http://www.elsevier.com/fundingbodies

POLYHEDRON

The International Journal for Inorganic and Organometallic Chemistry

Executive Editors

The Americas
G. Christou
Department of Chemistry, University of Florida,
Gainesville, FL 32611-7200, USA
E-mail: christou@chem.ufl.edu

Rest of the world
C.E. Housecroft
Department of Chemistry, University of Basel,
Spitalstrasse 51, CH-4056 Basel, Switzerland
E-mail: poly-chemie@unibas.ch

Associate Regional Editor for China
T.C.W. Mak
Department of Chemistry, University Science Centre,
The Chinese University of Hong Kong,
Shatin NT, Hong Kong, People's Republic of China
E-mail: tcwmak@cuhk.edu.hk

Polyhedron Reports
Editor
G. Christou *(Gainesville, FL, USA)*

Symposia-in-print
Editor
G. Parkin *(New York, NY, USA)*

Editorial Board

A.G. Blackman *(Dunedin, New Zealand)*
D.C. Bradley *(London, UK)*
A. Brodie *(Palmerston North, New Zealand)*
A. Castiñeiras *(Santiago de Compostela, Spain)*
X.-M. Chen *(Guangzhou, PR China)*
M.H. Chisholm *(Columbus, OH, USA)*
E.C. Constable *(Basel, Switzerland)*
L. Cronin *(Glasgow, UK)*
W.J. Evans *(Irvine, CA, USA)*
L.H. Gade *(Heidelberg, Germany)*
G. Girolami *(Urbana, IL, USA)*
J.-F. Halet *(Rennes, France)*
L. Hubert-Pfalzgraf *(Villeurbanne, France)*
C. Janiak *(Freiburg, Germany)*
C. Kepert *(NSW, Australia)*
P. Kruger *(Canterbury, New Zealand)*
I. Manners *(Bristol, UK)*
S. Perlepes *(Patras, Greece)*
P.P. Power *(Davis, CA, USA)*
T.B. Rauchfuss *(Urbana, IL, USA)*
J. Reedijk *(Leiden, The Netherlands)*
A.L. Rheingold *(Newark, DE, USA)*
M. Rosales Hoz *(Mexico, D.F., Mexico)*
P. Steel *(Christchurch, New Zealand)*
L.K. Thompson *(St John's, NF, Canada)*
M. Yamashita *(Sendai, Japan)*

Aims and Scope

Polyhedron will publish original, fundamental, experimental and theoretical work of the highest quality in all the major areas of inorganic chemistry. These include synthetic chemistry, coordination chemistry, organometallic chemistry, bioinorganic chemistry, and solid-state and materials chemistry. Papers should be complete pieces of work, and the inclusion of results from spectroscopic and/or physical techniques is encouraged. Papers merely reporting the preparation and X-ray structural characterization of only a single compound will not be considered appropriate unless the compound and its structure are particularly interesting.

Similarly, papers concerned solely with stability constants determined by potentiometric titration data unsupported by other e.g. spectroscopic techniques will not be acceptable nor will solvent extraction data unless supported by other data of interest to inorganic chemists. Unnecessary fragmentation of work is not acceptable.

In addition Polyhedron publishes specially commissioned review articles (Polyhedron Reports) and collections of original research papers (Polyhedron Symposia-in-Print) of appropriate timeliness.

Publication Information: Polyhedron (ISSN 0277-5387). For 2008, volume 27 is scheduled for publication. Subscription prices are available upon request from the Publisher or from the Regional Sales Office nearest you or from this journal's website (http://www.elsevier.com/locate/poly). Further information is available on this journal and other Elsevier products through Elsevier's website (http://www.elsevier.com). Subscriptions are accepted on a prepaid basis only and are entered on a calendar year basis. Issues are sent by standard mail (surface within Europe, air delivery outside Europe). Priority rates are available upon request. Claims for missing issues should be made within six months of the date of dispatch.

Orders, Claims and Journal Enquiries

(no manuscript enquiries)
Please contact the Customer Support Department at the Regional Sales Office nearest you:

Orlando
Elsevier
Customer Service Department
6277 Sea Harbor Drive
Orlando, FL 32887-4800
USA
Tel.: (877) 8397126
[toll free within the USA];
(+1) (407) 5636022
[outside the USA];
Fax: (+1) (407) 3631354
E-mail: JournalCustomerService-usa@elsevier.com

Amsterdam
Elsevier
Customer Service Department
P.O. Box 211
1000 AE Amsterdam
The Netherlands
Tel.: (+31) 20-485-3757
Fax: (+31) 20-485-3432
E-mail: nlinfo-f@elsevier.com

Tokyo
Elsevier K.K.
Customer Service Department
4F Higashi-Azabu, 1-Chome Bldg
1-9-15 Higashi-Azabu
Minato-ku, Tokyo 106-0044
Japan
Tel.: (+81) 3-5561-5037
Fax: (+81) 3-5561-5047
E-mail: jp.info@elsevier.com

Singapore
Elsevier
Customer Service Department
3 Killiney Road
#08-01 Winsland House 1
Singapore 239519
Tel.: (+65) 6349-0222
Fax: (+65) 6733-1510
E-mail: asiainfo@elsevier.com

USA mailing notice: *Polyhedron* (ISSN 0277-5387) is published triweekly by Elsevier Ltd. (P.O. Box 211, 1000 AE Amsterdam, The Netherlands). Annual subscription price in the USA US$ 8198.00 (valid in North, Central and South America), including air speed delivery. Periodical postage rate is paid at Rahway, NJ.
USA POSTMASTER: Send change of address to *Polyhedron*, Elsevier, 6277 Sea Harbor Drive, Orlando, FL 32887-4800.
AIRFREIGHT AND MAILING in the USA by Mercury International Limited, 365 Blair Road, Avenel, NJ 07001.

Advertising Information

Advertising orders and enquiries can be sent to: **South America:** Mr Tino DeCarlo, The Advertising Department, Elsevier Inc., 360 Park Avenue South, New York, NY 10010-1710, USA; tel.: (+1) (212) 633 3815; fax: (+1) (212) 633 3820; e-mail: t.decarlo@elsevier.com. **Europe, USA, Canada and ROW:** Miss Katrina Barton, Commercial Sales, Elsevier, 84 Theobald's Road, London, WCIX 8RR, UK; phone: (+44) (0) 20 7611 4117; fax: (+44) (0) 20 7611 4463; e-mail: commercialsales@elsevier.com

Funding body agreements and policies

Elsevier has established agreements and developed policies to allow authors who publish in Elsevier journals to comply with potential manuscript archiving requirements as specified as conditions of their grant awards. To learn more about existing agreements and policies please visit http://www.elsevier.com/fundingbodies

POLYHEDRON

The International Journal for Inorganic and Organometallic Chemistry

Executive Editors

The Americas
G. Christou
Department of Chemistry, University of Florida,
Gainesville, FL 32611-7200, USA
E-mail: christou@chem.ufl.edu

Rest of the world
C.E. Housecroft
Department of Chemistry, University of Basel,
Spitalstrasse 51, CH-4056 Basel, Switzerland
E-mail: poly-chemie@unibas.ch

Associate Regional Editor for China
T.C.W. Mak
Department of Chemistry, University Science Centre,
The Chinese University of Hong Kong,
Shatin NT, Hong Kong, People's Republic of China
E-mail: tcwmak@cuhk.edu.hk

Polyhedron Reports
Editor
G. Christou *(Gainesville, FL, USA)*

Symposia-in-print
Editor
G. Parkin *(New York, NY, USA)*

Editorial Board

A.G. Blackman *(Dunedin, New Zealand)*
D.C. Bradley *(London, UK)*
A. Brodie *(Palmerston North, New Zealand)*
A. Castiñeiras *(Santiago de Compostela, Spain)*
X.-M. Chen *(Guangzhou, PR China)*
M.H. Chisholm *(Columbus, OH, USA)*
E.C. Constable *(Basel, Switzerland)*
L. Cronin *(Glasgow, UK)*
W.J. Evans *(Irvine, CA, USA)*
L.H. Gade *(Heidelberg, Germany)*
G. Girolami *(Urbana, IL, USA)*
J.-F. Halet *(Rennes, France)*
L. Hubert-Pfalzgraf *(Villeurbanne, France)*
C. Janiak *(Freiburg, Germany)*
C. Kepert *(NSW, Australia)*
P. Kruger *(Canterbury, New Zealand)*
I. Manners *(Bristol, UK)*
S. Perlepes *(Patras, Greece)*
P.P. Power *(Davis, CA, USA)*
T.B. Rauchfuss *(Urbana, IL, USA)*
J. Reedijk *(Leiden, The Netherlands)*
A.L. Rheingold *(Newark, DE, USA)*
M. Rosales Hoz *(Mexico, D.F., Mexico)*
P. Steel *(Christchurch, New Zealand)*
L.K. Thompson *(St John's, NF, Canada)*
M. Yamashita *(Sendai, Japan)*

Aims and Scope

Polyhedron will publish original, fundamental, experimental and theoretical work of the highest quality in all the major areas of inorganic chemistry. These include synthetic chemistry, coordination chemistry, organometallic chemistry, bioinorganic chemistry, and solid-state and materials chemistry. Papers should be complete pieces of work, and the inclusion of results from spectroscopic and/or physical techniques is encouraged. Papers merely reporting the preparation and X-ray structural characterization of only a single compound will not be considered appropriate unless the compound and its structure are particularly interesting.

Similarly, papers concerned solely with stability constants determined by potentiometric titration data unsupported by other e.g. spectroscopic techniques will not be acceptable nor will solvent extraction data unless supported by other data of interest to inorganic chemists. Unnecessary fragmentation of work is not acceptable.

In addition Polyhedron publishes specially commissioned review articles (Polyhedron Reports) and collections of original research papers (Polyhedron Symposia-in-Print) of appropriate timeliness.

Publication Information: Polyhedron (ISSN 0277-5387). For 2008, volume 27 is scheduled for publication. Subscription prices are available upon request from the Publisher or from the Regional Sales Office nearest you or from this journal's website (http://www.elsevier.com/locate/poly). Further information is available on this journal and other Elsevier products through Elsevier's website (http://www.elsevier.com). Subscriptions are accepted on a prepaid basis only and are entered on a calendar year basis. Issues are sent by standard mail (surface within Europe, air delivery outside Europe). Priority rates are available upon request. Claims for missing issues should be made within six months of the date of dispatch.

Orders, Claims and Journal Enquiries

(no manuscript enquiries)

Please contact the Customer Support Department at the Regional Sales Office nearest you:

Orlando
Elsevier
Customer Service Department
6277 Sea Harbor Drive
Orlando, FL 32887-4800
USA
Tel.: (877) 8397126
[toll free within the USA];
(+1) (407) 5636022
[outside the USA];
Fax: (+1) (407) 3631354
E-mail: JournalCustomerService-usa@elsevier.com

Amsterdam
Elsevier
Customer Service Department
P.O. Box 211
1000 AE Amsterdam
The Netherlands
Tel.: (+31) 20-485-3757
Fax: (+31) 20-485-3432
E-mail: nlinfo-f@elsevier.com

Tokyo
Elsevier K.K.
Customer Service Department
4F Higashi-Azabu, 1-Chome Bldg
1-9-15 Higashi-Azabu
Minato-ku, Tokyo 106-0044
Japan
Tel.: (+81) 3-5561-5037
Fax: (+81) 3-5561-5047
E-mail: jp.info@elsevier.com

Singapore
Elsevier
Customer Service Department
3 Killiney Road
#08-01 Winsland House 1
Singapore 239519
Tel.: (+65) 6349-0222
Fax: (+65) 6733-1510
E-mail: asiainfo@elsevier.com

USA mailing notice: *Polyhedron* (ISSN 0277-5387) is published triweekly by Elsevier Ltd. (P.O. Box 211, 1000 AE Amsterdam, The Netherlands). Annual subscription price in the USA US$ 8198.00 (valid in North, Central and South America), including air speed delivery. Periodical postage rate is paid at Rahway, NJ.

USA POSTMASTER: Send change of address to *Polyhedron*, Elsevier, 6277 Sea Harbor Drive, Orlando, FL 32887-4800.

AIRFREIGHT AND MAILING in the USA by Mercury International Limited, 365 Blair Road, Avenel, NJ 07001.

Advertising Information

Advertising orders and enquiries can be sent to: **South America:** Mr Tino DeCarlo, The Advertising Department, Elsevier Inc., 360 Park Avenue South, New York, NY 10010-1710, USA; tel.: (+1) (212) 633 3815; fax: (+1) (212) 633 3820; e-mail: t.decarlo@elsevier.com. **Europe, USA, Canada and ROW:** Miss Katrina Barton, Commercial Sales, Elsevier, 84 Theobald's Road, London, WCIX 8RR, UK; phone: (+44) (0) 20 7611 4117; fax: (+44) (0) 20 7611 4463; e-mail: commercialsales@elsevier.com

Funding body agreements and policies

Elsevier has established agreements and developed policies to allow authors who publish in Elsevier journals to comply with potential manuscript archiving requirements as specified as conditions of their grant awards. To learn more about existing agreements and policies please visit http://www.elsevier.com/fundingbodies

POLYHEDRON

The International Journal for Inorganic and Organometallic Chemistry

Executive Editors

The Americas
G. Christou
Department of Chemistry, University of Florida,
Gainesville, FL 32611-7200, USA
E-mail: christou@chem.ufl.edu

Rest of the world
C.E. Housecroft
Department of Chemistry, University of Basel,
Spitalstrasse 51, CH-4056 Basel, Switzerland
E-mail: poly-chemie@unibas.ch

Associate Regional Editor for China
T.C.W. Mak
Department of Chemistry, University Science Centre,
The Chinese University of Hong Kong,
Shatin NT, Hong Kong, People's Republic of China
E-mail: tcwmak@cuhk.edu.hk

Polyhedron Reports
Editor
G. Christou *(Gainesville, FL, USA)*

Symposia-in-print
Editor
G. Parkin *(New York, NY, USA)*

Editorial Board

A.G. Blackman *(Dunedin, New Zealand)*
D.C. Bradley *(London, UK)*
A. Brodie *(Palmerston North, New Zealand)*
A. Castiñeiras *(Santiago de Compostela, Spain)*
X.-M. Chen *(Guangzhou, PR China)*
M.H. Chisholm *(Columbus, OH, USA)*
E.C. Constable *(Basel, Switzerland)*
L. Cronin *(Glasgow, UK)*
W.J. Evans *(Irvine, CA, USA)*
L.H. Gade *(Heidelberg, Germany)*
G. Girolami *(Urbana, IL, USA)*
J.-F. Halet *(Rennes, France)*
L. Hubert-Pfalzgraf *(Villeurbanne, France)*
C. Janiak *(Freiburg, Germany)*
C. Kepert *(NSW, Australia)*
P. Kruger *(Canterbury, New Zealand)*
I. Manners *(Bristol, UK)*
S. Perlepes *(Patras, Greece)*
P.P. Power *(Davis, CA, USA)*
T.B. Rauchfuss *(Urbana, IL, USA)*
J. Reedijk *(Leiden, The Netherlands)*
A.L. Rheingold *(Newark, DE, USA)*
M. Rosales Hoz *(Mexico, D.F., Mexico)*
P. Steel *(Christchurch, New Zealand)*
L.K. Thompson *(St John's, NF, Canada)*
M. Yamashita *(Sendai, Japan)*

Aims and Scope

Polyhedron will publish original, fundamental, experimental and theoretical work of the highest quality in all the major areas of inorganic chemistry. These include synthetic chemistry, coordination chemistry, organometallic chemistry, bioinorganic chemistry, and solid-state and materials chemistry. Papers should be complete pieces of work, and the inclusion of results from spectroscopic and/or physical techniques is encouraged. Papers merely reporting the preparation and X-ray structural characterization of only a single compound will not be considered appropriate unless the compound and its structure are particularly interesting.

Similarly, papers concerned solely with stability constants determined by potentiometric titration data unsupported by other e.g. spectroscopic techniques will not be acceptable nor will solvent extraction data unless supported by other data of interest to inorganic chemists. Unnecessary fragmentation of work is not acceptable.

In addition Polyhedron publishes specially commissioned review articles (Polyhedron Reports) and collections of original research papers (Polyhedron Symposia-in-Print) of appropriate timeliness.

Publication Information: Polyhedron (ISSN 0277-5387). For 2008, volume 27 is scheduled for publication. Subscription prices are available upon request from the Publisher or from the Regional Sales Office nearest you or from this journal's website (http://www.elsevier.com/locate/poly). Further information is available on this journal and other Elsevier products through Elsevier's website (http://www.elsevier.com). Subscriptions are accepted on a prepaid basis only and are entered on a calendar year basis. Issues are sent by standard mail (surface within Europe, air delivery outside Europe). Priority rates are available upon request. Claims for missing issues should be made within six months of the date of dispatch.

Orders, Claims and Journal Enquiries

(no manuscript enquiries)
Please contact the Customer Support Department at the Regional Sales Office nearest you:

Orlando
Elsevier
Customer Service Department
6277 Sea Harbor Drive
Orlando, FL 32887-4800
USA
Tel.: (877) 8397126
[toll free within the USA];
(+1) (407) 5636022
[outside the USA];
Fax: (+1) (407) 3631354
E-mail: JournalCustomerService-usa@elsevier.com

Amsterdam
Elsevier
Customer Service Department
P.O. Box 211
1000 AE Amsterdam
The Netherlands
Tel.: (+31) 20-485-3757
Fax: (+31) 20-485-3432
E-mail: nlinfo-f@elsevier.com

Tokyo
Elsevier K.K.
Customer Service Department
4F Higashi-Azabu, 1-Chome Bldg
1-9-15 Higashi-Azabu
Minato-ku, Tokyo 106-0044
Japan
Tel.: (+81) 3-5561-5037
Fax: (+81) 3-5561-5047
E-mail: jp.info@elsevier.com

Singapore
Elsevier
Customer Service Department
3 Killiney Road
#08-01 Winsland House 1
Singapore 239519
Tel.: (+65) 6349-0222
Fax: (+65) 6733-1510
E-mail: asiainfo@elsevier.com

USA mailing notice: *Polyhedron* (ISSN 0277-5387) is published triweekly by Elsevier Ltd. (P.O. Box 211, 1000 AE Amsterdam, The Netherlands). Annual subscription price in the USA US$ 8198.00 (valid in North, Central and South America), including air speed delivery. Periodical postage rate is paid at Rahway, NJ.
USA POSTMASTER: Send change of address to *Polyhedron*, Elsevier, 6277 Sea Harbor Drive, Orlando, FL 32887-4800.
AIRFREIGHT AND MAILING in the USA by Mercury International Limited, 365 Blair Road, Avenel, NJ 07001.

Advertising Information

Advertising orders and enquiries can be sent to: **South America:** Mr Tino DeCarlo, The Advertising Department, Elsevier Inc., 360 Park Avenue South, New York, NY 10010-1710, USA; tel.: (+1) (212) 633 3815; fax: (+1) (212) 633 3820; e-mail: t.decarlo@elsevier.com. **Europe, USA, Canada and ROW:** Miss Katrina Barton, Commercial Sales, Elsevier, 84 Theobald's Road, London, WCIX 8RR, UK; phone: (+44) (0) 20 7611 4117; fax: (+44) (0) 20 7611 4463; e-mail: commercialsales@elsevier.com

Funding body agreements and policies

Elsevier has established agreements and developed policies to allow authors who publish in Elsevier journals to comply with potential manuscript archiving requirements as specified as conditions of their grant awards. To learn more about existing agreements and policies please visit http://www.elsevier.com/fundingbodies

POLYHEDRON

The International Journal for Inorganic and Organometallic Chemistry

Executive Editors

The Americas
G. Christou
Department of Chemistry, University of Florida,
Gainesville, FL 32611-7200, USA
E-mail: christou@chem.ufl.edu

Rest of the world
C.E. Housecroft
Department of Chemistry, University of Basel,
Spitalstrasse 51, CH-4056 Basel, Switzerland
E-mail: poly-chemie@unibas.ch

Associate Regional Editor for China
T.C.W. Mak
Department of Chemistry, University Science Centre,
The Chinese University of Hong Kong,
Shatin NT, Hong Kong, People's Republic of China
E-mail: tcwmak@cuhk.edu.hk

Polyhedron Reports
Editor
G. Christou *(Gainesville, FL, USA)*

Symposia-in-print
Editor
G. Parkin *(New York, NY, USA)*

Editorial Board

A.G. Blackman *(Dunedin, New Zealand)*
D.C. Bradley *(London, UK)*
A. Brodie *(Palmerston North, New Zealand)*
A. Castiñeiras *(Santiago de Compostela, Spain)*
X.-M. Chen *(Guangzhou, PR China)*
M.H. Chisholm *(Columbus, OH, USA)*
E.C. Constable *(Basel, Switzerland)*
L. Cronin *(Glasgow, UK)*
W.J. Evans *(Irvine, CA, USA)*
L.H. Gade *(Heidelberg, Germany)*
G. Girolami *(Urbana, IL, USA)*
J.-F. Halet *(Rennes, France)*
L. Hubert-Pfalzgraf *(Villeurbanne, France)*
C. Janiak *(Freiburg, Germany)*
C. Kepert *(NSW, Australia)*
P. Kruger *(Canterbury, New Zealand)*
I. Manners *(Bristol, UK)*
S. Perlepes *(Patras, Greece)*
P.P. Power *(Davis, CA, USA)*
T.B. Rauchfuss *(Urbana, IL, USA)*
J. Reedijk *(Leiden, The Netherlands)*
A.L. Rheingold *(Newark, DE, USA)*
M. Rosales Hoz *(Mexico, D.F., Mexico)*
P. Steel *(Christchurch, New Zealand)*
L.K. Thompson *(St John's, NF, Canada)*
M. Yamashita *(Sendai, Japan)*

Aims and Scope

Polyhedron will publish original, fundamental, experimental and theoretical work of the highest quality in all the major areas of inorganic chemistry. These include synthetic chemistry, coordination chemistry, organometallic chemistry, bioinorganic chemistry, and solid-state and materials chemistry. Papers should be complete pieces of work, and the inclusion of results from spectroscopic and/or physical techniques is encouraged. Papers merely reporting the preparation and X-ray structural characterization of only a single compound will not be considered appropriate unless the compound and its structure are particularly interesting.

Similarly, papers concerned solely with stability constants determined by potentiometric titration data unsupported by other e.g. spectroscopic techniques will not be acceptable nor will solvent extraction data unless supported by other data of interest to inorganic chemists. Unnecessary fragmentation of work is not acceptable.

In addition Polyhedron publishes specially commissioned review articles (Polyhedron Reports) and collections of original research papers (Polyhedron Symposia-in-Print) of appropriate timeliness.

Publication Information: Polyhedron (ISSN 0277-5387). For 2008, volume 27 is scheduled for publication. Subscription prices are available upon request from the Publisher or from the Regional Sales Office nearest you or from this journal's website (http://www.elsevier.com/locate/poly). Further information is available on this journal and other Elsevier products through Elsevier's website (http://www.elsevier.com). Subscriptions are accepted on a prepaid basis only and are entered on a calendar year basis. Issues are sent by standard mail (surface within Europe, air delivery outside Europe). Priority rates are available upon request. Claims for missing issues should be made within six months of the date of dispatch.

Orders, Claims and Journal Enquiries

(no manuscript enquiries)

Please contact the Customer Support Department at the Regional Sales Office nearest you:

Orlando
Elsevier
Customer Service Department
6277 Sea Harbor Drive
Orlando, FL 32887-4800
USA
Tel.: (877) 8397126
[toll free within the USA];
(+1) (407) 5636022
[outside the USA];
Fax: (+1) (407) 3631354
E-mail: JournalCustomerService-usa@elsevier.com

Amsterdam
Elsevier
Customer Service Department
P.O. Box 211
1000 AE Amsterdam
The Netherlands
Tel.: (+31) 20-485-3757
Fax: (+31) 20-485-3432
E-mail: nlinfo-f@elsevier.com

Tokyo
Elsevier K.K.
Customer Service Department
4F Higashi-Azabu, 1-Chome Bldg
1-9-15 Higashi-Azabu
Minato-ku, Tokyo 106-0044
Japan
Tel.: (+81) 3-5561-5037
Fax: (+81) 3-5561-5047
E-mail: jp.info@elsevier.com

Singapore
Elsevier
Customer Service Department
3 Killiney Road
#08-01 Winsland House 1
Singapore 239519
Tel.: (+65) 6349-0222
Fax: (+65) 6733-1510
E-mail: asiainfo@elsevier.com

USA mailing notice: *Polyhedron* (ISSN 0277-5387) is published triweekly by Elsevier Ltd. (P.O. Box 211, 1000 AE Amsterdam, The Netherlands). Annual subscription price in the USA US$ 8198.00 (valid in North, Central and South America), including air speed delivery. Periodical postage rate is paid at Rahway, NJ.
USA POSTMASTER: Send change of address to *Polyhedron*, Elsevier, 6277 Sea Harbor Drive, Orlando, FL 32887-4800.
AIRFREIGHT AND MAILING in the USA by Mercury International Limited, 365 Blair Road, Avenel, NJ 07001.

Advertising Information

Advertising orders and enquiries can be sent to: **South America:** Mr Tino DeCarlo, The Advertising Department, Elsevier Inc., 360 Park Avenue South, New York, NY 10010-1710, USA; tel.: (+1) (212) 633 3815; fax: (+1) (212) 633 3820; e-mail: t.decarlo@elsevier.com. **Europe, USA, Canada and ROW:** Miss Katrina Barton, Commercial Sales, Elsevier, 84 Theobald's Road, London, WCIX 8RR, UK; phone: (+44) (0) 20 7611 4117; fax: (+44) (0) 20 7611 4463; e-mail: commercialsales@elsevier.com

Funding body agreements and policies

Elsevier has established agreements and developed policies to allow authors who publish in Elsevier journals to comply with potential manuscript archiving requirements as specified as conditions of their grant awards. To learn more about existing agreements and policies please visit http://www.elsevier.com/fundingbodies

POLYHEDRON

The International Journal for Inorganic and Organometallic Chemistry

Executive Editors

The Americas
G. Christou
Department of Chemistry, University of Florida,
Gainesville, FL 32611-7200, USA
E-mail: christou@chem.ufl.edu

Rest of the world
C.E. Housecroft
Department of Chemistry, University of Basel,
Spitalstrasse 51, CH-4056 Basel, Switzerland
E-mail: poly-chemie@unibas.ch

Associate Regional Editor for China
T.C.W. Mak
Department of Chemistry, University Science Centre,
The Chinese University of Hong Kong,
Shatin NT, Hong Kong, People's Republic of China
E-mail: tcwmak@cuhk.edu.hk

Polyhedron Reports
Editor
G. Christou *(Gainesville, FL, USA)*

Symposia-in-print
Editor
G. Parkin *(New York, NY, USA)*

Editorial Board

A.G. Blackman *(Dunedin, New Zealand)*
D.C. Bradley *(London, UK)*
A. Brodie *(Palmerston North, New Zealand)*
A. Castiñeiras *(Santiago de Compostela, Spain)*
X.-M. Chen *(Guangzhou, PR China)*
M.H. Chisholm *(Columbus, OH, USA)*
E.C. Constable *(Basel, Switzerland)*
L. Cronin *(Glasgow, UK)*
W.J. Evans *(Irvine, CA, USA)*
L.H. Gade *(Heidelberg, Germany)*
G. Girolami *(Urbana, IL, USA)*
J.-F. Halet *(Rennes, France)*
L. Hubert-Pfalzgraf *(Villeurbanne, France)*
C. Janiak *(Freiburg, Germany)*
C. Kepert *(NSW, Australia)*
P. Kruger *(Canterbury, New Zealand)*
I. Manners *(Bristol, UK)*
S. Perlepes *(Patras, Greece)*
P.P. Power *(Davis, CA, USA)*
T.B. Rauchfuss *(Urbana, IL, USA)*
J. Reedijk *(Leiden, The Netherlands)*
A.L. Rheingold *(Newark, DE, USA)*
M. Rosales Hoz *(Mexico, D.F., Mexico)*
P. Steel *(Christchurch, New Zealand)*
L.K. Thompson *(St John's, NF, Canada)*
M. Yamashita *(Sendai, Japan)*

Aims and Scope

Polyhedron will publish original, fundamental, experimental and theoretical work of the highest quality in all the major areas of inorganic chemistry. These include synthetic chemistry, coordination chemistry, organometallic chemistry, bioinorganic chemistry, and solid-state and materials chemistry. Papers should be complete pieces of work, and the inclusion of results from spectroscopic and/or physical techniques is encouraged. Papers merely reporting the preparation and X-ray structural characterization of only a single compound will not be considered appropriate unless the compound and its structure are particularly interesting.

Similarly, papers concerned solely with stability constants determined by potentiometric titration data unsupported by other e.g. spectroscopic techniques will not be acceptable nor will solvent extraction data unless supported by other data of interest to inorganic chemists. Unnecessary fragmentation of work is not acceptable.

In addition Polyhedron publishes specially commissioned review articles (Polyhedron Reports) and collections of original research papers (Polyhedron Symposia-in-Print) of appropriate timeliness.

Publication Information: Polyhedron (ISSN 0277-5387). For 2008, volume 27 is scheduled for publication. Subscription prices are available upon request from the Publisher or from the Regional Sales Office nearest you or from this journal's website (http://www.elsevier.com/locate/poly). Further information is available on this journal and other Elsevier products through Elsevier's website (http://www.elsevier.com). Subscriptions are accepted on a prepaid basis only and are entered on a calendar year basis. Issues are sent by standard mail (surface within Europe, air delivery outside Europe). Priority rates are available upon request. Claims for missing issues should be made within six months of the date of dispatch.

Orders, Claims and Journal Enquiries

(no manuscript enquiries)
Please contact the Customer Support Department at the Regional Sales Office nearest you:

Orlando
Elsevier
Customer Service Department
6277 Sea Harbor Drive
Orlando, FL 32887-4800
USA
Tel.: (877) 8397126
[toll free within the USA];
(+1) (407) 5636022
[outside the USA];
Fax: (+1) (407) 3631354
E-mail: JournalCustomerService-usa@elsevier.com

Amsterdam
Elsevier
Customer Service Department
P.O. Box 211
1000 AE Amsterdam
The Netherlands
Tel.: (+31) 20-485-3757
Fax: (+31) 20-485-3432
E-mail: nlinfo-f@elsevier.com

Tokyo
Elsevier K.K.
Customer Service Department
4F Higashi-Azabu, 1-Chome Bldg
1-9-15 Higashi-Azabu
Minato-ku, Tokyo 106-0044
Japan
Tel.: (+81) 3-5561-5037
Fax: (+81) 3-5561-5047
E-mail: jp.info@elsevier.com

Singapore
Elsevier
Customer Service Department
3 Killiney Road
#08-01 Winsland House 1
Singapore 239519
Tel.: (+65) 6349-0222
Fax: (+65) 6733-1510
E-mail: asiainfo@elsevier.com

USA mailing notice: *Polyhedron* (ISSN 0277-5387) is published triweekly by Elsevier Ltd. (P.O. Box 211, 1000 AE Amsterdam, The Netherlands). Annual subscription price in the USA US$ 8198.00 (valid in North, Central and South America), including air speed delivery. Periodical postage rate is paid at Rahway, NJ.
USA POSTMASTER: Send change of address to *Polyhedron*, Elsevier, 6277 Sea Harbor Drive, Orlando, FL 32887-4800.
AIRFREIGHT AND MAILING in the USA by Mercury International Limited, 365 Blair Road, Avenel, NJ 07001.

Advertising Information

Advertising orders and enquiries can be sent to: **South America:** Mr Tino DeCarlo, The Advertising Department, Elsevier Inc., 360 Park Avenue South, New York, NY 10010-1710, USA; tel.: (+1) (212) 633 3815; fax: (+1) (212) 633 3820; e-mail: t.decarlo@elsevier.com. **Europe, USA, Canada and ROW:** Miss Katrina Barton, Commercial Sales, Elsevier, 84 Theobald's Road, London, WCIX 8RR, UK; phone: (+44) (0) 20 7611 4117; fax: (+44) (0) 20 7611 4463; e-mail: commercialsales@elsevier.com

Funding body agreements and policies

Elsevier has established agreements and developed policies to allow authors who publish in Elsevier journals to comply with potential manuscript archiving requirements as specified as conditions of their grant awards. To learn more about existing agreements and policies please visit http://www.elsevier.com/fundingbodies

POLYHEDRON

The International Journal for Inorganic and Organometallic Chemistry

Executive Editors

The Americas
G. Christou
Department of Chemistry, University of Florida,
Gainesville, FL 32611-7200, USA
E-mail: christou@chem.ufl.edu

Rest of the world
C.E. Housecroft
Department of Chemistry, University of Basel,
Spitalstrasse 51, CH-4056 Basel, Switzerland
E-mail: poly-chemie@unibas.ch

Associate Regional Editor for China
T.C.W. Mak
Department of Chemistry, University Science Centre,
The Chinese University of Hong Kong,
Shatin NT, Hong Kong, People's Republic of China
E-mail: tcwmak@cuhk.edu.hk

Polyhedron Reports
Editor
G. Christou *(Gainesville, FL, USA)*

Symposia-in-print
Editor
G. Parkin *(New York, NY, USA)*

Editorial Board

A.G. Blackman *(Dunedin, New Zealand)*
D.C. Bradley *(London, UK)*
A. Brodie *(Palmerston North, New Zealand)*
A. Castiñeiras *(Santiago de Compostela, Spain)*
X.-M. Chen *(Guangzhou, PR China)*
M.H. Chisholm *(Columbus, OH, USA)*
E.C. Constable *(Basel, Switzerland)*
L. Cronin *(Glasgow, UK)*
W.J. Evans *(Irvine, CA, USA)*
L.H. Gade *(Heidelberg, Germany)*
G. Girolami *(Urbana, IL, USA)*
J.-F. Halet *(Rennes, France)*
L. Hubert-Pfalzgraf *(Villeurbanne, France)*
C. Janiak *(Freiburg, Germany)*
C. Kepert *(NSW, Australia)*
P. Kruger *(Canterbury, New Zealand)*
I. Manners *(Bristol, UK)*
S. Perlepes *(Patras, Greece)*
P.P. Power *(Davis, CA, USA)*
T.B. Rauchfuss *(Urbana, IL, USA)*
J. Reedijk *(Leiden, The Netherlands)*
A.L. Rheingold *(Newark, DE, USA)*
M. Rosales Hoz *(Mexico, D.F., Mexico)*
P. Steel *(Christchurch, New Zealand)*
L.K. Thompson *(St John's, NF, Canada)*
M. Yamashita *(Sendai, Japan)*

Aims and Scope

Polyhedron will publish original, fundamental, experimental and theoretical work of the highest quality in all the major areas of inorganic chemistry. These include synthetic chemistry, coordination chemistry, organometallic chemistry, bioinorganic chemistry, and solid-state and materials chemistry. Papers should be complete pieces of work, and the inclusion of results from spectroscopic and/or physical techniques is encouraged. Papers merely reporting the preparation and X-ray structural characterization of only a single compound will not be considered appropriate unless the compound and its structure are particularly interesting.

Similarly, papers concerned solely with stability constants determined by potentiometric titration data unsupported by other e.g. spectroscopic techniques will not be acceptable nor will solvent extraction data unless supported by other data of interest to inorganic chemists. Unnecessary fragmentation of work is not acceptable.

In addition Polyhedron publishes specially commissioned review articles (Polyhedron Reports) and collections of original research papers (Polyhedron Symposia-in-Print) of appropriate timeliness.

Publication Information: Polyhedron (ISSN 0277-5387). For 2008, volume 27 is scheduled for publication. Subscription prices are available upon request from the Publisher or from the Regional Sales Office nearest you or from this journal's website (http://www.elsevier.com/locate/poly). Further information is available on this journal and other Elsevier products through Elsevier's website (http://www.elsevier.com). Subscriptions are accepted on a prepaid basis only and are entered on a calendar year basis. Issues are sent by standard mail (surface within Europe, air delivery outside Europe). Priority rates are available upon request. Claims for missing issues should be made within six months of the date of dispatch.

Orders, Claims and Journal Enquiries

(no manuscript enquiries)

Please contact the Customer Support Department at the Regional Sales Office nearest you:

Orlando
Elsevier
Customer Service Department
6277 Sea Harbor Drive
Orlando, FL 32887-4800
USA
Tel.: (877) 8397126 or (800) 6542452 [toll free numbers for US customers];
(+1) (407) 3454020 or
(+1) (407) 3454000 [customers outside US]
Fax: (+1) (407) 3631354 or
(+1) (407) 3639661
E-mail: usjcs@elsevier.com or elspcs@elsevier.com

Amsterdam
Elsevier
Customer Service Department
P.O. Box 211
1000 AE Amsterdam
The Netherlands
Tel.: (+31) 20-485-3757
Fax: (+31) 20-485-3432
E-mail: nlinfo-f@elsevier.com

Tokyo
Elsevier K.K.
Customer Service Department
4F Higashi-Azabu, 1-Chome Bldg
1-9-15 Higashi-Azabu
Minato-ku, Tokyo 106-0044
Japan
Tel.: (+81) 3-5561-5037
Fax: (+81) 3-5561-5047
E-mail: jp.info@elsevier.com

Singapore
Elsevier
Customer Service Department
3 Killiney Road
#08-01 Winsland House 1
Singapore 239519
Tel.: (+65) 6349-0222
Fax: (+65) 6733-1510
E-mail: asiainfo@elsevier.com

USA mailing notice: *Polyhedron* (ISSN 0277-5387) is published triweekly by Elsevier Ltd. (P.O. Box 211, 1000 AE Amsterdam, The Netherlands). Annual subscription price in the USA US$ 8198.00 (valid in North, Central and South America), including air speed delivery. Periodical postage rate is paid at Rahway, NJ.

USA POSTMASTER: Send change of address to *Polyhedron*, Elsevier, 6277 Sea Harbor Drive, Orlando, FL 32887-4800.

AIRFREIGHT AND MAILING in the USA by Mercury International Limited, 365 Blair Road, Avenel, NJ 07001.

Advertising Information

Advertising orders and enquiries can be sent to: **South America:** Mr Tino DeCarlo, The Advertising Department, Elsevier Inc., 360 Park Avenue South, New York, NY 10010-1710, USA; tel.: (+1) (212) 633 3815; fax: (+1) (212) 633 3820; e-mail: t.decarlo@elsevier.com. **Europe, USA, Canada and ROW:** Miss Katrina Barton, Commercial Sales, Elsevier, 84 Theobald's Road, London, WCIX 8RR, UK; phone: (+44) (0) 20 7611 4117; fax: (+44) (0) 20 7611 4463; e-mail: commercialsales@elsevier.com

Funding body agreements and policies

Elsevier has established agreements and developed policies to allow authors who publish in Elsevier journals to comply with potential manuscript archiving requirements as specified as conditions of their grant awards. To learn more about existing agreements and policies please visit http://www.elsevier.com/fundingbodies

POLYHEDRON

The International Journal for Inorganic and Organometallic Chemistry

Executive Editors

The Americas
G. Christou
Department of Chemistry, University of Florida,
Gainesville, FL 32611-7200, USA
E-mail: christou@chem.ufl.edu

Rest of the world
C.E. Housecroft
Department of Chemistry, University of Basel,
Spitalstrasse 51, CH-4056 Basel, Switzerland
E-mail: poly-chemie@unibas.ch

Associate Regional Editor for China
T.C.W. Mak
Department of Chemistry, University Science Centre,
The Chinese University of Hong Kong,
Shatin NT, Hong Kong, People's Republic of China
E-mail: tcwmak@cuhk.edu.hk

Polyhedron Reports
Editor
G. Christou *(Gainesville, FL, USA)*

Symposia-in-print
Editor
G. Parkin *(New York, NY, USA)*

Editorial Board
A.G. Blackman *(Dunedin, New Zealand)*
D.C. Bradley *(London, UK)*
A. Brodie *(Palmerston North, New Zealand)*
A. Castiñeiras *(Santiago de Compostela, Spain)*
X.-M. Chen *(Guangzhou, PR China)*
M.H. Chisholm *(Columbus, OH, USA)*
E.C. Constable *(Basel, Switzerland)*
L. Cronin *(Glasgow, UK)*
W.J. Evans *(Irvine, CA, USA)*
L.H. Gade *(Heidelberg, Germany)*
G. Girolami *(Urbana, IL, USA)*
J.-F. Halet *(Rennes, France)*
L. Hubert-Pfalzgraf *(Villeurbanne, France)*
C. Janiak *(Freiburg, Germany)*
C. Kepert *(NSW, Australia)*
P. Kruger *(Canterbury, New Zealand)*
I. Manners *(Bristol, UK)*
S. Perlepes *(Patras, Greece)*
P.P. Power *(Davis, CA, USA)*
T.B. Rauchfuss *(Urbana, IL, USA)*
J. Reedijk *(Leiden, The Netherlands)*
A.L. Rheingold *(Newark, DE, USA)*
M. Rosales Hoz *(Mexico, D.F., Mexico)*
P. Steel *(Christchurch, New Zealand)*
L.K. Thompson *(St John's, NF, Canada)*
M. Yamashita *(Sendai, Japan)*

Aims and Scope

Polyhedron will publish original, fundamental, experimental and theoretical work of the highest quality in all the major areas of inorganic chemistry. These include synthetic chemistry, coordination chemistry, organometallic chemistry, bioinorganic chemistry, and solid-state and materials chemistry. Papers should be complete pieces of work, and the inclusion of results from spectroscopic and/or physical techniques is encouraged. Papers merely reporting the preparation and X-ray structural characterization of only a single compound will not be considered appropriate unless the compound and its structure are particularly interesting.

Similarly, papers concerned solely with stability constants determined by potentiometric titration data unsupported by other e.g. spectroscopic techniques will not be acceptable nor will solvent extraction data unless supported by other data of interest to inorganic chemists. Unnecessary fragmentation of work is not acceptable.

In addition Polyhedron publishes specially commissioned review articles (Polyhedron Reports) and collections of original research papers (Polyhedron Symposia-in-Print) of appropriate timeliness.

Publication Information: Polyhedron (ISSN 0277-5387). For 2008, volume 27 is scheduled for publication. Subscription prices are available upon request from the Publisher or from the Regional Sales Office nearest you or from this journal's website (http://www.elsevier.com/locate/poly). Further information is available on this journal and other Elsevier products through Elsevier's website (http://www.elsevier.com). Subscriptions are accepted on a prepaid basis only and are entered on a calendar year basis. Issues are sent by standard mail (surface within Europe, air delivery outside Europe). Priority rates are available upon request. Claims for missing issues should be made within six months of the date of dispatch.

Orders, Claims and Journal Enquiries

(no manuscript enquiries)

Please contact the Customer Support Department at the Regional Sales Office nearest you:

Orlando
Elsevier
Customer Service Department
6277 Sea Harbor Drive
Orlando, FL 32887-4800
USA
Tel.: (877) 8397126 or (800) 6542452 [toll free numbers for US customers];
(+1) (407) 3454020 or
(+1) (407) 3454000 [customers outside US]
Fax: (+1) (407) 3631354 or
(+1) (407) 3639661
E-mail: usjcs@elsevier.com or elspcs@elsevier.com

Amsterdam
Elsevier
Customer Service Department
P.O. Box 211
1000 AE Amsterdam
The Netherlands
Tel.: (+31) 20-485-3757
Fax: (+31) 20-485-3432
E-mail: nlinfo-f@elsevier.com

Tokyo
Elsevier K.K.
Customer Service Department
4F Higashi-Azabu, 1-Chome Bldg
1-9-15 Higashi-Azabu
Minato-ku, Tokyo 106-0044
Japan
Tel.: (+81) 3-5561-5037
Fax: (+81) 3-5561-5047
E-mail: jp.info@elsevier.com

Singapore
Elsevier
Customer Service Department
3 Killiney Road
#08-01 Winsland House 1
Singapore 239519
Tel.: (+65) 6349-0222
Fax: (+65) 6733-1510
E-mail: asiainfo@elsevier.com

USA mailing notice: *Polyhedron* (ISSN 0277-5387) is published triweekly by Elsevier Ltd. (P.O. Box 211, 1000 AE Amsterdam, The Netherlands). Annual subscription price in the USA US$ 8198.00 (valid in North, Central and South America), including air speed delivery. Periodical postage rate is paid at Rahway, NJ.
USA POSTMASTER: Send change of address to *Polyhedron*, Elsevier, 6277 Sea Harbor Drive, Orlando, FL 32887-4800.
AIRFREIGHT AND MAILING in the USA by Mercury International Limited, 365 Blair Road, Avenel, NJ 07001.

Advertising Information

Advertising orders and enquiries can be sent to: **South America:** Mr Tino DeCarlo, The Advertising Department, Elsevier Inc., 360 Park Avenue South, New York, NY 10010-1710, USA; tel.: (+1) (212) 633 3815; fax: (+1) (212) 633 3820; e-mail: t.decarlo@elsevier.com. **Europe, USA, Canada and ROW:** Miss Katrina Barton, Commercial Sales, Elsevier, 84 Theobald's Road, London, WCIX 8RR, UK; phone: (+44) (0) 20 7611 4117; fax: (+44) (0) 20 7611 4463; e-mail: commercialsales@elsevier.com

Funding body agreements and policies

Elsevier has established agreements and developed policies to allow authors who publish in Elsevier journals to comply with potential manuscript archiving requirements as specified as conditions of their grant awards. To learn more about existing agreements and policies please visit http://www.elsevier.com/fundingbodies

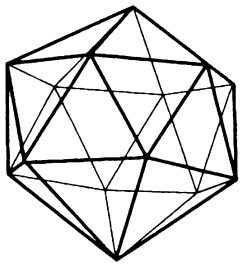

POLYHEDRON

The International Journal for Inorganic and Organometallic Chemistry

Founding Editor: **Sir Geoffrey Wilkinson**✠

Executive Editors

Regional Editors:

The Americas
G. Christou
Department of Chemistry, University of Florida, Gainesville, FL 32611-7200, USA
E-mail: christou@chem.ufl.edu

Rest of the world
C.E. Housecroft
Department of Chemistry, University of Basel, CH-4056 Basel, Switzerland
E-mail: poly-chemie@unibas.ch

Associate Regional Editor for China
T.C.W. Mak
Department of Chemistry, University Science Centre, The Chinese University of Hong Kong, Shatin NT, Hong Kong, People's Republic of China
E-mail: tcwmak@cuhk.hk

Polyhedron Reports Editor
G. Christou
Department of Chemistry, University of Florida, Gainesville, FL 32611-7200, USA
E-mail: christou@chem.ufl.edu

Symposia-in-print Editor
G. Parkin
Department of Chemistry, Columbia University, New York, NY 10027, USA
E-mail: parkin@chem.columbia.edu

Editorial Board

A.G. Blackman (Dunedin, New Zealand)
D.C. Bradley (London, UK)
A. Brodie (Palmerston North, New Zealand)
A. Castiñeiras (Santiago de Compostela, Spain)
X.-M. Chen (Guangzhou, PR China)
M.H. Chisholm (Columbus, OH, USA)
E.C. Constable (Basel, Switzerland)
L. Cronin (Glasgow, UK)
W.J. Evans (Irvine, CA, USA)
L.H. Gade (Heidelberg, Germany)
G. Girolami (Urbana, IL, USA)
J.-F. Halet (Rennes, France)
M.B. Hursthouse (Southampton, UK)
C. Janiak (Freiburg, Germany)
C. Kepert (NSW, Australia)
P. Kruger (Canterbury, New Zealand)
I. Manners (Bristol, UK)
S. Perlepes (Patras, Greece)
P.P. Power (Davis, CA, USA)
T.B. Rauchfuss (Urbana, IL, USA)
J. Reedijk (Leiden, The Netherlands)
A.L. Rheingold (Newark, DE, USA)
M. Rosales (Mexico, D.F., Mexico)
L.K. Thompson (St John's, NF, Canada)
M.D. Ward (Sheffield, UK)
M. Yamashita (Sendai, Japan)

ELSEVIER

Amsterdam — Boston — Jena — London — New York — Oxford — Paris — Philadelphia — San Diego — St Louis

Available online at www.sciencedirect.com
ScienceDirect
Polyhedron 27, issue 5, 7 April 2008
POLYHEDRON
www.elsevier.com/locate/poly

Contents

Papers

Magdalena Capó

Polyhedron 27 (2008) 1329

^{31}P NMR spectroscopy and discrete metallocycles from non-rigid ligands

Discrete M_2L_2 cyclic containing metal centers are thermodynamically favored over larger species. Depending on the different conformations of the non-rigid ligand, can display varied shapes in solution. ^{31}P NMR spectroscopy has been used in the determination of the isomeric *syn* an *anti* molecular rhombus.

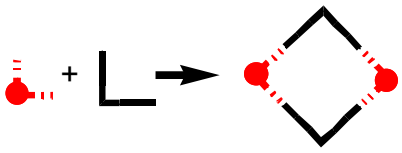

J. Kavalírová, M. Korabik, P. Stachová, J. Moncol, R. Sillanpää, T. Lis, D. Mikloš, M. Melník, J. Mroziński and D. Valigura

Polyhedron 27 (2008) 1333

Synthesis, spectral and magnetic properties of two different 2-nitrobenzoatocopper(II) complexes containing *N*,*N*-diethylnicotinamide

Two structurally different complexes $[Cu_2(2\text{-}NO_2Bz)_4(denia)_1]_n$ (**1**) $[Cu(2\text{-}NO_2Bz)_2(denia)_2(H_2O)_2]$ (**2**) were prepared from the same reaction (where 2-NO_2Bz = 2-nitrobenzoate, denia = *N*,*N*-diethylnicotinamide). In the polymeric chain of (**1**) the denia molecules serve as bridges between the dimeric $Cu_2(2\text{-}NO_2bz)_4$ units and in compound (**2**) the denia molecules serve as monodentate ligands with the pyridine nitrogen donor atom. The spectral and magnetic data of the complexes are analyzed in relation to their structures.

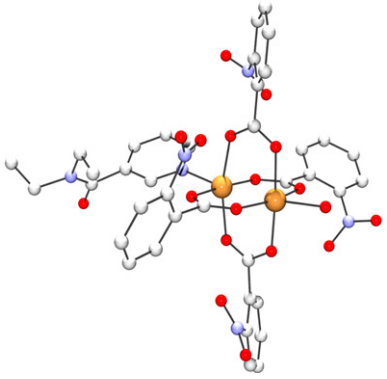

Ramakrishna Rao, Ashis K. Patra and P.R. Chetana

Polyhedron 27 (2008) 1343

Synthesis, structure, DNA binding and oxidative cleavage activity of ternary (L-leucine/isoleucine) copper(II) complexes of heterocyclic bases

The synthesis, characterization, DNA binding and "chemical nuclease" activity of ternary copper(II) complexes, $[Cu(AA)(B)(H_2O)](X)$ containing AA = L-leu/ile and planar phenanthroline bases (B), are described. The complexes are avid DNA binders and show oxidative DNA cleavage activity involving formation of a hydroxyl radical in the presence of a reducing agent.

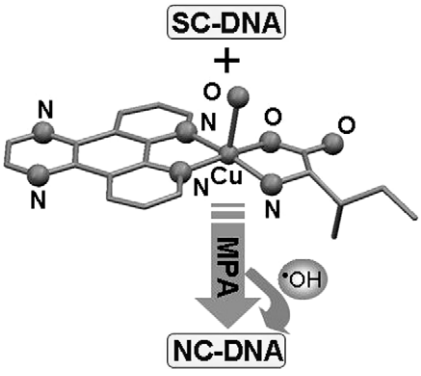

Elsevier Ltd.

L. Fuks, E. Gniazdowska, J. Mieczkowski and N. Sadlej-Sosnowska

Polyhedron 27 (2008) 1353

Structural features of tricarbonyl(*N*-methyl-2-pyridinecarboxyamide)chloro-rhenium(I)-potential precursor of radiopharmaceuticals

Structural characteristics of the novel complex, tricarbonyl(*N*-methyl-2-pyridinecarboxyamide)-chloro-rhenium(I), is presented. Molecular structure of the complex has been established by means of X-ray single crystal diffraction and compared with quantum mechanical calculations.

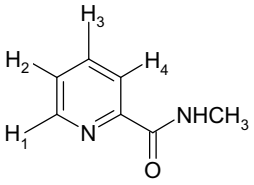

Marisa Belicchi-Ferrari, Franco Bisceglie, Giorgio Pelosi and Pieralberto Tarasconi

Polyhedron 27 (2008) 1361

Heterocyclic substituted thiosemicarbazones and their Cu(II) complexes: Synthesis, characterization and studies of substituent effects on coordination and DNA binding

New 5-formyluracilthiosemicarbazones (H_3ut) derivatives have been synthesised and characterized. In their complexes derived from copper chloride the metal atom is pentacoordinated, while in the nitrate derivatives the copper coordination is 4 + 2. The substituents on the thiosemicarbazidic moiety were varied. Interactions with DNA were studied and the nuclease activity was verified on plasmid DNA.

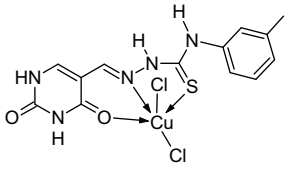

Petr Zimcik, Eva H. Mørkved, Trygve Andreassen, Juraj Lenco and Veronika Novakova

Polyhedron 27 (2008) 1368

Syntheses of octasubstituted zinc azaphthalocyanines with thiophene or thiophene combined with sulfanyl, amino or imido substituents: Influence of the substituents on photochemical and photophysical properties

New octasubstituted complexes of zinc azaphthalocyanines with thiophen-2-yl, thiophen-3-yl or benzo[*b*]thiophen-3-yl peripheral groups were synthesized and characterized. Unsymmetrically substituted ZnAzaPcs were also synthesized by cyclotetramerisations of pyrazine-2,3-dicarbonitriles attached to one thiophen-2-yl group and one alkylsulfanyl, thiomorpholinyl or imide group. Singlet oxygen and fluorescence quantum yields of these complexes were measured and the results were discussed.

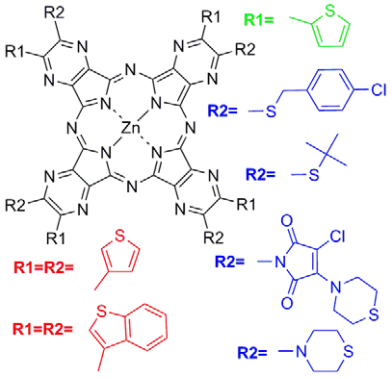

Tarlok S. Lobana, Rohit Sharma and Ray J. Butcher

Polyhedron 27 (2008) 1375

Pyridine-2-thione (pySH) derivatives of silver(I): Synthesis and crystal structures of dinuclear $[Ag_2Cl_2(\mu\text{-S-pySH})_2(PPh_3)_2]$ and $[Ag_2Br_2(\mu\text{-S-pySH})_2(PPh_3)_2]$ complexes

Pyridine-2-thione has yielded dinuclear complexes with silver(I) chloride/bromide in presence of PPh_3 (**1** and **2**).

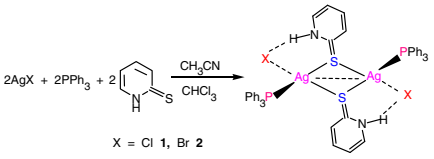

Veysel T. Yilmaz, Serkan Guney and Canan Kazak

Polyhedron 27 (2008) 1381

Copper(II)-saccharinato complexes with piperazine and *N*-(2-aminoethyl)piperazine ligands

Synthesis, characterization, crystal structure and thermal properties of two copper(II)-saccharinato complexes with piperazine (ppz) and *N*-(2-aminoethyl)piperazine, $[Cu(sac)_2(ppz)(H_2O)]_n$ (**1**) and *trans*-$[Cu(sac)_2(aeppz)_2]$ (**2**), have been reported. Complex **1** is a helical chain polymer assembled by bridging ppz ligands, while complex **2** is a centrosymmetric mononuclear compound.

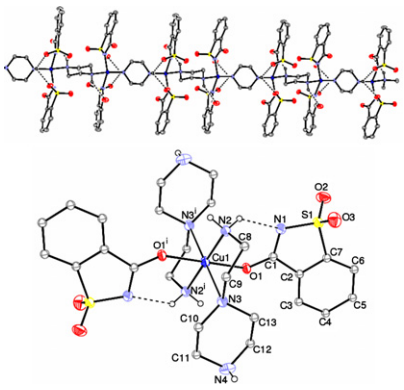

Vivek Bagchi and Debkumar Bandyopadhyay

Polyhedron 27 (2008) 1387

The porphyrin complex catalyzed dioxygen activation in presence of solid inorganic phosphates and small quantities of *t*-BuOOH.

The definitive role of several inorganic phosphates in the oxygenation of cyclohexene has been established where several iron(III) and manganese(III) porphyrins are used as a catalyst. Presence of *t*-BuOOH in the medium enhances the process further.

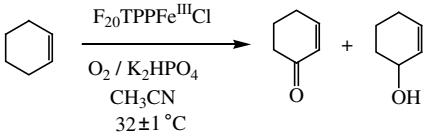

Yi Ding, Qing Chen, Jian-Chu Zhong, Megumu Munakata, Hisashi Konaka, Gui-Ling Ning and Hong-Zhi Wang

Polyhedron 27 (2008) 1393

Three-dimensional metal–organic frameworks: Two Ag(I) coordination polymers of TTF derivatives with axially chiral helical motifs

Two 3D TTF-silver(I) coordination polymeric networks with axially chiral helical motifs were obtained. Complex **1** has novel "8"-shaped channels and twisted double- helical structure. Polymer **2** exhibits an attractive "cds" network with a $6^5.8$ topology, and Ag_2S_2 rhombohedra subunits are formed which connect the ligands head to tail and result in fascinating helical structures.

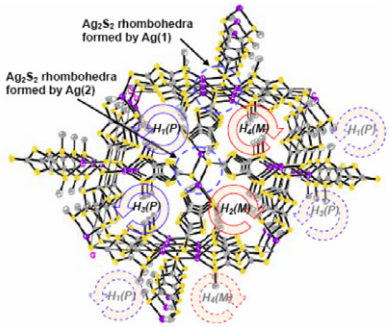

Jerzy Mroziński, Julia Kłak and Rafał Kruszyński

Polyhedron 27 (2008) 1401

Crystal structure and magnetic properties of the 1D bimetallic thiocyanate bridged compound: $\{(CuL_1)[Co(NCS)_4]\}$ (L_1 = *N-rac*- 5,12-Me_2-[14]-4,11-dieneN$_4$)

The synthesis, crystal structure and magnetic properties are reported for the new bimetallic compound $\{(CuL_1)[Co(NCS)_4]\}$ where L_1 = *N-rac*-5,12-dimethyl-1,4,8,11-tetraazacyclotetradeca-4,11-diene. The complex forms a one-dimensional zig-zag coordination polymer along the crystallographic *c* axis, with Co(II) and Cu(II) ions connected via thiocyanate bridges. The Co(II) centre in the $[Co(NCS)_4]$ fragment approximates a distorted tetrahedral symmetry. The Cu(II) geometry is a distorted tetragonal bipyramid with the apical position occupied by the bridging thiocyanate ligand and the basal ones by the four nitrogen atoms from the macrocyclic ring. The polymer chain nearest Cu(1)···Co(1) distances are 6.4152(9) and 6.0988(9) Å and the nearest Cu(1)···Co(1) interchain distances are 6.8609(9), 6.9628(9) and 6.0336(10) Å. The magnetization measurements for the examined compound have been carried out over the range 1.8–300 K. This data suggest ferromagnetic interactions through the thiocyanate bridge.

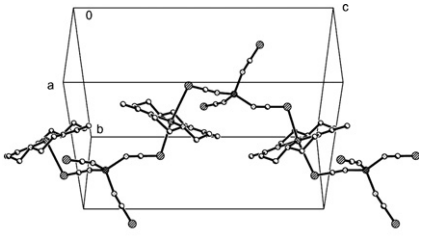

The coordination polymer of the $\{(CuL_1)[Co(NCS)_4]\}$ complex.

Susanta Hazra, Samit Majumder, Michel Fleck and Sasankasekhar Mohanta

Polyhedron 27 (2008) 1408

Synthesis, molecular and supramolecular structure, spectroscopy and electrochemistry of a dialkoxo-bridged diuranyl(VI) compound

The synthesis, molecular and supramolecular structure, spectroscopy and electrochemistry of a dialkoxo-bridged diuranyl (VI) compound $[(UO_2)_2(L)_2(\text{dimethylformamide})_2]$ (**1**) derived from the Schiff base ligand H_2L, obtained by condensation of 3-methoxysalicylaldehyde with 2-aminoethanol, have been described.

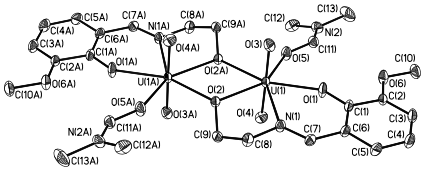

Marina González-Lorenzo, Carlos Platas-Iglesias, Marta Mato-Iglesias, David Esteban-Gómez, Andrés de Blas and Teresa Rodríguez-Blas

Polyhedron 27 (2008) 1415

Conformational study of lanthanide(III) complexes of *N*-(2-salicylaldiminatobenzyl)-1-aza-18-crown-6 by using X-ray and *ab initio* methods

An X-ray and computational (HF) structural study of nine-coordinate lanthanide complexes with an azacrown containing a 2-salicylaldiminato-benzyl pendant is presented.

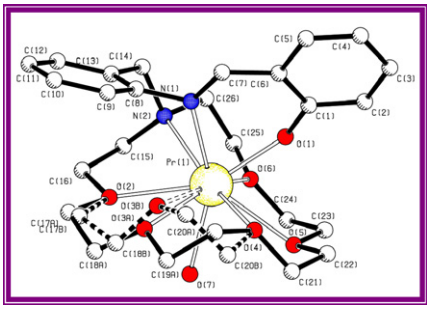

Mohamed A.S. Goher, Beate Sodin, Brigitte Bitschnau, Elmar C. Fuchs and Franz A. Mautner

Polyhedron 27 (2008) 1423

Ladders, rings and cubes as structural motifs in three new zinc(II) azide complexes: Synthesis, spectral and structural characterization

Ladders (1D), rings (2D) and cubes (3D) are the structural motifs of three new zinc(II) azide polymers, $\{[Zn_2(N_3)_4(\text{py-tetrazole})_2](\text{py-tetrazole})\}_n$, $\{[Zn_2(N_3)_4(3\text{-OHpy})] \cdot 2H_2O\}_n$, and $[Zn(N_3)_2(\text{pym})]_n$, with py-tetrazole = tetrazolo-[1,5-*a*]pyridine, 3-OHpy = 3-hydroxypyridine and pym = pyrimidine.

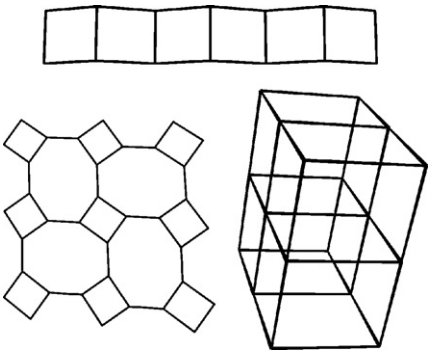

Kiyoshi Fujisawa, Ryosuke Kanda, Yoshitaro Miyashita and Ken-ichi Okamoto

Polyhedron 27 (2008) 1432

Copper(II) complexes with neutral bis(pyrazolyl)methane ligands: The influence of steric hindrance on their structures and properties

New mononuclear copper(II) complexes using the bidentate nitrogen-containing ligands bis(3,5-dimethyl-1-pyrazolyl)methane (L0″), bis(3,5-diisopropyl-1-pyrazolyl)methane (L1″), bis(3-tertiary-butyl-5-isopropyl-1-pyrazolyl)-methane (L3″), and bis(3,5-ditertiary-butyl-1-pyrazolyl)methane (L4″) were synthesized and structurally characterized. Structural and physicochemical studies of these complexes demonstrate the critical differences in the properties depending on the second coordination sphere of the coligands.

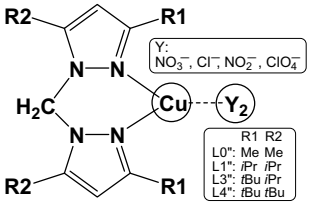

José Martínez-Lillo, Donatella Armentano, Giovanni De Munno and Juan Faus

Polyhedron 27 (2008) 1447

Magneto-structural study on a series of rhenium(IV) complexes containing $biimH_2$, pyim and bipy ligands

By reacting $(NH_4)_2[ReCl_6]$ and the chelating ligands $biimH_2$, pyim and bipy in *N*,*N*-dimethylformamide (DMF), three Re(IV) compounds namely $[ReCl_4(biimH_2)] \cdot 2DMF$ (**1**), $[ReCl_4(pyim)] \cdot DMF$ (**2**) and $[ReCl_4(bipy)]$ (**3**) are obtained, respectively. Magnetic susceptibility measurements show significant antiferromagnetic couplings in **1**–**3**, which are compared and discussed.

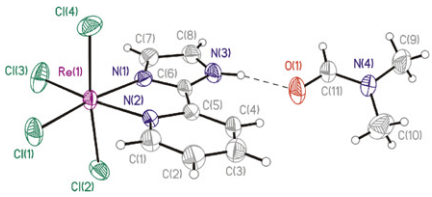

E.B. Seena, Nancy Mathew, Mini Kuriakose and M.R. Prathapachandra Kurup

Polyhedron 27 (2008) 1455

Synthesis, spectral and EPR studies of oxovanadium(IV) complexes incorporating tridentate ONO donor hydrazone ligands: Structural study of one oxovanadium(V) complex

Five oxovanadium(IV) complexes of 2-hydroxy-4-methoxybenzaldehyde nicotinic acid hydrazone (H_2L^1), 2-hydroxy-4-methoxyacetophenone nicotinic acid hydrazone (H_2L^2) and a binuclear oxovanadium(V) complex of H_2L^2 have been synthesized. These complexes are characterized by different physicochemical techniques like electronic, infrared and EPR spectral studies. The complexes $[VOL^1]_2 \cdot H_2O$ (**1**) and $[VOL^2]_2 \cdot H_2O$ (**4**) are binuclear and $[VOL^1bipy]$ (**2**), $[VOL^1phen] \cdot 1.5H_2O$ (**3**) and $[VOL^2phen] \cdot 2H_2O$ (**6**) are heterocyclic base adduct complexes and are EPR active. In frozen DMF at 77 K, all the oxovanadium(IV) complexes show axial anisotropy with two sets of eight line pattern. The complex $[VOL^2 \cdot OCH_3]_2$ (**5**) is an unusual product and having distorted octahedral geometry, as obtained by X-ray diffraction studies.

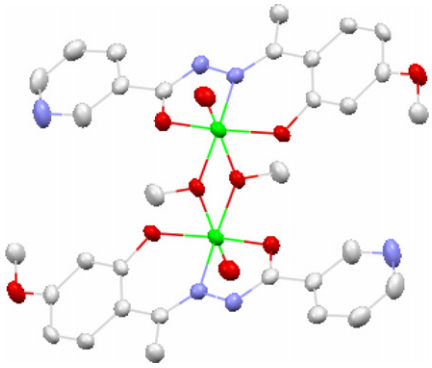

Christian R. Samanamú, Peter M. Lococo, William D. Woodul and Anne F. Richards

Polyhedron 27 (2008) 1463

Copper halide clusters and polymers supported by bipodal heteroelemental ligands

The flexible, multi dentate, heteroelemental, dipodal ligands; bis(2pyridylthio)methane, bis(2pyrimidylthio)methane and bipyrimidyldisulfide, afforded infinite polymeric chains when reacted with copper(II) chloride, copper(I) cyanide and copper(I) thiocyanate. Similar reactions with copper(I) iodide yielded tetranuclear clusters supported by two ligand molecules.

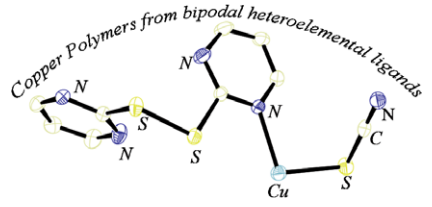

M.P. Juliarena, R.O. Lezna, G.T. Ruiz, M.R. Féliz, G.J. Ferraudi and E. Wolcan

Polyhedron 27 (2008) 1471

On the nature of the redox products of 4-$((CH_3)_2N)C_6H_4$–$CO_2^-$and 4-$((CH_3)_2N)C_6H_4$–CO_2–$Re(CO)_3$(1,10-phenanthroline): A spectroelectrochemical, pulse radiolysis and flash photochemical study

The UV–Vis absorption spectra of $DMAB^+$ and $phen^-$ were obtained by spectroelectrochemistry, flash photolysis and pulse radiolysis experiments on DMAB–CO_2–$Re^I(CO)_3$(phen) and DMAB–COOH.

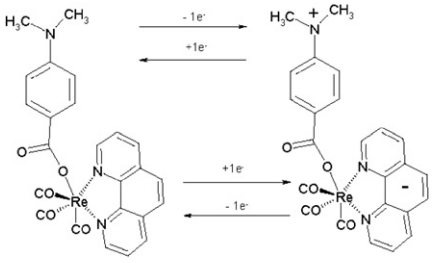

Boris-Marko Kukovec, Zora Popović, Gordana Pavlović, Marijana Vinković and Dražen Vikić-Topić

Polyhedron 27 (2008) 1479

Synthesis and characterization of some novel cadmium(II) complexes with 3-hydroxypicolinic acid (3-OHpicH): Crystal and molecular structures of $[CdI(3\text{-}OHpic)(3\text{-}OHpicH)(H_2O)]_2$, $[Cd(3\text{-}OHpic)_2(H_2O)_2]$ and $[Cd(3\text{-}OHpic)_2]_n$

Three new cadmium(II) complexes of 3-hydroxypicolinic acid were prepared and characterized by spectroscopic methods (IR, NMR) and their molecular and crystal structures were determined by X-ray crystal structure analysis. Three different coordination modes of 3-hydroxypicolinic acid were established in the solid state, but only monodentate one in the DMF solution.

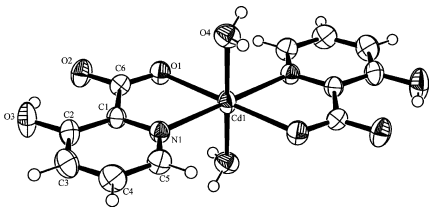

Danijela Čurman, Petra Živec, Ivan Leban, Iztok Turel, Anna Polishchuk, Karel D. Klika, Emiliya Karaseva and Vladimir Karasev

Polyhedron 27 (2008) 1489

Spectral properties of Eu(III) compound with antibacterial agent ciprofloxacin (cfqH). Crystal structure of $[Eu(cfqH)(cfq)(H_2O)_4]\text{-}Cl_2 \cdot 4.55H_2O$

A novel europium(III) complex of antibacterial agent ciprofloxacin (cfqH) with formula $[Eu(cfqH)(cfq)(H_2O)_4]Cl_2 \cdot 4.55H_2O$ was synthesized and its crystal structure was determined by X-ray crystallography. The spectral properties (IR, Raman, luminescence, NMR) of the isolated compound were studied and analysis of the Stark structure of the luminescence spectra was carried out.

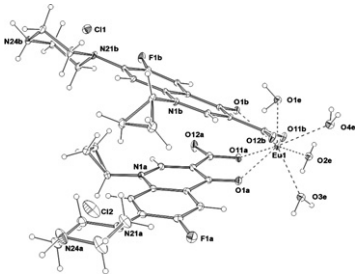

Marco Bortoluzzi, Giuliano Annibale, Gino Paolucci and Bruno Pitteri

Polyhedron 27 (2008) 1497

A DFT study on the interactions between the $[Pt(H_2O)(terpy)]^{2+}$ cation and the triflate and perchlorate counter-anions

The results of DFT calculations on the $[Pt(OH_2\cdots X)(terpy)]^{+}$ and $[Pt(OH_2\cdots S)(terpy)]^{2+}$ {terpy = 2,2′:6′,2″-terpyridine; X = ClO_4, SO_3CF_3; S = CH_3NO_2} models are reported. The computational results likely fit the previously reported X-ray and NMR data on the $[Pt(H_2O)(terpy)]X_2$ {X = ClO_4, SO_3CF_3} species and allowed to estimate the energy difference between the $[(terpy)Pt\text{–}OH_2\cdots OSO_2CF_3]^{+}$ and the $[(terpy)Pt\text{–}OH_2\cdots OClO_3]^{+}$ hydrogen-bond adducts. Finally, it was highlighted that also nitromethane is able to strongly interact with the aqua ligand of the $[Pt(H_2O)(terpy)]^{2+}$ cation.

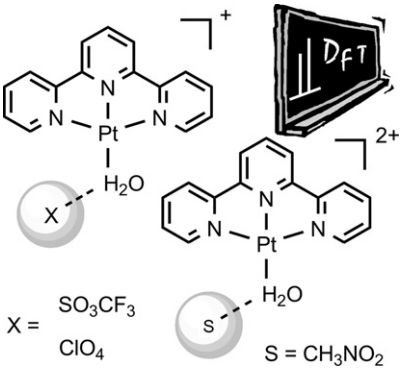

Youxuan Zheng, Majid Motevalli, Rendy H.C. Tan, Isaac Abrahams, William P. Gillin and Peter B. Wyatt

Polyhedron 27 (2008) 1503

Near IR luminescent rare earth 3,4,5,6-tetrafluoro-2-nitrophenoxide complexes: Synthesis, X-ray crystallography and spectroscopy

Tetrafluoro-2-nitrophenoxide coordinates to rare earth ions and provides a visible (orange-yellow) chromophore; IR emission from its Er(III) and Yb(III) complexes shows long lifetimes because of the lack of C–H and O–H bonds that could cause vibrational quenching.

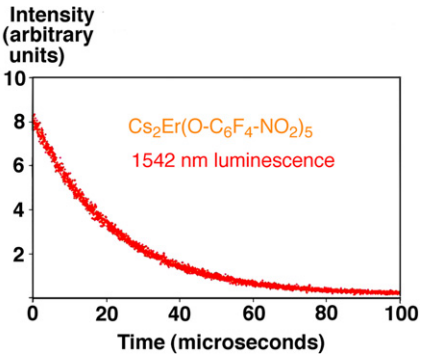

Anna Janicka-Klos, Paulina Juszczyk, Zbigniew Grzonka and Henryk Kozłowski

Polyhedron 27 (2008) 1511

Competition between the albumin and three histidine fragment of amyloid precursor protein sites to bind Cu(II)

The present paper reports the results of combined potentiometric and spectroscopic studies on the copper(II) complexes of two octadecapeptides (DAHQERMDVSETHLHWHT and Ac-DAHQERMDVSETHLHWHT-NH_2) having two distinct metal-binding-domains, the albumin-like N-terminal (DAH) and APP cysteine-rich three His. The -HXHYH- motif is very effective in binding metal ion although it is unable to compete with albumin-like coordination mode in unprotected peptide.

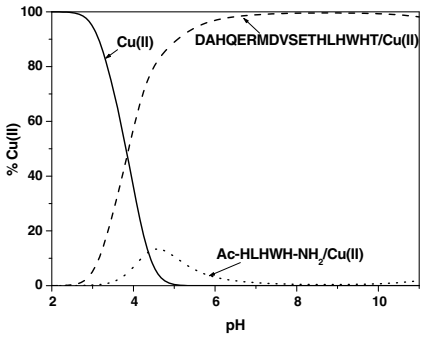

Lei Gou, Qing-Ran Wu, Huai-Ming Hu, Ting Qin, Gang-Lin Xue, Meng-Lin Yang and Zong-Xun Tang

Polyhedron 27 (2008) 1517

An investigation of the positional isomeric effect of terpyridine derivatives: Self-assembly of novel cadmium coordination architectures driven by N-donor covalence and π···π noncovalent interactions

The reaction of two pyridyl substituted terpyridine isomers L1 and L2 with Cd^{II} atoms resulted in different dimensional architectures. L1 as a mono-tridentate bridging ligand links Cd_3 and Cd_4 clusters into 1D grid-like and 2D wave-like polymers, respectively. However, L2 as a chelating ligand forms binuclear structures.

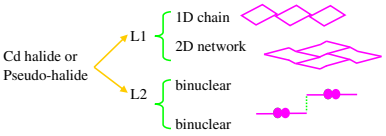

Christopher M. Fitchett and Peter J. Steel

Polyhedron 27 (2008) 1527

Synthesis and X-ray crystal structures of metal complexes of three isomeric bibenzodiazines: Discrete and polymeric assemblies

Thirteen complexes of three isomericbi benzodiazines were prepared and X-ray crystal structures were determined for seven of these. It is shown that 2,2′-biquinazoline prefers to form mononuclear complexes with chelation involving the less hindered nitrogen donors. 2,2′-Biquinoxaline is shown to offer two modes of coordination; in the first, it acts as a "stepped-linear" bridging ligand using the two less hindered nitrogens, while in the second mode it chelates to copper(I) centres using its more hindered nitrogens. The presence of the fused benzo rings leads to a higher propensity for π–π stacking of the heterocyclic ligands within such complexes.

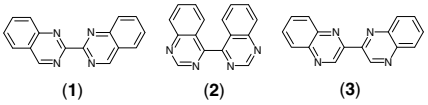

The Publisher encourages the submission of articles in electronic form thus saving time and avoiding rekeying errors. For detailed instructions on the preparation of manuscripts and of electronic artwork, consult the Author Gateway for Elsevier at http://authors.elsevier.com

ScienceDirect

Full text of this journal is available, on-line from **ScienceDirect**. Visit **www.sciencedirect.com** for more information.

Polyhedron 27, issue 16, 5 November 2008

Contents lists available at ScienceDirect

Polyhedron

journal homepage: www.elsevier.com/locate/poly

Contents

Papers

Yao-Cheng Shi, Hong-Jian Cheng and Su-Hua Zhang

Polyhedron 27 (2008) 3331

Syntheses and crystal structures of copper mixed-ligand complexes of multidentate enaminones and acetate anions

Reactions of ferrocenoylacetone with 2-(aminomethyl)pyridine and *N*-(2-hydroxyethyl)-1,2-diaminoethane afford the multidentate enaminones H**L**^{1} and H_3**L**^{2}, respectively. Reactions of copper acetate with the two enaminones generate the corresponding mixed-ligand complexes **I** and **II**, which are formulated as [Cu**L**^{1}(OAc)] and [Cu(H_2**L**^{2})(OAc)], respectively. The structures of H**L**^{1}, **I** and **II** have been determined by single-crystal X-ray crystallography. In complex **I**, H**L**^{1} acts as a monoanionic tridentate donor via the carbonyl oxygen, deprotonated enamine nitrogen and pyridyl nitrogen atoms, the acetate anion is monodentate and the coordination geometry of the central metal is square planar. In complex **II**, H_3**L**^{2} is a monoanionic tetradentate ligand via the carbonyl oxygen, deprotonated enamine nitrogen, secondary amine nitrogen and hydroxy oxygen atoms, the acetate anion is monodentate and the coordination geometry of the central metal is a distorted trigonal bipyramid.

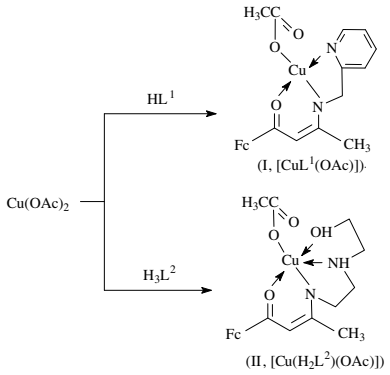

Muhammad Shahid, Muhammad Mazhar, Mohammad A. Malik, Paul O' Brien and James Raftery

Polyhedron 27 (2008) 3337

Fabrication of copper–zinc oxide composite thin films from single source precursor by aerosol assisted chemical vapour deposition

Heterobimetallic complex, $[Zn_2(OAc)_6(\mu\text{-}O)_2Cu_4(bdmap)_2Cl_2]$ (**1**), synthesized by direct reaction of $Cu(OCH_3)Cl$, $Zn(OAc)_2 \cdot 2H_2O$ and bdmapH in toluene was characterized by melting point, CHNS, FT-IR, TGA, mass spectrometry and single crystal X-ray diffraction. The complex (**1**) was tested to deposit Cu–ZnO composite thin films which were characterized by PXRD, SEM, EDAX, thickness and *V–I* measurements.

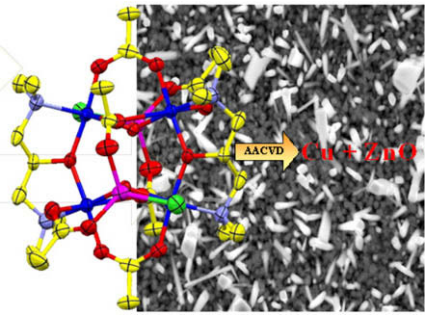

Pampa Mukherjee, Michael G.B. Drew, Albert Figuerola and Ashutosh Ghosh

Polyhedron 27 (2008) 3343

Incorporation of a sodium ion guest in the host of copper(II)-Schiff-base complexes: Structural characterization and magnetic study

Three Cu(II) complexes, [Cu**L**^{n}] where **L**^{n} (n = 1–3) are three tetradentate di-Schiff-base ligands prepared by the condensation of acetyl acetone and diamines (1,2-diaminoethane, 1,2-diaminopropane and 1,3-diaminopropane, respectively), on crystallization from methanol containing $NaClO_4$, give three sodium salt adducts having general formula $[(CuL^n)_2 Na(ClO_4)H_2O]$. Here, the [Cu**L**^{n}] units act as a host molecule and include guest sodium cation by bridging through the oxygen atoms of the ligand to form the tri-nuclear adducts.

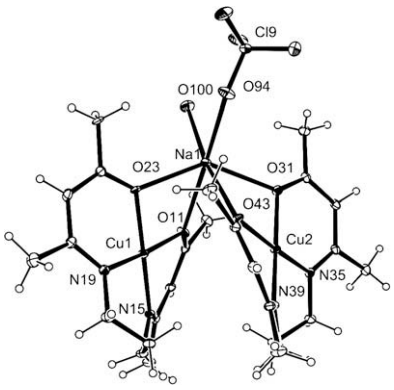

Wen-Li Zhang, Ying-Ying Liu, Jian-Fang Ma, Hui Jiang and Jin Yang

Polyhedron 27 (2008) 3351

Syntheses and characterizations of nine coordination polymers of transition metals with carboxylate anions and bis(imidazole) ligands

The simultaneous use of the transition metals, bis(imidazole) ligands and carboxylate anions affords nine intriguing compounds. The crystal structures of these compounds, along with the systematic investigation of the effect of the anions and the neutral ligands on the ultimate framework, are represented and discussed.

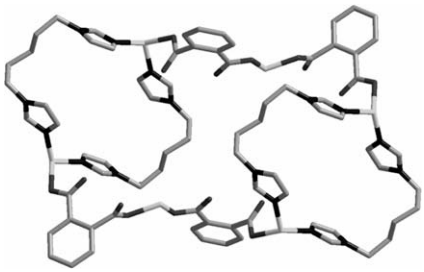

Saikat Sarkar, Susobhan Biswas, Meng-Sheng Liao, Tapas Kar, Yildirim Aydogdu, Fethi Dagdelen, Golam Mostafa, Asoke Prasun Chattopadhyay, Glenn P.A. Yap, Rui-Hua Xie, Abu T. Khan and Kamalendu Dey

Polyhedron 27 (2008) 3359

An attempt towards coordination supramolecularity from Mn(II), Ni(II) and Cd(II) with a new hexadentate $[N_4O_2]$ symmetrical Schiff base ligand: Syntheses, crystal structures, electrical conductivity and optical properties

The synthesis and physicochemical study of Ni(II), Cd(II) and Mn(II) compounds of a new hexadentate Schiff base ligand are presented. The complexes have been characterized by the single crystal X-ray diffraction method, IR, electronic spectroscopy and magnetic measurements. Optical properties and electrical conductivity have shown significant results. Theoretical calculations have also been performed using the DFT method. The optimized geometries are compared with the crystallographic data. The experimental spectra are assigned with the help of the calculated frequencies.

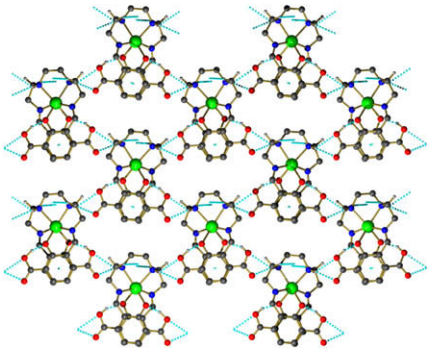

Yan-Hong Zhang, Ming Yu, Qing-Lun Wang, Gong-Feng Xu, Ming Hu, Guang-Ming Yang and Dai-Zheng Liao

Polyhedron 27 (2008) 3371

A macrocyclic oxamido vanadium(IV)-oxo ligand and its derivative $VO^{IV}{}_2M^{II}$ (M = Cu, Mn) trinuclear complexes: synthesis, structures and magnetic properties

A new oxamido-bridged vanadium(IV)-oxo complex ligand VOL (H_2L = 2,3-dioxo-5,6:13,14-dibenzo-7,12-diphenyl-1,4,8,11-tetraazacyclo-tetradeca-7,12-diene) (**1**) has been synthesized. Based on the mononuclear ligand, two trinuclear complexes $[Cu(VOL)_2(H_2O)_2](ClO_4)2 \cdot 1.5H_2O$ (**2**) and $[Mn(VOL)_2(CH_3OH)_2](ClO_4)_2 \cdot 5CH_3OH$ (**3**) have been prepared and structurally characterized by X-ray crystallography. Their spectroscopic properties and magnetic properties have also been investigated.

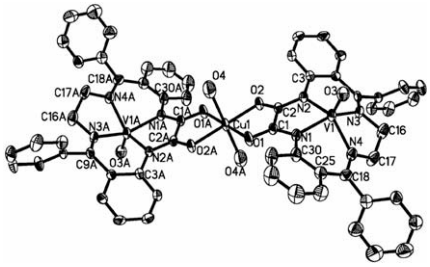

Horng Yi Juan, Wang Chin Lin, Ya Ling Wu and Jing-Huei Perng

Polyhedron 27 (2008) 3377

Substituent effects in porphyrin dimer complexes studied by IR spectroscopy

The IR spectra of a series of lanthanide porphyrin dimers are presented. These results indicate that the $\pi-\pi$ interactions of the porphyrin macrocycles intrinsically decrease the bond strength of the entire molecule. It is also observed that the ethyl vibrational modes of the OEP moiety can be used as characteristic bands to monitor the subtle deformations of the porphyrin rings.

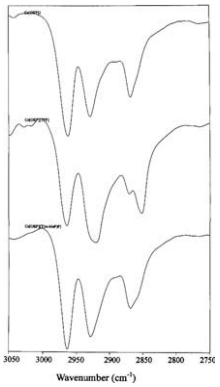

Dilek Dündar, Hatice Can, Devrim Atilla, Ayşe Gül Gürek, Zafer Ziya Öztürk and Vefa Ahsen

Polyhedron 27 (2008) 3383

Photoconductive novel mesomorphic oxotitanium phthalocyanines

The synthesis and photoconductivity properties of the alkylthia and triethyleneoxysulfonyl substituted oxotitanium (IV) phthalocyanines (**1a** and **2a**) are reported for the first time. The electrical dark conductivities (σ_d) and photoconductivities (σ_{ph}) of deposited films of **1a** and **2a** were investigated in various media. The photoconductivity mechanism and formation of Pc^+ which is positive charge carrier under the light irradiation of the phthalocyanine molecules are demonstrated using the theoretical calculations.

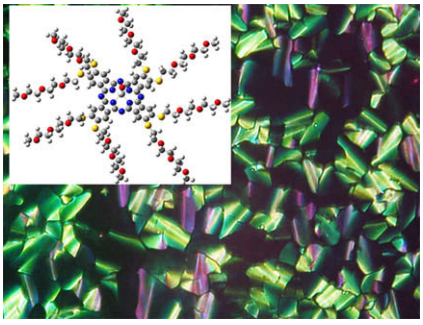

Antonio Sousa-Pedrares, Nuria Camiña, Jaime Romero, Maria L. Durán, José A. García-Vázquez and Antonio Sousa

Polyhedron 27 (2008) 3391

Electrochemical synthesis and crystal structure of cobalt(II), nickel(II), copper(II), zinc(II) and cadmium(II) complexes with 2-pyridinecarbaldehyde-(2′-aminosulfonylbenzoyl)hydrazone

Metal complexes, $[ML_2]$ M = Co, Ni, Cu, Zn or Cd, derivatives from a new hydrazonic Schiff base ligand have been synthesised by electrochemical oxidation of the anodic metal. The structural studies show that the metal is in a distorted octahedral environment with the monoanionic ligand acting as a meridional tridentate (N,N,O) chelate system.

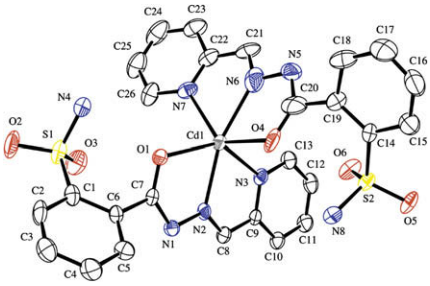

Adamantia Maniatakou, Christodoulos Makedonas, Christiana A. Mitsopoulou, Catherine Raptopoulou, Ioanna Rizopoulou, Aris Terzis and Alexandra Karaliota

Polyhedron 27 (2008) 3398

Synthesis, structural and DFT studies of a peroxo-niobate complex of the biological ligand 2-quinaldic acid

The $(gu)_2[Nb(O_2)_3(quin\text{-}2\text{-}c)] \cdot H_2O$ complex has been obtained in reaction of $(gu)_3[Nb(O_2)_4]$ with quinoline-2-carboxylate ion in the presence of an excess of hydrogen peroxide in aqueous medium. The crystal structure and the spectral characterization of the novel complex have been determined. The molecular orbital diagram of the triperoxo compound has been calculated with the density functional theory (DFT) method.

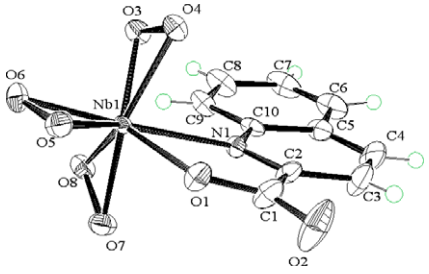

The Publisher encourages the submission of articles in electronic form thus saving time and avoiding rekeying errors. For detailed instructions on the preparation of manuscripts and of electronic artwork, consult the Author Gateway for Elsevier at http://authors.elsevier.com

ScienceDirect

Full text of this journal is available, on-line from **ScienceDirect**. Visit **www.sciencedirect.com** for more information.

Available online at www.sciencedirect.com
ScienceDirect
Polyhedron 27, issue 8, 6 June 2008
POLYHEDRON
www.elsevier.com/locate/poly

Contents

Papers

Ali Naghipour, Zahra Haji Ghasemi, David Morales-Morales, Juan M. Serrano-Becerra and Craig M. Jensen

Polyhedron 27 (2008) 1947

Simple protocol for the synthesis of the asymmetric PCP pincer ligand [C_6H_4-1-(CH_2PPh_2)-3-($CH(CH_3)PPh_2$)] and its Pd(II) derivative [PdCl{C_6H_3-2-(CH_2PPh_2)-6-($CH(CH_3)PPh_2$)}]

The asymmetric PCP pincer ligand [C_6H_4-1-(CH_2PPh_2)-3-($CH(CH_3)PPh_2$)] (**4**) has been synthesized in a facile manner in three simple steps in high yield. Metallation of PCP pincer ligand (**4**) with [$Pd(COD)Cl_2$] affords complex [PdCl{C_6H_3-2-(CH_2PPh_2)-6-($CH(CH_3)PPh_2$)}] (**7**).

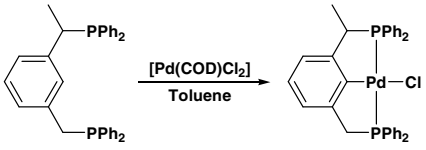

Sharon Moeno and Tebello Nyokong

Polyhedron 27 (2008) 1953

The photophysical studies of a mixture of CdTe quantum dots and negatively charged zinc phthalocyanines

Fluorescence resonance energy transfer (FRET) between CdTe quantum dots and negatively charged Zn phthalocyanines were studied; tetrasulfonated ZnTSPc gave the highest FRET efficiency (0.3), with tetra and octa carboxylated ZnPc giving a FRET efficiency of 0.2.

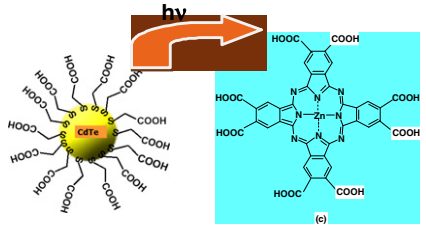

Laurence Carlton, Zikhona N. Tetana and Manuel A. Fernandes

Polyhedron 27 (2008) 1959

Thiolate complexes of iridium. Structures of [$Ir_2(\mu$-$SC_6F_5)_2(cod)_2$], [$Ir(SC_6F_5)(H)(SiPh_3)(XNC)_3$] and [$Ir_3(\mu$-$SC_6F_5)_2(SC_6F_5)(\mu,\mu'$-XNC)$(XNC)_4(cod)$] (XNC = xylyl isocyanide)

Complex **1** combines with Ph_3SiH in the presence of xylyl isocyanide (XNC) to form **2** in moderate yield. In the presence of XNC alone **3** is formed in low yield together with unidentified products.

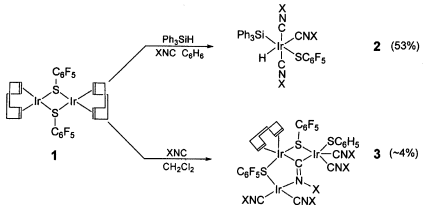

Seyyed Javad Sabounchei, Alireza Dadrass, Fateme Akhlaghi, Zabiholla Bolboli Nojini and Hamid Reza Khavasi

Polyhedron 27 (2008) 1963

Synthesis of a new carbbenzyloxymethylene-triphenylphosphorane ylide and the study of its reaction with mercury(II) halides: Spectral and structural characterization

The reaction of a new phosphorus ylide, carbbenzyloxymethylenetriphenylphosphorane, ($PPh_3CHCOOCH_2C_6H_5$), with mercury(II) halides yields dimeric complexes of the form $[(PPh_3CHCOOCH_2C_6H_5) \cdot HgX_2]_2$ (X = Cl, Br or I). Single crystal X-ray analyses of **3** reveals the presence of a centrosymmetric dimeric structure containing the ylide and HgI_2.

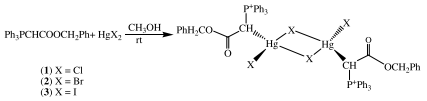

Fabio Marchetti, Guido Pampaloni and Stefano Zacchini

Polyhedron 27 (2008) 1969

The chemistry of niobium and tantalum halides, MX_5, with haloacetic acids and their related anhydrides: Anhydride C–H bond activation promoted by MF_5

The reactivity of MX_5 (M = Nb, Ta) with haloacetic acids or the corresponding anhydrides is strongly influenced by the nature of the halide: dinuclear carboxylates are obtained with chlorides and bromides, while the fluorides afford ionic compounds containing the $[MF_6]^-$ anion. The reaction of MF_5 with carboxylic anhydrides proceeds via C–O and C–H bonds activation.

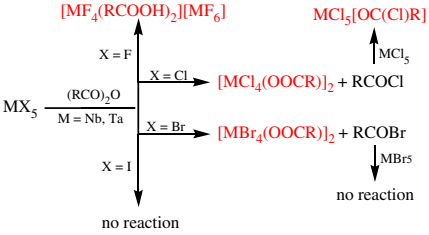

Junfeng Wang, Hongmei Sun, Yingming Yao, Yong Zhang and Qi Shen

Polyhedron 27 (2008) 1977

Bridged bis(amidinate) lanthanide complexes: Synthesis, molecular structure and reactivity

Four novel lanthanide complexes bearing bridged bisamidinate ligand $Me_3SiNC(Ph)N(CH_2)_3NC(Ph)NSiMe_3$, L were synthesized in high yields and fully characterized. Treatment of $LLnCl(sol)_x$ (Ln = Yb, sol = THF, x = 2 **1**; Ln = Y, sol = DME, x = 1 **2**) with the dilithium salt $Li_2L(THF)_{0.5}$ afforded lanthanide complexes supported by three ligands, $Ln_2(\mu_2\text{-}L)_3 \cdot DME$ (Ln = Yb **3**, Y **4**). Reaction of $LnCl_3$ (Ln = Yb, Y) with 2 equiv. of $Li_2L(THF)_{0.5}$ gave the anionic complexes $[Li(DME)_3][L_2Ln]$ (Ln = Yb **5**, Y **6**). The complexes **3** and **4** can also be synthesized by the reaction of $LnCl_3$ with 1.5 equiv. of $Li_2L(THF)_{0.5}$ or the reaction of **1** and **2** with the anionic complexes **5** and **6**. Complexes **3**, **4**, **5** and **6** were found to be high active catalysts for the ring-opening polymerization of ε-caprolactone (CL).

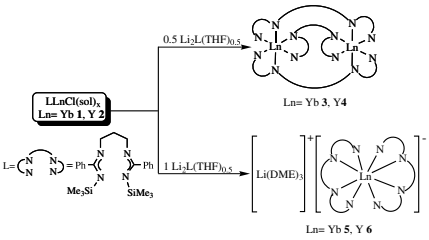

Amardeep Singh, Bolin Chetia, Saikh M. Mobin, Gopal Das, Parameswar K. Iyer and Biplab Mondal

Polyhedron 27 (2008) 1983

Ruthenium monoterpyridine complexes with 2,6-bis(benzimidazol-2-yl)pyridine: Synthesis, spectral properties and structure

Ruthenium monoterpyridine complexes $[1]^{2+}$ and 2, exhibit strong proton coupled electron transfer processes. The MLCT band for both the complexes is found to be dependent on the solution pH.

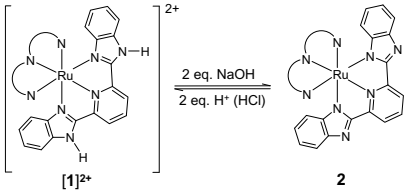

Manu Mehrotra and Raj N. Mehrotra

Polyhedron 27 (2008) 1989

The oxidation of carbohydrazide by the 12-tungstocobaltate(III) ion in acidic medium: Kinetics and mechanism

The redox reaction between the 12-tungstocobaltate(III) ion and carbohydrazide is first order with respect to both the oxidant and the substrate. The observed pseudo first-order rate constant, k_{obs}, is retarded by increasing the concentrations of H^+ and alkali metal ion (Li^+, Na^+ and K^+). There is a linear correlation between the k_{obs} and the concentrations of carbohydrazide and H^+ ion, but the plots of k_{obs} against the concentrations of the alkali metal ions is non-linear. However, the same data is applicable to the Davies equation for the effect of the ionic strength on the k_{obs}. Complex formation between the 12-tungstocobaltate(III) ion and carbohydrazide is indicated by optical density measurements, which increased with increasing H^+ concentration in the reaction mixture. This indicated that $^+H_3NNHCONHNH_2$ probably formed a complex with the 12-tungstocobaltate(III) ion. A suitable mechanism involving deprotonation of the complex and subsequent decomposition of the deprotonated complex as the rate limiting step is suggested.

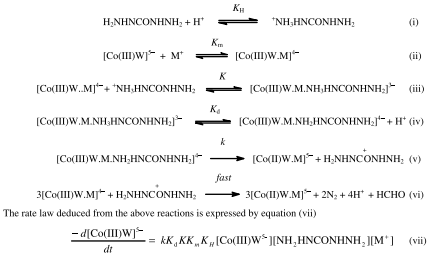

Damir A. Safin, Felix D. Sokolov, Łukasz Szyrwiel, Sergey V. Baranov, Maria G. Babashkina, Timur R. Gimadiev and Henryk Kozlowski

Polyhedron 27 (2008) 1995

Monodentate *S-vs*. bidentate 1,5-*O*,*S*-coordination of *N*-phosphoryl-*N*′-(R)-thioureas with Pd(II)

We reported three new complexes of the Pd(II) cation with *N*-phosphorylated thioureas RNHC(S)NHP(O)(O*i*Pr)$_2$ (R = *t*Bu, **HL^{I}**; R = Ph, **HL^{II}**; R = 4′-benzo-15-crown-5, **HL^{II}**). Reaction of *N*-phosphorylated thioureas of common formula RC(S)NHP(O)(O*i*Pr)$_2$ (R = Et$_2$N, **HL^{IV}**; R = morpholine-*N*-yl, **HL^{V}**) in the same conditions leads to complexes Pd(**L^{IV}**-*O*,*S*)$_2$ (**4**) and Pd(**L^{V}**-*O*,*S*)$_2$ (**5**), where the palladium(II) atoms are coordinated in a square-planar fashion by the C=S sulfur atoms and the P=O oxygen atoms of two anionic ligands. Structures of the obtained compounds were investigated by IR, ^{1}H and ^{31}P{^{1}H} NMR spectroscopy and elemental analysis. The crystal structure of complex *trans*-Pd(HL^{I}-*S*)$_2$Cl$_2$ has been investigated by X-ray crystallography. It was established that the thiourea ligands are in a *trans*-configuration and the palladium(II) cation is coordinated by the sulfur atoms of the C=S groups and the chlorine atoms. Complex *trans*-Pd(HL^{I}-*S*)$_2$Cl$_2$ is the first example of palladium(II) complex in which the potentially chelating *N*-phosphorylated thiourea ligand is bound through the sulfur atom only.

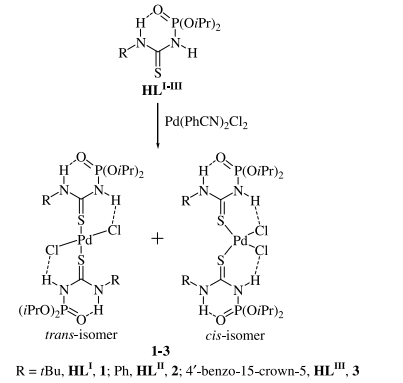

Sandra Rabaça, Maria Carolina Duarte, Isabel C. Santos, Laura C.J. Pereira, Marc Fourmigué, Rui T. Henriques and Manuel Almeida

Polyhedron 27 (2008) 1999

Thio-azo proligands based on 5,6-derivatives-1,10-phenanthroline and their use for iron(II) complexes: Synthesis, characterization and crystal structures

Two 5,6-substituted-1,10-phenanthroline ligands have been prepared and characterized. Theses two compounds can be direct precursors of 5,6-dithiolate-1,10-phenanthroline, which is an attractive thio-azo ligand. The diimine coordination ability of the proligands was explored with the synthesis of two Fe^{II}(L)$_3$ complexes.

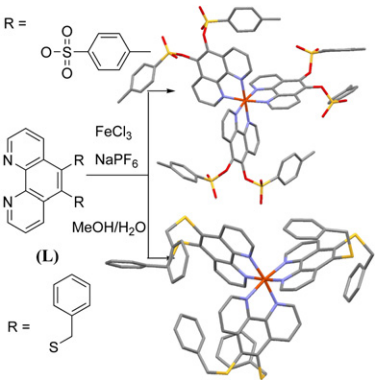

A.M. Fedosseev, M.S. Grigoriev, I.A. Charushnikova, N.A. Budantseva, Z.A. Starikova and Ph. Moisy

Polyhedron 27 (2008) 2007

Synthesis, crystal structure and some properties of new perrhenate and pertechnetate complexes of Nd^{3+} and Am^{3+} with 2,6-bis(tetramethylfurano)-1,2,4-triazin-3-yl)-pyridine, tris-(2-pyridylmethyl)amine and *N*,*N*′-tetraethylmalonamide

The structure of coordination complexes of trivalent f-element pertechnetates and perrhenates with some N-donor ligands were determined by using X-ray structural analysis: Nd^{3+} perrhenate with 2,6-bis(tetramethylfurano)-1,2,4-triazin-3-yl)-pyridine ([Nd(FBTP)$_3$-ReO$_4$]-(ReO$_4$)$_2$2H$_2$O (**I**)), tris(2-pyridylmethyl)-amine ([Nd(TPA)(ReO$_4$)$_3$] (**II**)) and *N*,*N*′-tetraethylmalonamide ([Nd(TEMA)$_4$](ReO$_4$)$_3$ (**III**)). The complexes of Nd^{3+} pertechnetate and Am^{3+} pertechnetate with TPA have been also synthesized [Nd(TPA)(TcO$_4$)$_3$] (**IV**) and [Am(TPA)-(TcO$_4$)$_3$] (**V**)).

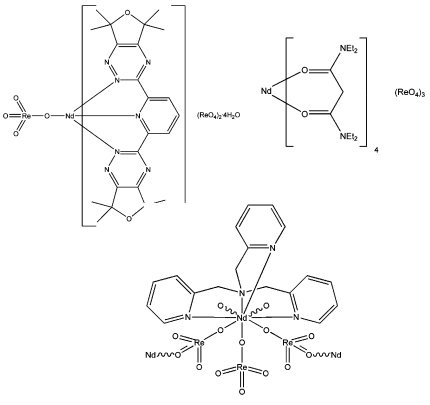

Seyyed Javad Sabounchei, Hassan Nemattalab, Sadegh Salehzadeh, Sima Khani, Mehdi Bayat and Hamid Reza Khavasi

Polyhedron 27 (2008) 2015

Structural, theoretical and multinuclear NMR study of mercury(II) complexes of phosphorus ylides: Mono and binuclear complexes

Reaction of some phosphorous ylides with Hg(II) halides in equimolar ratios using methanol as solvent leads to parent binuclear products. The bridge-splitting reaction of one of these binuclear complexes by DMSO yields the new mononuclear complex containing DMSO as ligand. Theoretical studies show that formation of mononuclear complexes in DMSO solution energetically is more favorable than that of binuclear complexes.

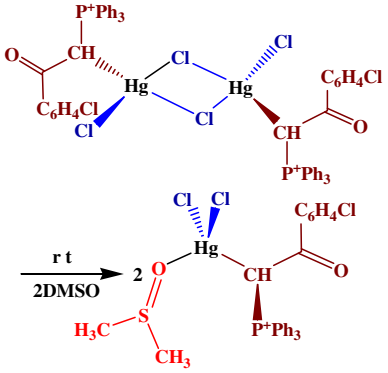

Damir A. Safin, Felix D. Sokolov, Heinrich Nöth, Maria G. Babashkina, Timur R. Gimadiev, Joanna Galezowska and Henryk Kozlowski

Polyhedron 27 (2008) 2022

Studies on zinc(II) complexes with *N*-thioacylamidophosphates: X-ray crystal structure of the $[Zn(RC(S)NP(O)(OiPr)_2)_2]$ (R = NH_2, *t*BuNH, *c*-$C_6H_{11}NH$)

We reported the photoluminescent properties of 17 zinc(II) chelates $[Zn(RC(S)NP(O)(OiPr)_2\text{-}O,S)_2]$ (R = Ph (**1a**), PhNH (**1b**), *p*-BrPh (**1c**), *p*-$MeOC_6H_4NH$ (**1d**), *p*-BrC_6H_4NH (**1e**), NH_2 (**1f**), *i*PrNH (**1g**), *t*BuNH (**1h**), Et_2N (**1i**), *c*-$C_5H_{10}N$ (**1j**), *c*-OC_4H_8N (**1k**), *c*-$C_6H_{11}NH$ (**1l**), aminobenzo-15-crown-5 (**1m**)) and $[Zn(B)(RC(S)NP(O)(OiPr)_2\text{-}O,S)_2]$ (R = Ph, B = 2,2′-bipyridine (**2a**); R = Ph, B = 1,10-phenanthroline (**2b**); R = PhNH, B = 2,2′-bipyridyne (**2c**); R = PhNH, B = 1,10-phenanthroline (**2d**)). Colorless and air/moisture stable chelate complexes of divalent zinc show blue emission in the solid state when excited with UV light. Complexes **1f**, **1h**, **1l** were investigated by single crystal X-ray diffraction. The zinc(II) atom in complexes **1f**, **1h**, **1l** is in a distorted tetrahedral O_2S_2 environment formed by the C=S sulphur atoms and the P=O oxygen atoms of two deprotonated ligands.

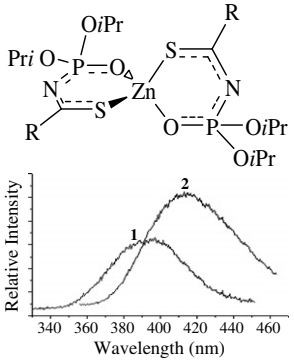

Erratum to "Copper(II) complexes with pyrazolyl-substituted nitronyl and imino nitroxides" [Polyhedron 27 (2008) 739–740] 2029

The Publisher encourages the submission of articles in electronic form thus saving time and avoiding rekeying errors. For detailed instructions on the preparation of manuscripts and of electronic artwork, consult the Author Gateway for Elsevier at http://authors.elsevier.com

ScienceDirect

Full text of this journal is available, on-line from **ScienceDirect**. Visit **www.sciencedirect.com** for more information.

Polyhedron 27, issue 17, 25 November 2008

Contents lists available at ScienceDirect

Polyhedron

journal homepage: www.elsevier.com/locate/poly

Contents

Papers

Anirban Karmakar and Jubaraj B. Baruah

Polyhedron 27 (2008) 3409

Synthesis and characterization of zinc benzoate complexes through combined solid and solution phase reactions

A combined solid and solution phase synthesis for a series of mononuclear and polynuclear zinc benzoate complexes is described. The substituents on the aromatic ring and solvent plays deciding role on the formation of such complexes.

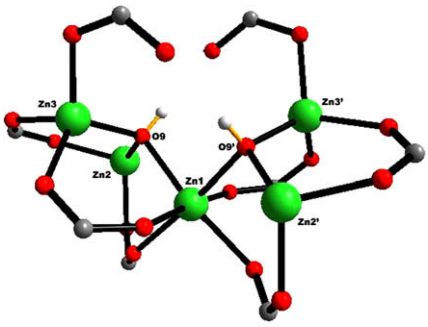

A pentanuclear zinc complex

Murugesan Velayudham, Muthuraman Rajkumar, Seenivasan Rajagopal and Perumal Ramamurthy

Polyhedron 27 (2008) 3417

Synthesis, characterization, electrochemical and photophysical properties of bimetallic complexes of rhenium(I) and osmium(II)

Monometallic and bimetallic diimine complexes of rhenium(I) and osmium(II), $[(CO)_3(bpy)Re(4,4'\text{-}bpy)](PF_6)$ **I**, $[(CO)_3(bpy)Re(4,4'\text{-}bpy)Re(bpy)(CO)_3](PF_6)_2$ **II**, $[Cl(bpy)_2Os(4,4'\text{-}bpy)](PF_6)$ **III** and $[Cl(bpy)_2Os(4,4'\text{-}bpy)Os(bpy)_2Cl](PF_6)_2$ **IV**, and a new heterobimetallic complex of rhenium(I) and osmium(II) $[(CO)_3(bpy)Re(4,4'\text{-}bpy)Os(bpy)Cl](PF_6)_2$ **V** (bpy = 2,2′-bipyridine; 4,4′-bpy = 4,4′-bipyridine) have been synthesized and characterized by various spectral techniques. The photophysical properties of all the complexes have been studied and a comparison is made between the heterobimetallic and corresponding monometallic and homobimetallic complexes. Emission and transient absorption spectral studies reveal that an excited state energy transfer from the rhenium(I) chromophore (*Re) to osmium(II) takes place. The energy transfer rate constant is found to be $8.7 \times 10^7\ s^{-1}$.

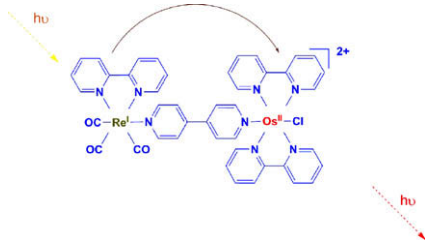

Kamla Sharma and Raj N. Mehrotra

Polyhedron 27 (2008) 3425

Kinetics and mechanism of the Os(VIII)-catalysed oxidation of hypophosphite and phenylphosphinite ion by alkaline hexacyanoferrate(III) ion

The OsO_4-catalysed oxidation of $RHPO_2^-$ by alkaline $Fe(CN)_6^{3-}$ is zero order in $Fe(CN)_6^{3-}$, first order in OsO_4 and Michaelis-Menten kinetics is observed with respect to $RHPO_2^-$. Consistent with this the suggested mechanism is:

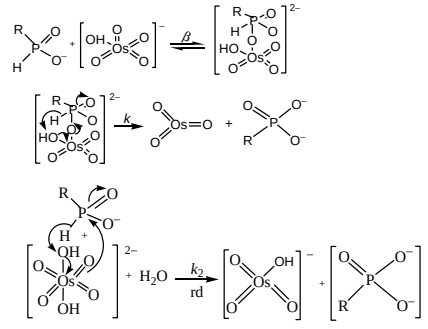

Pulakesh Bera, Chong-Hyeak Kim and Sang Il Seok

Polyhedron 27 (2008) 3433

Synthesis, spectroscopic characterization and thermal behavior of cadmium(II) complexes of *S*-methyldithiocarbazate (SMDTC) and *S*-benzyldithiocarbazate (SBDTC): X-ray crystal structure of $[Cd(SMDTC)_3] \cdot 2NO_3$

The reaction of *S*-methyl dithiocarbazate (SMDTC) and *S*-benzyl dithiocarbazate (SBDTC) with $Cd(NO_3)_2 . 4H_2O$ gave monomeric 1:2 complexes $[Cd(SMDTC)_3](NO_3)_2$ and $[Cd(SBDTC)_2](NO_3)_2$ respectively in which the ligands, in its neutral thione form, adopt bidentate chelating bonding mode to the metal center. The coordination geometry around cadmium(II) in $[Cd(SMDTC)_3](NO_3)_2$ is distorted octahedral, as obtained by X-ray diffraction study whereas $[Cd(SBDTC)_2](NO_3)_2$ is expected to be tetrahedral.

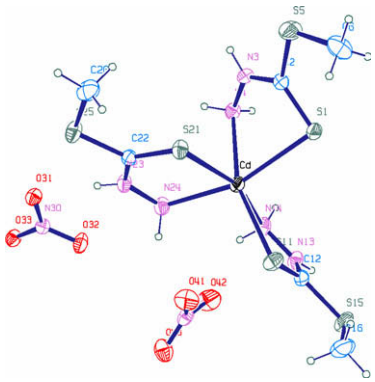

Xiaotai Wang, Haif Alshammary, Rongrong Zhang, Arezou Seifpour, Joe T. Villalva, Zili Xu, Chong Zheng, Jian-Rong Li and Xiao-Ying Huang

Polyhedron 27 (2008) 3439

3D Lanthanide–organic coordination polymers built upon infinite 1D secondary building units

Hydrothermal reactions of $Ln(NO_3)_3$ (Ln = La, Eu) with 1,4-phenylenedipropionic acid (H_2PDP) yield two isostructural coordination polymers of empirical formula $[Ln_2(PDP)_3(H_2O)_2]$, which show a 3D network structure consisting of infinite 1D $Ln(H_2O)$–OOC secondary building units (SBUs) that are cross-linked via $–CH_2CH_2C_6H_4CH_2CH_2–$ tethers of the PDP anions.

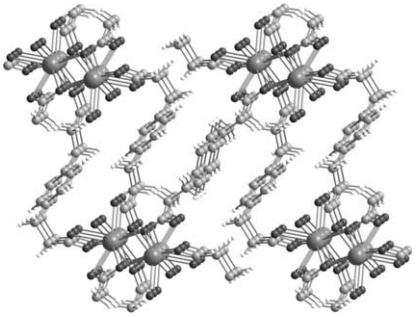

Ramasamy Indumathy, Mookandi Kanthimathi, T. Weyhermuller and Balachandran Unni Nair

Polyhedron 27 (2008) 3443

Cobalt complexes of terpyridine ligands: Crystal structure and nuclease activity

Synthesis, characterization and crystal structures of two new cobalt complexes with different oxidation states, containing tridentate ligand imidazole terpyridine have been reported. The complexes bind to DNA through intercalation and exhibit efficient nuclease activity.

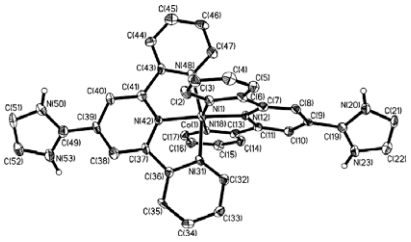

M. Singh, R.J. Butcher and N.K. Singh

Polyhedron 27 (2008) 3451

Synthesis and X-ray structural studies of *N*′-(pyridine-3-carbonyl) hydrazinecarbodithioic acid ethyl ester (H_2pchc) and [Mn(Hpchc)$_2$(*o*-phen)]

Complex [Mn(Hpchc)$_2$(*o*-phen)] formed with N′-(pyridine-3-carbonyl)-hydrazine-carbodithioic acid ethyl ester (H_2pchc) has MnN_4O_2 coordination and the ligand behaves as uninegative bidenate donor and forms a five membered chelate ring. In complex, the ortho C–H bond from *o*-phen ring forms an unusual C–H$\cdots\pi$ intramolecular interaction with $MnOCN_2$ chelate ring which gives structural support for metalloaromaticity in the complex.

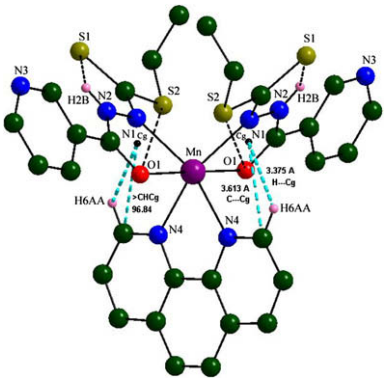

T.A. Reena, E.B. Seena and M.R. Prathapachandra Kurup

Polyhedron 27 (2008) 3461

Zinc(II) complexes derived from di-2-pyridyl ketone N^4-phenyl-3-semicarbazone: Crystal structures and spectral studies

Six zinc(II) complexes, $Zn(HL)Br_2$ (**1**), $Zn(HL)Cl_2$ (**2**), ZnL(OAc) (**3**), $ZnLN_3$ (**4**), ZnL_2 (**5**) and $ZnL_2 \cdot H_2O$ (**6**), have been synthesized and characterized by different physicochemical techniques. Complex **1** is five coordinated and has a distorted square pyramidal geometry. Complexes **5** and **6** are six coordinated and have distorted octahedral geometries. In complexes **1** and **2**, the ligand moieties are coordinated in the neutral form (HL), and in the other complexes they are monoanionic (L^-).

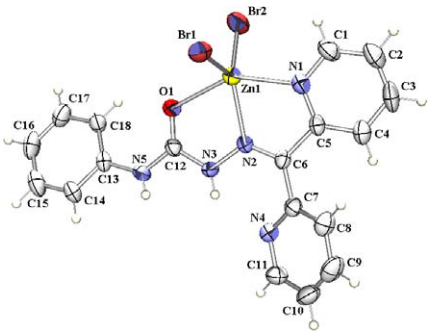

Masoud Salavati-Niasari, Fatemeh Davar and Mehdi Mazaheri

Polyhedron 27 (2008) 3467

Synthesis of Mn_3O_4 nanoparticles by thermal decomposition of a [bis(salicylidiminato)manganese(II)] complex

The present investigation reports on the novel synthesis of Mn_3O_4 nanoparticles using thermal decomposition and their physicochemical characterization. The Mn_3O_4 nanoparticle powder has been prepared using [bis(salicylidiminato)manganese(II)] as a precursor. The effect of oleyl amine and triphenylphosphine on the particle morphology has been investigated. Transmission electron microscopy (TEM) analysis demonstrated Mn_3O_4 nanoparticles with an average diameter of about 25 nm.

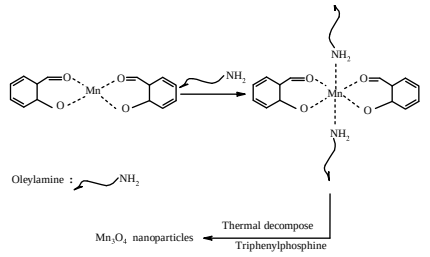

Anindita Sarkar and Samudranil Pal

Polyhedron 27 (2008) 3472

Decavanadates with $[Et_3NH]^+$ and $[Me_2HN(CH_2)_2NHMe_2]^{2+}$: Variation in protonation state and self-assembly

Syntheses, characterization and crystal structures of $[Et_3NH]_4[V_{10}O_{26}(OH)_2]$ (**1**) and $[Me_2HN(CH_2)_2NHMe_2]_3[V_{10}O_{28}] \cdot 4H_2O$ (**2**) are described. In the crystalline state, **1** forms dimeric aggregates via interanionic O–H···O hydrogen bonds, whereas a three-dimensional network of **2** is formed through intermolecular N–H···O and O–H···O hydrogen bonds.

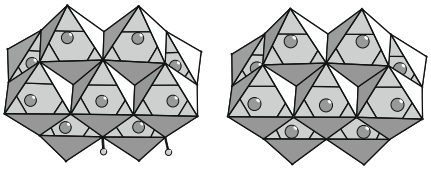

Milan Nádvorník, Vratislav Langer, Robert Jirásko, Michal Holčapek, Tomáš Weidlich, Antonín Lyčka and Alexander Popkov

Polyhedron 27 (2008) 3477

Syntheses, X-ray, MS^n, NMR and CD structure determination of nickel(II) complexes of Schiff bases of (*S*)-*N*-(2-benzoylphenyl)-1-benzylpyrrolidine-2-carboxamide and aromatic α-amino acids

A preparative procedure for the synthesis of an important chiral synthon of side-chain protected tyrosine was developed and optimised for the minimisation of nickel salts waste. While preparing a similar side-chain protected tryptophan synthon, an unexpected low stability was found of the Boc-protective group of the tryptophan aromatic nitrogen during purification on silica gel.

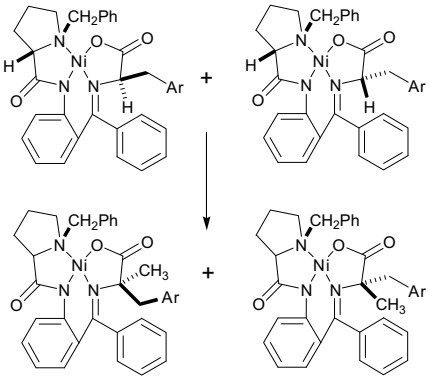

Han Kwak, Sun Hwa Lee, Soo Hyun Kim, Young Min Lee, Byeong Kwon Park, Eun Yong Lee, Yu Jin Lee, Cheal Kim, Sung-Jin Kim and Youngmee Kim

Polyhedron 27 (2008) 3484

Substituent effects of pyrazine on construction of crystal structures of Zn(II)-benzoate complexes and their catalytic activities (dinuclear, trinuclear, and pentanuclear to 1-D and 2-D)

Several substituted pyrazine ligands as well as simple pyrazine have been employed to investigate how the bridging pyrazine ligand influences on construction of Zn-benzoate complexes. The structural differences between such complexes reveal that the change of the substituents of the ligands has a great influence on the complex structures. The compounds catalyzed efficiently the transesterification of a variety of esters.

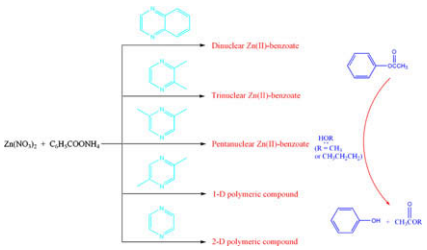

Zhi-Hui Liu, Yong-Cai Qiu, Ying-Hua Li, Hong Deng and Matthias Zeller

Polyhedron 27 (2008) 3493

Synthesis, structures and luminescent properties of 4d–4f heterometallic coordination frameworks based on lanthanide oxalate substructures with nicotinate bridging ligands

Four novel transition–lanthanide metal–organic coordination polymers, namely $[Ag_2Ln(nic)_4(H_2O)_4 \cdot (ClO_4) \cdot H_2O]$ [Ln = Eu (**1**), Gd (**2**)] and $[AgLn(nic)_2(ox)_{0.5}(H_2O)_2 \cdot (ClO_4) \cdot H_2O]$ [Ln = Tb (**3**), Yb (**4**)] (nic = nicotinate; ox = oxalate) have been synthesized by the hydrothermally reactions of 4d and 4f metal salts with N-/O-donor ligands. Furthermore, the luminescent properties of complexes **1** and **3** were studied.

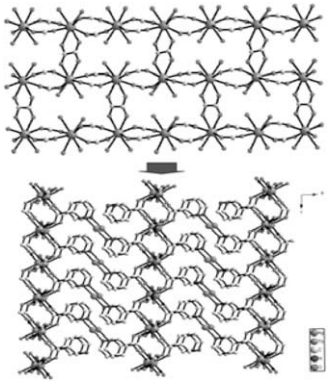

Barbara Barszcz, Agnieszka Jabłońska-Wawrzycka, Katarzyna Stadnicka and Julia Jezierska

Polyhedron 27 (2008) 3500

Coordination chemistry of 2-hydroxymethylbenzimidazole complexes with copper(II) and cadmium(II) ions: Similarities and differences

The new Cu(II) and Cd(II) complexes of the biologically relevant ligand 2-hydroxymethylbenzimidazole have been synthesized and characterized by UV–Vis, IR, Raman, EPR, NMR and X-ray. The polyhedra of metal complexes containing two ligands are different. The copper complex is a five-coordinated (tetragonal pyramid) but cadmium forms an eight-coordinated (CdN_2O_6) complex.

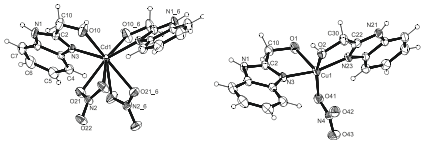

Laura Valencia Matarranz, Rufina Bastida, Alejandro Macías and Paulo Pérez-Lourido

Polyhedron 27 (2008) 3509

Synthesis and crystal structures of Cd(II) complexes with di-pyridyl hexa-azamacrocyclic ligands having cyano pendant-arms

The coordination capability of two pendant-armed azamacrocyclic ligands with cyanoethyl L^1 and cyanomethyl L^2 pendant groups towards cadmium nitrate and perchlorate salts was achieved. All metal complexes were characterized by elemental analysis, LSI-MS, IR, conductivity measurements and ^1H NMR spectroscopy. The X-ray crystal structure of the complexes $[CdL^1](NO_3)_2$, $[CdL^1](ClO_4)_2 \cdot CH_3CN$, and $[CdL^2](ClO_4)_2 \cdot H_2O$ were also determined. All the complexes are mononuclear with the metal ion in a distorted octahedral environment. The pendant groups are not coordinated to the metal due the linear nature of the cyano groups; however, different interactions between nitrate ions, nitrile groups and pyridine rings from the macrocycle have been observed in the Cd(II) complexes with L^1.

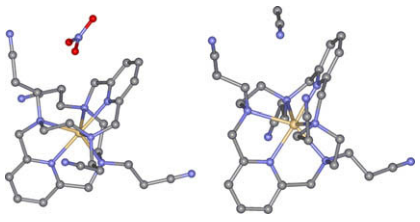

Masoud Salavati-Niasari, Fatemeh Davar and Noshin Mir

Polyhedron 27 (2008) 3514

Synthesis and characterization of metallic copper nanoparticles via thermal decomposition

Copper oxalate was used as a precursor to prepare metallic copper nanoparticles by thermal decomposition. The products were characterized by different techniques. X-ray diffraction pattern (XRD) analysis revealed broad pattern for fcc crystal structure of copper metal. The particle size of metallic copper nanoparticels was estimated about 40 nm.

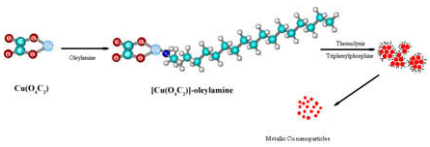

Pathik Maji, Setharampattu S. Krishnamurthy and Munirathinam Nethaji

Polyhedron 27 (2008) 3519

Palladium and platinum complexes of chiral and achiral calix[4]arene bisphosphite ligands

Chiral and achiral *p*-*tert*-butyl-calix[4]arene bisphosphites and their Pd and Pt complexes are reported. The crystal lattices of $PdCl_2$ complexes of chiral bisphosphites display hydrophobic channels and the molecules are held together by intermolecular C–H···Cl hydrogen bonds.

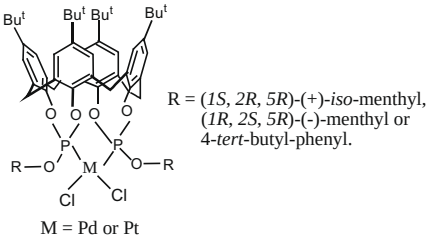

The Publisher encourages the submission of articles in electronic form thus saving time and avoiding rekeying errors. For detailed instructions on the preparation of manuscripts and of electronic artwork, consult the Author Gateway for Elsevier at http://authors.elsevier.com

ScienceDirect

Full text of this journal is available, on-line from **ScienceDirect**. Visit **www.sciencedirect.com** for more information.

Polyhedron 27, issue 14, 29 September 2008

Contents lists available at ScienceDirect

Polyhedron

journal homepage: www.elsevier.com/locate/poly

Contents

Papers

Claudia Rodrigues, Alzir A. Batista, Ricardo Q. Aucélio, Letícia R. Teixeira, Lorenzo do Canto Visentin and Heloisa Beraldo

Polyhedron 27 (2008) 3061

Spectral and electrochemical studies of ruthenium(II) complexes with N^4-methyl-4-nitrobenzaldehyde and N^4-methyl-4-nitrobenzophenone thiosemicarbazone: Potential anti-trypanosomal agents

N^4-Methyl-4-nitrobenzaldehyde thiosemicarbazone ($H4NO_2Fo4M$), N^4-methyl-4-nitrobenzophenone thiosemicarbazone ($H4NO_2Bz4M$) and their ruthenium(II) complexes $[Ru(4NO_2Fo4M)_2(PPh_3)_2]$ (**1**), $[Ru(4NO_2Bz4M)_2(PPh_3)_2]$ (**2**), $[Ru(4NO_2Fo4M)_2(dppb)]$ (**3**) and $[Ru(4NO_2Bz4M)_2(dppb)]$ (**4**) were obtained. The nitro anion radical, one of the proposed intermediates in the mechanism of action of nitro-containing anti-trypanosomal drugs, is formed at approximately −1.00 V in the free thiosemicarbazones as well as in their corresponding ruthenium(II) complexes, suggesting their potential to act as antitrypanosomal drugs. The natural fluorescence of $H4NO_2Fo4M$, $H4NO_2Bz4M$ and complexes (**1**)–(**4**) provides a way to identify and to monitor their concentration in biological systems.

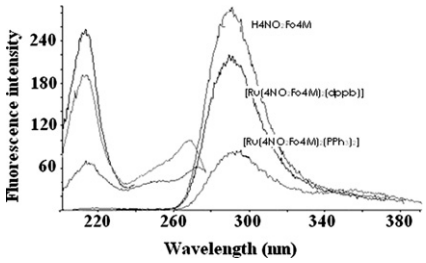

Leszek Pazderski, Jaromír Toušek, Andrzej Wojtczak, Jerzy Sitkowski, Lech Kozerski and Edward Szłyk

Polyhedron 27 (2008) 3067

The crystal and molecular structure of potassium aquapentachloroiridate(III) and the ^1H, ^{13}C, ^{15}N NMR coordination shifts in iridium(III) chloride complexes with 2,2′-bipyridine or 1,10-phenanthroline

X-ray structure of $K_2[Ir(H_2O)Cl_5]$ and ^1H, ^{13}C, ^{15}N NMR of Ir(III) chloride complexes with bpy and phen.

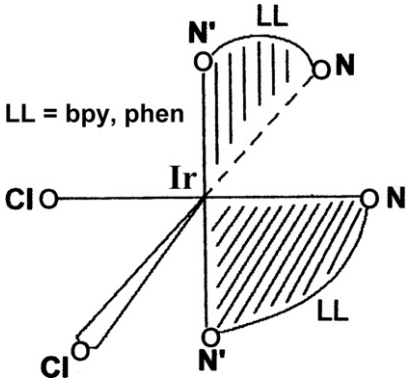

Timothy J. Boyle, Leigh Anna M. Ottley and Mark A. Rodriguez

Polyhedron 27 (2008) 3079

Structurally characterized group 4 metal alkoxides modified with the pyridyl-based ligands 2-mercapto pyridine *n*-oxide and 3,3′-dihydroxy-2,2′-bipyridine

The pyridine-based ligands 2-mercapto pyridine *n*-oxide (H-2MPO) and 3,3′-dihydroxy-2,2′-bipyridine (H_2-OBPy) were used to modify group 4 alkoxides forming: $(2MPO)_2Ti(OR)_2$ and $[(OR)_2M(\mu_c\text{-OBPy})]_3$ (M = Ti (shown), Zr). The synthesis and characterization of these compounds are presented.

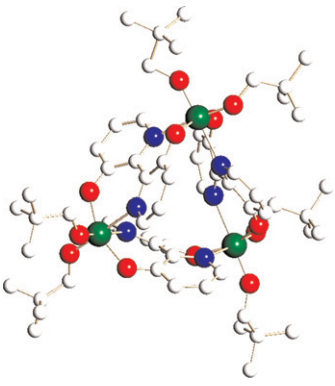

Partha Roy, Koushik Dhara, Mario Manassero and Pradyot Banerjee

Polyhedron 27 (2008) 3085

A new organic compound for the synthesis of gold nanoparticles

2,3,5,6-Tetrakis-(morpholinomethyl)hydroquinone has been synthesized by the aminomethylation of hydroquinone and characterized by single crystal X-ray diffraction. It acts as a reducing as well as a capping agent to generate gold nanoparticles with different morphologies.

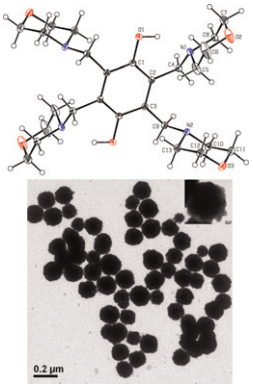

Mairéad E. Kelly, Santiago Gómez-Ruiz, Jürgen Schmidt, Christoph Wagner and Harry Schmidt

Polyhedron 27 (2008) 3091

Platinum(IV) complexes with α,ω-bis(pyrazol-1-yl) alkanediyl and diethyl ether/thioether ligands. Crystal structures of dibromodimethyl-[1,2-bis(pyrazol-1-yl)ethane]platinum(IV) and trimethyl-bis[2-(pyrazol-1-yl)ethyl]etherplatinum(IV) tetrafluoroborate

The reaction of flexible α,ω-bis(pyrazol-1-yl) alkanediyl and diethyl ether/thioether ligands with organometallic platinum precursors is described. Five new platinum(IV) complexes $[PtBr_2Me_2\{pz(CH_2)_{\boldsymbol{m}}pz\}]$, $m = 2$ (**1**) or 8 (**2**), $[PtI_2Me_2\{pz(CH_2)_2pz\}]$ (**3**), $[PtMe_3(pzCH_2CH_2OCH_2CH_2pz)][BF_4]$ (**4**) and $[PtMe_3(pzCH_2CH_2SCH_2CH_2pz)][CF_3SO_3]$ (**5**), where 'pz' is pyrazol-1-yl, are described.

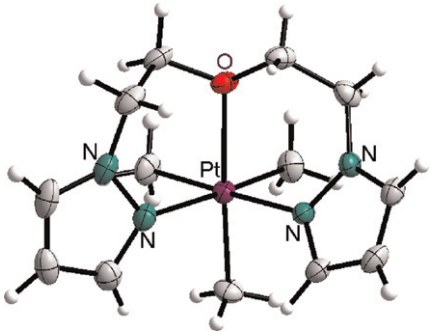

Gregory J. Grant, Maikel E. Botros, Jared S. Hassler, Daron E. Janzen, Craig A. Grapperhaus, Martin G. O'Toole and Donald G. VanDerveer

Polyhedron 27 (2008) 3097

Hg(II) and Cd(II) complexes with mixed donor macrocyclic thioethers: The oxophobicity of mercury(II)

We report a series of Hg(II) and Cd(II) complexes with mixed donor macrocyclic ligands. In contrast to Cd(II), Hg(II) does not form coordinate bonds to oxygen.

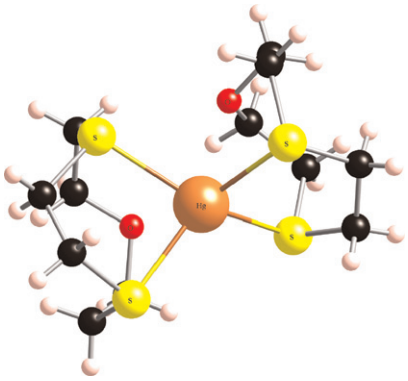

Xuan Shen, Hironori Miyashita, Li Qi, Dun-Ru Zhu, Mamoru Hashimoto and Kazunori Sakata

Polyhedron 27 (2008) 3105

Syntheses, crystal structure and electrochemical characterization of ferrocene-containing nickel(II) complexes with 4,11-dihydro-5,7,12,14-tetramethyldibenzo[*b*,*i*][1,4,8,11]tetraazacyclotetradecine

Two novel ferrocene-containing tmtaa (H_2tmtaa = 4,11-dihydro-5,7,12,14-tetra- methyldibenzo[*b*,*i*][1,4,8,11]tetraazacyclotetradecine) complexes $\{[(\eta\text{-}C_5H_5)Fe(\eta\text{-}C_5H_4)(CO)]\text{-}(C_{22}H_{21}N_4)Ni\}$ (**1**) and $\{[(\eta\text{-}C_5H_5)Fe(\eta\text{-}C_5H_4)\text{-}(CO)]_2(C_{22}H_{20}N_4)Ni\}$ (**2**) have been synthesized and characterized. The crystal structure of **1** shows that the symmetry axis of ferrocene is almost parallel to Nitmtaa. In **1** and **2**, the ferrocene groups act as electron acceptors, not electron donors.

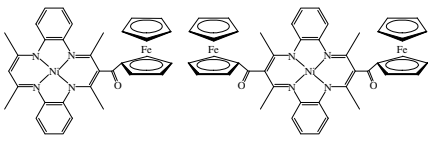

Ambarish Ray, Parikshit Chandra Mandal, Atish Dipankar Jana, William S. Sheldrick, Swastik Mondal, Monika Mukherjee and Mahammad Ali

Polyhedron 27 (2008) 3112

Cyanometallate incorporated supramolecular networks based on a nitroalkyl-substituted $Cu^{II}N_4$ precursor: Synthesis, crystal structure, thermal and electrochemical studies

Two new copper(II) complexes, *viz.* $[Cu(nelin)(H_2O)_2]_2[Fe(CN)_6] \cdot 6H_2O$ (**2**) and $[\{Cu(nelin)\}_2Ni(CN)_4](ClO_4)_2 \cdot 2H_2O$ (**3**), have been synthesized using $[Cu(nelin)](ClO_4)_2$ (**1**) as a nitroalkyl-substituted $Cu^{II}N_4$ precursor, and their supramolecular chemistry, thermal properties and comparative electrochemistry based on nitro-radical anion generation are fully explored.

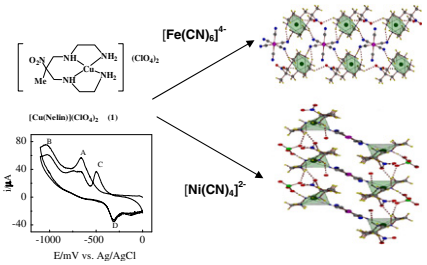

Ru-Fen Zhang, Qing-Feng Wang, Ming-Qing Yang, Yue-Rong Wang and Chun-Lin Ma

Polyhedron 27 (2008) 3123

Five new dicarboxylate organotin complexes under hydrothermal condition: Syntheses, characterization and crystal structures of 1D, 2D and 3D polymers constructed from dimeric tetraorganodistannoxane units

Five new diorganotin(IV) complexes have been synthesized under hydrothermal condition. All complexes were characterized by elemental analysis, IR, ^1H NMR, ^{13}C NMR, ^{119}Sn NMR, TGA and X-ray crystallography. The X-ray crystallography shows that all of the complexes possess 1D, 2D and 3D polymers constructed from dimeric tetraorganodistannoxane units.

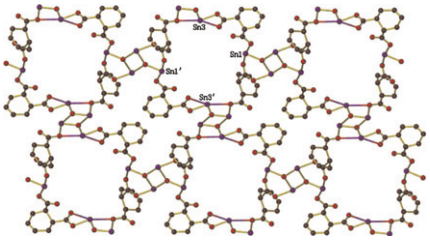

Masoud Salavati-Niasari

Polyhedron 27 (2008) 3132

Synthesis, characterization and catalytic oxidation of cyclohexene with molecular oxygen with host (nanopores of zeolite-Y)/guest (Ni(II) complexes of 14- and 16-membered tetraaza dioxo diphenyl macrocyclic ligands) nanocomposite materials

Ni(II) complexes of 14- and 16-membered tetraaza macrocycles have been encapsulated in the nanopores of zeolite-Y by a two-step process in the liquid phase: (i) adsorption of [bis(diamine)nickel(II)]; $[Ni(N\text{-}N)_2]^{2+}$-NaY; in the nanopores of the zeolite-Y, and (ii) in situ condensation of the nickel(II) precursor complex with ethylcinnamate. These complexes were used for oxidation of cyclohexene with molecular oxygen.

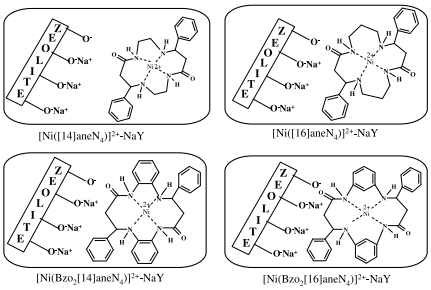

Felix D. Sokolov, Damir A. Safin, Michael Bolte, Elmira R. Shakirova and Maria G. Babashkina

Polyhedron 27 (2008) 3141

New bifunctional *N*-thiophosphorylated thiourea and 2,5-dithiobiurea derivatives. Crystal structures of $R[C(S)NHP(S)(OiPr)_2]_2$ (R = –N(Ph)-CH_2CH_2N(Ph)– and –NHNH–)

A new bifunctional *N*-thiophosphorylated thiourea and 2,5-dithiobiurea of the common formula $R[C(S)NHP(S)(OiPr)_2]_2$ [R = –N(Ph)-CH_2CH_2N(Ph)– (**H_2L^a**); –NHNH– (**H_2L^b**)] have been synthesized and characterized by IR, ^1H, ^{31}P spectroscopy and the single crystal X-ray diffraction method. The structure of the latter compound in $CDCl_3$ and acetone-d_6 solutions has been discussed in comparison with the monofunctional thiosemicarbazide PhNHNHC-(S)NHP(S)(O*i*Pr)$_2$ (**HL^c**).

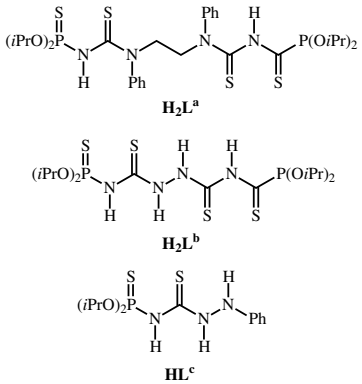

Takuya Akatsuka, Mayuko Ushiro, Shin-ichi Nagamatsu, Yoshio Takahashi and Takashi Fujikawa

Polyhedron 27 (2008) 3146

Multiple-scattering approach to Sn L_3-edge X-ray absorption near-edge structure (XANES) analyses for organic tin compounds

We apply multiple-scattering calculations to the analyses of Sn L_3-edge X-ray absorption near-edge structure (XANES) spectra for environmental organotin compounds such as $SnCl_{4-n}Me_n$, $SnCl_{4-n}Bt_n$, and $SnCl_{4-n}Ph_n$ (n = 0–4) where Me = CH_3, Bt = C_4H_9, and Ph = C_6H_5.

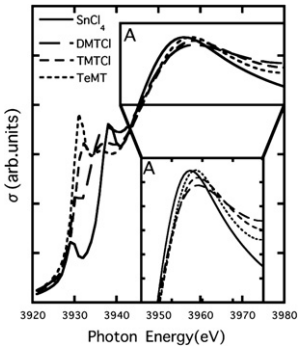

Mamata Singh, R.J. Butcher and N.K. Singh

Polyhedron 27 (2008) 3151

Syntheses and X-ray structural studies of the novel complexes $[Ni(en)_2(3\text{-pyt})_2]$ and $[Cu(en)_2](3\text{-pyt})_2$ based on 5-(3-pyridyl)-1,3,4-oxadiazole-2-thione

Two novel mononuclear mixed-ligand complexes $[Ni(en)_2(3\text{-pyt})_2]$ (**1**) and $[Cu(en)_2](3\text{-pyt})_2$ (**2**), based on 5-(3-pyridyl)-1,3,4-oxadiazole-2-thione $(3\text{-pyt})^-$, have been synthesized and their crystal structures reported. The ligand $(3\text{-pyt})^-$ is bonded through the oxadiazole nitrogen in the thione form in **1** and is ionically present in the thiolate form in **2**.

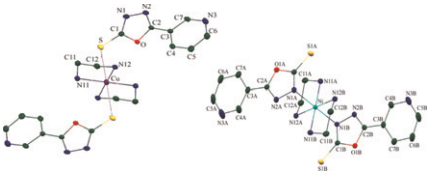

Fu-Ping Huang, Qing Yu, He-Dong Bian, Shi-Ping Yan and Hong Liang

Polyhedron 27 (2008) 3160

2-Benzothiazolylthioacetic acid and 4,4′-bipyridine as ligands in designing low-dimensional coordination polymers: Synthesis, architectures and magnetic properties

A series of coordination polymers (**1**–**6**) based on HBTTAA and 4,4′-bipy ligands have been prepared and characterized. There are weak antiferromagnetic interactions between the metal centers bridged by 4,4′-bipy in **1**, **2**, **5** and **6**.

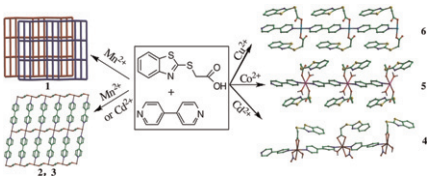

Svetlana G. Kozlova, Svyatoslav P. Gabuda, Vladimir A. Slepkov, Yuri V. Mironov and Vladimir E. Fedorov

Polyhedron 27 (2008) 3167

C^{4-} carbide ligand in the trigonal prismatic environment of rheniums in $[Re_{12}CS_{17}(CN)_6]^{n-}$ complexes

The electronic state of carbon in trigonal prismatic environment in $[Re_{12}CS_{17}(CN)_6]^{n-}$ complexes with variable redox state n = 6 ↔ 8 was characterized by sp^2-hybridisation and oxidation state –4 (arrow 1). It was revealed weak long-distance interaction between C and S in the group $[CS_3]$ for n = 6 (arrow 2).

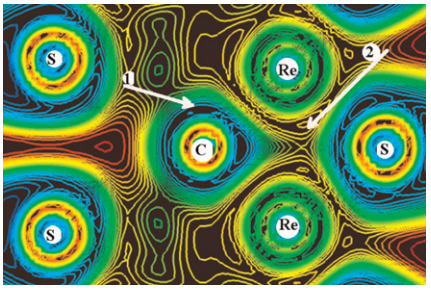

Hassan Keypour, Majid Rezaeivala, Laura Valencia and Paulo Pérez-Lourido

Polyhedron 27 (2008) 3172

Synthesis and crystal structure of Mn(II) complexes with novel macrocyclic Schiff-base ligands containing piperazine moiety

A series of Mn(II) macrocyclic Schiff-base complexes $[MnL^{n}Cl]^{+}$ (n = 1–4) have been prepared via the Mn(II) templated [1+1] cyclocondensation of 2,6-diacetylpyridine or 2,6-pyridinedicarbaldehyde with the symmetrical 1,4-bis(3-aminopropyl)piperazine or the novel asymmetrical *N*,*N*′(2-aminoethyl)(3-aminopropyl)piperazine linear tetraaza amines containing piperazine moiety.

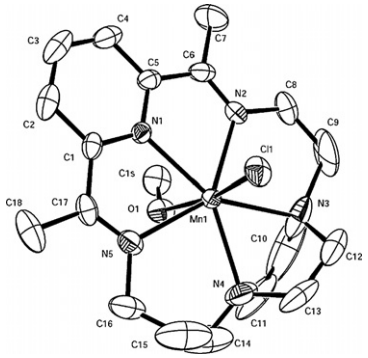

The Publisher encourages the submission of articles in electronic form thus saving time and avoiding rekeying errors. For detailed instructions on the preparation of manuscripts and of electronic artwork, consult the Author Gateway for Elsevier at http://authors.elsevier.com

ScienceDirect

Full text of this journal is available, on-line from **ScienceDirect**. Visit **www.sciencedirect.com** for more information.

Available online at www.sciencedirect.com
ScienceDirect
Polyhedron 27, issue 7, 20 May 2008
POLYHEDRON
www.elsevier.com/locate/poly

Contents

Papers

Anthony E. Wetherby Jr., Arnold L. Rheingold, Christa L. Feasley and Charles S. Weinert

Polyhedron 27 (2008) 1841

Synthesis and crystal structure of a germanium(II) calix[6]arene containing unusual diamidosilyl ether groups

The reaction of $Ge[N(SiMe_3)_2]_2$ with calix[6]arene generates a germanium(II) macrocyclic product where the six phenolic oxygen atoms are incorporated into either a Ge_2NO rhombus, a $-OSiMe_3$ silyl ether group, or two unprecedented $-OSi(H)(NH_2)_2$ groups. This species has been characterized by X-ray crystallography and multinuclear (^1H, ^{13}C, and ^{29}Si) NMR spectroscopy.

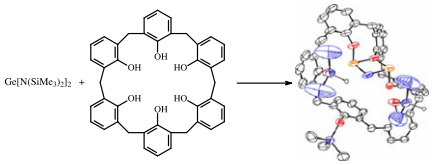

Hamid Reza Khavasi, Anita Abedi, Vahid Amani, Behrouz Notash and Nasser Safari

Polyhedron 27 (2008) 1848

Synthesis, characterization and crystal structure determination of zinc (II) and mercury (II) complexes with 2,2′-dimethyl-4,4′-bithiazole

The 2,2′-dimethyl-4,4′-bithiazole ligand, dm4bt, and its Zn and Hg complexes have been prepared. The X-ray structure determinations show that both complexes are four coordinated by two chlorine atoms and one bidentate 2,2′-dimethyl-4,4′-bithiazole ligand. In the Hg complex one of the two chlorides is set at a semi-bridging position.

$$MCl_2 + dm4bt \rightarrow [M(dm4bt)Cl_2]$$

M = Zn and Hg

Roushan Khoshnavazi, Rahmat Sadeghi and Liela Bahrami

Polyhedron 27 (2008) 1855

High stable sandwich-type polyoxometallates based on A-β-$SiW_9O_{34}^{10-}$. Synthesis, chemical properties and characterization of $[(A\text{-}\beta\text{-}SiW_9O_{34})_2(MOH_2)_3CO_3]^{13-}$ (M = Y^{3+} and Yb^{3+})

Highly hydrolytic and thermally stable sandwich-type polyoxometallates of $[(A\text{-}\beta\text{-}SiW_9O_{34})_2(MOH_2)_3CO_3]^{13-}$ (M = Y^{3+} and Yb^{3+}) have been synthesized and characterized by elemental analysis, IR, ^{13}C and ^{29}Si NMR, UV–Vis spectroscopy, TGA, DSC and single crystal structure analysis. The crystal structures of the complexes consist of two lacunary A-β-$SiW_9O_{34}^{10-}$ Keggin moieties which are linked by a $(H_2OMO)_3C$ belt into an assembly of virtual C_2 symmetry. Each M^{3+} ion adopts a mono-capped trigonal prismatic coordination. The hydrolytic and thermal stability conditions of the complexes and proving reasons for the retention of the isomeric form of the trilacunary A-β-$SiW_9O_{34}^{10-}$ ligand upon complexation are discussed.

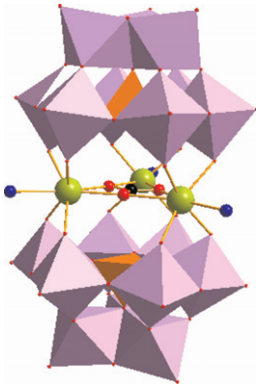

Glaico Chiericato Júnior and Ana Paula Saldanha Silva

Polyhedron 27 (2008) 1860

Spectroelectrochemistry and investigation of charge transport mechanisms of iron poly(pyridyl) redox polymers

In this work, we describe the characterization of the complex $[Fe(tpy\text{-}NH_2)_2](PF_6)_2$ (tpy-NH_2 = bis[4′-(3-aminophenyl)-2,2′:6′,2″-terpyridine] and report the electropolymerization and charge transport parameters. The results showed that poly-$[[Fe(tpy\text{-}NH_2)_2]^{2+}]_n$ can exhibit three regimes of charge transport as a function of film thickness and polymerization time. Morphological characterization was provided by atomic force microscopy.

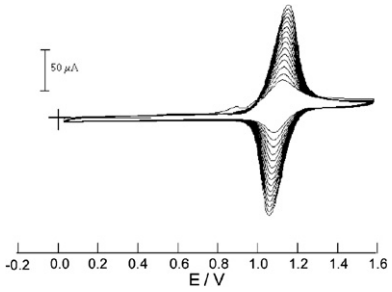

S. Sreedaran, K. Shanmuga Bharathi, A. Kalilur Rahiman, K. Rajesh, G. Nirmala, L. Jagadish, V. Kaviyarasan and V. Narayanan

Polyhedron 27 (2008) 1867

Synthesis, electrochemical, catalytic and antimicrobial activities of novel unsymmetrical macrocyclic dicompartmental binuclear nickel(II) complexes

A series of novel unsymmetrical dicompartmental binuclear nickel(II) complexes have been prepared by simple Schiff base condensation of the compound 1,8-[bis(3-formyl-2-hydroxy-5-methyl)benzyl]-l,4,8,11-tetraazacyclotetradecane (PC-1) with appropriate aliphatic or aromatic diamine, nickel(II) perchlorate and triethylamine. The effect of chain length on spectral, magnetic, electrochemical and catalytic studies was carried out.

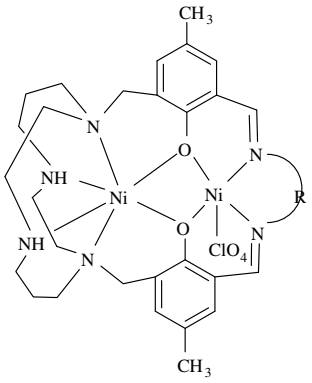

Sujittra Youngme, Achareeya Cheansirisomboon, Chanaiporn Danvirutai, Chaveng Pakawatchai, Narongsak Chaichit, Chainarong Engkagul, Gerard A. van Albada, José Sánchez Costa and Jan Reedijk

Polyhedron 27 (2008) 1875

Three new polynuclear tetracarboxylato-bridged copper(II) complexes: Syntheses, X-ray structure and magnetic properties

The synthesis, crystal structure and magnetic properties of a novel 1D complex $\{[Cu_4(phen)_2(\mu\text{-}O_2CC_2H_5)_8] \cdot (H_2O)\}_n$ (**1**) and two dinuclear paddle-wheel complexes $[Cu_2(\mu\text{-}O_2CC_6H_4OH)_4(C_7H_7NO)_2] \cdot 6H_2O$ (**2**) and $[Cu_2(\mu\text{-}O_2CCH_3)_4(C_7H_7NO)_2]$ (**3**) are reported. The magnetic interaction between Cu(II) ions inthe two classical paddle-wheel compounds are strongly antiferromagnetically coupled with $J = -278.5$ and $-287.0\ cm^{-1}$ for **2** and **3**, respectively. In compound **1** the magnetic susceptibility could be fitted with two different, independent Cu(II) units, one strongly coupled with a J value of $-299.5\ cm^{-1}$ and one weakly coupled with a J value of $-0.75\ cm^{-1}$. The magneto-structural correlations for complexes **1**, **2**, and **3** are discussed on the basis of the structural parameters and magnetic data.

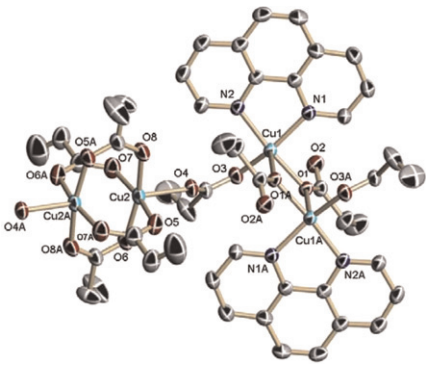

Mevlüde Canlıca, Ahmet Altındal, Ali Rıza Özkaya, Bekir Salih and Özer Bekaroğlu

Polyhedron 27 (2008) 1883

Synthesis, characterization, and electrochemical, and electrical measurements of novel 4,4′-isopropylidendioxydiphenyl bridged bis and cofacial bis-metallophthalocyanines (Zn, Co)

The new cofacial bis-phthalocyanines Zn(II) (**7**) and Co(II) (**8**) were synthesized. The electrochemical properties of the complexes were examined by cyclic voltammetry, differential pulse voltammetry and controlled potential coulometry in nonaqueous media. Measurements of capacitance showed a well defined decrease with increasing frequency and an increase with increasing temperature at lower frequencies.

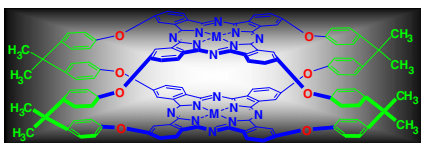

Raquel S. Amim, Marcelo R.L. Oliveira, Genivaldo J. Perpétuo, Jan Janczak, Liany D.L. Miranda and Mayura M.M. Rubinger

Polyhedron 27 (2008) 1891

Syntheses, crystal structure and spectroscopic characterization of new platinum(II) dithiocarbimato complexes

Three new complexes, potassium *N*-4-fluorophenylsulfonyldithiocarbimate dihydrate, and tetrabutylammonium bis(*N*-R-sulfonyldithiocarbimato)-platinate(II) (R = 4-IC_6H_4 and 4-FC_6H_4), were obtained in the crystalline form. The compounds were characterized by single crystal X-ray diffraction technique, and by IR, ^1H and ^{13}C NMR spectroscopies.

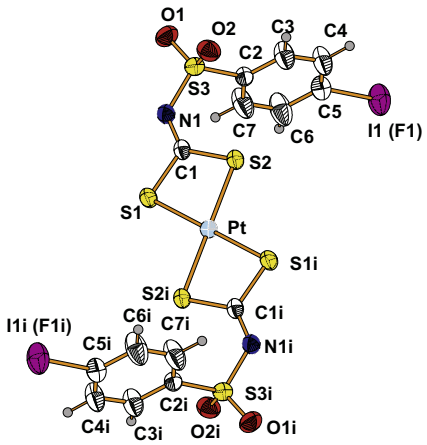

Ji-Hui Li, Jin-Tao Wang, Ping Hu, Li-Yi Zhang, Zhong-Ning Chen, Zong-Wan Mao and Liang-Nian Ji

Polyhedron 27 (2008) 1898

Synthesis, structure and nuclease activity of copper complexes of disubstituted 2,2′-bipyridine ligands bearing ammonium groups

A series of Cu(II) complexes of disubstituted 2,2′-bipyridine bearing ammonium groups at 5,5′- and 4,4′-positions were synthesized. All complexes, especially the two with 5,5′-ammonium groups, exhibit strong DNA cleavage abilities. The high nuclease activity may be attributed to the strong interaction of the metal moiety and two ammonium groups with three adjacent phosphate groups of DNA.

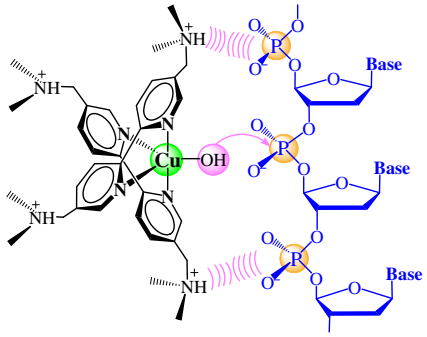

Vashishtha M. Gurame and Gavisiddappa S. Gokavi

Polyhedron 27 (2008) 1905

Kinetics and mechanism of oxidation of hypophosphite by Waugh-type enneamolybdomanganate(IV) in perchloric acid

The reaction between enneamolybdomanganate(IV) and hypophosphite occurs through prior complex formation between the reactants followed by its rate determining decomposition. The phosphitomolybdate was the product of reaction characterized by AAS and FTIR analysis.

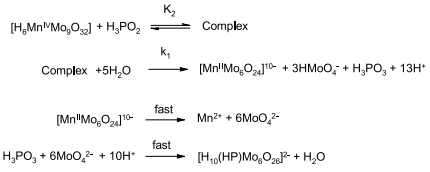

Akella Sivaramakrishna, Paul Mushonga, Ian L. Rogers, Feng Zheng, Raymond J. Haines, Ebbe Nordlander and John R. Moss

Polyhedron 27 (2008) 1911

Selective isomerization of 1-alkenes by binary metal carbonyl compounds

Selective isomerization reactions of various 1-alkenes have been carried out using several metal carbonyl complexes. The most efficient catalyst studied was found to be tri-rutheniumdodecacarbonyl.

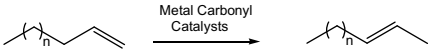

Viswanathan Mahalingam, Nataraj Chitrapriya, Frank R. Fronczek and Karuppannan Natarajan

Polyhedron 27 (2008) 1917

New Ru(II)–dmso complexes with heterocyclic hydrazone ligands towards cancer chemotherapy

A series of new Cl–Ru(II)–dmso complexes containing heterocyclic hydrazone ligands have been synthesized and characterized. The hydrazone ligands behave as neutral bidentate ligands. The redox properties of the complexes were studied by cyclic voltammetry. The substituents present in the hydrazone ligands affect the redox behavior. The antibacterial activity of the ligands and the complexes were studied in terms of minimum inhibitory concentration (MIC). The complexes were found to bind Herring sperm ds DNA in mixed modes.

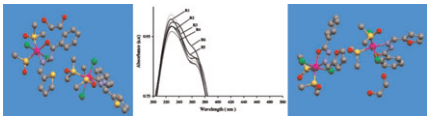

S. Sujatha, S. Balasubramanian, H.-K. Fun and K. Chinnakali

Polyhedron 27 (2008) 1925

Synthesis and characterization of nickel(II) and copper(II) complexes of hexaaza macrocycle, 4-methyl-1,3,5,8,11,14-hexaazatricyclooctadecane

Square-planar Ni(II) and Cu(II) complexes of macrotricyclic ligand 4-methyl-1,3,6, 8,11,14-hexaazatricyclooctadecane (PCHA) have been synthesized from the template condensation reactions of formaldehyde with triethylenetetraamine and 1,2-propanediamine in the presence of metal ion. The complexes have been characterized by spectroscopic, electrochemical and molar conductivity measurements. The crystal structure of $[Ni(PCHA)](ClO_4)_2$ determined by X-ray crystallography confirms a square-planar geometry around the metal centre.

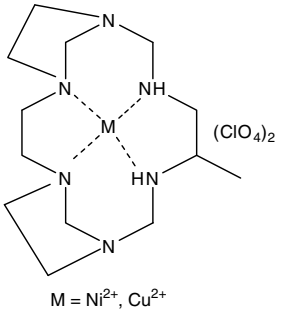

Anna Skarżyńska and Miłosz Siczek

Polyhedron 27 (2008) 1930

Reactivity of oxo-rhenium precursor *trans*-$ReOCl_3(OPPh_3)(SMe_2)$ with diaza heterocyclic congeners: Synthesis and spectroscopic characterization of mono and dinuclear compounds

A new class of mono and dinuclear oxo-complexes of Re(V) with N-heterocyclic bridged ligands: pyrazine and pyrimidine have been synthesized and isolated. The structure of the complexes were established based on spectroscopic methods: IR, NMR, UV–Vis, elemental analysis, and X-ray studies.

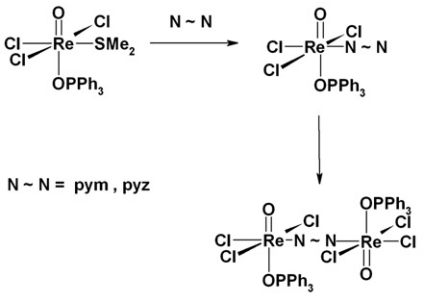

Angad Kumar Singh, Sanyucta Kumari, K. Ravi Kumar, B. Sridhar and T.R. Rao

Polyhedron 27 (2008) 1937

Ligational aspects of the hydrazide-based Schiff-base, *N*-(4″-pyridylcarboxamido)-4-(4′-hexyloxybenzoato)salicylaldimine towards some 3d metal ions and crystal structures of the Schiff-base and Zn(II) complex

A novel hydrazide-based mesogenic (nematic) Schiff-base, *N*-(4″-pyridylcarboxamido)-4-(4′-hexyloxyben-zoato)salicylaldimine, Hpychbsal (abbreviated as H_2L) was prepared and its structure studied by elemental analyses, mass, NMR and IR spectra and single crystal XRD (triclinic space group $P\bar{1}$ with $Z = 4$) techniques. The Schiff-base behaves as a uninegative bi/tridentate species in its non-mesogenic complexes of the general formula, $[M(HL)_2]$ [M = Mn, Co, Ni, Cu and Zn] and as a dinegative tridentate species with Zn(II) in the distorted square-pyramidal complex, [ZnL · 2py], for which the crystal structure was solved (triclinic space group $P\bar{1}$ with $Z = 2$). The IR and NMR spectral data imply bonding of HL^- and L^{2-} species through phenolate oxygen and/or amidic oxygen and azomethine nitrogen atoms.

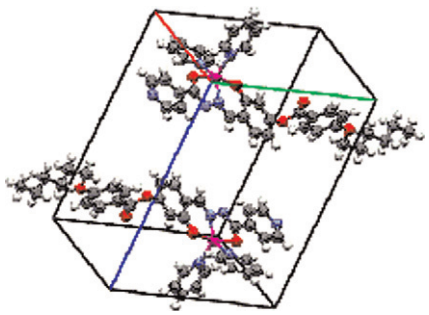

Rafał Janicki and Anna Mondry

Polyhedron 27 (2008) 1942

Structural and spectroscopic investigations of europium(III) entrapped by the ethylenediaminetetra(methylenephosphonate) ligand in $K_{12}H_8[Eu_4(EDTMP)_4] \cdot 45H_2O$ crystal

The structure and spectroscopy of the crystal of an anionic octacoordinate Eu^{3+} complex with a ethylenediaminetetra(methylenephosphonate) ligand, $K_{12}H_8[Eu_4(EDTMP)_4] \cdot 45H_2O$, is described; the crystal luminesces from both $^5D_0$ and $^5D_1$ states.

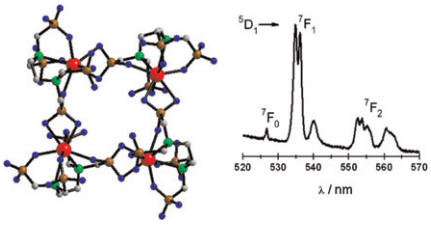

The Publisher encourages the submission of articles in electronic form thus saving time and avoiding rekeying errors. For detailed instructions on the preparation of manuscripts and of electronic artwork, consult the Author Gateway for Elsevier at http://authors.elsevier.com

ScienceDirect

Full text of this journal is available, on-line from **ScienceDirect**. Visit **www.sciencedirect.com** for more information.

Polyhedron 27, issue 15, 17 October 2008

Contents lists available at ScienceDirect

Polyhedron

journal homepage: www.elsevier.com/locate/poly

Contents

Review

Adam S. Veige

Polyhedron 27 (2008) 3177

Carbon monoxide as a reagent: A report on the role of *N*-heterocyclic carbene (NHC) ligands in metal-catalyzed carbonylation reactions

This report is a focused and critical essay on the effectiveness of M–NHC (NHC = *N*-heterocyclic carbene) catalysts in reactions that specifically utilize carbon monoxide as a C1-carbon source.

Papers

P. Bhunia, U.S. Ray, J. Cheng, T.-H. Lu and C. Sinha

Polyhedron 27 (2008) 3191

Nickel(II)-azido/thiocyanato complexes of 1-alkyl-2-(naphthylazo)imidazole

$[Ni(NaiR)_2(X)_2]$ (X = N_3 and NCS) are synthesized and characterized. One of them has been structurally characterized by single crystal X-ray diffraction study. Cyclic voltammogram exhibits quasireversible oxidation response at 0.3–0.4 V which is corresponding to Ni(III)/Ni(II) couple along with ligand reductions at negative potential to SCE reference electrode.

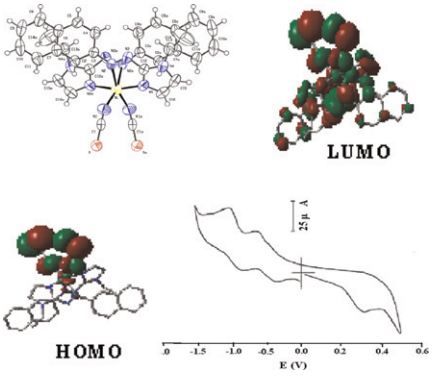

Bipul Mondal, Michael G.B. Drew, Rahul Banerjee and Tapas Ghosh

Polyhedron 27 (2008) 3197

Chemistry of mixed-ligand methoxy bonded oxidovanadium(V) complexes with a family of hydrazone ligands containing VO^{3+} core and their substituent controlled methoxy-bridged dimeric forms

Methoxy bonded mixed-ligand monomeric and methoxy-bridged dimeric VO^{3+} complexes with a family of benzoyl hydrazones have been synthesized and characterized by various techniques including structure determination by X-ray crystallography. Three of such monomeric complexes along with their methoxy-bridged dimeric forms have been structurally characterized for the first time.

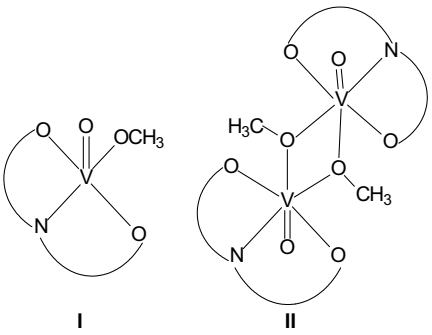

Masoud Salavati-Niasari

Polyhedron 27 (2008) 3207

Template synthesis and characterization of host (nanopores of zeolite Y)/guest (Co(II)-tetraoxodithiatetraaza macrocyclic complexes) nanocomposite materials

A series of Co(II) tetraoxodithiatetraaza macrocyclic complexes ([18]aneN$_4$S$_2$, [20]aneN$_4$S$_2$, Bzo$_2$[18]aneN$_4$S$_2$ and Bzo$_2$[20]aneN$_4$S$_2$) have been encapsulated in the nanopores of zeolite Y by template condensation reaction. Co(II) complexes with tetraoxodithiatetraaza macrocyclic ligand were entrapped in the nanopores of zeolite Y by a two-steps process in the liquid phase: (i) adsorption of [bis(diamine)cobalt(II)] (diamine = 1,2-diaminoethane, 1,3-diaminopropane, 1,2-diaminobenzene, 1,3-diaminobenzene); [Co(N-N)$_2$]$^{2+}$-NaY; in the supercages of the zeolite, and (ii) in situ template condensation of the cobalt(II) precursor complex with thiodiglycolic acid.

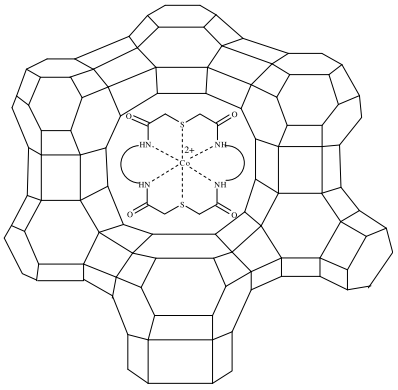

Nahed M.H. Salem, Laila El-Sayed and Magdi F. Iskander

Polyhedron 27 (2008) 3215

Metal complexes derived from hydrazoneoxime ligands: IV. Molecular and supramolecular structures of some nickel(II) complexes derived from diacetylmonoxime *S*-benzyldithiocarbazonate

Four new nickel(II) complexes, [{Ni(L)}$_2$], [NiL · HPyr], [NiL · HIm] and [Ni(HL)$_2$] · H$_2$O, derived from diacetylmonoxime-*S*-benzyldithiocarbazonate (H$_2$L) have been synthesized and characterized. The molecular and supramolecular structures of [NiL · HPyr], [NiL · HIm] and [Ni(HL)$_2$] · H$_2$O, were determined by single crystal X-ray analysis.

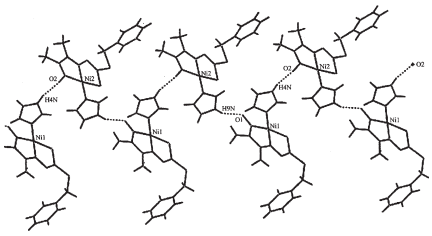

Quang Trung Nguyen and Jong Hwa Jeong

Polyhedron 27 (2008) 3227

Syntheses and X-ray structures of Cu(II) and Zn(II) complexes of *N*,*N*′-dibenzyl-(*R*,*R*)-1,2-diaminocyclohexane and application to nitroaldol reaction

X-ray crystal structures of these complexes reveal that Cu complex has the distorted square-planar geometry and the Zn one has the nearly tetrahedral fashion. The difference of the geometry around metals leads to the opposite preferential configuration of alcohol products using these chiral complexes as asymmetric catalysts in the presence of triethylamine or diisopropylethylamine.

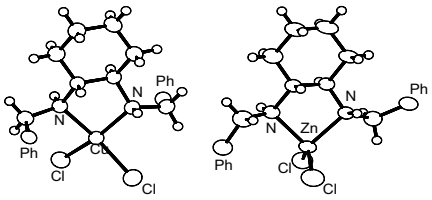

Geng-Geng Luo, Rong-Bin Huang, Na Zhang, Li-Rong Lin and Lan-Sun Zheng

Polyhedron 27 (2008) 3231

Structural diversity in the (Ag–NO_3^-–2-aminopyrimidyl derivatives) system: New zero-, one-, and two-dimensional inorganic–organic hybrids

Five new luminescent silver(I) complexes have been prepared by reactions of silver(I) nitrate with a family of 2-aminopyrimidine and its derivatives and characterized by X-ray single-crystal diffraction. The results reveal that the substituted groups of ligands and reaction solvent systems have great influence on the formation and structure of metal–organic frameworks. In addition, the secondary forces such as hydrogen bonds also play important role in the overall architecture and stabilization of the complexes.

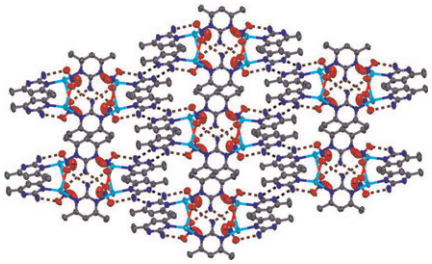

Mousa Al-Noaimi, Mohammad El-khateeb, Salim F. Haddad, Mahmoud Sunjuk and Robert J. Crutchley

Polyhedron 27 (2008) 3239

Synthesis, structural characterization, and DFT investigation of azoimine–ruthenium complexes containing aromatic-nitrogen ligands

Seven ruthenium(II) complexes continuing substituted diimine ligands and the azoimine ligand (Az: $C_6H_5N{=}NC(COCH_3){=}NC_6H_5$) are synthesized and characterized. *trans*-$[Ru(II)(Az)(L)Cl_2]$ are made by the reaction of $RuCl_3$ hydrate and the ligands in the presence of LiCl. These complexes have been characterized by cyclic voltammetry, UV–Vis spectroscopy, electrochemical measurements and X-ray diffraction analysis for two representative complexes. The electrochemical parameters (E_L(L)) of the substituted diimine ligands (L) are reported. The absorption spectrum of one complex in acetonitrile has been modeled by time-dependent density functional theory (TD-DFT) using a hybrid functional, B3LYP, as well as the LanL2DZ basis set.

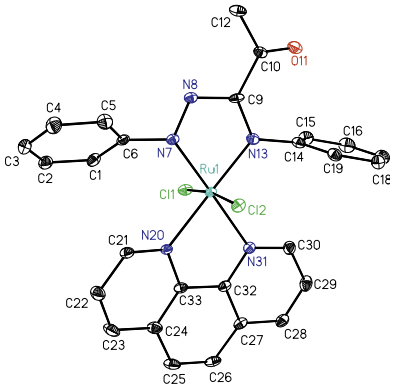

Rosa Carballo, Berta Covelo, Nuria Fernández-Hermida, Emilia García-Martínez, Ana Belén Lago and Ezequiel M. Vázquez-López

Polyhedron 27 (2008) 3247

Anion effect on the construction of copper(II) coordination polymers with the twisted ligand bis(4-pyridylthio)methane

We report the synthesis, crystal structures, thermal behaviour and analysis of the supramolecular association in one 1D and two 2D coordination polymers with the bis(4-pyridylthio)methane ligand. The 2D coordination polymers are pseudo-polymorphs, and one of them was obtained under microwave irradiation.

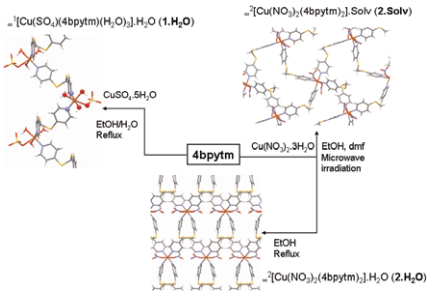

Ernesto Schulz Lang, Davi Fernando Back and Gelson Manzoni de Oliveira

Polyhedron 27 (2008) 3255

Improving the use of mercury bis(phenyltellurolate) as efficient start for the synthesis of ternary clusters and polymers

The synthesis, structural features and kinetic aspects of two Ag/Hg/Te compounds are discussed. The coordination polymer **1** builds layers which stack in the *c* plane. In the nanocluster **2** the occupation relationship for Ag and Hg is 40%/60%, respectively.

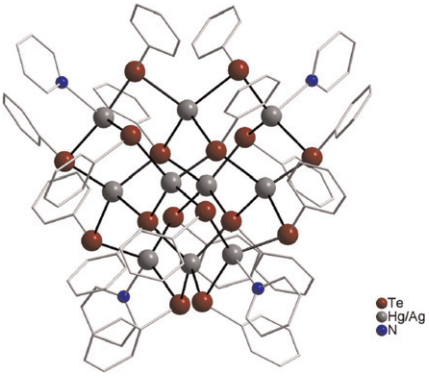

Maxim N. Sokolov, Pavel A. Abramov, Eugenia V. Peresypkina, Alexander V. Virovets and Vladimir P. Fedin

Polyhedron 27 (2008) 3259

In situ generation of H_2Se and hydrothermal synthesis of new polynuclear rhenium carbonyl polyselenides

Two new polyselenide-bridged rhenium carbonyl complexes, $[Re_5(CO)_{18}(Se_2)_3]^-$ and $[Re_4(CO)_{14}(Se_2)(Se_5)]$, were obtained by hydrothermal reaction of $[Re(CO)_5Cl]$ with in situ generated H_2Se and have been characterized by X-ray diffraction.

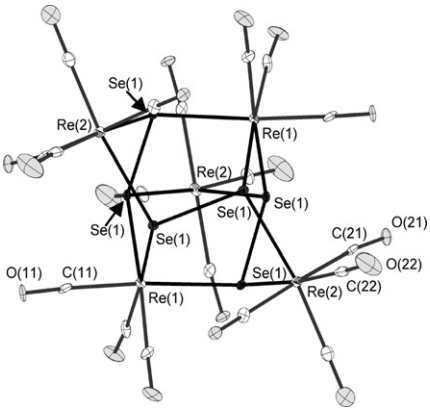

Hossein Dehghani and Maryam Shaterian

Polyhedron 27 (2008) 3263

Synthesis of intermediate sitting-atop complexes (i-SAT) from the reaction between free base *meso*-tetraarylporphyrins and phosphorus-(III) chloride in solvent free media

The reaction of *meso*-tetraarylporphyrins and PCl_3 produced intermediate sitting-atop (i-SAT) complexes where two pyrrolenine nitrogen atoms of the porphyrins act as electron donors to d orbitals of phosphorus atom in PCl_3.

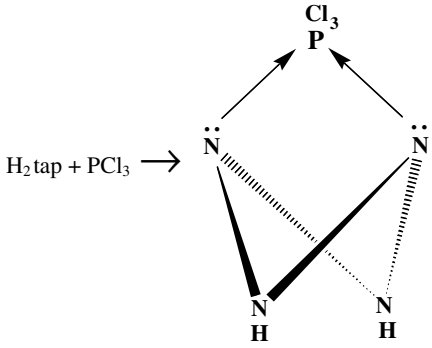

Tarak Nath Mandal, Somnath Roy, Anil Kumar Barik, Samik Gupta, Ray J. Butcher and Susanta Kumar Kar

Polyhedron 27 (2008) 3267

Synthesis and structural characterization of copper(II) and vanadium(V) complexes of pyridyl/pyrimidyl–pyrazole derived Schiff base ligands – Metal specific adjustment of ligand binding mode

Two Schiff base ligands HL_1 and HL_2 form two penta-coordinated square pyramidal Cu(II) complexes (**1** and **3**) and two V(V) complexes (**2** and **4**). The asymmetric unit of **2**, being comprised of two independent molecules has an square pyramidal and one distorted octahedral V(V) units differing in their conformation. The vanadium(V) atom in **4** is in distorted octahedral geometry with NO_5 chromophore.

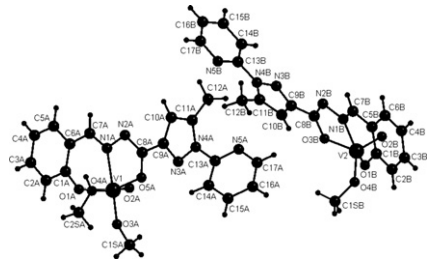

Seyyed Javad Sabounchei, Hassan Nemattalab, Fateme Akhlaghi and Hamid Reza Khavasi

Polyhedron 27 (2008) 3275

New orthopalladated complexes of phosphorus ylides: Crystal structure of [Pd{CH{P(C_7H_6)(*p*-tolyl)$_2$}$COCH_3$}Cl{P(*p*-tolyl)$_3$}]

Orthopalladation and C-coordination of the phosphorus ylide (*p*-tolyl)$_3$P$CHCOCH_3$ is demonstrated by the X-ray crystal structure of [Pd{CH{P(C_7H_6)(*p*-tolyl)$_2$}$COCH_3$}ClP(*p*-tolyl)$_3$].

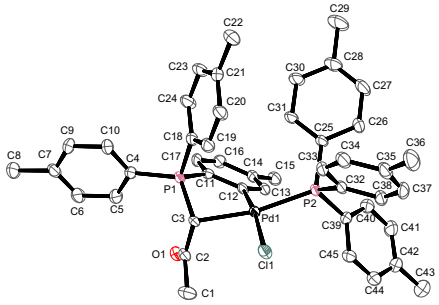

Selma Poturovic, Dongmei Lu, Mary Jane Heeg and Charles H. Winter

Polyhedron 27 (2008) 3280

Synthesis and structural characterization of heavier group 1 methyl tetrazolate complexes: New bridging coordination modes of the tetrazolate ligand

The group 1 methyl tetrazolate complexes Na(Metetz)$(H_2O)_2$, K(Metetz), Rb(Metetz), and Cs(Metetz) were prepared by deprotonation of methyl tetrazole by the metal hydroxides in water, and were characterized with respect to their spectral properties and thermal behavior. The X-ray crystal structures were also determined, and reveal several new coordination modes for the tetrazolate ligand.

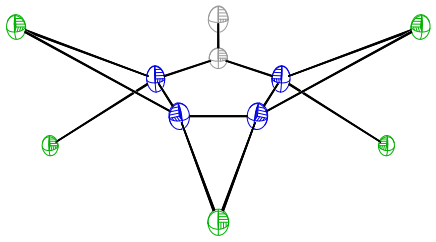

L.A.S. Ries, F.A. do Amaral, K. Matos, E.M.A. Martini, M.O. de Souza and R.F. de Souza

Polyhedron 27 (2008) 3287

Evidence of change in the molecular organization of 1-*n*-butyl-3-methylimidazolium tetrafluoroborate ionic liquid solutions with the addition of water

Specific conductivity of the IL solutions increases in the water-rich region and decreases in the salt-rich region, exhibiting a maximum at IL mole fraction ca. 0.9. Increasing specific conductivity has been attributed to the weakness of the intermolecular interaction of the [BMIm][BF4] structure provoked by adding water, increasing the dissociation and, consequently, increasing the ionic mobility of the ionic species. The decrease in the intermolecular interaction between the anionic and cationic species of [BMIm][BF4] due to the addition of water has been shown by IR.

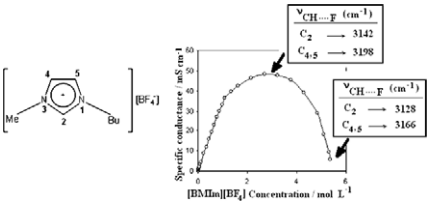

S. Renjusha and M.R. Prathapachandra Kurup

Polyhedron 27 (2008) 3294

Structural and spectral studies on manganese(II) complexes of di-2-pyridyl ketone *N*(4)-methyl and *N*(4)-ethyl thiosemicarbazones

Four manganese(II) complexes of two *N*(4)-substituted thiosemicarbazones derived from di-2-pyridyl ketone were synthesized and physico-chemically characterized by means of partial elemental analyses, molar conductance measurements, electronic, infrared and EPR spectral studies. The crystal structure of $[Mn(DpyMeTsc)_2]$ was established by single crystal X-ray diffraction studies. The compound crystallizes into a monoclinic lattice with $P2_1/n$ space group.

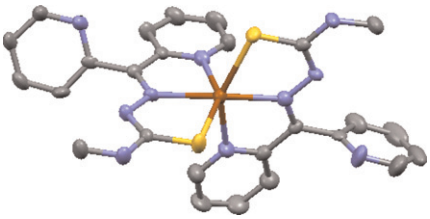

Bikshandarkoil R. Srinivasan, Santosh Y. Shetgaonkar, Jyoti V. Sawant and Pallepogu Raghavaiah

Polyhedron 27 (2008) 3299

Synthesis, X-ray structure and properties of a calcium(II) coordination polymer showing μ_2-η^1:η^1 and μ_3-η^2:η^1 coordination modes of 4-nitrobenzoate

In the one-dimensional coordination polymer $[Ca(N\text{-MeIm})(4\text{-nba})_2]_n$ (*N*-MeIm = *N*-methylimidazole; 4-nba = 4-nitrobenzoate) the two crystallographically independent 4-nba ligands function as μ_2-η^1:η^1 and μ_3-η^2:η^1 bridging carboxylate ligands.

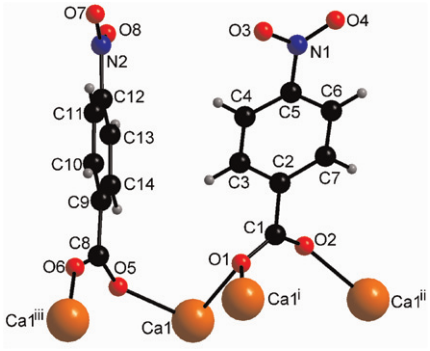

Maria Atanassova, Victoria Lachkova, Nikolay Vassilev, Boris Shivachev, Sabi Varbanov and Ivan Dukov

Polyhedron 27 (2008) 3306

Effect of *p*-*tert*-butylcalix[4]arene fitted with phosphinoyl pendant arms as synergistic agent in the solvent extraction of trivalent lanthanoids with 4,4,4-trifluoro-1-(2-thienyl)-1,3-butanedione and structural study of solid complexes by IR, NMR and X-ray

The synergistic solvent extraction of five selected lanthanoid ions with 4,4,4-trifluoro-1-(2-thienyl)-1,3-butanedione (HL) and 5,11,17,23-tetra-*tert*-butyl-25,26,27,28-tetrakis-(dimethylphosphinoylmethoxy)calix[4]arene, (S) in $CHCl_3$ has been studied. The solvent extraction data showed that the composition of the mixed complex is $[LnL_3S_2]$, while the composition of the synthesized solid complex is $[EuL_2S]Cl$. On the basis of the X-ray data, the structure of the Eu(III) complex with HL was determined.

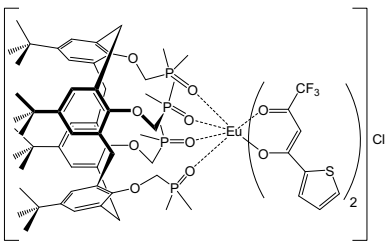

Adrienne M. Carver and Michael J. Knapp

Polyhedron 27 (2008) 3313

Electron and energy-transfer reactions of Ru-$(bpy)_3^{2+*/3+}$ with copper-phenolates

Copper-phenolate models of tyrosyl cofactors found in proteins undergo electron transfer or energy transfer with $Ru(bpy)_3^{2+*/3+}$. The self-exchange of Cu(phenolate)/Cu(phenoxyl) has a high reorganization energy, λ = 22 kcal/mol, suggesting that metal-associated tyrosyl cofactors may undergo slow electron transfer.

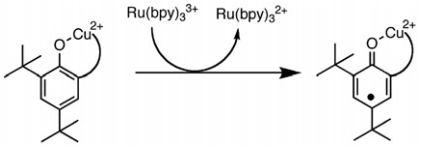

Marianna N. Xanthopoulou, Nikolaos Kourkoumelis, Sotiris K. Hadjikakou, Nick Hadjiliadis, Maciej Kubicki, Spyros Karkabounas and Thomas Bakas

Polyhedron 27 (2008) 3318

Structural and biological studies of organotin-(IV) derivatives with 2-mercapto-benzoic acid and 2-mercapto-4-methyl-pyrimidine

Di-organotin(IV) complexes of the formulae $[Ph_3Sn(MPMT)]$ (**1**), $[Me_2Sn(MPMT)_2]$ (**2**), $\{[(n\text{-}Bu)_2Sn(MBA)]_2\}_n$ (**3**), already reported in the literature, and $\{[Me_2Sn(MBA)]_2\}_n$ (**4**) ($H_2MPMT^+Cl^-$ = 2-mercapto-4-methyl-pyrimidine hydrochloride and H_2MBA = 2-mercapto-benzoic acid), with a different structure to the one already reported, have been synthesized and used to study their influence upon the catalytic peroxidation of linoleic acid by the enzyme lipoxygenase (LOX). The IC_{50} values were found to lie in the range 20–30 μM. A comparison of the structures of the helical polymeric complexes **3** and **4** with the already reported hexanuclear macrocycles complexes $\{[Me_2Sn(MBA)]_6\ H_2O\}$ (**5**) and $\{[(n\text{-}Bu)_2Sn(MBA)]_6\}$ (**6**) has been made. The results show that the self-assembly process of these type of complexes might be fortuity dependent and not based on intermolecular C_H···S weak hydrogen bonds and π–π interactions.

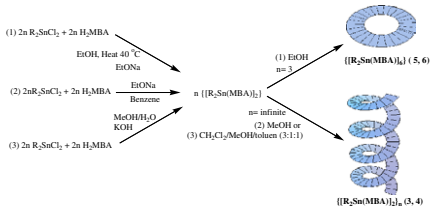

Fiona N.-F. How, Karen A. Crouse, M. Ibrahim M. Tahir, M.T.H. Tarafder and Andrew R. Cowley

Polyhedron 27 (2008) 3325

Synthesis, characterization and biological studies of *S*-benzyl-β-*N*-(benzoyl) dithiocarbazate and its metal complexes

S-Benzyl-β-*N*-(benzoyl) dithiocarbazate (SBNBODTC) a new disubstituted dithio-carbazate oxygen–sulfur (OS) donor ligand derived from reaction of *S*-benzyl dithiocarbazate with benzoyl chloride, formed bis-chelated complexes of general formula $[M(OS)_2]$ where M is Cu^{2+}, Ni^{2+}, Cd^{2+}, Co^{2+} or Pb^{2+} and OS is a uninegative bidentate ligand. The ligand and its metal complexes have been characterized by a variety of physico-chemical techniques. *S*-benzyl-β-*N*-(benzoyl) dithiocarbazate crystallized with $Z' = 2$ in its thione form in *cis*–*cis* conformation, with the N–N bond adopting a *cis* geometry with respect to C=S, while the *S*-benzyl group adopts a *cis* geometry with respect to the thione sulfur atom across the C–S bond. SBNBODTC, $Cu(OS)_2$, $Ni(OS)_2$ and $Pb(OS)_2$ display marked cytotoxicity against HL-60 (human myeloid leukemia) while $Cd(OS)_2$ and $Co(OS)_2$ are moderately cytotoxic. The compounds showed moderate but selective activity towards targeted pathogens.

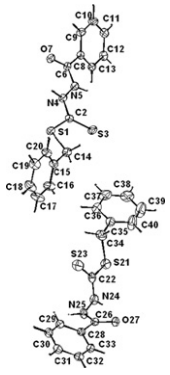

The Publisher encourages the submission of articles in electronic form thus saving time and avoiding rekeying errors. For detailed instructions on the preparation of manuscripts and of electronic artwork, consult the Author Gateway for Elsevier at http://authors.elsevier.com

ScienceDirect

Full text of this journal is available, on-line from **ScienceDirect**. Visit **www.sciencedirect.com** for more information.

Available online at www.sciencedirect.com

ScienceDirect

Polyhedron 27, issue 4, 15 March 2008

POLYHEDRON

www.elsevier.com/locate/poly

Contents

A tribute to Alfred Geoffrey (Geoff) Sykes FRS (1934–2007) 1139

Papers

Mun-Hoe Eddy Chan, Karen A. Crouse, M. Ibrahim M. Tahir, Rozita Rosli, Nasir Umar-Tsafe and Andrew R. Cowley

Polyhedron 27 (2008) 1141

Synthesis and characterization of cobalt(II), nickel(II), copper(II), zinc(II) and cadmium(II) complexes of benzyl *N*-[1-(thiophen-2-yl)ethylidene] hydrazine carbodithioate and benzyl *N*-[1-(thiophen-3-yl)ethylidene] hydrazine carbodithioate and the X-ray crystal structure of bis{benzyl *N*-[1-(thiophen-2-yl)ethylidene] hydrazine carbodithioate}nickel(II)

Cobalt (II), nickel (II), copper (II), zinc (II) and cadmium (II) complexes of general formula ML_2 were prepared using bidentate Schiff bases (SB2ATP and SB3ATP) synthesized by reaction of S-benzyldithiocarbazate with 2-acetylthiophene and 3-acetylthiophene. Single crystal X-ray crystal structure analysis of $Ni(SB2ATP)_2$ showed it to be a distorted square planar complex. SB2ATP and $Cd(SB3ATP)_2$ showed significant bioactivity towards human myeloid leukemia (HL-60) while SB2ATP, SB3ATP, $Co(SB2ATP)_2$, $Cu(SB2ATP)_2$, $Cu(SB3ATP)_2$, $Zn(SB2ATP)_2$ and $Cd(SB2ATP)_2$ showed significant chemotherapeutic activity against human breast carcinoma with positive estrogen receptor (MCF-7). With the exception of $Cu(SB3ATP)_2$, the Schiff bases displayed higher cytotoxic activity than their metal complexes. None of the compounds were active against human cervical cancer (HeLa) or human breast carcinoma with negative estrogen receptors (MDA-MB-231). $Cu(SB2ATP)_2$ showed strong activity towards *Candida lypolytica*.

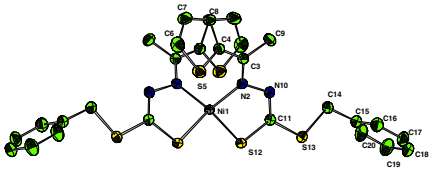

Jianxin Li, Fengying Zhai, Xiaohong Wang, Enmin Li, Shengdong Zhang, Quanliang Zhang and Xiguang Du

Polyhedron 27 (2008) 1150

Synthesis and biological activity of triorganogermanium substituted heteropolytungstates

Four new compounds, $[Me_4N]_4H_5[(RGe)_3(XW_9O_{34-n})_2]$ (R = $HOOCCH_2CH_2$, $HOOCCH_2(m\text{-}NO_2C_6H_4)CH$, X = P, $n = 0$; X = Sb, $n = 1$) have been prepared from trichlorogermanium precursors and lacunary polyoxometallates ($[PW_9O_{34}]^{9-}$ and $[SbW_9O_{33}]^{9-}$). The products were characterized by means of elemental analysis, IR spectroscopy, ^1H NMR and ^{183}W NMR spectroscopy. ^{183}W NMR spectra of the complexes support the stoichiometry of the new heteropolyanions and the probable retention of the XW_9 units in water. The organogermanium substituted complexes showed promising activity against two human tumor cell lines (leucocythemia Hela cells and S180 cells) in vitro and $[Me_4N]_4H_5[(HOOCCH_2CH_2Ge)_3(SbW_9O_{33})_2]$ exhibited some certain antitumoral activity in vivo and can increase the immune ability of the spleen.

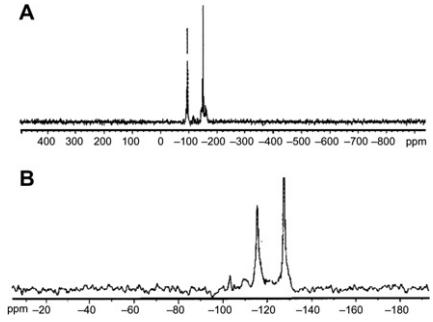

Bahadır Keskin, Yüksel Köseoğlu, Ulvi Avcıata and Ahmet Gül

Polyhedron 27 (2008) 1155

Synthesis and EPR studies of porphyrazines with bulky substituents

Magnesium porphyrazinate substituted with eight 4-tert-butylphenylthio-groups on the peripheral positions has been synthesized by cyclotetramerization of 1,2-bis(4-tert-butylphenylthio) maleonitrile. The novel metal porphyrazinates MPz (M=Cu(II), Zn(II), Co(II)) have been characterized by elemental analysis, together with FT- IR, ^1H NMR, UV–Vis spectral data. The EPR spectra of Cu(II) doped porphyrazine sample as powder and solution forms were measured at room temperature.

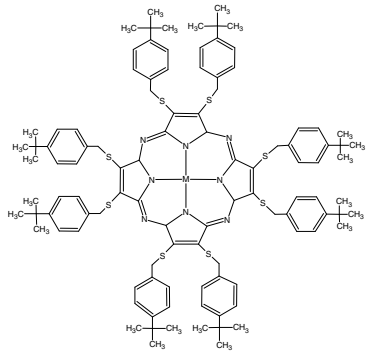

Sergiy O. Nikitin, Rostyslav D. Lampeka, Yulian M. Volovenko, Tetyana A. Volovnenko, Viktoria V. Dyakonenko, Svitlana V. Shishkina and Oleg V. Shishkin

Polyhedron 27 (2008) 1161

Synthesis and study of the structure of new 3d-metal coordination compounds with substituted 2-amino-4(5H)-ketothiophens

A series of 3d-metal complexes based on 2-amino-4(5H)-ketothiophens (HL^1) and (HL^2) were prepared and studied by spectroscopic and X-ray methods (for $[CuL^1{}_2] \cdot H_2O$). The coordination polyhedron of the copper atom is formed by four nitrogen atoms from two ligand anions and the geometry of the coordination sphere is intermediate between tetrahedral and square planar (Fig. 1).

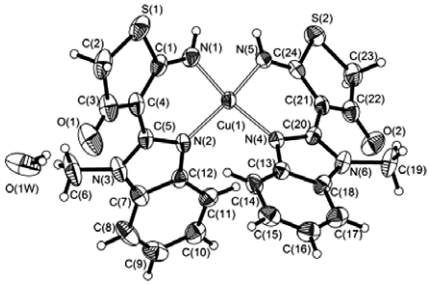

Wei Zhang, Jian-Hui Liu, Jing-Xi Pan, Ping Li and Li-Cheng Sun

Polyhedron 27 (2008) 1168

Synthesis and characterization of some new mononuclear ruthenium complexes containing 4-(un)substituted dipyridylpyrazole ligands

A mononuclear Ru complex $[Ru(bpy)_2(bpp)](PF_6)$ (**1**) and its halogenated and nitro derivatives $[Ru(bpy)_2(\mathbf{X}bpp)](PF_6)$ (bpy = 2,2′-bipyridine; bpp = 3,5-bis(2-pyridyl) pyrazole; X = Cl, **2**; X = Br, **3**; X = I, **4**; X = NO_2, **5**) have been synthesized and characterized by ^1H NMR, ^{13}C NMR, HRMS and elemental analysis. Complexes **2**–**5** have been further confirmed by X-ray diffraction. Their UV–Vis and emission spectroscopies, electrochemical measurements and acid–base properties are described.

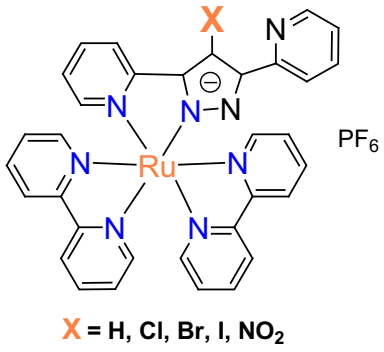

Yueh-Hua Wang, Hsun-Tsing Lee and Maw-Cherng Suen

Polyhedron 27 (2008) 1177

Syntheses and structures of Ag(I) complexes containing 1,4-bis(4,5-dihydro-2-oxazolyl)benzene

The syntheses and crystal structures of four new coordination polymers of the types $[Ag_2(\mathbf{L})(CH_3COO)_2]_\infty$ (**1**), $[Ag_2(\mathbf{L})_3(ClO_4)_2]_\infty$ (**2**), $[Ag(\mathbf{L})(CF_3SO_3)]_\infty$ (**3**), and $\{[Ag_2(\mathbf{L})_3(H_2O)_3][SO_4] \cdot 9H_2O\}_\infty$ (**4**) (L = 1,4-bis(4,5-dihydro-2-oxazolyl)benzene) are reported. Interestingly, the EA and IR have been recorded and all the complexes have been structurally characterized by X-ray crystallography, confirming that complexes **1**–**4** are two-dimensional coordination polymeric frameworks.

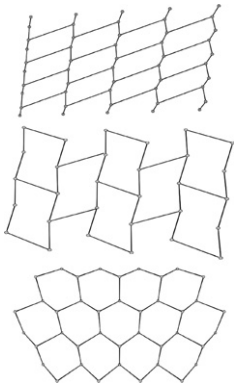

Phalguni Misra, Chun-Yuan Liao, Ho-Hsiang Wei and Sasankasekhar Mohanta

Polyhedron 27 (2008) 1185

Syntheses, molecular and supramolecular structures, and magnetic properties of a mononuclear Mn^{II} and a dicyanamide-bridged one-dimensional Cu^{II} compound derived from enolic 4-terpyridone

Syntheses, molecular and supramolecular structures, and magnetic properties of a mononuclear manganese(II) compound $[Mn^{II}(LH)_2](ClO_4)_2$ and a dicyanamide-bridged one-dimensional copper(II) compound $[Cu^{II}(LH)(\mu_{1,5}\text{-dca})]_n(NO_3)_n$ derived from enolic 4-terpyridone (LH) have been described.

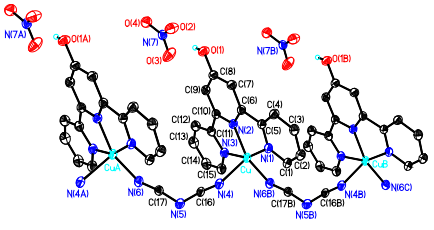

Subhra Basak, Soma Sen, C. Marschner, J. Baumgartner, Stuart R. Batten, David R. Turner and Samiran Mitra

Polyhedron 27 (2008) 1193

Synthesis, crystal structures and fluorescence properties of two new di- and polynuclear Cd(II) complexes with N_2O donor set of a tridentate Schiff base ligand

Two new di- and polynuclear Cd(II) complexes $[Cd_2(L)_2(Cl)_2]$ (**1**) and $[Cd_3(\mu_{1,1}\text{-}N_3)_4(L)_2\{H_2N(CH_2)_2N(C_2H_5)_2\} \cdot H_2O]_n$ (**2**) of the Schiff base ligand **LH** [**LH** = $(OCH_3)(OH)C_6H_3CHN(CH_2)_2N(C_2H_5)_2$] have been synthesized and characterized by elemental analysis, IR, ^1H NMR spectroscopy, TGA, fluorescence and single crystal X-ray diffraction studies. Both the synthesized complexes display intraligand $^1(\pi\text{–}\pi^*)$ fluorescence and can serve as potential photoactive materials.

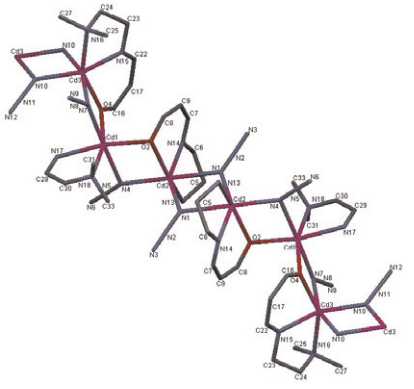

Malabika Nayak, Susanta Hazra, Pascale Lemoine, Rajesh Koner, C. Robert Lucas and Sasankasekhar Mohanta

Polyhedron 27 (2008) 1201

Self-assembled [2 × 1 + 1 × 2] heterotetranuclear $Cu^{II}_3Mn^{II}$/$Cu^{II}_3Co^{II}$ and [2 × 2 + 1 × 3] heptanuclear Cu^{II}_7 compounds derived from *N*,*N*′-*o*-phenylenebis(3-ethoxysalicylaldimine): Structures and magnetic properties

Syntheses, characterization, and magnetic properties of one mononuclear inclusion product $[Cu^{II}L^1 \subset (H_2O)]$, one interesting heptanuclear copper(II) compound $[\{Cu^{II}L^1Cu^{II}(H_2O)_3\}_2\{Cu^{II}L^1\}_3](ClO_4)_4 \cdot 2CH_3COCH_3$, and two heterotetranuclear $Cu^{II}_3M^{II}$ compounds $[\{Cu^{II}L^1M^{II}(H_2O)_3\}\{Cu^{II}L^1\}_2](ClO_4)_2 \cdot H_2O \cdot CH_3COCH_3$ (M = Co or Mn) derived from the hexadentate Schiff base compartmental ligand *N*,*N*′-*o*-phenylenebis(3-ethoxysalicylaldimine) (H_2L^1) have been described. Two monophenoxo-bridged dinuclear $[Cu^{II}L^1Cu^{II}(H_2O)_3]^{2+}$ cationic units are self-assembled and cocrystallized with three mononuclear $[Cu^{II}L^1]$ complex units in the Cu^{II}_7 compound, while the tetrametallic complexes consist of cocrystals of one diphenoxo-bridged heterodinuclear $[Cu^{II}L^1M^{II}(H_2O)_3]^{2+}$ cationic unit and two mononuclear $[Cu^{II}L^1]$ moieties. Formation of the mononuclear inclusion product and the dinuclear–mononuclear cocrystals are related to the tendency of a water molecule to be encapsulated in the O_4 compartment of the $[Cu^{II}L^1]$ moiety.

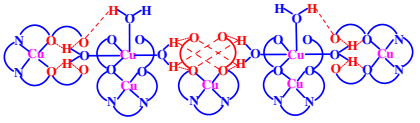

Almudena García-Fernández, Josefina Díez, Ángel Manteca, Jesús Sánchez, M. Pilar Gamasa and Elena Lastra

Polyhedron 27 (2008) 1214

Novel hydridotris(pyrazolyl)borate ruthenium(II) complexes containing the water-soluble phosphane 1,3,5-triaza-7-phosphaadamantane: Synthesis and evaluation of DNA binding properties

A series of water-soluble ruthenium(II) complexes containing $\kappa^3(N,N,N)$-hydridotris(pyrazolyl)borate ($\kappa^3(N,N,N)$-Tp) and the water-soluble phosphanes 1,3,5-triaza-7-phosphaadamantane (PTA) and [1-methyl-3,5-diaza-1-azonia-7-phosphaadamantane (m-PTA) triflate have been synthesized. DNA binding properties by using a mobility shift assay as well as cytotoxicity against a variety of microorganisms have been evaluated.

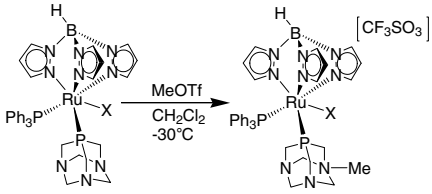

Hyun Sue Huh, Sung Hoon Kim, Sung Yol Yun and Soon W. Lee

Polyhedron 27 (2008) 1229

Silver coordination polymers and networks based on *O*- or *S*-heterocyclic linking ligands: $[Ag\mathbf{L}^1_2](PF_6)$, $[Ag_2\mathbf{L}^2_3](PF_6)_2$, $[Ag_2\mathbf{L}^2_3](ClO_4)_2$, $[Ag_2\mathbf{L}^2_2](BF_4)_2$, and $[Ag_2\mathbf{L}^2(NO_3)_2]$ ($\mathbf{L}^1$ = 1,2-bis(thiophen-2-ylmethylene)hydrazine; $\mathbf{L}^2$ = 1,2-bis(furan-2-ylmethylene)hydrazine)

One silver discrete compound $[Ag\mathbf{L}^1_2](PF_6)$ and four silver coordination polymers or networks, $[Ag_2\mathbf{L}^2_3](PF_6)_2$, $[Ag_2\mathbf{L}^2_3](ClO_4)_2$, $[Ag_2\mathbf{L}^2_2](BF_4)_2$, and $[Ag_2\mathbf{L}^2(NO_3)_2]$, were prepared by layer diffusion, where $\mathbf{L}^1$ is 1,2-bis(thiophen-2-ylmethylene)hydrazine and $\mathbf{L}^2$ is 1,2-bis(furan-2-ylmethylene)hydrazine.

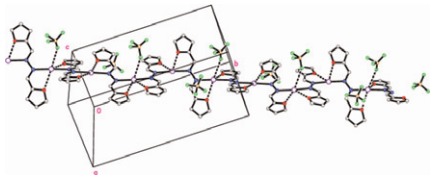

İbrahim Kani, Canan Darak, Onur Şahin and Orhan Büyükgüngör

Polyhedron 27 (2008) 1238

Synthesis, crystal structure and catalytic activity for H_2O_2 disproportionation of the manganese(II) coordination polymer $\{[Mn(O_2C(CF_2)_8CO_2)(phen)_2]H_2O\}_n$ (phen = 1,10-phenanthroline)

The synthesis, crystal structure and catalytic activity of the polymeric complex $[Mn(O_2C(CF_2)_8CO_2)(phen)_2]_nH_2O$ has been investigated. The complex catalyzes the disproportionation of hydrogen peroxide and kinetic studies revealed a first order dependence on the catalyst and it does not exhibit saturation kinetics with substrate.

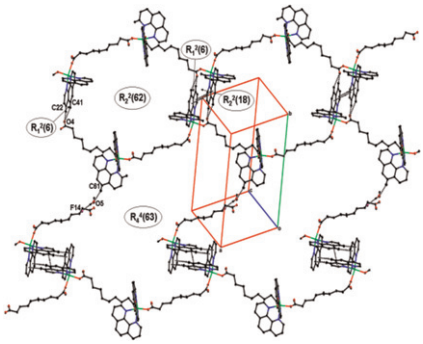

Lalit Rajput and Kumar Biradha

Polyhedron 27 (2008) 1248

Design and synthesis of coordination networks containing amide, pyridine and carboxylate functionalities

The reactions of bis(pyridinecarboxamido)alkane with copper(II) in the presence of mono or dicarboxylic acids resulted in discrete species, one-dimensional and two-dimensional networks. In the presence of *m*-nitrobenzoic acid the ligands with Cu(II) form 1D-coordination networks which include *m*-nitrobenzoic acid and water molecules as guests. The use of isophthalic acid resulted in discrete species while the use of succinic acid resulted in 2-fold interpenetrated two-dimensional layers containing rectangular grids of dimension 9.7×16.5 Å^2.

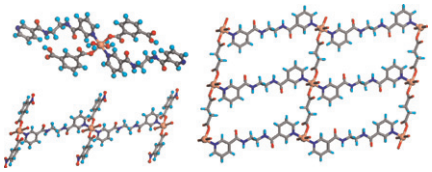

S.Y. Al-Raqa, A.S. Solieman, A.A. Joraid, S.N. Alamri, Z. Moussa and A. Aljuhani

Polyhedron 27 (2008) 1256

Preparation and optical properties of novel symmetrical hexadecachlorinatedphthalocyaninato zinc(II) spin coated thin films

Novel symmetrical 1,4,8,11,15,18,22,25-octahexyloxy-2,3,9,10,16,17,23,24-octa-(3,5- dichlorophenoxy)phthalocyaninato zinc(II) was synthesized and characterized by ^{1}H NMR, ^{13}C NMR, MS, UV–Vis, XRD, and IR spectrometry. The surface morphology of the thin films was investigated by atomic force microscopy, AFM, and showed that the molecules grow in stacks of rows.

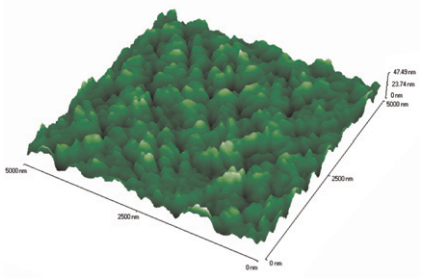

B. Machura, J. Miłek, R. Kruszynski, J. Kusz and J. Mroziński

Polyhedron 27 (2008) 1262

Synthesis, spectroscopic characterization, crystal and molecular structure of $[ReOX_2(bopyH)(PPh_3)]$ complexes: DFT calculations for $[ReOCl_2(bopyH)(PPh_3)]$

The reactions of $[ReOX_3(PPh_3)_2]$ (X= Cl, Br) with benzoylpyridine (bopy) have been examined and novel $[ReOX_2(bopyH)(PPh_3)]$ oxocompounds have been obtained. The complexes were structurally and spectroscopically characterised. In the both structures two-electron reduced form of benzoylpyridine is coordinated to the central ion. The electronic structure of $[ReOCl_2(bopyH)(PPh_3)]$ has been calculated with the density functional theory (DFT) method, and additional information about binding has been obtained by NBO analysis. The UV-Vis spectrum of the $[ReOCl_2(bopyH)(PPh_3)]$ has been discussed on the basis of TDDFT calculations.

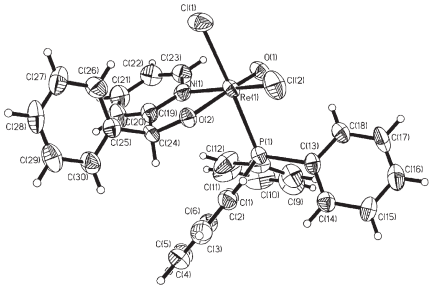

Adrian H. Murray, Zhang Yue, Andrew I. Wallbank, T. Stanley Cameron, Ramesh Vadavi, Brian J. MacLean and Manuel A.S. Aquino

Polyhedron 27 (2008) 1270

Synthesis, structure and electrochemistry of mononuclear and dinuclear ruthenium–thiophenecarboxylate complexes

Dinuclear diruthenium(II,III)-tetra-3-thiophenecarboxylate and -tetra-2,2′-bithiophene-5-carboxylate complexes of the form $[Ru_2(\mu\text{-}O_2CR)_4(MeOH)_2]PF_6$ and mononuclear ruthenium(II)-3-thiophenecarboxylate and -2,2′-bithiophene-5-carboxylate complexes of the form $[Ru(dppe)_2(\eta^2\text{-}O_2CR)]PF_6$ (where dppe = 1,2-bis(diphenylphosphino)ethane and R = $-C_4H_3S$, $-CH_2C_4H_3S$, $-CH{=}CHC_4H_3S$ and $-C_8H_5S_2$) were synthesized and characterized. The mononuclear complexes were studied using X-ray diffraction and the oxidative polymerization of the thiophene groups on all of the complexes was assessed via cyclic voltammetry.

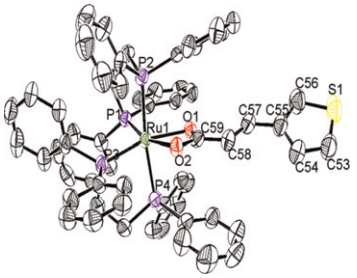

Subal Chandra Manna, Atish Dipankar Jana, Michael G.B. Drew, Golam Mostafa and Nirmalendu Ray Chaudhuri

Polyhedron 27 (2008) 1280

Polymorphism in $[Co(SCN)_4(ppz\text{-}H)_2]$ (ppz, piperazine)

A reactions of $[Co(NO_3)_2 \cdot 6H_2O$ and piperazine (ppz)] with NH_4SCN/NaSCN in water–methanol (1:1) solvent leads to two enantiotropically related polymorphs [(**I**) and (**II**)] of $[Co(SCN)_4(ppz\text{-}H)_2]$.

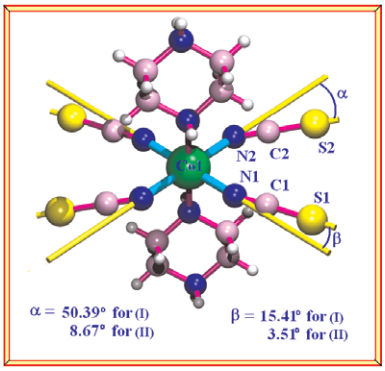

Lorena Barrientos, Carmen Araneda, Bárbara Loeb and Irma G. Crivelli

Polyhedron 27 (2008) 1287

Synthesis, spectroscopic and electrochemical characterization of copper(I) complexes with functionalized pyrazino[2,3-*f*]-1,10-phenanthroline

The present work reports the synthesis and the spectroscopic and electrochemical characterization of homoleptic copper(I) complexes with substituted pyrazino [2,3-*f* 1,10-phenanthroline, RpplR′, (R = H, Me, COOH or COOMe, and R′ = H, Me) as ligand. All the results are discussed in relation to the proposed flattened distortion of the ground state, as well in relation to the donor or acceptor character of the substituents on the ligand, and with the excited state distortion.

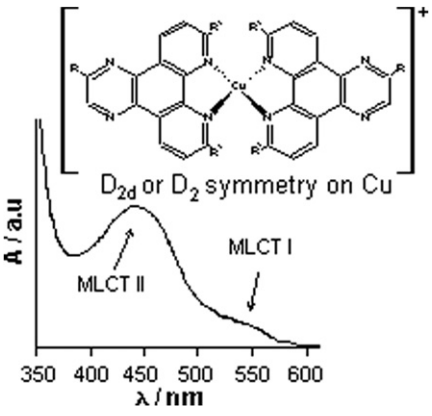

José S. Casas, Eduardo E. Castellano, Javier Ellena, María S. García-Tasende, Agustín Sánchez, José Sordo and Monica Toma

Polyhedron 27 (2008) 1296

Dimethylthallium(III) complexes with picolinic acid and its hydroxyl derivatives

The reaction of dimethylthallium(III) hydroxide with picolinic acid and its hydroxyl derivatives in an aqueous/methanol mixture afforded complexes that were studied in solid state by IR and Raman spectroscopy and by single-crystal X-ray diffraction and in solution by ^1H and ^{13}C NMR spectroscopy.

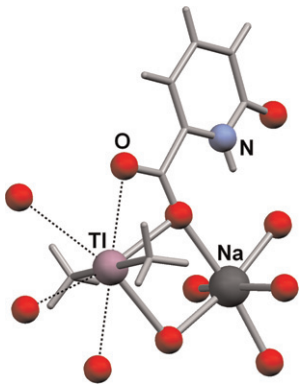

Roushan Khoshnavazi, Abdollah Salimi and Azra Ghiasi Moaser

Polyhedron 27 (2008) 1303

Complexes with carbonate as a tridentate ligand: Synthesis and characterization of sandwich-type polyoxometallates $[(A\text{-}\alpha\text{-}AsW_9O_{34})_2(MOH_2)_3(CO_3)]^{11-}$ (M = $Y^{(III)}$, $Yb^{(III)}$ and $Sm^{(III)}$)

Three new sandwich-type polyoxometallates $[(A\text{-}\alpha\text{-}AsW_9O_{34})_2(MOH_2)_3(CO_3)]^{11-}$ M = $Y^{(III)}$ **1**, $Yb^{(III)}$ **2** and $Sm^{(III)}$ **3** have been synthesized by the reaction of the trilacunary $[A\text{-}\alpha\text{-}AsW_9O_{34}]^{9-}$ ligand with $M^{(III)}$ in a carbonate solution, and characterized by elemental analysis, IR, ^{13}C NMR, UV–Vis spectroscopy, TGA, DSC and single crystal structure analysis. The crystal structure of the complexes consist of two lacunary $A\text{-}\alpha\text{-}[AsW_9O_{34}]^{9-}$ Keggin moieties which are linked by a M_3CO_3 belt into an assembly of virtual C_{3v} symmetry. The CO_3^{2-} anion acts as a tridentate ligand and fixes three $M^{(III)}$ centres together by its oxygen atoms. The syntheses of the complexes require the presence of a carbonate anion and their decomposition take place with the loss of it. Each $M^{(III)}$ cation adopts a mono-capped trigonal-prismatic coordination, the local 3-fold axis of the MO_6 group lying in the M_3CO_3 plane. The trigonal prismatic geometry is achieved by two the terminal oxygen atoms of an edge shared paired of WO_6 octahedra to each $A\text{-}\alpha\text{-}[AsW_9O_{34}]^{9-}$ moiety and two oxygen atoms from the belt, and the cap by one external water ligand.

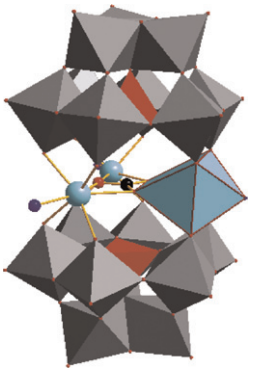

Ki-Young Choi and Ki-Jeong Kim

Polyhedron 27 (2008) 1310

Self-assembly of 1D coordination polymers from nickel(II) tetraaza macrocycle and carboxylate ligands

1D nickel(II) complexes $\{[Ni(L)(isoph)] \cdot 3H_2O\}_n$ (**1**) and $\{[Ni(L)(H\text{-}chtc)] \cdot H_2O\}_n$ (**2**) were synthesized and structurally characterized. The crystal structure of the 1D chain compounds **1** and **2** exhibits a weak antiferromagentic interaction and shows an elongated distorted octahedron about each nickel(II) ion.

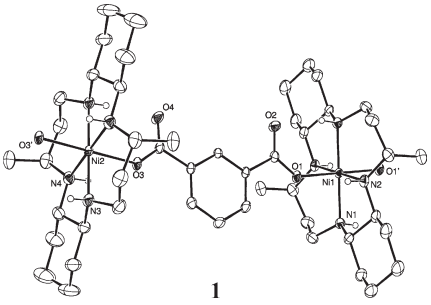

1

Ljerka Tušek-Božić, Marina Juribašić, Pietro Traldi, Vito Scarcia and Ariella Furlani

Polyhedron 27 (2008) 1317

Synthesis, characterization and antitumor activity of palladium(II) complexes of monoethyl 8-quinolylmethylphosphonate

Monoethyl 8-quinolylmethylphosphonate (8-Hmqmp) depending on pH and initial quinolinium and palladium salts forms four types of palladium(II) complexes. The complexes $[8\text{-}H_2mqmp]_2[PdX_4]$, $[8\text{-}H_2mqmp]_2[Pd_2X_6]$, $[8\text{-}H_2mqmp][Pd(8\text{-}Hmqmp)X_3]$ (X = Cl, Br) and $[Pd(8\text{-}mqmp)_2] \cdot 2H_2O$ were characterized by spectroscopic (IR, UV–Vis, ^1H NMR, FAB MS) and thermal (TG, DTA) studies. The antitumor activity *in vitro* of complexes was investigated against the human and murine cell lines.

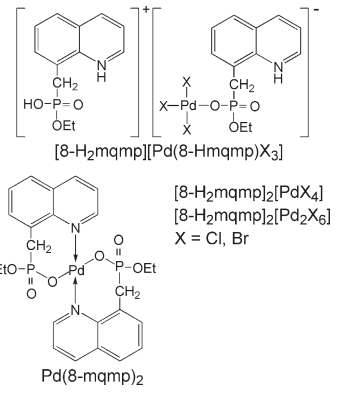

The Publisher encourages the submission of articles in electronic form thus saving time and avoiding rekeying errors. For detailed instructions on the preparation of manuscripts and of electronic artwork, consult the Author Gateway for Elsevier at http://authors.elsevier.com

ScienceDirect

Full text of this journal is available, on-line from **ScienceDirect**. Visit **www.sciencedirect.com** for more information.

Polyhedron 27, issue 18, 12 December 2008

Contents lists available at ScienceDirect

Polyhedron

journal homepage: www.elsevier.com/locate/poly

Contents

Papers

Chun-Yan Guo, Yao-Yu Wang, Kang-Zhen Xu, Hong-Li Zhu, Ping Liu, Qi-Zhen Shi and Shie-Ming Peng

Polyhedron 27 (2008) 3529

Crystal structures, bioactivities and fluorescent properties of four diverse complexes with a new symmetric benzimidazolic ligand

Four new supramolecular complexes based on a new ligand have been constructed and characterized. Interestingly, six or eight-membered hydrogen bonding rings play a key role in the assembly of high-dimensional networks extended by lower dimensional coordination polymers. Among them, complex 2 presents a 3D supramolecular structure with 1D open channels encapsulating NO_3^- ions.

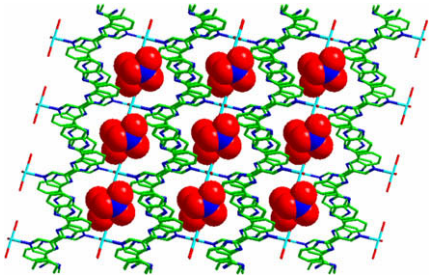

Alia C. Tenchiu, Monica Iliş, Florea Dumitraşcu, Adrian C. Whitwood and Viorel Cîrcu

Polyhedron 27 (2008) 3537

Synthesis, characterization and thermal behaviour of *ortho*-metallated Pd(II) complexes containing *N*-benzoylthiourea derivatives

A series of *ortho*-metallated Pd(II) complexes containing imine ligands and different types of *N*-benzoyl thiourea derivatives as co-ligands were prepared and investigated for their liquid crystal properties.
Three crystal structures are presented.

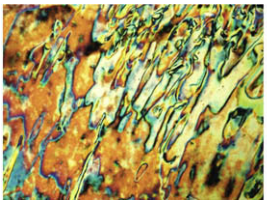

Štefan Lörinc, Jozef Švorec, Milan Melník and Marian Koman

Polyhedron 27 (2008) 3545

Structure and spectral characterisation of copper(II) meclofenamate complexes

Characterisation of $Cu(meclof)_2(2\text{-pyca})_2$ has been made based on elemental analyses, electronic, IR and EPR spectra. The crystal and molecular structures of $Cu(meclof)_2(2\text{-pyca})_2$ were measured. The carboxyl group of the meclofenamate anions coordinates to the Cu(II) atom as an unidentate or as a chelating ligand. On the basis of the spectroscopic parameters observed, a monomeric structure with a tetragonal bipyramidal geometry around the Cu(II) atom is deduced for $Cu(meclof)_2L_2$ and for $Cu(meclof)_2 \cdot H_2O$ a dimeric structure is predicted.

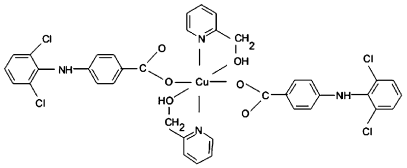

Elsevier Ltd.

Sadegh Salehzadeh, Reza Golbedaghi, Ian S. Tidmarsh, Nawal K. Al-Rasbi, Harry Adams and Michael D. Ward

Polyhedron 27 (2008) 3549

Cd(II) and Mn(II) complexes of a new hexadentate Schiff base ligand derived from an asymmetric tripodal tetraamine and 2-pyridinecarboxaldehyde

Two new complexes were prepared by the template condensation of a previously known ligand, (L22py), and 2-pyridinecarboxaldehyde in the presence of $Cd(NO_3)_2 \cdot 4H_2O$ or $MnCl_2 \cdot 4H_2O$ in equimolar ratios. The resulting compounds were characterized by elemental analysis, IR and single crystal X-ray diffraction, and by NMR in the case of the Cd(II) complex.

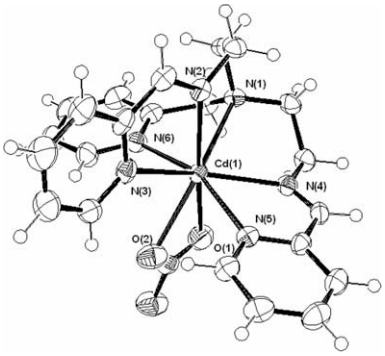

Kentaro Yamane, Satoko Hayashi, Waro Nakanishi, Takahiro Sasamori and Norihiro Tokitoh

Polyhedron 27 (2008) 3557

Fine structures of 8-G-1-(arylethynylselanyl)-naphthalenes (G = H, Cl, Br): Factors to control the linear alignment of five G···Se–C≡C–C_{Ar} atoms in crystals and the behavior in solution

The G-dependence for the change of the fine structures from **1** (G = H) to **2** (G = Cl) and **3** (G = Br) in 8-G-1-(*p*-$YC_6H_4C{\equiv}CSe)C_{10}H_6$ are clarified by X-ray analysis, theoretical calculations and NMR data in crystals and in solution.

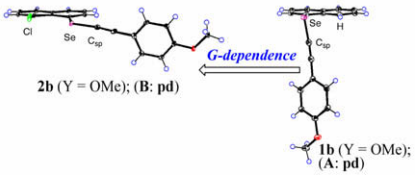

Prateek Tyagi, Pragya Gahlot and Rita Kakkar

Polyhedron 27 (2008) 3567

Structural aspects of the anti-cancer drug oxaliplatin: A combined theoretical and experimental study

The conformational behavior of the third generation antitumor drug, oxaliplatin, has been explored by GGA-PW91 density functional calculations and FT-IR spectra. The electronic properties have also been determined in order to understand its enhanced activity with respect to its first generation analogue, cisplatin.

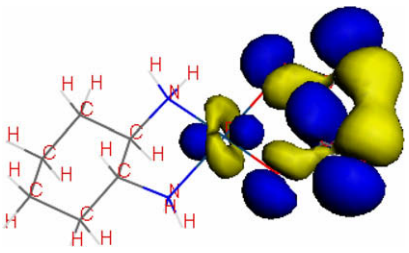

Catherine P. Raptopoulou, Athanassios K. Boudalis, Katerina N. Lazarou, Vassilis Psycharis, Nikos Panopoulos, Michael Fardis, George Diamantopoulos, Jean-Pierre Tuchagues, Alain Mari and George Papavassiliou

Polyhedron 27 (2008) 3575

Salicylaldoxime in manganese(III) carboxylate chemistry: Synthesis, structural characterization and physical studies of hexanuclear and polymeric complexes

Reactions of oligonuclear manganese clusters with salicylaldoxime in various solvents afforded hexanuclear and polymeric complexes. Slow magnetic relaxation phenomena have been observed for a hexanuclear complex as evidenced by dc and ac magnetic susceptibility measurements.

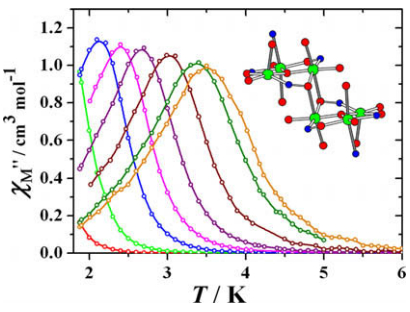

Sonia A. Saucedo Anaya, Adelheid Hagenbach and Ulrich Abram

Polyhedron 27 (2008) 3587

Tricarbonylrhenium(I) and -technetium(I) complexes with bis(2-pyridyl)phenylphosphine and tris(2-pyridyl)phosphine

$(NEt_4)_2[Re(CO)_3Br_3]$ or $(NEt_4)_2[Tc(CO)_3Cl_3]$ react with bis(2-pyridyl)phenylphosphine or tris(2-pyridyl)phosphine under formation of neutral tricarbonyl complexes of the composition $[M(CO)_3(halide)(phosphine)]$. The ligands coordinate solely via two of their nitrogen atoms. A reaction of $[Re(CO)_3(THF)_3](NO_3)$ with Ppy_3 yielded the complex $[Re(CO)_3(NO_3)(Ppy_3\text{-}N,N')]$ with a monodentate coordinated nitrato ligand.

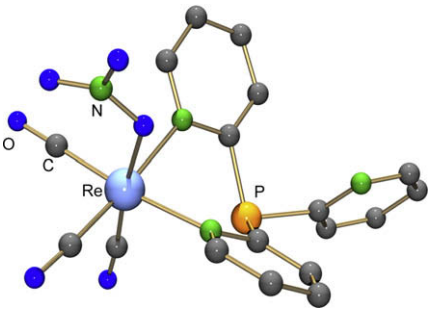

Murugan Indrani, Ramasamy Ramasubramanian, Sudalaiandi Kumaresan, Sung Kwon Kang, Min Chen and Miao Du

Polyhedron 27 (2008) 3593

Hydrothermal synthesis, crystal structures, and properties of Co^{II} and Ni^{II} supramolecular complexes with 2,4,6-trimethyl benzoate and 4,4′-bipyridyl

Two new supramolecular complexes $[Co(tmb)2(4,4'\text{-}bpy)2(H_2O)_2](Htmb)_2$ (**1**) and $\{[Ni(tmb)_2(\mu\text{-}4,4'\text{-}bpy)_2(H_2O)_2](4,4'\text{-}bpy)\}_n$ (**2**), have been prepared hydrothermally and characterized by single crystal X-ray diffraction, elemental analysis, IR, UV/Vis spectra, thermogravimetric analysis and magnetic susceptibility. With the aid of hydrogen bonds, **1** exhibits a square grid network structure and **2** shows the 2-fold interpenetrating framework with $CdSO_4$ topology. Both complexes exhibit antimicrobial activity.

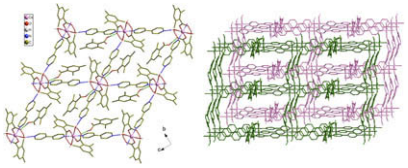

Edwin C. Constable, Egbert Figgemeier, Catherine E. Housecroft, Elaine A. Medlycott, Markus Neuburger, Silvia Schaffner and Sébastien Reymann

Polyhedron 27 (2008) 3601

Approaches to wired terpyridine: Bithienyl alkynyl derivatives of 2,2′:6′,2″-terpyridine and their ruthenium(II) complexes

Two approaches to the formation of ruthenium(II) complexes containing ligands with conjugated 2,2′:6′,2″-terpyridine (tpy), alkynyl and bithienyl units are described, starting with either 4′-(2,2′-bithien-5′-yl)-2,2′:6′,2″-terpyridine or 4′-ethynyl-2,2′:6′,2″-terpyridine. The single crystal structure of 4′-(5-bromo-2,2'-bithien-5′-yl)-2,2′:6′,2″-terpyridine is reported.

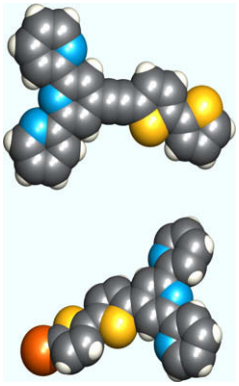

M. Emin Günay, Osman Dayan, Aytaç Gürhan Gökçe, Muhittin Aygün, Bekir Çetinkaya and Orhan Büyükgüngör

Polyhedron 27 (2008) 3607

Preparation and crystal structure of binuclear chloro{6-[[chloro(triphenylphosphine)platinum]-(mesitylimino)methyl]pyridin-2-yl}bis(triphenylphosphine)platinum(II)

Treatment of pyridine-2,6-dicarboxyimidoyl dichloride with $[Pt(PPh_3)]_4$ afforded the novel platinacyclic compound (**3**). Molecular and crystal structures of the compound have been determined by single crystal X-ray diffraction technique.

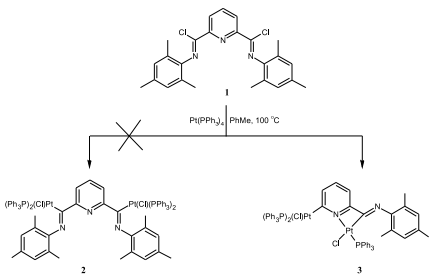

Chun-Wei Yeh, Jhy-Der Chen and Ju-Chun Wang

Polyhedron 27 (2008) 3611

Role of ligand conformation in the structural diversity of copper(II) and silver(I) coordination polymers containing the angular dipyridyl ligand bearing amide spacer

The new dipyridyl ligands *N,N′*-(methylenedi-*p*-phenylene)bis(pyridine-4-carboxamide), **L1**, and *N,N′*-(methylenedi-*p*-phenylene)bis(pyridine-3-carboxamide), **L2**, have been used to prepare complexes of the types $[Cu(\mathbf{L1})_2X_2]_\infty$ (X = Cl, **1** and X = Br, **2**), $\{[Cu(\mathbf{L1})_2(DMF)](NO_3)_2\}_\infty$, **3**, $\{[Ag_2(\mathbf{L1})_2](SO_4)\}_\infty$, **4**, and $\{[Cu(\mathbf{L2})(DMSO)_2(NO_3)](NO_3)\}_\infty$, **5**. Complexes **1**–**3** form 1-D double-stranded polymeric chains. Complex **4** forms 1-D zigzag polymeric chains, which are interlinked through a series of Ag–O interactions to form wavy 1-D ladder like chains, and complex **5** forms 1-D sinusoidal chains.

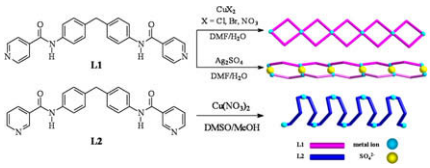

Brendan Gleeson, James Claffey, Daniel Ertler, Megan Hogan, Helge Müller-Bunz, Francesca Paradisi, Denise Wallis and Matthias Tacke

Polyhedron 27 (2008) 3619

Novel organotin antibacterial and anticancer drugs

Three benzyl-substituted bis(cyclopentadienyl)tin dichloride derivatives were synthesised through the hydridolithiation reaction of appropriately substituted fulvenes with $LiBEt_3H$. Within the synthesis of the three organotin compounds are reported along with a structural discussion of an isolated six co-ordinated tin(IV) species. Additionally, the compounds were tested for their antibacterial and anticancer activity.

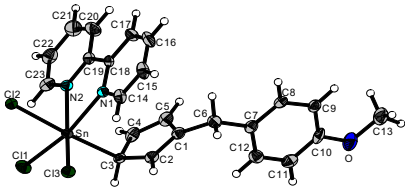

Habibe Çakıcı, Aliye Aslı Esenpınar and Mustafa Bulut

Polyhedron 27 (2008) 3625

Synthesis and characterization of novel phthalocyanines bearing quaternizable coumarin

The synthesis of novel metal-free and zinc phthalocyanines with four 3-[(2-diethylamino)ethyl]-7-oxo-4-methylcoumarin dye groups on the periphery were prepared by cyclotetramerization of the novel 3-[(2-diethylamino)ethyl]-7-[(3,4-dicyanophenoxy)]-4-methylcoumarin. The novel chromogenic compounds were characterized by elementel analysis, ^1H NMR, ^{13}C NMR, MALDI-TOF, IR and UV–Vis spectral data. The electronic spectra exhibit bands of coumarin identity along with characteristic Q and B bands of the phthalocyanine (Pc) core. The IR spectra of all the Pcs showed three characteristic intense bands, at 1704 cm^{-1} for the lactone carbonyl and two bands at 1489–1604 cm^{-1} for the conjugated olefinic system.

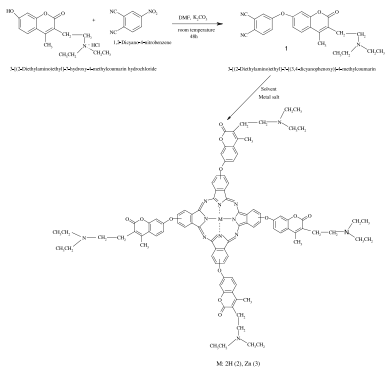

Boris-Marko Kukovec, Zora Popović, Bojan Kozlevčar and Zvonko Jagličić

Polyhedron 27 (2008) 3631

3D supramolecular architectures of copper(II) complexes with 6-methylpicolinic and 6-bromopicolinic acid: Synthesis, spectroscopic, thermal and magnetic properties

Three copper(II) complexes with 6-methylpicolinic and 6-bromopicolinic acid were prepared and characterized by spectroscopic (IR, EPR), thermal methods (TGA/DTA) and by magnetic susceptibility measurements. Their crystal structures were determined by X-ray structural analysis and their magnetic properties discussed in correlation with the structure.

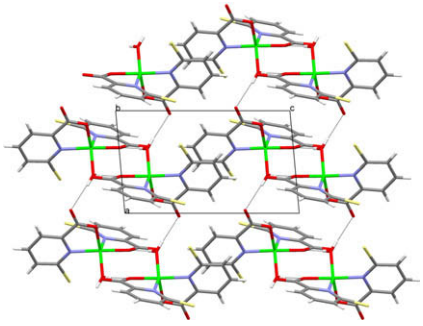

Hossein Naeimi and Mohsen Moradian

Polyhedron 27 (2008) 3639

Alumina-supported metal(II) Schiff base complexes as heterogeneous catalysts in the high-regioselective cleavage of epoxides to halohydrins by using elemental halogen

A highly regioselective method for the synthesis of β-iodohydrins and β-bromohydrins by direct ring opening of epoxides with elemental halogen in the presence of alumina-supported Mn(II), Co(II), Ni(II) and Cu(II) Schiff-base complexes as new catalysts is described. This method occur regioselectively under mild conditions with high yields in various aprotic solvents, even when sensitive functional groups are present.

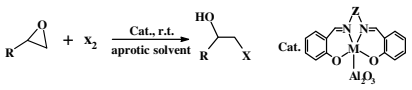

Bahri Ülküseven, Tülay Bal-Demirci, Mehmet Akkurt, Şerife Pınar Yalçın and Orhan Büyükgüngör

Polyhedron 27 (2008) 3646

Chelate structures of 5-(H/Br)-2-hydroxybenzaldehyde-4-allyl-thiosemicarbazones (H_2L): Synthesis and structural characterizations of $[Ni(L)(PPh_3)]$ and $[Ru(HL)_2(PPh_3)_2]$

The reactions of 5-*R*-2-hydroxybenzaldehyde-4-allyl-thiosemicarbazone {R: H (**L**^{1}); Br (**L**^{2})} with $[M^{II}(PPh_3)nCl_2]$ (M, *n* = Ni, 2 and Ru, 3) in a 1:1 molar ratio have given the stable solid complexes $[Ni(L)(PPh_3)]$ and $[Ru(HL)_2(PPh_3)_2]$. While the 1:1 nickel complexes are formed from an ONS donor set of the thiosemicarbazone and the P atom of triphenylphosphine in a square planar structure, the 1:2 ruthenium complexes consist of a couple from each of N, S and P donor atoms in a distorted octahedral geometry.

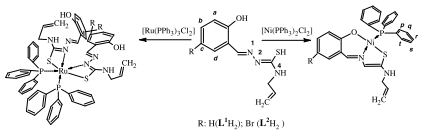

Masoud Salavati-Niasari, Seyed Nezamoddin Mirsattari and Mehdi Bazarganipour

Polyhedron 27 (2008) 3653

Synthesis, characterization and catalytic oxyfunctionalization of cyclohexene with *tert*-butylhydroperoxide over a manganese(II) complex covalently anchored to multi-wall carbon nanotubes (MWNTs)

The chemical modification of multi-wall carbon nanotubes (MWNTs) is an emerging area in material science. In the present study, hydroxyl functionalized manganese(II) Schiff-base has been covalently anchored on modified MWNTs. The new modified MWNTs have been characterized by transmission electron microscopy (TEM), X-ray diffraction (XRD), X-ray photoelectron (XPS), thermal analysis, UV–Vis, diffuse reflectance (DRS), FT-IR spectroscopy and elemental analysis. Multi-wall carbon nanotubes covalently anchored manganese(II) complex ($[Mn((OH)_2$-salen)]@MWNTs) catalyze the oxidation of cyclohexene with TBHP.

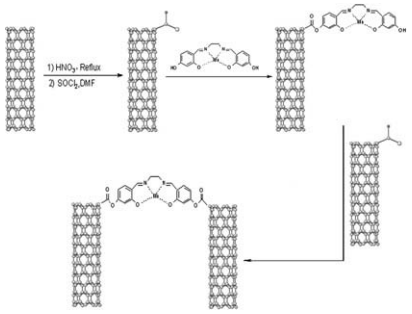

Bárbara L. Almeida, Joanna M. Ramos, Otávio Versiani, Marta Sousa, Claudio Alberto Téllez Soto, Ana Lúcia Ramalho Mercê, Antônio Sálvio Mangrich and Judith Felcman

Polyhedron 27 (2008) 3662

An integrated experimental and theoretical investigation of the vibrational modes and molecular structure of a new Cu(II)–phosphocreatine complex

This paper deals with the synthesis and characterization of a new complex of Cu(II) of stoichiometry $[Cu(PCr)(H_2O)]$. The calculated vibrational spectrum agrees well with the FT-IR experimental spectrum.

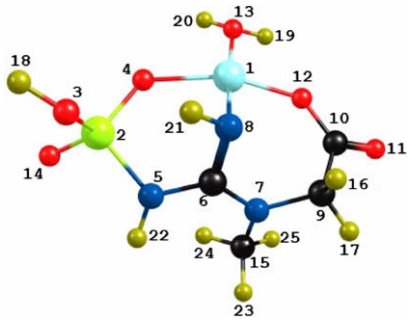

Xiao-Ming Lu, Pei-Zhou Li, Xiu-Teng Wang, Song Gao, Xiao-Jun Wang, Lei Zhou, Chen-Shu Liu, Xi-Na Sui, Jun-He Feng, Yu-Heng Deng, Qiong-Hua Jin, Jing Liu, Na Liu and Jing-Ping Lian

Polyhedron 27 (2008) 3669

pH-Directed assembly and magnetic properties of two polynuclear Mn^{II} complexes: (Δ, Λ)-$\{Mn_3(phen)_2(OOCCH_3)_6\}$ and 1-D $[Mn(phen)Cl_2]_n$

When the reaction conditions are deliberately controlled by the pH, two different polynuclear manganese complexes, (Δ, Λ)-$\{Mn_3(phen)_2(CH_3COO)_6\}$ (**1**) and $[Mn(phen)Cl_2]_n$ (**2**) (phen = 1,10-phenanthroline), have been synthesized from the same raw materials. The structural analyses show that **1** has a structure formed by neutral chiral linear trinuclear molecules, while **2** has a structure consisting of one-dimensional infinite chains. A study of the temperature dependent magnetic susceptibilities reveal that **1** is an antiferromagnetically coupled trimer molecule while **2** shows ferromagnetic interactions within the chain.

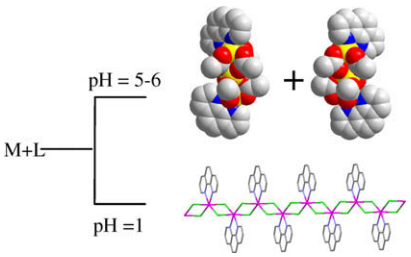

Nassera Tounsi, Laurent Dupont, Aminou Mohamadou, Emmanuel Guillon, Michel Aplincourt and Guillaume Rogez

Polyhedron 27 (2008) 3674

Synthesis of new Cu(II), Ni(II) and Co(II) complexes with a bis-amide ligand functionalized with pyridine moieties: Spectral, magnetic and electrochemical studies

The reaction of Cu^{2+}, Ni^{2+} and Co^{2+} ions with a bis-amide ligand functionalized with pyridine moieties gives square planar $Na[Cu_2(dmptH_{-3})(CO_3)]$ and octahedral $[Ni_2(dmptH_{-2})_2]$ and $[Co_2(dmptH_{-3})(\mu\text{-OH})]$ complexes. In all cases coordination occurs to the pyridyl and deprotonated amidic nitrogen atoms and to the oxygen atoms of an hydroxyl and a carbonato group for the copper complexes.

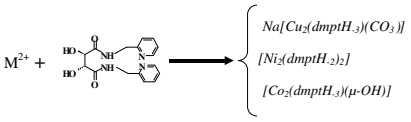

Giovanni B. Giovenzana, Zsolt Baranyai, Silvio Aime, Camilla Cavallotti, Daniela Imperio and Giovanni Palmisano

Polyhedron 27 (2008) 3683

NorDATA: An original ligand based on the norbornane skeleton. Synthesis and thermodynamic characterization of metal complexes

NorDATA: a new polyamino-carboxylic ligand based on the rigid bicyclic norbornane skeleton. Its expeditious four-step synthesis is reported with a study of some metal complexes in solution.

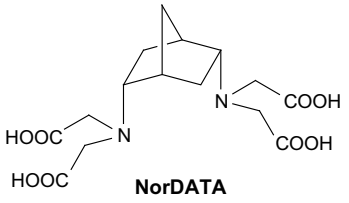

Michel M. Bélombé, Justin Nenwa, Evamarie Hey-Hawkins, Peter Lönnecke, Peter Strauch and Klaus R. Koch

Polyhedron 27 (2008) 3688

Synthesis, EPR spectrum and X-ray structure of tetra-*n*-butylammonium bis(benzene-1,2-dithiolato(2−)-κ^2S,S')platinate(III)

The reaction of tetra-*n*-butylammonium chloride (NBu_4Cl), dipotassium tetrachloroplatinate(II) ($K_2[PtCl_4]$) and benzene-1,2-dithiol (H_2bdt) in ethanol/water readily affords the 1:1 salt of general formula $[NBu_4][Pt(bdt)_2]$. Single crystal X-ray structure of this salt shows that the central platinum is in a square-planar coordination geometry of four S atoms, and the frozen solution EPR spectrum and the room temperature magnetic moment of μ_{eff} = 1.80 B.M. are in accord with the assignment of the Pt(III) oxidation state.

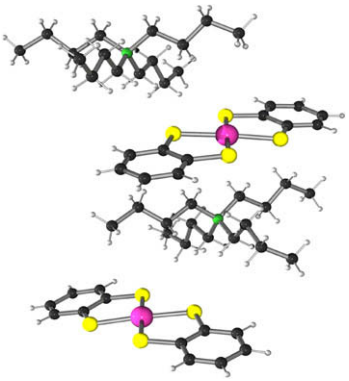

Bhaskar Poola, Sean W. Hunt, Xiaoping Wang and Michael G. Richmond

Polyhedron 27 (2008) 3693

New platinum compounds containing the diphosphine ligand 2-(ferrocenylidene)-4,5-bis-(diphenylphosphino)-4-cyclopenten-1,3-dione (fbpcd): Synthesis, redox behavior, and X-ray diffraction structures of $PtCl_2$(fbpcd) and Pt(mnt)(fbpcd)

The new compounds $PtCl_2$(fbpcd) (**2**) and Pt(mnt)(fbpcd) (**3**) have been synthesized and the redox properties investigated by cyclic voltammetry and extended Hückel MO calculations. Both **2** and **3** have been fully characterized in solution by IR, UV–Vis, and NMR spectroscopies, and their molecular structures established by X-ray crystallography.

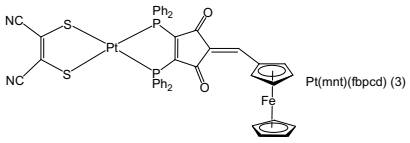

Eric Burkholder, Fenton Heirtzler, Laura Orian, Wayne Ouellette and Jon Zubieta

Polyhedron 27 (2008) 3700

Unusual hydrothermal synthesis of a heteroaromatic macrocyclic complex

Treatment of **1**, MoO_3 and $Cu(OAc)_2 \cdot H_2O$ in water under hydrothermal conditions gave planar macrocyclic $[\mathbf{2}Cu]^{2+}$ and $[bpy_2Cu]^{2+}$, imbedded within a matrix of $[\{Cu_2(benzotriazolate)\}_2Mo_8O_{26}]$ in modest yield. The $[\mathbf{2}Cu]^{2+}$ dication was structurally characterized and its electronic structure calculated using scalar relativistic ZORA DFT methods on ADF2005.01.

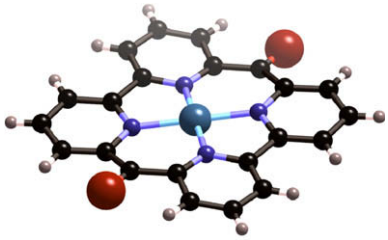

Constantinos C. Stoumpos, Theocharis C. Stamatatos, Vassilis Psycharis, Catherine P. Raptopoulou, George Christou and Spyros P. Perlepes

Polyhedron 27 (2008) 3703

A new $Mn^{II}_4Mn^{III}_4$ cluster from the use of methyl 2-pyridyl ketone oxime in manganese carboxylate chemistry: Synthetic, structural and magnetic studies

Various Mn benzoate sources/methyl 2-pyridyl ketone oxime reaction systems have led to a mononuclear Mn^{II} complex and an antiferromagnetically-coupled ($S = 0$) octanuclear cluster containing the $[Mn^{II}_4Mn^{III}_4(\mu_4\text{-}O)_2(\mu_3\text{-}OH)_2]^{14+}$ core.

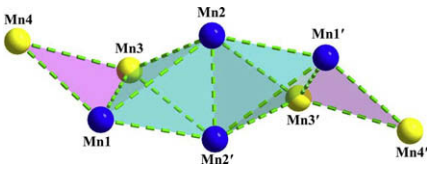

Angad Kumar Singh, Sanyucta Kumari, T.N. Guru Row, Jai Prakash, K. Ravi Kumar, B. Sridhar and T.R. Rao

Polyhedron 27 (2008) 3710

Coordination of a mesogenic Schiff-base with Mn^{II}, Co^{II}, Ni^{II}, Cu^{II} and Zn^{II}: Synthesis, spectral studies and crystal structures

The mesogenic (*nematic*) Schiff-base, *N,N′*-di-4-(4′-pentyloxybenzoate)salicylidene diaminoethane, H_2L^5, crystallizes in the non-centrosymmetric space group $Pna2_1$ with $Z = 4$, and the mesogenic (*nematic*) isomorphous nickel and copper complexes, $[NiL^5]_2$ and $[CuL^5]$, in the centrosymmetric space group $P2_1/c$ with $Z = 4$; both the Ni^{II} and Cu^{II} complexes possess *cis*-MN_2O_2 planes with a low-spin distorted square-pyramidal geometry involving Ni–Ni bonding in the former case and a square-planar geometry in the latter one.

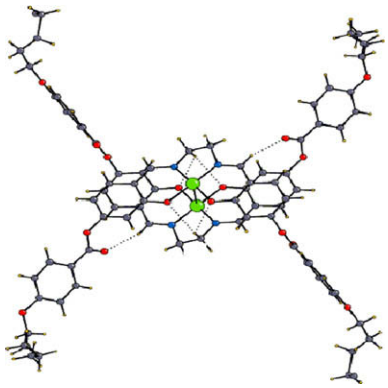

Erratum to "Template synthesis and characterization of host (nanopores of zeolite-Y)/guest (Co(II)–tetraoxodithiatetraaza macrocyclic complexes) nanocomposite materials" [Polyhedron 27 (2008) 15] 3717

The Publisher encourages the submission of articles in electronic form thus saving time and avoiding rekeying errors. For detailed instructions on the preparation of manuscripts and of electronic artwork, consult the Author Gateway for Elsevier at http://authors.elsevier.com

ScienceDirect

Full text of this journal is available, on-line from **ScienceDirect**. Visit **www.sciencedirect.com** for more information.

Polyhedron 27, issue 12, 21 August 2008

Contents lists available at ScienceDirect

Polyhedron

journal homepage: www.elsevier.com/locate/poly

Contents

Papers

Elena López-Torres, David G. Calatayud, César J. Pastor and M[a] Antonia Mendiola

Polyhedron 27 (2008) 2507

Unexpected differences in the reactivity between MPh_2Cl_2 (M = Pb or Sn) and benzil bis(thiosemicarbazone). X-ray crystal structure of benzil bis(thiosemicarbazonate)lead(II)

The differences in the reactivity of diphenyllead and diphenyltin dichloride with benzil bis(thiosemicarbazone) LH_6 are explored. The reaction of $PbPh_2Cl_2$ afforded the complex $[Pb(LH_4)]$ **1**. The reaction with $SnPh_2Cl_2$ in the absence of solvent yielded the complex $[Sn(LH_4)Cl_2]$ **2**. The lead(II) complex, also obtained by the reaction with lead(II) nitrate, was formed by a redistribution of the organolead derivative followed by a reductive elimination reaction, while the tin one was formed by a dephenylation process. Reactions in solution of the organotin derivative are complicated and depending on the working conditions other compounds could be isolated: the organostannoxane $[Sn_2Ph_4ClO(OH)]_2$, or $[SnPh_2(C_{15}H_{10}N_3S)Cl]$, was formed by the loss of one thiosemicarbazone arm with a subsequent cyclisation.

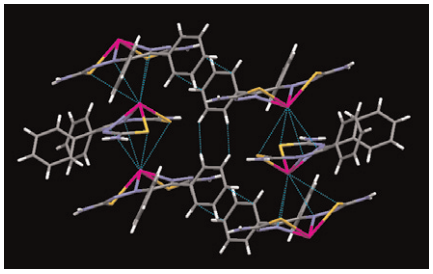

B. Machura, A. Świtlicka, R. Kruszynski, J. Kusz and R. Penczek

Polyhedron 27 (2008) 2513

Synthesis, spectroscopic characterization, X-ray structure and DFT calculations of five-coordinated chlorocopper(II) complex with bis(3,5-dimethylpyrazol-1-yl)methane

The reaction of copper dichloride dihydrate and bis(3,5-dimethylpyrazol-1-yl)methane affords $[Cu\{H_2C(3,5\text{-}Me_2pz)_2\}_2Cl]Cl \cdot 3H_2O$. The compound has been studied by IR, UV–Vis spectroscopy and X-ray crystallography. The electronic structure of the $[Cu\{H_2C(3,5\text{-}Me_2pz)_2\}_2Cl]^+$ cation has been calculated with the density functional theory (DFT) method. The spin-allowed doublet–doublet electronic transitions of $[Cu\{H_2C(3,5\text{-}Me_2pz)_2\}_2Cl]^+$ have been calculated with the time-dependent DFT method, and the UV–Vis spectrum of the title compound has been discussed on this basis.

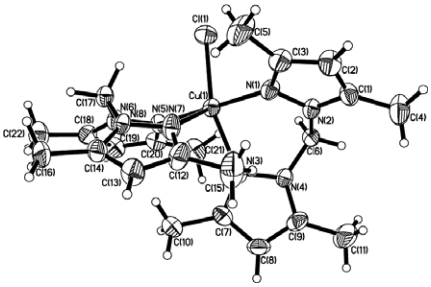

Samik Gupta, Sachindranath Pal, Anil Kumar Barik, Arijit Hazra, Somnath Roy, Tarak Nath Mandal, Shie-Ming Peng, Gene-Hsiang Lee, M. Salah El Fallah, Javier Tercero and Susanta Kumar Kar

Polyhedron 27 (2008) 2519

Synthesis, characterization and magnetostructural correlation studies on three binuclear copper complexes of pyrimidine derived Schiff base ligands

Two Schiff base ligands (HL_1 and HL_2) which are closely related in their donor environment only differing at one donor center (O versus S) have been utilized to synthesize a bis(μ-thiolato) and a bis(μ-phenoxo) binuclear Cu(II,II) complex(**1** and **2**) respectively. These two complexes are found to vary appreciably in their magnetic properties despite their structural similarities. Ligand HL_2 has been found to adapt well enough to form the (μ-4,4′-bipyridyl) Cu(II,II) binuclear complex (**3**).

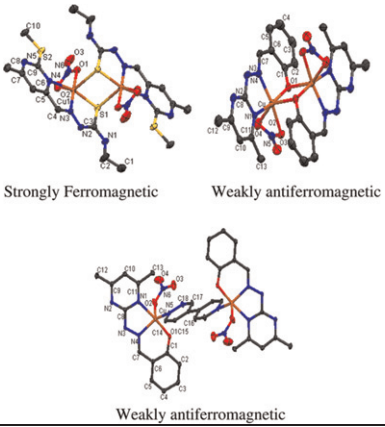

Graeme J. Gainsford, Andrew Falshaw, Cornelis Lensink and Michael Seth

Polyhedron 27 (2008) 2529

Density functional theory calculations of novel Rh(I) diphosphinite catalysts

Transition state energies were calculated by DFT methods for the asymmetric hydrogenation of three prochiral enamides using two novel Rh(I) chiral diphosphinite catalysts prepared from naturally-occurring resources. The predictive aspects of the calculations appear to be limited with starting models playing an important part in determining the final energy values.

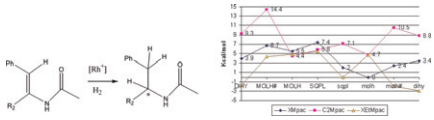

Wolfgang Petz and Bernhard Neumüller

Polyhedron 27 (2008) 2539

The carbodiphosphorane–CS_2 adduct as a complex ligand: Crystallographic characterization of $[I_2Pt\{S_2CC(PPh_3)_2\}] \cdot CH_2Cl_2$, $[Pt\{S_2CC(PPh_3)_2\}_2][SiF_5]_2 \cdot 2CH_2Cl_2$ and $[(Me)_2PtFI\{S_2CC(PPh_3)_2\}] \cdot 2CH_2Cl_2$

Various Pt^{II} and Pt^{IV} complexes with the betain-like ligand $S_2CC(PPh_3)_2$ (**1**) were studied by X-ray analyses. **1** is composed of CS_2 and the double ylide $C(PPh_3)_2$ and acts as a chelating ligand. The structures of $[I_2Pt\{S_2CC(PPh_3)_2\}]$ (**2**), $[Pt(Me)_2FI\{S_2CC(PPh_3)_2\}] \cdot 2CH_2Cl_2$ (**4**) and $[Pt\{S_2CC(PPh_3)_2\}_2][SiF_5]_2 \cdot 2CH_2Cl_2$ (**5**) were presented. Upon complex formation the C–S bond lengths of **1** are elongated accompanied by a slight shortening of the S_2C–CP_2 bonds.

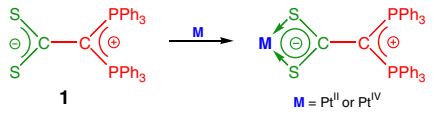

David P. Martin, Ronald M. Supkowski and Robert L. LaDuca

Polyhedron 27 (2008) 2545

Layered metal succinate/bis(4-pyridylmethyl)-piperazine coordination polymers featuring mutual inclined interpenetration

Isomorphous coordination polymers with formulation $[M(suc)(bpmp)(H_2O)_2]_n$ (M = Co, Ni, Cu; suc = succinate, bpmp = bis(4-pyridylmethyl)piperazine) have been prepared and structurally characterized. These possess $[M(suc)(bpmp)(H_2O)_2]_n$ mutually inclined interpenetrated 2D layer motifs.

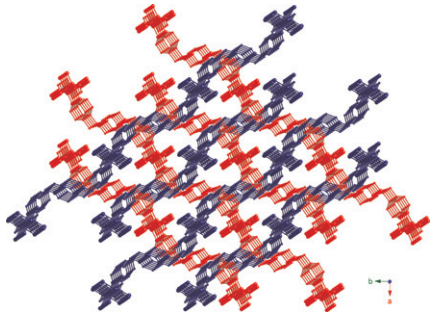

Davi Fernando Back, Gelson Manzoni de Oliveira, Ernesto Schulz Lang and Jaqueline Pinto Vargas

Polyhedron 27 (2008) 2551

Assembly of new Schiff base ligands derived from vitamin B6 and stabilization through complexation of *N*,*N*′-bis-(pyridoxylideneimine)-*o*-phenylene: Synthesis and X-ray structural features of pyridoxal/*o*-phenylenediamine adducts and of $[UO_2(H_2pyr_2phen)Cl]NO_3$ and $[UO_2(Hpyr_2phen)Cl]$ {pyr_2phen = *N*,*N*′-bis-(pyridoxylideneiminato)$^{2-}$phenylene}

The reaction of a new Schiff base ligand – obtained through reaction of vitamin B6 and *o*-phenylenediamine – with $UO_2(NO_3)_2 \cdot 6H_2O$ leads to the stabilization of *N*,*N*′-bis-(pyridoxylideneimine)-*o*-phenylene, giving $[UO_2(H_2pyr_2phen)Cl]NO_3$ (**3**) and $[UO_2(Hpyr_2phen)Cl]$ (**4**). In the new chelate compounds the uranium ions are the centers of distorted pentagonal bipyramides, characteristic for the coordination number 7.

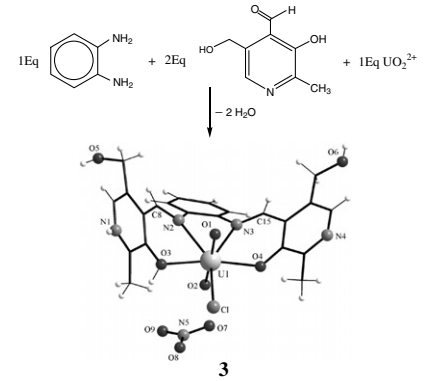

S. Kannan, Sadhan B. Deb, J.S. Gamare and M.G.B. Drew

Polyhedron 27 (2008) 2557

Coordination and separation studies of the uranyl ion with *iso*-butyramide based ligands: Synthesis and structures of $[UO_2(NO_3)_2(^iC_3H_7CON\{^iC_4H_9\}_2)_2]$ and $[UO_2(C_6H_5COCHCOC_6H_5)_2(^iC_3H_7CON\{^iC_3H_7\}_2)]$

Coordination studies of *iso*-butyramide based ligands show that they form 2:1 and 1:1 compounds respectively with the uranyl nitrate and uranyl bis(β-diketonates). These ligands act as monodentate ligand and bond through the carbamoyl oxygen atom to the uranyl moiety. These ligands can selectively precipitate uranyl ion from the mixture containing other ions such as thorium(IV) and lanthanum(III).

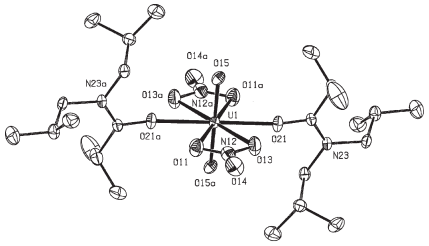

Amardeep Singh, Gopal Das and Biplab Mondal

Polyhedron 27 (2008) 2563

Ruthenium monoterpyridine complexes with 2,6-bis(benzoxazol-2-yl)pyridine as an ancillary ligand: Synthesis, structure and spectral studies

In the ruthenium monoterpyridine complexes $[\mathbf{1}]^+$ and $[\mathbf{2}]^{2+}$, the tridentate ancillary ligand L behaves as a bidentate and a tridentate ligand, respectively. Complex $[\mathbf{1}]^+$, in the presence of aqueous $AgNO_3$, affords $[\mathbf{2}]^{2+}$ through an intramolecular dissociative interchange pathway.

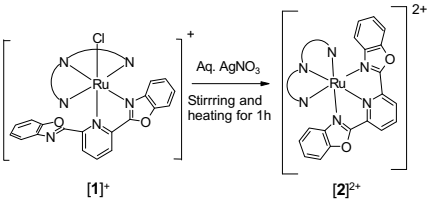

A. Abibat Salaudeen, Colin A. Kilner and Malcolm A. Halcrow

Polyhedron 27 (2008) 2569

Mononuclear and dinuclear iron thiocyanate and selenocyanate complexes of tris-pyrazolylmethane ligands

Reaction of $[\{Fe(NCE)(\mu\text{-}NCE)(tpm')\}_2]$ (E = S, Se) with the appropriate monodentate base yields $[Fe(NCE)_2(tpm')L]$ (L = $NCCH_3$, pyridine, imidazole) or $[\{Fe(NCE)_2(tpm')\}_2(\mu\text{-}4,4'\text{-bipy})]$. The iron centres in these products are high-spin between 5 and 300 K.

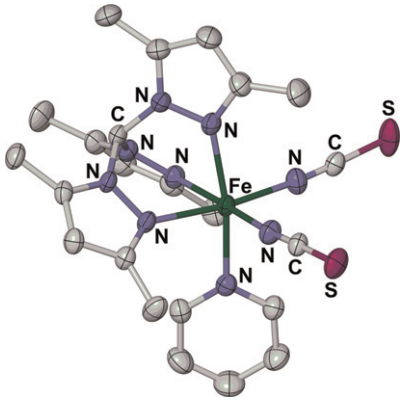

Consuelo Yuste, Danielle Cangussu de Castro Gomes, Harry Adams, Jim A. Thomas, Francesc Lloret and Miguel Julve

Polyhedron 27 (2008) 2577

Syntheses, crystal structures and magnetic properties of tricyanomethanide-containing bis-(2-pyrimidylcarbonyl)amidate copper(II) complexes

Three heteroleptic complexes $[Cu(bpcam)(tcm)(H_2O)] \cdot 2H_2O$ (**1**) (mononuclear), $[Cu(bpcam)(tcm)(H_2O)]$ (**2**) (mononuclear) and $[Cu(bpcam)(tcm)]_n$ (**3**) (zigzag chain) are obtained by the reaction of the stable $[Cu(bcam)]^+$ with the polynitrile ligand tcm^- in aqueous solution. Variable-temperature magnetic susceptibility measurements on **3** show a weak intrachain antiferromagetic interaction ($J = -0.39\ cm^{-1}$).

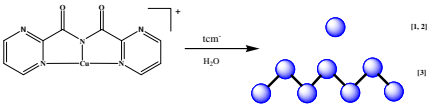

Matilde Fondo, Ana M. García-Deibe, Noelia Ocampo, Jesús Sanmartín and Manuel R. Bermejo

Polyhedron 27 (2008) 2585

Influence of some reaction conditions on the obtaining of tetra- and dinuclear zinc complexes of some Schiff bases derived from 2,6-diformyl-4-alkyl-phenols

The influence of the reaction conditions employed in the obtaining of di- and tetranuclear complexes derived from condensation of 2,6-diformyl-4-alkyl-phenol, triethylenetetramine, and zinc acetate have been studied.

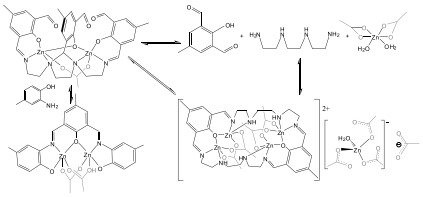

Hui Jiang, Ying-Ying Liu, Jian-Fang Ma, Wen-Li Zhang and Jin Yang

Polyhedron 27 (2008) 2595

Infinite chains constructed from flexible bis-(benzimidazole)-based ligands

The simultaneous use of the carboxylate and sulfonate anions, bis(benzimidazole) ligands to react with copper and silver ions affords seven intriguing frameworks. The results demonstrate that the neutral ligands and the coordination modes of anions may play important roles on the final frameworks.

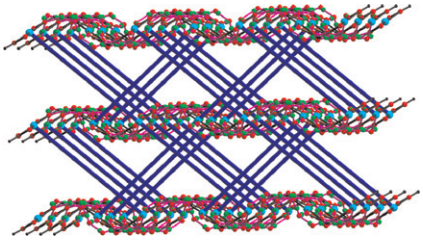

Margarita Crespo, Raquel Martín, Teresa Calvet, Mercè Font-Bardía and Xavier Solans

Polyhedron 27 (2008) 2603

Novel platinum(II) compounds with *N*-benzylidenebenzylamines: Synthesis, crystal structures and the effect of *cis* or *trans* geometry on cycloplatination

The reactions between *cis*-$[PtCl_2(dmso)_2]$ and ligands $ArCH{=}NCH_2(4\text{-}ClC_6H_4)$ (**L**) are reported and the influence of the *cis* or *trans* arrangement of the coordination compounds $[PtCl_2(\mathbf{L})dmso]$ on the success of the cyclometallation reaction is discussed.

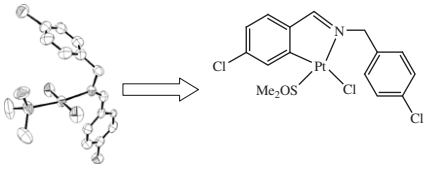

***trans* isomer** **Cyclometallated compound**

Iraj Mohammadpoor-Baltork, Majid Moghadam, Shahram Tangestaninejad, Valiollah Mirkhani and Arsalan Mirjafari

Polyhedron 27 (2008) 2612

12-Tungstophosphoric acid supported on inorganic oxides as heterogeneous and reusable catalysts for the selective preparation of alkoxymethyl ethers and their deprotections under different reaction conditions

A selective and efficient method for the protection of alcohols as MOM- and EOM-ethers and deprotection of these ethers to their parent alcohols using 12-tungstophosphoric acid supported on silica gel and zirconia as heterogeneous catalysts is reported.

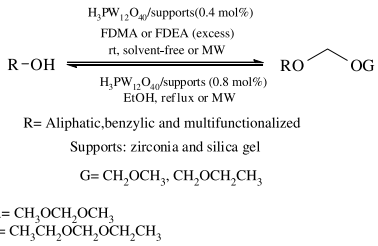

Biswarup Sarkar, Michael G.B. Drew, Marta Estrader, Carmen Diaz and Ashutosh Ghosh

Polyhedron 27 (2008) 2625

Cu^{II} acetate complexes involving N,N,O donor Schiff base ligands: Mono-atomic oxygen bridged dimers and alternating chains of the dimers and $Cu_2(OAc)_4$

Two N,N,O donor Schiff bases, yielded basal-apical, mono-atomic acetate oxygen bridging dimeric copper(II) complexes. Whereas two other similar tridentate ligands produced a mixture of the corresponding dimers and a one-dimensional alternating chain of the dimer and copper acetate moiety, formed by a very rare μ_3 bridging mode of the acetate ion. Variable temperature magnetic measurements of the dimers reveal a very weak antiferromagnetic coupling.

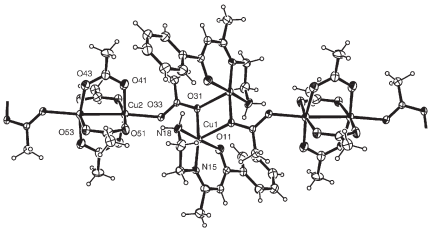

Xiu-Jian Wang, Hong-Xia Jian, Zi-Ping Liu, Qing-Ling Ni, Liu-Cheng Gui and Lin-Hua Tang

Polyhedron 27 (2008) 2634

Assembly molecular architectures based on structural variation of metalloligand [Cu(PySal)$_2$] (PySal = 3-pyridylmethylsalicylideneimino)

A metalloligand of [Cu(PySal)$_2$] (**1**) (PySal = 3-pyridylmethylsalicylideneimino) with structural versatility was exploited as a building unit to construct diverse structures in five complexes $\{Cu[Cu(PySal)_2]_2\}(ClO_4)_2$ (**2**), $\{Cd[Cu(PySal)_2]_2(H_2O)_2]\}(NO_3)_2 \cdot 2H_2O \cdot 4CH_3OH$ (**3**), $\{Zn[Cu(PySal)_2]Cl_2\}_n \cdot nCH_3OH$ (**4**), $\{Hg[Cu(PySal)_2]I_2\}_n$ (**5**) and $\{Cd[Cu(PySal)_2]Cl_2\}_n \cdot nCH_2Cl_2$ (**6**).

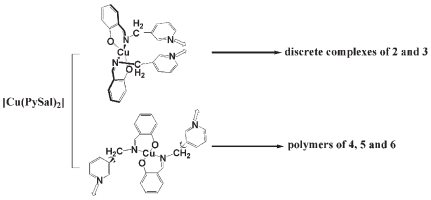

Dariusz Matoga, Janusz Szklarzewicz and Krzysztof Lewiński

Polyhedron 27 (2008) 2643

Cyanooxo molybdenum(IV) complexes with 2-pyrazinecarbonitrile and 2-pyrazinecarboxylate: Crystallographic and spectroscopic studies reveal metal-assisted nitrile hydrolysis

Crystallographic and spectroscopic studies have revealed metal-assisted hydrolysis of 2-pyrazinecarbonitrile on complexation with molybdenum(IV). The coordination versatility of 2-pyrazinecarboxylate (pca^-) toward cyanooxomolybdenum(IV) complexes is demonstrated by the IR and UV–Vis spectroscopy of solids with $[Mo(CN)_4O(Hpca)]^{2-}$ and $[Mo(CN)_3O(pca)]^{2-}$ ions, as well as by the X-ray crystal structure of the latter complex.

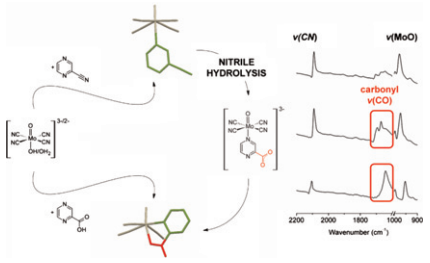

Jamie L. Manson, Jeffrey Donovan and Brendan Twamley

Polyhedron 27 (2008) 2650

Mono- and polynuclear Cu(II) coordination compounds that contain diazine ligands

$Cu(OTf)_2(2\text{-mepyz})_2(H_2O)_2$ (**1**) and $Cu(OTf)_2(H_2O)_2(pyz)$ (**2**) are two new Cu(II) coordination compounds comprised of diazine synthons organized into quasi-2D and 1D structures, respectively. While long-range magnetic ordering was not observed for either compound, significant Cu-pyz-Cu exchange interactions were found in **2**.

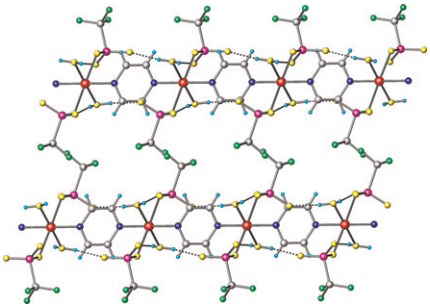

Attila Gyepes, Richárd Schäffer, Gábor Bajor, Ágnes Woller and Péter Fodor

Polyhedron 27 (2008) 2655

Synthesis and chromatographic study of methyl-2,3-*O*-isopropylidene-5-dimethyl-arsinoyl-β-D-ribofuranoside and methyl-2,3-*O*-isopropylidene-5-deoxy-5-dimethyl-thioarsinoyl-β-D-ribofuranoside

The synthesis of two riboside-containing arsenic compounds, methyl-2,3-*O*-isopropylidene-5-dimethyl-arsinoyl-β-D-ribofuranoside and methyl-2,3-*O*-isopropylidene-5-deoxy-5-dimethyl-thioarsinoyl-β-D-ribofuranoside is presented in this paper. Trimethylsilylation was used to volatilise the sugar compounds. GC, TLC and NMR spectroscopy were used for the identification and characterisation of the synthesised intermediates and products. The results affirmed the presence of tautomers in the case of the arsenosugars.

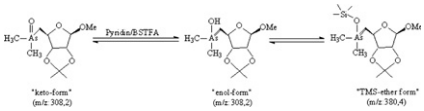

Sumanta Kumar Padhi and Rojalin Sahu

Polyhedron 27 (2008) 2662

Co(II/III) coordinated pyridine alcoholate ligand generated through metal assisted nucleophilic addition to a C=O function: Temperature dependent synthesis of a mononuclear complex and a neutral cubane cluster

Synthesis of $[Co\{OC(OH)(2\text{-pyridyl})_2\}_2][OAc] \cdot 4H_2O$ (**1**) and $[Co_4\{OC(OH)(2\text{-pyridyl})_2\}_4[OAc]_4] \cdot 7H_2O$ (**2**) are reported along with optical and magnetic studies.

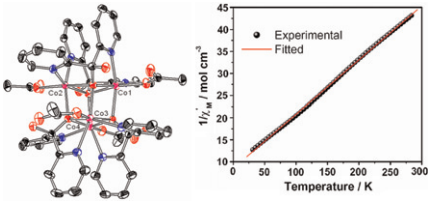

Micol Pasquali, Valeria Ferretti and Adriano Duatti

Polyhedron 27 (2008) 2667

Synthesis, characterization and X-ray crystal structure of the trigonal-planar copper(I) complex $[Cu(MIBI)_3]^+$ (MIBI = 2-methoxyisobutylisocyanide)

The trigonal-planar complex tris(2-methoxyisobutylisocyano) copper(I) tetrafluoroborate, $[Cu(MIBI)_3][BF_4]$ has been prepared and its spectroscopic and chromatographic properties determined. Full solid-state characterization has been carried out through X-ray crystallography and X-ray powder-diffraction spectra. This compound may have relevance for nuclear medicine applications where the tetrahedral Cu(I) complex, $[Cu(MIBI)_4]^+$, is currently used for the preparation of the commercial cardiac imaging agent ^{99m}Tc-MIBI (Cardiolite®).

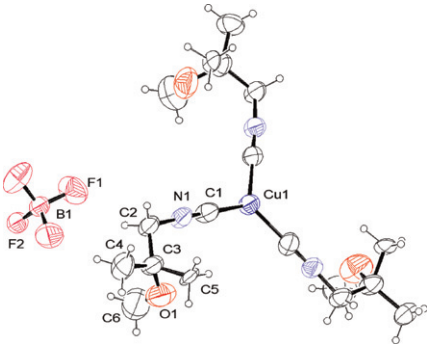

Zhao-Peng Qi, Zheng-Shuai Bai, Qing Yuan, Taka-aki Okamura, Kai Cai, Zhi Su, Wei-Yin Sun and Norikazu Ueyama

Polyhedron 27 (2008) 2672

pH-dependent self-assembly of copper(II) complexes with a new imidazole-containing polyamine ligand: Synthesis, structure and magnetic property

Four copper(II) complexes were synthesized by reactions of new imidazole-containing polyamine ligand with $Cu(ClO_4)_2 \cdot 6H_2O$ under different pH and their structures were found to be from protonated ligand, dinuclear, one-dimensional chain polynuclear to cyclic-tetranuclear coordination compounds by varying reaction pH from acidic to basic. The results indicate that the reaction pH has great impact on the formation and structure of the complexes. The magnetic property of the complexes was investigated.

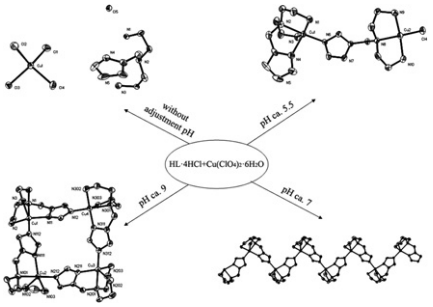

Chih-Yu Wu, Chen-Shiang Lee, Sachindranath Pal and Wen-Shu Hwang

Polyhedron 27 (2008) 2681

Anion dependent formation of Ag(I) complexes of multidentate azine ligands: Synthesis and structural study

Ag(I) complexes derived from pyridyl azine ligands have been synthesized and structurally characterized. The complexes possessed dinuclear, tetranuclear or linear chain structures. Hydrogen bonding and C–H···π interactions generate supramolecular frameworks.

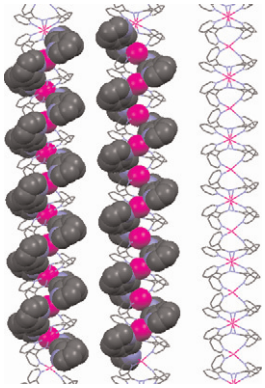

Jens Christoffers and Przemysław Starynowicz

Polyhedron 27 (2008) 2688

A europium(II) complex with bis-pyridino-18-crown-6

A new Eu(II) complex with a crown ligand was characterized structurally and its atypical spectroscopic properties were studied experimentally and theoretically (by DFT methods).

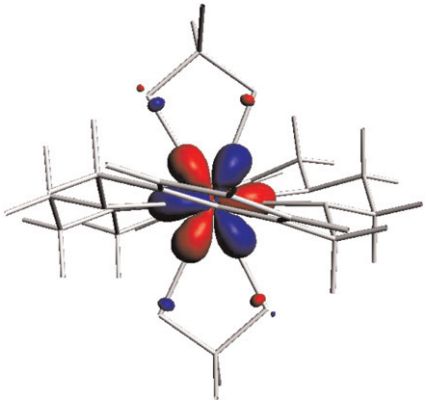

Chun-Yuan Liao, Malabika Nayak, Ho-Hsiang Wei and Sasankasekhar Mohanta

Polyhedron 27 (2008) 2693

Synthesis, crystal engineering, and magnetic properties of an anionic 4-terpyridone based copper(II) azide supramolecule containing dinuclear–mononuclear cocrystal

Synthesis, crystal engineering, and magnetic properties of an anionic 4-terpyridone (L) based three-dimensional supramolecule, $[Cu^{II}_2(L)_2(\mu_{1,1}\text{-}N_3)_2] \cdot 2[Cu^{II}(L)(N_3)(H_2O)] \cdot 6H_2O$, have been described. In this compound, one dinuclear $[Cu^{II}_2(L)_2(\mu_{1,1}\text{-}N_3)_2]$ unit is cocrystallized with two mononuclear $[Cu^{II}(L)(N_3)(H_2O)]$ units. Eight O–H···O type strong hydrogen bonds involving the oxygen centers of anionic 4-terpyridone ligand and water molecules link the components into a three-dimensional framework containing hydrogen bonded sheets interlinked by the dinuclear $[Cu^{II}_2(L)_2(\mu_{1,1}\text{-}N_3)_2]$ unit.

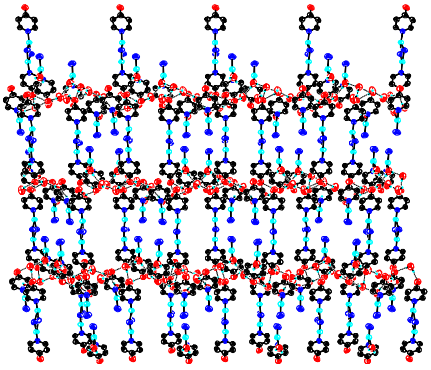

Mousa Al-Noaimi, Musa I. El-Barghouthi, Mohammad El-khateeb, Obada S. Abdel-Rahman, Helmar Görls and Robert J. Crutchley

Polyhedron 27 (2008) 2698

Synthesis and characterization of ruthenium(II) azoimine-diphosphine mixed-ligand complexes

A novel family of the general type *cis*-$[Ru^{II}(dppe)LCl_2]$ {L = $C_6H_5N{=}NC(COCH_3){=}NAr$, and dppe = $Ph_2P(CH_2)_2PPh_2$] has been synthesized. These complexes have been characterized through analytical, spectroscopic (IR, UV–Vis and NMR) and electrochemical (cyclic voltammetry) techniques. In addition, a representative complex has been further characterized by X-ray diffraction analysis. Crystallographic, electrochemical and electronic spectral data are all consistent with the azomethine ligand possessing strong π-acceptor properties. These π-acceptor properties can be "tuned" by a judicious choice of substituent on the azomethine ligand.

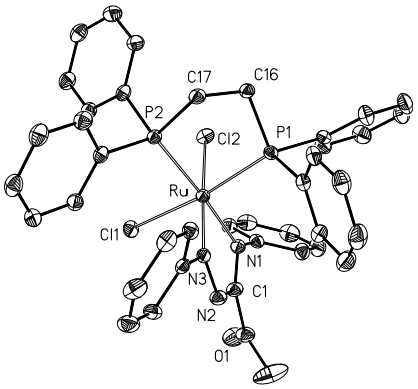

Wei Huang, Zhaolian Chu and Juechao Jiang

Polyhedron 27 (2008) 2705

Studies on an enantiomeric pair of dimeric copper(II) metallomacrocyclic complexes

An enantiomeric pair of [1+2] dimeric copper(II) metallomacrocyclic complexes (*S*,*S*)-**1** and (*R*,*R*)-**2**, prepared from the cleavage of Schiff base C=N double bonds and the ring-degradation of their respective chiral [3+3] macrocyclic ligands, are studied in this paper.

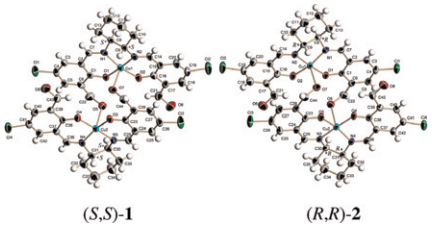

Lucie Szüčová, Zdeněk Trávníček, Igor Popa and Jaromír Marek

Polyhedron 27 (2008) 2710

Preparation and *cis*-to-*trans* transformation study of square-planar $[Pt(L_n)_2Cl_2]$ complexes bearing cytokinins derived from 6-benzylaminopurine (L_n) by view of NMR spectroscopy and X-ray crystallography

Mononuclear, square-planar platinum(II) complexes involving derivatives of aromatic cytokinins as the ligands, and having the general formula *cis*-$[Pt(L_n)_2Cl_2]$ (**1**–**3**) and *trans*-$[Pt(L_n)_2Cl_2]$ (**4**–**6**), where n = 1–3, L_1 = 2-chloro-6-(benzylamino)-9-isopropylpurine, L_2 = 2-chloro-6-[(4-methoxybenzyl)amino]-9-isopropylpurine and L_3 = 2-chloro-6-[(2-methoxybenzyl) amino]-9-isopropylpurine, have been synthesized and characterized. Dynamic *cis*-to-*trans* isomerization process of complex **1** in DMFA has been investigated by means of multinuclear NMR spectroscopy. The solid-state structures of **1**, **4** · 2DMF, and **5** have been determined by single crystal X-ray analysis. *In vitro* cytotoxicity of the prepared complexes against MCF7, G361, K562, and HOS has been evaluated.

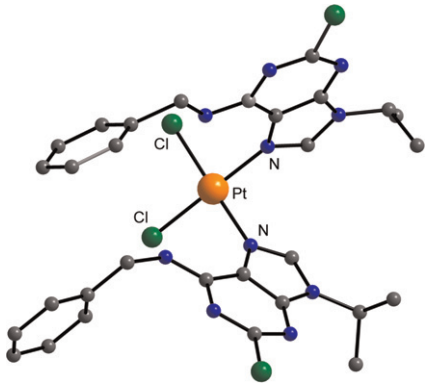

Emmanuel Zimmermman Moreira, Luiz Alberto Beraldo de Moraes, Marcos Nogueira Eberlin, Yassuko Iamamoto and Sofia Nikolaou

Polyhedron 27 (2008) 2721

The use of electrospray ionization tandem mass spectrometry on the structural characterization of novel asymmetric metallo-organic supermolecules, based on pentafluorophenylporphyrins and ruthenium complexes

This article focuses the development of a synthetic route to obtain the novel asymmetric triads *cis*- and *trans*-$[B(4\text{-py})BFPPH_2\{Ru_3O(Ac)_6(py)_2\}\{Ru(bpy)_2Cl\}](PF_6)_2$ and their structural characterization based on high resolution ESI mass spectrometry and ^1H and ^{19}F NMR spectroscopy. Preliminary photophysical essays showed that the porphyrinic core emission is being quenched by the modifying complexes, opening the possibility to use the triads as photophysical devices.

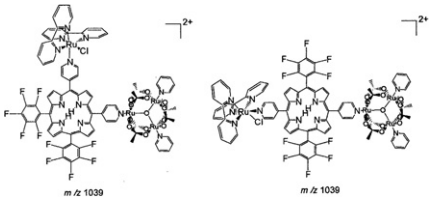

The Publisher encourages the submission of articles in electronic form thus saving time and avoiding rekeying errors. For detailed instructions on the preparation of manuscripts and of electronic artwork, consult the Author Gateway for Elsevier at http://authors.elsevier.com

ScienceDirect

Full text of this journal is available, on-line from **ScienceDirect**. Visit **www.sciencedirect.com** for more information.

Available online at www.sciencedirect.com
ScienceDirect
Polyhedron 27, issue 3, 26 February 2008
POLYHEDRON
www.elsevier.com/locate/poly

Contents

Papers

Maravanji S. Balakrishna, Ramalingam Venkateswaran and Shaikh M. Mobin

Polyhedron 27 (2008) 899

Silver(I) complexes of bis[2-(diphenylphosphino)-phenyl] ether

The reaction of AgOTf with bis(2-(diphenylphosphino)phenyl) ether affords a dinuclear complex $[Ag_2(\kappa^2\text{-}P,P'\text{-DPEphos})_2(\mu\text{-OTf})_2]$ (**1**), which on further reaction with 2,2′-bipyridine produces the mixed-ligand complex [Ag-(κ^2-*P*,*P*′-DPEphos)(2,2′-bipy)][OTf].

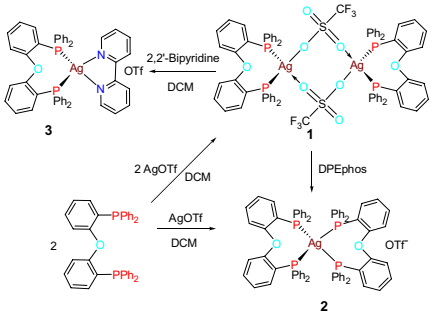

Okan Zafer Yeşilel, Cihan Darcan and Ertan Şahin

Polyhedron 27 (2008) 905

The first hydroxo-bridged saccharinate complexes: Syntheses, spectral, thermal, structural characterization and antimicrobial activities of $[Cu(\mu\text{-OH})(sac\text{-}N)(deten)]_2 \cdot 2H_2O$ and $[Cu(\mu\text{-OH})(sac\text{-}O)(tmen)]_2$

Two novel saccharinate complexes, $[Cu(\mu\text{-OH})(sac\text{-}N)(deten)]_2{\cdot}2H_2O$ (**1**) and $[Cu(\mu\text{-OH})(sac\text{-}O)(tmen)]_2$ (**2**) (deten = *N*,*N*-diethylethylenediamine, tmen = *N*,*N*,*N*′,*N*′-tetramethylethylenediamine and sac = saccharinate) have been synthesized and characterized. Although a lot of saccharinato complexes are well known, quite surprisingly, up to now hydroxo-bridged dimeric metal complexes of the saccharinate have not been reported. In the complexes, the sac ligands exhibit different coordination modes: in **1**, sac ligand is *N*-bonded, while the other complex is *O*-coordinated.

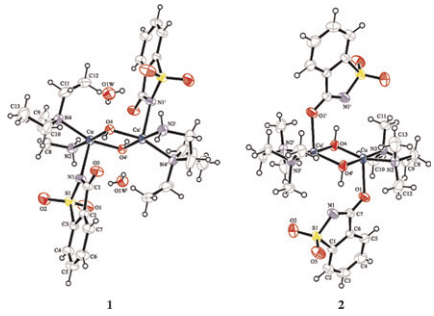

Ronald Lindner, Goran N. Kaluđerović, Reinhard Paschke, Christoph Wagner and Dirk Steinborn

Polyhedron 27 (2008) 914

Synthesis and characterization of dinuclear pyrazolato bridged platinum(IV) complexes

Dinuclear pyrazolato-bridged platinum(IV) complexes $(PPN)[(PtMe_3)_2(\mu\text{-pz})_3]$ (**3**) and $(PPN)[(PtMe_3)_2(\mu\text{-I})(\mu\text{-pz})_2] \cdot 1/2Et_2O$ (**4**) were prepared from the mononuclear pyrazole complexes $[PtMe_3(pzH)_3]$ (**1**) and $[PtMe_3I(pzH)_2]$ (**2**), respectively, by controlled deprotonation. NMR measurements, structural investigations and quantum chemical calculations gave insight into the bonding of bridging pyrazolato and iodo ligands in platinum(IV) complexes.

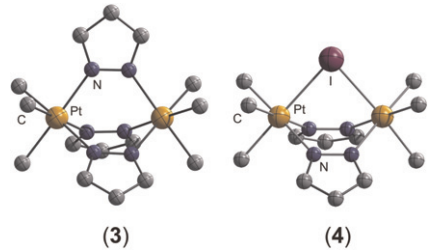

B. Machura and J. Kusz

Polyhedron 27 (2008) 923

Oxorhenium(V) complexes with 2-(1-H-pyrazol-3-yl)phenolato ligand. X-ray structures of $[ReOCl_2(C_9H_7N_2O)(PPh_3)] \cdot MeCN$ and $[ReOX_2(C_9H_7N_2O)(AsPh_3)] \cdot MeCN$ (X = Cl, Br) complexes. DFT and TD-DFT calculations for $[ReOCl_2(C_9H_7N_2O)(PPh_3)]$

Novel $[ReOX_2(C_9H_7N_2O)(EPh_3)]$ complexes (X = Cl, Br; E = As, P; $C_9H_7N_2O$ = 2-(1-H-pyrazol-3-yl)phenolato ion) have been prepared by treatment of $[ReOX_3(EPh_3)_2]$ with 2-(1-H-pyrazol-3-yl)phenol in acetone at room temperature. All the complexes were characterised by IR, UV-Vis spectroscopy and elemental analysis. The crystal and molecular structures have been determined for $[ReOCl_2(C_9H_7N_2O)(PPh_3)] \cdot MeCN$ (**1** · MeCN), $[ReOCl_2(C_9H_7N_2O)(AsPh_3)] \cdot MeCN$ (**3** · MeCN) and $[ReOBr_2(C_9H_7N_2O)(AsPh_3)] \cdot MeCN$ (**4** · MeCN) complexes, and electronic structure of **1** has been calculated with the density functional theory (DFT) method.

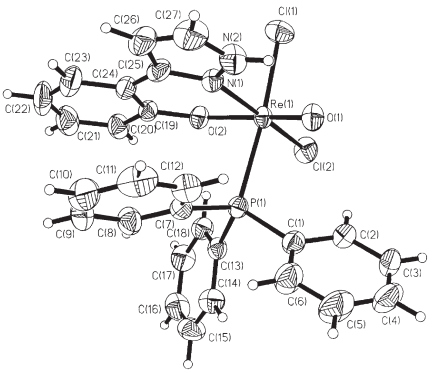

Rajeev C. Chikate, Ki-Won Jun and Chandrasekhar V. Rode

Polyhedron 27 (2008) 933

Nonaqueous synthesis and characterization of capped α-Fe_2O_3 nanoparticles from iron(III) hydroxy-oleate precursor

Non-aqueous synthesis of oelate capped iron oxide nanoparticles in different solvents results in the formation of cubical or spherical morphologies possessing appreciable dispersibility in organic solvents as a consequence of particles sizes in the range of 10–30 nm. These organosols exhibit photoluminescence properties owing to their organophilic character while XRD and XPS measurements reveal hematite formation having α-Fe_2O_3 structure.

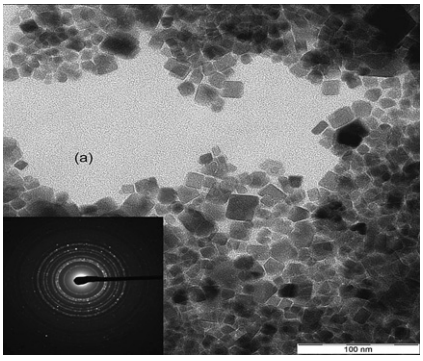

N. Chitrapriya, V. Mahalingam, M. Zeller, R. Jayabalan, K. Swaminathan and K. Natarajan

Polyhedron 27 (2008) 939

Synthesis, crystal structure and biological activities of dehydroacetic acid complexes of Ru(II) and Ru(III) containing PPh_3/$AsPh_3$

Six new Ru(II)/Ru(III) complexes of dehydroacetic acid (DHA) were synthesized and characterized. Single crystal X-ray structure determination of one of the Ru(III) complexes authenticated the monobasic bidentate (O,O) coordination of the DHA ligand. The complexes showed convincing antibacterial properties. The DNA-binding ability of the complexes has also been explored.

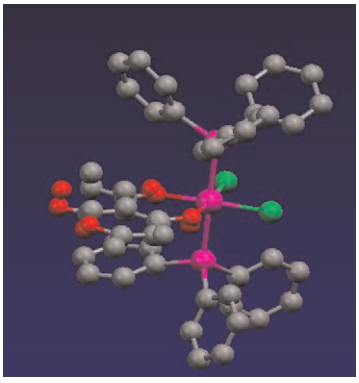

Da-Yu Wu, Gen-Hua Wu, Wei Huang and Chun-Ying Duan

Polyhedron 27 (2008) 947

Dinuclear double-helical cobalt complexes with two-armed terdentate ligands: Synthesis, structure and physical properties

Dinuclear double-stranded helicates $Co_2(\mathbf{L^1})_2(ClO_4)_2(C_2H_5OH)_2(H_2O)_2$ (**1**), $Co_2(\mathbf{HL^2})(\mathbf{L^2})(ClO_4)_3(C_2H_5OH)_2(H_2O)_2$ (**2**) and $Co_2(\mathbf{HL^3})(\mathbf{L^3})(ClO_4)_3(H_2O)_4$ (**3**) based on the ligands with flexible bis-terdentate coordination sites, $\mathbf{H_2L^{1-3}}$, respectively, have been obtained *via* self-assembly, their structures were identified by FT-IR, Elemental Analysis, ESI-MS and X-ray diffraction method.

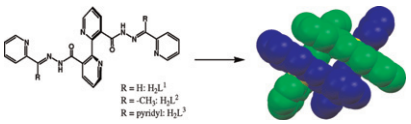

Roman Bobka, J. Nicolas Roedel, Bernd Neumann, Tobias Nigst and Ingo-Peter Lorenz

Polyhedron 27 (2008) 955

Spectroscopic and structural characterization of cationic *N*-(2-aminoethyl)aziridine-*N*,*N*′ chelate complexes of the d^6-metals Rh(III) and Ir(III)

The bis-aziridine complexes $[MCl(Cp^*)(az)_2]Cl$ (M = Rh (**1**), Ir (**2**), az = C_2H_4NH) react with AgO_3SCF_3 = AgOTf and an additional aziridine ligand (az) via a metal-mediated coupling reaction to give the compounds $[MCp^*(aeaz)(az)](OTf)_2$ (M = Rh (**4**), Ir (**5**), aeaz = $C_2H_4NC_2H_4NH_2$). The ORTEP plot of the Rh complex **4** is illustrated. The formed ligand aeaz is formally the dimer of az.

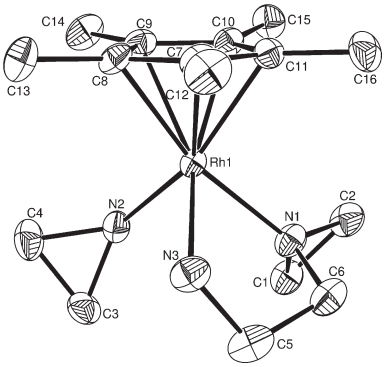

Wanda Ziemkowska, Romana Anulewicz-Ostrowska and Michał Cyrański

Polyhedron 27 (2008) 962

Synthesis and structural characterisation of alkylaluminium and alkylgallium pinacolates

The treatment of pinacol with $^tBu_3Al$ resulted in the formation of aluminium tripinacolate $^tBu_3Al_3[OC(CH_3)_2C(CH_3)_2O]_3$ (**2**) as the only product. In contrast, the reaction of the less reactive $^tBu_3Ga$ with pinacol stopped at the stage of the compound $^tBu_3Ga_2[OC(CH_3)_3C(CH_3)_2O][OC(CH_3)_3C(CH_3)_2OH]$ (**3**), which is an intermediate product of the reaction of 1,2-diols with group 13 trialkyls.

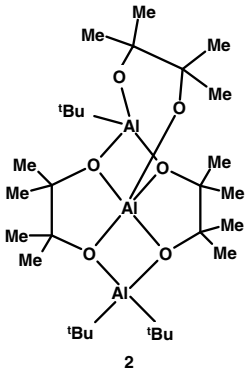

Jarosław Chojnacki

Polyhedron 27 (2008) 969

DFT and NBO theoretical study of protonation of tri-*tert*-butoxysilanethiol and its anion

Protonation on the sulfur atom gives elongation of the Si–S bond, while protonation on the oxygen atom causes shortening of the Si–S bond. Natural bond orbital (NBO) analysis was applied for justification of the changeability of the Si–S and Si–O bond lengths. Interaction of sulfur and oxygen lone pairs with anti-bonding Si–O orbitals may be a good explanation for the accounted trends.

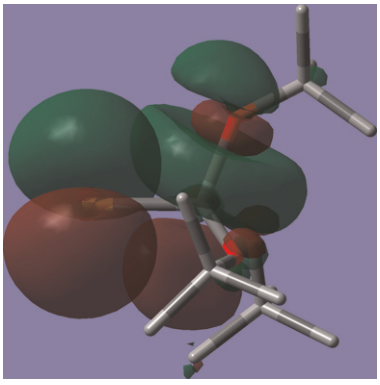

Mohammad Akbar Ali, Aminul Huq Mirza, Malai Haniti S.A. Hamid, Paul V. Bernhardt, Olaniran Atchade, Xueqing Song, George Eng and Leopold May

Polyhedron 27 (2008) 977

Synthesis, spectroscopic and structural characterization of diphenyltin(IV) complexes of acetone Schiff bases of *S*-alkyldithiocarbazates

The structures of the acetone Schiff bases of *S*-methyldithiocarbazate (Hacsme) and (Hacsbz) and $[Sn(C_6H_5)_2(NS)Cl]$ have been determined by X-ray diffraction. In the solid state, both the Schiff bases exist in their thioketo tautomeric forms with the azomethine nitrogen atom *trans* to the thione sulfur atom but in the tin(IV) complexes they are present in their deprotonated ene-thiolate forms. The tin atom adopts a five-coordinate, approximately trigonal bipyramidal geometry, with the thiolate sulfur atom of the Schiff base and the two phenyl groups occupying the equatorial positions. The azomethine nitrogen atom and the chlorine ligand occupy axial positions.

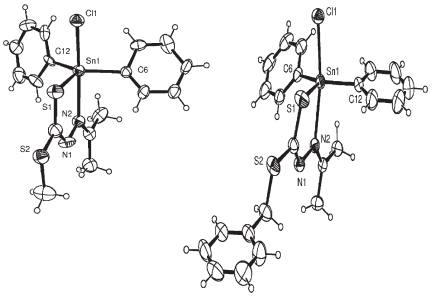

N.V. Loginova, T.V. Koval'chuk, N.P. Osipovich, G.I. Polozov, V.L. Sorokin, A.A. Chernyavskaya and O.I. Shadyro

Polyhedron 27 (2008) 985

Redox-active antifungal cobalt(II) and copper(II) complexes with sterically hindered *o*-aminophenol derivatives

Co(II) complexes with 4,6-di(*tert*-butyl)-2-aminophenol (R = H) and 2-anilino-4,6-di-(*tert*-butyl)phenol (R = Ph) have been synthesized and characterized. The reducing properties of the ligands and their Co(II) and Cu(II) complexes, as well as their antifungal activities, were found to decrease in the order: Cu-$(L^{I})_2$ > Cu$(L^{II})_2$ ⩾ Co$(L^{I})_2$ > Co$(L^{II})_2$ >HL^{I} > HL^{II}.

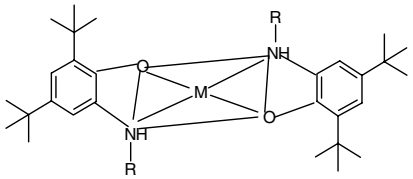

Nitinan Assavathorn, Robert P. Davies and Andrew J.P. White

Polyhedron 27 (2008) 992

On the role of anion templates for the self-assembly of octanuclear copper(I) dichalcogenophosph(in)ate clusters

The cubic octanuclear clusters $[Cu_8(S_2PPh_2)_6]^{2+}$ and $[Cu_8(\mu_8\text{-}Cl)(S_2PPh_2)_6]^{+}$ have been prepared from the reaction of $[Ph_2PS_2][HNEt_3]$ with $[Cu^{I}(CH_3CN)_4][PF_6]$ in hexane/CH_2Cl_2 or refluxing CH_2Cl_2, respectively. Both are rare examples of copper(I) dithiophosphinate clusters and $[Cu_8(S_2PPh_2)_6]^{2+}$ is the first example of a non-anion-centered dithiophosph(in)ate Cu^{I}_8 cluster. Theoretical calculations show that the stability of this 'empty' cluster can be attributed to the strong metal–ligand interactions.

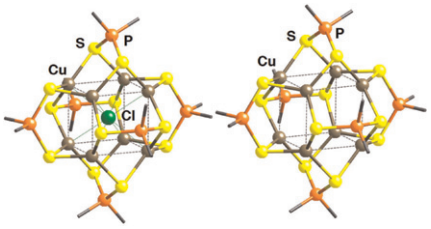

Yaşar Dürüst, Muharrem Akcan, Olli Martiskainen, Elina Siirola and Kalevi Pihlaja

Polyhedron 27 (2008) 999

Synthesis of new thiophene, furan and pyridine substituted 1,2,4,5-oxadiazaboroles

Twenty-two new 3,4,5-trisubstituted 1,2,4,5-oxadiazaboroles were prepared by the cyclo-condensation reaction of *N*-substituted thiophene, furan and pyridine carboxamidoximes with phenylboronic acid in refluxing toluene in good yields.The structures of the new oxadiazaboroles were elucidated by means of spectral measurements (IR, ^{1}H, ^{13}C, ^{11}B NMR, MS, X-ray) and physical data (melting points, elemental compositions by HRMS).

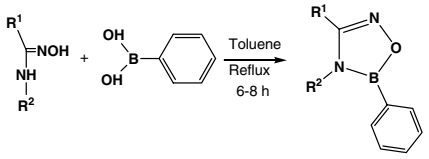

Tarlok S. Lobana, Razia Sultana and Geeta Hundal

Polyhedron 27 (2008) 1008

Heterocyclic thioamides of copper(I): Synthesis and crystal structures of copper complexes with 1,3-imidazoline-2-thiones in the presence of triphenyl phosphine

Reaction of copper(I) chloride with 1,3-imidazoline-2-thione (imzSH) in the presence of Ph_3P has yielded four coordinated [CuCl-(1κS-imzSH)$(PPh_3)_2$] (**1a**), and three coordinated [Cu$(PPh_3)_2$Cl] (**1b**) independent molecules in the same unit cell. Copper(I) bromide and iodide only formed four coordinated complexes, [CuX(1κS-imzSH)$(PPh_3)_2$] (X = Br, I), similar to **1a**.

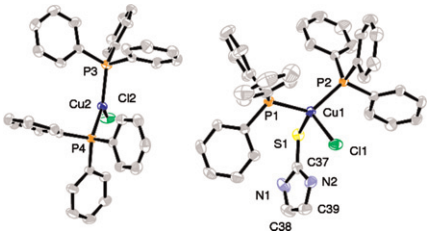

Kelin Li, M. Sarah Mohlala, Tebogo V. Segapelo, Poslet M. Shumbula, Ilia A. Guzei and James Darkwa

Polyhedron 27 (2008) 1017

Bis(pyrazole)- and bis(pyrazolyl)-palladium complexes as phenylacetylene polymerization catalysts

Syntheses and crystal structure of the pyrazolyl complex of the type [1,3-{3,5-R_2pzCO}$_2C_6H_4PdCl_2(\mu\text{-}Cl)_2$] (R = ^{t}Bu (**1**), Ph (**2**), Me (**3**)) and general application of these type of complexes in phenylacetylene polymerization is described. Two new compounds 1,3-(3,5-$Ph_2pzCO)_2C_6H_4$ (**L1**) and its corresponding complex [1,3-{3,5-Ph_2pzCO}$_2$-$C_6H_4PdCl_2(\mu\text{-}Cl)_2$] (**2**) were synthesized. Both compounds have structures that are monoclinic, with space group $P2_1/n$. This and similar pyrazolyl palladium complexes can be activated to catalyze the polymerization of phenylacetylene.

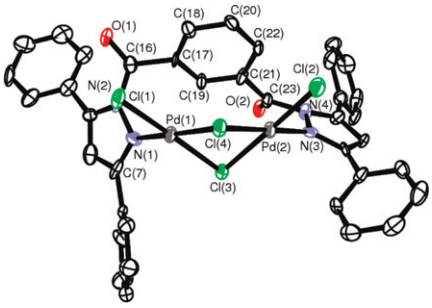

Esref Tas, Ahmet Kilic, Nazli Konak and Ismail Yilmaz

Polyhedron 27 (2008) 1024

The sterically hindered salicylaldimine ligands with their copper(II) metal complexes: Synthesis, spectroscopy, electrochemical and thin-layer spectroelectrochemical features

Three new dissymmetric bidentate salicylaldimine ligands containing a donor set of ONNO were prepared by reaction of different primary amine with 3,5-di-*t*-butyl-2-hydroxybenzaldehyde (3,5-DTB). Electrochemical and thin-layer spectroelectrochemical studies of the ligands and complexes were comparatively studied in the same experimental conditions. All copper complexes showed one quasi-reversible one-electron reduction process in the scan rates of 0.025–0.50 V s^{-1}, which are assigned to simple metal-based one-electron processes; $[Cu(2+)(L_n)_2] + e^- \rightarrow [Cu(1+)(L_n)_2]^-$.

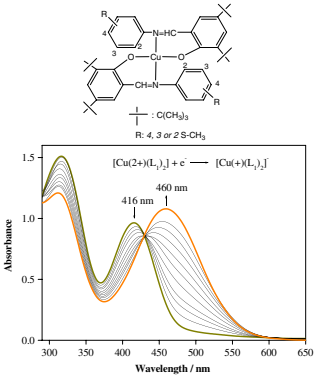

Ray L. Frost, Ashley Locke, B. Jagannadha Reddy and Matt C. Hales

Polyhedron 27 (2008) 1033

Synthesis and vibrational spectroscopic characterisation of nickel containing aurichalcite

Raman spectroscopy complimented with supplementary infrared spectroscopy has been used to characterise a synthetic nickel substituted aurichalcite a zinc/nickel hydroxy carbonate, (Zn, Ni^{2+})$_5(CO_3)_2(OH)_6$. This symmetry reduction results in multiple bands in both the symmetric stretching and bending regions. The intense band for the Ni-aurichalcite at 1070 cm^{-1} is assigned to the $_1(CO_3)^{2-}$ symmetric stretching mode. Three Raman bands assigned to the $_3(CO_3)^{2-}$ antisymmetric stretching modes are observed for Ni-aurichalcite at 1372, 1480 and 1543 cm^{-1}.

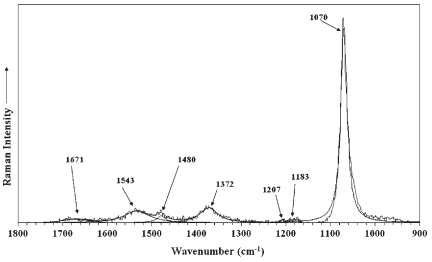

Plaboni Hasan, Stephen E. Potts, Claire J. Carmalt, Robert G. Palgrave and Hywel O. Davies

Polyhedron 27 (2008) 1041

Reactivity of $ZrCl_4$ and $HfCl_4$ with silylamines and thermal decomposition of the compounds [MCl_4{NH(R)(SiR'_3)}] (M = Zr, Hf, R = *t*Bu, R′ = Me; R = SiR'_3 = $SiMe_3$, $SiMe_2H$)

Pyrolysis of the Lewis acid/base adducts [MCl_4{NH(R)(SiR'_3)}] (M = Zr, Hf; R = *t*Bu, R′ = Me; R = SiR'_3 = $SiMe_3$, $SiMe_2H$) afforded powders of composition [ClMN] or [Cl_2MNH], where low pressure CVD yielded amorphous metal nitride films contaminated with oxide, C and Cl.

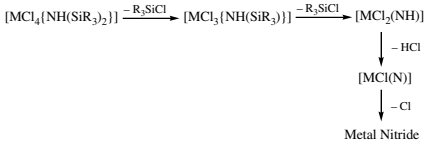

Rita Giovannetti, Vito Bartocci, Filippo Pucciarelli and Laura Petetta

Polyhedron 27 (2008) 1047

Remarks on the reactions of a tetracarboxylic porphyrin with gold and silver ions: A spectrophotometric, TEM and SEM study

The optical properties of the colloidal gold and silver forms obtained by coproporphyrin reactions with the corresponding ions have been investigated by UV–Vis spectrophotometry, and their morphology by TEM and SEM measurements. The structures and the size distributions of Ag and Au particles have been characterized and determined by computerized TEM images.

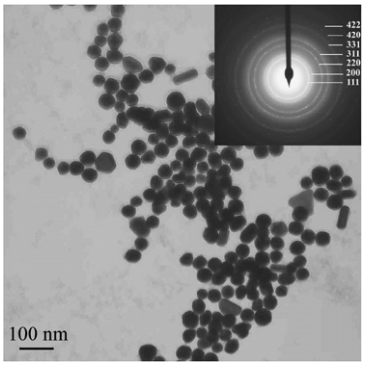

R.N. Patel, V.L.N. Gundla and D.K. Patel

Polyhedron 27 (2008) 1054

Synthesis, structure and properties of some copper(II) complexes containing an ONO donor Schiff base and substituted imidazole ligands

Five new mixed ligand coper(II) complexes, *viz.* [Cu(SAA)(H_2O)] (**1**), [Cu(SAA)(MeImH)] (**2**), [Cu(SAA)(EtImH)] (**3**), [Cu(SAA)-(BenzImH)] (**4**) and [Cu(SAA)(MebenzImH)] (**5**), have been synthesized and characterized by means of various physico chemical techniques. Single crystal X-ray analysis of **2** and **3** has revealed the presence of a distorted square planar geometry (N_2O_2) in the complexes. The superoxide dismutase (SOD) activity of the complexes has also been measured and discussed.

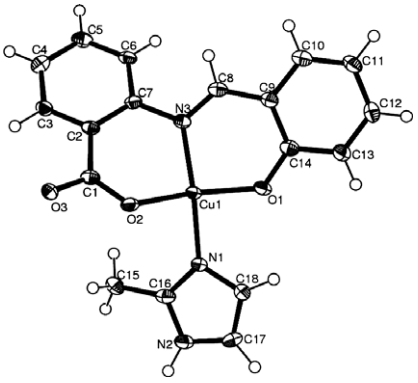

Shawn Swavey, Jeanette A. Krause, Daniel Collins, Deepika D'Cunha and Albert Fratini

Polyhedron 27 (2008) 1061

X-ray structure and temperature dependent luminescent properties of two bimetallic europium complexes

Homodinuclear europium complexes bridged by the polyazine ligand 2,2′-bipyrimidine display temperature dependent luminescent properties in toluene solutions.

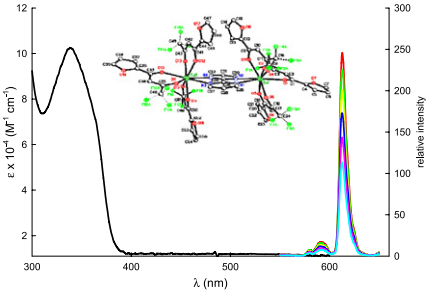

Ghodrat Mahmoudi and Ali Morsali

Polyhedron 27 (2008) 1070

Mercury(II) iodide coordination polymers generated from polyimine ligands

A series of new HgI_2 organic polymeric complexes, $[Hg_2(L1)I_4]_n$ (**1**), $[Hg(L2)I_2]_n$ (**2**), $[Hg(L3)I_2]_n$ (**3**), $[Hg_2(L4)I_4]_n$ (**4**), $[Hg(L5)I_2]_n$ (**5**), $[Hg(L6)I_3](HL6)$ (**6**) {L1 = 1,4-bis(2-pyridyl)-2,3-diaza-1,3-butadiene, L2 = 1,4-bis(3-pyridyl)-2,3-diaza-1,3-butadiene, L3 = 1,4-bis-(4-pyridyl)-2,3-diaza-1,3-butadiene, L4 = 2,5-bis(2-pyridyl)-3,4-diaza-2,4-hexadiene, L5 = 2,5-bis(3-pyridyl)-3,4-diaza-2,4-hexadiene and L6 = 2,5-bis(4-pyridyl)-3,4-diaza-2,4-hexadiene} was prepared from reactions of mercury(II) iodide with six organic nitrogen donor-based ligands under thermal gradient conditions using the branched tube method.

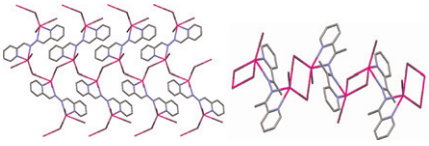

Zhaolian Chu, Wei Huang, Li Wang and Shaohua Gou

Polyhedron 27 (2008) 1079

Chiral 27-membered [3 + 3] Schiff-base macrocycles and their reactivity with first-row transition metal ions

The reaction of [3 + 3] chiral or achiral Schiff-base macrocycles with certain first-row transition metal salts [Cu(II), Zn(II), Fe(III)] under reflux condition led to the cleavage of Schiff-base C=N double bonds and the rearrangement of the macrocycles. We acquired [2 + 2], [2 + 1], [1 + 2] kinds of ring-contraction metal complexes in the process of metal ion complexation.

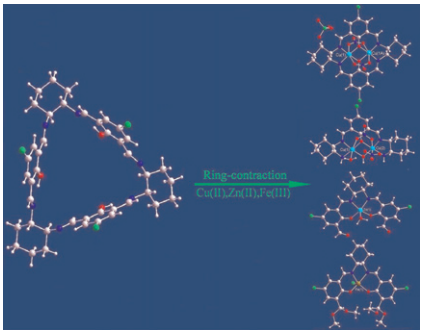

Florian P. Pruchnik, Hanna Pruchnik, Łucja Ostropolska and Leszek Z. Ciunik

Polyhedron 27 (2008) 1093

Tris(2-cyanoethyl)tin(IV) bromide and tris-(2-cyanoethyl)tin(IV) iodide, their structure, properties and reactions with adenosine, AMP and ATP

The organotin complexes $[Sn(CH_2CH_2CN)_3I]$ (**1**) and $[SnBr(CH_2CH_2CN)_3]$ (**2**) have been prepared. In the solid state they form zigzag single-strand chains with a bridging 2-cyanoethyl ligand. The calculated (with the DFT B3LYP method) interatomic distances agree well with those found crystallographically. The compounds in water solutions form trigonal bipyramidal complexes, which interact with 5′-adenosine monophosphate and 5′-adenosine triphosphate via the oxygen atom of the phosphate group.

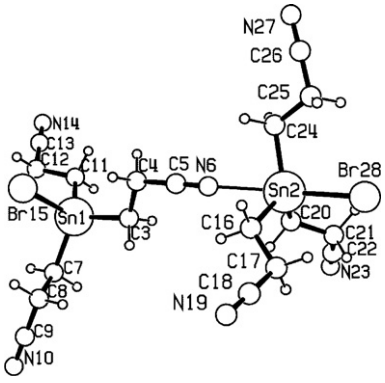

Desmond Kwena Modibane and Tebello Nyokong

Polyhedron 27 (2008) 1102

Synthesis and photophysical properties of lead phthalocyanines

For tetra- and octa-substituted lead phthalocyanines, the fluorescence spectra were different from excitation spectra due to demetallation upon excitation.

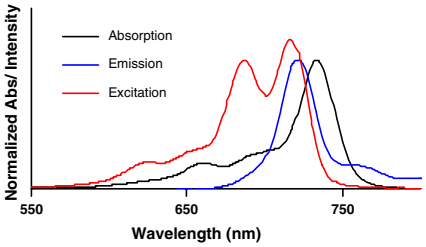

R. Senthil Kumar, S. Arunachalam, V.S. Periasamy, C.P. Preethy, A. Riyasdeen and M.A. Akbarsha

Polyhedron 27 (2008) 1111

Synthesis, DNA binding and antitumor activities of some novel polymer–cobalt(III) complexes containing 1,10-phenanthroline ligand

Some polymer–cobalt(III) complex samples (containing 1,10-phenanthroline ligand) with varying degree of cobalt(III) complex content in the polymer chain were prepared and characterized. DNA binding properties of these complex samples have been carried out using different physico-chemical methods. A sample of this polymer–cobalt(III) complex was tested for its antitumor activity. The antiproliferative and morphological effects of polymer–cobalt(III) complex sample with high degree of coordination appear to be target-specific killing of cells.

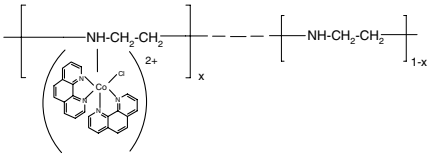

B. Machura, J. Miłek, J. Kusz, J. Nycz and D. Tabak

Polyhedron 27 (2008) 1121

Reactivity of oxorhenium(V) complexes towards quinoline carboxylic acids. X-ray structure of $[ReOCl_2(hquin\text{-}7\text{-}COOH)(PPh_3)] \cdot OPPh_3$, $[ReOBr_2(hquin\text{-}7\text{-}COOH)(PPh_3)]$ and $[ReOX_2(hmquin\text{-}7\text{-}COOH)(PPh_3)]$. DFT and TD-DFT calculations for $[ReOCl_2(hquin\text{-}7\text{-}COOH)(PPh_3)]$

The reactions of $[ReOX_3(PPh_3)_2]$ (X = Cl, Br) with 8-hydroxyquinoline-7-carboxylic acid (Hhquin-7-COOH) and 8-hydroxy-2-methylquinoline-7-carboxylic acid (Hhmquin-7-COOH) have been examined and $[ReOX_2(hquin\text{-}7\text{-}COOH)(PPh_3)]$ and $[ReOX_2(hmquin\text{-}7\text{-}COOH)(PPh_3)]$ complexes have been obtained. All the complexes were characterized by IR, UV–Vis spectroscopy and elemental analysis. The crystal and molecular structures have been determined for $[ReOCl_2(hquin\text{-}7\text{-}COOH)(PPh_3)] \cdot OPPh_3$, $[ReOBr_2(hquin\text{-}7\text{-}COOH)(PPh_3)]$ and $[ReOX_2(hmquin\text{-}7\text{-}COOH)(PPh_3)]$. The electronic structure of $[ReOCl_2(hquin\text{-}7\text{-}COOH)(PPh_3)]$ has been calculated with the density functional theory (DFT) method.

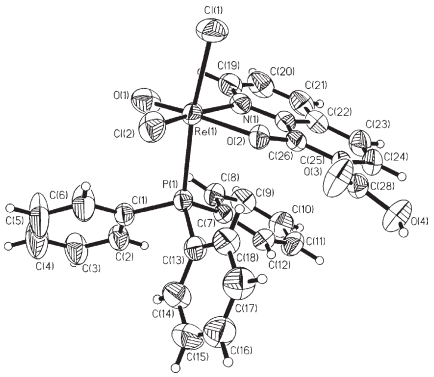

Geise Ribeiro, Marcel Benadiba, Alison Colquhoun and Denise de Oliveira Silva

Polyhedron 27 (2008) 1131

Diruthenium(II, III) complexes of ibuprofen, aspirin, naproxen and indomethacin non-steroidal anti-inflammatory drugs: Synthesis, characterization and their effects on tumor-cell proliferation

$[Ru_2(dNSAID)_4Cl]$ and novel $[Ru_2(dNSAID)_4(H_2O)_2]$ PF_6 complexes, where dNSAID = deprotonated carboxylate from the non-steroidal anti-inflammatory drugs (NSAIDs) have been prepared and characterized. Coordination of Ru_2(II, III) core led to synergistic effects that increased significantly the inhibition of C6 rat glioma proliferation in relation to the organic NSAIDs naproxen and ibuprofen.

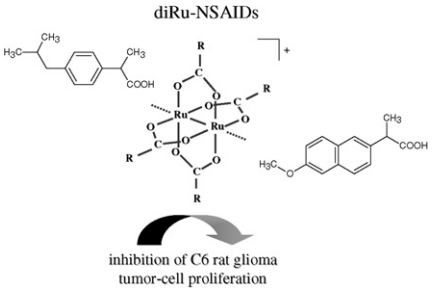

The Publisher encourages the submission of articles in electronic form thus saving time and avoiding rekeying errors. For detailed instructions on the preparation of manuscripts and of electronic artwork, consult the Author Gateway for Elsevier at http://authors.elsevier.com

ScienceDirect

Full text of this journal is available, on-line from **ScienceDirect**. Visit **www.sciencedirect.com** for more information.

Polyhedron 27, issue 11, 4 August 2008

Contents lists available at ScienceDirect

Polyhedron

journal homepage: www.elsevier.com/locate/poly

Contents

Papers

Tapan K. Si, Santu Chakraborty, Alok K. Mukherjee, Michael G.B. Drew and Ramgopal Bhattacharyya

Polyhedron 27 (2008) 2233

Novel supramolecular network in tri- and mono-nuclear oxovanadium(V)-salicyl-hydroximate: Synthesis, structure and catalytic oxidation of hydrocarbons using H_2O_2 as terminal oxidant

Two oxovanadium(V)salicylhydroximate complexes, $[VO(SHA)(H_2O)] \cdot 1.58H_2O$ (**1**) and $[V_3O_3(CSHA)_3(H_2O)_3] \cdot 3CH_3COCH_3$ (**2**) and a mono nuclear oxovanadium(V) complex $[VO(SHAH_2)(PyDC)]$ (**3**) with salicylhydroxamic acid ($SHAH_3$) and 2,6-pyridine dicarboxylic acid ($PyDCH_2$), a mono nuclear oxoperoxo vanadium(V)complex $H[VO(O_2)(PyDC)(H_2O] \cdot 2.5H_2O$ (**4**) with $PyDC^{2-}$, have been synthesized and structurally characterized. All the complexes exhibit supramolecular networks. Compound **1** and **2** behave as a good catalyst for functionalization of hydrocarbons.

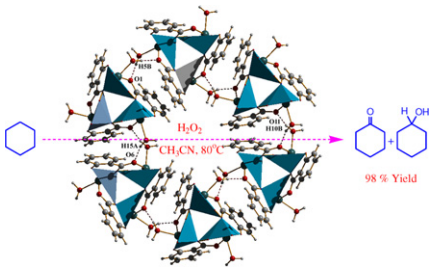

Mariana Dennehy, Ricardo M. Ferullo, Oscar V. Quinzani, Sandra D. Mandolesi, Norberto Castellani and Michael Jennings

Polyhedron 27 (2008) 2243

Unusual coordination in a silver thionate complex. Synthesis, structural characterization and theoretical calculations of dinuclear and polynuclear silver(I) thiosaccharinates with pyridine and 1,10-phenanthroline

New ternary silver(I) thiosaccharinates with pyridine and 1,10-phenanthroline are prepared and structurally characterized. The pyridine derivative is a dinuclear silver complex, $[Ag_2(tsac)_2py]$, with argentophilic interaction and very unusual metal environments. One Ag(I) is coordinated by two S atoms and the other silver atom by three N atoms.

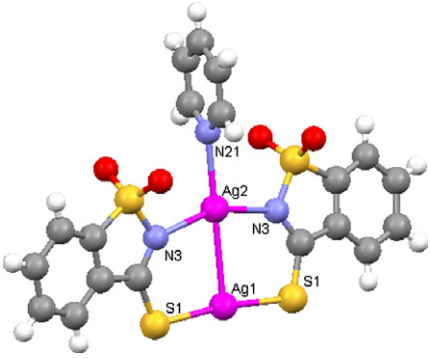

Tarlok S. Lobana, Sonia Khanna, Geeta Hundal, Ben-Jie Liaw and Chen W. Liu

Polyhedron 27 (2008) 2251

The influence of substituents at the C^2 carbon of thiosemicarbazones on bonding and nuclearity of silver(I) complexes

The substitution at C^2 carbon has led to a change in stoichiometry, nuclearity and dentacy of thiosemicarbazone complexes of silver(I). For example, 2-acetylpyridine thiosemicarbazone (HL^2) has yielded complex **1**, while 2-benzoylpyridine thiosemicarbazone (HL^1) has yielded a sulfur-bridged dimer **2**.

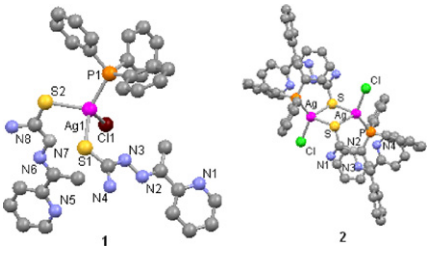

Bruno Pitteri and Marco Bortoluzzi

Polyhedron 27 (2008) 2259

Displacement of neutral nitrogen donors by chloride in $[Pt(SNS)(R\text{-}py)](ClO_4)_2$ (SNS = 2,6-bis(methylthiomethyl)pyridine; R-py = pyridines): A reactivity comparison between *meta*- and *para*-substituted pyridines

The kinetics of displacement by chloride of *meta*- and *para*-substituted pyridines (R-py) from $[Pt(SNS)(R\text{-}py)]^{2+}$ complexes {SNS = 2,6-bis(methylsulfanylmethyl)pyridine} are reported. The reactivity of the two groups of N-donors is different, the *meta*-substituted pyridines resulting less reactive than the *para*-substituted on growing their basicity. These results have been explained on the basis of a different π-acidity between the two groups of ligands which influences the reaction ground state.

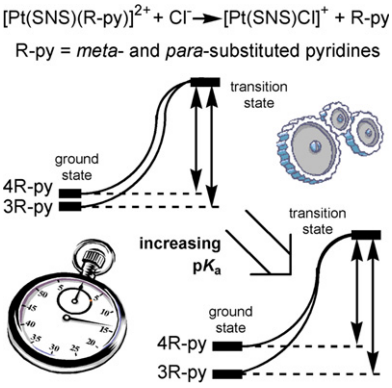

Krassimira P. Guerra and Rita Delgado

Polyhedron 27 (2008) 2265

Iron(III) complexes of the tris-(3-aminopropyl) derivative of a 14-membered tetraazamacrocycle: Potentiometric, spectroscopic and electrochemical studies

The potentiometric, UV–Vis, EPR and IR spectroscopic and electrochemical properties of mono- and dinuclear iron(III) complexes of 3,7,11-tris-(3-aminopropyl)-3,7,11,17-tetraazabicyclo[11.3.1]heptadeca-1(17),13,15-triene, L^1, were investigated in aqueous solution.

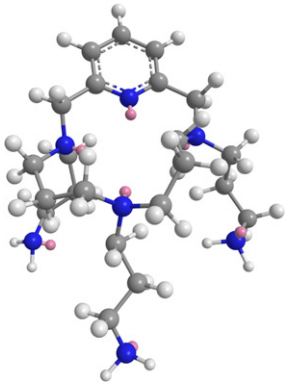

Damir A. Safin, Felix D. Sokolov, Łukasz Szyrwiel, Maria G. Babashkina, Timur R. Gimadiev, F. Ekkehardt Hahn, Henryk Kozlowski, Dmitriy B. Krivolapov and Igor A. Litvinov

Polyhedron 27 (2008) 2271

Nickel(II) complexes with *N*-(thio)phosphorylthioureas AdNHC(S)NHP(X)(O*i*Pr)$_2$: Versatile coordination of phosphoryl (X = O) and thiophosphoryl (X = S) derivatives

The reaction of the potassium salts of *N*-(thio)-phosphorylated thioureas of the common formula AdN(H)C(S)N(H)P(X)(O*i*Pr)$_2$ (X = O, $\mathbf{HL^I}$; X = S, $\mathbf{HL^{II}}$) with the Ni(II) cation in aqueous EtOH leads to $[\mathbf{Ni(L^{I,II})_2}]$ chelate complexes. The molecular structures of the thioureas $\mathbf{HL^{I,II}}$ and the complexes $[\mathbf{Ni(L^I}\text{-}\boldsymbol{N,S})_2]$ and $[\mathbf{Ni(L^{II}}\text{-}\boldsymbol{S,S'})_2]$ were elucidated by single crystal X-ray diffraction analysis, IR, ^{1}H and ^{31}P NMR spectroscopy and microanalysis. In the complex $[\mathbf{Ni(L^I)_2}]$, the metal center is found to be in a square-planar N_2S_2 environment formed by the C=S sulfur atoms and the P–N nitrogen atoms of two deprotonated $\mathbf{L^I}$ ligands. The ligands are in a *trans* configuration. The Ni(II) atom in complex $[\mathbf{Ni(L^{II})_2}]$, with the deprotonated thiourea $\mathbf{L^{II}}$, is coordinated in a square-planar fashion by the C=S and P=S sulfur atoms of two anionic ligands. The ligands are in a *cis* configuration.

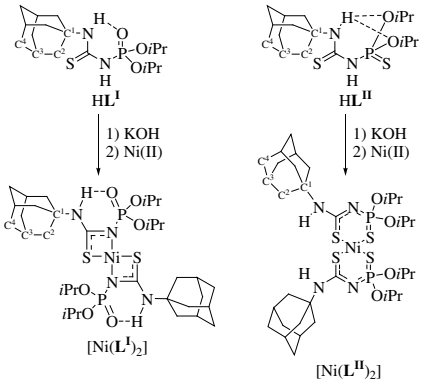

David G. Calatayud, Elena López-Torres and M. Antonia Mendiola

Polyhedron 27 (2008) 2277

Reactivity of benzil bis(4-methyl-3-thiosemicarbazone) with cadmium nitrate. Crystal structure of $[Cd(LMe_2H_4)(NO_3)_2][Cd(LMe_2H_4)(NO_3)(H_2O)]NO_3 \cdot H_2O$

Benzil bis(4-methyl-3-thiosemicarbazone) and cadmium nitrate form, depending on the pH, two new complexes: $[Cd(LMe_2H_4)(NO_3)_2]$-$[Cd(LMe_2H_4)(NO_3)(H_2O)]NO_3 \cdot H_2O$ (**1**) and $[Cd(LMe_2H_4)]_2$ (**2**). Complex **1** contains two different types of Cd(II) ions. The Cd(1) atom is seven-coordinate with a $S_2N_2O_3$ coordination sphere, but the coordination number of the Cd(2) atom expands to eight by an additional oxygen atom. Both units are linked by hydrogen bonds.

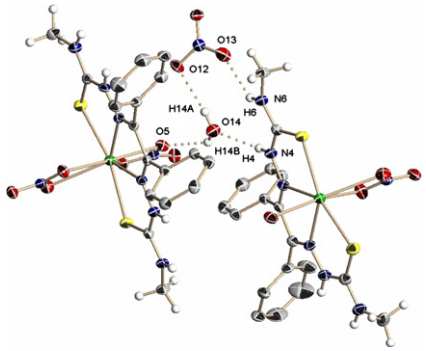

Saeed Rayati, Saeed Zakavi, Somayeh H. Motlagh, Vahid Noroozi, Maryam Razmjoo, Andrzej Wojtczak and Anna Kozakiewicz

Polyhedron 27 (2008) 2285

β-Tetra-brominated *meso*-tetraphenylporphyrin: A conformational study and application to the Mn-porphyrin catalyzed epoxidation of olefins with tetrabutylammonium oxone

In spite of the nearly planar structure of H_2TPPBr_4, the Soret and Q(0,0) bands of β-tetrabrominated porphyrin are significantly red shifted with respect to those of H_2TPP which is probably due to the electron-withdrawing effects of the substituents. $Mn(TPPBr_4)OAc$ is an efficient catalyst for the selective epoxidation of conjugated double bonds with tetrabutylammonium oxone.

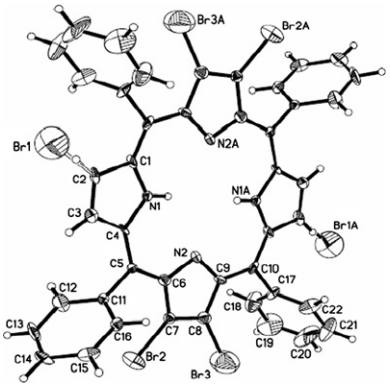

Maxwell A. Braverman, Richard J. Staples, Ronald M. Supkowski and Robert L. LaDuca

Polyhedron 27 (2008) 2291

Effect of pendant arm position and length on the structure and properties of nickel aromatic dicarboxylate coordination polymers incorporating a kinked organodiimine

Hydrothermal synthesis has afforded coordination polymers incorporating 4,4′-dipyridylamine (dpa) and flexible pendant arm aromatic dicarboxylate ligands. $[Ni(1,2\text{-phda})(dpa)(H_2O)]_n$ (1,2-phda = 1,2-phenylenediacetate) displays rhomboid grid 2D layers. $\{[Ni(hmph)(dpa)] \cdot 1.33H_2O\}_n$ (hmph = homophthalate) possesses (6,3) herringbone style 2D coordination layer motifs. $[Ni(1,3\text{-phda})(dpa)(\mu\text{-}H_2O)_{0.5}]_n$ (1,3-phda = 1,3-phenylenediacetate) manifests a 3D canted primitive cubic type coordination polymer lattice featuring antiferromagnetically coupled dinuclear kernels.

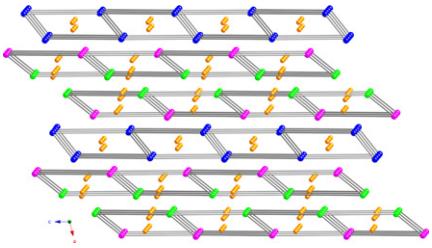

Mª del Carmen Fernández-Fernández, Rufina Bastida de la Calle, Alejandro Macías, Laura Valencia Matarranz and Paulo Pérez-Lourido

Polyhedron 27 (2008) 2301

Co(II), Ni(II) and Cu(II) complexes of new [1+1] and [2+2] macrocyclic ligands derived from 1,4-bis(2′-formylphenyl)-1,4-dioxabutane and *cis*-1,2-diaminocyclohexane

Two new macrocyclic ligands, L^1(14-membered, N_2O_2) and L^2(28-membered, N_4O_4) from [1+1] and [2+2] condensation, respectively, have been obtained in a one-pot synthesis starting from 1,4-bis(2′-formylphenyl)-1,4-dioxabutane and *cis*-1,2-diaminocyclohexane, in satisfactory yield and purity. Metal complexes of L^2 using hydrated nitrate and perchlorate salts of transitional Co(II), Ni(II) and Cu(II) metal ions have been synthesized and characterized by microanalysis, LSI-MS, IR and UV–Vis spectroscopy, magnetic measurements and conductivity measurements. Crystal structures of L^1 and the mononuclear $[Co(HL^2)(NO_3)_2(CH_3CN)](NO_3) \cdot 2CH_3CN$, $[NiL^2(NO_3)](NO_3) \cdot 2H_2O \cdot CH_3CN$ and the dinuclear $[Cu_2L^2(NO_3)_4] \cdot 4CH_3CN$ complexes have been determined by X-ray diffraction.

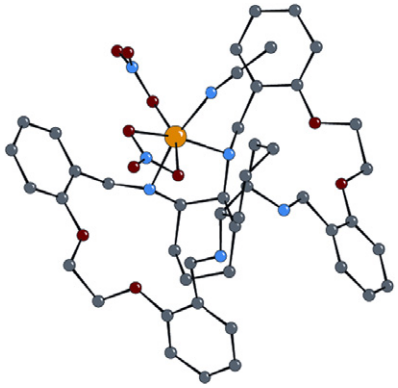

Cheng Chun Peng, Fuh-An Yang, Jyh-Horung Chen, Shin-Shin Wang and Jo-Yu Tung

Polyhedron 27 (2008) 2309

Mercury(II) complex of inverted *N*-methylated porphyrin: $HgPh(2\text{-}NCH_3NCTPP)$

The mercury phenyl complex bearing tridentate porphyrin ligand, *N*-methyl *N*-confused tetraphenylporphyrin, was prepared and its structure was established by X-ray crystallographic analysis.

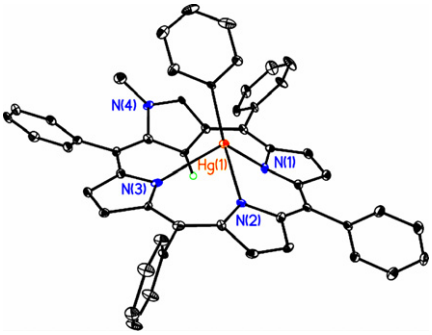

Catherine Gkioni, Athanassios K. Boudalis, Yiannis Sanakis, Leondios Leondiadis, Vassilis Psycharis and Catherine P. Raptopoulou

Polyhedron 27 (2008) 2315

A systematic investigation of the $CuCl_2/H_2mal/phen$ reaction system (H_2mal = malonic acid): Solution and solid state studies of its products

Variation of the $Cu^{II}/H_2mal/phen$ molar ratios and the crystallization methods employed afforded seven complexes either in pure form or as mixtures. All these species, and probably others not yet isolated, coexist in equilibrium in the reaction solution, a fact that has been further corroborated by using mass spectrometry.

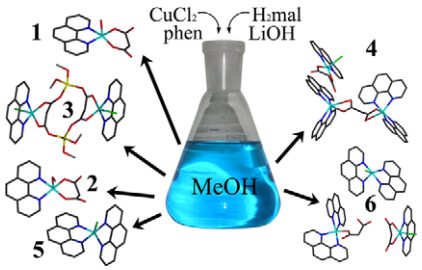

Guang-Xiang Liu, Rong-Yi Huang, Heng Xu, Xue-Jun Kong, Liang-Fang Huang, Kun Zhu and Xiao-Ming Ren

Polyhedron 27 (2008) 2327

Controlled assembly of zero-, one- and two-dimensional metal-organic frameworks involving in situ ligand synthesis under different reaction pH

A series of novel metal-organic frameworks have been fabricated by cadmium(II) salts with multi-carboxylate ligands and pdon ligands under different reaction pH. The differences of five metal-organic frameworks demonstrate that the reaction pH has an important effect on the structures of these complexes.

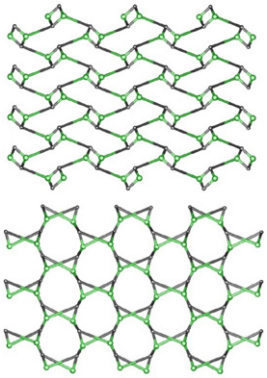

Andrew D. Sutton, James C. Fettinger, Brian D. Rekken and Philip P. Power

Polyhedron 27 (2008) 2337

Synthesis and characterization of low valent vanadium thiolate complexes

The addition of one or two equivalents of a lithium terphenyl thiolate ($LiSAr'$, $Ar' = C_6H_3$-2, 6(C_6H_3-2, 6-Pr^i_2)$_2$) to $VI_2(thf)_2$ afforded the V(II) and V(III) thiolates $[V(\mu\text{-}SAr')I]_2$ and $[V(SAr')_2I]$.

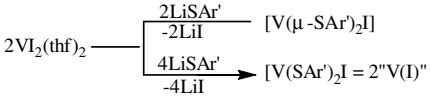

Nobumasa Koyama, Takayuki Ishida, Takashi Nogami and Tamizo Kogane

Polyhedron 27 (2008) 2341

A pyrazine-bridged linear pentanuclear copper(II) complex and related tri- and dinuclear complexes showing various coordination structures and magnetic couplings

Sterically bulky pyrazines are successfully utilized for the preparation of discrete oligo-nuclear TBP, SqP and Oh copper(II) complexes. A unique linear pentanuclear complex [{Cu-(hfac)$_2$}$_5$(μ-2-butyl-3-methylpyrazine)$_4$] is presented. Related tri- and dinuclear copper complexes were structurally and magnetically characterized. The σ-pathway is essential for the superexchange mechanism across the pyrazines.

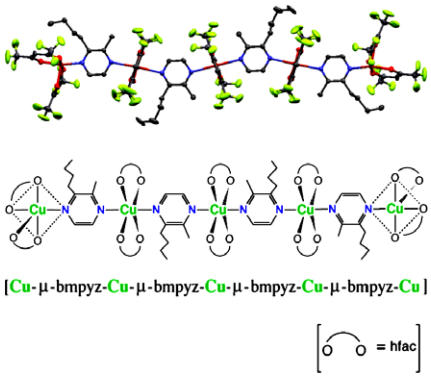

Evgen V. Govor, Andrey B. Lysenko, Alexander N. Chernega, Judith A.K. Howard, Andriy A. Mokhir, Joachim Sieler and Konstantin V. Domasevitch

Polyhedron 27 (2008) 2349

Copper(II)–lanthanide(III) 15-metallacrown-5 complexes based on pyrazinohydroxamic acid as new multiple-binding pentagonal platforms with Lewis amphoteric nature

Introducing of pyrazine hydroxamate into copper(II)–lanthanide(III) 15-metallacrown-5 core enhances the Lewis amphoteric properties leading to numerous structural types: from molecular monomeric and dimeric to the self-assembled polymeric motifs.

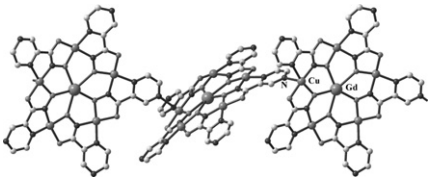

Maria S. Tarasenko, Nikolay G. Naumov, Dmitry Yu. Naumov, Sung-Jin Kim and Vladimir E. Fedorov

Polyhedron 27 (2008) 2357

A series of three-dimensional coordination polymers with general formula $[\{Ln(H_2O)_n\}\{Re_6Te_8(CN)_6\}] \cdot xH_2O$ (Ln = Eu, Gd, Tb, Dy, Ho, Er, Tm, Yb; n = 3, 4, x = 0, 2.5)

The eight three-dimensional coordination compounds $[\{Ln(H_2O)_4\}\{Re_6Te_8(CN)_6\}] \cdot 2.5H_2O$; Ln = Eu (**1**), Tb (**3**), Dy (**4**), Ho (**5**), Er (**6**), Tm (**7**), $[\{Gd(H_2O)_3\}\{Re_6Te_8(CN)_6\}] \cdot 2.5H_2O$ (**2**) and $[\{Yb(H_2O)_4\}\{Re_6Te_8(CN)_6\}]$ (**8**) were synthesized and X-ray characterized. Comparison of the structures **1**–**8** showed that despite of relatively small distinctions in atomic radii of lanthanides Eu–Yb in series of compounds **1**–**8** four types of structures are realized.

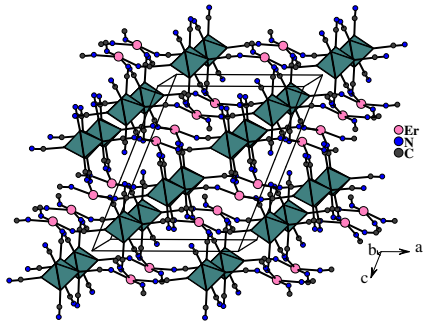

Michael Andrews, Rebecca H. Laye, Lindsay P. Harding and Simon J.A. Pope

Polyhedron 27 (2008) 2365

Quinoxaline sensitised lanthanide ion luminescence: Syntheses, spectroscopy and X-ray crystal structure of Na{1,4,7-tris[(*N*-diethyl)carbamoylmethyl]-1,4,7,10-tetraazacyclododecane-10-(2-methylquinoxaline)}I_3 C_7H_8

The syntheses and photophysical attributes of a series of quinoxaline-functionalised lanthanide complexes based on a tetra-aza macrocyclic architecture are described. Irradiation of the quinoxaline chromophore results in sensitised lanthanide emission from Nd^{III}, Eu^{III} and Yb^{III}. The coordinative ability and basicity of the quinoxaline unit were also exploited in the luminescent, pH responsive Eu^{III} complex.

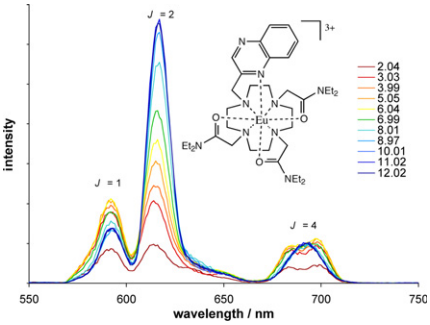

Debashree Mandal, Chang Seop Hong, Hyoung Chan Kim, Hoong-Kun Fun and Debashis Ray

Polyhedron 27 (2008) 2372

A new $[Ni^{II}_4]$ distorted cubane assembly on four solvent derived μ_3-OMe corners: Solvent dependent formation and cleavage of exogenous bridges

The solvent dependent course of formation and descend of Ni_4 cubane $[Ni_4(\mu_3\text{-}OMe)_4Q_4(MeOH)_4]$ (**1**) and mononuclear $[NiQ_2(Hgl)_2] \cdot 2H_2O$ (**2** · $2H_2O$) complexes have been examined in two similar solvents methanol and glycinol, respectively.

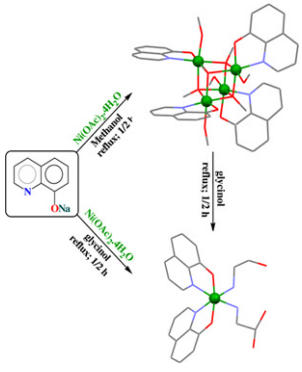

Sanaa M. Emam, Patrick McArdle, James McManus and Mary Mahon

Polyhedron 27 (2008) 2379

Ring opening complexation of nickel(II) and copper(II) by 2-phenyl-2-(2-pyridyl)imidazolidine: Synthesis, spectra and X-ray crystal structures

2-Phenyl-2-(2-pyridyl)imidazolidine undergoes metal induced ring opening with Ni(II) and Cu(II) salts and gives complexes containing the tridentate ligand (L). Crystal structures were obtained for (**1**), $[NiL_2][ClO_4]_2$, $[CuL(CH_3CN)][ClO_4]_2$, $[CuL(H_2O)][NO_3]_2$ and $[CuLN_3][ClO_4]$. DFT calculations at the 6-31G* level reproduce the X-ray crystal structure of the nickel dication but are less successful in the case of the aquo copper dication.

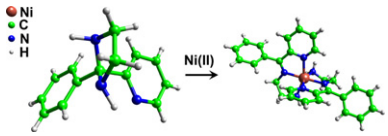

Jussara Lopes de Miranda, Jackeline da Silva Coelho, Luiza Cristina de Moura, Marcelo Hawrylak Herbst, Bruno Araújo Cautiero Horta, Ricardo Bicca de Alencastro and Magaly Girão Albuquerque

Polyhedron 27 (2008) 2386

Deamination process in the formation of a copper(II) complex with glutamic acid and a new ligand derived from guanidinoacetic acid: Synthesis, characterization, and molecular modeling studies

A binuclear copper(II) complex formed from a new ligand, biguanide-1,5-diethanoate (Bge) ($C_6H_9N_5O_4$) and glutamic acid (Glu), has been synthesized and characterized. Bge was formed from the deamination and condensation reaction between two Gaa species. The *trans–trans* isomer of the complex calculated by PM3/*d* method is shown in the figure.

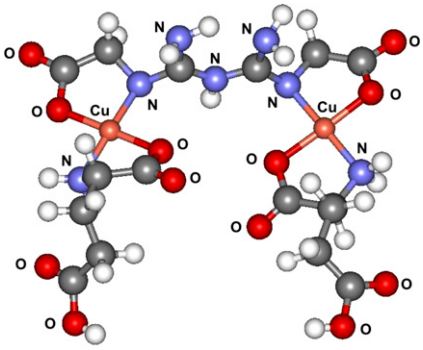

Jonathon E. Beves, Edwin C. Constable, Catherine E. Housecroft, Markus Neuburger and Silvia Schaffner

Polyhedron 27 (2008) 2395

A pyrazolyl-terminated 2,2′:6′,2″-terpyridine ligand: Iron(II), ruthenium(II) and palladium(II) complexes of 4′-(3,5-dimethylpyrazol-1-yl)-2,2′:6′,2″-terpyridine

The salts $[H_2\mathbf{2}][MeOSO_3]_2$ and $[H_2\mathbf{2}][EtOSO_3]_2$ where **2** = 4′-(3,5-dimethylpyrazol-1-yl)-2,2′:6′,2″-terpyridine, have been prepared and characterized; **2** is isolated by treating these salts with base. The syntheses and structural characterizations of the complexes $[Fe(\mathbf{2})_2][PF_6]_2$, $[Ru(\mathbf{2})_2][PF_6]_2$ and $[Pd(\mathbf{2})Cl][PF_6]$ are reported; $[H_2\mathbf{2}][ROSO_3]_2$ (R = Me or Et) is a more convenient precursor for complex formation than neutral ligand **2**.

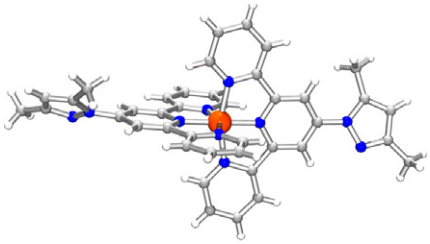

Xiao-Ming Lu, Pei-Zhou Li, Xiu-Teng Wang, Song Gao, Xiao-Jun Wang, Shuo Wang, Yu-Heng Deng, Yong-Jun Zhang and Lei Zhou

Polyhedron 27 (2008) 2402

Syntheses, crystal structures and magnetic behaviors of three Mn^{II}-terephthalate coordination polymers containing terminal ligands

Three coordination polymers have been synthesized and the structure analyses show that they are all composed of Mn atoms as nodes and terephthalate dianions as spacers. Interestingly, compound **1** consists of 1D infinite zigzag chains, while compound **2** consists of 2D sheets and compound **3** has a 3D framework structure. The study of the temperature dependent magnetic susceptibilities revealed that all of the polymers show antiferromagnetism.

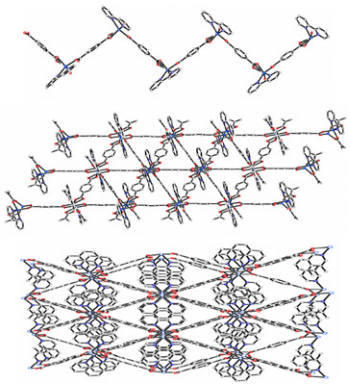

Aurkie Ray, Sambuddha Banerjee, Ray. J. Butcher, Cédric Desplanches and Samiran Mitra

Polyhedron 27 (2008) 2409

Two new end-on azido bridged dinuclear copper(II) and cobalt(III) complexes derived from the (*E*)-*N*′-((pyridin-2-yl)methylene) acetohydrazide Schiff base ligand: Characterisation, crystal structures and magnetic study

Single crystal structures of metal hydrazone complexes derived from an aliphatic hydrazide are very rare and still remain unexplored. In this paper we report two new end-on azido bridged dinuclear copper(II) (**1**) and cobalt(III) (**2**) hydrazone complexes derived from an aliphatic hydrazide. The structures of the complexes have been established by X-ray crystallography and variable temperature magnetic susceptibility measurement has been carried out for **1**.

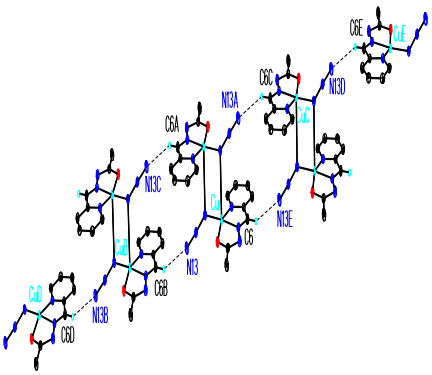

Hossein Dehghani, Majid Payam and Mohammad Reza Mansournia

Polyhedron 27 (2008) 2416

Sitting-atop complex formation of free base *meso*-tetraarylporphyrins with zirconium(IV) chloride

The reaction of *meso*-tetraarylporphyrin (H_2t(X)pp) and $ZrCl_4$ leads to the formation of the SAT complex, [(H_2t(X)pp)$ZrCl_4$], in which two pyrrolenine nitrogen atoms of the porphyrin act as electron donors to a zirconium atom, and two protons still remain on the pyrrole nitrogens.

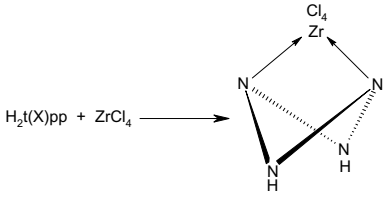

Rodrigo Arancibia, Fernando Godoy, Gonzalo E. Buono-Core, A. Hugo Klahn, Enrique Gutierrez-Puebla and Angeles Monge

Polyhedron 27 (2008) 2421

Cyrhetrenylimines and cyrhetrenylamines: Synthesis, characterization and X-ray crystal structure

New cyrhetrenylimine complexes **1a–c** have been synthesized and fully characterized. They exist as the *anti*-(*E*) conformation in solution and in solid state (**1b**). Reduction of **1a–c** with $NaBH_4$ produces quantitatively the corresponding cyrhetrenylamine derivatives **2a–c**.

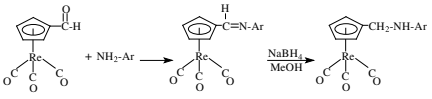

Vitalina M. Nikitina, Oksana V. Nesterova, Vladimir N. Kokozay, Evgeny A. Goreshnik and Julia Jezierska

Polyhedron 27 (2008) 2426

The first heterometallic Cu(II)/Cr(III) complex with an open-chain Schiff-base ligand self-assembled from copper powder, Reineckes salt, ethylendiamine and acetone

The one-pot self-assembly reaction of copper powder and Reineckes salt in an acetone/methanol solution of ethylendiamine in the open air affords the novel heterometallic complex [{Cu(enac)}$_2$Cr(NCS)$_4$(NH$_3$)$_2$][Cr(NCS)$_4$(NH$_3$)$_2$]$_3$ · 4(CH$_3$)$_2$CO (enac = 4,6,6-trimethyl-3,7-diazanon-3-ene-1,9-diamine). The structural features, as well as spectroscopic and magnetic properties, are reported.

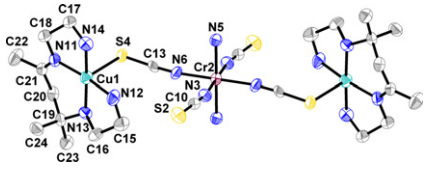

Ergün Gonca, Ümmü Gülsüm Baklacı and Hatice Akın Dinçer

Polyhedron 27 (2008) 2431

Synthesis and spectral properties of novel *seco*-porphyrazines with eight 4-biphenyl groups

Novel *seco*-porphyrazines with eight electron-rich 4-biphenyl groups on the periphery positions have been synthesized.

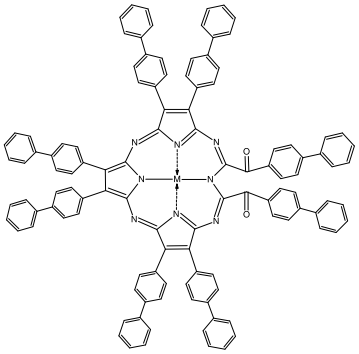

M= 2H, Cu, Zn, Co

José S. Casas, Alfonso Castiñeiras, María D. Couce, Manuel García-Vega, Manuel Rosende, Agustín Sánchez, José Sordo, José M. Varela and Ezequiel M. Vázquez López

Polyhedron 27 (2008) 2436

3-(Aryl)-2-sulfanylpropenoates of mercury(II) and phenylmercury(II)

The reactions of some 3-(aryl)-2-sulfanylpropenoic acids (H_2L) with mercury(II) acetate and diisopropylamine (Q), afford complexes of the type $[HQ]_2[Hg(L)_2]$, in which the Hg atom has an unusual HgO_2S_2 coordination kernel; the same reactions with phenylmercury(II) give compounds of the type [HQ][PhHg(L)], also with an unusual HgCOS kernel.

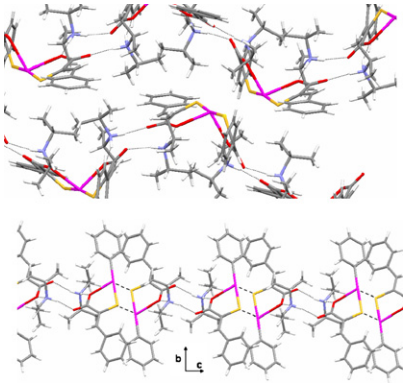

Pulak K. Dhara, Sandipan Sarkar, Michael G.B. Drew, Munirathinam Nethaji and Pabitra Chattopadhyay

Polyhedron 27 (2008) 2447

Nickel(II) complexes of tetradentate NSNO pyridylthioazophenol ligands: Synthesis, characterization and crystal structure

Two sets of nickel(II) complexes of a series of tetradentate NSNO ligands have been synthesized and isolated in their pure form. All these complexes were characterized by elemental and spectroscopic analyses. The solid-state structures of two complexes (**1a** and **2a**) were established by X-ray crystallography.

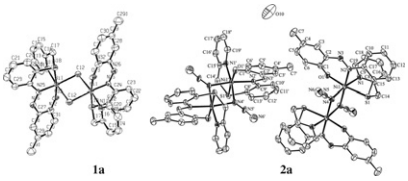

Tanmay Chattopadhyay, Arpita Banerjee, Kazi Sabnam Banu, Eringathodi Suresh, Munirathinam Netahji, Giovanni Birarda, Ennio Zangrando and Debasis Das

Polyhedron 27 (2008) 2452

Cadmium–halide and mixed cadmium–halide–dicyanamide polymers mediated by ancillary 2-aminoalkyl-pyridine ligands: Synthesis, X-ray single crystal structures and luminescence property

A series of mixed halide–dicyanamide and halide complexes of cadmium(II) mediated by 2-aminoalkyl-pyridine ligands [2-aminomethylpyridine (ampy) and 2-aminoethylpyridine (aepy)] have been synthesized and characterized. Although CdX_2, dca and the two py-ligands are not luminescent at room temperature all the complexes exhibit intense fluorescence in solution as well in solid state at room temperature.

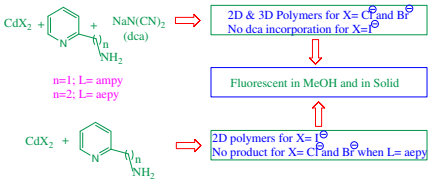

Valeriu Mereacre, Denis Prodius, Ayuk M. Ako, Narpinder Kaur, Janusz Lipkowski, Charles Simmons, Naresh Dalal, Ion Geru, Christopher E. Anson, Annie K. Powell and Constantin Turta

Polyhedron 27 (2008) 2459

Synthesis, structure and magnetic properties of unsymmetrical dodecanuclear Mn–Ln clusters

Reaction of manganese acetate and lanthanide nitrates in the presence of excess of PhCOOH affords highly asymmetric dodecanuclear mixed-metal $[Mn_{10}Ln_2(OH)(O)_8(PhCOOH)(PhCOO)_{19}]$ (Ln = Pr^{III} (**1**), Nd^{III} (**2**)) clusters. The similar reaction, but with only 2 equiv. of PhCOOH resulted in a compound with the higher nuclearity $[Mn_{11}Eu_4(O)_8(OH)_8(PhCOO)_{18}(NO_3)_2(H_2O)_6]\text{-}NO_3 \cdot 4CH_3CN$ (**3**). Variable-temperature solid-state magnetic susceptibility of **1** and **2** in the temperature range 1.8–300 K were carried out, and for both complexes predominantly antiferromagnetic exchange interactions between the metal centers were observed, giving an estimated $S = 17/2$ ground state. AC magnetic susceptibility data have revealed out-of-phase signals, which suggest that these complexes exhibit a slow relaxation of magnetization as observed in single-molecule magnets.

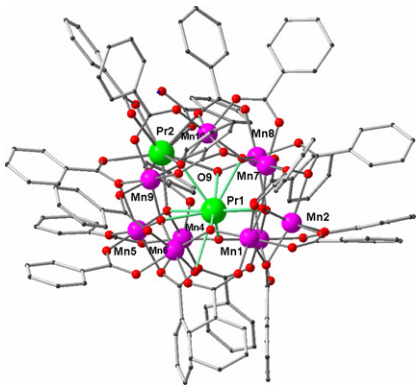

Alina Bieńko, Julia Kłak, Jerzy Mroziński, Rafał Kruszyński, Dariusz C. Bieńko and Roman Boča

Polyhedron 27 (2008) 2464

Rhenium(IV)–copper(II) heterobimetallic complexes: Synthesis, crystal structure and magnetic properties

Two Re(IV)–Cu(II) heterometallic complexes $\{(CuL_\alpha)[ReCl_4(ox)]\}_n$ (where L_α = *N-meso*-5,12-Me_2-7,14-Et_2-[14]-4,11-dieneN$_4$), **1**, and (CuL_β)-$[ReCl_4(ox)]$ (L_β = *N-rac*-5,12-Me_2-7,14-Et_2-[14]-4,11-dieneN$_4$*N-rac*-5,12-Me_2-7,14-Et_2-[14]-4,11-dieneN$_4$), **2**, were synthesized. The $[CuL^{2+}]$ macrocyclic cation is coordinated from above and below by $[ReCl_4(ox)]^{2-}$ units through the chloro-ligands and creates a chloro-bridged hetero-metallic Re^{IV}–Cu^{II} one-dimensional zig-zag chain. Compound **2** can be viewed as a hetero-bimetallic dinuclear unit, in which the Re(IV)–Cu(II) centers are linked by an oxalato bridge. The magnetic behavior of **1** and **2** has been investigated over the temperature range 1.8–300 K. Compound **1** behaves like a ferrimagnetic {Re(IV)–Cu(II)} bimetallic, one-dimensional chain with intrachain antiferromagnetic coupling. Compound **2** shows a weak antiferromagnetic interaction within the [Re(IV)–Cu(II)] unit along with a strong single-ion anisotropy, $D(Re) = -63\ cm^{-1}$.

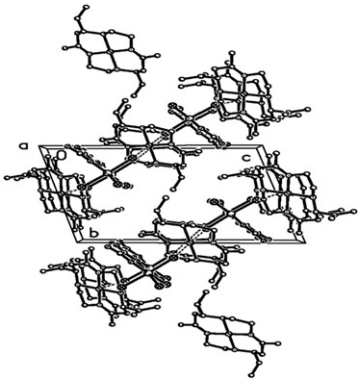

Okan Zafer Yeşilel, Aylin Mutlu and Orhan Büyükgüngör

Polyhedron 27 (2008) 2471

A new coordination mode of pyrazine-2,3-dicarboxylic acid and its first monodentate complexes: Syntheses, spectral, thermal and structural characterization of $[Cu(pzdca)(H_2O)(en)_2] \cdot H_2O$ and $[Cu(pzdca)(H_2O)(dmpen)_2]$

In the $[Cu(pzdca)(H_2O)(en)_2]\cdot H_2O$ and $[Cu(pzdc)(H_2O)(dmpen)_2]$ complexes, the pyrazine-2,3-dicarboxylate ligand exhibits new coordination mode and these complexes are the first example of the pzdca ligand exhibiting monodentate coordinated to the metal ions.

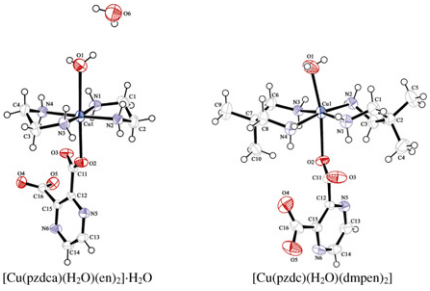

Kentaro Yamane, Satoko Hayashi, Waro Nakanishi, Takahiro Sasamori and Norihiro Tokitoh

Polyhedron 27 (2008) 2478

Fine structures of 1-(arylethynylselanyl)-naphthalenes: Characteristic features brought by the ethynylselanyl group

Fine structures of 1-(*p*-$YC_6H_4C{\equiv}CSe)C_{10}H_7$ (**1**) have been determined by X-ray analysis. The Y dependence of the fine structures are just the opposite to the case of 1-(*p*-$YC_6H_4Se)C_{10}H_7$ (**3**). The factor that controls the fine structures of **1** is called the "*ethynyl effect*". Structures in solution are also clarified.

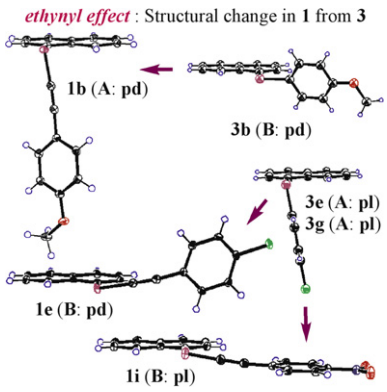

José Pérez, Luis García, Ramón Carrascosa, Eduardo Pérez and José Luis Serrano

Polyhedron 27 (2008) 2487

Solid state conformational preferences in transition metal complexes double bridged by phosphate and related ligands

The preferred conformations in the $\{M(\mu\text{-}OPO)\}_2$ core of transition metal complexes double bridged by phosphate and related ligands belong to a pseudorotation pathway (*chair* and *twist-chair* conformations).

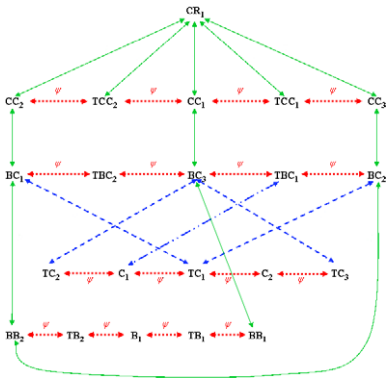

Xiao-Qiang Liang, Hong-Ping Xiao, Bao-Lin Liu, Yi-Zhi Li, Jing-Lin Zuo and Xiao-Zeng You

Polyhedron 27 (2008) 2494

Syntheses, structures and luminescent properties of four d^{10}-metal coordination polymers based on the 2,4,5-tri(4-pyridyl)-imidazole ligand

Four new d^{10}-metal coordination polymers based on 2,4,5-tri(4-pyridyl)-imidazole have been successfully synthesized and structurally characterized. All the complexes, together with the free ligand, display photoluminescence at room temperature.

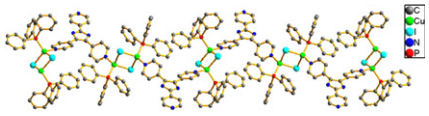

Yi-Ying Zhang, Yan Wang, Xian Tao, Ning Wang and Ying-Zhong Shen

Polyhedron 27 (2008) 2501

Synthesis and characterization of organophosphine/phosphite stabilized silver(I) methanesulfonates: Crystal structures of $[Ph_3PAgO_3SCH_3]$ and $[(Ph_3P)_2AgO_3SCH_3]$

Six phosphine/phosphite stabilized silver(I) methanesulfonates of type $[L_nAgO_3SCH_3]$ ($L = Ph_3P$, $n = 1$, **2a**; $n = 2$, **2b**; $n = 3$, **2c**; $L = (EtO)_3P$; $n = 1$, **2d**; $n = 2$, **2e**; $n = 3$, **2f**) were synthesized and characterized. Molecular structures of **2a** and **2b** have been determined by using X-ray single crystal analysis.

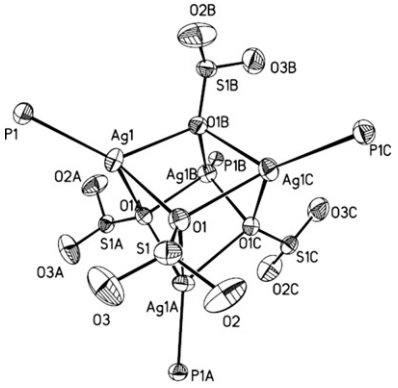

The Publisher encourages the submission of articles in electronic form thus saving time and avoiding rekeying errors. For detailed instructions on the preparation of manuscripts and of electronic artwork, consult the Author Gateway for Elsevier at http://authors.elsevier.com

ScienceDirect

Full text of this journal is available, on-line from **ScienceDirect**. Visit **www.sciencedirect.com** for more information.

Available online at www.sciencedirect.com
ScienceDirect
Polyhedron 27, issue 6, 25 April 2008
POLYHEDRON
www.elsevier.com/locate/poly

Contents

Papers

Agnieszka Matera, Justyna Brasuń, Marek Cebrat and Jolanta Świątek-Kozłowska

Polyhedron 27 (2008) 1539

The role of the histidine residue in the coordination abilities of peptides with a multi-histidine sequence towards copper(II) ions

The coordination of the group of protected and unprotected peptides containing three histidyl residues in the sequence were investigated towards Cu^{2+} ions. The investigations were performed by potentiometric, spectroscopic and computer calculations. Obtained results have determined a number of different binding modes strictly depending on position of histidyl residue.

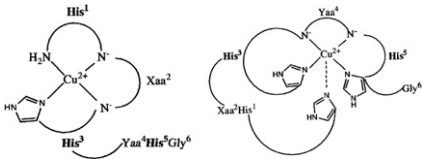

Chandan Adhikary, Rajesh Bera, Buddhadeb Dutta, Sreyashi Jana, Gabriele Bocelli, Andrea Cantoni, Siddhartha Chaudhuri and Subratanath Koner

Polyhedron 27 (2008) 1556

Catalytic efficacy of Schiff-base copper(II) complexes: Synthesis, X-ray structure and olefin oxidation

Copper(II) complexes containing tridentate and tetradentate Schiff-bases have been synthesized and characterized. Olefin oxidation reactions catalyzed by these complexes, in different solvent media, have been studied by using *tert*-BuOOH as an oxidant.

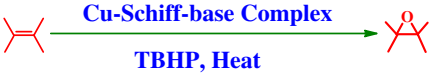

Halina Podsiadły

Polyhedron 27 (2008) 1563

Interaction of vanadium(III) with imidazole carboxylic acids

Complex formation between vanadium(III) and several imidazole carboxylic derivatives (urocanic acid, imidazole-4-carboxylic and imidazole-4,5-dicarboxylic acid) was studied using pH-potentiometric and spectroscopic (UV–Vis absorption and fluorescence) methods. The results show that urocanic acid is a weak ligand in aqueous solution and hydrolysis of vanadium(III) effectively competes with the complexation processes. Imidazole mono and di-carboxylate are relatively stronger donor (N,O) ligands and are able to prevent, to some degree, the hydrolysis processes. The main complex species in the vanadium(III)–imidazole-4,5-dicarboxylic acid system is the dinuclear μ-oxo bridged V_2OL_2 species.

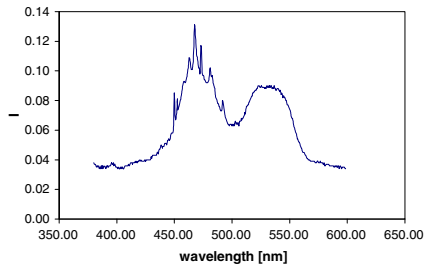

Elsevier Ltd.

Nataraj Chitrapriya, Viswanathan Mahalingam, Matthias Zeller and Karuppannan Natarajan

Polyhedron 27 (2008) 1573

Synthesis, characterization and crystal structures of cyclometallated Ru(II) carbonyl complexes formed by hydrazones

Six new cycloruthenated complexes have been synthesized and characterized. A mechanism has been proposed for C–H activation. The redox properties of the complexes have been studied by cyclic voltammetry.

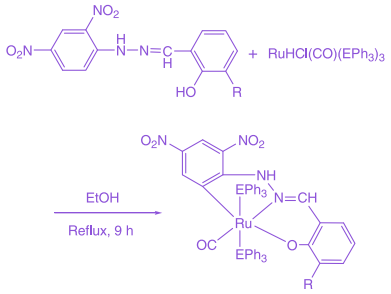

Laëtitia Dangleterre, Jean-Paul Cornard and Christine Lapouge

Polyhedron 27 (2008) 1581

Spectroscopic and theoretical investigation of the solvent effects on Al(III)–hydroxyflavone complexes

The complexation of Al(III) with some hydroxyflavones has been studied in methanol/water solution at pH 6. TD-DFT calculations have allowed the determination of the chelating site.

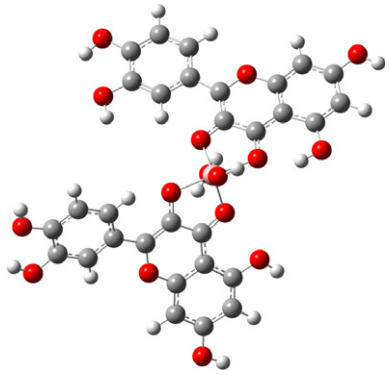

Deborah C. Bebout, Wei Lai, Sarah M. Stamps, Steven M. Berry and Raymond J. Butcher

Polyhedron 27 (2008) 1591

Bis-tridentate chelates of an asymmetric ligand: X-ray structures and solution NMR characterization of divalent zinc triad metal ion complexes of *N*-(2-pyridylmethyl)-*N*-(2-(methylthio)ethyl)amine

An asymmetric N_2S ligand formed *trans* facial bis-tridentate chelates of group 12 metal ions in the solid state. Unlike previously reported bis-tridentate chelates, slow exchange conditions on the δH time scale could be established in CD_3CN for the *trans* facial and slightly more thermodynamically stable *cis* forms.

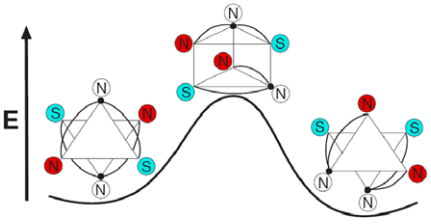

Grzegorz Romanowski, Edmund Kwiatkowski, Waldemar Nowicki, Marek Kwiatkowski and Tadeusz Lis

Polyhedron 27 (2008) 1601

Chiral dioxovanadium(V) Schiff base complexes of 1,2-diphenyl-1,2-diaminoethane and aromatic *o*-hydroxyaldehydes: Synthesis, characterization, catalytic properties and structure

Ten new chiral VO_2L complexes, where L is the deprotonated product of single condensation of SS(-)-1,2-diphenyl-1,2-diaminoethane and RR(+)-1,2-diphenyl-1,2-diaminoethane with aromatic *O*-hydroxyaldehydes, were synthesized and characterised by spectroscopic methods. Crystal structure of the $(VO_2L)_2 \cdot 2H_2O$ complex where L is the SS(–)-1-amino-2-N-[(2′,-oxido-κO-4′,6′,-dimethoxyphenyl)-methylene]amino-1,2-diphenylethane was determined. Complexes with ligands bearing methoxy substuents in positions 3 and 5 of the phenyl ring were found to act as catalysts in asymmetric oxidations of prochiral methyl phenyl sulfide to give the enantiometrically enriched sulfoxides.

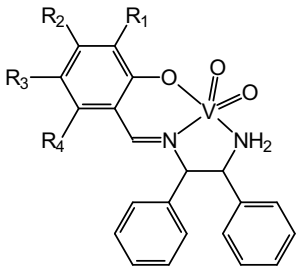

P. Raghavendra Kumar, Shailesh Upreti and Ajai K. Singh

Polyhedron 27 (2008) 1610

Schiff bases functionalized with PPh_2 and SPh groups and their Ni(II) and Pd(II) complexes: Synthesis, crystal structures and applications of a Pd complex for Suzuki–Miyaura Coupling

The Schiff bases 2-HO–$C_6H_4C(CH_3)$=N–CH_2CH_2Y (Y = SPh ($\mathbf{L}^1$) or PPh_2 ($\mathbf{L}^4$)) and 2,4-$(HO)_2$-$C_6H_4C(CH_3)$=N–CH_2CH_2SPh ($\mathbf{L}^2$) have been synthesized, and the compounds obtained by the borohydride reduction of $\mathbf{L}^1$ and $\mathbf{L}^2$, 2-HO–$C_6H_4CH(CH_3)$–$NHCH_2CH_2Y$ (Y = SPh ($\mathbf{L}^3$) or PPh_2 ($\mathbf{L}^5$)), have also been synthesized. The ligands $\mathbf{L}^1$–$\mathbf{L}^5$ coordinate in a uninegative tridentate mode (N, O^-, S/P) with Pd(II) and Ni(II). Single crystal structures of $\mathbf{L}^1$, $\mathbf{L}^2$, [PdCl($\mathbf{L}^1$–H)] (**1**), [PdCl($\mathbf{L}^3$–H)] (**3**) and [NiCl($\mathbf{L}^4$–H)] (**6**) have been solved. Pd($\mathbf{L}^2$–H)Cl] has been immobilized on silica gel and used as a catalyst for Suzuki–Miyaura C–C coupling reactions.

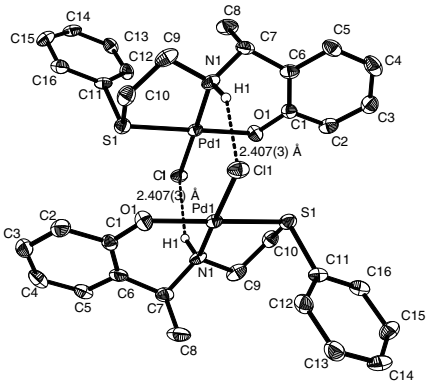

B. Żurowska and A. Brzuszkiewicz

Polyhedron 27 (2008) 1623

Co(II)-promoted transformation of diethyl-(quinolin-2-ylmethyl)phosphonate to quinoline-2-carboxylate (2-qca): Synthetic, structural and magnetic studies of [$Co(2\text{-qca})_2$-$(EtOH)_2$]

The synthesis and single-crystal X-ray structural characterization of a novel compound of the formula [$Co(2\text{-qca})_2(EtOH)_2$] (2-qca = quinoline-2-carboxylate) is reported. This compound has been synthesized by the oxidative decomposition of the diethyl(quinolin-2-ylmethyl)phosphonate ligand. In this reaction the cobalt(II) ion promotes C–P bond cleavage. Detailed characterization of $Co(2\text{-qca})_2$-$(EtOH)_2$ includes structural, spectroscopic and magnetic studies.

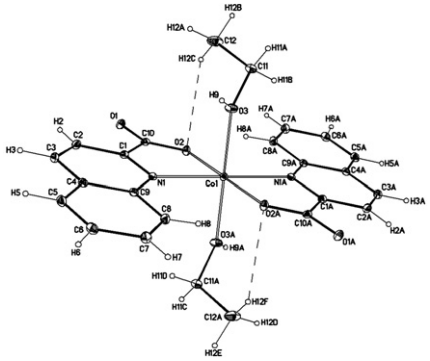

Hassan Keypour, Reza Azadbakht, Sadegh Salehzadeh, Hamid Khanmohammadi, Hamidreza Khavasi and Harry Adams

Polyhedron 27 (2008) 1631

Synthesis of two new tripodal ligands and their cyclocondensation with 2-[2-(2-formylphenoxy)ethoxy]benzaldehyde in the presence of manganese(II) and cadmium(II) metal ions

Two tetraamine tripodal ligands of 2-((bis(2-aminoethyl)amino)methyl)benzenamine (L^2) and 2-((2-amino-ethyl)(3-aminopropyl)amino)methyl)benzenamine were synthesized and their cyclocondensation with 2-[2-(2-formyl phenoxy)ethoxy]benzaldehyde (L4) in the presence of Manganes(II) and cadmium(II) ions were examined.

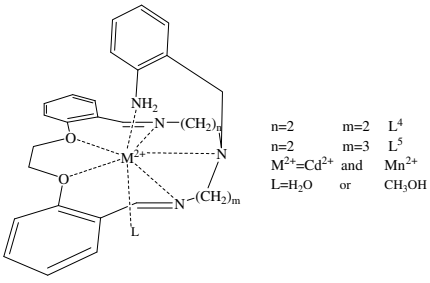

Khodayar Gholivand, Ahlam Madani Alizadehgan, Fresia Mojahed and Parviz Soleimani

Polyhedron 27 (2008) 1639

Crystal structures and mass spectral fragmentation studies of some new carbacylamidophosphate compounds

New carbacylamidophosphates, $R'_2P(O)NHC(O)R$ with *N*-benzoyl and *N*-acetyl derivatives were synthesized and their crystal structures and mass spectra were determined. The mass spectra showed that the greater intensities for 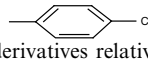 ions for *N*-benzoyl derivatives relative to R–C≡NH^+ ions for *N*-acetyl derivatives may due to different P=O, C=O, P–N_{amide} and C–N_{amide} bond lengths.

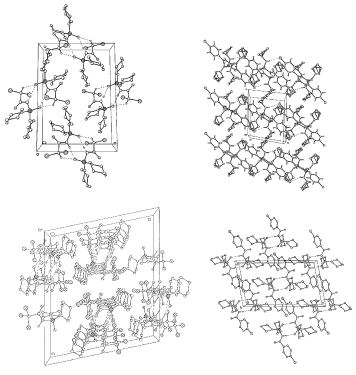

Zekeriya Bıyıklıoğlu and Halit Kantekin

Polyhedron 27 (2008) 1650

New long-chain-substituted polymeric metal-free and metallophthalocyanines by microwave irradiation: Synthesis and characterization

A tetranitrile monomer *N*,*N*-bis{2-[2-(3,4-dicyanophenoxy)ethoxy]ethyl}-4-methylbenzenesulfonamide (**3**) was synthesized by nucleophilic aromatic substitution of *N*,*N*-bis[2-(2-hydroxyethoxy)ethyl]-4-methylbenzenesulfonamide (**1**) onto 4-nitrophthalonitrile (**2**). The metal-free phthalocyanine polymer (**4**) was prepared by the reaction of a tetranitrile monomer **3** in 2-(dimethylamino)ethanol. Ni(II), Co(II) and Cu(II) phthalocyanine polymers were prepared by the reaction of the tetranitrile compound with the chlorides of Ni(II), Co(II) and Cu(II) in 2-(dimethylamino)ethanol (DMAE). The Zn(II)-phthalocyanine polymer was prepared by the reaction of the tetranitrile compound with the acetate of Zn(II) in DMAE. The new compounds were characterized by a combination of IR, ^{1}H NMR, ^{13}C NMR, UV–Vis, elemental analysis and MS spectral data.

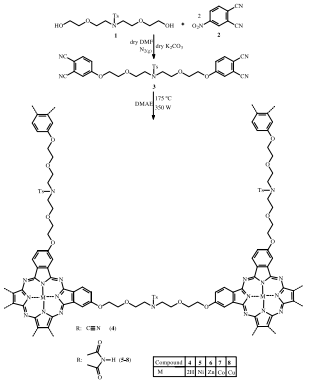

Mitra Ghassemzadeh, Leyla Fallahnedjad, Majid M. Heravi and Bernhard Neumüller

Polyhedron 27 (2008) 1655

Synthesis, characterization and crystal structure of new silver(I) and palladium(II) complexes containing 1,2,4-triazole moieties

The reaction of 4-amino-5-ethyl-2H-1,2,4-triazole-3(4H)-thione (AETT) with $AgNO_3$ in ethanol gave the ionic complex $[\{[Ag(AETT)]NO_3\}_2]_n$ with an interesting 10-membered silver–sulfur "mosaic" pattern. The behavior of Schiff-bases derived from AETT towards silver(I) and palladium(II) was also studied.

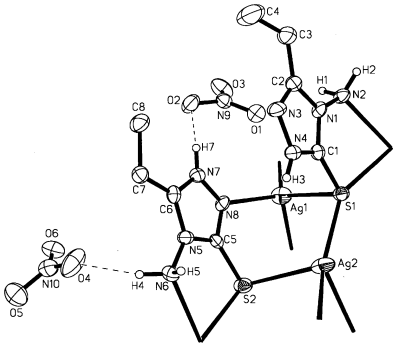

$[\{[Ag(AETT)]NO_3\}_2]_n$

Hong-Ting Sheng, Jun-Mei Li, Yong Zhang, Ying-Ming Yao and Qi Shen

Polyhedron 27 (2008) 1665

Synthesis and molecular structure of new heterometal alkoxide clusters $Ln_2Na_8(OCH_2CF_3)_{14}(THF)_6$ (Ln = Sm, Y, Yb): Highly active catalysts for polymerization of ε-caprolactone and trimethylene carbonate

The novel polynuclear heterometal alkoxide clusters $Ln_2Na_8(OCH_2CF_3)_{14}(THF)_6$ (Ln = Sm **1**, Y **2**, Yb **3**) have been synthesized by the reaction of anhydrous $LnCl_3$ with 7 equiv of $NaOCH_2CF_3$ in good yields. Clusters **1-3** show extremely high activity for the polymerization of -caprolactone (-CL) and trimethylene carbonate (TMC), and the reactivity is much higher than those found for the monometallic alkoxides lanthanide complexes previously reported.

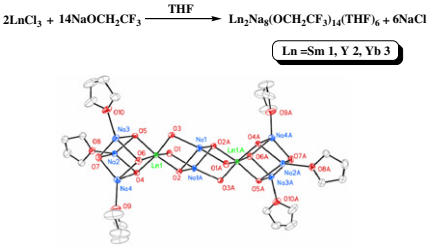

Ann L. Bingham, John E. Drake, Michael B. Hursthouse, Mark E. Light, Manisha Nirwan and Raju Ratnani

Polyhedron 27 (2008) 1673

Synthesis, characterization and spectral studies of bis(*O*,*O*-dialkylmonothiophosphato)cobalt(II) complexes and their adducts with nitrogen base ligands: Crystal structures of $[Co\{O(S)P(OPr^i)_2\}_2(C_5H_5N)_4]$ and $[Co\{O(S)P(OPr^n)_2\}_2(C_{10}H_8N_2)_2]$

Bis(*O*,*O*-dialkylmonothiophosphato)cobalt(II) complexes of the type $[Co\{O(S)P(OR)_2\}_2]$ (where R = Pr^n, Pr^i, Bu^n) and their nitrogen bases adducts, $[Co\{O(S)P(OPr^i)_2\}_2(C_5H_5N)_4]$, $[Co\{O(S)P(OPr^n)_2\}_2(C_{10}H_8N_2)_2]$ and $[Co\{O(S)P(OBu^n)_2\}_2(C_{10}H_8N_2)_2]$ have been prepared. These compounds were characterized by elemental analysis, IR spectroscopy, magnetic measurements and the single crystal X-ray diffraction structures of two of the adducts, $[Co\{O(S)P(OPr^i)_2\}_2(C_5H_5N)_4]$ and $[Co\{O(S)P(OPr^n)_2\}_2(C_{10}H_8N_2)_2]$.

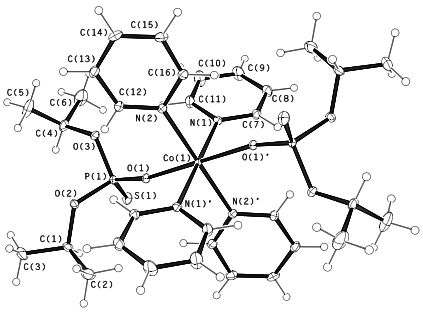

B. Machura, R. Kruszynski and J. Kusz

Polyhedron 27 (2008) 1679

Novel oxorhenium complexes with 2-(2′-hydroxyphenyl)-2-benzothiazolinato ligand: X-ray studies, spectroscopic characterization and DFT calculations

The $[ReOX_2(hbt)(EPh_3)]$ (X=Cl, Br; E=As, P) chelates have been prepared in the reactions of $[ReOX_3(EPh_3)_2]$ complexes (X=Cl, Br; E=P, As) with 2-(2'-hydroxyphenyl)-2-benzothiazole (hbtH) in acetone. From the reactions of $[ReOX_3(PPh_3)_2]$ with hbtH two kind of crystals $[ReOX_2(hbt)(PPh_3)] \cdot MeCN$ and $[ReOX_2(hbt)(PPh_3)]$ with different arrangement of halide ions (*cis* and *trans*) were isolated, whereas the $[ReOX_3(AsPh_3)_2]$ oxocompounds react with hbtH to give only *cis*-halide isomers. The complexes were structurally and spectroscopically characterised. The electronic structures of both $[ReOBr_2(hbt)(PPh_3)]$ isomers have been calculated with the density functional theory (DFT) method. The TDDFT/PCM calculations have been employed to produce a hundred of singlet excited-states starting from the ground-state geometry optimized in the gas phase of *cis*- and *trans*-halide isomers of $[ReOBr_2(hbt)(PPh_3)]$ and the UV–Vis spectra of these complexes have been discussed on this basis.

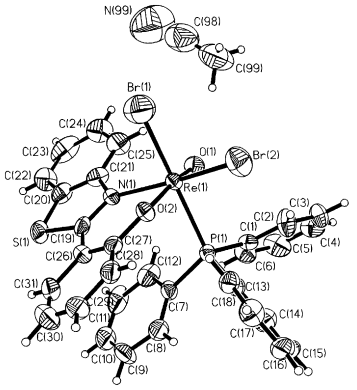

Muath Atmeh, Noel R. Russell and Tia E. Keyes

Polyhedron 27 (2008) 1690

Intramolecular photoinduced electron transfer in a ruthenium polypyridyl functionalised β-cyclodextrin capped with a hydroxo bridged Cu(II) dimer

The photophysics of a novel supramolecular donor–acceptor system comprising a ruthenium polypyridyl unit covalently linked to a hydroxo bridged dinuclear copper(II) β-cyclodextrin (CD) moiety indicates efficient photoinduced electron transfer is occurring. The parent ruthenium linked CD complex is readily quenched by copper ions at high pH whereas zinc ion has no impact on the photophysics of the complex. Although more commonly studied in the context of inclusion, such luminescently labelled CDs may have value in metal sensing.

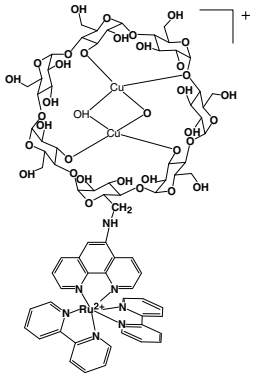

José Luis Serrano, Luis García, José Pérez, Eduardo Pérez, Joaquín García, Gregorio Sánchez, Gregorio López, Ian J.S. Fairlamb and Malva Liu

Polyhedron 27 (2008) 1699

Synthesis and characterization of new oxazoline-based palladacycles with bridging or terminal imidate ligands. Crystal structures of $[\{Pd(\mu\text{-dibromomaleimidate})(Phox)\}_2]$, [Pd(dibromomaleimidate)(Phox)(PPh_3)] and [Pd(glutarimidate)(Phox)(PPh_3)] (Phox = 2-(2-oxazolinyl)phenyl))

The dinuclear hydroxo complex $[\{Pd(\mu\text{-OH})(Phox)\}_2]$ has been used in the preparation of new cyclometallated palladium complexes $[\{Pd(\mu\text{-NCO})(Phox)\}_2]$ containing asymmetric imidate –NCO– bridging units. [–NCO– = succinimidate, phthalimidate, maleimidate, 2,3-dibromomaleimidate and glutarimidate]. The reaction of these complexes with tertiary phosphines provides novel mononuclear N-bonded imidate derivatives of the general formula [Pd(imidate)(Phox)(PR_3)]. The first X-ray crystal structures of complexes containing 2,3 dibromomaleimide as ligand, showing different coordination modes, are presented.

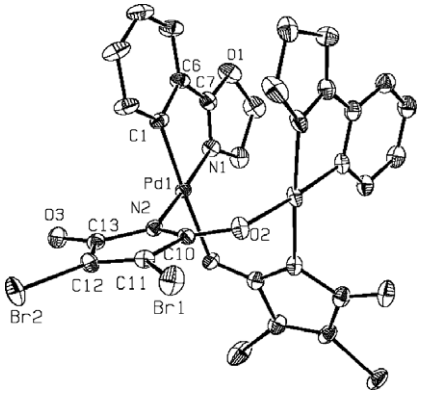

Zekeriya Bıyıklıoğlu, Ece Tuğba Güner, Saim Topçu and Halit Kantekin

Polyhedron 27 (2008) 1707

Synthesis, characterization and electrochemistry of a new organosoluble metal-free and metallophthalocyanines

4-[2-(phenylthio)ethoxy]phthalonitrile **3** was synthesized by nucleophilic displacement of nitro group in 4-nitrophthalonitrile with 2-(phenylthio)ethanol **1**. The metal-free phthalocyanine **4** was prepared by the reaction of a dinitrile monomer with 2-(dimethylamino)ethanol. Ni(II), Co(II), Cu(I)- phthalocyanines **5**, **7**, **8** were prepared by reaction of the dinitrile compound with the chlorides of Ni(II), Co(II), Cu(I) in DMAE. Zn(II)-phthalocyanine **6**, was prepared by reaction of the dinitrile compound with the acetates of Zn(II) in DMAE. Electrochemical behaviours of novel metal-free, Co(II) and Zn(II) phthalocyanines were investigated by cyclic voltammetry, potential differential pulse voltammetry techniques. The new compounds were characterized by a combination of IR, ^{1}H-NMR, ^{13}C-NMR, UV-vis, elemental analysis and MS spectral data.

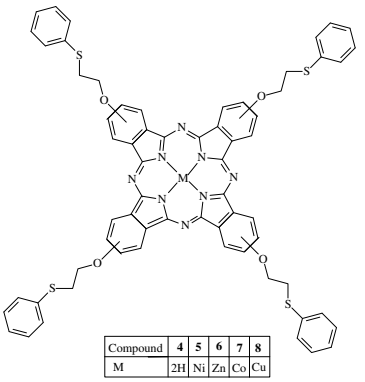

Sumanta Kumar Padhi, Dipankar Saha, Rojalin Sahu, Japyesan Subramanian and Vadivelu Manivannan

Polyhedron 27 (2008) 1714

Synthesis, structure, optical and magnetic properties of [Cr**L**$(X)_3$], {**L** = 4′-(2-pyridyl)-2,2′:6′,2″-terpyridine; X = Cl^-, N_3^-, NCS^-}

Three complexes of composition [Cr**L**$(X)_3$], where **L** = 4′-(2-pyridyl)-2,2′:6′,2″-terpyridine and X = Cl^-, N_3^-, NCS^-, are synthesized. Optical, magnetic and X-ray crystallographic studies are reported.

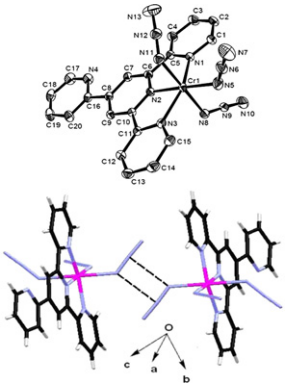

B. Żurowska, A. Brzuszkiewicz and J. Ochocki

Polyhedron 27 (2008) 1721

Ferromagnetic exchange coupling in phosphonato-bridged dinuclear copper(II) compound with monoethyl (pyridyn-2-ylmethyl)phosphonate ligand (2-mpmpe): Cu_2(2-mpmpe)$_2$-$(H_2O)_2(NO_3)_2$

Synthesis, spectroscopic and magnetic properties, and X-ray crystal structure of dinuclear copper(II) compound of formula Cu_2(2-mpmpe)$_2(H_2O)_2(NO_3)_2$, where 2-mpmpe = monoethyl (pyridyn-2-ylmethyl)phosphonate is described. Its structure consists of copper(II) ions doubly bridged by phosphate –OPO– groups. The magnetic properties of the compound revealed the occurrence of a weak ferromagnetic coupling through phosphonate bridge (J = 1.86 cm^{-1}) and interdimer superexchange coupling through H-bond network (zJ' = −0.17 cm^{-1}).

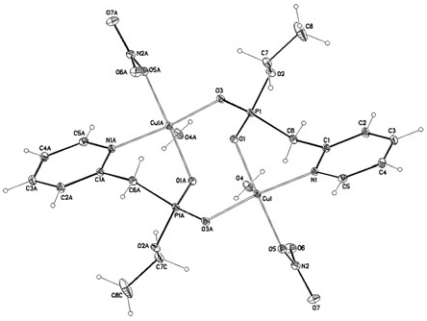

Eleni K. Efthimiadou, Alexandra Karaliota and George Psomas

Polyhedron 27 (2008) 1729

Mononuclear metal complexes of the second-generation quinolone antibacterial agent enrofloxacin: Synthesis, structure, antibacterial activity and interaction with DNA

The synthesis, the characterization, the antibacterial activity and the interaction with calf-thymus DNA of the novel mononuclear complexes of the second-generation quinolone antibacterial agent enrofloxacin with Mn^{2+}, Fe^{3+}, Co^{2+}, Ni^{2+}, Zn^{2+}, Cd^{2+} and UO22+ are presented.

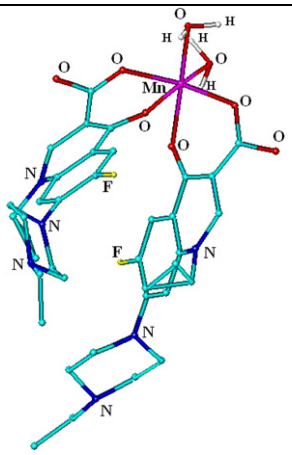

B. Machura, R. Kruszynski, J. Mroziński and J. Kusz

Polyhedron 27 (2008) 1739

Synthesis, spectroscopic characterization, X-ray structure and DFT calculations of rhenium(III) complex with 1-isoquinolinyl phenyl ketone

The $[ReCl_3(MeCN)(PPh_3)]$ complex reacts with 1-isoquinolinyl phenyl ketone (N–O) to give $[ReCl_3(N–O)(PPh_3)]$. The compound has been studied by IR, UV–Vis spectroscopy, magnetic measurements and X-ray crystallography. The magnetic behavior is characteristic of mononuclear octahedral Re(III) complex with d^4 low-spin ($^3T_{1g}$ ground state) and arises because of the large spin-orbit coupling, which gives diamagnetic ground state. The molecular orbital diagram of $[ReCl_3(N–O)(PPh_3)]$ has been calculated with the density functional theory (DFT) method, and TDDFT calculations have been employed in order to discussion of its spectroscopic properties in more detail.

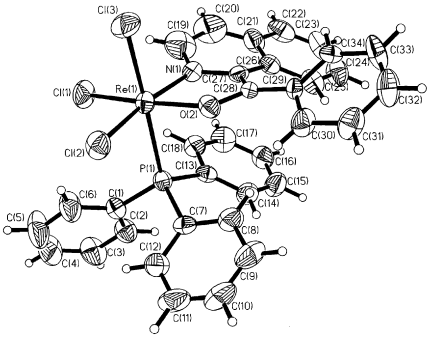

Ray L. Frost, B. Jagannadha Reddy and Sara J. Palmer

Polyhedron 27 (2008) 1747

The structure of mimetite, arsenian pyromorphite and hedyphane – A near-infrared spectroscopic study

A comparison of Raman spectra of pyromorphites with published infrared and Raman data of similar minerals has been made. Crystals of the pyromorphite- mimetite series are chemically zoned, resulting in changes in the crystal structure with the isomorphic replacement of phosphate by arsenate with the consequential change in crystal structure from monoclinic to hexagonal. Such dimorphic relationships are exemplified by the shift in the Raman spectral band positions of phosphate with increasing arsenate substitution.

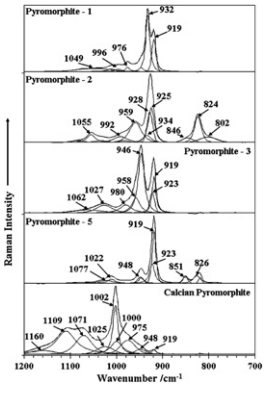

M.A.M.K. Sanhoury, M.T. Ben Dhia, K. Essalah, A. Guesmi and M.R. Khaddar

Polyhedron 27 (2008) 1754

Synthesis, spectroscopic and structural studies of 2,2,2-trifluoroethyl phosphorodiamidate complexes with tin(IV) chloride

The two octahedral complexes $SnCl_4 \cdot 2(O)P(NR_2)_2OCH_2CF_3$ (R = Me (**1**) or Et (**2**)) have been prepared and studied by a combination of experimental NMR and X-ray and theoretical DFT/B3LYP investigations.

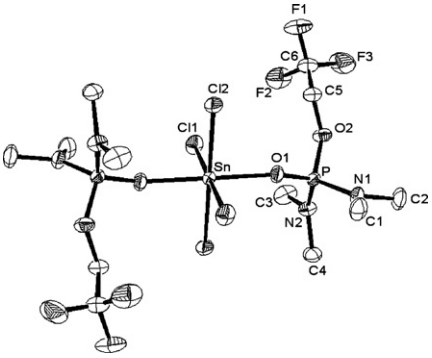

Veysel T. Yilmaz, Sevim Hamamci and Orhan Büyükgüngör

Polyhedron 27 (2008) 1761

One-dimensional silver coordination polymers generated from saccharinate, piperazine and *N*,*N*′-bis(2-hydroxyethyl)piperazine

The reaction of $Na(sac) \cdot 2H_2O$ and $AgNO_3$ in the presence of piperazine (ppz) or *N*,*N*′-bis(2-hydroxyethyl)piperazine (bheppz) results in the formation of the corresponding coordination polymers $[Ag(\mu\text{-sac})(\mu\text{-ppz})]_n$ and $[Ag(\mu\text{-sac})(\mu\text{-bheppz})]_n$. Silver(I) ions are doubly bridged by sac ligands, and further connected by ppz or bheppz bridges into one-dimensional linear chains. The chains are linked into 2D layers by hydrogen bonds.

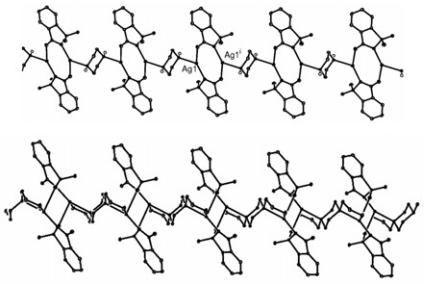

B. Machura, R. Kruszynski, M. Jaworska, P. Lodowski, R. Penczek and J. Kusz

Polyhedron 27 (2008) 1767

Tricarbonyl rhenium complexes of bis(pyrazol-1-yl)methane and bis(3,5-dimethylpyrazol-1-yl)methane – Synthesis, spectroscopic characterization, X-ray structure and DFT calculations

Two novel tricarbonyl rhenium complexes based on the bidentate heterocyclic N–N ligands [bis(pyrazol-1-yl)methane (bpzm) and bis(3,5-dimethylpyrazol-1-yl)methane (bdmpzm)] have been synthesized heating at reflux $[Re(CO)_5Cl]$ with the appropriate N–N ligand in toluene. The compounds have been characterised by IR, UV-Vis spectroscopy and X-ray analysis. The density functional theory (DFT) and time-dependent (TD) DFT calculations have been carried out for the $[Re(CO)_3(bdmpzm)Cl)]$ complex.

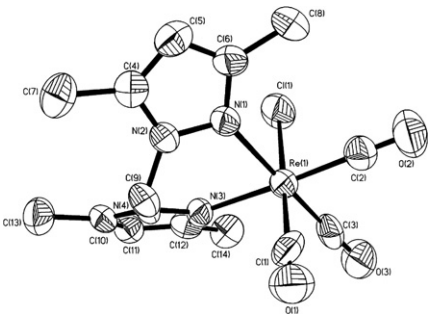

David R. Jansen, Jan Rijn Zeevaart, Zvonimir I. Kolar, Kristina Djanashvili, Joop A. Peters and Gerard C. Krijger

Polyhedron 27 (2008) 1779

^{31}P NMR study of the valence stability of tin in its 1-hydroxyethylene-diphosphonate (HEDP) and *N*,*N*′,*N*′-trimethylenephosphonate-polyethyleneimine (PEI-MP) complexes

^{31}P NMR study to determine the extent of oxidation – if any – of divalent tin when complexed with diphosphonate 1-hydroxyethylene-diphosphonate (HEDP) and polyphosphonate *N*,*N*′,*N*′-trimethylenephosphonate-polyethyleneimine (PEI-MP), respectively. In so doing evaluating the valence stability of complexed tin and the possibility of interconversion between tin(II) and tin(IV).

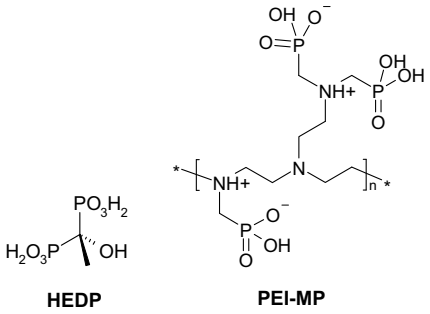

Ana Mena B. Bastos, Jeferson G. da Silva, Pedro Ivo da S. Maia, Victor M. Deflon, Alzir A. Batista, Adaliene V.M. Ferreira, Leida M. Botion, E. Niquet and Heloisa Beraldo

Polyhedron 27 (2008) 1787

Oxovanadium(IV) and (V) complexes of acetylpyridine-derived semicarbazones exhibit insulin-like activity

Reaction of 2-acetylpyridine (H2APS), 3-acetylpyridine (H3APS) and 4-acetylpyridine semicarbazone (H4APS) with $[VO(acac)_2]$ (acac = acetylacetonate) gave $[VO(H2APS)(acac)_2]$ (**1**), $[VO(H3APS)(acac)_2]$ (**2**) and $[VO(4APS)(acac)(H_2O)] \cdot 1/2H_2O$ (**3**). Oxidation of complex **1** gave $[VO_2(2APS)]$ (**4**). Complexes **1**–**3** were able to enhance glucose uptake and inhibit glycerol release from adipocytes.

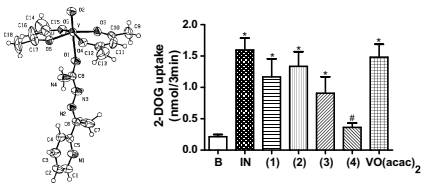

D. Andrew Knight, Jeffrey R. Deschamps, Ray J. Butcher, Christa Simmers and Eddie L. Chang

Polyhedron 27 (2008) 1795

A new coordination mode for tris(2-carboxyethyl)phosphine: Synthesis, crystal structure and characterization of the mixed-valence Co(III)/Co(II)/Co(III) complex $[Co\{P(CH_2CH_2COO)_2(CH_2CH_2COOH)\}_2]_2[Co(H_2O)_4][Na_2(H_2O)_4]Cl_2 \cdot 6H_2O$

Reaction of the water-soluble phosphine ligand tris(2-carboxyethyl)phosphine (TCEP) with cobalt(II) chloride to give a mixed-valence trimetallic Co(III)/Co(II)/Co(III) complex **1** in which the TCEP ligand adopts the previously unseen bidentate chelating binding mode to the metal center.

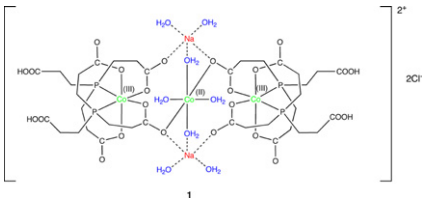

Wei Luo, Xiang-Gao Meng, Feng-Ping Xiao, Gong-Zhen Cheng and Zhen-Ping Ji

Polyhedron 27 (2008) 1802

Synthesis, characterization and bioactivity of a new Fe(III) 18-metallacrown-6 and a new trinuclear linear Ni(II) complexes

The chelating modes of these types of ligands to metal ions are the same. When we use bivalent nickel salt, we get a linear trinuclear complex; when we use trivalent iron salt, we get a new 18-metallacrown-6 compound.

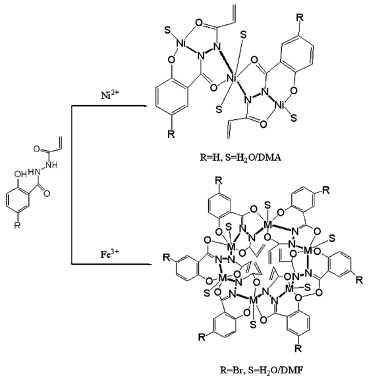

Hassan Hadadzadeh, Ali R. Rezvani and Hadi Esfandiari

Polyhedron 27 (2008) 1809

Dinuclear copper complexes with cyanamide derivatives as bridging ligands

Three mixed-valence copper complexes [{Cu(phen)$_2$}$_2$ (μ-L)](PF$_6$)$_2$ (where phen = 1,10-phenanthroline, L = 1,4-dicyanamidobenzene (dicyd)), 1,4-dicyanamido-2,5-dimethylbenzene (Me$_2$ dicyd) and 1,4-dicyanamido-2,5-dichlorobenzene (Cl$_2$ dicyd), and one dinuclear Cu(II) complex [{Cu(phen)$_2$}$_2$ (μ-apc)](PF$_6$)$_3$ (where apc = monoanion of 4-azo(phenylcyanamido)benzene) have been prepared and characterized by elemental analysis, IR and electronic absorption spectroscopies and cyclic voltammetry. [{Cu(phen)$_2$}$_2$(μ-apc)](PF$_6$)$_3$ · 2CH$_3$COCH$_3$ crystallized in the triclinic system and both five-coordinate Cu(II) ions in the dinuclear unit are linked through a bridging 4-azo(phenylcyanamido)benzene (apc) ligand.

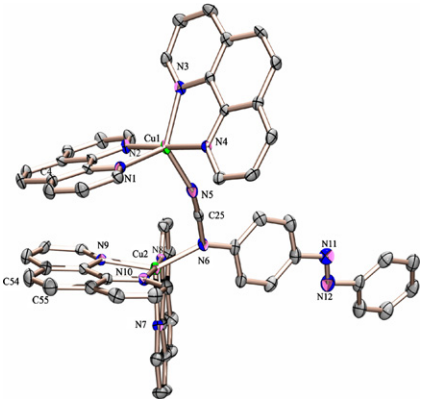

Ben-Jie Liaw, Leeyan Yu, Ju-Chun Wang and C.W. Liu

Polyhedron 27 (2008) 1818

Synthesis and characterization of metal diselenophosphates: M[Se$_2$P(OR)$_2$]$_2$ (M = Pd, Pt; R = Et, ^{n}Pr, ^{i}Pr)

The first square-planar Pd(II) and Pt(II) complexes incorporating diselenophosphate ligands have been reported. Structural elucidations indicate that minute differences exist in the M–Se bond distances and these were observed from solution ^{31}P and ^{77}Se NMR studies. A packing diagram showed a chain-like motif which was composed of square-planar M[Se$_2$P(OR)$_2$]$_2$ units and occurred via noncovalent Se···Se secondary interactions.

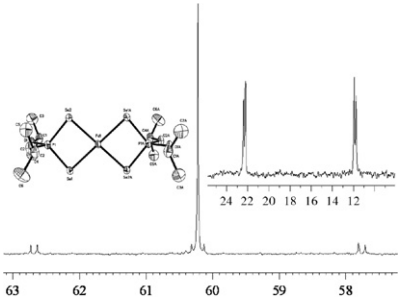

T.A. Reena, E.B. Seena and M.R. Prathapachandra Kurup

Polyhedron 27 (2008) 1825

Synthesis and spectral studies of cadmium(II) complexes derived from di-2-pyridyl ketone and N^4-phenylsemicarbazide: First structural report of a cadmium(II) complex of semicarbazone

A new semicarbazone based on di-2-pyridyl ketone and its three cadmium(II) complexes $[CdL(CH_3COO)]_2 \cdot 2CH_3OH$ (**1**), $Cd(HL)Br_2$ (**2**) and $[Cd_2L_2N_3]_2 \cdot H_2O$ (**3**) were synthesized and characterized by different physicochemical techniques. The complex, $[CdL(CH_3COO)]_2 \cdot 2CH_3OH$ (**1**) is having a dimeric structure. In complexes **1** and **3**, the ligand moieties are coordinated as monoanionic (L^-) forms and in complex **2**, the ligand coordinated as neutral (HL) one. The coordination geometry around cadmium(II) in **1** is distorted octahedral, as obtained by X-ray diffraction studies.

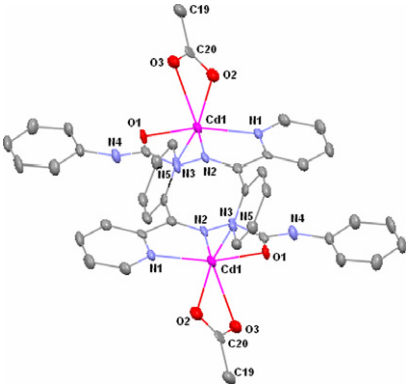

Landon C. Ziffle, Amanda P. Kenney, Seán T. Barry and Jens Müller

Polyhedron 27 (2008) 1832

Thermal fragmentation of the guanidinato aluminum amide precursor $[Me_2NC(N^{i}Pr)_2]Al(NMe_2)_2$: An investigation of reactive species by matrix-isolation FTIR spectroscopy and time-of-flight mass spectrometry

The guanidinato aluminum amide precursor **1** cleanly produces the reactive intermediate $Al(NMe_2)_3$ in gas-phase thermolyses. This monomeric aluminum amide was characterized in argon matrices by matrix-isolation FTIR spectroscopy supported by DFT calculations.

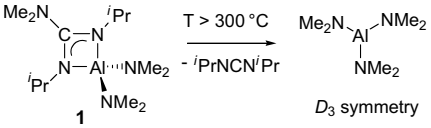

The Publisher encourages the submission of articles in electronic form thus saving time and avoiding rekeying errors. For detailed instructions on the preparation of manuscripts and of electronic artwork, consult the Author Gateway for Elsevier at http://authors.elsevier.com

ScienceDirect

Full text of this journal is available, on-line from **ScienceDirect**. Visit **www.sciencedirect.com** for more information.

Polyhedron 27, issue 13, 10 September 2008

Contents lists available at ScienceDirect

Polyhedron

journal homepage: www.elsevier.com/locate/poly

Contents

Papers

Dimitra Kovala-Demertzi, Alexandros Alexandratos, Athanassios Papageorgiou, Paras Nath Yadav, Panagiotis Dalezis and Mavroudis A. Demertzis

Polyhedron 27 (2008) 2731

Synthesis, characterization, crystal structures, *in vitro* and *in vivo* antitumor activity of palladium(II) and zinc(II) complexes with 2-formyl and 2-acetyl pyridine N(4)-1-(2-pyridyl)-piperazinyl thiosemicarbazone

The present paper includes synthesis and spectral characterization of the novel prepared palladium(II) and zinc(II) complexes with 2-formyl pyridine N(4)-1-(2-pyridyl)-piperazinyl Thiosemicarbazone, HFo4Npypipe, **1** and the 2-acetyl pyridine N(4)-1-(2-pyridyl)-piperazinyl thiosemicarbazone, HAc4Npypipe, **2**. The Pd(II) complexes [PdCl(Fo4Npypipe)], **3**, [PdCl(Ac4Npypipe)], **4** and the Zn(II) complexes [$ZnCl_2$(Fo4Npypipe)], **5** and [$ZnCl_2$(Ac4Npypipe)], **6** have been characterized by elemental analyses and spectroscopic studies. The crystal structure of the complexes [PdCl(Fo4Npippy)], **3** and [PdCl(Ac4Npippy)], **4**, have been solved by single-crystal X-ray diffraction. The results of the cytotoxic activity of **1**–**6** have been evaluated *in vitro* against the cells of three human cancer cell lines: MCF-7, T24, A-549 and a mouse L-929. For selected compounds **2** and **6** the acute toxicity and antitumor activity were evaluated on leukemia P388-bearing mice. The cytotoxic activity shown by these Zn(II) compounds **5** and **6** against MCF-7 and T24 cell lines indicate that coupling of **1** and **2** to Zn(II) metal center result in metallic complexes with important biological properties and remarkable cytotoxic activity, since they are display IC_{50} values in a μM range better to that of the antitumor drug *cis-platin*.

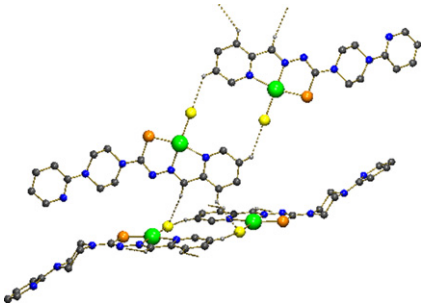

Hossein Dehghani and Mehrnoosh Babaahmadi

Polyhedron 27 (2008) 2739

Synthesis and characterization of intermediate sitting-atop (i-SAT) complexes of free base *meso*-tetraarylporphyrins and tin(IV) chloride

Meso-tetraarylporphyrins (H_2T(X)PP) and $SnCl_4$ leads to formation of intermediate sitting-atop (i-SAT) complexes, [$SnCl_4$(H_2T(X)PP)], that two nitrogen atoms of pyrrolic in the porphyrin core act as electron donors to a tin(IV) center and two pyrrolic protons remain on the macrocycle.

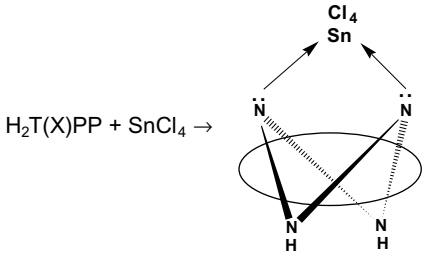

Viswanathan Mahalingam, Nataraj Chitrapriya, Frank R. Fronczek and Karuppannan Natarajan

Polyhedron 27 (2008) 2743

Dimethyl sulfoxide ruthenium(II) complexes of thiosemicarbazones and semicarbazone: Synthesis, characterization and biological studies

A family of new Cl–Ru(II)-dmso complexes of thiosemicarbazones along with benzaldehyde semicarbzone has been prepared and characterized. The benzaldehyde semicarbazone ligand has been obtained by the reaction of benzaldehyde and thiosemicarbazide in ethanol through water assisted conversion of C=S to C=O. The previously structurally uncharacterized [$RuCl_2$(dmso)$_2$(benzaldehyde semicarbazone)] complex has been characterized by single crystal XRD studies. The redox behavior of the complexes has been studied by cyclic voltammetry. The antibacterial activity and preliminary DNA-binding ability of the complexes has also been studied.

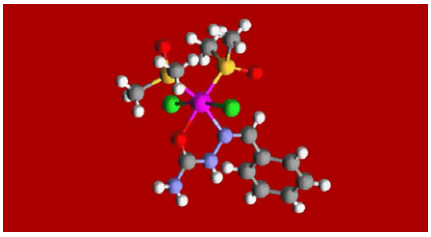

Elsevier Ltd.

Reena Singh, Coen de Graaf, Enrique Colacio and Kajal Krishna Rajak

Polyhedron 27 (2008) 2751

Mononuclear and binuclear iron(III) complexes incorporating N_4O_3 coordinating heptadentate ligand: Synthesis, structure and magnetic properties

The N_4O_3 coordinating heptadentate ligand afforded the mononuclear $[Fe^{III}(HL)][BPh_4]$ (**1**) and binuclear $[Fe_2^{III}L(OAc)_2][BPh_4]$ (**2**) complexes. In complex **1**, the ligand binds in a trianionic N_2O_3 fashion whereas in the case of **2** the ligand binds in the trianionic N_4O_3 form in which the iron ions are held together by μ-phenoxo and bis μ-acetato bridges. Complex **2** shows an intramolecular weak antiferromagnetic interaction. Gas phase geometry optimizations have been performed using density functional theory without any symmetry constraints.

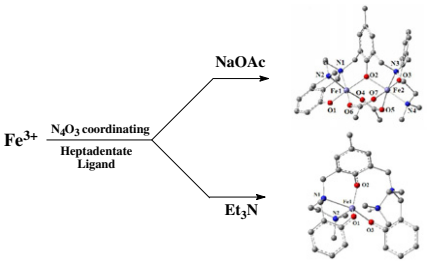

Shao-wu Wang, Hui-min Qian, Wei Yao, Li-jun Zhang, Shuang-liu Zhou, Gao-sheng Yang, Xian-cui Zhu, Jia-xi Fan, Yu-yu Liu, Guo-dong Chen and Hai-bin Song

Polyhedron 27 (2008) 2757

Synthesis of rare earth metal complexes incorporating amido and enolate mixed ligands: Characterization and reactivity

The reaction of 2,6-$(i\text{Pr})_2C_6H_3NHSiMe_3$ with excess *n*BuLi in THF, followed by treatment with $LnCl_3$, produced rare earth metal complexes incorporating amido and enolate mixed ligands.

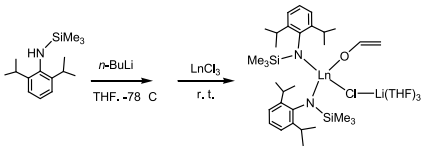

Iwona Łakomska, Andrzej Wojtczak, Jerzy Sitkowski, Lech Kozerski and Edward Szłyk

Polyhedron 27 (2008) 2765

Platinum(IV) complexes with purine analogs. Studies of molecular structure and antiproliferative activity *in vitro*

Here, we described the platimum(IV) complexes containing 1,2,4-triazolo[1,5-*a*]pyrimidine as carrier ligands. Their structures are characterized by multinuclear NMR, IR spectroscopy and X-ray analysis. The platinum(IV) complexation results in a large shielding of ^{15}N NMR signals of coordinated nitrogen atom (ca. 87–115 ppm) and proves that coordination of investigated 1,2,4-triazolo[1,5-*a*]pyrimidines occurs via N(3). In addition, $PtCl_4(dbtp)_2$ exhibits high cytotoxic activity and may be recommended for further preclinical studies.

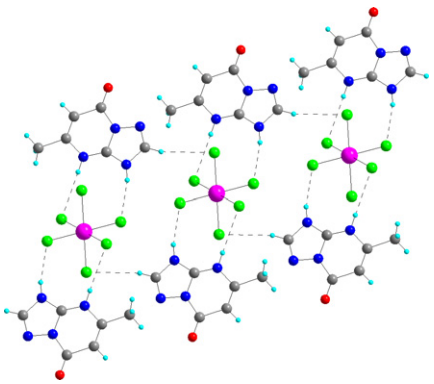

Soraia Meghdadi, Mehdi Amirnasr, Mohammad H. Habibi, Ahmad Amiri, Vahid Ghodsi, Azadeh Rohani, Ross W. Harrington and William Clegg

Polyhedron 27 (2008) 2771

Synthesis, structure, and electrochemistry of pyridinecarboxamide cobalt(III) complexes; the effect of bridge substituents on the redox properties

Co(III) complexes of two substituted pyridine carboxamide ligands, Mebpb and cbpb, with two axial amine ligands have been synthesized and structurally characterized. The effect of methyl and chloro substitution on the redox properties, and the sensitivity of the Co^{III}–Co^{II} redox potentials to the donor strength of the axial ligands have been investigated. The irreversible Co(III/II) redox process becomes quasi-reversible in the presence of excess amine. The two redox waves, resulting from the combination of Co^{II}–Co^{I} couple and the redox couple corresponding to one of the pyridyl rings, overlap in $[Co(Mebpb)(amine)_2]^+$, but are resolved in $[Co(cbpb)(amine)_2]^+$ complexes.

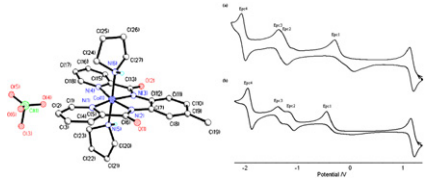

Carmen R. Maldonado, Miguel Quirós and Juan M. Salas

Polyhedron 27 (2008) 2779

Copper(II) complexes with 1,2,4-triazolo[1,5-*a*] pyrimidine and its 5,7-dimethyl derivative

The crystal structure of five mononuclear Cu(II) complexes containing 1,2,4-triazolo[1,5-*a*]pyrimidine (tp) or its 5,7-dimethyl derivative (dmtp) as main ligands and ethylenediamine or 1,10-phenanthroline as auxiliary ligands and the structure of a dinuclear compound with a μ-hydroxo and a N3,N4-bridging tp ligand are described.

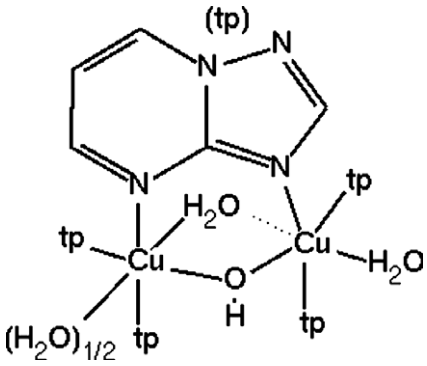

Yoshinobu Miyazaki, Hidenobu Matsuo, Takao Fujimori, Hiroyuki Takemura, Shiro Matsuoka, Tadashi Okobira, Kazuya Uezu and Kazuhisa Yoshimura

Polyhedron 27 (2008) 2785

Interaction of boric acid with salicyl derivatives as an anchor group of boron-selective adsorbents

The anion-exchange resin presorbed with 3,5-bis(hydroxymethyl)-4-hydroxybenzoate has a strong adsorbability of boron over a wide pH range. The boron species adsorbed onto the resin is predominantly present as the −3 charged 1:2 bischelate complex. The formation constant of the complex in the resin phase was estimated to be $10^{5.0}$, which almost agreed with those of the salicyl alcohol derivatives in aqueous solutions.

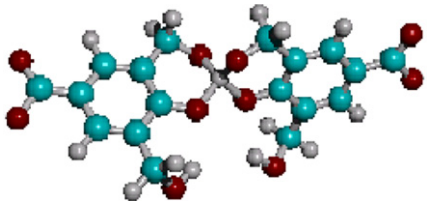

Geng-Geng Luo, Rong-Bin Huang, Jian-Hua Chen, Li-Rong Lin and Lan-Sun Zheng

Polyhedron 27 (2008) 2791

Diversity of coordination architecture of silver(I) complexes with different 2-aminopyrimidyl derivatives: Effect of counter anions and ligands

Five new luminescent silver(I) complexes have been prepared by reactions of varied silver(I) salts with a family of substituted 2-aminopyrimidyl and characterized by X-ray single-crystal diffraction. The results reveal that the nature of counter anions and the ligands have great influence on the formation and structure of metal–organic frameworks. In addition, the secondary forces such as hydrogen bonds also play important role in the overall architecture and stabilization of the complexes.

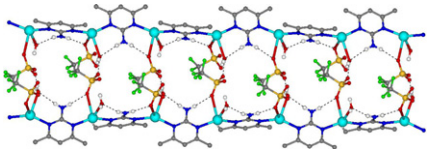

Gcineka Mbambisa and Tebello Nyokong

Polyhedron 27 (2008) 2799

Synthesis and electrochemical characterisation of a near infrared absorbing oxo vanadium(IV) octapentylthio-phthalocyanine

The cyclic voltammetry and spectroelectrochemistry of an α substituted phthalocyanine oxo vanadium(IV) octapentathiophthalocyanine which absorbs at 850 nm shows five redox couples which are all ring based.

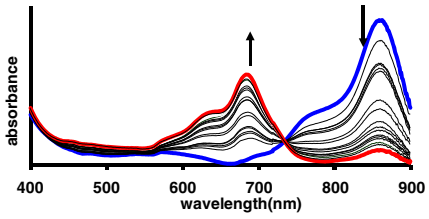

Selma Ünlü, Meryem N. Yaraşır, Mehmet Kandaz, Atıf Koca and Bekir Salih

Polyhedron 27 (2008) 2805

Synthesis, spectroscopy and electrochemical properties of highly soluble fluoro containing phthalocyanines

2(3),9(10),16(17),23(24)-Tetrakis-4′-[3,5-bis-(trifluoromethyl)phenoxy]-phthalocyanines, {M-[Pc-β(OBz-$(CF_3)_2$)$_4$]}, (M = Zn(II), Cu(II), Co(II) and Ni(II)) were synthesized and characterized by elemental analysis, FTIR, ^{1}H NMR, UV–Vis and MS (Maldi-TOF) spectral data. It is shown that 4-(3,5-bis(trifluoromethyl)-phenoxy) moieties on the periphery affect the solubility, spectroscopic data and electrochemistry of the tetrakis metallophthalocyanines. The electrochemical measurements of the complexes represent well-defined redox couples in harmony with common metallophthalocyanine complexes.

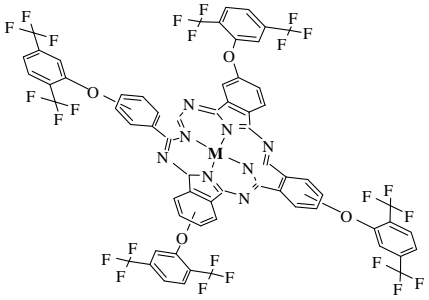

Natalia P. Kuzmina, Dmitry M. Tsymbarenko, Igor E. Korsakov, Zoya A. Starikova, Kostantin A. Lysenko, Olga V. Boytsova, Andrey V. Mironov, Irina P. Malkerova and Andrey S. Alikhanyan

Polyhedron 27 (2008) 2811

Mixed ligand complexes of AEE hexafluoroacetylacetonates with diglyme: Synthesis, crystal structure and thermal behavior

The synthesis, crystal structures and thermal behavior of the novel mixed ligand complexes [Ca(hfa)$_2$(diglyme)(H$_2$O)] (**I**), [Sr(hfa)$_2$(diglyme)(H$_2$O)] (**II**) and [Ba(hfa)$_2$(diglyme)$_2$] (**III**) (Hhfa – 1,1,1,5,5,5-hexafluoropentane-2,4-dione, diglyme – 2,5,8-trioxa-nonane) are described.

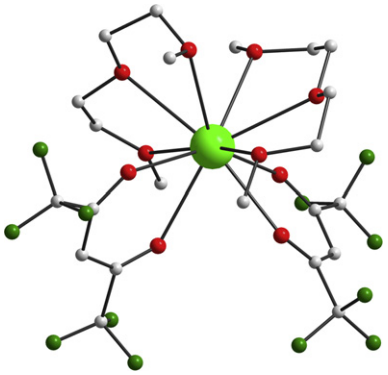

Klemens Noga, Piotr P. Romańczyk, Andrzej J. Włodarczyk and Ewa Broclawik

Polyhedron 27 (2008) 2819

Theoretical modeling of electrochemical interactions in bimetallic molybdenum nitrosyl complexes incorporating saturated bridges

DFT modeling for {Mo(NO)(Tp$^{3\text{-Me}}$)} binuclear complexes with ethane-1,2-diolate ligands provides direct evidence for electron localization in reduced species. Electron trapping is confirmed by geometric asymmetry, spin density distribution and the splitting of ν_{NO} stretching frequencies. In the doubly bridged complex 10% partial delocalization of unpaired electron occurs, while in the singly bridged one it is negligible.

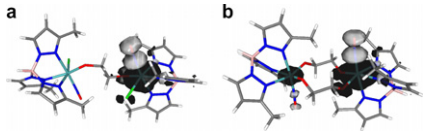

Olaf Kühl, Shanmuganathan Saravanakumar, Farman Ullah, Markus K. Kindermann, Peter G. Jones, Martin Köckerling and Joachim Heinicke

Polyhedron 27 (2008) 2825

Anellated *N*-heterocyclic carbenes: 1,3-Dineopentyl-benzimidazol-2-ylidene, structural aspects of C-protonated precursor salts and an AgCl complex

Access to 1,3-dineopentyl-benzimidazol-2-ylidene (**1**) by deprotonation of various benzimidazolium salts was studied. [Ag(**1**)Cl] was prepared from the corresponding benzimidazolium chloride. X-ray crystal structure analyses of benzo-, naphtho- and quinoxalino-anellated imidazolium salts are presented. Downfield shifts of the ^{13}C^{1}H(2) nuclei reflect the influence of electron-withdrawing anellation.

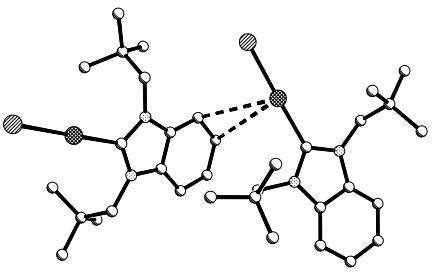

Bing-Qian Yao, Jia-Sen Sun, Zheng-Fang Tian, Xiao-Ming Ren, Da-Wei Gu, Lin-Jiang Shen and Jingli Xie

Polyhedron 27 (2008) 2833

Ion-pair charge transfer complexes with intense near IR absorption: Syntheses, crystal structures, electronic spectra and DFT calculations

Five ion-pair complexes, consisting of *R*-benzylidene-1-aminopyridinium derivatives with $[Ni(mnt)_2]^{2-}$ (R = *p*-nitro (**1**), *p*-methyl (**2**), *p*-bromo (**3**), *p*-chloro (**4**) and *m*-nitro (**5**); mnt^{2-} = maleonitriledithiolate), exhibit an intense absorption in near-IR region.

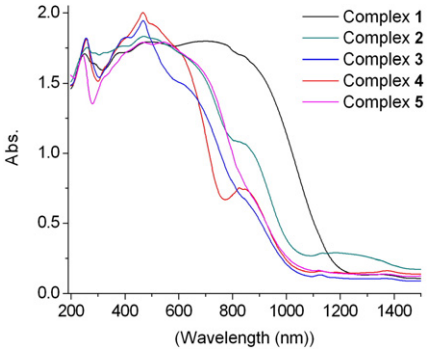

Jing Sun, Shuo Wu, Yan An, Jie Liu, Feng Gao, Liang-Nian Ji and Zong-Wan Mao

Polyhedron 27 (2008) 2845

Synthesis, crystal structure and DNA-binding properties of ruthenium(II) polypyridyl complexes with dicationic 2,2′-dipyridyl derivatives as ligands

Two new Ru(II) complexes with dicationic ligands, have been synthesized and structurally characterized. The interaction of both complexes with calf thymus DNA has been explored with UV–Vis, emission spectra, circular dichroic (CD) spectra, and viscosity measurements.

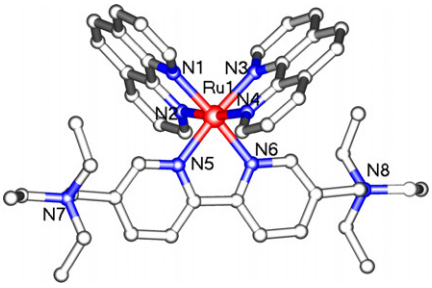

Juan J. Fiol, Angel García-Raso, Francisca M. Albertí, Andrés Tasada, Miquel Barceló-Oliver, Angel Terrón, María J. Prieto, Virtudes Moreno and Elies Molins

Polyhedron 27 (2008) 2851

Ruthenium(III) complexes with modified nucleobases: N^6-Substituted adenines

New chlorido-dimethylsulfoxide-ruthenium(III) complexes with different N^6-substituted adenines have been prepared and characterized. $[Ru^{III}Cl_4(DMSO)[H\text{-}(N^6\text{-pentyladenine})]]$, $[Ru^{III}Cl_4(DMSO)[H\text{-}(N^6\text{-hexyladenine})]]$ and $[Ru^{III}Cl_4(DMSO)[H\text{-}(N^6,N^6\text{-dibutyladenine})]]$ have been structurally characterized by single X-ray diffraction analysis. Preliminary electrophoretic mobility and atomic force microscopy (AFM) studies of the interaction between Ru(III) compounds and plasmidic DNA pBR322 have been performed.

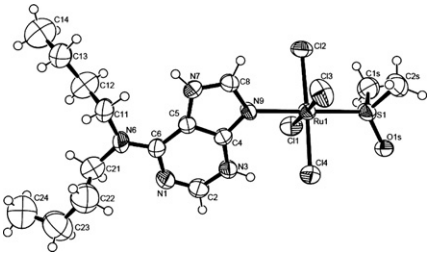

Patrina Paraskevopoulou, Eleftheria Petalidou, Alexandros Panas, Marinos Ioannou, Spyros Koinis, Nikolaos Psaroudakis, Nicholas Leventis, Pericles Stavropoulos and Konstantinos Mertis

Polyhedron 27 (2008) 2859

Redox reactivity and comprehensive synthetic chemistry of the perchloroditungstate $[W_2(\mu\text{-}Cl)_3Cl_6]^{n-}$ (*n* = 3, 2, 1) anions in organic media

New simple high-yield synthetic routes for complexes **2a**,**b** and **3a**,**b**, otherwise not easily accessible, have been developed and their redox chemistry in organic media is presented. Their facile chemical or electrochemical redox interconversion in conjunction to their stability and the ability of **3** to oxidize alcohols ($PhCH_2OH \rightarrow PhCHO$), while it is reduced to **2**, makes the W_2^{n+} (*n* = 6, 7) couple functional and of potential utility in catalytic oxidations of organic substrates.

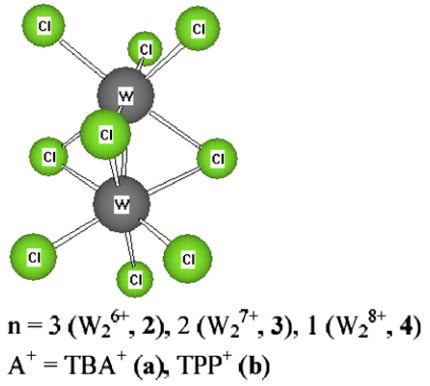

Ara Núñez-Montenegro, Rosa Carballo and Ezequiel M. Vázquez-López

Polyhedron 27 (2008) 2867

Synthesis and characterization of thiosemicarbazone derivatives of 2-ethoxy-3-methoxybenzaldehyde and their rhenium(I) complexes

New thiosemicarbazone ligands (HL) have been prepared and their reaction with *fac*-[ReX(CO)3(CH3CN)2] gave the adducts [ReX(CO)3(HL)] (**1**). The thiosemicarbazonate complexes [Re2(L)2(CO)6] (**2**) were also obtained by reaction of the adducts with NaOH. In both compounds ligand is S,N-bidentate and in **2**, dimer structures are formed by Re–S–Re bridges.

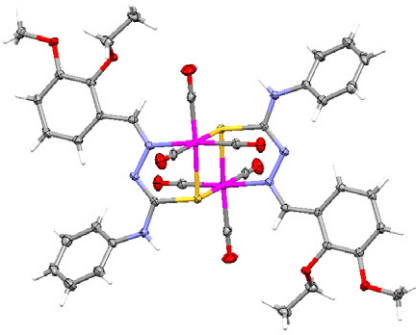

Sanjay Kumar Singh, Santosh Kumar Dubey, Rampal Pandey, Lallan Mishra, Ru-Qiang Zou, Qiang Xu and Daya Shankar Pandey

Polyhedron 27 (2008) 2877

Ruthenium(II), rhodium(III) and iridium(III) based effective catalysts for hydrogenation under aerobic conditions

The cationic mononuclear complexes [(η^6-arene)Ru(Ph-BIAN)Cl]BF_4 [η^6-arene = benzene (**1**), *p*-cymene (**2**)], [(η^5-C_5H_5)Ru(Ph-BIAN)PPh_3]BF_4 (**3**) and [(η^5-C_5Me_5)M(Ph-BIAN)Cl]BF_4 [M = Rh (**4**), Ir (**5**)] incorporating 1,2-bis(phenylimino)-acenaphthene (Ph-BIAN) have been prepared and characterized. Complexes **1**–**5** effectively catalyze the reduction of terephthalaldehyde in the presence of HCOOH/CH_3COONa in water under aerobic conditions.

Suman Mukhopadhyay, Jamal Lasri, M. Fátima C. Guedes da Silva, M. Adília Januário Charmier and Armando J.L. Pombeiro

Polyhedron 27 (2008) 2883

Activation of C–CN bond of propionitrile: An alternative route to the syntheses of 5-substituted-1*H*-tetrazoles and dicyano-platinum(II) species

Reaction of the tetrazolato complexes *trans*-[$Pt(N_4CR)_2(PPh_3)_2$] (R = alkyl, aryl) with EtCN gives *trans*-[$Pt(CN)_2(PPh_3)_2$] along with the corresponding 5-substituted-1*H*-tetrazoles N_4CR, *via* an unusual NC–C bond cleavage of propionitrile.

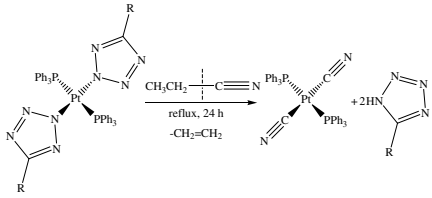

Bianca Antonioli, David J. Bray, Jack K. Clegg, Kerstin Gloe, Karsten Gloe, Anne Jäger, Katrina A. Jolliffe, Olga Kataeva, Leonard F. Lindoy, Peter J. Steel, Christopher J. Sumby and Marco Wenzel

Polyhedron 27 (2008) 2889

Interaction of copper(II) and palladium(II) with linked 2,2′-dipyridylamine derivatives: Synthetic and structural studies

The interaction of Cu(II) and Pd(II) with linked dipyridylamine derivatives in both the solid state and solution has been investigated; these ligands yield a diverse range of coordination geometries and lattice architectures.

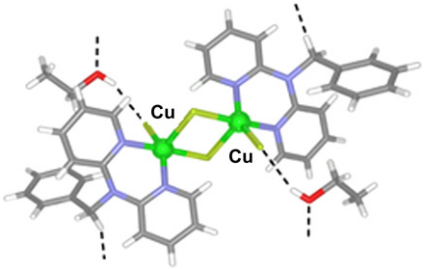

Biswajit Dey, Somnath Ray Choudhury, Suranjana Das, Atish Dipankar Jana, Li-Ping Lu, Miao-Li Zhu, Amitava Dutta and Subrata Mukhopadhyay

Polyhedron 27 (2008) 2899

A tridentate *in situ* generated ligand that directs the self-assembly of a transition metal complex: Synthesis and structural characterization of *cis*-dichloro[1-(2-aminoethyl)biguanide]copper(II) monohydrate

A tridentate ligand that can be prepared *in situ* in the presence of Cu(II) leads to an interesting crystalline solid. The single lattice water molecule played an important role in the formation of 2D supramolecular sheets and become an integral part of such self-assembled structure.

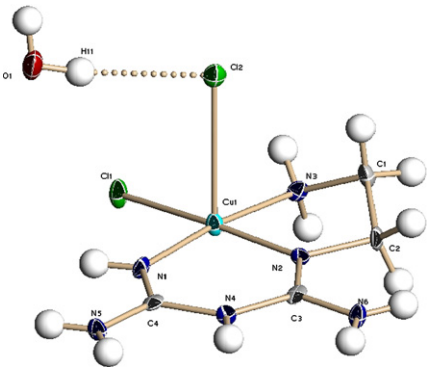

Ana Maria Preda, Anca Silvestru, Sorin Farcas, Alina Bienko, Jerzy Mrozinski and Marius Andruh

Polyhedron 27 (2008) 2905

New manganese(II) complexes with tetraorganodichalcogenoimidodiphosphinato ligands. Crystal and molecular structure of monomeric $Mn[(SPMe_2)(SPPh_2)N]_2$ and dimeric $[Mn\{(OPPh_2)\{OP(OEt)_2\}N\}_2(H_2O)]_2$

$Mn[(XPR_2)(YPR'_2)N]_2$ [X, Y = S, R = Me, R′ = Ph (**1**), X = S, Y = O, R = Ph, R′ = OEt (**2**)] and $M_n[(OPPh_2)\{OP(OEt)_2\}N]_2$ (H_2O) (**3**) were obtained from $MnCl_2 \cdot 4H_2O$ and $K[(XPR_2)(YPR'_2)N]$. The complexes were characterized by EPR, IR and MS, and the structures of **1** and **3** were established by single-crystal X-ray diffraction. The magnetic behaviour of **3** was investigated.

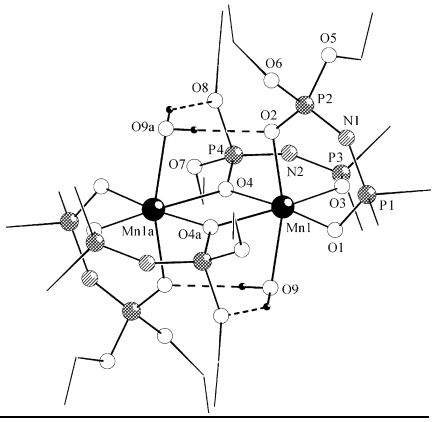

Catherine Gabriel, Melita Menelaou, Markos Daskalakis, Andrea Lakatos, Tamas Kiss, Constantin Mateescu, Raphael G. Raptis, Panagiotis Zoumpoulakis and Athanasios Salifoglou

Polyhedron 27 (2008) 2911

Synthetic, structural, spectroscopic and solution speciation studies of the binary Al(III)–quinic acid system. Relevance of soluble Al(III)–hydroxycarboxylate species to molecular toxicity

Reaction of Al(III) with D-(−)-quinic acid (pH 4.0), has led to the isolation of a new complex $K[Al(C_7H_{11}O_6)_3] \cdot (OH) \cdot 4H_2O$ (**1**). Complex **1** has been characterized by analytical, spectroscopic (FT-IR, NMR) and thermal techniques. X-ray crystallography reveals a mononuclear octahedral Al(III) bound by three quinates. The collective solid-state and aqueous solution studies formulate the physicochemical profile of **1** in the aqueous Al(III)–quinate speciation and shed light onto Al(III) binary interactions with O-containing substrates influencing molecular toxicity.

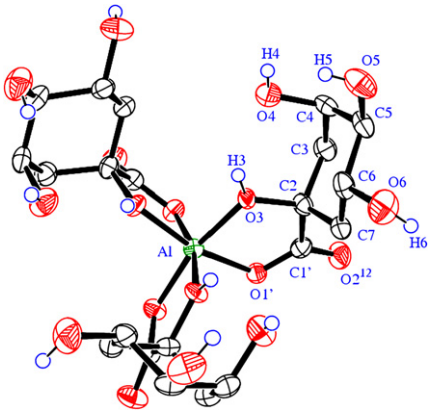

Susana Balboa, Rosa Carballo, Alfonso Castiñeiras, Josefa María González-Pérez and Juan Niclós-Gutiérrez

Polyhedron 27 (2008) 2921

Mononuclear, dinuclear and hydroxo-bridged tetranuclear complexes from reactions of Cu^{II} ions, mandelic acid and diimine ligands

Four novel coordination compounds $[Cu(bpy)(\mu_2\text{-MANO})]_2 \cdot 8H_2O$ (**1**), $[Cu(bpy)(MANO)] \cdot 4H_2O$ (**2**), $[Cu_4(\mu_3\text{-}OH)_2(\mu_2\text{-MANO})_2(bpy)_4](phglyo)_2 \cdot 8H_2O$ (**3**) and $[Cu_4(\mu_3\text{-}OH)_2(\mu_2\text{-}OH)_2(OH_2)_2(phen)_4](Bza)_2(OH)_2 \cdot 5H_2O$ (**4**) have been synthesized from diimine ligands, mandelic acid and Cu^{II} ions. In **3** and **4**, phenylglyoxylate or benzoate, respectively, are obtained by dehydrogenation or oxidative dehydrogenation followed by oxidative decarboxylation of mandelic acid.

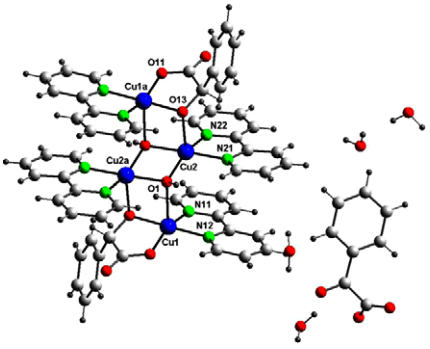

S. Sreedaran, K. Shanmuga Bharathi, A. Kalilur Rahiman, L. Jagadish, V. Kaviyarasan and V. Narayanan

Polyhedron 27 (2008) 2931

Novel unsymmetrical macrocyclic dicompartmental binuclear copper(II) complexes bearing 4- and 6-coordination sites: Electrochemical, magnetic, catalytic and antimicrobial studies

A series of novel unsymmetrical dicompartmental binuclear copper(II) complexes have been prepared by a simple Schiff-base condensation of the compound 1,8-[bis(3-formyl-2-hydroxy-5-methyl)benzyl]-l,4,8,11-tetraazacyclotetradecane (L) with the appropriate aliphatic or aromatic diamine, copper(II) perchlorate and triethylamine.

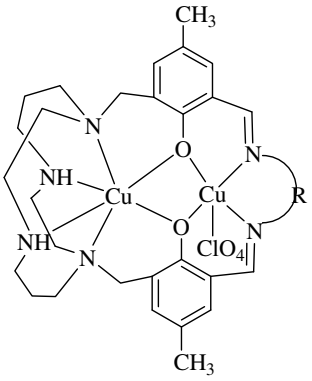

Kazuhiro Uemura, Akihisa Maeda and Hidetoshi Kita

Polyhedron 27 (2008) 2939

Syntheses and crystal structures of straight or zigzag one-dimensional coordination polymers based on Cu(II) square pyramidal or Cu(I) tetrahedral coordination environments

Two copper coordination polymers, $[Cu(SO_4)(pyz)(H_2O)]_n$ (**1**) and $[Cu_2(SO_4)(pyz)_2(H_2O)_2]_n$ (**2**) (pyz = pyrazine), have been synthesized in H_2O at different temperatures, and characterized by single X-ray analyses. Compounds **1** and **2** form one-dimensional chains with straight or zigzag configurations, which are attributed to their respective oxidation states, i.e., Cu(II) and Cu(I).

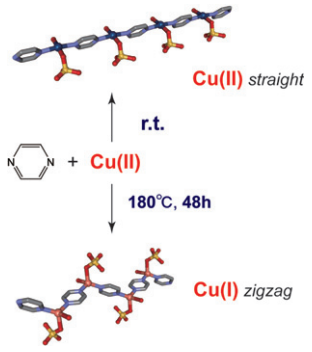

Semanti Basu, Sarmistha Halder, Indrani Pal, Saheli Samanta, Parimal Karmakar, Michael G.B. Drew and Samaresh Bhattacharya

Polyhedron 27 (2008) 2943

1-(2′-Pyridylazo)-2-naphtholate complexes of ruthenium: Synthesis, characterization, and DNA binding properties

Reaction of 1-(2′-pyridylazo)-2-naphthol (Hpan, **1**) with $[Ru(dmso)_4Cl_2]$, $[Ru(trpy)Cl_3]$, $[Ru(bpy)Cl_3]$ and $[Ru(PPh_3)_3Cl_2]$ in refluxing ethanol in the presence of a base (NEt_3) affords, respectively, the $[Ru(pan)_2]$, $[Ru(trpy)(pan)]^+$, $[Ru(bpy)(pan)Cl]$ and $[Ru(PPh_3)_2(pan)Cl]$ complexes, where the pan ligand is bound to ruthenium as monoanionic N,N,O-donor (**2**).

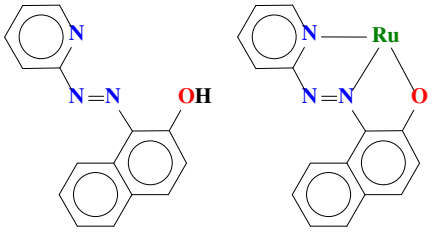

1 **2**

Barbara Kurzak, Anna Kamecka, Katarzyna Bogusz and Julia Jezierska

Polyhedron 27 (2008) 2952

Stabilities and coordination modes of histidine in copper(II) mixed-ligand complexes with ethylenediamine, diethylenetriamine or *N*,*N*,*N*′,*N*″,*N*″-pentamethyldiethylenetriamine in aqueous solution

Solution equilibrium studies on the Cu(II)–polyamine–histidine ternary systems (polyamine: ethylenediamine, diethylenetriamine, *N*,*N*,*N*′,*N*″,*N*″-pentamethyldiethylenetriamine) have been performed by pH-potentiometry, UV–Vis spectrophotometry and EPR methods. Our spectroscopic results indicate the tetragonal geometry for the $[Cu(en)(His)]^+$, the geometry slightly deviated from square pyramidal for the $[Cu(dien)(His)]^+$ and strongly deviated from square pyramidal towards trigonal bipyramidal for the $[Cu(Me_5dien)(His)]^+$ species.

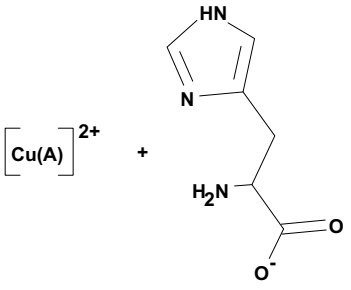

B. Machura, A. Świtlicka, R. Kruszynski, J. Mroziński, J. Kłak and J. Kusz

Polyhedron 27 (2008) 2959

Coordination studies of 5,6-diphenyl-3-(2-pyridyl)-1,2,4-triazine towards Cu^{2+} cation. X-ray studies, spectroscopic characterization and DFT calculations

The reactions of 5,6-diphenyl-3-(2-pyridyl)-1,2,4-triazine with $CuCl_2 \cdot 2H_2O$, $Cu(NO_3)_2 \cdot 3H_2O$ and $CuSO_4 \cdot 5H_2O$ have been examined, and four $[CuCl_2(dppt)]$ (**1**), $[CuCl_2(dppt)_2] \cdot 2MeOH$ (**2**), $[Cu(dppt)_2(H_2O)_2](NO_3)_2$ (**3**) and $[Cu(SO_4)(dppt)(H_2O)]_n \cdot nH_2O$ (**4**) complexes have been obtained. All the complexes have been structurally and spectroscopically characterized, and compound **4** has been additionally studied by magnetic measurement. The electronic structure of **1** has been calculated with the density functional theory (DFT) method, and the time-dependent DFT calculations have been employed to calculate the electronic spectrum of **1**.

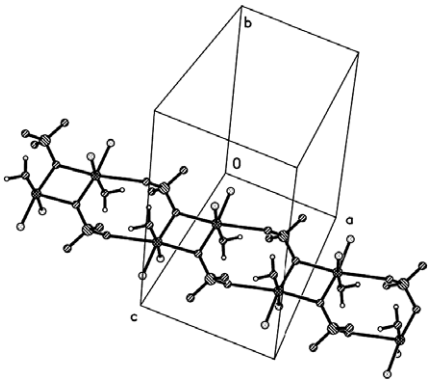

W. Marjit Singh and Jubaraj B. Baruah

Polyhedron 27 (2008) 2968

Nickel, copper and zinc complexes of (2-methoxycarbonylmethylimino-5-methyl-thiazol-3-yl)-acetic acid

A disodium salt of (2-methoxycarbonylmethylimino-5-methyl-thiazol-3-yl)-acetic acid has been prepared from a thiamine derivative. This salt forms mononuclear or polynuclear complexes with nickel(II), copper(II) and zinc(II). In the mononuclear complex the dicarboxylate acts as a tridentate ligand, whereas in the polynuclear complex it acts as a tetradentate ligand.

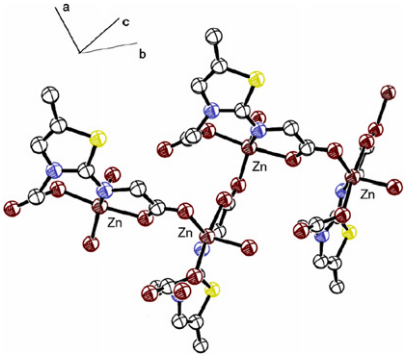

Abedien Zabardasti and Ali Kakanejadifard

Polyhedron 27 (2008) 2973

Theoretical study of hydrogen bonded clusters of water and cyanic acid: Hydrogen bonding in terms of the molecular structure

Ab initio and density functional calculations were used to analyze the interaction between a molecule of cyanic acid (HOCN) and up to 4 molecules of water at the B3LYP/6-311++G(d,p) and MP2/6-311++G(d,p) computational levels. The cooperative effect (CE) is increased with the increasing size of the studied clusters. Red shifts of the H–O stretching frequency for complexes involving HOCN as an H-donor were predicted. The strength of the hydrogen bonds in terms of molecular structures could be deduced from a comparison of HOCN–H_2O with HCNO–H_2O, HONC–H_2O and HNCO–H_2O HB clusters. The atom in molecules (AIM) method was used to analyze the cooperative effects on topological parameters.

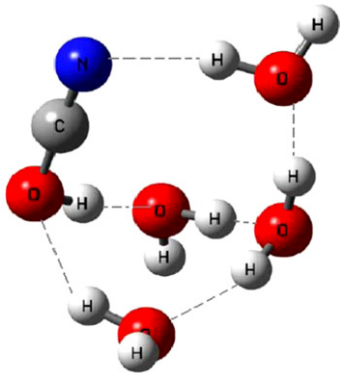

Damir A. Safin, Maria G. Babashkina, Timur R. Gimadiev, Michael Bolte, Marina V. Pinus, Dmitriy B. Krivolapov and Igor A. Litvinov

Polyhedron 27 (2008) 2978

Complexes of *N*-thiophosphorylthiourea $(EtO)_2P(O)CH_2C_6H_4$-4-[NHC(S)NHP(S)(O*i*Pr)$_2$] with Zn(II), Cd(II), Co(II) and $Cu(PPh_3)(I)$

Reaction of *O,O*'-diisopropylthiophosphoric acid isothiocyanate $(iPrO)_2P(S)NCS$ with diethyl 4-aminobenzylphosphonate $(EtO)_2P(O)CH_2C_6H_4$-4-NH_2 leads to the new *N*-thiophosphorylated thiourea $(EtO)_2P(O)CH_2C_6H_4$-4-[NHC(S)NHP(S)-(O*i*Pr)$_2$] (**HL**). Reaction of the potassium salt of **HL** with Zn(II), Cd(II) and Co(II) in aqueous EtOH leads to complexes of formula M(L-*S*,*S*')$_2$ (**ML$_2$**). Heteroligand copper(I) complex of **HL** and triphenylphosphine was prepared by the reaction of the potassium salt **KL** and $Cu(PPh_3)_3I$. Copper in complex **Cu(PPh$_3$)L** is bound by one PPh_3 and one SCNPS fragmnet of the chelating ligand. Compounds obtained were investigated by IR, UV–Vis, ^1H and $^{31}P\{^1H\}$ NMR spectroscopy, and microanalysis. The structures of **HL** and **Cu(PPh$_3$)L** were investigated by single crystal X-ray diffraction analysis.

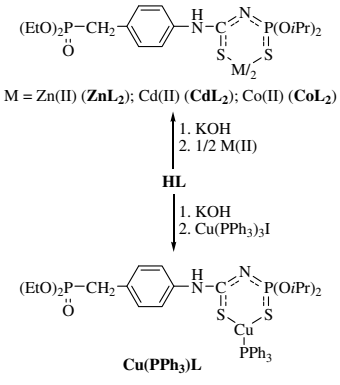

André Gustavo de A. Fernandes, Pedro Ivo da S. Maia, Elizeu J. de Souza, Sebastião S. Lemos, Alzir A. Batista, Ulrich Abram, Javier Ellena, Eduardo E. Castellano and Victor M. Deflon

Polyhedron 27 (2008) 2983

Rhenium chelate complexes with maltolate or kojate

A series of rhenium(V) complexes containing maltolate (mal) or kojate (koj) as ligand have been synthesized. The compounds [ReOCl(mal)$_2$], [ReOCl$_2$(mal)(PPh$_3$)], [ReOBr$_2$(mal)(PPh$_3$)], [ReOCl$_2$(koj)(PPh$_3$)] and [ReOBr$_2$(koj)(PPh$_3$)] were characterized by elemental analyses, IR, multinuclear NMR (^{1}H, ^{13}C and ^{31}P) and single crystal X-ray diffraction studies.

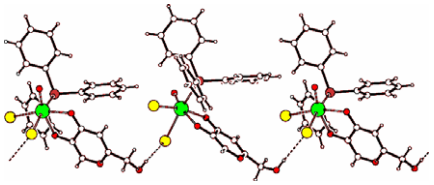

Gaston Pourrieux, Florencia Fagalde, Néstor E. Katz, Teodor Parella, Jordi Benet-Buchholz and Antoni Llobet

Polyhedron 27 (2008) 2990

Synthesis, spectroscopic and electrochemical characterization and molecular structure of polypyridyl ruthenium complexes containing 4,4′-azobis(pyridine)

New mononuclear and dinuclear polypyridyl ruthenium(II) complexes containing 4,4′- azpy have been synthesized and characterized by spectroscopic, X-ray diffraction and electrochemical techniques. In the mixed-valent asymmetric complex with pentaammineruthenium(III) as an electron acceptor, a relatively strong metal–metal coupling is disclosed, pointing to possible applications of 4,4′-azpy in "molecular wires".

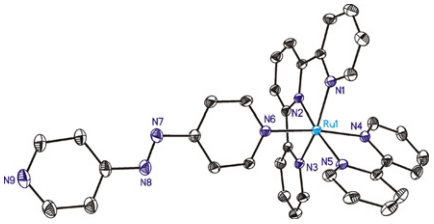

Matthew R. Montney, Ronald M. Supkowski and Robert L. LaDuca

Polyhedron 27 (2008) 2997

Three-dimensional acentric coordination polymers formed from the linkage of cobalt and nickel malonate quadratic layers through a kinked organodiimine: Synthesis, structure, thermal properties and magnetochemistry

A pair of isostructural acentric 3-D coordination polymers {[M$_2$(malonate)$_2$(dpa)(H$_2$O)$_2$] · 2H$_2$O}$_n$ (M = Co, **1**; M = Ni, **2**; dpa = 4,4′-dipyridylamine) with 3-D sqp network topology have been synthesized. Antiferromagnetic coupling was observed within the malonate-bridged layer motifs in **1**; in contrast, **2** exhibited ferromagnetic coupling.

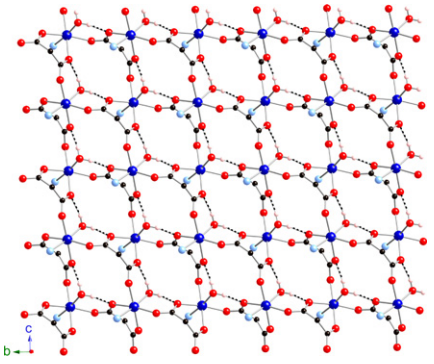

Ji-Eun Lee, Jai Young Lee, Joobeom Seo, So Young Lee, Hyun Jee Kim, Sunhong Park, Ki-Min Park, Leonard F. Lindoy and Shim Sung Lee

Polyhedron 27 (2008) 3004

Comparative structural study of the complexation behaviour of silver(I), cadmium(II), mercury(II), and palladium(II) with a 17-membered N_3O_2-donor macrocycle

An investigation of the coordination behaviour of the N_3O_2 macrocycle, **L**, with Ag(I), Cd(II), Hg(II), and Pd(II) is reported. The X-ray structures of 12 complexes were determined and a range of structural types, including mono- and dinuclear species, shown to occur.

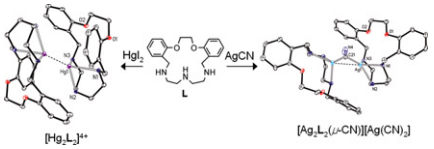

B. Machura, J. Mroziński, R. Kruszynski and J. Kusz

Polyhedron 27 (2008) 3013

Seven-coordinate rhenium(III) complexes of 1-(2-pyridylazo)-2-naphtholate: X-ray studies, spectroscopic characterization and DFT calculations

The reactions of $[ReX_3(MeCN)(PPh_3)_2]$ (X = Cl or Br) with 1-(2-pyridylazo)-2-naphthol (HPAN) have been examined and the $[ReBr(PAN)_2]\cdot 2CHCl_3$ (**1**) and $[ReCl(PAN)_2]$ (**2**) complexes have been obtained. The both complexes have been structurally and spectroscopically characterized, and compound **1** has been additionally studied by magnetic measurements. The magnetic behavior is characteristic of mononuclear seven-coordinated Re(III) complex with d^4 low-spin configuration, which gives diamagnetic ground state. The electronic structure of $[ReBr(PAN)_2]$ has been calculated with the density functional theory (DFT) method. The time-dependent DFT calculations have been employed to calculate the electronic spectrum of $[ReBr(PAN)_2]$, and the UV–Vis spectra of the $[ReX(PAN)_2]$ compounds have been discussed on this basis.

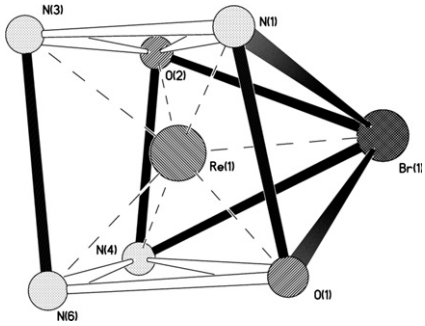

T.K. Mondal, S.K. Sarker, P. Raghavaiah and C. Sinha

Polyhedron 27 (2008) 3020

Ruthenium–carbonyl complexes of 1-alkyl-2-(arylazo)imidazoles: Synthesis, structure, spectra and redox properties

$[Ru(CO)_2Cl_2(PaiR/TaiR)]$ are described in this work where PaiR or TaiR are 1-alkyl-2-(arylazo)imidazoles, acting as imidazole-N, azo-N chelating agents. One of the structures, $[Ru(CO)_2Cl_2(PaiEt)]$, has been characterized by its X-ray structure determination, which shows a *trans*-(Cl,Cl) arrangement. Addition of excess Me_3NO has synthesized the mono-carbonyl complex, $[Ru(CO)Cl_2(PaiR/TaiR)(NCMe)]$. The electronic spectra and redox properties of the complexes have been supported by DFT and TD-DFT calculations.

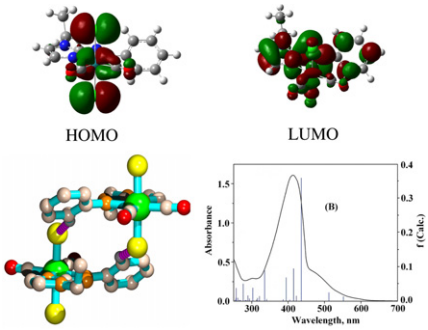

P. Aslanidis, P.J. Cox and P. Tsaliki

Polyhedron 27 (2008) 3029

Copper(I) halide complexes with 2,2′-bis(diphenylphosphano)-1,1′-binaphthyl (rac-binap) and heterocyclic thiones. Racemic compounds in chiral and achiral crystal space groups

Mixed-ligand complexes of the formula [CuX(binap)(thione)] are formed by the reaction between equimolar amounts of CuX, binap and a heterocyclic thione. The molecular structures of $[CuBr(rac\text{-}binap)(py2SH)]\cdot 2CH_2Cl_2$, $[CuBr(S\text{-}binap)(py2SH)]\ CH_2Cl_2$ and $[CuBr(S\text{-}binap)(dmpymtH)]\ CH_2Cl_2$, established by single-crystal X-ray diffraction, feature a rigid distorted tetrahedral copper(I) center with the diphosphane acting in a chelating fashion. The complexes are strongly luminescent at room temperature in the solid state.

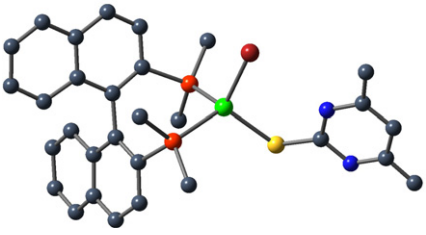

Aminou Mohamadou, Christian Gerard and Jérôme Marrot

Polyhedron 27 (2008) 3036

Syntheses, crystal structures, and properties of Ni(II) and Co(III) complexes derived from tripod polypyridine ligands containing N_7 or N_6 donor set atoms

The reaction of Ni^{2+} and Co^{2+} ions with tripod heptadentate pbpaen ligand in ethanol gives octahedral $[Ni^{II}(pbpaen)](ClO_4)_2$ and $[Co^{III}(pbpaen)](ClO_4)_3$ complexes. In acidic medium (pH ≈ 4), only the Co^{2+} ion gives an octahedral $[Co^{III}(bpaen)](ClO_4)_3$ compound in which one pyridylmethyl group of tripod pbpaen ligand has been eliminated giving new bpaen ligand.

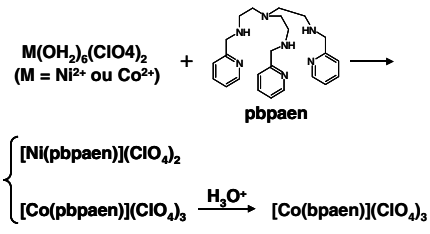

Neil F. Curtis, Rebekah Pawley and Ward T. Robinson

Polyhedron 27 (2008) 3041

The synthesis and structure of *trans*-di(cyano-κ^1)-(*trans*-6,13-dimethyl-6,13-bis(propionylamido)-1,4,8,11-tetraazacyclotetradecane-κ^4)cobalt(III) perchlorate dihydrate

The preparation and structure of *trans*-di(cyano-κ^1)-(*trans*-6,13-dimethyl-6,13-bis(propionylamido)-1,4,8,11-tetraazacyclotetradecane-κ^4)-cobalt(III) perchlorate dihydrate, formed by reaction of *trans*-$[Co(diam)(CN)_2]ClO_4 \cdot 2H_2O$ (diam = *trans*-6,13-diamino-6,13-dimethyl-1,4,8,11-tetraazacyclotetradecane) with propionic anhydride in DMF, are reported.

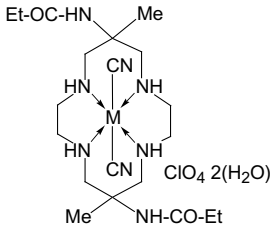

Ryszard Kubiak, Jan Janczak, Małgorzata Śledź and Ewa Bukowska

Polyhedron 27 (2008) 3044

Structural effect of the competition of 4-picoline and water molecules to form complexes with Be, Mg and Zn phthalocyanines

Crystals of monoaxially coordinated by 4-picoline BePc (BePc(4-Mepy)) and biaxially ligated MgPc (MgPc(4-Me)2) complexes transform in wet 4-picoline into aqua(phthalocyaninato) complexes, while monoaxially ligated ZnPc (ZnPc(4-Mepy)) transforms into microcrystalline β-ZnPc. Depending on the crystallisation condition two crystalline form of aqua(magnesium)phthalocyaninato complexes containing different number of 4-picoline molecules as a solvent in the crystalline network are obtained.

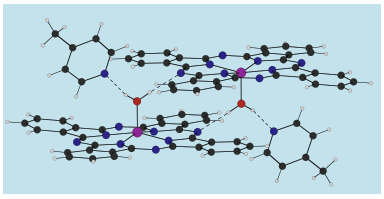

Barbara Kurzak, Agnieszka Woźna, Anna Kamecka and Krzysztof Kurzak

Polyhedron 27 (2008) 3053

Coordination properties of some nickel(II) monophosphono dipeptides species in aqueous solution: The role of phosphonic oxygen in complex stabilization and ligand-fields analysis

Equilibrium studies on the nickel(II) complexes of some monophosphono dipeptides were performed by potentiometric titration and NIR–Vis spectroscopy. The ligand-field parameters (CFM/AOM) were estimated and discussed. The lowest tetragonal distortion was observed in the case of the [NiHL] species, whereas the strongest in the $[NiL_2]$ species. In nickel(II) complexes with Gly-(Bz)Cys(P) additional interaction between sulfur and nickel(II) was suggested.

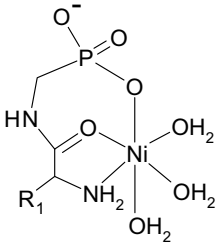

The Publisher encourages the submission of articles in electronic form thus saving time and avoiding rekeying errors. For detailed instructions on the preparation of manuscripts and of electronic artwork, consult the Author Gateway for Elsevier at http://authors.elsevier.com

ScienceDirect

Full text of this journal is available, on-line from **ScienceDirect**. Visit **www.sciencedirect.com** for more information.

Available online at www.sciencedirect.com
ScienceDirect
Polyhedron 27, issue 2, 6 February 2008
POLYHEDRON
www.elsevier.com/locate/poly

Contents

Papers

Moamen S. Refat, Lamia A. El-Zayat and Okan Zafer Yeşilel

Polyhedron 27 (2008) 475

Synthesis and spectroscopic characterization of piperidine/chloranil and piperidine/7,7′,8,8′-tetracyanoquinodimethane charge transfer complexes: X-ray crystal structure of a 7,7-dicyano-8,8-di-piperidinoquinodimethane adduct

Charge transfer reactions of piperidine with *p*-chloranil (CHL) and 7,7′,8,8′-tetracyanoquinodimethane (TCNQ) in chloroform have been synthesized and characterized. The asymmetric unit of 7,7-dicyano-8,8-di-piperidinoquinodimethane adduct composed of two crystallographic independent $[(pip)_2TCNQ]_2$. The piperidine rings of each of the two independent molecules exhibits a chair conformation, while TCNQ fragment is nearly planer.

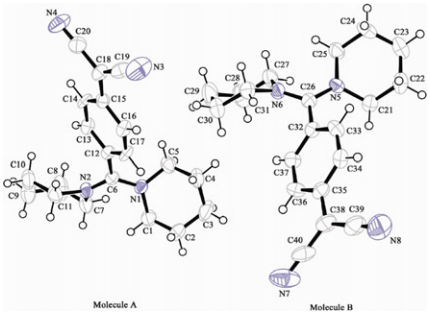

Arun Kumar, Monika Agarwal and Ajai K. Singh

Polyhedron 27 (2008) 485

Selenated Schiff bases of 2-hydroxyacetophenone and their palladium(II) and platinum(II) complexes: Syntheses, crystal structures and applications in the Heck reaction

Selenated Schiff bases 2-HO-$C_6H_4C(CH_3)$=$N(CH_2)_nSePh$ (n = 2, $\mathbf{L}^1$; n = 3, $\mathbf{L}^2$) and their complexes, [Pd($\mathbf{L}^1$–H)Cl] (**1**), [Pt($\mathbf{L}^1$–H)Cl] (**2**), [Pd($\mathbf{L}^2$–H)Cl] (**3**) and [Pt($\mathbf{L}^2$)Cl_2] (**4**), have been synthesized and characterized with proton carbon-13 and selenium-77 NMR spectra. On coordination of $\mathbf{L}^1$ and $\mathbf{L}^2$ the signals in the $^{77}Se\{^1H\}$ spectra undergo deshielding (by up to ~158 ppm). The single-crystal structures of $\mathbf{L}^1$, $\mathbf{L}^2$, **1** and **2** were solved. In the square planar complexes **1** and **2**, Pd/Pt–Se bond distances are 2.3683(11)–2.3654(10)/2.3549(15)–2.3536(17) Å. Complexes **1** and **2** are the first examples of crystal structures of Pd and Pt complexes of a (Se, N, O^-) ligand. Complex **1** catalyzes the Heck type C–C coupling reaction.

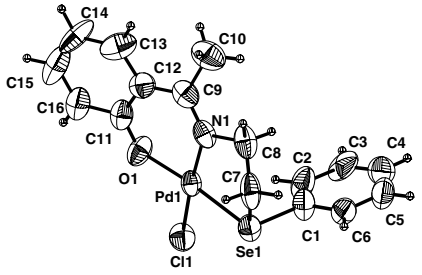

Elaine A. Medlycott, Garry S. Hanan, Tareque S.M. Abedin and Laurence K. Thompson

Polyhedron 27 (2008) 493

The effect of steric hindrance on the Fe(II) complexes of triazine-containing ligands

Fe(II) complexes based on ligands containing a 1,3,5-triazine core display dia- and paramagnetic behaviour depending on the triazine substituents.

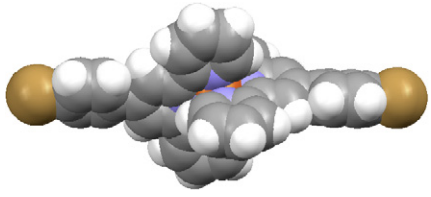

Ana C. González-Baró, Reinaldo Pis-Diez, Oscar E. Piro and Beatriz S. Parajón-Costa

Polyhedron 27 (2008) 502

Crystal structures, theoretical calculations, spectroscopic and electrochemical properties of Cr(III) complexes with dipicolinic acid and 1,10-phenantroline

The synthesis and physicochemical study of two chromium compounds of stoichiometry $Cr[(dipic)_2] \cdot 2H_2O$ and $[Cr(dipic)(phen)Cl] \cdot 1/2H_2O$ are presented. They were characterized by single crystal X-ray diffraction methods, FTIR, Raman, electronic spectroscopy and cyclic voltammetry. Theoretical calculations were also performed. The optimized geometries were compared with crystallographic data. The experimental spectra were assigned with the help of calculated frequencies.

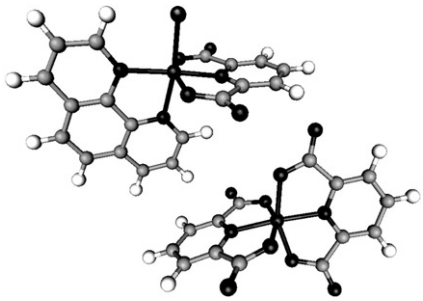

Seigi Suh, Liliana A. Mîinea, Saba Javed and David M. Hoffman

Polyhedron 27 (2008) 513

Synthesis of ethyl zinc fluoroalkoxide complexes and the crystal structure of $[EtZn(py)\{\mu\text{-}OCH(CF_3)_2\}]_2$

Diethyl zinc reacted with fluorinated alcohols to form $[EtZn(OR_f)]_n$ ($R_f = CH(CF_3)_2$, CMe_2CF_3, $CMe(CF_3)_2$) compounds, and the $[EtZn(OR_f)]_n$ compounds reacted with excess pyridine to yield the pyridine adducts $[EtZn(py)(\mu\text{-}OR_f)]_2$.

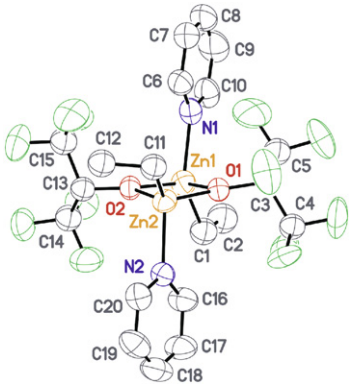

Samir Das

Polyhedron 27 (2008) 517

The chemistry of vanadate chelate esters of monoionized aromatic diols and methoxyphenolate

The synthesis, characterization and reactivities of a family of vanadate esters of monoionized aromatic 1,2-diols [catechol$^-$ (Hcat) and its 3,5-Bu^t_2 derivative (Hdbcat)] and 2-methoxyphenolate with diionized *N*-salicylidene/*N*-napthalidine-α-aminophenol (L) as coligands are reported. Molecular oxygen reacts smoothly with the vanadate esters quantitatively furnishing the corresponding *o*-quinone (Q) and in the presence of diol [catechol (H_2cat) or its 3,5-Bu^t_2 derivative (H_2dbcat)] or 2-methoxyphenol the reaction becomes catalytic.

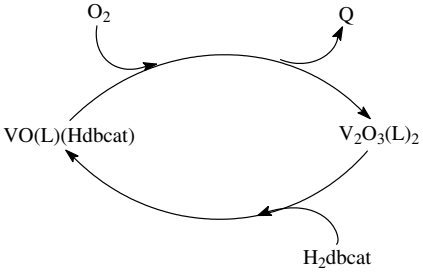

Chamindra S. Williams, Nelse C. Miller and John A. Collins

Polyhedron 27 (2008) 523

Single-crystal electronic spectra of some quadrate chromium(III) complexes

Polarised, single-crystal, electronic spectra of a number of *trans*-disubstituted bis(ethylenediamine) chromium(III) complexes have been measured at 77 K. The observed quartet bands have been given definitive quadrate assignments based on polarisation characteristics. The significance of the ligand field symmetry parameters and the translated angular overlap model parameters is discussed.

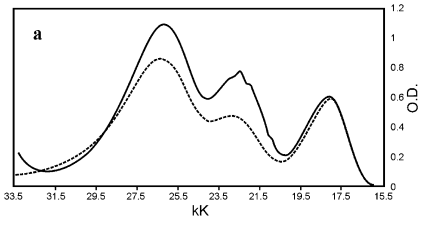

Merlín Rosales, Beatriz Alvarado, Federico Arrieta, Carlos De La Cruz, Ángel González, Karely Molina, Otto Soto and Yslamar Salazar

Polyhedron 27 (2008) 530

A general route for the synthesis of hydridocarboxylate complexes of the type MH(CO)-(κ^3-OCOR)(PPh_3)$_2$ [M = Ru, Os; R = CH_3, CH_2Cl, C_6H_5, $CH(CH_3)_2$] and their use as precatalysts for hydrogenation and hydroformylation reactions

Complexes MH(CO)(κ^3-OCOR)(PPh_3)$_2$ were obtained by reaction of the respective cationic complex [MH(CO)($NCMe$)$_2$(PPh_3)$_2$]BF_4 with the sodium salt of the corresponding carboxylic acid in a CH_2Cl_2/MeOH solution at room temperature. These complexes showed to be efficient precatalysts for the quinoline hydrogenation and for the hydroformylation of 1-hexene. The osmium complexes showed low activities for the benzothiophene hydrogenation whereas the corresponding ruthenium ones were inactive.

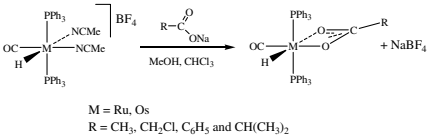

M = Ru, Os
R = CH_3, CH_2Cl, C_6H_5 and $CH(CH_3)_2$

Jean d'Angelo, Georges Morgant, Nour Eddine Ghermani, Didier Desmaële, Bernard Fraisse, François Bonhomme, Emma Dichi, Mehrez Sghaier, Yanling Li, Yves Journaux and John R.J. Sorenson

Polyhedron 27 (2008) 537

Crystal structures and physico-chemical properties of Zn(II) and Co(II) tetraaqua(3-nitro-4-hydroxybenzoato) complexes: Their anticonvulsant activities as well as related (5-nitrosalicylato)–metal complexes

The individual subunits of the (3-nitro-4-hydroxybenzoato) complexes of Zn(II) and Co(II) self-assemble via extensive hydrogen bonding involving water molecules leading to a 3D supramolecular architecture. The electrochemical impedance measurements show that these complexes are strong electrolytes in dilute aqueous solution. On the other hand, magnetic measurement of Co-complex indicates that the Co ions are ferromagnetically coupled. These complexes also show interesting anticonvulsant activities.

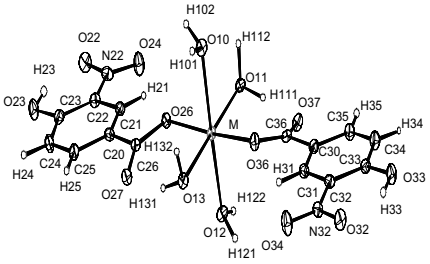

Angelica E. Graminha, Felipe S. Vilhena, Alzir A. Batista, Sonia R.W. Louro, Roberta L. Ziolli, Letícia R. Teixeira and Heloisa Beraldo

Polyhedron 27 (2008) 547

2-Pyridinoformamide-derived thiosemicarbazones and their iron(III) complexes: Potential antineoplastic activity

The iron(III) complexes [Fe(2Am4DH)$_2$]Cl (**1**), [Fe(2Am4Me)$_2$]Cl (**2**) and [Fe(2Am4Et)$_2$]Cl (**3**) with 2-pyridineformamide thiosemicarbazone (H2Am4DH) and its *N*(4)-methyl (H2Am4Me) and *N*(4)-ethyl (H2Am4Et) derivatives were obtained. The thiosemicarbazones and complexes (**1**) and (**2**) presented toxicity against *Artemia salina* at low concentrations, suggesting that the studied compounds might present antineoplastic activity.

Compound	LD_{50}* μmol L^{-1} ± SD against *Artemia salina*
H2Am4DH	35.24 ± 7.11
[Fe(2Am4DH)$_2$]Cl (**1**)	30.14 ± 1.93
H2Am4Me	26.09 ± 3.96
[Fe(2Am4Me)$_2$]Cl (**2**)	14.12 ± 0.98
H2Am4Et	31.89 ± 3.38
[Fe(2Am4Et)$_2$]Cl (**3**)	> 90

Livia Arizaga, Ricardo González, Raúl Chiozzone, Carlos Kremer, María Fernanda Cerdá, Donatella Armentano, Giovanni De Munno, Francesc Lloret and Juan Faus

Polyhedron 27 (2008) 552

Synthesis, crystal structure, electrochemical and magnetic properties of (NBu_4)[$ReCl_5$(L)] with L = pyrimidine and pyridazine

The reaction of $[ReCl_6]^{2-}$ with diazines in hot dmf affords the title compounds. Cyclic voltammetry studies show a one-electron reduction step for both complexes. Large zero-field splitting values and weak intermolecular antiferromagnetic interactions account for the observed magnetic behaviour.

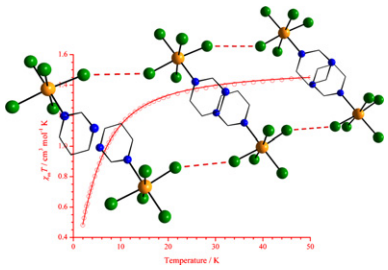

Danielle Cangussu de Castro Gomes, Luminita Marilena Toma, Humberto O. Stumpf, Harry Adams, Jim A. Thomas, Francesc Lloret and Miguel Julve

Polyhedron 27 (2008) 559

Syntheses, crystal structures and magnetic properties of mono- and polynuclear [bis-(2-arylcarbonyl)amidate]copper(II) complexes

The complexes [Cu(bpcam)(CN)(H_2O)] (**1**) (mononuclear), [Cu(bpcam)(N_3)(H_2O)]$_2$ (**2**) (mononuclear/dinuclear), [Cu(bpcam)(NCS)-(H_2O)] (**3**) (mononuclear), [Cu(bpcam)(dca)-(H_2O)]$_2$ (**4**) (dinuclear), and [Cu(bpca)(tcnm)]$_n$ (**5**) (chain) have been prepared and their crystal structures determined by X-ray diffraction. The magnetic properties of **2**, **4** and **5** reveal the occurrence of weak antiferromagnetic interactions in the range $-J = 0.5$–1.7 cm^{-1}.

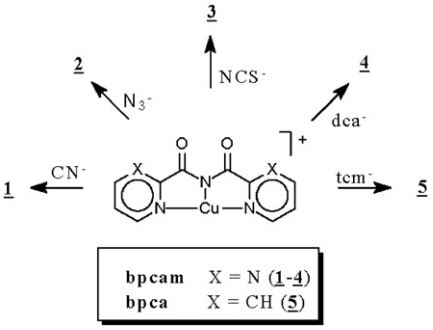

Cristian D. Ene, Floriana Tuna, Oscar Fabelo, Catalina Ruiz-Pérez, Augustin M. Madalan, Herbert W. Roesky and Marius Andruh

Polyhedron 27 (2008) 574

One-dimensional and two-dimensional coordination polymers constructed from copper(II) nodes and polycarboxylato spacers: Synthesis, crystal structures and magnetic properties

Four new coordination polymers were obtained by employing polycarboxylato spacers and cationic copper(II) complexes as nodes: $^{\infty}_{2}$[Cu_3(trim)$_2$(NH_3)$_6$(H_2O)$_3$] (**1**); $^{\infty}_{1}$[Cu(tmen)-(dhtp)] (**2**), $^{\infty}_{1}$[Cu(tmen)(hitp)](H_2O) (**3**), $^{\infty}_{1}$[Cu-(tmen)(nitp)] (**4**) (H_3trim = trimesic acid, H_2dhtp = 2,5-dihydroxy-terephthalic acid; H_2dhtp = 5-hydroxy-isophthalic acid, H_2nitp = 5-nitro-isophthalic acid; tmen = tetramethyl-ethylenediamine).

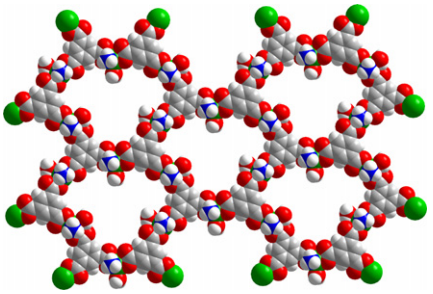

Ya-Hui Zhao, Zhong-Min Su, Yao-Mei Fu, Kui-Zhan Shao, Peng Li, Yong Wang, Xiang-Rong Hao, Dong-Xia Zhu and Si-Dong Liu

Polyhedron 27 (2008) 583

Syntheses and characterizations of four metal coordination polymers constructed by the pyridine-3,5-dicarboxylate ligand

Four new complexes based on divalent metal, pyridine-3,5-dicarboxylate acid ligand and two chelate ligands have synthesized under hydrothermal condition. The framework structures of these neutral polymeric complexes have been determined by the X-ray single crystal diffraction technique. In four complexes, pyridine-3,5-dicarboxylate acid ligand exhibits diverse coordination modes, which plays an important role in the construction of metal-organic frameworks. The thermal analyses of these four complexes are measured and discussed. In addition, complex **2** shows strong phosphorescent emission at room temperature and the magnetic measurement of polymer of **4** reveals that typical antiferromagnetic exchange.

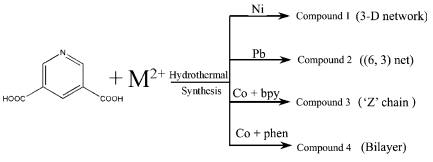

Somnath Roy, Tarak Nath Mandal, Anil Kumar Barik, Samik Gupta, Ray J. Butcher, Munirathinam Nethaji and Susanta Kumar Kar

Polyhedron 27 (2008) 593

Syntheses, characterization and X-ray crystal structures of Co(III) and Mn(II) complexes of pyrimidine derived Schiff base ligands

One Co(III) and two Mn(II) complexes (**1**–**3**) of two similar tridentate Schiff base ligands synthesized from 2-*S*-methylmercapto-6-methylpyrimidine-4-carbaldehyde and *S*-methyl/*S*-benzyl dithiocarbazate (HL_1 and HL_2) have been prepared and structurally characterized. All the three complexes have gross octahedral geometry with N_4S_2 chromophore. In all the complexes, the ligand molecule with ZEZ configuration binds the respective metal center as a uninegative tridentate one. The two Mn(II) complexes are found to be more distorted than corresponding Co(III) complex because of the steric interactions and asymmetric nature of the ligand molecules.

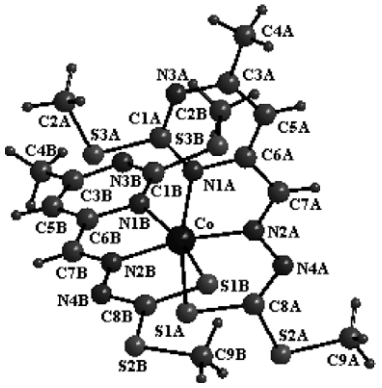

P. Piszczek, M. Richert and A. Wojtczak

Polyhedron 27 (2008) 602

Crystal structure and spectral characterization of hexanuclear oxo titanium(IV) clusters: $[Ti_6O_6(OSi(CH_3)_3)_6(OOCR)_6]$ (R = Bu^t, CH_2Bu^t, $C(CH_3)_2Et$)

Hexanuclear oxo titanium(IV) siloxo carboxylate complexes with the general formula $[Ti_6O_6(OSi(CH_3)_3)_6(OOCR)_6]$ (R = Bu^t (**1**), CH_2Bu^t (**2**), $C(CH_3)_2Et$ (**3**)) were synthesized in quantitative yield, by the reaction of $Ti(OSiMe_3)_4$ with the appropriate organic acid. Crystal structure determination revealed that molecules of **1**–**3** are composed of $[Ti_6\text{-}(\mu_3\text{-}O)_6]$ cores stabilized by six *syn–syn* carboxylato bridges and six terminal siloxide ligands. Each metal atom is surrounded by six oxo atoms, capping the triangular faces of the distorted octahedron. Spectral characterization (IR, NMR) of **1**–**3** revealed a significant non-equivalence of the carboxylate group interactions, resulting from the asymmetry of the Ti-μ-OOC bonds of the *syn–syn* bridges. The thermal stability of the studied compounds was determined from TGA/DTA analysis.

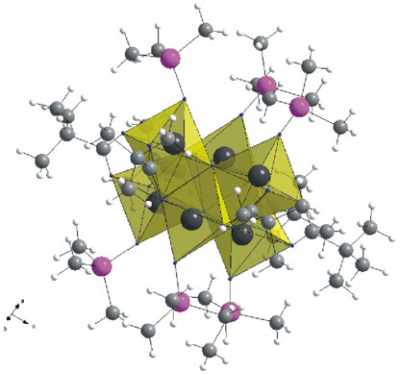

Manu Mehrotra, Vimal Soni and Raj N. Mehrotra

Polyhedron 27 (2008) 609

Oxidation of S(IV) by the dodecatungstocobaltate(III) ion over an extended pH range using acetic acid–acetate buffer: Different kinetics, oxidation product and mechanism

The reinvestigation of the title reaction over the extended pH range, 3.25 pH 6.3, has shown that the reaction is first-order in [Co(III)W]$^{5-}$, [SIV] and [M^+] where M^+ is the alkali metal ion, with SO_4^{2-} as the exclusive product. The alkali metal ions form ion-pairs with SO_3^{2-} and [Co(III)W]$^{5-}$ (abbreviation for 12-tungstocobaltate(III)) ions and also act as a bridge between the ion-pairs in the formation of the activated complex, the decomposition of which is rate limiting. A mechanism based on the above fact explains the kinetics results. Because of the nature of the rate dependence on M^+ and H^+, the application of the extended Marcus theory involving work terms could not be applied, but the application in its simple form does support that the reaction is outer-sphere.

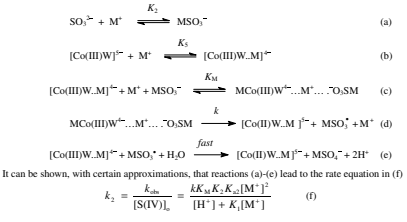

Gerard A. van Albada, Isja Dominicus, Marta Viciano-Chumillas, Ilpo Mutikainen, Urho Turpeinen and Jan Reedijk

Polyhedron 27 (2008) 617

A unique chain of trinuclear Cu(II) units containing both neutral and anionic *N*-(pyrimidin-2-yl) acetamide (Haapm, resp. aapm) as a ligand and dicyanamide (dca): Synthesis, characterization, X-ray structure and magnetism of $[Cu_3(\mu\text{-aapm})_2(\mu\text{-dca})_2(Haapm)_2]\text{-}(CF_3SO_3)_2$

A new trinuclear Cu(II) compound $[Cu_3\text{-}(\mu\text{-aapm})_2(\mu\text{-dca})_2(Haapm)_2](CF_3SO_3)_2$, containing the ligands *N*-(pyridin-2yl)acetamide (Haapm) and dicyanamide (dca) is reported. The dca anions are connected in an end-to-end fashion to a neighboring Cu(II) ion, forming in this way a chain of trinuclear units bridged by two dca anions.

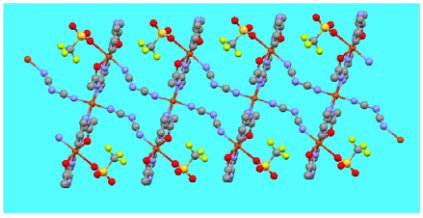

P. Arranz-Mascarós, M.D. Gutiérrez-Valero, R. López-Garzón, M.D. López-León, M.L. Godino-Salido, A. Santiago-Medina and H. Stoeckli-Evans

Polyhedron 27 (2008) 623

Study of protonation and Zn(II), Cd(II), Cu(II) and Mn(II) complexation with a glutamic acid *N*-pyrimidine derivative: Crystal structure of a neutral Cd(II) complex of the bianionic ligand

Aminoacids N-5-nitroso-pyrimidine derivatives behave as bifunctional ligands whose pyrimidine residue reveals bipolar nature that favours adsorption at the arene centres of graphitic activated carbon and their behaviour as versatile ligands. Water reaction of N-2-(4-amino-1,6-dihydro-1-methyl-5-nitroso-6-oxo-pyrimidinyl)-glutamic acid with Cd^{2+} yields a molecular layered compound with $\{[Cd(HL)H_2O] \cdot 3H_2O\}_n$ units containing three different coordination modes ($^1\eta$, $\mu\text{–}^2\eta$ and $\mu\text{–}^3\eta$).

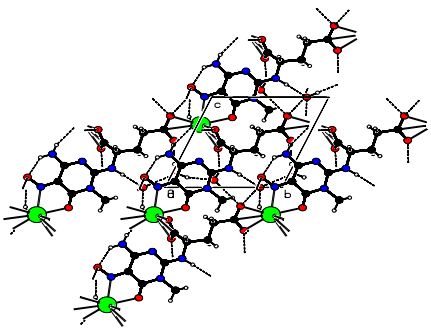

Hugo Núñez, Juan Server-Carrió, Emilio Escrivà, Lucía Soto, Julia García-Lozano, Amparo Sancho, Begoña Verdejo and Enrique García-España

Polyhedron 27 (2008) 633

Extended structures of copper(II) complexes with 2-di1*H*-2-imidazolylmethylmalonate (DIMMAL), a versatile bis(imidazole)–bis(carboxylate) ligand: Solution studies, crystal structures and spectroscopic characterization

Copper(II) complexes of 2-di1*H*-2-imidazolylmethylmalonate (DIMMAL) have been studied by potentiometric methods. Beside this, the synthesis, characterization and structure solution of two new complexes based on this novel bis(imidazole)–bis(carboxylate) ligand are reported. Non-covalent interactions (H-bonds and π–π) drive the build-up of infinite three-dimensional arrays in both compounds.

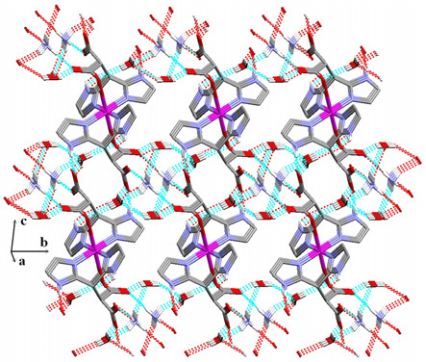

Jana Chrappová, Peter Schwendt, Dorota Dudášová, Jozef Tatiersky and Jaromír Marek

Polyhedron 27 (2008) 641

Synthesis, X-ray crystal structure and thermal decomposition of two peroxovanadium complexes with coordinated ammonia molecules: $[\{VO(O_2)_2(NH_3)\}_2\{\mu\text{-}Cu(NH_3)_4\}]$ and $[Zn(NH_3)_4][VO(O_2)_2(NH_3)]_2$

The compounds $[\{VO(O_2)_2(NH_3)\}_2\{\mu\text{-}Cu(NH_3)_4\}]$ (**1**) and $[Zn(NH_3)_4][VO(O_2)_2(NH_3)]_2$ (**2**) were characterized by infrared spectra and the X-ray structure analysis. Compound **1** consists of trinuclear molecules with rare heterobimetalic peroxo bridge. The final products of the thermal decomposition of **1** and **2** were $Cu(VO_3)_2$ and $Zn(VO_3)_2$, respectively.

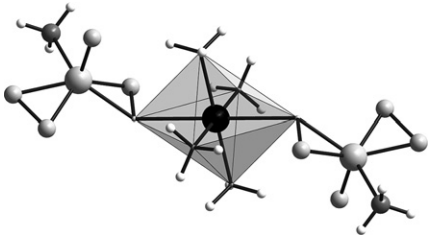

Hassan Keypour, Reza Azadbakht and Hamidreza Khavasi

Polyhedron 27 (2008) 648

Synthesis and characterization of three Cd(II) Schiff-base macrocyclic N_3O_2 complexes

Three polyamine ligands of N1-(2-nitrobenzyl)-N1-(2-aminoethyl)ethane-1,2-diamine (L_1), N1-(2-nitrobenzyl)-N1-(2-aminoethyl)-propane-1,3-diamine (L_2) and N1-(2-nitrobenzyl)-N1-(3-aminopropyl)propane-1,3-diamine (L_3) were synthesized and their cyclo-condensation with 2-[2-(2-formyl phenoxy)ethoxy]benzaldehyde (L_4) in the presence of various metal(II) ions was examined. These reactions only in the presence of a stoichiometric amount of cadmium(II) nitrate gave the related cadmium(II) macrocyclic Schiff-base complexes. In all the other cases no cyclic complexes have been obtained and metal(II) polyamines were the only products. The complexes have been studied with IR, ^1H NMR, ^{13}C NMR, DEPT, COSY, HMQC and microanalysis. The crystal structures of $[Cd(NO_3)(L_5)(\mu\text{-}NO_3)Cd(NO_3)(L_5)]0.5Cd(NO_3)_4$ (**1**) and $[CdL_5(NO_3)(CH_3OH)]ClO_4$ (**2**) have been also determined.

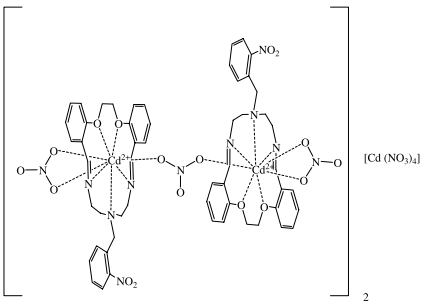

Raji Raveendran and Samudranil Pal

Polyhedron 27 (2008) 655

Ruthenium(III) complexes with *N*-(acetyl)-*N*′-(5-*R*-salicylidene)hydrazines: Syntheses, structures and properties

Syntheses, structures and physical properties of two series of ruthenium(III) complexes having the general formulae $[Ru(HahsR)(PPh_3)_2Cl_2]$ and $[Ru(ahsR)(PPh_3)_2Cl]$ with *N*-(acetyl)-*N*′-(5-*R*-salicylidene)hydrazines (H_2ahsR) are described. The rhombic EPR spectra of the complexes are typical of low-spin distorted octahedral ruthenium(III) species. All the complexes are redox active and display a ligand substituent sensitive metal centred reduction.

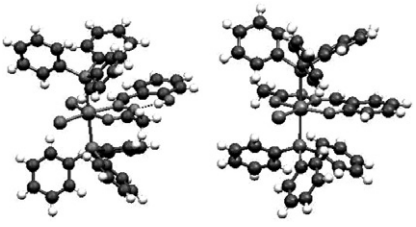

Han-Dong Yin, Jun Zhai, Yu-Ying Sun and Da-Qi Wang

Polyhedron 27 (2008) 663

Synthesis, characterizations and crystal structures of new antimony (III) complexes with dithiocarbamate ligands

A series of antimony (III) complexes with dithiocarbamate ligands $(R_2NCS_2)_2SbBr$ [R_2NCS_2 = $OC_4H_8NCS_2$ (**1**), $C_2H_5NC_4H_8NCS_2$ (**2**), Me_2NCS_2 (**3**), $C_4H_8NCS_2$ (**4**)] and $(R_2NCS_2)_3Sb$ [R_2NCS_2M = $C_5H_{10}NCS_2$ (**5**), Bz_2NCS_2 (**6**), Et_2NCS_2 (**7**), $(HOCH_2CH_2)_2NCS_2$ (**8**)] have been synthesized. These complexes have been characterized by elemental analysis, IR, ^1H and ^{13}C NMR spectra.

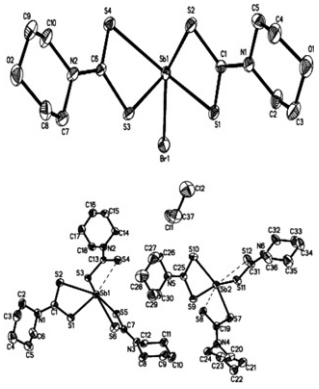

Shu-Xin Cui, Yu-Long Zhao, Bo Li, Jing-Ping Zhang, Qun Liu and Yan Zhang

Polyhedron 27 (2008) 671

Structural and magnetic properties of one-dimensional polymeric Co^{II} complexes

The twisting of polymer back bone and the corresponding decrease of antiferromagnetic interactions between Co^{II} ions can be tuned by the introduction of a substituent on the second ligand.

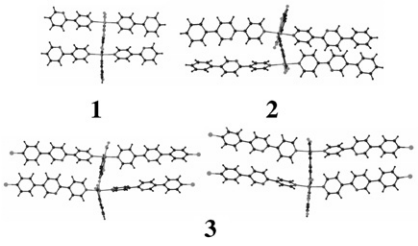

Sílvia Carvalho, Rita Delgado, Michael G.B. Drew, Vítor Félix, Mauro Figueira and Rui T. Henriques

Polyhedron 27 (2008) 679

Cascade dicopper architectures of a dibenzodioxatetraazamacrocycle

The Cu^{2+} and Pb^{2+} complexes of a dibenzodioxatetraazamacrocycle as well as the cascade species of the dicopper complex with dicarboxylate anions were studied by several techniques and the stability constants determined.

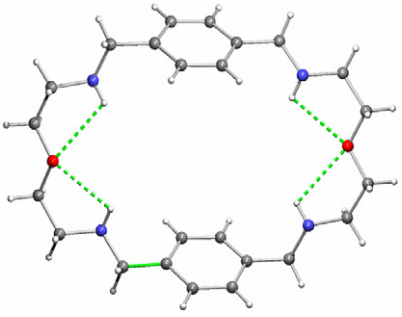

Mohammed Boujtita, Julien Boixel, Errol Blart, Cédric R. Mayer and Fabrice Odobel

Polyhedron 27 (2008) 688

Redox properties of hybrid Dawson type polyoxometalates disubstituted with organosilyl or organo-phosphoryl moieties

Three Dawson-type polyoxometalates (POMs) disubstituted with phenyl-phosphonate, phenyl silyl or tertbutylsilyl moieties have been characterized by cyclic voltammetry and on glassy carbon rotating disk electrode. We found that the grafted organic substituents modify the first and second reduction potential of the POM compared to the unsubstituted POM $[P_2W_{18}O_{62}]^{6-}$. The spectrum of the monoreduced and the bisreduced species of the polyoxometalate disubstituted with phenyl-phosphonate are also reported herein.

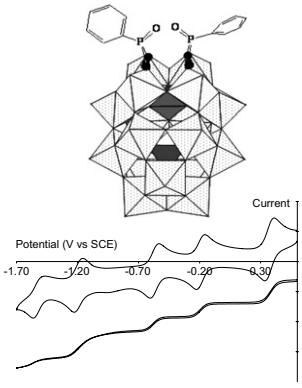

Biswarup Sarkar, Gabriele Bocelli, Andrea Cantoni and Ashutosh Ghosh

Polyhedron 27 (2008) 693

Copper(II) complexes of symmetrical and unsymmetrical tetradentate Schiff base ligands incorporating 1-benzoylacetone: Synthesis, crystal structures and electrochemical behavior

Three new copper(II) complexes $[CuL^1]_2(ClO_4)_2$ (**1**), $[CuL^2]ClO_4$ (**2**) and $[CuL^3]$ (**3**) where HL^1 and HL^2 are two tetradentate unsymmetric Schiff base formed by condensation of 1,3-diaminopropane with benzoylacetone and pyridine-2-carboaldehyde or 2-acetylpyridine and H_2L^3 the symmetrical di-Schiff base of 1,3-diaminopropane and benzoylacetone have been synthesized and structurally characterized. In complex **1**, the two units are associated weakly through ketonic oxygen of benzoylacetone part to form the dimeric entity. The square planar geometry of complex **3** is unusually distorted towards tetrahedral one. The *E*1/2 of **3** shows significant anodic shift due to the tetrahedral distortion around Cu(II).

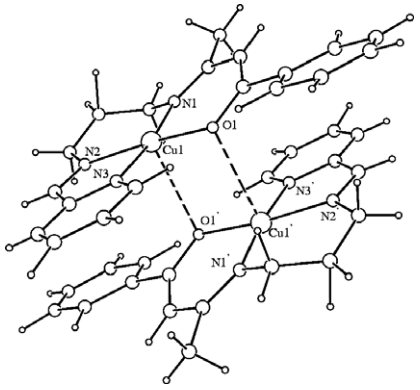

Sethuraman Kannan, K. Naresh Kumar and Rengan Ramesh

Polyhedron 27 (2008) 701

Ruthenium(III) complexes of amine-bis(phenolate) ligands as catalysts for transfer hydrogenation of ketones

Ruthenium(III) complexes of general formula $[Ru(L^1–L^3)(X)(EPh_3)_2]$ (where X = Cl (or) Br; E = P or As, $L^1–L^3$ are dianionic tridentate chelator) have been synthesized and characterized by analytical and spectral methods. The catalytic activity of one of the complexes $[Ru(pcr\text{-}chx)Br(AsPh_3)_2]$ (**7**) was examined in the transfer hydrogenation of ketones and was found to be an efficient catalyst with conversion up to 99% in the presence of isopropanol/KOH.

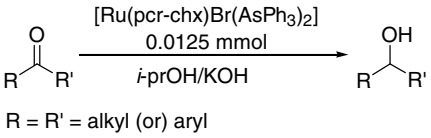

Bang-Yu Li, Ying-Ming Yao, Yao-Rong Wang, Yong Zhang and Qi Shen

Polyhedron 27 (2008) 709

Synthesis, reactivity and structural characterization of sodium and ytterbium complexes stabilized by a tridentate [*N*,*N*,*O*] Schiff base ligand

The first soluble monomeric ytterbium dichloride complex stabilized by a tridentate [*N*,*N*,*O*] Schiff base ligand was synthesized. This ytterbium dichloride can be used as a precursor for the synthesis of the corresponding ytterbium derivatives via general metathesis reactions. All of the complexes are well characterized including X-ray crystal structure determination.

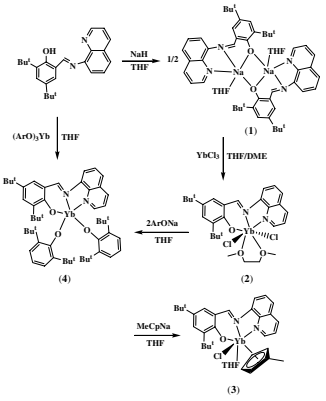

Feng-Qin Wang, Xiang-Jun Zheng, Yong-Hong Wan, Ke-Zhi Wang and Lin-Pei Jin

Polyhedron 27 (2008) 717

Architecture of zero-, one-, two- and three-dimensional structures based on metal ions and pyrazine-2,6-dicarboxylic acid

Metal pyrazine-2,6-dicarboxylic acid complexes with zero-, one-, two- and three-dimensional structures were obtained by hydro(solvo)thermal reactions. The assembly of structural versatility for the title complexes shows that the metal ions and the coordination modes of the pzda ligand play an important role in the dimensions and thus the structures of the complexes.

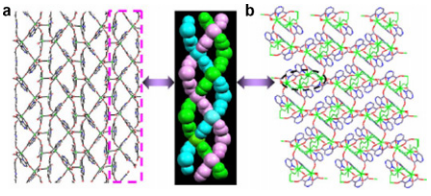

Marcelo R.L. Oliveira, Jorge Amim Jr, Ivan A. Soares, Vito M. De Bellis, Carlos Alberto de Simone, Celice Novais and Silvana Guilardi

Polyhedron 27 (2008) 727

Syntheses, crystal structure and spectroscopic characterization of novel 1,2-bis(diphenylphosphine)ethane(*N*-R-sulfonyldithiocarbimato)-nickel(II) complexes

Three new complexes of the general formula: $[Ni(RSO_2N{=}CS_2)(dppe)]$, where R = CH_3 (**1**), CH_3CH_2 (**2**), 2-$CH_3C_6H_4$ (**3**) and dppe = 1,2-bis(diphenylphosphine)ethane, were obtained by the reaction of potassium *N*-R-sulfonyldithiocarbimate dihydrate: $RSO_2N{=}CS_2K_2 \cdot 2H_2O$ and 1,2-bis(diphenylphosphine)-ethane with nickel(II) chloride hexahydrate. The square planar complexes were characterized by X-ray diffraction and by IR and NMR spectroscopies.

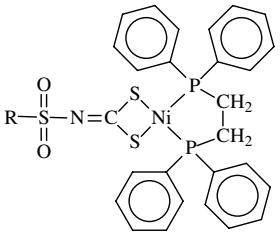

1 (R = CH_3), **2** (R = CH_3CH_2), **3** (R = 2-$CH_3C_6H_4$)

Hui Huang, Russell P. Hughes and Arnold L. Rheingold

Polyhedron 27 (2008) 734

Synthesis and structural characterization of a coordinatively unsaturated ruthenium complex, $Cp^*Ru(Ph_2nacnac)$, and its CO adduct

A half sandwich ruthenium complex with the Ph_2nacnac ligand has been synthesized, and characterized by X-ray diffraction as having a trigonal planar coordination geometry around ruthenium. It reacts with CO to give an air stable adduct, also characterized by X-ray diffraction, which has a *pseudo*-tetrahedral coordination geometry around the Ru(II) center.

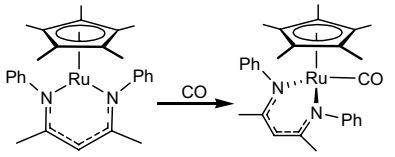

Eugene V. Tretyakov, Svyatoslav E. Tolstikov, Elena V. Gorelik, Matvey V. Fedin, Galina V. Romanenko, Artem S. Bogomyakov and Victor I. Ovcharenko

Polyhedron 27 (2008) 739

Copper(II) complexes with pyrazolyl-substituted nitronyl and imino nitroxides

Reactions of $Cu_2(OAc)_4(H_2O)_2$ with pyrazolyl-substituted nitronyl and imino nitroxides lead to tetra- and dinuclear copper(II) heterospin complexes, which tend to form polymer ribbons and layers in solids due to intermolecular H-bonding. In the case of pyrazole esters, the reaction with $Cu_2(OAc)_4(H_2O)_2$ causes cleavage of the ester bond and transformation of the starting nitroxides into the corresponding dianion.

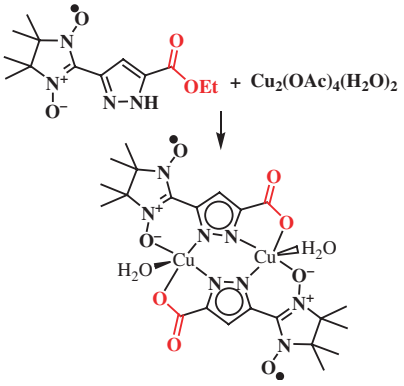

Iraj Mohammadpoor-Baltork, Majid Moghadam, Shahram Tangestaninejad, Valiollah Mirkhani and Seyedeh Fatemeh Hojati

Polyhedron 27 (2008) 750

Supported 12-tungstophosphoric acid as heterogeneous and recoverable catalysts for the synthesis of oxazolines, imidazolines and thiazolines under solvent-free conditions

12-Tungstophosphoric acid (TPA) supported on silica, activated carbon and poly(4-styrylmethyl)pyridinium chloride (PMP) were found as highly efficient catalysts for the synthesis of oxazolines, imidazolines and thiazolines from the condensation of various nitriles with aminoalcohols, ethylenediamine and cisteamine, respectively. Furthermore, these catalysts could be recovered and reused without significant loss of their activities.

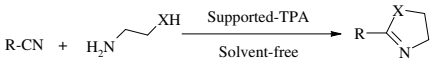

X= S, NH, O
R= Aryl

Chomchai Suksai, Chaveng Pakawatchai and Khajadpai Thipyapong

Polyhedron 27 (2008) 759

Unexpected Schiff-base complex formation from the oxidation reaction of a nickel(II) complex with the *meso*-HMPAO ligand by molecular oxygen

The oxidation of Ni(II) complex (**1**) can be easily oxidized to Schiff-base Ni(II) complex (**2**) by molecular oxygen in water.

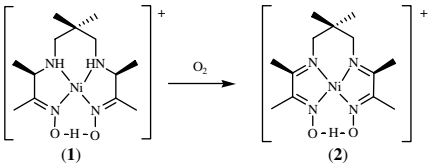

E. Szłyk, A. Wojtczak, L. Dobrzańska and M. Barwiołek

Polyhedron 27 (2008) 765

X-ray crystal structure and nuclear Overhauser effect studies of cerium(IV) complexes with Schiff bases obtained from *N*,*N*′-(1*R*,2*R*)(–)-1,2-cyclohexanediamine and benzaldehyde derivatives

Schiff bases, obtained by condensation of *N*,*N*′-(1*R*,2*R*)-cyclohexanediamine with 2-hydroxy-5-chlorobenzaldehyde or 2-hydroxy-3,5-dichlorobenzaldehyde and of (±)cyclohexanediamine and salicylaldehyde, have been used as ligands for cerium(IV). The complexes were characterized by circular dichroism (CD), ^{1}H NMR, ^{13}C NMR and nuclear Overhauser effect (NOE) studies. X-ray crystal structures determined for: [Ce(IV)((1*R*,2*R*)(−)chxn-(3,5-diClba)$_2$)$_2$] and [Ce(IV)(±)(chxn(salal)$_2$)$_2$] revealed different orientation of a pair of Schiff base ligands in the coordination sphere.

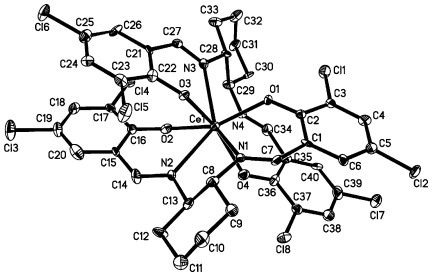

Azizolla Beheshti, William Clegg, Sophie H. Dale and Ahmad Solimankhani

Polyhedron 27 (2008) 777

Synthesis and structural characterization of copper–molybdenum–sulfur and copper–tungsten–sulfur cluster complexes (*n*-Bu$_4$N)[OMS$_3$-Cu$_3$Br$_2$L$_2$] with heterocyclic thiones as ligands

The anions of the title complexes have incomplete cubane core structures, in which the three Cu atoms have different coordination environments, being bonded, respectively, to a Br ligand, a thione ligand, and both of these. The isomorphous crystal structures display intramolecular and intermolecular hydrogen bonding.

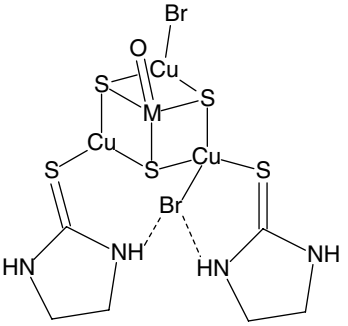

Andrzej J. Włodarczyk, Piotr P. Romańczyk, Stefan S. Kurek, Wojciech Nitek and Jon A. McCleverty

Polyhedron 27 (2008) 783

Electrochemical interactions in binuclear molybdenum and tungsten nitrosyl complexes incorporating saturated *n*-alkanediolate bridging ligands. Crystal structures of [Mo(NO)-(Tp^{Me2})I{O(CH$_2$)$_2$OCOCH$_3$}] and [W(NO)-(Tp^{Me2})I$_2$] · 0.5I$_2$ · 0.5C$_6$H$_5$CH$_3$

The electrochemical interactions, $\Delta E_{1/2}$, in bimetallic Mo and W complexes with saturated bridges being large for the complex with a C_2 bridge (310 mV, Mo···Mo distance > 6 Å) decrease by *ca.* 100 mV per CH_2 group with increased length for C_2 to C_4 bridges and become undetectable for complexes with bridges longer than C_4. The substitution of fluorine into the C_5 bridge causes the effect to become measurable due to easier polarisation of the σ-bond framework.

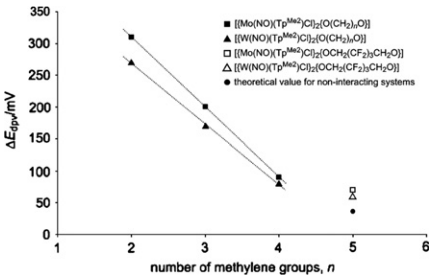

B. Machura, R. Kruszynski, R. Penczek, J. Mroziński and J. Kusz

Polyhedron 27 (2008) 797

Novel dioxorhenium complex with bis(3,5-dimethypyrazol-1-yl)methane ligand – Synthesis, spectroscopic characterization, X-ray structure and DFT calculations

The reactions of $[ReOBr_3(PPh_3)_2]$ and $[ReOBr_3(AsPh_3)_2]$ with bis(3,5-dimethypyrazol-1-yl)-methane (bdmpzm) have been examined and novel dioxo rhenium(V) complex $[ReO_2(bdmpzm)_2]Br \cdot HBr \cdot 2H_2O$ has been obtained. The compound has been studied by IR, UV-Vis, ^1H NMR spectroscopy, magnetization measurements and X-ray crystallography. The electronic structure of the $[ReO_2(bdmpzm)_2]^+$ cation has been calculated with the density functional theory (DFT) method. The spin-allowed electronic transitions of $[ReO_2(bdmpzm)_2]^+$ have been calculated with the TD-DFT/PCM method, and the UV-Vis spectrum of $[ReO_2(bdmpzm)_2]Br$ has been discussed on this basis.

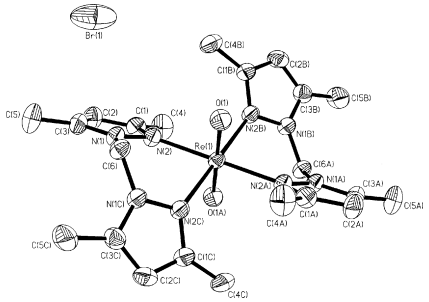

Sumanta Kumar Padhi, Rojalin Sahu and Vadivelu Manivannan

Polyhedron 27 (2008) 805

Synthesis, structure, thermal studies on Zn(II), Cd(II) complexes of N-(2-pyridylmethyl)pyridine-2-carbaldimine and N-(2-pyridylmethyl)-pyridine-2-methylketimine

Bivalent zinc and cadmium complexes based on two tridentate-N_3 ligand were synthesized and structurally characterized. The final residual part of thermal decompositions are ZnO and CdO, the SEM studies revealed, respectively, their porous and spherical natures. The activation parameters obtained from the Friedman fitting of the DSC profiles for the loss of pyridine rings are reported.

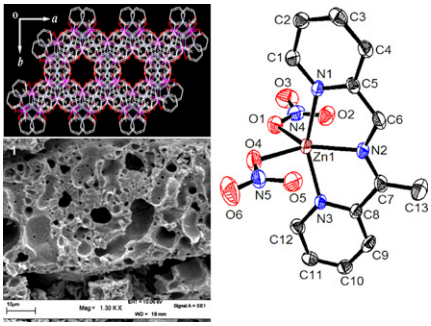

Qian Chu, Guang-Xiang Liu, Taka-aki Okamura, Yong-Qing Huang, Wei-Yin Sun and Norikazu Ueyama

Polyhedron 27 (2008) 812

Structure modulation of metal–organic frameworks via reaction pH: Self-assembly of a new carboxylate containing ligand *N*-(3-carboxyphenyl)iminodiacetic acid with cadmium(II) and cobalt(II) salts

New coordination frameworks were obtained by the reaction of a new carboxylate containing ligand, *N*-(3-carboxyphenyl)iminodiacetic acid (H_3L), with Cd(II) and Co(II) salts under different reaction pH, and their structures were determined by single crystal X-ray diffraction studies. The influence of the reaction pH on the structure of the complexes was discussed. The photoluminescence properties of the Cd(II) complexes were also investigated.

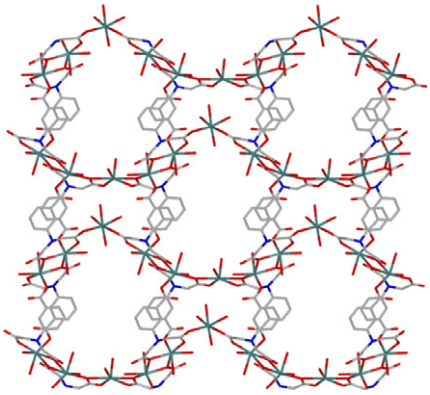

Subhashree Mallika Krishnan, Matthew R. Montney and Robert L. LaDuca

Polyhedron 27 (2008) 821

Two-dimensional divalent metal/pimelate coordination polymers incorporating dipodal organodiimines: Crystal structures, thermal properties, and magnetic studies

Hydrothermal synthesis has afforded coordination polymers incorporating the flexible pimelate ligand (pim) and either 4,4′-dipyridylamine (dpa) or 1,3-di-4-pyridylpropane (dpp). [M(pim)(dpa)(H_2O)] (M = Co, Ni) displays (4,4) rhomboid grids. {$[Cu_2(pim)_2(dpa)_2] \cdot 5H_2O$} (**2**) possesses slab motifs with water molecule chains. [Ni(pim)(dpp)] manifests doubly interpenetrated (4,4) grids. Thermal and magnetic properties are reported.

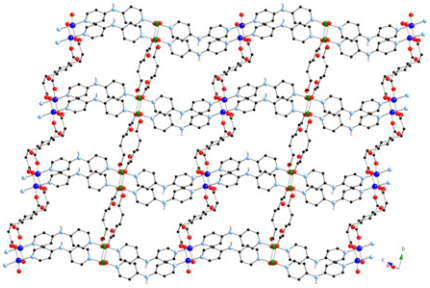

Prakash C. Srivastava, Sangeeta Bajpai, Roli Lath, Rajesh Kumar, Vikas Singh, Shrinkhala Dwivedi, Ray J. Butcher, Satoko Hayashi and Waro Nakanishi

Polyhedron 27 (2008) 835

X-ray characterization of $Te(S_2CNC_5H_{10})_2$ and $TeI_2[(C_{13}H_{10}N_2S)_2] \cdot 4C_4H_8TeI_2$; the first Te–C bond cleaved products obtained in the substitution reactions of organo(heterocyclic)-tellurium(IV) derivatives

Reaction of $C_8H_8TeI_2$ with ammonium piperidine dithiocarbamate gives the usual product $C_8H_8Te(S_2CNC_5H_{10})_2$ (**1**) and the first Te–C bond cleaved product $Te(S_2CNC_5H_{10})_2$ (**2**). The formation of **2**, in such type of substitution reaction, is unprecedented. The reaction of **2** with CH_3I yields the oxidative addition product $CH_3TeI(S_2CNC_5H_{10})_2$ (**8**). The various postulated processes leading to the formation of **2** are explained through Quantum Chemical calculations. Another Te–C bond cleaved product $TeI_2[(C_{13}H_{10}N_2S)_2] \cdot 4C_4H_8TeI_2$ (**9**) is obtained in the substitution reaction of $C_4H_8TeI_2$ with ammonium aniline dithiocarbamate.

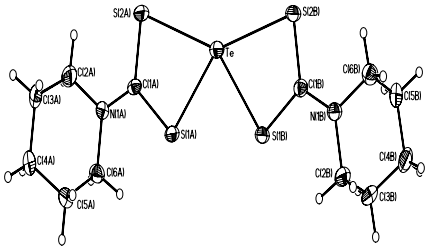

Hossein Dehghani and Mohammad Reza Mansournia

Polyhedron 27 (2008) 849

Novel sitting-atop complexation between uranyl and *meso*-tetraarylporphyrins under mild conditions

Reaction of *meso*-tetraarylporphyrins with $UO_2(NO_3)_2 \cdot 6H_2O$ under mild conditions in a 1:1 mole ratio lead to the formation of sitting-atop complexes, in which two pyrrolenine nitrogen atoms in the porphyrin core act as electron donors to an uranium(VI) center and two protons on the pyrrole nitrogens still remain.

$$H_2t(X)pp + UO_2^{2+} \rightarrow [(UO_2)H_2t(X)pp]^{2+}$$

Hongjian Sun, Lei She, Shimin Fang and Xiaoyan Li

Polyhedron 27 (2008) 854

Reaction of acyl(hydrido)cobalt(III) complexes with (2-diphenylphosphanyl)thiophenol and the influence of chelating ligands containing hard/soft donor atoms on the stability of cobalt complexes

The reaction of acyl(hydrido)cobalt(III) complexes **1**–**5** with (2-diphenylphosphanyl)thiophenol afforded a mixture products composed of compounds **6**–**7**, **11**–**15**, **16**, and **17**. A mechanism for the formation of these complexes is proposed. The influences of chelating ligands containing hard/soft donor atoms on the stability of the cobalt complexes in different oxidation states are discussed in terms of the HSAB concept.

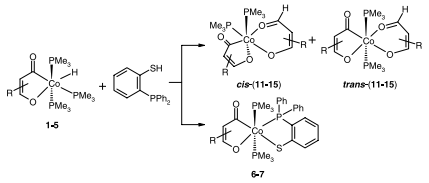

YounJung Jung, Kyung-In Son, Youl Eui Oh and Dong-Youn Noh

Polyhedron 27 (2008) 861

Ferrocenyl chalcones containing anthracenyl group: Synthesis, X-ray crystal structures and electrochemical properties

Two ferrocenyl chalcones with the anthracenyl group were synthesized by base-catalyzed solvent-free aldol condensation and analyzed by ^1H NMR and X-ray structure determinations. Their electrochemical properties were investigated by cyclic voltammetry and differential pulse voltammetry measurements, and compared to each other. Their fluorescent properties were also measured at room temperature.

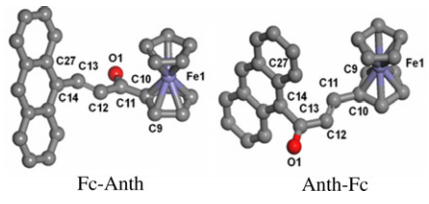

Abdullahi Mustapha, Krystoff Busch, Marta Patykiewicz, Alistair Apedaile, John Reglinski, Alan R. Kennedy and Timothy J. Prior

Polyhedron 27 (2008) 868

Multidentate ligands for the synthesis of multi-metallic complexes

A number of multi-metallic Schiff base complexes (M_3L_2, M = Ni, Zn; Ni_2PbL_2 and $Ni_2Pb_2L_2$) have been synthesised and crystallographically characterised. The attempted crystallisation of Ni_3L_2 leads to the production of two novel complexes: namely a partially hydrolysed Schiff base complex and an interesting nickel bromide–carbonate salt.

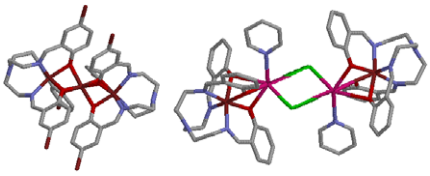

E. Viñuelas-Zahínos, M.A. Maldonado-Rogado, F. Luna-Giles and F.J. Barros-García

Polyhedron 27 (2008) 879

Coordination behaviour of Schiff base 2-acetyl-2-thiazoline hydrazone (ATH) towards cobalt(II), nickel(II) and copper(II)

Synthesis and characterization by physical measurements of cobalt(II), nickel(II) and copper(II) complexes with 2-acetyl-2-thiazoline hydrazone have been carried out. The X-ray crystal structures of $[NiCl_2(ATH)_2]$ and $[\{CuCl(ATH)\}_2(\mu\text{-}Cl)_2]$ have also been determined. Co(II) and Ni(II) complexes present a distorted octahedral geometry around the metal(II) ion, whereas the copper(II) complex presents a structure consisting of two square pyramids linked by one edge.

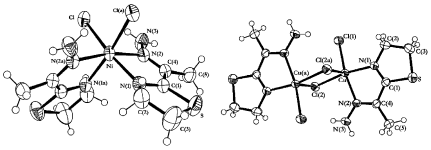

Ante Miličević and Nenad Raos

Polyhedron 27 (2008) 887

Estimation of stability constants of copper(II) and nickel(II) chelates with dipeptides by using topological indices

The ovelall stability constants β_1 of copper(II) and nickel(II) chelates with dipeptides were estimated from its constituents, K_1 and K_a. The chelate rings were treated as separate units in the model with the valence connectivity index of the 3rd order ($^3\chi^v$).

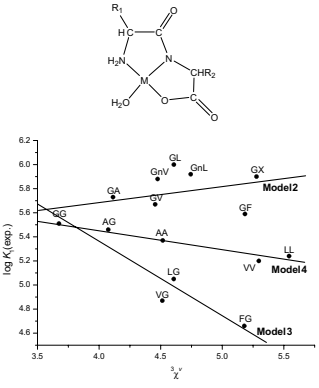

Najoua Belhaj Mbarek Elmkacher, Taha Guerfel, Igor Tkatchenko and Faouzi Bouachir

Polyhedron 27 (2008) 893

Synthesis and X-ray structure of cationic methallyl palladium complexes supported by unsymmetrical β-diimine ligands

New η^3-allyl cationic complexes of palladium (II) supported by new ligands, the unsymmetrical β-diimines, have been synthesized and characterized. The X-ray structure determination of the complex (**10**) $[PhCN(Ar)\text{-}CH_2CN(Ar)(Me)Pd(\eta^3\text{-}C_4H_7)]^+[PF_6]^-$ (Ar = 2, 6-iPr_2-C_6H_3) reveals a slightly distorted square planar arrangement around the metal and a unsymmetrical coordination of the β-iminoamine and allyl ligands.

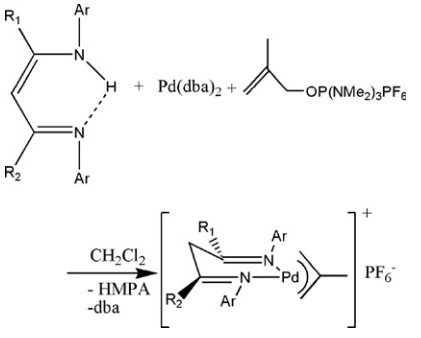

The Publisher encourages the submission of articles in electronic form thus saving time and avoiding rekeying errors. For detailed instructions on the preparation of manuscripts and of electronic artwork, consult the Author Gateway for Elsevier at http://authors.elsevier.com

Full text of this journal is available, on-line from **ScienceDirect**. Visit **www.sciencedirect.com** for more information.

Available online at www.sciencedirect.com
ScienceDirect
Polyhedron 27, issue 1, 20 Jaunary 2008
POLYHEDRON
www.elsevier.com/locate/poly

Contents

Papers

José S. Casas, Eduardo E. Castellano, Javier Ellena, María S. García-Tasende, Agustín Sánchez, José Sordo and Ángeles Touceda

Polyhedron 27 (2008) 1

New insights on the Lewis acidity of diorganolead(IV) compounds: Diphenyllead(IV) complexes with N,O,S-chelating ligands

New diphenyllead(IV) complexes have been synthesized and characterized by X-ray crystallography. Analysis of the Pb–S, Pb–N and Pb–O bond distances in these complexes suggests a borderline Lewis acid character for the diphenyllead(IV) cation.

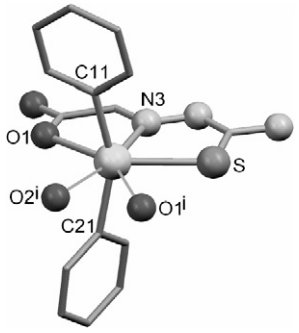

Guan-Cheng Xu, Li Zhang, Lang Liu, Guang-Fei Liu and Dian-Zeng Jia

Polyhedron 27 (2008) 12

Syntheses, characterization and crystal structures of mixed-ligand Cu(II), Ni(II) and Mn(II) complexes of *N*-(1-phenyl-3-methyl-4-propenylidene-5-pyrazolone)-salicylidene hydrazide containing ethanol or pyridine as a co-ligand

Five mixed-ligand complexes of Cu(II), Ni(II) and Mn(II) have been synthesized and characterized. The results show that the ligand undergoes isomerization in the reaction and acts as a double negatively charged tridentate chelating agent coordinated to the metal ion, other coordination sites of metal ions were completed either by the ethanol or pyridine molecules.

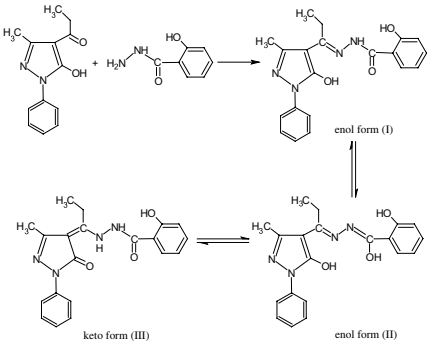

Bikshandarkoil R. Srinivasan, Sunder N. Dhuri, Ashish R. Naik, Christian Näther and Wolfgang Bensch

Polyhedron 27 (2008) 25

Crystallographic and thermal investigations of organic ammonium tetrathiomolybdates

The structures of *N*-methylethylenediammonium tetrathiomolybdate, *N*-(3-aminopropyl)-propane-1,3-diaminium tetrathiomolybdate, 4-(2-ammonioethyl)piperazin-1-ium tetrathiomolybdate hemihydrate consist of tetrahedral tetrathiomolybdate anions which are linked to the organic ammonium cations with the aid of weak hydrogen bonding interactions. A comparative study of the structural features of 28 tetrathiomolybdates is described.

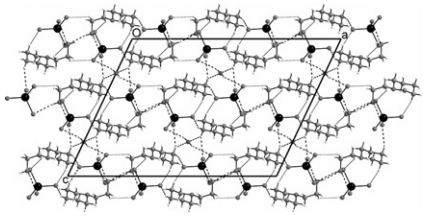

Elsevier Ltd.

Leji Latheef and
Maliyeckal R. Prathapachandra Kurup

Polyhedron 27 (2008) 35

Spectral and structural studies of nickel(II) complexes of salicylaldehyde 3-azacyclothiosemicarbazones

Four nickel(II) complexes of salicylaldehyde *N*(4)-hexamethyleneiminyl thiosemicarbazone (H_2L^1) and two nickel(II) complexes of salicylaldehyde *N*(4)-pyrrolidine thiosemicarbazone (H_2L^2) have been synthesized and characterized by different physicochemical techniques. The complexes were given the formulae $[Ni(HL^2)_2]$ (**1**), $[NiL^2py]$ (**2**), $[NiL^2\alpha\text{-pic}]$ (**3**), $[NiL^2\gamma\text{-pic}] \cdot H_2O$ (**4**), $[NiL^4py]$ (**5**) and $[NiL^4\gamma\text{-pic}]$ (**6**). In complex **1**, the ligand moieties are coordinated as monoanionic (HL^-). The other complexes posses the stoichiometry NiLB, where B represents different bases, *viz.* pyridine and α/β/γ-picoline. The coordination geometry around nickel(II) in **2** and **3** is found to be distorted square planar in geometry with coordination of azomethine nitrogen, thiolato sulfur, phenolato oxygen and pyridyl nitrogen atoms.

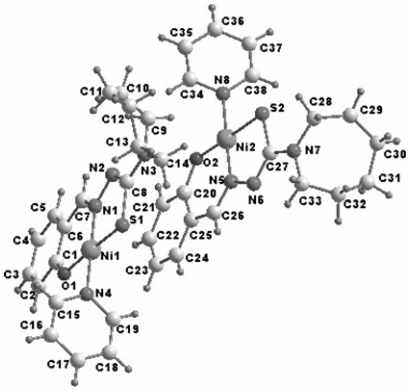

Akella Sivaramakrishna,
Banothile C.E. Makhubela, Feng Zheng,
Hong Su, Gregory S. Smith and John R. Moss

Polyhedron 27 (2008) 44

Synthesis, structure and reactivity of *cis*-$[PtL_2(1\text{-alkenyl})_2]$ complexes

The synthesis and characterization of several new bis(1-alkenyl)platinum(II) complexes have been carried out. The insertion of carbon monoxide into the metal–carbon bonds of the platinum alkenyl complexes and other reactions including transmetalation, intermolecular alkenyl migrations, and oxidative addition of methyl iodide are also described. The thermal decomposition studies of the bis(alkenyl) complexes are also reported.

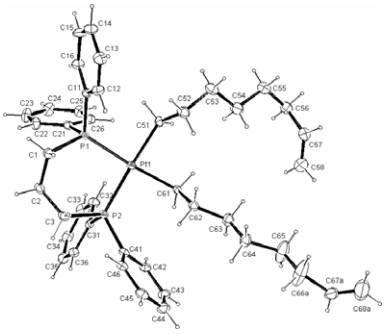

Lincoln Lucilio Romualdo, André Luis Bogado,
Eliana M.A. Valle, Icaro S. Moreira,
Javier Ellena, Eduardo E. Castellano,
Márcio P. de Araujo and Alzir A. Batista

Polyhedron 27 (2008) 53

Novel manganese (III) porphyrin containing peripheral "$[RuCl(dppb)(X\text{-bipy})]^+$" cations [dppb = 1,4-bis(diphenylphosphino)butane and X = $-CH_3$, –OMe, –Cl]. X-ray structure of the *cis*-$[RuCl(dppb)(bipy)(4\text{-Mepy})]PF_6$ complex

New tetraruthenated manganese (III) porphyrins were synthesized and characterized (^{31}P NMR, cyclic voltammetry, UV–Vis). This new system presents four units of cationic "$[RuCl(dppb)(X\text{-bipy})]^+$". The electrochemical and catalytic properties of the central manganese (III) show dependence on the characteristics of the peripheral ruthenium complexes as evidenced by the $Mn^{(III)}/Mn^{(II)}$ reduction potential.

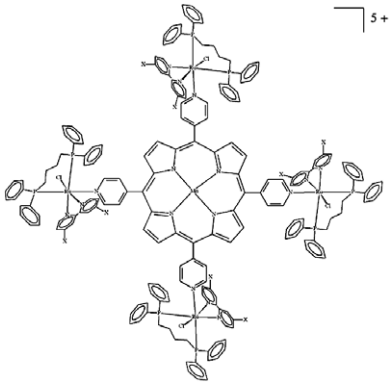

Ana C.D. Midões, Pedro E. Aranha,
Mirian P. dos Santos, Érica Tozzo,
Sandra Romera, Regina H. de A. Santos and
Edward R. Dockal

Polyhedron 27 (2008) 59

Synthesis, characterization, crystal structure and catalytic property of $[Cu(SalAHE)_2]$ (SalAHE = salicylaldehydeimine-1-hydroxyethane) complex for the oxidation of 3,5-di-*tert*-butylcatechol

A new Schiff base copper(II) complex $[Cu(SalAHE)_2]$ was synthesized and characterized. The crystal structure of this complex shows that it is almost coplanar with the two ligands in the *trans* configuration. This complex with a simple structure is able to oxidize 3,5-di-*tert*-butylcatechol to the respective *o*-quinone with molecular oxygen.

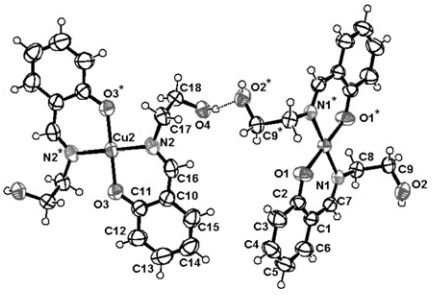

Edwin C. Constable, Catherine E. Housecroft, Markus Neuburger, Silvia Schaffner and Ellen J. Shardlow

Polyhedron 27 (2008) 65

Gold(I) phosphine-decorated 2,2′:6′,2″-terpyridine ligands

The synthesis and characterization of R_3PAu(**1**–H) (R = ^{n}Bu, Ph) and (**1**–H)Au(μ-dppe)Au(**1**–H) (**1** = HC≡CCH_2Otpy, tpy = 2,2′:6′,2″-terpyridine) are reported.

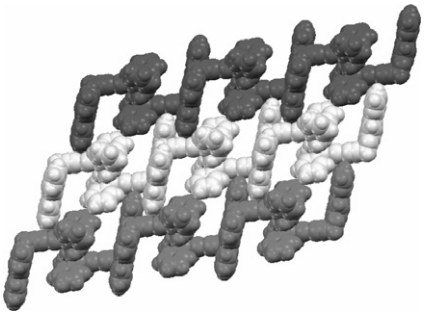

M. Akbar Ali, Hjh Junaidah Hj Abu Bakar, A.H. Mirza, S.J. Smith, L.R. Gahan and Paul V. Bernhardt

Polyhedron 27 (2008) 71

Preparation, spectroscopic characterization and X-ray crystal and molecular structures of nickel(II), copper(II) and zinc(II) complexes of the Schiff base formed from isatin and *S*-methyldithiocarbazate (Hisa-sme)

X-ray crystallographic structure determination of the $[Ni(isasme)_2] \cdot MeCN$ complex (isasme = monoanionic) form of the Schiff base formed by condensation of isatin with *S*-methyldithiocarbazate reveals a six-coordinate, distorted octahedral. Structure By contrast, $[Zn(isasme)_2] \cdot MeOH$ is four-coordinate and has a distorted tetrahedral geometry. The structure of the copper(II) complex $[Cu(isa\text{-}sme)_2] \cdot DMSO$ is complicated and comprises two different complexes in the asymmetric unit, one four- and the other five-coordinate.

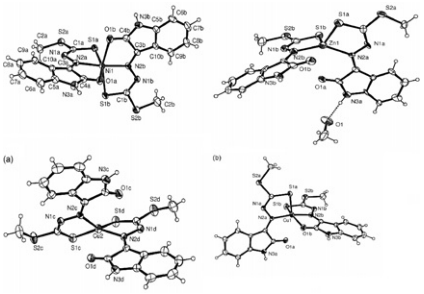

P. Chandrasekaran, Joel T. Mague and Maravanji S. Balakrishna

Polyhedron 27 (2008) 80

Synthesis and characterization of Ru^{II}/Au^{I}, Pd^{II}/Au^{I}, $Pd^{II}/2Au^{I}$, $Pt^{II}/2Au^{I}$ and $Cu^{I}/2Au^{I}$ heterometallic complexes of cyclodiphosphazane *cis*-{(*o*-$MeOC_6H_4O$)P(μ-N^{t}Bu)}$_2$

Selective monodentate coordination of the cyclodiphosphazane, *cis*-{(*o*-$MeOC_6H_4O$)P(μ-N^{t}Bu)}$_2$ with metal precursors such as $[RuCl_2(\eta^6\text{-cymene})]_2$, $[PdCl_2(PEt_3)]_2$ and $[MCl_2(COD)]$ (M = Pd, Pt) and bridging bidentate coordination with $[AuCl(SMe_2)]$ gives facile synthetic approach for Ru^{II}/Au^{I}, Pd^{II}/Au^{I}, $Pd^{II}/2Au^{I}$, $Pt^{II}/2Au^{I}$ and $Cu^{I}/2Au^{I}$ heterometallic complexes.

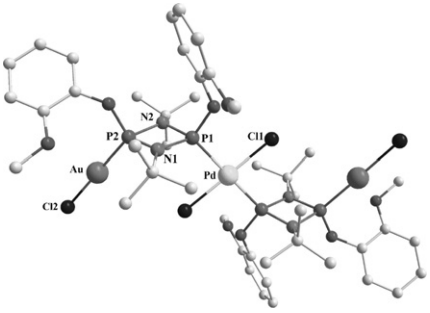

Qing-Xiang Liu, Li-Na Yin, Xiu-Mei Wu, Jin-Cheng Feng, Jian-Hua Guo and Hai-Bin Song

Polyhedron 27 (2008) 87

New *N*-heterocyclic carbene mercury(II) and silver(I) complexes

The complexes [1-(9-anthracenylmethyl)-3-octylimy]$_2$Hg[$HgCl_4$] (**2a**) (imy = imidazol-2-ylidene) and [1-(9-anthracenylmethyl)-3-butylbimy]$_2AgPF_6$ (**2b**) (bimy = benzimidazol-2-ylidene) have been prepared and characterized. Crystal packing of complex **2a** revealed that 1D polymeric chains are formed by [1-(9-anthracenylmethyl)-3-octylimy]Hg and $[HgCl_4]^{2-}$ through weak Hg…Cl bonds. The packing diagram of **2b** showed that 1D supramolecular chains are formed by both benzimidazole ring head to tail π–π stacking interactions and anthracene ring face-to-face π–π stacking interactions.

Harri Sopo, Ari Lehtonen and Reijo Sillanpää

Polyhedron 27 (2008) 95

Uranyl(VI) complexes of [*O*,*N*,*O*,*N*′]-type diaminobis(phenolate) ligands: Syntheses, structures and extraction studies

The reaction between uranyl nitrate hexahydrate and phenolic ligand precursors *N*,*N*-bis(2-hydroxy-3,5-dialkylbenzyl)-*N*′,*N*′-dimethylethylenediamine (alkyl = methyl or *t*-butyl) (H_2L1, H_2L2) in a 1:2 molar ratio (M to L) in acetonitrile afford a uranyl complex of the form $[UO_2(HLn)(NO_3)] \cdot xCH_3CN$ ($n = 1$, $x = 1$ and $n = 2$, $x = 2$) whereas H_2L1 and *N*-(2-pyridylmethyl)-*N*,*N*-bis(2-hydroxy-3,5-dimethylbenzyl)amine (H_2L3) in the presence of a base (triethylamine) afford the mononuclear, neutral uranyl complexes $[UO_2(HLn)_2] \cdot xCH_3CN$ ($n = 1$, $x = 0$ and $n = 3$, $x = 2$). Extraction studies of the uranyl ion from water to dichloromethane with these ligands are also presented.

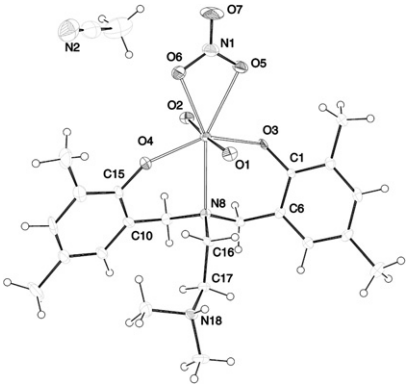

Somnath Roy, Tarak Nath Mandal, Anil Kumar Barik, Samik Gupta, Ray J. Butcher, Mohamed Salah El Fallah, Javier Tercero and Susanta Kumar Kar

Polyhedron 27 (2008) 105

A pyrazole-based orthogonal ferromagnetically coupled [2 × 2] homoleptic square Cu_4 grid: Magnetostructural correlations

Strategic and systematic positioning of polyfunctional groups within the backbone of a pyrazole derived ditopic ligand (PzOAPyz) leads to the formation of an aesthetically looking sophisticated supramolecular self-assembled homoleptic $Cu_4(\mu\text{-}O_4)$ square grid which exhibits intramolecular ferromagnetic exchange with an $S = 2$ magnetic ground state.

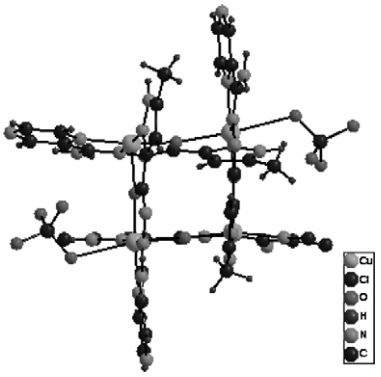

O.O.E. Onawumi, O.O.P. Faboya, O.A. Odunola, T.K. Prasad and M.V. Rajasekharan

Polyhedron 27 (2008) 113

Synthesis, structure and spectral studies on mixed ligand copper(II) complexes of diimines and acetylacetonate

The simplest member of the CASIOPEINAS® family of cytotoxic and antineoplastic compounds, $[Cu(acac)(bpy)(H_2O)]NO_3$ is prepared and characterized. The Cu(II) complex ion has a distorted square pyramidal coordination in the solid state and presumably also in solution.

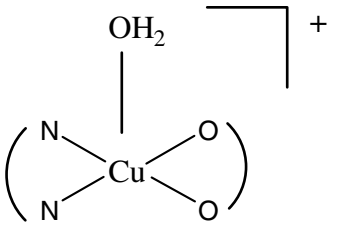

Andrea Lakatos, Tamás Kiss, Roberta Bertani, Alfonso Venzo and Valerio B. Di Marco

Polyhedron 27 (2008) 118

Complexes of Al(III) with D-gluconic acid

The complexation of Al(III) with D-gluconic acid has been studied in solution by pH-potentiometry, ESI mass spectrometry and one- and two-dimensional NMR spectroscopy. A solid complex $[AlL_2H_{-1}] \cdot 2H_2O$ was isolated as a microcrystalline powder and characterized. The structures of the complexes are discussed on the basis of spectroscopic results and MM force field calculations.

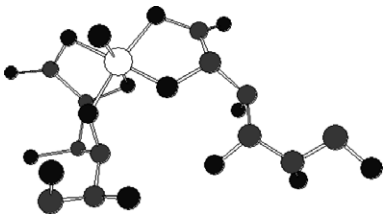

Ismail Yilmaz, Hamdi Temel and Hüseyin Alp

Polyhedron 27 (2008) 125

Synthesis, electrochemistry and *in situ* spectroelectrochemistry of a new Co(III) thio Schiff-base complex with *N*,*N*′-bis(2-aminothiophenol)-1,4-bis(carboxylidene phenoxy)butane

A new cobalt Schiff-base complex, [Co(L)(OH)(H_2O)] (where L = [*N*,*N*′-bis(2-aminothiophenol)-1,4-bis(carboxylidene phenoxy)-butane), was synthesized and its electrochemical and spectroelectrochemical properties were investigated using cyclic voltammetry (CV), differential pulse voltammetry (DPV) and thin-layer spectro-electrochemistry in solutions of dimethyl sulfoxide (DMSO) and dichloromethane (CH_2Cl_2).

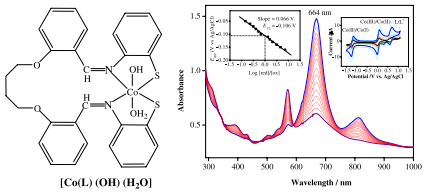

George Psomas, Alketa Tarushi and Eleni K. Efthimiadou

Polyhedron 27 (2008) 133

Synthesis, characterization and DNA-binding of the mononuclear dioxouranium(VI) complex with ciprofloxacin

The synthesis, characterization and interaction with calf-thymus DNA of the neutral mononuclear dioxouranium(VI) complex with the second-generation quinolone antibacterial agent ciprofloxacin are presented.

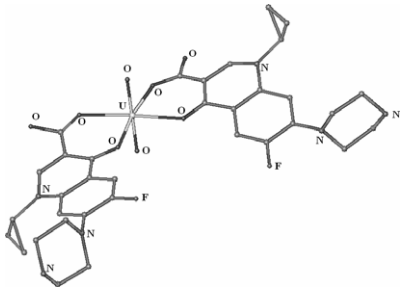

Moutusi Dasgupta, Sumon Nag, Gopal Das, Munirathinam Nethaji and Samaresh Bhattacharya

Polyhedron 27 (2008) 139

N,*N*′-Bis(aryl)pyridine-2,6-dicarboxamide complexes of ruthenium: Synthesis, structure and redox properties

Reaction of five *N*,*N*′-bis(aryl)pyridine-2,6-dicarboxamides (**1**) with [Ru(trpy)Cl_3](trpy = 2,2′,2″-terpyridine) in refluxing ethanol in the presence of triethylamine afforded a group of complexes of the type [Ru^{II}(trpy)(L-R)] (**2**, *n* = 0), which upon constant potential coulometric oxidation produced the corresponding [Ru^{III}(trpy)(L-R)]$^+$ complexes (**2**, *n* = 1), which have been isolated as the perchlorate salts.

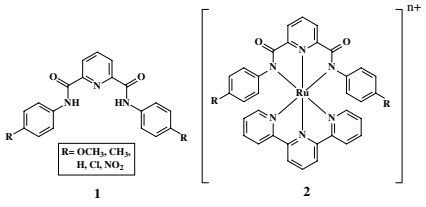

Matthias Linnert, Clemens Bruhn, Harry Schmidt, Renate Herzog and Dirk Steinborn

Polyhedron 27 (2008) 151

Synthesis, structure and characterization of [Mg_7(μ_3-OCH_2CH_2OMe)$_6$(μ-OCH_2CH_2OMe)$_6$]-[Al(*n*-Bu)$_4$]$_2$ – A cationic heptanuclear magnesium complex consisting of discrete cations and tetrabutylaluminate anions

Crystals of the title complex were found to consist of discrete heptanuclear magnesium complex cations built up from seven edge-shared MgO_6 octahedra (**I**) and [Al(*n*-Bu)$_4$]$^-$ anions (**II**). ^{1}H, ^{13}C and ^{27}Al NMR spectroscopic measurements showed that in THF solution the structures both of the cations and anions are preserved and that there are no cation–anion interactions reducing their symmetry (δ_{Al} = 151.6, $w_{1/2}$ = 5 Hz; $^1J(^{27}Al,^{13}C)$ = 72.3 Hz).

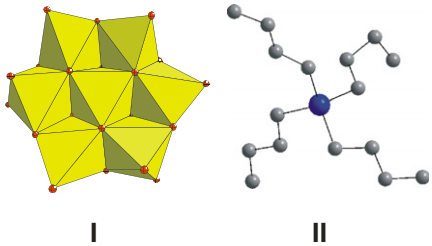

K. Naresh Kumar, G. Venkatachalam, R. Ramesh and Y. Liu

Polyhedron 27 (2008) 157

Half-sandwich *para*-cymene ruthenium(II) naphthylazophenolato complexes: Synthesis, molecular structure, light emission, redox behavior and catalytic oxidation properties

Five half-sandwich organoruthenium(II) naphthylazo phenolate complexes have been synthesized and characterized. All the complexes show luminescent property in the visible region. Complex **2** was structurally characterized by X-ray crystallography and was used as an efficient catalyst for oxidation of a range of primary and secondary alcohols in the presence of NMO.

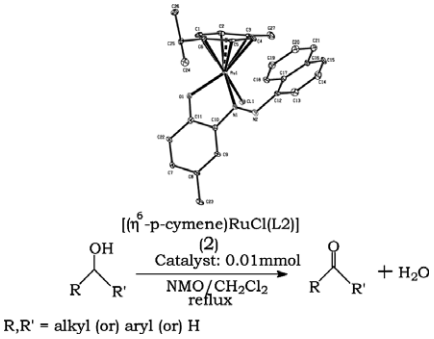

Vladimir B. Golovko, Martin J. Mays and Gregory A. Solan

Polyhedron 27 (2008) 167

Self-cyclisation versus diynediol-promoted ring closure during the construction of co-ordinated crown-type macrocycles

The ability of butyne-1,4-diol-$Co_2(CO)_6$ (**1a**) to undergo self-cyclisation reactions under acidic conditions to give both dimeric and trimeric crown-type macrocycles has been demonstrated; incorporation of a rigid 1,3-diyne unit into the macrocycle formed during self-reaction of **1a** is also reported.

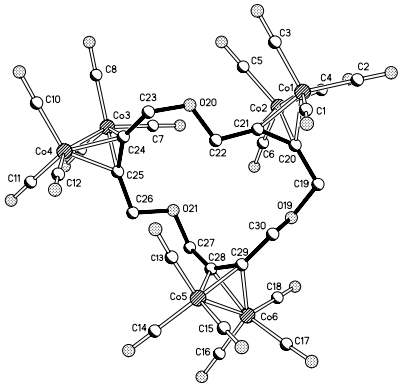

M. Mamais, P.J. Cox and P. Aslanidis

Polyhedron 27 (2008) 175

Three- and four-coordinate copper(I) halide complexes of 2-(diphenylphosphano)benzaldehyde: Dimerization induced by thione-S ligation

The coordination of 2-(diphenylphosphano)-benzaldehyde (PCHO) to copper(I) halides leads to the formation of trigonal planar complexes of type $[CuX(PCHO)_2]$ with the phosphane acting as a monodentate via the P atom. These complexes react with pyridine-2-thione or pyrimidine-2 thione forming dimeric species of type $[CuX(PCHO)(thione)]_2$ in which the two Cu^I centres are doubly bridged by thione-S atoms. The crystal structures of three examples of the novel complexes have been characterized by X-ray crystallography.

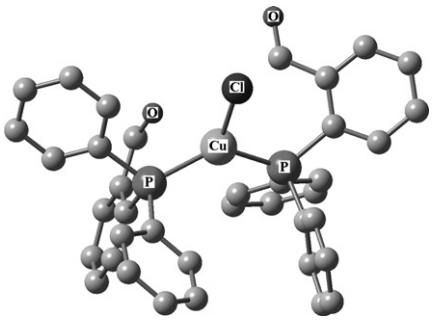

Angad Kumar Singh, Sanyucta Kumari, K. Ravi Kumar, B. Sridhar and T.R. Rao

Polyhedron 27 (2008) 181

Synthesis and spectral studies of the mesogenic Schiff-base, *N*,*N*′-di-(4′-pentyloxybenzoate) salicylidene-1,8-diamino-3,6-dioxaoctane and crystal structure of the Zn(II) complex

A novel Schiff-base, *N*,*N*′-di-(4′-pentyloxy-benzoate)salicylidene-1,8-diamino-3,6-dioxa-octane (H_2L_4) with the mesogenic phase, *nematic droplets*, was prepared and its structure studied by mass, NMR and IR spectra. The Schiff base reacts with Zn(II) as a di-negative tetra-dentate species, giving rise to a non-mesogenic tetrahedral complex, $[ZnL_4]$. The complex crystallizes in monoclinic $P2_1/n$ which possesses screw axis and *n*-glide and also inherent twofold axis by the combination of these two symmetry operations. Considerable torsion has been observed between benzoate ring and salicylaldimine ring on either side of the metal atom.

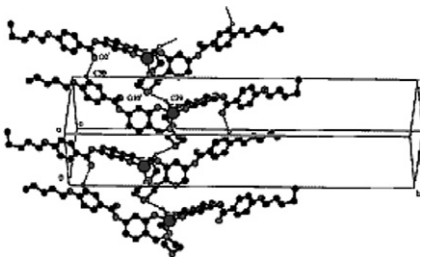

B. Machura and J. Kusz

Polyhedron 27 (2008) 187

Synthesis, spectroscopic characterisation, crystal and molecular structure of [ReOBr-(quin-2-c)$_2$] and [ReOCl(quin-2-c)$_2$] complexes: DFT and TD-DFT calculations for [ReOBr(quin-2-c)$_2$]

Novel [ReOX(quin-2-c)$_2$] complexes (X = Cl, Br; quin-2-c = quinoline-2-carboxylate ion) have been prepared by treatment of [ReOX$_3$-(AsPh$_3$)$_2$] with an excess of quinoline-2-carboxylic acid in acetonitrile. The complexes were characterised structurally and spectroscopically. The electronic structure of [ReOBr(quin-2-c)$_2$] has been calculated with the density functional theory (DFT) method, and additional information about binding has been obtained by NBO analysis. The TD-DFT/PCM calculations have been employed to produce a hundred of singlet excited-states, and UV–Vis spectrum of the [ReOBr(quin-2-c)$_2$] has been discussed on this basis.

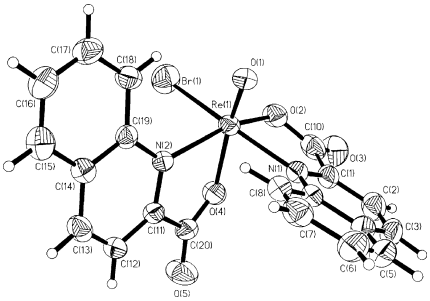

Feyyaz Durap, Nermin Biricik, Bahattin Gümgüm, Saim Özkar, Wee Han Ang, Zhaofu Fei and Rosario Scopelliti

Polyhedron 27 (2008) 196

Synthesis and characterizations of *N*,*N*-bis-(diphenylphosphino)ethylaniline derivatives and X-ray crystal structure of palladium (II), platinum (II) complexes

Transition metal complexes (Cu, Pd, Pt) and chalcogenides of N,N-bis(diphenylphosphino)ethylaniline derivatives have been synthesized and characterized.

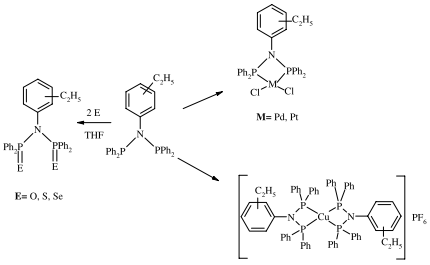

Xiao-Qing Shen, Hong-Chang Yao, Rui Yang, Zhong-Jun Li, Hong-Yun Zhang, Ben-Lai Wu and Hong-Wei Hou

Polyhedron 27 (2008) 203

Synthesis, structure and thermal properties of polynuclear complexes with a new multidentate ligand, *N*,*N*′-bis(5-ethyl-1,3,4-thiadiazol-2-yl)-2,6-pyridinedicarboxamide

Three polynuclear complexes based on *N*,*N*′-bis(5-ethyl-1,3,4-thiadiazol-2-yl)-2,6-pyridinedicarboxamide and inorganic Zn^{II} and Cd^{II} salts were prepared and their structures were characterized by single-crystal X-ray analysis. The thermal stabilities of all the complexes and the thermal decomposition kinetics of complex **2** have been studied.

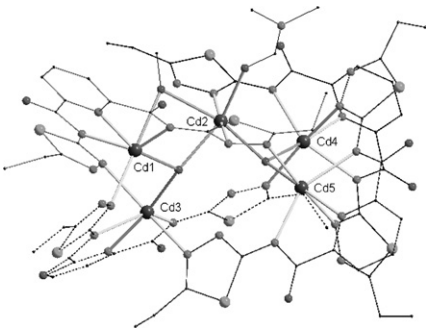

Marijana Đaković, Zora Popović, Gerald Giester and Maša Rajić-Linarić

Polyhedron 27 (2008) 210

Thiocyanate complexes of the group 12 metals with pyridine-2-carboxamide: Synthesis and structural characterization

The three new heteroleptic thiocyanato complexes of zinc(II) (**1**), cadmium(II) (**2**) and mercury(II) (**3**) with picolinamide (pia) have been prepared, and their structures determined by X-ray crystallography. In all cases pia acts as a chelating ligand. Compound **1** forms two polymorphs of monomeric [Zn(SCN)$_2$(pia)$_2$] units. The structure of compound **2** comprises of polymeric [Cd(SCN)$_2$(pia)]$_n$ and compound **3** of dimeric [Hg(SCN)$_2$(pia)]$_2$ units.

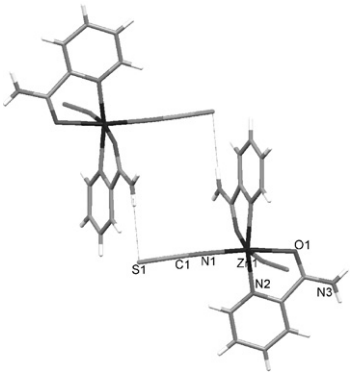

Ahmet Karadağ, İbrahim Önal, Ayşegül Şenocak, İbrahim Uçar, Ahmet Bulut and Orhan Büyükgüngör

Polyhedron 27 (2008) 223

Syntheses, IR spectra, thermal properties and crystal structures of novel cyano-bridged polymeric complexes of zinc^{II} and cadmium^{II} with tetracyanoplatinate^{II}

Using Zn(*hydeten*)$_2^{2+}$ or Cd(*hydeten*)$_2^{2+}$ as bricks and $[Pt(CN)_4]^{2-}$ anion as mortar, the novel binuclear one dimensional polymeric complexes **1** and **2** were prepared, and their structures were determined.

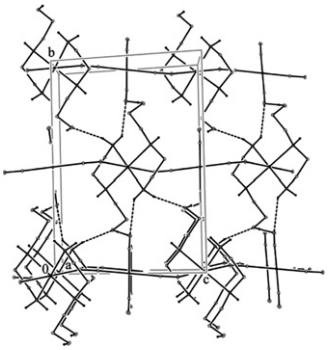

Zhi-Hua Li, Ping Lin and Shao-Wu Du

Polyhedron 27 (2008) 232

Syntheses and characterization of three novel W(Mo)/Cu/S cluster-based layered polymers with 1,3,4-thiadiazole-2,5-dithiolate (SSS): Intriguing coordination modes of SSS

Three novel 2D layered polymers, namely, $[Et_4N][WS_{3.5}O_{0.5}Cu_3(CN)_{0.5}(SSSH_{0.5})]$ (**1**), $[Et_4N][WS_4Cu_3(SSS)]$ (**2**) and $[Et_4N]_2[MoS_4Cu_4(CN)(SSSH_{0.5})_2]$ (**3**) have been prepared by solvothermal reactions of H_2SSS (H_2SSS = 1,3,4-thiadiazole-2,5-dithiolate) with CuCN and $[WOS_3CuCN]^{2-}$ or $[W(Mo)S_4]^{2-}$ in organic solvents. In these complexes, the nest-shaped $\{WS(O)S_3Cu_3\}$ core in **1**, the T-shaped $\{WS_4Cu_3\}$ core in **2** and the saddle-shaped $\{MoS_4Cu_4\}$ subunit in **3** serve as metal nodes whereas the SSS ligands function as multidentate linkers. The SSS ligand in both **1** and **2** coordinates to five Cu atoms via its exocyclic sulfur and endocyclic nitrogen atoms in an unprecedented fashion, while in **3**, it acts as a rare tridentate ligand to connect three Cu atoms. Complexes **1**–**3** show optical transitions with band gaps of 1.90–2.24 eV.

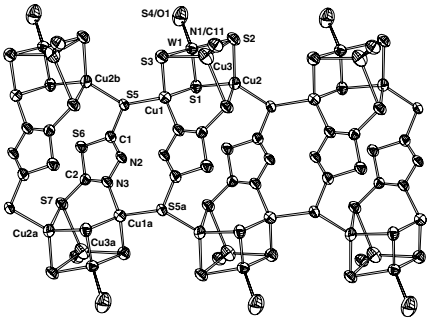

Part of the double chain in the anion of **1**

Niraj Kumari, Rishikesh Prajapati and Lallan Mishra

Polyhedron 27 (2008) 241

Reactivity of M(en)Cl_2 (M = Pd^{II}/Pt^{II}, en = 1,2-diaminoethane) with *N*,*N*′-bis(salicylidene)-*p*-phenylenediamine: Binding with hexafluorobenzene

The tetradentate Schiff base *N*,*N*′-bis(salicylidene)-*p*-phenylenediamine upon its complexation with Pd(en)Cl_2 and Pt(en)Cl_2 provides two different products. In the case of the Pt^{II} complex, (2 + 2) condensation provides a metallocyclophane which is found to bindan electron acceptor molecule like hexafluorobenzene, as monitored spectroscopically.

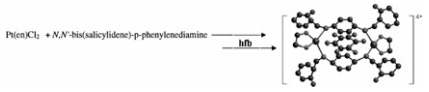

Hassan Hadadzadeh, S. Jamil A. Fatemi, Seyedeh Raziyeh Hosseinian, Hamid Reza Khavasi and Rainer Pöttgen

Polyhedron 27 (2008) 249

Synthesis, structure, spectroscopic, magnetic and electrochemical studies of a rare *syn–anti* acetate-bridged copper(II) complex

The structure, spectroscopy and electrochemical properties of a novel dinuclear copper(II) complex, $[\{Cu(phen)_2\}_2(\mu\text{-}CH_3COO)][PF_6]_3$, is reported. The crystal structure contains two independent Cu(II) ions with different geometries around each copper center which are bridged by an acetate anion. The acetate bridging ligand between the two Cu(II) centers shows a *syn–anti* coordination mode with a trigonal bipyramidal geometry for the Cu(1) center and a distorted square-based pyramidal geometry for the Cu(2) center.

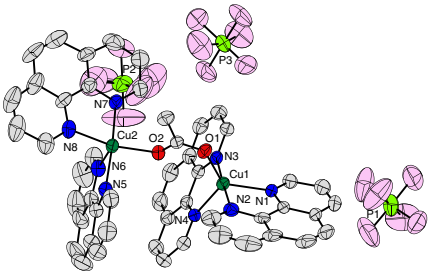

Vadapalli Chandrasekhar, Balasubramanian Murugesa Pandian and Ramachandran Azhakar

Polyhedron 27 (2008) 255

Synthesis, structure and metallation of spiro-$N_3P_3(O_2C_{12}H_8)(OC_5H_4N\text{-}2)_4$: A heptacoordinate Co(II) in the molecular structure of $N_3P_3(O_2C_{12}H_8)(OC_5H_4N\text{-}2)_4 \cdot Co(NO_3)_2$

Spiro-$N_3P_3(O_2C_{12}H_8)(OC_5H_4N\text{-}2)_4$ (**L**) is an efficient multi-site coordination ligand which binds with transition metal ions to afford the mononuclear complexes $[LCu(NO_3)_2]$, $[LCo(NO_3)_2]$ and $[LZnCl_2]$. The ligand **L** shows diverse coordination behavior towards these metal ions.

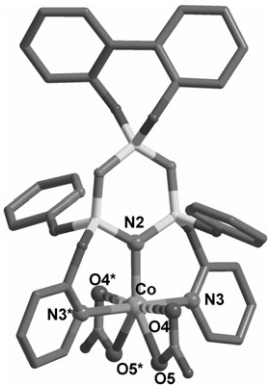

Susan A. Bourne and Lesego J. Moitsheki

Polyhedron 27 (2008) 263

Hybrid inorganic–organic layered structures of $[AuCl_4]^-$ and protonated bipyridyl derivatives

Complexes of $[AuCl_4]^-$ with 4,4′-dipyridylethane, 4,4′-dipyridylethene and 4,4′-bipyridine-*N*,*N*′-dioxide form hybrid organic–inorganic layered structures. The dipyridyl derivatives are stabilized by N–H···Cl and Au···Cl interactions. In the complex with and 4,4′-bipyridine-*N*,*N*′-dioxide the organic layers consist of hydrogen-bonded bipyridyldioxide cations, with a short O–H···O contact.

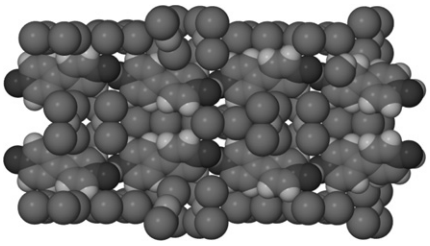

Pavel Drabina, Petr Valenta, Petr Jansa, Aleš Růžička, Jiří Hanusek and Miloš Sedlák

Polyhedron 27 (2008) 268

Copper(II) complexes derived from substituted 2,2′-bis-(4-isopropyl-4-methyl-4,5-dihydro-1*H*-imidazol-5-one) ligands: Synthesis, structure and catalytic activity

New chiral *N*,*N*-bidentate ligands derived from substituted 2,2′-bis-(4-isopropyl-4-methyl-4,5-dihydro-1*H*-imidazol-5-one) have been prepared and characterised by means of ^1H and ^{13}C NMR spectroscopy and optical rotation. Their Cu(II) complexes have been prepared and their structures have been studied by computational methods and by X-ray diffraction. The catalytic activity of some complexes have been studied.

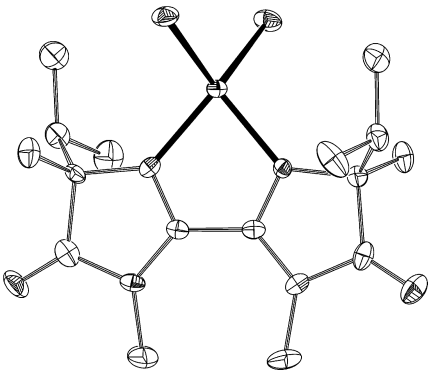

E. Manoj and M.R. Prathapachandra Kurup

Polyhedron 27 (2008) 275

Structural and spectral studies of nickel(II) complexes with *N*(4),*N*(4)-(butane-1,4-diyl) thiosemicarbazones

Nickel(II) complexes of quinoline-2-carbaldehyde *N*(4),*N*(4)-(butane-1,4-diyl) thiosemicarbazone (HL^1) and 2-benzoylpyridine *N*(4),*N*(4)-(butane-1,4-diyl) thiosemicarbazone (HL^2) were synthesized and physico-chemically characterized by means of partial elemental analyses, molar conductance measurements, magnetic measurements, electronic and infrared spectral studies. Three complexes were given the formulae $[Ni(HL^1)_2]Cl_2$ (**1**), $[Ni(HL^2)L^2]ClO_4 \cdot 7H_2O$ (**2**) and $[NiL^2Cl] \cdot 0.5H_2O$ (**3**). The structure of compound **1** has been solved by single crystal X-ray crystallography and is found to be distorted octahedral. Compound **2**, when crystallized in DMSO solution, got deprotonated to form a new compound $[Ni(L^2)_2]$ (**2a**), with a distorted octahedral Ni(II) center. In compound **1**, HL^1 coordinates to the metal in the thione form, while in compounds **2a** and **3**, HL^2 coordinates in its deprotonated thiolate form.

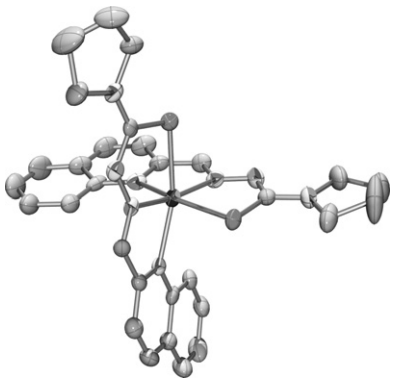

Zdenek Spichal, Vaclav Petricek, Jiri Pinkas and Marek Necas

Polyhedron 27 (2008) 283

Two-dimensional lanthanide coordination polymers with bis(diphenylphosphino)hexane dioxide. The determination of the polymeric structure from twinned crystals

Lanthanide salts and bis(diphenylphosphino)hexane dioxide ($dpphO_2$) formed under solvothermal conditions coordination polymers $[Ln(dpphO_2)_2(NO_3)_2](NO_3)$ and $[Ln(dpphO_2)_2Cl_2]Cl$, featuring two-dimensional network structures of the (4, 4) topology. The solution and refinement of the structures of the nitrate compounds was based on the data obtained on pseudo-merohedrally twinned crystals.

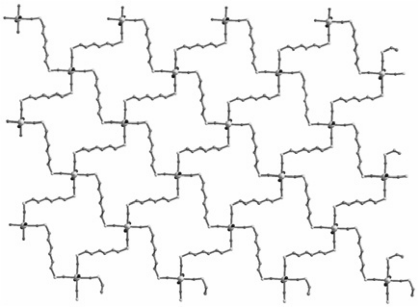

Athanassios C. Tsipis and Paraskevas A. Karipidis

Polyhedron 27 (2008) 289

Deciphering the bonding mode of the trihalide ligands in a series of halogen carrier homo- and hetero-trihalide Cu(II) Schiff base complexes

The molecular and electronic structure of the $[Cu(RdienR)(X)(XY_2)]$ complexes and their $[Cu(RdienR)(X)_2]$ precursors were analyzed in terms of charge decomposition analysis (CDA), natural bond orbital (NBO) population analysis, and percentage compositions of molecular orbitals in order to understand the nature of the bonding between the $[XY_2]^-$ ligands and the Cu(II) central metal ion, and unveil the effect of coordination on the bonding mechanism in the coordinated $[XY_2]^-$ ligands in comparison to that of the "free" $[XY_2]^-$ anions.

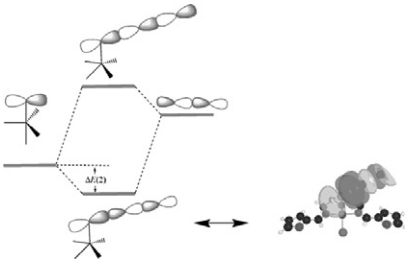

Jung Hak Lim, Houng Sik Yoo, Jung Hee Yoon, Eui Kwan Koh, Hyoung Chan Kim and Chang Seop Hong

Polyhedron 27 (2008) 299

Structure and magnetic properties of cyanide-bridged $Ni^{II}_9Mo^{V}_6$ cluster modified by bidentate capping ligands

A cyanide-bridged Ni_9Mo_6 cluster (**1**) capped with chelating bidentate ligands was prepared by self-assembling $[Mo(CN)_8]^{3-}$, Ni^{2+}, and bpy in a stoichiometric ratio. Compound **1** crystallized in the triclinic system with space group $P\bar{1}$ shows a body-centered Ni cube capped with six Mo entities. The non-covalent π–π stackings present in **1** lead to the extension of the molecule to a 2D sheet. Magnetic data exhibit that intracluster ferromagnetic interactions in **1** arise through the CN linkage coupled with zero-field splitting of the ground state.

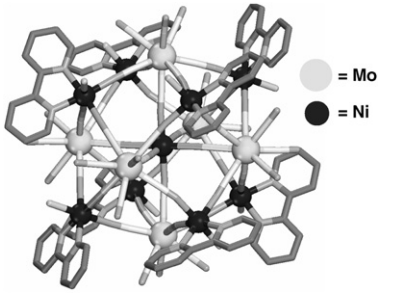

Sujittra Youngme, Jaturong Phatchimkun, Nanthawat Wannarit, Narongsak Chaichit, Siwaporn Meejoo, Gerard A. van Albada and Jan Reedijk

Polyhedron 27 (2008) 304

New ferromagnetic dinuclear triply-bridged copper(II) compounds containing carboxylato bridges: Synthesis, X-ray structure and magnetic properties

Six new triply-bridged dinuclear copper(II) complexes containing carboxylato bridges have been reported and their magnetic properties studied. A structural classification of this type of dimers has been performed, based on the local five-coordinate geometry with different degrees of distortion and the relative arrangement of the two basal planes, giving rise to different classes (A–F) of complexes. The most logical explanations have been made for each class describing different magnetic interactions. Practically, the correlations between structural data and *J* values are found for some classes of complexes. Extended Hückel calculations were preformed for class B complexes, the results are found to be useful for the proper interpretation and correlation of the magnetic data and dimer structure of the present complexes.

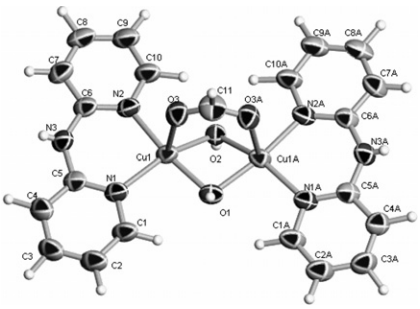

Jong Hwa Jeong, Young Hun An, Youn K. Kang, Quang Trung Nguyen, Hyosun Lee and Bruce M. Novak

Polyhedron 27 (2008) 319

Synthesis of polylactide using a zinc complex containing (*S*)-*N*-ethyl-*N*-phenyl-2-pyrrolidinemethanamine

The reaction between $ZnCl_2$ and (*S*)-*N*-ethyl-*N*-phenyl-2-pyrrolidinemethanamine (***S*-EPP**) as a chiral ligand affords [**$ZnCl_2$(*S*-EPP)**], whose structure has been determined by X-ray crystallography. [**$ZnEt_2$(*S*-EPP)**] has demonstrated high activity towards the polymerization of *rac*-lactide with a maximum turnover frequency (TOF) of 121. The observed heterotacticity was limited to under 0.6.

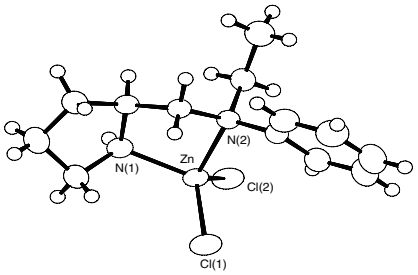

Yan Z. Voloshin, Oleg A. Varzatskii, Alexander S. Belov, Zoya A. Starikova, Alexander V. Dolganov and Tatiana V. Magdesieva

Polyhedron 27 (2008) 325

New antimony-capped iron(II) and cobalt(III) clathrochelate precursors of the polytopic hybrid cage complexes: Synthesis, X-ray structures and electrochemistry

Template macrocyclization on the iron(II) ion and the capping of K_3CoDm_3 complex with triethylantimony(V) derivatives afforded the triethylantimony-capped iron(II) and cobalt(III) tris-dimethylglyoximates, characterized using elemental analysis, mass, IR, UV–Vis, ^{57}Fe Mössbauer, NMR spectroscopies, and X-ray crystallography. The cyclic voltammograms show oxidation and reduction waves assignable to $Fe^{2+/3+}$ and $Co^{2+/3+}$ couples.

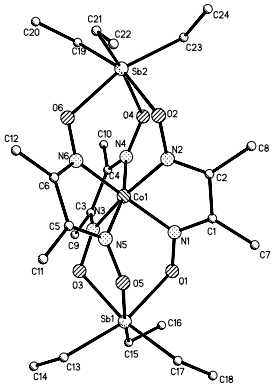

Eulália Pereira, Lígia R. Gomes, John N. Low and Baltazar de Castro

Polyhedron 27 (2008) 335

Synthesis, spectroscopic, electrochemical and structural characterization of Cu(II) complexes with asymmetric NN′OS coordination spheres

Copper Schiff base complexes with N2OS coordination spheres were synthesized and characterized electrochemically and by EPR spectroscopy. The molecular and the crystal structure have been determined by X-ray diffractometry.

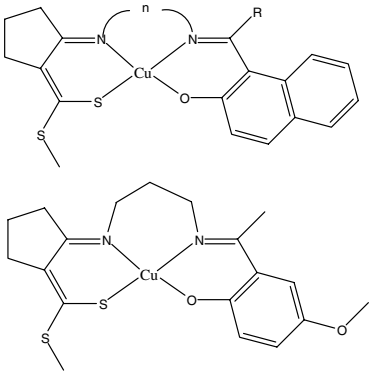

Ze-Li Yuan, Qi-Long Zhang, Xue Liang, Bi-Xue Zhu, Leonard F. Lindoy and Gang Wei

Polyhedron 27 (2008) 344

A new series of dinucleating macrocyclic ligands and their complexes of zinc(II)

The metal template synthesis of a new category of dinucleating macrocyclic Schiff base ligands with ring sizes from 34- to 52-membered and their interaction with zinc(II) are reported.

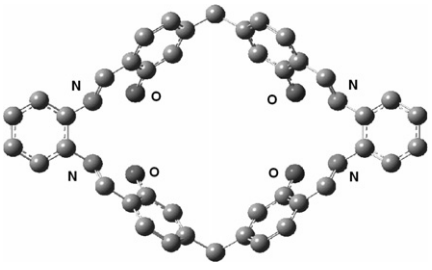

Eleni K. Efthimiadou, Alexandra Karaliota and George Psomas

Polyhedron 27 (2008) 349

Mononuclear dioxomolybdenum(VI) complexes with the quinolones enrofloxacin and sparfloxacin: Synthesis, structure, antibacterial activity and interaction with DNA

The synthesis, the characterization, the antibacterial activity and the interaction with calf-thymus DNA of the neutral mononuclear dioxomolybdenum(VI) complexes with the quinolone antibacterial agents enrofloxacin and sparfloxacin are presented.

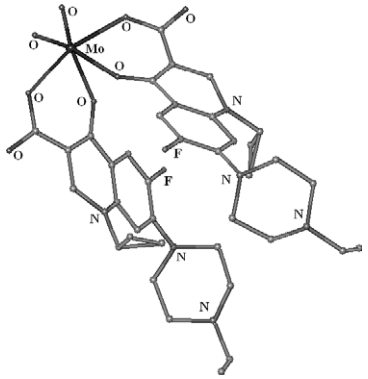

Sachindranath Pal, Anil Kumar Barik, Samik Gupta, Somnath Roy, Tarak Nath Mandal, Arijit Hazra, Mohamed Salah El Fallah, Ray J. Butcher, Shie-Ming Peng, Gene-Hsiang. Lee and Susanta Kumar Kar

Polyhedron 27 (2008) 357

Anion dependent formation of linear trinuclear mixed valance cobalt(III/II/III) complexes and mononuclear cobalt(III) complexes of a pyrazole derived ligand – Synthesis, characterization and X-ray structures

Co(II) mediated anion dependent Schiff base complex formation was studied. Depending upon the proportion of 5-methylpyrazole-3-carbaldehyde (MPA), 1,3-diamino-2-propanol (DAP) and metal salts with different anions, two trinuclear linear pyrazolate bridged mixed valence Co(III/II/III) complexes and a few mononuclear Co(III) complexes were characterized.

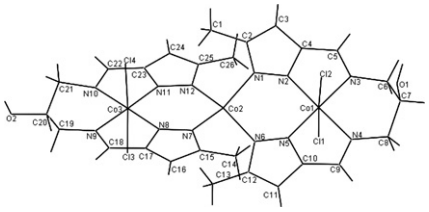

B. Machura and J. Kusz

Polyhedron 27 (2008) 366

Reactivity of oxorhenium(V) complexes towards 8-hydroxyquinoline-2-carboxylic acid: X-ray structure of $[ReOCl_2(hquin\text{-}2\text{-}COOH)(AsPh_3)] \cdot MeCN$ and $[ReOCl_2(hquin\text{-}2\text{-}COOH)(PPh_3)] \cdot MeCN$ complexes. DFT and TDDFT calculations for $[ReOCl_2(hquin\text{-}2\text{-}COOH)(AsPh_3)]$

The reactions of $[ReOX_3(EPh_3)_2]$ with 8-hydroxyquinoline-2-carboxylic acid (Hhquin-2-COOH) have been examined and $[ReOX_2(hquin\text{-}2\text{-}COOH)(EPh_3)] \cdot MeCN$ (X = Cl, Br; E = As, P) complexes have been obtained. All the complexes were characterised by IR, UV–Vis spectroscopy and elemental analysis. The crystal and molecular structures have been determined for $[ReOCl_2(hquin\text{-}2\text{-}COOH)(AsPh_3)] \cdot MeCN$ and $[ReOCl_2(hquin\text{-}2\text{-}COOH)(PPh_3)] \cdot MeCN$. The electronic structure of $[ReOCl_2(hquin\text{-}2\text{-}COOH)(AsPh_3)]$ has been calculated with the density functional theory (DFT) method, and TDDFT calculations have been employed to produce a hundred of singlet excited-states starting from the ground-state geometry optimized in the gas phase.

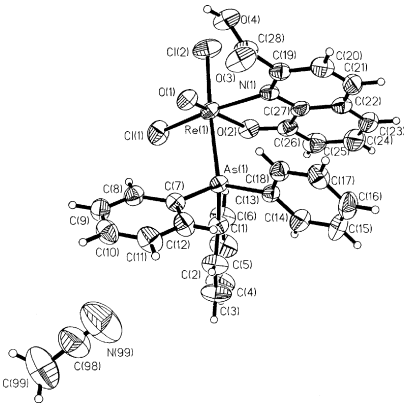

Nand K. Singh, Mamata Singh, Pratibha Tripathi, Ajay K. Srivastava and Ray J. Butcher

Polyhedron 27 (2008) 375

Synthesis of a new *N*,*N*′-ethane-1,2-bis-(4-methoxyphenyl)carbothioamide ligand and its Cu(I) and Ag(I) complexes

Complexes $[M(H_2L)(PPh_3)_2]NO_3 \cdot 0.5H_2O$, (M = Cu, Ag) formed with *N*, *N*′-ethane-1,2-bis(4-methoxyphenyl)carbothioamide (H_2L) have MS_2P_2 coordination and the ligand is bonded through the sulfur atoms forming a nine-membered chelate ring. The molecular packing in the copper(I) complex is dominated by hydrogen bonding offered by the NO_3^- ion and the basal plane of the CuS_2 chelate ring. The specific arrangement of two nitrate ions and two complex cations results in a rectangular shaped anionic channel.

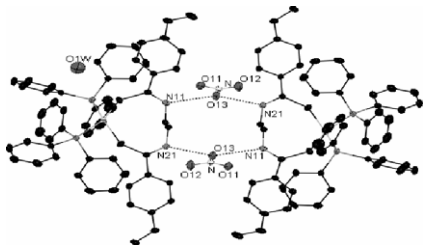

Richard J. Bushby, Colin Kilner, Norman Taylor and Rhidian A. Williams

Polyhedron 27 (2008) 383

Antiferromagnetic spin-coupling between Mn^{II} and amminium radical cation ligands: Models for coordination polymer magnets

A one-electron oxidation converts the triarylamine ligand of the complex $L_2Mn(hfac)_2$ (L = 4″,4‴-di-*tert*-butyl-2′,2″,2‴ trimethoxy-{4-(4′-diphenylaminophenyl)pyridine}) to the radical cation and gives an $S = 2$ system: $J/k_b = -1.5$ K. A two-electron oxidation converts both triarylamine ligands to the radical cation; $S = 3/2$: $J/k_b = -0.3$ K.

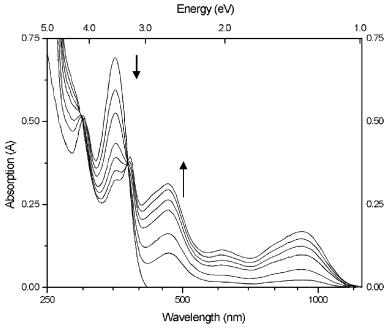

Agnieszka Mech

Polyhedron 27 (2008) 393

Crystal structure and optical properties of novel $(N(C_2H_5)_4)[Nd(hfa)_4(H_2O)]$ tetrakis complex

The novel $[Nd(hfa)_4(H_2O)](N(C_2H_5)_4)$ tetrakis complex has been synthesized and characterized using X-ray, DSC. An absorption spectrum of the single crystal were recorded and parameterized in terms of Judd-Ofelt theory.

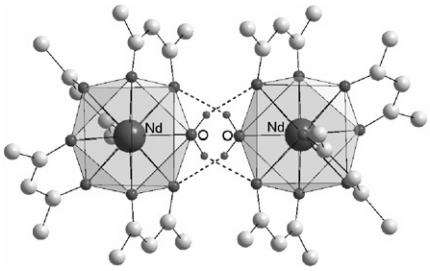

Zenixole R. Tshentu, Thomas I.A. Gerber, Ryan Walmsley and Peter Mayer

Polyhedron 27 (2008) 406

Imidazole-based bifunctional chelates for the "*fac*-$[Re(CO)_3]^+$" core

This paper presents the syntheses of tridentate bis-imidazole type ligands, and the study of their coordination chemistry with $[Re(OH_2)_3(CO)_3]Br$ or $(NEt_4)_2[ReBr_3(CO)_3]$ as Re(I) precursor compounds. Crystal structure evidence for one of the analogues shows that the tridentate ligand adopts a facial arrangement around the Re(I) ion, imposed by the *fac*-$[Re(CO)_3]^+$ core.

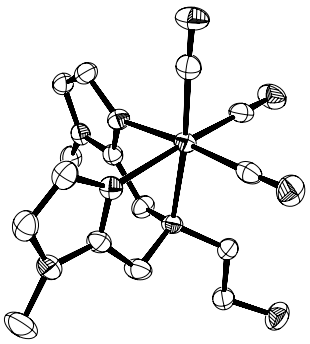

Zdeněk Trávníček, Richard Pastorek and Václav Slovák

Polyhedron 27 (2008) 411

Novel octahedral nickel(II) dithiocarbamates with bi- or tetradentate *N*-donor ligands: X-ray structures of $[Ni(Bzppzdtc)(phen)_2]ClO_4 \cdot CHCl_3$ and $[Ni(Bz_2dtc)_2(cyclam)]$

A series of novel octahedral nickel(II) dithiocarbamate complexes involving bidentate nitrogen-donor ligands (phen or bpy) or a tetradentate ligand (cyclam) of the composition $[Ni(BzMetdtc)(phen)_2]ClO_4$ (**1**), $[Ni(Pe_2dtc)(phen)_2]ClO_4$ (**2**), $[Ni(Bzppzdtc)(phen)_2]ClO_4 \cdot CHCl_3$ (**3**), $[Ni(Bzppzdtc)(phen)_2](SCN)$ (**4**), $[Ni(BzMetdtc)(bpy)_2]ClO_4 \cdot 2H_2O$ (**5**), $[Ni(Pe_2dtc)(cyclam)]ClO_4$ (**6**), $[Ni(BzMetdtc)_2(cyclam)]$ (**7**), $[Ni(Bz_2dtc)_2(cyclam)]$ (**8**) and $[Ni(Bz_2dtc)_2(phen)]$ (**9**) have been synthesized. Broad spectrum of physical techniques, including X-ray analysis of **3** and **8**, proved the octahedral geometry in the vicinity of the nickel atom in all cases. The catalytic influence of complexes **2**, **3**, **6**, and **7** on graphite oxidation was studied and discussed.

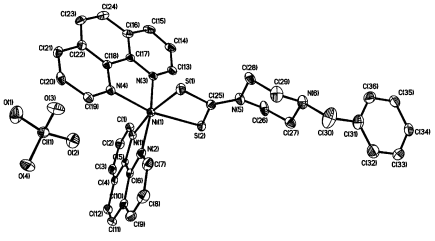

Chun-Lin Ma, Zhi-Fo Guo and Ru-Fen Zhang

Polyhedron 27 (2008) 420

Syntheses, characterizations and crystal structures of monomeric or macrocyclic compounds of di- or triorganotin (IV) moieties with 4,4′-thiodibenzenethiol

Six organotin compounds with 4,4′-thiodibenzenethiol (LH_2) of type $R_nSnL_{4-n}SnR_n$ (n = 3: R = Me **1**, Ph **2**, $PhCH_2$ **3**, n = 2: R = Me **4**, Ph **5**, $PhCH_2$ **6**) have been synthesized. All compounds were characterized by elemental analysis, IR and NMR (^1H, ^{13}C, ^{119}Sn) spectra. The structures of compounds **1**, **2**, **4**, **5** and **6** were also determined by X-ray diffraction analysis, which revealed that compounds **1** and **2** were monomeric structures, compounds **4**, **5** and **6** were centrosymmetric dinuclear macrocyclic structures, all the tin(IV) atoms are four-coordinated. Furthermore, supramolecular structures were also found in compounds **1**, **2**, **4**, **5** and **6**, which exist one-dimensional chains, two-dimensional networks or three-dimensional structure through intermolecular C–H···S weak hydrogen bonds (WHBs), non-bonded Sn···S interactions or C–H···π interactions.

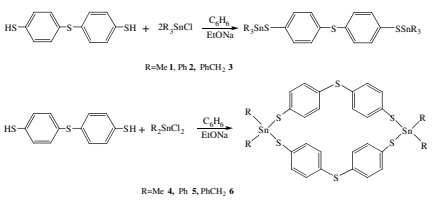

I.M. Ali, E.S. Zakaria, M.M. Ibrahim and I.M. El-Naggar

Polyhedron 27 (2008) 429

Synthesis, structure, dehydration transformations and ion exchange characteristics of iron-silicate with various Si and Fe contents as mixed oxides

Iron silicate was obtained from iron oxide impregnated with silica in different Fe/Si molar ratios. Kinetics of dehydration transformation indicated a 1st order process for different silicate ratios. Application of the materials as ion exchangers showed a high affinity for ions of different charges on increasing the solution pH as well as with the silica content increasing.

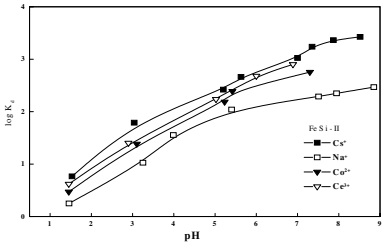

Tülay Bal-Demirci

Polyhedron 27 (2008) 440

Synthesis, spectral characterization of the zinc(II) mixed-ligand complexes of *N*(4)-allyl thiosemicarbazones and *N*,*N*,*N*′,*N*′-tetramethylethylenediamine, and crystal structure of the novel [ZnL_2(*tmen*)] compound

Mixed-ligand zinc complexes with *N*,*N*,*N*,*N*′-tetramethylethylenediamine (*tmen*) and R-salicylaldehyde N(4)-allyl thiosemicarbazones (R: 3-OCH_3 (L_1), 5-Br(L_2)), [$ZnL_{1,2}$(*tmen*)], were synthesized and the complexes were characterized by elemental, spectral and single crystal analysis. Crystal of [ZnL_2(*tmen*)] have a slightly distorted square pyramid involving O, N, S atoms of thiosemicarbazone and one N atom of *tmen* in basal plane and the other N atom of *tmen* in apex of the pyramid. The non-coordinated allyl group is disordered.

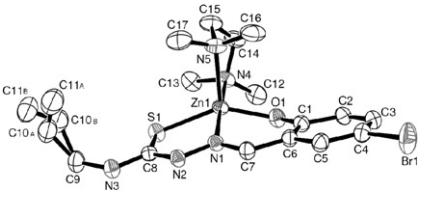

Dohyun Moon, Junghyun Kim, Minhak Oh, Byoung Jin Suh and Myoung Soo Lah

Polyhedron 27 (2008) 447

Synthesis and characterization of a bis-μ,η^1-carboxylate-bridged dinuclear manganese(II) complex containing a tetradentate tripodal ligand, *N*-(benzimidazol-2-ylmethyl)iminodiacetic acid

A dinuclear manganese(II) complex has been prepared using a tripodal ligand, where the complex mimics several important structural features of the manganese arginase core, such as the simultaneous presence of both μ,η^1 bridging carboxylate and non-bridging monodentate carboxylate binding modes, and an intramolecular hydrogen bond involving a coordinated water molecule.

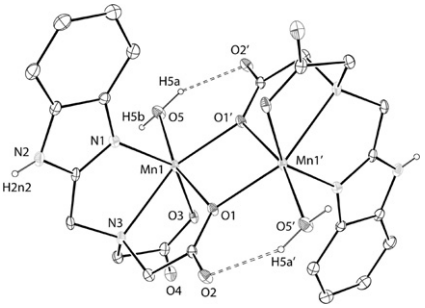

Sebusi Odisitse and Graham E. Jackson

Polyhedron 27 (2008) 453

In vitro and *in vivo* studies of *N*,*N*′-bis[2-(2-pyridyl)-methyl]pyridine-2,6-dicarboxamide–copper(II) and rheumatoid arthritis

Copper complexes of *N*,*N*′-bis[2(2-pyridyl)-methyl]pyridine-2,6-dicarboxamide have been evaluated as potential anti-inflammatory agents using potentiometry, biophysical measurements and animal studies.

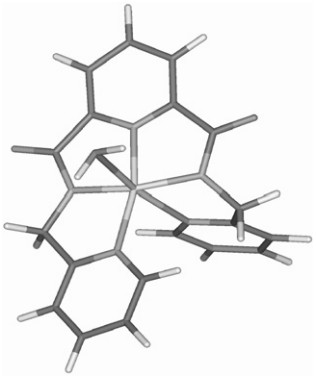

Marijana Đaković, Zora Popović, Gerald Giester and Maša Rajić-Linarić

Polyhedron 27 (2008) 465

Synthesis, spectroscopic and structural investigation of $Zn(NCS)_2(nicotinamide)_2$ and $[Hg(SCN)_2(nicotinamide)]_n$

The nicotinamido (nia) complexes of the thiocyanates of zinc (**1**) and mercury(II) (**2**) were prepared and spectroscopically and thermally characterized, and their structures were determined by X-ray crystallography. The nia ligand acts as a monodentate ligand through the pyridine nitrogen. Compound **1** comprises of monomeric $[Zn(SCN)_2(nia)_2]$, while compound **2** of polymeric $[Hg(SCN)_2(nia)]_n$ units. Centrosymmetric H-bond dimers of $R_2^2(10)$ type in **1** and of $R_2^2(8)$ type in **2** are formed.

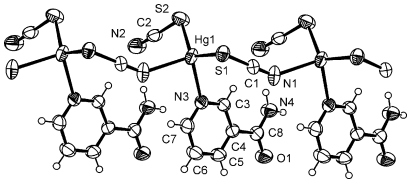

Corrigendum to "Three novel trinuclear zinc(II)/nickel(II) complexes with pentadentate ligands *N*-nitrobenzoylsalicylhydrazidate" [Polyhedron 26 (2007) 4793–4798]. 473

The Publisher encourages the submission of articles in electronic form thus saving time and avoiding rekeying errors. For detailed instructions on the preparation of manuscripts and of electronic artwork, consult the Author Gateway for Elsevier at http://authors.elsevier.com

ScienceDirect

Full text of this journal is available, on-line from **ScienceDirect**. Visit **www.sciencedirect.com** for more information.